THE 43rd ASMS CONFERENCE ON MASS SPECTROMETRY AND ALLIED TOPICS
May 21 - 26, 1995
TABLE OF CONTENTS

INTRODUCTION iii

ASMS BOARD OF DIRECTORS iii

ASMS INTEREST GROUP COORDINATORS iii

ASMS COMMITTEES iv

ASMS LOCAL DISCUSSION GROUPS iv

ASMS CORPORATE MEMBERS v

LISTING OF EXTENDED ABSTRACT TITLES BY SESSION vii

ABSTRACTS

Monday Orals
- Recent Dev. in the Characterization of Aerosol Microparticles 1
- Computational & Exp. Approaches to Ion Thermochem. & Structure 10
- Mass Spectrometry of Polymers 18
- Electrospray Ionization - Applications 28
- Elemental and Isotopic Analysis 40

Monday Posters
- Ion Molecule Reactions 50
- Ion Sources & Mass Spectrometer Design 96
- Organic Analysis 141
- Environmental Analysis 180
- Spray Ionization 233
- Proteins & Peptides 268

Tuesday Orals
- Mass Spectrometry in Pharmacology & Toxicology 327
- Mass Spectrometry in Environmental Research 337
- Chemistry of Multiply-Charged Ions 347
- Laser Desorption Ionization - Applications 357
- Mechanisms of Ion-Molecule Reactions 367

Tuesday Posters
- Ion Activation and Dissociation 376
- Separations/MS Techniques 422
- Combinatorial Libraries 483
- Toxicology 495
- Drugs and Metabolism 518
- Nucleic Acids and Constituents 579

- Proteins and Peptides 610

Wednesday Orals
- New Approaches to Quantitative Mass Spectrometry 658
- Electrospray Ionization - Fundamentals 667
- Fourier Transform Mass Spectrometry 675
- Laser Desorption Ionization - Fundamentals 683
- Mass Spectrometry and the Earth's Atmosphere 693

Wednesday Posters
- Ion-Molecule Reactions 696
- Computer Applications 717
- Materials Characterization 745
- Inorganic, Elemental & Isotope Ratios 767
- Trapped Ions 782
- Environmental Analysis 815
- Drugs & Metabolism 849
- Spray Ionization 884
- Laser Desorption/Ionization 915

Thursday Orals
- Hydrogen Bonding Interactions 969
- Mass Spectrometry in Immunology 975
- Ion Trap Mass Spectrometry 983
- Time-of-Flight Mass Spectrometry 994
- Energy & Petrochemicals 1005
- Organohalogens: New Issues & Techniques 1015

Thursday Posters
- Fundamental Studies 1025
- Ion Source & Mass Spectrometer Design 1068
- Trapped Ions 1100
- Lipids 1142
- Carbohydrates 1164
- Laser Desorption/Ionization 1204
- Proteins & Peptides 1257

Friday Orals
- Metal Ion Chemistry 1305
- Hyphenated Chromatography/Mass Spectrometry 1311
- Good Laboratory Practices for Mass Spectrometry 1319
- Mass Spectrometry to Study Higher Order Structure 1325
- Surface-Induced Dissociation 1332

INDEX OF AUTHORS 1338

INDEX OF KEY WORDS 1350

WORKSHOP AND INTEREST GROUP MEETING REPORTS
LC/MS Workshop 1356
Ion Trap Workshop 1357
FTMS: "Most Recent Results in FTMS" 1358
Good Laboratory Practices (GLP) Workshop 1359
Elemental: "Comparison of Mass Analyzers for ICP & GD Ion Sources" 1360
Process MS: "On-Line MS for Process Control and Diagnostics: 1361
Desorption/Ionization: "Micro-Electrospray: Can Less Give More?" 1362
Computer Applications: "Validation of MS Data Systems" 1363
TOF: "Progress and Prospects for TOF Mass Spectrometry" 1364
Historical Interest Group 1365
Biomedical Applications: "Probing Biomolecular Non-covalent Interactions: Tricks and Traps" 1366

MINUTES OF THE ASMS BUSINESS MEETING 1367

43rd ASMS Conference on Mass Spectrometry and Allied Topics

INTRODUCTION

This volume represents the official record of the 1995 Annual ASMS Conference and is designated as the Proceedings of the 43rd Annual Conference on Mass Spectrometry and Allied Topics.

The 1995 ASMS Conference was held May 21 - 26, at the Marriott Marquis Hotel in Atlanta, Georgia. The total number of conference attendees was 2,307. There were 1,451 scientific presentations, consisting of 5 plenary lectures, 260 orals, 1,182 posters and 4 tutorial lectures, which were new this year and very well attended. Some of the highlights included the presentation of the 1995 ASMS Award for a Distinguished Contribution in Mass Spectrometry to Prof. Keith R. Jennings of the University of Warwick for his discovery of collision-induced dissociation. In addition, the 1995 ASMS and Corporate Donor Awards were presented to Prof. Kermit K. Murray of Emory University and to Prof. Lee Sunderlin of Northern Illinois University. The plenary lectures were all unique, thought-provoking and spanned a broad range of topics relevant to our science, from mass spectrometric drug testing of Olympic athletes to the "geek factor" of science in the media.

This volume contains extended abstracts that provide brief descriptions of the research presented at the conference. In addition, reports from workshops, interest groups and the annual ASMS business meeting are included.

Special thanks go to Veronica Bierbaum for arranging the excellent scientific program and to Judith Sjoberg and her staff of Professional Association Management for coordinating the printing and distribution of the Proceedings.

Mark M. Ross
Editor and Member-at-Large
ASMS Board of Directors

CITATION NOTICE

This volume contains the extended abstracts of papers presented at the 43rd ASMS Conference on Mass Spectrometry and Allied Topics. The material is not copyrighted and appearance of material in this volume does not jeopardize the author's right to publish the information in scientific journals.

Reference to individual abstracts contained in this volume should be cited as follows:

Author(s); title; *Proceedings of the 43RD ASMS Conference on Mass Spectrometry and* Allied Topics, Atlanta, Georgia, May 21 - 26, 1995.

ASMS BOARD OF DIRECTORS 1994 - 95

President	Christie G Enke University of New Mexico Albuquerque, NM
Vice President for Programs	Veronica M. Bierbaum University of Colorado Boulder, CO
Vice President for Arrangements	Brian Musselman JEOL USA, Inc. Peabody, MA
Secretary	Thomas A Baillie Merck Research Labs West Point, PA
Treasurer	Charles A. Evans Charles Evans & Assoc. Redwood City, CA
Member at Large	Mark M Ross Naval Research Lab Washington, DC
Member at Large	Robert K Boyd Nat'l Research Council Halifax, Canada
Member at Large	Sharon G. Lias NIST Gaithersburg, MD
Past President	Henry M. Fales NIH Bethesda, MD
Executive Director	Judith A. Sjoberg ASMS 1201 Don Diego Avenue Santa Fe, NM 87505 (505) 989-4517
Staff	Cindi Lilly Michele Davenport Kim Leibman

INTEREST GROUP COORDINATORS

Automated MS	Mark F Beam SmithKline Beecham
Biomedical Applications	Pamela F Crain University of Utah
Computer Applications	David D. Stranz Fisons Instruments
Desorption Ionization	Richard B. Cole Univ of New Orleans
Elemental Analysis	Douglas C. Duckworth Oak Ridge Nat'l. Lab
Energy & Petrochemicals	Dean V Davis Unocal Science & Tech
Environmental Applications	M. Judith Charles Univ of North Carolina
FTMS	Carlito Lebrilla Univ of California (Davis)
Fundamentals	John Bartmess University of Tennessee
History of MS	Lawrence R. Phillips National Cancer Inst
Ion Trap MS	Gary L Glish Univ of North Carolina
Isotopic Applications	John Wacker Battelle Northwest Labs
Laboratory Managers	Andrew N Tyler Harvard University
LC/MS & Related Topics	ThomasCovey Sciex, Inc.
Metal Ion Coord. Chem	Jennifer Brodbelt University of Texas
Polymeric Materials	Phil Savickas Dow Chemical Company
Quantitation	Susan T. Weintraub University of Texas
Surface Science	Frasier Reich Charles Evans & Assoc
Time-of-Flight MS	Robert J. Cotter Johns Hopkins Univ
Young Mass Spectrometrists	David Dearden Brigham Young Univ

ASMS COMMITTEES

Asilomar Conference
R. Graham Cooks (Chair)
Purdue University
(317) 494-5263

Arnie Falick
Micheal L Gross
Mark M. Ross
Christie G Enke

Audit
Kelsey D. Cook (Chair)
University of Tennessee
(615) 974-8019

Frank H Field
Peter J. Todd

Education
Robert K. Boyd (Chair)
National Research Council
(902) 426-6503

Steven P Cepa
Jon Amster
Carol Haney
Alfred Yergey

Measurements & Standards
Sharon G Lias (Chair)
NIST
(301) 975-2562

John Bartmess
Phillip C. Price
Anne Giordani

Nominating
Douglas P Ridge (Chair)
University of Delaware
(302) 831-1197

Alan G Marshall
Ronald A Hites
Craig Whitehouse
Brian Chait

Sanibel Conference
Rebecca O'Malley (Chair)
University of South Florida
(813) 974-6375

Susan Graul
Sharon Lias
Lester Taylor

LOCAL MASS SPECTROMETRY DISCUSSION GROUPS

Arizona
Jim Lehman
Phone: 602/965-6193

Atlanta-Athens
Helen H Schurz
Phone: 404 488 4609

Atlantic Canada
W D Jamieson
Phone: 902/426-8279

Bay Area
Bud Buttrill, Jr
Phone. 415 424-5079

Boston
I. Papayannopouws
Phone. 617 253 7233

British Columbia
Guenter Eigendorf
Phone· 604/228-3235

Central Virginia
Terry Sumpter
Phone· 804/274-3537

Chicago Area
Grant B Kenion
Phone· 708 938 1821

Connecticut
Kenneth Rosnack
Phone 203/441 3126

Delaware Valley MS Group
Swapan K Chowdhury
Phone: 215/889-6025

East Tennessee
Greg Hurst
Phone· 615 576 6691

Louisiana
Richard Cole
Phone: 504/286-7412

Madison-Chic-Milwaukee
Alex Schilling
Phone 708/505 8880

Maryland
Lewis Pannell
Phone: 301 402 2196

Michigan
Dana E DeJohn
Phone· 313 996 7135

Mid-Ohio
Susan Olesik
Phone· 614/292-0733

Minnesota
Phil Lyon
Phone· 612/736-3525

North Jersey
Kelvin Chan
Phone 908 274 4337

Northeast Ohio
Frank Bockhoff
Phone· 216/357-3699

Ottawa
John Holmes
Phone 613/231-2239

Pittsburgh
Kasi Somayajula
Phone. 412/624-8406

Research Triangle Park
Don Chace
Phone· 919 549 0445

Southern California
Richard Kondrat
Phone: 714/787-5287

St. Louis MSDG
Fred Hileman
Phone: 314 694 5843

Toronto
Eric Reiner
Phone 416 235 5893

Washington DC-Baltimore
John Callahan
Phone· 202/767-3551

1995 CORPORATE MEMBERS

Allen Scientific Glass, Inc.
1752 55th Street
Boulder, CO 80301
Phone: 303/442-2141
FAX: 303/442-2260

Analytica
29 Business Park Drive
Branford, CT 06405
Phone: 203/488-8899
FAX: 203/481-0433

Bear Instruments
3645 Enochs Street
Santa Clara, CA 95051
Phone: 408 773 0461
FAX: 408 773 0463

Beckman Instruments, Inc.
2500 Harbor Boulevard
Fullerton, CA 92634
Phone: 714 773 8022
FAX: 714 773 8883

Bruker Instruments
15 Fortune Drive
Manning Park
Billerica, MA 01821-3991
Phone. 508/667-9580
FAX. 508/667-6406

C.S.S. Analytical
10306 W. 74th Street
Shawnee, KS 66203
Phone: 913 631 0864
FAX: 913 631 0864

C/D/N Isotopes
1000 Roche Avenue
Vaudreuill, Quebec
CANADA J7V 8P5
Phone: 514/424-4696

CIL
50 Frontage Road
Andover, MA 01810-5413
Phone: 508 749 8000
FAX: 617/932-9721

Chemical Concepts GmbH
PO Box 10 02 02
D-69442 Weinheim
GERMANY
Phone: 49 6201606437
FAX: 49 6201606430

Comstock, Inc.
1005 Alvin Weinberg Drive
Oak Ridge, TN 37830
Phone: 615/483-7690
FAX: 615/481-3884

Detector Technology, Inc.
66 Technology Park Road
Sturbridge, MA 01566
Phone: 508/347-5656
FAX: 508/347-5678

ETP Scientific Inc.
7 Midstate Drive
Auburn, MA 01501
Phone: 508/832-7030
FAX. 508/832-8022

Elsevier Science Publishers
655 Avenue of the Americas
New York, NY 10010
Phone: 212/633-3917

Extrel Corporation
575 Epsilon Drive
Pittsburgh, PA 15238-6578
Phone: 412 963 7530
FAX: 412 963 6578

Extrel, FTMS
6416 Schroeder Road
Madison, WI 53711-2424
Phone. 608 273 8262
FAX: 608 273 8719

Finnigan MAT
355 River Oaks Parkway
San Jose, CA 95134-1991
Phone: 408/433-4800
FAX. 408/435-1481

Fisons Instruments
55 Cherry Hill Drive
Beverly MA 01915
Phone: 508/524-1000
FAX. 508/524-1019

GB Scientific
PO Box 2831
Novato, CA 94948-9958
Phone. 415/898-7606
FAX: 415/898-7514

Galileo Electro-Optics
PO Box 550
Sturbridge, MA 01566-0550
Phone. 508/347-9191
FAX. 508/347-3849

HD Science Ltd.
4A Bessell Lane, Stapleford
Nottingham, NG9 7BX
United Kingdom
Phone: 44 1159491704
FAX: 44 1159491703

Hewlett-Packard
1601 California Avenue
Palo Alto, CA 94304
Phone: 415/857-6028
FAX: 415/852-8011

1995 CORPORATE MEMBERS

Hitachi Instruments Inc.
3100 No. First St.
San Jose, CA 95134
Phone: 408/432-0520
FAX: 408/432-0704

IM Publications
6 Charlton Mill
Charlton, Chichester
W. Sussex PO18 OHY, UK
Phone: 01243-811334
FAX: 01243-811711

Ionspec Corporation
Suite F
18009 Skypark Circle
Irvine, CA 92714-6516
Phone: 714/261-7743
FAX: 714/261-7743

Isotec Inc.
3858 Benner Road
Miamisburg, OH 45342
Phone: 513/859-1808
FAX: 513/859-4878

JEOL USA, Inc.
11 Dearborn Road
Peabody, MA 01960
Phone: 508/536-2271
FAX. 508/536-2205

John Wiley & Sons
605 Third Avenue
New York, NY 10158-0012
Phone: 212/850-6483
FAX. 212/850-6088

K and M Electronics
11 Interstate Drive
West Springfield, MA 01089
Phone: 413/781-1350
FAX. 413/737-0608

Kratos Analytical
535 East Crescent Avenue
Ramsey, NJ 07446
Phone: 201/825-7500
FAX: 201/825-8659

LC Packings, Inc.
80 Carolina Street
San Francisco, CA 94103
Phone. 415/552-1855
FAX: 415/552-1859

Linden-Chromasspec
PO Box 3451
Princeton, NJ 08542
Phone. 609/737-2859
FAX: 609 737 8949

Los Gatos Circuits (LGC)
2030 A Fortune Drive
San Jose, CA 95131
Phone: 408 456 0969
FAX: 408 456 0906

Mass Evolution, Inc.
330 Meadowfern, Suite 113
Houston, TX 77067-3227
Phone: 713/875-6219
FAX. 713/875-9658

Mass Spec. Svcs. Ltd.
Unit 2A
Mountheath Ind. Park
George Street, Prestwich
Manchester M25 8WB, U.K.
Phone: 44 61-7898611
FAX: 44 61-7732128

Meridian Instruments
2310 Science Parkway
Okemos, MI 48864
Phone: 517/349-7200

Michrom Bio Res., Inc.
1945 Industrial Drive
Auburn, CA 95603
Phone: 916 888 6498
FAX 916 888 8295

Micro-Tech Scientific, Inc.
140 S Wolfe Road
Sunnyvale, CA 94086
Phone: 408 730 3570
FAX: 408 730 3566

NIST
A260/222
Gaithersburg, MD 20899
Phone: 301/975-2505
FAX: 301/936-4513

NOVAMANN International
5540 McAdam Road
Mississauga, Ontario
Canada, L4Z 1P1
Phone: 905 890 2555
FAX: 905 890 0370

Oneida Research
One Halsey Road
Whitesboro, NY 13492
Phone. 315/736-3050

PE SCIEX
55 Glencameron Rd
Suite 202
Thornhill, Ontario L3T 1P2
CANADA
Phone: 905/881-4646

Palisade Corporation
31 Decker Road
Newfield, NY 14867
Phone: 607/277-8000
FAX: 607/277-8001

1995 CORPORATE MEMBERS

PerSeptive Biosystems/ Vestec
500 Old Connecticut Path
Framingham, MA 01701
Phone· 508/383-7700
FAX: 508/383-7880

Pernicka Corporation
112 Racquette Drive
Fort Collins, CO 80524
Phone· 303/224-0220

Phrasor Scientific
1536 Highland Ave
Duarte, CA 91010
Phone. 818/357-3201

Physical Electronics
6509 FLying Cloud Drive
Eden Prairie, MN 55344
Phone. 612 828 6100
FAX: 612 828 6322

Precision Instruments
P O Box 11235
Knoxville, TN 37939
Phone· 615 690 5608
FAX. 615 690 6730

Research Scientific Svcs.
3209 Gresham Lake Rd
Unit 131
Raleigh, NC 27615
Phone· 919/876-8689
FAX: 919/954-9079

Scientific Glass Eng.
2007 Kramer Lane
Austin, TX 78758
Phone: 512/837-7190
FAX. 512/836-9159

Scientific Instr. Svc.
1027 Old York Road
Ringoes, NJ 08551-9675
Phone: 908/788-8000
FAX: 908/806-6631

Shrader Analytical Lab
3814 Vinewood
Detroit, MI 48208
Phone: 313/894-4440
FAX: 313/894-4489

Spectroscopy
195 Main Street
Metuchen, NJ 08840
Phone: 503/343-1200
FAX: 503/344-3514

Teknivent Corporation
Suite 115
149 Weldon Parkway
Maryland Hghts., MO 63043
Phone: 314/994-0500
FAX. 314/994-0505

Teledyne Electronic Tech.
Scientific Instruments
1274 Terra Bella Avenue
Mountain View, CA 94043
Phone: 415 691 9800
FAX 415 967 4353

Varian Associates
2700 Mitchell Drive
Walnut Creek, CA 94598
Phone· 510/945-2235
FAX: 415/945-2335

Waters
34 Maple Street
Milford, MA 01757
Phone· 617 275 9200

43rd ASMS Conference on Mass Spectrometry and Allied Topics

Monday Orals
Recent Developments in the Characterization of Aerosol Microparticles

Ambient Aerosol Analysis Using Aerosol Time-of-Flight Mass Spectrometry; *Prather, Kimberly; Fergensen, David; Morrical, Bradley; Noble, Christopher; Nordmeyer, Trent; Salt.. 1
Rapid Single-Particle Mass Spectrometry of Aerosols and Aerosol Reactions; *Johnston, Murray; Carson, Peter; Mansoori, Bashir; Wexler, Anthony. 2
Tandem Mass Spectrometry of Airborne Particles; Yang, Mo; Whitten, William; *Ramsey, Michael. 3
Detection and Characterization of Ultrafine Particles; *Reents, William. 4
Sulfur Speciation of Single Aerosol Particles; *Neubauer, Kenneth; Johnston, Murray; Wexler, Anthony 5
Laser Microprobe Mass Spectrometry of Soot and Soot Precursor Particles; *Fletcher, Robert; Dobbins, Richard; Lu, Weining 6
Effects of MALDI and Solution Parameters on Aerosol MALDI Ion Signal; *Beeson, Michelle D.; Wei, Xiaona; Russell, David H. 7
Application of Two-Step Laser Mass Spectrometry to Kerogen; *Zhan, Qiao; Zenobi, Renato; Knochenmuss, Richard; Buseck, R. Peter. 8
A Reversed Geometry Organic Ion Microprobe; *Todd, Peter; Short, Rober.t 9

Monday Orals
Computational & Experimental Approaches to Ion Thermochemistry & Structure

A Computational Approach to Gas-Phase Ion Chemistry; *Radom, Leo 10
Recent Experimental Investigations of Gaseous Ion Thermochemistry; *McMahon, Terry. 11
Structure and Reactivity Of A Cyclopropyl Anion: Experiment and Theory; Baschky, Michael; Peterson, Kent; *Kass, Steven. 12
Neutral and ionic heats of formation; measurement and reliability; *Holmes, John L. 13
4-Member Cyclic Halonium Ions in Intramolecular 1,3-Fluoride Transfer; *Morton, Thomas Hellman 14
Theoretical Studies of Proton Transfer Potential Energy Surfaces.; *Gronert, Scott; Kimura, Cliff; Sadoun, Aladin. 15
Metal-Ligand Thermochemistry by Guided Ion Beam Mass Spectrometry; *Armentrout, Peter 16
Experimental and Ab Initio Studies of Second Row Radicals; *Turecek, Frantisek; Shaffer, Scott; Gu, Ming; Hop, Corneli. 17

Monday Orals - Mass Spectrometry of Polymers

Characterisation of synthetic polymer formulations using MALDI; *Scrivens, Jim; Yates, Hilary; Segal , John; Jackson, Tony; Taylor, Mike; Critchley, Glen; Maisey, Ann 18
Matrix-Assisted Laser Desorption Investigations of Industrial Polymers; *Hanton, Scott; Parees, David; **Goldschmidt, Robert; King, Richard; Owens, Kevin. 19
High Mass Resolution Imaging TOF-SIMS Analysis of Polymer Surfaces; *Reichlmaier, Stefan. 20
REVERSE ENGINEERING OF INDUSTRIAL POLYMER FORMULATIONS BY MALDI-MS; *Tang, X.; Vertes, Akos; **Dreifuss, Peter; Hull, Clifford, Dutton, Walter. 21
MALDI in Polymer Chem: Rapid Analysis of Chemical Modifications on Polymers; *Whittal, Randy M.; Li, Liang. 22
MW Determination of Synthetic Polymers from ESI & MALDI Mass Spectra; McEwen, Charles; Jackson, Christian; *Larsen, Barbara. 23
Mass Spectrometry of Otherwise Fragile Polymers by End Group REMPI; Anex, Deon S.; Hunziker, Heinrich E.; *de Vries, Mattanjah S. 24
A Polymer Library By In-Source Direct Pyrolysis Mass Spectrometry; *Qian, Kuangnan; Killinger, William E. 25
Polymer Analysis Using a Radio Frequency Glow Discharge Mass Spectrometer; *DePalma, Jr., Patrick; Shick, Jr., Charles, Marcus, R Kenneth.. 26
FD-MS Studies of Samarium-based Oligomerization of Ethylene; *Greaves, John; DeCoster, Donna M., Evans, William J. 27

Monday Orals - Electrospray Ionization-Applications

Protein & Peptide Analysis by A Low-Flow, High Sensitivity MicroES Source; *Wilm, Matthias; Mann, Matthias. 28
Biochemical Characterization of EGF Receptor-SRC SH2 Interactions; *Lombardo, Christian; Consler, Thomas; Luther, Michael; Kassel, Daniel. 29
RECEPTOR PEPTOID LIGANDS IN COMBINATORIAL MIXTURES: AFFINITY SELECTION ESMS; *Kaur, Surinder; Huebner, Vreni; Dollinger, Gavin; Tang, Dazhi; McGuire, Lisa 30
Proteins Associated with Cardiomyocyte Hypertrophy: 2D PAGE, LCMS AND MS/MS; *Arnott, David; King, Kathy; Bier, Mark; Land, Adrian; Stults, John. 31
Amino Acid Transformations during Oxidation of Peptides and Proteins; *Chowdhury, Swapan; Eshraghi, Jamshid, Wolfe, Henry; Forde, Diane; Hlavac, Allan; Johnston, David. 32
Identifying Proteins by Nanoelectrospray Tandem MS & Peptide Sequence Tags; M. Mann.; M Wilm; A Shevchenko; G Neubauer. 33

MALDI and ESI MS of Covalent Peptide-Oligonucleotide Hybrids; *Jensen, Ole N.; Kulkarni, Sandhya; Aldrich, Jane V.; Bennett, Samuel E.; Mosbaugh, Dale W.; Barofsky, Douglas F. 34
Studying Noncovalent Protein-Peptide Interactions by ESI Mass Spectrometry; *Loo, Joseph A.; Hu, Peifeng; Thanabal, Venkataraman 35
Mass Spectrometry in the Development of Recombinant Protein Drugs; Kubis, Alan; Chen, Tom; Ghosh, Kris; Natale, David; Nigam, Somesh; *Labdon, James 36
Application of Micro-ES/MS/MS for Monitoring the Effects of Drugs of Abuse; *Emmett, Mark R.; Caprioli, Richard M. 37
Sequencing Nucleotides (n>50) by Tandem Mass Spectrometry; *Little, Daniel P.; McLafferty, Fred W. 38
Searching Chemical Diversity for Molecular Recognition by ESI-MS; *Smith, Richard D.; Bruce, James E.; Chen, Ruidan; Cheng, Xueheng; Schwartz, Brenda L.; Anderson, Gordon A.; Hofstadler, Steven A.; Gale, David C. 39

Monday Orals - Elemental and Isotopic Analysis

Direct Connection of an ICP and an Ion Trap MS; *Barinaga, Charles J.; Eiden, Gregory C.; Koppenaal, David W. 40
Glow Discharge Ion Trap Mass Spectrometry Employing Filtered Noise Fields; *Duckworth, Douglas C.; Smith, David H.; Goeringer, Douglas E.; McLuckey, Scott A. 41
TIME-OF-FLIGHT MASS SPECTROMETRY WITH A PULSED GLOW DISCHARGE ION SOURCE; King, Fred; *Steiner, Robert. 42
Anodic Stripping Voltammetry Coupled On-line with ICP-MS; *Van Berkel, Gary; Zhou, Feimeng; Duckworth, Douglas; Morton, Shelby. 43
Laser Ablation ICP/MS Analysis of Real World Samples.; *Kahr, Michael; Brink, Christopher; Figg, Deborah. 44
Analysis of Nominally Flat Samples by Radio Frequency Powered GDMS.; *Shick, Jr., Charles R.; Marcus, R. Kenneth. 45
High Precision Continuous Flow D/H Measurement from Hydrogen Gas and Water; *Tobias, Herbert J.; Goodman, Keith J.; Blacken, Craig E.; Brenna, J. Thomas. 46
A Field Mass Spectrometric System for Isotopic Analysis of Actinides.; *Kahr, Michael; Olivares, Jose; Abney, Kent; Kinkead, Scott. 47
Nuclear Isotope Measurement in the Hanford Environment; *Stoffel(s), J. J.; Kelley, J. M.; Bond, L. A.; Kiddy, R. A.; Brauer, F. P. 48
High-sensitivity Thermal Ionization Cavity Source for Mass Spectrometry; *Olivares, Jose A.; Chamberlin, Edwin P.; Duan, Yixiang 49

Monday Posters - Ion Molecule Reactions

Thermochemical Studies of Halocarbenes and Halosilylenes; *Poutsma, John; Paulino, Jose; Squires, Robert. 50
Calculated and Measured Double-ionization Energies of Carbon Tetrachloride; *GRANT, RUSSELL. P.; HARRIS, FRANK M ; **ANDREWS, STUART. R.; PARRY, DAVID. E. 51
DETERMINATION OF Se-H BOND ENERGY OF BENZENESELENOL; Leeck, Diane T.; *Li, Ruomei; Chyall, Leonard; Kenttamaa, Hilkka I. 52
Alkali Metal Ion - Crown Ether Bond Strengths by FTICR Threshold CID ; *Pope, Marshall; Dearden, David. 53
Cation Affinities of Pyridine Bases: Steric Effects; *Isbell, John; Brodbelt, Jennifer. 54
Charge Repulsion in Peptides and Basicities of Different Charge States.; *Kaltashov, Igor; Fenselau, Catherine. 55
Polyatomic Cations Affinities of Pyridines Determined by the Kinetic Method; *Sheng S. Yang, ; Guodong Chen, ; Philip Wong, ; Shuguang Ma, , R. Graham Cooks, , **Fabio C Gozzo, ; Marcos Eberlin 56
Acidities of long chain diols: problems with the kinetic method; *Higgins, Priscilla; Bartmess, John. 57
Reactivity and Thermochemistry of Quadricyclane Anion; *Lee, Hack Sung; Bierbaum, Veronica M. 58
Temperature dependence of radiative association rates; *Ryzhov, Victor; Dunbar, Robert C. 59
A REACTION WINDOW IN CROSS-SECTIONS FOR DOUBLE ELECTRON CAPTURE REACTIONS.; *Griffiths, William; Langford, Marian; Harris, Frank. 60
Reactions and Laser Photofragmentation Processes of SiF2(2+) and SiF3(2+); **Lee, Yin-Yu; *Leone, Stephen R. 61
Partially Chlorinated Hydrocarbons: Gas-Phase Anion-Molecule Reactions ; *Grabowski, Joseph J.; Braun, Jennifer A. 62
Regioselectivity of oxygen addition on PCBs and DDT in ECNCI; *Lépine, François; **Mamer, Orval A.; Milot, Sylvain. 63
Dissociative Attachment in Sulfonate and Carboxylate Compounds; *Andrews, Kim; Bartmess, John; Sorensen, Daniel; Crowder, Cathy. 64
Experimental and Theoretical Characterization of the Gas-Phase SO2N- Anion; Morgon, Nelson H.; Linnert, Harrald V.; *Riveros, José M. 65
A NEGATIVE ION STUDY OF THE ISOMERS OF DINITROBENZENE USING A ASGDI SOURCE; Mo, Wenjun; Langford, Marian, L; Franklin, Anthony, M; *Todd, John, F. J. 66
Investigation of van der Waals clusters by a novel technique for ICR; *Garbade, Klaus ; Wanczek, Karl Peter. 67

Consecutive reactions of conjugated dienes; Rappmund, Andreas; *Wanczek, Karl Peter....68
Bulk Polymerization and Ion Chemistry of Crotonaldehyde, Studied with ICR; *Harder, Andreas; Spiess, Iris, Wanczek, Karl Peter....69
Reactivity of Ionized Carbonyl Compounds and Distonic and Enol Isomers; *Byrd, Michelle; Castro, Lori, Hwang, Thomas; Smith, Rebecca; Leeck, Diane; Kenttamaa, Hilkka....70
Generation and Reactivity of Charged Phenyl Radicals; *Smith, Rebecca; Kenttamaa, Hilkka....71
CHARGE TRANSFER REACTIONS OF THE CYCLOPROPENYL CATION; *Watkins, Layle; Rich, Jennifer; Frank, Samantha ; Hanson, Curtiss....72
Selective ion-molecule reactions of benzoyl ions in a quadrupole ion trap; Creaser, Colin; *Williamson, Brian; **Stockton, Brian....73
Gas-phase Ion-molecule Reactions of Methyl Tertbutyl Ether (MTBE); *Peterman, Scott; Rich, Michaela; Hanson, Curtiss....74
Ion/Molecule Reactions with Polyethylene Glycoles and PEG Ethers; *Onigbinde, Adebayo; Ridge, D. P., Munson, Burnaby, Zhang, Tianlan....75
GC/CIMS of Lipids with Benzene and Carbon Disulfide; *Evans, Jason, Nicol, Gordon; Munson, Burnaby....76
Gas-Phase Ion-Molecule Reactions of Amines with Carbonyl Compounds; Pykäläinen, Mika; *Vainiotalo, Pirjo....77
In-situ Investigation of Soot Formation; *Egsgaard, Helge....78
An Ion Trap MS/MS Study of [C14H10]+,[C10H10]+, and [C10H8]+ Ions.; *Wang, Xiaomin; **March, Raymond E., Hopkinson, Alan C.; Bohme, Diethard K....79
Isomeric Forms of the Products of Ion-Molecule Association Reactions; *Kerr, Kelly E.; Adams, Nigel G....80
Competitive SNi/SN2 from epimeric 1-2 hydroxyether and diether 1-2 indanes.; Christel , Bourhis; Vincent , Gervat; Marie-Claude, Perlat; Françoise, Fournier; *Acher, Mandelbaum; **Jean-Claude , Tabet....81
Ion-Molecule Reactions with Alkyl Cation Transfer by Electrospray FTICR-MS; *Burton, Richard; Watson, Cliff; Katritzky, Alan; Eyler, John....82
Association and Bimolecular Ion-Molecule Reactions of Sulfur Ring Systems; *James, Mary A.; Gidden, Jennifer; Peschke, Michael; Illies, Andreas J....83
ION/MOLECULE REACTIONS OF ALLYL CHLORIDE IN THE ION TRAP MASS SPECTROMETER; Mo, Wenjun; Franklin, Anthony, M; *Todd, John. F. J....84
Mechanism of H/D Exchange in the Reaction of BH2+ and Deuterium; *Hankin, Joseph; Davico, Gustavo; DePuy, Charles, Damrauer, Robert....85
Isotope Effects in the Dissociation of Aniline and Protonated Aniline; *Ranasinghe, Yasmin A.; Glish, Gary L....86
Hydrogen/Deuterium Exchange of Multiply-Protonated Cytochrome c Ions; *Wood, Troy D.; Guan, Ziqiang, Chorush, Russell A ; McLafferty, Fred W....87
Resolvation of Electrospray Ions in a Time of Flight Mass Spectrometer *Lasater, M. A.; Laude, D. A....88

Influence of Water and Structure on Coulomb Energy in Multiply Charged Ions; *Gross, Deborah S.; Rodriguez-Cruz, Sandra E ; Williams, Evan R....89
Acid/Base effect on FAB ionization process * L. Amado, Francisco; N. Domingues, Pedro ; O. Marques, M. Graa; Ferrer Correia, A. J....90
Ion/Molecule Reactions for Improved Effective Mass Resolution in ES/MS; McLuckey, Scott; *Goeringer, Douglas....91
Structure Elucidation of Peptides by Two-Dimensional FT-ICR MS; **Solouki, Touradj; *Ross III, Charles; Pasa-Tolic, Ljiljana; Marshall, Alan G....92
FT-ICR Observation of Metabolic Intermediates for Nephrotoxic Chloroalkenes; *Zhang, Tian-lan; Wang, Liping; Hahsmi, Mazzaz; Anders, M. W.; Thorpe, Colin; Ridge, Douglas....93
Study of Ion-Molecule Chiral Recognition by Amine Exchange Equilibria Dejsupa, Chadin; Liang, Yongjiang; *Dearden, David....94
Chiral Recognition in Molecular Host-Guest Complexations using FABMS; *Sawada, Masami; Takai, Yoshio; Yamada, Hitoshi; Hirayama, Shigeki, Kamada, Kimiko, Hirose, Keiji; Tobe, Yoshito; **Naemura, Koichiro....95

Monday Posters - Ion Sources & Mass Spectrometer Design

SFC/MS using a glow discharge ionization source; *Carazzato, Daniel; B langer, Patrick, Carrier, Alain; Bertrand, Michel J....96
A NOVEL LOW-POWER RF GLOW DISCHARGE ION SOURCE; *Langford, Marian L.; Povey, William T ; Todd, John F. J....97
Micro-electrospray on a Magnetic Sector Mass Spectrometer; *Woolfitt, Adrian; Bateman, Robert; Bordoli, Robert....98
ATMOSPHERIC PRESSURE CHEMICAL IONIZATION BY CORONA DISCHARGE.; *Andrien, Jr., Bruce; Dresch, Tomas; Haren, Patrick, Whitehouse, Craig, Shen, Shida....99
A New Atmospheric Presure MIP Ionization Source for Mass Spectrometry; *Moini, Mehdi, Xia, Ming; Hofmann, Bernhard, Mathews, Kimberly, Holbert, Anthony....100
MULTI-VACUUM STAGE HEXAPOLE ION GUIDE FOR ESI/MS INTERFACE; *Gulcicek, Erol E.; Whitehouse, Craig M....101
Ion Transmission Through Glass and Metal Tubes; *Cao, Jian-Ru; Rosell, Joan; Fenn, John....102
Design of a Composite Liquid-Junction/Electrospray Interface for CE/MS; *Wachs, Timothy; **Sheppard, Robin; Henion, Jack....103
A Versatile, Stable CE-ESI Source; *Kirby, Daniel P....104
Real Time UV Detection with On-Line CE-ESI-MS; *Foret, Frantisek; Muller, Odilo; Goetzinger, Wolfgang; Thorne, Jacqueline; Karger, Barry L.; Vouros, Paul; Kirby, Daniel P....105

Advanced Liquid Ionization Mass Spectrometry for Analysis of a Mixture; *Inoue, Masayuki; Kaneko, Takeo; Li, Yaming; Tsuchiya, Masahiko, **Niwa, Yoshio 106
Electric evaporation of ions from liquid in channels of polymer films; Balakin, A; Dodonov, A; Novikova, L; *Talrose, V; Yakovlev, B. 107
Molecular Weight Enhancement in GC-MS with Supersonic Molecular Beams; *Dagan, Shai; Amirav, Aviv. 108
Soft Ionization via Electron Impact on Free-Jet Clusters; *Wang, Dingneng; Evans, Robert. 109
Concentration Enrichment in High Pressure Ion Sources, Part II.; Williamson, D H.; *Knighton, W.B.; Grimsrud, E.P. 110
A Portable Mass Spectrometer to Measure Surface Contamination; *Gregg, Hugh; Meltzer, Michael; Lindsey, Jean; Edberg, Heather 111
Conversion of HP-5985 GC/MS to Automated, High-Volume ES-MS; *Kiesel, Jennifer R ; Jackson, Alan K.; Depperman, Kevin L.; Hileman, Fred D.; Duffin, Kevin L. 112
Improving Sensitivity in the HP MSD Mass Spectrometers; *Manura, John; Overton, Santford; Baker, Chris 113
Modification of an HP 5972 MSD to Accept a Direct Insertion Membrane Probe; *Bauer, Scott; 114
TWO QUADRUPOLE MASS SPECTROMETERS MODIFIED FOR PYROLYSIS-MS; *Wilkes, Jon G. ; **Voorhees, Kent J.; Lay, Jackson O. ; Volmer, Dietrich A. 115
EXAMINATION OF SEVERAL SHEET MATERIALS FOR USE AS MEMBRANES IN MI/MS; *Maden, Amy J , Hayward, Mark J 116
Optimal Design of a MALDI Time-of-Flight Instrument for MS/MS of Peptides; *Hoyes, John; Curbishley, Steve; Bateman, Robert. 117
Modulated Sample, Membrane Inlet MS: Theory and Practice; *Liu, Fei; Davenport, Michael, Enke, Christie G. 118
Ion storage study for a segmented-ring ion trap source for TOF-MS; *Ji, Qinchung; Davenport, Michael R.; Holland, John F. ; Enke, Christie G. 119
A new design of Ion Storage Accelerator for Time-of-Flight MS; Kraft, Andreas; *Wollnik, Hermann; Laiko, Victor; **Dodonov, Alexander. 120
A new MALDI Tandem QUISTOR Time-of-Flight Mass Spectrometer; *Stoeckli, Markus; Kofel, Peter, Krause, Joern, Schlunegger, Urs P 121
A New LC Electrospray Ion Trap Time-of-Flight Mass Spectrometer; *Mordehai, Alex; Karnicky, Joseph F., Limbek, Belá; Buttrill, Jr., S. E. 122
MALDI TOF/TOF of peptides: Past, Present and Future.; *Cordero, Marcela M.; Cornish, Timothy J.; Cotter, Robert J. 123
Progress in the design of a continuous flow - MALDI interface of a TOF - MS; *Grigorean, Gabriela; Wronka, John; Martin, Charles; Amster , I. Jonathan 124
An Inverted Perfectron Electrospray/Orthogonal TOF Mass Spectrometer; *Gao, Q ; Rockwood, A. L.; Udseth, H. R.; Follansbee, J. C.; Smith, R. D. 125

Collisional Focusing of Ions in the Electrospray TOF Mass Spectrometer; *Krutchinsky, A.N.; Chernushevich, I.V.; Ens, W.; Spicer, V , Standing, K.G. 126
The Laser Ionization GC-TOF/MS Analysis of Organometallics; *COLBY, STEVEN; HANSER, KENT; HARRIS, WILLIAM; REILLY, JAMES. 127
A new GC-TOF mass analyzer; Scherer, Stefan; Dormagen, Jonas; Horvath, Thomas; *Wollnik, Hermann. 128
Design of a GC/TOF MS System for the Analysis of Breath Components; *Miyares, Paul H.; Enke, Christie G. 129
Time-of-flight mirrors with ideal time-focusing in tandem mass-spectrometry; *Makarov, Alexander; Raptakis, Emmanuel; Derrick, Peter. 130
High Voltage Deflectors for Mass Selection on a Wire-Guide MALDI/TOF; *Bolanos, B. J.; Robinson, J. M.; Laude, D. A. 131
Improved Space-Focusing Using Non-linear Ion Acceleration Fields in TOFMS; *Gardner, Ben; **Artaev, Viatcheslav; Holland, John. 132
Design Optimization for Coaxial, Curved-Field Reflectron Time-of-Flight MS; *Cornish, Timothy J.; Cotter, Robert J 133
An Interleaved-Comb Ion Deflection Gate; *Beussman, Douglas J.; Vlasak, Paul R.; **Erickson, Tina A ; Davenport, Michael R.; Enke, Christie G 134
Ion Selection in TOF using a Bi-polar Pulsed Electrostatic Particle Guide; *Adams, Nathan; Just, Craig; Hanson, Curtiss. 135
Comparison of Ion Detectors for MALDI TOFMS; *King, Richard; Owens, Kevin; **Hanton, Scott. 136
Tandem MS Utilizing an Orthogonal Acceleration Time of Flight MS as MS-II; *Cerny, Ronald L , Wulser, Kurt W ; Smith, David L ; **Bateman, Robert H 137
MS & High Energy CID MS/MS of ESI & MALDI Ions on a Sector-TOF Instrument; *Bateman, Robert; Green, Martin; Scott, Gary. 138
A HYBRID TANDEM MASS SPECTROMETER III; *Duhr, Alexander; Stracke, Patric; Stadlmann, Jens; Wollnik, Hermann. 139
A new 2-D / 3-D-TOF MS; Linden, H. Bernhard; *Bamberg, Michael 140

Monday Posters - Organic Analysis

The Evaluation of a Comprehensive MS Reference Library; **Zaikin, Vladimir, Ausloos, Pierre; Lias, Sharon; Clifton, Carol; Mikaya, Anzor; *Stein, Stephen. 141
Odor analysis by GC/MS/FTIR using substructure based spectral libraries.; *Nikiforov, Alex; Remberg, Barbara; Buchbauer, Gerhard; Jirovetz, Leopold; Körnig , Stefan. 142
The Development of an Automated System for Routine MS Analysis; *Fink, Saul, W., Thompson, William, L.; Slayback, John, R. B. 143
Spectral Resolution of Isomeric Alkanes: A Process MS Application; *Haddix, Martin; Cook, Kelsey 144
Distinguishing between Isomeric C3H5 Moieties Using Daughter Ion Spectra; *Green, John Glass. 145

Structure Elucidation Using a Multi-Disciplinary Analytical Approach; *Russell, David J.; Fink, Saul W.; Mallis, Larry M.; Slayback, John R. B. 146
Practical Applications using Automated Mass Spectrometry in Drug Discovery; *Schaffter, L. M.; Spreen, R. C.; Morris, F. X.; Cureton, G. H. 147
Diversity Profiling: Rapid Pharmaceutical Development Based on ESI/MS; *Lee, Mike; Kerns, Edward; Hail, Mark; Rourick, Robyn; Starrett, Anne; Taylor, Susan; Thompson, William; Whitney, Jeffrey. 148
Changes in Volatile Organic Composition in Milk over Time; *Overton, Santford ; Manura, John. 149
Monitoring a Chemical Synthesis Using Flow Injection Mass Spectrometry; *Sheppard, Robin; **Hayward, Mark; Henion, Jack. 150
MI/MS USED IN SUPPORT OF THE MANUFACTURE OF QUINOLINEDICARBOXYLIC ACID; Lopata, Ronald J.; *Hayward, Mark J.; Thomson, Michael L.; Ruiz, Migdalia; Lafontaine, Felix; Marrero, Carlos. 151
On-line monitoring of an Organic Photochemical Reaction By MIMS; *Srinivasan, N.; Wong, P.; Kasthurikrishna, N.; Cooks, R. G.; **Grossert, S ; Pincock, J. A.; Wedge, P. 152
Analysis of Organic Analytes in Organic Matrices by Reverse Phase MIMS; *Bauer, Scott; Bauer, Jan. 153
Potential of the MAB ion source for routine analysis of organic compounds; *Faubert, Denis; Mireault, Pascal; Bertrand, Michel J. 154
UV Laser-Induced Selective Dissociation of Nitro Groups in Nitrocellulose; *Yang, Mo; Ramsey, J. Michael. 155
MS of Prepolymers 1,10-Undecadiyne & 1,2,10,11-C13-1,10-Undecadiyne; *Robbins, Ronny; Berg, Fred. 156
THE TMS-ESTERS OF DECENOIC ACID ISOMERS; DOUBLE BOND POSITION & GEOMETRY; *Jalonen, Jorma; **Mäkelä, Mauri; Hassila, Heikki; Haapaniemi, Esa; Joensuu, Päivi. 157
Development of GC-MS Determination of Nicotinic Acid and Nicotinamide; Dame, Amy D.; Wiberg, Karin; Jacobson, Myron K.; *Pyrek, Jan St. 158
Identifying Polyol Borate Ester Complexes by Negative Ion ESI MS/MS; *Shay, Brian J.; Falk, Nancy; Kalinoski, Henry T. 159
Electrospray / Ion Trap MSn for Structure Elucidation Of Cationics; *Strife, Robert; **Schwartz, Jae; Bier, Mark; Zhou, Joe. 160
Characterization of Monoazo Dyes by Chemical Ionization MS/MS.; *Wang, Jia-shen. 161
Analysis of Dibenzofuran and Dibenzo-p-dioxin in Diphenyl Oxide; *Sherman, Paul; Hileman, Fred; Wendling, Jay. 162
LC/TSP-MS of Hydroxy Compounds After Precolumn Derivatization with IMMC; *Phillips, Lawrence R.; Supko, Jeffrey G.; Wolfe, Tracy L.; Malspeis, Louis. 163
Specific Structural Features which Promote Cluster Formation in FAB-MS; *Sharp, T.R. 164

Study of Cobalt Complexes with Tetradentate Shiff Bases by IS- And FAB-MS; *Raffaelli, Andrea; Pucci, Sergio; Di Sacco, Sonia; Isola, Mauro. 165
Quantitative Analysis of ECF Derivatives of Non-protein Amino Acids; *Moini, Mehdi; Cao, Ping. 166
A Direct Method to Quantitate Fatty Acids in Complex Mixtures; *Ai, Jiu. 167
A NEGATIVE ION STUDY OF INDOLE AND QUINOLINE USING AN ASGDI SOURCE; *Cairns, Stuart N.; Langford, Marian L.; Todd, John F.J. 168
FAB-MS of Protected Steroids and Bile Acids Using Alkali Metal Addition; Aggarwal, Suresht K.; Pogue, Robert T.; *Pyrek, Jan St. 169
M[alkali metal]+ Ions in FAB Spectra of Protected Bile Acid Glucosides; Aggarwal, Suresht K.; Pogue, Robert T.; *Pyrek, Jan St. 170
Fragmentation of 1,5-dialkyl-3,7-diphenylbispidones under electron impact; *Tretyakova, Natalia; Vatsadze, Sergey; **Lebedev, Albert; Zyk, Nikolay; Zefirov, Nikolay; Hass, J. Ronald. 171
Trace Analysis of Degraded Antibiotics by ESI-LC/MS; *Yoo, Jong Shin; Kim, Jin Young; **Kim, Sung Ho. 172
Semi-Quantitative Analysis of Pharmaceutical Product Impurities by API/LCMS; *Wakefield, Michael; Sanders, Mark; Mylchreest, Iain. 173
Predictive Impurity Profiling of Pharmaceuticals Using LC/MS *Thompson, William L.; Venesky, John S.; Volk, Kevin (2); Klohr, Steven E. (2); Kerns, Edward H. (2); Lee, Mike S (3). 174
The Role of Mass Spectrometry in Stress-Testing of Pharmaceuticals; *Kemp, Craig; Cooke, Gary. 175
PROFILING SOTALOL IMPURITIES AND DEGRADANTS USING A STANDARD LC/MS METHOD *Volk, Kevin J.; Kerns, Edward H.; Hill, Susan E.; Wilson, Terry, Behme, Robert; Brooke, Dana; Lee, Mike S. 176
Identification of unknowns compounds in topiramate tablet by IC-ESI-MS; *Xiang, Xinzhen Jane; Ko, Chan Y. ; Guh, H. Y.; 177
Pharmaceutical Applications of IonSpray LC/MS for Cyclodextrin Analysis; *Visentini, Josie; Filosa, Angelo; Rousseau, Caroline; Winters, Conrad. 178
OLIGOMER DISTRIBUTION in PHOTOFRIN® PORFIMER SODIUM; *Siegel, Marshall; Tabei, Keiko; Berkenkamp, Stefan; **Hillenkamp, Franz; Tsao, Rushung; Ingedoh, Arnd; Pastel, Michael 179

Monday Posters - Environmental Analysis

Use of MS Coupled with a Solids Insertion Probe to Pre-Screen Soil Samples; *Check, Catherine E.; Bach, Stephan B.H. 180
Analysis of Soils - Part I: Soil Dynamics and Climatic Change; *Howald, Markus; Schuerch, Stefan; Schlunegger, Urs P. 181
Analysis of Soils - Part II: Determination of Saccharides by MALDI-TOF-MS; *Schuerch, Stefan; Howald, Markus; Schlunegger, Urs P. 182

Rapid Analysis of Fast GC Effluents by Time-of-Flight MS; *Borgerding, Anthony J.; Wilkerson, Charles W. 183
A STUDY OF AMBIENT AIR BY AEROSOL-TIME-OF-FLIGHT MASS SPECTROMETRY; *Lloyd, Patrick; Nordmeyer, Trent, Prather, Kimberly 184
Analysis of Single Inorganic Salt Particles Using TOF MS; *Salt, Kimberly; Prather, Kimberly. 185
Particle Size Analysis By Light Scattering and Aerodynamic Sizing Methods; *Noble, Christopher; Salt, Kimberly; Prather, Kimberly. 186
On-Line Single Particle Analysis of Environmental Tobacco Smoke; *Morrical, Bradley; Prather, Kimberly. 187
Gas-phase Modeling of Scrap Tire Pyrolysis Reactions; *Burrell, Tim; Phillips, Eugene; Rich, Michaela; Hanson, Curtiss. 188
Analysis of Carbonyls: Intermediates of Chemical Oxidation Reactions; *Feinberg, Thomas N.; Charles, M. Judith 189
A Study of the Oxidation of Heterocyclic Compounds using GC-MS Techniques; *Morris, Jackie; Clench, Malcolm; Allen, David. 190
A MEMBRANE INLET SYSTEM FOR MONITORING TRACE ENVIRONMENTAL POLLUTANTS; *Clarke, Nigel J.; Todd, John F.J. 191
Solid Phase Microextraction (SPME)-GC/MS of Proliferation Compounds; *Alcaraz, Armando; Andresen, Brian D. 192
The Detection of TNT and TNT Metabolites by Electrospray Mass Spectrometry; *Carlson, Joel; Vouros, Paul; Kaplan, David. 193
Environmental Analysis by Flow-injection Tandem Mass Spectrometry; *Filigenzi, Michael; Larson, Michael 194
Comparison of HPLC-MS Interfaces in the Determination of Heterocyclic PACs; *Thomas, Darren; Sim, P. Greig; **Benoit, Frank M. 195
Use of Two SPE-GC/MS Methods for Field Isolation and Quantitation of PAH; *Furlong, Edward T. ; Koleis, Janece C. ; Gates, Paul M. 196
VARIOUS MASS SPECTRAL TECHNIQUES FOR THE ANALYSIS OF NITRO-PAH; *Miles, Walter; Chiu, Chung; 197
Determination of Nitrated Polycyclic Aromatic Hydrocarbons in Tree Bark; *Clench, Malcolm; Douce, David; Pragnell, Charlton; Cooke, Michael. 198
Factors Effecting the Analysis of Organic Pollutants by Particle Beam LC-MS; *Clench, Malcolm, Leathard, David; **White, John; Brown, Richard. 199
Environmental Genotoxins by LC/TSP/MS of DNA-Adducts Formed In Vitro.; *Kuehl, Douglas; Serrano, Jose 200
Analysis of Serum PAHs and PAH Adducts by LC/MS; *McClure, P. Cheryl, Barr, John R.; Maggio, Vincent L.; Sirimanne, Sarath; Ma, Li; Patterson, Jr., Donald G. 201
MS Analysis of Pesticides by Combined On-line Photodegradation and LC-MS; *Volmer, Dietrich A ; Wilkes, Jon G. 202
Multiresidue Analysis of Pesticides by Electrospray LC-MS and LC-MS/MS; *Volmer, Dietrich A.; Wilkes, Jon G. 203

Determination of Carbendazim by Immunoaffinity Extraction and LC/LC/MS/MS; *Bean, Karen; Henion, Jack 204
Limitations and Challenges in LC/MS for the Analysis of Carbofuran; *Honing, M.; Barcelo, D.; van Baar, B. L. M.; Brinkman, U.A.Th. 205
Analysis of organophosphates using a trochoidal electron monochromator MS; *Mazurkiewicz, Paul; Laramee, Dr. James, Eichinger, Dr. Peter; Deinzer, Dr. Max. 206
Analysis of Soil Metabolites Utilizing Narrow Bore LC/MS/MS Techniques; *McGown, Steven; Delgado, Nelson 207
LC/MS of Atrazine and its Hydroxylation Metabolite Using Electrospray; *Cai, Zongwei; Cerny, Ronald; Spalding, Roy. 208
Determination of Atrazine and Metabolites Using GC/MS/MS.; *Heikes, David 209
Identification of Biodegradation Products of Carbazole by Mass Spectrometry; *Jayasimhulu, Koka, Schneider, Joanne; Xue, Weiling; Grosser, Robert; Warshawsky, David 210
Analysis of Carbamate and Phenylurea Pesticides by Particle Beam LC-MS.; *Ramesh, Rao. 211
Trace Determination of Sulfonyl Ureas in Soil.; *Li, Lily Y.T.; Campbell, Dale, Henion, Jack. 212
Comparison of Electrospray and Thermospray for the Analysis of Herbicides; *Lamaat, Shalaby, Robert, Croes; Michael, Wadsley; Debbie, Armbrust. 213
Determination of Myclobutanil by GC/MS, GC/HRMS, and MS/MS; Eitzer, Brian; Pylypiw Jr., Harry; **Moore, Colin; *Mattina, Mary Jane 214
NEGATIVE-ION UNIMOLECULAR DISSOCIATION OF ESTERS OF A HERBICIDE ACID; HEADLEY, JOHN V.; *PERU, KERRY M. 215
Determination of Hydrolysis Degradates of Cloransulam-Methyl by ESI LC/MS; *Balcer, Jesse L.; Brown, Stephen M.; Lewer, Paul. 216
The Dissipation of Cloransulam-Methyl in Soil as Determined by ESI LC/MS/MS; *Brown, Stephen M., Balcer, Jesse L.; Duebelbeis, Dennis, Thomas, Angela 217
GC/MS Analysis of Alkyl Methylphosphonic Acids; *Rohrbaugh, Dennis 218
DETERMINATION OF TRIADIMEFON AND IMIDACLOPRID IN WHITE PINE BY GC/MS; *MacDonald, Linda,M.; Rainbird, B.J.; Meyer, Timothy,R. 219
Determination of Triclopyr/Metabolites in Environmental Matrices by GC/MSD; *Olberding, Edward L.; Harnick, Barry J.; Foster, Dale R.; **McNett, Debra A. 220
Determination of Clopyralid in Water With Solid-Phase Extraction and GC/MSD; *Harnick, Barry; Olberding, Edward 221
Evaluation of a Benchtop API LC/MS/MS System for Environmental Analysis; *Bethem, Robert; **Sakuma, Takeo; Shushan, Bori 222
Analysis of Pyrethoid Insecticides by Ion Trap GC/MS/MS; *Bauerle, Gerald; Ray, Kenneth; Brodbelt, Jennifer. 223

Compounds Produced by Motor Burnouts of Refrigeration Systems; *Koester, Carolyn; Hawley-Fedder, Ruth; Foiles, Linda....224
Collisionally-Induced Fragmentation of Chlorinated n-Paraffins.; *Tomy, Gregg; Westmore, John; **Muir, Derek; Stern, Gary....225
LC-MS/MS identification of the major human urinary metabolite of alachlor.; *Driskell, William J.; Hill, Robert H.; Shealy, Dana B.; Hull, R. Delon....226
Structural Characterization of Toxaphene Congeners by GC/MS; *Benoit, Frank M.; Driega, Alex; **Malaiyandi, Murugan....227
Characterization of Major Clorinated Bornanes in Ring Seal Blubber; **Loewen, Mark; *Stern, Gary; Muir, Derek; Westmore, John; Parlar, H....228
Where in the Great Lakes is Toxaphene Going?; *Howdeshell, Mıchael; Glassmeyer, Susan; Myers, Tanya; Hites, Ronald....229
Optimal Ion Trap MS/MS Parameters for the Analysis of Dioxins and Furans; *Plomley, Jeffry B.; **Mercer, Roger S.; March, Raymond E....230
Elemental Compositions from Mass Peak Profiles of M, M+1 and M+2 Ions; *Grange, Andrew H., Donnelly, Joseph R.; **Sovocool, G. Wayne; Brumley, William C....231
Development of a Modernized HRMS Environmental Method for PCBs; *Donnelly, Joseph R.; Grange, Andrew H.; Nichol, Greg; Herron, Nelson; **Brumley, William C....232

Monday Posters - Spray Ionization

Validation of an HPLC-APCI-MS/MS Procedure for Diclofenac in Human Plasma; *Thomas, Darren; Draper, Sally; Hill, Howard; Richard, Martin; Robson, John....233
Effect of Solution Additives and Denaturants on Peptide and Protein ESI-MS *Smelyanskiy, Yanina; **Ogorzalek Loo, Rachel R.; Andrews, Philip C....234
Desolvation of Noncovalently-Bound Complex Ions for ESI-MS Analysis; *Loo, Joseph A.; **Ogorzalek Loo, Rachel R....235
Noncovalent Complex Formation of Cyclodextrins studied by ESI MS; *Penn, Sharron G.; Goodall, David M.; Monnig, Curtis A.; Loran, John S....236
Non-Covalent Complexes formed between Acyl CoA Binding Protein and CoAs; * Robinson, Carol ; Kragelund, Birthe; Knudsen, Jen; Aplin , Robin; Poulsen , Fleming; Dobson, Christopher....237
Source of the Ion at M/Z 622 in "TFA-Fix"; **Ijames , Carl F.; Markey, Sanford P ; Dutky , Robert C ; *Fales, Henry M....238
Electrospray of Borane Salts; High Molecular Weight Clusters and Reactions; *Hop, Cornelis E.C.A.; Saulys, Dovas A.; Gaines, Donald F....239
Comparison of ESI and LSI MS/MS in the Analysis of Newborn Blood Spots; *Chace, Donald; Hillman, Steven; Millington, David; Stevens, Robert....240
Monitoring reactions of nitric oxide with peptides and proteins by ESI-MS; *Mirza , Urooj A.; Lander , Harry M ; Chait, Brian T....241

43rd ASMS Conference on Mass Spectrometry and Allied Topics

Paired Ion ESI of Borane Neutron Capture Agents; *Singh, Padma; Swenson, David; **Schweingruber, Hans; Laine, Roger....242
Negative ESI/MS Enhancement of Primary Amines with TFA/TFE Derivatization; *Fujiwara, Hideji; Nadeau, Ronn G.; Chott, Robert C.; Solsten, R. Thomas....243
Selectivity and Binding Mode of DNA Interacting Molecules Studied by ESI-MS; *Gale, David C.; Camp II, David G.; Smith, Richard D....244
Characterization of Large Glycoproteins Using HPLC/ES-MS; *Huang, Lee; Paiva, Tony; Ramadas, Bhat; Wong, Mel....245
Fragmentation and CID Electrospray Spectra of Antineoplastic Agents.; *Roboz, John; Yu, Qitao....246
Factors Affecting ESI-MS of Nucleobases and Nucleosides; *Yen, Ten-Yang; Voyksner, Robert D.; Charles, M. Juidth....247
New Approach to Determine Modifications in DNA: CZE/MS of Oligonucleotides; Janning, P.; Schrader, W.; Pesch, R.; **Muenster, H.; *Linscheid, M....248
Structure Elucidation of Oligonucleotides Using CZE/ESI MS and Skimer CID; Siethoff, C.; Schrader, W.; Pesch, R.; **Muenster, H.; *Linscheid, M....249
Thermodynamical studies of metal self-assembled complexes by ES-MS *Dupont , Annick; Leize, Emmanuelle, Marquis-Rigault, Annie; Krmer, Roland; Funeriu, Daniel; Lehn, Jean-Marie; Van Dorsselaer, Alain....250
Ion Labeling Study of Self-assembled Supramolecular Species by ESMS *Leize, Emmanuelle; Russell, K.C ; Lehn, Jean-Marie; Van Dorsselaer, Alain....251
Retrospective Analysis of Hyperphenylalaninemias by LSI and ESI MS/MS; *Chace, Donald; Hillman, Steven; Sakuma, Takeo; LeBlanc, Yves; **Shushan, Bori....252
Electrospray Ionization Mass Spectrometric Study of Host-Guest Complexes; *Ramanathan, Ragulan; **Prokai, Laszlo....253
On-line Electrochemistry/Electrospray MS: Study of Oxidation of PAHs; *Xu, Xiaoming; Lu, Wenzhe; Suleiman, Ahmad A.; Cole, Richard B....254
Effects of Anion Encapsulation by Katapinates on Electrospray Mass Spectra; *Giordani, Anne B....255
PROBING THE OLIGOMERIC STRUCTURE OF 4OT USING "NATIVE" ESI-TOFMS; *Fitzgerald, Michael C.; **Chernushevich, Igor; Whitman, Chrıstian P.; Kent, Steven B.H....256
Investigation of Cyclodextrin-Metal Cation Complexes using ESI and FTICR MS; *Kage , David; Watson, Clıff; Prokai, Laszlo; Eyler, John....257
HPLC - Electrospray Mass Spectrometry of Flavonol Glycosides in Hops; *Saegesser, Martin; Deinzer, Max L....258
SULFATED OLIGOSACCHARIDES ANALYSIS : POTENTIALITY OF ESI-MS vs MALDI-TOF MS; *UZABIAGA, Françoise; MONTEIRO, Candida; PETITOU, Maurice; **PROME, Jean-Claude; PICARD, Claudine....259

Detection of Photosubstitution Intermediates of Ru(II) Diimine Complexes; *Arakawa, Ryuichi; Tachiyashiki, Satoshi, Matsuo, Takekiyo. 260
Complexes of Angiotensin II and Transition-Metal (II) Ions Formed By ESI; *Sullards, Cameron, Adams, Jeanette. 261
Amino Acid Coordination to Cu(II)-diimines: Structures and CAD Mechanisms; *Gatlin, Christine, L.; Turecek, Frantisek; Vaisar, Tomas. 262
Peptide Coordination to Cu(II)-diimines: Structures and CAD Mechanisms; *Gatlin, Christine L.; Turecek, Frantisek; Vaisar, Tomas. 263
Analysis of Metal Chelates by Electrospray Ionization Mass Spectrometry; *Wahl, Karen; Stromatt, Robert; Blanchard, David. 264
Production of Coordinated 3d Transition Metal Ions by ESMS; *Xu, Yaodong, Zhang, Xin; Yergey, Alfred L. 265
Characterization of Organometallic Complexes by ESI/Sector MS; *Tong, Huayi; Ng, Ken; Rodebaugh, Ron; Kuell, Chris; Shum, Sai; Pastor, Steve 266
Accurate Mass Measurement of Peptide Ions with a Magnetic Sector Instrument; *D'Agostino, Paul A.; Hancock, James R.; Provost, Lionel R. 267

Monday Posters - Proteins & Peptides

Some Important Effects of MALDI of Small Proteins and Peptides; *Zhu, Y. F.; Lee, K. L.; Tang, K.; Allman, S. L.; Taranenko, N. I.; Chen, C. H. 268
Matrix Solution Effects on the MALDI-MS of Peptides and Proteins; *Cohen, Steven L.; Chait, Brian T. 269
Study of Oxidation Reactions of Selenomethionyl Peptides by MS; *Wang, Rong, Mirza, Urooj A.; Birken, Steven; Chait, Brian T 270
Mapping of B-Amyloid Peptide using Gelatinase.; *Woods, Amina; Cotter, Robert; Ball, M.J.; Roher, Alex 271
Electrospray Mass Spectrometric Studies on Brain Delivery of Neuropeptides; *Prokai, Laszlo; Kim, Ho-Seung; Prokai-Tatrai, Katalin; Bodor, Nicholas 272
Characterization of Iron-binding Siderphores from M. tuberculosis; *Gibson, Bradford; Moore, Christopher; Wong, Diane; Gobin, Jovana; Reeve, Jr., Joseph; Horwitz, Marcus 273
HEMORPHINS IN BLOOD AND BRAIN STUDIED BY MICRODIALYSIS/ES/MS; *Andren, Per E.; Sandersson, Katarina; Caprioli, Richard M.; Nyberg, Fred 274
MS Detection of a new beta-Endorphin-containing Protein in Bovine Pituitary; *Desiderio, Dominic; Yan, Lin; Tseng, Jih-Lie. 275
A Quantitative LC/ESI/MS/MS Method for a Bioactive Peptide in Human Plasma; *White, Robert J.; Oglesby, Thomas D.; Taylor, Paul A.; Florance, James; Wilhelm, Jeffrey A.; Schwartz, Jae C.; Uhrich, Mark D. 276
Mass spectrometric analysis of impurities in peptide synthesis; Chao, Betty; Jiang, Kate; *Papayannopoulos, Ioannis A. 277

Analysis of Crude Synthetic Peptide Mixtures by IonSpray Mass Spectrometry; *Nuwaysir, Lydia; McCandless, Jacqueline; Noble, Dick; Banda, Phil; Chen, Ling; McLean, Matthew. 278
Tandem Mass Spectrometry of Metal-Peptide Complexes.; *Summerfield, Scott; Dale, Vanessa; Despeyroux, Dominique; Jennings, Keith. 279
Loss of the C-Terminal Amino Acid from Transition Metal-Peptide Complexes; *Reiter, Alex; Adams, Jeanette. 280
Intrinsic Coordination between Co(II) and Ni(II) and Histidine Peptides; *Reiter, Alex; Adams, Jeanette. 281
Peptide Adsorption at Gas-Liquid Interfaces Probed by FAB Mass Spectrometry; *van Breemen, Richard B.; Powers, Daniel D.; Kilpatrick, Peter K.; Carbonell, Ruben G. 282
FAB MS of Oxytocin, Deaminooxytocin and Arginine Vasopressin; *Pokrovskiy, Valeriy; Galagan, Natalia, Ostrovskaya, Galina; Rybal'chenko, Vladimir. 283
Processing of Dynorphin A (1-17) in Human and Monkey Blood Studied by MS; *Yu, Jim; **Butelman, Eduardo; Woods, James ; Kreek, Mary Jeanne ; Chait, Brian T 284
Analysis of heterogenous peptide mixtures with MALDI-MS and LC/MS; *Raida, Manfred; Heine, Gaby; Neitz, Susanne; Forssmann, Wolf-Georg. 285
MALDI MS as a Tool in the Characterization of E. Coli RNA Polymerase; *Fenyö, David; Severinov, Konstantin; Severinova, Elena; Darst, Seth; Chait, Brian T.; et al. 286
Pepetide Mapping and MS/MS Analysis of IgG2b containing 2H-Labeled Leucine; *Hirayama, Kazuo; Akashi, Satoko; Noguchi, Kazuyoshi; Yuji, Reiko, Tagami, Uno; Kato, Koichi; Shimada, Ichio; Arata, Yoji. 287
Structural Characterization of IgG Carrying Allotype-j; *Akashi, Satoko; Noguchi, Kazuyoshi; Yuji, Reiko; Tagami, Uno; Kato, Koichi; Shimada, Ichio; Arata, Yoji; Hirayama, Kazuo. 288
Monitoring Antibody Catalyzed Reactions and Interactions; *Siuzdak, Gary; Krebs, Joseph F. ; Benkovic, Stephen J.; Stewart, Jon D ; Strupp, Christian; Hilvert, Don; Dyson, H. Jane. 289
Investigation of Mouse Urinary Proteins Using Electrospray Ionization; *Cox, Kathleen A.; Gaskell, Simon J.; Robertson, Duncan H.L.; Beynon, Robert J. 290
Analysis of a Therapeutic Monoclonal Antibody by HPLC, MALDI-TOF and ESI/MS; *Chan, Stephen; Park, SungAe; Burinsky, David 291
Identifying Human Tear Cytokines by Immunoaffinity Chromatography/MALDI-TOF; *A. , Brockmann; S., Hirsh; R. , Kaswan; R. , Orlando 292
Characterization of Recombinant Human Interferon Alpha-2 by ESI LC/MS; *Heimark, L.; Huang, E.; Pramanik, B.; Nagabhushan, T.L. 293

Mass Spectrometric Characterization of the rhM-CSF Receptor Binding Site; Kalkum, Markus; Yamamoto, Ralph; Schreurs, Jolanda; Deinzer, Max L., *Glocker, Michael O ... 294
Comparison of the Crystallins from Normal and Cataractous Human Lenses; *S., He; S., Pan, K., Wu; R. , Orlando ... 295
Identification of Modified Human Water Insoluble Lens Crystallins by MS.; *Lund, Anders L ; Smith , Jean B.; Smith , David L. ... 296
Problems and Solutions in Sequencing a Mussel Foot Protein from M. edulis.; *Papov, Vladimir; Biemann, Klaus ... 297
Mass Spectrometry of Marine Biomolecules; *Ross, Mark; Waite, Herb; Taylor, Steven. ... 298
Structure elucidation of the sex-differentiation protein in Crustacea by MS; Martin, Gilbert, Sorokine, Odile; Moniatte, Marc; *Van Dorsselaer, Alain. ... 299
Sequence Characterization of a Spider Silk Protein by Electrospray MS/MS; *Yeung, Bernice; Vouros, Paul; **Mello, Charlene M.; Kaplan, David L. ... 300
Processing of avian sarcoma and leukemia virus precursor polyprotein.; *Papayannopoulos, Ioannis A.; Pepinsky, R. Blake; Chow, E. Pingchang; **Vogt, Volker M ... 301
PHOSPHORYLATION SITE IDENTIFICATION BY LC/MS/MS WITH AN ION TRAP MS; *Gillece-Castro, Beth; Arnott, David; Bier, Mark; Land, Adrian; Stults, John ... 302
Electrospray Ionization Mass Spectra of Recombinant Hirudin Byproducts.; *Lango, Jozsef; **Roboz, John; Salat, Janos; Yu, Qitao; Barta, Istvan; Ott, Istvan; Ambrus, Gabor; Simay, Antal. ... 303
Mapping of Brain Proteins Using MALDI/TOF-MS Combined with HPLC; *Ingendoh, Arnd; Seta, Kazuo, Kanai, Michiko; Nakayama, Hiroshi, Uchida, Kazuhisa; **Isobe, Toshiaki; Okuyama, Tsuneo. ... 304
Mass Determination of Large Proteins Exceeding 200 kDa by MALDI/TOF-MS; *Ingendoh, Arnd; Seta, Kazuo; Kanai, Michiko; Yamakawa, Yoshio, Omori-Satoh, Tamotsu; **Isobe, Toshiaki; Okuyama, Tsuneo. ... 305
CHARACTERIZATION and SEMI-QUANTITATION of CHONDROITINASE (MW 111 & 112 kDa); *Siegel, Marshall; Tabei, Keiko; Berkenkamp, Stefan; **Hillenkamp, Franz; Khandke, Kiran. ... 306
Dist. & Loading of Calicheamicin Derivatives Conjugated to Monoclonal...; Siegel, M; Keiko, T; Kunz, A; Berkenkamp, S; Hillenkamp, F. ... 307
MS Analysis of FILAMENTOUS HEMAGGLUTININ and MoAb-CALICHEAMICIN CONJUGATES; *SIEGEL, MARSHALL Ass; TABEI, KEIKO; KUNZ, ARTHUR; BERKENKAMP, STEFEN; **HILLENKAMP, FRANZ. ... 308
Observation of holoprotein molecular ions of several ferredoxins by ESI-MS; Ptillot, Yves; *Forest, Eric; Meyer, Jacques; Moulis, Jean-Marc; ... 309
PROTEOLYTIC PEPTIDES OF RHODOPSIN ANALYZED BY MALDI-TOF; *Barnidge, D. R.; Dratz, E. A.; Sunner, J.; Jesaitis, A. J. ... 310

Analysis of Hydrophobic Peptides and Proteins using ESI- and APCI-MS; *Pellascio, Bernhard; Schlunegger, Urs P.; Schaller, Johann, Kaesermann , Donald. ... 311
Heregulin/Epidermal Growth Factor Chimeras: A Structural Study; *Rosnack, Kenneth; Guarino, Bradley; Singleton, David; Barbacci, Elsa; Moyer, James; Andrews, Glenn; Stroh, Justin. ... 312
LC-MS peptide map of hirudin by using the unspecific protease thermolysin; *Zilg, Harald A.; **Schultz, Birgit. ... 313
Advances in Peptide Mapping by MALDI-TOF-MS; *Vorm, Ole; **Roepstorff, Peter; Mann, Matthias, Houthaeve, Tony ... 314
Use of ESMS for the study of the mechanism of resistance to beta-lactams; *Burlet-Schiltz, Odile; Saves, Isabelle; Samama, Jean-Pierre; Masson, Jean-Michel; Prom, Jean-Claude. ... 315
Analysis of Bovine Insulin (SBI) and Reduced SBI in Glucose Film by PDMS; *Song, Siqing; Cockrill, Steve; Macfarlane, Ronald, D. ... 316
Molecular Recognition in Drug Discovery; *Bell, David; West, Andrew. ... 317
ESI-MS/MS for the Identification of Modifications in Intact Proteins; Busman, M.; Wilcox, M. D.; McIntire, W. E.; Hamm, H. E.; Hildebrandt, J. D.; *Schey, K. L. ... 318
Mass Spectrometric Analysis of Recombinant Stromelysin and Collagenase; *Bauer, M.D.; Sun, Y., Anastasio, M.B., Snider, C.E. ... 319
Characterization of Recombinant NMDA Receptor Regions with ESIMS; *Eckart, Klaus; Koepke, Andreas K. E., Spiess, Joachim. ... 320
Enhanced Nucleophilicity of the N-terminal Proline in a Protease; *Yu, Zhonghua; Craik, Charles; **Jones, Patrick; Burlingame, Alma. ... 321
SEQUENCE AND Ca2+ BINDING PROPERTIES OF FROG (Rana tegrinka) PARVALBUMIN; *Hu, Peifeng; Buckel, Scott; Whitton, Margie; Loo, Joseph A. ... 322
Determination of the Sites of Non-Labile HNE-Adduction to Proteins; *Bolgar, Mark S.; Gaskell, Simon J. ... 323
Protease-catalyzed Incorporation of 18O into Protein Fragments; Schnolzer, Martina; Jedrzejewski, Paul; **Lehmann, Wolf ... 324
Methodology to Identify Proteins using LC-Ion Trap Mass Spectrometry; *Yates, John; Eng, Jimmy; Schieltz, David; Link, Andrew. ... 325
Cross linking of native protein complexes by organic mustards; *Hathout, Yetrib; Fenselau, Catherine. ... 326

Tuesday Orals
Mass Spectrometry in Pharmacology & Toxicology

Applications of MS/MS to the Study of S-Linked Conjugates of Isocyanates; *Davis, Margaret R.; Baillie, Thomas A ... 327
Strategies for Analyses of Drug Metabolite Mixtures by CE-MS and CE-MS/MS; *Naylor, Stephen; Benson, Linda M ; Tomlinson, Andy J. ... 328

Probing the Regioselectivity of Gas Phase Alkylation of Biomolecules; *O'Hair, Richard A.J ; Freitas, Michael A.; Gronert, Scott; Schmidt, Joseph A. R.; Williams, Todd D 329
Determination of ß-Agonists in Bovine Retina Using LC-APCI/MS and MS/MS; *Doerge, Daniel R., Bajic, Steve; Churchwell, Mona I. 330
The Use of GC-MS Techniques to Evaluate Biological Lipid Peroxidation; *Mathews, W. Rodney; Guido, David; McKenna, Rosemary; Laskey, Rachel.... 331
Macrolide Antibiotic Residues in Distiller's Grain and Milk by ESI LC/MS; *Flurer, Rick; Tomlinson, John; Satzger, Duane. 332
Isoprostane Families Following Free Radical Oxidation of Arachidonic Acid; *Waugh, Russell J.; Murphy, Robert C. 333
Beclomethasone Dipropionate and Metabolites in Plasma via HPLC-APCI/MS/MS; *Bryant, Matthew S.; Korfmacher, Walter A.; Nardo, Cymbelene L , Lapiguera, Amelia P.; Lin, Chin-Chung; **Langevin, Carolyn N.; Oglesby, Thomas D. 334
Column-switching sample preparation for quantitative analysis by LC-MS; *Hopfgartner, Gerard; Zell, Manfred; Husser, Christophe; Lausecker, Berthold.... 335
Direct Measurement of Steroid Glucuronides and Sulfates with HPLC/MS; Sanaullah, , *Bowers, Larry 336

Tuesday Orals - Mass Spectrometry in Environmental Research

Haloacetic Acid Drinking Water Disinfection By-Products; *Budde, William L.; Munch, Jean W.; Kryak, David D.; Behymer, Thomas D 337
Investigating Oxidation Reactions in Environmental Systems; *Charles, M Judith; Feinberg, Thomas N.; Richardson, Susan. 338
High Speed Analysis of TTHM Content in Drinking Water using MIMS; *Bauer, Scott, Bauer, Jan. 339
Chemistry and Toxicology of Poultry Chiller Water; *Haddon, William F., Binder, R.G., Harden, Leslie A., Wong, R Y , Stevens, K.L 340
Measurement of Verrucarol, a Product of Satratoxin, in Urine by APCI-MS/MS; *Schurz, Helen, Hill, Robert. 341
HPLC/MS & HPLC/MS/MS Analysis of Explosives in Environmental Samples; Gates, Paul M.; *Furlong, Edward T.; Lindley, Chris E.; Burkhardt, Mark R. 342
MS/MS CID FRAGMENTATION PROCESSES IN SOME PESTICIDES; *Yinon, Jehuda. 343
Quantification of Non-Persistent Pesticides in Human Serum; *Barr, John R.; Patterson, Donald G.; Jr.; Maggio, Vincent L.; McClure, P. Cheryl; Turner, Wayman E.; Newman, Carolyn M.; Needham, Larry L. 344
ESI MS/MS Determination of a New Cationic Surfactant in River Water; *Mertens, Thomas R.; Dunphy, Jocelyn C., Kershner, Karen M.; Morris, III, Samuel J. .. 345

Advantages and Applications of Mass Peak Profiles Plotted from SIR Data; *Grange, Andrew H.; Donnelly, Joseph R.; **Sovocool, G. Wayne, Brumley, William C. 346

Tuesday Orals - Chemistry of Multiply-Charged Ions

Protein Desalting via Gas-Phase Ion-Molecule Chemistry; *Pope, Marshall; Hofstadler, Steven; Dejsupa, Chadin; Dearden, David. .. 347
Importance of Charge-Separation Reactions in ESI/MS-MS; *Adams, Jeanette, Strobel, Fred; Reiter, Alex. .348
The Correlation of Fragmentation and Structure of a Protein; *Wu, Qinyuan ; Van Orden, Steven; Cheng, Xueheng; Bakhtiar, Ray; Smith, Richard D. .349
Quadrupole Ion Trap Study of Ion-Ion Chemistry of Multiply-Charged Ions; *Herron, William, J.; Goeringer, Douglas, E ; McLuckey, Scott, A. 350
Isomeric Structures for Ubiquitin Ions Produced by Electrospray FTMS; *Cassady, Carolyn J.; Ewing, Nigel. .351
Electrostatic Forces in Multiply Protonated Gas-Phase Ions; *Williams, Evan R ; Gross, Deborah S ; Schnier, Paul S , Rodrigez-Cruz, Sandra; Fagerquist, Clifton K. . 352
SID of Multiply-Charged and N-Terminal Fixed-Charge Derivatized Peptides; *Dongre, Ashok; Somogyi, Arpad; Wysocki, Vicki. .353
Deprotonation Reactions of Small Peptide Ions Produced by Electrospray; *Carr, Scott R.; Cassady, Carolyn J. .354
Characterization of Carbonic Anhydrase-Inhibitor Noncovalent Complexes; Cheng, Xueheng, *Chen, Ruidan, Bruce, James E , Schwartz, Brenda L , Anderson, Gordon A.; Hofstadler, Steven A.; Gale, David C.; Smith, Richard D . 355
Compounds That Elude FAB Analysis: It All Begins in Solution!; Noon, Kate; *Allison, John. ..356

Tuesday Orals - Laser Desorption Ionization-Applications

MALDI-MS in the Infrared: A critical evaluation; *Hillenkamp, Franz; Karas, Michael; Berkenkamp, Stefan. . 357
Sequencing Electroblotted Proteins by Tandem Mass Spectrometry; *Fabris, Dan; Vestling, Martha M.; **Cordero, Marcela M ; Doroshenko, Vladimir M ; Cotter, Robert J.; Fenselau, Catherine. 358
MALDI AND PSD CHARACTERIZATION OF RELEASED CARBOHYDRATES FROM GLYCOPROTEINS; *Rouse, Jason C.; Vath, James E.; Scoble, Hubert A. .359
MASS SPECTROMETRY IN PROTEIN AND GLYCOPROTEIN STRUCTURE ELUCIDATION.; Morris, Howard R.; Dell, Anne, Panico, Maria; *McDowell, Roy A. 360
Nucleotide analogs increase the stability of DNA for MALDI-MS analysis; *Schneider, Klaus; Chait, Brian T. 361

Molecular Diagnostics Via Mass Spectrometry of PCR-Amplified DNA Products; *Buchanan, Michelle V.; Doktycz, Mitchell J.; Hurst, Gregory B.; McLuckey, Scott A.; Habibi-Goudarzi, S. 362
Analysis of DNA and Modified Proteins with Resolution Improvements in MALDI; *COLBY, STEVEN; ARNOLD, RANDY; CHRISTIAN, NOAH, HOUSTON, CHRIS; REILLY, JAMES. 363
Applications of High Resolution MALDI TOF to Oligonucleotide Problems; *Juhasz, Peter; Vestal, Marvin; Martin, Stephen; Takach, Ed; Haff, Lawrence; Roskey, Mark; Smirnoff, Igor. 364
Applications of MALDI/TOF in Polymer Chemistry; *Danis, Paul O.; Huby, Francois. 365
Polymer Characterization: A Comparison of MALDI vs Direct Laser Desorption; *Weil, David A.; Jacoby, Cliffton B 366

Tuesday Orals - Mechanisms of Ion-Molecule Reactions

Chemical Reactions vs Collision-Induced Dissociation to Cleave Amide Bonds; *Williams, Tracie L.; Stephenson, James L.; Yost, Richard A. 367
Neutral Products From Ion-Molecule Reactions: F- + 5-Chloro-1,3-Pentadiene; Baschky, Michael; *Kass, Steven; Kass, Steven. 368
Ion-Molecule Reactions of Trimethylenemethane Radical Cation; *Chou, Phillip; Painter, Sherry; Blackstock, Silas; Kenttamaa, Hilkka. 369
Reactions of Small Carbon Clusters with Nitrogen Containing Compounds; *Dunbar, Robert C.; Pozniak, Boguslav P. 370
Ion-Molecule Reactions of 18-Crown-6 With its Fragment Ions Shen, Nanzhu; *Dejsupa, Chadin; Pope, Marshall; Dearden, David. 371
Reactions and Rearrangements of TMS Dimer Radical Cation.; *Peschke, Michael; Mckee, Michael; Illies, Andreas. 372
Ion Molecule Reactions of Organophosphorus Compounds; *Wensing, Michael W.; Snyder, A. Peter; Harden, Charles S. 373
State-selected reactions between N2+ molecular ions and atoms and molecules; *de Gouw, Joost A.; Ding, Li N.; Kato, Shuji; Bierbaum , Veronica M.; Leone , Stephen R. 374
Symmety Induced Kinetic Isotope Effects in the Formation of Ar¥CO2+; *Gellene, Gregory; Yoo, Ryong 375

Tuesday Posters - Ion Activation & Dissociation

Structural Aspects of Metal-Oligonucleotide Binding Studied by ESI-CID-MS *Cheng, Xueheng; Wu, Qinyuan; Gao, Quanyin; Hofstadler, Steven A.; Smith, Richard D.; 376
Gas Phase Chemistry of MX+ Ions (X= H, Na, Cu) from Glycine and Arginine; *Beranova, Sarka; Cerda, Blas; Wesdemiotis, Chrys 377
ESI MS-MS Using B/E vs MIKES Scans; *Sullards, Cameron; Adams, Jeanette. 378

43rd ASMS Conference on Mass Spectrometry and Allied Topics

Electrospray MS of Multiple Alkali Ion Complexes of Proteins and Peptides; Wang, Jianyao; Ke, Fu; Guevremont, Roger; *Siu, K.W.Michael. 379
INFLUENCE OF 2ND STRUCTURE ON PEPTIDE ION DISSOCIATION IN A TANDEM TOFMS; *Gimon-Kinsel, Mary; Russell, David. 380
Intra-ionic Acid/Base Interactions in the CID of Protonated Peptides; *Cox, Kathleen A.; Whiting, Andrew; Gaskell, Simon J. 381
A Multistep Pathway Leading to Peptide wn Ions Confirmed by MS3 and MS4; *Ballard, Kevin; Orkiszewski, Ralph; **Gaskell, Simon. 382
WHY ARE B IONS STABLE SPECIES IN PEPTIDE SPECTRA?; *Yalcin, Talat; Harrison, Alex. G. 383
Gas Phase Reactions of Protonated Biologically Active Peptides.; *MOSELY, JACKIE A; DERRICK, PETER J; GALLAGHER, RICHARD T; COOPER , HELEN J; CRAIG, ANTHONY G 384
Correlation of Energy Losses from CID with Observed Peptide Fragments; *Vachet, Richard W.; Winders, Andrew; Glish, Gary L. 385
Peptide Sequencing Using a Hybrid Magnetic Sector oa-TOF Mass Spectrometer; *Sun, Y.; Bauer, M.D.; Lacey, M.P.; Keough, T. 386
Peptide Fragment Mass Spectra: Comparison of PSD and CID spectra.; *Hines, Wade; Peltier, John; Hsieh, Frank; Martin, Steve. 387
CAD and Photodissociation of Multiply Charged Ions; *Watson, Clifford; Yang, Yarjing; Nawrocki, Joe; Eyler, John. 388
Impulsive Excitation of Ions during Surface-Induced Dissociation; Burroughs, John A.; *Wainhaus, Samuel B.; Hanley, Luke. 389
Electrospray Mass Spectra of Simple Aliphatic Diamines and Methiodides; *Zhang, X. Kate; **Fales, Henry M. 390
Thermal Radiation Induced Dissociation of Tetraethylsilane Cation; *Lin, Chuan-Yuan; Dunbar, Robert C. 391
Some More C3H6O2 Distonic Radical Cations; *An, Yan, Holmes, John L. 392
The Fragmentation of Geometric Isomer, Ionized Maleic and Fumaric Acids; *Chen, Hongwen; Holmes, John L. 393
Characterization of small, oxygen-rich ions.; *Aubry, Christiane; Holmes, John L. 394
The Identification of C3H6O+. from 2-Methoxyethanol.; *Polce, Michael J.; Wesdemiotis, Chrys. 395
N-substituted Benzisothiazolinons: Oxygen Rearrangement on Electron Impact.; *Lango, Jozsef. 396
Unimolecular Dissociation of Acetophenone by Thermal Radiation; Sena, Marcelo; *Riveros, José M. 397
Hyperthermal Surface Ionization of Organic Molecules: Alkyl Alcohols; *Kishi, Hiroshi; **Fujii, Toshihiro. 398
The Unimolecular Dissociation of Energy Selected 2, 5-Dihydrofuran; *Teklehaimanot, Bibi; Meisels, Gerry. 399

Influence of Substituents on Propene Loss from Aryl n-Propyl Ether Ions; *Matimba, Henri E. K.; Ingemann, Steen; Nibbering, Nico M M 400
Angle/Energy-Resolved CID of CS2+ ions at 8-35 eV Collision Energy; Shukla, Anil K.; *Tosh, R.E.; Futrell, Jean H. 401
Tandem crossed beam collision induced dissociation of CO2+; *Chawla, Rahul; Krishnamurthy, M.; Shukla, A. K. ; Futrell, J. H. 402
Investigation of Kinetic Trans Effect in Bis(platinum) Complexes by SID; *Schaaff, Thomas; Qu, Yun; Farrell, Nicholas; Wysocki, Vicki. 403
NI FAB and DCI-MS of Sulfonylurea Herbicides; CAD Spectra of (M-H)- Ions; *Winnik, Witold; Betowski, Leon; Brumley, William 404
DEP/CI-MS/MS Characterization of Sulfonylurea Herbicides; *Johnson, Jodie V.; Yost, Richard A. 405
Measurement of phosphonate proton affinities by using the kinetic method.; **Aline, Leroy; Françoise , Fournier; Jacquy, Dissard; Isabelle, Daoust-Maleval; André, Tambuté; *Jean-Claude, Tabet. 406
CID Studies of Inorganic Species Released During Biomass Combustion; *Dayton, David; Wang, Dingneng. 407
Photodissociation of Electrosprayed Ions in a Quadrupole Ion Trap; *Boue, Stephen M.; Stephenson, James L., Yost, Richard A 408
Pulsed Pressure Quadrupole Ion Trap for Tandem MS of Peptides; *Doroshenko, Vladimir M.; Cotter, Robert J. 409
Thermal Activation of Stored Ions in a Quadrupole Ion Trap; *Herron, William J.; Goeringer, Douglas E.; McLuckey, Scott A. 410
The Analytical Utility of Photodissociation in Tandem Mass Spectrometry; *Beussman, Douglas J.; Erickson, Tina A., Enke, Christie G. 411
SMIKES: A New Scan to Determine the Origin of Artefact Peaks in MIKE Scans.; *Mouget, Yves; Bertrand, Michel J. 412
Mapping Metastable Decays in a TOF MS with a Single-stage Ion Mirror; *Brinkmalm, Gunnar; HŒkansson, Per; Sundqvist, Bo U.R.; **Barofsky, Douglas F. 413
Tandem Mass Spectrometry Utilizing the Advantages of Both MALDI and FTMS; *Castoro, John; Shew, Sandy; Stout, Howard; Winger, Brian; Campana, Joseph 414
MS/MS Studies Using a Hybrid Magnetic Sector oa-TOF Mass Spectrometer; *Keough, T.; Lacey, M.P.; Bauer, M.D.; Sun, Y. 415
Surface Induced Dissociation of Biomolecules and Polymers by MALDI-FTMS; *Pastor, Salvador J.; Yao, Jie; Wilkins, Charles L. 416
Identifying Possible Sources of Ion Neutralization at SAM Surfaces; *Kane, Thomas; Angelico, Vincent; Nair, Hari; Somogyi, Arpad; Wysocki, Vicki. 417
Hydrogen-addition Reactivity of Ions on Odd vs Even Chain Alkanethiol SAMS; *Franklin, Rebecca; Zhong, Wenquing; Somogyi, Arpad; Wysocki, Vicki. 418
Derivatization Reactions for FAB, LSIMS, and Electrospray Ionization; *Carlson, Rich; Busch, Kenneth L. 419

EFFECT OF A MATRIX ON LSIMS-INDUCED FRAGMENTATION OF PHOSPHATE ESTER BOND; *Dass, Chhabil. 420
Parent Resolution in FFR1 MS/MS: Revelations from Ion Intensity Plots; *Ballard, Kevin; **Vachet, Richard; Orkiszewski, Ralph; Glish, Gary, Vrbanac, James; Gaskell, Simon 421

Tuesday Posters - Separations/MS Techniques

Identification of fullerenes in natural flames by APCI/LCMS; *Taghizadeh, Koli; Nauman, David; Lafleur, Arthur; Howard, Jack 422
Effect of Mobile Phase Buffers on Sensitivity in Negative APCI LC/MS; *Schaefer, William; Dixon, Frank, Jr 423
Analysis Of Selected Pharmacueticals Using Different API Techniques; *Goodley, Paul C.; Fischer, Steven. 424
Oscillating Capillary Nebulizer Interfacing with Mass Spectrometers; *Ho, Z. Stacy; Drew, Barry; Browner, Richard. 425
EVALUATION AND APPLICATION OF NEGATIVE ION ATTACHMENT LC/MS; *Norwood, Daniel; Fisher, Dixie, Mullis, James. 426
ANALYSIS OF CEFTIOFUR AND ITS METABOLITES IN MILK BY LC/API-MS; Voyksner, Robert; *Keevers, Jeff. 427
Electrospray Liquid Chromatography/Mass Spectrometry of Ginsenosides; van Breemen, Richard B.; *Huang, Chao-Ran; Rimando, Agnes; Lu, Zhi-Zhen, Fitzloff, John F. 428
Electrospray Liquid Chromatography/Mass Spectrometry of Carotenoids; *van Breemen, Richard B. 429
Multi-residue method of §-agonists by immunoaffinity extraction-LC/LC/MS/MS; *Cai, Jianyi, Henion, Jack. 430
An LC/MS Method Using Non-volatile Mobile Phases with Ionspray Ionization; *Mallis, Larry M.; Slayback, John R. B. 431
A Rapid Universal LC/ESI-MS Method for Profiling Drug Metabolites; Taylor, Susan; *Starrett, Anne, DiDonato, Gerald; Lee, Michael. 432
Electrospray LC/MS Profiling in Evolving Pharmaceutical R&D Strategies; *Kerns, Edward H.; Volk, Kevin J.; Klohr, Steven E.; Rourick, Robyn A., Thompson, William L.; Whitney, Jeffrey L.; Lee, Mike S. 433
Examination of Chiral Purity by HPLC-MS; Davidson, Susan; Pullen, Frank; *Richards, Don, Wright, Adrian 434
Quantitative Aspects of HPLC Peak Purity Determination by ESI/MS.; *Bryant, Duncan 435
Data Dependent Automated MS/MS Switching Methods for Routine LC/MS/MS; *Mylchreest, Iain; Campbell, Clay; Wheeler, Kevin; Wakefield, Michael. 436
Electrospray vs. Thermospray LC/MS for Analysis of Small Molecules; *Creasy, William R. 437

Enhanced Sensitivity LC/MS Using Low Resolution Quadrupole Mass Analysis; *Dodsworth, David W.; Alexander, Anthony J.; Blackledge, James A. 438
Electrospray Interface for Submicroliter LC/MS Analyses; *Davis, Michael T.; Lee, Terry D. 439
Separation and Analysis of Human Lens Alpha-Crystallins by LC-ESIMS *Lin, Peiping; Smith, Jean B., Smith, David L. 440
Preparative Applications of Microcapillary HPLC for Mass Spectrometry; *Hackett, Murray; Hendrickson, Ronald C.; Falchetto, Rocco; Walker, Carthene B.; Shabanowitz, Jeffrey; Hunt, Donald F. 441
Multi-Dimensional LC-MS and LC-MS/MS for Protein Sequencing and Mapping; *Hsieh, Frank, Elicone, Chris; Wang, HangQi; Tarr, George; Regnier, Fred; Martin, Stephen 442
Peptide Sensitivity by LC-ESI/MS as a Function of Column Diameter; *Ackermann, Bradley; Fields, Steven; Regg, Brian; **Dourdeville, Theodore. 443
ENHANCING API-MS PERFORMANCE THROUGH CHROMATOGRAPHY; *Voyksner, Robert; Keever, Jeff. 444
Effects of Salts and Trifluoroacetic Acid on Aerosol MALDI Ion Signal *Beeson, Michelle D.; Wei, Xiaona; Russell, David H. 445
Application of LC/IT/reTOF MS to Peptide Mapping and Drug Analysis; *Qian, Mark G , Liang, Li, He, Ling, Lubman, David M. 446
Continuous Flow MALDI MS in an Ion Trap/reTOF Mass Spectrometer; *Liang, Li; He, Ling; Chien, Benjamin; Lubman, David. 447
Structures of Bioploymers; A Combined MALDI - Ion Chromatography Approach; von Helden, G.; Wyttenbach, T.; Lee, S.; *Bowers, M.T. 448
CITP ESI-FTICR for the Study of X-Irradiation Damaged Tetranucleotides; *Hofstadler, Steven A; Zhao, Zhongxi, Bruce, James E; Smith, Richard D; Budzinski, Ed; Dawidski, Jean; Gobey, Jason, **Box, Harold. 449
Complex Mixture Analysis by using Liquid Chromatography Coupled with FTMS; *Winger, Brian, Castoro, John. 450
MALDI-TOF-MS of Organometallic Species: Comparison to FAB and ESI; *Grimm, Deborah A.; Baba, Aaron I ; Yongwu, Liang; Simon, Jerald; Schmehl, Russell H. 451
ATMOSPHERIC PRESSURE CHEMICAL IONIZATION FOR CE/MS; *Takada, Yasuaki; Sakairi, Minoru; Koizumi, Hideaki 452
DETERMINATION OF AMINO ACIDS BY ON-LINE CAPILLARY ELECTROPHORESIS - ESI/MS; *Lu, Wenzhe; Yang, George; Cole, Richard B. 453
CE-Ionspray-MS Analyses of Tryptic Peptides using a Benchtop Quadrupole MS; *Anacleto, Joseph F.; Allen, Mark. 454
CE/ES/MS of Peptides and Proteins Using A New Sheath-flow Probe; *Banks, J. Fred; Whitehouse, Craig M. 455
Analysis of Peptides, and Proteins Using CE/ESI/MS; *Moini, Mehdi; Cao, Ping; Ray, Kenneth; Holbert, Anthony. 456

On-line Characterization of Peroxidation Intermediates of NAD by CE-ESI-MS; *Zhao, Zhongxi (Zack); Udseth, Harold R.; Smith, Richard D. 457
Electrospray CZE/MS and LC/MS With An Ion Trap Mass Spectrometer; *Stacey, Catherine; Schubert, Michael; **Banks, J.Fred. 458
Direct Analysis of Cellular Proteins by Capillary Electrophoresis FTICR-MS; *Hofstadler, Steven A.; Swanek, Frank D.; Gale, David c.; Zhao, Zhongxi; Bruce, James E.; Ewing, Andrew , Smith, Richard D. 459
CE/ITMS: Achieving Ultra-low Detection Limits; *Ramsey, Roswitha S.; Goeringer, Doug E ; Van Berkel, Gary J.; McLuckey, Scott A. 460
A new setup for on-line CE-MS; *Li, Xuhui; Wu, Jingtao; Li, Hongwei; Lubman, David. 461
OFF-LINE COUPLING OF CAPILLARY ELECTROPHORESIS AND MALDI-TOF MS.; *Walker, Kathleen L.; Chiu, Rick W.; Monnig, Curtis A. ; Wilkins, Charles L. 462
Influence of the Source geometry on the Ion formation in LC/TSP-MS; *Honing, Maarten; Barcel, Damia; Abian, Joaquin; Gelp', Emilio; **Volmer, Dietrich; Levsen, Karsten. 463
Determination of Steroids by HPLC/UV-VIS/Particle Beam Mass Spectrometry; *Mesmer, Mantai; Satzger, R. Duane. 464
LC Particle Beam MS with Massive Cluster Impact; *Wang, T.-C. L.; Cornio, L J.; Markey, S.P. 465
Particle Beam LC/MS using a Glow Discharge Ionization Source; *DePalma Jr., Patrick; You, Jianzhang; Marcus, R. Kenneth; Willoughby, Ross C. 466
LC/MS for Identification of N-Nitrosamines in Cosmetic Raw Materials; *Billedeau, Stanley M ; Wilkes, Jon G ; Thompson, Harold C. 467
SFC/MS: Development and Problem Solving; *Pinkston, J. David; Smith, Claudia A.; Hentschel, Rosemary T.; Bowling, Donald J. 468
Separation and Identification of meso-substituted tetraphenylphorphyrins *M. Domingues, M. Rosario ; O. S. Marques, M. Gra a; Ferrer Correia, A. J. 469
Quantitative Analysis of Abscisic Acid in Plant Tissue Using LC/MS/MS; *Hogge, Lawrence; Abrams, Suzanne; Abrams, Garth; Bock, Cheryl; Dunstan, David; Olson, Douglas, Shaw, Angela. 470
Evaluation of GCMS and FABMS for Analysis of Fungicidal DTTT Degradation; Teesch, Lynn, Thorne, Peter S., *Subramanian, Periyasamy. 471
Pentafluorobenzyl Chloroformate as a Derivatization Reagent for NCI/MS *Simpson, J.T.; Torok, D.S.; Markey, S P. 472
Thermal Study of Glycyrrhizic Acid by On-line Thermogravimetry/GC/MS; *Chung, Henry; Aldridge, John; Dull, Gary; Shu, Chi-Kuen. 473
Characterization of Aromatized Biomarkers by GC/MS/MS with CI; *Hsu, Chang Samuel; Dechert, Gary J.; **Schaps, Marlene E., Hieshima, Glenn B. 474
Structure Elucidation of Trace Components in Pharmaceuticals Using GC/MSn; *Schachterle, Steve. 475
Isotopically Labeled Internal Standards Analysis Using Ion Trap GC/MS/MS; *Bolton, Barbara A.; Schachterle, Steve 476

Reproducibility Study of GC/MS/MS with an Ion Trap Mass Spectrometer; *Bolton, Barbara A.; Schachterle, Steve 477
High Speed Method Optimization For Routine GC/MS/MS In An Ion Trap; Wells, Greg; *Huston, Chuck. 478
Dual Oven Multidimensional Fast GC with Spectral Detection; *Sasaki, Tania A.; Wilkins, Charles L. 479
High-Speed GC/MS Using a Quadrupole Mass Filter; *Grimm, Casey; Lloyd, Steven; **Munchausen, Linda. 480
HIGH-SPEED GC/MS WITH A FAST DOUBLE-FOCUSSING MASS SPECTROMETER; Van Ysacker, Peter G.; Brown, Jeff; Phillips, Andy; Janssen, Hans-Gerd; *Leclercq, Piet A. 481
Fast, Very Fast and Ultra Fast GC-MS in Supersonic Molecular Beams; *Amirav, Aviv, Dagan, Shai. 482

Tuesday Posters - Combinatorial Libraries

Non-Peptide Libraries: Structure Determination by LC/MS/MS.; *Issakova, Olga; Ma, Nina; Kocis, Petr; Sepetov, Nikolai. 483
Optimization of MALDI Sequencing of Support-Bound Combinatorial Libraries; Youngquist, R. Scott; Fuentes, Gary R., Miller, Cathy M.; Ridder, Gregg M.; Lacey, Martin P.; *Keough, Thomas 484
Characterization of Small Molecules by ESI and APCI; *McKay, Richard; McEwen, Charles; Larsen, Barbara. 485
MS/MS of Thiazolidinones: Applications of MS in Combinatorial Chemistry; *Fitch, William, Shah, Nikhil, Holmes, Christopher, Look, Gary, Ni, Zhi-Jie. 486
Characterization of Complex Chemical Libraries Using LC/MS/MS; *Nugent, Kerry; Baldwin, Samuel W.; Land, Adrian P. **; Bier, Mark E. **; Wheeler, Kevin **; **Spear, Kerry L.; Figliozzi, Gianine M.; Zuckerman, Ronald N. 487
MS Analysis of Chemical Libraries Employing a Novel Photocleavable Linker; *Wagner, David; Geysen, H. Mario; Brown, Bradley 488
LC/MS Strategy for the Rapid Profiling of Solid Phase Synthetic Products *Rourick, Robyn, A.; Whitney, Jeffrey, L.; Klohr, Steven, E.; Volk, Kevin, J.; Kerns, Edward, H.; Lee, Mike, S. 489
MALDI-TOF-PSD Analysis of Peptides on Polymeric Beads; *Griffin, Patrick; Konteatis, Zenon; Klatt, Tracey. 490
Characterization of a Benzodiazepine Combinatorial Library By IAE/LC/MS/MS; *Nedved, Michael L.; **Ganem, Bruce; Henion, Jack D. 491
Analysis of Non-peptide, Bead-bound Combinatorial Libraries by MS; *Hemling, Mark; Hertzberg, Robert; Johnson, Walter; Mentzer, Mary; **Roberts, Gerald; Taylor, Paul; Weinsotck, Joseph; Carr, Steven. 492
Determination of the Diversity of Small-Molecule Libraries by ESI-MS; *Dunayevskiy, Yuriy; Vouros, Paul; Carell, Thomas; Wintner, Edward A.; Rebek, Julius Jr. 493

Mapping Chemical-Space: Application and Prediction Within LC/MS; Samuel, Mitrovich; *Willoughby, Ross. 494

Tuesday Posters - Toxicology

Alkylation of E. coli Thioredoxin by S-(2-chloroethyl)glutathione; *Erve, John, Barofsky, Lilo; Barofsky, Douglas; Deinzer, Max; Reed, Don. 495
Optimization of Instrumental Parameters used in HRMS of DNA Adducts; *Scheller, Nova; Ranasinghe, Asoka; Wu, Kuen Yuh; Swenberg, James A. 496
Quantitative Analysis of DNA Adducts by Using HPLC/ESI-MS; *Yen, Ten-Yang; Christova-Gueor, Nadia I ; Scheller, Nova, Swenberg, James A.; Charles, M. Judith. 497
Fragmentation of Thioether Conjugates by ESI and Low-Energy CID; *Oberth, C.H.; Jones, A.D. 498
ESI-LC-MS analysis of heterocyclic aromatic amines and their conjugates; *Stillwell, W. G.; Wishnok, J. S.; Kidd, L. R.; Tannenbaum, S. R.; **Turesky, R. J. 499
Characterization of Heterocyclic Amine Metabolites by Electrospray MS; *Eades, Donald; Malfatti, Michael; Felton, James. 500
Determination of Nitrosamines by ESI with Photochemical Enhancement; *Vollmer, David, Lay, Jack. 501
MS/MS Criteria for a Confirmatory Method for Sarafloxacin in Catfish Tissue; *Cepa, Steven; **Menacherry, Stanley; Bavda, Lalit. 502
ANALYSIS OF BREVETOXINS IN "RED TIDE" ALGAE BY ON-LINE LC - ELECTROSPRAY/MS; *Hua, Yousheng; Lu, Wenzhe; Henry, Michael S ; Pierce, Richard H., Cole, Richard B. 503
DIFFERENTIATION OF PACIFIC AND CARIBBEAN CIGUATOXINS BY APCI/LC/MS; *Musser, Steven M.; Grande, H. Ray; **Dickey, Robert. 504
Characterization 3,4-Dichloro-1-butene Metabolites in Rat by LC-MS-MS; Lam, Zamas; *Brach, Frank; Keller, Douglas; Carpenter, Stephen. 505
Preliminary Screen for Biodegradation of Xenobiotics; *Ottinger, Sean E.; Bach, Stephan B.H ; Guentzel, M. Neal. 506
Identification of Tamoxifen Metabolites in Patients; *Poon, G.K.; Lonning, P.E.; Phillips, D.H.; Jarman, M. 507
Biotransformation of 2,4-Dipyrrolidinylpyrimidine (2,4-DPP) In Vitro.; **Streeper, Rob; Pearson, Paul; Zhao, Zhiyang; *Vrbanac, James. 508
ANALYSIS OF PAHS IN HUMAN SERUM USING CLOUD POINT EXTRACTION AND LC/MS; *Sirimanne, Sarath R.; Ma, Li; McClure, P. Cheryl; Barr, John R., Patterson; Jr., Donald G. 509
HPLC-APCI-MS/MS for the Analysis of PAP Biotransformation Products; *Benson, Linda M ; Mayeno, Arthur N.; Gleich, Gerald J.; Naylor, Stephen. 510
GC-MS Analysis of Hydroxytestosterones to Measure Cytochrome P-450 Activity; *Purdon, Michael P.; Lehman-McKeeman, Lois D.; Caudill, Doug. 511

Determination of Clenbuterol in Retinal Tissue by Electrospray LC/MS/MS; *Tomlinson, John, Flurer, Rick; Satzger, R. Duane. 512
High Energy CID Spectra of Melphalan or Chlorambucil Adducted Peptides; *Zaia, Joseph; Fenselau, Catherine . .. .513
FAB-MS and MS-MS Studies of Extracts from Pinus Ponderosa; *Teesch, Lynn; Lamb, Diane; Al-Mahmoud, M. S., Rosazza, J. P. N. 514
Integrated Mass Spectrometric / Yeast Bioassay for Genotoxin Detection.; *Serrano, Jose; Kuehl, Douglas..... 515
MONITORING ACID- AND BASE-INDUCED "LIPID A" DEGRADATION BY ELECTROSPRAY MS; *Cole, Richard B ; Wang, Yan. 516
HPLC/IonSpray/MS/MS Analysis of Common and Illicit Drugs in Case Samples; *Picotte, Pierre; Sanchez, Gabriel; Shushan, Bori; **Sakuma, Takeo 517

Tuesday Posters - Drugs & Metabolism

IN VIVO METABOLISM OF PEPTIDE E IN RAT BRAIN BY MICRODIALYSIS/ES/MS; *Andren, Per E.; Emmett, Mark R.; Capriolí, Richard M 518
Characterization of Metabolites of a CCK Ligand on an Ion-Trap MS; *Moseley, Arthur; Tippin, Tim; Walsh, John; **Schwartz, Jay; Uhrich, Mark..... .. .. .519
Investigation of the Interactions Between Bicyclomycin and Rho Protein; *Cox, Kathleen A.; Gaskell, Simon J., Moon, Hong-sik; Park, Hyeung-geun; Widger, William R., Kohn, Harold. 520
Characterization of Limonene Metabolites in Advanced Human Cancer; **Vigushin, D ; Coombes, R.C.; *Somani, H.; Jarman, M.; Poon, G.K..... 521
An Electrospray Mass Spectrometric Study of the Gold Drug Myochrysine.; Lock, Colin J.L ; Howard-Lock, Helen E.; LeBlanc, Daren J.; *Smith, Richard W 522
IDENTIFICATION OF DIPHENHYDRAMINE METABOLITES USING DEUTERATED DCIMS; Heinze, T.M ; *Hansen, Jr., E.B.; Deck, J., Cerniglia, C.E. 523
LC/MS/MS detection of GSH-glucuronide conjugates of 2,4-diene VPA in rats; *Tang, Wei; Abbott, Frank..... 524
Characterization of a Novel Metabolic Reaction: The Metabolism of LY315535; *Gillespie, Todd; Goodwin, Mike; Catlow, John, Swanson, Steve. 525
Structural Elucidation of Bisbenzylisoquinoline Alkaloids by Ionspray MS/MS; *Wu, Wu-Nan; Moyer, Michael D. 526
Structures of Human Urinary Metabolites of Mazapertine by IonSpray MS/MS; *Wu, Wu-Nan; Gisclon, Lee G.; McKown, Linda A. 527
ANALYSIS OF TAMOXIFEN METABOLITES BY ON-LINE CE-ESMS USING NONAQUEOUS MEDIA; *Lu, Wenzhe; **Poon, Grace K ; Cole, Richard B. 528
Identification of Lotatadine Metabolites from Human Liver Microsomes.; *Cyr, Terry; Dawson, Brian; Ethier, Jean; Jurima-Romet, Malle; Menzies, Allan; Whitehouse, Larry.... 529
Biomarkers of OH radical formation in rat brain by microdialysis with MPP+; Ste-Marie, Line, **Vachon, Luc; Boismenu, Daniel, *Montgomery, Jane..... ... .530

2K3MVA Is Not An Obligate Intermediate Between Isoleucine & Allo-isoleucine; *Mamer, Orval A.; **Lepine, Francois L 531
Characterization of reactive drug intermediates by ESI Mass Spectrometry; *Lim, H.K.; Bhavsar, J. H ; Chan, K.; Sisenwine, S. 532
Capillary HPLC / CF-LSIMS Characterization of LTD4 Antagonist Metabolites; *Yergey, James; Nicoll-Griffith, Deborah, Chauret, Nathalie, Trimble, Laird. . . .. .533
CE-ES-MS Analysis of Drug Metabolites in Urine.; *Ashcroft, Alison E, Major, Hilary J; Lowes, Stephen; **Wilson, Ian D. 534
Analysis of B-Agonists Using Solid Phase Extraction and LC/APcI/MS/MS; *Preece, Steve, **van Vyncht, Gery. .... .535
Analysis of Cytochrome P-450 Metabolites of Arachidonic Acid by LC/MS/MS; *Garner, Carlos O.; Belas, Frank J.; Blair, Ian A. . .. .536
Characterization of Acylcarnitines by GC/MS/MS; *Carlson, Shannan; Johnson, Jodie; **Borum, Peggy; Bernier, Ulrich; Yost, Richard.. ... .537
Identification of in vitro and in vivo metabolites of Bosentan by LC-MS/MS; *Hopfgartner, Gerard, Zell, Manfred; Lausecker, Berthold; Husser, Christophe; Viger-Chougnet, Antoinette; Haas, Ruth..... 538
Mechanisms of Leukotriene B4 Metabolism: Negative ion ESI MS/MS analysis; *Wheelan, Pat; Murphy, Robert, C 539
Characterization of Acidic Triterpenes by HPLC/ESI/MS; *Weintraub, Susan T.; **Streeper, Robert T.; Satsangi, Neera; Stavinoha, William B 540
Microbore HPLC/MS/MS of CP-166,572 metabolites in the rat; *Avery, Michael; Ballinger, William; Zembrowski, William, Inskeep, Phil; Mylari, Larry, Fouda, Hassan 541
HPLC/ESI MS/MS for the Identification of in vitro Metabolites of CP-118,954; *Cui, Donghui; Prakash, Chandra..... 542
Inhibition of Aldehyde Dehydrogenase by Disulfiram and Metabolites; *Veverka, Karen A.; Johnson, Kenneth L.; Mays, Dennis C.; Lipsky, James J ; Naylor, Stephen. 543
A Study of the Metabolism of Rifabutin Using ESI-MS and Tandem MS; *Thompson, Toni; Vouros , Paul; Koudrikova, Tatiana; Gerber, Nicholas. 544
LC/IonSpray/MS/MS Analysis of Bile Acids; *LePage, Guy; Yousef, Ibrahim; Sanchez, Gabriel; Shushan, Bori; **Sakuma, Takeo..... 545
Detection of Trypanothione Conjugates in Cell Cultures by ESI Tandem MS; *Bolgar, Mark S ; Gaskell, Simon J.; Douglas, Kenneth T.; Wilton, Amanda N. 546
Characterization of Hemiketals of MDL 101146 by Normal Phase LC/ESI/MS; *Brown, Paul W. , Emary, W. Bart; Akbari, Nisar..... ... .547
Analysis of secondary metabolites in crude plant extracts by electrospray; *Wolfender, Jean Luc; Hostettmann, Kurt; **Wagner-Redeker, Winfried. .... .548
Angiotensin II Receptor Antagonist Metabolite Identification by MS/MS; *DeMaio, William; Morton, George. 549

In vitro metabolism of FK 506 (Tacrolimus) using MALDI mass spectrometry; *Gusev, Arkady I.; Muddiman, David C.; Proctor, Andrew; Hercules, David M.; Tata, Prasad; Venkataramanan, Raman. 550
Identification of levodopa and its metabolites by HPLC-Ion Spray-MS; *Koupai-Abyazani, Mohammed R.; Esaw, Barbara; Laviolette, Barbara. 551
Identification of the urinary metabolites of Brivudin in the rat *Triolo, Antonio; Agostara, Giuseppina; Bonelli, Fabio; Crea, Attilio; Freude, H.-Gerhard; Monteagudo, Edith. 552
Metabolism of the neuromuscular blocker NIMBEX by LC-RAM-API-MS; *Pleasance, Stephen; Dear, Gordon; Jones, Anne. 553
A Sensitive LC/ESI/MS/MS Assay for the Antineoplastic Agent Ifosfamide; *Goldthwaite, Charles A.; Belas, Frank J.; Phillips, Mark A.; Anthony, Lowell; Blair, Ian A 554
Identification and Quantitation of Cyclophosphamide Using LC/ESI/MS/MS.; *Belas, Frank J., Goldthwaite, Charles A.; Anthony, Lowell; Blair, Ian A. 555
Strategies for the Quantitative Analysis of Opioid Peptides in Plasma; *Streeper, Robert T., Weintraub, Susan T.; Marquez, Cristina D.; Smith, Philip C. 556
Electrospray LC/MS and LC/MS/MS of Ecdysteroids; *GRANT, RUSSELL P.; GAMES, DAVID.E.; **WILSON, IAN D.; MORGAN, E.D.; LAFONT, R. 557
HPLC/ESI-MS/MS Studies on the Metabolism of an Atherosclerosis Combatant; *Luther, Elbridge; Boyer, Scott; Cole, Mark; Fouda, Hassan; Destito, Rosalina; Liston, Theodore. 558
HPLC/APCI-MS/MS Method for Quantitation of a Cholesterol Absorption Inhibit; *Gauthier, Jeffrey, Butala, Pranay, Luther, Elbridge, Fouda, Hassan, Cole, Mark.. 559
HPLC/ESI-MS/MS of a LTB4 Receptor Antagonist; Glucuronide Acyl Migration; *Cole, Mark; Luther, Elbridge; Fouda, Hassan; Gauthier, Jeffrey; Destito, Rosalina; Liston, Theodore... 560
HPLC/MS/MS Determination of CP-118,954 in Human Serum; *Avery, Michael, Needham, Shane; Fouda, Hassan. 561
HPLC/DAD/ESI-MS/MS Studies on the Metabolic Fate of a Novel PDE4 Inhibitor; *Gauthier, Jeffrey; Bachert, Elizabeth; Liston, Theodore; Cole, Mark; Cole, Mark. 562
Characterization of metabolites of Ziprasidone in human by LC-MS/MS.; *Prakash, Chandra; Kamel, Amin; Anderson, Wayne; Wilner, Keith. 563
PRECLINICAL DRUG SELECTION - APPLICATION OF IONSPRAY LC-MS AND LC-MS/MS; *Kelly, Michele A.; Xiao, Guang; Greenberg, Gerald E., Kuzmich, Sandra; Robertson, Philmore... 564
In vivo and in vitro Metabolism of Immunomodulators by TOF-MS; *Muddiman, David C; Gusev, Arkady I; Proctor, Andrew; Hercules, David M; Venkataramanan, Raman; Tata, Prasad; Diven, Warren 565

Drug Metabolism Studies That Avoid the Use of Radioisotopes; *Hsieh, Feng-Yin; Goldthwaite, Charles A.; Nobes, Brian J.; Mayol, Robert F.; Klunk , Lewis J.; Chaudhary, A K. ; Blair, Ian A. 566
Orifice Voltage Dependent Oxidation of Dihydrolevobunolol to Levobunolol; *Luo, Wendy; Tang-Liu, Diane; Breau, Alan. 567
Metabolic Profiling Using LC/MS/MS With On-line Microdialysis Sampling; *Rourick, Robyn A.; Kerns, Edward H.; Volk, Kevin J.; Whitney, Jeffrey L.; Lee, Mike S. 568
Automated HPLC/MS/MS Approaches for Rapid Identification of Metabolites; *Cole, Mark; Gauthier, Jeffrey; Luther, Elbridge; Fouda, Hassan; Destito, Rosalina; Liston, Theodore. 569
Analysis of diuretics in urine by HPLC/APCI/MS; Yuan-Ping, Yang; *Jentaie, Shiea. 570
The Detection of Concealed Drugs by Field Portable IMS and GC/MS; *Fetterolf, Dean; Donnelly, Brian ; Jourdan, Thomas. 571
ANALYSIS OF "ECSTASY" AND OTHER DESIGNER DRUGS USING HPLC/APCI/MS; *Hansen, Jr , E B ; Churchwell, M.I.; Clark, C.R.; DeRuiter, J ; Noggle, F T , Doerge, D.R. 572
Immunoaffinity Extraction-LC/LC/MS/MS for analysis of LSD Analogs in Urine; *Cai, Jianyi; van Soest, Remco; Henion, Jack. 573
Identification of Previously Unreported Metabolites of LSD in Human Urine; *Nelson, Chad C.; Slawson, Matt H.; Reuschel, Scott A.; Foltz, Rodger L., **Brenneisen, Rudolf. 574
A Method for the Detection of Fluoxymesterone and metabolites by GC/ECNI; * Xu, Naxing; Watson, J. Throck. 575
Ion Trap GC/MS and GC/MS/MS Measurement of Cocaine and its Metabolites; *Bowers, Larry; Fregien, Kelly.. 576
Selected Ion Storage and Tandem Mass Spectrometry of Anabolic Steroids; *Bowers, Larry. 577
Quantification of the phosophodiesterase inhibitor CP-80,633 in human serum; *Kamel, Amin; Schneider, Rick; Navetta, Kim; Luther, El; Fouda, Hassan 578

Tuesday Posters - Nucleic Acids & Constituents

Protocols for DNA Mapping and Screening by MALDI MS; *Bai , Jian; Liu , Yan-Hui; Liang, Xiaoli; Qian, Mark G; Lubman, David M. 579
MALDI of Synthetic Oligonucleotides; *Bentzley, Catherine; **Larsen, Barbara; Johnston, Murray. 580
Improving Mass Resolution in MALDI/TOF Analysis of DNA; *Tang, Kai; **Worrall, Timothy; Cotter, Robert ; Koster, Hubert. 581
Probing the Stability of Phosphorothioate Oligonucleotides by MALDI-TOFMS; *Wang, Bing; Bourque, Andre; Belenky, Alexi; Cohen, Aharon. 582

6-Aza-2-Thiothymine: A Good Matrix for the Analysis of Oligonucleotides; *Lecchi, Paolo; Le, Han; Pannell, Lewis. 583
MALDI-MS - a New Tool to Monitor the Activ. of Nucl. Acid Modifying Enzymes; *Nordhoff, E.; **Cramer, R.; Kirpekar, F.; Hahner, S.; Roepstorff, P.; Haglund,Jr., R.F.; Hillenkamp, F. 584
Study of PAH-DNA adducts by CF-FABMS; *Plante, Sylvie; Bertrand, Michel, J. 585
MALDI-TOF Analysis of PAH-modified DNA Adducts at the Femtomole Level; *Gooden, Jonathon; Gross, Michael. 586
Tandem MS/MS for Determining Structural Isomers of PAH-DNA Adducts; *Byun, Jaeman; Vidavsky, Ilan; Gross, Michael; Mulder, Patrick; Li, Kai-Ming; Cavalieri, Ercole. 587
DNA Adduct and Probe Detection by Electrophore Mass Spectrometry; *Giese, Roger W ; Abushamaa, Amir; Naim, Abdul; Murugaiah, Veeravagu; Xu, Linxiao; Magiera, Daniel; Graner, Helena; Ismail, Yasser. 588
Analysis of Hydroxyl Radical Modification of DNA using LC/MS/MS; *Kowalski, E.M ; Chaudhary, A.K.; Blair, I.A. 589
The Application of CE/ESI/MS/MS for Detection of IQ Adducts of DNA; *Rindgen, Diane; Vouros, Paul; Turesky, Robert J. 590
GC/MS Quantitation of DNA Oxidation Products; Oh, Chang-Hwan; *Iden, Charles R. 591
Capillary Isotachophoresis-Mass Spectrometric Determination of DNA Damage; *Zhao, Zhongxi (Zack); Fuciarelli, Alfred F.; Smith, Richard D 592
Analysis of DNA base modifications in oligonucleotides using LC/ES MS.; *Chaudhary, A. K.; Reddy, G R., Compton, J. L.; Marnett, L. J.; Blair, I. A. 593
Micro electrospray MS/MS for the analysis of modified oligoribonucleotides; *Wolter, M. A.; **Wilm, M. S.; Mann, M.; Engels, J. W. 594
ESMS of oligonucleotides and non covalent interactions studies; *Potier, Noelle; Bischoff, Rainer; Van Dorsselaer, Alain. 595
Non-Covalent Associations of Metal Complexes with DNA Duplexes by ESI-MS; *Harms, Amy C.; Smith, Richard D., Jenkins, Yonchu; Barton, Jacqueline K. 596
Correlation Between ESI-MS, CID Data, and DNA Duplex Melting Temperature; *Gale, David C.; Morris, A. Kirk; Harms, Amy C.; Camp II, David G., Sisk, Ellen C.; Fusciarelli, Al F.; Udseth, Harold R.; Smith, Richard D.. 597
Characterization of oligonucleotide-peptide hybrids by MALDI and ESI MS; *Sochacki, Marek; Bergmann, Frank; Tam, Steve; Michel, Hanspeter. 598
Routine FAB Mass Spectra of Oliognucleotides: Enhancement by Crown Ethers; *Le, Han; Lecchi, Paolo; Sayer, Jane; Jerina, Donald; Pannell, Lewis. 599
Fragmentation of Multiply-Charged Oligonucleotides in Triple Quadrupoles; *Pomerantz, Steven C.; McCloskey, James A. 600
A New Approach for DNA Sequencing and Mutation Detection with ESI-MS; *Terunuma, Hideya; Naito, Yasuhiro; Tsuneyoshi, Toshihiro; Arakawa, Ryuichi; Ishikawa, Keiichiro; Koga, Yoshinori; Prockop, Darwin. 601

ESI-MS on a sector instrument for the analysis of oligonucleotides; *Wolter, M. A.; Engels, J W.; Montanarella, L ; Facchetti, S. 602
FAB/MS Confirmation of Modified Deoxynucleotides in Small Oligomers; Rieger, Robert A.; *Iden, Charles R. 603
The LCMS of Synthetic Oligonucleotides; Bothner, Brian; Chatman, Kelly, Sarkisian, Molly; *Siuzdak, Gary. 604
Analysis of DNA Analogues in Pharmaceutical Applications Using ESI-MS; *Chen, Ling, **Fearon, Karen; Nuwaysir, Lydia; McLean, Matthew. 605
Detection of Imidazoleacetic Acid Riboside by FAB/MS and ESI/MS; Rieger, Robert A. (1); Reddy, D. Meghanath(1); Thomas, Boban (2); Prell , George D (2); *Iden , Charles R. (1). 606
Characterization of 1,2,3,4-diepoxybutane purine adducts using LC/ESI/MS/MS; *Kambouris, S. J.; Chaudhary, A. K.; Blair, I. A. 607
A Study of Metal Ion Interactions With Nucleosides by LSIMS; *Paul, G. J. C.; Theophanides, T ; Anastassopoulou, J ; **Marcotte, I.; Bertrand, M. J. 608
Gas-Phase Chemistry of Metal(II)-Ion-Complexes of Monophosphates; *Adams, Jeanette; Hamilton, Jill. 609

Tuesday Posters - Proteins & Peptides

In situ digestion procedures and analysis of the digest by HPLC/ESI/MS *Falchetto , Rocco; Shabanowitz, Jeffrey; Owens, Gary; Hunt, Donald F. 610
Enzymatic fragmentation with immobilized enzymes and LC/MS analysis; *Raida, Manfred; Forssmann, Wolf-Georg. 611
Sepn/Manipulation of Proteins using Polymeric µ-HPLC On-line with ESI/MS *Hail, Mark; Warrack, Bethanne; Taylor, Susan; Baldwin, Sam; Stoney, Ken, Lee, Mike. 612
Comparison of a TSQ MS to a Reflectron TOF MS with Electrospray Ionization; *Verentchikov, Analoti; Hsieh, Frank; Tomany, Michael, Gabeler, Stephen; Vestal, Marvin; Martin, Stephen. 613
Peptide Mapping on a Nitrocellulose Membrane with Analysis by MALDI MS; *Bai, Jian; Qian, Mark G; Liu, Yan-Hui; Liang, Xiaoli; Lubman, David M. 614
Rapid Identification of Variant Enzymes from Commercial Detergent Products; *Lacey, M.P.; Keough, T.; Sun, Y.; Bauer, M.D.; Grant, R.A.; Bennett, C.B. 615
HPLC-ESI Ion Trap MS/MS Analysis of Proteins Separated by 2D-PAGE; *Kanai, Michiko, Seta, Kazuo; Land, Adrian; Bier, Mark; **Nakayama, Hiroshi; Isobe, Toshiaki; Okuyama, Tsuneo. 616
STRATEGIES FOR IDENTIFICATION OF 2D GEL PROTEINS BY MASS SPECTROMETRY; *Clauser, Karl R.; Hall, Steven C.; Andrews, Lori E.; Smith, Diana M.; Matsui, Neil; Tran, Huu M.; Epstein, Lois B.; Burlingame, Alma L 617
Mass Spectrometry of Proteins Directly Isolated from SDS Gels; *Schuhmacher, Martina; Wunderlin, Markus; Przybylski, Michael 618

Sequencing peptides: post-source decay MS without scanning the reflectron.; *Cordero, M.M., Cornish, T.J.; Cotter, R.J. 619
Evaluation of MALDI-PSD and MALDI-CID for Structural Analysis; *Carr, Steven; Hemling, Mark; Roberts, Gerald; Bean, Mark; Annan, Roland; Hilliard, George; **Hoyes, John. 620
Peptide Sequencing: MALDI Time-of-Flight vs Electrospray Triple Quadrupole; Overberg, A.; Ingendoh, A.; *Keane, A.; Sutton, C; Harrison, M.; Cottrell, J. S 621
Deuterated Terminating Agents for Ladder Sequence Analysis by MALDI-TOF MS; Holland, Ricky; *Lay, Jackson, Chiarelli, M. Paul; Vollmer, David. 622
Using ESI to Characterize Protein Sequencing Ladders; *Saha, Sanat; Beavis, Ronald C. 623
Sequence Analysis of C- and N-Terminal Blocked Peptides by PSD-MALDI; *Ingendoh, Arnd; Seta, Kazuo; Kanai, Michiko; **Yamakawa, Yoshio; Omori-Satoh, Tamotsu; Isobe, Toshiaki; Okuyama, Tsuneo 624
An Evaluation of Peptide Fragmentation by MALDI-TOF PSD and MALDI CID MS/MS; *Adams, Gregory W.; Medzihradszky, Katalin F.; Hall, Steven C ; Burlingame, Alma L.; **Bateman, Robert H; Green, Martin R; Maisey, Anne. 625
A Novel N-Terminal Derivative Designed to Simplify Peptide Fragmentation; *Sherman, Nicholas E.; Yates, Nathan A.; Jeffrey, William; Bartlet-Jones, Mike; Shabanowitz, Jeffrey; Hunt, Donald F., Pappin, Darryl. 626
High Energy CID Spectra of Peptides Containing Pyridylethylcysteines; *Wolf, Susan; Biemann , Klaus 627
Surface-Induced Dissociation of Cyclic Peptides; *Dongre, Ashok; Wysocki, Vicki; **Hayward, Mark. 628
Peptide Sequencing at the Low Femtomole Level Using PC-CE-MS/MS; *Tomlinson, Andy J.; Johnson, Kenneth L.; Naylor, Stephen. 629
Controlled fragmentation of derivatized peptides; *Lindh, Ingemar; Griffiths, William; Bergman, Tomas, Sjövall, Jan. 630
Fragmentation of Small Non-polar Peptides Containing NMe-Ala and Pro; *Vaisar, Tomas; Urban, Jan. 631
DETECTION OF PHOSPHORYLATED AND SULFATED PEPTIDES BY LC-ESI-MID; *Jedrzejewski, Paul; Schnolzer, Martina; Lorenz, Peter; Lehmann, Wolf D.; 632
Enzymatic Reactions on Membranes for the MALDI Analysis of Phosphoproteins; *Liao, Pao-Chi; Gage, Douglas A., Allison, John 633
Improved CID Spectra of Peptide Ions Using Stepped Collision Potentials. *Annan, Roland; Carr, Steven. 634
Location of peptide phosphorylation sites by use of (+) and (-)ESI-MS/MS; *Busman, M.; Schey, K. L.; Knapp, D. R. 635
Phosphorylation and N-terminal acetylation of phosrestin I in fly eyes; *Kinumi, Tomoya; Jackson, Kenneth; Kubota, Masayuki, **Ohashi, Mamoru; Matsumoto, Hiroyuki. 636

Electrospray FTICR Mass Spectrometry of Modified Peptides and Proteins; *Nawrocki, Joseph; Watson, Cliff; Eyler, John. 637
Mass Spectrometric Protein Identification in Completely Sequenced Genomes; *Mann, Matthias; Jensen, Ole N.; Vorm, Ole; Houthaeve, Tony; Wilm, Matthias; Mortensen, Peter; Shevshenko, Andrej. 638
Useful Tables of Possible and Probable Peptide Masses; *Mann, Matthias. 639
Analysis of Immunoprecipitated Proteins by Using Tandem Mass Spectrometry; *Schieltz, David M.; Eng, Jimmy K.; Yates, John R. 640
Protein Database Searching with Ion Trap MSn Spectra; *Eng, Jimmy; Yates, John; Schieltz, David. 641
Mass Accuracy Requirements to Map Proteolytic Peptides from a Protein; *Liao, Pao-Chi; Allison, John; Gage, Douglas A. 642
Protein Identification by Database Searching: A Bayesian Algorithm; *Zhang ,Wenzhu ; Chait, Brian T. 643
Applications of a New Algorithm for Deconvolving Multiply Charged Spectra; *Barclay, Victoria; Bonner, Ron; DeNoyer, Lyn; Dodd, Jack. 644
DATABASE FOR MASS SPECTRA OF PROTEINS; *Fenyó, David; **Beavis, Ron C.; Chait, Brian T. 645
Characterization of Protein Digests Using Novel Scanning (Funky Ramps); *Allen, Mark; Anacleto, Joseph; Bonner, Ron; Nuwaysir, Lydia; Bori, Shushan 646
Interpretation of Peptide CID Spectra using Artificial Neural Networks; *Scarberry, R E.; Zhang, Z. ; Knapp, D. R. 647
Peak Matching Techniques for Characterizing Protein Heterogeneity; *Johnson, Kenneth L., Tomlinson, Andy J., Naylor, Stephen 648
Identification of Proteins Using LC/MS/MS on an Ion Trap Mass Spectrometer; *Lane, W.S.; **Land, A.P.; Jardine, I.; Bier, M.E. 649
High Sensitivity Protein Sequencing with ESI-FTMS; *Guan, Ziqiang, Aaserud, David; Valaskovic, Gary; Kelleher, Neil; McLafferty, Fred 650
ESI/FTMS of Enzyme (>40 kDa) Sequence, Heterogeneity, and Inhibition; *Wood, Troy D.; **Kelleher, Neil L.; Little, Daniel P.; Begley, Tadgh P., McLafferty, Fred W., Chen, Lorenzo H.; Borders, Montie; Kenyon, George H. 651
Peptide Mapping by LC/MS/MS Using a Triple Quad or Ion Trap Spectrometer; *Baldwin, Samuel W.; Stoney, Ken; **Land, Adrian P., Bier, Mark E ; Wheeler, Kevin. 652
Protein Molecular Weight Determination on Quadrupole and Ion Trap Systems; *Land, A.P.; Mylchreest, I.C.; Bier, M.E.; Wheeler, K.P. 653
MS/MS in an Ion Trap/reflectron Time-of-flight Mass Spectrometer; *Qian, Mark G.; Zhang, Yu; Bai, Jian; Lubman, David M. 654
MS/MS of Alkali Cationized Peptides Using Quadrupole Ion Trap; *Lin, Tong; Glish, Gary L. 655
Tertiary Structure of Protein Ions in the Gas-Phase; *Fagerquist, Clifton; Schnier, Paul; Gross, Deborah; Rodriguez-Cruz, Sandra; Williams, Evan. 656

Strategies for Accurate Mass API LC-MS Analysis of Complex Mixtures; *Woolfitt, Adrian; Bateman, Robert; Pugh, Jonathon....657

Wednesday Orals
New Approaches to Quantitative Mass Spectrometry

Importance of Desalting Oligonucleotides in Quantitative Electrospray MS; *Greig, Michael J.; Klopchin, Patrick G ; Wheeler, Patrick D., Griffey, Richard H....658
Rapid Quantitation of Eicosanoids in Inflammation Models by ES/MS/MS; *Duffin, Kevin; Margalit, Alon; Isakson, Peter....659
Serum Albumin Determination Using LC/MS with Affinity Chromatography; *Bunk, David; Welch, Michael....660
Quantification of Pranlukast and SB218663 in Plasma Samples Using LC/MS/MS; *Bi, Honggang; Lundberg, David; Pirhalla, Jill; McHugh, Charles; Marchese, Alfredo....661
Application of Ionspray MS/MS Quantification of Beclomethasone Dipropionate; *Schorno, Karl S.; Winslow, L. D....662
Quantitative Analysis of Low Molecular Weight Biomolecules by MALDI-TOF; *Duncan, Mark W.; Lidgard, Ray....663
Quantitative Analysis of Angiotensin II by MALDI/TOF MS; *Nicola, Anthony J. Gusev, Arkady I.; Proctor, Andrew; Hercules, David M.; Jackson, Edwin K....664
Selection of Internal Standards for Quantification by MALDI; *Wilkinson, William R.; Gusev, Arkady I.; Proctor, Andrew; Houalla, Marwan; Hercules, David M....665
Use of Isotopic Surrogates in the Quantitation of Endogenous Analytes; *Alexander, Michael; Abolin, Craig....666

Wednesday Orals - Electrospray Ionization-Fundamentals

Electrochemical Aspects of Electrospray; *Zhou, Feimeng; Van Berkel, Gary....667
High-Frequency Synchronization of Electrospray Current using Pulsed Tension; *Beaugrand, C.; Charbonnier, F.; Rolando, C.; Sablier, M.; Saru, F....668
Characterization and Implementation of Micro-Flow Electrospray Nebulizers; *Covey, Thomas....669
How are electrospray Ions Born Free? - Dole vs. Iribarne Revisited; *Fenn, John B.; Rosell, Joan....670
Is Electrospray Ion Production Concentration Dependent?; *Coopersmith, Brad; Hamilton, Brenda; Abolin, Craig....671
DEPENDENCE OF CHARGE STATE DISTRIBUTION ON ANALYTE CONCENTRATION IN ESI/MS; Wang, Guangdi; *Cole, Richard B....672
PHYSICAL PROCESSES OF ELECTROSPRAY; *Willoughby, Ross; Sheehan, Edward; Mitrovich, Samuel....673
Ion Mobility Spectrometric / Mass Spectrometric Study of Electrospray Ions; *Guevremont, Roger; Siu, K.W.Michael; Wang, Jianyao....674

Wednesday Orals - Fourier Transform Mass Spectrometry

Principles and Design of Ion Traps for FT-ICR Mass Spectrometry *Marshall, Alan G.; Guan, Shenheng....675
Advantages of High Mass Accuracy MALDI-FTMS for Tryptic Mapping; *Stults, John; Li, Yunzhi; McIver, Jr., Robert....676
EVALUATION OF DISSOCIATION TECHNIQUES FOR MALDI-FTMS OF OLIGONUCLEOTIDES; *Hettich, Robert; Stemmler, Elizabeth....677
A Dual Chamber Approach to FT-MS Offering ESI, MALDI, FAB, and EI Sources; *Gard, Eric, Carroll, James; Green, Kirk; Fannin, Steve; Wu, Jiangyue; Camara, Elvira; Lebrilla, Carlito....678
FT-ICR Mass Spectrometry of Very Highly Charged Atomic Ions; *Schweikhard, Lutz; Becker, Stefan; Beiersdorfer, Peter; Beck, Bret; Elliott, Steve....679
ESI/FTMS Instrumentation for Tandem Mass Spectrometry; *O'Connor, Peter B.; Wood, Troy D., Little, Daniel P.; Guan, Ziqiang; Valaskovic, Gary A.; McLafferty, Fred W....680
Fragmentation of Labelled Lysozymes and Derivatives by FT MS; *Robinson, Carol; Miranker , Andrew; Kruppa, Gary; Dobson , Christopher....681
ESI-FTICR Methods for Bioaffinity Characterization Mass Spectrometry; *Bruce, James; Anderson, Gordon; Chen, Ruidan; Cheng, Xueheng; Gale, David, Hofstadler , Steven, Schwartz , Brenda; Smith, Richard....682

Wednesday Orals - Laser Desorption Ionization-Fundamentals

Fast Metastable Ion Fragmentation In MALDI; *Brown, Robert; Reiber, Duane, Lennon, John....683
Delayed Extraction of MALDI Ions in a Reflecting TOF Spectrometer; *Ens, W; Dworschak, R G; Spicer, V; Standing, K G....684
Investigation of Selective Detection in Peptide Mixtures by MALDI MS; *Yu, Wen; Vath, James, Scoble, Hubert....685
Examining MALDI Ion Formation at Various Laser Irradiances; *Campo, Karen K.; Edmondson, Ricky D., Russell, David H....686
Continuous Flow MALDI in an Ion Trap-ReTOF Mass Spectrometer; *He, Ling; Liang, Li; Li, Xuhui; Lubman, David....687
Lanthanide Oxide Cluster Ions Produced by Laser Ablation; *Gibson, John K....688
Role of Solubility in the Preparation of Synthetic Polymer Samples; King, Richard; Goldschmidt, Robert; Xiong, Yansan; *Owens, Kevin; Hanton, Scott....689
Mechanistic Implications of MALDI Ion Signal Profiles; *Kinsel, Gary; Edmondson, Ricky; Russell, David....690
Dissecting MALDI-TOF Mass Spectra; *Allison, John; Liao, Pao-Chi; Lavine, Gary; Hiller, Joseph....691
MALDI Sample Preparation Techniques By X-ray Photoelectron Spectroscopy; *Thompson, Stephen; Jones, David; Robinson, Kevin....692

Wednesday Orals - Mass Spectrometry & the Earth's Atmosphere

Sift Studies of the Reactions of H3O+ with a Series of Sulfides and Thiols; Williams, Ted L.; Babcock, Lucia M.; Adams, Nigel G., Decker, Brian K.; *Nigel Adams 693
The Study of HCFC Radicals Decomposition by NR Mass Spectrometry; *Sadilek, Martin; Turecek , Frantisek 694
Astrophysical Thermochemistry: The Heats of Formation of C3H2 isomers.; *Chyall, Leonard; Squires, Robert 695

Wednesday Posters - Ion-Molecule Reactions

Oxidation Reactions of Cationic Vanadium Clusters; *Rodgers, M. T., Griffin, J. B., Armentrout, P. B. 696
Chemisorption of Hydrogen Molecules on Vanadium Cluster Cations; **Dietrich, G.; Dasgupta, K. ; Kluge, H.-J.; Lindinger, M.; Lützenkirchen, K. ; *Schweikhard, L. ; Ziegler, J. 697
Metal Ion/Molecule Chemistry using a Radio Frequency Glow Discharge Source; *Eanes, Ritchie C ; Christopher, Steven J ; Marcus, R. Kenneth 698
GENERATION AND CHARACTERIZATION OF SILACYCLOPENTADIENYL COMPLEXES OF IRON; *Kardash, Dawn; Kloos, Steve; Boudjouk, Phil; Jacobson, Denley 699
Structure & Reactivity of (FeCNC3H5Cl)+ Complexes; Capron, L., Mestdagh, H.; *Rolando, C., Sablier, M. 700
Ethylene Insertion and Hydrogenolysis Rates of [(C5Me4)SiMe2(n-t-Bu)]ZrMe+; *Hayes, T W , Alameddin, N G ; Richardson, D E , Eyler, J R , Watson, C. H. 701
Gas Phase Reactions of +1 and +2 Chlorotitanium Ions With Isobutene; *Kneen, Kurt; Leroi, George E.; Allison, John 702
Electrospray Mass Spectrometry (ESI-MS) of Metal Chelates; *Ross, Andrew R.S , Ikonomou, Michael, G , Orians, Kristin J. 703
Gas-Phase Actinide Ion Chemistry: Reactions of Th+ and U+ with CH4 and C2H6; *Marçalo, Joaquim, Leal, João Paulo, Pires de Matos, António 704
Gas-Phase Reactivity of Transition Metal Cations with Atomic Species; Angeli, C.; Leymarie, N ; Mestdagh, H.; *Rolando, C.; Sablier, M. 705
Organometallic Distonic Ions: +FeC6H4.; *Xu, Young; Lee, Sam; Freiser, Ben, Bauschlicher, Charles 706
Gas-Phase Isomeric Differentiation Study of FeC7H7+; *Xu, Young, Garcia, Edna; Freiser, Ben; Bauschlicher, Charles 707
Experimental and Theoretical Studies on Nb6C7+; *Lee, Samuel; Kan, Steven; Freiser, Ben S. 708
Generation and Reactivity of Yttrium-Carbon Clusters; *Kan, Steven Z.; Lee, Sam A.; Freiser, Ben S 709

FT-ICR Studies of the Structures and Reactivities of Metal-Carbon Clusters; *Byun, Yong G.; Yeh, Chen-Sheng; Afzaal, Sunia; Lee, Samuel A , Kan, Steven Z., Xu, Young; Freiser, Ben S. 710
Gas-Phase Ion-Molecule Reactions of Lanthanide Ions with Crown Ethers; *White, Forest M.; Solouki, Touradj; Xin, Tianpei; Marshall, Alan G. 711
Gas Phase Reactions of Pt+, Au+, and Hg+ with Small Hydrocarbons; *Taylor, William; Rippy, Allyson; **Babcock, Lucia; Linder, Christopher 712
Glow Discharge/SIFT Studies of Some Gas Phase Metal Ion Reactions; *Linder, Christopher; **Taylor, William; Dalton, A. Leigh; Babcock, Lucia. 713
Reactions of singly-charged transition metal ions with cyclopentene; *Ni, Jinsong; **Harrison, Alex. G. 714
C5H8 isomer distinctions by metal ion reactions; *Ni, Jinsong; **Harrison, Alex. G. 715
Radiative association rate and bond strength of metal ion-neutral complexes; *Ho, Yen-Peng; Dunbar , Robert C. 716

Wednesday Posters - Computer Applications

SIMION 3D Version 6.0; *Dahl, David, ... 717
MacSimion past, present and future; *McGilvery, D. C., Morrison, R J S 718
The Practical Application of Data Controlled Mass Spectral Analysis. *Stahl, Douglas C., Swiderek , Kristine M ; Davis, Michael T ; Lee, Terry D. 719
Possible use of a time domain signal inverse algorithm in FTICR-MS; *Gorshkov, Michael V., Kouzes, Richard T. 720
Homologous Series Plots: A New Slice Through the GC/MS Data Set; *Dolnikowski, Gregory, **Smith, Brian 721
The Determination of Elemental Composition by Low Resolution MS/MS.; *Wang, Jia-shen. 722
USE OF PM3 MOPAC TO PREDICT PHOTOINDUCED H+-TRANSFER IN H-BONDED CLUSTERS; *Gimon-Kinsel, Mary; Huang, Yong; Russell, David 723
Application of a Fuzzy Logic peak-finding algorithm for GC/MS Analysis; *Sander, Peter. 724
New Software Tools for the Analysis of High Resolution Mass Spectra; *Price, John M.; Rockwood, Alan W ; Myers, James D.; Van Orden, Steven 725
Processing MALDI-Time-of-Flight Data: A Maximun Entropy Approach; Reynolds, David J., *Gallagher, Richard T.; Scrivener , Elaine, Derrick, Peter J 726
Hybrid Neural Network for Mycobacterial Detection and Speciation by GC-MS; *Herold, Christopher; Fitzgerald, Robert; Herold, David; **Lu, Taiwei, Zhao, Sean; Lerner, Jeremy. 727
Evaluating EI Mass Spectral Library Search Results; *Sparkman, David 728
Substructure Identification by Library Searching; *Stein, Stephen E , Tchekhovskoi, Dmitrii V 729

Sharing Corporate Mass Spectral Databases; *Little, James L.; McSpadden, William M. 730
Artificial Neural Networks for Identifying Components in Mixtures by MS; *Lay, Jackson; **Darsey, Jerry. 731
Design of a Computer Controlled Magnetic Sector Mass Spectrometer; *Cody, R. B. ; Makino, S. ; Asada, T.; **Yoshidome, K. 732
High-Performance FT-ICR Data System; *Senko, Michael W.; Guan, Shenheng; Marshall, Alan G. 733
High Performance Data System for Ion Trap Mass Spectrometry; *Overney, Gregor; **Hart, Kevin; Wise, Marc B.; Enke, Christie G. 734
PROGRAMMING THE TELEDYNE FILTERED NOISE FIELD SYSTEM; *Clarke, Nigel J.; Todd, John F.J ; Hoekman, Don J. 735
A HIGH SPEED DATA ACQUISITION FOR FAST GC-MS; *Gilbert, Anthony; Atherton, Paul; Hanson, Stewart; Lu, Lin; **Preston, Andrew; Smith, Steve. 736
Display and Manipulation of Three-Dimensional Plots of Ion Trap Data; *Li, Rebecca; Hoekman, Don, Wilson, Ray; McHugh, Sean; Karr, Dane. 737
Interactive Setup and Control of Ion Trap Mass Spectrometry Experiments; *Wilson, Ray; Hoekman, Don; McHugh, Sean; Li, Rebecca. 738
Automating Mass Spectrometry with AppleScript and QuickKeys; *Bonner, Ron; Burton, Lyle; **Mann, Matthias; Wilm, Matthias. 739
A New Mass Spectrometry Data Processing Program; *Bonner, Ron; Burton, Lyle. 740
Automating Pharmaceutical API/LC/MS/MS Quantitation; *Wakefield, Michael; Weissenberg, Klaus. 741
A New Multi-Vendor "CLP-Like" Report Generator for GC/MS Data; *Patkin, Adam. 742
Matrix Assisted Laser Desorption for R&D and automated QC applications; *Humphrey, Paul; Dingley, David; Jones, David. 743
Evaluation of TICFILT as a Software used in LC/MS Analysis.; *Carrier, Alain; Zidarov, Dimo; Bertrand, Michel J. 744

Wednesday Posters - Materials Characterization

Mass Spectrometry as a Tool to Study Painted Art.; *Boon, Jaap J.; van der Doelen, Gisela; Pureveen, Jos; van Ocht, J.; van Grevenstein, A. 745
HPLC-FAB-MS and GCMS study of aromatic components of "gum benzoin" resins; *Pastorova, Ivana; de Koster, Chris G.; Boon, Jaap J. 746
GC/MS Analysis of Vegetal Adhesive Material from Archaeological Origin; Delacotte, J.-M.; *Regert, M.; Rolando, C.; Sablier, M. 747
The Effect of the Terminal Group on the TOF-SIMS Spectra of PDMS; *Dong, Xia; Proctor, Andrew; Hercules, David. 748
Application of ESI MS to the Analysis of Polysulfide Polymers; *Buzy, Armelle; Mahon, Andrea, Kemp, Terry; Jennings, Keith. 749

The Analysis of Polymer Additives by Tandem Mass Spectrometry; *Jackson, Tony; Jennings, Keith; Scrivens, Jim. 750
Average Mass and End-Group Information on Polymers Using MALDI and MS/MS.; *Jackson, Tony; Jennings, Keith; Scrivens, Jim. 751
MS Analysis of Alkylated Benzothiophenes...; Budzikiewicz, H; Drabner, G. 752
Characterisation of Cyclic PET Oligomers by LC-MS; *Yates, Hilary; Scrivens, Jim; Hedley, Julie; Taylor, Mike. 753
LC-MS Characterisation of a Surfactant Complex Mixture; *Yates, Hilary; Scrivens, Jim; Hedley, Julie. 754
Mass Spectrometry of Polyoxyalkylene Block Copolymer Surfactants; *Kalinoski, Henry T.; Hargiss, Leonard O., Shay, Brian J.; **Schuyl, P.J.W. 755
Diffusion of argon in K3B polyimide and its carbon fiber laminates*; *Grayson, Michael. 756
The characterisation of commercial lubricant formulations; *Scrivens, Jim; Yates, Hilary; Bunn, Alan; Tayler, Paul; Beckett, Malcolm; Taylor, Mike; Jennings, Richard. 757
Transformation of Feedstock Molecules in FCC Studied by Mass Spectrometry; *Qian, Kuangnan; Harding, Robert H.; Zhao, Xinjin. 758
Quantitative Analysis of Reformulated Gasoline by Mass Spectrometry; *Drinkwater, Donald; Nero, Vince. 759
Characterization of Asphaltenes from Midway Sunset Crude Oil; *Haas, George W.; Ellis, Leroy; Hunt, Jerry E.; Winans, Randall E. 760
Pyrolysis-Photoionization Mass Spectrometry; *Bookwalter, Craig; Zoller, David; Johnston, Murray. 761
The Accuracy of Chemical Type Analysis Using a Dynamic Batch Inlet System; *Roussis, Stilianos, G.; Cameron, Andrew, S. 762
Improving the Reproducibility of Pyrolysis MS Techniques; *Roussis, Stilianos, G.; Fedora, Jim, W. 763
Analysis of Pyrolysis Residues from Poly (vinyl alcohol); *Pogue, Robert; Ackley, Kathryn; Majidi, Vahid 764
TPD MS of Chemically Modified Ultrafine Oxides; *Pokrovskiy, Valeriy 765
Thermogravimetric Analysis-MS with Data Logging on a Teknivent Data System; *Hileman, Fred; Grote, William; Johnson, Deborah; Tria, John; **Norberg, Peter. 766

Wednesday Posters - Inorganic, Elemental & Isotope Rations

Improved Performance of a Quadrupole Based-Glow Discharge Mass Spectrometer; *Valiga, Robert E.; Duckworth, Douglas C.; Smith, David H.; 767
Elemental Quantification Based on Secondary Species in the Glow Discharge; **Goodner, Kevin L.; Eyler, John R.; Barshick, C. M.; Smith, David H. 768
Reduced Mass Range Ion Trap MS for Atomic Ions; *Barinaga, Charles J.; Eiden, Gregory C.; Koppenaal, David W.; **Hemberger, Philip H. 769

Reducing Energy Dispersion in Plasma-Source Sector-Field Mass Spectrometry; *Burgoyne, Thomas; Hieftje, Gary; Hites, Ronald. 770
Insulator Surface Potential Measured by TOF SIMS; *Guo, X. Q.; Short, R. T. 771
Resonant Laser Ablation - Thin Film and Multilayer Analysis; *Allen, T. A ; **Gill, C. G.; Anderson, J. E.; Kelly, P. B.; Nogar, N. S. 772
High sensitivity LC-combustion-IRMS based on a moving belt; *Caimi, Richard J.; Brenna, J. Thomas. 773
LC Combustion Interface for High Precision Isotope Ratio Mass Spectrometry; Brand, Willi; *Dobberstein, Peter. 774
Optical versus Mass Spectrometry: The Race for Fieldable Isotopic Analysis; *Barshick, C.M.; Young, J.P ; Shaw, R.W.; Smith, D.H.; Ramsey, J.M. 775
Alumatrane Revisited: Distribution of Oligomeric Ions in EI, CI, and LSIMS; *Bartlett, Michael; Burns, Scot; Bruce, David; **Busch, Kenneth. 776
Characterization of Supported and Unsupported Transistion Metal Complexes; *Bartlett, Michael; Bruce, David; **Busch, Kenneth; Thomas, Susan; White, Mark, Bertrand, J. Aaron 777
A STUDY OF THE CLUSTER ION DISTRIBUTION FROM METAL NITRATES USING PDMS; *Ferrell, William; Van Stipdonk, Michael, da Silveira, Enio, Schweikert, Emile 778
Electrospray Ionisation of Polyoxoanions of W, Mo and Si in Aqueous Soln.; *Summerfield, Scott; Howarth, Oliver; Jennings, Keith 779
Study of the Stability of Metal Ion-Macrocycle Complexes by ESI-MS/CID/MS; *Znamirovschi, Calin G.; **Frutos, Dinorah; Enke, Christie G. 780
Atmospheric Pressure Chemical Ionization of Novel Bismuth Compounds; *Yhard, G Bradley *, Curtis, Jonathan M ^, Agocs, Lisa *, Burford, Neil * 781

Wednesday Posters - Trapped Ions

Comparison of ICR cells with open geometry for FT-ICR; *Kuhnen, Florian; Spiess, Iris; Wanczek, Karl-Peter. 782
A comparison of fundamental principles and properties of ion traps; Engelmohr, Peter; *Wanczek, Karl Peter 783
A new structure for a FT Ion Trap used in electrical and combined modes; Engelmohr, Peter; *Wanczek, Karl Peter. 784
Characterisation of a multi-purpose open endcap ICR-Cell; *Spiess, Iris; Kuhnen, Florian; Wanczek, Karl-Peter. 785
Examples in Hierarchies of Optimally Triple Frequency Focused FTMS Traps; *Rempel, D. L.; Gross, M. L. 786
Short-Bore Concentric Tube Source for Coupling HPLC to ES/FTICR; *Harper, C. J.; Drader, J. J., Campbell, V. L.; Laude, D. A. 787
Experimental Effects of the Radial Electric Field in Open Cells; *Vartanian, V. H.; Laude, D. A 788

Investigation of Gas Phase Ion-Ion Reactions in an FTICR Trapped Ion Cell; *Torres, T. A., Laude, D A. 789
FTICR/TOF for Measuring Large Ion Populations in Penning Traps; *Schmidt, E. G , Laude, D. A. 790
Improved Ion Injection in a Single Trap Electrode Cell for FTICR; *Anderson, J. S.; Torres, T. A.; Vartanian, V H.; Laude, D. A. 791
Quadrupolar Excitation Efficiency in Non-Ideal FTICR Trapped Ion Cells; *Drader, J. J.; Hendrickson, C. L., Campbell, V. L ; Laude, D. A. 792
MALDI/FTICR Using Quadrupolar Excitation in a Single Trapped Ion Cell; *Anderson, J. S.; Laude, D. A 793
ESI/FTICR Analysis of Protein Conformation; *Campbell, V. L ; Laude, D. A. 794
A New Approach for Stabilizing Ion Radial Motion in FT-ICR; Vartanian, V H., *Laude, D. A. 795
Facile Implementation of Quadrupolar Axialization in FTMS; *Ijames, C. F. 796
Electron Bean Induced Axialization of Ions in FT-ICR; Amster, Jon; *Easterling, Michael. 797
Experimental and Theoretical Studies of Broadband Quad Excite in FT-ICR; *Pitsenberger, Cynthia; Amster, I. Jonathan 798
Quadrupole Excitation Trapping during Electron Beam Events in ICR; Hatcher, Joey; *Bartmess, John. 799
Studies of Large Individual Ions by FTICR Mass Spectrometry; *Chen, Ruidan; Bruce, James E ; Cheng, Xueheng, Dale, Mitchell W., Hofstadler, Steven A.; Anderson, Gordon A.; Smith, Richard D 800
A New Dual Cell for Selective Ion Accumulation and Separation in FTICR/MS; *Chen, Ruidan, Bruce, James E ; Cheng, Xueheng, Hofstadler, Steven A , Anderson, Gordon A.; Rockwood, Alan L , Udseth, Harold R., Smith, Richard D 801
Enhanced Selective Ion Accumulation with Dipolar Magnetron Excitation; *Bruce, James; Anderson, Gordon; Chen, Ruidan; Cheng, Xueheng; Gale, David; Hofstadler, Steven; Schwartz, Brenda; Smith, Richard 802
Selective Ion Excitation and Isolation in Trapped-Ion Mass Spectrometry; *Guan, Shenheng , Marshall, Alan G. 803
A Unified Description of Space Charge Effects in FT - ICR; *Mitchell, Dale W.; Smith, Richard D. 804
Minimization of Frequency Shifts for Improved Mass Accuracy in FT-ICR MS; *Gillig, Kent; Bluhm, Brian; Solouki, Touradj; Russell, David 805
FT-ICR Mass Spectral Analysis of Unevenly-Sampled Biomolecule Data; Guan, Shenheng, *Senko, Michael W.; Huang, Yulin; Marshall, Alan G., McLafferty, Fred W. 806
Optically Detected Electron Spin Resonance of Trapped Mass-Selected Ions; *Li, Guo-Zhong, Guan, Shenheng; **Dalal, Nar S; Marshall, Alan G. 807
A Combined rf Quadrupole/Magnetic Ion Trap for FT-ICR MS; *Huang, Yulin ; Li, Guo-Zhong , Guan, Shenheng , Marshall, Alan G. 808

Delayed Photofragmentation of Size Selected Gold and Silver Cluster Ions; Lindinger, M. ; Dietrich, G.; Kluge, H.-J.; **Lützenkirchen, K. ; *Schweikhard, L. , Walther, C.; Ziegler, J. 809
Instabilities of Ion Motions in Ion Cyclotron Resonance Traps; *Schweikhard, L. ; Ziegler, J. ; Bopp, H. ; **Lützenkirchen, K. 810
Single- and Two-Photon Fragmentation of Stored Gold Cluster Ions; Walther, C ; Becker, St.; Dietrich, G.; Kluge, H.-J., Lindinger, M. ; **Lützenkirchen, K. ; *Schweikhard, L. ; Ziegler, J. 811
Substituent distribution analysis in O-methyl celluloses by MALDI-FT-ICR-MS; *De Koster, Chris G.; Duursma, Marc C.; Arisz, Peter W ; Heeren, Ron M.A.; Boon, Jaap J. 812
Characterisation of electrosprayed polymers with MALDI-FT-ICR-MS; *Heeren, Ron M.A. ; van Rooij, Gerard J.; Duursma, Marc; de Koster, Chris G.; Boon, Jaap J. 813
FT/MS Analysis of Block and Random Polyester-Urethane Polymers; *Ludicky, Robert. 814

Wednesday Posters - Environmental Analysis

Halogenated Aromatic Compounds in Air Particulates SRM 1648 & 1649; *Xu, Ming; **Kim, Hyun Sik; Guan, Shenheng; Marshall, Alan G.; Dougherty, Ralph C. 815
A New Approach for the Analysis of Volatiles in Complex Matrices; *Barshick, Stacy-Ann; Buchanan, Michelle; Guerin, Michael 816
EPA Method 8270 (semivolatiles) using a GC/Ion Trap Spectrometer; *Barshick, Stacy-Ann; Griest, Wayne; Worthy, Suzanne. 817
Factors Affecting Membrane Introduction Mass Spectrometry; *Ohorodnik, Susan; Callahan, John; Anderson, Mark; McElvany, Steve. 818
Direct Sampling Ion Traps vs. GC/MS for Monitoring VOCs in Groundwater*; *Wise, Marcus; Merriweather, Roosevelt; Guerin, Michael. 819
RAPID SAMPLING FOR RAPID ANALYSIS: A NEW METHOD FOR VOCs IN DRINKING WATER; *Gardner, Ben; Johnson, Jennifer; **Artaev, Viatcheslav; Sparkman, O. David; Holland, John. 820
Monthly Variations of Haloacetic Acids in Drinking Water by GC/MS; *Benoit, Frank M.; Williams, David T.; LeBel, Guy L. 821
Determination of Haloacetic Acids in Drinking Water by Electrospray LC/MS; *Kryak, David D.; Behymer, Thomas D. 822
Analysis of VOCs in water at the Parts-per-Quadrillion Level using MIMS; *Bauer, Scott; Bauer, Jan 823
Analysis of Pesticide Residues in Drinking Water using Megaflow ESI; *Rontree, John; Lowes, Steve; Claereboudt , Jan; Ackermans, P.; Van Hoof, F. 824
Formation of Organochlorine Compounds during Water Chlorination; *Lebedev, A.T.; Moshkarina, N.A.; Brodsky, E.S.; Klujev, N.A.; Petrosyan, V.S. 825

43rd ASMS Conference on Mass Spectrometry and Allied Topics

Multispectral Identification of Ozonation By-products in Drinking Water; *Richardson, Susan D.; Thruston, Jr., Alfred D.; Collette, Timothy W.; **Patterson, Kathleen S.; Lykins, Jr.,Benjamin W. 826
Identification of Brominated Organics in Ozonated Drinking Water; *Thruston, Jr., Alfred D.; Richardson, Susan D.; Collette, Timothy W.; **Patterson, Kathleen S.; Lykins, Jr.,Benjamin W. 827
Isotope Ratio Monitoring for Stable Isotope Analysis on CH4 and N2O in Air; *Brand, Willi A.; Seedorf, Ronald. 828
Evaluation the Air-Quality in Mass Spectrometry Labs. by SPTD/GC/MS; Anren, Hu; *Jentaie, Shiea. 829
GC-MS-MS a novel approach for monitoring the bacterial load in air.; *Krahmer, Mark; Fox, Alvin; Fox, Karen. 830
Transfer Line on MS Sampling and Analysis of VOCs in Air; *Thompson, Cyril; Wise, Marcus; Guerin, Michael. 831
MONITORING TRACE CONTAMINANTS IN AIR VIA ION TRAP MASS SPECTROMETRY; *Palmer, Peter T ; **Karr, Dane, Pearson, Richard; Valero, Gustavo; Wong, Carla. 832
Air Analysis for VOCs: Tenax Collection vs. On-Line Membrane Sampling; *Cisper, M.E.; Gill, C.G ; Kok, G.L.; Hemberger, P.H. 833
Characterization of Volatile Organic Compounds by Thermal Desorption-GC-MS; *Ma, Cheng-Yu; Skeen, Todd T ; Dindal, Amy B.; Higgins, Cecil E.; Jenkins, Roger A. 834
Analysis of Air Samples from Polypropylene Film Plants using Thermal Desorp; *Chuang, C.H. William; Arnold, Elizabeth; Roy, Tim 835
Volatile Organic Compound (VOC) Analysis in Blood Using Spray Extraction; *St-Germain, François; Vachon, Benoit; Brunet, Julie; **Mamer, Orval; Des Rosiers, Christine ; Montgomery, Jane. 836
A Study of Semi-Volatile Organic Emissions of Polymer Combustion by GC/MSD; *Carlson, Joel; Dunayevskiy, Yuriy; Atal, Ajay; Panagiotou, Thomai; Vouros, Paul; Levendis, Yiannis. 837
STRATEGIES FOR IDENTIFICATION OF OFFGASSED VOLATILE ORGANIC COMPOUNDS; *Yang, Lily; Leano, Hector; Martin, Millie; Limero, Thomas; James, John. 838
Electrospray Ionization and Tandem Mass Spectrometry of Dyes; *Fencl, Jennifer B.; Glish, Gary L.; **Voyksner, Robert D. 839
Analysis of Surfactants and Their Metabolites by HPLC-IS-MS and MS-MS; *Raffaelli, Andrea; Pucci, Sergio; Campolmi, Laura; Salvadori, Piero 840
Determination Surfactants In Water by LC and LC-MS; *Scullion, Simon; Clench, Malcolm; Cooke, Michael. 841
Biodegradation Kinetics and Pathways; *Morrall, Stephen W.; Lawrence, David L.; Federle, Thomas W. 842

Detection of Adsorbed Atmospheric Contaminants Using Static SIMS; *Groenewold, Gary; Harrison, Evan; Delmore, James; Ingram, Jani; Appelhans, Anthony; Dahl, David. 843
DETERMINATION OF RADIATION STABILITY OF CROWN ETHERS; *CAMPBELL, JAMES A ; GRANT, KAREN E.; WESTER, DENNIS W.; ABASHKIN, V.M.; JOHNSTON, PAUL F. 844
GC/MS Analyses of Hanford Waste Tank Vapors Using SUMMA[a] Canisters; *Lucke, Richard B; McVeety, Bruce D; Klinger, George S; Clauss, Therese W; Fruchter, John S; Goheen, Steve C 845
MASS SPECTROMETRY ANALYSIS OF TANK WASTES AT THE HANFORD SITE; *CAMPBELL, JAMES A.; LUCKE, RICHARD B.; MONG, GARY M.; CLAUSS, SCOTT A. 846
GC/MS Method for the Chemical Speciation of Arsenic and Selenium Compounds; *Cameron, Douglas; Brozovich, Tara; Watts, Heath; Wang, Jin. 847
Organoarsenic and Organotin Speciation by Ionspray-MS-MS and LC-MS-MS; *Corr, Jay J.; Siu, K.W. Michael. 848

Wednesday Posters - Drug & Metabolism

Quantitation of a CCK Ligand Using LC/MS/MS on Traps and Quadrupoles *Moseley, Arthur, Tippin, Tim, Hart, Robert; St. Claire, Bob; **Schwartz, Jay, Uhrich, Mark. 849
Concomitant Detection of Tazarotene and Three Metabolites from Human Urine; *Luo, Wendy; Matsumoto, Richard; Tang-Liu, Diane; Breau, Alan. 850
Quantification of Dofetilide and its N-desmethyl metabolite in Human Serum *Schneider, Rick, Fouda, Hassan. 851
Measurement of CO2 Exchange Rates in Transferrin by Mass Spectrometry; *Brown, Todd; Hileman, Fred; **Harris, Wes. 852
Analysis of 2-Butoxyethanol and Metabolites in Human Urine by GC & ESI/MS; *Markham, Dan A ; Bartels, Micheal J.; Corley, Richard A.; **Rettenmeier, Albert W. 853
Evaluation of Nalmefene Metabolism in Rats and Dogs Using Thermospray LC/MS; *Mathur, Chandra; Murthy, Satya S ; Kvalo, Loretta T.; Wilhelm, Jeffrey A 854
Quantitation of Ritalin and Ritalinic Acid in Human Plasma by API LC/MS/MS; Cassidy, Ken C.; *Matassa, Luca C. 855
Automated LC/ESI/MS/MS Quantitation of a Phospholipid Drug in Human Plasma; *Hamilton, Brenda; Graham, Elizabeth, Abolin, Craig; **White, Robert, Oglesby, Thomas. 856
Ultra Trace LC/MS/MS Determination of Reserpine in Plasma.; **Anderson, Melissa; *Wachs, Timothy; Henion, Jack. 857
Lovastatin and Hydroxy-acid Lovastatin in Dog Plasma via LC-APCI/MS/MS; *Korfmacher, Walter A.; Lapiguera, Amelia P.; Lin, Chin-Chung; **Langevin, Carolyn N.; Oglesby, Thomas D. 858

LC/MS/MS QUANT. OF LOVASTATIN & ITS HYDROXY ACID IN MOUSE & RAT PLASMA; *Wu, Henry, Y, Henion, Jack , Zhao, Jamie; Korfmacher, Walter A ; Lin, C.C. 859
QUANTITATION OF LTE4 IN HUMAN URINE BY ION SPRAY LC/MS/MS; *Wu, Henry Y.; Li, Lily Y.-T ; Henion, Jack; Krol, George J. 860
Automation of Rapid, High Sensitivity Pharmacokinetic Assays by LC/MS/MS; *Stoney, Ken; Nugent, Kerry; **Land, Adrian P., Bier, Mark E.; Schwartz, Jae, Wheeler, Kevin. 861
Semi-automated Electrospray LC/MS/MS Quantitation of CGS 20286A in Plasma; *Hayes, Michael J.; Joshi, Jill C.; Carlsen, Steve; Powell, Mark L. 862
Quantitation of Cefoxitin in plasma by LC/MS Negative Ion Electrospray; *Zamecnik, Jiri; Florio, Eugene. 863
Determination of Novel Thrombin Inhibitors in Animal Plasma by LC/API-MS; *White, Dineen J.; Russell, John W.; Wang-Iverson, David. 864
LC/MS/MS Method for the Determination of Nicotine & Cotinine in Plasma; *Xu, Allan; Havel, Jim; Petersen, Mary; Hulse, James. 865
Tetracyclines in Honey, Eggs and Animal Tissues by ESI MS and MS/MS.; Snider, Neil S ; *Malis, Greg M 866
Determination of a 4-Azasteroid in Serum Using Negative Ion APCI LC/MS *Halm, Kathy; Lloyd, Thomas, Moss, M. Lee. 867
Determination of a 5-HT receptor agonist by LC-APCI-MS-MS; *Pleasance, Stephen; Fraser, Ian; Allanson, John; Jones, Anne. 868
Quantitative Analysis of Tirilazad Mesylate in Plasma by APCI/MS-MS.; *Hauer, Michael J.; Moore, Theresa A.; Steenwyk, Rick C.; Bombardt, Paul A , Pearson, Paul G 869
GC/MS and LC/MS Confirmation of Malachite Green Metabolites in Catfish; *Turnipseed, Sherri; Roybal, Jose; Hurlbut, Jeff; Long, Austin. 870
ESI-MS Analysis of Bioactive Isoleukotrienes; *Harrison, Kathleen; Murphy, Robert C. 871
LC-ESI-MS/MS of polyamines and basic amino acids.; *Feistner, Gottfried J 872
LC/LC/MS/MS ANALYSIS OF HUMAN PLASMA FOR A "STICKY" PEPTIDE; *Li, Lily Y.-T., Zhao, Jamie, Henion, Jack; Newman, Michael 873
Detection of the Endogen NO Gas from Living Animals by Mass Spectrometry; Delacotte, J -M.; Faye, T.; *Regert, M.; Rolando, C.; Sablier, M 874
MACROMOLECULE ISOTOPE-RATIO MEASUREMENTS WITH HPLC/CRIMS; *Osborn, Blaire L.; Abramson, Fred P. 875
QUANTITATIVE ASPECTS OF MASS SPECTROMETRIC IMMUNOASSAY; *Nelson, Randall W.; Krone, Jennifer R.; Lewis, J. Kathleen; Williams, Peter 876
The Analysis of Flunixin Residues in Animal Tissues by NICI-GC-MS; *Kwok, David; Chow, Pauline; Young, Larry; Mori, Brian. 877
GC/MS Determination of Perillyl Alcohol Metabolism After Oral Dose in Dog; *Phillips, Lawrence R , Supko, Jeffrey G.; Malspeis, Louis 878

Positive chemical ionisation GC-MS analysis of nicotine and continine; *Loftus, Neil; Skarping, Gunnar; Dalene, Marianne; Speakman , Alison ; Bukowski, Nick... 879
Analysis of anagrelide in human plasma by GC/ECNCI MS.; *Yeola, Suresh N.; Saleh, Samir A.; Sanchez, Stephanie C.; Kambouris, Sara J.; Chaudhary, Ajai K.; Migdalof, Bruce H.; Blair, Ian A... 880
QUANTITATIVE DETERMINATION OF ZK 118372 IN HUMAN PLASMA USING NCI-GC/MS; *BRUDNY-KLOEPPEL, Margarete; GUENTHER, Clemens; WEISS, Christian... 881
Quantitation of Odd-Numbered Long Chain Fatty Acids in Red Cell Membranes; *Giordano, G.; Burlina, A., Magarotto, M.; Edini, C.; Zacchello, F. ... 882
A Novel Approach for Analysis of Fadrozole Pseudoracemates in Human Plasma; *Iannucci, Robert; Linberg, Leonid; Powell, Mark... 883

Wednesday Posters - Spray Ionization

Sonic Spray Ionization Method for API Mass Spectrometry; *Hirabayashi, Atsumu, Sakairi, Minoru; Takada, Yasuaki; Koizumi, Hideaki ... 884
Electrospray LC/MS With Orthogonal TOFMS and Ion Trap TOFMS *Purves, Randy; Li, Liang... 885
Sensitivity Advances In Electrospray FTMS; *Kruppa, Gary; Stacey, Catherine; Speir, J. Paul; **Whitehouse, Craig; Laukien, Frank... 886
High Sensitivity Electrospray With A Fourier Transform Mass Spectrometer; *Stacey, Catherine; Kruppa, Gary; Spier, J. Paul; **Mann, Matthias... 886
Characterization of in vitro Metabolites of Ziprasidone by Mass Specrometry; *Kamel, Amin; Prakash, Chandra... 887
Reduction of Ambient Air Contaminants; Aebi, Beat; *Henion, Jack... 888
Pulsing Electrospray and Selecting Ions from Electrospray by Ion Mobility; **Li, Guo-Zhong; Wang, Weimin; Kim, Tamen; *Moore, Robert B... 889
Achieving High Sensitivity LC/MS with an API-Ion Trap Mass Spectrometer; *Habibi-Goudarzi, Sohrab; Henion, Jack; **Duffin, Kevin, L.; Hileman, Fred D.;... 890
Capillary, Multicapillaries or Porous Tube for Electrospray Ion Sources; *Beaugrand, C.; Charbonnier, F.; Rolando, C.; Sablier, M.; Saru, F... 891
Transport of Electrospray Particles through the Interfaces; *Bondarenko, Pavel; Macfarlane, Ronald... 892
Ion Distribution of Electrospray and Efficiency of Transferring Ions; Wang, Weimin; **Li, Guo-Zhong; Kim, Tamen; *Moore, Robert B... 893
Stability of a Liquid Jet Emerging from an Electrospray Cone-Jet; *Sheehan, Edward; **Willoughby, Ross... 894
Secondary Droplet and Ion Formation in Electrospray: The Teardrop Model; *Sheehan, Edward; **Willoughby, Ross... 895
Role of Peptide Structure in the Production of Ions from Charged Droplets; *Downard, Kevin; Biemann, Klaus... 896

43rd ASMS Conference on Mass Spectrometry and Allied Topics

Tuning Parameters: Their Dominant Role in Electrospray Ion Intensities; *Cunniff, John; Vouros, Paul... 897
The Characterization of m/z Deviates and Molecular Mass Uncertainty; *Juneau, Paul L.; Giordani, Anne B., Pyne, David A... 898
Chemical Redox Reactions in ES-MS: Study of Electrode Reactions; *Zhou, Feimeng; Van Berkel, Gary... 899
Electrochemistry Combined On-line with Electrospray Mass Spectrometry; *Van Berkel, Gary; Zhou, Feimeng... 900
Formation of Protonated Ions from Acidic Species at High pH in Electrospray; *Smith, Richard W... 901
Electrospray Ionization, Maximum Charge States to Multiplexing; *Schnier, Paul D.; Williams, Evan R... 902
Protein Cations from Basic Solutions with an API III and an API 100.; *Le Blanc, J.C. Yves; Shushan, Bori; **Siu, K.W. Michael; Guevremont, Roger... 903
Effects of Organic Solvents on Aerosol MALDI Ion Signal *Beeson, Michelle D ; Wei, Xiaona; Russell, David H... 904
Analyzing Thermally Labile Compounds in ESI Sources with Heated Capillaries; *Kleintop, Brent; Lim, H.K.; **Oglesby, Thomas; Chan, Kelvin; Sisenwine, Samuel... 905
Peptide Mixture Analysis by Combining Electrospray-CID-MS and Chemometrics; *Cusworth, III, William; Turecek, Frantisek... 906
Ion Solvation in Electrospray Generated SDS Clusters; *Gao, Q; Zhang, J; Harms, A. C.; Udseth, H. R.; Rockwood, A. L ; Sherman, M. G.; Smith, R. D... 907
Rapid Molecular Weight Determination Using Electrospray Ionization; *Gedamke, Rich; DiDonato, Gerald; Hail, Mark; Lee, Mike... 908
Adventures in the Positive Ion ESIMS of Acids and Neutral Molecules; *Shah, Nikhil; Fitch, William... 909
Electrospray Ionization of Neutral Complexes from Non-Polar Solvents; *Cheng, Xueheng; Gao, Quanyin; Smith, Richard D.; Simanek, Eric E.; Mammen, Mathai; Whitesides, George M... 910
Electrospray Mass Spectra of Less Polar Compound Dissolved in n-Hexane; Wang, Wen-shyang; Huang, S-wan ; *Shiea, Jentaie... 911
Low Temperature Electrospray Mass Spctra of Thermally Unstable Compound; Wen-Shyang, Wang; Chin-Hsiung, Wang; *Jentaie, Shiea... 912
Multi-channel ESI source for directly coupling to HPLC; Chinghsiung , Wang, *Jentaie, Shiea... 913
Negative ESI Mechanism of TFA/TFE Derivatives of Glyphosate and AMPA; *Fujiwara, Hideji; Singh, Rajendra. K.; Nadeau, Ronn; Chott, Robert C... 914

Wednesday Posters - Laser Desorption/Ionization

MALDI of Non-Covalently Bound Complexes.; *Woods, A.S.; Buchsbaum, J.C., Berg, J.M.; Cotter, R.J. 915
Primary Structure of Proteins Determined by MALDI Mass Spectrometry; Yang, Hou-Jun; Amft, Matthias; Grundwuermer, Johann M.; Li, Yiao-Ling, *Grotemeyer, Juergen. 916
MALDI/TOF/MS and Recombinant HIV Protein Expression; *Parker, Carol; Papac, Damon; Tomer, Kenneth. 917
MALDI-TOF Analysis of Peptide Digestion Mixtures with Detergents; *Gharahdaghi, Farzin, Fernandez, Joseph; Mische, Sheenah, M. 918
Sample Preparation for Protein Fingerprinting of Bacteria Using MALDI MS; *Liang, Xiaoli; Cain, Teresa C.; Bai, Jian, Liu, Yan-Hui; Lubman, David M. 919
MALDI Combined with Chemical Reaction Methods for Studying Protein Folding; *Zhang, Jian; Wang, Yajun; Edmondson, Rick; Gillig, Kent; Hayes, Timothy; Russell, David 920
Carboxyl-Terminal Ladder Sequencing of Peptides and Proteins; *Wang, Rong; Chait, Brian T 921
PROTEIN CONFORMATION, HYDROGEN BONDING, AND ENERGY TRANSFER IN MALDI; Bencsura, Akos; *Vertes, Akos. 922
Mass Tracer Methods based on MALDI; *Whittal, Randy M.; Schriemer, Dave C.; Li, Liang 923
MALDI Mass Spectrometry of Tissue Extracts ; *Ogorzalek Loo, Rachel R , Andrews, Philip C 924
Evaluation of Maldi.MS For Agricultural Applications; *Shalaby, Lamaat; Hubbard, Natalie; Stahl, Bernt; Hillenkamp, Franz; Zeng, Jianru. 925
CID studies of MALDI generated peptide ions by RETOF MS; *Holle, Armin; Köster, Claus. 926
Effective Methods for Characterization of Membrane Proteins by MALDI-MS; *Shyong, Bao-Jen, Mitchell, Charles; Andrews, Philip 927
Assessment of Photoaffinity Crosslinking of Macromolecules by MALD MS; *Farmer, Terry B.; Caprioli, Richard M. 928
DESALTING PROCEDURE FOR HIGH SENSITIVITY ANALYSIS OF PEPTIDES BY MALDI-MS; *Zhang, Haiying; Caprioli, Richard M. 929
DIFFERENTIATION OF MULTIMERIC ANTIGENS BY MSIA AND ENZYMATIC MODIFICATION; *Nelson, Randall W.; Krone, Jennifer R.; Dogruel, David; Lewis, J. Kathleen; Williams, Peter 930
Sequence Specific Fragmentation Generated by MALDI in Ion Trap/reTOF; *Lee, Heewon; Lubman, David. 931
Strategy to Locate Cysteine Residues by Specific Cleavage and MALDI-TOF MS; *Wu, Jiang; Gage, Douglas A ; Watson, J Throck. 932

MALDI-MS of Proteins Electroblotted onto Membranes after 2D-PAGE Separation; *Strupat, Kerstin, **Eckerskorn, Christoph; Karas, Michael; Hillenkamp, Franz. 933
Oligonucleotide And Protein Analyses Using Membranes And MALDI-MS; *Stevenson, Tracy I ; Loo, Joseph A. 934
LDMS for Fast DNA Analysis and Disease Diagnosis; *Chen, C. H.; Taranenko, N I.; Allman, S. L.; Tang, K ; Matteson, K. J.; Ch'ang, L. Y. 935
Oligonucleotide Analysis by MALDI MS via Ion Trap/reTOF MS; *Liu, Yan-Hui; Bai, Jian; Qian, Mark G.; Liang, Xiaoli; Lubman, David M. 936
Synthesis and MALDI Characterization of Electrophore-Labeled DNA; *Hurst, Gregory B.; Britt, Phillip F.; Buchanan, Michelle V 937
Use of a Polymeric Substrate in MALDI MS for DNA Mapping and Screening; *Liu , Yan-Hui; Bai, Jian, Liang, Xiaoli; Lubman, David M 938
The Effect of Impurities on the Analysis of Oligodeoxynucleotides by MALDI; *Shaler, Thomas; Wu, Kuang Jen; Wickham, Juanita; Becker, Christopher 939
Analysis of DNA Dideoxy-Sequencing Reaction Products by MALDI-TOFMS; *Shaler, Thomas; Wu, Kuang Jen, Sannes, Kristin; Becker, Christopher. 940
Protocols for improved laser ejection/ionization TOFMS of oligonucleotides; *Srinivasan , Jannavi, R.; Levis, Robert, J., Narayanaswami, Gowri. 941
IMPROVEMENT IN OLIGONUCLEOTIDE ANALYSIS BY ADDUCT FORMATION; *Tang, Xiaodong, **Callahan, John; Zhou, Ping; Hayes, Joe; Vertes, Akos*1-1. 942
MALDI Post-Source Decay of Oligonucleotides; *Deterding, Leesa; Tomer, Kenneth. 943
NEW INSTRUMENTAL APPROACHES TO TOF MASS SPECTROMETRY OF DNA; *Dogruel, David; Nelson, Randall W.; Williams, Peter. 944
PROGRESS IN DNA SEQUENCING AND FUNDAMENTAL STUDIES USING MALDI-TOFMS; *Chou, Chau-Wen; Nelson, Randall W.; Williams, Peter. 945
MALDI of Drug Compounds from Intact Biological Tissue; *Reddick, Christopher, Yost, Richard. 946
Application of MALDI TOFMS for Quantitative Analysis; *Hensel, Russell; King, Richard, Owens, Kevin. 947
Analysis of Synthetic Polymers and Copolymers by MALDI-MS; *Schaer, Martin. 948
Characterization of Polyesters by Transesterification Using MALDI TOF MS; *Williams, John B.; Gusev, Arkady I.; Hercules, David M. 949
Accuracy of MALDI for Mol. Weight Characterisation of Synthetic Polymers; *Overberg, A.; Ingendoh, A., Keane, A.; Sutton, C ; Cottrell, J S. 950
High Resolution MALDI Studies of Polymer Mixtures and Copolymers; *Schriemer, Dave C; Li, Liang. 951
Analysis of GPC Standards by Matrix-Assisted Laser Desorption/Ionization; Hanley, Brian; Parees, David; *Hanton, Scott; **King, Richard; Owens, Kevin. 952

Structural Determination of Azo Dyes by Photoionisation Mass Spectrometry; *Wright, Scott; Dale, Michael; Jones, Anita; Langridge-Smith, Patrick. 953
Two Step Laser Mass Spectrometry of Copolymerised Indole Derivatives; *Mackintosh, J. Gordon; Mount, Andrew; Wright, Scott; Redpath, Craig; Dale , Michael; Langridge-Smith, Patrick. 954
Molecular Analysis From Organic Substrates Using Laser Mass Spectrometry; *Dale, Michael; Langridge-Smith, Patrick; **Zhan, Qaio; Zenobi, Renato; Costello, Kevin. 955
Wavelength Dependent Photo-ionization of some Amines at Metal Surfaces; *Goldschmidt, Robert; Owens, Kevin. 956
Enhanced Detection Limits of High Molecular Weight PAHs Using LD-TOF MS; *Soloveytchik, Boriana; **Miller, John; Vertes, Akos. 957
Real-Time Monitoring of Aerosol Reactions; *Carson, Peter; Johnston, Murray; Wexler, Anthony. 958
Laser Desorption/FTMS For Polymer Microstructure Characterization; *Qian, Kuangnan; Tianlan, Zhang; Ridge, Douglas P. 959
The electronic spectroscopy of some p-alkylphenols and catechols *Grace, Louis I.*; Barstis, Toni L.O.**; Lubman, David M.; Dunn, Thomas M. 960
Laser Desorption/Ionization of Size-Resolved Liquid Microdroplets; *Mansoori, Bashir; Johnston, Murray; Wexler, Anthony. 961
Laser Desorption Mass Spectrometry of Hydroxy-Nitro-PAHs; *Bezabeh, Dawit; Jones, A. Daniel; Kelly, Peter B. 962
Infrared spectroscopy of methanol attached to gold tetramer cluster ions; **Dietrich, G.; Walther, C.; Kluge, H.-J.; Lützenkirchen, K. ; *Schweikhard, L. ; Ziegler, J. 963
Laser Desorption/Resonant Laser Ablation - Trace Analysis of Solid Matrices; *Gill, C. G.; Earl, W. L. ; Garrett, A. W.; Nogar, N. S.; Hemberger, P. H. 964
Lanthanide, Thorium, and Uranium Oxide Clusters Formed by DLV/FTICR; *Pires de Matos, António; Marçalo, Joaquim; Leal, João Paulo. 965
Photolabalisation of Fe Bound Phosphine Ligands: Laser Desorption FTI CR MS; *Aplin, Robin; Davies, Stephen; McMarthy, Tom; Watkins, Carl; Evard, Dwight. 966
Laser ablation mass spectrometry of sodium penetrated petroleum cokes; *Willett, Gary; Hopwood, Femia; Fisher, Keith; **Greenhill, Paul. 967
Laser Mass Spectrometry of Synthetic Linear and Dendritic Polymers.; *Mowat, Ian; Donovan, Robert; Bruce, Morag; **Monaghan, John. 968

Thursday Orals - Hydrogen Bonding Interactions

Effects of Protonation on Structure and Entropy of Bifunctional Molecules; Szulejko, Jan; *McMahon, Terry; **Audier, Henn; Milliet, Ariel. 969
Detection and Characterization of Gas Phase Cyclodextrin Complexes Dejsupa, Chadin; Dearden, David. 970
Probing Hydrogen-Bonding Interactions in an Ion Trap; *Brodbelt, Jennifer; Colorado, Armando; Vartanian, Victor; Chen, Jim. 971
Studies of Photoinduced Proton Transfer Reaction in H-Bonded Clusters; *Huang, Yong; Russell, David H. 972
Protonated Dimethyltartrate Dimer Decomposition Chirality Effects in FTMS; *Nikolaev, Eugene; McMahon, Terry. 973
In Search of Non-Classical Ethyl Cation Stabilized by Organic Molecules.; *Zagorevski, Dmitri; Holmes, John L. 974

Thursday Orals - Mass Spectrometry in Immunology

Schistosome Surface Oligosaccharides Modulate Immune Response; *Reinhold, Vernon N.; Reinhold, Bruce B.; Velupillai, Palanivel; Harn, Donald A. 975
Identification of a Graft-vs-Host Disease Associated Human Minor Antigen; *Sherman, Nicholas E.; den Haan, Joke M.M.; Hunt, Donald F.; Shabanowitz, Jeffrey; Engelhard, Victor H.; Goulmy, Els. 976
CE-MS and MS-MS analyses of lipopolysaccharides from Pseudomonas aeruginosa; Auriola, Seppo I-1; *Thibault, Pierre; Sadovskaya, Irina I-2; Masoud, Hussein I-2; Altman, Elenora I-2; Richards, James I-2. 977
A Human Melanoma Antigen which Results from Post-Translational Modification; *Hendrickson, Ronald C.; Skipper , Jonathan A.; Gulden, Pamela H.; Shabanowitz, Jeffrey; Chen, Y.; Slingluff, C. L.; Englehard, V H.; Hunt, Donald F. 978
Tandem Mass Spectrometry & Data Analysis of Immunological Peptide Mixtures; *Yates, John R. III; McCormack, Ashley L.; Eng, Jimmy K.; DeRoos, Paul C.; Rudensky, Alexander Y. 979
ES and MALDI MS Analysis of Glycosylation-Engineered a-1 Acid Glycoprotein; *Bean, Mark; Huddleston, Michael; O'Shannessy, Daniel; Carr, Steven. 980
Epitope Determination by Mass Spectrometry: HIV p24; *Tomer, Kenneth; Papac, Damon; Parker, Carol. 981
Probing the antibody-antigen interaction by affinity-mass spectrometry; *Zhao, Yingming; Muir, Tom; Kent, Stephen H.B.; Chait, Brian T. 982

Thursday Orals - Ion Trap Mass Spectrometry

Resonant Excitation of Injected Atomic Ions in an Ion Trap MS; *Eiden, Gregory C.; Barinaga, Charles J.; Koppenaal, David W 983
Ion Remeasurement in the RF Quadrupole Ion Trap; *Goeringer, Douglas; McLuckey, Scott; Crutcher, Richard. 984
Buffer Gas and q-eject Effects on the Performance of an Ion Trap; *Lammert, Stephen A.; Wells, J. Mitchell. 985
Effect of Ion population Upon MS/MS Parameters in a Quadrupole Ion Trap; *Griffin, Timothy; Yost, Richard. 986
Fragmentation of Peptides by MicroES/ Quadrupole Ion Storage (QUISTOR) MS; Kšrner, Roman; *Wilm, Matthias; Mann, Matthias; Houthaeve, Tony. 987
Peptide Sequencing Using Fast MS and MS/MS Scans on a Quadrupole Ion Trap; *Bier, Mark E ; Schwartz, Jae C.; Zhou, Joe; Taylor, Dennis; Syka, John; Fies, Bill; Borchers, Torsten; James, Mike. 988
Practical Matrix-Assisted Laser Desorption Ion trap MS for Peptide Analysis; *Qin, Jun; Chait, Brian T 989
Analyzing Mixtures With a Hybrid Quadrupole/Ion Trap Mass Spectrometer; *Jonscher, Karen R.; Yates, John R. 990
A Portable Atmospheric Sampling QUISTOR/reTOF- MS for Air Monitoring; *Grace, Louis I.; Chambers, David M.; Thomas, Stan W.; Andresen, Brian D. 991
Identification of in vitro Bupropion Metabolites by APCI LC-Ion Trap MS; *Taylor, Lester; Singh, Romi, Chang, Sai; Johnson, Robert, Schwartz, Jae; Barber, Michael. 992
Analytical Protocols for Environmental Substances using an Ion Trap; Plomley, Jeffry B , Koester, Carolyn J., Lausevic, Mila, Xuewu, Jiang, *March, Raymond E.; Londry, Frank A. 993

Thursday Orals - Time of Flight Mass Spectrometry

Time-of-Flight (TOF) Mass Spectrometry--Nearing the Half Century; * Standing, K. G. 994
Organic Secondary Ion Imaging by Time-of-Flight Secondary Ion MS (TOF-SIMS); *Lindley, Patricia M.; Reich, Fraser. 995
Important Aspects Concerning the Quantification of Biomolecules by TOF-SIMS; *Muddiman, David C; Nicola, Anthony J, Proctor, Andrew; Hercules, David M. 996
Peptide Sequencing by Carboxypeptidase Digestion Coupled with MALDI-TOF; *Patterson, Dale; Tarr, George; Martin, Stephen; Regnier, Fred. 997
MALDI electrostatic analyzer TOF mass spectrometry studies of biopolymers; *Wu, Kuang Jen; Marsh, Eugene; Odom, Robert. 998
A Mass Analyzer for High Speed Liquid Chromatography; Andrien, Jr., Bruce; Boyle, James, Banks, Fred; *Dresch, Thomas; Haren, Patrick, Whitehouse, Craig. 999

ACHIEVING LINEAR DETECTOR RESPONSE IN TOF-MS; *Stresau, Dick, Hunter, Kevin; Gray, John 1000
A Time Focusing Equation and a Classical Uncertainty Relation in TOFMS; *Stein, Ronald. 1001
Analytical Form of Position Focusing in the Parabolic Electrostatic Field; *Stein, Ronald. 1002
Space-Velocity Correlation Focusing; COLBY, STEVEN; *REILLY, JAMES; 1003
Tandem Mass Spectrometry on a Triple-ESA Time-of-Flight SIMS Instrument; *Kristo, Michael; Odom, Robert. 1004

Thursday Orals - Energy & Petrochemicals

Mass Spectrometric Studies on Porphyrins and Geoporphyrins; *Quirke, J. Martin E.; Yost, Richard A.; Van Berkel, Gary J. 1005
Mass Spectrometry of Porphyrins: Ionization and Appearance Energies; *Ferguson, James A.; Quirke, J. Martin E ; Johnson, Jodie V., Yost, Richard A. 1006
Heavy Resid Characterization using High Resolution and Laser Desorption MS; *Hunt, Jerry E.; Kim, Yeonhee; Winans, Randall E.; Anderson, Ken B , Miller, Jeffery. 1007
The New EPA GC/MS Method for Total Aromatics in Reformulated Gasoline; *Drinkwater, Donald, Nero, Vince. 1008
Analysis of Gasoline for Aromatic Hydrocarbons by GC/MS and by Low eV-HR/MS; *Grigsby, Ronald D.; McWilliams, Ted B. 1009
Hydrocarbon Analysis Using An Ion Trap/MS With External Ionization; *Teng, Siu. 1010
Industrial Applications of FTMS: A Present and Future Prospectus; *Campana, Joseph. 1011
The Identification of Zinc Dialkyldithiophosphates in Lubricating Oils; *Nero, Vincent; Drinkwater, Donald. 1012
FLUID CATALYTIC CRACKING PRODUCTS CHARACTERIZED BY GCMS; *Cheng, Michael, Hudson, James. 1013
Coupling FI-MS with LC for the Characterization of Heavy Sat'd Hydrocarbons; Liang, Zhenmin, *Hsu, Chang Samuel, Blum, Saul, Robbins, Winston; Grosshans, Peter. 1014

Thursday Orals - Organohalogens:New Issues & Techniques

Why Do We Still Care about Dioxins?; *Hites, R.A., Brzuzy, L., ... 1015
Ultrasensitive and Very Fast Analysis of Halogenated Toxicants; *Patterson, Donald G.; Jr; Liu, Zaiyou; Green, Vaughn E., Barr, John R 1016
Inventories of Toxic Organochlorine Compounds in the Great Lakes' Sediments; *Swackhamer, Deborah L., Pearson, Roger; Eisenreich, Steven J ; Long, David T. 1017

Characterization of Major Taxophene Components in Lake Sediments & Aquatic; *Stern, G.A.; Lowen, M.; **Miskimmin, B.M.; Muir, D.C.G.; Parlar, H.; Schindler, D.W.; Westmore, J.B. 1018
Dioxin and Furan Analysis by Ion Trap, Triple Quadrupole MS/MS, and HRMS; *Mercer, Roger S.; Plomley, Jeffry B.; Townsend, Jennifer A.; Waddell, Dave S.; Plomley, Jeffry B.; March, Raymond E. 1019
An Isotope Dilution Method for the Analysis of Chlorinated Diphenyl Ethers; *Ralitsch, Milan; Gottschalk, Russell; Birkholz, Detlef. 1020
Photoelectron Capture Negative Ion Mass Spectrometry of Organohalogens; *COLBY, STEVEN; HARRIS, WILLIAM; HANSER, KENT; REILLY, JAMES. 1021
Determination of Pesticides on Agricultural Samples by Static SIMS Analysis; *Ingram, Jani; Groenewold, Gary; Appelhans, Tony; Miller, David; Delmore, James. 1022
Real-time Analysis of Breath for Carbon Tetrachloride and its Metabolites; *Kenny, Donald; Thrall, Karla; Callahan, Patrick. 1023
TUNABLE ENERGY (0.03-60 eV) ELECTRON CAPTURE NEGATIVE ION SPECTROMETRY; *Laramee, James; Deinzer, Max. 1024

Thursday Posters - Fundamental Studies

STRUCTURES AND ELECTRONIC PROPERTIES OF FULLERENE-RELATED COMPOUNDS; *Hettich, Robert; Ying, Z. Charles; Compton, Robert. 1025
Reactions of Fullerene Oxides in a FT-Mass Spectrometer; *Holliman, Christopher; McElvany, Stephen 1026
Collision experiments with fullerene ions and molecular gases; *Cooper, Helen J; Gallagher, Richard T; Derrick, Peter J; Vulpius, Tore. 1027
Intermolecular Nitrile Oxide Transfer in Fullerene Isoxazolines; *Pogue, Robert; Meier, Mark; Thomas, Craig; Majidi, Vahid 1028
Ion Mobilities from FT-ICR Mass Spectral Peak Widths; *Pasa-Tolic, Ljiljana; Guan, Shenheng; Marshall, Alan G. 1029
Gas Phase Protonation of Aniline; *Nold, Michael ; Wesdemiotis, Chrys. 1030
Synthesis and Characterization of the 3,5-dehydrophenyl Anion; *Hu, Jun; Squires, Robert. 1031
Reactions of Radical Anions Having Formally Distinct Radical & Anion Sites; *Grabowski, Joseph J.; Owusu, Daniel. 1032
Photodetachment of Solvated Ions; *Yang, Yarjing; Peiris, Dil; Riveros, Jose M.; Eyler, John R. 1033
Advances in Applications of the Kinetic Method; *Cooks, R. Graham; Horn, Lynn; Chen, Guodong; Yang, Sheng; Patrick, Jeffrey. 1034
Gas Phase Ion Chemistry of Sulfonate Anions. *Smith, Jacob D.; O'Hair, Richard A.J.; Schmidt, Joseph A.R.; Williams, Todd D. 1035
Bond-Selective Photodissociation: Mechanisms and Applications; *Bookwalter, Craig; Ross, Philip; Johnston, Murray. 1036

43rd ASMS Conference on Mass Spectrometry and Allied Topics

Collision Spectroscopy Involving Charge Permutation and Light Emission; *Wesdemiotis, Chrys; Beranova, Sarka; Polce, Michael J.; Wiedmann , Fred A. 1037
Collisionally Induced Emission Spectroscopy; *Wiedmann, Fred; Wesdemiotis, Chrys. 1038
Matrix Isolation of Mass-Selected Ions for Analysis by FTIR Spectroscopy; *Allison, John; Halasinski, Thomas; Godbout, Jerry; Leroi, George E. 1039
Spectroscopic Studies of the Electron Recombination of Several Small Ions; *Foley, B. Lachele; Adams, Nigel G.; Babcock, Lucia M.; Butler, Jeffery M.; Drucker, Mark B. 1040
Ab Initio Calculations of the Ar¥CO2+ Cluster Ion; *Gellene, Gregory 1041
Symmetry Breaking and Electron Correlation in (O2)-, O2, and (O2)+; Chandrasekher, Charu A., *Griffith, Kelly S.; **Gellene, Gregory I. 1042
Accurate Ionization Energies And Heats of Formation of Simple Enols; *Turecek, Frantisek. 1043
Theoretical Study of the Ring Closure of the 1,7-Octadiyne Cation; *Robbins, Ronny; Jensen, James; Berg, Fred. 1044
The Presence of Hydrogen Trioxide in the Gas Phase; *Fujii, Toshihiro; **Kishi, Hiroshi. 1045
Structure of isomeric Gly-Pro b2 ions calculated by ab-initio methods; *Eckart, Klaus; Holthausen, Max C., Koch, Wolfram; Spiess, Joachim. 1046
Fragmentation of Benzalacetones: Theory and Experiment; Heinicke, Ralf; Moritz, Fritz; *Grotemeyer, Juergen. 1047
Ion Pair Formation and Fragmentation in EIMS of Methyl Octadecanoate; *TAKAYAMA, Mitsuo; HIRAOKA, Kenzo; NAKATA, Hisao. 1048
Gas Phase Decomposition of Dimethyl(hydroxy)silyl Radical; *Nguyen, Viet; Shaffer, Scott, A; Hop, Marcel, C.E.C.A; Turecek, Frantisek. 1049
Evolution of the m/z91:92 ratio during CAD of Butylbenzene Molecular Cation; Beaugrand, C ; Rolando, C.; *Sablier, M. 1050
Can Protonated Peptides Fragment from Their Triplet States?; *Somogyi, Arpad; Wysocki, Vicki; **Mayer, Istvan. 1051
Study Of MS Decomposition Mechanisms In 2,3-Difluoro-dimethyl Succinates; *Parees, David. 1052
Energy Resolved Mass Spectrometry of Organophosphonates; *Wensing, Michael W.; Forch, Brad E.; Fifer , Robert A.; Snyder, A. Peter; Harden, Charles S. 1053
Energy Resolved Mass Spectrometry of Organophosphorus Esters; *Wensing, Michael W.; Forch, Brad E.; Fifer, Robert A.; Snyder, A. Peter; Harden, Charles S. 1054
Effect of Collision Gas on FAB-MS/MS Spectra from Calibration Point Method; *Lemire, Sharon; Busch, Kenneth. 1055
Considerations about the FAB ionization process of a-aminoacids *N. Domingues, Pedro ; L. Amado, Francisco ; F.Barros, Cristina; O. S. Marques, M. Graa; Ferrer Correia, A. J. 1056

PDMS Analysis of Frozen Cycloalkenes Betts, Robert; **da Silveira, Enio; *Schweikert, Emile. 1057
Biomolecular Cluster Formation in PDMS; *Demirev, Plamen; Eriksson, Jan; Hkansson, Per; Papaleo, Ricardo, Sundqvist, Bo; Zubarev, Roman. 1058
252Cf-PDMS of New Pyrazole Derivatives; Ponciano, Cassia; Lin, Whei; Pereira, Neila; Freitas, Antonio; Barrelro, Eliezer; *da Silveira, Enio. 1059
Matrix Effects on the Fragmentation of Vitamin B12 in PDMS *Blankenship, James; Van Stipdonk, Michael; Schweikert, Emile 1060
DESORPTION OF PEPTIDE IONS USING MALDI MATRICES IN CONJUNCTION WITH PDMS; *Van Stipdonk, Michael; Blankenship, James; Schweikert, Emile. 1061
Evaluation of Solvent Effects on MALDI Matrix Crystal Formation; *Sumner, Lloyd W.; Edmondson, Ricky D.; Campo, Karen K.; Russell, David H 1062
Infrared Matrix-Ass. Laser Des./Ion. (IR-MALDI) using a Free-Electron Laser; *Cramer, Rainer; **Haglund, Jr., Richard F.; Hillenkamp, Franz. 1063
Effect of analyte hydrophobicity on beam-induced dehalogenation in LSIMS; *Th berge, Roger; Bertrand, Michel, J 1064
Cluster Ion Formation in LSIMS for a Series of Quaternary Ammonium Salts; *Paul, G. J. C.; Anastassopoulou, J., Arkas, M.; Paleos, C. M., **Marcotte, I , Bertrand, M. 1065
Organic Secondary Ion Emission from Solids and Liquids; *McMahon, John; Todd, Peter, Caimi, Richard; **Brenna, Thomas 1066
Mechanistic Studies of High Valent Iron Catalysts; *Weintraub, Susan T.; Bartos, Michael J , Gordon-Wylie, Scott, Wright, L James, Noon, Kathleen R.; Collins, Terrence J. 1067

Thursday Posters - Ion Source & Mass Spectrometer Design

New Axial Energy Analyzer For Secondary Ion Mass Spectrometry; *Wei, Jian; Schaeffer, Richard 1068
Resolution and Transmission of Quadrupoles: RF-DC and RF-Only Operation; *Pedder, Randall E.; Schaeffer, Richard A. 1069
Quadrupole Mass Spectrometry Using the Second Mathieu Stability Region; *Pedder, Randall E.; Schaeffer, Richard A. 1070
A.M. versus F.M. Quadrupole Mass Spectrometer; *Beaugrand, C.; Rolando, C.; Sablier, M.; Simonneau, G. 1071
Influence of a Low Frequency Component on the Standard RF of a Quadrupole; Beaugrand, C.; Poisson, L.; *Rolando, C.; Sablier, M. 1072
CHARACTERISTICS OF A HIGH-PRESSURE QUADRUPOLE COLLISION CELL; *Thibault , Pierre ; Whalen, Kevin I-1; Boyd, Robert I-1; **Shushan, Bori , Sakuma, Takeo I-2; 1073
A New Detector for Magnetic Sector Instruments Based on a Scanning CCD; *Finch, Jeffrey W.; Musselman, Brian D.; Sims, Gary R., **Kunihiro, Fumio. 1074

Secondary electron multiplier operating at forvacuum pressure; *Makarov, Alexander; **Yablokov, Michail 1075
The Direct Imaging of Ions Using a Charge Injection Device (CID) Detector; *Christopher, Steven J.; Parker , Mark A., Marcus, R. Kenneth. 1076
Development of an Hybrid Mass Spectrometer for Ion Investigations.; Mueller, Matthias; Wilhelm, Ulf; Aicher, Klaus-Peter; *Grotemeyer, Juergen. 1077
An API-Quistor-Quadrupole Mass Spectrometer for Ambient-Air Analysis; *Gaelli, Markus; Schlunegger, Urs P. 1078
Applications of Notched Broadband Waveforms in Ion Trap Mass Spectrometry; *Karr, Dane; Hoekman, Don, Koski, Alice. 1079
Design of a High Field FTICR for MALDI and LD/CI Studies; *Pitsenberger, Cynthia; Lei, Qing Paula; Easterling, Michael; Amster, I. Jonathan. 1080
Construction of a New External Source FTMS Instrument; *Carroll, James; Fannin, Steve, Wu, Jiangyue; Lebrilla, Carlito 1081
In-Cylindrical-Cell Maldi with FT ICR Spectrometer; *Knobeler, Markus, Wanczek, Karl Peter; Laukien, Frank. 1082
An Electrostatic Ion Guide Interface for Electrospray FTMS; *Tang, Liang; Buchanan, Michelle V , Hettich, Robert L ; Hurst, Gregory B 1083
Interchangeable Electrospray Source for Study of Biomolecules using FTMS *Green, M. Kirk; Gard, Eric; Camara, Elvira; Penn, Sharon G., Lebrilla, Carlito B. 1084
High-Field Electrospray FT-ICR Mass Spectrometer for Biopolymer Analysis; *Pasa-Tolic, Ljiljana; Marto, Jarrod A., Senko, Michael W , White, Forest M.; Guan, Shenheng; Marshall, Alan G 1085
The Design and Performance of an In-Field ESI-FTICR Instrument; *Wu, Qinyuan , Udseth, Harold R , Anderson, Gordon A , Van Orden, Steven, Sherman, Michael G. ; Chen, Ruidan ; Hofstadler, Steven A.; Smith, Richard D 1086
Performance of an External Cluster Ion Source and Electrostatic Ion Guide; *DeSantolo, Anthony M.; Mandich, Mary L., Reents , William D 1087
Construction of an ICP-FTICR Mass Spectrometer; *Milgram, Eric; Watson, Cliff; Eyler, John. 1088
Characterisation of a Novel Ion-Emitter for FT-ICR; *Spiess, Iris, Maass, Imke, Görtler, Bernd, Glasmachers, Albrecht; Wanczek, Karl Peter 1089
Fluorescence and Absorption Spectra of Mass-Selected Trapped Ions; *Jackson, George S.; Huang, Yulin; Guan, Shenheng; Kim, Hyun Sik; Marshall, Alan G. 1090
FTICR Performance of a 5.3 Tesla Split-Pair Magnet; *Reents, William; Mandich, Mary, DeSantolo, Anthony. 1091
Performance of a small Low-field FT/ICR Mass Spectrometer; *Perez, James; Leeck, Diane; Beasley, Brandon; Kenttamaa, Hilkka. 1092
Low Noise FTICR Detection Electronics *Anderson, Gordon; Bruce, James; Hofstadler, Steven, Rockwood, Alan; Smith, Richard. 1093

Improved Performance of a LabVIEW-Based FTICR Data Station; *Drader, J. J.; Hendrickson, C. L.; Laude, D. A 1094
A New ICR-Cell for Simultaneous Trapping of Positive and Negative Ions; *Malek, Robert; Wanczek, Karl-Peter. 1095
A scheme for feedback excitation in FTICR-MS based on multielectrode trap; *Gorshkov, Michael V.; Kouzes, Richard T. 1096
Hypercube: ICR Ion Trap Optimized for Excitation, Detection, and Trapping; *Jackson , George S.; Guan, Shenheng; Marshall, Alan G 1097
Extending the Functionality of Ion Trap Spectrometers; *McHugh, Sean; Hoekman, Don; Bradshaw, Stephen; Wilson, Ray, Li, Rebecca... 1098
Performance Enhancement of the HP 5971/5972; *Roy, Laura; Jehnsen, Chris; Hamerly, Thomas; Graves, Peter. 1099

Thursday Posters - Trapped Ions

Matrix-Assisted Laser Desorption Ion Trap Tandem MS of Peptides; *Qin, Jun; Chait, Brian T. 1100
Filtered Noise Fields in a Paul Ion Trap for Multiple MS Analyses; *Karr, Dane; Kelley, Paul; Bradshaw, Steve; Louris, John..... 1101
Advanced SWIFT Technique for MALDI/Quadrupole Ion Trap Mass Spectrometer; *Doroshenko, Vladimir M.; Cotter, Robert J.... 1102
Application of Tailored Waveform Generation to the Quadrupole Ion Trap; *Taylor, Dennis; Schwartz, Jae; Zhou, Joe; James, Mike; Bier, Mark; Korsak, Andy; Stafford, George. 1103
Selective Ion Accumulation in an ICP/ITMS using a Filtered Noise Field *Eiden, Gregory C.; Barinaga, Charles J.; Koppenaal, David W..... 1104
AUTOMATED RESONANCE EJECTION IN A QUADRUPOLE ION-TRAP MASS SPECTROMETER.; Murrell, Jason; *Todd, John F.J.; Watts, Peter. 1105
Enhancement of Ion Trapping Efficiency in an Ion Trap with a Pulsed Valve; *Wang, Yang; Schubert, Michael; Franzen, Jochen. 1106
New Method for Signal Generation; **Schubert, Michael; Nagel, Marcus; Wang, Yang; *Franzen, Jochen. 1107
Ion Cloud Structure In A Quadrupole Ion Trap; *Bach, Gloria A.; Dynin, Efim A.; Kirchner, Nicholas J. 1108
A Field-Portable Ion Trap for the Detection of Chemical Weapons Compounds; *Lammert, Stephen A.; Merriweather, Roosevelt; **Sarver, Emory W.; Wasserman, Michael B..... 1109
Ion Traps as Chemical Sensors; *Hart, Kevin J. 1110
Electron-Capture by Ions in a Quadrupole Ion Trap; *Vachet, Richard W.; Clark, Steven D.; Glish, Gary L. 1111
Experimental Studies of Space Charge Effects in an Ion Trap MS; *Shaffer, Barrie A.; Karnicky, Joseph F.; Buttrill Jr., S. E. 1112

Negative Ion Electrospray / Ion Trap MSn For Structure Elucidation; *Strife, Robert; **Schwartz, Jae; Bier, Mark; Zhou, Joe;. 1113
Technological Aspects of a New LC/MSn Quadrupole Ion Trap; *Schwartz, Jae; Bier, Mark; Taylor, Dennis; Zhou, Joe; Syka, John; James, Mike; Stafford, George; Stafford, George. 1114
Novel Technologies and Enhanced Features for GC/MS/MS; *Johnson , Eric, Schwartz, Jae; Taylor, Dennis; Bier, Mark; Ragsdale, John. 1115
Quadrupole Ion Trap Control Language - Power in the Hands of Researchers; *Zhou, Joe; Schwartz, Jae. 1116
Ion Optics and Design Considerations for a New LC/Quadrupole Ion Trap; *Bier, Mark E.; Schwartz, Jae C.; Zhou, Joe; Taylor, Dennis; Stafford, George; Syka, John; James, Mike; Borchers, Torsten. 1117
Particle Resonances in "Monopole" and Quadrupole Electric Ion Traps; *Wuerker, Ralph; **Kelley, Paul; Louris, John. 1118
Implications of Ion Population for GC/MS/MS on a Quadrupole Ion Trap; *Quarmby, Scott T.; Yost, Richard A. 1119
Investigations of Mass Shifts in the Ion Trap Mass Spectrometer; *DeGnore, Jon P.; Yost, Richard A. 1120
Effect of Scan Direction on Mass Resolution in Stretched & Compressed Traps; *Wang, Mingda. 1121
High Resolution Selective Ion Monitoring In An Ion Trap; *Wells, Greg; Huston, Chuck. 1122
Field Modulated Selective Ion Storage In An Ion Trap; *Wells, Greg; Huston, Chuck. 1123
Mass Displacements Measured in a Quadrupole Ion Trap; *Londry, F.A.; March, R.E. 1124
Collisional cooling effects on the ion relaxations in an ITMS instrument.; Philippe, Lière; Stephane, Bouchonnet; Thierry, Blasco; **Ray , March; *Jean-Claude , Tabet. 1125
QIT/TOF Analysis of Space Charge Effects in a Quadrupole Ion Trap; *Ventura, M. C.; Laude, D. A. 1126
OPTICAL TOMOGRAPHY INSIDE QUADRUPOLE ION TRAPS; *Garrett, Aaron; Nogar , Nicholas; Hemberger, Philip; **Cleven, Curtis; Cooks, R. Graham..... 1127
Ion Trap MS: Variations in Electrode Size and RF Drive Frequency; *Garrett, Aaron W.; Hemberger, Philip H.... 1128
New Modes of Operation in an Ion Trap Mass Spectrometer; *Cleven, C.D.; Frankevich, V.; Horn, L., Nappi, M.; Soni, M.H., Weil, C.; Cooks, R.G.; **Garrett, A.W.; Hemberger, P.H.; Amy, J., Stafford, G. 1129
Calculation of Parametric Resonance For Non-Linear Ion Trap; *Dynin, Efim A.; Kirchner, Nicholas J. 1130
The Use of Ion Trap Mass Spectrometry with FNF Waveforms for MS of Drugs; *Miller, Mark L. 1131

BIOMARKER DETECTION LIMITS USING A PRYOLYSIS-QUADRUPOLE ION TRAP SYSTEM; *Basile, Franco; Mowry, Curtis; Voorhees, Kent. 1132
Reactions of NO+ in a QITMS: Implications for Biological Metabolic Studies; *Silverton, Susan F.; Basic, Cecilia; **Johnson, Jodie V.; Yost, Richard A. 1133
Barbiturate Analysis In A Quadrupole Ion Trap:Borinium Adduct Ion Formation; *Colorado, Armando; Brodbelt, Jennifer..... 1134
Measurement Of Critical Energies In A Quadrupole Ion Trap.; *Colorado, Armando; Brodbelt, Jennifer. 1135
Gas-Phase Basicities and Metal Ion Affinities of Quinones in a QIT; *Hall, Brad; Brodbelt, Jennifer. 1136
Metal Complexation of Quinolone Antibiotics in a Quadrupole Ion Trap; *Alvarez, Erwin J.; Tang, Ming; Brodbelt, Jennifer S.; Vartanian, Victor. 1137
The QUISTOR as a Pulsed-Extraction Source for TOF-MS of VOCs in Air; *Chambers, David M.; Thomas, Stan W.; Grace, Louis I.; Andresen, Brian D. 1138
Oxidation of Azo Dyes: Gas Phase Reactions in an Ion Trap MS; *Voyksner, Robert ; **Betowski, L. Don. 1139
Developments in Explosives Vapor Detection by Glow Discharge/Ion Trap MS; *Asano, Keiji; Vaidyanathan, Gopalakrishnan, Goeringer, Douglas; McLuckey, Scott. 1140
CAD Spectra of PAHs by Ion Trap and Triple Quadrupole Mass Spectrometry; *Winnik, Witold; Betowski, Leon; Pyle, Steven; Marcus, Alvin; Brittain, Robert. 1141

Thursday Posters - Lipids

FRAGMENTATION PATHWAYS OF TRIACYLGLYCEROLS DEDUCED FROM MODEL COMPOUNDS; **STROOBANT, Vincent; *DE HOFFMANN, Edmond; 1142
Ag-phase HPLC-MS of tri acyl glycerides; *Schuyl, P.J W.; Joode, T. de, Duchateau, G.S.M.J.E.; Vasconcellos, M.A 1143
Characterization of a Family of Brain Lipids with Sleep-Inducing Potential; *Siuzdak, Gary; Cravatt, Benjamin F.; Prospero-Garcia, Oscar, Henrikson, Steven J , Boger, Dale L., Lerner, Richard A 1144
EI Mass spectra of Monounsaturated w3 Fatty Acid Nicotinates and SQMGs.; Keusgen, Michael; *Curtis, Jonathan M.; Ayer, Stephen W. 1145
Identiification of Eicosanoids Using Electrospray Mass Spectrometry; *Kerwin, James; Ericsson, Lowell. 1146
ESI-MS Analysis of PAF Precursors in Human Keratinocytes and Cell Line; *Harrison, Kathleen; **Travers, Jeffrey; Murphy, Robert C. 1147
IDENTIFICATION OF 20-HETE IN RAT KIDNEY PHOSPHATIDYLINOSITOL; *Zhu, Ying; McGiff, John C.; Balazy, Michael. 1148
Phospholipid Analysis by MALDI FT-ICR MS/MS; *Marto, Jarrod A.; White, Forest M., Marshall, Alan G. 1149

Detection of Phospholipid Molecular Species in U937 Cells using CF-LSIMS; *Li, Chun; Yergey, James. 1150
Analysis for Analogs of Phospholipids by FAB Mass Spectrometry; *Yu, Chungping; Huang, Jianxing; Widlanski, Theodore S. 1151
Analysis of Polyunsaturated Phospholipid Turnover by Electrospray LC/MS; *Ma, Yee-Chung; Ward, Glen; Wang, Tao-Chin; Salem, Jr, Norman; Kim, Hee-Yong. 1152
Isolation and Identification of Phospholipids in Lipid Extracts by ES/MS/MS; *Duffin, Kevin; Obukowicz, Mark; Shieh, J.J. 1153
Massie Cluster Impact Ionization of Phospholipids; *Dookeran, Nyla; Todd, Peter. 1154
Formation of the [M-H]+ Ion in the LSIMS Mass Spectrum of Sphingosine; *Chevis, Eddie A.; Busch, Kenneth L. 1155
Characterization of GS-15 and Biomarkers of the Helderberg Formation; *Ospina, Maria; Powell, David, Yost, Richard, **Channell, James 1156
PY/MS FAME EXTRACT PROFILING OF PATHOGENIC MICROORGANISMS; *Basile, Franco; **Hadfield, Ted L.; Sickenberger, Dave W.; Voorhees, Kent J. 1157
SPECIES DIFFERENTIATION OF BEESWAXES USING PYROLYSIS MASS SPECTROMETRY; **Beverly, Michael, Kay, Paul, *Voorhees, Kent J. 1158
GC-MS TECHNIQUES USED IN EVALUATING ALCOHOL AFFECTS ON LIPID METABOLISM; *Pawlosky, Robert, Salem, Norman 1159
A COMPARISON OF HIGH- AND LOW- ENERGY CID OF DERIVATIZED LIPIDS; *Griffiths, William; Yang, Yang, Zhang, Jie; Lindgren, Jan Åke; Sjövall, Jan 1160
Electron Capture MS Analysis of Lipid Peroxidation Products; *Grimsrud, A.J., van Kuijk, F J.G.M. ; Thomas, D.W., Sears, L J 1161
Analysis of Neurosteroids by Liquid Chromatography/Mass Spectrometry; *Kim, Hee-Yong; Romeo, Elena; Ma, Yee-Chung 1162
MS/MS Study of PBN Spin Adducts from Rat liver Microsomal Dispersions; *Sang, Hong, Janzen, Edward, G; Arimura, Masana; Kotake, Yashige; DuBose, Coit M ; Poyer, J Lee 1163

Thursday Posters - Carbohydrates

Characterisation of Glycosylation Sites in Recombinant Proteins by ES-MS/MS; Truong, Long; Eng, Marian; Canova-Davis, Eleanor, *Ling, Victor. 1164
Determination of glycosylation in external invertase by MALDI-TOF MS; *Zeng, Chenhui; Biemann, Klaus 1165
Characterizing the N-Glycosylation of CRF-Binding Protein; *Craig, A. G., Sutton, S. W., Vaughan, J.; Koerber, S.C.; Fischer, W.H. 1166
Characterization of a Plasminogen Activator with LC, CE, ESI-MS and MALDI; Apffel, A.; *Chakel, J ; Hancock, W S ; Holloway, B.; Swedberg, S ; Udiavar, S ; Pungor Jr , E., Souders, C. 1167

Analysis of parotid gland oligosaccharides by MALDI mass spectrometry; Wing, David R.; O'Donnell, Niall; Naven, Thomas J P.; *Harvey, David J. 1168
Analysis of the N-linked oligosaccharides of human C1s using ESI-MS; **Ptillot, Yves; *Thibault, Pierre; Thilens, Nicole; Rossi, Vronique; Lacroix, Monique; Coddeville, Bernadette; Spik, Genevive, Schumaker, Verne. 1169
GLYCOSYLATED END-PRODUCTS OF Beta-2-MICROGLOBULIN IN SERUM BY MALDI-MS; *Dreifuss, Peter; Vertes, Akos; **Tang, X; Braatz, James; Hull, Clifford. 1170
Characterization of human Chorionic Gonadotropin Using HPLC/MS; Liu, Chuanliang; *Bowers, Larry. 1171
Glycosylation Site Mapping by MALDI-TOF; *Yang, Y.; Orlando, R. 1172
Characterizing the Carbohydrate Moieties of EPGs and PGIPs by MALDI-TOF; *Kolli, V.S.K.; Bergmann, C.; Mohn, C.; Albersheim, P.; Darvill, A.; Orlando, R. 1173
Characterization of the Nodulation Factors Produced by Bradyrhizobium; *Kolli, V.S.K.; Carlson, R.W ; Peters, N.K.; Orlando, R. 1174
FAB and ESIMS of Acidic Glycosphingolipids—Lex- and Lea-derivatives; *Ohashi, Yoko; Ii, Tadashi; Kurono, Sadamu; Ogawa, Tomoya; Nagai, Yoshitaka. 1175
MALDI-MS ANALYSIS OF GANGLIOSIDES FROM HUMAN GRANULOCYTES; *Peter-Katalinic, Jasna; **Stahl, Bernd; Karas, Michael; Hillenkamp, Franz; Hanisch, Franz-Georg; Egge, Heinz; Muething, Johannes; Spanbroek, Rainer. 1176
SIALYLATION OF GANGLIOSIDES FROM DEVELOPING CHICKEN BRAIN BY ES-MS; *Peter-Katalinic, Jasna; Ashcroft, Alison; Green, Brian; Hanisch, Franz-Georg; Muething, Johannes. 1177
ESI-MS and ESI-CID-MS/MS of Complex neoLacto-Series Glycosphingolipids; *Levery, Steven B.; **Salyan, Mary Ellen K.; Stroud, Mark R. 1178
GLYCOSPHINGOLIPIDS FROM BOVINE RED BLOOD CELLS AND FOETAL CALF BRAIN; *Perreault, Helene; Koul, Omanand; Street, Jacqueline; McCluer, Robert; **Costello, Catherine. 1179
Detailed Characterization of Glycosphingolipids by ES-MS-CID-MS; *Reinhold, Bruce B.; Song, Ye; Reinhold, Vernon; Brigande, John V.; Seyfreid, Thomas, N. 1180
Determination of the Glycosylation Position in Mono-O-glycosyl Flavonoids; Li, Qimin; Van den Heuvel, Hilde; *Claeys, Magda. 1181
Mass Spectrometry and LC/MS of Polyphenols; *Williams, Jon; **Belanger, Ronald; Cohen, Gerald. 1182
Low-energy Fragmentation of Protonated Glycoalkaloids and Related Aglycones; *Claeys, Magda; Van den Heuvel, Hilde; Chen, Su; Derrick, Peter J.; Mellon, Fred A.; Price, Keith R. 1183
MALDI-MS of Bacterial Glucans; *Stahl, Bernd; **Talaga, Philippe; Zeng, Jianru; Karas, Michael; Steup, Martin; Hillenkamp, Franz; Bohin, Jean-Pierre 1184

Examination of Chitin-Metal Interactions by ESI and MALDI Mass Spectrometry; *Callahan, John H.; Shahgholi, Mona; Ross, Mark M. 1185
FAB-MS/MS of Immunoreactive Tetrasaccharides from Chondroitin Sulfate; *Ohashi, Mamoru; Ii, Tadashi; Kubota, Masayuki; Hirano, Takashi; Yoshida, Keiichi; Suzuki, Sakaru. 1186
Mass Spectromeric Characterisation of Sulfated Oligosaccharides.; *Watson, Eric; Termin, Andreas; Shah, Bhavana; Bhide, Anjali; Zamborelli, Tom; Venot , Andre. 1187
ES-MS of Heparin-Derived Glycosaminoglycan Disaccharides.; *Watson, Eric; Yao, Flora. 1188
CE/MALDI-MS of Mixtures of Heparin Derived Oligosaccharides; *Rhomberg, Andrew; Juhasz, Peter; Biemann, Klaus. 1189
Ionspray (lc-)ms of synthetic sulphated oligosaccharides; *Jacobs, Peter L.; Westerduin, Pieter; **Silvestro, Luigi; 1190
Massive Cluster Impact Ionization of Saccharides; *Dookeran, Nyla; Todd, Peter. 1191
LC-ESIMS and in-source CID of derivatized oligosaccharides.; *Aduru, Subhodaya; **Faull, Kym F. 1192
Improved MS Analysis of Oligosaccharides as Fluorinated Glycosylamines; *Huang, Zhi-Heng; Gage, Douglas A. 1193
MALDI and ESI mass spectrometry of cationic oligosaccharide derivatives; *Naven, Thomas J. P.; Harvey, David J. 1194
MALDI/FTMS of Oligosaccharides; *Fannin, Steve; Wu, Jiangyue; Carroll, James; Lebrilla, Carlito. 1195
MALDI-MS Applications on Carbohydrates; *Börnsen, Klaus Olaf ; Mohr, Martin; Widmer, H. Michael. 1196
ANOMERIC CONFIGURATION OF SUGAR NUCLEOTIDES BY FAB/MS/MS; WOLUCKA, B. A.; *de HOFFMANN, E. 1197
LC-MS/MS of Carbohydrates with Post Column Addition of Metal Salts; *Kohler, Martin; Leary, Julie, A. 1198
KER of Oligosaccharide/Metal/Ligand Isomers Using FAB and ES Ionization; Smith, Glenn; Bott, Geoffrey; *Leary, Julie, A. 1199
ESI-MS/MS Study of Co, Zn, Mn, Cu, Ca and Mg Complexes of Oligosaccharides; *Sible, Emily, M.; Brimmer, Steven, P.; Leary, Julie, A. 1200
Post-source decay fragmentation of oligosaccharides ionized by MALDI; *Maisey, E. Anne; **Harvey, David J. 1201
Oligosaccharide Structure Determination On An Ion Trap.; *Asam, Michael; Glish, Gary. 1202
High energy CID spectra of complex oligosaccharides ionized by MALDI; *Bateman, Robert H.; **Harvey, David J. 1203

Thursday Posters - Laser Desorption/Ionization

Using Aerosols for MALDI Liquid Introduction; Wei, Gang; Fei, Xun; He, Lin; *Murray, Kermit K. ... 1204
Design parameters of a gridless ion mirror for post source decay analysis; *Zeng, Jianru, Karas, Michael; Hillenkamp, Franz ... 1205
A Method for Acquiring Daughter-Ion Spectra in a Reflecting TOF Instrument; *Westmacott, G R; Ens, W; Standing, K G. ... 1206
Time of Flight PSD measurements with pre-cursor ion selection; *Kowalski, Paul; Hauer, Charles; Cornett, DS; Park, Melvin; Stack, Robert; Wronka, John. ... 1207
High Resolution Precurson Ion Selection for Post Source Decay Experiments; *Holle, Armin; Park, Melvin; Detlev , Suckau. ... 1208
Probing the Outer Limits of Performance for MALDI-TOF MS and MS-MS; *Vestal, Marvin, Juhasz, Peter; Blakley, Calvin, Martin, Stephen. ... 1209
HIGH RESOLUTION LINEAR MALDI-TOFMS OF PEPTIDES AND OLIGONUCLEOTIDES; **WEINBERGER, SCOT; KENNY, JAMES; *KORNFELD, RICH. ... 1210
Strategies for LDI/MALDI on a Sector Instrument; *Lennon, III, John D.; Shinn, David; Vachet, Richard W., Glish, Gary L. ... 1211
High Resolution Array Detection of the Ions Formed by MALDI; *Itagaki, Yasuhiro; Fujita, Tsuyoshi; Naoki, Hideo; Nakajima, Terumi ... 1212
Accurate Mass Determination in MALDI/FTMS using Internal Standards; *wu, Jiangyue; Fannin, Steve; Franklin, Melanie A. ; Molinski, Tadeusz F. ; Lebtrilla, Carilto. ... 1213
Ion Coupling in High-Resolution MALDI FT-ICR Mass Spectra of Biopolymers; *Pasa-Tolic, Ljiljana, Guan, Shenheng, Huang, Yulin, Jackson, George S.; Kim, Hyun Sik ; Marshall, Alan G. ... 1214
Peptide Mapping and Sequence Analysis of Proteins by MALDI FT-ICR MS *Solouki, Touradj; Pasa-Tolic, Ljiljana; Jackson, George S.; Guan, Shenheng; Marshall, Alan G. ... 1215
Femtomole Biomolecule Detection by Remeasured MALDI FT-ICR MS; *Solouki, Touradj; Guan, Shenheng; Marto, Jarrod A.; White, Forest M.; Marshall, Alan G. ... 1216
HIGH MASS ANALYSIS IN FOURIER TRANSFORM MASS SPECTROMETRY; *Yao, Jie; Pastor, Salvador J ; Wilkins, Charles L. ... 1217
Further Improvement of Mass Accuracy in MALDI reTOF MS of Peptides; *Vorm, Ole, Mortensen, Peter; Mann, Matthias. ... 1218
Orthogonal-Injection MALDI; *Dworschak, R G, Ens, W; Spicer, V; Standing, K G; Verentchikov, A V ... 1219
A Charge Detector for High Mass MALDI Ions; *Lautz, Carsten; Bahr, Ute, Roehling, Ulrich; Hillenkamp, Franz ... 1220

Application of Maximum Entropy to MALDI; *Zhang, X Kate; **Ferrige, Anthony G., Fales, Henry M. ... 1221
SEM as a Tool to Investigate Sample Morphology Effects in MALDI MS; *Westman, Ann; Barofsky, Elisabeth. ... 1222
Nanoscale Sample Manipulation and Preparation Method for MALDI MS; *Golding, Rafael E ; Whittal, Randy M.; Li, Liang. ... 1223
Methods for Modifying the MALDI Process; *Bai, Jian; Liang, Xiaoli; Liu, Yan-Hui; Lubman, David M. ... 1224
Novel Sample Preparation for MALDI; *Kochling, Heinrich; Biemann, Klaus. ... 1225
Investigation of Sample/Matrix Preparation in MALDI by Confocal Microscopy; *Li, Liang; Whittal, Randy M.; Dai, Yuqin. ... 1226
Influence of Sample Preparation on Time-Dependent MALDI MS of Proteins; *Lavine, Gary; Allison, John. ... 1227
Dependence of Resolution on Laser Power in MALDI-TOF MS; *Liao, Pao-Chi; Allison, John. ... 1228
Big Spot MALDI - Advantages of Irradiating Large Portions of the Target; *Hiller, Joseph; Szekely, Gabriella; Allison, John ... 1229
The Behavior of Peptide Mixtures in MALDI-MS; *Hiller, Joseph F , Lavine, Gary; Micke, Mel; Szekely, Gabriella, Allison, John ... 1230
MALDI Calibration and the Effect of Layered Sample and Standard; *Zhou, Jie; Lee, Terry D ... 1231
Charge State Distribution Shifting of Protein Ions Observed in MALDI; *Zhou, Jie; Lee, Terry D. ... 1232
Optical Characterization of the MALDI Plume; *Hurst, Gregory B. ... 1233
Optoacoustical Monitoring of Laser Absorption of MALDI Matrices; *Taranenko, N. I , Golovlev, V V.; Puretzky, A A.; Allman, S. L.; Chen, C. H ... 1234
The Wavelength Dependance of MALDI in the Range 350-450 nm; *Chen, Xiangjun; Beavis, Ronald C ... 1235
Influence of esterification and target preparation in MALDI of polyesters; *Joëlle, Guittard, Martine, Tessier; **Jean-Claude , Blais, Gérard, Bolbach, Laurence, Rozes; Alain, Brunot; Ernest, Maréchal; Jean-Claude, Tabet. ... 1236
Cationization Mechanism of Synthetic Polymers by Alkali Metals in MALDI; *King, Richard; Goldschmidt, Robert; Xiong, Yansan; Owens, Kevin ... 1237
Separation of the Desorption and Ionization Events in the MALDI Experiment; King, Richard, *Owens, Kevin, **Hanton, Scott. ... 1238
Evaluation the matrices used in MALDI by their FAB mass spectra; Hsing-Long, Chei; *Jentaie, Shiea. ... 1239
Comparisons of Proton Transfer Reactions of MALDI Matrices; *Kinsel, Gary, Land, Mark; Li, Nan. ... 1240
SEMI-EMPIRICAL STUDY OF PROTON TRANSFER IN MALDI-MS OF SMALL PEPTIDES; *Sadeghialavijeh, Mehrnoosh; Vertes, Akos ... 1241
INTERNAL ENERGIES OF IONS FORMED BY MALDI; *Gimon-Kinsel, Mary; Gillig, Kent; Sumner, Lloyd; Edmondson, Ricky; Russell, David. ... 1242

Factors influencing metastable fragmentation in MALDI TOF/MS; COLBY, STEVEN; Houston, Chris; Christian, Noah; Arnold, Randy; *REILLY, JAMES.....1243
Ion Formation and Photodissociation in MALDI-Mass Spectrometry; Amft, Matthias; Grundwuermer, Johann M.; Yang, Hou-Jun; *Grotemeyer, Juergen. 1244
Photochemical versus Thermal Mechanism for MALDI; Ehring, Hanno; Costa, Cesar; *Demirev, Plamen; Sundqvist, Bo. 1245
Probing The Dynamics of MALDI Ion Formation; *Edmondson, Ricky D.; Campo, Karen K.; Russell, David H. 1246
Water as a Matrix in Infrared MALDI-MS; *Berkenkamp, Stefan; Karas, Michael; Hillenkamp, Franz. 1247
Inorganic Matrix uses for MALDI - TOF - MS; *Tanaka, Koichi; Kawabata, Shin-ichirou; Resch, Martin; Paulus, Gert; **Humphrey, Paul; Dingley, David.....1248
Hydroxy Benzophenones: A New Class Of MALDI Matrices For Proteins/Peptides; *Reiber, Duane; Brown, Robert. 1249
Synthesis of MALDI Matrices and Correlation with Ion/Neutral populations; *Sumner, Lloyd W.; Hipp, Travis L.; Edmondson, Ricky; Gimon-Kinsel, Mary; Russell, David H. 1250
New matrices for Matrix-Assisted Laser Desorption/Ionization (MALDI) MS *Krause, Joem L.; Schlunegger, Urs P. 1251
Amino Acid Composition and Wavelength Effect on MALDI-MS of Small Peptides; *Olumee, Zohra; Vertes, Akos. 1252
Investigation of Selective Peptide Ionization with Various MALDI Matrices; *Blackledge, James A.; Alexander, Anthony J.; Dodsworth, David W. 1253
Effects of Substrates on the Ion Yields for Mixture Analysis by MALDI MS; *Liang, Xiaoli; Bai, Jian; Liu, Yan-Hui; Lubman, David M 1254
Surface Modification of Active Substrate Applied in MALDI MS; *Liu , Yan-Hui; Bai, Jian; Liang, Xiaoli; Lubman, David M 1255
Polymers as a Probe Element for Surface Enhanced Neat Desorption (SEND); *Bardel, Patrick; Hutchens, T.William 1256

Thursday Posters - Proteins & Peptides

Conformation of cytochrome c2 mutants studied by H/D exchanges using ESIMS; Halgand, Frdric; Jaquinod, Michel; Caffrey, Michael; Fitch, John; Cusanovitch, Michael; *Forest, Eric. 1257
Probing Conformation and Dimerization in Yeast Hexokinase with ESIMS; *Eckart, Klaus; Spiess, Joachim. 1258
ESI-TOF-MS Studies of Refolding and Assembly of Soybean Agglutinin; *Tang, Xue-jun; Saha, Sanat; Brewer, C. Fred; Chernushevich, Igor; Standing, Kenneth G. 1259
Rapid Deuterium Exchange-in Time for Probing Protein Conformational Change; *Dharmasiri, Kuruppu; Smith, David L. 1260

ESI-MS of Protein Noncovalent Tetrameric Associations at High m/z; *Schwartz, Brenda L.; Gale, David C.; Smith, Richard D., Chilkoti, Ashutosh; Stayton, Patrick S.; Smith, Virginia F.; Randall, Linda L. 1261
ESI-MS Analysis of the Transthyretin Tetramer & Some Non-Covalent Adducts.; *Green, Brian N.; **Oliver, Ronald W.A. 1262
Conformational Changes of Proteins Detected by MALDI-MS; Yang, Hou-Jun; Li, Xia-Ling; *Grotemeyer, Jürgen. 1263
Unusually Strong Binding of A Noncovalent Spermine-Peptide Complex; *Feng, Rong. 1264
Conformation of Chaperone Bound Ligands Probed by ESI MS; *Robinson, Carol; Gross, Michael; Dobson, Christopher; Radford, Sheena. 1265
Studies of H/D exchange of peptides and proteins by using aerosol MALDI *Wei, Xiaona; Beeson, Michelle D.; Russell, David H. 1266
Probing High Order Structure of Proteins by H/D Exchange/ESI-MS; *Maier, Claudia S.; Kim, Ok-Hee; Deinzer, Max L. 1267
Studies of Partially Folded Proteins by H/D Exchange and ESI-MS; *Tang, Xue-jun; Wang, Fang; 1268
Disulfide bridges assignments of homologous vegetable proteins; Guy, Philippe; Gagnon, Jean; Marion, Didier; *Forest, Eric. 1269
Characterization and Location of Disulfide Bonds in Proteins with ABD-F; *Rajamani, Umamaheswari; Pannell, Lewis; Sackett, Danny; Le, Han; Lecchi, Paolo. 1270
Determination of Disulfide Bonds in Proteins from AIDS Related Research; *Pannell, Lewis; Rajamani, Umamaheswari; Le, Han; Lecchi, Paolo. 1271
Identification of Cross-Linking Peptides Using ESI and MALDI-TOF MS *Le, John C.; Haniu, Mitsuru; Horan, Thomas; Katta, Viswanatham; Arakawa, Tsutomu; Rohde, Michael. 1272
Synthesis of Disulfide Linked B-Actin Peptides.; *Bencsath, F. Aladar; Shartava, Archil; Monteiro, Carlos A.; **Goodman, Steven R. 1273
DETERMINATION OF THE LOCATION OF CYS IN PEPTIDES BY TANDEM MS/MS; *NEMIROVSKIY, OLGA; GROSS, MICHAEL. 1274
Identification of a Cysteine Substitution in GCSF by Peptide Mapping-ESI-MS; *Yeh, Che-Hung; Tedeschi, Nicole; Herman, Alan. 1275
The Location of S-S Bonds in Proteins by Partial Acid Hydrolysis and MS; *Aplin, Robin; Anderson, Kerry. 1276
Disulfide Structure Study of EGF domain of Neu Differntiation Factor (NDF); *Katta, Viswanatham; Liu, Naili; Meng, Shi-Yuan; Zamborelli, Tom; Mayer, John; Lu, Hsieng; Hara, Shinichi. 1277
Identification of Venomous Snakes using Electrospray Mass Spectrometry. *Perkins, John R.; Despeyroux, Dominique; Gallagher, Richard T.; Derrick, Peter J.; Jennings, Keith R.; Newton, Russell P. 1278
MS Investigation of the Molecular Mechanism of Action of Cytotoxin B; *Wilm, Matthias; Just, Ingo; Selzer, J; Aktories, Klaus; Mann, Matthias. 1279

Tandem Mass Spectrometry of Cyanobacterial Toxins; Dale , Vanessa, *Jennings, Keith. 1280
Structural Analysis of Conotoxins by Mass Spectrometry; *Nakamura, Takemichi; Fainzilber, Michael; Zlotkin, Eliahu; Burlingame, A. L. 1281
STRUCTURE-FRAGMENTATION CORRELATIONS OF PROTONATED ACTINOMYCINS; *Thomas, Darren; Morris, Michael; Curtis, Jonathan; Boyd, Robert. 1282
Characterization of Recombinant Forms of Adenylate Cyclase Toxin, CyaA; *Hackett, Murray; Walker, Carthene B.; Shabanowitz, Jeffrey; Sebo, Peter; Guo, Lin; Hewlett, Erik L.; Hunt, Donald F. 1283
Identification of Post-translational Modifications for Cytochrome P450lin; *Huang, Rong; Ghosh, Dipak; Gunsalus, Irwin ; Rinehart, Kenneth. 1284
An ESI MS Study of the Soluble Methane Monooxygenase Enzyme System; *Buzy, Armelle; Jennings, Keith; Amarbalita, Marvy; Wilkins, Pat; Dalton, Howard. 1285
ES-MS analysis of resorcinol suicide substrate binding to cyt c peroxidase.; *Doerge, Daniel R; Divi, Rao L; **Hutton, Therese. 1286
Characterizing Peptides Isolated from Conus Venoms by Ionspray HPLC/MS & MS; *Jones, Alun; Bingham, Jon-Paul; **Lewis, Richard J.; Alewood, Paul F 1287
ANALYSIS of CYTOMEGALOVIRUS (CMV) PROTEASE (MW 28 kDa); *Siegel, Marshall; Tabei, Keiko; Berkenkamp, Stefan; **Hillenkamp, Franz; Bebernitz, Geraldine; Ding, Wie-Dong, Baum, Ellen. 1288
Effects of pH on the MALDI MS of Class I MHC Peptide Antigens.; *Woods, A S.; Huang, A Y.; Cotter, R.J.; Pardoll, D.; Jaffee, E.M. 1289
Identification of Peptides Associated with Class II MHC Molecules; *Addona, Theresa A.; Shabanowitz, Jeffrey, Hunt, Donald F. 1290
Characterization of the Major Peptide Components in Subcellular Fractions; *McCormack, Ashley L.; Eng, Jimmy K., DeRoos, Paul C., Rudensky, Alexander Y.; Yates, John R. III. 1291
A Method of Analyzing Peptides with Continuous-Flow FAB; *Whitehill, Andy; Vidavsky, Ilan; Gross, Michael. 1292
Identification of Influenza Epitopes and Insight into Antigen Processing; *Gulden, Pamela H., Shabanowitz, Jeffrey; Hunt, Donald F., Tykodi, Scott; Wang, Wei, Skipper, Jonathon; Engelhard, Victor H. 1293
Proteolytic Processing of Ovalbumin by the Murine Proteasome; *King, Gina M.; Shabanowitz, Jeffrey; Hunt, Donald F., Neidermann, Gabi; Eichmann, Klaus. 1294
Identification of endo-HEL Peptide Fragments Presented by MHC Molecules.; *Vidavsky, Ilan; Whitehill, Andy B.; Gross, Michael L ; Nelson, Christopher A , Viner, Nicholas J.; Unanue, Emil R. 1295
Analysis of Invertebrate Hemoglobin Chains by ESI-MS and ESI-MS-MS.; *Green, Brian N ; Kuchumov, Askar R.; Oliver, Ronald W. A.; **Vinogradov, Serge N 1296

Characterization of the hemoglobin of Cebus apella by ESI- and MALDI-MS; *Shen, Tun-Li; Johnson, Robert B.; Buck, Steven; Goodman, Morris; Gage, Douglas A. 1297
Characterization of the hemoglobin from the backswimmer Buenoa scimitra; *Kong, Zhengrong; Rinehart, Kenneth; **Vossbrinck, Charles; Huang, Rong; Sun, Furong. 1298
HEMOGLOBIN ANALYSIS BY ESI MASS SPECTROMETRY: QUADRUPOLE vs MAGNETIC SECTOR; *White, Earl; Uhrig, Mary; Reed-Bombick, Betsy; Chu, Inhou. 1299
Electrospray Tandem Mass Spectrometry of Normal and Abberant Haemoglobins.; *Summerfield, Scott; Jennings, Keith; **Johnson, Andrew. 1300
ISOLATION AND IDENTIFICATION OF HEMOGLOBIN GLOBULIN CHAINS BY HPLC/ESI-MS; *Chu, Inhou; **White, Earl. 1301
A Structural Assignment for a Stable Acetaldehyde-Lysine Adduct; *Braun, Karen P.; **Cody, Robert B. ; Jones, Dane R.; Peterson, Charles M. 1302
Variant hemoglobin characterisation by ES-MS/MS of intact globin chains; *Morris, Mike; Green, Brian N, Shackleton, Cedric H L; Witkowska, H Eva. 1303
Protein Mapping of Human Plasma using Off-Line HPLC-MALDI/TOF-MS; *Ingendoh, Arnd; Seta, Kazuo; Kanain, Michiko; Nakayama, Hiroshi; Uchida, Kazuhisa; **Isobe, Toshiaki; Okuyama, Tsuneo. 1304

Friday Orals - Metal Ion Chemistry

The Metal Ion Affinities of Biomolecules Determined by the Kinetic Method; *Cerda, Blas; Wesdemiotis, Chrys. 1305
Metal Ion Assisted Derivatization of Buckminsterfullerene; *Kan, Steven Z , Byun, Yong G., Lee, Sam A.; Freiser, Ben S. 1306
Amino Acid and Peptide Reactions with Ground State Metal Ions by FTICR; *Lei, Qing Paula; Amster, I. Jonathan 1307
MS & MS/MS OF COORDINATION BETWEEN ALKALI METALS AND NATIVE GANGLIOSIDES; *Ngoka, Lambert; Costello, Catherine. 1308
Electron Affinity and Catalytic Activity of Fe(octethylporphyrin (NO2)n); *Jin, Lei; Ellis, P E.; Lyons, L.E.; Ridge, D.P. 1309
Tandem Mass Spectrometric Study of C5H5FeR(+) Ions.; *Zagorevski, Dmitri; Holmes, John L 1310

Friday Orals - Hyphenated Chromatography

Rapid and Sensitive Sequencing of Proteins isolated by Gel Electrophoresis; *Mann, Matthias; Wilm, Matthias; Shevshenko, Andrej, Houthaeve, Tony 1311
In Situ Chemical Modification, Digestion and Characterization of Proteins; *Blackburn , R K., Mark, J; **Kassel, D.B. 1312

Identification of Peptides from Combinatorial Libraries with ACE-ESI-MS; *Kirby, Daniel P.; Chu, Yen-Ho; Dunayevskiy, Yuriy, Karger, Barry L.; Vouros, Paul.....1313
CZE-MS analysis of peptides and proteins using a sheathless interface; *Kelly, John ; Thibault, Pierre I-1; Ramaley, Louis I-2. 1314
Novel Modifications and Clinical Applications of PC-CE-MS; *Tomlinson, Andy J.; Braddock, W. David; Benson, Linda M.; Oda, Robert P.; Riggs, B. Lawrence; Katzmann, Jerry A.; Naylor, Stephen.....1315
LC/MS Using an Ion Trap/reflectron Time-of-flight Mass Spectrometer; *Qian, Mark G.; Bai, Jian; Liu, Yuanhui; Zheng, Kefei; Luman, David M.....1316
Direct Coupling of TLC with MALDI mass spectrometry; *Gusev, Arkady I.; Proctor, Andrew; Rabinovich, Yakov I.; Hercules, David M.....1317
Flow Injection Analysis - MS for In-Process Control of Drug Synthesis; Colgan, S.T.; *Sharp, T R.; Hammen, P.D.; Reed, R.H ; Horan, G.J.; Gwiazda, P.W.....1318

Friday Orals
Good Laboratory Practices for Mass Spectrometry

GLP for Qualitative Mass Spectrometry from an Academic Perspective *Henion, Jack.....1319
Providing Evidence of Structural Validity As Part Of GALP Compliance; *Canales, Ph.D., Mark; Hall, Trevor; Shofstahl, James; Coyle, Robert.....1320
GOOD LABORATORY PRACTICE AND DATA MANAGEMENT; *Musser, Steven M., Sphon, James A.; Browning Jr., Martin; Woolen, Stan W.....1321
Validation of an On-Line Archiving System for Quantitative Mass Spec Data; *Coleman, Patricia M.; Oglesby, Thomas D.; White, Robert J.; Werdel, Lisa P.....1322
An Electronic Lab Notebook System for the VG 11/250J Data System; Rosnack, K.J.; *Sharp, T.R.....1323
Validation of Mass Spectrometry Data Systems in a Regulatory Environment; Palmer, Cynthia A.; *Alexander, Michael S.; Abolin, Craig R.....1324

Friday Orals
Mass Spectrometry to Study Higher Order Structure

Probing Noncovalent Interactions by Ion Spray MS *Ganem, Bruce, Henion, Jack D.....1325
Characterization of Protein-DNA Complexes using ESI-MS Cheng, Xueheng; *Harms, Amy C.; Smith, Richard D.; Morin, Paul E.; Goudreau, Paul N.; Terwilliger, Thomas C.....1326
Studies of Non-Covalent Interactions by Time-of-Flight Mass Spectrometry; *Chernushevich, I. V.; Ens, W.; Standing, K. G.....1327

Detecting conformational Changes in Cytochrome C Upon binding Membranes; Stoker, Paul; Ng-Ilag, J; Smith, D.....1328
Protein Conformational Changes Studied by Hydrogen Exchange and MS; *Zhang, Zhongqi; Smith, David L.....1329
Mass Spectrometric Characterization of Non-covalent TT Ef-Tu/Ts Complexes; *Glocker, Michael O.; Nock, Steffen, Sprinzl, Mathias; Przybylski, Michael.....1330
Mass Spectrometry as a Tool for Protein X-ray Crystallographic Analysis; *Cohen, Steven L., Xie, Xiaoling; Mirza, Urooj A.; Burley, Stephen K ; Chait, Brian T.....1331

Friday Orals - Surface-Induced Dissociation

In-line SID Modes: Characterization and Comparison with High-Energy CAD; Durkin, David A.; *Schey, Kevin L.....1332
Influence of Peptide Sequence, Size and Basicity on ESI/SID Spectra.; *Jones, Jennifer; Dongre, Ashok; Nair, Hari; Somogyi, Arpad, Wysocki, Vicki.....1333
Ion/Surface Reactions: Towards a Better Understanding of Mechanisms; *Cooks, R. Graham; Rohrs, Henry, Miller, Scott; Feng, Bingbing; Jiang, Xudong; Pradeep, Thallapil; Patrick, Jeffrey; Ast, Teodor.....1334
Construction of a TQMS for the Study of Ion Surface Interactions Occurring; *Hayward, Mark J.; Park, Frederick D S.; Manzella, Lynn M.; **Bernasek, Steven L.....1335
A Surface Sensitive Super TOF-SIMS Technique Using Very Highly Charged Ions; Briere, Michael A.; *Schenkel, Thomas; von Wittenau, Alexis Schach; Schneider, Dieter H.....1336
Ion Neutralization for Surface-Induced Dissociation at Ni(111) and NiO(111); *Wainhaus, Samuel B. ; Burroughs, John A.; Hanley, Luke.....1337

Ambient Aerosol Analysis Using Aerosol-Time-of-Flight Mass Spectrometry

*Kimberly A. Prather, C Noble, K. Salt, T Nordmeyer, D Fergenson, and B. Morrical,
Department of Chemistry, Riverside, CA 92521

Particulate pollution is an area of growing concern in light of recent studies which suggest a link between high concentrations of ambient PM_{10} (particles with diameters equal to or less than 10 μm) and adverse health effects ranging from respiratory ailments to premature death. However, analytical chemistry techniques aimed at sampling and analysis of atmospheric aerosols are extremely limited in comparison to the number of methods that exist for studying gas phase smog components. As a result, current government regulations for levels of ambient particulates are necessarily general, lacking any chemical specificity

We have recently developed a technique, Aerosol-Time-of-Flight Mass Spectrometry (ATOFMS), which is capable of real-time determination of the size and chemical composition of individual aerosol particles [1-3] In order to obtain such information, the techniques of aerodynamic particle sizing and time-of-flight mass spectrometry are combined in a single instrument In one of the aerosol studies being performed in our laboratory, this instrument is being used for the direct analysis of ambient aerosols with the goal of establishing correlations between particle size and chemical composition. To date, we have observed very distinct size/composition correlations for organic and inorganic particles Two type of particles representative of the more common chemical classes of particles we observe are shown in Figures 1 and 2. Figure 1 shows an example of a single particle spectrum of a 2 2 micrometer particle of marine origin Figure 2 shows a single particle spectrum of a 2 9 micrometer particle we classify as organic soot The majority of particles in both of these chemical classifications fall in very distinct particle size ranges

Current measurements are being made to establish potential links between the presence of particular types of particles with such factors as the time of day, weather conditions, and concentration levels of gaseous smog components such as NO_x and ozone This data will allow a better understanding of tropospheric gas-aerosol processes to be established. Clearly, if one begins to establish links between chemical species in different particles for a particular size range, this will contribute significantly to our understanding fundamental atmospheric mechanisms. In addition, such information will yield information of potential sources of aerosols of biological and environmental concern Accurate characterization of the sources of particles is a necessary step in efforts towards the establishment of adequate pollution control strategies

1 K. A. Prather, T. Nordmeyer, and K Salt, Anal. Chem , **66**, 1403-1407 (1994)
2 C A. Noble, T. Nordmeyer, K. Salt, B Morrical, and K A. Prather, Trends in Anal Chem., **13**, 218-222 (1994)
3. T. Nordmeyer and K. A. Prather, Anal. Chem., **66**, 3540-3542 (1994).

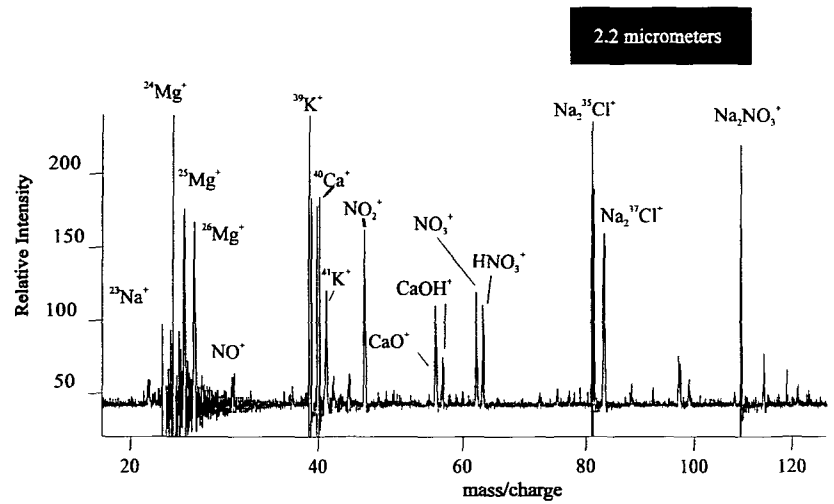

Figure 1: Laser desorption mass spectrum of a single 2.2 micrometer particle of marine origin

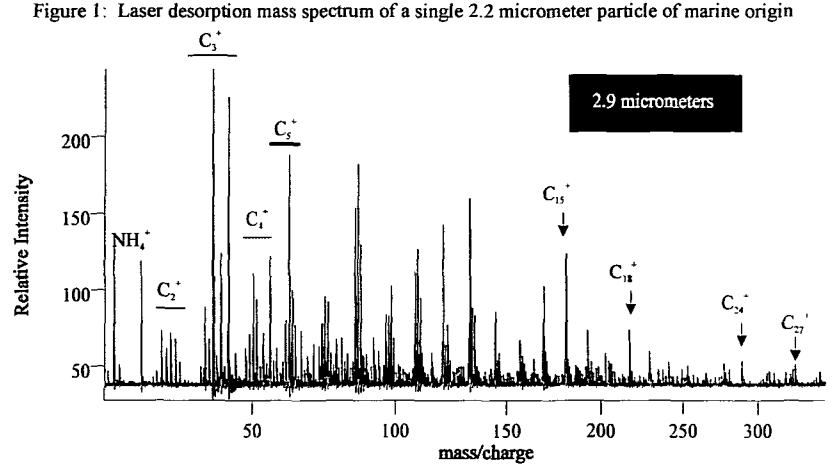

Figure 2: Laser desorption mass spectrum of an individual 2.9 micrometer soot-type particle.

RAPID SINGLE-PARTICLE MASS SPECTROMETRY OF AEROSOLS AND AEROSOL REACTIONS

M.V Johnston, P.G. Carson, and B A. Mansoori, Department of Chemistry and Biochemistry
A.S. Wexler, Department of Mechanical Engineering
University of Delaware, Newark, DE 19716

Many applications in aerosol science and technology require on-line, real-time chemical characterization of individual particles. Although several techniques are available for off-line single particle analysis, suitable on-line methods have been developed only recently. In our work, individual aerosol particles are analyzed by rapid single-particle mass spectrometry (RSMS) The experimental apparatus is shown in Figure 1. Particles are sampled directly into the source region of a time-of-flight mass spectrometer through a nozzle which forms a tight particle beam. Individual particles in the beam are detected by the light scattered from a continuous laser beam The particle size can be determined from the intensity and/or width of the scatter peak. The scattered radiation also triggers an excimer laser which performs laser desorption/ionization (LDI) of the particle in-flight. Ions generated from the particle are mass analyzed, and its chemical composition is determined from the mass spectrum. Thus, both size and composition are obtained for each particle. Since the total time between sampling and analysis is approximately one millisecond, chemical transformation by reaction, condensation, evaporation, or phase change is minimized.

We have used RSMS to study aerosol reactions The basic setup for this application is also shown in Figure 1. Aerosol particles having a known size and composition are generated with a vibrating orifice aerosol generator These particles flow into a reaction chamber where they are exposed to one or more reactive gases. After an adjustable reaction time, the particles are sampled directly into the mass spectrometer. An aerodynamic particle sizer is also available to separately monitor the particle size distribution With this setup, a variety of experiments can be performed to address both the kinetics and thermodynamics of aerosol reactions. Current applications in our laboratory include redox reactions of particulate chromium or sulfur with gaseous oxidizing and reducing agents, chemical equilibria in liquid droplets, and condensation reactions of gases onto particles.

The success of this work is directly related to the analytical capabilities of LDI. Unfortunately, LDI is only a semiquantitative technique owing to shot-to-shot irreproducibilities of the laser pulse energy and beam profile and to complex dependences of the signal intensity on matrix composition and morphology. However, much of the work we do involves liquid droplets and we have found that these samples act as ideal media for LDI. Liquids provide a reproducible local environment around the analyte, the droplet morphology is reproducible and well-defined, and the preparation of calibration aerosols is straight forward.

Since particle-to-particle variations of the signal intensity typically range from 20 to 60% for particles having similar size and composition, quantitative information cannot be obtained from the mass spectrum of a single particle ablated by a single laser pulse. When the aerosol consists of

particles having uniform size and composition, the precision can be improved by averaging the spectra of several particles. For example, inorganic cation and anion concentrations can be determined to better than +/- 10% by averaging the spectra of twenty particles. In each case, the absolute signal intensity of the appropriate quantitation ion in the mass spectrum scales linearly with concentration. When the aerosol consists of particles having different composition, particles are first grouped into classes having similar composition (via discriminant analysis, the classification and regression tree algorithm, etc.) and then the average analyte concentration within each group is determined. Particle size is also an important parameter. Although the relative signal intensities usually do not change significantly with particle size, the absolute signal intensites scale linearly with either surface area or volume depending upon the nature of the analyte and the laser fluence used to obtain the mass spectrum. Thus, quantitation can be achieved, but the mass spectra must be averaged over many "similar" particles and several parameters must be controlled or accounted for over the course of the experiment

References

McKeown, P.J.; Johnston, M.V., Murphy, D M. *Analytical Chemistry* **1991**, 63, 2069.

Mansoori, B.A ; Johnston, M.V , Wexler, A S *Analytical Chemistry* **1994**, 66, 1994

Carson, P.G.; Neubauer, K R , Johnston, M V., Wexler, A S. *Journal of Aerosol Science* **1995**, in press.

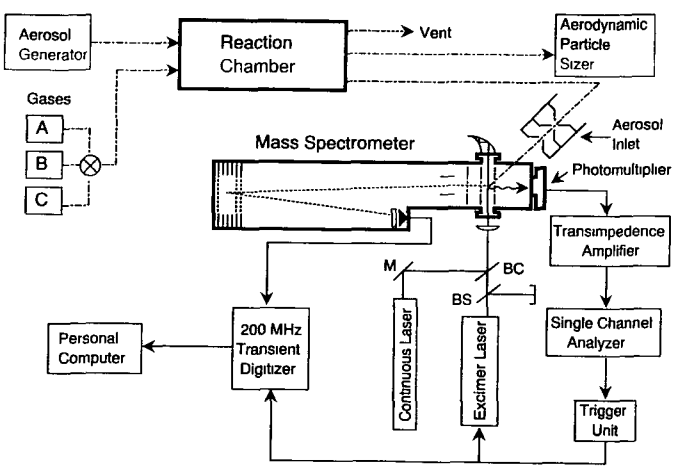

Figure 1

Tandem Mass Spectrometry of Airborne Particles

J. Michael Ramsey, Mo Yang, Peter T. Reilly, William B. Whitten
Oak Ridge National Laboratory, Oak Ridge, TN 37831-6142

Most manufacturing or processing activity produces solid emissions in the form of airborne particulates. Low vapor pressure liquids condensed on ambient particulate matter is indicative of the materials and processes being used. Laser Desorption mass spectrometry of single microparticles in an ion trap provides a capability to analyze the airborne particles as well as condensed phase materials on a microparticle surface without any instrument manipulation. On-line, single particle analysis allows detection of microscopic variations in sample compositions in real time. In this experiment, a quadrupole ion trap mass spectrometer coupled with a particle injection system is demonstrated for laser desorption mass spectrometry and MS/MS analysis of single microparticles. The device can be used for detection of controlled substances and investigation of harmful airborne particles such as pollens, fibers, microorganisms, etc.

Chemical analysis of individual microparticles using laser desorption mass spectrometry in our ion trap system has been described elsewhere.[1] Briefly, the particles are introduced into the ion trap by a particle hopper or a particle launcher mounted in the vacuum chamber. When a particle arrives at the center, a YAG laser (532 nm) desorbs and ionizes the molecules adsorbed on the microparticle surface. The ions are trapped and subsequently mass analyzed using the mass-selective instability mode of operation of the ion trap.[2] A detection limit of 0.7 fm per particle was determined for tetraphenyl-phosphonium bromide (TPPB) adsorbed on 100 μm silicon carbide microparticles.[1] Also, direct isotope ratio measurements of nickel particles with a size of 50 μm has been demonstrated using the same method.[1]

For the measurements of MS/MS fragmentation, all masses of ions are expelled except the parent ions. These parent ions are excited with an additional low RF voltage between the two end cap electrode, resulting in dissociation through collision with buffer gas atoms. The fragmented ions dissociated from the parent ions are again mass analyzed. This additional information, which cannot be obtained with a conventional time-of-flight mass spectrometer, enhances the specificity of a chemical determination.

The measured primary mass spectrum of TPPB laser-desorbed from a SiC microparticle and the fragmentation mass spectrum dissociated from the mass selected parent ions of $(C_6H_5)_4P^+$ are displayed in Figure 1 and 2 respectively. While the primary mass spectrum shows a large number of fragmentation peaks and inorganic background peaks with the parent ion peak, the fragmentation mass spectrum exhibit a recognizable fragmentation pattern in which the peaks correspond to the loss of one, two, or three phenyl groups from the parent ions. This measurement may be interpreted by pattern recognition algorithms for chemical determinations. For example, if the fragmentation pattern of an unknown sample demonstrated a similar fragmentation pattern to that in Figure 2, then we would suspect that the sample molecule consists of four phenyl groups surrounding a base block that also may be determined from the fragmentation pattern.

To apply the MS/MS technique to real-time chemical analysis of aerosol particles, an atmospheric particle sampling system and a dual particle detection system were designed and examined with a particle generator that simulates airborne particulates. Figure 3 illustrates the overall systems including the ion trap, particle detector, atmospheric sampling interface, and

particle generator. The fiberoptic particle counter enables one to detect the injected particles and to trigger the desorption laser to intercept the particle. Figure 4 shows the real-time positive ion mass spectrum of 15 μm KNO_3 particles injected directly from the air into the ion trap. The peaks are the isotopes of potassium with a measured ratio of 6.7. The natural abundance ratio is 6.9.

The demonstrated real-time spectra of the KNO_3 particles and MS/MS measurements of the organic chemicals desorbed from a microparticles surface indicates that chemical composition of aerosol particles can be analyzed directly from the air without any sample manipulation. Detailed information about the particle transmission efficiency, minimum detectable particle size, ratio of neutral to charged particles, and mass spectroscopic investigation of various aerosol particles will be available in the near future.

1. J. M. Dale, M. Yang, W. B. Whitten, and J. M. Ramsey, "Chemical Characterization of Single Microparticles by Laser Ablation/Desorption in a Quadrupole Ion Trap Mass Spectrometer", *Analytical Chemistry*, Vol. 66, No. 20, pp 3431-3435, Oct. 1994 .

2. R.E. March, R. J. Hughes, In *Quadrupole Storage Mass Spectrometry, Vol. 102, Chemical Analysis*, J. K. Wineforder, Ed., Wiley-Interscience, New York, 1989.

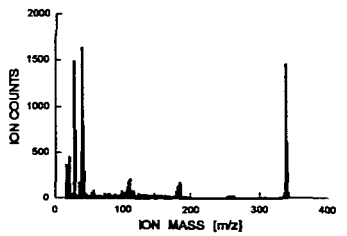

Figure 1. Primary mass spectrum of TPPB laser desorbed from the surface of a SiC microparticle.

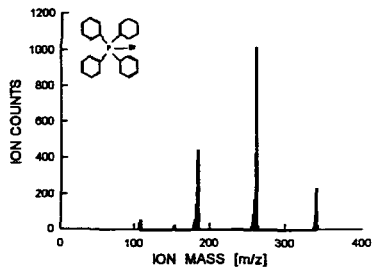

Figure 2. Secondary mass spectrum of fragments dissociated from the parent ions of TPPB.

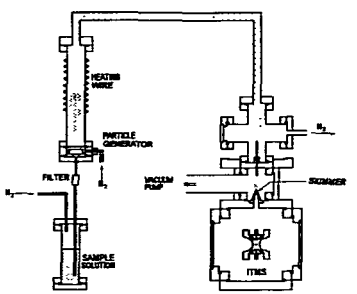

Figure 3. Experimental setup for real-time chemical analysis of aerosol particles including sample particle generator.

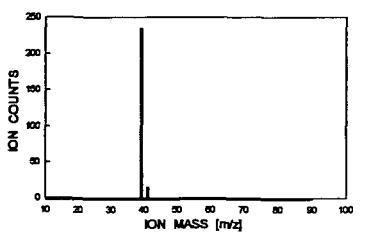

Figure 4. Measured mass spectrum of KNO_3 microparticles (15 um) injected directly from the air into the ion trap.

Detection and Characterization of Ultrafine Particles

W. D. Reents, Jr.
AT&T Bell Laboratories, Murray Hill, NJ 07974 USA

Particles present in the environment have significant affects in many areas from personal health due to atmospheric particles to various industrial processes that can be ruined due to particulate contamination such as semiconductor device manufacture and manufacture of sterile health products. The ability to detect deleterious contamination requires appropriate instrumentation to detect these particles. To prevent such contamination, the particle source must be identified by determining the composition of the offending particles.

In a controlled environment, particle contamination often occurs in transients. In order to identify unknown particles, a technique must obtain compositional and size information regardless of particle identity, and perform this analysis in real-time so as to separate "background" particles from those produced in the transient event. Since processes are sensitive to certain particle size regimes and, possibly, compositions, the instrumentation must be designed with these needs in mind. I have developed an instrument, the Ultra-Sensitive Particle Analysis System (USPAS) for situations where ultrafine particles, down to 0.002 micron, are of concern, such as the semiconductor manufacturing industry and the ambient environment.

Particle characterization occurs via pulsed laser ablation/ionization of individual particles with time-of-flight mass spectrometric detection of the created positive ions. Particle composition can be determined only if sufficient information is contained in the ion population; discrimination against elements due to their high ionization potentials reduces compositional information Negative ion detection can be used to compensate for this discrimination, but correlating negative and positive ion intensities to obtain relative abundances is difficult. Instead, by heating the particle to extremely high temperatures, ionization of all elements approaches 100%. This is shown in Figure 1 for NaCl where the relative *positive ion* intensities match the actual elemental ratio present.

Further characterization is obtained from sizing the particle. In some processes, particles smaller than a critical size do not harm the process. In semiconductor device manufacturing, device line widths approaching 0.18-0.35 micron will be affected by particles >0.05 micron whereas gate oxides with thicknesses of 0.002 - 0.08 micron will be affected by correspondingly smaller particles. Since ionization is efficient with the USPAS, the ion signal should correlate with particle mass and, for dense particles, their diameter. This is the case when the cube root of ion signal is plotted vs. particle diameter (see Figure 2). These particles represent not only different sizes, but also different compositions. They are 0.2 micron NaCl, 0.15 micron polystyrene latex spheres, 0.1 micron NaCl, and 0.017 micron silicon particle. Based upon the noise level of the USPAS, the particle size characterization limit is below 0.002 micron.

Detection efficiency and real-time characterization are also very important capabilities. The USPAS detects 3-4% of particles entering the capillary inlet; evaluated using 0.074 nm polystyrene latex spheres and calibrated against a Condensation Particle Counter. All of these characteristics of the USPAS are available during real-time characterizations.

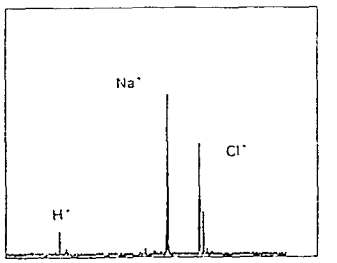

Figure 1
USPAS mass spectrum of single 0.1 micron NaCl particle

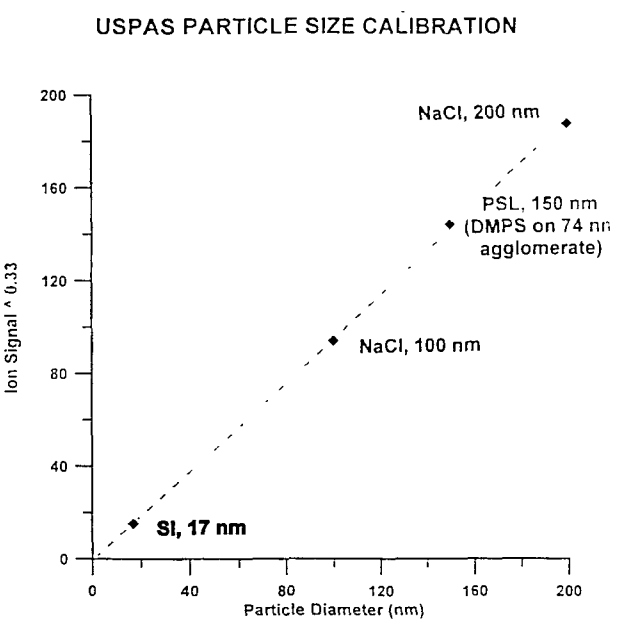

Figure 2
Particle size calibration of USPAS for particles from 0.017 to 0.2 micron in diameter

Sulfur Speciation of Single Aerosol Particles

K.R. Neubauer, S.T. Sum, M.V. Johnston, Department of Chemistry and Biochemistry
A.S. Wexler, Department of Mechanical Engineering
University of Delaware, Newark, DE 19716

Sulfur enters the atmosphere as gaseous species emitted from both natural and anthropogenic sources. These species can undergo a variety of oxidation reactions that ultimately yield hexavalent sulfur aerosols Since the final products play an important role in acid rain production and the earth's energy balance, it is important to distinguish tetravalent and hexavalent sulfur aerosols, as well as differentiate those arising from natural and anthropogenic sources. To attain these goals we chose to examine five target compounds that are present in the atmosphere: sodium sulfate, ammonium sulfate, ammonium sulfite, methanesulfonic acid (MSA), and the sodium salt of hydroxymethanesulfonic acid (NaHMSA). Sodium sulfate is observed in oceanic aerosols, while both ammonium salts are observed over land. MSA is found only in the marine environment and originates solely from natural emissions, while HMSA is formed in urban hazes and primarily arises from anthropogenic sources Thus, MSA and HMSA serve as tracers for distinguishing natural and anthropogenic sulfur emissions.

To differentiate these compounds, we used Rapid Single-Particle Mass Spectrometry (RSMS), a method that allows single particles to be analyzed on-line and in real time. With RSMS, particles are drawn directly into the source region of a reflectron time-of-flight mass spectrometer where they are detected by light scattering of a continuous laser beam and then ablated by an excimer laser pulse. With this sequence of events, each mass spectrum results from a single laser pulse ablating a single particle

Our results indicate that these sulfur compounds can be distinguished on the basis of peak area ratios and threshold laser fluences; the relevant portions of representative spectra are shown in Figure 1 MSA is characterized by $SO_4^-/CH_3SO_3^-$ and $HSO_4^-/CH_3SO_3^-$ area ratios much less than one, while Na_2SO_4 possesses a dominant SO_4^- peak, an HSO_4^-/SO_4^- ratio less than 1, and no $CH_3SO_3^-$ signal. NaHMSA is characterized by a strong SO_2^- peak, weak SO_4^- and HSO_4^- peaks, and, under certain conditions $HOCH_2SO_3^-$ is observed. Ammonium sulfate and ammonium sulfite yield similar spectra, both possessing HSO_4^-/SO_4^- area ratios greater than one. These latter two compounds can only be distinguished on the basis of excimer fluence: ammonium sulfate has a lower threshold for ion production than ammonium sulfite.

Because ambient particles likely contain mixtures of various sulfur species, it is important to distinguish the relative amounts of these compounds in multicomponent particles. To address this issue we produced particles consisting of varying amounts of MSA, Na_2SO_4, NaHMSA, and NaCl and monitored the peak area ratios of ions characteristic of each species. Although the average peak area ratios scale with relative concentration, quantitative information cannot be obtained due to large particle to particle spectral variations.

To improve quantitation, we subjected the sulfur mixtures to classification and regression trees (CART) analysis. CART examines a given data set and decides which variables best distinguish the different classes within the data set. Once CART has been trained, it can then analyze unknown data sets. When the sulfur mixtures were analyzed by CART at least 80% of the particles were correctly classified, with the majority of the errors resulting from classifications in the adjacent concentration ranges The results for the three mixtures analyzed are shown in Figure 2. Thus, CART analysis allows the concentration distribution within a group of particles to be determined.

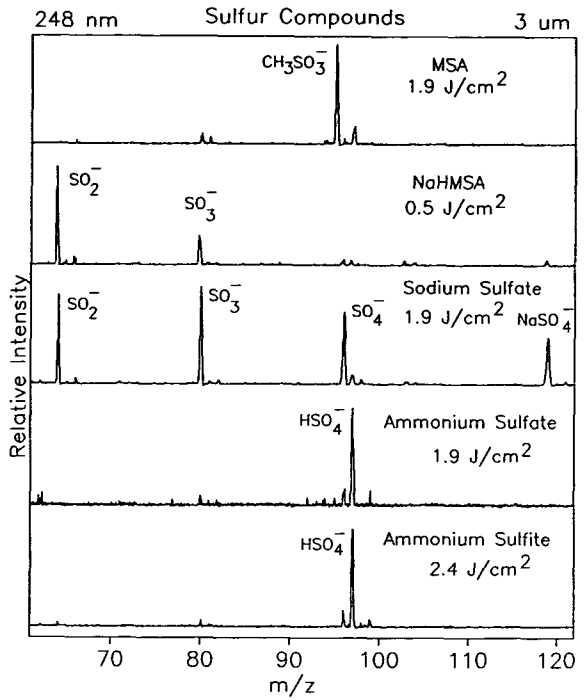

Figure 1

CART Results

Mixture	% MSA or NaHMSA	Number of Variables Used	Number of Spectra (Particles)	Number Correctly Classified	% Correctly Classified
MSA/Na_2SO_4	1.5, 7.3, 14, 23, 33, 39, 50	22	162	140	***83***
50% NaCl MSA/Na_2SO_4	0.1, 1.6, 10, 17, 21, 25	16	120	96	***80***
NaHMSA/ $(NH_4)_2SO_4$	1, 10, 20, 30, 40, 50	17	120	102	***83***

Figure 2

Laser Microprobe Mass Analysis of Soot and Soot Precursor Particles

R.A. Fletcher[1], R.A. Dobbins[2] and W. Lu[2]

[1]Surface and Microanalysis Science Division
National Institute of Standards and Technology, Gaithersburg, MD 20899.
[2]Division of Engineering, Brown University, Providence, RI 02906

In flame combustion research the study of gas-to-particle conversion and the subsequent aerosol evolution occurring in or above flames is important for providing fundamental understanding of the flame combustion processes and developing control strategies to limit combustion products relevant to health and environmental concerns. Laser microprobe mass spectrometry and transmission electron microscopy (TEM) have been applied to particles collected in the flame to characterize particle chemical composition and morphology.

Brown University developed a quick-collection (~10ms) method, shown in Figure 1, to sample particles at various heights (20, 30, 40, 50, and 70 mm) in an ethene diffusion flame where the temperature and oxidation conditions differ.[1,2] The particles are captured on plasma-etched TEM grids. The precursor particles found low in the flame (20 and 30 mm) have the appearance of individual spherules, approximately 5 nm in diameter, and have low electron opacity when viewed by TEM.[3] Particles collected using the same technique at higher regions in the flame have a distinctly different morphology; they show classic soot aggregation and exhibit higher opacity with respect to the transmitted electron beam. To learn more about the chemical composition of these two types of particles, a commercial transmission laser microprobe mass analyzer having the time-of-flight spectrometer was used in a defocused mode to obtain characteristic mass spectra and to identify chemical differences of samples collected at different heights.[4] The positive ion mass spectra of the precursor particles collected low in the flame (typical spectrum Figure 2a) are characteristic of mid-mass range polycyclic aromatic hydrocarbons (m/z 202 to 302). The hydrogen mole fraction for the precursors is approximately 0.36. Spectra of particles collected high in the flame contain primarily the carbon cluster series, $C_mH_n^+$ where m = 1 to 15 and n = 0 to 2, characteristic of carbonaceous material devoid to a large extent of hydrogen (typical spectrum in Figure 2b). The hydrogen mole fraction based on peak areas corrected for ^{13}C abundance is 0.15. In a small fraction of the spectra, we observed mass peaks that correspond to polycyclic aromatic hydrocarbon-like compounds in the range m/z 418-444 and high mass fullerene-like peaks. At this time, the source of these large ions is not clear - whether they are inherent in the sample or are formed in the laser ablation process. Work is progressing to help determine the source.

The mass spectrometric technique is sensitive to unseparated PAH's as found by Mauney in his analysis of shale oil soot with laser microprobe[5] and more recently by Zare and co-workers in their analysis of meteoritic samples.[6] The peaks that we have identified are the ones predicted by Stein and Fahr to be the most thermodynamically stable (stabilomer) structures possible in the flame under the conditions prevailing in these experiments.[7] The results of our experiments suggest that PAH or PAH-like compounds are formed low in the flame and contribute to the composition of the precursor particles. As the small particles are processed at higher temperatures in the upper regions of the flame, hydrogen is lost and the soot is transformed into a more carbonaceous material.

References

1. Dobbins, R.A. and C.M. Megaridis, *Langmuir* (1987)3, 254.
2. Megaridis, C.M. Ph.D. thesis(1987), Division of Engineering, Brown University, Providence RI
3. Dobbins, R.A., Glassman Symposium (1993) (in press)
4. Dobbins, R.A., R.A. Fletcher and W. Lu, *Combust. and Flame* (1994) (in press)
5. Mauney, T., Ph.D. thesis (1984) Colorado State University, Fort Collins, CO.
6. Clemett, S.J., C.R. Maechling, R.N. Zare, P.D. Swan, and R.M. Walker. *Science* (1993)262, 721.
7. Stein, S.E. and A. Fahr, *J. Phys. Chem.* (1985)89, 3714.

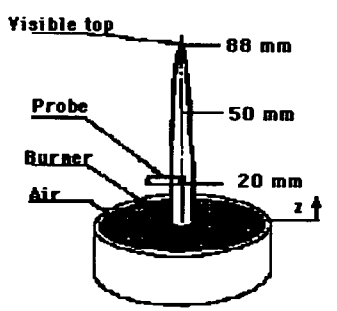

Figure 1. Schematic of coannular burner.

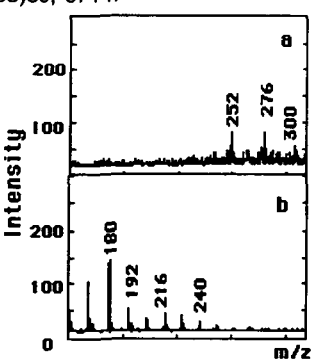

Figure 2. Positive ion mass spectra of (a) precursor particles collected z = 20 mm and (b) soot aggregated particles collected at z = 50 mm.

Effect of MALDI and Solution Parameters on Aerosol MALDI Ion Signal

Michelle D. Beeson, Xiaona Wei, and David H. Russell,
Laboratory for Biological Mass Spectrometry, Department of Chemistry
Texas A&M University, College Station, TX 77843

We have recently described a technique that uses a pneumatic aerosol generator to combine liquid introduction with matrix-assisted laser desorption ionization (MALDI) mass spectrometry.[1] This technique is called aerosol MALDI to differentiate it from the more common surface MALDI experiment. In the aerosol MALDI technique, the matrix and analyte-containing solution is delivered using a syringe pump to a pneumatic aerosol generator and sprayed into the vacuum as an aerosol. The aerosol first passes through a heated drying tube at 500 C to remove solvent and then ionization is performed using 355 nm from a frequency tripled Nd:YAG laser. The ions are orthogonally accelerated at 10 kV, mass separated in a 1.1 m flight tube, and detected with a microchannel plate particle multiplier. The mass spectra are collected by a digital oscilloscope and downloaded to a microcomputer for analysis.[1]

We have examined the effect of several MALDI and solution parameters on the aerosol MALDI ion signal. One of the more interesting observations concerns the effect of analyte concentration on ion signal. The aerosol MALDI ion signal is non-linear in analyte concentration (Figure 1). We attribute this observation to residual solvent in the aerosol particles.[2] We have also examined the effect of adding

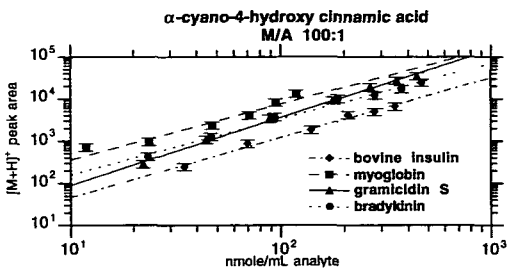

Figure 1. Aerosol MALDI ion signal as a function of analyte concentration.

water to organic solvents (Figure 2). For over 80 % of the analyte/matrix/organic solvents studied, maximum analyte ion signal is obtained from organic solvent/water mixtures. However, the composition of this mixture is not the same for all analytes or all matrices studied. We interpret this to mean that analyte/matrix/solvent interactions within the aerosol particle are important for obtaining optimum aerosol MALDI ion signal.

References:

1. K. K. Murray and D. H. Russell, *J. Am. Soc. Mass Spectrom.*, **5**, 1, (1994).
2. M. D. Beeson, K. K. Murray, D. H. Russell, *Anal Chem.*, in press.
3. J. A. Borowiec, A. W. Boorn, J. H. Dillard, M. S. Cresser, R. F. Browner and M. J. Matteson, *Anal. Chem.*, **52**, 1054 (1980).
4. H. Kornahrens, K. D. Cook and D. W. Armstrong, *Anal. Chem.*, **54**, 1325 (1982).

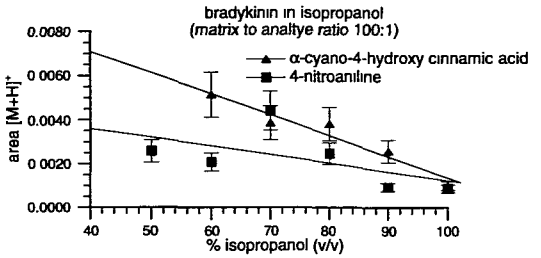

Figure 2. Bradykinin ion signal from solutions of isopropanol and water.

Based on our observations and the work of Browner and co-workers[3] and Cook and co-workers,[4] we have developed a model describing the microphysical aspects of aerosol MALDI. For aerosol particles produced from solutions containing multiple solutes, it is possible for aerosol particle composition to vary with particle size. After initial formation, (Figure 3a) aerosol particles continue to break-up, as depicted in Figure 3c. During the break-up process, small particles are ejected from the surface of the original particle and the composition of these small particles may not be identical to the composition of the initial particle due to aerosol ionic redistribution (AIR).[3,4] AIR can occur in aerosol particles that are inhomogeneous due to the more hydrophobic solutes migrating to the air interface. In the process of AIR, the inhomogeneous aerosol particles break up and form "daughter" aerosol particles. The smaller particles ejected from the surface of the initial aerosol particle are enriched in the *more* hydrophobic species whereas the larger particles are enriched in the *less* hydrophobic species at the center of the initial aerosol particle. This AIR effect may influence the aerosol MALDI ion signal. For example, if the hydrophobicities of the matrix and analyte are not the same, AIR may separate the matrix and analyte into different particles, resulting in reduction or loss of ion signal. Other species in the aerosol particle will also affect the matrix/analyte interactions and thus AIR. For example, when trifluoroacetic acid is present, matrix/analyte interactions are increased, resulting in improved aerosol MALDI ion signal.

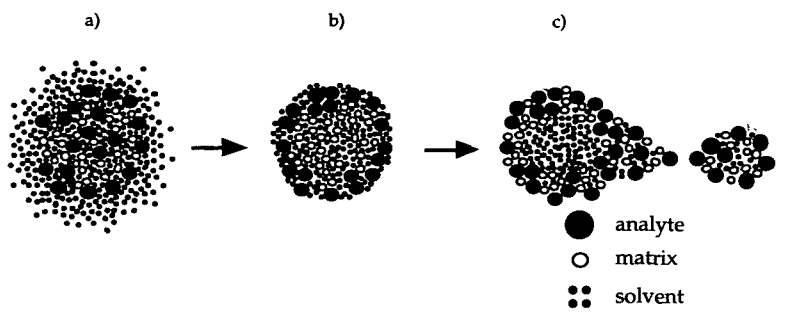

Figure 3. Aerosol Ionic Redistribution for aerosol MALDI

Analysis of Polycyclic Aromatic Hydrocarbons (PAHs) in Kerogens using Two-step Laser Mass Spectrometry

QIAO ZHAN[1], RENATO ZENOBI[1,*], RICHARD KNOCHENMUSS[1], PETER R. BUSECK[2], and STAN TEERMAN[3]

[1]Lehrstuhl für Analytische Chemie, Department of Chemistry, Swiss Federal Institute of Technology Zurich, Universitätstr. 16, CH-8092 Zürich, Switzerland

[2]Depts. of Geology and Chemistry/Biochemistry, Arizona State University, Tempe, AZ 85287-1404, U.S.A.

[3]Western Australian Petroleum Pty. Limited Perth, W. Australia 6001, Australia

Two-step laser mass spectrometry (L2MS) is a modern analytical method that features intact vaporization and efficient soft ionization of high molecular weight compounds. It utilizes a pulsed CO_2 laser for desorption of intact neutral molecules, a pulsed, tunable UV laser for resonance-enchanced multiphoton postionization, and a reflectron time-of-flight mass spectrometer for mass analysis [1]. L2MS is a highly sensitive and optically selective analysis method. It can serve as very powerful tool for the direct chemical analysis of selected compounds in complex sample mixtures, such as tissue, polymers, environmental samples, and geo/cosmochemical materials.

Kerogen is the oldest carbonaceous matter found on Earth. It formed from the residues of biological organisms and land-plant material that degraded into complex carbon-rich structures. During burial, thermal processes progressively convert the organic material into oil, gas, polycyclic aromatic hydrocarbons (PAHs), and ultimately graphite [2]. For conventional analysis methods, e.g., pyrolysis chromatography [3], a time-consuming kerogen acid digestion process is used (several days) In this work we studied Green River, Phosphoria, and Mowry kerogens, all form Wyoming, U.S.A. We recorded the L2MS spectra of digested samples, as well as untreated rock and rock powder directly.

Figure 1 shows the L2MS spectra of a *post-mature* sample (Phosphoria formation). The peak at m/z = 178 results from anthracene, phenanthrene, or both. All spectra show a series of peaks with mass intervals of 14 starting from m/z = 178. They arise from alkyl-substituted 178, e.g., peaks at m/z = 192, 206, and 220 are from methyl-, dimethyl-, or ethyl-178 etc.

Figure 2 shows the L2MS spectra of different forms of an *immature* sample (Green River formation). The series of peaks with mass intervals of 14 starting from m/z = 178 is again observed most strongly in the spectrum of the untreated rock sample. Peaks at m/z = 202 and 228 result from pyrene and chrysene (or their isomers). There are other examples of peak groups, i.e. 274, 288, and 245, 259, etc.

For *post-mature* and *immature* samples, the acid-digested kerogens and the pulverized rock give almost identical L2MS spectra. This similarity demonstrates that acid digestion does not introduce any artifacts, e.g., from chemical alteration of the PAH contents of these samples. It also shows that grinding the rock suffices for sample preparation for L2MS analyses.

In the spectra of the *post-mature* samples (Fig.1), there are only slight differences among the spectra of intact rock, rock powder, and digested samples. Acid treatment or grinding did not liberate the higher mass PAHs from bulk material. But for *immature* samples (Fig. 2), acid treatment or grinding induce a dramatic shift in the mass distribution relative to the intact rock data. We suspect that this difference is related to the lower

molecular weight PAHs that accumulate along fissures or cracks in the material, whereas higher molecular weight molecules stay trapped in the rock matrix.

1. VOUMARD P., ZHAN Q.and ZENOBI R. (1993) *Rev. Sci. Instrum.* **64**, 2215-2220.
2. TISSOT B. P., WELTE D. H. (1978) *Petroleum Formation and Occurrence.* Springer-Verlag,148p.
3. DURAND B. (1980) *Kerogen, insoluble organic matter from sedimentray rocks.* Editions Technip. Chap. 1, pp. 13-34.

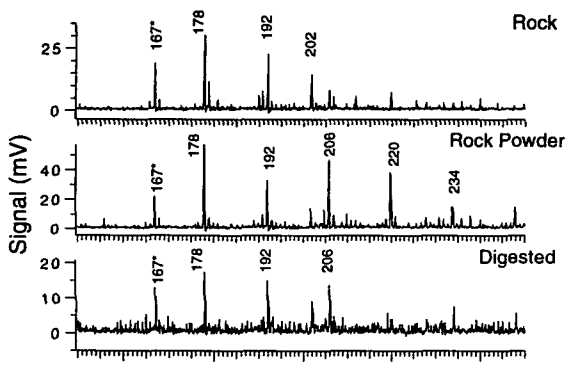

Figure 1 m/z

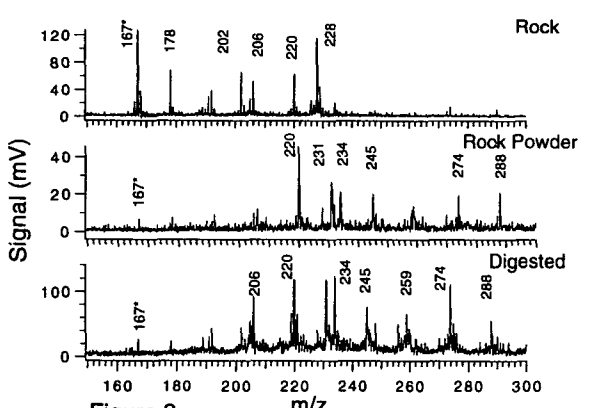

Figure 2 m/z

A REVERSED GEOMETRY ORGANIC ION MICROPROBE

Peter J. Todd, John M. McMahon and Robert T. Short
Chemical & Analytical Sciences Division
Oak Ridge National Laboratory
PO Box 2008, Bldg. 5510A
Oak Ridge, Tennessee 37831-6365

Secondary ion microprobes perform mapping of sample surfaces by measuring the intensity of selected secondary ions while a beam of high energy primary ions are rastered across the sample surface. Transmission of secondary ions through the mass spectrometer depends in part on the careful focus of the secondary ion optics. This focusing requirement limits the size of the sample (i.e., the field of view) that can be mapped to about 100 - 200 μm in diameter. This field of view can be enlarged by use of deflectors inside the secondary ion source. By coordinated operation of deflectors in both the primary and secondary ion sources, fields of view in excess of 1 cm. dia. can be demonstrated. The process of employing coordinated primary and secondary ion deflectors is called dynamic emittance matching (DEM).

With microprobes, only secondary ions from a single point on a sample can be transmitted, regardless of how broad the primary ion beam is. Consequently, if the deflectors of the secondary ion source are operated in the usual DEM mode, but (a) the primary ion beam is defocused and (b), the deflectors of the primary ion beam are disengaged, then a secondary ion image can be created. Figures 1 and 2 demonstrate this capability. Figure 1 shows a secondary ion image of choline (m/z 104) obtained from two spots on a gold sample. It was obtained by using our microprobe in normal fashion. Figure 2 shows the secondary ion image generated by using a defocused Cs+ primary ion beam, with primary deflectors turned off, and only secondary ion deflectors operated. Clearly, there is some loss in spatial resolution in Figure 2, but the image is unmistakably from the same sample as that is Figure 1. The spatial resolution is, in fact, determined by the quality of the secondary ion optics, rather than the primary ion spot size, the latter being the more conventional requirement for spatial resolution. Because the secondary ion optics, rather than the primary ion optics, determine spatial resolution, we call our method, a reversed geometry ion microprobe.

The utility of a reversed geometry microprobe is related to the fact the some primary sources cannot be focussed. These include the traditional fast Xe atom bombardment (FAB) source, and the massive cluster ion impact (MCI) source. The latter cannot be focussed because the cluster ions generated by it possess a broad distribution of mass, kinetic energy and charge states. Unique features of the MCI

as a primary ion source include the ability to generate abundant secondary ions from high molecular weight compounds and such emission persists well beyond the dose known as the static SIMS limit. In short, the MCI gun can be used exactly like a FAB gun except that secondary ions can be emitted from dry samples, including biologic tissue, without sample preparation. By combining the capabilities of the MCI gun with the reversed geometry ion microprobe, characteristic secondary ions can be emitted directly from a specific place on a sample of biologic tissue.

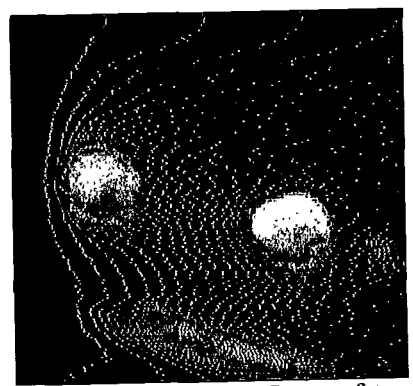

Figure 1 Secondary Ion Image of two choline spots obtained using the Cs+ primary ion beam

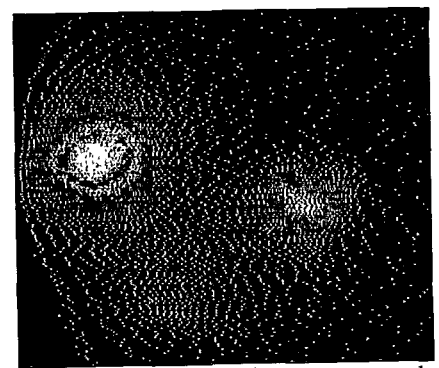

Figure 2 Image of the same sample obtained by rastering the deflection plates of the secondary ion source while defocusing the primary beam.

A COMPUTATIONAL APPROACH TO GAS-PHASE ION CHEMISTRY

Leo Radom

Research School of Chemistry, Australian National University, Canberra, ACT 0200, Australia

Ab initio molecular orbital theory today can straightforwardly produce information about the structures and thermochemistry of ions and on the mechanisms of the reactions that they undergo. For small systems, the calculations are now able to provide quantitatively reliable data, that may be used to assist in the interpretation of experimental results and, occasionally, to resolve discrepancies. Particularly useful in this regard are variants of a level of theory called G2 theory, introduced by Pople and co-workers in 1991 with the aim of being able to predict thermochemical data to so-called chemical accuracy: roughly 10 kJ mol^{-1}, 2 kcal mol^{-1} or 0.1 eV.

The first example presented concerns **gas-phase proton affinities** (PAs).[1] The background to the story is the suggestion in 1991 by Mautner and Sieck (MS) and Szulejko and McMahon (SM), on the basis of high quality variable temperature proton-transfer equilibrium measurements, that the standard proton affinity scale of Lias and co-workers (LBLHLM) should be revised. It was of interest to test this challenge theoretically. What we find from a comparison of our calculated G2 proton affinities with the LBLHLM values spanning a range of more than 500 kJ mol^{-1} is that there is generally good agreement, the mean absolute deviation between theory and experiment for 31 comparisons being just 6.2 kJ mol^{-1}. Thus, there is no support for a wholesale revision of the LBLHLM scale. The largest and only serious discrepancy occurs for isobutene where the G2 proton affinity (802 kJ mol^{-1}) lies significantly below the LBLHLM value (820 kJ mol^{-1}). Significantly, isobutene was the molecule chosen as the anchor point in the MS and SM scales!

On the other hand, there *are* a number of significant discrepancies between the G2 proton affinities and the MS values at the upper end of the scale. However, if we examine the proton-transfer enthalpies *directly measured* by MS, we find uniformly good agreement between theory and experiment, including reactions involving the "problem" molecules. The mean absolute error is 2.3 kJ mol^{-1} and the maximum error is 6.9 kJ mol^{-1}. Again, noting that the MS PA scale was derived using the PA of isobutene as an absolute standard, it is of interest to examine the effect of removal of this absolute standard by evaluating the theoretical and experimental proton affinities at the upper end of the scale *relative to isobutene*. The resulting values are all in very good agreement!

Our analysis points us in one obvious direction: virtually all the results can be reconciled if we trust the theoretical predictions and lower the standard proton affinity for isobutene by about 18 kJ mol^{-1} from its current value, i.e. from 820 to 802 kJ mol^{-1}. Our G2 results also suggest that the currently accepted experimental $\Delta H_{f\,298}$ value for *t*-butyl cation may be too low by about 15–20 kJ mol^{-1}.

Subsequent to the completion of our calculations, a new and independent proton affinity scale has been reported by Szulejko and McMahon (SM), and related new measurements have been reported by Traeger. The agreement between our theoretical results and the new experimental data is quite remarkable. The 20 comparisons show a mean absolute deviation of just 2.3 kJ mol^{-1} and a maximum deviation of less than 7 kJ mol^{-1}. But, in particular, the new SM results also suggest a downwards revision in the proton affinity of isobutene to about 802 kJ mol^{-1}. In addition, new experiments by Traeger and by Baer also suggest a proton affinity for isobutene in the vicinity of 802 kJ mol^{-1}.

In addition to calculating proton affinities or proton-transfer enthalpies, theory may be used to calculate **proton-transfer entropies**[2] using standard statistical thermodynamics procedures Comparisons of calculated and experimental absolute entropies reveal excellent agreement, with a mean absolute deviation of 0.3 J mol^{-1} K^{-1}. All values agree to within 0.7 J mol^{-1} K^{-1}, lending confidence to the theoretical predictions in those cases where the experimental information is less precise.

Because absolute entropies are generally not available for ions, it is commonly assumed in the experimental literature that the entropy for the ion is the same as that for an isoelectronic neutral analogue. We have examined this assumption and find that in many cases (e.g. NH_3 vs H_3O^+) that this involves an error of 1–2 J mol^{-1} K^{-1} but in some cases, particularly for those species containing hindered rotors, the error is 5–10 J mol^{-1} K^{-1}, i.e. is unacceptably large.

Examination of entropies for proton-transfer reactions show that there is a significant scatter between experimental measurements from different laboratories, with differences of up to 9 J mol^{-1} K^{-1}. If we take this as representing roughly the sort of accuracy available from such experimental determinations, the agreement between theory and experiment may be considered generally reasonable, but there are a few cases of significant discrepancies. We believe that the determination of reaction entropies may be an area where it is currently more straightforward to obtain precise results from theory than from experiment.

The **tropylium and benzyl cations**[3] have been widely studied by mass spectrometrists but their precise thermochemistry is still uncertain. Our calculated heat of formation for benzyl cation (907 kJ mol^{-1}) is in good agreement with recent experimental results (910 kJ mol^{-1}) but for tropylium cation our $\Delta H_{f\,298}$ (878 kJ mol^{-1}) suggests that experimental re-examination would be desirable. Our best estimate of the energy difference between the two $C_7H_7^+$ isomers is 29 kJ mol^{-1} in favor of tropylium cation.

Recent work from Beauchamp's laboratory on the silicon analogues of the tropylium and benzyl cations has given indirect evidence for the production of both species from the ionization of silatoluene. The experiments also suggested that the stability ordering in the silicon systems is the same as in the $C_7H_7^+$ systems, i.e. silatropylium is more stable than silabenzyl cation. Our calculations do not support this conclusion. We find a clear-cut energy preference of 38 kJ mol^{-1} in favour of silabenzyl cation.[3]

Finally, **nucleophilic substitution reactions**[4] are discussed as an example of the use of theory to study gas-phase ion reactions. Overall barriers for identity S_N2 reactions of X^- with CH_3X (X = F, Cl, Br and I), taking place via backside attack and resulting in inversion of configuration, are found to be small and to lie in a narrow range between -11 (X = F) and +10 (X = Cl) kJ mol^{-1}. In contrast, frontside attack, resulting in retention of configuration, needs to overcome large barriers of between 170 and 195 kJ mol^{-1}. The theoretical results provide an explanation for a second pathway for exchange, observed at about 193 kJ mol^{-1} by Bierbaum and coworkers in the case of X = Cl. The observed barrier is very close to that calculated (195 kJ mol^{-1}) for the frontside attack.

The summary take-home message is that theory can play an important and complementary role to experiment in studying the structure and thermochemistry of gas-phase ions and the mechanism of reactions involving such species.

(1) (a) Smith, B.J.; Radom, L. *J. Am. Chem. Soc.* **1993**, *115*, 4885; (b) Smith, B.J.; Radom, L. *Chem. Phys. Lett* **1994**, *231*, 345, and references therein.

(2) East, A.L.L., Smith, B.J.; Radom, L. to be published, and references therein

(3) Nicolaides, A ; Radom, L. *J. Am. Chem. Soc.* **1994**, *116*, 9769, and references therein.

(4) (a) Glukhovtsev, M.; Pross, A.; Radom, L *J. Am. Chem. Soc.* **1995**, *117*, 2024; (b) Glukhovtsev, M.; Pross, A ; Schlegel, H.B.; Radom, L. to be published, and references therein.

Recent Experimental Investigations of Gaseous Ion Thermochemistry

T.B. McMahon; Department of Chemistry; The University of Waterloo;
Waterloo, Ontario; CANADA N2L 3G1

Thermochemical data for gas phase ions provide a valuable means for assessing intrinsic stabilities and reactivities of charged species in the absence of complications due to solvation and ion-pair interactions. Pulsed ionization high pressure mass spectrometry (HPMS) is one of the most valuable techniques for obtaining such thermochemical data, through examination of the temperature dependence of ion-molecule equilibrium processes.

For example, from an examination of proton transfer equilibrium, eqn. (1), the *relative* base

$$B_1H^+ + B_2 \rightleftharpoons B_2H^+ + B_1 \qquad (1)$$

strengths of the species B_1 and B_2 can be determined. If the *absolute gas phase basicity* of either B_1 or B_2 is known then the other is automatically determined. Alternatively an absolute basicity may be determined from the free energy change for an association reaction. For example the basicity of methyl *t* butyl ether my be obtained from a measure of the equilibrium constant for association of the *t*-butyl cation with methanol, eqn. (2).

$$t\text{-}C_4H_9^+ + CH_3OH \rightleftharpoons [CH_3Ot\text{-}C_4H_9]H^+ \qquad (2)$$

In recent attempts to carry out such experiments for the association of small organic cations with neutral molecules it was discovered that temperature dependence of the equilibrium constant (van't Hoff plot) revealed the existence of two isomeric forms of the association adducts of *t*-butyl cation and several small organic molecules. For example, the data for methanol (Figure 1.) show an adduct at low temperature characterised by a strong enthalpy of association ($\Delta H°$=-29 kcal/mole) but an unusually unfavourable entropy of association ($\Delta S°$=-54 cal/(mole-K)). In contrast, the adduct formed at high temperature has a much weaker enthalpy of association ($\Delta H°$=-15 kcal/mole) but a less unfavourable entropy of association ($\Delta H°$=-21 cal/(mole-K)). As can be seen from the data summarized in Table 1., this pattern is repeated for a number of other species. The low temperature structures are thought to be covalently bound adducts (*i.e.* protonated methyl *t*-butyl ether in the case of methanol, **I**) while the higher temperature structures are, most probably, weakly hydrogen bonded species in which the proton of a protonated base interacts with the π system of *i*-butene (*i.e.* **II** in the case of methanol). These two types of structure have been found, by *ab initio* calculation, to correspond to stable minima on the potential energy surfaces of several of the adducts. In addition, the data are also consistent with a further stabilizing interaction in the low temperature adducts of ethanol and diethyl ether, in which a hydrogen on the carbon adjacent to the basic oxygen site forms a hydride bridge to the *t*-butyl cation centre. Such an interaction would serve to explain the peak due to protonated acetaldehyde (+ *i*-butane) in the metastable spectrum of ethanol adducts.

Analogous experiments have been carried out involving adducts of transition metal ions generated *via* laser ablation with rare gases and small molecules. For example the data shown in Table 2. for argon adducts reveal a predominantly electrostatic character for such species.

Table 1 Experimentally obtained thermochemical data for the association reaction of $t\text{-}C_4H_9^+$ onto several bases (B).

B	$\mu(B)^a$	PA(B)	High temperature $-\Delta H^{\circ\,e}$	High temperature $-\Delta S^{\circ\,e}$	Low temperature $-\Delta H^{\circ\,e}$	Low temperature $-\Delta S^{\circ\,e}$	$-\Delta S^{\circ}$ (estimate)^f
	D	kcal/mol	kcal/mol	cal/mol·K	kcal/mol	cal/mol K	cal/mol K
CH_3OH	1 70	181.7^b	15 1	21 1	29 1	54.0	50 1
CH_3CN	3.92	187 0^c	20 4	20.5	35 0	45.4	46 0
C_2H_5OH	1 69	187.0^d	20 4	27 6	38 6	72.9	50 4
$(CH_3)_2O$	1.30	189 6^b	23.2	36.0	33.2	62 1	49 6
$(CH_3)_2CO$	2 88	194.2^c	19 2	24 2	33.5	54 4	45 2
$(C_2H_5)_2O$	1 15	199.2^b	33.7	52.4	46.3	86 4	50.2

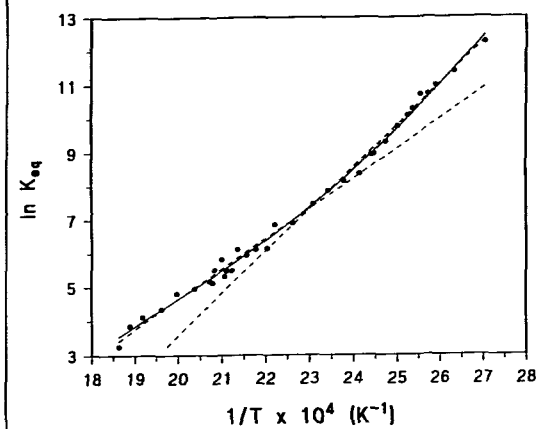

Table 2

Product	ΔH (kcal/mol)	ΔS (cal/mol/K)	DBE (kcal/mol)
Mg·Ar$^+$	-5.0	-16 4	3.67/3.25*
Al Ar$^+$	-6.5	-21 9	
Sn Ar$^+$	-8 3	-14 7	
Ti Ar$^+$	-8 8	-16 9	6 92*
V Ar$^+$	-8 1	-13.8	8 76/7 22*
V Ar_2^+	-7 9	-15 7	6 85*
Fe Ar$^+$	-5.3	-13.7	4 04*
Fe·Ar_2^+	-9 2	-17 2	5.10*
Fe Ar_3^+	-6 5	-16.8	
Nb Ar$^+$	-8 5	-14 2	
Nb Ar_2^+	-10 3	-21 3	
Mo·Ar	-7.1	-13.9	
Mo Ar_2	-9 6	-24 1	

Figure 1.

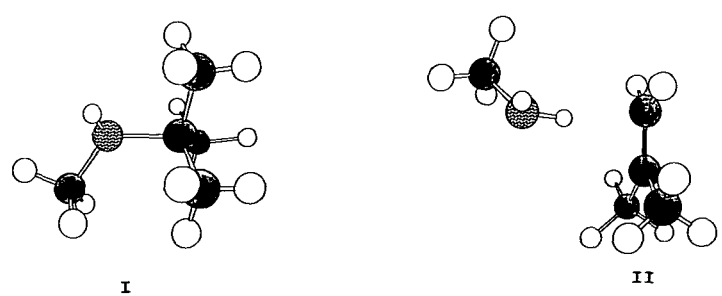

Structure and Reactivity Of A Cyclopropyl Anion: Experiment and Theory

Michael Baschky, Kent Peterson and Steven Kass
Department of Chemistry
University of Minnesota, Minneapolis, MN 55455

Cis and *trans*-2-(trimethylsilyl)formylcyclopropane react in our variable temperature flowing afterglow device at room temperature to afford distinct, noninterconverting, cyclopropyl anions (eq 1).[1] The structure, reactivity and

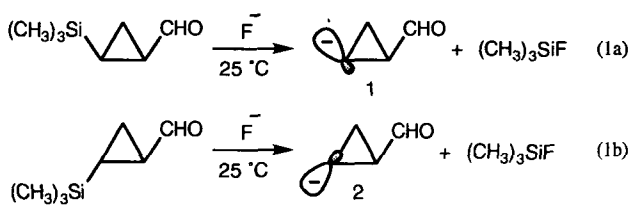

thermodynamic properties of these homoenolates have been probed experimentally and computationally. For example, the formyl group is found to have a large stabilizing influence (Figure 1).

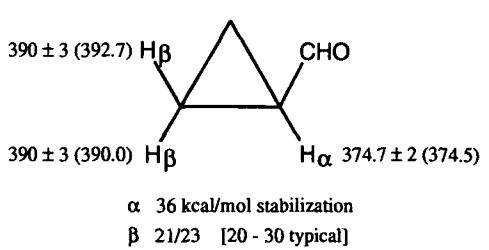

Figure 1. Experimental and calculated (in parentheses) acidities in kcal/mol.

Cyclopropyl anions **1** and **2** isomerize at elevated temperatures; inversion and ring-opening processes take place (eqs 2 and 3). The latter rearrangement can proceed, in principle, via eight different transition states, six of which were found

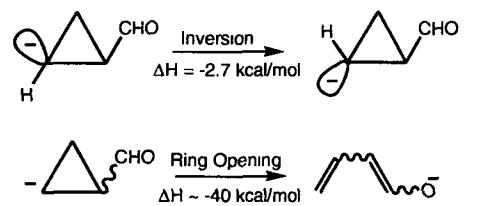

computationally. The theoretical (Table 1) results are in accord with experiment and indicate that there is a large preference for inward rotation (torquoselectivity) of the *trans* anion and essentially no bias for the *cis* species. These results can readily be explained in terms of orbital and electrostatic interactions.

Table 1. Calculated (MP2/6-31+G(d)) barriers for the ring-openings of *cis* and *trans*-2-formylcyclopropyl anions.[a]

cis		*trans*	
exo-inward	17.6	exo-inward	14.5
exo-outward	16.8	exo-outward	-
endo-inward	-	endo-inward	19.3
endo-outward	19.2	endo-outward	30.6
experiment	~19	experiment	~21

[a]All values in kcal/mol.

Reference

1. Baschky, M. C.; Peterson, K. C.; Kass, S. R. *J. Am. Chem. Soc.* **1994**, *116*, 7218.

Neutral and Ionic Heats of Formation; Their Measurement and Reliability for Ketenes.

J.L. Holmes, J.K.Terlouw *, C. Aubry and D. Suh *

Chemistry Department, University of Ottawa, Ottawa, Ontario, K1N 6N5, Canada
** Chemistry Department, McMaster University, Hamilton, Ontario, L8S 4M1 Canada*

The heat of formation, $\Delta_f H°$, of ketene, CH_2CO, is an important thermochemical quantity, leading to $\Delta_f H°$ estimates for many substituted ketenes, R_1R_2CCO. $\Delta_f H°[CH_2CO]$ was measured in 1971 from the heat of the reaction $CH_2CO(g) + NaOH(aq) \dashrightarrow CH_3COONa(aq)$ and the resulting value of -11.4 ± 0.4 kcal mol^{-1} has been widely quoted.

There are no data for methyl or dimethyl ketenes and only the former has been investigated by *ab initio* MO theory [1], $\Delta_f H°[CH_3CHCO](calc) = -15.6 \pm 2.4$ kcal mol^{-1}. This value implies a most unusually small (-4 kcal mol^{-1}) $\Delta(\Delta_f H°)$ for methyl substitution, which in olefins and allenes is -8 ± 1 kcal mol^{-1} and in carbonyl compounds -13 ± 1 kcal mol^{-1}.

To investigate this problem by experiment the AE values for the reactions (1)-(3) were measured using energy selected electrons.

$$CH_3COOC_6H_5 \dashrightarrow C_6H_5OH^+ + CH_2CO \quad (1)$$
$$CH_3CH_2COOC_6H_5 \dashrightarrow C_6H_5OH^+ + CH_3CHCO \quad (2)$$
$$(CH_3)_2CHCOOC_6H_5 \dashrightarrow C_6H_5OH^+ + (CH_3)_2CCO \quad (3)$$

The fragment ion was easily demonstrated to be ionized phenol by its metastable ion and collision induced dissociation behaviour. The three reactions showed very small kinetic energy releases from the metastable ionized phenyl esters. The AE values were 9.83, 9.58 and 9.50 ± 0.05 eV respectively and the $\Delta_f H°$ values for the esters were -66.8, -70.8 and -77.6 kcal mol^{-1} respectively. With $\Delta_f H°[C_6H_5OH^{+\cdot}]$ as 172.3 kcal mol^{-1}, the ketene enthalpies of formation were:

$$\Delta_f H°[CH_2CO] = -12.4 \pm 1.3 \text{ kcal mol}^{-1};$$
$$\Delta_f H°[CH_3CHCO] = -22.2 \pm 1.3 \text{ kcal mol}^{-1},$$
$$\Delta_f H°[(CH_3)_2CCO] = -30.8 \pm 1.3 \text{ kcal mol}^{-1}.$$

The average $\Delta(\Delta_f H°) = -9$ kcal mol^{-1}, the same as for allenes and olefins and so the results of the calculations may be in error.

The neutral heats of formation, combined with the IE values of Bock [2], lead to ionic heats of formation of 211, 185 and 165 kcal mol^{-1} respectively, in excellent agreement with independent values determined from the production of $CH_2CO^{+\cdot}$, $CH_3CHO^{+\cdot}$ and $(CH_3)_2CCO^+$ as fragment ions. The present results therefore appear to be consistent.

1. M.L.McKee and L.Radom, *Org. Mass Spectrom.*, **28**, 1238 (1993).
2. H.Bock, T.Hirabayashi and S.Mohmand, *Chem. Ber.*, **114**, 2595 (1981).

43rd ASMS Conference on Mass Spectrometry and Allied Topics

4-MEMBER CYCLIC HALONIUM IONS IN INTRAMOLECULAR 1,3-FLUORIDE TRANSFER

Viet Nguyen and Thomas Hellman Morton
Department of Chemistry, University of California, Riverside

When an ion and molecule encounter one another in the gas phase, they do not necessarily fall into a potential well, even if the well is deep and accessible with no energetic obstacle other than the centrifugal barrier. An instance is provided by the reaction of CF_3^+ with C_3H_6O carbonyl compounds. Eyler, Ausloos, and Lias reported the transposition of F^+ for O two decades ago,[1] and our experimental results show that simple metathesis operates regardless of whether the neutral reactant is acetone or propionaldehyde.

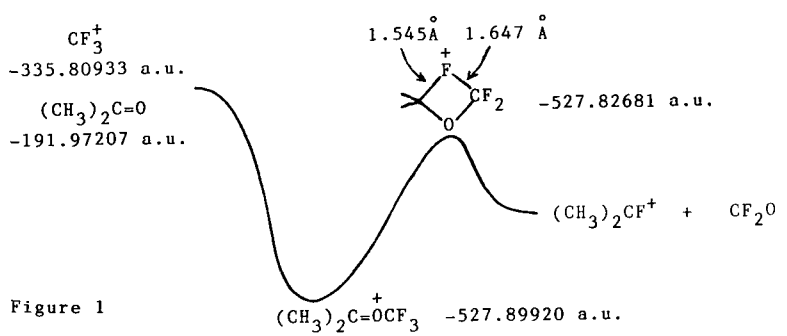

Figure 1

The peculiarity of this outcome can be grasped by first considering the high barrier corresponding to the 4-member cyclic transition state represented in Figure 1 for the reaction of CF_3^+ with acetone. As portrayed by the reaction coordinate diagram above, Hartree-Fock based SCF calculations (6-31G**//6-31G**) indicate that the simple Lewis acid-base adduct has an electronic energy more than 3 eV below that of the isolated reactants (Zero Point Energy correction <0.1 eV). We find no other potential energy minima corresponding to alternative approach geometries. The transition state for F-O metathesis lies nearly 2 eV above the Lewis acid-base adduct.

Does the reaction perforce pass through a Lewis acid-base adduct

Figure 2

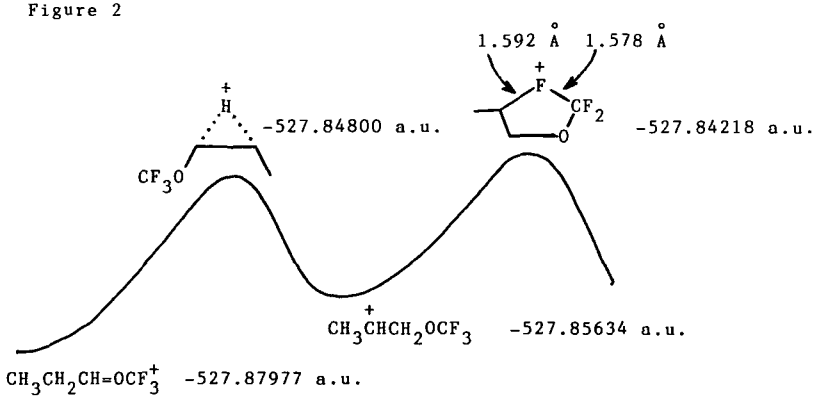

en route to the transition state? Consideration of the potential energy surface for CF_3^+ plus propionaldehyde offers a test of that hypothesis. Barriers for rearrangement of $CH_3CH_2CH{=}\overset{+}{O}CF_3$ are considerably lower than the 4-center transition state for F-O metathesis. As the reaction coordinate diagram in Figure 2 depicts, the barrier for a vicinal hydride shift is 1 eV lower than for F-O metathesis. Although the resulting isomeric ion, $CH_3\overset{+}{C}HCH_2OCF_3$, is 0.6 eV higher than the Lewis acid-base adduct, it has a low barrier for subsequent fluorine transposition via a 5-center transition state, 0.3 eV. Therefore the intermediacy of a Lewis acid-base adduct would predict that $(CH_3)_2CF^+$ ought to result from the reaction of propionaldehyde with CF_3^+.

EBFlow experiments show that $(CH_3)_2CF^+$ is produced when CF_3^+ reacts with propionaldehyde,[2] but ^{13}C-labeling reveals that this is not a consequence of the rearrangement portrayed in Figure 2. Instead (as confirmed by a comparison of the CAD fragmentation of the product ion from $CD_3CH_2CH{=}O$ and CF_3^+ with the CAD of authentic $CH_3\overset{+}{C}FCH_3$) simple metathesis occurs followed by (on the msec timescale of the EBFlow experiment) a rearrangement of free $CH_3CH_2CHF^+$ by competing methyl and fluorine shift.

Acknowledgment. Computation supported, in part, by UCR Academic Senate.

1. J.R. Eyler, P. Ausloos, S.G. Lias, J. Am. Chem. Soc. (1974) 96, 3673
2. T.A. Shaler and T.H. Morton, J. Am. Chem. Soc. (1991) 113, 6771.

Theoretical Studies of Proton Transfer Potential Energy Surfaces

Scott Gronert, Cliff Kimura, and Aladin Sadoun
Department of Chemistry and Biochemistry,
San Francisco State University, San Francisco, CA 94132

Introduction

Proton transfer plays a critical role in a variety of processes and provides a model for more complicated bond transformations. Gas phase studies can be the most illuminating because the potential energy surface is not perturbed by solvation or ion pairing effects. Although experimental gas phase studies have provided a wealth of thermochemical data, there are critical limitations. For example, the relatively narrow dynamic range of the present mass spectroscopy technology limits the range of activation barriers that can be characterized accurately. As a result, computational studies provide an important complement to experimental studies of gas phase proton transfers. To be useful, the calculations must provide results that are reliable and accurate. In the present contribution, we present a new computational protocol that yields very accurate ΔHacid values for a series of simple acids. In particular, the hydrides of the first and second row non-metals are investigated (CH_4 => FH and SiH_4 => ClH) as well as HCCH and NCH. In addition, a set of high-level calculations are presented for the reactions of these species with their conjugate bases. Transition states as well as ion dipole complexes have been located and the activation barriers have been correlated to the reaction exothermicities *via* a Marcus Theory approach.[1,2]

Results

Radom and Smith[3] have shown that the Pople's G2 approach[4] can reproduce experimental gas phase acidities with good accuracy. For the series in this study, an RMS error of 0.9 kcal/mol is observed; however there are large discrepancies in some cases. For example the acidity of CH_4 is underestimated by 1.8 kcal/mol. In an earlier study, we showed that the errors can be reduced (RMS error = 0.7 kcal/mol) by augmenting the basis sets of the conjugate bases with a set of ghost functions centered at the position of the missing proton.[5] Although successful, this approach suffers from arbitrariness (where to position the ghost functions) and it is difficult to generalize to reaction systems. A preferable approach would be to supplement the basis sets of the heavy atoms with diffuse, atom-centered functions. The exponents of a second set of diffuse sp functions for the first and second row non-metals have been defined in this study by minimizing the calculated proton affinities of the conjugate bases at the MP4/6-311++(+)G(d,p) level (the third '+' refers to the second set of diffuse functions on heavy atoms). The exponents as well as the calculated acidities are given in Table 1. As before, we have adopted a modified version of the G2 protocol. The major differences are the addition of the second set of diffuse sp orbitals on heavy atoms and a single set of diffuse s orbitals on hydrogens. Optimizations are completed at the MP2/6-31+G(d,p) level and energies are corrected for zero-point vibrations (HF scaled by 0.91). Finally, the values are converted to 298 K by the usual methods. Overall, the process gives energies that approximate the QCISD(T)/6-311++(+)G(3df,2p) level.

G2+++ = MP4/6-311++(+)G(2df,p) + ZPE

+ QCISD(T)/6-311++(+)G(d,p) - MP4/6-311++(+)G(d,p)

+ MP2/6-311++(+)G(3df,2p) - MP2/6-311++(+)G(d,p)

Table 1 Exponents for Extra Diffuse Functions and Calculated Gas Phase Acidities.

System	Exponent	ΔHacid(298 K) Exp.	G2+++	G2	Becke3P86
CH_4	0.0142	416.7 ± 0.7	416.6	418.5	417.6
NH_3	0.0192	404.0 ± 0.4	403.4	403.9	404.9
OH_2	0.0337	390.7 ± 0.1	390.4	390.0	391.4
FH	0.0570	371.5 ± 0.2	371.0	370.9	370.7
SiH_4	0.0163	373.0 ± 0.9	373.0	374.0	372.8
PH_3	0.0170	368.2 ± 0.5	367.2	368.1	367.7
SH_2	0.0332	351.4 ± 0.7	351.5	352.3	352.2
ClH	0.0355	333.4 ± 0.1	333.9	334.6	333.9
HCCH		378.0 ± 0.6	377.2	377.9	378.8
NCH		351.4 ± 0.5	351.4	350.8	352.5

Energies in kcal/mol. Experimental values from Berkowitz, Ellison, and Gutman, *J. Phys. Chem.* **1994**, *98*, 2744. G2 from Smith and Radom, *J. Phys. Chem.* **1991**, *95*, 10549.

The values in Table 1 indicate that the G2+++ method can give excellent results with a smaller RMS error than the G2 method (0.5 kcal/mol vs. 0.9 kcal/mol). Moreover, none of the errors is greater than 1 kcal/mol. DFT calculations have also been investigated.[6] The best values come from the Becke3P86/6-311++(+)G(3df,2p) level and they are included in Table 1. The RMS error is 0.9 kcal/mol.

Our earlier studies of identity proton transfers[5] have been extended to a series of exothermic proton transfers: OH^- + FH, SH^- + ClH, PH_2^- + SH_2, CH_3^- + H_2, NH_2^- + OH_2, CH_3^- + NH_3, HCC^- + FH, SiH_3^- + PH_3, HCC^- + SiH_4, NH_2^- + H_2, SiH_3^- + FH, and NC^- + SH_2. In most cases, there is no barrier to proton transfer and a stable, hydrogen-bonded complex is formed. For the systems where both reaction partners have significant intrinsic barriers to proton transfer, a double-well potential with a barrier is observed (CH_3^- + H_2, CH_3^- + NH_3, NH_2^- + H_2, HCC^- + SiH_4, SiH_3^- + PH_3, and NC^- + SH_2). The barriers do not correlate with the exothermicity of the reaction or the difference in energy of the reactant and product ion-dipole complexes. Marcus Theory leads to a reasonable correlation for this small data set; however, analysis of the contributions from each of the terms in the Marcus equation indicates that the correlation is somewhat fortuitous and that the Marcus approach can provide no more than a crude description of the potential energy surface.[7]

References

(1) Cao, H. Z.; Allavenna, M.; Tapia, O.; Evleth, E. M. *J. Phys. Chem.* **1985**, *89*, 158
(2) Marcus, R. A. *J. Chem. Phys.* **1956**, *24*, 966.
(3) Smith, B. J.; Radom, L. *J. Phys. Chem.* **1991**, *95*, 10549.
(4) Curtiss, L. A.; Raghavachari, K.; Trucks, G. W.; Pople, J. A. *J. Chem. Phys.* **1991**, *94*.
(5) Gronert, S. *J. Am. Chem. Soc.* **1993**, 10258.
(6) As implemented in the DFT version of Gaussian92.: GAUSSIAN92 : Frisch, M. J.; Trucks, G. W.; Head-Gordon, M.; Gill, P. M. W.; Wong, M. H.; Foresman, J., B.; Johnson, B. D.; Schlegel, H. B.; Robb, M. A.; Replogle, E. S.; Gomperts, R.; Anfres, J. L.; Raghavachari, K.; Binkley, J. S.; Gonzalez, C.; Martin, R. L.; Fox, D. J.; DeFrees, D. J.; Baker, J. J. P.; Pople, J. A., Gaussian, Inc., Pittsburgh, PA, 1992.
(7) Murdoch, J. R. *J. Am. Chem. Soc.* **1983**, *105*, 2159.

METAL-LIGAND THERMOCHEMISTRY by GUIDED-ION BEAM MASS SPECTROMETRY

Y.-M. Chen, N. F. Dalleska, S. Goebels, C. Haynes, F. A. Khan, F. Meyer, M. B. More, M. T. Rodgers, R. H. Schultz, M. Sievers, B. L. Tjelta and P. B. Armentrout
Chemistry Department, University of Utah, Salt Lake City, UT 84112

In the last several years, a versatile approach has been developed to determine accurate sequential bond dissociation energies (BDEs) for a multitude of metal-ligand systems. This is accomplished by generating individual ML_x^+ (or ML_x^-) complexes in the gas phase and monitoring reaction (1), collision-induced dissociation (CID), as a function of the kinetic energy of the collision in a mass spectrometer.

$$ML_x^+ + Rg \longrightarrow ML_{x-1}^+ + L + Rg \qquad (1)$$

Such studies can include virtually any metal and ligands ranging from familiar species such as CO,[1,2,3,4,5,6,7] H_2O,[8,9] NO,[4] alkenes,[10,11] and benzene[12,13] to the unusual but potentially important such as N_2,[4] CH_4,[8,14] and other alkanes.[15,16] Most recently, we have begun to examine the interactions of alkali ions with crown ethers,[17] nucleic acid bases and amino acids.[18]

The studies described here have been performed on a guided ion beam tandem mass spectrometer described in detail elsewhere.[19] Cationic transition metal complexes are generated in a high pressure flow tube source,[20] where the ions undergo ~10^5 collisions with the room temperature bath gasses, which provide three-body stabilization and thermalization of the metal-ligand complexes. The ions are then mass analyzed and focused into a collision cell. Here the ions react with a neutral reagent (at sufficiently low pressures that single ion-neutral encounters are the rule) at a kinetic energy, E_T, that can be varied over a wide range (3-4 orders of magnitude). Product ions are analyzed in a second mass spectrometer and detected by single particle counting. Ion intensities are converted to absolute reaction cross sections, $\sigma(E_T)$, a direct measure of the probability of reaction at E_T.

There are several important factors that must be considered in order to extract accurate thermochemistry from threshold CID data. These include complete thermalization of the ions, analysis that explicitly considers the kinetic and internal energy distributions of the reactants, the choice of collision gas (Xe is used almost exclusively in our studies), and the effects of multiple ion-neutral collisions (before analysis, our data are extrapolated to zero neutral pressure, rigorously single collision conditions).[1] In addition, as the metal-ligand complexes become larger, the probability increases that they do not dissociate before detection (a time window of ~10^{-4} s). We account for this effect by using RRKM theory to calculate a dissociation probability as a function of the ion internal energy.[2]

Examples of our CID data are shown in Figure 1 for the case of $Na^+(H_2O)_4$ and Figure 2 for Na^+-Adenine. The first example shows the influence of the internal and kinetic energy distributions. It is obvious that the 0 K threshold (dotted line) of ~0.5 eV differs appreciably from the apparent threshold exhibited by the data (open circles). The threshold determined in this analysis agrees well with an energy derived from equilibrium methods,[21] indicated by the arrow. Figure 2 shows that even complicated ligands yield good quality threshold CID spectra. Interpretation of such systems is in progress.[18]

This research is supported by the National Science Foundation.

References

1) Schultz, R. H.; Crellin, K. C.; Armentrout, P. B. *J. Am. Chem. Soc.* **1991**, *113*, 8590.
2) Khan, F. A.; Clemmer, D. E.; Schultz, R. H.; Armentrout, P. B. *J. Phys. Chem.* **1993**, *97*, 7978.
3) Sunderlin, L. S.; Wang, D.; Squires, R. R. *J. Am. Chem. Soc.* **1992**, *114*, 2788; **1993**, *115*, 12060.
4) Khan, F. A.; Steele, D. A.; Armentrout, P. B. *J. Phys. Chem.* **1995**, *99*, 7819.
5) Meyer, F.; Chen, Y.-M.; Armentrout, P. B. *J. Am. Chem. Soc.* **1995**, *117*, 4071.
6) Sievers, M.; Armentrout, P. B. *J. Phys. Chem.* in press.
7) Goebel, S.; Haynes, C. L.; Khan, F. A.; Armentrout, P. B. *J. Am. Chem. Soc.* accepted for publication.
8) Schultz, R. H.; Armentrout, P. B. *J. Phys. Chem.* **1993**, *97*, 596.
9) Dalleska, N. F.; Honma, K.; Sunderlin, L. S.; Armentrout, P. B. *J. Am. Chem. Soc.* **1994**, *116*, 3519.
10) Schultz, R. H.; Armentrout, P. B. *Organometallics* **1992**, *11*, 828.
11) Haynes, C. L.; Armentrout, P. B. *Organometallics* **1994**, *13*, 3480.
12) Chen, Y.-M.; Armentrout, P. B. *Chem. Phys. Lett.* **1993**, *210*, 123.
13) Meyer, F.; Khan, F. A.; Armentrout, P. B. *J. Am. Chem. Soc.* submitted for publication.
14) Haynes, C. L.; Armentrout, P. B.; Perry, J. K.; Goddard, W. A., III *J. Phys. Chem.* **1995**, *99*, 6340.
15) Schultz, R. H.; Armentrout, P. B. *J. Am. Chem. Soc.* **1991**, *113*, 729.
16) Schultz, R. H.; Armentrout, P. B. *J. Phys. Chem.* **1992**, *96*, 1662.
17) More, M. B.; Glendening, E. D.; Ray, D.; Feller, D.; Armentrout, P. B. work in progress.
18) Rodgers, M. T.; Armentrout, P. B. work in progress.
19) Ervin, K. M.; Armentrout, P. B. *J. Chem. Phys.* **1985**, *83*, 166.
20) Schultz, R. H.; Armentrout, P. B. *Int. J. Mass Spectrom. Ion Processes* **1991**, *107*, 29.
21) Dzidic, I.; Kebarle, P. *J. Phys. Chem.* **1970**, *74*, 1466.

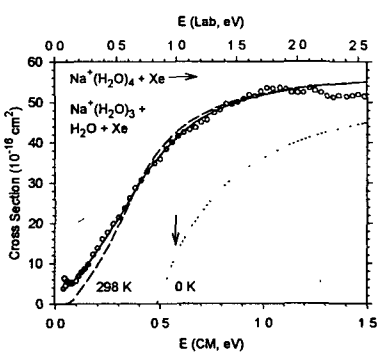

Figure 1.

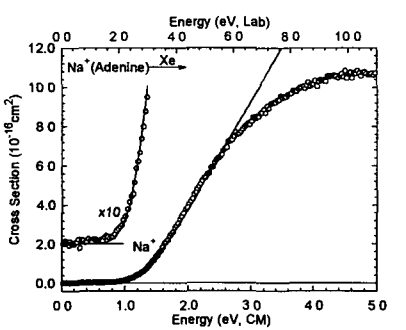

Figure 2.

EXPERIMENTAL AND AB INITIO STUDIES OF SECOND ROW RADICALS

František Tureček, Scott A. Shaffer, Ming Gu and Cornelis E. C. A. Hop
Department of Chemistry, Box 351700, University of Washington, Seattle, WA 98195-1700
Department of Chemistry, University of Wisconsin, Madison

Radicals centered at second-row atoms appear as possible intermediates of several chemical reactions. The $(CH_3)_2S^{\bullet}OH$ radical has been presumed by atmospheric chemists to be formed transiently in the tropospheric oxidation of dimethylsulfide, but it has never been detected *(1)*. Hydroxyl radical attack on phosphines is presumed to involve hydroxylated phosphoranyl radicals that have been studied by theory but eluded detection. We combine neutralization-reionization mass spectrometry with ab initio calculations to investigate the formation of hypervalent sulfuranyl and phosphoranyl radicals by fast electron transfer, and examine their stabilities and unimolecular dissociations.

$(CH_3)_2S^{\bullet}OH$ represents a (9-S-3) hypervalent radical with formally nine electrons at the central sulfur atom. We prepared it transiently by collisional neutralization of its stable cation, $(CH_3)_2S^{+}OH$, which in turn was made by gas-phase protonation of dimethyl sulfoxide with $t\text{-}C_4H_9^{+}$ *(2)*. The sulfuranyl radical was found to decompose completely on the 4.5 μs time scale of the experiment to yield CH_3SOH, $(CH_3)_2S{\rightarrow}O$, and $(CH_3)_2S$, which underwent consecutive dissociations. Ab initio investigations of $(CH_3)_2S^{\bullet}OH$, carried out at the MP2(FULL)/6-31+G(d) level of theory, found no potential energy minimum for the sulfuranyl radical *(3)*. At typical S-O and C-S bond lengths the radical shows large negative gradient for dissociation by S-O bond cleavage. A shallow potential energy minimum of 13-17 kJ mol^{-1} was found at various levels of ab initio theory for a dipole-dipole complex of $(CH_3)_2S$ with $HO^{\bullet}$, in which the hydroxyl hydrogen is oriented toward the sulfur atom. No bonding interaction between S and O was found at various S-O distances. Closer approach of the hydroxyl oxygen atom to the sulfur atom resulted in a substantial increase of potential energy, indicating a large activation barrier (Figure 1). By contrast, we found an activation barrier of only 4 kJ mol^{-1} for the hydrogen abstraction to yield $CH_3SCH_2^{\bullet}$ and water, which is exothermic by 105 kJ mol^{-1} at 298 K *(2)*. Hydrogen abstraction is predicted to be the favored channel in the dimethyl sulfide-hydroxyl radical reaction.

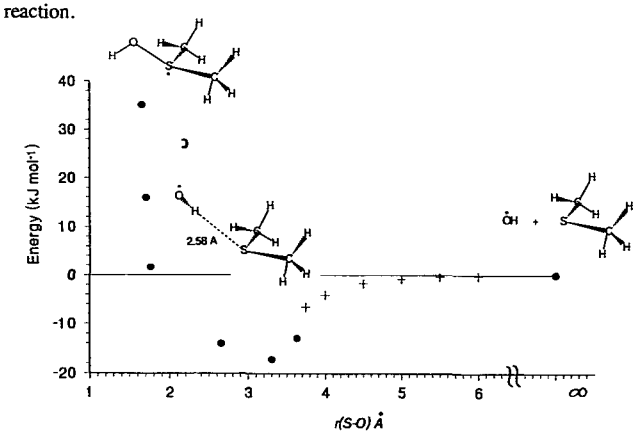

The tetrahydroxyphosphoranyl radical, $P^{\bullet}(OH)_4$, represents a hypervalent (9-P-4) species with formally nine electrons at the central phosphorus atom. The radical was prepared transiently by collisional neutralization of the $P(OH)_4^{+}$ ion, which is a common dissociation product of electron ionization of trialkyl phosphates. The $P^{\bullet}(OH)_4$ radical dissociates completely on the μs time scale. The observed dissociations involve loss of hydrogen atom, and formations of H_2PO_3, HPO_3, HPO_2, PO_2, PO, P, and OH. Isotope effects were found favoring the formation of $P(OD)_3$ and D_2O from $P^{\bullet}(OD)_4$. Ab initio calculations at the MP4(SDQ)/6-31+G(d)//MP2(FULL)/6-31+G(d) level of theory found $P^{\bullet}(OH)_4$ to be metastable with respect to exothermic dissociations by loss of $H^{\bullet}$ ($\Delta H_{f,298}$ = -30 kJ mol^{-1}) and elimination of water ($\Delta H_{f,298}$ = -7 kJ mol^{-1}). The loss of $H^{\bullet}$ overcomes a barrier of 90 kJ mol^{-1}. The optimized geometries of $P(OH)_4^{+}$ and $P^{\bullet}(OH)_4$ greatly differ (Figure 2).

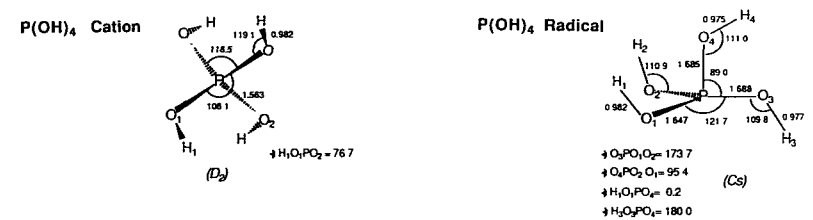

Consequently, vertical electron transfer forms the hypervalent radical with non-relaxed geometry of 129 kJ mol^{-1} internal energy that drives fast dissociation by loss of $H^{\bullet}$. The H_3PO_4 molecules are formed with >160 kJ mol^{-1} internal energy due to the dissociation exothermicity. This and further energy deposition upon reionization drives the loss of $OH^{\bullet}$ from $H_3PO_4^{+\bullet}$, which is only 223 kJ mol^{-1} endothermic. The loss from $P^{\bullet}(OH)_4$ of $OH^{\bullet}$ is 108 kJ mol^{-1} endothermic and requires an activation energy estimated at >160 kJ mol^{-1}. The calculated electron distribution in $H_3PO_4^{+\bullet}$ indicates separation of the radical and charge sites *(5)*. The ion can be viewed as an oxy radical with an adjacent positive charge on the phosphorus atom. This explains the large hydrogen atom affinity of oxygen atoms in phosphate cation-radicals and the ensuing isomerizations by exothermic intramolecular hydrogen transfer.

Relative energies were also calculated for the $P(OH)_3$ and $HPO(OH_2)$ isomers, which were prepared by neutralization of their cations and found to be distinct species. Neutral phosphorous acid is 45 kJ mol^{-1} more stable than trihydroxyphosphine. Collisional activation of the $P(OH)_3$ brings about isomerization to $HPO(OH)_2$, which is calculated to have 225 kJ mol^{-1} activation energy. An opposite order of stabilities is found for the cation-radical of which $P(OH)_3^{+\bullet}$ is 136 kJ mol^{-1} more stable than $HPO(OH)_2^{+\bullet}$. The latter ion dissociates readily by loss of $H^{\bullet}$ which requires only 119 kJ mol^{-1}.

References

(1) A. A. Turnipseed and A. R.Ravishankara, In *Dimethylsulphide: Oceans, Atmosphere and Climate*, G. Restelli and G. Angeletti, Eds, Kluwer, Dordrecht, 1993, pp 185-196.
(2) M. Gu and F. Turecek, *J. Am. Chem. Soc.* **1992**, *114*, 7146.
(3) F. Turecek, *J. Phys. Chem.* **1994**, *98*, 3701.
(4) S. M. Gustafson and C. J. Cramer, *J. Phys. Chem.* **1995**, *99*, 2267.
(5) F. Turecek, M. Gu and C. E. C. A. Hop, *J. Phys. Chem.* **1995**, *99*, 2278.

CHARACTERISATION OF SYNTHETIC POLYMER FORMULATIONS USING MALDI

Jim H Scrivens*, Hilary Yates, John Segal, Tony Jackson, Mike Taylor
ICI, Wilton Research Centre, Po Box No 90, Wilton, Cleveland, England, TS90 8JE

Glen Critchley, Ann Maisey
VG Organics, Floats Road, Wythenshawe, Manchester, England

INTRODUCTION

The use of mass spectrometry in the characterisation of synthetic polymer formulations has, until recently, been restricted to the characterisation of monomers, oligomers, additives and performance enhancers. Secondary ion mass spectrometry (SIMS) and field desorption (FD) have been used to characterise synthetic polymers in excess of 10,000 Da but the study of intact polymer systems of commercial interest has been extremely limited. The technique of matrix assisted laser desorption/ ionisation mass spectrometry (MALDI), although initially used almost exclusively in biological applications offers significant potential for the study of synthetic polymer systems.

EXPERIMENTAL

A VG Organics TofSpec MALDI-TOF spectrometry was used in the work. Both linear and reflectron modes were employed with the linear mode using a hybrid microchannel plate/ electron multiplier detector and the reflectron mode a dual channel plate detector. A nitrogen laser (337nm) was employed. Polystyrene spectra were obtained in dithranol with CF_3COO^- Ag^+ added. Polymethylmethacrylate (PMMA) samples were run in indole acrylic acid (IAA) having been dissolved in acetone.

RESULTS

A number of systems have been studied including PMMA with varying end groups, polystyrenes, commercial phenol formaldehyde resins, complex esters used in lubricant formulations and polybutadienes. Considerable care was taken with calibration since a conventional two point external calibration using a compound of different chemical class and with varying experimental conditions such as laser power etc. leads to a mass measurement accuracy of ~ 0.2%. This can be adequate for profile determination or general scouting experiments but is not adequate for the determination of end groups. For this work a multi-point external calibration using either a combined sample of polystyrene 1700, 5050 and 10200, or PMMA 2010, 5270 and 9200 was used. Where possible experimental conditions were maintained. This resulted in mass accuracies of ~ 0.04% for linear operation and ~ 0 025% for reflectron operation. Further accuracy could be obtained using internal standards but this was not always possible or desirable.

43rd ASMS Conference on Mass Spectrometry and Allied Topics

END GROUPS IN PMMA SAMPLES

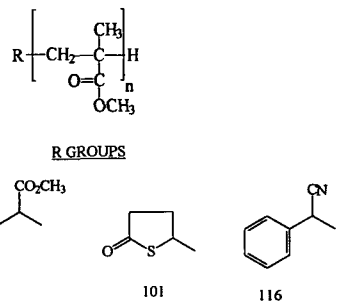

Figure 1

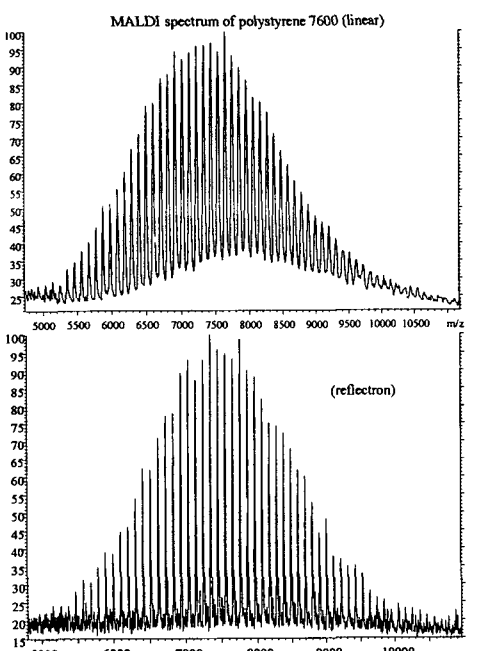

Figure 2

Figure 2 shows the MALDI spectra of a polystyrene 7600 sample in both linear and reflectron modes. The reflectron data gave improved mass accuracy data over the linear. Care needs to be taken with cationised species where the individual species are not always resolved.
The MALDI data have been compared with that obtained by field desorption and give good agreement for polystyrene samples although the obtainable resolution is greater with FD. For many samples however thermal fragmentation is a problem with FD and MALDI gives superior results. MALDI gives promising results for synthetic polymers particularly for those with low polydispersity in the 10-50 KDa region which is of commercial significance Further work is needed to extend the applicability of the approach to other polymer systems and to samples of widely varying dispersity.

Matrix-Assisted Laser Desorption/Ionization Investigations of Industrial Polymers

Scott D. Hanton and David M. Parees,
Air Products & Chemicals, Inc., Allentown, PA 18195
Robert Goldschmidt, Richard C. King and Kevin G. Owens,
Department of Chemistry, Drexel University, Philadelphia, PA 19104

Matrix-assisted laser desorption/ionization (MALD/I) mass spectrometry is being applied to measure the chemical structure of industrial polymers.[1] The chemical structure information is used to better understand the structure/property relationships of these materials. MALD/I experiments produce data allowing us to measure the molecular weight distributions, determine the end groups and clearly observe the masses of the oligomer repeat units of individual polymers. MALD/I can analyze some materials that are difficult for more traditional analyses like gel permeation chromatography (GPC), either because of solvent or column incompatibilities. The molecular weight distribution information is used in the verification of synthetic pathways, product comparisons, vendor product specification and quality control of materials.

The successful application of MALD/I analysis to industrial polymers is greatly dependent on the chemical structure of the polymers. Different chemical structures may require significantly different sample preparation. The sample preparation step is perhaps the most important component of a MALD/I experiment. We developed a sample preparation strategy that enables us to analyze a wide range of polymer chemistries. The strategy consists of four primary steps:

* Identify the chemistry of the material,
* Choose an appropriate solvent based on the solubility parameters of the sample,
* Choose an appropriate matrix based on the polarity of the sample,
* Ensure efficient ionization with the addition of an ionization reagent.

To aid in choosing the appropriate matrix, we break the role of the matrix into five components: separation of the individual oligomers, isolation of the oligomers, absorption of the laser radiation, desorption of the oligomers, and ionization of the oligomers. The appropriate matrix does not need to be a single molecule, as long as the matrix role is accomplished. By using combinations of different molecules we can tune the matrix to the sample chemistry. This can provide the flexibility necessary to analyze new sample chemistry.

The new sample preparation strategy has helped us analyze a wide range of polymers, including: isocyanate based prepolymers, formamides, polyesters, acrylates, polyols and silicones. These experiments were completed on a non-commercial, 1-M linear time-of-flight mass spectrometer with 18 kV extraction potential and a nitrogen desorption laser (337 nm). The data were analyzed with a software package developed in-house.

One example, of this work is the analysis of poly(ethenylformamide (PEF). Figure 1 shows a MALD/I mass spectrum of a low molecular weight PEF polymer. In the development of PEF products we need to understand the impact of different synthesis conditions on polymer molecular weight. In this case we measured PEF produced at three different reactor temperatures. Figure 2 shows the average molecular weights for three temperatures. Over the range measured, molecular weight of PEF is linearly dependent on reactor temperature.

Figure 1

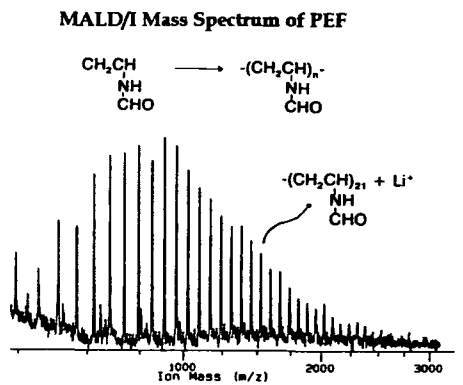

Figure 2

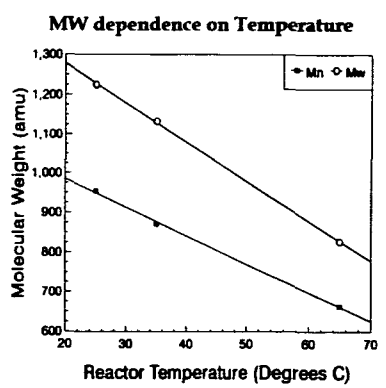

[1] P. O. Danis and D. E. Karr, Org. Mass Spectrom. 1993, 28, 923-925.

High Mass Resolution Imaging TOF-SIMS Analysis of Polymer Surfaces

Stefan Reichlmaier, Physical Electronics Inc.
6509 Flying Cloud Drive, Eden Prairie, MN 55344, USA

Introduction

Industrial polymer surfaces contain a variety of substances including additives, process aids, protective coatings and oligomeric materials. Adhesion, wetability, printing properties and physical properties like friction are affected by these organic and inorganic compounds on the surface of the polymer. Analyzing the spatial distribution of these materials on a solid surface of a polymer is frequently crucial in industrial problem solving Secondary Ion Mass Spectrometry (SIMS) utilizes a finely focused scanned primary ion beam and a Time-of Flight (TOF) mass analyzer offers great opportunities for these challenging analyses.

Imaging of organic compounds on polymer surfaces down to micron sized features has become possible with the recent advances in Time-of-Flight SIMS (TOF-SIMS) [1-4]. Most recently the application of retrospective data analysis for small oligomeric particle analysis has proven to be an important next step in the application of organic imaging with TOF-SIMS [5] These imaging applications, however, suffered from chemical ambiguity due to the low mass resolution mode the instruments had to be operated in when performing TOF-SIMS imaging analysis. With a carefully optimized bunching scheme in the primary ion optical column it is now possible to obtain good spatial resolution and good mass resolution simultaneously. This allows the resolution of mass interference in the fragmentation region (m/z=0-350) most commonly used for organic imaging applications

Experimental

Two different kind of samples were investigated in this study. A poly (ethylene terephthalate) (PET) film coated with a solvent cast glyceryl monostearate (GMS) layer and a polycarbonate bulk material with poly (vinyl alcohol) dots on it. In both cases the samples were cut to size for mounting on a one inch sample mount and then directly analyzed in the mass spectrometer. A PHI 7200 model TOF-SIMS instrument equipped with a Ga liquid metal ion (LMI) gun was used for the analysis This instrument utilizes a double stage reflectron type time-of-flight mass analyzer. A low energy electron flood gun was used for charge compensation during the measurements Images were acquired using the LMI gun in the conventional (low mass resolution) mode and also in the bunched mode of operation (high mass resolution) Utilizing the retrospective analysis of the obtained data (a complete mass spectrum is stored at any image pixel), reconstruction of images of specific mass peaks and recreation of local area mass spectra was carried out after data acquisition was completed.

Results and Discussion

A mass interference at m/z=341 between ions originating from the GMS coating and ions from the PET substrate was found in a previous study [3], but could only be mass resolved using the

instrument in the high mass resolution spectroscopy mode without sufficient spatial resolution. By analyzing this sample utilizing the new high mass resolution imaging capability it was confirmed that the observed GMS islands on the sample surface give rise to a mass peak at m/z=341 31 whereas the exposed PET surface between the islands only showed a peak at m/z=341.07
The PVA dots on polycarbonate were first imaged using a low mass resolution "fingerprint" (peak pattern) of the spectra of the two polymers to locate a PVA dot (figure 1).

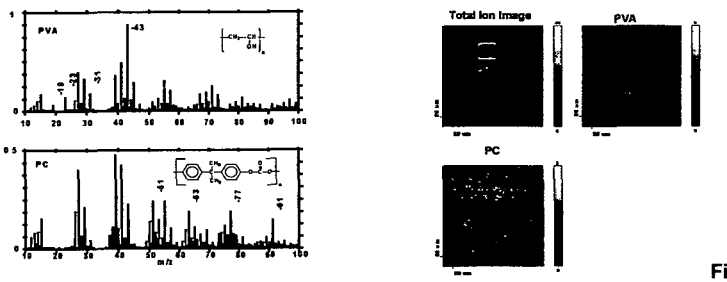

Figure 1.

Using a data set acquired in the high mass resolution imaging mode and reconstructing mass spectra from on and off the PVA dot show an oxygen containing fragment ion clearly resolved from the hydrocarbon peak (figure 2a) The images created using only these two peaks respectively, clearly show the different spatial distribution (figure 2b).

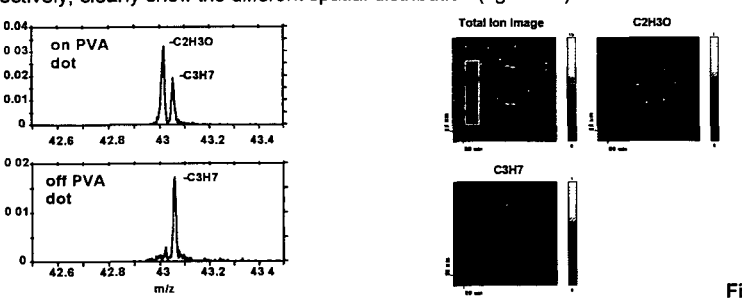

Figure 2.

This new capability resolves previously existing ambiguities in assigning chemical species to the observed mass peaks. The spatially resolved chemical spectroscopy strongly enhances the problem solving capability of the technique for polymer surface chemistry.

References

1 D. Briggs and M J. Hearn, Surf and Interface Anal. Vol. 15, 62-65 (1990)
2. J. Zehnpfenning, H.G. Kramer, T. Heller, U Jurgens, E. Niehuis, J Schwieters and A Benninghoven, Proceedings SIMS VIII, John Wiley and Sons (1991), p 501-504
3. S. Reichlmaier, J.S. Hammond, M.J. Hearn and D. Briggs, SIA Vol. 21 739-746 (1994)
4 D Briggs and M J Hearn, SIA Vol. 13, 181-185 (1988)
5. S. Reichlmaier, S.R. Bryan and D. Briggs, to be published JVST A May/June 1995

REVERSE ENGINEERING OF INDUSTRIAL POLYMER FORMULATIONS BY MALDI-MS

Xiaodong Tang[1]*, Akos Vertes[1], Peter Dreifuss[2], Clifford Hull[2], Walter Dutton[2]
[1] Department of Chemistry, The George Washington University, Washington, D. C. 20052
[2] Washington Research Center, W. R. Grace & Co., 7379 Route 32, Columbia, MD 21044

Matrix-Assisted Laser Desorption/Ionization Mass Spectrometry (MALDI-MS) has recently been viewed as a useful technique for synthetic polymer analysis [1-4]. However, industrial applications are still somewhat limited because operational parameters require further optimization. For this report, we sought to maximize the information obtained by MALDI-MS analysis on polymer standards and applied this to the analysis of actual industrial samples. Variables under investigation included choice of matrix, sample pretreatment and accelerating voltage. We also looked at potential interferences from polymer mixtures. Experiments were carried out on a linear time-of-flight mass spectrometer equipped with a compact nitrogen laser.

Choice of Matrix: Over 15 potential matrices were tested; 9-anthracenecarboxylic acid (9-ACA) was found to be particularly sensitive both to polar and to some non-polar polymers. Good quality spectra were readily obtained from the following polymer standards: PEG 610, 3300, 5000, 8000, 10225, 10730, 15000; PPG 450, 1000, 1200, 2000, 5000; PMMA 2000, 6000, 12000; Jeffamine 2000; polybutadiene 1000; and polydimethyl siloxane (PDMS) 1500. Additional experiments were carried out using matrix mixtures of varying composition. Excellent results could be obtained from a composite matrix ("super" 9-ACA) of 9-ACA and 5-methoxysalicylic acid (molar ratio 5:2) (see Figure 1a).

Sample Pretreatment: The presence of both sodium and potassium cationized ions results in an apparent loss of resolution in a MALDI analysis. To overcome this problem, two sample pretreatments were found to be useful: (a) both analyte and matrix solutions were purified by ion-exchange, followed by addition of a controlled amount of sodium or potassium ions to the matrix. This resulted in homogeneously cationized polymer ions; (b) To remove some of the cations, 18-crown-6 was added to the matrix/analyte solution on the probe. This method often resulted in better mass resolution. The concentration of the crown ether depended on the amount of alkali impurity in the matrix/analyte mixture.

Accelerating Voltage: In MALDI-MS analysis, the detector efficiency is known to fall off with decreasing velocity of the ions, especially for high mass particles. Figure 1 shows a comparison of the mass spectra of PPG 5000 in "super" 9-ACA matrix at 30 kV and 15 kV accelerating voltages. We observed that decreasing the accelerating voltage decreased the ion intensity by a factor of 5, decreased the mass resolution from 275 to 125 (at m/z 5078) and truncated the high mass end of the spectrum.

Polymer Mixtures: The MALDI spectrum of a PPG 2000/PEG 3300 mixture in 9-ACA matrix is shown in Figure 2. Both polymers are readily recognized by repeating mass differences of m/z 58 and m/z 44, derived from the repeating PPG [$-OCH_2CH(CH_3)-$] and PEG [$-OCH_2CH_2-$] monomers, respectively. No fragmentation or interaction between these two samples were observed, indicating the potential of MALDI for the analysis of synthetic polymer mixtures.

Applications on Industrial Samples: Based on the above studies, we investigated the use of MALDI-MS for problem solving, as well as for characterization and quality control of industrial polymers. Information could be obtained by MALDI-MS on samples that were not well characterized, but for which corroborating analytical data was available, including GPC, FTIR, NMR, and electron ionization, APCI and K^+IDS MS.

Figure 3 shows an example of MALDI-MS analysis of an unknown polyurethane component in a commercial product isolated by HPLC. From GPC measurements, only one component with average MW 6,000 could be readily discerned. In the MALDI spectrum, we observed two components with

averages centered at m/z 5,300 and m/z 8,000. The peaks in the 4,000 to 6,000 mass range were sufficiently resolved to indicate PPG bonded to a single toluene diisocyanate. Despite various attempts, the higher mass component centered at m/z 8,000 is not sufficiently resolved to be able to determine its composition. The solution to these challenges is still required.

[1] Karas, M. and Hillenkamp, F. (1988) *Anal. Chem.* **60**, 2299-2301.
[2] Tanaka, K.; Waki, H.; Ido, Y.; Akita, S.; Yoshida, Y. and Yoshida, T. (1988) *Rapid Commun. Mass Spectrom.* **2**, 151-153.
[3] Vertes, A.; Gijbels, R., In: Laser Ionization Mass Analysis, Vertes, A.; Gijbels, R.; Adams, F. (eds), John Wiley & Sons, New York, 1993. pp. 127-175.
[4] Danis, P.; Karr, D.; Mayer, F.; Holle, A.; and Watson, C. (1992) *Org. Mass Spectrom.* **27**, 843.

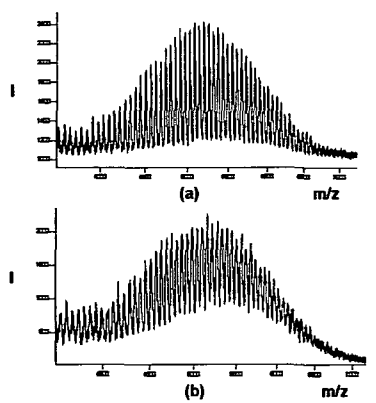

Figure 1. PPG 5000 in "super" 9-ACA matrix at (a) 30 kV and (b) 15 kV accelerating voltages.

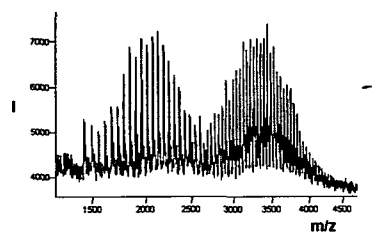

Figure 2. MALDI mass spectrum of the mixture of PPG 2000 and PEG 3300 in 9-ACA matrix.

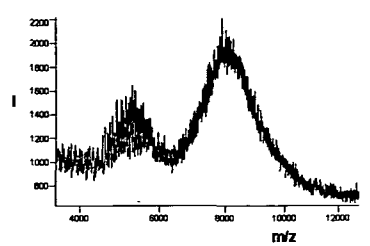

Figure 3. Mass spectrum of polyurethane using 2-(4'-hydroxyazobenzene) benzoic acid matrix.

MALDI in Polymer Chemistry: Rapid Analysis of Chemical Modifications on Polymers

Randy M. Whittal and Liang Li
Department of Chemistry, University of Alberta, Edmonton, Alberta, Canada
T6G 2G2

Chemical modification of polymers is a common practice in polymer chemistry. Assessing the success of a chosen chemical modification usually requires several analytical methods for unambiguous assignment. Among these analytical tools, matrix-assisted laser desorption ionization (MALDI) mass spectrometry can provide strong evidence of structural modification. The objective of this work is to assess the feasibility of analyzing end-group modified polymers with MALDI in our linear time-lag focusing time-of-flight (TOF) instrument [1].

A linear TOF mass spectrometer, combined with time-lag focusing, provides mass resolution in the range of 3000-6000 fwhm for peptides up to 3000 Da [1]. In this technique, MALDI ions are generated in a field-free source and then pulsed out of the source after a 280 ns delay. For polymer analysis, a sample preparation method capable of providing good external mass accuracy, reproducibility, resolution and uniform analyte distribution is necessary.

The matrix 2-(4-hydroxyphenylazo)benzoic acid (HABA) introduced by Juhasz et al. [2] is found to provide the best external mass accuracy, highest resolution and reproducibility of the molecular weight distribution. HABA is dissolved in 1,4-dioxane at a concentration of 0.05 M. Polyethylene glycol and modified polymers are dissolved in methanol ($\approx 10^{-3}$ M). The polymer solution and HABA solution are premixed to provide a final polymer concentration of 10^{-4} M. To 100 μL of polymer/HABA solution, 1.0 μL of 0.02 M NaCl is added. 1.0 μL of this mixture is added to the sample probe and allowed to dry. The HABA crystals formed from the 1,4-dioxane solution are small (1 to 3 μm) and uniform. The analyte is evenly distributed throughout.

Figure 1A is the MALDI mass spectrum of PEG 3350 using a pulse voltage of 1.80 kV. This is the optimal pulse voltage for ions of ≈3300 Da. The resolution for the polymer ions in this spectrum is 950 to 1050 fwhm across the whole distribution. This resolution is limited by the isotope peaks of the polymer at this mass. The kinetic energy of MALDI generated ions increases with mass. It is thus necessary to increase the pulse voltage to focus ions of higher mass at the detector plane. Figure 1B shows the mass spectrum of PEG 3350 using a pulse voltage of 2.19 kV. This pulse voltage is appropriate for focusing ions of ≈5000 Da. However, the pulse voltage change does not affect the determination of the molecular weight distribution. The number average (M_n) and weight average (M_w) molecular weight for three repeat experiments at each pulse voltage vary by only 0.1%.

Figure 2 is the MALDI spectrum of PEG 3350 bis(Acetaminophen). The mass accuracy is 53±35 ppm across the entire distribution using external calibration with PEG 3350. Good mass accuracy is necessary for this compound to distinguish unlabeled, singly labeled and doubly labeled polymer which vary by 1 amu (see Figure 2). The peaks on the low mass end of the distribution demonstrate that during synthesis the polymer may undergo hydrolysis as all peaks correspond to doubly labeled product but some oligomers are of lower mass than starting material oligomers. The dispersity of the polymer is changed during modification. As a result, the shift in M_n and M_w does not accurately reflect the chemical modification.

Accurate molecular mass assignment is necessary to confirm the expected structure from chemical modification. Relying on the shift in M_n and M_w to demonstrate the success of a modification may not be reliable.

[1] Whittal, R. M.; Li, L. *Anal. Chem.* in press.
[2] Juhasz, P.; Costello, C. E.; Biemann, K. *J. Am. Soc. Mass Spectrom.* **1993**, *4*, 399-409.

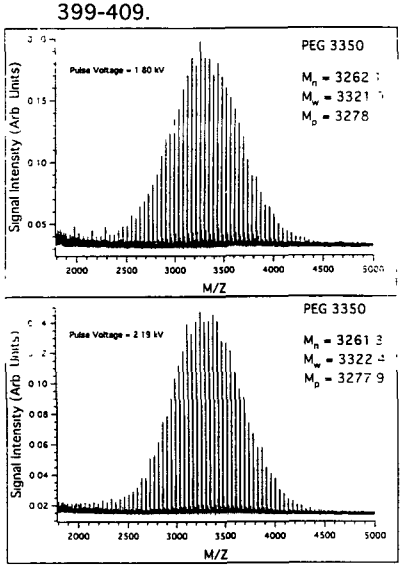

Figure 1

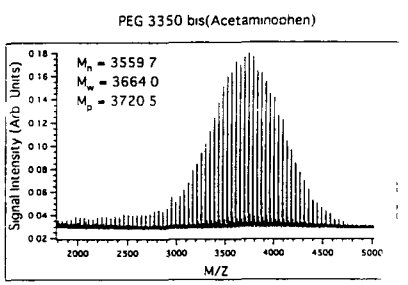

Mass Accuracy = 56 ± 38 ppm external

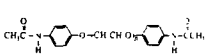

Theoretical Mass (M + Na)+		Observed Mass
1 end group n = 83	2 end group n = 80	
3830.57	3831 56	3831 44
		error = 31

Figure 2

MW DETERMINATION OF SYNTHETIC POLYMERS FROM ESI & MALDI MASS SPECTRA

Charles McEwen, Christian Jackson, and Barbara Larsen
DuPont Central Research Department, P.O. Box 80228, Wilmington, DE 19880-0228

Electrospray ionization (ESI) and matrix assisted laser desorption ionization (MALDI) are capable of ionizing a variety of polymers. ESI mass spectra of oligomer distributions are complicated by the propensity of each oligomer to carry multiple charges. But ESI has the advantage of better mass resolution and mass accuracy than MALDI TOF. With MALDI on the other hand, a wider variety of solvents can be used than with ESI and thus applicable to a wider variety of polymers. In addition, multiple charging is limited resulting in higher mass ranges obtained and less complicated spectra.

In this report, we are attempting to determine the value of these ionization techniques in providing unique or more accurate polymer characterization than is available through GPC, light scattering, nmr, osmometry, etc.. Individual oligomers of t-butyl end-capped polymethylmethacrylate (isotactic and syndiotactic 25 and 50 mers) were collected by SFC and weighed to provide equimolar solutions.[1] By ESI, peak areas and peak heights of the multiply charged ions underestimated the molar concentration of the 50 mers relative to the 25 mers. However, after accounting for peak area compression of multiple charging (i.e. a double charge peak will have only 1/2 the area of a singly charge peak, a triply charged peak only 1/3 the area, etc.) the areas of the 25 mers and 50 mers were the same for equimolar concentrations within experimental error. MALDI produced only singly charged ions for these oligomers and the peak areas were equal for equimolar solutions. Fragmentation of the molecular ions were not observed with either technique.

The above data suggests that for narrow distributions, ESI and MALDI should produce accurate values for the weight and number average molecular weights (Mw, Mn) as well as polydispersity (Mw/Mn), D, and Mp (most probable mass as measured by GPC) for low molecular weight PMMA polymers. Comparing MALDI values with the GPC data for narrow distribution PMMA standards showed reasonably good agreement, but MALDI values were consistently low, particularly the Mp values. Low Mp values for MALDI data of PMMA standards has recently been reported.[2]

A narrow polymer distribution can be simulated by a Poisson distribution of oligomers using the following equations for a weight average and number average distribution where x is the degree of polymerization and v is the number of monomers reacted per initiator.

$$W_x = \frac{x\, e^{-v}\, v^{x-1}}{(v+1)\,(x-1)} \qquad N_x = \frac{e^{-v}\, v^{x-1}}{(x-1)!}$$

The weight fraction distribution, W_x, is measured by GPC while mass spectrometry measures number fraction, N_x. Plotting these distributions on a linear scale shows that for a Poisson distribution Mp will be one monomer mass lower for a number average distribution than for a weight average distribution over any mass range. When the weight fraction distribution is plotted on a logrithmic scale as in GPC, the Mp value is two monomer masses higher than the Mp number fraction plotted on a linear scale. Clearly showing that the Mp values as determined by M.S. will be at least two monomer masses below the Mp values determined by GPC.

Mp values determined by mass spectrometry are measured over just a few oligomer species and thus over a narrow mass range. The results from the PMMA 25 and 50 mers show reasonable (± 5%) molar ion abundance's can be measured over a 2X mass

difference. Therefore, the much smaller mass difference needed to determine Mp would suggest that Mp values measured by mass spectrometry are accurate.

Wide distribution PMMA standards have been reported not to give reliable data by mass spectrometry based partly on Mp values.[2] MALDI of a standard with a reported Mp of 33,000 gave an Mp of only 2200 by MALDI. Our experiments show a similar discrepancy, (see Figure) but not as large for a PMMA Mp=17,000 (American Standards Laboratory) resulted in a Mp by MALDI of 7500. Because MALDI of narrow distribution PMMA standards gave results close to those reported by the manufacturer (Polymer Laboratories, Ltd.), we mixed equimolar amounts (based on Mn values) of PMMA 2400, 6950, and 21,600. Peak areas were measured for the 2400, and 6950 distributions and summed (the area under the 21600 distribution was estimated). Surprisingly, the total distribution areas were in the approximate ratio of 1.0:2.0:3.0 for PMMA 2400, 6950, and 21600, respectively (107 picomoles of each distribution loaded on the target). Reducing the concentration to 7 picomoles/distribution gave a ratio closer to expected (1.0:1.07:1.15). These surprising results suggested that at least for the Finnigan Vision 2000 MALDI instrument, MW distribution values should be skewed higher mass rather than lower mass.

The 17 K wide-distribution polymer standard was run by GPC with refractive index and light scattering detectors and the results plotted on a linear mass scale as both weight fraction and number fraction distributions. The GPC was calibrated using narrow distribution PMMA standards. Mp and Mw determined by GPC and by light scattering were found to be ca. 12600. However, when plotted on a linear scale, Mp was ca. 6500 as a weight fraction distribution and ca. 3000 as a number fraction distribution. These results indicate that comparing weight fraction Mp values obtained by GPC with number fraction values obtained by mass spectrometry is not appropriate. The Mp number average depends on polymerization and termination mechanisms whereas Mp from GPC is almost independant of these mechanisms and close to Mw for linear polymers.

Mn obtained by mass spectrometry (Mn = 7900) for the 17 K PMMA was in good agreement with the GPC (Mn = 7200) and LS (Mn = 8000) values. Mw by MALDI was only 10300 and compared to 12600 by GPC and LS. The difficulty is in the high mass tail above 25K where the signal obtained by mass spectrometry is not discernable above the noise but the contribution to the weight fraction in the GPC results is significant. Recalculating the GPC results by eliminating the signal above 25000 Da, results in a Mw value of 10400 in agreement with MALDI without significantly changing Mn. These results suggests that mass spectrometry can obtain reasonable molecular weight distribution values from polymers with a wide polydispersity only if the signal-to-noise ratio can be enhanced so that high mass tails of polymer distributions can be observed.

[1]McEwen, Simonsick, Larsen, Ute, and Hataba, Accepted J. Am. Soc. Mass Spectrom.
[2]Montaudo, Montaudo, puglisi, Samperi, Rapid Commun. Mass Spectrom., (1995), 9, 453.

Mass Spectrometry of Otherwise Fragile Polymers by Resonant Multiphoton Ionization of End Group Chromophores.

Deon S. Anex, Heinrich E. Hunziker, and Mattanjah S. de Vries
IBM Almaden Research Center, 650 Harry Road, San Jose CA 95120-6099

Perfluorinated polyethers are polymers of practical importance, yet are difficult to characterize mass spectrometrically because they fragment when analyzed by conventional techniques. To overcome this problem we demonstrate the use of laser desorption with separate photoionization of end group chromophores. In this way we have (a) obtained complete parent molecular weight distributions in a mass range of up to 8000 amu, (b) characterized compositions of copolymers in detail, (c) studied polymer degradation products, and (d) performed wavelength dependent spectroscopy on mass selected polymers.

We studied polymers with repeat units $\mathbf{R_i}$ of the form $-O-(CF_2)_i-$ with i = 1, 2, or 3, and with one or both end groups containing a phenyl chromophore. The chromophore can either be part of the original polymer or it can be chemically attached. Laser desorbed neutral molecules were entrained in a pulsed, supersonic expansion, which leads to vibrational and rotational cooling. Downstream the molecules were resonantly two-photon ionized and subsequently detected in a reflectron time of flight mass spectrometer. We obtained complete parent molecular weight distributions, showing no fragmentation and in good agreement with averages obtained from NMR. When using this technique to characterize copolymers of the type $-(\mathbf{R_1})_n-(\mathbf{R_2})_m-$, the parent mass spectrum makes it possible to map the relative abundance of all possible combinations of n and m, providing a characterization with unprecedented detail. This information is crucial for

elucidating degradation products and selective adsorption characteristics of such polymers. We obtained further information by scanning the ionization laser wavelength over the electronic origin of the S_{0-0} transition while observing specific mass to charge ratios of the resulting ions. From the spectra we deduce the formation of van der Waals dimers between chromophore end groups. While polymers with a single chromophore form inter-molecular dimers, our results also show the formation of internal dimers in bifunctional polymers.

Finally these results must be discussed relative to the general problem of photoionization of large molecules. This issue is important both theoretically and because of the question how generally the technique of separate laser desorption and laser ionization with minimal fragmentation can be applied to high mass molecules.

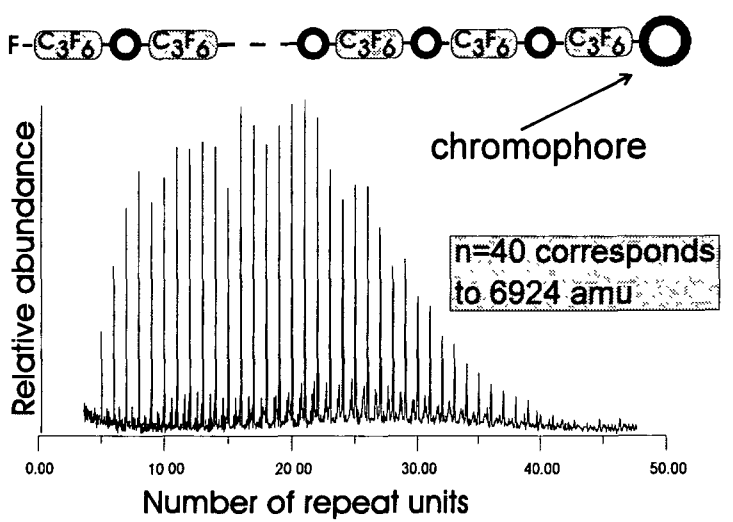

IN-SOURCE DIRECT PYROLYSIS MASS SPECTROMETRY AND LIBRARY MATCHING TECHNIQUES FOR DIRECT ANALYSIS OF POLYMERS IN INDUSTRIAL PRODUCTS

[a]Kuangnan Qian*, [a]William E. Killinger and [b]Gordon Nicol
[a]W.R. Grace & Co.--Conn., Washington Research Center, Columbia, MD 21044; [b] Department of Chemistry and Biochemistry, University of Delaware, Newark, DE 19716

INTRODUCTION

Direct pyrolysis mass spectrometry (DP/MS) has been found particularly valuable in industrial product analysis where matrix interference and detection limit may present challenges to the application of other techniques. Polymers can be pyrolyzed within an ion source of a mass spectrometer using a resistively-heated insertion filament. Compared to conventional DP/MS, in-source DP/MS avoids the condensation of pyrolysis products during transportation, and therefore is able to provide unbiased polymer mass spectra suitable for library matching purposes. In addition, since the temperature of the filament is scanned at a controlled rate, non-polymeric material can be removed prior to the pyrolysis of polymer components. Thus, it is possible to directly analyze polymers in industrial products with minimum sample preparation.

EXPERIMENTAL

The DP/MS experiments were carried out on a Finnigan MAT TSQ 700 mass spectrometer using a direct exposure probe (DEP) for polymer pyrolysis. The filament current of the DEP was increased from 250 to 700 mA at a constant rate of 75 mA/minute. The polymer library was created using a library editor provided by the Finnigan software. The electron energy was fixed at 70 eV to maximize the reproducibility of the polymer spectra. The mass analyzer was scanned from m/z 33 to 600 at a scan rate of 1 sec/scan. The integrated mass spectrum across the TIC peak top (90% of the peak height) of the pyrogram was used to create the library entry.

RESULTS AND DISCUSSION

Most polymers studied in this work were found to fall into three categories based on their pyrolysis patterns. In the first category, the polymers degrade via backbone scission and produce mostly monomers and low molecular weight oligomers. The mass spectra of these polymers are similar to that of their monomers and are normally easy to interpret. The second type of polymer, although also showing a single peak in the pyrogram, degrades via the random chain cleavage mechanism. The polymer spectra of this type therefore are very different from their monomer spectra. The third type of polymer contains thermally labile sidechains and pyrolyzes via two steps. The mass spectra of this type of polymer are normally very complicated and less characteristic of their monomer structures.

The impact of various experimental parameters on polymer mass spectra was studied. Within a wide range, polymer mass spectra were found to be unaffected by the heating rate, sample loading and polymer molecular weight.

The temperature resolved in-source DP/MS offers a possibility to differentiate polymers by their pyrolysis temperatures. This has been found particularly successful in the analyses of polymer blends and co-polymers with a large degree of blockness in monomer distribution. Figure 1 illustrates the total ion current (TIC) pyrogram of an industrial copolymer of styrene/isoprene. There are two clearly separated peaks corresponding to the pyrolysis of polystyrene and polyisoprene, suggesting that there is a certain degree of blockness in the monomer distribution. High quality library matches can be obtained by background subtraction as shown in Figure 2. In most cases, however, different polymer components may not be differentiable by their pyrolysis

temperatures. Spectrum-subtraction of top library hits has been found very useful in these cases to deconvolute the polymer spectra.

The library currently contains more than seventy polymer entries and is still in rapid expansion as this paper goes into print. Our next step is to test the compatibility of the polymer spectra on different instrumentation at different labs.

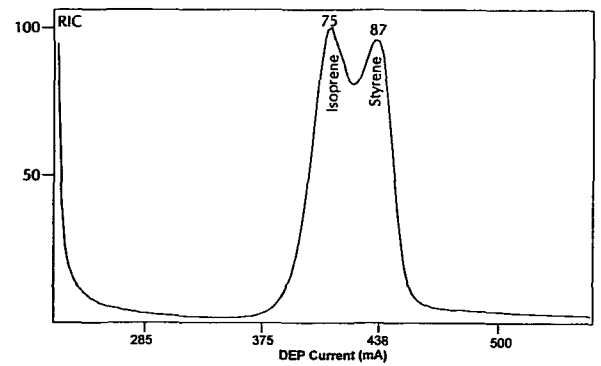

Figure 1. Total ion current pyrogram of a styrene/isoprene copolymer

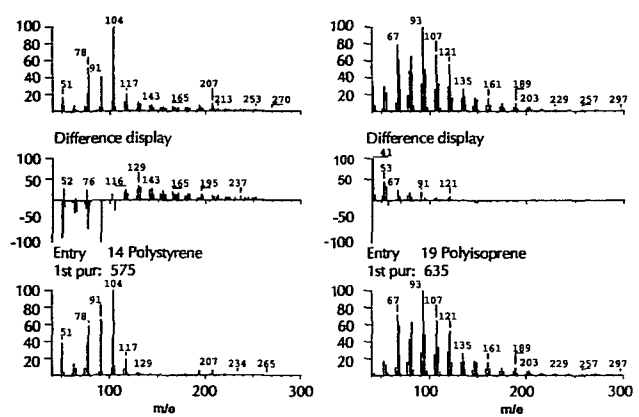

Figure 2. Mass spectra of the styrene/isoprene copolymer after background subtraction and their library matches

Polymer Analysis using a Radio Frequency Glow Discharge Mass Spectrometer

Patrick A. DePalma, Jr., Charles R. Shick, Jr.,
and R. Kenneth Marcus

Department of Chemistry
Howard L. Hunter Laboratory
Clemson University
Clemson, SC 29634-1905

Glow discharge (GD) sources have been widely applied for the direct solids elemental analysis of metals, alloys, and semiconductors. The inherent ability of the radio frequency (rf) powered glow discharges to sputter/atomize nonconductors allows for the analysis of polymer and composite materials. From a recent study, different types of adhesives were employed to mount glass particles for elemental rf-GDMS analysis, and upon spectral evaluation the mounting materials produced predictable spectral features of polymer films. This suggested that the rf sputtering process was sufficient to bring substantial amounts of the polymer fragments into the gas phase for subsequent ionization in the glow discharge plasma. In this presentation, the preliminary observations of polymeric material analysis by rf-GDMS are described in terms of discharge parameters, signal intensity, stability, sample thickness, and topology. Comparison to static SIMS spectra is also described.

For this presentation a copolymer of polytetrafluorethylene (PTFE) and perfluoroalkoxy (PFA), in addition to three Teflon sheets of thickness 1 mm, 1.5 mm, and 3.0 mm were studied and reported by the use of this rf-GD source, and the characteristic ion fragments monitored in a peak jumping mode of the quadrupole mass filter. Figure 1 is a typical rf-GD mass spectrum of Teflon. Figure 2 shows the temporal response curves of selected fragments during the analysis of Teflon, which exemplifies the stability of the rf-GD source. The primary scope of this research is to assess the feasibility of this technique for the analysis of various polymeric materials. A preliminary evaluation of the role of discharge parameters and sample thickness on the fragment intensities was also preformed. Scanning electron micrographs of the sputtered region of 1.5 mm thickness Teflon provided some insight on the effects of sputtering on polymeric materials. A similar experiment was conducted on a terpolymer consisting of tetrafluorethylene, hexafluoropropylene, and vinylidene fluoride, and the resulting rf-GD mass spectrum was in good agreement with the static SIMS spectra of the individual polymer components. All of the results obtained herin suggest that the implementation of this rf-GDMS system is a viable technique for the analysis of polymeric material.

43rd ASMS Conference on Mass Spectrometry and Allied Topics

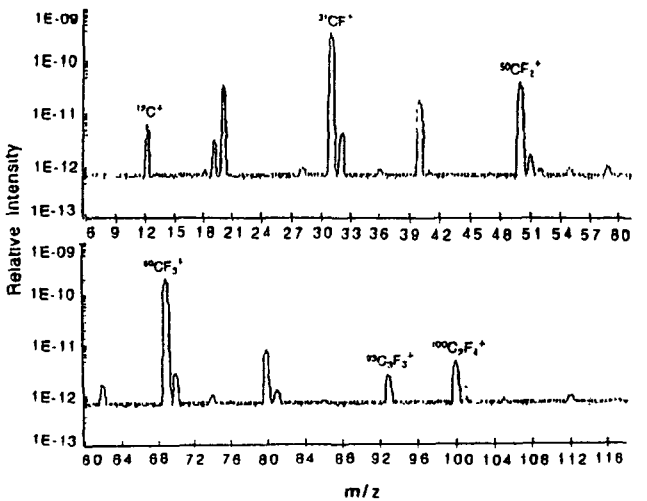

Figure 1. RF-GD mass spectrum of Teflon acquired under the operating conditions of 20 W power, 1.5 sccm Ar, and 8 mm anode plate.

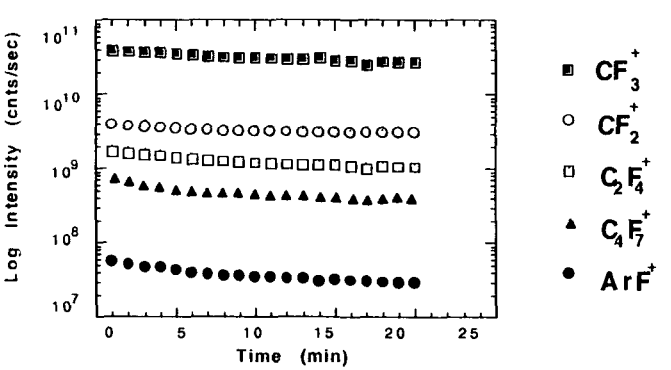

Figure 2. Temporal response curves for selected fragments of PTFE using the rf-GD source.

FD-MS Studies of Samarium-Based Oligomerization of Ethylene.

John Greaves, Donna M. DeCoster and William J. Evans.

Department of Chemistry, University of California, Irvine CA 92717-2025

Bis(pentamethylcyclopentadienyl) samarium complexes such as $(C_5Me_5)_2Sm$, $[(C_5Me_5)_2Sm(\mu\text{-}H)]_2$ and $(C_5Me_5)_2Sm(THF)_2$ can be used to catalyze polymerization of ethylene without a co-catalyst such as trialkylaluminum compounds or methylalumoxanes as required in the Ziegler-Natta systems. The polyethylene produced is insoluble and therefore of high molecular weight (>150,000 daltons). It is difficult to understand the basic steps in the polymerization processes and the influence that reaction conditions have on the process and the products because of the rapid polymerization rate of the reaction. In addition, while analysis of the molecular characteristics would assist in this understanding, the high molecular weight and insolubility of the product renders it particularly difficult to analyze. However, in the presence of hydrogen the molecular weight of the polyethylene produced is limited by hydrogenolysis. The resulting ethylene oligomers have molecular weights in approximately the 300-1000 dalton range and thus are amenable to characterization by FD-MS.

Analyses were conducted on a Fisons Autospec with a high field (4,500 dalton) magnet. The acceleration and extraction voltages were 8 kV and 4 kV respectively. A 4400 - 100 dalton scan was used with a scan rate of 7 sec/decade. Spectra were collected in continuum mode and all scans collected were averaged to obtain the profile of the oligomers being investigated. The emitter (Linden ChroMasSpec) current was programmed from 0-50 mA at 1 mA/min.

The efficiency of FD-MS was assessed using narrow molecular weight range polyethylene and polystyrene standards. Analyses of 800, 1100 and 2000 molecular weight polyethylene standards showed that all three molecular weight ranges could be could be analyzed by FD-MS and gave primarily the molecular ions although some loss of H_2 was observed which became dominant at higher masses. There was a significant loss of sensitivity for the 2000 dalton standard (factor of 50) as compared to the 800 dalton standard which could not be accounted for by the difference in molarity or the increased number of oligomer chains in the 2000 standard. This is in contrast to the analysis of 800 and 1800 dalton polystyrene standards which showed much less of a reduction in sensitivity for the higher molecular weight standard most of which could be accounted for in the molarity and number of oligomer chains. The reason for the difference between the two types of standards is not known but may relate to items such as volatility, or ability to stabilize a charge. It should be noted that when a highly branched poly(1-octene) was characterized by FD-MS, under the same conditions, ions up to the limit of the scan (4400 daltons) were observed. The ability to analyze samples in the low mass region was also assessed using a mixture of single hydrocarbons; $C_{20}H_{42}$, $C_{30}H_{62}$ and $C_{34}H_{70}$. The results showed that little of the $[C_{20}H_{42}]^+$ ion was observed although it comprised more than 50% of the mixture. In addition, it was only observed in the first few scans, before there was a significant emitter current, indicating that the C_{20} was being lost to vacuum during its introduction into the instrument. The overall result of the standard analyses was that FD-MS is an effective approach for analyzing polyethylene providing highly diagnostic molecular ions but that there are limitations to the technique for assessing the average molecular weight distribution of the polymer samples because of the rapid loss of low molecular weight components (<300 daltons) and loss of sensitivity at higher masses (e.g., 2000 daltons).

The lanthanide compounds used in the polymerization reactions are air- and moisture sensitive. They require handling under nitrogen or argon with the rigorous exclusion of air and water using high-vacuum, Schlenk and glove-box techniques. Typical reaction conditions used 0.04 mmol of the organolanthanide in 40 mL toluene. Measured ratios of ethylene and hydrogen were

introduced to the solution at atmospheric pressure. The reaction started immediately and was allowed to proceed until gas uptake had ceased. The reaction was terminated by addition of water and the polymer precipitated with 150 mL methanol. The precipitate was recovered by filtration and dried overnight prior to analysis.

The averaged FD-MS spectra of the polyethylene produced by this technique showed a distribution of polymer chains. The molecular ions, $[M]^+$, were separated by 28 mass units as expected. There were some ions at $[M\text{-}2]^+$ but by NMR the presence of olefins could not be detected. This data supports the report of Heine and Geddes (Org. Mass Spectrom. 29, 277-282, *1994*) that the formation of the $[M\text{-}2]^+$ was because of the loss of an H_2 fragment. The mechanism of formation of the ethylene oligomers was investigated using deuterated gases and D_8-toluene. When the synthesis was carried out utilizing CD_2CD_2:H_2 mixtures the resulting polymer gave $[H(CD_2CD_2)_nH]^+$ molecular ions separated by 32 mass units. Whereas, synthesis with CH_2CH_2 under D_2 gave $[D(CH_2CH_2)D]^+$ ions separated by 28 mass units. When CH_2CH_2 under H_2 was reacted in D_8-toluene there was no evidence of the introduction of deuterium into the polymer chain. The conclusion from this data is that the polymerization process is through the elongation of the chain by clean insertion of ethylene and termination by hydrogenolysis. There was no evidence of radical processes which would be expected to result in branching and the abstraction of D from the D_8-toluene into the oligomer. The choice of samarium II compounds, e.g. $(C_5Me_5)_2Sm$ and $(C_5Me_5)_2Sm(THF)_2$, did not appear to alter the composition or distribution of the polyethylene generated. The catalytic cycle may involve a samarium III hydride is the active species and reactions with isolated $[(C_5Me_5)_2Sm(\mu\text{-}H)]_2$ also gave the same results.

In order to test for the possibility of altering the composition of the polymer produced various olefins were introduced into the reaction mixture at differing concentrations. A typical example was 1-pentene which was used at 8.8, 36 and 210 equivalents per samarium. The FD-MS of the products showed the presence of an odd number carbon envelope at 15%, 50% and 85% of the mixture for the three concentrations. The results were indicative of the inclusion of only one pentene per oligomer chain but this was not certain because the inclusion of two pentene molecules would have resulted in an even carbon chain. When the reaction was carried out with CD_2CD_2 and D_2 there was no evidence of the inclusion of two pentenes, which would have had a unique molecular weight. However, when styrene was added to the reaction, the FD-MS data comprised three envelopes with different molecular compositions. The major envelope consisted of oligomers into which one styrene had been incorporated giving $[H(CH_2CH_2)_n(C_8H_8)H]^+$ ions. The second envelope was the homo-polymer, $[H(CH_2CH_2)_nH]^+$, while the smallest envelope consisted of oligomers into which two styrenes had been incorporated thus giving $[H(CH_2CH_2)_n(C_8H_8)_2H]^+$ ions. It was also noted that for the chains into which styrene had been incorporated ions could be observed at higher molecular weights (m/z > 2,500).

The overall conclusion is that even though FD-MS appears to be limited in mass range for polyethylene discriminating against higher masses, i.e., outside the 300-1000 mass range, the ability of FD-MS to provide molecular ion data means that the technique is particularly suited to investigating the polymerization of ethylene, enabling labeling experiments and other synthetic manipulation experiments to be carried out which would not be possible with other analytical techniques such as NMR or GPC. Manipulations that result in alterations in the structure (e.g., co-polymers or branching) extend the mass range over which FD-MS can be used.

Protein & Peptide Analysis by A Low-Flow, High Sensitivity NanoES Source

Matthias Wilm, and Matthias Mann

European Molecular Biology Laboratory, Meyerhofstr. 1, 69 012 Heidelberg, Germany

Following a theoretical investigation[1] into the electrospray mechanism we built an electrospray ion source with a very low flow rate of 20 - 30 nL/min and implemented the source on a triple quadrupole instrument (API III, Sciex, Ontario, Canada). The low flow rate leads to an initial droplet diameter of 180 nm. The small diameter of the initial droplets exposes 100% of the analyte molecules in the sprayed solution to the mass spectrometer in a form accessible to desolvation. Nothing of the sample is lost in the form of large droplets. This feature of our "NanoElectrospray" source (NanoES) allows us to center the ion source with respect to the axis of the quadrupole at a distance of 1 - 2 mm in front of the orifice. The small droplet size and the geometry of the set-up insures a high transmission. The NanoES source consists of a finely drawn metal coated glass capillary (fig.1). The sample is sprayed out of an 1 - 2 µm orifice. The flow rate is established by the electrostatic force. In the case of samples with high viscosity a small air pressure of less than 0.8 bar supports the flow. No pumps are used and no nebulizing gas is needed nor an electron scavenger to prevent discharge.

The NanoES source is a stable electrospray ion source which allows to do extensive MS/MS investigations on 1 µl sample. The low flow rate does not compromise the concentration sensitivity and peptide measurements on 10 fmol/µl are possible. The small droplet size facilitates the desolvation for glycosilated proteins. 11 different glycosilation states on ovalbumin could be resolved. The stability of the source makes it possible to add more than 800 scans to compensate for electronical fluctuations in the ion signal. The C-terminal sequence of a 40 kDa protein digested with a carboxypeptidase could be confirmed by this technique (fig.2). The NanoES is also very tolerant towards buffers, thus the buffer can be optimized to the needs of the sample. This facilitates the analysis of non-covalent interactions. Complementary DNA strands are observed as a double stranded DNA when sprayed in negative mode in an aqueous buffer after annealing. The main advantage of this stable, low flow ion source is the routine availability of the MS/MS mode on virtually every sample which can be analyzed by ES. Combined with efficient cleaning and desalting techniques proteins can be identified via MS/MS sequencing of their tryptic peptides[2] (fig.3).

(1) Wilm, M. S. and M. Mann (1994), Int J Mass Spec Ion Processes **136**. 167 - 180

(2) Mann, M. and M. S. Wilm (1994), Anal Chem **66**: 4390-4399.

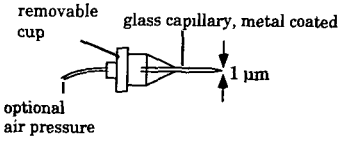

Figure 1 The NanoElectrospray with a stable flow rate of 20 - 30 nL/min.

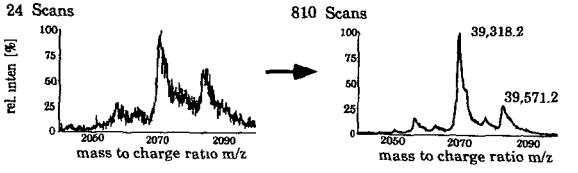

Theoretical Mass: 39 571.5 Da

C-terminal pattern :	D	N	M	R	P
Expected Masses :	115.1	114.1	131 2	156.2	97.1
Measured :	114.0	114.4	132.5	155.1	97 9

Figure 2 C-terminal characterization of a protein. The protein was digested with carboxypeptidase. The partially digested protein was analyzed with a NanoES source on a triple quadrupole instrument. Only the acquisition of more than 800 scans resulted in a spectrum where the C-terminal amino acids could be confirmed.

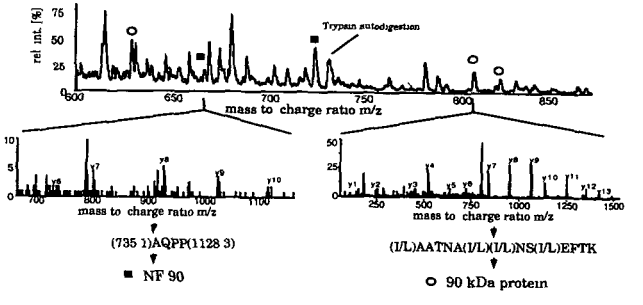

Figure 3 Protein identification by NanoES MS/MS sequencing out of an unseparated tryptic peptide mixture of two different protein (o ; ■).

Biochemical Characterization of EGF receptor-SRC SH2 Interactions

Christian R. Lombardo, Thomas G. Consler, Michael Luther, and Daniel B. Kassel, Glaxo Research Institute, Research Triangle Park, NC 27706

Introduction

The epidermal growth factor receptor (EGFR) is a prototypic member of a family of receptor tyrosine kinases. Upon binding EGF, receptor autophosphorylation on tyrosine residues creates high affinity interaction sites for several SH2 containing proteins including c-src, PLC-g, grb2, the p85 regulatory subunit of PI3-kinase , shc and GAP. These proteins act in concert to effect a cascade signal transduction ultimately responsible for the control and regulation of mitogenesis. The role of *c-src* binding to autophosphorylated EGFR in EGF mediated signal transduction is not well understood. Cell lines overexpressing src have increased EGF induced mitogenesis which requires myristylation, and active SH2 and kinase domains. In addition, v-src expressing cell lines have elevated levels of receptor phosphorylation. These findings implicate c-src in the upregulation of EGFR signalling. Current efforts are focused detailed bioanalytical and biophysical studies of the interaction of the EGF receptor with the SH2 domain of c-src.

Results and Discussion

ESI/MS in conjunction with microaffinity chromatography is being utilized to study *in vitro* protein-protein interactions involved in signal transduction. LC/MS of the purified EGF receptor autophosphorylation domain (aa residues 976-1186) demonstrates that it is a substrate for both the EGFR and c-SRC tyrosine kinase activities. Tryptic phosphopeptide mapping and the technique of negative ion orifice potential stepping of the phosphorylated domain has enabled the sites of tyrosine phosphorylation by c-src to be rapidly identified. Several of the sites were phosphorylated by both kinases. c-SRC also was capable of phosphorylating additional sites distinct from EGFR tyrosine kinase activity. This analysis directly identified Y1086, Y1148 and Y1173 of the EGFR C-terminal domain as c-src phosphorylation sites. Tryptic peptides containing two putative phosphorylation sites were subjected to analysis via Edman sequencing or secondary digestion with Asp-N and LC/MS to identify the phosphorylated residue. Y992, Y1068 and Y1101 were identified as c-src phosphorylation sites by these methods. Kinetic analysis of site specific phosphorylation demonstrated that Y992, Y1086 and Y1173 are the most rapidly and extensively phosphorylated residues. LC/MS/MS was also performed to confirm the assignment of these phosphorylation sites. These data are summarized in Table I.

These phosphorylation sites have been demonstrated to interact with the c-src SH2 domain. Synthetic phosphopeptides derived from the 8 potential phosphorylation sites of the C-terminal domain of EGFR were evaluated for their ability to bind to the SH2 domain of c-src. Microaffinity chromatography of these EGFR phosphopeptides on SH2 columns coupled with LC/ESI/MS has enabled the amino acid sequences contributing to EGFR-SH2 interactions to be determined. Phosphopeptides derived from Y992, Y1086, Y1101, and Y1148 bound directly to the c-src SH2 domain (Fig. 1). Finally, extensive c-src phosphorylation of EGFR is

demonstrated to promote its conversion to a form that exhibits high affinity (K_D= 380 nM) and co-operative binding to the SH2 domain of c-src as measured by BIAcore™ . These model studies offer that the approach of microaffinity chromatography and ESI/MS will be generally applicable for the affinity selection and identification of novel protein-ligand and protein-protein interactions. The identification of c-src phosphorylation sequences on EGFR C-terminal domain as c-src SH2 binding sites supports the notion that this interaction plays a key role in the biology of mitogenic signal transduction.

Table I. *Summary of Phosphorylation and SH2 Binding Sites*

P-Tyr Site	Sequence	c-SRC-TK (%)	EGFR-KD (%)	SH2 Binding
Y992	DADEY*LIPQQ	46 %	46 %	yes
Y1045	FLQRY*SSDPT	0 %	0 %	no
Y1068	PVPEY*INQSV	11 %	30 %	no
Y1086	QNPVY*HNQP	64 %	15 %	yes
Y1101	RDPHY*QDPH	8 %	0 %	yes
Y1114	GNPEY*LNTV	nd	nd	no
Y1148	DNPDY*QQDF	26 %	41 %	yes
Y1173	ENAEY*LRVA	67 %	66 %	no

Fig. 1. *Identification of EGFR Binding Sites for src SH2 by Affinity Chromatography/HPLC/Mass Spectrometry*

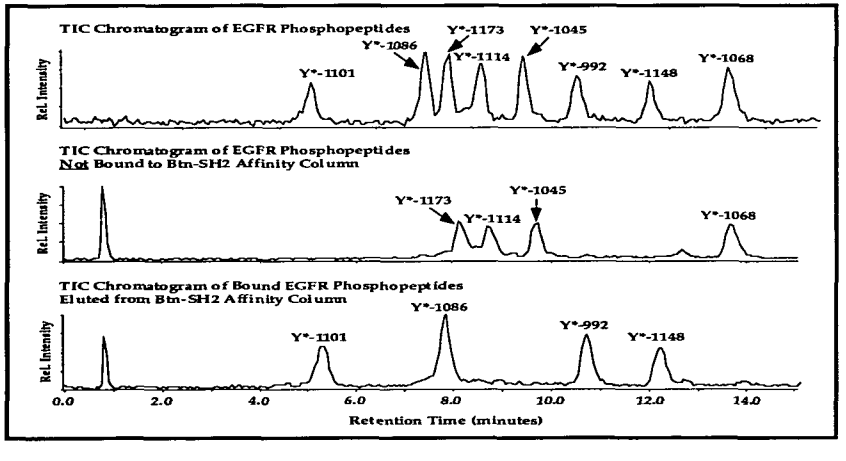

IDENTIFICATION OF SPECIFIC RECEPTOR PEPTOID LIGANDS IN COMBINATORIAL MIXTURES BY AFFINITY SELECTION AND MASS SPECTROMETRY.

S. Kaur, V. Huebner, D. Tang, L. McGuire, R. Drummond, J. Csetjey, J. Strattton-Thomas, S. Rosenberg, G. Figliozzi, S. Banville, R. Zuckermann and G. Dollinger.

Chiron Corporation, 4560 Horton Street, Emeryville, CA 94608-2916.

For many years, new drugs have been discovered by the systematic screening of diverse chemical compounds isolated from plants, marine organisms and synthetic reactions. This approach suggests that the screening of chemical compounds prepared by combinatorial synthetic methods similarly could provide lead compounds for drugs. In combinatorial chemistry, peptides are ideal candidates for generating molecular diversity because of their modular structure; parallel and mixing synthetic strategies can be used to generate rapidly libraries of tens of thousand of compounds. Furthermore, once active structures have been identified, they can be prepared easily in a pure form for detailed pharmacological studies. To date, peptide libraries have been used to find ligands for cellular receptors, to determine substrate specificities of enzymes and map epitopes for antibody binding (1-4). While peptide libraries offer great potential in drug discovery, the poor pharmacokinetic properties of peptides make them less than ideal drug candidates. The poor pharmacokinetic properties of peptides can be circumvented if metabolically stable "unnatural" monomers are used to synthesize peptide-like oligomers. Such "unnatural" peptides, known as peptoids, e.g., oligo(N-substituted)glycines, have been prepared by automated solid-phase synthesis (5, 6). In a drug design strategy, diverse mixtures of peptoids can be used to screen for components with favorable binding characteristics to enzymes or receptors. Once target compounds have been identified, chemically similar mixtures can be generated to optimize binding characteristics.

We have developed an affinity selection and mass spectrometry-based strategy (7) to identify resin-free peptoids with favorable binding characteristics in combinatorial mixtures containing multiple compounds (Fig. 1). This strategy uses the receptor to "fish out" the peptoids of interest from the mixture and directly identify the structures by mass spectrometry. The procedure involves incubation of the peptoid mixture with the receptor of interest, at various levels of molar excess. The incubation mixture is rapidly fractionated by size exclusion chromatography; the receptor with bound ligand is excluded from the column and the excess unbound ligands are eluted in the included volume. An aliquot of the bound peptoids is introduced to an electrospray triple quadrupole mass spectrometer using an on-line reversed phase trap cartridge. Under the conditions used for elution off the reversed phase cartridge, the receptor-peptoid complexes dissociate readily. The molecular weight range of the peptoid mixture is scanned to determine the molecular weight of the peptoid ligands. As a control, the binding experiment is repeated in the presence of a natural receptor ligand with high binding affinity. The peptoids that bind specifically are hence identified readily, since they are observed only in the absence of the natural ligand. The remaining peptoid sample is used to confirm the structure of the peptoids that bind using collision-induced-dissociation (CID) MS/MS. The sensitivity of the mass spectrometry experiments (low pmol peptoid) allows ligands of a variety of affinities to be identified in the combinatorial mixtures.

Fig. 2a-c shows the electrospray mass spectra from an affinity selection experiment using soluble human urokinase plasminogen activator receptor (uPAR) and a combinatorial mixture containing 576 peptoid trimers. The complexity of the starting peptoid mixture is shown in Fig. 2a, where numerous singly charged molecular ions are observed in the range m/z 350-800. Fig. 2b shows the mass spectrum of the peptoids binding to uPAR in the absence of the receptor binding domain (residues 1-48) of human uPA(1-48) and identifies protonated molecular ions m/z 708 and 676. Fig. 2c shows the mass spectrum for the control experiment and indicates that compounds m/z 708 and 676 do not bind in the presence of uPA(1-48); only multiply-charged ions from uPA(1-48) are observed. Since compounds m/z 708 and 676 compete with uPA(1-48), these peptoids presumably bind specifically at the receptor binding site. The structures of compounds m/z 708 and 676 were confirmed by low energy CID MS/MS and comparison with the structures predicted in the mixture. Using structural features from the ligands identified in initial experiments, further combinatorial mixtures were generated to attempt to optimize binding characteristics. Using this strategy, a number of ligands were readily identified.

References

1. Gallop M. A., Barrette R. W., Dower W. J., Fodor S. P. A. & Gordon E. M. (1994), *J. Med. Chem.*, **37**, 1233.
2. Petithory J. R., Masiarz F. R., Kirsch J. F. and Santi D. V. (1991) *Proc. Natl. Acad. Sci. USA*, **88**, 11510.
3. Till J. H, Annan R. S., Carr S. A. and Miller W. T. (1994) *J. Biol. Chem.*, **269**, 7423.
4. Zuckermann R. N., Kerr J. M., Siani M., Banville S. C. and Santi D. V. (1992) *Proc. Natl. Acad. Sci. U. S. A.* **89**, 4505.
5. Simon R. J. Kania, R. S., Zuckermann R. N., Huebner V. D., Jewell D. A., Banville S., Ng, S., Wang L., Rosenberg S., Marlowe C. K., Spellmeyer D. C., Tan R., Frankel A. D., Santi D. V., Cohen F. E. and Bartlett P. A. (1992) *Proc. Natl. Acad. Sci.*, **89**, 9367.
6. Zuckermann R. N., Kerr J. M., Kent S. B. H. and Moos W. H. (1992) *J. Am. Chem. Soc.*, **114**, 10646.
7. Dollinger G. "Exploiting Molecular Diversity." oral presentation, Cambridge Healthtech Institute, San Diego, January, 1995

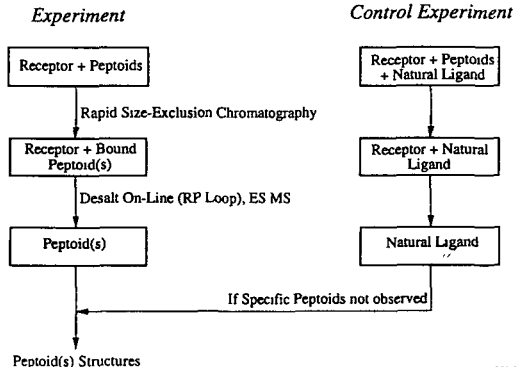

Fig. 1. Experimental Scheme.

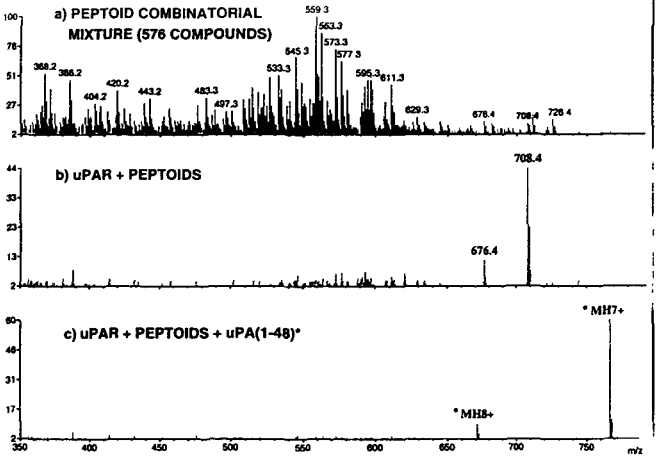

Fig. 2. Electrospray mass spectra showing, a) Peptoid combinatorial mixture containing 576 compounds. b) Peptoids observed after affinity selection experiment using uPAR, and c) Peptoids not observed after affinity selection experiment using uPAR in the presence of the natural ligand uPA(1-48).

The Identification of Proteins Associated with Hypertrophy of Cardiomyocytes by 2D Gel Electrophoresis Combined with Microcapillary LCMS and Tandem MS

David Arnott, Kathy King, Mark Bier*, Adrian Land*, and John T. Stults
Genentech, Inc., 460 Point San Bruno Blvd., South San Francisco, CA 94080, and *Finnigan MAT, 355 River Oaks Parkway, San Jose, CA 95134

Congestive heart failure is a serious health threat which caused the deaths of 39,000 Americans in 1991. One manifestation of heart disease is enlargement (hypertrophy) of the heart, resulting in a loss of pumping capacity. Cardiac hypertrophy is an adaptive response to hypertension and damage from myocardial infarction, but eventually becomes pathological. The search for heart disease treatments would benefit from a better understanding of cardiac hypertrophy at the molecular level. Several model systems have been developed; hypertrophy in cultured myocytes (muscle cells), for example, can be induced by phenylepherine. Two dimensional polyacrylamide gel electrophoresis (2D-PAGE) and electrospray ionization mass spectrometry were used to identify proteins associated with cardiac hypertrophy.

Methods

2D Page: The cell pellet from a single 60 mm plate of cultured cardiac myocytes was dissolved in 10-25 µL O'Farrel's lysis buffer,[1] and centrifuged at 4°C. The supernatant was diluted with sample buffer[1] and 2D PAGE was carried out on a Pharmacia Multiphor II system. The isoelectric focusing step used 18 cm immobilized pH 3-10 gradient strips. The second dimension used SDS-PAGE gels (245x180x0.5 mm, 12-14% polyacrylamide gradient, pre-cast on a plastic support). Proteins were silver stained[2] or electroblotted onto PVDF membranes which were stained with Coomassie Blue.[3]

***In Situ* Digestion:** Protein spots were cut out of the blot, wet with MeOH and destained by vortexing in 70% MeCN. Disulfide bonds were reduced by addition of 100 µL of 10 mM DTT, 5 mM EDTA, 500 mM Tris HCl with incubation for one hour at 45°C. Cys residues were carboxymethylated by addition of 10 µL 200 mM iodoacetic acid in 0.5 M NaOH, with incubation in the dark for 20 min. The membranes were washed 3x with 10% MeCN, shaken 20 min. in 0.5% w/v PVP-360, 0.1% HOAc. The membranes were washed 2x with 10% MeCN, 1x with 20% MeCN, and 1x with digestion buffer (50 mM NH_4HCO_3, 10% MeCN). Proteins were digested 16 hr @ 37 °C with 0.05 µg endo Lys-C in 15 µL digestion buffer. The membrane was removed and washed with digestion buffer. The pooled samples were acidified with HOAc, reduced to <5 µL by vacuum centrifugation, diluted to 10 µL with 0.1 M HOAc, and frozen.

Mass Spectrometry: Samples were introduced to the ESI source of the mass spectrometers by capillary HPLC. Reverse phase microcolumns with 15 cm of POROS R2 10 µm beads packed in 75 µm i.d. x 190 µm o.d. x 30 cm fused silica were constructed.[4] Samples were loaded hydrostatically and peptides were eluted by a 15 minute gradient of 0-80% MeCN in 0.1 M HOAc from an ABI model 140A dual syringe pump. A pre-column split of the mobile phase was used to obtain column flow rates of 0.2 - 0.5 µL/min.

Mass spectra were recorded on a Finnigan TSQ-7000 triple quadrupole MS with an API-ESI ion source. A liquid sheath of 70% MeOH/0.1 % HOAc @ 1.5 µL/min. was used. The spray was assisted by N_2 gas flow from sheath and auxiliary gas ports. Spectra were acquired every 1.5 sec. from 300-1600 Da. CAD experiments were carried out at 2.5 mTorr Ar in the collision cell; collision energies of 13-20 eV, 20-30 eV were used for CAD of triply, and doubly charged peptides. Q3 was scanned at 500 amu/sec in MS/MS mode. Sensitivity was enhanced by operating at less than unit resolution (FWHM =1.5 amu).

Spectra were also acquired using a prototype Finnigan LCQ ion trap mass spectrometer. The ESI source and its operating conditions were the same as for the triple quadrupole. One virtue of this instrument is the ability to rapidly change scan modes in a data-dependent manner. Samples were introduced by LCMS as before, and spectra acquired under computer control. A full mass range scan was taken, followed by a high resolution narrow range scan of the base peak. A charge state was calculated from the isotope spacing, and CAD was carried out. This cycle repeated throughout the HPLC run.

Database Searching. Proteins were identified from the mass spectral data by searching a compilation of protein and DNA databases using the program FRAGFIT, developed at Genentech.[4] For each protein spot, the masses of the peptides were input along with partial sequences from MS/MS. Additional parameters include enzyme specificity, mass tolerance, approximate protein MW, Cys alkylation regent, allowance for Trp and Met oxidation, allowance for incomplete digestion, and the number of matching masses required.

Results and Discussion

Proteins were extracted from neonatal rat cardiac myocytes with or without phenylepherine induced hypertrophy (~ 150 µg protein from ~ $2x10^5$ surviving cells), and resolved by 2D PAGE. Analytical gels were silver stained, and scanned with a flat bed scanner. Spots were located and matched among gels with BioImage 2D analysis software. For mass spectrometry, 3 samples were pooled, and blotted onto PVDF membranes after 2D PAGE. Spots were identified by *in situ* digestion and analysis by LC-ESI-MS.

Figure 1 illustrates the experimental method for one protein spot from normal cardiomyocytes. Ten percent of the digested sample was injected on a capillary HPLC column and eluted into the mass spectrometer (1A). Molecular weights were measured for each peptide (1B), and MS/MS performed on major peptides (1C). The TSQ7000 required two or more injections to accomplish both MS and MS/MS; the ion trap required only one HPLC run when the data dependent experiment was performed. Both instruments were capable of CAD on tens of fmol of peptide. The use of partial sequence information along with MW data resulted in highly discriminating database searches; frequently a single mass with 3-4 residues of sequence was sufficient to uniquely identify a protein.

Initial experiments to validate the method focused on the more abundant proteins found in cardiac myocytes; 12 such proteins were identified and are listed in Table 1. Each is a protein which would be expected in heart cells, although two had not previously been sequenced in rats. Preliminary results indicate that myosin light chain 1 (atrial isoform) was found in 100% greater abundance in hypertrophic cells than in normal cells. A number of similarly upregulated proteins are under investigation.

[1]O'Farrell P.H., J. Biol. Chem. (1975) 250: 4007-21.
[2]Rabilloud T., Vuillard L, Gilly C., Lawrence J-J. Cell. Mol. Biol. (1994) 40: 57-75.
[3]Henzel, W.H. et al. J. Biochem. (1993) 90. 5011-5015.
[4]Kennedy R.T., and Jorgenson, J.W., Anal. Chem (1989) 61:1128.

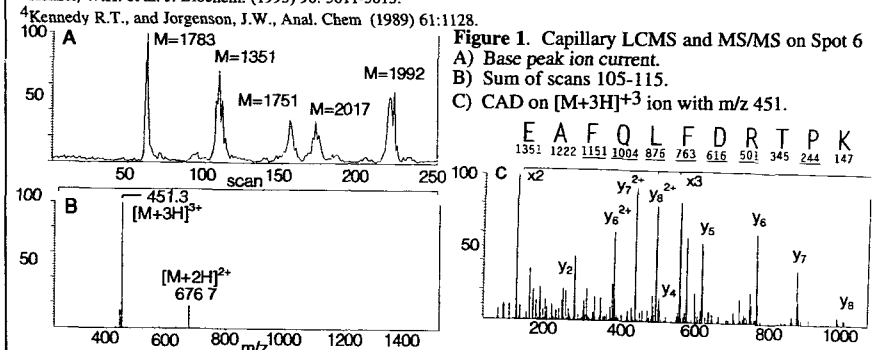

Figure 1. Capillary LCMS and MS/MS on Spot 6
A) Base peak ion current.
B) Sum of scans 105-115.
C) CAD on $[M+3H]^{+3}$ ion with m/z 451.

Spot	Protein name	Mr calc	pI calc
1	actin	42 kD	5.3
2	mitochondrial matrix protein p1 precursor	61 kD	6.1
3	ATP synthase alpha chain, mitochondrial precursor	59 kD	9.4
4	myosin regulatory light chain 2, cardiac muscle isoform	19 kD	4.9
5	aconitate hydratase precursor, sequence from pig	86 kD	8.4
6	myosin light chain 1, ventricular isoform	22 kD	5.1
7	78 kDa glucose regulated protein precursor	73 kD	5.1
8	ATP synthase beta chain, mitochondrial precursor	56 kD	5.3
9	ATP synthase d chain, mitochondrial	19 kD	6.0
10	isocitrate dehydrogenase, sequence from cow	50 kD	9.1
11	HSP70, mitochondrial homolog	74 kD	6.2
12	myosin light chain 2, atrial isoform	21 kD	5.0

Table 1. Proteins from Cardiac Myocytes Identified by HPLC-ESI-Tandem MS

Identification of Amino Acid Transformations during Oxidation of Peptides and Proteins: Modifications of Methionine and Tyrosine

S.K. Chowdhury, J. Eshraghi, H. Wolfe, D. Forde, A.G. Hlavac, and D. Johnston, Sanofi Winthrop, Inc., 9 Great Valley Parkway, Malvern, PA 19355

Liquid chromatography/electrospray ionization mass spectrometry (LC/ESI-MS), tandem mass spectrometry with on line liquid chromatography (LC/ESI-MS-MS) and high resolution mass spectrometry with liquid secondary ionization (LSIMS) were utilized to identify the modified amino acids in peptides and proteins formed during oxidation with performic acid. The procedure of protein oxidation was chosen to assist in protein unfolding by oxidizing the cystines to cysteic acids to allow for more complete proteolytic digestion and to create additional cleavage sites for endoproteinase Asp-N. Investigation of the Asp-N peptide map of oxidized superoxide dismutase (SOD) by LC/ESI-MS revealed that an expected proteolytic fragment of the protein was missing. In its place, two peptides with molecular weights (MWs) 66 and 100 higher than that calculated for the missing peptide were observed. To identify the modified amino acids in the unexpected peptides, a model peptide with some amino acid similarities (tyrosine, arginine, methionine, and lysine) to the missing peptide was chosen and was subjected to the similar oxidation and enzymatic digestion steps, conditions and reactions. After oxidation and digestion, the model peptide (TAP, sequence: Ac-MDKVLNRY) showed 3 major peaks in LC/MS (Figure 1). The peptides in the three peaks were identified to be the unmodified peptide (peak a) and two peptides whose MWs were 66 (peak c) and 100 (peak d) higher than that of TAP. The LC/ESI-MS-MS of these reaction products demonstrated that in the two modified peptides the N-terminal methionine has been transformed into methionine sulfone (MW increase of 32), whereas m/z values of all the fragment ions containing C-terminal arginine and tyrosine were 34 (peak c) and 68 (peak d) higher than those in the unmodified peptide (figure 2 and Chart 1). To establish whether the arginine or tyrosine or both were modified, another peptide Neuromedin N (sequence: KIPYIL) was chosen that contains tyrosine but no arginine or methionine. The LC/MS analysis of the oxidized peptide again showed three peaks (Figure 3). The early eluting peak corresponds to residual unmodified peptide (peak a) and the MW of the two later eluting peptides are respectively 34 (peak b) and 68 (peak c) higher than that of Neuromedin N. The LC/ESI-MS-MS of the peptides confirmed that the tyrosine underwent transformations with an increase of MW by 34 or 68 (Chart 2). Accurate m/z of the monoprotonated molecules of the two peptides were determined to 780.44294 (calculated m/z 780.44267 for $C_{38}H_{63}N_7O_8Cl$) and 814.40391 (calculated m/z 814.40369 for $C_{38}H_{62}N_7O_8Cl_2$). The measured values agree with those calculated to 0.35 and 0.27 ppm, respectively). We believe that sodium chloride used as buffer in peptides and SOD solutions produced electrophiles in the oxidizing medium that caused electrophilic aromatic substitution in tyrosine (scheme I). This observation was further supported by the identification of mono and dibromo peptides when chloride salts were replaced with bromides.

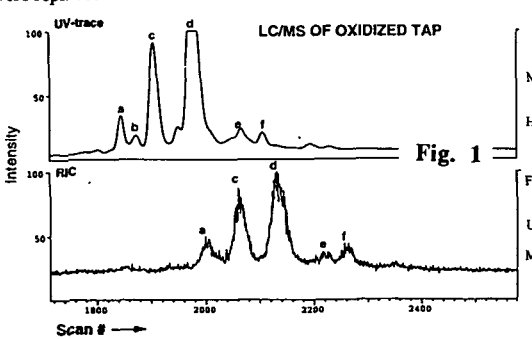

Fig. 1

LC/MS/MS Instrumentation

Mass Spectrometer	Finnigan TSQ-700 Analytica Electrospray Source
HPLC.	Waters 600 MS 320 µm i.d x 15cm Vydac C-18
Flow Conditions (Gradient)	4 µl/min (1:100 split) 3 µl/min (sheath liquid)
UV detection	214 nm
MS/MS	2.5-3 mTorr (Ar) Collision energy = 15-20 eV

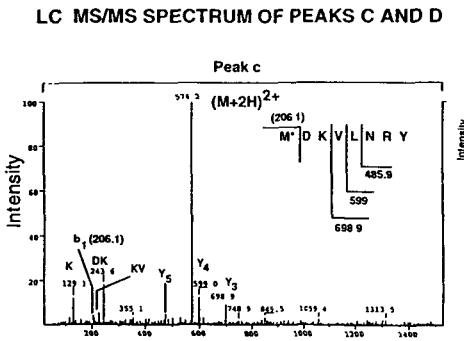

Fig. 2

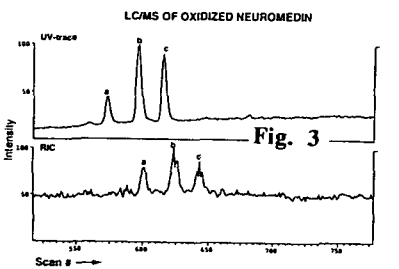

Fig. 3

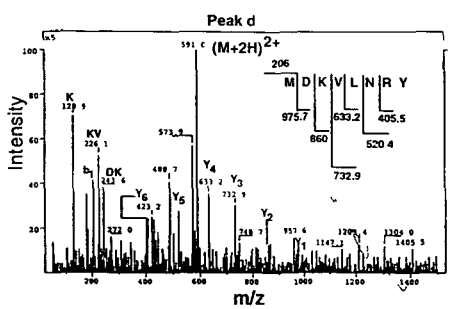

Chart 2

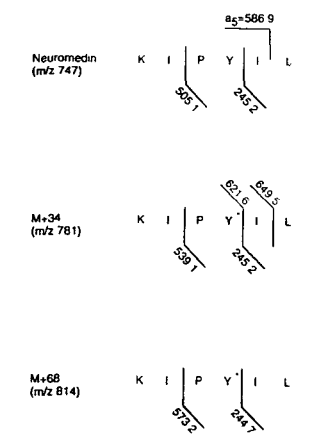

Chart 1

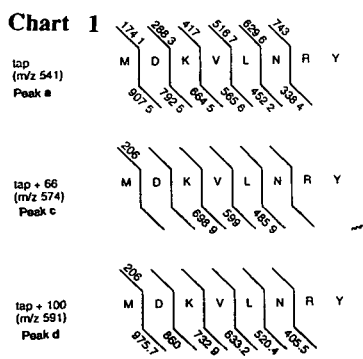

Scheme 1

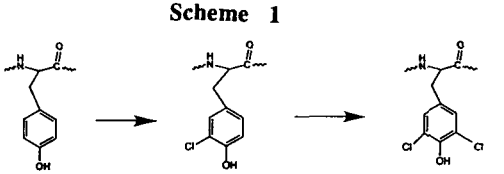

IDENTIFYING PROTEINS BY NANOELECTROSPRAY TANDEM MASS SPECTROMETRY AND PEPTIDE SEQUENCE TAGS

M. Mann, M. Wilm, A. Shevchenko and G. Neubauer
European Molecular Biology Laboratory (EMBL)
Postfach 10.2209, D-69012 Heidelberg, Germany

Identification of proteins is an important analytical challenge in molecular biology. Peptide Sequence Tags have recently been introduced as a highly specific probe for the identification of proteins in sequence databases[1]. A fragmentation spectrum usually contains a short, easily identifiable series of sequence ions, yielding a partial sequence. This partial sequence, together with its starting and end mass is a signature of the peptide which we term a "peptide sequence tag". Peptides can be identified even in the presence of unknown post translational modifications or amino acid substitutions between an expected sequence and the measured peptide. Just two to three amino acid residues derived by fragmentation are usually enough to identify the peptide. Using Apple Scripts, the process of finding a protein in the database has been reduced to selecting three fragment peaks in the tandem mass spectrum.

Peptide Sequence Tags can be obtained in various ways including ES MS/MS, ES orifice fragmentation or MALDI post source decay (PSD). Examples from NanoES[2] of unseparated mixtures of peptides, such as the one shown in fig 1 demonstrate the power of the technique. Even the minimal information present in the partial spectrum is enough to uniquely locate the protein. As a "second pass" the found sequence is loaded and compared to the rest of the MS/MS spectrum giving an additional unambiguous selection step. When several other peptide sequence tags are added identification is positive (fig 2). The sequence of the protein (see caption to fig. 2) only contains very few peptides which would have been in the preferred mass range between 1000 and 2500 Da for identification by mass fingerprinting.

When compared to identification by "mass fingerprinting", peptide sequence tags are vastly more specific even when using very few peptides. Indeed, in almost all cases, a single peptide is enough to obtain a unique hit in the database. In practice, we have found several proteins which could not be identified by mass fingerprinting but were readily identified by peptide sequence tags. Sequence tags can furthermore readily resolve proteins mixtures. The concept applies also to an extended form of peptide mapping in which partial tandem mass spectra are taken of each of the components in a peptide mixture of a protein of (putatively) known sequence. This approach is orders of magnitude more specific than peptide mapping by masses alone, yet does not entail the difficult complete interpretation of tandem mass spectra.

1. Mann, M. & Wilm, M.S. *Anal. Chem.* **66**, 4390-4399 (1994).
2. Wilm, M.S. & Mann, M. *Int. J. Mass Spec. Ion Processes* **136**, 167 - 180 (1994).

A Tag on a Yeast Protein

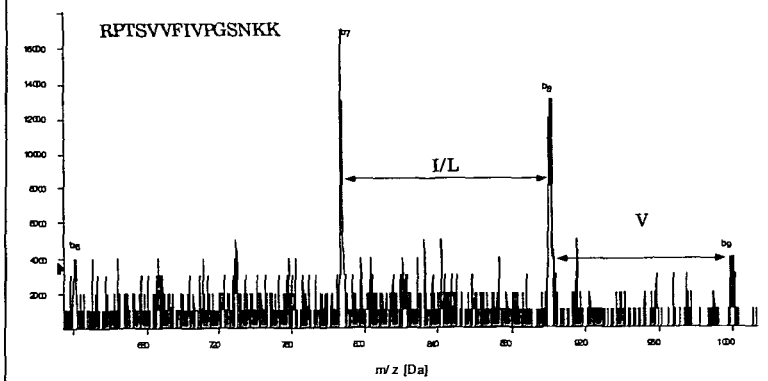

Figure 1. Partial region of the MS/MS spectrum of one peptide in a mixture sequenced by NanoES.

Second Tag on Yeast Protein

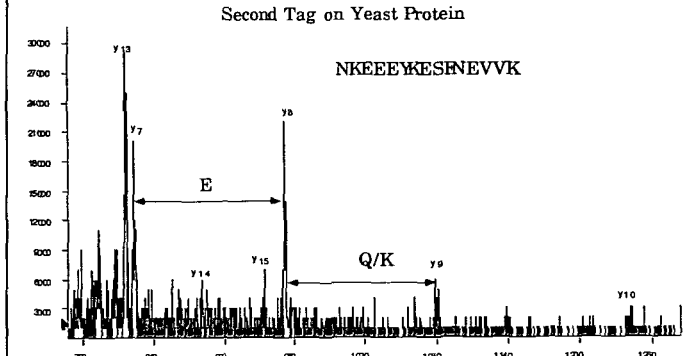

Figure 2. Partial region of the MS/MS spectrum of a second peptide, uniquely identifying the same protein as the tag in figure 1. The sequence of the protein makes it very difficult to be identified by mass fingerprinting (very few peptides in "preferred" mass range):

MVNGSLGSRETETSAVKMGKDNKEHKESKESKTVDNYEARMPAVLPFAKPLAS KKLNKKVLKTVKKASKAKNVKRGVKEVVKALRKGEKGLVVIAGDISPADVISHI PVLCEDHSVPYIFIPSKQDLGAAGATKRPTSVVFIVPGSNKKKDGKNKEEEYKES FNEVVKEVQAL

MALD AND ES MASS SPECTROMETRY OF COVALENT PEPTIDE-OLIGONUCLEOTIDE HYBRIDS

Ole N. Jensen[1], Sandhya Kulkarni[2], Jane V. Aldrich[4], Samuel E. Bennett[1], Dale W. Mosbaugh[3], and Douglas F. Barofsky[3]. [1]Department of Biochemistry and Biophysics, [2]College of Pharmacy, and [3]Department of Agricultural Chemistry, Oregon State University, Corvallis, OR 97331. [4]Department of Pharmaceutical Sciences, University of Maryland at Baltimore, 20 North Pine St., Baltimore, MD 21201.

INTRODUCTION. We are in the process of developing and implementing a novel protocol for characterization of protein-nucleic acid interactions. The protocol employs photochemical cross-linking techniques followed by mass spectrometric analyses of protein primary structure [1]. We have previously demonstrated that intact, UV-crosslinked protein-nucleic acid complexes can be analyzed by MALD mass spectrometry [2, 3]. In the study presented here, we have investigated how peptide-oligonucleotide hybrids behave during MALD and ES mass spectrometric analyses.

EXPERIMENTAL. Photochemically crosslinked peptide-dT_{20} hybrids were obtained by tryptic digestion of Escherichia coli uracil-DNA glycosylase (Ung) photochemically crosslinked to dT_{20} followed by anion-exchange chromatography [3]. Synthetic hybrids were prepared by reacting an eleven residue synthetic peptide containing an internal carboxyl-group (Asp side chain) with an amino-linker-5'pdT_6 or an amino-linker-5'pdT_{10} oligonucleotide [4]. The synthetic hybrids were purified by RP-HPLC. MALD mass spectrometry was performed on a custom-built linear time-of-flight instrument equipped with a frequency tripled (355 nm) Nd:YAG laser. Peptide-oligonucleotide hybrids were prepared for MALD by mixing them with a matrix consisting of 2,4,6-trihydroxyacetophenone in 50 mM diammoniumcitrate/50% acetonitrile. ES mass spectrometry and ES tandem mass spectrometry were performed on a Sciex API III Plus mass spectrometer system. Samples (5 uL) were flow injected in 5 mM ammonium acetate/50% acetonitrile at a flow rate of 3 uL/min.

RESULTS AND CONCLUSIONS. We have demonstrated that MALD MS is a facile means for ascertaing the identities of photochemically crossslinked and synthetic peptide-oligonucleotide hybrids. We have further demonstrated that sufficiently pure synthetic peptide-oligonucleotide hybrids can be easily analyzed by ES MS.

Scrutiny of MALD mass spectra of tryptic peptide mixtures of Ung indicates that the presence of free peptides completely suppress ionization of the peptide-oligonucleotide hybrids. However, separation of the hybrids as a group from the free peptides by anion-exchange chromatography is sufficient to allow MALD mass spectra of the peptide-dT_{20} hybrid mixtures to be obtained with only 5-10 pmol of sample. We have been able to deduce the DNA binding domain of Ung from such mass spectra and complementary sequence information obtained by Edman degradation [3].

The sensitivities of MALD MS and ES MS for peptide-oligonucleotide hybrids are similar to their respective sensitivities for pure oligonucleotides. The presence of free peptides or oligonucleotides in a sample suppresses ionization of the hybrids - this is especially marked in the case of ES MS. In general, MALD MS is less affected by sample impurities and more sensitive than ES MS for these compounds, while ES MS has greater

mass accuracy and resolution than MALD linear TOF MS, e.g. salt adducts can be resolved by ES MS on a triple quadrupole instrument. The behavior of peptide-oligonucleotide hybrids in solvent systems (matrix in MALD, spray solvent in ES) seems to be governed mainly by the oligonucleotide, whereas their ionization seems to be predominated by the peptide, i.e. the peptide seems to promote positive ion formation in both MALD MS and ES MS.

Positive ion ES tandem mass spectrometry yielded the complete oligonucleotide sequence and more than 50% of the peptide sequence of a peptide-dT_6 hybrid (Figure 1). Thus, ES MS/MS has the potential for localizing sites of crosslinking or branching, i.e. for identifying the modified amino acids, in peptide-oligonucleotide hybrids. Mass spectrometric structural characterization of covalent peptide-oligonucleotide hybrids should find widespread application in photochemistry/photobiology, in molecular biology, and in antisense research.

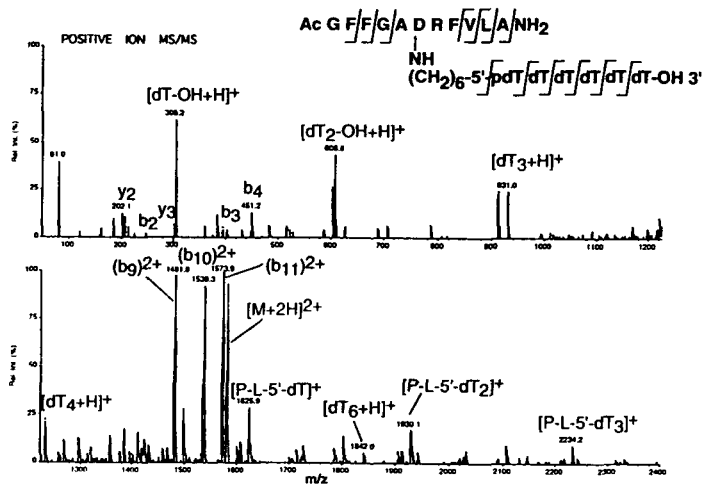

Figure 1. Positive ES-CID spectrum of the doubly charged ion of the peptide-dT_6 hybrid.

REFERENCES.

1. Jensen et al. (1994) In *Techniques in protein Chemistry, V* (JW Crabb, Ed) pp 27-37, Academic Press.
2. Jensen et al. (1993) *Rapid Commun. Mass Spectrom.* **7** 496-501.
3. Bennett et al. (1994) *J. Biol. Chem.* **269** 21870-21879.
4. Jensen et al. (199x, submitted).

ACKNOWLEDGEMENT. This work was supported by National Institutes of Health Grants RR07079, GM32823, and ES00210, and by Medical Research Foundation Grant 9146. O.N.J. was supported by fellowships from the Danish Research Academy and the Carlsberg Foundation, Denmark.

Studying Noncovalent Protein-Peptide Interactions by Electrospray Ionization Mass Spectrometry

Joseph A. Loo, Peifeng Hu, and Venkataraman Thanabal
Parke-Davis Pharmaceutical Research, Division of Warner-Lambert Company, 2800 Plymouth Road, Ann Arbor, MI 48105

Electrospray ionization mass spectrometry (ESI-MS) has been applied for detection of noncovalently-bound biochemical complexes, including peptide-peptide, protein-cofactor, and protein subunits. The detection of these complexes is the first step of an MS-based methodology. The next steps are to relate the observations back to the more relevant solution phase studies and to determine how the molecules are interacting on a structural level. To assess the usefulness of ESI-MS for studying noncovalent interactions, we have examined the binding of various peptide inhibitors to v-src SH2 (Src homology 2) domain protein (12.9 kDa). SH2 motifs in proteins are critical in the signal transduction pathways of the tyrosine kinase growth factor receptors. SH2 domains bind to the phosphotyrosine-containing growth factor receptors. Electrospray ionization mass spectrometry with a magnetic sector instrument and array detection has been used to detect the protein-peptide complex with subpicomolar sensitivity.

The relative abundances of the src protein complex with several nonphosphorylated and phosphorylated peptides were compared and were found to correlate well to the known binding constants derived from solution-based methods, indicating that the mass spectrometry-based method can be used to assess the specificity of such interactions. Covalent modification by a nonpeptide inhibitor of the putative binding site of the protein inhibits detection of the protein-peptide complex. Peptide inhibitors studied include those based on the -pTyrGluGluIle- motif that has been demonstrated to bind to src SH2 domain with high specificity (K_d ~ 0.6 μM). Peptides without a *phospho*tyrosine residue exhibits very little binding in ESI mass spectra (except at very high peptide concentrations) (Figures 1 and 2). Other phosphopeptides examined include sequence stereoisomers with a wide range of binding affinities. For example, peptides based on the sequence Ac-Gln-pTyr-Glu-homoPhe-NH_2 have a wide range of IC_{50} values (concentration required to inhibit specific binding by 50%).

There are several ESI-MS methods to differentiate peptide binding affinities that differ in IC_{50} values by as little as a factor of 2. Titration experiments and measuring the amount of relative binding shows differential binding to src SH2. However, a more straightforward method is to perform competitive binding experiments with another inhibitor of known affinity. For example, ESI-MS of tertiary mixtures of src SH2 protein, a phosphopeptide with an IC_{50} ~ 4 μM (*I*), and either the D- or L-homoPhe[4] peptide (see above) at a molar ratio of 1:3:3 respectively show that the D-homoPhe[4] peptide (IC_{50} ~ 6 μM) has nearly equal affinity to peptide *I*, whereas the L-homoPhe4 peptide (IC_{50} ~ 15 μM) has a lower affinity to src SH2 than *I* (i.e., does not competitively bind to src SH2 against peptide *I*).

Solution-phase equilibrium constants may be determined by measuring the amount of bound and unbound species as a function of peptide inhibitor concentration for construction of a Scatchard graph. Preliminary analysis of peptide Ac-Gln-pTyr-Glu-Glu-Ile-Pro-NH_2 shows a binding constant of ~ 0.5 μM measured by ESI-MS, in good agreement with the literature value of 0.55 μM (K_d) for the larger peptide Ac-Lys-Gly-Gly-*Gln-pTyr-Glu-Glu-Ile-Pro*-Ile-Pro-NH_2 (Ladbury et al., *Proc. Natl. Acad. Sci. USA* **1995**, *92*, 3199).

Electrospray ionization MS may have potential for analyzing complex mixtures for finding potent inhibitors. Possible candidates derived from mixtures from combinatorial chemistry (e.g., peptide libraries) may be initially screened by the method. ESI-MS of src SH2 protein with a mixture of phosphopeptides (where [total peptide] > [src SH2]) showed the expected complex(es) as the dominant species in the mass spectrum.

Many examples have been reported to suggest that some aspects of solution phase interactions are retained in the gas phase. Careful control of all experimental parameters is necessary for studying noncovalently-bound complexes by ESI mass spectrometry. Particular attention to the variables affecting droplet/ion desolvation needs to be taken. Source temperature, countercurrent gas flow rate, collision energy in the ESI interface, ESI spray angle, and many other variables can affect the relative amount of noncovalent binding to proteins indicated in a mass spectrum. However, by establishing experimental conditions to provide consistent desolvation behavior, relative binding affinities can be determined.

Acknowledgments. The authors wish to thank T. K. Sawyer, E. Lunney, M. Plummer, and K. Para (Parke-Davis) for providing the peptide inhibitors and helpful discussions.

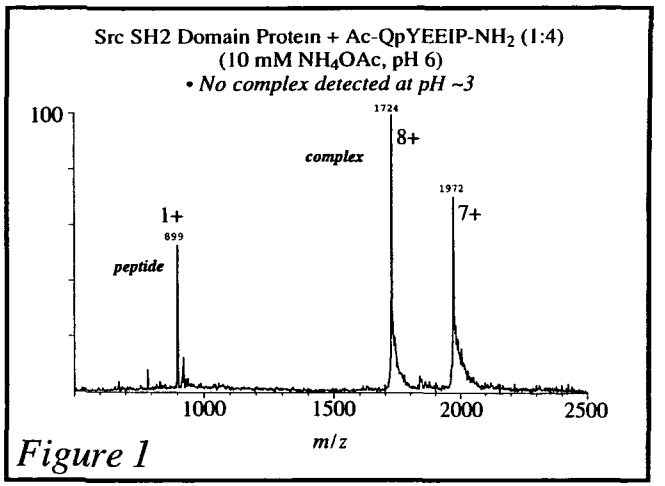

Figure 1

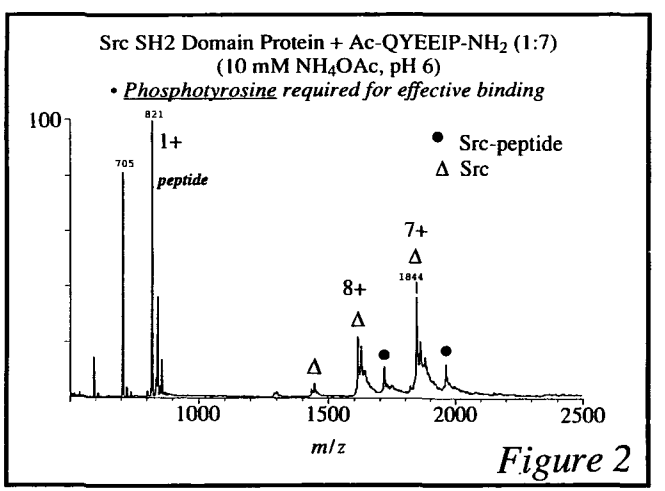

Figure 2

Mass Spectrometry in the Development of Recombinant Protein Drugs

Alan Kubis, Tom Chen, Krishendu Ghosh, David Natale, Lynette Settles, Somesh Nigam and
*James E. Labdon, Regeneron Pharmaceuticals, 777 Old Saw Mill River Road, Tarrytown, NY 10561

During the course of development of pharmaceuticals from recombinant DNA technology, it is necessary to fully characterize the structure of the candidate proteins and determine the nature of any modified forms. Mass spectrometry is an indispensable tool for the development of therapeutic proteins in the biotechnology industry. ESIMS and MALDI-TOF methods are used to investigate the primary structure (sequence), tertiary structure (folding), stability and modified forms of therapeutic proteins prior to toxicology studies or clinical trials. This is illustrated by the analysis of recombinant brain-derived neurotrophic factor (rHuBDNF)[1], a homodimeric, neuronal growth and survival factor with therapeutic potential in certain neurological disorders.

BDNF elutes as three peaks by reversed-phase HPLC, depending upon prior treatment with denaturants or reducing agents. The second peak represents an partially unfolded form of the first peak which retains the disulfide bonds. The fully reduced molecule elutes with greatest retention time. E. coli-derived human BDNF (mass 13,505) is extremely heat stable (Td=87°C) and is resistant to trypsin without prior heat denaturation. The disulfide arrangement was determined by LCMS and a sequential digestion technique using trypsin and thermolysin at pH 8.0. Capillary LC-ESIMS peptide mapping revealed all expected tryptic peptides from the protein, including disulfide-linked peptide ions indicating a 1-4, disulfide arrangement (Figs. 1,1a). In addition, a disulfide tripeptide was observed (Figs. 1,1b), which was consistent with a 2-5, 3-6 or 3-5, 2-6 arrangement ("x "in Fig .1a). In order to determine the arrangement of cystine pairing within the tripeptide, a thermolysin fragment of the tripeptide was generated which cleaved the peptide bond between Cys-109 and Val-110. The detection of an ion at m/z 783 (Fig. 2) demonstrated that the BDNF disulfide arrangement was consistent with the crystal structure of NGF, another homologous member of the neurotrophin family.[2] These peptides were not observed in BDNF in which the cystine residues were reductively alkylated.

Several heterodimer variants comprising 1-2% of total protein were observed in in the manufacture of rHuBDNF High-temperature (60°C) HPLC with online ESIMS analysis allowed the separation and mass determinations of variant forms of the protein (Fig. 3). The approximate mass differences from unmodified BDNF were deduced from accumulated scans in Fig. 3 as follows: a=+16 amu, b=BDNF, c= - 340 and +43 amu, d= -664, e,f= -18 and g= - 36 amu.

LCMS tryptic mapping and Edman sequencing revealed the nature and location of several covalent modifications of the protein and supported the interpretation of the variants from Fig. 3. as follows: Oxidized methionine (a), N-terminal deletions of 3 (c) and 6 (d) amino acids from the N-terminus, and carbamylation of lysine side chains (c). In addition, a -18 amu form of tryptic peptide 5 from the digest of variant (e) was found to shift to a later retention time in LCMS. Edman sequence analysis and fluorometric amino acid analysis of the peptide confirmed the substitution of norleucine for methionine at position 31 (M31Nle, DM -18 amu predicted) arising from the mistranslation of one (e,f) and possibly two (g) modifications of methionine residues.

Stability studies of BDNF in phosphate buffered saline, pH 7.0 showed extensive degradation after several weeks at 45°C, but little change at 4°C. HPLC of the degraded product showed increased levels of variant peaks 1 and 2, consistent with oxidation of the protein, along with a shoulder peak on the trailing edge of the main BDNF peak. LC/ESIMS of the degraded products showed three cleaved forms (Fig. 4) corresponding to removal of 1 3 and 4 amino acids from the N-terminus of BDNF. Edman sequence analysis also detected a sequence beginning with residue 60, indicating a cleavage between residue 59 and 60. This modification would not be expected to appear as discrete peptides in LCMS analysis without prior reduction of the disulfide bonds linking these fragments together. Figure 5 summarizes the modification sites.

1Barde, et. al. EMBO J. 1:549-553 (1982)
2. Macdonald, N. Q. et al., Nature 354(6352) 411-4 (1991).

43rd ASMS Conference on Mass Spectrometry and Allied Topics

Figure 1

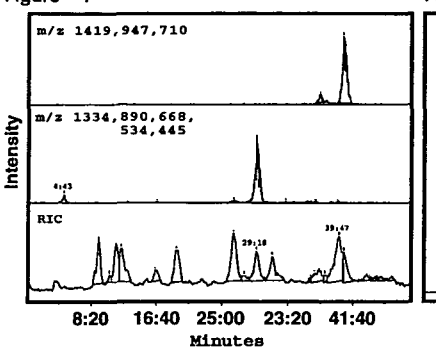

Figure 2

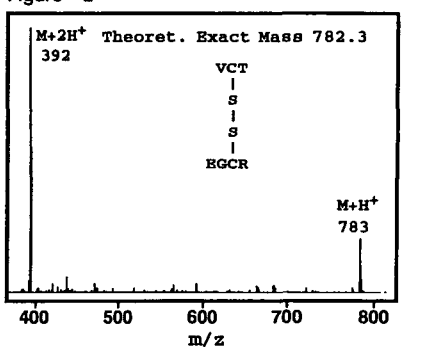

Figure 3

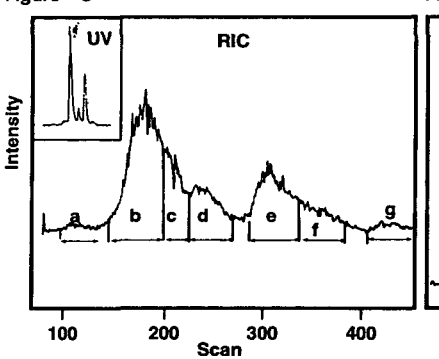

Figure 4

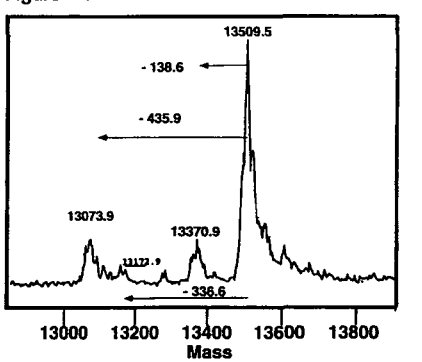

Figure 1a

```
GELSVCDSISEWVTAADK
      |   1-4
HWNSQCR
```

Figure 1b

```
CNPMGYTK   EGCR
    \      /
     X (3-6,2-5 or 3-5,2-6)
     /\
IDTSCVCTLTIK
```

Figure 5

```
   Δ3  (HPLC induced?)
   |  Δ6                                M31Nle
   |  | 10          20          30 |        40          50
HSDPARRGEL SVCDSISEWV TAADKKTAVD MSGGTVTVLE KVPVSKGQLK
 || |
Δ1| |        (45 C Stability Study)
  Δ2|
   Δ4     Met-S=O
        60 |        70          80          90          100
QYFYETKCNP MGYTKEGCRG IDKRHWNSQC RTTQSYVRAL TMDSKKRIGW
           | |
           | Possible M31Nle
         Δ59 (45 C Stability Study)
       110
RFIRIDTSCV CTLTIKRGR
```

Application of Micro-ES/MS/MS for Monitoring the Effects of Drugs of Abuse. Mark R. Emmett* and Richard M. Caprioli, Dept. of Biochemistry and Molecular Biology and the Analytical Chemistry Center, The University of Texas-Houston Medical School, P.O. Box 20708, Houston, Tx 77225.

In vivo microdialysis (Md) is a sampling technique that has been used to monitor a variety of endogenous neurotransmitters (1). Md has not been widely used in the study of endogenous neuropeptides due to low extracellular concentrations coupled with poor recoveries of these larger molecules and their contamination with high concentrations of salts. Because of the dilute nature of the microdialysate (attomole/μl), previous experiments have been performed with antibody radioimmunoassays of wide specificity which interact with all proteins/peptides containing homologous sequences (2).

The opiate neuropeptide, [Met]^5-enkephalin (ME) belongs to a family group that share homologous amino acid sequences. ME has been proposed to be involved in the natural reward pathway which is thought to contribute to the addictiveness of many drugs of abuse (3). To test this idea, we have developed a highly sensitive and specific mass spectrometric assay that is used to analyze and quantitate ME from *in vivo* brain dialysates. **In this presentation, we show the effects of various drugs of abuse on endogenous ME release in the globus pallidus/ventral pallidum region of rat brain.**

MATERIALS AND METHODS

ES/MS/MS: ES spectra were generated using a modified Vestec Electrospray Ion Source (PerSeptive Biosystems-Vestec Corporation) mounted on a Finnigan TSQ 70 mass spectrometer (Finnigan Corporation) with a 20 kV dynode. MS/MS data were gathered with Q_1 focused on the parent ion of 574.4 m/z with a resolution of approximately 2.5 AMU. The collision gas was Xenon at a pressure of 1.4 mT. Q_3 was scanned over the mass range of 390-405 AMU every 0.4 sec.

Microelectrospray: The micro-ES interface (4,5) was specifically developed for the detection of the endogenous release of neuropeptides via microdialysis. Packed micro-ES needles (50 μ i.d., packed with a 40 nL bed volume of 10 μ C18 particles [YMC Corp.]) were used to desalt and concentrate samples.

Microdialysis: CMA/10 microdialysis probes (CMA/*Microdialysis*, Acton, MA) were used in the *in vivo* experiments. Cannulae were stereotaxically implanted into the brain of male Sprague/Dawley rats under pentobarbital anesthesia; such that, when the microdialysis probe was inserted it extended into the Globus Pallidus/Ventral Pallidum region of the brain. The animals were allowed to recover for at least four days after the surgery. The experiments were all performed on freely moving animals using an Instech (Plymouth Meeting, PA) freely moving animal apparatus. Freely-moving animals were necessary for these experiments due to the inhibition of neurotransmitter release by anesthetics (6). After insertion of the probe, the animal was allowed a 3 hr equilibration time before beginning the experiment. During this time and all during the experiment artificial CSF (5 mM KCl, 120 mM NaCl, 1.2 mM $MgCl_2$, 1.8 mM $CaCl_2$, 0.15% phosphate buffered saline, pH 7.4) was perfused through the probe at a rate of 436 nL/min. A control injection of drug vehicle was administered I.P. and two, 30 min dialysates were collected. The drug of abuse (Morphine, Methamphetamine, Cocaine or Diazepam) was administered I.P. and 30 min samples were collected over the next 3 hrs. Perfusate samples were analyzed by micro-ES/MS/MS.

43rd ASMS Conference on Mass Spectrometry and Allied Topics

RESULTS

Previous data showing the release of endogenous ME by local depolarization and systemically administered morphine has been reported (7,8).

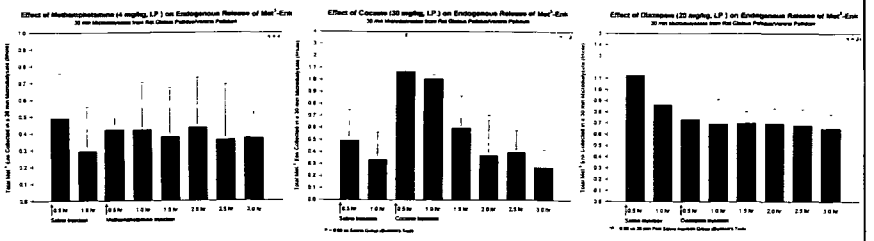

DISCUSSION

1) Micro-ES/MS/MS permits the identification and quantitation of endogenous [met]^5-enkephalin collected from rat brain by *in vivo* microdialysis.
2) Morphine (10 mg/kg, I.P.) and Cocaine (30 mg/kg, I.P.) activate an enkephalinergic pathway that releases [met]^5-enkephalin in the Globus Pallidus/Ventral Pallidum region of rat brain, supporting the hypothesis that endogenous opiates may be involved in the reward pathway.
3) Diazepam (20 mg/kg, I.P.) does not activate an enkephalinergic pathway to the Globus Pallidus/Ventral Pallidum region of rat brain.
4) Methamphetamine (4 mg/kg) unexpectedly does not activate an enkephalinergic pathway to the Globus Pallidus/Ventral Pallidum region of rat brain. This data infers that the mechanism of addiction for methamphetamine differs from that of morphine or cocaine.

REFERENCES

1. Ungerstedt, U., In Marsden, C.A. (Ed.), Measurement of Neurotransmitter Release *In Vivo*, **1984**, John Wiley, Chichister, pp. 81-105.
2. Maidment, N.T., Brumbaugh, D.R., Rudolph, V.D., Erdely, E. and Evans, C.J., *Neuroscience*, **1989**, 33:549-557.
3. Koob, G.F., *Trends in Pharm. Sci.*, **1992**, 13:177-184.
4. Emmett, M.R. and Caprioli, R.M., *J. Am. Soc. Mass Spectrom.* **1994**, 5:605-613.
5. Andrén, P.E., Emmett, M R. and Caprioli, R.M., *J. Am. Soc. Mass Spectrom.* **1994**, 5:867-869.
6. Llorens-Cortes, C., Gros, C.,and Schwartz, J., *Proc. Natl. Acad. Sci.*, **1986**, 83:6226-6230.
7. Emmett, M.R. and Caprioli, R.M., Proceedings of the 42nd ASMS Conference on Mass Spectrometry and Allied Topics, Chicago, IL, May 29-June3, 1994.
8. Emmett, M.R. and Caprioli, R.M., *J. Neurosci. Meth.* in press.

Nucleotide (n = 10^1-10^2) Sequencing and Screening Using ESI/FTMS

Daniel P. Little, David J. Aaserud, Gary A. Valaskovic, Peter B. O'Connor, Fred W. McLafferty

Chemistry Department, Baker Laboratory, Cornell University, Ithaca, NY 14850-1301

The presence of a single DNA base mutation or deletion within a gene is often sufficient to incapacitate an organism. Clinical diagnostics will demand sensitive analytical methods to verify the integrity of loci known to contain disease sites, as well as to identify new ones The advantages of Fourier transform mass spectrometry (FTMS), including ppm mass measuring accuracy, fmol sensitivity, speed, and ultrahigh resolution make it ideal for this, especially when coupled with electrospray ionization (ESI). Synthetic DNA strands as large as 100-mers have been measured with 1 Da accuracy, with minor (<5%) N - 1 and N + 1 failure sequences easily characterized.[1]

For small (n≤14) oligonucleotides, dissociation products of the multiply charged ions from ESI give consecutive backbone cleavages providing full sequence in <1 minute[2] With nozzle-skimmer (NS) and infrared multiphoton (IRMPD) dissociation, fragmentation patterns consistent with those of McLuckey were observed,[3] with w (3') and a - BH (5') ions predominating For longer strands (50- to 108-mers), however, we now find that NS yields exclusively 5' sequence (b, d, and a - B ions), while IRMPD (MS/MS, MS^3) provides w, a - BH, and internal region fragments determining most of the remaining sequence The advantage of predictable fragmentation types made of only four building blocks (A, T, C, G) make it possible to determine a fragment's type and composition with only accurate MW determination A computer program has been developed to exploit this; a separate program searches for fragments differing by the mass of a single nucleotide unit, generating overlapping partial sequences

Thus we outline a strategy for sequencing oligonucleotides using tandem FTMS: 1) Accurate MW determination, 2) IRMPD for 3' and internal stretches and 5'-3' pairs, 3) MS^n to establish each of these as w or a - BH, 4) NS for 5' stretches, 5) overlap of 5', 3', and internal regions from steps 2-4, and 6) verification of determined sequence considering all fragments, including those not identified by mass alone Using this methodology, the full sequence of a 50-mer DNA was determined, except for order ambiguity in one region of three bases and in four regions of two bases (Figure 1). An unknown mutated 50-mer gave a 9.04 Da lower MW, consistent with A→T, IRMPD pinpointed the mutation at base 27 (Figure 2) With conventional ESI, each experiment requires 1-3 pmol, interfacing through a microelectrospray source decreases this by more than an order of magnitude.[4,5]

(1) Little, D P, Thannhauser, T. W ; McLafferty, F W *Proc Natl. Acad. Sci USA* **1995**, *92*, 2318-2322
(2) Little, D P.; Chorush, R A, Speir, J. P.; Senko, M W.; Kelleher, N. L ; McLafferty, F. W. *J Am. Chem Soc.* **1994**, *116*, 4893-4897.
(3) McLuckey, S. A., Habibi-Goudarzi, S. *ibid.* **1993**, *115*, 12085-12095.
(4) Wilm, M.; Mann, M *Int J. Mass Spectrom. Ion Processes* **1994**, *136*, 167-180
(5) Valaskovic, G A ; McLafferty, F. W. Submitted.

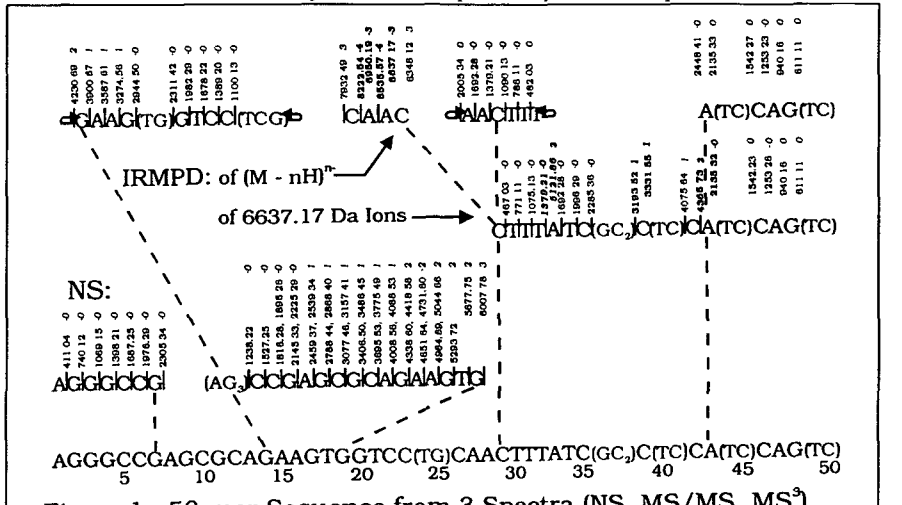

Figure 1. 50-mer Sequence from 3 Spectra (NS, MS/MS, MS^3)

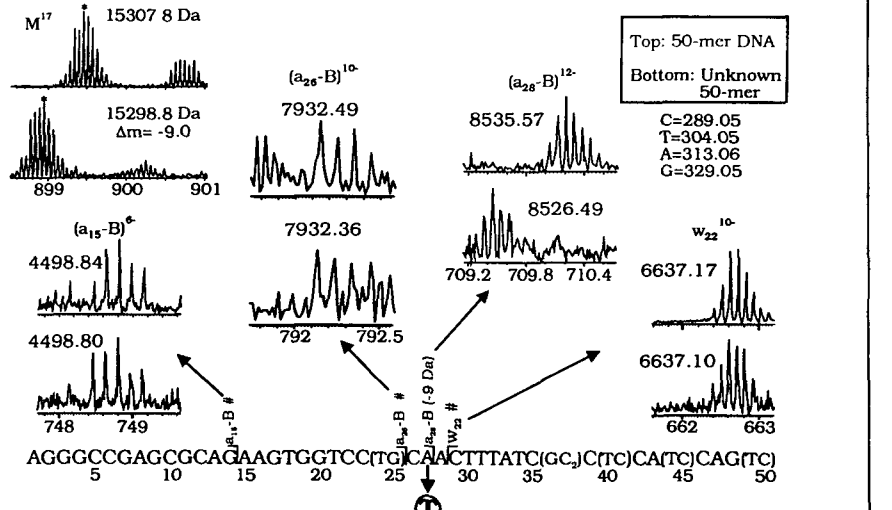

Figure 2. Locating Point Mutations

SEARCHING CHEMICAL DIVERSITY FOR MOLECULAR RECOGNITION BY ESI-MS

Richard D. Smith, James E. Bruce, Xueheng Cheng, Gordon A. Anderson, Ruidan Chen, David C. Gale, Steven A. Hofstadler and Brenda L. Schwartz

Chemical Sciences Department, Pacific Northwest Laboratory, Richland, WA 99352

The traditional approach to drug lead development has generally involved the synthesis or high purity isolation of individual compounds followed by their screening and evaluation through a series of chemical and biological assays. A key step in the screening process may involve identification of candidate compounds that display high binding affinity *in vitro* to a targeted biopolymer, e.g., a specific protein or DNA segment. More recently, the *in vitro* selection of pharmacologically active molecules from mixtures of compounds has been shown effective, leading to the development of potential new drugs. Identifying the biologically most active compounds, often those displaying the highest affinity of noncovalent binding, from such "libraries" has become a major enterprise. In particular, the generation and searching of large "combinatorial" libraries has become popular for certain classes of compounds. In the "combinatorial" approach, many compounds are synthesized to deliberately produce a complex mixture, and then subsequently examined for their affinity to the targeted biopolymer, often by partitioning subsets of the library so as to facilitate the identification of the most active components. This is commonly performed by binding either the target or library molecules to a solid support, often in some fashion designed to facilitate identification of the active components. The combinatorial approach has proven attractive since it allows much larger numbers of compounds to be screened more rapidly than other serial approaches involving the individual synthesis and assay of each prospective affinant.

An essential aspect of screening large libraries of compounds is the ability to identify the active components, often on the basis of their strong binding to the selected target. The ability to screen very large libraries is obviously attractive, and essential if a broad range of molecular diversity is to be explored. For example, in the case of tripeptides, a library containing all variations for three amino acid residues will consist of 8,000 peptides (twenty possible for each of three residues, i.e., 20^3). The number of possible hexapeptides is 6.4×10^7 (i.e., 20^6). The conventional screening of combinatorial libraries is most effective when the synthesis is well behaved (i.e., components are generated in nearly equimolar quantities, unsuspected components are not present, etc.), the general composition is well established, and suitable analytical methods are available. From this viewpoint, libraries consisting of polypeptides or oligonucleotides are attractive, since the well-developed tools of biochemistry and molecular biology may be invoked for their synthesis and analysis. On the other hand, such libraries offer only a limited range of structural diversity and can have limited utility as drugs due to their generally rapid degradation by enzymatic processes. Thus, there is considerable interest in chemically more diverse libraries, where the synthetic and analytical advantages that apply for linear biopolymers do not currently exist. Furthermore, as much as the combinatorial approach can speed drug screening, it may still require weeks or months (even for libraries based upon linear biopolymers) to generate a library, develop a combinatorial selection scheme, and then identify potential candidates for more extensive evaluation.

The new approach we demonstrate, "bioaffinity characterization mass spectrometry" (BACMS), may potentially aid studies involving conventional libraries by providing much more rapid and direct analysis, as well as applicability to chemically more diverse libraries. Current methods that involve the use of solid supports, such as affinity chromatography, can suffer from contributions due to modified or nonspecific binding, as well as the need for time-consuming retrieval and purification of the selected

species prior to analysis, and the accompanying loss in sensitivity introduced by the additional sample handling required. The BACMS approach would exploit the ability of electrospray ionization (ESI) for the transfer of noncovalent complexes from solution[1-4] as a key step for the rapid screening of combinatorial libraries, and could greatly speed the initial screening process.

The BACMS approach exploits several newly developed Fourier transform ion cyclotron resonance (FTICR) methods, as well as the high sensitivity and gentle nature of the electrospray process. These technologies, when coupled to electrospray ionization (ESI), allow the investigation of specific noncovalent complexes formed in solution. BACMS utilizes the well-known attributes of FTICR, such as the high resolution mass analysis and $(MS)^n$ ($n \geq 2$) capabilities, as well as the recently developed techniques involving quadrupolar excitation (e.g., selected-ion accumulation[5,6]). Also crucial is the extraordinary sensitivity achievable ($<10^{-9}$ M) without the use of separations. Recent studies by Cheng et al at our laboratory, conducted in collaboration with Professor George Whitesides and co-workers (Harvard University), have shown the capability for measuring binding for two inhibitor mixtures with bovine carbonic anhydrase (BCA)-inhibitor dissociation constants (K_D's) spanning 2-3 orders of magnitude (approximately 10^{-6} M^{-1} to 10^{-9} M^{-1})[7]. The ESI-MS measurements showed the complexes contained one Zn(II) cation (which is known to bind to three histidine residues in the active site of BCA, and is involved in the catalytic process). The results showed that neither ESI nor the FTICR detection methods caused any significant dissociation of the complexes, and that structural information for the noncovalently bound inhibitors could be obtained in one FTICR experiment. The most important aspect of this work was that the individual inhibitors could be isolated from the dissociated complexes, and their relative abundances were shown to correlate well with the known binding constants. Beyond this, the isolated inhibitors could be dissociated and the products measured with high resolution to aid in their identification. Thus, these methods appear to offer the potential to rapidly evaluate the binding of sets of compounds to a specific target molecule in one experiment that consumes only very limited amounts of both the target compound and the ligand "library."

These results and others have indicated that even relatively weak associations are amenable to study (K_D's of $> 10^{-6}$ to 10^{-7}) with the proper selection of ESI and solution conditions. These results also support the potential for obtaining semi-quantitative or quantitative information about relative binding constants when no dissociation of the complexes is observed during the ESI process. It is reasonable that gas phase abundances of the complexes under such conditions will most directly reflect relative abundances in solution, and provide conditions under which relative binding affinities can be derived from appropriately designed studies.

1. R. D. Smith and K. J. Light-Wahl, *Biol. Mass Spectrom.* **1993**, *22*, 493-501.
2. B. L. Schwartz, J. E. Bruce, G. A. Anderson, S. A. Hofstadler, A. L. Rockwood, R. D. Smith A Chiloki and P. S. Stayton, *J. Am. Soc. Mass Spectrom.*, in press.
3. D. C. Gale and R. D. Smith, *J. Am. Chem. Soc.* **1994**, *116*, 6027-6028.
4. K. J. Light-Wahl, B. L. Schwartz, R. D. Smith, *J. Amer. Chem. Soc.*, 1994, *116*, 5271-5278.
5. J. E. Bruce, G. A. Anderson, S. A. Hofstadler, S. L. Van Orden, M. G. Sherman, A. L. Rockwood and R. D. Smith, *Rapid Commun. Mass Spectrom.* **1993**,*7*, 914-919 .
6. J. E. Bruce, S. L. Van Orden, G. A. Anderson, S. A. Hofstadler, M. G. Sherman, A. R. Rockwood and R. D. Smith, *J. Mass Spectrom.* **1995**, *30*, 124-133.
7. X. Cheng, R. Chen, J. E. Bruce, B. L. Schwartz, D. C. Gale, G. A. Anderson, S. A. Hofstadler, R. D. Smith J. Gao, G. B. Sigal, M. Mammen and G. M. Whitesides, submitted for publication.

This research was supported by Pacific Northwest Laboratory (PNL) exploratory research through the U.S. Department of Energy. PNL is operated by Battelle Memorial Institute for the U.S. Department of Energy, through Contract No. DE-AC06-76RLO 1830.

Direct Connection of an Inductively Coupled Plasma and an Ion Trap Mass Spectrometer

C.J. Barinaga, G.C. Eiden, D.W. Koppenaal
Pacific Northwest Laboratory*,
PO Box 999, Richland WA 99352

The good sensitivity and tandem mass spectrometric capability of the quadrupole ion trap mass spectrometer (ITMS) has made it a useful instrumental technique for organic analysis. These same qualities might be useful for elemental analysis, including techniques like inductively coupled plasma mass spectrometry (ICP-MS). Two existing ITMS capabilities, prolonged ion injection and MS/MS could be immediately helpful. Long ion trapping times could be advantageous for determination of trace level elements and isotopes. MS/MS could be used to resonantly excite and collisionally dissociate polyatomic ions that arise from the plasma gas (argon) and sample matrix (water, various acids, and high concentration sample components) and that are nominally isobaric with analyte ions below 81 m/z. In addition slow scanning techniques suggested that greater mass resolution was possible. The most direct approach would be to couple the ICP and ITMS directly with minimal intervening vacuum interface and ion optic hardware. However the limited ion capacity of the ion trap before onset of significant space charge effects and the intense Ar ion current from the plasma raised concerns that the direct connection would quickly fill the trap with Ar ions, rendering the trap useless for detection of trace ions. Therefore, in our first instrument system (denoted as ICP-Q_L-Q_T), a linear quadrupole was employed between the vacuum interface and the ion trap to act as as an RF-only high pass filter, an RF/DC selective mass filter, or as a notch filter to.reduce or eliminate the Ar and matrix ion currents to the ion trap.

This instrument approach (ICP-Q_L-Q_T) was successful (1,2). Surprisingly a significant reduction in the intensity of the Ar ion signal was noted as was the nearly complete absence of matrix related polyatomic ions. Auger neutralization processes have been invoked to explain the reduction in Ar ion beam intensity during injection. Further loss of Ar ions occurs by charge exchange with background water in the trap. The loss of matrix related polyatomics is due to collision induced dissociation of these ions by the helium bath gas. Detection limits for the heavier elements is in the ten's of ppt range with a pronounced decrease in sensitivity for lighter mass ions. Also noted was the time and water vapor pressure dependent formation of metal oxides and hydroxides especially for the strong oxide-bond forming metals, e.g. lanthunum, thorium, uranium, etc. Greater than 90% of the metal ion signal could be recovered by the selective removal of water from the trap atmosphere.

The strong attenuation of the Ar ion beam suggested that the direct connection of an ICP and ion trap was feasible. This work reports the first direct connection ICP/ITMS instrument (denoted ICP-Q_T), assembled as illustrated in Fig.1. The result is a much smaller and less complex instrument. Preliminary data indicate performance very comparable to the ICP-Q_L-Q_T instrument. The Ar ion beam is still strongly attenuated in the ICP-Q_T system so that it does not immediately fill the trap. Plasma and sample matrix related polyatomic ions are also eliminated during trapping, Fig. 2. (2% HCl). Certain metal oxides and hydroxides are seen but the better pumping arrangement of the trap chamber results in lower levels than the original ICP-Q_L-Q_T system. Sensitivity remains in the low ppt region for the new ICP-Q_T system. A significant reduction in instrument size and complexity has also resulted from this new approach.

1. C. J. Barinaga and D. W. Koppenaal, Rapid Comm. Mass Spectrom. **8**, 71 (1994).
2. D. W. Koppenaal, C. J. Barinaga, and M. R. Smith, J. Anal. At. Spectrom. **9**, 1053 (1994).

* Pacific Northwest Laboratory is operated for the U.S. Dept. of Energy by Battelle Memorial Institute under contract DE-AC06-76RLO 1830.

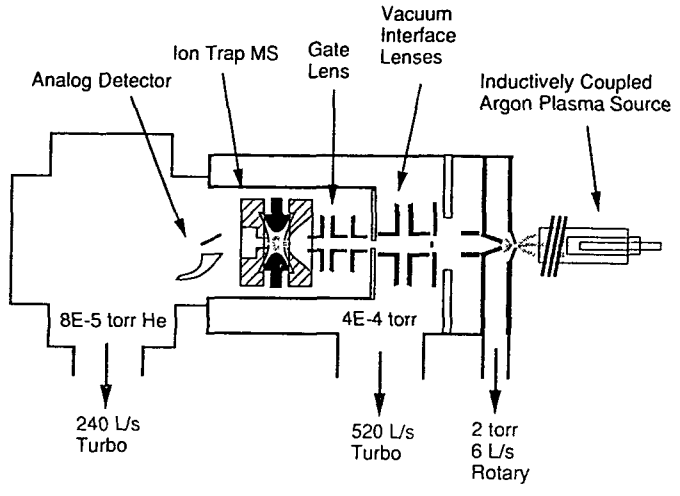

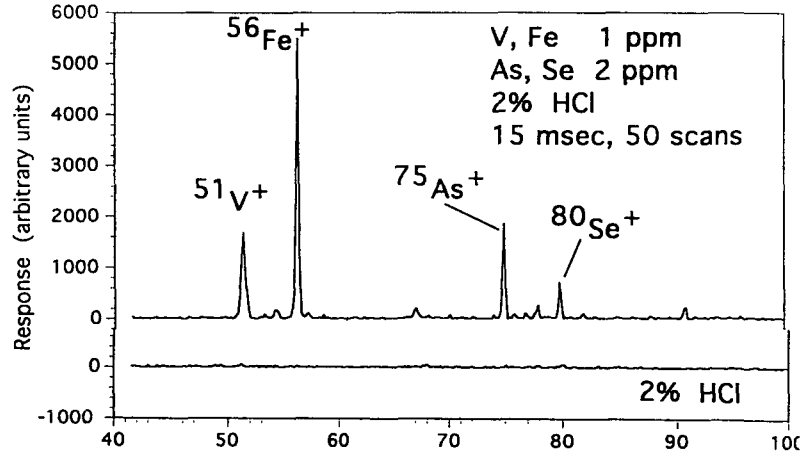

Glow Discharge Ion Trap Mass Spectrometry Employing Filtered Noise Fields

Douglas C. Duckworth, David H. Smith, Douglas E. Goeringer, Scott A. McLuckey
Oak Ridge National Laboratory, Oak Ridge, TN 37831-6375

Introduction

In previous work we have shown quadrupole ion traps to be promising mass analyzers for glow-discharge-generated ions. Among the benefits are the spontaneous dissociation of weakly bound polyatomics and the ability to dissociate more strongly bound polyatomic ions through the application of a resonance excitation frequency. To date, this has been accomplished using single frequency excitation. In this work, we use digitally synthesized broadband noise fields for simultaneous resonance excitation of several m/z species. Because they are digitally synthesized, these filtered noise fields (FNF's) can be single or multiple notch filters which can be employed for selective ion accumulation and mass isolation.

Experimental

An argon direct-current glow-discharge ion source was interfaced to a Teledyne HST-2000 quadrupole ion trap mass analyzer. Ions extracted from the cell passed through an ion exit orifice and were focussed through the entrance endcap with a three-element lens system. The second element was a pair of half-plates, which were used to gate ions into the trap.

Results

Figure 1 shows mass spectra from NIST SRM 1103 Free Cutting Brass. In the absence of a FNF notch filter (Figure 1a), space charge effects are evident from the lack of mass resolution. When the FNF notch filter is used during ion injection, only the Sn ions undergo stable trajectories in the trap, resulting in selective ion accumulation, improved sensitivity, and improved mass resolution.

Two filtered noise fields are shown in Figure 2. Figure 2a shows the frequencies applied to the endcaps to isolate the polyatomic species assigned as CuO^+ and $CuOH^+$. These ions were generated from Cu in a brass matrix. The resulting spectrum is shown in spectrum 3a. Upon the application of a broadband resonance excitation field (109 - 120 kHz) shown in 2b, the polyatomic ions dissociate. The product ions, ^{63}Cu and ^{64}Cu, are recovered with ~80% efficiency (Figure 3b).

Conclusion

Filtered noise fields have proven to be an effective means of selective ion accumulation, which will be necessary for routine detection at low concentration levels. The ability easily tailor waveforms with high selectivity will be essential as matrices change. The ability to dissociate polyatomic ions may allow purely atomic spectra to be observed.

Acknowledgment

U.S. Department of Energy, Office of Basic Energy Sciences, under Contract DE-AC05-84OR21400 with Martin Marietta Energy Systems, Inc.

"The submitted manuscript has been authored by a contractor of the U.S. Government under contract No. DE-AC05-84OR21400. Accordingly, the U.S. Government retains a nonexclusive, royalty-free license to publish or reproduce the published form of this contribution, or allow others to do so, for U.S. Government purposes."

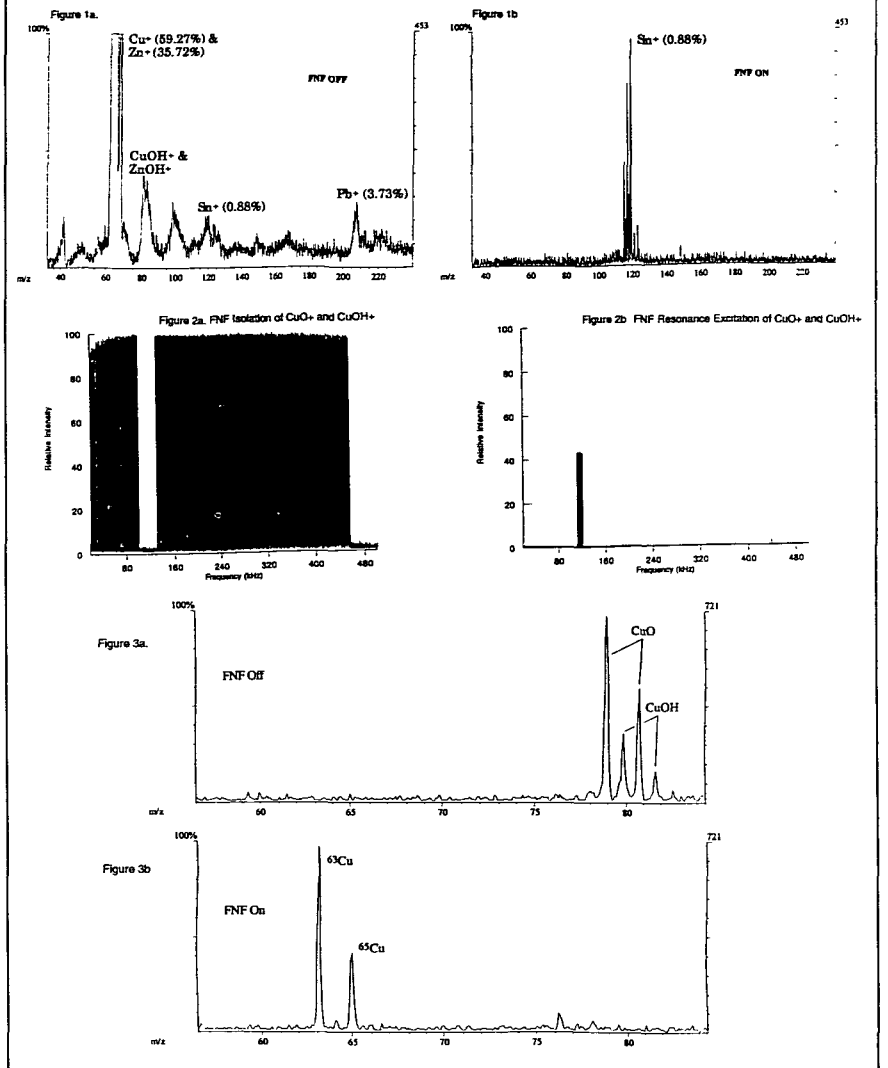

TIME-OF-FLIGHT MASS SPECTROMETRY WITH A PULSED GLOW DISCHARGE SOURCE

Robert E. Steiner, Cris L. Lewis, and Fred L. King
Department of Chemistry, West Virginia University, Morgantown, WV 26506

A pulsed glow discharge plasma makes a nearly ideal ionization source for time-of-flight mass spectrometry. This combination exhibits distinct advantages for the direct determination of trace elements in solid state samples. Improvements in sensitivity and selectivity result from the pulsed operation of the glow discharge. These improvements arise from the selective enhancement of the Penning ionization processes occurring during the time period immediately following the termination of the discharge power[1].

$$Ar^m + M \rightarrow Ar + M^+ + e^-$$

Time-of-flight mass spectrometry uniquely affords the ability to monitor a narrow temporal window for a time varying process such as ion formation in the pulsed glow discharge plasma. Because electron ionization processes terminate with applied power termination, the ion extraction into the ToF-MS after power termination yields a mass spectrum that is free from contributions arising from electron ionized species.

Variation of the temporal location of the repeller pulse within the 20 ms discharge pulse cycle permits investigation into the temporal evolution of the ion formation within the plasma. Moving this pulse to a time window after the termination of the discharge power results in improved analytical performance because the analyte ion signals are at a maximum while the discharge gas ion signals are at a minimum. Such sampling eliminates the saturation of the detector arising from the strong argon ion signal. Spectra representative of this temporal selectivity are shown below. ToF mass spectra for the plateau and afterpeak time regimes are shown in Figure 1 for a copper-iron-silver pressed disk. The plateau region spectra exhibits signals from both analyte and discharge gas species. The spectra aquired during afterpeak region shows no contribution from discharge gas species and is dominated by the Fe, Cu, and Ag signals.

Pulsed radio-frequency glow discharge ionization sources may also be interfaced to the time-of-flight mass spectrometer. The pulsed operation mode of the RF power source again makes temporal selectivity possible. Another distinct advantage of the pulsed RF source is its ability to sputter nonconducting materials. This capability allows analytes such as glasses or ceramics to be analyzed via ToF mass spectrometry.

The pulsed GD-TOFMS system implemented in our laboratory suffered from poor resolution. One method known to improve resolution is the implementation of a narrow slit place behind the skimmer cone and oriented in an orthogonal geometry with respect to the flight tube[2]. In theory this slit will narrow the ion beam entering

the accelerator region and therefore like analyte ions pulsed into the flight tube will have a narrower range of flight distances. However, a problem arises when the width of this slit becomes too narrow or too great as shown in Figure 2. At narrow widths, species at low concentrations may not provide sufficient signals to trigger the detector, resulting in lower observed signal intensities. This is evident for the $^{63}Cu/^{65}Cu$ ratio. At narrow slit widths this isotope ratio may increase as much as two fold over the actual value. When no slit is utilized, the isotope ratio actually falls below the known value. This observation can be attributed to saturation of the detector. Spectra collected with no slit also have characteristic low energy tails for analyte signals with high intensities that degrade resolution.

[1] Pan, C.; King F.L. Anal. Chem. 1993, 65, 3187-3193.
[2] Myers, D.P.; Yang, G.L.P.; Hieftje, G.M. J. Am. Soc. Mass. Spec. 1994, 5, 1008-1016.

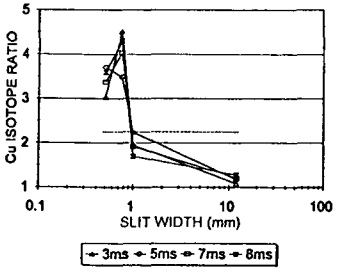

Figure 1 $^{63}Cu/^{65}Cu$ isotope ratio vs. slit widths

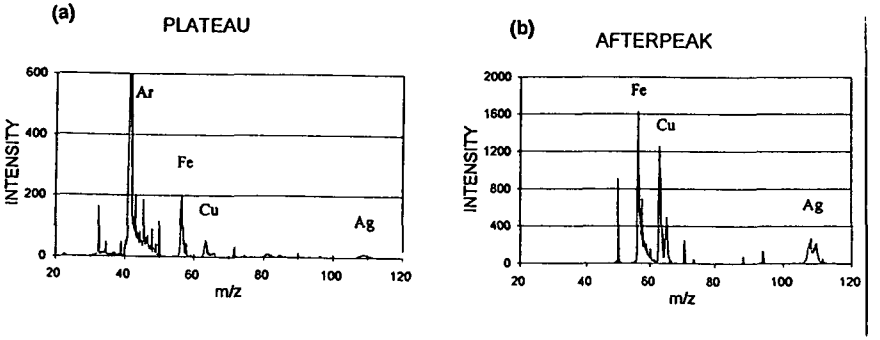

Figure 2 ToF spectra of Fe, Cu, Ag disk in (a) plateau and (b) afterpeak regions

ANODIC STRIPPING VOLTAMMETRY COUPLED ON-LINE WITH ICP-MS

Gary J. Van Berkel, Feimeng Zhou, Douglas C. Duckworth, and Shelby J. Morton
Chemical and Analytical Sciences Division
Oak Ridge National Laboratory, Oak Ridge, TN 37831-6365

Inductively coupled plasma-mass spectrometry (ICP-MS) is a sensitive technique for elemental analysis which provides submicrogram-per-liter (sub-ppb) detection limits (DLs) for most elements. The drive towards lower DLs in response to regulatory mandates and the need to eliminate problems imposed in quantitative analyses by sample matrices are research areas of active pursuit in ICP-MS. A generic means to effectively lower concentration detection limits and eliminate matrix effects is an on-line preconcentration/matrix elimination device In our hands, anodic stripping voltammetry (ASV) coupled on-line with ICP-MS has proven to be an effective and relatively simple method for on-line preconcentration and matrix elimination [1,2].

ASV utilizes an electrochemical deposition step to preconcentrate metal species from solution into the small volume of a mercury electrode. After deposition, the metal is electrochemically oxidized, thereby stripping it from the electrode back into solution. In previous work [1,2], we have shown that concentration detection limits for our VG Plasma Quad, equipped with a conventional nebulizer and spray chamber, could be lowered by at least an order-of-magnitude for some elements (e.g., Tl) with on-line ASV-ICP-MS using a thin-layer, low-dead volume (i.e., 1.0 µL) flow-by electrochemical cell. This flow cell consists of a 6-mm dia glassy carbon working electrode, a s.s. auxiliary electrode, and a Ag/AgCl reference electrode. We also showed that quantification was feasible at metal concentration levels below the normal detection limits of our ICP-MS and that matrix interferences could be effectively eliminated with problem samples such as urine. The linear calibration curves for Tl shown in Figure 1 demonstrate the large dynamic range of the combination and the low detection limits (3σ/sensitivity).

Even though the quality of the data obtained with our prior experimental setup was good, there were two major limitations imposed by the high flow rates (near 1.0 mL/min) necessary for operation of the conventional spray chamber and nebulizer. First, the electrolytic efficiency of the thin-layer cell was low thus requiring longer plating times (and sample volumes of a few milliliters) to achieve the desired level of preconcentration. Second, the mercury thin-film electrode used for preconcentration was not physically stable for longer than a few experimental runs (e g., about 30 min). Therefore, frequent stripping and replating of the film was necessary which decreased sample throughput. These problems have recently been circumvented by incorporation of a direct injection nebulizer (CETAC Technologies, Inc.) into our system which operates at much lower flow rates. ASV-ICP-MS experiments are now carried out at 50-60 µL/min and film lifetimes are greater than 8 hrs. The increased electrolytic efficiency of the cell (ca. 80 %) has reduced sample consumption to a few hundred microliters or less for elements present at or above the low ppt level. Another area being explored with this new system is multi-element analysis. As illustrated by the data in Figure 2, we can now analyze for at least six elements simultaneously by first plating all six (180 s, -1 25 V) then simultaneously stripping them (0.25 V) from the film. Each of the six elements shown was present in the sample at the low ppb level.

(1) Zhou, F , et al Proceedings of the 42nd ASMS Conference, p. 844. (2) Zhou, F., et al. Special ASTM Symposium Publication, in press.

Research Sponsored by the United States Department of Energy, Office of Basic Energy Sciences under contract DE- AC05-84OR21400 with Martin Marietta Energy Systems, Inc.

FIGURE 1

Linear Dynamic Range for Tl Detection by ASV-ICPMS

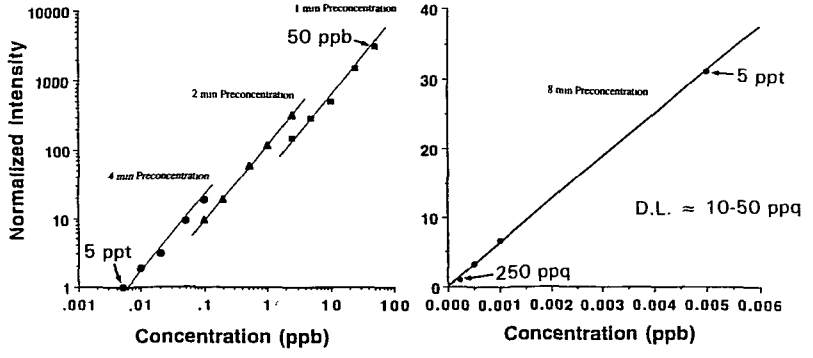

FIGURE 2

Determination of Multiple Elements in Synthetic Urine

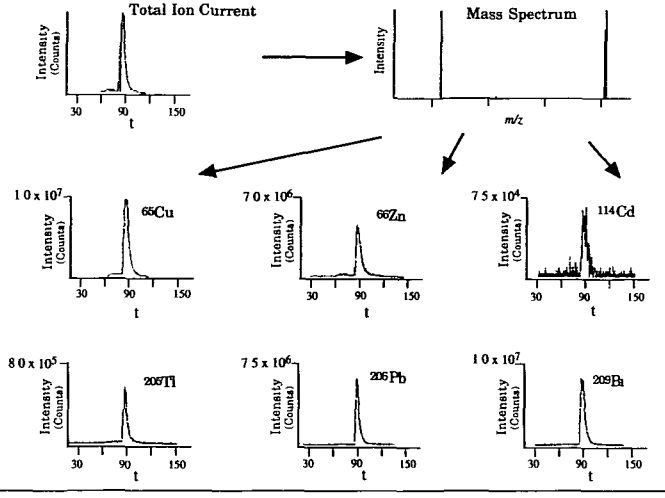

LASER ABLATION ICPMS ANALYSIS OF REAL WORLD SAMPLES.

Michael S. Kahr, Christopher Brink, Deborah Figg
Chemical Science and Technology Division
Los Alamos National Laboratory
Los Alamos NM 87545

INTRODUCTION

There is a need to develop a rugged, rapid, accurate in-situ technique to provide elemental data for solid radioactive (hot) samples. Laser ablation inductively coupled plasma mass spectrometry (LA/ICPMS) is an attractive method for application to this problem. LA/ICPMS provides rapid analyses without the need for sample preparation or digestion. LA/ICPMS is also capable of providing in-situ analysis with spatial information for elemental composition. Laser ablated material can be introduced remotely via tubing into an inductively coupled plasma mass spectrometer (ICP/MS) system. This allows the mass spectrometer and operator to sit away from the actual sample, which is ideal for hot sample analysis. Mass spectrometric detection allows positive identification for elements with less spectral interferences than for atomic emission spectroscopy (AES).

EXPERIMENTAL

The fundamental, frequency doubled, and frequency quadrupled output of a Nd:YAG laser at 1064 nm, 532 nm, and 266 nm, respectively, was employed for ablation. Power can be varied by changing the voltage of the laser flashlamp or by employing a laser power attenuator. Particle size distributions were measured using a commercially available laser Raman scattering particle size instrument which has a useful analysis range of 0.1 μm to 2.0 μm. Laser powers were measured after the last mirror in the optics set-up prior to focusing the laser beam for ablation. The glass sample employed for these experiments was West Valley 205, a waste glass simulant. The sample cell was mounted to an x,y,z computer controlled positioning stage. Ablated material was carried into the ICP mass spectrometer by argon flowing through the sample cell.

RESULTS AND DISCUSSION

The relative change in elemental fractionation was monitored by taking the ratio of the raw counts for each isotope to the raw counts for Zr 90. This was calculated at each z position and then normalized to the ratio determined at the focus point. This fractional change of the ratios is shown in Figures 1 and 2 for 1064 nm and 266 nm, respectively. Lower ablation powers at 266 nm produced ratios that were relatively constant throughout the range of z motion (+/- 20% throughout a delta z of 15-20 mm).

Elemental fractionation as a function of z position was observed for both the 532 and 1064 nm wavelengths. In addition to the elemental fractionation, an elemental bias becomes obvious at higher ablation powers. It appears that for the elements studied there are two groups of behavior. The first group includes Ba, Ce, Nd, La, and Al. These elements behave similar to Zr with ratios to Zr that are laser focus independent. The second group includes Si, Ru, Ni, Na, and Fe. The relative elemental responses for the second group, unlike the first group, are laser focus dependent. As this sample is a glass, it is expected that most of the constituent elements are in their oxide form. The oxides of the first group of elements (similar to Zr) have high melting points, while those of the second group have low melting points, decompose or sublimate. The second group is thus more sensitive to the local heating of the surface by infrared and visible light which presumably ablates via a thermal mechanism.

43rd ASMS Conference on Mass Spectrometry and Allied Topics

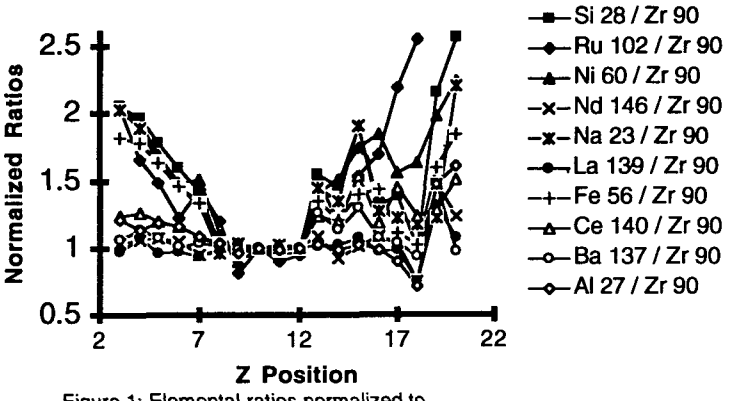

Figure 1: Elemental ratios normalized to their value at the focus point (z=12 mm) for ablation using a1064 nm laser beam.

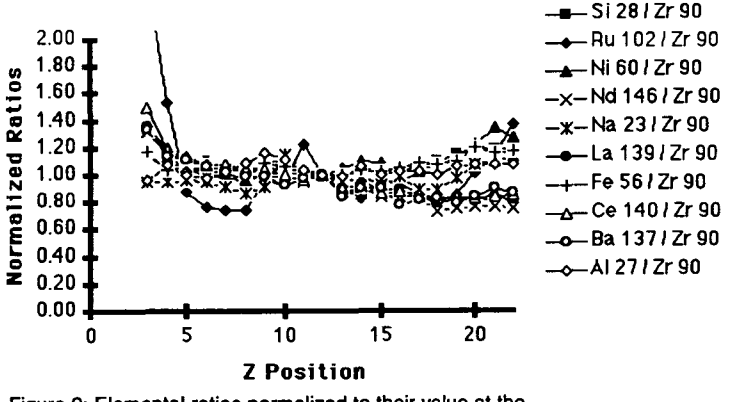

Figure 2: Elemental ratios normalized to their value at the focus point (z=12 mm) for ablation using a 266 nm laser beam.

ANALYSIS OF NOMINALLY FLAT SAMPLES BY RADIO-FREQUENCY POWERED GDMS

Charles R. Shick, Jr. and R. Kenneth Marcus

Clemson University, Department of Chemistry, Howard L. Hunter Laboratory, Clemson, SC 29634-1905.

INTRODUCTION.

Glow discharge mass spectrometry (GDMS) has persevered through the years to become a widely accepted method for performing sensitive direct solids analysis of metals, alloys, and semiconductors. Non-conducting samples are required to be made conducting by either mixing with a conducting binder like copper powder or utilizing a secondary, sacrificial metal cathode to initiate a GD at the surface of the non-conducting sample. In this laboratory, radio-frequency (rf) powered GD sources have been developed for the analysis of non-conducting samples. These sources can atomize both conducting and non-conducting samples and produce stable ion beams leading to reliable mass spectrometric analysis. The objectives of this work were to optimize rf-GD parameters, provide figures of merit, and investigate rf power losses through non-conducting samples for a flat-type sample rf-GDMS source.

EXPERIMENTAL.

With only slight modifications, a VG GloQuad (Fisons Instruments, Elemental) has been developed into an rf-GDMS system. This system is a quadrupole-based instrument with two detectors installed: a Faraday cup for ion currents typical of matrix species and an electron multiplier for minor and trace measurements. A novel flat sample holder was designed to mount onto the end of a direct insertion probe (DIP).

RESULTS AND DISCUSSION.

Optimization study. A series of parametric studies for both conducting and non-conducting samples were performed towards identifying an optimum source geometry and set of discharge conditions. Three discharge cells, which varied in length from 6 to 10 mm (cell length is the distance from the edge of the discharge cell to the ion exit orifice) were evaluated according to the response of analyte signal to changes in the rf power, Ar flow rate (cell pressure), and limiting anode orifice plate. The optimum conditions for conducting samples were a 10 mm discharge cell length, 10 mm anode orifice plate, 2.50 - 3.00 sccm Ar flow rates, and 30 - 35 W rf powers. For the non-conducting samples, the optimum conditions were also with the 10 mm discharge cell length and 10 mm anode orifice plate; however, the better analytical ion beams were found between 1.50 - 2.00 sccm Ar flow rates and 35 - 40 W rf power range.

Non-conducting sample considerations. Temporal stability and external repeatability of non-conducting samples are hindered because most of these samples are either porous or contain significant amounts of trapped gases. These residual gases have the undesired effects of producing isobaric interferences, irreproducibility (stemming from the variability in the "wetness" from glass sample to glass sample), and discharge instability. In order to achieve some consistent level of sample preparation and to reduce residual gas/contaminant contributions, non-conducting samples must be pre-sputtered for approximately an hour. The dielectric nature of the non-conducting samples causes rf power losses as a function of sample thickness and in turn affects the ion beam intensity. Figure 1 demonstrates the linear relationship between $^{55}Mn^+/^{28}Si^+$ as a function of sample thickness. A correction could be obtained for this effect where $R_{corrected} = R_{measured}$ + (slope*change in thickness).

Figure 1.

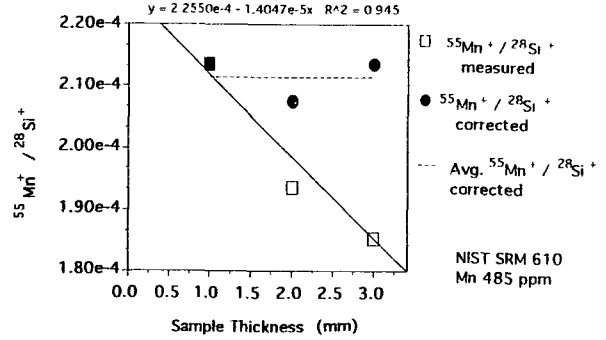

SUMMARY.

A complete optimization and evaluation study of this rf-GDMS system has determined the optimum conditions for both conducting and non-conducting samples. Plasma stabilization times are < 5 minutes for conductors and < 60 minutes for non-conductors. The overall internal (< 5 %RSD) and external (< 12 %RSD) repeatabilities were reported. RSF variations for non-conductors was shown to be due to rf power losses through different sample thicknesses. Preliminary observations for rf-GDMS depth profile analysis were also presented.

ACKNOWLEDGEMENTS.

Financial and instrumentation support from the National Science Foundation and Fisons Instruments are greatly appreciated.

High Precision Continuous Flow D/H Measurement from Hydrogen Gas and Water

H. J. Tobias; K. J. Goodman; C. E. Blacken; J. T. Brenna
Division of Nutritional Sciences, Cornell University, Ithaca NY 14853

High precision gas isotope ratio mass spectrometry (GIRMS) has been the technique of choice for determination of isotopes of the light elements, H, C, N, O, and S for several decades. Fast, continuous flow techniques have been developed for all the classic IRMS elements except for H. A system capable of determining D/H ratios via continuous flow is presented here.[1]

A Varian 3400 gas chromatograph (GC) with a split/splitless injector set at 250°C equipped with 10 meters of fused silica capillary, is interfaced with an IRMS. Hydrogen gas samples are swept by Ar or He carrier through the capillary and directed to a Pd foil held at 330°C (Fig 1). The Pd foil is mounted on a tube that leads into the mass spectrometer ion source. At elevated temperatures, the Pd absorbs and transfers only hydrogen isotopes into the vacuum, and so serves as a hydrogen filter. Purified H_2 and HD then flow to the ion source and *m/z* 2 and 3 are continuously monitored. Precision for repeated injections of H_2 gas is S.D. (δD) < 6 ‰ over a range of δD = -200 to 340 ‰. Linearity over this range for gas injections corresponds to an r^2 > 0.99996 and accuracy is < 2 ‰, when referenced to dual inlet analysis.

Liquid water samples (100 nL) are injected into a He carrier, are passed through the capillary and directed into a reduction furnace loaded with Ni metal and held at about 850°C (Fig 1). A combustion furnace filled with CuO and Pt metal can be positioned before the reduction furnace for potential extension to hydrocarbon analysis. A Nafion™ (DuPont) water trap removes trace quantities of unreduced water from the stream and flow is directed to a Pd foil. Source nonlinearities were characterized for hydrogen analysis in which no carrier gas enters the ion source. These nonlinearities can be corrected; water sample analyses with precisions of S.D. (δD) < 10 ‰ over a range of δD = 400 ‰ and accuracy of < 4 ‰ are obtained. A significant problem with water analysis is that of sample memory.[2] Memory effects were assessed for repeated water injections over a larger range of δD from about -50 to 4700 ‰. Consecutive injections show no signs of memory effects, even for injection of tap water (sample a) after five consecutive injections of δD ~ 4700 ‰ water (sample j) as shown in Fig 2.

This work was supported by the NIH (GM49209) and pre-doctoral support for KJG (DK07158).

1. Tobias, H. T.; Goodman, K. J.; Blacken, C. E.; Brenna, J. T. in press to *Anal. Chem.*
2. Wong, W. W.; Cabrera, M. P.; Klein, P. D. *Anal. Chem.* 1984, *56*, 1852-1858.

FIGURE 1:

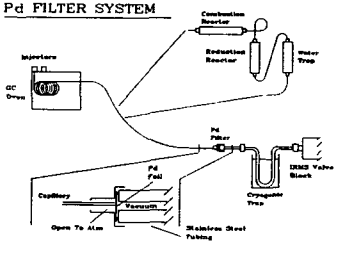

FIGURE 2:

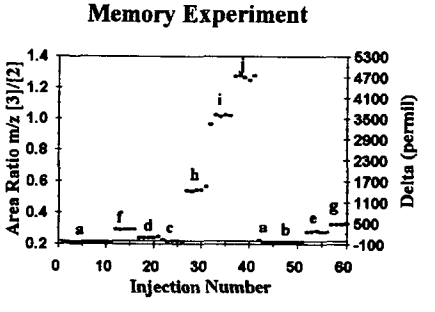

A FIELD MASS SPECTROMETRIC SYSTEM FOR ISOTOPIC ANALYSIS OF ACTINIDES.

Michael S. Kahr, José A. Olivares, Kent D. Abney and Scott Kinkead
Chemical Science and Technology Division
Los Alamos National Laboratory
Los Alamos NM 87545

INTRODUCTION

An important need exists for field instrumentation capable of providing isotopic analysis of uranium and plutonium samples. Currently, the time required for actinide isotopic analysis of field samples is weeks to months. Clearly this delay is too long to make appropriate decisions by inspectors. This data could be obtained rapidly on site by employing the transportable field mass spectrometer system which has been developed and tested by our group.

EXPERIMENTAL

A compact transportable mass spectrometric system based upon a commercially available quadrupole residual gas analyzer has been developed and evaluated. The system has been minimized for size and weight and currently fits into a large suitcase.

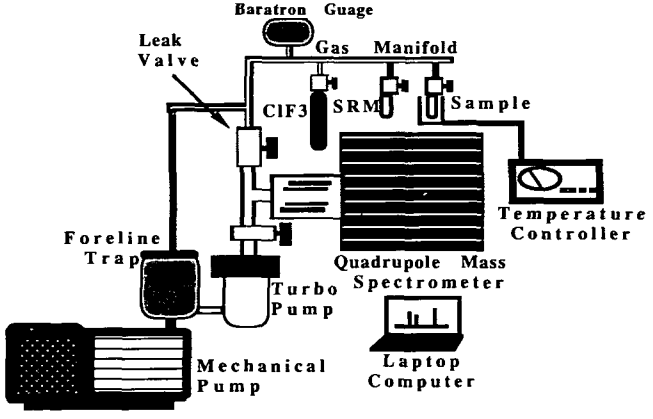

FIGURE 1: Block diagram of the transportable mass spectrometer system for actinide analysis.

For these studies, uranium samples are converted into volatile hexafluorides by reaction with chlorine triflouride. Chlorine trifluoride rapidly converts all uranium compounds studied to UF_6, including high fired uranium pellets. The uranium hexafluoride is then introduced into the mass spectrometer for isotopic analysis. Isotopic ratios are measured from the doubly charged uranium ion signal using peak heights.

RESULTS

Standard (NIST) reference uranium samples and a highly enriched sample from Los Alamos National Laboratory were analyzed for their isotope ratios. The quantitative results are reported in Table 1. Without calibration or mass bias correction the differences between the measured and reported values for the standards was better than 10% in all cases.

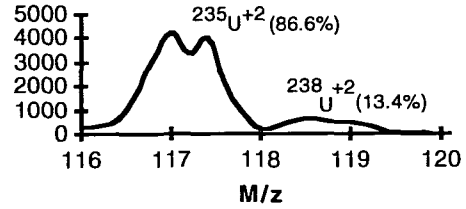

Figure 2: Mass spectrum of a highly enriched sample (The Alpa Wing sample, see Table 1 below) This sample was measured to be 86.6% 235U.

Table 1: Quantitative Results

Sample	%U235 (NBS)	%U235 (Best Value)	Average Error (%)	RSD
U950a	0.7	0.8	12.3	N.A.
Depleted Uranium	<0.7	0.4	N.A.	N.A,
U030	3.0	3.1	6.1	7.3
U500	50.0	48.1	6.6	4.6
Alpha Wing	N.A.	86.6	N.A.	N.A.

CONCLUSION

A small transportable mass spectrometer system has been constructed and employed to analyze a range of uranium samples with various isotopic compositions including a highly enriched sample which was measured to be 86.6% ^{235}U. Accuracy is currently better than 10% without calibration or mass bias correction employing a simple peak height algorithm. Accuracy is expected to improve by employing calibration, mass bias correction and peak areas with background subtraction.

Nuclear Isotope Measurement in the Hanford Environment

J.F. Wacker, J.J. Stoffel(s), J.M. Kelley, L.A. Bond, R.A. Kiddy, and F.P. Brauer
Pacific Northwest Laboratory, Richland, WA 99352

The Pacific Northwest Laboratory (PNL) is located at the federal government's Hanford Site in southeastern Washington State, which was built during World War II as part of the secret Manhattan Project to develop the atomic bomb. Hanford produced the plutonium for the Trinity test and for the bomb exploded on Nagasaki on August 9, 1945. The war ended six days later.

Monitoring of the Site itself and surrounding environs for Hanford-related radionuclides has been a routine part of the operations since 1944. One of the most sensitive analytical methods used is thermal ionization mass spectrometry (TIMS) with triple-sector mass spectrometers. Our normal geometry instruments have an abundance sensitivity of 10^{-9} for uranium while our newest Triple-Sector Isotope Mass Spectrometer (TRISM), utilizing a new ion-optical design developed at PNL, has an abundance sensitivity of 10^{-11} [1]. In favorable cases, sensitivity is such that complete isotopic analyses are obtained on total samples in the femtogram range; and minor isotopes in the attogram range are measured.

Plutonium Measurement

Plutonium is a highly toxic element that has been distributed over the earth's surface by atmospheric testing of nuclear weapons. To distinguish plutonium from a second source, such as Hanford production facilities, it is necessary to resolve the contribution of that source from the global burden of fallout plutonium in soil Soil and sediment samples of typically 1 gram are dissolved by microwave digestion. The plutonium is chemically separated, purified, and loaded into an ion-exchange resin bead for analysis by positive thermal ionization.

Table 1 shows the concentration and isotopic composition of plutonium in soil as a function of distance from the Hanford source in the center of the Site. Distant from the Site, the plutonium isotopic composition, as characterized by the $^{240}Pu/^{239}Pu$ ratio, is the global mean value for fallout. At a distance of two miles from the plant, the plutonium concentration is elevated and has an isotopic composition that is a mixture of Hanford product and fallout. Only one mile from the plant, the plutonium concentration is higher and has an isotopic composition characteristic of weapons-grade material. Beyond the Site boundary, Hanford plutonium is not detectable in soil.

Table 1. Plutonium concentration and isotopic composition in soil, fallout and Hanford product

Distance from plant (miles)	Replicate samples	Pu concentration (fg/g ± 1σ)	Isotopic composition ($^{240}Pu/^{239}Pu$ ± 1σ)
200	3	91 ± 7	0.1785 ± 0.0095
2	4	212 ± 16	0.0957 ± 0.0013
1	2	263 ± 31	0.0522 ± 0.0005

Radioiodine Measurement

Another important application of TIMS at Hanford is measurement of the long-lived (half-life=16 million years) fission product, ^{129}I Groundwater beneath the Hanford Site is contaminated with ^{129}I as a result of past waste disposal practices. The contaminated groundwater seeps into the Columbia River along the Site boundary. The Columbia River is monitored quarterly with samples from locations above the Hanford Site and at the pumphouse for the City of Richland's water system downstream of the Site.

Iodine samples are spiked with ^{125}I to obtain the concentrations of both ^{129}I and natural ^{127}I by isotope dilution, and are analyzed by negative thermal ionization. Two ion detectors are required for measurement of the large isotope ratios, a Faraday cup to measure the intense beam of natural ^{127}I (typically 10^{-9} A) and a pulse-counting electron multiplier for the minor isotopes. The minor isotope measurement limit, due to contaminant interference in the mass spectrum, is 10^7 atoms (2 fg) of ^{129}I.

Table 2 gives data for 1993. The concentration of natural ^{127}I in the river was the same above and below Hanford, ~1 μg/L. Although the concentration of ^{129}I below Hanford, 678 fg/L, was 26 times greater than above Hanford, the amount is still negligible The ^{129}I concentration downstream from Hanford corresponds to an activity of 1.2×10^{-4} pCi/L. This is 8,000 times lower than the EPA Drinking Water Standard of 1 pCi/L for ^{129}I.

Table 2. Annual average iodine concentrations in Columbia River water during 1993

Location	^{127}I (μg/L ± 1σ)	^{129}I (fg/L ± 1σ)
Above Hanford	1.04 ± 0.30	26 ± 7
Below Hanford	1.06 ± 0.40	678 ± 147

TEAMS

The objective of the TEAMS project is to combine the efficiency of a thermal emission (TE) ion source with the isobaric selectivity of an accelerator mass spectrometer (AMS) for measurement of ^{129}I and other nuclides in small (less than microgram) samples. We have completed construction of a thermal emission ion source module that is being installed on the AMS at Lawrence Livermore National Laboratory. The module is equipped with the same commercial thermal ion source that is used on our new TRISM mass spectrometer. We have also built and installed a low-current Faraday cup for small sample measurements.

In our collaboration with LLNL, we have been developing a small sample capability with their existing Cs^+ sputter ion source. We have already reduced the sample size that can be run by a factor of 100--from 3 mg down to 30 μg--with reproducible results. The AMS measurement limit for ^{129}I is 10^6 atoms. We expect the TEAMS system to push that limit down to 10^5 atoms.

1. J. J. Stoffel(s), D. R. Ells, L. A. Bond, P. A. Freedman, B. N. Tattersall, and C. R. Lagergren, Int. J. Mass Spectrom. Ion Processes 132, 217 (1994).

Thermal Ionization Cavity Source for Mass Spectrometry

José A. Olivares, Edwin P. Chamberlin, and Yixiang Duan, Los Alamos National Laboratory, Chemical Science and Technology Division, Los Alamos, NM 87545

Thermal ionization mass spectrometry (TIMS) is widely used for isotopic determination, and elemental concentration measurements by isotope dilution. TIMS is applicable to over 70 elements in the periodic table, often, with very high sensitivity, low detection limits, high precision, and high accuracy.[1] Probably due to its success and simplicity, the traditional resistively heated filament type ion source, used in TIMS, has remained relatively unchanged in the past 50 years Only minor changes in the number of filaments used for vaporization and ionization, and the shape of the filament have been employed. Much of the science of thermal ionization has focused on sample preparation, and chemical ionization enhancers.

Beyer et al.[2], in the USSR, and Johnson et al.[3], later in the US, introduced a new high temperature cavity-type thermal ionization source for isotope separation on-line (ISOL) projects. Delmore et al.[4] introduced a similar cavity-type source for the study of thermal emission of primary ions for secondary ionization mass spectrometry (SIMS)

A new thermal ionization cavity-type source for mass spectrometry has been developed in our laboratories. The source is based on the sources developed for isotope separation but, has been miniaturized for use on small quadrupole and sector mass spectrometers, see Fig. 1. The redesign of the source has kept, as the main objective, the high sample utilization efficiency for which the original sources are well known. The new source has been characterized on an isotope separator and on a quadrupole mass spectrometer The source gives ionization efficiencies of 2% for thorium, 8% for uranium, and rare-earths and other elements can exhibit around 50% ionization efficiency. This is 10-100 times better sample utilization efficiency than achieved by conventional filament type thermal ionization sources.

Vaporization and ionization of the sample is governed by the temperature required to give a substantial vapor pressure (~10^{-4} Torr) of the element of interest in the source cavity. This is exemplified in Figure 2, showing a spectrum of Eu, Sm, and Lu taken from the oxide powders loaded into the source. Note the absence of MO^+ ions in these spectra. For the actinides the MO^+ ions are more prominent and must be controlled, typically with the use of graphite. The enhanced ionization is caused by the multitude of atom to surface interactions as the atoms evaporate and leave the source cavity

[1] Herzog, L. F. *Int. J. Mass Spectrom. Ion Phys* **1970**, 4, 253-265.
[2] Beyer, G. J., E. Herrmann, A. Piotrowski, V. J. Raiko, and H. Tyrroff *Nucl. Instrum. and Meth.* **1971**, 96, 437-439.
[3] Johnson, P G., A. Bolson, and C. M. Henderson *Nucl. Instrum. and Meth.* **1973**, 106, 83-87.
[4] Delmore, J. E., A. D. Appelhans, and E. S Peterson *Int. J. Mass Spectrom. Ion Phys.* **1991**, 108, 179-187

Internal isotopic precision measurements have been made on various rare-earths The precision varies with the element, and source conditions. Typical precisions for short measurement periods (~10 min) are around 1% Yet, some measurements with precisions in the 10's of ppm have been observed, see Table I.

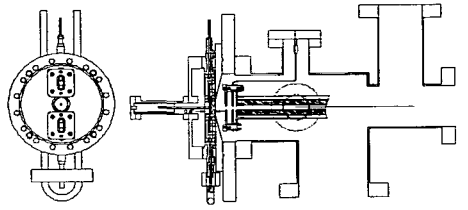

Figure 1. Thermal ionization cavity source on a quadrupole mass spectrometer

Table I. Internal isotopic precision for 10 min measurements

Ratio	Average Value	Standard Deviation	%RSD
	Europium Isotopic Ratios		
151/153	0.98620	0.000034	0.0034
	Samarium Isotope Ratios		
144/152	0.1749	0.0032	1.8
147/152	0.6678	0.0093	1.4
148/152	0.5015	0.0064	1.3
149/152	0.5871	0.0068	1.2
150/152	0.3227	0.0031	0.97
154/152	0.8091	0.0051	0.62

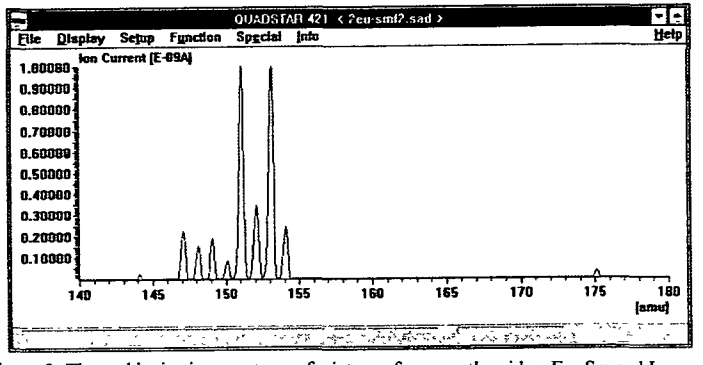

Figure 2. Thermal ionization spectrum of mixture of rare-earth oxides, Eu, Sm and Lu.

Carbenes represent an important class of reactive intermediates in organic chemistry.[1] Their reactivity is determined, in part, by their spin multiplicity. Methylene, the simplest of all carbenes, is a ground state triplet and reacts via radical-type multi-step reactions which produce biradical-type intermediates. Substitution of one or more hydrogens by π-donating, σ-withdrawing groups can stabilize the singlet state relative to the triplet state. Singlet carbenes react via single-step concerted pathways with retention of stereochemistry.

Recently, our laboratory determined the heats of formation of CF_2 and CCl_2, both ground state singlets, by measuring the threshold energy for collision-induced halide loss from CF_3^-, and CCl_3^-.[2] We complete the chlorine and fluorine containing carbene series by measuring thermochemical properties for CHF, CHCl, and CFCl, molecules that are of interest due to their possible role as intermediates in the stratospheric degradation of chlorofluorocarbons (CFC's).

CH_2Cl_2, CH_2ClF and $CHCl_2F$ were allowed to react with OH^- in the room temperature flow tube. The ions $CHCl_2^-$, $CHClF^-$, and CCl_2F^- were then mass selected by Q1. Collision-induced dissociation occurs in Q2 with argon serving as the collision target. An appearance curve is generated by monitoring the intensity of the Cl^- product as a function of collision energy in the center of mass frame.

The appearance curve is fit with an assumed model function which explicitly accounts for ion internal energy and the possibility of a kinetic shift due to slow dissociations.[3] From this model, average energy thresholds for collision-induced chloride loss of 1.57 ± 0.11, 0.96 ± 0.09 and 1.07 ± 0.06 eV were determined for $CHCl_2^-$, $CHClF^-$ and $CFCl_2^-$ dissociations.

Gas phase acidities of the parent neutral halocarbons CH_2ClF and $CHFCl_2$ were determined by bracketing techniques. Gas phase acidities of $\Delta H_{acid}(CH_2ClF)$ = 386.1 ± 2.0 and $\Delta H_{acid}(CHFCl_2)$ = 360.9 ± 2.0 kcal/mol were measured. A value for the gas phase acidity of methylene chloride of 369.0 kcal/mol was derived from gas phase equilibrium studies with t-butyl alcohol. The gas phase acidities of the halocarbon precursors were estimated using *ab initio* molecular orbital theory. Acidities calculated from the G2[4] and G2MP2[5] procedures produce are in excellent agreement with our experimental acidities.

The gas phase acidities were then combined with the threshold energies and supplemental thermochemistry to derive the final heats of formation of $\Delta H_{f,298}(CHCl)$ = 80.1 ± 2.8, $\Delta H_{f,298}(CHF)$ = 34.9 ± 3.4 and $\Delta H_{f,298}(CFCl)$ = 7.6 ± 2.6 kcal/mol.

Theoretical estimates for the heats of formation of the halocarbene were calculated using G2 and G2MP2 methods. Heats of formation were determined from the G2 heats of atomization, and from the energies of the isodesmic dihydrogen transfer reaction shown in reaction 1. The values for the heats of formation of the

$$CXY + CH_4 \longrightarrow CXYH_2 + {}^1A_1\ CH_2 \qquad (1)$$

halocarbenes predicted from these methods are in excellent agreement with the heats of formation derived from the threshold energy experiments.

Analogous procedures were used to determine the absolute heats of formation of $SiCl_2$ and SiClF. Average threshold energies for collision-induced chloride loss from $SiCl_3^-$ and $SiCl_2F^-$ were determined to be 2.38 ± 0.05 and 1.99 ± 0.08 eV.

G2MP2 theory was used to predict the gas phase acidities of $SiHCl_3$ and $SiHCl_2F$. Values of $\Delta H_{acid}(SiHCl_3)$ = 338.2 and $\Delta H_{acid}(SiHCl_2F)$ = 344.3 kcal/mol were determined. Combining these energy thresholds with the acidities give values for the heats of formation of $\Delta H_{f,298}(SiCl_2)$ = -37.2 ± 2.5 and $\Delta H_{f,298}(SiClF)$ = -93.8 ± 2.5 kcal/mol. G2 and G2MP2 predictions for the heats of formation of the halosilyleneswere were also carried out and are in good agreement with the experimental values.

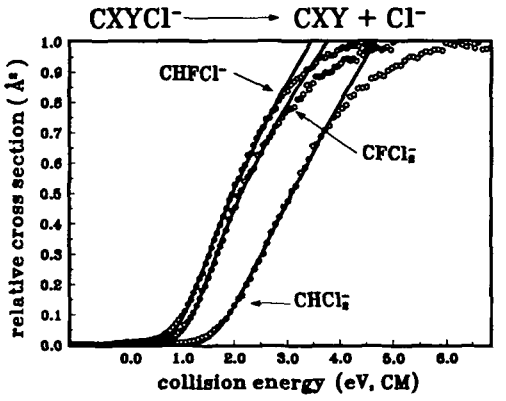

References

1. (a) Kirmse, W. *Carbene Chemistry*; 2nd ed, Academic Press, New York, N.Y., 1971;(b) *Carbenes*; Jones, M. Jr., Moss, R.A., Eds; J. Wiley and Sons: New York, N.Y., 1973.
2. Paulino, J.A., Squires, R.R. *J. Am. Chem. Soc.* **1991**, 113, 5573.
3. Data was analyzed using the CRUNCH program developed by Peter Armentrout and co-workers.
4. Curtiss, L.A.; Raghavachari, K.; Trucks, G.W.; Pople J.A. *J. Chem. Phys.* **1991**, 94, 7221.
5. Curtiss, L.A.; Raghavachari, K.; Pople J.A. *J. Chem. Phys.* **1993**, 98, 1293.

Calculated and Measured Double-ionization Energies of Carbon Tetrachloride

[1] Russell P. Grant,[1] Frank M. Harris,[2] Stuart R. Andrews,[2] David E. Parry,
[1] Mass Spectrometry Research Unit,[2] Chemistry Department, University of Wales
Swansea, Swansea, SA2 8PP, Wales, U.K.

Introduction

Previous investigations of the carbon tetrachloride molecule using Auger-electron (AE) spectroscopy [1] and double-charge-transfer (DCT) spectroscopy [1-3] have yielded considerable information regarding singlet and triplet state energies of CCl_4^{2+}. The theoretical study reported here using the multiple scattering X alpha (MSXalpha) computational method in a semi-empirical form [4], however, predicted that considerably more states exist than had previously been revealed by experimentation. To confirm these predictions, DCT spectroscopy studies of the double-ionization energies (DIEs) to the singlet and triplet electronic states of CCl_4^{2+} were undertaken in the present investigation.

Experimental

3 keV H^+ and OH^+ projectile ions interacted with CCl_4 molecules contained in the collision-gas cell situated in the second field-free region of a Finnigan MAT 8230 mass spectrometer. Double-electron-capture (DEC) reactions generated CCl_4^{2+} and H^-/OH^- ions, the translational energies of which depended on the electronic states of the dication being populated. The H^-/OH^- translational-energy scale was calibrated using xenon, the DIEs to states of Xe^{2+} being known. Because of spin conservation in DEC reactions, the use of H^+ and OH^+ projectile ions populated singlet and triplet electronic states, respectively, of CCl_4^{2+}.

Results

A typical DCT spectrum for H^+/CCl_4 is shown in figure 1. A considerable number of peaks are evident and the DIEs determined from their positions are shown in table 1. Also shown in this table are the DIEs to singlet states of CCl_4^{2+} predicted using the MSXalpha computational method. It can be seen that the predicted and measured DIEs are in good agreement. The increased resolution of the mass spectrometer yields information where previous studies had yielded little, particularly in the 29.1-30.9 eV region, where only one state had been previously reported but four had been predicted.

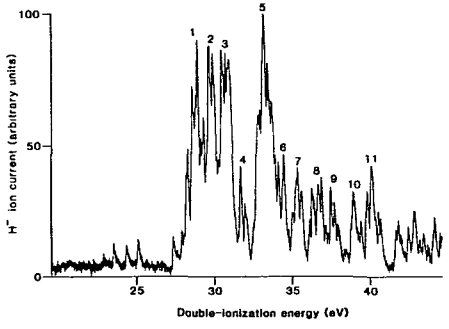

Figure 1

Typical H^+/CCl_4 spectrum.

The data for the OH^+/CCl_4 DCT spectroscopy study is shown in table 2. The predicted data correlates well with the measured data although the density of states from 30.5-32.2 eV is too high for the predicted peaks to be revealed experimentally.

Table 1 Measured and calculated DIEs to singlet states of CCl_4^{2+}.

Peak	Measured[a] (eV)	Calculated[b] (eV)	State configuration	State designation
1	29.1 ± 0.1	29.1	$1t_1^{-2}$	$^1A_1, ^1E, ^1T_2$
2	30.0 ± 0.1	30.0	$1t_1^{-1}3t_2^{-1}$	$^1A_2, ^1E, ^1T_1, ^1T_2$
3	30.9 ± 0.1	30.8 }	$1t_1^{-1}1e^{-1}$	$^1T_1, ^1T_2$
		30.9 }	$3t_2^{-2}$	$^1A_1, ^1E, ^1T_2$
4	32.2 ± 0.2	31.7	$3t_2^{-1}1e^{-1}$	$^1T_1, ^1T_2$
5	33.2 ± 0.1	32.5	$1e^{-2}$	$^1A_1, ^1E$
6	34.2 ± 0.1	34.2	$1t_1^{-1}2t_2^{-1}$	$^1A_2, ^1E, ^1T_1, ^1T_2$
7	35.2 ± 0.1	35.2	$3t_2^{-1}2t_2^{-1}$	$^1A_1, ^1E, ^1T_1, ^1T_2$
8	36.0 ± 0.1	35.9	$1e^{-1}2t_2^{-1}$	$^1T_1, ^1T_2$
9	37.1 ± 0.1	37.3	$1t_1^{-1}2a_1^{-1}$	$^1T_1$
10	38.2 ± 0.2	38.3	$3t_2^{-1}2a_1^{-1}$	$^1T_2$
11	39.1 ± 0.2	39.0	$1e^{-1}2a_1^{-1}$	^1E

Table 2 Measured and calculated DIEs to triplet states of CCl_4^{2+}.

Peak	Measured[a] (eV)	Calculated[b] (eV)	State configuration	State designation
A	29.5 ± 0.2	29.5	$1t_1^{-2}$	$^3T_1$
B	30.7 ± 0.3	30.5	$1t_1^{-1}3t_2^{-1}$	$^3A_2, ^3E, ^3T_1, ^3T_2$
-	-	31.2 }	$1t_1^{-1}1e^{-1}$	$^3T_1, ^3T_2$
		31.4 }	$3t_2^{-2}$	$^3T_1$
-	-	32.2	$3t_2^{-1}1e^{-1}$	$^3T_1, ^3T_2$
C	33.1 ± 0.2	32.9	$1e^{-2}$	$^3A_2$
D	34.5 ± 0.3	34.8	$1t_1^{-1}2t_2^{-1}$	$^3A_2, ^3E, ^3T_1, ^3T_2$
E	35.6 ± 0.3	35.7	$3t_2^{-1}2t_2^{-1}$	$^3A_1, ^3E, ^3T_1, ^3T_2$
F	36.7 ± 0.2	36.5	$1e^{-1}2t_2^{-1}$	$^3T_1, ^3T_2$
G	37.9 ± 0.3	38.0	$1t_1^{-1}2a_1^{-1}$	$^3T_1$
H	39.0 ± 0.3	38.9	$3t_2^{-1}2a_1^{-1}$	$^3T_2$
-	-	39.7 }	$1e^{-1}2a_1^{-1}$	^3E
-	-	40.0 }	$2t_2^{-2}$	$^3T_1$
-	-	43.2	$2t_2^{-1}2a_1^{-1}$	$^3T_2$

Conclusions

The present study has greatly enhanced the information regarding the electronic-state energies of CCl_4^{2+}. The accuracy of the predictions is confirmed by the consistently good agreement obtained between the measured and calculated double-ionization energies.

References

1 P.G. Fournier, G. Comtet, J. Fournier, S. Svensson, L. Karlsson, M.P. Keane and A. Naves de Brito, Phys. Rev. A, 40 (1989) 163.
2 W.J. Griffiths and F.M. Harris, Rapid Commun. Mass Spectrom., 2 (1988) 28.
3 M.L. Langford, F.M Harris, C.J. Reid, J.A. Ballantine and D.E Parry, Int. J. Mass Spectrom. Ion Processes, 112 (1992) 630.
4 S.R Andrews and D.E. Parry, Chem. Phys. Lett., 196 (1992) 630.

Determination of Se-H Bond Energy of Benzeneselenol

Diane T. Leeck, Ruomei Li, Leonard J. Chyall, and Hilkka I. Kenttamaa*

Department of Chemistry, Purdue University
West Lafayette, IN 47907-1393

Benzeneselenol is a useful trapping agent for distonic ions because it transfers a hydrogen atom to distonic ions faster than any other reagent studied. The rate of the trapping reaction depends on the reaction enthalpy. Unfortunately, the Se-H bond dissociation energy of benzeneselenol is unknown. Hence, it is not possible to accurately predict and interpret the outcome of reactions involving benzeneselenol. The objective of this study was to determine the homolytic Se-H bond energy of benzeneselenol.

The experiments were carried out in a dual-cell Fourier-transform ion cyclotron resonance mass spectrometer (FT/ICR). The instrument consists of a differentially pumped dual cell that is aligned collinearly with a magnetic field produced by a 3 T superconducting magnet. Reactant ions were generated in one side of the dual cell, transferred into the other side, and collisionally cooled with argon. The ion of interest was isolated and allowed to react with the desired neutral reagent for a variable period of time.

The homolytic Se-H bond energy of benzeneselenol was determined experimentally by using two independent routes. The hydrogen-selenium bond strength was directly bracketed to be $\leq 82 \pm 2$ kcal mol^{-1} by measuring the efficiency of hydrogen atom abstraction by several radical cations (Figure 1). Another estimate for the Se-H bond energy was obtained from the thermochemical cycle shown in Scheme 1. The ionization energy of benzeneselenol was determined to be 8.3 ± 0.1 eV by measuring the efficiencies of various electron transfer reactions (in the forward and reverse directions; Figure 2). Similarly, the proton affinity of $C_6H_5Se\bullet$ was bracketed to be $201 \pm$ kcal mol^{-1} (Figure 3). Using the thermochemical cycle, the homolytic Se-H bond energy was calculated to be 79 ± 3 kcal mol^{-1}.

The second method is considered to give the better value for the homolytic Se-H bond energy than the first method since the barrier height is not known for hydrogen atom abstraction from benzeneselenol by radical cations. Hence, the value recommended for the Se-H bond energy is 79 ± 3 kcal mol^{-1}. Based on this value, hydrogen atom abstraction from benzeneselenol by most distonic ions is concluded to be highly exothermic.

$$D(\text{Se-H; kcal mol}^{-1}) = IE(C_6H_5SeH) + PA(C_6H_5Se\bullet) - IE(H\bullet) \quad (1)$$

43rd ASMS Conference on Mass Spectrometry and Allied Topics

Scheme 1

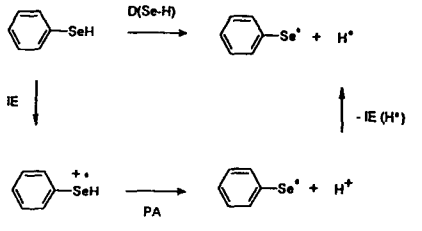

Figure 1

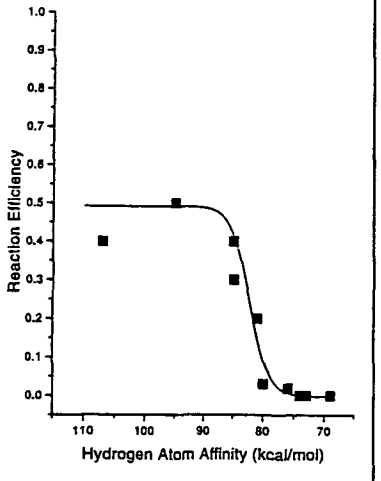

Figure 2

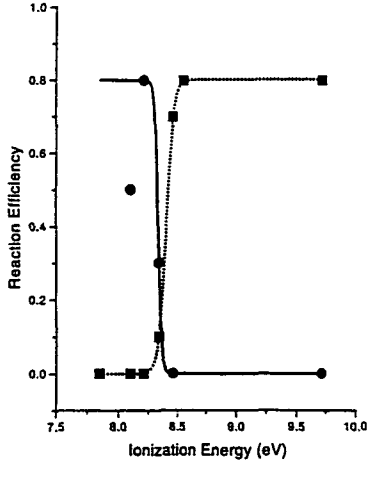

Figure 3

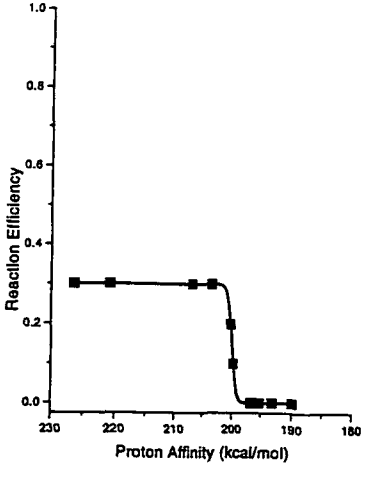

SINGLE COLLISION CID STUDIES OF ALKALI-METAL, 12-CROWN-4 COMPLEXES BY FTICR

Marshall Pope and David V. Dearden
Brigham Young University, Dept. of Chemistry and Biochemistry, Provo, Utah 84602

Introduction

Gas phase studies of the chemistry of multidentate ligation offer opportunities to observe metal-ligand systems in the absence of the interfering effects of solvent. Several studies have determined the *relative* bond strengths of various ligands for a given metal, using equilibrium techniques. *Absolute* bond strengths, which are of fundamental importance, have proven more difficult to determine. One study has appeared which used threshold CID in a Fourier transform ion cyclotron resonance instrument to determine a few alkali metal ion / 18-crown-6 bond strengths,[1] but agreement between this work and recent high-level theory[2] is poor. Experimental studies are hampered by the very large number of internal degrees of freedom in these systems, leading to large kinetic shifts. Rapid radiative stabilization leads to a so-called *intrinsic shift* which also complicates the measurement of bond strengths. We begin our work on this problem by investigating the smallest readily-available member of the crown ether series, 12-crown-4, to minimize kinetic shifts. Likewise, to maximize observation time and decrease the kinetic shift problem, our experiments have been performed in the low-pressure (1-3 x 10^{-8} mbar) environment of a Fourier transform ion cyclotron resonance mass spectrometer.

Experimental

All experiments were performed in a Fourier transform ion cyclotron resonance mass spectrometer (model APEX 47e, Bruker Instruments) equipped with an ion source external to the high-field region of a 4.7-Tesla superconducting magnet. Electrospray ionization from 49:49:2 methanol:water: acetic acid, spiked with alkali metal acetates or nitrates, was used to generate the ions. Electrostatic focusing and injection techniques were used to transfer ions from the source to the field-corrected ("Infinity") trapping cell of the instrument. Isolation of the parent ion was by conventional FTICR techniques (chirp and shot ejection of unwanted ions). The CID target was Ar, and neutral pressures were measured using a magnetically-shielded ionization gauge (Balzers). Fragment spectra at a given excitation duration were collected in narrowband mode. Sixteen identical scans were accumulated in memory for each activation duration. The same experiment was then repeated to permit narrowband acquisition of the remaining parent ion abundance. The excitation duration was incremented, and the cycle was repeated. The data are reported as fragment/parent intensity ratios as a function of center-of-mass kinetic energy (calculated following McMahon.[3])

Results and Discussion

Figure 1 illustrates a set of trials for 12-crown-4 / K^+. Data are plotted as the ratio of fragment ion intensity to parent abundance. The ordinate scale is proportional to center-of-mass energy,

$$E_{com} = \frac{m_t}{m_t + m_p} \frac{E_{rf}^2 t_{rf}^2 e}{8 m_t}$$

where m_t is the mass of neutral argon background, m_p is the mass of the parent crown, E_{rf} is measured in volts per meter and t_{rf} is the duration of the acceleration pulse prior to a 20 msec delay to allow collisional activation. Recent ab-initio calculations on the Na^+/ 12-crown-4 complex suggest a bond strength of 60 kcal mol^{-1};[4] we would expect this to be an upper limit for K^+ bond strengths. Our current results for 12-crown-4 / K^+ set an appearance threshhold for fragmentation at ~64 ± 17 kcal mol^{-1} if the onset region is extrapolated. However, the high energy region of our data, which appears to have better precision, extrapolates to 109 ± 8 kcal mol^{-1}. These fragment appearence threshholds do not represent bond strengths. We expect, but did not observe, competative fragmentations at these energies (but fragmentation may be unobservable if it occurs in the neutral product).

When the alkali metal is varied, the relative order of fragment appearence energies is in good agreement with the expeeted order of alkali metal-crown bond strengths. There exists, however, a stark contrast between the absolute magnitudes and our expectations based on simple chemical intuition. Because

experimental scatter seems to increase for the lighter fragments, we suspected a mass-dependent instrumental response. To check for this we performed CID on 12-crown-4/K^+ at three electric field intensities. The data show good correlation in the onsets and similar scatter.

Other features of the data suggest that even our longest CID delay, 100 msec, was insufficient to overcome the sizable kinetic and intrinsic shifts in these systems. The energy onsets for K^+ cation fragmentation from 12-crown-4/K^+ were compared at several different CID delays. It is interesting that the three different delays give different slopes but that, within experimental error (± 8 kcal/mole), they yield the same intercept. The slope does not vary if the pressure•CID delay product is fixed. Both kinetic shift and multiple collisions would shift the intercept. Kinetic shifts however, have a more pronounced effect on the slope. Though kinetic shifts for these large systems are beyond our control, we believe that a more accurate calibration of the energy scale (against a reference system) may redeem the onsets as a fair estimate of the relative bond strengths of two metals for a given crown.

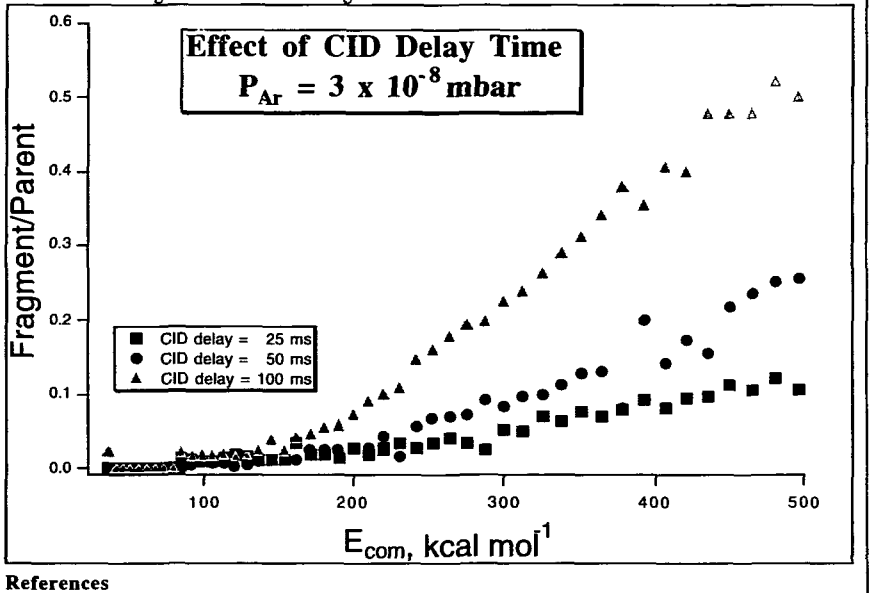

References

(1) Katritzky, A. R.; Malhotra, N.; Ramanathan, R.; Kemerait, R. C.; Zimmerman, J. A.; Eyler, J. R. *Rapid Commun. Mass Spectrom.* **1992**, *6*, 25-27.
(2) Glendening, E. D.; Feller, D.; Thompson, M. A. *J. Am. Chem. Soc.* **1994**, *116*, 10657-10669.
(3) Hop, C. E. C. A.; McMahon, T. B.; Willett, G. D. *Int. J. Mass Spectrom. Ion Proc.* **1990**, *101*, 191-208.
(4) Ray, D., private communication.

CATION AFFINITIES OF PYRIDINE BASES: STERIC EFFECTS

John J. Isbell* and Jennifer S. Brodbelt, Deparment of Chemistry, University of Texas at Austin
Austin, TX 78712-A5300

INTRODUCTION

The nature of hydrogen-bonding has been studied extensively in solution and in the gas phase due to the importance of these forces in both intra- and intermolecular interactions.[1] In solution hydrogen-bonding interactions comprise the dominant intermolecular interaction responsible for drug-receptor recognition. In the solvent-free environment of the mass spectrometer it is possible to examine the intrinsic reactivities of the proton without the interference of solvent effects. We have begun several systematic studies of hydrogen-bonding interactions in a variety of ion-molecule complexes, and in this report we describe the evaluation of gas-phase basicities and boronium ion affinities of a series of substituted pyridines. The pyridines are strong bases in which the nitrogen can be effectively blocked by neighboring substituents. The borinium ion serves as a model of a 'steric proton', thus allowing a second means of probing steric effects on cation affinities and hydrogen-bonding interactions.

EXPERIMENTAL

All experiments were performed in a Finnigan MAT ITMS. The manifold temperature was maintained at 393K (uncorrected) The pyridines mixture was admitted to the chamber through heated leak valves at pressures ranging from $3x10^{-7}$ torr to $3x10^{-6}$ torr Trimethyl borate was introduced at a static pressure of $5x10^{-7}$ to $5x10^{-6}$ torr (uncorrected) and helium buffer gas was added to increase the total pressure to one millitorr There was no fluctuation in K_{eq} over these pressure ranges.

RESULTS and DISCUSSION

Rationale

Several workers have shown the influence of entropy on the relative proton affinities of similar molecules.[2] However, to the best of our knowlege, little gas-phase work has quantitatively addressed the effects of sterics on electron-deficient addition reactions.[3] Such a study could provide the foundation for obtaining a better understanding and a method for quantifying ion bulk with reactivity. Protons are not very large, and simply adding a ligand to a proton to increase its bulk is not sufficient to ensure that the liganded proton is the one transfered in subsequent reactions. In addition, the use of a 'derivatized proton', such as $P1H^+$, would require the formation of a heterodimer complex as a precursor to transfer of the bulky proton, and such a complex may not readily form if the proton affinity of P2 is much larger than that of P1. It was for these reasons that an alternative model of a steric proton was chosen.

Monomethyl- and dimethylpyridines proved to be ideal bases for the examination of the influence of sterics on ion affinity due to the availability of all the isomers

Determination of Relative Borinium Ion Affinities

The quadrupole ion trap, due to its ability to trap and store ions for seconds, is nearly ideal for equilibrium determinations. However, the main problem with the ion trap for these types of measurements is the temperature uncertainty [4] To compensate for this shortcoming, the relative gas-phase basicities were determined for each pair of pyridines studied in order to normalize them with respect to the known gas-phase basicities of the neutrals.[5] The gas-phase basicities at 393K were extrapolated from those at 300 or 320 K and the corresponding proton affinities. Thus the relative free energy of dimethoxy borinium binding was calculated using the equation: $\Delta G_{(Borinium)} = (\Delta G_{(Borinum)expt}) * (\Delta GB_{lit}/\Delta GB_{expt})$

Examination of the relative borinium ion affinities in Table 1 shows that $(3,5\text{-lutidine/B(OMe)}_2)^+$ is favored over $(3\text{-Picoline/B(OMe)}_2)^+$ by 4.4 kcal/mole, while the basicity of the latter is 3.1 kcal/mole greater. The 3,4-lutidine/3-picoline pair yielded similar results. Since the methyl groups are removed from the site of ion attachment for these pyridines, it was anticipated that there would be no steric influence on binding, and, therefore, this system should provide relative binding energies for the dimethoxyborinium ion that are most similar to the relative proton affinities. An examination of Table 1 shows that for similarly-hindered systems, the borinium ion affinity parallels the gas-phase basicity.

Steric inhibition of binding was pronounced for the 2,6-lutidine/pyridine and 2,3-lutidine/3-picoline systems. These reactions were essentially thermoneutral even though the lutidines have greater basicities, demonstrating the repulsive interactions between the methyl groups and the dimethoxy borinium ion.

TABLE 1

System	$\Delta G\ (B(OMe)_2)^+$ (kcal/mole)[a]	$\Delta G\ B^b$ 393K
3,5-Lutidine/3-Picoline	4.4 ± 0.2	3 1
3,4-Lutidine/3-Picoline	3.2 ± 0.6	3.8
2,3-Lutidine/3-Picoline	-0.2 ± 0.5	3.8
2,4-Lutidine/2-Picoline	1.8 ± 0.4	1 8
2,6-Lutidine/Pyridine	0.2 ± 0.5	7.1

a. ΔG for transfer from lutidine to picoline or Pyridine. b. GB = gas-phase basicity (in kcal/mole)

CONCLUSIONS

The data presented herein supports the idea of using trialkylborates as models of 'steric protons' and such models may prove to be a better probe of reactivity for explaining why certain reactions do not occur For instance, this comparison can be done by simply chosing the appropriate alkoxy borinium ion as a probe so that it is comparable in size to the ion used in the ion-molecule reaction Since the borinium ions bind strongly to heteroatoms, the lack of an addition product would provide strong evidence for steric inhibition of the reaction. In addition, the use of a series of increasing dialkylborinium ions would permit bracketing of the range of 'sizes' of the ion permitted for an addition reaction to occur.

SELECTED REFERENCES

1. a. Meot-Ner (Mautner), M., J. Am. Chem. Soc. **1992** *114* 3312.; b. Lau, Y.K ; Kebarle, P., Can J. Chem. **1980** 151 ; c. Gorman, G S , Amster, I.J., J. Am. Chem Soc. **1993** *115* 5729 , d Liou, C -C ; Brodbelt, J.S., J. Am. Chem. Soc. **1992** *114* 6761.; e. Vinogradov, S.N ; Linnel, R.H., Hydrogen-Bonding; Van Nostrand, NY 1971. **2.** Ausloos, P.; Lias, S G., eds., Structure/Reactivity and Thermochemistry of Ions, (NATO Series C: Mathematical and Physical Sciences), Vol 193, p. 381 **3.** a. Houriet, R.; Rolli, E., Nouv. J. Chim. **1987** *11* 221., b Buker, H.-H ; Grutzmacher, H.-F , Int. J. Mass Spectrom. Ion Proc. **1991** *109* 95. **4.** McLuckey, S A., Glish, G.L., Asano, K.G.; Bartmess, J.E., Int. J. Mass Spectrom. Ion Proc. **1991** *109* 171, and references therein. **5.** Lias, S.G.; Bartmess, J.E.; Liebman, J.F ; Holmes, J L., Levin, R.D.; Mallard, W.G., J. Phys. Chem. Ref. Data **1988** *17*, Supplement No. 1.

Acknowledgements: We thank the following agencies for their financial support: NIH, NSF, Welch Foundation, Dreyfus Foundation, and the Sloan Foundation. We also gratefully acknowledge helpful conversations with Dr Jan E Szulejko and Dr. John E. Bartmess

Charge Repulsion in Peptides and Basicities of Different Charge States.

Igor A. Kaltashov, Catherine Fenselau*
Department of Chemistry and Biochemistry
University of Maryland Baltimore County
5401 Wilkens Ave., Baltimore MD 21228

Values of gas phase basicities of different charge states of the same peptide or protein are influenced by both electrostatic repulsion and conformational changes. Careful experimental determination of thermochemical parameters may provide insight on the three dimensional structure of peptides and proteins in the gas phase and its relation to conformations in solution.

A modified kinetic method[#1] has been used to measure gas phase basicities of protonated peptides. Unimolecular decomposition of a doubly charged dimer, formed by M (a peptide) and B (a reference base):

$$^{+}HM\cdots H^{+}\cdots B \begin{cases} \xrightarrow{k_1} MH_2^{2+} + B & (1) \\ \xrightarrow{k_2} MH^{+} + BH^{+} & (2) \end{cases}$$

in a third field-free region of a four sector mass spectrometer (JEOL HX110/HX/110, Tokyo, Japan) provides information on both "apparent" second gas phase basicity $GB_{app}(MH^+)$ (see Fig. 1) and electrostatic repulsion between the two protons δ (as kinetic energy release in (2), see Fig. 2). A true value of the second gas phase basicity can be calculated as $GB(MH^+) = GB_{app}(MH^+) - \delta$.

In the present work a second gas phase basicity of bradykinin fragment [1-8] (RPPGFSPF) was determined to be $GB(MH^+)$=191.7±1.2 kcal/mol. The value of Coulombic repulsion δ=22.4±1.2 kcal/mol (Fig. 2, insert) was independently confirmed by KER experiments with metastable MH_2^{2+} ions. The first gas phase basicity of the peptide was determined by the classical kinetic method[#2] to be GB(M)= 254.8± 0.4 kcal/mol (see Fig. 1).

Two models were considered for localization of protons in the doubly charged peptide RPPGFSPF: the Arg[1] side chain and the N-terminal amino group (maximum "local" proton affinity) or, alternatively, the Arg[1] side chain and the C-terminal carboxylic group (maximum charge separation). The two models ($R^{\oplus\oplus}$PPGFSPF and $R^{\oplus}$PPGFSPF$^{\oplus}$) were subjected to molecular dynamics calculations using the CHARMm22 semi-empirical force field. The calculations revealed that the most probable intercharge distance in $R^{\oplus\oplus}$PPGFSPF is 7.00 Å (Coulombic repulsion of 47.1 kcal/mol, which is twice as high as the experimentally measured value). In contrast, the most probable intercharge distance for $R^{\oplus}$PPGFSPF$^{\oplus}$ is 14.55 Å (Coulombic energy of 22.8 kcal/mol, which is strikingly close to the experimentally measured value of δ). Also, the lowest energy conformation of $R^{\oplus}$PPGFSPF$^{\oplus}$ is 16.9 kcal/mol lower than that of $R^{\oplus\oplus}$PPGFSPF. This suggests that in doubly protonated RPPGFSPF the "extra" protons are located so as to maximize the distance between them, not to occupy the sites with highest "local" proton affinities.

Bradykinin fragment [2-9] (peptide PPGFSPFR) has the same aminoacid composition as bradykinin fragment [1-8], but differs by the position of the Arg residue along the chain. The second gas phase basicity of this peptide has been determined to be $GB(MH^+)$=197.6±1.4 kcal/mol ($GB_{app}(MH^+)$=220.2±1.0 kcal/mol and δ=22.6±1.0 kcal/mol). This is significantly higher (by 5.9 kcal/mol) than the second gas phase basicity of bradykinin fragment [1-8], because the two most basic sites of PPGFSPFR (Arg[8] side chain and N-terminus) are separated much further, and the second proton is not forced to a more distant site with a lower local proton affinity.

(1) I.A. Kaltashov, D. Fabris, C.C. Fenselau. *J. Phys. Chem.* **1995**, in press.
(2) S.A. McLuckey, D. Cameron, R.G. Cooks. *J. Amer Chem. Soc.* **1981**, *103*, 1313.

43rd ASMS Conference on Mass Spectrometry and Allied Topics

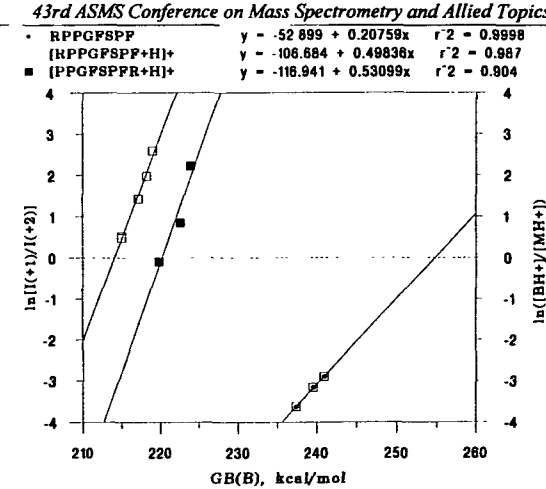

Figure 1. Plots of the logarithms of relative rates of unimolecular dissociation of proton-bound dimers $[M+B+2H]^{2+}$ (left) and $[M+B+H]^+$ (right).

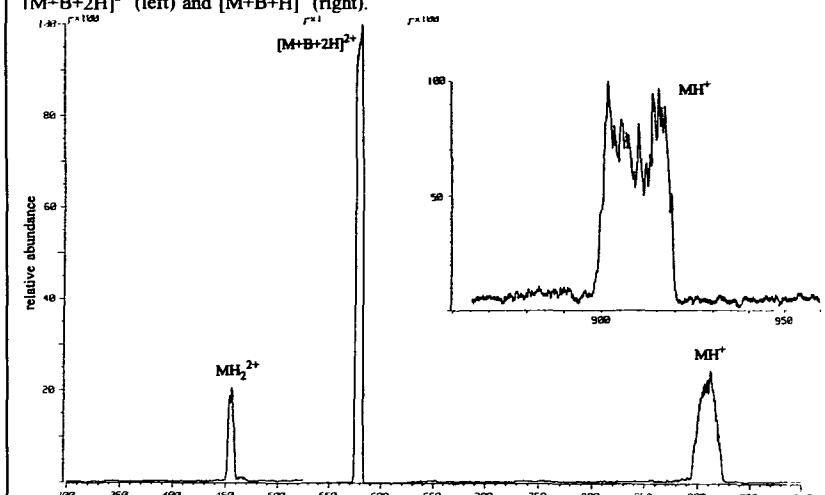

Figure 2. A MIKE spectrum of unimolecular dissociation of a metastable proton-bound dimer $[M+B+2H]^{2+}$ formed by bradykinin fragment [1-8] (M) and GLG (B). Energy slit of the second electrostatic analyzer β_2=4.0 mm. The insert: the MH^+ peak shape. Energy slit β_2=0.8 mm.

Polyatomic Cations Affinities of Pyridines Determined by the Kinetic Method

Yang, S. S.; Chen, G.; Wong, P.; Ma, S.; Cooks, R. G.
Department of Chemistry, Purdue University, IN 47907

Gozzo, F. C.; Eberlin, M. N.
State University of Campinas, Institute of Chemistry, CP 6154 Campinas, SP 13081-970, Brazil

The affinities of polyatomic cations, like those of protons, can be measured by the kinetic method [1] This is done by using ion/molecule reactions in a pentaquadrupole mass spectrometer[2] to generate dimeric clusters in which neutral pyridine molecules are bound to such cations as $OCNCO^+$, $SiCl_3^+$, and $SiCl^+$ ions The dimeric adducts, viz. $Py_1[X]^+Py_2$ where Py_1 and Py_2 represent substituted pyridines, where X represents $OCNCO^+$, $SiCl_3^+$ or $SiCl^+$, are dissociated to yield the corresponding monomeric adducts All polyatomic cation complexes of meta- and/or para-substituted pyridines display excellent linear correlations between the fragmentation abundance ratio, $\ln[Py_1[X]^+/Py_2[X]^+]$, and the proton affinity difference of the pyridines (Figures 1, 2) The relationships between the affinities of $[OCNCO]^+$, $SiCl_3^+$, and $SiCl^+$ and the proton affinities of the pyridine are relative $[OCNCO]^+$ affinity (kcal/mol) = 0 96ΔPA, relative $[SiCl_3^+]$ affinity (kcal/mol) = 0.86ΔPA, and relative $[SiCl^+]$ affinity (kcal/mol) = 0.55ΔPA, with the assumption of an effective temperature as 555 K (i.e. the same as those of the corresponding Cl^+-bound dimers) [3] The smaller constant in the relationship between the relative $SiCl^+$ affinity and the relative proton affinity is ascribed to the influence of the non-bonding electrons on Si atom in producing a weaker inductive interaction with the pyridine

The MS/MS/MS[4] experiments and the linear relationships observed for all three polyatomic cations show the complexes are loosely-bound with the pyridines symmetrically attached to the central polyatomic cations Ab initio calculations show that the $[OCNCO]^+$-bound pyridine dimer has a structure where nitrogen atoms on pyridines are bound to the carbon atoms on $[OCNCO]^+$ Structures for $[SiCl_3^+]$- and $[SiCl^+]$- bound pyridine dimers are proposed to have nitrogen/silicon bonding.

Steric interactions between ortho-substituted pyridines and the central $OCNCO^+$ and $SiCl_3^+$ ions reduce the bond strengths for these cations The magnitude of the steric acceleration of fragmentation allows gas phase steric parameters (S^k) to be determined (Table 1) Dimers consisting of ortho-substituted pyridines in the $OCNCO^+$ and $SiCl_3^+$ systems, display steric effects which are similar to those observed previously for the chlorine cation.[3] The $OCNCO^+$ bound dimers have the largest steric parameters due to the bulky central $OCNCO^+$ (Table 1)

Anomalous behavior is observed in the $SiCl^+$ clusters with ortho-substituted pyridines All of the ortho-substituted pyridines, except 2-methylpyridine and 2,4-dimethylpyridine, show abundance ratios which lie above the linear correlation line (Figure 2) This enhanced stabilization in the case of $SiCl^+$ is believed to be due to the sterically favorable orientation of the ortho-substituted methyl group, which promotes intramolecular auxiliary bonding between the methyl group and the central silicon atom It is worthy of note that the deviation from the linearity in the cases of the ortho-substituted pyridines is the combined result of the electronic and steric effects and that both effects apparently cancel in the 2-methylpyridine and 2,4-dimethylpyridine cases

References

1 Patrick, J S , Kotiaho, T , Mcluckey, S A , Cooks, R G Mass Spectrom Rev Submitted for publication
2 Schwartz, J. C , Schey, K L , Cooks, R G Int J. Mass Spectrom. Ion Processes 1990, 1, 101
3 Eberlin, M N , Kotiaho, T ; Shay, B J , Yang, S. S , Cooks, R G J Am Chem. Soc 1994, 116, 2457
4 Schwartz, J. C.; Wade, A. P , Enke, C G., Cooks, R. G Anal Chem 1990, 62, 1809.

Table 1. Steric Parameters S^k for Cl^+, $OCNCO^+$, $SiCl_3^+$ and $SiCl^+$ Cations vs. Solution S^0 Values.

Pyridine	S^k Cl^+	S^k $OCNCO^+$	S^k $SiCl_3^+$	S^k $SiCl^+$	S^0
Py	0	0	0	0	0
2-MePy	-0.43	-1 39	-0.47	0.15	-0 73
2,5-diMePy	---	-3.02	-0 32	0.78	---
2,4-diMePy	---	-3 15	-0.71	-0 17	---
2,3-diMePy	-0.64	-3.29	-0.22	0.55	-0.85
2,6-diMePy	-1.6	-5.09	-0 94	1 62	-1.98
2,4,6-triMePy	-1 7	-6 13	---	1 44	---

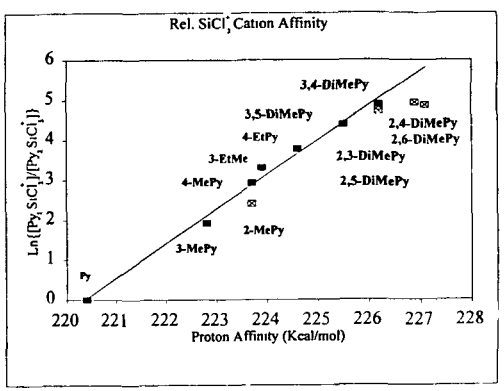

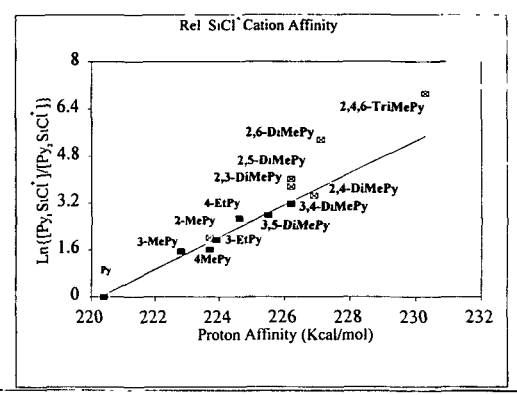

Acidities of Long Chain Alcohols: Kinetic versus Equilibrium Methods

Priscilla R Higgins,* John E Bartmess, Dept of Chemistry, University of Tennessee, Knoxville TN 37996-1600

Cooks' method of dissociation of dimers[1], when used by Boand and co-workers to determine the acidities of long chain n-alkanols,[2] showed a monotonic strengthening in acidity of these from the C-4 to the C-9 case. The increase per methylene group was 0 9 kcal/mol at C-4 decreasing to 0 5 kcal/mol at C-9.

Haas and Harrison[3] found that the acidities obtained by this method for small and highly-branched alcohols were insensitive to conditions of preparation and internal energy, but that long chain alcohols were appreciably weaker in acidity under low energy CID conditions, relative to the other alcohols.

To resolve this difference, we have carried out equilibrium measurements of the gas phase acidities of many of these alcohols using the ICR mass spectrometer.

Equilibrium studies were carried out in a homebuilt Ion Cyclotron Resonance (ICR) mass spectrometer. The instrument was operated both at 25°C and 75°C, in which the temperature was measured outside the analyzer manifold. Methoxide was generated from methyl nitrite.

The acidity ladder below reveals that there is a non-monotonic trend in the n-alkanol acidities· C4<C7<C8<C5<C6. The C7 alcohol is appreciably <u>weaker</u> as an acid than C6 We are unsure of the C9 value at present due to volatility problems. At 75°C, all these alcohols were more acidic by ca 0.8 kcal/mol, relative to the nitriles This implies that ΔS_{acid} for the long chain alcohols is >25 eu; they are <u>less</u> ordered on ionization than small alcohols.

The actual temperature of the cell with the instrument operated hot was not well regulated. This is currently being corrected, to obtain accurate equilibria at higher temperatures.

The fit of the acidities of the branched alcohols to the CID data indicates that the kinetic method is working for such structures. It is only for the longer alcohols, where the distal end can interact with the reactive site, that we see deviations.

A similar case for diol acidities has been noted,[4] where the diols are appreciable <u>stronger</u> in equilibrium acidity than indicated by the kinetic method. That effect was assigned to an enthalpic interaction not present in the precursor dimer in the kinetic method transition state.

The effect observed here may be due to the "straight chain anomaly" of Brown, seen in all aqueous pKas (Table 1) and in gaseous dimerizations.[5] At a certain chain length, entropic factors become important when one form in an equilibrium has interactions between the ends of the chain, not present in the other form. For shorter chains, these interactions are not present in either form; for longer chains, in both forms. A non-monotonic increase in reactivity is not surprising, therefore.

Catalan[6] has attributed the non-regular increase in long chain alcohol acidities, seen in the low energy CID work, to intramolecular hydrogen bonding, rather than a general coiling/polarizability interaction.

Some preference for hydrogen bond donation by the terminal methyl, relative to methylene groups, is expected based on the stronger gas phase acidity of primary versus secondary alkanes

Although we still must obtain accurate temperature dependent data to sort out these entropic effects, there is a real non-monotonic change in acidities observed here. The kinetic method must be used with caution when there are possible interactions between two functional groups, or the reactive site with the end of a long chain, in the structures under investigation.

Table 1. The "Straight Chain Anomaly"
Aqueous pKas, 25°C

	RCO_2H	RNH_3^+
H-	3.75	9 24
Me-	4.75	10 64
Et-	4.88	10.67
nPr-	4.82 <-	-> 10 57
nBu-	4.84	10 63
nPn-	4.87	10.64
nHx-	4.89	10.64
nHp-	4.90	

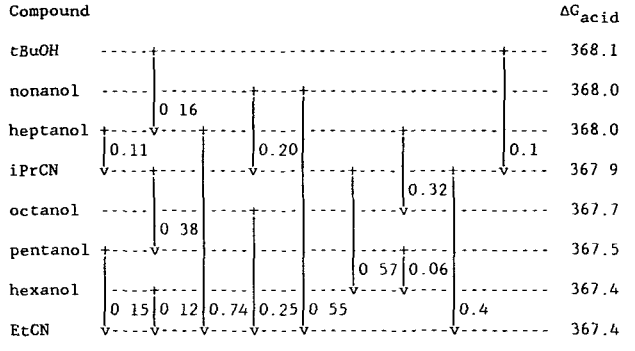

References
1 McLuckey, S.A ; Cameron, D ; Cooks, R.G ; *J Am. Chem. Soc.* **1980** *103*, 1313
2 Boand, G ; Houriet, R., Gaumann, T.; *J. Am. Chem. Soc.* **1983** *105*, 2203.
3. Haas, M. J ; Harrison, A G , *Int. J. Mass Spectrom. Ion Proc* **1993** *124*, 115
4. Crowder, C., Bartmess, J E., *J Amer. Soc Mass Spectrom* **1993** *4*, 723.
5. Brown, H. C., M D Taylor, and S. Sujishi, *J Am. Chem Soc* **1951** *73*, 2464
6. Catalan, J., *Chem. Phys Letter* **1994** *221*, 68.

Reactivity and Thermochemistry of Quadricyclane Anion

Hack Sung Lee and Veronica M. Bierbaum

Department of Chemistry and Biochemistry
University of Colorado, Boulder, CO 80309-0215

A flowing afterglow - selected ion flow tube instrument has been used to measure the rates of reaction of amide ion with quadricyclane(QC) and deprotonated quadricyclane anion($C_7H_7^-$) with ammonia. Use of the established gas phase acidity of ammonia and the equilibrium rate constant yields a value, $\Delta_{acid}G_{300}(QC) = 395\ 0 \pm 0.5$ kcal/mol. Combined with *ab initio* calculations, the enthalpy change, $\Delta_{acid}H_{300}(QC) = 403.3 \pm 0\ 8$ kcal/mol, has been derived. Electron transfer reactions of $C_7H_7^-$ ion with several neutrals set a limit on the electron affinity of C_7H_7 radical, which agrees with the results of photoelectron spectroscopy (PES) study (0.96 ± 0.01 eV)[1] Using these thermochemical values one can derive C-H bond dissociation energy (111.9 ± 1.0 kcal/mol). Gas-phase acidity of QC measured against monomethylamine and benzene also agrees within experimental uncertainties (see Table)

To generate the $C_7H_7^-$ ion in the source flow tube, QC was added downstream of amide ion. If hydroxide ion is used instead, the mass 91 ion shows very different reactivity. This ion turns out to be benzyl anion, confirmed by PES study. It is not clear whether the benzyl anion is produced in the collision complex of hydroxide and QC, or from toluene impurity in QC.

Reaction of the $C_7H_7^-$ ion with ND_3 shows 3 fast and 2 slow H/D exchanges, implying that two structures of anion may be present (less than 3 kcal/mol energy difference according to *ab initio* calculations). This result collaborates with the reaction of amide ion with dideuterated QC (63 %/ 37 % loss of H^+/D^+). It is interesting to note that, in the case of norbornadiene, only 3 H/D exchanges were observed[2]. However, when $C_6D_5^-$ ion reacts with QC, no H/D exchange occurred. This suggests a barrier for H/D scrambling within the collision complex. Reactions with CS_2 and COS gives $C_7H_7S^-$, N_2O gives HC_2O^-, CO_2 gives $C_5H_5^-$ and numerous other products including adducts. S_N2 reaction with methyl chloride is fast, whereas E2 reaction with diethyl ether is slow, although it is exothermic.

Several isomers of $C_7H_7^-$ ion show distinct collision induced dissociation (CID) mass spectra . C_2H^-(74 %), $C_5H_5^-$(18 %), $C_3H_3^-$(8 %) for QC, C_2H^-(98 %), $C_5H_5^-$(2 %) for norbornadiene, and no CID for benzyl anion.

When O^- ion reacts with QC, $C_7H_6^-$ ion is formed. Dideuterated QC (two D's on the bridge of 5 - and 4 - membered rings) reacts with the oxygen anion to give 32 %/ 54 %/ 14 % loss of H_2^+/ HD^+/ D_2^+. This seems to suggest that almost all hydrogens are involved in this reaction. Further study is needed to elucidate the structure of the $C_7H_6^-$ ion.

Table. The gas-phase acidity of quadricyclane determined from ammonia, monomethylamine and benzene.

$$B^- + QC \underset{k_r}{\overset{k_f}{\rightleftharpoons}} (QC - H)^- + BH$$

Base	$\Delta_{acid}G(BH)$ (kcal/mol)	k_f / k_r (cm^3/sec)	$\Delta_{acid}G(QC)$ (kcal/mol)
NH_3	396.4 ± 0.4	8.1 ± 0.2 (-10) 8.0 ± 1.0 (-11)	395.0 ± 0.5
CH_3NH_2	395.8 ± 0.5	7.2 ± 0.8 (-10) 9.7 ± 0.6 (-11)	394.6 ± 0.6
C_6H_6	392.9 ± 0.4	2.2 ± 0.8 (-12) 3.2 ± 0.4 (-11)	394.5 ± 0.6

References :

1. Gunion, R. F. and Lineberger, W. C. , private communication.
2. Lee, R. E. and Squires, R. R., J. Am. Chem. Soc., **1986**, 108, 5078.

Temperature Dependence of Radiative Association rates

Victor Ryzhov and Robert C. Dunbar*
Department of Chemistry, Case Western Reserve University, Cleveland, OH 44106

Introduction

Radiative association is an important part of the chemistry of interstellar molecule-building as well as a common process in ion trapping experiments. The bimolecular rate constant for radiative association at zero pressure limit is given by

$$k_2 = k_{ra} = k_f k_r/(k_b + k_r), \qquad (1)$$

where k_f is the bimolecular rate constant for the collisional complex formation, k_b is the unimolecular redissociation rate constant, k_r is the unimolecular rate constant for IR photon emission from the energized complex. k_{ra} is expected to depend strongly on the temperature. Despite the fact that some theoretical modelling has attempted to rationalize the observed trends[1], a universal theory to explain the temperature dependence of radiative association rate constants is yet to be developed.

In the present work the temperature dependence of NO^+ associating with 3-pentanone was studied. This system has been shown[2] to have a fairly fast association at room temperature that makes it convenient for a thermal behavior study. The experimental results were compared with phase space theory and simple RRKM modelling.

Methods

Rates of radiative association were measured in the temperature regime from 300K to 400K. The pressure of 3-pentanone varied from 1×10^{-8} to 3×10^{-7} torr while the pressure of NO was 3×10^{-8} torr. The ion gauge pressure readings were calibrated to match the known proton transfer rate constant between methane molecular ion and neutral methane[3].

Experiments were performed on a FT-ICR spectrometer with a 2.54 cm cubical cell. After the electron beam pulse (electron energy 15 eV), the parent ion of pentanone and any other ion species except NO^+ were ejected. Then a thermalization time was provided to give 5-6 ion-neutral collisions. After one more ejection sequences NO^+ ions were allowed to react for a time which ranged from 400ms to 8s and the extent of association and charge transfer was measured as a function of the reaction time. The temperature in the cell was measured by a copper-constantan thermocouple located inside the chamber on the trapping plate. To avoid extra heating by the filament, it was turned off before the thermalization period, and an idle time up to 5 s was provided in each working cycle.

Results

The reaction consists of two channels, radiative association (ra) and charge transfer (ct):

$$C_5H_{10}O + NO^+ \xrightarrow{k_{ra}} C_5H_{10}ONO^+ \qquad (2)$$

$$C_5H_{10}O + NO^+ \xrightarrow{k_{ct}} C_5H_{10}O^+ + NO \qquad (3)$$

An illustrative time plot is shown in Fig.1. The overall rate constant for the NO^+ disappearance, $k_{rx} = k_{ra} + k_{ct}$, was obtained for each individual pressure and averaged for each temperature. After that the individual bimolecular rate constants for both channels were easily obtained. The lack of pressure dependence in each case (Fig. 2) indicates clearly that our association is purely radiative. As expected, the radiative association is fairly fast at room temperature (collisional efficiency of radiative stabilization about 8%). As temperature goes up the association rate drops very fast and at 400K almost vanishes (Fig. 3 and 4). The charge transfer is very efficient (about 25% of the Langevin rate) in this temperature range.

Comparison with theory

A high level phase space approach to radiative association reactions developed by prof. S.J.Klippenstein was used to describe the temperature dependence of the reaction of interest. The geometry of the association adduct $C_5H_{10}ONO^+$ was calculated *ab initio* along with its vibrational frequencies and IR intensities. This led to a calculation of the photon emission rate k_r which is otherwise not known. Subsequent canonical phase space treatment of Eq. 1 at different temperatures gave excellent agreement with the experimental values (see Fig. 3 and 4). The simple "standard hydrocarbon" model[4] that was found useful in describing the size dependence of radiative association[2] predicts a faster decrease of the association rates as the temperature goes up compared to the experimental data (Fig.5 and 6). This crude model, however, still gives a good qualitative picture of the temperature dependence.

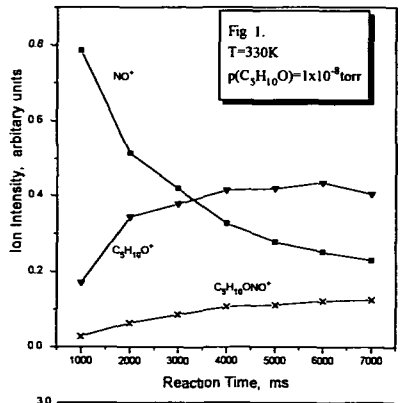

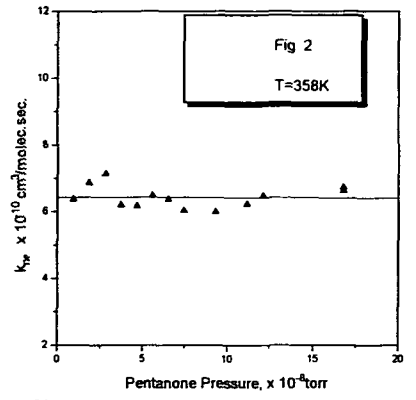

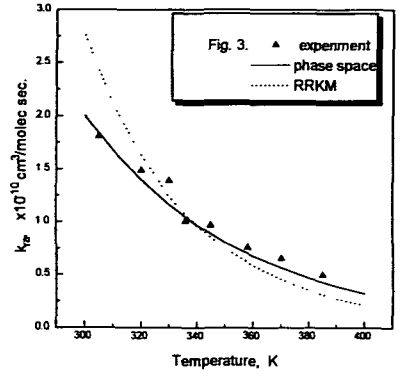

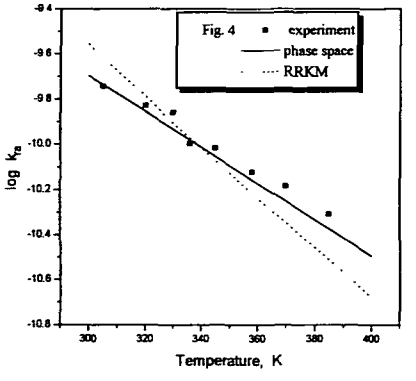

Conclusions

- The NO^+ + 3-pentanone system represents a suitable object for the thermal behavior study of radiative association over a wide range of temperatures.
- The phase space calculations applied here show excellent agreement with the observed experimental temperature dependence.
- The simple RRKM modelling predictions are somewhat less exact but give a very easy and acceptably accurate estimate of the temperature dependence.

References

1. Lin, Yi. Ph.D.Thesis, University of Delaware, Newark, Delaware, 1992.
2. Weddle, G.; Dunbar, R.C. *Int. J. Mass Spectrom. Ion Processes* 1994, *134*, 73-82.
3. Huntress, W.T.,Jr. *et al. Int. J. Mass Spectrom. Ion Phys.* 1974, *13*, 331-334.
4. Dunbar, R.C. *Int. J. Mass Spectrom. Ion Processes* 1990, *100*, 423-443.

A REACTION WINDOW IN CROSS-SECTIONS FOR DOUBLE ELECTRON CAPTURE REACTIONS

W. J. Griffiths, M. L. Langford and F M. Harris.
Mass Spectrometry Research Unit, University College of Swansea, Singleton Park, Swansea SA2 8PP, Wales.

Double charge transfer (DCT) reactions of the type

$$A^+ + B \longrightarrow A^- + B^{2+} \qquad (1)$$

where A^+ is a fast moving projectile ion and B a collision gas molecule, can be discussed in terms of a reaction window model The conversion of reactants to products can be considered in terms of two quasimolecules (i) A^+,M and (ii) A^-,M^{2+}. The long-range potential energy functions may be described as a function of the internuclear separation, r, of A and M For the reactants

$$V_{A^+,M}(r) = -\frac{Z^2e^2\alpha(M)}{2r^4} \qquad (2)$$

where $\alpha(M)$ represents the dipole polarizability of the collision gas molecule. For the products the potential energy function is dominated by the strong coulombic attraction between A^- and M^{2+}, but also has a weaker attractive component owing to the polarizability of A^- and M^{2+}

$$V_{A^-,M^{2+}}(r) = -\frac{2Ze^2}{r} - \frac{Z^2e^2[\alpha(A^-) + \alpha(M^{2+})]}{2r^4} \qquad (3)$$

A schematic representation of these potential energy functions is shown in fig. 1. Although the double electron capture (DEC) reaction (1) is strongly endoergic (as the energy to doubly ionize M is greater than that released in the charge inversion of A^+), avoided crossing of the potential-energy function can occur with the resulting double electron transfer from M to A^+. It has been shown that the cross-section for a DEC reaction is strongly dependent on a quantity β This is a complex function but is strongly dependent on the endoergicity of the reaction It is predicted that the cross-section passes through a maximum at a particular value of β. This means that a reaction window exists in which the endoergicity must fall in order that a reaction can take place. The endorergicity (ΔE) of the DEC reaction (1) is described by equation (4)

$$\Delta E = IE_2(M) - E(A^+ \rightarrow A^-) \qquad (4)$$

where $IE_2(M)$ is the energy required to convert M into M^{2+}, and $A \rightarrow A^-$ is the energy released in converting A^+ to A^- .

We have attempted to determine the endoergicity at which the maximum cross-section occurs for the DEC reactions between both 6-keV OH^+ and F^+ projectile ions and a series of halogenated benzene collision gas molecules. The experiments were carried out using a ZAB-2F reverse-geometry double focusing mass spectrometer (VG Analytical Ltd., Manchester, England).

A reaction window has been found, the lower limit of which has a ΔE value of approximately 8eV and the upper limit a value of approximately 20eV. The centre of the window where the cross-section for DEC is at a maximum is in the range 10 - 14eV.

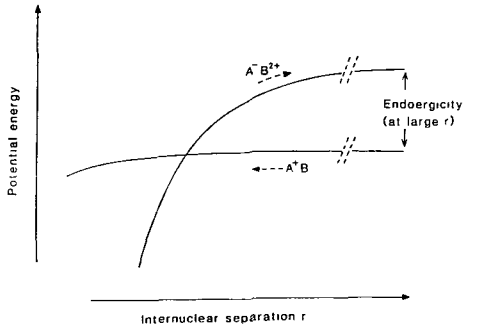

Reactions and laser photofragmentation processes of SiF_2^{2+} and SiF_3^{2+}

Yin-Yu Lee, Stephen D Price,* and Stephen R. Leone
Joint Institute for Laboratory Astrophysics, National Institute of Standards and Technology and University of Colorado, and Department of Chemistry and Biochemistry, University of Colorado, Boulder, CO 80309-0440
and
*Chemistry Department, University College London, 20 Gordon Street, London WC1H 0AJ, UK

Multiple product channels are observed for the reactions of SiF_2^{2+} and SiF_3^{2+} with the rare gases at 49 eV laboratory collision energy. The dication beam is generated in an electron impact ion source and mass selected using a quadrupole mass spectrometer. The ion beam is focused into a collision region and a time-of-flight mass spectrometer is used to monitor the reaction products. Reactions of SiF_2^{2+} produce SiF_2^+, SiF^{2+}, SiF^+, Si^{2+}, Si^+, and F^+ ions and reactions of SiF_3^{2+} produce SiF_3^+, SiF_2^{2+}, SiF_2^+, SiF^{2+}, SiF^+, Si^+, and F^+ ions (Fig. 1).

The corresponding rare gas ions are formed when charge transfer occurs. The relative yields of these products are quantified. For reactions of both dications, there is a substantial increase in the total reaction cross section as the collision partner is varied from He to Xe. The collision induced neutral loss reactions are observed to be a major product channel for reactions of SiF_3^{2+} or SiF_2^{2+} with the lighter rare gases, He and Ne. However, collision induced dissociation and charge transfer processes dominate when the ions react with the heavier collision partners, Kr and Xe. The doubly charged product yield is largest for systems in which charge transfer does not compete effectively with the collision induced process The atomic dication Si^{2+} produced in those collision reactions implies that the chemical structure of SiF_2^{2+} has most of the electron deficiency on the silicon atom.

Experiments to measure the product channels by laser photodissociation of SiF_2^{2+} and SiF_3^{2+} show that both dications readily absorb near infrared radiation and are promoted to excited states which dissociate by neutral-loss or charge-separation (Fig. 2). Detailed studies show that the dissociation occurs by single-photon absorption, which promotes the molecule to unbound excited states. Energetic thresholds for the photoinduced neutral-loss and charge separation reactions of SiF_3^{2+} are obtained from the data. A simple electron transfer mechanism was used successfully to explain the competition of neutral-loss and charge-separation reactions from the same electronic state of SiF_3^{2+} following excitation.

(Fig. 1) SiF_3^{++} + Rare gas

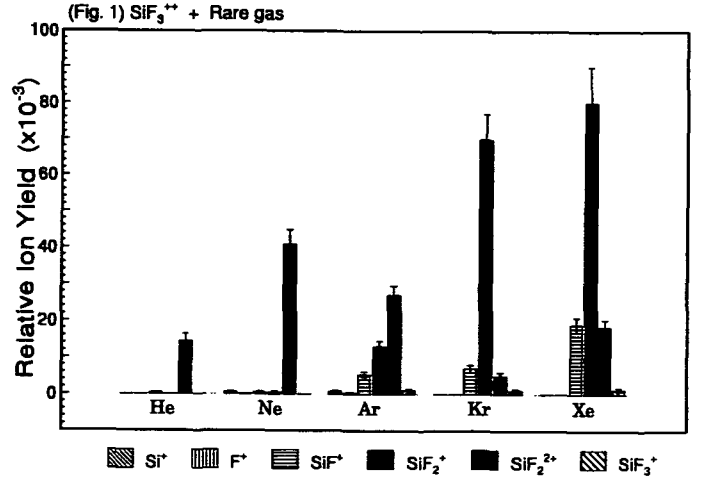

(Fig. 2) SiF_2^{2+} and SiF_3^{2+} Photodissociation at 1064 nm

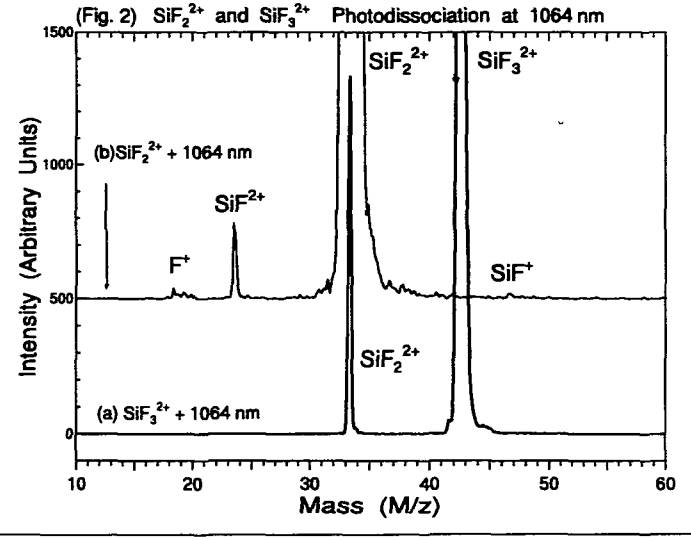

Partially Chlorinated Hydrocarbons: Gas-Phase Anion-Molecule Reactions

Joseph J. Grabowski and Jennifer A. Braun
Department of Chemistry
University of Pittsburgh, Pittsburgh, PA 15260

The hazardous effects of chlorinated organic compounds on the ozone layer limit the use of these species in our society. We previously studied the anion-molecule reactions of chlorofluorocarbons, and in these reactions carbanions are formed by chloride transfer. These results led us to investigate similar pathways for chlorinated hydrocarbons.

We have examined the reactions of hydroxide and allyl anion with several chlorinated ethanes and toluenes at 300 K in a 0.30 Torr He buffer gas using the flowing afterglow. Other anions were only examined peripherally. We chose hydroxide and allyl anion as our nucleophiles because they have similar proton affinities but differ in their localization. The chlorinated toluenes studied include 1,1,1-trichlorotoluene, 1,1-dichlorotoluene, and 1-chlorotoluene and the chlorinated ethanes studied include 1,1,1-trichloroethane, 1,1-dichloroethane, and chloroethane.

The distribution of products for the reactions of chlorinated toluenes with hydroxide and allyl anion is shown in Figure 1. The proton transfer product $(M\text{-}H)^-$ is always the major product when HO^- is used as the base. Of the three neutrals, only 1,1,1-trichlorotoluene undergoes S_N2 as well as PT to produce Cl^- as a minor product. A significant difference in product distribution occurs when allyl anion is used as the nucleophile instead of hydroxide; the major pathway when $PhCCl_3$ is used as the neutral is chloride transfer. As is also evident in Figure 1, the competition between PT and S_N2 increases (as compared to hydroxide reaction) when allyl anion is the base

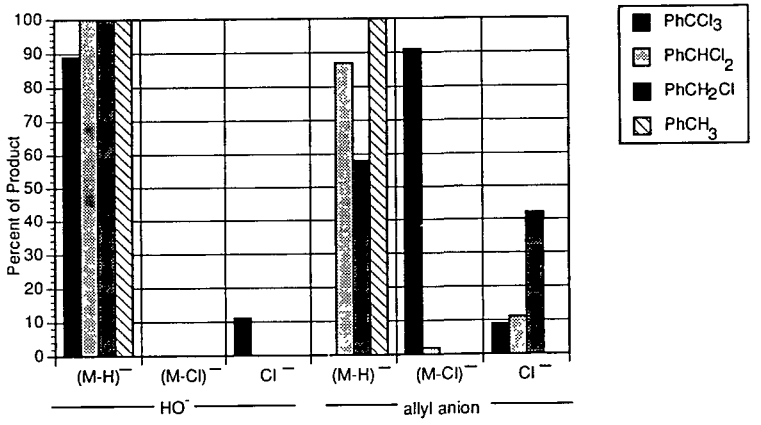

Figure 1. Product distribution for the reaction of Nu^- + $PhCH_nCl_{3-n}$.

Figure 2 gives the product distribution for the reactions of hydroxide and allyl anion with the chlorinated ethanes. For the hydroxide reactions, PT dominates when it is thermodynamically feasible, otherwise Cl^- is produced presumably through elimination. With allyl anion, once again the trichlorinated hydrocarbon gives the chloride transfer product as the major product. As can be noted in Figure 2, chloroethane and 1,1-dichloroethane give similar results with both hydroxide and allyl anion.

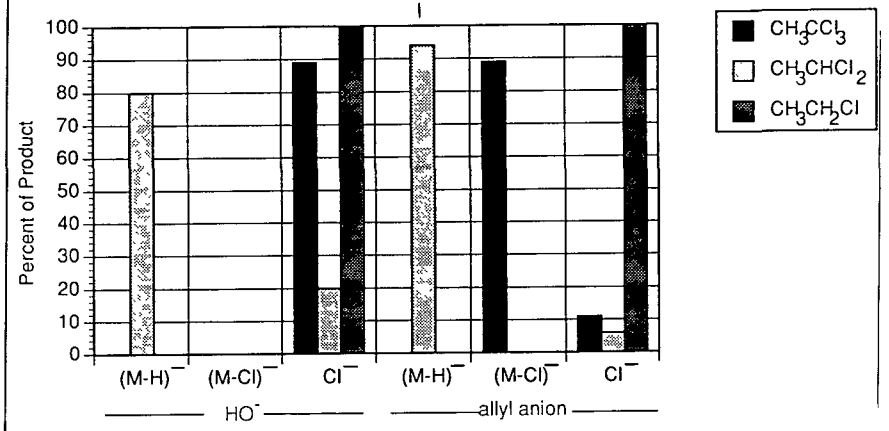

*HO^- + CH_3CCl_3 also gives 11% $Cl^-(H_2O)$.

Figure 2. Product distribution for the reaction of Nu^- + $CH_3CH_nCl_{3-n}$.

Several conclusions can be drawn about the competition between various pathways for the reaction of an anion with a chlorinated hydrocarbon. First, chloride transfer is the major pathway for $RCCl_3$ ($R \neq H$) compounds with allyl anion. For all hydroxide reactions, chloride transfer is endothermic; therefore it is not observed. The exclusive reaction for CH_3CCl_3 with hydroxide is E2 (we assign E2 as the mechanism based on 11% $Cl^-(H_2O)$ formed), which is also a minor channel with CH_3CHCl_2. Proton transfer dominates whenever it is thermochemically allowed. With the exception of ethyl chloride, S_N2 is essentially unobserved in HO^- reactions. S_N2 is a major channel for allyl anion with benzyl chloride (and possibly ethyl chloride), but with the other four substrates S_N2 is a minor pathway. The reaction of allyl anion with CH_3CCl_3 is an excellent source of the carbanion, $CH_3CCl_2^-$ for future CID studies to determine the heat of formation of the corresponding carbene. The reaction of Me_3Si^- + CH_3CCl_3 may be a better source of $CH_3CCl_2^-$, however more quantitative studies are needed in order to determine the best source of the carbanion

REGIOSELECTIVITY OF OXYGEN ADDITON INDUCED DECHLORINATION ON PCBs AND DDT ANALOGS IN ECNCI

F. Lépine[1], O. A. Mamer[2] and S. Milot[1]
[1] Institut Armand-Frappier, 531 des Prairies Blvd., Laval, Can. H7N 4Z3
[2] Biomedical Mass Spectrometry Unit, Mc Gill University, 1130 Pine ave., Montreal, Can.,H3A 1A3

INTRODUCTION

The Electron Capture Negative Chemical Ionization (ECNCI) spectrum of many chlorinated compounds presents ions at 19 Da lower than the molecular ion. These ions are due to reactions between the organochlorine and trace amounts of oxygen present in the source. They correspond to the addition of one oxygen with the simultaneous loss of one chlorine atom.

Because we observed previously that the dechlorination reactions of PCBs and various DDT metabolites in a mass spectrometer were very regioselective, especially under ECNCI, we were interested to see if such regioselectivity could be observed for the oxygen addition induced dechlorination of these organochlorines in ECNCI.

MATERIAL AND METHODS

The synthesis of the various labelled PCBs and DDT analogs was described previously (Lépine et al, *Org. Mass Spectrom.*, **27**, 1311, 1992 and Lépine et al., *J. Mass Spectrom.*, in press). The labelled compounds were obtained as mixtures and were analyzed by GC/MS with a Hewlett-Packard 5988A using a 30 m. DB-5 column. The PCBs analyses were performed in triplicate. The moderator gas was a 1/5 mixture of oxygen in methane. The source pressure was 0.3 Torr and the source temperature was 150 °C. The DDT analogs were analyzed under the same conditions.

RESULTS

In order to evaluate the regioselectivity of the dechlorination, various penta- and hexachloro- PCBs labelled at various positions with one or two ^{35}Cl were used. With oxygen present in the moderator gas, the mass spectra of all the PCBs consist almost exclusively of M-19 ions.

The regioselectivity of the dechlorination reactions is reflected by the residual amounts of label in the M-19 ion cluster. This value is calculated by measuring the isotopic distribution of the cluster (Lépine et al., *Org. Mass Spectrom.*, **27**, 1311, 1992). The structure of the labelled PCBs and the percentage of the label retained in the M-19 ion are presented. The M-19 ions of all the pentachloro- PCBs retained between 77 and 78 percent of the label. For the hexachloro-PCBs this value varies between 81 and 84 percent.

The DDT analogs were labelled with one ^{37}Cl on each aromatic ring. Because of the extensive fragmentation and the corresponding low intensities of the ions of interest, accurate quantification of the residual label cannot be achieved. However qualitative information could be deducted from these spectra.

Ions corresponding to M-19 were observed for p,p'- DDMU and p,p'-DDE. The mass spectrum of p,p'-DDD show many similarities with the one of p,p'-DDMU. An intense 254 ion can be observed for every compound, except for o,p'-DDD.

43rd ASMS Conference on Mass Spectrometry and Allied Topics

DISCUSSION

In a previous publication (Lépine et al., *Org. Mass Spectrom.*, **29**, 133, 1994) using pure methane as moderator gas, the labelled PCBs all presented molecular and M-35 ions in ECNCI. This dechlorination reaction was found to be highly regioselective. With oxygen in the source, the results presented indicate that the dechlorination is completely non regiospecific. The percentage retention of the label are very close to 80 and 83 percent for the penta- and hexachloro congeners, respectively. These two values correspond to random loss of one chlorine atom out of the five or six initially present. This lack of regioselectivity could be due to the relatively high concentration of oxygen in the source. Under these conditions, oxygen probably picks up electrons preferentially over the PCBs and the $^{-}O_2$ radical then reacts non regioselectively with the neutral PCBs. The fact that the molecular ions of PCBs were generally not observed would tend to confirm this hypothesis.

The spectrum of DDMU (MW=286) presents ions at M-4 (282 Da) and M-19 (267 Da). The former fragment probably represents addition of O_2 with the loss of HCl. An intense ion appears at 254 which probably corresponds to 4,4'-dichloroacetophenone. The 282 Da ion could be a precursor of 254 trough loss of CO. The isotopic distribution of all these ions indicate that the aromatic chlorines are retained.

The spectrum of p,p'-DDE (MW=316) presents ions at M-19, M-35, M-47 and the 254 ion. The M-47 ions are probably generated through loss of CO from the M-19 ions. The chlorine atoms retained in these ions were the aromatic ones.

The spectrum of o,p'-DDD shows ions at M-40, M-55 and M-70. These fragments corresponds to M-2HCl+O_2, M-HCl+O-Cl and M-2Cl, respectively. The isotopic distribution of the clusters indicates that the aromatic chlorine are retained in every ions.

The spectrum of p,p'-DDD presents ions at M-282, M-267 and the 254 ions. This spectrum is almost identical to the one of p,p'-DDMU. It is likely that in a first step, p,p'-DDD undergoes loss of HCl to produce p,p-DDMU. Because the spectra of these two compounds are completely different when pure methane was used as moderator gas, the initial loss of HCl observed here must be due to hydrogen abstraction of the alpha hydrogen, possibly by a $^{-}O_2$ radical anion or related species, followed by loss of chlorine anion. The degradation pathways of the o,p'- and p,p'-DDD are then quite different although dechlorination proceeds only at the aliphatic chlorines in both cases.

Formation of 4,4'-dichlorobenzophenone in the decomposition pathways of many DDT analogs is also interesting, as this compound is also observed upon gamma irradiation of these compounds in aliphatic solvents in presence of oxygen (Lépine et al., *J. Agric. Food Chem.*, **42**, 2012, 1994). Formation of this compound in both cases is probably due to an attack at the alpha position by the $^{-}O_2$ radical.

CONCLUSION

The regioselectivity of the dechlorination reaction of various organochlorines in ECNCI in the presence of oxygen is very dependent of the structure of the organochlorine. Contrary to what was observed previously with pure methane as moderator gas, PCBs, under the conditions used, were not regioselectively dechlorinated. DDT analogs however, where regioselectively dechlorinated at the aliphatic chlorines.

Dissociative Attachment in Sulfonate and Carboxylate Compounds

Kim Andrews,* John E. Bartmess, Daniel N Sorensen, Cathy A. Crowder,
Department of Chemistry, U. of Tennessee, Knoxville TN 37996-1600

The generation of cations by electron ionization is straightforward: above the ionization energy, all compounds form some cations, with only ca. two orders of magnitude variation in the ionization cross-section. Formation of anions, however, is much more variable The cross-section for the dissociative attachment process:

$$A\text{-}B + e^- \longrightarrow [AB^-]^* \longrightarrow A^- + B^\cdot$$

varies over more than seven orders of magnitude, and in a non-monotonic fashion with electron energy. Few compounds fall in the high-cross-section end of the range.

There are numerous small molecules such as H_2O, NH_3, NF_3, CCl_4, MeONO, etc. that yield anions of interest by dissociative attachment. The cross sections for anion production from these, however, vary widely. For use in ICR spectrometry, we need compounds in the high-cross-section range for production of anions, due to the limited pressure range of the ICR spectrometer.

Approaches to this problem include, in descending order of cost:
- external ion sources
- pulsed valve admittance of the precursor gas (see poster WPE111)
- design of appropriate chemical precursors

We focus on the last choice here.

A Rational Design Strategy:
Based on the known cases, we predict that dissociative attachment will be favored by:
- a bound or low-lying LUMO in AB, for capture of the electron, to form an intermediate with enough excess energy to fragment, but not too much, to minimize electron detachment
- a weak A-B bond, that thermochemically favors fragmentation of the intermediate, as opposed to electron loss.
- a stable A^- anion (large electron affinity)

Compounds of the type $PhN{=}NC(Me)_2G$, where G is a good electron acceptor group like nitro, cyano, etc. were targeted as possible dissociative attachment sources of $Me_2C{=}G^-$ carbanions These possess the desired pi system (PhN=N-) to capture the electrons, easily broken bonds (N_2 is the best leaving group in chemistry), and can be tailored to form a variety of carbanions. The methyl groups are desired to prevent the carbanion from deprotonating the more acidic precursor. This approach was successful for G = $-NO_2$ and $-CF_3$, but for G = -COMe, a pNO_2- group on the phenyl ring was necessary to increase the cross section; the parent compound gave negligible amounts of anions. The cross section σ is ~1 $Å^2$, similar to NF_3. PhN=NNHPh gave $PhNH^-$ comparably.

Not all azo compounds are good dissociative attachment candidates: AIBN, $NC\text{-}C(Me)_2\text{-}C(Me)_2\text{-}CN$, with no aromatic pi system to capture the electron, gives no anions.

Methyl methanethiosulfonate, MeSO2SMe, yields principally $MeSO_2^-$, plus some $MeSO_2S^-$ and MeS^- due to ion-molecule reactions of $MeSO_2^-$ with the neutral. The σ at 0 eV is ca. 1 $Å^2$. This makes use of the fact that $RSO_2\text{-}X$ BDEs are among the weakest known

The acidity of $MeSO_2H$ is bracketed as between CF_2HCO_2H and CF_3CO_2H, or ΔG_{acid} = 319.2 kcal/mol We are unsure if the conjugate acid formed has the hydrogen bound to sulfur or oxygen, no reliable MO calculations appear to have been carried out PM3 predicts the -OH isomer to be 18 kcal/mol more stable than the -SH form.

Similarly, dimethyl sulfate, $MeO\text{-}SO_2\text{-}OMe$, yields primarily $MeOSO_3^-$, with small amounts of $MeOSO_2^-$, and SO_3^{--}.

A wide variety of MeCOX and PhCOX compounds yield X^- anions in large σ of ~1 $Å^2$, including X = OAc, Cl, Br, and CN. The first case, typically acetic anhydride, is our preferred method of generating carboxylate anions. These are thus available over a 30 kcal/mol range of basicity. Interesting, formic acetic anhydride yields only formate on dissociative attachment, the thermochemically favored product by 5 kcal/mol

No anions were observed from PhCONHPh, MeO_2Me, or MeCOF The last is intriguing, in that the thermochemistry is favorable.

Although semi-empirical calculations will not be exceptionally accurate in describing these structures, as general guides to the thermochemistry (±10-15 kcal/mol) they are useful in designing structures, and evaluating performance

	LUMO,eV	ΔH_{rxn},eV	ΔG_{acid}
$PhN{=}NC(Me)_2CN$	-0 8	+0 5	368
$PhN{=}NC(Me)_2NO_2$	-1.1	-0.5	350
$PhN{=}NC(CF_3)_3$	-1.8	-1 3	344
$PhN{=}NC(Me)Ac_2$	-0.5	-1 2	337
$MeSO_2SMe$	-2 1	-1 4	319
$(MeO)_2SO_2$	-2 0	-1 3	303 (est)
MeCOCl	-0 1	-0 1	333
MeCOCN	-0.4	0 3	349
$MeCO_2OCOMe$	0.4	0 4	345

The Gas-Phase SO_2N^- Ion: Experiment and Theory

Nelson H. Morgon, Harrald V. Linnert, and José M. Riveros

Instituto de Química, Universidade de São Paulo, Caixa Postal 26077, São Paulo, Brazil, CEP 05599-970

Experiments carried out in a homemade FT-ICR spectrometer reveal that the reaction of NH_2^- with SO_2F_2 proceeds rapidly through the two channels as shown below with their respective branching ratios. The overall rate constant could not be measured accurately because of the competing reaction of NH_2^- with the background water present in the instrument. Yet, this rate constant is comparable to that of OH^- with SO_2F_2, determined to be close to the ADO collision limit.

$$NH_2^- + SO_2F_2 \rightarrow HF + HNSO_2F^- \quad 0.15$$

$$NH_2^- + SO_2F_2 \rightarrow 2\,HF + NSO_2^- \quad 0.85$$

Ion isolation experiments for either product ion, $HNSO_2F^-$ and NSO_2^-, reveal that both ions are unreactive towards the parent SO_2F_2.

The above reaction represents an easy way to generate the sulfonyl imide ion, NSO_2^-, isoelectronic with SO_3 and hereto an elusive anionic species. In fact, the successful isolation of NSO_2^- had not been reported until the synthesis of $Cs^+NSO_2^-$ was claimed in 1982.[1] Yet, the evidence for the actual existence of $Cs^+NSO_2^-$ was disputed by Chivers *et al*[2] based on the analysis of infrared, Raman and NMR spectra which were shown to be consistent with an NSO^- anion.

The proton affinity of the NSO_2^- species cannot be directly measured from the usual gas-phase acid-base equilibrium experiments since the conjugate acid, $HNSO_2$, is not known as a stable species. Thus, an estimate of the proton afinity of NSO_2^-, or the gas-phase acidity of $HNSO_2$, was obtained by bracketing techniques. For these experiments, NSO_2^- ions were first isolated in the cell after all the NH_2^- ions had reacted (typically 200 to 250 ms), and were then allowed to react with volatile compounds of known gas-phase acidities to establish the occurrence and ease of proton abstraction. Reactions were followed up to 5 s at substrate of pressures ranging from 5×10^{-8} to 2×10^{-7} Torr. No proton abstraction was observed for HCOOH, $CH_2(COMe)_2$, or MeCHClCOOH whereas rapid and complete proton transfer was observed with CF_3COOH. No attempt was made to study proton abstraction from due to the fact that the NH_3, used to generate the reactant NH_2^- ions, is flowed together with the reagent gas. Our measurements therefore allow us to estimate,

$$\Delta H^\circ_{acid}(HNSO_2) = 330 \pm 5 \text{ kcal/mol}$$

Preliminary experiments revealed the ability to photodetach the electron with the fourth harmonic of the Nd:YAG laser at 266 nm but not with the third harmonic at 355 nm. Thus,

$$EA(NSO_2) > 3.49 \text{ eV}$$

Ab initio calculations were carried out with the GAUSSIAN/92 program in the cluster of work stations available at the Computer Center of the Unversity of Campinas (CENAPAD-SP). Starting with a DZVPD basis set, the Generator Coordinate Method[3] (GCM) was used to improve the description of the diffuse character of the electron cloud of negative ions. Diffuse functions were added to the H, O, N and S by analysis of the weight functions following the procedure outlined in Ref. 3.

The theoretical calculations performed at the MP4SDTQ level with the geometries optimized at the MP2 level predict the N atom to be the preferred protonation site in NSO_2^- and yield the following thermochemical parameters.

$$\Delta H^\circ_{acid}(298\text{ K}) \text{ for } O_2SN\text{-}H = 331 \text{ kcal/mol}$$

$$\Delta H^\circ_{acid}(298\text{ K}) \text{ for } NS(O)O\text{-}H = 306 \text{ kcal/mol}$$

$$EA(NSO_2) = 3.76 \text{ eV}$$

$$D_0(O_2SN\text{-}H) = 104.6 \text{ kcal/mol}$$

The uncertainty in the distinction between NSO_2^- and NSO^- in condensed phases lead us to carry out a similar calculation on NSO^-. The experimental ΔH°_{acid} (298 K) for HNSO was determined earlier[4] to be 344 ± 5 kcal/mol. Our calculated values for this species yield

$$\Delta H^\circ_{acid}(298\text{ K}) \text{ for } OSN\text{-}H = 347 \text{ kcal/mol}$$

$$\Delta H^\circ_{acid}(298\text{ K}) \text{ for } NSO\text{-}H = 327 \text{ kcal/mol}$$

$$EA(NSO^\cdot) = 3.53 \text{ eV}$$

$$D_0(OSN\text{-}H) = 115 \text{ kcal/mol}$$

This work was supported by the São Paulo Science Foundation (FAPESP) and the Brazilian Research Council (CNPq).

[1] Roesky, E.; Schmieder, W. E.; Isenberg, W , Böhler, D.; Sheldrick, G. M., *Ang. Chem. Int. Ed. Engl.* **1982**, *21*,153.

[2] Chivers, T.; Schmidt, K. J.; McIntyre, D. D.; Vogel, H. J. *Can. J. Chem.* **1989**, *67*, 1788

[3] Morgon, N. H., Custodio, R.; Riveros, J. M., *Chem. Phys. Letters* (in press)

[4] Bierbaum, V.M., Grabowski, J.J.; DePuy, C.H., *J. Phys. Chem.* **1984**, *88*, 1389.

A Negative Ion Study of The Isomers of Dinitrobenzene Using an ASGDI Source

W. Mo, M.L. Langford, A.M. Franklin and J.F.J. Todd
The Chemical Laboratory, University of Kent at Canterbury
Canterbury Kent, CT2 7NH, UK

The differentiation of isomers on Mass Spectrometers has always been a difficult task: the spectra of the isomers from the standard data bases are always nearly identical. In this investigation of all three isomers of dinitrobenzene (DNB) has been carried out using an Air Sampling Glow Discharge Ionization (ASGDI) source coupled to an Finnigan MAT ITMS quadrupole ion trap mass spectrometer.

In the ASGDI source the sample is drawn into the glow discharge by an ambient air stream and thus the sample constitutes a low percentage of the total gas sample. To produce a DC glow discharge a voltage of 350-400 volts was applied across plates 1 and 2, at a pressure of ca. 8×10^{-1} Torr. Samples were introduced into the source by placing them on a glass spoon in the sampling chamber and any vapour from the sample was drawn into with the stream of air. The ASGDI source is rich in ion/molecular reagent anions formed from the background, which helps the identification of isomers through the dissociation of product ions.

The anions of interest are isolated and then subjected to collisional dissociation (MS/MS) in order to observe the fragmentation pathways. The same values of the tickling period (10 milliseconds) and tickling voltage (350 millivolts) are applied in each of the MS/MS experiments.

Differences in pathways of the dissociation of the molecule ions have been observed (the CID pathways deduced for the molecular ions of the isomers are shown in Fig. 1). For all three isomers, an NO neutral molecule is first detached from the molecular ion 168^- forming 138^- (the loss of NO and CO are known to occur in similar systems under negative ionization[1]) ; when the CID of 138^- ions is performed 108^- ions are observed as the result of losing a second NO group. Differences in the spectra have been observed in

the CID of the 138^- ions which are formed from each of the isomers: in the dissociation of 138^- ions formed from 1,3- DNB, 80^- ions have been observed (as a result losing an NO and a CO group), as well as the 46^- and 108^- ions; in the spectra from the same experiment on 1,2- and 1,4- DNB, no ion 80^- has been observed. When 108^- ions formed from each isomer are subjected to CID, differences in pathways have been observed: the 108^- ions formed from 1,2- DNB and 1,3- DNB are further dissociated losing a CO molecule and producing 80^- ; the 108^- ions formed from 1,4- DNB cannot be dissociated any further, indicating a relatively stable structure.

REFERENCE:

1. Langford, M.L. and Todd, J.F.J. *Org. Mass Spectrom.* **28** (1993), 773.

ACKNOWLEDGEMENT:

One of us (W.M.) thanks the Committee of Vice-Chancellors and Principals (CVCP) and the University of Kent for funding the tuition fees and Fisons Instruments plc for "goodwill" sponsorship.

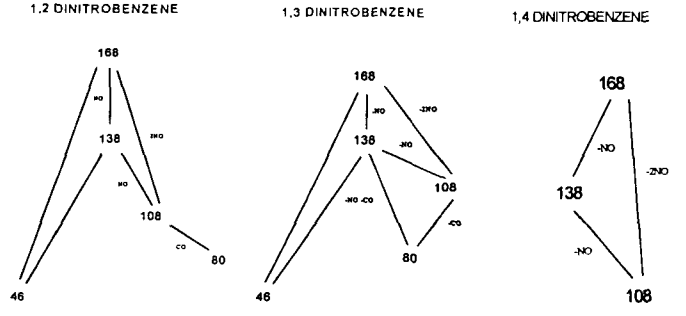

Figure 1. The dissociation pathways of molecular anions of dinitrobenzene isomers

INVESTIGATION OF VAN DER WAALS CLUSTERS BY A NOVEL TECHNIQUE FOR ICR

K. GARBADE, K.P. WANCZEK
University of Bremen, POBox 33 04 40, D-28334 Bremen, Germany

Introduction

Research on clusters is of growing interest in present mass spectrometry. However different things are understand by the term cluster: Metal clusters and atom clusters like S_8 or C_{60} are more or less stable and classified as molecules. By contrast clusters of the van der Waals type, for example $(CO_2)_n$ or Ar_n, are fragile aggregates and only available by special techniques like ion-molecule association reactions, an adiabatically gas expansion or evaporation of liquids or solids. This poster deals only with van der Waals clusters.

The investigation of weakly bound clusters is important for understanding molecular interactions, chemical reactions, condensation and solvation processes.

In our work group in Bremen van der Waals clusters of carbon dioxide have been subject of research for a long time. G. ROMANOWSKI examined clusters generated in a supersonic beam instrument by means of a quadrupole mass spectrometer observing cluster sizes up to ten molecules, vaporization and fragmentation reactions. Reaction kinetics and lifetimes could be studied [1].

M. BAMBERG coupled the supersonic cluster source to an ICR spectrometer with an external ion source. With this system the first ICR spectra of small cluster ions of carbon dioxide are obtained [2].

The next idea presented at this poster is a simplification of the experiment. We tried to place the supersonic gas expansion directly in front of the ICR cell. To realize this a special inlet system with a pneumatic valve working inside the magnet has been constructed.

Methods

The ICR spectrometer is modified CMS-47 FT-ICR spectrometer (Spectrospin AG Fällanden, Switzerland) with cylindrical cell. A grid as a trapping plate ensures minimal irritation of the supersonic jet. The ICR experiments are controlled by an Aspect 3000 microcomputer. Internal ionization by electron impact or chemical ionization can be used. The magnetic field of the superconducting magnet (Oxford Instruments) is 7.02 Tesla. The vacuum system is home build and pumped by an oil diffusion pump (Edwards Kniese & Co, Marburg) with a liquid nitrogen cooled baffle. The capacity of the pump is 150 l/s. The pressure is measured by an IMR 132 hot cathode ion gauge (Balzers) in combination with the Balzers IMG 050 vacuummeter

The gas inlet system (Fig. 1) has been built by EMG, Bremen. A tube of 2 cm diameter made of a non-magnetic alloy is placed inside the ICR vacuum chamber. Its mean part is a pneumatic valve at its end facing the ICR cell. The cluster beam is passing directly through the cell. The distance to the front of the cell can be varied. The sample gas reaches the valve passing through a capillary circuit guaranteeing good flushing of the system. An electron microscopic lens serves as a nozzle for the gas expansion. The diameter of the orifice is 100 µm. Lenses with different orifice diameters can be used. The valve is controlled by pulses from the ICR console used in automation programs. The stagnation pressure of the gas is 2 bar.

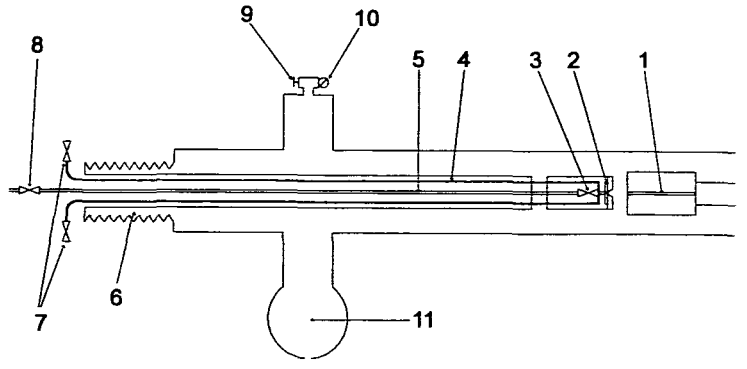

Fig. 1: Vacuum and inlet system

1. ICR cell
2. electron microscopy lens
3. pneumatic valve
4. sample gas circuit
5. compressed air pipe
6 correction of the distance valve – ICR cell
7. valves controlling the sample gas flow
8. valve controlling the compressed air
9. leak valve
10. pressure gauge
11. diffusion pump

Investigations planned

Generation of ICR spectra with sample inlet right in front of the cell is possible. Unfortunately spectra with cluster peaks have not yet been obtained. The following experiments are in progress:

- Change of the design of nozzle, cell and holding device or use of an open endcap cell avoids negative influence on the supersonic jet and allows shorter distance between valve and cell
- Use of higher stagnation pressure adjusts pressure reduction inside the capillary system
- Cooling of the cell reduces the influence of thermal radiation of the ICR cell
- Investigations on different van der Waals clusters and ion molecule reactions of clusters

First results will soon be published.

References

1. G. ROMANOWSKI, K.P. WANCZEK: Studies of reactions of ionized carbon dioxide microclusters, Int. J. Mass Spectrom. Ion Proc. 95(1989)223
2 M. BAMBERG, K.P. WANCZEK: A supersonic beam ion cyclotron resonance instrument for the study of van der Waals cluster ions, Z. Phys. D. - Atoms, Molecules and Clusters 20(1991)433

Consecutive reactions of conjugated dienes

Rappmund A., Wanczek K. P., Institute of Inorganic and Physical Chemistry, University D-28334 Bremen, Germany

The present study examined the consecutive reactions of 2-methyl 1.3-butadiene and 1 3-butadiene with the Fourier-tansform mass spectrometer (FTMS) after electron impact ionisation. Both related systems reacted with its neutral precursor in several stages. The reaction channels of these reactions were proved by double resonance experiments.

2-methyl 1.3-butadiene

At a pressure pressure of $1*10^{-7}$ peaks of C_6H_9 (m/z 81), C_7H_9 (m/z 93), C_7H_{11} (m/z 94), C_8H_{11} (m/z 107), C_8H_{13} (m/z 108)and C_9H_{13} (m/z 121) are visible This is the significant pattern in the first stage reaction between 2-methyl 1.3-butadiene with the neutral precursor. But no ion/molecule dimer complex was detected. This observation is consistent with the results of earlier authors.
Ejection of this ion/molecule complex during the reaction time results in decreasing of the relative abundances of the pattern for this system. At the pressure of $2*10^{-6}$ mbar peaks of $C_{11}H_{17}$ (m/z 149), $C_{12}H_{17}$ (m/z 161), $C_{12}H_{19}$ (m/z 163), $C_{14}H_{17}$ (m/z 185), $C_{15}H_{19}$ (m/z 199) and $C_{16}H_{20}$ (m/z 212) were detected. The formation of these masses can be explained by series of double resonance experiments The pattern of the ion/molecule dimer complex reacted with the neutral isoprene to form these masses (see scheme1). No reaction pathway was found to form the fragment ion $C_{11}H_{12}$ (m/z 144).
We assume this ion was formed by decomposition of a meta stable ion. Finally this ion reacted with the neutral to $C_{16}H_{20}$ (m/z 212) Ejection of C_8H_9 (m/z 105) results in decreasing of $C_{10}H_{11}$ (m/z 131).This observation can interpreted by the reaction of:

$$C_8H_9 \text{ (m/z 105)} + \text{Isoprene} \rightarrow C_{13}H_{17} \text{ (m/z 173)} \rightarrow C_{10}H_{11} \text{ (m/z 131)} + C_3H_6$$

At a pressure of $1*10^{-5}$, the main fragment ion of $C_{11}H_{17}$ (m/z 149) can undergo further reaction with isoprene to form the product ion $C_{16}H_{24}$ (m/z 217).

1.3 butadiene

The spectrum of 1 3 butadiene at a pressure of $2*10^{-6}$ is similar to that of isoprene. Also these ion reacted in several stages with the neutral butadiene, but the explanation of these consecutive reaction is difficult and succeded only in a few cases by double resonance experiments. The main fragment ion of C_5H_7 (m/z 67), C_6H_7 (m/z 79), C_6H_8 (m/z 80), C_6H_9 (m/z 81), C_7H_7 (m/z 91) and C_7H_9 (m/z 93) are decomposition products of the ion/molecule dimer complex. Permanent excitation of the dimer complex during the reaction time results not in decreasing of the relative abundance of these pattern. The life time of this metastable ion is not long enough to remove the ion before it decomposes. These primary ions also reacted with the neutral. The ion of $C_{11}H_{13}$ (m/z 145) was formed by the reaction of:

$$C_7H_7 \text{ m/z 91} + \text{butadiene} \rightarrow C_{11}H_{13} \text{ m/z 145}$$

Ejection of $C_{11}H_9$ (m/z 141) decreased the abundance of $C_{14}H_{27}$ (m/z 195), ejection of $C_{10}H_{11}$ (m/z 131) that of m/z 141 and m/z 195, so we propose the reaction pathway of

$$C_{10}H_{11} \text{ m/z 131} \rightarrow (C_{14}H_{17} \text{ m/z 185})^{\#} \rightarrow C_{11}H_9 \text{ m/z 141} \rightarrow C_{14}H_{27} \text{ m/z 195}$$

The rection pathway to form the product ion C_8H_9 (m/z 105) and C_9H_9 (m/z 117) were not found But also these ions reacted in consecutive reactions:

$$C_8H_9 \text{ m/z 105} + \text{butadiene} \rightarrow C_{12}H_{11} \text{ m/z 159}$$

$$C_9H_9 \text{ m/z 117} + \text{butadiene} \rightarrow C_{13}H_{15} \text{ m/z 171}$$

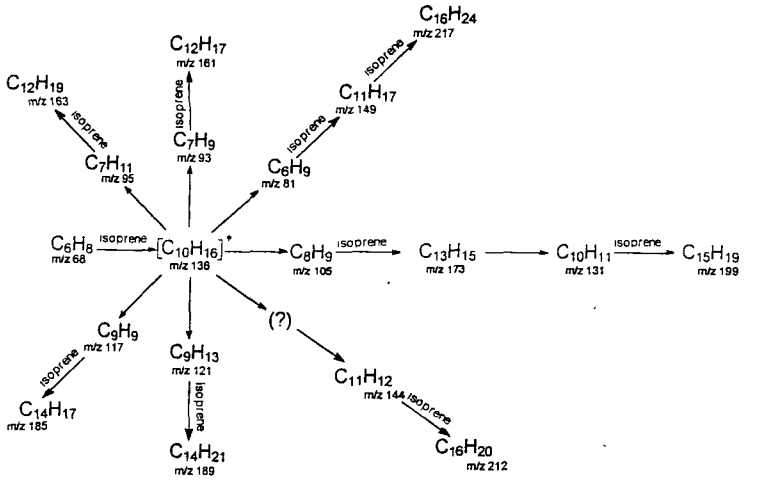

Scheme 1. Reaction pathways of isoprene radical cation with the neutral

References

[1] Groenewold G. S.; Gross M.L., J. Am. Chem. Soc., 106 (1984) 6569.
[2] Barker R.; Hamill W. H.; Williams R. R., J. Phys. Chem., 63 (1959) 825
[3] Kascheres C.; Cooks R. G., Anal. Chim. Acta, 215 (1988) 223.
[4] Lu L.; Yang S.; Wang Z.; Cooks R. G., J. Mass Spectrom. 30 (1995) 581.

Polymerisation and Ion Chemistry of 2-Butenal, studied with ICR

Harder A., Spiess I. Institute of Inorganic and Physical Chemistry
University of Bremen, Germany

Introduction:

The double bonds of α,β-unsaturated aldehydes shows a characteristic chemistry in polymerization processes. We investigated the oligomerization and oxidation of 2-butenal with FT-ICR spectroscopy. In purpose to understand the aging processes in polymeres, the chemistry of aged bulk 2-butenal in the gas phase is examined.

Experimental:

The pure 2-butenal is investigated with a gas inlet system and ionized with electron impact with an electron energy of 70 eV.

A new improved electric pulse induced desorption EPID method is used to characterize the ion chemistry of bulk 2-butenal. The emitter is a thin aluminium filament deposited on a plate which also contains the two electrical connections. Ionization is induced by a discharge of a capacitor with a short current pulse of 2 ns duration . Because of the high heat capacity of the emitter we excluded the possibility of thermal ionization. The emitter is fixed on a push rod of 900 mm length. The push rod is used to place the sample more directly in front of the ICR cell. A cylindrical sreened ICR cell of 50 mm diameter is employd to improve yield of ion collection. The investigation is performed with a Bruker Spectrospin FT-ICR spectrometer equipped with a superconducting magnet of 7.02 T.

Results and discussion:

Pure 2-Butenal, Ion Chemistry in the gas phase

Figure 1 shows an ICR spectrum of pure 2-butenal introduced by gas inlet and ionized by electron impact with an electron energy of 70 eV The most abundant peaks are the molecule $[M+H]^+$ m/e= 71 and the molecule $[M-H]^+$ m/e=69. We observed no fragment ions or ion-molecule reaction products with a reaction delay of D3=0 s.

Figure 2 shows an ICR spectrum of 2-butenal with a reaction delay of D3=10 s We observed the dimer $[M_2+H]^+$ m/e=141. After a reaction delay of D3=15 s the trimer $[M_3+H]^+$ m/e=211 occured.

Bulk 2-Butenal, condensed phase

We investigated bulk 2-butenal with the EPID ionization method [1]. From the bulk material, several types of polymerization and oxidation products could be characterized: m/e= 87, $C_4H_7O_2^+$ protonated 2-butene acid, m/e=139, $C_8H_{11}O_2^+$ $[M_2-H]^+$of 2-butenal, m/e=155, $C_8H_{11}O_3^+$ oxidated dimer of 2-butenal. Under our experimental conditions with a reaction delay of D3=0 s we observed mainly these molecule-molecule reaction products which are produced during the aging process in the condensed phase (see Fig. 3) We increased the reaction delay for observation ion-molecule-reaction products. After a reaction delay D3=2 s we detected the oligomers m/e=211 $[M_3+H]^+$and m/e=279 $[M_4-H]^+$. Using a reaction time of 15 s we observed m/e= 419, $[M_6-H]^+$. It is a surprise that we could not detect the oligomer M_5.

Conclusions:

In the ion-molecule chemistry experiments with pure 2-butenal in the *gas phase*, we could examine the beginning processes of the polymerization. The stepwise increase of dimer and trimer was observable as result of extending the reaction time.

The aged bulk 2-butenal is a mixture of mainly monomer, dimer and their oxidation products such as acids and ketones This mixture shows a more complicated chemistry in the *condensed phase* The products can be detected with EPID method and a reaction delay D3=0 s. The extension of the reaction time causes the formation of many new compounds, because many reaction pathways exist. Their molecular masses grow with the increase of the reaction time. We could observe the formation of the oligomeres M_2, M_3, $M_4$and M_6 Unexpectedly the oligomere M_5 could not be found. The peak m/e=391, probably a fragment of M_6, had a noticeable high abundance In comparision with the results of the experiments in the gas phase, we could observe advanced steps of the polymerization in the condensed phase

References:

[1] I. Spiess, University of Bremen, to be published

43rd ASMS Conference on Mass Spectrometry and Allied Topics

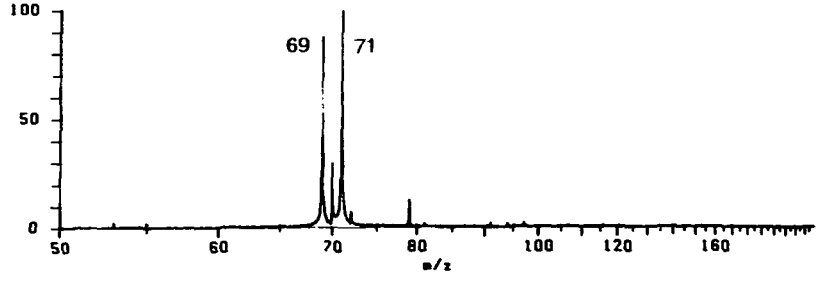

Figure 1

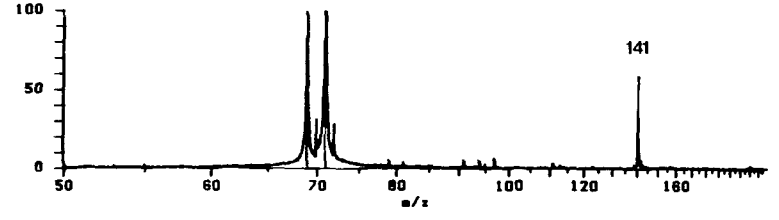

Figure 2

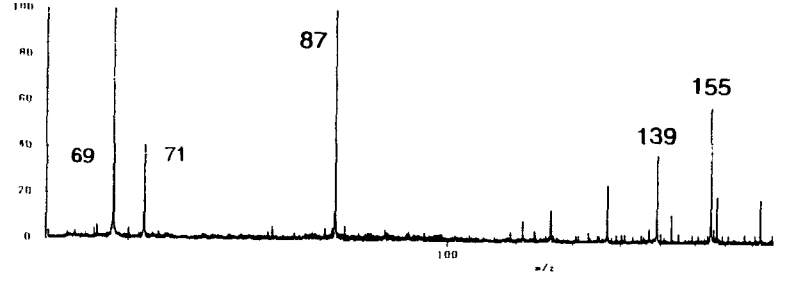

Figure 3

Reactivity of Ionized Carbonyl Radical Compounds and Their Distonic and Enol Isomers

H.C. Michelle Byrd, Lori C. Castro, C. Thomas Hwang, Rebecca L. Smith, Diane T. Leek, and Hilkka I. Kenttämaa
Department of Chemistry
Purdue University, West Lafayette, Indiana

Many long-lived (> 300 ms), low energy organic molecular ions isomerize to energetically more stable species in the gas phase. Ion-molecule reaction experiments in the Fourier-transform mass spectrometer are a well-known method for studying the structures of radical cations. Surprisingly, this technique has not been applied to the structural characterization of simple long-lived, nondecomposing aldehyde and ketone radical cations. Therefore, the ion-molecule reactions of acetaldehyde, acetone, acrolein, vinyl methyl ketone, benzaldehyde, acetophenone, propanal, and 2-pentanone radical cations were examined in the Fourier-transform mass spectrometer. This investigation focused on the comparison of the reactivity of aldehyde and ketone radical cations with cyclopentanone and the application of this information to the structural characterization of larger aldehyde and ketone radical cations.

Typical reaction experiments in the Fourier-transform mass spectrometer have been described elsewhere [1]. The change in abundances of the reactant and product ions are measured as a function of time. In the presence of excess neutral reagent, pseudo first-order kinetic laws can be applied to ion-molecule reaction kinetics. This assumption simplifies the process of determining the experimental rate constant (k_{exp}) from the measured data. Information about the structure of radical cations is learned by examining the type of products formed, the reaction rates, and the energy dependencies of reactions.

The heats of reaction for the charge exchange and proton transfer and reactivity of the aldehyde and ketone radical cations are summarized in Tables 1 and 2. The keto and/or enol forms of acetaldehyde, acetone, acrolein, vinyl methyl ketone, benzaldehyde, and acetophenone radical cations were of known structure and used as references in this investigation. Based on the exothermicity of charge exchange and proton transfer processes, the keto form of aldehyde and ketone radical cations investigated could react with cyclopentanone by both charge exchange and proton transfer. The keto forms of the aldehyde radical cations indeed react by both processes; however, the ketone radical cations only react by charge exchange in spite of the exothermicity for proton transfer(See Table 1).

Charge exchange is endothermic for the reaction between the enol form of the aldehyde and ketone radical cations and cyclopentanone; therefore, no charge exchange reaction was expected to occur. In agreement with the thermochemical prediction, no charge exchange products were observed. The heats of reaction for the enol form of acetaldehyde and acetone radical cations are exothermic for proton transfer. As expected, only proton transfer was observed. The results from the reactions with cyclopentanone indicate that keto and enol forms of aldehyde and ketone radical cations can be distinguished based on their reactivity with cyclopentanone. This information was applied to the structural characterization of the long-lived, nondecomposing propanal and 2-pentanone radical cations, which structures are not known.

Propanal radical cations react with cyclopentanone mainly by proton transfer. The enol from of propanal radical cation, generated from the molecular ion of 2-methylbutanal, reacts with cyclopentanone exclusively by proton transfer and displays linear kinetics. A small portion of the propanal reactant ions reacts by charge exchange, and an even smaller portion remains unreactive towards cyclopentanone resulting in non-linear kinetics. These findings suggests that some of the propanal radical cations isomerize to the enol form and another structure.

Although charge exchange and proton transfer are thermochemically favorable for the reaction of 2-pentanone radical cations, slow charge exchange and production of m/z 143 were the only processes that were observed. This finding suggests that a portion of the population 2-pentanone radical cations retains its keto form. At least 90% of the 2-pentanone radical cations appear to remain unreactive. Deviations from linear kinetics indicates that the long-lived molecular ions of 2-pentanone exists as a mixture of keto form and isomeric structure other than the enol form.

1) a) Chyall, L J.; Byrd, H.C.M.; Kenttämaa, H.I. J. Am. Chem. Soc. **1994**, 116, 10767. b) Stirk, K.M.; Kiminkinen, L.K.M.; Kenttämaa, H.I Chemical Reviews **1992**, 92, 1649.

Table 1 Thermochemical and Kinetic Information for Charge Exchange (CE) and Proton Transfer (PT) Reactions of the Keto Forms of Aldehyde and Ketone Radical Cations with Cyclopentanone

Ionized Molecule ($HA^{+\bullet}$)	ΔH_{rxn}^{298}(CE)	ΔH_{rxn}^{298}(PT)	k^a	k_{coll}^b	k/k_{coll}^c	%CE	%PT
$CH_3CHO^{+\bullet}$	-95	-146	2 1	3 0	1 2	50	50
$(CH_3)_2CO^{+\bullet}$	-44	-69	2 1	2 7	0 78	100	0
$C_6H_5CHO^{+\bullet}$	-24	-70	0.32	2 3	0.14	40	60
$C_6H_5COCH_3^{+\bullet}$	-4	~ -27	ND[d]	2 2	ND[d]	100	0
$CH_2{=}CHCHO^{+\bullet}$	-83	-125	0 77	2 7	0 28	70	30
$CH_2{=}CHCOCH_3^{+\bullet}$	-38	~ -63	2 3	2 6	0.90	100	0
$CH_3CH_2CHO^{+\bullet}$	-68	-115	(NL[e])	2 7	(NL[d])	15	85
$CH_3CH_2CH_2COCH_3^{+\bullet}$	-13	-37	(NL[e])	2 4	(NL[e])	100	0

a) Reaction rate constant; $x10^{-9}$ $cm^3molecule^{-1}s^{-1}$
b) Collision rate constant, $x10^{-9}$ $cm^3molecule^{-1}s^{-1}$
c) Rate Efficiency
d) Not yet determined
e) Non-linear kinetics

Table 2 Thermochemical and Kinetic Information for Charge Exchange (CE) and Proton Transfer (PT) Reactions of the Enol Forms of Aldehyde and Ketone Radical Cations with Cyclopentanone

Ionized Molecule ($HA^{+\bullet}$)	ΔH_{rxn}^{298}(CE)	ΔH_{rxn}^{298}(PT)	k^a	k_{coll}^b	k/k_{coll}^c	%PT
$CH_2{=}CHOH^{+\bullet}$	11	-46	2 1	3 0	0 70	100
$CH_2{=}C(OH)CH_3^{+\bullet}$	56	-11	1 7	2 7	0 64	100
$CH_3CH{=}CHOH^{+\bullet}$ (E) $CH_3CH{=}CHOH^{+\bullet}$ (Z)	59 53	15 15	2 4	2 7	0 90	100
$CH_3CH_2CH{=}C(OH)CH_3^{+\bullet}$ $CH_3CH_2CH_2C(OH){=}CH_2^{+\bullet}$	> 0	64 16	ND[e]	2 4	ND[e]	ND[e]

a) Reaction rate constant, $x10^{-9}$ $cm^3molecule^{-1}s^{-1}$
b) Collision rate constant; $x10^{-9}$ $cm^3molecule^{-1}s^{-1}$
c) Reaction Efficiency
d) Generated from 2-methylbutanal radical cations
e) Not yet determined

Generation and Reactivity of Charged Phenyl Radicals

Rebecca L. Smith, Hilkka I. Kenttämaa
Department of Chemistry, Purdue University, West Lafayette, IN 47907.

Distonic ions (species with spatially separated charge and radical sites) may be a useful tool for the examination of free radical reactivity in the gas phase, provided that the charge site of the ion is unreactive. A method was developed that allows the synthesis of a series of charged phenyl radicals with different unreactive charge sites.

The charged phenyl radicals were formed by nucleophilic *ipso*-substitution of a halogen atom in an ionized dihalobenzene[1] followed by CAD to remove the second halogen atom (Figure 1). The charged phenyl radicals (Figure 2) were structurally characterized by CAD, ion-molecule reactions and comparisons with isomeric ions. For example, the ions were identified to be distonic ions on the basis of the observation of $^{\bullet}SCH_3$ abstraction from dimethyl disulfide and $^{\bullet}SeCH_3$ abstraction from dimethyl diselenide. Conventional radical cations do not undergo these reactions. The *ortho*, *meta*, and *para* isomers of the ion **d** were differentiated on the basis of their reactivity toward allyl iodide.

The charged phenyl radicals react with neutral reagents in a manner analogous to that of the neutral phenyl radical and other neutral radicals. For example, ion **a** reacts with allyl bromide predominately by allyl radical abstraction as is observed for the phenyl radical.[2] Ion **b** reacts with trimethyl phosphite similarly as the phenyl radical, by elimination of $^{\bullet}OCH_3$ from an adduct.[3] Like neutral free radicals, the ions **a**, **b**, and **d** react with cyclohexene by addition to the carbon-carbon double bond and by hydrogen atom abstraction. Further, ion **a** reacts with benzeneselenol by adduct formation and hydrogen atom abstraction and this occurs approximately ten times faster than with thiophenol, in agreement with the reactivity of neutral alkyl radicals toward these two reagents.[4]

The reactivity of the charged phenyl radicals toward electron rich reagents was found to be enhanced by additional electron-withdrawing substituents. Substituting one of the hydrogen atoms adjacent to the radical site with an electron withdrawing group (a fluorine atom) (ion **h**) enhances the reactivity of the ion toward dimethyl disulfide by a factor of 23. Four fluorine atoms on the phenyl ring (ion **i**) cause even a larger rate enhancement: ion **i** reacts with dimethyl disulfide 69 times faster than ion **c**. A similar rate enhancement has been observed in solution for neutral phenyl radicals substituted with electron withdrawing substituents. For example, *p*-nitro phenyl radical reacts with dimethyl disulfide 11 times faster than neutral phenyl radical.[5]

References

1. Thölman, D.; Grützmacher, H.-F. *J. Am. Chem. Soc.* **1991**, *113*, 3281.
2. Takayama, K.; Kosugi, M.; Migita, T. *Chem. Lett.* **1973**, 193.
3. Fu, J.-J.L.; Bentrude, W.G. *J. Am. Chem. Soc.* **1972**, *94*, 7710.
4. Newcomb, M.; Manek, M.B. *J. Am. Chem. Soc.* **1990**, *112*, 9662.
5. Migita, T.; Takayama, K.; Abe, V.; Kosugi, M. *J. Chem. Soc., Perkin Trans. 2* **1979**, 1137.

43rd ASMS Conference on Mass Spectrometry and Allied Topics

Figure 1

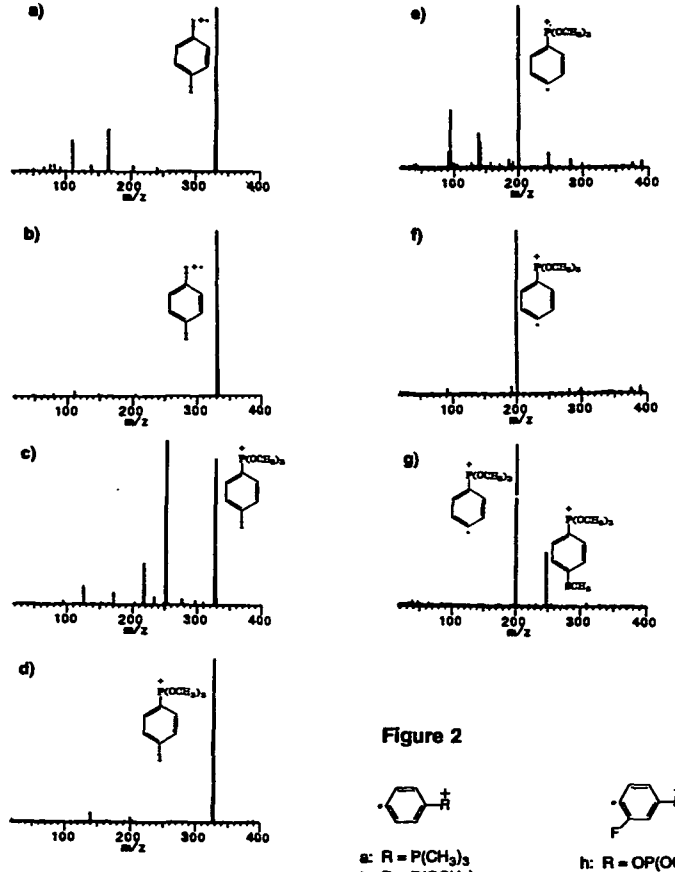

Figure 2

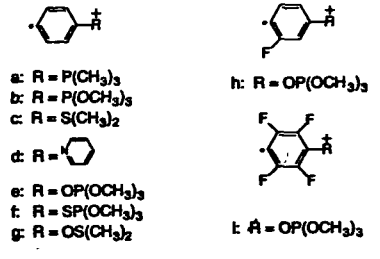

Charge Transfer Reactions of the Cyclopropenyl Cation

Samantha Franck, Jennifer Rich, Layle Watkins, and Curtiss Hanson
University of Northern Iowa, Department of Chemistry
Cedar Falls, IA 50614

INTRODUCTION

The propargyl $C_3H_3^+$ cation (m/z 39) has been extensively studied as a precursor ion to the formation of soot in the pyrolysis of fuels and other hydrocarbons (1,2,3). Studies involving soot nucleation in flames point to an ionic mechanism, versus a neutral free radical mechanism, driving the formation of aromatic hydrocarbons. These aromatic hydrocarbons are believed to continue the transformation process from a molecular level to particulate systems to soot aggregates (1) These studies show that the propargyl $C_3H_3^+$ cation is critical to this transformation.

Studies by Eyler et al. have involved modeling the soot particle initiation process through reactions of $C_3H_3^+$ with acetylene and diacetylene using FT-ICR (2,3). Using Fourier transform ion cyclotron resonance (FT-ICR), the gas phase reactions arising during the pyrolysis of hydrocarbons can be modeled. In these types of experiments, two forms of $C_3H_3^+$ are observed: i) The reactive linear propargyl cation (l-$C_3H_3^+$), and ii) the unreactive cyclopropenyl cation (c-$C_3H_3^+$). Theoretical calculations reported by Wong and Radom (4) shows a significant activation energy of 97.6 kcal/mole required for rearrangement of the propargyl form to the cyclic form. It is estimated that under flame conditions that the concentration of the propargyl cation is less than 1% of the total $C_3H_3^+$ concentration. Therefore, the reactions of the cyclic form is critical to the proposed mechanism.

The scope of the following research centers around developing an understanding of the mechanisms driving the formation of products during the pyrolysis (thermal decomposition in the absence of oxygen) of hydrocarbons, i e styrene butadiene rubber (SBR). Among those systems studied using FT-ICR was and 1,3-butadiene which produces $C_3H_3^+$ upon electron impact of the neutral target gas. Although this work examines the endothermic charge transfer reactions of cyclopropenyl with small conjugated dienes, the scope of this research centers around developing an understanding of the gas phase reactions of $C_3H_3^+$ during the pyrolysis process and the implications of these reactions performed on a large scale.

EXPERIMENTAL

An IonSpec Omega 50 Fourier transform mass spectrometer (FTMS) based on the concept of ion cyclotron resonance was employed for the experiments described in this report.he Omega 50 FTMS instrument uses a Walker Scientific resistive electromagnet which was set with a magnetic field strength of 1 03 T. Samples were introduced through a Varian Series 951 leak valve into a single vacuum chamber Background pressure was maintained at 8 x 10^{-10} torr using a Balzers 330 liter/second turbomolecular pump backed by an Alcatel direct drive roughing pump. Pressures were monitored using a Bayard Alpert ionization gauge, with average experimental pressures set between 2 0-3.0 x 10^{-7} torr. The temperature was monitored using a calibrated thermocouple attached to the vacuum chamber and the neutral gases were allowed to equilibrate prior to kinetic measurements. Ionization followed a 20 ms electron beam with ion current set between 1.2-1 5 μA and electron energy of 60 eV. Values for the excitation time required for the mass and energy selective partitioning of the molecular ion of butadiene was obtained and compared to the dimensions of the skimmer orifice in the rear trap plate.(5). This data was used to calibrate the amplitude of the rf ejection fields used

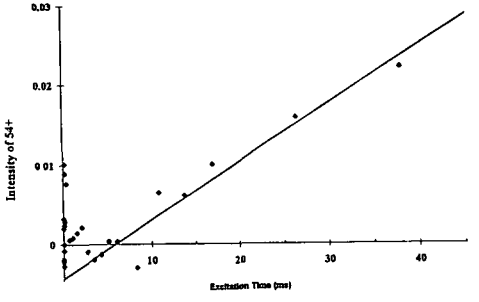

Results and Disscussion

To study the charge exchange reactions between the cyclopropenyl isomer A stable population of the cyclic isomer of C3H3 cation was trapped and thermallized int the FT-ICR mass spectrometer by allowing the more reactive linear propoargyl isomer to react away prior to the isolation of ions of m/z 39 The cyclopropenyl isomer was then allowed to collisionally relax to thermal internal energies by collisions with background neutrals of 1,3 butadiene These ions were then given increasing amounts of translational energy using resonant rf bursts,and the products were observed. As seen in figure 1, there is no initial intensity of m/z 54 which corresponds to a charge exchange product between the cyclopropenyl cation and the neutral 1,3-butadiene. However, following the resonant acceleration of the ions of m/z 39, the formation of ions of m/z 54 is observed indicating the occurance of an electron transfer. The emperical threshold was determined to be ca. 6 9 eV. This emperical data was then compared to differences in ionization potential which were calculated at the MP2/6-31G level using Gaussian 92. The results of these calculations are seen in Figure 2. The good corelation between the calculated ionization potentials and the emperical data suggests that in the collision both the neutral 1,3-butadiene and the cyclopropenyl cation are destabilized, resulting in the endothermic charge transfer reaction.

Structure	HF STO-3G	MP2 3-21G	MP2-631G*
	-113.620	-114.327	-115.004
	-113.760	-114.527	-115.192
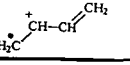	-152.808	-153.573	-154.448
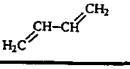	-153.017	-154.057	-154.917
IP 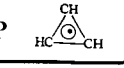	-0.140	-0.200	-0.188
IP 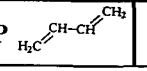	-0.209	-0.484	-0.469

Acknowledgements
We would like to express our gratitude for the funding provided by the Small Business Association Grant #SB-BD-92-007-01, the Reuse Recycling and Technology Transfer Center, the Department of Chemistry at the University of Northern Iowa, Environmental Programs at the University of Northern Iowa, and the Intercollegiate college fund.

Literature Cited

1. Calcote, H. F. *Combustion and Flame*. 1981. *42*, 215-242.

2. Wiseman, F. L.; Ozturk, F.; Zerner, M. C.; Eyler, J. R. *Int. J. of Chem. Kinet.* **1990**, *22*, 1189-1209.

3. Ozturk, F.; Baykut, G.; Moini, M.; Eyler, J. R. *J. Phys. Chem.* **1987**, *91*, 4360-4364.

4. Wong, M. W.; Radom, L. *J. Am. Chem. Soc.*, **1989**, *111*, 6980.

5. Beauchamp, J. L.; Armstrong, T. J. *Rev. Sci. Instrum.* **1969**, *40*, 123-128.

SELECTIVE ION-MOLECULE REACTIONS OF BENZOYL IONS IN A QUADRUPOLE ION TRAP: APPLICATION TO SAMPLES OF PHARMACEUTICAL INTEREST.

Colin S. Creaser and Brian L. Williamson, Deparment of Chemistry and Physics, Nottingham Trent University, Clifton Lane, Nottingham, NG11 8NS, UK.
Brian M. Stockton, Department of Analytical Sciences, SmithKline Beecham Pharmaceuticals, Old Powder Mills, Nr Leigh, Tonbridge, Kent, TN11 9AN, UK.

The benzoyl ion, $[C_6H_5CO]^+$, has been shown to undergo ion-molecule reactions with hydroxy related compounds in a quadrupole ion trap.[1] This ion shows limited reactivity towards other oxygenated compounds and therefore has potential as a selective reagent for chemical ionisation. An ion trap mass spectrometric study has been undertaken on the selectivity of the ion-molecule reactions of the benzoyl ions of the type $[C_6X_nH_{5-n}CO]^+$, (X= H, F, 4-CH_3), with analytes of pharmaceutical interest containing hydroxy, double bond and amine functional groups.

Experiments were performed using a quadrupole ion trap mass spectrometer (Finnigan MAT ITMS), operated at 120 °C. In a typical experiment, the benzoyl ion was generated as an electron ionisation fragment of acetophenone, isolated and allowed to react with neutral sample vapour for 100 ms. Reagent pressure was 2×10^{-6} torr and typical sample pressures were 5×10^{-6} torr. Helium bath gas was maintained at 1×10^{-4} torr measured using the vacuum chamber ion gauge.

The reactions of the benzoyl ion with hydroxy containing compounds produce the characteristic product ions; $[M+105]^+$ (adduct), $[M-OH]^+$, and $[M-H]^+$. Product distributions are determined by the structure of the hydroxy compound, making it a potentially useful probe for establishing the presence and chemical environment of hydroxy groups.

(i) *Keto-enol tautomers of methylacetoacetate*
Methylacetoacetate is an analogue of a β-diketo ester used in the synthesis of the drug candidate SK&F96067 (SmithKline Beecham). The EI GC/MS chromatogram of methylacetoacetate is shown in Figure 1a. It shows two well resolved peaks assigned to the keto-enol tautomers of methylacetoacetate, but the EI spectra do not allow these tautomers to be distinguished. The corresponding benzoyl ion selective CI GC/MS chromatogram of methylacetoacetate is shown in Figure 1b. Reaction with the double bond of the enol tautomer is observed, giving the spectrum shown in Figure 2, but there is no reaction with the keto tautomer.

(ii) *The product related intermediates of 2-(8-phenyloctyl)benzaldehyde*
2-(8-Phenyloctyl)benzaldehyde (POB)[2] is the precursor of SK&F104353,[3] a high affinity peptidoleukotriene antagonist (SmithKline Beecham). The $[C_6H_5CO]^+$ ion reacts with the hydroxy and double bond containing intermediates of POB, forming electrophilic addition product ions. Both benzyl alcohol and phenylheptyl alcohol undergo hydroxy abstraction to produce $[M-OH]^+$ ions, where as phenylheptene reacts to form a $[M+105]^+$ adduct ion. Bibenzyl undergoes a side reaction, which leads to the formation of $M^{+\cdot}$ by charge exchange. The pentafluorobenzoyl ion, $[C_6F_5CO]^+$, a much stronger electrophile than $[C_6H_5CO]^+$, reacts with chloride, hydroxy, carbonyl and double bond containing intermediates of POB, to produce $[M+105]^+$, $[M-H]^+$, $[M-Cl]^+$ and $[M-OH]^+$ ions. The 4-methylbenzoyl ion, a much weaker electrophile than $[C_6H_5CO]^+$, only reacts with benzyl alcohol, to produce $[M-OH]^+$ hydroxy abstraction ions.The electrophilic nature of the benzoyl ion can therefore be controlled easily,

allowing its selectivity to be varied. It therefore has potential for trace analysis as a selective chemical ionisation technique and product ion distributions may allow functional group assignment.

References

1) C. S. Creaser and B. L. Williamson, J. Chem. Soc., Chem. Comm., 1677, 1994.
2) M. A. Forth, M. Mitchell, S. A. C. Smith, K. Gombatz and L. Snyder, J. Org. Chem., 1994, 59, 2616.
3) J. G. Gleason, R. F. Hall et al, J. Med. Chem., 1987, 30, 959.

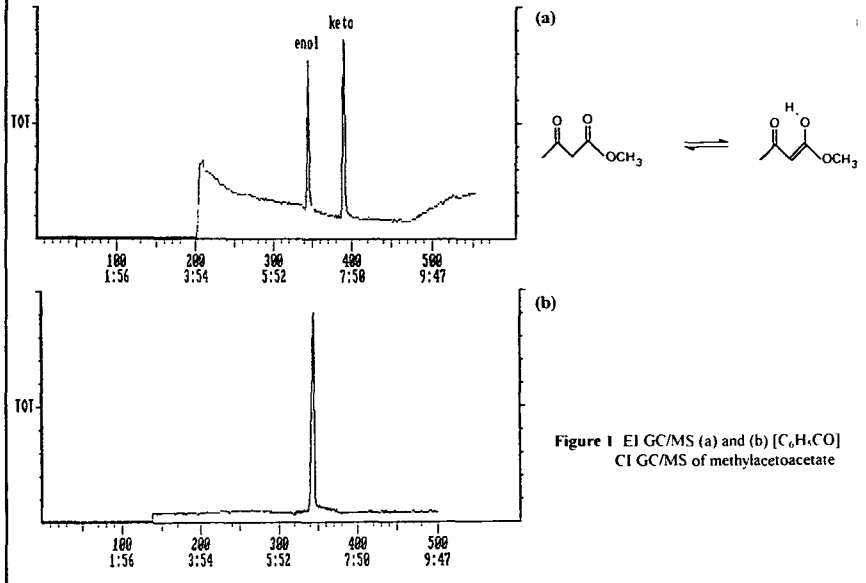

Figure 1 EI GC/MS (a) and (b) $[C_6H_5CO]^+$ CI GC/MS of methylacetoacetate

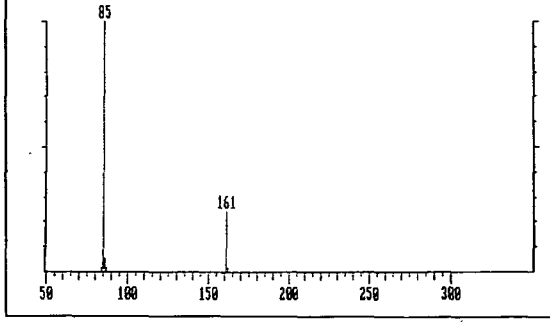

Figure 2. Mass spectrum resulting from the $[C_6H_5CO]^+$ ion reaction with the enol tautomer of methylacetoacetate

Gas-Phase Ion-Molecule Reactions of Methyl tertButyl Ether (MTBE)

Scott Peterman, Michaela Rich, and Curtiss Hanson
University of Northern Iowa, Cedar Falls, Iowa 50613

The evaluation of Methyl-tert Butyl Ether has been intensively studied since its initial use in the late 1970's. In general, there has been fewer studies concerning the fragement ions formed under combustion conditions. MTBE has been the fastest growing chemical in production during the past decade[1]. Its major use is an octance inhancer. Since MTBE is a labile molecule, the energy of combustion does produce chemical reactions that must be recognized. With the health complaints associated with blended gas, the need for an understanding of the chemical reactions occurring from combustion must be understood.

The use of a Fourier transform ion cyclotron resonance mass spectrometer was used for all experimental work. The FT-ICR was chosen due to the ability to model combustion conditions at an ideal rate for observation. All theoretical calculations were done on the Spartan RISC 6000 system calculated at the MP2 6-31g* theory level Using both methods, a complete picture was provided of the fragmentation patterns and bi- and unimolecular reactions of MTBE

The intial spectrum of MTBE displayed fragmentation at minimal energy into two primary ion, m/z 73 and m/z 57, with no cold molecular ions Spartan was used to calculate the thermochemical energy relationship for the unimolecular ion decomposition of MTBE

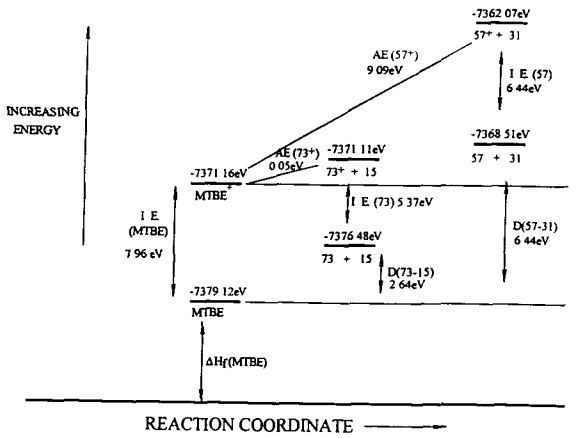

Becuase of the lability and the time frame of combustion, the chemical reactions of these fragment ions were studied. Time delays were implemented to distinguish bimolecular reactions occurring. Through this study, a gas-phase acid was determined to be the t-butyl ion, m/z 57. Studies done

by Gray and Westbrook focused on MTBE in a shock tube experiment, determining that the primary product was the t-butyl radical[2]. The heat of formation for this radical was 6.92 eV, the ion was calculated to be 7.13 eV[3]. Spartan calculations for the ionization energy of the t-butyl ion was determined to be 6.44 eV.

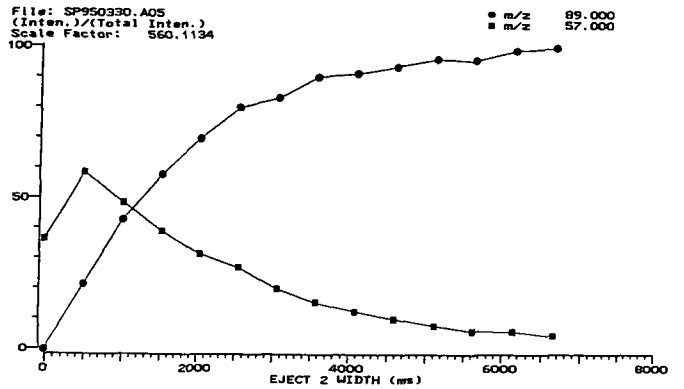

From the delay scan, a rate of proton transfer was calcautaed to be 3.24 x 10^{-10} cc/(molecules x sec) This rate was compared to similar systems and evaulated to be a strong gas-phase acid

The t-butyl ion also functioned as base. The strenght of the ion coupled with the lability of the neutral allowed the ion to abduct an electron from the neutral, causing fragmentation. From this, the formation of the m/z 73 ion was observed. Through labelled experiments, the isomer of this ion was identified.

Collisional activation of the protonated MTBE ion shows the formation of two ions, m/z 57 and m/z 74. The amount of energy imparted on m/z 89 was calculated to be 1 75 eV for the m/z 57 ion, and 2 72 eV for the m/z 74 ion Spartan calculations gave theoretical values of 1.69 eV and 3.03 eV for the m/z 74.

Literature Cited

1.Heylin, M ; *Chem. & Eng. News,* **1994,** July 4 28-34

2.Gray, J. A., Westbrook, C. K., *Int. Journ. Chem. Kinetics,* **1994,** *26,* 757-770

3.Traeger, J. C., McLoughlin, R. G ; *J. Am. Chem. Soc.* **1981,** *103(13),* 3847-3653

Ion/Molecule Reactions with Polyethylene Glycols

Adebayo Onigbinde, D. P. Ridge, Tianlan Zhang, and Burnaby Munson
Department of Chemistry and Biochemistry
University of Delaware
Newark, DE 19716-2522

Polyethylene glycols have many industrial applications. The compounds also show strong evidence for intramolecular interactions in ion chemistry. The electron ionization (EI) mass spectra of homologous compounds are very similar and contain no molecular weight information for identification of the compounds. The CH_4 CI mass spectra contain structurally useful fragment ions and MH^+ ions. The abundance of MH^+ ions, however, depends on the PEG concentration, which increases across the chromatographic peaks and result from sample ion/sample molecule reactions, probably from $C_2H_5O^+$, the dominant ion in the CH_4 CI mass spectra of PEG.

FT/ICR/MS was used to study the ion/molecule reactions of $C_2H_5O^+$ from three sources with PEG to determine the reaction products and the rate constants for the ion/molecule reactions. $C_2H_5O^+$ ions were produced by electron ionization of PEG; by ion/molecule reactions in ethylene oxide, C_2H_4O; and by electron ionization of dimethyl ether.

The glycols were introduced with the probe. The ethylene oxide and dimethyl ether were introduced through the pulsed valve and the $C_2H_5O^+$ ions were transferred from the analyzer to the source to react with PEG. The source temperature was approximately 27 °C. Pressures were of the order of 10^{-7} -10^{-8} torr (gauge). Rate constants were calculated using the indirect method of pressure determination of Pan and Ridge (J. Am. Chem. Soc. 1992, **114**, 2773).

The products and their abundances from ion/molecule reactions with PEG of $C_2H_5O^+$ made by electron ionization of PEG were very similar to the products and abundances obtained in CH_4 CI of PEG. The dominant $C_2H_5O^+$ ion decreased in relative abundance with increasing sample concentration in the CH_4 CI studies and with increasing time in the FT/ICR/MS studies. Essentially no MH^+ ions were present at low concentrations or zero time and the abundance of MH^+ increased with increasing concentration in CH_4 CI studies and with increasing time in the FT/ICR/MS experiments. Therefore, $C_2H_5O^+$ is the primary source of MH^+ ions in the CH_4CI spectra of PEG.

Studies were made on the time dependences of product ions from reactions of $C_2H_5O^+$ made from three different sources with PEG in order to differentiate between the structures of the ions. $C_2H_5O^+$ ions made from ethylene oxide and by electron ionization of PEG were expected to be the same and different from $C_2H_5O^+$ ions made from dimethyl ether. Plots of the relative abundances of product ions from the reactions of $C_2H_5O^+$ ions from PEG and from ion/molecule reactions in ethylene oxide were very similar. Some of the major product ions from the reactions of $C_2H_5O^+$ from dimethyl ether with PEG were different from those observed from reactions of $C_2H_5O^+$ from the other two sources. Consequently, we believe that the $C_2H_5O^+$ ions from electron ionization of PEG have the protonated ethylene oxide structure, not $CH_3OCH_2^+$.

The rate constants for reactions of $C_2H_5O^+$ from PEG and of $C_2H_5O^+$ from ethylene oxide were very similar for ethylene glycol, diethylene glycol, triethylene glycol, and tetraethylene glycol and relatively close to the calculated ADO values. The rate constants for the reaction of $CH_3OCH_2^+$ with ethylene glycol and diethylene glycol were significantly lower than rate constants for reaction of $C_2H_5O^+$ from PEG or ethylene oxide. The rate constants for reaction of $CH_3OCH_2^+$ with tri- and tetraethylene glycols were approximately the same as the calculated ADO values.

The observation of protonated dimers, $(PEG)_2H^+$, in the CH_4 CI spectra of ethylene glycol and diethylene glycol at high concentrations, but not in the spectra of tri- and tetraethylene glycol suggests that the proton is internally solvated in MH^+ ions of the higher glycols.

CS_2 AND BENZENE CI OF METHYL ESTERS AND PARAFFINS

Jason J. Evans, Burnaby Munson, Gordon Nicol
Chemistry and Biochemistry
University of Delaware
Delaware, 19716 DE

Charge exchange chemical ionization (CI) can sometimes provide mass spectra containing primarily molecular ions. Advantages that can be realized include enhanced sensitivity and ease of quantitation. Benzene CI, for example, has been used for the analysis of gasoline samples with a moderate degree of success.

Saturated esters and paraffins have ionization potentials around 10.0 eV, slightly below IP(CS_2). The CS_2 CI spectra of saturated esters and paraffins contain essentially no fragment ions. Benzene has an ionization potential of 9.25 eV. Therefore, a charge exchange reaction does not take place. The proton affinity of benzene is 7.8 eV. The $C_6H_7^+$ will not transfer a proton to a paraffin, but proton transfer is observed with saturated esters.

The EI spectra of unsaturated esters contain low abundance molecular ion peaks. The CS_2 CI spectra of unsaturated esters show some fragmentat ions but the molecular ions are the most abundant peaks in the spectra. The C_6H_6 CI spectra of unsaturated esters contain only the molecular ions.

The EI spectra of acetals do not contain molecular ions. Benzene CI gives $(M-H)^+$ ions at about ten percent of the base peak, which can aid in identification.

Studies of the CS_2 CI GC/MS system were performed on a VG 7070E mass spectrometer modified for high pressure work. CS_2 CI spectra can be obtained at source pressures between 0.25 and 0.40 torr of a 70:30 He/CS_2 mixture. He and CS_2 were introduced through separate inlet lines. The GC column was brought into the source through a Vespel plug. A manometer was connected to the source through Tygon tubing and a Vespel plug. There is a broad maximum in sensitivity between 0.25 and 0.40 torr. However, with pure CS_2 the TIC decreases signficantly quickly with time during continuous operation. Such declines in sensitivity are not observed with He/CS_2 mixtures. The sensitivities are also higher using He/CS_2 mixtures as the CI reagent gas than using pure CS_2 at the same pressure.

Benzene and CS_2 CI spectra obtained with a VG Autospec mass spectrometer under normal CI operating conditions contain much more fragmentation than is observed with the 7070E mass spectrometer at 0.3 torr. It appears that the source pressure is low and some direct electron ionization is occurring in addition to the charge exchange CI reactions. The CS_2 and benzene CI spectra obtained with the Autospec are still useful for identification purposes and show enhance abundances of $M^{+\cdot}$ compared with EI spectra.

Benzene and CS_2 CI GC/MS can be useful in the analysis of fatty acids as the methyl esters. Assignment of molecular weights is much easier from CI spectra of unsaturated esters with both reagent gases than from the EI spectra.

43rd ASMS Conference on Mass Spectrometry and Allied Topics

Benzene CI is perhaps the best technique for identifying acetals. Quantitation of the saturated esters using CS_2 appears promising since the spectra contain only molecular ions. Also, the rate constants for charge exchange of CS_2^+ with C14 through C20 methyl esters should very similar, scaling only slightly with molecular weight; therefore, the compounds should have similar molar sensitivities.

Benzene CI is not a sensitive technique for the analysis of methyl esters of saturated fatty acids. However, quantitation of the methy esters of unsaturated fatty acid using benzene CI is promising. It can be informative to use both reagent gases in GC/CIMS analyses of complex mixtures of methyl esters of fatty acid sample. The CS_2 chromatogram will show all methyl esters with approximately equal ionization efficiencies. In benzene CI, however, the unsaturated esters peaks are enhanced relative to the peaks for the saturated esters peaks. One can, therefore, identify some unsaturated esters which are present only in trace amounts. In the EI and CS_2 chromatograms these peaks may be masked by intense peaks of saturated esters.

CS_2 CI appears to be a powerful tool for the analysis of paraffins. The molecular ions of paraffins are often barely detectable in EI mass spectra. Determining the molecular weights from the fragment ions is impossible. Quantitation of paraffin mixtures using CS_2 is also promising.

GAS PHASE ION-MOLECULE REACTIONS OF AMINES WITH CARBONYL COMPOUNDS

Mika Pykäläinen and Pirjo Vainiotalo

Department of Chemistry, University of Joensuu, P.O. Box 111, FIN-80101 Joensuu, Finland

Both imines and enamines are important intermediates in many synthetically significant reactions. In solution, the nucleophilic addition of ammonia, amine, hydroxylamine or hydrazine to a carbonyl-containing substrate followed by the elimination of water gives rise to the formation of an imine or enamine (Scheme 1). However, the reaction of primary amines to carbonyl compounds produces imines rather than enamines.

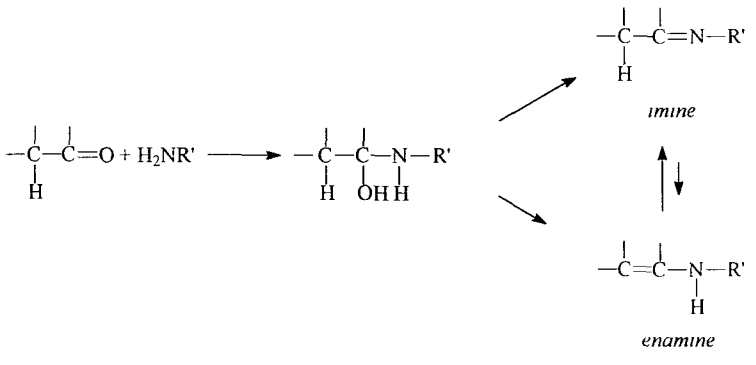

Scheme 1

In this work, ion-molecule reactions of several mono- and diamines with acetone and 3-pentanone were investigated under chemical ionization (CI) using the carbonyl compound as reagent gas. The main aim was to establish whether the nucleophilic addition-elimination reaction takes place under these conditions and what is the structure of possible product ions.

In addition to protonation, the most important ionization reactions were the formation of the $[M+43]^+$, $[M+59]^+$ and $[M+57]^+$, $[M+87]^+$ adduct ions under acetone and 3-pentanone CI, respectively. All the primary amines gave rise to the $[M+59-18]^+$ and $[M+87-18]^+$ ions which at least formally correspond to the products of the nucleophilic addition-elimination reaction either with imine or enamine structure. Comparison of the collision induced dissociation (CID) mass spectra of the $[M+59-18]^+$ ions with those of authentic imines showed that imine formation really takes place in the gas phase. However, under 3-pentanone CI the nucleophilic addition-elimination products, the $[M+87-18]^+$ ions, in most cases formed a mixture where portion of the enamine structure was considerable in addition to the imine structure (Fig. 1) Further experiments showed that the amount of enamine formed was strikingly dependent on the structure of ketone.

The principal reactions of diamines were the same observed for monoamines The formation of the product ions of the nucleophilic addition-elimination reaction was, however strikingly more favourable with diamines than with monoamines both under acetone and 3-pentanone CI In some cases these ions even gave rise to the base peak in the spectrum. Comparison of the CID mass spectra of the $[M+59-18]^+$ and $[M+87-18]^+$ ions generated from diamines with the corresponding spectra of primary monoamines showed that fragmentations in both cases are quite similar.

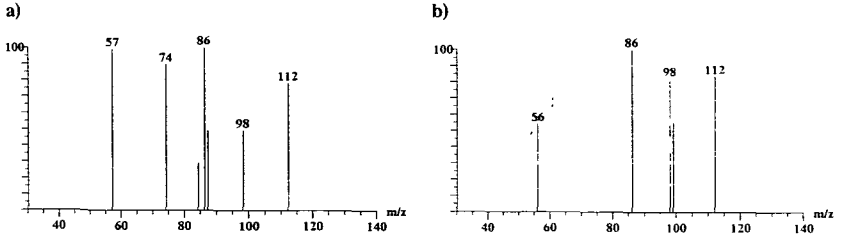

Figure 1. a) The CID mass spectrum of the product ion m/z 142 under 3-pentanone CI

b) The CID mass spectrum of the authentic protonated imine m/z 142 under isobutane CI.

In Situ Investigation of Soot Formation

Helge Egsgaard

Department of Combustion Research, Risø National Laboratory,
DK-4000 Roskilde, Denmark

Soot as collected from flames is likely to be more well-defined that commonly realized as consisting of chainlike aggregates of spherical units with a diameter of 10-50 nm. The spherical units are characterized by having a hexagonal substructure and a very high carbon to hydrogen ratio.

The soot formation involves a series of distinct steps namely nucleation, growth to spherical particles, and the final agglomeration. The most widely accepted mechanism for soot formation is based on free radical reactions and the other on an ionic mechanism, i.e. the Calcote mechanism [1]. The ionic mechanism is initiated by the $C_3H_3^+$ chemi-ion, which rapidly grows by the addition of, e.g. acetylene. It should be noted that a flame may regarded as a weak plasma being the result of highly energetic *chemical* reactions, e.g. between the parent methylidyne, CH, and atomic oxygen.

Very recently we have demonstrated the application of tandem mass spectrometry to chemi-ions based on supersonic molecular beam sampling [2]. This methodology gives unique possibilities for studying the reactivity of isolated chemi-ions [3]. Thus, our studies on soot formation are experiments involving the species actually present in the flame and conceivable reactants under highly controlled conditions.

Our studies of the first step of the Calcote mechanism may serve as an illustrative example. The mass spectra following the reaction of the $C_3H_3^+$ chemi-ion with C_2H_2 and C_2D_2 are shown in Figure 1. The primary adduct $[C_5H_5^+]^*$, m/z 65, is directly observed (Fig. 1a). A very high deuterium content is observed in this complex (m/z 65 - m/z 70) as well as in the C_3-species (m/z 39 - m/z 42) in the C_2D_2 experiments (Fig 1b). An unique feature of the reaction is that if the C_5-complex breaksup the $C_3H_3^+$ ion is re-formed in an mixture of linear and cyclic C_3-species [4]. Thus, the reaction causes a distribution of the isotopic label originating from acetylene in the products, i.e. the ionic C_3-species and acetylene. This leads ultimately to the very high deuterium content of the C_5-complex.

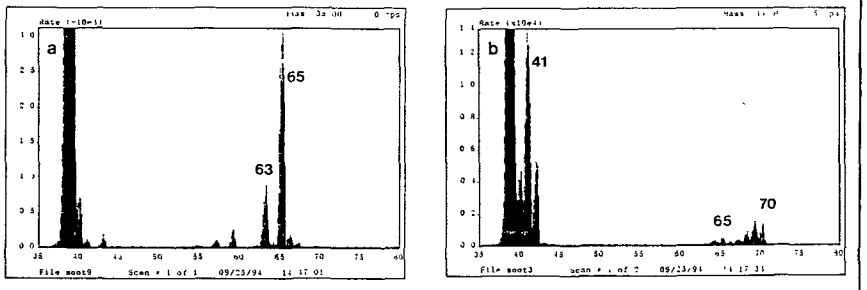

Figure 1. Ion distribution following reaction of the $C_3H_3^+$ chemi-ion with a) acetylene and b) D_2-acetylene. The $C_3H_3^+$ chemi-ion was selected by the first quadrupole, and following reactive collisions in the second quadrupole, the ionic products were analyzed by the final quadrupole.

The translatory energy is in general kept low, i.e. ≤ 0.5 eV. Raising the energy has a pronounced influence as the complex is not traced. The isotopic pattern of the C_3-ions indicates, on the other hand, that the complex does form as evidenced by deuterium inco-operation. Thus, the complex breaks up before collisional deactivation takes place as a result of a possible weak, but sufficient transformation of translatory energy to ro-vibrational energy, causing a much more rapid fragmentation of the encounter complex than observed near thermal kinetic energies. Finally, it should be noted that the product distribution is very dependent on pressure. Thus, the intensity ratio of the $C_5H_5^+$ and $C_5H_3^+$ ions increases with increasing pressure. The comprehensive studies on the ion-molecule reactions related to the ionic soot mechanism will be published elsewhere.

References

1. H.F. Calcote; *Combust. Flame*, 42 (1981) 215.
2. H. Egsgaard, M. S. Thomsen and E. Larsen; *42nd ASMS* (1994) 1091.
3. H. Egsgaard and L. Carlsen; *Chem. Phys. Letters*, 236 (1995) 78.
4. M. Moini; *J. Am. Soc. Mass Spectrom.*, 3 (1992) 631.

An Ion Trap Tandem Mass Spectrometric Study of $[C_{14}H_{10}]^{+\cdot}$, $[C_{10}H_{10}]^{+\cdot}$ and $[C_{10}H_8]^{+\cdot}$ Ions formed in Ion/Molecule Reactions

Xiaomin Wang, Raymond E. March[1], Alan C. Hopkinson and Diethard K. Bohme, Department of Chemistry and Centre for Research in Earth and Space Science, York University, North York, ON, CANADA M3J 1P3,

[1]Department of Chemistry, Trent University, Peterborough, ON, CANADA K9J 7B8

The experimental results presented here are complementary with those obtained with a Selected-Ion Flow Tube (SIFT) wherein it was observed that diacetylene condenses rapidly with benzene cations;[1] the structure proposed for $C_{10}H_8^{+\cdot}$ product ions was that of the naphthalene cation. In experiments performed in a modified ion trap detector, it was observed that diacetylene and vinylacetylene condense with benzene cations and that vinylacetylene condenses with vinylacetylene cations in the gas phase as shown in reactions (1-3), respectively.

$$C_6H_6^{+\cdot}+C_4H_2 \rightarrow C_{10}H_8^{+\cdot}, C_{10}H_6^{+\cdot}+H_2 \quad (1)$$

$$C_6H_6^{+\cdot}+C_4H_4 \rightarrow C_{10}H_{10}^{+\cdot}, C_{10}H_9^{+}+H^{\cdot}, C_{10}H_8^{+\cdot}+H_2, C_9H_7^{+}+CH_3^{\cdot} \quad (2)$$

$$C_4H_4^{+\cdot}+C_4H_4 \rightarrow C_6H_6^{+\cdot}+C_2H_2,\ C_8H_7^{+}+H^{\cdot} \quad (3)$$

$$C_6H_6^{+\cdot}+C_4H_4 \rightarrow C_{10}H_9^{+}+H^{\cdot}, C_{10}H_8^{+\cdot}+H_2$$

$$C_{10}H_8^{+\cdot}+C_4H_4 \rightarrow C_{14}H_{10}^{+\cdot}+H_2$$

The rate constants for the reactions of benzene cations with both diacetylene and vinylacetylene, and of vinylacetylene cation with vinylacetylene were determined to be 3.69×10^{-10}, 2.70×10^{-10} and 7.59×10^{-10} $cm^3 molecule^{-1} s^{-1}$, respectively. The principal product ions detected from these reactions were $C_{10}H_8^{+\cdot}$, $C_{10}H_{10}^{+\cdot}$ and $C_{14}H_{10}^{+\cdot}$. These experiments were carried out in argon at 10^{-4} Torr and at 475 K; both benzene and vinylacetylene cations were produced by electron impact(~70 eV). Three possible modes of formation of $C_{10}H_8^{+\cdot}$ by ion/molecule reactions are illustrated in Scheme 1. A comparison of collision-induced dissociation mass spectra of $C_{10}H_8^{+\cdot}$ produced in reactions (1-3) is shown in the Table 1. This comparison of the CID mass spectra of $C_{10}H_8^{+\cdot}$, together with an evaluation of thermochemical data and observation of chemical reactivity permit the relatively unambiguous determination of the $C_{10}H_8^{+\cdot}$ ion structures. $C_{10}H_8^{+\cdot}$ produced from the reactions of benzene cation with diacetylene(1) and vinylacetylene cation with vinylacetylene(3), have been proposed as ionized naphthalene; while $C_{10}H_8^{+\cdot}$ produced from reaction of benzene cation with vinylacetylene(2) has been proposed as ionized 1-methylene-1-H-indene. Using the same method as described above, ions of $C_{10}H_{10}^{+\cdot}$ (from reaction (2)) and $C_{14}H_{10}^{+\cdot}$ (from reaction (3)), have been proposed as ionized 3-methylindene and 9H-9methylene-fluorene, respectively.

Scheme 1. Formation and Collision-Induced Dissociation of $C_{10}H_8^{+\cdot}$

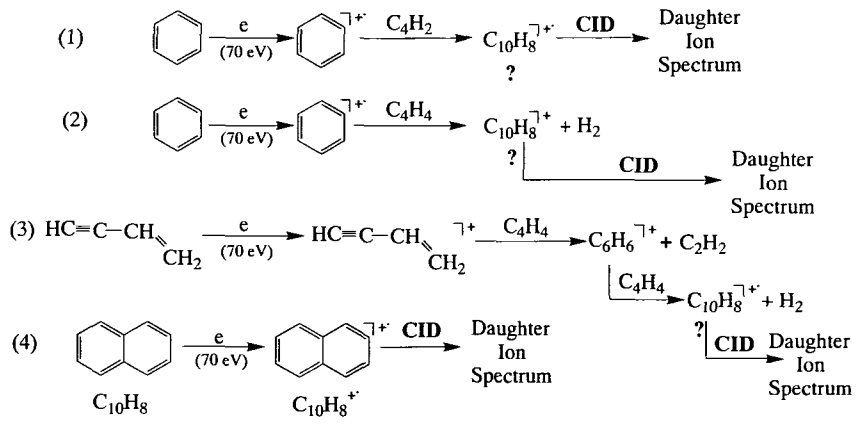

Table 1. Relative abundances of fragment ions of the product ions formed from (1) $C_6H_6^{+\cdot}+C_4H_2$, (2) $C_6H_6^{+\cdot}+C_4H_4$ and (3) $C_4H_4^{+\cdot}+C_4H_2$ and the collision-induced dissociation efficiency, E_f[a]

Parent Ion	Fragment Ion	Relative Abundance %	E_f %
(1) $C_{10}H_8^{+\cdot}$	$\rightarrow C_{10}H_7^{+}+H^{\cdot}$	9	60
	$\rightarrow C_{10}H_6^{+\cdot}+H_2$	45	
	$\rightarrow C_8H_6^{+\cdot}+C_2H_2$	32	
	$\rightarrow C_6H_6^{+\cdot}+C_4H_2$	14	
(2) $C_{10}H_8^{+\cdot}$	$\rightarrow C_9H_7^{+}+CH^{\cdot}$	78	40
	$\rightarrow C_6H_6^{+\cdot}+C_4H_2$	22	
(3) $C_{10}H_8^{+\cdot}$	$\rightarrow C_{10}H_7^{+}+H^{\cdot}$	15	35
	$\rightarrow C_{10}H_6^{+\cdot}+H_2$	5	
	$\rightarrow C_8H_6^{+\cdot}+C_2H_2$	50	
	$\rightarrow C_6H_6^{+\cdot}+C_4H_2$	30	

[a] E_f is a fragmentation efficiency, which is the sum of the daughter ions collected following CID divided by the sum of all ions detected following CID.

Reference

[1] Bohme, D.K.; Wlodek, S.; Zimmerman, J.A.; Eyler, J.R., *Int. J. Mass Spectrom. Ion Processes*, **1991**, *109*, 31.

ISOMERIC FORMS OF THE PRODUCTS OF ION-MOLECULE ASSOCIATION REACTIONS

Kelly K. MATTHEWS and Nigel G. ADAMS, Department of Chemistry, University of Georgia, Athens, GA 30602

Product ions of many association reactions could have different isomeric forms. The identity of the product ion is important for understanding the chemistry occurring in interstellar clouds as well as gaining insight into mechanisms of the reactions by which the more complex species observed there are formed. For example, $(CH_3)_2O$ and C_2H_5OH have been detected.

It has been suggested[1] that radiative association reactions of the type:

$$CH_3^+ + CH_3OH \rightarrow (CH_3)_2OH^+ + h\nu \quad (1a)$$

$$\rightarrow C_2H_5OH_2^+ + h\nu \quad (1b)$$

followed by dissociative electron-ion recombination could produce these species. The collisional association analog of the reaction

$$H_3O^+ + C_2H_4 \rightarrow (CH_3)_2OH^+ + h\nu \quad (2a)$$

$$\rightarrow C_2H_5OH_2^+ + h\nu \quad (2b)$$

has been suggested as an alternative production route by Jarrold et al[2], which they believe proceeds by channel (2b)

We have used a selected ion flow tube (SIFT) to study the isomeric forms of the ionic products of the collisionally stabilized analogs of reactions (1) and (2). To distinguish between the isomeric forms, differences in reactivities of the isomers have been used as a diagnostic. Though reactants were initially chosen on the basis of proton affinities, other reaction channels are possible. Reactions of $C_2H_5OH_2^+$ and $(CH_3)_2OH^+$ with the chosen species are also being studied to help identify the form of the association product ions. The ions CH_3^+, H_3O^+, and $C_2H_5OH_2^+$ were separately produced in low and high pressure ion sources and injected into flowing He at 0.5 Torr. The $C_2H_7O^+$ association ions were produced by adding CH_3OH and C_2H_4 into the flowing ion swarm. Reactant gases and vapors were added further downstream. All measurements were made at 300K. Rate coefficients obtained for the collisional analogs of reactions (1) and (2) compare favorably with previous values (2.6×10^{-9} cm^3s^{-1} for reaction (1) and 7.8×10^{-11} cm^3s^{-1} for reaction (2)).[1,3,4]

Our results indicate that the $C_2H_7O^+$ produced from $CH_3^+ + CH_3OH$ is different from the $C_2H_7O^+$ from $H_3O^+ + C_2H_4$. For example, the rate coefficients measured in reaction with toluene differ by more than 50%. Though the study is not yet complete, results from the protonated ethanol reactions suggest that the $C_2H_7O^+$ (CH_3^+/CH_3OH) is not $C_2H_5OH_2^+$ Allene reacts slowly with $C_2H_7O^+$ (CH_3^+/CH_3OH) ($k = 6.8 \times 10^{-12}$ cm^3s^{-1}) while the reaction with $C_2H_5OH_2^+$ is closer to gas-kinetic ($k = 4.8 \times 10^{-10}$ cm^3s^{-1}). Additional evidence is based on the reactions of these ions with cyclopropane. In the reaction with $C_2H_5OH_2^+$, two products corresponding to different association-type products were observed. However, only one product ($C_4H_9^+$, possibly a weakly bonded association ion of CH_3^+ and cyclopropane) was observed for the reaction with $C_2H_7O^+$ (CH_3^+/CH_3OH). The observed product suggests that the $C_2H_7O^+$ (CH_3^+/CH_3OH) is the association ion $CH_3^+{\cdot}CH_3OH$ rather than $(CH_3)_2OH^+$ as suggested previously.[1,3] Support for our conclusion comes from an ICR study[5] in which 14% of the products from the isotopically labeled $^{13}CH_3^+ + CH_3OH$ reaction were produced via the intermediate complex $^{13}CH_3^+{\cdot}CH_3OH$. Stabilization of these complexes will be likely to occur in the higher pressure SIFT Comparisons with results from $(CH_3)_2OH^+$ reactions in progress will better ascertain the identity of the ion.

Jarrold, et al,[2] concluded from collisional induced dissociation that the $C_2H_7O^+$ (H_3O^+/C_2H_4) was $C_2H_5OH_2^+$, though energies involved could have been high enough to overcome the barrier (10 kcal mol^{-1}) from a stable minimum, corresponding to a proton-bound dimer structure (H_2O---H^+---C_2H_4), as calculated by Radom[6]. Protonated ethanol was found to be the most thermodynamically stable structure in that investigation Comparison of results between $C_2H_7O^+$ (H_3O^+/C_2H_4) and $C_2H_5OH_2^+$ is less definitive, and no final conclusions have been reached about the form of the $C_2H_7O^+$ (H_3O^+/C_2H_4).

During the studies of $C_2H_7O^+$, interesting products have been observed from reactions of $C_2H_5OH_2^+$ never before investigated. Reactions with cyclopropane and acetic acid produce cluster ions as primary products in addition to simple proton transfer products. Only a cluster product ion is observed in reaction with allene

References:

(1) Smith, D.;Adams, N. G Astrophys. J. **1978** 220, L87.
(2) Jarrold, M. F.; Kirchner, N. J.; Liu, S.; Bowers, M. T. J. Phys. Chem. **1986** 90, 78.
(3) Smith, D.; Adams, N. G. Chem. Phys. Lett. **1978** 54, 535.
(4) Bohme, D K.; Mackay,G I. J. Am. Chem. Soc. **1981** 103, 2173.
(5) Audier, H.E.; Koyanagi, G. K.; McMahon, T. B.; Tholmann, D 42nd ASMS Conference on Mass Spectrometry, Chicago, 1994.
(6) Radom, L. Int. J. Mass Spectrom. Ion Processes **1992** 118/119, 339.

COMPETITIVE SNi/SN2 FROM EPIMERIC 1-2 HYDROXYETHER AND DIETHERS 1-2 INDANES IN AMMONIA CHEMICAL IONISATION .

Gervat V.[1], Perlat M.-C.[1], Bourhis C.[1], Fournier F.[1], Mandelbaum A.[2], Tabet J.-C.[1*]

[1]Laboratoire de Chimie Structurale Organique et Biologique, EP 103, U.P.M.C., FRANCE,
[2]Department of Chemistry, Technion, Institut of Technology, ISRAEL.

In a recent study[1], the comparative reactivity of the epimeric diether derivatives of the 1-2 indanediols towards the NH_3/NH_4^+ system has been investigated under CI-NH_3 conditions First, competitive MH^+ and $[M+NH_4-ROH]^+$ (noted as MsH^+) ions are generated as well as fragment ions The abundance of these ions depends upon the stereochemistry The occurrence of these reactions reflectes the similarity of PA values of ammonia and substrat In addition, submitted low collision energy , MNH_4^+ fragments into MH^+ and MsH^+ as well as by consecutive processes yielding the $[MH-ROH]^+$ ions and/or $[MsH-NH_3]^+$ ions. Note that formation of the substituted MsH^+ ions is stereospecific of the trans epimers since it is not produced from the cis epimers Alternatively, this reaction occurs regioselectively at the benzylic position independantly of the size of the ether group located at this reactive position (from heterogeneous diethers, e g ethyl-methyl or methyl-ethyl diethers) This behavior is unexpected since proton affinity of benzylic ethers has been shown higher than that of ammonia and this PA effect should hinder formation of the substituted ion formation The relative high PA values for diethers is confirmed by the absence of NH_4^+ ions from CID of the selected adduct ions which prefer to lead to formation of the MH^+ ions in contrast with that observed from the epimeric indanediols which fragment mainly into ammonium ion However, very likely, the particular polarisability of the benzylic ether group must allow the nucleophilic substitution process which occurs from the trans epimers in CID conditions by SNi mechanism associated with configuration retention From the cis isomers, function exchange being observed in ion source and not in the collision cell, the mechanism of the MsH^+ formation must follow a like-SN2 pathway with configuration inversion From the former isomers, the enhanced fragmentations leading to the benzylic leaving group loss under collisions is due to an anchimeric assistance induced by the homobenzylic group[2] The CI mass spectra of the 1-methylether 2-hydroxy indanes (2'c and 2't) as well 1-methylether 2-hydroxy indanes (3'c and 3't) display the adduct ions as base peak These ions react according to different pathways as shown in the following Table 1

Table 1. *Major ions diplayed in ammonia CI mass spectra of the epimeric cis trans hydroxy ethers.*

cis epimer	MH^+	$Ms''H^+$	MsH^+	$[MH-H_2O]^+$ $[M''sH-NH_3]^+$	$[MH-CH_3OH]^+$ $[MsH-NH_3]^+$
2'c (MNH_4^+, m/z 182)	165 (4)	—	150 (17)	—	133 (2)
3'c (MNH_4^+, m/z 182)	—	164 (67)	—	147 (12)	—
trans epimer					
2't (MNH_4^+, m/z 182)	165 (5)	—	150 (31)	—	133 (15)
3't (MNH_4^+, m/z 182)	—	164 (62)	—	147 (35)	—

The adduct ions are produced as base peak in CI mass spectra of four isomers However, observation of MH^+ is only observed from the cis and trans 1-2 indane methylether alcohols (2'c and 2't) This suggests that protonation is due to the increase of the benzylic group PA On the orther way, from these 2'c and 2't epimers, competition between the protonation and the SN processes is reinforced the latter one in the trans 2't epimer (PA(trans) < PA(cis)) Absence of MH^+ ion from the hydroxy ethers (3'c and 3't) is comparable to that observed from indanediols Then, it can be considered that NH_4^+ solvation in source takes place mainly by the benzylic position This assumption is confirmed by CID of the MNH_4^+ ions since only the benzilic site is lost independantly to the PA value of the leaving group However, from the latter pairs of isomers, the importance of the stereochemical effects is some what lowering which contrasts with that observed in low energy collision conditions, since enhancement of stereochemical effects is observed from fragmentations of the selected MNH_4^+ ions (*Figure 1*)

Figure 1. *CID spectra (E_{lab}=10eV, single collision) of MNH_4^+ ions (m/z 182) from the pair of the 2'c/2't and 3'c/3't epimers.*

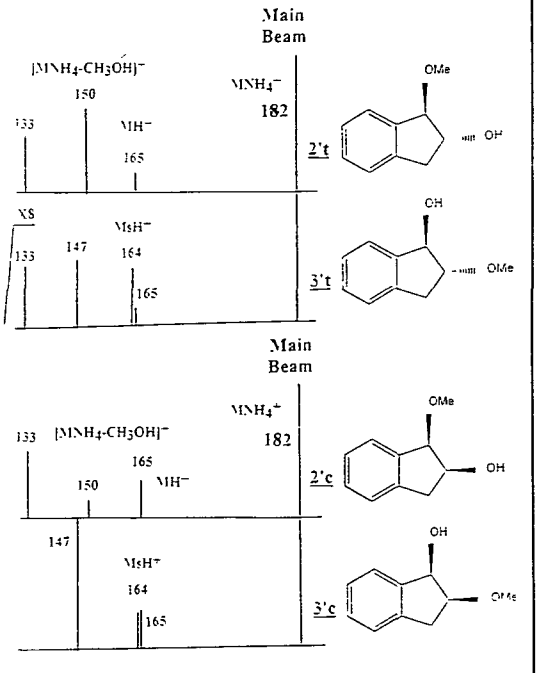

Spectacular stereochemistry influence on relative ion abundances is observed for MH^+ and MsH^+ The observed protonation is explained by considering the relative frequency factors allowing competition between simple cleavage and group substitution (via rearrangement) in contrast with that occurs in source from the lower internal energy $[M+NH_4]^+$ ions SNi occurs from cis and trans isomers as for the corresponding diols This results to the lowering of PA of hydroxy-ethers relative to the diethers Likely, the hydrogen bond is not sufficiently strengh to hinder formation of the four center nucleophilic transition state of SNi which occurs regioselectively at the benzylic position. All these results are consistent with calculation approachs and estimated PA values.

(1) (a) C. Bourhis, M.C. Perlat, F. Fournier, J.C. Tabet, 41th Conference on Mass Spectrometry, 1993 and (b) C. Bourhis, M.C. Perlat, F. Fournier, A. Mandelbaum and J.C. Tabet, 42th Conference on Mass Spectrometry, 1994. (2) A. Etinger, A. Idina, A. Mandelbaum, J. Am. Chem. Soc. 115, 7397, 1993

Ion-Molecule Reactions with Alkyl and Acyl Cation Transfer by Electrospray FT-ICR-MS

R D.Burton, P Shipkova, A.R. Katritzky, C.H. Watson, and J.R. Eyler
Department of Chemistry, University of Florida, Gainesville, FL 32611-7200

In the past, we have been interested in examining the gas phase chemistry of several alkylpyridinium cations.[1,2] Collisionally-Activated Dissociation (CAD) of these molecules was performed using FT-ICR mass spectrometry in order to determine bond dissociation energies. In addition, the bimolecular chemistry of several 1-benzylpyridiniums was studied in the presence of various neutral nucleophiles Nucleophilic substitution products were formed via S_N1 reaction pathways, however, no evidence was seen for products formed from an S_N2 pathway In order to generate an S_N2 reaction, it seemed logical to replace the benzyl group with an alkyl group of poorer leaving ability. Certainly a 1-methyl pyridinium is not a good candidate for S_N1 chemistry (due to the instability of a methyl cation) and should provide a better substrate for an S_N2 reaction.

It was therefore our intention to generate a gas phase S_N2 reaction between a 1-methylpyridinium and a neutral nucleophile thus effecting a transfer of the methyl cation. Using electrospray ionization, these organic salts were transferred from a 50/50 H_2O-MeOH solution into the gas phase where the pyridinium cations were trapped in the ICR analyzer cell Next, all other ions were ejected from the cell leaving only the substrate cation and the neutral nucleophile, which was leaked in to a constant background pressure of ca. 1 x 10^{-7} Torr. Although no S_N2 reactions were seen, several other reaction pathways were detected upon RF heating.

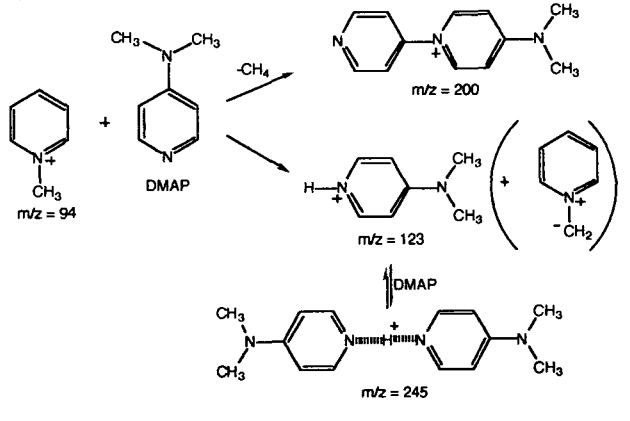

In one of these reactions, 1-methylpyridinium cation reacted with dimethylaminopyridine (DMAP) to form aromatic nucleophilic substitution product(s), protonated DMAP, and a proton-bridged structure containing two DMAPS (see figure above). The reaction mechanism was determined by doing a series of individual ion ejection experiments. From these experiments it is clear that the product at m/z 200 is most likely formed from the parent ion and a neutral DMAP with loss of methane. Our assignment of para rather than ortho aromatic substitution comes from a second reaction which we examined where methylviologen dication was used as the substrate

Despite the fact that the methylviologen dication should have been even more reactive than the 1-methylpyridinium, only protonation of the DMAP was seen. In this case, the para position is blocked to nucleophilic attack indicating the likelihood that the aforementioned aromatic nucleophilic substitution on 1-methylpyridinium occurs at the para position

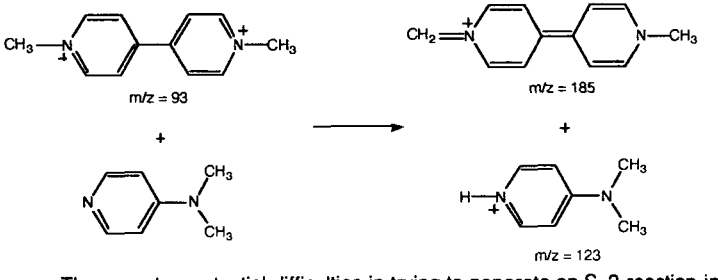

There are two potential difficulties in trying to generate an S_N2 reaction in the gas phase The first is the existence of large transition state barriers in the absence of solvent which, according to Brauman et. al, are likely.[3] The other is an entropy effect Since this work was done at extremely low pressures (< 5 x 10^{-7} torr), few collisions will occur where the reactants' molecular orbitals are in the correct orientation to generate the reaction. Despite the fact that no S_N2 reactions were seen for any of the systems studied, we will continue to search for this type of gas phase chemistry.

References

1) Katritzky, A.R.; Watson, C H.; Dega-Szafran, D.; Eyler, J R. *J. Am. Chem Soc.* **1990**, *112*, 2471

2) Katritzky, A.R.; Malhotra, N.; Dega-Szafran, D , Savage, P.G.; Eyler, J R. *J. Am. Chem. Soc.* **1992**, *27*, 1317.

3) Wilbur, J.L.; Brauman, J.I. *J. Am. Chem. Soc* **1991**, *113*, 9699.

Association and Bimolecular Ion-Molecule Reactions of Small Sulfur Ring Systems

Mary A. James, Jennifer Gidden, Michael Peschke and Andreas Illies*
Auburn University
Department of Chemistry
Auburn University, AL 36849-5312

The association and bimolecular reactions of thiirane with trimethylene sulfide radical cation are presented here. In the neat thiirane system, m/z 92, m/z 124 and m/z 156 were experimentally observed and computationally studied.[1] m/z 92 is a four membered ring with two endocyclic sulfur atoms. Subsequent sulfur atom addition occurs until a six membered ring is formed. In neat trimethylene sulfide, m/z 106, a five membered ring with two endocyclic sulfur atoms, was observed. This ion however, did not undergo further sulfur addition to form a six membered ring (m/z 138) containing three sulfur atoms.[2] These results indicated the bimolecular reactions lead to ring expansion via incorporation of sulfur atoms into the ring.

In the present study on the mixed system of thiirane (cSC_2H_4) reacting with trimethylene sulfide radical cation ($cSC_3H_6^+$), unique product ions were observed at m/z 134, m/z 166, m/z 138 and m/z 198. Interestingly, the six membered ring (m/z 138) was observed in the mass spectrum of the mixed system, suggesting that the driving force behind the ring expansion mechanism may be in the thiirane moiety.

The ion-molecule experiments were done with a highly modified Dupont mass spectrometer with a hybrid drift tube / ion source. The metastable and collision induced dissociation experiments were done with a modified ZAB-1F. These modifications included a variable temperature source and a collision zone in the second field free region.

The metastable and CID studies of m/z 134 indicate that this species fragments into m/z 92 (a four membered ring with two sulfur atoms) and m/z 106 (a five membered ring with two sulfur atoms). This suggests the following pathways occur.

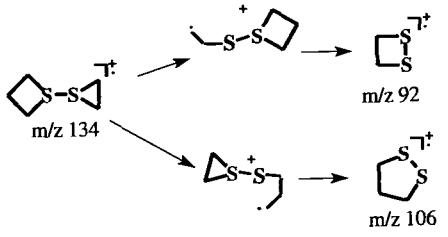

m/z 166 is the intermediate leading to m/z 138 (the six membered ring). m/z 92 and m/z 106 are observed in the metastable and CID experiments on m/z 166, suggesting that the two structures shown below contribute to the ion intensity.

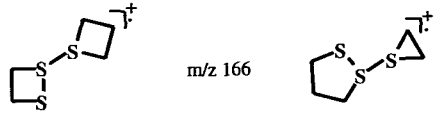

m/z 138 (the cyclic ion) undergoes association reactions with thiirane and/or trimethylene sulfide to produce interesting cluster ions. Possible structures for some of the observed clusters are shown below. Determination of the structure of these clusters are still under investigation.

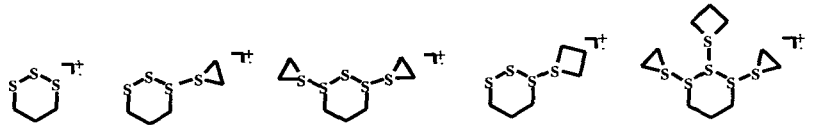

m/z 138 m/z 198 m/z 258 m/z 212 m/z 332

[1]Ekern, S.; Illies, A ; McKee, M. L., Peschke, M. *J. Am. Chem. Soc* **1993**, *115*, 12510.
[2]Peschke, M.; McKee, M L.; Illies, A. To be submitted for publication.

Ion/Molecule Reactions of Allyl Chloride in The Ion Trap Mass Spectrometer

W. Mo, A.M. Franklin and J.F.J. Todd
The Chemical Laboratory, University of Kent at Canterbury
Canterbury Kent, CT2 7NH, UK

This presentation covers the ion/molecule reactions of the ions formed from allyl chloride with neutral allyl chloride and with air present in the ion trap mass spectrometer (ITMS). The ITMS is an ideal instrument for the investigation of ion/molecule reactions due to the long residence time of the reactant and product ions before the detection and the range of techniques available to aid structure and pathway elucidation.

All experiments were carried out on a modified Finnigan MAT ITD (San Jose, CA, USA) system, which is given the capability of an ITMS. Dynamically Programmed Scanning [1] was utilised in the data acquisition after the DC isolation of a certain species of ions: the parameters of reaction time, or tickle time, or tickle voltage were dynamically scanned in the investigation of the ion/molecule reactions and the relevant pathways.

The ion/molecule reactions between the fragments of allyl chloride and allyl chloride neutral are widely observed during the trapping period. Typically, reactions between 41^+ ($C_3H_5^+$) and allyl chloride neutral are observed when the reaction time is dynamically scanned after the DC isolation, resulted in producing 55^+, 79^+, 81^+ and 91^+.

In the experiments when tickle voltages or tickle frequencies (corresponding to tickle mass) are dynamically scanned, it is observed that when different amounts of energy are deposited in the ions, the reaction can be switched to different pathways.

As a result of the isolation of specific ions and dynamically scanning one of the above parameters, the reaction pathways have been fully investigated. Ion Trap Mass Spectrometry, combined with Dynamically Programmed Scanning is a powerful method with which to investigate the ion/molecule reactions in a complex chemical system.

REFERENCE:

1. Todd, J.F.J. Penman, A.D. Thomer, D.A. and Smith, R.D. *Rapid Commun. Mass Spectrom.* **5**, 491 (1991).

ACKNOWLEDGEMENT:

One of us (W.M.) thanks the Committee of Vice-Chancellors and Principals (CVCP) and the University of Kent for funding the tuition fees and Fisons Instruments plc for "goodwill" sponsorship.

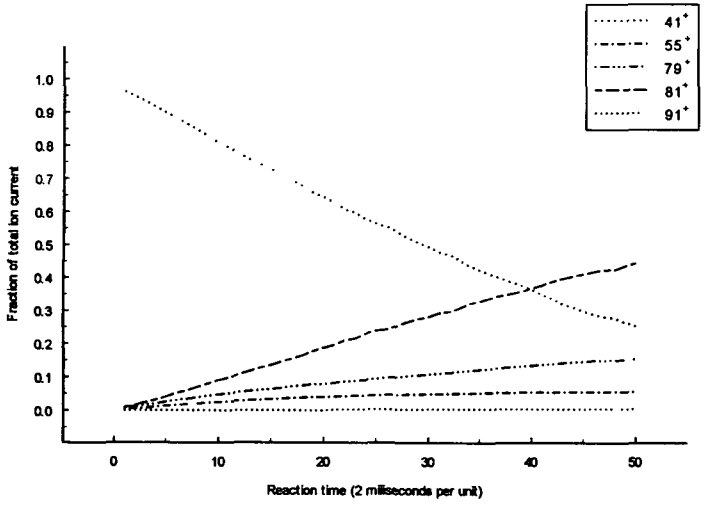

Figure 1. Ion current plots recorded when the reaction time is dynamically scanned after the isolation of 41^+ ($C_3H_5^+$) ions.

Mechanism of H/D Exchange in the Reaction of BH_2^+ + Deuterium

Joseph A. Hankin, Gustavo E. Davico, Charles H. DePuy, and Robert Damrauer
Department of Chemistry and Biochemistry
University of Colorado
Boulder, CO 80309-0215

Ionization of diborane by electron impact in the source of a Flowing Afterglow-Selected Ion Flow Tube (FA-SIFT) gives rise to an enormous number of borohydride anions and cations. Many of these ions have been identified by earlier studies in an ICR[1], or analyzed using *ab initio* computations[2-6].

Because boron consists of appreciable amounts of two isotopes, ^{10}B and ^{11}B, several different ionic species may appear at the same mass. The ion at *m/z=13 is purely the* $^{11}BH_2^+$ *isotopomer. The FA-SIFT enables selection of this* ion out of the source mixture using a source quadrupole.[7] This "SIFTed" ion can then be injected into a second flow tube for reaction studies.

The chemistry of BH_2^+ has been initially probed by studying the mechanism and energetics of H/D exchange in the reaction of $BH_2^+ + D_2$. BH_2^+ is the boron analog of methyl cation, and it is hoped that comparisons of the chemistry of these two ions will elucidate mechanistic aspects of the reactions of methyl cation. *Ab initio* computations have been carried out to help define the reaction pathway.

The reaction of $CH_3^+ + D_2$ is a fast, efficient reaction that results in random mixing of H/D.[8] The analogous reaction of BH_2^+ is slower, less efficient, and involves less exchange **(Figure 1)**.

$$CH_3^+ + D_2 \longrightarrow CH_2D^+ + HD \quad 65\%$$
$$CHD_2^+ + H_2 \quad 35\%$$

$k_r = 6.8 \times 10^{-10}$ cc/molecule-sec; efficiency = 58%

$$BH_2^+ + D_2 \longrightarrow BHD^+ + HD \quad 91\%$$
$$BD_2^+ + H_2 \quad 9\%$$

$k_r = 4.1 \times 10^{-11}$ *cc/molecule-sec;* efficiency = 3.4%

Figure 1: Reaction data for $CH_3^+ + D_2$,[8] and $BH_2^+ + D_2$.

The reaction, $BD_2^+ + H_2$ was also studied, and was found to have a slower rate ($k_r = 3.9 \times 10^{-11}$ cc/molecule.sec) than $BH_2^+ + D_2$. This was expected as this reaction proceeds in the endothermic direction ($\Delta H_r = +0.4$ kcal/mol) of the forward and reverse reactions. $^{11}BD_2^+$ was made in the FA-SIFT by adding D_2 into the flowing afterglow source along with B_2H_6. No other ions or isotopically substituted ions were present at this mass (m/z=15).

The potential energy surface for the reaction of $BH_2^+ + D_2$ has been determined computationally using Gaussian 92 (MP4//6-311G**//MP2(full)/6-311G**).[9] The energetics of the reaction of $CH_3^+ + H_2$ were determined experimentally by Kebarle[10] and various CH_5^+ intermediate and transition state structures have been calculated by Schleyer et. al.[11] A comparison of the two systems reveals that both form 3-centered 2 electron bonded complexes as low energy adduct structures. However, the entrance channel for $CH_3^+ + H_2$ is much larger than for $BH_2^+ + D_2$ (-40 vs. -14.8 kcal/mol), and the transition state for exchange of H/D is much smaller (relatively) for CH_3^+ than for BH_2^+ ($\Delta G^{\dagger\dagger}$= -+2 kcal/mol ($CH_3^+$) vs. +16.3 kcal/mol ($BH_2^+$). These differences in reaction energetics account for the experimental differences in rates, efficiencies, and amounts of H/D exchange observed.

1. Dunbar, Robert C. *J. Am. Chem. Soc.* 1968, 90 (21), 5676-5682.

2. Curtiss, Larry A.; Pople, John A.; *J. Phys. Chem.,* 1988, 92, 894-899.

3. Ruscic, B.; Schwarz, M.; Berkowitz, J.; *J. Chem. Phys.* 1989, 91 (7) 4183-4188.

4. Jemmis, E. D.; Subramanian, G.; Srinivas, G. N.; *J. Am. Chem. Soc.* 1992, 114, 7939-7941.

5. Sana, M.; Leroy, G.; Henriet, Ch.; *Theor. Chim. Acta* 1989, 76, 125-135.

6. Olah, George A.; Aniszfeld, Robert; Prakash, G. K. Surya; Williams, Robert E. *J. Am. Chem. Soc.* 1988, 110, 7885-7886.

7. VanDoren, J. M.; Barlow, S. E.; DePuy, C. H.; Bierbaum, V. M. *Int. J. Mass Spectrom. Ion Processes* 1987, *81,* 85-100.

8. Smith, David; Adams, Nigel G.; Alge, Erich; *J. Chem. Phys.* 1982, 77 (3) 1261-1268.

9. Frisch, M. J.; Head-Gordon, M.; Trucks, G. W.; Foresman, J. B.; Schlegel, H. B; Raghavachari, K; Robb, M. A.; Binkley, J. S.; Gonzales, C.; DeFrees, D. J.; Fox, D. J.; Whiteside, R. A.; Seeger, R.; Melius, C. F.; Baker, J.; Martin, R. L.; Kahn, L. R.; Stewart, J. J. P.; Topiol, S.; Pople, J. A.; *Gaussian 92,* Gaussian Inc.: Pittsburgh, PA, 1990.

10. Hiraoka, Kenzo; Kebarle, Paul; *J. Am. Chem. Soc.* 1976, 98 (20), 6119-6125.

11. Schreiner, Peter R.; Kim, Seung-Joon; Schaefer, Henry F. III; Schleyer, Paul von Ragué; *J. Chem. Phys.* 1993, 99 (5) 3716-3720.

Isotope Effects in the Dissociation of Aniline and Protonated Aniline

Yasmin A. Ranasinghe and Gary L. Glish
Department of Chemistry, University of North Carolina, Chapel Hill, NC 27599

The essence of mass spectrometric analysis is structure characterization and the determination of fragmentation pathways. Exchange of 'active' hydrogens with deuterium in an ion is a widely recognized technique for structure elucidation. The number of acidic/exchangeable hydrogens can be determined by using many different types of mass spectrometers.

However, discrepancies are often observed between different mass spectrometers depending on the internal energy deposited into the ion during formation in the ion source. In addition, different time frames for reactions lead to difference in spectra between instruments. At low internal energies, isotope effects can contribute significantly to the observed results. In this work we are investigating isotope effects in a quadrupole ion trap compared to a sector mass spectrometer.

ND_3 was leaked into the ion trap using a Varian leak valve and chlorobenzene was pulsed in using a pulsed solenoid valve. Helium was used as a buffer gas and was maintained at a pressure of 1.4×10^{-3} torr. CID was performed by kinetically exciting the parent ions by applying a resonance excitation voltage to the endcaps. The experiments in the sector was performed by introducing chlorobenzene using the injection port or the solids probe. The reagent gas ND_3 was leaked in through the CI gas inlet and the pressure is estimated to be ~ 0.5 torr. The ions formed from the reaction of $C_6H_5^+$ with ND_3 were observed by performing a magnetic scan. Metastable ion spectra dissociations occurring in the first field free region were obtained by performing a linked scan at constant B/E to detect the product ions.

$C_6H_5^+$ reacts with ND_3 to give three product ions. The ion trap showed an increased propensity for H vs. D loss compared to the sector. The H:D loss ratios were found to be 6:1 for the trap vs. 2:1 for the sector. Greater isotopic discrimination observed could be due to the different time frames of the experiment which could lead to sampling of the ions of different internal energies.

			Relative Abundance		
			m/z	Trap %	Sector %
$C_6H_5^+ + ND_3$	$\rightarrow C_6H_{5-n}D_nNH_{3-m}D_m^+$		97	73	85
	$\rightarrow C_6H_{5-n}D_nNH_{2-m}D_m^+$	+ H	96	23	10
	$\rightarrow C_6H_{5-n}D_nNH_{3-m}D_{m-1}^+$	+ D	95	4	5

$n+m = 3$

A substantial amount of H/D scrambling between the ring and substituent hydrogens is observed. This results in different isomeric structures. Evidence for the interchange of aromatic and ring hydrogens have also been observed by Dookeran et al. in the reactions of protonated aniline with ND_3.[1] Because of the time frame of the experiment, a nearly statistical distribution of H/D exchange is observed in the ion trap, whereas that is not the case with the sector.

The MS/MS results show that the isotope effect observed for the ion trap is 2.7 as opposed to a value of 3.0 for the sector. The smaller difference in the secor vs. the ion trap is attributed to the lower internal energies of the metastable ions in the sector as opposed to the increased internal energies of the resonantly excited ions in the trap, vs. the ion source generated ions. For the ions formed by H loss from the adduct (m/z 96) DNC loss is 1.5 times more favorable than HNC loss. This isotope effect is a secondary effect related to transfer of H or D from the nitrogen to the ring.

References

1. N. N. Dookeran; A. G. Harrison, J. Am. Soc. Mass Spec. *6*, 19, 1995

Hydrogen/Deuterium Exchange of Multiply-Protonated Cytochrome *c* Ions

Troy D. Wood, Ziqiang Guan, Peter B. O'Connor, Russell A. Chorush, and Fred W. McLafferty, Department of Chemistry, Baker Laboratory, Cornell University, Ithaca, NY 14850-1301.

Low resolution measurements show gaseous multiply-protonated cytochrome *c* ions undergo hydrogen/deuterium (H/D) exchange with pseudo first-order kinetics [1] at three distinct exchange levels, suggesting the co-existence of gaseous protein conformations. Although exchange levels first increase with increasing charge values, they decrease at the highest charge values, consistent with solution-phase behavior of cytochrome *c*, where the native structure unfolds with decreasing pH until folding into a compact A-state at lowest pH. High resolution measurements indicate the presence of at least six H/D exchange levels [2]. Infrared (IR) laser heating and fast collisions via quadrupolar excitation (QE) increase H/D exchange levels (unfolding) while charge-stripping ions to lower charge values can increase or decrease H/D exchange levels (unfolding or folding). Wolynes has suggested studying proteins *in vacuo* could play an important role in delineating the contributions various forces play in the protein folding process, provided appropriate comparisons can be made between gas-phase and solution-phase structures [3].

Tandem mass spectrometry of multiply-protonated cytochrome *c* ions produces up to 35 sequence informative fragment ions. Sustained off-resonance irradiation/ collisionally-activated dissociation of gas-phase deuteriated species representing the previously identified states I (16+, 112 exchange level), II (16+, 129, and 9+, 138), and V' (15+, 121) reveal subtle structural differences between the different species. The low (I) and high (II) exchanging conformers of 16+ have almost identical exchange levels in the N-terminal 25 residues, but differ by 9 D's in the C-terminal 35 residues. State II 16+ and 9+ show identical H/D exchange everywhere except between residues 26-50. Clearly, tandem mass spectrometry can provide considerable insight into subtle structural differences between these species and may be used to identify additional conformations. Exchange in individual amino acid residues can be tracked in regions where fragmentation occurs at adjacent amide bonds (Figure 1). H/D exchange levels for cytochrome *c* under prolonged high velocity collisions (by QE) approach the denatured level (190 out of 198), giving further evidence of gas-phase unfolding (Figure 2). Possible mechanisms of H/D exchange have recently been proposed for oligopeptides [4]. For cytochrome *c*, the role of protonated sites was probed by removing charges from gas-phase deuteriated 16+ (to 9+); the 16+ exchanged ~77 D's after 5 minutes, while charge-stripped 16+ --> 9+ exchanged ~75 D's. Thus, H^+'s (and not D^+'s) were primarily removed, suggesting H/D mechanisms requiring H^+'s do not predominate for multiply-protonated cytochrome *c* ions. This work was supported by the National Institutes of Health (GM16609).

References

1. Suckau, D.; Shi, Y.; Beu, S. C.; Senko, M. W.; Quinn, J. P.; Wampler, F. M., III; McLafferty, F. W. *Proc. Natl. Acad. Sci. USA* **1993**, *90*, 790-793.
2. Wood, T. D.; Chorush, R. A.; Wampler, F. M., III; Little, D. P.; O'Connor, P. B.; McLafferty, F. W. *Proc. Natl. Acad. Sci. USA* **1995**, *92*, 2451-2454.
3. Wolynes, P. B. *Proc. Natl. Acad. Sci. USA* **1995**, *92*, 2426-2427.
4. Campbell, S.; Rodgers, M. T.; Marzluff, E. M.; Beauchamp, J. L. *J. Am. Chem. Soc.* **1994**, *116*, 9765-9766.

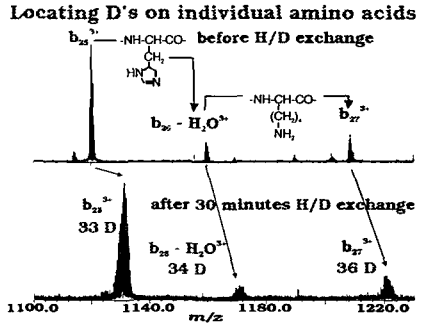

Figure 1. Fragments differing by one amino acid residue produced from SORI-CAD of 9+ cytochrome *c*(top) before and (bottom) after 30 min H/D exchange.

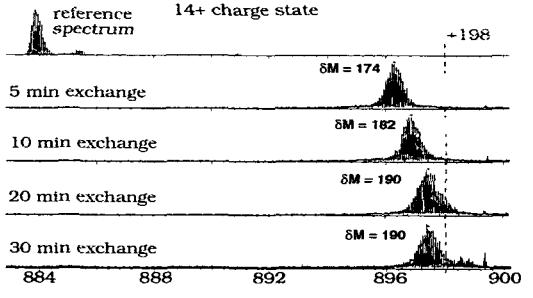

Figure 2. H/D exchange vs time for 14+ cytochrome *c* under high velocity quadrupolar excitation conditions.

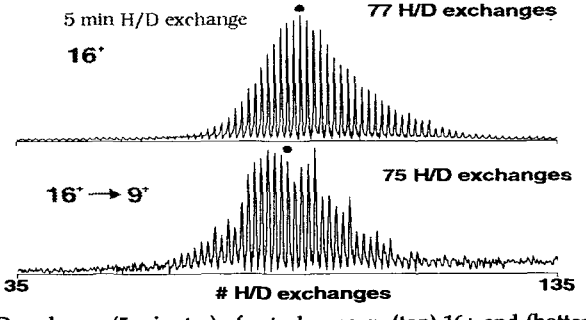

Figure 3. H/D exchange (5 minutes) of cytochrome *c*: (top) 16+ and (bottom) 16+ charge-stripped to 9+.

Ion Resolvation in a Time of Flight Mass Spectrometer

*M. A. Lasater and D. A. Laude

Department of Chemistry, The University of Texas at Austin, Austin, TX 78712

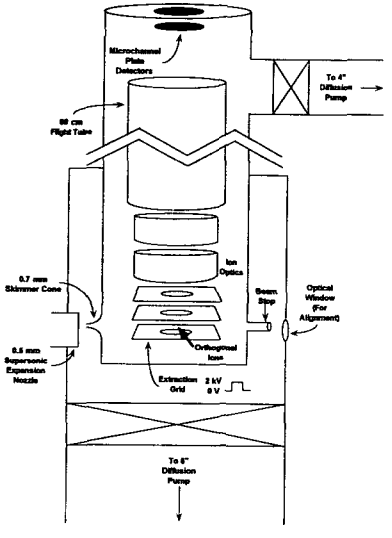

Schematic of Time-of-Flight Region

Figure 1

Supersonic expansions of molecular beams have been used to create clusters of molecules Clusters are of an intermediate size between individual gas phase molecules and the bulk solution. As such, the properties of the clusters span this potentially fruitful area.

In this work, a study of alcohol clusters were intersected with alkali metal cations and then accelerated by use of a very fast high voltage pulser into a TOF mass spectrometer. Also, an electrospray source of ions has been added to explore the nature of the electrospray ionization process itself

A general schematic of the system is shown in Figure 1. A pulsed expansion valve (Newport Corporation) was used to create a supersonic expansion of an alcohol from vapor saturated nitrogen. The saturated vapor was formed by bubbling the gas through dried solvent and taking the resultant vapor into the supersonic expansion chamber. The resulting collection of internally cooled clusters was skimmed and then allowed to react with thermally desorbed sodium ions. The heat of solvation from the reaction was dissipated by evaporation of the alcoholic clusters. The resulting internally warm clusters were orthogonally accelerated by using a 2 kV extraction pulse from a fast (25 ns rise time) high voltage pulser (Directed Energy, Inc.). The ions were then focused with electrostatic lenses and detected using a

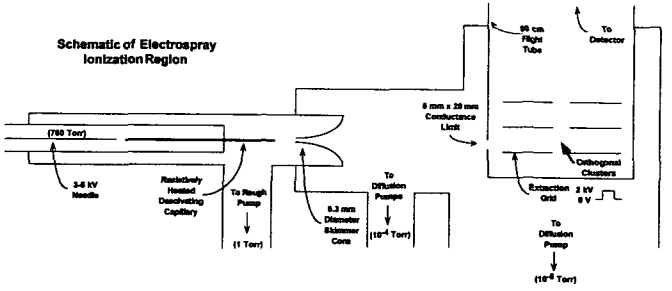

Figure 2

25 mm microchannel detector (R.M. Jordon Corporation). The extraction pulse was varied between 100 ns and 1 μs to maximize the resolution and signal. A delay generator (Interstate Electronics Corporation) was used to vary the time between the pulsed expansion valve opening and the high voltage extraction pulse to accommodate the travel time between the valve and the middle of the ion extraction region. An electrospray probe mount has also been recently added in addition to the thermal ion source This design is shown in Figure 2. The data were collected on a 150 MHz Digital oscilloscope (LeCroy Instrumentation). With methanol clusters, there was a distinct preference for both $Na(MeOH)_3^+$ and $Na(MeOH)_4^+$, as well as a preference for the $Na(MeOH)_6^+$. The $Na(MeOH)_5^+$ cluster was also seen. $Na(MeOH)^+$ and $Na(MeOH)_2^+$ were uncommon. The higher order clusters were rarely seen. An example of the methanol data is seen in Figure 3a. Moving up to ethanol, the 3 and 4 cluster is still preferred but the 2 cluster was also frequently observed. Again the 1 cluster was uncommon, and the higher order clusters were not observed. When isopropanol is used, the incidence of successful clustering is sharply reduced. However, the lower clusters (1-4 IPA's) were all observed with approximately equal frequency. Again, higher order clusters were not observed. An example of this data is in Figure 3b. The resolution of the individual peaks is good for a time-of-flight, with a resolution of 974 for Na^+. In increasing size from methanol to alcohols of larger size, the maximum common cluster size shifts from 6 to 4. This is somewhat counterintuitive as the heat of vaporization trends upward with larger alcohols (This would mean that fewer molecules of solvent would have to evaporate to dissipate as much energy.) However, bulkier side chains may prevent as many molecules from binding into the inner solvent sphere. There is also a trend towards smaller S/N as the solvent size increases. This is probably due to the decreasing efficiency of the ion focusing at higher masses. Future work includes improving the cluster source, optimizing electrospray ionization for this system, and improving the constancy of the thermal ion source The adaptation of this technique to a Fourier transform mass spectrometer will be attempted to study structural information. The electrospray ion source will allow the exploration of fundamental questions involving this ionization process

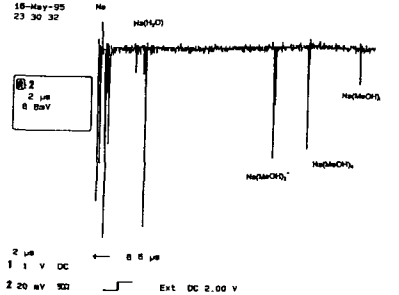

Figure 3a

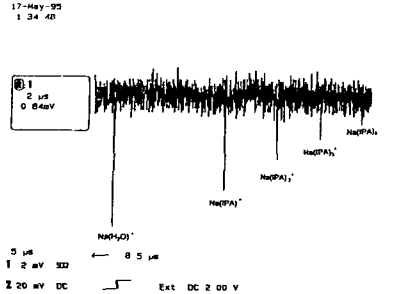

Figure 3b

The Influence of Ion Structure on Coulomb Energy in Multiply Charged Ions

Deborah S. Gross, Sandra E. Rodriguez-Cruz, and Evan R. Williams
Department of Chemistry, University of California, Berkeley, CA 94720

Multiply protonated ions formed by electrospray ionization (ESI) provide a unique opportunity to study the effects of charge on the conformation and reactivity of highly charged gas-phase ions in the absence of solvent. Highly charged ions are more reactive toward proton transfer and dissociation. We have developed a method to quantitatively measure the Coulomb repulsion between charges in gas-phase ions through measurements of their proton transfer reactivity. Because of the 1/r distance dependence of the Coulomb energy, these measurements provides information about the gas-phase conformation of these multiply charged ions. From the kinetics of proton transfer reactions with neutral reference bases, the apparent (or kinetic) proton affinity (PA^{app}) of a site of protonation can be assigned. The difference between the PA^{app} and the intrinsic PA of the site of protonation in the neutral molecule ($PA_{Intrinsic}$) can be fit to a point-charge model (1). In situations where the entropic terms cancel, the Coulomb energy can be obtained by measurement of gas-phase basicities:

$$\text{Coulomb Energy} = GB_{Intrinsic} - GB^{app} \qquad (1)$$

This method has been demonstrated for 1,*n*-diaminoalkanes (n = 7 - 10, 12) in which the distance between charges varies (this distance is obtained from molecular modeling) (2). Because the singly protonated ion cyclizes to solvate the proton in the gas-phase, monoaminoalkanes of equivalent chain length are used as a reference of the intrinsic reactivity (3). For these ions, the measured GB^{app} values fit eq. 1 with a dielectric polarizability $\varepsilon_r = 1.01 \pm 0.07$, indicating that these reactions follow a point-charge Coulomb potential, and that -(CH_2)- groups provide negligible shielding in the gas-phase. In order to determine the effects of functional groups between the charges, we are investigating a series of analogous diamine molecules in which there are branched hydrocarbon chains and ether groups between the charges. The proton transfer rates and the Coulomb energy are given in Table 1 for $CH_3CH(NH_2)CH_2[OCH_2CH(CH_3)]_nNH_2$, n = 2, 3. $CH_3OCH_2CH_2NH_2$ (GB = 215.0 kcal/mol (4), on an adjusted GB scale (5)) is used as a reference for the $GB_{Intrinsic}$ value. For the n = 2 and n= 3 species, we measure CE = 19.0 and < 17.0 kcal/mol, respectively, and, when combined with the distance between charges, we obtain dielectric polarizabilities of $\varepsilon_r = 1.4$ and $\varepsilon_r > 1.2$, respectively. This indicates that branched alkanes and ether functionalities more efficiently shield the charges in the gas-phase than the straight-chain alkanes.

In order to test the point-charge Coulomb model presented here, we have extended our measurements on the cyclic peptide gramicidin s (6) to a series of $(M + H + X)^{2+}$ ions of the gramicidin s, where X = Li^+, Na^+, and K^+. The proton transfer rates are slower than those of the doubly protonated ion. Kinetic curves obtained for the reactions of the X = Li^+ ions are shown in Figure 1. The proton-transfer rate constants for all of these ions are given in Table 2. The GB^{app} of the singly charged gramicidin s $(M + X)^+$ ions are found to be 223.3 kcal/mol for all X, compared to 219.1 kcal/mol obtained for the $(M + H)^+$ ion (using the revised GB scale (5)). The GB of the neutral peptide is > 243.3 kcal/mol. Using the previously determined dielectric polarizability of $\varepsilon_r < 1.4$ (GB scale from reference 5) for gramicidin s, we calculate the distance between the charge sites to be 11.9 Å in these

43rd ASMS Conference on Mass Spectrometry and Allied Topics

metal ion systems. This value is greater than the 9.5 Å obtained for the doubly protonated ion indicating that the alkali metal cation is attached to the exterior surface of the peptide and is most likely not as efficiently solvated as the protons in the doubly protonated ion.

(1) Schnier, P. D.; Gross, D. S.; Williams, E. R. *J. Am. Chem. Soc.*, in press.
(2) Gross, D. S.; Rodriguez-Cruz, S. E.; Bock, S.; Williams, E.R. *J. Phys. Chem.* **1995**, *99*, 4034.
(3) a) Aue, D. H.; Webb, H. M.; Bowers, M. T. *J. Am. Chem. Soc.* **1973**, *95*, 2701. b) Yamdagni, R.; Kebarle, P. *J. Am. Chem. Soc.* **1973**, *95*, 3504.
(4) Lias, S. G.; Liebman, J. F.; Levin, R. D. *J. Phys. Chem. Ref. Data* **1984**, *13*, 695.
(5) Meot-Ner, M. Sieck, W. *J. Am. Chem. Soc.* **1991**, *113*, 4448.
(6) Gross, D. S.; Williams, E. R. *J. Am. Chem. Soc.* **1995**, *117*, 883.

Figure 1. Normalized ion abundance as a function of time for the reactions of the $(M + H + Li)^{2+}$ and $(M + 2H)^{2+}$ ions with two reference bases.

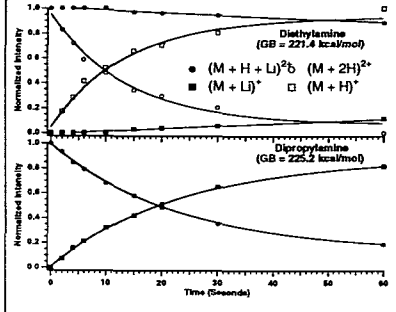

Table 1. Proton transfer rates (x 10^{-11} cm^3/mol-s) and CE for functionalized diaminoalkanes. The GB^{app} is assigned between the reference bases which bracket the absolute proton transfer rate of 1 x 10^{-11} cm^3/mol-s.

	n = 2	n = 3
Base: cyclohexanone (GB = 194.0 kcal/mol)	0.026	< 0.01
Base: acetophenone (GB = 198.0 kcal/mol)	37	<0.01
charge separation	12.95 Å	16.71 Å
Coulomb energy (kcal/mol)	19.0	< 17.0
dielectric polarizability ε_r	1.4	> 1.2

Table 2. Proton transfer rates (x 10^{-11} cm^3/mol-s) and CE for gramicidin s $(M + H + X)^{2+}$ ions, X = Li^+, Na^+, K^+, H^+. The GB^{app} is assigned between the reference bases which bracket the absolute proton transfer rate of 1 x 10^{-11} cm^3/mol-s.

	X = Li^+	X = Na^+	X = K^+	X = H^+
Base: t-butylamine (GB = 216.7 kcal/mol)	<0.0013	<0.0040	<0.0039	<0.0046
Base: diethylamine (GB = 221.4 kcal/mol)	0.16 ± 0.02	0.034 ± 0.01	<0.036	4.4± 0.4
Base: dipropylamine (GB = 225.2 kcal/mol)	1.3 ± 0.2	1.2 ± 0.2	0.9 ± 0.1	>52
Base: triethylamine (GB = 227.5 kcal/mol)	>52	>52	>52	>52
Coulomb Energy (kcal/mol)	>20.0	>20.0	>20.0	>24.4

Acid/Base effect on FAB ionization process

Francisco L. Amado, Pedro N. Domingues,
M. Graça O. Santana Marques and A. J. Ferrer Correia

Department of Chemistry
Mass Spec. Lab., University of Aveiro, Portugal

In this work, we have tried to understand the effect of the addition of acids or bases, in both FAB positive and negative ionisation processes. In face of our results, different interpretations had to be used for a comprehensive approach of the acid/base effect.

Figure 1 shows the variation of the $[M+H]^+$ (FAB+) and $[M+H]^-$ (FAB-) ion signals in the presence of the different acids and bases. Generally it can be seen that there is an increase of the $[M+H]^+$ ion yield production with acid addition and an increase of the $[M-H]^-$ ion yield production with NH_3. From the results we can suggest the following mechanistic interpretations.

Its not possible to speak about a direct effect due to AcOH. The signals of AcOH ions disappear from the spectra within approximately two minutes. Volatile compounds will disappear quickly, as it occurs with the cosolvents normally used like water or methanol, and an enrichment of the ionised forms is obsserved. As we are in the presence of a weak acid it is possible that it passes to the gas phase in the neutral form acting as a coanalyte. This explanation its also possible for tris-(hydroxymetyl)-aminomethane (Tris). Signal divergence could also be caused by variation of physical properties of the matrix, namely viscosity.

In the negative ion mode, when NH_3 is added there is a signal increase of the analyte, whatever analyte is used. However, in the gas phase NH_3 behaves simultaneously as an acid and as a base. This feature explains the quasi molecular ion improvement both in positive and negative FAB.

In the positive ion mode whatever the analyte used there is a signal increase when. trichloroacetic acid (TCA), hydrochloric acid (HCl) or trifluoroacetic acid (TFA) is added. In the negative mode, in the presence of TFA there is always a decrease on the $[M-H]^-$ ion yield production. Cluster formation between the acid and the analyte is observed. In the TPP/TFA spectrum do not see these clusters. Glutathione/TFA or TCA (Figure 2) spectra only show one cluster each. Arginine clusters with one and two acid ions. This feature could be interpreted as a experimental evidence of a possible general mechanism of the acid effect. At the pH values of the different solutions all the amino acids glutathione and TPP molecules are on their ionised form. Acids act as counter-ions and the passage to the gas-phase occurs via ion pair formation. Therefore, in the gas phase one of the three situations can occur: the ion pair doesn't dissociate; the ion pair loses one proton and appears in the negative FAB spectra; the ion pair dissociates producing analyte positive ions and acid negative ions.

Signal improvement can be explained because as there are more molecular ions in the gas phase, more protons are available for $[M+H]^+$ ion production.

With extensive ion-ion recombination in the gas phase, it is likely that ion pairs pass through intermediate neutralisation and reionisation steps. With this mechanistic picture it is understandable that the number of basic groups within each analyte molecule determines the different negative cluster ions formed when the carboxylic group of the basic compound loses a proton. Molecular structure, ionic bond strength, volatility and matrix viscosity diminution are also factors that should determine the final ion mass spectra.

Figure 1-

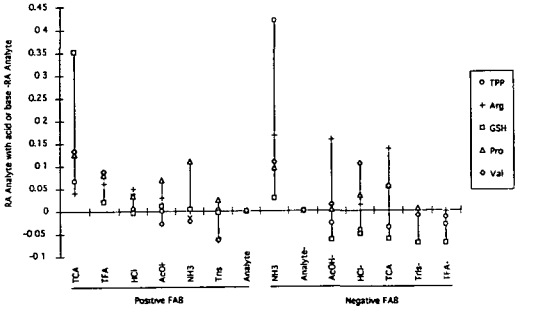

Figure 2-

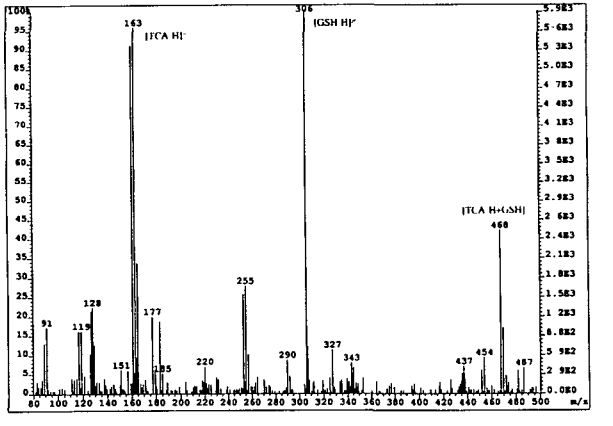

ION/MOLECULE REACTIONS FOR IMPROVED EFFECTIVE MASS RESOLUTION IN ES/MS

Scott A. McLuckey and Douglas E. Goeringer
Chemical and Analytical Sciences Division
Oak Ridge, TN 37831-6365

Tandem mass spectrometry can improve the effective mass resolution in electrospray mass spectrometry of multiply-charged ions. The technique involves selecting a population of ions within a narrow range of mass-to-charge values and allowing the ions to undergo proton transfer reactions. The shifts in mass-to-charge associated with product ions formed by proton transfer allow for mass and charge assignment. The success of the technique relies on the relative enrichment of ions of a particular charge state that occurs in the mass-to-charge selection step. This approach can be used to extend the polymer mass range amenable to measurement, analyze mixtures that might otherwise be too complex for reliable mass measurements, and improve mass measurement precision when a mixture of cations is present within a given charge state. The technique is illustrated with a quadrupole ion trap.

The use of proton transfer reactions in conjunction with tandem mass spectrometry to improve effective mass resolution in electrospray MS is illustrated conceptually in **Figure 1**. **Figure 1a** shows a simulated electrospray mass spectrum of a hypothetical biopolymer of M_r = 15 kDa in which ions of charge states 14+-10+ are present. For the purpose of illustration, the isotopic distribution associated with each charge state is shown as an envelope the width of which was arbitrarily defined to be sufficiently broad to result in significant overlap between charge states. **Figure 1b** shows a peak profile for a mass-to-charge-selected portion from the most intense part of the spectrum shown in **Figure 1a**. It is critical to the success of this approach that the selected region be narrow enough to ensure that it is significantly enriched in one component of the mixture of ions present in the mass spectrum. **Figure 1b** also shows the peak profiles associated with each component present in the selected region along with the total peak profile. Note that the 12+ charge state is by far the most important contributor to the total peak intensity. **Figure 1c** simulates the spectrum observed after a 400 ms reaction period in which a strong base, present at a number density of 3×10^9 cm^{-3}, undergoes proton transfer reactions with the rate constants on the order of 1×10^{-9} cm^3-$molecule^{-1}$-s^{-1}. **Figure 1d** shows the mass spectrum obtained when no mass selection step precedes the ion/molecule reaction period. Comparison of the spectra of **Figures 1c** and **1d** illustrates the utility of ion/molecule reactions as part of an MS/MS experiment. The mass selection step serves to simplify the mixture of ions that undergo proton transfer reactions. The proton transfer reaction provides part of the m/z information necessary for a mass assignment. The resolution of the analyzer itself is unaffected.

Figure 2 shows the results from a negative ion application in which trifluoroacetic acid was used to transfer protons to anions of E coli tuna, strain W. **Figure a** shows the electrospray mass spectrum derived in the absence of trifluoroacetic acid. The spectrum of **Figure a** reflects a complex mixture of species, arising from sample heterogeneity and a mixture of cations, which precludes a mass measurement. **Figure b** shows the results obtained when a relatively narrow portion of the ion population was mass-to-charge-selected and allowed to react with trifluoroacetic acid for 200 ms. Two charge states at higher mass-to-charge clearly emerge allowing for both charge and mass assignment. Although it was

not possible to determine the most probable charge of the ion population initially selected for reaction, the shifts in mass-to-charge associated with the product ions indicated that the mass-to-charge selection process yielded an enriched relative concentration of the 17-charge state. The total signal is greatly reduced due to the fact that the majority of the analyte ions was ejected. However, such a sacrifice is clearly warranted given the fact that no mass information could be obtained from **Figure a**.

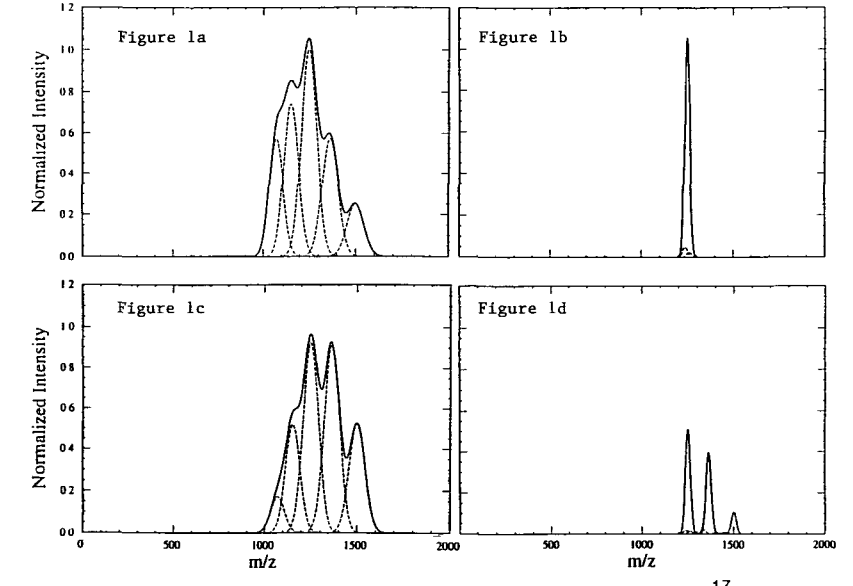

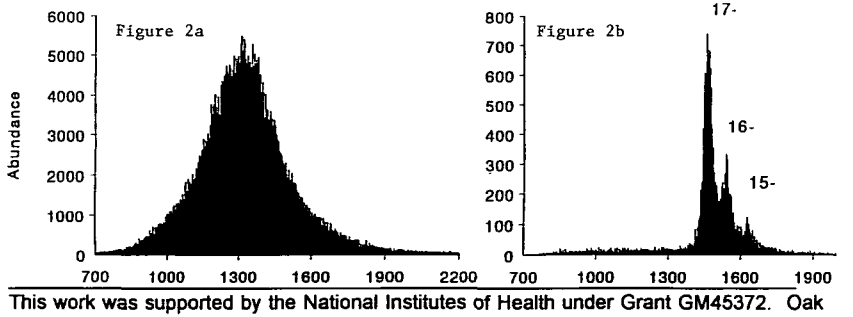

This work was supported by the National Institutes of Health under Grant GM45372. Oak Ridge National Laboratory is managed for the United States Department of Energy by Martin Marietta Energy Systems, Inc. under Contract DE-AC05-84OR21400.

Structure Elucidation of Peptides by Two-Dimensional FT-ICR Mass Spectroscopy

Touradj Solouki, Charles W. Ross III†, Ljiljana Paša-Tolić, and Alan G. Marshall*

Center for Interdisciplinary Magnetic Resonance, National High Magnetic Field Laboratory, Florida State University, 1800 E. Paul Dirac Dr., Tallahassee, FL 32310

†DuPont Marshall Laboratories, Grays Ferry Avenue, Philadelphia, PA 19146

* Department of Chemistry, Florida State University

Stored Waveform Ion Modulation (SWIM) two-dimensional FT-ICR MS/MS[1] offers an automated method for identifying connectivities between primary and secondary ions for all ion-neutral reactions in a single experiment. The Stored Waveform Inverse Fourier Transform (SWIFT) excitation waveforms of the SWIM experiment modulate primary ion speed and hence the number of secondary ions derived from those primary ions by means of ion-molecule collisions and/or reactions. Peaks along the diagonal line of the 2-D spectrum represent the conventional one-dimensional FT-ICR mass spectrum. Each off-diagonal peak corresponds to a unique ion-molecule reaction whose reactant ion and product ion can be identified by horizontal and vertical projections to the diagonal.

Previously we have shown that the SWIM technique may be used with laser desorption ionization.[2] Here we show that the SWIM technique can help to elucidate the structures of biological molecules in multi-component samples in an automated fashion. Preliminary results obtained for MALDI generated quasi-molecular ions of bradykinin and angiotensin II, a two-component system with similar fragmentation patterns, are reported and discussed. A key component in two-dimensional analyses is reproducibility in total signal intensities. For mass spectrometry by use of MALDI, 2D requires minimal shot to shot ion production variations. Results reported herein indicate promise for 2D analysis of biochemical complex mixtures.

This work was supported by NIH (GM-31683) and the National High Magnetic Field Laboratory at Florida State University. We thank Michael Dunk of Waters Extrel-FTMS for valuable discussions concerning implementation of the SWIM waveforms.

References

1. C. W. Ross III, S. Guan, P. B. Grosshans, T. L. Ricca, and A. G. Marshall, *J. Am. Chem. Soc.* **1993**, 115, 7854-7861.
2. C. W. Ross III, and A. G. Marshall, *Proc. 42nd ASMS Conf., Chicago, III* **1994**, p. 1060.

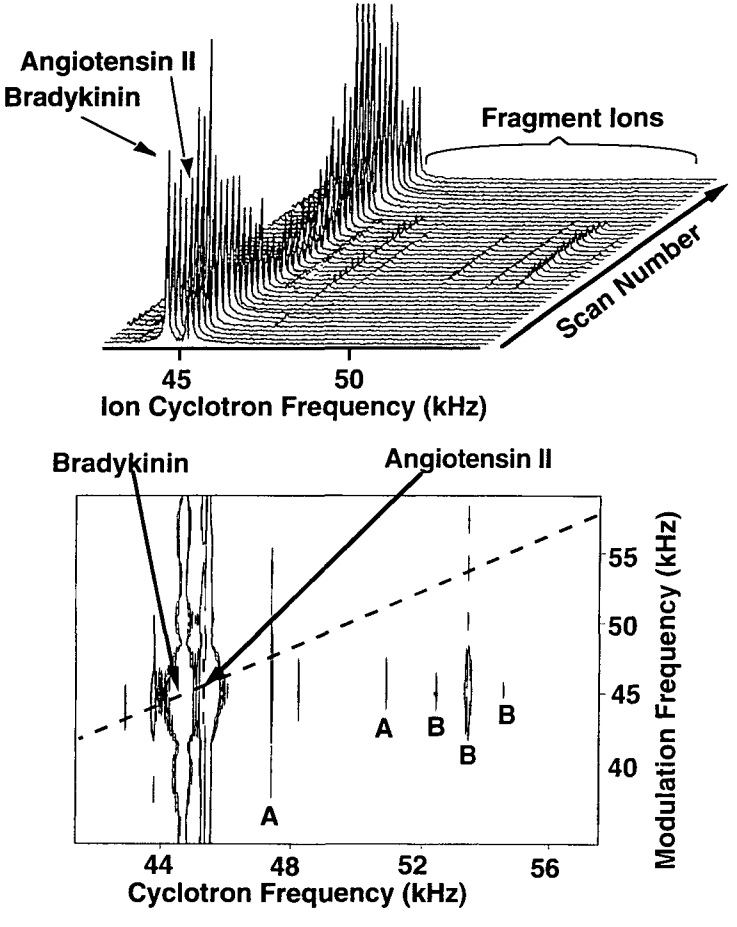

Portion of MALDI FT-ICR magnitude mode frequency spectra of angiotensin II and bradykinin from scan one through 50 (top). Fragment ions are observed at specific quasimolecular ion modulation frequencies (shown as "scan number"). Iso-power contours are shown at bottom after the second FT. Off-diagonal signals correspond to fragments from angiotensin II (A) and bradykinin (B). Enhanced resolving power in both dimensions will simplify off-diagonal peak assignments.

Ion Cyclotron Resonance Evidence for the Formation of α-Chloroethenethiolates and Thioketenes during Biotransformation of Chloroalkene-Derived, Cytotoxic 4-Thiaalkanoates

Tian-lan Zhang,[†] Liping Wang,[†] Mazzaz Hashmi,[‡] M.W. Anders,[‡] Colin Thorpe,[†] and Douglas P. Ridge.[†,*]

[†]*Department of Chemistry and Biochemistry, University of Delaware, Newark, DE 19716*
[‡]*Department of Pharmacology, University of Rochester, Rochester, NY 14642*

Characterization of the reactive intermediates formed during the bioactivation of xenobiotics is an important step in understanding their cytotoxicity. Nephrotoxic chloroalkenes generate cysteine S-conjugates that are proposed to undergo ß-lyase-dependent bioactivation affording α-chloroenethiolates and thioketenes as reactive intermediates. Formation of thioketenes has also been proposed during the metabolism of 5,6-dichloro-4-thia-5-hexenoic acid **1** (Scheme 1) and related analogues. This report describes the use of ion cyclotron resonance to provide the first direct evidence for the formation of thiolate and thioketene species from a cytotoxic 4-thia-carboxylic acid.

Bioactivation of **1** involves conversion to the corresponding CoA thioester **2** and oxidation by the medium chain acyl-CoA dehydrogenase to **3** is followed by hydration to the thiohemiacetal **4**. Elimination of 1,2-dichloroethenethiolate **6** would give malonylsemialdehyde-CoA **5**. Thiolate **6** and related α-chloroalkenethiolates have not been observed directly in aqueous solution. However, their formation as precursors to thioketenes (*e.g.* **7**) has been inferred from indirect evidence

Our recent studies with the acyl-CoA dehydrogenase suggest that removal of a C-2 proton from **2** can also lead to the direct elimination of **6** (Scheme 2). The present report shows the utility of Fourier Transform ion cyclotron resonance (FT-ICR) in modelling this enzymatic reaction. FT-ICR provides unequivocal evidence for the formation 1,2-dichloroethenethiolate **6** and for the subsequent elimination of chloride to yield the putative chlorothioketene **7**.

The propyl thioester analogue of **2**, **9** (Scheme 3) was introduced on an unheated probe inserted into the reaction chamber of a dual cell FTMS 2000 FT-ICR mass spectrometer. The volatility of **9** and the pumping rate maintained a sample pressure of ca. 10^{-7} torr. The instrument has two differentially pumped ion analyzer-traps. OH^- was formed by electron impact on water vapor admitted into one of the analyzer-traps through a valve opened for 15 msec. OH^- formed by electron impact on the water vapor was transferred to the adjacent analyzer-trap where it was exposed to neutral reactant **9** in the adjacent analyzer. The results of the gas-phase encounter of **9** with OH^- were interrogated at various delay times by FT-ICR analysis of the resulting ions.

Figure 1 illustrates typical results. As the reaction time increases the OH^- ion concentration decreases exponentially with a corresponding increase in two product ions. The neutral reactant, **9**, is present in large excess so these pseudo first-order kinetics unambiguously demonstrate that the bimolecular reaction between OH^- and **9** produces an anion of the stoichiometry of **6**, $C_2HCl_2S^-$, and the chloride anion (Scheme 3). Thus, while **6** has been deduced as a cytotoxic intermediate from indirect evidence in condensed phase studies, it is directly observed here in the gas phase as a product of the action of base on **9**.

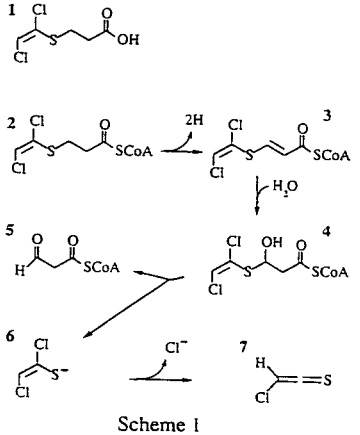

Scheme 1

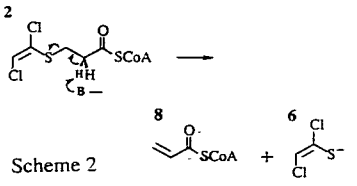

Scheme 2

The postulate that **6** loses chloride to give thioketene **7** was tested using collision induced decomposition (CID) FT-ICR. The results showed that elimination of Cl^- from **6** is facile and suggest that the neutral product of the elimination is the expected thioketene **7**. These studies support earlier proposals for the cytotoxicity of **6** and suggest that FT-ICR may be generally useful in modelling enzymatic elimination reactions.

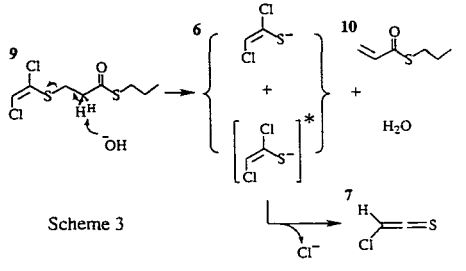

Scheme 3

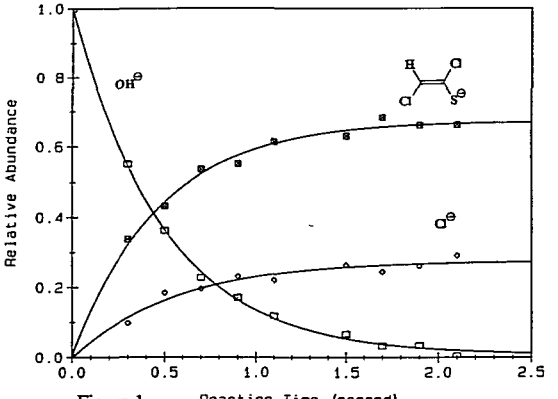

Figure 1.

ION-MOLECULE CHIRAL RECOGNITION BY AMINE EXCHANGE EQUILIBRIA

Chadin Dejsupa, Yongjiang Liang, and David V. Dearden
Brigham Young University, Department of Chemistry, Provo, Utah 84602

Introduction

Like other analytical techniques for chiral species, successful mass spectrometric methods rely on differences in the reactivity of enantiomers with a chiral reagent. Recently, fast atom bombardment (FAB) mass spectrometry has been used to examine the relative intensities of adduct peaks arising from interactions of chiral species.[1-4] Fourier transform ion cyclotron resonance mass spectrometry was used several years ago to measure equilibrium populations of clusters of chiral molecules such as L- and D-dimethyl tartrate.[5,6] The equilibrium approach has the advantage that equilibrium constants are easily related to free energy changes, so the degree of chiral recognition can be quantified.

Our own prior gas phase studies of chiral recognition in gas-phase ion-molecule reactions[7] use similar equilibrium techniques. The host molecule, dimethyldiketopyridino-18-crown-6 (hereafter designated "**1**"), has two stereocenters. The guest, α(1-naphthyl)ethylammonium, is designated $NapEtNH_3^+$. The chiral host, *S,S*-**1**, and an achiral host, 18-crown-6, were both admitted into the trapping region of a Fourier transform ion cyclotron resonance mass spectrometer. Either *R*- or *S*-$NapEtNH_2$ was also admitted into the trapping region, and $NapEtNH_3^+$ was formed by self-CI. Reaction of $NapEtNH_3^+$ with the neutral ligands afforded the host-guest complexes. The exchange of the guest between the chiral and achiral hosts, reaction (1), was allowed to proceed to equilibrium. The attainment of equilibrium was verified by monitoring ion intensities as a function of reaction time until the ratio of the 18-crown-6•$NapEtNH_3^+$ and *S,S*-**1**•$NapEtNH_3^+$ ion intensities became constant. Perturbation of the system away from equilibrium by ejection of either of the complexes always resulted in re-establishment of the same equilibrium ratios after an appropriate delay, attesting to the fact that true equilibrium was reached.

$$S,S\text{-}\mathbf{1}\bullet(R\ or\ S)\text{-}NapEtNH_3^+ + 18C6 \rightleftharpoons S,S\text{-}\mathbf{1} + 18C6\bullet(R\ or\ S)\text{-}NapEtNH_3^+ \quad (1)$$

These were difficult experiments. First, *S,S*-**1** is fairly involatile, so that usable vapor pressures were barely attainable when the ligand was inserted into the high vacuum region of the instrument on a direct-exposure solids probe. Second, achiral 18-crown-6 binds $NapEtNH_3^+$ much more strongly than the chiral ligand, making equilibrium difficult to observe unless there is a large excess pressure of the less volatile, chiral *S,S*-**1**. Finally, measurement of the partial pressures of the ligands, which is crucial to the results, is difficult and introduces a great deal of uncertainty into the results.

Amine Exchange Equilibria

Our new experiments were performed using a model APEX 47e (Bruker Instruments) external source Fourier transform ion cyclotron resonance mass spectrometer. Rather than observing equilibria for exchanging an *ammonium guest* among *neutral hosts*, we observe the exchange of *neutral amines* by a *protonated host* ion, reaction (2). One enantiomer of the chiral amine, as well as an achiral reference amine, are introduced into the trapping cell as neutrals. One of the host enantiomers is electrosprayed in the external source, and the resulting protonated host ions are guided into the trapping cell and captured. Reaction of the protonated host with the neutral amines results in formation of complexes. Exchange of the chiral and achiral amines on the protonated chiral host is allowed to proceed to equilibrium, which is verified as before. The experiments are then repeated with the other enantiomer of the host or the guest.

$$(S,S)\text{-}\mathbf{1}H^+\bullet R\text{-}NapEtNH_2 + \text{cyclohexylamine} \rightleftharpoons (S,S)\text{-}\mathbf{1}H^+\bullet\text{cyclohexylamine} + R\text{-}NapEtNH_2 \quad (2)$$

It is interesting to note that not all protonated host molecules form complexes with neutral amines. Of the ligands we studied, only 18-crown-6 and *S,S*-**1** were observed to form amine adducts, while neither protonated dicyclohexano-18-crown-6 nor protonated dibenzo-18-crown-6 formed amine complexes. These differences have not yet been explained.

When both host enantiomers are available (as is the case for host **1**), switching between the two enantiomers can be done rapidly enough (by simply flushing the solution of one enantiomer out of the electrospray needle, and replacing it with a solution of the other enantiomer) that pressure conditions in the trapping region do not change appreciably between the two measurements. Since the results for the degree of chiral recognition depend on a ratio of the two equilibrium constants for the two enantiomers, if the partial pressures of the amines do not change the pressures cancel in the ratio and pressure is no longer a variable in the measurement. This is a very significant advantage, since the pressure measurements are the largest potential sources of error in the experiments.

The approach of the system to equilibrium was observed from both "forward" and "reverse" directions. In these experiments, the achiral reference amine was cyclohexylamine, the chiral amine was *R*-$NapEtNH_2$, and the chiral ligand was *R,R*-$\mathbf{1}H^+$. Ejection of either the complex of *R,R*-$\mathbf{1}H^+$ with the chiral amine (at m/z 525) or with the achiral amine (at m/z 453) was followed by re-establishment of the equilibrium ratio of about 1 for these two peaks. At equilibrium, the *R*-$NapEtNH_2$•*S,S*-$\mathbf{1}H^+$ complex peak is much more intense relative to the reference than the *R*-$NapEtNH_2$•*R,R*-$\mathbf{1}H^+$ complex peak. This corroborates our earlier results, obtained with the more difficult experimental method, that indicated stronger complexation between *R*-$NapEtNH_3^+$ and *S,S*-**1**.

Quantitatively, the difference in equilibrium constants corresponds to the free energy of binding in the *R*-$NapEtNH_2$•*S,S*-**1** complex being 3.1 ± 0.4 kJ mol^{-1} (at 300 K) greater than in *S*-$NapEtNH_2$•*S,S*-**1**. The results obtained using amine exchange equilibrium are in good agreement with those obtained earlier using ligand exchange (4.2 ± 0.4 kJ mol^{-1} at 350 K), especially when it is noted that the two experiments were done at different temperatures.

The simplicity of the new experiments, along with the ease of electrospraying large, enantiomeric crowns, has now enabled us to examine a number of other chiral guests for recognition by **1**. The results, shown in Table 1, reveal some of the structural requirements for recognition in this system. Both enantiomers of *sec*-butylamine and cyclohexylethylamine reacted identically with respect to the achiral reference; the chirality of both these guests was not recognized. Recognition was observed for phenylethylamine, but the difference in free energy of binding for the two enantiomers was only about 0.7 kJ mol^{-1}. This suggests that the π-π stacking interaction is essential for recognition in this system. No recognition is seen in guests lacking the π system, and recognition is much weaker for phenylethylamine than for naphthylethylamine, because the former is too small to simultaneously allow optimal hydrogen bonding and π system overlap

Table 1. Difference in Free Energy of Binding Chiral *R*-amines by *S,S*-1 vs. *R,R*-1 at 300 K.

amine	ΔΔG°, kJ mol^{-1}
sec-butyl	0
cyclohexylethyl	0
phenylethyl	0.7 ± 0.4
naphthylethyl	3.1 ± 0.4

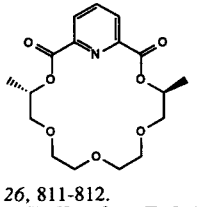

References

(1) Hofmeister, G.; Leary, J. A. *Org. Mass Spectrom.* **1991**, *26*, 811-812.
(2) Sawada, M.; Shizuma, M.; Takai, Y.; Yamada, H.; Kaneda, T.; Hanafusa, T. *J. Am. Chem. Soc.* **1992**, *114*, 4405-4406.
(3) Sawada, M.; Okumura, Y.; Shizuma, M.; Takai, Y.; Hidaka, Y.; Yamada, H.; Tanaka, T.; Kaneda, T.; Hirose, K.; Misumi, S.; Takahashi, S. *J. Am. Chem. Soc.* **1993**, *115*, 7381-7388.
(4) Sawada, M.; Okumura, Y.; Yamada, H.; Takai, Y.; Takahashi, S.; Kaneda, T.; Hirose, K., Misumi, S. *Org. Mass Spectrom.* **1993**, *28*, 1525-1528.
(5) Nikolaev, E. N.; Goginashvili, G. T.; Tal'rose, V. L.; Kostyanovsky, R. G. *Int. J. Mass Spectrom. Ion Proc.* **1988**, *86*, 249-252.
(6) Honovich, J. P.; Karachevtsev, G. V.; Nikolaev, E. N. *Rapid Commun. Mass Spectrom.* **1992**, *6*, 429-433.
(7) Chu, I.-H.; Dearden, D. V.; Bradshaw, J. S.; Huszthy, P.; Izatt, R. M. *J. Am. Chem. Soc.* **1993**, *115*, 4318-4320.

Chiral Recognition in Molecular Host-Guest Complexations using FABMS

Masami Sawada, Yoshio Takai, Hitoshi Yamada, Shigeki Hirayama
The Institute of Scientific and Industrial Research,
Osaka University, Ibaraki, Osaka 567, Japan
Kimiko Kamada, Keiji Hirose, Yoshito Tobe, and Koichiro Naemura
Department of Chemistry, Faculty of Engineering Science,
Osaka University, Toyonaka, Osaka 560, Japan

Chiral recognition in molecular host-guest complexations is one of the highlights in modern organic chemistry. Various chiral crown ethers have been synthesized and various degrees of chiral recognition have been achieved. Several methods were used for determining chiral recognition of chiral crown ether hosts. Examples are extraction/NMR, extraction/polarimetry, titration NMR, variable temperature NMR methods and so on. Mass spectrometry is highly sensitive, but primarily uninformative for this purpose because of the absence of these mass differences.

We report here the successful detection of chiral recognition by a simple and direct method using FAB mass spectrometry. The method particularly uses a 1:1 mixture of a labeled and an unlabeled guest enantiomer, which is called as FABMS/EL (Enantiomer Labeled) method. Diastereomeric host-guest complex ions, $[(H + G_R)^+$ and $(H + G_{S\text{-}d3})^+]$, produced by a chiral crown ether host (H) and an enantiomeric pair of guests (G_R and $G_{S\text{-}d3}$: deuterium-labeled) have different masses and then, simultaneously appear as a pair of host-guest complex ion peaks. Since the complex ions are identified by the aid of the isotope tag, both the degree and the direction of the chiral recognition properties of a given crown host toward a given amino acid ester ammonium ion guest can be directly determined using the relative peak intensities of the corresponding host-guest complex ions in one spectrum as $I[(H + G_R)^+]/I[(H + G_{S\text{-}d3})^+]$, which is abbreviated as $I_R/I_{S\text{-}d3}$. A typical FABMS spectrum is shown in Fig. 1 (NBA matrix).

Application and applicability of this methodology are presented. Among several crown ether hosts and the related natural compounds, it is found that host **2** possesses a high degree of chiral recognition ability and shows remarkably large guest's structure-dependency upon the chiral recognition properties: the $I_R/I_{S\text{-}d3}$ values vary from 0.7 to 5.4. Typical results of the $I_R/I_{S\text{-}d3}$ values are illustrated in Fig. 2.

Very importantly, the $I_R/I_{S\text{-}d3}$ values determined by the FABMS/EL method are compatible with the relative thermodynamic stabilities (K_R/K_S) in solution.

For example,

host **2** + (*R*)-Met-OMe in $CD_3OD/CDCl_3$(10/1) at 25°C, $K_R = 78.6\ M^{-1}$
host **2** + (*S*)-Met-OMe $K_S = 15.9\ M^{-1}$

Then, $K_R/K_S = 4.9$ by the titration NMR method.
$I_R/I_{S\text{-}d3} = 5.4$ by the FABMS/EL method.

As a summary, the FABMS/EL method is a novel and practically useful technique for determining chiral recognition properties in the highly structured host-guest complexations.

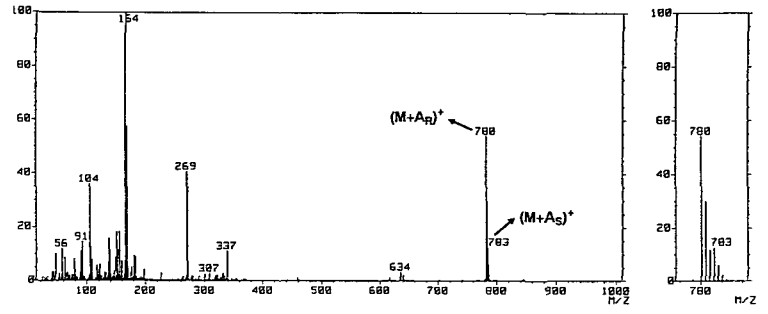

Fig. 1. A FAB mass spectrum (NBA) of a mixture of host **2** with guest Met-OMe(Cl⁻).

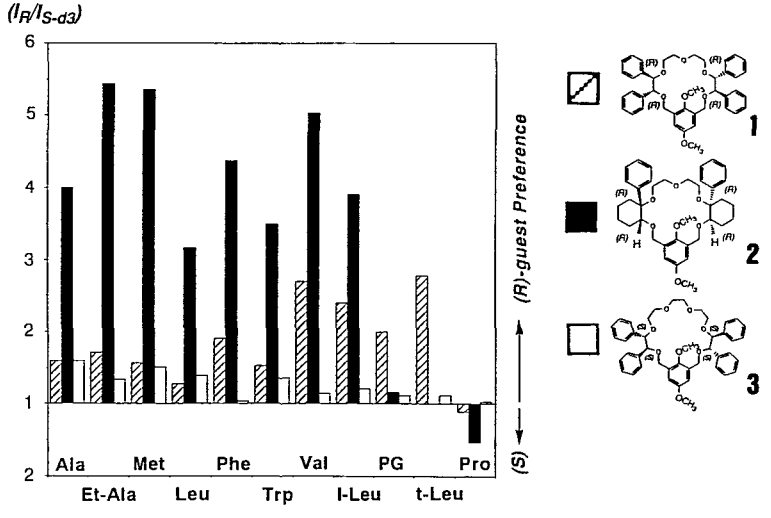

Fig. 2. Chiral recognition properties of hosts **1** - **3** toward various amino acid methyl ester ammonium ion guests determined by the FABMS/EL method.

References: M. Sawada et al., *J. Chem. Soc., Chem. Commun.*, **1994**, 2497.

SFC/MS using a glow discharge ionization source

D. Carazzato, P. Bélanger, A. Carrier and M.J. Bertrand
Department of chemistry, University of Montreal, Montreal, Canada, H3C 3J7

Many organic pollutants and drugs are thermo-labile compounds or have a low volatility and, therefore, are analysed by liquid chromatography. These compounds can also be handled by supercritical fluid chromatography. From an instrumental point of view, interfacing SFC to mass spectrometry seems to be simple as compared to HPLC, because carbon dioxide is easily vaporized at low temperature. The use of a thermospray-type interface (TS) seems quite simple and more appropriate than the moving belt, which appears to be more adapted to packed columns, as well as particle beam interfaces which suffers from a lack of sensitivity. A TS interface requires simple instrumentation and is relatively easy to operate, provided that an efficient back pressure restrictor is used. For the present work, several types of thermospray restrictors have been utilized and very few are capable to widthstand the tendency to clog. The most effective, involved the use of a pinched stainless steel needle attached to a capillary column.

Amongst the ionization techniques that have been routinely used for SFC detection, CI has shown greater sensitivity than EI. Attempts at obtaining pure EI spectra have mostly resulted in combined EI and CI processes. Most of the problems associated with the use of these sources concern the contamination of their inner components and the reduced lifetime of the filament. In previous work[1] we have developed and evaluated the analytical potential of a glow discharge source. Recently we have investigated the usefulness of the same prototype as an ion source for capillary SFC introduction. Until now, the work that was been done mainly involved isothermal and isoconfertic operation with pure carbon dioxide. It has already been shown that the charge and proton transfer are important processes leading to the ionization of organic molecules in glow discharges operating at moderate pressures. The contribution of electron ionization is found to be relatively low and, there is no high energy metastable states capable of ionizing organic molecules. The ion distribution in the background plasma appears to be strongly anisotropic and apart from the carbon dioxide ion, only a few others are observed. Because of the intensity of CO_2^+ it is expected that charge exchange involving carbon dioxide ions will play a major role at a short distance from the cathode while it's importance will be significantly lower at longer distances, where protonated water (not shown on the spectrum) and water clusters (m/z 37) are present.

An interesting feature of the glow discharge technique is its ability to also sample negative ions. The high densities of low energy electrons favour electron attachment to molecules having positive electron affinities and ion lifetimes of a few microseconds. The "background" spectrum of the CO_2 discharge in the negative ion mode exhibits a large CO_3^- ion as well as some oxygen based, chlorine and C_xO_y ions. Since the use of glow discharge devices for organic analysis is uncommon, various substances have been injected through the SFC system in order to obtain an idea of the spectral features in both positive and negative ion mode. Different chemical classes were analyzed and mass spectra of 2 compounds are presented in Figure 1 and 2. In the positive ion mode they exhibit spectral features compatible with charge exchange with carbon dioxide and fragments characteristic of the chemical structures are observed. It is believed that the spectral features could change drastically from EI to CI characteristics upon the addition of a

modifier in the CO_2 phase. Although this will result in the loss of structural information by reducing fragmentation, the CI ionization process usually provides better sensitivities. In the negative ion mode, molecules with high electron affinities such as 5-nitroacenaphtene (Fig 1) show a dominant $M^{-\cdot}$. Ions resulting from ion-molecule reactions such as $(M+15)^-$ are the result of the $M+O_2\text{-}OH\cdot$ process that is usually found in oxygen containing discharges. Since more than one oxygen atom can be added to the molecule, such common reactions often complicate the interpretation of the mass spectra. Calibration curves for estrone (positive ion mode) and 5-nitroacenaphtene (negative ion mode) are presented in Figure 3. Detection limits close to 10^{-12} g have been found with linearity extending over 4 orders of magnitude. In conclusion, results obtained indicate that charge transfer is the main process leading to the ionization of organic molecules. The measured sensitivity and linearity with the prototype indicate that it can be used for organic analysis. Spectral features shows molecular peaks as well as some fragmentations carateristic of the structure of the compound.

References

1-D Carazzato, M.J. Bertrand; J. Am. Soc. Mass Spectrom. 5, 305, (1994).

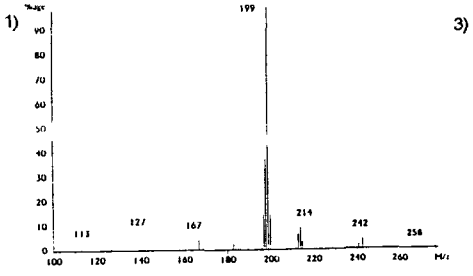

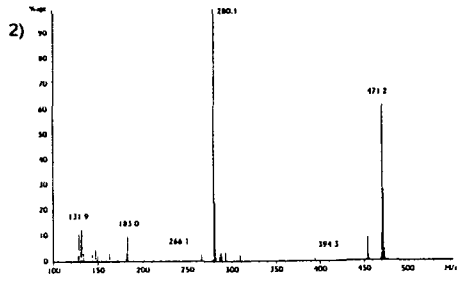

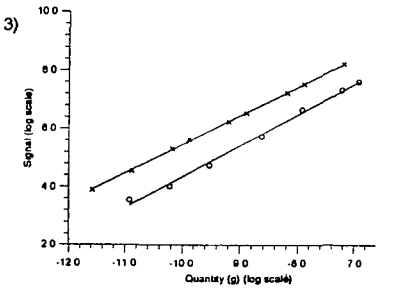

Figure 1) Mass spectrum of 5-nitroacenaphtene (negative ion mode)

Figure 2) Mass spectrum of terfenadine (positive ion mode)

Figure 3) Sensitivity curves for estrone (O) (positive ion mode) and 5-nitroacenaphtene (X) (negative ion mode)

A novel low-power rf glow discharge ion source

*ML Langford, WT Povey and JFJ Todd

Chemical Laboratory, University of Kent, Canterbury, Kent CT2 7NH, UK
**Building S18, DERA Fort Halstead, Sevenoaks, Kent TN14 7BP, UK*

A novel radio frequency ion source has been constructed. Positive and negative ions are produced in a rf plasma and extracted using a pressure differential into a lensing system which directs a positive or negative ion beam into a mass spectrometer.

The structure and configuration of the discharge electrodes was designed to favour low power operation. This was successfully achieved and spectra were obtained using powers less than 0.5 Watts. This enabled the source to be driven by a wide-band transistorised rf power amplifier with associated signal generator and miniaturised matching circuit.

One of the outstanding features of this low power ion source is its versatility. The source is able to operate in a variety of gaseous environments including air and under a wide range of pressure conditions including atmospheric pressure. The plasma conditions can be altered to achieve different purposes. It can be run at different rf frequencies, different rf peak-to-peak amplitudes, different source pressures, in different source environments and it can produce both positive- and negative-ion spectra.

Figure 1 shows a spectrum which was collected by allowing the airstream to pass over a glass spoon containing water before it passed through an aperture into the ion source. The intensities of water cluster peaks in air were recorded as a function of rf amplitude, rf frequency and source pressure. Cluster formation was facilitated at higher source pressures, fragmentation reactions were increased at higher rf amplitudes and lower rf frequencies. Both positive and negative-ion spectra were obtained.

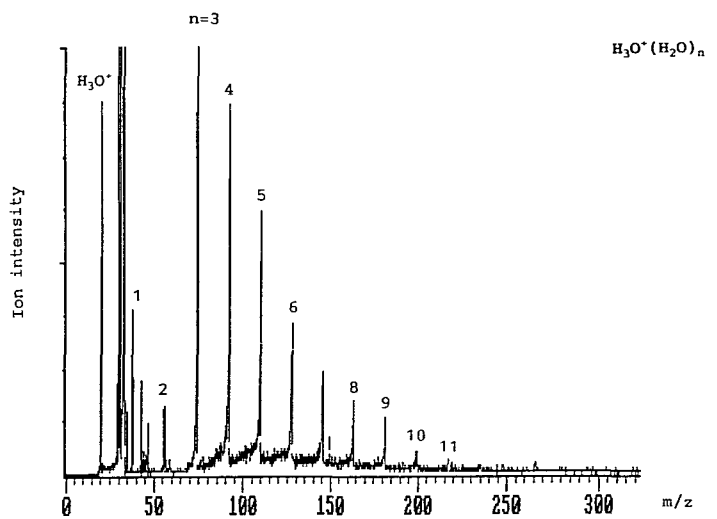

Background mass spectrum plus $H_3O^+(H_2O)_n$ cluster spectrum. each cluster is identified by its value of n.

MICRO - ELECTROSPRAY ON A MAGNETIC SECTOR MASS SPECTROMETER

R.S. Bordoli, A. R. Woolfitt and R. H. Bateman,
VG ORGANIC, Floats Road, Wythenshawe, Manchester M23 9LZ, U.K.

The micro - electrospray (μ-ESI) interface developed by Mann's group [1] which utilises drawn and gold coated glass capillaries has been shown to have significant advantages over higher flow rate interfaces.

In this presentation we describe the use of fine stainless steel capillaries operating at a flow of 50 nl/minute, which are considerably more robust than drawn glass [1] or ground fused silica [2] capillaries. They are produced by grinding a 25 μm ID x 178 μm OD stainless steel needle to a fine point, with a tip diameter of around 50 - 70 μm.

To take full advantage of magnetic sector instrumentation we have developed a dual spray system for making high precision μ-ESI accurate mass measurements, Figure 1. The sample sprayer, operated at 50 nl/minute, is mounted directly on a syringe, so as to minimise dead volumes. The second sprayer, containing the mass reference, in this case PEG 400 or PEG 600, is operated at 500 nl/minute. The second sprayer is advanced or withdrawn in order to produce mass spectra of the reference or sample material, respectively. Figure 2 shows one measurement on the M^+ ion of rhodamine B, at a resolution of 8000 (10% valley definition), obtained by summing the sample and reference spectra A total of 8 similar measurements were made over a 15 minute period (0 75 μl consumed), yielding an overall RMS error of 1 62 ppm.

A new first field free region gas cell has been designed for use with electrospray, to facilitate more efficient fragmentation of the relatively cold ions It incorporates a much longer collision region to give increased collision frequency, while at the same time giving negligible formation of product ions outside of the cell. This design also has the advantage that there is increased sensitivity towards the low mass part of the spectrum, and better product ion resolution

In order to try to assess the likely performance of the μ-ESI system with precious samples, we have attempted to complete both accurate mass analyses and B/E linked scans during a period of 20 minutes, corresponding to the total consumption of 1 μl of sample at 50 nl/minute The results from the analysis of 1 μl of leucine enkephalin are shown in Figure 3 The RMS error is within 3 ppm, and the linked scan spectrum is characteristic of that obtained using a high energy collision regime The two spectra were obtained using a combined total of 6 pmol in 200 nl, leaving up to 80% of the sample available for optimising the tuning or for other measurements

References

1 Wilm, M S & Mann, M , (1994) Int. J Mass Spectrom Ion Processes 136 167-180.
2 Kriger, M S , Cook, K.D., & Ramsey, R.S., (1995) Anal. Chem. 67, 385-389

Acknowledgements

We gratefully acknowledge the helpful discussions with Dr Walter Blackstock, of Glaxo, Stevenage, U K , at the early stages of this project.

Figure 1.

Schematic of Accurate Mass Micro Electrospray
Using Alternating Sprayers

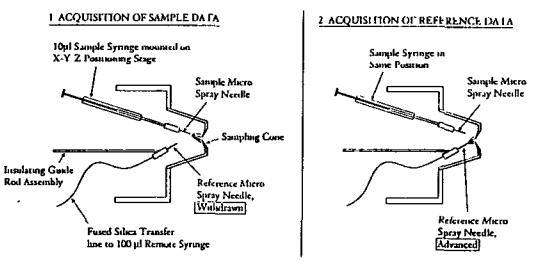

Figure 2.
Accurate Mass Micro Electrospray, one measurement at 8000 Resolution

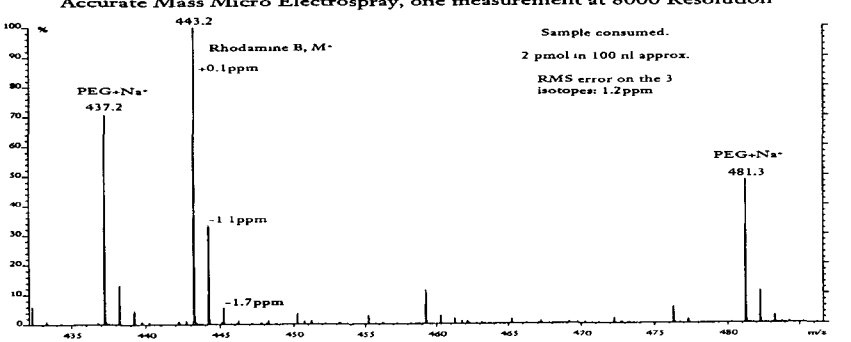

Figure 3.
Accurate Mass and B/E Daughter Scan of 1μl of Leucine Enkephalin

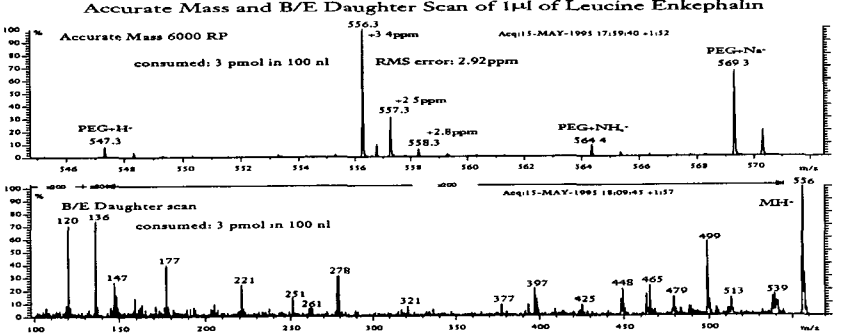

ATMOSPHERIC PRESSURE CHEMICAL IONIZATION BY CORONA DISCHARGE.

B. A. Andrien, T. Dresch, P. J. Haren, C. M. Whitehouse, and S. Shen.
Analytica of Branford Inc., 29 Business Park Dr., Branford, CT 06405.

An atmospheric pressure chemical ionization (APCI) source using corona discharge for promoting chemical ionization has been combined with Quadrupoles, Sectors, and time-of-flight (TOF) mass spectrometers (MS). This APCI source uses a pneumatic nebulizer to form droplets of the liquid sample and solvent which are entrained and collimated by the focusing carrier gas. This sample and solvent mixture is then evaporated and vaporized in the APCI heater and is subsequently ionized in the corona discharge region. A portion of the sample and solvent related ions formed in the corona discharge region are focused into the dielectric capillary entrance by high voltages and subsequently swept into vacuum. Some of these ions are accelerated and focused through a series of skimmers, electrostatic lenses and vacuum pumping stages before entering the MS platform. Singly charged compounds from less than 100 daltons to singly charged compounds well over 2000 daltons can be analyzed by APCI. Two examples are, Alanine (90 daltons) and Polyethylene Glycol 2000 (2400 daltons).

SIM and Scan data taken on a Quadrupole (HP5988), Sector (VG ZAB), and TOF (Analytica) mass spectrometer have been analyzed and all found to be linear in peak height and peak area as a function of total mass injected with linear correlation coefficients (r>0.990). The total mass sensitivity limits differ for these platforms by a factor of twenty whereas, the concentration sensitivity limits only vary by a factor of five. This being caused by the scan speed of the MS platform, which requires a larger injection loop size for slower scan speeds. Thus, both the total mass injected along with the concentration need to be compared when evaluating performance of a system.

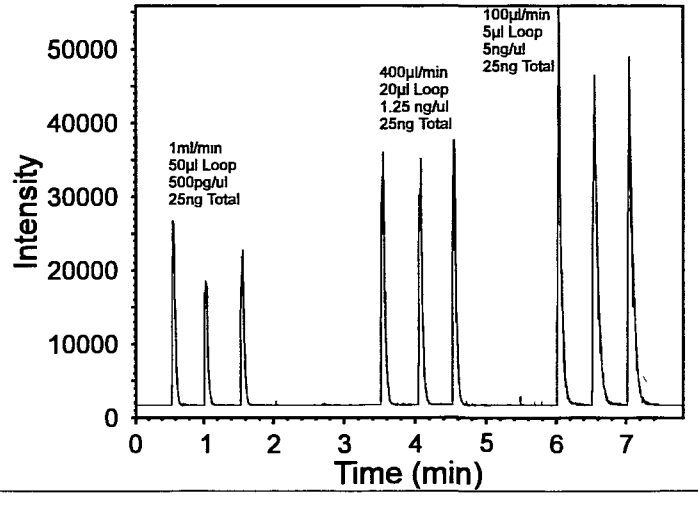

Signal of Reserpine versus flowrate was obtained by flow injection analysis on all the platforms from 100µl/min to 2ml/min. Each of these sets of data where similar and showed an increased in peak signal with flowrate but a decrease in peak area with flowrate. This flowrate data is ambiguous, however, the ratio of loop size/flowrate was not constant since the same size injection loop was used. To shed some light on this two experiments where performed. Figure 1, shows data at different flowrates but with the same ratio of loop size/flowrate with the same total mass injected. This makes the injection slug pass the corona needle in the same time frame for each flowrate. Thus, it is expected that there is the same gas phase concentration at the corona needle. Both peak height and peak area increase with lower flowrates and higher concentration. This shows for a fix scan speed that better sensitivity can be achieved with smaller loop sizes and higher concentrations.

Figure 2, show data at 1ml/min but with different loop sizes with the same total mass injected. This makes the injection slug pass the corona needle in a different time frame for each loop. Both peak height and peak area increase with lower loop sizes and higher concentration. This also shows for a fixed scan speed that better sensitivity can be achieved with smaller loop sizes and higher concentrations. It was also found that loop size is almost linear with peak area and that concentration is linear with peak height. If the system was a mass detector we would expect that the peak area would be constant for each of these injections. Thus, we reconfirm that APCI-MS is a concentration detector. These results suggest that for a given total mass and mass spectrometer scan speed that the best sensitivity that can be obtained is when the highest concentration and smallest loop size is used with the highest flowrate which does not compromise the sampling of the injection peak.

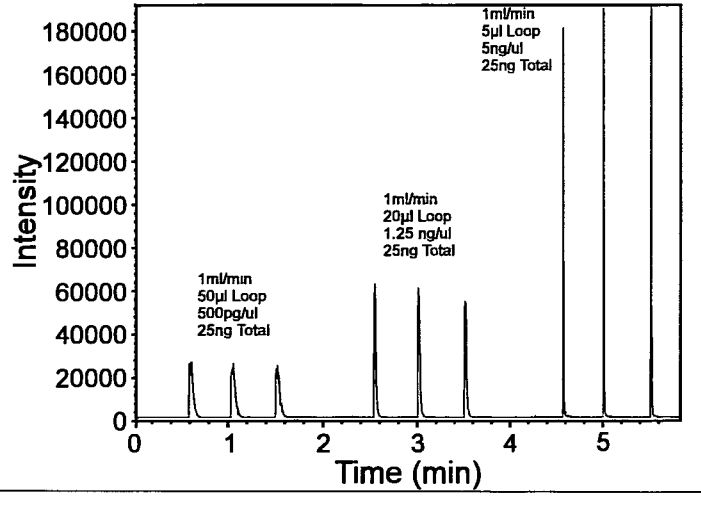

A New Atmospheric Pressure Microwave Induced Plasma Ionization Source for Mass Spectrometry

Mehdi Moini, Ming Xia, Bernhard Hofmann, Anthony Holbert, Kimberly Mathews

Department of Chemistry and Biochemistry, University of Texas at Austin
Austin, TX 78712

Historically, microwave induced plasmas (MIP) have been used in conjunction with spectral or mass analyzers for elemental analysis. More recently, attempts have been made to use the MIP as a soft ionization source for mass spectrometry. The initial examples of the MIP as a soft ionization source for mass spectrometry were accomplished by introducing the sample into the expansion stage of a low pressure plasma. This technique, however, was applicable only to compounds which were gaseous at the plasma pressure, and thus it was not possible to interface these sources with separation techniques such as HPLC. More recently, Shen and Satzger[1] have developed an atmospheric pressure MIP ionization source for mass spectrometry using a new torch design. With this design they were able to observe quasi-molecular and molecular fragment ions of a number of organic vapors as well as an ion pair in aqueous solution. In addition they were able to control the degree of fragmentation by adjusting the microwave power.

Because Shen and Satzger's source was able to desolvate and ionize tetrabutylammonium hydroxide in aqueous solution, it shows promise for the use of MIP as an interface between liquid chromatographic techniques and mass spectrometry. They obtained quasi-molecular peaks with a signal stability of approximately 40% relative standard deviation. Since the primary use of HPLC is the separation of thermally labile and/or non-volatile compounds, in order for MIP to be used as an interface it must be able to desolvate and ionize such compounds intact. This paper presents an improved torch design for atmospheric pressure MIP and demonstrates its use for the quantitative analysis of a number of non-volatile and thermally labile compounds.

The microwave induced plasma (MIP) ionization source consists of three sections, the MIP torch, the MIP cavity, and the vacuum interface. The design of the torch is outlined in Figure 1 The liquid sample passes through the torch in the inner glass capillary and a carrier gas flow (typically at 40 psi) passes through the outer glass capillary. The plasma gas passes through the outer quartz tube. The ceramic tube is positioned so that the sample is introduced into the afterglow region of the plasma.

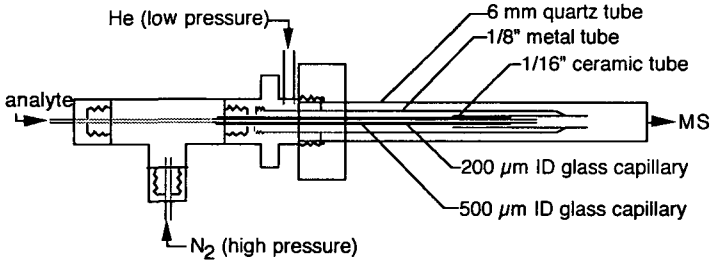

Figure 1. Schematic diagram of the MIP torch.

[1] Shen, W.-L.; Satzger, R. D. *Anal. Chem.*, **1991**, *63*, 1960.

Good sensitivity was obtained for the protonated molecular peaks of all 20 amino acids as well as several other thermally labile and/or non-volatile compounds. The flow rates, solvent composition, and sample types were consistent with those used in HPLC. The stability and reproducibility of this ionization source is sufficient for quantitative study, as is demonstrated by the injection of four consecutive 20 μl aliquots of a 0.1 M lysine solution shown in Figure 2. The spectrum obtained for lysine is shown in Figure 3.

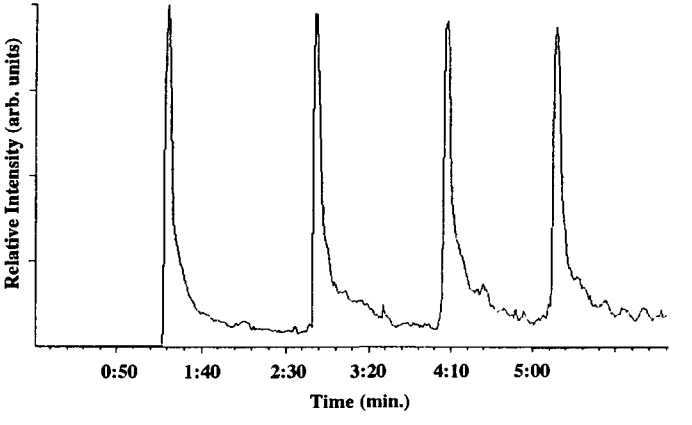

Figure 2. Total ion chromatogram for 4 consecutive 20 μl injection of 0 1 mg/ml solution of lysine in 50/50 v/v water + methanol solution using the MIP MS condition.

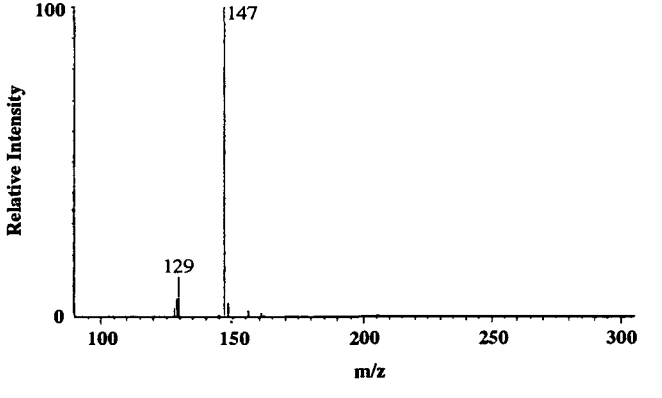

Figure 3. Mass Spectrum of lysine (MW 146) using MIP- MS.

MULTI-VACUUM STAGE MULTIPOLE ION GUIDE FOR ESI/MS INTERFACE

Erol E. Gulcicek, and C. M. Whitehouse
Analytica of Branford, Inc., Branford, CT 06405

A small size hexapole ion guide operated in a Radio Frequency-only (RF-only) mode has been incorporated into an electrospray ion source to interface with variety type of mass spectrometers. The ion guide was especially designed to go through two or three differentially pumped vacuum stages without any interruptions inside the longitudinal dimensions of the rods (ie. without any apertures or cuts in between the stages). In an ESI MS interface, typically, a capillary is used to transfer electrospray generated ions from atmospheric pressures into a viscous flow and/or intermediate flow pressure regions pumped by mechanical pumps. Then, through a series of ion optics in the following high vacuum stages, the ions are accelerated and focused into a final vacuum stage that contains the mass analyzer and the detector. In the present work, we show that an ion guide is used in place of a number of ion optics and skimmers to effectively capture substantial part of the ions emanating from a capillary in a viscous flow/intermediate flow pressure regions and efficiently transfer them inside of a mass analyzer contained in a high vacuum area.

As it will be presented, when an ion guide is used in the present configuration, the focusing, density, intensity, and the kinetic energy distribution of the ions are improved substantially compared to widely used static lens configurations. The main reason for these improvements come from the fact that the ions are entrained inside the ion guide at relatively higher pressures of the gas expansion before they reach free molecular flow pressure region. Since the ions are accelerated directly into a mass analyzer from the ion guide, The kinetic energy of the ions can be controlled to any practical level and can be decreased almost to the thermal kinetic energy levels. This feature is highly desirable for many type of mass analyzers, for it improves the mass resolution of the overall instrument without loosing much of the ion intensity.

Due to its high ion transmission, and tight ion focusing features, typical sensitivity gains for small molecular weight ions, ie.less than 300, have been observed to vary from 10 to 20 over the previous conventional ion optic lens assemblies. The observed sensitivity gains for higher singly and multiply charged molecular weight compounds were between a factor of 2 to 10. Figure 1 shows a three compound mixture mass spectra obtained with static lens and hexapole ion guide configurations under the same experimental conditions on a HP 5989 quadrupole mass spectrometer. The increase in signal sensitivity can be seen in all of the 3 compounds, although it is more pronounced for the 177 amu ion. Similar gains in sensitivity are also seen with other type of mass analyzers. Figure 2 shows not only signal sensitivity improvement for the doubly charged gramicidin S peaks (a factor of 2 to 3 between 3kV spectra), but also improvement of the natural resolution on a JEOL 102 SX magnetic sector instrument with the ion guide configuration. The gramicidin S concentration was 17 pmole/µl in 1:1 MeOH:water. Similarly, FTMS (Bruker Analytical Systems) results also show signal sensitivity improvements with the utilization of the ion guide over the static lens configurations as evidenced from Figure 3.

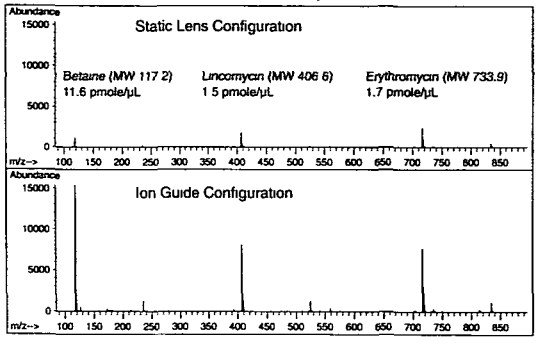

Figure 1.

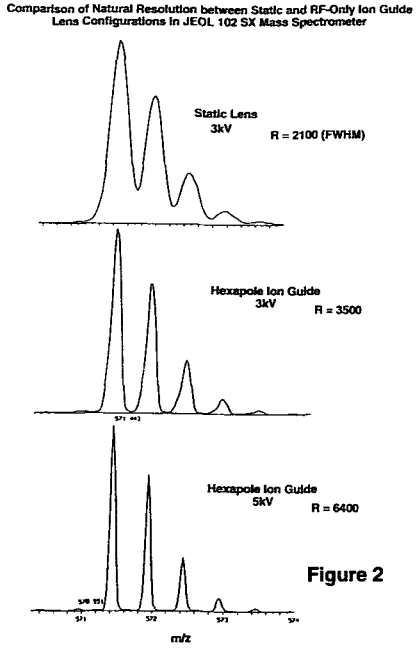

Figure 2

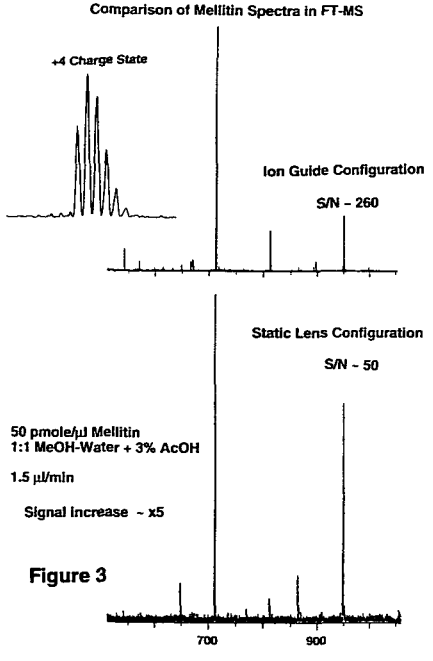

Figure 3

ION TRANSMISSION THROUGH GLASS AND METAL TUBES.

Jian-Ru Cao, Joan Rosell and John B. Fenn
Virginia Commonwealth University, Richmond, VA 23284-2006

Many electrospray mass spectrometers depend upon tubes of glass [1] or metal [2] for the transfer of ion-bearing gas from the source at atmospheric pressure to the first stage of the vacuum system where pressures range from a few torr to a few millitorr. Lin and Sunner recently presented data on the efficiency of such transfer from corona and electrospray sources with both metal and glass tubes of various dimensions over a wide range of flow conditions [3] We present results from a similar and supplementary study. Early in our work we found that total transmitted current measured with a collecting electrode and a picoammeter as used by Lin and Sunner, did not relate consistently to the ion flux, total or mass selected, measured by the multiplier detector in a triple quadrupole mass spectrometer (Delsi Nermag R3010). Therefore, all results reported here relate to "realistic" conditions in which the tubes performed in their intended roles as conduits for ions from an ES source into a mass analyzer. The MS detector output was taken as the measure of the flux of free ions, whether total or mass selected, entering the mass analyzer from the source via the tube

Three different tubes were used, each mounted in an ES source from Analytica of Branford· (1) A standard glass capillary 18 cm in length with a bore of 0.57 mm, an OD of 6.5 mm and metalized on the outside at each end; (2) A solid metal tube whose dimensions, bore and external shape were identical with those of the glass tube; (3) A typical Chait-type source capillary of stainless steel hypodermic tubing with length and bore the same as for tubes (1) and (2) but with an OD of only 0 8mm Data were collected with all three tubes unheated except by the small flow of hot gas "inhaled" from the bath gas (room air or carbon dioxide) flowing annularly around the tube inlet, counter-current to the flux of charged droplets and ions from the ES injection needle. Data were also obtained with the Chait tube heated but without a counter-current flow of bath gas. Analytes included tetrabutyl ammoniumbromide (TBAB), bovine insulin (INS), and cytochrome C (CYT) at micromolarities respectively of 190, 22 and 2.9 in 50.50 methanol-water which for the protein solutions contained 0 5 % acetic acid All were infused at a flow rate of about 2 uL/min.

The figures shows some examples of the spectra obtained with the cyctochrome C solution. Panels a and b relate to the unheated glass and Chait tubes respectively with desolvation by counter-current gas Panel c is for the Chait tube with desolvation by heating the tube to 493 K. Interesting but not shown were the differences in the mass spectra as the tube temperature rose from 323 K to 493K The abundance of small ions attributable to protonated clusters of solvent molecules decreased markedly as the temperature rose. Not immediately obvious are how those ions were formed and whether this temperature dependence was due to incomplete desolvation in the tube, resolvation during the free jet expansion, or some combination of the two. Somewhat provocative is the absence of any cytochrome C ions except at the high tube temperatures, eventhough some TBA+ ions (due to residual traces of TBAB from runs with that solute) appear at the lowest temperatures Essential results are summarized in the Table The take-home message is that overall the signal strength is about the same for all three tubes when desolvation is effected by a counter-current flow of heated gas The Chait tube provides somewhat less signal when desolvation is by heating alone, without counter-current bath gas.

TABLE OF RESULTS

Tube (Desolv. by)	TBAB Total	TBAB Selected	Insulin Total	Insulin Selected	Cytochrome C Total	Cytochrome C Selected
	Analyte Signal in Megacounts					
Metal (cc CO_2)	10.5	1.38	10.0	1.43	36.0	4.98
Glass (cc CO_2)	7.0	1.20	10.0	1.58	38.0	5.71
Chait (cc CO_2)	7.4	1.88	9.0	1.30	33.0	5.84
Chait (hot) (air-not cc)	7.3	1.05	5 7	0.37	14.0	1.29
(CO_2-not cc)	-	-	3.7	0.65	-	-

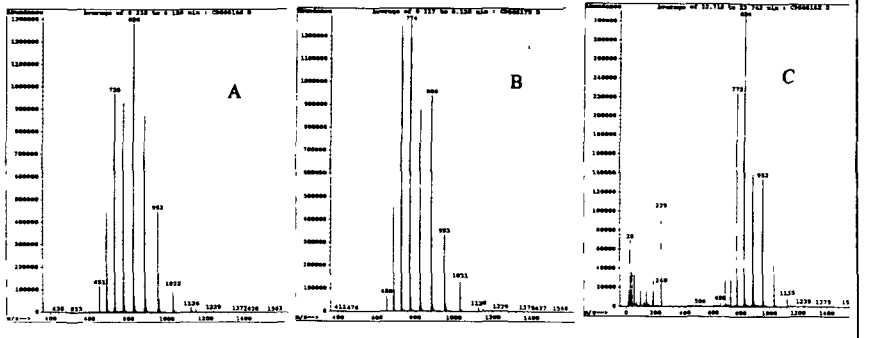

[1] C.M.Whitehouse, M. Yamashita, C.K Meng, J B Fenn, RarefiedGas Dynamics, (H Oguchi, ed) v 2, p 733, Univ. Tokyo. Press (1985)
[2] S.K. Chowdhury, V Katta, B T. Chait, Rapid Commun. MassSpectrom 4, 81 (1990)
[3] Baiwei Lin and Jan Sunner, JASMS 5, 873 (1994)

Design of a Composite Liquid-Junction/Electrospray Interface for CE/MS

Timothy Wachs, Robin L. Sheppard, and J.D. Henion, Analytical Toxicology, Diagnostic Laboratory, Cornell University, 927 Warren Drive, Ithaca, NY 14850

Coupling a capillary electrophoresis system to an atmospheric pressure ionization mass spectrometer entails challenges that are more demanding than those for coupling an LC system to a mass spectrometer. Of the two "coupling" systems, Olivares' et al. (1) "sheath-flow" interface is generally easier to implement than Lee's et al. (2) "liquid junction" interface. The latter system generally requires a high degree of precision in aligning and spacing the CE capillary and the sprayer capillary. In contrast, the sheath-flow approach can suffer from incomplete mixing of the sheath and analyte leading to ion current instability.

We have developed a simple composite liquid-junction/electrospray interface system for the precise alignment of the capillaries combined with a positive make-up flow. The capillary from the CE instrument and the sprayer capillary are held in a single piece of PEEK tubing, the internal diameter of which matches the outside diameter of the entrance and exit capillaries. Prior to assembly, a notch or "window" is cut half-way into the PEEK tubing. The CE and sprayer capillary are butted together with the junction centered in the window. The PEEK tubing is held in a drilled-out PEEK Tee (Figure 1) with the window aligned with the side-arm of the Tee. When the ferrules are tightened, the capillaries are held tightly and in proper alignment. A continual flow of solvent is added to the side-arm of the Tee, providing a continuous sweep of the junction with the majority of flow exiting the sprayer capillary. This also prevents contamination of the junction solvent while flushing the capillary. With a controlled continuous positive flow, band broadening is minimized and the solvent flow and/or composition can even be varied during a CE run by using a programmable micro LC pump. Because the analyte from the CE capillary is picked up by the flowing make-up, there is less problem with mixing than in the sheath flow interface. The device is used in the electrospray mode thus providing a small and simple interface. Electrical connection is either via the side-arm of the Tee (when fused silica is used for the sprayer) or directly to a metal sprayer capillary.

This interface has been used on both a Sciex API-III mass spectrometer system and on a PE-Sciex API-300 LC/MS/MS system. Figure 2 is a comparison

of the sheath flow and composite interfaces for the chiral separation of terbutaline. Although the sensitivity by infusion of the composite interface is higher than that of the sheath flow interface, the opposite is true in this example. This is probably due to the slightly lower (~5%) resolution in the composite liquid-junction interface. However, the signal-to-noise ratio for the composite liquid-junction interface is better by a factor of 3 to 4 for both the infusion and CE experiments. We attribute this to better mixing which results in better spray stability.

Longer migration times are sometimes reported when using a liquid-junction interface vs. a sheath flow interface. The positive pressure used to deliver the make-up solvent can "push" the analyte backwards in the capillary. Using a Hewlett-Packard model ^{3D}CE system, a pressure of a few millibars was applied to the inlet of the capillary to counteract this flow. The interface has been used to obtain SRM-CE/MS data on low (20-130) femtomole quantities (injected) of beta-agonists extracted from spiked human urine.

The authors acknowledge the generous loan of equipment from Hewlett-Packard Co. and PE-Sciex, Inc. Financial support of PE-Sciex, Inc. and the National Institutes of Health (GM47931) is appreciated. RLS thanks Xerox Corp. for providing this educational opportunity.

1) Olivares, J.A., et al., Anal. Chem., 59 (1987) 1230-1232.
2) Lee, E.D., et al., Biomed. Environ. Mass Spectrom., 18 (1989) 844-850.

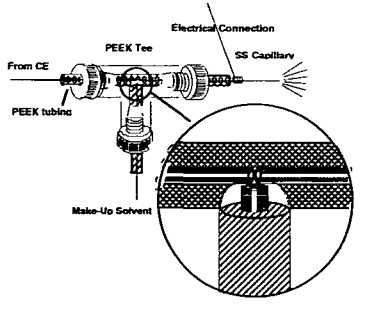

Figure 1

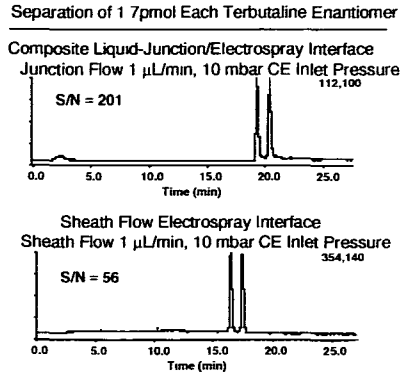

Figure 2

A Versatile, Stable CE-ESI Source

Dan Kirby, The Barnett Institute, Northeastern University, Boston, MA

With the increased availability of ESI-MS, the stimulus to interface it with liquid-based separations systems has likewise increased One of most exciting areas of ESI-MS interfacing is that with capillary electrophoresis (CE) and its offer of fast, efficient separations using extremely small sample quantities. Since the first report of CE-ESI-MS interfacing in 1987, many laboratories have contributed to its growth. Numerous reports have discussed interface improvements to overcome difficulties obtaining and maintaining a stable electrospray, especially at low flow rates, to correct poor reproducibility, and to improve sensitivity Use of pointed/tapered capillaries and the need to match liquid sheath tube and capillary geometries have been noted Occasionally in print, but more frequently in conversation, is discussed the fact that sensitivity and stability benefit from, and in many cases demand, correct placement of the capillary within the liquid sheath tube Our experience has been that correct positioning can be determined by (time consuming) trial and error, and once found is satisfactory as long as other experimental parameters are not changed too much.

We have modified two commercial ESI sources to incorporate the above ideas and, most importantly, to permit dynamic adjustment of the capillary with respect to the liquid (and gas) sheath tube(s) during CE-ESI-MS operation In practice this procedure enables one to establish a stable electrospray quickly and reliably over a wide range of flow rates, liquid compositions and component geometries Liquid sheath flows of less than 1uL/min are readily accommodated. Use of this system permits one to choose experimental parameters, such as capillary and liquid sheath flow rates, liquid sheath composition, and others, and then adjust the capillary position to achieve stability As a result, one is able to choose experimental parameters independently of stability requirements (we had often been forced to use liquid sheath flow rate to achieve stability) and, for example, optimize peak efficiency or sensitivity through optimal choice of liquid sheath flow rate

Figure 1 shows examples of electrospray instabilities often encountered in CE-MS· periodic "dropouts", where ESI and MS ion current are momentarily lost, and high noise in the MS ion current Both of these instabilities are reduced or eliminated by adjustment of the capillary position while observing, for example, the total ion current In practice one can chose experimental parameters, such as liquid sheath flow rate, then use capillary adjustment to stabilize the system Figure 2 shows the effect of liquid sheath flow rate on separation sensitivity and efficiency In general we have found that increased liquid sheath flow results in improved peak efficiency but increased S/N because of the dilution effect of the sheath liquid

CE-MS Instabilty Problems

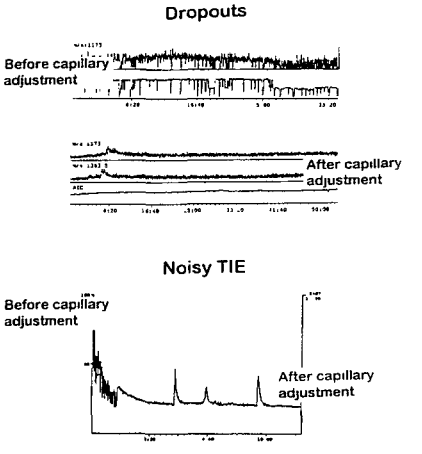

Figure 1. Examples of instabilities often encountered in CE-MS. Both have been corrected with very minor adjustment of the CE capillary with respect to the liquid sheath tube Efffective adjustments are often as small as 10-20μM.

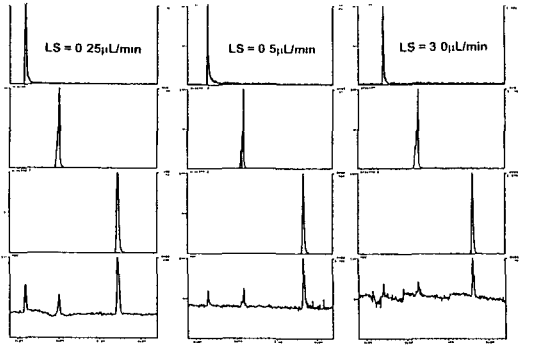

Figure 2. CE-MS analysis of a mixture of peptides with varying liquid sheath flow rates **Capillary:** 34cm x 285μM O D x 50μM I.D with a neutral coating, **Liquid sheath tube:** 24 gauge needle; **Buffer:** 20mM e-amino caproic acid, pH 4.5; **Liquid sheath:** 25-75-0.1:H_2O-MeOH-HAc, **Sample:** KRTLRR, Substance P [1-4] and Substance P [1-9], 100pM/μL each

REAL TIME UV DETECTION WITH ON-LINE CE-ESI-MS

F. Foret*, O. Mueller, W. Goetzinger, J. Thorne, B.L. Karger, P. Vouros and D.P. Kirby.
Barnett Institute, Northeastern University, Boston, MA 02115.

Coupling of capillary electrophoresis (CE) to electrospray mass spectrometry (ESI-MS) is one of the most powerful separation techniques for analysis of biologically important mixtures. In developing a CE-ESI-MS separation, one typically optimizes off-line the CE operational parameters (buffer composition, field strength, sample injection, etc.) without tying up the mass spectrometer. Most CE-ESI-MS systems do not include an optical detector since this addition usually requires increased capillary length resulting in long analysis times. Furthermore, when the detector is located relatively far from the ESI interface only limited information about separated species exiting the capillary can be obtained. Hence, there can be an uncertainty involved in transferring an off-line separation to on-line CE-ESI-MS. Also, since many important ions contain a chromophore or fluorophore, optical detection may be more sensitive than ESI-MS detection in the scanning mode. Hence, simultaneous use of optical detection close to the ESI interface can facilitate on-line CE-ESI-MS analysis. First, the presence of a real time optical signal permits rapid troubleshooting of applications that have been developed off-line. The presence (or absence) of an optical signal just prior to migration into the MS quickly differentiates CE or MS related problems. Next, precise knowledge of the exit times of low concentrated species, visible to optical detection but not in the total ion current, allows one the ability to locate the relevant MS information. Finally, simultaneous optical detection can provide additional, useful information about migration of the sample matrix ions as well as the presence of disturbances due to electroosmosis, hydrodynamic flows and/or migration of ionic boundaries.

In this work we have constructed and evaluated a miniaturized integrated CE-UV-ESI interface. Mass spectrometry was done with a TSQ 700 (Finnigan MAT, San Jose, CA). The original electrospray interface was removed and substituted with a laboratory built interface for capillary electrophoresis. The interface operated in the liquid sheath flow mode [1], with an optional gas sheath [2]. The scheme of the interface is in Fig. 1. The CE as well as the ESI high voltage power supplies were connected through the sheath liquid tube. The position of the CE capillary was adjustable with respect to both the electrospray tip and the fiber optic detection cell. The position of the detection point close to the capillary exit was achieved using a fiber optic-based UV detector. The performance of the interface was evaluated in separations of proteins, peptides and nucleotides in both zone electrophoresis and isoelectric focusing mode.

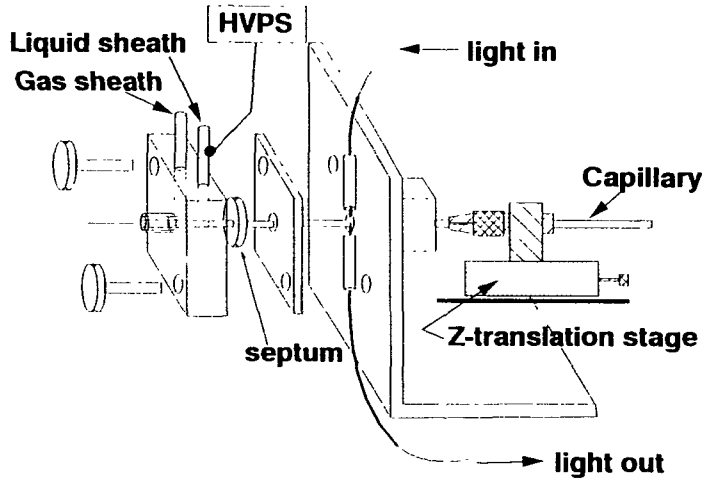

Figure 1.
The scheme of the CE-ESI interface.

References:

1. Smith, R. D., Barinaga, C. J. and Udseth, H. R., Anal. Chem., 1988, 60, 1948-1952.

2. Lee, E. D., Muck, W., Henion, J. D. and Covey, T. R., J. Chromatogr., 1988, 458, 313-321.

Advanced Liquid Ionization Mass Spectrometry for Analysis of a Mixture

Masayuki Inoue, Takeo Kaneko, Li Yaming, Masahiko Tsuchiya, *Niwa Yoshio
Yokohama National University, Tokiwadai, Hodogaya, Yokohama, 240, Japan
*National Institute of Material and Chemical Research, Tsukuba, 305, Japan

Although polar compounds are easy to measure by soft ionization techniques, it is not to measure a mixture containing less polar compounds and rather hard job for ordinary chemists to select a solvent and an adequate chromatographic column for analysis of an unknown sample.

Liquid Ionization (LI) mass spectrometry 1,2], a kind of atmospheric pressure ionization, is applicable to analysis of a mixture containing either polar or non polar compounds. Therefore, LI ion source is complementary for ESI and APCI. Several improvements were performed to improve the reproducibility and sensitivity of the LI method. Those are;

1) use of Teflon coated sample holder for ionizing a sample effectively, 2)use of computer-controlled temperature programming for better separation of analytes, 3) use of matrix (referred to as vapor-matrix) continuously supplied through a vapor phase, 4) devices for introducing a liquid for measuring clusters.

Use of a needle (sample holder) coated by thin Teflon film, except its very sharp end, gives much better reproducibility and sensitivity to the to the LI method.Since a sample is concentrated on the needle tip, the sample loaded can be ionized with much higher efficiency than before.

It was confirmed that the temperature at which the desorption of MH^+ ions begins is characteristic of each compound and almost constant, regardless of heating rate. The computer controlled power supply is useful for adequate temperature programming for the analytes. The desorption profiles (selected ion profile) of characteristic ions give useful information about separation and thermal property of analytes.

Vapor-matrix introduction technique is very useful to analyze a mixture and observe MH^+ of analytes with high desorption temperature, because matrix molecules are continuously supplied to disperse analyte molecules up to the end of the experiment.

Chemical reactions occurred in solution are observed by LI method. Figure 1 shows LI mass spectra of an aqueous solution of paraformaldehydes mixed with methanol (1:1 by volume). The spectra were measured 5 min after mixing. Top of Fig.1 shows total ion profile, in which abscissa indicate scan numbers, corresponding to temperature. The temperature of the sample was ambient up to scan No.15 and increased almost linearly. Protonated polyoxymethylene glycol, $HO(CH_2O)_nH(H_2O)_mH^+$ (refer to as $A_nW_mH^+$) desorb at about 40-80 C (scan No.17-26) as shown in Fig.1 (bottom right). LI mass spectrum (bottom left) observed at ambient temperature (scan No. 1-10) indicate that protonated monomethyl ether oligomers, $CH_3O(CH_2O)_nH(H_2O)_mH^+$ were produced soon after mixing. About 15 min after mixing, almost no polyoxymethylene glycol oligomers remained in the solution.

Collision induced fragmentation is useful. In the case of ZDTP, fragment peaks corresponding to the successive loss of alkyl groups appeared as shown in Fig.2. These peaks were unable to observe by FAB and ESI.

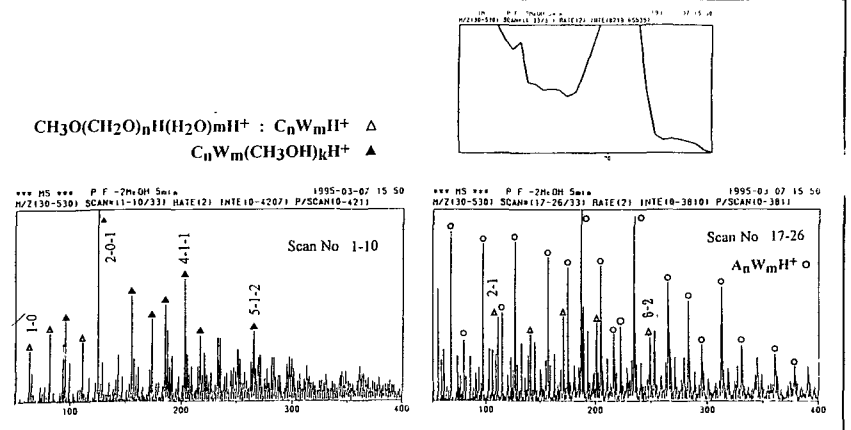

Fig.1 LI mass spectra of an aqueous solution of paraformaldehydes mixed with methanol (1:1 by volume), measured 5 min after mixing.

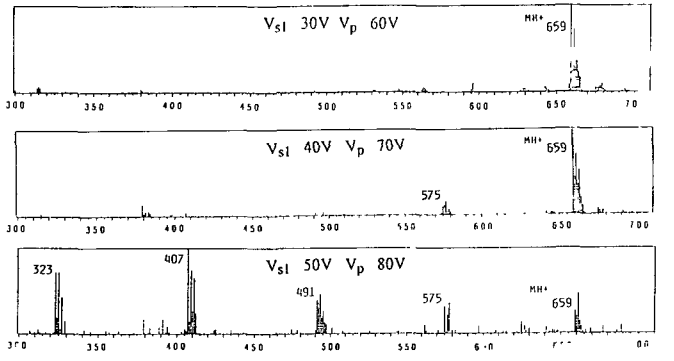

Fig.2 CID (Collision-Induced Dissociation) occurs between Skimmer-1 and Skimmer-2. Fragment peaks correspond to the successive loss of alkyl groups (C6H12 = 84). These disociation is novel in comparison with other ionization method.

1] M.Tsuchiya, H.Kuwabara,, K.Musha, Anal Chem., 58, 695 (1986)
2] M.Tsuchiya,Advances in Mass Spectrometry Volume13,(1995) John Wiley in press.

ELECTRIC EVAPORATION OF IONS FROM LIQUID IN CHANNELS OF POLYMER FILM

A.A.Balakin, A.F.Dodonov, L.I.Novikova, V.L.Talrose, B.S.Yakovlev†
(†Deceased May 19, 1993)
Institute of Energy Problems of Chemical Physics, Russian Academy of Sciences, Moscow, Russia

In spite of the attractive feature, the method of electric evaporation of ions from molecular liquids (EHDI) [1] has not been developed as well as thermospray or electrospray methods. Recently a new method of ion extraction from liquids was proposed by B S.Yakovlev, V.L Talrose et al.[2,3] The method uses polymer films densily perforated with channels as an interface between a solution at atmospheric pressure and a vacuum chamber of MS A goal of the present report is elucidation of the main physical processes driving work of the membrane ion source

For a liquid with adequate conductance the stability of the surface in an external electric field is determined by the Rayleigh criterion [4] The estimation for glycerol shows that the radius of capillary needle used in EHDI is too large to prevent destruction of the surface of a liquid by electric field strange $>10^6$ V/cm. To provide stability for a liquid surface at p=1 atm, and $E \approx 10^6$ V/cm one would need for glycerol a capillary with radius < 0,1 μm Many difficulties creating by this requirement overcame by using a system of thin channels in a polymer film The channels have much lower radii than those used in EHDI, nevertheless their number provides a huge ion current from the liquid [5]

The membrane investigated in present work· a) prevents air flow into the MS vacuum chamber, b) provides ion transport to liquid/vacuum boundary, c) makes conditions for ion extraction

Major questions are 1) what physical processes do control the operation of membrane ion source? 2) what of primary charge particles are extracted from the liquid?

Methods. A liquid sample is placed on the atmospheric side of nonconductive polymer film. The 10 μm thick film contains multiple narrow channels To create the electric field two electrodes are used. The one is sunk in the liquid and the other is placed in vacuum in form of a grid. The distance between vacuum side of membrane and the extracting grid was 0,3÷3 mm The channels density was about 10^7 cm^{-2} They were made by irradiation poly (ethylene terephthalate) film by high energy Xe ions with a special chemically treatment of tracks [6]

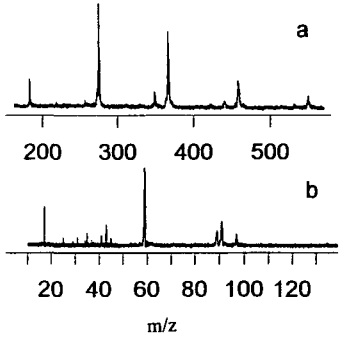

Fig 1

The Dodonov's orthogonal ion optics [7] was used to MS measurements The TOF MS device was supplied with the membrane ion source, which is similar in physical arrangement to the one described in [3,5]

RESULTS. The degree of fragmentation in spectra obtained depends on variation of potential difference between liquid and the accumulator. Fig 1a shows the mass spectra obtained from glycerol when MS indicates particles which have the maximal energy There are cluster ions in this case only. The energy dependence for intensity of mass picks observed for "pure" glycerol is shown in fig 2 Fig 1b shows mass spectra of ions with the energy less than that corresponding to potential difference between liquid and accumulator of MS. In this case, declustered ions can be observed as well as clusters and their fragments.

DISCUSSION

What conditions do provide of ion extraction? The channel filling of conducting liquid is like to a very sharp

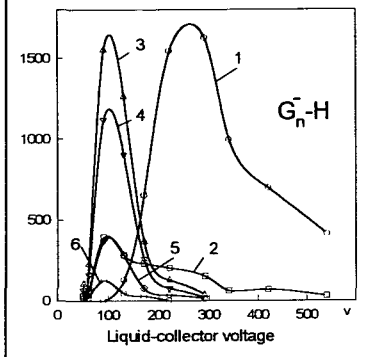

Fig 2

needle in insulating polymer, if the surface density of channels is low enough. So the localelectric field strange at liquid surface of membrane used is significantly higher than U/d, were U is extracting voltage, d is the liquid-extracting grid distance

The choice of channel radius affords the implementation of the Rayleigh criterion

The transport of ions The voltage drop across the channels of the membrane is equal to $\Delta U_{channel} = U_{liquid} - U_0$ where U_{liquid} is potential supplied to the liquid sample, U_0 is collector potential corresponding to appearance of current in the accumulator of MS It was shown that the electric field strange in channel is about $10^4 \div 10^5$ V/cm at film thickness about 10 μm The electric field helps ions to enter from sample the channels and clears the channels from ions of other sign

The nature of charge particles extracted. The ions extracted are formed due to dissociation of molecules of solvent and solute, considered as a subject of chemical analysis. The energy of ions extracted from liquid is equal to $\varepsilon = e\,(U_{liquid} - U_{collector} - \Delta U_{channel})$ were $U_{collector}$ is the potential of collector

The gas pressure in vacuum chamber of MS was too low to promote dissociation of ions by gas phase collision Therefor one can anticipate that the particles extracted from liquid have the energy distribution $\sim k_B T$ As one can see, the energy distributions all of ions observed are appreciably broader then the energy resolution of MS (~5 eV) The ions with n equal to zero or one are observed only if the energy of particles entering the accumulator is more than that for ions detected by MS Those ions are detected probably after collisions of primary ions with electrodes of the accumulator [5]

CONCLUSIONS. The electric evaporation of ions from liquid in channels of polymer film is controled by many physical processes, the main from which are . a) the emission from liquid, b) the ions transport through channels, c) the way of a strong electric field formation

The possibilities of investigation of particles extracted from liquid were demonstrated by analysis of energy distribution of ions detected

It was shown that the cluster ions only are extracted from solutions expected.

Acknowlegment. The research was suppored by the grant N95-03-09083 of Russian Basic Reseaches Foudation.

REFERENCES

1 Simons,D S ; Colby,B.N.; Evans, C.A Int. J. Mass Spectrom Ion Phys. 1974, 15, 291-302
2 Balakin, A.A., Mchedlishvili, B.V , Flerov, G N , Talrose, V.L ,Yakovlev, B S ;1984 , av sy N4382445 Authors application number N 1542322 (1989)
3 Yakovlev, B S ; Talrose, V L ,1991, Patent of Russia N 4879085 Bull N3,27.01 95
4. Lord Rayleigh, Philos. Mag 1882, 14, 184-190
5 Yakovlev, B S , Talrose, V L ,Fenselau, C Anal Chem. 1994, v.66, p 1704-1707.
6 Flerow, G N.; Baraschenkov, V S , Usp. Phys Nauk (USSR) 1971,114, 351-373
7 Dodonov, A F., Chernushevich, I V.; Laiko, V V , 1993, Electrospray Ionization on a Reflecting Time-of-flight Mass Spectrometer in "Time of Flight Mass Spectrometry", Cotter, R.J , Ed , American Chemical Society, Washington, DC.

MOLECULAR WEIGHT ENHANCEMENT IN GC-MS WITH SUPERSONIC MOLECULAR BEAMS

Shai Dagan and Aviv Amirav
School of Chemistry, Tel Aviv University, Tel Aviv 69978, Israel, Fax: 972-3-6409293

Supersonic molecular beams are characterized by the supercooling of the molecular vibrational temperature, a controlled unidirectional kinetic energy in the hyperthermal range (0.1-30 eV) and a high flow atmospheric pressure sample inlet with optimal jet separation capability. The vibrational supercooling induces a considerable enhancement in the relative abundance of the molecular weight peak under 70 eV electron impact (EI) ionization, combined with tail free GC-MS traces, regardless of the sample volatility.

The elimination of the intramolecular thermal energy makes the electron energy the only parameter that governs the degree of ion dissociation. Therefore, at reduced electron energies such as 18 eV, the molecular weight peak in n-alkanes and in many other compounds, is the dominant mass spectral peak, being higher by more than a factor of 10 than any other peak. Due to the diminished fragmentation, the sensitivity reduction at reduced electron energies is minimal. Improved library search is achieved with 70 eV EI-MS in SMB by limiting the search using the molecular weight peak information, while ignoring its intensity. EI-SMB provides EI and chemical ionization (CI) information simultaneously, as well as accurate isotopic and elemental information, taken from the peak height ratios of the M, (M+1), (M+2) ions.

In the rare cases where the M^+ peak is missing, a unique Cluster CI can be employed. It is based on the co-expansion of methanol (or water) vapor and the sample molecule, forming clusters of the sample molecule with few methanol molecules. The EI ionization of the cluster is followed by energy removal through cluster desolvation and intra cluster proton transfer to form a protonated molecular ion. This method is demonstrated with aldicarb sulfone as shown in figure 1. The addition of deuterated methanol (or heavy water) to the supersonic expansion induces an effective deuterium exchange of all the labile OH and NH hydrogens. In this routine mode of EI-SMB, in contrast to conventional CI, the EI fragmentation pattern contains labile hydrogen information as shown in figure 2 for 17-β-estradiol. Note also the dominant M^+ peak in this 70 eV EI mass spectrum of 17-β-estradiol.

An additional ionization method used with SMB is Hyperthermal Surface Ionization (HSI). The hyperthermal sample molecules are ionized through scattering from a suitable surface such as rhenium oxide. HSI is an ultra sensitive ionization method, providing sub-femtogram detection limits. It is also a tunable selective method for molecules with low ionization potential,

such as the polycyclic aromatic hydrocarbons (PAH's) (exhibiting mass spectra with a molecular peak only in HSI), or nitrogen containing molecules. HSI is selective against aliphatic hydrocarbons, a fact that helps in the GC-MS analysis of complex mixtures such as screening of drugs in urine. This selectivity is achieved by reducing the molecular kinetic energy using helium as a carrier gas. At this low kinetic energy, HSI becomes a soft ionization method.

Recommended References on SMB-MS:

1. A. Amirav., Org. Mass Spectrom. 26, 1-17 (1991),
2. S. Dagan and A. Amirav., Int. J. Mass. Spectrom. & Ion. Proc., 133, 187-210 (1994).
3. S. Dagan and A. Amirav., J. Am. Soc. Mass. Spectrom. 6, 120-131 (1995).

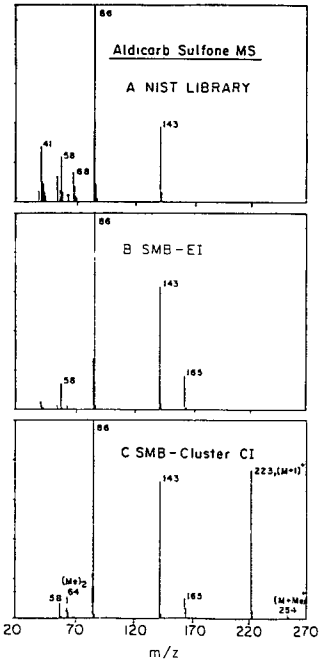

Fig.1 - Cluster CI-MS of Aldicarb sulfone

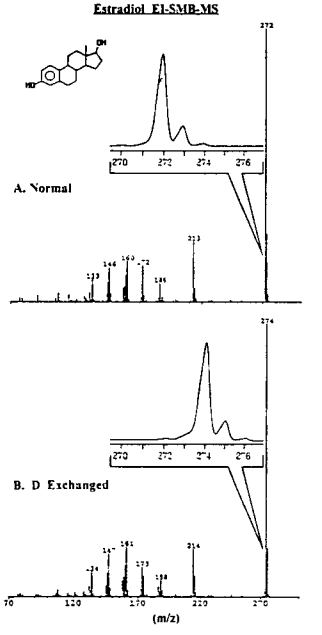

Fig.2 - Deuterium exchange in SMB-MS

SOFT IONIZATION VIA ELECTRON IMPACT ON FREE-JET CLUSTERS

Dingneng Wang and Robert J. Evans
National Renewable Energy Laboratory, 1617 Cole Boulevard, Golden, CO 80401

The combination of a molecular beam sampling source with mass spectrometric detection provides a versatile tool for studies of high temperature processes to produce renewable energy resources, such as pyrolysis, gasification and the combustion of biomass.[1] Among the many advantages of molecular beam mass spectrometry (MBMS) is its ability to detect a wide range of products simultaneously, rapidly and in real time. Even fragile species can be detected because of the extensive cooling as a result of the supersonic free-jet expansion during the molecular beam formation. However, the popular configuration of using an electron-impact ionization source makes it difficult to obtain molecular ion information for pyrolysis products of carbohydrates, which are an important component of biomass. For example, only a weak molecular ion ($M^{+\cdot}$) peak is observed for levoglucosan with low energy EI ionization using the MBMS instrument, while no $M^{+\cdot}$ signal is found in its 70 eV library spectrum.

We have developed a novel technique to achieve soft ionization in a molecular beam mass spectrometer (MBMS), ensuing a conceptual discussion at a recent MBMS meeting.[2] It employs the cluster formation ability of a molecular beam source, and the local high density (or pressure) within clusters provides an ideal environment for intramolecular chemical ionization as well as the release of excess energy on ionization. We report some preliminary results in this paper and compare this technique with other common soft ionization techniques

Experimentally, this soft ionization technique involves the following procedure The gaseous sample or a stream of product vapors is mixed with a helium carrier gas and a clustering agent such as water or methanol in a heat-traced zone at atmospheric pressure. The gaseous mixture is then extracted through an orifice into three consecutive vacuum stages. During the supersonic, free-jet expansion, a molecular beam is formed that contains a series of clusters of the analyte molecule (M) with the agent molecules (A), MA_n, n=1,2,3,.. The molecular beam enters the electron impact (EI) ionization region of a triple quadruple mass analyzer, where the clusters, MA_n, are ionized to produce positive ions. The mass spectrum of the analyte contains not only an enhanced molecular ion ($M^{+\cdot}$) peak, but also intense signals for MH^+, $MA_{n-i}^{+\cdot}$, and $MA_{n-j}H^+$ (i,j=0,1,2,.. ,n-1).

$$M + nA \xrightarrow[\text{clustering}]{\text{free-jet}} MA_n \xrightarrow[e^-]{\text{EI}} MA_i^{+\cdot} \;\&\; MA_jH^+$$

Shown in Figure 1 are mass spectra obtained for levoglucosan with MeOH, H_2O and D_2O as clustering agents There is more than an order of magnitude enhancement in the formation of the molecular ion and cluster ions that contain the intact molecule. The ionization of free-jet clusters leads to the enhanced formation of molecular ion products but at the low operating pressure of the EI source, which is about five orders of magnitude lower than that required for chemical ionization in a quadrupole mass spectrometer. Fragment ions are still observed but the extent of fragmentation is reduced because of the free-jet cooling and the removal of energy from the ionized cluster by boiling off molecules of the clustering agent. In addition, facile H/D exchanges occur prior to detection with D_2O as the agent, thus revealing the number of hydroxyl groups present in the molecule (a shift of four amu for levoglucosan, which has three HO groups) Where the H/D exchange takes place is unclear H/D exchanges both before and after ionization are likely to occur

The mass spectra of ionized free-jet clusters are further simplified, but at the expense of reduced sensitivity, by carrying out collision-induced dissociation (CID) experiments in the neutral-loss (NL) mode.

---

[1] Evans, R.J. and Milne, T.A. *Energy and Fuels* **1987**, *1*, 123 and 311

[2] Dagan, S. and Amirav, A. *J. Am. Soc. Mass Spectrom* **1995**, *6*, 120-131 and references therein

Only product ions that lose a molecule of the clustering agent are detected, thus filtering out almost all the fragment ions of any remaining unclustered analyte molecules Figure 2 shows such mass spectra of levoglucosan, glycerol, and a mixture of aromatic compounds, demonstrating the selectivity for detecting molecular ions of polar species. We are examining the effects of experimental parameters, including clustering agent type, partial pressure, temperature, orifice shape and size, ionization energy, and collision energy to achieve optimum sensitivity. Applications of both techniques to the analysis of products derived from pyrolysis of lignocellulosic materials are also under investigation

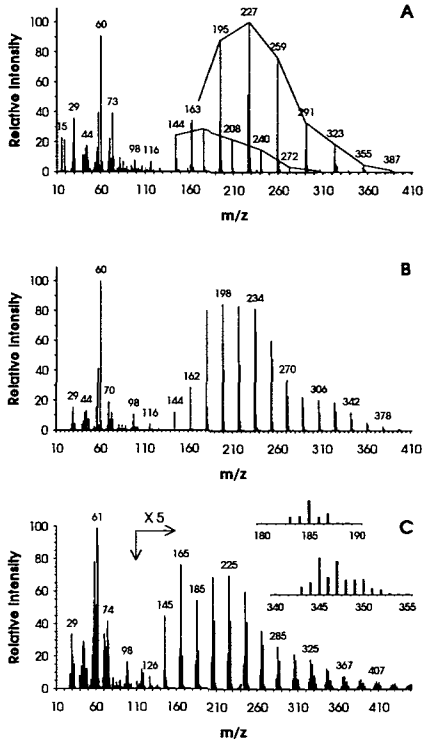

Figure 1 Molecular beam mass spectra of free-jet clusters of levoglucosan (25 eV EI). Clustering agent: (a) MeOH at 350°C, (b) H_2O and (c) D_2O at 500°C.

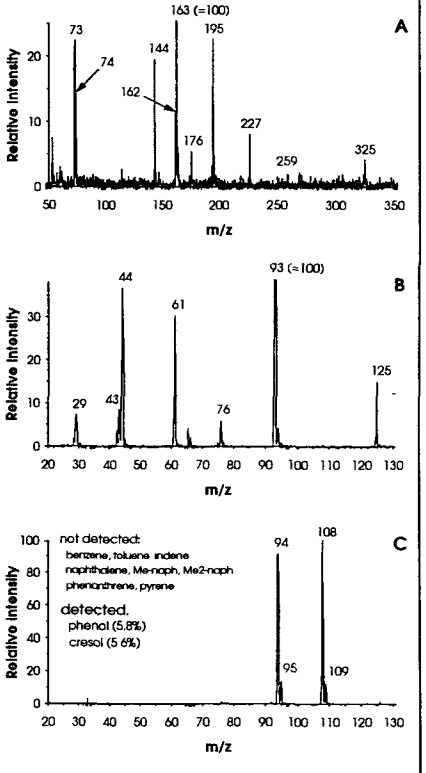

Figure 2. CID neutral-loss mass spectra of free-jet clusters of (a) levoglucosan, (b) glycerol, (c) a mixture of aromatics. Clustering agent: MeOH at 500°C, 25 eV EI, Ar CID, NL=32

Concentration Enrichment in High Pressure Ion Sources, Part II.

D. H. Williamson, W. B. Knighton and E. P. Grimsrud,
Department of Chemistry, Montana State University, Bozeman, MT, 59717

INTRODUCTION

The pulsed high pressure mass spectrometry technique has proven to be the most successful method available for the measurement of ion-molecule equilibria in the gas phase and has also been extensively used for the determination of rate constants for ion-molecule reactions (1). The accuracy of the measurements obtained with this or other techniques which use mass spectrometry to sample a high pressure gas depends on the validity of two assumptions:

1. The relative ion abundances measured by the mass spectrometer must accurately reflect the actual ion abundances present within the ion source. Accurate ion sampling typically demands the use of very small ion sampling orifices which provide near molecular flow conditions (1).

2. The concentrations of the neutral reagents within the ion source must also be known.

The use of molecular flow conditions, however, can lead to a concentration enrichment of the heavier reagent neutrals within the ion source due to mass dependent ventilation rates of the ion source contents through the ion source orifices (2). Thus, a contradiction between the two criteria for accurate measurements appears to exist, since conditions that satisfy one of the criteria seem to violate the other. In a previous study (2) we characterized the effect that near molecular flow conditions had on the observed rate constant measurements of the S_N2 nucleophilic displacement reaction,

$$F^- + CH_3I \rightarrow I^- + CH_3F \qquad (1)$$

In the present study, we examine the use of viscous or near viscous flow conditions on the same kinetic system. It will be shown that certain combinations of source pressure and aperture size provide accurate rate constant determinations of Reaction 1 The effect of employing viscous or near viscous flow conditions on association equilibria measurements will also be discussed.

INSTRUMENTATION

All the measurements reported here were obtained using a pulsed e-beam high pressure mass spectrometer (PHPMS) which was constructed in our lab. This instrument consists of two major component systems a gas handling plant and a mass spectrometer Gas samples were prepared in CH_4. The total pressure of the gas mixture was typically 800 torr The contents of the GHP were leaked into the ion source at a rate sufficient to maintain source pressures from 0.5 to 8 Torr. The mass spectrometer consists of a commercial quadrupole instrument equipped with a specialized high pressure ion source. A unique feature of this ion source is that its contents exit solely through the ion exit and electron entrance apertures. In this study, two sets of apertures having diameters of 150 μm and 200 μm were used. Negative ions formed within the ion source were monitored by a quadrupole mass filter and an ion counting detector. The time-dependence of each ion signal was recorded with a multichannel scaler.

ION SOURCE FLOW DYNAMICS

The nature of the flow of a gas through an aperture can be estimated by calculating the ratio of the mean free path of the gas (L_a) to the critical dimension (a) of the aperture as follows (3): $L_a/a > 1.0$ molecular flow; $0.01 > L_a/a < 1.0$ transition region; $L_a/a < 01$ viscous flow. Figure 1 shows a plot of L_a/a versus ion source pressure where the term, a, corresponds to the aperture radius and L_a is the mean free path of either the CH_4 buffer gas or the CH_3I minor component. The L_a/a values for CH_3I are included in Figure 1 because previously (2), this quantity was found to be a better indicator of the nature

of the flow out of the ion source. Regardless of which series of L_a/a values are considered, the flow conditions within the ion source are clearly in the transition region over the pressure range of 1 to 10 torr.

RATE CONSTANT MEASUREMENTS

Figure 2 shows a plot of the apparent rate constants for the reaction of F^- with CH_3I at 150°C over the pressure range of 0.5 - 8.0 torr. At low pressures, 2 torr and below, the apparent rate constants increase significantly with decreasing pressure. This effect is attributed to the concentration enrichment phenomena which occurs as molecular flow conditions are approached. Also shown in Figure 5 is the limiting value of the rate constant expected under pure molecular flow conditions where $k_{obs} = k(M_{CH3I}/M_{CH4})^{1/2}$. However, at higher ion source pressures the rate constants determined here become less pressure dependent and essentially equal to the known value of the rate constant.

CONCLUSIONS

Accurate kinetic measurements can be obtained with the use of large ion sampling apertures when near viscous flow conditions exist within the ion source. This success is attributed to the elimination of the concentration enrichment phenomena by providing convective flow of the contents out of the ion source. No problems associated with convective flow of gas through the relatively large apertures (Point 1 - Introduction) were observed. We do not, however, recommend performing cluster equilibria measurements under viscous flow conditions. This is because of the potential for increased cluster growth which can result from the cooling of the gas as it expands through the ion exit aperture. This effect can be quite significant and has been previously documented in a PHPMS ion source (1).

REFERENCES

1. P. Kebarle, in J.M. Farrar and W. Saunders (eds.), Techniques for the Study of Ion Molecule Reactions, John Wiley and Sons, Inc., New York, 1988, p. 221.
2 D.S. McGrew, W.B. Knighton, J.A. Bognar, E.P. Grimsrud, Int J. Mass Spectrom Ion Proc., 139 (1994) 47.
3 S Dushman, Scientific Foundations of Vacuum Technique, John Wiley and Sons, Inc., New York, 1989.
4 T. Su, R A Morris, A.A. Viggiano and J F. Paulson, J Phys. Chem., 94 (1990) 8426.

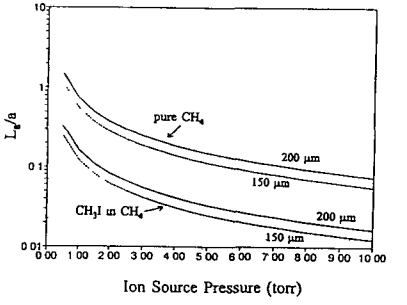

Figure 1. Plot of the ratio of molecular mean free path to aperture radius as a function of ion source pressure for pure CH_4 buffer gas and CH_3I in CH_4 at 150 °C

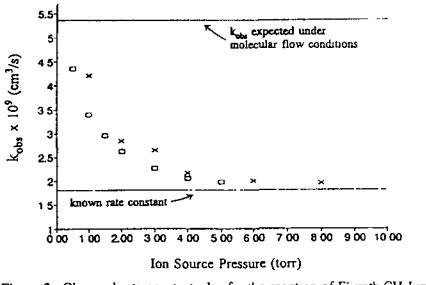

Figure 2. Observed rate constants, k_1, for the reaction of F^- with CH_3I in methane at 150°C as a function of ion source pressure, 150 μm diameter apertures (triangles), 200 μm diameter apertures (squares) The dotted line indicates the known rate constant, k_1, for this reaction reported by Su et.al (4) The dashed line shows the limiting value of the rate constant expected under conditions of pure molecular flow where $k_{obs} = k_1(M_{CH_3I}/M_{CH_4})^{1/2}$

Using a Portable Mass Spectrometer to Measure Surface Contamination

Hugh Gregg, Michael Meltzer, Jean Lindsey, and Heather Edberg
Lawrence Livermore National Laboratory, PO Box 808, L-310, Livermore, CA 94550

One of the major sources of hazardous waste and VOC air emissions throughout the manufacturing industry is parts and equipment cleaning operations. Modification of the cleaning process to use non-hazardous cleaning agents may be the best way to eliminate these sources, but some operations still require the use hazardous solvents. Monitoring the contamination levels during cleaning operations can provide useful feedback for reducing waste generation and air emissions due to over- or under-cleaning. Near real-time evaluation of cleaning operations can help reduce pollution in a wide variety of industries, including aerospace, electronics, and metal finishing industries.

Two common techniques for the verification of cleanliness include the water break test (very crude and subjective), and non-volatile residue (NVR) analysis. NVR analysis utilizes solvents (freon, 1,1,1-trichloro-ethane) to further "clean" the surface; the solvent is flash evaporated and the residue weighed. NVR analysis is quantitative, but is dependent on the sampling solvent being able to remove the expected contaminant. In addition to NVR, a number of instrumental methods are commonly used to measure surface contamination, including ellipsometry and FTIR. These techniques are sensitive to the surface conditions (smooth or rough?) and composition (aluminum, quartz, other?), and can be difficult to calibrate.

We have developed a mass spectrometry based analyzer that has similar or better sensitivity than ellipsometry or FTIR and is more tolerant of surface conditions and composition. In addition, the instrument is relatively portable and can be used to help identify unknown surface contamination. Our method uses vacuum and thermal desorption to remove volatile and semi-volatile contaminants from the surface. A quadrupole mass spectrometer is used to identify and measure the contamination. A bench-scale model of our "contamination analysis unit" employs a residual gas analyzer (RGA) mated to a small, internally heated inlet that samples a surface.

The current version of the instrument has the following features:

- ~7 cm^2 sampling surface with a Viton O-ring seal (maximum temperature of 240°C)
- resistance heater (constant temperature ramp, maximum rate 1.4°C/sec)
- spring loaded thermocouple in contact with surface
- residual gas analyzer (quadrupole mass spectrometer) with an open ion source, 1 to 200 dalton mass range and both a Faraday cup and an electron multiplier
- LabView control of the RGA, heater, and thermocouple

Trimsol, a machine tool coolant, was the contaminant used in these tests. Test coupons (aluminum) were cleaned with methylene chloride and baked in a vacuum oven at 150°C for two hours. Trimsol was brushed onto the surface and wiped off. The cleaning solutions were prepared according to the manufacturer's specifications. The coupons were cleaned in an ultrasonic bath for five minutes, then were washed twice with deionized water. Air drying completed the test coupon preparation. Coupons used for calibration were cleaned, and spotted with a known amount of Trimsol diluted in methylene chloride, and allowed to air dry.

The intensity at three m/z values (95, 97, 109), characteristic of Trimsol, were recorded as the temperature was ramped from ambient to 230°C. The area under an intensity vs. temperature curve was integrated from 65°C to 225°C, and this integrated value provided the basis for quantitation.

Several aqueous based cleaners were obtained from our waste minimization group, and they all produced excellent results. Freon TE is a common degreaser used in industry, and is presented here as a baseline cleaning product. The CO_2 cleaned samples were "CO_2 blasted" (similar to sandblasting) using CO_2 pellets (~2 to 4 mm) and snow (~0.5 to 1 mm).

Cleaning solvent /method	µg Trimsol	µg/cm² Trimsol
Brulin 1793	< 4.	< 0.6
Brulin 1990GD	< 4.	< 0.6
CitriSafe	< 4.	< 0.6
Hurisafe	< 4.	< 0.6
JALSAC	< 4.	< 0.6
Brulin 815GD	4.3 ± 1.6	0.6 ± 0.2
Freon TE	5.1 ± 1.9	0.7 ± 0.3
CO_2 pellet	14. ± 1	2. ± 0.1
CO_2 snow	120. ± 2	17. ± 0.3
4.5 µg check sample	4.0 ± 0.6	0.6 ± 0.1

One of our goals is to travel to an assembly line (e.g. for aircraft components) and measure parts before and after cleaning operations. While the work to date proves that this method works, there are three aspects of this technique that we hope to improve.

1) Increase the sensitivity of the instrument
   a) Change the open ion source to a closed ion source, creating a higher pressure region in the new source
   b) Make a smaller sample interface which is directly coupled to the closed source

2) Make the instrument more portable
   a) Smaller pumping system
   b) More compact control system

3) Incorporate better data analysis methods
   a) Acquire full scan mass spectra (vs. selected ions)
   b) Create a library of common contaminants
   c) Identify and deconvolute multiple contaminants

Conclusions

The system, as currently configured, has comparable performance to an FTIR. It is not a universal tool for measuring surface contamination (some surfaces cannot be heated up to 200°C; non-volatile contaminants cannot be desorbed), but it can be used in a wide variety of applications not suitable to ellipsometry or FTIR analysis. With the modifications outlined above, the instrument should be more sensitive, allowing for the determination of smaller amounts of surface contaminants.

Heather Edberg is now attending the University of Washington.

Work performed under the auspices of the U. S. Department of Energy by the Lawrence Livermore National Laboratory under contract W-7405-ENG-48.

Conversion of HP 5985 GCMS to Automated, High-Volume ESMS

Jennifer Kiesel, Alan Jackson, Kevin Depperman, Fred Hileman, Kevin Duffin
Monsanto Corporate Research, Monsanto Company
700 Chesterfield Parkway North, St Louis, Missouri 63198

INTRODUCTION

A retired Hewlett-Packard 5985 gas chromatograph/mass spectrometer (GC/MS) was modified to operate as an electrospray mass spectrometer (ESMS) The gas chromatograph was removed and a new ionization source was fabricated to replace the existing electron ionization (EI) source The mass spectrometer has a mass range of 1,000 amu and can be operated in the positive or negative ion mode For the past two years this system has been used for routine structural confirmation of synthetic, pharmaceutical samples

A PC-based Teknivent data system was incorporated to 1) enhance instrument control and consequently performance, 2) control satellite liquid chromatography (LC) and flow injection autosamplers (AS) resulting in increased sample throughput, and 3) automate data acquisition and processing to reduce operator-instrument interaction

To enhance instrument sensitivity, conversion from a high-energy dynode multiplier to a pulse-counting multiplier was done

INSTRUMENT CONFIGURATION

Mass Spectrometer HP 5985 Quadrupole Mass Spectrometer, Electrospray Ionization (ESI), Pulse-counting multiplier

Data System Teknivent - Vector Two Version 2.02.02

Computer 486 IBM Compatible, 32 MB RAM, 200 MB Hard Drive
IEEE-488 Instrument Interface

Operating System IBM OS-2 Version 2.1, Multitasking, Windows User Interface, Local area network (OS-2 LAN Server) with additional instruments to permit remote data processing.

Instrument Interface The data system and interface provide digital control of all instrument functions This permits real time computer driven manipulation of selected ion focus elements even during a scan.

CONCLUSIONS

Good sensitivity
Detection limits of approximately 500 pg/ul for reserpine in the positive ion mode with the pulse-counting multiplier Detection limits of approximately 5 ng/ul for adenosine triphosphate in the negative ion mode with the pulse-counting multiplier. Noticeable sensitivity improvement, particularly in the negative ion mode, with the pulse-counting multiplier vs. the HED multiplier

Degree of fragmentation can be controlled
The potential between the capillary and the skimmer is variable. Higher values induce the formation of fragment ions which becomes useful in structure elucidation. Lower values enhance formation of intact molecular ions for molecular weight determination of compounds in solution. This is particularly good for mixtures, because it provides semi-quantitative data based on relative ion count intensities

Easy to use
Data system can be tailored to run multiple vendor instrumentation which lends itself to networking and remote data retrieval and reporting. Operator training is minimized due to universally applied software.

Autosampler increases sample throughput and reduces redundant, manual operator tasks ESI useful for a wide variety of compounds in pharmaceutical research. The upgrades are cost effective.

Sensitivity of the HP 5985 Electrospray Mass Spectrometer
Positive Ion Mode Detection Limits for Pulse-Counting and High-Energy Dynode Multipliers

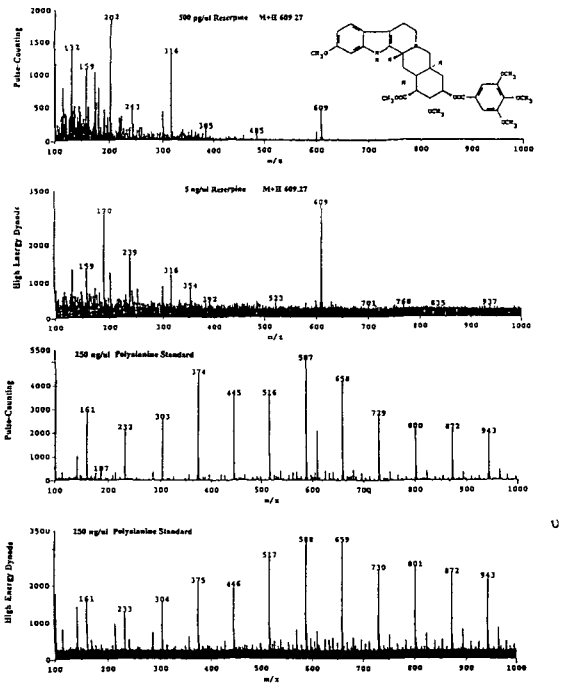

Improving Sensitivity in the H.P. MSD Mass Spectrometers

John J. Manura
Scientific Instrument Services, Inc., 1027 Old York Road, Ringoes, NJ 08551

The H.P. MSD instruments (Models 5970, 5971 and 5972) have proven to be very efficient, low cost, highly sensitive and versatile mass spectrometers. Sensitivity in the MSD's can be improved by decreasing the background or noise level, increasing the sensitivity of the mass spec or detector or by improving the resolution of the GC peak for the analyte of interest. The 5971 MSD sensitivity has increased at least 10 fold by incorporating the improvements in the GC and the MSD as described below.

GC/MS Transfer Line

In the standard GC/MS transfer line on the HP 5971, the GC capillary column bottoms out inside the transfer line tip inside the MSD source. The GC column flow elutes at 90° to the normal GC flow. This design does not provide for an efficient straight through flow of the GC effluent into the MSD source and the analytes eluting off the GC capillary column are exposed to hot metal surface. A straight through transfer line tip eliminates the exposure of the GC analytes to this metal surface and provide for a straight through flow of the capillary column effluent into the MSD source. Therefore the analytes are eluted off the GC column directly into the MSD source without exposure to any metal surface.

Mass Spectrometer Source

Over the last 20 years we have continued to improve on our source cleaning methodology. These cleaning methods have been perfected to provide the cleanest source possible and therefore the optimum sensitivity of the mass spectrometer. Highly polished metal (mirror like) surfaces help to maintain cleaner sources since they do not contain the small scratches and uneven surfaces that are prone to contamination.

Electron Multiplier

Electron Multipliers have improved significantly over the last few years. The newest multipliers from Galileo have with 2 to 10 times increase in sensitivity. Galileo has improved the electron multiplier sensitivity, reduced extraneous noise, increased the dynamic range and increased electron multiplier life. The new Galileo Model 5778 for the HP 5971, 5972 and GCD and the corresponding Model 5772 for the HP 5970 series of MSD's have recently been introduced as the latest enhancements to sensitivity and performance. These newest multipliers improved sensitivity at least 5 fold as compared to the original multipliers supplied with these instruments.

Vacuum System

HP installed either an Alcatel UM2002 or a small Edwards E2M1 or E2M2 in the MSD's. Both of these vacuum pumps are small, run at high RPM's, run very hot and have a history of limited life. They have a pumping speed of about 30 to 50 liters per minute. In our lab, we wanted to move the rough vacuum pumps on the other side of the wall from the MSD in order to reduce the noise level in the mass spec lab, therefore we chose to use the Alcatel UM2015. This pump has a pumping speed of 300 liters per minute. These larger rough pumps result in a much faster pumping speed which is especially noticeable during initial pump down after the system has been vented. In addition the system runs at a lower vacuum level due to this increased pumping efficiency.

Proper care of the rough pumps is very important. The rough pump oil should be changed every 3 to 6 months. Dirty or contaminated oils, increase the wear on the metal shafts of the pump and the pump runs much hotter. This higher temperature escalates pump wear. If the rough pump oils are routinely changed, the rough pump should have a life of about 5 years before an overhaul is required.

In the last two years, a new rough oil has been introduced called Inland 45. It is a highly refined and distilled oil with a low vapor pressure that will provide for increased performance in the rough pumps used on mass spectrometers. This oil will provide a much lower vacuum level, reduced hydrocarbon background and increased performance from the vacuum pump and mass spectrometer.

Santovac 5 has a history of being the best vacuum pump oil for use in diffusion pumps. This oil is a highly refined polyphenyl ether fluid that can achieve vacuum levels of 1×10^{-10} torr in research grade mass spectrometers. Santovac 5 is routinely used in the diffusion pumps on most mass spectrometers manufactured over the last 25 years. Other lower grade diffusion pump fluids are available such as the Dow Corning diffusion pump fluids, but will not provide the vacuum levels achievable by Santovac 5.

GC Septum

The most common source of GC background is the GC septum. Most GC septum are constructed of silicone. The common mass spec background peaks appearing at mass values of 207, 281, 267 and 355 can all originate from the siloxanes in the GC septa. We performed a series of studies to determine the degrees of background contamination that can originate from the GC septum from different manufacturers. The Supelco Thermogreen LB-2 septa were determined to be the best GC septa on the market. They produced the lowest septa bleed.

Cleaning the GC Injection Port

The GC injection port should be cleaned on a regular basis or when it becomes contaminated. The recommended procedures involves the physical cleaning of the injection port with small wire brushes and solvents followed by the baking out of the GC injection port at high temperature with preheated carrier gas and no column installed. This high temperature flow conditioning of the GC injection port purges all parts of the injection port with gas at the highest temperature possible. The hot gas flushes the injection port area including the septum area and also flushes the septum purge and split vent lines. Areas of the injection port that are not normally cleaned are thoroughly cleaned and purged during this high temperature flow conditioning.

GC Capillary Columns

The manufacturers of GC capillary columns are continuing to produce columns with lower column bleed. Since the introduction of bonded phase capillary columns, column bleed has been steadily reduced by the manufacturers. At Pitt Con this year J&W introduced an even lower bleed DB5 column for mass spec use called the DB-XLB column. This new non-polar capillary column provides for the lowest column bleed and is the recommended non-polar column for GC/MS analysis.

Conclusion

A number of changes in the mass spec and GC that have been made to the HP 5971A MSD in order to improve performance. These changes will increase the sensitivity by a factor of between 5 to 10 fold over the original instruments performance.

Modification of a Hewlett Packard 5972 MSD to Accept a Direct Insertion Membrane Probe

Scott Bauer, Jan Bauer, MIMS Technology Inc.
1900 S. Harbor City Blvd. Suite 115
Melbourne, FL 32901

Much of the previous work in the field of membrane introduction mass spectrometry (MIMS) has been performed on expensive research grade mass spectrometers equipped with direct insertion probe interfaces, or with modified ion traps. There are thousands of Hewlett Packard 5971 and 5972 mass spectrometers in use in laboratories throughout the world. Most of these are relegated to gas chromatographic use by design. Often chromatography is a sideline and the mass spectrometer sits idle in the laboratory where it may be put to better use in other investigations. Although these spectrometers are inexpensive, the quality of results is quite good. Modifications incorporated into the 5972 model make it very attractive for membrane inlet or solids probe use.

Modification of the 5972 to accept direct insertion probes is troublesome due to the lack of an internal source heating mechanism. The 5972 source is heated by the GC transfer line and temperature controls are incorporated into the GC operating system. The experiments described here demonstrate a relatively simple modification to heat the source in the absence of a GC transfer line.

An auxiliary heater block was attached to the 5972 source frame. Wires to the heater cartridge are routed down through the calibration gas port to a modified vacuum feed-through fitting. An external power circuit with a high / low switch setting controls power to the heater cartridge. At the low setting, the source will operate at approximately 90°C. The high setting provides a 180°C source temperature more suitable for solids probe work. A vacuum interlock assembly from MIMS Technology Inc. was fitted to the side KF flange of the 5972. This completed the direct probe modification. Although source temperature is controlled externally, the actual source temperature can still be monitored through the MSD operating system. The modified 5972 was configured for membrane introduction mass spectrometry (MIMS) use. A 1900-C1 capillary membrane probe and FIA-TC1 flow injection module obtained from MIMS Technology Inc. was installed to complete the system as shown in the diagram.

The mass spectrometer was tuned with the membrane probe inserted and water running through the system. Volatile organic standards were prepared in laboratory de-ionized water at 0.5, 1, 5, and 10 parts-per-billion by weight. The four standards for each compound were injected into the 5972 MIMS system to assess linearity of response and detection limits. All of the compounds studied demonstrated good linearity over the concentration range that was used. Detection limits were good with many of them at or below one part-per-billion. A table of compounds studied and their detection limits was displayed.

This relatively simple modifications will allow the use of direct insertion probes in the Hewlett Packard 5971/5972 MSD. The present study demonstrated that the 5972 can perform very well in MIMS mode and future experiments are planned to investigate solids probe use.

5972 MIMS Instrument Diagram

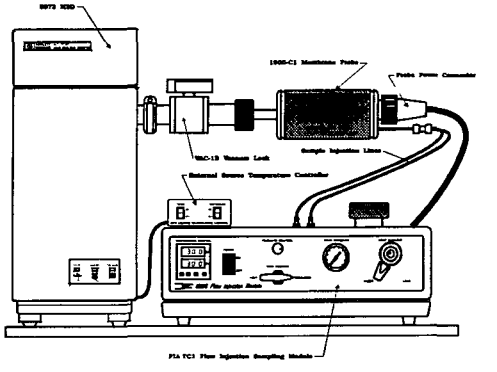

o-Chlorotoluene Analysis by HP 5972 MIMS

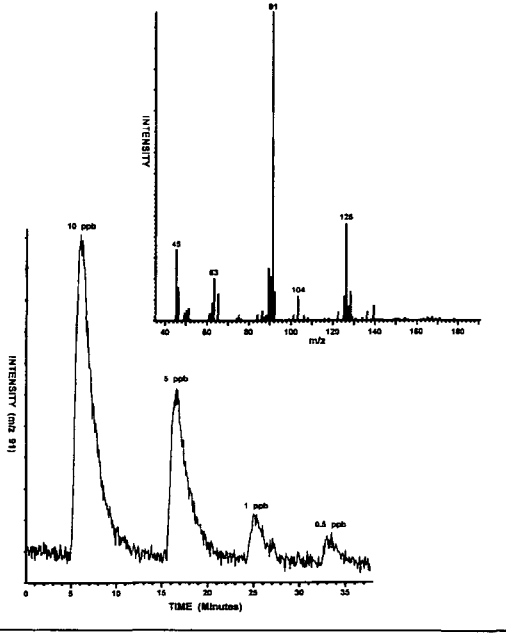

TWO VINTAGE QUADRUPOLE MASS SPECTROMETERS MODIFIED FOR COORDINATED PYROLYSIS-MS

Jon G. Wilkes[1], Kent J. Voorhees[2], James P. Freeman[1], Dietrich A. Volmer[1], and Jackson O. Lay, Jr.[1]

[1]FDA, National Center for Toxicological Research, NCTR Drive, Jefferson, AR 72079
[2]Colorado School of Mines, Golden, CO 80401

ABSTRACT

Two vintage quadrupole mass spectrometers were modified and upgraded to create an integrated system for identification of bacteria using pyrolysis mass spectrometry (Py-MS) with computerized pattern recognition. If, using one of the instruments, pyrolysis spectra of bacteria were produced that were essentially identical to those collected on the other instrument, the feasibility of Py-MS data bases for unknown identification would be demonstrated.

Modifications to both instruments included fitting them with flexible, mutually compatible data acquisition systems (Galaxy2000 by LGC, San Jose, CA), cold traps to reduce background, and 5 kV conversion dynodes for increased high mass sensitivity. A pyrolysate introduction system, including a probe vacuum lock and high temperature transfer line (350 °C), was developed which could be used on either instrument.

Comparison of calibration gas and Py-MS bacterial spectra both demonstrated the successful achievement of the goal.

INTRODUCTION

Pyrolysis mass spectrometry (Py-MS) with computerized pattern recognition (PRec) has been used successfully 1) for rapid identification of microbial agents responsible for infectious outbreaks in hospitals and also 2) for "fingerprinting" well-defined chemical mixtures to detect product adulteration. Particularly in the first case, production of sufficiently reproducible pyrolysate patterns has only been possible within batches: standard and unknown bacteria inoculated together on media from the same lot, cultured in the same incubator, and analyzed on the same day on the same pyrolysis mass spectrometer. These constraints significantly restrict potential large-scale implementation of the technique in a regulatory setting - screening for food-borne pathogens, for example, an application of particular interest to the FDA.

The cost/benefit relationship dictates both economy of design and high productivity to justify a high-tech solution involving mass spectrometry for such an analytical problem.

EXPERIMENTAL

Two older quadrupole mass spectrometers having significantly different secondary design features were available: a Finnigan-MAT (San Jose, CA) model 5100 GC/MS (1985) and a Vestec (Houston, TX) model 201 LC/MS (1985; quadrupole rods 1977). The differences between these two instruments presented substantial challenges to the goal of producing near-identical spectra. Once modifications were complete, the integrated use of the instruments was tested by comparing PFTBA calibration gas spectra (Table 1) and by performing Py-MS with PRec on bacteria. Species tested [and 1 digit symbols used in FIGURE 2] included *Shigella flexneri*(1), *Staphylococcus aureus*, *Pseudomonas*

fluorescens(3), *Bacillus cereus*(4), *Escherichia coli* 078:H11(6), *Salmonella typhimurium*(7), *Serratia marcescens*(X), *Bacillus circulans*, and *Mycobacterium pyr-1*(Z).

PYROLYSIS VACUUM INLET DESIGN/PERFORMANCE

Specifications for the heated transfer line included indefinite, stable operation at temperatures up to 340 °C with no cold spots, containment within a probe of no greater than 0.25" o.d., and sufficient length to be inserted into the vacuum manifolds of the 5100 or the 201 or (eventually) a Hewlett-Packard 5970 MSD.

The design adopted is shown schematically in Figure 1. Ceramic tubes served as electrical insulation between the probe shaft and transfer line. A thermocouple with fiberglass insulated leads was spot welded to the transfer line and read by a thermocouple thermometer. Also, the pyrolyzer sample probe was redesigned to traverse an upstream vacuum lock. *Results*: Temperature of the pyrolysate transfer line adjustable to 300 ± 1 ° C. The probe vacuum lock performed easily. Time/pyrolysis: < 4 min. [Compare 35 - 40 min. @ for a MIDI (GC-based) system.] Equipment acquisition and modification costs for the two mass spectrometers and the PRec system totaled only $98.2K

Figure 1.Pyrolysis-MS Vacuum Inlet System

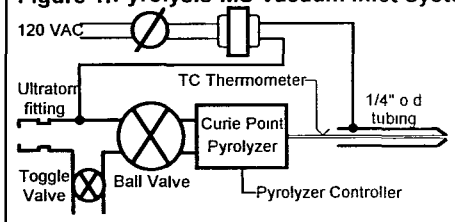

Figure 2.

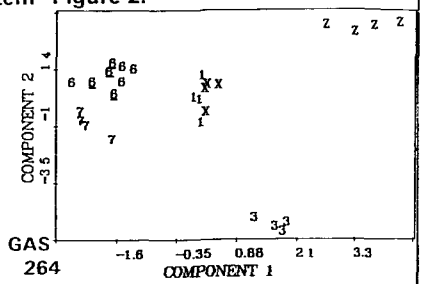

TABLE 1: PEAK RATIOS (%) FOR PFTBA CAL. GAS

MASS SPEC *m/z*→ ↓	69	131	219	264
5100	*100*	*41.60*	*63.76*	*16.15*
201 (autotune)	100	38.54	53.55	13.72
201 (manual tune)	*100*	*41.44*	*63.82*	*16.70*

PY-MS APPLICATION RESULTS

Bacteria were pyrolyzed on the 5100 and 201 with data subject to both Principal Component and Canonical Variate Analyses. Figure 2 is a discriminant component factor plot in which four replicates of each bacteria from the 5100 were used except for *E. coli* (symbol 6), with eight replicates. The four underlined symbols (6) came from 201 runs. The other four were from the 5100. *Results*: well-defined clusters for replicates in which the *E. coli* spectra from the different instruments were classified into the same factor space.

CONCLUSIONS

Py-MS with PRec is possible with coordination between different mass spectrometers and with operation on different days if there is sufficient instrumental and sampling control.

EXAMINATION OF A VARIETY OF SHEET MATERIALS FOR USE AS MEMBRANES IN MEMBRANE INTRODUCTION MASS SPECTROMETRY

Amy J. Maden‡ and Mark J. Hayward*
American Cyanamid - Agricultural Research Division
P.O. Box 400 - Princeton, NJ 08543-0400

Abstract: Several polymers including silicone, latex, PVC, Teflon®, polyurethane, polyimide, polyethylene, and nitrile have been utilized as membranes for membrane introduction mass spectrometry (MI/MS) in order to explore the relative performance of each material for MI/MS analyses. Each of the membrane materials were tested by exposing them to separate aqueous solutions containing the analytes benzene and ethanol in order to represent the results that may be achieved for environmental analyses and fermentation monitoring (respectively). These solutions were used to measure the relative analyte quantification limits, response times, and permeation of water as a function of temperature for each membrane material. It was observed that natural latex and polyurethane yield similar MI/MS performance characteristics (in aqueous matrix) to the commonly used silicone membranes for both benzene and ethanol solutions. Polyethylene was observed to work well with benzene as an analyte and simultaneously provides very high selectivity over water. While the other materials allowed aqueous matrix MI/MS to be performed, poor quantification limits or slow response times made these materials undesirable for this purpose. Two membrane materials which showed especially low organic permeability and higher water permeability, polyimide and Teflon, were briefly tested with polar analytes and non-polar solvent. For the polyimide material, the analytes acetone, acetic acid, chloroform, ethanol, ethylacetate, and water were readily observed in hexane solvent.

MI/MS Membrane Materials Which Yield Best Performance For Aqueous Matrix Samples

Performance Characteristic	[a]Fermentation Monitoring	[b]Environmental Analyses	Selectivity Over Water (30 °C)	Selectivity Over Water (60 °C)
[c]Membrane Materials Giving Best Performance	Polyurethane (ether) Latex Silicone	Silicone Latex Polyethylene Polyurethane (ether)	Latex Silicone	Polyethylene Silicone

[a]Based on quantification limits and response times for ethanol.
[b]Based on quantification limits and response times for benzene
[c]Listed in order of performance level with the best listed first.

‡*Visiting intern from Chemistry Department, Mount Holyoke College, South Hadley, MA .*
**Author to whom correspondence should be addressed.*

Table 2. MI/MS Characteristics at 60 °C for 10 membranes

Membrane Material	Ethanol Quantification limit[a] (ppm)	Ethanol Response Time[b] (sec)	Selectivity Ethanol[c]	Benzene Quantification limit[a] (ppb)	Benzene Response Time[b] (sec)	Selectivity Benzene[c]	Water Response[c]
Silicone	36	19	1.0	2.8	20	1.0	1.0
Latex (Flexam)	58	16	0.90	13	22	0.31	0.56
Latex (Hygenic)	32	19	0.90	56	23	0.031	1.1
Nitrile[d]	310	22	0.045	83	63	0.015	1.5
PVC	4200	82	0.011	1900	180	0.0019	2.0
Polyimide	180	120	0.082	not observed	not observed	not observed	0.27
Teflon	2600	550	0.013	13000	56	0.00020	2.4
Polyurethane (ether)	19	16	0.69	49	18	0.017	1.9
Polyurethane (ester)	19	16	0.96	60	22	0.029	1.4
Polyethylene	440	37	5.5	41	18	4.8	0.010

[a] Quantification limits are the concentration that yields S/N = 15 for a 200 µL injection into a 1 mL/min carrier stream of water
[b] Response times are measured as FWHM for a 200 µL injection into a 1 mL/min carrier stream of water
[c] Values are relative to those for the silicone membrane.
[d] Values are given for the 40 °C experiment. Nitrile is not mechanically stable at 50 °C and above

OPTIMAL DESIGN OF A MALDI TIME-OF FLIGHT INSTRUMENT FOR MS-MS OF PEPTIDES

J.B. Hoyes, J. M. Brown, R.H. Bateman, S.G. Curbishley
VG ORGANIC, Floats Road, Wythenshawe, Manchester, M23 9LZ, UK

Introduction A high performance MALDI-TOF instrument for MS and MS-MS of proteins and peptides has been designed and built. The TofSpec SE consists of a three stage source, gas cell for CID work, a Bradbury-Nielson ion gate for precursor ion selection and a single stage reflectron.

The source consists of a target sitting at the acceleration voltage of the instrument (up to 30 KV in linear mode and 26KV in reflectron mode), a field extraction electrode and a focusing lens for high ion transmission through the analyser. A high extraction field leads to high PSD yield with monoisotopic resolution possible on product ions, whereas lowering the extraction field reduces the PSD ion yield. A gas cell installed close to the ion source yields high energy CID.

A Bradbury-Nielson ion gate gives precursor ion selection for MS-MS operation with parent ion selection resolution in excess of 100 being achievable. The co-axial geometry coupled with a single stage reflectron gives high transmission and simple linear calibration law for product ions. Full product ion spectra can be taken with fewer voltage steps on the reflectron than with two stage "V" geometry designs.

Experimental To characterise the performance of the instrument a number of well characterised peptides were run. An example of the high resolution attainable on the daughter ions is show in figure 1 for a synthetic peptide MW 1498.7 (M+H = monoisotopic). Here two species differing by only two mass units the B10 and Y9 fragments are clearly resolved.The resolution is enhanced by using the ion gate to narrow the energy width of the parent (and associated fragments).

The PSD process generates fragment ion spectra that resemble those taken on triple-quadrupole instruments. The process is a function of both matrix and extraction field strength. Carr et al [TPG259 ASMS 95] have shown that the degree of CID with respect to PSD depends on the matrix choice.

A practical approach to observe CID is to allow the PSD process to occur and then to admit gas into the gas cell. Figure 2a shows a spectrum of the Glu-Fibrinopeptide-B under normal PSD conditions with the majority of ions being backbone cleavages more reminiscent of low energy collisions . Figure 2b shows a mass spectrum under the same voltage conditions as 2b but with the addition of air as a collision gas into the cell. It can be seen that new species are present in this spectrum, specifically side chain cleavages that are traditionally associated with the high energy collisions produced on magnetic sector instruments.

Conclusions A high performance MALDI-TOF machine has been developed with enough resolution to see single isotopes upto 3000 daltons. This means 1 Da differences such as would occur in a de-amidation reaction can be distinguished. PSD spectra +-0.1Da mass accuracy can be produced with parent ion selectivity sufficient to eliminate the sodium adduct at masses 2500Da (for example) permitting MS/MS on individual components in complex mixtures.A collision cell introduces high energy CID products that are superimposed on the low energy like PSD spectra. Switching between pure PSD and mixed PSD/CID modes is accomplished simply by turning the gas on and there is no need to recalibrate the instrument. For peptides the high energy CID process produces side chain cleavages that permit important differentiation between isobaric residues such as leucine and isoleucine.

43rd ASMS Conference on Mass Spectrometry and Allied Topics

PSD of Peptide MW 1498.7, Sequence AEGETTTFTALTEK

Figure 1.

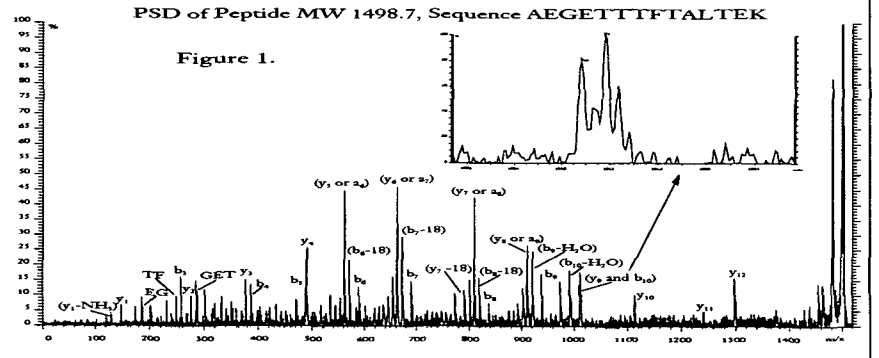

Post Source Decay of [Glu]fibrinopeptide - B

Figure 2.

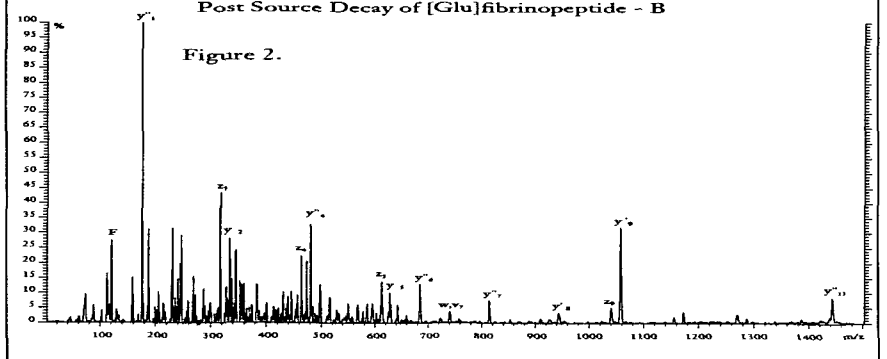

Post Source Decay + CID of [Glu]fibrinopeptide - B

Figure 3.

normal source extraction field

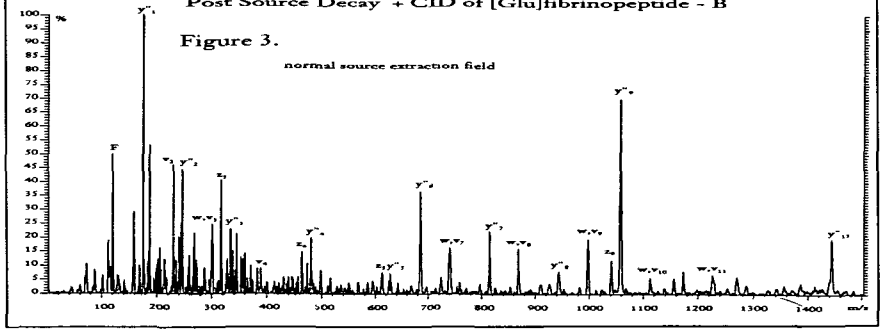

Modulated Sample Membrane Inlet MS: Theory and Practice

Fei Liu, Michael Davenport, and Christie G. Enke
Department of Chemistry, The University of New Mexico, Albuquerque, New Mexico 87131

Most membrane inlet work to date has employed steady-state diffusion through the membrane[1,2,3]. In order to utilize the diffusion coefficient (diffusivity) D as a distinguishable property of organic compounds, we have investigated modulated sample introduction.

We have developed a computer program to simulate the diffusion process through a membrane with a modulated sample stream. In our simulation, the motion of the alternating valve is modeled as, or close to, a periodic step function. The resulting diffusion flux profile for each component converges to a periodical function for which the time lag, shape, and magnitude are related to the diffusivity and concentration of that component[4]. The deviation between the flux profile obtained from our simulation and the results calculated from analytical solutions[5] for steady-state cases is within 2%. The shape of the flux profile, but not the magnitude is independent of membrane geometry. For the same membrane thickness and surface concentration, the diffusion through a flat sheet membrane gives a higher flux than that through a hollow fiber membrane where the diffusion in from the inside out The proportionality constant is 0.707 for 2:1 ratio of inner and outer diameters.

An experimental system to implement modulated sample introduction has been assembled. The membrane inlet is switched periodically between the sample and background streams. The sample components are detected by a Finnigan MAT Ion Trap Detector. A time-dependent response pattern, called a chronogram such as seen in the figure, is produced for each m/z value in the mixture spectrum. The profile of each chronogram depends on the concentrations and diffusivities of the components contributing to the response at that m/z value. The theoretical flux profiles and the experimental chronograms have been compared separately for the rising and falling edges using slightly different diffusivities for single m/z values and agreements have been reached. The difference in apparent diffusivities between sample turn-on and turn-off is due to a corresponding pressure change in our present apparatus. For multiple component sample, the significant difference has been observed among the channels to which only signal component contributes and those to which multiple components contribute.

Sample modulation and chronogram analysis provides a useful second dimension for mixture analysis. Although modulated sample introduction with the membrane provides less temporal separation than normal speed GC, the modulated membrane is simpler than

a GC and achieves faster update rates. Due to its simplicity and rapid update rate, the sample modulation at membrane inlet mass spectrometry should find useful applications for relatively simple mixture such as in process control.

We gratefully acknowledge Sponsorship of the U.S. Army Environmental Center, Interagency Agreement No. 1769-A073-A1, Under United States Department of Energy Contract DE-AC05-84OR21400 with Martin Marietta Energy Systems, Inc. and partial financial support from Dow Chemistry Company.

1 (a) Bier, M. E.; Cooks, R. G.; Tou, J C.; Westover, L. B. *U.S Patent* 4, **1989**, 791, 292.
(b) Bier, M. E.; Cooks, R. G. *Anal Chem.* **1987**, 59, 597.

2 LaPack, M. A.; Tou, J. C.; Enke, C. G.; *Anal. Chem.* **1991**, 63, 1631.

3 Cameron, D.; Hemberger, P.H.; Alarid, J. E.; Lerbman, C. P., and Williams, J. D.; *J Am Soc Mass Spectrum.* **1993**, 4, 774

4 Liu, F.; Enke, C., G.; submitted for publication.

5 Crank, J. *The Mathematics of Diffusion,* 2ed; Clarendon Press: Oxford, 1975, pp47-50.

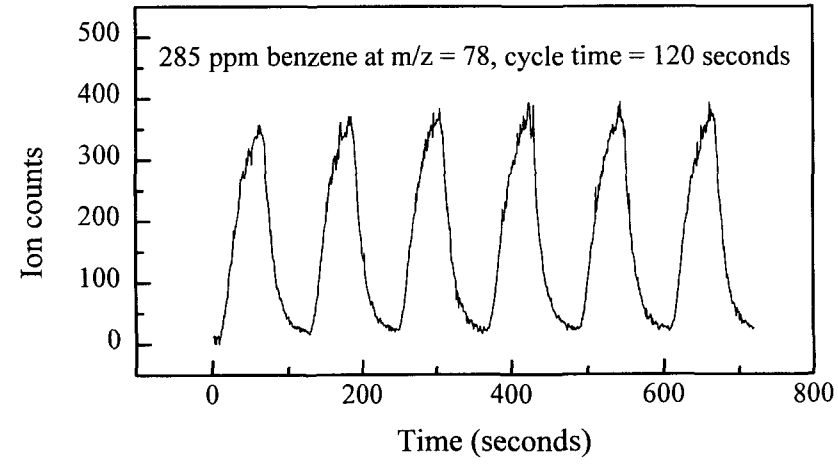

Ion storage study for a segmented-ring ion trap source for time-of -flight mass spectrometry

Qinchung Ji[1,3], M R Davenport[3], J F. Holland[2], and C G Enke[1,3]
Department of Chemistry[1], Department of Biochemistry[2], Michigan State University, East Lansing, MI 48824
Department of Chemistry[3], University of New Mexico, Albuquerque, NM 87131

For time-of-flight mass spectrometry (TOF-MS) analysis of continuously introduced samples, continuous ion generation and storage of ions between ion extractions is an effective method to achieve good sample utilization efficiency [1,2] We are developing a segmented-ring ion trap source for time-of-flight mass spectrometry to achieve ion storage without losing the resolution and spectrum generation rate of conventional TOF-MS[3] During the ion extraction period, a linear, uniform extraction field is generated in this source by applying a set of dc voltages proportional to the positions of the ring and extraction electrodes Between ion extractions, ions will be accumulated and stored in this ion source by applying radio frequency (rf) field between the rings and caps

A time-of-flight mass spectrometer with this segmented-ring ion trap source has been constructed. This instrument is composed of a segmented ring ion storage source, a broad energy range reflectron and a microchannel plate detector Electron impact ionization is used to generate sample ions inside ion source Ion storage is evaluated by measuring the ion peak area for various values of the delay time between sample ionization and ion extraction When operated without an rf field applied to the ring electrodes of the segmented ring ion storage source, 85% of $[CH_3C{=}O]^+$ ions generated in the ion source remain there for 1 4 μs based on their thermal velocity and the physical dimensions of the ion source As shown in Figure 1, only 10% of the ions will remain 4 6 μs after ionization has ceased For continuously introduced samples, and a 200 μs extraction cycle time, 99% of the sample ions will lost between extractions. Enhanced ion storage is obtained when the rf field is applied to this segmented-ring ion trap storage source between ion extractions The peak area profile in Figure 2 shows that $CHCl_2^+$ ions are stored efficiently for at least 12 μs when an rf field is applied Lower mass ions are removed for delay times of 500 ns and 12 μs due to the dc offset, frequency, and amplitude of the rf applied as shown in Figure 3 This demonstrates the possibility of selective ion storage. Extensive collisional cooling is not required to achieve either ion storage or good mass resolution as the $CHCl_2^+$ ion peaks in the spectra is unchanged from 500 ns to 12 μs storage The ability to extract ions without delay allows frequent ion extraction (2500 Hz) and thus greatly improves ion statistics

Rf operation of the segmented-ring ion source acts as a kind of cylindrical ion trap between ion extractions This ion trap source is providing efficient, long term storage of ions generated in the source as well as good resolution with frequent extraction The development of this approach to TOF-MS source design should greatly improve sample utilization efficiency for analysis of gaseous samples by time-of-flight mass spectrometry.

[1] Grix, R , Gruner, U ; Li, G , Stroh, H, Wollnik, H , Int J Mass Spectrometry and Ion Process, 1990, 96, 267-274
[2] Michael, S M , Chen, B M ; Lubman, D M Anal Chem , 1993, 65, 2614-2620
[3] Ji, Q , Vlasak, P R., Holland, J. F , Enke, C G., ASMS, Chicago, 1994

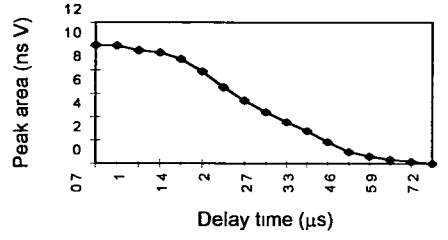

Figure 1. Peak area of $[CH_3C{=}O]^+$ ion vs delay time without rf field

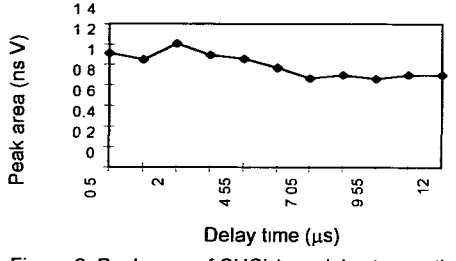

Figure 2. Peak area of $CHCl_2^+$ vs delay time with rf field

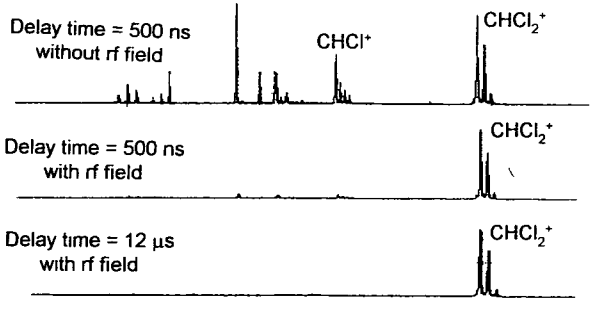

Figure 3 The mass spectra of $CHCl_3$

A new design of Ion Storage Accelerator for Time–of–Flight MS

A. Kraft, H. Wollnik
II.Physikalisches Institut, Justus–Liebig–Universität, 35392 Giessen,Germany
V. Laiko, A.F. Dodonov
Institute of Energy Problems of Chemical Physics, Russian Academy of Sciences, 142432 Chernogolovka, Russia

A new Time–of–Flight MS (fig.1) for orthogonal extraction has been constructed. It consists of a API–source, the orthogonal extraction optic and a single stage reflectron as well as a detector with two MCP's in Chevron–arrangement. The extraction optic has a new design in respect to the prevention of disturbing fields. Such fields take influence on the primary beam during accumulation mode and causes noise as well as broadening of mass peaks. This fields arises from the penetration of field through the grid between the two stages of the extraction optic. In our construction these penetration is compensated by the introduction of an additional electrode which is hold at the average virtual potential of the separation grid (fig.2).
By adjusting all electrical parameters of the mass spectrometer (extraction-pulser, backplane of reflector, focussing optics) the peakwidth had been otimized. It has been shown that the peakwidth strongly depends on the potential of the compensation electrode (fig.3). The optimal value corresponds in good agreement with the calculated value (1.7V instead of 1.56V).
In the case of Gramicidin S (m=1140) a resolving power of 2000 is achieved (fig.4).

[1] : A.F. Dodonov, I.V. Chernushevich and V.V. Laiko
in "Time-of-Flight Mass Spectrometry"
Ed. R.J. Cotter, ACS Pubs. 1994, p.108

[2] : V.V. Laiko and A.F. Dodonov
Rapid Communications in Mass Spectrometry , Vol.8, 720–726(1994)

[3] : I. Chernushevich, A. Verentchikov, K.G. Standing and W. Ens
42nd ASMS Conference on Mass Spectrometry

[4] : K.G. Standing, I. Chernushevich, W. Ens and A. Verentchikov
42nd ASMS Conference on Mass Spectrometry

43rd ASMS Conference on Mass Spectrometry and Allied Topics

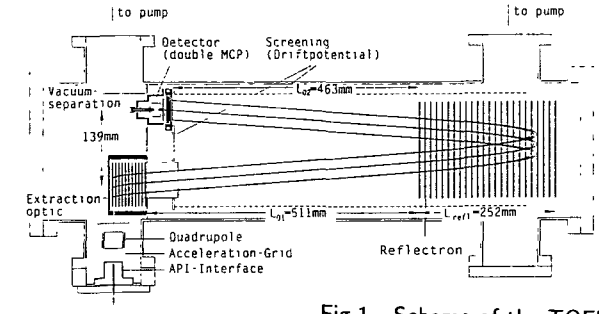

Fig.1 Scheme of the TOFMS

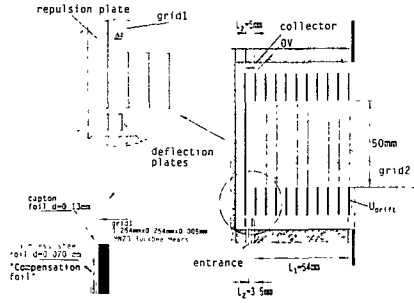

Fig.2 Scheme of the extraction optics

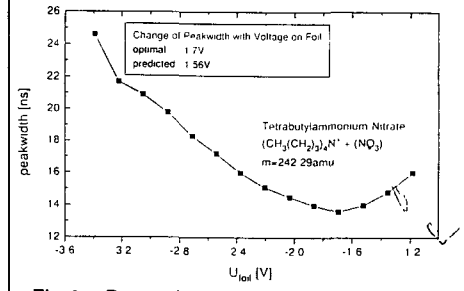

Fig.3 Dependence of the peakwidth on the compensationvoltage

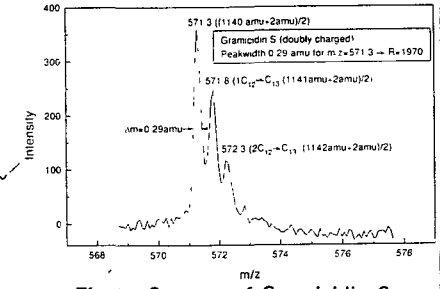

Fig.4 Spectra of Gramicidin S

A New MALDI Tandem QUISTOR, Time-of-Flight Mass Spectrometer

Markus Stoeckli, Peter Kofel, Joern Krause, Urs P. Schlunegger,
Institute of Organic Chemistry, University of Berne, Freiestr. 3, CH-3012 Berne, Switzerland

Matrix-assisted laser desorption/ionization (MALDI) is a powerful technique to get molecular ions of large molecules. Because of the pulsed nature of the ionization process, mass analysis is best done with an analyzer capable to accept a broad range of m/z values simultaneously. Especially suited to this need are time-of-flight, ion trap and ICR instruments. For the standard MALDI/time-of-flight system mass resolution is low and few structural information is obtained [1,2]. To gain more insight into and possibly overcome these limitations we have constructed a new MALDI/QUISTOR/time-of-flight instrument.

The instrument is built around a QUISTOR (QUadrupole Ion STORage trap) with 1 cm ring electrode radius (same design as [3]). The trap is placed inside an ultra-high vacuum system with a 100 cm flight tube. The design of axial ion production allows to operate the instrument also in direct linear time-of-flight mode, which is useful for control and tuning purposes.

Samples were prepared by mixing on a stainless steel probe tip 0.5 µl of a 0.5 mM aqueous solution of the proteins with 0.5-1.0 µl of a 1 M solution of the matrix in a 1:1 acetonitrile /ethanol mixture, followed by rapid drying in vacuum. Using this procedure a total amount of 250 pmol of sample was deposited on the probe tip, which lasted for up to 1000 laser shots. The probe was inserted into the instrument, the probe tip parked at the QUISTOR end cap and the probe removed. Then the trap was floated to 1.5 kV, and the rf voltage (20 to 200 V, 50 kHz) was applied to the ring electrode of the trap.

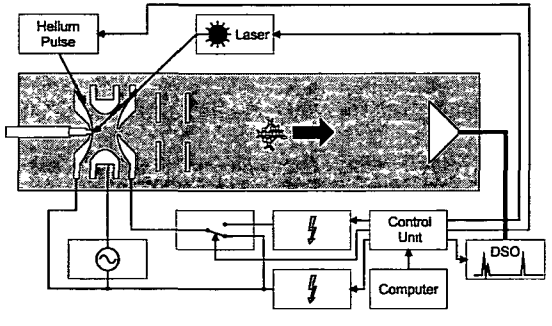

The experiment is characterized by a pulse sequence from a purpose built control unit. Helium was pulsed in for 1 ms to a peak pressure of $>10^{-2}$ Pa. 1 ms later the nitrogen laser was fired. After 1 s for collisional cooling the *extraction end cap was pulsed to* 1.3 kV for time of flight analysis of the stored ions. 20 kV post-acceleration and averaging on a digital storage oscilloscope (1000 sweeps) were used for ion detection.

Sensitivity and resolution were found to be strongly dependent on the phase angle of the laser shot and the extraction pulse, buffer gas pressure, storage time and extraction amplitude. Good sensitivity and resolution were always obtained when both the laser shot and the extraction were done at 270 deg, i.e. when the maximum negative amplitude was at the ring. The longer the ions are stored, the better the resolution gets. The initial axial spread of the ions in the QUISTOR can be time focussed by tuning the extraction amplitude. Further examination of this effect may allow to improve the limited resolution obtained so far.

[1] Chambers et al., Anal. Chem. 65, 14 (1993).
[2] Michael et al., Anal. Chem. 65, 2614 (1993).
[3] Kofel et al., Org. Mass Spectrom. 26, 463 (1991).

In contrast to earlier predictions the results prove that large mass ions may be trapped with very small trapping fields (as low as 20 V amplitude on the ring electrode and trapping well depths down to 1 eV), as long as the frequency is suitably adjusted. At least a significant part of the molecular ions produced by MALDI are trapped intact in the QUISTOR. Comparison with measurements in the direct linear mode suggests that the observed molecular ions are identical. At q_z values around 0.5 the ions can be stored in the trap for several minutes. During storage clustering reactions of Melittin ions with background DHB matrix molecules have been observed. This may open the possibility for selective determination of specific functional groups by ion/molecule reactions.

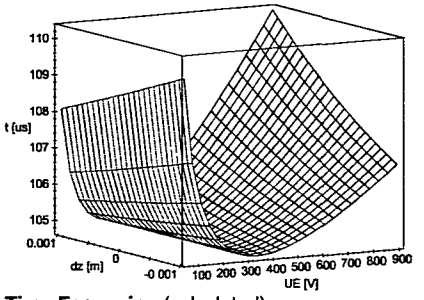

Time Focussing (calculated)

Calculated time of flight t for an ion with m/z 2'846 in dependence of the extraction voltage UE and the distance dz from the trap center. For UE ≈ 200 V all the ions have nearly the same time of flight independent of their initial *dz-location in the trap.*

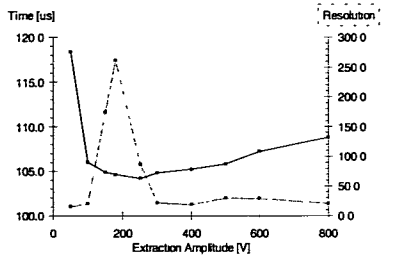

Time Focussing (measured)

Measured time of flight (solid line) and time resolution (dotted line) for m/z 2'846 as a function of the extraction amplitude. By combining these data with the calculation results (see at left), the axial spatial distribution of the ions at the start of extraction was calculated to be dz = +/- 3 mm.

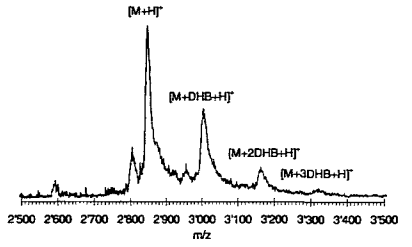

Melittin from honey bee venom (MW 2'846.5)
Matrix: DHB; trapping voltage: 40 V.

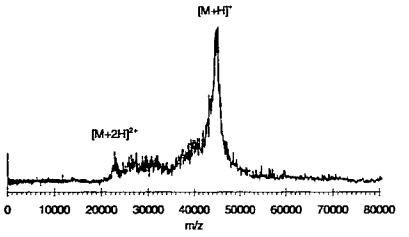

Albumin from chicken egg (MW ~45'000)
Matrix: Sinapic acid; trapping voltage: 180 V.

Financial support from Ciba-Geigy Corporate Analytical Research and the Swiss National Science Foundation is gratefully acknowledged.

A NEW LC ELECTROSPRAY ION TRAP TIME-OF-FLIGHT MASS SPECTROMETER

Alex Mordehai, Joe Karnicky, Béla Limbek, and S. E. Buttrill, Jr.
Varian Associates - Ginzton Research Center
3075 Hansen Way, Palo Alto, CA 94304-1025

The recent work by David Lubman and his students [1] has highlighted the advantages of the ion trap time-of-flight (IT TOF) mass spectrometer. This arrangement has high sensitivity because of its large duty factor. When ion currents are weak, ions may be accumulated in the trap for 100 milliseconds or longer. The ions are then pulsed out into the TOF for mass analysis, which typically requires less than 200 microseconds. The duty factor for mass analysis and detection of all ions from a continuous ion source can therefore in principle be greater than 99%. In practice, the time for ion cooling in the trap and the reset time for the electronics limits the duty factor to about 95%. The purpose of this project is to explore the potential of IT TOF MS, and especially its suitability for electrospray LC/MS.

Our system uses pneumatically assisted electrospray (ion spray) together with a two stage differentially pumped API interface with a heated stainless steel capillary. The ion trap reflectron time-of-flight mass spectrometer was purchased from R. M. Jordan Co., Grass Valley, CA and uses a 20 mm two stage microchannel plate detector. The 500 megasample per second transient digitizer is a Model 9846-500 from Precision Instruments.

We have found that the performance of the IT TOF can be improved by using a symmetrical or nearly symmetrical pair of extraction voltage pulses applied to the ion trap end caps. The two plots below from a SIMION analysis of the ion trajectories shows that the beam quality with symmetrical extraction is much better than with the use of a single pullout pulse. Use of a push out pulse results in a diverging ion beam (not shown).

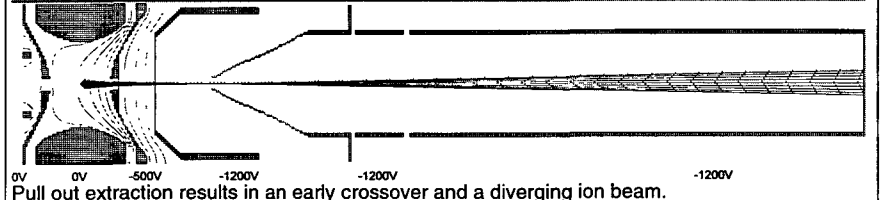

Pull out extraction results in an early crossover and a diverging ion beam.
Contours shown at -10, -100, -200, -300, -400, -600, -800, and -1000 volts.

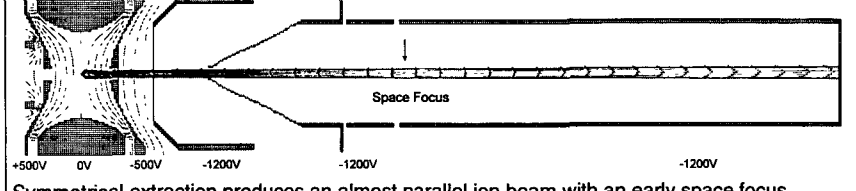

Symmetrical extraction produces an almost parallel ion beam with an early space focus.
Contours shown at 400, 300, 200, 100, 0, -100, -200, -300, -400, -600, -800, and -1000 volts.

The performance of the LC/MS system is shown below. A 15 pg sample of reserpine was injected using a 5 microliter injection loop. The mass chromatograms and the Total Ion Current plot were obtained from the mass spectral peak areas. The raw data for the scan at the top of the reserpine LC peak are shown on the right. The 15 pg injection contains about 10 pg of pure C12 reserpine, about 4 pg of reserpine C13 and less than one pg of reserpine with two atoms of C13 at m/z 611.

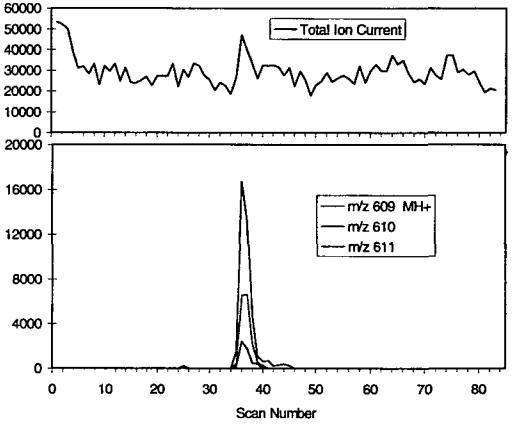

LC column: 2.1 mm i.d. C8
Flow rate: 0.20 ml/minute
75% acetonitrile: 25% water
0.1% acetic acid
20 mM ammonium acetate

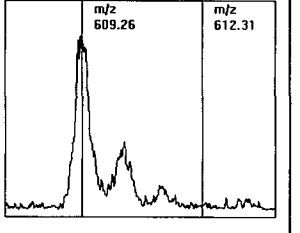

Raw data from scan 36

Mass resolution of over 2200 FWHH is shown below for the bradykinin MH+ ion at m/z 1060 and the sodium ion adduct peak at m/z 1082.

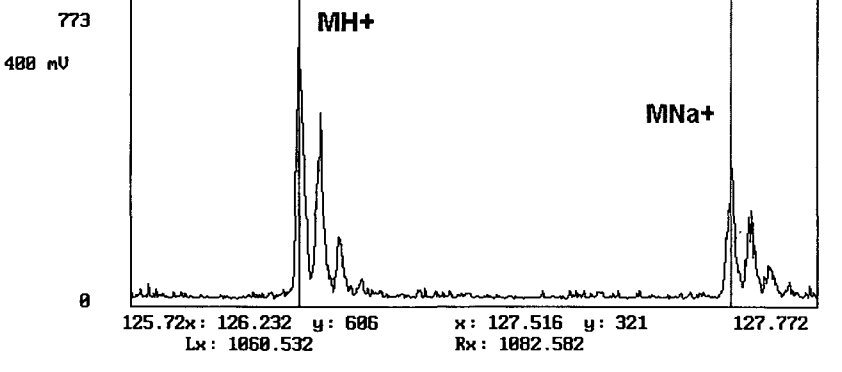

[1] Benjamin M. Chien, Steven M. Michael, and David M. Lubman, 'The design and performance of an ion trap storage-reflectron time-of-flight mass spectrometer,' Int. J. Mass Spectrom. Ion Processes 131 (1994) 149-179 and references therein.

MALDI-TOF/TOF of peptides: Past, Present and Future.

Cordero M.M.; Cornish, T.J.; Cotter, R.J.
The Johns Hopkins University School of Medicine, Baltimore, MD 21205

The ability to perform *high* energy collisional-induced dissociation (CID) in a low-cost, compact instrument is very appealing. Recently this laboratory has produced several versions of an instrument that combines MALDI with CID: a tandem time-of-flight mass spectrometer.[1] An overview of its performance is presented here.

The initial instrument design contained two linear reflectrons: one for mass selection and the other for product ion dispersion. A pulsed valve introduced He required for the CID process. A nitrogen laser was used for ionization. CID results for dermorphin and Met-enkephalinamide, among others, indicated that *only* those ions close in mass to the precursor ion achieve maximum resolution at the position of the detector. A new version of the instrument was built incorporating a curved field reflectron (CFR) which energy focuses all ions to within a small region near the detector. (Fig. 1) A striking improvement in the resolution was noted when using the CFR to disperse CID products.

CID mass spectra obtained for RYLGYLE and FERFEIFPKE (Fig. 2) presented many sequencing ions. These peptides, however, were difficult to detect at low concentration due to loss of sensitivity by metastable decay of the precursor.

As expected, post-source decay (PSD) MS obtained with a coaxial curved field reflectron TOF-MS also developed in this laboratory [2] gave both higher sensitivity and resolution for the same peptides. (Fig.3)

The next generation of MALDI-TOF/TOF will probably have:
i) A shorter first reflectron and drift region, to minimize metastable decomposition of the precursor ion.
ii) A coaxial curved field reflectron to energy-focus the product ions and maximize ion transmission.

(1) Cornish, T.J.; Cotter, R.J. *Rapid Comm. Mass Spectrom.* **1993**, 7 1037-140 and references therein.
(2) Cornish, T.J.; Cotter, R.J. *Rapid Commun. Mass Spectrom.* **1994**, 8, 781-785

43rd ASMS Conference on Mass Spectrometry and Allied Topics

Fig.1

MALDI-TOF/TOF ver. 2

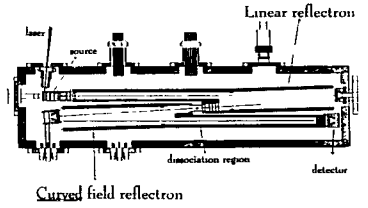

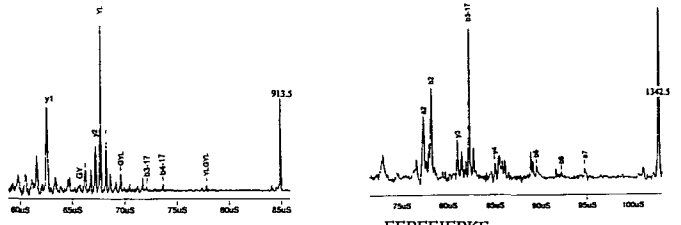

RYLGYLE (α–casein frg.90-96)
matrix: α-cyano-4-hydroxycinnamic acid
1 nmol, 369 shots

FERFEIFPKE
matrix: α–cyano-4-hydroxycinnamic acid
1 nmol, 569 shots

Fig. 2 CID (He) MS spectra

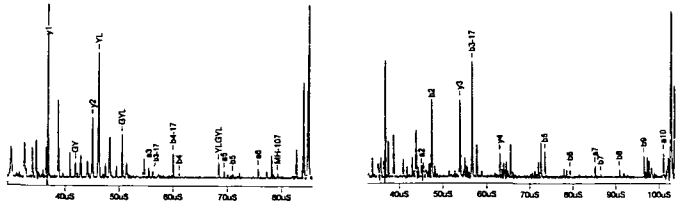

RYLGYLE (a-casein frg.90-96)
matrix: α-cyano-4-hydroxycinnamic acid
3 pmol, 500 shots

FERFEIFPKE
matrix: α-cyano-4-hydroxycinnamic acid
300 fmol, 400 shots

Fig. 3 PSD MS spectra

PROGRESS IN THE DESIGN OF A CONTINUOUS FLOW - MALDI INTERFACE OF A TOF - MS

Gabriela Grigorean, *John Wronka, *Charles Martin, *Frank Laukien, I Jonathan Amster
Department of Chemistry, University of Georgia, Athens, GA 30602
*Bruker Instruments, Inc., Billerica, MA, 01821

Laser desorption of proteins and peptides using liquid matrices is an alternative strategy to conventional MALDI experiments Previously we have reported use of binary liquid matrices for which a light absorbing molecule is mixed with a vacuum compatible liquid matrix [1] Light absorber molecules like Rhodamine 6G, sinapinic acid and alpha-cyano-4-hydroxy cinnamic acid have been used successfully These experiments were performed in a static fashion, where the analyte - liquid matrix droplet was placed on a stainless steel probe surface and introduced in a TOF. Recently we began investigating dynamic liquid MALDI, where both the analyte and the matrix are continuously introduced in the TOF Our goal was to develop an interface which will couple the technique of capillary electrophoresis to TOF-MS So far, well-known developments in CE-MS interfacing have been based either on electrospray ionization or CF-FAB The main advantages of using a TOF as a CE detector is that (theoretically) there is no upper mass limit for analytes, and that much higher scan rates can be used

The interface we have constructed, Fig 1, consists of a metal cylinder housing two fused silica capillaries, 15 µm i d , one for the introduction of a liquid matrix and the other for the introduction of the analyte The capillaries are attached with epoxy onto the back of a stainless steel probe and terminate flush with the probe surface, where the sample and matrix mix The interface fits the standard vacuum interlock of a Bruker Reflex TOF, and the probe tip makes electrical contact with the acceleration plate We have examined a number of experimental parameters, including matrix viscosity, capillary diameter, flow rates of the matrix and the analyte, and composition of the binary matrix mixture Alpha-cyano-4-hydroxy cinnamic acid was found to perform better for these experiments than sinapinic acid. With it, we obtained better resolution, increased sensitivity and reduction of capillary clogging. To maintain low pressures in the TOF, we originally used glycerol as the liquid matrix Memory effects were observed, thus we eliminated glycerol, the present working matrix consists of water / acetonitrile / TFA saturated with alpha-cyano-4-hydroxy cinnamic acid

Shown in Fig 2 are spectra of bradykinin and insulin, $1x10^{-10}$ mol/µl, in reflectron mode Flow rates into the TOF are 1 5 µl/min for matrix and 100 nl/min for analyte The bradykinin resolution in linear mode is 130, in reflectron 368 Adduct formation observed in such techniques as aerosol MALDI [2] are not present here Limit of detection was $1x10^{-11}$ mol/µl for bradykinin At this concentration the insulin peak did not appear due to supression effects Currently, we are investigating the use of the analyte delivery capillary as a capillary electrophoresis column for performing CE - MALDI mass spectrometry

REFERENCES

1. Cornett, S D., Duncan M. A , Amster I J , *Anal. Chem* 1993, **65**, 2608
2 Murray, K. K , Lewis, T M , Beeson, M. D ; Russel, D H , *Anal Chem.* 1994, **66**, 1601.

43rd ASMS Conference on Mass Spectrometry and Allied Topics

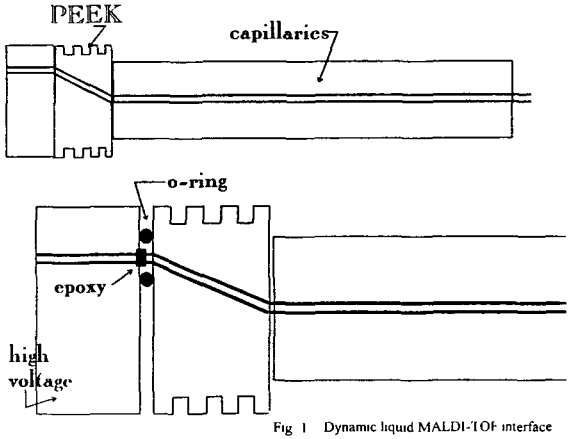

Fig 1 Dynamic liquid MALDI-TOF interface

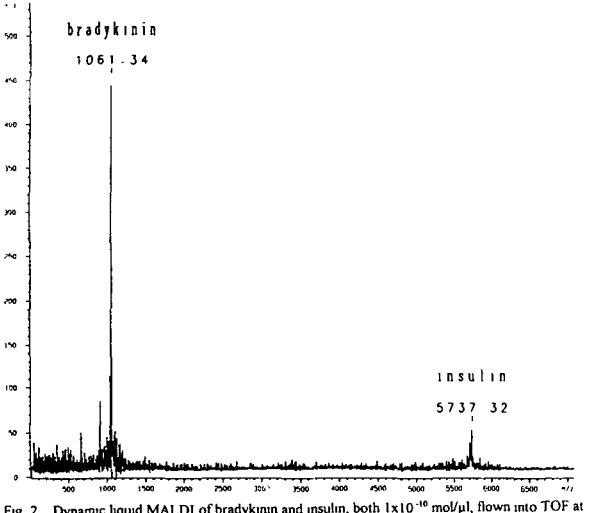

Fig 2 Dynamic liquid MALDI of bradykinin and insulin, both $1x10^{-10}$ mol/µl, flown into TOF at 100 nl/min Matrix water/acetonitrile/TFA saturated with alpha-cyano-4-hydroxy cinnamic acid, flown in at 1 5 µl/min

An Inverted Perfectron Electrospray/Orthogonal TOF Mass Spectrometer and On-Line Analysis with Capillary Electrophoresis

Q. Gao, A. L. Rockwood, H. R. Udseth, J. C. Follansbee,
J. C. Severs, D. C. Muddiman and R. D. Smith

Chemical Sciences Department
Pacific Northwest Laboratory, Richland, WA 99352

Based on the principle of "inverted perfectron"[1], we have designed and constructed [2] an electrospray ionization (ESI) orthogonal time-of-flight mass spectrometer. Ions are injected into the mass spectrometer orthogonal to the ion flight-path. A novel "beam dump" for the molecular beam permits large loading of ion beams while maintaining high vacuum in the flight tube. Using a molecular beam to introduce a well collimated ion beam minimizes the degradation of the theoretically perfect focusing of the "inverted perfectron" geometry. An extremely large detector (20 cm x 8 cm multichannel plates) permits the efficient acceptance of the ion packet and drift compensation. A novel detection system consisting of opto-electric coupling of the floating detectors (10 kV) and a custom data system designed in conjunction with Sensar (Salt Lake City, Utah) permit high sensitivity, high resolution and fast data acquisition of either positive or negative ion signals.

Preliminary results indicate an instrumental resolution of ~ 930 at m/z~2045 (Fig. 1a) for lyzozyme (egg white) 7+ charge state and a signal-to-noise ratio of ~ 50 for single-shot spectrum of Angiotensin I at 200 pmole/μL concentration (Fig. 1b). For the latter, the sample consumption is about 300 attomoles and the acquisition time is about 300 μs. Furthermore, capillary electrophoresis has been coupled with the inverted perfectron TOF instrument. A model mixture system of neurotensin, angiotensin I and mellitin (Fig. 2) was analyzed successfully demonstrating the potential of TOF-MS for on-line fast separation analysis.

Acknowledgments: We thank Mr. J. Price and Dr. A. Proctor for their technical help. Pacific Northwest Laboratory is operated by Battelle Memorial Institute for the U.S. Department of Energy, through Contract No. DE-AC06-76RLO-1830

1. A. L. Rockwood, Proc. 34th Annu. Conf. Mass Spectrom. & Allied Topics, 1986, Cincinnati, Ohio, p173.
2. A. L. Rockwood, H. R. Udseth, Q. Gao and R. D. Smith, Proc. 42nd Annu. Conf. Mass Spectrom. & Allied Topics, 1994, Chicago, Illinois, p1038.

43rd ASMS Conference on Mass Spectrometry and Allied Topics

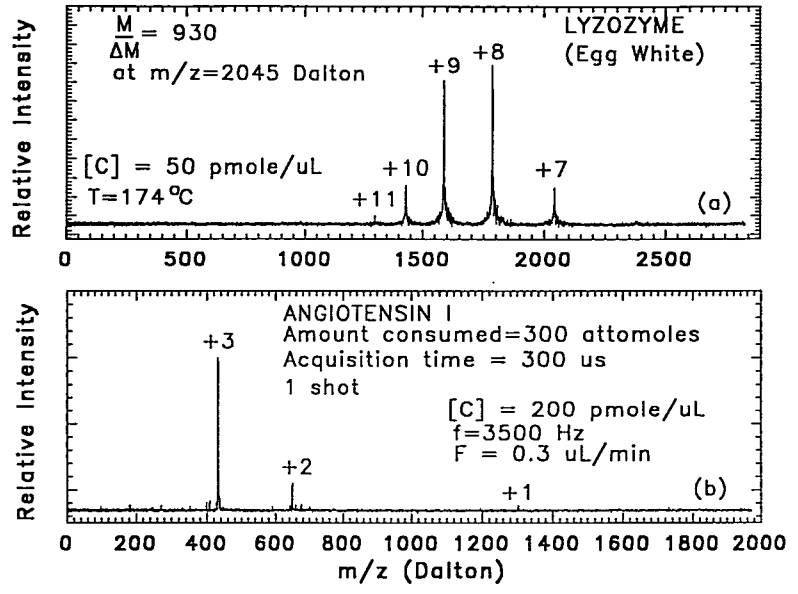

Fig. 1 Orthogonal ESI–TOF–Mass Spectra

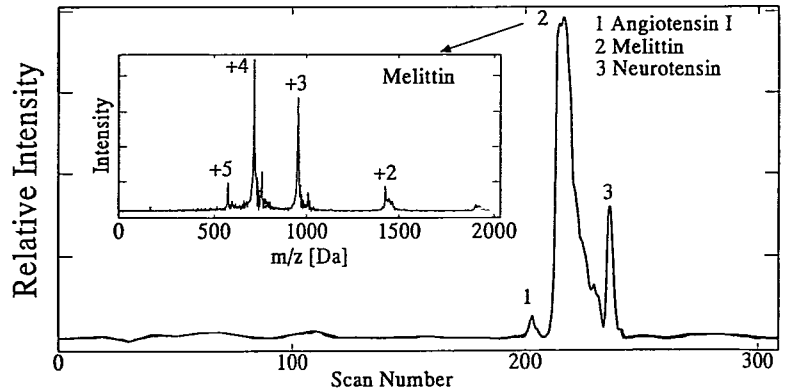

Figure 2: Capillary Electrophoresis Electrospray Ionization Time-of-Flight Mass Spectrometry

Collisional Focusing of Ions in the Electrospray TOF Mass Spectrometer.

A. N. Krutchinsky, I. V.Chernushevich, V. Spicer, W. Ens and K.G. Standing.
Physics Department, University of Manitoba, Winnipeg, Canada R3T 2N2

The formation of a beam of electrosprayed ions is a very important process in any gas-dynamic interface. While undergoing expansion into a vacuum with subsequent acceleration by the declustering potential, the ions acquire large velocities and spatial dispersion, i.e. they occupy a large volume in phase-space. However, it is possible to improve the ion beam quality by subsequently passing the ion beam through an RF quadrupole or sextupole operating at relatively high pressure [1,2]. Collisions with molecules of the buffer gas damp the velocities of ions, while the RF field constrains them close to the axis of the quadrupole.

We have redesigned the previous ES gas-dynamic interface for orthogonal ion injection into our TOF III mass spectrometer [3] and installed a new section containing a small RF quadrupole. The schematic diagram of the ion source interface is shown in Figure 1. The new section is evacuated by a 30 l/s Leybold mechanical pump. The small diameters of the skimmer orifices (0.35 mm for s1 and 0.75 mm for s2) are sufficient to keep the pressure at ~ 0.1Torr in the quadrupole and at $2x10^{-7}$ Torr in the main chamber of the TOF III. The quadrupole rods are driven by a small sine-wave signal generator coupled through an ENI broadband RF power supply providing operating frequencies from 100 kHz to 2 MHz and output voltages from 0 to 750 volts peak-to-peak.

The RF quadrupole has significantly increased the sensitivity of the TOF III mass spectrometer. Figure 2 shows a spectrum of soybean agglutinin (SBA, M.W. ~ 116,000u) recorded in 10 seconds, using a conventional electrospray technique; 120 femtomoles of the sample was consumed. Much higher sensitivity for the same sample (in the attomole range [4]) was obtained using the nanospray technique [5].

The new interface allows us complete control over the energy of the orthogonally injected ions by applying the appropriate potential to the second skimmer, whereas previously this energy depended strongly on *m*, *m/z* and the declustering potential. A numerical simulation performed by our group to study the operating principles of the quadrupole verify the phase-space reduction. This provides a number of advantages in instrument performance. Figure 3 shows the deconvoluted mass spectrum of bovine insulin (average M.W. 5733.58u), demonstrating that a resolution of ~ 10,000 can be achieved when no deflection potential is required to steer the orthogonally injected ions to the detector. Figure 4 shows the spectrum of a mixture of four compounds, Substance P (M.W. =1346.74u, molar concentration 1 μM), Cytochrome C (12,360u, 1 μM), SBA (~116,000u, 3 μM) and Catalase HP II (~ 339,100u, 5 μM), which was prepared in a water/0.08% acetic acid solution. The spectrum reveals no mass discrimination over a wide range of m/z.

1. Douglas, D. J., French, J. B. *J. Am. Soc. Mass Spectrom.* 1992, **3** 398-408.
2. Xu, H. J. *et al*, *Nucl. Instrum. and Meth.* 1993, **A333**, 274-281.
3. Verentchikov, A. N. *et al*, *Anal .Chem.* 1994, **66** 126-133.
4. Chernushevich I. V. *et al*, 43rd ASMS Conference, FOD 10:30.
5. Wilm, M. S. and Mann M. *Int. J. Mass Spectrom. Ion Processes* 1994, **136** 167-180.

43rd ASMS Conference on Mass Spectrometry and Allied Topics

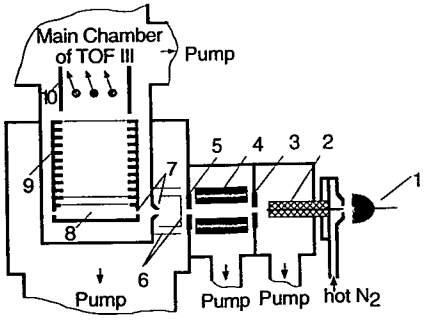

1 - electrospray source
2 - heated metal capillary
3 - skimmer 1
4 - RF quadrupole
5 - skimmer 2
6 - grids
7 - slits
8 - ion storage region
9 - accelerating column
10 - deflection plates

Fig. 1. Schematic diagram of the ion source interface.

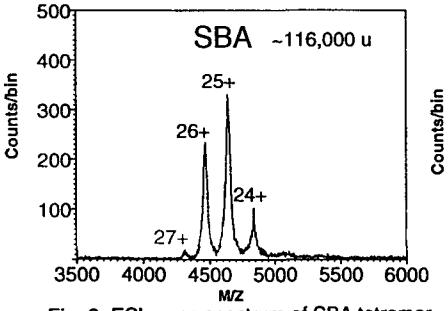

Fig. 2. ESI mass spectrum of SBA tetramer (M.W.~ 116,000 u) recorded in 10 s, 120 fmole of the sample consumed.

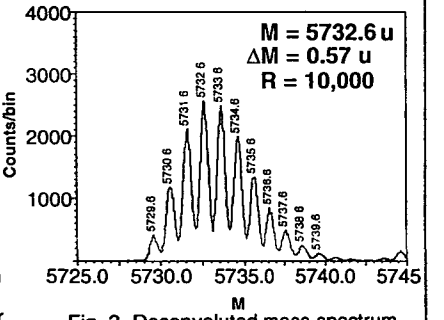

Fig. 3. Deconvoluted mass spectrum of bovine insulin with partially resolved isotopic peaks.

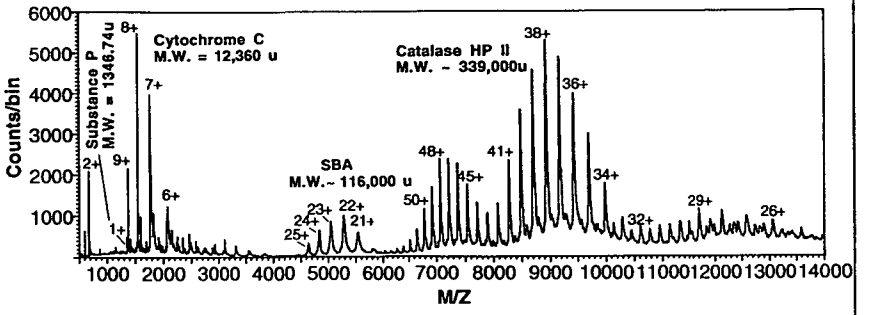

Fig. 4. The mass spectrum of a mixture of four compounds: Substance P, Cytochrome C, SBA tetramer and Catalase HP II tetramer prepared in water/0.08% acetic acid.

THE LASER IONIZATION GC-TOF/MS ANALYSIS OF ORGANOMETALLICS

Steven M. Colby, Kent H. Hanser, William A. Harris, and James P. Reilly
Dept. of Chemistry, Indiana University, Bloomington, IN 47405

In previous work we illustrated the sensitivity of laser ionization GC-TOF/MS by demonstrating a detection limit of 1.5 fg for tetraethyltin[1]. In this method ultra-violet laser light is used to atomize organometallic compounds eluting from a gas chromatograph and ionize the atomic fragments. The ions are then detected using a time-of-flight mass spectrometer. The method was primarily limited by the relatively small duty cycle of the laser. As a consequence of the short (8 ns) laser pulse only a fraction (~ 1 in 10^5) of the GC effluent was exposed to light. Two approaches to increasing sensitivity have recently been examined. The first involves a TOF/MS source in which the GC effluent was partially confined and therefore had more than one chance to pass through the laser beam[2]. While this method increased the signal obtained from concentrated samples (e.g. 10 pg in 1 µl), sensitivity to more dilute samples was not enhanced because the GC carrier gas was also confined. The He or Ar gas increased the pressure in the source region and became the source of a large number of ions produced by photoemission electron impact ionization[3].

A second approach to increasing sensitivity has been more successful. As illustrated in Figure 1 it employs a cryogenically cooled 12 cm diameter drum to trap the analyte as it exits the GC column. The drum rotates so that the sample is transported into the source region of the TOF/MS where it is laser desorbed and ionized. The advantage to this approach is that most of the analyte is trapped on the drum and then exposed to the laser while the nitrogen carrier gas is not trapped on the liquid nitrogen cooled surface. We are thus able to increase the interaction of the ArF laser with the analyte while reducing the concentration of carrier gas within the ionization region.

An important aspect of this new system is that background signals reappear in the chromatogram with each rotation of the drum. (140 sec. period) Figure 2 displays a chromatogram with a number of peaks separated in time the one drum rotation period. These signals are due to the injection of a concentrated sample (1 µg) of tetraethyltin that was used to align the laser light with the trapped analyte. We have found that samples over ~400 ng remain on the drum for many days even after it has been warmed to room temperature. The same sample spot can therefore be used for daily alignment over an extended period. Unlike the higher concentration depositions, smaller samples are removed from the drum by each pass of the laser. A sample on the order of 10 ng will be detected for 5 or 6 rotations while those below 10 pg will only be seen once. Using this new system we have recorded chromatograms by injecting samples as small as 100 attograms of tetraethyltin in 1 µl. An example is shown in Figure 3. The width of the peak is due to a poorly heated valve between the chromatographic column and the GC-MS interface. One advantage of the repetitive nature of the background is that they it easily be subtracted from the chromatogram. Figure 4, for example, displays the same data as in Figure 3 except that the latter part of the chromatogram has been subtracted from the first part. This is valid because the latter part of the data contains only signals that are correlated with the drum and therefore reappear every 140 seconds. These signals can therefore be used as a legitimate background for the first part

The 100 ag sample peak is seen only once in the first part of the data and therefore is the only strong peak remaining after background subtraction.

The method is currently being applied to organolead compounds.

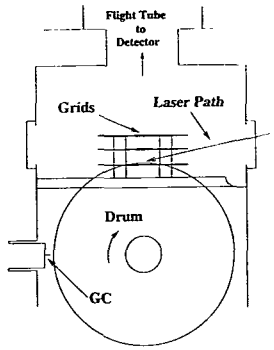

Figure 1

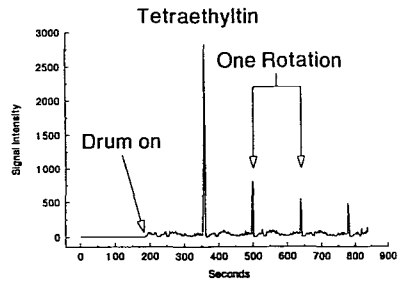

Figure 2

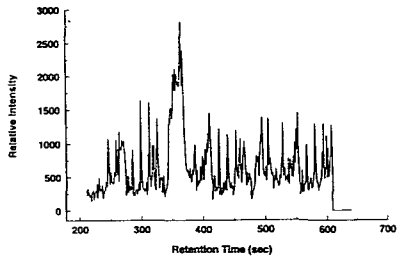

Figure 3

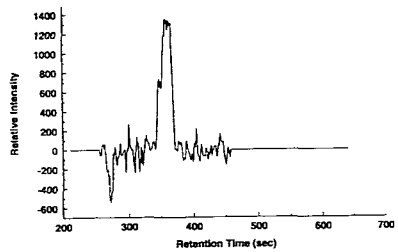

Figure 4

Refs:
1. S. M. Colby, M Stewart, and J. P. Reilly; Anal Chem. 62 (1990) 2400-3.
2. S M. Colby and J. P. Reilly 42nd ASMS Conference on Mass Spectrometry, Chicago, 1994, pg 854
3. S. M. Colby and J. P. Reilly; Int J. Mass Spectrom. Ion Process. 131 (1994) 125-138.

Sensitive GC-TOF mass analyzer

M Andreessen, U Czok, J.Dormagen, T.Horvath, S.Scherer, H,Wollnik
II Physikalisches Institut der Justus-Liebig-Universität, Heinrich-Buff-Ring 16, 35392 Giessen, Germany
V.V.Raznikov
Institute of Energy Problems of Chemical Physics of Russian Academy of Sciences, 142432 Chernogolovka Moscow region
Russia

A Time-of- Flight Mass Spectrometer (TOF-MS) coupled to a Gas-Chromatograph (GC) yields just the retention time of the eluation components but also the accompanying mass spectras. Monitoring the intensities of ions of several masses as function of time on find the GC-spectrum as the sum of all ion signal In contrast to scanning mass spectrometers a GC-TOF-MS system permits also to calculate a GC-chromatogram under consideration of a single mass or selected characteristic masses, which are recorded under exactly the same conditions. Further the available datas of the mass spectras give the possibilities to process these mathematically and separate unresolved GC peaks effectively.
The time spread in a TOF-system with an electron impact ion source is caused mainly by the energy distribution owing to the different start positions in the ionisation region and the turn-around-time depending on the initial ion energy and the extraction field strength.
The TOF-system operates with ion energies of 2keV and extraction field strength of 250V/mm, so that a mass resolving power (FWHM) of about 2000 has been achieved routinely. The overall flight distance of the system lies in the range of 1500mm and facilitates to record a full mass spectrum in less than 100µs
A chromatogram was taken by injecting 0 2µl of a 5-component mixture of hydrocarbons diluted in hexane at concentrations of 15ng/µl per component. For a split range of 1:1700 the amount on column of the substances was in a range of 2pg. The signal-to-noise ratio calculated by the quotient of peak-intensity to the standard deviation of the noise level shows a ten times better result for the Selected-Ion-Chromatogram (SIC) compared to the Total-Ion-Chromatogram (TIC) in our experiment (see table and Fig 1 and Fig. 2)

No	compound	amount A [pg]	TIC noise ΔA [fg]	SIC noise ΔA [fg]
1	Toluene	2 11	± 148	± 12
2	Chloro Benzene	2 18	± 121	± 12
3	Nonane	1.97	± 121	± 23
4	Chloro Heptane	2.27	± 352	± 84
5	Tert. Butyl-Benzene	2.39	± 127	± 16

To specify an explicit component of the injected substance we use a filter algorithm [2], which folded the accompanying mass spectra and the chromatogram in a mathematical way and allows to identify exactly the interesting component during the rest will be suppressed (see Fig 3). This filter will be also helpfull to differ clearly overlapping peaks of a sample with nearly equal retention times, but different mass spectras.

43rd ASMS Conference on Mass Spectrometry and Allied Topics

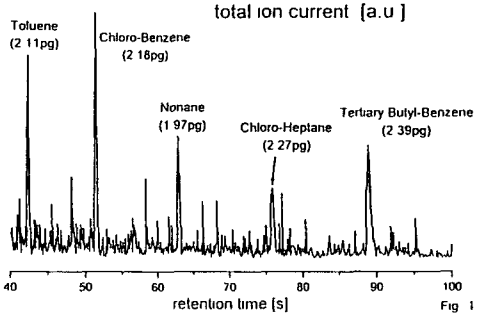

Fig 1

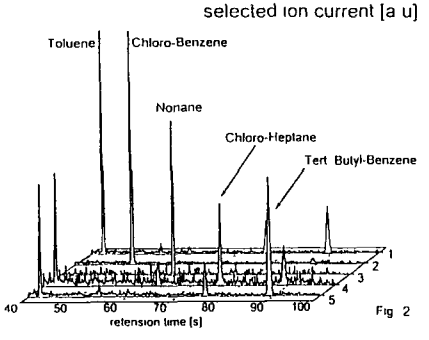

Fig 2

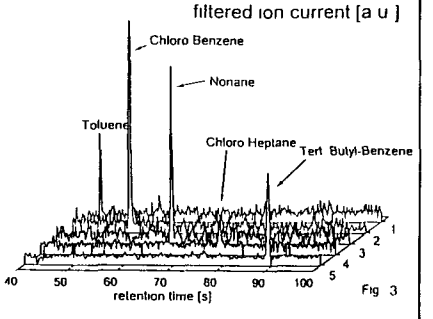

Fig 3

Results:
A **mass resolving power** of more than 2000 has been achieved routinely
The mass spectrometer shows a **linear response** from a few nanogram down to well below picogram.
Improvement of the signal-to-noise ratio by a factor of ten in the Selected-Ion-monitoring mode
Explicite **Separation** of eluation peaks by a mathematical filter algorithm

References:
[1] H Wollnik, R Becker, H Goetz, A.Kraft, H Jung, C.Chen
P Van Ysacker, H Jansen, H Snijders, P.Leclercq, c.Cramers
Int. J. Mass Spectrom. Ion Processes, 130 (1994) L7-L11
[2] V.V.Raznikov, M.O Raznikova
Information-analytical mass spectrometry (computer enhanced mass spectromtry),
Nauka, Moscow, 1992,
(ISBN 5-02-001547-4)

Design Criteria for a GC-TOF/MS Analyzer for Human Breath

Paul H. Miyares and Christie G. Enke
Department of Chemistry, University of New Mexico
Albuquerque, NM 87131

The human breath contains a vast amount of information about metabolic processes occurring in the body. The analysis of human breath, though, is a difficult and challenging task. As many as 400 volatile organic compounds have been observed[1]. Breath analysis is complicated by the presence of a high concentration of water, up to 40 mg/L at 37°C, and the large concentration range over which the components may be present. For medical diagnostic purposes, both qualitative and quantitative analysis of trace components is required. Furthermore, the speed of analysis must be such that results can be obtained within the span of a normal office visit.

The system required to perform breath analysis consists of six major components; sample collection, water removal, sample preconcentration, analyte separation, detection, and data analysis. Design criteria have been developed for each of the individual components of the breath analyzer.

The sample collection system serves to both collect the breath sample as well as introduce the sample into the analyzer. The system is equipped with a mouth piece through which a sample can be collected directly from the subject. A glass chamber serves as the collection vessel. A unidirectional valve allows the subject to exhale breath into the chamber and inhale clean air from a supply tank. Large diameter tubing is used to allow the subjects breathing to be uninhibited. The glass chamber is fitted with a draw tube where the sample is withdrawn via vacuum into the instrument. A purge gas supply and purge vent are used to clean the chamber between sample collections. A syringe port is added to allow for the addition of internal standards after sample collection. The chamber and tubing are heated in order to prevent condensation and subsequent loss of analyte along the surfaces.

The water removal device is used to reduce the physical and chemical interferences present due to the high concentration of water in the breath sample. It uses a silicone hollow fiber membrane[2] has a higher rate of permeation for organic compounds than for water. A pump is used to draw the sample into the hollow fiber. A constant vacuum applied to the chamber around the hollow fiber maintains the concentration gradient across the membrane.

The preconcentration system is used to enhance to detection capability of the system for trace component analysis. It utilizes a thick film, wide bore capillary trap. The trap is maintained at liquid nitrogen temperature in order to trap even highly volatile components. Flash heating is used to desorb the trapped compounds. The wide bore tubing is used to allow rapid flow

rates and to help prevent blockage from formation of any ice crystals that may form. The thick film stationary phase is used to increase the capacity of the trap resulting in greater preconcentration, thus better detection capability.

A gas chromatographic system is used to the first level of selectivity in the sample analysis and serves as the introduction system to the mass spectrometer. The chromatograph is equipped with a dual column configuration; a standard 100% methylsilicone (DB-1) column (5m x 0.53mm ID) and an aluminum oxide porous layer open tubular (PLOT) column (5m x 0.53mm). The PLOT column will separate low molecular weight compounds that are normally unretained on a DB-1 column. The columns are connected through a valve system that splits the low molecular weight fraction toward the PLOT column while routing the remainder of the sample directly to the mass spectrometer. The short, wide bore capillary columns allow for rapid flow rates thus decreasing the analysis time and better utilizing the capabilities of the detector. Cryogenic focusing[3] is used the ensure a narrow injection band required for rapid gas chromatography.

Detection by time-of-flight mass spectrometry (TOF/MS) with time array detection (TAD) is used due to the inherent "full-scan monitoring" mode and rapid spectral generation rate. This allows for rapid detection, excellent sensitivity and effective deconvolution of overlapping chromatographic peaks. The TOF/MS is a home-built reflectron time-of-flight instrument equipped with an electron impact (EI) source, a two stage gridded reflectron[4] and an active film electron multiplier detector (Model AF820 ETP-PTY Limited, Ermington, Australia). The reflectron design coupled with a flight tube length of 1.5 m and a small reflectron turnaround angle of three degrees enhances the resolution of the mass analyzer. The active film electron multiplier is used to provide high signal response with little noise.

A data system is used to provide control over the instrument including the sample collection and processing systems, the valve system of the chromatograph and the electronics of the mass spectrometer. It also serves to collect, process and store the data. Deconvolution algorithms will be developed to extract the desired quatitative and qualitative information from the spectral data.

The integration of these six systems results in an analyzer designed for the rapid analysis of human breath. Quantitative and qualitative information should be obtainable over a dynamic range of 10^4 to 10^5 with ppb detection limits.

---

[1] Phillips, M., *Scientific American*, July 1992.
[2] Westover, L.B.; et al., *Anal Chem*, 46(4), 1974.
[3] Ewels, B.A. and Sacks, R.D.; *Ansl Chem*, 57, 1985.
[4] Vlasak, P., et al.; *in preparation*, November, 1995.

TIME-OF-FLIGHT MIRRORS WITH IDEAL TIME-FOCUSING IN TANDEM MASS SPECTROMETRY

Alexander A. Makarov*, Emmanuel N Raptakis, Peter J Derrick
Institute of Mass Spectrometry and Department of Chemistry, University of Warwick, Gibbet Hill Road, CV4 7AL, Coventry, UK

Widespread usage of matrix-assisted laser desorption (MALDI) as a tool for producing impulse packs of protein ions has resulted in a real renaissance of time-of-flight (TOF) mass-spectrometry. To expand the analytical capabilities of MALDI TOF for structural analysis, tandem instruments are employed. The second or both stages may employ TOF and molecular structure elucidation of high-mass molecules is most favourably carried out using high-energy collision-induced dissociation

As velocities of fragment ions are close to the parent ion velocity while the differences in masses may be up to orders of magnitude, fragment ions have energies from <1 to 100% from parent ion energy, i e from hundreds to ten(s) kiloelectronvolts for high-energy collisions

The challenge of providing at least unit mass resolution for all these ions simultaneously can not be successfully met by traditional reflectrons Instead, quadratic-field mirrors providing independence of TOF from initial energy and angular spreads over wide ranges (i e *ideal time-focusing*) are required.

The most practically feasible quadratic fields possess some type of symmetry, e.g planar [1]

$$U(x, y, z) = k_{/2}\,(z-a)^2 - k_{/2}\cdot(x-b)^2 + d\,y + C \qquad (1)$$

where x, y and z form a Cartesian coordinate system, or rotational symmetry [2-4].

$$U(r, z) = k_{/2}\cdot(z-a)^2 - k_{/4}\,r^2 + e\cdot\ln(r_{/f}) + C \qquad (2)$$

where r is radius, z is the initial ion direction and k, a, b, C, d, e, f>0 are constants (in [2-3] e=0)

The objective of the present theoretical work has been to reveal in general how close to the ideal the characteristics of quadratic-field mirrors may approach for fragment mass analysis, i e what are the general limitations inherent to mirrors of this class

The following classifications of limitations have been revealed

A. Limitations on sensitivity.

In simple quadratic-field mirrors (i e with field (1) or (2) with e=0), such limitations arise from defocusing in the transverse direction (x or r) In quantitative terms, it means that the detector size should be made about four times larger along x for field (1) and about two times larger along r for field (2) than would be necessary for a linear drift tube with the same TOF dispersion.

B. Limitations on mass resolution.

Though at first glance mass resolutions of quadratic-field mirrors seems to be unlimited, more careful investigation reveals a number of general limitations on TOF resolution. These are of two main types.

1) fundamental, i.e unavoidable even when the electrostatic field is perfectly defined, such as:

- Small drift region, unavoidable in practice due to the need to separate spatially elements of construction (e.g. detector from collision cell), results in poor resolution at lower masses. This may be corrected by "shifting" the fragment ion energies to higher values (by less than 5-20% of the maximum energy) through introducing a slight acceleration after the collision cell This factor becomes practically negligible provided that the acceleration gap is <5-10% of the drift region which is, in its turn, <10-20% of the mirror length
- The uncertainty in the co-ordinate of ion fragmentation inside the collision cell limits resolution. On the basis of the impulsive collision transfer theory [5], we have developed a model of high-energy ion

scattering and dissociation in the collision cell Fig 1a, b shows the dependence of mass resolution on the mass of the fragment ions for two different collision gases and compares the results with these for an idealised orthogonal scheme (100% transmission in both cases, 3 kDa singly-charged precursor ions, 10 keV collision energy, 0 1 eV energy release, 2 m effective flight path, 20 mm collision cell length and, in orthogonal scheme, 10 mm wide push-out gap with a 1 kV pulse followed by a 4 kV static acceleration). This figure demonstrates that the latter is superior to quadratic-field mirrors only for fragment ion masses <10-20% of the precursor ion mass and does not compare favourably at higher masses

- The metastable decay of ions inside the mirror limits resolution. In this case, "ghost" peaks will does appear Due to the inherent smoothness of quadratic fields, these peaks will be smoother and much lower in intensity than analogous peaks in any traditional reflectron

2) practical, i e. arising due to imperfections in the field approximation when using the multi-electrode systems:

- The long-range field sag due to field non-linearity limits resolution. This sag may be minimised by shifting electrodes potentials in such a way that the weight-averaged integral of the difference between ideal and real potentials vanishes Then introducing, for example, a flat detector on the flange of the mirror (i.e. distorting field near the plane z=0) does not result in any significant loss of mass resolution provided all ions penetrate into the mirror to a distance deeper than 3-5 times size of the detector
- Short-range field perturbations due to "granularity" of boundaries limit resolution Their influence becomes negligible as soon as the ion trajectories lie at distances from the boundaries of more than 3-5 times the centre-to-centre separation of adjacent electrodes

It has been concluded that quadratic-field mirrors are capable of providing better than unit mass-resolution over the wide mass range up to 3-5 kilodaltons

Acknowledgements· This work has been supported under LINK TAPM EPSRC grant GR/H 20091

1. Davis S. C., US Patent # 5,077,472, 1991
2. Yoshida Y., US Patent # 4,625,112, 1986
3 Rockwood A L , Proc 34th ASMS Conference on Mass Spectrometry, June 8-13, 1986, Cincinnati, Ohio, p.173
4. Gall L N , Golikov Y K , Aleksandrov M L , Pechalina Y E , Holin N A , USSR Pat #1,247,973, 1986
5. Uggerud E and Derrick P.J , J.Phys.Chem , 95 (1991) 1430

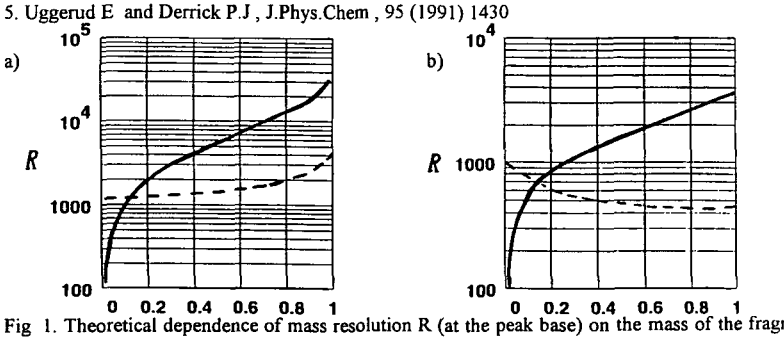

Fig 1. Theoretical dependence of mass resolution R (at the peak base) on the mass of the fragment ions m for a) helium and b) xenon collision gases
——— quadratic field mirror, – – – orthogonal scheme

HIGH VOLTAGE DEFLECTORS FOR MASS SELECTION ON A WIRE GUIDE MALDI/TOF

B.J. Bolanos, D.A. Laude, Department of Chemistry and Biochemistry,
The University of Texas, Austin, TX, 78712

Wire ion guides are employed to improve ion transport in matrix assisted laser desorption and ionization(MALDI)/time-of-flight(TOF) mass spectrometry as a means to enhance instrument sensitivity. Unfortunately, the wire guide is not mass selective and a large abundance of low-mass ions generated by MALDI can saturate standard microchannel plates(MCP) and mask the detection of the later arriving biomolecules. A number of research groups have employed techniques to combat detector saturation. However, for the most part success is limited by reduced ion deflection efficiency and poor mass selectivity(1,2). In the work to be presented, a high voltage deflection ring positioned at the end of the flight tube is demonstrated to provide the selective ion deflection needed to prevent MCP saturation. This approach is shown to have superior mass selectivity and sensitivity compared to the alternative bipolar pulsed wire method(2).

Experiments were performed on a 1.43 m linear TOF mass spectrometer with a dual microchannel plate detector.. MALDI ions formed by a 4.5 ns, 2 x 10^7 W/cm^2 354 nm pulse from a Nd:YAG laser are accelerated to between 5 and 30 kV before entering the flight tube. The wire guide consists of an electrically isolated 0.53 mm diameter stainless steel wire aligned along a 7.62 diameter stainless steel tube support. A deflection ring, 8 cm long and 4 cm in diameter, was mounted at the end of the wire guide tube support 10 mm away from the detector. In order to drive the deflection ring, a GRX 3.0K-H switching circuit from DEI was used in combination with a 5 kV power supply to allow for 3 kV pulses with no greater than 35 ns rise and fall times. Samples were prepared as a 2000:1 mixture of sinapinic acid to protein deposited on a sample probe tip and allowed to crystallize. Acceleration potential remained constant at 20 kV and wire guide potentials ranged from 0 V to -500 V. Spectra were generated from the coadding of ten laser firings on the same sample spot.

A typical MALDI spectrum which exhibits high-mass signal suppression due to detector saturation is shown in Figure 1. The baseline noise is pronounced even up to 25 µs due to enormous matrix and K^+ signals, and obscured desired sample signals up to several kDa. The use of bipolar pulsing techniques to correct for saturation can be successful in deflecting low-mass ions away from the detector, and increasing the signal/noise of the protein. For example, shown in Figure 2 is the spectrum for a a 5 µs, +100 V deflection pulse on the wire guide followed by a static -200 V potential prevents detector saturation and improves the bovine insulin signal/noise five-fold.

There are important limitations in mass selection when applying the bipolar technique. This is because the bipolar method requires that all ions, including analyte ions, experience the deflection voltage on the wire. A strong correlation between the magnitude of the deflection pulse used to eliminate the matrix ions and the decreased intensity of the protein signal was observed. Another problem with the bipolar technique is the difficulty in defining the conditions for optimal low-mass deflection without pronounced loss of bovine insulin signal.

The effectiveness of the deflection ring is demonstrated in Figure 3 for increased bovine insulin signal. As shown, a 2.5 kV 50 µs pulse on the deflection ring is acceptable to permit low-mass deflection without influencing the bovine insulin ions, which have a flight time of approximately 58 µs. The deflection ring allows protein ions to experience wire guide focusing

for their entire flight times for better signal/noise enhancement. Employing this technique provides a fifteen-fold increase in signal/noise, three times that of the bipolar spectrum in Figure 2, as well as a more efficient deflection of low-mass ions. Additionally, the deflection ring technique allows for more flexibility in optimizing focusing conditions since ions of interest don't experience competitive deflection and focusing voltages.

A deflection ring positioned at the end of the flight path allows for increased mass selective deflection of ions well-separated by time-of-flight. The mass selectivity of the deflector technique is demonstrated in Figure 4 in profiles of bovine insulin and gramicidin S signal with varied length of deflection pulse. Both profiles demonstrate a wide range of deflection conditions for optimal protein signal, in addition to well defined deflection windows for increased mass-selectivity. In the case of bovine insulin a deflection pulse of 30 µs is sufficient to deflect abundant low-mass ions for a dramatic increase in signal intensity, which remained constant through a 55µs pulse. Complete loss of protein signal occurred at a 60 µs pulse length due deflection of the protein ions prior to arrival at the detector at 58 µs.

1. R.S. Brown, N.L. Gilfrich *Rapid Comm. Mass Spec.* 6 (1992) 697.
2. C.D. Hanson, C.L. Just *Anal. Chem.* 66 (1994) 3676.

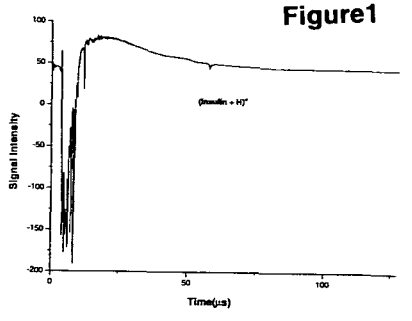

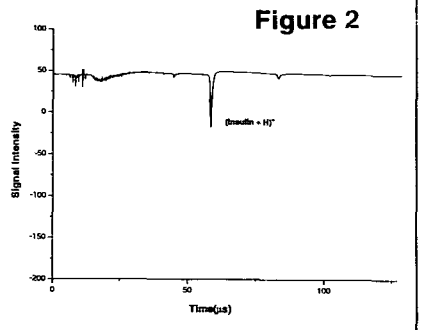

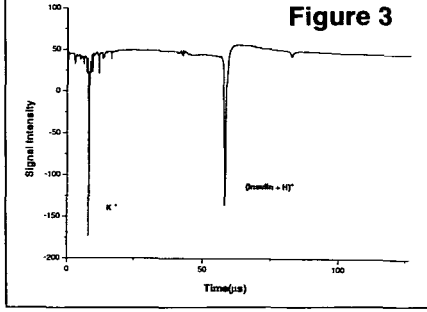

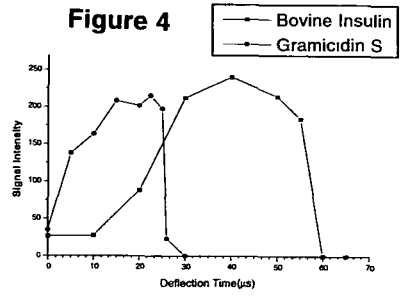

Improved Space-Focusing Using Non-linear Ion Acceleration Fields in Time-of-flight Mass Spectrometry

Ben D. Gardner[1] and John F. Holland[2]

Departments of Chemistry[1] and Biochemistry[2], Michigan State University, East Lansing, MI 48824

Viatcheslav B. Artaev

Meridian Analytical Systems, Inc., 2310 Science Parkway, Okemos, MI 48864

In time-of-flight mass spectrometry (TOFMS), the resolution parameter is, by definition, the temporal coincidence of iso-mass ion arrivals at the detector surface Deviations from coincidence are, in essence, manifestations of variations in energy along the transmission axis The primary factors responsible for these deviations are the initial spatial and energetic (including turn-around effect) distributions of ions in the source at the moment of extraction. For ionization methods where the axial spatial distribution is quite narrow, the ion energy distribution will be the dominant factor However, for three-dimensional ionization techniques acting on gas phase molecules, the initial ion location in the source determines the axial energy induced by the extraction field which, in turn, is the dominant cause of ion energy variation

Compensation for the spatial distribution is achieved by placing the detector at the position along the flight path where the temporal distribution of iso-mass ions is minimized, a position known as the space-focus plane [1] Space focusing is currently achieved using linear extraction fields. Unfortunately, the use of linear fields does not provide the optimal focus condition Theoretically, ideal space-focusing may be achieved through the use of non-linear ion acceleration in the extraction region of the ion source We have previously described a computational model based on numerical analysis for determining the potential profile required to provide complete space focusing in a given instrument geometry [2] This model includes calculations of short linear electric field segments along the flight axis within the ion source, beginning at the ion source exit, following the equation

$$t=\sqrt{\frac{2m}{q}}\left[\sum_{n=1}^{i}\frac{\sqrt{U_0+q\sum_{j=n}^{i}x_jE_j}-\sqrt{U_0+q\sum_{j=n+1}^{i}x_kE_k}}{E_n}\right]+D\frac{\sqrt{2m}}{2\sqrt{q\sum_{i=1}^{i}x_iE_i}}$$

where t is the time required for an ion, beginning at some axial location within the source, to arrive at the space-focus plane, and is a function of mass m, charge q, initial energy U_0, electric field E, and field-free distance D Subsequent to the entry of a predefined t, the computation outputs an iteratively solved solution for a series of electric fields E_j having x_j width. When the applied width of these fields is short relative to the ion source dimension, a non-linear field distribution is approximated

We have fabricated a TOF instrument, illustrated in Figure 1, to test the validity of the computational model and experimentally evaluate the performance of various non-linear source geometries.

The ion source of this instrument consists of several parallel, grid-free, ring electrodes spanning the ionization region, and two gridded electrodes defining the acceleration region Photoionization of gas-phase molecules is accomplished using a Nd YAG laser operating at λ=355 nm. The laser beam is guided to the ionization region using a mirror assembly and is focused into the center of the ionization volume using a cylindrical lens By laterally adjusting the mirror assembly, the ionization volume is shifted along the ion source transmission axis

Figure 1

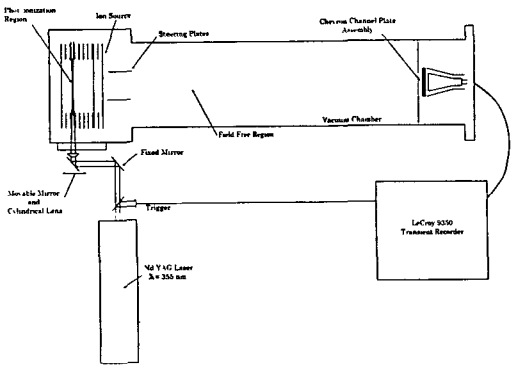

Using this instrument, the arrival-time dependence of iso-mass ions on initial ion position can be tomographically mapped throughout the source Initial results have substantiated the temporal limitations of ion sources utilizing linear electric fields, with the experimental results closely matching theoretically predicted behavior Our current efforts center on optimization of the non-linear ion source configuration A major challenge has been the application of appropriate voltages to the source electrodes in order to achieve the optimal electric field along the cylindrical axis Non-linear electric fields are not strictly orthogonal to the cylindrical axis, yielding an offset between the applied electrode voltage and the axial potential. Both the offset and field curvature must be accounted for in the ion source design.

Ultimately, tomographic mapping of the computationally designed non-linear ion source will reveal the extent to which the mathematical model is applicable We expect that the use of extended ionization regions may require the use of non-linear extraction fields

[1] W C Wiley and I. H McLaren, *Rev. Sci. Instrum* , **1955**, *26*, 1150

[2] B.D.Gardner, V.Artaev and J.F.Holland, *Proc. 42nd ASMS Conf. on Mass Spec* , **1994**, 1040

DESIGN OPTIMIZATION FOR A COAXIAL, CURVED FIELD REFLECTRON TIME-OF-FLIGHT MASS SPECTROMETER

Timothy J. Cornish and Robert J. Cotter, The Johns Hopkins University, Baltimore, Maryland, 21205

A coaxial time-of-flight mass spectrometer utilizing a curved field reflector has been developed in order to facilitate both high speed and high sensitivity analysis of bio-polymers These performance enhancements over conventional reflectron TOF designs can be realized because the complete sequence information of MALDI generated ions is obtained without the requirement of voltage stepping or scanning of the reflector

Shown in Figure 1 is a diagram of the instrument In contrast to a single stage constant field reflector, which focuses only stable ions and requires that L= 4D, the curved field reflector will focus all ions, both stable and metastable, if L ≅ D.

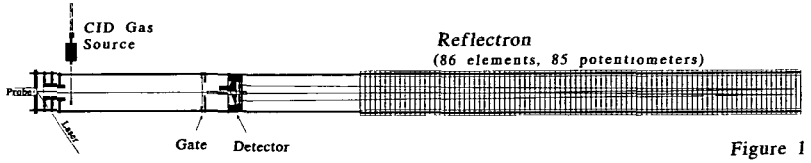

Figure 1

The MALDI generated ions are produced by the pulse of a nitrogen laser and extracted using a low voltage (4 kV) drawout potential Gating elements and a center-hole detector are located midway down the drift tube in order to allow sufficient time dispersion of the precursor ions in the first linear TOF region. A pulsed valve (Iota One General Valve Corp), capable of producing pulses of 250 μs duration, has been installed so that the collision gas intersects the ion beam near the beginning of the first drift region

Performance of the gate assembly is shown in Figure 2. Using PEG as a test compound, it was found that the minimum effective gate width is ± 50 Da at mass 1000 Da (±5% of the target mass) While not as selective as the gate of a true tandem MS, this configuration allows, in many cases, the isolation of single components from within a mixture.

Figure 3 shows the CID product ion spectrum of caffeic acid. The 163 Da peak was gate selected and fragmented using helium as the collision gas Instantaneous calibration of the product ion spectrum is accomplished using the time-of-flight data processing program TOFWARE© (ILys Software, Pittsburgh, PA) Based on the curve depicted in Figure 4, the entire procedure requires only the mass assignment of the parent ion. This calibration curve, which closely resembles the arc of a circular function, represents a plot of the normalized product ion data. The deadtime is mass dependent and represents the total time the parent ion spends in the field free regions

A single post source decay (PSD) spectrum of a polyproline derivative (P_{14}-R 20 data points total) was used to produce the calibration curve presently in use In Figure 5, these sequence ions are shown comparing the TOFWARE generated masses with those expected from theoretical calculations Further refinement by incorporation of data from many known product ion spectra is currently in progress

43rd ASMS Conference on Mass Spectrometry and Allied Topics

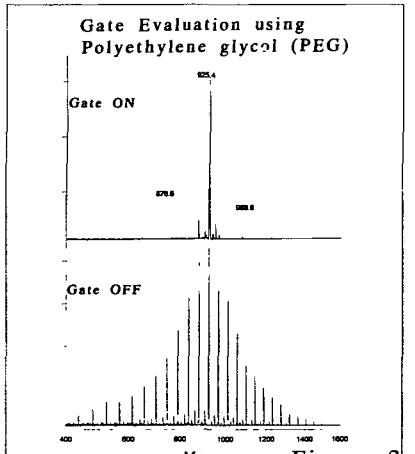

Figure 2

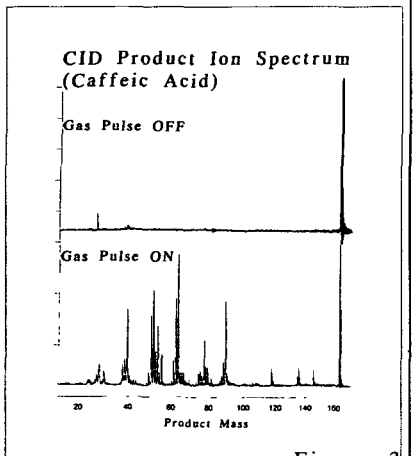

Figure 3

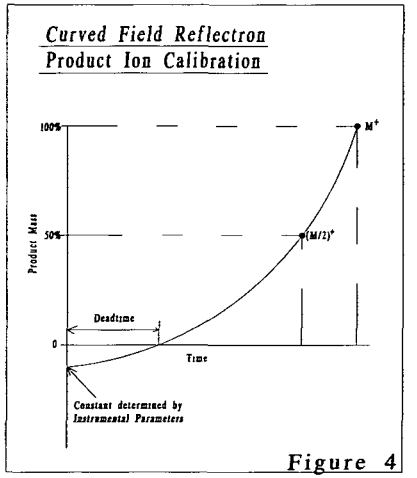

Figure 4

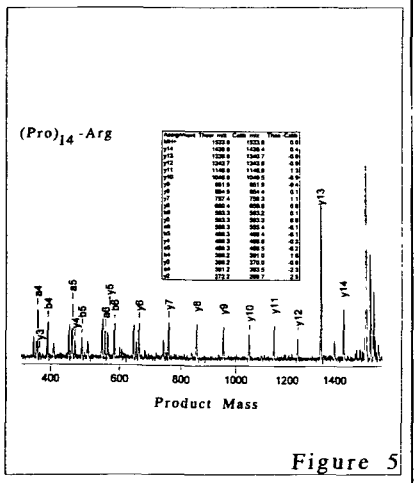

Figure 5

An Interleaved-Comb Ion Deflection Gate

D. J. BEUSSMAN[1,2], P. R. VLASAK[2], T. A. ERICKSON[1], M. R. DAVENPORT[1], and C. G ENKE[1,2]
[1]Department of Chemistry, University of New Mexico, Albuquerque, NM 87131
[2]Department of Chemistry, Michigan State University, East Lansing, MI 48824

We have designed and constructed an ion deflection gate and implemented it in a time-of-flight (TOF) mass spectrometer This gate is based on the ion gate, adapted from the electron filter design of Loeb[1], and first implemented in a TOF mass spectrometer by Schlag[2] This gate can be used to select a single *m/z* ion packet for further fragmentation in a tandem mass spectrometer, as well as to eliminate a range of ions such as those due to the matrix in MALDI or the carrier gas in GC-MS. Since time-of-flight mass spectrometers are batch array detectors, with all ions that are extracted from the source reaching the detector, a gate device is crucial for tandem time-of-flight instruments using post-dissociation acceleration. The gate allows a single *m/z* ion packet from the normal spectrum to be transmitted while deflecting all others This ensures that the product spectra are not convoluted with ions from the normal mass spectrum

Our interleaved-comb ion deflection gate is constructed from two stainless steel wires that are strung back and forth through alternate holes in an insulating material, thus creating a plane of wire segments approximately 1 mm apart. The two wires are attached to separate high-voltage pulsers such that equal but opposite voltages can be applied with pulse widths as narrow as 135 ns

The gate is 'open' when the wires are at the field-free voltage, allowing ions to pass through the gate unimpeded. The gate is 'closed' when one of the wires is pulsed to 250 V above the field-free voltage, while the other is pulsed to 250 V below the field-free value This creates a strong field between alternate wires, causing ion deflection from the normal ion trajectory Since the wire segments are interleaved and only 1 mm apart, the deflection field does not extend a significant distance into the field-free region from the gate device, as opposed to conventional deflection plates For example, in order to deflect *m/z* 167 ions by the same amount using either the interleaved-comb deflection gate or conventional 1 5 cm deflection plates, ±5 V field lines extend 1 3 mm into the field-free flight path from the center of the gate device, while they extend 28 mm from the center of the deflection plates This allows better gating resolution to be achieved in pulsed-field mode using the interleaved-comb ion deflection gate

A practical electronic pulsing system has been designed and implemented. Pulse amplitude and duration are adjustable from 0 to ±500 V and from 135 ns to dc respectively Circuitry for minor timing control and voltage offset of each of the pulsers has been designed to ensure that the two pulse shapes complement each other. The rise- and fall-times for the ±250 V pulses have been measured to be approximately 20ns (10%-90%)

The ability to transmit or eliminate a single *m/z* ion packet is demonstrated below using the molecular ion region of diphenylmethane (*m/z* 168) Figure A below shows the entire molecular

[1] Loeb, L. B *Basic Processes of Gaseous Electronics*, University of California Press Berkeley, CA, 1995.
[2] Weinkauf, R., Walter, K.; Weickhardt, C.; Boesl, U ; Schlag, E W *Z. Naturforsch*, **1989**, *44a*, 1219-1225.

ion region of diphenylmethane from *m/z* 163 to 169 This was obtained with the gate 'open' for 2.5 µs, allowing the entire region to be transmitted. Figure B shows the selected transmission of *m/z* 167 with the deflection of all other ions. This spectrum was obtained with the gate 'open' for 135 ns, and the delay timed to transmit the desired ion packet. Figure C indicates the ability to deflect a single *m/z* ion packet while transmitting all others by keeping the delay the same as in figure B but reversing the gate so that it is 'closed' for 135 ns.

A)

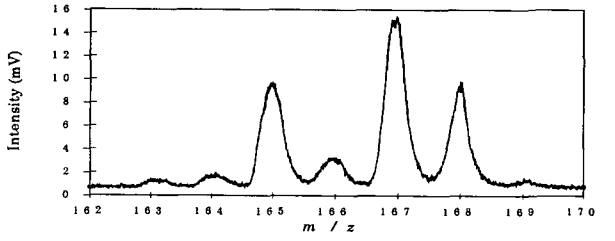

B)

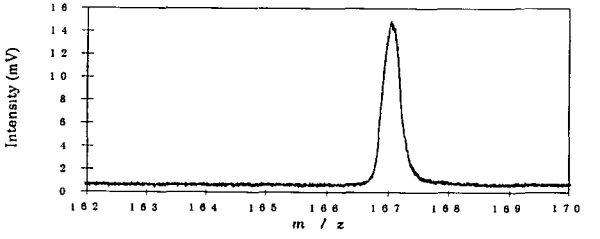

C)

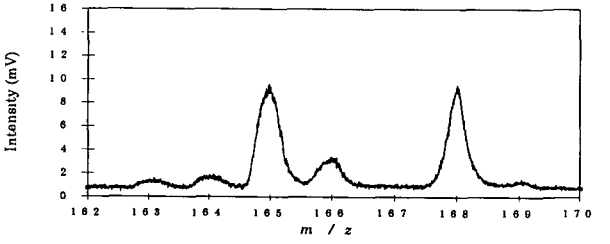

Ion Isolation in MALDI-TOF Mass Spectrometry Using a Bipolar Pulsed EPG

Curtiss D. Hanson and Nathan A. Adams
University of Northern Iowa Chemistry Department, Cedar Falls, IA 50614

Time of flight mass spectrometry (TOF-MS) has come to the forefront of high-mass analysis due to the high sensitivity and extended mass range offered by the instruments.[1-3] These techniques have shown superb sensitivity for sample sizes within the range of a few hundred attomoles,[3,4] and the mass range of TOF-MS is theoretically unlimited.[5] Although the high sensitivity and mass range of MALDI-TOF provide strong arguments for its use, the spectra are complicated by the high-intensity background peaks that result from the matrix which limit both the resolution and detector response, reducing the effectiveness of the technique for high molecular weight biomolecule analysis.

Microchannel Plate (MCP) detectors are ideally suited for high-sensitivity applications due to the rapid response coupled with a very high gain.[2,6] However, these same characteristics make the MCP detectors susceptible to saturation resulting from the low mass ion component in the MALDI spectrum. An individual channel of the microchannel plate array becomes saturated following generation of the electrode cascade, and a recovery of up to several milliseconds is required before the channel is restored to an active state. Because a large component of the ion flux in MALDI is composed of low-mass ions (m/z<300), and because the time scale of the experiment is in the microsecond range, early saturation of the detector occurs frequently, resulting in a reduced capacity to detect high-mass ions.[2]

One approach to selective elimination of low molecular weight matrix ions was demonstrated by use of a bipolar pulsed EPG.[7] The ability to apply pulsed positive and negative voltages on the EPG allows one to combine the deflection capability of an EPG that traverses the full length of the flight region. The bipolar pulsed EPG not only deflects undesired ions away from the detector but recaptures divergent high molecular weight ions into an elliptical, spiraling orbit about the EPG back toward the detector. This mode of operation permits the selective elimination of low-mass ions by operating the bipolar pulsed EPG as a high-pass filter.

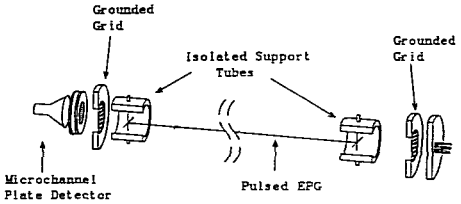

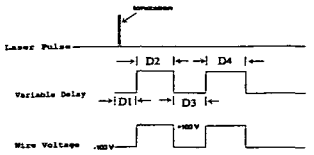

The mechanism and selectivity of the ion elimination can be described on the basis of ion motion about the EPG derived by Oakey and Macfarlane.[8] A particle injected into the potential field of a centrally located EPG will have a velocity with vector components parallel and perpendicular to the ion axis. The perpendicular component of the ion's velocity, vp, results in an eccentric spiral motion around the EPG. Ions trapped by the radial electric field are transported to the detector by the velocity component parallel to the ion axis. It is important to note that the parallel component of the velocity is unchanged by the radial electric fields and therefore does not alter the time of flight of the ion. When the polarity of the EPG is made positive to create a repulsive electric field, the ions are accelerated toward the flight tube walls. Ions are therefore eliminated by collision with the walls of the flight tube. If the polarity of the applied voltage is changed to create an attractive electric field (i.e., negative) prior to collision with the flight tube, the ion will by recaptured into a stable orbit. This ability to recapture and detect deflected ions results in a highly selective ion elimination technique. This technique was shown to be an effective method of selected reduction of unwanted background peaks and provides an increase in both dynamic range and sensitivity.[9]

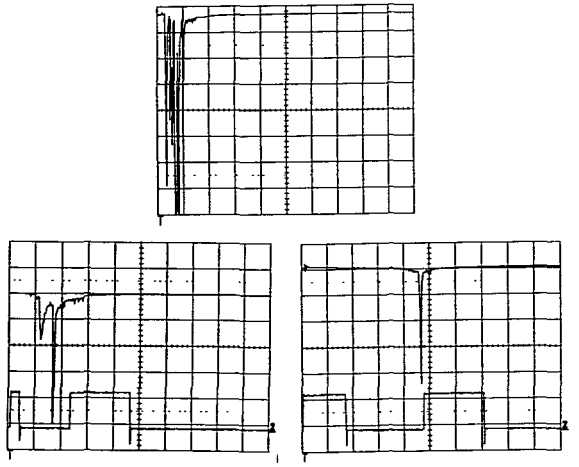

The work presented here demonstrates the effects of the addition of a second pulse to the pulsing sequence to allow for ion isolation. This allows the EPG to be used as a band-pass filter for the ions Ion isolation using an EPG permits a method of selecting specific ions for structural analysis. Because the EPG has no field vectors along the flight axis, ion selection does not effect the TOF of the selected ions. However, presently the resolution of the second pulse is fairly low because the initial pulse gives the ions a radial velocity distribution. If coherency could be induced in the ions prior to the second pulse, the resolution of this technique would increase dramatically.

Literature Cited

(1) Karas, M.; Bahr, U.; Ingendoh, A.; Hillenkamp, F. *Angew Chem, Int. Ed. Engl.* **1989**, 28, 760
(2) Beavis, R., Chait, B. *Rapid Commun. Mass Spectrom.* **1989**, 3, 233-237.
(3) Beavis, R.; Chait, B. *Anal. Chem.* **1990**, 62, 1838.
(4) Strobel, F H.; Solouki, T.; White, M. A.; Russell, D H. *J. Am. Soc. Mass Spectrom.* **1991**, 2, 91-94.
(5) Opsel, R.; Owens, K., Reilly, *J. Anal. Chem.* **1989**, 57, 1884-1889.
(6) Wolf, B.; Mudget, P.; Macfarlane, R. J. *Am. Mass Spectrom.* **1990**, 1, 28-36
(7) Just, C. L.; Hanson, C. D. *Rapid Comm. Mass Spectrom* **1993**, 7, 502-506
(8) Oakey, N.; Macfarlane, R. *Nucl. Instrum. Methods* **1967**, 49, 220-228
(9) Hanson, C. D.; Just, C. L *Anal. Chem* **1994**, 66, 3676-3680.

Comparison of Ion Detectors for Matrix-Assisted Laser Desorption/Ionization Time-of-Flight Mass Spectrometry

Richard C. King and Kevin G. Owens, Department of Chemistry, Drexel University, Philadelphia, PA 19104
Scott D. Hanton, Air Products & Chemicals, Inc., Allentown, PA 18195

Time-of-Flight mass spectrometry (TOFMS) is a pulsed technique requiring ion detectors with special properties. These detectors must have fast response times to resolve closely-spaced ior packets, high gain to amplify weak ion signals, high current capability to prevent saturation, and a sensitive conversion surface. Two different types of detectors are commonly used in TOFMS: continuous dynode microchannel plate (MCP) detectors[1-3] and discrete dynode electron multipliers (EM). The MCP detector is valued for its fast response time, but is prone to saturation even for relatively low ion current. EM detectors have become popular recently due to improvements in their rise times.

In most MCP and EM detector configurations the secondary electron gain is directly coupled to the ion post-acceleration potential. Post-acceleration is often used to increase the sensitivity of detection[4] while maintaining the mass resolving power gained through low voltage ion extraction. Additionaly, low voltage extraction reduces the risk of ion fragmentation through collisions with neutral material in the expanding plume and decreases the probability of detection for any neutrals formed from these fragmentation processes. Post-acceleration increases the ion kinetic energy, improving the detection of high mass ions by improving the ion/electron conversion efficiency. Unfortunately, this can lead to saturation by lower mass materials (both ions and neutrals) incident on the detector. Decoupling the detector post-acceleration and gain poses some experimental difficulties: providing separate electric fields to decouple the ion conversion from the electron gain in the detector, the addition of coupling capacitors to recover the signal from high post-acceleration potentials and protecting the signal amplifiers from high voltage spikes.

To address the problems of using MCP or EM detectors, a scintillation detector (SD) is constructed that employs a fast scintillator to convert electrons to photons that are then detected with a fast photomultiplier tube (PMT)[5]. The performance of the SD (schematic shown below) is compared to the tandem MCP detector and a commercially available EM detector (model AF820 ETP Scientific, Inc. Auburn MA). Factors investigated include the mass response, rise time, detector saturation, and ion (and neutral) kinetic energy effects. The SD has advantages, particularly for the analysis of polymers by matrix-assisted laser desorption mass spectrometry compared to the MCP and EM detectors. The performance of the detectors will be compared and the advantages and disadvantages of each detector will be presented.

Results

The tandem microchannel plate detector, although it possesses extremely high temporal resolution, was found to suffer from severe saturation effects. Low mass blanking was always necessary in order to observe higher mass analyte ion signals during the MALDI analyses.

The ETP EM was found to yield excellent results when used for synthetic polymer analyses. The significantly flatter ion/electron conversion characteristics allowed for the faithful reproduction of low mass (<2000 MW) polymer oligomer distributions. The lack of saturation obviated the need for using low mass beam blanking, which was found to significantly shift the flight times of ions experiencing the falling edge of the blanking pulse. Elimination of the need for beam blanking also significantly simplifies the experimental setup.

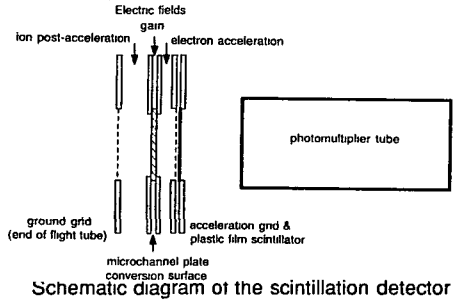

Schematic diagram of the scintillation detector

Excellent results were obtained with the scintillation detector, even when used with a less than optimum PMT. The sensitivity of the detector was high, enabling much lower desorption laser intensities to be employed for the MALDI experiments. The time response, although slower than that of the ETP multiplier or tandem MCP, is acceptable for ion signals observed in the MALDI experiment. The detector does seem to suffer from the same low mass signal enhancement (high mass discrimination) as the tandem MCP detector. This is likely due to the use of the MCP ion/electron conversion surface Future work on the scintillation detector will involve combination of the active surface used in the ETP Scientific AF820 discrete dynode multiplier with the scintillator/PMT combination.

Experimentally, there are significant advantages to the SD. Under normal operating conditions for both positive and negative ion detection the front of the MCP is held at ground potential and the rear is biased at up to -1000V The Ni mesh grid in front of the PFS is held at -3000V, defining the electron acceleration region. The photocathode of the PMT is biased at up to -1100V while the anode is held at ground potential (the standard operating conditions). Each of the potentials can be changed independently, optimizing the ion/electron conversion and initial electron amplification, the electron/photon conversion, and subsequent photon collection and signla amplification. In order to post-accelerate either positive or negative ions, the MCP and grid/PFS combination can be floated at any potential. As the signal is coupled out of this portion of the detector via photons, the overall detector signal is always recovered at ground potential. This eliminates the need for signal coupling capacitors under any conditions, simplifying the electronic setup, decreasing the noise pickup in the circuit, and adding a measure of protection for the signal conditioning and recording devices.

References

1 J.L. Wiza, "Microchannel Plate Detectors", Nucl. Inst. Meth., 162, 587-601, (1979).
2 P.W. Geno, R.D. MacFarlane, "Secondary Electron Emission Induced by Impact of Low-Velocity Molecular Ions on a Microchannel Plate", Int. J. Mass Spectrom. Ion Proc., 92, 195-210, (1989).
3 R. Meier, P. Eberhardt, "Velocity and Ion Species Dependence of the Gain of Microchannel Plates", Int. J. Mass Spectrom. Ion Proc., 123, 19-27, (1993).
4 S.A. Ruatta, J. Perel, J.F. Mahoney, "Improved Ion Detectrion for Mass Spectrometers. Advantages of using Post-Acceleration in Conjunction with Particle Multipliers", Mass Spec Source, January 1992.
5 R.S. Brown, S.S. Hermsen, J.J. Lennon, Proceedings of the 41st ASMS Conference on Mass Spectrometry, 669a-b, 1993.

TANDEM MS UTILIZING AN ORTHOGONAL ACCELERATION TIME OF FLIGHT MS AS MS-II

R. L. Cerny, K. W. Wulser and D. L. Smith Deparment of Chemistry, University of Nebraska Lincoln, NE 68588
R. H. Bateman Fisons Instruments Manchester, U.K.

The use of tandem mass spectrometry in the structure determination of biomolecules is well established. There continues to be, however, need for improvements in both detection limit and mass accuracy to allow routine characterization of molecules derived from *iv-vivo* studies. We have recently installed a new VG Autospec hybrid magnetic sector-orthogonal acceleration time of flight (oa-TOF) mass spectrometer in our laboratory. This instrument is being used in conjunction with continuous flow FAB or electrospray ionization (ESI) for the structure determination of peptides resulting from the enzymatic digestion of proteins.

EXPERIMENTAL CONDITIONS All data were obtained using continuous flow FAB as the ionization method. The solvent system used was a 1:1 mixture of water:acetonitrile to which was added 1.5% glycerol, 1.5% thioglycerol and 0.1% TFA (by volume). The flow rate was 5 µl/ minute. An 8125 Rheodyne injector with a 5 µl loop was used to introduce the samples. The source temperature was 50 C. A Cs^+ ion gun operated at 25 keV was used to provide the primary beam. The instrument was operated at an accelerating voltage of 8000 v. Xenon was used as the collision gas and was admitted to the collision cell at a level to attenuate the precursor ion by 50 to 75%. Spectra were obtained at 30 to 90 kHz depending on the mass of the precursor ion. Spectra were bunched and stored as a single spectrum every 3 seconds.

HEMOGLOBIN A 10 nmole sample of human hemoglobin was digested with an equal amount of pepsin for 5 min at 0 C and a pH of 2.4. The resulting peptides were fractionated using reversed phase HPLC with an analytical C-18 column. A gradient of 0 to 40% acetonitrile over 40 min followed by 40 to 60% over 10 min was used for the separations. Fractions were collected and then dried using a Speed Vac system. Samples were reconstituted with 50 µl of water containing 0.1% TFA. The MS/MS spectra were obtained on 5 µl of these solutions. The incomplete digest results in pmole amounts of peptides. A representative MS/MS spectrum is shown in Figure 1.

EYE LENS CRYSTALLINS Three normal human lenses were homogenized with .05 M NaCl, centrifuged, and the precipitate redissolved in urea. The protein monomers were isolated using size exclusion chromatography. The crystallins were further purified by ion exchange and reversed phase chromatography. Two nmoles of α B protein isolated from the monomer fraction were digested using AspN for 4 h at 37 C and pH of 7.8. The resulting peptides were fractionated using reversed phase HPLC with a microbore C-8 column. HPLC fractions were collected based on UV absorbance at 215 nm. The collected fraction volumes ranged from 40 to 60 µl. The MS/MS spectra were obtained on 5 µl of these solutions. It is estimated that 40 to 80 pmoles of peptide were used in the analysis. A representative MS/MS spectrum is shown in Figure 2.

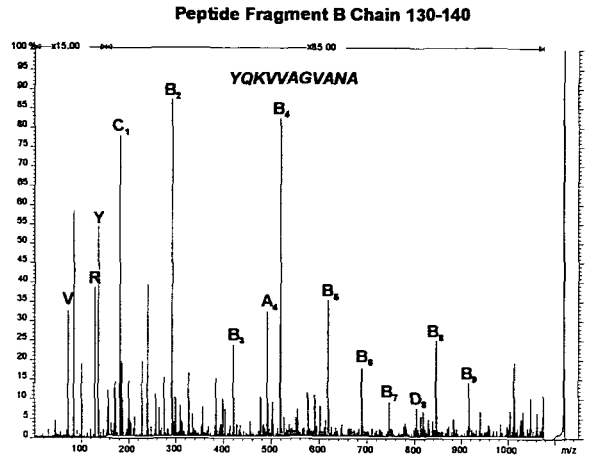

Figure 1 Tandem MS spectrum of peptide fraction isolated from pepsin digest of human hemoglobin.

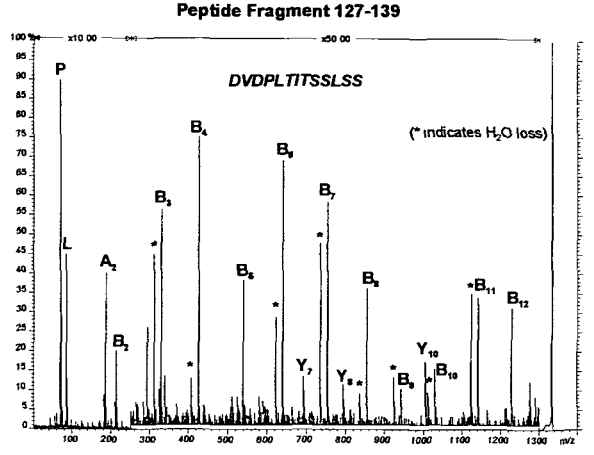

Figure 2 Tandem MS spectrum of peptide fraction isolated from AspN digest of α-B lens crystallin.

MS and high energy CID MS/MS of ESI and MALDI ions on a Magnetic Sector - TOF instrument

R H Bateman, M R Green, G Scott, VG Organic, Manchester, M23 9LE, UK.

Low and high energy CID MS/MS of singly charged ions from LSIMS and continuous flow LSIMS ion sources have been shown to yield different and complementary mass spectra which can be used to aid structural determinations of biomolecules. To date most MS/MS spectra using Electrospray ionisation (ESI) and MALDI ion sources have been acquired using low energy collisions on a triple quadrupoles in the case of ESI and by the techique of post source decay (PSD) on MALDI time-of-flight instruments. In this work high energy CID spectra for ESI and MALDI ions are investigated. The instrumentation used is a combined magnetic sector - TOF tandem MS/MS instrument, employing orthogonal acceleration time-of-flight In addition a "magnet by-pass" has been fitted to the magnetic sector which allows the whole of the ion beam to be transported, without mass analysis, from the ion source directly to the TOF analyser. This allows the high sensitivity spectrum acquisition characteristics of the TOF analyser to be used for MS as well as MS/MS Fast switchover between MS and MS/MS is achieved simply by switching the "magnet by-pass" on and off.

Figure 1 shows a plan view of the combined magnetic sector -TOF instrument MS-1 is a VG AutoSpec magnetic sector mass spectrometer fitted with two additional electrostatic deflection systems, situated before and after the magnet, and an interconnecting straight flight tube. Switching these deflectors on, and the magnet off, transmits the total ion beam without mass selection through this *magnet by-pass* to the oa-TOF for fast high sensitivity acquisition of full mass spectra.

Figure 2 shows the electrospray mass spectrum from 16 fmol of Lysozyme acquired on the oa-TOF via the magnet by-pass at a solvent flow rate of 10 ul/min. The spectrum over the mass range from 1 to 3500 dalton was acquired in 1 second.

The AutoSpec may be fitted with a MALDI ion source which operates at 8kV. A Nitrogen 337 nm UV laser is used in the MALDI source and operated at 10 Hz pulse rate. The precursor ions selected by MS-1 arrive at the gas collision cell some microseconds after the laser is fired. These ions are decelerated to 800 eV energy before entering the gas collision cell, which is operated at a pressure such as to give an average of one or two precursor ion collisions. These and the resulting product ions travel with essentially the same velocity, and therefore arrive at the orthogonal acceleration chamber at the same time. The oa-TOF extraction field is applied just at this moment so that the sampling efficiency is 100 %. This required delay time is calculated and controlled by the data system. The ion signal from the MCP detector is acquired using a 1 GHz time to digital convertor. The TOF detector is long enough to detect the whole product ion spectrum for each laser pulse.

Figure 3 shows the product ion spectrum from the $(M+H)^+$ ion from a 10 pmol loading of [Glu]-Fibrinopeptide B (m/z 1570.7) for 800 eV Xenon CID. Unlike PSD data, the spectrum exhibits the side chain cleavage ions expected for high energy CID MS/MS.

43rd ASMS Conference on Mass Spectrometry and Allied Topics

Figure 1.

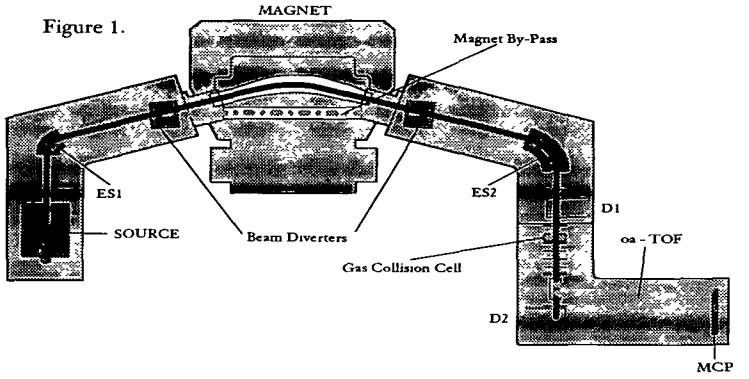

Figure 2.

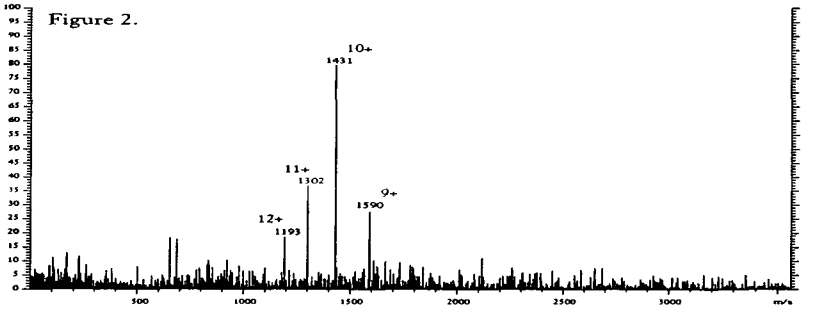

Figure 3.

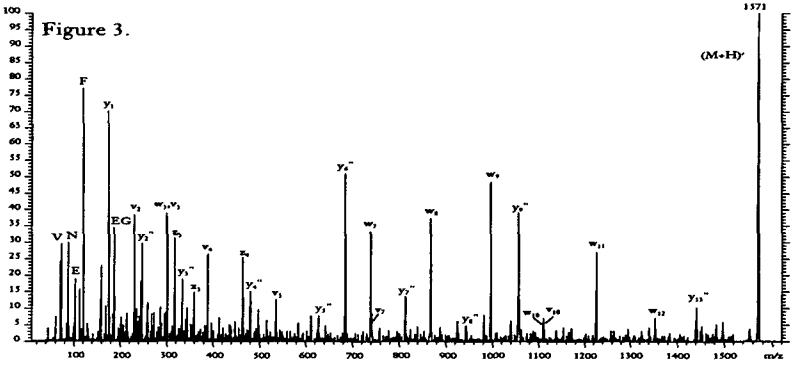

A HYBRID TANDEM MASS SPECTROMETER II.

A. Duhr, J. Stadlmann, P. Stracke and H. Wollnik

2. Physikalisches Institut der Justus–Liebig–Universität, Heinrich-Buff-Ring 16, 35392 Gießen, Germany.

A hybrid tandem mass spectrometer (Tandem–MS) was build for the study of molecular fragmentation reactions (see lower Fig. on opposite page). The first stage of the Tandem–MS is a high resolution sector field type. The second one is a Time–of–flight(TOF) instrument which allows a simultaneous detection of fragmented ions. The interface between the two different mass spectrometers was build with a microchannel plate as a collision target which yields a high fragmentation efficiency and a high ion transmission [1,2,3]. The resulting spectrum is recorded by counting single ions in the collision cell as well as at a stop detector located at the end of a drift tube or a reflectron, respectively, and measuring their time difference by a time to digital converter (TDC).

The electron released by the ion that hits the channel wall is guided by electric and magnetic fields to a MCP chevron assembly. There it is amplified and finally detected as start pulse for time counting. The collision cell is operated in high vacuum and can be heated up to 250 °Centigrades, resulting in less dark noise in the electron detector and far less surface impurities on the fragmentation channel plate. As a result of these changes SIMS products that are frequently mentioned by other authors in the fragmented ions spectrum are now reduced to invisibility.

By floating the collision cell in potential the collision energy is varied and the probable energy transfer variates. The collision cell works simultaneously as a detector for the first stage mass spectrometer. No moveable parts, therefore, are contained in the setup. In particular, this allows scanning of the first stage MS and switching to tandem mode at the same moment. The use of thos collision cell does not influence the properties of the first stage MS. The time for data aquisition in the second stage depends on the required statistic accuracy and may be as small as 10 seconds or less for an intense primary ion.

The mass resolution of the second stage depends on the time-of-flight MS used. In linear mode with 5 keV post accelleration it is limited to approx. 10 (see top Fig. on opposite page).

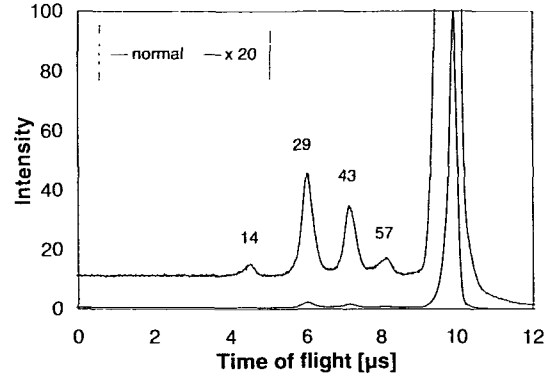

The spectrum of Hexane aquired in pulsed mode of the linear TOF is shown in the upper picture. The whole tandem mass spectrometer in an overview (bottom).

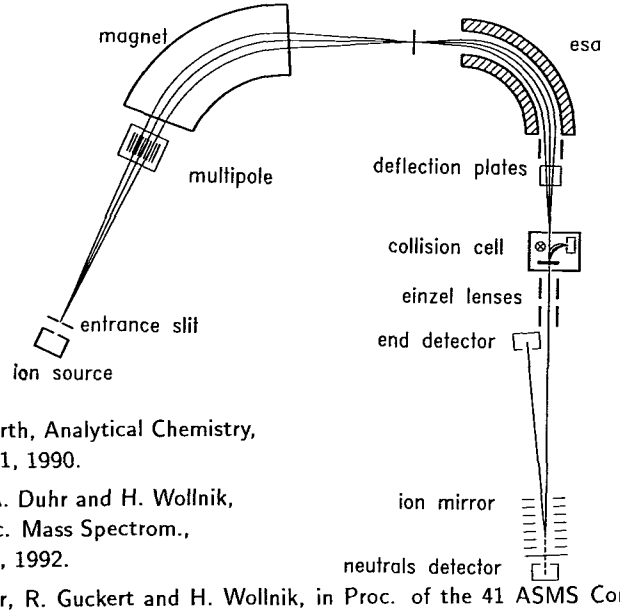

[1] W. Aberth, Analytical Chemistry, 62, 609–611, 1990.

[2] G. Li, A. Duhr and H. Wollnik, J. Am. Soc. Mass Spectrom., 3, 487–492, 1992.

[3] A. Duhr, R. Guckert and H. Wollnik, in Proc. of the 41 ASMS Conf. on Mass Spec. and Allied Topics. page 929, 1993.

A new 2-D / 3-D-TOF MS

H. Bernhard Linden and Michael Bamberg;
Linden ChroMasSpec GmbH, Auf dem Berge 25,
D-28844 Leeste, Germany

In recent years time-of-flight mass spectrometry (TOF MS) has become very popular. TOF-instruments have the basic merits of simplicity, high sensitivity, and unlimited mass range. Improvement is desired with respect to mass resolution and fragment ion analysis [1-4].

In order to improve these draw-backs, we have developed a new type of TOF MS equipped with dispersion electrodes the potentials of which vary with time [5]. Ions penetrating said electrodes after each other, experience different fields and are respectively dispersed:

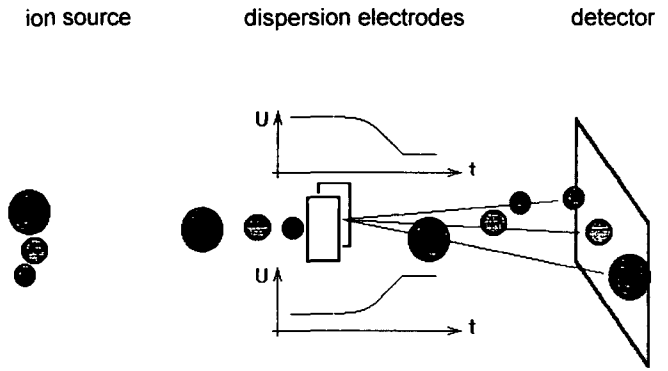

Fig. 1 Basic 2-D / 3-D TOF mass separation with $U \sim t^2 + t_d$

Dispersion potentials varying with the square of the flight time generate linear mass scales on the detector plate. To compensate for different energy, an electrical sector is added:

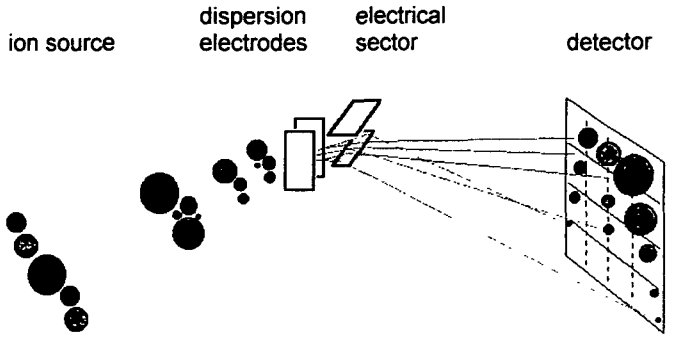

Fig. 2 Advanced 2-D / 3-D TOF mass and energy separation: every shot exhibits the entire information on precursors and related fragments

The experimental setup has an effective TOF flight path of 17 cm, kinetic ion energy of 150 V, chevron type detector with postacceleration and phosphor screen, and a high resolution CCD-camera with video image processing software.

Spectra are presented confirming the theory that at constant mass unit distances the resolution increases with the mass. Simplicity of handling is preserved: Mass range and resolution are individually selectable by setting 1 specific parameter only.

The new 2-D / 3-D-TOF MS is able to disclose information on several precursor ions and their fragment families simultaneously in every shot.

References:

1) W.C. Wiley, I.H. McLaren, Rev.Sci.Instrum., 26 (1955) 1150
2) B.A. Mamyrin, Russian Patent No. 198034 (1966)
3) R. Kaufmann, D. Kirsch, B. Spengler, Int.J.Mass Spectrom.
4) M. Oron, Y. Paiss, US pat. No. 3,953,732 (1976)
5) H.B. Linden, US Patent No. 5,420,423 (1995)

The Evaluation of a Comprehensive MS Reference Library

V Zaikin*(1-1), P Ausloos, C. Clifton, S. Lias, A Mikaya, D. Sparkman, S.Stein*(1-2)
1-1 Topchiev Institute of Petrochemical Synthesis, Moscow, Russia
1-2 NIST, Gaithersburg, MD, USA

The confidence in correctly identifying a compound by matching its spectrum with a reference library spectrum depends directly on the quality of the library. Since it has become clear that automated quality control algorithms are unreliable, a spectrum-by-spectrum evaluation of the source archive of the NIST/EPA/NIH Mass Spectral Library has been undertaken over the past four years. This archive, containing over 110,000 spectra, has been exhaustively examined by individuals well trained in mass spectrometry. Once 20,000 recently obtained spectra are also subjected to this evaluation, NIST will release a fully evaluated collection of spectra. Because of unavoidable uncertainties in judging the quality of a spectrum, an important requirement has been the agreement on both the analysis and the remedy (correction or deletion) for each spectrum by at least two individuals. An exact record of any modifications to the spectra has been maintained. Where possible, suspect spectra have been remeasured.

Below are the criteria for inclusion in the distributed database and the factors used to evaluate spectra, along with examples of difficult evaluations

Criteria For Spectrum Inclusion

- Spectra consistent with structure and containing all the most characteristic peaks
- Incomplete spectra with 10 or more of the most characteristic peaks
- Monoisotopic spectra of compounds which cannot be remeasured
- Modified spectra (correction of nonspectral data, peak coordinates, deleting peaks, adding isotope peaks, etc.)

In some cases, the spectrum will be excluded from use in the distributed database because it is obviously incorrect. However, in other cases, it may be desirous to take corrective action. Whenever possible, compounds with suspect spectra are remeasured There are some spectra where this is not possible. Listed below are the corrective actions that can be taken Peaks are never added except in the case of monoisotopic spectra of compounds containing chlorine and/or bromine or multiple atoms of silicon and/or sulfur Then, only characteristic isotope peaks are added at high mass to help in the visual identification of the spectrum.

When mass assignment or transcription errors are detected in a spectrum, peaks are never shifted more than one m/z unit

A critical requirement is that the evaluation and any corrections must be agreed on by at least two experienced, independent evaluators.

Evaluation Factors

- Consistency of name, structure, formula, molecular weight and CAS registry number
- Identification and analysis of molecular ion and important fragment peaks
- Consistency of formula with presence of significant isotope peaks (for Cl, Br, Si & S)
- Interpretation of spectrum based on mass spectral rules.
  - Nitrogen
  - Even-Electron
  - Stevenson-Audier
  - Bond Cleavage Adjacent to Unsaturation
  - Primary Fragmentation Rules
    - Simple cleavages
    - Rearrangement processes, including skeletal rearrangement
- Identification of background, impurity and other phantom peaks
- Visual and computerized comparison to other spectra
  - Replicate spectra of the same compound
  - Stereoisomers
  - Homologous Series
  - Derivatives
  - Spectra of the same compound in other collections
- Comparison of observed isotope peak intensity to calculated (performed with software specially developed by NIST)
- Comparison of calculated neutral losses to observed values (performed with software specially developed by NIST)

If a spectrum is labeled as a certain compound and the evaluation does not agree with the label, the identity of the compound is never changed The spectrum is excluded from use in the distributed database. If the source of the data is available, such as spectra taken from the literature, the changes will result in a spectrum with a new NIST number, which will then be reevaluated.

If two independent examiners agree the spectrum meets all evaluation criteria or that corrections can be made within the restrictions enumerated above, the spectrum will be included in the distributed version of the NIST/EPA/NIH Mass Spectral Library. Where there is more than one spectrum available for a given compound, the best spectrum (covering the widest mass range, requiring the least corrections and having the largest number of plausible peaks) will be selected for the Main Library Depending on the overall quality of the remaining spectrum or spectra for a given compound, inclusion in the Selected Replicates Library will be considered.

This fully evaluated mass spectral database will contain approximately 100,000 spectra for over 80,000 compounds. This version of the NIST/EPA/NIH Mass Spectral Main and Selected Replicates Libraries will have 7,000 to 8,000 spectra measured by NIST by GC/MS. This process of measuring spectra of commercially available compounds will continue and allow further growth of the database. As in the past, NIST solicits the donation of other collections of mass spectra for either recognized or anonymous inclusion in the database after evaluation

Odor Analysis by GC/MS/FTIR using Substucture Based Spectral Libraries.

A Nikiforov[1], Barbara Remberg[1], G Buchbauer[2], L.Jirovetz[2] and S.Kórnig[3]

[1] Inst. Org Chem , Univ.Vienna, Wahringerstr 38, 1090 Vienna, Austria, Fax· 011-43-1-31367-2280
[2] Inst of Pharmaceutical Chemistry, Univ.Vienna, Althanstr. 14, 1090 Vienna, Austria,
[3] Chemical Concepts GmbH, Boschstr 10, Weinheim, Germany

The odor attributes of complex odor systems, which exhibit distinct effects in medical and aroma applications (aromatherapy, perfumery), could not be predicted until today. Thus it was the aim of this work to investigate, whether there is a correlation between the concentration displacement of the volatiles and the odor attributes of such complex systems.

In the first part of this work, the selection of appropriate odor systems, the preparation of olfactorically representative samples and the instrumental analysis were performed. The dynamic headspace method was used for the preparation of 25 samples of the following odor systems flowers. apple, grape, Exacum affine, different plant parts of Aesculus hippocastanum, leaves of Plectranthus coleoides, different mushrooms, sunflower stems, peels of Juglans nigra, Chenopodium botrys plant, SCF-extract of shellac, needles and twigs of Douglas Fir, as well as old books and fragrance candles with different notes Sensoric evaluation was performed by professional perfumers who classified the samples in terms of "flowery", "fruity", "fresh", "green" and "mushroomlike" odor notes Investigation by means of GC-FID, GC-FTIR-MS and GC-Sniffing technique allowed the identification of more than 350 different components in total, mostly terpenes, ketones, lactones and esters

In the second part, the structures of 61 796 components of NIST/EPA/NIH mass spectra library and of approx 130 000 entries of Wiley (R) Spectral Library were transferred (authorized work), together with the corresponding ID numbers, as MOL-files in the commercially availably structure and substructure based "ISIS/BASE (R)" of MDL Information Systems. Using this data files, substructure

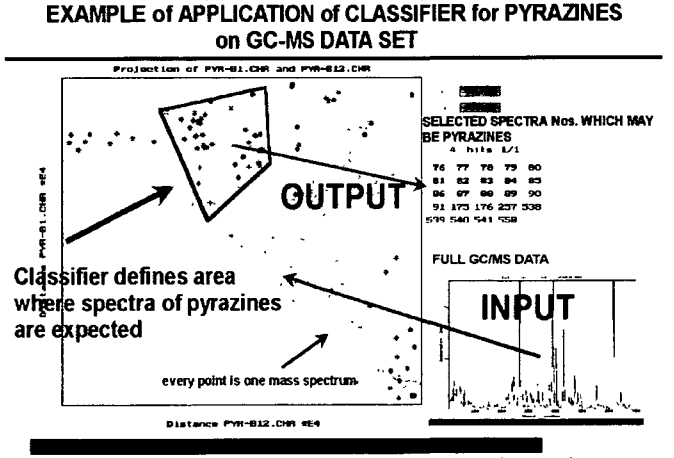

Fig.1: Example of a planar classifier based on MS-data for pyrazines

search (queries) subsequently enabled, via the ID library numbers, the selection of mass spectra (as contained in the spectral libraries of NIST/EPA/NIH resp Wiley) for training data sets These training MS data sets, in turn, were used for the development of classifiers for semiautomatic preselection, via multivariate analysis, of groups of target compounds in instrumental data of the odor systems investigated. The classifier's performance is mostly essentially improved if classifying criterions based on IR data are also included An example of planar classifier for pyrazines, based on MS data exclusively is given in Fig. 1

The structure files in MOL formate have additionally proved to be useful as a structure pool for input in a variety of programs which use MOL formates (see MDL Information Systems "Affinity" Group), e g MOLGEN (R) structure generator of Chemical Concepts GmbH, Weinheim, Germany, etc.

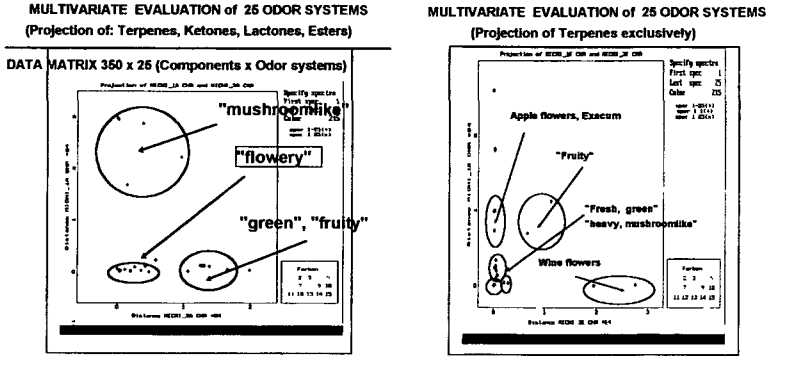

Fig.2: Correlation of MS-data of combined substance classes (terpenes, ketones, lactones and esters) and of terpenes alone with the odor notes of 25 aroma systems

In the third part of this work, multivariate evaluations, via PCA (projection in plane of the 1st and 2nd eigenvector), of 350 selected components, which were identified in investigated odor samples, based on a 350 x 25 (volatiles identified x odor systems) data matrix, were performed in order to find out if the displacement of the components concentrations of the samples correlates with their odor notes, as defined by professional perfumers. As a result of this, it became clear that the odor notes "flowery", "fruity", "fresh", "green" and "mushroomlike" may be correlated with a certain distribution of terpenes, alcohols, aldehydes and ketones, but not with the group of terpenes alone (Fig 2) Nevertheless, the prediction of odor notes based on instrumental data via multivariate analysis of the volatiles of complex mixtures is principally possible.

Experimental: The GC/FTIR/MS data were registered in a serial arrangement of IR and MS (HP-5965B IRD with 5970C MSD). The recorded data was converted into own data arrays for subsequent data processing All calculations were made as desktop applications using a Highscreen 60 MHz Pentium PC For multivariate analysis own programs MSIR (written in TurboPascal) were used.

Acknowledgement: The support of the „**Hochschuljubiläumstiftung der Stadt Wien**" (**Project H-78/94**) is gratefully acknowledged.

A FULLY AUTOMATED SYSTEM FOR CONFIRMATIONAL MASS SPECTROMETRIC ANALYSIS

Saul W. Fink, William L. Thompson, and John R. B. Slayback
Bristol-Myers Squibb Pharmaceutical Research Institute
One Squibb Drive, P. O. Box 191, New Brunswick, NJ 08903

Mass spectrometry (MS) is a vital tool in the development of novel pharmaceutical compounds. There are benefits of automating an MS system for routine analysis in the laboratory. First, rapid turnaround of analytical data is necessary as the results may be used to determine the next step of the synthesis. An automated MS system can support a turnaround time of one day or less of data without creating a "sweatshop" atmosphere in the laboratory. Second, routine MS analysis without automation requires many personnel hours. The time consuming elements of these routine samples can be substantially lightened using an automated MS system which provides more time for the operator to work on other challenging MS experiments.

Although GC/MS systems have been automated successfully for many years, instrument manufacturers have been slow in their progress towards automating other hyphenated chromatography (e.g. liquid, supercritical fluid) and MS techniques. A few laboratories have invested a significant amount of time to develop automated systems for MS analysis.[1,2,3,4] Described herein is an automated system for preparing and analyzing samples, and processing MS molecular weight data with a minimal amount of "hands-on" time.

EXPERIMENTAL

A Zymark Benchmate™ II Workstation equipped with an injection port, is used to prepare the sample solutions. There are two 2-tube methods running in series to prepare the samples. One method prepares solid samples (powders and crystals) and another prepares liquid samples (oils and solutions). There is a capacity of 100 samples/run.

A schematic diagram of the instrumental setup for the automated system is shown in Figure 1. A Waters 600 MS HPLC pump is connected to a Zymark Benchmate™ II which prepares and injects sample solutions into the Sciex API III triple quadrupole mass. The mass spectrometer is operated in the flow injection mode at 50 µL/min using the ionspray LC/MS interface and a mobile phase of 50/50 (acetonitrile/2 mM ammonium acetate, pH 6.0 using acetic acid). The mass spectrometer is equipped with the AutoGate option which allows the cryo-pumped vacuum system to be recycled (shutdown) in the absence of an operator.

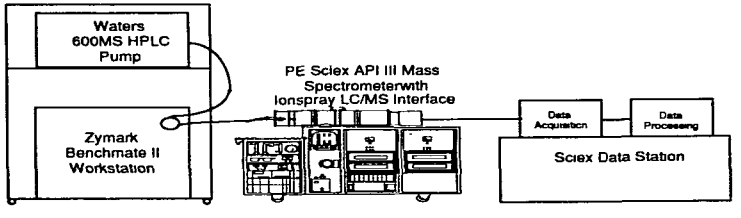

Figure 1. Schematic diagram of the instrumentation for the fully automated MS system.

The analyst inputs the sample information into a file in the automated acquisition program (RAD) and determines whether to analyze the samples using the positive or negative ion mode. A script code has

been written to automate the MS data processing. The macro, developed with the assistance of Dr. Ron Bonner of PE Sciex, processes a batch of files, sums the data from a specified range of MS scans, and background subtracts scans prior to the scans of interest. The MS spectra are then printed to a local printer for distribution to the submitting chemist.

RESULTS and DISCUSSION

Repetitive injections of standards were made to show the reproducibility and ruggedness of the automated system. Figure 2 displays the ISP-MS total ion chromatogram (m/z 300-1100) and selected mass chromatograms for injections of 200 ng of paclitaxel and reserpine using the solid method for sample preparation. The MS data show little, if any, carry over of sample between injections demonstrating the ruggedeness of the system. The standard deviations for the repetitive injections of reserpine and paclitaxel standards are 5.38% and 5.79%, respectively. Although the automated system is used for qualitative purposes exclusively, the results demonstrate the reproduciblity of the system.

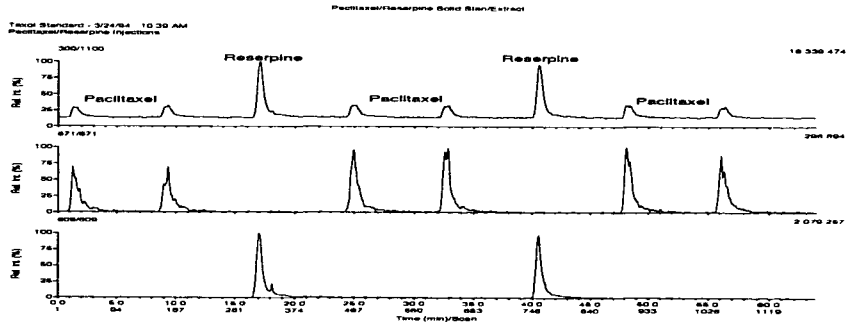

Figure 2. ISP-MS total ion chromatogram (m/z 300-1100) and mass chromatograms (m/z 871 and 609) for injections of 200 ng of paclitaxel and reserpine, respectively.

SUMMARY

An automated system has been developed which allows us to prepare, analyze and process molecular weight data for routine confirmational MS samples. A minimal amount of analyst time is necessary giving the operator time to work on other experiments while the routine samples are analyzed. The system is capable of analyzing the samples overnight, generating more instrument time during the day to conduct more challenging MS experiments or to increase MS sample throughput. The automated system yields reproducible results and there is little, if any, noticeable carry-over. To date, 94% of all samples analyzed using this system have produced good quality MS spectra with minimal operator intervention. In a one year period, we estimate that the enhancement in productivity has saved at least 600 direct labor hours.

1. M. J. Hayward, J. T. Snodgrass, and M. L. Thomson, *Rapid Commun. Mass Spectrom.*, 7(1993), p. 85.
2. D. J. Martin and P. M. Bond, "Automated Probe Mass Spectrometry," *Biomed Environ Mass Spectrom.*, 18(1989), p. 733.
3. D. E. DeJohn and A. B. Giordani, *Proceedings of the 40th ASMS Conference on Mass Spectrometry and Allied Topics*, Washington, D.C., 1992, p. 852.
4. L. C. E. Taylor, *Proceedings of the 42nd ASMS Conference on Mass Spectrometry and Allied Topics*, Chicago, IL, 1994, p. 322.

SPECTRAL RESOLUTION OF ISOMERIC ALKANES: A PROCESS MASS SPECTROMETRY APPLICATION

Martin L. Haddix and Kelsey D. Cook, Department of Chemistry, University of Tennessee-Knoxville, TN 37996-1600

Isomer resolution by mass spectrometry (MS) is not widely practiced, in large part due to the strong similarity among isomer mass spectra. However, the need for such an application has arisen, in attempting to exploit the speed of MS for monitoring a process isoprene stream (a complex mixture of C_4-C_6 alkanes, alkenes, and alkynes) being examined in collaboration with a member of the University of Tennessee Measurement and Control Engineering Center. As a first step in assessing feasibility and reliability, mixtures comprised of two components from the isoprene stream (pentane and isopentane) have been examined by EI MS using an Extrel quadrupole-based process analyzer. Reference spectra of these two components (Figure 1) show expected overlap (*i.e.*, all ions in one spectrum are also in the other), but there are distinct differences in relative abundances, suggesting that resolution should be feasible. The problem of optimizing the accuracy, precision, and speed of determination of the relative concentrations of the two compounds in a mixture then becomes a problem of *parameterization*, selecting which part of the spectrum to use for deconvolution. Since much of the spectrum contains only noise (*i.e.*, at those m/z ratios where there is no significant signal), it is clear that deconvoluting the *entire* spectrum will not provide optimum efficiency. At the other extreme, two concentrations can, in principle, be determined by monitoring as few as two ion signals, provided that the intensity ratios for those ions differ in the spectra of the pure components. If consideration is limited to ions of relative abundance greater than 10% in the pure component spectra (thus the eight most intense peaks in a spectrum from a 50/50 v/v mixture of pentane and isopentane), there are 28 such pairs possible. Similarly, there are 56 possible combinations of three ion signals selected from among the eight peaks, 70 combinations of four, *etc.*, comprising a total of 247 possible combinations of two to eight peaks The utility of any of these parameter choices for providing the needed deconvolution depends on the signal-to-noise ratio of the signals monitored and the differentiation among the intensity ratios in the pure component spectra. Even ions of high abundance may not be useful for deconvolution if their intensities do not differ in the reference spectra.

There is little guidance in the statistics literature to facilitate optimum parameterization in cases like this For a relatively simple case (such as this prototype binary system), it is feasible to employ a "brute force" approach, wherein all possible combinations are tested for accuracy and precision. As spectra become more complex, the number of combinations increases rapidly, making this exhaustive approach impractical. Therefore, it is instructive to examine the impact of various parameterization alternatives in an exhaustive treatment, to try to discern guidelines that may provide short-cuts to optimum parameterization as we move from the two-component prototype to the more complex process mixtures of real interest. This is the main goal of the current study.

In the exhaustive treatment of the 8-peak mixture spectrum, data for each m/z ratio can be used to obtain 124 different estimates of the vapor composition. Figure 2 presents the accuracy and precision (standard deviation of 5 replicate determinations) of each of these estimates for each m/z, using data obtained from a binary mixture estimated to provide vapor comprised of 45.1% pentane. (The preponderance of positive errors suggests that there may have been a systematic error in preparing the sample or estimating its vapor composition.) Figure 3 shows the average and range of values obtained using 2-, 3-, . ., up to 8-parameter fits. The largest error (1400%) occurred for a 2-parameter estimate (m/z 29 and 41), although these two parameters gave reasonable results in other 2-parameter combinations . Some 2-parameter estimates were quite accurate (*e.g.* 2% error using m/z 15 and 43). Use of all eight peaks did not afford the most accurate (6% error) or precise (std. dev. = 0.009) results. In general, however, the accuracy of the

determination did increase with the number of peaks used for prediction. In contrast, the precision varied widely and erratically (0.004 < standard deviation < 1.8) (Figure 2b).

From the spread of values in Figure 2, it is evident that the ion at m/z = 57 gave accuracy and precision generally better than that obtained with most other ions. This can be rationalized based on fragmentation pathways, as shown in Figure 4. The methyl-loss products at m/z 57 and 15 are the only major fragments which can be formed by more equivalent pathways starting with isopentane (three), than starting with n-pentane (two). Clearly, if such rules can be placed on a more quantitative basis, they can greatly facilitate parameterization. A "scoring system" aimed at quantitating the distinguishing ability of ions in a spectrum is under development. Failing that, more empirical approaches (*e.g.*, neural networks, partial least squares, or principal components analysis) will be invoked as we move from prototype to more complex process systems.

Figure 1

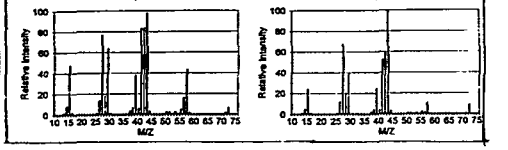

Figure 3a **Accuracy summary**

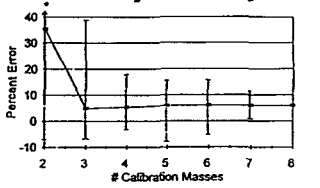

-line connects average of all estimates based on indicated number of calibration masses
-preponderance of positive errors suggests "target" value (54.9% isopentane) may be in error
*Outlier at 1400% error

Accuracy of all concentration estimates involving indicated mass
Figure 2a (average of 5 replicate determinations)

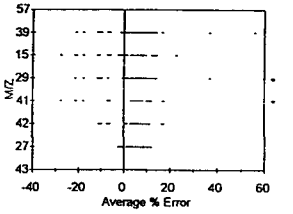

*Estimate based on intensities at m/z 29 and 41 is actually an outlier with 1400% error (Offscale)

Figure 3b **Precision summary**

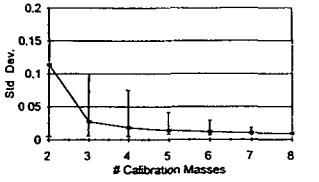

-line connects average values, error bars represent full range of precision values for given number of calibration masses

Standard Deviation of all concentration estimates involving indicated mass
(Standard deviation of 5 replicate determinations)

Figure 2b

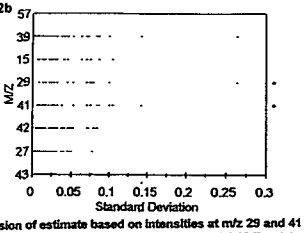

*Precision of estimate based on intensities at m/z 29 and 41 is actually an outlier with standard deviation = 1.8 (Offscale)

Figure 4

Ion with m/z 57 tends to give "superior" results.

Tentative explanation: Fragmentation schemes for Pentane & Isopentane

2 pathways to m/z 57 — 3 pathways to m/z 57

Only m/z 57 (and 15) have more equivalent pathways for Isopentane than pentane.

DISTINGUISHING BETWEEN ISOMERIC C3H5 MOIETIES USING DAUGHTER ION SPECTRA

John Glass Green

Louisiana Division Analytical Sciences Laboratory
Research and Development, B-2503
Plaquemine, Louisiana 70765-0400

During the analysis of a complex mixture resulting from the reaction of various chloropropanols with propylene oxide, a compound was detected that apparently had molecular weight 134 u. Isobutane chemical ionization confirmed the molecular weight. Based on the m/z 134,136 cluster, the compound contained one chlorine atom. The EI spectrum let to the conclusion that the compound was a propenyl 1-chloro-2-propyl ether. The question then arose as to which propenyl isomer was present. The m/z 58 base peak held the key to the structure of this portion of the molecule. Proton transfer from the chloropropyl moiety to the ether oxygen gave the m/z 58 ion.

The daughter in spectrum of the m/z 58 ion was obtained. (Figure 1) This spectrum was compared to the spectra for three model compounds, acetone, propanal, and allyl alcohol. (Figures 2-4) McLafferty has shown that the tautomers of acetone give similar CAD spectra.[1] This is also true for propanal. Regardless of which tautomer is involved, the CAD spectra of acetone and propanal are quite easily distinguished.

The CAD spectrum for acetone shows a significant m/z 43 daughter. The base daughter peak in the CAD spectra for both allyl alcohol and propanal is m/z 57 with essentially no m/z 43 present. McLafferty reported that the spectra for allyl alcohol and propanal are identical.[1]

The m/z 58 ion from the unknown was thus determined to be of the 2-propenyl structure.

Experimental

These experiments were conducted with a Finnigan MAT 95 high performance mass spectrometer using the linked scan capability. Collisional activation was done using helium in the collision cell in the first field-free region with 5kV accelerating voltage. Helium pressure was adjusted to give a 50% reduction in the parent ion intensity.

[1]C.C. Van de Sande and F.W. McLafferty, JACS, 97(16), 4617-20(1975)

Daughter Ion Spectrum of m/z 58 from Unknown

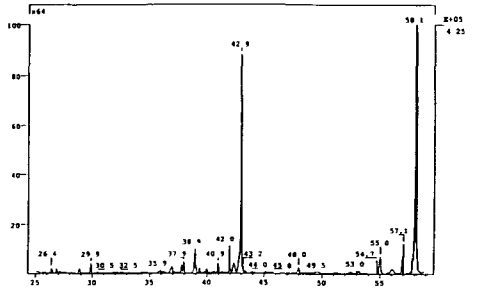

Figure 1

Daughter Ion Spectrum of m/z 58 from Acetone

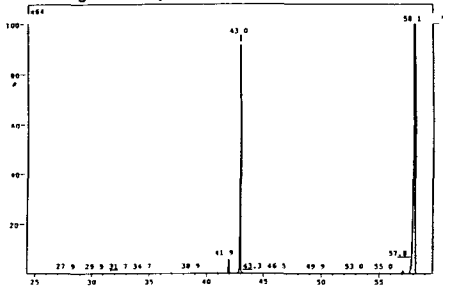

Figure 2

Daughter Ion Spectrum of m/z 58 from Allyl Alcohol

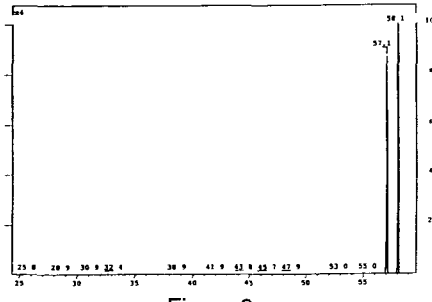

Figure 3

Daughter ion Spectrum of m/z 58 from Propionaldehyde

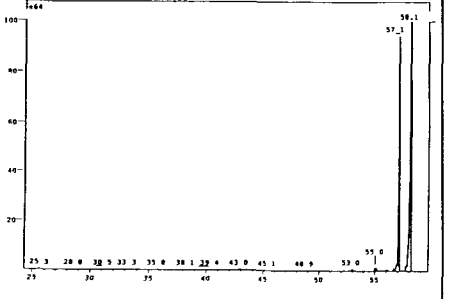

Figure 4

Structure Elucidation Using a Multi-Disciplinary Analytical Approach

D. J. Russell, S. W. Fink, L. M. Mallis, and J. R. B. Slayback

Bristol-Myers Squibb Pharmaceutical Research Institute
1 Squibb Dr., Building 90
New Brunswick, NJ 08903

The traditional role of an analytical spectroscopy group is to provide technical expertise in areas related to specific disciplines. Structure characterization problems are then carried out as independent problems within the different disciplines. This fragmentation of effort leads to the inefficient use of both the instrumentation and expertise available in the analytical environment. In our department, the focus has been moved away from analytical techniques and centered on problem solving. Our approach to structure elucidation is use of all available techniques in a concerted, cohesive fashion to solve the problem.

To show how this approach is applied, we present the structure elucidation of a chlorinated intermediate of the thromboxane antagonist, BMS-180291. Ionspray mass spectrometry (ISP-MS) and ISP-MS/MS techniques were used to determine the molecular weight of the compound and to verify the presence of a chlorine atom. Interpretation of the MS/MS data provided some substructure information about the molecule, but the position of the chlorine atom was ambiguous. Interpretation of ^{1}H and ^{13}C NMR data showed that during the chlorination reaction a quaternary carbon was formed from a methine carbon in the preceding reaction intermediate. Classical 2D NMR analysis provided unambiguous information regarding the site of substitution. Thus, it was the combination of disciplines, using one and two-dimensional NMR, ISP-MS, and MS/MS techniques, which allowed the unambiguous assignment of structure.

Our approach improves the efficiency of small molecule structure elucidation by driving the project exclusively within the analytical domain while maintaining a high level of confidence in the result through the use of teamwork between the various disciplines.

43rd ASMS Conference on Mass Spectrometry and Allied Topics

Practical Applications using Automated Mass Spectrometry in Drug Discovery

L.M. Schaffter*, R.C. Spreen, G.H. Cureton and F X. Morris
Zeneca Pharmaceuticals, A Business Unit of Zeneca, Inc.
Wilmington, Delaware 19850-5437

Our laboratory is currently using a VG Platform mass spectrometer (Fisons Instruments) with ApCI (atmospheric pressure chemical ionization) for molecular weight analysis of small molecules in drug discovery. The instrument has been automated and utilizes "Open Access" software as discussed previously by Taylor *et al* The system allows chemists to directly submit a prepared sample to a large tray autoinjector for flow analysis. Name and sample ID are input into a log-in computer and choice of positive or negative ionization is selected Sample ions are formed, the mass analyzer measures the spectrum, the MS computer processes the acquired data and prints the spectrum in both graphical and tabular form

The objective of the study discussed in this presentation was to optimize instrumental variables to facilitate automated production of abundant molecular ion signal (relative to fragment or adduct ion formation) for a wide range of chemical compounds.

Table 1. Qualitative Comparison of Positive and Negative ApCI

Compound Name	isotopic MW	Molecular Ions	
		Positive	Negative
[illegible]	651 3 amu	Yes	Yes
Creatinine	113.1 amu	Yes	Yes
2-acetyl-5-bromothio-phene	203 9 amu	Yes	No
aurintricarboxylic acid	422.1 amu	No	Yes
[illegible]	744 4 amu	No	Yes
5-acetyl-2,3-isopropylidene-adenosine	349 1 amu	Yes	Yes
9-acetyl anthracene	220 1 amu	No	Yes
2-amino-7-methyl-5-oxo-5H-[1] benzopyrano [2,3-b] pyridine-3-carbonitrile	251 3 amu	Yes	Yes
2,5-dichloropurine	188 0 amu	No	Yes
2-(trifluoromethyl)- phenothiazine	267 0 amu	Yes	Yes
(S,R)- Noscapine	413 1 amu	Yes	Yes
(S)-(+)-Camptothecin	348 1 amu	Yes	Yes

[1]L.C.E Taylor, R.L. Johnson, L. St. John-Williams, T. Johnson and S.V Chang, *42nd ASMS Conf. on Mass Spectrom. Allied Topics,* **1994**, p. 322.

Table 1 is a list of the twelve standard, non-proprietary compounds that were used in the study. A qualitative comparison was made of positive versus negative molecular ion formation using these compounds, to determine if providing the option of automated negative ion analysis in addition to positive ion analysis would be of benefit. The data shown above illustrates that if only positive ion analysis had been performed for four of the twelve standard compounds, no molecular ion would have been identified.

Several carrier solvent systems were examined but it was found that pure methanol gives the most consistent results in the flow injection system A variety of solvents may be used to dissolve the analyte prior to auto-injection into the carrier solvent flow, without a deleterious effect on the molecular ion signal (*e.g.* methanol, methylene chloride, acetone, DMSO, THF, DMF)

From this study it is clear that appropriate choice of both probe temperature and cone voltage is important. Too high of a setting for either of these two variables causes most analytes to fragment to a high degree. However, too low of a setting (< 350 degrees, Celsius for probe temperature and $\leq$ 15 volts for cone voltage) can also be a problem. Some analytes will not form molecular ions at these low settings, and when the probe temperature is this low it causes carry over between samples. Compromise values for both of these variables were selected for the final automated experiment. A value of 400 degrees, Celsius allows formation of molecular ions that are not particularly thermally labile and prevents significant carry over. A value of 20 V for cone voltage is high enough to produce molecular ions of most analytes, without causing too much fragmentation of compounds with more labile bonds.

Because of the short analysis time (approx. 4 minutes for each analysis) the instrument's high success rate at producing molecular ions and the system's overall versatility, many of the chemists in Zeneca's Medicinal Chemistry Department have more than doubled their use of mass spectrometry as an analytical tool In addition to analysis of isolated products and intermediates, the chemists commonly use the system for reaction monitoring, screening of fractions and analysis of TLC spots

Diversity Profiling: Rapid Pharmaceutical Development Based on ESI/MS

Mike S. Lee[1], Edward H. Kerns[2], Gerald C. DiDonato[1], Richard Gedamke[1], Mark E. Hail[1], Steven E. Klohr[2], Robyn Rourick[2], Anne M. Starrett[1], Susan C. Taylor[1], William L. Thompson[3], Kevin J. Volk[2], Bethanne M. Warrack[1] and Jeffrey L. Whitney[2]
Bristol-Myers Squibb Pharmaceutical Research Institute, [1]Princeton, NJ 08543-4000, [2]Wallingford, CT 06492, [3]New Brunswick, NJ 08903-0191

Electrospray ionization/mass spectrometry (ESI/MS) is ideally suited for the structural analysis of mixtures. Recent trends which highlight the utility of this tool for the analysis of pharmaceuticals have focused on biomolecule structure analysis and the identification of metabolites, impurities and degradants contained in complex matrices. These tasks are representative within the dynamic scope of drug discovery and pharmaceutical development and are often repetitive in that identical or similar assays are performed throughout the lifetime of the program.

Currently, our approach for rapid structure analysis utilizes liquid chromatography/mass spectrometry (LC/MS) based profiling protocols. Our strategy emphasizes early "lock-in" of analytical methods, a template motif for the generation of structure based libraries and proactive methods for the predictive structure analysis of mixtures. Here we describe our ESI/MS approach for supporting the rapid development of drugs and provide insight into further extensions of this valuable analytical tool for pharmaceutical applications, in particular, applications involving the micro-scale generation of diverse mixtures of compounds.

Early Method Lock-In

Perhaps the cornerstone of any analysis is the analytical method. The early development of analytical methods which are "universal" to all samples within the particular study (and beyond!) provide distinct advantages for drug development and product support. Standardized methods allow for quick response to diverse needs and changing priorities. Universal methods also allow for the easy transfer of methods from laboratory to laboratory.

A key to the successful launch and implementation of these methods is the realization that not all studies will be amenable to these methods. We streamline this approach by using an "80/20 rule" which provides realistic constraints. This rule provides a benchmark of method success to 80 percent of the samples and helps to avoid unnecessary and time-consuming method refinement. Thus, some detail such as resolution and specificity is sacrificed for increased speed of analysis.

Traditional molecular weight determinations using ESI/MS methods successfully incorporate this strategy. Utilized exclusively as a "front-line" ionization method, structural prescreen ESI/MS approaches have also been developed which provides useful relationships between structural features (i.e., compound class, functional groups, basicity) and ionization. Generally, small molecule analysis involves the use of conventional LC columns with volatile buffers and modifiers (optimized for sample concentration, solvents, eluent modifiers, pH and flow rates) while biomolecule analysis utilize polymeric microbore LC columns in combination with "trap cartridges" for rapid desalting or preconcentration. The rapid molecular weight profiling of flavones in fermenation broths represents an example of this early method lock-in approach.[1]

Generation of Structure Based Libraries

A template motif is utilized to generate structure based libraries using our universal LC/MS methods in conjunction with tandem mass spectrometry (MS/MS). This strategy makes use of substructural templates which are generated for each standard compound (impurity or metabolite) using on-line LC/MS/MS techniques. Structures are proposed based on differences between diagnostic ions in the MS/MS product ion spectra. Structural libraries are created which provide quick reference to proposed structure, relative retention time, molecular weight and diagnostic functional groups.

Structure libraries are generated for impurities, degradants and metabolites as well as for combinatorial libraries. Combined libraries can be used to facilitate selection of a drug candidate for development and correlate structure with activity, bioavailability, lipophilicity or solubility. These libraries can also be used to indicate potential problems associated with long-term storage (stability) and scale-up (impurities). The structure based library generated for taxanes is an accurate illustration of the utility of this approach.[2]

Application of Predictive Models

Predictive models allow for a proactive approach to establish a structural data base. These methods involve the use of chemical modification and solid phase synthesis to simulate realistic conditions and provide a diverse ensemble of potential metabolite, impurity or degradant structures. Structures are obtained from these models using micro-scale LC/MS methods consistent with our current profiling methods allowing for the ultimate incorporation with the structure libraries generated from actual samples.

Chemical modification methods employ a general scheme of conditions representing oxidation, reduction and hydrolysis as well as acylation, alkylation and halogenation. The standard compound, typically the final product, is subjected to these conditions and the products are monitored. Related compounds or a standard corresponding to a strategic structural analog (i.e., key intermediates, known impurities) are also subjected to these chemical modification conditions. Reagents such as HOAc, NaOH, K_2CO_3 and $KMnO_4$ provide abundant information with preliminary investigations dealing with modified captopril analogs.

Solid phase synthesis of analogs represents a potentially powerful approach for obtaining a head-start with metabolite, impurity and degradant structure analyses. Our protocols have been refined using captopril on a N-Fmoc-L-proline resin ester solid support. Analogs were generated from the coupling of the deprotected Fmoc-proline Rink acid resin with a variety of carboxylic acids followed by the release from the resin. This approach has promise for other compounds containing a carboxylic acid or amine functional groups.

Conclusions

The early identification of potential metabolites, impurities and degradants as well as the early lock-in of analytical methods provides a streamline continuum within the drug discovery-pharmaceutical development interface and provides benchmarkable measures of consistency. Current ESI/MS based methods provide an excellent tool for profiling a diverse array of structures. Combined with early method lock-in strategies, structure based libraries and proactive models utilizing chemical modification or solid phase synthesis, ESI/MS approaches can be developed to facilitate the discovery and development process. In combination with combinatorial chemistry methodologies, this type of analytical approach may be applicable to the rapid screening and characterization of small organic molecules with specific enzymes.

References

1. M.S. Lee, D.J. Hook, E.H. Kerns, K.J. Volk and I.E. Rosenberg, *Biol. Mass Spectrom.*, **22**, 84-88 (1993).
2. E.H. Kerns, K.J. Volk, S.E. Hill and M.S. Lee, *J. Nat. Prod.*, **57**, 1391-1403 (1994).

Changes in Volatile Organic Composition in Milk over Time

Santford V. Overton and John J. Manura
Scientific Instrument Services, Inc.
1027 Old York Road, Ringoes, NJ 08551

Volatile and semi-volatile organic compounds present both in the matrix and the headspace aroma are largely responsible for the flavor qualities of the foods we eat. Flavor is always considered the most important factor of any of the quality categories when comparing various dairy products. Because milk possesses a bland and soft flavor, the appearance of an objectionable off-flavor or off-odor is readily noticeable. There is a delicate balance between many flavor compounds that produce a desirable milk flavor and if this balance is disturbed, off-flavors may occur. In assessing its overall flavor quality, it would be extremely advantageous to have a reliable and efficient method for the detection, identification and quantification of the volatile organic compounds responsible for the degree of freshness in milk. Analytical techniques are needed to profile a wider range of volatile and semi-volatile organics in milk and to identify the flavors, off-flavors, off-odors and potential contaminants that may be present. The purpose of this investigation is to develop an analytical technique that could detect and identify a wide range of volatile and semi-volatile compounds in milk over time and relate the differences in volatile organic composition to the quality of milk. For this study, volatile organic compounds were purged from samples of milk followed by trapping onto Tenax TA adsorbent resin using a dynamic purge and trap technique (P&T). The adsorbent traps were subsequently analyzed by thermal desorption-gas chromatography-mass spectrometry (TD-GC-MS)

Several brands of milk that were freshly opened and allowed to sit at room temperature for two days were analyzed by a Purge and Trap technique to relate the off-flavor/off-odor to changes in the volatile organic composition of milk. In addition, several milk cartons were analyzed by "Direct Thermal Extraction" to determine if any volatile organics from the cartons contributed to the flavor profiles of milk. Sample sizes of 0 5 ml of the various milks were pipetted into a 10 ml test tube and heated to 60°C for 90 minutes. The surface of the samples was purged with high purity helium at 20 ml/min with an additional 25 ml/min dry purge using the S.I.S. Purge and Trap System. Volatile analytes were purged from the liquid matrix and carried to a preconditioned 4.0 mm i.d glass-lined stainless steel desorption tube packed with 200 mg of Tenax™TA. Approximately 25 mg of each of the milk carton samples with different colored inks were inserted into a 4.0 mm i d glass-lined stainless steel desorption tube and purged for 2 minutes at 80 ml/min to remove any moisture from the sample The desorption tube with sample was then attached to the Short Path Thermal Desorption System and a syringe needle attached. The desorption tube was injected into the GC injection port at desorption block temperatures of 250°C for 10 minutes and a flow rate of 1 ml/min for samples collected via purge and trap For samples to be analyzed by "Direct Thermal Extraction", the desorption block temperatures were set at 220°C.

Three different manufacturers of milk (Grade A, Half & half and a glass bottled milk) as well as samples from milk cartons with different colored inks were analyzed by Purge and Trap techniques and "Direct Thermal Extraction" to identify and compare the volatile organics present, and from the data, relate off-flavor/off-odor to the differences in composition of the volatile organic compounds Over 100 volatile organics were identified in the fresh and two day old milk. Most of the milk studied

produced 50 or more volatile organics which were identified in addition to many more that were either too weak to identify or in which a good NBS library match was not achievable. The milk samples were found to contain numerous straight and branched chain hydrocarbons, aldehydes, alcohols, ketones, fatty acids, esters, phenolic compounds, lactones and other miscellaneous compounds. Significant differences in the volatiles present occurred in the fresh milk samples versus the 2 day old samples. Although many of the same volatiles are present in all of the milk samples, there is a distinct variation in the quantities as well as the variety of volatile organics present. This variation could be due to the cow's diet, environment, heat treatment, bacterial spoilage, storage and the oxidation of lipids. In addition, the milk packaged in carton containers contained several volatile organic compounds that appear to be derived from the ink used in the manufacturing of the milk cartons

Among the hydrocarbons identified, tetradecane, pentadecane, hexadecane and heptadecane were the most abundant. They are derived either from the autooxidation of free fatty acids or from plants used in cow feed. Limonene was the predominant terpene hydrocarbon identified in the milk samples. Because only plants and some microorganisms synthesize terpenes, they must be transferred to the milk through the rumen The aliphatic compounds octanal, nonanal and decanal which are typical products of lipid oxidation were identified in each of the milk samples When these compounds pass a certain threshold, they are considered significant contributors to the development of rancid flavor Among the ketones, 4-methyl-3-penten-2-one, 4-hydroxy-4-methyl-2-pentanone, 3-methyl-2-cyclohexen-1-one, 3,5,5-trimethyl-2-cyclohexen-1-one and 2-nonanone were identified However, 1-phenyl-ethanone was only detected in the 2 day old milk samples packaged in carton containers In addition, 1-butanol, isoamyl alcohol and acetic acid, propanoic acid and butanoic acid were identified in the 2 day old milk samples. The differences in composition of the alcohols between the fresh and 2 day old samples may contribute to the difference of odor characteristics between the samples Most of the esters were found in the 2 day old milk samples. 2,6-Di-*tert*-butyl-*p*-cresol (BHT) was the predominant phenolic compound detected in each of the milk samples and may have been added as an antioxidant. The compounds 2-(2-methoxyethoxy)-ethanol and 2-(2-butoxyethoxy)-ethanol were only found in the milk samples packaged in the carton containers and not in the glass bottled sample. These compounds are believed to be derived from the ink used in the manufacturing process of the cartons Both of these compounds were also detected in carton samples containing different colored inks using the "Direct Thermal Extraction" technique. In addition, the milk cartons contained numerous straight and branched chain hydrocarbons, aldehydes, alcohols and terpene compounds.

The dynamic P&T technique together with TD-GC-MS has been utilized for the detection and identification of volatile organics, aromas and flavor components in milk over time and how these differences in volatile organic composition relate to the quality of milk. This analytical technique can be utilized for the quality control during the production of milk as well as a technique for the detection of potential contaminants in milk. The dynamic P&T technique offers several unique advantages over static headspace including greater sensitivity and the detection of a wider range of volatile organics including higher molecular weight compounds and is more sensitive by a factor of at least 100 as compared to the static headspace technique. This technique can easily be incorporated into troubleshooting techniques to detect problems in a wide variety of commercial food products, to compare various competing manufacturers' products as well as the implementation of a quality control program for the food industry.

MONITORING A CHEMICAL SYNTHESIS USING MASS SPECTROMETRY

Robin Sheppard, Mark Hayward* and Jack Henion, Analytical Toxicology,
Diagnostic Laboratory, Cornell University
927 Warren Drive, Ithaca, NY 14850
* American Cyanamid Company, Agricultural Research Center
P.O. Box 400, Princeton, NJ 08543-0400

The chemical synthesis of *o*-anilinocyclopropylketone was investigated using flow injection ion spray mass spectrometry and direct probe mass spectrometry. The reaction outline is shown in Figure 1. The goal is to monitor the by-products of the reaction and to identify reaction intermediates leading to the by-products in order to eventually understand and optimize the reaction parameters to improve the yield of the desired product.

This is a challenging application for ion spray mass spectrometry since the reaction is mediated with boron trichloride thereby requiring that it be carried out in non-aqueous conditions in a chlorinated solvent. The mass spectrometer used is a Sciex TAGA 6000E triple quadrupole upgraded to an API III with a home-made ion spray interface. We have monitored the reaction mixture as the reactants were added and at hourly intervals to characterize the reaction dynamics and to attempt to observe the reaction intermediates for this reaction. Full-scan spectra were collected for each sample and MS/MS was used to obtain product ion scans of abundant ions although essentially no fragmentation was obtained for the boron containing compounds. Figure 2 shows representative spectra obtained in these experiments. The major ions are identified to be protonated aniline (m/z 94), the protonated borazole by-product (m/z 187), the methyl ester of 187 caused by reaction with the methanol sheath (m/z 201), and the $[2M+H-H_2O]^+$ of the borazole (m/z 355).

In separate experiments, samples of the reaction mixture were analyzed by both EI and CI direct probe mass spectrometry using isobutane for ionization on a Finnigan MAT 95. MS/MS data was also obtained for many of the species monitored. Several ions of interest were identified to be: the amidine (m/z 161) which is formed after aniline addition, the acylation product (m/z 205) formed after $AlCl_3$ addition, a new intermediate (m/z 241), and the same m/z 355 ion seen in the ion spray data. The amidine formation does not depend on $AlCl_3$ or reflux. The mechanism for the borazole formation is shown in Figure 3. The MS/MS spectrum of m/z 241 is shown in Figure 4. This intermediate (m/z 241) helps explains the preferred charging order which favors the borazole intermediate: (1) cyclopropylnitrile, (2) BCl_3, (3) aniline, (4) $AlCl_3$. Formation of this intermediate (m/z 241) leaves the nitrile CI positioned for $AlCl_3$ catalyzed Freidel-Crafts acylation to an ortho position on the phenyl ring. The data suggests that formation of the m/z 241 is the rate limiting step as it is only observed prior to $AlCl_3$ addition and not during the several hours of reflux afterward.

This work shows the feasibility of using off-line mass spectral monitoring of this chemical synthesis for the optimization of reaction yield and shows promise that on-line monitoring could also be used to study such reactions. While ion spray mass spectrometry was not as useful for qualitative analysis of the actual reaction species because of reaction quenching in the sheath solution, it successfully allowed monitoring of reaction by-products. Direct probe mass spectrometry successfully identified important reaction species; however it is not

amenable to possible on-line analysis. Particle beam mass spectrometry may be a good choice for on-line analysis where both qualitative and quantitative information is desired. Preliminary experiments using particle beam with flow injection sampling show that the same qualitative results obtained with direct probe are easily achieved.

Figure 1

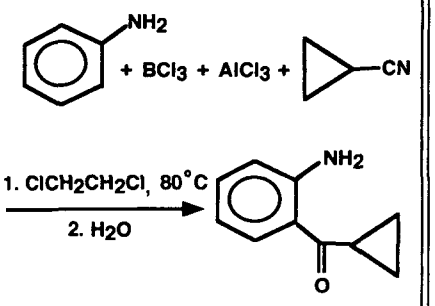

Figure 2

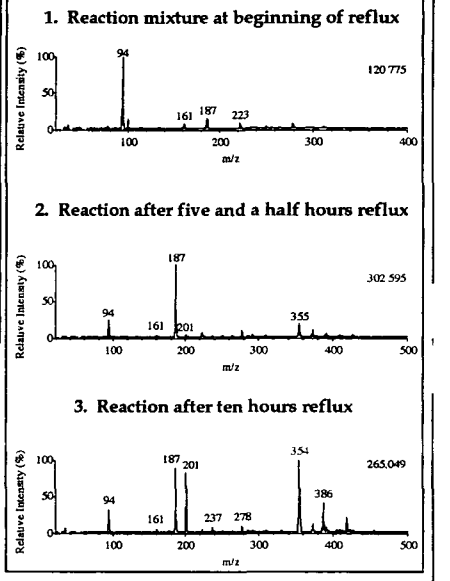

Figure 3

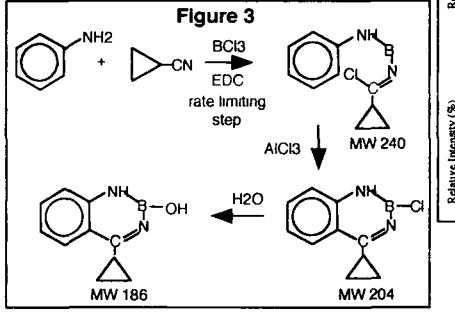

Figure 4

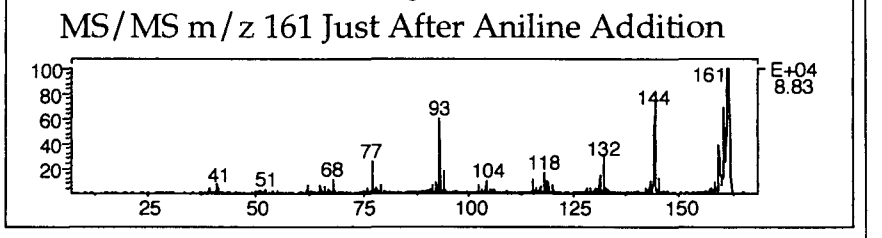

MEMBRANE INTRODUCTION MASS SPECTROMETRY USED IN SUPPORT OF THE MANUFACTURE OF QUINOLINEDICARBOXYLIC ACID

Ronald J. Lopata, Mark J. Hayward, and Michael L. Thomson
American Cyanamid - Agricultural Products Research Division
P.O. Box 400 - Princeton, NJ 08543-0400
and
Migdalia Ruiz, Felix Lafontaine, and Carlos Marrero
Cyanamid Agricultural of Puerto Rico
P.O. Box 243 - Manati, PR 00674

Membrane introduction mass spectrometry (MI/MS) has been used to identify, quantify, and locate the source of a low level volatile unknown that was observed by routine gas chromatography analyses of the vent stacks for all tanks containing toluene at a company manufacturing plant. Samples including the reaction streams, fresh toluene, recycled toluene, and the starting material for the process were all examined in order to understand the nature of the unknown. Sample preparation required only diluting each sample 1000 fold in water. Electron impact mass spectra permitted identification of the unknown as benzene and quantification of the benzene in each of the samples. Confirmation of the identification of benzene was carried out using tandem mass spectrometry. All analyses were readily carried out in one day by using totally automated flow injection sample introduction techniques as shown in the accompanying figure. The results obtained provided two key pieces of information: (i) the source of the benzene was the starting material, and (ii) that simple distillation of the toluene during the recycle part of the process raises the benzene concentration in the retentate because it is carried through with the toluene. When presented with these results, the supplier of the starting material acknowledged the presence of benzene and agreed, in the future, to provide starting material without significant levels of benzene. The primary benefit of using MI/MS (as opposed to other analytical techniques) to solve this problem was the unprecedented high speed at which the results were obtained. The high speed can be attributed to the following two qualities of MI/MS: (i) the ease of automation using flow injection sample delivery and, (ii) the ability to analyze complex mixtures without complicated sample preparation or method development. Based on these results, we view MI/MS as an important tool that should be included among the arsenal of interfaces utilized by mass spectrometrists to rapidly solve chemical problems.

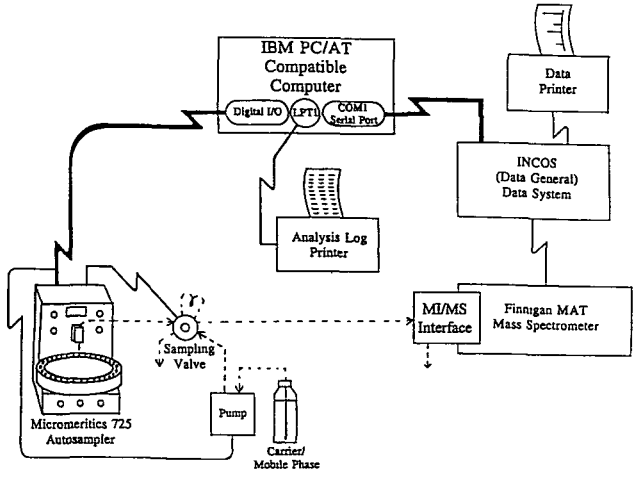

MEMBRANE INTERFACE

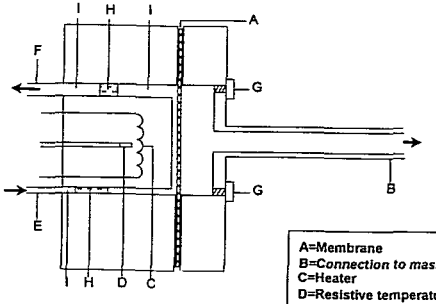

A=Membrane
B=Connection to mass spectrometer ion source
C=Heater
D=Resistive temperature sensor
E=Liquid sample inlet
F=Sample outlet (to waste)
G=Carrier gas inlet
H=Flowing sample solution
I=Flowing water (carrier)

Close Up of Membrane Interface

On-line Monitoring of the Photolysis of Benzyl Acetate by Membrane Introduction Mass Spectrometry (MIMS)

N. Srinivasan, P. Wong, N. Kasthurikrishnan and R.G. Cooks*
Aston Laboratory, Department of Chemistry, Purdue University, West Lafayette, IN 47907.
&
P. Wedge, J. A. Pincock, and J.S. Grossert
Department of Chemistry, Dalhousie University, Halifax, Nova Scotia, Canada, B3H4J3.

Exploration of the photochemistry of many organic compounds in water is difficult because the low solubility makes product characterization and determination of their yields difficult. We have applied MIMS [1] to such reactions because its high sensitivity overcomes the problem of low solubility and its capability for on-line monitoring potentially adds detailed insights into the course and kinetics of the process.

All the on-line photolysis monitoring experiments used a triple quadrupole mass spectrometer (Finnigan TSQ 4500) equipped with a sheet direct-insertion membrane probe.[2] The membrane employed was a dimethyl vinyl silicone sheet membrane with a thickness of 0.0125 cm. A solution of 400 mg/L benzyl acetate in 1:1 methanol-water in an 8 mL quartz tube was irradiated in a Rayonet photoreactor at a wavelength of 254 nm. The solution was recirculated by a peristaltic pump at a rate of 1 mL/min *via* Teflon transfer lines The probe, inserted directly into the source of the mass spectrometer, was heated to 80 °C. Analytes permeating the membrane were chemically ionized by either ammonia or isobutane. External calibration was accomplished by aspirating 500 μL of either sample or standard solutions into the membrane probe.

Scheme 1 shows the general mechanism for the photolysis of benzyl acetate in methanol-water [3]. Under isobutane CI conditions, several characteristic ions (m/z 107, 123, 183) are formed. The ion at m/z 123 is identified as protonated benzylmethyl ether by collision induced dissociation experiments (argon 17 eV) The ion at m/z 183 (bibenzyl, $[M+H]^+$) has a very low abundance indicating that this is a very minor product The ion at m/z 107 cannot be uniquely assigned due to the fact that both ethylbenzene and benzyl alcohol yield this ion.

Under ammonia CI conditions, ethylbenzene and benzyl alcohol yield characteristic ions of different mass-to-charge ratio. All the products yield the respective ammonium adduct ions $[M+NH_4]^+$ except ethylbenzene which yields M^+ at m/z 106. Benzyl alcohol was not observed under these conditions. Figure 1 shows that the ion abundance at m/z 168 (benzyl acetate, $[M+NH_4]^+$) decreases with time while the abundance of m/z 140 (benzylmethyl ether, $[M+NH_4]^+$) shows a corresponding rise with time. Figure 2 exhibits the ammonia CI mass spectrum of benzyl acetate after photolyzing for 20 minutes.

The concentration of benzyl acetate, benzylmethyl ether, bibenzyl and ethylbenzene were found to be 32, 44, 7.6, 32 mg/L respectively, after about 20 minutes of photolysis. These measurements were made by calibration using external standard solutions as shown in Figure 3. This corresponds to 92% conversion of benzyl acetate and the corresponding yields of benzylmethyl ether, ethylbenzene and bibenzyl are 14%, 11% and 3.1% respectively. Previous experiments in methanol solvent showed yields of 26%, 19% and 23% respectively [3]. The differences may be ascribed to the change in solvent. The initial rates of formation of benzylmethyl ether, ethylbenzene and bibenzyl were found to be 4.0×10^{-7}, 3.7×10^{-7} and 5.8×10^{-8} Ms^{-1} respectively. Hence, the relative rate constant ($k_{ethylbenzene} / k_{benzylmethylether}$) is about 0.93.

In conclusion, MIMS can be applied for on-line monitoring of an organic photochemical reaction due to its high sensitivity and selectivity and appears to be a very promising technique in studying reaction kinetics. The results show that the yields are dependent on the solvent and the products formed are consistent with earlier demonstrations by Pincock *et al.* [3] that the photolysis proceeds through both ion and radical pair intermediates.

REFERENCES

1 (a) Kotiaho, T., Lauritsen, F.R., Choudhury, T.K.; Cooks, R.G, Tsao, G T *Anal Chem.* **1991**, 63, 875A. (b) Cooks, R G.; Kotiaho, T *ACS Symp. Ser* **1992**, 508, 126
2 (a) Bier, M E, Cooks, R.G. *Anal. Chem* **1987**, 59, 597. (b) Bier, M E; Kotiaho, T; Cooks, R G., *Anal. Chem.* **1990**, 231, 175.
3 Hilborn, J W., MacKnight, E.; Pincock, J. A., Wedge, P. J. *J. Am.Chem.Soc.* **1994**, 116, 3337

Acknowledgement

We thank Dr. Philip Fuchs and Dr Harry Morrision for the loan of a Rayonet photoreactor The work at Purdue was supported by the Office of Naval Research.

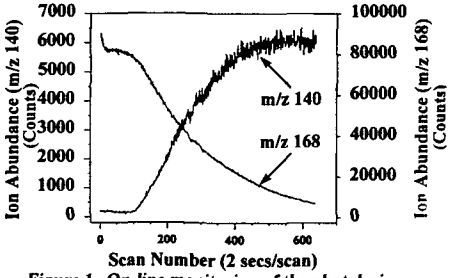

Figure 1. On-line monitoring of the photolysis of benzyl acetate (NH_3 CI).

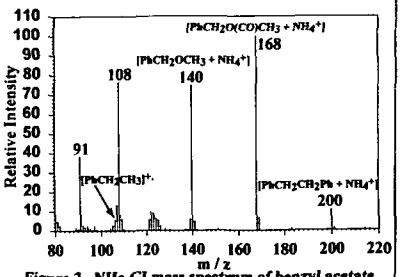

Figure 2. NH_3 CI mass spectrum of benzyl acetate after photolyzing for 20 minutes.

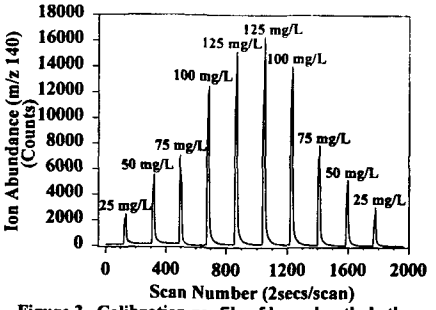

Figure 3. Calibration profile of benzylmethyl ether (NH_3 CI).

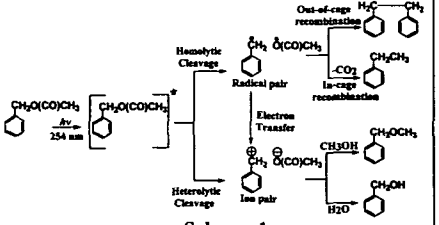

Scheme 1.

General mechanism for the photolysis of benzyl acetate in methanol-water.

Direct Analysis of Organic Compounds in Organic Matrices by Reverse Phase Membrane Introduction Mass Spectrometry (MIMS)

Scott Bauer, Jan Bauer, MIMS Technology Inc.

1900 S. Harbor City Blvd. Suite 115

Melbourne, FL 32901

Membrane introduction mass spectrometry (MIMS) has been applied to the direct analysis of volatile organic compounds in water with great success for many years. The high speed, low maintenance, inexpensive nature of MIMS makes it a natural choice for industrial monitoring applications. Unfortunately, most industrial processes take place in organic phases. In 1992 a method for the direct analysis of polar organic compounds in organic phases was demonstrated at Purdue University This method employed microporous membranes in a direct insertion membrane probe installed in a Finnigan TSQ 4500 spectrometer. This spectrometer has a differentially pumped source and can handle the high sample matrix flow across the microporous membrane. Unfortunately, the high cost of these spectrometers precludes their use in process monitoring applications. Bench-top mass spectrometer vacuum systems can not cope with the high flow of sample entering through a microporous membrane.

This presentation describes a method for the direct analysis of polar volatile organic analytes dissolved in non-polar organic solvents. Pervaporation membranes have long been used for direct analyses of organic compounds in water. They work well in benchtop mass spectrometers because the flux across the membrane can be managed by the instrument vacuum system. Polyvinyl alcohol (PVA) membranes are selective toward very polar compounds like water and reject less polar organic compounds. A PVA membrane was installed in a 1900-S1 sheet membrane probe from MIMS Technology Inc. The probe was installed in a Finnigan Magnum ion trap mass spectrometer. Sample introduction was performed using flow injection analysis techniques with an FIA-TC1 flow injection module from MIMS Technology Inc. Samples of volatile organic compounds such as acetone, methylethyl ketone, methanol, and THF were prepared at the low part per million level in hexane The flow injection module was filled with hexane and the flow rate through the system was set to 1 5 mL/minute. Although the PVA membrane discriminated against the non-polar hexane stream, enough of the matrix flowed through the pervaporation membrane to be used as a chemical ionization (CI) reagent gas.

Solutions of polar organic compounds were injected into the system to assess instrument response Parts-per-million level samples were easily detected and the mass spectra are clearly identifiable. All of the samples analyzed were protonated by the hexane CI reagent gas

43rd ASMS Conference on Mass Spectrometry and Allied Topics

10 PPM Acetone in Hexane by RPMIMS

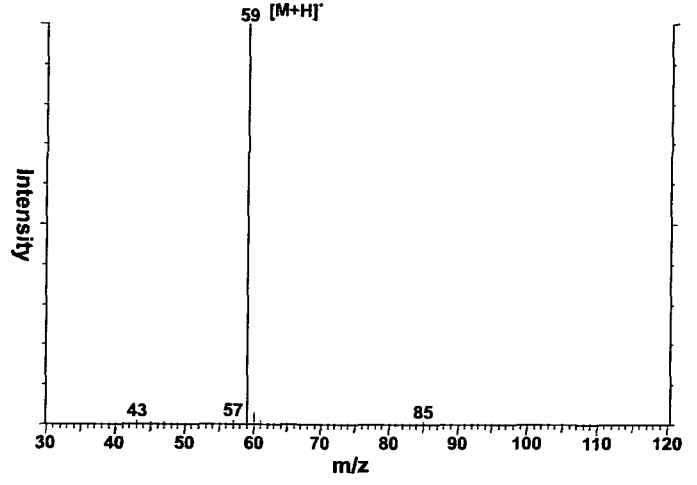

Extracted Ion Current for Protonated Acetone

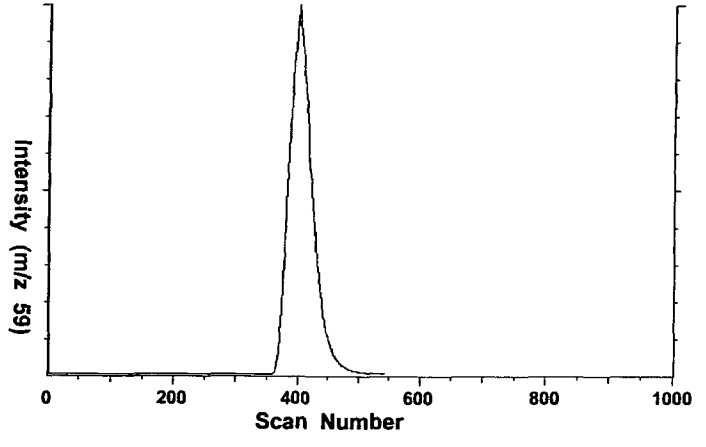

Analytical Potential of the MAB source for routine analysis of organic compounds

D. Faubert, P Mireault and M J. Bertrand.
Department of Chemistry, University of Montreal, Canada, H3C 3J7.

Electron ionization (EI) and chemical ionization (CI) have long been used for the analysis of thermally stable and volatile organic compounds. The former is known to induce fragmentation and often provides molecular weight information. However, many compounds do not provide intense molecular ions in EI and it is common for those to resort to CI that yields protonated parent species but relatively weak fragment ions Penning ionization (PI), which has been rather neglected as a common ionization technique for organic analysis, can offer many of the combined advantages of EI and CI while eliminating some of the limitations of those techniques Using different rare-gases, a range of internal energies can be transferred to the analyte providing spectral information that can be very specific or extremely general. We have recently developed a series of ionization sources based on the principle of Penning ionization. These sources use Metastable Atom Bombardment (MAB) to ionize molecules in the gas phase. The commercial version of the MAB ion source was provided by Dephy Technology (Quebec, Canada) The MAB source acts as an energy tunable ionization source, since different rare-gases can be employed The accessible energies are in the range of 8 32-20 61 eV depending on the metastable atoms used (Xe, Kr, Ar, Ne and He) By selecting the appropriate rare gas, the MAB source can achieved both hard and soft EI-like ionization. Thus, MAB is an excellent energy tunable ion source.

Most mass spectrometry techniques such as accurate mass measurement, MS/MS, LC/MS and GC/MS are used in chemical analysis of complex mixtures. Reproducibility of quantification is important in most applications Electron ionization is the preferred ionization technique but it is often used in the so-called "low-eV" mode In this mode the electron energy is reduced to minimize fragmentation and generate mostly molecular ions. This results in a lost of sensitivity and in low reproducibility. In order to solve some analytical problems more analysts are resorting to MS/MS techniques. It is desirable in this technique to generate only one ion per component in the mixture so as to reduce the number of species and have most of the ion current in the molecular ion to increase sensitivity In view of the ionization features required, it appears that MAB can offer advantages in terms of ionization and fragmentation selectivity To illustrate this, a mixture of 15 compounds (Figure 1) has been analyzed with the MAB source using Krypton and the mass spectrum shows 15 major peaks each corresponding to a compound in the mixture Thus, the MAB source affords softer ionization then EI giving an exclusive or a predominant molecular ion signal. This characteristic makes the MAB source ideally suited for MS/MS experiments In another experiments, a mixture containing typical compounds present in petroleum samples and compounds having amino groups has been analyzed with the MAB source using Xenon Results (Figure 2a) show that only molecules containing an amino group are ionized by the Xenon metastable atoms. For comparison, the mass spectrum of the same mixture obtained with electron ionization is shown at Figure 2b. The molecular peaks characteristic of compounds containing amino group are lost among all the fragments spawned by aliphatic chains The MAB source using Xenon can selectively ionize certain classes of compounds with low ionization energies such as amines, thioethers, polycyclic aromatic hydrocarbons (PAH), some polysubstituted aromatic compound, etc By using Krypton or Xenon gas, the MAB source can generate intense molecular ion even for extremely labile compounds

as methoxychlor, while electron ionization does not provide intense molecular ion. Figure 3 shows the case of a molecule synthesize in laboratory The MAB source using Krypton generates a mass spectrum with the molecular ion as major peak (Figure 3a), while the molecular ion is weak in electron ionization (Figure 3b). Thus, MAB is an excellent ionization source for routine analysis Furthermore, the MAB source has the advantage of requiring no maintenance for many months.

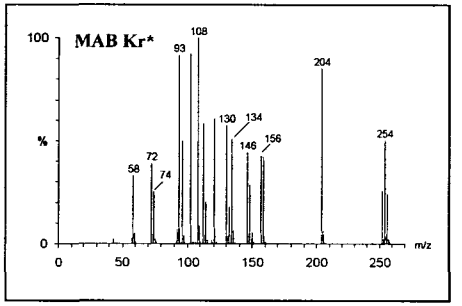

Figure 1 Mass spectrum of a mixture of 15 compounds obtained with the MAB source using Krypton

Mixture (m/z): Acetone (58), 2-butanone (72), Ether (74), Aniline (93), Fluorobenzene (96), Phenylacetylene (102), Anisole (108), Chlorobenzene (112), Propylbenzene (120), 1-chloro-3-fluotobenzene (130), Butylbenzene (134), 1,2-dichlorobenzene (147), Bromobenzene (156), Iodobenzene (204), 2 4-dibromo-1-florobenzene (254)

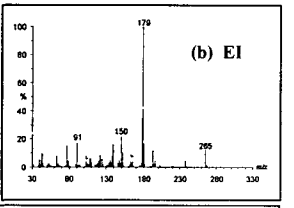

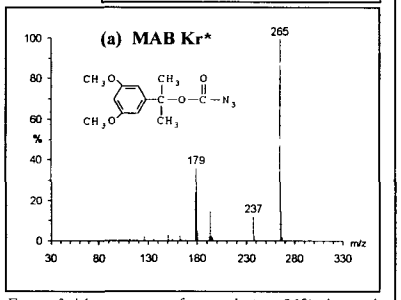

Figure 3 Mass spectra of an azide (m/z 265) obtained by the MAB source using Krypton (a), and with EI (b)

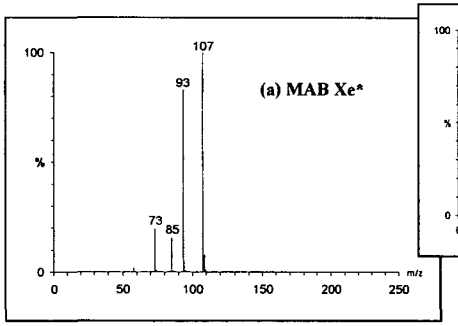

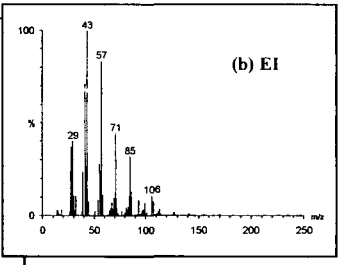

Figure 2 Mass spectrum of a mixture of 13 compounds obtained with the MAB source using Xenon (a), and with EI (b)

Mixture (m/z): Pentane (72), **Diethylamine (73), Piperidine (85),** Hexane (86), **Aniline (93), Toluidine (107),** Octane (114), 1-octanol (130), 1,9-decadiene (122), Decane (144), Dodecane (170), Pentadecane (212), Hexadecane (226)

UV Laser-Induced Selective Dissociation of Nitro Groups in Nitrocellulose

Mo Yang*, J. Michael Ramsey*, and Byung J. Kim**
* Oak Ridge National Laboratory, Oak Ridge, TN 37831-6142
** U.S. Army Construction Engineering Research Laboratory, Champaign, IL 61826-9005

Photon-induced dissociation of organic molecules is becoming an useful method for destruction of toxic or hazardous materials in the environment, since the absorption of a photon often results in selective dissociation of radicals that make the materials toxic or hazardous. In this case, mass spectrometric measurement of the dissociation products can also be a detection method that verifies the presence of those materials. In this paper, UV laser-induced dissociation of nitro groups in nitrocellulose (high explosive material known as smokeless gun powder) and its dependence on the laser parameters have been investigated using an ion trap mass spectrometer.

Figure 1 shows the experimental setup. The nitrocellulose sample with a nitrogen content of 13.56 % was spread on a glass plate in a vacuum chamber and irradiated by laser beams through a quartz window. The gaseous products released from the sample were ionized by an electron gun and the ion masses were analyzed by the ion trap mass spectrometer. The distance from the sample to the ion trap was 12 cm, so that the ions produced primarily by the laser irradiation were excluded in the ion mass analysis.

Figure 2 shows a typical mass spectrum of the gaseous products from nitrocellulose by irradiation with a pulsed UV laser. Only two significant mass peaks were observed, dominantly at m/z = 30 (nitric oxide) and a small one at m/z = 48. MS/MS analysis through ion mass selection and collision induced dissociation in the ion trap confirmed that ions of m/z = 48 were composed of nitric oxide attached by water vapor ($NO{\cdot}H_2O$). In conclusion, irradiation of nitrocellulose with pulsed UV laser produces primarily nitric oxide and a small amount of water vapor, implying that the nitro groups in nitrocellulose are selectively dissociated.

The quantity of gaseous NO produced by 266 nm irradiation was four times greater than the amount produced at 355 nm, as shown in Figure 3. Irradiation of nitrocellulose with 532 nm laser light did not produce any measurable level of gaseous products. The wavelength dependence of denitration measured with a tunable dye laser in the vicinity of 320 nm shows a linear decrease in NO yield with increasing laser wavelength. The weight loss rate of the sample (nitrogen content 13.6 %) due to denitration induced by 266 nm laser light was measured to be 3.9 ± 0.4 μg/J. This indicates hat the photon to nitro group conversion efficiency may be up to 6 %. Increased laser intensity and repetition rate resulted in thermal decomposition of nitrocellulose rather than selective denitration. The laser intensity threshold for sample detonation was found to be 7 mJ/cm² at 266 nm and 10 Hz repetition rate.

Direct dissociation of nitrocellulose into NO without producing NO_2 or other gaseous products suggests that nitrocellulose may have a peroxide structure (R-O-O-NO) rather than an ester structure (R-O-NO_2). UV induced selective denitration demonstrated with nitrocellulose in this paper can be applied for the safe destruction of explosives and the treatment of waste water containing explosive materials without using any chemical or biological reagents.

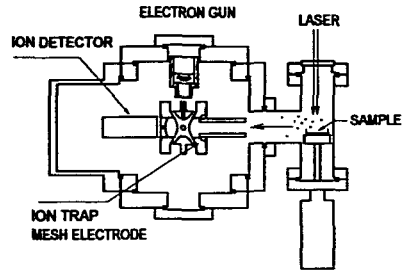

Figure 1. Experimental setup for measurement of laser-induced dissociation products.

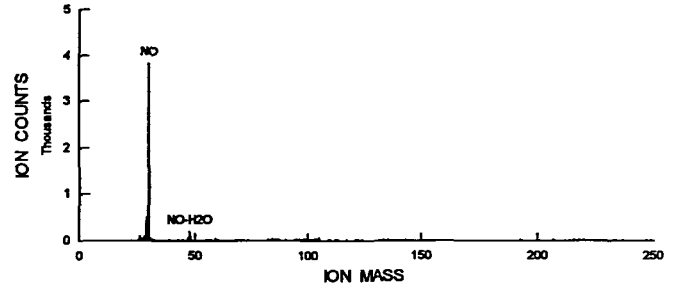

Figure 2. Gaseous products by irradiation of nitrocellulose with a pulsed UV laser (266 nm, 5 mJ/cm², 10 Hz).

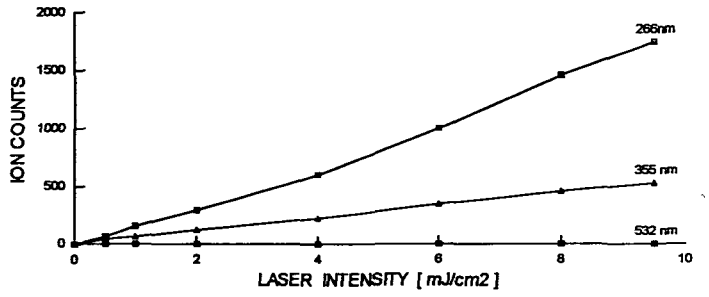

Figure 3. Nitric oxide yields with laser intensity at various wavelengths (3.3 Hz, 1 cm²).

MS of Prepolymers 1,10-Undecadiyne & 1,2,10,11-^{13}C-1,10-Undecadiyne

Robbins, Ronny C.; Berg, Fred J.
U.S. Army
ERDEC, SCBRD-RTE
E3549, Berger Laboratory
Aberdeen Proving Ground, Maryland 21010-5423

Alpha-omega diynes are very useful compounds in the production of poly-acetylene type polymers. The mass spectra of both short chain and long chain terminal mono-alkynes contain an intense ion at mass m/Z 95. The mass spectra of short chained alpha-omega diynes contain an intense ion at m/Z 91 and a minor peak at m/Z 45.5 indicating an aromatic type of structure for the m/Z 91 ion. Carbon-13 labeling experiments for 1,7-octadiyne, 1,8-nonadiyne and 1,9-decadiyne also indicate the formation of some type of ring system before fragmentation. Ring formation may be of some utility in the study of long chain prepolymers that are alpha-omega diynes.

	Mass to Charge								
m/Z	89	90	91	92	93	94	95	96	97
1,7-Octadiyne	1%	0%	100%	8%	0%	0%	0%	0%	0%
1,2,7,8-^{13}C-1,7-Octadiyne	0%	0%	0%	0%	4%	84%	68%	2%	0%
1,10-Undecadiyne	0%	0%	77%	20%	21%	3%	3%	0%	0%
1,2,10,11-^{13}C-1,10-Undecadiyne	0%	0%	0%	17%	39%	30%	44%	11%	0%
1,23-Tetraeicosa-diyne	0%	0%	12%	11%	31%	28%	49%	20%	11%

Table 1: EI Mass Spectra on Perkin-Elmer Q-Mass 910 Mass spectrometer connected to a Perkin-Elmer Autosystem Gas Chromatograph Model 1020, Mass To Charge versus Relative Intensity in the range of m/Z 89 to 97

The mass spectra of alkynes with only one terminal triple bond have a large peak at m/Z 95 and very minor peak at m/Z 91. The mass spectrum of 1,10-undecadiyne contains an intense m/Z 91 ion. Carbon-13 labeling experiments indicate that this ion is produced from cyclic precursors. The difference in intensity of the 91 m/Z ion in the 1,10-undecadiyne to that of the m/Z 95 ion in the 1,2,10,11-^{13}C-1,10-undecadiyne indicates that the four carbon atoms in the two triple bonds are retained.

The data in table one indicates that prepolymers the length of 11 carbons in the case of 1,10-undecadiyne and 24 carbons in the case of 1,23-tetra eicosadiyne undergo ring formation. In the case of 1,23- tetraeicosadiyne, the prepolymer is acting more like two terminal mono-alkyne molecules bonded together giving a large m/Z 95 ion. As the chain length of the alpha-omega diyne increases, the m/Z 91 ion should greatly decrease in intensity.

Experimental

All mass spectra were collected on a Perkin-Elmer Q-Mass 910 Mass spectrometer connected to a Perkin-Elmer Autosystem Gas Chromatograph Model 1020.

Future work

The 1,2,23,24-^{13}C-1,23-tetraeicosadiyne will be synthesized and the mass spectrum taken to determine the degree of ring formation.

References

Lifshitz, C., Gefen, S., "Time-Dependant Mass Spectra and Breakdown Graphs. I. 1,5-Hexadiyne", Int. J. Mass Specatrom. Ion Phys., 35, (1980), 31-37

Nagy-Felsobuki, E., Peel, J.B., Willett, G.D. Chem. "The Photoelectron Spectra of Some Non-Conjugated Acyclic Diynes", Phys. Lett. Vol. 68, No. 2,3, Pages 523-526, 1979

THE TMS-ESTERS OF DECENOIC FATTY ACID ISOMERS. CHARACHTERIZATION OF DOUBLE BOND POSITION AND GEOMETRY IN ROUTINE GC/MS.

J.E. Jalonen, M.J. Mäkelä*, H.O. Hassila, P.H. Joensuu and E. Haapaniemi
Chemistry Department, University of Oulu, POB. 333, FIN-90571 Oulu, Finland
*** Oulu Regional Institute of Occupational Health, FIN-90220 Oulu, Finland.**

Many different approaches have been utilized in the mass spectral characterization of fatty acids.(1) A major problem in the analysis of unsaturated fatty acids has been reliable determination of the position and geometry of a double bond in electron impact (EI) mass spectrometry because of the easy isomerization of the double bond. Available methods often require multistep synthesis or special MS instrumentation and therefore simple and reliable method for routine GC/MS applications is still needed.
In order to study these problems systematically, we prepared *cis*- and *trans*- 2-, 3-, 4- and 5-**decenoic acids (DA)**.(2) We then tested the behavior of corresponding TMS (trimethylsilyl-) esters, used widely in GC-work to improve the volatility of polar organic compounds.
In **TMS-2-DA** the differentiation between *cis* and *trans* isomers was easily done by comparing RI (relative intensity) of peaks in molecular ion (m/z 242) region. In the spectrum of TMS-*cis*-2-DA, RI of m/z 242 is 25% of the m/z 227, i.e. $(M\text{-}Me)^+$ ion. This peak itself is about 60% of the base peak (m/z 73) as seen in Fig. 1 A. In *trans*-isomer m/z 227 is the base peak while molecular peak itself is hardly detectable. We subsequently used this observation to study enzymes catalyzing dehydration of D-3-hydroxydecanoyl-CoA to *trans*-2-decenoyl-CoA. (3)
The spectra of **TMS-3-DAs** differ very much from the corresponding spectra of 2-DAs. The base peak is m/z 73 with only two peaks of some importance; m/z 117 and m/z 227 both about 5% RI. See Fig. 1B (TMS ester of *cis*-3-DA). Determination of a double bond geometry was not possible.
In the spectra of **TMS-4-DAs** the base peak is also m/z 73. Fragment ion m/z 117 is now about 65% RI and $(M\text{-}Me)^+$ is 20%.(Fig. 1C) Molecular ion is also clearly detectable. No unambiguous identification of *cis* and *trans* isomers was possible.
In the case of **TMS-5-DAs** the base peak is m/z 117. The ion at m/z 75 is about 65% RI and both molecular peak and $(M\text{-}Me)^+$ intensities are significant. (Fig. 1D) Once again the differences between geometrical isomers were minimal.
Since TMS esters of cis and trans-2-DAs were easily differentiated from each other, we examined how general is this feature. TMS esters of following cis- and trans-2-enoic fatty acids were selected: 2-dodecenoic, 2-hexenoic, 2-pentenoic and 2-butenoic acids. In *trans*-TMS-2-enoates intensity ratios of $(M\text{-}Me)^+$ ion to molecular ion varied from 40 to 200. In *cis* isomers the corresponding ratios were from 4 to 15. In addition, in all *trans* TMS-2-enoates examined m/z 227 was the base peak.
Other important structure specific ions in *cis* TMS-2-enoates were m/z 155 and m/z 171. They were 4- 20 times greater in intensity than corresponding fragments in *trans* isomers. Exact mass measurement gave composition of $C_4H_9O_2Si$ for m/z 117 and $C_7H_{11}O_2Si$ for m/z 155. The ion at m/z 117 is probably CO_2SiMe_3.

43rd ASMS Conference on Mass Spectrometry and Allied Topics

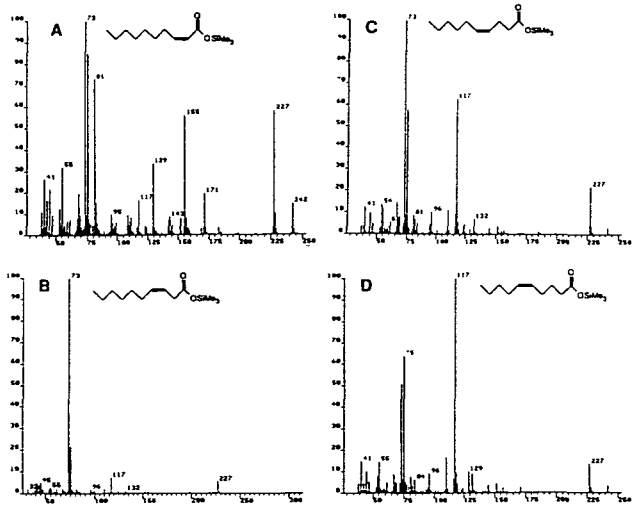

Figure 1. 70 eV EI-spectra of TMS *cis*-decenoates. See text.

AM1 MO calculations gave further insight to the structures of these specific ions. It is suggested that cyclic ions are often most stable and the charge at Si site will effectively direct the formation of these stable ions. However, the very recent results of another silyl derivative, TBS (t-butyldimethylsilyl) esters of *cis* and *trans*-2-decenoic acid showed that the mass spectra of these compounds are identical. The base peak is again at m/z 227 corresponding elimination of t-butyl group, not methyl group.
MS/MS study of $M^{+\cdot}$ showed m/z 226 i.e methane elimination as for $(M\text{-}Me)^+$ ions mainly m/z 129 fragment and some other nonselective fragmentations were observed depending on the CA conditions (res./nonres.). Structure specific ions m/z 155 and 171 were not noticed.
As a conclusion these simple TMS derivatives, used generally in GC work, can be utilized easily for the determination of double bond position of decenoic fatty acids. In the case 2-enoates the geometry of the double bond can be solved as well. This novel method is based on the ordinary EI spectra produced by routine GC/MS, e.g. bench-top instrument.

Experimental: All spectra were recorded with a Kratos MS80RF mass spectrometer: The esters were introduced through a Carlo Erba 4160 capillary chromatograph. MS/MS measurements were done using a Varian Saturn 4D GC/MS/MS instrument. AM1 calculations were carried out using Spartan 3.1 program on a Silicon Graphics workstation.

References.

1. R.P. Evershed in Mass Spectrometry, Vol 9, ed. M.E. Rose, R.S.C. London, 1987, p.197
2. H.O. Hassila, M.Sc. Thesis, University of Oulu, Oulu, Finland, 1992
3. L. Malila, K. Siivari, M. Mäkelä, J. Jalonen, P. Latipää, W. Kunau, K. Hiltunen, J. Biol. Chem. 268 (1993) 21578.

DEVELOPMENT OF GC-MS DETERMINATION OF NICOTINIC ACID AND NICOTINAMIDE

Amy J. Dame, Karin Wiberg, Myron K. Jacobson, and Jan St. Pyrek,
MS-Facility, College of Parmacy, University of Kentucky,
Lexington, KY 40536-0082

Nicotinic acid (niacin) and nicotinamide serve as precursors for the synthesis of NAD. At high therapeutic doses, nicotinic acid is well known as hyperlipidemic agent while nicotinamide may prevent diabetes (e.g. German Nicotinamide Intervention Study (DENIS)). The involvement of NAD as a substrate for poly(ADP-ribose) polymerase, an enzyme involved in DNA repair, may also indicate a preventive role of these two vitamins in cancer. In this context, the relation of a dietary intake of nicotinic acid and nicotinamide, their metabolism, blood levels, and the content of tissue NAD is of importance but is poorly understood. Current analytical methods (primarily HPLC with UV detection) used for quantitation of blood levels of nicotinic acid and nicotinamide are sufficiently sensitive to monitor their levels following large therapeutic doses (e.g. 0.5 to 3.0 g of nicotinic acid per day used for the treatment of cholesterolemia). Their sensitivity, however, is not sufficient to monitor a small dietary intake, fasting levels, and levels resulting from the sustained release dosage formulations.

Following the only example of the GC-MS analysis of nicotinic acid [1] we examined this method for the determination of both nicotinic acid and nicotinamide in human and canine plasma employing respective deuterated compounds as internal standards. The standard of d_4-nicotinic acid was obtained from ISOTEC and was transformed to nicotinamide in our laboratory via standard reactions. Although the GC-MS analysis of trimethylsilyl derivatives (TMS) was straightforward, its application to relatively low levels in plasma required two consecutive purification stages (ion exchange "SO_3H cartridge" and reverse phase C_{18} HPLC separation) prior to the derivatization (BSTFA-Pyridine) and gas chromatography (splitless injection on 15M, 0.3μ, DB-5MS capillary; temperature program 60° for 1 min to 280°, 10° per min). For the definitive identification both "full scan" and SIM of M-15 ions 180/184 and 179/183 for TMS of nicotinic acid and nicotinamide respectively. Importantly, the TMS derivative of nicotinamide (probably acting as a silylating agent) was found to be very sensitive even to a minor column deterioration producing serious peak broadening and even peak splitting.

This analytical approach was verified with radiolabeled compounds (per cent recovery measured for six samples: nicotinic acid 93 ±5, nicotinamide 94 ±1). This method provided full agreement with the HPLC determination of nicotinic acid in canine plasma following a therapeutic dose. Most importantly, it allowed to measure fasting levels of nicotinic acid (about 40 ng/nl) and nicotinamide (about 15 ng/ml) in the human plasma [Figure 1].

REFERENCE 1: L. Sautebin, G. Galli, L. Puglisi, M. G. Ciapponi and R. Paoletti. Analysis of free nicotinic acid released by a polymeric preparation preparation using a mass fragmentographic technique. **Pharm. Res. Commun., 13**, 141-149 (1981).

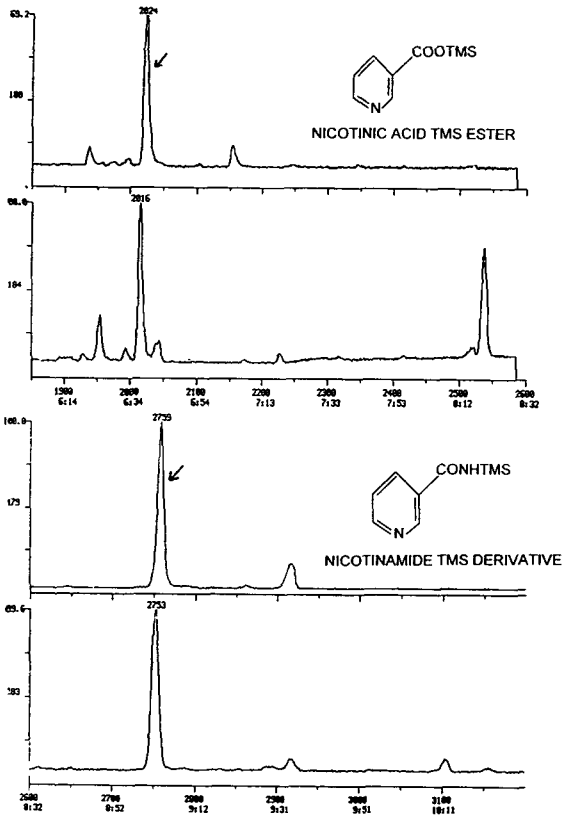

FIGURE: Example of the SIM determination of nicotinic acid (TOP GRAPH) and nicotinamide (BOTTOM GRAPH) in a fasting plasma. Deuterated internal standards were added in the amount of 20 ng each per 0.5 ml plasma sample. After a two-stage purification, about 4% of the silylated sample was injected (splitless mode). Note D_4 compounds preceding D_0 compounds by about 7 scans.

Identifying Polyol Borate Ester Complexes by Negative Ion ESI MS

Brian J. Shay, Nancy Falk, and Henry T. Kalinoski
Unilever Research US, Edgewater, New Jersey, 07020, USA

In water solution borate (BO_3) is known to complex covalently with polyhydroxy molecules such as glycerol and various sugars to form borate esters. Formation of these complexes is a reversible process for which pH titration data has been employed to obtain equilibrium constants. Modelling of the pH titration data to obtain equilibrium constants requires knowing the identities of the borate esters formed. This led us to apply electrospray mass spectrometry to confirm the presence of the complexes assumed in the model and to identify any other species. Several carbohydrate-based surfactants were evaluated with data for one compound shown here. Trends in the polyol concentration dependance on complex formation and pH will be discussed.

Sample solutions of .005 to .025 M N-dodecanoyl-N-methylglucamide ("polyol") were prepared by dissolving the polyol at .025 M in .0013 M sodium tetraborate aqueous borate with brief heating to 40 °C then diluting with .0013 M tetraborate to the desired concentration. These polyol and borate concentrations are much higher than one normally requires for electrospray analysis but were chosen to study systems with high polyol/borate complexation and to simulate practical levels in liquid detergents. N-dodecanoyl-N-methylglucamide was synthesized in-house, sodium tetraborate decahydrate was purchased from Fisher Scientific, and ethoxylated alkylsulfate from ChemService Standards.

Electrospray data were collected using a Finnigan TSQ Mass Spectrometer with a Finnigan electrospray interface, employing a heated capillary design. The analyte sample volumes of polyol/tetraborate were kept small (1 μL) and were injected into a 20 μL/min deionized water stream to keep the system relatively clean. The spray voltage was adjusted to -3 kV by flow injecting 1 μL samples of .005 M polyol in .0013 M tetraborate to give a reasonable discharge current of *ca.* 1-2 μA as opposed to the 8 μA observed at -3.4 kV. Other parameters were 35 psi N_2 sheath gas, 150 and 180 °C capillary temperatures, and 0 V octapole voltage. No organic modifiers, such as methanol, were added to the samples themselves and no sheath liquids or auxiliary gases, such as SF_6 or O_2 (to prevent discharges) were used.

Electrospray mass spectrometry was chosen for this analysis as it has been used previously as a fairly accurate probe of solution phase species. Carbohydrate based surfactants $(P\text{-}H)^-$ and their borate esters BP^- and BP_2^- (and for certain analytes $B_2P_2^-$ and $B_2P_3^-$) are easily and selectively detected by negative ion electrospray-MS. Expected and novel borate containing species are identified by boron's distinctive ^{10}B and ^{11}B isotope pattern of the anions containing these isotopes. The negative ion mode preferentially detects the borate-containing species since they readily form anions in solution. Positive ion spectra also yield information on free polyol and borate esters, but contained intense sodium bound dimers of the polyol and of the borate esters. Hence, the positive ion mode was not the method of choice.

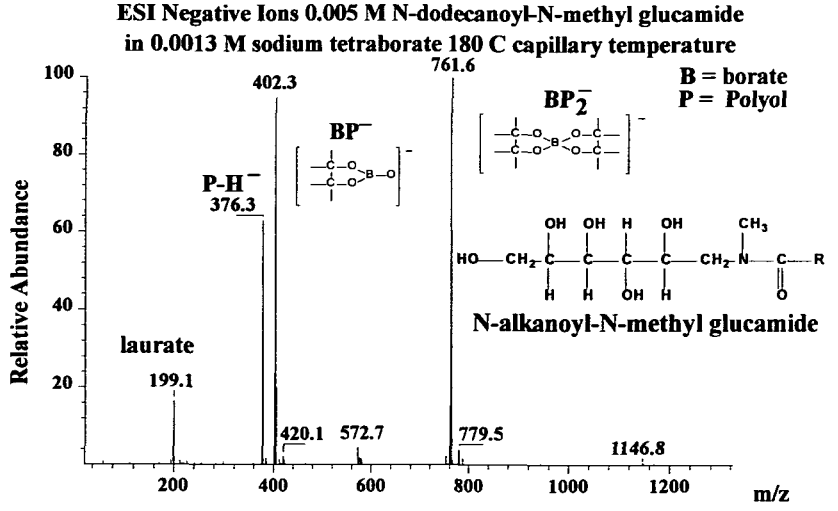

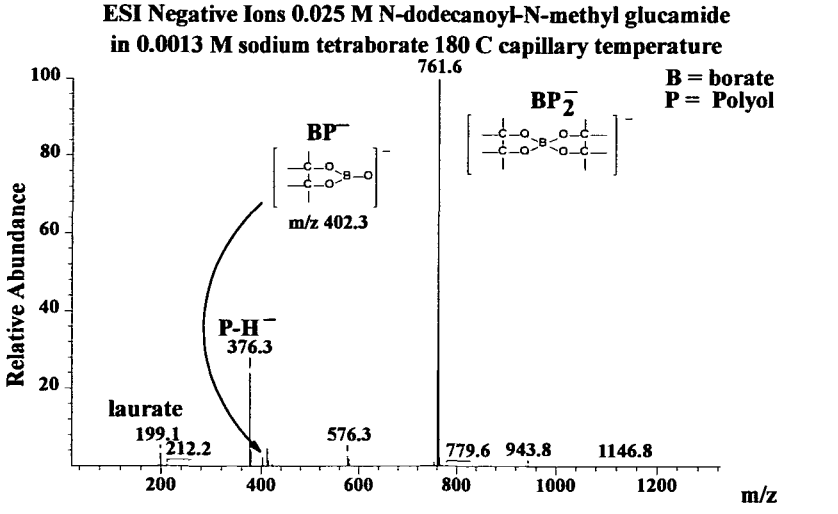

ELECTROSPRAY / ION TRAP MS^n FOR STRUCTURE ELUCIDATION OF SURFACTANTS

Robert J. Strife, The Procter & Gamble Co, Miami Valley Laboratories,
P.O. Box 538707, Cincinnati, OH 45253-8707
&
Jae Schwartz, Mark Bier and Joe Zhou, Finnigan-MAT, 355 River Oaks Pkwy.
San Jose CA 95134

Electrospray ionization (ESI) produces predominantly pseudo molecular ions of organic compounds. While compounds that provide pre-formed ions in solution (e.g., "quats") exhibit the highest relative molar response factors, even neutral components may be ionized if the matrix contains appropriate ions (e.g., cationization of ethoxylates). In the case of ESI of a complex mixture, like a crude extract of a shampoo for consumer use, a qualitative array of ions representing many of the individual components is produced (Fig. 1).

The combination of the ion trap with ESI provides several distinct advantages over linear arrays of quadrupoles including: 1) ion integration capabilities, ideal for a "dim" ion source like ESI; 2) sequential product ion experiments in the time domain (MS^n) so that ions may be refragmented and probed for their organic structure; 3) efficient mass selective storage, via "notched" wave forms, for isolating a component from a mixture and 4) very efficient observed CID efficiencies.

EXPERIMENTAL -- Pure standards were diluted to 1-2 ng/µL for analysis using a prototype of the Finnigan-MAT LCQ. Shampoo extracts which had previously been analyzed using an ESI / triple quadrupole instrument were diluted 100x for analysis on the LCQ prototype. Samples were infused through the electrospray device at 220°C at 5 µL/min. Ion injection periods from 1 ms to 500 ms were used, with longer times being applied at higher stages of MS^n. Mass selective storage was accomplished by adjusting the q_z value of ions of the desired m/z value to 0.83. A notched wave form of variable amplitude was applied to eject ions of unwanted m/z values. CID was carried out at q_z of the parent ion of 0.2 - 0.3.

RESULTS & DISCUSSION -- The ESI / Ion Trap analysis of a shampoo extract is shown in Fig. 2. The injection parameters were intentionally tuned to emphasize the region of interest, where m/z 345 and 373 represent a surfactant of "unknown" structure. MS/MS on both instruments produced one main daughter ion of m/z 226 or 254, respectively. To probe the structure of these ions further, the ESI / ion trap offered the possibility of refragmentation. MS^3 of m/z 226 revealed a series of ions separated by methylene units (m/z 67, 81, 95, 109, 123) and refragmentation (MS^4) of some of these ions showed preferred losses of 42 and / or 28 u. The s/n at the MS^4 stage is greater than 20 (Fig. 3).

Since CID of pseudo molecular ions generated by electrospray should be dominated mainly by even-electron fragmentation processes, the ion of m/z 226 should contain at least one nitrogen center. Likewise, since the MW's are 344 and 372 (even), the total number of nitrogens present must be at least two. Furthermore, the product ions of m/z 226 have odd m/z's and if they are even-electron species, likely represent combinations of C, H, O. Further studies in our lab (data not shown here) have led us to propose that the 67, 81, 95, 109, 123 series represent carbonium ions of the empirical formula C_nH_{2n-3}. The ions are derived from species containing a fatty acyl function and may be derived by rearrangement and dehydration of the even-

electron acylonium ion. The MS^4 fragmentations are losses of ethylene and propene. Given the nature of the sample (shampoo-derived), it was quite likely that the alkyl chain was C_{12}/C_{14} fatty acyl amide and that the partial structure of m/z 226 was $C_{11}H_{23}CONCH_2CH_2$-X. MS^2 studies using (-) ES yielded a key fragment ion of m/z 161, containig the remaining portion of the molecule. Higher orders of MS^n gave evidence that X = N (CH_2COOH)(CH_2CH_2OH), 118 u (344 = 226 + 118) and 161^- is HNCH2CH2X. When a standard of the proposed material was obtained, its spectral properties were found to match those of the "unknown."

In conclusion, refragmentation played an essential role in the elucidation of these structures, which was not achieved by MS/MS alone. While electrospray MS^n experiments have been reported previously, the major advantages here are: 1) the ease with which such experiments are now programmed, being easily executed in a one-hour time frame, and 2) mass selective storage of desired parent ions via "notched" wave forms with unit resolution and no loss in sensitivity. Finally, other strucutural hypotheses were possible during the elucidation process. Our experience with CID of surfactants was an important factor in suggestions we made.

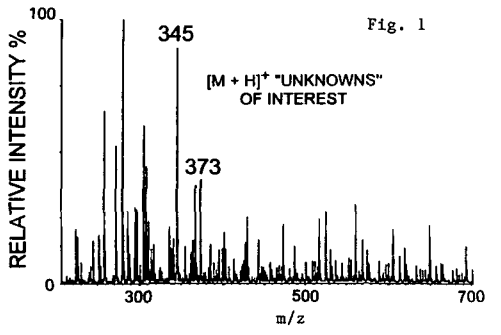

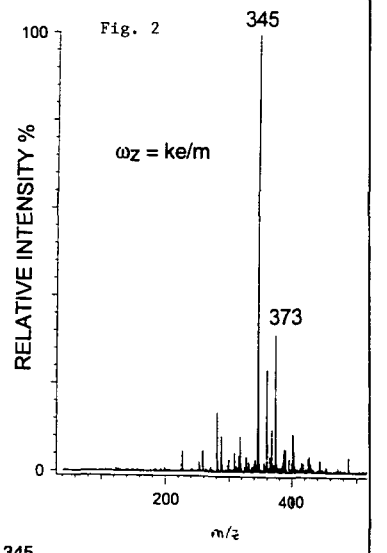

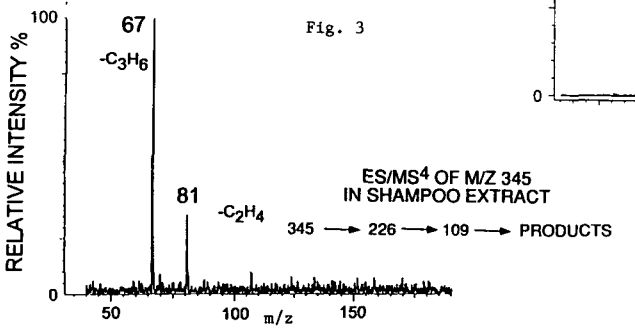

CHARACTERIZATION OF MONOAZO DYES BY CHEMICAL IONIZATION MS/MS.

Jia-shen Wang
Clairol Inc., Stamford, CT 06922

INTRODUCTION

Many azo dyes have been successfully characterized by traditional electron impact (EI) MS, since very often the spectral patterns of this type of dyes correlate well with the azo unit (Ar-N=N-Ar'). A typical example is shown in Figure 1. For dyes with complex aromatic rings, however, the spectral patterns tend to show the partial structures and provide very little information about azo unit. An example is shown in Figure 2. In this spectrum, the base peak (269) clearly indicates the presence of an alkylamino group ($-NCH_2CH_2OH$), but not much information on other structural features. This program, therefore, was developed to determine the structures of azo dyes using the analytical capabilities of (CI)MS/MS.

Figure 1.

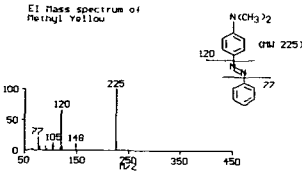

Figure 2.

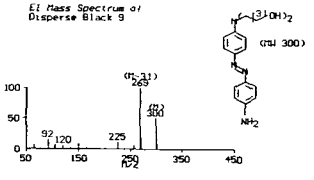

EXPERIMENTAL

In this study, all analyses were carried out using a Finnigan TSQ-7000 triple quadrupole mass spectrometer. Samples were introduced by a solid probe. All of the samples are commercial available.

RESULTS & DISCUSSION

Unlike most CI spectra of other compounds which show mainly the protonated molecular ions, we have observed two features in the CI spectra of azo dyes which are quite interesting. An example is shown in Figure 3a. The intensity of molecular ion $[m]^+$ (by charge exchange reactions, presumably) is relatively high, and the presence of two ion clusters (197 and 109) is rather unusual. The $[m]^+$ with high intensity enables us to perform MS/MS analyses.

Figure 3a.

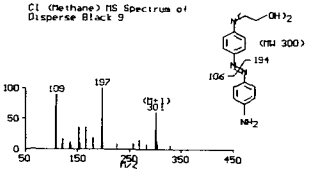

The daughter spectrum of $[m]^+$ (m/z 300) is shown in Figure 3b. The similarity of this spectrum and that of the EI spectrum (Figure 2), suggests that the fragmentation pathways to produce both spectra are similar (by odd-electron ion fragmentation mechanisms, presumably). This characteristic allows us to utilize the library search capability of the data

system. The daughter spectrum of the protonated molecular ion is shown in Figure 3c. As expected, the spectral patterns of 3b and 3c are quite different since $[m+1]^+$ is an even-electron ion. Here the important part is that neither 3b nor 3c shows evidence for the 300 and 301 ions to be the precursors of 109 and 197 clusters.

Figure 3b.

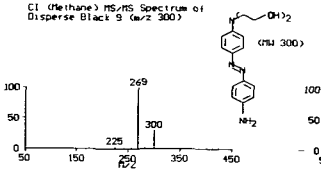

Figure 3c.

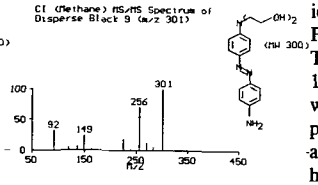

The daughter spectra of the 196 and 108 ions are shown in Figures 3d and 3e. The structures of the 108 and 196 ions were elucidated to be phenylenediamine and N,N-bis(2-hydroxyethyl)-phenylenediamine. The authentic EI spectra of the respective compounds are shown in Figures 3f and 3g. Indeed, we have found that all MS/MS spectra of these cluster ions are consistent with those of reference compounds. We, therefore, concluded that under CI ionization conditions, reactions may occur for azo dyes at the azo unit sites to form the respective amino compounds.

Figure 3d.

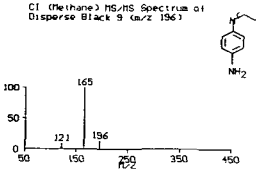

Figure 3e.

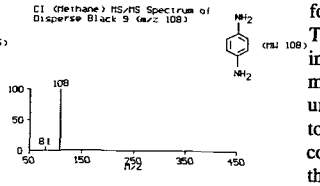

We have observed similar phenomena for other azo dyes. The relative ion intensities of the CI mass spectra are unavoidably sensitive to the experimental conditions, especially the source pressure. It, however, does not cause problems in this application.

Figure 3f.

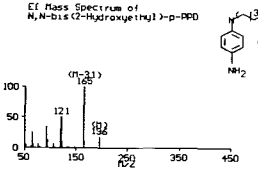

Figure 3g.

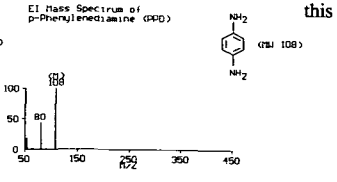

CONCLUSION

The characterization of azo dyes by CI/MS/MS is demonstrated. A CI mass spectrum provides the sub-structural information related to the azo unit of a compound. An $[m]^+$ MS/MS spectrum allows one to perform structural elucidation with the readily available mass spectral data bases and searching capabilities of the system.

Analysis of Dibenzofuran and Dibenzo-p-dioxin in Diphenyl Oxide

Paul L. Sherman, Fred D. Hileman, and Jay M. Wendling
Monsanto Corporate Research, 800 N. Lindbergh Blvd., St. Louis, MO 63167

Diphenyl oxide (DPO) is a common agent used as a substrate for the production of brominated flame retardants Dibenzofuran (DBF) is a contaminant in DPO and is structurally very similar to DPO. Pressure to reduce trace levels of halogenated dibenzofuran and halogenated dibenzo-p-dioxin (DBD) in halogenated products such as DPO has resulted in demands for lower levels of nonhalogenated DBF and DBD in DPO As an example, the Environmental Protection Agency and various European agencies have begun to set standards for the levels of brominated DBFs and DBDs in brominated DPOs at the low part per billion (ppb, ng/g) level. Facilities producing DPO can typically measure DBF in DPO to a detection limit of 1 part per million (ppm, ug/g) using capillary column gas chromatography with flame ionization detection. However, it is desirable to measure for both DBF and DBD to low ppb levels to be in compliance with the new standards. An analytical procedure has been developed which uses a column chromatography sample isolation procedure followed by gas chromatography chemical ionization mass spectrometry to achieve these desired levels of detection.

The procedure (Figure 1) involves the dissolving of one gram of DPO in 10 mL of hexane and this solution is then spiked with both D_8-DBF and $^{13}C_{12}$-DBD The hexane solution is passed through a Woelm basic alumina column, which is then eluted with 8 mL of 10% CH_2Cl_2/hexane which strips the DPO from the column while allowing the DBF and DBD to remain. The DBF and DBD are eluted from the column using 10 mL of CH_2Cl_2 to which is added 20 uL of undecane to serve as a keeper and the eluate is concentrated under a steam of dry nitrogen This concentrate is then analyzed by gas chromatography (see Figure 2) on a 60 m SP-2330 capillary column with detection by chemical ionization (CH_4) mass spectrometry with selected ion monitoring for the protonated molecular ions for DBF (m/z 169), D_8-DBF (m/z 177), DBD (m/z 185), and $^{13}C_{12}$ DBD (m/z 197) It is necessary to use chemical ionization rather than electron impact ionization (EI) since EI results in the fragmentation of DPO (loss of H_2) to form an ion with the same mass as DBF which contributes to the background noise and thus raises the detection limits for DBF. The highly polar SP-2330 was also essential in providing a high degree of separation of DBF and DBD from DPO and from each other The key to the success of this method is the use of stable labelled DBF and DBD as internal standards. The alumina column chromatography separation is effective but inexact in its ability to separate DBF and DBD from DPO. These labelled materials allow compensation for any losses during the sample preparation and analysis The detection limits for DBF and DBD are somewhat variable due to the variability in recovery from the alumina column. Typical detection limits for DBF and DBD in DPO using this method are 1-5 ppb and 5-10 ppb respectively

43rd ASMS Conference on Mass Spectrometry and Allied Topics

Figure 1. Sample preparation for the analysis of dibenzofuran and dibenzo-p-dioxin in diphenyl oxide.

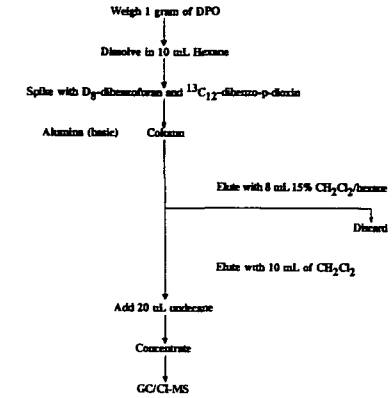

Figure 2. Selected ion traces for DBF and DBD for an unspiked and spiked DPO sample.

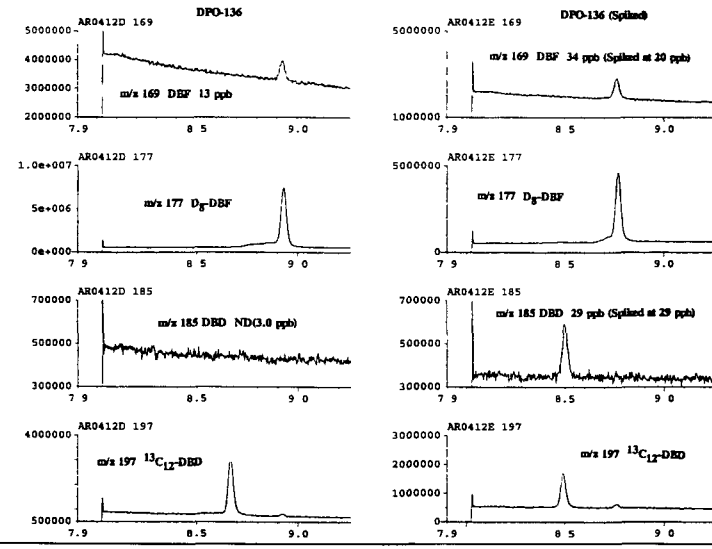

Precolumn Derivatization of Hydroxy Compounds with 7-[(Imidazolemethanoyl)methoxy]-4-methylcoumarin (IMMC) and LC/TSP-MS of the Resulting Esters

Lawrence R. Phillips, Jeffrey G. Supko, Tracy L. Wolfe and Louis Malspeis

Laboratory of Pharmaceutical Chemistry
Developmental Therapeutics Program
Division of Cancer Treatment
National Cancer Institute
Frederick, Maryland 21702-1201

7-[(Chlorocarbonyl)methoxy]-4-methylcoumarin (CMMC) is a fluorescent reagent for precolumn derivatization of hydroxy compounds in liquid chromatography [1]. The synthesis of the acyl chloride involves the use of thionyl chloride, which has been subsequently shown to unexceptably introduce highly fluorescent impurities due to over-chlorination. An improved derivatization reagent utilizes a reactive acyl imidazole, instead of the acyl chloride, offering a purer product while maintaining desirable reagent characteristics such as ease of handling, mild derivatization conditions, etc. Reaction of 7-[(imidazolemethanoyl)methoxy]-4-methylcoumarin (IMMC) with various hydroxy compounds produces esters which are readily separable under reversed-phase HPLC conditions compatible with detection by thermospray mass spectrometry.

Synthesis of 7-[(Imidazolemethanoyl)methoxy]-4-methylcoumarin (IMMC). To a stirred solution of 102.3 mg (0.44 mmol) of 7-(carboxymethoxy)-4-methylcoumarin in 7 ml of tetrahydrofuran was added 1,1'-carbonyldiimidazole (70.9 mg, 0.44 mmol) in one portion. The stirred reaction mixture was heated to reflux for 30 min, whereupon heating was discontinued but stirring continued an additional 5 hours; as the reaction mixture cooled, a white precipitate formed. The white solid was isolated by filtration and then freed of solvent *in vacuo*, yielding 84.1 mg of crystals (0.30 mmol, 68%) mp 161-162°C (melts with decomposition). MS (EI, 70 eV) *m/z* (% relative abundance): 284 (M^+,94), 189(32), 159(30), 103(24), 81(100). HRMS: *m/z* 284.0793 (calcd for $C_{15}H_{12}N_2O_4$: 284.0797).

Sample Derivatization and Analysis. IMMC was reacted with several 1° and 2° alcohols, as well as *tert*-butyl alcohol. A typical procedure is as follows: to a solution of IMMC (0.60 mg (2.1 μmoles)) in 2.5 ml of toluene and 0.75 ml of acetonitrile was added benzyl alcohol (20 μl, 20.9 mg, 194 μmoles) and 0.15 ml of acetonitrile containing 4-dimethylaminopyridine (0.014 mg (0.11 μmole). The resulting solution was vigorously mixed, heated to 60°C for 1.5 hr, cooled, concentrated to dryness under a stream of nitrogen gas at room temperature. The sample was then reconstituted in 0.3 ml of acetonitrile-0.1*M* ammonium acetate buffer, pH 5.5-methanol (50:48.5:1.5, v/v/v). A 5-μl aliquot of this solution was injected onto the chromatographic system. Separations were conducted at ambient temperature under isocratic reversed-phase conditions on a 3.9 mm I.D. x 15 cm stainless steel column packed with 4 μm Nova-Pak C_{18}. A mobile phase composed of acetonitrile-0.1*M* ammonium acetate buffer, pH 5.5-methanol (50:48.5:1.5, v/v/v) was employed at a flow rate of 0.7 ml/min. The effluent was introduced directly into a Hewlett-Packard 5989A mass spectrometer equipped with a thermospray LC-MS interface. The thermospray interface was operated in the filament-assisted ionization mode with either positive- or negative-ion detection. The operating temperatures for the interface were as follows: ion source, 280°C; probe stem, 112°C; and probe tip, 235-245°C.

Results. Although initially intended as a fluorescent label for hydroxy compounds, IMMC smoothly reacts with primary and secondary hydroxyl compounds to produce esters which have been found to be

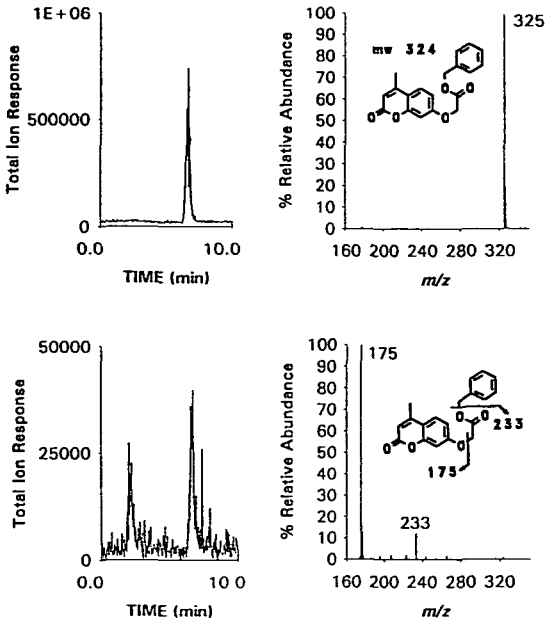

Figure 1. Total ion response chromatograms and averaged TSP mass spectra acquired during the elution of 1.2 μg of the ester product of IMMC with benzyl alcohol by continuous scanning over a mass range of 160-350 u with positive (top) and negative-ion (bottom) detection.

quite responsive to thermospray ionization. When observed by positive ion thermospray mass spectrometry, these compounds give [M+H]+ ions as the base peak of their mass spectra with no discernible fragmentation. In the negative ion thermospray mass spectra of these compounds, the proton-abstracted anion of 7-hydroxy-4-methylcoumarin (appearing at *m/z* 175) is, without exception, the base peak. A quantity of 7-[((methoxy)-carbonyl)methoxy]-4-methyl-coumarin (the ester resulting from reaction of IMMC with methanol) was synthesized and its response to thermospray ionization was evaluated by LC/MS using filament-assisted, positive ion thermospray ionization. Using selected ion monitoring, we found that this compound gave a response curve which was linear over a range of < 10 ng to over 100 ng injected on-column. Easily detectable to 0.8 ng (S/N = 3), a 10-15 ng sample produced an integratable peak in the ion chromatogram that possessed a signal-to-noise ratio of about 10.

The response to thermospray ionization thus makes these compounds extremely useful in derivatization and post-column detection of hydroxy compounds. Following initial precolumn derivatization, a sample may first be examined by LC/MS using negative ion thermospray detection to identify all compounds possessing the coumarin-based fluorescent tag. From the subsequent LC/MS analysis using positive ion thermospray, molecular weight information can be easily deduced for derivatizable hydroxy compounds present in the original sample. Once the molecular species has been determined, the analyst is then presented with the option of performing low-level quantitation using selected ion monitoring thermospray mass spectrometry.

Reference. 1. K.-E. Karlsson, D. Wiesler, M. Alasandro, and M. Novotny (1985) *Anal. Chem.* **57**, 229-234.

Specific Structural Features which Promote Cluster Formation in FAB Mass Spectra

Thomas R. Sharp
Analytical R&D, Central Research, Pfizer Inc., Groton, CT 06340 U.S.A.

FAB mass spectrometry of a series of compounds, represented by the genral structure shown below, indicates that certain of the hydroxyl groups on the molecule play a determinant role in their tendency to form abundant proton-bound dimers and counterion-containing dimers of the formula $[2M+counterion+2H]^+$. The parent molecule for which this study was initiated is compound 1, a drug substance under development as an antiischemic compound [1], in which all three R groups are hydroxyls.

Observations were made on a VG 70-S magnetic sector instrument using a 7 kV fast xenon beam generated by a saddle field gun. The matrix used was the dithiothreitol-dithioerythritol mixture of Witten *et al.*[2] Samples of compounds were dissolved in methanol. Aliquots of this solution were added to the matrix on the FAB probe target. Five compounds, the structures of which are indicated in Table 1, were examined in addition to the free base and two salt forms of 1.

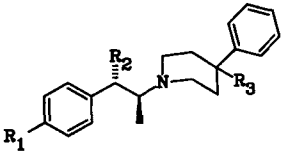

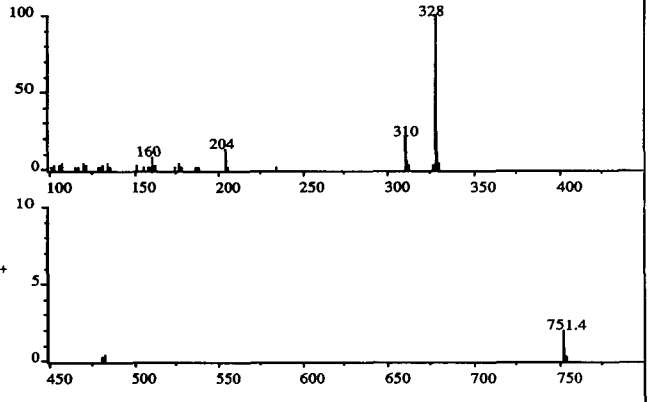

Figure 1: FAB mass spectrum of compound 1 methanesulfonate salt. $[M+H]^+$ at m/z 328. The m/z 751.4 species corresponds to a methanesulfonic acid-containing proton-bound dimer of the empirical formula $(C_{20}H_{25}NO_3)_2(CH_3SO_3H)H^+$ Note that the lower panel y-axis is 10% relative abundance.

The FAB mass spectrum of compound 1 methanesulfonate salt is shown in Figure 1. All three R groups on compound 1 are free hydroxyls. In addition to the abundant $[M+H]^+$ at m/z 328, the two structurally significant ions are m/z 310 and m/z 204. The m/z 310 species results from neutral loss of H_2O from $[M+H]^+$. Examination of structural analogs 2 and 3 (Table 1) indicates that either the benzylic hydroxyl or the piperidinyl hydroxyl can be lost, although the data suggest that loss of the benzylic hydroxyl is the more fascile reaction. The m/z 204 fragment corresponds to loss of *p*-hydroxybenzyl alcohol from

$[M+H]^+$. This point is also corroborated by observations on the analogs. FAB accurate mass measurements on ions of compounds 1, 2 and 3 support these assignments.

The approximately 2% relative abundance peak in Figure 1 at m/z 751.4 corresponds to a van der Waals dimer containing two molecules of compound 1, a proton which carries the electrostatic charge, and a molecule of methanesulfonic acid. The empirical formula for this ion would be $(C_{20}H_{25}NO_3)_2(CH_3SO_3H)_1H^+$. Investigation of the behavior of the hydrochloride salt form of compound 1, and of the free base, indicates that these forms of compound 1 also produce the van der Waals dimer, although to a lesser extent.

Structural analogs were obtained in which the various hydroxyl groups were removed, blocked or replaced with a different oxygen oxidation state. Compounds 2 through 5 (Table 1) are structural analogs which retain various combinations of two of the three hydroxyl groups. Data suggest that two specific hydroxyls of the three are necessary for formation of these clusters. The only analog which retains the ability to form an observable dimer is compound 5, in which both R_2 and R_3 are present as hydroxyl groups. Further, the presence of an attached oxygen in these positions is insufficient. The group cannot be a carbonyl group, but must be a hydroxyl group, as demonstrated by compound 4.

The compounds form proton-bound dimers when observed as the free bases of the compounds. The tendency to form counterion-containing clusters appears to be independent of the identity of the counterion. Both hydrochloride salts and methanesulfonate salts form counterion-containing clusters.

Table 1:
Correlation of Dimer Formation with Presence of Free Hydroxyl Groups

Compound & Salt Form	R_1	R_2	R_3	Dimer Formation	Dimer Abundance % of $[M+H]^+$
1 free base	OH	OH	OH	+	0.5%
1 hydrochloride salt	OH	OH	OH	+	1.0%
1 mesylate salt	OH	OH	OH	+	2.0%
2 free base	OH	OH	H	-	0
3 free base	OH	H	OH	-	0
4 free base	$OCH_2C_6H_5$	=O	OH	-	0
5 free base	OCH_2C_6H5	OH	OH	+	0.2%

References:
1. B.L. Chenard *United States Patent 5,185,343,* 9 February 1993.
2. J.L. Witten, M.H. Schaffer, M. O'Shea, J.C. Cook, M.E. Hemling, K.L. Rinehart (1986). **Biochem. Biophys. Res. Commun.** 124,350-8.

STUDY OF COBALT COMPLEXES WITH TETRADENTATE SHIFF BASES BY IS- AND FAB-MS

by Andrea RAFFAELLI, Sergio PUCCI, Sonia DI SACCO, Mauro ISOLA

Centro di Studio del CNR per le Macromolecole Stereordinate ed Otticamente Attive, Dipartimento di Chimica e Chimica Industriale, Università di Pisa, Via Risorgimento 35, 56126 PISA, Italy.

Nitrosyl derivatives of transition metals, M(NO), have recently drawn the attention of several researchers, as they are involved in some biological processes and in some catalytic cycles. Oxidation by molecular oxygen of nitrosyl complexes of cobalt containing tetradentate Shiff bases, in the presence of pyridine, affords cationic Co complexes of the type $[Co(L\frown L\frown L\frown L)(Py)_2]^+NO_3^-$. We report here the results obtained in the MS study of a series of such complexes, with different tetradentate Shiff bases. Ionspray (IS) and Fast Atom Bombardment (FAB) ionization techniques were used in order to get complementary information and to compare the two techniques for the study of these compounds.

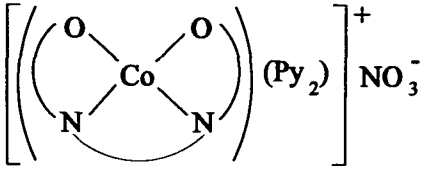

General structure of the Co complexes examined

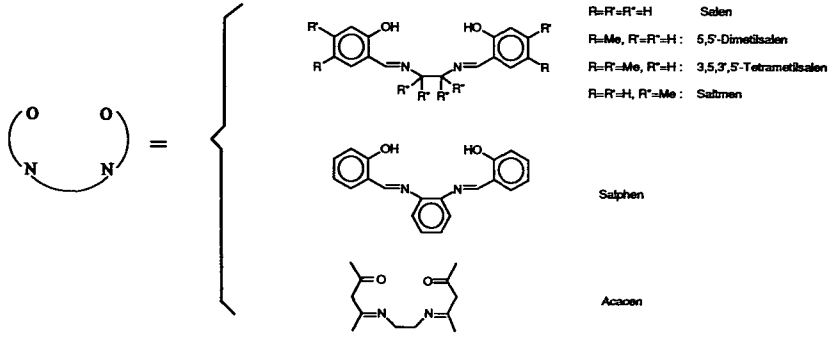

FAB-MS measurements have been performed on a VG 70-70E double focussing mass spectrometer, while IS-MS and IS-MS-MS measurements have been carried out on a Perkin Elmer Sciex API III plus triple quadrupole mass spectrometer. The main MS data for the complexes examined are summarized in the table. The structure of the complexes has been completely confirmed, both by IS and FAB ionization. The comparison between the two techniques showed some interesting differences. Under FAB conditions, it was possible to observe the formation of clusters, whereas using IS ionization these clusters could not be detected. It is worthy to note that the molecular cation peak was usually very weak with

FAB, and practically not present for the less stable complexes of the series, the base peak being the $[M\text{-}2Py]^+$ ion. Under IS conditions, the fragmentation afforded the $[M\text{-}Py]^+$ and $[M\text{-}2Py]^+$ species together with the molecular cation M^+, even working with a low orifice potential (35 V), but the M^+ peak was present in all cases, even if it was very weak for the less stable complexes.

Table. Main MS Data of the Cobalt Complexes Examined

Ionization	Ligand	M^+ (*m/z*-%)	$[M\text{-}Py]^+$ (*m/z*-%)	$[M\text{-}2Py]^+$ (*m/z*-%)	"Dimer" (*m/z*-%)
F.A.B. MS	Di-Me-SALEN	511 - 2	432 - 9	353 - 100	706 - 7
	SALTMEN	539 - 0	460 - 2	381 - 100	762 - 11
	ACACEN	439 - 8	360 - 30	281 - 100	562 - 0
	Tetra-Me-SALEN	539 - 3	460 - 8	381 - 100	762 - 5
	SALEN	483 - 14	404 - 38	325 - 100	650 - 5
	SALOPHEN	531 - 35	452 - 42	373 - 100	746 - 0
Ionspray MS (OR 35 V)	Di-Me-SALEN	511 - 11	432 - 66	353 - 100	==
	SALTMEN	539 - 2	460 - 76	381 - 100	==
	ACACEN	439 - 92	360 - 100	281 - 60	==
	Tetra-Me-SALEN	539 - 90	460 - 100	381 - 59	==
	SALEN	483 - 100	404 - 77	325 - 40	==
	SALOPHEN	531 - 100	452 - 5	373 - 0	==
Ionspray MS-MS (EC 10 eV)	Di-Me-SALEN	511 - 7	432 - 32	353 - 100	==
	SALTMEN	539 - 1	460 - 41	381 - 100	==
	ACACEN	439 - 3	360 - 100	281 - 85	==
	Tetra-Me-SALEN	539 - 1	460 - 98	381 - 100	==
	SALEN	483 - 1	404 - 63	325 - 100	==
	SALOPHEN	531 - 25	452 - 100	373 - 95	==

IS-MS-MS spectra, at different values of collision energy, allowed to figure out the relative stability of the complexes examined. The stability scale obtained was perfectly in keeping with the electronic and steric stabilization effects of the substituents present on the tetradentate ligand.

The general fragmentation pattern involved the initial loss of the two molecules of pyridine consecutively. This loss takes place already with low values of collision energy (10-15 eV) and also in the source. Further fragmentation of the $[M\text{-}2Py]^+$ species were more difficult, and it could be observed only with relatively high values of collision energy (40-50 eV).

Quantitative Analysis of Fluorinated Ethylchloroformate Derivatives of Non-protein Amino Acids and Hydrolysis Products of a Tripeptide Using Positive and Negative Chemical Ionization Gas Chromatography / Mass Spectrometry

Ping Cao and Mehdi Moini*
Department of Chemistry and Biochemistry,
University of Texas at Austin, Austin , Texas 78712

Recently, Husek introduced a derivatization procedure for gas chromatographic (GC) analysis of protein amino acids using ethylchloroformate(ECF) [1]. The main advantages of this technique include: 1) *simultaneous N(O,S)-derivatization of amino acids in one step*, 2) *derivatization of amino* acids in aqueous solution, 3) reaction time of only a few seconds, 4) derivatization with inexpensive reagents, and 5) GC or GC/MS identification of products.

To date, most of the reported data shows the application of ECF derivatization to protein amino acids. Here we report the application of the ECF derivatization to non-protein amino acids using trifluoroethanol as the esterifying agent. GC/MS was used to analyze the products using positive and/or negative chemical ionization (CI) mode.

The procedure for the derivatization of non-protein amino acids is the same as before [1] except trifluoroethanol is used as the esterfying agent. An equimolar solution of twenty-three non-protein amino acids (2.5 μmol/ml) was diluted by two to six orders of magnitude using 0.1 N HCl solution for the qualitative analysis. Other experimental conditions are reported elsewhere [2,3].

The reconstructed total ion chromatogram (RIC) of the twenty-one ECF + trifluoroethanol + pyridine derivatives of non-protein amino acids under positive chemical ionization mode is shown in Figures 1. Mass spectra of these non-protein amino acid derivatives showed characteristic $[M-19]^+$, $[M+1]^+$, $[M+29]^+$, and $[M+41]^+$ peaks in the positive CI mode, and $[M-1]^-$, and $[M+35]^-$peaks in the negative CI mode. Three non-protein amino acids containing an aromatic ring, anthranilic acid, *m*-aminobenzoic acid , and *p*-aminabenzoic acid, gave relatively strong peaks in negative CI mode compared to positive CI mode.

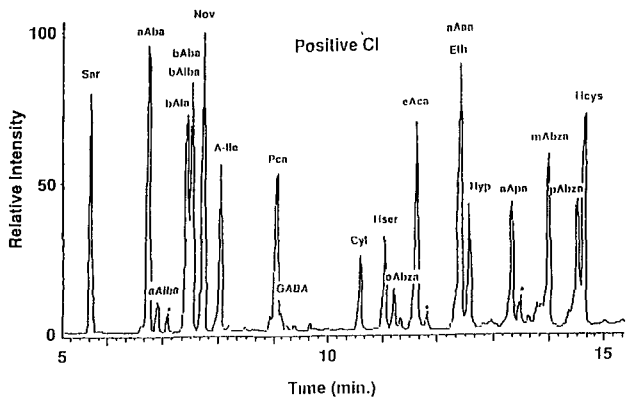

Figure 1. Reconstructed TIC of positive chemical ionization GC/MS of the trifluoroethanol ECF derivatized non-protein amino acids. Peaks marked with an asterisk were mostly ethyl derivatives.

The detection limits and linear dynamic range of the ethylchloroformate derivatives of non-protein amino acids were studied using chemical ionization in the positive ion mode. The results are given in Table 1. As is shown, the detection limits are mostly in the femtomole range.

Furthermore, to investigate the application of the ethylchloroformate + trifluoroethanol derivatization of amino acids to the hydrolysis products of peptides, a tripeptide diprotin B (VAL-PRO-LEU) was used. A solution of the three amino acids in diprotin B was identically treated for comparison. The relative ratios of derivatization and ionization efficiencies of three amino acids from the peptide and amino acid mixture after hydrolysis from 72 hr at 110°C were 100:73:92 and 100:67:83, respectively.

Table 1. Detection limits and linear dynamic ranges of trifluoroethyl ester ECF derivative non-protein amino acids.

Non-protein amino acid	Detection limit (ng)	Linear dynamic range (orders of magnitude)	Correlation coefficient
α-aminobutyric acid (aAba)	5.00E-03	3.7	0.988
L-norvaline (Nov)	5.00E-03	3.7	0.9848
β-alanine (bAla)	5.00E-03	3.7	0.9854
DL-homocystein (Hcys)	5.00E-03	3.7	0.992
m-aminobenzoic acid (mAbza)	5.00E-03	3.7	0.9747
p-aminobenzoic acid (pAbza)	5.00E-03	3.7	0.9914
DL-ethionine (Eth)	5.00E-02	3	0.9917
DL-α-aminopimelic acid (aApa)	5.00E-02	3	0.9986
Sarcosine (Sar)	5.00E-02	3	0.982
Hydroxy-L-proline (Hyp)	5.00E-02	3	0.98
α-aminoisobutyric acid (aAiba)	5.00E-02	3	0.9933
DL-homoserine (Hser)	5.00E-02	3	0.9877
Pipecolinic acid (Pca)	5.00E-02	3	0.9916
Cycloleucine (Cyl)	5.00E-02	3	0.9924
L-allo-isoleucine (Alle)	5.00E-02	3	0.9975
ε-amino-η-caproic acid (eAca)	0.25	2.7	0.9948
DL-α-aminoadipic acid (aAaa)	0.25	2.7	0.9988

References

[1] P. Husek, *J. Chromatogr.*, 552 (1991) 289.
[2] M. Vatankhah and M. Moini, *Biological Mass Spectrom.*, 23 (1994) 277-282.
[3] P. Cao and M.Moini, J. Chromatogr. (in press).

A Direct Method for the Quantification of Free Saturated Fatty Acids in Tobacco

Jiu Ai

US Tobacco Manufacturing Company, Inc., 800 Harrison Street, Nashville, TN 37203

GC methods for quantitative determination of free fatty acids require tedious sample preparation steps such as derivatization and clean-ups before injection. Without sample preparations, a GC chromatogram of underivatized fatty acids shows poorly resolved peaks that can be interfered by enormous chemical background when a complex mixture is injected. It is very difficult to quantify such peaks. In this study, a new direct method is developed to quantify free fatty acids in complex mixtures without sample cleaning and derivatization by selecting an appropriate GC column to improve peak shapes and by choosing a highly selective detection method to eliminate the chemical background.

The peaks of underivatized saturated fatty acids eluted from a bonded phase polyethylene glycol GC column (DB-WAX of J&W) are better resolved than those eluted from a non-polar column (DB-5 from J&W). Mass spectrometers with multiple analyzing devices, such as triple quadruples, etc., provide great selectivity when used at tandem scanning mode. It is possible to selectively detect a specific compound or a specific group of compounds from a complex mixture using the selected reaction monitoring (SRM) scanning mode. Thus, the chemical background in the complex mixture can be completely eliminated.

A Finnigan TSQ700 mass spectrometer was used in this study and the SRM scanning was set for the m/z 129^+ to m/z 87^+ fragmentation pathway during the collision. With this SRM scanning, all the saturated straight chain fatty acids having more than eight carbons were selectively detected. Figure 1 shows two MS chromatograms of a CH_2Cl_2 tobacco extract. The total ion scan chromatogram was very complex and the SRM chromatogram of the same extract was much simpler and clearer. Only those underivatized saturated fatty acids showed up in the SRM chromatogram and their peaks were completely resolved for quantitative integration.

Since the volatility of underivatized fatty acids is low, there is always concern that they might be detained in the GC column. A study was performed to compare ratios of the peak intensities of saturated fatty acids eluted from the DB-WAX GC column with those measured from a direct probe insertion. Intensity ratios of C16, C17 and C18 acids to C14 acid from the GC/MS/MS measurement were very close to those of the Probe/MS/MS measurement, respectively. This indicates that the introduction of underivatized fatty acids into the mass spectrometer ion source through a DB-WAX GC column is comparable to the direct probe insertion.

Table 1 Fatty acid concentrations of acid spiked and un-spike tobacco

Fatty Acids	Spiked Samples		Un-spiked samples		Concen. Difference
	Concen. (μg/ml)	*RSD*	*Concen. (μg/ml)*	*RSD*	*(μg/ml)*
decanoic acid	11.6	2.5%	0.7	7.4%	10.9
dodecanoic acid	11.4	2.4%	0.8	10%	10.6
tridecanoic acid	11.5	3.7%	0.6	12%	10.9
tetradecanoic acid	13.8	4.1%	2.6	6.0%	11.2
pentadecanoic acid	14.1	5.4%	2.9	6.5%	11.2
hexadecanoic acid	51.7	5.2%	41.5	6.1%	10.2
heptadecanoic acid	14.2	8.2%	3.6	6.6%	10.6
octadecanoic acid	24.1	10%	13.4	6.9%	10.7

Six calibration solutions were prepared containing C10 to C18 straight chain saturated fatty acids with C11 acid as the internal standard. The amount of acids injected ranged from 4.0 ng to 120 ng and the correlation coefficients for all the eight fatty acids were 0.999 or higher. Two tobacco samples were spiked with a mixture of standard fatty acids before CH_2Cl_2 extraction. The spiked concentration was 10 μg/ml for each one of the acids. Table 1 lists saturated fatty acid concentrations in CH_2Cl_2 extracts of the spiked and un-spiked tobacco samples. The concentration differences between the spiked and un-spiked samples quantified by the GC/MS/MS method were very close to 10 μg/ml for all the eight fatty acids studied. The data were the averages of six measurements from two different pairs of spiked and un-spiked samples prepared in the same way.

Concentrations of the eight saturated fatty acids were determined in two types of tobacco and two types of Chinese green tea (Longchin and Gun powder). The results are shown in Table 2. In both tobaccos and green teas, hexadecanoic acid (palmitic acid) was the major saturated fatty acid, followed by the octadecanoic acid (stearic acid). Other prominent fatty acids were tetradecanoic acid, pentadecanoic acid and heptadecanoic acid. There were trace amounts of decanoic acid, dodecanoic acid and tridecanoic acid. Several other fatty acids found in tobaccos with the SRM scanning, but not yet quantified, were nonanoic acid, 13-Me-tetradecanoic acid, 12-Me-tetradecanoic acid, 14-Me-pentadecanoic acid, 14-Me-hexadecanoic acid, 16-Me-heptadecanoic acid, oleic acid, nonadecanoic acid and eicosanoic acid.

Table 2 Fatty acids in tobacco and green tea samples

Fatty Acid	Tobacco no. 1	Tobacco no. 2	Longchin green tea	Gun powder
	(ppm)	*(ppm)*	*(ppm)*	*(ppm)*
decanoic acid	0.5	1.8	0.3	-
dodecanoic acid	0.7	2.9	1.0	1.2
tridecanoic acid	0.2	2.0	0.6	-
tetradecanoic acid	17.4	19.2	7.2	5.6
pentadecanoic acid	22.0	23.0	5.1	5.2
hexadecanoic acid	242.6	371.8	78.6	171.1
heptadecanoic acid	18.8	26.7	-	9.4
octadecanoic acid	77.5	110.4	18.5	25.8

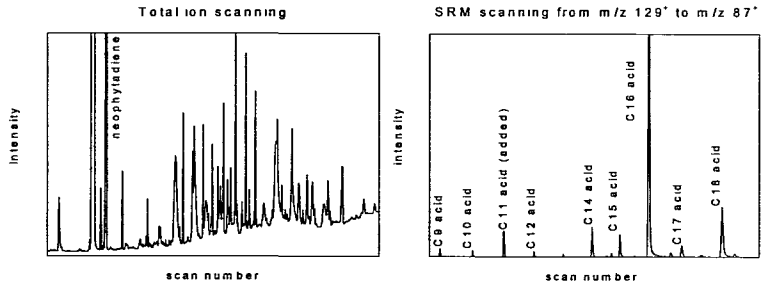

Figure 1 GC/MS and GC/MS/MS chromatograms of the same tobacco extract

A NEGATIVE ION STUDY OF INDOLE AND QUINOLINE USING AN ASGDI SOURCE

S. N. CAIRNS, M. L. LANGFORD, A. M. FRANKLIN AND J.F.J.T. TODD
The Chemical Laboratory, The University of Kent, Canterbury, Kent, CT2 7NH, UK

Introduction

Indole and quinoline both have a significant part to play in petroleum chemistry and are found in alkaloids frequently observed in nature. In this study quinoline and indole have been investigated using an Air Sampling Glow Discharge Ionization (ASGDI) source coupled to an ion trap mass spectrometer. The ability of the ion trap to carry out high efficiency tandem mass spectrometry was utilized to illuminate some of the fragmentation pathways present.

The processes involved in an ASGDI source can produce a complex array of chemical reactions which often lead to the spectra being difficult to interpret. In order to complement the interpretation of the complex spectra semi-empirical AM1 calculations were carried out to give qualitative thermodynamic stabilities of the possible adducts and fragments.

Experimental

All the experiments were carried out using a Finnigan MAT Ion Trap Mass Spectrometer (ITMS) coupled to an Atmospheric Sampling Glow Discharge. To produce a DC glow discharge a potential of 350-400 V was applied at a pressure of ca 800 mTorr. Samples were introduced into the source by placing them on a glass spoon in the sampling chamber and any vapour from the sample was drawn into source with the stream of air.

In a DC glow discharge the energies of the electrons present range from thermal (immediately following ejection on electron impact) to energies defined by the source voltage, source pressure and the ionization of energy of the discharge gas. Collisionally induced dissociation reactions between energetic electrons and sample molecules give rise to the production of neutral fragments. These fragments and the sample molecules may form negative ions by the capture of low energy electrons. The anions formed in the source are extracted and are injected into the ion trap via a lensing system.

In addition, because of the high proportion of background air which is taken in to the source, a large number of small, highly reactive anions of air molecules are produced which react with the sample to form anionic adducts which are characteristic of this technique.

Computational Chemistry All the computational chemistry was carried out using the molecular modeling package HyperChem™. Semi-empirical AM1 SCF calculations were used. The Restricted Hartree Fock (RHF) approximation was employed for the neutrals and Unrestricted Hartree Fock (UHF) for the anions. The molecules were first geometry-optimised and then a single point calculation was carried out on the ion or neutral to evaluate the heat of formation. The adiabatic electron affinity of a particular species was calculated by subtracting the heat of formation for the optimised neutral species from the heat of formation of the corresponding geometry-optimised anion.

Results and Discussion

Ion Formation The anions appear to react in three main ways with the indole and quinoline:

1. Removal of a proton to form $(M\text{-}H)^-$ (hydrogen atom abstraction): this can occur by reaction with a BrØnsted base e.g. O^-, O_2^-, NO^- e.g. $O^- + M \longrightarrow (M\text{-}H)^- + OH^-$
2. Formation of an adduct ion e.g. $(M+O\text{-}H)^-$ (H-atom displacement): this can be occur by reaction with O^- e.g. $O^- + M \longrightarrow (M+O\text{-}H)^- + H^-$
3. The anions or molecules present can undergo a loose association with the sample to form a cluster ion. The formation of a cluster can occur with neutral and a charged particle, e.g. $(M\text{-}H)^-{:}O_2$ or $(M\text{-}H){:}O_2^-$

Electron Affinities In the negative ion spectra it is not just the ions that are the most abundantly formed but also the ions that are most stable that will be more dominant in the spectrum. In the glow discharge the ions that will accumulate and hence be dominant in the mass spectrum are the ions with the largest electron affinities. The electron affinity plays a very large role in the abundance of peaks seen in the spectra obtained. The ratios of the $(M\text{-}H)^-$ and the $(M+O\text{-}H)^-$ peaks for three methyl quinolines are shown to be correlated to the electron affinities of the ions theoretically obtained.

Position of Adducts The semi-empirical calculation results can also give an indication of the position of adducts. . For the negative ions the strongest force will be the electron affinity of the final adduct. The knowledge of where the adduct has attached to the sample or where the greatest proportion of adduct attached is useful in interpreting and predicting the chemistry of the ions.

Clusters There is evidence in the results obtained of both cluster formation and of reaction of the indole and quinoline with the oxygen molecule.. The molecule is therefore likely to initially form a cluster or tight ion pair that allows the oxygen molecule to migrate around the deprotonated quinoline. The oxygen then over a period of time reacts with the quinoline to give the covalent interactions which lead to the reaction pathways observed. This set of conditions governing the production of ions makes there interpretation complex.

Conclusion

The way in which the ions are formed in a glow discharge, where many reactive ions and neutrals present at different energies and excited states, makes it an almost impossible task to try to predict a mass spectrum. However, Semi-empirical calculations can be used successfully as an aid to the interpretation of the complex spectra produced from ASGDI sources The most useful information for use in interpretation being gained in the area of electron affinities.

Acknowledgments

SNC wishes to thank EPSRC and BP Ltd. for their sponsorship through the award of a CASE studentship.

FAB-MS OF PROTECTED STEROIDS AND BILE ACIDS USING ALKALI METAL ADDITION

Suresht K. Aggarwal, Robert Y. Pogue, and Jan St. Pyrek, MS-Facility, College of Pharmacy, University of Kentucky, Lexington, KY 40536-0082

Metal attachment ions are frequently observed in FAB-MS and LD-MS spectra [1]. Their formation may be induced by the dissolution of suitable salts in a FAB matrix. Very early, the combination of sulfolane with group I iodides, silver (I) and thallium (I) have been used to characterize compounds such as antibiotics and peptides [2,3]. Metal attachment ions, especially MLi^+, are frequently used in the FAB-MS-MS analysis. This is exemplified by macrolide antibiotics [4], flavonoid and steroidal glucosides [5], free and acetylated triterpenoid acids [6], and carbohydrates [7]. Similarly, salt addition may be used in LD-MS as also exemplified for the underivatized steroid glucosides [8].

In relation to our interest in the area of bile acid, the evaluation of FAB-MS in a nitrobenzyl alcohol (NBA) matrix saturated with alkali metal iodides was undertaken for 84 fully acetylated steroidal (C_{27}, C_{24}, C_{21}, and C_{19}) glucosides and methyl glucuronides. Most (69 compounds) originated from the collection of Dr. Harry E. Hadd, others were either previously obtained in our laboratory or especially prepared for this study. In addition, a series of fully acetylated major C_{24} bile acid methyl esters and tetrahydropyranyl ethers (THP) of selected steroids and bile acid methyl esters have also been tested.

Such highly non-polar derivatives are frequently used both in the chemical synthesis and characterization of natural compounds. As a rule, such multiply blocked compounds produce great difficulties in the MS analysis by EI, CI and FAB due to extremely facile eliminations of acetic acid or dihydropyrane moieties.

EXPERIMENTAL: Spectra were measured using CONCEPT IH (Kratos). In most cases, the mass spectrometer was scanned from 100 to 2,500 u (at 4 kV), 3 sec/decade, with a 3 kHz filter and the "raw" data were acquired at resolution of about 2,000-2,500. Solutions of CsI and CsI-RbI were applied for mass calibration using a "home made" SS double sided FAB probe (one side for sample another for the standard). Matrices were prepared by saturation of NBA with LiI, NaI, KI, RbI, and CsI to give stable solutions. About 1 μl of a selected matrix was mixed on the probe tip with ethyl acetate solution of a sample (1 to 10 μg).

RESULTS AND DISCUSSION: For mono-, di- and tri-THP ether of several available steroids and C_{24} bile acids variable intensity of $\mathbf{MLi^+}$ and $\mathbf{MCs^+}$ ions was observed. Only a few compounds produced fully diagnostic and lucid spectra. On the other hand, MeAc of C_{24} bile acid, MeAc derivatives of all tested steroidal glucosides and glucuronides produced prevalent metal attachment ions and a highly suppressed fragmentation. In addition to the prevalent $\mathbf{MLi^+}$, the following

ions were also present (usually below 2%) with a decreasing intensity $\mathbf{MLiILi^+}$, $\mathbf{M_2Li^+}$, $\mathbf{M_2(LiI)Li^+}$, and $\mathbf{M_2(LiI)_2Li^+}$. In some cases, however, the ion $\mathbf{M_2(LiI)Li^+}$ was more abundant than $\mathbf{M_2Li^+}$. Moreover, for the NBA-CsI matrix such cluster ions were usually less pronounced. Relatively simple daughter ions scans were observed and included a prominent elimination of one AcOH and lithiated sugar fragments.

The lasting signal of $\mathbf{MMetal^+}$ ion allowed long spectral registration. The spectra were especially clear at toward the end of acquisition when most of transient signals disappeared. This was especially valuable for the accurate mass peak-matching. For this NBA-PEG-CsI was used as a matrix and $PEGCs^+$ ions as mass reference ions.

This extensive survey demonstrated general applicability of a FAB measurement with group I iodides dissolved in a NBA matrix to non-polar derivatives of glycosylated sterols, steroids and bile acids. All compounds investigated produced dominant $\mathbf{MMetal^+}$ **ions** with sensitivity allowing a facile characterization of a μg and below, sufficiently sensitive for many applications such as synthesis and isolation. Many functional groups incorporated in the structure did not interfere. This included free hydroxyl groups, ketones and acetonides with no influence on the MS response. Semicarbazones, especially when two were present, lowered the response considerably. For 17Ā-hydroxy compounds with 20-ketone, the additional weak ion was always observed at M+13 [$\mathbf{(M-H)LiLi^+}$].

Preliminary data obtained by MALDI FT-MS (4.7 Tesla magnet, external LD ion source with a N_2 laser) showed also abundant formation of MNa+, MK^+ ions (no salt addition). These ions were completely suppressed by MCs^+ with the addition of CsI to the DHB matrix. Ions MNa-AcOH and M-2xAcOH were observed but these eliminations were completely absent for MK^+ and MCs^+ ions. We thank to Dr. Richard L. Hunter, IonSpec Corporation, for the help in these measurements.

REFERENCES:

(1) L. M. Teesch and J. Adams, **J. Org. Mass Spectrom.**, **27**, 931-943 (1992).
(2) G. R. Pettit, C. W. Holzapfel, and G. M. Cragg. **J. Nat. Prod.**, **47**, 941-946 (1984).
(3) G. R. Pettit, C. W. Holzapfel, and G. M. Cragg, C. L. Herald, and P. Williams. **J. Nat. Prod.**, **46**, 917 (1983).
(4) R. L. Cerny, D. K. McMillan, M. L. Gross, A. K. Mallams, and B. N. Pramanik. **J. Am. Soc. Mass Spectrom.**, **5**, 151 (1994).
(5) M. Takayama, T. Fukai, T. Nomura, and T. Yamauchi. **Org. Mass Spectrom.**, **26**, 655 (1991).
(6) K. P. Madhusundanan, and C. Singh. **Org. Mass Spectrom.**, **27**, 1329 (1992).
(7) G. E. Hofmeister, Z. Zhou, and J. A. Leary. **J. Am. Chem. Soc.**, **113**, 5964 (1991).
(8) M. L. Coates and C. L. Wilkins. **Biomed. Environ. Mass Spectrom.**, **13**, 199 (1986).

M[ALKALI METAL]$^+$ IONS IN FAB SPECTRA OF PROTECTED BILE ACID GLUCOSIDES

Suresht K. Aggarwal, Robert Y. Pogue, and Jan St. Pyrek, MS-Facility, College of Pharmacy, University of Kentucky, Lexington, KY 40536-0082

Increased plasma level and urinary excretion of bile acid (BA) are augmented in certain diseases and involve conjugation with sulfuric and glucuronic acids and recently revealed glucosamine and glucose conjugation [1,2]. Toxic lithocholic acid represents an important example. It is 6α-hydroxylated to hyodeoxycholic acid (3α,6α-dihydroxy-5ß-cholan-24-oic, HDCA), 6-glucuronidated [3], and (probably) 3- and 6-glucosidated by distinct enzymes. Following detection of BA glucosides, the site of a sugar substitution was addressed by chemical and enzymatic synthesis and MS [4-6]. We isolated the product of UDP-Glc-specific glucosyltransferase (from human liver microsomes) formed with HDCA. It was characterized as its MeAc derivative by proton NMR indicating that sugar is attached at C-6 [7]. Now, we synthesized all three possible glucosides of HDCA. Analysis by (+)FAB in the NBA matrix saturated with alkali metal iodides provided an excellent method for characterization of this and others blocked BA derivatives.

EXPERIMENTAL: Synthesis of BA glucosides was performed as described for BA glucuronides [8]. All FAB spectra were measured using CONCEPT IH (Kratos), scanned from 100 to 2,500 u, 3 sec/decade, "raw" data were acquired with the mass resolution of about 2,000. Matrices were prepared by saturation of NBA with LiI, NaI, KI, RbI, and CsI to give stable solutions. About 1 μl of a selected matrix solution was mixed on the probe tip with ethyl acetate solution of a protected BA. A long lasting response was obtained using about 1 μg samples.

RESULTS AND DISCUSSION: We favor handling and spectral characterization of MeAc derivatives of BA glucosides and glucuronides. This is because: (a) MeAc derivatives are easily formed by Koenigs-Knorr reaction; (b) MeAc derivatives are stable and can be separated and purified by different chromatographic methods; can be analyzed by high temperature GC and by low eV EI-MS [9]; NMR of MeAc derivatives indicates the point of a sugar attachment in the most unambiguous way; (c) isomeric glucosides and glucuronides have the same MW (e.g. the same $(M-H)^-$ ion in (-)FAB spectra) but for MeAc derivatives of hydroxyl and carboxyl attached isomers the number of Me and Ac groups differs leading to a different MW; (d) blocked ester-glucosides/glucuronides are deprotected with breakage of the glycosidic bond. Because of all these reasons, it is easier to derivatize metabolic products and to perform their comparison with the direct synthetic product. Consequently, we searched for a suitable MS method allowing unambiguous measurements of their MW.

We measured FAB spectra of the MeAc derivatives of BA glucosides listed in the **TABLE** below. In NBA alone, only a barely detectable MH^+ ion was accompanied by an extensive fragmentation consistent with a presumption that these non-polar compounds are not compatible with the FAB analysis. However, encouraged by many reports of the use of metal ion attachments for FAB and LD-MS, we found that all these MeAc derivatives produce intense alkali metal attachment ions and highly

suppressed fragmentation when analyzed in the NBA matrix saturated with LiI, NaI, KI, RbI, and CsI.

BILE ACID	3	6	7	12	glucose position	MLi^+
lithocholic	α				3	727
lithocholic	α				COOH	755
chenodeoxycholic	α		α		3	785
ursodeoxycholic	α		ß		3	785
deoxycholic	α			α	3	785
hyodeoxycholic	α	α			3	785
hyodeoxycholic	α	α			6	785
hyodeoxycholic	α	α			COOH	813
cholic	α		α	α	3	843
cholic	α		α	α-OH	3	801

Peracetylated cholesterol ß-D-glucoside is another good example. In NBA-LiI, it shows the predominant MLi^+ ion (m/z 723), followed by $MLiILi^+$ (857) and weak ions corresponding to M_2Li^+ (1439), M_2LiILi^+ (1574), and $M_2(LiI)_2Li^+$ (1708), elimination of AcOH (663), steroid derived fragments (369, 368, 367) and lithiated and non-lithiated "sugar ions" (355, 331, 295, and 169). Linked scan (daughter ions) indicated the formation of ions 663, 355, and 295 from the MLi^+ ion. Ions 369, 368, 367, and 331, however, were more abundant when MH^+ (of a negligible intensity) was selected as a precursor. These ions were also detected in NBA matrix and their presence suggests that the lithiation may not be complete.

REFERENCES: (1) H. Matern, S. Matern, and W. Gerok. **PNAS**, 81, 7036-7040 (1984). H.-U. Marschall, B. Egstad, H. Matern, S. Matern, and J. Sjovall. **JBC**, **264**, 12989-12993 (1989). H. Matern, R. Bolz, H.-U. Marschall, J. Sjovall, and S. Matern. **FEBS**, **270**, 11-14 (1990). **(2)** H.-U. Marschall, G. Green, B. Egestad, and J. Sjovall. **J. Chromat.**, **452**, 459-468 (1988). H. Wiethholtz, H.-U. Marshall, R. Reuschenbach, H. Matern, and S. Matern. **Hepatology**, **13**, 565-662 (1991). **(3)** Radominska-Pyrek, A., Zimniak, P., Irshaid, T.M., Lester, R., Tephly, T.R., and Pyrek, J. St., **J. Chem. Invest.**, **80**, 234-241 (1987). **(4)** T. Niwa, T. Koshiyama, J. Goto, and T. Nabara. **Steroids**, **57**, 522-529 (1992). T. Iida, S. Tazawz, Y. Ohshima, T. Niwa, J. Goto, and T. Nambara. **Chem. Pharm. Bull**, **42**, 1479-1484 (1994). **(5)** H. Matern, R. Boltz, and S. Matern. **Eur. J. Biochem.**, **190**, 99-105 (1990). **(6)** H.-U. Marschall, W. J. Griffiths, J. Zhang, H. Wietholtz, H. Mater, S. Matern, and J. Sjovall. **J. Lipid Res.**, **35**, 1599-1610 (1994). **(7)** A. Radominska, J. Little, J. St. Pyrek, R. R. Drake, Y. Igari, S. Fournel-Gigleux, J. Magdalou, B. Burchell, A. D. Elbein, G. Siest, and R. Lester. **JBC**, **268**, 15127-15135 (1993). (8) A. Radominska-Pyrek, P. Zimniak, M. Chari, E. Golunski, R. Lester, and J. St. Pyrek. **J. Lipid Res.**, **27**, 89-101 (1986). K. E. Shattuck, A. Radominska-Pyrek, P. Zimniak, E. W. Adcock, R. Lester, and J. St. Pyrek. **Hepatology**, **6**, 869-873 (1986). (9) Pyrek St. J. **Recent Advances in Phytochemistry**, H. A. Stafford Editor, pp 175-249. Pergamon Press (1991).

Fragmentation of 3,7-dialkyl-1,5-diphenyl-3,7-diazabicyclo[3,3,1]-nonan-9-ones under electron impact

Natalia Yu. Tretyakova, J. Ronald Hass

Department of Environmental Science and Engineering, University of North Carolina, Chapel Hill, NC 27599, USA

Sergey Z. Vatsadze, Albert T. Lebedev, Nikolay V. Zyk, Nikolay S. Zefirov

Department of Chemistry, Lomonosov University of Moscow, Moscow, 119899, Russia

3,7-Diazabicyclo[3,3,1]-nonan-9-ones (bispidones) are of interest to organic chemists due to their conformational behavior. A wide range of bispidones has been recently examined as new biologically active agents. 1,5-Diphenylbispidones were shown to have the properties of local anesthetics. In the present paper, various 3,7-dialkyl-1,5-diphenyl-3,7-diazabicyclo[3,3,1]-nonan-9-ones have been prepared, and the details of their mass fragmentation under electron impact have been elucidated.

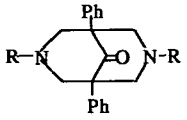

1, R = Me
2, R = Et
3, R = i-Pr
4, R = $-CH_2-CH=CH_2$
5, R = $CH_2-CH_2-O-CH_3$

The molecular ions of each compound under consideration were observed in their EI spectra. Full-scan spectra exhibited a number of fragment ions which were clearly assigned using substituent shifts, collision-induced dissociation spectra of selected ions B/E and B^2/E scans) and accurate mass measurements (for compound 1). From these results, the fragmentation process in the scheme below is suggested.

C1-C2 bond cleavage results in the formation of intermediate A. Hydrogen migration through a six-membered-ring intermediate similar to the odd-electron McLafferty rearrangement leads to abundant ions B. This can be accompanied by charge migration yielding cyclic species (ion C). According to the Stevenson Rule (1951), the favored ion product should form from the fragment of lower ionization energy. Since both

ions are observed at comparable intensity, B should have close ionization energies. Alternatively, A can eliminate an imine molecule giving ion D. The latter probably rearranges to a more stable ion D' which gives rise to abundant ions at m/z 234 present in the EI spectra of all the compounds.

The results of the present work can be useful in selecting the fragment ions suitable for identification and quantitation of 1,5-diphenylbispidones in biological matrices.

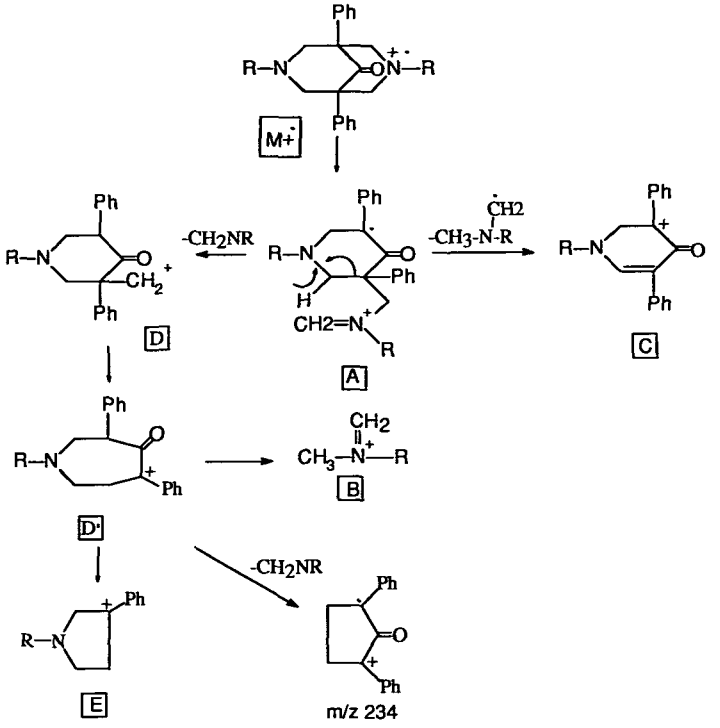

Trace Analysis of Degraded Antibiotics by ESI-LC/MS

Jong Shin Yoo[1], Jin Young Kim[1], Sung Ho Kim[2]
1. Korea Basic Science Institute, Taejon, Korea
2 Department of Chemistry, Soonchunhyang Univ., Asan, Korea

Amoxicillin is one of the important classes of β-Lactam antibiotics. During its preparation, the presence of trace amount of degradation products or by-products, however, is thought to be responsible for its adverse effects in clinical use. Because these compounds exist in less than 1% of total weight and are very unstable in solution with various solvent composition, and pH conditions, it was hard to collect and detect them individually for analytical characterization. In this study amoxicillin and its unknown residues were separated and identified by HPLC/MS system using electrospray ionization(ESI) technique.

All samples were dissolved in 40% aqueous methanol solution with 0.05% formic acid to make 1mg/mL solution. They were kept less than an hour to prevent any compositional change in the solvent before analysis. The optimum separation condition for the analysis of amoxicillin products in HPLC system was determined by using a 2.1×200mm×5μm, C_{18} column. The end of the column was connected through an electrospray LC/MS interface into a mass spectrometer. Due to the low flow-rate limitation for successful electrospray ionization, a post-column split ratio of 20:1 for the eluent from a column was chosen to provide the required flow-rate(approximately 20μL/min). ESI-MS and ESI-MS/MS spectra of the compounds were obtained on a VG Quattro Triple Quadrupole Mass Spectrometer under the operation conditions as follows; capillary tip voltage, 3.5kV; cone voltage, 20V; N_2 curtain gas flow rate, 250L/h; source temp., 70℃; Ar as collision gas. The mass spectrometer was scanned from mass-to-charge ratio(m/z) 300 to 800 for 3 seconds.

For the amoxicillin sample aged 4 years since preparation, the trace compounds in it were considered to be the degraded products of amoxicillin In LC/MS analysis shown in Figure 1, they were monitored at the retention time of 9 and 25 min, and represented with the $[M+H]^+$ peaks at m/z 340 and 705 respectively. The peak at m/z 366 indicates amoxicillin which has a molecular weight of 365. The structural identification through fragmentation pattern of the degraded products was further obtained by the use of collision induced dissociation technique in the second collisional chamber of the triple quadrupole mass spectrometer(Figure 2). In all of the spectra we could see the loss of 17 mass unit from pseudomolecular ion $[M+H]^+$, which is the typical pattern for the amoxicillin. They also showed various fragmentation, mostly within the β-Lactam ring and the amide group. Usually, the fragmentation followed the pattern of amoxicillin and most of penicillin type of antibiotics, showing a characteristic cleavage product of the β-Lactam ring, $[C_6H_9HSO_2+H]^+$ at m/z 160, and a further loss of COOH at m/z 114. The fragmentation pattern of the compounds with molecular weight of 339 and 704 showed the possible spectrum for amoxicillin derivatives. In addition, from the same UV maxima at 195 nm and 230 nm in diode array spectra of each compound, they could be expected to have the same structure as amoxicillin.

From these results the compounds with molecular weight of 339 and 704 were assigned to be the penilloic acid of amoxicillin and its additional product. And the compounds which have exactly the same peak at m/z 340 but different LC retention time were thought to be two possible empimers of the penilloic acid of amoxicillin. In conclusion the LC/MS approach with electrospray ionization showed good sensitivity and selectivity for the detection of trace amounts of degradation products by selected ion monitoring of pseudomolecular ion peaks of amoxicillin derivatives. It was proven to be one of the most suitable methods for the analysis of trace mixture of labile compounds such as β-Lactam antibiotics.

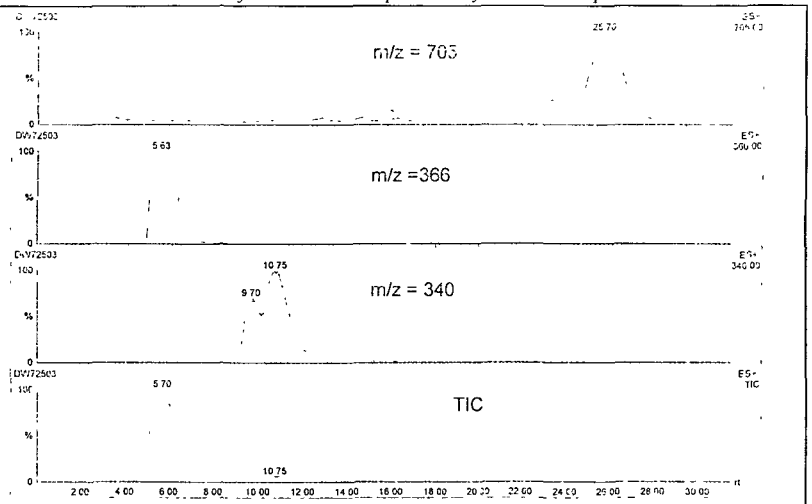

Figure 1. LC/MS TIC of Aged Amoxicillin

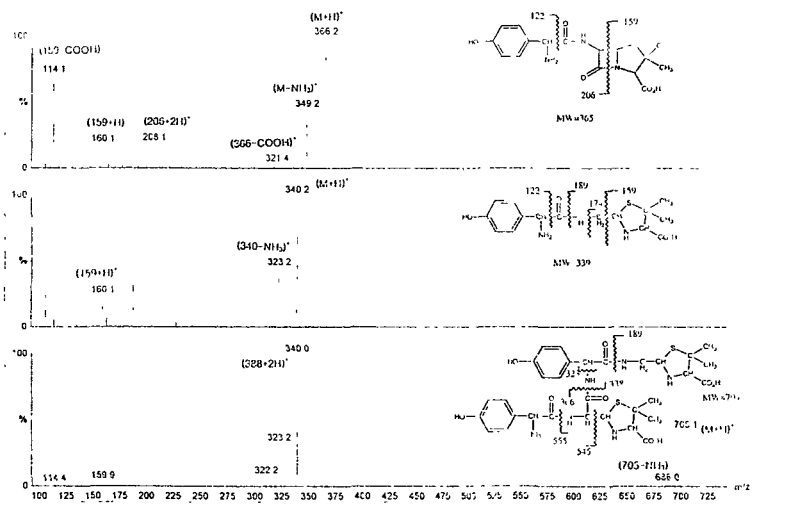

Figure 2. MS/MS Fragmentation of Amoxicillin and Its Degradation Products

Semi-Quantitative Analysis of Pharmaceutical Product Impurities by API/LCMS

Michael R. Wakefield, Mark Sanders, Jonathan L. Josephs and Iain Mylchreest
Finnigan MAT, 355 River Oaks Parkway, San Jose CA 95134

FDA regulations require pharmaceutical companies to identify impurities present at >0.1% in their products. Recent technological advantages in atmospheric pressure ionization (API) now permit LC/MS analysis of low level impurities in pharmaceutical products on conventional 4.6mm id columns. In addition the LC/MS/MS process may be automated, thereby streamlining the identification of the product impurities. Two examples of automated Smart MS/MS of product impurities are presented.

For a conventional MS/MS experiment first a Q1MS LC/MS chromatogram is obtained, the peaks are analyzed and molecular ions in each peak are determined. A second chromatogram is then run in which the instrument is programmed to change the parent mass with retention time in order to obtain MS/MS product ion spectra. The experiment requires that retention times do not shift and that the list of allowable parent set masses is greater than the number of impurity peaks. Additional experiments may then be performed, *e.g.* a neutral loss/parent scan LC/MS/MS run will reveal compounds which have a common structural motif. This may well uncover minor impurities not obvious from the Q1MS data. To obtain product ion MS/MS data on these peaks would then require yet another chromatographic run, once more programming the mass spectrometer to change the parent set mass with retention time.

The concept behind Smart MS/MS is a simple one[1]. The mass spectrometer does in real time what the chemist would do post acquisition. The instrument detects an HPLC peak when an ion signal exceeds a preset threshold. Depending on the incoming data a parent ion is selected, the appropriate mass ranges are set and an MS/MS product ion spectrum is recorded. The Smart MS/MS experiment takes one of three basic forms. 1) Q1MS mode - all peaks above threshold have product ion spectra recorded. 2) Parent mode - only compounds with a common product ion have their product ion spectra recorded. 3) Neutral loss mode - only compounds exhibiting a certain neutral loss would have their product ion spectra recorded.

One example is the analysis of fumonisin B_1, a member of a family of mycotoxins isolated from *Fusarium moniliforme* which is found on corn. The other is the analysis of the analgesic, anti-convulsant carbamazepine which was spiked with known levels of impurities. Both analyses were performed on a Finnigan MAT TSQ 7000 using electrospray ionization (ESI). In order to accommodate the high column loading required to see impurities at the 0.1% level normal bore HPLC columns (4.6mm) were employed at a flow rate of 1ml/min with no presource splitting. For the analysis of fumonisin B_1 Q1MS spectra of low level impurities are illustrated along with the semi-quantitative results. The parent mode Smart MS/MS experiment was performed. Screening for parents of m/z 352 reveals impurities with an unmodified backbone, specifically fumonisin B_1 at m/z 722 and four compounds showing monomethyl side chain modifications at m/z 736. The associated product ion spectra are also shown. The carbamazepine analysis showed impurities at the 0.02% level. A neutral loss to product ion MS/MS experiment screened for compounds with the carbamate moiety, and produced the associated product ion spectra for these impurities.

In conclusion automating semi-quantitative assays of chemical impurities in pharmaceutical compounds has become a routine task. Using the Smart MS/MS technology of the Finnigan MAT TSQ 7000, sample throughput and information acquired per analysis are increased. In addition impurities not revealed by conventional HPLC detectors can be detected.

1. Stahl, D.C., Martino, P.A., Swiderek, K.M., Davis, M.T. and Lee, T.D., *Automated LC/MS/MS Analysis of Peptide Mixtures Using Capillary HPLC and Electrospray Ionization on a Triple Sector Quadrupole Mass Spectrometer*, Proc. of the 40th ASMS Conf. on Mass Spectrometry and Allied Topics, Washington, DC, **1992**

Fumonisin B_1 Q1 MS Chromatogram
ESI 4.6mm x 150mm Column at 1 ml / min

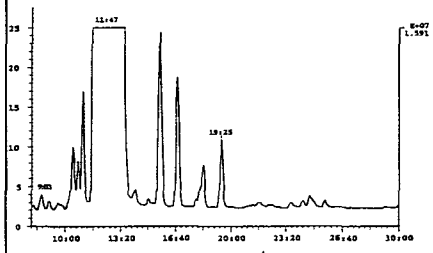

Q1 MS Spectra of Fumonisin B_1 Impurities

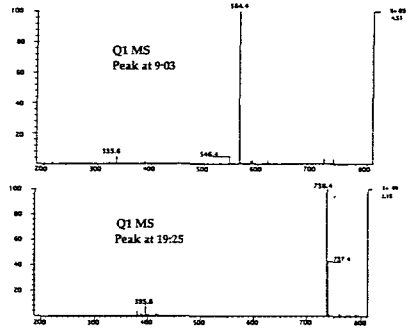

Semi - Quantitative Results

Fumonisin B_1

Scan #	Actual Time	Area	Percent Total
308	10:29	60182	0.01
321	10:57	10005354	1.07
338	11:32	336804	0.04
375	12:50	8.66E+08	92.21
413	14:11	621882	0.07
462	15:54	33660524	3.58
492	16.58	23958152	2.55
525	18:06	107348	0.01
562	19.23	30250	0.01
723	24.55	4309154	0.46

Parent Mode Detection ⟶ Product Ion MS/MS

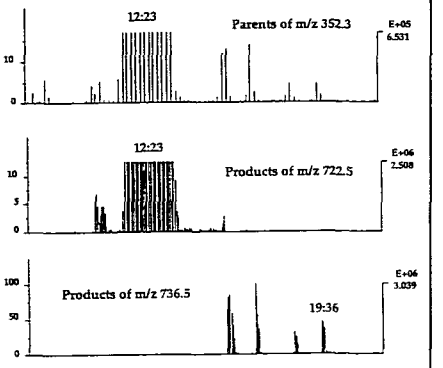

Product Spectra of Compounds Detected by Parents of m/z 352.3

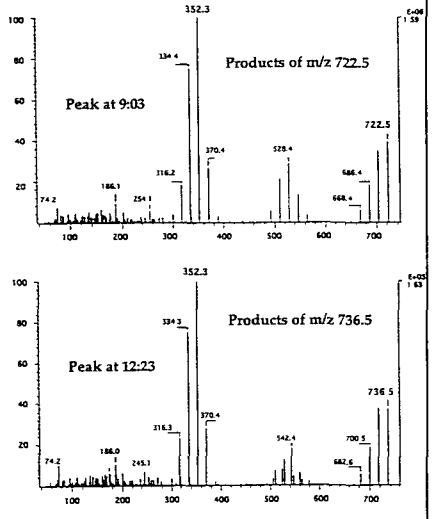

Predictive Impurity Profiling in Pharmaceutical Research Utilizing Rapid LC/MS and Chemical Degradation

William L. Thompson[1], John S. Venesky[1], Kevin Volk[2], Steven E. Klohr[2], Edward H. Kerns[2] and Mike S. Lee[3]

Bristol-Myers Squibb Pharmaceutical Research Institute, [1]New Brunswick, NJ 08903-0191, [2]Wallingford, CT 06492, [3]Princeton, NJ 08543-4000

The profile analysis of degradants and other impurities present in pharmaceuticals plays a key role in pharmaceutical research. Unfortunately, this role is frequently a "just in time" activity and can negatively impact critical development timelines. In addition, this responsibility may be performed by multiple groups throughout the company and lead to redundancy due to lack of effective technology transfer strategies.

Here we describe our efforts to develop mass spectrometry-based methods and analytical approaches for the predictive profiling of potential impurities in pharmaceuticals. This approach utilizes intentional chemical degradation of a drug with a variety of reagents followed by LC/MS analysis to determine the structures of the impurities formed. This experiment will be conducted at the stage when a potential drug candidate passes from drug discovery to pharmaceutical development and the results will be cataloged in a structure based impurity library. This predictive library will then be made available to all investigators who work on the drug as it passes through development. This streamlined analytical approach is demonstrated with a model compound captopril.

The protocol is as follows:

1. React the final drug substance or the penultimate intermediate in its synthesis with various reagents.

2. Analyze the reaction mixture by HPLC/UV to find new impurities and to collect photo-diode array spectra.

3. Use LC/MS to characterize the impurities and propose structures.

4. Catalog the relative retention times (RRT), UV spectra, molecular weight, and proposed structure for each new impurity. This library will then be used later in the development process as an aid in identifying these impurities when they arise.

The following results were obtained for captopril:

Relative RT	Blank	HCl	HOAc	NaOH	NH4OH	K2CO3	NaHCO3	KMnO4	Air	Heat (75 °C)	CH3OH
0.33				7.26							
0.34			3.03	40.63							
0.37				1.6							
0.911						10.31					
0.970						27.46					
1.000	99.47	100	94.82	5.32	98.93	9.99	99.78	4.13	99.33	99.44	99.76
1.109				1.35							
1.210						2.1					
1.230						21.01					
1.237	0.53		2.15		1.07	14.98	0.22	0.09	0.67	0.56	0.24
1.300				34.42		14.15		55.08			
1.370				9.43							

The table above shows the relative retention times (RRT) and area percents of the impurities formed under the various chemical conditions (LC/UV). LC/MS studies gave ions ($M+H^+$) at m/e of 236, 449, 465, and 433 for peaks at RRT 0.45, 0.34, 1.10, and 1.18, respectively. The peak with mass 432 corresponds to captopril disulfide, a known compound. The peaks at 448 and 464 would correspond to the disulfide plus 1 and 2 oxygens, respectively. The peak at m/e 236 is unassigned.

The LC/MS phase is still in progress, and is expected to yield more information. In addition, LC/UV studies have been performed on the penultimate intermediate in the synthesis of captopril, the thioacetate. This work, when complete, should yield much additional information, since many "real life" impurities derive from the penultimate during the last step of the synthesis.

This procedure can also be applied to other areas of pharmaceutical development, including preliminary stability studies.

THE ROLE OF MASS SPECTROMETRY IN THE STRESS TESTING OF PHARMACEUTICALS

Craig Kemp, Gary Cooke, and The Chemical Characterization Team
Pharmaceutical and Analytical DevelopmentEli Lilly and Company,
Lilly Research Laboratories, Indianapolis, IN 46285

Part of the process of pharmaceutical development is a thorough characterization of the degradation products of the active drug substance. Accelerated degradation conditions are set up in accordance with predetermined protocols to satisfy specified regulatory requirements. The characterization scheme in our laboratory uses a MS technique to establish the molecular weight and the molecular formula of isolated degradation products. Since the impurities are true unknowns at this stage of the structure elucidation process, careful consideration must be given to information generated by the mass spectrometer. It is accepted that no one technique will always produce an unambiguous molecular ion and frequently the results from several techniques must be collected and compared to establish a true molecular ion. Three examples from recent projects have been selected to demonstrate the often critical contribution MS techniques make in solving difficult structure elucidation problems.

Compound A is an N-oxide formed by oxidative degradation of the parent drug molecule.

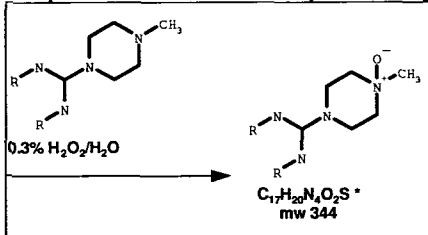

FAB	Intense M-O
FD	Intense M-O, weak M+
EI+	M-O
EI Accurate Mass	No Molecular Ion, M-O lost in baseline noise
ES+	M-O

* Determined by Accurate Mass FAB measurements after sample was acidified

Compound B is a dimer produced by basic degradation of the parent compound.

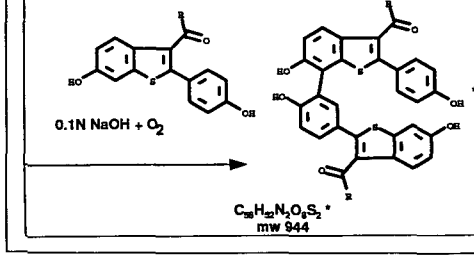

FAB	Very weak [M+H]+
*Accurate Mass FAB	Calculated: 945.3243 Measured: 945.3249
ES+	$[M+2H]^{2+}$ and $[M+H]^+$

Compound C is a process impurity produced in the final step of the synthesis of the bulk drug.

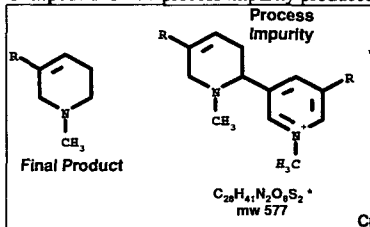

*Accurate Mass FAB	Calculated: 557.2732 Measured: 557.2752
EI+	M^+
ES+	M^+

Cmpd C + D2O ⟶ No Exch Protons
Cmpd C + NaI ⟶ $[M^+ + M^+ + I^-]^+$

Since NMR data of this unknown showed no protons on the nitrogen in the aromatic ring the assumption was made that a **quaternary nitrogen** was present in the molecule. A recent paper[1] describes methods for recognizing quaternary ammonium compounds and this unknown presented an ideal opportunity to test these ideas.

A solution of the unknown was made up with sodium iodide and infused into the electrospray source. Figure 1 is the resulting ES spectrum showing the incorporation of iodide in the molecule and confirming the presence of a quaternary nitrogen in the structure of the unknown. The ion at *m/z* 557 is the *true* molecular ion for this unknown.

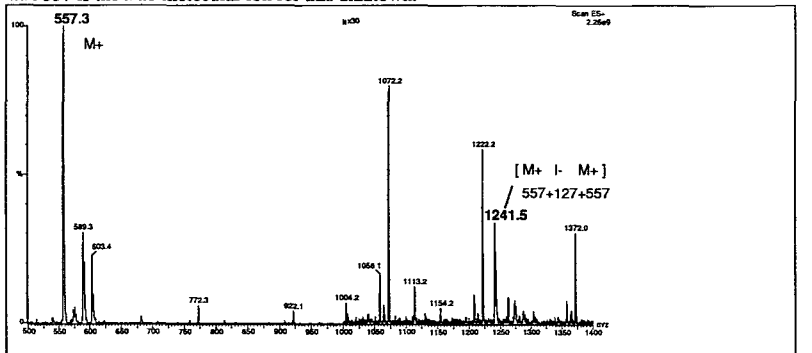

Figure 1: Positive Ion electrospray spectrum of compound C in 50/50 ACN/H2O 0.1mg/mL NaI

The vast majority of the compounds analyzed in our laboratory give an ion that can be established as the true molecular ion by a single ionization technique. The array of ionization techniques used for Compounds A, B, and C are the exception rather than the rule and are implemented only when the NMR spectrum cannot be reconciled with the molecular ion proposed by the mass spectroscopist from a single ionization technique. When these situations occur it is prudent to utilize all the ionization tools available for the MS experiment.

[1] D.L. Fisher, M.A. Mosely, J.O. Mullis and D.L. Norwood: Rapid Communications in Mass Spectrometry 8 65-70 (1994)

Profiling Sotalol Impurities and Degradation Products Using a Standard LC/MS and LC/MS/MS Method

Kevin J. Volk, Edward H. Kerns, Susan E. Hill, [2]Terry Wilson, [2]Robert Behme, [2]Dana Brooke, and [3] Mike S. Lee,
Bristol-Myers Squibb Pharmaceutical Institute
5 Research Parkway, Wallingford, CT 06492
[2]2400 W. Lloyd Expressway, Evansville, IN 47721
[3] P.O. Box 4000, Princeton, NJ 08543-4000

During the pharmaceutical drug discovery and drug development process, we employ a strategy using standard LC/MS profiling and LC/MS/MS substructural analysis methodologies to rapidly elucidate the structures of degradants and impurities. The analytical strategy includes a systematic approach for the identification of unknown impurities and degradants which retain key substructures of the parent drug. We utilize standard LC/UV conditions on-line for comparability to collaborating labs as well as standard LC/MS profiling conditions to determine molecular weight of unknowns in samples. Comparison of an unknown to known analogs provides additional information about relative polarity and difference in molecular weights. Structures of impurities and degradants are elucidated based on relative retention time, UV spectra, molecular weight, and MS/MS substructure analysis (Figures 1 and 2). In these studies, various sotalol preparations possessing distinct degradant and impurity profiles were examined using standard profiling conditions which facilitated the development of a structural database of sotalol impurities. We have examined long term storage stability samples of bulk drug, forced degraded bulk drug (oxygen and heat), and various formulated drug products using these methodologies and have proposed structures for 12 impurities and degradants.

Our standard profiling conditions utilize a Sciex API III tandem mass spectrometer equipped with an ionspray interface. For small molecule work we typically scan from m/z 100 to m/z 1200 using a step size 0.4 Dalton and a dwell time of 1.0 mSec. The choice of polarity modes is based on the structures of the parent drug as well as expected impurities and degradants. However, acquisition of data in both the positive and negative ion modes provides complementary information. A gradient HPLC with diode array UV detector (HP 1090) and a C-18 column (Zorbax, 2mm X 150 mm X 5 µm) with the gradient programmed from 90/10 (A/B) where solvent A is acetonitrile and solvent B is 2 mM ammonium acetate, pH 5.3 to 10/90 in 25 minutes at a flow rate of 200 µL/min. The LC/MS and LC/MS/MS strategies were developed to rapidly and accurately provide structural data which would have been time-consuming using traditional methods of structure elucidation. The use of standard LC/MS profiling conditions permits the development of a database consisting of molecular structures, chromatographic behavior, molecular weight, UV spectrum, and substructure specific (product ions) information. Structures and information are added to the database in support of one area of pharmaceutical development research and are often found to be critical in other areas of development. Ideally, an LC/MS structural database will have its origin in drug discovery research. It will be utilized and enhanced during the pharmaceutical development process, and provide support for future activities such as patent interference, product failures, and new generations of drug analogs.

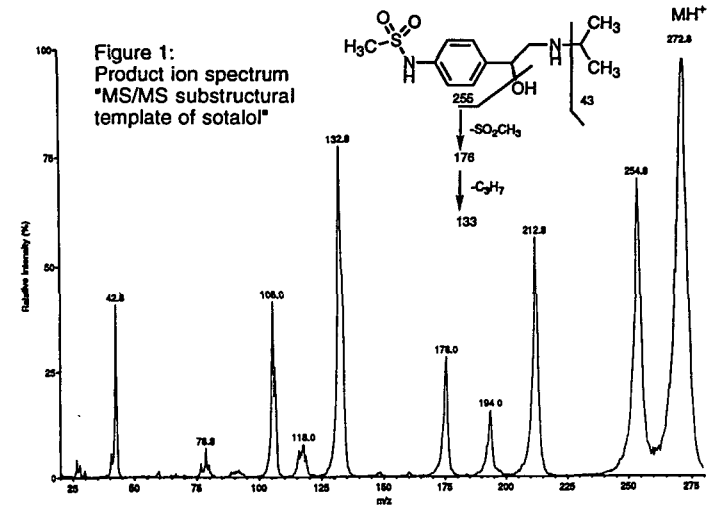

Figure 1: Product ion spectrum "MS/MS substructural template of sotalol"

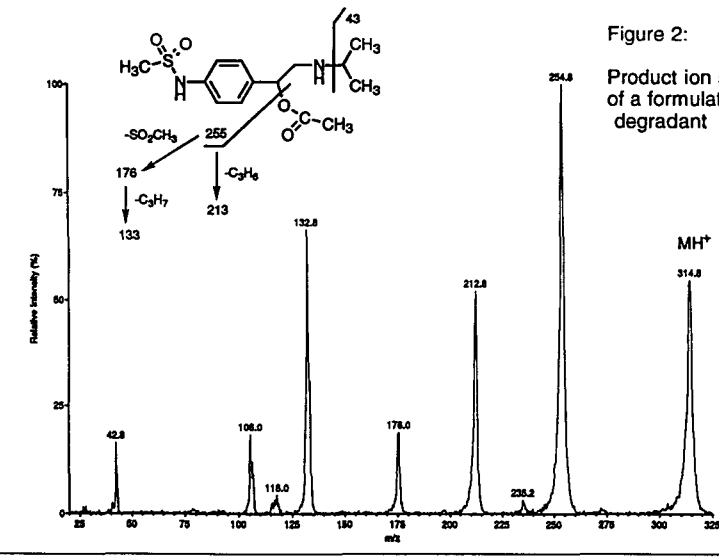

Figure 2: Product ion spectrum of a formulation degradant

Online ion-exchange chromatography/electrospray mass spectrometry for the identification of organic and inorganic species in topiramate tablets

Xinzhen Xiang, Chan Y. Ko, H. Y. Guh

Analytical Research and Development
The R.W. Johnson Pharmaceutical Research Institute
Welsh and McKean Roads, Spring House, PA 19477-0776

Topiramate is a novel anticonvulsant drug under development [1,2]. Under normal storage conditions (ambient temperature and humidity), topiramate in the solid state is stable. However, it can degrade under stress conditions (elevated temperatures and humidities) and produce organic degradation products and inorganic sulfamate and sulfate as shown in Scheme 1. Since sulfamate and sulfate are: (a) produced stoichiometrically during topiramate degradation; (b) stable and nonvolatile; and (c) extractable quantitatively from the degraded drug tablets, a stability-indicating ion chromatographic method has been developed for monitoring topiramate degradation in topiramate tablets by quantifying sulfamate and sulfate [3]. When the topiramate tablet sample was analyzed on the anion-exchange column, many unknown peaks which are not obviously related to the excipients were detected. It is important to identify these peaks in order to control the chromatography effectively and to better understand the sample matrix. Since those unknown peaks could be either organic or inorganic species, a technique capable of providing elemental and molecular information for both organic and inorganic species is necessary.

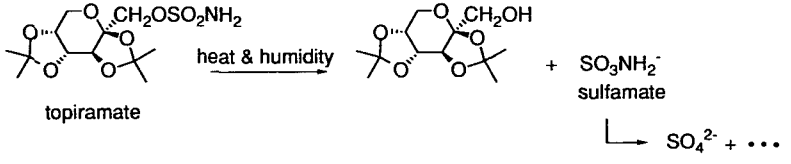

Scheme 1

In the present work, an on-line ion-exchange chromatography/electrospray ionization mass spectrometer (IC-ESI-MS) was used successfully to identify organic and inorganic species present in topiramate tablets. An ion suppressor is placed between the column and detectors to replace sodium ions in the mobile phase with hydrogen ions supplied by the suppressor. The combination of the hydrogen ions with mobile phase hydroxide ions produces nonconducting water, thus first greatly reducing the baseline conductivity for the ion conductivity detector; and secondly, preventing nonvolatile sodium salts from clogging the heated capillary and contaminating the ion source of the mass spectrometer. The ability to detect analytes in solvents with a water content up to 100 % was demonstrated. The analytes, including lactate, glycolate, chloride, formate, sulfate, and oxalate were unambiguously identified by comparing their mass spectra and retention times with those of the authentic compounds as summarized in Table 1. IC-ESI-MS proved to be a convenient and powerful tool for the detection and characterization of a variety of organic as well as inorganic species of low to moderate molecular weight. Though the coupling of ion exchange chromatography to mass spectrometry has been reported previously with ion spray ionization [4], thermospray ionization [5], and particle beam ionization [6] respectively, this is the first experimental demonstration of IC-ESI-MS for the identification of unknown species in real samples, especially for the identification of both organic and inorganic species in the low mass range.

Table 1: Summary of retention times, m/z, and identities of the unknown peaks present in the placebo tablet, obtained from the analysis of IC-ESI/MS (in negative ion mode).

Peak	Retention time (minute)	Corresponding m/z	Species identified
A	4.4	89	lactate
B	4.9	75	glycolate
C	6.6	45, 89	formate
D	11.1	35, 37	chloride
E	15.7	97	sulfate
F	17.4	89	oxalate

ACKNOWLEDGMENT:
Valuable discussions with David J. Burinsky are gratefully acknowledged. We thank Arthur P. Micheel for his assistance in setting up the IC instrument.

REFERENCES:

(1) Rangel, R. J.; Penry, J. K.; Wilder, B. J.; Riela, A.; Margul, B. L. *Neurology* **1988**, *38*, 234.
(2) Reitz, A. B.; Tuman, R. W.; Marchione, C. S.; Jordan, A. D.; Bowden, C. R.; Maryanoff, B. E. *J. Med. Chem.* **1989**, *32*, 2110-2116.
(3) Guh, H. Y.; Micheel, A. P.; Ko, C. Y., *6th International Symposium on Pharmaceutical and Biomedical Analysis*, St. Louis, Missouri, T-P/E7, April, 1995.
(4) Conboy, J. J.; Henion, J. D.; Martin, M. W.; Zweigenbaum, J. A. *Anal. Chem.* **1990**, *62*, 800-807.
(5) Simpson, R. C.; Fenselau, C. C.; Hardy, M. R.; Townsend, R. R.; Yee, Y. C.; Cotter, R. J. *Anal. Chem.* **1990**, *62*, 248-252.
(6) Hsu, J. *Anal. Chem.* **1992**, *64*, 434-443.

Pharmaceutical Applications of IonSpray LC/MS for Cyclodextrin Analysis

Josie Visentini, Angelo Filosa, Caroline Rousseau and Conrad Winters,
Merck Frosst Centre for Therapeutic Research,
P.O. Box 1005,Pointe Claire-Dorval, P.Q. H9R 4P8 Canada

Cyclodextrins are cyclic oligosaccharides in which the number of glucose units increases from 6 to 7 to 8 for α–, β–, and γ-cyclodextrin respectively. Figure 1 shows the molecular structure of the parent β-cyclodextrin (BCD) and some BCD derivatives. The size of the cavity within the ring structure also increases from α (5.1Å) to β (6.3 Å) to γ-cyclodextrin (8.0 Å) and it is believed that the cavity size is a key factor in determining the degree to which cyclodextrins can form inclusion complexes with different molecules. This non-covalent complexation can potentially modify the physical and chemical nature of the included compound. These inclusion complexes are of particular interest to the pharmaceutical industry for improving the aqueous solubility of poorly water soluble drugs. The solubility of drugs can often be further increased by using substituted cyclodextrins such as hydroxypropyl-β-cyclodextrin (HPBCD) or methyl-β-cyclodextrin (Me-BCD) (Figure 1) which have a greater intrinsic solubility than the unsubstituted parent cyclodextrin. Since cyclodextrins do not contain chromophores, their HPLC analysis using conventional spectroscopic detectors is limited to methods involving the inclusion of chromophoric modifiers. These methods, however, often lack sensitivity and are vulnerable to interferences caused by the inclusion of impurities rather than the intended chromophore. The potential use of IonSpray LC/MS was explored for the detection of cyclodextrins and their drug-included complexes in both positive and negative ion modes. All inclusion complexes were prepared in a 1:1 molar ratio of drug to cyclodextrin except for spironolactone (SPL) which was prepared in a 1:2 ratio. The drug was dissolved in methanol and the cyclodextrin in water to give a 30:70 methanol:water cosolvent system. The mixtures were stirred for at least 8 hours, filtered using 0.22 μm filters and then diluted using water to 0.5 mg/mL cyclodextrin concentrations. Analyses were conducted by flow injection HPLC on a Hewlett Packard HP1090 coupled to a PE/Sciex API III+ mass spectrometer.

Preliminary work in the characterization of drug-included complexes was conducted using the parent BCD since the HPBCD and Me-BCD showed ranges of ion peaks for both the cyclodextrin and drug complexes while the spectra obtained for the parent BCD contained fewer peaks and were thus easier to interpret. Once the complexes had been characterized using the parent cyclodextrin, later work was conducted using the the more water-soluble and potentially more useful substituted cyclodextrins. Results from different drug-cyclodextrin systems showed the complex in both positive and negative ion modes corresponding to a 1:1 drug:cyclodextrin stoichiometric ratio. The relative amount of complex to cyclodextrin, however, was generally seen to be higher in negative ion mode than in positive mode. In some cases, such as that for the spironolactone+BCD complex, ions corresponding to the complex of drug fragments as well as the intact drug molecule were observed in both positive and negative ion modes. For example, as shown in the positive ion mass spectrum in Figure 2, complexes were observed for BCD+SPL and for BCD+fragments (m/z 43 and m/z 374) which are designated in the structure above the spectrum. Generally, mass spectra obtained for different drug-cyclodextrin combinations showed that only the types of ions observed for the drug alone are observed as complexes. It appears therefore that the ionization behaviour of the drug molecules alone is intimately related to that of the cyclodextrin complex. In the case of spironolactone, however, the methyl keto fragment (m/z 43) was only observed in the inclusion complex ion and not as a fragment of the drug. The absence of this fragment alone indicates that either this group is not ionized under the present conditions or that the BCD+intact drug

ion fragments to produce the BCD+fragment ion. This phenomenon is the subject of ongoing studies. Other studies were also conducted to study the relative affinities of ibuprofen (IBP) for unsubstituted α, β and γ cyclodextrins and the results are shown in Figure 3. The relative affinities of IBP for each cyclodextrin were approximated by calculating the relative ion intensities of complexed to uncomplexed cyclodextrin. The relative affinities of IBP for α and β cyclodextrins were 1.06 and 0.92 respectively while that for γ cyclodextrin was only 0.23 thereby indicating that the cavity size is indeed related to the degree of complexation.

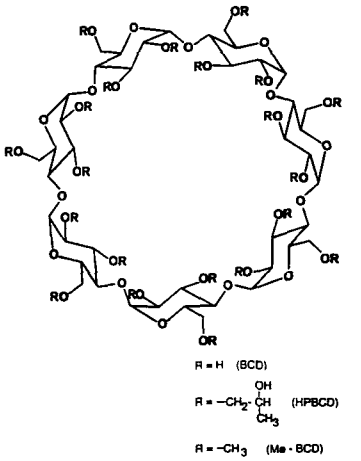

Figure 1 Schematic Representation of parent BCD and substituted HPBCD and Me-BCD

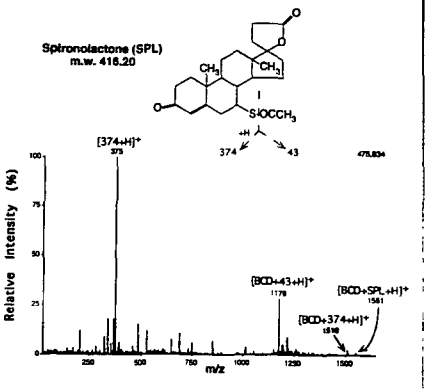

Figure 2: Positive Ion Mass Spectrum obtained for BCD+SPL

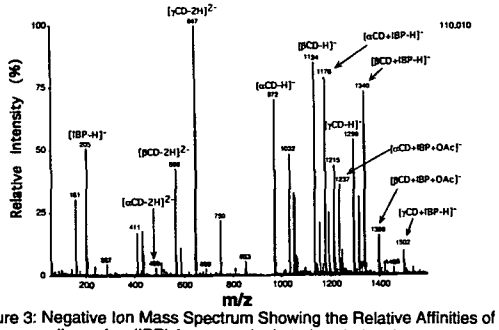

Figure 3: Negative Ion Mass Spectrum Showing the Relative Affinities of Ibuprofen (IBP) for non-substituted cyclodextrins

DETERMINATION of OLIGOMER DISTRIBUTION in PHOTOFRIN® PORFIMER SODIUM by FAB/MS, UV- & IR-MALDI/MS, ESI/MS and LD/JET-REMPI/MS

Marshall M. Siegel[1], Keiko Tabei[1], Rushung Tsao[1], Michael Pastel[1], Ravindra K. Pandey[2], Mattanjah de Vries[3], Stefan Berkenkamp[4], Arnd Ingedoh[4], Franz Hillenkamp[4]

[1]American Cyanamid Company, Medical Research Division, Lederle Laboratories, Pearl River, NY 10965
[2]Roswell Park Cancer Institute, Department of Radiation Biology, Buffalo, NY 14263
[3]IBM, Almaden Research Center, San Jose, CA 95120
[4]Institute of Medical Physics, University of Münster, D-4400 Münster, FRG

INTRODUCTION PHOTOFRIN porfimer sodium is a porphyrin derivative used in the treatment of a variety of cancers by photodynamic therapy. In earlier work, FAB/MS was used to characterize PHOTOFRIN which was found to be a mixture of oligomers containing up to eight porphyrin units [1]. A FAB matrix was developed to suppress the effect of the salt present in PHOTOFRIN (~6% w/w NaCl) which consisted of glycerol:thioglycerol:TFA (1:1:1%). In recent work, Zhan *et. al* [2], using a 2LD/MS instrument, observed only PHOTOFRIN porphyrin monomers, so they suggested that PHOTOFRIN consists of micelles of monomeric porphyrin species. To resolve the structural issues related to PHOTOFRIN, the newer mass spectral ionization methods of ESI, UV- and IR-MALDI and LD/Jet-REMPI/MS [3], besides FAB, were used to analyze PHOTOFRIN, its permethyl ester and porphyrin monomers, dimers and trimers related to PHOTOFRIN.

RESULTS Desalted PHOTOFRIN was analyzed by FAB/MS (matrix: glycerol:thioglycerol:TFA [1:1:1%]), ESI/MS (solvent: for positive/negative ions: water:acetonitrile:acetic acid [1:1:30%]/ water:acetonitrile:ammonium hydroxide [2:1:15%])) and UV- and IR-MALDI/MS (matrix: 2,5-dihydroxybenzoic acid). In the FAB/MS, UV- and IR-MALDI/MS positive ionization modes, only singly charged porphyrin oligomers were observed with masses up to about 4,100 daltons (Figure 1). The distributions of the oligomers were nearly identical for all these mass spectra (Figure 2). The average oligomer length for PHOTOFRIN was about 2.7 porphyrin units.

In the ESI/MS positive and negative ionization modes, singly and multiply charged porphyrin oligomers were observed with corresponding masses up to 5,000 daltons. When the ESI/MS nozzle-skimmer voltage in the positive ionization mode is elevated from 20 to 200 volts, the abundances of multiply charged ions were significantly reduced and nearly all of the observed ions were singly charged (Figure 1), dehydration of the individual oligomers increased with increasing voltage and the oligomer distribution (≥100 volts) closely resembled that of the distributions observed in the FAB/MS and MALDI/MS spectra (Figure 2). The high voltage nozzle-skimmer experiments demonstrated that PHOTOFRIN is a mixture of covalently bound porphyrin oligomers since the observed components only partially dehydrated and did not break down into monomeric species which would be expected if PHOTOFRIN were a micelle mixture of porphyrin monomers.

Figure 1

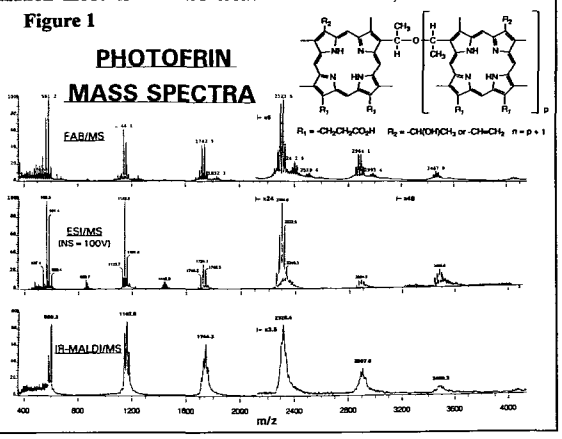

ESI/MS positive ion spectra of PHOTOFRIN samples differing in concentration by over three orders of magnitude (~1.3 ng/μL - ~1.3 μg/μL) were obtained and showed no significant change in oligomer distribution as a function of concentration (Figure 3). These observations are consistent with the behavior of a mixture of covalently bound oligomers rather than micelles of non-covalently bound monomers.

The permethyl ester of PHOTOFRIN was analyzed by ESI, UV- and IR-MALDI, FAB [1] and LD/Jet-REMPI. Oligomers containing from 6 to 9 porphyrin units were observed in the mass spectra. Figure 4 illustrates the LD/Jet-REMPI mass spectrum, obtained at unit resolution and ionized at 193 nm (6.3 eV), demonstrating the presence of up to 6 porphyrin methyl ester units. The average oligomer length was calculated from the LD/Jet-REMPI distribution (Figure 2) as 2.9 porphyrin units.

All PHOTOFRIN spectra (Figure 1) exhibited ions originating from the monomeric species hematoporphyrin (MW 598), hydroxyethylvinyldeuteroporphyrin (MW 580) and protoporphyrin (MW 562). When mixtures of these pure monomers were analyzed by FAB/MS, UV- and IR-MALDI/MS and ESI/MS, no new higher mass oligomeric species related to PHOTOFRIN were generated. Likewise, the FAB, UV- and IR-MALDI, ESI and LD/Jet-REMPI mass spectra of synthetic methyl ester porphyrin dimers and trimers, components believed to be present in PHOTOFRIN as carboxylates, produced molecular ions and some fragment ions of lower mass oligomers. These results as well as the dilution and high voltage nozzle-skimmer ESI/MS experiments with PHOTOFRIN demonstrate that PHOTOFRIN is a mixture of porphyrin oligomers and is not micelles of the monomeric species as recently suggested by Zhan *et. al* based upon 2LD/MS experiments [2].

[1] R.K. Pandey, M.M. Siegel, R. Tsao, J.H. McReynolds, T.J. Dougherty, *Biomed. Environ. Mass Spectrom.* **1990**, 19, 405-414.
[2] Q. Zhan, P. Voumard, R. Zenobi, *Anal. Chem.* **1994**, 66, 3259-3266.
[3] G. Meijer, M. de Vries, H.E. Hunziker, H.R. Wendt, *App. Phys. B* **1990**. 51, 395-403.

Figure 2

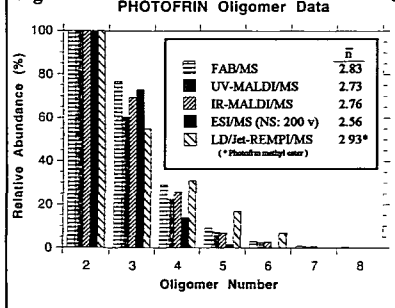

Figure 3

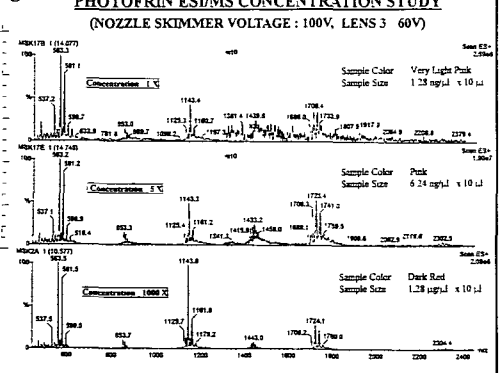

Figure 4

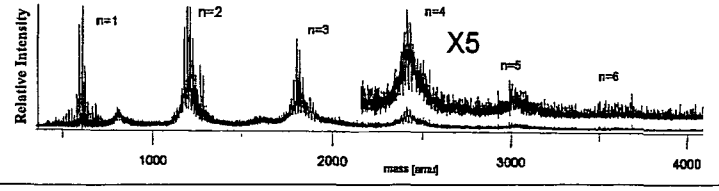

Use of Mass Spectrometry Coupled with a Solids Insertion Probe to Prescreen Soil Samples for Environmental Samples

Catherine E. Check and Stephan B H Bach, Chemistry Program, Div. of Earth and Physical Sciences
The University of Texas at San Antonio, San Antonio, Texas 78249-0663

INTRODUCTION

The contamination of air, water, and soils by a myriad of sources generates a large sample volume. Currently, sample volume for hazardous constituent analyses is approximately half a million samples per year [1] The total analytical costs associated with this are astronomical. The analysis of these samples is vital in terms of assessing the types of contamination present and to what degree a site has been contaminated. The results of these analyses are very important for making an informed, knowledgeable decision as to the need for remediation and what type of remediation processes should be initiated based on site suitability vs non-action for the various sample sites. With an ever growing environmental consciousness in todays society, the assessment and subsequent remediation of a site needs be accomplished promptly despite the time constraints traditional methods place on such actions.

In order to facilitate a rapid assessment, it is desirable to utilize instrumentation and equipment which afford the most information about a site allowing for optimization in environmental assessment while maintaining a realistic time schedule for the resulting remediation process Because there are various types of environmental samples that can be taken at a site, different combinations of instrumentation and methods are required for assessing the level and type of contamination present whether it is in air, water, or soils. This study is limited to analyzing soil-like media that would normally fall under EPA Method 8270 which is used to analyze solid waste matrices, soils, and groundwater for semi-volatile organic compounds.

One method currently under development at USEPA is a thermal vacuum desorption method. A vacuum distillation procedure which is currently in the approval process for becoming an EPA test method has been reported by Hiatt, Youngman, and Donnelly [2] Their study is on the use of vacuum distillation of water, soil, oil, and fish samples. The analyte recoveries were found to relate to the boiling points of the compounds unless solubilities of the compounds exceeded 5 mg/L. Also being investigated and developed as alternatives to standard extraction methods are supercritical fluid extraction (SFE) methods using carbon dioxide.[3,4] SFE is generally performed at low temperatures between 40 °C and 100 °C) but at high pressures (between 170 atm and 400 atm)

A fundamental obstacle in the analysis of soil samples is the time and labor intensive procedure necessary for the extraction of target compounds from the soil matrix It would be advantageous if samples, that did not contain target compounds above the minimum detection limits stipulated by the EPA, could be identified before they were subjected to the entire extraction and evaluation process. This project investigates the use of a solids insertion probe coupled with a quadrupole mass spectrometer. This investigation is designed to determine the feasibility of analyzing soil samples by loading a portion into a small tube, mounting the tube into a direct insertion probe, inserting the probe into the ionizer of the mass spectrometer, and analyzing the contents by running a temperature program on the solids probe If no compounds of interest are detected using this procedure then no further analysis would be necessary. Otherwise, the remainder of the sample could be analyzed routinely.

Initial runs were unbaked sea sand used as blanks. These experiments were conducted to establish a baseline for the blank soil matrix. The initial runs of the blank unbaked sea sand indicated the presence of contaminants when the solids probe was heated ballistically to 200 °C The sea sand was baked at 200 °C to remove the contaminants. The baked sea sand did not produce significant quantities of contaminants upon the heating of the solids probe. The relative ion counts for the baked sea sand were

less than one-sixth of the counts observed for the unbaked sea sand After establishing the baked sea sand as a blank soil matrix, the next step was to determine if organic chemicals contained within the sand could be detected using the solids probe The figure shows spectra taken immediately upon insertion (compounds are from the Ultra GBN-2 mix) The spectra clearly indicate the presence of these compounds.

Further investigations will involve using other target organic compounds as well as environmental reference standards. Determining reproducibility limits is also a high priority. Developing temperature profiles for various classes of compounds is also necessary Different soil-like media will also be studied as the relatively inert property of the sea sand has allowed for the simplest of analyses. For instance, a clay presence in the soil mixture may keep the semi-volatile compounds from coming off as readily as well as dropping the detection limits to well below that of the signal to noise ratio Another point to be addressed in future investigations will be the homogeneity of the soil sample This is a major concern since only a small fraction of the sample is being examined. Initial efforts will study methods of homogenizing the soil sample to ensure a representative sample for loading into the sample vial and to minimize contaminant loss.

The authors would like to acknowledge the following support· Col V. Dunovant and Col K. Locke of Armstrong Laboratories, Brooks AFB - for the Finnigan 4600 and 5100 GC/MS, S. Jones, Texas Instruments, Dallas, TX and R Swaim, Finnigan MAT - for the Finnigan 4500 GC/MS; Dr. J Adams and the Graduate Env. Sci. Prog , College of Sci. and Eng , UTSA - for the Small Grant Award

1. Analytical Service Program Five Year Plan; Laboratory Management Division Office of Env Restoration and Waste Management. U.S. DOE· Washington, DC, (1992); 2 M.H Hiatt, D R Youngman, J R. Donnelly, Anal. Chem , 66, 905 (1994) 3. A.P. Emery, S.N. Chesler, W A MacCrehan, J. Chrom., 606, 221 (1992) 4. D.R Gere and E M. Derrico. LC-GC. 12. 334 (1994).

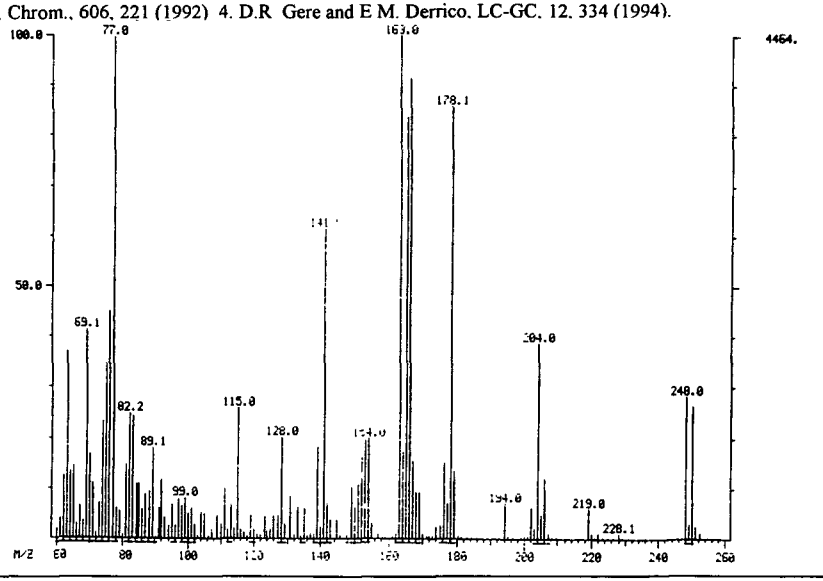

Analysis of Soils - Part I: Soil Dynamics and Climatic Change

M. Howald, S. Schuerch and U.P. Schlunegger, Department of Organic Chemistry, University of Berne,Freiestrasse 3, CH-3012 Bern

Introduction

The reaction of soil characteristics to vegetative alterations as a simulation of the effects of a climatic change are investigated, because the organic matter of soils reflects the condition of nature. The search for suitable acreages is a basic condition, since the stage of being fallow, i. e. the time since the last agricultural use, is supposed to be the only variable. That is why a test area has to fulfil different criteria, as e. g. altitude, soil, slope, exposition, evapotranspiration, amount, intensity and duration of rainfall, amount of sunshine, humidity, temperature, definability and an only extensive use.

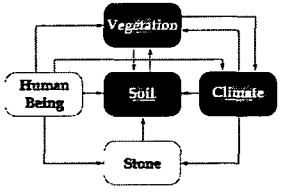

Six soils with different ages of fallow land fulfil all the postulated criteria and are dated with the aid of maps, aerial photographs and dendrochronolgy.

Analysis of the Soil Organic Matter

Organic Fragments (Py-GC-MS)

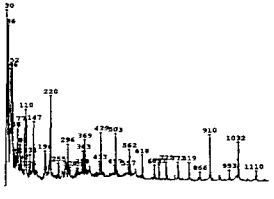

The vegetative change in the middle areas is shown by a slight decrease in the organic fragments, while in the two soils with the longest time of laying fallow especially the bigger fragments are heavily increasing.

The fact that the fragments for each soil are very similar proves that the evaluation concerning the criteria mentioned above was successful.

Hydrocarbons (GC-MS)

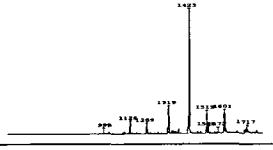

Here human intervention into nature is clearly visible, for after laying fallow for about twenty years the soil is seen in its original state in the pattern.

Inorganic Ions (Capillary Electrophoresis)

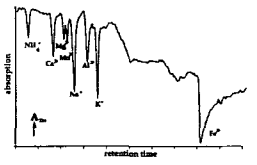

The distribution of eight inorganic cations seems to rely rather on incident for the sequence of laying fallow. In contrast, a strong overloading of the soil being used at present by nitrate shows with the three essential anions.

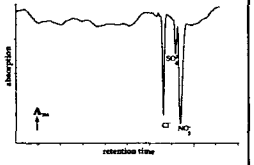

Oligosaccharides (MALDI-ToF-MS)

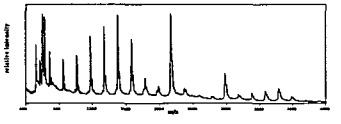

Once again, the amount of oligosaccharides shows the human influence on soil structures. For only with the end of agricultural use microorganisms and bacteria are able to produce larger cyclic sugar molecules.

Humic and Fulvic Acids

The amounts of humic and fulvic acids again point to human intervention, because in soil Collo, used at present, the production of humic acids is disturbed and therefore clearly too low. Also the amounts of humic acids of fractions of the six soils (sand, clay, schluff, 1mm, 500um, 250um, 125 m m and 53 mm) give evidence of the disturbtion in soil being used at present. The clay fraction plays a special role for the soil fertility as ion exchanger and water or nutrien reservoir. Under that aspect the small portion of humic acids in this fraction in the soil being used at present is alarming. The functional groups are analyzed by fourier transform infrared spectroscopy. It can be shown that with the rising age of fallow land the humic acids become bigger and therefore their acidity and the amounts of functional groups decrease. In contrast more aliphatic structures, e.g. saccharides, are built in.

Conclusions

The soil seems to have recovered after laying fallow for about 20 years, because from this time on the organic matter of the soil is in balance again. If we reflect this perception to a climatic change in company with a vegetative alteration, we can draw three conclusions concerning the effects: a climatic change will heavily disturb the state of the ground, this disturbtion will last relatively long, but after a convalescence of the climate nature has still the power for regeneration.

This work was supported by the Swiss National Science Foundation

Analysis of Soils - Part II: Determination of Oligosaccharides in Soils by MALDI-Time-of-Flight Mass Spectrometry

S. Schuerch, M. Howald and U.P. Schlunegger
University of Berne, Department of Organic Chemistry
Freiestrasse 3, CH-3012 Berne, Switzerland

Polysaccharides are the most abundant organic compounds in nature. Decomposition of plant and animal residues leads to a high polysaccharide content in soils. The decomposition of carbohydrates and subsequent mineralization of the products are part of the cylce of life on earth. In extracts of soils collected in the Valle Onsernone (Ticino, Switzerland), oligosaccharides of different size and structure have been identified by matrix-assisted laser desorption/ionization time-of-flight mass spectrometry (**MALDI-TOF-MS**). The selected soils show identical climatic parameters and pedological factors, whereat the age of fallow land is the only varying factor. Identification and structure elucidation of the oligosaccharides is performed by substrate-specific **enzymatic hydrolysis**. Moreover the appearance and the distribution of the oligosaccharides is correlated to soil genesis.

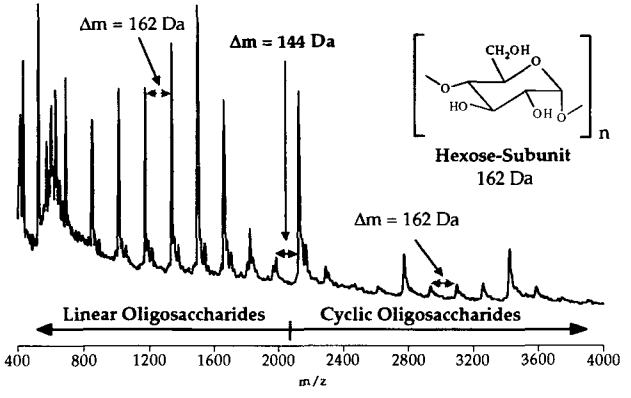

MALDI-TOF spectrum of a soil sample The spectrum shows two sequences of oligosaccharides: linear structures up to 2000 Dalton and cyclic oligosaccharides from 2000 to 4000 Dalton.

The MALDI-TOF spectra show periodically appearing peaks with a mass difference of 162 Dalton. They are attached to linear and cyclic hexose oligosaccharides consisting of up to 24 monomers. The MALDI-TOF spectra of the original soil samples do not give any information about the nature of linkage between the hexose-subunits and the degree of branching of the oligosaccharides. To get more structural information the oligosaccharides are exposed to degradation by substrate-specific enzymes.

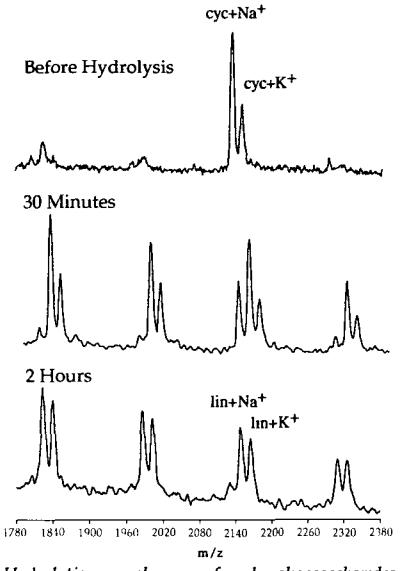

Hydrolytic ring cleavage of cyclic oligosaccharides by cellulase. The peaks are shifted to higher masses

The spectra show good reproducibility and allow to compare samples of fallow land of different age. A direct correlation of the age of fallow land to the oligosaccharide distribution is observed. The intensities of peaks corresponding to cyclic oligosaccharides increase with the age of fallow land. Therefore the MALDI-TOF spectra allow to estimate the age of fallow land in this series of samples. Cyclic oligosaccharides are formed by micro-organisms in the soil. Their activity is depth-dependent and reflected by the MALDI-TOF spectra as well.

The enzyme **cellulase** randomly hydrolyses the β-(1,4)-linkages between glucose monomers. The oligosaccharides found in soils are attacked by cellulase as well. Cyclic structures are opened by the enzyme after a short reaction time. The hydrolytic ring cleavage is accompanied with the addition of water. The reaction leads to a slightly increased molecular weight which is detected by the MALDI-TOF mass spectrometer.

The enzyme **glucoamylase** subsequently hydrolyses α-(1,4)-linked glucose units. **Isoamylase** cleaves β-(1,6)-glycosidic linkages appearing at branching positions in the molecules. In spite of very long reaction time no hydrolysis was observed in both cases. Therefore β-(1,4)-glycosidic linkages are present in the oligosaccharides only and the existence of β-(1,6)-linked side chains is excluded.

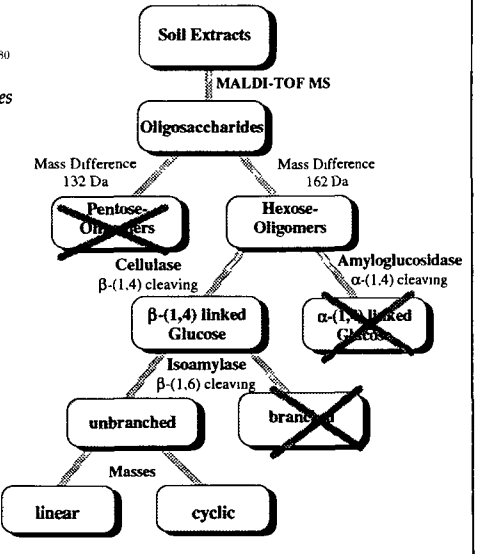

Structure elucidation of oligosaccharides by enzymatic hydrolysis.

RAPID ANALYSIS OF FAST GC EFFLUENTS BY TIME-OF-FLIGHT MS

Anthony J. Borgerding* and Charles W. Wilkerson, Jr.
Chemical Science and Technology Division
Los Alamos National Laboratory, Los Alamos, NM 87545

Recent studies in gas chromatography, utilizing short columns and increased flow rates, have reduced analysis times by a factor of 10 or more (1). Fast GC analysis of this type has great potential for improving environmental measurements. In addition to the improved sample throughput and resulting gains in productivity, rapid monitoring of various environmental systems is possible. There are, however, some difficulties interfacing Fast GC with mass spectrometry. Specifically, analyte peaks from Fast GC systems are usually less than a few hundred milliseconds, preventing the use of scanning instruments. In addition, the high volumetric flow rates from the GC can cause difficulties in maintaining a sufficient vacuum. In this paper, we study the potential of time-of-flight mass spectrometry along with the use of narrow bore GC columns to overcome these limitations. Early examples of the capabilities of this instrumentation for the analysis of volatile compounds in atmospheric samples are shown.

When doing rapid separations, the achievable chromatographic resolution often is limited by the initial temporal width of the injected analytes. Our instrument uses an injection system that cryogenically traps compounds from air onto a 25 cm length of 50 µm i.d. GC column. The tube is then isolated, heated to revaporize the analytes, and injected into the flow stream. This system serves both to concentrate dilute air samples, and also to allow rapid injection onto the column, resulting in narrow injection bands. A 4 meter DB-5 microbore column with an inner diameter of 100 µm was used. This column has two advantages relative to columns with diameters of 250 µm or more. Since chromatographic plate height is related to the square of the radius of the column, more theoretical plates per length of column are obtained. In addition, similar linear flow rates can be obtained with much lower volumetric flow rates, easing the pumping requirements of the mass spectrometer. For example, a 4 meter, 100 µm i.d. column has as many theoretical plates as a 25 meter column with a 250 µm i.d. and has volumetric flow rates over 6 times less at equivalent linear flow.

Fast GC peaks are usually less than a few hundred milliseconds and cannot be measured accurately using quadrupole or other scanning instruments. Several laboratories have used time-of-flight mass spectrometry, which can record 1000 or more mass spectra per second (2, 3). Our gas chromatographic system was interfaced to a reflectron time of flight mass spectrometer (2 meter flight path) by passing the column directly into a pulsed electron impact ion source via a heated transfer line. The source is pulsed at a rate of at least 100 Hz. Signal from a microchannel plate detector was digitized on a Sonix model 864 board (64 MHz). Waveform averaging was done to the extent possible. For example, compounds which are poorly retained and elute early

in a chromatogram usually have peak widths of less than 100 msec, making averaging difficult. Compounds which are retained better have peaks that are often as much as 5 times as wide, allowing several waveforms to be averaged without sacrificing chromatographic integrity.

The potential of this instrumentation for environmental studies was studied. Analyses that typically take a few minutes using conventional GC-MS were finished in less than 5 seconds using Fast GC-TOFMS. In addition, our injection system allows compounds to be samples while separation is taking place, allowing rapid reinjection immediately after the separation is complete. The example below shows repeat injections of a gaseous mixture of chlorodifluoromethane, dichloromethane, chloroform, and carbon tetrachloride. Eleven separations are accomplished in less than one minute, showing the ability of this instrument to monitor rapidly changing concentration levels in a system.

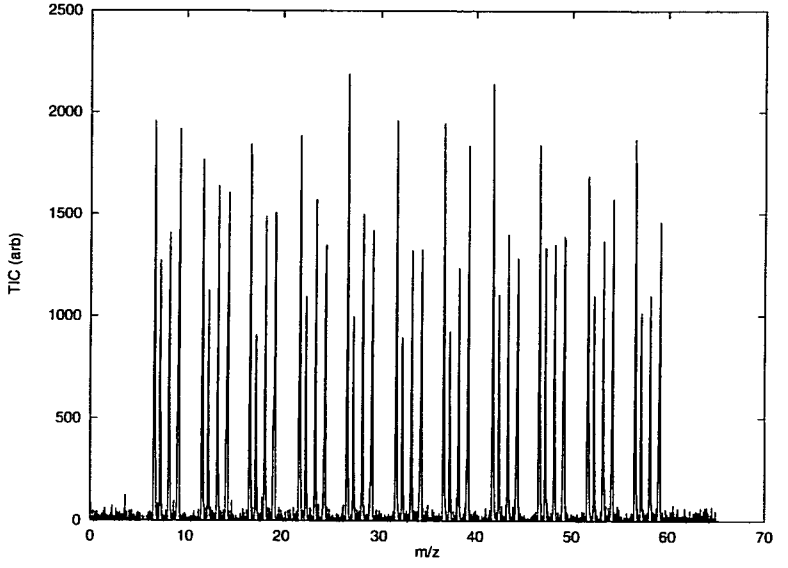

References

1. Klemp, M.; Peters, A.; Sacks, R. *Environ. Sci. Technol.* **1994**, 28, 369A.
2. Wollnik, H., et al. *Int. J. Mass Spectrom. Ion Proc.* **1994**, 130, L7
3. Holland, J., et al. *Rev. Sci. Instrum.* **1991**, 62, 69

Real-Time Characterization of the Size and Chemical Composition of Individual Particles in Ambient Aerosol Systems in Riverside, California

Christopher A. Noble and Kimberly A. Prather*
Department of Chemistry, University of California, Riverside, California 92521

Atmospheric aerosols, although ubiquitous, are highly diverse and continually fluctuating systems A typical aerosol system may consist of particles with diameters between ~0.002 µm and ~200 µm Even in rural or pristine areas, atmospheric particle concentration is significant, with concentrations up to 10^8 particles/cm^3 not being uncommon. Chemical composition of atmospheric particles vary from simple water droplets or acidic ices to soot particles and cigarette smoke. Due to changes in atmospheric conditions, processes such as nucleation, coagulation or heterogeneous chemistry may effect both physical and chemical properties of individual particles over relatively short time intervals

Recently, aerosol measurement techniques are focusing on determining the size and/or chemical composition of individual aerosol particles Our research group has recently developed aerosol time-of-flight mass spectrometry (ATOFMS), a technique which allows for real-time determination of the size and chemical composition of individual aerosol particles. Single particle measurements are performed in one instrument using dual laser aerodynamic particle sizing and time-of-flight mass spectrometry

Aerosol-time-of-flight mass spectrometry is briefly described in several other abstracts in this publication [1-4]

Results and Discussion

A simple size distribution of all particles analyzed in one aerosol sample is shown as a histogram in Figure 1 This aerosol sample consists of 500 individual particles sampled from ambient conditions on 16May 1995, from 5 02 PM through 5.21 PM It can be seen in this sample that two distinct size modes occur, the smaller mode is centered at 1 1 µm, while the larger mode for this sample is at 1.4 µm

Particle distributions change over time as Figure 2 demonstrates. These ambient samples are from 11 May 1995, each histogram represents a sample of 500 particles Figure 1a shows that the earlier sample analyzed has a significant mode at 1.0 µm, with over 160 particles shared between two bins Only one hour later (as shown in Figure 2b), this mode is noticeably reduced, the particle count in the same two bins has dropped to less than half, with only 70 particles analyzed while the total sample size has remained unchanged Also in Figure 2b, there is a higher particle count of particles under 1 0 µm in diameter, with the highest number of particles in the 0.6 µm bin.

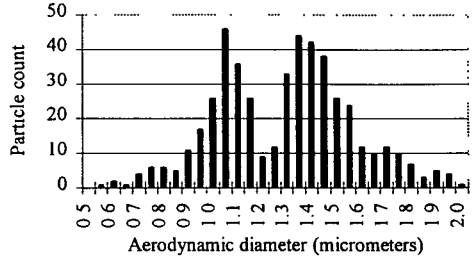

Figure 1: Particle size distribution of ambient aerosol.

A complete mass spectrum of each of these particles is also acquired, using a single pulse from a Nd:YAG laser to desorb/ionize individual particles in flight. Because the mass spectrum for each particle is acquired, particles may be divided into simple groups defined by chemical composition Ambient particles types which are observed in Riverside, CA are classified as organic, inorganic (non-marine), marine and soot.

Typically, smaller particles are more prevalent in the morning, larger size modes tend to grow in during the afternoon. The smaller mode, centered at ~0 6 µm, is mainly due to organic particle, which decrease in concentration in the afternoons. Larger size modes are representative of inorganic or soot particles

Figure 3 is the mass spectrum of an individual inorganic particle from ambient sampling It was analyzed on 11 May 1995 at 12.53 PM in Riverside, CA This spectrum is the result of a single laser desorption/ionization pulse impinged on the particle while it is in flight. Species commonly found in inorganic particles are labeled. The aerodynamic diameter of this particle is 1 4±0 2 µm

Mass spectra for other particles are also acquired along with corresponding particle size

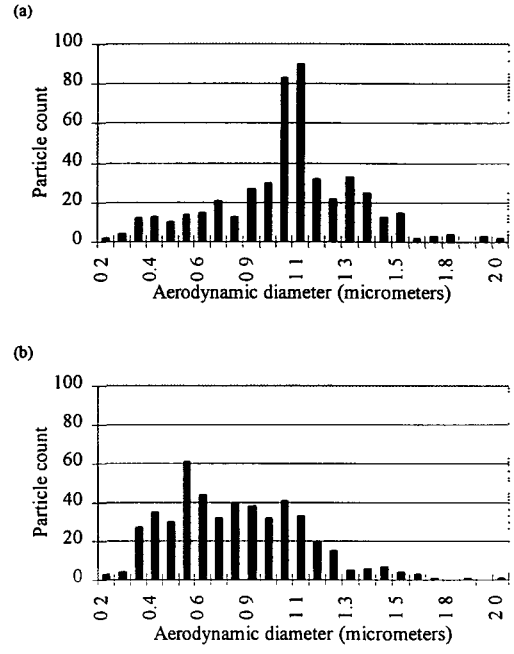

Figure 2: Total particle size distribution of ambient aerosol sample. (a) Sampling period: 9:19-9:33 AM. (b) Sampling period: 10:13-10:31 AM

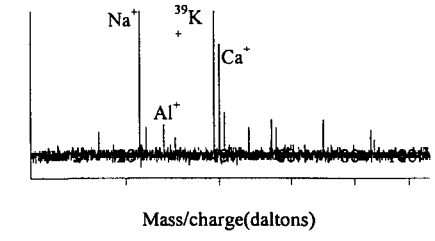

Figure 3: Mass spectrum of single inorganic particle.

1 Morrical, B D , Prather, K A , *Proceedings of the 43rd ASMS Conference on Mass Spectrometry and Allied Topics*
2. Noble, C A., Salt, K , Prather, K. A., *Proceedings of the 43rd ASMS Conference on Mass Spectrometry and Allied Topics*
3. Prather, K. A., *Proceedings of the 43rd ASMS Conference on Mass Spectrometry and Allied Topics*
4. Salt, K , Prather, K. A., *Proceedings of the 43rd ASMS Conference on Mass Spectrometry and Allied Topics*

Analysis of Single Inorganic Salt Particles Using TOF MS

Kimberly Salt and Kimberly A Prather*
Department of Chemistry, University of California, Riverside, CA 92521

Particles containing inorganic salts, such as sulfoxy and nitrogen oxide salts, play a vital role in atmospheric chemistry and air pollution and are of great environmental concern Sulfuric and nitric acid are the main acids responsible for the environmental effects of atmospheric acidity The deleterious effects of acid deposition on aquatic biota, vegetation and materials are well established while health effects from the inhalation of acidic aerosols is currently under investigation One goal of our research is to be able to determine the forms of sulfur and nitrogen present in atmospheric particles This determination may ultimately aid in developing an understanding of the mechanism of sulfate and nitrate transformation in the atmosphere

We have recently reported the technique of aerosol time-of-flight mass spectrometry (ATOFMS) which combines aerodynamic particle sizing with time-of-flight mass spectrometry for the determination of both size and chemical composition of individual aerosol particles [1-3] ATOFMS has proven to be a viable means to characterize particles containing sulfoxy salts and nitrogen oxide salts in real time

Particles of known size and composition were generated using a vibrating orifice aerosol generator (TSI Inc) The results obtained using ATOFMS to study sodium sulfoxy salts, namely Na_2SO_3 (Figure 1), Na_2SO_4, and $Na_2S_2O_3$, were compared to those obtained using laser microprobe mass analysis (LAMMA) (Figure 2) There is good agreement in the major mass peaks observed between the two techniques Relative peak heights give an indication of exactly which sulfur species is present and can be used even when the particles are composed of a mixture of the sulfoxy salt and another inorganic salt

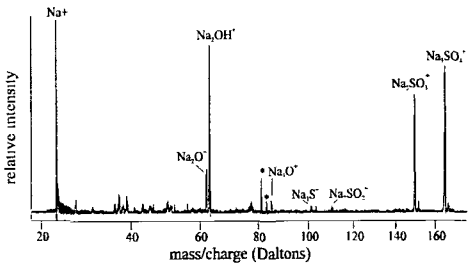

Figure 1: Typical positive ion mass spectrum for a single 2.12 μm Na_2SO_3 particle. The relative intensity of the peak at 149 to 165 is a major indication of which sulfoxy salt is present.

Particles of nitrogen oxide salts, $NaNO_3$ and $NaNO_2$, were also investigated The results for these samples are not in agreement with the LAMMA results as the mass spectra for the nitrate containing particles can only be observed when the nitrate salt is mixed with another inorganic salt species (Figure 3) Nitrite salts can be determined without another species being present and the results for the negative ion spectra are consistent with those reported by LAMMA

[1] Prather, K A., Nordmeyer, T , Salt, K *Anal Chem* , **1994**, *66*, 1403
[2] Noble, C A., Nordmeyer, T , Salt, K, Morrical, B , Prather, K A. *Trends Anal Chem*, **1994**, *13*, 218
[3] Nordmeyer, T , Prather, K A *Anal Chem* . **1994**, *66*, 3540

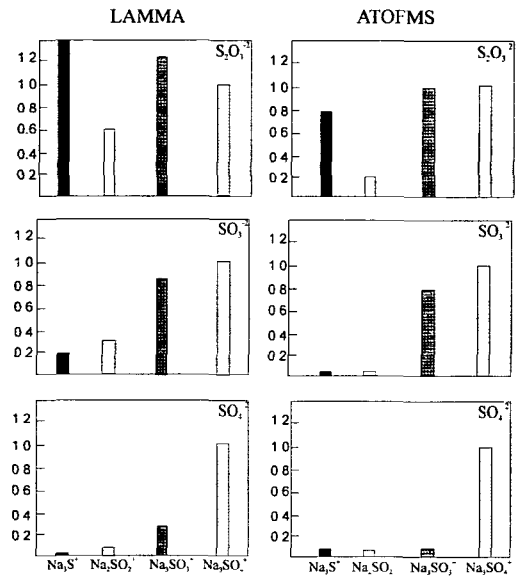

Figure 2: A comparison of the relative intensities of the major mass peaks seen the positive ion mass spectra of different sulfoxy containing particles observed using laser microprobe mass analysis (LAMMA) and aerosol time-of-flight mass spectrometry (ATOFMS). The particle size is 2 μm and the wavelength of the desorption/ionizaiton laser is 266 nm.

The effects of laser power, the wavelength of the desorption/ionization laser, and the particulate size on the mass peaks observed have also been investigated for both sulfur and nitrogen containing particles

From these studies, criteria for the determination of sulfur and nitrogen species have been established Future studies aim at examining ambient samples for these sulfur and nitrogen species and then quantifying the total amount of sulfur and nitrogen in the individual particles

Figure 3: Negative ion mass spectrum of a 2 μm particle containing $NaNO_3$ and Na_2SO_3 in a 2:1 molar ratio.

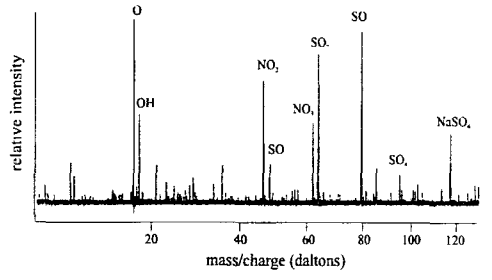

Aerodynamic Particle Sizing Versus Light Scattering Intensity Measurements as Methods for Real-Time Particle Sizing Coupled with Time-of-Flight Mass Spectrometry

Christopher A Noble, Kimberly Salt and Kimberly A. Prather*
Department of Chemistry, University of California, Riverside, California 92521

One emphasis in aerosol research includes the development of methods capable of single particle analysis in real time. Single particle measurements cover a broad range of both physical and chemical properties, such as size, shape, temperature and elemental or chemical composition. Various instruments have been developed which focus on the measurement of one or more of these properties. Particle size influences particle transportation and reactivity, while chemical composition determines which reactions may take place on the particle surface. Therefore, various researchers have placed an emphasis on determining the size and composition of individual aerosol particles. The two most common particle sizing methods coupled with mass spectrometry are light scattering intensity measurements and aerodynamic particle sizing

Our research group has recently developed aerosol time-of-flight mass spectrometry (ATOFMS), a technique which allows for real-time determination of the size and chemical composition of individual aerosol particles. Single particle measurements are performed in one instrument using dual laser aerodynamic particle sizing and time-of-flight mass spectrometry ATOFMS is a unique experimental platform capable of evaluating both of these sizing techniques This study is to aid in determining which particle sizing method will provide better results for a field portable ATOFMS system

Experimental Section

Figure 1 shows a schematic diagram of the light scattering region which determines the size of individual particles using either light scattering intensity measurements or aerodynamic particle sizing.

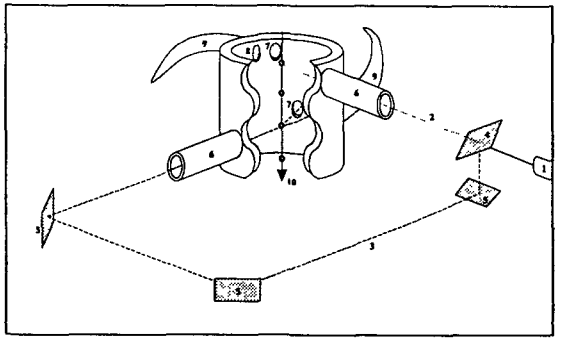

Figure 1: Cut away view of *light scattering region of* ATOFMS system. (1) Ar^+ laser. (2) 514 nm Ar^+ line. (3) 488 nm Ar^+ line. (4) Dichroic mirror. (5) Mirror. (6) Laser window and spatial filters. (7) Exit port for scattered light into light detection system. (8) Exit port for non-scattered light into light horn. (9) Light horn. (10) Particle beam trajectory.

Using a vibrating orifice aerosol generator, particles of known size (±1%) are produced to compare these two methods of particle size analysis. Particles of both NaCl and 2,4-dihydroxybenzoic acid (DHB) were used for this study. For determining particle size based on light scattering intensity

43rd ASMS Conference on Mass Spectrometry and Allied Topics

measurements, the peak height of each scattering pulse caused by a particle passing through the 514 nm laser line is recorded from a photomultiplier tube Aerodynamic sizing employs an electronic timing/logic circuit to measure the time between light scattering signals produced at both laser lines; the transit time of an individual particle is a function of its size.

Results and Discussion

The comparison of size measurements for DHB particles is shown in Figure 2 Because the number of data points taken for each measurement varied, all data sets are normalized to one hundred percent Typically, a minimum of 200 measurements are taken for the light scattering intensity method and 1000 measurements for aerodynamic sizing. Bin sizes used for all histograms were chosen to correspond to the range of the data measurements divided by ten Particles ranging from 1 to 3 μm were chosen for particle size measurement comparisons because particles in this size range will be the targets of future ambient monitoring studies

Figure 2a shows a frequency distribution of the light scattering signal intensity signals produced from particles passing through the 514 nm laser line for 1 0, 2.2, and 3.2 μm DHB particles. As shown in this plot, it is difficult to distinguish between these three different particle sizes based solely on the scattering signal intensity resulting from the single laser. This same trend may also be observed with NaCl particles

Frequency distributions for the transit times of individual particles are summarized in Figure 2b Clearly, the relative spread in transit times collected for aerodynamic sizing is narrower than the spread in the measured light scattering intensities. The narrow measured transit time distributions allow for accurate determination of particle size using this method.

Figure 3 shows the relationship between measured transit time and known diameter for NaCl particles within the range of 0.8 to 8.0 μm. As is evident, transit time is a linear function of particle diameter over the range shown, allowing for simple size determination of unknown samples.

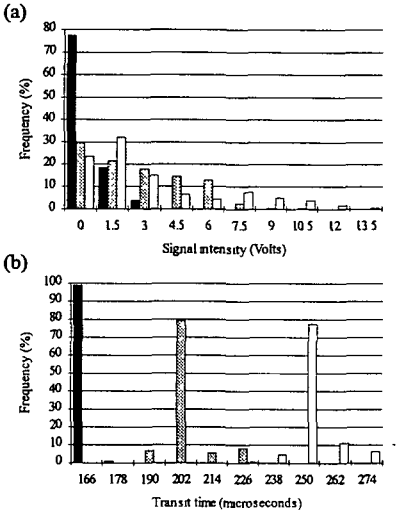

Figure 2: Frequency distribution for ■ 1.0, □ 2.2, and □ 3.2 μm DHB particles. (a) Light scattering intensity measurements. (b) Aerodynamic sizing.

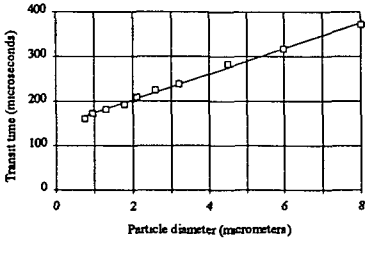

Figure 3: Transit time for NaCl particle as a function of time.

Size and Composition Determination of Sidestream Cigarette Smoke in Real-Time by Aerosol Time-of-Flight Mass Spectrometry (ATOFMS)

Bradley D. Morrical and Kimberly A. Prather*
University of California, Riverside
Riverside, CA 92521
*To whom correspondence should be addressed

Introduction

Exposure to cigarette smoke in both indoor and outdoor environments has become a major concern to the public over the past decade Sidestream and exhaled main stream cigarette smoke constitute a large portion of household, and public indoor air pollution It has also been determined that approximately 2 7% of anthropogenic air pollution in the Los Angeles basin is a result of cigarette smoking(1) I t has been difficult to clearly assess the extent to which pollution occurs from cigarette smoking primarily because of the complexity of the sample and the difficulty this presents when it comes to qualitative and quantitative analysis

Until now, particulate analysis of cigarette smoke has been performed using off-line techniques, such as GC/MS, that do not provide the real-time information of size and composition for individual particles As a result, off-line techniques cannot monitor environmental changes that occur in real-time Aerosol Time-of-Flight Mass Spectrometry (ATOFMS) is a real-time technique that has been used to obtain size and composition information from single particles and has been used to watch changes that occur in time

Experimental

The ATOFMS system (figure 1) consists of three main sections, an interface region, a light scattering region, and the mass analysis region. Particles are introduced into the interface region in which the undergo supersonic expansion into vacuum. The aerosol beam is collimated by the use of skimmer cones and then passed on into the light scattering region

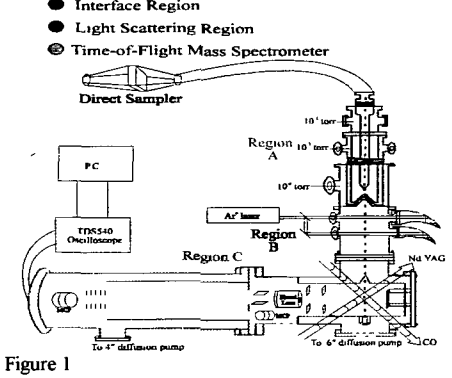

Figure 1

In this region an individual particles velocity is determined by the time it takes for the particle to pass through two scattering lasers 5cm apart The two Ar^+ lasers enter the region orthogonal to one another to insure that only particles traveling through the center of the system will be timed A timing circuit determines the particle velocity and also controls the firing of the Nd YAG desorption/ionization laser

1 Rogge,W F ,Hildemann,L.M.,Mazurek, M.A, Cass,G R, *Sources of fine Organic Aerosol 6 Cigarette Smoke in the Urban Atmosphere* Envirom Sci Technol 1994,28,1375-1388

43rd ASMS Conference on Mass Spectrometry and Allied Topics

When a particle reaches the center of the ion source in the TOFMS, the timing circuit causes the Nd.YAG to fire desorbing and ionizing the particle The ions are then detected by a reflectron time-of-flight mass spectrometer.

Results

Cigarettes were sampled directly into the ATOFMS system and a histogram was obtained (figure 2) for the size distribution of cigarette smoke particulates. The histogram consists of 1500 individual particles and shows the aerodynamic sizing capability of this instrument. A mass spectrum was obtained for each of the 1500 particles as well as the aerodynamic size of that particle. From figure 2 it can be seen that there are at least three major size modes with the composition of the particles within each mode differing. The histogram demonstrates the complexity of cigarette smoke as being heterogeneous in size, and the different size modes in general contain different chemical compositions. The chemical composition difference that is present in the different size modes is shown in figure 3. The top spectrum is from a particle with a aerodynamic diameter of approximately 0.4μm, putting it in the smallest size mode of this histogram. The particle was desorbed and ionized from a single pulse from an Nd:YAG operating at 266nm. This particle contains primarily organic carbon and has an interesting peak at m/z = 185 due to nicotine+Na^+. The bottom spectrum is from 1.17μm particle and contains primarily elemental carbon as evidenced by carbon envelopes extending to C_{13}.

ATOFMS has the capabilities for monitoring real-time size and composition changes for a complex system such as cigarette smoke The advantages this technique provides include the ability to obtain a complete mass spectrum per individual particle. This eliminates the need for depositing particles on a surface and averaging multiple shots together. Future work includes better qualitative characterization and quantitative determination of tracer components such as nicotine.

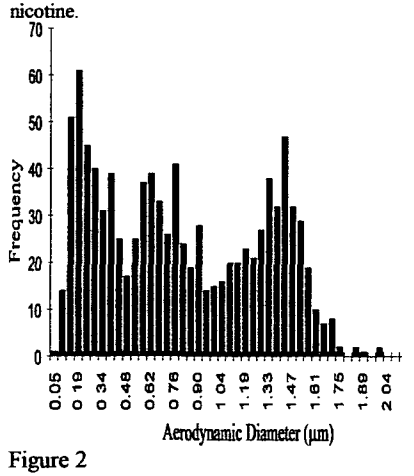

Figure 2

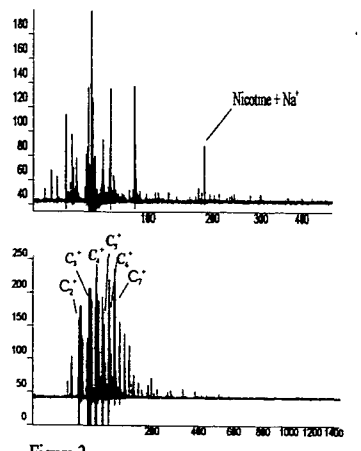

Figure 3

Modeling Scrap Tire Pyrolysis

Tim Burrell, James Haworth, Eugene Phillips,
and Curtiss D. Hanson
University of Northern Iowa, Department of Chemistry
Cedar Falls, IA 50614

Estimates of the generation of scrap tires in the United States are on the order of 2 million tons per year. Although these tires contain a high percentage of useful hydrocarbons of these 2 million tons only 30 percent are converted to other uses. The remaining 70 percent are simply disposed of in land fills, accumulated in large quantities at questionable concentration sites or they are illegally disposed of in such places as roadside ditches or river and stream beds. This 1.4 million tons of scrap tires better represent a resource for valuable and recyclable materials. The bead and belt steel has value and should be recycled. The rubber itself can be processed pyrolyticly and yield light hydrocarbon products such as limonene. The resulting solid char can be the starting material from which activated carbon is produced. Recently, pyrolytic recycling of scrap tires (thermal decomposition in the absence of oxygen) is receiving renewed interest because of its ability to produce valuable products which can dramatically offset the costs of the pyrolytic process. Our process is an improvement over current processes and procedures. Since pyrolysis is decomposition in the absence of a combustible atmosphere many processes evacuate their systems and use complex machinery to maintain this sealed system. We prefer to displace the combustible atmosphere with steam. At the same time we eliminate the need for evacuation we also eliminate the need for complex hard seals to seal and isolate the system. Since we operate at ambient air pressure we are able to use simple water traps to isolate our system from the atmosphere. This separation allows us to control emission releases in to the environment. This water trap sealing system also allows for material to easily and continuously be fed in to our system and for the solid products

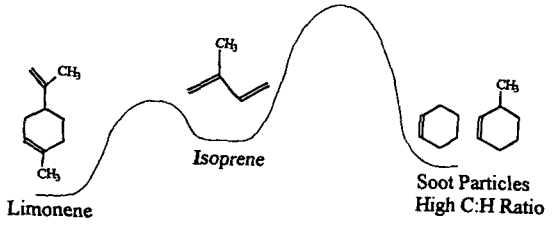

43rd ASMS Conference on Mass Spectrometry and Allied Topics

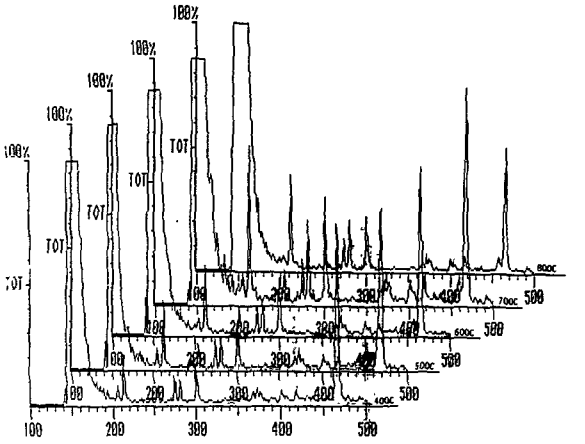

to just as easily exit our system. Vapors generated are quickly and easily condensed along with the steam preventing a build up of pressure. The small amount of gases generated ar contained and easily removed from a collection tower also attached to the system. This process increases the affiance and control over present approaches and lowering the energy requirements while maximizing the collection and generation of valuable products. What we are presenting are some of the results of bench set ups which are also briefly described.

One of the more interesting results from our work is the proposed idea of that the residence time that the generated vapors spend in the heat of the reaction chamber influence the type of liquid products formed. As can be seen in the attached figure we propose that secondary reactions occur relative to the amount of energy the isoprene and products gain while in the reaction chamber. If the vapors do not escape the reaction chamber quickly they will obtain enough energy to form less desirable hydrocarbons having a high C:H ratio rather the more valuable saturated hydrocarbons, such as limonene. The chromatogram below shows the limonene peak at 468 is stable for the 4 temperatures prior to 800 degrees. But the limonene peak drops significantly at 800 degrees which corresponds to a change in the products formed due to increased gas phase reactions occuring in the pyrolysis reactor.

Analysis of Carbonyls: Intermediates of Chemical Oxidation Reactions

Thomas N. Feinberg and M. Judith Charles
Department of Environmental Sciences and Engineering
University of North Carolina at Chapel Hill
Chapel Hill, NC 27599-7400

Introduction

The identification of atmospheric photooxidation products of isoprene and toluene has been the subject of laboratory investigations over the last 20 years, but the products and mechanisms have yet to be completely explained[1]. The reasons for the uncertainty has been the lack of appropriate analytical methods to identify the highly polar intermediates. Previous work has shown that derivatization of carbonyls with Girard's Reagent P and analysis by Fast Atom Bombardment Mass Spectrometry is a sensitive method for molecular weight determination of carbonyls[2], but this method is limited to mixture analysis. We are developing an electrospray ionization mass spectrometry (ESI/MS) method for the identification of carbonyls in photochemical smog chamber impinger samples using Girard's Reagent P.

Experimental Methods

Aqueous standards of 15 carbonyl compounds were reacted with Girard's Reagent P in 50/50 acetonitrile/water with 0.5% acetic acid. Each standard carbonyl was mixed with the reagent to produce final concentrations of 5mM carbonyl and 1mM reagent. Tetraethylammonium bromide was used as an internal standard and spiked into each reaction mixture to a final concentration of 20μM. Solutions were allowed to react overnight. A syringe pump infused each solution at a rate of ~2μL/min into an Analytica of Branford electrospray ionization source retrofitted on a Finnigan 4000 mass spectrometer. The mass spectrometer was under computer control using the Teknivent Vector/Two data system. A calibration curve was constructed by determining the ratio of the ESI/MS signal for Girard's Reagent P (m/z 152) to that of the internal standard (m/z 130). Linearity of signal was observed over 3 orders of magnitude of reagent concentration (1μM-1mM). Derivatization yields for the carbonyls were determined by quantifying excess reagent by ESI/MS in reaction mixtures of known initial concentrations of reagent and carbonyl.

In order to alleviate ion suppression from using a high reagent concentration, an affinity column clean-up procedure was developed to remove excess reagent in samples by finding a suitable solid substrate with free aldehyde groups. A 1:10 w/v mixture of chopped Type 1 collagen and clean sand was packed into short disposable pipets to provide 6mL of column material. A 350μL aliquot of a 1mM solution of Girard's Reagent P was eluted from one column and a 350μL aliquot of a 500μM glyoxal and 1mM reagent solution was eluted from a second column. Fractions were collected from each column, pooled to 2mL volumes and the UV absorption at 260nm (reagent λ_{MAX}) was measured by a Hitachi U-2000 scanning spectrophotometer.

Results and Discussion

ESI/MS spectra of many carbonyl standards were dominated by molecular ion peaks 134u higher than the molecular weight of the carbonyl substrate. Dicarbonyls such as glyoxal (molecular weight of 58u) produced singly charged derivatives when the reagent was at low concentrations, while doubly charged ions were formed when reagent was in excess (Figure 1).

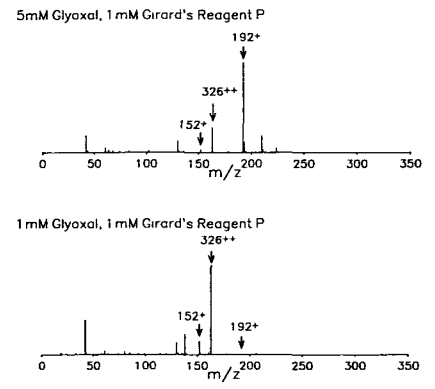

Figure 1

At carbonyl concentrations below 10μM, a high (>1mM) concentration of the reagent is necessary for greater than 90% derivatization yield of all tested analytes. This high reagent concentration is not necessary for aldehydes as derivatization equilibrium constants for aldehydes were generally greater than ketones by a factor of 10.

The affinity column technique was effective in removing over 90% of Girard's Reagent P from samples (Figure 2). The absorbance plateau of the glyoxal derivative suggests that derivatized carbonyls will freely exit the column (Figure 3).

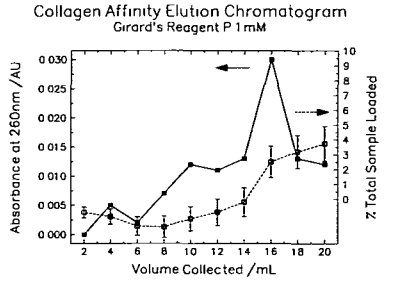

Figure 2

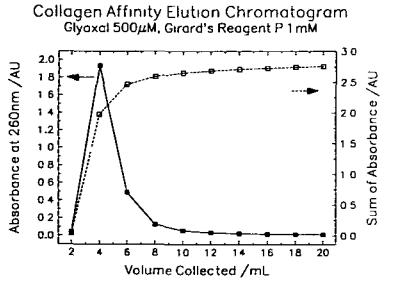

Figure 3

The high ionization efficiencies for electrospray ionization along with future implementation of a liquid chromatography interface such as capillary electrophoresis (CE) suggests an excellent potential for the determination of gas-phase carbonyl photooxidation products. This method is also applicable to identify carbonyl intermediates of oxidative processes in aqueous and biological systems.

1. Tuazon, E. C.; Atkinson, R. *Int. J. Chem. Kinet.* **1990**, *22*, 1221.
2. Ross, M.M.; Kidwell, D.A.; Colton, R.J. *Int. J. Mass Spectrom. Ion Proc.* **1985**, *63*, 141

A Study of the Oxidation of Heterocyclic Compounds using GC-MS Techniques

J Morris, M. R. Clench & D. W. Allen, Environmental Research Centre, Sheffield Hallam University, Pond Street, Sheffield, S1 1WB, UK.

The Wet Air Oxidation process has considerable attractions for the disposal of toxic organic wastes(1) A fundamental study is being made of the mechanism of oxidation under Wet Air and related conditions of a series of well defined substances known to occur as components of industrial wastes and which are known to present difficulties in the Wet Air Oxidation process. The progress of the oxidation reactions has been followed using GC-MS techniques, so as to establish the nature of the oxidation products formed. The oxidation of 2-, 3-, and 4-picoline was carried out under simulated Wet Air Oxidation plant conditions in a laboratory autoclave operating at 270°C and 750psi air pressure. The literature and some of the oxidation products observed so far suggest that the formation of the hydroxyl radical (•OH) under Wet Air conditions may be responsible for the initiation of the radical oxidation reactions(2). Therefore, the possibility of catalysis of the above systems by reagents known to generate •OH has been explored. Much literature suggests that Fenton's reagent (Fe^{II} + H_2O_2) provides a source of •OH(3), and so the oxidation of the picolines using Fenton's reagent under laboratory conditions and also as a catalyst in the autoclave process has been explored. Work has also involved comparisons of the effectiveness of other metal ion/hydrogen peroxide systems e.g. iron(III), copper (I) and (II), vanadium (IV), and titanium(III) as there is evidence from the literature of their involvement in oxidation chemistry(4). All of these systems were used as catalysts in the autoclave oxidation reactions of each of the picolines and in laboratory oxidation studies.

A wide range of oxidation products has been characterised from the oxidation of 2-picoline under both uncatalysed and catalysed autoclave conditions and from those catalysed oxidation experiments carried out in the laboratory. Similar observations were made in the oxidation of both 3- and 4-picoline, although the extent of oxidation varied in each case. Under the various conditions adopted there was evidence of destructive oxidation of the heteroaromatic ring. However, in addition to ring destruction products, a range of intermediate compounds were also observed, including a variety of dimeric structures. One that was identified from the Fenton Catalysed oxidation of 2-picoline was 1,2-bis(2-pyridyl)ethane at a retention time of 16.65 mins exhibiting an apparent molecular ion of 184.

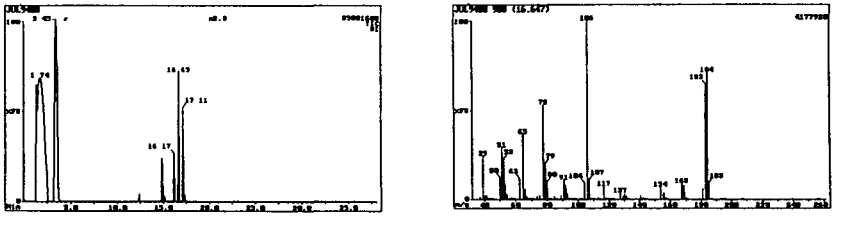

Figure 1 - GC trace from the Fenton Catalysed Oxidation of 2-Picoline and a Mass Spectrum of the Oxidation Product at a Retention Time of 16.65 mins

The study has also involved an investigation of the kinetics of the Fenton catalysed oxidation of 2-picoline. The data obtained illustrated that there is a first order dependence of the rate of the reaction on the concentration of 2-picoline.

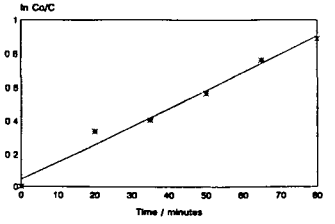

Figure 2 - First Order Kinetic Plot for the Fenton Catalysed Oxidation of 2-Picoline

GC/MS has been successfully used to identify products arising from the oxidation of picolines using a variety of oxidising conditions and investigate the kinetics of a typical Fenton catalysed oxidation reaction The radical responsible for the reactions occurring is thought to be the hydroxyl radical However, a recent suggestion in the literature(5) postulates that Fenton's reagent is not a principal source of hydroxyl radicals. The major oxidising species is thought to be a high oxidation state iron complex.

The aim of this work is now to establish if Fenton's Reagent and other metal ion/hydrogen peroxide oxidising systems are initiating radical chemistry, or not Studies are to continue involving the use of TEMPO, a radical trap, and EDTA, a complexing agent to compare the effect on the oxidation of each of the picolines. Essentially, the aim is to establish if incorporation of such catalytic systems into the WAO process will enhance the oxidation reaction occurring effectively.

1. Jackman A. P & Rowell R. L., Hazardous Waste Treatment Technologies, Noyes Publications, 1991, 90-135 and references therein.
2. Allen D. W , Clench M. R. & Morris J., *Analyst*, 1994, **119**, 903-907.
3. Walling C., *Accounts of Chemical Research,* 1975, **8**, 125-131.
4. Strukul G., Catalytic Oxidations with Hydrogen Peroxide as Oxidant, Klumer Academic Publishers, 1992, 97-151
5 Sawyer D.T., Kang C., Llobet A & Redman C., *J. Am. Chem Soc.*, 1993, **115**, 5817-5818.

A Simple Gas/Liquid Membrane Interface for a Mass Spectrometer (GLMIMS)

N.J.Clarke and J.F.J. Todd
The Chemical Laboratory, University of Kent, Canterbury, Kent, CT2 7NH, Uk

I. Introduction

The idea of using a selectively permeable membrane which would allow volatile organic molecules to pass through but actively hinder the passage of water and polar molecules was first suggested by Hock and Kok[1]. Such a membrane provides a simple and cheap means of transferring samples directly from their surrounding liquid medium into the gas phase and thence into the mass spectrometer More recently systems based on this idea have been used to examine a wide variety of samples, from fermentation vats to olive oil [2,3].

I.1 Description of standard MIMS system

The Membrane Inlet Mass Spectrometer (MIMS) interface described by Cooks et al [4] has become a standard design and uses silastic hollow fibre tubing inside a metal or glass casing. The membrane is normally around 15 cm long and is attached to deactivated silanised silica capillary tubing at each end through which helium gas is passed. Water containing the sample(s) is pumped through the gap between the outer casing of the interface and the membrane, in the opposite direction to the flow of helium. A silicone membrane is commonly used as this is a hydrophobic material which helps to prevent water passage through the membrane into the helium flow and ultimately the instrument. The volatile organic compounds in the sample are also hydrophobic and diffuse easily into the membrane which effectively concentrates them. Once a sufficient concentration of the compounds has been reached within the membrane they will naturally pass through into the hollow centre of the fibre by a process known as pervapouration and are swept into the mass spectrometer by the helium flow. The interface is placed inside a GC oven and heated to around 85°C, in order to facilitate the flow of organic compounds through the membrane.

I.2 Description of Gas/Liquid MIMS system

The system designed at Kent employs the same membrane as mentioned earlier, however instead of the system being encased inside a metal or glass tube, the membrane is wrapped in a helical manner around the outside of a glass sheath. (See Fig. 1) Because of this method of attachment the probe has a greatly increased surface area of membrane whilst still remaining very compact. Typically a membrane of 1 metre or greater is used and this increase in surface area leads to much faster response times and sensitivity.

The glass sheath is placed over a solids probe which has a built in heater and thermocouple, allowing the temperature to be easily monitored and controlled. Helium is then passed through the inside of the membrane into the mass spectrometer via silica capillary tubing as in the standard system but without passing through a jet separator.

Since the interface is now on a hand-held probe it can be easily manipulated and placed into confined spaces or containers, opening up the possibility of using the system for environmental monitoring either in the laboratory or as a portable, handheld unit for sensing in the field.

II. Experimental

All experiments were carried out on a modified Finnigan MAT ITD Quadrupole Ion Trap Mass Spectrometer and the results were acquired using dynamically programmed scanning software written at the University of Kent [5]. An investigation of the relationship between the concentration of ethanol in the headspace and liquid of a series of known concentrations in water was undertaken. An examination of compounds leaching from plastic cups in contact with hot or boiling liquid was also undertaken as an extension of work into detection of estrogenic materials, such as anti-oxidants, passing into foodstuffs from plastic containers. Finally an examination of car exhaust gases and volatile organics present in roadside soil was attempted.

III. Conclusions

1). The new probe can accommodate a much larger surface area of membrane compared to the existing interface.

2). The new probe design can sample both gaseous and liquid samples easily. Although it is possible to examine gaseous samples using the standard interface, the design is inappropriate to the requirements of such a task and the results are disappointing. Further the probe enables quantitative data to be gathered for samples in both the liquid and gaseous state.

3) The gas/liquid probe has been designed to be portable. The entire interface is only as large as the heated probe used. It is ideal for handheld use as well as a fixed atmosphere sensors within buildings etc. The standard MIMS system is extremely cumbersome, requiring a pumping system as well as a large oven.

4). The probe membrane is heated specifically meaning the environment experiences very little heat gain. By comparison the standard MIMS interface requires the entire interface plus sample to be heated which will affect any equilibria and as well as the system being sampled.

5). Less sample is needed to allow the experiment to be completed. Since a flow of sample is required using the standard interface a relatively large volume of liquid is needed. If one examines the headspace gas above a sample very little liquid need be used.

6). Gaseous examination of a system reduces the chance of contamination. This is especially useful when working with sterile environments such as fermenters.

References

[1] G. Hock and B. Kok, Arch. *Biochem. Biophys.* (1963), 101 pp160-70
[2] F.R. Lauritsen, N.T. Nielsen, H. Degn, D. Lloyd and S. Bohátka, *Biol. Mass Spectrom.* (1991), **20** pp253-258
[3] T. Kotiaho, S. Gylling, A. Lunding and F.R. Lauritsen, *J. Agric. Food Chem.* (1994), (Pending)
[4] T. Kotiaho, F.R. Lauritsen, T.K. Choudhury, R.G. Cooks and G.T. Tsao, *Anal. Chem.* (1991), **63** pp875A

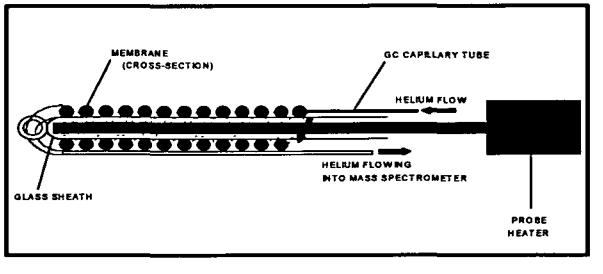

Figure 1: Gas/Liquid MIMS Interface

A Rapid Srceening Procedure for the Analysis of Proliferation Compounds in Complex Matrices Using Solid Phase Microextraction (SPME) and SPME With *In-Situ* Derivatization

Armando Alcaraz*, Suzy S. Hulsey, and Brian D. Andresen
Lawrence Livermore National Laboratory, P.O. Box 808, Livermore, CA 94550

Introduction

A variety of methods have been established using advanced chromatographic techniques and new detection systems for the analysis of chemical signatures associated with nuclear and chemical weapon (CW) proliferation. Most of these analytical methods are used in the laboratory and seldom applied in the field. The Chemical Weapons Convention (an international treaty to ban chemical weapons) may require the rapid on-site analysis of environmental samples which contain CW agents, their precursors, and/or their degradation products. In addition to the fact that certain countries are involved in CW non-compliance, there is a current uncertainty regarding nuclear proliferation. This also creates new demands on sample work-up and analytical instrumentation use in the field. The isolation and identification of unique chemical signatures in complex samples such as soils, waste tanks, and decontamination solutions would determine non-compliance. However, a primary area of detection research continues to be sample preparation. Most of the established sample cleanup technologies involve liquid/liquid, Soxhlet, or most recently, solid phase extraction (SPE). Despite the success of these traditional sample preparation techniques, they are time consuming and require multi-step procedures (especially when preparing samples for gas chromatographic mass-spectrometric analysis). The goal of this work is to demonstrate the advantages of utilizing SPME and SPME in-situ derivatization techniques to eliminate time consuming steps necessary to prepare a sample for on-site GC-MS [1]. Our approach was to compare two SPME fibers and to develop methods to facilitate the isolation of polar and moderately polar proliferation compounds from complex environmental samples. This work will help to evaluate current SPME technologies for use during on-site environmental monitoring analysis.

Experimental

Two types of SPME fibers (Supelco, Inc.) were evaluated for each analyte: 100-um polydimethyl-siloxane and 85-um polyacrylate coatings. Samples were then analyzed directly by GC-MS (Varian Saturn III) or derivatized "on fiber" first, then analyzed by GC-MS. The "on-fiber" derivatization procedure is accomplished by gently coating the SPME fiber with N,O-bis(trimethylsilyl)-trifluoroacetamide (BSTFA) prior to GC-MS analysis. The sample matrices analyzed in this study included soil leachate (sandy loam, Livermore, CA), simulated sea water (Instant Ocean, Aquarium Systems Co., Mentor, OH), and canal water (rain runoff). The chemical signatures we selected for the proliferation of CW and nuclear weapons included dimethyl methylphosphonate (DMMP), diisoproplyl methylphosphonate DIMP), 1,4-dithiane, thiodiglycol (TDG), 2-(diisoproplylamino)ethanol (DIAE), and tributyl phosphate (TBP).

SPME Conditions for Analysis

SPME Fiber: Polyacrylate 85-µm coating

Sample: 10 mL of spiked solution*

Extraction: 10 min, fiber immersed in solution, rapid stirring, and heat to 55°C

Desorption: 3 min, 250°C

Desorption: 5 min, 250°C ("*on-fiber*" derivatization)

**Simulated Sea Water:* Added 10% NaCl, adjusted pH to 9.0 (NH_4OH)
Canal Water and Soil Leachate: Added 10% Na_2CO_3, resulting pH of 11

References

[1] K.D. Buchholz and J. Pawlisyn, *Anal. Chem.* 1994, *66* , 160-167.

GC-MS Conditions

Oven: 50°C (1 min) to 300°C at 8°C/min

Injector: Splitless/split closed initial 3 min, set at 200°C and at 10 psi
Column: DB-5MS, 30m x 0.25mm, 0.25um film (J&W Scientific), helium carrier gas

Scan: 50 to 400 Daltons, 1 scan/sec, 3 min EM delay, transfer line at 280°C

SPME (*On-fiber*) Derivatization GC-MS Conditions

Oven: 70°C (8 min) to 300°C at 8°C/min, Injector: Splitless/split closed initial 1 min, and set at 250°C. Scan: 50 to 400 Daltons, 1 scan/sec, 8 min EM delay

Results

The polyacrylate 85-um coated SPME fiber appears to extract DMMP, DIMP, TDG, 1,4-dithiane, DIEA, and TBP best. The polydimethyl-siloxane 100-um fiber does not extract DMMP, TDG, and DIAE as effectively. The use of SPME "on-fiber" derivatization increases the detection of DIAE, figure 1.

Thiodiglycol could be identified only by using "on-fiber" derivatization. Heating at 55°C, stirring, and adjusting the sea water pH to 9 (with NH_4OH) enhances the extraction of the polar analytes. These sample modifications do not significantly effect the extraction of moderately polar compounds (DMMP, DIMP, 1,4-dithiane, and TBP). Heating at 55°C, stirring, and adjusting the canal water and soil leachate pH to 11 (with Na_2CO_3) enhances the extraction of the polar analytes. These sample modifications do not significantly effect the extraction of moderately polar compounds. In the case of 1,4-dithiane pH adjustment by Na_2CO_3 appears to increase its extraction efficiency.

Lower Limits of Detection

Compound	Sea Water	Canal Water	Soil Leachate
Tributylphosphate (TBP)	10 ppb	0.5 ppb	50 ppb
Diisopropylmethylphosphonate (DIMP)	0 5 ppm	0 1 ppm	0.5 ppm
Dimethyl methylphosphonate (DMMP)	1 ppm	1 ppm	0.25 ppm
1,4-Dithiane (1,4-D)	5 ppb	5 ppb	12 ppb
2-(Diisopropylamino)ethanol (DIAE)	5 ppm	0.5 ppm	0.10ppm
Thiodiglycol (TDG)	Not detected	Not detected	Not detected
"On-Fiber"* Derivatization			
2-(Diisopropylamino)ethanol (DIAE)	50 ppb	50 ppb	50 ppb
Thiodiglycol (TDG)	30 ppm	30 ppm	50 ppm

* Derivatization with N,O-bis(trimethylsilyl)-trifluoroacetamide (BSTFA)

Conclusions

Solid-phase microextraction (SPME) can isolate target analytes in complex environmental samples rapidly for field analysis. Previously developed SPME methods (in the laboratory) will greatly optimize the analyte's partition between the sample matrix and fiber coating for field work. A set of systematic SPME procedures can be developed to extract sequentially a variety of analytes onto the solid-phase coating. This can be accomplished by varying pH, temperature, and using salting-out techniques. The use of SPME "on-fiber" derivatization greatly reduces the time required to analyze polar compounds. This technique offers a solution for the rapid field screening of polar compounds by GC-MS. New SPME fibers are needed for the extraction of small very polar compounds from polar solvents.

Thiodiglycol does not adsorb on the 100-µm polydimethyl siloxane or 85-µm polyacrylate fiber efficiently.

*Work performed under the auspices of the U.S. Department of Energy by Lawerence Livermore National Laboratory under contract W-7405-ENG-48.

The Detection of TNT and TNT Metabolites by Electrospray Mass Spectrometry

J. Carlson[1], P. Vouros[1], D. Kaplan[2]
[1]Department of Chemistry, Northeastern University, Boston, MA 02115
[2]U.S Army Natick, Research, Development and Engineering Center Natick, MA 01760

There exists great interest in determining the fate of TNT residues in soils at munitions plants and testing facilities throughout the United States. The storage, spillage, testing and usage of 2,4,6-trinitrotoluene (TNT) for well over a century has resulted in the introduction of TNT into the environment at numerous military installations and contractor facilities Aerobic and anaerobic methods of TNT degradation have been studied, but detailed information on reaction intermediates and mechanisms have not been thoroughly explored. Mechanisms for the transformation products and intermediates of TNT have been postulated, but these materials are often difficult to separate and identify in the complex matrices from which they originate. Several of the TNT intermediates are thermally unstable and cannot be analyzed by gas chromatography. Since electrospray mass specrtometry does not expose the intermediates to harsh conditions it is expected that these intermediates may be isolated and identified. In addition, once separated some of these materials are unstable and readily undergo degradation to more stable structures. In most cases TNT undergoes a long-term reduction in the environment to form the principal metabolites 2-amino-4,6-dinitrotoluene, 4-amino-2,6-dinitrotoluene, 2,4-diamino-6-nitrotoluene, 2,6-amino-4-nitrotoluene, 2,2',6,6'-tetranitro-4,4'-azoxytoluene, 2',4,6,6'-tetranitro-2,4'-azoxytoluene, and 4,4',6,6'-tetranitro-2,2'-azoxytoluene1.

TNT and the principal TNT metabolites were studied by direct injection electrospray ionization mass spectrometry (ESI-MS). In addition to the observed $[M+H]^+$ ion the collisionally induced dissociation (CID) of each of these analytes was conducted in order to determine the primary fragments. Under these conditions, fragments representing the loss of 46 amu are easily observed for each of the NO_2 group(s) present in the aromatic ring.

TNT and TNT metabolites with no functional groups on the aromatic ring other than NO_2 often require negative ion detection modes because of the strong electron withdrawing characterisitics of the NO_2 group(s). Collisionally Induced Dissociation (CID) of these compounds requires high pressures in the gas cell and low dissociation energies in order to fragment these molecules. This suggests that multiple reactions are required within the gas cell in order to produce stable fragments.

TNT metabolites with amine functionalities can be observed in the positive ion mode during electrospray, but the matrix must sometimes be acidified prior to analysis as is the case with the monoaminodinitrotoluenes.

The use of methylene chloride/water/methanol in a 2:3:5 ratio with direct flow injection produces a stable electrospray particularly in the negative ion modes. This solution matrix is desirable because of the limited solubities of the tetranitroazoxytoluenes in typical methanol/water solution matrices.

The comparison of negative and positive ion detection modes has shown the potential for improved selectivity in more complex matrices.

The collisionally induced dissociation (CID) mass spectra of 4,4',6,6'-tetranitro-2,2'-azoxytoluene and 2,2',6,6'-tetranitro-4,4'-azoxytoluene are shown in Figures 1 and 2 respectively. These isomers produce fragments only at high gas cell pressures (2.8 E-3 torr) and relatively low collisional energies (15V). The resulting mass spectra show entirely different fragmentation patterns due in part to the position of the methyl group relative to the azoxy

functionality. In addition, fragments representing the loss of NO (m/z 30) and NO_2 (m/z 46) are observed for the -4,4'-azoxytoluene which are not readily observed with the -2,2'-azoxytoluene.

Figure 1

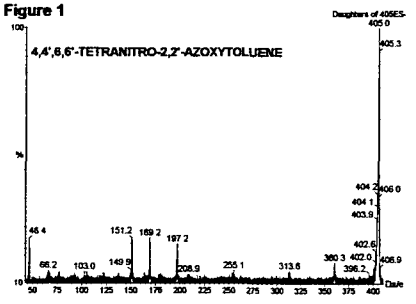

Figure 2

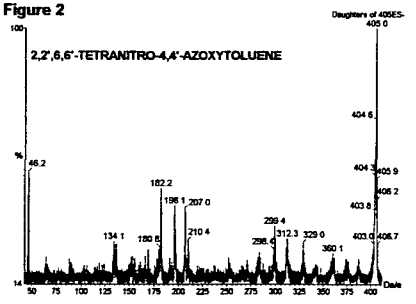

Reference

1. Kaplan, D.L., Kaplan, A.M., *App. and Envir. Microbiol.*, **44**, 3, 757-760 1982.

Environmental Analysis by Flow-injection Tandem Mass Spectrometry

Michael Filigenzi and Michael Larson
Quanterra Environmental Services
880 Riverside Pkwy, West Sacramento, CA 95605

Flow-injection thermospray MS/MS (FIA-TSP/MS/MS) was used for the rapid screening of environmental samples to detect the presence of diethanolamine (DEA) and N-Nitrosodiethanolamine (NDEA).

Water samples were prepared by dilution with ammonium acetate to a level of 0.20M, and addition of d5-atrazine to a level of 50 ng/ml. Soil, wipe, and vegetation samples were prepared by shaking with 0.20M ammonium acetate. The ammonium acetate was withdrawn, filtered, and spiked to a level of 50 ng/ml. A method blank and a pair of spiked method blanks were extracted with each set of 20 samples of a given matrix. Matrix spike samples were also extracted with some sample sets.

All analyses were performed using Finnigan TSQ-70 mass spectrometers with TSQ-700 data systems, Finnigan TSP-2 thermospray interfaces, Waters 600 LC pumps, and Waters 717 autosamplers. Instrument conditions such as vaporizer temperature, source block temperature, and instrument tuning paramaters were optimized by continuous infusion of a 1 ug/ml DEA solution into the instrument. Argon was used as the collision gas with a collision pressure of 1.0 mtorr. The instrument was run in selective reaction monitoring mode, with m/z 106 as the precursor ion and m/z 70 as the product ion for DEA. For sample analysis, the LC pumps were set to deliver 1.2 ml/minute of 0.20M ammonium acetate solution. The spray was turned on several minutes prior to analysis in order to allow source conditions to equilibrate. Analytical runs were initiated by starting acquisition and starting the autosampler (in manual mode) simultaneously. The autosampler was set to inject each sample or standard in duplicate at a rate of approximately one injection every two minutes.

d5-Atrazine response in samples was monitored in order to detect any overall drop in response due to co-eluting compounds Its precursor ion was at m/z 221 and the product ion was at m/z 179.

Quantitation was performed using the external standard method. Three-point standard curves at levels of 1000, 100, and 10 ng/ml were run at the beginning of each day. These curves were required to show <30% relative standard deviation to be considered valid. The mid-level standard was re-injected after every 10 samples. It was quantified using the average response factor from the curve, and was required to give a value within 30% of the expected concentration. Exceeding these limits resulted in reinjection of the standard curve and reanalysis of any associated samples. DEA concentrations in samples were calculated using the average response factor from the associated standard curve.

The associated chromatogram shows a complete analytical run for DEA (m/z 70), NDEA (m/z 74), and d5-Atrazine (m/z 179), including a 3-point calibration curve, quality control extracts, sample extracts (some diluted), and continuing calibration standards.

Response was good for DEA and NDEA at the 10 ng/ml level (>5:1 signal to noise). d5-Atrazine peak heights were stable in all samples. There was no evidence of suppression of response due to co-eluting compounds in any sample. Spike recoveries in

the spiked method blanks were routinely good. Matrix spike recoveries were somewhat lower, particularly in soil samples, reflecting differences in soil types and the gentle extraction technique which was utilized. Several background (uncontaminated) soil samples were also analyzed in order to evaluate the possibility that we could get false positive results from uncontaminated soils. These samples showed no evidence of DEA or NDEA.

Over 340 samples were analyzed using this method. Analyses were run quickly, with results for many samples provided within the 48-hour time frame. Quality control specifications were routinely met, although re-analyses were sometimes required due to drifting instrument response.

This data shows the viability of FIA-TSP/MS/MS for high throughput analysis of real-world environmental samples. The gentle extraction procedure combined with the sensitivity and specificity provided by TSP-MS/MS gives data which meets QC criteria consistent with those of common environmental mass spectrometry methods. The speed of the analysis provides the quick results necessary for some cleanup projects.

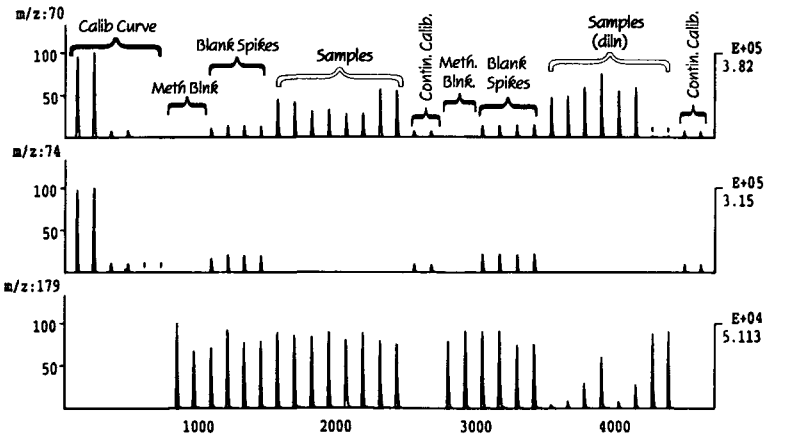

COMPARISON OF HPLC-MS INTERFACES IN THE DETERMINATION OF HETEROCYCLIC POLYCYCLIC AROMATIC COMPOUNDS*

Darren Thomas, P. Greig Sim, Institute for Marine Biosciences, National Research Council of Canada, Halifax, NS, Canada, B3H 3Z1 and**
Frank M. Benoit, Health Canada, Tunney's Pasture, Ottawa, ON, Canada, K1A 0L2

Polycyclic aromatic compounds (PACs) are generally regarded as one of the most widely disseminated groups of chemical carcinogens[1]. In our work we are interested in the determination of some of the heteroatom substituted PACs, particularly those containing nitrogen (PANHs) or sulfur (PASHs) in the aromatic ring structure. The reason for our interest in these compounds is the extreme carcinogenicity of many of them[2]. Further, the relative carcinogenicity can vary markedly between different members of a set of isomeric compounds. Any reliable assessment of the hazards associated with exposure to mixtures of PACs must, therefore, include analysis of the levels of these compounds in the mixture. The analytical technique used must also yield information about the relative amounts of different isomeric compounds.

The sample chosen for this study is an extract of PACs from the Sydney Tar Ponds, Sydney, Nova Scotia, Canada. The Tar Ponds represent the end result of approximately 80 years of the uncontrolled discharge of effluent from an industrial coking operation into a tidal lagoon. It is thus a rich source of complex PAC mixtures.

In general, PAC analysis is restricted to the determination of a preselected group of PAHs using well established GC-MS techniques. The determination of the PANH and PASH content of a sample is more complex and involves some form of preconcentration step to isolate the target group from the more abundant PAHs, followed by some form of chromatographic-mass spectrometric analysis. We have developed a technique using immobilized copper (II) on silica[3] (open column) or strong cation exchange resin[4] (preparative scale HPLC), and applied it to extracts from the Tar Ponds to separate the PAC fraction into three subfractions. The latter contain PAHs and PASHs (Fraction 1), carbazoles (Fraction 2) and other PANHs (Fraction 3).

In the present work, we have applied two HPLC-MS methods to the characterization of the PASH content of Fraction 1 and the PANH content of Fraction 3. The methods differed in the nature of the interface between the HPLC and the MS, and in the ionization process. The two techniques studied were the moving belt with EI ionization, and the heated nebulizer with APCI. We were interested in comparing the relative performance of these two techniques. The comparison was made on the basis of a number of criteria, including ease of use (and of automation), quality of mass spectra provided, preservation of chromatographic integrity, and sensitivity.

The heated nebulizer had considerable advantages in terms of ease of use, and of automation: we were able to leave it operating unattended for considerable periods of time, an advantage for the repetitive analysis of many similar samples. The heated nebulizer was also advantageous in the ionization of relatively involatile compounds. With the heated nebulizer, however, ionization is effected by at least two competing processes: charge exchange (to produce M^+ ions) and proton transfer (to produce MH^+ ions). The relative abundances of the ions produced by these two processes is dependent on a variety of factors. These include the molecular weight of the compound, in that lower mass compounds tend to yield ions formed from both processes whereas higher mass compounds yield predominantly protonated molecular

* NRCC # 38067
**Present address: Hazleton Europe, Otley Road, Harrogate, North Yorkshire, England, HG3 1PY

also be affected by other conditions in the laboratory environment, higher humidity favouring proton transfer ionization, for example. Both factors may come into play when the analyst is attempting to profile the isomeric content of a given sample, and may also affect the apparent sensitivity of the method.

The moving belt has a significant advantage in the nature of the mass spectra afforded. Under EI conditions almost all PACs yield simple spectra, dominated by an abundant molecular ion. Further, the relative sensitivity of ionization of different isomers is affected solely by properties of the compounds themselves, and not by external conditions. However, the moving belt has a well-known disadvantage in the analysis of less volatile compounds, since the ionization process cannot proceed without prior thermal desorption of the analyte from the material of the moving belt.

The analysis of dibenzo-, benzonaphtho- and phenanthro-thiophenes in Fraction 1, and of acridine, benzacridines and methyl benzacridines in Fraction 3 offers an opportunity to illustrate these features of the two techniques. Under normal laboratory conditions, the ionization of all PASH compounds using the heated nebulizer is dominated by the formation of molecular ions, in other words, they act as lower mass PAHs do in the same environment. However, when the moisture content of the laboratory air is extremely high, several of the higher mass compounds, particularly the phenanthrothiophenes, form relatively more abundant protonated molecular ions. Thus the analyst must constantly check the nature of the ionization process, if reliable results are to be obtained. The PANH compounds generally do not exhibit the same variability in behaviour. The higher mass PASHs also tend to give lower apparent sensitivity with the moving belt interface, which may be caused by difficulty in desorption from the surface. In general, the heated nebulizer does tend to give superior performance in the analysis of these compounds, but the analyst must be aware of factors affecting the ionization process.

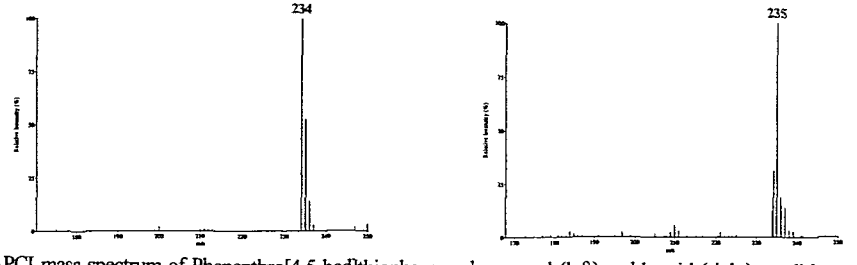

APCI mass spectrum of Phenanthro[4,5-bcd]thiophene under normal (left) and humid (right) conditions

1. M.L. Lee, M.V. Novotny and K.D. Bartle. in *Analytical Chemistry of Polycyclic Aromatic Hydrocarbons*, Academic Press, New York (1981)

2. G. Grimmer in *Polycyclic Aromatic Compounds: Synthesis, Properties, Analytical Measurements, Occurrence and Biological Effects*, Proceedings of the 13th International Symposium on Polynuclear Aromatic Hydrocarbons, Bordeaux, P. Garrigues and M. Lamotte, Eds., Gordon and Breach, (1993) pp. 31-41.

3. P.G. Sim, H. Perreault, F.M. Benoit, L. Ramaley, S.M. Crain, G.K. McCully and D.Thomas, *Polycyclic Arom. Compounds*. Submitted for publication, May 1995.

4. D. Thomas, S.M. Crain, P.G. Sim and F.M. Benoit, *J. Chromatogr. (A)*, 695, (1995), 1.

USE OF TWO SPE-GC/MS METHODS FOR FIELD ISOLATION AND QUANTITATION OF POLYCYCLIC AROMATIC HYDROCARBONS

Edward T. Furlong, Janece C. Koleis, and Paul M. Gates,
U.S. Geological Survey, 5293 Ward Road, Arvada, Colorado 80002.

Increasing sensitivity and subsequently improving method-detection limits for a variety of organic contaminant compounds is an ongoing effort in environmental analytical chemistry [1]. Several field-deployable isolation techniques have been developed for concentrating hydrophobic organic contaminants from large (> 1 liter) volumes of aqueous samples [2-3]. The capacity of large-volume solid-phase extraction (LV-SPE) was used as part of a simple, efficient, field-operable technique for isolating microgram-per-liter to nanogram-per-liter quantities of polycyclic aromatic hydrocarbons (PAH) in 4- to 8-liter ground-water samples from a petroleum-contaminated aquifer near Bemidji, Minn. [4].

The analytical sensitivity (~100 picograms injected) and specificity of selected-ion monitoring gas chromatography/mass spectrometry (SIM-GC/MS) was coupled with two LV-SPE field isolation techniques compared in this study. The two approaches were as follows: (1) large (145 millimeter) diameter solid-phase extraction (SPE) membranes (M-SPE), and (2) 10-gram SPE cartridges (C-SPE). Both SPE types contain silica-bonded octadecylsilane as the solid-phase sorbent. These two SPE types were compared to determine which LV-SPE technology provided the most accurate and precise PAH concentration measurements. PAH recoveries from both M-SPE and C-SPE isolation methods were compared using (1) reagent water fortified with 18 individual PAH at 1.23 micrograms per kilogram, and (2) ground-water samples with trace (microgram per liter or less) quantities of ambient PAH in the presence of other hydrocarbons and hydrocarbon degradation products. In studies with M-SPE, samples were collected and the PAH isolated at the wellhead; with C-SPE, a separate, simultaneously collected sample was processed in a field laboratory. In the analytical laboratory, the SPE membrane or cartridge was extracted using dichloromethane and analyzed by SIM-GC/MS using electron-impact ionization. PAH were quantified by isotope dilution and internal injection standard methods.

In laboratory tests, PAH recoveries ranged from 78 to over 100 percent for lower molecular weight PAH (naphthalene to pyrene) using either C-SPE or M-SPE (Fig 1). M-SPE recoveries for higher molecular PAH (chrysene to benzo[*ghi*]perylene) ranged from 18 to 56 percent, greater than those measured for C-SPE (0 to 25 percent). The loss of higher molecular weight PAH, observed for both native PAH and perdeuterated PAH, may result from sorption onto surfaces in the sample processing equipment. Comparable amounts of lower molecular weight PAH, at concentrations as low as 20 nanograms per kilogram, were isolated by both M-SPE and C-SPE in oil-contaminated ground-water samples (Fig. 2.).

Although the data are variable, elevated ground-water PAH concentrations at Bemidji appear associated with elevated dissolved organic carbon (DOC) concentrations (Fig. 3), particularly downgradient of the emplaced oil. This suggests that DOC formed *in situ* from microbial degradation of oil in the aquifer [5] is sufficiently hydrophobic that it acts as a cosolvent dissolved in ground water and consequently facilitates aqueous transport of insoluble hydrophobic organic contaminants, including PAH [6].

References:

[1] Pankow, J.F., *Environ. Sci. Tech.* **1988,** *22*, 1372-1373.
[2] Foster, G.D., Gates, P.M., Foreman, W.T., McKensie, S.W., and Rinella, F.A., *Environ. Sci. Tech.* **1993,** *27*, 1911-1917.
[3] Foreman, W.T., and Foster, G.D. , **1988** Water-Resources Investigation Report 91-4034; 530-533.
[4] Eganhouse, R.P., Baedecker, M.J., Cozzarelli, I.M., Aiken, G.R., Thorn, K.F., and Dorsey,T.F., *App. Geochem.* **1993,** *8*, 551-567.
[5] Thorn, K.A., and Aiken, G.R., Phoenix, Arizona **1988**; U.S. Geological Survey Water-Resources Investigations Report 88-4220; 41-51.
[6] Wijayaratne, R.D., and Means, J.C., *Environ. Sci. Tech.* **1984,** 18, 121-123.

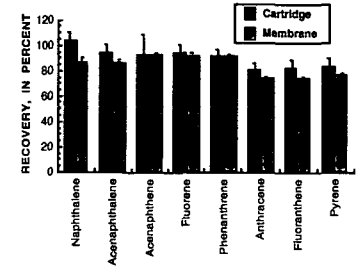

Fig. 1 Recovery of PAH from HPLC-grade water using cartridge and membrane SPE (by isotope dilution).

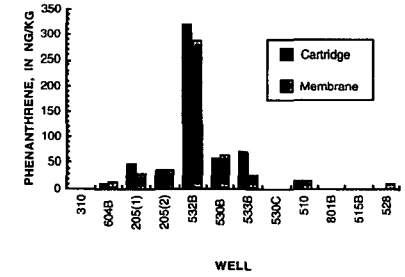

Fig. 2 Phenanthrene concentrations in contaminated ground water from Bemidji, isolated with M-SPE and C-SPE

[ng/kg nanograms per kilogram]

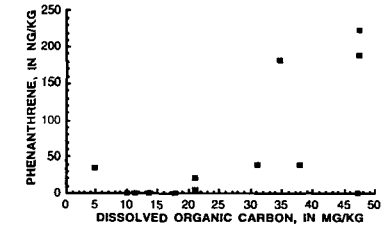

Relation between phenanthrene and organic carbon concentration in contaminated ground water - Bemidji, MN.

[Points are combined C-SPE & M-SPE data. Concentrations at 0 are below method detection limit. MG/KG, milligrams per kilogram; NG/KG, nanograms per kilogram]

VARIOUS MASS SPECTRAL TECHNIQUES FOR THE ANALYSIS OF NITRO-PAH

W. Miles and C.Chiu, Environment Canada, Environmental Technology Centre, Ottawa, Ontario, Canada K1A 0H3

Introduction

Nitro-polycyclic aromatic hydrocarbons are of environmental concern because of their mutagenic and carcinogenic properties(2). They are found in both combustion emission particulate matter and ambient air but at much lower levels than other organic compounds such as polycyclic aromatic hydrocarbons(2). Since the nitro-PAH are much more toxic than most other substances in these types of sample, there is a need for a sensitive and specific method for the accurate determination of this class of compounds.

Methods

All the data shown were obtained with a VG Autospec Q mass spectrometer equipped with a VAX 4000 model 60 data system using OPUS software. Negative chemical ionization was accomplished using methane as reagent gas at $3X10^{-5}$ torr indicated source pressure and resolution of 10000. MS/MS monitoring the loss of m/z 46 from the molecular ion utilized xenon as the collision gas at $4X10^{-6}$ torr indicated in the collision cell. The sector was set at 1000 resolution and the quad to unit mass resolution. The adduct experiments were conducted in EI positive mode with pyridine as collision gas at $3X10^{-6}$ torr indicated in the collision cell, sector resolution 1000,quad unit mass resolution. Tuning for adducts was done by introducing nitrobenzene to the septum inlet and monitoring the formation of the m/z 156 ion. Collision energy was the most critical parameter for good adduct yield and had to be optimized on a daily basis. GC separations were carried out on either a 30m DB5-MS (J&W) column or a 60m Quadrex 007-2 column using a Hewlett Packard 5890 series II GC.

Results and Discussion

Negative chemical ionization was examined as both a sensitive and selective analytical technique, avoiding a tedious and labour intensive sample clean-up procedure. Figure 1 shows the mass chromatograms of m/z=223 run by low resolution EI, low resolution NCI and high resolution selected ion recording NCI of an urban air sample. It can be seen that high resolution NCI eliminates many interferences and offers about three orders of magnitude better sensitivity than EI. Tandem mass spectrometry monitoring the loss of NO2 from the molecular ion was also examined as an alternative to high resolution. In some cases this was more selective than high resolution and in others the opposite was the case. Both methods demonstrated similar sensitivity and we find it convenient to use high resolution for routine analysis and MS/MS as a confirmation tool since this avoids the variables of collision gas pressure and quadrupole transmission. A calibration table prepared using seven native nitro-PAH's and three deuterated surrogates

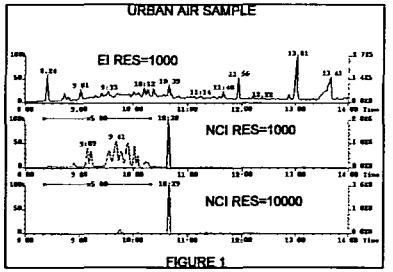

FIGURE 1

over a 100 fold concentration range gave a maximum relative standard deviation of 17% using the high resolution NCI method.

Pyridine Adducts of Nitro-PAH

In 1994 Freeman et al (1) published a paper describing a new instrumental technique to screen environmental samples for chemical contaminants having the propensity to covalently bond to biomacromolecules such as DNA. Since some nitro-PAH's are known mutagens, it was decided to investigate this technique for screening exhaust samples for potential mutagenic or carcinogenic compounds. Figure 2 shows the mass spectrum of neutral pyridine with 3-nitrofluoranthene which is representative of most of the nitro-PAH's studied in that the major and in this case only adduct ion, is due to the loss of the nitro group and the addition of pyridine. The reaction is given in figure 3 and was used for screening air samples. Figure 4 shows a chromatogram of a diesel exhaust sample analyzed by high resolution, loss of 46 from the molecular ion and adduct formation of m/z=247 with pyridine. It can be seen that only two of the peaks give adducts and that both adduct peaks are of similar size while the peak at 14:12 is about 30 times less than the one at 14:41 by both high resolution and loss of 46. Comparison with standards shows the first peak is 3-nitrofluoranthene and the second is 1-nitropyrene. Their mutagenicities for Salmonella typhimurium TA98 are 5,439 and 453 mutants per nmole respectively(2). This demonstrates that pyridine adducts can be used not only to indicate the presence of a mutagenic substance but also to provide a measure of its potency.

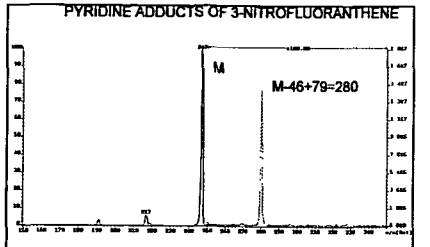

FIGURE 2

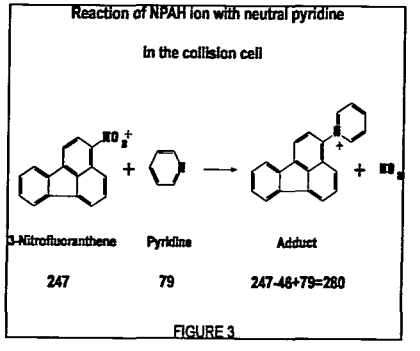

FIGURE 3

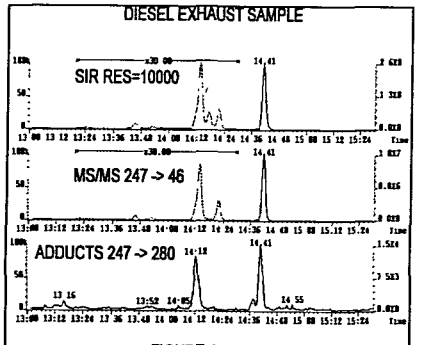

FIGURE 4

References

1. Freeman J.A.;Johnson J.V.;Yost R.A., Anal. Chem.,1994, 66,1902-1910
2. White C.M., Nitrated Polycyclic Aromatic Hydrocarbons, Huthig, 1985

DETERMINATION OF NITRATED POLYCYCLIC AROMATIC HYDROCARBONS IN TREE BARK

DAVID. S DOUCE, MALCOLM. R. CLENCH, MICHAEL. COOKE.
Environmental research centre, Division of science, Sheffield Hallam University, Pond Street, Sheffield, S1 1WB.

INTRODUCTION

Nitrated polycyclic aromatic hydrocarbons (nitro-PAHs) are released into the enviroment from a variety of sources, including the combustion of diesel, gasoline and other organic fuels.

The most important source or nitro'PAHs, is believed to be the emissions from diesel fuelled vehicles. Monitoring of this class of compound is important due to their carcinogenicity (1), and mutagenicity (1).Sturaro et al (2)have shown that tree bark acts as a passive absorbant for polycyclic aromatic hydrocarbons (PAHs). They proposed that the use of a natural and passive sampler such as tree bark might lead to a less complex overall analytical strategy for environmental measurements.It was decided to modify the method proposed by Sturaro et al (1), in an attempt to monitor nitro-PAH levels absorbed into the tree bark from diesel emissions.

METHODOLOGY

Samples

1) Tree bark A. Adjacent to city bus station
2 Tree bark B. A park on the city outskirts

Tree samples were taken from between 1-2 metres above the base of the tree The fragments were stored in amber screw topped vials.

Extraction.

The bark was cut into small pieces and extracted with Dichloromethane in a soxhlet apparatus. The solvent was removed to produce a residual weight

Clean-up procedure.(3)

An hplc system, using an Alumina column - activated, basic, Brockman 1 (150 mesh) was used to separate the mixture into four distinct fractions:-

n-Hexane -Alkanes, Dichloromethane -PAHs,

Acetonitrile-Polar PAHs, Acetonitrile·Methanol (3·1) -Multi polar PAHs

Nitro-PAHs were detected in the acetonitrile fraction.

SEPARATION AND DETECTION

Gas chromatography, using either an electron capture detector or a mass spectrometer using negative ion chemical ionisation in selective ion monitoring mode (NICI-SIM) were used.

Figure 1 - Nitro-PAH standard.

Figure 2 - Acetonitrile fraction of tree bark A, from hplc procedure.

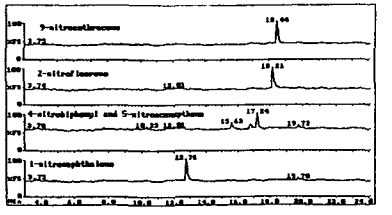

Figure 1.

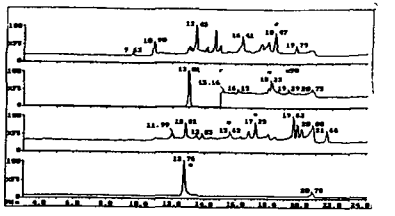

Figure 2.

QUANTITATIVE RESULTS

	1-Nitronaphthalene	4-Nitrodiphenyl	5-Nitroacenaphthene	2-Nitrofluorene	9-Nitroanthracene
GC/ECD TREE A	220 7 ng/g	Trace	Trace *	Trace	156 98 ng/g *
GC/ECD TREE B	103.0 ng/g	17 94 ng/g	10.12 ng/g	-	Trace *
NICI-SIM TREE A	154 8 ng/g	36 12 ng/g	50 62 ng/g	35 63 ng/g	177 09 ng/g

* Levels not seen in chromatograms provided

CONCLUSION

The NICI-SIM method of detection was highly specific, producing very clear quantitative results The result obtained from the electron capture detector are a little more difficult to interpret, due to the large quantity of interfering compounds still present in the cleaned up extract. Further steps need to be taken to improve the clean up fraction to concentrate and separate the nitro-PAH's from the other organics present in the tree bark sample.

However, we have shown that tree bark can be used as a passive monitor for the level of diesel pollution, both in the urban and rural environment.

REFERENCES.

1) Rosenkrantz. H. S. in Nitrated Polycyclic Aromatic Hydrocarbons White C. M. (ed) Heidelburg. New York and Basel 1986. 267-297
2) Sturaro A et al. Journal of Chromatography. 643. (1993) 435-438
3) Ciccioli P et al Journal of Chromatography. 1986, 351, 451-464.

Factors Effecting the Analysis of Organic Pollutants by Particle Beam-Liquid Chromatography-Mass Spectrometry

Mr.J.White and Dr.R.H.Brown
(Health and Safety Laboratory, HSE, Sheffield, S3 7HQ, U.K.)
Dr.M.R.Clench and Dr.D.A.Leathard
(Sheffield Hallam University, Ponds St. Sheffield, U.K.)

Liquid chromatography (LC) is probably the most versatile of chromatographic techniques as it can be used for compounds with a wide range of polarity and for compounds of low thermal stability or low volatility that are not amenable to gas chromatography. Additionally, many types of LC packing materials are available with varying surface chemistries to achieve the desired separation and a large amount of research has been carried out on the technique.

Mass spectrometry (MS) is probably the most versatile of detectors currently available. Using electron impact ionisation (EI-MS) generates characteristic fragmentation patterns ("fingerprints") which are of particular use for identification in forensic situations. Selected Ion Monitoring (SIM) can be used to simplify "noisy" or complicated chromatograms this is particularly of use for environmental samples.

An LC-MS system would therefore give the analyst an extremely powerful tool for the determination of unknown or trace compounds.

As part of a joint project between Sheffield Hallam University and HSL the use of particle beam-liquid chromatography-mass spectrometry (PB/LC/MS) for the analysis of environmental samples has been examined. The particle beam interface is perhaps the simplest PB/LC/MS interface available but has certain disadvantages. These are limited tolerance to some chromatographic buffers, non-linearity of response under certain conditions, poor sensitivity for some compounds (particularly those of low molecular mass) and operational difficulties due to interface blocking (particularly for "dirty" samples).

To investigate means of reducing these disadvantages a series of poly nuclear aromatic hydrocarbons (PAHs), the "EPA-16" **(1)** was chosen as trial compounds. Various methods of increasing sensitivity were examined, such as, instrumental factors (e.g. altering nebulizer position, increasing nebulizer gas pressure etc.), varying interface temperature and the addition of additives post column. These results were compared with those obtained from analysis by LC with diode array (UV) and programmed fluorescence detection and estimated detection limits compared. A variety of mobile phases, LC columns and gradient profiles was examined to give baseline resolution within an acceptable run time. Using the methods developed above PAH samples from environmental samples (refractory brick dust) were analysed. Various extraction and clean up procedures were examined for these samples.

Based on the above experiments a few comments may be made. Instrumental factors and interface temperature were shown to have an effect on sensitivity although this effect was not common throughout the sixteen compounds used as probes. Limits of detection obtained for PB/LC/MS were generally worse than those obtained by LC/DAD or LC/F . Detection for low molecular mass compounds (< 200) were generally very poor or undetectable. For higher molecular mass compounds detection limits improved until at RMM >270 similar limits to the other techniques were found. Further work shows this trend continues with coronene (RMM ~300). The post column addition of additives did improve sensitivity and linearity especially at low concentrations but again this effect was not uniform for all the PAHs and no single additive can be recommended. These findings are in accordance with the work of Apffel and Perry **(2)** who proposed a "low mass filter" model to account for this finding.

The use of solid phase extraction cartridges for the clean up of the brick dust extracts raised the following points. For both the silica gel (Si) and octadecyl silica (C18) cartridges used recoveries varied for each PAH. Again the lower RMM compounds were lost completely (up to mass 202). However preliminary work with gel permeation chromatography (GPC) also shows this effect which is probably due to sample work up after GPC or SPE e.g. drying down in the turbovap. Recovery work carried out on spiked SPE tubes (Si gel and C18) showed that C18 tubes gave slightly higher recoveries and better reproducibility than Si gel. In general it may be said that his type of sample proved to be difficult to analyse. LC/DAD traces in particular were very noisy and the PB interface was prone to being blocked by what were presumably brick dust particulates. GC/MS and LC/F gave acceptable chromatograms.

In conclusion it can be said that although PB/LC/MS shows great potential certain difficulties still remain especially low sensitivity for certain compounds. Further work in this study will look at GPC vs SPE clean up, different post column additives, and comparison of PB with electrospray, field and thermospray ionisation interfaces The use of PB-LC-MS for other classes of pollutants, such as pesticides and pharmaceuticals will also be investigated

References

(1) *"Polynuclear Aromatic Hydrocarbons"* United States Environmental Protection Agency. Method 610 (EPA-610) . Federal Register, Friday October 26th, Vol. 49, No. 209, p112-115 Rules and Regulations.

(2) *"Quantitation and Linearity for PB/LC/MS"* Apffel A and Perry M.L., J.Chrom. 1993,Vol. 554, p103-118

Environmental Genotoxin Characterization by LC/MS Analysis of DNA-Adducts formed *In Vitro*.

Douglas W. Kuehl and Jose Serrano
U.S. Environmental Protection Agency
Duluth, MN 55804
(218) 720-5559

The a priori identification of those environmental chemical contaminants with the propensity to be genotoxic (covalently bond to DNA) from the total of those that may be present in a sample has been the subject of study for some time. Methods of assessment have ranged from multi-generation life cycle mammal dosing studies to the use of short term predictive methods, including quantum chemical calculations and analytical models. None of the short-term predictive methods provides a complete assessment of potential hazard; however, each can be complementary to another and provide an alert for further testing. We have proposed and evaluated another assessment technique, the use of liquid chromatography/mass spectrometric characterizations of chemical adducts of DNA formed *in vitro* to detect and identify those contaminants in the aquatic environment which have the propensity to be genotoxic The technique was evaluated using, first, a series of direct acting chemicals which have different electrophilic reactivities; and second, indirect acting chemicals, i.e., those that require metabolic activation to become reactive. LC/MS was done by C_{18} RP-HPLC and both thermospray and electrospray MS and MS/MS.

Allyl reagents (isothiocyanate, chloride, bromide and iodide) were used to demonstrate that LC/MS characterization of DNA-adducts formed with direct acting chemicals was linear with the concentration of toxicant (allylbromide) (r^2=0.995 for the formation of the N-7 adduct) and proportional to relative reactivity of each toxicant as measured by the nucleophilic reagent 4-(4-nitro-phenyl)pyridine (NBP) and to Ames mutagenicity test results (Table 1). It was also possible to determine from LC/MS the proportion of adduct formation of N-7 vs O^6 of deoxyguanosine. N vs O bonding is an important parameter in the assessment of the carcinogenic potential of many genotoxins. For low concentrations of allylbromide (25 nmol/µg DNA) the N:O product ratio was 69:1, indicating that the allyl reagent was a soft electrophile and most likely possess little carcinogenic potential.

Table 1

Allyl reagent	LC–TSP-MS, 7-A-Gua/dGuo	Alkylating activity, NBP (ΔE_{560})*	Mutagenic activity (revertants/µmol)
Thiocyanate	<0 0001	0.03	1
Chloride	0 002	0 3	9
Bromide	0 012	54	700
Iodide	0 018	164	2000

Formation of 7-A-Gua relative to dGuo was estimated from $[M+H]^+$ TSP peak area, not quantitative Reaction conditions· 37°C, pH 7 0, 2 h, 5 µmol allylbromide, 100 µg DNA

alkylating (NBP) and mutagenic activity obtained by Eder et al ·

B[a]P was selected as a model compound for indirect acting chemicals, such as PAHs. Standard microsomal incubation reactions were developed which provided sufficient B[a]P/DNA adduct formation for LC/MS characterizations when environmentally realistic concentrations of B[a]P were used. Standard reaction conditions were: 2 mg trout liver microsomes; 0.4 mg NADPH, 2 hr; 25° C; and 200 mg calf thymus DNA. LC/MS characterization of the formation of the anti- isomer adduct of B[a]P/DNA was linear (r^2=0.990) at doses of B[a]P < 50 pmol/µg DNA; but it was later shown that higher doses could exceed the range of linear response (Figure 1). This observation agrees with the hypothesis that B[a]P arylation of DNA is highly base site specific and that the dose of B[a]P can exceed available reaction sites. It was also shown that LC/MS analyses were sensitive to the ratio of anti- to syn-isomer formation when altered by the presence of co-contaminants in the microsomal incubation reaction mixture (Table 2).

Figure 1

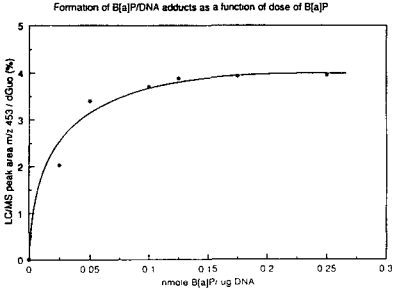

Table 2

Variation of formation of BPDE-dGuo in simple mixtures of B[a]P with B[e]P and pyrene LC/TSP/MS response presented as percent of peak area of m/z 453/192

Dose nmole PAH/100µg DNA			LC/TSP/MS peak area%
B[a]P	B[e]P	Pyrene	m/z 453/152
0 5			0 23
0 5		0 5	0 44
0 5	0 5		0 47
0 5	0 5	0 5	0 25

References

- Serrano, J., Kuehl, D.W., and Naumann, S. *J. Chromatogr. B 615(1993)203.*
- Kuehl, D.W., and Serrano, J. *J. Chromatogr. A 684(1994)113.*
- Kuehl, D.W., and Serrano, J. *J. Chromatogr. A submitted 1995.*
  Identification of potentially mutagenic contaminants in the aquatic environment by LC/MS characterization of in vitro DNA adducts formed during microsomal incubation.
- Serrano, J, and Kuehl, D.W. *J. Chromatogr B submitted 1995.*
  Liquid Chromatography-Mass Spectrometric characterization of B[a]P/fish liver DNA adducts formed in vitro during microsomal incubation.

Analysis of Serum PAH's and PAH Adducts by LC/MS

P Cheryl McClure, John R Barr, Vincent L. Maggio, Sarath Sirimanne, Li Ma, Donald G Patterson, Jr

Centers for Disease Control and Prevention, 4770 Buford Highway, Atlanta, GA 30341

Polycyclic aromatic hydrocarbons are an important class of chemical carcinogens There is potential for extensive chronic human exposure and EPA has listed many of these compounds as priority pollutants It is believed that PAH's can enter the body from a variety of environmental sources and then are metabolized by cytochrome P-450 to highly reactive electrophylic intermediates These intermediates can then react and form adducts with a variety of biopolymers such as DNA and proteins It is thought that the reaction of the electrophylic PAH metabolite with cellular DNA yields an adduct that is the initial step in the induction of mutants and neoplastic cell transformation Benzo[a]pyrene is the most extensively studied and best understood carcinogenic PAH. It is believed that Benzo[a]pyrene is metabolized *in vitro* to the diol epoxide, Benzo[a]pyrene-7,8-dihydrodiol-9,10-epoxide which then can react with various nucleophilic centers on DNA. The major alkylation product appears to be the reaction of the Benzo[a]pyrene diol epoxide with the N^2 position of guanine sites on DNA. Methods that can measure exposure and biological response to carcinogens such as PAH's are needed Human Blood can be separated into plasma, lymphocytes, and red blood cells The plasma should contain native PAH's which may yield some useful information about recent exposure The red blood cells contain hemoglobin and adducts of PAH's. Hemoglobin has an average lifetime of 120 days so quantification of hemoglobin adducts should give an average of a persons exposure over four months Also, the electrophilic metabolites that react with hemoglobin to form adducts are the same metabolites that form DNA adducts which can lead to mutations and cancer Lymphocytes contain DNA and therefore DNA adducts DNA adducts can be repaired by a series of enzymes so quantification of these adducts will only yield information about recent or non-repairable adducts. DNA adduct formation is believed to be the first important step in chemical carcinogenesis so quantification of these adducts should yield some information on exposure and a great deal of important data on biological response and risk from specific PAH's

The levels of various PAH's in plasma can determined by isotope dilution high resolution mass spectrometry Two separate approaches are currently under development These are solid phase extraction of serum followed by high resolution GC/high resolution mass spectrometry and cloud point extraction with LC/MS analysis.

Hemoglobin has an average lifetime of 120 days The measurement of Hemoglobin-PAH adducts will therefore yield information of exposure over a four month period. Whole blood will be separated into plasma, lymphocytes, and red blood cells Hemoglobin will then be isolated from the red blood cells and the heme will be removed to yield globin. Acid hydrolysis will then release the adducts which can be partially purified by an organic extraction The final analysis and quantification will then be achieved by LC/MS or CE/MS The PAH-Hemoglobin adduct study started with the analysis of Benzo[a]pyrene adducts. The products released from hemoglobin for Benzo[a]pyrene are four different Benzo[a]pyrene tetrols Positive ion APCI yielded primarily an M^+ and negative ion yielded an $(M-H)^-$ We also have found from the analysis of the released heme that adduct formation on this portion of the protein can be

determined Treatment of hemoglobin with Benzo[a]pyrene followed by analysis with ESI MS showed that the initial adduct formation was actually on the heme (See Figure) Ions for the heme (m/z 617), Heme + dioxygen (m/z 649), heme + DMSO (m/z 695) and heme + B[a]P adduct (m/z 919) are all present. Treatment of hematin with Benzo[a]pyrene diol epoxide also produced these adducts

DNA adducts have a much shorter lifetime than Hemoglobin adducts due to the DNA repair mechanism, but are the most significant biological response for cancer risk The DNA adduct study would use DNA obtained from human lymphocytes isolated from blood The DNA would then be processed so that individual nucleotides with adducts could be isolated and analyzed by CE/ESI-MS.

The development of methods for the analysis of human exposure to PAH's in serum is important for the determination of health risk for the general population and exposed groups The extent of the risk to both low and high level exposures can only be determined by a correlation of health effects to measured body burden levels in humans. To aid in the understanding of human health effects due to PAH's, we are currently developing methods for the analysis of serum/plasma PAH's, PAH-Hemoglobin adducts, and PAH-DNA adducts.

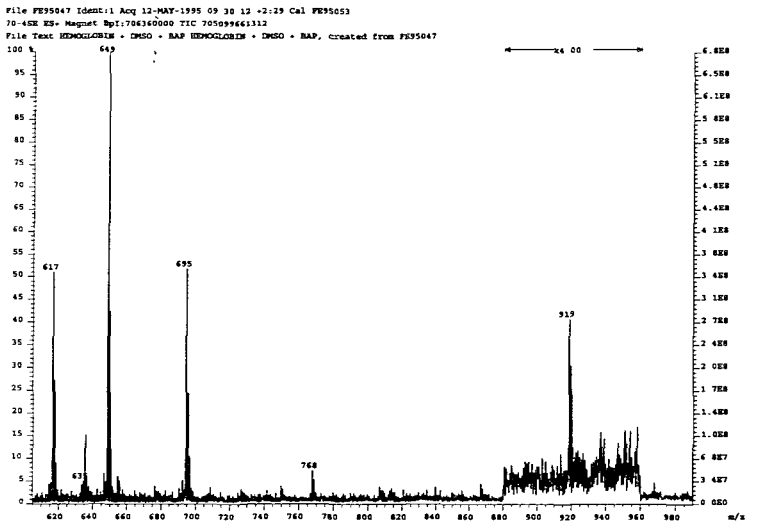

MS Analysis of Pesticides by Combined On-line Photolysis and LC–MS

Dietrich A. Volmer* and Jon G. Wilkes

Food and Drug Administration, National Center for Toxicological Research, 3900 NCTR Drive, Jefferson, AR 72079

1. Introduction. The LC–MS spectra of many pesticides consist in general only of $[M+H]^+$ ions or simple adducts. The lack of structurally significant fragments limits the specificity of analysis. The problem can be overcome by the application of collision-induced dissociation (CID) either in MS/MS systems or by using in-source octapole lenses and cone-voltage fragmentation in API systems in conjunction with APCI and ESI. However, MS/MS systems are not readily available and inducing fragmentation with other ionization techniques such as thermospray (TSP) is more complicated. Furthermore, the sensitivity with CID is often not sufficient for trace level monitoring of pesticides. In this study we have used a different approach to overcome these limitations. An on-line photolysis ESI LC–MS system has been utilized for the analysis of several pesticide compound classes, *e.g.* carbamates, phenylureas and triazines.

2. Experimental. ESI LC–MS work was done with an Ultracarb 5 ODS 30, 5 μm, 150 × 3.2 mm column at a flow of 0.6 ml/min. The mobile phase consisted of a methanol-water gradient (initial 20% methanol; in 45 min to 95% methanol). An additional postcolumn flow (0.4 % formic acid in methanol) of 0.2 ml/min was applied. The mass spectrometer, a Finnigan TSQ 7000 equipped with an ESI source, was operated in the positive ion mode. Collision-induced dissociation (CID) was accomplished with argon at a collision-offset voltage of 20V and an argon pressure of 1.3 mTorr. The photolysis experiments were carried out in 5, 10 and 15 m × 0 25 mm knitted-reactor coils at irradiation wavelengths of $\lambda = 254$ nm and 366 nm. A mobile phase consisting of methanol/water = 50:50 (v/v) was used. Acetone and benzophenone were added postcolumn as photosensitizers at a concentration level of 1 % and 1 mM, respectively.

3. Results. An on-line photolysis electrospray LC–MS system has been used for the analysis of several pesticides with respect to the sensitivity and specificity of their ESI–MS detection. Experimental parameters such as irradiation time, irradiation wavelength and solvent composition have been investigated. Furthermore, the effect of postcolumn addition of photosensitizers on the degree and mechanism of photochemical degradation of the analytes and on the sensitivity of their detection has been investigated.

Carbamates: All investigated N-methylcarbamates produced significant amounts of methylamine after photolysis. Addition of acetone and benzophenone as photosensitizers significantly enhanced photolysis; i.e. the isocyanate and methylamine formation was greatly enhanced. Photosensitized UV degradation led to a > 90 % transformation in these experiments.

Phenylureas: LC-MS Analysis of photolysis products of phenylureas indicated a large number of degradation products with an unsatisfactory high noise level in the mass spectra. The major degradation pathway was loss of halogen and subsequent replacement by a hydroxyl group or hydrogen. Furthermore, loss of amines and formation of isocyanates was observed. By using photosensitizers, the noise level was substantially reduced. In general, photosensitized photolysis led to significantly reduced noise levels in all experiments conducted.

s-Triazines: Photolysis of *s*-triazines in the presence of solvent led to a number of photodegradation products. The chlorinated *s*-triazines readily underwent replacement of the chloro group by a methoxy or hydroxyl group, while in alkylthiotriazines the alkylthio group is replaced by hydrogen. Moreover, reactions in the alkylamine sidechain enabled characterization of isomers, *e.g.*, the isomeric triazines propazine/terbutylazine and prometryn/terbutryn could be distinguished by their photolysis LC–MS spectra. Photosensitizers can enhance the yield of these reactions (Figure 1a). Since the ESI sensitivity was not reduced in the photolysis mode, the system could readily be used for a very sensitive confirmatory analysis of triazines in sample extracts (Figure 1b).

4. Conclusions. It is demonstrated in this study, that the on-line combination of photolysis and LC–MS can increase spectral information for most pesticides and thus the specificity of their LC–MS analysis without loosing sensitivity, as is often observed in CID experiments. This is important for an unambiguous identification of pesticides in environmental or food samples, since several additional fragment ions are required for proof of presence. Most LC–MS ionization techniques, however, provide only mass spectra with little structural information, *i.e.* only $[M+H]^+$ ions or simple adducts are formed. Moreover, the utilization of on-line photolysis and LC–MS, especially in combination with tandem mass spectrometry, offers distinct possibilities for structure elucidation of transformation products formed by photochemical reactions, as is demonstrated in this paper.

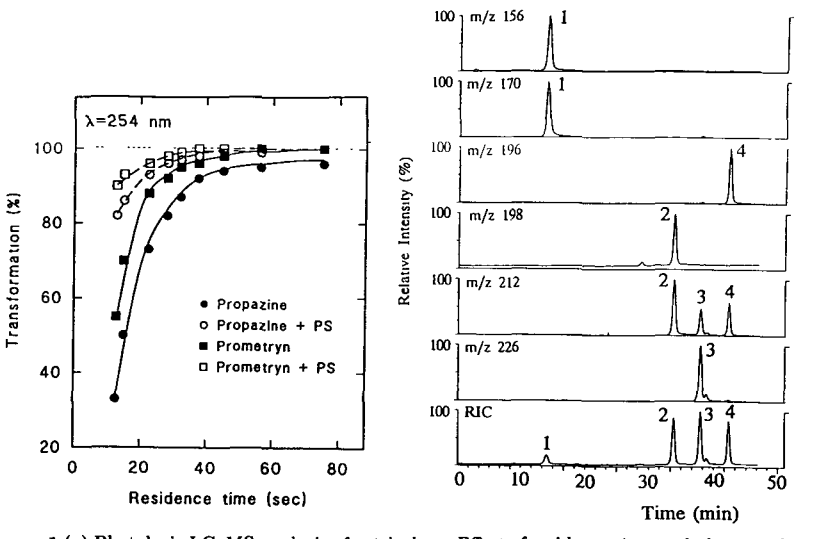

Figure 1 (a) Photolysis LC–MS analysis of *s*-triazines. Effect of residence time and photosensitizer (acetone) on phototransformation. (b) Photolysis ESI chromatogram of a spiked blueberry extract: **1** Atrazine–desisopropyl; **2** Atrazine; **3** Propazine; **4** Terbutryn. Injeccted amount, 5 ng each.

Multiresidue Analysis of Pesticides by Electrospray LC–MS and LC–MS/MS

Dietrich A. Volmer* and Jon G. Wilkes

Food and Drug Administration, National Center for Toxicological Research, 3900 NCTR Drive, Jefferson, AR 72079

1. Introduction. The very low concentration limits set for pesticides in food and water has prompted the development of analytical techniques to determine these compounds at trace levels. Analysis of pesticides is not only complicated by the low detection limits required, but also by the fact that the regulated pesticides belong to very different compound classes which vary widely in their polarity. More important standard methods are an HPLC method with UV detection and a GC method with confirmation by GC–MS. Confirmatory analyses, however, are even more important for HPLC methods since the selectivity of these methods is lower compared to GC. Confirmation by UV is difficult because the UV spectra are often very similar and many thermally labile pesticides lack a strong UV chromophore for UV detection. Furthermore, co-eluting compounds cannot be distinguished by means of conventional UV or diode-array detection. When two compounds co-elute, LC–MS allows the identification and quantification of both, provided each has different characteristic ions. LC–MS has demonstrated its potential for analyzing a broad spectrum of pesticides [1-4]. At present, thermospray is most widely used because of its compatibility with conventional HPLC systems. In this study electrospray ionization (ESI) and tandem mass spectrometry (MS/MS) were evaluated with respect to their suitability for the LC–MS determination of a broad range of pesticides.

2. Experimental. ESI LC–MS work was done with an Ultracarb 5 ODS 30, 5 μm, 150 × 3.2 mm column at a flow of 0.6 ml/min. The mobile phase consisted of a methanol-water gradient (initial 20% methanol; in 45 min to 95% methanol). An additional postcolumn flow (0.4 % formic acid in methanol) of 0.2 ml/min was applied. The mass spectrometer, a Finnigan TSQ 7000 equipped with an ESI source, was operated in the positive ion mode. Collision-induced dissociation (CID) was accomplished with argon at a collision-offset voltage of 20V and an argon pressure of 1.3 mTorr. Liquid/liquid extraction was used for the preparation of food sample extracts.

3. Results. Electrospray ionization was evaluated in the LC–MS determination of a large number of pesticides having a wide range of chemical structures and polarities. The multiresidue method employs HPLC separation on a narrow-bore reversed-phase column with postcolumn addition of a reagent solution. An examples of an LC–MS separation of several triazines in the time-scheduled selected-ion monitoring (SIM) mode is shown in Figure 1a.

The multiresidue method is linear over at least 3 orders of magnitude with correlation coefficients $r > 0.998$. That is, quantitation is readily possible by using external standards. The precision is excellent, usually $< 5\%$ RSD, and the detection limits (LOD) are in the lower pg-range, typically 1–10 pg (time-scheduled SIM) thus enabling ultratrace analysis in environmental or food samples. Figure 1b shows the analysis of a lettuce extract.

Tandem mass spectrometry techniques such as constant-neutral-loss (CNL) scan and time-scheduled reaction monitoring (SRM) were applied to certain pesticide compound classes. The SRM detection limits obtained are in the range of 50–1000 pg.

4. Conclusions. The purpose of the present work was to evaluate a multiresidue electrospray LC–MS method used for determination and confirmation of a large number of pesticides with widely different chemical structures and polarities. The precision, linearities and detection limits obtained are adequate for monitoring a broad spectrum of pesticides by using reversed-phase gradient LC in combination with time-scheduled selected-ion-monitoring (SIM) or selected-reaction monitoring (SRM). For an unambiguous identification of pesticides in environmental or food samples, several additional fragment ions are needed, required for proof of presence. Because ESI is a soft ionization technique, mass spectra of almost all investigated pesticides usually consist of only $[M+H]^+$ and $[M+Na]^+$ ions. The selectivity of the method can, however, readily be enhanced by inducing fragmentation *via* the application of a collision-offset voltage to the built-in octopole rods of the source or by using MS/MS as demonstrated in this paper.

References.

(1) Volmer, D.; Levsen, K.; *J. Am. Soc. Mass Spectrom.* **1994**, 5, 655
(2) Volmer, D.; Levsen, K.; Wünsch, G.; *J. Chromatogr.* **1994**, A660, 231
(3) Volmer, D.; Levsen, K.; *Vom Wasser* **1994**, 82, 335
(4) Sennert, S.; Volmer, D.; Levsen, K.; *Fresenius J. Anal. Chem.* **1995**, 351, 642

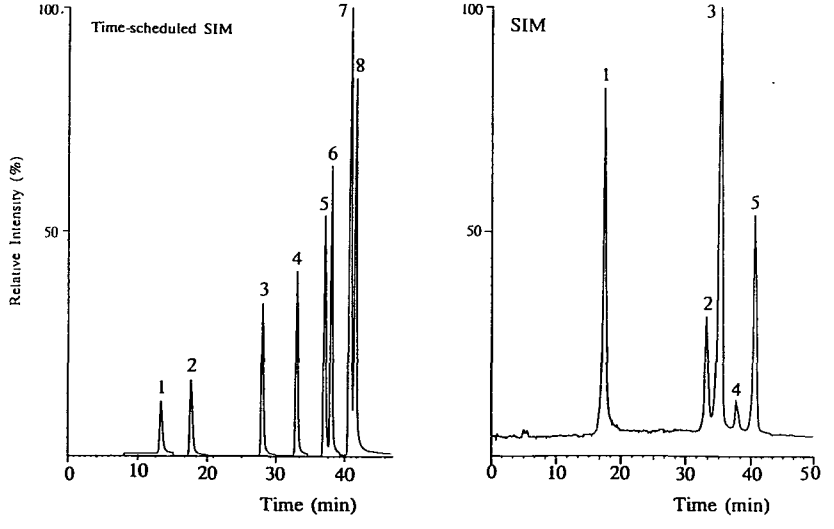

Figure 1 (a) ESI LC–MS analysis of triazines. Time-scheduled SIM chromatogram; injected amount, 1 ng each: **1** Atrazine-desisopropyl; **2** Metamitron; **3** Simazine; **4** Atrazine; **5** Propazine; **6** Terbutylazine; **7** Prometryn; **8** Terbutryn. (b) ESI SIM chromatogram of a spiked lettuce extract: **1** Fenuron; **2** Metobromuron; **3** Difenoxuron; **4** Linuron; **5** Chloroxuron.

DETERMINATION OF CARBENDAZIM BY IMMUNOAFFINITY EXTRACTION AND LC/LC/MS/MS

Karen Bean and Jack Henion, Analytical Toxicology,
Diagnostic Laboratory, Cornell University, 927 Warren Drive,
Ithaca, NY 14850

Benomyl has been widely used as a systemic fungicide for disease control in crops for many years. Its mode of action and movement in the environment, however, are not clearly understood[1]. The primary reason for this is because benomyl readily decomposes in many common organic solvents[2] and also in water[3]. For this reason, benomyl is commonly determined as its primary degradation product, carbendazim The title method employs a high performance protein G immunoaffinity column coupled to a reversed-phase analytical column through the use of a trapping column and INTEGRAL™ Micro-Analytical Workstation. Carbendazim is enriched from soil extracts at the 100 ppb level and from lake water at the 25 pptr level and characterized by on-line mass spectrometric analysis

EXPERIMENTAL

Immunoaffinity extraction and coupled column chromatography were achieved using a PerSeptive Biosystems INTEGRAL™ Micro-Analytical Workstation equipped with an autosampler, two reciprocating HPLC pumps, and two automated switching valves The extraction itself was accomplished on a 2 1 mm i d. x 33 mm ChromatoChem Hi Pac Protein G column through which phosphate buffered saline (0 15 M NaCl, 0.01 M NaH_2PO_4) was pumped at 2.0 mL/min by pump 1 A 3 mm i d x 10 mm Regis Technologies SPS C_{18} guard column was used as the analyte trapping column when the 2% (v/v) acetic acid stripping buffer was pumped through the protein G column. Pump 2 delivered 40/60 MeCN/H_2O, 10 mM NH_4OAc at a flow rate of 200 µL/min through a Keystone Scientific Betasil C_{18} 2 mm i d x 150 mm column The effluent from the column was directly transferred to the ion spray interface which was maintained at 3 95 kV without post-column split The mass spectrometer, a PE-Sciex API-300, was operated in the positive ion detection mode Collision-induced dissociation (CID) reactions were accomplished with nitrogen and the collision energy was 23 eV in the laboratory frame Soil samples were extracted according to the procedure of Itak et al.[4] and 100 mL of the extract were pumped through the protein G column at 10 mL/min. Lake water samples were filtered prior to extraction.

RESULTS AND DISCUSSION

The specificity of immunoaffinity extraction makes it possible to detect low levels of carbendazim in soil samples without interference from matrix components The extracted ion current profile resulting from the SRM IAE/LC/LC/MS/MS analysis of soil fortified at 100 ppb with carbendazim is found in Figure 1 At sub-ppb levels, however, it is found that recovery of carbendazim from soil becomes more difficult This is most likely due to adsorptive losses of analyte on the soil The use of selected reaction monitoring allows for the achievement of the highest possible sensitivity with a minimum of chemical interference.

Figure 2 demonstrates that it is possible to detect trace levels of carbendazim in lake water samples This is probably due to fewer matrix interferences in water than in soil Very little sample preparation is required for environmental water samples The lake water samples analyzed for this work required only filtration prior to analysis to

remove particulate matter which could cause damage to the HPLC pumps and to the columns used for extraction and chromatography. The ability to pump sample through the protein G column at high flow rates (10 mL/min) and to automate the column-switching procedure makes the method rapid and efficient. Many samples can be analyzed in a relatively short period of time with minimum sample preparation Three samples can be analyzed per hour without operator intervention

ACKNOWLEDGEMENTS

We wish to thank PerSeptive Biosystems for the generous loan of the INTEGRAL™ Micro-Analytical workstation. Our gratitude also extends to PE-Sciex for the loan of the API-300 mass spectrometer We also thank Dr Richard Hammond of Chromatochem for providing the Protein G immunoaffinity column and Dr Robin Charlton of E I DuPont de Nemours for the use of the anti-carbendazim IgG Funding for this work is made possible by E I DuPont de Nemours.

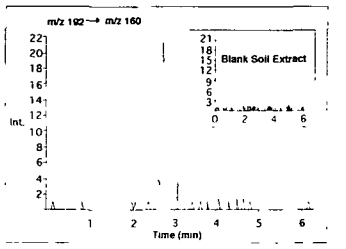

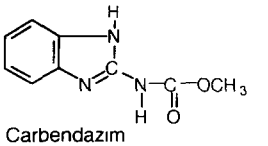

Carbendazim
MW = 191

Figure 1: Result of SRM IAE/LC/LC/MS/MS analysis of soil fortified at 100 ppb with carbendazim Blank soil extract is shown in the inset

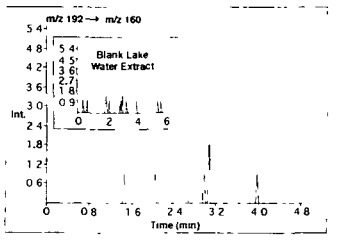

Figure 2: Result of SRM IAE/LC/LC/MS/MS analysis of lake water fortified at 25 pptr with carbendazim Blank lake water extract is shown in the inset

REFERENCES

1 Singh, R P. et al *J. Agric Food Chem* 38 (1990) 1759
2 Chiba, M *J Agric Food Chem.* 25 (1977) 368
3. Clemons, G.P , Sisler, H.D. *Phytopathology* 59 (1969) 705
4 Itak et al in *J. Agric Food Chem* 41 (1993) 2329

Limitations and Challenges in the Determination of Carbofuran with Various LC/MS Interfacing Systems

Maarten Honing* and Damià Barceló, Ben L.M. van Baar[1], and Udo A.Th. Brinkman[2], Department of Environmental Chemistry, CID CSIC, Jordi Girona 18-26, 08034 Barcelona, Spain and Departments of Organic[1] and Analytical[2] Chemistry, Free University, De Boelelaan 1083, 1081 HV Amsterdam, The Netherlands

Most reports on LC-MS of carbamates deal with the use of thermospray (TSP) as the interfacing system. Problems with this type of interface may arise from the gas phase ion-molecule reactions between analyte molecules and ammonium ions. The abundances of the ions formed from these reactions appear to be dependent upon the ion source geometry in TSP-MS [1]. This especially holds true for the carbamate carbofuran. LC-TSP mass spectra of carbofuran reported in the literature, show large differences in the relatives intensities of the $[M+H]^+$ and $[M+NH_4]^+$ ions. It has earlier been proposed that the adduct ion formation observed is due to pH differences of the solvent stream [2]. For verification we analyzed 30 carbamates at pH values from 7 to 3 of the methanol-water (50:50) with 100 mM ammonium acetate as solvent stream. Table 1 shows the summarized results for carbofuran and dioxacarb and represents the our findings for carbamates in general: pH variation does not result in significant differences in relative abundances of protonated and ammoniated molecules.

Table 1 Relative abundances of $[M+H]^+$ and $[M+NH_4]^+$ ions of two carbamates at pH 3 and 7.

Compound	m/z	pH 3	pH 7
Carbofuran			
$[M+H]^+$	222	79	69
$[M+NH_4]^+$	239	100	100
Dioxacarb			
$[M+H]^+$	224	21	16
$[M+NH_4]^+$	241	100	100

An alternative explanation for the variance among literature reports lies in the variable effectiveness of the protonation or adduct ion formation in TSP-MS, which depends on the partial pressure of ammonia in the ion source and, therefore, on the ammonium salt concentration in the eluent. This was demonstrated by varying the eluent ammonium acetate concentration in the methanol-water (50:50) LC eluent(figure 1). Varying the concentration between 100 (A), 25 (B) and 1(C) mM results in a strong change of the $[M+H]^+$ ion (m/z 222) to $[M+NH_4]^+$ (m/z 239) abundance ratio. These results are in agreement with literature reports, where the $[M+NH_4]^+$ ion intensity was much lower at 8 mM than at 50 or 80 mM. A pressure dependence of the relative intensities of the $[M+H]^+$, and the, $[M+NH_4]^+$, ions of carbofuran was also observed in ammonia CI experiments (with a PB-MS system or desorption CI)[3]. An increase of the ion

source pressure resulted in a decrease of the total ion current and a strong increase of the relative abundance of the ammonium adduct ion. Ionisation in the API techniques takes place at atmospheric pressure. Thus no pressure dependence of the ion formation of carbofuran is expected. With regard to precision of the data, identification capability and sensitivity, the API techniques (APCI and ISP) have shown promising results [4, 5]. For some selected carbamates, and organophosphorus pesticides, combination of the LC/ISP-MS with novel preconcentration techniques results in detection limits between 10 and 50 pg [6, 7].

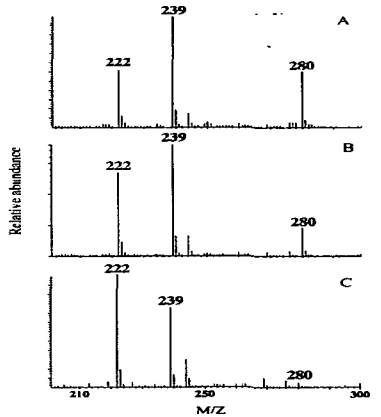

Figure 1 The full-scan (m/z 200-350) thermospray mass spectra (filament-assisted buffer ionization) of carbofuran, using a methanol-water (50:50) effluent with (A) 100, 2(B) 5 and (C) 1 mM ammonium acetate, 10 µl of a 50 mg/l standard solution in methanol-water (50:50) were injected.

References

[1] D. Volmer, K. Levsen, M. Honing, D Barceló, J Abían, E. Gelpí, B.L.M. van Baar and U.A.Th. Brinkman, *J. Am. Soc Mass Spectrom.*, in press

[2] S. Chiron, S. Dupas, P Scribe and D. Barceló, *J. Chromatogr.*, 665 (1994) 295

[3] M. Honing, D Barceló, M.E. Jager, J. Slobodnik, B.L M. van Baar and U.A.Th Brinkman, *J Chromatogr.*, In press

[4] S Pleasance, J.F. Anacleto, M.R. Bailey and D.H. North, *J Am. Soc. Mass Spectrom.*, 3 (1992) 378

[5] J.A. Schoemaker, T D. Behymer, J.W. Eichelberger and W L. Budde, *42nd ASMS Conference on Mass Spectrometry and Allied Topics*, Chicago, IL, 1994 p. 257

[6] M. Honing, J. Riu, D Barceló, B L M. van Baar and U A.Th. Brinkman, *J Chromatogr.*, Submitted

[7] C. Molina, M. Honing and D. Barceló, *Anal. Chem.*, 66 (1994) 4444.

The Analysis of Organophosphate Pesticides by a Trochoidal Electron Monochromator/Mass Spectrometer System

Paul H. Mazurkiewicz, James A. Laramee and Max L. Deinzer
Department of Agricultural Chemistry
and Environmental Health Sciences
Oregon State University
Corvallis Oregon

Organophosphate pesticides are in widespread use throughout the world making their low-level determination in environmental matrices and degradation mechanisms of utmost importance. Standard Electron Capture Negative Ion Mass Spectrometry (ECNIMS) is well suited for this task, but understanding of the electron capture processes is difficult because a buffer gas is present. The Electron Monochromator/Mass Spectrometer system (EM/MS) eliminates the need for a buffer gas, simplifies the number of electron-molecule and ion-molecule reactions present within the ion source and allows the experimentalist to tune to a specific electron energy allowing a more quantitative analysis than is possible with traditional ECNIMS[1]. EM/MS measurements of Negative Ion Resonances (NIRs) provide a new understanding of negative ion formation and have applications in biological, environmental and theoretical sciences.

Mechanisms of electron capture were probed by examining a series of novel parathion derivatives which possessed different electrophilicities. Pesticide samples were acquired from AccuStandard, tested for purity, and were found to be >99% pure. Derivatives of parathion were prepared using a classical coupling procedure[2].

Since parathion derivatives only differ in their *para* substitution, therefore they lend themselves to analysis using the Hammett equation which relates *para* substituents of aromatic compounds with the empirical Hammett substituent constant[3]. The constant represents all substituent electronic effects including resonance, through-space and inductive effects.

A linear correlation between electron energy and the Hammett constant implies a similar mechanism in the process under consideration. In the case of the parathion derivatives, all but one substitution correlates (Figure 1). A Hammett correlation was also discovered for the formation of fragment ion m/z 169. The di-ethoxythiophosphate anion is formed by cleavage of the phenolic oxygen carbon bond (Figure 2). Several of the derivatives correlate showing that the di-ethoxythiophosphate anion is formed in a similar mechanism for compounds that contain halogens and the unsubstituted derivative. Derivatives containing highly electron withdrawing or electron releasing substituents do not correlate. This fragment is important as it is the most intense spectral feature in most of the ion yield curves and appears in every derivative and compound similar to parathion. This fragment is not very intense in gas-mediated ECNIMS suggesting that the buffer gas interferes with its formation and lifetime.

Phosphothioate pesticides can capture a low-energy electron into a pi orbital to produce a radical anion which can rearrange to a spiro intermediate and can then fragment via pathway ***A*** to give the thiophenolate ion or pathway ***B*** to produce the phenolate ion (Figure 3). Since rearrangement mechanisms involve bond formation along with bond cleavage, the thiophenolate ion should have a lower activation energy than the phenolate ion. Indeed the NIRs for rearrangement ions occur at lower energies than for simple cleavage ions.

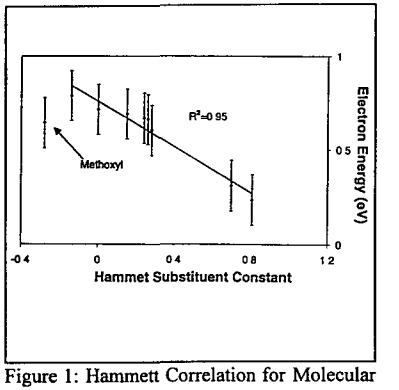

Figure 1: Hammett Correlation for Molecular Ions of Parathion Derivatives.

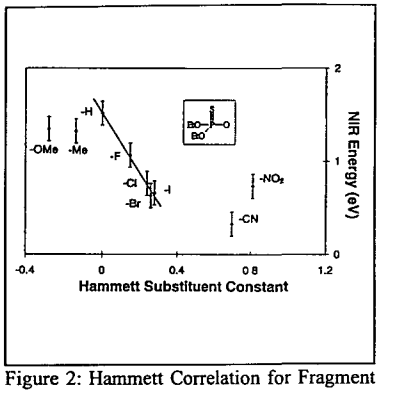

Figure 2: Hammett Correlation for Fragment Ion M/Z 169 of Parathion Derivatives.

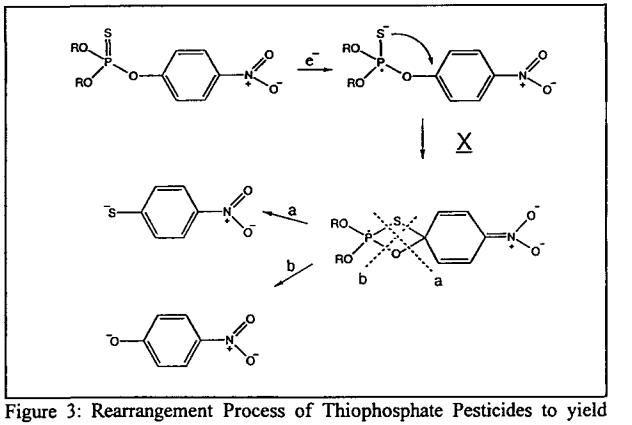

Figure 3: Rearrangement Process of Thiophosphate Pesticides to yield Thiophenoxide and Phenoxide Fragments.

1) Laramee J.A. Kocher, C.A. Deinzer, M.L. **Application of a Trochoidal Electron Monochromator/Mass Spectrometer System to the Study of Environmental Compounds.** *Anal. Chem* 1992 *64* pp. 2316-2322
2) Thurston, **FIAT Final Report No. 949**, October 14, 1946 (PB-60890)
3) Johnson, C.D. **The Hammett Equation** Cambridge University Press, 1973

Analysis of Soil Metabolites Utilizing Narrow Bore LC/MS/MS Techniques

Steven R. McGown, Nelson Delgado
BASF Corporation
26 Davis Drive
Research Triangle Park, NC 27709

The trend for decreasing application rates of modern crop protection agents poses continuous new challenges for residue analysis. The agrochemical industry performs a wide variety of residue analyses, studies and tests so that the safety of agrochemicals to the consumer and the environment can be ensured. Metabolite analysis of crop protection agents in complex matrices, such as soil, poses difficulties for traditional analytical methods using HPLC/UV detection. The traditional methods can sometimes be long and tedious, requiring several days for sample preparation and analysis for more than one component. The use of API LC/MS/MS techniques on appropriate analytes can substantially reduce the analysis time per sample, increase LOD's, and raise confidence in data due to the added specificity of the mass spectrometer. The overall effect can also be a substantial cost savings for the analysis in terms of manpower and time. Here, we present an extraction and analysis scheme comparing two analytical approaches; the traditional HPLC/UV method and the API LC/MS/MS method.

The mass spectrometer used in these experiments was a PE/SCIEX API III Plus system manufactured in Thornhill, Canada. All HPLC analyses were performed using a Varian Star 9010 HPLC pump(Varian, Walnut Creek, CA), or a Thermoseparations P-4000 pump, and a Thermoseparations AS3000 autosampler, (Thermosepartions, Riviera, FL). Separations were performed on one of two types of narrow bore columns, either a 1 mm x 50 mm BDS-Hypersil C18, 5 µm or a 1 mm x 50 mm Prism, 3 µm, both supplied from Keystone Scientific, INC (Bellefonte, PA). The mobile phase was made using B & J HPLC grade methanol and water each containing 1% formic acid (Aldrich Chemical Co., INC), and 4 mM ammonium formate (Fluka Biochemika, Ronkonkoma, New York).

The mass spectrometer was operated in the MRM mode and was optimized by infusing a mixture of the 3 target molecules (Fig 1). Analytical standards were prepared in the mobile phase and extracts were prepared according to the extraction scheme shown. An isocratic system was used with a flow rate of 50 µl/min of the mobile phase. Injection volumes were normally 1µl.

Utilizing this type of approach to residue analysis has significant benefits when compared to traditional approaches. The LC/MS/MS method is capable of high through put (three analytes in under 5 minutes), has better limits of detection (LOD) than UV (<10 ppb vs 100ppb), and increased specificity. Normally an improvement in any one of these areas would be considered significant, but the combination makes this technique extremely powerful.

A traditional HPLC/UV method for each component was initially attempted since this type of equipment is generally more accessible to enforcement and contract laboratories. It should be noted that in the soil extract the 10 ppb fortification was totally masked by background interference. The extraction workup required about 16 man hours to complete and then each analyte had to be analyzed separately under two different chromatographic systems, approximately 20-30 min. each to satisfy federal regulations. The system worked well at the 100 ppb level but failed at the required 10 ppb lower limit.

Rather than spend additional effort on clean-up, a mass spectral solution was sought.Utilizing the power of MS/MS, appropriate parent/product ion transitions were chosen for each analyte. Analytical standards were prepared in the needed concentration range and analyzed. The three analytes are clearly separated in under 5 minutes with signal to noise ratios>25 :1 (Fig 2).Then control soils were extracted and analyzed to verify that there were no co-eluting components with similar transitions. These control soils were then spiked with known amounts of the analytes, extracted, and then analyzed (Fig 3). The end result was a short extraction/workup, about 4 manhours and a short HPLC run on a C18 BDS Hypersil narrow bore column, 1 mm x 50 mm, utilizing an isocratic mobile phase (80:20 MeOH/water, 4mM NH4CO2H, 1% Formic Acid). The recoveries were lower than expected for P-14 and this was probably due to suppression, since P-14 eluted in the void volume on the C 18 column After consulting with Keystone Scientific representatives, a 1 mm x 50 mm Prism RP column was tried and a more desirable separation was achieved (Fig 4). The mobile phase was altered to 90:10 (v/v) MeOH/water, 4mM NH4CO2H, 1% Formic Acid. There was a notable improvement in signal to noise ratio for all components, the suppression problem alleviated, a change in elution order, and some band broadening of the last component, PB-14.

The performance of the HPLC MS/MS methodology is far superior to that of the more traditional HPLC/UV methodology. Recent regulations require mass spectral confirmation of UV data making the analysis using traditional methods impractical. This method of analysis is more than fifty times faster than the traditional approach resulting in considerable savings in time and manpower. Data generated from the MS/MS approach has a higher confidence level due to the nature of the data. In addition to the retention times, there is the specificity of an MS/MS transition which gives the data an orthogonal dimension. In conclusion, the MS/MS approach has demonstrated its value in residue analysis.

Figure 1

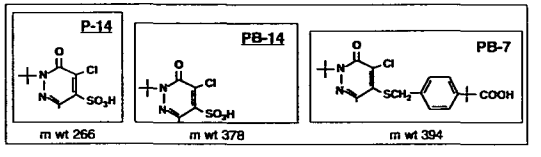

Figure 2

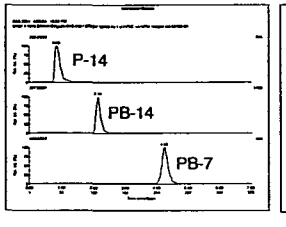

Figure 3

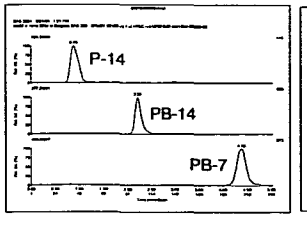

Figure 4

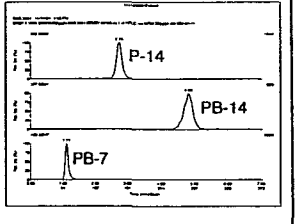

Acknowledgments

The Authors would like to acknowlege the previous work by Hiroshito Yoshida, NISSAN Chemical Industries, Ltd., on the HPLC/UV method. Additionally, we would like to thank Keystone Scientific for the loan of the 1 mm x 50 mm Prism RP column utilized in the final portion of the LC/MS/MS work.

LC/MS of Atrazine and its Hydroxylated Metaboilite by Using Electrospray

*Zongwei Cai[1], Ronald L. Cerny[1], and Roy F. Spalding[2], (1) Nebraska Center for Mass Spectrometry, (2) Water Center, University of Nebraska-Lincoln, Lincoln, NE 68588.

Atrazine (ATR) is one of the most widely used agricultural herbicides in the United States and has been identified along with its metabolites as contaminants in surface and ground water. Field-applied atrazine is known to undergo abiotic hydrolysis reactions leading to dechlorination and formation of hydroxyatrazine (HA). Methods currently used for the analysis of ATR and HA in water include HPLC (*1*) and fast atom bombardment mass spectrometry (*2*).

Liquid chromatography/mass spectrometry with electrospray ionization (LC/ESI-MS) has been employed for the quantification of small molecular species (*3*). However, LC/MS capability for atrazine and its metabolites as well as the quantitative aspects of the technique have not been investigated. The goal of this study is to develop a method using ESI-MS coupled with HPLC for the quantitative analysis of atrazine and its metabolites.

The electrospray mass spectra of ATR and HA are shown in Figures 1-2. In addition to the protonated molecular ions sodiated molecular and dimer ions were also observed at the mass spectrometric condition. Selected ion recording chromatograms for ATR and HA and their ^{13}C-labeled internal standards are demonstrated in Figure 3. The analytical method provides for a high throughput of samples as less than 6 min is needed per sample analysis.

A linear dynamic range over two orders of magnitude was obtained. The concentration of the calibration standards used ranged from 5 to 500 pg/uL and 25 to 1000 pg/uL for ATR and HA, respectively. The detection limits (S/N = 3) are 10 pg and 50 pg for ATR and HA, respectively, with the sample injection volume of 5 uL. Lower detection limits may be achieved if a larger volumes is injected. Injections of more than 30 uL, however, resulted in tailing of the HPLC peaks.

The quantification is based on the use of isotopically labeled internal standards, which increases accuracy and reliability of the analysis. Relative response factor for each of the native compounds relative to its corresponding internal standard was used to minimize the analytical error. Table 1 shows the analytical results for the surface water samples collected from York River, Nebraska after runoff events by using both electrospray LC/MS and FAB/MS methods. The results from both methods agree with less than 15% variation. The data profile shows that the levels of HA are approximately 5 times lower than those of ATR.

The method using solid-phase extraction with the carbon black cartridge and LC/ESI-MS is satisfactory for the trace analysis of atrazine and hydroxyatrazine in water. Quantification by using corresponding $^{13}C_3$-labeled compounds as internal standards was accurate and precise at ppt to ppb level. The method was successfully used to analyze ground and surface water samples for atrazine and its hydroxylated metabolite. The procedure can be expanded to other metabolites as well as to other related herbicides present in the environment.

References:

1. Lerch, R.N.; Donald; W.W.; *J. Agric. Food Chem.*, **1994**, *42*, 923.
2. Cai, Z.; Ramanujam, V.M.S.; Gross, M.L.; Monson, S.J.; Cassada, D.A.; Spalding, R.F. *Anal. Chem.*, **1994**, *66*, 4202.
3. Kim H.Y.; Wamg, T.L.; Ma, Y.C. *Anal. Chem.*, **1994**, *66*, 4202.

Figure1: ESI Mass Spectrum of ATR.

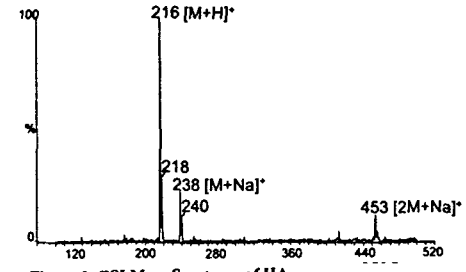

Figure 2: ESI Mass Spectrum of HA.

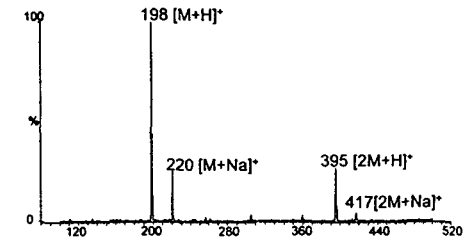

Figure 3: Selected Ion Chromatograms.

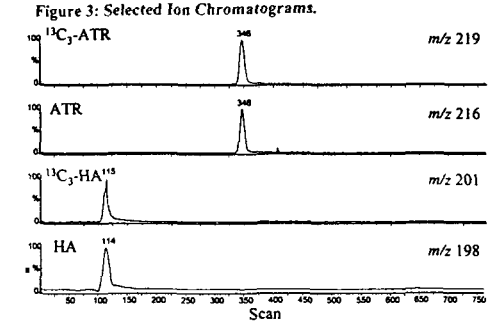

Table 1. Levels (ppb) of ATR and HA in Surface Water Collected From York River, Nebraska.

	LC/ESI-MS		FAB-MS		Dev.,%	
Sample ID	ATR	HA	ATR	HA	ATR	HA
94-2667	13.2	3.0	12.7	2.8	3.9	6 9
94-2671	12.7	2.5	11.5	2.6	9 8	4.0
94-2674	12.6	2.3	11.0	2.4	13	4.3
94-2679	10.9	2.3	12.5	2.6	-14	-12

DETERMINATION OF TRIAZINE HERBICIDES AND THEIR METABOLITES USING GC/MS/MS

DAVID L. HEIKES, Total Diet Research Center, Food and Drug Administration, P.O. Box 15905, Shawnee Mission, KS, 66285-5905

Triazine herbicides are some of the most widely applied pesticides in the U.S. The most common member of this class, atrazine, was the most heavily used pesticide in recent years. Many cleanup procedures with GC detection have been developed for the determination of these compounds in agricultural products. Several nitrogen-specific detectors have been utilized. However, a stringent cleanup procedure is required since nitrogen-containing compounds are ubiquitous in plant material.

The important practical benefits of ion trap MS/MS are it's inherent selectivity, sensitivity, and ease of routine operation. This unique and sensitive technique provides an approach to residue analysis which holds the very real potential to dramatically reduce labor-intensive cleanup and isolation steps while enhancing specificity.

Supercritical fluid extraction techniques have been employed to rapidly obtain an extract suitable for GC/MS/MS analyses. Although the parent triazine herbicides are relatively easily extracted using SFE, the more polar metabolites require more stringent conditions. Figure 1 depicts the extraction profiles of atrazine, desethylatrazine, desisopropylatrazine, and desethyl-desisopropylatrazine SFE-CO_2 at various pressures, 80° C, and a static-dynamic approach.

A Varian Saturn III has been upgraded to MS/MS capabilities. Unit mass isolation coupled with collision induced dissociation produced unique daughter ion spectra for each of eight triazine herbicides and three metabolites. After development of GC and MS/MS parameters (Figure 2) on a standard mixture, fortified samples were examined. Recoveries ranged from 89 to 103% at levels as low as 20 ppb on extracts of celery, pineapple, and wheat.

43rd ASMS Conference on Mass Spectrometry and Allied Topics

SFE EXTRACTION PROFILES

Atrazine and Metabolites

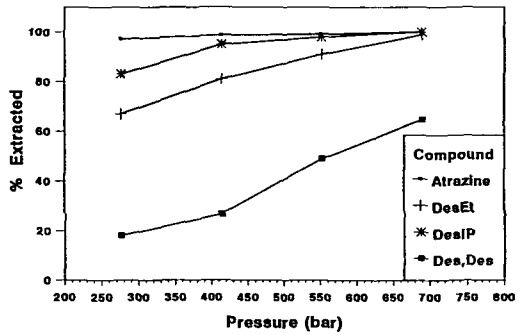

ATRAZINE MS/MS

Product Ion Formation vs. Excitation RF for 200 m/z

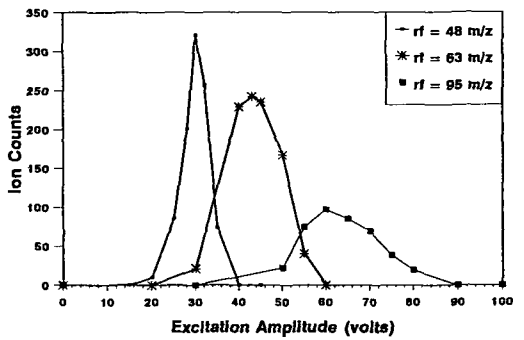

IDENTIFICATION OF BIODEGRADATION PRODUCTS OF CARBAZOLE BY MASS SPECTROMETRY

Jayasimhulu, K., Schneider, J., Xue, W., Grosser, R. and Warshawsky, D.
University of Cincinnati, Department of Environmental Health, Cincinnati, OH

ABSTRACT

Microbial degradation of harmful compounds opens the way for biodegradation of contaminated soils. A *Xanthomonas* sp. from former coal gasification site was isolated and its ability to mineralize carbazole was studied. The microorganism was incubated with carbazole for approximately two weeks. The resulting metabolites of carbazole were extracted from the media with ethyl acetate under acidic conditions. The pooled extract was concentrated and aliquots were injected on to a HPLC column for separation and collection of the fractions containing UV absorbing metabolites. The fractions were evaporated to dryness, methylated with diazomethane and analyzed by gas chromatography and mass spectrometry (GC/MS). The pooled total extract, after dryness, was also methylated and analyzed by GC/MS without prior separation by HPLC. A portion of the metabolite extract was also acetylated and methylated and analyzed by GC/MS. Elemental compositions obtained by high resolution mass spectral analysis and mass spectral fragmentation patterns made it possible for the identification of major metabolites detected in this study.

INTRODUCTION

Sites of former coal gasification plants constitute major health and environmental concerns in the U.S. These areas contain high levels of polycyclic aromatic hydrocarbons (PAH) and N-heterocyclic aromatic compounds (NHA) many of which are carcinogenic and/or mutagenic. Our overall aim is to isolate organisms which are capable of degrading these compounds, to elucidate degradative pathways and enhance the biodegradation rates. Towards that objective, we have isolated an organism, *Xanthomonas* sp. from a former coal gasification site which is capable of mineralizing ^{14}C-carbazole to $^{14}CO_2$. In this study we present data showing the metabolites of carbazole formed by this *Xanthomonas* sp.

MATERIALS AND METHODS

The bacterium was isolated from soil and growth and maintenance procedures have been published previously. Bacterial cells were maintained in minimal basal salts medium (MBS) with 37.5 $\mu g\ ml^{-1}$ of carbazole as the sole source of carbon. In order to obtain sufficient quantities of metabolites for mass spectral analyses, the bacterium *Xanthomonas* sp. was incubated in 1 liter of MBS with 900-1000 μg of carbazole. After two weeks of growth, the cultures were centrifuged to remove bacterial cells and the media was extracted twice with ethyl acetate (1:0.5, vol/vol) under acidic conditions. The ethyl acetate layers were pooled and evaporated to dryness. A portion of the isolated metabolites were derivatized with gaseous diazomethane to convert the carboxyl groups present to methylesters. Another portion was methylated and acetylated to methylate the carboxyl groups and acetylate the hydroxyl groups and amino groups. These derivatives were analyzed by gas chromatography and high resolution mass spectrometry. The samples were introduced onto a DB-5, 0.53 i.d., 30 m, 1 μm film thickness, capillary column of a Carbo Erba gas chromatograph interfaced with a Kratos MS-80 high performance mass spectrometer. The initial temperature of the oven is kept at 40°C and then is raised to 160°C after the introduction of the sample and is kept at that temperature for 3 minutes. The temperature was then raised to 280°C at a rate of 4°/min and kept at that final temperature for 20 min. The mass spectrometer was operated in the high resolution mode and the electron voltage, beam

current and the source temperature were maintained at 70 eV, 100 μA and 200°C respectively. The scan rate was 3 sec/decade and the data acquisition and processing was accomplished by DS-55 data system based on a Data General NOVA-4X computer.

RESULTS

The GC chromatograph indicates the presence of at least 16 peaks. GC-MS identified and confirmed 11 of these as metabolites of carbazole formed by *Xanthomonas* sp. The elemental compositions of the molecular ion ($M^{+\cdot}$) and fragment ions for these metabolites are consistent with the metabolites identified. Three of the peaks on GC (peaks 1,3,6) remain unidentified and are not products of biodegradation of carbazole by the bacterium. The identified metabolites include anthranilic acid, 2-aminophenyl acetic acid, 3-(2-aminophenyl)propionic acid, 4-(2-aminophenyl)butanoic acid, (1H)-4-quinolinone, 3-methylene-2-indole-carboxylic acid, 5-oxo-5-(2-aminophenyl)pentanoic acid, 6-oxo-6-(2-aminophenyl)hexanoic acid, indole-2,3-dicarboxylic acid and indole-2-carboxylic-3-acetic acid. The metabolite identified as anthranilic acid has been identified as a biodegradation product of carbazole by another bacterium, *Pseudomonas* sp. High resolution MS data of this metabolite formed by *Xanthomonas* sp. matches that of the standard anthranilic acid after methylation. Similarly, the MS data of the *Xanthomonas* sp. metabolite identified as indole-2-carboxylic acid matches that of the authentic standard after methylation. The carbazole metabolites of *Xanthomonas* sp. were also acetylated and methylated and these derivatives were analyzed by GC/MS. The data (not shown) further corroborated the assignments made for the methylated metabolites formed by *Xanthomonas* sp.

SUMMARY

GC-MS analyses identified at least eleven metabolites of carbazole formed by *Xanthomonas* sp. The formation of these metabolites by the bacterium is similar to other reports for another closely related bacterium, *Pseudomonas* sp. In particular, the formation of anthranilic acid was reported for this other bacterium. The formation of these carbazole metabolites by *Xanthomonas* sp. indicates that this species biodegrades carbazole and may be capable of degrading larger ring compounds.

ANALYSIS OF CARBAMATE AND PHENYLUREA PESTICIDES BY PARTICLE BEAM LC/MS

Ramesh Rao, VG Organic, Crewe Road, Wythenshawe,
Manchester, M23 9BE

Introduction

Carbamate and Phenylurea pesticides were introduced worldwide in the 1950's for use on a wide range of crops including potatoes, cotton and cereals.
In the following examples, HPLC is used combined with a dedicated benchtop Particle Beam Mass Spectrometer as the detector to obtain positive identification and structural information. The reproducibility and typical sensitivity is also shown along with an investigation of the linearity of response.

Methods

All analyses were carried out using the MD800 LCD (Liquid Chromatography Detector), a dedicated Particle Beam-LC-MS instrument. The MD800 LCD was operated in Electron Impact mode (EI+) scanning at 300amu/sec. The source temperature was set at 200°C and the desolvation temperature at 80°C.

Results

Reproducibility

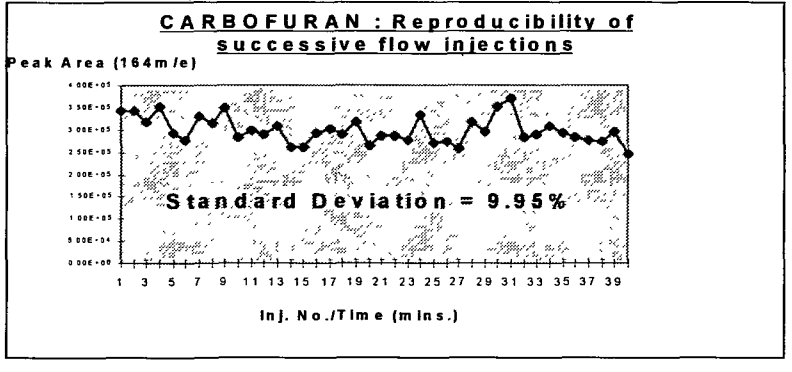

Sensitivity

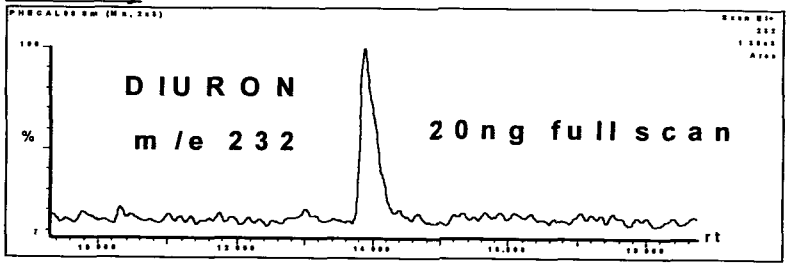

Linearity

The linearity of response can been shown to be compound dependent; for certain carbamates/phenylurea pesticides the response is linear, however, for others a non-linear response is seen.

Methomyl : linear

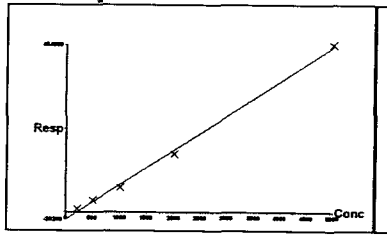

Linuron : non-linear

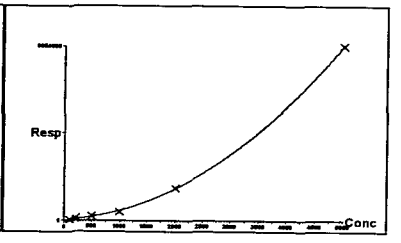

Conclusions

The combination of EI+ mass spectra and isotope distribution patterns from compounds containing naturally occurring isotopes gives excellent information for the identification of target analytes and other unexpected analytes in environmental analyses.
Typical detection limits are from about 5 to 50ng in full scan, equivalent to a 20µl injection of a 0.25-2µg/ml solution.
Particle Beam LC-MS using the MD800 LCD is a practical solution for the qualitative and quantitative analysis of carbamate and phenylurea pesticides as well as other common environmental contaminants.

Trace Determination of Sulfonyl Ureas in Soil

Lily Y.T. Li, Dale Campbell, Patrick Bennett, and Jack Henion
Advanced BioAnalytical Services, Inc., 15 Catherwood Rd., Ithaca, NY 14850

INTRODUCTION

The trace analytical determination of polar, involatile compounds in environmental samples remains a demanding analytical problem. The isolation, identification, and quantitation of labile analytes such as sulfonylureas (SU's) in soils is a representative challenge. Eight commonly used sulfonyl ureas (Accent, Harmony, Ally, Oust, Glean, Londax, Express, and Classic) and deuterium-labeled Accent (D6-Accent), used as an internal standard, were isolated from soils, and identified by ion spray LC/MS/MS under selected reaction monitoring (SRM) conditions. After several technical modifications (e.g., using a TurboIonSpray adapted LC/MS interface without a pre-column split and optimizing different MS/MS conditions for individual SU's), these eight SU's were qualitatively and quantitatively identified at the 0.05 ppb level in soil. This LC/MS/MS method demonstrates a twenty-fold increase in sensitivity from our earlier work and at least a four-hundred-fold improvement in sensitivity over other reports.[1]

EXPERIMENTAL

Soil samples were fortified with known levels of each of the eight SU's plus a fixed level of the internal standard. All analytes and the internal standard were then isolated from soils by a liquid/liquid extraction procedure. A gradient reversed-phase HPLC system using Keystone Betasil C_{18} columns (1 x 150 mm or 2 x 150 mm) provided separation of the eight SU's.

The LC/MS/MS analysis of the soil extracts was carried out using a PE Sciex API III ^{plus} tandem triple quadrupole mass spectrometer (MS) under SRM conditions in the positive ion mode. Data were acquired in four separate periods to optimize sensitivity for each analyte.

RESULTS AND DISCUSSION

The eight SU's were successfully isolated from soils by a liquid/liquid extraction procedure and were separated by an LC gradient program. Originally, a microbore Betasil C_{18} column (1 x 150 mm) was used to separate the SU's by running an eluent gradient with a pre-column split (~ 50 µL/min flow rate into column). The LC/MS/MS data were acquired using one period for the entire analysis to quantify and identify the eight SU's in soils at the 1 ppb level (Figure 1). Technical modifications, including the use of a TurboIonSpray adapted LC/MS interface, a 2 x 150 mm Betasil C18 column with an unsplit gradient and 200 µL/min flow rate directly to the mass spectrometer, and using four SRM periods to optimize the sensitivity for individual SU's, improved the method to allow the qualitative identification and quantitative measurement of the eight SU's at the 0.05 ppb level (Figure 2). This modified LC/MS/MS method demonstrates high selectivity, specificity, and sensitivity to unequivocally identify and quantify the eight SU's in soils.

REFERENCES

1. R.W. Reiser, A.C. Barefloot, R.F. Dietrich, A.J. Fogiel, W.R. Johnson, and M.T. Scott, "Application of microcolumn liquid chromatography-continuous-flow fast atom bombardment mass spectrometry in environmental studies of sulfonylurea herbicides", J. Chromatogr., 1991, 554, 91-101.

43rd ASMS Conference on Mass Spectrometry and Allied Topics

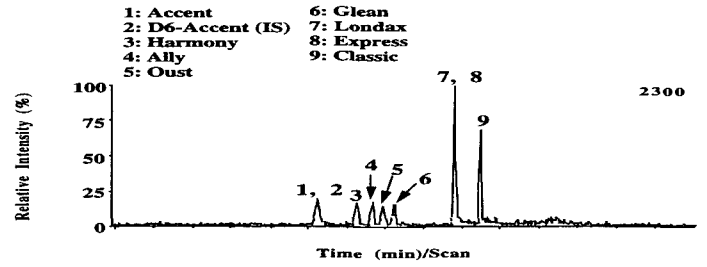

Figure 1. Total Selected Ion Current Chromatogram of 1 ppb SU's in Soil from Previous Work

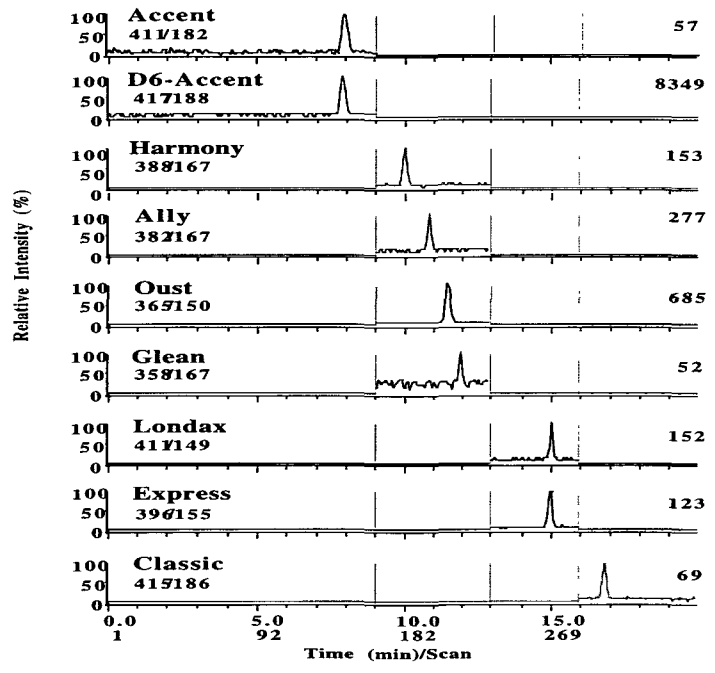

Figure 2. Selected Ion Current Chromatogram of 0.05 ppb SU's in Soil with Described Changes

Comparison of Electrospary and Thermospray for the Analysis of Herbicides

L. M. Shalaby, R. A. Croes, M. P. Wadsly and D. A. Armbrust, L. J. Mulderig and K. W.Ledeker
DuPont Agricultural Products, Wilmington, Delaware

The electrospary and thermospray LC/MS techniques have been evaluated for the study of the thermally labile sulfonylurea herbicides and metabolites. Both techniques were found to ionize those compounds and metabolites efficiently but the electrospary ionization enhances the protonated molecular ion and provides a complementary fragmentation pattern to thermospary. A typical thermospray mass spectrum of a sulfonylurea indicates a weak molecular ion and fragmentation ions characteristic of the sulfonamide and the heterocyclamine moieties. The sulfonamide moiety is detected in the protonated and ammonium adduct form. On the other hand the heterocyclamine and heterocyclurea are detected in the form of the protonated ion. A typical electrospray mass spectrum of sulfonylurea indicate the protonated molecular ion , the sodium and potassium adduct. Using the source collision induced dissociation produces mainly the protonated heterocycl isocyanate and heterocyclamine ion. The two ionization techniques were evaluated in the positive and negative ion mode. Results indicated that the negative ion electrospray ionization is more efficient than negative ion thermospray ionization for this class of compounds. Electrospray ionization was found to be more efficient in the ionization of metabolite conjugate as glucose, glucuronic acid, glutathione , amino acid and sulfate.

A typical spectrum for the sulfonylurea conjugate indicates the protonated molecular ion, the aglycone and few fragment ions. Preliminary evaluation of atmospheric pressure chemical ionization (APCI) has been carried out for sulfonylurea. Results indicated that both positive and negative ion APCI is applicable and spectral pattern indicated more intense fragmentation compared to electrospray ionization.

The electrospray ionization indicated an order of magnitude increase in sensitivity compared to themospray. The quantitative aspects of the two techniques were also evaluated for trace multi-residue analysis of several sulfonylurea and metabolites using conventional gradient LC and the selected ion mode for the mass detector. Eight sulfonylurea, rimsulfuron, bensulfuron, tribenuron, chlorimuron, nicosulfuron, thifensulfuron, metsulfuron methyl, and sulfmeturon methyl were separated and detected within 30 min in a single method(Figure 1). We used a

conventional 4.6mm o.d.x 250 mm Partisil 5 ODS column at a flow rate of 0.8 mL/min for the thermospray analysis and a 2.1 mm o.d.x 200 mm hypersil ODS at a flow rate of 0.3 mL/min and a 1:1 split with electrospray LC/MS. The selected conditions were found to give comparable separation while optimizing the sensitivity of each technique. While electrospray ionization is more sensitive and universal, thermospray was found to be more tolerant to matrices. Several instruments have been used to generate the electrospray LC/MS data, a Finnigan TSQ 700 , a Finnigan SSQ7000 and a Hewlett Packard Model 5989. For the thermospray LC/MS data we used a Finnigan SSQ700.

A study of the trace level thermospray and electrospray method precision indicated a relative standard deviation of 8-12% for thermospray and 4-8% for electrospray. The linear dynamic range for thermospray .and electrospray is in the 2-3 order of magnitude.

The method was evaluated for the analysis of those compounds in soil and wheat crop. The soil samples were extracted using 80% acetonitrile and the wheat grain samples was extracted using a C18 Empore disc. Using a simple sample preparation and eliminating the need for sample clean-up saved time and maximized the method efficiency The multiresidue method was applicable for all compounds down to 50 ppb. A method was developed to analyze for rimsulfuron, nicosulfuron and metabolites in Sassafras soil using electrospray LC/MS and simple extraction. The method was evaluated at fortification level of 0.02-0.2ppm and the average recovery was 94%. The mfThermospray LC/MS has been validated and used by several industrial and regulatory labs for multiresidue analysis the last few years. Multiresidue method validation using electrospray LC/MS is underway.

Figure 1

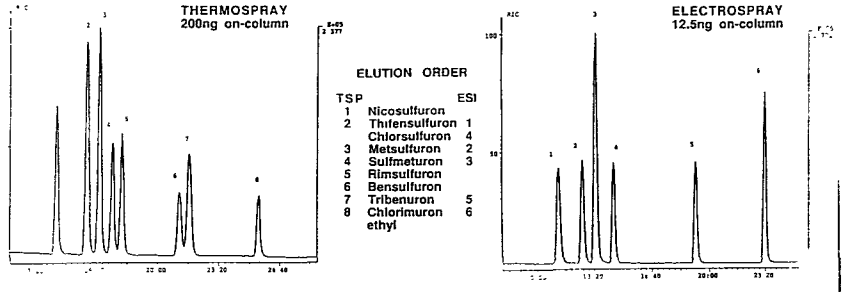

DETERMINATION OF MYCLOBUTANIL BY GC/MS, GC/HRMS, AND MS/MS

Brian D Eitzer, Harry M Pylypiw, Mary Jane I. Mattina*
Department of Analytical Chemistry
The Connecticut Agricultural Experiment Station
123 Huntington Street
New Haven, Connecticut 06511
and
Colin Moore
Uniroyal Chemical Company
Benson Road
Middlebury, Connecticut 06749

The Analytical Chemistry Department at The Connecticut Agricultural Experiment Station analyzes large numbers of food samples annually for the presence of pesticide residues. The routine screening is conducted using conventional GC detectors such as electron capture (ECD), electrolytic conductivity (ELCD), and flame photometric (FPD) Recently we have been utilizing benchtop mass spectrometry to screen increasing numbers of samples

During a routine analysis, an unidentified peak was observed in the ECD and ELCD chromatograms of the extract from table grapes, suggesting the presence of a non-standard halogenated compound The extract was, therefore, analyzed using GC-MSD. The mass spectrum of the peak with the same RRT as the unknown peak from the ECD and ELCD analyses had a library match with a chlorinated triazole compound (see Figure 1) Discussions with colleagues at US FDA and California Department of Food and Agriculture indicated that the unknown compound might be Myclobutanil (Systane), a relatively new fungicide approved for use on grapes The RT and the mass spectrum of the unknown compound matched those of authentic Myclobutanil (see Figure 2)

There remained several unanswered questions from the low resolution mass spectrum which prompted us to investigate this fungicide in more detail. In particular (1) the library spectrum for the chlorinated triazole is missing the chlorine isotope pattern around m/e 179-181, (2) several alternate fragmentation schemes of Systane are possible to yield an m/e 179 ion, (3) several different structures for the m/e 179 fragment ion are possible

High resolution mass spectrometry of Systane provided data which showed that numerous m/e values observed as single ions in the low resolution mass spectrum are, in fact, resolved into two or more distinct fragment ions under high resolution. In particular the base peak is composed of two clearly resolved fragment ions at high resolution, each of which corresponds to a different fragmentation pathway (see Figure 3) In addition the cluster of ions at m/e 150-152 can be partially resolved into three different fragments (see Table 1)

In conclusion this study strongly suggests that fragmentation patterns deduced from low resolution mass spectra may be erroneous High resolution data are necessary to characterize fully compounds included in mass spectral libraries

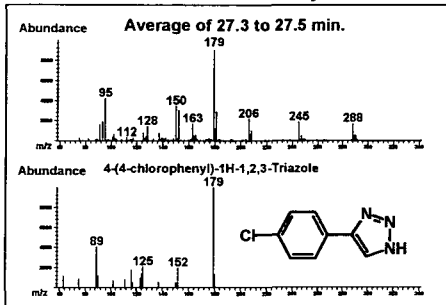

Figure 1 Top panel· mass spectrum from extract
Bottom panel library match

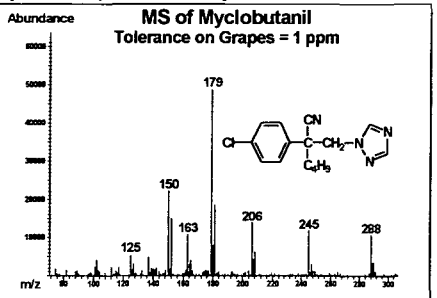

Figure 2 Mass spectrum of authentic Myclobutanil.

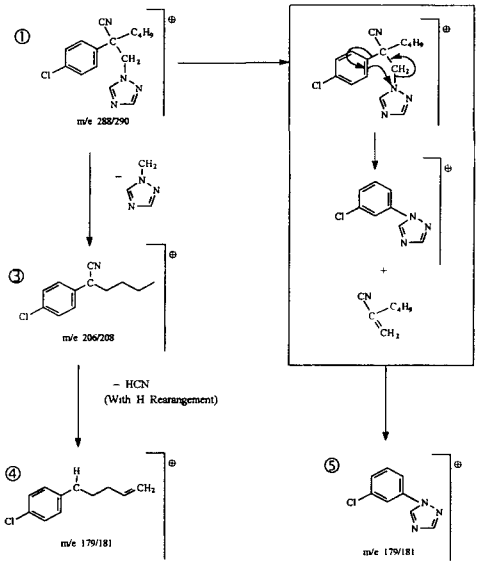

Figure 3. Suggested fragmentation scheme for m/e 179 ions.

Table 1. Exact Masses and Atomic Compositions

Mass	Deviation (PPM)	Composition	Structure No
181.0582	-8.86	$C_{11}H_{12}{}^{37}Cl$	4
181.0210	-5.94	$C_8H_9N_3{}^{37}Cl$	5
180.9888	Reference Mass	C_6F_7	
179.0617	-5.88	$C_{11}H_{12}{}^{35}Cl$	4
179.0244	-3.49	$C_8H_9N_3{}^{35}Cl$	5
154.0672	9.90	$C_{11}H_8N$	
154.0370	4.36	$C_9H_6{}^{37}Cl$	
154.0120	5.35	$C_7H_5N_2{}^{37}Cl$	
152.0391	-1.17	$C_9H_6{}^{35}Cl$	
152.0099*	11.82	$C_8H_5N{}^{37}Cl$	
152.0099*	-27.8	$C_7H_5N_2{}^{35}Cl$	
150.0116	3.65	$C_8H_5N{}^{35}Cl$	

* It would require a resolution of 25,000 to separate these two structures

NEGATIVE-ION UNIMOLECULAR DISSOCIATION OF ESTERS OF THE HERBICIDE DICLOFOP ACID IN A MASS SPECTROMETER SOURCE

J.V. Headley, and K. Peru. National Hydrology Research Institute,
11 Innovation Boulevard, Saskatoon, Saskatchewan, CANADA, S7N 3H5

INTRODUCTION

The transformation of some contaminants in the environment has been shown to correlate with unimolecular dissociations of gas-phase ions[1,2]. It is suspected that the internal energy (E) dependence of the transformation of chlorinated contaminants in the gas-phase may also correlate with the chemistry of neutral molecules in geological materials. To investigate the dependence of gas-phase transformations of a chlorinated herbicide relative to E, the unimolecular dissociations of three derivatives of diclofop acid (2-[4-(2,4-dichlorophenoxy)-phenoxy]propionate) were studied using electron capture negative-ion mass spectrometry (ECNIMS). Dissociation of the methyl, trimethylsilyl (TMS) and pentaflurobenzyl (PFB) esters in the ion-source was used to form a common precursor-ion, the carboxylate anion.

EXPERIMENTAL

Diclofop-methyl was purchased from Caledon Laboratories and the other two esters were prepared using derivatization procedures described in the literature[3,4].

The GC/MS experiments utilized a VG AUTOSPECQ mass spectrometer equipped with a 4000 VAX data system and OPUS 3.1X software. Identification of the derivatives for ECNIMS studies was based on retention time data, electron impact data and positive-ion chemical ionization data obtained for commercial and synthetic standards[2]. GC/MS experimental conditions were established as per Method 8270 guidelines : 30 m DB-5 column, internal diameter 0.33 mm, film thickness 0.25 μm, helium carrier gas 1 ml/min, injector 250°C, transfer line 300°C, temperature program 35°C/5 min at 10°C/ min - 280°C/7 min. For ECNIMS studies the ion-source was operated at 150°C, 35 eV and 0.3 μA emission current, using argon as the buffer gas at 2.0 - 2.5 x 10^{-5} torr.

RESULTS AND DISCUSSION

The carboxylate anion of the herbicide esters was observed to be stable to low energy collision induced dissociations (15-250 eV, laboratory frame of reference). However, the relative distribution of the E of the carboxylate ions formed in the ion-source was dependent on the chemical nature and size of the ester group. For the highest E (methyl ester) there was preferential formation of a chlorodibenzofuran oxide ion. In contrast, this dissociation was only a minor pathway for relatively low E (PFB ester) where loss of HCl only, was the preferred pathway. The distribution of E arising from dissociation of the TMS ester resulted in no preferred pathways. For this ester, the carboxylate ion was formed with E overlapping the range of E available for both the methyl and PFB esters. Dissociation of the carboxylate ion derived from the TMS ester was observed to be a mixture of the pathways for the methyl and PFB esters including a third pathway leading to full dechlorination.

The GC/ECNIMS data can be summarized by the mechanism given in Figure 1. This mechanism

highlights the importance of internal energy in switching on and off specific transformations. There was however, no evidence of chlorodibenzofuran as a metabolite in actual soil samples. Previous studies reported transformation of diclofop-methyl to chlorinated metabolites of benzoic acid, involving complex rearrangements and /or reactions with other contaminants present in the soil[5].

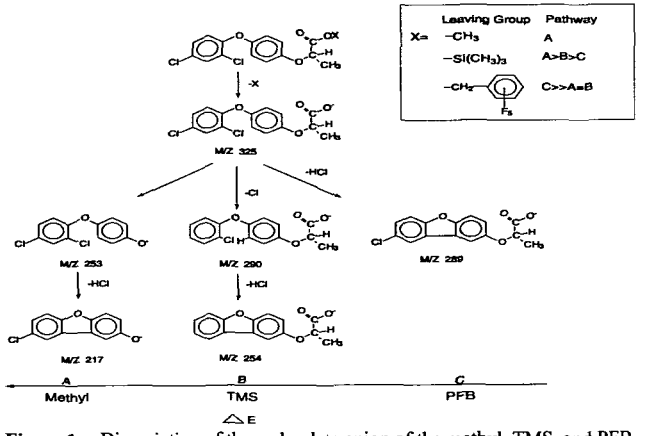

Figure 1 Dissociation of the carboxlate anion of the methyl, TMS, and PFB esters

CONCLUSION

For relatively high internal energies (methyl ester) there was preferential formation of a chlorodibenzofuran oxide ion, however at relatively low internal energies (PFB ester), elimination of HCl was the preferred pathway. In the case of the TMS ester there were no preferred pathways. Further work is warranted to develop models to predict the conditions under which the internal energy of contaminants can be manipulated to enhance remediation of contaminated sites.

ACKNOWLEDGEMENTS

Nicholas Bradshaw's provided technical assistance Financial support was provided by PESTPLAN.

REFERENCES

1. McLafferty F.W., in Mass Spectrometry of Organic Ions, F.W. McLafferty (Ed.), Academic Press, New York, 1963, p.309.
2. Headley J.V., K.M. Peru and P.W. Brooks, RCMS, Vol. 8, 484-486 (1994)
3. Sulpelco Canada Ltd., Cat. #30, 428 (1992).
4. Kawahra F.K., Anal. Chem. 40, 2073 (1968).
5. Headley, J.V., J.R. Lawrence, B.N. Zanyk and P.W. Brooks. Water Poll. J. Canada 29(4):557-567

Determination of Hydrolysis Degradates of Cloransulam-Methyl by Electrospray Liquid Chromatography Mass Spectrometry

Jesse L. Balcer, Stephen M. Brown, Paul Lewer
DowElanco, Indianapolis, IN 46268

During the course of plant metabolism studies, it is frequently necessary to extract the tissues under acidic and/or basic conditions. A necessary assumption of this approach is that the analytes of interest are not degraded by the extraction procedure. Cloransulam-methyl (CM), a new triazolo-pyrimidine sulfonanilide herbicide targeted for the control of broadleaf weeds in soybeans, and several of its known metabolites, were subjected to relatively severe acidic and basic hydrolysis conditions to validate this assumption in support of a nature of the residue study of CM in soybeans.

When extracting under severe conditions, compounds of interest may be converted to a single component or mixture of components. Since cloransulam-methyl was known to be both acid and base labile, standards of parent and several related compounds were treated separately with both acid (0.5M-hydrochloric acid) and base (0.5M-sodium hydroxide), reacted for two hours at 100°C, and the resulting products identified.

Cloransulam-methyl (CM), cloransulam-methyl-cysteine (CM-CYS), triazolopyrimidine sulfonic acid (TPSA), and methyl 3-chloroanthranilate (MCA) standards were chosen for testing. CM-CYS and TPSA had been identified as degradates of CM in soybeans. MCA was a hypothetical product from the bridge cleavage of CM.

Electrospray-LC-MS coupled with UV detection was performed on the reaction mixtures. Electrospray conditions consisted of a spray voltage at 4.5 kV, capillary temperature of 235°C, and nitrogen gas pressures of 70 psi and 20 mL/min for the sheath and auxiliary flows, respectively. A typical chromatogram showing products from the acid hydrolysis of CM is shown in figure 1. A typical spectrum derived from the chromatogram is shown in figure 2.

In all cases acid hydrolysis resulted in a mixture of more polar products plus a variable amount of residual starting material. In contrast, base hydrolysis gave a single product in high yield (> 94%) from each starting material. Therefore, these reactions showed that each test material was converted in high yield to a single product under basic, but not under acidic, conditions, and that the basic reaction was, therefore, preferred for the extraction of compound-related residues due to the formation of the fewest side-products. Figure 3 summarizes the basic reaction products.

The use of electrospray LC/MS allowed for the identification of all the major acid and base hydrolysis products of cloransulam-methyl without the need to isolate each individual component. This rapid screening experiment insured that products resulting from acidic or basic extractions of treated tissues were correctly identified.

43rd ASMS Conference on Mass Spectrometry and Allied Topics

FIGURE 1 CLORANSULAM-METHYL ACID HYDROLYSIS

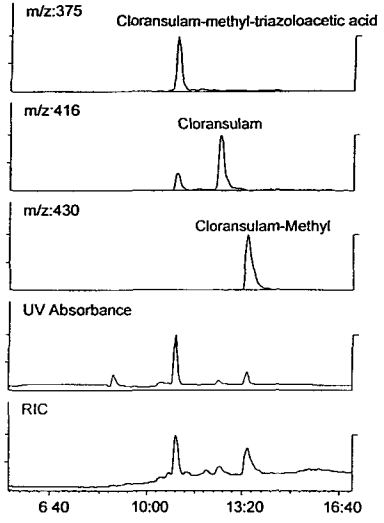

FIGURE 2 ELECTROSPRAY MASS SPECTRUM OF CLORANSULAM-METHYL

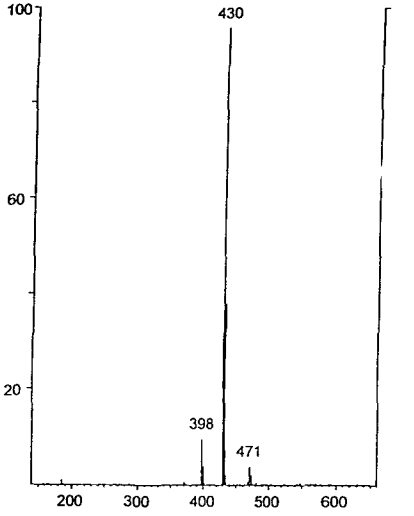

FIGURE 3 - PRODUCTS FROM BASE HYDROLYSIS

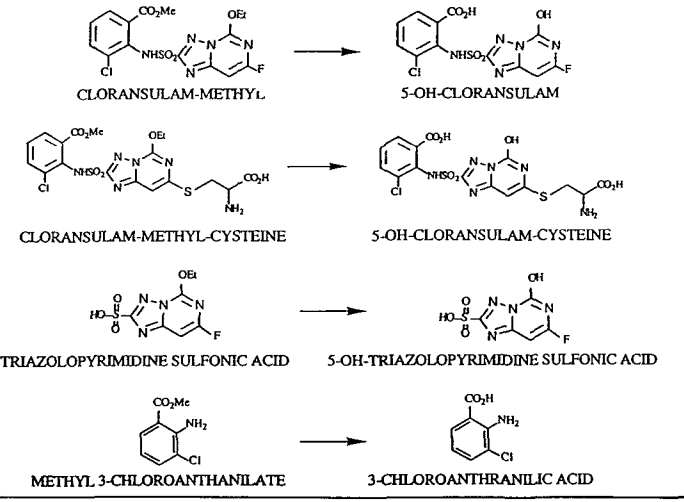

DETERMINATION OF CLORANSULAM-METHYL AND ITS METABOLITES IN SOIL BY ESI LC/MS/MS

Stephen M. Brown, Jesse L. Balcer, Dennis O. Duebelbeis, and Angelea Thomas
Environmental Chemistry Laboratory, DowElanco, Indianapolis, IN 46268

Cloransulam-methyl is a new triazolopyrimidine sulfonanilide herbicide for the control of broadleaf weeds in soybeans. In order to register this new agricultural product for sale in the United States, a large number of metabolism, environmental, toxicological, and residue studies must be conducted. One of the required environmental studies follows the dissipation of the active ingredient and any known soil metabolites under actual field conditions. Usually, only the parent molecule and one or two similar metabolites need to be monitored throughout the soil core. Because of the small number (and similarity) of analytes, a derivatization procedure can usually be developed and GC/MS is often feasible for the analysis. However, cloransulam-methyl which has a more complex chemistry, breaks down in the environment to 5 different degradates (see **Figure 1**). Therefore, the parent molecule and 5 different metabolites may need to be determined. Due to the extreme variations in the nature and polarity of these metabolites, a single cleanup and derivatization scheme could not be developed. Because of this, electrospray LC/MS/MS was investigated for its feasibility as a possible analytical technique for cloransulam-methyl and metabolites in soil.

The extraction that we were forced to use due to analyte adsorption to the soil matrix, while very efficient at solubilizing the analytes of interest, also removed a significant amount of the organic matter present in the soil, resulting in a very viscous, "dirty" extract. The high background contamination precluded the use of LC/MS and necessitated the use of LC/MS/MS.

In order for an analytical method to be used for a soil dissipation study, it must meet certain reproducibility, linearity and sensitivity criteria. For reproducibility, the relative standard deviations of the method throughout the entire range of expected concentrations must be less than 20%. **Figure 2** shows typical reproducibility with this method for the six analytes. These data were not corrected through the use of an internal standard, and, with the exception of one analyte, meet the reproducibility requirements. The use of an internal standard was shown to improve this reproducibility by an average of about 5%.

In terms of sensitivity, it is mandated that the method must be sensitive enough to quantify an analyte at 10% of application rate. For cloransulam-methyl, that means our method must have a limit of quantitation (LOQ) no greater than approximately 2 ppb. Therefore, a target LOQ was set at 1 ppb in soil. A chromatogram at the proposed LOQ of 1 ppb is given in **Figure 3**. The lowest signal to noise ratio seen in the chromatogram is about 20:1. The LC/MS/MS method, therefore, has more than adequate sensitivity for the analysis.

However, when control soil extracts that have been spiked with the six analytes are analyzed, the calculated LOQ suffers dramatically due to increased background from the soil matrix. **Figure 4** shows the chromatogram of an actual spiked sample at 1 ppb. It is quite obvious that there is a significant suppression of the signal by the soil matrix. In fact, the peak for 5-OH cloransulam cannot be detected. The calculated LOQ for this analyte has been determined to be about 5 ppb. However, the other analytes meet our target LOQ of 1 ppb.

To conclude, the use of electrospray LC/MS/MS has allowed the determination of 6 analytes in a standard mixture in one run. The detection limit of the analysis is 1 ppb or better. The precision of the determination meets the mandated guideline of RSD<20%, with typical RSD's ranging from 3-20%. The use of isotopically labelled internal standards should lower this number.

However, when soil extracts are analyzed by this method, the high background of the soil matrix (arising from our severe extraction procedure) causes significant signal suppression or enhancement. It should be noted that for other molecules where we used less severe extraction solvents (0.1N vs 1N HCl) the matrix effect was drastically reduced.

Although further clean-up will be necessary for this analytical method to be used in an actual study involving cloransulam-methyl and its metabolites, ESI LC/MS/MS has nonetheless proven itself to be a feasible alternative to the more traditional methods of residue analysis.

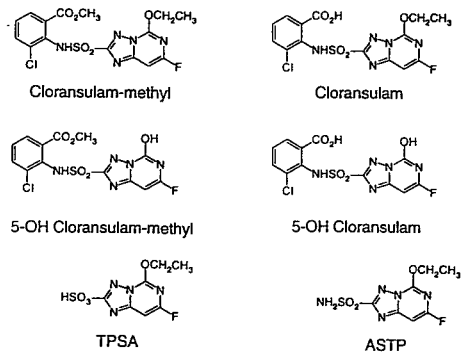

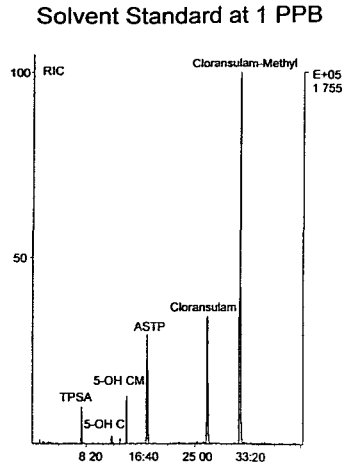

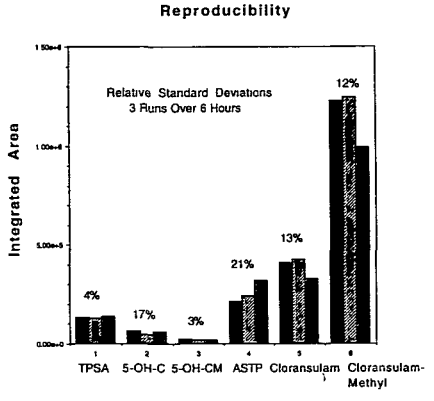

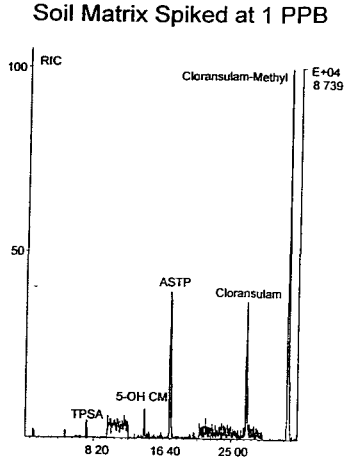

GC/MS ANALYSIS OF ALKYL METHYLPHOSPHONIC ACIDS

Dennis K. Rohrbaugh
U.S. Army Edgewood RD&E Center, APG, MD 21010-5423

Detection of chemical warfare agent degradation products is important for assuring treaty verification compliance as part of the Chemical Weapons Convention and for monitoring chemical stockpile demilitarization efforts. Alkyl methylphosphonic acids [Me-P(O)(OR)OH], the primary environmental degradation products of organophosphorus agents, are not detected by direct GC/MS injection because of their acidity and low volatility and require derivatization prior to analysis. In this study, five acids resulting from the degradation of Schedule 1 compounds (R = Et, *i*Pr, *i*Bu, pinacolyl, and cyclohexyl) were converted to their trimethylsilyl (TMS) derivatives and analyzed using three methods of ionization (electron ionization, methane chemical ionization, and ammonia chemical ionization).

Each acid was derivatized by addition of 1 mg to 0.1 mL pyridine and 0.1 mL bis(trimethylsilyl)trifluoroacetamide (BSTFA) containing 1% trimethylchlorosilane (TMCS) and heating for 20 minutes at 60°C.

Derivatized samples were analyzed on a Finnigan 5100 GC/MS equipped with a 15m x 0.25mm DB-1701 or Rtx-5 capillary column. The oven was ramped from 60°C to 270°C at 10°C per minute. The injection port temperature was 200°C and the interface temperature was 230°C. Both methane and ammonia were used as CI reagent gases with a source pressure of 0.5 Torr. The mass range was scanned at 1 scan/sec from 45-450 amu for EI and from 60-450 amu for CI. The electron energy was 70 eV and the emmision current was 750 μA for both EI and CI. Retention times obtained for the TMS derivatives where R = Et, *i*Pr, *i*Bu, pinacolyl, and cyclohexyl were 263, 279, 370, 433 and 572 seconds, respectively, with the DB-1701 column, and 171, 188, 269, 337 and 465 seconds, respectively, with the Rtx-5 column.

The EI, methane CI, and ammonia CI mass spectra of the TMS derivatives of the 5 alkyl methylphosphonic acids are shown in Figure 1. The EI spectra of this class of compounds are characterized by ions at m/z 153 (base peak) and m/z 169 (10-50% of base peak), resulting from loss of OR and R, respectively, with subsequent protonation. The molecular ion is observed only for the ethyl ester. The similarity in spectra can make identification based on EI spectra alone difficult, especially at low concentrations. CI is particularly useful for the detection of these compounds. A protonated molecular ion is observed for all five compounds using methane CI, but the intensity decreases with increasing size of the R group and is only about 10% of the base peak for the cyclohexyl and pinacolyl esters. Ammonia CI is a superior method of ionization for detection of this class of compounds and provides enhanced protonated molecular ion formation, with the protonated molecular ion being observed as the base peak for all five compounds. A strong adduct ion $[M+NH_4]^+$ is also observed in all cases (20-50% of base peak).

FIGURE 1. EI, METHANE CI AND AMMONIA CI MASS SPECTRA OF ALKYL METHYLPHOSPHONATES

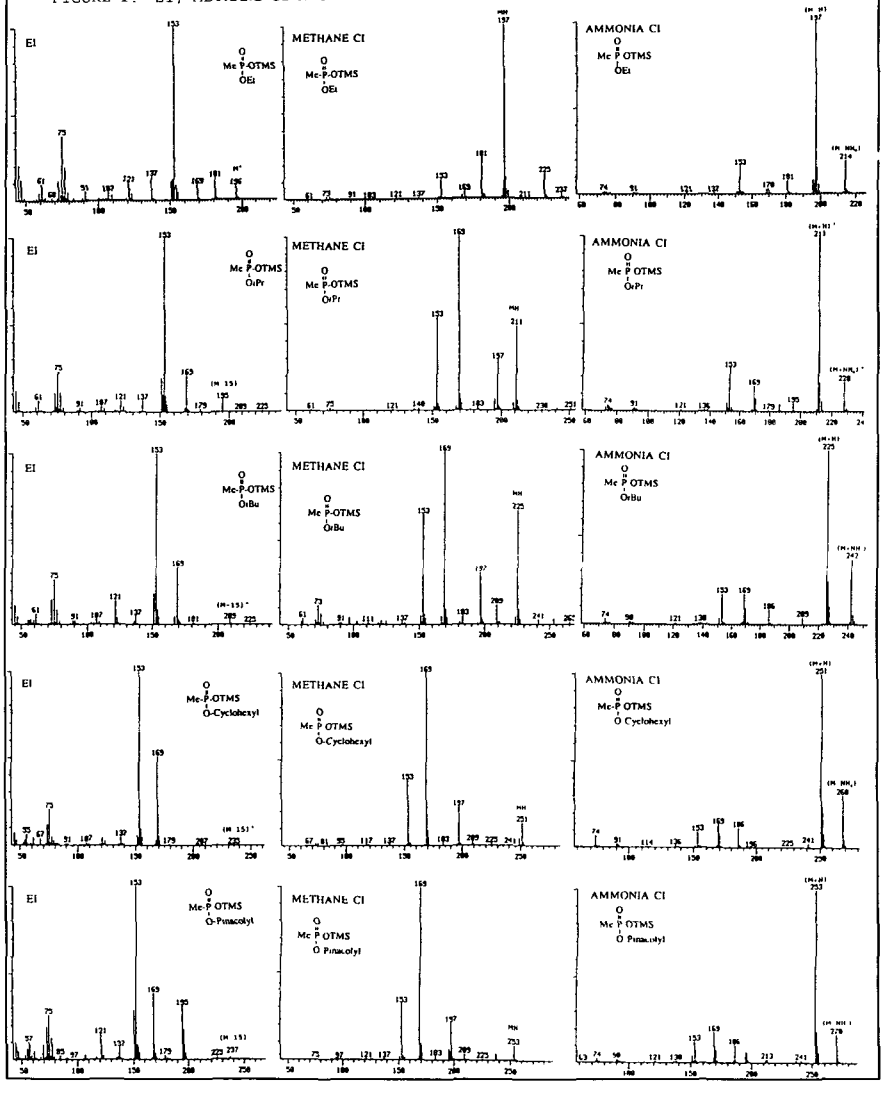

DETERMINATION OF TRIADIMEFON AND IMIDACLOPRID IN WHITE PINE BY GC/MS

Linda M. MacDonald[1], Bobbi-Jo Rainbird[1], Timothy R. Meyer[2]

Canadian Forest Service, Natural Resources Canada, Sault Ste. Marie, Ontario, Canada[1]
Ontario Forest Research Institute, Ontario Ministry of Natural Resources, Sault Ste. Marie, Ontario, Canada[2]

INTRODUCTION:

The white pine blister rust fungus (Cronartium ribicola Fisch.) and the white pine weevil (Pissodes strobi Peck) are the two most serious pest management problems in the production and reforestation of eastern white pine (Pinus strobi L.) in Canada. White pine weevil is also an important pest on other pines and spruces. To date reliable, cost-effective and environmentally acceptable methods of prevention and/or control are not available

In 1993, a major field study was undertaken by the Ontario Ministry of Natural Resources to evaluate the potential of applying, at the time of planting, a pesticide-impregnated, timed-release tablet containing the systemics triadimefon (fungicide) and imidacloprid (insecticide). The pesticides were incorporated into the tablet, individually and in combination, at various concentrations. Some treatments also contained a specially formulated fertilizer.

The triazoles triadimefon and its' major metabolite, triadimenol, are sterol-biosynthesis inhibiting fungicides which also exhibit plant growth regulating properties. The reduction of triadimefon to triadimenol may be regarded as an activation since the alcohol possesses greater fungicidal activity. Both have been registered for some time under the trade names Bayleton and Baytan respectively.

Imidacloprid is a new "nitroguanidine" insecticide with properties that make it very attractive as a tool in integrated pest management in today's world that demands enhanced environmental safety. These properties include favourable environmental/toxicological characteristics, excellent systemic activity against a wide range of insects on a wide range of crops, and a novel mode of action necessary to address the problem of insect resistance-it is an agonist of the nicotinic acetylcholine receptor

The timed-release tablet provides a delivery mechanism within the root zone, maximizing uptake of the chemicals while minimizing contamination of the surrounding soil volume and exposure of non-target organisms.

Pesticide distribution and persistence, over a period of several years, will be correlated with disease and insect incidence as well as with growth response data.

An analytical method has been developed for extraction of these pesticides from white pine needles, subsequent separation and quantitation by GC/MS. Triadimefon and triadimenol, are determined directly while imidacloprid is converted to the heptafluorobutyryl derivative. Quantification of all the analytes is performed by external standard comparison, in matrix, in selected ion monitoring mode.

METHODS:
SAMPLE PREPARATION:

White pine needles (1-5g) are macerated in acidified 7:3 methanol:water, filtered and the filtrate concentrated to the aqueous remainder under vacumn. The aqueous remainder is diluted with water then loaded onto a preconditioned C18 Sep-Pak. Co-extractives are removed by washing with 0.05M potassium carbonate. Following thorough drying, all analytes are eluted from C18 with methylene chloride.

Separation of triadimefon and triadimenol from imidacloprid is accomplished on activated Florisil. The triazoles are eluted in 20mL 75.25 ethyl acetate:hexane No attempt was made to separate the two on Florisil since they are easily resolved by GC. Imidacloprid, if present, is then eluted with 5mL of acetonitrile.

The 75:25 fraction is evaporated to dryness with nitrogen and triadimefon and/or triadimenol recovered in ethyl acetate for direct analysis by GC/MS.

The acetonitrile fraction containing imidacloprid is concentrated to 1.0mL and reacted with HFBA and pyridine (100uL each) at 60°C for 2hr. After cooling to room temperature, excess reagent is removed by evaporation to dryness with nitrogen and the derivative recovered in ethyl acetate for GC/MS.

ANALYTICAL CONDITIONS:

Analyses were performed on a Hewlett-Packard 5989A GC/MS. Samples were injected onto a DB-5ms column (J&W Scientific, 30m x 0.25mm ID x 0 1um film) with a deactivated fused silica guard column (1.0m x 0.32mm ID) at an injection port temperature of 250 °C.

For triadimefon and triadimenol the column temperature was programmed from 60 °C to 235 °C at 25 °C/min, then to 250 °C at 5 °C/min, and finally to 300 °C at 30 °C/min where it was held for 10 minutes.

For the HFB derivative of imidacloprid the column temperature was programmed from 150 °C to 300 °C at 12 °C/min and held for 10 minutes.

The transfer line and source temperatures were 280 °C and 275 °C, respectively

Confirmation and quantification were performed by selected ion monitoring of structurally significant ions.

Ions selected in the determination of triadimefon and triadimenol are indicated in Fig 1(a) and (b) with m/z 208 and m/z 168, respectively, used for quantification. Ion m/z 112, the base peak of triadimenol, could not be used reliably at low residue levels (<50ppb) due to the presence of this fragment ion at the same retention time in some matrix extracts

The EI spectrum of imidacloprid-HFB is shown in Fig 2. The ion pairs m/z 126/128, 210/212 and 407/409 were selected for confirmation, with m/z 407 used for quantitation.

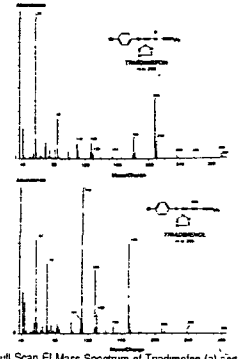

Figure 1 Full Scan EI Mass Spectrum of Triadimefon (a) and Triadimenol (b)

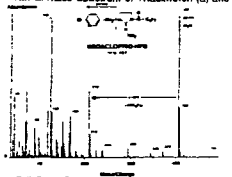

Figure 2 Full Scan EI Mass Spectrum of Imidacloprid - HFB

RESULTS and DISCUSSION:

This method has been validated for triadimefon and triadimenol in fortified white pine foliage at 10ppm, 1pmm and 100ppb. Limits of quantitation are 100pg on-column, with limits of detection conservatively set at 50pg.

Quantitation of imidacloprid was validated at the above levels as well as at 10ppb, equivalent to 10pg injected. LOD has been set at 5pg.

Overall mean recoveries were 84.14% + 6.22 (7.4%), n=50.

Figures 3 and 4 illustrate chromatograms obtained at 100ppb and 10ppb for triadimenol/triadimefon and imidacloprid-HFB, respectively.

During the course of our investigations, a variety of derivatization reactions were attempted with imidacloprid, including methylation, silyation and acylation. Acylation with HFBA provided the derivative most suitable for GC/MS, that is free from matrix interferences at environmentally significant concentrations.

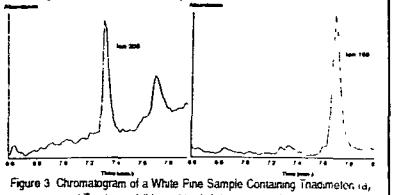

Figure 3 Chromatogram of a White Pine Sample Containing Triadimefon (a), and Triadimenol (b) at 100ppb (100pg injected)

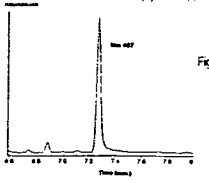

Figure 4 Chromatogram of a White Pine Sample Containing Imidacloprid at 10ppb (10pg injected as HFB derivative)

CONCLUSIONS:

Although this method was developed for a very specific application, we are confident it can be applied with little or no modification to the determination of triadimefon/triadimenol and imidacloprid in a variety of environmental matrices. It is our intention to extend it to seeding stem and root samples as well as to soils. Quantification of triadimefon and triadimenol by SIM at levels below 100ppb in white pine may be achievable with additional cleanup of the Florisil eluate to remove co-extractives. MS/MS to filter out the chemical background is certainly an option and could lower the LOQ to ppt levels.

Determination of Triclopyr and Metabolites in Environmental Matrices Using Solid-Phase Extraction and Capillary Gas Chromatography/Mass Spectrometry

E. L. Olberding, B. J. Harnick, and D. R. Foster

DowElanco, North American Environmental Chemistry Laboratory,
Indianapolis, Indiana 46268

D. A. McNett

The Dow Chemical Company, Health and Environmental Sciences Laboratory,
Midland, Michigan 48674

INTRODUCTION

Triclopyr (3,5,6-trichloro-2-pyridinyloxyacetic acid) is a frequently used herbicide for the control of a variety of woody plant and broadleaf weed species. The compound is also under development for use as an aquatic herbicide. As such the chemical is active against a wide range of introduced aquatic nuisance species such as purple loosestrife and Eurasian milfoil, without adverse effect on desirable native plant species such as rushes and cattails (1). To support the registration for triclopyr as required under Subdivision N of the U.S. EPA Pesticide Assessment Guidelines, methodology is required for the determination of triclopyr and its two major metabolites in soil, sediment, and water.

Methods for the determination of triclopyr, 3,5,6-trichloro-2-pyridinol (TCP) and 2-methoxy-3,5,6-trichloropyridine (MP) were developed and validated over the concentration range 10-1000 ng/g in soil and sediment, and 0.10-10 ng/mL in water. This paper describes the methodology developed for the analysis of soil and sediment samples.

ABSTRACT

Residues of triclopyr, TCP, and MP are extracted from soil and sediment samples using acidified acetone. Aliquots of the soil extracts are purified by C_{18} solid-phase extraction (SPE) for triclopyr and TCP determination, while the MP determination requires a hexane extraction with an optional silica gel SPE. Following recombination of the purified extracts, the samples are derivatized to form the *tert*-butyldimethyl silyl (TBDMS) ethers, and analyzed by gas chromatography with mass selective detection.

For water samples, MP is first extracted with hexane and then purified using a silica gel SPE. Residues of triclopyr and TCP are then extracted using a C_{18} SPE. The subsequent sample preparation is the same as for the soil and sediment samples.

Analyses were performed by capillary GC/MS employing selected ion monitoring using a Hewlett-Packard Model 5971A benchtop mass selective detector. A splitless injection onto a J&W Scientific Durabond-1701 column was used for resolution of triclopyr and its metabolites from sample matrix components.

RESULTS

Compound	Validated Range, µg/g	Percent Recovery	Standard Deviation
Triclopyr	0.01-1.0	106	7 (n=32)
TCP	0.01-1.0	90	4 (n=32)
MP	0.01-1.0	95	7 (n=32)

CONCLUSIONS

The above method has proven reliable for the analysis of several thousand environmental samples from aquatic dissipation and field dissipation studies. Compared to existing methods (2,3), the advantages of this method include easier sample preparation, the formation of the TBDMS ethers for both the triclopyr and TCP (4), and the simultaneous determination of all three compounds in a single chromatographic run.

Because of the high specificity achieved for triclopyr and its metabolites by the use of capillary GC/MSD coupled with multiple ion detection, the usual requirement for a second independent confirmatory method for enforcement purposes is not necessary.

REFERENCES

1) Woodburn, K B ; Green, W R ; Westerdahl, H E. Aquatic dissipation of Triclopyr in Lake Seminole, Georgia. *J. Agric. Food Chem.* 1993, 41, 2172-2177.

2) McKellar, R. L.; Brown, W. C. "Determination of Triclopyr and 3,5,6-Trichloro-2-pyridinol in Soil by Gas Chromatography", Method ACR 84.2, unpublished method of DowElanco, 1984.

3) McKellar, R. L. "Determination of 2-Methoxy-3,5,6-Trichloropyridine in Soil by Gas Chromatography", Method ACR 86.4, unpublished method of DowElanco, 1986.

4) Evershed, R. P. In *Handbook of Derivatives for Chromatography*; 2nd edition; Blau, K; Halket, J. M., Ed; Wiley, New York, 1993, Chapter 4.

TITLE: Determination of Clopyralid in Soil Using Solid-Phase Extraction and Capillary GC/ECD and GC/MSD

AUTHORS: B. J. Harnick and E. L. Olberding
DowElanco, North American Environmental Chemistry Laboratory

INTRODUCTION

Clopyralid is the active ingredient in several broadleaf weed control products in use throughout the United States. As part of the reregistration process, methodology must be developed to determine clopyralid residues in various environmental and agricultural matrices.

A method for the determination of clopyralid residues in soil was developed and validated in the Residue Chemistry Group of DowElanco North American Environmental Chemistry Laboratories. The methodology employed a solid-phase extraction (SPE) with analysis by GC/ECD or GC/MSD.

ABSTRACT

Residues of clopyralid were extracted from soil samples using acidified acetone. A portion of each extract was evaporated to aqueous, diluted, and purified using C_{18} and alumina solid-phase extractions (SPE). After derivatization with acidified 1-propanol, the 1-propanol was evaporated and the clopyralid 1-propyl ester derivative (clopyralid PE) was partitioned from an aqueous sodium chloride solution into hexane containing clopyralid 1-butyl ester (clopyralid BE) as an internal standard. A portion of the hexane extract was then analyzed by capillary gas chromatography with electron capture detection (GC/ECD).

Capillary GC/ECD was performed using a Hewlett-Packard Model 5890 gas chromatograph equipped with an electron capture detector. A splitless injection onto a J&W Scientific Durabond-17 column was used for resolution of clopyralid from sample matrix components. The method was validated over concentration ranges of 5-250 ng/g in soil.

Capillary GC/MSD employing selected ion monitoring was used for confirmation of clopyralid residues. Capillary GC/MSD was performed using a Hewlett-Packard Model 5971A benchtop mass selective detector. A splitless injection onto a J&W Scientific Durabond-17 column was used for resolution of clopyralid from sample matrix components.

RESULTS

Validation of the above method produced the following results:

Matrix	Instrument	Validated Range	Percent Recovery	Standard Deviation
Soil	GC/ECD	5.0-250 ng/g	83	8 (n=29)

CONCLUSIONS

The use of solid-phase extraction with GC/ECD or benchtop GC/MSD for routine residue analysis has been demonstrated to produce excellent results. The above methods will be used for the analysis of environmental samples from field dissipation studies to provide data for re-registration of clopyralid.

Control Sample

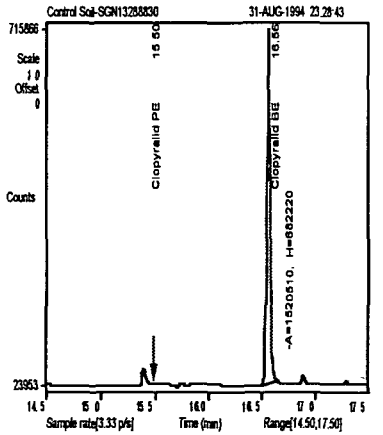

Fortified Sample

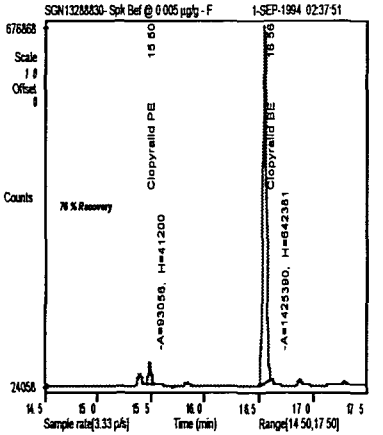

THE EVALUATION OF A BENCHTOP API LC/MS/MS SYSTEM FOR ENVIRONMENTAL ANALYSES

Robert Bethem, ALTA Analytical Lab, 5070 Robert J. Mathews Pkwy., El Dorado Hills, CA 95762
and Takeo Sakuma and Bori Shushan*, Perkin-Elmer SCIEX Instruments, 71 Four Valley Drive, Concord, Ontario, Canada, L4K 4V8

INTRODUCTION

Atmospheric pressure ionization LC/MS is becoming a generally accepted and widely used analytical tool for quantitative environmental analysis. We have validated several environmental methods for the quantitation of pesticides and herbicides using a PE SCIEX API III+. We are currently using this data to assess the quantitative performance of the PE SCIEX API 300, a newly introduced benchtop LC/MS/MS system Two methods were chosen for the instrument comparisons The first method described is for the analysis of one carbamate (carbofuran) and two organophosphorous pesticides (methyl parathion and malathion) in rice field drainage water by LC-API/MS/MS These difficult samples provide us with an excellent opportunity to test method specificity and ruggedness. Although the quantitative statistics for the APCI method validation are excellent, methylparathion is thermally labile and does not give a molecular ion while in APCI mode. For this reason, we are also evaluating IonSpray™ for this analysis. We have generated instrument comparison data using APCI and IonSpray on the PE SCIEX API III+ and API 300. Sensitivity and linearity comparisons demonstrate similar performance. The second method is the analysis of hydroxytriazine degradates in groundwater by LC-APCI/MS/MS. The analysis provides quantitative analysis for all five analytes in a single injection with excellent sensitivity. The method uses strong cation exchange (SCX) chromatography and requires the use of volatile buffers for chromatographic retention. Due to the low molecular weight of the analytes (<200 amu), the use of ammonium acetate in the mobile phase, and the need to quantitate versus external standards, this method is a good candidate for evaluation of small molecule sensitivity, precision, accuracy and ruggedness. Comparison of APCI data from the API III+ and API 300 once again showed similar performance characteristics.

ANALYSIS OF RICE FIELD DRAINAGE WATER BY LC-APCI/MS/MS

This example describes the preparation of water extracts by liquid-liquid extraction followed by the determination of the following compounds by LC-APCI/MS/MS. The method has been validated with rice field drainage water and is being used to assess the toxicity of rice field releases. Seven control sample aliquots were fortified with the analytes listed below at an estimated method detection limit (EMDL; fortification amounts varied for each analyte based on the sensitivity from standard injections). The samples were extracted using a concentration factor of 200 mL/2 mL and analyzed. The Method Detection Limit (MDL) for each analyte was calculated by multiplying the standard deviation of the seven replicate analyses by the Student value of 3.143. The Limit of Quantitation (LOQ) represents 10 times the standard deviation. See Figure 1 for the product ion mass spectra and Table I for a summary of results used for MDL and LOQ calculations.

An acidified water sample is extracted three times with methylene chloride. The combined aliquots are concentrated by rotary evaporation to less than 10 mL. The aliquot is transferred with methanol to a calibrated tube and concentrated to ~0.5 mL using nitrogen. The concentrate is diluted to a 2 mL final volume using 0.1% formic acid. Stable isotope internal standards for Carbofuran and Malathion are added prior to the extraction procedure. An internal standard for Methylparathion (d_{10}-Diethylparathion) is added just prior to bringing the extract to its final volume. For the analytical injection, all compounds are separated by reversed phase liquid chromatography (75mm x 4mm Nova-Pak C18) and introduced directly to the mass spectrometer using a heated nebulizer APCI probe. The analytes are analyzed by positive ion MS/MS using either the protonated molecular ions (carbofuran and malathion) or thermal degradation ions (Methylparathion and d_{10}-Deethylparathion) as precursors. See Figure 2 for a chromatogram of a matrix fortification analysis at the estimated MDL. A linear regression ($1/x^2$) is used for quantitation. Samples were quantitated using the area response ratios of the analytes/internal standards (y) versus the concentration of the native compounds (x) from all standards injected. Each analysis requires approximately 13 minutes. See Figure 3 for a comparison of results between API III ^{plus} and API 300.

TABLE I: LC-APCI/MS/MS Method Detection Limit Study

EMDL Spike Level (ppb)	Methylparathion ppb	Methylparathion % Rec	EMDL Spike Level (ppb)	Malathion ppb	Malathion % Rec	EMDL Spike Level (ppb)	Carbofuran ppb	Carbofuran % Rec
N/A	ND		N/A	ND		N/A	0.01604	
0.1	0.1042	104	0.05	0.04549	91	0.01	0.01038	104
	0.08594	86		0.04422	88		0.01057	106
	0.07678	77		0.04976	100		0.01087	109
	0.09075	91		0.04053	81		0.01103	110
	0.07927	79		0.04794	96		0.01070	107
	0.07640	76		0.04718	94		0.01028	103
	0.08475	85		0.04589	92		0.01024	102
Mean	0.08544	85	Mean	0.04586	92	Mean	0.01058	106
SD	0.0098		SD	0.0030		SD	0.00030	
MDL	0.031		MDL	0.0093		MDL	0.00094	
LOQ	0.098		LOQ	0.030		LOQ	0.003	

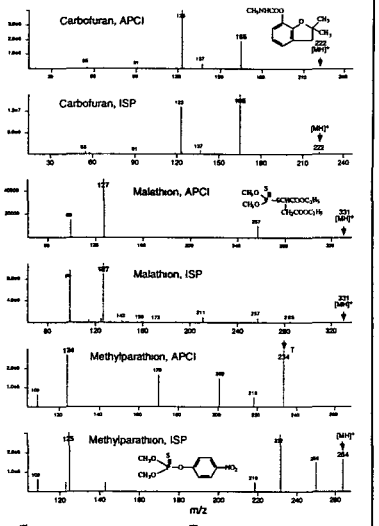

Figure 1: (right)
Product ion Spectra for Carbofuran, Malathion, and Methylparathion under APCI and IonSpray conditions
Precursor ions are indicated by an arrow. The Ion labeled "T" indicates a thermal fragment of Methylparathion used as the precursor ion.
The product ions used in the MRM analysis are indicated in bold

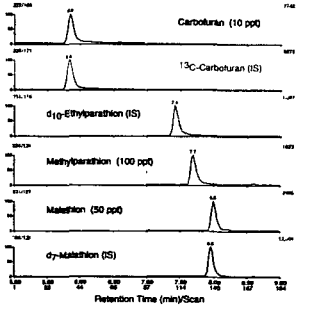

Figure 2:
APCI-LC/MS/MS (MRM) of rice drainage water matrix fortified at the indicated EMDL levels.

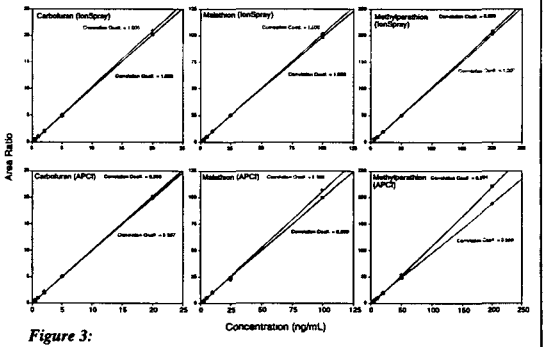

Figure 3:
Comparison of quantitative results between API III ^{plus} and API 300 (data shown in grey).All calibration curves use a $1/x^2$ linear regression and all correlation coefficients were between 0.997 and 1.000.

CONCLUSION

Atmospheric pressure ionization LC/MS/MS has been successfully applied to environmental analysis of several compound classes. Method Detection Limit studies demonstrate that accuracy and precision data equals or exceeds that obtained from traditional GC and LC methodologies with quantitative reporting limits in the low ppt level for water. The need for sample cleanup is dramatically reduced due to the inherent specificity of the technique. The methods are rugged and are capable of providing reliable results on a routine basis.The comparison of the results from the API III ^{plus} and the API 300 indicated similar response characteristics for the analyte classes studied.

Analysis of Pyrethoid Insecticides by Ion Trap GC/MS/MS

Gerald F. Bauerle, Jr., Kenneth L. Ray, and Jennifer S. Brodbelt*
Univerisity of Texas at Austin
Department of Chemistry
Austin, TX 78712

Pyrethoids are derivatives of pyrethrin, an extract of the Chrysanthemum family of plants, and are used as insecticides worldwide [1]. Many different methods have been used to analyze them including HPLC [2,3], and more commonly GC with appropriate detectors. Recent advances in ion trapping technology have promoted the development of sensitive and versatile bench-top gas chromatograph/tandem mass spectrometers which permit electron and chemical ionization of components in addition to collisionally activated dissociation of ions [4-6]. Detection limits as low as 0.5 ppb have been reported for standardized reference components, and complete mass spectra can be accumulated in a little as 80 ms [7].

Chemical Ionization and Collisionally Activated Dissociation of Compounds

The reactant ions of 43 and 57 u from isobutane were isolated after ionization, and were then allowed to react with the pyrethoids. For the CAD experiments typically the protonated pyrethoid was activated unless its abundance was too small, as for the cases of tetramethrin (331) and bifenthrin (422). Protonated tetramethrin dehydrated very efficiently and was used for CAD studies. For bifenthrin, none of the protonated structure remained intact. The ion at 361 u had a large intensity as well as a high mass to charge ratio, so it was used for CAD as well.

Since the Saturn 4D ion trap mass spectrometer is capable of performing CAD in real time on ions of different mass to charge ratios as they elute from the capillary column, experiments were performed to test the ability of the instrument to isolate and dissociate ions of different mass to charge ratios which elute closely. It was demonstrated that it was possible to successfully activate the dehydrated tetramethrin ion at 314 u, activate the ion from bifenthrin at 361 u, and switch back to activation of the 314 u ion.

Comparison of SECI/CAD to SECI and Interpretation of CAD spectra

The SECI/CAD spectra show several significant differences from the SECI spectra. For example, the SECI and the SECI/CAD spectra for bioallethrin (302) show several new ions, such as a fragment ion at 203 u which is one of the most abundant products in the CAD spectrum. Present in the SECI and SECI/CAD spectra is an ion at 285 u which indicates a loss of water. Ions appearing at 151 u and 123 u can be explained by a mechanism previously reported by Holmstead and Soderlund [8]. This cleavage to give a oxonium ion and an alcohol is characteristic in the CAD spectra of all the protonated pyrethoids.

A comparison of the SECI spectrum to the SECI/CAD spectrum, activation of $(M + H - 62)^+$, of bifenthrin shows numerous differences, having only the 181 u ion in common.

In the CAD spectrum of protonated cypermethrin (415), only two fragment ions are produced, 191 and 388 u. The ion at 191 u is from the ester cleavage of the protonated species [9]. The other is due to a loss of 28, possibly CO from the carbonyl group of the ester giving an ion at 388 u.

Tetramethrin does not show drastic differences in the SECI and SECI/CAD spectra as does bifenthrin. Thus, it is likely that many of the fragmentation processes include dehydration as the first step. Ions at 151 u and 123 u in the SECI spectrum, corresponding to the characteristic ester cleavage from protonated tetramethrin followed by the loss of carbon monoxide, are present. This combination is identical to the one seen for bioallethrin.

Limits of Detection

Limits of detection for bioallethrin and deltamethrin (503), corresponding to the first and last peak of the separation as well as the highest and lowest molecular weights, were determined. Upon isolation of the protonated bioallethrin analyte, the detection limit decreased to 50 ppb from 5 ppb, a loss of an order of magnitude, which can be explained by several factors. First, the ion at 303 u only represents 46 percent of the sum of the three most predominant ions used for determining the SECI limit of detection. In addition, upon isolation, the waveform generator incidentally ejects a portion of the desired ion. Using the CAD mode, the limit of detection decreases by a factor of four from the isolation mode. Since the three most predominant ions in the SECI/CAD spectrum comprise 46 percent of the total signal , it appears that half of the ions were lost.

The SECI limit of detection for deltamethrin was 0.5 ppm which represents an order of magnitude improvement over the detection limit previously reported for a quadrupole mass analyzer system [9]. The SECI-isolation technique showed a deterioration in the limit of detection similar to that of bioallethrin, but the fact that selected isolated ion only represented 2 percent of the total ion current in the original SECI product spectrum indicates an efficient isolation procedure. The SECI/CAD limit of detection was identical to that of the SECI-isolation technique, indicating nearly quantitative dissociation of the isolated precursor ion to the product ion at 281 u.

References

[1] W. Blaß, Chem. of Plant Prot., 3 (1990) 1.
[2] P. G. Baker and P. Bottomley, Analyst, 107 (1982) 206.
[3] S.G. Lisseter and S. G. Hambling, J. Chromatogr., 539 (1991) 207.
[4] M. Wang. and G. Wells, Proceedings of the 41st ASMS Conference on Mass Spectrometry and Allied Topics, (1993) 463.
[5] B. Bolton, G. Wells and M. Wang, Proceedings of the 41st ASMS Conference on Mass Spectrometry and Allied Topics, (1993) 474.
[6] B.A. Shaffer, J. Karnicky and S.E. Buttrill, Proceedings of the 41st ASMS Conference on Mass Spectrometry and Allied Topics, (1993) 802.
[7] J.B. Plomley, C.J. Koester and R.E. March, Org. Mass Spectrom., 29 (1994) 372.
[8] R.L. Holmstead and D.M. Soderlund, J. Assoc. Off. Anal. Chem., 60 (1977) 685.
[9] R.O. Lidgard, A.M. Duffield and R.J. Wells, Biomed. Environ. Mass Spectrom. 18 (1986) 677.

Compounds Produced by Motor Burnouts of Refrigeration Systems

Carolyn J. Koester*, Ruth A. Hawley-Fedder, and Linda Foiles
Lawrence Livermore National Laboratory, Livermore, CA 94568

Introduction: The phase-out of chlorofluorocarbons has necessitated the introduction of alternate refrigerants. R22 (CF_2ClH), R134a (CF_3CH_2F), and R507 (50/50 CHF_2CF_3/CF_3CH_3) are newer fluids which are used in cooling systems. Recently, concern over the possible formation of toxic compounds during electrical arcing through these fluids has prompted us to identify their electrical breakdown products by electron ionization GC/MS. For example, it is known that perfluoroisobutylene (PFIB), which has an threshold limit value of 10 ppb (set by the American Conference of Government Industrial Hygienists), is produced from the thermal and electrical breakdown of some refrigerants. We have used specially designed test cells, equipped with electrodes, to simulate the electrical breakdown of R22, R134a, and R507 in refrigeration systems.

Experimental: R22, R134a, or R507 were introduced into a test cell as gases. The test cell used for experiments at 15 PSI was made of epoxy, had a 93 mL volume, and had brass electrodes having a surface area of 0.8 in^2. The cell used for experiments at high pressure and temperature was made of vespel, had a volume of 77 mL, and had brass electrodes with a surface area of 0.3 in^2. The test cell had been previously filled with 1% by weight of the appropriate oil--Calgon C4 was used with R22 and EM Karate RL-327 was used with R134a and R507 Oil was added to the cells to simulate conditions expected in motors--oils are used to lubricate pistons in compressors and it is known that some contamination of the refrigerant by this oil will occur. The cell was then evacuated to 20 mtorr before being filled with the selected refrigerant. The refrigerant, as a gas, was subjected to up to 200,000 electrical pulses (30 µsec, 20 kV pulsed-breakdown at 100 Hz) and the resulting gas mixture was sampled and analyzed by GC/MS with a Hewlett-Packard 5989. The GC column (Restek RTX-1, 105 m, 250 µm i.d., 1 µm film thickness) was temperature programmed as follows: -30°C for 13 min, ramped at 5°C/min to 150°C, held for 10 min, ramped at 10°C to 300°C, and held for 10 min. The MS was operated in the electron ionization mode and scanned from 30u to 650u in 1.1 sec.

Results: The formation of many new compounds was observed; Table 1 shows the major compounds produced when R22 was subjected to electrical breakdown at 15 PSI and 20°C. Compounds were tentatively identified by using mass spectral data bases. Many of the compounds that were produced at 15 PSI and 20°C were also produced at 200°C and at higher pressures; however, the distribution of products changed slightly. The total amount of breakdown products increased with increasing arc exposure for experiments performed at 15 PSI and for experiments performed at higher pressures.

Conclusions: Many different compounds are formed at parts-per-thousand concentrations as electrical arcs are passed through refrigerants. PFIB was not present in sufficient quantities to be detected by GC/MS; thus, we plan to use the more sensitive GC/ECD to look for its presence. The variety of compounds produced suggest that interesting chemistry is occurring, including the formation and recombination of radicals to produce species which are larger than their parents. The electrical burnout of actual refrigeration motors will be performed to determine how well our test cells simulate processes that can occur in refrigeration systems.

Table 1. Major compounds present after 100,000 arcs passed through R22 at 15 PSI and 20°C. Each number represents the average of duplicate measurements.

Tentative Identification	mg/g R22
tetrafluoroethene	300
dichlorodifluoromethane (R12)	200
dichlorotetrafluoroethane	50
hexafluoropropene	40
dichlorohexafluoropropane	10
dichlorodifluoroethene	10
trichloropentafluoropropane	9
chloropentafluoropropene	8
chlorotrifluoropropyne	8
dichlorodifluoroethene	8
trichloropropene	8
dichlorodifluoroethene	7
chlorine & fluorine containing hydrocarbon	7
trichlorofluoromethane	6
dichloroethyne	6
trichlorofluoroethylene	6
chlorodifluoromethane	5
dichlorotetrafluorocyclobutene	5

Acknowledgments: We thank Dave Goerz, Gary Mease, Ken Leighton, and John Sze for support in the construction and operation of the test cells. We also thank the Air Conditioning and Refrigeration Technology Institute for funding.

Work performed under the auspices of the U.S. Department of Energy by the Lawrence Livermore National Laboratory under contract W-7405-ENG-48.

Collisionally-Induced Fragmentation of Chlorinated *n*-Paraffins.

G.T. Tomy[a,b], J.B. Westmore[b], D.C.G. Muir[a] and G.A. Stern[a].
[a] Fisheries and Oceans, Winnipeg, MB. R3T 2N6, Canada.
[b] Department of Chemistry, University of Manitoba, Winnipeg, MB. R3T 2N2, Canada

Introduction. Chlorinated *n*-paraffins (CPs) are used as fire retardants, plasticisers in PVC, adhesives, and as extreme pressure additives in lubricants and cutting oils. They have also found use as replacement chemicals for more toxic and persistent chemicals such as PCBs.

There have been a few reports of the mass spectrometric behavior of CPs[1,2]. In these studies, efforts were made to resolve commercial mixtures by capillary gas chromatography (gc) columns, prior to introduction into the ion source. Because of the inherent complexity of commercial mixtures, most peaks eluting off the gc-column contained multiple components, and thus mass spectra were not of individual congeners.

Clearly then, there is a need for individual CP congeners. Methods of synthesizing individual CP congeners have already been developed in our laboratory[3]. In addition, the positive electron ionization (EI) and the electron capture negative ion (ECNI) mass spectrometry of these synthesized CP congeners have been described.

In this report, we describe the fragmentation behavior of two individual CP congeners by examining the results of a detailed study of metastable and collisionally induced dissociation (CID, argon) processes. Fragmentation pathways were determined by B/E, B^2/E and CNL linked-field scanning.

Mass Spectrometer. All studies were carried out on a Kratos Concept high resolution mass spectrometer controlled by a Mach 3 data system. EI mass spectra were scanned from 40 to 500 daltons at a scan rate of 0.7 seconds per decade. The ion source was maintained at a temperature of 220°C, the trap current was 500µA and the ion acceleration voltage was 8kV. The electron beam energy was adjusted for maximum sensitivity (~50eV). Ion decomposition was enhanced by collisional activation by introducing argon into the collision cell at a pressure sufficient to attenuate the m/z 231 ion of PFK by 50%.

Chromatography. GC separations were performed with a Hewlett Packard 5890 Series II gas chromatograph using a 60 m x 0.25 mm DB5 column, with He as the carrier gas. The initial column temperature was set at 80°C; it was ramped to 280°C at a rate of 10°C/minute and held there for 10 minutes. The injector and transfer interface were set at 200°C and 280°C respectively.

Results and Discussion. The EI positive ion mass spectra of one of the congeners, 1,2,9,10-tetrachlorodecane, $C_{10}H_{18}Cl_4$ (M_4) is shown in Figure 1. As reported earlier, the EI mass spectra of CP congeners do not show the presence of molecular ions; however, many fragment ions resulting from one, or several, losses of HCl and Cl· are observed[3].

Several fragmentation mechanisms for this compound have been determined (***Scheme I***). For the M_4 species, consecutive losses of 2 molecules of HCl lead to the $C_{10}H_{16}Cl_2^+$ ion, m/z 206, which is the precursor of a number of other significant ions. The mechanisms proposed involve known six-membered cyclic transition structures for the HCl losses, and 1,2 H-shifts for the subsequent decompositions. The dominant m/z 139 ion, $C_5H_9Cl_2^+$, had no identifiable precursor, so is assumed to be formed by rapid decomposition of $M_4^{+\cdot}$ in the ion source; the formation of a five-membered cyclic ion, as shown, is known to be a favored process.

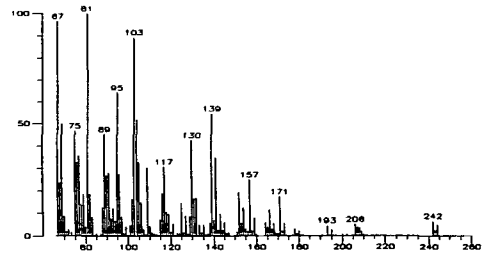

Figure 1. EI positive ion mass spectrum of M_4.

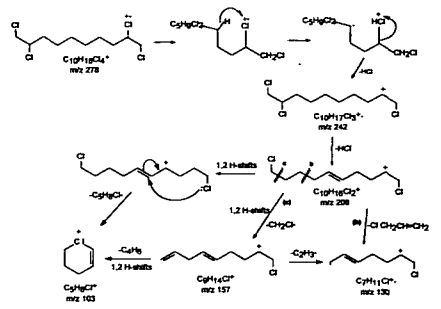

Scheme I. Decomposition mechanisms for M_4.

It is interesting to note that at low mass in the mass spectrum of M_4 there exist many even-electron odd mass ions To date, the precursors of many of these ions have not been established. The ions at m/z 117, 103, 89 and 75 correspond to the series $C_nH_{2n-2}Cl^+$. Proposed structures are shown below

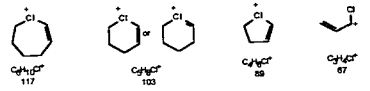

Conclusions. The EI and CID mass spectrum of M_4 shows characteristic losses of HCl and Cl atoms, as well as some structure-specific ions. These results are a necessary step in the development of analytical techniques for characterization of complex CP mixtures.

References.

1 Schmid, P P., Muller, M.D **1985**. *J. Assoc. Off. Anal. Chem.* 68, 427-430
2. Gjos, N.; Gustavsen, K.O. **1982**. *Anal. Chem.* 54, 1316-1318.
3. Tomy, G.T., Muir, D C.G., Westmore, J.B.; Stern, G.A. 42nd Annual Conference on Mass Spectrometry and Allied Topics, Chicago, **1994**, pg 263.

LC-MS/MS Identification and Analysis of a Major Human Urinary Metabolite of Alachlor

William J. Driskell[1], Robert H. HIll, Jr.[1], Dana B. Shealy[1], and R. Delon Hull[2]
[1]National Center for Environmental Health and Injury Control, Centers for Disease Control and Prevention, U.S. Department of Health and Human Services, Atlanta, Georgia 30333 USA
[2]National Institute for Occupational Safety and Health, U.S. Department of Health and Human Services, Cincinnati, Ohio 45242 USA

Alachlor (2-chloro-2',6'-diethyl-N-(methoxymethyl)acetanilide) is a commonly used preemergence herbicide on soybeans, corn and other crops. It is rapidly and completely metabolized to products that have not been characterized in human urine. Alachlor exposure has commonly been estimated by quantifying the base hydrolysis product, 2,6-diethylaniline (DEA), of alachlor metabolites in urine (Cowell et al 1987). In this study we attempted to identify alachlor metabolites by LC-MS/MS analysis of extracts of urine samples from subjects who were occupationally exposed to alachlor.

Four 25 ml samples from workers occupationally exposed to alachlor were obtained from the Environmental Protection Agency (EPA). To estimate the total concentration of alachlor metabolites in the samples, we used a base-pressure hydrolysis method, based on that of Cowell et al, 1987, that converts alachlor metabolites to 2,6-diethylaniline. We analyzed ethylacetate extracts of urine samples from the occupationally exposed subjects and unexposed control subjects with the Finnigan TSQ-7000 mass spectrometer by LC-MS/MS in the APCI mode. Our approach for identifying alachlor metabolites was to look, by means of MS/MS parent scanning, for parents of alachlor daughters with the presumption that some alachlor daughters would also be produced by alachlor metabolites. Two major alachlor daughters were present: A 238 amu dau was produced by a loss of a CH_3OH moiety and the 162 amu dau was produced by the loss of a $CH_3OC{=}OCH_2Cl$ moiety. There was a peak with a retention time of 5 min when the 162 amu daughter was analyzed in the parent scan mode in the samples from exposed subjects but no peak in the controls. Changing to daughter scanning, we found, in addition to the 162 amu daughter, two other major daughters of 365 amu and 130 amu. The 365 amu dau is a loss of methanol analogous to the 238 dau of alachlor; this implies that the amine methoxymethyl sidechain is still intact. We postulated that the 130 amu dau might be a product of an N-acetylcysteine moiety in which the sulfur-carbon bond is cleaved. From these data, a likely structure, analogous to that of some other pesticide metabolites, is the N-acetylcysteine displacement of the chlorine atom of alachlor to produce alachlor mercapturate. Based on mass spectrometry and chromatographic behavior of synthetic alachlor mercapturate, we identified this human metabolite of alachlor as alachlor mercapturate.

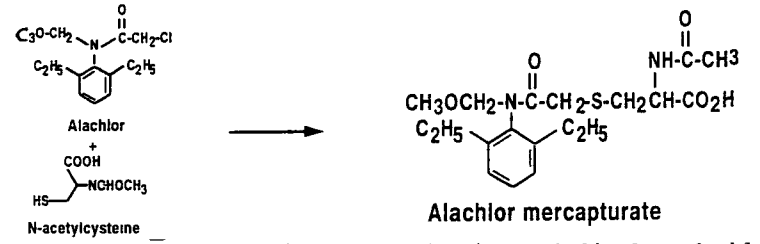

To estimate what proportion of alachlor is metabolized to alachlor mercapturate in humans, we analyzed exposed urine samples using the base hydrolysis method that quantitates DEA and, also, quantitated alachlor mercapturate in the same samples.

Sample	DEA (nanomolar)	Alamerc (nanomolar)
A	930	350
B	470	120
C	4320	2750
D	1120	475

In these four urine samples, alachlor mercapturate ranges between 25% and 62% of the concentration of DEA, the hydrolysis product that probably almost all alachlor metabolites produce.

In monkeys injected with radioactive alachlor, alachlor mercapturate was the major metabolite accounting for about 40% of the metabolite concentration (Carr et al, 1986). No free alachlor was detected in urine. Other pesticides besides alachlor, including lindane, cyanatryn (Aizawa 1982) and atrazine (Lucas et al 1993), and xenobiotics, including acrolein, benzene, vinyl chloride, and various allylic and benzylic halides (Stanek 1993), are metabolized to thioethers like alachlor.

References

Cowell JE, Danhaus RG, Kunstan JL, Hackett AG, Oppenhuizen ME, Steinmetz JR (1987). Arch. Environ. Contam. Toxicol. 16, 327-332.
Carr, KH, Chott, RC, Howe, RK, Malik, JM (1986). The Sixth International Congress of Pesticide Chemistry, IUPAC, Ottawa, Canada, Abstract 7c-06.
Stanek W, Krenmayr P, Scherer G, Schmid ER (1993) . Biol. Mass Spec. 22, 133-142.
Aizawa H (1982) In Metabolic Maps of Pesticides. Academic Press Inc.: New York. p 76 and p 216.
Lucas AD, Jones AD, Goodrow MH, Saiz SG, Blewett C, Seiber JN, Hammock BD (1993). Chem. Res. Toxicol. 6, 107-116.

Structural Characterization of Toxaphene Congeners by GC/MS

Frank M. Benoit[1], Alex Driega[2] and Murugan Malaiyandi[2]
[1]Environmental Health Directorate, Health Canada, Ottawa, Canada, K1A 0L2
[2]Centre for Analytical and Environmental Chemistry, Ottawa, Canada, K1S 5B6

Technical toxaphene is produced by chlorination of C10 terpenes and contains a highly complex mixture of polychlorinated bornane congeners that are difficult to isolate and characterize by GC/MS. Mass spectral characterization is hampered by the sheer number of congeners eluting into the ion source within a narrow time window, rendering it impossible to obtain a pure mass spectrum of an individual congener. Chlorination of 2-exo-,10-dichlorobornane produced a less complex mixture from which individual hepta-, octa- and nona-chlorobornanes were selectively isolated from the chlorinated mixture using a multistage purification scheme based on column chromatography and preparative HPLC. The nature and purity of each fraction were monitored by GC analysis at each stage of the fractionation until the purity of the sample was sufficient (> 90%) for congener characterization by GC/MS (EI and ECNI). Of the eight fractions isolated in this manner, six contained a single toxaphene congener and two contained minor components as well as one major toxaphene congener. Generally toxaphene congeners do not show molecular ions under electron impact ionization, however, very weak molecular ions may be observed when larger amounts are injected. ECNI (methane) produced simpler mass spectra consisting primarily of one cluster of ions resulting from the loss of chlorine from the molecular ion. The chlorine content of the original molecule was determined from the distribution of peaks within the fragment ion cluster. There is little structural information available in the ECNI mass spectra but the EI mass spectra of toxaphenes provides a complex array of ions which contains a wealth of structural information.

Table 1. Percent Distribution of Fragmentation Streams in High Mass Region

Congener (Knowns)	# of Chlorines	M-Cl -nHCl	M-HCl $C_2H_{4-x}Cl_x$	M-CH_2Cl -nHCl	M-$CHCl_2$ -nHCl
TOXB	7	55	15	30	0
TOX8	8	31	14	0	54
TOX9	9	45	21	0	34
A1750	8	64	0	10	26
(Unknowns)					
G1380	7	46	40	14	0
I1482-1	7	49	10	0	41
I1482-2	7	42	30	0	28
01677-1	8	78	0	0	22
01677-2	8	68	15	0	17
J1648	8	49	28	23	0
R1728	8	59	18	23	0
01677-3	9	47	21	0	32
U1836	9	88	0	0	12

The primary fragmentations were the losses of Cl, HCl, CH_2Cl and $CHCl_2$ from the molecular ion and the secondary fragmentations were the losses of Cl, HCl, CH_2Cl, $CHCl_2$ and $C_2H_{4-x}Cl_x$ (Retro Diels-Alder). The major fragmentation streams consisting of a primary fragmentation followed by a series of secondary fragmentations were: M-HCl-$CH_{4-x}Cl_x$, M-CH_2Cl-nHCl, M-$CHCl_2$-nHCl and M-Cl-nHCl. Unlike other isomeric compounds, the isomeric chlorinated bornane congeners presented distinctive EI mass spectra; hence, the structural integrity of the ions was retained, at least through the initial fragmentation steps. The structure of the chlorinated bornane could not be completely determined from the EI mass spectrum alone. However, some structural features, such as the distribution of chlorine in the three possible locations within the molecule (ring, C10 and C8/C9) could be established. Based on the mass spectra of known toxaphene congener structures, the structures of unknown congeners were assigned as follows: The Retro Diels Alder fragmentation occured from either ring segment and provided information on the ring chlorine distribution: M-HCl-$C_2H_2Cl_2$ only indicated symmetric ring chlorines (2:2) whereas M-HCl-C_2H_3Cl indicated asymmetric ring chlorines (2:1). The Retro Diels Alder fragmentationwas absent in fractions A1750, O1677-1 and U1836 (Table 1). The structure of A1750 (as determined by x-ray crystallography - 2,2',5,5',8,9,10,10'-octachlorobornane) suggested that the loss of HCl from the molecular ion was forbidden when all the ring chlorines were geminal (CCl_2). The loss of $CH_{3-x}Cl_x$ provided information on the C10 chlorine distribution. Both CH_2Cl (C8) and $CHCl_2$ (C9 and C10) groups were present in TOX9. C8 and C9 are essentially equivalent positions and the loss of $CH_{3-x}Cl_x$ would be expected to occur from either position with equal probability. However, only the loss of $CHCl_2$ was observed. Therefore the loss of $CH_{3-x}Cl_x$ must occur primarily from the C10 position. The C8/C9 substitution was deduced by difference between the total number of chlorines and the sum of the ring and C10 chlorines. The structural features of the isolated toxaphene congeners are summarized in Table 2.

Table 2. Structural Features of Isolated Toxaphene Congeners

Congener	#Cl	C10	Ring	C8/C9
G1380	7	CH_2Cl	2:2	2Cl
I1482-1	7	$CHCl_2$	2:2	CH_2Cl/CH_3
I1482-2	7	$CHCl_2$	2:1	2Cl
A1750	8	$CHCl_2$	2:2 (g)	$CHCl/CH_2Cl$
01677-1	8	$CHCl_2$	2:2 (g)	2Cl
01677-2	8	$CHCl_2$	2:1	3Cl
J1648	8	CH_2Cl	2:2	3Cl
R1728	8	CH_2Cl	2:2	2Cl
U1836	9	$CHCl_2$	2:2 (g)	3Cl

(g) all chlorines are geminal

Characterization of Three Major Toxaphene Components in Ringed Seal Blubber

M.D. Loewen[1], G.A. Stern[2], D.C.G. Muir[2], J.B. Westmore[1], H. Parlar[3].

[1]Department of Chemistry, University of Manitoba, Winnipeg, MB, R3T 2N2, Canada. [2]Freshwater Institute, Department of Fisheries and Oceans, Winnipeg, MB, R3T 2N6, Canada. [3]Lehrstuhl fur Chemisch-Technische Analyse und Chemische Lebensmitteltechnologie der TU Munchen, D-85350 Freising-Weihenstephan, Germany.

Toxaphene, a complex pesticidal mixture consisting primarily of chlorinated bornanes (CHBs), was widely used in the US, Canada and other parts of the world before its ban in the early 1980's[1]. It's primary use was as an insecticide for cotton and soybean crops, and briefly as a piscicide in the late 1950's, and 1960's[1]. Although technical toxaphene is thought to consist of between two and three hundred penta- to undecachlorobornanes, a much more limited number have been shown to be environmentally significant[1]. At present only one Cl_9 compound, T12, and one Cl_8 compound, T2, have been structurally identified in marine environmental samples.[2,3]

We report here the isolation of three more environmentally significant CHB congeners, TS2, TS3 and TS4, extracted from Ringed seal blubber, and their structures as determined by mass spectrometry (GC-ECNIMS (CH_4), low resolution EIMS, and linked field scanning).

A Kratos Concept high resolution mass spectrometer, yielded mass spectra of TS2, TS3, and TS4. From ECNIMS we have determined that TS2, 3, and 4 are octachlorobornanes. Three major ion degradation pathways in the positive ion spectra, can be used to identify a given CHB congener First, is the loss of C_2H_3Cl, $C_2H_2Cl_2$, or C_2HCl_3 after an initial loss of HCl or Cl_2 from the molecular ion. This gives rise to an even mass odd-electron ion that is characteristic of the number of chlorine atoms located on C2-C3 and C5-C6. Elimination of a neutral fragment comprised of C7 and it's two attached substituents yields information regarding the bridging group's (C7, 8, 9) chlorine content. Observation of decompositions involving the elimination of CH_2Cl or $CHCl_2$ (eg $[M-CH_2Cl]^+$) gives evidence as to the identity of the substituted chloromethyl groups on C7, while the presence of CH_2Cl^+ or $CHCl_2^+$ ions at m/z 49 and 83 respectively provide information with regard to the chlorine substitution on C10.

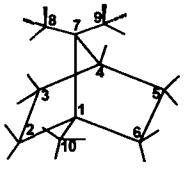

Bornane skeleton

In the positive ion mass spectrum of TS2 the even mass odd-electron ion of m/z 244 is the result of two processes. Successive losses of Cl_2 and $C_2H_2Cl_2$, or of HCl and C_2HCl_3, from M^{+o} indicate that there must be five chlorine atoms on the ring, two on one side and three on the other. The exact positioning of these ring chlorines however could not be determined by mass spectrometry. An ion

giving rise to a peak at m/z 195 results from loss of $C_3H_4Cl_2$ from $[M-Cl_2-Cl]^+$ (m/z 305), indicating there is a total of two chlorines on the of successive losses of HCl and $C_2H_2Cl_2$ from M^{+o}. There is no other significant pathway resulting in an even mass odd electron ion and we can therefore conclude that there must be two chlorine atoms on bridging group. The observed losses of CH_2Cl from M^{+o} and $[M-Cl_2]^{+o}$ and not of $CHCl_2$, suggest the presence two monochloromethyl substituents on C7. The one remaining chlorine atom must be positioned on C10.

In the positive ion mass spectrum of TS3 a peak observed at m/z 278 is the result each of the C2-C3 and C5-C6 sides of the ring. By the high relative abundance of $[M-HCl]^+$ we can conclude that the chlorine substitution pattern on the ring is trans staggered (e.g. 2-exo,3-endo,5-exo,6-endo), but the actual substitution pattern cannot be verified by mass spectrometry. Loss of the neutral fragment $C_3H_4Cl_2$ from $[M-HCl-Cl]^+$ indicates the presence of two chlorine atoms on the bridging group. Loss of CH_2Cl from M^{+o} and $[M-HCl]^{+o}$ and the absence of losses involving $CHCl_2$ verify that the two chlorines in the bridging group are the result of two monochloro substituents on C7. The remaining two chlorine atoms must be positioned on C10. Support for a dichloromethyl group at C10 is shown by the presence of a peak corresponding to $CHCl_2^+$ at m/z 83.

A significant feature of the positive ion mass spectrum of TS4 is the very low relative abundance of the even mass, odd-electron ion at m/z 278, which results from the loss of $C_2H_2Cl_2$ from $[M-HCl]^{+o}$. As with TS3, the observed loss of $C_2H_2Cl_2$ indicates the presence of two chlorine atoms on both C2-C3 and C5-C6. Lack of a predominant even mass odd-electron ion would be consistent with a ring structure having a geminal dichloro-substitution and an adjacent unchlorinated carbon. Elimination of HCl in this case would be less likely while loss of Cl would be favoured. We cannot, however, verify the actual chlorine substitution pattern on the ring by mass spectrometry. Loss of $C_3H_3Cl_3$ is observed from $[M-HCl-Cl]^+$ This confirms the presence of three chlorine atoms on the bridging group. Decompositions involving the loss of CH_2Cl and $CHCl_2$ from M^+ and $[M-HCl]^{+o}$ indicate the presence of a dichloromethyl and monochloromethyl substituent on C7. The remaining chlorine must be located on C10.

Recently, Parlar *et al* were successful in isolating, and characterizing a number of CHBs in the technical mixture using mass spectrometry and NMR spectroscopy[4]. Based on their GC retention times and by comparison of full scan positive EIMS spectra, we found TS2, 3 and 4 to correspond to Parlar #39, 2,2,3-exo,5-endo-6-exo,8,9,10-octachloroborane; Parlar #40, 2-exo,3-endo,5-exo,6-endo,8,9,10,10-octachlorobornane; and Parlar #42, which is a mixture of 2,2,5-endo,6-exo,8,8,9,10-octachlorobornane, and 2,2,5-endo,6-exo,8,9,9,10-octachlorobornane respectively. The two compounds in Parlar #42 are identical except for the proximity of the substituted chloromethyl groups on C7 to the ring substituents. Since these two compounds would likely give the same mass spectrum we cannot conclude whether we have a single congener or a mixture of the two compounds.

(1) M.A. Saleh, Reviews of Environmental Contamination and Toxicology. Springer-Verlag New York. 1991, 118, 1-83.
(2) G.A. Stern, D.C.G. Muir, C.A. Ford, N.P. Grift, E. Dewailly, T.F. Bidelman, M.D. Walla, Environ Sci. Technol. 1992, 26, 1838-1840.
(3) G.A. Stern, D.C.G. Muir, J.B. Westmore, W.D. Buchannon, Biological Mass Spec. 1993, 22, 19.
(4) H. Parlar, *et al.* Unpublished data.

WHERE IN THE GREAT LAKES IS TOXAPHENE GOING?

Michael J. Howdeshell, Susan T. Glassmeyer,
Tanya R. Myers, and Ronald A. Hites
School of Public and Environmental Affairs and Department of Chemistry
Indiana University, Bloomington, IN 47405

Toxaphene is a broad range pesticide which was used primarily on cotton in the southeastern United States. Its use was banned by the US Environmental Protection Agency in 1986 because of its persistence. Residues of technical toxaphene are found in biota far removed from sites of its application. Because toxaphene is an extremely complex mixture of hexa- to decachlorinated norbornanes and norbornenes and because few of its numerous congeners have been synthesized, toxaphene can only be analyzed effectively with a selective analytical technique. Various methods have been used; however, electron capture gas chromatographic mass spectrometry (EC GC/MS) gives the most reproducible results due to its selectivity and sensitivity. To determine the fate of this pesticide in the Great Lakes, we have used EC GC/MS to determine total toxaphene concentrations and chlorination level profiles in fish and sediment. In all cases, it was necessary to correct the toxaphene concentrations by subtracting contaminant contributions by using isotopic abundances for toxaphene and for the expected interferences.

Lake Erie walleye and trout from the other four Great Lakes were collected in 1982 and 1992. While both species occupy the same relative level in the food chain, they show markedly different bioaccumulation mechanisms. Additionally, the chlorination level profile for the fish from Lake Erie is significantly different from that of fish from the other four Lakes, suggesting that some unique process is occurring in Lake Erie. Figure 1 shows the average toxaphene concentrations for Great Lakes fish in 1982 and 1992. The error bars represent one standard deviation. The overall decrease in toxaphene concentrations can be attributed to the ban of its production in 1982. The increase in Lake Superior concentrations indicates that there are additional unknown sources.

We have also analyzed Lake Ontario sediment and found that toxaphene fluxes maximize in 1973 ± 6 years with a horizon year of 1945 ± 6 years. This compares well with the small amount of production and usage data that is available. Total toxaphene concentration profiles for the eight Lake Ontario sediment cores are plotted in Figure 2. From these profiles, sediment *in situ* density, and overall sedimentation rate for each core, fluxes to the lake were calculated. The maximum flux to Lake Ontario sediment was 22 ± 8 $\mu g/m^2$ yr in 1973 and the total toxaphene load in the lake is 10 ± 3 metric tonnes. By comparing the toxaphene burdens for the cores, we conclude that toxaphene is deposited to Lake Ontario sediment from both the Niagara River and from the atmosphere. We have developed a simple toxaphene decay model by using the ratios of the concentrations of hexachlorinated toxaphene (6-Cl) to heptachlorinated (7-Cl) toxaphene. By plotting the natural logarithm of 6-Cl to 7-Cl abundance ratios *versus* time since deposition, one obtains a pseudo first-order kinetic plot. Figure 3 shows this function plotted for all the core data and the overall regression line; in this case, the slope is 0.017 yr^{-1}. Taking the reciprocal of this slope gives a time constant of about 60 years.

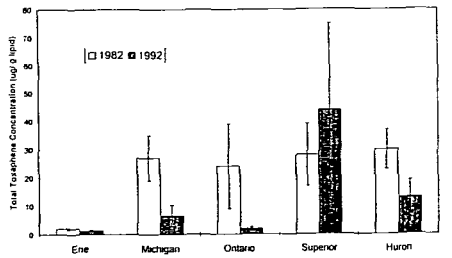

Figure 1. Average toxaphene concentrations in 1982 and 1992 Great Lakes fish.

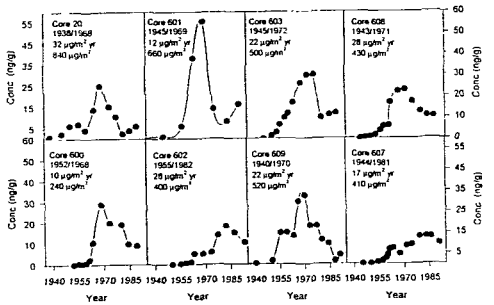

Figure 2. Toxaphene concentration profiles in Lake Ontario sediment cores with core identification, maximum and horizon years, maximum flux, and total burden listed on the plot. The cores are from the Niagara (core 20, 600), Mississauga (601, 602), Rochester (603, 609), and Kingston (607, 608) Basins.

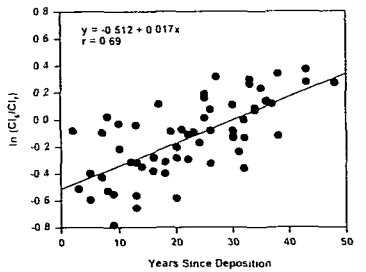

Figure 3. Plot of natural logarithm of the 6-Cl abundance divided by the 7-Cl abundance as a function of time since deposition for each core station; the regression is shown.

OPTIMAL ION TRAP MS/MS PARAMETERS FOR THE ANALYSIS OF DIOXINS AND FURANS

J.B. Plomley, R. S. Mercer* and R.E. March
Trent University, Department of Chemistry, Peterborough, ON. Canada K9J 7B8
***Dioxin/Furan Unit, Laboratory Services BranchOntario Ministry of Environment and Energy Etobicoke, ON, Canada M9P 3V6**

Introduction. Previously, one of the software limitations of non-research grade ion traps for analytical applications was the inability to quantitate using internal standards which chromatographically co-elute with their native analytes.[1] Further, the analysis by MS/MS of a number of different analytes which differ in parent ion mass was impossible in a single chromatographic run, since only one scan function could be applied per acquisition. These two impediments to quantitation have been alleviated on a number of commercially available GC/ion traps, thus making the ion trap suitable for dioxin and furan analysis using isotopic dilution techniques. An examination of those factors necessary for the optimization of an ion trap for dioxin and furan analysis by GC/MS/MS has been carried out. Specifically, three modes of resonant excitation were examined in an attempt to optimize the major dissociative channel (loss of COCl) from isolated parent ions. These modes were single-frequency irradiation (SFI), secular-frequency modulation (SFM), and multi-frequency irradiation (MFI). The last two resonant excitation modes obviate the laborious procedure required for empirically matching an applied single-frequency waveform to the fundamental secular frequency ($\omega_{z,0}$) of the ion.

Experimental. All data were acquired on a Varian Saturn 4D GC/ion trap with an EI/MS/MS scan function which consisted of (a) ionization at a low mass cut-off of 160 u, (b) waveform isolation of parent ions, (c) CAD using various modes of resonance excitation described below, and (d) mass analysis *via* an rf ramp. Saturn version 5.0 software was used for data acquisition while prototype software ("Toolkit") was required for the application of multiple-scan functions across a GC peak The ion trap was operated at 260°C with He buffer gas present at ≈1 mTorr. GC conditions for the separation of dioxins and furans have been described elsewhere.[1] The following were the conditions used for each mode of resonant excitation examined:
(a) **SFI**: Parent ions were irradiated at $q_z \approx 0.4$ for 30 ms with a single-frequency sine waveform.
(b) **SFM**: The rf applied to the ring electrode was varied over ranges of $4V_{0-p}$ and $6V_{0-p}$,with an ion dwell time of 5 ms/V_{0-p}. A single frequency sine waveform was applied at $\omega_{z,0}$ for an ion at $q_z \approx 0.4$.
(c) **MFI**: 1 kHz and 2 kHz bandwidth waveforms were applied to an ion at $q_z \approx 0.4$ for 30 ms.

Results and Discussion. Parent ion isolation efficiencies were on the order of 90% for all congener groups examined. Overall, each resonant mode of excitation accessed, to varying degrees, the energy channel corresponding to the loss of COCl. Under SFI conditions, waveform amplitudes required for optimal conversion efficiency (CE), corresponding to the loss of COCl, were larger for the furans (≈ $1.0V_{p-p}$) compared to the dioxins by as much as 400 mV_{p-p}; CE is defined as the sum of the daughter ion current divided by the abundance of the parent ion prior to dissociation. The larger waveform amplitude required for furan fragmentation compared to dioxin suggests that a larger activation energy barrier exists for the loss of COCl in the former species. Moreover, higher activation energy channels corresponding to the loss of $COCl_2$ and $COCl_3$ were observed for the furans;this contrasts with the high energy loss of 2(COCl) in dioxin. One noteworthy difference between the fragmentation channels of the dioxins and furans concerns the lowest energy channel, the loss of Cl. As much as 15% of the dioxin parent ion current (6% in furan) is conserved in the daughter ion resulting from loss of Cl. Thus the ion trap is more sensitive for furan detection than dioxin when the COCl channel is monitored. All the dissociation channels observed in the ion trap confirm those reported in earlier TSQ studies.[2]
Optimization of SFM required an examination of the ion dwell time and modulation range. For all congeners, a 5 ms ion dwell time/V_{0-p} was required for optimal CE, regardless of the modulation range. Furthermore, less than 5 CAD scan segments resulted in the incomplete dissociation of parent ions. The distribution of daughter ion current in SFM paralleled that of SFI when the optimal modulation range was used, and larger waveform amplitudes were required for furan dissociation compared to dioxin. In contrast to SFI, larger amplitudes were required for COCl loss using SFM, since the irradiating process was not continuous; $\omega_{z,0}$ is constantly changing. This can be rationalized as follows: When the frequency components of the ion are off-resonance with the applied waveform, collisional de-excitation can occur for internally excited ions which would otherwise undergo dissociation. Of course there will be instances when frequency components other than $\omega_{z,0}$ will be on-resonance. Since the amplitude of the applied waveform influences the collision energy by affecting the rate of increase in the amplitude of an ions trajectory, excitation at a frequency other than $\omega_{z,0}$ requires a larger waveform amplitude to achieve the same rate of increase in the amplitude of the trajectory. The optimal modulation range for SFM was not predictable. A $\pm 1V_{0-p}$ rf change corresponds to a ±200 Hz shift in $\omega_{z,0}$ at $q_z \approx 0.4$. Since empirically determined values of $\omega_{z,0}$ were never greater than +400 Hz from the waveform calculator utility, a $6V_{0-p}$ modulation range is extreme, though required in many instances for optimal CE. This suggests that a complex relationship exists between energy deposition and the ratio of time that an ion spends on- and off- resonance, and is the subject of further investigation using a thermometer molecule.

The following experimental observations characterize the MFI of dioxins and furans: (a) higher activation energy channels are more highly populated, (b) in contrast to SFI and SFM, larger amplitudes are required for optimal CE since each frequency component in the waveform only receives a portion of the specified voltage, (c) larger amplitudes are required to effect COCl loss in the furans (d) CE's for COCl loss are on average 5-15% less than observed with optimized SFI and SFM. Although the frequency pattern used to generate the waveform is designed to distribute the excitation power evenly over the bandwidth, the true power spectrum may contain an irregular power distribution that can lead to ion losses and reduced CE.

Preliminary results for the quantitation of dioxins and furans using toolkit software and optimal SFI conditions are impressive. The daughter ion extracted chromatograms for 1 pg of native 2,3,7,8-tetrachlorodibenzofuran and 1 pg of 2,3,7,8-tetrachlorodibenzo-*p*-dioxin, with their respective co-eluting $^{13}C_{12}$-internal standards) exhibited a Gaussian appearance, even though 4 scan functions were applied across each GC-peak (at a scan time of 0.5 s). S/N ratios of 15:1 for 1 pg of native analyte on the ion trap compared favourably with those observed on a TSQ 70 for the same calibration standard. Plots of response *vs* concentration were linear for many of the congener groups. For example, 2,3,4,7,8-pentachlorofuran analyzed with the ion trap by MS/MS over a concentration range of 2.5 pg-2,000 pg, had a correlation co-efficient of 0.99973 with a 17% RSD; analysis with the TSQ 70 also furnished a linear response, with a correlation co-efficient of 0.99975 and an RSD of 11%.

Conclusions. Both SFM and MFI represent resonant excitation techniques designed to overcome the shortcomings of automated frequency calibration and secular frequency shifting. The application of SFM for the analysis of dioxins and furans by MS/MS is unlikely; the CAD episode is too long (100-150 ms) and thus lowers the number of scan functions which can be applied across a GC-peak, as well as the number of μscans/scan. Parenthetically, we have found that a minimum of 4 μscans/scan are required to maintain the accuracy of each chromatographic data point. MFI is an alternative to SFM and satisfies the need for short CAD episodes, but CE's are lower and this may ultimately effect sensitivity.

While some fine tuning of the offset in SFI is required even after automated frequency recalibration, SFI with optimal irrradiating frequency offsets has initially produced satisfactory calibration results.

References

1. Plomley, J.B., Koester, C.J., and March, R.E. *Org. Mass Spectrom.* **29** 372-381 (1994).
2. Reiner, E.J., Schellenberg, D.H., and Taguchi, V.Y. *Env. Sci. and Technol.* **25** 110-117 (1991).

Determination of Elemental Compositions from Mass Peak Profiles of M, M+1 and M+2 Ions

Andrew H. Grange* and Joseph R. Donnelly
Lockheed Environmental Systems and Technologies, 980 Kelly Johnson Drive, Las Vegas, NV 89119
William C. Brumley and G. Wayne Sovocool
U.S.E.P.A., Environmental Monitoring Systems Laboratory, PO Box 93478, Las Vegas, NV 89193-3478

Mass peak profiles plotted from selected ion recording (SIR) data provide masses accurate to within 2.5 ppm for ions from trace components in complex mixtures. The number of elemental compositions with a mass within this error range increases rapidly with the ion's mass. At high mass resolution, 5 criteria for the M+1 and M+2 profiles are used to reject all but 1 composition.

Five criteria. At 20,000-25,000 resolution, interferences are usually separated from the M, M+1 and M+2 profiles. Four criteria, the relative abundances and masses of the M+1 and M+2 ions, are determined by using a split SIR descriptor to monitor across 60% of the M, M+1 and M+2 profiles simultaneously. The fifth criterion is the shape of the M+2 profile, which is observed using a SIR descriptor that monitors the full M+2 profile. SIR descriptors are prepared and data are processed by procedures written in Reflection™ 4.2, Lotus 1-2-3™ (2.2) and WordPerfect™ 5.1.

An example. An accurate mass of 423.2953 Da was obtained for an unknown compound in an environmental sample from a superfund site. Allowing up to 35 C, 74 H, 6 O, 6 N, 4 P, 4 S and 4 Si atoms and an error of ±2.5 ppm, 13 possible compositions were calculated. Of these, 5 were eliminated by invoking the nitrogen rule. The 8 remaining compositions are listed in Table I.

Table I. Error; M, M+1 & M+2 mass defects; relative abundances & ranges for 8 possible compositions

Error (ppm)	Composition	M	M+1		M+2	%M+1	%M+1 Range		%M+2	%M+2 Range		Shape M+2
-1.0	$C_{19}H_{45}O_4N_3Si_2$	.2949	.2969	x	.2937	30.2	(26.2-31.2)		8.8	(6.2-8.7)		x
-0.5	$C_{19}H_{45}O_3N_3SSi$	.2951	.2976	x	.2930	27.4	(25.0-28.6)	x	9.4	(5.8-9.1)		x
+2.5	$C_{19}H_{47}ON_3P_2Si$	.2964	.2989		.2968	26.7	(25.0-28.5)	x	4.8	(4.4-5.3)	x	x
+0.1	$C_{20}H_{45}O_2N_3S_2$	.2953	.2983		.2920	24.8	(23.6-25.8)	x	9.8	(4.6-8.9)		x
-1.4	$C_{20}H_{42}N_3PSi$	.2947	.2972	x	.2959	29.3	(26.7-30.3)	x	5.0	(5.0-5.2)	x	x
-1.0	$C_{20}H_{42}ONP_3$	.2949	.2982		.3014	24.2	(23.4-25.2)	x	2.9	(1.8-3.2)	x	x
+1.0	$C_{20}H_{41}ONSi$	.2957	.2986		.2993	35.0	(33.2-36.6)	x	6.5	(5.9-7.1)		x
+1.6	$C_{20}H_{40}NS$	.2960	.2992		.2980	32.5	(31.6-33.5)		6.0	(5.9-6.6)		

Hypothetical composition. A composition must be chosen before masses are calculated for the M, M+1 and M+2 profiles and used in a split SIR descriptor. After obtaining an M+2 profile, its shape and exact mass are compared to those predicted by the model to choose a hypothetical composition. If wrong, another composition with a similar M+2 profile will be identified as correct.

Model. A model was written in QuickBASIC™ and executed on a PC to calculate masses of M, M+1 and M+2 ions, estimates of the areas monitored by only 6 points about the center of the M, M+1 and M+2 profiles and a graphical representation of M+1 and M+2 profiles. The model also provides estimates of the range of %M+1 and %M+2 for the hypothetical and other compositions when the masses in the SIR descriptor are based on the hypothetical composition for shifts of ±5 ppm in the partial profiles' positions and ±10% changes in the resolution occur. The ranges also include the isotopic abundance errors possible for each element. The masses, relative abundances and their predicted ranges are listed in Table I at 21,400 resolution. An "x" next to an entry indicates that the criterion is useful for rejecting the composition based on an error of $\pm 2\sigma$.

Shape of the M+2 profile. In Figure 1 are shown M+2 profiles for 3 compositions from Table I calculated for 20,400 resolution. Each profile is plotted as the sum of contributions from all M+2 ions; those containing an M+2 isotope, two atoms of a single M+1 isotope or pairs of M+1 isotopes. The profiles for the compositions containing a S or Si atom are broad due to the large mass difference between the positive mass defect difference of ^{13}C vs ^{12}C and the negative mass defect differences of the M and M+2 isotopes (e.g., 2x0.00335-(-0.00420)=0.0109 Da for ions containing $^{13}C_2$ & ^{34}S). The shapes of the M+2 profiles shown are unique. The profiles obtained in Figure 2, acquired at (a) 20,400 and (b) 37,600 resolution, are similar to those predicted by the model (c) and (d) and identified the last composition as correct.

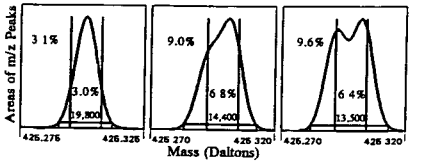

Figure 1.

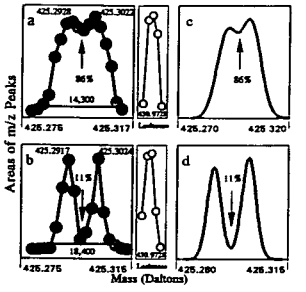

Figure 2.

Data. In Figure 3, partial profiles for the M, M+1, M+2 and PFK calibration ions plotted from SIR data acquired at (a) 10,100 and (b) 21,400 resolution are shown. After correcting the M+1 and M+2 masses for the error in the M mass, 1 and 3 compositions were rejected for falling outside the range of the observed M+1 mass ± 2.5 ppm at 10,100 and 21,400 resolution, respectively. Similarly, 4 compositions were rejected by the M+2 mass criterion at 10,100 resolution, but at 21,400 resolution, two maxima in the profile confused the issue.

In Figure 4 are plotted predicted ranges for (a) %M+1 and (b) %M+2 at 21,400 resolution for the 8 compositions. The dotted line marks the average %M+1 or %M+2 observed and the dashed box encloses 2σ. At 10,100 and 21,400 resolution, 5 and 7 compositions were rejected, respectively, by the %M+1 criterion. For the %M+2 criterion, 6 and 3 compositions were culled at 10,100 and 21,400 resolution.

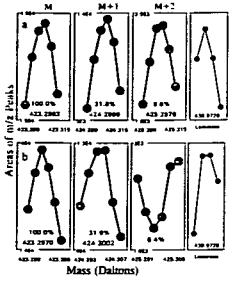

Figure 3.

Summarizing, at either resolution the correct composition was also identified by rejection of 7 of 8 compositions based on data acquired using the split SIR descriptor. Had another composition been correct, the 5 criteria would have confirmed the composition. These criteria can also be used to identify fragment ions.

Conclusion. Full and partial mass peak profiles plotted from data acquired with normal or split SIR descriptors at high mass resolution were used to identify the correct composition for a compound in a complex environmental extract. This technique is a valuable addition to the capabilities of double focusing mass spectrometers and is made possible by simple procedures executed on an ancillary computer.

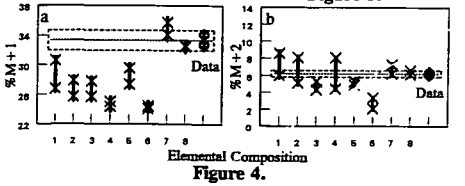

Figure 4.

References: *Anal. Chem.*, **1994**, *66*, 4416-4421; *Anal. Chem.*, Submitted; Oral TOB 05:00

Notice: This abstract was funded by the U.S. Environmental Protection Agency (EPA), through its Office of Research and Development (ORD), but does not necessarily reflect the views of the EPA or ORD.

DEVELOPMENT OF A MODERNIZED HRMS ENVIRONMENTAL METHOD FOR PCBS

J. R. Donnelly, A. H. Grange, G. R. Nichol, N. R. Herron,
J. L. Jeter, R. J. White, and W. C. Brumley*

Lockheed Martin-Environmental Systems & Technologies, 980 Kelly Johnson Dr., Las Vegas, NV 89119;
*U.S. Environmental Protection Agency (EPA), P.O. Box 93478, Las Vegas, NV 89193-3478.

The EPA Characterization Research Division at Las Vegas is developing a comprehensive screening and confirmatory method for monitoring PCBs, both as Aroclors and as individual congeners. About 130 PCB congeners are found in Aroclors.[1] This method includes extraction, extract cleanup, and analysis modules. Compatibilities of the modules are under investigation, and expected data quality and applicability for each technique will be included so researchers can select method features meeting cost, time, and data quality requirements.

Soxhlet, supercritical fluid (SFE), and accelerated solvent extractions (ASE) have been tested, and their performance characteristics have been determined. Both Soxhlet and the Dionex ASE™ provided high and reproducible recoveries. SFE required careful control of experimental variables, such as percent modifier (methanol) and cell temperature (not merely oven temperature), for adequate reproducibility. SFE also was less able to recover tightly-bound analytes from some soil matrices.

Carbon chromatographic cleanup procedures were elaborated with AX-21 (Anderson) and SK-4 (Alltech) to provide a chromatographic fraction enriched in the more toxic non-ortho and mono-ortho substituted congeners. Enrichment was realized with both types of carbon, however, SK-4 enabled a significant reduction in solvent usage.

The TCDD-like toxicity of an individual PCB congener is expressed as its toxicity equivalency factor (TEF) multiplied by its concentration in the sample. TCDD-like toxicity may be associated with structures that contain Cl atoms at both para positions, at least 2 meta positions and at no more than 2 ortho positions.[2] The 21 congeners suggested for TEF monitoring have assigned TEFs and are believed to contribute to TCDD-like toxicity in the Aroclors. Of these congeners, 14 have been found in human milk or blood serum.[3,4] The 21 congeners include three non-ortho substituted PCBs: 3,3',4,4' (#77); 3,3',4,4',5 (#126); 3,3',4,4',5,5' (#169); seven mono-ortho substituted PCBs: 2,3,3',4,4' (#105); 2,3',4,4',5 (#118); 2',3,4,4',5 (#123); 2,3,3',4,4',5 (#156); 2,3,3',4,4',5' (#157); 2,3',4,4',5,5' (#167); 2,3,3',4,4',5,5' (#189); and eleven di-ortho substituted PCBs: 2,2',3,3',4,4' (#128); 2,2',3,4,4',5 (#137); 2,2',3,4,4',5' (#138); 2,2',4,4',5,5' (#153); 2,3,3',4,4',6 (#158); 2,2',3,3',4,4',5 (#170); 2,2',3,4,4',5,5' (#180); 2,3,3',4,4',5,6 (#190); 2,3,3',4,4',5',6 (#191); 2,2',3,3',4,4',5,5' (#194); 2,3,3',4,4',5,5',6 (#205).

Congeners having IUPAC numbers 77, 126 and 169 are considered the most toxic, with TEFs of 0.01, 0.1 and 0.05, respectively. These congeners are present at trace levels in Aroclors and must be separated from interferences before they are quantified against carbon labeled standards. The separation of these congeners from mono-ortho and di-ortho PCBs was achieved as follows. The ortho congeners eluted in 20 mL of 2:1 CH_2CH_2:hexane from a 1 mL pipet packed with 60 mg of SK-4 carbon. The non-ortho congeners were then back-flushed off the

column with 20 mL of toluene. TEFs for the mono-ortho and di-ortho PCBs are 0.001 and 0.00002, respectively.

Immunoassay results using the Ohmicron RaPID™ PCB Assay kit were found to be comparable with GC-ECD results in the range 500 ppb to 100 ppm, when the appropriate Aroclor calibrator was used. A "decision tree" was developed to aid in Aroclor identification by low resolution mass spectrometry (LRMS). The LRMS detection limit for Aroclors was approximately 10 ppm. Linearity of response was verified to the level corresponding to 500 ppm in the sample.

A histogram-based technique was designed to allow visual Aroclor identification based on isomer-total areas. Automated high resolution mass spectrometry (HRMS) quantitations are conveniently based on areas of individual major peaks. Using HRMS, at least ten measurements are made across each chromatographic peak while using a 0.18 mm ID, 0.2 μm film, 40 m, RT_x-5 (or equivalent) GC column with an analysis time of under 50 minutes. Seven SIR descriptors are used to monitor 2 or 3 levels of chlorination each. Either non-labeled PCBs that are not found in Aroclors, or carbon-13 labeled standards may be used as internal standards. Most or all congeners should be quantitated against an internal standard within the same SIR window. For PCBs with three or more chlorines, two ion ratios from the molecular ion cluster are used for confirmation.

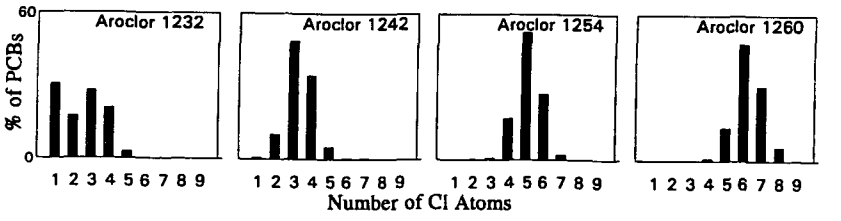

Figure 1. Example Isomer-Total Histograms for Aroclor Identification

References

[1]Schulz, D.E; Petrick, G.; Duinker, J.C. *Environ. Sci. Technol.* 1989, *23*, 852-859.
[2]Safe. S. *Environmental Health Perspectives* 1992, *100*, 259-268.
[3]Duarte-Davidson, R.; Harrad, S.J.; Allen, S.C.; Jones, K.C. *Chemosphere* 1992, *25*, 1653-1663.
[4]Patterson, D.G.; Lapeza, C.R., Jr.; Barnhart E.R.; Groce, D.F.; Burse, V.W. *Chemosphere* 1989, *19*, 127-134.

Notice

The U.S. Environmental Protection Agency (EPA), through its Office of Research and Development (ORD), partially funded and collaborated in the research described in this abstract for a proposed poster. It does not necessarily reflect the views of the EPA or ORD.

Validation of an HPLC-APCI-MS/MS Procedure for Diclofenac in Human Plasma

D. Thomas, S. Draper, H. Hill, M. Richards and J. Robson

Corning Hazleton, Otley Road, Harrogate, North Yorkshire, HG3 1PY, UK

Introduction

Diclofenac is a non-steroidal anti-inflammatory drug usually dosed at 75-100 mg/day. The drug is metabolized mainly via oxidative pathways followed by glucuronide conjugation. The resulting plasma levels are low, and therefore a sensitive and specific assay is needed to evaluate its pharmacokinetics.

In the present work, a method was developed and validated using high-performance liquid chromatography (HPLC) with tandem mass spectrometry (MS/MS) for the determination of diclofenac in human plasma following a single oral dose of 50 mg. The analytical procedure was validated according to current guidelines acceptable to international regulatory authorities i.e. inter- and intra-day precision and accuracy of calibration and quality control samples (QCs), stability to freeze/thaw cycles, stability at room temperature, recovery, sensitivity and specificity. Concentration of diclofenac in calibration standards and study samples was determined using least squares linear regression with a 1/x weighting factor to improve accuracy at low levels.

Experimental

Diclofenac and Indomethacin (used as internal standard) were purchased from Sigma. Standard solutions (1 mg/mL) of each analyte in methanol were used to fortify the calibration standards. A second set of solutions were prepared in the same manner and used to fortify the QCs. Control human plasma was obtained from Hazleton volunteers, pooled and used to prepare the calibration standards, QCs and plasma blank samples.

Extraction Procedure

Samples were removed from a freezer (-20°C), allowed to thaw at room temperature and mixed by vortex. Plasma (1 mL) was transferred to a borosilicate centrifuge tube and internal standard (50 μL, 10 μg/mL) added. Orthophosphoric acid (4 mL, 2.5 M) and hexane/IPA (5 mL, 90:10) were added and the tubes capped and mixed on a horizontal shaker. After mixing, the tubes were centrifuged for 5 min. The aqueous layer was frozen in dry ice/acetone and the upper organic layer transferred to a clean tube. The samples were evaporated to dryness under a stream of N_2 at 35°C. The extracts were dissolved in mobile phase (150 μL) and submitted for analysis.

HPLC-MS

HPLC-MS/MS quantitation was performed using a Perkin Elmer Series 400 LC pump, with a Perkin Elmer ISS 200 Autosampler. Aliquots (100 μL) of extract were injected onto a reversed phase column (10 mm x 4.6 mm i.d. with 3 μm particle size) and eluted with methanol:acetonitrile:water at a flow rate of 1 mL/min. The eluent from the column was conveyed into a SCIEX API *III* triple quadrupole mass spectrometer equipped with an APCI source. Mass spectra were acquired in the positive ion mode with the heated pneumatic nebulizer interface at a temperature of 480°C, the nebulizer pressure (UHP N_2) at 80 psi, a make-up flow of 1.5 L/min of UHP N_2, and the corona discharge needle maintained at a current-controlled 3 μA discharge. For the MS/MS experiments, Ar collision gas was used at a target thickness of 300 atoms/cm^2. The (laboratory frame) collision energy (nominal) was 10 eV for the singly charged ions studied here. The mass spectrometer was operated in the multiple reaction monitoring (MRM) mode with a dwell time of 100 ms per channel for diclofenac and the internal standrd.

43rd ASMS Conference on Mass Spectrometry and Allied Topics

Results

Calibration Curve

Calibration curves were obtained using the ratio of peak areas for the analyte and IS using a linear regression with a 1/x weighting factor over the concentration range 10 - 1000 ng/mL.

Specificity and Sensitivity

The chromatograms of six samples of control matrix from different individuals were examined, and the regions in the chromatograms corresponding to the retention time of the analyte and the internal standard checked for interferences. From these experiments, no interferent compounds were found in any of the control plasma samples analysed. Sensitivity (the lower limit of quantification (LLOQ)) was set at the concentration of the lowest calibration standard (10 ng/mL).

Recovery

Recovery was assessed using six replicates at each of the three QC levels used for the study. The peak areas of extracted samples were compared with the peak areas of direct injections of pure standards containing equivalent amounts of analyte and internal standard. The recovery of diclofenac from human plasma was approximatley 90% over the concentration range studied.

Stability

The stability of diclofenac was evaluated under various conditions: 1, 2, 3 freeze/thaw cycles; 1, 4, 24 h storage; stability of extracts in the autosasmpler. No apparent degradation of diclofenac was evident up to 3 f/t cycles or after storage described above.

Intra- and Inter-Day Validation

The procedure was validated as follows:-

Intra-Day - 1 x calibration standards, 6 x QC samples, 6 x matrix blanks from different individuals, 6 x calibration samples, matrix blank + IS, 2 x high standards and 2 x blanks to assess carry over, and a reagent blank.

Inter-day - 1 x calibration standards, 6 x QC samples, matrix blank, matrix blank + IS, reagent blank.

Intra-day precision of the calibration standards was determined from the coefficients of variation of the observed concentrations at each level. Intra-day precision of the calibration standards ranged from 13.2% at 10 ng/mL to 5.6% at 1000 ng/mL. Carry over was assessed by analysing blanks immediatley following high calibration standards and was found to be negligible.

Inter-day precision of the calibration standards and the quality control samples was determined from the coefficient of variation of the observed concentrations at each level from the three inter-day batch runs and from the intra-day validation. Inter-day precision for the calibration standards varied from 16.3% at the 10 ng/mL level to 3.0% at the 900 ng/mL level. Accuracy for the calibration standards ranged from 96.6 - 106.0% over the concentration range. The mean coefficient of determination of the inter-day calibration curves was 0.997905. The inter-day precision of the quality control samples was 6.7% at 30 ng/mL, 12.8% at 200 ng/mL and 6.7% at 800 ng/mL. Inter-day accuracy of the quality control samples was 109% at 30 ng/mL, 108% at 200 ng/mL and 95.6% at 800 ng/mL.

Conclusion

The method described was validated to current internationally accepted criteria and is capable of quantitating diclofenac in plasma which allows its pharmacokinetics to be described following a single oral dose of 50 mg to man.

Effects of Solution Additives and Denaturants on Peptide and Protein Electrospray Ionization Mass Spectrometry

Y. Smelyanskiy, R. R. Ogorzalek Loo, and P. C. Andrews
University of Michigan, Department of Biological Chemistry, Ann Arbor, MI 48109

Frequently detergents, urea or other additives are added to proteins to solubilize them and it is not always possible to avoid their use. Denaturants such as urea and formamide can be used to probe protein structure (e.g., in stability studies). It is of interest to understand the effects of these denaturants on charging and whether these reagents can be effectively used in conjunction with ESI-MS to probe protein conformation. We examine a practical issue: how much of a particular additive can be tolerated in electrospray ionization mass spectrometry (ESI-MS), and a fundamental issue: how do these additives affect charging.

Urea has a reputation for destroying protein signals in mass spectrometry, but its reputation may be overly tarnished, at least where ESI is concerned. We have employed urea to obtain spectra from inclusion bodies, formed when overexpressed proteins precipitate in the cell. Urea's performance with a standard protein is illustrated in Figure 1. Figure 1a was obtained with a 6 pmol/μL solution of myoglobin in 4% acetic acid/50% acetonitrile. Figures 1b and 1c were obtained under the same conditions, but with 0.1 M and 1.0 M urea, respectively. Note the reduction in ion signal, as well as the shift to lower charging with urea. Ion intensities and charging were reduced similarly when urea was added to hemoglobin and ubiquitin in 4% acetic acid/50% acetonitrile. Reduced charging in the presence of urea is also observed for peptides.

Charging is already reduced when ubiquitin or cytochrome *c* is sprayed from 100% H_2O relative to that observed when either protein is sprayed from 4% acetic acid/50% acetonitrile. When urea is added to a 100% aqueous solution, surprisingly no shift to higher charge was observed for either protein, even at up to 5 M urea. We had expected denaturation with its concomitant higher charging. It is possible that urea denaturation does not display higher charging for these proteins. Alternatively, the proteins may not have denatured in 5-6 M urea; other techniques must be applied to determine the protein conformation under these conditions. Still another possibility is that the urea breaks down to ammonia in the heated ion source. Gas phase proton transfer from the highest charge states to ammonia would yield similar spectra. Further studies were performed with formamide. Concentrations up to 1 M did not shift charge distributions for hemoglobin sprayed from 4% acetic acid/50% CH_3CN in contrast to the urea studies. Either formamide decomposes less to ammonia than urea or another explanation must be found.

Myoglobin spectra were acquired in 5 mM NH_4OAc/H_2O, showing the heme-associated (*holo*) protein. Addition of formamide denatured the protein, yielding at least 2 forms, the *holo*-protein and the *apo*-protein (without heme). Higher charging was observed in the presence of formamide for both *apo*-myoglobin and *holo*-myoglobin, probably reflecting the denaturation.

ESI mass spectra obtained following addition of the nonionic saccharide surfactant n-hexyl glucoside at 0%, 0.01%, and 0.1% (w/v) to a solution of horse heart cytochrome *c* in H_2O showed increased charging as the amount of surfactant increased. Increased charging is general to nonionic saccharide surfactants for concentrations below and above surfactant

CMC's. Thus, the increased charging appears not to be a consequence of micelle formation or of its absence. Because surface tension does not continue to decrease with increasing concentration for concentrations exceeding a surfactant's CMC, the charge shifts cannot be attributed solely to surface tension effects, either.

It was demonstrated that the charge shift induced by addition of nonionic saccharide surfactants is not a consequence of protein unfolding, by examining solutions yielding 2 conformations (Figure 2). If the surfactant addition caused the analyte protein to unfold, the bimodal conformation would have collapsed to a single, high charge state distribution. Instead, the surfactant caused charge shifts without regard to higher order structure; both portions of the bimodal charge envelope shifted to higher charge (lower *m/z*). Circular dichroism studies have also provided no indication of denaturation for cytochrome *c* and ubiquitin in nonionic saccharide surfactant solutions.

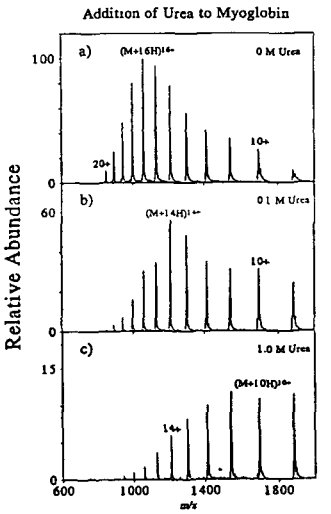

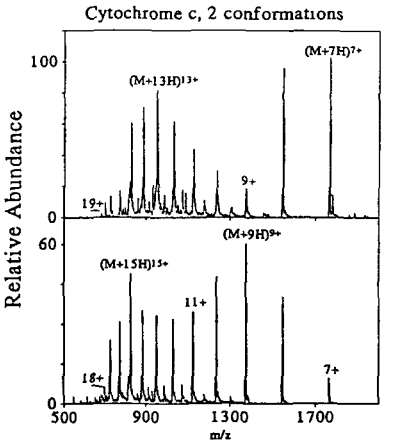

Desolvation of Noncovalently-Bound Complex Ions for ESI-MS Analysis

Joseph A. Loo, Parke-Davis Pharmaceutical Research, Division of Warner-Lambert Company, 2800 Plymouth Road, Ann Arbor, MI 48105

Rachel R. Ogorzalek Loo, Department of Biological Chemistry, University of Michigan, Ann Arbor, MI 48109

INTRODUCTION. The gentleness of electrospray ionization (ESI) has allowed MS to detect several examples of noncovalently-bound complexes. To preserve the proper protein conformation and/or complexation upon transfer from solution to the gas phase, ESI of aqueous solutions is often necessary. Although the ESI process depends on efficient desolvation of the highly charged droplets prior, it is sometimes difficult to completely remove *all* solvent molecules from the protein complex ions without affecting the gas phase complex (i.e., dissociation of the complex may occur). The resulting mass spectra can show variable amounts of solvation, depending on several experimental factors, such as collisional activation in the atmosphere/vacuum interface, drying gas flow rate and temperature, pressure in the high vacuum region, and ESI needle position.

EXPERIMENTAL. ESI-MS analyses were performed with a Finnigan MAT 900Q (EBqQ) mass spectrometer equipped with a PATRIC focal plane array detector. An ESI interface based on a heated glass capillary inlet was used. Droplet desolvation was aided by a countercurrent stream of warm nitrogen and by collisions in the interface controlled by adjustment of the voltage difference between the tube lens at the metalized exit of the glass capillary and the first skimmer element (ΔV_{TS}).

RESULTS AND DISCUSSION

Effect of Nitrogen Countercurrent Flowrate. For many ESI interfaces, the use of a gas flow (e.g., N_2) countercurrent to the electrospray axis is necessary for efficient ion desolvation. The N_2 flowrate can influence not only ESI sensitivity, but also the amount of solvation observed for the multiply charged ions, especially for ESI of aqueous solutions. For avidin, a 64 kDa tetrameric protein, peaks for the protein tetramer are broad and shifted to higher *m/z* than expected with the N_2 flowrate of 2.5 L min^{-1}. Increasing the N_2 flowrate to 10 L min^{-1} produces sharper peaks and shifts the peaks to lower *m/z*, consistent for more desolvated ions.

Effect of Energetic Collisions and Pressure in the ESI Interface. Optimizing the voltage difference between the various lens elements in the vacuum region of the ESI interface is critical for removing remaining solvent molecules from the ions. Solvated ions can also be desolvated by increasing the pressure in the vacuum region of the interface. Residual solvation can be effectively stripped from the molecules with only a slight loss in sensitivity (factor of ~ 2).

Effect of Electrospray Position. The position of the electrospray source can also influence the amount of solvation observed for the protein ions. Optimum sensitivity with our system for the myoglobin complex (16.9 kDa polypeptide noncovalently-bound to heme) is achieved with the spray situated ca. 5.2 degrees "off-axis" (off the axis of the capillary inlet). Directing the ESI source "on-axis" results in very broad peaks and an increase in low *m/z* background ions. The use of an on-axis electrospray results in "wet" ions because larger droplets are sampled by the MS inlet. Similar results were obtained for trypsin (23.3 kDa) complexed with an inhibitor (BPTI, 6.5 kDa).

Spray conditions also play a role in the analysis of peptide mixtures. For an equimolar mixture of two similar mass peptides, $P(K_2G)_9K_2$ and dipalmitoyl-$K(KG)_{13}K$, high flow rates and on-axis spraying favor desorption of the surface active peptide (the dipalmitoyl-modification is extremely hydrophobic, making the dipalmitoyl-peptide surface active). Lower ESI voltages and lower countercurrent desolvation flows also favor desorption of the dipalmitoyl-peptide. All of these conditions yield larger droplets.

Solvation Shielding Effect? The amount of dissociation of the noncovalently-bound complex observed in a mass spectrum is affected by a variety of factors, including the solvation state. Figures 1 and 2 compares the effect of increasing ΔV_{TS} at two different spray angles for myoglobin. Starting off with "wet" ions and subjecting them to energetic collisions results in less solvated ions for the myoglobin complex (Fig. 1). Starting with "dry" ions and subjected them to the same energy collisions results in dissociation of the complex (Fig. 2). *Solvation can act as a shield around the protein complex, "protecting" them from further dissociation in the ESI interface.*

CONCLUSION. For a more accurate molecular weight determination of protein complexes, efficient desolvation is required. Solvated ions can yield higher mass values than expected. However, there is a fine balance in experimental conditions for producing desolvated complex ions versus the dissociated complex. Careful control of all experimental factors affecting droplet/ion desolvation is necessary for successful detection of weakly-bound complexes by ESI-MS.

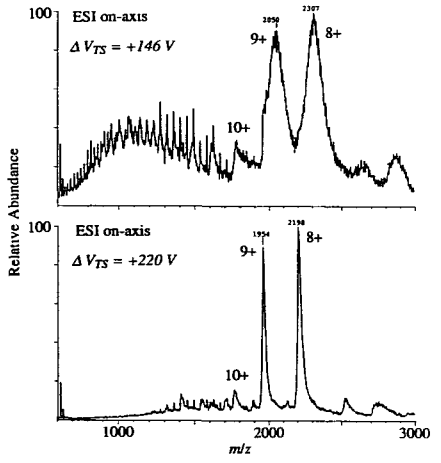

Fig. 1

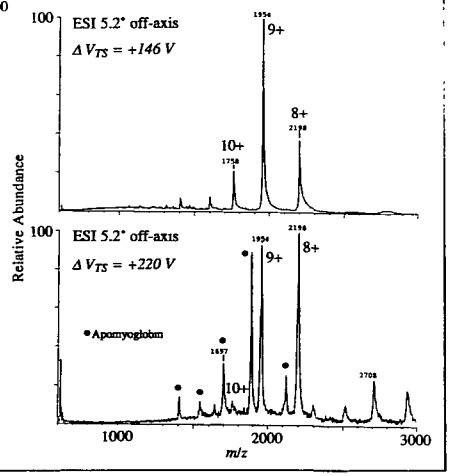

Fig. 2

Noncovalent Complex Formation of Cyclodextrins studied by Electrospray Ionization Mass Spectrometry

Sharron G. Penn[a*], David M. Goodall[a], Curtis A. Monnig[b] and John S. Loran[c]
a Department of Chemistry, University of York, Heslington, York, YO1 5DD, UK.
b Department of Chemistry, University of California, Riverside, CA 92521.
c Analytical Research and Development, Pfizer Central Research, Sandwich, Kent, UK.

We are interested in the use of cyclodextrins (CDs) as chiral selectors in capillary electrophoresis (CE) and HPLC. We have studied the chiral separation of tioconazole using these techniques, and determined the binding constants for the complex[1]. Tioconazole is a racemic pharmaceutical, used in the topical treatment of fungal infections. Tioconazole has been shown by NMR to form a 1:1 complex with CD. When tioconazole was analyzed in solution with α-, β- and γ-CD by ESI-MS, host-guest complexes were observed in each case (Figure 1). For each CD, the fraction complexed was calculated from the ratio of the peak height of the complex to the sum of the heights of the complexed and free CD. In Figure 1 these are 0.28, 0.53 and 0.73 for α- β- γ-CD respectively. This implies an order of binding strength of $\alpha > \beta > \gamma$.

CE is an analytical technique in with ionic species in solution are separated according to their mobilities, μ. When there is a dynamic equilibrium, μ is the weighted average value of the bound and unbound forms of the analyte. The mobility of tioconazole was measured with 5 mM of α- β- and γ-CD in the background electrolyte This provides a measure of the extent of binding in the liquid phase, for comparison to the mass spectrometry data With no cyclodextrin in the background electrolyte the mobility was 1.18×10^{-8} $m^2 V^{-1} s^{-1}$. With α-, β- and γ-CD the mobilities were 1.04×10^{-8} $m^2 V^{-1} s^{-1}$, 0.83×10^{-8} $m^2 V^{-1} s^{-1}$ and 0.71 10^{-8} $m^2 V^{-1} s^{-1}$ respectively. The order of mobilities CE therefore agrees with the ratios observed in the mass spectrometer. This provides strong evidence that we are, indeed, observing true inclusion complexes and not just associations in the gas phase.

Mass spectra were collected at constant tioconazole concentration (1.1 mM) and varying β-CD concentration (0.5 mM to 1.9 mM), and the peak height of tioconazole was measured. By only monitoring this single species, differences in the ionization efficiency of the complex could be ignored. The peak height of tioconazole diminished with increasing β-CD concentration. The concentration of the complexed and free β-CD was then calculated using mass balance, and used to estimate K, the binding constant. The average binding constant of the complex from the data points was found to be 230 ± 50 M^{-1}. Binding constants from CE for a 50:50 aqueous:methanol buffer were calculated to be 68 ± 1 M^{-1}. From previous work[1] it is known that the binding constant of the tioconazole:β-CD complex increases with decreasing methanol content. Therefore can we postulate that at the time of expulsion of the complex from the droplet, the composition of the droplet was 25 % methanol?

1. S.G. Penn, E.T. Bergstrom, D.M. Goodall and J.S. Loran, *Anal. Chem.* (1994) 66 2866.

43rd ASMS Conference on Mass Spectrometry and Allied Topics

Figure 1

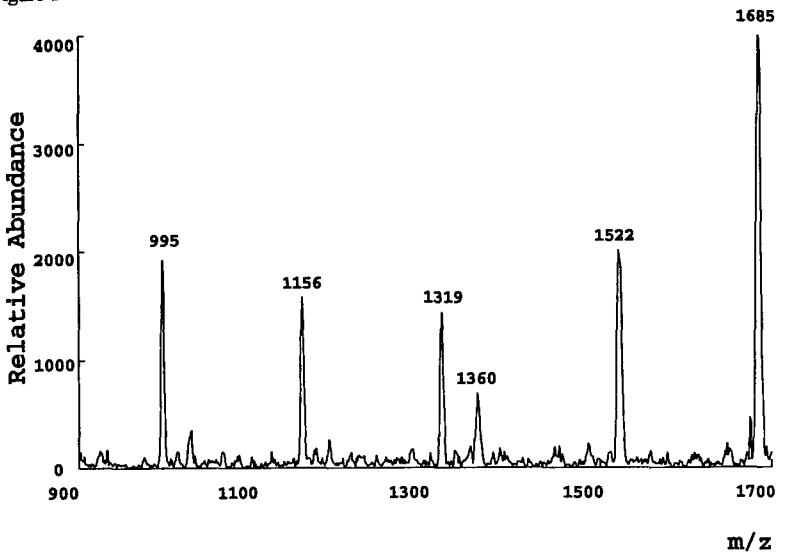

Electrospray ionization mass spectrum of tioconazole (6 5 mM) with equimolar quantities of α-, β- and γ-CD (1.0 mM) in a 50 50:1 water:methanol:acetic acid solution. Mass assignments given in table below.

Mass	Assignment
995	$[\alpha\text{-CD} + Na]^+$
1156	$[\beta\text{-CD} + Na]^+$
1319	$[\gamma\text{-CD} + Na]^+$
1360	$[\alpha\text{-CD} + \text{tioconazole} + H]^+$
1522	$[\beta\text{-CD} + \text{tioconazole} + H]^+$
1685	$[\gamma\text{-CD} + \text{tioconazole} + H]^+$

Non-Covalent Complexes formed between Acyl CoA Binding Protein and CoAs

Carol V. Robinson, Birthe Kragelund, Jens Knudsen,
Robin T. Aplin and Christopher M. Dobson
Oxford Centre for Molecular Sciences,
South Parks Road, Oxford, OX1 3QT, UK.

Introduction

Acyl coenzyme A binding protein (ACBP) is an 86 residue protein present in a wide range of eukaryote organisms. Since the protein binds long chain acyl-coenzyme A esters (acyl CoAs) with high affinity, it is thought to have a role in the transport and storage of acyl CoAs in the cell. The protein and acyl CoA associate by electrostatic and non-polar interactions and have been the subject of an investigation by NMR.(B.B. Kragelund *et al* ,.J. Mol. Biol. 1993, **230**, 1260-1277).

The non-covalent complexes formed between ACBP and a variety of acyl CoAs have been studied by electrospray ionization mass spectrometry (ESI MS). Whilst initial experiments clearly demonstrate an interaction between the protein and its non-covalent CoA ligand a number of control experiments were used to examine the specificity of the interaction.

Results and Discussion

The following experiments were used to study the interaction between the binding protein and its ligand:

(1) Increasing the ratio of ligand to protein from 1:1 up to 1:10.

(2) Denaturing the protein or disrupting the complex using heat, organic solvent or a high voltage difference between the needle and skimmer.

(3) Varying the binding affinity of the ligand.

(4) Monitoring the hydrogen exchange of the *apo* and *holo* proteins.

(5) A competition experiment in which a mutant protein which lacks a critical residue involved in the binding interaction is mixed in a 1:1 ratio with the wild type protein and the CoA ligand added to the protein mixture.

In the first control experiment the effect of increasing the ratio of the ligand to the free protein was examined using a stepwise increment from 1:1 to 1:10. In all cases increased amounts of the complex were observed with increased concentrations of the ligand. This observation suggests that even with the high binding affinity of the palmitoyl CoA ligand, K_D = 0.5+/-0.2x10^{-13}M, dissociation in the gas phase is a relatively

facile process. Furthermore, increasing the concentration of the ligand in the electrospray droplets increases the probability of observing the complex.

In the second experiment 50% acetonitrile was added to the aqueous solvent to denature the protein and the interface heating increased to 50C. Under these conditions no complex was observed in the ESI mass spectrum indicating that the tertiary structure of the protein is indeed required for observation of the complex.

Further evidence for the preservation of tertiary structure was obtained from hydrogen exchange kinetics. If a fully deuterated sample of ACBP and a deuterated complex formed between ACBP and an acyl CoA ligand are diluted into water at pH 5 and the hydrogen exchange kinetics monitored over a period of 10 hours, increased protection from exchange is observed for the complexed protein. This increase in protection from exchange was observed for both the palmitoyl and the octanoyl CoA ligands (K_D=0.2+/-0.1x10^{-6}M) and was not found to differ despite the large difference in binding affinities measured for these two ligands in solution.

If the electrospray mass spectrum was a reflection of the situation in solution it would be predicted that a mixture of acyl CoAs added to the protein would yield a complex for the highest binding affinity CoA. However, addition of a 1:1:1 mixture of CoAs with ACBP gave rise to complexes for all three acyl CoAs despite their widely differing binding constants. This result was surprising and indicated a lack of specificity in complex formation or some interaction between the CoAs. However, if a mutant of ACBP is prepared in which the essential tyrosine residue is mutated for an asparagine residue and mixed with the wild type protein a molar equivalent of palmitoyl CoA added; the complex is only observed for the wild type protein. This is in complete agreement with observations in solution.

Conclusion

The observation of the intact complex and the increased hydrogen exchange protection, detected for the *holo* protein in comparison with the *apo* protein, indicate that the ligand is indeed in the correct binding site of the protein. However, the lack of specificity observed for the different acyl CoA ligands suggests that the complex in the spectrum is not a reflection of the relative binding affinities of the ligands but infers some non-specific association or interaction of the ligands in the mixture. Nevertheless, the lack of a complex for the mutant protein indicates some specificity. Further work will establish if the observations made on this system are applicable to the study of a wider range of non-covalent complexes by ESI MS.

An Iron Carboxylate Oxygen-Centered-Triangle Complex Detected During Use of "TFA-Fix": A Comment on the Finnigan TSQ-700 Electrospray Inlet System

Carl F. Ijames, Robert C. Dutky*, and Henry M. Fales*

Section on Analytical Biochemistry, Laboratory of Clinical Science, National Institute of Mental Health, and * Chemical Structure Section, Laboratory of Biophysical Chemistry, National Heart, Lung, and Blood Institute, Bethesda, Maryland 20892

The deleterious effect of small amounts of hydrochloric, sulfuric, phosphoric, and especially trifluoroacetic acid (TFA) on electrospray mass spectra of basic compounds such as peptides is well known, although its cause is still a matter for some speculation. With TFA the effect is particularly unfortunate since many of the most useful HPLC systems rely on this additive. Apffel et al. (abstracts # 642 and #772, Proceedings of the 42nd ASMS Conference on Mass Spectrometry and Allied Topics, Chicago, Illinois, May 29-June 3, 1994, Hewlett-Packard "Ion Notes", **1994**, 9, #2, 4-5) reported last year that addition of a solution of 75:25 propionic acid-isopropanol ("TFA-Fix"), added one-third by volume post-column via a mixing tee at a total flow rate of 300 μL/min before the pneumatic nebulizer nozzle, increases by 15-30 fold the signal of basic compounds (peptides and alkaloids) whose signals had been drastically reduced by 0.1-0.2% TFA.

We attempted to extend the technique to simple infusion analysis of peptides at low flow rates (1-3 μL/min) by adding the ingredients of "TFA-Fix" to peptides prior to analysis. After tuning our triple quadrupole instrument with a standard mixture of 5 μM equine apomyoglobin and 20 μM MRFA in 50% aqueous methanol containing 0.5% acetic acid, we observed the not unexpected loss of maximum apomyoglobin signal by a factor of 19 and MRFA by 13 after addition of TFA to a final concentration of 0.1%. Addition of 25% v/v of "TFA-Fix" reduced the signal loss of apomyoglobin to a factor of 14 even though the degree of adduct tailing became severe. The effect of "TFA-Fix" on the MRFA component of the tuning solution was impressive, actually increasing its intensity by a factor of 1.8 over the original solution. However, an intense peak was noted at m/z 622 and inspection of its isotope pattern suggested it contained three atoms of iron. This was confirmed by mass measurement on an FTMS instrument yeilding 621.9722 ($C_{18}H_{30}O_{13}Fe_3$). The presence of at least 4 propionoxy groups in the cluster is clear from its fragmentation pattern in the TSQ. Six propionoxy groups would account for twelve of the oxygen atoms while the presence of the extra oxygen suggests the ion at m/z 622 is derived from a "basic iron carboxylate" as shown in structure **1**. These compounds are known as "oxygen centered triangles" since their three metal atoms and lone oxygen form a nearly planar triangular unit, and they have the general formula $Fe_3O(O_2CR)_6(L)_3$ where L is a ligand such as water or pyridine. They are thought to have relevance to the ferritin iron storage protein. When acetic acid was substituted for propionic acid in the above experiment an analogous ion formed at m/z 538. As the tube lens-skimmer potential

was reduced from 66 to zero volts, ions containing up to three acetic acid ligands replaced m/z 538 as expected for its structure. Similar results were obtained with a wide variety of other cosolvents including water, acetonitrile, and tetrahydrofuran all of which adducted in combinations with the carboxylic acid totalling three molecules of ligand. The intensity of these adducted ions is affected not only by reduction of the tube lens potential, but also by the presence of auxiliary gas in the spray region. The ion is most likely derived from dissolution of iron from the stainless steel needle surrounding the fused silica capillary, either by direct or subsequent reaction with the carboxylic acid. The inlet system of our Finnigan TSQ-700 spectrometer regularly produces a more conventional electrolytic process which greatly exceeds the true electrospray current. Indeed, the current displayed on the computer terminal is actually a combination of the true electrospray current plus a conventional electrolysis current running back through the solvent-filled fused silica capillary to the grounded stainless steel fitting. When the grounding connection is removed from the stainless steel fitting virtually no current is observed even in the presence of a strong electrospray ion signal since the first small division on the software current display represents 0.32 μA, which greatly exceeds the true electrospray current. With the ground connection in place as recommended by Finnigan, solutions of moderate conductivity supply an erratic ion signal and spray due to formation of hydrogen gas bubbles by electrolysis of the solution at the grounded fitting We now routinely operate with the ground connection removed, although this presents a safety concern when the high voltage is on.

Returning to the evaluation of "TFA-Fix" for the infusion electrospray of peptides, we analyzed a 50 μM solution of a mixture of peptides (angiotensin I, angiotensin II, physalaemin, aprotinin, and insulin) in 50% aqueous methanol. As with the tuning solution, making this solution 0.1% in TFA reduced the average signal (sum of all intensities) by a factor of ~69. Addition of 25% by volume of the "TFA Fix" solution increased the signal strongly so that it was now only reduced by an average factor of 2.3 from the original, confirming the results of Apffel et al. Addition to the TFA solution of the same volume of a 1:1 mixture of methanol and acetic acid was not as effective as "TFA-Fix", and the signal was still reduced by a factor of 28 from the original intensity (not shown).

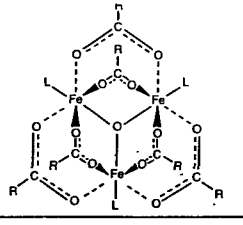

Electrospray of Borane Salts; High Molecular Weight Clusters and Reactions

Cornelis E.C.A. Hop,* Dovas A. Saulys and Donald F. Gaines, Department of Chemistry, University of Wisconsin-Madison, 1101 University Avenue, Madison, WI 53706.

The recent development of electrospray ionization (ESI) has revolutionized the biochemical applications of MS. In comparison, much less attention has been paid to the use of electrospray for analysis of inorganic compounds. Here,[1] we will demonstrated that ESI is a valuable technique for identification of borane salts, which cannot be analyzed with conventional MS ionization methods such as EI, CI and liquid SIMS.

A VG AutoSpec triple sector (EBE) mass spectrometer equipped with the mark II ESI source was operated in the - or + ion mode. The samples were dissolved in CH_3CN, CH_3OH, H_2O or THF (200 ng.μl^{-1}) and the flow rate was 15 μl.min^{-1}. All experiments were performed with a resolution of 1,250 to obtain maximum signal strength. N_2 was used as both the nebulizer gas and the bath gas. The following borane salts were examined: $[(Me)_4N][B_3H_8]$, **I**; $Cs[B_3H_8]$, **II**; $Na[B_{10}H_{13}]$, **III**; $[Ph_3PMe][B_{11}H_{14}]$, **IV**; $[Ph_3PMe][B_{11}H_{13}\text{-}C_6H_{13}]$, **V**; $Na_2[B_{12}H_{12}]$, **VI**. The ^{11}B NMR spectra of these compounds showed only resonances attributable to the cations and/or anions.

The most remarkable feature of the - ion mode ESI mass spectrum of $[(Me)_4N][B_3H_8]$, **I**, in CH_3CN is the extensive clustering displayed by **I**. Up to 1,000 Dalton all signals correspond to cluster ions having the formula $[C_{x-1}A_x]^{1-}$ (C = cation; A = anion). Indeed, the observed isotope patterns of these signals match the calculated patterns. Above m/z 1,000, multiply charged ions are visible and the onsets of the various charge states are listed below.

charge	2-	3-	4-	5-
m/z	1015	1454	1903	2425
composition	$[C_{17}A_{19}]^{2-}$	$[C_{37}A_{40}]^{3-}$	$[C_{65}A_{69}]^{4-}$	$[C_{104}A_{109}]^{5-}$

In contrast, the - ion mode ESI mass spectrum of $Cs[B_3H_8]$, **II**, in CH_3CN shows mainly singly and doubly charged cluster ions; the first doubly charged cluster ions are observed at m/z 1688 ($[C_{19}A_{21}]^{2-}$). Thus, the onset of doubly charged cluster ions in terms of the number of $B_3H_8^-$ units is similar for **I** and **II**. The + ion mode ESI mass spectra of CH_3CN solutions of **I** and **II** are compatible with those obtained in the negative ion mode. Again, the most remarkable feature of the spectra is the formation of singly and multiply charged cluster ions; the onsets of the various charge states for **I** are listed below.

charge	2+	3+	4+
m/z	1049	1488	2052
composition	$[C_{19}A_{17}]^{2+}$	$[C_{40}A_{37}]^{3+}$	$[C_{73}A_{69}]^{4+}$

The + mode ESI mass spectrum of a CH_3CN solution of **II** shows mainly singly and doubly charged cluster ions; the first of the doubly charged cluster ions is observed at m/z 1954 ($[C_{23}A_{21}]^{2+}$). Thus, again the onset of doubly charged cluster ions in terms of the number of $B_3H_8^-$ units is similar for **I** and **II**.

The + ion mode ESI mass spectra of the CH_3OH solutions of **I** and **II** differ substantially from those of the corresponding CH_3CN solutions: cluster ions containing B_3 units are not present in these spectra! (Degassing the solution with Ar prior to use did not change the spectra, implying that the presence of residual O_2 is irrelevant.) Since ^{11}B and ^1H NMR spectra clearly indicated that the methanol solutions of **I** and **II** are stable and pure, an electrochemical reaction during the ESI process is implied. To resolve this issue, we removed the electrospray needle

assembly from the source [2] and collected an electrosprayed CH_3OH solution of **II** in a flask mounted around the needle. The CH_3OH was then pumped away and the residual solid was dissolved in CD_3OD. The NMR spectrum of the latter solution exhibits resonance positions corresponding to the presence of $B(OCH_3)_4^-$ (37 molar %) as well as $B_3H_8^-$ (63 molar %). Complete conversion of $B_3H_8^-$ into $B(OCH_3)_4^-$ under ESI conditions explains all signals observed in the + ion mode ESI mass spectra of the CH_3OH solutions of **I** and **II**. Differences in nucleophilicity and/or basicity alone are insufficient to rationalize the observed reactivity; more specific aspects of the solvents must be invoked. As the hydrogen atoms in the borane anions are negatively polarized with respect to the boron atoms, protic bases, such as CH_3OH, are capable not only of nucleophilic attack on boron, but also of concurrent elimination of H_2, a pathway not available to aprotic reagents, such as CH_3CN.

The - mode ESI mass spectra of CH_3CN solutions of $[Ph_3PMe][B_{11}H_{14}]$ (**IV**), $[Ph_3PMe][B_{11}H_{13}\text{-}C_6H_{13}]$ (**V**) and $Na_2[B_{12}H_{12}]$ (**VI**) and a THF solutions of $Na[B_{10}H_{13}]$ (**III**) gave spectra characteristic for the borane salts, even though some of these borane salts are extremely air sensitive. The borane anions as well clusters of these anions with the corresponding cations were observed. The - mode ESI mass spectrum of $Na_2[B_{12}H_{12}]$), **VI**, in CH_3CN is presented below; the onsets of the various charge states (2-, 3-, 4-, 5-, 6- and 7-) are indicated. The most intense signals are due to $[B_{12}H_{12}]^{2-}$ and $\{Na[B_{12}H_{12}]\}^{1-}$. Cluster ions with a charge of 6- or 7- are clearly visible. The enhanced ability of cluster ions from **VI** to support negative charges correlates with the larger size of the closo $[B_{12}H_{12}]^{2-}$ anions in **VI** compared to the arachno $[B_3H_8]^{1-}$ anions in **I** and **II**.

In conclusion, we have shown that electrospray is a valuable technique for identification of borane salts. However, it is crucial to consider the influence of various experimental parameters (e.g. the solvent) on the electrospray mass spectra.

1. For more details see (a) Hop, C.E.C.A; Saulys, D.A.; Gaines, D.F. *Inorg. Chem.* **1995**, *34*, 1977 and (b) Hop, C.E.C.A; Saulys, D.A.; Gaines, D.F. *J. Am. Soc. Mass Spectrom.* **1995**, *6*, in press.

2. In this experiment the charge on the needle was reduced to prevent discharges.

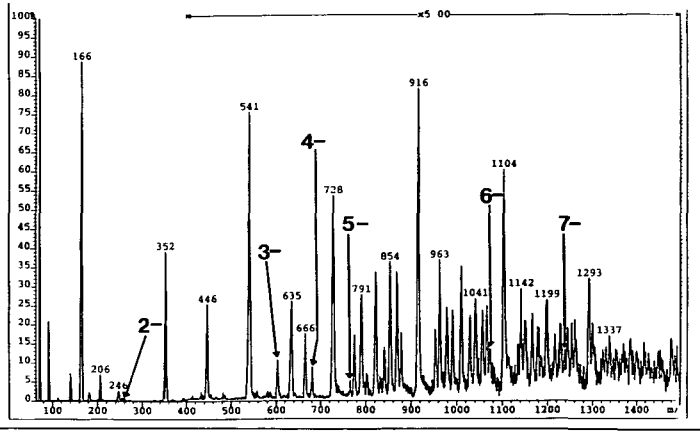

COMPARISON OF ESI AND LSI MS/MS IN THE ANALYSIS OF NEWBORN BLOOD SPOTS

Donald H Chace, Steven L. Hillman, David S Millington, Robert D. Stevens
Duke University Medical Center, MS Facility, RTP, NC, USA

Analysis of amino acids and acylcarnitines by liquid secondary ionization MS/MS (manual introduction FIB) has previously been shown to be a simple, rapid, accurate, and reliable method for the early detection of numerous metabolic diseases (Chace et al ASMS '93 & '94). Much of the sample preparation has been successfully automated using simple, commercially available equipment. Automation of the MS/MS analysis using dynamic LSI MS/MS (Flow FIB) for amino acids was achieved. However, this method was seriously compromised by sample retention, sample carry-over, frequent cleaning of the probe tip and difficulty maintaining reproducible conditions Electrospray ionization offers the potential to overcome many of these problems. A preliminary investigation of the ability of electrospray ionization to attain full automation of these analyses for newborn blood spots is presented as well as a quantitative comparison of acylcarnitine and amino acid profiles by ESI MS/MS with LSI MS/MS.

Filter paper blood spots from normal patients (newborns or adults) were used in this comparative study Sample preparation consisted of extracting two 3/16" diameter filter paper blood spots with 400 µL of methanol containing 13 stable isotopically enriched (99 9%) internal standards (9 amino acids and 4 acylcarnitines) and esterifying with 3N HCl in *n*-butanol at 65°C for 15 min For the comparison study of static LSI MS/MS and ESI MS/MS, 10 control blood spots were prepared These samples were split into two aliquots and either 35µL of 50:50 methanol:glycerol + 0 1% Na-Octylsulfate (LSI) or 50-100µL of 50:50 acetonitrile:water + 0.02% Formic acid (ESI) was used For comparison studies of dynamic LSI MS/MS with electrospray, random blood spots for each analysis were used. A VG Quattro I fitted with a Cesium Ion gun was used to analyze samples by LSI. A VG Quattro II was used to analyze samples by ESI. An amino acid profile (*m/z 125-300)* was obtained by each tandem mass spectrometer using the neutral loss (NTL) of 102 amu scan function An acylcarnitine profile (*m/z 250-550)* was obtained by each tandem mass spectrometer using the parents (PAR) of 85 amu scan function A Gilson 231 automated sample injector fitted with an interchangeable low dispersion Rheodyne loop (1, 2 or 5µL) was used for automated analysis An ISCO Model 500D syringe pump delivered solvent at 10 -15 µL/minute.

Acylcarnitine profiles obtained by ESI MS/MS and LSI MS/MS are presented in Figures 1a and b. A comparison of amino acids produces similar results (see accompanying ASMS poster, Chace et. al) This comparison of acylcarnitine and amino acid profiles by LSI and ESI MS/MS shows that these modes of ionization produce similar results. Different absolute intensities of many amino acids and acylcarnitines are observed. However, there are few differences in the intensities of specific amino acids or acylcarnitines relative to their internal standards. Detection of long chain fatty acylcarnitines (C14-C18) is approximately 10 fold greater by ESI. Higher molecular weight amino acids are better detected in ESI whereas lower molecular weight amino acids are better detected using LSI. Automated analysis of 60 blood spots is significantly better by ESI. Using ESI, the sample analysis time is 1 sample per minute versus 1 sample per 2 minutes using dynamic LSI. Excellent peak shape and sensitivity were maintained throughout the ESI analysis. Good sensitivity for the detection of amino acids was observed using both ionization modes. A satisfactory acylcarnitine analysis by dynamic LSI could not be achieved because of low sensitivity.

The analysis of newborn blood spots using electrospray ionization compares well with static (manual) LSI and is superior to dynamic LSI. Each method produces similar qualitative and quantitative data in normal patients. We have demonstrated that electrospray ionization clearly

offers the potential to fully achieve automated analyses of blood spots for amino acids and acylcarnitines Other improvements of the assay, such as increased sensitivity of diagnostically important long chain acylcarnitine metabolites, were noted. This study shows that either mode of ionization can be used in the application of tandem mass spectrometry to diagnose disease

We thank Fisons-VG for the temporary loan of a Quattro II MS/MS. Financial support was from the State of North Carolina, Division of Maternal and Child Health, Department of Environmental Health and Natural Resources (Raleigh, NC grant No. C-05070)

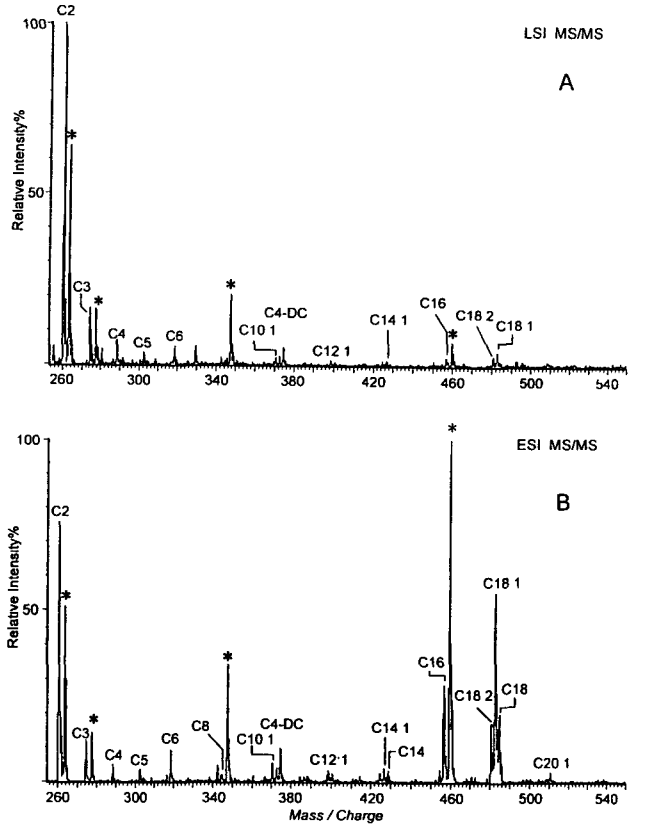

Figure 1 Acylcarnitine Profiles from a normal blood spots obtained by Par 85 scan function using LSI (A) and ESI (B). Asterisks represent internal standards

Monitoring Reactions of Nitric Oxide with Peptides and Proteins by Electrospray Ionization Mass Spectrometry.

*Urooj A. Mirza[φ], Harry M. Lander[δ] and Brian T. Chait[φ]
[φ]The Rockefeller University, 1230 York Ave, New York, NY. 10021,
[δ]Cornell University Medical College, 1300 York Ave, New York, NY. 10021

Introduction: The interaction of nitric oxide (NO) with proteins is known to play a critical role in regulating blood pressure, host defense and neurotransmission. Known targets of NO on proteins are cysteine and tyrosine residues and metals such as heme-Fe^{2+}. Although much work has been performed in characterizing NO-Fe interactions there is considerably less data on the reaction of NO with cysteine. One reason for this paucity of data is the labile nature of the nitrosothiol (RSNO) bond. In an effort to observe these labile products, we have employed the gentle technique of electrospray ionization mass spectrometry (ESI-MS)[1].

Experimental: 20mM bicarbonate solution (pH 8.0) was sparged for 15 min with N_2 then for 15 min with NO gas to produce a saturated solution of NO. Electrospray ionization mass spectra were obtained on a Finnigan-MAT TSQ-700 quadrupole instrument.

Results. A peptide (KNNLKECGLY MW = 1181.4) (Fig. 1a) was treated (Fig. 1b) with a 10 fold molar excess of NO. Treatment with NO for 5 min at pH 3.0 resulted in formation of new species with mass 29 Da greater than the starting peptide, indicative of a substitution reaction. Derivatization of the cysteine sidegroup of the peptide with N-ethyl maleimide (NEM) a blocked all reaction of NO with the peptide. This result indicates the cysteine residue is the primary site of NO reaction. We also carried out a detailed ESI-MS examination of the reaction of NO with the peptide as a function of time over extended time periods. The results demonstrated that NO reacts with the cysteine thiol to form a nitrosothiol (RSNO) derivative. Additional chemical modifications such as oxidation of cysteine to sulfonic acid and nitration of tyrosine residue are also observed but these are much slower processes. The order of formation of reaction products was RSNO >> Tyr-NO_2 = SO_3H. We also studied the nature of the RSNO bond by varying the energy input into the peptide ions during transit through the metal capillary transfer tube of the electrospray ionization source. Our results showed that very gentle mass spectrometric conditions are required for the detection of intact nitrosated derivatives, and that elevated transfer capillary temperatures lead to homolytic cleavage of the nitrosothiol bond to produce thiyl radical (R-S$^{\bullet}$) with the loss of NO$^{\bullet}$. Reactions of NO with the peptide at physiological pH demonstrated that dimerization of the peptide is the favored process. Bacterially expressed $p21^{ras}$ has 5 reduced cysteines residues available for nitrosation. ESI-MS analysis (Fig. 2a,b) demonstrates that only one of the five free cysteines in $p21^{ras}$ is nitrosated. Thus, this technique also allows for the determination of stoicheometry of the nitrosothiol formation in proteins.

Ref. 1) Urooj A. Mirza, Brian T. Chait and Harry M. Lander.; J. Biol. Chem. (in press)

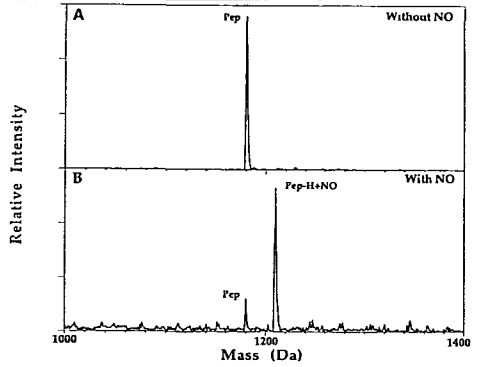

Fig. 1. Analysis of nitrosothiols. **A**; Peptide KNNLKECGLY MW = 1181.4 in the absence of NO, **B**; Peptide in the presence of NO (100uM peptide:NO 1:10)

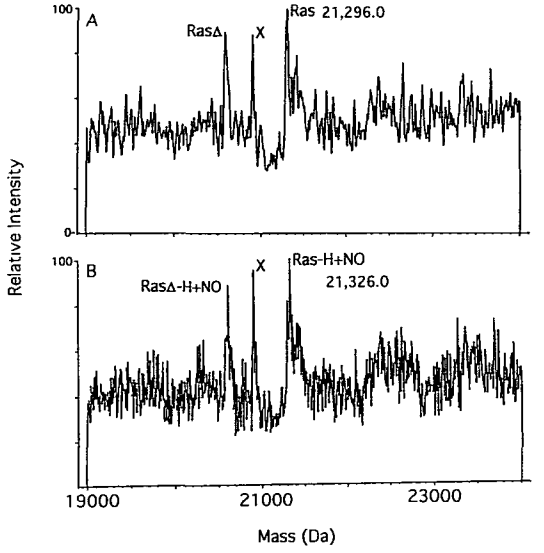

Fig. 2. ESI-MS of NO-treated $p21^{ras}$. $P21^{ras}$ was treated without (**A**) or with (**B**) NO (100uM) for 5min prior to mixing with H_2O:CH_3OH:CH_3COOH (1:1:0.05 v/v/v, pH 3.0). RasΔ indicates truncated $p21^{ras}$, Ras indicates full-length $p21^{ras}$ and X indicates an unidentified impurity whose mass did not shift upon NO treatement.

Paired Ion ESI of Borane Neutron Capture Agents

Padma S. Singh[1,**]; David H. Swenson[2,**]; Hans Schweingruber*, Roger A Laine[3,*,**].
Departments: [1]Chemistry, [2]Vet Physiology, [3]Biochemistry.
**Louisiana State University Baton Rouge, LA 70803
*Glycomed, Inc., Alameda, CA 40503

INTRODUCTION

Imidocaptate (IC) was developed for experimental boron neutron capture therapy for cancer. Electrospray ionization mass spectrometry(ESI-MS) was used to characterize the IC by using various counter ion pairs. The best results were obtained with ion paired with triethylamine, and tetraethylammonium cations.

EXPERIMENTAL

Imidocaptate was prepared by coupling the dicesium salt of dodecaborane sulfhydryl with 1-(2-bromoethyl)-5-nitroimidazole in dimethylformamide-water (1:1) buffered with sodium bicarbonate. The molecule was purified by reversed - phase HPLC using a triethyl ammonium acetate methanol solvent system. Different salt forms were obtained by Dowex 50 exchange. ESI-MS was done on a Finnigan -MAT 900 equipped with Analytica Source, and PATRIC array detector Sample was dissolved in 1 1 0.01 in methanol water. acetic acid at a concentration of 30pmol/ul. The flow rate was set at 1.7 ul/min and 1.5ul/min, the skimmer voltage at 65v, and 55v, and the needle voltage at -2.7kV and -2.6kV for triethyl ammonium and tetraethyl ammonium cations respectively. In the IC with the triethyl ammonium cation pair, isopropyl alcohol was used as a sheath liquid with a flow rate of 1 7ul/min, the skimmer voltage set at 65v, and the needle voltage at 2.5kV for negative ion detection. The tetraethyl ammonium did not require sheath liquid for negative ion detection The skimmer was set at 55v, and the needle at 2.2 kV. The data was acquired at the scan rate of 30sec/decade.

RESULTS

The IC with the three different counter ion pairs showed complementary results. The triethyl ammonium ion pair Imidocaptate in negative ion detection showed an ion at 317 daltons $[M-2(102)]^-$ or IC minus the ion pair triethyl ammonium, and the ion at 419 daltons represents the IC minus one triethyl ammonium. In positive ion detection $[M+H]^+$ was present at 522 daltons. The IC (with the cation pair) plus sodium or $[M+Na]^+$ gave an ion at 544 daltons. The Imidocaptate ion pair molecule which was treated with excess of triethyl ammonium indicated a base peak at 624 daltons, which corresponds to $[M+Triethyl]^+$ ion In the tetraethyl ammonium Imidocaptate we observed a peak at 707 daltons corresponding to $[M+Et4n]^+$ ion.

DISCUSSION

The result obtained for the IC with the various paired ion indicated the presence of whole molecules (ion pairs plus the molecule) as the dominant ionic specie in ESI-MS. In the sample which the triethyl ammonium was exchanged with the tetra ethyl ammonium the base peak was at 707 daltons. This peak showed the successful exchange of paired triethyl ammonium moiety with a paired tetraethyl ammonium specie, plus a tetraethyl ammonium ion $[M+tetraethyl]^+$. The initial IC showed a base peak at 544 daltons or $[M+Na]^+$ [M= molecule +2(triethyl ammonium), after a successful exchange of the sodium with a triethyl ammonium ion the base peak shifted to 624 daltons or $[M+triethl\ ammonium]^+$. The labile IC was preserved with its adduct ion paired species in ESI-MS and was the dominant specie.

REFERENCE

1. Col, R.D., Silvestro, L , Naggi, A.; Torri, G., Baiocchi, C.; Moltrasio, D ; Cedro, A , Viano, I *Journal of Chromatography* 1993, 647, 289-300.
2 Juhasz, P., Biemann, K. *proc Natl. Acad. Sci.* 1994, 91, 433-4337
3 Suzuki-Sawada, J , Umeda, Y , Kondo, A , Kato, I *Analytical Biochemistry* 1992, 207, 203-207

Structure of Imidocaptate

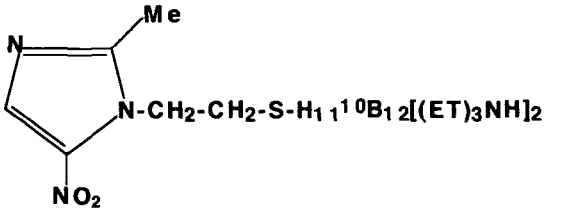

Negative-Ion ESI/MS of Primary Amines with TFA/TFE Derivatization

Hideji Fujiwara, Ronn G. Nadeau, Robert C. Chott, R. Thomas Solsten

Life Sciences Research Center, Monsanto Company
700 Chesterfield Parkway St. Louis, MO 63198

The study of glyphosate metabolism over the past 20 years, has been complicated by the difficulties associated with obtaining pure samples. Typically, identification required many chromatographic separations and purifications prior to MS analyses. Derivatization of these herbicidal compounds significantly improves the ease of MS analyses.

The derivatization of glyphosate and AMPA for GC/MS was initially developed at Monsanto. Several additional studies have since reported quantification of these compounds through derivatization. The derivatization makes these compounds to be less polar and volatile. The derivatization, however, is not always complete and some of the partial derivatives are not volatile enough for GC analysis. It is, therefore, desirable to use HPLC for the analysis.

Recently, we discovered that a trifluoroacetyl and trifluoroethanol (TFA/TFE) derivative of glyphosate was about 25 to 50 times more sensitive to negative ion electrospray ionization mass spectrometry (ESI/MS) than underivatized glyphosate. The derivatization increased the molecular weight of the metabolite and also improved the reverse phase LC chromatographic properties.

Since herbicides are generally metabolized in soils, plants, and animals into carboxylic (or sulfonic) acids, amino acid (or peptide) conjugates, and sugar conjugates, we have now extended this derivatization technique to amino acids & small peptides, nucleosides, amino alkyl(or aryl) sulfonic acids, and primary amines. We anticipate that this technique will be a valuable tool for analyzing metabolites of chloroacetanilide and sulfonylurea herbicides.

43rd ASMS Conference on Mass Spectrometry and Allied Topics

Negative Ion ESI Sensitivity Enhancement of TFA/TFE Derivatives

Compounds	No Sensitivity Improvement	Moderate Sensitivity Improvement	Great Sensitivity Improvement
		x 10	x 50 or Greater
glyphosate			x
AMPA			x
AMPA-dimethylester			x
Amino Acids			
Glycine			x
Sarcosine	x		
Alanine			x
Valine			x
Leucine			x
Glutamine			x
Glutamate			x
Phenylalanine			x
Lysine			x
Peptides			
Glutathione		x	
NO2-Phe-GSH		x	
Aminoalkyl(aryl)sulfonic Acids			
Aminoethylsulfonic Acid		x	
8-NH2-naphthalene-SO3H		x	
Aminoalkylphosphonic Acids			
2-NH2-3-phosphonopropionic Acid			x
2-NH2-4-phosphonobutyric Acid			x
2-NH2-5-phosphovalic Acid			x
Nucleosides			
Guanosine			x
Adenosine			x
Herbicide Metabolites			
2,6-diethylaniline			x
Halosulfuron			x
Aminopyrimidine			x
Propachloroxanilide	x		

Selectivity and Binding Mode of DNA Interacting Molecules Studied by ESI-MS

David C. Gale, David G. Camp II, and Richard D. Smith
Chemical Sciences Department, Pacific Northwest Laboratory, Richland WA, 99352

An area of interest to a number of scientists are small organic molecules that bind to or interact with DNA, thereby exhibiting antitumor, antiviral, or antibacterial activity.[1] Recently, the noncovalent complex formed between an oligonucleotide duplex and a minor groove binder was observed by electrospray ionization mass spectrometry (ESI-MS).[2] In this report, we address two important areas where by ESI-MS may be utilized in the study of minor groove binding molecule/oligonucleotide duplex noncovalent complexes. First, can the binding motif of a minor groove binding molecule be determined by ESI-MS? Second, can differences in the solution binding affinity of minor groove binding molecules to different duplexes, be observed in ESI mass spectra?

Shown in Figure 1 is the ESI mass spectrum of a self complementary oligonucleotide, 5'-dCGCAAATTTGCG-3' (M), with the minor groove binder distamycin (Dm). A charge state distribution for the 1:1 Dm/oligonucleotide duplex is observed. Shown in Figure 2 is the ESI mass spectrum of a duplex comprised of two sequence specific oligonucleotides, 5'-dCGCCTCGTCCGC-3' (T1) and 5'-dGCGGACGAGGCG-3' (T2), with Dm. No peaks for a 1:1 Dm/oligonucleotide duplex are observed in Figure 2. A charge state distribution for a 2:1 Dm/oligonucleotide duplex is however observed in Figure 2. It is important to note that the concentration of Dm and duplex are approximately the same in both Figures 1 and 2. These results demonstrate that Dm has a different binding motif with the two different oligonucleotide duplex sequences.

It is known that Dm has a high binding affinity for long AT regions (4 to 6 base pairs in length).[3] Shown in Figure 3 is the ESI mass spectrum of a solution containing the self complementary oligonucleotide, 5'-dCGCAAATTTGCG-3' (M), and two sequence specific oligonucleotides, 5'-dCGCCTCGTCCGC-3' (T1) and 5'-dGCGGACGAGGCG-3' (T2), without Dm Peaks composed of **both** Duplexes are observed at *m/z* 1214, 1457, and 1822. Distamycin was added to the solution used to acquire Figure 3, this data is shown in Figure 4. In comparing Figures 3 and 4, a charge state distribution for the 1:1 Dm/oligonucleotide duplex is observed. This is consistent for the binding of Dm to the 5'-dCGCAAATTTGCG-3' oligonucleotide duplex, as observed in Figure 1.

These results indicate that ESI-MS may be useful as an analytical technique in the analysis of small molecule/oligonucleotide duplex noncovalent complexes. As demonstrated in Figures 1 and 2, different binding motifs can be observed for different oligonucleotide duplex sequences. In addition, with carefully constructed experiments, binding affinity information of at least qualitative utility can be obtained by ESI-MS. This can be observed in Figure 4, where Dm binds only to the oligonucleotide duplex containing the long AT base pair region, as expected based on solution binding affinities.[3]

1. Zimmer, C.; Wahnert, U. *Prog. Biophys. Mol. Biol.* **1986**, 47, 31-112.
2. Gale, D. C.; Goodlett, D. R.; Light-Wahl, K. J.; Smith, R. D. *J. Am. Chem. Soc.* **1994**, 116, 6027-6028.
3. Dervan, P. *Science*, **1986**, 232, 464-471.

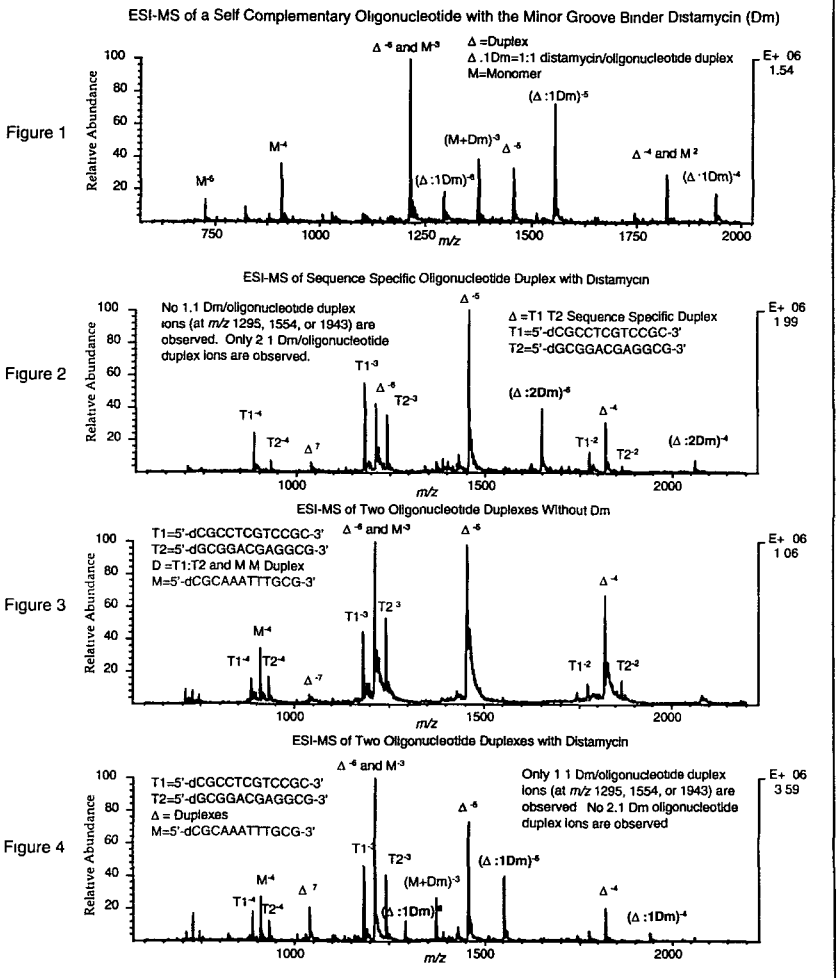

Pacific Northwest Laboratory is operated for the U.S. Department of Energy by Battelle Memorial Institute under contract DE-AC06-76RLO 1830

CHARACTERIZATION OF LARGE GLYCOPROTEINS USING HPLC/ELECTROSPRAY MASS SPECTROMETRY

Lee Q. Huang, Anthony Paiva, Ramadas Bhat*, Mel Wong*, Bayer Research Center, Pharmaceutical Division,Bayer co., 400 Morgan Lane, West Haven, CT 06516,
*Biological Division, Bayer co., Berkeley, CA 94701

HPLC coupled to mass spectrometry (MS) using electrospray ionization (ESI) has been widely used recently in the biological sciences for the characterization of proteins and peptides. Analysis of large glycoproteins by MS is, however, still challenging due to heterogeneity of the cabohydrates on the proteins. In this presentation, we describe the successful application of HPLC/ES/MS to the analysis of glycoproteins as large as 150,000 Da, determining not only the molecular weight, but also detailed heterogeneity for the first time. It is found to be crucial to use a synthetic peptide of MW 3259.6 for the optimiztion and calibration of the instrument in the high mass range up to 4000 amu, where the multiply charged envelopes of the 150,000 Da proteins are found. Further tuning of the instrument at relatively high mass resolution enabled us to resolve single monosaccharide deletions for the glycoproteins.

Electrospray ionization was performed on a Finnigan TSQ 7000 triple quadrupole mass spectrometer (Finnigan MAT, San Jose, CA) fitted with a Finnigan ESI source. Protein samples were introduced without any splitting into the electrospray source through a 0.10 mm id untreated fused silica column coupled to the HPLC with a PEEK zero dead-volume union (Upchurch Scientific, Oak Harbor, WA). A voltage of 4500 V - 5000V for the positive ions was maintained on the ESI electrode throughout all the experiments. The capillary was heated to 220° C. Nitrogen was introduced as a sheath gas at a pressure of 50 psi. Auxilliary Nitrogen gas at 40 cm/min was also introduced to improve sensitivity and reproducibility.

Q1 was operated in high mass range and was scanned from 1800-4000 amu over 5 seconds. The electron multiplier was run at 1200 - 1400 V. This resulted in a typical TIC (total ion count) of 1×10^{8} counts. A DEC 5000/25 data system running Finnigan ICIS software (version 8.0) was used to control the TSQ 7000. All spectra for proteins were acquired in profile mode. Profile data was averaged using a peak width of 100 mmu on a DEC 5000/133 data system. A mass defect of 0 mmu at 0 AMU and 300 mmu at 1000 AMU was used for data processing. Mass deconvolution of multiply charged ions was performed using Finnigan Biochemistry software.

With the improvement of instrumentation and sample introduction, it is demonstrated here that HPLC coupled to a quadrupole mass spectrometer with electrospray ionization can detect both molecular weight and microheterogeneity for 150,000 Da glycoproteins. High mass capability of the instrument facilitates the studies and is of importance for the characterization of large glycoproteins. Complementary information from Carbohydrate Analysis or Amino Acid Analysis are important to understand the glycosylation of large proteins. Together, the application of this method should have an impact on future glycoproteins research.

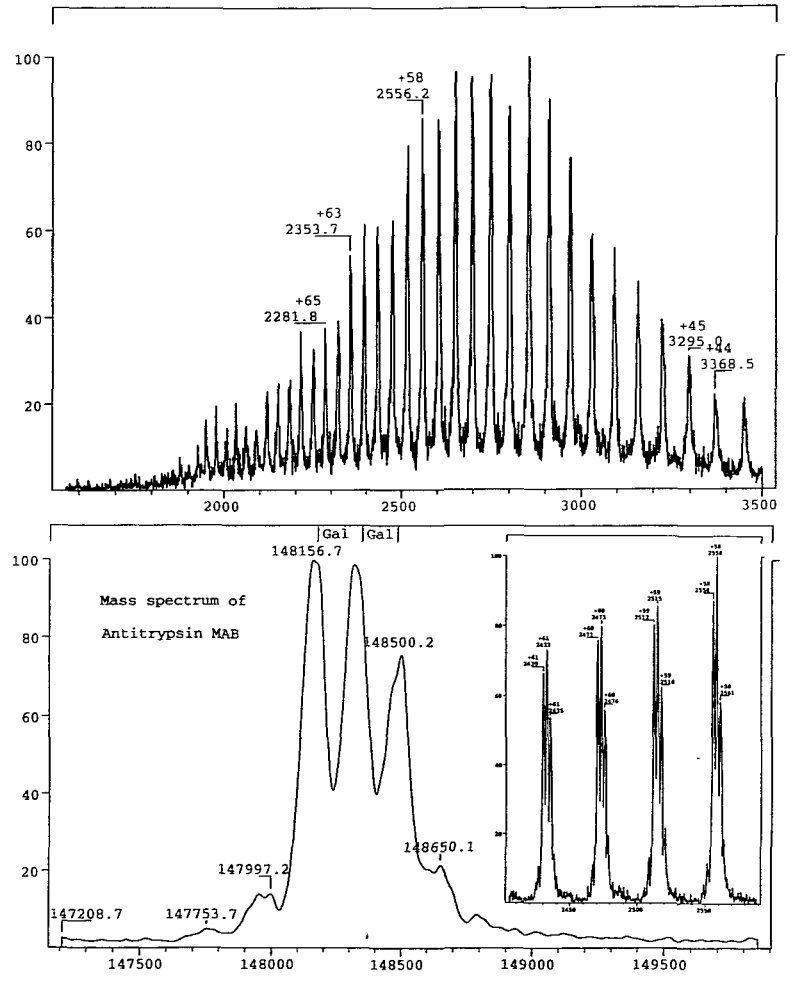

Cone Voltage Fragmentation and Collision-Induced Decomposition Electrospray Mass Spectra of Antineoplastic Drugs.

John Roboz, Longhua Ma and Qitao Yu, Division of Neoplastic Diseases, Department of Medicine, Mount Sinai School of Medicine, New York, NY, 10029, USA

OBJECTIVES. The prospective objective has been to explore electrospray ionization as a general technique for the quantification of antineoplastic drugs and for the identification of their metabolites in body fluids and tissues. The present objective was to obtain comparative data on the cone voltage fragmentation (CVF) and collision-induced decomposition (CID) electrospray (ESP) spectra of 12 compounds, selected to represent different classes of antineoplastic agents.

EXPERIMENTAL. Samples: 5-Fluorouracil (247 Da), cis-platin (298 Da), mitomycin C (335 Da), tamoxifen (371 Da), medroxyprogesterone acetate (387 Da), amsacrine (394 Da), doxorubicin (544 Da), homoharringtonine (545 Da), etoposide (589 Da), vincristine (825 Da), dactinomycin (1256 Da), bleomycin (1427 Da) Samples were dissolved in methanol/water (1:1 v/v) containing 1 % formic acid, to yield 5-100 ng/uL analyte concentration. ESI: Positive ESI spectra were obtained using a triple quadrupole mass spectrometer (Model Quattro, Fisons). Sample flow rate into the source was 5 µl/min. In CVF experiments spectra were obtained in the 70-300 V cone voltage range in 7 steps of 20-50 V increments. In CID experiments, argon was used as collision gas, using 50 V and 150 V collision energy Scan speed was 10 sec/scan, mass range from 100 to 500-1500 depending on the analyte. Spectra were obtained by summing 5 scans for CVF and 10 scans for CID.

RESULTS At 70 V cone voltage (normal condition) all drugs gave protonated molecules, actinomycin, bleomycin and vincristine gave both singly and doubly charged ions Medroxyprogesterone acetate and tamoxifen have relatively rigid structures with MH^+ at base peak intensity even at cone voltages of 220 V and 300 V, respectively. For bleomycin, high cone voltage (220 V) permitted identification of all analogs in the drug mixture. Increasing cone voltage led to considerable fragmentation providing structural information comparable to CID, e.g., doxorubicin (Fig. 1) and amsacrine (Fig. 2). High voltage CVF was often fully compatible with CID but with 2-5 times higher sensitivity, e g , etoposide. When fragment ions obtained at 250-300 V cone voltage were subjected to CID, additional structural information could be obtained from second and third generation product ions, e.g , mitomycin C, dactinomycin.

DISCUSSION. In the ESI of antineoplastic drugs, the CVF technique often produces structural information complementary to that provided by CID. Advantages of CVF include: simplicity (programmable), high sensitivity, both molecular and fragment and isotopic ions detectable, MS/MS-like spectra with single quadrupoles, intense fragments for second generation subsequent CID, and no loss of resolution. Disadvantages of CVF include less specificity than CID, and inapplicability to mixtures.

CONCLUSIONS. Judicious selection of experimental conditions provide intense protonated molecules for quantification by selected ion (CVF) or reaction (CID) monitoring, as well as structurally significant fragment ions to be used in strategic schemes for metabolite detection. (Supported by the T.J. Martell Memorial Foundation for Leukemia, Cancer and AIDS Research).

43rd ASMS Conference on Mass Spectrometry and Allied Topics

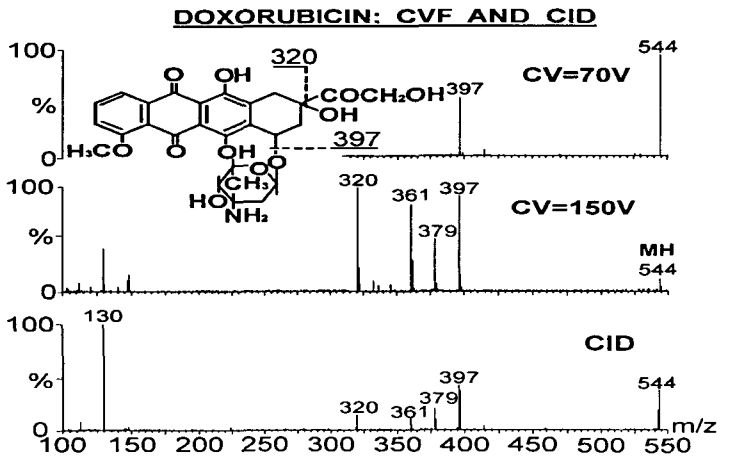

Fig. 1.

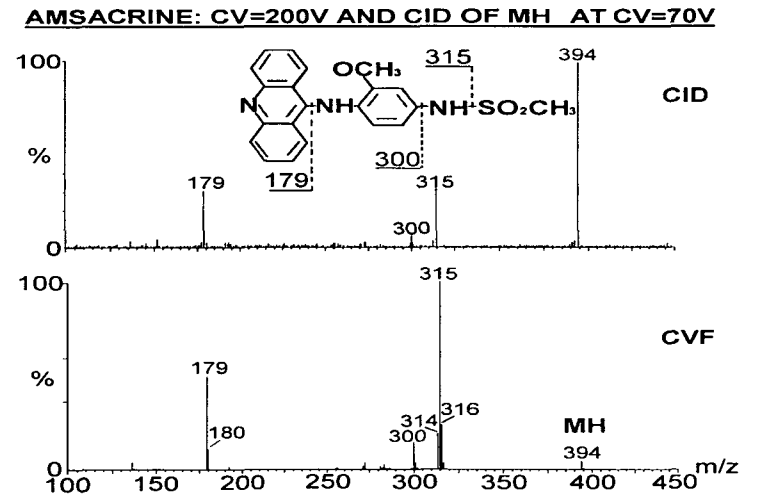

Fig. 2.

Factors Affecting ESI-MS of Nucleobases and Nucleosides

Ten-Yang Yen[1], Robert D. Voyksner[2] and M. Judith Charles[1]
[1]Department of Environmental Sciences and Engineering, University of North Carolina Chapel Hill, NC 27599-7400
[2]Analytical and Chemical Sciences, Research Triangle Institute, Research Triangle Park, NC 27709-2194

Introduction:

Electrospray ionization mass spectrometry (ESI-MS) has enhanced our capability to analyze thermally labile polar biomolecules including nucleobases and nucleosides, but the mechanism of electrospray ionization is not well understood. The ESI response is greatly affected by several physico-chemical parameters such as the concentration, pK_a of analytes and acids, as well as the nature of solvent[1]. Further understanding these factors can help us to improve the sensitivity of ESI needed for its application to analyze DNA adducts. In this study, we present data to demonstrate that the $(M+H)^+$ ion does not greatly increase (< 2 fold) by acidifying the solution, and a dramatic decrease in response was observed from organic bases in solutions acidified with HCl or CF_3COOH. From conductivity measurements data, we propose that the dramatic suppression of response is due to the ion-pair interactions between the $(M+H)^+$ ion of organic bases and the anion of HCl or CF_3COOH. A model for the ESI droplets formation of acidified solution related to the $(M+H)^+$ ion response is also proposed.

Experimental:

Solutions of analytes (500 μM) dissolved in 50% methanol/water were infused into ESI source at a flow rate of 2 μL/min. The ESI-MS mass spectra were acquired on a Finnigan 4000 quadrupole mass spectrometer retrofitted with an Analytica of Bradford, Inc. ESI source and a Teknivent Vector 2 data system. A tensiometer (CSC scientific Company, Inc.) was used to measure the surface tension of the solution. The conductance measurements were performed with an YSI conductivity meter and an YSI dip cell.

Results and Discussion:

Analytes with higher pK_a generally have greater response of the $(M+H)^+$ ion in ESI. The response of 1-methyladenosine, N^6-methyladenosine, thymine and uracil as a function of concentration of acetic, formic, hydrochloric and trifluoroacetic acid showed that the $(M+H)^+$ ion does not greatly increase (< 2 fold) by acidifying the solution. Moreover, a rapid decrease in response for organic bases such as 1-methyladenosine and N^6-methyladenosine was observed in solutions acidified with HCl or CF_3COOH. This dramatic suppression was not observed for neutral compounds such as thymine or uracil. According to results of conductivity measurements, the concentration of H^+ ion are nearly equal for those acidified solution with the same conductivity. The response of $(M+H)^+$ ion as a function of the solution conductivity for organic bases in solutions acidified with HCOOH or CH_3COOH is different than for solutions acidified with HCl or CF_3COOH (Figure 1). We propose that the dramatic suppression of response for organic bases is due to the ion-pair interactions between the

43rd ASMS Conference on Mass Spectrometry and Allied Topics

$(M+H)^+$ ion and anion of HCl or CF_3COOH. Because we did not observe a rapid decrease in response either from the solution acidified with HCOOH or CH_3COOH containing the same concentration of H^+ ion, or from neutral compounds (thymine, uracil) in any of acidified solution examined (Figure 2). The surface tension determined by tensiometer in any of acidified solutions was similar (33-34.5 dyne/cm). From these data, we infer that the response of $(M+H)^+$ ion is related to the ESI droplet formation processes. The competition of excess charge on the droplet surface between $(M+H)^+$ of analyte and H^+ of acid affects the observed response in ESI. Higher concentration of H^+ suppresses the $(M+H)^+$ ion signal and also reduces the size of droplet[2]. The decrease in response for neutral analytes in high conducting solutions is possibly due to the formation of smaller droplets during ESI processes. Fewer coulombic explosions occur in smaller droplets[3], and thus less response in the $(M+H)^+$ ion.

Figure 1

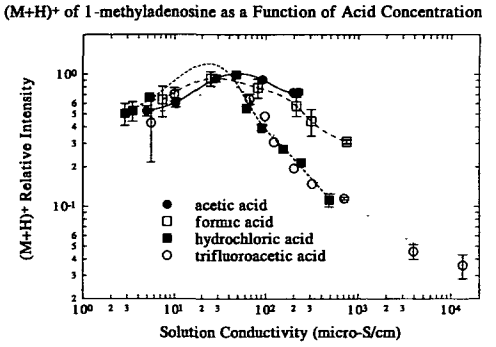

Figure 2

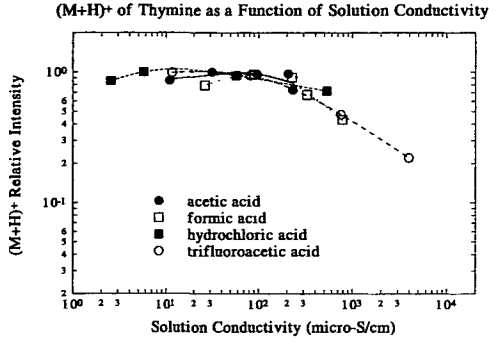

References: 1. Kebarle, P. and Tang, L. ***Anal. Chem.*** **1993**, ***65***, 972A-986A.
2. Rosell-Llompart, and Fernández de la Mora, J. ***J. Areosol Sci.*** **1994**, **25**, 1093-1119.
3. Gomez, A. and Tang, K. ***Phys. Fluids A*** **1994**, **6**, 404-414.

Acknowledgements:

This research was supported in part by a grant from NIEHS P42 ES05948. We gratefully acknowledge Dr. Craig M. Whitehouse of Analytica of Bradford, Inc. for his assistance with ESI source.

A NEW APPROACH TO DETERMINE MODIFICATIONS IN DNA CZE/MS OF OLIGONUCLEOTIDES

P. Janning[1], W. Schrader[1], R.Pesch[2], H. Münster[2] and M. Linscheid[1]
[1]*ISAS - Institut für Spektrochemie, P.O.Box 10 13 52, D - 44013 Dortmund, Germany*
[2]*Finnigan MAT Bremen*

Chemical modifications of DNA by xenobiotic compounds are regarded to play a major role in mutagenicity and carcinogenesis. The structural determination of such modifications of covalent and non covalent nature is difficult, since the compounds are normally rather polar and labile and the amount of material is small. In addition, the development of convincing experimental models was handicapped by the normal procedures, which require to cleave the DNA into nucleosides or nucleobases. Thus, all the sequence and topological information of the modification reaction is lost. We have now established a procedure which allows the *investigation of DNA modifications on the* oligonucleotide level. An unspecific nuclease is used to cleave DNA into mainly di-, tri-, tetra- and some penta- and hexanucleotides. In the next step, the 5'- phosphate is removed with alkaline phosphatase. The resulting mixture can be separated using CZE into groups of the same chain length. With electrospray MS, the different species are detected within the groups[1].

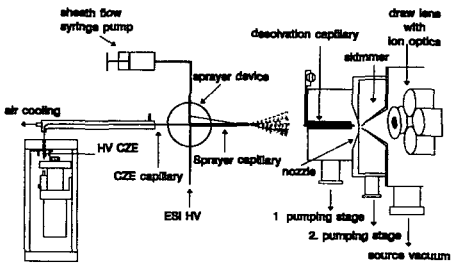

Fig. 1: Home build ESI source for a MAT 90 comprising static quadrupoles as focusing elements; interfaced to a CZE instrument

We have used this approach in two studies. In the first, the reaction of the potentially carcinogenic styrene oxide with DNA is explored aiming at the determination of nucleobase preferences and sequence specificity. In a second study the known reaction of cisplatin with DNA is used to detect the limits of this approach with respect to applications in drug development. For both, the detection power of the system is of major concern due to very low levels of adducts formed in DNA. Thus we have compared the results from a MAT 90 with a home built ESI source and from a MAT 900 equipped with an ESI II ion source and a PATRIC detector as one of simultaneous detections systems available.

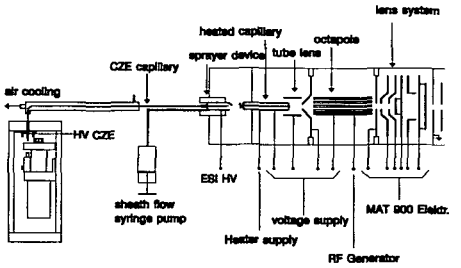

Fig.2: *ESI II ion source interfaced to the laboratory built CZE instrument*

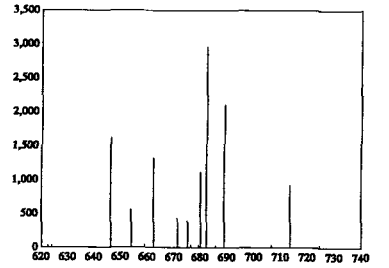

Fig.3: *Single scan of the mass range for adducts of styrene oxide to dinucleotides, home build ion source, MAT 90*

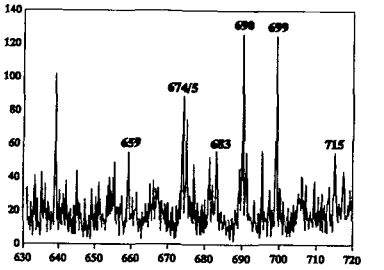

Fig.4: *Adducts of styrene oxide to dinucleotides, single scan, PATRIC detector*

The same capillary zone electrophoresis instrument was interfaced to the mass spectrometers. In figures 1 and 2, the schematics of both sources are given. For the styrene oxide adducts we have been able to detect the styrene oxide adducts (negative ions) at low levels with the PATRIC detector, whereas with the MAT 90 no signal at all was to discover. As an example a single spectrum from the MAT90 (Figure 3) covering the mass range in question and of a MAT 900 (Figure 4) is shown. In principle the same effect was obtained with the positive ions for the detection of cisplatin adducts to oligonucleotides, although the higher chemical background limited the gain in sensitivity to some extend. We were able to detect previously unknown complexes of the drug with two and three dinucleotide moieties. It is evident that the use of simultaneous detection systems can be crucial for the method to become a viable tool for the determination of modifications at the low level, which are to expect in real world samples. On the basis of these experiments it appears feasible to use this approach for biomonitoring programs e.g. for the control of occupational hazards. A second field of application envisaged is the study of genotoxic reactions of drugs in early stages of the development. But it seems inevitable that it is not sufficient only to use the best detection systems available; rather, the development of optimized sample introduction schemes for the CZE separation such as combinations with isotachophoresis or liquid chromatography and sample stacking procedures are required and experiments along that line are under way[2].

References:

1. P. Janning, W. Schrader, M. Linscheid, Rapid Commun. Mass Spectrom. 8, 1035 (1994)
2. W. Schrader, M. Linscheid, J. Chromatogr., accepted for publication (1995)

Acknowledgements
Financial support by the German Bundesminister für Forschung und Technologie and the Ministerium fürWissenschft und Forschung des Landes Nordrhein-Westfalen is gratefully acknowledged.

STRUCTURE ELUCIDATION OF OLIGONUCLEOTIDES USING CZE/ESI-MS AND SKIMMER CID

Chr. Siethoff[1], W. Schrader[1], R.Pesch[2], H. Münster[2] and M. Linscheid[1]
[1]*ISAS - Institut für Spektrochemie, P.O.Box 10 13 52, D - 44013 Dortmund, Germany*
[2]*Finnigan MAT Bremen*

The determination of adducts of xenobiotic compounds in DNA is one of the major steps towards an understanding of chemical carcinogenesis as well as of the role of DNA modifying cytostatic drugs. We have developed a mass spectrometric approach using enzymatic digestion of DNA into oligonucleotides and the separation with CZE/ESI-MS into groups of the same chain length[1]. The oligonucleotides are detected as negative ions with the number of charges depending on the chain length.

In a study with the potential carcinogen styrene oxide and DNA we have been able to separate the adducts to dinucleotides and trinucleotides and to obtain the molecular weight information with ESI-MS on sector field mass spectrometers (MAT 95/MAT 900). From the molecular ions the location of the reaction with respect to the nucleobases, riboses or phosphates cannot be determined, only the preference to the purine bases is evident (see Figure 1). To obtain a more detailed view of the reactions at the different oligonucleotides, we have attempted to use skimmer CID to get fragments from modified nucleotides[2] and from several di- and trinucleotides as well.

In analogy to earlier studies we have optimized the fragmentation conditions with a series of dinucleotides[3]; in Figure 2, as one example the fragments of the dinucleotide d(ApC) as a function of the skimmer voltage are shown. It is possible to distinguish isomeric dinucleotides on the basis of the intensity of fragments. We have then used skimmer CID during a CZE separation of oligonucleotides to detect the fragments of the di- and trinucleotides and of the modified species. Since the modification occurs in a few percent of the unmodified material only, we have used single ion detection at the relevant m/z values only to determine the adducts of the nucleobases. In Figure 3, the result for the purines is given; reactions at Cytosine was very low, Thymine did not react at all.

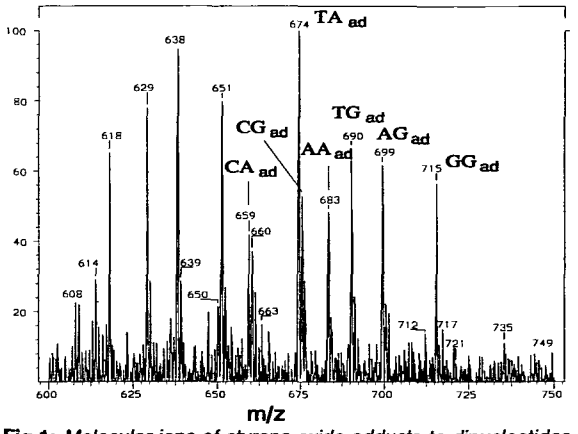

Fig.1: *Molecular ions of styrene oxide adducts to dinucleotides*

The first peak in both electropherograms appears always and is a result of N-7 adduct formation causing chemical depurination of the oligonucleotides. The second broader peak is a CID fragmentation product and indicates the reaction at the purines at site yielding chemically stable products. The loss of a modified nucleobase cannot be detected with our current procedure, because the signals are identical to those of unmodified dinucleotides. Since with the separation scheme used so far the oligonucleotides are separated according to the number of nucleobases only, it can become difficult to further elucidate the relation of the different precursor and product ions. To solve this problem, two approaches are conceivable: either using MS/MS experiments or a refinement of the electrophoretic separation.

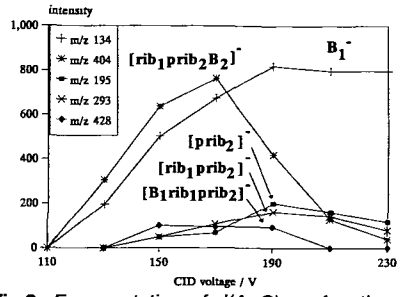

Fig.2: *Fragmentation of d(ApC) as function of skimmer voltage; [M-H] was omitted*

We have begun to modify the separation scheme in order to isolate the different oligonucleotides within the groups. First experiments confirm that this is possible at least at the di- and trinucleotide level, which makes the interpretation of skimmer CID experiments straight forward. Since the levels of adducts in real samples are low, the superior detection capabilities of skimmer CID compared to linked scan makes this a very valuable option to obtain further structural information on the modified DNA components.

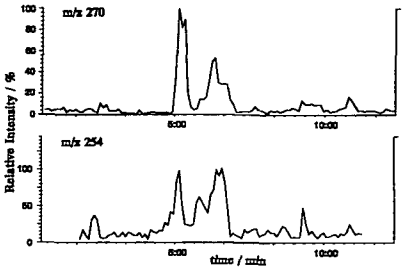

Fig.3: *Single ion electropherograms ESI/CID MS of adducts of guanine (upper trace) and adenine (bottom trace)*

With an improved separation scheme and the superior detection capabilities of a PATRIC detector this approach may allow to discover adducts in DNA down to the level required for the analysis of samples from people exposed to occupational hazards and to determine endogenous modifications.

References:

1. P.Janning, W.Schrader, M.Linscheid, Rapid Commun. Mass Spectrom. 8,1035(1994)
2. W.Schrader, M.Linscheid, J. Chromatogr., accepted for publication (1995)
3. a)D.R.Phillips,J.A.McCloskey, Int.J.Mass Spectrom.128,61(1995);
b)M.T.Rogers et al, Int.J.Mass Spectrom.137,121(1994);
c)S.Habibi-Goudarzi, S.A.McLuckey, J.Am.Soc.Mass Spectrom.6,102(1995)

THERMODYNAMIC STUDIES OF METAL SELF-ASSEMBLED COMPLEXES BY ESMS.

A. Dupont[1], E. Leize[1], A. Marquis-Rigault[2], D. Funeriu[2], J.-M. Lehn[2], and A. Van Dorsselaer[1]
[1] Laboratoire de Spectrométrie de Masse Bio-Organique, URA 31 CNRS-Université Louis Pasteur Strasbourg, France. [2] Laboratoire de Chimie Supramoléculaire, URA 422 CNRS-Université Louis Pasteur, Strasbourg, France.

INTRODUCTION :

Self-assembly, which consists of the spontaneous formation of a well-defined architecture from a given set of molecules able to recognize, orient and assemble themselves, is one of the basis of life chemistry [1]. Polynuclear metal complexes formed by self-assembly of different small synthetic ligands around metal ions are models allowing to approach the driving forces involved in self-assembly. ESMS has already been successfully used for the characterization of these molecules [2]. Quantization of **all ionic species present in a solution** is necessary to determine the thermodynamic parameters of a system and are important to understand the basic principles of the formation of these complexes.
In this work, we will evaluate the possibilities of ESMS for quantitative studies. We first study alkali ions solutions to determine key parameters for the response factors in ESMS. We show then an example of copper self-assembled complexes with identical desolvation energies. Their formation is studied by ESMS and results compared with NMR.

RESULTS :

1. Comparison of ESMS response factors of alkali ions : In this simple model, all the ions (same state of charge, very close m/z values, no fragmentation in the interface) are in equimolar concentration but show very different response factors (fig. 1). Such differences in response factors necessary originate from the ion evaporation itself. It is possible to correlate the response factor k of each cation and its hydration energy E, with a simple mathematical relationship (fig. 2). Such an effect of the hydration energy has already been qualitatively mentionned [3] but never mathematically described.

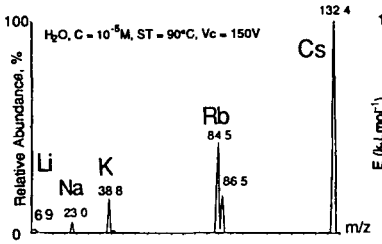

Fig. 1 : ESMS of an equimolar mixture of LiCl, NaCl, KCl, RbCl and CsCl.

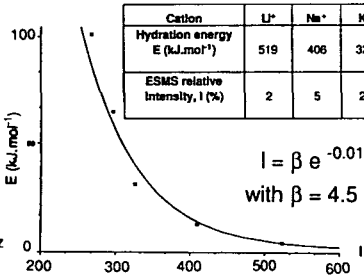

Cation	Li+	Na+	K+	Rb+	Cs+
Hydration energy E (kJ.mol-1)	519	406	322	293	264
ESMS relative intensity, I (%)	2	5	20	60	100

Fig. 2 : Correlation between desolvation energy and ESMS response factors of the alkali ions.

This result demonstrates that the **solvation energy of the ions is a key parameter** for the response factors of ionic species by ESMS. A quantitative study is then only possible whether the solvation energies of the different compounds under study are known or if they are identical.

2. Application to the study of Cu(I) self-assembled complexes : We have investigated **molecular recognition** between 2 types of ligands which are expected to form homohelicates [4] rather than

heterohelicates (fig. 3). For this study the ES mass spectrum is expected to give an exact image of the different species in solution because they have very close structure and hence comparable desolvation energies and response factors. Figure 4 shows the ES mass spectrum of the mixture of the heterodimer ($L^1L^2Cu_3$) and the homodimers ($(L^1)_2Cu_3$, $(L^2)_2Cu_3$) obtained by mixing 2 equiv. of L^1 and L^2 with 6 equiv. of $CuPF_6$. From this spectrum it is clear that ligands L^1 and L^2 are capable of self-recognition. Indeed a statistical repartition would have led to 50% of the heterohelicate instead of 23% as measured by ESMS.
This quantization obtained by ESMS is in perfect agreement with a quantization performed by NMR (at 10^{-3}M), which validates the use of ESMS for quantization of this series of compounds. A similar work has been performed on another model : a self-assembled capped complex [5], where the ESMS quantization of the intermediate species is in good agreement with the UV-Vis spectrophotometric data.

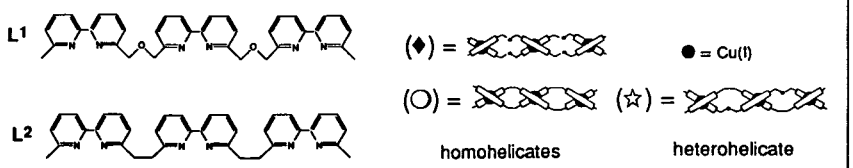

Fig. 3 : Structure and symbolism of the helicates

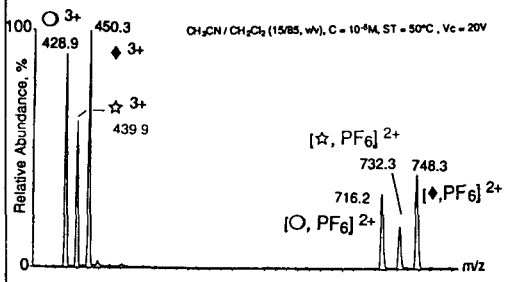

Species	% ESMS	% NMR
O	37	40
♦	41	40
☆	23	20

Fig. 4 : ES-mass spectrum of a mixture of 2 eq. L^1, L^2 and 6 eq. $CuPF_6$: comparison with NMR data.

CONCLUSION :

ESMS appears to be a very valuable technique for the analysis of metal complexes in thermodynamic equilibrium in diluted solutions. Indeed, in each case either NMR or UV-vis spectrophotometry could correlate with the relative intensities on the ES mass spectra for each molecular species present in solution. However it appears that quantization is possible only provided some precautions : no fragmentation, same charging rules and same solvation energy of all molecular species.

REFERENCES :

[1]. J.-M. Lehn, *Angew. Chem. Int. Ed. Engl.* (1990), **29**, 1304-1319.
[2]. V. Katta, S.K. Chowdury, B.T. Chait, *J. Am. Chem. Soc.* (1990), **112**, 5348-5349. F. Bitsch, G. Hegy, C.O. Dietrich-Buchecker, E. Leize, J.-P. Sauvage, A. Van Dorsselaer, *New J. Chem.* (1994), **18**, 801-807.
[3]. P. Kebarle, L. Tang, *Anal. Chem.* (1993), **65**, 972A.
[4]. R. Krämer, J.-M. Lehn, A. Marquis-Rigault, *Proc. Natl. Acad. Sci. USA* (1993), **90**, 5394-5398.
[5]. E. Leize, A. Van Dorsselaer, R. Krämer, J.-M. Lehn, *J. Chem. Soc., Chem. Comm.* (1993), 990-993.

ION LABELING STUDY OF SELF-ASSEMBLED SUPRAMOLECULAR SPECIES BY ESMS

Leize E.[1], Russell K.C.[2], Lehn J.M.[2] and Van Dorsselaer A.[1]
1 Laboratoire de Spectrométrie de Masse Bio-Organique,URA 31 CNRS-Université Louis Pasteur,
2 Laboratoire de Chimie Supramoléculaire, URA 422 CNRS-Université Louis Pasteur, Strasbourg, France.

INTRODUCTION :
ESMS has recently emerged as a suitable technique for understanding supramolecular self-assembly processes by following their formation. [1]
When supramolecular assemblies formed by hydrogen bonds are neutral, their study by ESMS is difficult because charges cannot be brought by protonation since acidity would disrupt the supramolecular complexes. In this case the study of these assemblies by ESMS needs the use of an ion label as ionization agent. The ion label used is a triaminotriazine attached to a crown-ether able to complex metal cations (ligand A) and allows the detection by IL (Ion Labelling)-ESMS of the species formed through hydrogen bonding with a complementary barbituric acid derivative (ligand B) without destroying the species obtained.

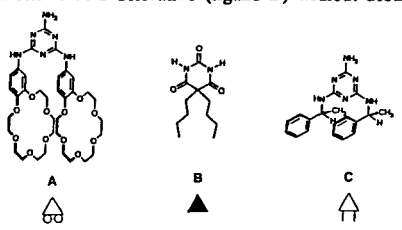

RESULTS AND DISCUSSION :
Characterisation by IL-ESMS of the complexes obtained by self-assembly of A and B :
The ES mass spectrum of S_1 (= equimolar mixture of A and B in CH_2Cl_2 at 10^{-2} M, saturated with KPF_6) shows major peaks corresponding to the different charged states of the ligand A and the A_3B_3 complex (Fig. 1). As ligand B was not ionized, it was not detected. A less intense peak is also observed corresponding to the doubly-charged ion of A_2B_3.
The charge state of these peaks was confirmed by the ESMS study of S_2 (= equimolar mixture of A and B in CH_2Cl_2 at 10^{-2} M, half saturated with KPF_6). S_2 contains half the KPF_6 than does S_1 and this fact increases the number of peaks (Table 1) corresponding to species, by the loss of one and several KPF_6 units. A m/z difference of 61.2 Da/e (= KPF_6 molecular weight/3) obtained between the peaks indicates that these peaks are indeed triply-charged ions, a m/z difference of 92.5 Da/e (= KPF_6 molecular weight/2) confirmed the doubly-charged state of the corresponding ions.
These ESMS studies have thus allowed the characterization of three complexes in solution: A_3B_3, A_2B_3 and A_3B_2. A_3B_3 was the predominant species detected. Since no larger complexes were observed, we can attribute to A_3B_3 a closed structure of the supramolecular macrocycle D, similar to that observed in the crystal for related systems.[3] Such a structure could explain the higher stability of A_3B_3 in comparison to A_3B_2 and A_2B_3. Three possible structures for A_3B_2 and A_2B_3 in solution again could be a linear ribbon (a), a bent ribbon (b), or a partial rosette (Fig. 1).
Characterisation by diluted IL-ESMS of the complexes obtained by self-assembly of B and C :
By extension, the IL-ESMS could be applicable to the study of any self-assembled structure in solution capable of incorporating the labelling agent A added in trace amounts. In the presence of a salt, A coordinates a cation and label ion containing species become visible by ESMS. This was tested by the introduction of five percents of A into a preformed assembly of B•C to obtain information by ESMS about the neutral entities formed (solution S_3 = 1 eq. A (5.10^{-4} M), 20 eq. B (10^{-2} M) and 20 eq. C (10^{-2} M), in CH_2Cl_2 saturated with KPF_6). The ES mass spectrum of S_3 (Fig. 2) shows two major species : the ion label A and the AB_3C_2 complex, as well as two other complexes : the ABC complex and AB_2C_2 complex. Again in this case, the six-components complex is the major species observed, suggesting that the assembly of B and C also prefers a macrocyclic rosette architecture.

CONCLUSION :
In conclusion, the IL-ESMS that we describe in this work allows the characterization of non-covalent complexes involving few hydrogen bonds which corresponds to particulary low energy interactions. Thanks this new IL method, it is possible to use ESMS for the investigation of the self-assembly processes of neutral and labile complexes.

REFERENCES:
1. E. Leize, A. Van Dorsselaer, R. Krämer, J.M. Lehn, *J. Chem. Soc., Chem. Commun.*, 990 (1993).
2. K.C. Russell, E. Leize, A. Van Dorsselaer, J.M. Lehn, *Angew. Chem. Int. Ed. Engl.*, **34**, 209 (1995).
3. J.A. Zerkowski, C.T. Seto, G.M. Whitesides, *J. Am. Chem. Soc.*, **114**, 5473 (1992).

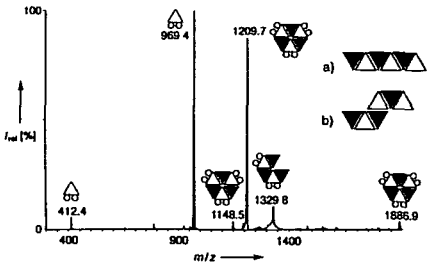

Fig. 1 : ES mass spectrum of S_1.
The observed ions are summarized in Table 1.

	A	A_2B_3	A_3B_3	A_3B_2
M [b]	746.8	2214.5	2721.0	2961.3
M + K^+	785.5	–	–	–
M + K^+ + KPF_6	969.4	–	–	–
M + 2K^+	412.4	–	1399.0	1519.1
M + 2K^+ + KPF_6	–	1237.9	1491.0	1611.0
M + 2K^+ + 2KPF_6	–	1329.8	1582.9	1703.0
M + 2K^+ + 3KPF_6	–	–	1674.9	1794.9
M + 2K^+ + 4KPF_6	–	–	–	1886.9
M + 3K^+	–	–	–	1025.7
M + 3K^+ + KPF_6	–	–	–	1087.3
M + 3K^+ + 2KPF_6	–	–	–	1148.5
M + 3K^+ + 3KPF_6	–	–	–	1209.7

Table 1 : Summary of m/z values of ions detected by ESMS for S_1 and S_2.

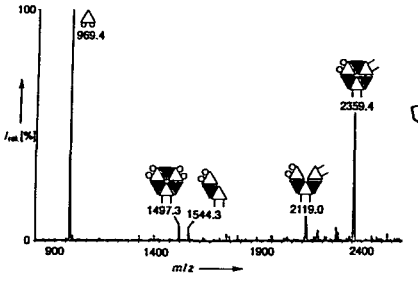

Fig.2 : ES mass spectrum of S_2.
m/z = 969.4, [A + 2 K^+ + PF_6^-]
m/z = 1497.1, [A_2B_3C + 4 K^+ + 2PF_6^-]
m/z = 2359.2, [AB_3C_2 + 2 K^+ + PF_6^-]
m/z = 1544.3, [ABC + 2 K^+ + PF_6^-]
m/z = 2119.0, [AB_2C_2 + 2 K^+ + PF_6^-]

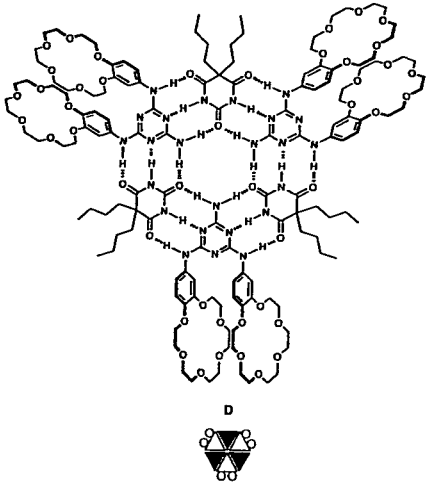

RETROSPECTIVE ANALYSIS OF HYPERPHENYLALANINEMIAS BY LSI AND ESI MS/MS

Donald H. Chace[†], Steven L. Hillman[†], Takeo Sakuma*, Yves Le Blanc*, Bori Shushan*
[†]Duke University Medical Center, MS Facility, RTP, NC, USA;
*PE Sciex, Concord, Ontario, Canada

Phenylketonuria (PKU) is a genetic disorder of phenylalanine (Phe) metabolism that results from the accumulation of this amino acid in blood. Early detection through infant screening and subsequent dietary changes prevents mental retardation. Presumptive diagnosis of this disorder relies on the quantitative measurement of an elevated Phe in blood Most methods used currently have a false positive rate that is at best 0.1%. Tandem mass spectrometry with liquid secondary ionization (LSI) has been used recently to screen for this form of hyperphenylalaninemia (1). Using isotope dilution techniques, this method is very accurate and precise for Phe quantitation. Calculation of Phe to Tyr ratios improves the diagnostic accuracy such that false positive analysis are reduced to less than 0.1% In this study, we have compared in retrospective analyses the accuracy of both LSI and ESI MS/MS to diagnose PKU.

Sixty filter paper blood spots containing normal, positive, and false positive samples were analyzed in a blinded fashion Sample preparation has been described previously(1) The samples were divided in two equal aliquots, dried, and the following matrices were added:

LSI: 35µL of 50.50 methanol:glycerol + 0.1% Na-Octylsulfate.
ESI: 50µL of 50:50 acetonitrile:water.

A VG Quattro I fitted with a Cesium Ion gun was used to analyze 2 µL aliquots by manual sample introduction. A PE Sciex API III was used to analyzed 5µL aliquots by flow injection techniques. An amino acid profile (*m/z 125-300)* was obtained by each tandem MS using the neutral loss (NTL) of 102 amu scan mode

Amino acid profiles from a blood spot of a patient with PKU using LSI and ESI MS/MS is shown in Figures 1a and b, respectively For each profile, internal standards are marked with an asterisk. A quantitative comparison for all samples that were analyzed by LSI and ESI MS/MS for measurement of Phe concentration and the µmolar ratio of Phe to Tyr was made A plot of Phe concentration by LSI versus Phe concentration by ESI showed that these two ionization modes produced similar results and closely correlate with each other (r = 0.97). The slope of the concentration data set is 0 66, which suggest that a higher estimate of the Phe concentration by LSI MS/MS is a observed when compared to ESI MS/MS. It is unlikely that different ionization efficiencies of Phe would account for this difference because the concentration is calculated from the ratio of Phe to d_5-Phe. Differences in the data processing software (baseline subtraction, smoothing, centroiding) could account for some of these differences Correlation of the Phe:Tyr ratios is also excellent (r=0.95) while the slope of the data set is 1 08 suggesting that these two ionization methods are producing similar Phe:Tyr ratios We have found previously that calculating Phe/Tyr ratios is the best method for diagnosing PKU resulting in a reduction in false positive diagnosis (1) In each case, both techniques differentiated normal patients from patients with PKU This comparative analysis demonstrates that it is MS/MS and its application to selective detection of key diagnostic amino acids that is the basis for the diagnosis of phenylketonuria regardless of the ionization method.

Financial support was from the State of North Carolina, Division of Maternal and Child Health, Department of Environmental Health and Natural Resources (Raleigh, NC grant No. C-05070)

43rd ASMS Conference on Mass Spectrometry and Allied Topics

REFERENCE

[1]Chace DH, Millington DS, Terada N, Kahler SG, Roe CR, Hofman LF. Rapid diagnosis of phenylketonuria by quantitative analysis for phenylalanine and tyrosine in neonatal blood spots by tandem mass spectrometry. Clin Chem 1993,39:66-71.

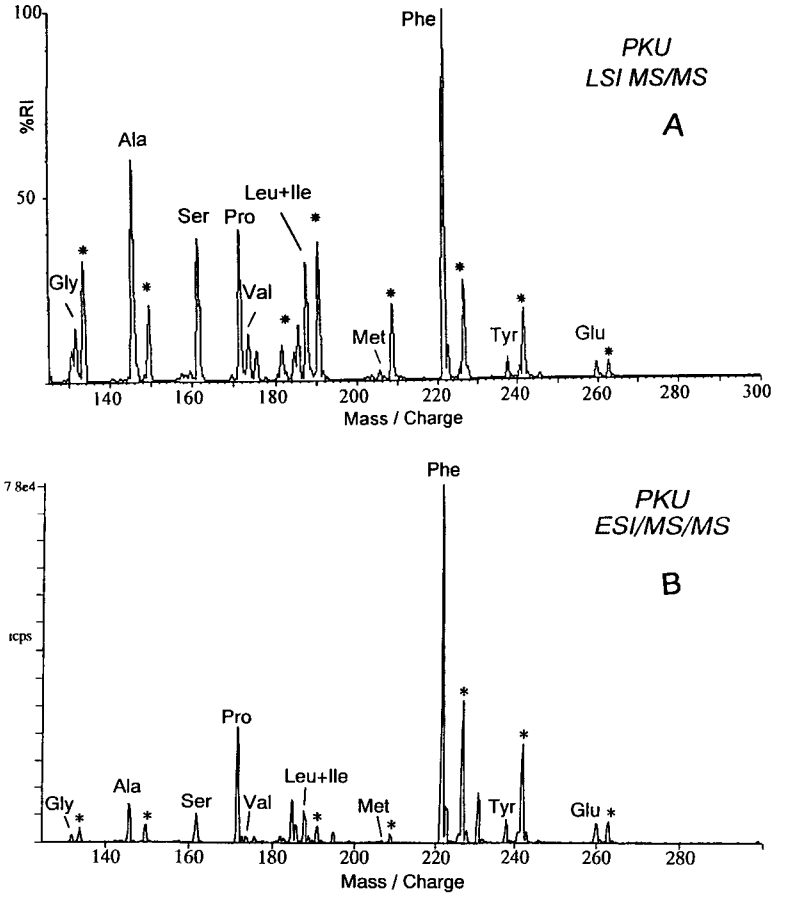

Figure 1 Amino acid MS/MS profiles of a blood spot of a newborn previously diagnosed with phenylketonuria using the neutral loss of 102 scan mode. a. Liquid Secondary ionization b. Electrospray ionization.

Electrospray Ionization Mass Spectrometric Study of Host-Guest Complexes

Ragulan Ramanathan and Laszlo Prokai

University of Florida, Center for Drug Discovery, Gainesville, FL 32610-8186

Recent studies have shown, that noncovalently-bound receptor-ligand, enzyme-substrate, and heme-protein complexes, formed in solution can be studied in the gas-phase using electrospray ionization (ESI) mass spectrometry (1). In the experiments reported here, an ESI mass spectrometer was used to demonstrate the applicability of this technique in the study of host-guest complexes. Cyclodextrins (α-, β-, γ- and heptakis(2,6-di-O-methyl)-β-CD) were selected as host molecules along with protonated amino acids (AA) (*L*-tryptophan, *L*-phenylalanine, *L*-tyrosine, and *L*-valine) as guest molecules. For the second part of this study, we selected protonated Ala-Leu-Gly [(TP)H^+] and Tyr-Gly-Gly-Phe-Leu [(PP)H^+] as guest molecules in order to investigate whether the peptide with all aliphatic amino acid residues formed less stable complexes than the peptide with aromatic amino acid residues.

All experiments were performed using a Vestec 200 ES single quadrupole mass spectrometer, equipped with an ESI source (2). The ESI was achieved by applying 2-2.5 kV to a flat tipped stainless steel needle. Sample solutions were delivered to the ESI source via syringe pump at a flow rate of 2-5 μL/min. The mass spectrum shown in Figure 1 was obtained via electrospraying equimolar mixtures of α-, β- and γ-CD's (1.0×10^{-4} M) with (Trp)H^+ (1.0×10^{-5} M). The results suggested that a better match between the cavity diameter of the host and the size of guest molecules increases the net complex stabilization. Mass spectra obtained by electrospraying equimolar mixtures of *L*-Trp, *L*-Phe, *L*-Tyr, *L*-Val and β-CD suggested that β-CD encapsulates protonated AA's in the order of Trp > Phe > Tyr > Val. The striking difference between ESI mass spectra obtained by using β-CD and DM-β-CD is the enhanced complexation (>90%) of protonated amino acids by DM-β-CD. However, the trends observed in complexation are similar for both host molecules. The encapsulation of (Trp)H^+ by both CD's is favored greatly over (Val)H^+, (Phe)H^+ and (Tyr)H^+. In order to understand the relationship between complex stability in solution versus gas-phase, a series of experiments were performed varying the DM-β-CD concentrations. Figure 2 represents a graph obtained by plotting the normalized ion intensities of each amino acid complexed as a function of the log of DM-β-CD concentration in the sample solution. The concentration of the amino acid was kept constant at 5.0×10^{-5} M and the concentration of DM-β-CD was varied between 3.7×10^{-8} and 7.5×10^{-4} M. Analysis of the curve indicates that the selectivity of DM-β-CD for protonated amino acids is (Trp)H^+ > (Phe)H^+ > (Tyr)H^+ > (Val)H^+.

Repeller/collimator CID experiment was performed on each (DM-β-CD)--(AA)H^+ to obtain relative stabilities and fragmentation information. For example, at lower repeller/collimator potential difference (2-10 V), collisional activation is low, and peaks due to (DM-β-CD)--(AA)H^+, (DM-β-CD) + (CH_2)--(AA)H^+ and (DM-β-CD) + $(CH_2)_2$--(AA)H^+ were observed. when the repeller/collimator potential difference was increased to 15 V, peaks due to the loss of $[(CH_3)_2C_6H_8O_5]_n$ (n = 1-2) units from the protonated host molecule (formed during or after the dissociation) were observed at *m/z* 1142 and 952. However, direct loss of the protonated AA, such as (Trp)H^+, from the complex, is not predominant. Step-wise loss of glucopyranose units from protonated DM-β-CD was common at higher repeller/collimator CID potentials with all the (DM-β-CD)--(AA)H^+ complexes studied. Increasing the potential difference >90 V produced $[(\text{DM-}\beta\text{-CD})\text{-}[(CH_3)_2C_6H_8O_5]_6\text{-}(H_2O)_2 + H]^+$ at *m/z* 155 as the most abundant fragment ion. The energy required for the dissociation of the complexes varied in the order of (DM-β-CD)--(Trp)H^+ > (DM-β-CD)--(Phe)H^+ > (DM-β-CD)--(Tyr)H^+ > (DM-β-CD)--(Val)H^+.

Repeller/collimator CID was performed on (DM-β-CD)--(TP)H^+, (DM-β-CD)--(PP)H^+, (TP)H^+ and (PP)H^+. At lower repeller/collimator potential difference, direct loss of the protonated peptide from complex was detected. At higher repeller/collimator potential difference, step-wise loss of glucopyranose units from the protonated (DM-β-CD) and the appearance of sequence ions were predominant. As shown in Figures 3-4, the appearance of sequence ions was monitored as a function of the repeller/collimator potential difference. The shift, between the fragmentation curve obtained from the complexed and uncomplexed peptide, correlates to the energy required to dissociate the host from the DM-β-CD cavity.

FIGURE 1

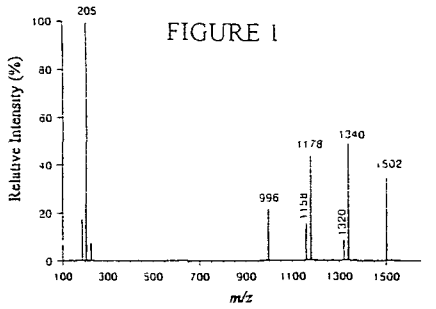

FIGURE 2

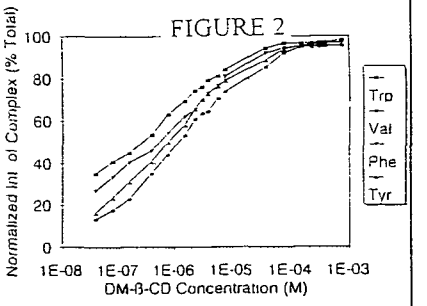

FIGURE 3

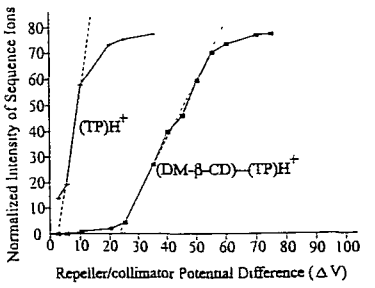

FIGURE 4

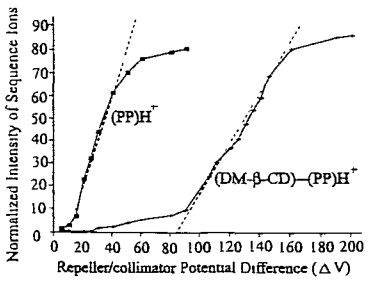

References

(1) Li, Y. T.; Hsieh, Y. L.; Henion, J. D.; Ocain, T. D.; Schiehser, G. A.; Ganem, B. *J. Am. Chem. Soc.* **1994**, *116*, 7487-7493.

(2) Allen, M. H.; Vestal, M. L. *J. Am. Soc. Mass Spectrom.* **1992**, *3*, 18-26.

On-Line Electrochemistry / Electrospray Mass Spectrometry: Studies of Oxidation of Polycyclic Aromatic Hydrocarbons (PAHs)

Xiaoming Xu[1], Wenzhe Lu[1], Ahmad A. Suleiman[2], and Richard B. Cole[1]*

1. Department of Chemistry, University of New Orleans, New Orleans, LA 70148
2. Dept. of Chemistry, Southern University-Baton Rouge, Baton Rouge, LA 70813

Studies of on-line coupling of electrochemistry with mass spectrometry, i.e., "electrochemical mass spectrometry" (EC/MS) date back to work by Bruckenstein et al. in the 1970's [1]. In these and other early experiments, porous working electrodes or permeable membranes were usually used as the interface between the cell and the MS ionization source which exclusively employed electron ionization (EI). As a result, only volatile products of electrochemical reactions could be detected by the mass spectrometer.

An important development in on-line electrochemistry/mass spectroscopy was the coupling of an electrochemical cell to a thermospray (TS) mass spectrometer (EC/TS/MS) reported by Hambitzer and Heitbaum [2], and Volk et al. [3]. Employing an aqueous ammonium acetate thermospray buffer solution, all detected species appeared as either protonated or ammoniated species in the positive ion mode or as deprotonated or acetate adduct species in the negative ion mode. Radical cations or anions were not detected.

Although "electrochemically assisted electrospray mass spectrometry" has been progressing for a few years, chiefly due to the pioneering efforts of Van Berkel and coworkers [4,5], on-line coupling of electrochemistry with electrospray mass spectrometry (EC/ESMS) is still a developing area because of the experimental difficulties involved, such as high voltage hazard to the electrochemistry hardware (e.g. potentiostat), and MS signal suppression caused by the presence of high concentrations of supporting electrolytes.

We report the coupling of an electrochemical device on-line with electrospray mass spectrometry (EC/ESMS) to extend the potential of ESMS to detect non-polar neutral compounds, and to monitor and identify intermediates and products generated by electrochemical reactions. Under favorable conditions, EC/ESMS can be used for the detection of radical cations of polycyclic aromatic hydrocarbons (PAHs) as first reported by Van Berkel et al. [5]. We find that PAHs can be divided into three groups according to the stability of the radical cations. The first group of compounds includes anthracene, phenanthrene and pyrene. Their radical cations are extremely reactive and undergo rapid irreversible reactions with solvent or impurities. Therefore, these radical cations were not detectable, or were only barely detectable under the applied potential. The second group includes 9,10-diphenylanthracene, perylene and rubrene. Their radical cations are very stable because the most reactive sites (e.g., carbon atoms at 9, 10 positions of anthracene) have been blocked by substituents. In addition, the resonance effect of phenyl substituents greatly increases the stability of radical cations. As a result, the radical cations of this group of compounds were detected by ESMS, even without use of the electrochemical cell (cell off). In this case, the electrospray capillary and counterelectrode functioned as an electrochemical cell which generated detectable amounts of radical cations. With an applied potential (+1.5 V), however, the radical cation abundance increased about 3-6 fold. The third group includes 9-methylanthracene, 9,10-dimethylanthracene, chrysene and benzo[a]pyrene. The stability of their radical cations lies between the above two groups. The radical cations could not be detected or were only barely detectable with the cell off, but high abundances of radical cations appeared in ESMS spectra with the cell on (+1.5 V).

One of the most important applications of the EC/ESMS system is to determine intermediates and products from solution chemical reactions of radical ions. Here we report the EC/ESMS study of the electrochemical oxidation of benzo[a]pyrene an extremely carcinogenic PAH.

[1] Bruckenstein, S.; Gadde, R. R., *J. Am. Chem. Soc.*, 1971, 93, 793.
[2] Hambitzer, G.; Heitbaum, J., *Anal. Chem.*, 1986, 58, 1067.
[3] Volk, K. J.; Yost, R. A.; Brajter-Toth, A., *Anal. Chem.*, 1989, 61, 1709.
[4] Van Berkel, G. J.; McLuckey, S. A.; Glish, G. L., Proc. 39th ASMS Conf., 1991, p. 1237.
[5] Van Berkel, G. J.; McLuckey, S. A.; Glish, G. L., *Anal. Chem.*, 1992, 64, 1586.
[6] Jeftic, L.; Adams, R. N., *J. Am. Chem. Soc.*, 1970, 92, 1332.

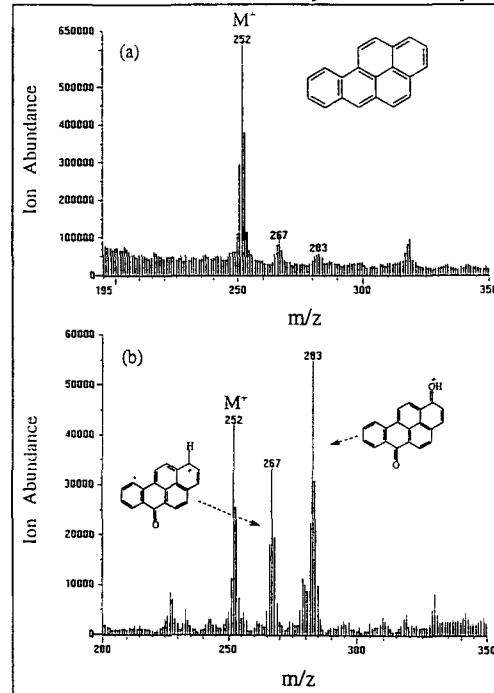

Figure 1. EC/ESMS studies of the oxidation of benzo[a]pyrene. (a) In dried 95% CH_2Cl_2 + 5% CH_3CN solvent, a high abundance of BaP $M^{+\cdot}$ (m/z=252 was detected with +1.5 V applied). (b) After adding 0.1 M H_2O to the solution, the abundance of m/z 267 and 283 increased sharply while $M^{+\cdot}$ abundance decreased.

Table 1. EC / ESMS Data for PAHs

Compound (M.W.)	$E_{1/2}$ (ox) vs. SCE (V)	$M^{+\cdot}$ abundance cell off	$M^{+\cdot}$ abundance cell on
Anthracene (178)	1.09	-	25,000
Pyrene (178)	1.16	-	-
Phenanthrene (178)	1.50	-	22,000
9-methyl-anthracene (192)	0.96	-	40,289
9,10-dimethyl-anthracene (206)	0.87	-	653,615
Chrysene (228)	1.35	-	93,473
Benzo[a]pyrene (252)	1.27	-	577,557
9,10-diphenyl-anthracene (330)	1.22	13,782	35,500
Perylene (252)	0.85	10,500	59,620
Rubrene (532)	0.77	5,100	24,500

This result demonstrates that the solvent composition plays an important role in determining the pathway of electrochemical reactions. Addition of a small amount of water introduced a series of solution chemical and electrochemical reactions which led to the formation of the ionic intermediate 6-oxobenzo[a]pyrene cation (m/z=267), and the "final" products 1,6- 3,6- and 6,12- benzo[a]pyrene quinone in accordance with the mechanism of Jeftic and Adams [6]. One should note that 6-oxobenzo[a]pyrene and the benzo[a]pyrene quinones are not radical cations implying that they cannot be detected by EPR spectrometry, but they are readily detected by ESMS.

This study demonstrates that on-line coupling of electrochemical / electrospray mass spectrometry allows identification of intermediate ions (radical or even electron) and products generated from electrochemical and ensuing solution-phase reactions. EC/ESMS offers much potential as a novel tool for studying the mechanism of complicated electrochemical reactions such as those occurring in biological redox systems or in electrochemical organic synthesis. EC/ESMS also enables the analysis of neutral compounds which are otherwise difficult to analyze by ordinary electrospray mass spectrometry.

THE EFFECTS OF ANION ENCAPSULATION BY KATAPINATES ON ELECTROSPRAY MASS SPECTRA

Anne B. Giordani
Parke-Davis Pharmaceutical Research, Division of Warner-Lambert Company
2800 Plymouth Road, Ann Arbor, MI 48105

Introduction Numerous factors affect the sensitivity of electrospray (ES) mass spectrometry and the appearance of ES spectra. The presence of salts in ES solutions may cause a reduction in analyte signal. Mirza and Chait have shown that the nature of the anionic species present in the analyte solution can influence charge state distributions in positive ES spectra.[1]

Addition of a cation-binding-macrocyclic compound, 18-crown-6 ether, to sodium-chloride-contaminated electrospray solutions decreases the sodium-cationized analyte levels and can increases sensitivity through an improvement in analyte signal-to-noise.[2] Katapinates are macrobicyclic diamines. Doubly protonated katapinate molecules form ion pairs with halide ions by encapsulation of the anion into the macrobicyclic hydrocarbon cavity.[3]

This poster reports the use of electrospray mass spectrometry to observe interactions of halide ions with the C_{10} katapinate: 1,12-diazabicyclo[10.10.10]decacosone,**1**, extends the study of Mirza and Chait to encompass the full halide anion series and reports the effects of ion pair formation by this katapinate with halide anions on positive electrospray mass spectra.

Observation of katapinate binding to halide anions ES-MS spectra of 1,12-diazabicyclo[10.10.10]decacosone are consistent with the literature NMR data showing facile Cl^-, Br^- and I^- ion pair formation with the doubly-protonated diamine.[3] The relative intensity of the peak corresponding to the $[M + 2H^+ + I^-]^+$ ion is lower than that of the chloride or bromide, which may be due to the larger ionic radius of I^-. Iodide ion was not observed to bind with the *[9.9.9]*diamine in the NMR studies, and this was attributed to the size of the hydrocarbon cavity relative to the radius of I^-. Fluoride ion binding to the katapinates was not observed. The lack of fluoride ion binding has been attributed to the high heat of hydration of fluoride ion, and bifluoride ion formation.[3] Product ion spectra of the $[M + 2H^+ + X^-]^+$ ions show ready losses of neutral HX to form the singly-protonated bicyclic diamine.

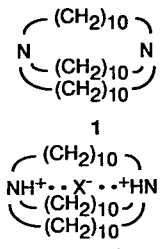

Halide anion- katapinate ion pair

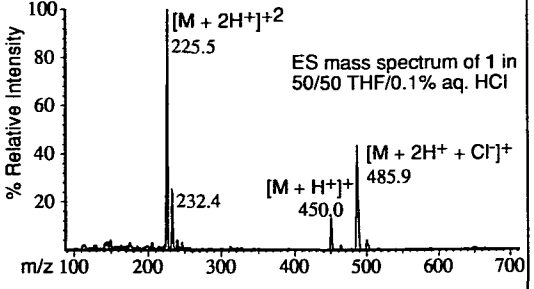

The effects of halide anions on ES mass spectra of some peptide and proteins ES mass spectra of peptides and proteins from solvent solutions of 50/50 THF/0.1% aqueous HX show a decrease in the average charge state across the halogen acid series. (The measured pH of the hydrochloric, hydrobromic and hydriodic acid solutions was 2.2.) The observed order of halide anion effectiveness in shifting charge state distributions to lower charge states is: $I^- > Br^- > Cl^- > F^-$. This order parallels the acetate

anion series studied by Mirza and Chait.[1] The trend was consistent for TRH precursor peptide, melittin, ubiquitin and myoglobin, although the mean charge states observed from HCl/aqueous THF solutions were lower than those reported by Mirza and Chait for the same peptides and proteins from HCl/aqueous methanol.

The ES spectrum of ubiquitin exhibits the narrowest peak widths from HCl solution compared to HF, HBr and HI, indicating that there is the least amount of adduction. Adduction of HI and HBr is particularly apparent for the +5 peaks in the spectra from their respective solutions. An overall increase in ion current and decrease in the average charge state is observed in the spectra of ubiquitin from HI-containing solution, as the degree of adduction is reduced at higher repeller voltages.

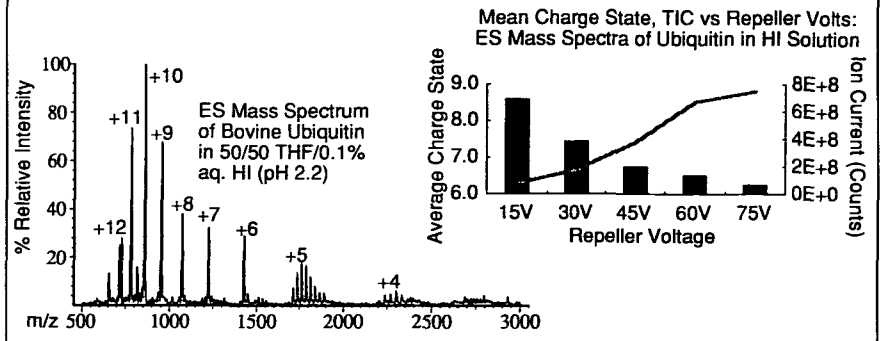

Effects of halide anion-katapinate ion pair formation on positive electrospray mass spectra Considerable suppression of ES signal is observed in the presence of a relatively large concentration of katapinate. The average charge states are lower than in solutions without katapinate, probably because the diamine's presence causes an increase in the solution pH. Despite the halide anion-katapinate ion pair formation and the severely suppressed protein signal, the trend toward decreasing mean charge across the halogen ion series is still evident.

Conclusions

- Halide anion-katapinate ion pair formation is readily observed by electrospray mass spectrometry.
- The observed order of halide anion effectiveness in shifting charge state distributions to lower charge states is: $I^- > Br^- > Cl^- > F^-$.
- Katapinate addition to ES solutions does not diminish the effectiveness of halide ions in shifting charge state distributions to lower charge states.

References

[1]Mirza, U.A. and Chait, B.T.; *Anal. Chem.* **1994**, *66*, 2898-2904.

[2]Giordani, A.B.; "Use of Crown Ethers to Enhance Electrospray Ionization Mass Spectra of Samples Containing Alkali Metal Salts;" Proceedings of the 41st ASMS Conference on Mass Spectrometry and Allied Topics, San Francisco, CA, May 30-June 4, 1993.

[3]Park, C.H. and Simmonds, H.E.; *J. Am. Chem. Soc.* **1968**, *90*, 2431-2.

[4]Simmonds, H.E. and Park, C.H.; *J. Am. Chem. Soc.* **1968**, *90*, 2428-9.

Acknowledgement The author is grateful to Dr. Gary Bolton of Parke Davis for the synthesis of the 1,12-diazabicyclo[10.10.10]decacosone.

PROBING THE STRUCTURE OF 4OT USING "NATIVE" ESI-TOFMS

M.C. Fitzgerald[1], I. Chernushevich[2], C.P. Whitman[3], and S.B.H. Kent[1]

1.Department of Cell Biology, The Scripps Research Institute, La Jolla, CA 92037
2.Department of Physics, University of Manitoba, Winnipeg, Manitoba, Canada R3T2N2
3. College of Pharmacy, University of Texas, Austin, Texas 78712

4-Oxalocrotonate (4OT) tautomerase is an enzyme used by certain soil bacteria to help degrade aromatic hydrocarbons to intermediates in the Krebs cycle. The enzyme is a hexamer of identical 62 amino acid subunits which catalyzes the 1,3-allylic isomerization of 2-oxo-4-trans-hexenedioate to 2-oxo-3-trans-hexenedioate through the intermediate 2-hydroxymuconate. We have established access to 4OT by total chemical synthesis and are interested in studying the structure and function of this highly efficient enzyme by exploiting the advantages afforded by total chemical synthesis. Here we have used electrospray ionization time of flight (ESI-TOF) mass spectrometry to establish the multimeric state of our synthetic enzyme. The technique has also proven very useful in studying the non-covalent nature of several 4OT analogs including the D-enantiomer of the enzyme as well as several analogs containing modifications to the active site at the N-terminus of the enzyme.

All mass spectra were acquired using an ESI-TOF instrument constructed at the University of Manitoba and described previously(1). ESI-TOF analysis was performed under both native (5 mM ammonium bicarbonate, pH 7.0) and denaturing (5 mM ammonium bicarbonate, 0.02% formic acid, pH 4.0) conditions at concentrations of approximately 10 µM.

Under native electrospray conditions strong ion signals corresponding to the multiply charged monomer and hexamer complex of the enzyme (MW 40,866) were observed in the ESI-TOF mass spectrum of synthetic 4OT (Fig. 1A). Only weak signals representative of the dimer and pentamer were detected and there was no evidence for trimer or tetramer in the spectra. Analysis of the enzyme under denaturing conditions yielded only multiply charged monomer ions and confirmed the specific, noncovalent nature of the hexamer that is formed under native conditions (Fig. 1B). Increasing the declustering voltage from 120 V to 250 V also fragmented the hexamer. Significantly, however, the major decomposition product (the pentamer) appears to be unusually stable.

We have also used native ESI-TOF to assess the structural integrity of several 4OT analogs including the D-enantiomer, a truncated construct (2-62), and a derivative where the N-terminal proline was replaced with cyclopentane carboxylate (CP). Native ESI-TOF mass spectra of D-4OT and CP were similar to those obtained with L-4OT and show that these analogs appropriately fold to form a hexameric enzyme complex resembling that of L-4OT (Figs. 2A and 2B). Only monomer ions were observed in the native mass spectrum of (2-62) indicating that this 4OT construct does not fold appropriately (Fig.2C).

Our native ESI-TOF results with L-4OT, D-4OT, (2-62), and CP were also consistent with structural data obtained from circular dichroism experiments on these samples. Multimeric (hexamer) complexes were only observed in the native mass spectra of samples that showed significant helical content by CD spectroscopy (Fig. 3). Furthermore, our ESI-

TOF results with (2-62) and CP were instrumental in establishing the mechanistic and structural significance of the catalytically important Pro1 residue in 4OT. The absence of multimeric (hexamer) complexes in the native mass spectrum of (2-62) suggests that Pro1 is essential for enzyme folding. From our studies with CP we also conclude that 4OT requires an N-terminal amine for activity as the CP analog apparently folds correctly but is inactive (Table 1). Therefore, we conclude that the N-terminal proline residue of 4OT is both chemically and structurally significant.

Reference:

(1) A.N. Verentchikov, W. Ens, K.G. Standing, *Anal Chem.*, **66** p.126 (1994).

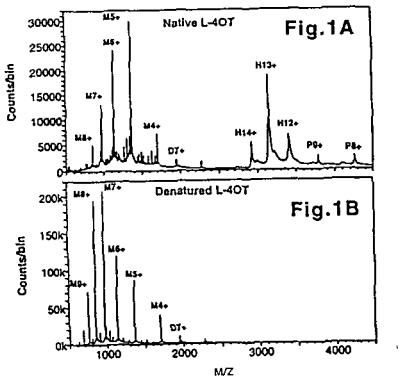

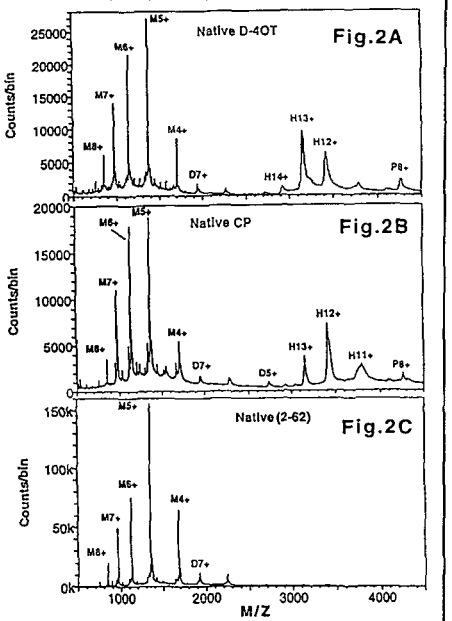

TABLE 1: Kinetic Parameters for Synthetic 4OT and Analogs

Analog	K_M, µM	k_{cat}, s^{-1}	k_{cat}/K_M, $M^{-1}s^{-1}$
L-4OT	38	290	7.6×10^6
D-4OT*	56	450	8.0×10^6
(2-62)**		Not Active	
CP***		Not Active	

*D-4OT=4OT analog containing 62 amino acid polypeptide chains made up entirely of D-amino acids

**(2-62)=Truncated L-4OT where Pro-1 has been omitted

***CP=4OT construct where cyclopentane carboxylate (a proline isostere lacks an amine functionality) has been coupled to the N-terminus of 4OT(2-62).

Fig.3 Far UV-CD Results for L-4OT and Analogs

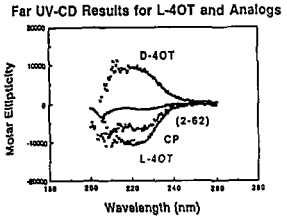

Investigation of Cyclodextrin-Metal Cation Complexes Using ESI/FTICR-MS

David E. Kage, Clifford H. Watson, [1]Laszlo Prokai, John R. Eyler
Department of Chemistry, University of Florida, Gainesville, FL 32611-7200
[1]Center for Drug Delivery, University of Florida, Gainesville, FL 32611

Cyclodextrins were discovered by Villiers near the turn of the twentieth century. They were isolated as enzymatic degradation products of starch.[1] Not long after their discovery, Schardinger characterized them as cyclic oligosaccarides.[2] Freudenberg et al. revealed that the cyclodextrins were held together by the formation of α(1,4)-linked glucose units[3] (Figs. 1 and 2). The products of the enzymatic degradation contain α-, β-, and γ-cyclodextrins with traces of cyclodextrins ranging up to thirteen glucose units. The three that are produced to an appreciable extent are α-, β-, and γ-cyclodextrin which contain six, seven, and eight glucose units, respectively.

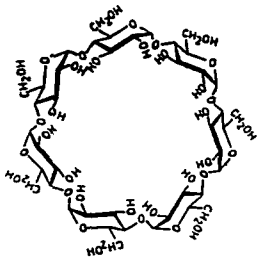

Figure 1

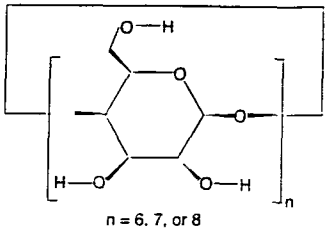

Figure 2

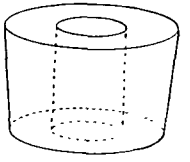

Figure 3

Figure 1 depicts the chemical structure of α-cyclodextrin where the glucose units are in the C1 chair conformation and are linked by α(1,4) bonds. Their overall geometry leads to a shape that is described as a truncated cone (a lamp shade if you will). The wider side of the molecule contains the secondary hydroxyl groups, while the narrower side contains the primary hydroxyl groups. The dimensions of the cavity are governed by the number of glucose units in the ring (Fig. 3). Due to the arrangement of the functional groups, the cavity created by the cyclodextrins is hydrophobic (relative to water), while the external faces of the cone are hydrophilic.

Cyclodextrins have a number of unique properties as a result of their structural features. The most important property, or at least the one that has generated the bulk of the literature, is the ability of cyclodextrins to form inclusion complexes with a large variety of guest molecules. The guests can be organic or inorganic, neutral or ionic, or even gaseous in nature. The limiting factor is that the guest must "fit" (even if only partially) into the host cavity created by the cyclodextrins. The alkali and alkaline earth metal cations are well suited for the formation of inclusion complexes based on their size.

In these studies, cyclodextrins (α-, β-, and γ-) have been investigated as potential host molecules for small metal cation guests ($M^{+1,2}$). Our interests start with understanding and measuring the affinity and binding strengths of different metal guests to different cylodextrin hosts. The experiments were performed on a 7-T

FTICR mass spectrometer equipped with an external electrospray ionization source. Samples of cyclodextrins were dissolved in 50/50 ($MeOH/H_2O$) and brought to ca. 1-5x10^{-4} M. Salt solutions were prepared using the same solvent system. The capillary, cylinder, and needle of the ESI source were kept near -4kV, -3kV, and 0V, respectively Standard pulse sequences written into the software were used to detect ions in the ICR cell.

Preliminary results have shown that alkali and alkaline earth metal cations (specifically Li^+, Na^+, K^+, Cs^+, and Ca^{+2}) will bind to α-cylodextrin (see Figs. 4 and 5 for examples). The results are promising and prove to us that our instrumental design is suitable for studying these species in the gas phase. Work on this project is ongoing in our laboratory. We are working toward a better understanding of the binding of these metal guests to the cylodextrin hosts. Are the metal cations truly encapsulated within the host cavity, or merely stuck to the outside walls electrostatically as recently suggested by Vouros et al?[4] Collisionally activated dissociation (CAD), laser photodissociation, and ion-molecule reaction experiments will be conducted on these host-guest complexes.

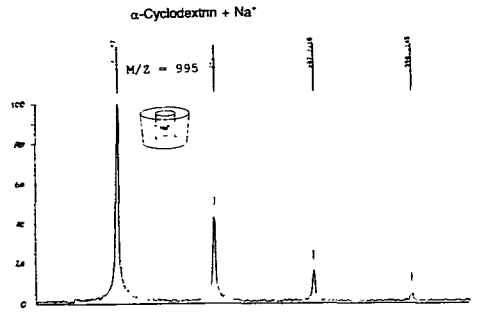

Figure 4

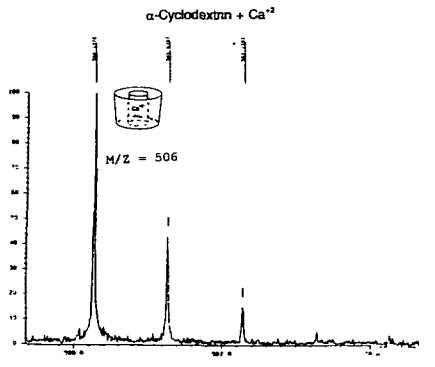

Figure 5

References:
1. *C. R. Acad. Sci.* **1891**, *112*, 536.
2. *Wien. Klin. Wochenschr.* **1904**, *17*, 207.
3. *Ber. Dtsch. Chem. Ges.* **1938**, *71*, 1596.
4. *J. Am. Soc. Mass Spectrom.* **1995**, *6*, 437.

HPLC - ESI - MS of Flavonoid Glycosides in Hops

Martin Sàgesser and Max L. Deinzer, Oregon State University, CORVALLIS, OR

INTRODUCTION

The objective of this work was to determine the content of flavonoids in hops (*humulus lupus*).

Flavonoids[1], also known as tannins or polyphenols, include a wide range of compounds, suchs as catechins, anthocyanidins, flavonols, flavones and their different glycosides. They are widely distributed in the plant world and are common in the human diet. They ere found in barley and hops[2,3], in honey, black tea, fruit, vegetables and other plants These naturally occurring flavonoids (aglycones and glycosides) can be separated using reversed-phase HPLC[4].

RESULTS

Extraction and HPLC

One gram of dried hop pellets and 50ml of water were placed in a flask and homogenized. The extract was filtered after 24h and used for the following RP-HPLC Initial experiments by HPLC showed differences in flavonoid content of different hop varieties

Mass Spectrometry

The mass spectrometry analyses were performed using a SCIEX API III triple-quadrupole mass spectrometer (Thornhill, Ontario, Canada) with an ionspray interface and a Macintosh data system The MS was operated in the positive ion mode under conditions of unit mass resolution. Profile spectra were obtained by acquiring data points every 0.2 Da with a dwell time of 2ms. Purified air was used as the nebulizing gas at 24-48 psi and the ionspray voltage was to +5000V. The curtain gas was nitrogen and the orifice voltages were set at +80 -120V. Collision induced dissociation (CID) experiments were performed using argon as target gas with a thickness of 2-3x10^{14} atoms cm^{-2}. The step size was 0.5 amu and the mass range 400-900 Dalton. The mass spectrum of Rutin in Fig. 1 shows not only the protonated molecular ion, but also information about the glycosidic residue - glucose (Δm. 162Da) and deoxyglucose(Δm· 146 Da) - and also the aglycone unit of the molecule.

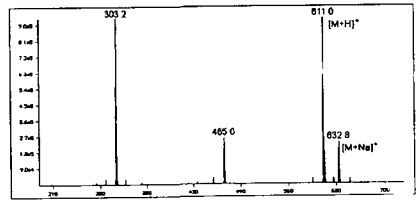

Fig 1: ESI-MS of Rutin (Quercetin-3-rutinoside)

LC - ESI - MS

A typical LC-MS basepeak chromatogram (BPC) of a hop extract is shown in Figure 2

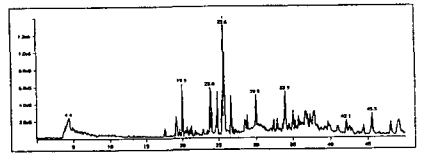

Fig 2· BPC of Hallertau hop extract

The mass spectra of the different HPLC peaks show molecular ion and fragments which could be derived from proanthocyanidins and flavonol glycosides.

LC - Tandem Mass Spectrometry

The mass spectra in the positive ion mode of glycosides of quercetin and kaempferol show signals for the protonated molecular ion and for the different possible losses of the sugar residues as shown in Figure 1. All spectra have in common a peak with m/z 303 Da or 287 Da, both of which are due to the protonated aglycones. These ions were scanned in order to identify the parent ions. To get the most useful information out of one LC run, both the parent ion scans of kaempferol and quercetin were performed simultaneously

By analysing these scans we found 12 different glycosides related to these flavonols The amount of each glycoside was different in the various hop varieties.

The mass spectrum of compound A is shown in Figure 3 This compound must have quercetin as the aglycone because it is a parent scan of m/z 303 The peak at m/z 757 Da could be the $[M+H]^+$-ion of quercetin with one hexose and two desoxyhexose sugar units. The difference between m/z 757 and 611 and between m/z 611 and 465 is in both cases 146, which corresponds exactly to a desoxyhexose unit. The remaining fragment has a mass of 162, a hexose unit The mass spectrum alone is not enough to determine the correct structure. Either reference compounds or further isolation and NMR analysis would help to get the right structure.

Direct analysis of beer samples

Without any concentration or purification, samples of beer were directly injected into the LC-MS. The same type of scan as described above (parent ion scan)

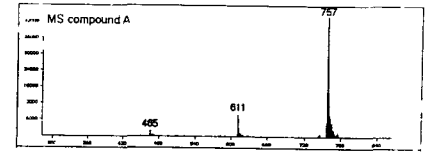

Fig 3 Mass Spectrum of compound A

was used to search for flavanol glycosides in these samples. Figure 4 shows a fraction of the chromatogram of a commercial beer.

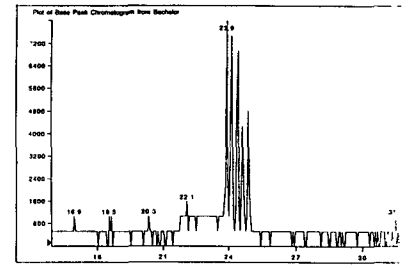

igure 4 Chromatogram of a commercial beer

The intensity is about ten times smaller than in the hop extracts, but the mass spectra allow one to determine the different compounds

CONCLUSION

- HPLC-electrospray mass spectrometry is a powerful method for the investigation of these polyphenols in hops The technique provides molecular mass information and some structural data with a minimum of sample preparation
- Tandem mass spectrometry is even more useful to get specific information on one class of compounds, as shown here with the flavanol glycosides

POTENTIALITY OF MASS SPECTROMETRY FOR THE ANALYSIS OF SULFATED POLYSACCHARIDES OF HIGH POLYMERIZATION DEGREE

F. UZABIAGA[1], C. MONTEIRO[1], M. PETITOU[1], C. PONTHUS[1], J.C. PROME[2] and C. PICARD[1]

INTRODUCTION

Mass spectrometry analysis of highly sulfated oligosaccharides derived from Heparin is complicated by their strongly ionic and hydrophilic character. Because of their strong interaction with the surrounding (solvent, matrix), it is very difficult to volatilize these molecules intact from the sample, in particular when increase polymerization degree (PD), degree of sulfation (SD) and number of anionic charges (AC)

Attachment of small cations to the anionic groups also interferes with molecular weight determination.

In a previous study (1), we first demonstrated the potentiality of mass spectrometry using LSIMS AND ESI-MS for the analysis of synthetic sulfated oligosaccharides (up to 10 mer with a degree of sulfation 16).

We concluded that ESI-MS was a more sensitive technique which allowed molecular weight determination of oligosaccharides with higher polymerization and sulfation degree than LSIMS did.

In this study, we present the ESI-MS results obtained for several new synthetic sulfated oligosaccharides with higher polymerization degree (PD - up to 20 mer) higher sulfation degree (SD - up to 31) and higher number of anionic charges (AC - up to 41) However when the size, number of sulfate groups and number of anionic charges increased, interpretation of the ESI data were becoming more and more intricate due to overlaps between multicharged molecular species and multicharged fragments (loss of Na^+ or $NaSO_3$ groups).

Thus, it seemed interesting to evaluate the potentiality of MALDI-TOF-MS applied to the MS analysis of such higher charged and higher masses oligosaccharidic compounds with the hope that this technique could lead to more comprehensive experimental data and, hence, could be more routinely applied to synthesis follow-up of these compounds by mass spectrometry.

MATERIALS AND METHODS

Chemicals

The various compounds were obtained from one of us (M. Petitou). They were analysed in aqueous solution.

- LSIMS : Negative LSIMS analyses were performed on a ZAB-2E (VG Organic Fisons) using a magnet scanning over a mass range of 600 to 2400 amu. Spectra were acquired in the continuum mode and 4 to 8 scans were summed. The caesium ion gun energy was set to 35 keV and the source accelerating voltage was 8 kV

Oligosaccharides were analysed in this mode up to 6- mer (SD = 10 , AC = 13). 1 µl of 100 µg/µl solution (*45 nmoles*) was added to 2 µl of triethanolamine matrix.

- ESI-MS : Negative ESI spectra were obtained on a VG-Platform instrument (VG Organic Fisons). 10 µl loop injections were performed using a mobile phase isopropanol/water (8/2) at 10 µl/min

Polysaccharides (from 12-mer and up to 20 mer) were injected at a concentration ranging from 1 to 2 µg/µl in water (*7 nmoles* injected). A 3 kV ESI potential was applied to produce the spray .

Spectra were acquired in the MCA mode over a mass range of 200-1200 amu with a scanning rate of 10 sec/scan. Sample cone voltage was optimised in the 15-30 V range

- MALDI-TOF-MS : Negative MALDI-MS was tried on a VG-TOF-SPEC (VG Organic Fisons) in linear mode. A N2 laser radiating at 337 nm with 4 ns pulses was used

Ions were accelerated to 18 KeV. Spectra were acquired over 0-5000 amu and the calibration performed with Glucagon and Bombesin

The various matrices tested were used at a concentration of 50 mM in H_2O/CH_3CN (2/1) Only a pentamer compound (average MW = 1731 , PD = 5 ; SD = 8 ; AC = 10) was tested at a concentration ranging from 10 pmol/µl to 100 pmol/µl in H_2O/CH_3CN (2/1) 2 µl of the tested matrix and 2 µl of the sample were premixed 2 µl of the mixture were then deposited on a stainless steel target and then dried at atmospheric pressure and room temperature before analysis.

RESULTS

- LSIMS

⇨ LSIMS spectra for polysulfated polysaccharides showed a base-peak pseudo molecular ion $[M - Na]^-$ and a fragment ion corresponding to the loss a sulfate group $[M - Na_2SO_3 + H]^-$. *Increasing polymerization and sulfation* degrees up to the hexasaccharide decasulfated leads to very weak ion signal showing losses of sulfate groups without evident pseudo molecular ion.

- ESI-MS

⇨ ESI spectra : On the well defined spectrum (obtained for the 12 mer with 19 sulfates and 25 anionic charges), we observed multiply charged ions from the 4^- up to the 11^-. On this spectrum, each multiple charged state shows a rather complex profile in which the desodated ion dominates. After deconvolution with sodium adduct ion, the obtained molecular weight is 4296.8 which is very closely related to the expected molecular weight (Table 1) *Increasing polymerization and sulfation degrees leads to more intricate spectra.*

The ESI spectrum obtained for the 20 mer is presented on figure 1 The spectrum presents ions from 6^- to 14^- giving an experimental molecular weight of 7077 amu as expected.

In this case, the polycharged ions coming from the only losses of Na^+ counter-ions do not appear as the most intense ones within a defined polycharged state profile. Indeed ions resulting from an additional loss of a sulfate *group predominate. Other ions corresponding to the losses of 2 or 3 sulfate groups are also observed, thus giving* overlaps between multicharged molecular species and multicharged fragments

The maximum state charge observed in the ESI spectra decreased as the anionic charge number increased. The measured molecular weights were always found comprised between the monoisotopic and the average values. A few nanomoles were necessary to obtain these results by ESI-MS

- MALDI-TOF-MS

In the present work, we tried to obtain a direct MALDI-TOF mass spectrum of a pentasaccharide compound (average MW 1731 , PD = 5 ; SD = 8 , AC = 10). This compound was analysed either directly in different matrices (2.5-dihydroxybenzoic acid, 3-amino-quinoline, sinapinic acid, caffeic acid, anthranilic acid) or after treatment with cation exchange beads (AGMP50, Biorad) to convert the salts into free acids In neither case a direct MALDI spectrum could be obtained and trials were not extended to other higher molecular weight derivatives.

These negative results were in good accordance with the work of Juhasz et al (2) who also failed to obtain direct MALDI spectra from polysulfated oligosaccharides. These authors suggested an indirect measurement by the observation (in positive MALDI-TOF-MS) of complexes between these highly acidic compounds and highly basic proteins and peptides (with high Arginine content).

Hence, the "complex formation" concept appears to be the only alternative for using MALDI-TOF-MS as a tool for mass measurement of polysulfated oligosaccharides

DP	SD	AC	Expected MW monoisotopic average	Measured MW	State Charge observed
12 (dodeca)	19	25	4297.5 4300.7	4296.8 +/- 0.9 amu	$5^- \rightarrow 11^-$
14 (tetradeca)	22	29	4991.4 4995.2	4993.0 +/- 2.2 amu	$5^- \rightarrow 12^-$
16 (hexadeca)	25	33	5685.3 5689.6	5687.6 +/- 2.3 amu	$5^- \rightarrow 13^-$
18 (octadeca)	28	37	6379.2 6384.1	6381.4 +/- 3.2 amu	$6^- \rightarrow 13^-$
20 (icosa)	31	41	7073.1 7078.5	7077.3 +/- 3.2 amu	$6^- \rightarrow 14^-$

Table 1 : **Main characteristics of the various oligosaccharides analysed by ESI-MS.**

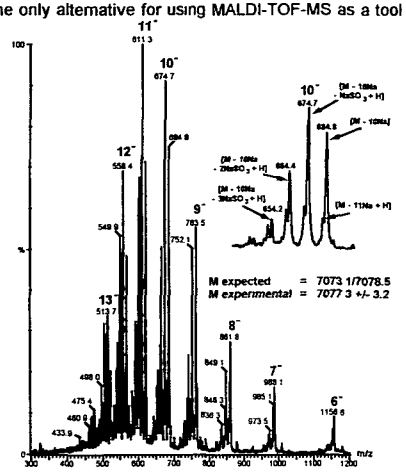

Figure 1 : **ESI mass spectrum of the 20 mer compound (DP 20, DS 31, 41 Na).**

CONCLUSION

This comparative study of LSIMS, ESI-MS and MALDI-MS for the analysis of sulfated polysaccharides shows that :

⇨ LSIMS give the most accurate mass determination but could be only used up to the hexamer with 8 sulfate groups.

⇨ ESI allows direct observation of molecular weight up to 20 mer (SD = 31 ; AC = 41) with good accuracy and sensitivity We have not reach the limits of this technique. However the spectrum becomes more intricate with higher polymerization degree.

⇨ MALDI failed to give any interpretable data by direct measurement in accordance with Juhasz. P et al. (2)

REFERENCES

(1) F. Uzabiaga, C. Ponthus, M Petitou and C. Picard 13th Int. Mass Spectrometry Conference ; 29 August-2 September 1994. Budapest (Hungary). Abstract book p. 67 (MOD14).

(2) P. Juhasz and K. Biemann - PNAS 91 (1994) - 4333 - 4337.

Detection of Photosubstitution Intermediates of Ru(II) Diimine Complexes using On-line Electrospray Mass Spectrometry

Ryuichi Arakawa, Satoshi Tachiyashiki,[a] and Takekiyo Matsuo[b]
Department of Applied Chemistry, Osaka University, 560 Japan
[a]Laboratory of Chemistry, Kagawa Nutrition University, 350-02 Japan
[b]Department of Physics, Osaka University, 560 Japan

In thermal- and photo- ligand substitution of a metal complex with bidentate ligands the substitution is considered to proceed stepwise and thus an intermediate with a η^1 bidentate (one-legged) ligand is proposed (Fig. 1). However it has not yet been possible to demonstrate the existence of such an intermediate, at least for tris(bidentate)type chelates. However, we have recently been able to identify an intermediate with a one-legged bidentate ligand in the photosubstitution of $Ru(bpy)_2(dmbpy)^{2+}$ (Fig. 2a) by ^1H nmr and HPLC separation.

Here, we report studies of photosubstitution of Ru(II) diimine complexes by on-line ES-MS in order to obtain direct evidence of intermediate formation and to observe some mechanistic details of the photoreaction, such as the effects of solvent and intensity of irradiation. Through this study it is hoped that on-line electrospray mass spectrometry will be demonstrated to be a powerful tool for the study of photochemical reactions in solution.

Two different modes of irradiation (λ >420nm) were used for photoreaction: cell mode and spray mode irradiation. For the cell mode irradiation a cylindrical quartz cell (1mm i.d.) was installed in the middle of a syringe needle. The spray mode irradiation was carried out 3mm from the tip of the electrospray needle, i.e., the charged droplets were irradiated.

Figure 2a shows an ES mass spectrum of the complex in acetonitrile (AN) solution without photoirradiation. The spectrum is simple, showing only two peaks of RuL_2B^{2+} and RuL_2BX^+, where L, B, and X represent bpy, dmbpy, and ClO_4^-, respectively. No apparent difference in the photosubstitution reaction was observed either in the cell mode (Fig. 2b) or in the spray mode (Fig. 2c), although the photoreaction enviroments were fifferent (ordinary solution vs. microscopic charged droplets). The photoproducts were divalent $RuL_2(AN)_n^{2+}$ (n=0-2), monovalent $RuL_2(AN)_2X^+$, and BH^+, the protonated dmbpy liberated

Figure 1. Photosubstitution

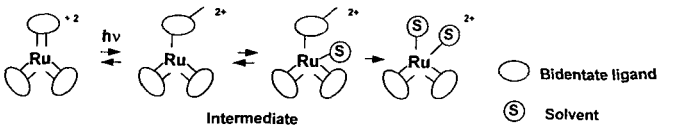

Figure 2.

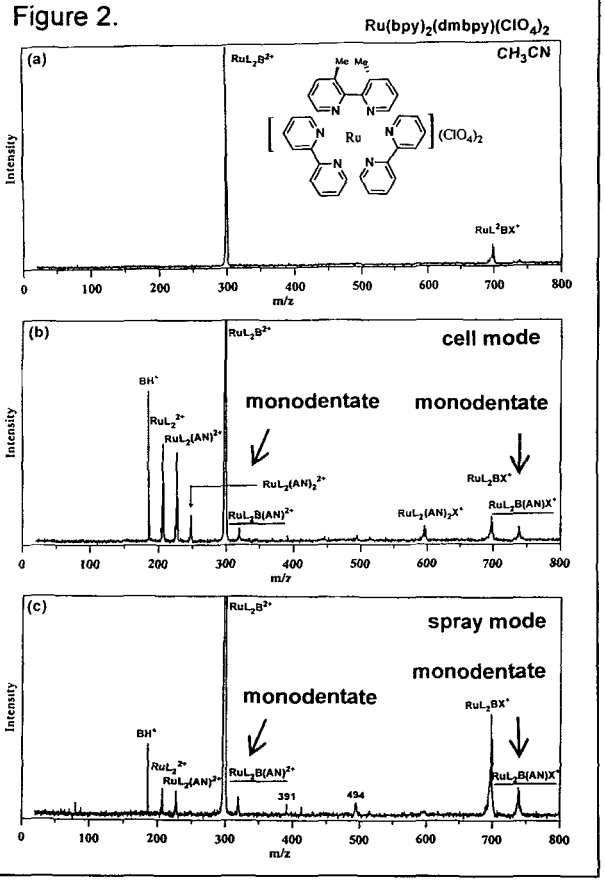

from the complex. $RuL_2B(AN)^{2+}$ and $RuL_2B(AN)X^+$ were also observed; they must be reaction intermediates with a monodentate B ligand since AN is expected to coordinate to Ru in these species. Such a signal was not detected in the on-line ES mass spectra obtained after photoreaction of $Ru(bpy)_3^{2+}$ and $Ru(bpz)_3^{2+}$.

The larger intensities observed for the 4- and 5-coordinate ions than for the 6-coordinate ion must be due to a facile dissociation of acetonitrile molecules from the 6-coordinate ion by collision-induced dissociation (CID).

FORMATION OF COMPLEXES BETWEEN ANGIOTENSIN II AND FIRST-ROW TRANSITION-METAL(II) IONS BY ESI: SOLUTION VS GAS PHASE

M. Cameron Sullards, Jeanette Adams, and Alex Reiter, Department of Chemistry and the Emory University Mass Spectrometry Center, Emory University, Atlanta, GA 30322

Experiments were conducted to determine: (1) the binding affinities between first-row transition metal(II) ions and angiotensin II; (2) whether angiotensin II-Me^{2+} complexes in which Me^{2+} = Mn^{2+}, Co^{2+}, Ni^{2+}, Cu^{2+}, and Zn^{2+} reflect solution or gas-phase formation. Narrow scan range (*m/z* 515-615) electrospray ionization (ESI), full scan range (*m/z* 200-1200) ESI, and MS^2 experiments were performed using a JEOL JMS-SX102/SX102A/E five-sector tandem mass spectrometer.

The narrow scan range data show that the relative ion abundances of $(M + Me)^{2+}$ ions change with metal(II) ion. Furthermore, the absolute ion intensities of the $(M + Me)^{2+}$ ions change with metal(II) ion. The absolute ion intensities increase from Mn^{2+} to Cu^{2+} then decrease sharply from Cu^{2+} to Zn^{2+}. This follows the Irving-Williams series of transition metal(II) ion binding to ligands [1].

The full scan range data reveal that the $(M + Me)^{2+}$ ions are the predominant metal ion-peptide species (Figure 1). The singly charged $(M + Me - H)^{+}$ ions are not detected. Furthermore, the triply charged $(M + Me + H)^{3+}$ ions are only weakly abundant. The absolute ion intensities of $(M + Me)^{2+}$ ions are the same as in the narrow-scan data (brackets in Figure 1).

MS^2 metastable ion decomposition spectra of the $(M + Me)^{2+}$ precursor ions show abundant product ions (Figure 2). Singly charged product ions arise from complexes that contain zwitterionic peptides coordinated to the metal ion. Spectra of Co^{2+}, Ni^{2+}, and Zn^{2+} complexes show abundant $(b_6 + Me - H)^{2+}$ ions. Complexes that contain Cu^{2+} bind differently than other transition metal(II) ions.

In solution at pH 5-8, complexes between angiotensin II and Mn^{2+} contain no deprotonated amides [2]. The Mn^{2+} is bound to either the Asp or C-terminal carboxylate. The resulting solution complex is doubly charged, and thus highly abundant $(M + Mn)^{2+}$ ions are expected by ESI if ESI reflects solution. In this same pH range, Ni^{2+} and Cu^{2+} form 3N complexes with the His side chain and two deprotonated amides toward the N-terminus [3,4]. The resulting solution complexes have no net charge. Thus, highly abundant $(M + Ni)^{2+}$ or $(M + Cu)^{2+}$ ions are not expected by ESI if ESI reflects solution. The ESI data, however, do not reflect these expected solution results.

The ESI data reveal that complexes between angiotensin II and first-row transition metal(II) ions are readily formed. The $(M + Me)^{2+}$ ions are the predominant metal ion-peptide species. The complex formed with Cu^{2+} is of significantly greater abundance than that formed with Mn^{2+}. The ion abundance trends are not related to solution chemistry. Furthermore, the MS^2 data show that the gas-phase complexes of Cu^{2+} and Ni^{2+} do not reflect expected solution species.

References

1. Irving, H.; Williams, R. J. P. *J. Chem. Soc.* **1953**, 3192.
2. Basosi, R.; Gaggelli, E.; Valensin, G. *J. Inorg. Biochem.* **1984**, *20*, 263.
3. Pettit, L. D.; Pyburn, S.; Kozlowski, H.; Decock-Le Reverend, B.; Liman, F. *J. Chem. Soc. Dalton Trans.* **1989**, 1471.
4. Decock-Le-Reverend, B.; Liman, F.; Livera, C.; Pettit, L. D.; Pyburn, S.; Kozlowski, H. *J. Chem. Soc. Dalton Trans.* **1988**, 887.

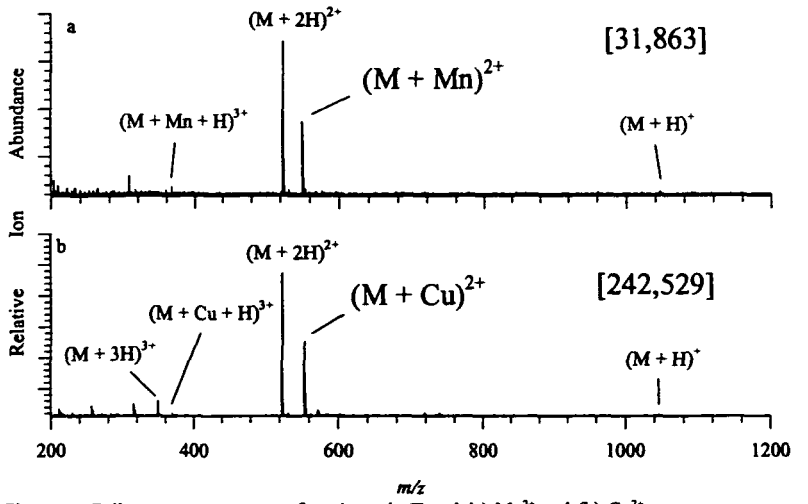

Figure 1. Full scan range spectra of angiotensin II and (a) Mn^{2+} and (b) Cu^{2+}.

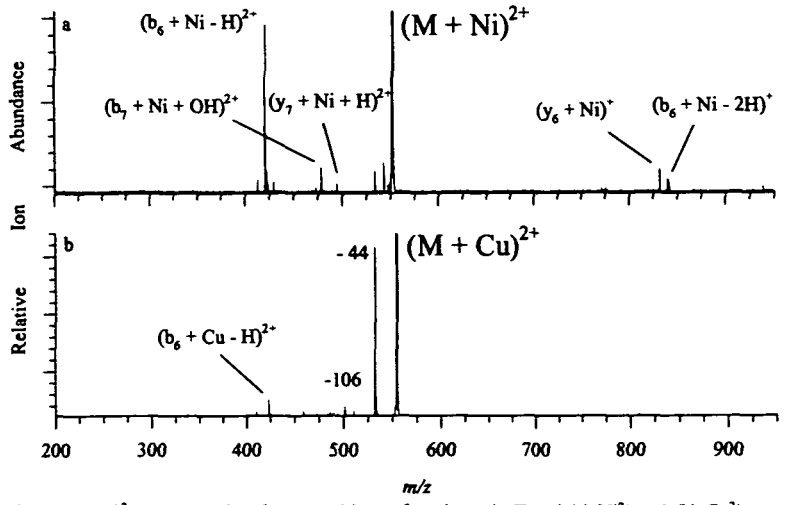

Figure 2. MS^2 metastable ion decompositions of angiotensin II and (a) Ni^{2+} and (b) Cu^{2+}.

Amino Acid Coordination to Cu(II)-Diimines: Structures and CAD Mechanisms

Christine L. Gatlin,[1] *Frantisek Turecek,*[1] *Tomas Vaisar*[2]
[1]Chemistry Dept., Box 351700, University of Washington, Seattle, WA 98195-1700
[2]Molecumetics, Ltd , Bellevue, WA 98102

Coordination of Cu(II) to amino acid residues (eg. His, Cys, Met) in highly ordered protein structures has been well documented. However, much less is known about the intrinsic properties of Cu(II) interactions with free amino acids Tetracoordinate complexes of Cu(II) and diimines with amino acids are known to be stable in solution.[1] We report[2-4] the ES-MS detection of singly and doubly-charged ions of Cu(II)-diimines with all 20 essential amino acids Low-energy CAD of the resulting gas-phase ternary complexes ($[Cu(AA-H)L]^+$, L=bpy, phen, dmphen) show several common features which can be rationalized in terms of free radical-induced dissociations and used to distinguish isomers (Leu and Ile) and isobars (Gln and Lys).

REDUCTIVE DECARBOXYLATION

Reductive decarboxylation to form stable $(M-CO_2)^+$ ions is a common first step resulting in an aminoalkyl radical residue coordinated to Cu(I) by the amino group $Cu(bpy)^+$ complexes of other carboxylic acids do not form stable $(M-CO_2)^+$ ions stressing the importance of the α-aminoalkyl radical for binding to copper.

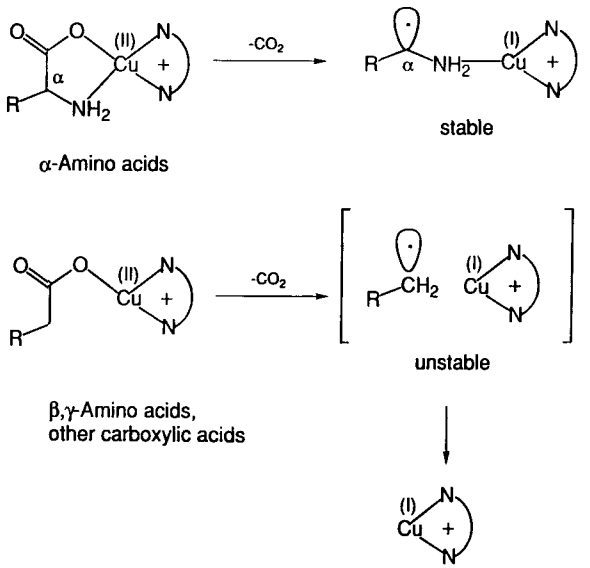

RADICAL β-FISSION

For aliphatic amino acids, further dissociations of the aminoalkyl radical complex involve β-fission of the alkyl chain which gives information on its branching, as shown for Leucine and Isoleucine

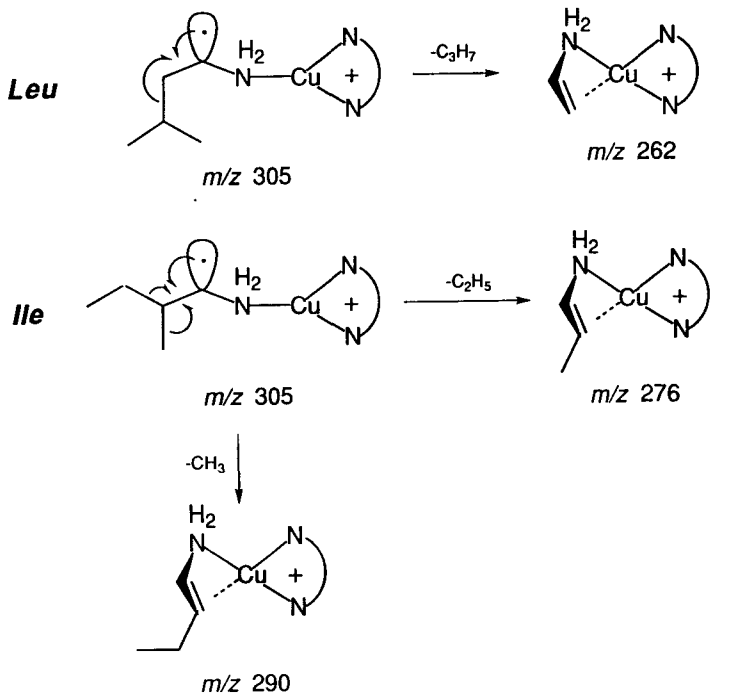

REFERENCES

(1) Yamauchi, O ; Odani, A *J. Am. Chem Soc* **1985**, *107*, 5938
(2) Gatlin, C L , Turecek, F , Vaisar, T *J. Am. Chem. Soc* **1995**, *117*, 3637
(3) Gatlin, C. L., Turecek, F , Vaisar, T *J Mass Spectrom.*, accepted 1995
(4) Gatlin, C. L.; Turecek, F., Vaisar, T *J. Am. Chem. Soc* , submitted 1995

Peptide Coordination to Cu(II)-diimines: Structures and Sequence Information

Christine L. Gatlin,[1] Ramesh D. Rao,[1] Frantisek Turecek,[1] Tomas Vaisar[2]*
[1]Chemistry Dept., Box 351700, University of Washington, Seattle, WA 98195-1700
[2]Molecumetics, Ltd., Bellevue, WA 98102

The analytical utility for peptide sequencing by MS has been of growing interest.[1] Most studies have been based on the gas-phase fragmentations of *protonated* peptide ions. Sequencing of these ions is based on a series of charge-induced fragmentations ideally occurring at random along the peptide backbone Difficulties have been encountered, however, with peptides containing amino acids with basic side groups which can impede backbone fragmentation.[2] In contrast to "random" fragmentations, *metallated* peptide ions have shown specific fragmentations depending on the nature of the metal ion and its binding site. Most studies have involved FAB-induced (*high energy*) fragmentations of negatively-charged alkali or alkaline-earth cationized peptides.[3] However, there are a few reports discussing gas-phase peptide interactions with *bare* transition-metal ions which typically provide a few sequence fragment ions upon CAD.[4]

We report the formation of gas-phase ternary complexes of the transition-metal Cu(II), and a diimine co-ligand (such as bpy) with a number of isomeric dipeptides[5] and tripeptides upon electrospraying their methanol-water solutions. Low-energy CAD of the resulting Cu-diimine-peptide complexes show (1) the distinction of peptide isomers differing in their amino acid positions, (2) the sharp differentiation of C-terminal leucine and isoleucine, and (3) specific fragmentations that can be induced starting at either the N- or C-terminus of the coordinated peptide.

Three dipeptide isomeric pairs (LF, FL; AL, AI; MF, FM) and three tripeptide isomers (GGI, GGL, LGG) were selected for detailed comparison For the $Cu(bpy)^+$ of Ala-Leu and Ala-Ile (*next page*), low energy CAD clearly distinguishes the isomers The $'a_1$ fragment at *m/z* 262 is indicative of N-terminal Ala. Reductive decarboxylation followed by β-fission of the C-terminal aliphatic side chain distinguishes Leu (loss of C_3H_7) from Ile (loss of C_2H_5).

REFERENCES

1a) Biemann, K.; Martin, S. A. *Mass Spectrom. Rev* **1987**, *6*, 1
b) Roepstorff, P. *Trends Anal. Chem* **1993**, *12*, 413.
2) Tang, X -J ; Thibault, P., Boyd, R. K. *Anal. Chem* **1993**, *65*, 2824
3a) Hu, P.; Gross, M L. *J. Am. Soc. Mass Spectrom* **1994**, *5*, 137.
b) Zhao, H., Reiter, A ; Teesch, L. M., Adams, J *J. Am. Chem. Soc* **1993**, *115*, 2854.
4a) Reiter, A.; Adams, J ; Zhao, H. *J. Am. Chem. Soc.* **1994**, *116*, 7827.
b) Hu, P ; Gross, M. L *J. Am. Chem. Soc* **1993**, *115*, 8821
5) Gatlin, C L.; Rao, R. D.; Turecek, F., Vaisar, T , submitted to ***Anal. Chem.***, 1995

43rd ASMS Conference on Mass Spectrometry and Allied Topics

CAD of {Cu(AL-H)bpy}+

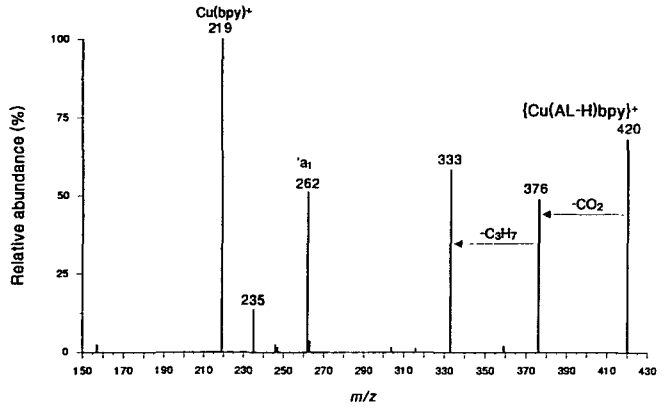

CAD of {Cu(AI-H)bpy}+

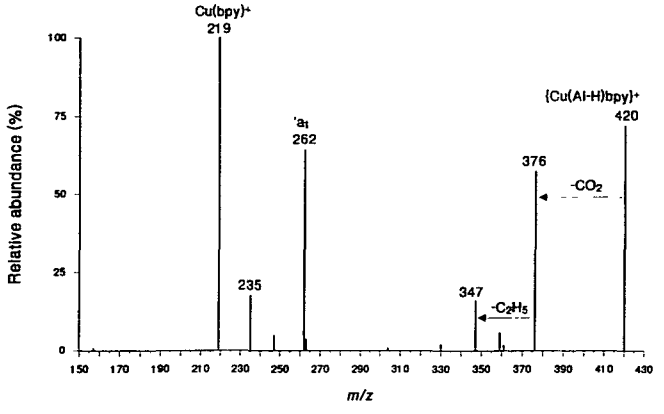

ANALYSIS OF METAL CHELATES BY ELECTROSPRAY IONIZATION MASS SPECTROMETRY

K. L. Wahl, R. W. Stromatt, and D. L. Blanchard
Pacific Northwest Laboratory, P.O. Box 999 Richland, WA 99352

Solubilized metal ions pose a potential environmental threat for many waste-disposal sites. Understanding the behavior of metal ions in complex organic matrices and the possible metal-chelate complexes that could form may aid in developing remediation techniques. For example, waste tanks on the Hanford Site are known to contain large amounts of chelators such as ethylenediaminetetraacetic acid (EDTA). These chelators may be responsible for difficulties in removing some of the radioactive metals, such as ^{90}Sr. One possible method for examining these metal-chelate complexes is electrospray ionization mass spectrometry (ESI-MS). The goal of this project is to examine the behavior of strontium (Sr) in complex mixtures containing a variety of inorganic and organic components that simulate tank waste constituents. Preliminary results presented suggest that ESI-MS can be used to study the behavior of chelators, such as EDTA, N-(2-hydroxyethyl)ethylenediaminetriacetic acid (HEDTA), and nitrilotriacetic acid (NTA), in the presence of metals such as iron (Fe) and Sr.

Negative ESI-MS of a solution containing EDTA and Sr in a 20:1 molar excess of EDTA exhibits ions from the Sr-EDTA complex, in addition to doubly and singly charged EDTA with various amounts of sodium (Na) adduction. These concentrations were chosen because they resemble those estimated to be present in the waste tanks at the Hanford Site. Increasing the concentration of Sr relative to EDTA increases the intensity of the Sr-EDTA ion relative to the Na adducted EDTA. As expected, adjusting the capillary-skimmer offset voltage in the interface region affects the observation of the Sr-EDTA ion. Adding $Fe(NO_3)_3$ to the solution mixture creates a competition between Fe and Sr for complexation with EDTA. Both metal-EDTA complexes are observed by negative ESI-MS as shown in Figure 1. The relative ratios of Fe, Sr, and EDTA were chosen to represent typical relative concentrations in tank waste. Further studies of adjusting the solution conditions to verify that ESI-MS is probing solution specific complexation behavior are in progress.

When citrate, another potential chelator that is present in the tank wastes, is added to a solution of EDTA and Sr, only the Sr-EDTA complex is observed by ESI-MS (Figure 2). No evidence of a Sr-citrate complex is observed. The order that the solution components are added and the solution pH needs to be adjusted to substantiate these preliminary results Other chelators, such as NTA and HEDTA, show significant complexation with Sr when individually studied. The next step is to combine different chelators in the same solution to determine if competition for complexation based on known stability constants of different metal-chelate complexes can be observed by ESI-MS.

Preliminary results indicate that negative ESI-MS can provide insight into the chelation of Sr by compounds such as EDTA and HEDTA. The next step is to study the effects of solution conditions, such as pH, mixing order, and solvent composition, in addition to the electrospray conditions on the complexes observed by ESI-MS. Future work will expand these studies to more complex solutions and focus on adding on-line separations such as capillary electrophoresis.

Pacific Northwest Laboratory is operated for the U.S. Department of Energy by Battelle Memorial Institute under Contract DE-AC06-76RLO 1830.

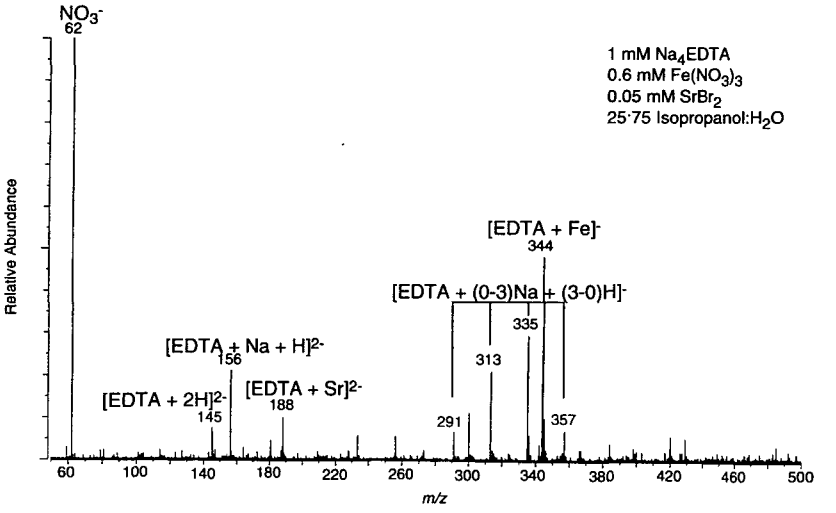

Figure 1. Observation of EDTA Complexation with Fe and Sr by Negative ESI-MS.

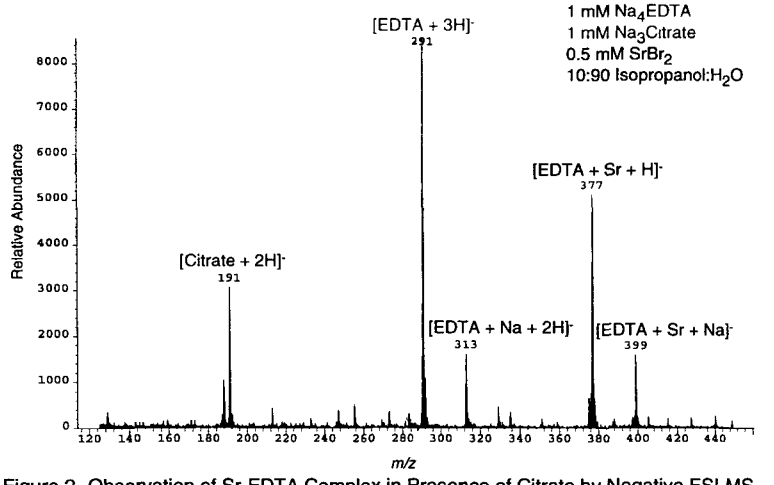

Figure 2. Observation of Sr-EDTA Complex in Presence of Citrate by Negative ESI-MS.

PRODUCTION OF COORDINATED 3D TRANSITION METAL IONS BY ESMS

Yaodong Xu, Xin Zhang, Alfred L. Yergey
LTPB, NICHD, National Institutes of Health, Bethesda, MD 20892

We have investigated first-row transition metal ions, Cu(II), Ni(II), Zn(II) and Co(II), coordinated with model amino acid and/or simple peptide systems, glycine (gly) and glycylglycine (gly-gly), by means of electrospray ionization mass spectrometry (ESMS). The purpose of this investigation is to study the formation of these complex ions under electrospray ionization conditions and the relationship between the electrospray mass spectra of these ions and their solution chemistry. These preliminary results will serve as the basis for more detailed studies of the coordination chemistry and interactions of proteins with transition metal ions by ESMS.

Experiments were carried out in the apparatus consisted of a home-built electrospray ionization source interfaced to a component based quadrupole mass analyzer. A 500 mm ID, 26 cm long stainless steel capillary that is resistively heated were employed. Multiply charged droplets were produced from solutions flowing at 1.8 μL/min from a syringe pump through the discharge needle held at +2.6kV. The capillary was maintained at the lowest temperature possible consistent with detection of ions. The discharge needle is separated from the capillary by about 6.0mm. The 0.5mm aperture skimmer is 3.5mm away from the capillary end. The average pressure in the region between the capillary and skimmer is 1.2 torr maintained by a 600 l/min mechanical pump. The ion beam exiting the skimmer passes through an einzel lens held in a differentially pumped chamber evacuated by a 4-in., 1200 liter/sec oil diffusion pump. The ion beam passes through a 5mm diameter aperture into the quadrupole analyzer. Operating pressure in the latter is 1x10-6 torr. A Model 4752-G continuous dynode electron multiplier is used for ion detection.

The electrospray mass spectrum of a mixture of Cu(II) and gly solutions is shown in Fig. 1a. We have identified the pairs of ions at 138/140, 173/175, 212/214 and 287/289 Da as the singly-charged ions $[Cu(I)\cdot gly]^+$, $[Cu(II)\cdot(H_2O)_2\cdot(gly^-)]^+$, $[Cu(II)\cdot gly\cdot(gly^-)]^+$ and $[Cu(II)\cdot(gly)_2\cdot(gly^-)]^+$. In addition, we have identified the pairs of peaks at m/z 87/88 and 106.5/107.5 Da as the doubly-charged ions $[Cu(II)\cdot(H_2O)_2\cdot gly]^{2+}$ and $[Cu(II)\cdot(gly)_2]^{2+}$. The fractional abundances of ^{63}Cu and ^{65}Cu at 0.692 and 0.308 were reflected in the ion intensities of these species. Replacing gly with gly-gly led to analogous singly- and doubly-charged ions. When a mixture of the solutions containing Cu(II) and equal amounts of both ligands was used, the singly- and doubly-charged ions of both ligands as well as mixtures were observed. The mass spectrum of Ni(II)/gly solution is shown in Fig. 1b.

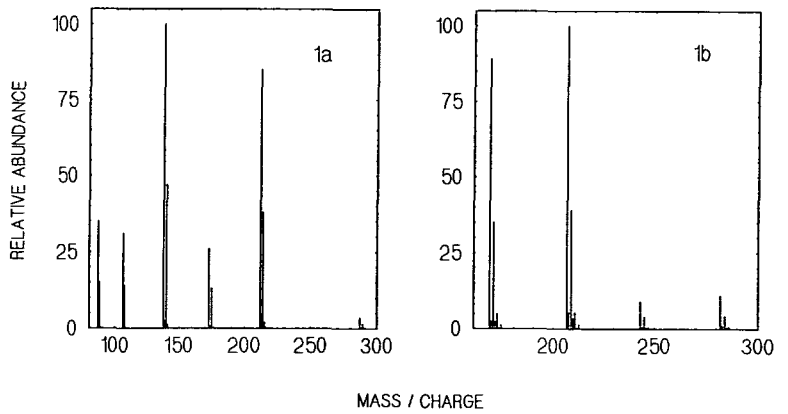

Figure 1. Electrospray ionization mass spectrum of complex ions. flow rate = 1.8 μL/min, the capillary was heated to 60°C. (a) 5.0×10^{-4} M Cu^{2+} and 1.0×10^{-3} M glycine in deionized water. pH=3.92. (b) 5.0×10^{-4} M Ni^{2+} and 1.0×10^{-3} M glycine in deionized water. pH=5.00.

The metal·gly and metal·gly-gly complex ions can be divided into two groups that differ in their formation mechanisms. The first group is a novel type of ion for ESMS, and is taken to be a consequence of direct desorption of a complex that originated in the solution and was protonated [1], if necessary, during ESI. The second group results from a number of possible gas phase reactions including charge transfer and ligand replacement [2]. Most of the complex ions we observed are believed to belong to first group.

The aqueous solution chemistry of 3d transition-metal ions and gly and gly-gly has been well established in electrochemical studies. Comparing our results with previous data, we conclude that the electrospray spectrum may not be a quantitative representation of the aqueous solution for these complex ions, but it does show that the spectrum is a qualitative representation of the bulk phase compositions.

Reference

1. Fenn, J.B.; *J. Am. Soc. Mass Spectrom.* **1993**,*4*, 524-535.
2. Blades, A.T.; Jayaweera, P.; Ikonomou, M.G.; Kebarle, P.; *J. Chem. Phys.* **1990**,*92*, 5900-5906.

Characterization of Transition Metal Organometallic Complexes by ESI/Sector MS

H. Tong, K. Ng, R. Rodebaugh, C. Kuell, S. Shum and S. Pastor
Ciba-Geigy Corporation, 444 Saw Mill River Road, Ardsley, NY 10502-2699

The study of organometallic chemistry is important to life science, catalysis and many other fields. Mass spectrometry, especially via FAB, has been a useful tool for these studies. But FAB has serious limitations, particularly in ionizing large molecules while preserving their fragile bonds. The emergence of ESI/MS, with its unique ion formation mechanism and its "softness", has provided an unprecedented opportunity for the characterization of a small amount of large organometallic compounds in solution. This is demonstrated through the study of cyclic phosphite-Rh complexes in solution at pmole levels.

The metallic complexes in this study were synthesized in the Ciba Additives research laboratories. The ESI/MS analyses were performed on a Fisons AutoSpecQ hybrid (EBEqQ) MS with a m/z range up to 9,000 under the ESI condition. High- and low-energy collision-induced dissociation (CID) MS/MS techniques were also used in the analyses. The NMR data of these complexes were obtained from Varian Gemini 300 and UNITY 500 MHz NMR instruments.

The target complex of this study was the [A-Rh-Cl_2-Rh-A] dimer (see the diagram). The NMR data (P31, 1 and 2D) of the synthetic product in $CDCl_3$ clearly showed the P-Rh-P binding unit, but could not affirm the presence of Cl as a ligand The P31 NMR explicitly failed to show the dimer because the increased P31 spectral complexity expected from the virtual coupling of the two rhodium was not seen. The dimer structure was proposed on the basis of the synthetic path followed and literature precedent.

In the ESI/MS spectrum I of the sample in CH_2Cl_2/MeOH, the major complex component is $[A'Rh]^+$ observed at m/z 1,583 (A' = A with one P oxidized, only the structures associated with Rh are given in all the spectra) No complex dimer was detected When the sample solution was acidified with 0 5% CH_3COOH, an ion at m/z 1,620 emerged (spectrum II), indicating that Cl has rejoined the complex. At the same time, an ion was observed at m/z 3,239 (spectrum III), corresponding to the Cl-bridged dimer. Both [A'RhCl] and the dimer were able to be charged via protonation, but produced weak signals. However, the spectra of the complex can be dramatically changed when the solvent is altered. This is illustrated in spectra IV and V which arose upon a replacement of CH_3COOH with a small amount of CH_3CN. The chloride is displaced; an intense ion at m/z 1,666 and weak ion at 3,284 represent [A'Rh+2CH_3CN] and [dimer+2CH_3CN], respectively. The easy detection of these four-coordinate species of Rh^I is likely due to their stabilities in the solution. Under the CID conditions, as shown in spectra IV and V, the CH_3CN ligands can be consecutively removed, and other bonding properties can be explored (which will be detailed in the full paper) *To ensure that the dimers detected were not the result of ion* clustering phenomena commonly encountered in ESI, the sample solution was scanned up to m/z 9,000 and no species above m/z 4,000 was observed.

The ESI/MS data provide a "dynamic" picture of these complexes in solution, as opposed to a static one from X-ray crystallography. The phosphite ligand binds to Rh^I tightly, whereas Cl associates with Rh^I loosely. The role of Cl within the complex, and its participation in formation of the "dimer bridge" can be manipulated through careful control of solvation. Furthermore, we were able to successively displace Cl with other ligands more strongly electron donating in nature. Through these, an array of novel, subtly varied, charged species in solution can be realized by ESI/MS. The volatile nature of Cl participation in these complexes may explain the difficulties of NMR in developing evidence for the dimer.

43rd ASMS Conference on Mass Spectrometry and Allied Topics

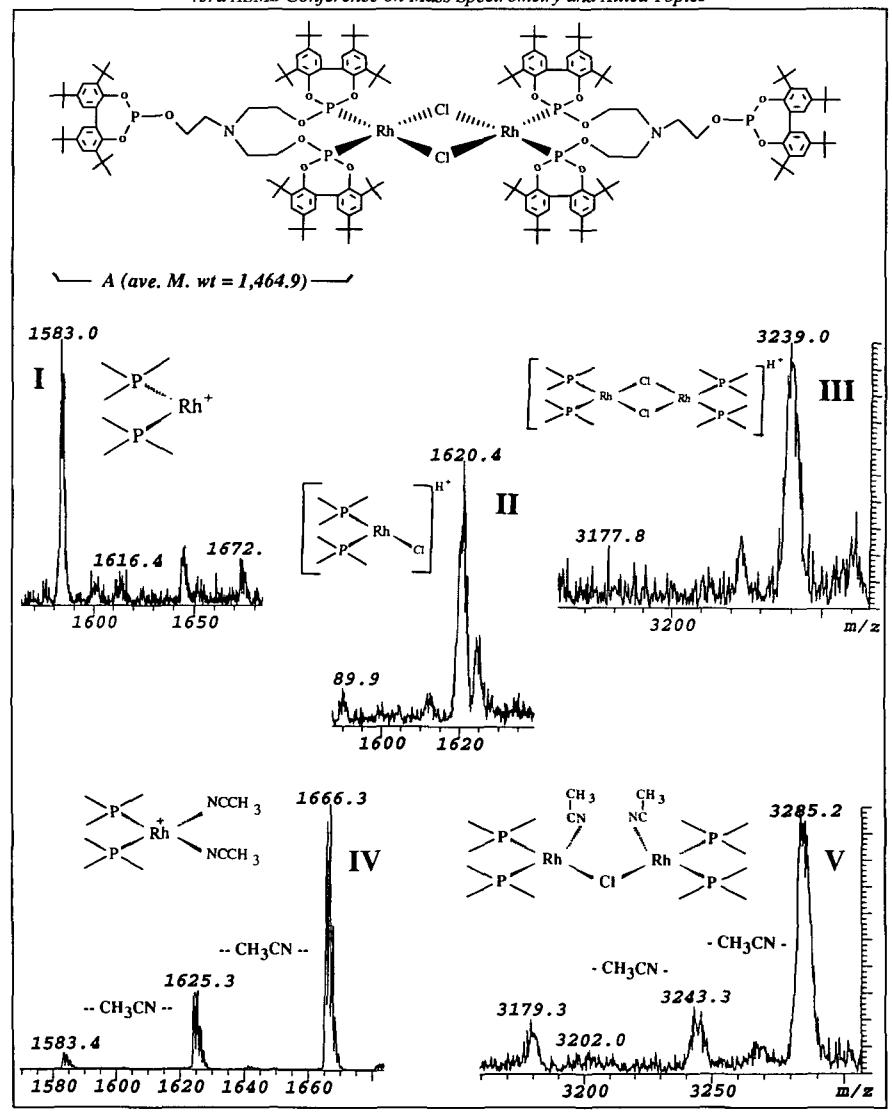

Accurate Mass Measurement of Peptides Ions with a Magnetic Sector Instrument

P.A. D'Agostino, J.R. Hancock and L.R. Provost, Defence Research Establishment Suffield, P.O. Box 4000, Medicine Hat, Alberta, CANADA, T1A 8K6

The use of magnetic sector instruments for high resolution mass measurement of peptide molecular and product ions is limited, with prior publications dealing with the electrospray (ESI) analysis of pure peptides available from commercial sources. High resolution ESI-MS enables the confident assignment of charge state to multiply charged isotope clusters, the calculation of monoisotopic molecular weights, and aids in the interpretation of primary sequence data following collisional activated dissociation (CAD) in the ESI interface.

ESI-MS Conditions follow: Instrument, Autospec-Q with Mark II ESI interface; Electrospray needle, 7.8 kV; Acceleration voltage, 4 kV; Sampling cone voltage, 0 to 250 volts; Nitrogen bath gas (80°C), 500 L/hr; Nitrogen nebulizer gas, 14 L/hr; Source/Analyser vacuum, $2x10^{-6}$ / $3x10^{-8}$ Torr; Scan functions, 1550 to 400 Da (25 sec/dec) or 1000 to 400 Da (30 sec/dec); Resolution, 2500 to 9000 (10% valley); Calibration, external calibration with PEG; LC, Applied Biosystems 140B pumping 1:1 mixture of water (with 0.05% TFA) and 20% water/80% acetonitrile (with 0.05% TFA). Samples: 0.02 to 0.1 mg/mL range in distilled water.

High resolution ESI-MS data were obtained for unknown synthetic peptides and toxic peptides of particular interest to the defence community. Accurate monoisotopic molecular weights were obtained for peptides up to 7500 Da during magnetic sector scanning over a wide mass range. Figure 1 illustrate the ESI-MS data obtained for one of the Conus snail toxins, w-Conotoxin MVIIC. Figure 2 illustrates the ESI-MS data obtained for synthetic peptide #29 at a sector resolution of 6000. A 37 ppm difference between the theoretical and observed molecular weight was obtained. Errors between observed and theoretical monoisotopic molecular weights were typically in the 5 to 60 ppm range at sector resolutions between 2500 and 9000 (10% valley definition).

CAD/MS was investigated under a number of different cone voltage settings, LC flow rates and bath gas temperatures in an attempt to increase product ion formation. Product ion formation, as anticipated, increased with increasing cone voltage settings. Cone voltages above 175 volts resulted in significantly reduced signal strengths. LC flow rates of 20 μL/min and bath gas temperatures of 80°C, recommended for the ESI interface, were used successfully during loop injections. Increasing the LC flow rate to 50 μL/min, to be compatible with 1 mm I.D. LC, resulted in a lack of product ion formation. Incomplete desolvation in the ESI interface was suspected. Increasing the bath gas temperature to 100°C (maximum) resulted in only a modest improvement in product ion formation. The best CAD/MS analyses were obtained at lower flow rates, 10 to 20 μL/min., with cone voltage settings in the 100 to 150 volt range. Full or partial sequencing of unknown peptides below 2000 Da was demonstrated for the synthetic and bioactive peptides used in this study. The complete primary sequence for an unknown was determined and the value of high resolution MS was demonstrated by the differentiation of Lysine from Glutamine, two amino acids differing in residue mass by 0.0364 Da.

Acknowledgement: The authors thank Dr. R. Hodges and Mr. P. Semchuk (University of Alberta) for the unknown synthetic peptides used in this study.

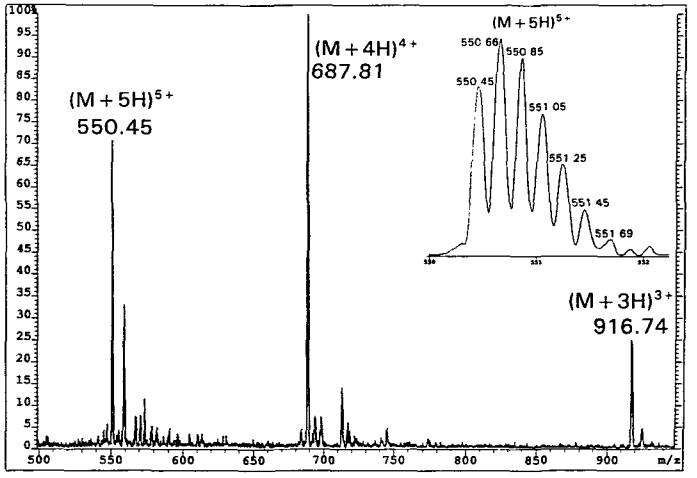

Figure 1: ESI-MS of w-Conotoxin MVIIC at a sector resolution of 4000 (MWt. 2747.16).

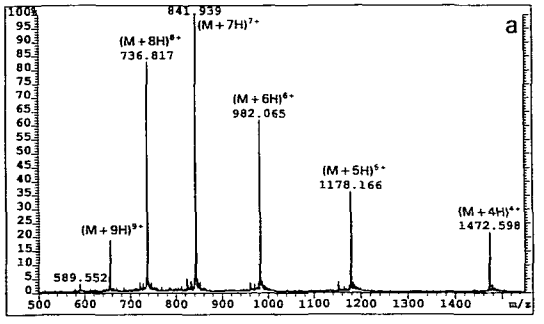

Figure 2: ESI-MS of synthetic peptide #29 at a sector resolution of 6000 (Calculated MWt. 5883.44 ± 0.12, Theoretical MWt. 5883.2247).

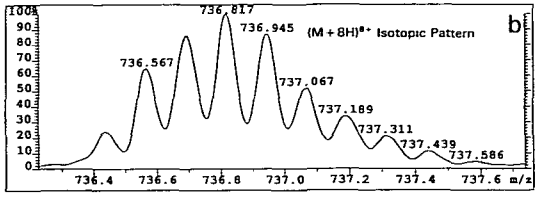

Some important effect in protein and peptide analysis by MALDI*

Y.F. Zhu, K.L. Lee, K. Tang, S.L. Allman, N I. Taranenko, and C.H. Chen

Oak Ridge National Laboratory
P.O. Box 2008, Bldg 5500, Oak Ridge, Tennessee 37831-6378, U.S.A.

During the past few years, tremendous progress has been achieved in the analysis of proteins and peptides by Matrix-Assisted-Laser Desorption Ionization spectroscopy (MALDI). Observations of protein ions with molecular weights greater than 100,000 Da by MALDI have been reported. The detection of peptides and proteins by MALDI is beginning to be accepted as an effective analytical technique. But, on the other hand, the desorption and ionization mechanisms of MALDI process are not well understood despite extensive study. Many questions in this area remain unanswered, and the selection of good matrices for MALDI analysis of biomolecules relies on "experience" rather than scientific analysis. For example, is there any specific ionization channel which is enhanced by the presence of a certain functional group in a protein or peptide chain? If there is, what is the preferred ion form (positive or negative), and how does it relate to the molecular weight? In this work, we present the MALDI results of proteins and peptides to answer some of these questions.

The MALDI experiments were conducted in a recently built reflectron time-of-flight mass spectrometer (Jordan) with 15 and 16 kV for linear and reflectron voltages respectively Two ion detectors have been installed, one for the linear signal and an other for the reflected signal. An interesting effect was observed in our preliminary MALDI results of insulin, insulin A chain and insulin B chain. The MALDI signal of insulin B chain was found to be much larger than the one of insulin A chain under identical experimental condition even though the molecular weight of the B chain is much larger than that of A chain. Further experimental results imply that the weak MALDI signal of insulin A chain was not due to suppression by contaminants, insulin B chain, or matrix molecules This intensity difference between A and B chains indicates that the ionization efficiency depends on the molecules themselves, i.e. the type of amino acids they contain. In comparing the types of amino acids in insulin A and B chains, we notice that there are several basic amino acids (arginine, histidine, and lysine) in B chain which are not in A chain. To confirm the effect of enhanced ionization efficiency by these basic amino acids, we made MALDI measurements of many small peptides which contain either one basic amino acid or none in their chains. These small peptides are similar in molecular weight and amino acids other than the basic amino acid. Comparing the ionization efficiencies of these peptides in MALDI spectroscopy, we discovered several important effects.

1) For positive ion detection, the MALDI intensity of the peptides containing one basic amino acid are generally 10-100 times greater than the MALDI intensity of the peptides containing no basic amino acid. This conclusion is based on the measurement of 15 peptides which contain one basic amino acid, and 6 peptides which do not contain any basic amino acid Figure 1 shows the MALDI spectra of Allatostatin IV (contains one arginine) and Allatostatin III (no arginine).
2). For negative ion detection, the MALDI intensity of the peptides containing one basic amino acid are almost negligible. The ratios of positive ions vs negative ions of these peptides are approximately $10\text{-}10^2$ using laser energies of 1 to 4 mJ/cm^2. (See Figure 2)
3). No double charged peptide ions have been detected in the peptides containing one basic amino acid even under high laser energy (~10 mJ/cm^2). On the other hand, double charged peptide ions have been detected in the peptides containing more than one arginine at the threshold laser energy (1 mJ/cm^2).
4) The ratios of the positive ion vs negative ion signals for matrix molecules are approximately $10\text{-}10^{-2}$, which is opposite to the ratio of peptides that contain one basic amino acid.
5). The positive ion signals of peptides containing one basic amino acid are greatly suppressed when a small amount of NH_3 is used to neutralize 25% of H^+ in matrix molecule. This result indicates that the ionization of these peptides containing basic amino acid is H^+ related.

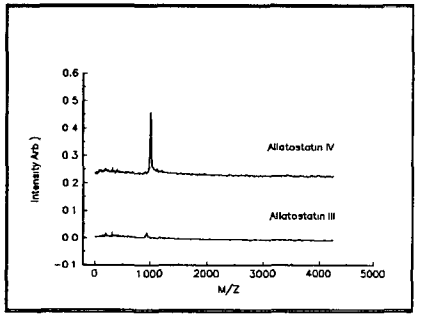

Figure 1 The MALDI spectra of Allatostatin IV and Allatostatin III.

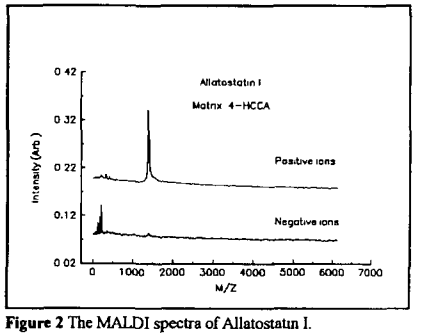

Figure 2 The MALDI spectra of Allatostatin I.

All these results strongly indicate that the ionization mechanism of the peptides or proteins containing basic amino acid is different from that of the peptides or proteins containing no basic amino acid The basic amino acid in protein or peptide chains can react with the protons of matrix molecules to form stable ions during the MALDI process. The ionization mechanism is dominated by the proton transfer from matrix molecule to peptide. Due to the low energy barrier of the acid and base reaction, large numbers of peptide ions are formed and the MALDI intensities of these peptides are greatly enhanced. When a peptide only contains one basic amino acid, the single charged ion is formed. When a peptide contains more than one basic amino acid, both the single charged ion and the double charged ion are observed. Due to the mechanism of proton transfer, if the H^+ concentration of the matrix solution is reduced by the presence of an other base, the MALDI intensity of these peptides should be greatly decreased, which is consistent with experimental results

*Research sponsored by the Office of Health and Environmental Research,
U. S Department of Energy under contract DE-AC05-84OR21400
with Martin Marietta Energy Systems, Inc

Matrix Solution Effects of the MALDI-MS of Peptides & Proteins

*S. L. Cohen and B. T. Chait
The Rockefeller University, 1230 York Avenue, NY, NY 10021

MALDI-MS is a powerful tool for evaluating mixtures of peptides and proteins. In this study we have found that the details of the sample/matrix preparation have profound effects on the quality of the MALDI response using 4HCCA (4-hydroxy-*alpha*-cyano cinnamic acid).

First, the matrix solution composition strongly influences the MALDI response. We investigated sixteen different matrix solution compositions and have determined that there are solution-dependent mass discrimination effects. **Fig. 1** shows the positive ion MALDI-MS of a partial V8 digest of an 11 kDa recombinant protein (the transcription factor Max; five Glu residues) [**1**]. The spectra were run in two matrix preparations using the conventional dried drop method [**2**] with a linear time-of-flight instrument. The top spectrum was taken with a saturated 4HCCA solution made from formic acid-water-isopropanol (FWI) (1:3:2 v/v), pH 1.3. Note the strong presence of intermediate- and high-mass components of the digest. The bottom spectrum of **Fig. 1** was run with 4HCCA made with water-acetonitrile (2:1 v/v), pH 2.5. In contrast to the FWI spectrum, note the dominance of low mass peptide fragments and the distinct lack of components above m/z 6000. These results, along with our studies of other 4HCCA matrix solutions, suggest that the observed mass discrimination effects are strongly pH-dependent.

A second matrix solution effect involves the time scale of matrix/analyte crystallization. **Fig. 2** shows the MALDI-MS of a complete V8 digest of the protein Max. A total digest of the protein results in six V8 fragments (labeled 1-6). The matrix solution used was 4HCCA / water-acetonitrile (2:1 v/v). Two different crystallization procedures are compared. In the dried drop technique [**2**] (TOP spectrum) the matrix/analyte solution droplet air dries on the MALDI probe in about two minutes. Using this method, all six V8 fragments are observed. In the slow crystallization method [**3**], analyte-doped matrix crystals where grown for 12 hr. in the matrix solution. For this method (BOTTOM spectrum) only the two high-mass V8 fragments (5 and 6) appear in the spectrum. We have found this low-mass discrimination effect to occur regardless of the composition or pH of the matrix solution.

In conclusion, we have shown that there are pH-, solution composition-, and time-dependent mass discrimination effects observed in MALDI-MS using the matrix 4HCCA. These effects add a "chromatographic" dimension to the sample/matrix preparation procedures that can be suitably exploited to optimize the analysis of mixtures of peptides and proteins.

References
1. Cohen, S. L. *et al. Protein Sci.* **1995** (in press).
2. Karas, M.; Hillenkamp, F. *Anal. Chem.* **1988**, *60*, 2299-2301.
3. Xiang, F.I.; Beavis, R. C. *Org. Mass Spectrom.* **1993**, *28*, 1424-1429.

43rd ASMS Conference on Mass Spectrometry and Allied Topics

FIGURE 1

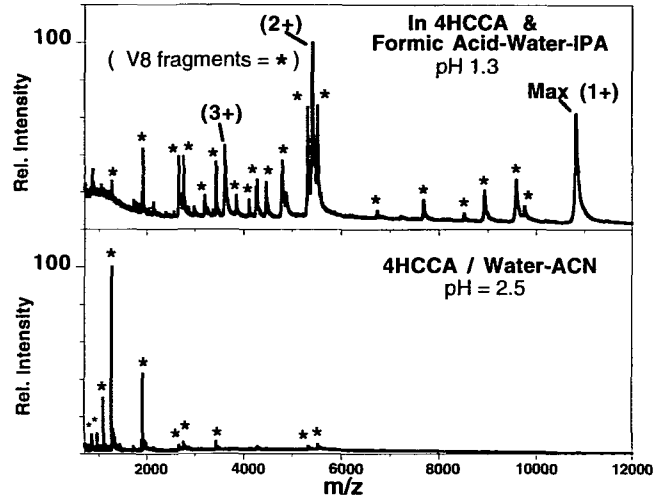

FIGURE 2

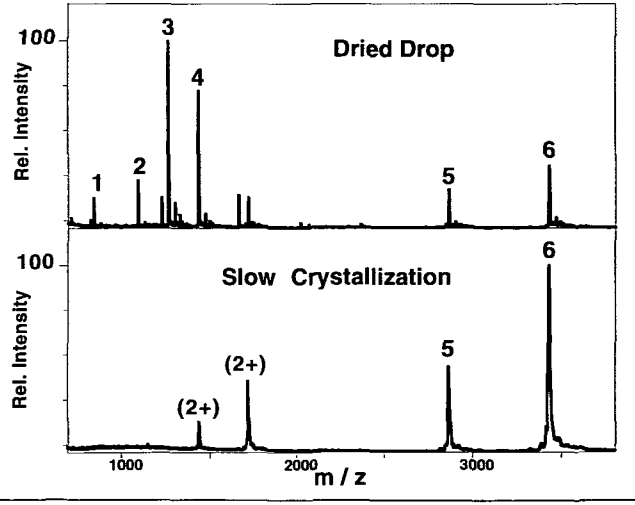

STUDY OF OXIDATION REACTION OF SELENOMETHIONINE PEPTIDES BY MASS SPECTROMETRY

Rong Wang[1], Urooj A. Mirza[1], Steven Birken[2], and Brian T. Chait[1]
The Rockefeller University, New York, NY 10021
College of Physicians & Surgeons of Columbia University, New York, NY 10032

A powerful variation of multiwavelength anomalous diffraction that is extremely useful for determining the three-dimensional structures of proteins involves the substitution of selenomethionine for methionine in the proteins of interest[1]. Unfortunately, selenomethionine has a high sensitivity to oxidation. Because protein crystals take a long time to grow, this sensitivity to oxidation may produce a heterogenous product that diffracts poorly. Therefore, it is important to have a reliable method for analyzing the oxidation of selenomethionine residues in proteins -- to ensure that a homogenous product is produced. oxidation of free selenomethionine was studied in the early 70's.[2] The oxidation product was identified as selenoxide by NMR. However, it is much more difficult to analyze oxidation of selenomethionine residues in peptides and proteins. In the present study, we tested several mass spectrometric approaches for assaying the oxidation of selenomethionine in peptides, which includes matrix-assisted laser desorption/ionization mass spectrometry (MALDI-MS), californium-252 plasma desorption mass spectrometry (PDMS) and electrospray ionization mass spectrometry (ESI-MS).

Selenomethionine-containing peptide (SeMet-peptide, Arg-Ala-Ala-Ala-SeMet-Asn-Pro-Thr-Leu-Glu) and methionine-containing peptide (Met-peptide, Arg-Ala-Ala-Ala-Met-Asn-Pro-Thr-Leu-Glu) were chemically synthesized by the solid phase method. The Oxidation was induced by hydrogen peroxide. Peptides were reacted with hydrogen peroxide in the molar ratio of 1:100 to 1:1000 (peptide/hydrogen peroxide) and the reaction products were either directly analyzed by mass spectrometry or separated by reverse-phase high performance liquid chromatography (HPLC) and analyzed by mass spectrometry.

MALDI-MS results indicate that the Met-peptides undergo oxidation to the Met-sulphoxide and a small amount of sulphone, while oxidation of the SeMet-peptides gives no selenoxide. Rather, the original peptide is observed together with product that arises from loss of the selenomethyl group and homoserine derivative (Figure 1).

PDMS gives the same results as MALDI-MS. In addition, when the selenomethionine peptide is exposed as a solid film to air, loss of the selenomethyl group is observed. The major product from an oxidation of the Met-peptide is the Met-sulfoxide.

The oxidation reaction products were analyzed by ESI-MS. When the reaction mixture was infused into the mass spectrometer in the presence of hydrogen peroxide, a selenoxide derivative of the peptide and a fragment arising from the loss of the oxidized methylseleno group were detected (Figure 2). The presence of hydrogen peroxide in the spray solution appears to accelerate the loss of the oxidized methylseleno group. The ratio of the fragment to the selenoxide increases in proportion to the concentration of hydrogen peroxide.

Two product peaks were readily resolved in reverse-phase HPLC from the oxidation reaction mixture (Figure 3). These two peaks were analyzed by MALDI-MS and gave almost identical spectra. By doing LC/ESI-MS, these two peaks were identified as methionine selenoxide peptide derivative and original SeMet-peptide (Figure 4).

Our experiment results shown that great care should be taken when studying labile compounds by mass spectrometry. For selenomethionine residue oxidation studies, electrospray ionization mass spectrometry is the method of choice.

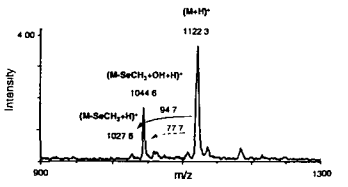

Figure 1 *MALDI-MS spectrum of oxidized SeMet-containing peptide.*

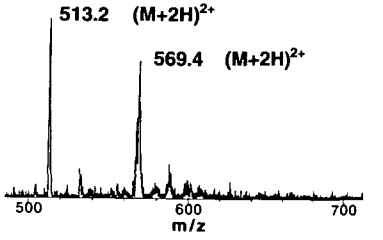

Figure 2 *ESI-MS spectrum of oxidized SeMet-containing peptide.*

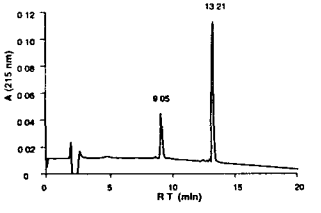

Figure 3 *Reverse-phaseHPLC separation of the oxidized reaction mixture.*

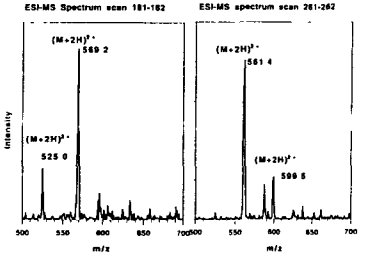

Figure 3 *ESI-MS spectra of HPLC fractions from oxidation reaction mixture.*

References

1 Wei Yang, Wayne A. Hendrickson, Robert J. Crouch, Yoshinori Satow (1990) "Structure of ribonuclease H phased at 2 A resolution by MAD analysis of the selenomethionyl protein" *Science*, **249**, 1398-1405.

2. Roderich Walter, J. Roy (1971) "Selenomethionine, a potential catalytic antioxidant in biological systems" *J. Org. Chem.*, **36**, 2561-2563.

Mapping of the β-Amyloid Peptide from Alzheimer Disease Brain by Gelatinase A using MALDI.

A.S. Woods and R.J. Cotter
Johns Hopkins School of Medicine Baltimore, MD 21205

M.J. Ball A.E. Roher
Wayne state University School of Medicine Detroit, MI 48201.

In Alzheimer disease (AD), the β-Amyloid (Aβ) peptide accumulates in the gray matter, leading to destruction of brain cells, cortical vessels, and occlusion of capillary networks resulting in dementia (1). The 39-42 amino acid long Aβ polymerizes into 10 nm filaments which are very insoluble and resistant to proteolytic degradation. The Aβ peptide is derived from a larger molecule that resembles a cell surface receptor, the β-amyloid precursor protein (βAPP), is expressed by a gene in chromosome 21. By alternative mRNA splicing molecules made of 695, 751 or 770 amino acid residues (aa res) are generated. The N-terminus of the 42 aa res form of Aβ results from hydrolysis between Met_{596}-Asp_{597} of the 695 aa res βAPP ($βAPP_{695}$) by β-secretase. The C-terminus of Aβ is produced by hydrolysis of the bond Ala_{638}- Thr_{639} located within the transmembrane domain of βAPP. An alternative cleavage of $βAPP_{695}$ can be made by the enzyme α-secretase between Lys_{612}- Leu_{613}, generating a secreted large N-terminal βAPP domain and a non-amyloidogenic C-terminal peptide(3).

It was reported that the proteolytic enzyme gelatinase hydrolyzed the Lys_{16}-Leu_{17} peptide bond of a synthetic peptide (YEVHHQKLVFF) representing the soluble Aβ sequence of amino acid residues 10-20. The proteolytic activity of gelatinase A appears to be inhibited by a 28 kDa domain located at the C-terminal region of the secreted βAPP. Thus βAPP seems to have a dual role in its interaction with gelatinase A since it can function as its enzymatic substrate and its proteolytic inhibitor(4).

The purpose of this work was to test if this enzyme could also degrade the insoluble 40-42 residues long Aβ peptides purified from AD brain.

Human brains with severe deposits of vascular amyloid as well as large numbers of neurofibrillary tangles were used to extract the insoluble 40-42 residues long Aβ peptides (2). The extract's supernatant was applied to a FPLC-Superose 12 column. Fractions containing Aβ were pooled, dialyzed and concentrated. Digestion of Aβ by gelatinase was done at an S:E ratio of 20:1, at 37°C, for both 4 and 16 hours. The fragments generated by the digest were separated by reverse phase HPLC using a C_4 column.

Aliquots of the fractions were lyophilized and resuspended in 10 ul 20% CH_3CN, 0.1% TFA. 0.3 ul of each fraction was spotted on a target site of a a sample slide, followed by addition of 0.3 ul of matrix solution (saturated alpha-cyano-4-hydroxy-cinnamic acid in 1:1 ethanol:water). The sample-matrix mixture was allowed to dry at room temperature. The samples were analyzed by matrix assisted laser desorption/ionization (MALDI) mass spectrometry using a Kompact MALDI III(Kratos Analytical, Manchester, England).

Aβ peptide was purified, digested with gelatinase A, the resulting peptides were separated by Reverse phase HPLC using a C_4 column and characterized by MALDI (Table I). The results indicated that within the hydrophobic sequence of res 30-38 (AIIGLMVV) of both $Aβ_{1-40}$ and $Aβ_{1-42}$ numerous peptide bonds were hydrolysed. Gelatinase A preferentially cleaves hydrophobic sequences. Gelatinase A hydrolyzed $Aβ_{1-40}$ and $Aβ_{1-42}$ peptides at Lys_{16}-Leu_{17}, Leu_{34}-Met_{35} and Met_{35}-Val_{36} peptide bonds. These results suggest that Gelatinase A is capable of degrading the purified Aβ by hydrolysing this peptide *(in vitro)* at the α-secretase site and even more efficiently in the middle of its C-terminal domain. If This hydrolysis occured in the brain's extracellular matrix, the enzymztic action of gelatinase A could prevent generation of amyloidogenic $Aβ_{1-40(42)}$. The proteolytic activity of enzymes that occur natyrally in the extracellular space and that are capable of degrading Aβshould be further investigated in the search for a possible therapeutic tool in the treatment of Alzheimer's disease.

DAEFRHDSGYEVHHQK_{16}--L_{17}VFFAEDVGSNKGAIIGL_{34}--M_{35}--V_{36}GGVVIA

The amino acid sequence of the β-amyloid peptide.

REFERENCES

1. Selkoe, D.J. (1994) Ann. Rev. Neurosci. **17**:489-517.

2. Roher, A.E., Lowenson, D.J., Clarke, S., Woods, A.S., Cotter, R.J., Gowing, E. and Ball, M.J. (1993) Proc. Natl. Acad. Sci. USA **90**:10836-10840.

3. Mc Dermot, J.R. and Gibson, A.M. (1991) Biochem. Biophys. Res. Comm. **179**:1148-1154.

4. Roher, A.E., Kasunic, T.C., Woods, A.S., Cotter, R.J., Ball, M.J. and Fridman R. (1995) Biochem. Biophys. Res. Comm. **205**:1755-1761.

Electrospray Ionization Mass Spectrometric Studies on Brain Delivery of Neuropeptides

Laszlo Prokai, H.-S. Kim, K. Prokai-Tatrai, and N. Bodor
Center for Drug Discovery, College of Pharmacy
University of Florida, Gainesville, FL 32610-0497

The major obstacle to the use of neuropeptides in the pharmacotherapy of brain diseases is their delivery to the central nervous system (CNS) because of the existence of the blood-brain barrier (BBB -- a continuous lipid bilayer in the brain capillary endothelium). To cross this physical component of the BBB, the solute must possess sufficient lipid solubility. Most peptides are water soluble and, without specific transport system, are excluded from the brain. The BBB also contains highly active neuropeptide-degrading enzymes forming an enzymatic barrier that rapidly cleaves peptides and prevents them to reach the brain.

We have recently developed a strategy for brain delivery of neuropeptides by chemical/enzymatic means [1,2]. Covalent modifications are employed to the peptides (**P**) such as an enkephalin analog (Tyr-Ala-Gly-Phe-Leu) and the progenitor sequence of a thyrotropin-releasing hormone (TRH) analog (Gln-Leu-Pro-Gly) to increase lipophilicity through biolabile functional groups susceptible to enzymatic removal: a bulky, lipophilic ester (**L**) at the C-terminus, and a lipoidal 1,4-dihydrotrigonellyl (**T**) at the N-terminus that also serves as a redox targetor, because it is converted to a membrane-impermeable pyridinium ion (**T**$^+$) by enzymatic oxidation ($NAD^+ \leftrightarrow$ NADH coenzyme). A spacer (**S**) residue is applied that allows for the removal of **T**$^+$ by specific peptidase(s). In addition, the molecular architecture of the chemical delivery system (CDS) also disguises the peptide nature preventing the recognition and degradation by the enzymatic component of the BBB. Brain delivery occurs by the following sequence: (1) the CDS crosses the BBB by passive transport, and within the CNS (2) the targetor is converted to a membrane-impermeable form, and (3) the lipophilic protection (**L**) is removed to yield a relatively stable peptide conjugate that is retained (locked-in) in the CNS. Finally, (4) peptidases process the conjugate to release the desired peptide.

Electrospray ionization (ESI) mass spectrometry (Vestec/Perseptive Biosystems 200 ES quadrupole instrument) was used to verify that the peptide derivatives reach the brain in significant concentration after intravenous administration to rats [1]. However, the release of the peptide could not be directly determined because of the complexity of the (*post mortem*) rat brain samples. Therefore, metabolism of the peptide conjugate accumulated in the brain was studied *in vitro* (incubation in rat brain homogenate) and *in vivo* (microdialysis in living tissue [3]). Fig. 1 and 2 show that the sustained release of the biologically active peptide (Tyr-D-Ala-Gly-Phe-D-Leu, YAGFL, *m/z* 570) is confirmed. The advantage of cerebral microdialysis has been that the samples are free from interfererence by the brain tissue (endogenous peptides/proteins, self-proteolysis during incubation, etc.). Hence, metabolites can be easily identified (Fig. 2).

References

[1] N. Bodor, L. Prokai, W.M. Wu., S. Jonnalagadda, H. Farag, M. Kawamura and J. Simpkins, *Science* **257,** 1689 (1992).
[2] L. Prokai, X. Ouyang, W.M. Wu, and N. Bodor, *J. Am. Chem. Soc.* **116**, 2643 (1994).
[3] P.E. Andren, M.R. Emmett, B.B. Dague, and R.M. Caprioli, *Proceedings of the 41st ASMS Conference on Mass Spectrometry and Allied Topics*, May 30-June 4, 1993, p. 41.

43rd ASMS Conference on Mass Spectrometry and Allied Topics

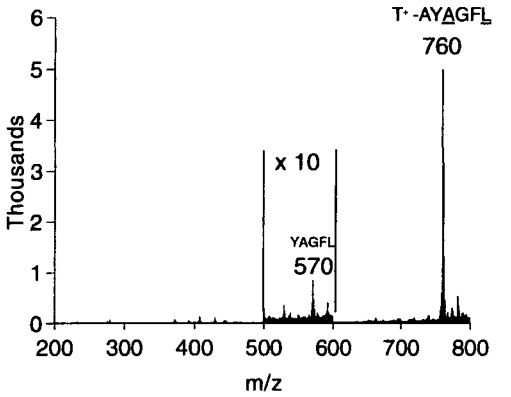

Figure 1.
ESI mass spectrum showing the release of the enkephalin analog from the peptide conjugate (m/z 760) in vitro (rat brain homogenate, 37°C, 1 hour incubation).

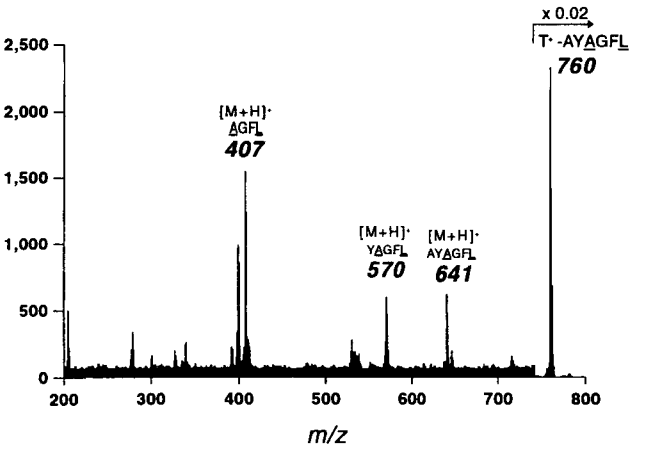

Figure 2.
ESI mass spectrum of T$^+$-Ala-Tyr-[D-Ala]-Gly-Phe-[D-Leu] solution (5 mM) after in vivo cerebral microdialysis (rat striatum).

Characterization of Iron-Binding Exochelins of *Mycobacteria tuberculosis*

Bradford W. Gibson[1], Christopher H. Moore[1], Diane Wong[1], Jovana Gobin[2], Joseph R. Reeve Jr.[2], and Marcus A. Horwitz[2], [1]Department of Pharmaceutical Chemistry, University of California, San Francisco CA and [2]Department of Medicine, University of California, Los Angeles CA

Mycobacterium tuberculosis, the primary agent of tuberculosis, is a human pathogen that infects up to one-third of the world population. Recent cases caused by multiple-drug resistant strains of *M. tuberculosis* has made this organism a particular lethal pathogen, especially for immunocompromised patients. In order to better combat this re-emerging pathogen, a better understanding of the molecular mechanisms of *M. tuberculosis* host-pathogen interactions needs to be obtained.

Almost all bacteria need to acquire iron from their environment for the proper functioning of a number of key enzymes necessary for growth and survival. This requirement poses a significant problem for infectious bacteria which must meet their iron needs from the host where iron is quite limited. In an effort to understand the molecular basis of how *M. tuberculosis* acquires iron from the host, we have isolated and characterized a class of secreted iron-binding compounds, or "siderophores", from *M. tuberculosis*.

We have shown that these secreted siderophores, called "exochelins" (1), exist as a complex group of related compounds that are similar to the iron-binding molecules immobilized in the cell wall, the "mycobactins". Our studies include data from LSIMS, MS/MS, GC/MS and HPLC/electrospray ionization mass spectrometry (2). LSIMS of the HPLC separated exochelin mixture initially identified two separate series of potential iron-binding species. In most fractions, peaks were observed in pairs of roughly equal abundance 53 Da apart that was indicative of the iron-free and iron-bound molecular forms, i.e., $(M + H)^+$ and $(M - 2H + Fe^{III})^+$, in addition to other metal-containing species such as Mg and Al adducts. High energy CID MS/MS analysis of the non-iron binding forms of the exochelins was critical in defining the conserved core and variable components of these structures (see Figure 1A), and these des-ferri forms were only observed under LSIMS conditions. Under HPLC/ESI-MS conditions, the exochelins appear almost exclusively as their iron-bound forms (see Figure 1B) which do not undergo CID fragmentation nearly as readily as the iron-free forms. The lack of fragmentation and single ion species per component observed under ESI-MS conditions, however, provided an ideal method to identify the complete set of exochelins.

Overall, the exochelins were found to be more polar and smaller in mass compared to the water-insoluble mycobactins due the presence of a methyl ester terminating small alkyl chain attached to the N^{ε}-hydroxylysine group, i.e., $-N-CO-(CH_2)_nCOOCH_3$, compared to the much longer unmodified alkyl chain of the mycobactins, i.e., $-N-CO-(CH_2)_nCH_3$. We also observed some amounts of the corresponding free acid exochelins, $-N-CO-(CH_2)_nCOOH$, which likely arise through ester hydrolysis. However, we also observed that the methyl ester-containing exochelins could be quantitatively converted to the free acids forms by esterase treatment, suggesting the possibility of their *in vivo* conversion these acidic forms. These structural difference are likely to be important factors relating to the extracellular transport of exochelin through the *Mycobacteria* cell wall and their presumed interactions with the human host iron-binding proteins such as lactoferrin and transferrin. Moreover, the structural similarity of these two iron-binding compounds suggests that the mycobactins and exochelins share a common core biosynthetic pathway.

Figure 1. Opposite page. Top (**A**) MS/MS spectrum under high energy CID conditions of the major saturated serine-containing exochelin with $(M+H)^+$ at m/z 720.3. Fragment ions are assigned as structural moieties ***A-F*** arising from one or more cleavages about the amide or ester bonds. Bottom (**B**) On-line HPLC-ESI/MS analysis of exochelins. Note that only ferri-exochelin species are seen by ESI-MS, i.e., $(M-2H+Fe^{III})^+$, while LSIMS analysis yield numerous species for each exochelin component.

References:

1. L. P. Macham, C. Ratledge, *J. Gen. Micro.* **89**, 379 (1975).
2. J. Gobin, C. Moore, D. Wong, J. Reeve Jr., B. W. Gibson, M. A. Horwitz, *Proc. Natl. Acad. Sci. USA*, in press (1995).

Acknowledgment: This work was supported by grants from the National Institutes of Health (NIAID AI33790; BWG and MAH). We also acknowledge support by the Mass Spectrometry Facility through the National Center for Research Resources (RR 01614; ALB).

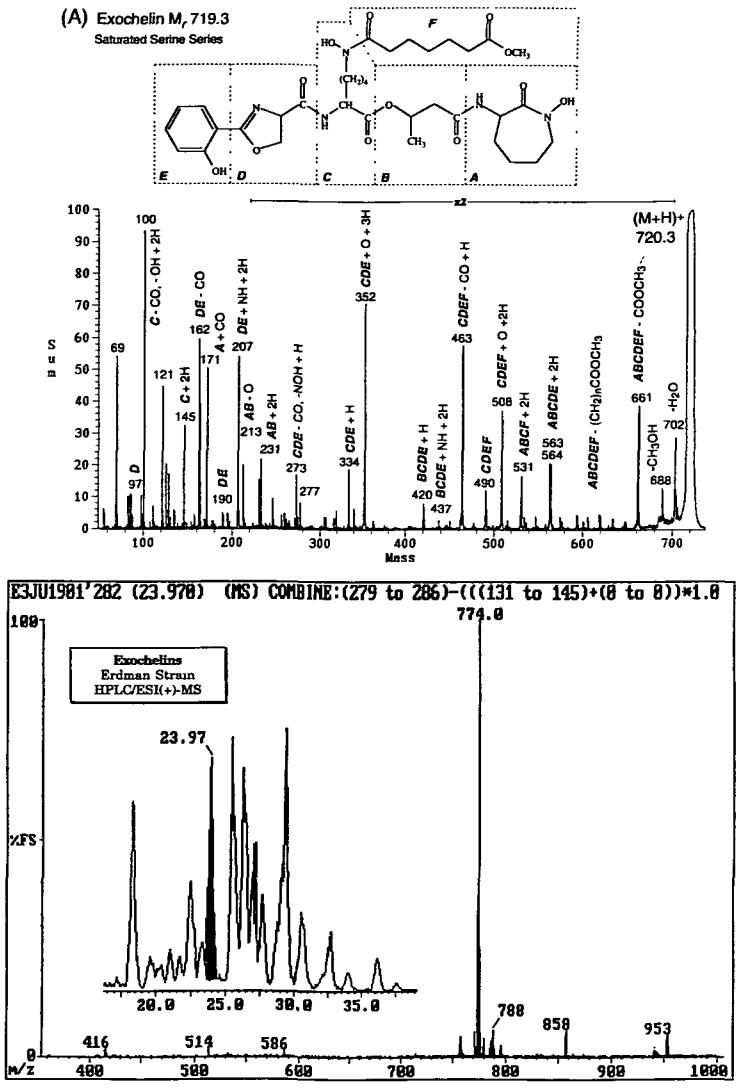

HEMORPHINS, HEMOGLOBIN-DERIVED PEPTIDE FRAGMENTS, IN BLOOD AND BRAIN STUDIED BY IN VIVO MICRODIALYSIS/MICRO-ELECTROSPRAY MASS SPECTROMETRY

Per E. Andrén[1], Katarina Sanderson[2], Fred Nyberg[2], Richard M. Caprioli[1],
[1]Analytical Chemistry Center and Dept. of Biochemistry and Molecular Biology, University of Texas Medical School, 6431 Fannin, Houston TX 77030, and [2]Div. of Biological Research on Drug Dependence, Uppsala University, Box 591, S-75124 Uppsala, Sweden

INTRODUCTION

The hemorphins are peptides with opioid activity, which are enzymatically released from hemoglobin. They have an inhibitory effect on the angiotensin converting enzyme (ACE)-activity, an enzyme known to be involved in blood pressure regulation. The hemorphins are quite stable in tissue extracts containing ACE, and are therefore proposed to be naturally occuring ACE inhibitors. A decapeptide, LVV-hemorphin-7, identical to the sequence 32-41 of the beta-chain of hemoglobin has been isolated from human ventricular cerebrospinal fluid (CSF).

In the present experiments we have studied the *in vivo* metabolism of LVV-hemorphin-7 (LVVYPWTQRF) in rat blood and brain by using microdialysis in combination with micro-electrospray mass spectrometry (micro-ES MS). In addition, we have examined the metabolism of LVV-hemorphin-7 in human plasma and CSF by using *in vitro* microdialysis and micro-ES/MS.

METHODS

In vivo metabolism of LVV-hemorphin-7 in rats

Rats were anesthetized with an intraperitoneal (ip) injection of pentobarbital (45 mg/kg) and a microdialysis probe was implanted either in the jugular vein or the striatum of the brain by stereotaxic technique (coordinates were AP +2.4, ML +3.0, DV -6.5 mm). The microdialysis probes used were CMA/20, 4mm membrane (blood) and CMA/10, 4 mm membrane (brain). The probes were perfused with artificial CSF at a flow-rate of 0.3 µL/min and were allowed a two hour equilibration period before the experiment was started.

LVV-hemorphin-7, 1.0 or 10 pmol/µL was infused for 10 min at a flow-rate of 0.3 µL/min and samples were taken every 10 min. The microdialysis probes were used to both introduce LVV-hemorphin-7 into the blood and brain as well as to collect reaction products.

In vitro metabolism of LVV-hemorphin-7 in human plasma and CSF

Microdialysis probes (CMA/10, 4 mm) were placed in 1.0 mL of human plasma or CSF. The probes were perfused with artificial CSF at 0.3 µL/min. LVV-hemorphin-7 was added to plasma and CSF to yield a concentration of 1.0 pmol/uL. Samples were taken every 30 min for 2 hours.

Capillary liquid chromatography/micro-electrospray mass spectrometry

Mass spectra were obtained with a TSQ70 triplequadrupole mass spectrometer (Finnigan MAT, San Jose, CA) equipped with a modified micro-ES source. A capillary-LC/C18-packed column (50 µm i.d., 40 nL bed volume) was used for the concentration and desalting of the peptides. The dialysate samples were loaded on to a 10 µL loop on a 10-port valve and washed onto the capillary C-18 column at a flow rate of 2 µL/min. The mobile phase contained 2% methanol/0.25% acetic acid in distilled water. After washing at 2 µL/min, LVV-hemorphin and its fragments were eluted with 50% methanol/0.25% acetic acid in distilled water at 0.82 µL/min directly into the mass spectrometer.

CONCLUSIONS

This study has demonstrated that LVV-hemorphin-7 is metabolized *in vivo* by proteolytic enzymes in the brain extracellular fluid as well as the blood.

The result showed that LVV-hemorphin-7 was metabolized mainly from the N-terminal end of the peptide. The fragments found were N-terminal fragments 2-10, 3-10, 4-10, 5-10, 7-10, C-terminal fragment 1-9, and internal fragments 5-8 and 4-9.

LVV-hemorphin-7 was relatively stable in human CSF, but more readily metabolized in human plasma.

Microdialysis in combination with micro-ES/MS is advantageous in studying dynamic chemical processes in vivo in that microdialysis provides a highly filtered, low-volume, aqueous solution of polar analytes. This technology is clearly advantageous and is the method of choice because of its unique mass specificity.

***IN VIVO* METABOLISM OF LVV-HEMORPHIN-7 IN RAT STRIATUM**

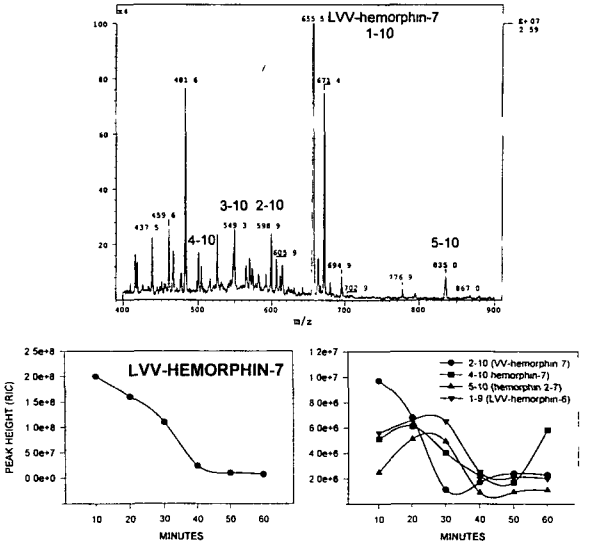

Mass Spectrometric Detection of β-Endorphin-containing Proteins in Bovine Pituitary

Dominic M. Desiderio, Lin Yan, and Jih-Lie Tseng

Charles B. Stout Neuroscience Mass Spectrometry Laboratory, University of Tennessee, Memphis, 800 Madison Avenue, Memphis, TN, 38163.

Non-secreting pituitary tumors provide difficult clinical problems because no hormone is excessively secreted. During the past several years, we found in non-secreting human anterior pituitary tumors a hypometabolism of the β-endorphin (BE)/proopiomelanocortin (POMC) system by our MS/MS quantification of BE. This significant discovery will facilitate future clinical diagnosis for non-secreting human anterior pituitary tumors.

To clarify the molecular processes that are involved in the formation of human anterior pituitary tumors and to indicate any defects in the metabolism of the BE/POMC system in tumors versus control pituitaries, we have developed a new analytical strategy,[1-3] including chromatography separation, enzyme and chemical digestion, RIA detection, and mass spectrometry characterization, to analyze endogenous BE-containing peptides and proteins that derive from POMC. The bovine pituitary is chosen as the model tissue for this research.

Trypsin digestion of BE-containing proteins will produce the following specific "marker" tryptic peptides: BE_{20-24} (=$POMC_{254-258}$, molecular weight = 557) and BE_{10-19}(=$POMC_{244-253}$, molecular weight = 1133) have favorable LSIMS properties. Therefore, the MS detection of the $(M+H)^+$ ions of those marker peptides in the trypsin-digested gel permeation (GP) and RP-HPLC fractions would guide us to find new BE-containing proteins. For the first time, two putative intermediate-sized BE-containing proteins, with molecular weight of *ca.* 9855 and 8350, were found in bovine pituitary.

A partially-purified fraction, which was different from the BE fraction, but which also showed BE-li (Figure 1), was obtained by C_{18} Sep-Pak and RP-HPLC. ESIMS analysis of this immunoreactive fraction showed the presence of a mixture of peptides and proteins. Trypsin digestion of this mixture, when analyzed by LSIMS, yielded the ions at *m/z* 558 and 1134 (among others); those two ions correspond to the $(M+H)^+$ of tryptic peptides BE_{20-24} (=$POMC_{254-258}$) and BE_{10-19}(=$POMC_{244-253}$). That immunoreactive fraction was subjected to further HPLC separation, and two components in different fractions, corresponding to molecular weight of *ca.* 9855 and 8350, showed the presence of the ions at *m/z* 558 and 1134 after treatment with trypsin (Figure 2 and 3). The component with a M.W. of *ca.* 9855 has been reported previously as a putative BE-containing protein[1]. The other component with a M.W. of *ca.* 8350 is a new putative BE-containing protein in bovine pituitary. NIH GM26666

1. L. Yan, G. Fridland, J.-L. Tseng and D. M. Desideno, *Biochem. Biophys. Res. Commun.* **196**, 521(1993).
2. L. Yan, J.-L. Tseng, G. Fridland, and D M. Desiderio, *J. Am. Soc. Mass Spectrom.* **5**, 377(1994).
3. L. Yan, J -L. Tseng, and D. M Desiderio, *Life Sci.* **55**, 1937(1994).

cDNA-derived amino acid sequences

Preproenkephalin $A_{bovine,\ 1-263}$ (263 amino acids)

MARFLGLCTWLLALGPGLLATVRAECSQDCATCSYRLARPTDLNPLA
CTLECEGKLPSLKTWETCKELLQLTKLELPPDATSALSKQEESHLLAK
KYGGFMKRYGGFMKKMDELYPLEVEEEANGGEVLGKRYGGFMKKDA
EEDDGLGNSSNLLKELLGAGDQREGSLHQEGSDAEDVSKRYGGFM
RGLKRSPHLEDETKELQKRYGGFMRRVGRPEWWMDYQKRYGGFLKR
FAEPLPSEEEGESYSKEVPEMEKRYGGFMRF

The underlined sequences equal methionine enkephalin (ME).

Preproopiomelanocortin, $POMC_{bovine,\ 1-265}$ (265 amino acids)

MPRLCSSRSGALLLALLLQASMEVRGWCLESSQCQDLTTGSNLLACI
RACKPDLSAETPVFPGNGDEQPLTENPRKYVMGHFRWDRFGRRNGS
SSSGVGGAAQKREEEVAVGEGPGPRGDDAETGPREDKRSYSMEHFR
WGKPVGKKRRPVKVYPNGAEDESAQAFPLEFKRELTGERLEQARGPE
AQAESAAARAELEYGLVAEAEAEAAEKKDSGPYKMEHFRWGSPPKDK
RYGGFMTSEKSQTPLVTLFKNAIIKNAHKKGQ

The underlined sequence equals β-endorphin (BE).

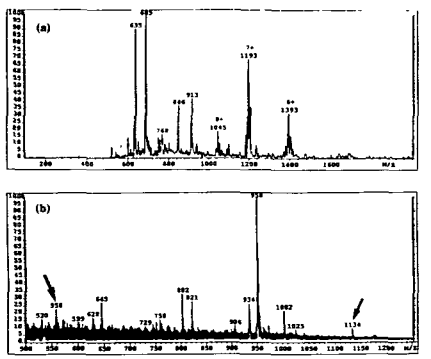

Fig. 2. Mass spectra of one of the fractions separated by a second stage of RP-HPLC of the BE-li fraction I (Fig. 1b): (a) ESI mass spectrum. The ions [1045(8+), 1193(7+), and 1393(6+)] correspond to a protein with a M.W. of 8350. (b) LSIMS spectrum obtained from trypsin digestion.
(It has been verified that the ions at m/z 558 and 1134 were derived from the tryptic peptides from only the component with M.W. 8350, and not from the tryptic peptides of the other component shown in Fig. 2a.)

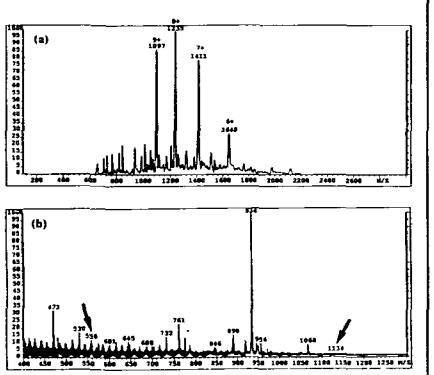

Fig. 3. Mass spectra of another fraction separated by a second stage of RP-HPLC of the BE-li fraction I (Fig. 1b): (a) ESI mass spectrum. The ions [1097(9+), 1235(8+), 1411(7+), and 1648(6+)] correspond to a protein with a M.W. of 9855. (b) LSIMS spectrum obtained from trypsin digestion.

A Quantitative LC/ESI/MS/MS Method For A Bioactive Peptide In Human Plasma

Robert J. White[1], Thomas D. Oglesby[1], Paul A. Taylor[1]
James Florence[2], Jeffrey Wilhelm[2]

[1]Taylor Technology, Inc., 107 College Road East, Princeton, NJ 08540
[2]Ohmeda, The BOC Group Technical Center, 100 Mountain Avenue, Murray Hill NJ 07974

Introduction

Endogenous Motilin is a gastrointestinal peptide hormone containing 22 amino acid residues that is involved in the regulation of fasting motility of the small intestine. A fourteen amino acid Motilin analog has been synthesized which seems to produce similar effects on the small intestine. A sensitive and selective LC/ESI/MS/MS method for the quantitative determination of a Motilin analog, extracted from human plasma, has been developed and validated. The fourteen amino acid residue peptide was quantitated using a d_{10}-analog as the internal standard. The validated method was linear from 100 to 5000 pg/mL. A three day study was performed to assess linearity, precision, and accuracy for intra-and inter-day assays.

Experimental

The peptide was isolated from 1.0 mL of heparinized human plasma using Spec microcolumn solid phase extraction. Reverse Phase chromatography of 200 µL of sample extract was performed on a Hewlett Packard Series II 1090 liquid chromatograph using a YMC Basic column (2 x 100 mm) with a flow rate of 0.5 mL/min. Mobile phases consisted of 0.01% TFA in Water (A) and 0.01% TFA in Acetonitrile. A gradient, with an initial 1 minute hold, from 0% B to 100% B in 3 minutes, followed by a 2 minute hold and a 3 minute re-equilibration. Co-elution of the test article and the internal standard was achieved at a temperature of 60°C with a typical retention time of 4.5 minutes. Detection was achieved on a Finnigan MAT TSQ700 equipped with a Finnigan electrospray interface. The mass spectrometer was operated in the positive daughter ion mode with 1.6-2.0 mtorr of argon as the collision gas. The collision energy was set at -40 ev. SRM of the singly charged product ions, formed from the triply charged parent ions, were used for quantitation.

Results

The limit of quantitation was defined as that concentration having intra-day variability less than 20%, mean accuracy of back-calculated values which was within 20% of the expected values and provided a signal to noise ratio greater than 5:1 . The signal-to-noise (baseline) ratio was always greater than 5:1. A representative chromatogram for a 100 pg/mL standard is displayed in Figure 1. The mean back-calculated value for the 100 pg/mL standards analyzed within the same day in replicate (n=4) was 98.4 pg/mL; within 2% of the expected value. The relative standard deviation was 17.4% for the 100 pg/mL Standard.

Linearity and sensitivity were assessed by replicate (n=5) analyses of extracted analytical standards over the range 100 to 5000 pg/mL for the Motilin analog using a d_{10}-analog at 2000 pg/mL. All acceptable standard concentrations produced a %CV and a mean difference from expected value (accuracy) of no greater than 15% except at the LOQ where 20% was acceptable. The method was linear from 100 to 5000 pg/mL of the Motilin analog in extracted human plasma using analytical standards from duplicate determinations at seven concentrations. The mean correlation coefficient (r^2) from the regression analysis was 0.996. The mean slope and slope %CV for 9 individual standard curves performed over three days for the Motilin analog were 6.83E-04 and 4.6%, respectively.

The precision and accuracy were evaluated in both intra- and inter-day studies. Intra-day and inter-day precision and accuracy data were provided by replicate analyses (n=5) of QC samples prepared at 250, 800, and 4000 pg/mL plasma for the Motilin analog on three separate run days. Reported concentrations of the QC's were calculated from an "aggregate" regression of duplicate standard curves (n=2 at each of seven concentrations for the Motilin analog) which were analyzed daily at the beginning and end of each analytical run. The intra-day precision (%CV) for the Motilin analog at the medium and high QC levels on each of the three days never exceeded 6%, except for the Day 1 medium QC level which was 16.2%. The intra-day precision (%CV) for the Motilin analog at the low QC level on each of the three days never exceeded 17%.The inter-day precision was less than 12% for the medium and high QC levels and less than 14% for the low QC level. Intra- and inter-day precision for replicate QC standards at low, medium, and high concentrations of the Motilin analog are displayed graphically in Figures 2. The intra- and inter-day mean values for the low, medium and high QC levels were always within ±10% of the expected concentration for the QC's.

Discussion

A specific and sensitive method for the quantitation of a Motilin analog in human plasma using solid phase extraction followed by HPLC-ESI/MS/MS has been validated. The method was linear between 100 and 5000 pg/mL. It was demonstrated that accurate and precise quantitation using freshly prepared standards in plasma and stored QC samples (-70°C) could be accomplished in a production fashion (80 or more samples/24 hr). The validity and reproducibility of the assay was determined by examining precision and accuracy in the QC's. Intra-day and inter-day precision were acceptable at all concentrations of QC's between 100 and 5000 pg/mL for the Motilin analog. The LOQ was determined to be 100 pg/mL on the basis of acceptable bias and variability, and acceptable signal-to-noise ratio.

S/N Greater Than 5:1

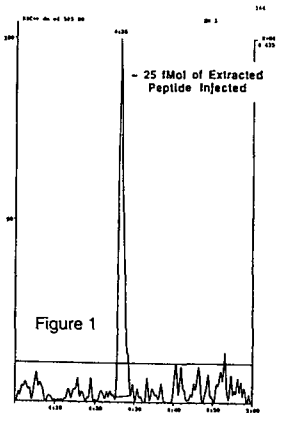

Figure 1

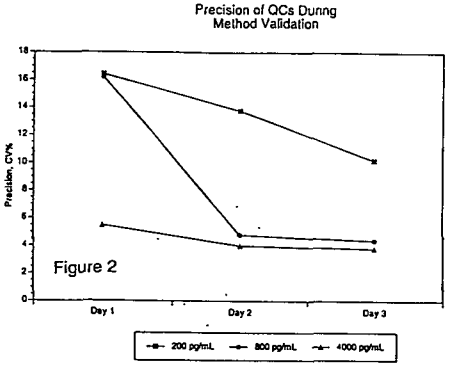

Figure 2

Mass spectrometric analysis of impurities in peptide synthesis

I.A. Papayannopoulos, B. Chao, K Jiang
Biogen Inc., 14 Cambridge Center, Cambridge, MA 02142

The eicosapeptide Phe-Pro-Arg-Pro-Gly-Gly-Gly-Gly-Asn-Gly-Asp-Phe-Glu-Glu-Ile-Pro-Glu-Glu-Tyr-Leu (Hirulog™) was built by rational design as a direct thrombin inhibitor using the protein hirudin as a model (1,2). For the purposes of evaluating the therapeutic potential for this peptide in the management of thrombotic disease with regard to its tolerability and anticoagulant activity, studies in humans were carried out (3). The material used for the clinical trials was made by solution-phase synthesis, the final step of which involved the coupling of two fragments, each of which had, in turn, been made from smaller fragments. The product, including all impurities, was characterized in detail.

All impurities present at the 0.1% level or higher compared (by UV absorption) to the main product were first analyzed by neutral gradient reversed-phase (rp) high performance liquid chromatography (HPLC) and fractions were collected Each of these fractions was re-injected into a rp-HPLC and eluted using an acidic gradient; often the second round of HPLC resulted in further separation of peaks which had co-eluted under the neutral gradient conditions For all HPLC separations a C-18, 0 46 x 25 cm column was used. Typically, a substantial amount of material (*ca.* 0 25 mg) was loaded onto the column in order to generate enough (50-200 pmol) of the low-level impurities for further analysis.

The fractions collected by HPLC were analyzed by fast atom bombardment (FAB) or electrospray ionization (ESI) mass spectrometry In cases where the measured molecular weight did not allow for unambiguous assignment of an impurity to the eicosapeptide amino acid sequence, collision-induced dissociation (CID) tandem mass spectrometry was employed. FAB mass spectrometric analyses were carried out on a four-sector magnetic deflection tandem mass spectrometer (JEOL HX110/HX110) installed at the M.I.T. mass spectrometry facility. ESI mass spectrometric analyses were carried out on a triple quadrupole instrument (VG Quattro II) installed at Biogen.

The commercial scale product was directly analyzed by ESI mass spectrometry as well as by FAB mass spectrometry. In the FAB spectrum in addition to an ion at m/z 2180, due to the protonated peptide molecule, an ion at m/z 650 was also present, which, from its CID tandem mass spectrum, was found to be a peptide with the sequence Pro-Glu-Glu-Tyr-Leu; these are the last five amino acids of the eicosapeptide being analyzed. In order to establish whether the ion at m/z 650 were due to fragmentation during FAB ionization, or to an impurity, the sample was acetylated with a mixture of acetic acid and acetic anhydride (10:1) and the FAB mass spectrum of the acetylated material was acquired. An ion at m/z 2222, corresponding to the acetylated eicosapeptide (the only possible acetylation site is the peptide N-terminus), was present, but the pentapeptide Pro-Glu-Glu-Tyr-Leu, was shown not to have been acetylated, because the ion at m/z 650 did not shift by 42 u (as a control, synthetic Pro-Glu-Glu-Tyr-Leu was readily acetylated under the same conditions). It is clear that the ion at m/z 650 was a fragment, generated during FAB ionization, and this situation illustrates the difficulty of attempting to establish purity of peptide samples by mass spectrometric analysis alone.

Mass spectrometric analysis of the fractions collected (and, when it was necessary, tandem mass spectrometry) allowed for the identification of a number of impurities, most of which could be readily matched by their molecular weights to contiguous amino acid segments of the eicosapeptide sequence.

Tandem mass spectrometry was utilized when it was not possible to identify a contiguous amino acid segment in the eicosapeptide amino acid sequence, that corresponded to a peptide with molecular weight matching the value measured by mass spectrometry. For example, comparison of the low-energy tandem collision-induced dissociation (CID) mass spectra of the correct peptide (Figure 1A) and of an impurity 71 u higher in mass (Figure 1B), revealed that Phe-12 in the impurity had been modified by the addition of a group, either by alkylation of the amine nitrogen, or by a Friedel-Crafts type acylation of the aromatic ring during the highly acidic conditions employed for the removal of amino acid protecting groups at the end of the synthesis

In conclusion, mass spectrometry has been used to carry out the identification of impurities, isolated by two different HPLC gradients and present at very low levels, of a synthetic eicosapeptide. It was possible to assign all impurities that were missing one or more amino acids to the expected peptide sequence either from their molecular weights alone or from their tandem CID mass spectra, and to obtain, from the latter data, information on impurities containing modified amino acids.

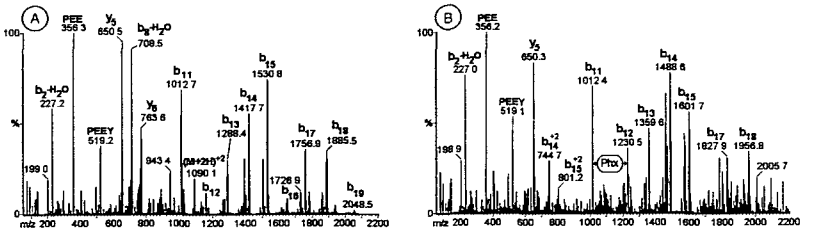

Figure 1. Low-energy, tandem mass spectra of the eicosapeptide Phe-Pro-Arg-Pro-Gly-Gly-Gly-Gly-Asn-Gly-Asp-Phe-Glu-Glu-Ile-Pro-Glu-Glu-Tyr-Leu (**A**) and an impurity 71 u higher in mass (**B**). Both spectra were obtained after CID of the respective doubly protonated molecules. The impurity contains a modified Phe at position 12 (indicated as "Phx" in the spectrum).

References

1. Maraganore, JM; Bourdon, P; Jablonski, J; Ramachandran, KL; Fenton, JW *Biochemistry* **1990**, *29*, 7095-7101.
2. Cannon, CP; Maraganore, JM; Loscalzo, J; *et al.* *The American Journal of Cardiology* **1993**, *71*, 778-782.
3. Fox, I; Dawson, A, Loynds, P, Eisner, J; Findlen, K, Levin, E; Hanson, D, Mant, T, Wagner, J, Maraganore, J *Thrombosis and Haemostasis* **1993**, *69*, 157-163.

ANALYSIS OF CRUDE SYNTHETIC PEPTIDE MIXTURES BY IONSPRAY MASS SPECTROMETRY

Lydia M. Nuwaysir, Jacqueline McCandless, Richard Noble, Ling Chen
Perkin Elmer Applied Biosystems Division, Foster City, CA 94066

INTRODUCTION

The characterization of synthetic peptides is straightforward using mass spectrometry. Since the sequence of the desired product is known, an accurate mass can be calculated and compared to the mass spectrometric results. Frequently, however, the synthetic peptide product will contain additional products produced *via* side-reactions, incomplete deprotections, and/or insufficient couplings. Often times it is desirous to characterize these side products in order to eliminate or minimize their production in the future. Normally, these products are collected from an HPLC purification and submitted for mass spectrometric analysis. An easier solution is to submit the entire crude peptide mixture for LC/MS analysis. This, in combination with high/low orifice scanning, allows the entire mixture to be analyzed for molecular weights, possible contaminants, and confirmation of structure. High/low orifice scanning entails using a programmed set of scan conditions such that intact ions and fragment ions are alternately generated every other scan. Thus, both molecular weight information and sequence information are obtained within the same LC/MS run. In this study, several examples are shown of the use of alternate high/low orifice scanning for the LC/MS analysis of crude synthetic peptides.

EXPERIMENTAL

A PE SCIEX API 300 benchtop triple-quadrupole mass spectrometer was used for this study and operated in the single MS mode. Data were acquired using a step size of 0.25 mass units, a dwell time of 0.5 ms, and a scan range from 100 Daltons to 1500 Daltons. An orifice potential of either 50 or 150 Volts was used, alternating the voltage every other scan. On-line LC/MS was accomplished using a PE ABI 140B LC pump. Crude peptide mixtures were dissolved in an aqueous solution of 5% acetic acid and injected onto an Aquapore OD-300 1 x 100 mm C18 column and eluted using a gradient from 5% to 75% B. Buffer A = 95% H_2O, 5% ACN, 0.05% TFA; Buffer B = 80% ACN, 20% H_2O, 0.0425% TFA. Peptides #1, #2, and #3 were synthesized on a PE Synergy® Peptide Synthesizer using HBTU activation and the Fmoc protecting strategy. Peptides were cleaved according to the ABD User Bulletin No. 40. All reagents were from PE Applied Biosystems Division Peptide #4 was from an outside source.

RESULTS

Figure 1 displays the LC/MS analysis of crude peptide #1. Two main products were produced during the synthesis, the expected peptide (DN1) and a peptide 15 Daltons less than the expected peptide (DN1*). Inspection of the sequence data generated by the high orifice scans reveals that the DN1 peptide has the correct sequence while the DN1* peptide contains a residue in place of the lysine with a nominal mass of 113 Daltons, indicating a leucine, isoleucine, or norleucine in this position (Figure 2). Edman sequencing revealed that this residue was in fact a leucine, and was due to the use of a degenerate cartridge containing equal amounts of Fmoc-Lys(Boc)-OH and Fmoc-Leu-OH during the synthesis.

As further observed in the TIC, Both DN1 and DN1* undergo side reactions to produce additional products. These side reactions result in the formation of a peptide 18 Daltons lower than the expected molecular weight, and a peptide 67 Daltons higher than the expected molecular weight. Closer inspection revealed that this was due to aspartimide formation at the Asp residue (loss of 18 Daltons) followed by formation of a piperidide adduct during the piperidine deprotection steps of the synthesis (addition of 67 Daltons).[1,2] In order to test the sensitivity of the -DN- sequence for aspartimide and piperidide formation, peptide #2, "DN2", was generated (a truncated peptide containing only the first five residues DNGKA). Piperidide formation was suppressed as a result of fewer deprotection steps (only one) following coupling of the Asp residue. However, a small amount of the aspartimide-containing peptide was still observed.

Aspartimide formation and piperidide adduction were also observed for peptide #3. In fact, virtually all of the peptide had reacted during the synthesis to produce these two side products. Treatment of the mixture with base opened up the aspartimide to reform the desired peptide. However the piperidide peptide was unaffected. Thus, in order to limit piperidide formation, the aspartimide must be limited first.

Many peaks were observed to elute very closely in the TIC for the analysis of crude peptide #4. High/low orifice scanning during the LC/MS run indicated that the peptide with the correct sequence eluted last, while other peaks were due to oxidation of methionine and insufficient couplings.

CONCLUSION

Alternating low and high orifice scans during a single LC/MS run speeds analysis of peptides by providing both molecular weight information and sequence information of entire crude mixtures within the same time frame. The technique is easily implemented using the standard software and provides sequence data without the need for a triple-quadrupole instrument.

REFERENCES

1. R. Dolling, M. Beyermann, J. Haenel, F. Kernchen, E. Krause, P. Franke, M. Brudel, M. Bienert *J. Chem. Soc. Chem. Commun.*, (1994) 853-854.
2. J.L. Lauer, C.G. Fields, G.B. Fields *Letters in Peptide Science*, 1 (1994) 197-205.

ACKNOWLEDGMENTS

We gratefully acknowledge Dave Dupont for Edman sequencing and Dave Jackson for helpful discussions

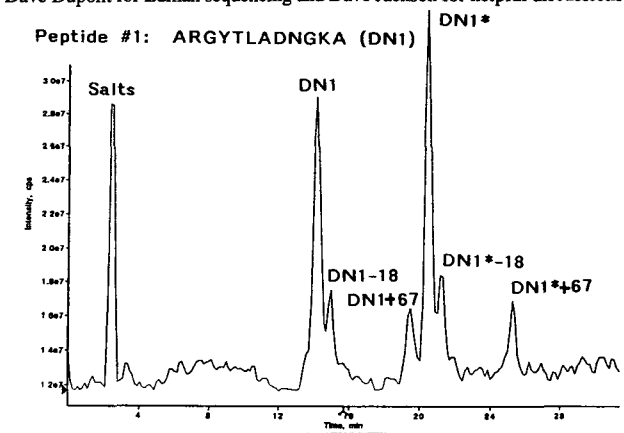

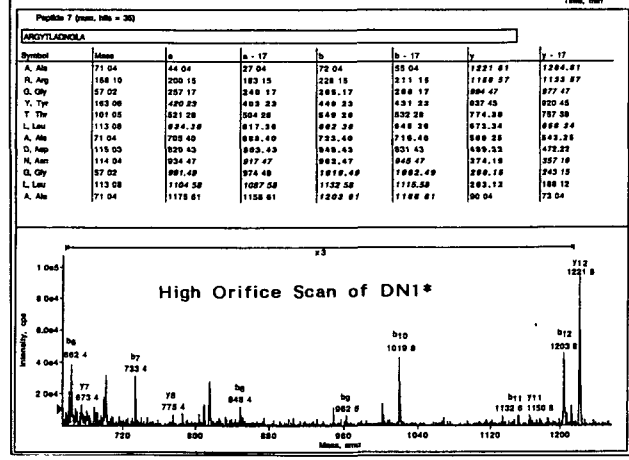

Tandem Mass Spectrometry of Metal-Peptide Complexes.

Scott G. Summerfield, Vanessa C. M. Dale, Dominique Despeyroux and Keith R. Jennings.
Department of Chemistry, University of Warwick, Coventry, CV4 7AL, U.K.

Collisional activation of metal-peptide complexes provides a complementary source of information to the more traditional studies of the $[M+H]^+$ ion. Charge remote fragmentations are common from protonated peptide complexes when highly basic residues are present. This study has been undertaken to gain more information about the charge remote processes occurring in Group 1 metal complexes of the type $[M+Cat]^+$ and $[M-H+2Cat]^+$. High energy collision induced dissociation has been performed using a Kratos 'Concept' Four-sector instrument equipped with a liquid SIMS source, floated collision cell and scanning array detector. The results described suggest that at high collision energies, small losses from the side chains of certain amino acids occur *via* charge remote processes. These losses can be characteristic of the presence of residues such as those of arginine, lysine and methionine [1].

Collision induced losses from the arginine residue are typified by the behaviour of the metal complex shown in Figures 1a and 1b. The $[M+K]^+$ complex of Arg-Pro-Pro-Phe-Leu-Ser-Pro-Phe, m/z 942.4 Da. (Figure 1a), generates a number of sequence-specific product ions including the N-terminal a_n series and the C-terminal y_6 and y_7 ions. Figure 1b shows the upper mass range of the spectrum where the neutral losses of the **100**, **87**, **73** and **59** Da from the precursor ion are due to fragmentation along the pendant chain of the arginine residue.

These observations may be rationalised by postulating a series of elimination reactions. Loss of **87** Daltons from the metal complex occurs by a 1,4 elimination where the α-hydrogen of the arginine side chain is involved in the rearrangement. The losses of **73** (inset) and **59** Daltons arise from similar reactions further along this side chain. As a result, the arginine side chain, $-(CH_2)_3NHC(NH)NH_2$ is converted to a shorter alkene chain. Loss of **100** Daltons occurs by radical cleavage of the α-β bond of the pendant chain and results in the loss of the entire $[C_4H_{10}N_3]^+$ group.

Many cation peptide complexes undergo analogous rearrangements [1]; the methionine residue may lose **62** or **48** Da; the side chain of the lysine residue may lose **59**, **45** or **31** Da.

Similar fragmentations occur on CID of certain $[M+H]^+$ ions such as for the peptide Tyr-Phe-Met-Arg-Phe-NH_2. The expected site of protonation is the arginine residue and the high energy collision induced decomposition results in losses of **62** and **48** Daltons from the methionine side chain. These data suggest that these fragmentations occur remote from the site of proton attachment and similarly, fragmentations of this type from metal complexes may also be charge remote in nature. This suggestion is consistent with other studies of alkali metal-peptide complexes where the major interactions are thought to occur between the metal and the carbonyl oxygens of the peptide backbone [2], leaving the amino acid side chains playing a less important role in charge stabilisation.

1 S. G. Summerfield, V. C. M. Dale, D. Despeyroux and K. R. Jennings, *Eur. Mass Spectrom.*, in Press.
2. L. M. Teesch, R. C. Orlando, J. Adams, *J. Am. Chem. Soc.*, **113**, 3668-3675 (1991).

43rd ASMS Conference on Mass Spectrometry and Allied Topics

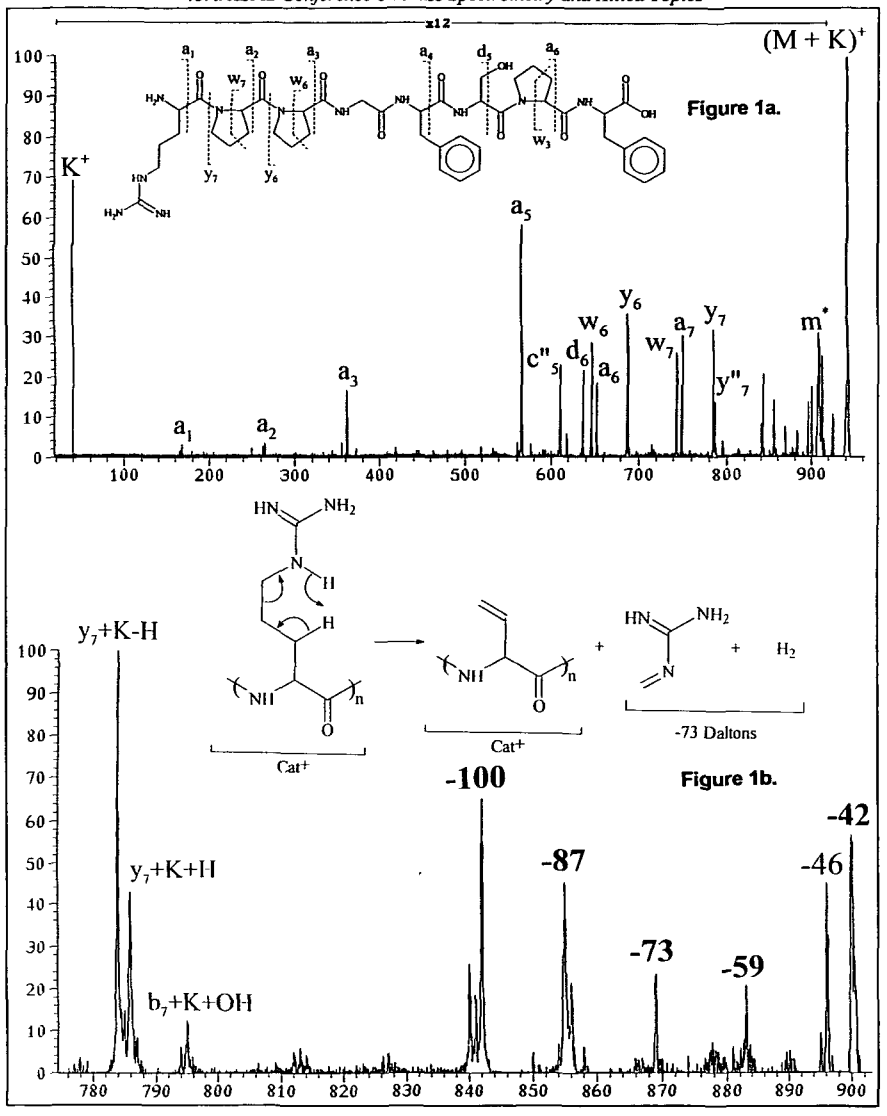

LOSS OF THE C-TERMINAL AMINO ACID FROM COMPLEXES BETWEEN TRANSITION METAL IONS AND PEPTIDES

Alex Reiter, Jeanette Adams, and M. Cameron Sullards, Department of Chemistry and the Emory University Mass Spectrometry Center, Emory University, Atlanta, GA 30322

Experiments are conducted: (1) to investigate the mechanism for metastable ion loss of the C-terminal amino acid from complexes between transition metal ions and peptides; (2) to relate this chemistry to that of complexes between alkali metal ions and peptides; and (3) to demonstrate the occurrence of this chemistry for multiply-charged complexes between peptides and transition metal ions formed by electrospray ionization (ESI). ESI, MS^2, and MS^3 experiments are performed using a JEOL JMS-SX102/SX102A/E, five-sector tandem mass spectrometer.

Loss of the C-terminal amino acid results in formation of $(b_{n-1} + OH)$ ions. MS^2 spectra show that precursor $(M + H)^+$ ions give $(b_{n-1} + OH)^+$ ions [1]; $(M + Li)^+$ ions give $(b_{n-1} + Li + OH)^+$ ions [2,3]; and $(M + Me^{2+} - 3H)^-$ ions give $(b_{n-1} + Me^{2+} - 3H + OH)^-$ ions. MS^3 experiments show that first-generation $(b_{n-1} + Me^{2+} - 3H + OH)^-$ ions have the same structures as $(M_{n-1} + Me^{2+} - 3H)^-$ ions of peptides that are missing the C-terminal amino acid (Figure 1). Furthermore, the $(b_{n-1} + Me^{2+} - 3H + OH)^-$ ions decompose to give second-generation $(b_{n-2} + Me^{2+} - 4H)^-$ products [4] (Figure 1A). The only mechanism that can explain formation of both first- and second-generation product ions is the mechanism originally proposed by Westmore [5] (Scheme I).

Loss of the C-terminal amino acid to give $(b_{n-1(2)} + Me^{2+} + OH)^{2+}$ ions also occurs for $(M + Cu)^{2+}$ complexes of angiotensin II that are formed by ESI (Figure 2A). Although these ions are weakly abundant in the MS^2 spectrum (Figure 2A), they are predominant in the MS^3 spectrum of the first-generation $(M + Cu - 44)^{2+}$ ions. The $(M + Cu - 44)^{2+}$ ions arise by loss of CO_2 from the precursor complexes. The MS^3 spectrum indicates that $(b_7 + Cu + OH)^{2+}$ and $(b_6 + Cu + OH)^{2+}$ ions must arise from precursor structures that contain the metal ion bound toward the N-terminus but not to the deprotonated Asp side chain. Furthermore, the precursors must contain a neutral C-terminal carboxylic acid.

The mechanism in Scheme I explains all the data for $(M + H)^+$, $(M + Li)^+$, $(M + Me^{2+} - 3H)^-$, and $(M + Cu)^{2+}$ ions. In contrast, the mechanism originally proposed by Renner and Spiteller [6] cannot explain all the data. This strongly suggests that the Westmore mechanism [5] is the correct one.

References

1. Thorne, G. C.; Ballard, K. D.; Gaskell, S. J. *J. Am. Soc. Mass Spectrom.* **1990**, *1*, 249-257.
2. (a) Teesch, L. M.; Adams, J. *J. Am. Chem. Soc.* **1991**, *113*, 812-820. (b) Teesch, L. M.; Orlando, R. C.; Adams, J. *J. Am. Chem. Soc.* **1991**, *113*, 3668-3675.
3. (a) Grese, R. P.; Cerny, R. L.; Gross, M. L. *J. Am. Chem. Soc.* **1989**, *111*, 2835-2842. (b) Grese, R. P.; Gross, M. L. *J. Am. Chem. Soc.* **1990**, *112*, 5098-5104. (c) Hu, P.; Gross, M. L. *J. Am. Soc. Mass Spectrom.* **1994**, *5*, 137-143.
4. Reiter, A.; Adams, J.; Zhao, H. *J. Am. Chem. Soc.*, **1994**, *116*, 7827-7838.
5. Tang, X.; Ens, W.; Standing, K. G.; Westmore, J. B. *Anal. Chem.* **1988**, *60*, 1791-1799.
6. Renner, D.; Spiteller, G. *Biomed. Environ. Mass Spectrom.* **1988**, *15*, 75-77.

43rd ASMS Conference on Mass Spectrometry and Allied Topics

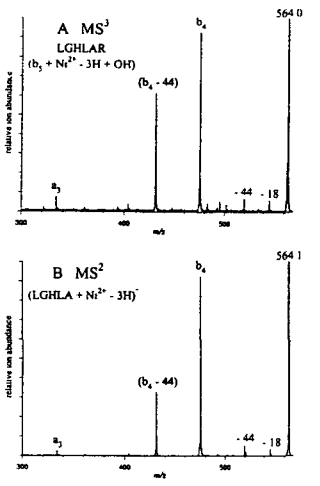

Figure 1. MS^3 spectrum of $(b_5 + Ni^{2+} - 3H + OH)^-$ ions from $(M + Ni^{2+} - 3H)^-$ complexes of LGHLAR (A), and MS^2 spectrum of $(M + Ni^{2+} - 3H)^-$ complexes of LGHLA.

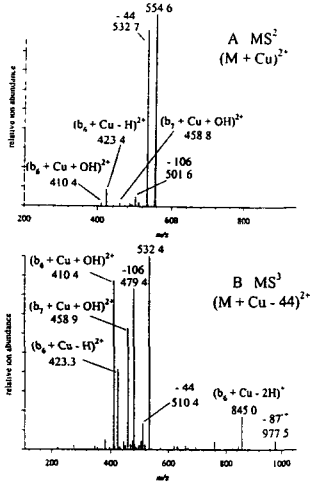

Figure 2. MS^2 spectrum of $(M + Cu)^{2+}$ ions (A), and MS^3 spectrum of $(M + Cu - 44)^{2+}$ ions (B) of angiotensin II.

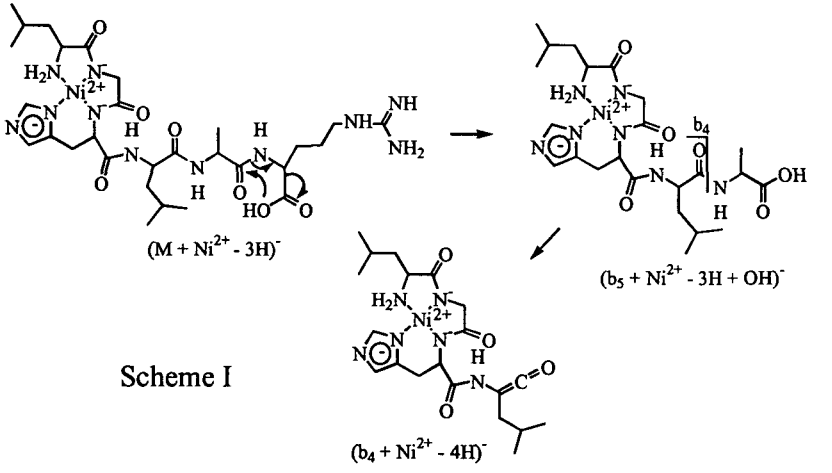

Scheme I

INTRINSIC COORDINATION BETWEEN CO(II) AND NI(II) AND HISTIDINE PEPTIDES

Alex Reiter and Jeanette Adams, Department of Chemistry and the Emory University Mass Spectrometry Center, Emory University, Atlanta, GA 30322

We previously studied gas-phase anionic complexes between Co^{2+} and Ni^{2+} and peptides that contain hydrocarbon amino acids.[1] The complexes decompose metastably to give abundant $(b_4 + Me^{2+} - 4H)^-$ ("b_n") ions. It was shown by MS^3 experiments that precursor ions that give rise to the $(b_4 + Me^{2+} - 4H)^-$ ions contain the Me(II) ion in a N-terminal square planar complex.

We extend this study to investigate the gas-phase anionic complexes between Co^{2+} and Ni^{2+} and peptides that contain His side chains. Seven hexapeptides (HLGLAR, LHGLAR, LGHLAR, LGLHAR, LGLAHR, DTHAAA, and ADTHAA) that contain His in varying positions are investigated by MS^2 and MS^3 experiments using a JEOL JMS-SX102/SX102A/E, five-sector tandem mass spectrometer.

For the HLGLAR series, Ni^{2+} complexes metastably decompose to give more abundant b_n ions than Co^{2+} complexes. Co^{2+} complexes generally decompose to give more abundant $(y_n + Me^{2+} - 2H)^-$ ("y_n") ions than Ni^{2+}. These trends demonstrate that Ni^{2+} prefers N-terminal binding more so than Co^{2+}. Complexes of LGLHAR and LGLAHR show an increase in $(y_3 + Me^{2+} - 2H)^-$ and $(y_4 + Me^{2+} - 2H)^-$ ions. MS^3 experiments show that these ions arise from precursor structures that contain the metal ion bound internally to the His side chain. Unique $(a_3 + Me^{2+} - 4H)^-$ ions are observed for LGHLAR (Figure 1). These ions arise from N-terminal square planar complexes. Precursor ions that give rise to $(b_4 + Me^{2+} - 4H)^-$ ions contain the metal ion bound to the N-terminus and three deprotonated amides. Precursor ions that give rise to $(a_3 + Me^{2+} - 4H)^-$ ions, however, contain the metal ion bound to the N-terminus, two deprotonated amides, and a deprotonated His side chain. This type of binding by His is similar to that which occurs in solution.[2]

The only cleavages of the peptide backbone that occur for Co^{2+} and Ni^{2+} complexes of DTHAAA and ADTHAA give b_n and y_n ions (Table I). Ni^{2+} complexes (Figure 2A and 2B) give both b_n and y_n ions, whereas Co^{2+} complexes give only y_n ions (Table I). The lack of b_n ions for Co^{2+} complexes indicates that no N-terminally bound complexes are formed. MS^3 experiments show that the precursor ions that give y_n ions have the metal ion bound internally to the His side chain.

This study shows that three major factors determine the extent and type of binding that occurs for complexes between Co^{2+} and Ni^{2+} and His-containing peptides: metal ion, position of His, and neighboring residues. Co^{2+} binds to the His side chain more than it binds to the N-terminus. Ni^{2+}, however, generally prefers to bind to the N-terminus more than it binds to the His side chain. Effects of neighboring residues are illustrated by comparing the MS^2 spectra of Ni^{2+} complexes of LGHLAR and DTHAAA (Figure 1 and 2A). LGHLAR binds simultaneously to both the His side chain and the N-terminus to form a square planar complex, whereas the metal ion binds internally to the His side chain of DTHAAA. These structures are verified by MS^3 experiments.

References

1. Reiter, A.; Adams, J.; Zhao, H. *J. Am. Chem. Soc.* **1994**, 116, 7827-7838.
2. Kiss, T.; Sóvágó, I. In *Biocoordination Chemistry: Coordination Equilibria in Biologically Active Systems;* Burger, K. (Ed.); Ellis Horwood: New York, 1990, pp 162-164.

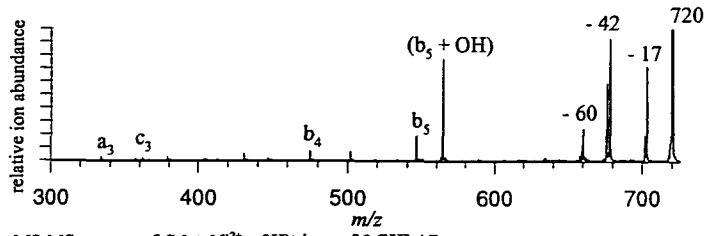

Figure 1. MS-MS spectra of $(M + Ni^{2+} - 3H)^-$ ions of LGHLAR.

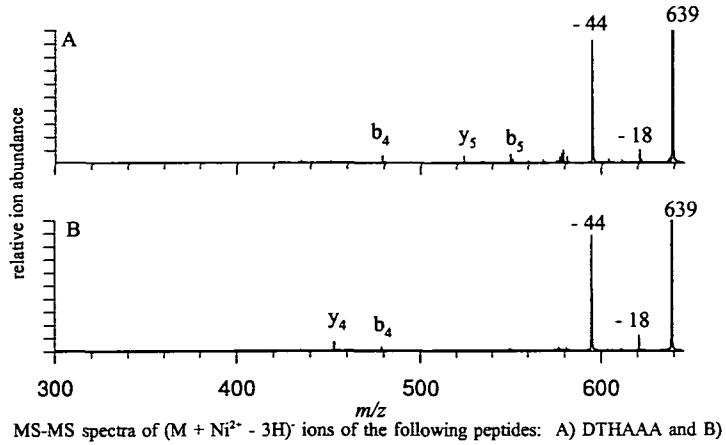

Figure 2. MS-MS spectra of $(M + Ni^{2+} - 3H)^-$ ions of the following peptides: A) DTHAAA and B) ADTHAA.

	b_5	y_5	b_4	y_4	- 18	- 44
DTHAAA						
Co^{2+}	-	0.20	-	-	1 85	2.93
Ni^{2+}	0.12	0.10	0.10	-	0.17	1.46
ADTHAA						
Co^{2+}	-	-	-	0.18	0.57	2.86
Ni^{2+}	0.05	-	0.08	0.21	0.34	2.58

Table 1. Relative abundances (%) of ions from Co^{2+} and Ni^{2+} complexes of DTHAAA and ADTHAA.

PEPTIDE ADSORPTION AT GAS-LIQUID INTERFACES PROBED BY FAB MASS SPECTROMETRY

Richard B. van Breemen, Department of Medicinal Chemistry & Pharmacognosy, College of Pharmacy, University of Illinois at Chicago 833 S. Wood Street, Chicago, IL 60612-7231

Daniel D. Powers, Peter K. Kilpatrick and Ruben G. Carbonell, Department of Chemical Engineering, Box 7905, North Carolina State University, Raleigh, NC 27695

Any compound that will adsorb preferentially to an interface is surface active. In particular, amphiphilic molecules may adsorb at the interface between hydrophilic and hydrophobic bulk phases, such as the air-water interface. The only method which can directly quantify adsorbed molecule concentrations is the radiotracer method.[1] The basis for this technique is that the radiation emitted by a weak β-emitting nuclide is attenuated much more by solvent than by air. This results in surface-adsorbed radiolabeled species contributing more to the radiation measured by a detector directly above the solution than do species in the bulk solution. The disadvantages of this technique are the requirement of tritiated or ^{14}C labeled solute and length of time (several hours) per measurement. In this investigation, fast atom bombardment (FAB) was evaluated as a method for probing the surface activity of peptides or other surfactants in a glycerol matrix, and the surface activities of several peptides were compared in glycerol and water.

Although several studies have investigated the mechanism of FAB ionization, none have compared the abundance of analyte ions desorbed by FAB directly to their surface excess concentrations. The only related study was carried out by Allmaier,[2] who used a de Nouy ring tensiometer to measure surface tension of several peptide solutions in glycerol and then from these measurements estimated surface excess concentration. Allmaier found a rough correlation between estimated surface concentration and abundance of protonated peptide.

METHODS

The isomeric peptides, $Gly_4Lys_4Phe_4$ and $(GlyLysPhe)_4$, were synthesized using Fmoc chemistry using a solid support and then deprotected and released from the resin. Radiolabeled peptides were synthesized using ^{14}C-labeled Fmoc-glycine. Semi-preparative reversed-phase HPLC was used to purify each synthetic peptide. Positive ion FAB mass spectrometry with collision induced dissociation and linked scanning at constant B/E were used to confirm peptide molecular weights and sequences.

Standard solutions of each peptide in glycerol or water were prepared by serial dilution. Peptide concentrations ranged from 7.0 mg/ml to 0.35 μg/ml. Radiotracer measurements were carried out using a Teflon sample cell in a thermostatted environmental chamber. A solid scintillator β-detector was positioned immediately above the glycerol (or water) surface. The radiotracer apparatus has been described in detail.[3]

Positive ion FAB mass spectra were acquired using a Finnigan MAT 90 double-focusing mass spectrometer at 1000 resolution. Aliquots of 1 μl each were loaded onto the FAB probe, inserted into the ion source, and analyzed by FAB using xenon fast atoms at 8 kV. The FAB gun was turned on exactly 10 s after the sample was introduced into the vacuum system.

RESULTS

In order to determine if peptide surface activities in glycerol differ significantly from those in water, the surface excess concentrations of several peptides were measured in water and glycerol using the radiotracer method. The radiotracer measurements demonstrated that surface activities of peptides in glycerol are considerably different than in water. Therefore, the surface excess concentration of a peptide in glycerol may not be predicted based on its properties in water. For example, the two isomeric peptides, $Gly_4Lys_4Phe_4$ and $(GlyLysPhe)_4$, showed different surface activities in water, but the isotherms measured in glycerol were indistinguishable.

Isotherms were plotted showing surface excess concentration (determined using the radiotracer technique) or intensity of protonated peptide signal (obtained using positive ion FAB) versus bulk concentration. Whether obtained using the radiotracer method or FAB mass spectrometry, each pair of isotherms showed that same slopes and inflection points, which indicated that the mechanism of FAB desorption/ionization of peptides is primarily a surface desorption technique (see Figure 1).

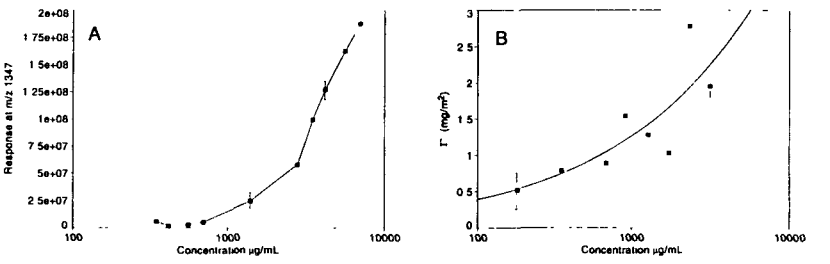

Figure 1. (A) Positive ion FAB SIM of $[M+H]^+$ at m/z 1347 of peptide $Gly_4Lys_4Phe_4$ in glycerol. (B) Surface excess concentration of $[^{14}C]$-$Gly_4Lys_4Phe_4$ in glycerol using the radiotracer method.

Additional evidence supporting FAB as a surface desorption technique was provided by the shape of the FAB isotherm. If FAB primarily sampled the bulk of the peptide solution instead of the surface, than the mass spectrometer response should increase linearly with increasing bulk concentration of peptide in glycerol. Instead, the mass spectrometer response increased sharply at high concentrations as the peptide surface excess concentration increased more rapidly than the bulk concentration. Finally, these results suggest that FAB mass spectrometry can be used as a much faster technique than the radiotracer method to compare surface activity of peptides in glycerol solutions.

ACKNOWLEDGEMENTS

This material is based upon work supported by grant BIR-9204042 from the National Science Foundation. The authors wish to thank Richard Dvorak at the University of Illinois at Chicago and George Dubay at Duke University for assistance with mass spectrometry.

REFERENCES

1. Muramatsu, M. *Surf. Colloid Sci.* **1973**, *6*, 101.
2. Allmaier, G. M. *Rap. Commun. Mass Spectrom.* **1988**, *2*, 74-76.
3. Hunter, J. R.; Kilpatrick, P. K.; Carbonell, R. G. *J. Colloid Interface Sci.* **1990**, *137*, 462-482.

FAB MS OF OXYTOCIN, DEAMINO-OXYTOCIN AND ARGININE VASOPRESSIN

Valeriy A. Pokrovskiy , Natalia P. Galagan
Laboratory of Mass Spectrometry,
Institute for Surface Chemistry, Academy of Sciences of Ukraine
Pr. Nauki 31, Kiev 252022, Ukraine

Galina V. Ostrovskaya, Vladimir K. Rybalchenko
Laboratory of membranology, Taras Shevchenko University
Vladimirskaya 60, Kiev 252033, Ukraine

Neurohypophysial hormones oxytocin (OT) and arginine vasopressin (VP) belong to a class of peptide hormones. The main function of VP is the regulation of diuresis and blood pressure; OT regulates birth action and lactation. In the last decade attention was paid to a synthetic analog of OT namely deamino- oxytocin (d-OT) which differs from natural hormone by absence of NH_2 group at the Cys-1. The biological oxytocin-like activity of d-OT on tissues-targets is 2-4 times higher than that of natural hormone [1].

Recently the experimental proofs appeared which allow to explain the biological activity of neurohypophysial peptides by their direct action on the membrane lipid phase. In particular, the formation of ion channels was observed in model lipid membranes under effect of peptides [2,3]; the change of phase transition temperatures [4,5] and the direct effect of peptides on membrane bound enzymes [6]. The idea of the present work is the FAB MS study of individual peptide hormone molecules and their equimolar mixtures in comparison with physico-chemical properties and biological activity.

The samples of oxytocin, (1006.5 dalton for the lowest isotope), deamino-oxytocin (991,5 dalton) and arginine vasopressin (1083,6 dalton) samples were synthesized and purified in the Institute of Organic Synthesis (Riga, Latvia). FAB mass spectra were obtained on a MX-1310 double focusing instrument (Chernogolovka, Russia) of 2000 dalton mass range at 5 KV accelerating voltage and resolution 10 000. The design and performance of original FAB MS ion source using argon atom beam were published earlier elsewhere [7]. The details of experimental procedure of peptide studies were described previously [8]. Parameters of peptide surface activity were studied according to the well known Wilhelmy method in a glass trough [9].

RESULTS AND DISCUSSION

"Monoisotopic" FAB spectra in the mass interval (M-H), (M+4H) were computed, for which all elements are represented by their lowest isotopes only. The deconvolution procedure of obtaining "monoisotopic" mass spectra proposed by K. Vekey [10] was used, including the substraction of "chemical" background (usually 2-4% of main peak intensity).

The most interesting feature of oxytocin FAB mass spectrum is abundant (about 40% to protonated molecule) satellite group of lines 15 dalton heavier than molecular cluster ions. The distribution of relative ion intensities in this group is similar to distribution of molecular cluster ions. Observed effect may be explained by replacement of a hydrogen atom by an amino group in molecular cluster.

The only source of amino groups availiable in a FAB liquid matrix (glycerol + water) is the nearby peptide molecule. It seems that under FAB conditions the disproportion reaction between two peptide molecule may occur resulting in attaching eighther a proton or a charged amino group ion to a peptide molecule. No analogous satellites were observed for deamino-oxytocin and arginine vasopressin.

The experiments with equimolar mixtures of peptides in all possible combinations were proceeded in order to discover possible ionization of intermolecular associates and/or products of their decomposition. No such species was observed. In all cases the mass spectra of mixtures looked like a superposition of individual peptide mass spectra and relative abundances of species observed did not depend on pH value. But contributions of different peptides to the mass spectrum of mixture was not equal. The mean ratio of molecular ions abundances estimated from all the equimolar experiments was approximately 5:4:1 in the raw OT:d-Ot:VP; the same ratio was 7:4:1 if satellite ion of OT (M+15) was taken into account.

The maximum Gibbs adsorption Γ on (KCl solution)-atmosphere interface and on the azolectine monolayers (integral phospholipide fraction of soy-bean with lipid composition similar to biological membranes) gave in both cases the sequence OT>d-OT>VP which coincide with ion yield in FAB mass spectra of mixtures.

The comparison of the effects of natural neurohypophysial hormones on lipide membranes shows good correlation with physiological activity, surface activity and abundance of cluster ions in FAB mass spectra of mixtures. It was found out, for example, that OT, in contrast to VP, is able to create ion channals in bilayer lipid membranes [11] and that VP action is limited by vesicles surface [12] whereas OT effects the whole structure of bilipid layer [13]. This may be the reason of dramatic difference in effect of OT and VP on liposomes: both peptides increase the permeability of phosphatidylcholine liposomes to Ca ions, but to uncommensurate levels.

CONCLUSIONS

In FAB study of d-OT, OT and VP and their equimolar mixtures the resulting mass spectra of mixtures were the superposition of individual peptide mass spectra. No intermolecular association of different peptides was observed. The ion yield from mixtures in FAB glycerol matrix decreased in the row OT> d-OT>VP, similar to their surface activity. The ion yield from natural peptides mixtures in glycerol (OT and VP) correspond both to surface and membranotropic biological activity. The ion yield in the pair of natural (OT) and synthetic (d-OT) peptides was inverse to biological activity. Natural hormone (OT) posesses less physiological and membranothropic activity in spite of its higher surface activity. The specific behaviour of OT may be explained by structure peculiarities of OT molecule resulting in dimer formation and aminogroup exchange in the surface layer of glycerol matrix.

1. B. M. Ferrier, D. Jarvis, V. du Vigneaud, J. Biol. Chem. 40, 4264 (1965).
2. V. Singh, D. B. Raju, Ravindram C. Srivastava, J. of Colloid and Interface Science. 139, 337 (1990).
3. K. Anzai, M. Hamasuma, H. Kadono et. al., Biochim. and Biophis Acta Biomembr. 1064, 256 (1991).
4. R. S. Phadke, S. Srivastava, G. Govil, J. Biosci. 15, 153 (1990). 5. C. Mollay, FEBS Letters. 64, 65 (1976).
6. V. K. Rybalchenko, G. V. Ostroskaya, XXIII Europ. Muscle Congress. Bohum, 11-14 Sept., 1994, 08/10P.
7. V. A. Pokrovskiy, V. I. Borisevich, A. M. Gluhoy, Pribori i tekhnika eksperimenta. 1, 156 (1987).
8. K. B. Yatsimirskiy, V. A. Pokrovskiy, A. G. Kolchinskiy, V. V. Mosin, Teor. Eksper. Khim. 5, 634 (1987).
9. J. J. Bickerman, Surface Chemistry for Industrial Research. New York. Academic Press (1948).
10. K. Vekey, Int. J. Mass Spectrom. Ion Processes. 97, 265 (1990).
11. V. K. Rybalchenko, G. V. Ostrovskaya, N. E. Kucherenko. Bul. Exp. Biol. Med. 108, 1729 (1989).
12. G. V. Ostrovskaya, S. I. Shevchenko, B. R. Mogilevich, V. K. Rybalchenko, Bul. Exp. Biol. Med. 114, 1600 (1992).
13. V. K. Rybalchenko, G. V. Ostrovskaya (unpublished data).

PROCESSING OF DYNORPHIN A (1-17) IN HUMAN AND MONKEY BLOOD STUDIED BY MS

Jim Yu, Eduardo R. Butelman*, James H. Woods*,
Mary Jeanne Kreek, and Brian T. Chait
The Rockefeller University, New York, NY 20021, and
*The University of Michigan, Ann Arbor, MI 48109

Studies of the endogenous neuropeptide dynorphin A [Dyn A (1-17)] have indicated that this peptide may attenuate the behavioral signs and objective measurements of the opioid withdrawal syndrome in morphine-dependent rodents and may be useful as a therapeutic agent for the treatment of opioid dependent patients [1,2]. It has also been shown that Dyn A peptides can modulate morphine tolerance in morphine-dependent mice [1,2]. Dyn A peptides have been demonstrated to have analgesic properties and may have potential application in the management of chronic pain [3]. Also both opioid and non-opioid dynorphin peptides have been shown to alter the immune function of natural killer cell activity [4].

Isolation and characterization of the processing of dynorphin A in tissues and brain regions [5-8], spinal cord [9] and cell cultures [10] have been studied. However, there is still relatively little information about the dynamics and nature of dynorphin A biotransformation in biological systems [11,12]. The processing of Dyn A (1-17) produces various opioid and non-opioid peptides, which are potentially biologically active. In order to find a suitable model for invasive studies of the biotransformation of Dyn A (1-17), and to further evaluate the potential therapeutic effects of this peptide, the rhesus monkey was chosen as a primate model. Comparative studies of *in vitro* biotransformation of Dyn A (1-17) in rhesus monkey and in human blood were conducted.

Human blood was obtained from eight healthy volunteers, 6 males and 2 females with an average age of 30.8 years (range 22-47). Monkey blood was obtained from three healthy adult female rhesus monkeys, average age 8.3 years (range 7-10). Dyn A (1-17) in an amount of 0.59 mg/ml was added to freshly drawn blood from each subject and incubated at 37°C. Samples were taken from the incubated blood at specific time intervals. Plasma was separated from blood cells by centrifugation at 4°C for 5 min (4,000 rpm). Two hundred-µl of plasma containing the biotransformed dynorphins was added to 1.8 ml of 1% trifluoroacetic acid (TFA) aqueous solution, along with 100 µl of 315 µM somatostatin in 0.05% aqueous TFA as the internal standard. The solution containing plasma, biotransformation products from Dyn A (1-17), somatostatin and TFA, was centrifuge-filtrated with concentrators (Centricon-SR3, Amicon Inc., Beverly, MA), having molecular weight cutoff of 3,000 Da. After filtration, 100 µl of filtrate was evaporated in a Speed Vac concentrator (Savant Instruments, Farmingdale, NY) for 20 min to reduce the total volume to approximately 40 µl. Twenty-µl of the solution was mixed with 10 µl of acetonitrile. Ten-µl of this solution was mixed with 20 µl of matrix (α-cyano-4-hydroxycinnamic acid) solution. The mass spectrometer employed in this study is a matrix-assisted laser desorption ion source and a linear time-of-flight mass analyzer, which was constructed at the Rockefeller University. Every MS spectrum employed an average of 200 laser shots.

It has been demonstrated that Dyn A (1-17) *in vitro* biotransformation in human and rhesus monkey blood is very similar. One major pathway is the non-specific or specific enzymic cleavage of tyrosine from position one of Dyn A (1-17) to yield Dyn A (2-17). This is a slow process with prolonged presence of Dyn A (1-17) in both human and rhesus monkey blood. Intact Dyn A (1-17) was detected in human and rhesus monkey blood at 180 min and 90 min, respectively. Dyn A (2-17) is the major and long-lasting biotransformation product of Dyn A (1-17) *in vitro* both in human blood and in rhesus monkey blood. However, there are some variations in the formation of minor products between human and monkey and among individual subjects. It has been shown that Dyn A (2-17), which is a non-opioid peptide, has many effects including prevention or reversal of opioid withdrawal in rodent models; analgesic properties for chronic pain; and alteration of natural killer cell activities [1,2,4]. Another major pathway is the specific enzymic cleavage between Arg(6) and Arg(7) to produce the opioid peptide, Dyn A (1-6), and the non-opioid peptide, Dyn A (7-17). Our results indicate that rhesus monkey may be a good model for further *in vivo* pharmacological studies. However, dynorphin A processing occurred at a faster rate *in vitro* in monkey blood than that in human blood, indicating any use of rhesus monkey as a model for pharmacokinetic studies for humans will need to be carefully evaluated.

References

1. A.E. Takemori, H.H. Loh and N.M. Lee, Eur. J. Pharmacol., 221: 223-226, 1992.
2. A.E. Takemori, H.H. Loh and N.M. Lee, J. Pharmacol. Exp. Therap., 266: 121-124, 1993.
3. A.P. Smith and N.M. Lee, Ann. Rev. Pharmacol. Toxicol., 28: 123-140, 1988.
4. G. Bodner, S. Pinto, H. Albeck and M.J. Kreek, Problems of Drug Dependence 1991: Proceeding of the 53rd Annual Scientific Meeting, NIDA Research Monograph Series, Vol. 119, pp. 331.
5. A. Goldstein, S. Tachibana, L.I. Lowney, M. Hunkapiller and L. Hood, Proc. Natl. Acad. Sci. U.S.A., 76: 6666-6670, 1979.
6. B.H. Herman, F. Leslie and A. Goldstein, Life Sci., 27(10): 883-892, 1980.
7. L. Devi and A. Goldstein, Proc. Natl. Acad. Sci. U.S.A., 81: 1892-1896, 1984.
8. L. Devi, P. Gupta and L.D. Fricker, J. Neurochem., 56: 320-329, 1991
9. J. Silberring, M.E Castello and F. Nyberg, J. Biol. Chem., 267: 21324-21328, 1992.
10. S. Petanceska, J. Zikherman, L.D. Fricker and L. Devi, Mol. Cell Endocrinol., 94. 37-45, 1993.
11. J.Z. Chou, S. Pinto, M.J. Kreek and B.T. Chait, Problems of Drug Dependence 1992: Proceeding of the 54th Annual Scientific Meeting, NIDA Research Monograph Series, Vol. 132, pp. 380.
12. J.Z. Chou, M.J. Kreek and B. T. Chait, J. Am. Soc. Mass Spectrom., 5: 10-16, 1994.

ANALYSIS OF HETEROGENOUS PEPTIDE MIXTURES BY LC/MS

Manfred Raida, Gabi Heine, Peter Schulz-Knappe, Wolf-Georg Forssmann
Lower-Saxony Institute for Peptide Research (IPF)
Feodor-Lynen-Strasse 31, D - 30 625 Hannover, Germany

The analysis of heterogenous peptide mixtures, as present in blood or urine, by immunological methods has become an important technique in diagnostics to detect markers which are present or absent due to disease or a genetic variation. Immunological detection is limited to known markers, thus an overview of the peptide pattern to compare healthy and sick persons cannot be performed by this method Nevertheless, a comparative analysis of the peptide pattern with respect to a certain disease could help to detect those peptides which are related to the disease. This comparative analysis can lead to the detection of new markers which are helpful for early diagnosis.

The main problem in the comparative analysis of the peptide pattern of serum is the presence of high concentrations of proteins, like albumin and globulins, the large number of peptides up to appr 30 kD, and their low concentration in the solution. More than several 100 000 different peptides are present in the serum, besides bioactive peptide hormones these are mainly fragments of larger proteins like albumin, fibrinogen or collagen, ranging from low fM / l to nM / l in concentration. The analysis of complex mixtures has to be performed by the combination of different chromatographic or electrophoretic separation techniques with highly sensitive detection methods, like electrospray mass spectrometry

Two dimensional techniques, like consecutive chromatographic separation by ion exchange chromatography and chromatography of subfractions by reversed-phase chromatography are suitable to resolve even very heterogenous mixtures. A third independent parameter is introduced to every component in the mixture by electrospray mass spectrometric detection. Therefore every single peptide in a complex mixture can be defined by three parameters, the charge, the hydrophobicity, and the molecular weight. This method will be denoted as 2D-LC/MS in the following

Firstly 2D-LC/MS analysis has been performed using the peptides from human hemofiltrate. Human hemofiltrate was obtained by blood filtration of patients with final stage renal disease. The hemofiltrate contains all peptides present in the blood, but no larger proteins, cells and cell fragments which are retained by the filter with a 20,000 D cut-off. For further analysis the hemofiltrate was desalted by batch extraction using alginic acid as a week cation exchanger and the peptides lyophilized. This crude extract served as the starting material for further analysis.

In the first separation step, the hemofiltrate is fractionated by strong cation exchange chromatography using volatile buffer systems Fractions were collected and lyophilized prior to reversed-phase chromatography The reversed-phase chromatography was connected on-line with the electrospray interface of the mass spectrometer. In the experiments shown here 1 x 250 mm C-18 columns (YMC, Japan) were used for the separation. The flow rate was 20 µl / min, the column outlet was directly connected through a variable UV-detector equipped with a capillary flow cell with the electrospray interface of the mass spectrometer (API III, SCIEX, Toronto, Canada) No postcolumn splitting was performed. The mass spectrometer was run in single MS mode.

About 40 fractions from cation exchange chromatography of human hemofiltrate peptides were analyzed by LC/MS. The raw data were analyzed manually. More than 1.000 peptides could be determined with respect to their charge, hydrophobicity and molecular weight. These peptides represent the abundant peptides in the hemofiltrate, equivalent to concentrations in the pM / l. The molecular weights of the peptides detected ranges from about 600 D to over 25,000 D, and even low amounts of serum albumin, due to large pores in the hemofiltrate membrane and restraint filtration were detected

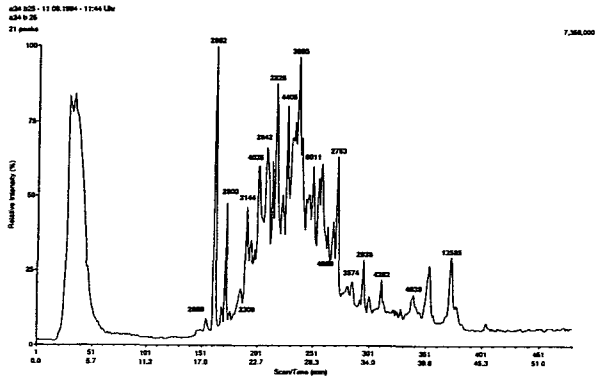

Figure Total ion chromatogram of one fraction from human hemofiltrate (see text) The molecular weights indicate those peptides which could be clearly identified.

The 2D-LC/MS analysis allows the detection of a single peptide in the complex mixture As shown with human hemofiltrate the total analysis of the peptide pattern becomes possible ussing this method In addition, peptides which could be obtained as pure fractions were identified by N-terminal sequencing or other methods.

Nevertheless, efforts have to be made to increase the sensitivity, reduce the time of analysis, and increase the separation in the second step With the 2D-LC/MS method, very heterogenous mixtures can be analyzed and data bases, equivalent to the 2D-gel electrophoresis databases can be created allowing the comparison of peptide patterns.

We wish to thank Ulrike Ballnus, Jutta Barras-Akhnoukh, and Ilka Uhrlandt for their excellent and experienced help in the analysis shown here

Matrix-Assisted Laser Desorption/Ionization Mass Spectrometry as a Tool in the Characterization of E. Coli RNA Polymerase

D. Fenyő [†], K. Severinov[‡†], E. Severinova[†], H. Tang[¥], A. Mustaev[‡], A. Goldfarb[‡], R.H. Ebright[¥], S. Darst[†], B. T. Chait[†].
[†]The Rockefeller University, New York, NY 10021
[‡]Public Health Research Institute, New York, NY 10016
[¥]Dept. of Chemistry and Waksman Institute, Rudgers University, New Brunswick, NJ

The core enzyme of Escherichia coli RNA Polymerase (RNAP) has the subunit composition of ($\alpha_2\beta\beta'$). The α subunit is a 329 amino acid long protein which consists of two domains each capable of independently folding and dimerizing: αCTD (C-terminal domain) and αNTD (N-terminal domain). The αNTD dimer plays an important role in initiating RNAP assembly by binding to the beta subunit. The αCTD dimer makes specific protein-DNA interactions with promoters containing an UP element (e.g., *rrnB P1*) and specific protein-protein interactions with activator proteins at promoters with activator sites (e.g., *lac{CAP}*). For specific binding to promoters and initiation of transcription the core enzyme has to bind to a σ factor. The σ factors, in addition to binding specifically to promoters, also responsible for melting of the DNA double helix. In this paper we present results exemplifying how mass spectrometry can be used in combination with molecular biological techniques to increase the understanding of the structure and function of RNAP.

Limited proteolysis using trypsin was performed on the σ^{70} factor and the β subunit to determine domain boundaries. The SDS-PAGE gel of tryptic fragments of σ^{70} using different trypsin concentrations is shown in Figure 1a. The fragment at 40 kDa was purified and its mass was measured with Matrix-Assisted Laser Desorption/Ionization Mass Spectrometry (MALDI MS). It consisted of two components with molecular masses of 39785 Da and 38651 Da (Figure 1b). The relative intensity of the peaks was very sensitive to trypsin concentration and digestion time. To determine the identity of the fragments, they were digested with CNBr in 0.1 N HCl for 30 minutes. The positive ion MALDI spectrum of the digest of a sample dominated by the larger fragment is shown in Figure 1c (the corresponding spectrum of a sample dominated by the smaller fragment is very similar). The peaks in the mass spectrum are labeled with the position number of the first and last residues of the corresponding peptide in the σ^{70} sequence Peaks corresponding to peptides between residues 278 to 448 were identified. Since residue 448 is an arginine, it is likely the C-terminal of the fragment to be identified. The only N-terminal agreeing with the molecular weight measurement of the larger and the smaller fragments are 104 and 114, respectively. That residue 104 is the N-terminal of the larger fragment was confirmed in another experiment where the sample was digested with endoproteinase Glu-C. We conclude that the 40 kDa fragment of σ^{70} is residues 104-448 or 114-448. Other tryptic fragments of σ^{70} [1] and of β were also identified using MALDI MS in combination with N-terminal sequencing. The polypeptide corresponding to residues 114-448 of σ^{70} was expressed and is being crystallized to determine its 3D structure.

To confirm and quantify in vivo experiments that show that the side chain of amino acid 261 of αCTD is essential for CAP-dependent transcription, in vitro transcription experiments with wild type RNAP ([Glu^{261}]α) and with RNAP reconstituted using [Gly^{261}]α and [Lys^{261}]α were performed [2]. In order to produce mutant RNAP substantially free from wild-type α, the mutant α genes were subcloned into T7 RNAP expression vector pET3a and the mutant α's were overproduced to the extent of ~30% of total cell protein. The mutant α's were purified and the mutant RNAP was reconsituted from purified mutant α and purified wild-type β, β', and σ^{70}. The contamination of wild-type RNAP was measured by MALDI MS. The wild-type and mutant α subunits were prepared from the reconstituted RNAP by denaturing centrifugal ultrafiltration and digested with endoproteinase Glu-C and the reaction products were analyzed with MALDI MS. Since residue 261 is a glutamic acid in wild-type α but not in the mutants endoproteinase, Glu-C can digest wild-type α but not the mutants at residue 261. Figure 2 shows a part of the mass spectra of wild-type α and of [Gly^{261}]α. Peaks labeled A and B correspond to residues 289-319 and 287-319, respectively and the peak labeled C correspond to residues 230-261. The intensity ratio of peaks A and B does not change significantly between the mass spectra of wild-type α and of [Gly^{261}]α while the relative intensity of peak C is dramatically different. This is expected since the mutant α cannot be digested by endoproteinase Glu-C at residue 261. Therefore the ratio of the relative intensities of peak C and B is taken as a measure of

the content of wild type α in RNAP. In Figure 2C the measured content of wild-type α is shown together with the CAP-dependent transcription initiation activity at the lac promoter for wild type and mutant RNAP. The activity of the mutant RNAP can be explained with the contamination of wild-type RNAP. From this result we conclude that amino acid 261 is essential for CAP-dependent transcription.

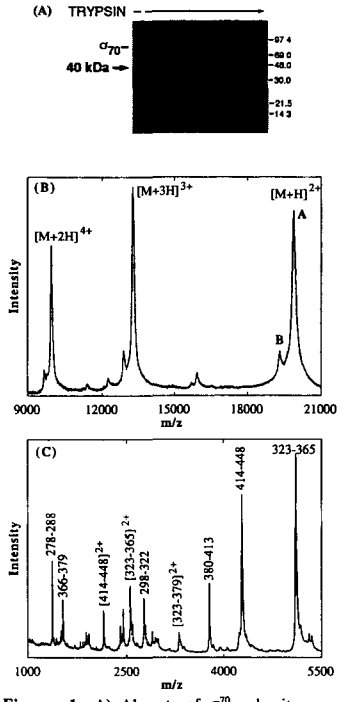

Figure 1. A) Aliquots of σ^{70} subunit were treated with increasing amounts of trypsin and the reaction products were separated on a 10% Tris-Tricine SDS-polyacrylamide gel. B) MALDI spectrum of the purified 40 kDa fragment. C) MALDI spectrum of the purified 40 kDa fragment digested with CNBr.

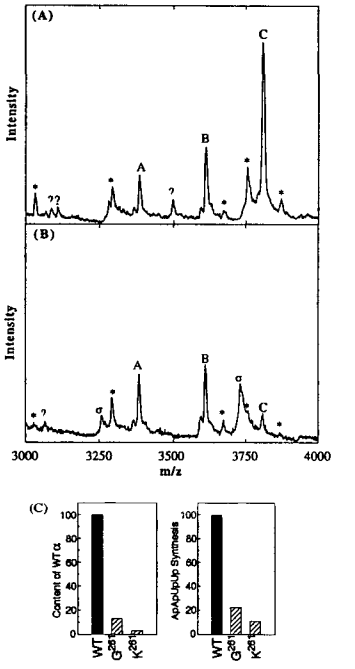

Figure 2. Endoproteinase Glu-C digest of the α subunit purified from reconstituted RNAP. A) Wild type α subunit. B) α subunit with glutamic acid at residue 261 replaced with glycine. Peaks A, B, and C correspond to residues 289-319, 287-319, and 230-261, respectively. Other fragments of the α subunit are marked with * and fragments due to contamination of σ^{70} are marked with σ C) Purity and in vitro CAP-dependent transcription activity at lac promotor for wild-type RNAP, [Gly^{261}]α-RNAP, and [Lys^{261}]α-RNAP.

1. K. Severinov, D Fenyő, E. Severinova, A. Mustaev, B T Chait, A. Goldfarb & S Darst, Journal of Biological Chemistry, 269 (1994) 20826-8.
2. H. Tang, K. Severinov, A. Goldfarb, D. Fenyő, B T Chait & R. Ebright, Genes Dev., 8 (1994) 3058

Peptide Mapping and MS/MS Analysis of IgG2b Containing ^{2}H-Labeled Leucine

Kazuo Hirayama, Satoko Akashi, Kazuyoshi Noguchi, Reiko Yuji, Uno Tagami, Koichi Kato§, Yoshiki Yamaguchi§, Jun-ichi Enokizono§, Ichio Shimada§ and Yoji Arata§, †

Cent. Res. Labs., Ajinomoto Co., Inc., 1-1 Suzuki-cho, Kawasaki-ku, Kawasaki 210, JAPAN
§Faculty of Pharmaceutical Sci., University of Tokyo, Hongo, Bunkyo-ku, Tokyo 113, JAPAN
†Water Research Institute, 2-1-6 Sengen, Tsukuba-shi, Ibaraki 305, JAPAN

Introduction

Peptide mapping using mass spectrometry, especially MALDI-TOFMS and LC/ESIMS, are now widely used for the structural characterization of proteins. Mass spectrometric peptide mapping can be carried out well when the molecular weight of a protein is not so large. In the case of a large protein, such as IgG, however, molecular weight of a peptide generated by the cleavage is sometimes attributed to more than two positions of the amino acid sequence only by its molecular weight and the specificity of the cleavages. One more serious problem is that the differentiation of leucine and isoleucine residues is impossible only by the molecular mass information. Leucines and isoleucines cannot be differentiated by low-energy MS/MS, too. From this point of view, new methodology utilizing ^{2}H-labeled leucine (Leu(D10)) was developed and applied for the peptide mapping of mouse monoclonal IgG2b.

Methods

^{2}H-Labeled leucine was purchased from Euriso-top. Labeled and unlabeled mouse monoclonal anti-dansyl antibody IgG2b were obtained by the cultivation of a culture fluid containing a Leu or a Leu(D10). Labeled and unlabeled mouse IgG2b was reduced and carboxymethylated, and then digested with lysyl-endopeptidase. RCM-IgG2b(mix), an equivalent mixture of the labeled and the unlabeled RCM-IgG2b was prepared in the same manner. FABMS (JEOL HX110/HX110) was applied for the confirmation of the number of the ^{2}H-labeled atoms. Peptide mapping by MALDI-TOFMS was carried out by Shimadzu-Kratos Kompact. Peptide mapping by capillary LC/ESIMS was achieved by Finnigan-MAT TSQ700. MS/MS experiments were carried out by JEOL HX110/HX110 (high-energy CID) and Finnigan-MAT TSQ700 (low-energy CID).

Results

It was recognized that the mass difference between the labeled and the unlabeled leucine residue in the protein was 9 mass units, not 10 mass units, by FABMS analysis, while the mass difference between a Leu and Leu(D10) was 10 mass units. One mass unit decrease of the molecular mass of a leucine residue must be derived from a deuterium-hydrogen exchange caused by the racemization by racemase during the cultivation. Figure 1 shows MALDI-TOF mass spectrum of the lysyl-endopeptidase digested peptides of RCM-IgG2b(mix). Considerably many splitted twin peaks could be observed. For example, twin peaks were observed at *m/z* 2333.5 and *m/z* 2360.4. Mass value of *m/z* 2333.5 could be attributed to the protonated molecular mass of two peptides, TDSFSCNVRHEGLKNYYLK (H420-438) and GLVRAPQVYILPPPAEQLSRK (H341-361), by the specificity of the enzyme. It was impossible to assign the mass value to the peptide certainly only by molecular mass information. On the other hand, the mass difference of the observed twin peaks indicated the number of the leucine residues in the peptide. In the case of the above mentioned peptide, the mass difference of the twin peaks were 26.9, which suggested that this peptide contained three

leucine residues in the sequence. The peptide H420-438 contained three leucine residues while the peptide H341-361 contained two leucine residues. Accordingly, it could easily be determined that the peak at *m/z* 2333.5 was a protonated molecular ion of the peptide H420-438, not H341-361. Similarly, certain assignment of all the observed mass values in MALDI-TOFMS peptide mapping could be carried out by referring the number of leucine residues. The differentiation of leucine and isoleucine residues could be achieved by MS/MS. Tandem mass spectrum with high energy collision, of course, could differentiate a leucine and an isoleucine residue in a peptide. When a leucine residue was labeled by deuterium, clearer differentiation could be carried out by MS/MS with high energy collision, and in addition, these two amino acid residues could be distinguished by MS/MS with low energy collision. Figure 2 shows ESI-MS/MS spectra of the isolated peptides DVLNISLTPK (H249-258) and DVL*NISL* TPK (H249-258) with low energy collision. The y series ions were clearly observed and the sequence could easily be identified.

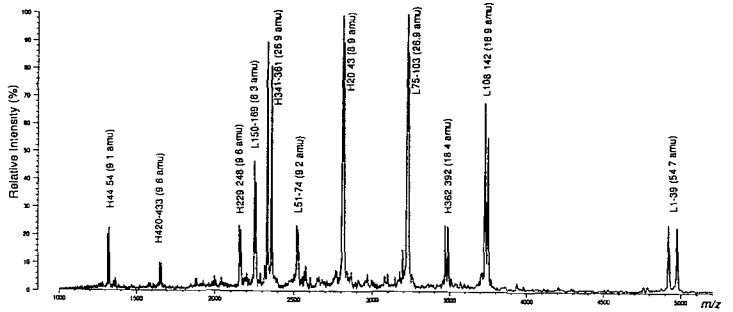

Fig. 1 MALDI-TOF mass spectrum of the lysyl-endo-peptidase digest of RCM-IgG2b(mix).

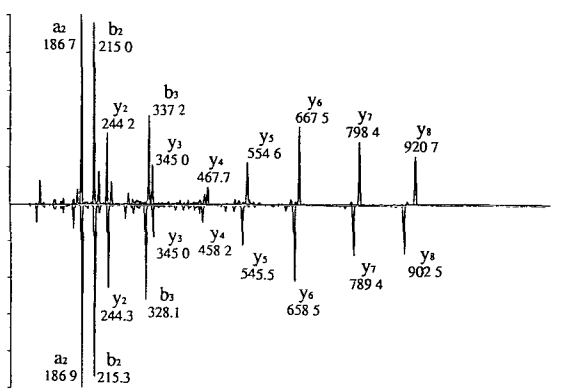

The mass difference between y_5 and y_6 ions in the both spectra is 113 amu. This indicates the exsistence of a Ile residue at the 5th position from the N-terminus.
The mass difference between y_3 and y_4, and y_7 and y_8 ions in the upper spectrum is 122 amu while those in the lower spectrum is 113 amu. This indicates the existence of a Leu residue at the 3rd and 7th positions from the N-terminus.

Fig.2 ESIMS/MS spectra of the labeled (upper) and the unlabeled (lower) peptides DVLNISLTPK.

Structural Characterization of IgG Carrying Allotype-j

Satoko Akashi, Kazuyoshi Noguchi, Reiko Yuji, Uno Tagami, Koichi Kato, §
Kazuhiro Tokioka, § Ichio Shimada, § Yoji Arata§, † and Kazuo Hirayama

Cent. Res. Labs., Ajinomoto Co., Inc., 1-1 Suzuki-cho, Kawasaki-ku, Kawasaki 210, JAPAN
§Faculty of Pharmaceutical Sci., University of Tokyo, Hongo, Bunkyo-ku, Tokyo 113, JAPAN
†Water Research Institute, 2-1-6 Sengen, Tsukuba-shi, Ibaraki 305, JAPAN

Introduction

A family of switch variant, which produce mouse anti-dansyl monoclonal antibodies with the identical V_H, V_L and C_L in conjunction with different heavy chain constant regions, have been generated by Dangl et al.. This family of switch variant antibodies contains IgG1, IgG2a, IgG2b and IgG2a(s). This paper reports the structural characterization of switch variant IgGs produced by haplotype-j mice. Among these four IgGs, only IgG2a is classified into allotype-j and the other IgGs are classified into allotype-a by the serological properties. It has been believed that there must be some structural difference which suggests the existence of allotypic markers.

Methods

The cells which produced mouse switch variant IgGs were from C3H/SW mice (haplotype-j). Switch variant IgGs were reduced and carboxymethylated prior to the peptide mapping. Peptide mappings were carried out by MALDI-TOFMS (Shimadzu-Kratos KOMPACT) and capillary-LC/ESIMS (Finnigan-MAT TSQ700) after the digestion with lysyl-endopeptidase or *S. aureus* V8 protease. When a peptide with an unexpected molecular weight calculated from the reference sequence was found, it was isolated by HPLC and subjected to the amino acid sequencer and FABMS analysis (JEOL HX110). After the determination and confirmation of the sequences of switch variant IgGs, investigation on the allotypic markers was carried out by computer graphics.

Results

Figure 1 shows MALDI-TOF mass spectra of lysyl-endopeptidase digest of RCM-IgG1. A peak at *m/z* 6559.7 could not be attributed to any peptide, by referring the sequence of IgG1 of the other allotype. It was impossible to detect all of the protonated molecular ions of the peptides by MALDI-TOFMS. The peptide with molecular weight of 6558.7 was isolated and sequenced after the capillary-LC/ESIMS analysis. It was clarified that Pro193H and Arg194H were substituted by Thr and Trp, respectively. In like manner, all of the sequences of other switch variant antibodies produced by haplotype-j mice could be confirmed, by referring the sequences of IgG grouped in other allotypes. It was recognized that the C-terminal Lys residue of the heavy chain was sometimes missing in the sequences of switch variant IgGs. Several amino acid residues in the CH1 domain of IgG1 and IgG2a were found not identical to the reference sequences. No other modification except for the above mentioned could be recognized.

In IgG1, Thr and Trp were found instead of Pro193H and Arg194H, respectively, and Ser was found instead of Thr136H in IgG2a. Considering the fact that only IgG2a is classified into allotype-a, Ser136H was supposed to be related to the allotypic marker. The environment of Ser136H was investigated by computer graphics (Fig. 2), using the atomic coordinates of the human immunoglobulin molecule obtained from the Protein Data Bank (code:2IG2).

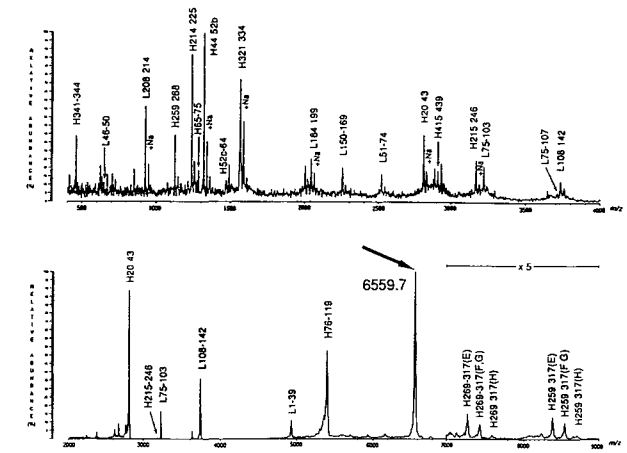

Fig. 1 MALDI-TOF mass spectra of the lysyl-endopeptidase digest of RCM-IgG1.
(a) reflector mode (matrix:DHBA) (b) linear mode (matrix:sinnapinic acid+HABA)

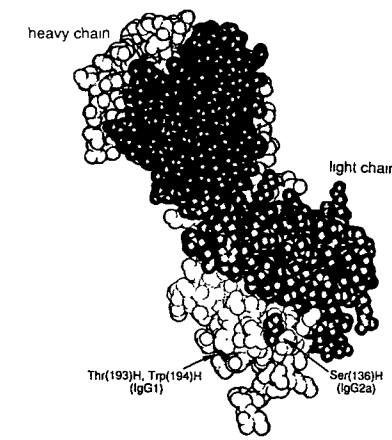

Fig.2 A space-filling model of the Fab region of IgG1 (PDB code:2IG2).

Monitoring Antibody Catalysis

Gary Siuzdak, Joseph F. Krebs, Christian Strupp, Don Hilvert, Jon D. Stewart
Rodrigo Chavez, Brian Bothner, Stephen J. Benkovic, and H. Jane Dyson,

Departments of Chemistry and Molecular Biology
The Scripps Research Institute & Pennsylvania State University

Antibodies are components of the basic defense mechanism in our immune system, their formation being an immunological response to the presence of foreign substances (antigens). In general, the interaction of an antibody with an antigen results in the noncovalent formation of an antigen/antibody complex. An antibody elicited by a specific antigen (hapten) exhibits shape and charge complementasity to that hapten. This was exploited by chemists to design catalytic antibodies capable of catalyzing specific chemical transformations. Catalytic antibodies are produced by introducing haptens that structurally resemble a reactions transition state species into mice. Antibodies produced by accordingly immunized mice may, in effect, catalyze the reaction by binding and stabilizing the true metastable transition state.

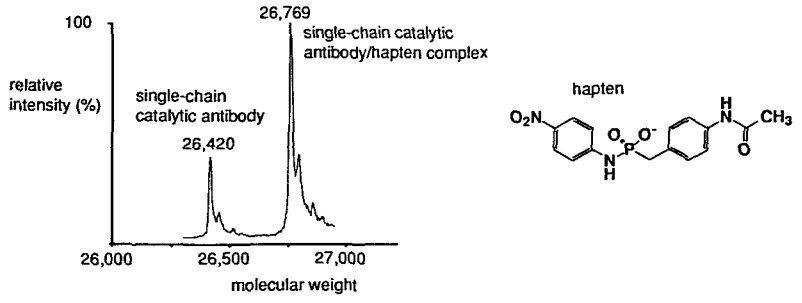

Figure 1. ESI of catalytic antibody and noncovalently bound hapten.

In the first study, a single-chain catalytic antibody was used with a molecular weight of 26,419.9 Da. Although ESI (API III PE SCIEX) cannot be used for the intact catalytic antibody due to its high molecular mass (~ 150 kDa), it is ideally suited for examining smaller fragments such as the single-chain Fv fragment. Antibodies generally exhibit high affinities (<1 nM) for the haptens they were elicited by and are excellent candidates for the study of noncovalent gas phase interactions. The antibody-hapten complex observed with ESI is shown in Fig. 1.

43rd ASMS Conference on Mass Spectrometry and Allied Topics

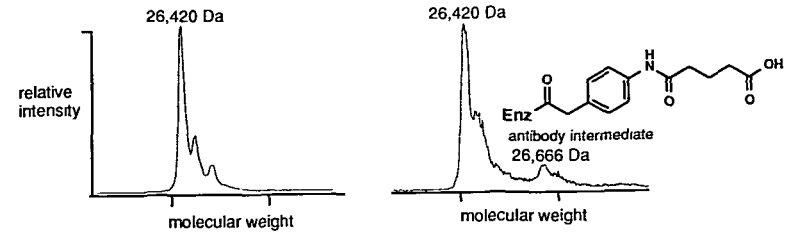

Figure 2. ESI of catalytic antibody and acyl intermediate.

The same catalytic antibody was used to study the hydrolysis of an anilide for which this antibody was designed (Fig. 2). The antibody was first analyzed alone, and then in the presence of substrate. Upon addition of substrate, a peak consistent with an adduct mass of 26,666 Da was observed. The observed mass increase of 247 Da is identical (within error) to the mass of the acyl functionality of the substrate. These spectra were acquired with declustering potentials of 175 - 250 V, under conditions where even high affinity (≤ 1 nM) noncovalent complexes are separated. Additional experiments with an antibody mutant, devoid of catalytic activity, showed no accumulation of the intermediate. These experiments provided the first direct evidence for the acyl-antibody intermediate previously proposed for this antibody.

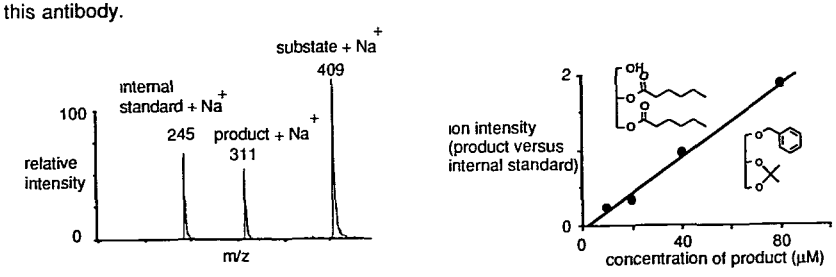

Figure 3. Reaction catalyzed by lipase quantitatively monitored by electrospray ionization.

Electrospray was also used to investigate the reaction kinetics of lipid hydrolysis, Fig. 3. Selected ion monitoring was used to perform the calibration and kinetic studies. The electrospray measurement of the rate of triacylglycerol hydrolysis by the lipase was consistent with rates determined through colormetric and derivatization techniques.

References: G. Siuzdak, J.F. Krebs, S.J. Benkovic, and H.J. Dyson, *JACS*, **1994**, 116, 7937.
J.F. Krebs, G. Siuzdak, H J. Dyson, J.D.Stewart, and S.J Benkovic, *Biochemistry*, **1995**, *34*, 720.

Investigation of Mouse Urinary Proteins Using ESI and MALDI

[1]K.A. Cox, [2]D.H.L. Robertson, [2]R.J. Beynon, [3]R.P. Evershed and [1]S.J. Gaskell

[1] The Michael Barber Centre for Mass Spectrometry; UMIST; Manchester, U.K.
[2] Department of Biochemistry and Applied Molecular Biology; UMIST; Manchester, U.K.
[3] School of Chemistry; University of Bristol; Bristol, U.K.

One of the most important forms of communication in mice is through the use of olfactory signals originating from the mouse urine. Mouse urine has been shown to mediate many behavioral responses such as inter-male aggression and mate selection. Although the actual scents are caused by small hydrophobic ligands (pheromones),[1] the regulation of the pheromones is controlled by a series of proteins known as major urinary proteins (MUPs). These acidic proteins, in the molecular weight range of 18.6 to 18.9 kDa, are the products of a multi-gene family, and variation exists in the types and amounts of proteins found in different mouse strains.[2] This results in mixtures of closely related proteins in the urine. Electrospray ionization mass spectrometry (ESI-MS) is highly amenable to the analysis of these mixtures.[3] Direct analysis of MUPs from the urine is possible with only minimal sample preparation and MaxEnt processing allows resolution of two proteins separated by only 15 Da at mass 18,700 Da. Although the mechanisms involved in ligand binding are not yet fully understood, small differences in the primary structures of individual MUPs may influence binding specificity. Selected proteolytic digests have been used to probe the primary structure of two MUPs. MALDI-Reflectron TOF is highly suited for the analysis of these peptide mixtures, resulting in detection of all major fragments and allowing the identification of a novel MUP.

Proteolysis Study

MUP mixtures from the species BALB/C and BALB/K consist of primarily three proteins (MW 18,647, 18,710 and 18695 Da). Initial studies involving the proteins from BALB/C mice indicated that the proteins degraded when incubated over time (37°C, 1 mM MES buffer). Although an FTIC-Casein proteolytic assay confirmed that proteolysis was occurring in the protein mixtures, gel electrophoresis was insufficient to characterize the nature or extent of proteolysis. However, analysis of these samples by ESI-MS and processing by MaxEnt showed the progression of proteolysis, revealing clear formation of lower mass products after 7 days corresponding in mass to the loss of the first 4 N-terminal amino acids in each sequence.

Initially proteolysis was believed to occur due to the endogenous protease, meprin, in the urine. Incubation of the mutant MUP strain BALB/K (no meprin) should have shown no cleavage. However, variable amounts of cleavage were observed throughout the incubation time. Further duplicate incubations showed variable amounts of cleavage. When the incubation study was repeated using sterile conditions, no cleavage was observed, indicating that the source of the proteolytic activity was not endogeneous to the protein mixture.

Identification of Allelic Variation

An anion exchange profile of the MUPs found in the C57BL/6 mouse strain showed four prominent peaks. The masses of these species (determined by ESI-MS) indicated that the two later eluting peaks (III and IV) had the same mass, suggesting an isobaric amino acid substitution, which changed the overall charge properties of these species, but not the mass. The Swissprot database contained one relevant cDNA sequence corresponding to the mass observed. An isobaric substitution of lysine to glutamine would sufficiently change the overall charge properties of these species to allow their chromatographic resolution. This substitution was investigated by the use of a selective proteolytic agent, endoproteinase Lys-C, which cleaves at the C-terminal side of the lysine residues in the proteins.

The digestion mixtures were analyzed by reflectron-MALDI-TOF with only minimal sample preparation. The resulting spectra (below) showed Lys-C fragments encompassing 96% of the protein structure. MUP III (Figure 1) contained a Lys residue at position 140 and gave a cleavage product at m/z 1123 corresponding to residues 132-140. A smaller peak is also observed at m/z 2535 corresponding to residues 141-162. In contrast, digestion of MUP IV (Figure 2) resulted in a prominent peak at m/z 3642 corresponding to residues 132-162, confirming a $Lys_{140} \rightarrow Glu_{140}$ substitution, and therefore identifying a new MUP species.

References

1) Robertson, D.H.L.; Beynon, R.P.; Evershed, R.P. *J Chem. Ecol.*, **1993**, *19*, 1405-1416.
2) Finlayson, J.S.; Potter, M.; Runner, C.R. *J Natl. Cancer Inst.*, **1963**, *31*, 91-107.
3) Evershed, R.P.; Robertson, D.H.L.; Beynon, R.J.; Green, B.N. *Rapid Commun Mass Spectrom.*, **1993**, *7*, 882-886.

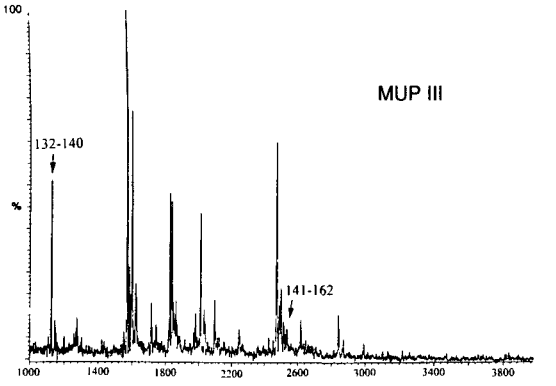

Figure 1

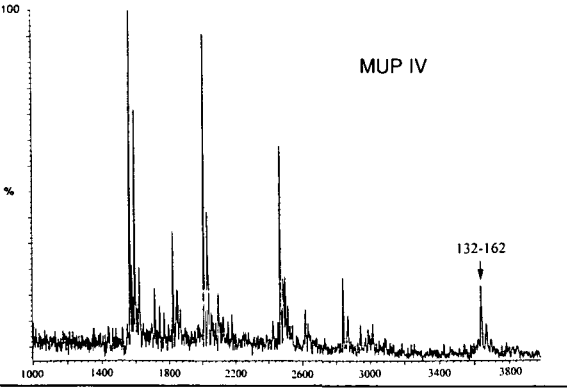

Figure 2

The Analysis of a Therapeutic Monoclonal Antibody by HPLC, MALDI-TOF/MS and ESI/MS

Stephen Chan* @, SungAe Park# and David J. Burinsky @

Department of Analytical Research & Development @ and Biopharmaceutical Development#
R.W. Johnson Pharmaceutical Research Institute
Route 202, P.O. Box 300, Raritan, New Jersey 08869

The analysis of monoclonal antibody molecules, with a typical molecular weight at around 150,000 amu, generally requires many months of labor-intensive laboratory work involving multiple steps of tedious sample separation, sample collection and Edman degradation sequencing. For the purpose of screening specific sites of modification due to product aging and other causes, sequencing the entire antibody molecule may not be necessary. In this work, we have explored an analytical strategy based largely on enzymatic digestion, HPLC and mass spectrometry to quickly extract the critical information about the amino acid sequence of these molecules.

We have analyzed therapeutic monoclonal antibody samples using a combination of HPLC and mass spectrometry (MS) involving both matrix-assisted laser desorption (MALDI) and electrospray ionization (ESI). The ESI/MS experiments were performed on a Finnigan-MAT TSQ-70/0 triple stage quadrupole mass spectrometer. All the MALDI experiments were done on a Finnigan-MAT LaserMAT linear time-of-flight mass spectrometer using sinapinic acid as the ionization matrix. The MALDI laser power was optimized for maximum signal to noise ratio. For HPLC/ESI/MS, the solvent flow rate of 1.00 ml/min was split 1:1 for both UV and mass spectrometric traces.

The antibody samples were first checked by MALDI for sample integrity. Each sample was then reduced and alkylated with 4.5 mM dithiothreitol and 10 mM iodoacetamide, respectively. These samples were found to produce intense ions at m/z 51,000 and 23,000 which correspond to the reduced and alkylated heavy and light chain molecules, respectively (Figure 1). The method of using disodium 2-nitro-5-thiosulfobenzoate (NTSB) as a sulfitolysis reagent was also attempted to reduce the heavy and light chain molecules. When separating the heavy and light chain molecules by size exclusion chromatography (SEC), molecules undergone reactions with the sulfitolysis reagent appears to have a much better resolution for the heavy and light chain molecules than other reagents (Figure 2). For amino acid sequence analysis, the reduced and alkylated antibody molecules were subjected to either tryptic or lys-C digestion. In our case, the tryptic peptide map provided fragments which are more compatible with the mass spectrometric characterization.

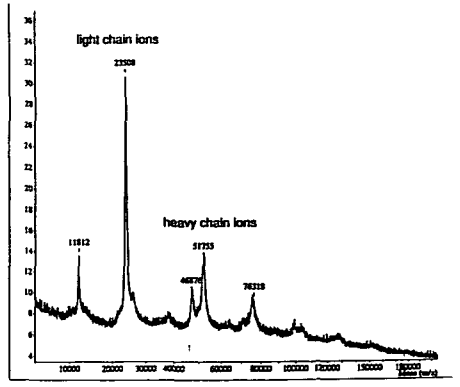

Figure 1 MALDI mass spectrum of the reduced and alkylated heavy and light chain molecules

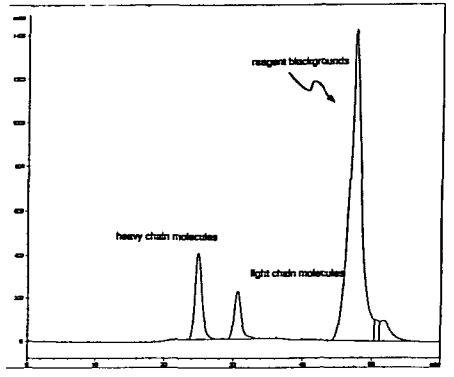

Figure 2 Size exclusion chromatography for antibody molecules undergone reactions with the sulfitolysis reagent. The heavy and light chain molecules are clearly baseline separated.

Identifying Human Tear Cytokines By Immunoaffinity Chromatography/MALDI-TOF

Adam H. Brockman*, Susan Hirsh**, Renee Kaswan**, Ron Orlando*
*Complex Carbohydrate Research Center, and the Department of Biochemistry and Molecular Biology
**College of Veterinary Medicine
The University of Georgia
220 Riverbend Road, Athens GA 30602, USA

Introduction:

Indirect evidence has linked the presence or absence of certain cytokines in tears to a number of pathological events that occur in the anterior segment of the eye. Despite the apparent clinical importance of identifying these proteins, techniques for their direct detection in tears have not been developed. Multiple problems are encountered in the detection of these proteins in tears. For example, a large number of proteinaceous components (>100) are known to be present in tears. Furthermore, the quantity of these cytokines is extremely limited. Current thinking places the concentration of these cytokines at roughly the attomole to femtomole per microliter level. However, only a few microliters, (2-5) of tears can be obtained from each collection, and the total quantity of each cytokine that can be obtained from an individual tear sample is limited to at most ~500 femtomoles. Although we have not yet achieved the sensitivity necessary to detect cytokines reproducibly and with acceptable intensity, we have developed a new technique that provides affinity separations directly on the surface of the matrix assisted laser desorption/ionization mass spectrometer (MALDI-MS) probe. This strategy which we call "probe affinity MS" (PAMS) provides both *in situ* identification of biomolecules through biospecific antibody/antigen interactions and molecular weight information in a rapid and facile manner.

Methods:

Separation:

Capture agents specific for molecules of interest are immobilized on a gold surface by covalent attachment through reductive amination with a self assembled monolayer of dithiobis succinymidylpropionate (DSP), (see Figure 1).

MALDI Detection:

The mass spectrum shown here (Figure 2) was acquired on a Hewlett Packard LDI 1700XP MALDI TOF mass spectrometer, using α-cyano-dimethoxy-4-hydroxy cinnamic acid. Each dried sample on our eight mesa gold plated probe tip was reconstituted using 80% acetonitrile, 19% ultra pure water, (Continental), and 1% TFA. The instrument was operated at an accelerating voltage of 30 kV and an extractor voltage of 9 kV. The goat anti-biotin and the DSP was purchased from Sigma, and the human anti lysozyme was purchased from BTI.

Results and Discussion:

A conventional MALDI spectrum of a mixture of biotinylated insulin and myoglobin is shown in Figure 2A. The MALDI spectrum obtained following PAMS analysis is shown in figure 2B, with ion peaks corresponding to singly, doubly, and triply biotinylated insulin. Comparison between the PAMS spectrum and the normal MALDI spectrum of the protein mixture serve to illustrate the success of the PAMS experiment in separating an analyte of interest. Figure 2C illustrates the minimal amount of non-specific binding seen of analyte on the gold surface.

Figure 1

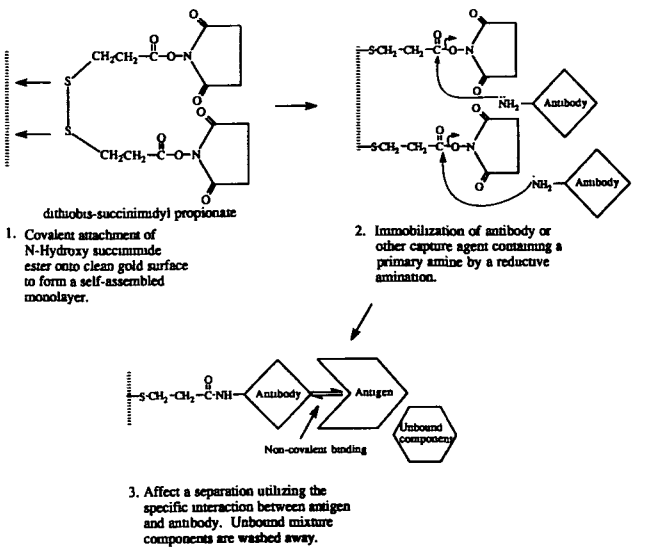

Figure 2

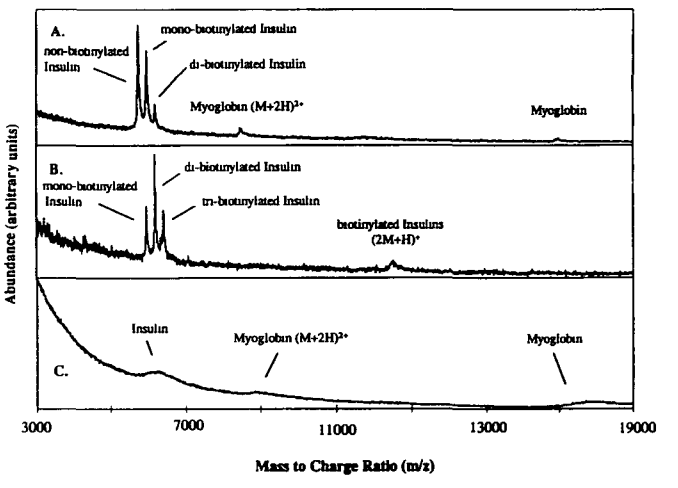

Characterization of Recombinant Human Interferon α-2 by Electrospray LC/MS

Larry Heimark, Eric Huang, Birendra Pramanik
Schering-Plough Research Institute, 2015 Galloping Hill Road, Kenilworth, NJ 07033

The recombinant protein, human interferon α-2 (Hu-IFN), marketed under the trade name Intron A, is an important cytokine with broad spectrum antiviral, antiproliferative and immunomodulatory properties. As a result, Intron A has been approved for the treatment of hairy cell leukemia, selected cases of condylomata acuminata, AIDS-related Karposi's Sarcoma, chronic hepatitis B and chronic hepatitis non-A , non-B/C. In this work, Hu-IFN is characterized by ESI of the intact protein and ESI LC/MS of the trypsin digest using 1.0 mm and 0.5 mm I.D. columns, and a 0.32 mm I.D. packed capillary column.

Hu-IFN is a 165 amino acid protein with 2 disulfide bonds and no other post-translational modification. The theoretical average molecular weight for the reduced protein is 19,266 Da. An observed MW of 19, 265.4 Da was recorded by ESI analysis (Figure 1). Figures 2-4 present the base peak chromatograms of the Hu-IFN trypsin digest separated on 1.0 mm, 0.5 mm and 0.32 mm ID columns, respectively. The chromatographic peaks representing the various tryptic peptides are labeled in each chromatogram. The molecular weight and amino acid sequence of all expected tryptic fragments are shown in Table 1. The scan range was m/z 500-2400, therefore, all digest fragments below 500 Da representing one or two amino acids were not detected.

An examination of the chromatograms for the 1.0 mm, 0.5 mm and 0.32 mm columns reveals that most of the expected tryptic peptide fragments, except T-10, are detectable regardless of column dimension. Fragment T-10 was not eluted under the gradient conditions used for this study. The chromatograms differ primarily in peak resolution. All chromatograms were run using the same gradient program with no attempt to optimize elution conditions for each column. These results demonstrate that, even without extensive optimization of elution conditions, similar information can be obtained using both conventional microbore and packed capillary columns. The major difficulty encountered with smaller diameter columns is in column setup, plumbing and maintenance of a stable flow rate and reliable gradient mixing. The 1.0 mm ID column required no special setup. The flow rate and gradient stability were provided by using a pump with small piston volume (250 µl) and a small volume (10 µl) mixer. The 0.5 mm and 0.32 mm columns required pre-column flow splitting after the gradient mixer then post-column flow measurement and adjustment of the pump flow rate to achieve the optimal flow rate for the two columns. Despite the additional setup time required with the smaller columns, the enhanced sensitivity provided by the lower flow rates used with smaller diameter columns can be especially advantageous when sample amount is limited.

Figure 1.

Deconvoluted Mass Spectrum of Hu IFN-α

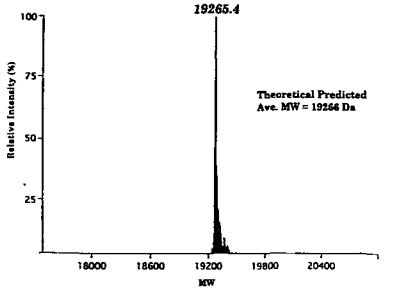

Figure 2

ESI LC/MS of IFN-α Tryptic Digest (1-mm i.d. column)

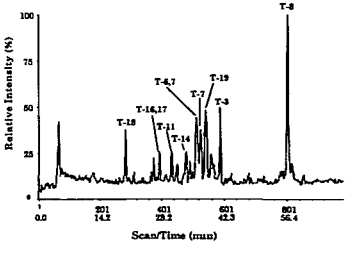

Figure 3.

ESI LC/MS of IFN-α Tryptic Digest (0.5-mm i.d. column)

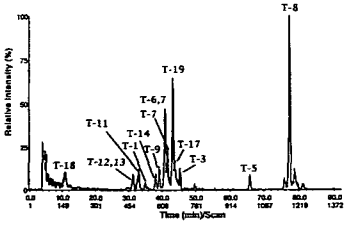

Figure 4.

ESI LC/MS of IFN-α Tryptic Digest (0.32-mm i.d. column)

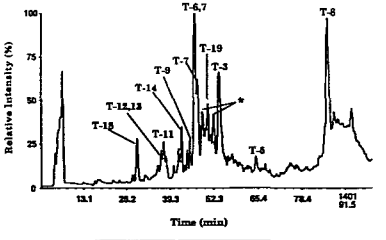

Table 1.

Peptide Fragments from Tryptic Digestion of Hu-IFN-α2

	Position	MW	Sequence
T-12	121--121	146 106	K
T-16	134--134	146.106	K
T-21	165--165	147.053	E
T- 2	13--13	174 112	R
T- 4	23--23	174 112	R
T-20	163--164	233 138	SK
T-1	132--133	275 148	EK
T- 6	32--33	289 139	DR
T-13	122--125	612.302	YFQR
T-18	145--149	618.316	AEIMR
T-14	126--131	749 469	ITLYLK
T-11	113--120	901 487	EDSILAVR
T- 5	24--31	909 499	ISLFSCLK
T- 3	14--22	1075.588	TLMLLAQMR
T-17	135--144	1208.565	YSPCAWEVVR
T- 1	1--12	1312.619	CDLPQTHSLGSR
T- 9	71--83	1450.522	DSSAAWDETLLDK
T-19	150--162	1481 626	SFSLSTNLQESLR
T- 7	34--49	1955 074	HDFGFPQEEFGNQFQK
T- 8	50--70	2459.893	AETIPVLHEMIQQIFNLFSTK
T-10	84--112	3303 803	FYTELYQQLNDLEACVIQGVGVTETPLMK

Mass Spectrometric Characterization of the rhM-CSF Receptor Binding Site

M. Kalkum[1], R. Yamamoto[2], J Schreurs[2], M.L. Deinzer[3] and M O Glocker[1]

[1]Faculty of Chemistry, P.O. Box 5560M732, University of Konstanz, 78434 Konstanz, Germany. [2]Chiron Corp 4560 Horton Street, Emeryville, CA 94608, USA. [3]Department of Agricultural Chemistry, Oregon State University, Corvallis, OR 97331, USA.

Macrophage Colony Stimulating Factor (M-CSF) is a cytokine of pharmaceutical interest because of its ability to stimulate innate host defenses in immunocompromised patients It is a hematopoietic growth factor that stimulates the survival, proliferation, differentiation, and function of mononuclear phagocytes. Three human cDNA clones, each encoding a M-CSF polypeptide of different length, have been isolated and expressed as active protein. The recombinant human M-CSF (rhM-CSF) studied here was cloned and expressed from *E. coli* as a truncated form (aa4-221) of the longest cDNA clone (M-CSF ß) [1]. rhM-CSF forms a disulfide linked homodimer with a molecular weight of 49029 Da The inter- and intramolecular disulfide bonds were assigned using mass spectrometric methods [2]. M-CSF dimers contain the cytokine-specific four-helix bundle in each monomer at their N-terminal regions [3] In order to investigate substructures of the receptor interacting four-helix bundles, histidine residues, which occur in the A-helix of the molecule and not in one of the other three helices (B - D), were selected as targets for chemical modification

In this study we report the use of diethyl pyrocarbonate (ethoxyformic anhydride, diethyl dicarbonate, DEP) for selective modification of histidine residues, combined with mass spectrometric peptide mapping analyses, as a tool for the characterization of the receptor recognition region of rhM-CSF. DEP is a commonly used reagent for the specific modification of histidine residues in proteins [4] The product of the modification is considered to be an N-carbethoxy-histidine derivative (CEt-His) Mass spectrometric analyses have shown that with excess DEP the reaction of imidazole or histidine residues in peptides proceeds through Bamberger cleavage to N,N'-dicarbethoxy-N-formyl-1,2-diaminoethenes (FCEt) which then slowly decompose to urethane-derivatives, N,N'-dicarbethoxy-1,2-diamino-ethenes, (UCEt) DEP reacts with protein histidine-residues in a narrow pH range Below pH 5 5 the imidazolyl-nitrogens will be protonated and reaction is very slow, and above pH 7 5 hydrolysis of both, DEP and the CEt-His derivative will play a major role Our investigations have shown, that modification of histidine residues in proteins with DEP best be carried out in ammonium acetate buffer at pH 6.5 in which the selectivity of the reaction, the stability of the product, and the hydrolysis-side reactions, all

43rd ASMS Conference on Mass Spectrometry and Allied Topics

are optimized to yield in a 1 . 1.16 stoichiometry of the CEt-His derivative, with respect to the starting amount of imidazolyl groups.

Using the above mentioned conditions, the chemical reactivities of the histidine residues of rhM-CSFß (5 His / monomer; His9, His15, His98, His176, His210) were monitored. Increasing conversion of histidine-residues was observed with increasing excess of DEP by MALDI-MS molecular weight determination. After tryptic digest of the modified protein derivatives MALDI-MS peptide-mapping analyses showed that histidines were converted to CEt-His and UCEt-His, respectively The degree of the chemical modifications at His9/15 are correlated to the biological activity of the protein derivatives. A substantial decrease (>60%) of the biological activity and receptor binding of rhM-CSF was found in *in-vitro* bioassays. Although histidines 176 and 210 were modified to a comparable extent than the histidines 9 and 15, only the latter two are located in the A-helix of the 4-helix bundle and, thus, the histidine residues from the C-terminal areas are not important for biological activity. Site specific mutagenesis experiments in wich His8 and His15 were replaced by alanine residues exhibited a decrease in specific bioactivity [5]. Also, His98 seems not necessary for biological activity, as was deduced by comparison of human and mouse M-CSF, where His98 is replaced by Gln [6].

Two types of histidine residues were differentiated by chemical modification reactions. His176 and His210 were found to react to UCEt-derivatives to a greater extent than His9 and His 15 For the formation of UCEt both nitrogen atoms of the imidazolyl-group must be accessible to the reagent In rhM-CSF the surface accessibilities (SA) of the imidazolyl-nitrogen atoms of His9, His15, and His98 are very asymmetric, indicating, that only one of the two nitrogens is accessible The predominant mono-derivatization to CEt-His of these residues is in agreement with the calculated values from the X-ray structure [3] SA values from nitrogen atoms of His176 and His210 are not available, however, our results suggest that both nitrogen atoms should be accessible to the surface.

1) R. Halenbeck, E. Kawasaki, J Wnn and K. Koths (1989) Bio/ Technology 7, 710-715.
2) M O. Glocker, B. Arbogast, J Schreurs and M L. Deinzer (1993) Biochemistry 32, 482-488.
3) J Pandit, A Bohm, J. Jancarik, R. Halenbeck, K. Koths and S -H. Kim (1992) Science 258, 1358-1362
4) E W. Miles (1977) Methods Enzymol. 48, 431-443
5) E.W. Taylor, A L Fear, A. Bohm, S.-H. Kim, K. Koths (1994) J. Biol. Chem. 269, 31171-31177
6) E S Kawasaki and M.B Ladner (1990) in Colony-Stimulating Factors: Molecular and Cellular Biology, eds T M Dexter, J.M. Garland and N G Testa (Dekker, N.Y.), pp. 155-176.

COMPARISON OF THE WATER-SOLUBLE CRYSTALLINS FROM NORMAL AND AGE-RELATED CATARACTOUS HUMAN LENSES

S. He,[1] S. Pan,[2] K. Wu[2] and R. Orlando[1*]
1. Complex Carbohydrate Research Center and Department of Biochemistry and Molecular Biology, University of Georgia, Athens, GA
2. Zhongshan Ophthalmic Center, Sun Yat-sen University of Medical Science, Guangzhou, China

To better understand the mechanism(s) for cataractogenesis, we have begun an investigation into the *in vivo* transformations that occur to the primary structure of human lens crystallins upon cataract formation. In this study, the *in vivo* post-transtlational modifications found in the water-soluble lens crystallins from a 65-year-old cataractous individual were compared to those of a normal human fetus by high performance liquid chromatography/mass spectrometry (HPLC/MS).

The water-soluble crystallins, prepared by homogenization of the lenses, were directly analyzed by HPLC/MS. This technique permits separation of crystallins while simultaneously determining the molecular weight of each component to within a few Daltons.

These HPLC/MS experiments determined that the molecular weights of the water-soluble crystallins in the normal and age-related cataractous lenses were virtually identical (table 1, figure 2), implying that there are no significant differences between the *in vivo* post-translational modifications found in the water-soluble crystallins of normal and age-related cataractous lenses. These experiments also demonstrated that the quantity of βB1 and several γ-crystallins are significantly reduced in the water-soluble fraction of the age-related cataractous lenses (figure 1), presumably these crystallins have become water-insoluble.

These result demonstrate that post-translational modifications do not appear to accumulate in the water-soluble crystallins fraction, providing evidence that alterations in the primary structure of the crystallins that remain water soluble do not play a role in age-related cataract formation. Alternatively, the disappearance of several crystallins appears to be associated with age-related cataractogenesis; however, the fate of these missing crystallins could not be determined by these experiments.

43rd ASMS Conference on Mass Spectrometry and Allied Topics

Table 1: Molecular Weight and assignments of the crystallins found by HPLC/MS analysis of the fetal lens and the cataractous lens.

Peak	MWfetus	MWcataract	Assignment
1	23289	23291	βB2
	23157		β
	23409		β
	23591	23591	β
2	25304	25303	βA3
	25198		β
	25433		β
	25492		β
	25613		β
3	20911	20911	γS
	21029		γ
	21041		γ
4	20726		γ
	20981		γ
	21212		γ
5	20866		γ
6	20606		γ
7	20200	20200	αB2
	20073	20072	αB2-lys
		20283	αB1
8	20747		γC
9	27933	27933	βB1
10	19950	19950	αA2
		20028	αA1
	19859	19860	α
	20067		α
	20256	20255	α

Figure 1: Total ion chromatrograms of the HPLC/MS analysis of the fetal lens (—) and the cataractous lens (—).

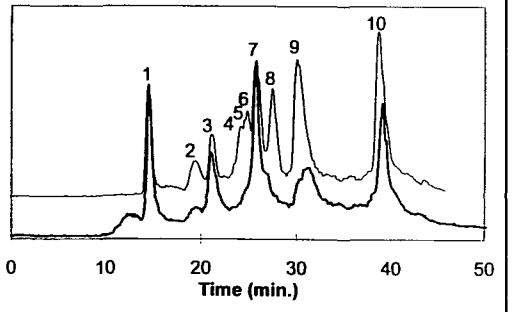

Figure 2: Reconstructed MW plot of the peak 7 found from HPLC/MS analysis of the fetal lens (—) and the cataractous lens (—).

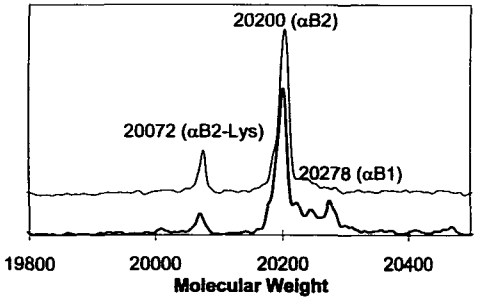

Identification of Modified Human Water Insoluble Lens Crystallins by MS

Anders L. Lund, Jean B. Smith and David L. Smith
Department of Chemistry, University of Nebraska-Lincoln, Lincoln, NE 68588-0304

Cataract is the number one cause of blindness worldwide, and the cost of cataract surgery is 11 % of the Medicare budget. One hypothesis for the formation of cataract is that opacification arises from aggregation of the modified lens crystallins. The eye lens crystallins can be separated into water soluble and water insoluble fractions. Initial work on the water insoluble fraction indicates that there are multiple modifications of several crystallins in this fraction.

The water insoluble monomers are very complex mixtures. Two dimensional polyacrylamide gel electrophoresis can resolve the mixture into its components, but the proteins cannot be easily removed for analysis. We were unable to use ESIMS to analyze the fractions solely isolated by reversed phase HPLC. The crystallin composition of the fractions was too complex. Ion exchange chromatography is needed prior to the reversed phase separation to add another dimension to the fractionation of the monomers.

Many of the modified crystallins constitute a very small portion of the total protein in the water insoluble fraction. To increase the amount of trace components in the monomer fraction, the monomers from three lenses were combined. Prior to combining the monomers, the UV traces from the three lenses were compared to examine the variability of the lenses. The combined sample was fractionated on a Pharmacia Mono Q 5/5 ion exchange column.

The fractions collected from ion exchange chromatography were further purified by reversed phase HPLC on a Vydac C4 column. The gradient was started at 30% B to ensure the crystallins would stay in a denatured state after the urea was removed. The peaks were collected and concentrated.

ESIMS was used to analyze the fractions isolated from reversed phase HPLC. The ESI mass spectrum in Figure 1 is of the fraction designated α-A. (The inset spectrum in Figure 1 is of water soluble α-A crystallin.) The water insoluble protein in this fraction coelutes with water soluble α-A crystallins on reversed phase HPLC. The MW of unmodified α-A is 19952. Approximately 10 pmol of sample was analyzed by on-line LC/ESIMS. The effective resolution was enhanced three fold with the maximum entropy algorithm. Two ions corresponding to novel *in vivo* degradation products were immediately observed. The minor components of this fraction are still associated with the parent crystallin after extensive chromatography. The mass difference between the water soluble and water insoluble α-A crystallin is 2 mass units.

To determine where the water insoluble crystallin was modified, the sample was digested with trypsin. To perform LC/ESIMS, the effluent from a C8 microbore column was split 10:1, 5μl was directed into a Fisons VG Platform quadrapole mass spectrometer with an ESI source. The other 45μl was directed into a UV detector and fractions were collected for later analysis.

The information obtained from the digest includes: two sites of deamidation, confirmation of the loss of serine from the C-terminus, a doubly charged ion and triply charged ion that correspond to the peptide sequence 120-145 (this sequence may contain a disulfide bond), and possibly an oxidized methionine in the amino terminus.

To determine the amount disulfide bonding present in the peptide 120-145 we analyzed 5 μl of the fraction containing the peptide 120-145 on a Fisons VG AutoSpec. This fraction was collected during the LC/MS analysis described previously. The array detector of the AutoSpec provided increased sensitivity at the resolution required to analyze the sample. The spectrum was compared to the calculated isotopic pattern (Figure 2). The doubly charged ion from the spectrum matched the isotopic pattern of the disulfide bonded peptide, suggesting that all of the protein is disulfide bonded.

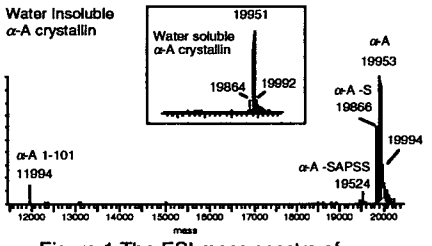

Figure 1 The ESI mass spectra of water soluble and water insoluble α-A crystallins.

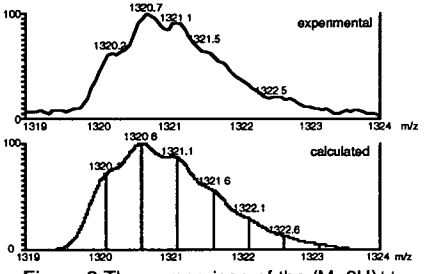

Figure 2 The comparison of the $(M+2H)^{++}$ peak from the ESI mass spectrum of the peptide 120-145 to the calculated isotopic distribution at the same resolution.

Additional evidence for the complete disulfide bonding of α-A was obtained from the AspN digest of the crystallin. The digest was analyzed by on-line LC/ESIMS; the total ion current is displayed in Figure 7. A selected ion plot for the peptide 125-135 (DQSALSCSLSA) disulfide bonded to 136-150 (DGMLTFCGPKIQTGL) shows a strong single peak at scan 165. Selected ion plots for the individual peptides 125-135, and 136-150 did not show any peak in the chromatogram.

The following modifications are found in both the water soluble and water insoluble α-A crystallins: deamidation of several asparagine and glutamine residues, phosphorylation of serine 45 and 122 (either or both), and partial loss of the C-terminal serine. Two major modifications of the α-A crystallins in the water insoluble fraction were identified. First, the water insoluble fraction is completely disulfide bonded, whereas the water soluble fraction is less than 10 % disulfide bound. Next, peptide bond cleavage occurred between Asn 101 / Glu 102 and Thr 167 / Ser 168 only in the water insoluble fraction. These modifications may cause the transfer of the crystallins from the water soluble fraction to the water insoluble fraction. Deamidation at Asn 101 was readily observed in the water insoluble fraction. Peptide bond cleavage at this site may be associated with this event. It is not known if this site is just prone to hydrolysis, or if there are external factors catalyzing the hydrolysis at this site.

PROBLEMS AND SOLUTIONS IN SEQUENCING A MUSSEL FOOT PROTEIN FROM *MYTILUS EDULIS*

Vladimir V. Papov and Klaus Biemann
Dept. of Chemistry, Mass. Inst. of Technology, Cambridge, MA 02139

The marine mussel, *Mytilus edulis*, is particularly adept at attaching its foot to underwater surfaces through the byssus, which can be described as a bundle of threads ending in adhesive pads or plaques.[1] The process of this surface bonding is of considerable technological and scientific interest since it is quite strong, rugged, persists while completely immersed in seawater, and finally, is naturally occurring and presumably environmentally benign. Waite and coworkers at the University of Delaware have previously isolated at least four distinct families of polymorphic proteins thought to be involved in this adhesion process.[2] These proteins are derived from *Mytilus edulis* foot and byssal adhesive plaques and have been named mefp (for *Mytilus edulis* foot protein).

The third protein family (mefp-3) is unusual in that all of its variants (at least nine have been isolated) contain short sporadic repeat sequences. In addition, mefp-3 is composed almost exclusively of 3,4-dihydroxyphenylalanine (DOPA), Gly, Asn, Trp, Arg, and an unknown basic amino acid. The unusual composition of these proteins, no doubt due to their unusual biological role, complicated the sample handling and analysis of mefp-3. The primary sequence of mefp-3 is based on a variant F (mefp-3F) which appeared to be the most chromatographically pure as determined by acid-urea-PAGE analysis.

Although the identity of 4-hydroxyarginine (the unknown basic amino acid) was ultimately determined by fast atom bombardment (FAB) tandem mass spectrometry, peptides derived from mefp-3F ionized poorly by FAB due to their high content of DOPA, Arg, and 4-hydroxyarginine. Conversely, both mefp-3F and peptides derived thereof ionized well by matrix-assisted laser desorption ionization time-of flight mass spectrometry (MALDI-TOF-MS). The MALDI mass spectrum of native mefp-3F contained a cluster of $(M+H)^+$ ions that differed from the most highly hydroxylated form, $(M+H)^+ = m/z$ 6135.2, in multiples of -16 mass units due to incomplete post-translational hydroxylation.

Endoproteinase cleavage of mefp-3F was complicated by the tendency of this protein to oxidize, polymerize, and degrade while in solution, especially at alkaline pH. Trypsin digestion in particular resulted in an inordinate amount of peptides making analysis difficult. On the other hand, Endo-Lys-C retained its specificity producing a very simple digest consisting of only three peptides. Although the Endo-Lys-C peptides (LC-1, 2, and 3) were partially sequenced using automated Edman degradation (Waite *et al.*), the unusual composition of mefp-3F did not allow unambiguous determination of the C-terminus by this method. Ultimately, the C-terminal sequences of peptides LC-2 and LC-3 were identified by separately digesting each peptide with carboxypeptidase P and directly analyzing aliquots at different time points by MALDI-TOF mass spectrometry. For example, Figure 1 shows a MALDI-TOF mass spectrum of peptide LC-3 [$(M+H)^+ = m/z$ 1606.7] incubated with carboxypeptidase P for 30 seconds. All of the C-terminal lysine has been released at this time but the four major peaks at m/z 1478.6, 1421.4, 1249.3, and 1077.1 (loss of 128.1, 57.2, 172.1, and 172.2 Da) correspond to the consecutive loss of K, G, **R**, and **R** (where **R** is 4-hydroxyarginine), respectively.

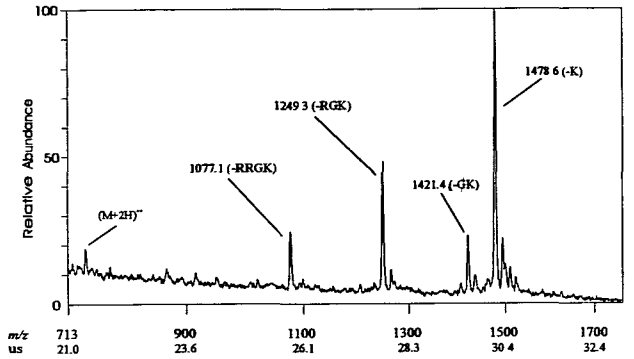

Figure 1. MALDI-TOF mass spectrum acquired after 30 sec of carboxypeptidase P digestion of peptide LC-3 from mefp-3F. The mass differences indicate that **RRGK** are the last four C-terminal residues of this peptide (undigested LC-3 has $(M+H)^+ = m/z$ 1606.7 as measured with an internal standard).

Similarly, the N-terminal peptide sequence was determined (and confirmed) by incubating the peptide with aminopeptidase M and analyzing the aliquots by MALDI-TOF-MS. In this manner, it was possible to determine the sequence of peptide LC-3 entirely by mass spectrometry. The alignment of the peptides in the final sequence was accomplished by digesting native mefp-3F with carboxypeptidase P in combination with MALDI-TOF-MS.

In conclusion, the mussel foot protein, mefp-3F, presented unique challenges to the determination of the amino acid due to its unusual composition. Furthermore, the post-translational hydroxylation of mefp-3F complicated the conventional sequencing method of Edman degradation. The complete sequence of the most highly hydroxylated form of mefp-3F was finally determined to be (where **Y** and **R** are DOPA and 4-hydroxyarginine, respectively)

ADYYGPNYGPP**RRY**GGGNY**NRY**NRY**GRRY**GGYKGWNNGWNRGRRGKYW

by using a combined approach of Edman degradation sequencing and mass spectrometry.

References:

1. Benedict, C.V. and Waite, H.J. *J. Morphol.*, **189**, 261 (1986).
2. Diamond, T.V. Ph.D Thesis, University of Delaware (1993).

Acknowledgments:
This work was supported by the National Institutes of Health (grant No. GM05472 and RR00317). Mefp-3F was provided by H.J. Waite at the University of Delaware.

MASS SPECTROMETRY OF MARINE BIOMOLECULES

Mark M. Ross[1], Steven W. Taylor[2] and J. Herbert Waite[2]
[1]Code 6113, Naval Research Laboratory, Washington, DC 20375
[2]Dept. of Chemistry, University of Delaware, Newark, DE 19716

The growth of marine organisms on surfaces in the ocean is a serious problem for the Navy. This "biofouling" phenomenon is the focus of chemical, biological and materials science research aimed at determining the adhesive agents, adhesion chemistry and strategies or new materials that will prevent the adhesion.

This project is focused on marine mussels, which stick to surfaces via a strong, durable thread and a versatile plaque. Some of the proteins produced and secreted by mussels have been characterized, and some of these are speculated to be involved in the adhesion [1]. However, the exact identities of the binding molecules and the adhesion chemistry are unknown.

In this work, the marine mussel, *Mytilus edulis*, is grown on different substrates, cold-shocked, harvested and the feet or plaques are extracted [2]. These extracts are fractionated by HPLC, and the components of these complex mixtures are analyzed using MALDI and ESI mass spectrometry. The objective is to identify the proteins that are contained in the mussel foot and plaque. Because it is the plaque that sticks to a substrate, the biomolecules in this part of the mussel are of primary interest. One unique aspect of this work is that the adhesive side of intact plaques were subjected to MALDI in an attempt to probe directly the species used to adhere.

The HPLC fractions of an extract of 5,000 plaques showed a wide variety of species by MALDI, from 2-15 kDa. Of particular interest are variants of Mefp-3 (the 3rd family of Mytilus edilus foot proteins), which have molecular weights in the 5-6 kDa range and are suspected adhesive agents. Figure 1 shows the MALDI mass spectrum of one plaque extract fraction, which contains many species and some with masses in the correct range for Mefp-3.

It is known that the plaque contains Mefp-3 proteins, but it is not known which of the many variants are used in adhesion. Figure 2 shows a MALDI mass spectrum taken directly of the adhesive side of a plaque. Some of the most abundant ions are in the 5-6 kDa range, and the narrower peak widths, relative to those of the extract species, indicate specific variants.

The next step is to determine the sequence of those species observed directly from the plaque. It may then be possible to determine if the adhesive agents used by the mussel vary with the substrate.

[1] J.H. Waite, Comp. Biochem. Physiol., 97B, 19, 1900.
[2] J.H. Waite et al., Biochemistry, 24, 1038, 1985.

MALDI/MS of a Plaque Extract Fraction (GPE-41)

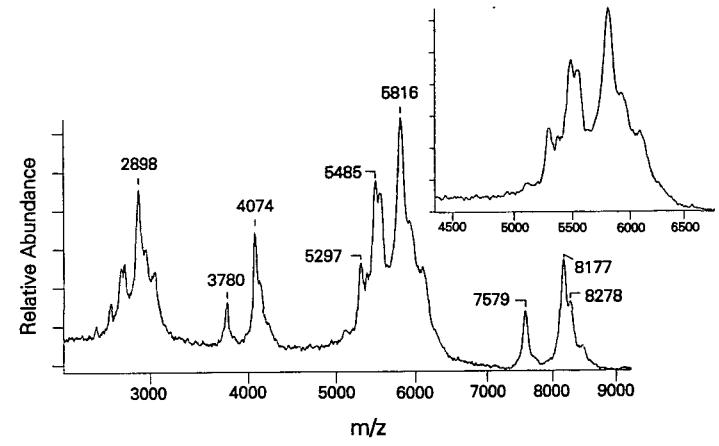

Figure 1

MALDI/MS of a "Glass" Plaque - Underside

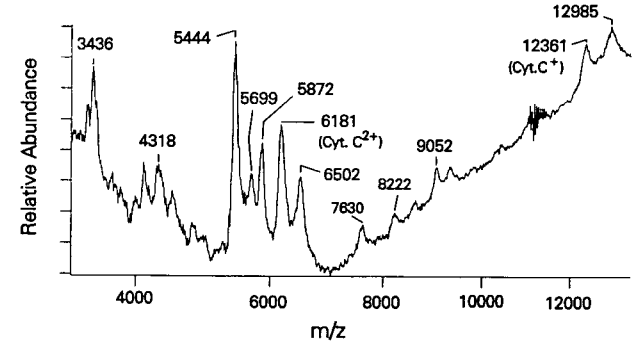

Figure 2

STRUCTURE ELUCIDATION OF THE SEX-DIFFERENTIATION HORMONE IN CRUSTACEA BY MASS SPECTROMETRY

G. MARTIN[1] - O. SOROKINE[2] - M. MONIATTE[2] and A. VAN DORSSELAER[2]
1. Laboratoire de Biologie Animale URA CNRS 1975, 40, Avenue du Recteur Pineau, 86022 POITIERS Cedex , France.
2. Laboratoire de Spectrométrie de masse bioorganique UA CNRS 31, Faculté de Chimie, 1, rue B. Pascal 67008 Strasbourg Cedex, France.

INTRODUCTION :

Molecular machinery of sex determination is understood in details only in few cases. In crustacea the sex differentiation of young animals is totally under control of the androgenic glands (AG). It has been clearly demonstrated that a protein isolated from AG was responsible from sexual differentiation. This protein is the Androgenic Hormone (AH).(1,2)

Our goal was to determine the primary structure of AH. We have used mass spectrometry and Edman degradation in conjonction to determine not only the sequence but also the possible post-translational modifications. We have also isolated and characterized its precursor (prohormone) and a C-peptide. To follow the biological activity of AH on female woodlouse, two kinds of bioassay were performed. A rapid one, which revealed a biological response within 8 to 10 days and a second one (sex reversal and mating experiments), which required several months but which led to the complete convertion of females to sexually active males.

RESULTS :

1-MALDI-TOF spectrum from a single crude Androgenic Gland. (Fig 1)

A single gland was isolated and directly submitted to MALDI-TOF analysis.

2-Purification and characterization of the androgenic hormone. (Fig 2)

The extract from 1200 androgenic glands was injected on a phenyl rp-HPLC column (4 x 300 mm). Three peaks were shown to be active. After several chromatography, each peak was analysed by MALDI-TOF. The MALDI spectrum of peak 1 and 2 were characterized by a broad peak ranging from 10 to 12 kDa. Peak 3 showed a large peak ranging from 16.5 to 18.5 kDa and a strong peak at 5kDa.

For Peak 1 and 2 the same primary structure was observed by Edman Degradation and MALDI-TOF. Both proteins are heterodimers made of 2 chains linked by 2 disulfide bonds. The 2 highly active proteins named AH1 and AH2 were only differentiated by the size and the heterogeneity of glycan chain on Asn 18 from chain A. This glycosylation was characterized by MALDI-TOF.

3-MALDI-TOF characterization of the glycan moiety of AH. (Fig 3)

Chains A, from AH1 and AH2 were isolated by reduction-alkylation and analysed by MALDI-TOF. Digestion with Lys-C allowed to isolate a small peptide (17-29) with the glycan chain. Fig 3 shows the MALDI-TOF spectrum after partial hydrolysis with MeOH/HCl 0.5N of the peptide 17-29 of chain A. Different peaks could be attributed to the core structure of the complex type N-glycosylation. GC-MS data confirmed the presence of N-acetylglucosamine, galactose and fucose.

CONCLUSION:

We have determined for peak 1 and 2 the same primary structure. AH1 and AH2 were both an heterodimer N-glycosylated on Asn 18 of chain A. The glycosylation is heterogeneous. From active peak 3, we have isolated the precursor of AH (17kDa) and the C-peptide (45 residues) linking chain B to chain A. All the peptides characterized after purification could be observed in the preliminary MALDI-TOF analysis of a single crude Androgenic Gland.

Ref:
1-Courrier, R. *C.R. Acad. Sc. Paris* 173 668-671 (1921)
2-Martin, G., Juchault, P., Sorokine, O. and Van Dorsselaer, A. *Gen. Comp. Endocrinol.* 80 349-354 (1990)

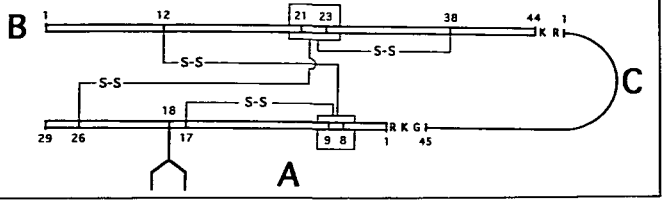

Fig 1:

MALDI-TOF spectrum from a single crude Androgenic Gland
Several major peaks were observed. Their masses are similar to those obtained for all the active products purified and characterized showing low degradation during the multistep purification. Mass measurements were performed on a Biflex™ (Bruker) MALDI-TOF spectrometer in the linear mode.

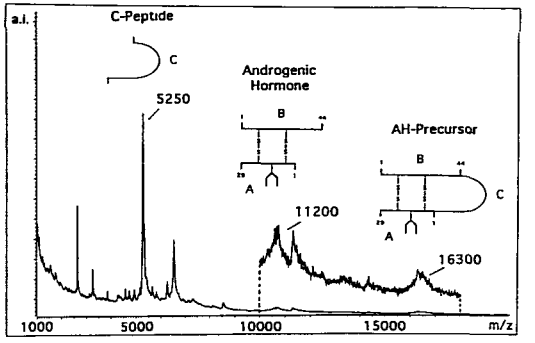

Fig 2:

rp-HPLC of a crude extract of AG and MALDI-TOF characterization of Peak 1 and 2
The MALDI spectrum shows the heterogeneity and the difference of glycosylation between peak 1 and 2. Edman degradation was performed in liquid pulsed mode on a ABI 473 (Perkin Elmer) sequencer.

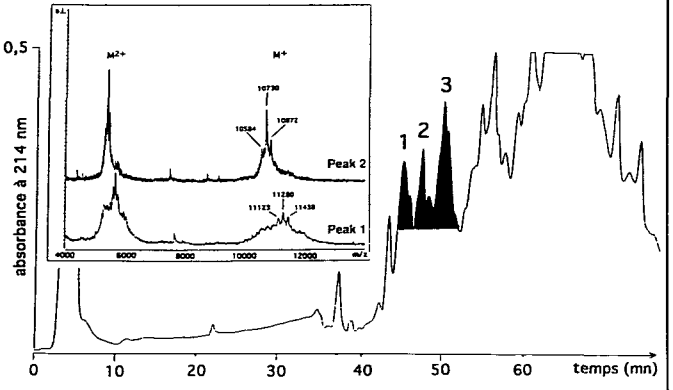

Fig 3:

MALDI-TOF characterization of the glycan moiety by MeOH/HCl 0.5N hydrolysis of peptide 17-29 of chain A.
The N-glycosylation is of the complex type.

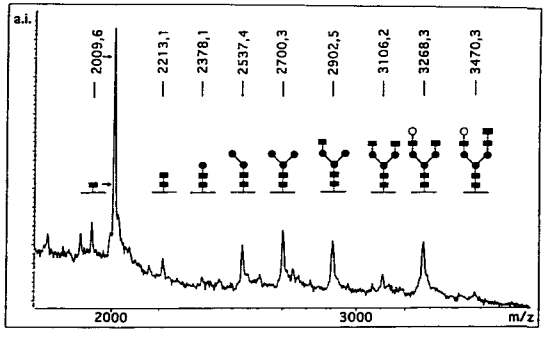

SEQUENCE CHARACTERIZATION OF PEPTIDES FROM A SPIDER SILK PROTEIN BY ELECTROSPRAY MS/MS

Bernice Yeung & Paul Vouros
Chemistry Department and Barnett Institute, Northeastern University, Boston, MA 02115
Charlene M. Mello & David L. Kaplan
Biotechnology Division, US Army RD& E Center, Natick, MA 01760

INTRODUCTION Silks are fibrous proteins spun by biological systems. Unlike silkworms, spiders produced a variety of silks which has not been well characterized. The dragline silk of *Nephila clavipes* is the most studied of all spider silks, and it has been found to possess a unique balance of mechanical strength and elasticity [1]. Sequence characterization of this silk will lead to an understanding of its structure-function relationship, and ultimately to its application as bioengineered materials.

The focus of our work is on the direct sequencing of this dragline protein. Due to difficulties with solubility and the lack of basic amino acids in its composition, a chemical digest using N-bromosuccinimide (NBS) was opted over the conventional enzymatic methods for the digest of this protein. Digest protocol using NBS has been optimized for generating peptides suitable for sequencing by MS/MS and Edman degradation. The results are presented below.

EXPERIMENTAL

(1) Sample Preparation: Digest protocol and sample preparation are outlined in Figure 1.

(2) SDS-PAGE: All electrophoresis was carried out using precast 10-20% Tricine gels (Novex), running under a constant voltage of 125V for 100 minutes.

(3) HPLC: Peptide mapping was done on a Waters 625 LC system, using a H_2O/ACN/TFA gradient system on a Delta-Pak C18 column. Fractions were collected manually and concentrated to a final volume of ~50μL each.

(4) ESI MS: All work was done using a Fisons Quattro triple quadrupole instrument coupled to a Carlo Erba Phoenix 20 capillary HPLC system. A C18 packed capillary LC column (LC Packings) was utilized in the gradient mode, using a H_2O/IPA/TFA system.

RESULTS

Fraction 26: The full scan ESI mass spectrum is shown in Figure 2. CID analysis of m/z 768 and m/z 455 were performed, and their sequences were determined to be (Q/K)GGAGGHG(Q/K) and GGY, respectively. The CID spectrum of the latter peptide is displayed in Figure 3, where the tyrosine residue is shown to be NBS-modified and bears the characteristic fragmentation pattern as previously discussed [2].

Fraction 13: Figure 4 shows the full scan mass spectrum of this fraction, where an MH^+ ion is seen at m/z 304, along with its $[2M+H]^+$ and $[3M+H]^+$ ions. CID data of m/z 304 (Figure 5) indicates two possible sequence assignments: GGGGG and GG(L/I)G. Finally, Edman degradation of this fraction established the sequence to be GGLG.

REFERENCES

[1] Cunniff, P.M., Fossey, S.A., Auerbach, M.A. and Song, J.W., in *Silk Polymers: Materials Science and Biotechnology*, D. Kaplan *et al.* ed., pp. 234-251, ACS Symposium 544, Washington, D.C. (1994).

[2] Yeung, B., Vouros, P., Mello, C.M. and Kaplan, D.L., in *Proc. of 41st ASMS Conferences*, p. 369a (1993).

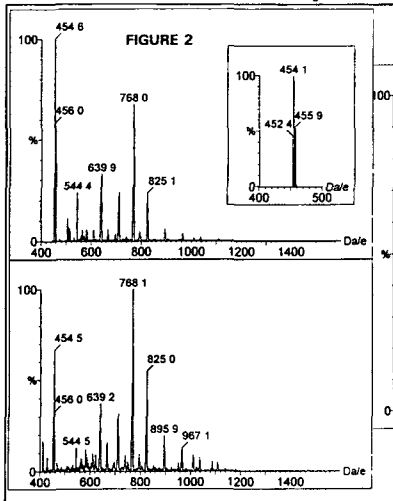

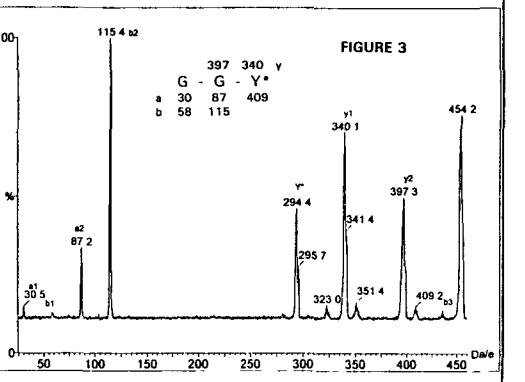

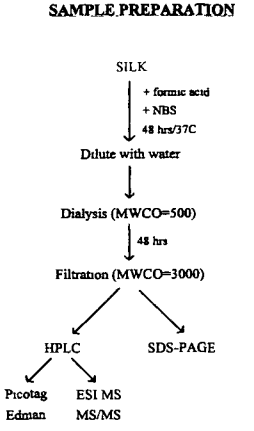

FIGURE 1

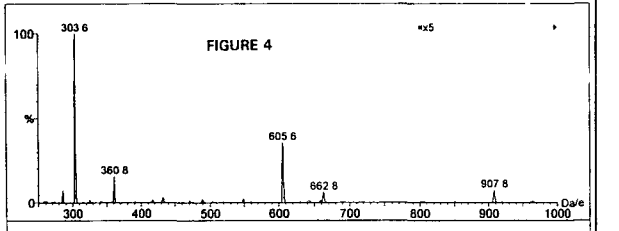

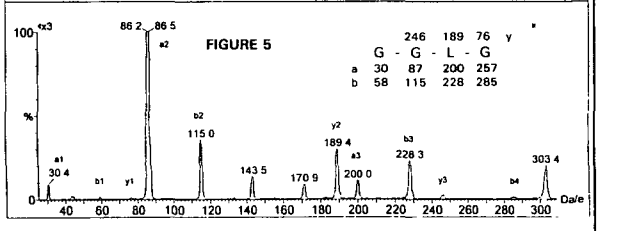

Processing of avian sarcoma and leukemia virus polyprotein

I.A. Papayannopoulos[1], R.B. Pepinsky[1], E.P. Chow[1], V.M. Vogt[2]
[1]Biogen Inc., 14 Cambridge Center, Cambridge, MA 02142
[2]Section of Biochemistry, Cornell University, Ithaca, NY 14853

The internal structural proteins of retroviruses are formed by proteolytic processing of the Gag precursor polyproteins in the last stages or after budding of the virus particle from the infected cell. In all retroviruses the proteins into which Gag is proteolyzed include (in order from the Gag N-terminus) MA (matrix protein), CA (capsid protein), and NC (nucleocapsid protein). In avian retroviruses the Gag precursor also encodes the protease (PR) that is responsible for processing the precursor (for a review on the form, function, and use of retroviral Gag proteins see reference 1). Cleavage of Gag leads to a morphological change in the virus particle called maturation, which is essential for the virus to become infectious.

In the mature virus particle, CA forms the protein shell or "core" that encapsulates the viral RNA genome and RNA-associated proteins, including NC and the replication enzymes reverse transcriptase and integrase. In the newly infected cell, the core is delivered to the cytoplasm, where reverse transcription (replication of the genome) occurs. In the avian sarcoma and leukemia viruses, typified by Rous sarcoma virus (2), the major Gag proteins are MA, p10, CA, NC, and PR. In addition, several small peptides are produced, from Gag proteolysis between MA and p10 (peptide p2), and between CA and NC (spacer peptide).

In earlier studies (3) it was found that mature viruses contain multiple forms of the CA protein that differ by proteolytic processing of the C-terminus. We have now definitively identified three forms of CA in mature virions, and have investigated the proteolytic processes by which these forms are generated *in vivo*, using electrospray ionization mass spectrometry (carried out on a VG Quattro II instrument) to analyze various Gag-derived proteins of the Prague C strain Rous sarcoma virus (PrC-RSV) and avian myeloblastoma virus (AMV). Each protein generated from *in vivo* processing of Gag was collected and analyzed by ESI MS. The results for PrC-RSV are tabulated as follows:

Protein	Position[1]	Calculated MW	Measured MW
MA	[1-153]	16574.1	16653[2], 16574
p10	[176-237]	6044.6	6044
CA	[238-477]	25815.9	25815, 25684[3], 25543[3]
NC	[487-575]	9492.6[4]	9492
PR	[586-699]	13609.9	13609

1 Positions refer to the sequence of the Gag precursor polyprotein.
2 MA is known to be phosphorylated; MW 16653 corresponds to the phosphorylated protein
3 The CA variability is discussed below.
4 The calculated MW corresponds to one of the known isoforms of this protein.

The ESI mass spectra of PrC-RSV and AMV CA proteins, along with the corresponding transformed data, are shown, in Figure 1. PrC-RSV (Figure 1A) consists of two major components of MW 25542 and 25815; the latter agrees with the molecular weight predicted for CA from the nucleotide sequence, while the former corresponds to the predicted sequence minus the last three amino acids (Ala-Ala-Met). A minor component of MW 25684 corresponds to the predicted CA sequence minus the C-terminal Met residue. All three components are generated during proteolysis of the Gag precursor molecule. Unlike PrC-RSV,

AMV is a mixture of closely related viruses, thereby resulting in a mixture of CA species, consisting of at least three CA proteins (Figure 1B). Nevertheless, for each component the same processing, including relative abundances, was observed as for the PrC-RSV CA protein.

Recombinant viruses that were designed to contain the CA protein missing its last three amino acids (AAM) were found to undergo proteolytic maturation but were non-infectious. Earlier results (4) had demonstrated that deletion of the nine amino acids (spacer) that are present between CA and NC sequences in Gag (see Figure 1) had a similar effect (i e., CA is not processed further to the shorter form lacking the three C-terminal amino acids).

The processing of Gag to CA minus the C-terminal three amino acids was a previously unrecognized event. Two experiments were designed to test if this shorter form of CA were indeed a Gag PR product. The first experiment involved *in vitro* cleavage with the PR protease of a synthetic peptide (LTDGIAAAMSSAI) consisting of the last nine amino acids of CA and the first four amino acids of the spacer sequence. The second experiment involved digestion with PR of a fusion protein encompassing CA, the spacer peptide, and NC In both cases cleavage analogous to that observed *in vivo* took place. Furthermore, the synthetic peptide (LTDGIAAAM) comprising the last nine amino acids of CA did not cleave with the PR protease. These results clearly demonstrate that if the spacer region between CA and NC is present (as in Gag) then the protease will process CA *in vitro* in a manner similar to the *in vivo* processing, and that the shorter form of CA is not generated from C-terminal trimming of CA.

Although the full significance of multiple processing sites between CA and NC is not known, it is apparent from our experiments that the region between CA and NC is required for proper processing of the CA protein and, presumably, the interactions between the various CA forms affect the infectivity of the virus. It is interesting that certain features of the CA maturation in PrC-RSV are also found in other retroviruses, such as HIV-1 (5,6).

1. Wills, JW; Craven, RC *AIDS* **1991**, *5*, 639-654.
2. Schwartz, DE; Tizard, R; Gilbert, W *Cell* **1983**, *32*, 853-869.
3. Pepinsky, RB Ph.D. Thesis, **1984**, Cornell University.
4. Craven, RC; Leure-duPree, AE; Erdie, CR; Wilson, CB; Wills, JW *Journal of Virology* **1993**, *67*, 6246-6252.
5. Henderson, LE; *et al.* *Journal of Virology* **1992**, *66*, 1856-1865.
6. Henderson, LE, *et al.* In: Human retroviruses, cancer, and AIDS: Approaches to prevention and therapy (Bolognesi, D Ed.) Alan R. Liss Inc, New York, **1988**, pp. 135-147.

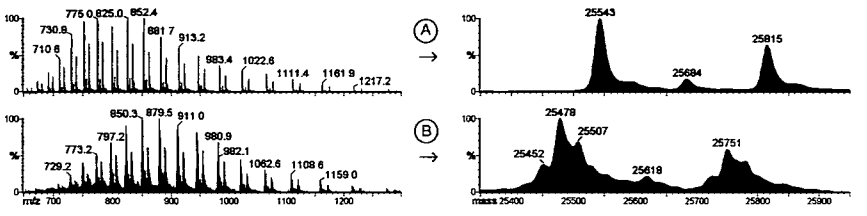

Figure 1. ESI mass spectra (left) and transformed molecular weight spectra (right) of CA proteins generated from *in vivo* processing of Gag proteins from PrC-RSV (**A**) and AMV (**B**).

Peptide phosphorylation site identification: A new method based on ion trap mass spectrometry.

Beth L. Gillece-Castro, David P. Arnott, Mark E. Bier*, Adrian P. Land*, and John T. Stults ; Genentech, Inc., 460 Point San Bruno Blvd., South San Francisco, CA 94080 and *Finnigan MAT, 355 River Oaks Parkway, San Jose, CA 95134

Phosphorylation of proteins is an enzymatically-controlled method of signal transduction within cells. Importantly, the sites and level of phosphorylation determine the activity of these signals. To identify these sites, a number of mass spectrometric methods have been developed in recent years. Many of the methods rely measuring Δ 80 Da on peptides or proteins, and have been demonstrated using LSIMS (1), ESI (2) and MALDI ionization techniques. Alternatively, phosphopeptides can be isolated from non-phosphorylated species by TLC or affinity chromatography (eg. iron binding) (2). Some characteristic fragments may be produced in tandem mass spectra which further confirm the presence of phosphorylation on particular peptides. In positive ion mode phosphoric acid is often lost from phosphoserine and phosphothreonine residues (- 98 Da). Fragment ions of this type have been observed in high-energy CID (1), low-energy CID (3) and MALDI-TOF post-source decay. In negative ion mode, low mass fragments of $H_2PO_4^-$ and HPO_3^- (97 and 80 Da, respectively) are produced by CID, and have been used for on-line LC/MS identification of phosphorylated peptides (4). Finally, the sequence of *phosphorylated peptides can be determined from CID to identify the specific site within a peptide (1).*

We developed a new method for identification of protein phosphorylation sites using a single LC/MS run on an ion trap mass spectrometer (Finnigan LCQ). Ion trap mass spectrometers can acquire multiple mass spectra in a data dependent manner in which ions detected in a full scan mass spectrum are selected by the data system for further MS experiments. The presence of an intense ion in the normal mass spectrum triggers the aquisition of scans further identifying this ion. These MS experiments include determination of charge state by narrow mass scan at high (>1000) resolution. Unique to the ion trap method is the MS^3 scan, shown in Figure 3. The double protonated peptide ion (m/z 418.9, Figure 1) was isolated and induced to dissociate (MS^2 scan, Figure 2). The abundant fragment ion at *m/z* 370 was selected for the MS^3 scan (Figure 3) from which the P-Thr site was deduced.

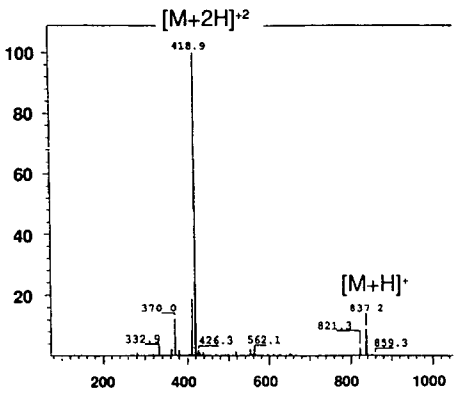

Figure 1. Peptide LKRA(p)TLG-amide analyzed by ESI-ion trap mass spectrometry.

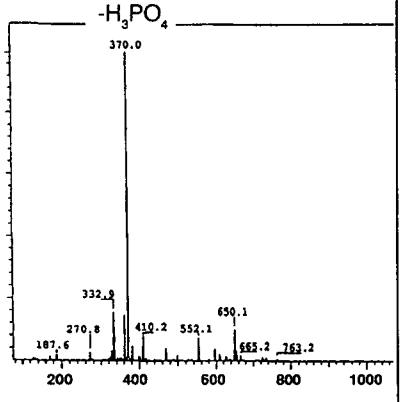

Figure 2. MS^2 scan of the doubly charged peptide LKRA(p)TLG (*m/z* 418.9) shown in Figure 1.

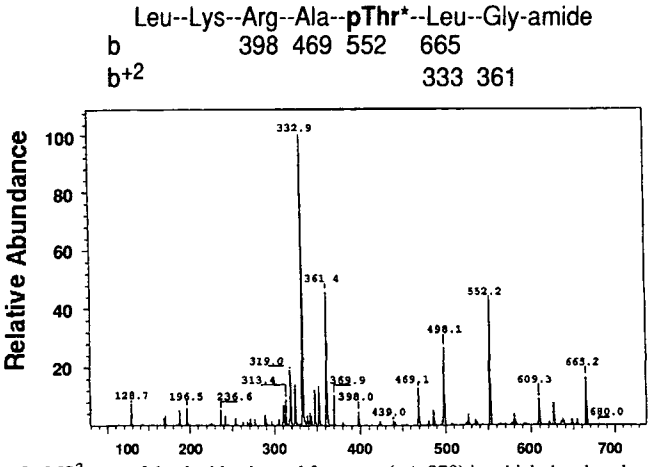

Figure 3. MS^3 scan of the doubly charged fragment (*m/z* 370) in which the phosphate group was lost by elimination forming a new residue, dehydroaminobutyric acid (pThr*).

Capillary HPLC was connected for on-line electrospray ionization mass spectrometry with a quadrupole ion trap analyzer. Peptides, including those produced by protein digestion were injected using from 0.1 to 10 pmol of each. Four types of mass spectra were obtained in a sequential manner with data-dependent scans First a scan from *m/z* 300-2000 is obtained. The most abundant ion detected in the MS scan above a preset threshold was selected for a second narrow higher resolution scan to determine the charge state of this ion. This same ion is then isolated for CID and the third, product ion spectrum (MS^2) obtained with the scan width calculated from the MW determined from the m/z and charge state. Finally, the most abundant ion observed in the MS^2 spectrum was isolated for a MS^3 scan. Total time for the series of MS scans was 3 to 4 seconds depending on the MW of the peptides observed. The MW of peptides was determined from the full scan mass spectrum and charge state determination. From the MS^2 scan the sequences of P-Tyr containing peptides were determined by the residue mass difference of 243 Da. Partial sequence of P-Ser and P-Thr containing peptides were also observed in MS^2 spectra, but the most abundant species were the $[M-H_3PO_4]^{+2}$ ions. These fragment ions now have dehydroalanine or dehydroaminobutyric acid where the P-Ser or P-Thr residues resided. MS^3 scan of this product ion typically gives sequence information with the phosphorylation site identified by residue mass differences of 69 Da or 83 Da. Occasionally, the MS^2 scan produces sufficient sequence ions to identify a site of phosphorylation in addition to the loss of phosphoric acid.

Advantages to the ion trap method for phosphopeptide identification are that the complete identification can be done in a single LC/MS run with peptides in any charge state. Singly, doubly and triply charged ions have been identified as phosphopeptides by the loss of phosphoric acid (98, 49, or 32.67 Da respectively) and/or sequence ions in the MS/MS spectra.

1. B. W. Gibson, P. Cohen, *Methods Enzymol.* **193**, 480-500 (1990).
2. L. M. Nuwaysir, J. T. Stults, *J. Am. Soc. Mass Spectrom.* **4**, 662-669 (1993).
3. T. Covey, B. Shushan, R. Bonner, W. Schroder, F. Hucho, in *Methods in Protein Sequence Analysis* H. Jörnvall, J. O. Höög, A. M. Gustavsson, Eds. (Birkhauser Press, Basel, 1991) pp. 249-256.
4. M.J. Huddleston, R. Annan, M. Bean, S.A. Carr, *J. Am. Soc. Mass Spectrom.* **4**, 710-717 (1993).

Electrospray Ionization Mass Spectra of Recombinant Hirudin Byproducts

József Langó[1], John Roboz[2], János Salát[1], Quitao Yu[2], István Barta[1], István Ott[1], Gábor Ambrus[1], Antal Simay[1]

[1] Institute for Drug Research Ltd. P.O. Box 82, Budapest, Hungary, H-1325

[2] Mount Sinai School of Medicine, One Gustave L. Levy Place, New York, N.Y. 10029

BACKGROUND AND OBJECTIVE

Hirudin [1] is a natural antithrombotic peptide of 65 amino acids containing three disulfide bridges. Recombinant hirudin (rHV-1) is produced by a process using genetically modified saccharomyces microorganisms. The biotechnological process also yields some byproducts with chemical properties similar to those of rHV-1. Six peaks named M(1)-M(6) in order of their retention time were separated by preparative HPLC and their major and minor constituents analyzed by electrospray ionization (ESI) mass spectrometry.

EXPERIMENTAL

Liquid chromatography: The byproducts were separated on a reversed phase C-18 type column (Vydac) using gradient elution. The mobile phase was water-acetonitrile (with 0.1% TFA). Flow rate was 1 ml/min, UV detector was at 220 nm. The collected samples were dissolved and introduced directly into the ESI source in acetonitrile-water (1:1, v/v) containing 1% formic acid. Mass spectrometry: ESI source in positive mode (Model Quattro, Fisons). Settings: capillary 3.50 kV, source temperature 80 °C, mass range 700-1900 Da, scanning speed: 0.1 sec/decade. The peak intensities reported are the averages from 5-10 consecutive spectra.

RESULTS AND DISCUSSION

Fig.(1) shows the HPLC separation of the raw sample: ESI spectra were obtained for all separated components. Fig.(2) shows, from up to down, the ESI spectra of samples rHV-1, M(1), M(2), M(3), M(4) and M(6), respectively. In addition to the base peaks, sodium addition peaks were also detected in all samples. The molecular mass of rHV-1 was 6963.33 Da, within 0.20 Da from the theoretical value. The molecular mass of major component of M(1), was 5059.49 Da (within 0.16 Da) corresponding to the 1-49 fragment of rHV-1, starting from the N terminal. Two minor components of M(1) were identified as 1C, the fragment of 1-51 of rHV-1 (m/z5284.08 Da, 0.27 Da from theoretical) and 1D, the fragment of 1-53 of rHV-1, (m/z5512.55 Da, 0.46 Da from theoretical) a third minor component, 1B was not identified. HPLC peak M(2), a single component, corresponded to the fragment 1-46 of rHV-1 (m/z4706.21 Da, 0.00 Da from theoretical). HPLC peak M(3) had three components, the first (3A) corresponding to fragment 1-61 of rHV-1 (m/z6429.95 Da, 0.0 Da from theoretical), the second (3B) corresponding to 1-62 fragment of rHV-1 (m/z6558.43 Da, 0.63 Da from theoretical), 3C was not identified. HPLC peak M(4), a single component, was identified as fragment 1-63 of rHV-1 (m/z6723.06 Da, 0.82 Da from theoretical). HPLC peak M(5) did not show ESI activity. The major constituent of HPLC peak M(6) was fragment 1-64 of rHV-1(m/z 6834.88 Da, 0.52 Da from the theoretical), a minor constituent had the molecular mass of rHV-1. A pictorial summary of the results with the structural significance is shown in Fig.(3).

CONCLUSION

The ESI technique was suitable for the determination of byproducts obtained in preparation of recombinant hirudin. The results suggest that the presence of carboxypeptidase and/or carboxydipeptidase enzymes may be responsible for the formation of byproducts during the biotechnological process.

ACKNOWLEDGMENT

J. Langó supported by the Soros Foundation, J. Roboz and Q. Yu supported by the T. J. Martell Memorial Foundation for Leukemia, Cancer and AIDS Research.

REFERENCES

[1] Markwad, F., Thromb. Haemostasis, 66(1), 141-152, 1991

43rd ASMS Conference on Mass Spectrometry and Allied Topics

Fig.(1): HPLC chromatogram of the raw sample

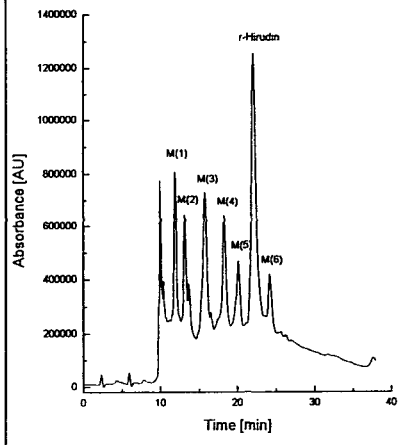

Figure (2): ESI spectra of samples studied

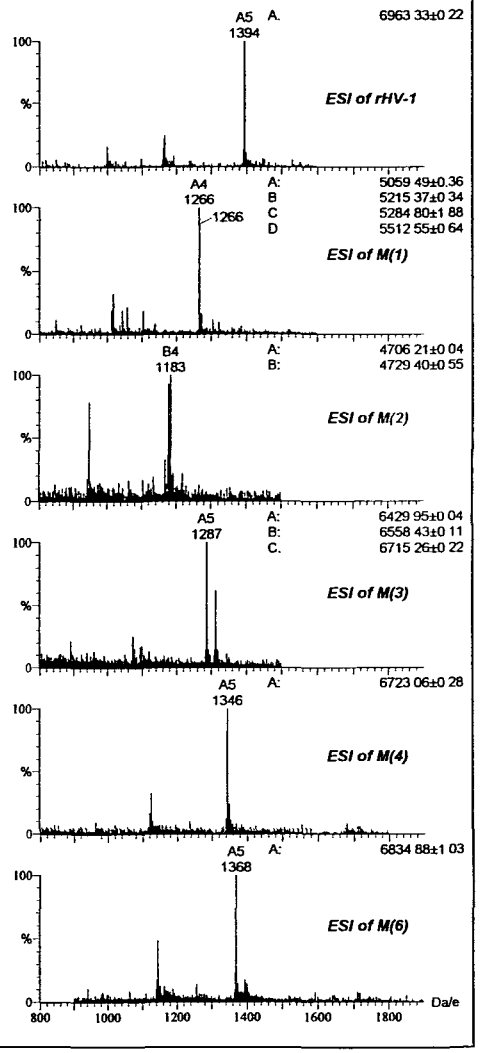

Figure (3): Schematic summary of the results

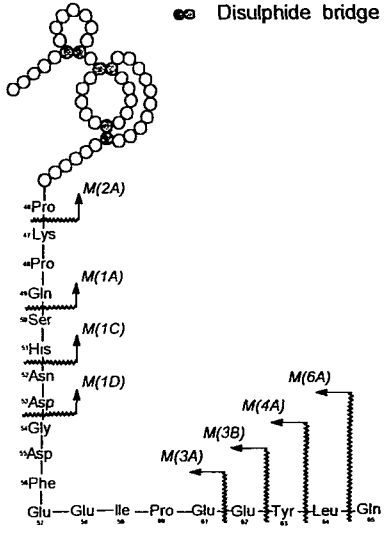

Mapping of Brain Proteins Using MALDI/TOF-MS Combined with HPLC

A. Ingendoh, H. Ikezawa, K. Seta, M. Kanai, H. Nakayama, K. Uchida, T. Isobe, T. Okuyama
Finnigan MAT Instruments Inc , 2-5-8 Hatsudai, Shibuya-ku, Tokyo 151, Japan
Tokyo Metro University, Department of Biochemistry, Hachioji-shi, Tokyo 192-03, Japan

Introduction

A certain strength of Matrix-assisted Laser Desorption/ Ionization Time-of-Flight Mass Spectrometry (MALDI/TOF-MS) compared to other MS techniques is its capability to analyze very heterogeneous mixtures of biopolymers Therefore, it is very suitable for investigations on extracts of biological material We applied MALDI for mapping of bovine and rat brain proteins. Conventionally, this is done by 2D-PAGE. However, the identification of the different components is often difficult there because of the limited accuracy of the MW determination. We fractionated an extraction of brain rougly by HPLC and analyzed the resulting fractions subsequently by MALDI. HPLC was coupled off-line to MALDI, i e. the different fractions have been collected and mixed with matrix outside of the MS instrument. To perform the mapping time-efficiently and to avoid a too excessive dilution, that might lead to the loss of components with low concentrations, each fraction still contained a smaller number of different components How effectively can a protein map of the many brain proteins, having very different concentrations in the extract, be established by the combination of HPLC and MALDI? Besides the number of detected proteins also the accuracy of their mass determination is a main criterion

Methods

1. Homogenization of bovine/ rat brain with 4 vol. of 0 1M potassium phosphate buffer (pH 7 1), 1.38M $(NH_4)_2SO_4$, 1mM EDTA ("solution 1") Centrifugation at 10,000g (30 min) Adding of powdered $(NH_4)_2SO_4$ to 85% saturation at pH 4 7 Collection of the precipitate by centrifugation, redissolution in a minimal volume of solution 1.
2. Desalting. injection of 50 µl crude brain extract into a reversed-phase C18 HPLC column and elution with a linear gradient from 0 1% aequeous TFA to acetonitrile Collection of the eluates into 42 different fractions (fig 1) Adjustment to equal volumes with 0.1% TFA / MeCN.
3. Mixing of 0.5 µl of each fraction with 0 5 µl matrix solution on the MALDI target. Matrix was a 9 1 mixture of salicylic acid and 5-methoxysalicylic acid, dissolved at 10 g/l in 9·1 0.1% TFA / MeCN
4. Mass analysis of the fractions in a VISION 2000 reflector-type MALDI/TOF-MS (Finnigan MAT) MALDI spectra were calibrated by Insulin, Cytochrome C or BSA due to the measured sample MW

Results

Each HPLC fraction analyzed by MALDI contained up to 10 different peptides and proteins (fig 2) MALDI provides for a high sensitivity for the detection of all components, which were in the fractions with quite different concentrations. Summarizing all MS spectra, about 160 different brain proteins were detected, of which ca 70% could be identified by comparison with databases. So, a detailled and accurate map of brain proteins and peptides could be established that is more detailed and more accurate than the conventioal 2D-PAGE (fig.3) The identification of all components is easier because of the much higher mass accuracy of MALDI-MS that was about 0 04% in average over the entire mass range. By comparison of the respective maps of different species, similiarities and differencies between their peptides and proteins can easily be revealed Off-line HPLC/MALDI has been demonstrated to be a powerful tool for mapping of complex biological samples like a brain extract.

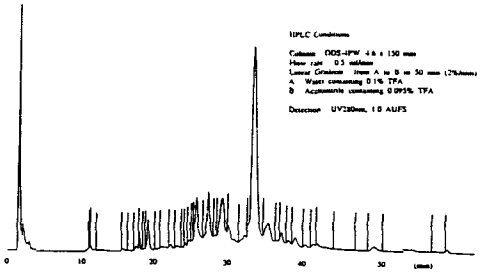

Fig. 1: Fractionation of Brain proteins using a Reversed-Phase HPLC Injection of 50 µl of Brain Extract into the column 42 fractions have been collected

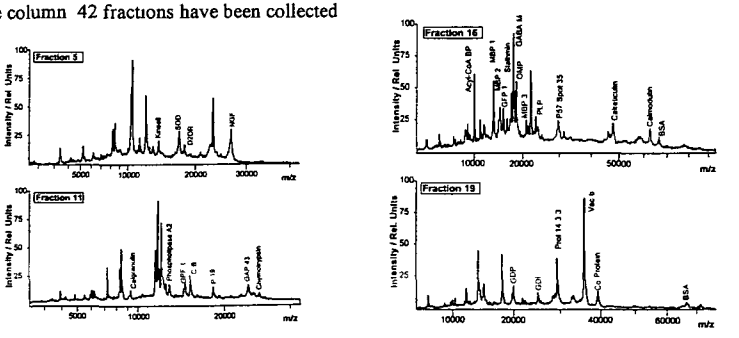

Fig. 2: MALDI spectra of the HPLC fractions #5, 11, 16, 31 from bovine brain as examples. Sum of 50 shots As can be seen, each fraction still contained up to 10 different proteins

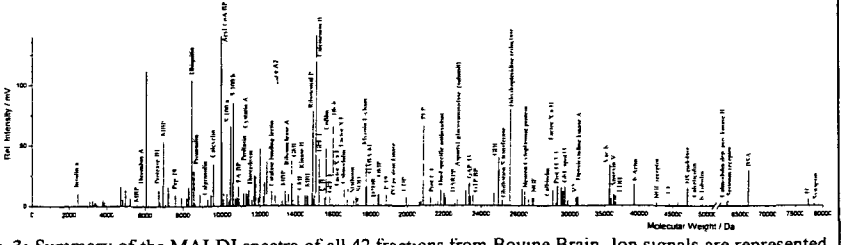

Fig. 3: Summary of the MALDI spectra of all 42 fractions from Bovine Brain Ion signals are represented by columns. About 160 different components have been detected which we tried to identify by comparison with databases The proposals for about 70% of all components are written on the columns

Mass Determination of Large Proteins Exceeding 200 kDa by UV-MALDI/TOF-MS

A. Ingendoh, H. Ikezawa, K. Seta, M. Kanai, Y. Yamakawa*, T. Omori-Satoh*, T Isobe# and T. Okuyama#
Finnigan MAT Instruments Inc., 2-5-8 Hatsudai, Shibuya-ku, Tokyo 151, Japan
*Japanese National Institute of Health, Shinjuku-ku, Tokyo 162, Japan
#Tokyo Metropolitan University, Department of Biochemistry, Hachioji-shi, Tokyo 192-03, Japan

Introduction

Molecular weight determination of large molecules is widely still done by SDS-PAGE, regardless of its by far insufficient accuracy. Moreover, by SDS-PAGE it is impossible to determine the MW of proteins above 200 kDa, as those large molecules cannot migrate sufficiently in the gel. GPC-HPLC, that is used more often in that case, is also very inaccurate and influenced by many factors Among today's MS methods, only Matrix-assisted Laser Desorption/ Ionization (MALDI) is able to analyze molecules with a mass exceeding 200 kDa. Few attempts have been made by ESI-MS also, but as most large biomolecules contain a distribution of carbohydrates or consist even of different species, the various highly charged ion signals of each species overlap and cannot be separated sufficiently. Moreover, MALDI has advantages in terms of a quite high sensitivity in the upper mass range and of a high tolerance against contaminants or biochemical additives which often cannot be removed completely from the sample solution. Here, we report about the successful analysis of biomolecules with MW between 200 and 400 kDa by MALDI.

Methods

Sample Preparation: Bov Catalase (Sigma), SCRI, Human α_2-Macroglobulin and Protease Inhibitor (Erinaceus europaeus) were dissolved at about 10^{-6} M in 0.1% aequeous TFA (some mM of phosphate buffer in some cases). Sample amount loaded onto the target was about 1pmol. Matrix was 9:1 salicylic and 5-methoxysalicylic acid, dissolved at 10 g/l in 9:1 0.1% aequeous TFA / acetonitrile.

Experimental Setup: The MALDI instrument used was a VISION 2000, Finnigan MAT, equipped with a N_2-laser emitting at a wavelength of 337 nm. All spectra have been taken in the reflectron mode. As even in the high mass range the transmission of the used reflectron is in the range of at least 80%, its advantage of a higher resolution compared to the linear mode can still be utilized. A specially designed post-acceleration dynode in front of a SEM is used for an effective detection of the striking large ions. All spectra have been calibrated externally by using BSA (MW 66,430 Da) as a calibrant.

Results

The MW determination of different macromolecules up to a mass of 350 kDa by MALDI has been demonstrated (fig.1). Most of the investigated macromolecules consist of several identical, non-covalently bond subunits. Although an acidic matrix solution has been used, in some cases at least a part of these subunits remained associated, giving ion signals of the entire biomolecule. Dimer ions up to at least 500 kDa have been clearly detected, proving the unrivaled high mass range of MALDI/ TOF-MS (fig.2). Because of the non-uniformity of most large biomolecules due to different species or a heterogeneous glycosylation, it is difficult to specify the accuracy of mass determination in this high mass range. However, by a careful estimation it was presumed in the range of 0.5%. Because this still means a deviation of 1500 Da at a molecular weight of 300 kDa, it is obvious that the mass accuracy has to be improved to give more reliable results. As the reproducibility of the calibration could be shown to be already within 0.2%, better calibration standards with MW closer to those of the large biopolymers might improve the mass accuracy easily. Such standards are highly demanded.

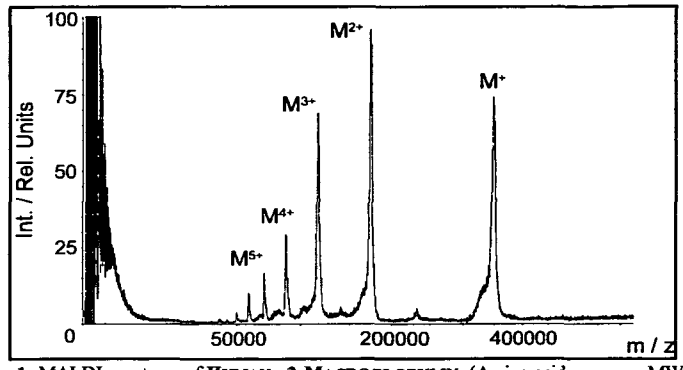

Fig. 1: MALDI spectrum of **HUMAN α2-MACROGLOBULIN**. (Amino acid sequence MW 643,148 Da). 100 laser shots. α2-MG consists of 4 non-covalently bond subunits and is a highly glycosylated protein. Averaged measured MW 349,730 Da, i.e. 2 of 4 subunits stay together despite of the acidic matrix solution. The mass difference between the measured and the amino acid sequence value indicates a glycosylation of Human α2-Macroglobulin in the range of 8 5%.

Subunit amino acid sequence of the **HUMAN α2-MACROGLOBULIN** (MW 160,787 Da - 1450 AA):

```
SVSGKPQYMV LVPSLLHTET TRKGCVLLSY LNETVTVSAL ESVRGNRSLF TDLEAENDVL HCVAFAVPKS SSNEEVMFLT VQVKGPTQEF KKRTTVMVKN
EDSLVFVQTD KSIYKPQQTV KFRVVSMDEN FHPLNKLIPL VYIQDPKGNR IAQWQSFQLE GGLKQFSFFL SSEPFQQSYK VVVQKKSGGR TEHPFTVEEF
VLPKFEVQVT VPKIITILES EMNVSVCGLY TYGKPVPGHV TVSICRKYSD ASDCHGEDSQ AFCEKFSGQL NSHGCFYQQV KTKVFQLKRK EYEMKLHTEA
QIQEEGTVVE LTGRQSSEIT RTITKLSFVK VDSHFRQGIP FPGQVRLVDG NGVPIPNKVI FIRGNEANYY SNATTDEHGL VQFSINTTNV MGTSLTVHVN
YKDESPCYGY QWVSEEHEEA EHTAYLVFSP SKSFVHLEPM SHELPCGHTQ TVQAHYILNG GTLLGLKKLS FYYLDMAKGG IVRTGTHGLL VEQEDMKGHF
SISIPVKSDI APVARLLIYA VLPTGDVTGD SAEYDVENEL ANKVDLSFSP SQSLPASHAH LEVTAAPQSV CALEAVDQSV LLMKPDAELS ASSVYNLLPE
KDLTGFPGPL EDQDDEDCIN EHNVYINGIT YTPVSSTNEK DMYSFLEDMG LKAFTNSKIR KFEMCPQLQQ YEMHGPEGLR VGFYESDVMG EGHARLVHVE
EPHTETVRKY FPETWIWDLV VVNSAGVAEV GVTVPDTITK WKAGAFCLSE DAGLGISSTA SLRAFQPFFV ELTMPYSVIR GEAFTLKATV LNYLPKCIEV
SVQLEASPAF LAVPVEKEQA PHCICANGHQ TVSWAVTPKS LGNVNFTVSA EALESQELCG TEVPSVPEHG RKDTVIKPLL VEPEGLEKET TFNSLLCPSG
GSVSEKLSLK LPPNVVKESA RASVSVLGDI GSAMQETQNY LLQMPYGCGE ENMVLFAPNI YVLDYLNETQ QLTPEIKSKA IGYLNTGYQR QLNYKHYDGS
YSTPGERYGE NQGNTWLTAF VLKTFAQARA YIFIDEAHIT QALIWLSQEQ EDEGCFRSSG SLLNNAIKGG VEDEVTLSAY IKIALLSIPL TVTHPVVEEA
LPCLESAWKT AEKGDHQSHV TTKALLAYAF ALAGNQDKRK EVLKSLNKEA VKKDNSVHWE RPQKPKAPVG HFYEPQAPSA EVEMTSYVLL AYLTAQPAPT
EDLTSATNIN VKNITKQQNA QGGFSSTQDK VVALHALSKY GAATFTKTGK AAQVTIQSSG TFSSKFQVDN NNRLLLQQVS LPELPGRYSM KVTGEGCVYL
QTSLKYNILP EKEEFPFALG VQTLPQTCDE PKAHTSFQIS LSVSTTGSRS ASKMAIVDVK MVSGFIPLKP TVKMLERSNH VSRTEVSSNH VLIYLDKVSN
QTLSLFFTVL QDVPVRDLKP AIVKVYDYYE TDEFAIAEYN APCSKDLGNA
```

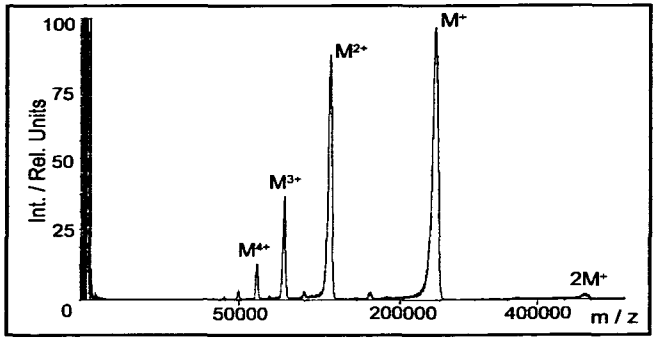

Fig. 2: MALDI spectrum of **SCRI**, a highly glycosylated protein. 60 laser shots, MW unknown. Avrgd. measured MW 246,070 Da. A $2M^+$ signal peak at 492 kDa is clearly observed.

CHARACTERIZATION and QUANTITATION of CHONDROITINASE I (MW 112.5 kDa) and II (MW 111.7 kDa) by ESI/MS and MALDI/MS

Marshall M. Siegel[1], Kiran M. Khandke[1], Keiko Tabei[1], Stefan Berkenkamp[2], Arnd Ingendoh[2], Franz Hillenkamp[2]

[1]American Cyanamid Company, Medical Research Division, Lederle Laboratories, Pearl River, NY 10965
[2]Institute of Medical Physics, University of Münster, D-4400 Münster, FRG

INTRODUCTION Chondroitinase is an enzyme that digests chondroitin sulfate (a sulfated polysacchride) which is part of a proteoglycan that binds the vitreous humor to the retina. Chondroitinase is being developed as a chemical scalpel to separate the vitreous humor from the retina for medical purposes by replacing the conventional scalpel used for this ophthalmic surgery.

RESULTS Two forms of chondroitinase have been discovered and are referred to as chondroitinase I and II. Wide scan ESI and IR-MALDI mass spectra for chondroitinase II are illustrated in Figures 1A and 1B, respectively. Similar spectra were obtained for chondroitinase I. Likewise, mixtures of chondroitinase I and II can be resolved and analyzed by both ESI/MS (Figure 2A: narrow scan data; Figure 2B: transformed maximum entropy data) and IR-MALDI/MS (Figure 2C and 2D: singly and doubly charged molecular ions, respectively). The molecular weights for chondroitinase I and II, computed from the ESI and IR-MALDI mass spectral data, are 112.5 kDa and 111.7 kDa, respectively, which are consistent with predicted molecular weights based upon DNA sequencing data. The estimated molecular weights obtained from SDS-PAGE gels were of the correct magnitude but in reverse order. Table 1 summarizes the measured molecular weight for chondritinase I and II. The mass difference between chondoitinase II and I is 795 Da.

Chondroitinase I and II are produced simultaneously during bacterial fermentation. The relative amounts of both materials were quantitated by ESI/MS and MALDI/MS. Concentration studies by ESI/MS showed that each of the pure chondroitinases had similar linear responses from 0 to 4 pmoles/μL and saturated above 5 pmoles/μL. ESI/MS studies of chondroitinase mixtures of known concentrations, falling within the linear or saturated response regions, showed that the relative responses for chondroitinase I and II are always proportional to the relative concentrations of the components. The saturation effect coupled with a linear relative response is due to the limited number of charges available in the ESI source which randomly ionize the analytes. The rate of formation of chondroitinase mixtures was

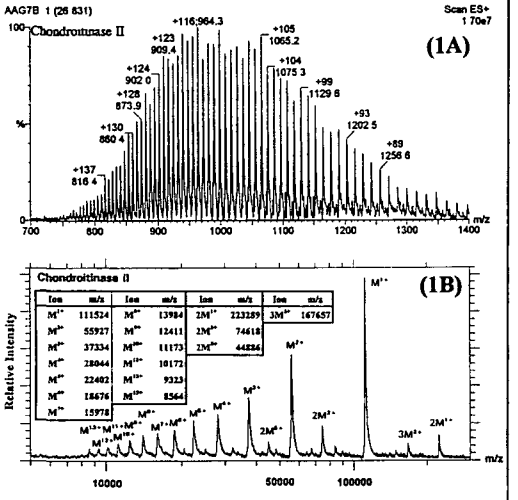

Table 1

Method	Chondroitinase I MW	Δ (Error)	Chondroitinase II MW	Δ (Error)	I - II
DNA	112,507.82	-	111,713.33	-	+795
ESI/MS	112,553 ± 3 (0.003%)	+45 (0.04%)	111,750 ± 1 (0.001%)	+37 (0.03%)	+803
IR-MALDI/MS	112,324	-183 (0.16%)	111,525	-188 (0.17%)	+799
GELS	110 kDa		112 kDa		

Δ = Observed MW - Theoretical MW
I - II = Chondroitinase I MW - Chondroitinase II MW

quantitatively studied by ESI/MS as illustrated in Figure 3. Preliminary quantitative studies by IR-MALDI/MS were consistent with the ESI/MS results.

Degradation products of chondroitinase I were characterized by UV-MALDI/MS (MW 95,370±60; MW 16,630±50) and correlated with corresponding amino acid residues of chondroitinase I (AA 158-997, MW 95,022.4; AA 1-157, MW 17,503.4). Note that these two fragment ions correspond to cleavage of the amide linkage between AA residues 157 and 158 of chondroitinase I.

Chondroitin sulfate was degraded by chondroitinase. Isolated fractions were analyzed by ESI/MS and found to be only sulfated disaccharides and tetrasaccharides with from 1 to 3 sulfate moieties present.

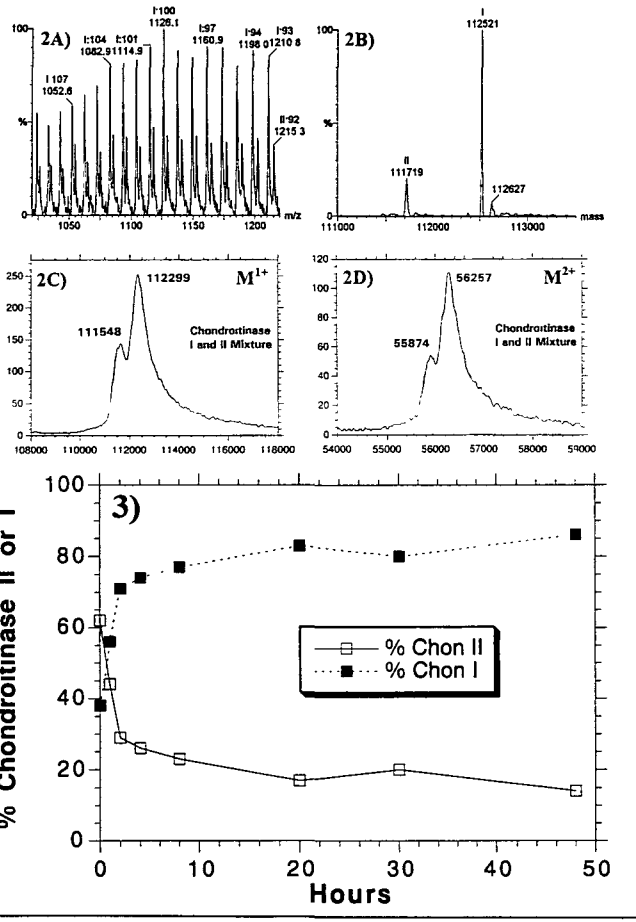

DISTRIBUTION and LOADING of CALICHEAMICIN DERIVATIVES CONJUGATED to MONOCLONAL ANTIBODIES by IR-MALDI/MS and ESI/MS

Marshall M. Siegel[1], Keiko Tabei[1], Arthur Kunz[1], Stefan Berkenkamp[2], Franz Hillenkamp[2]
[1]American Cyanamid Company, Medical Research Division, Lederle Laboratories, Pearl River, NY 10965;
[2]Institute of Medical Physics, University of Münster, D-4400 Münster, FRG

INTRODUCTION Calicheamicin and its derivatives are potent enediyne-containing antitumor antibiotics which function by cleaving DNA. Calicheamicin derivatives (MW ~1.5 kDa) conjugated to monoclonal antibodies (MoAbs, MW ~150 kDa) are being developed as targeting agents for anticancer therapy and have shown promising results in irradicating solid cancer tumors in laboratory animals and are presently undergoing clinical trials in leukemia patients. The average loading values for calicheamicin conjugates studied to date by UV-MALDI/MS were 2-5 times less than the values obtained by UV absorption spectrometry, immunoassay and biological assays [1]. In addition, the distribution of calicheamicin derivatives conjugated to MoAbs were not obtainable from these assays. These poor correlations with accepted biochemical assays prompted us to seek out the causes of these failures. Previous work [2] demonstrated the lability of calicheamicin derivatives and calicheamicin MoAb conjugates under UV-laser irradiation and that calicheamicin loading values as well as drug distributions can be obtained using IR-lasers in the MALDI/MS experiments with succinic acid. We now demonstrate that neutral glycerol is a better IR-MALDI matrix and the limitations of ESI/MS for determining accurate loading values and distributions for calicheamicin conjugates with stable linkers.

EXPERIMENTAL The IR-MALDI mass spectrometer was a reflector-type time-of-flight mass spectrometer. The IR laser system used was an Er-YAG, wavelength 2.94 mm (3401 cm^{-1}), pulse width 150-180 ns (electro-optically Q-switched) (Schwartz Electro Optics, Orlando, FL). The spot size diameter was ~200 μm (focused by a ZnSe lens having a 127 mm focal length) with irradiance of about 10^{+6} - 10^{+7} W/cm^2. The acceleration voltage was 12.3 kV. Electrospray ionization mass spectra were obtained with a VG Quattro triple quadrupole mass spectrometer equipped with a VG electrospray source, rf hexapole lens and Megaflow gas nebulizer probe.

RESULTS Figures 1A-1 and 1A-2, respectively, illustrate the singly and doubly charged parent ion peaks for pure gCTM01 MoAb using (frozen) glycerol as the matrix. An unusual feature of the MALDI mass spectra of MoAbs is that resolutions up to ~200 are achieved routinely in the IR-MALDI mode which is

Figure 1

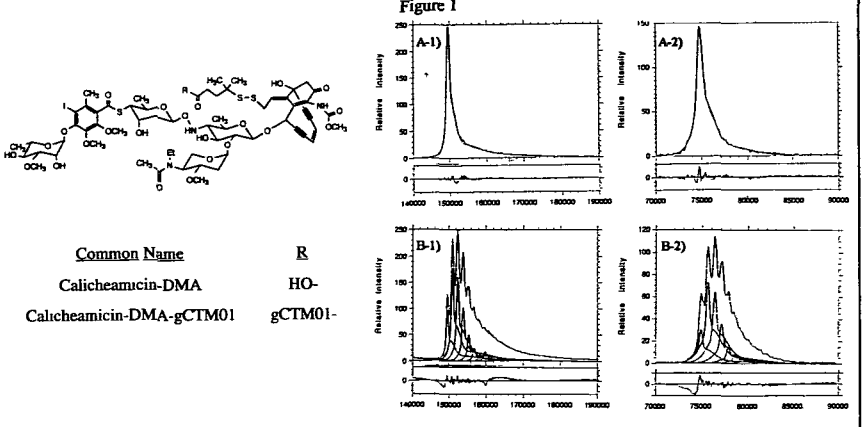

Common Name	R
Calicheamicin-DMA	HO-
Calicheamicin-DMA-gCTM01	gCTM01-

about 2 times greater than can be achieved in equivalent measurements in the UV-MALDI mode. Figures 1B-1 and 1B-2, respectively, illustrate the singly and doubly charged parent ion peaks for low levels of calicheamicin-DMA conjugated to gCTM01 MoAb using (frozen) glycerol as the matrix. All the IR-MALDI/MS peak profiles in the observed spectra of the MoAbs conjugated to calicheamicin derivatives are broadened relative to the pure MoAb peak widths and are modulated. The mass difference between each maximum in the modulated peak corresponds to 1,460 daltons which is the mass change for the covalent addition of different numbers of calicheamicin-DMA molecules to the MoAb. The distributions of the calicheamicin derivatives conjugated to the MoAbs were calculated by deconvoluting the modulated peak profiles of the IR-MALDI spectra of the MoAb conjugates (See Figures 2A and 2B) using the peak profiles of the pure MoAbs as the basis functions. IR-MALDI/MS (with glycerol matrix) average distribution loading values (1.95) computed for MoAb conjugates made with the stable DMA linker were very similar to those computed from UV absorption spectrometry data (2.00). UV absorption spectrometry loading values correlated poorly with ones obtained using UV-MALDI/ MS with nicotinic acid matrix and using IR-MALDI/MS with succinic acid matrix [2].

Wide and narrow scan ESI/MS spectra are illustrated respectively in Figures 2 and 3 for pure gCTM01 MoAb and for low levels of calicheamicin-DMA conjugated to gCTM01 MoAb. Unique features of the spectra are the broad charge distribution and partial resolution (modulation) of the peaks. The transformed and integrated maximum entropy (resolution enhanced) spectra are illustrated in Figure 3. The modulation of the molecular ion peak is due to the heterogeneity of the polysaccharide present in the MoAb which corresponds to mass increments of 162 Da consistent with the addition of mannose or galactose units to the lowest mass immunoglobulin glycan. For the MoAb-conjugate sample, note the appearance of a new series of peaks each ~1,460 Da apart. relative to the peaks in the corresponding spectra for pure gCTM01 MoAb. This mass difference corresponds to the mass change of the MoAb after the covalent addition of calicheamicin-DMA via an amidation reaction. These ESI/MS distribution average loading value (1.28) is lower than the UV absorption average loading value (2.00) and less reliable than the IR-MALDI/MS result (1.95) due to the difficulty in resolving the overlapping multiply charged peaks arising from the heterogeneity of the covalently bound calicheamicin-DMA drug and the polysaccharide in the monoclonal antibody.

[1] Siegel, MM.; Hollander, I.J.; Hamann, P.H.; James, J.P.; Hinman, L.; Smith, B.J.; Farnsworth, A.P.H.; Phipps, A.; King, D.J.; Karas, M.; Ingendoh, A.; Hillenkamp, F. *Anal. Chem.* (1991) **63**, 2470-2481.
[2] Siegel, M.M.; Kunz, A.; Bell, D.; Berkenkamp, S.; Karas, M.; Ingendoh, A.; Hillenkamp, F. *Proceedings of the 42nd ASMS Conference on Mass Spectrometry and Allied Topics,* (1994) Chicago, IL, May 29 - June 3, p. 967.

Figure 2 Top: gCTM01
Bottom: Calicheamicin-DMA-gCTM01

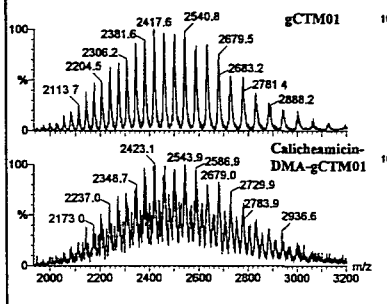

Figure 3 Top gCTM01 Bottom: Calicheamicin-DMA-gCTM01

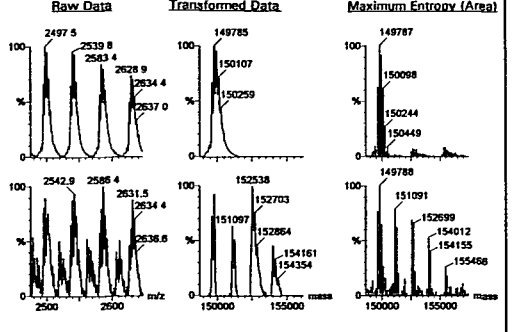

CHARACTERIZATION of FILAMENTOUS HEMAGGLUTININ (FHA) (MW 230 kDa), LYSYL-FHA and FRAGMENT A by ESI/MS and MALDI/MS

Marshall M. Siegel[1], Dai-Fang Liu[2], Keiko Tabei[1], Stefan Berkenkamp[3], Franz Hillenkamp[3]

[1]American Cyanamid Company, Medical Research Division, Lederle Laboratories, Pearl River, NY 10965
[2]American Cyanamid Company, Lederle-Praxis Biologicals Division, West Henrietta, NY 14586
[3]Institute of Medical Physics, University of Münster, D-4400 Münster, FRG

FHA is a major adhesion protein of *Bordetella pertussis*, the etiological agent of whooping cough. This protein is a component of a number of acellular pertussis vaccines. The MW of FHA was estimated from SDS-PAGE gels to be approximately 220 kDa. FHA was analyzed by ESI/MS (Figure 1A) and IR-MALDI/MS (Figure 2A) and found to have a molecular weight of 230,544±11 and 230,240±60 kDa, respectively. The ESI/MS MW value was computed from narrow scan data (Figure 1B) by minimizing the average mass error in the average MW by systematically varying the charge assignments to the observed multiply charged peaks (Figure 1C). Figure 1D illustrates the transformed ESI mass spectrum for FHA.

Lysyl-FHA, developed as a more soluble form of FHA, was prepared by mixing FHA with a very large molar excess of L-lysine followed by titration with formaldehyde. Lysyl-FHA was formed by linking lysine to FHA via a methylene group by the reaction of the addition product of lysine and formaldhyde with the active hydrogen atoms in FHA. The amount of lysine covalently bound to the FHA was quantitated by IR-MALDI/MS. Figure 2A, 2B and 2C illustrate respectively the singly, doubly and triply charged molecular ion regions of the IR-MALDI mass spectra for the pure FHA and the Lysyl-FHA components. (SDS-PAGE was incapable of distinguishing between FHA and Lysyl-FHA.) Mass centroids were computed for both components. (The mass centroid for Lysyl-FHA was computed from the sharp peak in the spectrum. The ions on the low mass side of the sharp peak are degradation products present in the impure FHA used in this preparation and were ignored for this calculation.) The IR-MALDI/MS loading values for lysine is computed from the difference in the mass centroids between Lysyl-FHA and pure FHA divided by the mass change upon the addition of one methylene-linked lysine moiety to FHA (158 Da). Figure 2D illustrates the data used for the loading calculations. The lysine loading value by IR-MALDI/MS was found to be 15.2±2.3 and the average MW for this batch of Lysyl-FHA was 232,640±360.

Fragment A, a recombinant protein containing the putative carbohydrate recognition domain of FHA which is critical for bacterial adherence, was purified from *E. coli*. ESI mass spectra obtained at the pH's of 3 and 10 (Figures 3A and 3B, respectively) revealed that Fragment A has a molecular weight 29,659.0±1.0 which is about twice that of the 14,812.4 kDa MW predicted from the DNA sequence. The ESI experiment was performed at the basic pH to demonstrate that the experiment at the acidic pH did not induce dimerization. Upon reducing the protein with dithiothreitol, the molecular weight computed from the ESI mass spectrum (Figure 3C) was 14,822±2.0, confirming that Fragment A is produced as a dimer.

1A)

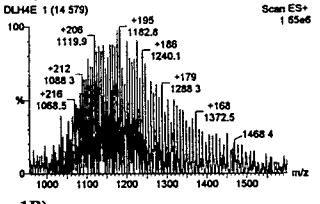

1C)

Observed M/Z	Calculated Mass	Z	Calculated Mass	Z	Calculated Mass	Z
1177.3	229382.4	195	230558.7	196	231735.0	197
1183.3	229368.2	194	230550.3	195	231732 8	196
1189.4	229353.5	193	230541.8	194	231730.2	195
1195 6	229361.2	192	230535.9	193	231750 5	194
1201.6	229322.3	191	230522.9	192	231723.5	193
1207.9	229316.7	190	230523.6	191	231730 6	192
1214.4	229336.4	189	230549.8	190	231763.2	191
1220.8	229329 9	188	230549.8	189	231769.6	190
AV MASS	229346.3		230544.1		231741.9	
AV ERROR	20 0		11.0		14 4	

1B)

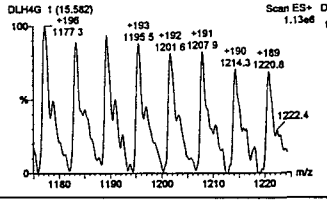

1D)

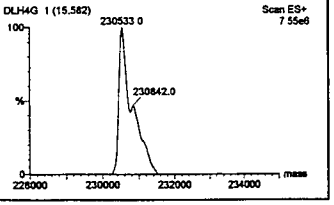

43rd ASMS Conference on Mass Spectrometry and Allied Topics

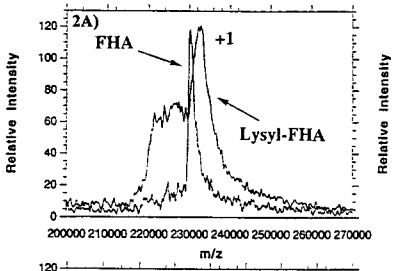

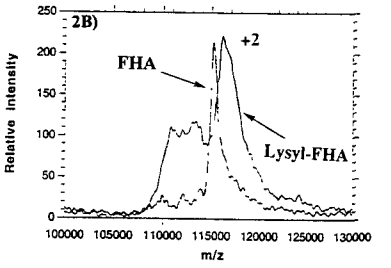

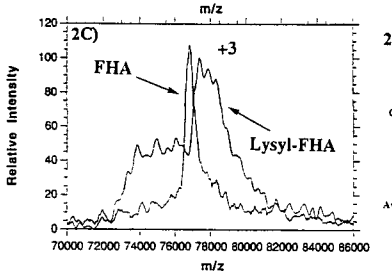

2D)

Lysyl-FHA Loading Calculation

Charge (z)	Lysyl-FHA (m/z)	MW Lysyl-FHA z*(m/z)	FHA (m/z)	MW FHA z*(m/z)	MW Lysyl-FHA - MW FHA (Δ)	IR-MALDI Loading (Δ/158)
+1	232,350	232,350	230,190	230,190	2,160	13 7
+2	116,270	232,540	115 110	230 220	2,320	14 7
+3	77,680	233 040	76,770	230,310	2 730	17 3
Average Value		232,640±360		230,240±60		15 2±2.3

Raw Data | **Transformed Data**

3A) Fragment A at pH 3

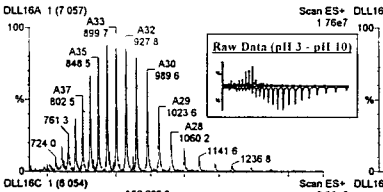

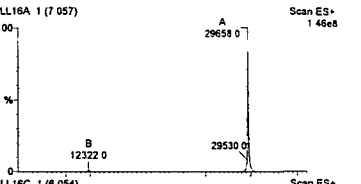

3B) Fragment A at pH 10

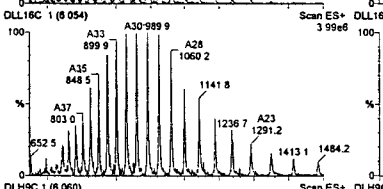

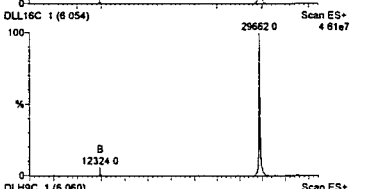

3C) Fragment A + Dithiothreitol (DTT)

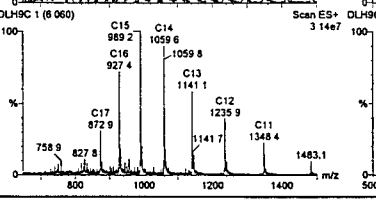

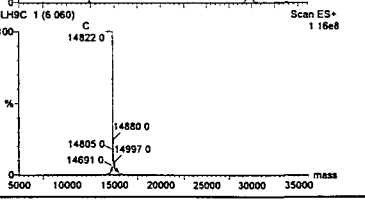

Observation of holoprotein molecular ions of several ferredoxins by electrospray-ionization mass-spectrometry .

Yves Pétillot[1], Eric Forest[1], Jacques Meyer[2], Jean-Marc Moulis[2]
[1]Institut de Biologie Structurale (CEA/CNRS), [2]Departement de Biologie Moleculaire et Structurale (CEA), 38 Grenoble, France.

In order to characterize **iron-sulfur proteins**, we have defined experimental conditions leading to their holoprotein state detection by **ESI-MS**. For this purpose we took advantage of the fact that most ferredoxins and rubredoxins are negatively charged at neutral pH, where their stability is highest. Thus, the implementation of the negative-ion detection mode (**ESI⁻**) at neutral pH has already proved to be more successful than the positive-ion detection mode (**ESI⁺**) at acidic pH: in negative-ion detection mode, the mass spectra displayed contributions of only the protein with its bound metallic ion (1). We report here an extension of these studies to several proteins containing iron-sulfur clusters(2).
High-potential [4Fe-4S] ferredoxin (HiPIP) extracted from *Chrom. vinosum* (Cv. Fd) was analysed in **ESI⁺** and in **ESI⁻**, as shown in **Fig.1a** and **1b**, respectively. The relatively low charge state observed in **ESI⁻**, indicates that the deprotonation sites react less easily in this slightly basic solution than the protonation sites under the conditions of **ESI⁺**. The measured masses are in good agreement with the calculated mass of the holoprotein (M=9252.6)
Low potential 2[4Fe-4S] ferredoxins extracted from *Clostr. pasteurianum* (Cp. Fd), *Clostr. acidurici* (Cau.Fd), *Chrom. vinosum* (Cv.Fd), did not yield satisfactory results in **ESI⁺**, but in **ESI⁻** no evidence for degradation of these unstable proteins was found and the mass mesured for each protein fits closely with the calculated mass of the holoforms (M=6194.5, M=6234.5 and M=9750.4, respectively).
[2Fe-2S] spinach ferredoxins: two isoforms (Sp.Fd-I and Sp.Fd-II) have been evidenced in spinach chloroplasts. In **ESI⁺**, both isoforms give a coherent series from 6 to 11 charges which could correspond to the protonation of all basic residues plus the four glutamines; these data suggest a complete unfolding of the polypeptide chain with the loss of the iron-sulfur cluster. The reconstrusted spectra in insets yielded molecular masses which are in good agreement with the calculated values (M=10,482.5 and M=10,334.4, respectively) for the apoproteins. In **ESI⁻**, the mass spectra of the two isoforms are different and display a serie from 5 to 12 charges for Sp.Fd-I and only two charge states for Sp.Fd-II which are both well below the number of potential negative sites (23 and 22, respectively): this can be explained by the proteins remaining folded and limiting acces of the solvent to the deprotonation sites. Reconstructed mass spectra indicate molecular mass in good agreement with those calculated (M=10,654.3 and M=10,506.2, respectively) for the holoforms .

1. Pétillot, Y., Forest, E., Mathieu, I., Meyer, J., and Moulis, J.-M. (1993) *Biochem. J.*, **296**, 657-661.
2. Pétillot, Y., Forest, E., Meyer, J. and Moulis, J.M. *Anal. Biochem.* in press.

43rd ASMS Conference on Mass Spectrometry and Allied Topics

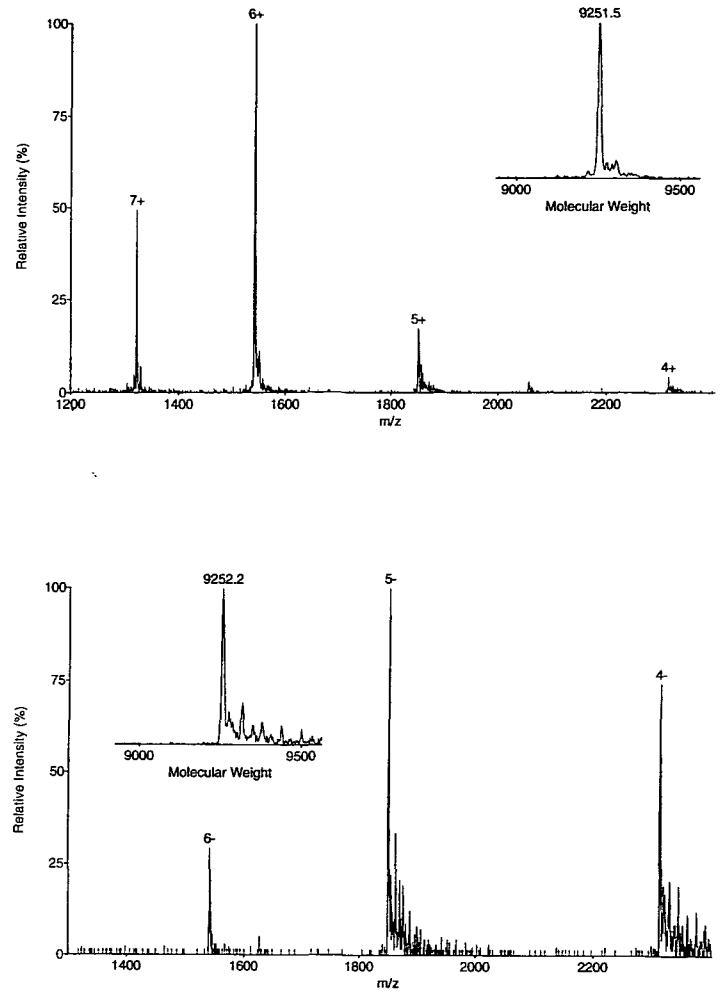

Figure 1: ESI mass spectrum of *C. vinosum* HiPIP:
a)in positive-ion mode; b) in nagative mode.

PROTEOLYTIC PEPTIDES OF RHODOPSIN ANALYZED BY MALDI-TOF

David Barnidge, Ed Dratz, and Jan Sunner
Dept. of Chemistry and Biochemistry
Al Jesaitis
Dept. of Microbiology
Montana State University, Bozeman, MT 59717
email: UCHJS@EARTH.OSCS.MONTANA.EDU

Integral membrane proteins play a vital role in a variety of cell functions. Their part in signal transduction has prompted a great deal of research into the mechanisms involved in transporting a signal across a membrane and in promoting cell response to stimuli such as chemotaxis. In order to study these events, techniques including affinity labelling, fluorescent probes, and peptide mapping have been used.

The use of mass spectrometry to identify proteolytic peptides from integral membrane proteins modified by biological techniques has been limited due to the hydrophobicity of the fragments. Digestion of an integral membrane protein followed by analysis of the mixture using MALDI-TOF does not produce an adequate map of the protein due to aggregation of the peptides and the subsequent loss of ionization. The use of LC-ESI with standard water:acetonitrile gradients will not elute hydrophobic fragments.

In order to utilize mass spectrometry as a tool to analyze a mixture of proteolytic peptides we have been using a technique that separates a mixture of hydrophobic peptides prior to mass analysis. The separation method was developed by Tomich et. al. *[1]* and involves RP-HPLC using a C_4 column and mobile phase containing octyl-β-glucoside (OG). The digest is made 20mM (2 x CMC) in SDS and 2% formic acid prior to injection to reduce aggregation and loss of peptides to the column.Samples are fractionated, concentrated, and analyzed by MALDI-TOF using ACHCA matrix.

The objective of this method is to have a mass analysis technique that will allow the identification of modified sites on an integral membrane protein including post-translational modifications. It will also be used to identify structural information such as transmembrane fragments and extramembrane loops. We present here identification of transmembrane segments and the heterogeneously glycosylated N-terminus of the G protein-coupled receptor rhodopsin.

Table 1 is a list of tryptic peptide fragments from rhodopsin. The model by Dratz and Hargrave [2] list each fragment as having at least one transmembrane sequence. The peptides with an asterisk * have been identified using detergent modified RP-HPLC and MALDI-TOF.

Figure 2 is a chromatogram from a tryptic digest of affinity purified rhodopsin in 0.1% OG. The peptides represented are listed next to the retention times.

Figure 3 is a MALDI-TOF spectra from the peak at 48.59 min. It is from the #1 transmembrane peptide. The peak at 5462.46Da is the #1 fragment plus an additional lysine due to incomplete digestion. Late eluting hydrophobic peptides having the mass of transmembrane peptide #5 were found however due to the closeness in mass to fragment #1 the true identity of the fragment was not conclusive. Work with absorbance spectra of these fragments is ongoing. Spectra

containing the mass of fragment #2 plus a formyl group were found but the parent ion was not. This may be fragment #2 due to the formic acid used in this procedure.

1. J. M. Tomich, L. Carson, K. Kanes, N. Vogelaar, M. Emerling, and J. Richards (1988) *Anal. Biochem.* **174**, 197-203.
2. E. A. Dratz and P. A. Hargrave (1983) *Trends Biochem. Sci.* **8**, 128-131.

Table 1
List of transmembrane fragments from a tryptic digest of rhodopsin

Number	From -To	Mass	Sequence
1*	22 - 66	5331.33	*SPFEAPQYYLAEPWQFS*
			...LGFPINFLYLYVTVQHK
2	70 - 135	7233.40	*TLPNYILLNLAVADLFMV*
			...ATLGGEIAWSLVVAIER
3*	148 - 177	3259.82	*FGENHAIMGVAFTWVMA*
			...LACAAPPLVGWSR
4*	178-231	6528.52	*YIPEGMQCSCGIDYYTPH*
			..IIPLIVIFFCYGQLVFTVK
5	253 -296	5329.11	*MVIIMVIAFLICWLPYAGV*
			GSDFGPIFMTIPAFFAK

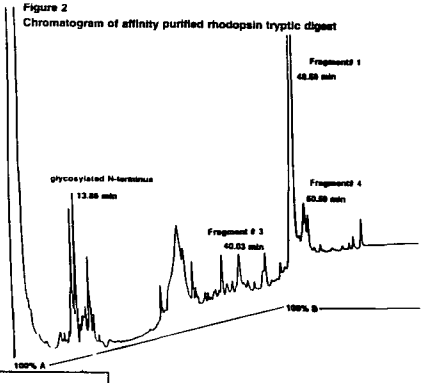

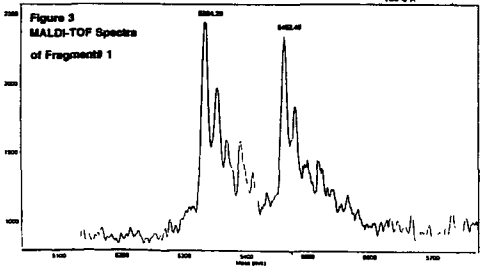

Analyses of Hydrophobic Peptides and Proteins using ESI- and APCI-MS

Bernhard C. Pellascio, Urs P. Schlunegger, Institute of Organic Chemistry, University of Berne, Berne, Switzerland

Johann Schaller, Donald Kaesermann, Institute of Biochemistry, University of Berne, Berne, Switzerland

INTRODUCTION: Over the past few years electrospray (ESI) and atmospheric pressure chemical ionization (APCI) have been playing an increasing role in the characterization of biomolecules. Up to day analyses have been performed mainly with biopolymers soluble in aqueous solutions; therefore data of hydrophobic peptides and proteins are seldomly reported in the literature [lit. 1].

The hydrophobic membrane protein bacteriorhodopsin (BR) forming the proton pump in the lipid bilayer of the bacterium *Halobacterium halobium* consists of the chromophore retinal and the protein bacterioopsin (BO). We present here mass spectrometric data of BO and its fragments. BO was cleaved with protease V8 from *Staphylococcus aureus* into two fragments, V-1A/B (Glu-1 to Glu-161/166) and V-2A/B (Glu-161/166 to Glu-232). Cyanogen bromide cleavage of V-2 at Met-209 produces two fragments ψ, ψA (Ser-162 to Hse-209) and ψB (Val-167 to Hse-209) and a fragment ω (Val-210 to Glu-232).

MATERIALS AND METHODS: The spectra were acquired on a VG Platform II (Fisons/VG, Manchester UK). The mass spectrometer was scanned from m/z 700 to 2500 in 10 s. For one analysis ten scans were used. The samples were dissolved either in the carrier solvents or in hexafluoroisopropanol. The flow rate was 10 µl/min. Typical used sample quantities were 100-200 pmol per analysis. The separations were carried out on a HPLC system from Applied Biosystems with a 759A absorbance detector, a 140B solvent delivery system and a phenyl aquapore column. After the isolation of BR the chromophore retinal was removed by bleaching to leave the protein BO. BO was cleaved with protease V8 and cyanogen bromide to produce the fragments V-1, V-2, ψA/B and ω (according lit. 2).

RESULTS: Influence of carrier solvents: The samples BO, V-2A/B, ψ and ω were dissolved in hexafluoroisopropanol and subjected to ESI-MS and APCI-MS with three different carrier solvents: **1. neat formic acid; 2. chloroform:methanol:water (2:5:2, v/v/v) with 2% HOAc; and 3. acetonitrile:water (1:1, v/v).** The carrier solvent chloroform:methanol:water gave excellent results for V-2A/B whereas neat formic acid was best for BO. With the carrier solvent usually used in ESI-MS, acetonitrile:water (1:1, v/v) no good spectra could be obtained. FIG. 1 and FIG. 2 show the maximum entropy processed spectra and in the inset the transformed

mass (calculated mass: V-2A 7147.6 Da; V-2B 7747.3 Da; BO 26785 Da).

Similar experiments were also carried out with APCI-MS but no good results could be obtained. It seems that APCI-MS is not the appropriate method for hydrophobic peptides and proteins.

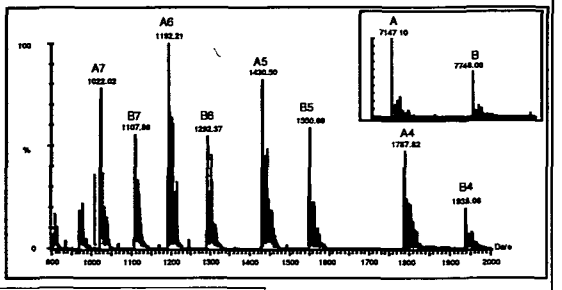

FIG. 1 Electrospray mass spectrum of the fragments V2-A/B (A calculated mass: 7147.6 Da; B calculated mass: 7747.3 Da) with chloroform:methanol:-water (2:5:2, v/v/v) containing 2% HOAc as carrier solvent. The transformed spectrum is shown in the inset.

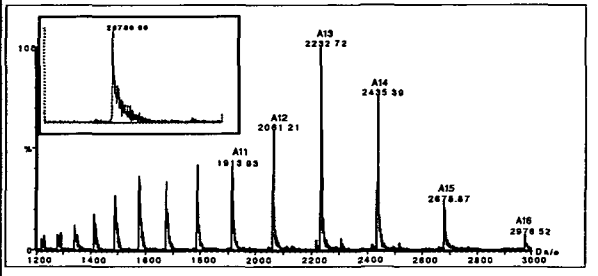

FIG. 2 Electrospray mass spectrum of bacterioopsin with neat formic acid as carrier solvent (calculated mass: 26785 Da). The transformed spectrum is shown in the inset.

Influence of source temperature: All fragments of BR were measured under the same conditions as described above except the source temperature: **a) 60°C; b) 100°C**. For all fragments the results were better at a source temperature of 60°C (spectra not shown).

CONCLUSIONS: Formic acid is well known to be an excellent solvent for hydrophobic peptides and proteins. We were able to show that formic acid is as well a very powerful carrier solvent for ESI-MS. However, care must be taken not to allow samples to remain in neat formic acid. The chloroform:methanol:water mixture is especially useful for smaller fragments and peptides. The solvents usually used in ESI are useless for hydrophobic peptides and proteins because of their insolubility in conventional solvents without detergents. The results of the APCI-MS experiments show that this method is not yet fully developed to analyse hydrophobic peptides and proteins. It will be an aim in the future to continue the development of the APCI-MS technique. A source temperature of more than 60°C is disadvantageous with a substantial loss of sensitivity.

LITERATURE: 1. P.A. Schindler, A. Van Dorsselaer, A.M. Falick *Anal. Biochem.* **213**, 256-263 (1993); 2. C. Longstoff, R.R. Rando, *Biochem.* **26**, 6107 (1987)

HEREGULIN / EPIDERMAL GROWTH FACTOR CHIMERAS: A STRUCTURAL STUDY

K.J. Rosnack, J.G. Stroh, B.C. Guarino, D.H. Singleton, E.G. Barbacci, J.D. Moyer, G.C. Andrews
Pfizer Inc, Central Research, Eastern Point Road, Groton, CT 06340

The heregulins (HRGs) are a family of proteins that stimulate the tyrosine phosphorylation of p185^{erbB2} and have a region of high homology to EGF. Although HRG was initially proposed to act as a ligand for p185^{erbB2}, subsequent studies revealed that binding of HRG did not correlate with p185^{erbB2} expression. Further studies have demonstrated that *erb*B4, *erb*B3, and their heterodimers are receptors for HRG. These receptors and EGFR have substantial homology both in the intracellular and extracellular domains and therefore may bind ligands that also share common structural features.

Although there are multiple receptors for the HRGs, both EGF and HRG bind to breast cancer cells with complete specificity (EGF does not block HRG binding nor does HRG block EGF binding.). This specificity is obtained despite topological similarity generated by three conserved disulfide bonds in their core domains. A 65 amino acid EGF-like domain of heregulin β1, amino acids 177-241, was shown to be sufficient for high affinity binding. The receptor binding domain of heregulin β and heregulin α have been synthesized, and a series of truncated synthetic HRGs and EGF/HRG chimeric peptides were utilized to determine the essential structural elements of HRG receptor binding.

Mass Spectrometry was used in this project to determine molecular weight for each peptide using direct infusion electrospray ionization (ESI) mass spectrometry (MS). Disulfide bond determination was accomplished for HRG and HRG chimeras using chemical and enzymatic digestion followed by liquid chromatography mass spectrometry (LCMS).

Direct Infusion ESI Mass Spectrometry was used to confirm the molecular weights of each of the synthesized peptides. Disulfide bond analysis was accomplished using chemical and enzymatic digestion followed by LCMS analysis. Two peaks of interest were observed in the LCUV trace from a Heregulin α (177-227) tryptic digest. The observed MW (1679 1 Da) for Peak #1 corresponds to the tryptic fragment shown in Figure 1C (right) while the observed MW (2131.3 Da.) for Peak #2 corresponds to the tryptic fragment shown in Figure 1C (left). From the information contained in this experiment, one disulfide bond was confirmed. A Glu-C digest of the tryptic digested material was necessary to confirm the remaining disulfide bonds.

The LCUV trace from the Glu-C digest of the previous sample gave one peak of interest. The observed molecular weight (1349.6 Da.) corresponds to the fragment shown in Figure 1D (right). Results from this experiment confirmed a second disulfide bond. The third disulfide bond shown in Figure 1D (left) was not observed but can be inferred.

Other Heregulin chimeras were analyzed in the same fashion. Complete disulfide bonding patterns could not be determined for EGF and EGF chimeras by this method. These compounds were then subjected to the binding and phosphorylation testing.

For both HRGα and HRGβ, a 50 amino acid region (177-226) was fully active both for binding to cellular receptors and for stimulation of p185 phosphorylation. Further truncation by a single amino acid or two amino acids reduced both the receptor binding and phosphorylation by > 100-fold. Thus the critical binding and activation are contained within a 50-amino acid portion of the heregulins beginning at amino acid 177 and ending with amino acid 226.

Alignment of the core regions of HRGα with HRGβ and EGF with HRGβ shows the extensive homology within this family. On the basis of the results with the truncated HRG's, we examined chimeras of EGF 1-48 and the core 50-amino acid region of HRGβ to determine the essential structural elements of HRG receptor binding and the basis for receptor binding selectivity.

Substitution of any single cysteine bound region of EGF or the EGF C-terminus into HRG produced a chimera that retained full affinity for the HRG receptor and the ability to stimulate the p185 phosphorylation in cell. It had no affinity for the EGF receptor. All the HRG chimeras were potently active. Even the region 197-209 of HRG, postulated to be involved in receptor binding, can be replaced with EGF 21-30 without loss of binding affinity. Results indicate that neither the regions between cysteine residues nor the C-terminus contribute to the specificity of binding for EGFR vs. HRGR.

Substitution of the HRG 177-181 (SHLVK) for the N-terminus of EGF produced a chimera which bound both receptors with high affinity. Specific binding of both EGF and HRG could be completely blocked by this chimera. This chimera was as active as EGF in the EGFR autophosphorylation and was highly active in the stimulation of p185 phosphorylation. The EGF chimera with the HRG 191-195 had moderate affinity for both receptors.

Substitution of individual amino acids had little effect on the affinity for the HRG receptor. However, removal of amino acids 177 & 178 reduced affinity for the HRG receptor by >10-fold, without a corresponding effect on affinity for the EGF receptor. This supports the conclusion that amino acids 177-181 are of specific importance for binding to the HRG receptor. While the region comprising residues 177-181 of HRG are important elements for binding specificity, additional regions are also necessary for high affinity binding -- most notably, loss of the C-terminal residues at 225-226 ablated activity.

Mass Spectrometry confirmed the molecular weights of all synthesized products. Sequential digestion followed by LCMS analysis confirmed the disulfide bond pattern of the heregulins and heregulin chimeras. The complete disulfide bond analysis of Epidermal Growth Factor and EGF chimeras was not possible. Substitutions of EGF sequences for HRG regions bound by conserved cysteine residues, or substitution of the EGF C-terminus for that of HRG, had no effect on binding affinity for the HRG receptor. Several amino acids in EGF shown to be important in EGFR binding such as Tyr13, Tyr37, and Arg41, are either conserved or replaced with conservative substitutions (Tyr to Phe) in the HRG's Results suggest that the conserved residues in the intracysteine regions of EGF and HRG together with the unique HRG N-terminus are essential elements of HRG binding. Results suggest that the specificity for the HRG receptor is entirely generated by the HRG N-terminus. Findings also suggest that it may be possible to design compounds that combine activity for the two receptors at various ratios.

Figure 1
Tryptic & Glu-C Fragments

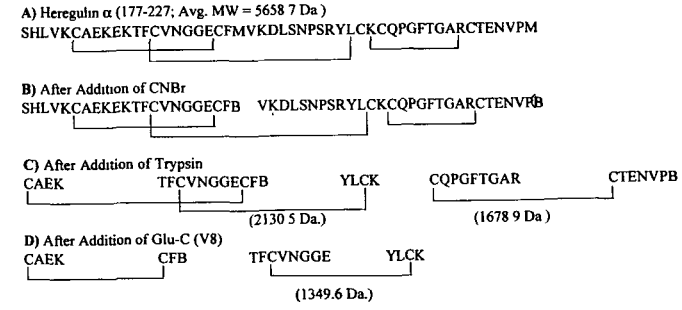

LC-MS PEPTIDE MAP OF HIRUDIN BY USING THE UNSPECIFIC PROTEASE THERMOLYSIN

Harald A. Zilg * and Birgit Schultz **
*Research laboratories of Behringwerke AG, D- 35001Marburg, Germany
**FH Ostfriesland, Dept. of Biotechnology,D- 26723 Emden, Germany

Peptide mapping of a recombinant therapeutic protein generally is performed using highly specific proteases. The ruggedness of the method justifies its use for quality control, as any structural deviation is most probably seen in the peptide map, e.g. by appearance of a new peptide peak.However limitations sometimes are: a) the peptides obtained are not small enough to reveal structural deviations, b) the cleavage sites are not domains of the protein where they are mostly needed, e.g. when analysing disulfide pairing in native protein digest.

Hirudin, the highly potent thrombin inhibitor from the leech HIRUDO MEDICINALIS *is also* being expressed in yeast. Part of our aim to confirm the structure of a variant of hirudin was devoted to cystine bridge positions. These should link the cysteines in amino acid position 6-14, 16-28 and 22-39 in the core domain of the 65 amino acid peptide. The only protease found to cleave the hirudin amino acid chain between C(14) and C(16) was thermolysin with its broad specificity to cleave at the N-terminus of the following amino acids in the order of decreasing activity: L > F > I, V, M, A > Y, G, T, S. Some cystine bridge containing peptides have been described (1).

Complete identification of hirudin peptides obtained by thermolysin digest was possible *using reversed phase HPLC combined with Electrospray MS. The large number of* cleavage sites including some unexpected sites allowed the identification of numerous cystine bridged peptides and to prove correct disulfide pairing. Due to slow and fast cleavage reactions along the amino acid chain a pathway in the formation of individual peptides can be derived from thermolysin digest kinetics followed by LC- MS:

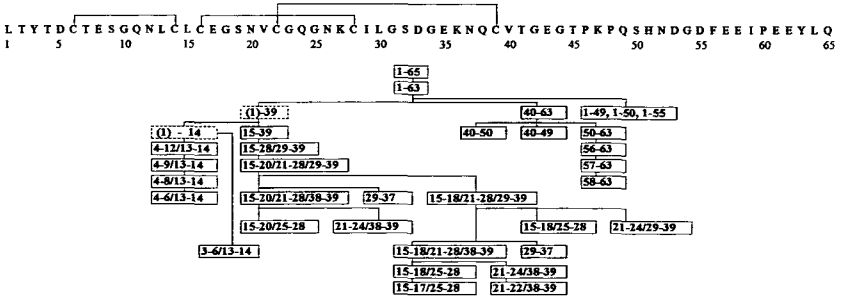

Some of the intermediates were not found as indicated by dotted lines, but were derived from occurrence of others. A number of peptides were identified with the expected cystine bridges. A few peptides exhibited even two. It is evident that the correct disulfide pairing in hirudin is confirmed by these results.

For a therapeutic protein absence of structural variants with mismatched cystine bridges has to be shown. Thermolysin digest yield is nearly quantitative for cystine bridge C(6)- C(14) containing peptides. However peptides derived from the domain of the molecule containing the intertwined two other cystine bridges C(16)- C(28) and C(22)- C(39) are either not formed in considerable amount by the digestion or the digestion did produce peptides too small to be seen in Electrospray- MS. The identification cut- off is near 300 amu which means that penta- to hexapeptides with two charges are not detectable by and large. Thus digest yield is no promising approach.

We then focussed our attention on the positive identification of structural variants with mismatched disulfide pairing. This was based on the observation that rapid reoxidation of completely reduced hirudin is leading to structure variants with higher retention than hirudin in RP- HPLC, but identical molecular mass by direct Electrospray- MS. Similar behaviour was described for a hirudin core peptide, which indeed exhibited structural properties of a mismatched variant (2).

When the thermolysin peptide map is performed on the higher retention fraction of hirudin according to the procedure for hirudin itself, we observed several unusual peptides in the chromatogram. To identify these peptides we used a list of all thermolysin peptides derived from the 14 structural variants of hirudin with mismatched disulfide pairing (F1- F14). Some of the peptides found definetely are not expected with hirudin. For example at 30.77 min retention an m/z signal of 824 originates most probably from a peptide with C(16)- C(22) or C(22)- C(28) disulfide pairing:

Peptide analysis of a mismatched hirudin variant - chromatogram segment 27- 33 min

RT (min)	Mass (theory)	variant	peptide	m/z found	Intensity	m/z found	Intensity
27,667	639,30	F2, F11, F14	15-18<->21-22	639,00	127500		
		F1, F5, F12	21-22<->25-28				
	937,40	F3, F10, F13	10-14<->21-24	469,50	8333		
		F1, F5, F12	21<->29				
	995,50	Hir, F4, F9	21-22<->34-40	498,00	7500		
	1014,10	Hir, F1- F14	40-49	507,50	111000	1013,50	146000
		F12, F13, F14	04-06<->34-39				
	1253,50	Hir, F4, F9	18-22<->34-40	627,50	6667		
		Hir, F4, F9	21-22<->31-40				
	1625,70	Hir, F4, F9	18-22<->30-40	813,50	18750		
29,060	1099,50	Hir, F1, F2	04-08<->10-14	551,00	15000	1100,50	11667
30,765	644,00	Hir, F1- F14	50-55	644,00	16667		
	1287,50	F9, F10, F11	13-18<>21-24<>38-39				
	819,40	Hir, F1- F14	30-37	-	-		
	824,40	**F1, F5, F12**	**21-24<->25-28**	412,50	3571	824,50	17857
		F2, F11, F14	**15-18<->21-24**				
32,351	1473,60	F9, F10, F11	13-17<>21-22<>34-39	737,50	31667		

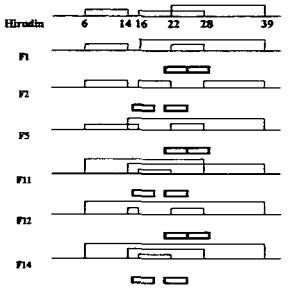

However a straigthforward assignment of these peptides to one specific mismatched variant was not possible at this stage of the analysis. Probably the search for simultaneous appearance of specific peptides shall lead to the final interpretation. An appropriate software could possibly ease the evaluation.

In our view the question raised can be answered at the level reached, since high retention peptides can easily be monitored by standard RP- HPLC once their identification as mismatched variants is achieved.

1) Dodt, J. et al. (1985) Biol. Chem. Hoppe- Seyler 366, p.379- 385.
2) Chatrenet, B., Chang, J.-Y.(1993) J. Biol. Chem. 268, p. 20988- 96

Advances in Peptide Mapping by MALDI-TOF-MS

O. Vorm, P. Roepstorff and M. Mann
European Molecular Biology Laboratory

Mass Spectrometric peptide mapping is often a necessary step in protein characterization. It follows the molecular weight determination of the intact protein (where possible) and precedes sequencing (where needed). Matrix assisted laser desorption ionization (MALDI) time-of-flight (TOF) mass spectrometry holds great promise for peptide mapping because it is fast, sensitive, and relatively tolerant against many buffers. Furthermore, spectra of peptide mixtures are simple to interpret since each component is present only as the singly charged species. Disadvantages of peptide mapping by MALDI TOF MS have been its moderate mass accuracy and resolution. More seriously, we and others have frequently noticed the absence of peptides that were expected to be seen in the MALDI spectrum when compared to HPLC and/or LC-MS data. Here we show how all three drawbacks are alleviated by some recent improvements in sample preparation techniques for MALDI MS.

We obtain much better resolution, mass accuracy, sensitivity, and a more qualitative representation of peptide components in MALDI TOF than previously possible (ref 1-3). Reflector TOF data enable routine peptide mixture analysis with better than 0.01% mass accuracy without the use of internal calibration standards and isotope resolution up to 2 kDa and beyond. The total peptide amounts needed for mapping are around 10 fmole per component making the method competitive with LC-MS and in any case attractive as a prescreening technique. With the new methods we observe significantly less variability between peptide maps when analyzed under different experimental conditions as well as a higher degree of consistency between MALDI spectra and data obtained by other forms of analysis such as LC-ES-MS and HPLC.

These results have enabled us to quickly pinpoint sites of suspected sequence inaccuracy without the use of LC/MS. Apart from greatly facilitating the mapping of known sequences, the increased mass accuracy also increases the specificity of database searches of previously unidentified proteins by a large factor. In many cases the new techniques lead to certain rather than probable assignment of a protein on the basis of a peptide map alone. Examples show a large sequence coverage and unambiguous protein identification achieved from isotope resolved, high mass accuracy peptide maps of small amounts of peptides obtained from 2 dimensional protein gels.

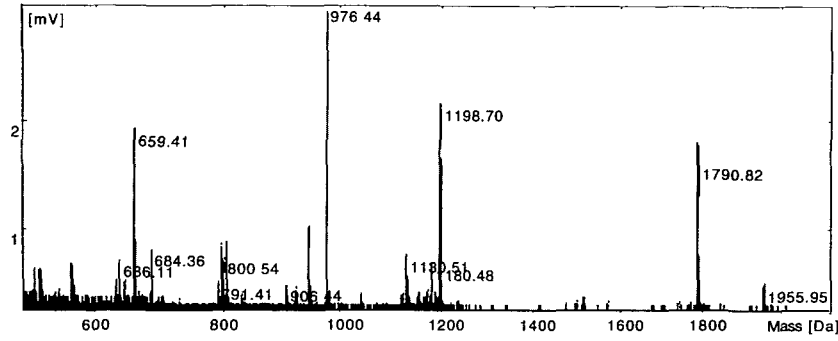

Fig. 1 MALDI reflector TOF mass spectrum of peptide map obtained by tryptic digestion of a protein isolated by SDS-PAGE. The measured peptide masses were used for database search, which lead to unambiguous identification of actin.

Measured	Calculated	Diff.	Residues	Sequence
515.32;	515.31 Da (mono);	0.01;	209-212	(R)EIVR(D)
630.37;	630.37 Da (mono);	0.00;	194-198	(K)ILTER(G)
643.41;	643.43 Da (mono);	-0.02;	65-70	(R)GILTLK(Y)
643.41;	643.37 Da (mono);	0.04;	180-185	(R)LDLAGR(D)
790.42;	790.37 Da (mono);	0.05;	287-292	(K)CDIDIR(K)
794.47;	794.47 Da (mono);	0.00;	331-337	(K)IIAPPER(K)
799.54;	799.53 Da (mono);	0.01;	64-70	(K)RGILTLK(Y)
922.59;	922.56 Da (mono);	0.03;	331-338	(K)IIAPPERK(Y)
975.44;	975.44 Da (mono);	-0.00;	21-30	(K)AGFAGDDAPR(A)
1129.52;	1129.54 Da (mono);	-0.02;	199-208	(R)GYSFVTTAER(E)
1170.61;	1170.56 Da (mono);	0.04;	42-52	(R)HQGVMVGMGQK(D)
1197.70;	1197.70 Da (mono);	0.01;	31-41	(R)AVFPSIVGRPR(H)
1499.68;	1499.70 Da (mono);	-0.02;	362-374	(K)QEYDEAGPSIVHR(K)
1789.83;	1789.89 Da (mono);	-0.06;	241-256	(K)SYELPDGQVITIGNER(F)
1954.95;	1955.04 Da (mono);	-0.09;	98-115	(R)VAPEEHPTLLTEAPLNPK(A)

These peptides cover 120 out of 377 AAs (31.8%)

Matching with Met(ox) and Cys (Acrylamid)

804.45; 804.38 Da (mono); 0.07; 287-292 (K)CDIDIR(K) Cys(acrylamide)

Table 1 Assignment of the peptides identified in the map above. The data shows excellent mass accuracy (mean absolute error 0.03 Da, std. 0.03 Da) and high sequence coverage for this demanding sample.

1 O. Vorm, P. Roepstorff and M. Mann, *Anal. Chem.* **1994**, 66, 3281-3287.
2 O. Vorm and M. Mann, *J. Am. Soc. Mass Spectrom.* **1994**, 5, 955-958.
3 O. Vorm, B. T. Chait and P. Roepstorff, *Manuscript in preparation.*

USE OF ESMS FOR THE STUDY OF THE MECHANISM OF RESISTANCE TO β-LACTAMS

O. Burlet-Schiltz, I. Saves, J.-P. Samama, J.-M. Masson, and J.-C. Promé
Laboratoire de Pharmacologie et Toxicologie Fondamentales, C.N.R.S., 205 Route de Narbonne, 31077 Toulouse Cedex, FRANCE

Resistance to β-lactam antibiotics is becoming an increasingly alarming problem for the treatment of bacterial infections. Resistant strains generally appear a few years after the extensive use of a new β-lactam, such as a penicillin or a cephalosporin. The major cause of resistance of Gram-negative bacteria is the production of enzymes, β-lactamases, which hydrolyze the β-lactam ring of these antibiotics, and thus inhibit their action. The class A β-lactamase TEM-1 and mutants derived from TEM-1 represent the most frequently encountered β-lactamases in clinical isolates.

The emergence of resistance is usually due to point mutations at one or a few positions on TEM-1 sequence. Thus, the mutation of a glycine into a serine at position 238 (G238S) is responsible for cefotaxime resistance, a third-generation cephalosporin. It has also been shown that this mutation decreases the penicillinase capacity of TEM-1. At the molecular lever, however, the effect of the G238S mutation remains unclear. We have developed an approach, based on electrospray mass spectrometry (ESMS), to access elementary rate constants of the catalytic mechanism. Comparison of these constants for the hydrolysis of penicillins and cefotaxime by TEM-1 and the G238S mutant provides valuable information to understand the global effect of the mutation on the resistance to cefotaxime.

Enzymes were produced by *Escherichia coli* strain XaC-1 transformed by the plasmids pAra 15 and T28C2+ for TEM-1 and the G238S mutant, respectively. They were then extracted, concentrated, desalted, and purified. Michaelis-Menten constants, k_{cat} and K_m, were determined by UV measurements. ESMS analyses were performed with a TRIO 2000 quadrupole mass spectrometer equipped with an electrospray source. Enzymatic reactions were quenched by acidification to pH 2.5 before analysis by ESMS.

The general mechanism for the hydrolysis of penicillins or cephalosporins by class A β-lactamases may be decomposed into three elementary reactions. After formation of a reversible non covalent complex, conversion of this complex into a covalent acyl-enzyme intermediate (acylation), and then hydrolysis of the acyl-enzyme to liberate the free enzyme and the hydrolyzed product (deacylation). The deacylation rate constant, k_3, can be determined knowing the concentration of acyl-enzyme at the steady-state of the reaction (ESMS and UV) and the rate of product formation (UV). The acylation rate constant, k_2, can then be calculated knowing the catalytic rate constant, k_{cat}.

ESMS analyses of the hydrolysis of penicillins by TEM-1 (oxacillin and cloxacillin) and the G238S mutant (oxacillin and penicillin G) show that the acyl-enzyme intermediate is the only enzyme species in solution during the steady-state. The determination of acylation and deacylation rate constants

for these reactions indicates that the rate-determining reaction is deacylation (Table). ESMS analyses of cefotaxime hydrolysis by TEM-1 and the G238S mutant show that the free enzyme is the only enzyme species observed during the steady-state. However, the product of the reaction is formed, as it is observed by ESMS (Figure). Thus, hydrolysis occurs and acylation is rate-determining for cefotaxime hydrolysis. These results, combined to the catalytic properties and to computer modeling of TEM-1 and the G238S mutant, allow to understand the effect of this mutation at the molecular level. Modeling of the G238S mutant suggests an enlargement of the active site and a misplacement of the deacylating residue (E166). These structural hypotheses are in agreement with a better catalytic efficiency of the G238S mutant toward cefotaxime by facilitating its access to the active site, and with a less efficient deacylation of penicillins due to the misplacement of the E166 residue.

TABLE: ELEMENTARY RATE CONSTANTS FOR TEM-1 AND THE G238S MUTANT

	TEM-1					G238S				
Substrate	T (°C)	K_m (μM)	k_{cat} (s^{-1})	k_2 (s^{-1})	k_3 (s^{-1})	T (°C)	K_m (μM)	k_{cat} (s^{-1})	k_2 (s^{-1})	k_3 (s^{-1})
Penicillin G	-	-	-	-	-	2.5	7	16	>> 16	16
Oxacillin	2.5	25	30	143	38	37	9	0.7	>> 0.7	0.7
Cloxacillin	2.5	30	6	24	8	2.5	-	< 0.1	-	-
Cefotaxime	37	1100	1.8	$k_2 < k_3$		37	180	20	$k_2 < k_3$	

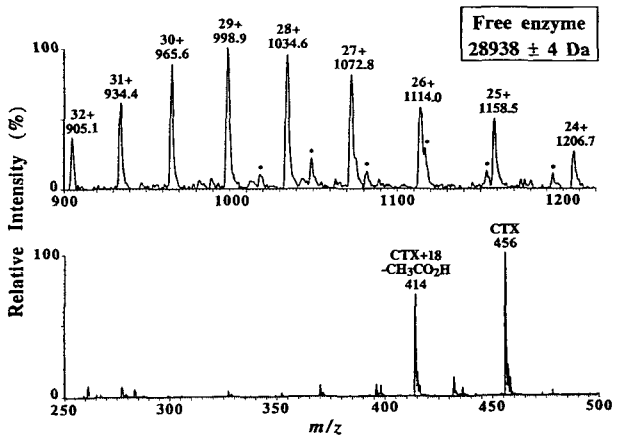

Figure: ESMS spectra of the reaction mixture of the G238S mutant (10 μl, 6 μM) and cefotaxime (2 μl, 20 mM) at 2.5°C, pH 7 after 3 minutes of reaction.
(* indicates a higher mass contaminant)
CTX: protonated substrate, CTX+18: protonated product.

Analysis of Bovine Insulin (SBI) and Reduced SBI in a Glucose Film by ^{252}Cf-Plasma Desorption Mass Spectrometry (PDMS)

S. Song, S. Cockrill, R. D. Macfarlane, Department of Chemistry, Texas A&M University, College Station, TX 77843

Glucose films have been developed as a liquid matrix for sample analysis in PDMS.[1] The deposition of sample molecules in a well defined chemical environment results in high sensitivity and efficiency for PDMS detection. Salts, amino acids and peptides have been analyzed in the glucose films. Glucuronic acid as co-matrix provides higher molecular ion yield for peptide samples.

The positive ion spectra of SBI using Nitrocellulose (NC) or glucose/glucuronic acid film give the molecular ion peaks (MH^+, MH_2^{2+}), and B chain and A chain ion peaks. The negative ion spectrum of SBI in NC matrix gives little information, the negative ion spectrum of SBI in glucose/glucuronic acid gives the A chain ion peak with low intensity.

The analysis of reduced SBI was conducted by mixing the sample solution into the matrices (electrosprayed NC, glucose/glucuronic acid film, and glucose/TFA film), or directly depositing the sample solution onto the aluminized Mylar foil. Bovine insulin was reduced by 0.06 M ammonium bicarbonate and 0 08 M dithiothreitol at room temperature for 30 minutes.[2]

The positive molecular ion region for reduced SBI is shown in Figure 1 Using the NC matrix the B chain molecular ion is observed The spectra for the glucose/TFA film and the directly deposit sample show both A chain and B chain molecular ions. The spectrum for the glucose/glucuronic acid film shows high intensity A chain molecular ions, the B chain molecular ion intensities were suppressed by the presence of the A chain molecules. The observation of a B chain molecular ion in the glucose/TFA indicates that the surface activity is affected by the matrix component.

In the negative ion mass spectra, the A chain and B chain ion peaks are observed using the glucose/TFA film. Only the A chain ion peak is present in the spectra for the glucose/glucuronic acid film and the directly deposit sample. No informative ion peaks are observed in the negative ion spectrum for the NC matrix.

The fragment ions from the NC matrix originate from the B chain which has basic residues. It has been proposed that the Arg residues direct the fragmentation process by a charge-remote mechanism.[3] The same positive fragmentation pattern is observed in the glucose/glucuronic acid film. For the reduced bovine insulin, the NC matrix produces only B chain positive fragment ions and no negative fragment ions. When glucose/glucuronic acid is used as the matrix, fragment ion peaks from the A chain are present in both the positive and negative ion mass spectra, although there is no Arg residue in the A chain. The glucose/TFA film produces positive fragment ions from the B chain and negative fragment ions from the A chain. The details on fragment ion type from all those matrices are listed in Figure 2.

In conclusion, glucose films with a co-matrix provide a matrix system capable of producing different molecular ion profiles and fragmentation patterns for reduced SBI sample. The negative fragment ions, which is not observable with the NC matrix, are present in the spectra with glucose matrix for negative fragmentation mechanism study.

References:

1. Song, S.; Macfarlane, R. D. *J. Mass Spectrom.*, accepted.
2. Chait, B. T.; Field, F. H. *Biochem. Biophys. Res. Commun.*, **1986**, *134*, 420-426.
3. Bunk, D. M.; Macfarlane, R. D. *Proc. Natl. Acad. Sci. USA*, **1992**, *89*, 6215-6219.

43rd ASMS Conference on Mass Spectrometry and Allied Topics

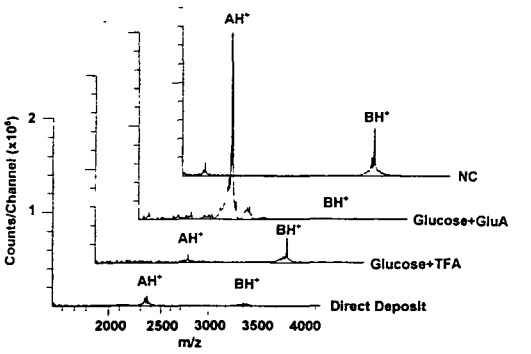

Figure 1. Positive molecular ion regions of reduced SBI from different matrices. (GluA-glucuronic acid)

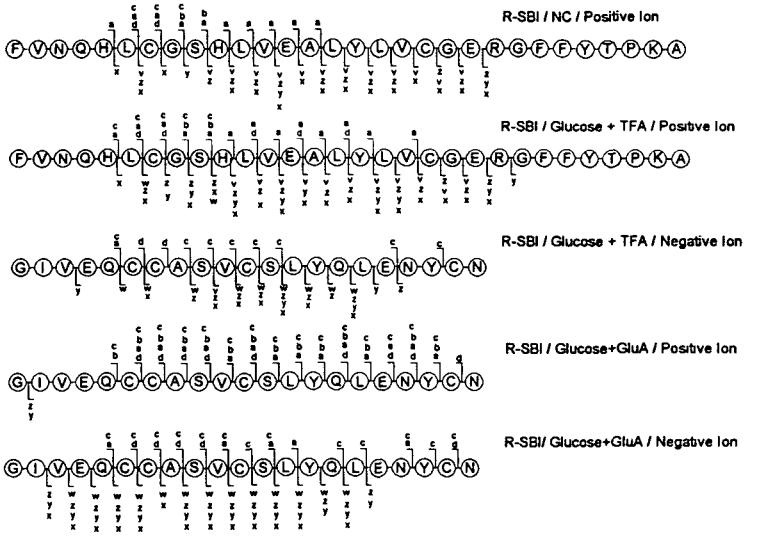

Figure 2. Fragment ions of reduced SBI from different matrices.

This reseach was supported by the National Institutes of Health (GM-26096)

MOLECULAR RECOGNITION IN DRUG DISCOVERY

David J Bell and A.West, SmithKline Beecham Pharmaceuticals, Great Burgh, Epsom, Surrey KT18 5XQ, UK.

In addition to the characterisation of both potential therapeutic agents and target proteins, mass spectrometry can be used to study the interactions between such entities. The formation of a covalent inhibitor-enzyme complex can be studied by electrospray ionisation mass spectrometry to yield information relating to rate of formation and/or stability of the complex by monitoring the change in molecular mass as a function of time. We have found that certain steps must be taken when using high ratios of inhibitor:enzyme, i.e. 10:1 or greater, as the formation of adducts in the mass spectrometer ion source can give rise to ambiguous data. Prior separation of excess inhibitor by reverse phase HPLC or size exclusion methods will avoid such effects, the latter being essential for the determination of complex stability. Other data that can be readily determined by mass spectrometry is the point of binding by the use of proteolytic digestion of the complex followed analysis of the resulting peptides using mass spectrometic techniques and Edman sequencing. Conformational changes in proteins upon binding can be observed by comparing the rate of change in molecular masses of the complex and the native enzyme as a result of hydrogen/deuterium exchange when dissolved in deuterated buffer solution.

Non-covalent interaction can be characterised by the formation of free inhibitor upon denaturation, i.e. such a complex will give rise to separate protein and inhibitor spectra when analysed by reverse phase HPLC/MS. To ensure that the origin of the inhibitor is from the complex, unbound material were removed by non-denaturing techniques prior to such analyses. Determination of the binding sites is however more difficult but the methodolgies that have been developed based on the protection of the area around the binding sites from modifications. The techniques used included the comparison of the degree and rate of deuterium exchange by monitoring the change in molecular mass using electrospray ionisation. Whilst the deuterium exchange experiments can produce a profile that will differentiate complexes, chemical modification of the complex by the use of selective reagents produced information relating to the sites of interaction as the amino acid residues protected from derivatisation were identified.

43rd ASMS Conference on Mass Spectrometry and Allied Topics

ESI-MS/MS for the Identification of Modifications of Intact Proteins

M. Busman, M.D. Wilcox, W.E. McIntire, J. Millsap*, H.E. Hamm*, J.D. Hildebrandt, and K.L. Schey, Dept. of Pharmacology, Medical University of South Carolina, Charleston, SC 29425, *Dept. of Physiology and Biophysics, University of Illinois, Chicago, Chicago IL

Posttranslational modifications play important roles in cellular processes including cell signalling and molecular recognition. Biochemical methods for identifying these covalent structures are often laborious. With the introduction of electrospray mass spectrometry, ionization of large proteins is easily achieved. Furthermore, the use of tandem mass spectrometry (MS/MS) provides an opportunity for structural studies on these large ions. Previously, proteins as large as bovine serum albumin have been dissociated by the ESI-MS/MS method[1].

Heterotrimeric GTP-binding proteins play critical roles in signal transduction pathways. The gamma subunits of these proteins have been reported to be isoprenylated by farnesyl group in the case of retinal γ_t (transducin) and geranylgeranylated in the case of brain γ subunits. Based on MALDI mass measurements, predictions of posttranslational modifications of brain γ subunits have been published[2]. In this report we utilize ESI-MS/MS on intact protein ions to identify posttranslational modifications. In addition, a sample preparation method for generating ESI signals for proteins provided in complex matrices including salts, detergents, DTT and glycerol is presented.

Samples were acetone precipitated by adding 9 volumes of ice cold acetone and placing on ice for 20 minutes. After centrifuging for 10 min. at 10,000 rpm, the supernatant was removed and excess acetone blown off. Pellets were resuspended in water/methanol/acetic acid 48/48/4. MS/MS experiments were carried out using an API-III Sciex triple quadrupole instrument.

Figure 1 shows the ESI mass spectrum of bovine transducin. Strong signals are observed for the γ subunit having a molecular weight of 8330. The $[M+8H]^{8+}$ ion at m/z 1042 was selected by Q1 and the product ion spectrum is shown in Figure 2. The most abundant product ion, m/z 1161, can be assigned to loss of the farnesyl group and loss of one charge. In addition, in the low mass range, a series of b ions is observed. These b ions confirm that the N-terminus begins with a proline residue. Finally, a series of multiply charged y ions is observed corresponding to cleavage at proline residues. The facile loss of farnesyl group is also observed in nozzle/skimmer collisions.

Figure 3 shows an ESI-MS/MS spectrum of the $[M+8H]^{8+}$ ion, m/z 968 of the bovine brain γ_2 subunit. As was observed for γ_t, facile loss of the isoprenyl group, geranylgeranyl, is the most prominent product ion observed. The low mass b ions confirm that the N-terminal methionine is cleaved and the resulting glycine is acetylated. Also, cleavage at proline residues is observed in the form of multiply charged y ions.

In summary, acetone precipitation allows proteins presented in complex matrices to be examined by ESI-MS. Significant structural information can be obtained from ESI-MS/MS experiments on intact proteins. More specifically, facile loss of isoprene modifications is observed. In addition, low mass b ions confirm N-terminal sequence and y ions confirm C-terminal sequence.

References

1. Loo, J.A., Edmonds, C.G., and Smith, R.D., Anal. Chem. 63:2488-2499, 1991.
2. Wilcox, M.D., Schey, K.L., Finch, J.W., Halushka, M., Dingus, J., and Hildebrandt, J.D., J. Biol. chem. 269:12508-12513, 1994.

Figure 1. ESI mass spectrum of bovine transducin.

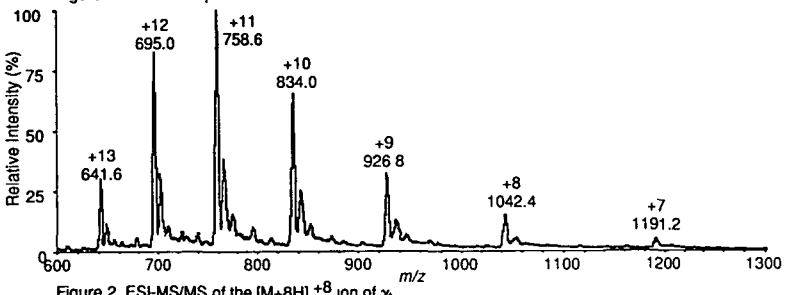

Figure 2. ESI-MS/MS of the $[M+8H]^{+8}$ ion of γ_t.

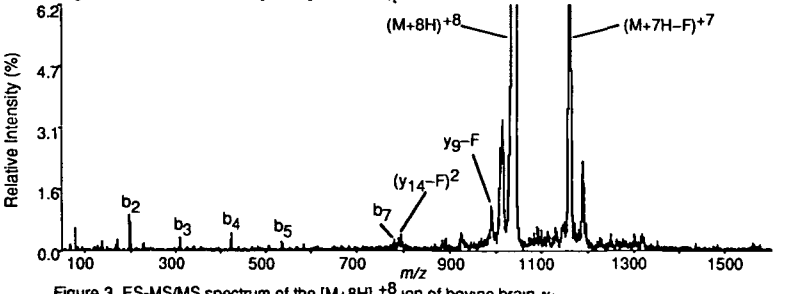

Figure 3. ES-MS/MS spectrum of the $[M+8H]^{+8}$ ion of bovine brain γ_2.

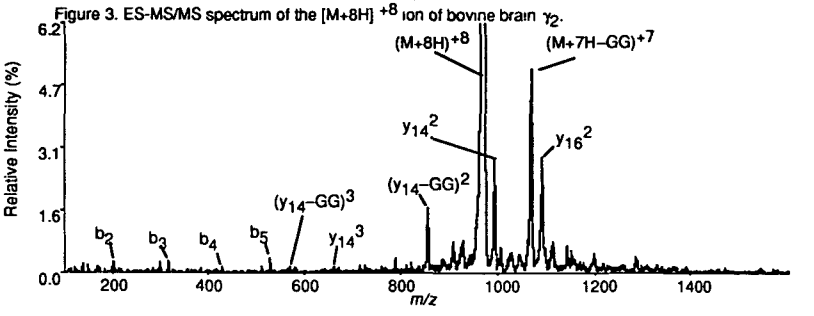

Mass Spectrometric Analysis of Recombinant Stromelysin and Collagenase

Mark D. Bauer, Yiping Sun, Melanie V. Anastasio and Cathy E. Snider
The Procter and Gamble Company, Miami Valley Laboratories
P.O. Box 538707, Cincinnati, OH 45253-8707

Introduction Stromelysin and collagenase are metalloproteases that are key targets for osteoarthritis therapy. Ionspray mass spectrometry is a powerful analytical technique for the structural characterization of these proteins. Ionspray MS provides high sensitivity (low picomoles), high mass accuracy (0.01%) and high speed (5-10 min. for flow injection analysis and 30-60 min. for on-line LC-MS analysis). In this presentation, the structural characterization of recombinant, truncated human collagenase, stromelysin, $^{13}C/^{15}N$-labeled stromelysin, and biotinylated stromelysin is demonstrated. In addition, the detection of non-covalent stromelysin-metal complexes under non-denaturing conditions is presented.

Experimental Both stromelysin and collagenase were expressed in *E. coli* grown in LB broth containing ampicillin. Protein expression was IPTG induced. p-aminophenyl mercuric acetate was used for protease activation. CNBr digestions were carried out in 0.1N HCl for 2 hours at 37°C in the dark and stopped by the addition of 4 volumes of H_2O. Biotinylation was performed using the NHS-LC-Biotinylation Kit (No. 21430, Pierce). Isotope enriched stromelysin was generated by substituting M9 minimal salts media composed of $^{13}C/^{15}N$ labeled components in place of LB broth. All ionspray MS analyses were carried out on a PE-Sciex API-III LC/MS/MS triple quadrupole instrument (PE-Sciex, Thornhill, Canada). On-line microbore LC-MS analysis was carried out on a Waters 600-MS system at a flow rate of 0.8 ml/min in the gradient mode. A pre-injector split ratio of 9:1 was established by splitting one side to a balance column (Waters Delta Pak C18, 3.9x150 mm) and splitting the other side to a 1x150 mm C4 microbore column (Vydac, 300 Å, 5 µ) with an in-line Rheodyne injector (model 7125). For the detection of non-covalent stromelysin-metal complexes, the delivery solvent was neat water at 5 µl/min. Sample solutions, which were passed through a 10,000 MW cut off microconcentrator, were introduced using a Rheodyne loop injector (model 7125).

Results and Discussion On-line microbore LC-MS was used to accurately measure the molecular weights for both recombinant, truncated human stromelysin (MW=19396.6) and recombinant, truncated human collagenase (MW=18992.8) to within 0.01%. Although collagenase gave a single peak by HPLC (RT = 19.6 min), it was found to be a mixture of intact material and two N-terminal truncated forms involving the loss of either the first residue or the first and second residues (Figure 1). CNBr mapping, along with on-line microbore LC-MS, confirmed the native structures of both stromelysin and collagenase. On-line microbore LC-MS analysis confirmed that biotinylation of stromelysin was successful. Furthermore, from one to five biotin molecules were added to the native protein (Figure 2). The degree of $^{13}C/^{15}N$ incorporation into stromelysin was measured to be 98% (Figure 3). That is, the mass of native stromelysin increased by 1087 Da out of a possible 1110 Da mass unit shift if all of the ^{12}C and ^{14}N atoms were replaced by their ^{13}C and ^{15}N counterparts. Figure 4 is the mass spectrum for stromelysin complexed with 2 Zn and 2 Ca atoms (Measured MW=19597.7). The binding of two zinc atoms to stromelysin is consistent with NMR data (1). There is, however, still some debate as to whether stromelysin (or other metalloproteases) binds one or two calcium atoms (2,3). In addition to the non-covalent complex, an autolytic fragment corresponding to residues 1-80 (MW=9250.5) was observed. This fragment was generated during the filtration step where stromelysin spent several minutes in conditions ideal for autolytic processes.

43rd ASMS Conference on Mass Spectrometry and Allied Topics

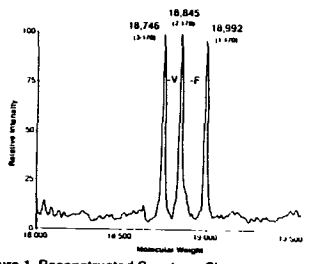

Figure 1 Reconstructed Spectrum Showing N-terminal Truncated Forms of Collagenase from the Peak at 19 6 min

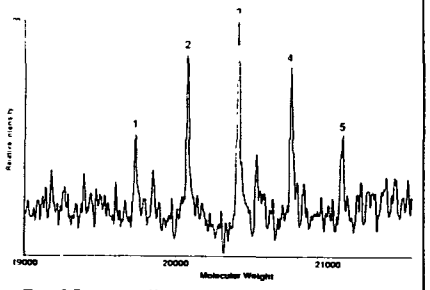

Figure 2 Reconstructed Ionspray mass spectrum of biotinylated stromelysin. Each labelled peak represents the addition of 1, 2, 3, 4 and 5 biotin molecules to stromelysin.

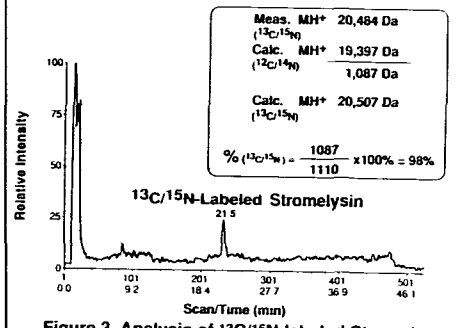

Figure 3 Analysis of 13C/15N-labeled Stromelysin Showing a 98% Incorporation Ratio

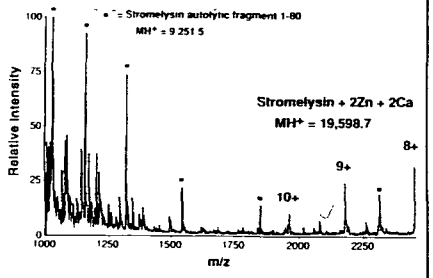

Figure 4 Detection of Stromelysin-Metal Complexes by Ionspray MS

References

1. Gooley, P.R.; et. al., (1994) Structural Biology **1**, No. 2, 111-118.
2. Spurlino, J.C.; et. al., (1994) Proteins **19**, 98-109.
3. Bode, W.; et. al., (1994) EMBO **13**, No. 6, 1263-1269.

Characterization of Recombinant NMDA Receptor Regions with ESIMS

Klaus Eckart, Andreas K. E. Koepke, and Joachim Spiess; Department of Molecular Neuroendocrinology, Max Planck Institute for Experimental Medicine, Hermann-Rein- Str. 3, D-37075 Goettingen;

INTRODUCTION

NMDA receptors (NR) are involved in diseases such as epilepsia and scizophrenia and may also play an important role in memory and learning. For a functional understanding the three-dimensional structure including the transmembrane localization is of great interest. These questions were approached by using regiospecific antibodies directed against different domains of various NMDA receptor subunits (1). These receptor regions were produced using an *E. coli* overexpression system. All receptor regions carry an N-terminal leader sequence. This includes a His_6 sequence used for affinity purification on a Ni^{2+}-chelate column and an enterokinase cleavage site. The A-regions are expected to represent the N-terminus of the receptor subunit, whereas the location of the D-region is discussed controversially (2). These fusion proteins are analyzed with electrospray ionization mass spectrometry (ESIMS).

METHODS

Overexpression and purification of the proteins were described recently (1). The purity of the proteins was initially assessed by SDS polyacrylamide gel electrophoresis. In cases of low expression rates the Ni^{2+}-chelate column purification was repeated one time. Dialyzed proteins were completely desalted by 5 successive water washes on microcon 10 (amicon) ultrafiltration devices. Electrospray ionization mass spectra were recorded on a Fisons VG AutoSpec-T mass spectrometer equipped with the Fisons electrospray interface. Measurements were carried out using the following parameters: spray chamber temperature: 60°C, needle voltage: 8000 V, counter electrode voltage: 5000 V, accelerating voltage/skimmer voltage: 4000 V, bath gas: 300 l/h nitrogen. The sampling cone voltage and ring electrode voltage were adjusted according to the best conditions of each sample. Samples were continuously infused with 1 µL/min from an infusion syringe pump (Harvard model 22). The D-region proteins were dissolved in a mixture of 49.5% water, 49.5% methanol and 1% acetic acid, whereas the A-region proteins were measured and desalted in a mixture of 47.5% water, 47.5% methanol and 5% acetic acid. ESI mass spectra were recorded with an exponential magnet down scan from m/z 6000 to m/z 600 using a scan rate of 5 seconds/decade. Mass spectra were calibrated with 0.1 mg/ml myoglobin or a 1 mg/ml polypropylen glycol 2000 solution The instrument was operated with a fully opened collector slit. Data acquisition and analysis including the maximum entropy deconvolution were performed with the OPUS data system.

RESULTS

The purity of the overexpressed proteins assessed by SDS polyacrylamide gel electrophoresis was usually better than 80%. Nevertheless further purification for ESIMS using ultrafiltration on microcon devices was necessary to remove the excess of urea, which gave rise to extensive clustering and suppression of the protein ions.

Table 1: NR protein regions subjected to ES mass spectrometry

Protein	Subunit	Region	MW measured	MW calculated	Difference
NR1a-D	1a	D	20,290 Da	20,288 Da	+0.10 ‰
NR2A-A	2A	A	31,039 Da	31,079 Da	-1.28 ‰
NR2C-A	2C	A	29,648 Da	29,594 Da	+1.83 ‰
NR2C-D	2C	D	23,752 Da	23,746 Da	+0.25 ‰

The molecular masses for both D-region proteins determined by maximum entropy charge deconvolution (Tab. 1) showed the typical experimental errors. In contrast to this the molecular masses for both A-region proteins (Fig. 1) deviate significantly from the calculated values. The molecular masses of the overexpressed proteins were calculated on the basis of the DNA sequence of the plasmid used for overexpression. The mass differences are therefore most likely to be the result of posttranslational processing in the *E. coli* overexpression system.

Figure 1: Electrospray Ionization Mass Spectra of the NMDA Receptor Regions NR2C-A and NR2C-D

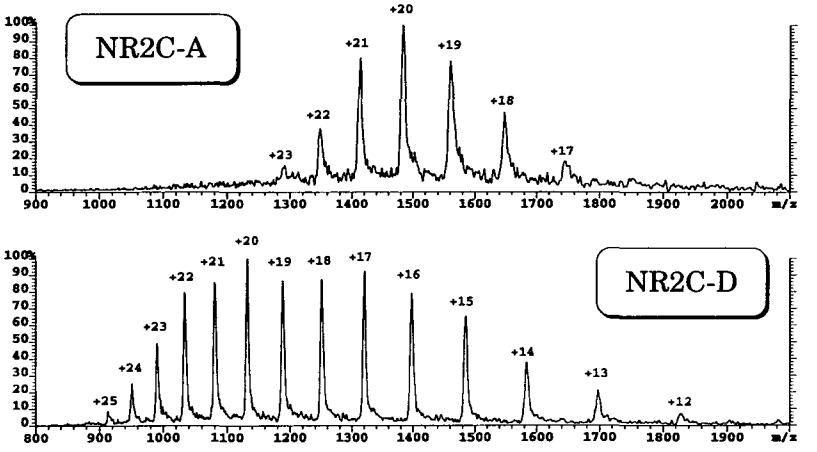

Both A-region proteins were insoluble in a methanol water mixture containing 1% acetic acid. Therefore, the handling of these proteins had to be carried out in a methanol water mixture containing 5% acetic acid after the proteins were predissolved in pure acetic acid. The hydrophylicity analysis reveals a relatively high degree of hydrophobicity of these proteins. This property is also reflected in the ESI mass spectra (Fig. 1). Both A-region proteins exhibit a larger ratio of molecular mass per proton attached to the proteins compared to the D-region proteins. Furthermore, the number of different charge states is relatively small. Both effects may be interpreted as less unfolding induced by solvent and pH of the A-region proteins compared to the D-region proteins.

It must be pointed out that the proteins were purified by a simple and straightforward one-step procedure. The essential step is the affinity purification of the proteins using the specific binding of the His_6 sequence to Ni^{2+} ions. The incomplete removal of urea from the 8M urea containing elution buffer by dialysis presented some difficulty to ESIMS. Desalting of the proteins on microcon ultrafiltration devices provided salt-free proteins which produced much more abundant and less broadened signals in ESIMS.

References:
1) Köpke, A. K.; Bonk, I.; Sydow, S.; Menke, H.; Spiess, J., *Prot. Sci.* **2**, 2066-2076 (1993).
2) Barinaga, M., *Science* **267**, 177-178 (1995).

Enhanced Nucliophilicity of N-terminal Proline. Zhonghua Yu[1,2], Charles Craik[1], Patrick Jones[2], Alma L. Burlingame[1], Dept. of Pharmaceutical Chemistry, UCSF, San Francisco, CA 94143, and [2]Dept. of Chemistry, Univ. of the Pacific, Stockton, CA 95211

Proteolytic activity is high in living organisms and the activities of the many proteases must be balanced to maintain normal physiological conditions of homeostasis. Strategies to stop the maturation of the HIV virus include efforts to block the action of the HIV protease, a homodimeric aspartate protease, with a 99 amino acid monomer.

Various peptide based inhibitors and nonpeptide inhibitors of HIV protease have been considered. A non-selective inhibitor of aspartate protease, EPNP, was shown to be effective in binding covalently to HIV-1, HIV-2 and SIV proteases (Yu, 1995). Various workers have sought selective inhibitors. Haloperidol was found to be highly complementary to the binding pocket of HIV-1 protease (DesJarlais, 1990) and was shown to have an 8:1 selectivity for HIV-1 protease over cellular proteases (Rose and Craik, 1994). Irreversible inhibitors of the HIV-1 protease based on the haloperidol framework have been developed (see **Figure 1**).

The products of the irreversible inhibition reaction were separated by HPLC. Electrospray mass spectra of the intact HIV-2 and the UCSF-86 modified protease showed an increase in mass of 354 corresponding to the addition of one molecule of the haloperidol. The modified protease molecules were subjected to a digest, separated by HPLC, and the masses of the peptides were determined by mass spectrometry. The peptides including covalently bound modifiers were separated using a C-18 analytical column. The HPLC fractions containing the inhibitor were analyzed by tandem mass spectrometry as shown in **Figure 2.** In this case, the inhibitor was found only to be attached to the proline at the N-terminus. Mass fragment assignments were confirmed by selecting first the ^{35}Cl and then the ^{37}Cl containing parent ion using MS1. High energy CID provided the unambiguous assignments shown in Figure 2. Other CID spectra demonstrated irreversible binding of the haloperidol derivatives to Cys-95 of the HIV-1 protease and to Cys-67 and Pro-1. Pro-1 was not modified as much in HIV-1 protease as in HIV-2 and SIV. Possible mechanisms for the attachment of the haloperidol derivatives suggest the involvement of hydrogen binding between the haloperidol and the N-terminal proline.

In conclusion, we note that (1) Certain haloperidol derivatives prove to be efficient inhibitors of HIV-1, HIV-2 and SIV proteases. X-ray studies show the N-terminal proline to be at the surface. This work demonstrates the access of the modifier to Pro-1 and not to other nucleophilic centers under these conditions. The attachment to Pro-1 may inhibit protease activity by interfering with dimer formation or by altering the tertiary structure. (2) Mass spectrometry is very useful in the development of selective and potent irreversible inhibitors of targeted enzymes by unambiguously identifying the sites of binding. (3) Binding at the N-terminus is not as effective as binding at the cysteines of HIV-1, but suggests another strategy for designing drug molecules to inhibit the protease activity.

This work was supported by NIH Grant RR01614 and NIEHS Grant ES04705 (to A.L.B.) and NIH Grant GM39552 (to C.S.C.). The support is gratefully acknowledged.

REFERENCES:

- Yu, Zhonghua W., (1995), *Characterization of Irreversible Inhibition of Proteases by Mass Spectrometry*, Ph.D. dissertation, University of the Pacific.
- DesJarlais, R. L., Seibel, G. L., Kuntz, I. D., Furth, P. S., Alvarez, J. C., Ortiz de Montellano, P. R., DeCamp, D. L., Babe, L. M., and Craik, C. S., (1990), *Proc. Natl. Acad. Sci., USA*, **87**, 6644 - 6648.
- Rose, J. R., Salto, R., and Craik, C. S., (1993), *J. Biol. Chem.* **268**, 11939.

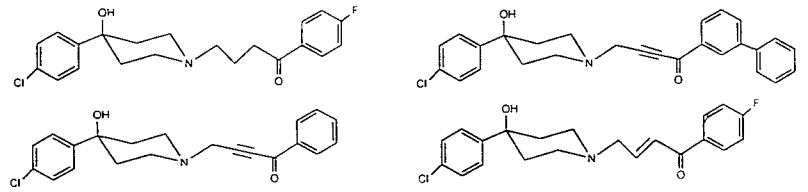

Figure 1 Haloperidol and derivative compounds: haloperidol, UCSF-86, UCSF-142, UCSF-191

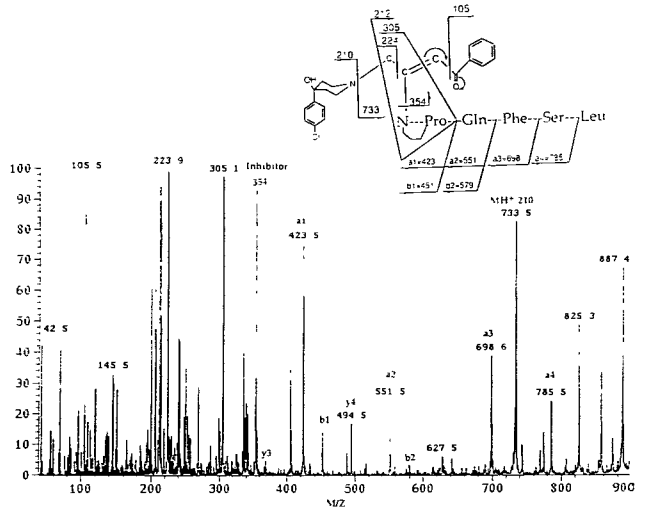

Figure 2. CID MS of UCSF-86 modified HIV-2 protease, ^{35}Cl

Calcium Binding Properties and Sequence of Frog (*Rana tegrinka*) Parvalbumin as Determined by Electrospray Ionization - Mass Spectrometry

Peifeng Hu, Scott D. Buckel, Margaret M. Whitton and Joseph A. Loo Chemistry Department, Parke-Davis Pharmaceutical Research, Division of Warner-Lambert Company, 2800 Plymouth Road, Ann Arbor, MI 48105

Recently, we applied ESI-MS to the analysis of Ca^{2+} - binding proteins.[1] The Ca^{2+}-binding stoichiometries for calmodulin, parvalbumin, and α-lactalbumin were readily determined to be 4, 2, and 1 respectively, in agreement with results obtained by other methodologies. Of particular interest, the distribution of Ca^{2+} ions among the protein molecules were also revealed. Rabbit and rat parvalbumins were found to bind either zero or two Ca^{2+} ions, suggesting strong cooperativity between the two calcium- binding sites.[1] The ESI-MS analyses of frog parvalbumin (R. tegrinka), however, showed that the protein retains one Ca^{2+} ion and binds to two Ca^{2+} ions only at high Ca^{2+} concentration levels (Figure 1). The sequence of this parvalbumin remained unknown and therefore, should be of interest for future studies on the structure - Ca^{2+} binding relationships for calcium - binding proteins.

The strategy used to determine the protein primary structure was to sequence the tryptic peptides and the protein with a free N-terminus by Edman degradation to obtain the majority of the protein sequence, and to use ESI-MS to screen Asp-N and Protease V8 digests for peptides that provide overlapping sequences (Figure 2). Mass spectrometry was used in three areas: 1) confirming the sequences of peptides by measuring the molecular weight of the peptides; 2) determining the C-terminal residue of peptides left out by Edman chemistry; 3) determining the N-terminal blocking group of the protein. The mass accuracy provided on our sector instrument is generally better than 0.3 amu. Thus, the masses of the peptides provided information that confirms the sequence assignments. For peptides whose C-terminal residue is missing the mass difference between the measured mass and the mass deduced from the known part of the seqence reveals the identity of that residue. The N-terminal blocking group was determined by tandem mass spectrometry. The N-terminal tetrapeptides with/without the blocking group were separated from Asp-N digest. All N-terminal product ions produced by the $(M+H)^+$ ion of the modified peptide are 42 u higher than those produced from the tetrapeptide. The C-terminal product ions from both peptides have the same mass to charge ratios.

The protein contains two cysteines, with one conserved at position 34 and the other located at the C-terminus (residue 110). This justifies its propensity to dimerizes. However, the question whether this structure chracteristics affects the Ca^{2+} affinity and the interacting relationships of the two Ca^{2+} sites awaits to be addressed.

1. P.F. Hu, Q. Ye, J. A. Loo, *Anal. Chem.* **1994**, *66*, 4190-4194.

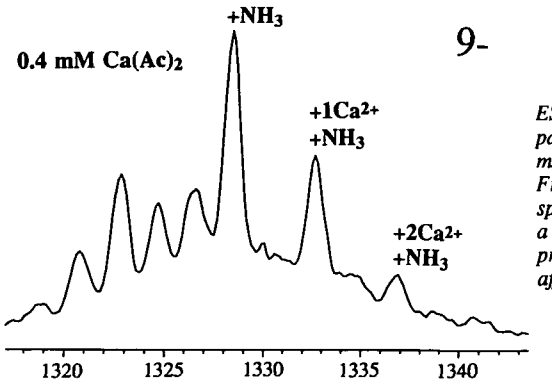

9-

Figure 1

ESI-MS spectrum of frog parvalbumin in the presence of 0.4 mM calcium acetate acquired on Finnigan MAT 900Q mass spectrometer. The protein binds to a maximum of two Ca^{2+} ions. The protein also appears to have some affinity towards ammonium ion.

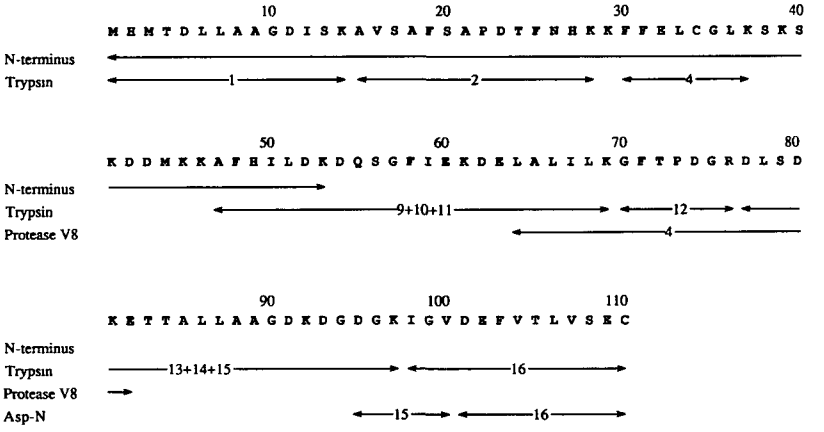

Figure 2 *Peptide map of frog parvalbumin. The C-terminal cysteine residue of trypsin peptide 16 and Asp-N peptide 16 were determined by MS. The non-tryptic peptides that provided overlapping sequences were screened out by MS.*

Determination of the Sites of Non-Labile HNE-Adduction to Proteins

Mark S. Bolgar and Simon J. Gaskell

The Michael Barber Centre for Mass Spectrometry, UMIST, Manchester, M60 1QD, U.K.

Structural changes that accompany oxidation of low density lipoprotein (LDL) are believed to be responsible for the increased atherogenicity of oxidized LDL. Among the modifications demonstrated to occur are adduction of protein amino acids by lipid peroxidation products. One of the lipid oxidation products implicated in the modification of LDL is 4-hydroxy-2-nonenal (HNE). In vitro studies have suggested that HNE modifies primarily lysine, histidine and cysteine residues of proteins (1-2). In a previous study we demonstrated that histidine and cysteine residues of a series of short model peptides are readily modified by HNE and that adduction occurs via an addition type reaction (3). In the current study, techniques have been developed for the identification of the number and sites of non-labile HNE-adductions to protein using apomyoglobin as a model system.

Data presented here from the analyses of apomyoglobin provides clear evidence that histidine residues are the major sites of non-labile HNE-adduction to protein. Electrospray MS analysis revealed that incubation of apomyoglobin with 2 mM HNE for 2 hours resulted in the addition of up to 10 HNE adducts, consistent with adduction solely to apomyoglobin's 11 histidine residues. A mass increase of 156 Da per HNE-adduct was observed indicating modification occurred by an addition reaction. Examination of the unfractionated tryptic digest by ESI MS (Fig 1) provided a rapid technique for the localization of the sites of HNE-adduction. The spectrum was extremely complex due to the presence of 19 identifiable components, most of which were represented by more than one charge state. This analysis, which consumed 45 pmol of sample, yielded coverage of ca. 80% of the amino acid residues and revealed a precise correlation between the number of histidine residues contained in the fragment and the maximum number of HNE-adducts. For all of the tryptic fragments the number of HNE-adducts detected equaled the number of histidine residues. We previously reported that peptides which contained an HNE- adducted histidine residue, when subjected to collisional activation, gave an abundant fragment ion at m/z 266 (3). This ion corresponded to the HNE-adducted histidine immonium ion and we demonstrated that scanning a mixture for precursors of m/z 266 was an effective method for selectively detecting peptides which contained an HNE-adducted histidine residue. Analysis of the tryptic digest of HNE-adducted apomyoglobin by scanning for precursor of m/z 266 (Fig 2) resulted in the detection of all of the HNE-modified tryptic fragments observed in the full scan spectrum (Fig 1). In addition to providing conclusive evidence for extensive adduction specifically to histidine residues, the precursor ion spectrum was greatly simplified compared to the full scan mass spectrum due to elimination of the ions from native tryptic fragments.

1) Jurgens, G.; Lang, J.; Esterbauer, H.; Biochimica et Biophysica Acta 1986; 875, 103-114.
2) Bruenner, B.A.; Jones, A.D.; German, J.B.; Rapid Commun. Mass Spectrom. 1994, 8, 509-513.
3) Bolgar, M.S.; Gaskell, S.J.; Proceedings of the 42nd Annual Conference on Mass Spectrometry and Allied Topics, Chicago, 1994.

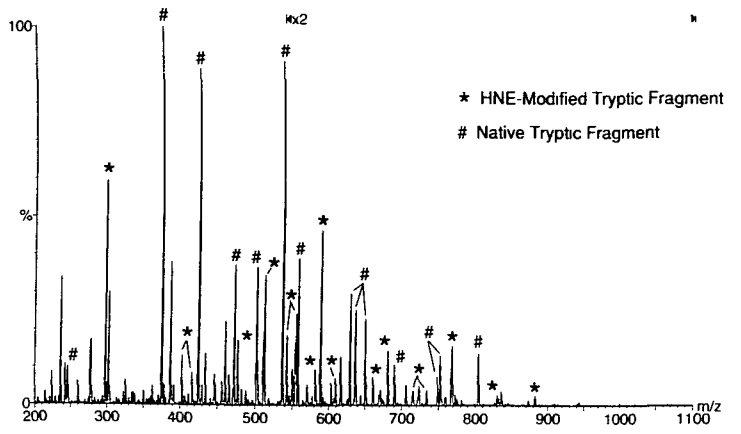

Figure 1. ESI mass spectrum of the unfractionated mixture from the tryptic digestion of apomyoglobin incubated with HNE.

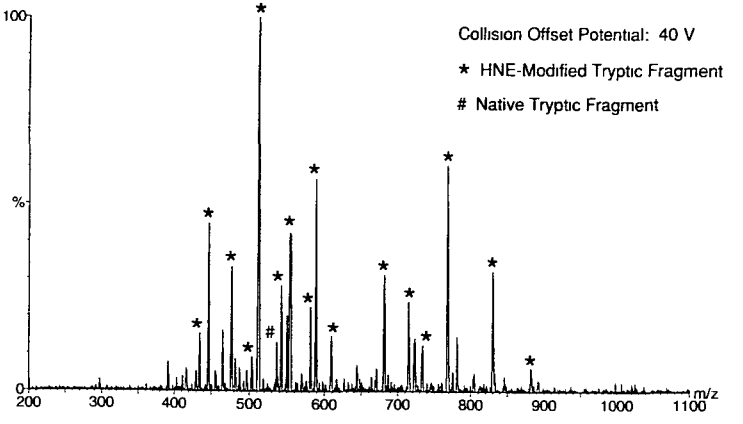

Figure 2. ESI precursors of m/z 266 spectrum of the tryptic digest of apomyoglobin incubated with HNE.

Protease-catalyzed Incorporation of ^{18}O into Protein Fragments

Martina Schnölzer, Paul Jedrzejewski,* Wolf D. Lehmann*

Dept. of Cell Biology and *Central Spectroscopy Dept.
German Cancer Research Center, Im Neuenheimer Feld 280,
D-69120 HEIDELBERG, Germany

Normally, the preparation of an enzymatic digest containing a set of smaller peptide fragments is the first step in protein sequence analysis. Since proteolytic cleavage proceeds via incorporation of oxygen from water into the newly formed peptides, the reaction can be used to generate a set of carboxyl-^{18}O labeled peptides by using buffers containing $H_2{}^{18}O$. MALDI- and ESI-MS are the most powerful techniques for studying the incorporation of ^{18}O in digest mixtures with or without LC separation of the peptide mixture.

Proteolytic digests in $H_2{}^{18}O$ buffers can be analyzed using FAB-MS, and the C-terminal peptide can in general be recognized as the only nonlabeled peptide fragment in such digests.[1-3] However, the extent of ^{18}O-incorporation catalyzed by endoproteinases has not been studied in detail. We report here on an investigation of endoproteinases commonly used for protein sequence analysis and their incorporation of ^{18}O into peptide fragments. Analytical applications for this approach are shown.

Enzyme-catalyzed protein cleavage in highly enriched $H_2{}^{18}O$ buffers (>95 atom% ^{18}O) using various endoproteinases results in two distinctly different ^{18}O incorporation patterns (Table 1).

Table 1: Incorporation of ^{18}O from highly enriched $H_2{}^{18}O$ buffers into enzymatic protein fragments catalyzed by some endoproteinases frequently used for peptide sequencing.

enzyme		no. of ^{18}O atoms incorporated after 18 h
trypsin		2
Lys-C	(major activity Lys/)	2
Lys-C	(minor activity Arg/)	1
chymotrypsin		1
Glu-C		1
Asp-N		1

Trypsin and the major activity of Lys-C lead to incorporation of 2 atoms of ^{18}O into the newly formed carboxyl group. This indicates that following hydrolytic cleavage this labeled fragment undergoes repeated covalent binding/hydrolysis cycles on the enzyme leading to a complete equilibration of ^{18}O between solvent and both oxygens of the carboxyl group. In contrast chymotrypsin, Glu-C, Asp-N and the minor activity of Lys-C only incorporate 1 atom of ^{18}O under identical experimental conditions, indicating that these enzymes only interact with their substrates in a single covalent binding/hydrolysis step with incorporation of 1 atom of ^{18}O.

43rd ASMS Conference on Mass Spectrometry and Allied Topics

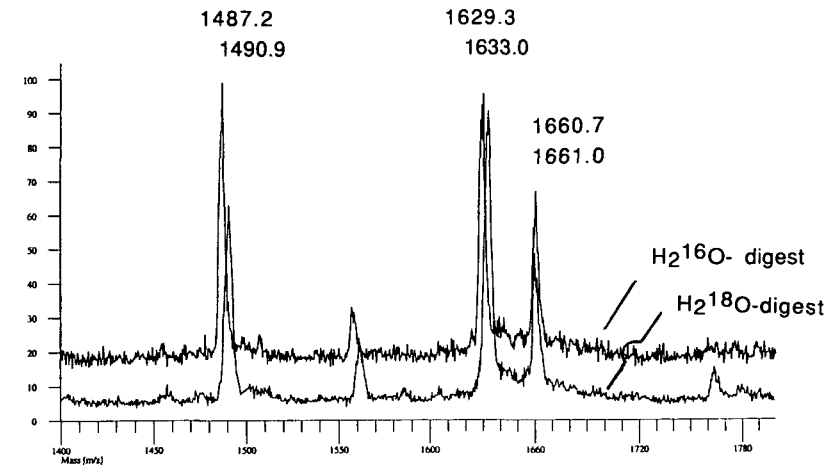

Fig. 1: Partial positive-ion MALDI spectra of a total tryptic digest of ß-lactoglobulin performed in $H_2{}^{16}O$ and $H_2{}^{18}O$, respectively. The C-terminal fragment at m/z 1661 (LSFNP TQLEE QCHI, calculated average m/z for $[M+H]^+$ = 1659.86) is recognized by the absence of a mass shift, whereas all other proteolytic fragments in the $H_2{}^{18}O$-digest show a mass shift of + 4 D. The sample amount was 0.25 pmol.

For determination of the C-terminal peptide, tryptic digests of ß-lactoglobulin were prepared in both $H_2{}^{16}O$ and $H_2{}^{18}O$ buffers and a 0.25 pmol aliquot of each digest was investigated by positive-ion MALDI-MS (Figure 1). The ion signal at m/z 1661, which has the same position for the $H_2{}^{16}O$ and $H_2{}^{18}O$ digests, can be clearly identified as the C-terminal peptide LSFNP TQLEE QCHI. Two other ion signals in Figure 1 show a mass shift of + 4 D, typical for peptide fragments generated by trypsin digestion in $H_2{}^{18}O$ buffer.

The use of $H_2{}^{18}O$ buffers for enzymatic digests has two additional applications in protein sequence analysis: (i) identification of MS/MS fragment ions as either C-terminal or N-terminal fragment ions, since exclusively the C-terminal fragment ions are shifted, and (ii) recognition of the charge state of ions in ESI-MS.

References

1. Rose, K.; Simona, M.G.; Offord, R. E.; Prior, C. P.; Otto, B.; Thatcher, D. R. *Biochem. J.* 215:273-277; 1983.
2. Rose, K.; Savoy, L.-C.; Simona, M. G.; Offord, R. E.; Wingfield, P. *Biochem. J.* 250:253-259; 1988.
3. Takao, T.; Hori, H.; Okamoto, K.; Harada, A.; Kamachi, M.; Shimonishi, Y. *Rapid Commun. Mass Spectrom.* 5:312-315; 1991.

Methodology to Identify Proteins using LC-Ion Trap Mass Spectrometry

John R. Yates, Jimmy Eng, David Schieltz, Andrew Link
Department of Molecular Biotechnology, University of Washington, Seattle, WA 98195

The ability to obtain sequence information from peptides contained in a complicated mixture by MS/MS analysis enables the identification of individual proteins in the mixture. Proteolysis of the entire mixture of proteins creates peptide "identities" for each protein. In addition to the determination of the amino acid sequence of antigens or other peptides, an MS/MS spectrum can be used to search protein databases directly, to determine the protein origin of the peptide. This approach benefits from instrumentation capable of rapidly acquiring large numbers of tandem mass spectra. The LC/Q ion trap was examined for its ability to rapidly acquire tandem mass spectra of LC separated peptides. Results are presented for the identification and characterization of proteins from *E. Coli* and *S. Cerevisiae* by using the Ion trap mass spectrometer to generate MS/MS data and correlation analysis of the ion trap data with sequences in the databases (Eng et. al. JASMS **5**, 976 (1994), Yates et al *Analytical Chemistry* **67**, 1426 (1995)). The peptide sequence represented in the tandem mass spectrum serves as a pointer to the protein sequence in the database. This allows proteins contained in a mixture to identified.

Proteins were isolated from the periplasmic membranes of *E. Coli* and by heparin chromatography of *S. cerevisiae* lysates. Selected fractions were digested with trypsin subjected to LC/MS/MS analysis on the LC/Q. Peptides were separated on a 1 mm x 150 mm C_{18} column with a 50 µL/min flow rate and a 0-65% 20 min linear gradient (water/acetonitrile/TFA; 10/90/0.09). Peptides eluted over 700 scans and MS/MS data were collected, on average, every other scan.

Tandem mass spectra were acquired on a newly designed and built tandem mass spectrometer, LC/Q (Finnigan MAT, San Jose, CA). Ions are trapped in the RF field and selected by creation of broad field with a frequency notch at the frequency corresponding to the m/z value of the ion of interest. This ion is then excited by resonance excitation and the resulting fragmentation products are scanned out of the trap. High resolution mass spectra are obtained by ion selection, and slowing the scan speed over a narrow mass range as previously described by Schwartz et al (*J. Am. Soc. Mass Spectrom.* **2**, 198 (1991)) This process is automated with Ion Trap Control Language (ICTL).

Database searches were conducted with previously described software on a DecStation 3000/900 computer (Eng et. al. *J. Am. Soc. Mass Spectrom.* **5**, 976 (1994), Yates et al *Analytical Chemistry* **67**, 1426 (1995)) using the OWL database.

As part of an effort to identify proteins from *E. coli* and correlate the results from the genome (A. Link, Ph.D. Dissertation, Harvard University, 1994), proteins from the periplasmic space were fractionated on a Mono Q column. Fraction 24 was digested with trypsin and analyzed by using LC/MS/MS on the LC/Q. A representative tandem mass spectrum and the amino acid sequence represented therein is shown in Figure 1. By searching the database with this tandem mass spectrum a sequence of ELNADDVVFSFDR was found to belong to the periplasmic dipeptide transport protein. Proteins enriched from S. cerevisiae cells by using heparin chromatography were also digested and analyzed. A list of peptide sequences and their proteins sources are listed in Table 1.

In both analyses approximately 250-350 tandem mass spectra were acquired over the course of a 35 minute reversed-phase HPLC analysis. Due to limitations in the prototype data acquisition software and data file formats, only a hand full of the spectra were retrieved and submitted for data analysis. A majority of the peptides represented in the spectra were identified. Analyzing the large volume of data that can now be acquired

requires more sophisticated data analysis techniques. By pre-filtering all spectra through the databases spectra matching known sequences can be identified. Those spectra not matching any known sequences can be submitted to de novo computer interpretation software for further analysis.

Acknowledgements

This work was supported by the University of Washington's Research Royalty Fund. Partial support was derived from the National Science Foundation, Science and Technology Center (DIR 8809710), NIH (GM52095), and Digital Equipment Corporation.

Table 1. Proteins Identified S. Cerevisiae Heparin column

Peptide Sequence	Protein Sequence
AKQSLDVSSBR	60s Ribosomal Protein
AGLKDVVTR	60S Ribosomal protein
VLEQLSGQTPVQSK	60s Ribosomal protein
QKYDADVLDK	60s Ribosomal protein
FAVQVDKVTK	S. CEREVISIAE XII COSMID
ALVEHIIQAK	60s Ribosomal protein
TYAAEIAHNISAK	60s Ribosomal protein
IGIVEISPK	40s Ribosomal protein
TTKEDTVSWFK	60s Ribosomal protein
QGKLEVPGYVDIVK	40S Ribosomal protein
KQFVVDVLHPNR	S. cerevisiae IX complete sequence
ARFEDLNAALFK	Heat Shock Protein SSB1
VAAVETLYQDMAAR	EST101549 cDNA

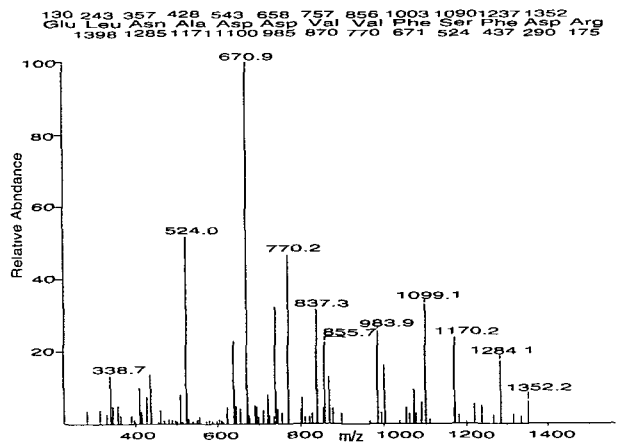

CROSS LINKING OF GLUTATHIONE-S-TRANSFERASE pi DIMER BY ORGANIC MUSTARDS

Yetrib Hathout and Catherine Fenselau
Structural Biochemistry Center, Dept of Chemistry and Biochemistry,
University of Maryland Baltimore County, Baltimore, MD 21228

Glutathione-S-transferases (GST's) are a family of protein which catalyze the conjugation of reduced glutathione to a large variety of electrophilic compounds. Numerous studies (1) suggest that overexpression of GST's in tumor cells may contributes in resistance to nitrogen mustards (alkylating agents) used in chemotherapy. GST class pi is one of the overexpressed protein in many human tumors (2). Human placenta GST class pi is formed by two identical subunits. Each subunit has a molecular mass of 23.2 Kda and contains four reduced cysteines residues. The objective of the present study is to test the hypothesis that pi class GST can inactivate the therapeutic mustard chlorambucil (CHB) by covalent sequestration.
Human placenta GST pi (43 μM) was treated with CHB (172 μM) in vitro at pH 7. The complex formed was purified by HPLC and characterized by Matrix Assisted Laser Desorption (MALDI) using 2-(4'-hydroxyazobezen)-benzoic acid as a matrix and bovine α-chymotrypsinogen (M.W. 25657 Da) as internal calibrant. To test reproducibility products from 5 different reactions were analyzed. The molecular mass obtained from the complex was 46676 Da while molecular mass obtained from GST control was 23223 Da. This result indicates that one CHB molecule has cross linked two subunits of GST. Based on the difference between molecular mass of the complex obtained and molecular mass of GST dimer without the drug attached (46446 Da) one molecule of CHB bonds each protein dimer. To characterize the chlorambucil alkylation site on GST, the protein was digested with trypsin and the resulting peptides were separated by HPLC. One chlorambucil modified peptide was detected. Close examination of this peptide using MALDI and FAB/MS/MS indicates that the alkylation site occurs on the Cys47 of one subunit and Cys101 of the second subunit. This result can be explained by the fact that these two cysteine residues are proximal in the three-dimensional structure of the dimeric protein (3). This result is consistent with the idea that covalent sequestration of this and other drugs by GST's contributes to the acquired resistance of tumors to chemotherapy.

References :

1. Shea, T.C., Kelly. S.L. and Henner, W.D. (1988) Cancer Res. 48, 527-533.
2. Colvin, O.M.,Friedman, H.S., Gamcsik, M.P., Fenselau, C. and Hilton, J. (1993). Advances in Enzyme Regulation, (G. Weber ed), Pergamon Press, New York, NY, Vol 33, pp19-26.
3. Wilce, M.C. and Parker, M.W. (1994) Biochim. Biophys. Acta 1205, 1-18.

Acknowledgments

Daniele Fabris and Martha Vestling are gratefully acknowledged. This work was supported by the National Institutes of Health.

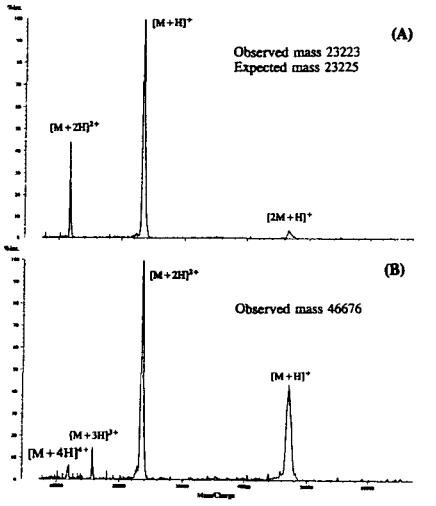

Figure 1. MALDI spectra : (A) GST control and ; (B) GST-CHB complex

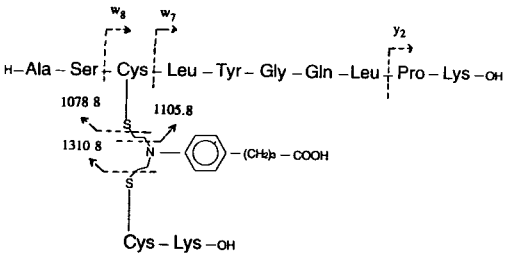

Figure 2. FAB/MS/MS characterization of CHB-alkylated peptide.

Applications of MS/MS to the Study of *S*-Linked Conjugates of Isocyanates

Margaret R. Davis* and Thomas A. Baillie*
Department of Medicinal Chemistry, School of Pharmacy, University of Washington, Seattle, WA 98195

Isocyanates (R-N=C=O) are highly reactive, electrophilic compounds which are formed as products of the metabolic activation of certain drugs and other xenobiotics. In general, conjugation of electrophiles with the tripeptide, glutathione (GSH) serves as an important detoxification process. In certain cases, however, conjugation of a xenobiotic with GSH results in the formation of a reactive, and thus potentially toxic, conjugate. The GSH adducts of isocyanates represent one such class in that they are formed reversibly and thus may serve as *in vivo* "carriers" of the isocyanates from which they are derived.

N,N'-bis(2-chloroethyl)-*N*-nitrosourea (BCNU) is a widely-used antineoplastic agent which decomposes under conditions of physiological temperature and pH to alkylating and carbamoylating intermediates (Figure 1). The carbamoylating species, 2-chloroethyl isocyanate (CEIC), is believed to be responsible for the pulmonary toxicity associated with the parent drug through its ability to covalently modify the active site of glutathione reductase (GR). Inactivation of this enzyme, which is crucial to maintaining a normal cellular redox state, produces oxidative stress which, in turn, has been linked to the development of the potentially-fatal pulmonary fibrosis associated with long-term BCNU therapy.

GR is a 118 kDa protein, the sequence of which has not yet been fully elucidated. It is known, however, that two cysteine residues are present in the active site and are directly involved in the catalytic conversion of glutathione disulfide (GSSG) to GSH. It has been proposed that carbamoylation of one of the active site sulfhydryl groups by CEIC is responsible for the inactivation of the enzyme observed following administration of BCNU.[1] Interestingly, the GSH conjugate of CEIC (SCG, Figure 2) has been shown to be an inhibitor of GR, equipotent to BCNU, in isolated rat hepatocytes.[2] In the present studies, oxytocin, a nonapeptide with two cysteine residues, was chosen as a peptide model of the active site of GR to probe the reactivity of BCNU, CEIC and SCG towards nucleophilic centers. Ionspray MS provided molecular weight information on the products of reaction between these carbamoylating agents and oxytocin *in vitro*. These adducts afforded doubly-protonated molecular ions, CID of which provided product ion spectra which were characterized by many doubly- and singly-charged fragment ions which resulted primarily from cleavages of the peptide bonds in the oxytocin-derived backbone. From these spectra, the structures of a number of products formed by the reaction of BCNU, CEIC and SCG with the peptide were characterized, thus providing valuable insight into the potential nature of the covalent interaction of these carbamoylating agents with GR.

References:
1. P.A. Karplus *et al.*, *Eur. J. Biochem.* **171**, 193-198 (1988).
2. M.R. Davis *et al.*, *Chem. Res. Toxicol.* **6**, 376-383 (1993).

*Present Address: Department of Drug Metabolism, Merck Research Laboratories, West Point, PA 19486

43rd ASMS Conference on Mass Spectrometry and Allied Topics

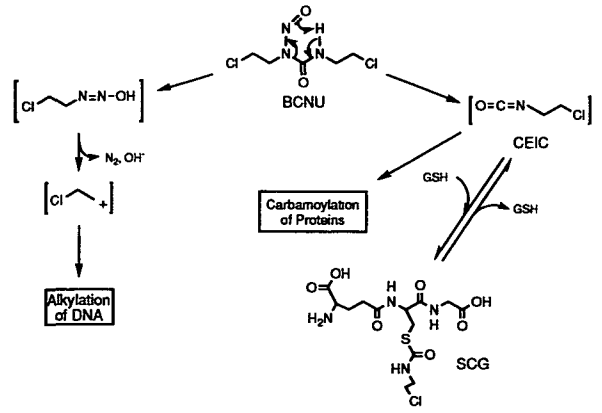

Figure 1. Decomposition of BCNU to alkylating and carbamoylating intermediates. The carbamoylating product, 2-chloroethyl isocyanate (CEIC) reacts with GSH to form SCG.

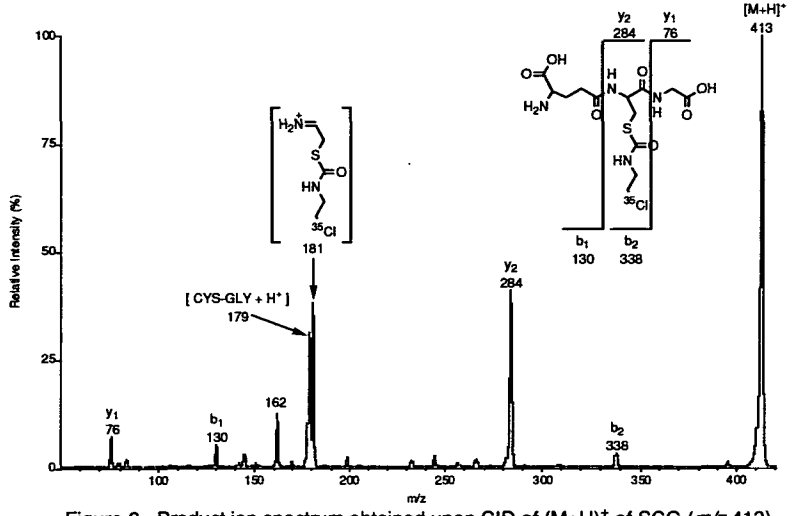

Figure 2. Product ion spectrum obtained upon CID of $(M+H)^+$ of SCG (*m/z* 413).

Supported by NIH grant ES05500.

Strategies for Analyses of Drug Metabolite Mixtures by CE-MS and CE-MS/MS

Stephen Naylor, Linda M. Benson, and Andy J. Tomlinson, Biomedical Mass Spectrometry Facility and Department of Biochemistry and Molecular Biology, Mayo Clinic, Rochester, MN 55905, USA

Investigation of the metabolic fate of therapeutic agents ultimately requires structural characterization of unknown metabolites. However, such products are often minor components of a complex biologically derived mixture that may also contain a large excess of parent drug. Good sensitivity and high dynamic range are basic requirements of the analytical methods to be used in these studies. In the present study, we demonstrate a systematic method development of CE separation media and describe the instrumental requirements of on-line CE-MS. Furthermore, we discuss the practical aspects of performing CE-MS and CE-MS/MS in the structural characterization of drug metabolites.[1] We investigate the *in vivo* metabolism of haloperidol which is a widely used neuroleptic agent to treat psychiatric disorders such as schizophrenia.

Various CZE conditions for the separation of haloperidol and six structurally similar analogs were investigated involving consideration of 1) pH; 2) % organic modifier (MeOH); and 3) ionic strength. Optimal separation conditions were determined to be 50 mM NH_4OAc, 10% MeOH and 1% AcOH. Furthermore for CE to be coupled to the MS, the following points must also be considered: 1) good electrical contact at the outlet of the CE capillary in the MS; 2) position of the CE capillary within the ion source; 3) use CE separation media of low ionic strength containing volatile salts.

Using this CE-MS approach, we have previously determined the metabolic fate of haloperidol after guinea pig and mouse hepatic microsomal incubations. However, due to the limited loading capacity of a conventional CE capillary, only limited information was obtained. In order to overcome this problem, we have developed on-line preconcentration-CE-MS (mPC-CE-MS)[2]. This allows both on-line analyte concentration as well as sample cleanup prior to elution and subsequent electrophoretic analysis. This is demonstrated in Figure 1 for a mPC-CE-ESI-MS analysis of a rat microsomal incubation of haloperidol where six metabolites were detected.

The isolation and analysis of haloperidol metabolites by mPC-CE-MS only results in a tentative identification. However, by employing tandem MS (MS/MS) where a molecular ion is selected and subjected to collision with an inert gas and the subsequent fragment (product) ions are analyzed can result in a more compelling determination.

We report for the first time the use of mPC-CE-MS in conjunction with high energy (5 kV) fast linked scanning (FLS) to obtain structural information of metabolites. The use of mPC-CE-FLS-MS/MS enables selection of a specific molecular ion and also allows detection of isotope ions. This is demonstrated in Figures 2 and 3 for the haloperidol metabolite HP^+ (M^+= 354) found in both a rat liver microsomal incubation and human urine sample respectively.

[1]Tomlinson *et al., J. Cap. Electrophoresis,* **1**, 127,1994.
[2]Tomlinson *et al., J. Cap. Electrophoresis,* **2**, 97, 1995.

Figure 1 mPC-CE-ESI-MS Analysis of a Rat Microsomal Incubate of Haloperidol

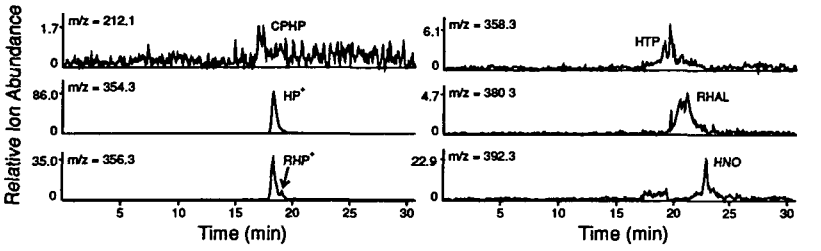

Figure 2 mPC-CE-ESI-MS/MS FLS of M^+= 354 from Rat Liver Microsomal Incubation of Haloperidol

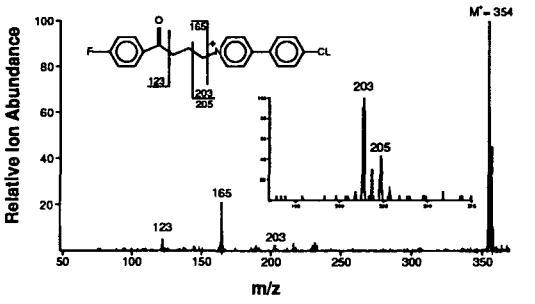

Figure 3 mPC-CE-ESI-MS/MS FLS of M^+= 354 from On-Line Analysis of Human Urine

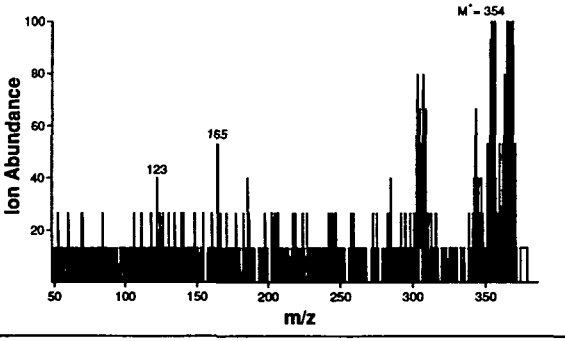

Probing the Regioselectivity of Gas Phase Alkylation of Biomolecules.

Richard A. J. O'Hair* [(a)], Michael A. Freitas [(a)], Scott Gronert [(b)], Joseph A. R. Schmidt [(a)] and Todd D. Williams[(c)].

(a) Department of Chemistry, Kansas State University, Manhattan, KS 66506-3701

(b) Department of Chemistry and Biochemistry, San Francisco State University, San Francisco, CA 94132

(c) Mass Spectrometry Laboratory, University of Kansas, Lawrence, KS 66405

It has been recognized that mutagenic and carcinogenic chemicals tend to be reactive electrophiles capable of modifying biological macromolecules such as DNA and proteins.(1) Despite much progress, a full understanding of the mechanisms of modification of biomolecules by reactive electrophiles at the molecular level remains elusive.(2,3) This is due to the complexity of these systems, whereby the actual electrophile(s) responsible for modification are often uncertain, the roles of solvent and counter ions are usually unknown, and the exact fate of the initially formed adduct(s) between the biological macromolecule and electrophile is unclear. In our work, two of the complicating factors, viz. the solvent and the counter ions are removed.(4) Thus the *intrinsic* reactivity of biomolecules with electrophiles in the gas phase are determined. The regioselectivity of these reactions are determined by analyzing the unimolecular fragmentation reactions of the product ions formed by reacting biomolecules with electrophiles in the CI source of a tandem mass spectrometer (all experiments were performed on a Fisons/VG (Manchester, UK) Autospec-Q; for details see ref. 4). Further insights into the thermodynamics and mechanisms of these reactions are gained by performing *ab initio* calculations on both the reactants and products of these reactions.

Specifically, we have determined that glycine undergoes a non- regioselective S_N2 reaction with $(CH_3)_2Cl^+$, with methylation occurring at both nitrogen and oxygen. This is consistent with the relative methyl cation affinities (MCAs) of CH_3Cl (MCA (CH_3Cl) = 62.0 kcal /mol) and those calculated via *ab initio* calculations (at the MP2/6-31G*//HF/6-31G* level) for the three nucleophilic sites in glycine: MCA (H_2N group) = 116.0 kcal/mol, MCA (C=O group) = 90.8 kcal/mol and MCA (HO group) = 80.6 kcal/mol. In contrast, the ambident electrophile $CH_3OCH_2^+$ reacts almost exclusively via a regiospecific pathway involving addition at nitrogen followed by elimination of CH_3OH to form a $[M + CH]^+$ ion with the structure $CH_2{=}NHCH_2CO_2H^+$. The experimental results are consistent with the *ab initio* calculated (at the MP2/6-31G*//HF/6-31G* level) relative stabilities of isomeric $[M + CH]^+$ ions.(4)

$(CH_3)_2Cl^+$ methylates cysteine (**1**) and the 2-hydroxypyridine (**2a**)/ 2-pyridinone (**2b**) system (a model for the tautomerism exhibited by nucleobases) at the sites indicated with a * in Scheme 1. The largest system studied to date is glutathione (Figure 1), which seems to be

methyated by $(CH_3)_2Cl^+$ at the sulfhydryl group. Our work is currently being extended to include the reactivity of other electrophiles (such as NO^+) and other biomolecules.

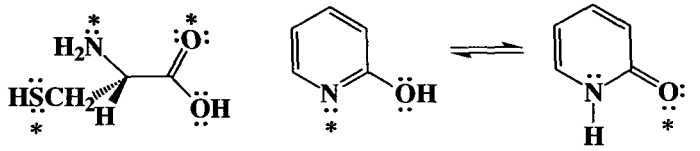

(1) (2a) (2b)

Scheme 1

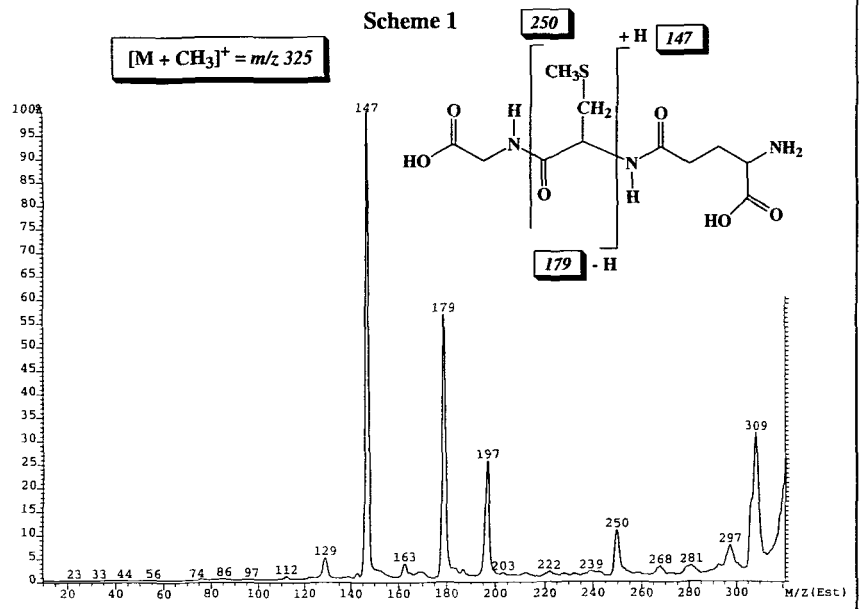

Figure 1: MIKE spectrum of gas phase methylated glutathione.

(1) Miller, J. A. Cancer Res., 1970, 30, 559.
(2) Lawley, P. D. in "Chemical Carcinogens", ACS Monograph 182, 1984; Chapter 7.
(3) Weisburger, J. H. et. al. in ref 2; Chapter 22.
(4) O'Hair, R. A. J.; Freitas, M. A.; Gronert, S.; Schmidt, J. A. R.; Williams, T. D., *J. Org. Chem.*, **1995**, *60*, 1990.

DETERMINATION OF β-AGONISTS IN BOVINE RETINA USING LC-APCI/MS AND MS/MS

Daniel R. Doerge[1], Steve Bajic[2], Mona I. Churchwell[1] and C. Lee Holder[1]
[1]National Center for Toxicological Research, Jefferson, AR 72079
[2]VG Organic, Altrincham, Cheshire WA14 5RZ, U.K.

INTRODUCTION

β-Adrenergic agents are used illegally to enhance the lean body mass of livestock by repartitioning metabolic energy from fat deposition to muscle accretion. This creates the potential for misuse in commercial meat production. These compounds, commonly referred to as β-agonists, have produced acute toxicity (cardiac, central nervous system) in humans consuming liver from illegally treated cattle. Because of high potency, the doses of β-agonists used in treating farm animals are in the μg/kg range and very low residue levels remain in tissues. Residues are cleared from the plasma, urine and muscle before liver and pigmented retinal epithelium, roughly in that order. The high potency, rapid elimination from animal tissues, and the large number of β-agonists available for misuse requires multiresidue screening methods that incorporate efficient extraction from tissues with long clearance times, chromatographic separation and sensitive, selective detection coupled with unequivocal identification.

EXPERIMENTAL

Untreated bovine eyeballs were obtained from a slaughterhouse and eyeballs from clenbuterol-treated animals were obtained from a pharmacokinetic study conducted by USDA. β-Agonist standards were obtained from commercial sources. Pigmented retinal epithelium was dissected and residues were extracted using sonication in aqueous HCl (0.01M) and solid-phase extraction using C18 cartridges. Recoveries of clenbuterol, salbutamol and terbutaline spiked into control tissue were 80-110%. Incurred residue levels of clenbuterol in treated eyeballs were comparable to those found by USDA researchers who used liquid-liquid extraction and GC/MS quantification. LC separations were made using a C18 NovaPak cartridge or C4E column flowing at 1.0 ml/min with 90% acetonitrile/10% 1 mM ammonium acetate or 20% acetonitrile/80% 20 mM ammonium acetate, respectively. MS measurements were performed using a VG Platform single quadrupole mass spectrometer or a VG Quattro II triple quadrupole mass spectrometer (VG Organic, Altrincham, U.K.). The entire effluent from the LC column was introduced into the mass spectrometer using an APCI interface and positive ion data collected. MS/MS measurements were obtained using Ar as the collision gas at a pressure of 2×10^{-3} mbar. A collision energy of 15 eV was used for multiple reaction monitoring (MRM).

RESULTS AND DISCUSSION

We previously developed a multiresidue extraction and separation of 5 β-agonists from plasma using LC-APCI/MS and MS/MS (*J. Mass Spectrom.*, in press). In the present study, we extend these results to bovine retinal epithelium, a tissue with an extended clearance time for β-agonist residues, to provide a method that can support regulatory surveillance of livestock. The basis for the method is an isocratic LC separation of 9 currently available β-agonists. In this study, we focused on three t-butyl-substituted compounds thought to be used in livestock: terbutaline, salbutamol and clenbuterol. A goal of this work was to develop MS and MS/MS methods with high sensitivity and the specificity required for regulatory confirmation. In the MS experiments, data from a minimum of three ions: $(M+H)^+$, $(M+H-H_2O)^+$ and $(M+H-t\text{-}Bu-H_2O)^+$ were acquired for each compound in selected ion monitoring mode (SIM). The cone voltage was varied throughout the acquisition such that a particular ion was monitored under the condition that maximized the respective intensity (e.g., acquisition of MH^+ ions was made at a low cone voltage, etc.). In this way, the intensity ratios for a given compound were approximately equivalent (i.e., as close to 1.0 as possible). This minimized the influence of data variation, especially on low intensity peaks. This technique was used to confirm the presence of incurred clenbuterol residues in eyeballs (72-100 ppb). Table 1 shows the ion intensity ratios for injection of standards (1 ng) vs. those from clenbuterol-dosed eyeballs. The high degree of reproducibility and the close agreement between ratios for standards and incurred samples meets current regulatory guidelines for confirmation (≥ 3 ions, ± 10%). Furthermore, the estimated LOD (S/N = 3) was 1-2 ppb (100-200 pg on-column) in retina using the method described here.

TABLE 1. Ion intensity ratios determined from the areas under the respective SIM chromatogram for clenbuterol residues from dosed cow retina (72-100 ppb) and an equivalent amount of clenbuterol standard.

RATIO	277/277	259/277	203/277
Standards (n=4)	1.0	0.82 ± 0.01	0.95 ± 0.06
Incurred Retina (n=4)	1.0	0.79 ± 0.02	0.90 ± 0.03

On-line LC-MS/MS techniques were also used to increase specificity and sensitivity of detection for the 3 t-butyl-substituted compounds. Constant neutral loss (CNL) of 74 ($-H_2O$, - t-Bu) was monitored to perform class-specific detection. Similar scans could be performed for iPr-substituted compounds using loss of 60. The estimated detection limit for this technique was 8-16 ppb (1-2 ng on-column) in retina. MRM of the most prominent transition for each t-butyl-substituted compound yielded the highest sensitivity detection (16-80 ppt, 2-10 pg) of β-agonist residues in retina.

These techniques can be combined in a strategy to detect, confirm and quantify misuse of β-agonists in livestock: 1) use retinal tissue because of long clearance times for residues; 2) employ the multiresidue extraction and LC separations described; 3) use CNL scans to identify t-Bu or i-Pr substituted compounds; 4) quantify target residues using low cone voltage MS-SIM using external standards or isotope dilution; 5) confirm target residues using intensity ratios of at least 3 characteristic ions or transitions in comparison with those from standards using MS-SIM or MRM, respectively; 6) for very low level detection, use MS/MS with MRM to monitor one specific transition and quantify residues using external standards or isotope dilution.

THE USE OF GC-MS TECHNIQUES TO EVALUATE BIOLOGICAL LIPID PEROXIDATION

W. Rodney Mathews, David Guido, Rose McKenna, Rachel Laskey.
Biochemistry, The Upjohn Company, Kalamazoo MI.

Reactive oxygen species such as superoxide anion, hydrogen peroxide and hydroxyl radical have been implicated in a variety of human diseases. Reactive oxygen species attack biological membranes resulting in a chain reaction referred to as lipid peroxidation. Lipid peroxidation results in damage to cellular membranes as well as the production of toxic compounds. The role of reactive oxygen species in many human pathologies remains speculative however since most currently used methods for quantifying lipid peroxidation lack adequate sensitivity and specificity. We have developed two GC-MS methods for quantifying lipid peroxidation products that can be used both in vitro and in vivo. The first method involves the use of electron impact GC-MS to measure various hydroxy-arachidonic acids (HETE assay,(1)). This method is especially useful for tissue samples. The second method employs negative ion chemical ionization GC-MS to quantify F2-Isoprostanes as first described by Roberts and coworkers (2) and is especially useful for measuring lipid peroxidation in plasma and urine samples. These assays have been used to determine lipid peroxidation in a variety of different systems.

The HETE assay has been used to investigate the role of nitric oxide (NO) in lipid peroxidation. NO has been reported to be a pro-oxidant by virtue of its reaction with superoxide anion to generate the powerful oxidant peroxynitrite anion ($ONOO^-$). Phosphatidylcholine (2 mg/ml) liposomes were incubated at 37 C with various NO sources (NO gas, Sin-1, diethylamine NONOate) or $ONOO^-$. After one hour, internal standard (25 ng 16-hydroxy-heneicosatetraenoic acid) was added and the samples analyzed by GC-MS as described previously(1). The results are shown in figure 1. Ferrous ammonium sulfate (FAS) used as a positive control and $ONOO^-$ caused significant lipid peroxidation. The NO donor Sin-1 which generates NO and O_2^- simultaneously with subsequent $ONOO^-$ formation caused a slignt increase in lipid peroxidation. Interestingly NO not only does not cause lipid peroxidation of PC liposomes but blocks iron-induced lipid peroxidation. Therefore, whether NO acts as a pro- or anti-oxidant in vivo will depend on the nature of the biological milieu into which it is released.

The HETE assay has been used to evaluate the role of lipid peroxidation in an in vitro model of oxidant induced damage to vascular function. Rings of rabbit aorta were suspended in bioassay baths and exposed to hydrogen peroxide or $ONOO^-$ and tested for endothelium dependent relaxation in response to acetylcholine. Both oxidants completely abolished ACh relaxations. Strips of rabbit aorta were exposed to the same concentration of oxidant species and the endothelial cells removed and assayed for HETE content. As shown in figure 2, the functional damage to the endothelial cells caused by these oxidants was not associated with a significant increase in lipid peroxidation. These results indicate that oxidant stress can cause significant alterations in cell function by mechanisms other than membrane lipid peroxidation.

43rd ASMS Conference on Mass Spectrometry and Allied Topics

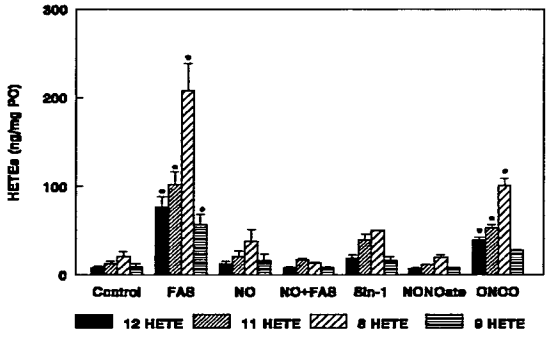

Figure 1

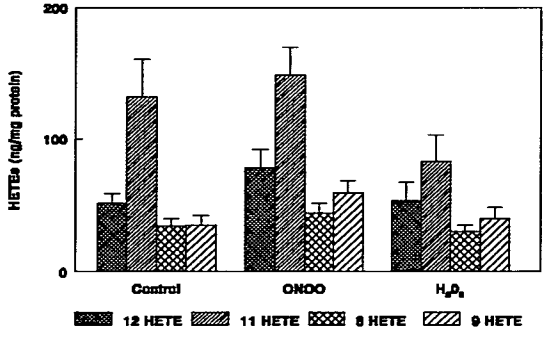

Figure 2

References:
1. GUIDO, D. M., MCKENNA, R. AND MATHEWS, W. R. Quantitation of hydroperoxy-eicosatetraenoic acids and hydroxy-eicosatetraenoic acids as indicators of lipid peroxidation using gas chromatography-mass spectrometry. Anal. Biochem. **209:123-9**: 123-129, 1993.
2. MORROW, J. D. AND ROBERTS, L. J.,II: Quantification of noncyclooxygenase derived prostanoids as a marker of oxidative stress. Free Radic. Biol. Med. **10:195-200**: 195-200, 1991.

MACROLIDE ANTIBIOTIC RESIDUES IN DISTILLER'S GRAIN AND MILK BY ESI LC/MS

Rick A. Flurer, John A. Tomlinson, and R. Duane Satzger
Forensic Chemistry Center, U.S. Food and Drug Administration
1141 Central Parkway, Cincinnati, OH 45202

The Forensic Chemistry Center has recently been involved in the investigation of large numbers of beef cattle deaths in several midwestern states. The factor linking these deaths is currently thought to be the consumption of contaminated dried distillers grain (DDG), a feed additive. During the course of this investigation, it was determined that the DDG had been contaminated with antibiotic residues at an ethanol production facility. These residues originated from waste stream ethanol that had been sent to the ethanol production facility for removal of high levels of dissolved solids before use in the production of gasohol. The solids remaining after distillation of the waste stream ethanol were then combined with the DDG produced by the firm's standard process for production of ethanol. The residues consisted of erythromycin A, clarithromycin, and a variety of side-reaction products or decomposition products (analogs) from a process wherein clarithromycin is synthesized from erythromycin A. Ethanol is used as a solvent in this synthetic process. We have developed an electrospray LC/MS method for the analysis of these antibiotic residues in DDG. The investigation also revealed that dairy cattle were also fed the contaminated DDG; however, they did not suffer any effects from exposure to the macrolide residues. In spite of this fact, it was necessary to check several tank trucks of milk from these cows for macrolide antibiotic residues to prevent possible exposure of the public to these residues. The level of concern was approximately 10 ppb. Therefore, we have also developed an electrospray LC/MS/MS method for confirmation of macrolide antibiotic residues in bovine milk at the 1-10 ppb level.

The total ion chromatogram (TIC) and several reconstructed ion chromatograms (RIC) for a contaminated DDG sample are shown in Figure 1. More than two dozen components are present, and the RIC's indicate that many components share the same nominal masses. The product ion spectra for erythromycin A, clarithromycin, and decladinosyl-clarithromycin (Declad) standards contain an ion at m/z 158. The commonality of the presence of the ion at m/z 158 suggests that a precursor ion LC/MS/MS experiment for precursors of m/z 158 would be useful as a screen for clarithromycin analogs. The precursor ion LC/MS/MS TIC and the LC/MS TIC for contaminated DDG are compared in Figure 2. Clearly, there is one-to-one correspondence between the chromatographic peaks in each TIC, indicating that virtually all of the peaks represent macrolide antibiotic species. Most have been identified through their product ion spectra, the mass of their $[M+H]^+$ ions, and knowledge of possible side-reactions or decomposition pathways. In general, the analogs in the DDG samples were present at the 1-100 ppm level, as determined by a single point calibration versus a clarithromycin standard.

The selected reaction monitoring (SRM) data for a mixed 25 ppb clarithromycin and declad standard are shown in Figure 3. Declad elutes at retention time 7:23 and clarithromycin elutes at retention time 9:32. The corresponding data for a 1 ppb milk spike are shown in Figure 4. The data exhibit a signal-to-noise ratio > 3:1, and the peak maxima in the RIC for each reaction monitored occur at the retention time of the corresponding standard. The SRM data for a negative control milk sample are shown in Figure 5; they demonstrate the absence of interferences at the retention times of the standards. The average recoveries for declad at the 1 ppb and 10 ppb spike levels are 79±12% and 82±5 (n=5), respectively. The corresponding recoveries for clarithromycin are 69±5% and 77±2% (n=5). Clearly, this method is more than adequate for the determination of macrolide residues in milk at the 1-10 ppb level.

43rd ASMS Conference on Mass Spectrometry and Allied Topics

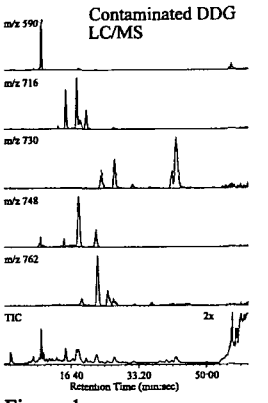

Figure 1

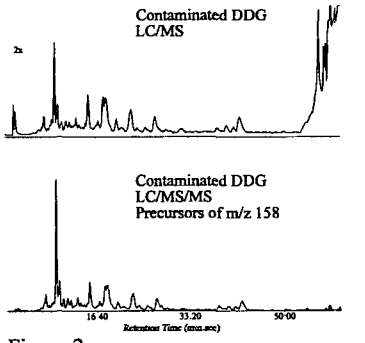

Figure 2

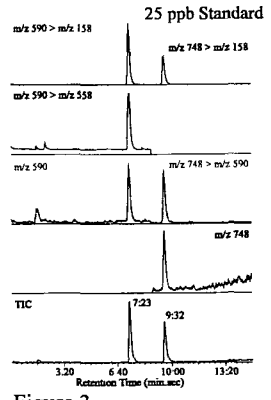

Figure 3

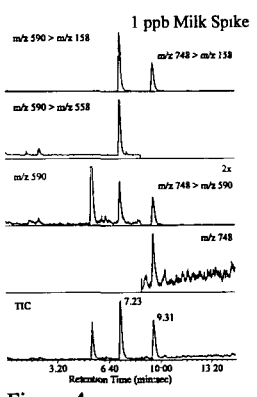

Figure 4

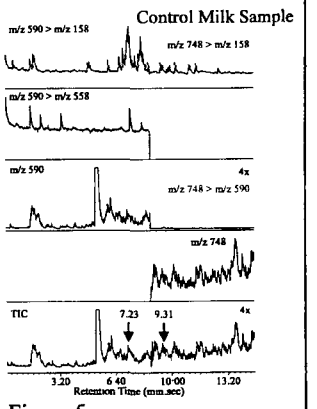

Figure 5

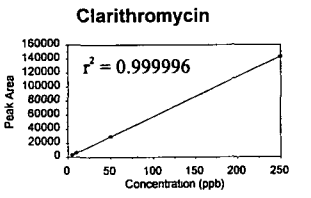

Figure 6

ISPROSTANE FAMILIES FOLLOWING FREE RADICAL OXIDATION OF ARACHIDONIC ACID

Russell J. Waugh and Robert C. Murphy
National Jewish Center for Immunology and Respiratory Medicine
1400 Jackson Street, Denver, CO 80206

INTRODUCTION

A great deal of interest has centered around the role of lipid peroxidation in diseases which range from cancer, atherosclerosis to ischemia reperfusion injury (1). Typically, very small molecules have been measured to assess lipid peroxidation; these small molecules include pentane, malonyldialdehyde, and 4-hydroxynonenal (2). Recently, structures of more complex free radical oxidation products have been identified, in particular the compounds isomeric to the cyclooxygenase-derived prostaglandins that have been termed *isoprostanes* (3). As seen in Figure 1, the free radical formation of these isoprostanes are initiated by formation of a stable bisallylic product which reacts with triplet oxygen to form a hydroperoxy adduct. This can cyclize and further react with another molecule of triplet oxygen yielding a hydroperoxy endoperoxide. Arachidonic acid has three bisallylic positions which can form, in theory, four different structural family subtypes of hydroperoxy cyclic endoperoxides (Figure 1). We have undertaken studies to investigate the formation of these families by free radical oxidation of arachidonic acid and obtained mass spectra of different family subtypes.

RESULTS

Using Fenton chemistry (4), oxidation of arachidonic acid with hydrogen peroxide and Cu^{++} was carried out to form a host of free radical products. Following HPLC separation of these products, catalytic reduction using Rh/Al_2O_3 with hydrogen gas, methylation, and trimethylsilylation products were analyzed by electron ionization GC/MS. One component from the initial HPLC separation is shown in Figure 2A which was identified as a Type-IV family member based upon the characteristic α-cleavage ions identical to authentic $PGF_{2\alpha}$ derivatized in the same manner. Another HPLC fraction yielded a component with the EI mass spectrum shown in Figure 2B. The α-cleavage ions were identical to those predicted for a Type I family member.

A method for direct detection of isoprostanes eluting from the HPLC was developed using electrospray ionization mass spectrometry. Isoprostanes have a unique structural characteristic, namely a 1,3-diol moiety within a cyclopentane ring. The carboxylate anion from $PGF_{2\alpha}$ (*m/z* 353) was previously shown to decompose with the loss of 44 u (C_2H_2O) to form *m/z* 309 (5,6). Selected reaction monitoring was employed for *m/z* 353 during HPLC/MS/MS analysis of the oxidation products of arachidonic acid as described above. The elution of isoprostanes were readily detected and three major HPLC peaks identified (Figure 3). Structural analysis of these isoprostanes using the GC/MS techniques of the reduced methyl ester trimethylsilyl ether derivative described above, revealed the presence of two predominant family members, Type IV and Type I.

The free radical oxidation of arachidonic acid using Fenton chemistry conditions resulted in the predominate formation of family Type IV (cylooxygenase-like products) and family Type I which has the free hydroxyl group at carbon 5 of arachidonic acid. This latter family type is structurally unique in that members are not enzymatically derived from cyclooxygenase-mediated oxygenation of arachidonic acid.

ACKNOWLEDGEMENT - This work was supported by a grant from the National Institutes of Health (HL34303).

REFERENCES

1. *Oxygen Free Radical in Tissue Injury*, Tarr, M., Samson, F., Eds., Boston, Birkhauser (1993).
2. Shimizu, T., Kondo, K., and Hayaishi, O. (1989) *Arch. Biochem. Biophys.* **206**, 271.
3. Morrow, J. D., Hill, K. E., Burk, R. F., Nammour, T. M., Badr, K. F., and Roberts, L. J. (1990) *Proc. Natl. Acad. Sci. U. S. A.* **87**, 9383-9387.
4. Halliwell, B. and Gutteridge, J. M. (1984) *Biochem. J.* **219**, 1-14.
5. Contada, M. J., Adams, J., and Gross, M. L. (1989) *Adv. Mass Spectrom.* **11B**, 1034-1035.
6. Kayganich, K. A., Rose, D. M., Murphy, R. C., Morrow, J. D., and Roberts, L. J. II (1993) *J. Lipid Res.* **34**, 1229-1235.

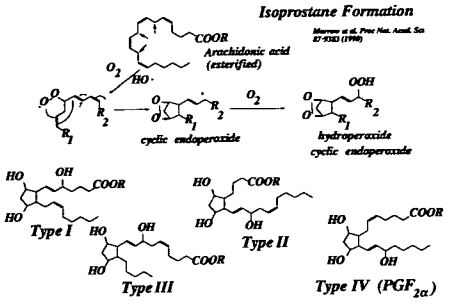

Figure 1 *Mechanism of free radical oxidation of arachidonic acid leading to isoprostanes.*

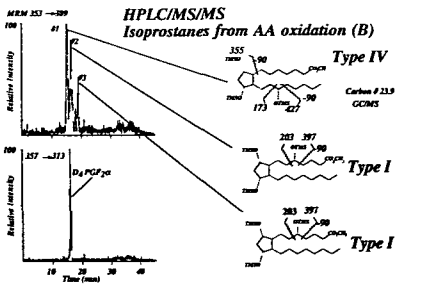

Figure 3 *ESI/MS/MS for the loss of 44 u from m/z 353 to form m/z 309 characteristic of F_2-isoprostanes. Subsequent structural analysis of HPLC fractions reveal elution of the structures indicated.*

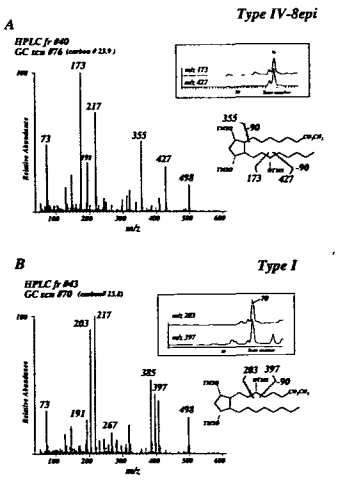

Figure 2 *Electron ionization GC/MS of isoprostanes separated by HPLC following catalytic reduction and derivatization to the methyl ester trimethylsilyl ether derivative. Selected ion recording traces for specific α-cleavage ions are indicated as insets.*

DETERMINATION OF BECLOMETHASONE DIPROPIONATE AND THREE METABOLITES IN HUMAN, DOG AND RAT PLASMA VIA HPLC-APCI/MS/MS.

Matthew S. Bryant, Walter A. Korfmacher, Cymbelene L. Nardo, Amelia P. Lapiguera and Chin-Chung Lin.
Department of Drug Metabolism and Pharmacokinetics
Schering-Plough Research Institute, 2015 Galloping Hill Road, Kenilworth, NJ 07033-0539

Carolyn N. Langevin and Thomas D. Oglesby.
Taylor Technology Inc.
350 Alexander Road, Princeton, NJ 08540

Introduction. Beclomethasone 17,21-dipropionate (BDP; figure 1) is an anti-inflammatory steroid used for the control of the symptoms of rhinitis or bronchial asthma. A sensitive assay was needed for the simultaneous determination of BDP and three potential metabolites, beclomethasone (BEC), beclomethasone 17-propionate (17-BMP) and beclomethasone 21-propionate (21-BMP) in plasma of several species. The technique of HPLC combined with atmospheric pressure chemical ionization (APCI) tandem mass spectrometry (MS/MS) was found to provide the necessary sensitivity and selectivity to develop and validate this analytical methodology.

Experimental. A Finnigan-MAT TSQ 700 or 7000 triple stage quadrupole mass spectrometer equipped with the Finnigan APCI source was used for the study. Plasma samples (0.4 to 1.0 ml; depending on species) containing mometasone furoate as an internal standard (IS) were subjected to liquid-liquid extraction. Separation of the four analytes and the IS was achieved by a reverse phase HPLC column connected directly to the APCI inlet. The MS analysis was performed using the selected reaction monitoring (SRM) technique. In each case, the protonated molecule $[MH]^+$ was chosen as the parent ion by Q1 and a molecule-specific fragment ion selected for the progeny ion by Q3. Collision gas energies in Q2 were optimized for each of the compounds (see figure 2.)

Results and Discussion. The HPLC-APCI/MS/MS analytical methodology was sensitive and specific for the simultaneous determination of BDP and three metabolites. The method was validated and found to be linear over the range of 50 to 5000 pg/ml for BDP and 17-BMP and 100 to 5000 pg/ml for BEC and 21-BMP in 1.0 ml human plasma samples. Accuracy and precision of the method were evaluated using quality control (QC) samples. Back calculated values for all analytes at each concentration of the standard curve were within 8% of the expected values. Relative standard deviation was less than 13% for standards below 100 pg/ml and less than 11% for values 100 pg/ml or higher. Samples were found to be stable during multiple freeze-thaw cycles.

The assay was also validated in dog and rat plasma. Lower limits of quantitation were 2-fold higher due to smaller sample volumes of 0.5 and 0.4 ml, respectively.

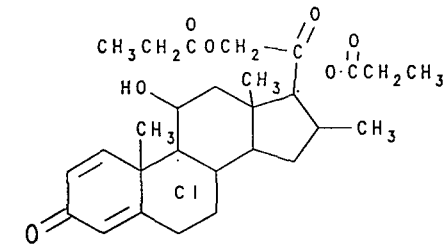

Figure 1. Structure of Beclomethasone 17,21-Dipropionate

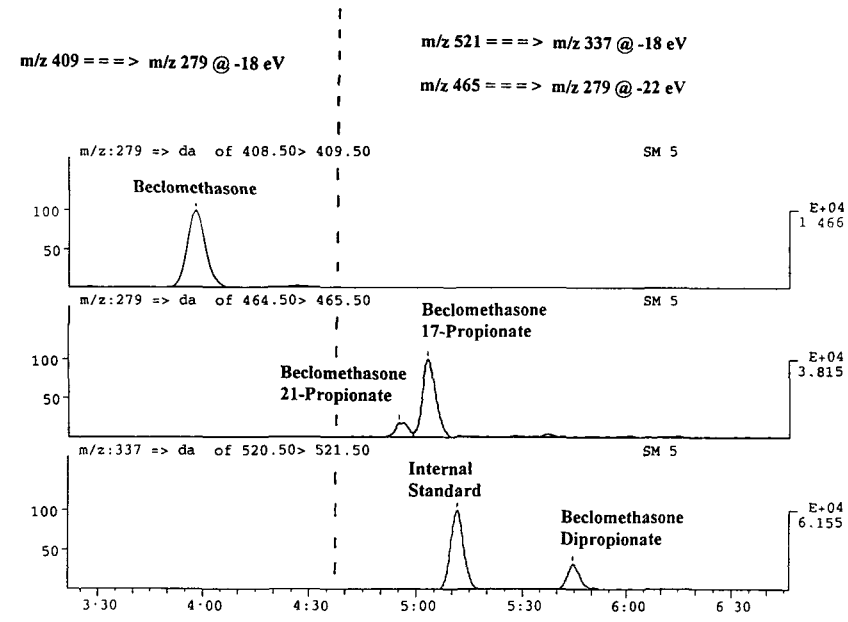

Figure 2. Extract of plasma spiked with 4 analytes, showing SRM parameters.

Column-Switching sample preparation for quantitative analysis by LC-MS

G. Hopfgartner, M. Zell, C. Husser
F. Hoffmann-La Roche, Pharma Division, Department of Drug Metabolism & Kinetics, CH-4002 Basel

Introduction

Atmospheric pressure ionisation (API) tandem mass spectrometry combined with liquid chromatography (LC-MS/MS), becomes a powerful analytical tool in respect to sensitivity and selectivity that arising with the use of HPLC with UV-detection for the quantification of pharmaceutical compounds.

Due to high selectivity of tandem mass spectrometry fast analysis time in the range of one to five minutes are possible and over 300 samples can be analysed on a daily basis assuming that several people or automates are involved with sample preparation. Limiting factors became sample preparation and data handling. For sample preparation the following techniques are widely used : liquid-liquid extraction or solid-phase extraction.

An elegant alternative to off-line sample preparation is column-switching (1,2), where large amount of samples (up to 1 ml) were injected onto a standard bore pre-column where the analytes are retained while salts and endogenous compounds were washed out. After this preconcentration and wash step the analytes are eluted in backflush onto a standard, narrow or microbore analytical column. Plasma or plasma samples after protein precipitation can directly be injected into the fully automated system. The setup is simple, low cost, universal and can be used either with ion spray or the heated nebuliser interface reducing development and optimisation time of a given analytical problem.

Using the same strategy two assays have been developed for the quantification of the benzodiazepine agonist Ro 48-6791 and its depropyl metabolite Ro 48-6792 or the platelet aggregation inhibitors : Ro 48-3856 and Ro 44-3888 in human plasma.

Experimental

The HPLC system used in this work was constituted by two Merck Hitachi L6200A and 6000 pump and an AS-4000 autosampler (Merck) equipped with a 2 ml injection loop. For column switching a high speed Reodhyne six port switching valve was used. The analytes were separated on a 150 x 2 mm or a 150 x 1 mm i.d. Inertsil ODS-2, 5 µm column.The eluant was 1% HCOOH/MeOH (60/40, v/v and the flow rate was 0.2 ml/min for 2 mm i.d. column or 0.05 ml/min for the 1 mm i.d. column. For the analysis of Ro 48-6791 and Ro 48-6792 plasma proteins (0.5 ml plasma) were precipitated with acetonitrile. After partial evaporation of acetonitrile, a buffer solution was added and 1 ml of the supernatant was injected into the HPLC system.

All analyses were performed on an API III^{plus} (PE Sciex) triple quadrupole mass spectrometer equipped with a home-made autogate for automated recycling.
The MS analysis was performed using ion spray in positive mode with selected reaction monitoring (SRM). The following precursor-to-product ions reactions were monitored with dwell times of 200 and 400 msec : m/z 371 to 300 (Ro 48-6792), m/z 375 to 300 (d4 IS) and m/z and m/z 413 to 114 (Ro 48-6791), m/z 417-118 (d4 IS). The collision energy was set at 10 eV and argon was used at a collision gas thickness of 270 x 10^{13} atoms/cm^2.

43rd ASMS Conference on Mass Spectrometry and Allied Topics

Results

The column-switching approach was found to be robust and sensitive. Over 700 samples could be analysed with the same trapping pre-column. The lower limit of quantification was 20 pg/ml for Ro 48-6791 and 50 pg/ml for Ro 48-6792, respectively. The assay was liner for both compounds up to 20 ng/ml. The precision and accuracy derived from QC samples, concomitantly assayed along with unknown samples from clinical studies, was found to be better than 8.1 % and 94.7 % in the concentration range of 100 pg/ml to 10ng/ml, respectively. By adding a second switching valve and a second trapping pre-column the sample throughput can be increased from 100 samples per day to 150 samples per day without compromising analytical performance. A quantification limit of 2 pg/ml in human of plasma was achieved by transfering from the standard bore trapping column to a microbore (1 mm i.d.) analytical column.

The column-switching system can be used with analytes of different polarities and a sensitive method was also developed with the same strategy for the quantification of the platelet aggregation inhibitors (Ro 48-3856 and Ro 44-3888) in human plasma.

1) U. Timm, G. Hopfgartner and R. Erdin, J. Chromatogr., 456, (1988), 21-31.
2) K.A. Ramsteiner, J. Chromatogr., 456 (1988), 3-20.

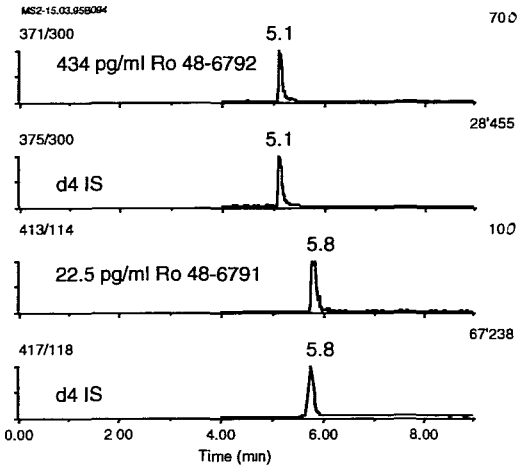

Figure 2: SRM Chromatogram of a human plasma sample 4H after i.v. administration of 0.1 mg Ro 48-6791

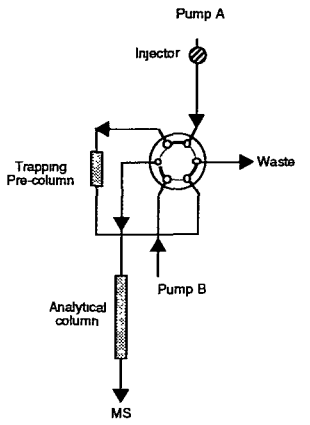

Figure 1 : Column -switching setup

Direct Measurement of Steroid Glucuronides and Sulfates with HPLC/MS and HPLC/MS/MS

Sanaullah and Larry D. Bowers
Department of Pathology and Laboratory Medicine
Indiana University Medical Center
Indianapolis, IN 46202-5120

The measurement of steroids in urine is an important aspect of doping control in sports, as well as diagnosis of disease and genetic metabolic disorders. Steroids are excreted in urine as conjugates with glucuronate and sulfate. The present analysis of steroids requires hydrolysis, derivatization, and GC/MS detection; this approach has a number of limitations. One area of steroid measurement which is of great interest in doping control is measurement of the testosterone-epitestosterone (T/E) ratio. The IOC requires sanctions for T/E ratios greater than six. Recent work by Dehenin and Matsumoto suggests that differences in glucuronidation and sulfation could result in variability of the T/E ratio. We have developed HPLC/MS and HPLC/MS/MS methods for direct quantitation of T-sulfate, T-glucuronide, E-sulfate, and E-glucuronide in urine.

We have synthesized ES, EG, d_3-TG, and d_3-ES in our laboratory. The T labeling procedure began with androstendione. d_3-E was synthesized from d_3-T using the Mitsunobu reaction. We have used a modified version of the Köenig-Knorr reaction to improve the yield of glucuronidation. Using the synthesized standards and deuterated internal standards, we have developed a method for extraction and quantitation using HPLC/MS. The steroid conjugates were extracted from urine using a modification of the reported by Weidolf and Henion.

The HPLC/MS method makes use of a PE Sciex API III tandem mass spectrometer. The IonSpray interface was used in conjunction with both 1 mm id and 320 um id HPLC columns. Using the packed capillary, detection limits of 20 pg on column were achieved. The orifice voltage is very important in achieving a sensitive analysis. TG and EG behave very differently, with EG fragmenting to yield predominanatly the aglycone at orifice voltages of 60 V. The sulfate conjugates are much more rugged. In fact, the inability to significantly fragment these compounds in the positive ion mode is a drawback in terms of the utility of the technique to provide information about the identity of the steroid.

Measurement of the T and E conjugates in urine showed that although significant inter-individual differences in the conjugation do occur, they do not appear to affect the T/E ratio.

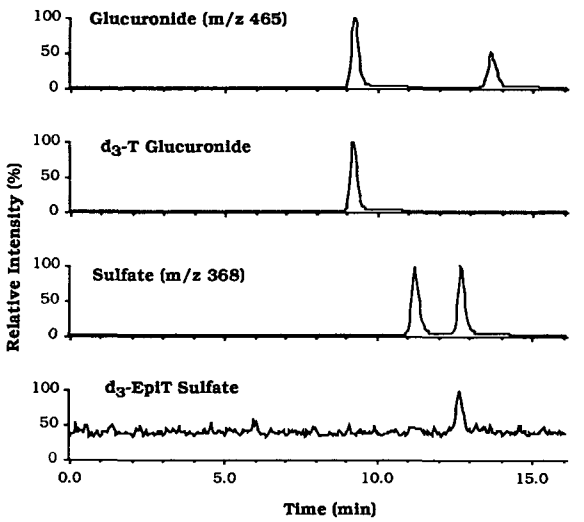

Haloacetic Acid Drinking Water Disinfection By-Products

William L. Budde, Jean W. Munch, David D. Kryak, and Thomas D. Behymer

U. S. Environmental Protection Agency, Office of Research and Development, National Exposure Research Laboratory, Aquatic Research Division, 26 W. Martin Luther King Drive, Cincinnati, OH 45268

Humic material from decaying vegetation, etc. in surface and ground waters reacts with chlorine which is added to drinking water for microbiological disinfection. A series of well-characterized drinking water disinfection by-products (DBPs) are formed including the well-known trihalomethanes, mono-, di-, and trihaloacetic acetic acids, haloacetonitriles, and other substances. Depending on the concentration of bromide ion in the water, brominated and mixed bromochloro DBPs are also produced.

$$\text{humic substances in source water} \xrightarrow[Br^-]{Cl_2} Br_xCl_yC\text{-}COOH + Br_xCl_yCH + Br_xCl_yC\text{-}CN + \text{others}$$

This work focused on the haloacetic acids which are usually determined with EPA Methods 552 or 552.1. In Method 552, a 100 mL drinking water sample is extracted with methyl tert-butyl ether (MTBE), the acids are converted to methyl esters with diazomethane in MTBE, the esters are separated with capillary column GC, and measured with an electron capture detector (ECD). Because it is highly desirable to reduce laboratory worker exposures to solvents like MTBE and reagents like diazomethane, alternative Method 552 1 was developed. In this method, a 100 mL drinking water sample is passed through an anion exchange column, the retained acids are eluted with acidic methanol, the acids esterified by heating with a small amount of MTBE, partitioned into MTBE, separated with capillary column GC, and measured with an electron capture detector (ECD). Unfortunately, haloacetic acids are not extracted efficiently by the ion exchange column from waters with a high ionic strength, and particularly from those waters with relatively high concentrations of sulfate ion which displaces the acid anions from the resin Both methods suffer from a reliance on retention times for identifications and the potential for many coeluting electron capturing substances.

We are exploring alternative approaches to the measurement of haloacetic acids which have been proposed for regulation in drinking water. Use of a high sensitivity mass spectrometer in place of the ECD would eliminate at least one of the shortcomings of Methods 552 and 552.1. High sensitivity in the full mass scan mode is required to ensure that the concentrations of acids are below proposed regulatory levels and to ensure correct identifications of the haloacetic acids. An instrument detection limit of 20 pg or less was obtained for the methyl esters using an ion trap mass spectrometer. The methyl esters of mono-, di-, and trichloroacetic acids, mono-, and dibromoacetic acids, and bromochloroacetic acid chromatograph on standard bonded phase fused

silica capillary columns with retention times in the 5-15 min range. Tribromoacetic acid and several other mixed bromochloroacetic acids may be present in some drinking waters but were not included in our studies because of problems with stability, purity, availability of standards, and chromatography. The methyl esters of the compounds studied are readily identified by their 70 eV electron ionization spectra, although molecular ions are very weak or not observed.

A completely different approach is being investigated as a means of overcoming all the deficiencies in Methods 552 and 552.1. In this approach, no extraction is used but the water sample is concentrated by a factor of 10-20 by lyophilization. The acid anions are separated at pH > 10 by ion chromatography , introduced into the mass spectrometer (MS) by pneumatically assisted negative ion electrospray, and measured by time scheduled selected reaction monitoring (SRM) in a tandem MS system The ions used in the SRM mode are given below:

Anion	Q_1 m/z		Q_3 m/z
$ClCH_2\text{-}COO^-$	93		35
$BrCH_2\text{-}COO^-$	137		79
$Br(CH_2)_2\text{-}COO^-$ (IS)	151		79
$Cl_2CH\text{-}COO^-$	127	$\xrightarrow{-CO_2}$	83
$Br_2CH\text{-}COO^-$	217	"	173
$BrClCH\text{-}COO^-$	173	"	129
$Cl_3C\text{-}COO^-$	161	"	117

On collision induced decomposition (CID), chloroacetate, bromoacetate, and the internal standard 2-bromopropionate give primarily chloride and bromide ions respectively, and these reaction products are monitored in Q_3. On CID, the other haloacetate molecular anions lose carbon dioxide and the residual anions are monitored in Q_3. Instrument detection limits are in the range of 0.1-3 ng which may be adequate for monitoring these acids in drinking water. Further details on this approach are given in Wednesday poster (WPF) 136.

Investigating Oxidation Reactions in Environmental Systems

M. Judith Charles[1], Thomas N. Feinberg[1], and Susan D. Richardson[2]
[1]Department of Environmental Sciences and Engineering, University of North Carolina at Chapel Hill, Chapel Hill, NC 27599-7400; [2]U.S. Environmental Protection Agency, Environmental Research Laboratory, Athens, Georgia 30605-2720.

Introduction: Research in the environmental sciences strives to understand processes such as chemical oxidation reactions that influence the formation transport and transformation of chemicals in environmental systems. Explorations of chemical mechanisms is a critical component of these studies. We present two research stories highlight the contribution of mass spectrometry to understanding environmental issues affecting everyday life, and exemplify the interplay between the emergence of significant environmental issues and the development of analytical technologies to cope with these issues.

Chemical mechanisms affecting the formation of worrisome chemicals in disinfected waters: In 1974, the finding that halogenated methanes are present in chlorinated waters by Rook and Bellar *et al.*, (1,2) led these and other researchers to investigate the formation of these compounds. Bellar *et al.*, 1974 suggested that chloroform resulted from the step-wise oxidation of ethanol to acetaldehyde, chloral and chloral hydrate. This hypothesis failed to account for the ubiquity of disinfection by-products as little evidence was found to support the notion that ethanol is present in all natural waters (3). Rook was the first to suggest that humic substances are precursors for trihalomethanes in drinking waters. Rook evoked the "haloform reaction", a series of base-catalyzed halogenation and hydrolysis reactions explains the production of chloroform from methyl ketones such as acetone (4,5). The half-life for haloform formation for acetone at pH 7 is too long (almost a year; 7500 hr) (4) and the concentration of acetone in waters is insufficient to account for the high levels (200 μg/L) of chloroform (1). Rook then suggested, based on chlorination studies of model compounds that fast chlorination occurs on resorcinol or resorcyclic acid moieties incorporated causes ring rupture of the humic macromolecule to produce methylene chloride, dichloroacetic acid, chloroform and butenoic acid (6). Chemical degradation studies advanced the idea that humic substances are comprised of aromatic and aliphatic components and the identification of unchlorinated aliphatic and aromatic compounds highlights the oxidation capabilities of chlorine (7,8). The identification of saturated molecules and 3,5,5-trichlorocyclopent-3-ene-1,2-dione as the primary intermediate in the reaction of chlorine with resorcinol led Christman and co-workers (7) to dispute Rook's hypothesis. Ring rupture mechanisms similar to those proposed by Rook effect the formation of unsaturated molecules and OCl^- attack on side chains of aromatic molecules produces saturated molecules (9). Tretyakova *et al.*, (10) observed the formation of cyclopentadione intermediates, compounds observed to occur during the formation of chloroform from resorcinol and thought to be too unstable to be reaction intermediates by Rook. The identification of toxicologically worrisome chemicals has fostered research on the use of disinfectants, such as monochloriamine, ozone, chlorine dioxide, and TiO_2/UV. These disinfectants do not produce high levels of trihalomethanes, but do produce polar oxygenated molecules that may be hazardous to human health.

Chemical mechanisms for the transformation of volatile organics affecting tropospheric ozone formation: Volatile organic hydrocarbons participate in the photochemical cycle by reacting with the hydroxyl radical to form organic radicals that combine with molecular oxygen and nitric oxide to form other radical species and nitrogen dioxide. The photodissociation of nitrogen dioxide releases ground state oxygen that recombines with molecular oxygen to form ozone. Because ozone dissociates to form hydroxyl radicals, this process is a chain reaction. On a global scale the emissions of biogenic hydrocarbons exceed that of all anthropogenic sources of non-methane organic gases. Isoprene (2-methyl-1,3-butadiene) constitutes a major fraction of all vegetative non-methane hydrocarbon emissions. Hence, the atmospheric photochemistry of isoprene is a critical component of understanding tropospheric ozone formation. Gu *et al.* (11) proposed that 1,2- and 3,4-addition reactions leads to the formation of alkoxy radicals that degrade to form methacrolein and methylvinylketone. 3-methylfuran and formaldehyde, also reaction intermediates were proposed to form by other chemical mechanisms. Subsequent FTIR work done by Tuazon and Atkinson (12) confirmed the formation of intermediates previously observed and second generational species, including hydroxyacetone, methylglyoxal and glycoaldehyde. The total product yield uncertain because only $\approx$55% of the carbon containing products can be positively identified. The remaining "unknown" composition was determined from its IR spectrum to consist of carbonyls and only a small fraction from organic nitrates. From data obtained by using PFBHA derivatization in combination with ion trap mass spectrometry, Yu *et al.* (13), established that hydroxyl radical oxidation of isoprene process by many types of addition reactions. 1,2-addition of ·OH to isoprene forms alkoxy radicals that degrade to methylvinylketone and hydroxymethylketone. Second generational species formed include methylglyoxal, glycoaldehyde and hydroxymethyl glyoxal. 3,4-addition, 2,1-addition and 4,3-addition reactions are also important and also leads to the formation of multi-functional carbonyl compounds.

Summary: After 20 years of research, we now know that humic substances are complex materials that cannot be elucidated by a simple drawing; and that chlorination of these materials effects chlorination and oxidation reactions that degrade humic substances. At present more than 50% of the total organic halogen in chlorinated humic samples and in chlorinated water supplies remain unidentified. After 9 years of research, we now understand that many types of addition reactions effect degradation of isoprene. The "missing carbon" formed from degradation of the humic macromolecule or photooxidation of isoprene is believed to be low-molecular weight polar and oxygenated molecules. New analytical methodologies are needed to further advance our understanding of chemical mechanisms in aquatic and atmospheric systems. Electrospray mass spectrometry, derivatization techniques in combination with ion trap mass spectrometry and the development and application of novel chemical ionization reagents will likely allow deeper and better research questions to be answered in the environmental sciences.

References Cited: **1.** Rook, J. J. *Water Treat. Exam.* **1974**, 23 (Part 2, 234); **2.** Bellar and Lichtenburg, J. J.; Kroner, R. C. *Jour. AWWA.* **1974, 703.**; **3.** Symons *et al.*, *Jour AWWA*, **1975**, 634.; **4.** Morris, J. C., Baum, B. In *Water Chlorination, Environmental Impact and Health Effects*, Vol. 3, **1980**, Ann Arbor Science Publishers; **5.** Rook, J. J. *ES&T* **1977**, 5:478.; **6.** Rook, J. J. *et al.* In *Water Chlorination, Environmental Impact and Health Effects*, Vol. 2, **1977**, Ann Arbor Science Publishers; **7.** Christman, R. F. *et al.*, In *Water Chlorination, Environmental Impact and Health Effects*, Vol. 2., **1977**, Ann Arbor Science Publishers; **8.** Liao, W. *et al.*, *ES&T.* **1982**, 16, 403.; **9.** Christman, R. F. *et al.*, In *Humic Substances II*, **1989**, John Wiley & Sons.; **10.** Tretyakova, N. Y. *et al.*, *ES&T.* **1994**, 28, 606.; **11.** Gu, C. *et al.*, *ES&T.* **1985**, 19, 151; **12.** Tuazon, E.C. and Atkinson, R. *Int. J. Chem. Kinet.* **1990**, 22, 1221. **13.** Yu, J. *et al.*, **1995**, accepted for publication, *ES&T.*

High Speed Analysis of Total Trihalomethane (TTHM) Content in Drinking Water using Membrane Introduction Mass Spectrometry (MIMS)

Scott Bauer, Jan Bauer, MIMS Technology Inc.
1900 S. Harbor City Blvd. Suite 115
Melbourne, FL 32901

Traditional methods for the determination of total trihalomethane content in drinking water by purge and trap gas chromatography (GC) is slow, expensive, and requires specialized training to interpret the results. An alternative method using membrane introduction mass spectrometry (MIMS) is presented here. MIMS provides an analysis method that is fast, simple, inexpensive, and requires little training to derive meaningful results. Furthermore, due to the high speed nature of MIMS analyses, use of this technique on-line as a drinking water treatment process monitor is also discussed. Dedicated software is under production to automate the analysis and provide a means for feed-back control of the treatment process. Simultaneous use of the MIMS system to screen for the presence of other volatile organic compounds of environmental interest is also discussed.

Traditionally, trihalomethane analysis is performed by gas chromatography wherein the individual trihalomethanes, chloroform, bromodichloromethane, dibromochloromethane, and bromoform are separated in time, individually quantified, and the results are added together to arrive at the total trihalomethane content of the sample. This procedure is intuitively inane. One may ask, why bother separating the compounds in time by GC/MS and then add the results together again at the end of the analysis? The answer lies in the fact that at the time this method was written, there was no other way to remove the analytes from the water matrix for introduction into a detector. Today, there is MIMS.

MIMS is a direct introduction sampling method that utilizes a semi-permeable membrane which separates the liquid sample from the vacuum of the mass spectrometer. Volatile organic compounds, like trihalomethanes, diffuse across the membrane into the source of the mass spectrometer where they are ionized and mass analyzed. Water is excluded from passage across the membrane so there is an increase in analyte concentration in the mass spectrometer source compared to that in the bulk sample solution. This makes the technique very sensitive. Detection limits at or below 100 parts per trillion are routine. Additionally, other potential interfering components of the sample such as acids, bases, salts, metals, suspended solids, and biological materials are also excluded from passage into the mass spectrometer. This means that no sample preparation of any kind is required to achieve optimum performance. This is one of the chief advantages in MIMS. Other direct inlet technologies such as capillary direct, thermospray, and electrospray techniques are plagued by constant problems associated with the build-up of salts and other non-volatiles on the mass spectrometer source and inlet components.

The presented experiments demonstrate the ability to directly determine total trihalomethane content in drinking water using MIMS and flow injection analysis techniques. Samples are injected into the FIA-TC1 flow injection module where they are carried to the 1900-C1 capillary membrane probe. Trihalomethanes diffuse across the membrane directly into the mass spectrometer source. All of the volatile components of the sample enter at the same time. Extraction of the ion current chromatograms for m/z 83, 129, and 173 in summation form allows for direct determination of the total trihalomethane content in one step. Identification of the trihalomethanes is easily accomplished without separation from the mass spectrum.

Experiments described here demonstrate that trihalomethane analysis may be performed by MIMS in less than five minutes per sample, with percent RSDs of 1.12%, detection limits of 100 parts-per-trillion, and average percent recoveries of 98.9%. This performance rivals that of the best purge and trap GC systems and details productivity as much as one order of magnitude higher than conventional systems.

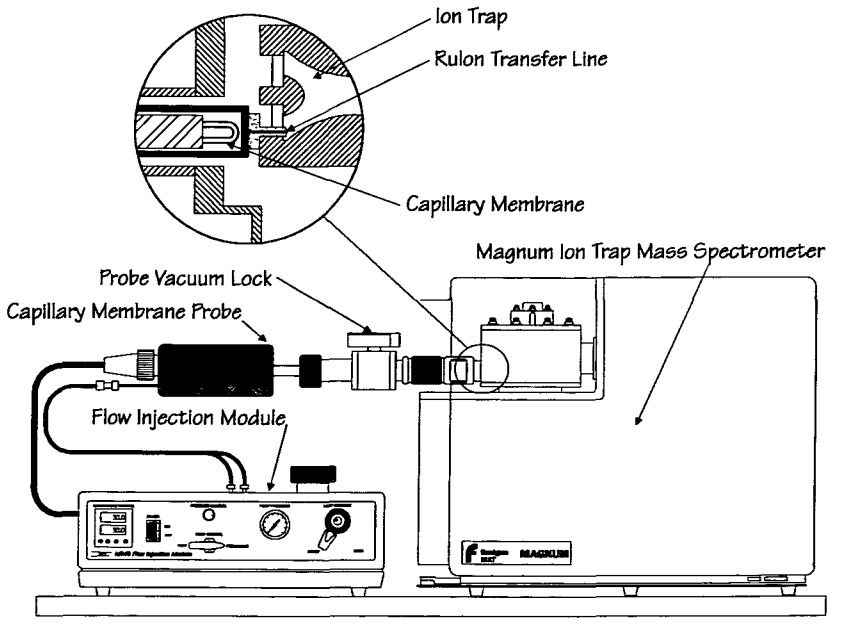

CHEMISTRY AND TOXICOLOGY OF POULTRY CHILLER WATER

WILLIAM F. HADDON, R. G. Binder, Leslie A. Harden, R.Y. Wong, R. Wilson and K. L. Stevens, Western Regional Research Center, USDA, Albany, CA 94710. e-mail haddon@pw.usda.gov

Introduction: Chlorination of poultry chiller water using hypochlorous acid (bleach) is an effective sanitation process for reducing the levels of pathogenic bacteria in poultry chiller water (PCW). However the chemistry of chlorination of PCW and the toxicology of its many chlorine disinfection by-products have not been thoroughly studied, and there has been some concern that bacterial mutagens may be formed at increased chlorination levels (Masri, 1986). As in water disinfection, there is interest in alternative disinfectants (Richardson, et al, 1994), and use of chlorine dioxide has recently been approved for poultry processing.

Results and Discussion: There is a dose-response relationship between the level of chlorination and the bacterial mutagenicity of PCW in several Ames tester strains. Systematic fractionation and chromatographic purification of chiller water from a simulated PCW, followed by mass spectrometry, has allowed us to characterize the Ames-active components that are formed. Remarkably, a single compound, 2,5-pyrrolidinedione-3,3-dichloro-4-dichloromethylene, 2, accounts for most of the mutagenicity in tester strain TA-100 for the pH 2 extract of the simulated chiller water after chlorination. A related compound, 3,4-dichloromaleimide 1, appears to co-occur in the chlorination mixtures (Haddon, et al, 1995).

An especially interesting aspect of the work is the similarity in molecular structure between 2 and the chlorofuranone "MX", which is the principal mutagenic product formed in when chlorine is used to bleach paper. This relationship links our toxicology study of PCW to the much larger area of drinking water, where chlorination in the presence of humic material produces "**MX**".

The Ames mutagenicity for 2 in TA-100, without metabolic activation, is 1850 revertants per nanomole, making it the second most potent bacterial mutagen so-far discovered from chlorination; the mutagenicity of MX under comparable conditions of testing is about 5500 rev/nmole. Both **MX** and 2 should be potent electrophiles.

We are exploring these toxicology relationships through computational chemistry approaches which attempt to link molecular structure information to biological activity. For 2 (E), and a related synthetic tri-chloro imide 3 (D), the computed (negative) energy of the lowest unoccupied molecular orbital correlates with molecular mutagenicity and falls on the same curve developed by Lalonde, et al for MX and several of its structure analogs. ECNI mass spectra may provide a similar indication of electrophilicity for these molecules.

43rd ASMS Conference on Mass Spectrometry and Allied Topics

References:

W. F. Haddon, R. G. Binder, R.Y. Wong, L. A. Harden, R. Wilson, M. Benson and K. L. Stevens, *J. Ag. Food Chem.* **1995** (Submitted)

Masri, M. S. *Food Chem. Toxic.* **1986**, *24*, 923-930.

Richardson, S. D. et al *Environ. Sci. Technol.* **1994**, *28*, 592-598.

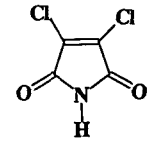

DCMI, 1

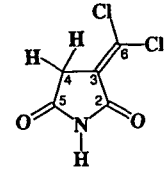

Cmpd B, 2

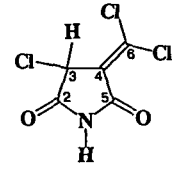

Cmpd D, 3

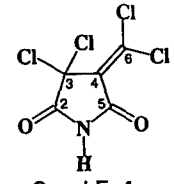

Cmpd E, 4

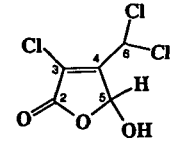

MX, 5

Measurement of Verrucarol, a Product of Satratoxin, in Urine by APCI-MS/MS

Helen H. Schurz, Robert H. Hill, Ruth Etzel, Eduardo Montana, Clarice Green
Centers for Disease Control and Prevention, Center for Environmental Health, Toxicology Branch, Atlanta, Georgia
Dorr Dearborn, Rainbow Babies and Children Hospital, Cleveland, Ohio

Pulmonary hemosiderosis is a rare and serious disease characterized by spontaneous pulmonary hemorrhage and associated with iron deficiency anemia. The disease is so rare that from 1983 to 1993 only three cases were identified at a referral hospital in Cleveland, Ohio. Despite the low incidence of this disease, in January 1993 to November 1994, eight cases of idiopathic pulmonary hemorrhage/hemosiderosis (IPH) were identified among previously healthy infants at the same hospital mentioned above .[1] During the investigation of the Cleveland cases, an additional seven cases of IPH were identified at a children's hospital in Chicago, IL (from April 1992 - November 1994).[2] Cases have continued to be reported since then, with a total of 15 cases in Cleveland and 12 cases in Chicago. Examination of the infants at the hospital and laboratory testing did not indicate the cause of the illness. Urine samples from infants with IPH and some of their parents were collected, frozen and stored at CDC for analysis.

A black mold was found in homes of some of the sick infants. The mold was growing on walls, wall paper, ceiling or other areas in the homes that had been water-damaged and remained moist. Samples were collected with scotch tape and the tape fixed on glass slides. A mold called *stachybotrys* was identified on some of the slides. *Stachybotrys atra* (*S. atra*) produces a macrocyclic trichothecene called satratoxin (Figure 1) that has been shown to be toxic. It was proposed that the IPH occurring in the infants may be associated with satratoxin or another previously unidentified toxicant produced by *S. atra*. Human and animal illnesses have been associated with *S. atra* in the past (Stachybotrytoxicosis); however, illnesses involving infants have not been reported previously.

Based on the hypothesis that satratoxin was linked to IPH, our laboratory developed a method to measure the satratoxin exposure. Little is known about the metabolism of satratoxin in the human body. Metabolism usually involves attachment of glucuronides or sulfates to a toxicant in an attempt to increase its solubility in urine and thereby increase its excretion. We assumed that at minimum glucuronide attachment occurred during the metabolism of satratoxin, and that satratoxin and all its metabolites were hydrolyzed to verrucarol (Figure 1). Since the number of glucuronides that may associate with any toxicant is unknown, it is usually helpful to strip the glucuronides from the analyte prior to analysis. Removal of glucuronides from metabolized compounds is normally accomplished using acid, base or enzyme hydrolysis. Further base hydrolysis of satratoxin produces verrucarol. Since verrucarol production from satratoxin is an easy reaction, it was chosen to be the target analyte to determine whether satratoxin had been present.

The sample preparation method for hydrolysis of urine and satratoxin urinary metabolites is described in Figure 2. Initial experiments with verrucarol-spiked urine showed that verrucarol is not destroyed by this method and is recovered between 60-70%. Strong base hydrolysis was used to hydrolyze satratoxin in the urine to verrucarol. Recovery for satratoxin converted to verrucarol is approximately 40%. Atmospheric pressure chemical ionization and tandem mass spectrometry was used to measure verrucarol in the extracts. The molecular ion of verrucarol $(M+H)^+$ 267 and its daughter ion at m/z 219 were monitored. This fragmentation constitutes the loss of OH and CH_2OH from the molecular ion. An isotopically labeled internal standard was unavailable and a suitable non-labeled internal standard could not be identified, therefore urine samples spiked at varying concentrations were used to construct a standard curve and determine the limit of detection and limit of quantitation for this method. The LOQ for verrucarol is 59 ppb in urine, or 11.8 ng on-column injection, the LOD for verrucarol in urine is 23.6 ppb, or 4.72 ng on column injection.

Very small volumes of urine from infants were available, therefore we decided to first analyze urine collected from the parents of the ill infants. The parents should be exposed to the same environment as the infants, and their urine specimens should document this. Four parental urine samples were available, and ten milliliters of each was hydrolyzed and extracted. There were no positive detects made for verrucarol in these urine samples.

The results imply that these parents were not exposed to *S. atra* or satratoxin in amounts large enough to result in detectable amounts of verrucarol in these urine samples. There are however, many assumptions that have been made throughout the course of these analyses: a) exposure to *S.atra* occurred; b) *S. atra* produced satratoxin; c) satratoxins are metabolized to compounds which hydrolyze to verrucarol (in basic solution); d) concentrations of satratoxin are great enough to be detected. In addition to these assumptions, we do not know if in fact satratoxin is the prinsiple toxicant in *S. atra*. It has been suggested that other compounds could be present in *S. atra* (spirolactones and lactams), or that a synergistic effect may be occurring with these compounds or other environmental factors that may be associated with this illness. Presently, fungus samples from the homes of ill infants are being analyzed to determine the types of toxicants present in them. Once these results become available, that information will be used to improve our present method, and provide direction for future studies to identify the cause of IPH.

References

1. Morbidity and Mortality Weekly Report 1994; 43:881-883
2. Morbidity and Mortality Weekly Report 1995; 44:67-74
3. "Mycotoxins and Phytoalexins" R.P. Sharma and D. K. Salunkhe, Eds., CRC Press, Inc., 1991

Figure 1

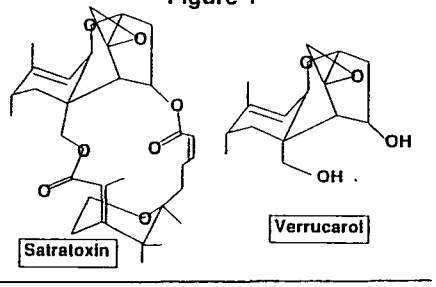

Figure 2

Sample Prep for Verrucarol Analysis

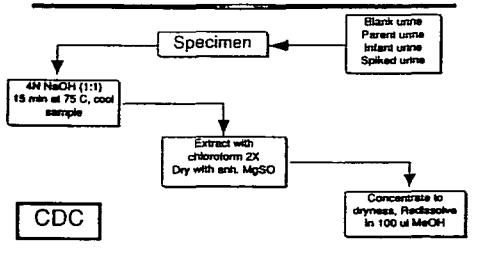

HPLC/MS and HPLC/MS/MS Analysis of Explosives in Environmental Samples

P.M. Gates, E.T. Furlong, C.E. Lindley, and M.R. Burkhardt
U.S. Geological Survey, National Water Quality Laboratory
Arvada, CO 80002

The production, storage, and disposal of nitroaromatic and nitramine explosives and propellants at military installations worldwide present serious environ-mental problems. Several of these explosives and their degradation products are hazardous to human and ecosystem health [1,2] and are subject to Federal regulatory statutes. These water-soluble compounds have been demonstrated to be environmentally mobile by their presence in ground-water samples [3]. Thus, nitroaromatic and nitramine explosives and propellants are significant site-specific water contaminants.

Typically, explosives are separated by high-performance liquid chromatography (HPLC) and identified by ultraviolet photodiode-array detection (PDA). Consequently, the identification of most explosives is not definitive, particularly for the determination of unknown degradation products in environmental matrices. A new analytical method was developed to (1) improve the specificity and reliability of identification, and (2) develop an experimental design to en-hance identification of unknown compounds in surface-water, ground-water, and soil matrices.

An HPLC with PDA was coupled to a triple-stage-quadrupole mass spectrometer using a thermospray interface. Selected compounds were separated under isocratic conditions using an octadecylsilane liquid-chromatographic column (5-micrometer particle size, 4.6-millimeter internal diameter, 250-millimeter length). Electron-capture negative ionization (ECNI) HPLC-thermospray mass spectrometry (HPLC/MS) and HPLC-thermospray tandem mass spectrometry (HPLC/MS/MS) were applied to determine molecular weight and confirm molecular structure.

For optimal detection of known compounds, selected-ion-monitoring (SIM) MS was used. Calibration curves fit quadratic models, with correlation coefficients typically exceeding 0.995 over two orders of magnitude. Instrument-detection limits ranged from 2.5 to 10 nanograms per injection, resulting in estimated method-detection limits from 50 to 200 nanograms per liter for typical water samples. The identities of nitroaromatic explosives were confirmed by combining optical absorbance and ECNI/SIM/MS spectral evidence, improving reliability and selectivity.

Mass spectra produced by HPLC/MS were characteristically simple, usually consisting of molecular ions and acetic acid or acetate ion adducts (Figure 1). In order to elucidate com-pound structures, MS/MS spectra of many explosives were collected. Product-ion (PI) MS/MS spectra were dominated by neutral losses of OH, NO, and 2(NO). Nitrobenzene, 2-, 3-, and 4-nitrotoluene, and 4,6-diamino-2-nitrotoluene PI spectra were dominated by the presence of NO_2^-. 2,4,6-Trinitrotoluene, 2-amino-4,6-dinitrotoluene, and 2,4-dinitrotoluene exhibit a pri-mary loss of OH, characteristic of ortho-substituted nitrobenzene ions [4]. 1,3,5-Trinitroben-zene, 3,5-dinitroaniline, 1,3-dinitrobenzene, 4-amino-2,6-dinitrotoluene, and 2,6-dinitrotoluene PI spectra are dominated by the loss of NO. 2-

Amino-4,6-dinitrotoluene also has an approx-imately 50 percent larger 2(NO) loss relative to total-ion-current intensity than 4-amino-2,6-dinitrotoluene. PI/MS/MS spectra and the relative abundances of specific ion fragments provide tools for unknown compound identification, including isomer specific identification.

Unknown compounds were first indicated by optical spectra. Molecular ions were identified by full-scan MS on the sample extract. A PI/MS /MS experiment was performed to elucidate structure when molecular ions were identified. Following tentative identification, a compound's identity was confirmed with a standard, if available. Molecular ions for compounds from a settling-pond sample are shown in Figure 2. These compounds were tentatively identified as 2-amino-6-nitrotoluene, 4-amino-2-nitrotoluene, and 2-amino-4-nitrotoluene.

Low detection limits and reliable identification of explosives and related degradation products using SIM/HPLC/MS were developed into an analytical method applicable to ambient concentrations in surface-water, ground-water, and soil matrices. Using ECNI, this method is relatively free of interferences restricting detection to compounds capable of electron capture. An experimental design is proposed to facilitate the identification of unknown nitroaromatic compounds and degradation products. The suitability of selected-reaction-pair HPLC/MS/MS as a detection method for selected compounds is also discussed.

[1] Won, W.D., Desalvo, L.H., and Ng, J., 1976. Appl. Environ. Microbiol., **31**, 576-580.
[2] Office of Water, November 1994. U.S. Environmental Protection Agency, Drinking Water Regulations and Health Advisories, Washington, D.C.
[3] Pereira, W.E., Short, D.L., Manigold, D.B., and Roscio, P.K., 1979. Bull. Environ. Contamin.Toxicol., **21**, 554-562.
[4] McLuckey, S.A , and Glish, G.L., 1987. Org. Mass Spectrom., **22**, 224-228.

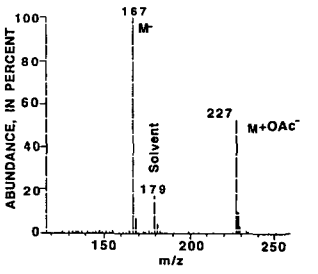

Fig. 1. The ECNI/HPLC/MS spectrum of 4,6-diamino-2-nitrotoluene.

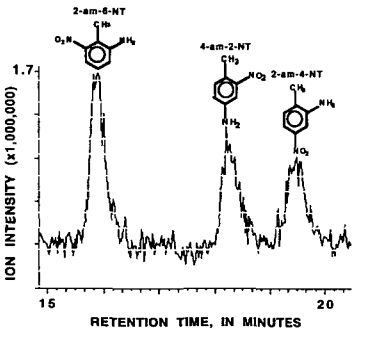

Fig 2. Tentative identification of unknowns in a settling pond sample, selected-ion chromatogram m/z 152.

MS/MS CID FRAGMENTATION PROCESSES IN SOME PESTICIDES

Jehuda Yinon

Weizmann Institute of Science, Department of Environmental Sciences and Energy Research, Rehovot 76100, Israel.

Because of their widespread use, pesticide residues and their degradation products are currently detected in various environmental matrices, such as soil, water and air. Analytical methods for trace detection of these pesticides and their degradation products require high sensitivity and selectivity. Tandem mass spectrometry (MS/MS) with collision induced dissociation (CID) is able to identify trace amounts of organic pollutants in a variety of matrices with a high degree of selectivity. The recorded daughter-ion spectrum will enable the characterization of the analyzed compound by providing structural information leading to its unambiguous identification.
We have studied the MS/MS CID fragmentation processes of a series of pesticides, including atrazine, simazine, linuron, diuron, alachlor, aldicarb and carbofuran. CID mass spectra of the molecular and major fragment ions were recorded with a Finnigan MAT TSQ 70 triple quadrupole.
Fig. 1 shows the CID fragmentation map of simazine, which was deducted from the CID mass spectra. An example of the use of the CID data is the GC/MS/MS of carbofuran, which has a very small molecular ion. Fig. 2a shows the MS/MS mass chromatograms of the EI fragment ion at m/z 164 (precursor ion), and the main daughter ion at m/z 149. Fig. 2b shows the the CID mass spectrum of the ion at m/z 164. These were recorded on a Varian 3D GC/MS -ion trap, equipped with MS/MS capability and a Septum Programmable Injector (SPI).

Spray application is one of the most familiar operations connected with pesticide use, resulting in large losses of pesticides to the atmosphere. Photodecomposition or photochemical stability are important factors influencing the pesticide composition and residence time in the atmosphere, and determining the distance over which pesticides are transported in the atmosphere. It is therefore of great interest to be able to predict the stability and/or decomposition of pesticides exposed to UV sunlight.
We have found that there seems to be a possible similarity between UV chemical degradation products of pesticides and CID fragment ions of the same compounds. An example is given in Fig. 3 which shows the UV decomposition [1] and CID fragmentation of atrazine. A similar UV decomposition product [2] and CID fragmentation ion was also found in alachlor.
More work has to be done on UV chemical degradation in order to determine whether CID mass spectra can be used to predict the decomposition of pesticides exposed to sunlight.

References

1. J. Kempney, D. Kotzias and F. Korte, *Chemosphere*, **10**, 487 (1981).
2. C. E. Rostad, W. E. Pereira and T. J. Leiker, *Biomed. Environ. Mass* Spectr., **18**, 820 (1989).

Acknowledgement
This work has been supported by the European Union, Avicenne Project AVI-CT92-0004

43rd ASMS Conference on Mass Spectrometry and Allied Topics

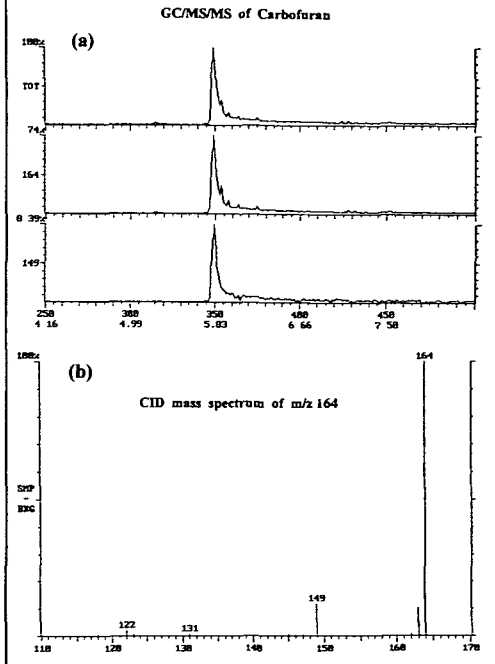

Fig. 2

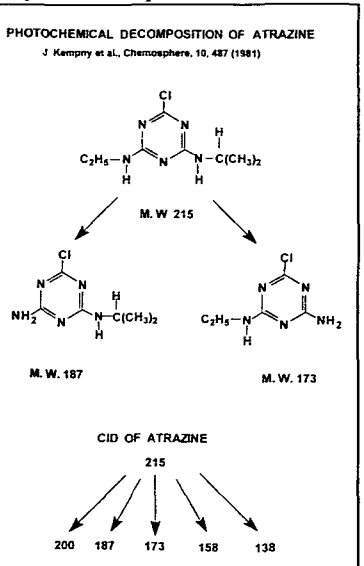

Fig. 3

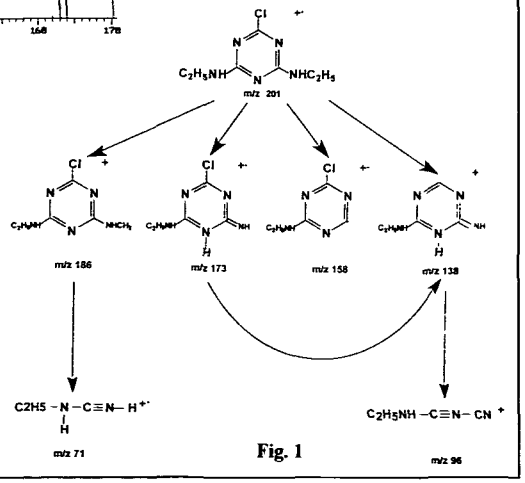

Fig. 1

Quantification of Non-Persistent Pesticides in Human Serum

John R. Barr, Donald G. Patterson, Jr., Vincent L. Maggio, P. Cheryl McClure, Carolyn M. Newman, Wayman E. Turner, and Larry L. Needham

Centers for Disease Control and Prevention
4770 Buford Highway, NE
Atlanta, GA 30341

The widespread use of pesticides in agriculture has led to a ubiquitous presence of these compounds in the environment. The health effects of non-persistent pesticides in exposed and general human populations is not yet known. The extensive use of these compounds has created a great interest in developing laboratory and epidemiology studies on possible health risks. We have recently developed methods for a pilot study to analyze blood samples collected from farmers and their families in two states. These samples were collected before, during, and after pesticide application. A target group of non-persistent insecticides, herbicides, and fungicides have been identified and isotope dilution mass spectrometric methods have been developed.

The analysis of these pesticides in serum requires an efficient sample preparation procedure followed by high resolution chromatography and high resolution mass spectrometry so that interferences do not hinder the analysis. The method developed for the quantification of this complex mixture of non-persistent pesticides includes a solid phase extraction of serum that has been treated with an equal amount of saturated ammonium sulfate (Figure 1). This procedure yields an extract which is analyzed by GC/MS. A DB-1701 column is employed for the GC separations and the pesticides are recorded on a high resolution magnetic sector mass spectrometer (VG 70-4SE). Specificity and sensitivity are obtained by ionization with low energy electron impact (30 eV) and selective ion monitoring at a resolution of 10,000. Employing this procedure with isotope dilution mass spectrometry allows for an accurate and sensitive method of quantification. Parts-per-trillion (ppt) levels of many of the non-persistent pesticides were found in the serum pools from the general population . An example of the data from a farm is shown in Figure 2. Serum levels tended to be in the low ppt for pre-application season. During application, pesticide levels typically rose to parts-per-billion in applicators and were then eliminated from the body in subsequent days. Spouses levels also tended to rise during the pesticide application. In addition to the current analytical methods, new approaches such as ultra-sensitive, fast, multidimensional GC/high resolution MS (2DGC/MS) are currently being developed. An example of a 2DGC/MS chromatogram of a pesticide mix is shown in Figure 3

43rd ASMS Conference on Mass Spectrometry and Allied Topics

Figure 1

Sample Cleanup Method
For Nonpersistent Pesticides

Serum
↓
Add Labeled Standards
↓
Add Saturated Ammonium Sulfate
↓
Empore C-18 Disk
↓
Dry Solvent
↓
Elute with CH_2Cl_2
↓
Concentrate
↓
Add Dodecane
↓
Evaporate
↓
Add Recovery Standard
↓
Analyze by GC/MS

Figure 2

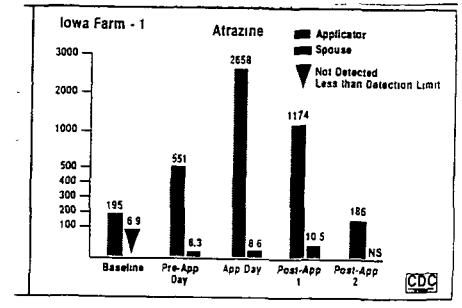

Figure 3

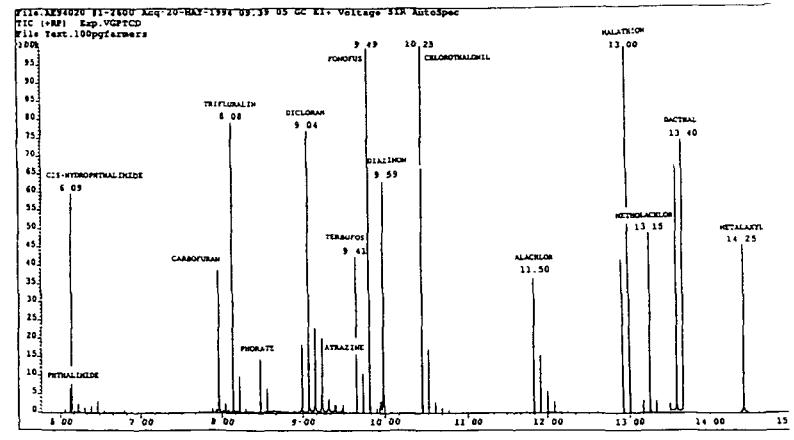

ESI MS/MS Determination of a New Cationic Surfactant in River Water

Thomas R. Mertens, Jocelyn C. Dunphy[1], Karen M. Kershner, and Samuel J. Morris, III
Laundry & Cleaning Products Development, Analytical Sciences Department
The Procter & Gamble Company
5299 Spring Grove Avenue, Cincinnati, OH 45217

Introduction: The need to quantify trace levels of surfactants in environmental samples is critical for the environmental safety assessments of new laundry and cleaning product chemicals and the long-term environmental defense of existing chemicals. New liquid introduction MS techniques (Flow-FAB, electrospray) have significant advantages over conventional methods (usually pre-concentration followed by HPLC) for measuring trace levels of surfactants in environmental samples. These include high throughput, high selectivity, less sample preparation required, and ultimately lower detection limits, especially for compounds that lack a chromophore, like most cationic surfactants. We needed to develop a rapid, sensitive method to determine the new cationic, di-(ethanolester)dimethylammonium chloride (DEEDMAC), in river water to support exposure levels of this biodegradable material during aquatic toxicity studies. (DEEDMAC structure given in Figure 1).

Experimental: Using a Finnigan TSQ-700 with a Finnigan API source in the ESI mode, ESI/MS/MS conditions were developed and optimized to determine DEEDMAC in river water samples. DEEDMAC gave excellent ESI response in the positive ion mode using 50:50 v/v mixture of n-propanol and water containing 7.5 mM $NH_4^+HCOO^-$. Figure 1 shows a spectrum of DEEDMAC derived from soft tallow fatty acid. The C16,C18:1 homolog (most abundant) was chosen to act as a tracer for the complex mixture of homologs that are present in commercial grade DEEDMAC. Low energy MS/MS (29 ev) of DEEDMAC (parent ion 636.6) and a pure deuterated (C16,C18) homolog (parent ion 641.6) provided fragments corresponding to the esterified fatty acids. M/z 308.3 and 310.3, respectively, were chosen for selected reaction monitoring (SRM). Typical ESI conditions for this instrument, (4500v ESI spray) were used. Due to the selectivity of SRM, no chromatography or extensive sample preparation was needed for the river water samples. Thus, a simple scheme was developed in which river water samples are taken, acidified to pH 3, filtered using 0.45 um filters, and diluted 1:1 with n-propanol with 15 mM $NH_4^+HCOO^-$, and injected using an HPLC pump (100 uL inj. volume, flow rate 0.1 mL/min) following addition of the deuterated internal standard. Quantitation (peak areas) is performed using a linear fit to calibration curves constructed to bracket expected sample levels. A typical calibration curve is shown in Figure 2.

Results: We have found that the simple sample preparation serves both to prevent any adsorption to containers (due to addition of organic solvent) and also preserves samples for at least two weeks when stored frozen. We make the use of a low and high calibration curve to ensure optimal quantitation of DEEDMAC by having the standards and internal standards at a concentration near the concentration of each sample. Blanks must be injected between each sample/standard injection to minimize carryover. Validation (spike/recovery) results are outlined in the following table. The MS detection limit was found to be ~0.020 ppm, which corresponds to 0.040 ppm in river water samples.

	10 ppm Sample	1.6 ppm Sample	0.05 ppm Sample
Avg. Concentration	10.7	1.67	0.064
Percent Recovery	107.1	104.1	127.5
Std. Dev.	0.18	0.045	0.005
Relative Error %[1]	3.0	4.97	9.02
number of samples	4	4	6

[1]Calculated as $100(t' s_n)/n$*avg. conc., where t' is at the 95% confidence level

Conclusions: A rapid, sensitive method was developed for DEEDMAC at trace levels in river water. The specificity of selected-reaction monitoring makes sample preservation simple, and the sensitivity obviates the need for sample concentration techniques, which are challenging for cationic surfactants. This method was successfully used for the analysis of over 300 samples for 5 river water aquatic studies. Variations of this methodology can be used for other environmental applications with cationic surfactants.

Figure 1: Electrospray MS Spectrum of DEEDMAC.

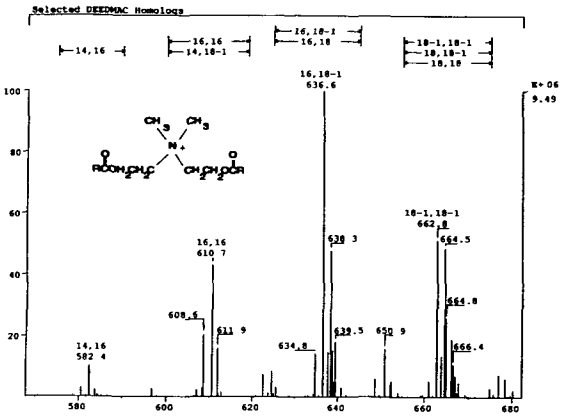

R is a linear alkyl chain ranging from 11 to 17 (conforms generally to a tallow distribution where the most abundant homologs are derived from C16, C18, and C18:1 fatty acids.

Figure 2: DEEDMAC calibration curve measured against d3-DEEDMAC

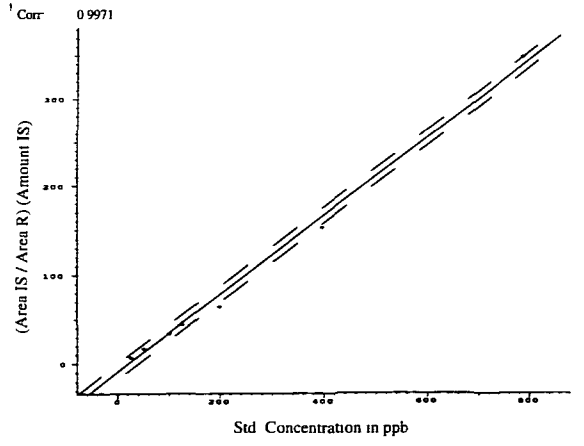

Advantages and Applications of Mass Peak Profiles Plotted from Selected Ion Recording Data

Andrew H. Grange* and Joseph R. Donnelly
Lockheed Environmental Systems & Technologies Co., 980 Kelly Johnson Dr., Las Vegas, NV 89119
William C. Brumley and G. Wayne Sovocool
U.S.E.P.A., Environmental Monitoring Systems Laboratory, PO Box 93478, Las Vegas, NV 89193-3478

Advantages. Exact masses of molecular ions can provide unequivocally, the elemental composition of unknown compounds, provided the error and precision in the mass determinations are small. In Figure 1, a mass peak profile is plotted as the areas under the chromatographic peaks in the ion chromatograms for m/z ratios monitored across the profile. Compared to KVE scanning at a mass resolution of 10,000 using a VG70-250SE double focusing mass spectrometer, plotting mass peak profiles from selected ion recording data (MPPSIRD) provides 3 times greater scan speed with 17 times more sensitivity while operating at 20,000 resolution. Error limits for exact masses computed as the weighted average of several points across the profile are ±2.5 ppm, ±1.5 ppm and ±1.0 ppm when 3, 7 or 15 determinations are made. This high precision greatly reduces the number of possible compositions, which increase rapidly with the mass and number of elements an ion might contain. Preparation of SIR descriptors and processing of the data are done automatically by procedures written in the RSX and VG languages on the data system and in Lotus 1-2-3™, Reflection 4.2™ and WordPerfect 5.1™ on an ancillary personal computer.

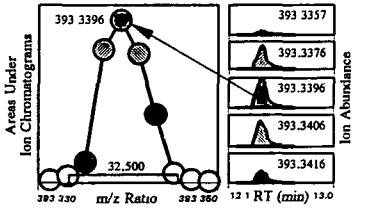

Figure 1.

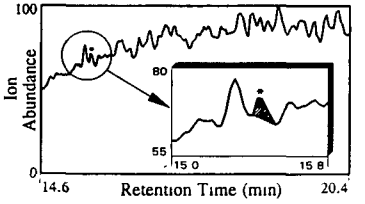

Figure 2.

Applications. Shown in Figure 2 is part of the total ion chromatogram for a GC/MS run of an extract from a Superfund site sample that contained a high level of PCBs. Four poor library matches were found for the background subtracted mass spectrum of the trace component responsible for the chromatographic peak marked with an asterisk. For each match, the molecular ion weighed 266 Da.

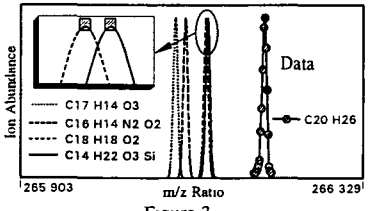

Figure 3.

The profiles for the four molecular ions were calculated at 20,000 resolution and plotted in Figure 3. The boxes on top of the two profiles closest in mass shown in the insert correspond to an error limit of ±2.5 ppm. Hence, any of the 4 compositions could have been identified from its exact mass. The profile obtained and shown in Figure 4 was also plotted in Figure 3 and corresponded to $C_{20}H_{26}$, which might be an alkylated biphenyl. This composition for the trace component in the complex mixture rejected all four library matches. Thus, MPPSIRD is a powerful technique for proving that no compounds with targeted compositions are present to a very low detection limit.

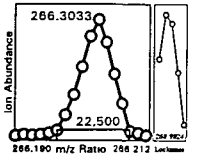

Figure 4.

MMPSIRD is an important quality assurance tool. It can be used to document the resolution required to avoid interference from coeluting compounds that yield ions with masses similar to an analyte ion. In Figure 5, the profiles for the molecular ions of acridine on the left and of anthracene and/or phenanthrene containing a ^{13}C atom on the right are well separated at 22,000 resolution. Lower resolution would result in interference for quantification of acridine in creosote containing soils if a single m/z ratio atop the acridine profile were monitored. In addition, the resolution during elution of each analyte is routinely determined from the profile width at 5% of its maximum.

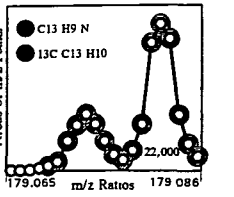

Figure 5.

M+1 and M+2 profiles. Multiple compositions are often calculated for large ions within the error range for exact mass determinations. The shape of the M+2 profile, the exact masses of the M+1 and M+2 profiles, and the relative abundances of the M+1 and M+2 profiles provide 5 criteria for rejection of erroneous compositions. Because only 22 m/z ratios are used, a split SIR descriptor simultaneously monitors the top 60% of the M, M+1 and M+2 profiles with 6 m/z ratios each and the top 40% of the lock mass profile with 4 m/z ratios. A model based on the Gaussian distribution, written in QuickBASIC™, provides plots of the full M+1 and M+2 profiles, labeled with predicted masses and relative abundances for the partial profiles. For an unknown compound found in an extract of a Superfund site sample, one of eight compositions ($C_{28}H_{41}NS$) was identified based on the unique shape of the M+2 profile and confirmed by rejection of the other seven compositions based on the exact masses and relative abundances of the M+1 and M+2 profiles. For a minor component in another environmental extract, a good library match suggested the compound was bis(2-bromophenyl)diazene ($C_{12}H_8N_2Br_2$). But the exact mass and %M+1 identified $C_{13}H_8OBr_2$ as the composition and the full scan spectrum was consistent with a dibromomethylfuran.

Larger Mass Ions. For four standards with molecular weights between 536 and 766 Da, 15 mass and relative abundance determinations were made using probe introduction into the ion source. The mass error was <1.0 ppm for the M, M+1 and M+2 profiles for all 4 standards. This table shows the errors in averaged masses and relative abundances for the correct compositions and the compositions most difficult to reject, which are italicized. The emboldened errors failed the criteria and eliminated incorrect compositions.

Mass of M (Da)	Composition	ΔM	ΔM+1	ΔM+2	Δ%M+1	Δ%M+2
		----(ppm)		-----	(% %M+1 &	%M+2)
536.2621	C28 H40 O10	-0.3	-0.0	+0.5	+0.1	-0.1
536.2635	*C29 H36 O6 N4*	-2.9	-2.1	-2.1	-1.9	+0.1
536.3151	C34 H40 O2 N4	+0.1	-0.2	-0.2	+0.1	-0.0
536.3138	*C33 H44 O6*	+2.5	+1.8	+2.5	+2.1	-0.1
622.2791	C36 H38 O6 N4	+0.6	+0.2	-0.95	-0.0	+0.0
622.2796	*C38 H45 N2 P3*	-0.2	-0.7	-2.2	-1.5	+0.4
766.3942	C44 H54 O8 N4	-0.6	+0.1	+0.5	-0.7	+0.1
766.3946	*C46 H61 O2 N2 P3*	-1.02	-0.6	-0.4	-2.2	+0.3

When multiple compositions remain possible for a large molecular ion, fragment (F), F+1 and F+2 profiles are monitored. Because their masses and the masses of neutral loss fragments obtained by difference are smaller, unique compositions are obtained and the molecular ion is identified as the sum of its parts. Compositions are determined without knowledge of the sample's history.

Conclusion. MPPSIRD is an important new analytical technique for double focusing mass spectrometers. The basic capabilities needed to perform MPPSIRD are already included in the data system software. Custom procedures permit automation of the technique, and a simple model allows planning of experiments and interpretation of the data obtained.

References: *Anal. Chem.*, 1994, *66*, 4416-4421; *Anal. Chem.*, Submitted; Poster MPD 202

Notice: This abstract was funded by the U.S. Environmental Protection Agency (EPA), through its Office of Research and Development (ORD), but does not necessarily reflect the views of the EPA or ORD.

BIMOLECULAR GAS-PHASE EXCHANGE OF ALKALI METALS BETWEEN CATIONIZED BIOMOLECULES AND NEUTRAL CROWN ETHERS

Marshall Pope*, Steven Hofstadler‡ and David V. Dearden
Department of Chemistry and Biochemistry, Brigham Young University, Provo, UT
‡Pacific Northwest Laboratories, Battelle, Richland, WA

Introduction

Electrospray ionization of polypeptides and nucleic acids often yields ions containing sodium or potassium charge carriers. These alkali adducts are frequently the residue of ionic buffers used to preserve protein conformation in solution or artifacts of a natural matrix such as blood plasma. Measures taken in solution to desalinate these samples are hindered by the desire to maintain native conformation. We show here that ion-molecule chemistry is an alternate means of removing alkali metal ions from multiply-charged biomolecules. Ion-molecule reactions of multiply charged polypeptides with crown ethers result in adduction of the crown if protons are the only charge bearing species, or desalting (removal of an alkali cation) if alkali metals are among the attached charge carriers. Both product ions, the desalted peptide and the crown/alkali metal complex, are observed in the latter case.

Experimental

All experiments were performed in a Fourier transform ion cyclotron resonance mass spectrometer (model APEX 47e, Bruker Instruments) equipped with an Analytica electrospray ion source external to the high-field region of a 4.7-Tesla superconducting magnet. Neutral crowns (12-crown-4, 15-crown-5, 18-crown-6) were purchased from Parish Chemical (Orem, UT). 12-crown-4 and 15-crown-5 were purified by sequential freeze-pump-thaw cycles prior to introduction on a Varian leak valve. 18-crown-6 was used unaltered and introduced on an unheated solids probe. Twelve hours of gentle bake out were sufficient to eliminate methanol and reach a stable pressure of ~6 x 10^{-8} mbar. Proton transfer kinetics for the reaction of acetone and 18-crown-6 (assuming unit efficiency) have been used to coarsely determine a response factor for our Balzers IMG 233 ionization gauge[1]. Nozzle skimmer voltages varied from 50 to 80 V. Extensive adduction may be observed in neutral water solutions containing millimolar concentrations of alkali metals. Electrostatic focusing and injection techniques were used to transfer ions from the source to the field-corrected ("Infinity") trapping cell of the instrument. Ion-molecule kinetics experiments were performed with ions isolated using conventional FTICR techniques (chirp and shot ejection of unwanted ions).

Results and Discussion

The trapped-ion mass spectrum of electrosprayed gramicidin S (GS) c[Val-Orn-Leu-Phe-Pro-Val-Orn-Leu-Phe-Pro] shown in figure 1 is typical of peptides sprayed from alkali metal containing solutions. To the far right, the envelope of the +1 charge state is dominated by $NaGS^+$ at 1163 m/z. Protonated gramicidin S appears at 1141 m/z. Impurities resulting from leucine or isoleucine substitution for valine shadow each peak at +14 m/z in the +1 charge state and +7 in the +2 charge state. Although the magnification of the inset clips the isotopic distribution of H_2GS^{2+}, four sodium adducts are easily identified within the +2 charge state. A .5 m/z isotopic spacing confirms a net charge of +2. The individual metal adduct states are separated by 11 m/z, indicating that each adduct displaces a proton.

The progress of the charge shifting reaction following isolation of the +2 charge state is illustrated in figure 2. Each of the doubly-charged, multiply-sodiated peaks gives rise to a corresponding singly-charged gramicidin with one less metal adduct. In addition, the other stripping product, the crown-sodium complex, accumulates. If sodium is not present as in H_2GS^{2+}, adducts of the crown ether and peptide ion form.

Gross and Williams[2] have demonstrated that the protons attached to gas phase H_2GS^{2+} are on the terminal amine groups of the two ornithine side chains. It is possible that these functional groups also participate in alkali metal binding, however the smaller extent of charge transfer associated with alkali metal cations suggests that these metals prefer harder Lewis bases or multidentate bases. Another explanation for the loading we observe is coordination to tautomerized peptidic oxygen. Proton displacement from amide sites along the peptide backbone would result in a zwitterionic cation without a shift in charge state. If such sites actually exist, the group I binding affinity of the peptidic oxygen anion is expected to exceed that of 12-

43rd ASMS Conference on Mass Spectrometry and Allied Topics

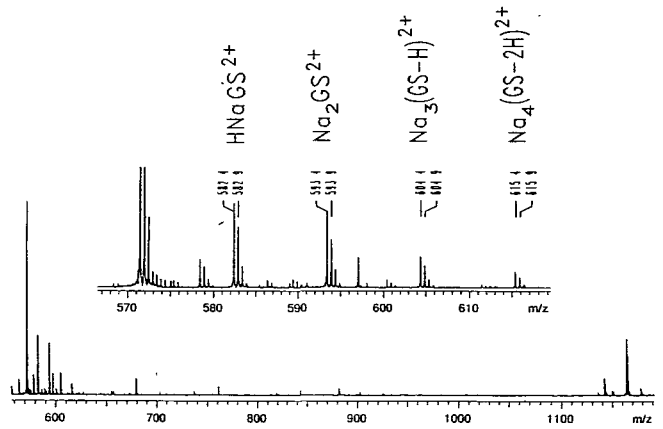

Figure 1. Electrosprayed gramicidin S from a sodiated water/methanol solution.

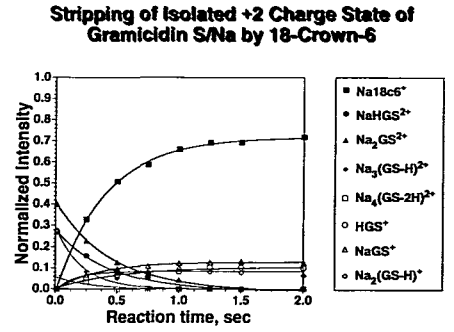

Figure 2. Reactions of the isolated H_2GS^{2+} (571.4 m/z), $NaHGS^{2+}$ (582.4 m/z), Na_2GS^{2+} (593 4 m/z) and $Na_3(GS\text{-}H)^{2+}$ (604.4 m/z) with 18-crown-6. P_{18C6} = 6 x 10^{-8} mbar.

crown-4. The charge shifting behavior we observe must then be facilitated by intramolecular proton transfer. Such an isomerization involving protonated ornithine would release sodium cation by neutralizing the peptidic oxygen anion.

We are grateful for the support of NSF, PRF and the many helpful suggestions of Professor T. Hellman-Morton.

[1] Chu, In-Hou; Zhang Hong; Dearden, David V. *J. Am. Chem. Soc* **1993**, *115*, 5736-5744
[2] Gross, D. S., Williams, E. R. *J. Am. Chem Soc*, **1995**, *117*, 883-890.

THE IMPORTANCE OF CHARGE-SEPARATION REACTIONS IN ELECTROSPRAY IONIZATION TANDEM MASS SPECTROMETRY

Jeanette Adams, Fred H. Strobel, and Alex Reiter, Department of Chemistry and the Emory University Mass Spectrometry Center, Emory University, Atlanta, GA 30322

Research was conducted to determine: (1) why low-mass complementary ions from charge-separation reactions are missing in ESI/MS-MS spectra acquired using B/E scans; (2) whether the kinetic energy release (KER) in metastable ion charge-separation reactions can be related to intercharge distance; and (3) whether the information from the KER can be used to understand structure and reaction mechanisms. MS-MS B/E and MS-MS MIKES experiments of $(M + 2H)^{2+}$ ions of angiotensin II were performed using a JEOL JMS-SX102/SX102A/E five-sector, tandem mass spectrometer.

The MS-MS B/E spectrum shows abundant doubly charged product ions and one weakly abundant b_6^+ singly charged product ion (Figure 1). The low-mass $y_2^{\cdot+}$ complementary ion is missing. In contrast, the MS-MS MIKES spectrum shows a highly abundant b_6^+ ion and a relatively highly abundant $y_2^{\cdot+}$ ion (Figure 1). Narrow MIKES scans of these two ions show that they are broad and dished (Figure 2). The kinetic energy release distributions (KERDs) give a most probable KER (T_{mp}) of 0.902 eV (Figure 3).

Using Coulomb's Law and assuming a dielectric constant of 1.0, the T_{mp} gives an intercharge distance of 16.0 Å. This value can be compared to distances obtained from SYBYL molecular dynamics calculations when one proton is fixed on the C-terminal amino acid and the other is placed in various positions in the peptide (Figure 4). The calculations give an intercharge distance of 15.8 Å for having one proton on the Arg side chain, which is in accord with the experimental measurement.

The intercharge distance can be used to address possible mechanisms for formation of the $b_6^+/y_2^{\cdot+}$ complementary ion pair. The accepted mechanism for formation of b^+ ions, which gives an N-terminal acylium ion, is not in accord with the experimental data In contrast, a "charge-remote" rearrangement mechanism, which is commonly accepted for formation of y^+ ions, is in agreement.

The experimental data reveal that product ions from charge-separation reactions are severely discriminated against in B/E scans, and partially discriminated against in MIKES experiments. Consequently, MIKES experiments provide a better, but not accurate, estimate of relative product ion abundances. The agreement between the measured KER and the calculated value suggests that these types of charge separation reactions can be used to address structure and reaction mechanisms.

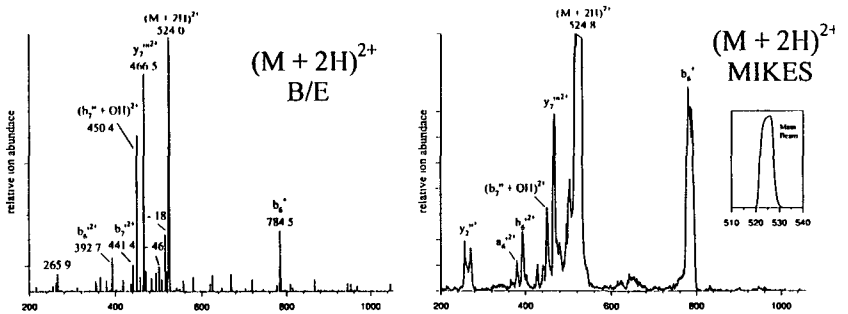

Figure 1. MS-MS B/E and MS-MS MIKES spectra of $(M + 2H)^{2+}$ ions of angiotensin II.

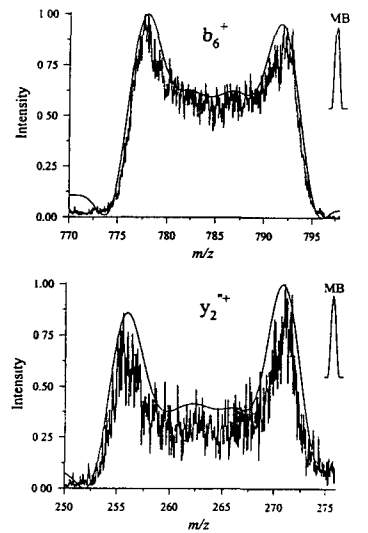

Figure 2. Narrow-scan MIKES spectra of b_b^+ and $y_2^{\cdot+}$ ions.

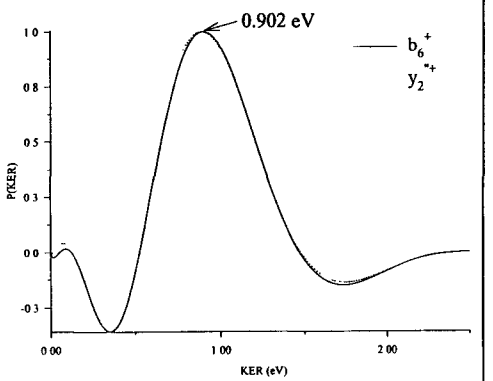

Figure 3. KERDs for b_6^+ and $y_2^{\cdot+}$ ions.

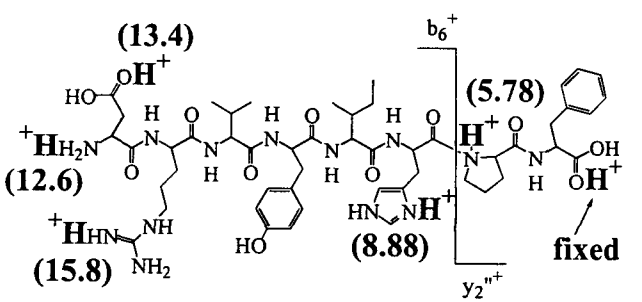

Figure 4. Intercharge distances calculated from SYBYL molecular dynamics.

The Correlation of Fragmentation and Structure of a Protein

Qinyuan Wu, Xueheng Cheng, Steven Van Orden, Ray Bakhtiar and Richland D. Smith*
Pacific Northwest Laboratory, Richland WA 99352

Characterization of proteins of similar structures is important to understanding the biological function of the proteins and the processes with which they are involved. Cytochrome *c* variants typically have similar sequences, and have similar conformations in solution with almost identical absorption spectra and redox potentials. We chose cytochrome *c* 's from bovine, tuna, rabbit and horse as a model system in studying large biomolecules using MS^n of multiply charged ions generated from electrospray ionization (ESI).

All of the experiments reported here used an external source ESI-FTICR (7 T) instrument. SORI-CID pulses were placed at +/- 1500 Hz of the cyclotron frequency of the parent ions and the irradiation time was 300 ms. N_2 gas was pulsed into the cell for trapping and dissociation. For each stage of MS, the precursor ions were isolated using SWIFT. Cytochrome *c* samples were dissolved in 5% HOAc and the 15+ state ions were studied.

Due to the high resolution capability, we can assign over 95% of the product ion peaks from SORI-CID with an accuracy better than 10 ppm. All four variants were effectively dissociated and showed distinctive, but complicated MS/MS spectra. Fig. 1 shows the relative probability of fragmentation along the amino acid sequences for bovine and horse cytochrome *c*, whose sequences are only different by three residues at position 47, 60, and 89. In general, fragmentation does not appear at charge sites (basic residues, shown as full length lines in Fig. 1). The silent regions in residues 10-20 and around residue 80 correspond to the heme-binding pocket. Fragmentation mainly occurs at the N-, C-, 60's helices and residues 40-50. Such a fragmentation pattern seems to correlate to the known feature of denatured cytochrome *c* in solution, and is consistent with gas phase H/D exchange results. We tentatively attribute the dramatic difference (Fig. 1) between bovine and horse cytochrome *c* patterns as arising mainly from replacing Gly with a charged Lys at the 60th position. Lys^{60} and Lys^{79} have been shown to be close in space in X-ray structures of the native state cytochrome *c*. Our observation suggest that their charge repulsion causes changes in 3-D structure, resulted in the changes in fragmentation at Pro^{76} and residues 40-70.

We have also succeeded in performing up to four stage of MS without using quadrupole cooling technique. In Fig. 2, 15+ state tuna cytochrome *c* ions are dissociated and the resulting b_{102} fragment is then selected to be further dissociated. At MS^4, b_{98} ions generate complimentary ions with isotopic resolution. Such MS^n techniques are very useful not only in identifying internal fragmentation of the known structures, but also in analysis of proteins having small structural modification or unknown sequences.

These results indicate that the dissociation of the cytochrome *c*'s is influenced by the higher order structures and charge location, in addition to the amino acid sequence. Low energy CID may be useful in probing small structural differences of proteins in the gas phase.

This work was supported by Laboratory Directed Research and Development funds by Pacific Northwest Laboratory through the U.S. Department of Energy. Pacific Northwest Laboratory is operated by Battelle Memorial Institute for the U.S. Department of Energy under Contract DE-AC06-76RLO 1830.

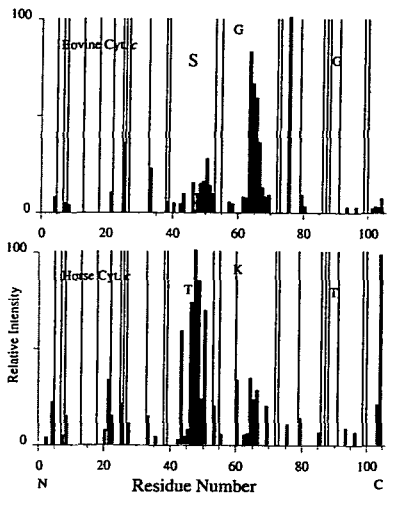

Fig. 1 MS/MS of bovine and horse cytochrome *c*. Basic residues are shown as 100% lines.

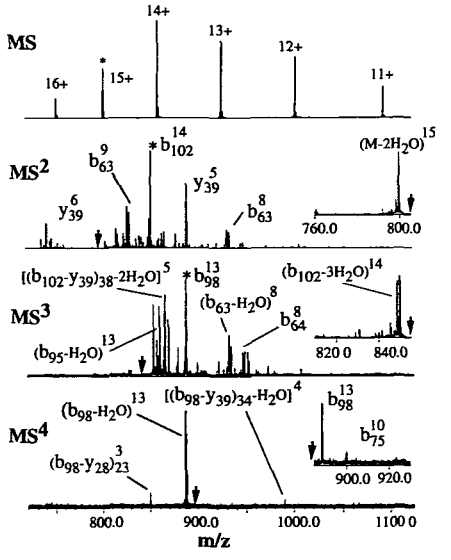

Fig. 2 MS^4 of Tuna cytochrome *c*. Arrows stars indicate the position of irradiation and precursor ions, respectively.

Quadrupole Ion Trap Study of Ion-Ion Chemistry of Multiply-Charged Ions

William J. Herron, Douglas E. Goeringer, and Scott A. McLuckey
Oak Ridge National Laboratory

The gas phase ion chemistry of multiply-charged biological polymers, such as oligonucleotides and proteins is a new and growing field of research. Understanding the gas phase chemistry of these species is important both to obtaining information on ion mass, structure and reactivity and to determining the relationship between gas phase and condensed phase chemistry. Gas phase ion chemistry studies to date have principally emphasized unimolecular fragmentation following some form of activation and ion-molecule chemistry, primarily proton transfer and hydrogen/deuterium exchange. The experiments described here constitute an important first step in understanding the ion-ion chemistry associated with the reactions of multiply-charged ions with oppositely charged ions in the gas phase.

We have adapted an electrospray/quadrupole ion trap combination to incorporate a means for generating positive ions in the ion trap to interact with negative ions injected into the ion trap from an external source. The reaction (mutual neutralization) of O_2^+ and NO_2^- provided an initial confirmation of ion-ion recombination in the ion trap. (1) However, our long range interest lies in observing ion-ion reactions between singly-charged positive ions and multiply-charged negative ions. The unique advantage of studying such reactions is the ability to observe and further study both the reactants and the product ions.

We have studied ion-ion proton transfer reactions (Figure 1) involving protonated pyridine and multiply-charged anions of short single-stranded poly A deoxynucleotides. (2) More recently we have expanded the scope of our studies to include ion-ion electron transfer reactions (Figure 2). We have examined multiply-charged anions of short single-stranded poly A deoxynucleotides with singly-charged rare gas radical cations. (3)

Figure 1. Isolated multiply-charged oligonucleotide anions were allowed to react with protonated pyridine cations for 1 s within a quadrupole ion trap mass spectrometer. The isolated triply-charged reactant anions $d(A_4 - 3H)^{3-}$ (a) undergo ion-ion proton transfer with protonated pyridine to form doubly-charged product anions $d(A_4 - 2H)^{2-}$ and (b) isolated doubly-charged product anions from the first ion-ion proton transfer, react with protonated pyridine to form singly-charged product anions $d(A_4 - H)^{1-}$.

Figure 2. Isolated multiply-charged oligonucleotide anions were allowed to react with xenon radical cations for 200 ms within a quadrupole ion trap mass spectrometer. The isolated triply-charged reactant anions $d(A_4 - 3H)^{3-}$ undergo ion-ion electron transfer with Xe^+ to form doubly-charged product anions $d(A_4 - 3H)^{2-\cdot}$. Although in this example, the doubly-charged product anion is not observed, the extensive fragmentation is consistent with the doubly-charged radical anion fragmenting either by charged base loss and subsequent fragmentation along the phosphodiester linkage or by neutral base loss and fragmentation along the phosphodiester backbone.

Reference:
(1) Herron, W. J.; Goeringer, D.E.; McLuckey, S.A. Proceedings of the 42nd ASMS Conference on Mass Spectrometry and Allied Topics, Chicago, Illinois, May 29-June3, 1994.
(2) Herron, W. J.; Goeringer, D.E.; McLuckey, S.A. J. Am. Soc. Mass Spectrom. In Press.
(3) Herron, W. J.; Goeringer, D.E.; McLuckey, S.A. In preparation.

43rd ASMS Conference on Mass Spectrometry and Allied Topics

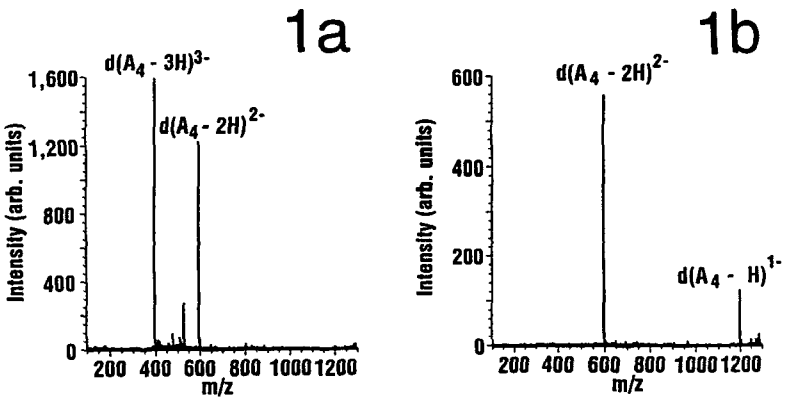

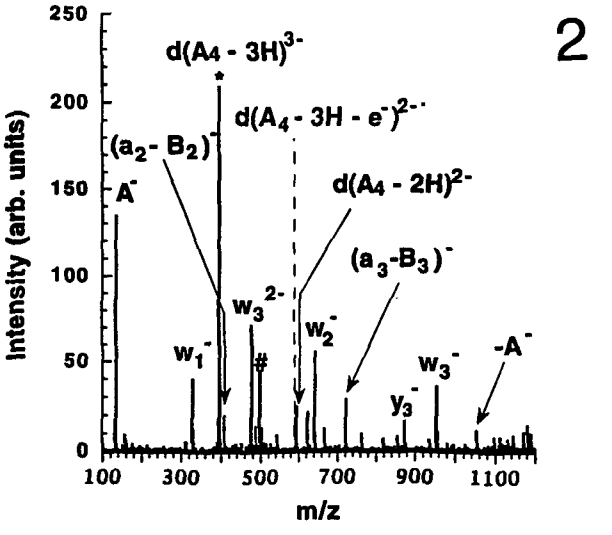

Credit:
Research sponsored by the National Institutes of Health under Grant GM45372 with Martin Marietta Energy Systems, Inc.

ISOMERIC STRUCTURES FOR UBIQUITIN IONS PRODUCED BY ELECTROSPRAY FTMS

Carolyn J. Cassady and Nigel Ewing
Department of Chemistry, Miami University, Oxford, OH 45056

The determination of gas-phase ion structures is an active area of research which increases our understanding of the processes that occur inside a mass spectrometer. Historically, this work has been limited to singly charged ions because these species were readily generated by common ionization techniques. The recent development of electrospray ionization mass spectrometry (ESI MS), however, has made possible the formation of large multiply charged ions from samples such as proteins and peptides. The current investigation demonstrates that the same MS/MS techniques utilized to elucidate isomeric structures of singly charged ions can be successfully applied to multiply protonated ions, $[M+nH]^{n+}$, generated by ESI. Conclusive evidence for at least two structures of $[M+12H]^{12+}$ from the protein ubiquitin has been obtained by deprotonation reactions, hydrogen/deuterium (H/D) exchange reactions, and collisionally activated dissociation (CAD). In addition, it is found that the $[M+12H]^{12+}$ population generated directly by ESI is not identical to the $[M+12H]^{12+}$ population formed by gas-phase deprotonation of $[M+13H]^{13+}$.

Electrospray ionization was achieved using an Analytica of Branford source in the external ion source of a Bruker CMS-47X Fourier transform mass spectrometer. Ubiquitin ions, $[M+nH]^{n+}$, containing 7-13 attached protons were produced. $[M+12H]^{12+}$ were m/z-selected by resonant frequent ejection techniques. For ion/molecule reaction studies these ions were allowed to react with static pressures of neutral reagents present in the FTMS cell. In CAD experiments, sustained off-resonance irradiation (SORI)[1] was used to induce low energy fragmentation.

Ubiquitin (M_r = 8564.8) is a monmeric peptide containing 76 amino acid residues. It has 13 basic sites that may be preferentially protonated in the gas-phase. We recently reported that $[M+12H]^{12+}$ of ubiquitin were rapidly deprotonated by compounds having gas-phase basicities (GB) greater than or equal to that of n-propylamine (GB = 210.1 kcal/mol^2).[3] These reactions exhibit linear pseudo-first-order kinetic behavior and provide no evidence for more than one $[M+12H]^{12+}$ structure. In contrast, deprotonation reactions of ESI-generated $[M+12H]^{12+}$ with the less basic ammonia (GB = 195.6 kcal/mol^2) and 2-fluoropyridine (GB = 202.8 kcal/mol^2) reveal non-linear pseudo-first-order kinetic behavior that suggests the presence of at least two ion structures. With ammonia, 60.4($\pm$9.6)% of $[M+12H]^{12+}$ react with a rate constant (k_{exp}) of 8.4($\pm$4.4) x 10^{-12} cm^3 molecule^{-1} s^{-1}, while the remaining 39.6($\pm$9.6)% of the ions are slower to react with k_{exp} = 5.4($\pm$2.0) x 10^{-13} cm^3 molecule^{-1} s^{-1}. For 2-fluoropyridine the difference is more pronounced: fast-reacting ions account for 45.8($\pm$4.5)% of the $[M+12H]^{12+}$ and have k_{exp} = 3.8($\pm$1.5) x 10^{-10} molecule^{-1} s^{-1}, while 54.2($\pm$4.5)% of the ions react with k_{exp} = 2.8($\pm$0.2) x 10^{-12} cm^3 molecule^{-1} s^{-1}. Interestingly, this behavior appears to be unique to n = 12 and was not seen with n = 13 and 11.

In addition to production directly by ESI, $[M+12H]^{12+}$ were formed by removal of a proton from "fully protonated" $[M+13H]^{13+}$ with 2-fluoropyridine. Surprisingly, these ions show kinetic evidence for only one $[M+12]^{12+}$ population and react with a rate constant of 5.1($\pm$0.8) x 10^{-12} cm^3 molecule^{-1} s^{-1}. This suggests that deprotonation of $[M+13H]^{13+}$ (which yields exclusively slow-reacting ions) produces a more homogeneous and energetically stable ion population than the ESI process itself. Thus, ESI is less selective than ion/molecule reactions at protonating (or deprotonating) basic sites on proteins.

The presence of two ubiquitin $[M+12H]^{12+}$ populations is also indicated by reactions with D_2O and CD_3OD. These species do not deprotonate $[M+12H]^{12+}$; instead, H/D exchange occurs. The ions that are rapidly deprotonated also rapidly exchange the first 11$\pm$1 hydrogens. The ions that are slower to deprotonate are slower to H/D exchange. Again, this behavior is not found with n = 13 and 11.

Additional confirmation of at least two different $[M+12H]^{12+}$ structures was provided by SORI CAD experiments performed as a function of reaction time with ammonia and with 2-fluoropyridine. The reaction time, during which ubiquitin's fast-reacting $[M+12H]^{12+}$ is selectively depleted, occurs before SORI activation. The spectra reveal a gradual shift in the relative abundances of several fragment ions as the deprotonation reaction progresses. After the reaction has removed the fast-reacting $[M+12H]^{12+}$ population, this shift ceases and the CAD spectra remain virtually unchanged as the reaction time is increased. For example with the y_{58} product ions, the first 1.0 second of the reaction time yields marked changes in the relative abundances of y_{58}^{8+}, y_{58}^{9+}, and y_{58}^{10+}; however, beyond 1.0 second the ratios remain relative stable. Based upon k_{exp} and the experimental conditions, 94 % of the fast-reacting $[M+12H]^{12+}$ should be removed within the first 1.0 second. Therefore, after longer reaction times only the slow-reacting $[M+12H]^{12+}$ still remains for study by SORI CAD. In addition, the CAD spectra do not change as a function of reaction delay when the amine is replaced with argon. This is important because it indicates that collisional thermalization is not responsible for the phenomenon of changing product intensities as a function of reaction — and thus collision — time.

The SORI CAD spectra for $[M+12H]^{12+}$ formed by deprotonation of $[M+13H]^{13+}$ resemble the spectra of the slow-reacting ions and are independent of reaction delay with 2-fluropryidine or ammonia. This agrees with the deprotonation reaction results that indicated that protonation of $[M+13H]^{13+}$ produces only the slow-reacting $[M+12H]^{12+}$.

The two ubiquitin $[M+12H]^{12+}$ ion structures may be conformational isomers, isomers related to differences in protonation site, or both. In considering the CAD spectra for $[M+12H]^{12+}$, several notable changes occur as the fast-reacting ions are selectively removed by deprotonation reactions. For example, the abundances of y_{58}^{8+} and y_{24}^{4+} are highest when both $[M+12H]^{12+}$ isomers are present at short reaction times but decrease as the fast-reacting ions are depleted. In contrast, production of y_{58}^{9+}, y_{58}^{10+}, and y_{24}^{5+} increases as the reaction progresses, meaning that these fragments are formed in greater abundance from slow-reacting $[M+12H]^{12+}$. The y_{58} fragment contains amino acid residues 19 through 76 of ubiquitin, which have 10 of the preferred basic sites; y_{24} contains residues 53 through 76 with 5 basic sites. In the CAD spectrum of "fully protonated" $[M+13H]^{13+}$, y_{58} has a maximum charge of 10+ and y_{24} has a maximum charge of 5+. Thus, the preferential formation of y_{58}^{10+} and y_{24}^{5+} for slow-reacting $[M+12H]^{12+}$ suggests that these ions may be protonated at all 10 basic sites of residues 19 through 76 and all 5 sites of residues 53 through 76, respectively. That is, for slow-reacting ions the absent proton is near the N-terminus. For fast-reacting $[M+12H]^{12+}$, the more abundant y_{58}^{8+} supports loss of a proton from a basic site between residues 19 and 76, while the more abundant y_{24}^{4+} suggests that a proton is absent between residues 53 and 76. Therefore, fast-reacting ions may be missing a proton near the C-terminus. These changes in protonation site could also induce changes in 3-dimensional conformation.

Ubiquitin $[M+12H]^{12+}$ is the only multiply charged ion systems to date that has been subjected to structural studies that combine ion/molecule reactions and CAD. This combination should be a powerful tool for solving structural problems for proteins relating to sequence, conformation, and protonation site.

References

(1) Gauthier, J.W.; Trautman, T.R.; Jacobson, D.B. *Anal. Chim. Acta* **1991**, *246*, 211-225.
(2) Lias, S.G.; Liebman, J.F.; Levin, R.D. *J. Phys. Chem. Ref. Data* **1984**, *13*, 695-808.
(3) Cassady, C.J.; Wronka, J.; Kruppa, G.H.; Laukien, F.H. *Rapid Commun. Mass Spectrom.* **1994**, *8*, 394-400.

Electrostatic Interactions in Multiply Protonated Gas-Phase Ions

Evan R. Williams, Deborah S. Gross, Paul D. Schnier, Sandra E. Rodriguez-Cruz, Clifton K. Fagerquist
Department of Chemistry, University of California, Berkeley, CA 94720

Coulomb repulsion in multiply protonated gas-phase ions, such as those produced by electrospray ionization, dramatically increases the reactivity of these ions. Increased rates of proton transfer (1) and dissociation (2) are observed with higher charge state ions. We have developed a method for determining the Coulomb energy in multiply protonated ions through measurements of apparent gas-phase basicities (GB^{app}, equation 1).

1) $$GB^{app} = GB_{Intrinsic,t} - \sum_{i=1}^{n} \frac{q^2}{(4\pi\varepsilon_o)\varepsilon_r r_{it}}$$

where ε_r is the effective shielding between charges in these gas-phase ions, and $GB_{intrinsic}$ is the basicity of a molecule protonated at a site *t*. All experiments are performed in an external ion source Fourier-transform mass spectrometer that uses electrostatic ion lenses to guide the electrospray generated ions through the fringing fields of a 2.7 T superconducting magnet into the ion cell (3). Ions are thermalized with N_2 gas introduced through a pulsed valve and mass selected with SWIFT. Reactions with reference bases at a pressure of ~1 x 10^{-7} Torr are measured with varying reaction times. Rates of proton transfer are obtained from these data and the GB^{app} of the ions is obtained.

Initial evaluation of this method was done with doubly protonated 1,*n*-diaminoalkanes (*n* = 7-10, 12) (4) and doubly protonated gramicidin s (3). For the diaminoalkanes, singly protonated monoaminoalkanes were used as references to obtain values for $GB_{intrinsic}$; distances between charge sites were obtained from molecular modeling. Measured GB^{app} values for this series fit equation 1 using an ε_r = 1.01 ±0.07 indicating that these reactions accurately follow a point charge Coulomb potential. For gramicidin s, intramolecular charge solvation occurs. We make the approximation that if charges are independently solvated, that the difference, $GB^{app}(MH_n^{n+})$ - $GB_{intrinsic}$ will reflect differences in Coulomb energy and that entropies and enthalpies of cyclization will cancel. For this peptide, we find ε_r < 1.2. (3).

For larger more complicated ions, such as proteins, information about where charges are located must be obtained so that an estimate of the $GB_{intrinsic}$ of the site of deprotonation can be obtained. For this, we model the most energetically favorable configuration of charges using a pseudo random-walk algorithm (5,6). By comparison of these calculated values to our measured values, ε_r for proteins is obtained. For the 3+ to 15+ charge states of cytochrome c, we find a best fit to our experimental values using a fully denatured ion structure and an ε_r = 2.0 (5). Our calculations show that the charge state for which our calculated GB^{app} is lower than the GB of the solvent from which the ion is formed corresponds to the maximum charge state observed experimentally. For 15 proteins commonly analyzed by ESI, our calculated maximum charge state based on gas-phase reactivity is within 6% of the maximum charge state observed in the literature (6). The maximum charge state for peptides (ε_r = 1.3) with many basic sites also appears to be determined by the gas-phase chemistry. For peptides with few basic residues, we find that the maximum charge state is better correlated to the charge state in solution.

Because of the long range 1/*r* distance dependence (where *r* is the intercharge separation), accurate measurements of Coulomb interactions should provide a sensitive probe of ion conformation. Lysozyme contains four disulfide linkages that are readily cleaved in solution. The GB^{app} of the 3+ - 15+ ions formed from denaturing and native solutions was measured (7). For some charge state, the proton transfer kinetics required two or more rate constants for an accurate fit (Figure 1), indicating the presence of more than one ion conformation for the charge state. Significant differences in reactivity between ions formed from "native" and denaturing solutions are observed for several charge states (Figure 2) For example, the most reactive isomer of the 9+ ion formed from a "native" solution is 23 kcal/mol more reactive than the least reactive isomer of the 9+ ion formed from a denaturing solution. The reactivity of these two ion structures is consistent with our calculated values for ions that are in a crystal structure and

fully denatured conformation, respectively. Lower charge state ions are formed by proton transfer to neutral base. The low charge state ions formed from denaturing solutions are *more* reactive than those formed from native solutions. This indicates that these ions have a more compact structure than disulfide intact ions. Since these low charge state disulfide reduced ions are formed by removal of protons from higher charge states that are initially denatured in the gas-phase, this indicates that these ions must be *folding in the gas-phase.*

REFERENCES

1. McLuckey, S. A.; Van Berkel, G. J.; Glish, G. L. *J. Am. Chem. Soc.* **1990**, *112*, 5668-5670.
2. Little, D. P., Speir, J. P., Senko, M. W.; O'Connor, P. B., McLafferty, F. W. *Anal. Chem.* **1994**, *66*, 2809-2815.
3. Gross, D.S.; Williams, E.R. *J. Am. Chem. Soc.* **1995**, *117*, 883-890.
4. Gross, D.S.; Rodriguez-Cruz, S.E.; Bock, S.; Williams, E.R. . *Phys. Chem.* **1995**, *99*, 4034-4038.
5. Schnier, P.D.; Gross, D.S.; Williams, E.R. *J. Am. Chem. Soc* , in press.
6. Schnier, P. D.; Gross, D. S.; Williams, E. R., submitted.
7. Gross, D.S.; Schnier, P.D.; Rodriguez-Cruz, S.E.; Fagerquist, C.K.; Williams, E.R., submitted.

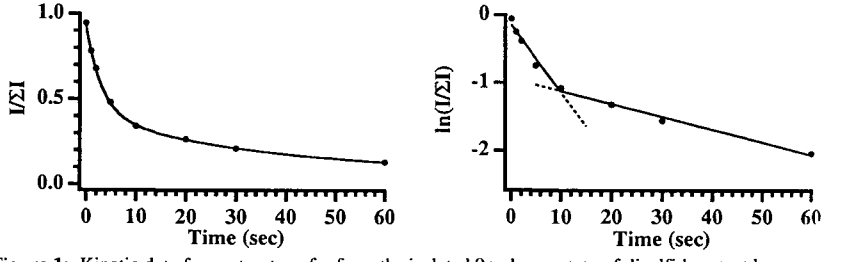

Figure 1: Kinetic data for proton transfer from the isolated 9+ charge state of disulfide-intact lysozyme to neutral triethylamine (GB = 227.5 kcal/mol). The decrease of 9+ ion abundance with time is fit using three rate constants (semi-log plot of these date are shown on right).

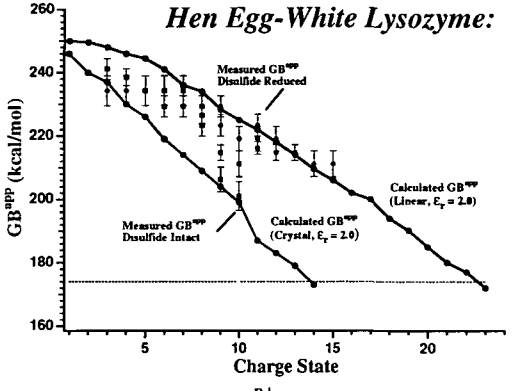

Figure 2: Apparent gas-phase basicities of $(M+nH)^{n+}$ ions of disulfide-intact and disulfide-reduced hen egg-white lysozyme. Calculated values of apparent GB of these ions modeled using the X-ray crystal structure coordinates, and modeled as a fully denatured one dimensional string are shown. The dashed line indicates the GB of methanol (174.1 kcal/mol).

Surface-Induced Dissociation of Multiply-Charged Peptides

Ashok R. Dongré, Árpád Somogyi and Vicki H. Wysocki

Department of Chemistry, Virginia Commonwealth University, Richmond VA 23284-2006

Surface-induced dissociation has proved to be an effective technique to elucidate structure and study mechanisms of peptide fragmentation for peptide <2000 u.[1] Side-chain specific sequence namely "d" and "w" ions which are high energy charge remote fragmentation processes, are observed in low energy SID spectra of peptides. The advantages afforded by SID such as high energy deposition can also be utilized to study fragmentation of large (>2000 amu) protonated peptides. The goal of the current investigation is to study fragmentation of multiply-protonated peptides in the molecular weight range of (2000-5000 amu). The experiments were carried out on a custom designed tandem mass spectrometer for ion surface collisions.[2] A fluorinated alkanethiolate monolayer surface was used in the current investigation, as it yields higher energy deposition and greater scattered ion efficiency than observed on the octadecanethiolate monolayer surface.

All the different charge states from the electrosprayed peptide solution were mass selected, in separate experiments and made to collide with the surface to observe fragmentation and obtain sequence information. Figure 1 illustrates a SID spectrum of doubly-charged insulin B-chain (oxidized). The SID spectrum yields a complete series of "b" and "y" type ions. Complete sequence information for insulin B-chain can be obtained from this spectrum. Other peptides, such as glucagon, melittin, human parathyroid hormone, and ACTH 1-39 were also investigated. Except for Insulin B-chain, the spectra for all the other peptides are either dominated by a "b" ion series or a "y" ion series. The position of the basic amino acid residues (namely Lys and Arg) along the peptide backbone affects which of the ion series predominates. If the basic amino acids are towards the C-terminus as in melittin, a "y" ion enevlope is observed. The charge state of ions observed in SID spectra are one lower than the mass selected ion, even the mass selected ion losses a proton on collision with a surface to yield a lower charge state intact peptide ion. The fragment ion

intensities may also be dictated by the sequence and conformation of these multiply protonated peptide ions.

In summary, surface-induced dissociation can be utilized to obtain sequence information from these large (>2000 amu) peptides and also to study the fragmentation mechanisms of these multiply-protonated peptides.

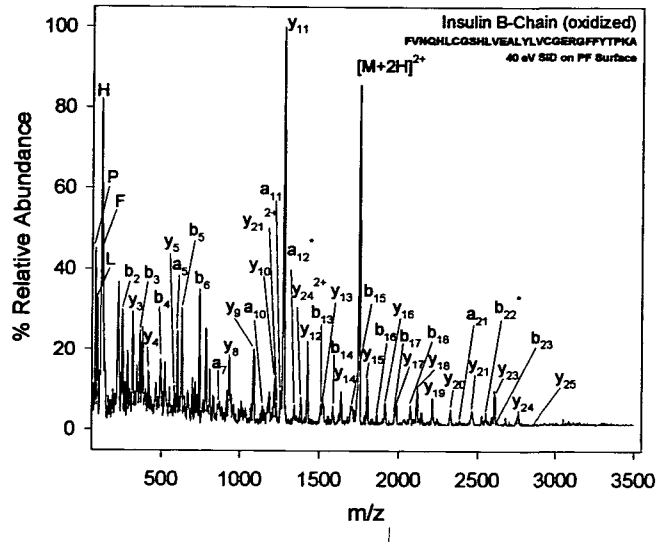

Figure 1

References:

(1) (a) McCormack, A. L.; Somogyi, Á.; Dongré, A. R.; Wysocki, V. H., *Anal. Chem.* **1993**, *65*, 2859-2872. (b) Jones J. L.; Dongré, A. R.; Somogyi, Á.; Wysocki, V. H., *J. Am. Chem. Soc.*, **1994**, *116*, 8368-8369

(2) V. H. Wysocki, J.-M. Ding, J. L. Jones, J. H. Callahan and F. L. King, *J. Am Soc. Mass Spectrom.* **1990**, *1*, 473.

DEPROTONATION REACTIONS OF SMALL PEPTIDE IONS PRODUCED BY ELECTROSPRAY

Scott R. Carr and Carolyn J. Cassady
Department of Chemistry, Miami University, Oxford, OH 45056

Gas-phase reaction chemistry of multiply charged small peptide ions produced by electrospray ionization (ESI) has been examined. These ions were allowed to undergo gas-phase deprotonation reactions with neutral bases in a Fourier transform ion cyclotron resonance mass spectrometer (FT-ICR). The peptides that were examined had 13 or 14 amino acid residues, but varied in composition as well as sequence of the residues These include· ACTH (11-24), fibrinopeptide B, human gastrin I (1-14), renin substrate (1-14), somatostatin, and tyrosine protein kinase. Deprotonation reactions have been done by this lab on a larger peptide, namely, ubiquitin[1], under similar conditions.

The peptides were dissolved in a 49.49.2 mixture of methanol, water and acetic acid Individual solutions of ~10^{-5} M were delivered by a syringe pump at 2-3 μL/min. The solution then passed through an electrospray needle and across ~5 kV A Bruker CMS-47X FT-ICR was used for all experiments. The Analytica of Branford ESI source was at atmospheric pressure and the analyzer cell at ~10^{-9} Torr. The m/z-selected peptide ions were reacted with various amines held at a static pressure (2-20 × 10^{-8} Torr) in the cell. These amines had a wide range of varying known gas-phase basicities (195.6 to 232 6 kcal/mol)[2] and are listed in order of increasing gas-phase basicity· ammonia, 2-fluoropyridine, n-propylamine, di-n-propylamine, tri-n-propylamine, and N,N,N′,N′-tetramethyl-1,4-diaminobutane. See the example spectra on the following page.

The number of charges that were present on the individual multiply charged peptide ions produced by ESI had a close correlation with the number of inherently basic amino acid residues, namely, histidine, lysine, arginine and the N-terminal residue. For example, ACTH has two arginines and four lysines, one of which was at the N-terminus, and was seen to have six different charge states

Upon examination of the rates of deprotonation, it is seen that as the charge state of the peptide and the gas-phase basicity of the amine increased, the rate did likewise. Most of the peptides exhibited linear pseudo-first-order kinetics with only a few exceptions The reactions occurred very fast and often approached the collisional rate as calculated from ADO theory The small peptides with the same number of residues and charge appeared to be deprotonated at nearly equivalent rates once the reactions had become thermodynamically favorable (see neighboring figure). This implies that, with the possible exception of adjacent residues, composition and sequence is not actually a determining factor in the deprotonation rate based on the studied peptides

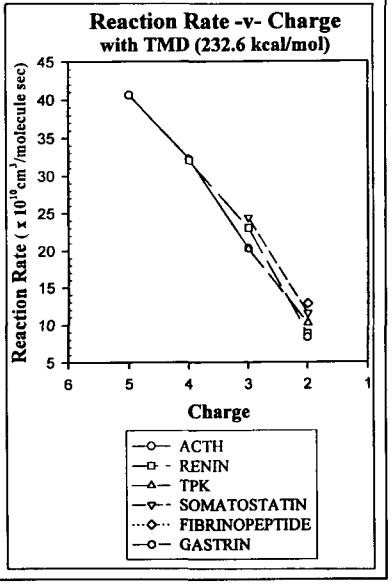

Example spectra are shown **A**, all ions in a reaction of somatostatin with n-propylamine are being detected without isolation The large peak present is the +3 charge state **B**, all ions except that of the +3 state have been removed by resonant frequency ejection techniques **C**, the product ions of the deprotonation reaction after 0 2 seconds at a static pressure of 4 8 × 10^{-9} Torr.

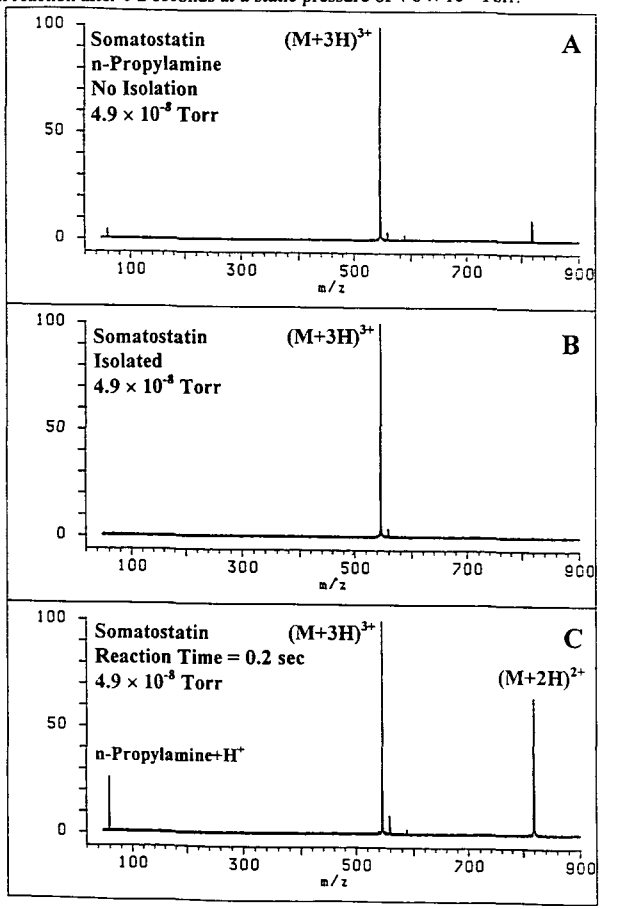

References
(1) C J Cassady, J Wronka, G H. Kruppa, and F H Laukien, *Rapid Commun Mass Spectrom* 8, 394, (1994)
(2) S G Lias, J. F. Liebman, and R. D Levin, *J. Phys. Chem. Ref Data* 13, 695, (1984)

Characterization of Carbonic Anhydrase-Inhibitor Noncovalent Complexes

Xueheng Cheng, Ruidan Chen, James E. Bruce, Brenda L. Schwatz, Gordon A. Anderson, Steven A. Hofstadler, David C. Gale, Richard D. Smith, #Jinming Gao, #George B. Sigal, #Mathai Mammen, and #George M. Whitesides
Pacific Northwest Laboratory, Richland, WA 99352
#Department of Chemistry, Harvard University, Cambridge, MA 02138

Competitive binding of two mixtures of inhibitors to bovine carbonic anhydrase II (BCAII) was studied using electrospray ionization mass spectrometry (ESI-MS). The first mixture contained inhibitors with hydrocarbon/fluorohydrocarbon linker groups and with an 800 fold span of binding constants. The second contained inhibitors with dipeptide extensions synthesized using the solid phase method. Noncovalent enzyme-inhibitor complexes were observed from solutions in 10 mM ammonia acetate having abundances consistent with their relative binding constants measured in solution. The inhibitor with highest affinity was readily identified in an equimolar mixture. The inhibitors with very low affinity were identified to form specific complexes as well. Several control experiments including acidifying the solution or removing the Zn metal from the enzyme resulted in the disappearance of the enzyme-inhibitor complexes, demonstrating the specificity of the (mass spectrometrically) observed complexation and the reliability of ESI-MS in the characterization of biomolecular binding. Good correlation between gas phase inhibitor ion abundances and their binding constants in solution were observed (Fig. 1). Structural information and relative binding constants of inhibitors of close or degenerate masses were obtained using Fourier transform ion cyclotron resonance mass spectrometry (FTICR-MS) through multi-stage dissociation experiments (Fig. 2). These results support the role of ESI-FTICR-MS in the study of specific noncovalent associations from solution, and show that its unique capabilities can be exploited to extend studies to large mixtures of inhibitors in drug leads discovery.

Pacific Northwest Lab is operated by Battelle Memorial Institute for the U.S. Department of Energy under Contract DE-AC06-76RLO 1830.

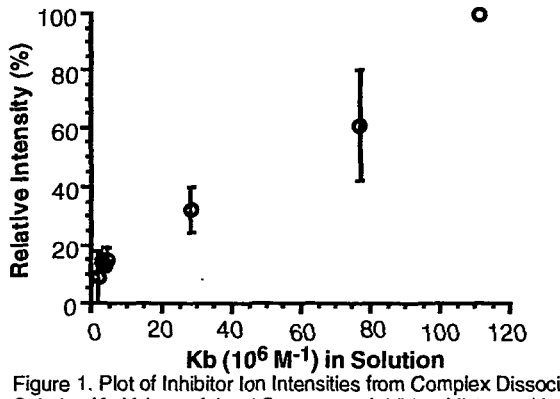

Figure 1. Plot of Inhibitor Ion Intensities from Complex Dissociation vs. Solution K_b Values of the 7-Component Inhibitor Mixture with BCA(II).

43rd ASMS Conference on Mass Spectrometry and Allied Topics

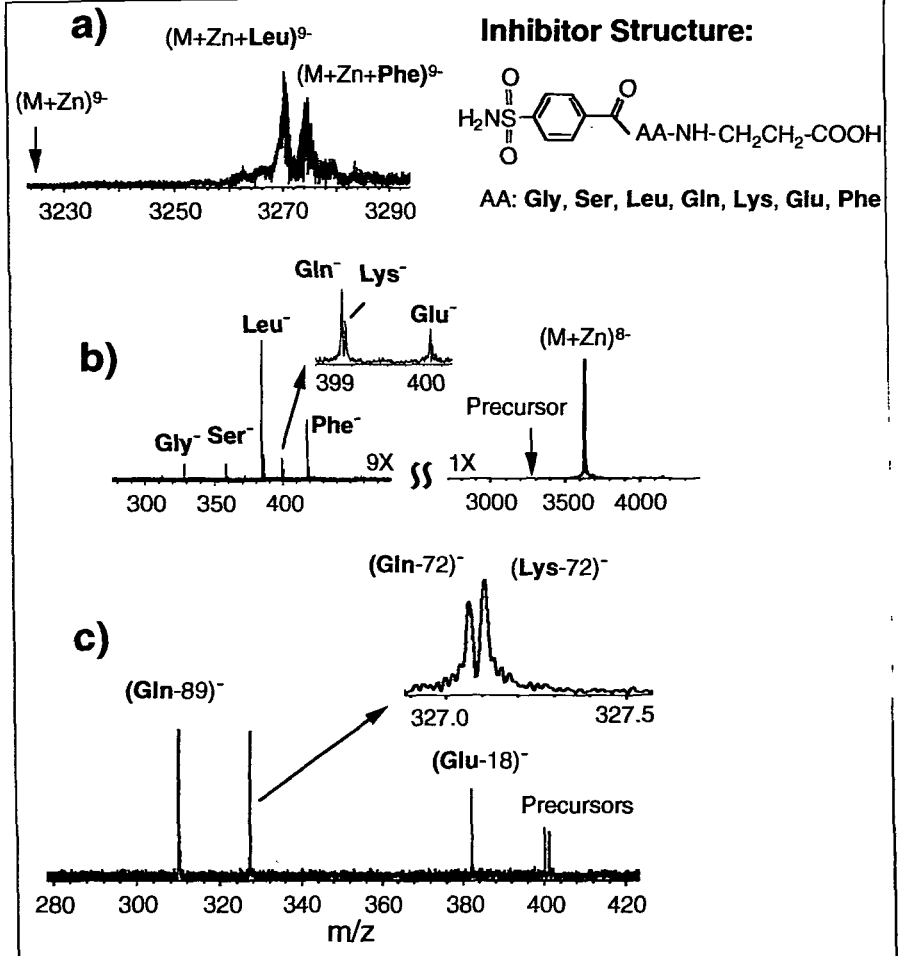

Figure 2. Accumulation, separation, and dissociation of BCAII-Inhibitor Complexes. a) MS: Selective accumulation of the 9th charge state of the complexes; b) MS/MS: SORI CID of the complexes. Inhibitors break off with one negative charge; c) MS/MS/MS: Structure information can be obtained by isolation and dissociation of the broken-off inhibotor ions.

Compounds That Elude FAB Analysis: It All Begins in Solution!

Kate Noon and John Allison
Department of Chemistry, Michigan State University, East Lansing, Michigan

This presentation is an unusual one for this session on multiply-charged ions in that it does not concern electrospray ionization, but fast atom bombardment. Also, it is a story about "compounds that don't work", those that traditionally elude analysis by FAB. In FAB, some have reported that if an analyte is ionic in solution, a "preformed ion", then it is more likely to result in a successful FAB analysis, with strong analyte signals. One group of molecules for which FAB does not yield strong signals are those which form anionic species in solution. One would predict that negative ion FAB would be the method of choice, but it is not. The most challenging compounds form *polyanionic* species in solution, and include molecules such as inositol hexaphosphate, glutathione coenzyme A (sodium salt), and gangliosides, expecially those that contain multiple sialic acid residues. To enhance our ability to detect these compounds, as well as to investigate the relationship between the ionic species formed in solution and those observed in the negative ion mass spectra, we use the matrix additive octylnicotinium bromide, ON^+Br^-. It is believed that the octylnicotinium cation, ON^+, is surface active. Because it is cationic, it attracts negatively charged analytes to the surface, increasing the desorption probability and altering the environment from which the analyte desorbs.

It is not unreasonable to assume that, if an analyte exists in a glycerol matrix in a polyanionic form, it will not appear in the gas phase as a multiply charged species. Consider for example the phosphate ion, PO_4^{3-}. We estimate that approximately 285 kJ/mol is required to desorb the singly charged speices, $H_2PO_4^-$, from glycerol, but an energy of more than 2500 kJ/mol would be required to desorb the intact phosphate anion in the 3- form. A variety of other experiments suggest that energies of that magnitude are not available in the desorption process in FAB.

While many compounds that form polyanionic species in solution do not form strong signals in negative ion FAB experiments, we observe that citric acid does. Citric acid is a small triprotic acid, which we will designate as H_3Cit. We have introduced citric acid into the glycerol matrix via various citric acid/trisodium citrate mixtures, each keeping the total citrate concentration constant. The spectra are complex because the citrate ion appears in many forms such as H_2Cit^-, $HNaCit^-$ and Na_2Cit^-. From this work it is clear that the sodium ion concentration in the solution influences the form in which the citrate desorbs, so we have studied a range of citric acid/sodium citrate mixtures (buffers) with a constant sodium concentration, to minimize the variables influencing the ions formed. In the "buffer" solutions prepared at various pH's, the ionic forms observed in the mass spectra do change with pH. The H_2Cit^- form always dominates over those containing sodium. It appears that, at low pH values, the analyte mainly forms H_3Cit in the FAB sample solution. It may desorb in neutral form, and react via ion/molecule reactions with ions such as $(G\text{-}H)^-$ to form H_2Cit^-. At high pH, when the dominant solution form is Cit^{3-}, direct desorption is not energetically possible. At high pH's where multiply charged forms of the citrate dominate the solution, more H_2Cit^- is formed in the gas phase. The 3- ion can form an ion pair with Na^+ to lower its charge, or react with neutral glycerol and extract a proton. Both lead to species with lower charge. The process can again happen, yielding 1- ions that can desorb (see Figure 1). For the systems studied, the concentration of the glycerol matrix is higher than any ionic species such as Na^+, and this may influence the relative rates of H^+ vs Na^+ capture by the polyanionic citrate.

When the same systems are studied in the presence of ONBr, the major ion at all pH's is H_2Cit^-. ONBr creates a very different environment for desorption of the anions, and in the process it appears to displace alkali ions from regions close to the surface. With ONBr present , citrate signals are highest at high pH values, suggesting that the 1- ions observed evolve from the 3- ions in the solution. We have performed similar studies with the tartaric acid/sodium tartrate system (Figure 2). Tartaric acid, H_2Tar, is a diprotic acid. While the Tar^{2-} ion need not undergo as many steps to obtain a 1- state as citrate, the results are quantitatively similar.

The collected results and observations indicate that polyanionic molecules in the FAB matrix glycerol have a rich chemistry during the desorption process. Atom bombardment results in local temperature increases. As T increases, density and dielectric constant decrease, and rates for ion pair formation (involving Na^+) become high. The polyanionic materials also can extract protons from the matrix. This process is endothermic, but the resulting anion has a lower net charge and requires less energy for desorption. Presumably, polyanionic species can scavenge positive charges through a variety of mechanisms to lower their net charge, can become completely neutralized, and can even acquire a net positive charge through similar processes. The rate for each process seems to reflect relative reactant concentrations in a straightforward way. Thus, while "preformed ions" may in some cases yield strong signals, this is not necessarily the case for many polyanionic species in solution These compounds appear to undergo charge-changing reactions at high rates, and may be extensively neutralized by the time they leave the interfacial region (the space above the FAB target between the solution and high vacuum).

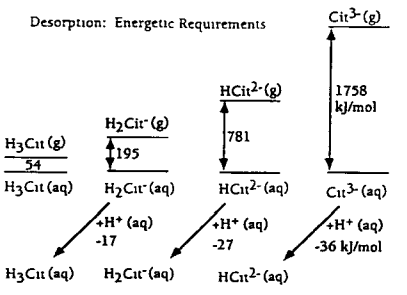

Figure 1. Thermochemical estimates for energies required for the desorption of the various forms of citric acid from glycerol. Also shown, protonation during the desorption process from an acidic environment leads to lower charge states, which require less energy to desorb.

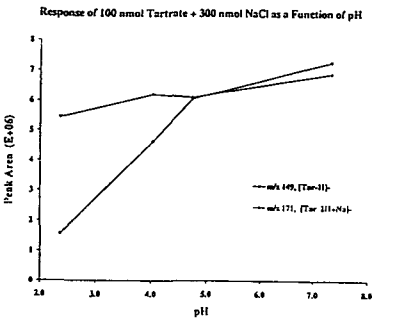

Figure 2. Changes in the ionic species of tartaric acid observed in the mass spectrum as the pH of the analyte solution is varied.

MALDI-MS IN THE INFRARED: A CRITICAL EVALUATION

Franz Hillenkamp, Michael Karas and Stefan Berkenkamp
Institute for Medical Physics and Biophysics, University of Muenster, Germany

Matrix-Assisted Laser Desorption/Ionization Mass Spectrometry (MALDI-MS) has become a widely used technique for the analysis of large biological molecules Lasers emitting in the ultraviolet (UV) wavelength range of 260 - 360 nm and matrices absorbing strongly in this range are almost exclusively used in MALDI instruments. First reports about the use of lasers emitting in the infrared (IR) at wavelengths around 3 µm (ER-lasers) and 10 6 µm (CO_2-lasers) have appeared as early as 1990 (1, 2) A host of potential matrices are available with a strong absorption at these wavelengths, mainly that resulting from O-H and N-H vibrational modes at 3 µm. Several of them such as succinic acid, glycerol or urea have been proven to be functional matrices yielding spectra of a quality comparable to those obtained in the UV The current state of our knowledge on the experimental parameters and the performance data of IR-MALDI with Er YAG lasers will be presented.

An in-house built single stage reflectron TOF instrument of 3.5 m equivalent flight length and a 12 kV acceleration potential was used for all experiments (3) Working pressure in the sample chamber is 3×10^{-4} Pa Ions are detected by a conversion dynode (ion impact energy 20 - 27 kV, depending on ion mass) mounted 1 cm in front of a venetian blind secondary electron multiplier (EMI R2362). Signals are processed by a transient recorder with a time resolution of 10 ns (LeCroy 9400A) and then transferred to a PC for storage and further evaluation Single pulses of two different ER.YAG lasers (SEO 1-2-3, Schwartz Electro Optics, USA, Spektrum GmbH, Berlin, Germany) of respectively ca 150 ns and ca. 80 ns duration at a wavelength of 2 94 µm are focused to a spot diameter of 180 µm (with a 45° angle) onto the sample The instrument is equipped with a liquid nitrogen (LN) cooling stage The temperature of the stainless steel substrate is monitored with a thermocouple with an absolute accuracy of ± 5 K; it may be possible that the actual temperature of the top layer, even of very thin samples, is slightly higher than the measured substrate temperature. As in UV-MALDI, the results depend strongly on matrix and preparation techniques chosen for a given analysis. Different combinations will be discussed For the results obtained with an ice matrix, the reader is referred to poster abstract ThPF233 (this volume)

The reproducibility of IR-MALDI spectra from shot to shot has been a major concern in the past This reproducibility depends predominantly on two factors the variation of the laser pulse energy from shot to shot and the sample homogeneity. For ER.YAG lasers of recent design, the energy variation can be minimized at ±2%, comparable to that of the best UV-lasers. Sample homogeneity depends critically on the type of matrix and the preparation technique Solid matrices such as succinic acid typically form heterogeneous microcrystalline patterns. This can be more problematic in IR- vs. UV-MALDI, because only 3-4 single spectra can typically be obtained from a given sample spot due to the IR-radiation penetration into the sample between 1 and 10 micrometers. Liquid matrices such as glycerol or water form very homogeneous layers and for these matrices the reproducibility is as good, if not better, than for comparable UV-preparations.

All other parameters being equal, at least a factor of 100 - 1000 more material is consumed per spectrum as compared to the UV, because of the deeper penetration of the radiation into the sample. For succinic acid, this does not necessarily result in more material needed for a single preparation, but less spectra can be obtained from any given sample Normally 0.5 µl of a 10^{-5} M protein solutions are used, but the minimum amount of sample material necessary has not yet been explored for this matrix Substantially higher amounts of protein are needed for preparations with liquid matrices such as glycerol The ion signal intensity of IR-MALDI spectra is quite comparable to that of UV-MALDI spectra. Considering that much more material is ablated per laser pulse in the IR, the material is either primarily removed as clusters and

small particulate matter, or the ion yield is smaller by two to three orders of magnitude.

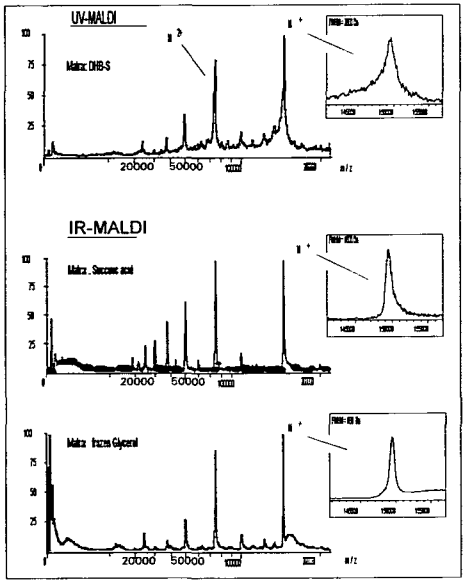

Figure 1 Mass spectra of a Monoclonal Antibody (MW ca 150,000Da)

In the mass range below ca 20 kDa the mass resolution for most of the matrices was equal to that found in UV-MALDI spectra recorded with the same instrument Above 20 kDa the mass resolution of the IR-MALDI spectra is substantially better than that of comparable UV-MALDI spectra as demonstrated in Figure 1 for spectra of an IgG monoclonal antibody It is interesting to note that mass resolution increases for glycerol if the temperature is lowered to 150 K. This increased mass resolution has been used to determine the distribution of a specific conjugate to monoclonal antibodies (4). The superior mass resolution of the IR-MALDI spectra is mainly a result of significantly less metastable fragmentation as evidenced by less low mass tailing og the peaks. the steep low mass edge of the peaks Succinic acid and glycerol tend to form adducts, broadening the peaks on the high mass side. For frozen glycerol these adducts appear to separated from the protein peak, leading to the above mentioned increase in mass resolution An important task for future work will be the search for other matrices with less tendency for adduct formation. Preliminary results indicate that, for yet unknown reasons, the decrease in metastable decay is accompanied by an increase in prompt fragmentation. The different fragmentation behavior is also the suspected reason for fact that the upper mass limit appears to be higher for IR-MALDI. A spectrum of Gramicidin S synthease at mass 510,000 Da has been recorded with a quite acceptable S/N-ratio and a mass resolution of ca. 50.

So far the absolute mass accuracy has been limited to 10^{-3} - 5×10^{-4} for two main reasons First, only external mass calibration has been used for example with lysozyme clusters. The second problem has been the jitter of the trigger signal for the transient recorder due to the shot to shot variation of the laser pulse energy The latter problem seems to be resolved with the new 80 ns ER:YAG laser A major advantage of IR-MALDI over UV-MALDI is the availability of physiological matrices such as TRIS-HCl. Excellent spectra of myoglobin samples have been recorded, showing peaks of the apoprotein as well as the protein itself. Particularly in combination with this buffer matrix, physiological concentrations of NaCl are tolerated without a significant degradation of the spectrum quality.

1. Overberg, A.; Karas, M.; Bahr, U ; Kaufmann, R , Hillenkamp, F ,*Rapid Commun. Mass Spectrom*, 4, 293 (1990)
2. Overberg, A , Karas, M , Hillenkamp, F ; *Rapid Commun. Mass Spectrom*, 5,128, (1991)
3. Overberg, A.,Hassenbürger, A ; R.; Hillenkamp, F, in *Mass Spectrometry in Biological Science - A Tutorial*, M.L Gross Ed (Kluwer Acad Publ) 182-197 (1992)
4. Siegel, Marshall M., A. Kunz, D. Bell, S. Berkenkamp, M Karas, A. Ingendoh, F. Hillenkamp, *Proceedings of the 42nd ASMS Conference on Mass Spectrometry and Allied Topics, May 29 - June 3, 1994, Chicago IL. pg. 967.*

Sequencing electroblotted proteins by tandem mass spectrometry

D. Fabris[1], M.M. Vestling[1], M.M. Cordero[2], V.M. Doroshenko[2], R.J. Cotter[2], and C. Fenselau[1]

1) Structural Biochemistry Center, University of Maryland Baltimore County, Baltimore, MD 21228
2) Middle Atlantic Mass Spectrometry Laboratory, Johns Hopkins University, Baltimore, MD 21205

Gel electrophoresis, particularly SDS-PAGE, is routinely used to separate protein mixtures. Electroblotting the separated proteins to membranes makes available small amounts of relatively pure samples for further analysis. Specific antigen detection (Western blotting), *in situ* reduction, alkylation, digestion, Edman sequencing, and mass spectrometric analysis can be performed directly on the membrane or after extraction. On-membrane cleavage followed by accurate molecular weight determination of a few tryptic peptides allows the identification of a protein if it is present in an appropriate database. The objective of the present work was to further support the database identification with sequence information obtained from the tryptic peptides by tandem mass spectrometry. The broad applicability of this approach was evaluated using MALDI on both a curved field reflectron (CFR) TOF-MS[1] and a quadrupole ion trap[2] developed "in house" at the Middle Atlantic Mass Spectrometry Laboratory of the Johns Hopkins University. High energy collision-induced dissociations (CID) were performed at the Structural Biochemistry Center of the University of Maryland Baltimore County on a HX110/HX110 (JEOL, Tokyo, Japan) high performance four sector mass spectrometer equipped with both a FAB (JEOL) and a massive cluster impact (MCI) ion gun (Phrasor Scientific Inc., Duarte, CA).

Following SDS-PAGE of 1.2 nmoles of cytochrome C, the protein was blotted onto nitrocellulose and digested *in situ* with trypsin. The peptides were extracted with 60:40 iso-propanol·water, 0.1% TFA. Tryptic peptides were mapped by MALDI CFR TOF-MS and eight molecular weights were used to search the MOWSE[3] protein database succesfully. For sequencing, precursor ions were selected by a voltage gate and post source decay (PSD) spectra were obtained by analyzing the decomposition products on the CFR TOF-MS. The fragmentation observed in PSD spectra of peptide [88-91] (m/z 533.3) and peptide [28-38] (m/z 1168.6, Fig. 1) showed good correlation with the known sequences. The PSD spectrum of m/z 659.3 confirmed its identification as a trypsin autolysis peptide [44-49].

In an analogous manner, the tryptic digest was mapped by MALDI in a quadrupole ion trap. Precursor ions were selected using the SWIFT[4] technique and collided with Xe for 50-500 msec. The MS/MS spectra of cytochrome C peptide [28-38] (m/z 1168.6, Fig. 2) and trypsin peptide [44-49] (m/z 659.3) showed good agreement with the expected patterns.

For the sector analyses, cytochrome C was deposited on PVDF (polyvinylidene difluoride), digested on-membrane, and directly loaded onto the FAB probe. Both FAB and MCI gave good mapping and sequencing data. The m/z values of the fragments observed for cytochrome peptide [28-38] (m/z 1168.6) were in good agreement with the calculated values.

1) T. J. Cornish and R. J. Cotter, *Rapid Commun. Mass Spectrom.* 8, 781 (1994)
2) V. M. Doroshenko, T. J. Cornish and R. J. Cotter, *Rapid Commun. Mass Spectrom.* 6, 756 (1992)
3) D. J. Pappin, P. Hojrup and J. Bleasby, *Current Biology* 3, 327 (1993)
4) V. M. Doroshenko and R. J. Cotter, *Anal Chem* in press

ACKNOWLEDGEMENTS: T.J. Cornish is gratefully ackowledged. Financial support was offered by NSF, NIH, GM 33967

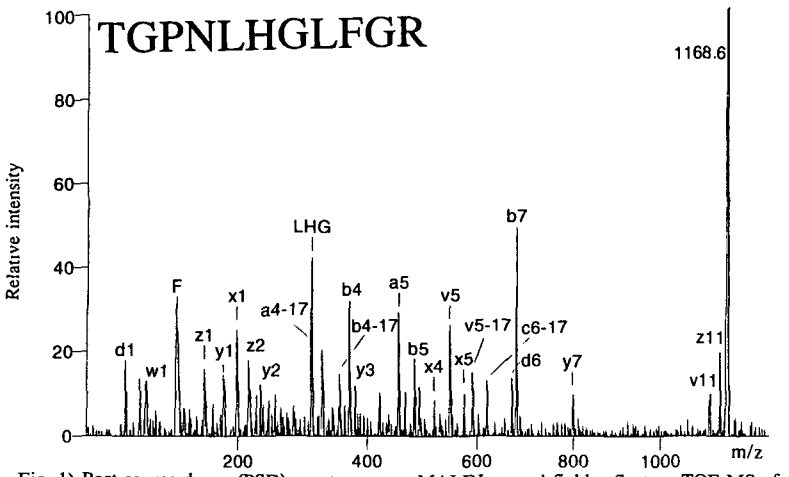

Fig. 1) Post source decay (PSD) spectrum on a MALDI curved field reflectron TOF-MS of peptide [28-38] prepared by tryptic digestion on membrane of cytochrome C electrophoresed and electroblotted

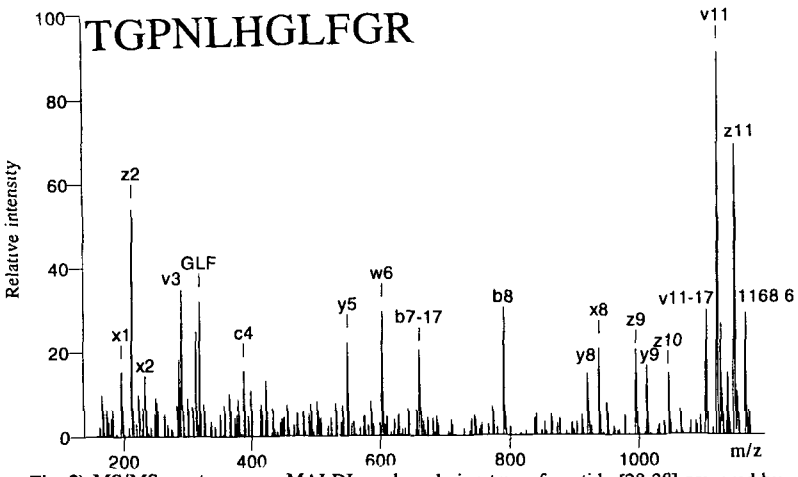

Fig. 2) MS/MS spectrum on a MALDI quadrupole ion trap of peptide [28-38] prepared by tryptic digestion on membrane of cytochrome C electrophoresed and electroblotted

MALDI AND PSD CHARACTERIZATION OF RELEASED CARBOHYDRATES FROM GLYCOPROTEINS

Jason C. Rouse, James E. Vath, and Hubert A. Scoble, Genetics Institute, Inc., One Burtt Road, Andover, MA 01810*

The potential for carbohydrate structural heterogeneity at individual glycosylation sites on a glycoprotein is vast due to the permutations generated from differing monosaccharide compositions, branching sites, and linkages. In the case of CHO-expressed glycoproteins, the heterogeneity typically observed experimentally is not as large as theoretical considerations would suggest. Many common carbohydrate structures can be recognized based on composition information (i.e., molecular mass) provided one has prior knowledge regarding the glycosylation phenotype(s) of the host cell. While this approach is often structurally conclusive, a remaining challenge for carbohydrate analyses utilizing mass spectrometry is the differentiation of isomeric structures. MALDI-post-source decay (PSD) (i.e., gas-phase ion fragmentation) of carbohydrates has the potential to quickly provide isomeric structural information on small amounts of underivatized, minimally purified material.

The heterogeneous carbohydrate structures from a particular protein glycosylation site were enzymatically released and directly analyzed as a mixture by MALDI-MS to prevent sample handling loss and to speed analysis time (see Scheme 1). On-the-probe sample clean-up strategies employing small in situ amounts of chromatographic media, instead of traditional protein removal and desalting procedures, were applied to minimize interferences from cations, anions, and/or detergents. In Figure 1, on-the-probe chelex treatment (or small cation removal) shifts the distribution of multiple sodium adduct ions to $[M+Na]^+$ and improves the signal-to-background ratio greater than 2 fold. For MALDI-PSD, each carbohydrate component in the mixture can be mass spectrometrically isolated with a precursor ion selection device in place of traditional chromatography.

A library of MALDI-PSD spectra was assembled using a variety of highly purified, previously characterized N-linked complex, hybrid, and oligomannose carbohydrates, and interpreted as a whole to identify the rules and trends associated with carbohydrate $[M+Na]^+$ low-energy fragmentation. The primary structural information extracted from these spectra was carbohydrate branching patterns. The key fragmentation that reveals the branching patterns are branch loss ion types ($y_{\alpha/\beta n}$) and internal ion types ($b_{\alpha/\beta n/n}$) which arise from single and multiple glycosidic bond cleavages at branch points, respectively (see Figure 2). For the oligomannose 7 library spectra in Figure 3, the peak intensity ratios among the branch loss ion types and among the internal ion types are consistent with expected isomeric structures and ratios. This knowledge base of MALDI-PSD carbohydrate fragmentation was successfully applied to the interpretation of oligomannose 7 with unknown isomeric structures and distributions. The distribution of isomers in this unknown mixture was validated by HPAE isolation and PSD of each individual isomer. This "PSD knowledge-based isomeric differentiation" strategy allows comparison of fragment ion abundance ratios in unknown and library MALDI-PSD spectra to identify the location of structural variations, to recognize isomerically pure carbohydrates from isomeric mixtures and estimate the distribution of isomers.

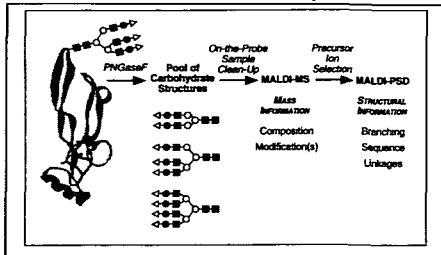

Scheme 1. MALDI-MS based characterization of N-linked carbohydrates.

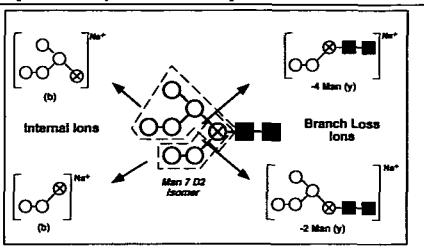

Figure 2. The key fragment ions in oligomannose carbohydrates that contain the isomeric information are the branch loss ion types ($y_{\alpha/\beta n}$, Na^+ retained on reducing end) and internal ion types ($b_{\alpha/\beta n/n}$, Na^+ retained on non-reducing end), which arise from single and multiple glycosidic bond cleavages at branch points, respectively

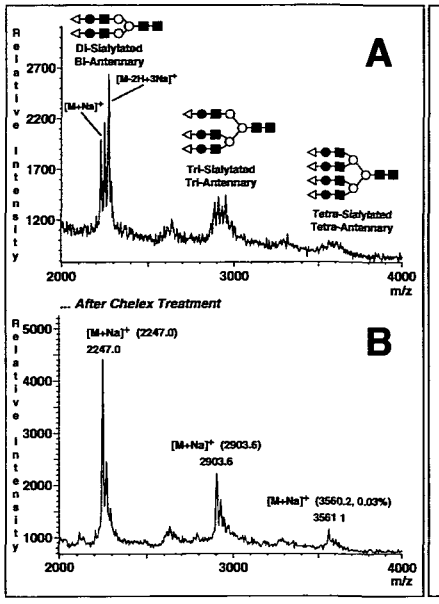

Figure 1. In both spectra, an equimolar mixture of commercially available, sialylated complex carbohydrates (7 pmol each) were analyzed by MALDI. These acidic carbohydrates have a high affinity for Na^+ given the signal for each component is divided by the multiple sodium adduct ions in (A). After on-the-probe chelex treatment (small cation removal) in (B), $[M+Na]^+$ becomes the dominant form and the S/B increases two fold or greater

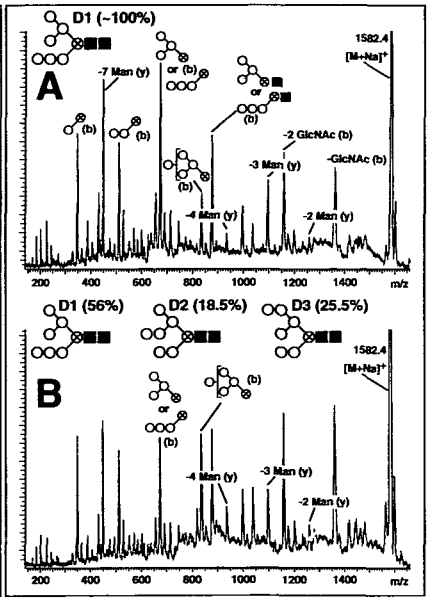

Figure 3. Both oligomannose 7 library MALDI-PSD spectra above were obtained from 40 pmol (i.e., material on the probe) of commercially available material in super DHB matrix. For the D1 isomer of Man 7 in (A), the -3 Man (y) branch loss fragment ion abundance is greater than that of -2 and -4 Man (y), and the internal "b" type ion containing the 3 mannose branch plus mannose core is more abundant than the 4 mannose branch plus mannose core "b" internal ion, which is consistent with the branching structure of the D1 isomer. For the Man 7 isomeric mixture in (B), the abundances of the 4 mannose branch plus mannose core "b" internal ion and the -4 Man (y) branch loss ion increase 2 fold indicating the D2 and D3 isomers represent ~50% of the total isomeric content while D1 represents the other 50%. The ratios listed are derived from chromatographic separation.

MASS SPECTROMETRY IN PROTEIN AND GLYCOPROTEIN STRUCTURE ELUCIDATION

Howard R Morris, Anne Dell, Maria Panico and Roy McDowell
Department of Biochemistry, Imperial College, Exhibition Rd., London SW72AZ, U K.

Whilst the relatively new ability to determine an intact protein or glycoprotein molecular weight has value, for example in determining whether or not a protein may be post-translationally modified, the critically important objective of determining the precise covalent structures involved is still dependent upon the "mapping" of low molecular weight (approx 3kD) fragments from digest mixtures, a strategy first introduced in the late 1960's and early 1970's - then called "mixture analysis" mass spectrometry (1,2) What has changed in modern research is the ability through instrumentation development to execute this strategy at the pico or femtomole level rather than the tens of nanomole level necessary for studying unknowns twenty five years ago. The intervening years have seen instrumentation developments of FAB, Electrospray and MALDI ionisation techniques, as well as High Field Magnet, Quadrupole, TOF and Cyclotron separation methods, and the introduction of MCP Array Detection. Various combinations of these technologies seem to work better or worse for solving particular problems with respect to sensitivity, mass accuracy, mass range and resolution.

Some years ago (1987) we suggested the building of a wide angle (1 5 mass ratio) magnetic sector focal plane detector instrument for mapping studies with high sensitivity and mass accuracy, and although the raising of funds for that instrument proved impossible, sufficient funding was available to commission a pseudo-focal plane version built to our specifications around ZAB2SE optics (3). This novel "dual array" mass spectrometer is compatible with most if not all ionisation methods including FAB, FD, Electrospray and MALDI, and the combination of Array Detection with Double Focusing allows high sensitivity with good resolution and mass accuracy Our instrument incorporates a low resolution wide-angle survey array for "mapping" and post-translational modification analysis of unknowns, and most data is first acquired on Array 1. This allows single shot data at a mass ratio of 1 5.1 e.g. 4,000 to 6,000 daltons, with wide mass range (up to 15 kD) data created in real time (interscan) by software stitching of consecutive shots. Peaks of interest may then be consecutively switched to a second high resolution array (Array 2) at the conventional double focusing point of the instrument within the timeframe of a single sample loading to give isotopically resolved data (>8,000 RP) with mass measurement accuracy of better than 0.2 Daltons for biopolymer characterisation.

Some examples of the instrument performance taken from our biopolymer research studies are shown below FAB remains probably the simplest and fastest way of mapping biopolymers if partial suppression or sample quantity are not limiting, giving good data down to 1 picomole on pure samples. The resolution of our instrument on Array 2 is illustrated in Figure 1 showing a FAB spectrum of Insulin giving a resolution of around 8,000 (FWHM). To exploit the inherent sensitivity of the Array it is of course necessary to chose a relatively low chemical background noise ionisation technique such as F D. or MALDI. Here, the quality of data far exceeds FAB with respect to signal to noise, even with relative sample loadings of less than one per cent Figure 2 shows the MALDI spectrum on this magnetic sector instrument (MAGNETIC MALDI to distinguish it from conventional MALDI TOF) of a relatively impure sample of 1 picomole of a human Calcitonin Gene Related peptide. The fully resolved data showing good mass accuracy illustrate some advantages of this MAGNETIC MALDI double array technique. In our studies of carbohydrate and peptide mapping by MALDI, we have determined that for small sample loadings in the 10 femtomole to 1 picomole range, the variability of ion beam intensity for consecutive laser firings on the same spot is incompatible with collection of wide mass range (multi-step) array data. However, excellent MALDI mapping data can be achieved simply by collecting array data in individual

steps, and switching the laser to different sample spot locations as and when sample is consumed An example of Array 1 low resolution MAGNETIC MALDI data acquired in this way is shown in Figure 3 allowing the location of the N-terminal polypeptide (F-1 to R-30), in one of the steps of a seven step experiment, in a digest of a glycoprotein from N. meningitidis

We thank the Wellcome Trust, MRC and BBSRC for financial support.

(1) Morris H. R. et al. (1969) Biochem. J. 114, 695-702
(2) Morris H. R. et al. (1971) Biochem. J. 125, 189-201
(3) Morris H R., McDowell R., Dell A and Panico M. Proc. 39th. ASMS Conf. on MS and Allied Topics, Nashville, (1991), 1693-1694.

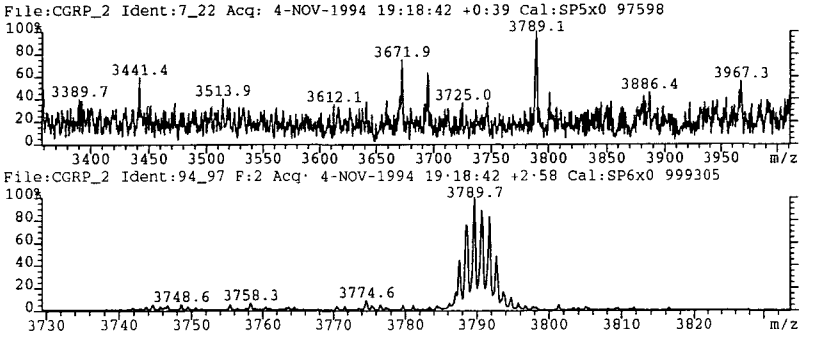

Fig. 2

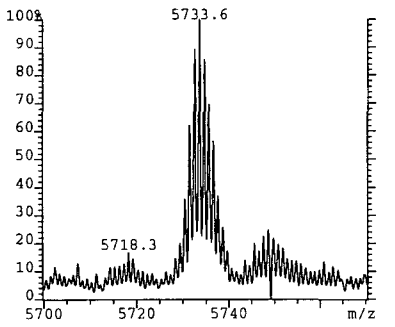

Fig. 1

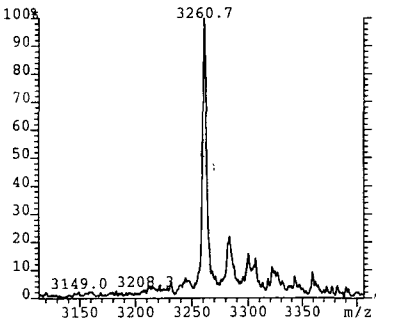

Fig. 3

Nucleotide analogs increase the stability of DNA for MALDI-MS analysis

Klaus Schneider and Brian T. Chait

The Rockefeller University, 1230 York Ave., New York, N.Y. 10021

The use of matrix-assisted laser desorption mass spectrometry (MALDI-MS) has been suggested as an ultrafast readout of Sanger DNA sequencing ladders in a manner analogous to that used with sequencing gels. Currently, a serious limitation of MALDI-MS for the analysis of DNA results from the tendency for oligonucleotides to undergo facile fragmentation in the gas phase. The present study was undertaken to gain an understanding of the influence of various chemical structural features of purine bases on the stability of oligodeoxynucleotide ions produced by MALDI. The study focused on the stability of model compounds of the type d(TTTTT TTTTT X TTTTT TTTTT TTTT), where T designates deoxythymidine and X a purine-containing 2'-deoxynucleotide analog.

In a first set of experiments, we chose guanine, hypoxanthine, adenine, and 2-amino-purine as the base in the nucleotide X. Two types of mass spectrometric fragments were observed. The first was a fragment occurring through the loss of the purine base from the intact molecule. The second were fragments that arise by cleavage of the sugar-phosphate backbone. We found that the relative tendency for fragmentation of the four model compounds decreased in the order of the bases guanine > hypoxanthine > adenine = 2-amino-purine. This order correlates with the decrease in basicity of the N7 nitrogen of the purine.

We therefore carried out a second set of experiments in which the nucleotide X contained bases with the N7 nitrogen replaced by carbon C7, i.e., 7-deaza-guanine and 7-deaza-adenine. The mass spectra of the model compounds containing 7-deaza analogues of guanine and adenine reveal a significantly increased stability compared to the 7-aza analogues under the conditions of MALDI-MS. The previously reported incorporation of the 7-deaza-2'-deoxy-adenosine triphosphate and the 7-deaza-2'-deoxy-guanosine triphosphate into DNA by polymerases suggests their use in a Sanger dideoxy sequencing experiment. The dideoxy termination products with the 7-deaza-purines instead of the 7-aza-purines might be sufficiently stable to allow the separation and detection of the sequencing ladder by MALDI- MS. Thus an ultrafast (seconds) read-out of DNA may become feasible.

References

Klaus Schneider and Brian T. Chait *Nucleic Acids Research* (1995) in press

43rd ASMS Conference on Mass Spectrometry and Allied Topics

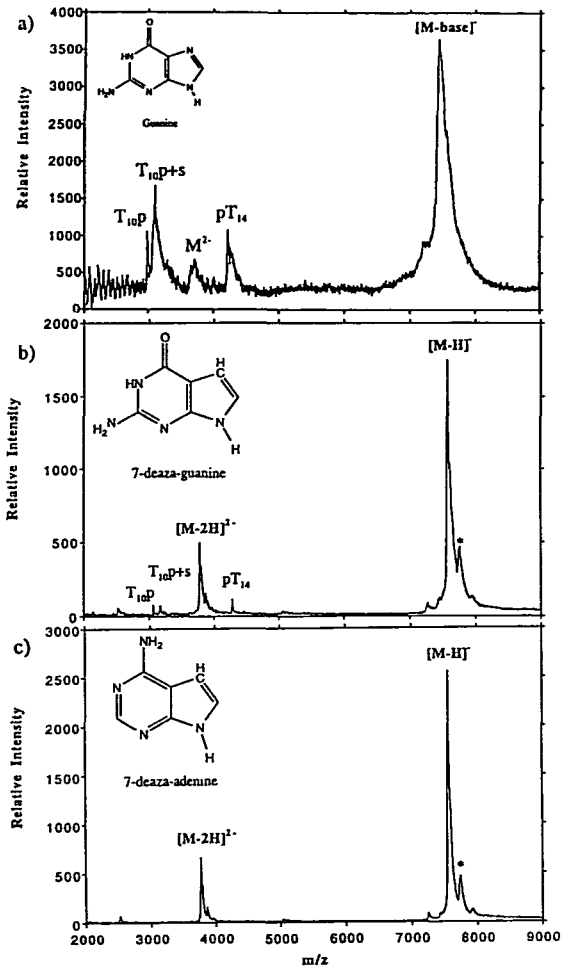

Figure

Matrix-assisted laser desorption mass spectrum of model compounds d(T10XT14) with a) X = guanine, b) X = 7-deaza-guanine, c) 7-deaza-adenine. (matrix: ferulic acid in 150 mM Ammonium citrate/acetonitrile 1:1

Molecular Diagnostics Via Mass Spectrometry of PCR-Amplified DNA Products

Michelle Buchanan, Mitch Doktycz, Greg Hurst, Scott McLuckey, and S. Habibi-Goudarzi
Chemical and Analytical Sciences Division
Oak Ridge National Laboratory, Oak Ridge, TN 37831-6365

Identifying the presence of a specific DNA fragment is becoming increasingly critical to many applications in medical, clinical, forensic and other research laboratories. At present, regions of interest in DNA are amplified using the Polymerase Chain Reaction (PCR) or other reactions to produce fragments containing a specific number of nucleotide units that are diagnostic for the targeted genetic disease, person, or pathogen. These fragments are then typically analyzed by slab gel electrophoresis. Mass spectrometry has the potential of characterizing the DNA fragments faster and more confidently than chromatography-based methods

We have evaluated matrix assisted laser desorption (MALDI) time-of-flight (TOF) and electrospray (ES) quadrupole ion trap (QIT) mass spectrometry for the rapid analysis of PCR fragments. Synthetic oligomers and PCR products from human and bacterial genomic DNA were used in these initial studies. The human samples studied represent a mutation, ΔF508, in a gene that involves the cystic fibrosis transmembrane conductance regulator; this mutation is caused by a three base deletion. PCR primers containing 18 bases were prepared that would result in a 75-base fragment for a normal individual and a 72-base fragment for an individual with the 3-base deletion. The bacterial sample was isolated from a region from the gene that codes for 5S rRNA in bacteria of the genus *Legionella*, and the amplified product contained 108 bases

ES spectra of synthetic oligomers and $tRNA^{Phe}$ showed that methanol solutions generally yielded 100 to 1000 fold lower detection limits than aqueous solutions. Removal of alkali metal counter-ions was found to significantly improve sensitivity and resolution of charge states. Figure 1 shows the ES spectra of synthetic 75-base single-stranded oligonucleotides in which alkali counter-ions have been replaced by ammonium ions. Double stranded DNA fragments, which are produced by the PCR amplification, could be analyzed intact by ES.

MALDI spectra, using 3-hydroxypicolinic acid as the matrix, were also obtained on the synthetic 72- and 75-base oligomers, Figure 2. Removal of alkali metal counter ions was also found to be necessary to enhance both sensitivity and resolution. For DNA of this size, oligomers that differed in mass by three bases (approximately 900 Daltons), could be readily distinguished, resolution of single base differences, however, was limited to oligomers containing about 40 bases. Because MALDI sensitivity falls off with mass, it was also necessary to remove the PCR primers. A spectrum of a 75-base PCR product from human genomic DNA (after removal of a majority of the 18-base primers and salt) is shown in Figure 3. We have used similar approaches to detect the 108-base PCR fragment that is diagnostic of the *Legionella* species (not shown)

In general, it was found that both ES and MALDI are capable of analyzing of DNA fragments; however, several areas need to be addressed before either may be used in a routine method.

Both techniques are useful for analysis of DNA fragments containing at least 100 bases at present. To extend this technology to larger PCR fragments, current limitations in mass resolution and mass range need to addressed. As stated previously, both ES and MALDI require removal of cations and primers for optimum detection of the DNA fragments. Finally although detection of low- to sub-picomoles of the DNA fragments is currently achievable, higher sensitivity is desirable to reduce the extent of PCR amplification required for the analysis. We are currently developing approaches to circumvent these limitations, including enhancements in instrument performance, investigation of microsample handling techniques, and development of methods for rapid on-line sample preparation.

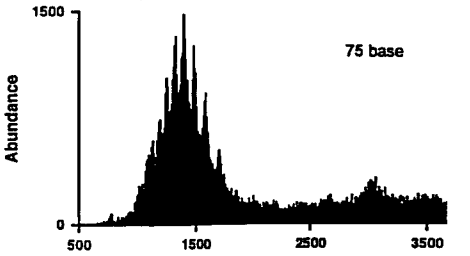

Figure 1. ES QIT negative ion mass spectrum of a synthetic 75-base single strand oligomer

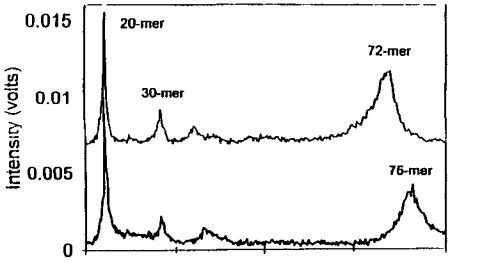

Figure 2. MALDI-TOF negative ion mass spectrum of synthetic 72- and 75-base single strand oligomer; 20- and 30-mer used as mass markers.

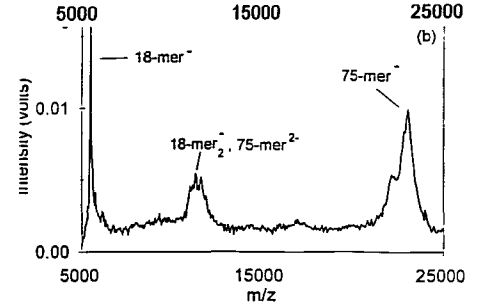

Figure 3. MALDI-TOF negative ion mass spectrum of PCR product of human genomic DNA after removal of salts and PCR primers

Research was supported by the Oak Ridge National Laboratory Director's Research and Development Program, under contract No. DE-AC05-84OR21400 with Martin Marietta Energy Systems, Inc.

THE ANALYSIS OF DNA AND MODIFIED PROTEINS BY EXPLOITING RESOLUTION IMPROVEMENTS IN MALDI-TOF MASS SPECTROMETRY

Steven M. Colby, Randy J. Arnold, Noah P. Christian, Chris T. Houston , and James P. Reilly
Dept. of Chemistry, Indiana University, Bloomington, IN 47405

One of the most time consuming steps of current DNA sequencing methods is the separation of DNA oligomers that have been prepared via the Sanger method[1]. This process is an important part of the Human Genome project which proposes to sequence the entire human genome. Current technology employs gel electrophoresis (PAGE) although other separation methods such as capillary electrophoresis are also being developed. An exciting alternative would be the separation of oligomers by mass spectrometry. This approach could be significantly more rapid than other techniques. A considerable amount of effort has therefore been directed at detecting oligonucleotides via mass spectrometry. Considerable progress has already been made. As pointed out by Tang et. al.[2] there are three principal advances required for DNA sequencing by mass spectrometry: 1. The detection of DNA fragments larger than 300 nucleotides; 2. Femtomole sensitivity for the detection of PCR products; and 3. Sufficient mass spectral resolution to distinguish a 500-mer from a 501-mer. Tang[2] and Bai et. al.[3] have already demonstrated the detection of large oligomers with significant sensitivity using Matrix Assisted Laser Desorption/Ionization and point out that the only element required for mass spectral sequencing of DNA is sufficient mass resolution.

We report the application of a mass resolution enhancement technique to the study of single stranded DNA oligomers ranging in size from 27 to 68 bases. This technique, called Space-Velocity Correlation Focusing, has been previously reported and is further described in another abstract at this conference.[4-6] It reduces the effect of the initial velocity distribution on the peak width of the detected signal. This distribution is one of the major factors affecting mass resolution. Others may include the presence of counter ions, metastable decay, gas phase collisions, and electronic limitations. The reduction of the effect of the initial velocity distribution permits for the first time the careful examination of these other factors. The work reported herein focuses on the study of counter ions in the analysis of DNA oligomers, specifically the use of desalting and ion exchange techniques.

We have explored the use of drop dialysis for the desalting of oligomers as well as the addition of the following salt solutions: ammonium chloride, ammonium citrate, and ammonium acetate. We have also used EDTA buffered with ammonium hydroxide as a chelating agent and examined the effect of aluminum and stainless steel substrates.

The effect of ammonium citrate on DNA mass spectra has been examined previously[7-9]. However, except for very short oligomers[7], the MALDI work was done without sufficient resolution to observe specific counter ions. The changes in peak width that were observed could therefore not be fully characterized. Fig. 1 compares the mass spectra of a 27-mer recorded with and without the addition of ammonium citrate. Counter ions or adducts corresponding to Na (b) , K (c), and Fe (d) are observed. Fig. 2A shows

another example of the effect of ammonium citrate. The counter ion distribution has changed slightly and potassium is now the strongest. This change is simply due to variations in handling of the sample. (The flight times are shifted due to differing operating conditions.) Fig. 2B illustrates the effects of drop dialysis (0.025μm) on the same sample. The signal intensity is dramatically reduced and we would appear to have lost the analyte in the membrane. However, Fig. 2C shows the result of subsequent re-addition of ammonium citrate. The resulting peak intensity is now almost 3 times greater than without membrane treatment. While we were originally concerned only with the cation in the buffer, we have found that the anion is also important. The use of ammonium acetate and chloride each produced progressively worse results. The use of dialysis and ammonium citrate on larger oligomers is shown in Fig. 3. As seen the treatment is less effective with longer polymers. This is to be expected since the number of counter ion sites increases with length. It should be noted that the change in peak width is not due to Space-Velocity Correlation Focusing. We are able to record mass spectra of proteins (trypsinogen) with mass similar to the 68-mer with 12 nanosecond wide peaks[5].

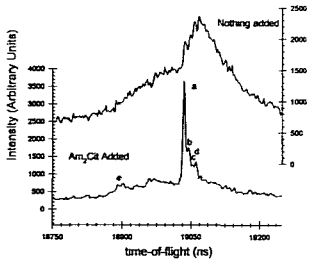

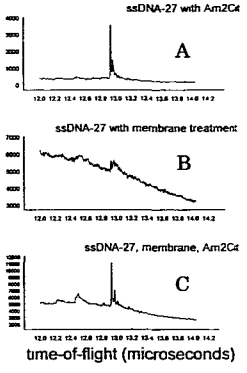

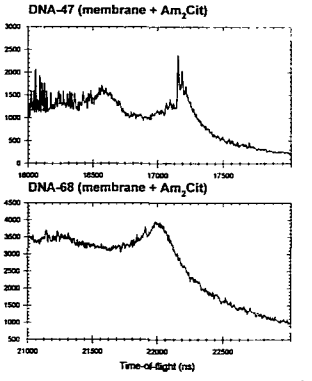

Figure 1 **Figure 2** **Figure 3**

1. F. Sanger, S. Nicklen, and A. R. CoulsonProc. Natl. Acad. Sci. USA 74 (1977) 5463-5467.
2. K. Tang, N I. Taranenko, S. L. Allman, L. Y. Chang, and C. H. Chen; RCMS 8 (1994) 727-730.
3. J. Bai, Y. H. Lin, D. M. Lubman, and D. Siemieniak; Rapid Comm. Mass. Spectro 8 (1994) 687-691
4. S. M. Colby, T. B. King, and J. P. Reilly; Rapid Comm. Mass Spectrom. *8*, (1994) 869-75
5. T. B King, S. M Colby, and J. P. Reilly; Int. J. Mass Spectr. Ion Process. In Press.
6. S. M. Colby and J P. Reilly; "Space-Velocity Correlation Focusing" ASMS 1995, Atlanta,
7. U. Pieles, W. Zurcher, M. Schär, and H. E. Moser; Nucleic Acids Research, 21 (1993) 3191-3196.
8. D. P. Little, T. W Thannhauser, and F. W. McLafferty; Proc. Natl. Acad. Sci. USA 92 (1995) 2318-2322.
9. J. Bai, Y. H. Liu, and D. M. Lubman; Rapid Comm. Mass Spectrom. 8 (1994) 687-691.

Applications of High Resolution MALDI TOF to Oligonucleotide Problems

Peter Juhasz, Marvin Vestal, Ed Takach, Mark Roskey, Igor Smirnoff,
Lawrence Haff and Stephen Martin
PerSeptive Biosystems, Inc., 500 Old Connecticut Path, Framingham, MA 01701

Matrix-assisted laser desorption ionization (MALDI) mass spectrometry has been vigorously explored recently for its potential use in high throughput DNA sequencing. Although speed of analysis is the main appeal of mass spectrometry, there are a number of issues which need to be addressed for mass spectrometry to be competitive with established biochemical methods. Major difficulties in MALDI which have to be overcome are the inherently low sensitivity of oligonucleotide desorption and ionization, and relatively poor mass resolution, in particular in the case of very complex mixtures such as sequencing ladders. Sensitivity of oligo- and polynucleotides to fragmentation is an additional complication rendering accurate molecular weight determination of large polynucleotides very difficult.

By means of a new ion source design considerable improvement of mass resolution has been achieved Inspired by the success of previous research on delayed ion extraction [1], an ion source was constructed utilizing three high voltage sources. In the two-stage ion source an extraction grid had constant electric potential while potential on the sample holder could be rapidly switched between the other two high voltage supplies. Thereby a well controlled extraction pulse could be applied following the ionization event which took place in a nearly field free environment. This ion source was used on two commercially available instruments - 1.3m and 2.1m long - both equipped with a coaxial, single stage reflector.

I. Basic performance. When tuned properly a mass resolution in excess of 1000 was obtained in the linear mode for mixed base oligomers up to 50mer. As a general rule, mass accuracy and sensitivity also increased in proportion with the resolution. Reproducibility of data was improved substantially, and high quality data could be readily generated with 3-hydroxypicolinic acid matrix: a matrix well known for hard to find sweet spots. Figure 1 demonstrates the typical performance on the delayed extraction (DE) linear instrument: a baseline separated pair of synthetic 31mers of different 3' termini but otherwise of identical sequence. C-T substitution corresponds to 15 Da mass difference, and the mass resolution in the figure is around 1,200. Even more dramatic increase in mass resolution was observed in the reflector mode. Figure 2 presents an RNA 12mer with 7500 mass resolution at *m/z* 3839.

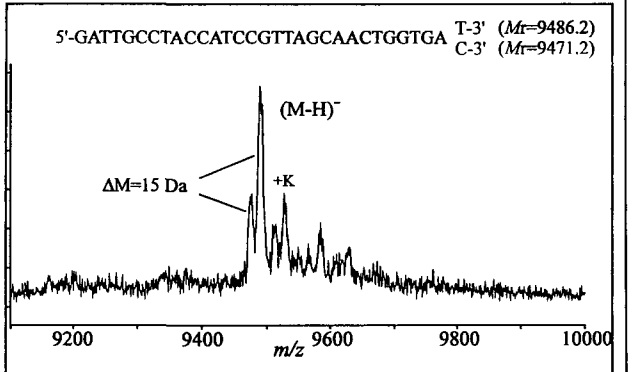

Figure 1 Pair of DNA 31mers differing by 15 Da. Mass resolution is 1200.

II. Sequencing applications. Improved performance by DE was extremely useful in sequencing applications dealing with complex mixtures. Sequence analysis of oligonucleotides up to 31mer was demonstrated based on failure sequences. Fast fragmentation processes were also reported earlier in delayed extraction experiments [1] and an 11mer could be completely sequenced based on its fast fragmentation when proper experimental conditions were used: picolinic acid matrix and 266nm irradiation.

Exonuclease degradation is the to be method of choice for sequencing ssDNA up to the 40mer range. 3'-Phosphodiesterase reactions exhibited more uniform digestion rates than those with 5'-phosphodiesterase. With a simple protocol, combination of the two digests yielded the sequence in less than 10 minutes when using delayed extraction (DE) MALDI with improved mass resolution. The strategy was successfully demonstrated on a 33mer and a 40mer.

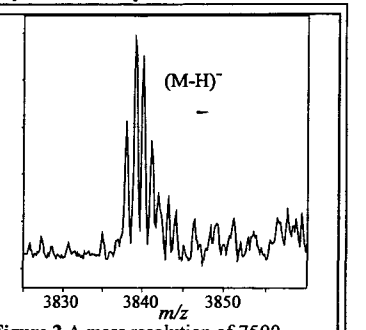

Figure 2 A mass resolution of 7500 observed in the reflector on an RNA 12mer at *m/z* 3839.

The Sanger method is used exclusively for high throughput sequencing of genomic DNA. A sequencing reaction amplified by thermocycling was devised to generate dideoxynucleotide terminated fragments at the 20-100 fmol level on a 40mer and 50mer template. While conventional MALDI failed on these samples, delayed extraction MALDI successfully reproduced almost the complete sequences. Mass spectrum of the "T" reaction of the 40mer is shown in Figure 3. From these applications it was obvious that adequate mass resolution has been obtained leaving sensitivity as the limiting factor for the routine use of mass spectrometry in DNA sequencing

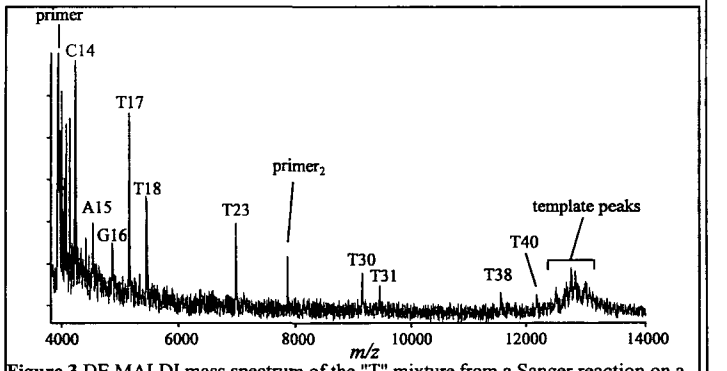

Figure 3 DE MALDI mass spectrum of the "T" mixture from a Sanger reaction on a 40mer template. The components are present at a 20-100 fmol/μL concentration.

References:

1. J. J. Lennon and R. S. Brown in *Proceedings of the 42nd ASMS Conference on Mass Spectrometry and Allied Topics,* May 29 - June 3, 1994, Chicago, IL, p. 501.

Applications of MALDI/TOF in Polymer Chemistry

Paul O. Danis and Francois J. Huby
Research Laboratories, Rohm and Haas Company, Spring House, PA 19477

The application of MALDI to problems in polymer science is growing rapidly.(1-7) With molecular weight measurements as the obvious primary application, other areas where MALDI can play a role is in the structure elucidation of copolymers and the determination of end groups for the elucidation of polymerization mechanisms. Additionally coupling MALDI with a technique such as gel permeation chromatography [GPC] allows one to obtain direct measurement of polymer solution properties. From the comparison of MALDI data with GPC a greater understanding of the capability of both methods can be realized.

While aqueous(1) and non-aqueous(3) polar polymers can be readily analyzed, hydrocarbons are more difficult due to their low matrix solubility and lack of a dipole site for cation attachment. Using the matrix 1,4-di-(2-(5-phenyloxazolyl))benzene [POPOP] with silver acetoacetonate for cationization, polymers of styrene as well as isoprene and butadiene can be analyzed, Figure 1.

From the MALDI of poly(methyl methacrylate) [pMMA] prepared with a di-anion initiator several pathways of initiation are observed. These corresponding to the di-, tri-, and tetra-α-methylstyrene di-anion. It is also shown that the rate of initiation for the tetra- species is slower than that for the di-species.

From well-characterized standards of poly(methyl methacrylate), a comparison of MALDI data to that obtained from gel permeation chromatography, Figure 2, has allowed us to directly determine the band-broadening function of the chromatographic system. This important parameter is usually calculated with an analytical function containing assumptions of its independence on retention time and analyte composition. With MALDI the assumptions are removed and direct measurement is possible. The band broadening function for poly(methyl methacrylate) of 28k, 59k, 127k, and 260k Da is shown if Figure 3, and the lack of mass dependence on this function is obvious.

1. P. O. Danis, D. E. Karr, F. Mayer, A. Holle, C. H. Watson, *Org. Mass Spectrom.* 1992, *27*, 843.
2. U. Bahr, A. Deppe, M. Karas, F. Hillenkamp, U. Giessmann, *Anal. Chem.* 1992, *64*, 2866.
3. P. O. Danis and D. E. Karr, *Org. Mass Spectrom.* 1993, *28*, 923.
4. H.S. Creel ,*Trends Polymer Sci.* 1993, *1*, 336.
5. R. Abate, A. Ballistreri, G. Montaudo, D. Garozzo, G. Impallomeni, G. Critchley, K. Tanaka, *Rapid Comm. Mass Spectrom.* 1993, *7*, 1033.
6. H.M. Burger, H.-M. Muller, D. Seebach, K.O. Bornsen, M. Schar, H.M. Widmer, *Macromolecules*, 1993, *26*, 4783.
7. P. O. Danis, D. E. Karr, W. J. Simonsick, and D. T. Wu, *Macromolecules* 1995, *28*, 1229-1232.

43rd ASMS Conference on Mass Spectrometry and Allied Topics

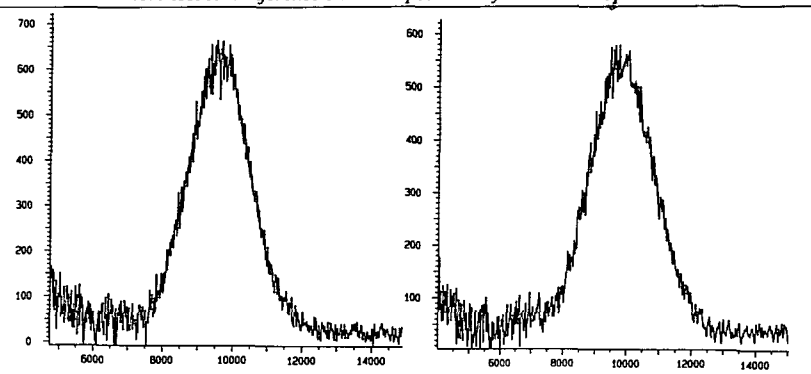

Figure 1. The MALDI/TOF mass spectra of polybutadiene 10k Da (left) and polyisoprene 11k obtained with POPOP matrix and silver acetoacetonate.

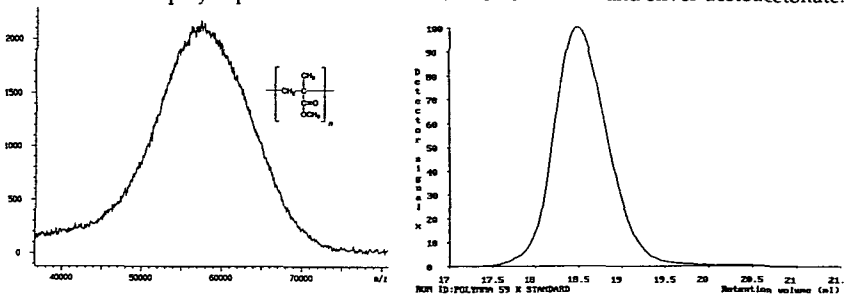

Figure 2. The MALDI/TOF mass spectrum (*t*-3-indoleacrylic acid matrix) and GPC (refractive index detection) trace of poly(methyl methacrylate) 59k Da.

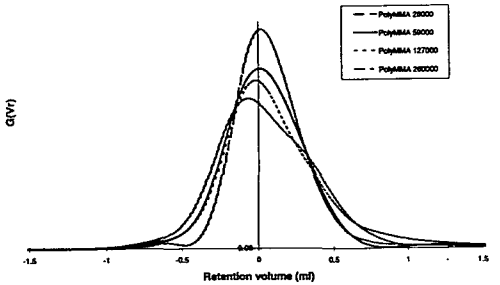

Figure 3. The band broadening functions determined for pMMA 28k, 59k, 127k, and 260k Da.

Polymer Characterization: A Comparison of MALDI vs Direct Laser Desorption

David A. Weil* and Cliffton B. Jacoby, 3M Company, St. Paul, MN 55144-1000

The characterization of high-mass polymers by MALDI have generally been from single component samples with narrow molecular weight distributions, and not from synthetic polymers routinely encountered in industry. A problem encountered in MALDI of high-mass, polydispersive polymers, is that the ion current is spread over a wide mass range, where as proteins have their ion current concentrated in a narrow mass range. Unlike reference standards, synthetic polymers encountered in industry are often mixtures of various molecular-weight distributions, monomers, initiators and end-cappers. At 3M we've found that present expectations are much higher than routine performance. The limitations in sample preparations, instrumentation, software and the fundamentals of MALDI-TOF may limit the practical application of MALDI to polymers with M_w < 50K Daltons. Both MALDI/TOF and LD/FTMS are extremely useful in characterizing low-molecular weight polymers, surfactants and oligomers. A comparison of the techniques was completed to determine the current strengths and weaknesses of the ionization methods and mass spectrometers. We have also compared the performance of MALDI/TOF and MALDI /FTMS systems.

The direct laser desorption ionization experiments were performed by using a pulsed high-powered CO_2 laser, at 10.6 micron, coupled to an EXTREL FTMS 3.0T, dual-cell system. Additional FTMS experiments were completed by using a similar system equipped with the nitrogen laser interface. The MALDI-TOF experiments were completed by using a Fisons TOFSPEC or TOFSPEC E systems, that utilize a pulsed N_2 laser. Standard sample preparation methods were utilized for the comparison.

In general, the strengths of MALDI/TOF are the ease-of-use, simple design, and wide mass range; while the weaknesses are the sample preparation, low-resolving power and high-chemical background at low mass. The strengths of LD/FTMS are high-resolving power, high mass accuracy, and ion manipulation methods; while the weaknesses are the space-charge effects, mass range limitations and more complex instrument design. The performance of the TOF mass spectrometer (dynamic range, mass resolution, detector type) in reflectron and linear mode may inhibit the identification of low-level components present in oligomer mixtures. In comparison, the high-resolution Fourier transform mass spectrometer can identify these low-level components, at the expense of mass range

MALDI has been shown to be a rapid and routine method for characterizing low-molecular weight polyethylene and polypropylene oxides in polymer extracts. With just a few micoliters of a solution of the polymer extract (even from an NMR sample tube), both the average molecular weight and the chemical composition information can be obtained within a few minutes from an extract. The MALDI/TOF mass spectrum (Figure 1) shows the presence of four different polymers. In LD/FTMS, one can detect low-mass fragment ions indicative of the initiator and monomer. While in MALDI, the chemical background from the matrix may inhibit the detection of these fragments.

The strengths and weakness of MALDI/TOF and LD/FTMS are illustrated in the characterization of modified polydimethyl siloxanes oligomers which contain end groups that vary by one mass unit and have overlapping isotope patterns. The broad mass-range capabilities of MALDI/TOF easily provide absolute M_w values (Figure 2), but the low resolving power inhibit determination of diamine and dibutyl levels from the isotope patterns. In comparison, the high-resolving power capabilities of LD/FTMS were used to determine the percent of monoamine, diamine and dialkyl end groups present (Figure 3). The mass spectral data was important since the proton NMR data can tell the ratio of the amine and the alkyl end groups, but not the amount of the dialkyl or

diamine groups. The LD/FTMS mass spectra also showed evidence for variations in the oligomerization process of these modified polydimethylsiloxanes (Figure 4).

Figure 1. MALDI mass spectrum of a polymer extract showing the detection of four different PEO and PPO polymers.

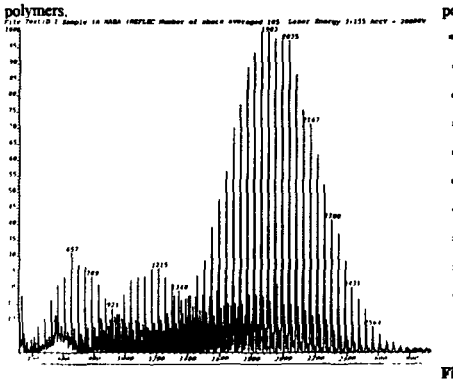

Figure 2. MALDI mass spectrum of a modified polydimethyl siloxane polymer with differing end groups. The low resolving power of MALDI/TOF makes end group polymers

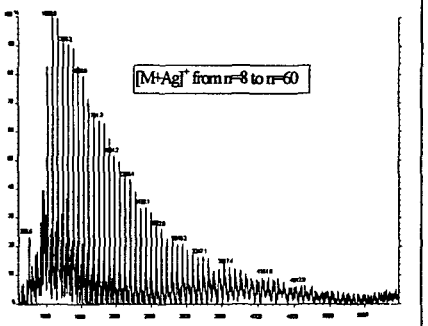

Figure 3. A narrow portion of the LD/FTMS mass spectra of a modified polydimethyl siloxane. The relative amounts of the different end groups can be estimated from the isotope ratios.

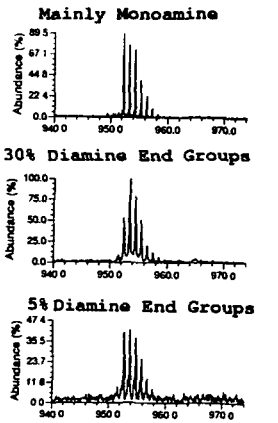

Figure 4. LD/FTMS mass spectra showing the characteristic differences in oligomerization processes of polydimethylsiloxanes

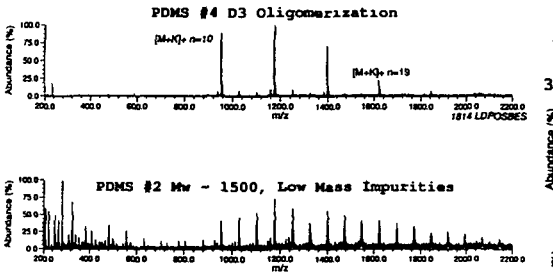

In summary, both MALDI and direct laser desorption ionization techniques are useful, routine and rapid methods for characterizing low-molecular weight oligomers and surfactants. The high-mass expectations of polymer chemists overshadow the current capabilities of the techniques. More research into sample preparation, mechanisms, and improvements in MALDI/TOF systems are needed to make MALDI a routine analytical tool for polymer characterization.

CHEMICAL REACTIONS VS. CID TO CLEAVE AMIDE BONDS

Tracie L. Williams, James L. Stephenson, and Richard A. Yost
Department of Chemistry, University of Florida, Gainesville, Florida

The structural analysis of biological molecules by tandem mass spectrometry has relied primarily on collision-induced dissociation (CID), in which precursor ions undergo low-energy collisions with a neutral target gas. This technique, however, suffers as the m/z of singly charged ions increases due to the limited energy available in center-of-mass coordinates. Therefore, collisions with low mass collision gas is unable to deposit sufficient internal energy to cause fragmentation. An attractive alternative to CID would be the use of a chemical reagent which would drive an exothermic bimolecular reaction to cleave selected bonds to form fragments bearing structural information specific to both the analyte and the reagent used. Cheng and coworkers have shown in a flowing-afterglow study that S-ethyl trifluorothioacetate and hexafluorobenzene react with deprotonated anions of model amide compounds to cleave the carbonyl-nitrogen bond (1). This reaction scheme is shown in Figure 1. In work to be presented, we investigate the feasibility of using these chemical reagents to selectively cleave the amide bond of peptides.

Figure 1

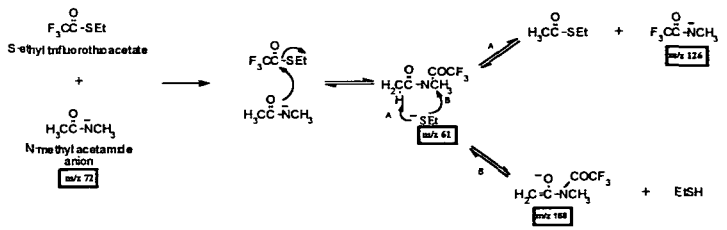

All experiments were performed on a quadrupole ion trap. The rationale for using this instrument is its ability to mass-select the ion of interest and its capability of controlling ion/molecule reactions by varying the storage time. In addition, MALDI and electrospray ionization sources can be interfaced with the ion trap. In our preliminary studies, negative chemical ionization in the trap was used to ionize small model amide compounds. An electrospray/ion trap instrument was then utilized to extend the reactions to small peptides.

NEGATIVE CHEMICAL IONIZATION

The negative CI experiment involves the use of the hydroxide ion from water as the reagent ion. The hydroxide ion abstracts a proton from the neutral amide molecule generating the $[M-H]^-$ ion. This ion is mass isolated and allowed to react with the neutral reagent which is introduced through a pulsed valve

mounted within the vacuum manifold. A negative DC voltage is placed on the endcaps of the ion trap in order to operate outside the stability region of positive ions (2). This eliminates the possibility of ion-ion recombination which would occur if the trap were operated in its normal mode in which both positive and negative ions are stable and efficiently stored. The spectra illustrating the sequential steps for the reaction between S-ethyl trifluorothioacetate and $[M-H]^-$ ion of N-methyl acetamide are shown in Figure 2.

ELECTROSPRAY IONIZATION

In order to extend these studies to peptides, it is necessary to use an ionization technique suitable for labile molecules. However, forming the anion of the peptide in which the negative charge is present on the amide group poses a problem. Instead, the most likely site of deprotonation is the terminal carboxylic acid or side chain of an acidic amino acid. If the reaction of the anion formed from an underivatized peptide is allowed to react with S-ethyl trifluorothioacetate, the product ion is that shown in Figure 3. Derivatization of the acidic groups with tert-butyl ester will protect these acidic functionalities, but the ability to subsequently deprotonate the amide group by electrospray has yet to be demonstrated.

Figure 2

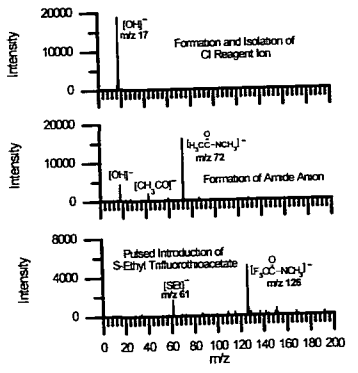

Figure 3

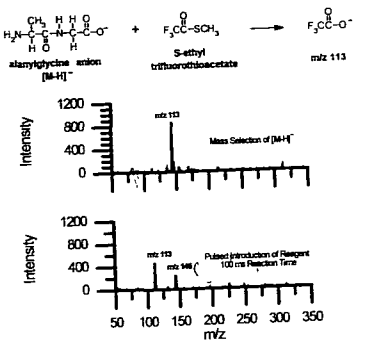

(1) Cheng, X. and Grabowski, J. J. *Proceedings from the 39th ASMS Conference on Mass Spectrometry and Allied Topics*, 1991, 477-478.
(2) Berberich, D.W. and Yost, R.A., *JASMS*, 1994, 757-764.

Neutral Products From Ion-Molecule Reactions: F^- + 5-Chloro-1,3-Pentadiene

Michael Baschky and Steven Kass
Department of Chemistry
University of Minnesota, Minneapolis, MN 55455

Ion-molecule reactions generate new ionic species which are readily detected with mass spectrometers. The neutral byproducts, however, often contain the information of interest, but they are much more difficult to identify. In this paper we describe how these compounds formed in a flowing afterglow device can be collected and identified.

Cyclohexyl isocyanate reacts readily with fluoride to afford isocyanate ion (eq 1). Analysis of the neutral products from this reaction reveals that cyclohexene is formed and that cyclohexyl fluoride is not observed (i.e. elimination is favored over substitution).

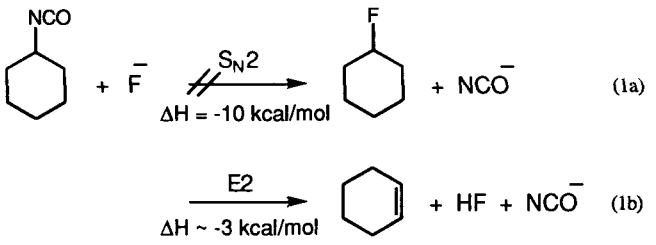

(1a)

(1b)

5-Chloro-1,3-pentadiene reacts with fluoride at the collision controlled rate to afford chloride ion (eq 2). Several different reaction channels can readily be envisioned to be responsible for the formation of the chloride ion. Identification of the neutral products from this reaction indicates that all three pathways (i.e. S_N2, S_N2', and E2) take place, and that $S_N2 > S_N2' > E2$. Molecular orbital calculations (Table 1) are consistent with this observation. They also reveal that the double bond does not activate the nucleophilic substitution reaction, and that it has a flexible orientation (i.e. conjugation of the double bond with the incipient p-orbital of the carbon atom bearing the leaving group is unimportant in contrast to conventional

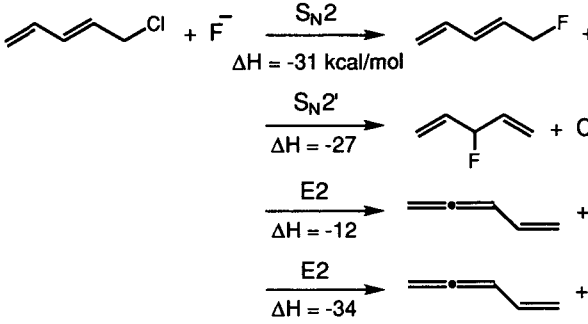

(2a)

(2b)

(2c)

(2d)

wisdom based upon liquid phase studies).

Table 1. Calculated barriers for nucleophilic substitution reactions.[a]

substrate	HF	MP2
C_3H_5Cl	-10.8	-6.4
CH_3Cl	-11.5	-7.8
CH_3CH_2Cl	-10.5	-4.8
anti-$CH_3CH_2CH_2Cl$	-7.9	-2.6
gauche-$CH_3CH_2CH_2Cl$	-11.4	-6.5
$CH_3CHClCH_3$	-10.6	-3.1

[a]All values are given in kcal/mol, and most of the data comes from S. Gronert, *J. Am. Chem. Soc.* **1991**, *113*, 6041 and **1993**, *115*, 652.

Ion-molecule Reactions of Trimethylenemethane Radical Cations

Phillip K. Chou[1], Sherry L. Painter[2], Silas C. Blackstock[2], and Hilkka L. Kenttämaa[1]

[1]Department of Chemistry, Purdue University, 1393 BRWN Building, West Lafayette, IN 47907-1393. [2]Department of Chemistry, Vanderbilt University, Nashville, TN 37235.

Radical cations that have charge and radical sites separated by one or more atoms are defined as distonic ions. Utilizing an Extrel Model 2001 Fourier transform ion cyclotron resonance mass spectrometer, studies were carried out on an unusual class of distonic ions (**1-3**) possessing the trimethylenemethane radical cation ($TMM^{+\bullet}$) structure.

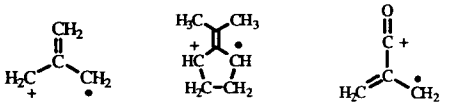

1 **2** **3**

These ions are unique in that both the radical and charge sites are potentially delocalized throughout the ion. Electron impact ionization of methylenecyclopropane (MCP) produces an ion corresponding to the molecular formula of $TMM^{+\bullet}$ (**1**), $C_4H_6^{+\bullet}$. Recombination energy (RE) bracketing experiments indicated that $RE(C_4H_6^{+\bullet})=9.3 \pm 0.1$ eV. In comparison, the ionization energy (IE) of MCP was bracketed to be 9.4 ± 0.1 eV. These results suggest that most of the $C_4H_6^{+\bullet}$ ions generated from MCP have a cyclic structure. The $C_4H_6^{+\bullet}$ ions react with CH_3SSCH_3, $CH_3SeSeCH_3$, and benzeneselenol to yield abundant charge exchange products. However, a small amount of radical abstraction products were also observed in each case. This suggests that the $C_4H_6^{+\bullet}$ ions consist of a mixture of ionized MCP and $TMM^{+\bullet}$.

A cyclic derivative of $TMM^{+\bullet}$, the radical cation of isopropylidenecyclopentan-1,3-diyl ($IPC^{+\bullet}$, **2**) was generated from the fragmentation of an azo precursor (eq 1). In contrast to $TMM^{+\bullet}$, $IPC^{+\bullet}$ does not react with CH_3SSCH_3 and benzeneselenol. The RE of $IPC^{+\bullet}$ was

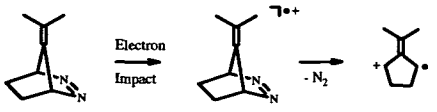

(1)

bracketed to be 7.8 ± 0.3 eV. This is consistent with the expected RE for $TMM^{+\bullet}$-type radical cations.

Dimethyleneketene radical cation ($DMK^{+\bullet}$, **3**) was formed from the fragmentation of α-methylene-γ-butyrolactone. The reactivity of $DMK^{+\bullet}$ was consistent with that of a distonic species; radical abstraction reactions were observed with CH_3SSCH_3, $CH_3SeSeCH_3$, and benzeneselenol. These reactions are very efficient, $Eff.(CH_3SSCH_3)=0.61$, $Eff.(CH_3SSCH_3)=1$, Eff.(benzeneselenol)=1, which is likely due to a mechanism that involves charge catalysis. Molecular orbital calculations (BVWN5/6-31G*//BVWN5/6-31G*) indicate that in $DMK^{+\bullet}$ the unpaired electron is delocalized over the allylic carbon atoms while the charge is localized on the carbonyl carbon. Clearly, delocalization of the radical does not diminish ion reactivity. The $DMK^{+\bullet}$ ion also displays unique reactive behavior in that it can undergo sequential abstraction of up to three $CH_3S^{\bullet}$ groups during reactions with CH_3SSCH_3 (Scheme 1).

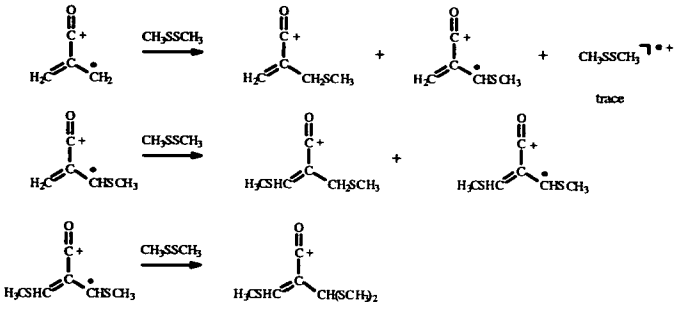

Scheme 1

Reactions of Small Carbon Cluster Ions with Nitrogen Containing Compounds

Robert C. Dunbar and Boguslav P. Pozniak
Chemistry Department, Case Western Reserve University, Cleveland, OH 44106

Introduction

Reactions of carbon cluster cations in the range C_{10}^+ to C_{24}^+ were studied,

$$C_n^+ + M \rightarrow C_n^+ \cdot M \; [\rightarrow \text{Fragmentation products}]$$

These cluster ions are believed to be monocyclic, and could be expected to obey Huckel-type aromaticity rules Previous work has showed striking cluster-number selectivity and aromaticity effects in reactions with benzene[1], and in some partial reaction series with acrylonitrile[2] and crotononitrile[3]. A more extensive set of nitrogen-containing substrates was examined here, using the complete series of cluster ions.

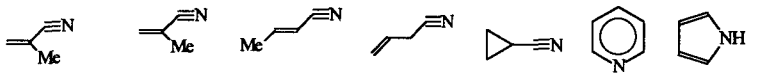

Acrylonitrile ACN | Methacrylonitrile MeCN | Crotonitrile CRN | Allyl cyanide ALC | Cyclopropyl cyanide CCN | Pyridine | Pyrrole

Experimental

Ions were produced by laser desorption/ionization of graphite at 532 nm, and trapped in the FT-ICR cell (Fig 1). Fig 2 shows a typical cluster ion production spectrum. After isolation of the desired cluster ion by rf ejection pulses, the reactions were followed by FT-ICR detection Pressures ranged from 1-100 x 10^{-8} Torr. Early in the reaction period ions had excess kinetic and internal energy ("hot ions"), while later, after 5-10 ion-neutral collisions, the ions were presumed to be thermalized Reaction rates and products were different in these two time regimes, and were recorded separately

Results

In most cases, the only reaction of thermalized cluster ions was simple association with neutral Exceptions were C_{10}^+, C_{12}^+ and C_{14}^+reacting with ALC and CRN, which gave some fragmentation products. Figs. 3 and 4 show the rate constants. Hot ions showed a wide variety of fragmentation products, and a greatly reduced association channel. CID of C_{11}^+ C_4H_5N and C_{15}^+ C_4H_5N gave only regeneration of the carbon cluster ion.

Discussion

Aromaticity effects. For the nitrile substrates, strongly enhanced reactivity is seen for the antiaromatic series of ions C_{13}^+, C_{17}^+, C_{21}^+ (Fig 3). This extends the previous observation of antiaromaticity enhancement of reactivity seen for benzene.[1] Enhanced ion production was seen for the aromatic series C_{11}^+, C_{15}^+, C_{19}^+, C_{23}^+ (Fig 2).

Mechanism. For thermal ions, the rate-limiting process is believed to be association to form an electrostatically bound complex, while rearrangements, insertions and fragmentation channels open up for hot ions. Supporting the complex-formation mechanism are (1) the fact that all the C_4H_5N isomers react at similar rates, (2) the tenfold lower reactivity of C_3H_3N than C_4H_5N, and (3) the CID results suggesting retention of carbon cluster ion identity in the complex. Pyrrole and pyridine showed fast reactions and little selectivity, and a different mechanism is believed to govern these kinetics.

Conclusions

Very large selectivity of reaction rates was observed depending on the size of the cluster ion, but little selectivity based on neutral substrate isomeric form. The selectivity strongly supports the hypothesis of aromaticity effects in carbon cluster ions, and reactivity enhancement for the antiaromatic cluster ions

References

1. Pozniak, B. and Dunbar, R. C , J. Am. Chem. Soc., 116, 4113 (1994).
2. Sun, J., Grutzmacher, H. F and Lifshitz, C , J. Am. Chem. Soc 115, 8382 (1993).
3. Sun, J., Grutzmacher, H F. and Lifshitz, C., J. Phys. Chem. 98, 4536 (1994).

Figure 1

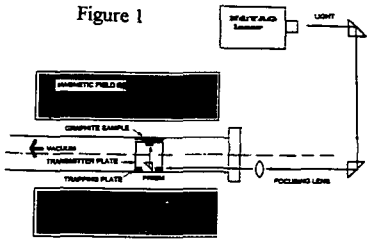

Figure 2

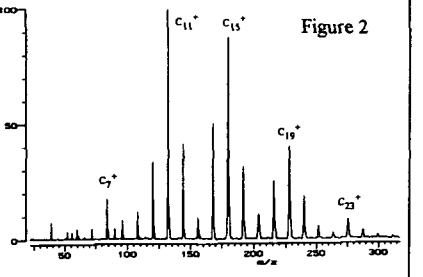

Figure 3

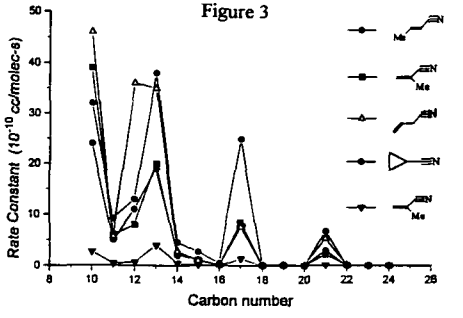

Figure 4

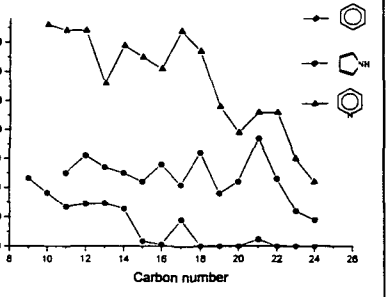

ION-MOLECULE REACTIONS OF 18-CROWN-6 WITH ITS FRAGMENT IONS

Nanzhu Shen, Chadin Dejsupa, Marshall Pope, and David V. Dearden
Brigham Young University, Department of Chemistry, Provo, Utah 84602

Introduction

The mass spectrum of the macrocyclic ligand 18-crown-6 is well-known.[1-3] Under 70 eV EI, the protonated molecular ion M+1 peak (m/z 265) is not observed, while under more gentle conditions such as NH_3 CI or ESI it is prominent. The remainder of the spectrum is dominated by fragment ions characterized by losses of $(C_2H_4O)_n$ from the protonated parent. Notably, the loss of C_2H_4O to yield m/z 221 is not observed, consistent with losses of neutral *p*-dioxane.[4] This pattern of fragmentation results in fragment ions which are isobaric with protonated molecular ions of smaller members of the simple crown ether family, such as 12-crown-4 (m/z 177), 9-crown-3 (m/z 133), and *p*-dioxane (m/z 88). Our interest in 18-crown-6 stems from our use of proton attachment kinetics to measure the pressure of the neutral ligand. In this paper we probe some of the chemistry of 18-crown-6 chemical ionization, both using ammonia as a reagent and using "self-CI."

Experimental

All experiments were performed in a Fourier transform ion cyclotron resonance mass spectrometer (model APEX 47e, Bruker Instruments) equipped with an ion source external to the high-field region of a 4.7-Tesla superconducting magnet. EI, CI, and ESI were all performed with ion sources provided by the manufacturer, and which are readily interchangable. Electrostatic focusing and injection techniques were used to transfer ions from the source to the field-corrected ("Infinity") trapping cell of the instrument. Ion-molecule kinetics experiments were performed using ions isolated using conventional FTICR techniques (chirp and shot ejection of unwanted ions). Studies of the reactivity of m/z 177 also involved extensive collisional cooling by pulsing 10^{-5} mbar Ar into the trapping cell immediately after ion injection, followed by 90 sec cooling / pumpdown delay prior to isolation. Neutral pressures were measured using a magnetically-shielded ionization gauge (Balzers).

Results and Discussion

The molecule is surprisingly fragile. Reaction of NH_4^+ with 18-crown-6 gives extensive fragmentation, even though the proton affinity of 18-crown-6 is only 26 kcal mol^{-1} greater than that of NH_3.[5] The most prominent ion initially is a fragment at m/z 89, but fragments at m/z 133 and 177 are also produced. All eventually decay so at long reaction times the protonated molecular ion dominates. A small amount of 18-crown-6•NH_4^+ adduct also forms.

The pattern in self-CI is similar, but with some intriguing twists. The m/z 133 fragment reacts with the parent neutral to yield m/z 45, 89, 177, and, eventually, 265. Similarly, m/z 177 reacts with 18-crown-6 yielding m/z 45, 89, 133, and 265 (Figure 1). No adduction is evident in the reactions of either m/z 133 or m/z 177. Closer examination of the decay of these fragment ions shows that neither can be described by simple exponentials. A double exponential fits the decay of m/z 133 reasonably well, but fails to fit the decay of m/z 177. This suggests two or more isobaric ions at m/z 133, and three or more at m/z 177.

The observation of both smaller and larger fragment ions, as well as the inability to fit the decay curves using single exponentials, suggest that reactions of m/z 133 result in products at m/z 133, and that reactions of m/z 177 yield products at m/z 177. Since 18-crown-6 is a stable molecule, it follows that the structures of the isobaric reactant and product ions must differ.

We will focus on the m/z 177 fragment. It has generally been assumed that this fragment is protonated 12-crown-4. Is this really so? Collision-induced dissociation of the m/z 177 fragment, generated using 70 eV EI, NH_3 CI, and ESI from 49:49:2 methanol:water:trifluoroacetic acid, are similar. When EI is used to generate it, m/z 177 fragments to yield m/z 89, 45, and 40. From CI-generated m/z 177, only the m/z

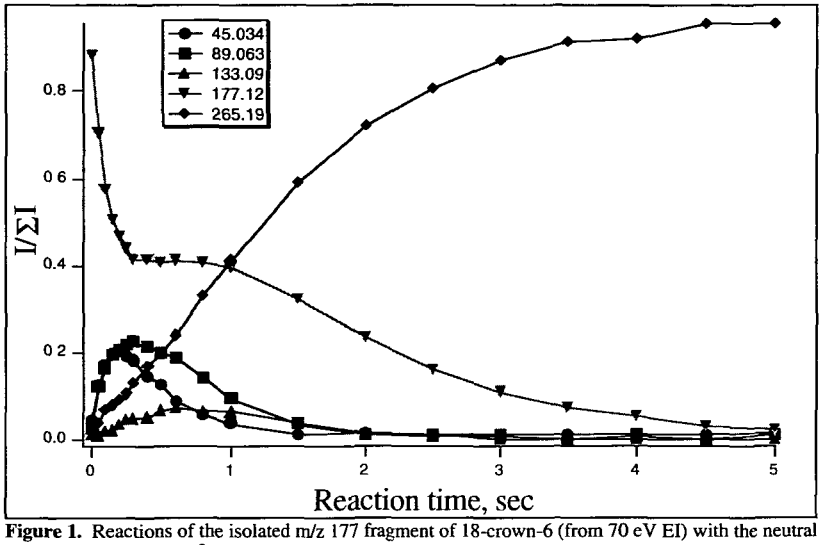

Figure 1. Reactions of the isolated m/z 177 fragment of 18-crown-6 (from 70 eV EI) with the neutral parent. $P_{18C6} = 5 \times 10^{-8}$ mbar.

89 fragment is seen, while the ESI-generated m/z 177 yields both 89 and 45. Thus, the CID spectra suggest that the three ionization methods produce ions which are energetically or structurally different.

Reactivity can be a sensitive probe of ion structural differences. We investigated the chemistry of protonated 12-crown-4, generated by electrospray from 49:49:2 methanol:water:acetic acid, with NH_3. In all of these experiments, $P_{NH_3} = 5 \times 10^{-8}$ mbar. The only observed reaction was formation of a 12-crown-4•NH_4^+ adduct at m/z 194; no proton transfer was observed, consistent with the fact that the proton affinity of NH_3 is 17 kcal mol^{-1} less than that of 12-crown-4.[6] (Similarly, the acyclic analog of 12-crown-4, triglyme, reacts exclusively by adduct formation.) EI-generated m/z 177, on the other hand, reacts primarily by proton transfer, with a very slow reaction to yield adducts. CI-generated m/z 177 also proton transfers to ammonia, but adducts were not observed. The ESI-generated fragment ion is unreactive even after 120 sec.

The structure of the m/z 177 fragment ion is still not known, but it is clearly *not* protonated 12-crown-4, and its reaction kinetics suggest ions of two or perhaps three different structures are present. Further interpretation awaits investigation of possible structures using theory.

We are grateful for support of this work by NSF, PRF, and Alcon Laboratories.

References

(1) Van Gaever, F.; Van de Sande, C. C.; Bucquoye, M.; Goethals, E. J. *Org. Mass Spectrom.* **1978**, *13*, 486-488.
(2) Johnstone, R. A. W.; Rose, M. E. *J. Chem. Soc., Chem. Commun.* **1983**, 1268-1270.
(3) Lee, Y. C.; Popov, A. I.; Allison, J. *Int. J. Mass Spectrom. Ion Phys.* **1983**, *51*, 267-277.
(4) Selby, T. L.; Wesdemiotis, C.; Lattimer, R. P. *J. Am. Soc. Mass Spectrom.* **1994**, *5*, 1081-1092.
(5) In NIST Positive Ion Energetics Database: Gaithersburg, MD, 1990.
(6) Sharma, R. B.; Blades, A. T.; Kebarle, P. *J. Am. Chem. Soc.* **1984**, *106*, 510-516.

Structural Rearrangements and Reactions of the Trimethylene Sulfide Dimer Radical Cation. An Experimental and Theoretical Study

Michael Peschke, Michael L. McKee and Andreas J. Illies
Department of Chemistry
Auburn University

Abstract:

An experimental and computational study of the ion-molecule reactions of the trimethylene sulfide dimer radical cation, formed from the monomer and its monomer cation, has been carried out. The experiments were done mainly in a hybrid drift tube / ion source under chemical ionization conditions. MS/MS experiments were also done in a modified VG ZAB-1F mass spectrometer. The most abundant species under virtually all conditions is m/z 106 $S_2C_3H_6^+$. Computations suggest a cyclic structure with the sulfur inserted into the ring rather than an exocyclic sulfur attached to the trimethylene sulfide ring or an open chain. This is analogous to an earlier study of thiirane in which m/z 92 $S_2C_2H_4^+$, m/z 124 $S_3C_2H_4^+$, and m/z 156 $S_4C_2H_4^+$ were observed in the mass spectra. Those masses were attributed to sulfur insertion into one of the rings of the thiirane dimer parent cluster and subsequent ejection of ethylene followed by further ring expansion up to the six membered ring. In the present case, computations indicate a mechanism in which the trimethylene sulfide dimer cation undergoes several rearrangements resulting in sulfur insertion into the trimethylene sulfide ring. After a few more steps, including two hydrogen transfers, propylene is ejected. All of the intermediates and transition states are exothermic with respect to the monomer plus monomer cation (Figure 1). In addition, computations indicate a very stable eight-

membered ring, 1,5-dithiacyclooctane radical cation, as an intermediate which has the same mass as the dimer, m/z 148. MS/MS results support the presence of 1,5-dithiacyclooctane radical cation as well as the hydrogen transfer steps in the dimer rearrangement. Further ring expansion, analogous to the thiirane case, is not observed. Computationally, it is found that the six-membered ring $S_3C_3H_6^+$ plus propylene is endothermic with respect to m/z 106 cation plus trimethylene sulfide monomer neutral, explaining the end of the ring expansion with the five-membered ring.

Figure 1:

Trimethylene Sulfide Dimer Cation Reaction Surface at the PMP2/6-31G(d)//HF/6-31G(d) + 0.9ZPC level

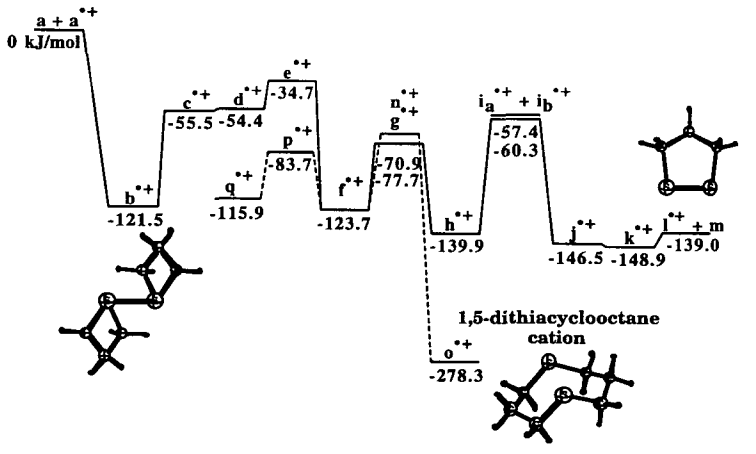

Ion Molecule Reactions of Organophosphorus Compounds

Michael W. Wensing, Brad E. Forch, Robert A. Fifer
U.S. Army Research Lab, Aberdeen Proving Ground, MD 21005
A. P. Snyder and C. S. Harden
U.S. Army, Edgewood Research, Development and Engineering Center
Aberdeen Proving Ground, MD 21010

Organophosphorus compounds (OPCs) have many important commercial applications: in plasticizers, pharmaceuticals, nerve gas agents, and pesticides. Their detection and differentiation is becoming of great commercial importance.

Sensitive detection of OPCs is achieved by atmospheric pressure chemical ionization triple quadrupole mass spectrometry (APCI-TQMS) due to the high proton affinities associated with these compounds. Characterization of the dissociation pathways of these compounds can result in selective detection schemes, and ion molecule reactions may be used to differentiate the dissociation pathways of different organophosphorus compounds. It has been observed that selected product ions produced from the dissociation of phosphonate and phosphate parent ions are subject to nucleophilic attack, while no product ions of phosphites are subject to nucleophilic attack. Ion molecule reactions may therefore be used to distinguish certain classes of compounds. In addition, these ion molecule reactions may be to differentiate isobaric daughter ions produced in the the dissociation of phosphonate, phosphate, and phosphite compounds. This work focused on characterizing different classes of compounds based on the interaction of their daughter ions with water.

The compounds analyzed included dimethyl methyl phosphonate (DMMP), diethyl ethyl phosphonate (DEEP), diethyl methyl phosphonate (DEMP), diethyl propyl phosphonate (DEPP), diethyl butyl phosphonate (DEBP), diisopropyl methyl phosphonate (DIMP), trimethyl phosphate (TMP), triethyl phosphate (TEP), tripropyl phosphate (TPP), tributyl phosphate (TBP), trimethyl phosphite (TMPI) and dimethyl phosphite (DMPI).

Neat samples were introduced by headspace analysis, protonated via a corona discharge, and travelled through a 2 mm orifice, N_2 curtain gas, a smaller 0.1 mm orifice, and into the high vacuum of the triple quadrupole mass spectrometer. Parent ions were selected with Q1, and product ions were detected with Q3. Collisions between water molecules and the product ions occured in Q2. The intensity of the product ions were monitored at increasing Ar pressures in the collision cell. The water was present as an impurity in the UHP 99.999% Ar gas. As the CAD gas thickness increased the amount of H_2O increased as well as the amount of product ions.

Selected phosphonate and phosphate product ions both show a great tendency to form water adducts. Phosphonate product ions form water adducts more extensively, phosphate product ions form water adducts less extensively. The phosphite product ions analyzed do not form water adducts. From the results obtained it appears that quadvalent phosphonate and phosphate ions react with water extensively. Product ions that have a lone electron pair on the phosphorus atom do not form water adducts.

43rd ASMS Conference on Mass Spectrometry and Allied Topics

Vibrational-energy dependence of the reactions of N_2^+ with Ar, Kr, O_2 and H_2 at thermal energies

Joost A. de Gouw, Li Ning Ding, Shuji Kato, Veronica M. Bierbaum and Stephen R. Leone

JILA, National Institute of Standards and Technology and University of Colorado, Department of Chemistry and Biochemistry, University of Colorado, Boulder, Colorado 80309-0440

In the study of ion-molecule reactions much attention has been paid in recent years to the role of the initial state of the molecular ions. Depending on the vibrational or electronic excitation of the ion, the reaction rate constants may vary considerably.

The apparatus used to study these processes consists of a selected-ion flow tube (SIFT) combined with either laser-induced fluorescence detection of the molecular ions, or mass spectrometric analysis of the reactant and product ions[1]. The quadrupole mass spectrometer identifies the reaction pathways, and the LIF technique provides a state-selective measurement of rate constants at thermal energies.

In reactions between $N_2^+(v)$ and Ar or Kr the charge transfer,

$$N_2^+(v) + \mathrm{Ar\ (or\ Kr)} \longrightarrow N_2 + Ar^+\ (\mathrm{or}\ Kr^+), \qquad (1)$$

is the most important channel[2] The rate constants measured for reaction (1) are shown in Fig. 1a. Charge transfer between $N_2^+(v)$ and Ar is endothermic for $v = 0$, but becomes exothermic for $v = 1$, which explains the increase of the rate constant by two orders of magnitude. Although charge transfer between $N_2^+(v)$ and Kr is exothermic for all v, the rate constant increases, though more gradually, by a factor of 100 in going from $v = 0$ to $v = 4$. These observations can be explained qualitatively by considering the Franck-Condon overlap and the energy difference between the possible initial and final states, but the calculations give no quantitative agreement.

In the $N_2^+(v) + O_2$ system both charge transfer and the vibrational deactivation process,

$$N_2^+(v) + O_2 \longrightarrow N_2^+(v') + O_2 \qquad \text{with } v' < v, \qquad (2)$$

are important reaction channels[3]. The rate constants for reaction (2) even exceed the charge-transfer rates. Unlike rare gas atoms a diatomic molecule can easily absorb the vibrational energy of N_2^+, especially if the vibrational frequencies of the ion and the molecule are similar.

In the $N_2^+(v) + H_2$ reaction the dominant channel is the transfer of a hydrogen atom[4]:

$$N_2^+(v) + H_2 \longrightarrow N_2H^+ + H. \qquad (3)$$

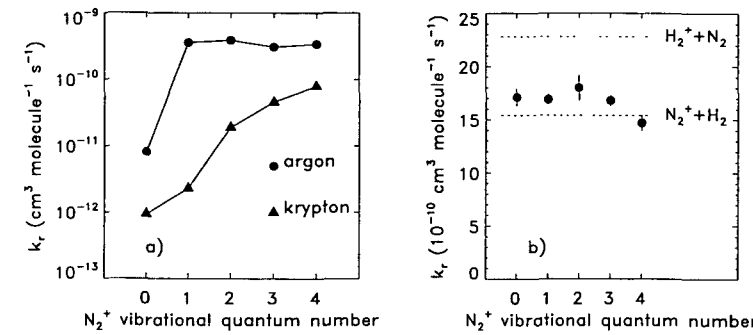

Figure 1: The rate constant as a function of the vibrational excitation of N_2^+. a) for the charge-transfer reaction with Ar and Kr, and b) for the hydrogen-atom transfer reaction with H_2.

The two other reaction channels, charge transfer and vibrational deactivation, are of minor importance. The measured rate constants for reaction (3) are shown in Fig. 1b The rate constant is almost independent of the vibrational excitation of the N_2^+ ion. The lower dashed line represents the classical Langevin rate for this system and it is clear that the results exceed this rate These observations are explained by a simple reaction model in which the first step of the hydrogen-atom transfer consists of a charge transfer at large internuclear distances. After this first step the Langevin rate is higher, since the polarizability of N_2 is larger than of H_2. The experimental results are below this second Langevin rate, as indicated in Fig. 1b. Moreover, as a result of the first step, a number of different intermediate states can be reached, which qualitatively explains the weak state-dependence of the rate constant.

References

[1]S. Kato, M.J Frost, V.M. Bierbaum, and S.R. Leone, Rev. Sci. Instrum. **64**, 2808 (1993).

[2]S. Kato, V.M. Bierbaum, and S.R. Leone (to be published).

[3]S. Kato, M.J Frost, V.M. Bierbaum, and S.R. Leone, Can. J. Chem. **72**, 625 (1994).

[4]J.A. de Gouw, L.N. Ding, M.J. Frost, S. Kato, V.M. Bierbaum, and S.R. Leone, Chem Phys. Lett. (in press).

Symmetry Induced Kinetic Isotope Effects in the Formation of $Ar{\bullet}CO_2^+$

R. K. Yoo and Gregory I. Gellene
Department of Chemistry and Biochemistry
Texas Tech University, Lubbock, TX 79409-1061

During the past decade evidence has been mounting for the existence of a new type of kinetic isotope effect which is dependent on symmetry considerations and is thus qualitatively and quantitatively different from those usually considered in chemical kinetics. Our interest in Symmetry Induced Kinetic Isotope Effects (SIKIE) was motivated by the observation of SIKIE in the formation of O_4^+ from O_2 and O_2^+. In that study [Griffith and Gellene, JCP **96**, 4403 (1992)], ^{17}O and ^{18}O were equivalently incorporated into O_4^+ to levels up to 100 times their natural abundance. This result could not be explained by any existing theory and a new theoretical approach [Gellene, JCP **96**, 4387 (1992)] was developed which both rationalized the O_4^+ results and provided a framework for identifying new systems where SIKIE might be observed. In particular, a potential system is required to have an asymptotic electronic degeneracy arising from either (1) one or both of of the reactants being in a degenerate electronic state or (2) identical reactants in different electronic states. Application of this theory to the association reaction: $He^+ + 2He \rightarrow He_2^+ + He$, lead to the prediction that $^7He_2^+$ formation should be enhanced by SIKIE which was subsequently experimentally observed [Gellene, JPC **97**, 34 (1993)].

A particularly interesting conclusion of the application of the theory to the O_2/O_2^+ system, was the prediction different SIKIE for the loss of molecular centrosymmetry and the loss of the asymptotic degeneracy. That point was addressed by the study of $(CO_2)_2^+$ formation where ^{13}C substitution lifts the asymptotic degeneracy while preserving molecular centrosymmetry and $^{17,18}O$ substitution removes both symmetries. The results confirmed the theoretical predictions with unique and independent SIKIE being observed for ^{13}C and ^{18}O [Yoo and Gellene, JCP **102**, 3227 (1995)]. Because the observed ^{18}O SIKIE is attributed to the loss of the centrosymmetry of CO_2^+ ion, it was suggested that an ^{18}O SIKIE might still be observed if CO_2 is replaced by another closed shell species. This conjecture is explored in the present study.

CO_2^+ was produced by 21 eV electron ionization of Ar/CO_2 mixtures (with natural isotopic abundances) at an ion source inlet pressure of 10-150 mTorr and an ion source temperature of -55° C. The ions were accelerated to 5 keV, magnetically mass resolved and detected by a Channeltron electron multiplier operating in the single ion counting mode.

The primary data was used to calculate the statistically normalized enhancement fac[illegible] EF) for ^{13}C and ^{18}O by the procedure described previously [Yoo and Gellene, JCP **102**, 3227 (1995)]. The results are shown in Fig. 1. In agreement with the theoretical predictions no enhancement of ^{13}C is observed (i. e., $EF(^{13}C) = 1$) whereas a substantial enhancement of ^{18}O is observed (e. g. $EF(^{18}O) > 20$ for $Ar:CO_2 = 1:15$). Because the measurements were taken under conditions where Ar^+ can be produced, the loss of $EF(^{18}O)$ with increasing $Ar:CO_2$ ratio suggests that CO_2^+ ions produced by $Ar^+/CO2$ charge transfer are preferentially produced in those states for which no symmetry restrictions to $Ar{\bullet}CO_2^+$ cluster formation are

predicted. Noting that these quantum states of CO_2^+ are precisely those for which no symmetry restrictions to $(CO_2)_2^+$ formation were predicted [Yoo and Gellene, JCP **102**, 3227 (1995)], the present results imply that CO_2^+ ions produced by Ar^+/CO_2 charge transfer will more efficiently produce $(CO_2)_2^+$ cluster ions than will CO_2^+ ions produced by electron impact. This remarkable prediction was tested by monitoring the intensity of $(CO_2)_2^+$ cluster ions produced in the presence of Ar under conditions where Ar^+ could (E_e = 21 eV) and could not (Ee = 15 eV) be produced. The results shown in Fig. 2 clearly demonstrate that $(CO_2)_2^+$ are strongly promoted when the CO_2^+ ion is produced by Ar^+/CO_2 cha ge transfer.

Fig. 1. Isotopic Enhancement Factors (EF) in $Ar{\bullet}CO_2^+$ Formation

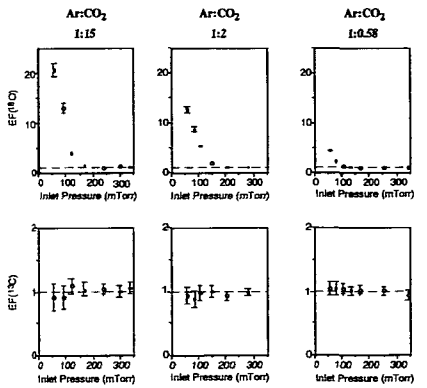

Fig. 2. Effect of Ar on $(CO_2)_2^+$ Formation

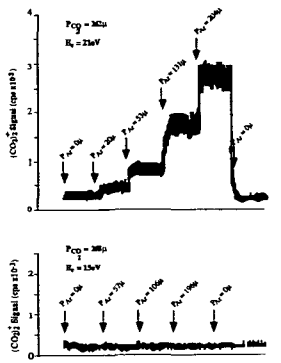

Conclusions

1. SIKIE has been observed for the first time in a chemical system where the reactants have no atoms in common. This effect can be understood (indeed, it was anticipated) by the theory of the phenomena being developed in this laboratory.

2. Unanticipated quantum state propensities are inferred for Ar^+/CO_2 charge transfer.

3. Ar acts as a catalyst for $(CO_2)_2^+$ cluster ion formation.

Structural Aspects of Metal-Oligonucleotide Binding Studied by ESI-CID-MS

Xueheng Cheng, Qinyuan Wu, Quanyin Gao, Steven A. Hofstadler, Richard D. Smith
Chemical Sciences Department and Environmental Molecular Sciences Laboratory,
Pacific Northwest Laboratory, Richland, WA 99352.

INTRODUCTION

Metal ions play important roles in biological system. Not only are they often required as cofactors for enzymes, but they also associate with RNA and ribozymes (i.e. catalytic RNA). Similarly, interaction of the negatively charged DNA backbone with certain metal counterions have been known to affect the DNA's polyelectrolyte behaviors and to stabilize certain structures such as DNA quadruplexes. Some metal complexes have also been used for DNA cleavage as potential methods for DNA sequencing or as alternatives for DNA-protein footprinting. On the other hand, the effects of cation binding on dissociation behaviors of oligonucleotides in mass spectrometry are closely related to the fragmentation mechanism and the application of MS to characterization of oligonucleotide structures.

EXPERIMENTAL

Multiply-charged ions of oligonucleotides and their complexes with Na^+, Mg^{2+} and UO_2^{2+} ions were generated by electrospray ionization (ESI). The collision induced dissociation (CID) experiment was done on a 7-T FTICR instrument (IonSpec). The experiments on tRNA were done on a Finnigan MAT TSQ 7000 triple-quadrupole mass spectrometer. A home-built microspray emitter optimized for very low sample infusion rate (0.2-0.5 ul/min) was used on both instruments. The DNA and tRNA samples was desalted using Centricon 3 or Centricon10 filters twice with 100 mM triethylammonium acetate or 10 mM ammonium acetate. The amount of residue metals in the DNA and RNA was determined using ESI-MS before addition of specific metal ions to be studied.

RESULTS

We have probed the structures of metal-bound oligonucleotides using collision CID. The CID of negative ions from two oligonucleotides (8mer: 5'-pGCTTGCATp-3' and 12mer: 5'-TTGGCCCTCCTT-3') with and without metal adduction were studied. The results of the 8mer DNA indicate that cleavage at the 3'-side of T is the least facile process. In the CID of metal containing species, the position of the metal can be inferred from an analysis of the distribution of the metal containing fragments. The results suggest that in the 8mer DNA, UO_2^{2+} is localized in the middle of the sequence possibly binds to the TT position while Na^+ is more mobile. The 12mer DNA also showed a clear absence of 3'-side dissociation for all the T residues while abundant fragments were observed for all other positions. The low dissociation propensity of T will impose certain limitations on the use of CID for DNA sequence determination. The CID spectra of the metal adducted ions of the 12mer DNA (Mg^{2+} and UO_2^{2+} studied) also suggested that the metals are localized in the middle of the sequence involving the T_8 position. Multi-step dissociation experiments (up to MS^4) revealed the dissociation sequence and aided the assignment of fragment ions. These results on the dissociation of metal-bound DNA showed the potential of using CID to determine binding location and possibly higher order structures of metal-bound DNA in the gas phase. The effect of divalent metal Mg^{2+} and monovalent cation NH_4^+ on the conformation of tRNA was also examined. The addition of both cations induced a charge state shift of tRNA from around m/z 1500 to m/z 2500, indicaitng the formation of a folded structure, while triethylammonium cation did not show such an effect. These results are consistent with the effect of cations on the conformation of tRNA studied in solution and suggest that gas phase dissociation of metal adduct of tRNA may eventually reveal the position of cation binding in tRNA.

Pacific Northwest Laboratory is operated by Battelle Memorial Institute for the U.S. Department of Energy, through Contract No. DE-AC06-76RLO 1830.

43rd ASMS Conference on Mass Spectrometry and Allied Topics

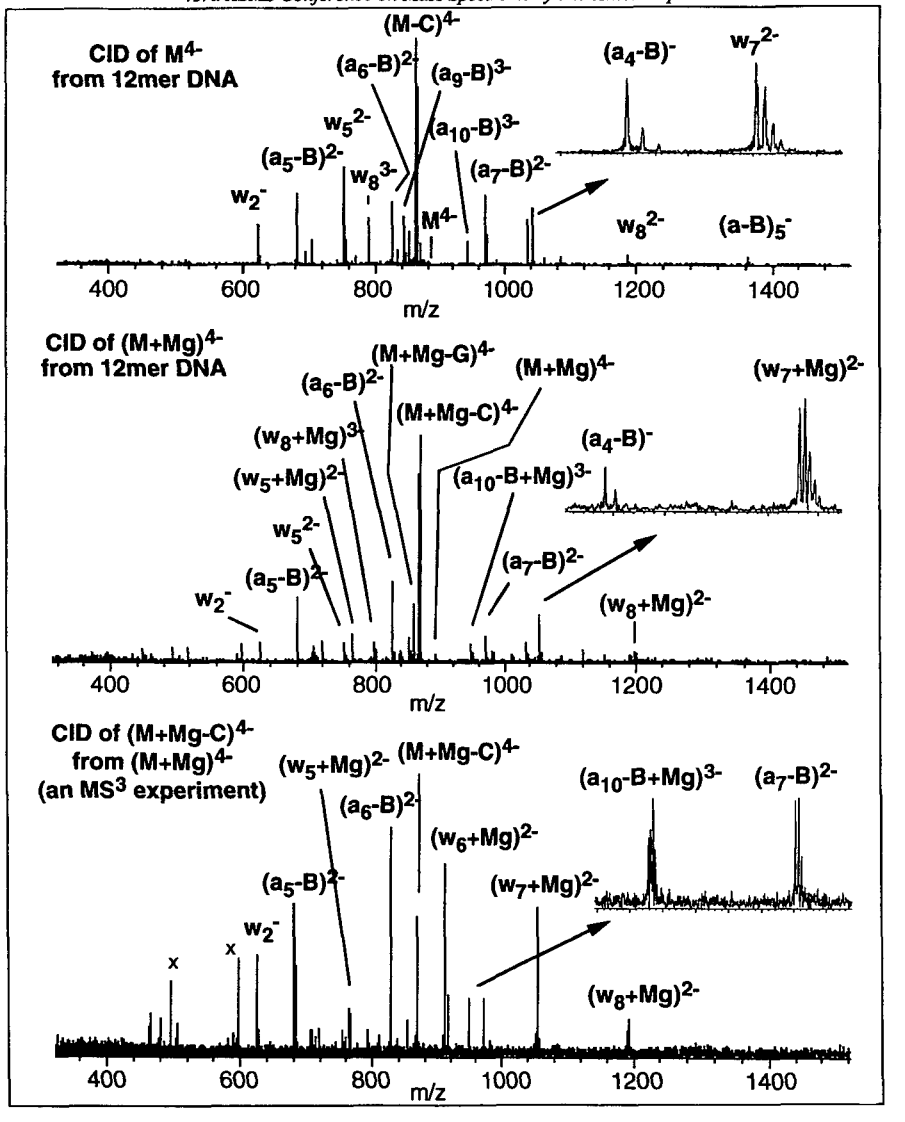

GAS PHASE CHEMISTRY OF MX$^+$ IONS, (X = H, Na, Cu), FROM GLYCINE

Sarka Beranova, Blas A. Cerda, and Chrys Wesdemiotis

Department of Chemistry, The University of Akron, Akron, OH 44325-3601.

Interactions of biomolecules with cations play a crucial role in biological systems. Mass spectrometry has been established as a powerful tool for studies of these interactions in a solventless environment. Elucidation of detailed gas phase chemistry of cationized amino acids can help understand the behavior of peptides and proteins and is, therefore, of fundamental interest. This investigation concerns the unimolecular reactivity of the FAB generated glycine complexes with three different cations: H^+ [1], Na^+, or Cu^+. Their chemistry is probed by collisionally activated dissociation (CAD), and neutralization-reionization mass spectrometry (NRMS). The NRMS methodology allows (a) the evaluation of the complementary neutral fragments generated upon CAD of the precursor ion under investigation, or (b) the generation and characterization of the ion's neutral counterpart, accessible by charge-exchange reduction, which can provide additional structural and mechanistic information.

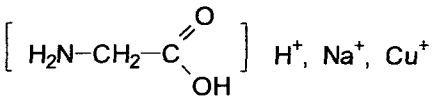

Collisionally activated $GlyH^+$ dissociates by several competitive pathways, giving rise to the CAD spectrum of Figure 1a. The most prominent decomposition yields the $H_2N^+{=}CH_2$ ion (*m/z* 30) by consecutive losses of H_2O and CO. The alternative pathway, i.e., direct cleavage of $:C(OH)_2$ (or HCOOH) is ruled out from the absence of a sizable amount of these molecules among the coproduced neutral fragments. Other primary CAD fragments include $H_3NCHCOOH^+$ (*m/z* 75), $CH_2C(OH)_2^+$ (60), H_2NCHCO^+ (57), $H_2N^+{=}CH_2$ OH_2 (48), ^+COOH (45), and $H_3NCH_2^+$ (31). Either of the functional groups in glycine can bind the added proton. The CAD data point out that the ionic products commence from both the N- and the O-protonated species. Examination of the neutralized form of $GlyH^+$ shows that both isomers are present at the moment of neutralization. Since glycine neutrals should prefer direct dissociation over rearrangement, the initial protonation process most probably occurs at both the amino and the carboxyl functionality.

When subjected to dissociating collisions, $GlyNa^+$ and $GlyCu^+$ produce mainly the metal ion Na^+ and Cu^+, respectively (viz. Figure 1b and 1c). The majority of additional fragments has organometallic character. The glycine-sodium adduct eliminates H, H_3N, H_2O, H_2NCH_2, CH_5N, COOH to give Na^+-containing ions at *m/z* 97, 81, 80, 68, 67, and 53, $GlyCu^+$ produces ions at *m/z* 120 (H_2O loss), 108 ($-H_2NCH_2$), 92 ($-CH_2O_2$), and 90 ($-CH_4O_2$). Both complexes generate the immonium ion $H_2N^+CH_2$. The other

significant organic product ion arising from $GlyNa^+$, namely ^+COOH (*m/z* 45), is not reproduced in the $GlyCu^+$ spectrum, which displays an abundant $CH_2O_2^+$ at *m/z* 46, instead.

In summary, despite their small size, glycine-cation adducts exhibit rather complex dissociation characteristics. Combining tandem mass spectrometry techniques provides a valuable means to investigate the unimolecular chemistry and binding sites of such species.

REFERENCES:

1. Beranova, S.; Wesdemiotis, C. *J. Am. Chem. Soc.*, submitted February 1995.

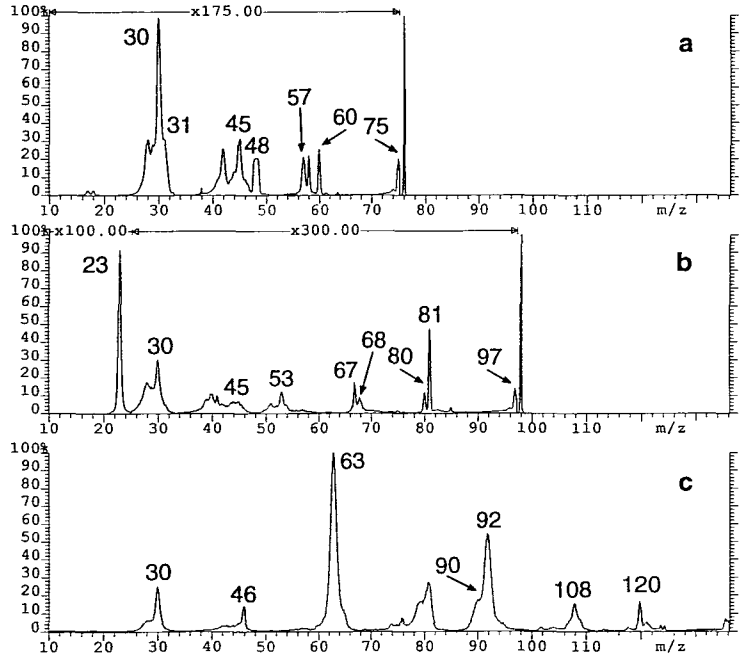

Figure 1. CAD spectra of: a) $GlyH^+$
b) $GlyNa^+$
c) $GlyCu^+$

MULTIPLY CHARGED COMPLEXES BETWEEN PEPTIDES AND TRANSITION METAL IONS: ESI MS-MS AND MS-MS-MS USING B/E VS MIKES SCANS

M. Cameron Sullards and Jeanette Adams, Department of Chemistry and the Emory University Mass Spectrometry Center, Emory University, Atlanta, GA 30322

Experiments were conducted to determine if product ions from $(M + Me)^{2+}$ complexes of angiotensin II, in which $Me^{2+} = Co^{2+}$, Ni^{2+}, Cu^{2+}, and Zn^{2+} are are discriminated against in B/E scans. MS^2 and MS^3 experiments were performed using electrospray ionization (ESI) and a JEOL JMS-SX102/SX102A/E five-sector, tandem mass spectrometer.

MS^2 B/E spectra of the $(M + Me)^{2+}$ precursors reveals abundant doubly charged product ions (Figure 1a). Singly charged product ions are either weakly abundant or not observed. MS^2 MIKES scans, however, reveal the presence of singly charged product ions of higher *m/z* than the precursor (Figure 1b). The low-mass complementary ions are significantly less abundant than their high-mass counterparts.

Narrow signal-averaged MIKES scans show that the complementary ion pairs exhibit a large kinetic energy release. Virtually identical kinetic energy release distributions (KERDs) indicate that the ions are indeed complementary. Increased dishing and decreased detectability occurs for the low-mass ions.

MS^3 B/E spectra of the first-generation product ions that arise from $(M + Me)^{2+}$ precursors reveal abundant doubly charged second-generation product ions (Figure 2a). Singly charged product ions are either weakly abundant or not detected. MS^3 MIKES scans, however, show a greater abundance of singly charged product ions (Figure 2b). The low-mass complementary ions are not observed.

Metastable ion and collision-induced dissociations (CID) are traditionally used for structure determination of singly charged gas-phase complexes between peptides and metal(II) ions [1,2]. Singly charged product ions that arise from doubly charged precursors must be formed via charge separation reactions. These reactions are characterized by a large kinetic energy release (KER). Sector instruments discriminate against ions that have a large KER, and this discrimination is proportionately greater for low-mass ions. This discrimination is caused by the finite heights and widths of slits, and the limited kinetic energy bandpass of the magnet and ESA.

Consequently, double-focusing B/E scans give misleading relative ion abundances for product ions formed by charge-separation reactions. MIKES experiments can be used to either detect or to estimate relative ion abundances. Furthermore, accurate mass calibration is vital for correct *m/z* determination and product ion assignment in B/E scans.

References

1. (a) Teesch, L. M.; Adams, J. *J. Am. Chem. Soc.* **1990**, *112*, 4110-4120. (b) Zhao, H.; Reiter, A.; Teesch, L. M.; Adams, J. *J. Am. Chem. Soc.* **1993**, *115*, 2854-2863. (c) Zhao, H.; Adams, J. *Int. J. Mass Spectrom. Ion Processes* **1993**, *125*, 195-205. (d) Reiter, A.; Teesch, L. M.; Zhao, H.; Adams, J. *Int. J. Mass Spectrom. Ion Processes* **1993**, *127*, 17-26. (e) Reiter, A.; Zhao, H.; Adams, *J. Org. Mass Spectrom.* **1993**, *28*, 1596-1601. (f) Reiter, A.; Adams, J.; Zhao, H. *J. Am. Chem. Soc.* **1994**, *116*, 7827-7838.

2. (a) Hu, P.; Gross, M. L. *J. Am. Chem. Soc.* **1992**, *114*, 9153-9160. (b) Hu, P.; Gross, M. L. *J. Am. Chem. Soc.* **1992**, *114*, 9161-9169. (c) Hu, P.; Gross, M. L. *J. Am. Chem. Soc.* **1993**, *115*, 8821-8828.

43rd ASMS Conference on Mass Spectrometry and Allied Topics

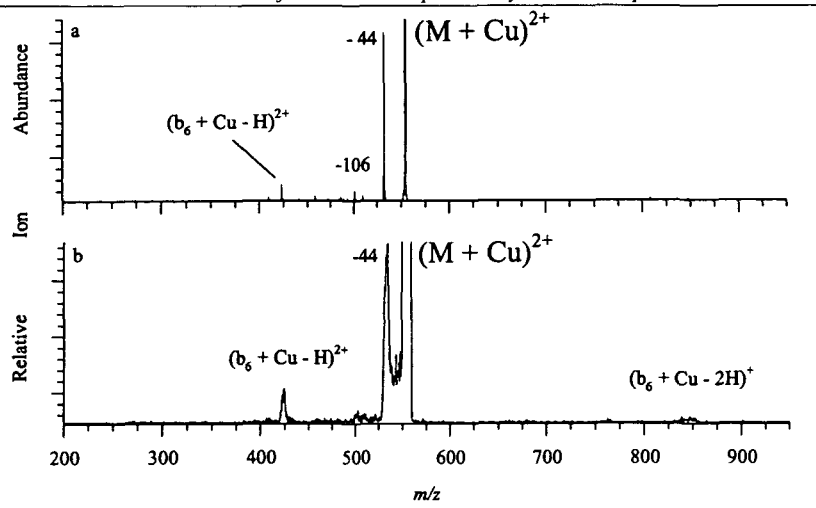

Figure 1. MS^2 metastable ion decompositions of $(M + Cu)^{2+}$ ions using (a) B/E scans (b) MIKES scans.

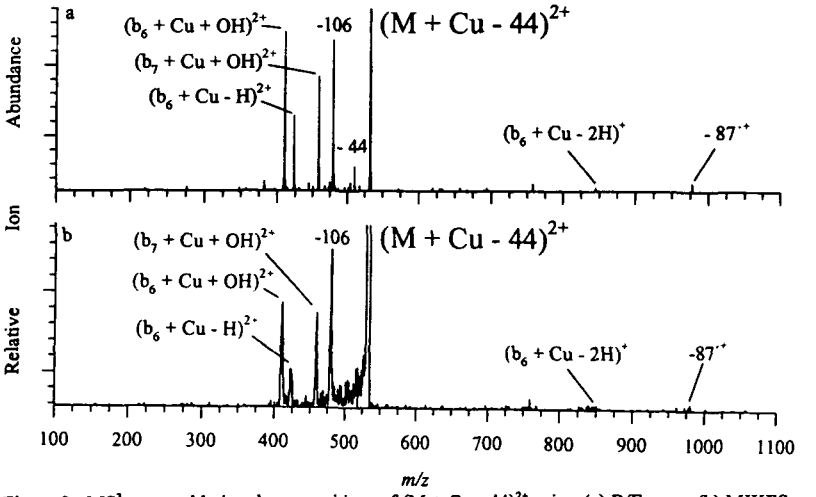

Figure 2. MS^3 metastable ion decompositions of $(M + Cu - 44)^{2+}$ using (a) B/E scans (b) MIKES scans.

ELECTROSPRAY MASS SPECTROMETRY OF ALKALI-METAL ION COMPLEXES OF PROTEINS AND PEPTIDES

Jianyao Wang, Fu Ke, Roger Guevremont and K.W. Michael Siu, Institute for Environmental Research and Technology, National Research Council of Canada, Ottawa, Ontario, Canada, K1A 0R6; J.C. Yves Le Blanc, SCIEX, 71 Four Valley Drive, Concord, Ontario, Canada, L4V 4V8.

Gas-phase alkali-metal ion complexes of proteins and peptides that contain one to tens of metal ions can readily be produced in electrospray mass spectrometry from peptide/protein solutions containing the appropriate alkali metal hydroxides. For tripeptides, the $[M-H+2X]^+$ and the $[M-2H+3X]^+$ ions (where X is the alkali metal ion) are the most intense species observed in the positive ion detection mode {1}, while the $[M-H]^-$, the $[M-2H+X]^-$ and the $[M-3H+2X]^-$ ions are those observed in the negative ion detection mode. Collision-induced dissociations of these adduct ions showed that the alkali metal ions attach to one or several of the following moieties, the C-terminal carboxylate anion, the amide nitrogen atom, the amide carbonyl oxygen, and the N-terminal nitrogen atom {1}. The above adduct ions may be expressed in the general form $[M+nH+mX]^{(n+m)}$; e.g. the $[M-2H+3X]^+$ ion is a $[M+nH+mX]^{(n+m)}$ ion where n = -2 and m = 3. $[M+nH+mX]^{(n+m)}$ ions in which n and m are relatively large are observable from longer peptides and proteins. Figure 1 shows the electrospray mass spectrum of a 20 μM bradykinin (RPPGFSPFR) solution in 50/50 water/methanol adjusted to pH 12 with potassium hydroxide. The most abundant cluster is doubly charged, (n+m) = 2, with n = 1 to -7 and m = 1 to 9. Similar results for ubiquitin are displayed in Figure 2. For the 8+ cluster, cluster ions with n = -5 to -10 and m = 13 to 18 are evident.

$[M+nH+mX]^{(n+m)}$ ions, especially those of oligopeptides, are revealing in that they show "substitution" of peptide protons that are not conventionally considered acidic by alkali-metal ions. These protons are likely to be the amide protons on the peptide backbone. We have argued that a gas-phase ion-ion reaction to form the positively charged $[M+nH+mX]^{(n+m)}$ ions is unlikely as non-complexed peptides are anionic in a pH 12 solution, and anions are not expected to desorb when the electric field is directed outward from the air/solution interface {1}. As a result, we speculated that the $[M+nH+mX]^{(n+m)}$ ions or their "precursor" ions must exist in solution and desorb into the gas phase during the electrospray experiment. The precursor ions that desorb are transformed into the $[M+nH+mX]^{(n+m)}$ ions in the front end of the mass spectrometer and measured {1}. The mechanistic limitations on the formation of the $[M+nH+mX]^{(n+m)}$ ions are identical for the scenarios in which desorption takes place from a droplet formed from solvent evaporation and Rayleigh fission and in which desorption takes place from the surface of the Taylor cone.

{1} J. Wang, R. Guevremont and K.W.M. Siu, Eur. Mass Spectrom., in press.

43rd ASMS Conference on Mass Spectrometry and Allied Topics

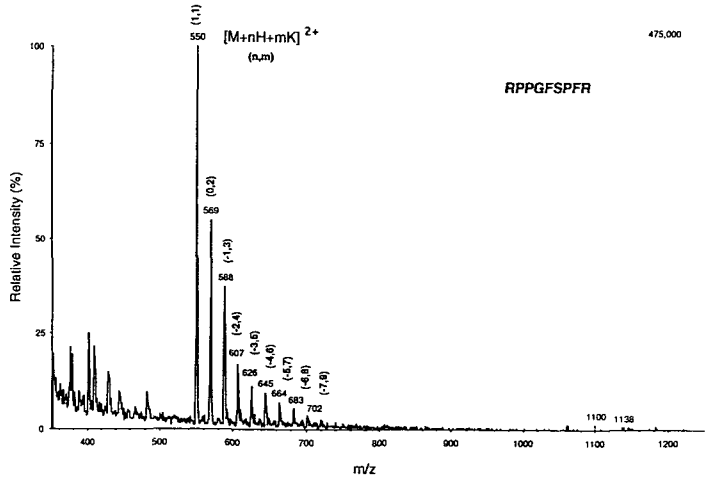

Fig 1 : 20uM bradykinin in 50/50 water/methanol adjusted to PH12 with potassium hydroxide

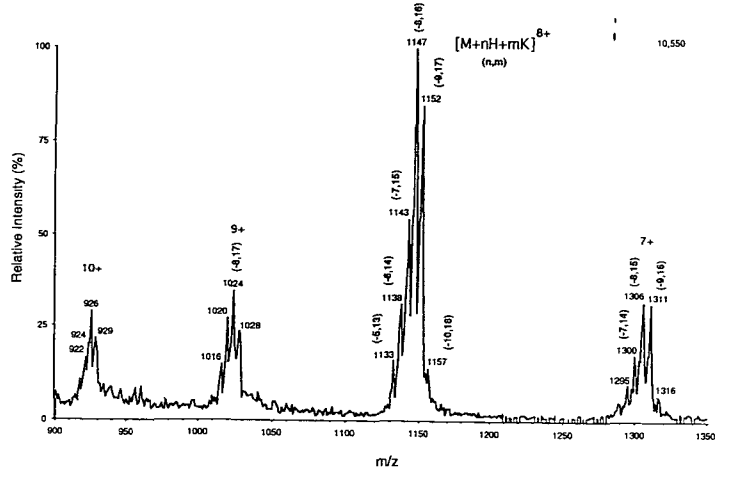

Fig 2 : 20uM ubiquitin in 50/50 water/methanol adjusted to PH10.3 with potassium hydroxide

INFLUENCE OF SECONDARY STRUCTURE ON PEPTIDE ION DISSOCIATION IN A TANDEM TOFMS

Mary Gimon Kinsel, Damon C. Barbacci, and David H. Russell, Laboratory for Biological Mass Spectrometry, Department of Chemistry, Texas A&M University, College Station, Texas 77843

The non-covalent interactions experienced by biomolecule ions in the gas-phase may or may not be similar to those which determine their solution-phase conformations. It has been suggested that these interactions have an effect on ion dissociation. A series of peptides, Bradykinin and fragments containing amino acid residues 1-5, 1-6, 1-7, 1-8, and 2-9, has been studied in a TOF/ ReTOF mass spectrometer. Fragment ions are produced by metastable decay of the cationized peptide $[M+H]^+$ ion ($[M+Na]^+$ ion) or by 193-nm photodissociation of the cationized peptide ion. We have evaluated the information content of these spectra in terms of (i) sight of cationization, (ii) stability of fragment ion as well as neutral fragment lost, and (iii) relationship, if any, to the known solution phase structure of bradykinin determined by circular dichroism (CD)[1].

The metastable decay product ion spectra for bradykinin is shown in Figure 1. All spectra were recorded using the MALDI matrix α-cyano-4-hydroxycinnamic acid, 337-nm output of a nitrogen laser, 15.0 kV acceleration voltage, and -2.35 kV detector voltage. The $[B_8 + H_2O]^+$ product ion is the dominant fragment. Less abundant signals arise from a-type, b-type, and internal cleavages To investigate the nature of the effect ion structure, we examined the dissociation of 5 commercially available fragments of bradykinin: Pro-Pro-Gly-Phe-Ser-Pro-Phe-Arg (fragment 2-9); Arg-Pro-Pro-Gly-Phe-Ser-Pro-Phe (fragment 1-8); Arg-Pro-Pro-Gly-Phe-Ser-Pro (fragment 1-7); Arg-Pro-Pro-Gly-Phe-Ser (fragment 1-6); and Arg-Pro-Pro-Gly-Phe (fragment 1-5)

Compositional effects have an influence on the relative abundances of internal fragment ions in metastable decay spectra. The relative abundances of these product ions are shown in Figure 2. The competition between formation of the various product ions is a function of the stabilities of the product ions formed and the neutral(s) lost. Photodissociation of bradykinin $[M+H]^+$ ions yields an increase in the abundance of N-terminus containing product ions. However, the most dramatic increase is in the abundance of internal fragment ions (see Figure 3). This result is not unexpected because the internal energy of

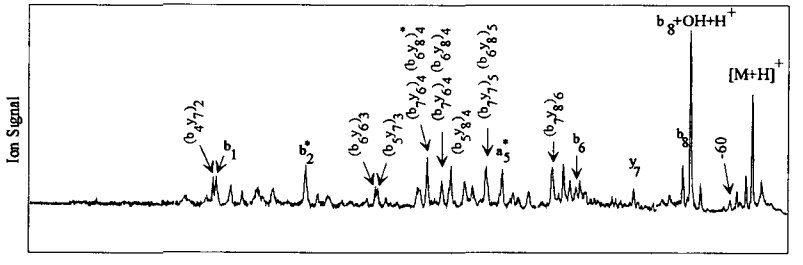

Figure 1: Metastable decay mass spectrum obtained for bradykinin using the α-cyano-4-OH-cinnamic acid matrix. An '*' following a sequence ion indicates loss of 17 mass units.

ions excited by absorption of a 193-nm (6.42eV) is high and the formation of internal fragments requires that two bonds break. Loss of the N-terminal Arg, Arg-Pro, and Arg-Pro-Pro appear to be common dissociation pathways. Metastable decay and photodissociation of the bradykinin and related fragment $[M+H]^+$ ions and $[M+Na]^+$ ions (results not shown) suggests that the sequence Pro-Gly-Phe (and/or Pro-Gly) has a high cation affinity.

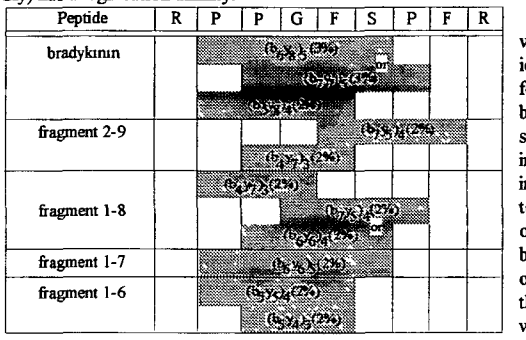

Figure 2: Relative abundances of internal fragment ions observed from the metastable decay of MALDI generated peptides.

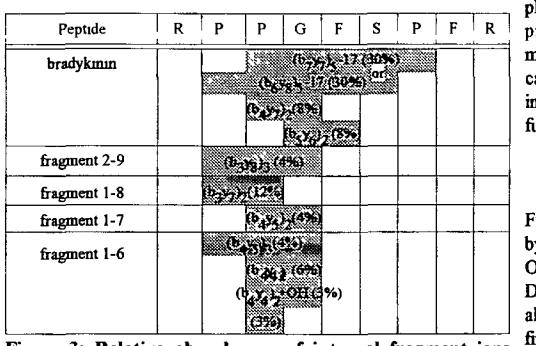

Figure 3: Relative abundances of internal fragment ions resulting from the 193-nm photodissociation of MALDI generated peptide ions.

From the results of this study, we find no indication that the gas-phase ion retains the secondary structural features (*i.e.*, intramolecular H-bonding) observed in solution-phase studies. We are currently investigating in detail the mechanism of dissociation, in particular, the role played by the N-terminal Arg. For example, the effect of exchanging Arg[1] for Lys[1] in bradykinin. If the mechanism for loss of the N-terminal residues depends on the length of the quananine side chain, we expect to see less efficient production of product ions by this mechanism. The identity of the neutral(s) lost can be further investigated by isolation followed by photoionization of the neutral products We are also exploring in more detail the use of semiempirical calculations as a tool to aid the interpretation of fragmentation as a function of peptide structure.

Acknowledgments

Funding for this research is provided by the U.S. Department of Energy, Office of Basic Energy Science, Division of Chemical Science. MGK also thanks W.R. Grace & Co. for its financial support through a 1994-1995 College of Science Graduate Fellowship.

References

[1] Cann, J.R., Stewart, J.M., Matsueda, G R. *Biochemistry* 1973, *12*, 3780

Intra-ionic Acid/Base Interactions in the CID of Protonated Peptides

[1]K.A. Cox, [2]A. Whiting, [3]M. Morris, [1]S.J. Gaskell
[1]The Michael Barber Centre for Mass Spectrometry; UMIST; Manchester, United Kingdom
[2]Department of Chemistry; UMIST; Manchester, United Kingdom
[3]VG Organic, Tudor Road, Altrincham, Cheshire, United Kingdom

There has been a strong driving force to understand the factors which determine low energy dissociation processes of peptides.[1,2] The poor fragmentation efficiencies observed in the low energy CID of peptides containing strongly basic residues[3] is of particular interest because of widespread analyses involving tryptic peptides which contain C-terminal basic residues.

The nature of product ions derived from the dissociation of a precursor peptide ion is highly dependent on the primary structure of the peptide, particularly on the number and location of the basic amino acid residues.[4] In the presence of a highly basic amino acid residue, a precursor ion population is generated in which the ionizing proton is localized on this residue in a high proportion of the ions. The presence of the strongly localized charge is a detriment to the low energy CID of these peptides, and suppresses efficient and varied backbone cleavages.

The work described here represents a systematic investigation of the effects of charge heterogeneity in the precursor ion population of model peptides in low energy CID experiments. The nature and extent of low energy decompositions of peptides which contain highly basic arginine residues are compared to dissociations of analogous peptides in which acidic groups have been incorporated to balance the protonated arginines, allowing further protonation at less basic sites. In addition, molecular modelling has been utilized to determine preferred low energy conformational states of these gas-phase peptide ions.

Figure 1 shows the product ion spectra of doubly protonated RLCIFSCFR and RLC*IFSC*FR (where C* indicates cysteic acid) under identical conditions. In the first case, both ionizing protons reside on the highly basic arginine side chains, creating a precursor ion population which is homogeneous with respect to charge site; thus suppressing low energy fragmentation, which occurs primarily via charge directed mechanisms. Incorporation of the cysteic acid residues allows the generation of a heterogeneous charge population; these residues remain negatively charged upon ionization and effectively balance the positive charges incorporated on the arginines. The ionizing protons locate along the amide bonds of the peptide backbone and efficient low energy fragmentation is observed.

Molecular modelling was incorporated to provide insight into broad structural features of these peptides. In the case of RLCIFSCFR, the energy minimized structure is highly compact, with the hydrophobic backbone on the inside of the structure and the hydrophillic side chains on the outside. In contrast, the incorporation of cysteic acids results in a more open structure in which the negatively charged cysteic acid groups adopt a position proximal to the positively charged guanidino groups, giving clear evidence of electrostatic interactions.

RLCIFSCF can also produce a doubly charged precursor ion population which is heterogeneous with respect to charge site. Here, one proton remains on the N-terminal arginine, but the other site of protonation is variable. A predominant series of b-type ions is observed due to the charge retention on the arginine. In contrast, CID of tryptic peptides, where a strongly basic amino acid residue is at the C-terminus, generally yields more abundant y-type ions.[5] The present data suggest that the stability of the product ion is not solely due to its type (y or b), but to whether it retains its charge on the side chain of the basic residue, remote from the peptide backbone, making it resistant to further charge proximal dissociations.

In an effort to investigate the specificity of the electrostatic interactions and their influence on observed fragmentation patterns, we analyzed the peptides RLAIFSCFR and RLCIFSAFR which differ only in the relative positions of the amino acids at position 3 and 7. CID of the $(M+2H)^{2+}$ ions resulted in virtually identical fragmentation spectra. However, CID of the oxidized forms of these species resulted in strikingly different product ion spectra, apparently due to the specificity of the electrostatic interactions. This was substantiated by molecular modelling, which indicated distinct structural conformations for these species.

References:
1) Tang, X.-J.; Thibault, P.; Boyd, R.K. *Anal. Chem* **1993**,*65*, 2824-2834.
2) McCormack. A.L; Somogyi, A.; Dongre, A.R.; Wysocki, V.H. *Anal. Chem.* **1993**, *65*, 2859-2872.
3) Poulter, L.; Taylor, L. *Int. J. Mass Spectrom. Ion Processes*, **1989**, *91*, 183-197.
4) Burlet, O.; Yang, C.-Y.; Gaskell, S.J. *J. Am. Soc. Mass Spectrom.* **1992**, *3*, 337-344.
5) Tang, X.-J.; Boyd, R.K. *Rapid Commun Mass Spectrom.*, **1992**, *6*, 651-657.

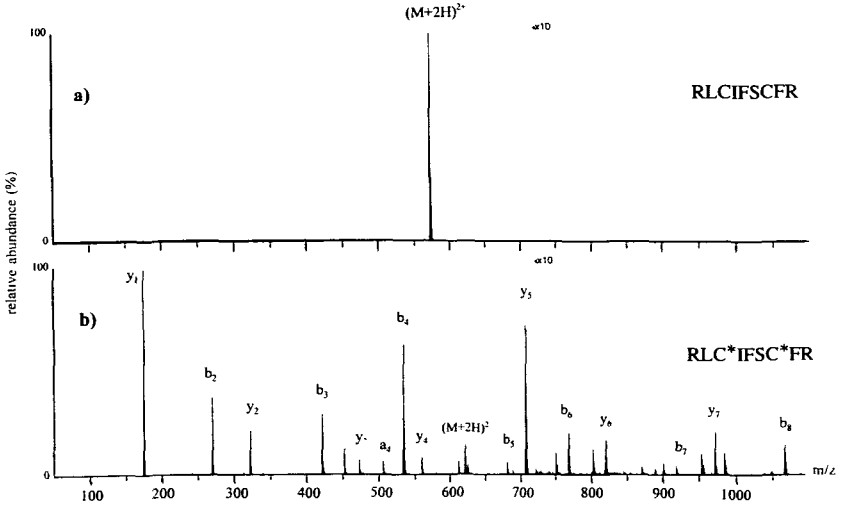

Figure 1

A MULTISTEP PATHWAY LEADING TO PEPTIDE w_n IONS CONFIRMED BY MS^3 AND MS^4

Kevin D. Ballard, Ralph S. Orkiszewski and Simon J. Gaskell[1]
Center for Experimental Therapeutics, Baylor College of Medicine, Houston, TX 77030
[1]Centre for Mass Spectrometry, UMIST, Manchester, M60 1QD UK

Fragment ions of the d_n, w_n, and v_n types from peptide $[M+H]^+$ ions represent concomitant side-chain and peptide backbone cleavages. Such ions are often observed during tandem mass spectrometric analyses of peptides under high energy collisionally activated decomposition (CAD) conditions. These types of ions facilitate amino acid sequencing of peptides, particularly the distinguishing of isobaric amino acid residues such as leucine and isoleucine. The formation of each these types of ions necessarily requires the cleavage of at least two covalent bonds, and thus involves at least one reaction intermediate in each of the fragmentation pathways leading to the formation of these ions. Previous studies from these and other[1] laboratories have shown that the activation energy requirement for the formation of w_n ions may be substantially lower than the corresponding requirements for the formation of the d_n and v_n species. Based on some elegant modelling studies, Wysocki and co-workers[1] suggested that one possible pathway for the formation of w_n ions from $[M+H]^+$ species involves the initial formation of an x_n+1 ion, which then decomposes to form a z_n+1 ion, which then further fragments to form the w_n species (Figure 1). The present studies were undertaken to test this hypothesis experimentally.

Results. Previous studies from these laboratories using reaction intermediate scanning demonstrated that z_n+1 species are involved as intermediates in w_n ion formation. The z_n+1 ions are not the only intermediates involved, however. Figure 1 presents a reaction intermediate scan representing the $[M+H]^+ \rightarrow$ intermediates $\rightarrow w_6$ reaction sequence for the peptide SIGSLAK. The first stage of decomposition occurred under high energy CAD conditions, with low energy CAD conditions for the second stage. It is clear from the spectrum that other intermediates, in addition to the z_6+1, are involved in the formation of the w_6 ion, including the $[M+H-H_2O]^+$ ion. The observation that an $[M+H-H_2O]^+$ intermediate, subjected to low energy CAD, can give rise to a w_n species again suggests that the energy requirements for w_n ion formation may be comparatively low. A reaction intermediate scan obtained under strict unimolecular decomposition conditions for the $[M+H]^+ \rightarrow$ intermediates $\rightarrow w_3$ reaction sequence for neurotensin (1-6) showed that the z_3+1 ion from this peptide can derive through unimolecular decomposition of the $[M+H]^+$, then subsequently decompose unimolecularly to form the w_3 ion *m/z*-deconvoluted MIKES analysis of the peptide VHLTPVEK representing the $[M+H]^+ \rightarrow w_6$ fragmentation (by all possible pathways) occurring in FFR2 under unimolecular decomposition conditions gave similar findings. These data thus demonstrate unequivocally that w_n ions can be formed unimolecularly from FAB desorbed peptide $[M+H]^+$ ions.

In order for the proposed multistep pathway for the formation of w_n ions to occur, it must be possible for z_n+1 ions to derive through the initial formation of x_n+1 intermediates. Reaction intermediate and sequential product ion scans with several peptides demonstrated that z_n+1 ions can be formed through x_n+1 intermediates. The third generation product ion spectrum (MS^4) depicted in Figure 2 explicitly demonstrates the occurrence of the $[M+H]^+ \rightarrow x_6+1 \rightarrow z_6+1 \rightarrow w_6$ reaction sequence for the peptide VHLTPVEK. The first two stages of decomposition occurred in the absence of added collision gas, with low energy CAD conditions employed for the third stage. The signal detected was very weak but was nevertheless reproducible The multistep mechanistic pathway for the formation of w_n ions, delineated as $[M+H]^+ \rightarrow x_n+1 \rightarrow z_n+1 \rightarrow w_n$, which was proposed by Wysocki and co-workers[1] based upon modelling studies, has thus been experimentally demonstrated to occur. As a serendipitous finding, new internal cleavage fragmentations, representing concomitant w-type and either B-type or A-type cleavage, have been identified during MS^3 analyses of FAB desorbed peptide $[M+H]^+$ ions.

Reference. [1] McCormack, A.L.; Somogyi, A.; Dongre, A.R.; Wysocki, V.H. *Anal. Chem.* 1993, *65*, 2859.

43rd ASMS Conference on Mass Spectrometry and Allied Topics

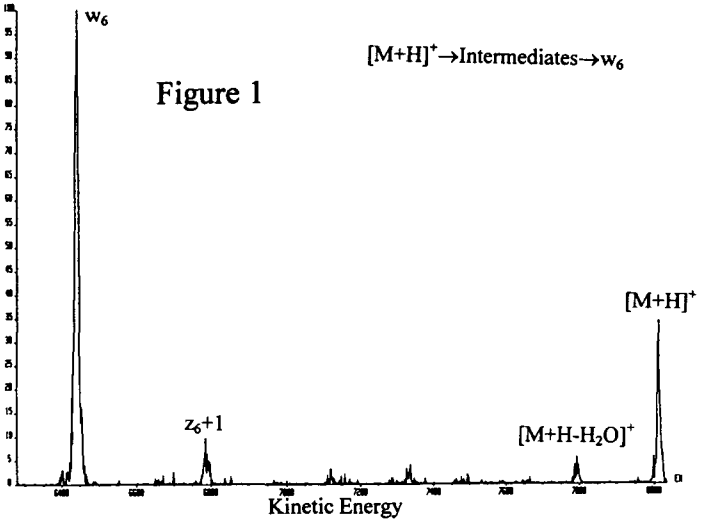

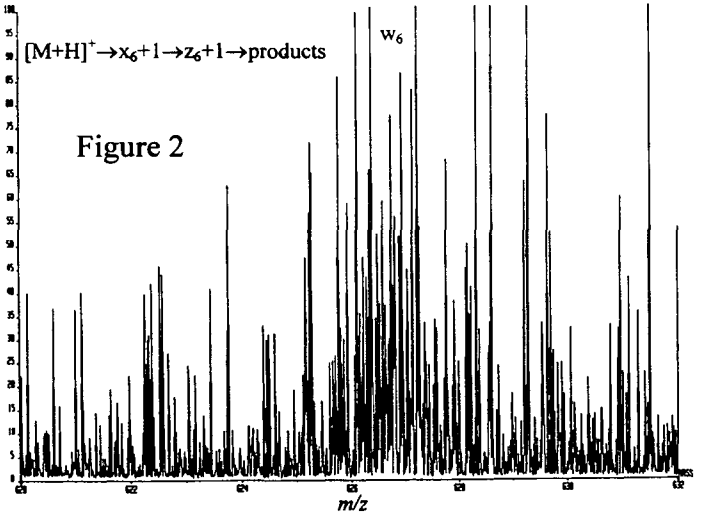

WHY ARE B IONS STABLE SPECIES IN PEPTIDE SPECTRA?

T. Yalcin, I.G. Csizmadia, M.R. Peterson and A.G. Harrison
Department of Chemistry
University of Toronto
Toronto, Canada

Protonated amino acids and derivatives do not form stable acylium ions on fragmentation, rather the incipient acylium ion exothermically eliminates CO to form the immonium ion

$$RCH(NH_2)C(=O)X.H^+ \longrightarrow [RCH(NH_2)CO^+] \longrightarrow RCH{=}NH_2^+$$

On the metastable ion time scale the overall reaction occurs with substantial release of kinetic energy ($T_{1/2} \approx 0.2$-0.4 eV).

By contrast, protonated peptides and derivatives frequently show abundant B_n ($n \geq 2$) ions, which nominally are acylium ions, in their FAB and CID mass spectra. The present work addresses the question of why these B_n ions (nominally acylium) are stable when the acylium ions derived from protonated amino acid derivatives are unstable. We have used metastable ion studies, CID studies and *ab initio* molecular orbital calculations in these investigations.

We have observed that protonated dipeptide derivatives $H_2NCH(R')C(=O)NHCH(R)C(=O)X.H^+$ and protonated N-acyl amino acid derivatives $R'C(=O)NHCH(R)C(=O)X.H^+$ show a very similar behaviour in that HX is lost to form stable B_2 ions. These B_2 ions fragment metastably, in part, by loss of CO with substantial release of kinetic energy

$$B_2 \longrightarrow A_2 + CO \quad T_{1/2} = 0.3 - 0.5 \text{ eV}$$

In the same way, the B_3 and B_4 ions observed in the FAB mass spectra of larger peptides fragment unimolecularly, in part, by elimination of CO with a similar release of kinetic energy.

These results indicate that there exist stable configurations (S) of the B_n ions which fragment by way of reacting configurations (RC) which are higher in energy than the fragmentation products A_n + CO. Some of the exothermicity of the final fragmentation step is partitioned into kinetic energy of the separating fragments leading to the large $T_{1/2}$ values.

Both experimental results and theoretical calculations indicate that the stable structures (S) are protonated oxazolones formed by interaction of the next-adjacent carbonyl oxygen with the developing charge as HX is eliminated from the protonated species.[1] Experimentally we observed that the B_2 ion, nominally $C_6H_5C(=O)NHCH_2CO^+$, derived by loss of neutral glycine from protonated hippurylglycine shows the same metastable ion and CID behaviour as protonated 2-phenyl-5-oxazolone (Figure 1).

Theoretical calculations (3-21G and 6-31G**) for the simplest B ions nominally

$HC(=O)NHCH_2CO^+$	B_2
$HC(=O)NHCH_2C(=O)NHCH_2CO^+$	B_3
$HC(=O)NHCH_2C(=O)NHCH_2C(=O)NHCH_2CO^+$	B_4

show, in each case, that the global energy minima correspond to protonated oxazolone structures. Those for B_2 and B_3 are shown in Figure 2. Calculations for the acyclic acylium form of the B_2 ion showed one imaginary frequency indicating that the structure corresponded to a

saddle point or transition state on the potential energy hypersurface. These calculations showed that the acyclic structure (the reacting configuration, RC) was 1.5 eV higher in energy than the stable cyclic structure (S) and 0.9 eV higher in energy than the fragmentation products $HC(=O)NHCH_2^+$ + CO, consistent with the measured kinetic energy releases.

For the B_3 and B_4 ions the calculated structures indicate that there is a strong interaction of the next-adjacent carbonyl oxygen with the site of the positive charge in the oxazolone ring. Thus, a concerted electron shift can readily lead (Scheme) to the fragmentation reaction $B_n \longrightarrow B_{n-1}$ as is observed experimentally for B_3 and higher B ions.

This work will be published (hopefully) in J. Am. Soc. Mass Spectrom.

1. A protonated oxazolone structure has been proposed earlier for B ions, D. Arnott, D. Kottmeir, N. Yates, J. Shabanowitz and D.F. Hunt, *42nd ASMS Conference on Mass Spectrometry*, Chicago, June, 1994, p.470.

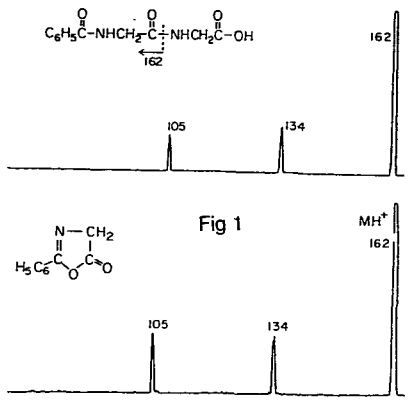

Fig 1

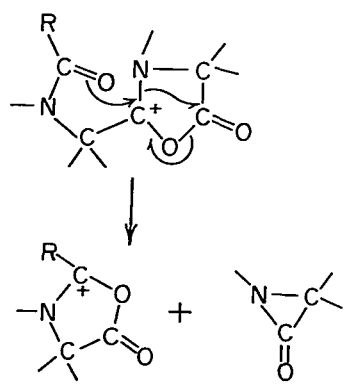

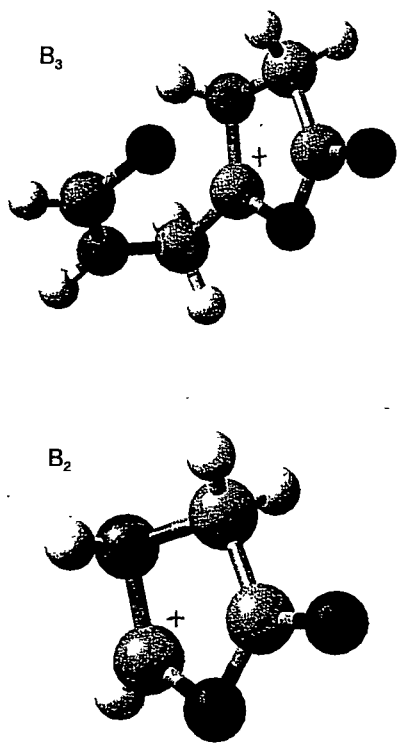

Fig 2

GAS PHASE REACTIONS OF BIOLOGICALLY ACTIVE PEPTIDES.

By Jackie A.Mosely, P J.Derrick, R T.Gallagher and H J.Cooper.
Institute of Mass Spectrometry and Department of Chemistry, University of Warwick, Coventry, CV4 7AL. UK.

Anthony G.Craig.
Salk Institute of Biological Sciences, PO BOX 85800, San Diego, La Jolla, California 92186-5800, USA.

Bombesin is a tetradecapeptide with thermoregulatory and gastric effects in mammals. There are 39 other biologically active peptides closely related to bombesin[1], alytesin being one such example and so the importance of understanding how these compounds breakdown or form adducts is significant. The creation of a peptide/gas adduct was first proposed by Neumann et al[2] who said that under the correct collision conditions the system would have the maximum internal energy.

The peptides were analysed on a Kratos Concept IIHH four sector tandem mass spectrometer with EBEB type geometry. Ions were generated using static probe liquid secondary ion mass spectrometry (LSIMS) and were detected after MS2 by a scanning array detector.
The ions produced at the source were accelerated to 7.9kV (V_{acc}) and passed through MS1. The collision cell was floated to a potential (V_{cell})in order to create the desired laboratory frame energy (E_{LAB}) such that:

$$E_{LAB} = (V_{acc} + V_{cell})e \qquad (1)$$

Ions now travelling with an energy of (E_{LAB}) entered the second electric sector whose potential had been manually reduced to account for the centre-of-mass collision energy (E_{COM}).

$$V_{ESA\ potential\ used} = V_{full\ ESA\ potential} - E_{COM} \qquad (2)$$

$$E_{COM} = E_{LAB} \times m_{gas}/(m_{ion}+m_{gas}) \qquad (3)$$

Equation 3 gives the centre-of-mass collision energy (E_{COM}) provided the entire gas molecule joins the peptide. If fragmentation of the adduct occurs, the electric sector potential will be greater depending on the mass of the fragment.

The second magnet was scanned in order to produce a spectrum.

The target gas was allowed into the collision cell at such a pressure that the adduct could be seen. This value reduced the parent peak to about 80-90% its original size.

When the alytesin parent ion is collided with CH_4 an adduct appears at a +14Da mass shift from the molecule-ion, CD_4 produces a +17Da mass shift and $C^{13}H_4$ produces a +15Da mass shift. Results for CH_4 and CD_4 reactions are consistent with work done on renin substrate by Fenselau et al[3]. The +15Da mass shift obtained using $C^{13}H_4$ confirms that one proton (or in the case of CD_4, one deuterium) is lost from the target gas and one proton is lost from the parent molecule-ion, thus producing $(CH_3M)^+$, $(CD_3M)^+$, $(C^{13}H_3M)^+$ species as shown in figure 1

(1) J E. Rivier and M R. Brown.
Biochemistry(ACS) 17, 1766-1771, (1978).
(2) G M. Neumann, M M. Sheil, and P J. Derrick.
Z. Natursforsch 39a, 584-592, (1984).
(3) X. Cheng and C. Fenselau.
J. Am. Chem. Soc. 115, 10327-10333, (1993).

Figure 1. Alytesin/gas adduct ions produced with different isotopic forms of methane.

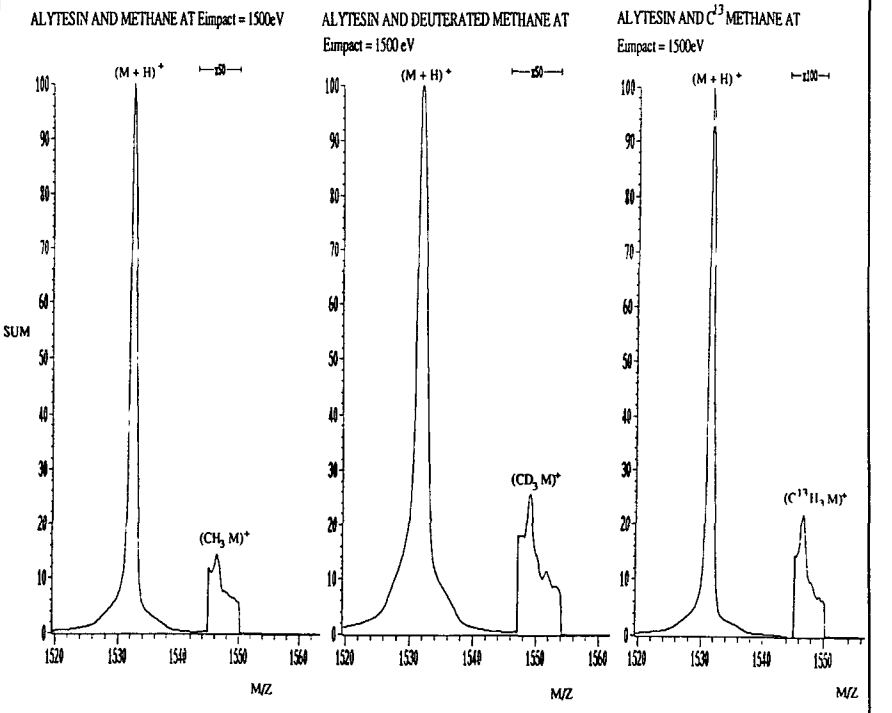

Correlation of Energy Losses from CID with Observed Peptide Fragments

Richard W. Vachet, Andrew D. Winders, and Gary L. Glish
Department of Chemistry, University of North Carolina, Chapel Hill 27599-3290

Introduction: Collision- induced dissociation (CID) has been used quite extensively in mass spectrometry to bring about the dissociation of ions and allow for the elucidation of analyte structure. In CID, some of an ion's kinetic energy is converted into internal energy upon collision with a neutral target. It is known that the kinetic energy lost upon collision(s) is proportional to mass.[1] The kinetic energy lost is also related to the amount of internal energy taken up by any individual ion. To see dissociations of different critical energies on the same time scale, different amounts of internal energy need to be deposited into the parent ion. This should be evident in the kinetic energy lost by the parent ion in the formation of different product ions.

Thus we postulate that measuring the energy losses in the formation of product ions may provide a means for identifying product ion types in complex spectra. Also, the magnitude of the energy loss may provide some insight into the mechanism of the fragmentation pathway and intramolecular interactions.

Experimental: Experiments were performed using a Finnigan MAT 900 instrument which has the normal (EB) geometry. Ions were generated by FAB using an 8 keV Argon beam and glycerol as the liquid matrix. Various peptide were used including leucine enkephalin and analogues, bradykinin, des- Arg[1]- bradykinin, and Substance P. Data was obtained using a B^2/E linked scan which provided the desired energy information of a parent ion when a particular product ion was selected. Helium was used as a collision gas and enough was added to attenuate the beam 60-70%. To determine the energy loss during CID, two experiments were performed. Observing the metastable decomposition of the parent ion to a particular product ion served as the reference to compare the energy lost by a parent during CID. Mass values reported by the data system were converted to energies and energy losses were calculated.

Results and Discussion: The rate of dissociation of an ion is a function of a number of parameters:

$$k=\nu\left(\frac{\epsilon-\epsilon_o}{\epsilon}\right)^{N-1}$$

where ν is a frequency factor, ε is the internal energy of the ion, ε_o is the critical energy of a particular decomposition, and N is the number of degrees of freedom of the ion. In our experiments the time scale is fixed, and for a given ion, N is fixed. Since product ions of a particular type presumably have the same mechanism for formation and thus similar critical energies, they should show similar energy losses. This is indeed evident for a number of peptides. For example the $\mathbf{y_2}$, $\mathbf{y_3}$, and $\mathbf{y_4}$ ions of leucine enkephalin (YGGFL) show energy losses of 4.59, 3.57, and 3.74 eV respectively. A general trend that is also seen is that **a**- and **b**- type ions have greater energy losses than do **y**- type ions. Likewise, **a**- type ions show greater energy losses than **b**- type ions. These results make sense in view of the accepted mechanism for the formation of these type ions. Also note that the energy losses for a particular fragment type increase with increasing mass (Figure 1).

An ion that shows a particularly interesting result is the $\mathbf{b_8}$+ OH ion of bradykinin (RPPGFSPFR). Previous studies have shown that this ion results from the loss of the C-terminal arginine and not the N- terminal arginine which would give the isomeric $\mathbf{y_8}$ ion.[2] The formation of this ion involves a rearrangement, and ion decompositions that involve rearrangements generally have lower critical energies than simple cleavages. This seems evident in the energy loss measurement for this ion, since the value is substantially lower than for other values for bradykinin.

Another general trend in the energy losses can be noticed in the peptides that contain arginine

(R). Product ions that correspond to fragmentations on the amino acid adjacent to the arginine tend to show surprisingly large energy losses. The trend can be noticed for the $\mathbf{b_8}$ ion of bradykinin and the $\mathbf{y_4}$ and $\mathbf{a_4}$ ions of YGRFL and can possibly be attributed to the side chain of the arginine interacting with the carbonyl oxygen on the adjacent amino acids and forming some type of second order structure. More energy is needed to disrupt this interaction and cause the resulting dissociation. Efforts to use computer modeling to verify this are underway.

Conclusions: The amount of energy loss by a particular ion during CID is related to the type of fragmentation that occurs. These variations in energy losses are attributed to the differences in critical energy and mechanisms of the fragment types. The size of the energy loss may help elucidate mechanisms in the formation of various product ions. Furthermore, the energy loss of a parent ion in the formation of a particular product ion may serve as a means of classifying fragment types. This should facilitate the interpretation of the MS/MS spectra of peptides and thus simplify the sequencing of peptides by mass spectrometry.

Table 1
Energy losses of selected peptides (eV)

YGGFL	YGRFL	RPPGFSPFR
a_5 = 4.26	a_4 = 13.00	a_8 = 15.05
a_4 = 5 48	b_4 = 5.61	a_6 = 19.74
b_4 = 3.52	b_3 = 7.03	a_5 = 22.93
b_3 = 7.36	y_4 = 8.83	b_8 = 17.87
y_4 = 3.74	y_3 = 4.89	b_6 = 12.78
y_3 = 3.57	b_4+H_2O = 2.98	y_7 = 11.06
y_2 = 4.59		b_8+OH = 5.56

Figure 1

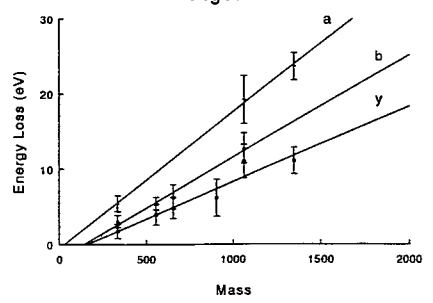

1. Neumann, G. M.; Derrick, P. J.; *Org. Mass Spectrom.*, **1984**, 19, 165-170.
2. Thorne, G. C.; Ballard, K. D.; Gaskell, S. J.; *J. Am Soc. Mass Spectrom.*, **1990**, 1, 249-257.

Peptide Sequencing by MS/MS Using a Hybrid Magnetic Sector-Orthogonal Acceleration Time-of-Flight Mass Spectrometer

Yiping Sun, Mark D. Bauer, Martin P. Lacey and Thomas Keough, The Procter and Gamble Company, Miami Valley Laboratories, P. O. Box 538707, Cincinnati, OH 45253-8707

Introduction MS/MS sequencing using a triple quadrupole mass spectrometer has proven to be a powerful technique for the structural characterization of peptides. However, because of the low-energy collision process, it generates very few side-chain fragments (d, w, and v ions). High-energy collision-induced dissociation (CID) using four-sector mass spectrometers provides side-chain fragmentation, unit mass selection of precursor ions and accurate mass measurement of product ions. However, these instruments are very expensive and relatively difficult to operate. A novel combination of a magnetic sector and orthogonal acceleration time-of-flight (oa-TOF) mass spectrometer is an alternative approach offering several advantages: high sensitivity, high mass accuracy and both low- and high-energy CID (1, 2). In this study, peptide sequencing using the VG Zabspec instrument is demonstrated. Data obtained from both fast atom bombardment and electrospray ion sources is presented.

Experimental oa-TOF MS/MS experiments were performed on a VG ZabSpec instrument. Peptides were ionized with either fast atom bombardment (FAB) or electrospray ionization (ESI). For FAB ionization, the instrument was operated at 8 kV acceleration voltage and 800 V collision energy. The TOF detector was set at 2350 V. The collision gas used was xenon, helium or methane. The product ions from CsI cluster ions were used for calibrating the instrument. For electrospray ionization, ions were decelerated from initial energies (4000 V) to 400 V for singly, 200 V for doubly, and 133 V for triply charged ions.

Results and Discussion Detailed evaluations on optimal collision gas pressure, sensitivity, mass accuracy, peptide size, and peptide type (e.g. linear, cyclized, difulfide-bonded, and phosphorylated), were performed. Good spectra were obtained with as little as 10 picomoles of material using FAB. Oxidized bovine insulin B chain (MH^+=3496.9) was fragmented extensively (Figure 1), while bovine insulin (MH_2^{2+}=2867.6) showed only two major fragment ions corresponding to both A chain and B chain, with Xe as the collision gas (Figure 2). Using renin tetradecapeptide (MH^+=1758.7) as a model peptide, the optimum collision gas pressure was 6.5-8.5x10^{-7} mbar for xenon, 4-5x10^{-7} mbar for helium, and 1-2x10^{-6} for methane. In addition, a variety of peptides were tested. Data indicated that oa-TOF MS/MS can be used to sequence phosphorylated peptides (e.g. $PP^{60C\text{-}SRC}$ carboxyl-terminal phosphoregulatory peptide) and cyclic peptides (e.g. gramicidin-S and cyclosporin-A). For intramolecular disulfide-bonded peptides like oxytocin, MS/MS of the (MH^+) peak showed weak fragmentation. MS/MS of the $(MH+2)^+$, the reduced form generated during FAB analysis, showed good fragmentation. Intermolecular disulfide-bonded peptides like glutathione (oxidized form) can be also sequenced. Figure 3 is a plot of the ratio of relative intensity of d11/a11 of renin tetradecapeptide as a fuction of the collision energy in FAB mode. This plot is similar to high energy CID data from four sector type MS/MS systems (3). Figure 4 is the ESI-oa-TOF MS/MS spectrum of the doubly charged ion (MH_2^{2+}=769.0) of fibrinopeptide A. The side-chain fragment ion W8 indicates the amino acid residue at position 9 is Leu, not Ile. Because of much lower ion transmission for multiply charged ions, a few hundred picomoles of peptides were needed to obtain a good spectrum in the electrospray mode.

Conclusions The combination of a sector instrument and an oa-TOF mass analyzer for peptide sequencing provides: 1. good mass accuracy for product ions, better than ± 0.3Da; 2. high sensitivity at low picomole levels for both FAB and ESI; 3. both high- and low-energy CID; 4. choice of different collision gases; 5. good mass selection of precursor ions; 6. good product ion resolution, 1000-1500 (FWHM); 6. sequencing peptides up to 4000 Da; and 7. easy to use.

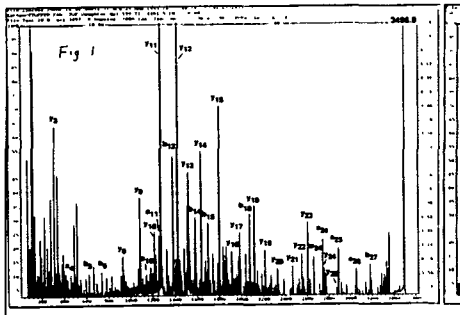

FAB-oa-TOF MS/MS Spectrum of Oxidized Insulin B-Chain

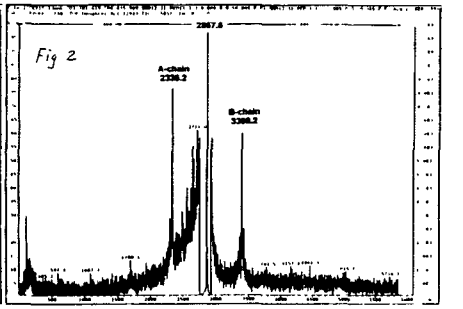

FAB-oa-TOF MS/MS Spectrum of the Doubly Charged Ion (m/z =2867.6) of Bovine Insulin (Mwt=5733)

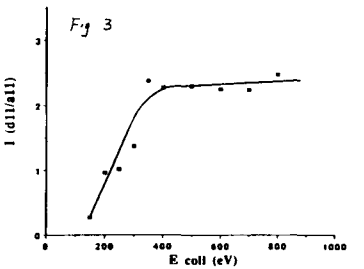

Plot of the ratio of relative abundance of product ions (d11 and a11) as a function of the collision energy (E_{coll}) in the FAB-oa-TOF MS/MS spectra of renin substrate using xenon as collision gas. Each data point represents the average of three runs.

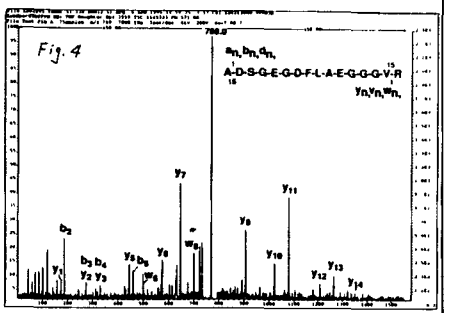

ESI-oa-TOF MS/MS Spectrum of Fibrinopeptide A from the peak $(M+2H)^{2+}$ Showing a Side-Chain Fragment Ion of Leucine (W_8)

References 1. R.H. Bateman, M.R. Green and G. Scott, Proc. 42nd ASMS, p. 1034, 1994; 2. R.H. Bateman, R.S. Bordoli and C. Braybrook, Proc. 41st ASMS, p. 928, 1993; 3. S.A. Martin, Proc. 37th ASMS, p. 858, 1989.

Peptide Fragment Mass Spectra: Comparison of PSD and CID

Wade Hines, John Peltier, Frank Hsieh and Stephen A. Martin
PerSeptive Biosystems Inc., 500 Old Connecticut Path, Framingham, MA 01701

Protein sequence determination is essential to a broad range of disciplines including a critical role in linking cellular phenomena to their genetic origins. We are pursuing strategies which integrate sample purification, enzymatic digestion, chemical derivatization and sequence ladder creation with mass spectrometric based detection to enable rapid and reliable sequence identification of peptides and proteins Matrix-assisted laser desorption (MALDI) post-source decay (PSD) analysis of peptides is one key feature of this program. PSD allows for peptide sequence determination from the mass analysis of gas-phase fragment ions in a manner very similar to collision induced dissociation (CID) commonly done with triple quadrupole, multisector or hybrid tandem mass spectrometers. In analysis of peptides by MALDI, PSD fragmentation occurs spontaneously within the time frame of a reflector time-of-flight (TOF) mass spectrometry experiment. The fragmentation pathways observed in PSD analysis are familiar from both high and low energy CID of peptides but the mix of immonium ions, internal sequence fragments, and other sequence ions requires new strategies in order to capitalize on this route to discover sequence information.

Using commercially available peptides and peptides from mixtures produced by enzymatic digestion, we acquired the PSD spectra by MALDI and in some cases compare this to that obtained by low-energy CID on a triple quadrupole with electrospray ionization. PSD spectra included those obtained with timed ion selection from peptide mixtures.

PSD spectra provided extensive sequence data from a wide mass range of peptides including the oxidized B chain of bovine insulin (Ave. MH^+ 3496.9) and the hemoglobin tryptic peptide representing the sickle cell mutation (monoisotopic MH+ 922.54). The insulin B chain spectrum obtained from sinnapinnic acid as a matrix includes an extensive y ion series from y9 to 28 (Figure 1). It further includes b ions with both complementary and additional sequence information. Somewhat suprizingly, PSD spectra obtained from alpha cyano as a matrix yielded less overall sequence information but it did yield more extensive immonium and lower mass fragments. The insulin B chain sequence data was complete for internal regions of sequence but lacking near the termini. This is common among the larger peptides studied. The difficulty with terminal regions is inherent in the technic because even when sequence ions are present, internal fragment ions can offer false sequence trails near low mass region. The tendency to detect strong b2 and bn+18 ions may in part compensate for this difficulty. In all cases, additional sequence information, perhaps from ladder sequencing techniques is expected to prove useful to assist and extend sequence interpretation (Patterson et al. ASMS 95). Suppresion of the sample ion signal can also be a problem in MALDI resulting in poor signal to noise and little or no PSD information, eg. the unmodified peptide ALILTLVS yield no signal. When this peptide was derivitized with a quartenary ammonium functionality (reagent a gift from Darrel Pappin) a strong molecular ion and extensive PSD was obtained (Figure 2).

In general, PSD spectra were found to include much more internal sequence fragments and more immonium ions. The extent of immonium ion data for PSD appears to be between that found in high and low energy CID. Strong signals, for example His at 110, are common in PSD and document some of the amino acids present in a peptide but the lack of an immonium ion for an amino acid does not appear to be a reliable indication that a given amino acid is absent. This is especially true for competing cases. While Phe normally yields a peak at 120, this signal is absent in the peptide DRVYIHPFHLLVYS. Finally, precharged derivatives can offer a method to enhance the primary ion yield and PSD information.

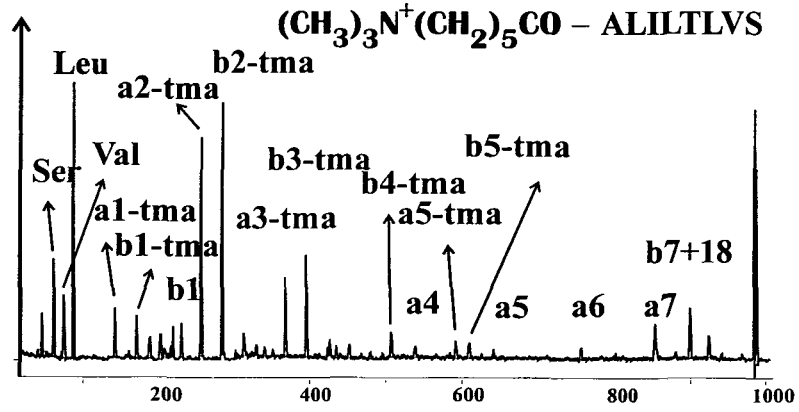

Figure 2. PSD MALDI-TOF mass spectrum of ALILTLVS derivitized with a quartenary ammonium functionality (reagent a gift from Darrel Pappin) exhibiting a strong molecular ion and extensive sequence specific fragment ions.

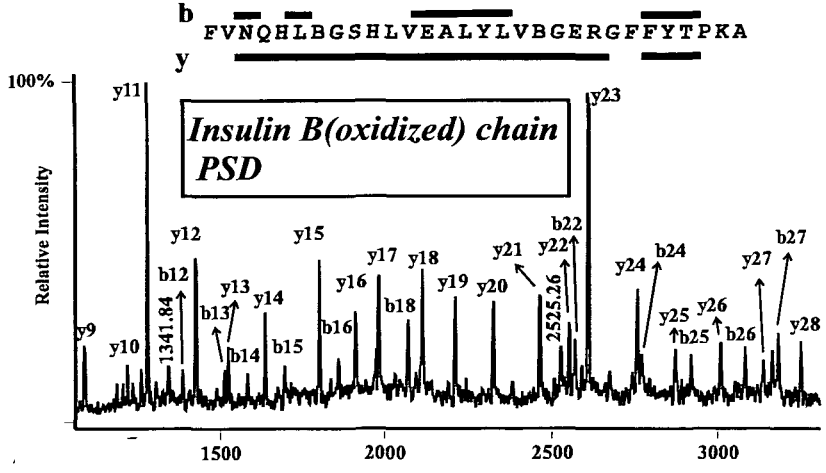

Figure 1. PSD MALDI-TOF mass spectrum of oxidized B chain of bovine insulin (Ave. MH^+ 3496.9) obtained from sinnapinnic acid as a matrix showing an extensive y ion series from y9 to 28.

COLLISONALLY ACTIVATED DISSOCIATION AND PHOTODISSOCIATION STUDIES OF MULTIPLY CHARGED IONS

Clifford H. Watson, Petia Shipkova, Richard D. Burton, Alan R. Katritzky, and John R. Eyler, Department of Chemistry, University of Florida, Gainesville, FL 32611-7200

In principle, multiply charged ions should be less stable than their singly charged analogs due to the inter-molecular strain resulting from columbic repulsions associated with two or more charged sites on an individual molecule. Prior to the emergence of electrospray ionization (ESI), detection of intact multiply charged ions was difficult because: (i) the intrinsic instability of such ions often leads to fragmentation; (ii) doubly charged ions often cluster with a counter-ion; and (iii) the loss or gain of a single electron is often favored[1]. Techniques used previously to study selected multiply charged organic halide and diquaternary ammonium salts have included FDMS[2], SIMS[3], LDMS[4], PDMS[5], and FAB[6] We report our initial results on the generation and dissociation of multiply charged organic cations using ESI coupled with Fourier transform ion cyclotron resonance (FTICR) mass spectrometry.

Previously, we have reported the production of singly charged cations using LD/FTICR and determined the CAD dissociation thresholds and infrared multiphoton dissociation pathways for a number of substituted alkyl pyridinium cations. These results are being extended using ESI to produce a series of doubly charged substituted alkyl pyridinium di-cations for study in the gas phase.

The di-cations are generated using an external ESI source, transferred to the FTICR analyzer cell using electrostatic ion optics, and trapped in the analyzer cell where they can be allowed to react with neutral molecules or fragmented using either collisional activation or laser-induced infrared multiphoton dissociation. In addition, we are also interested in studying multiply charged peptide molecules in a similar fashion.

The organic di-cation salts were dissolved in 50:50 (v:v) water/methanol solution at a concentration of 10^{-3} to 10^{-5} M and infused into the ESI source at a rate of 1 µl/min The relative intensity of the doubly charged cations for these organic salts was found to be concentration dependent. Lower concentrations tended to form a higher relative abundance of the doubly charged species while higher concentrations tended to favor production of "cluster" ions. Cluster ions consisted of one or more cations (CAT^{++}) associated with one or more anions (AN^-).

Shown in Figure 1 are portions of a typical ESI/FTICR mass spectrum of N-benzyl-2,4-diphenyl-6-[(N-methyl)-3-pyridinium] pyridinium di-perchlorate. When analyzed by ESI this compound tends to form two "cluster" ions $[2(CAT^{++})3(AN^-)]^+$ at m/z 1127 and $[(CAT^{++})(AN^-)]^+$ at m/z 513, a singly charged cation at m/z 413, and the doubly charged cation at m/z 207 as shown in Scheme 1 The doubly charged cation at m/z 207 undergoes dissociation via loss of $C_7H_7^+$ to produce the singly charged ions at m/z 91 and m/z 323 Similar dissociation patterns, i.e. loss of a singly charged alkyl cation and formation of a singly charged pyridinium cation, were observed for the other doubly charged pyridinium cations.

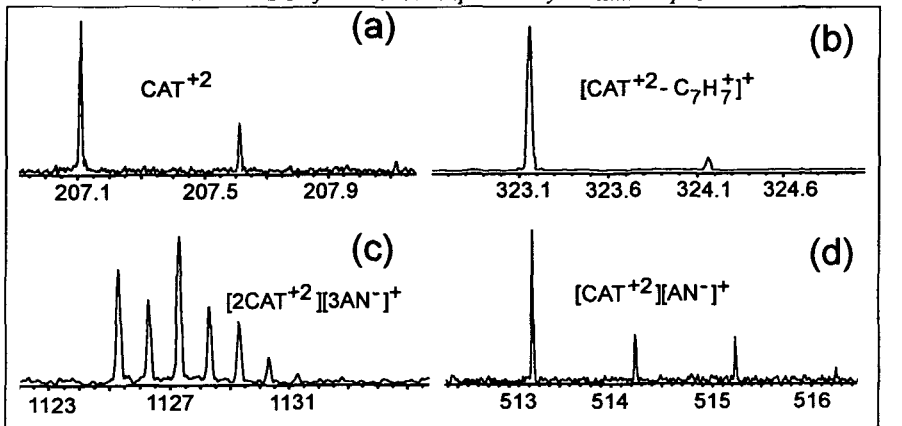

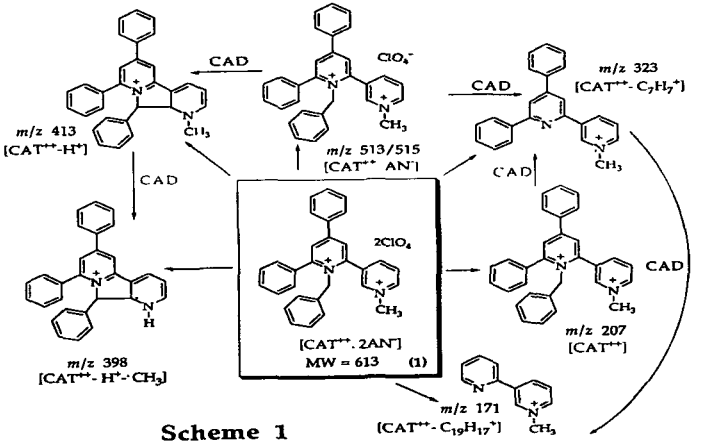

Scheme 1

1. KL Laali, J Phys Org. Chem. 7, 465, 1994.
2. DN Heller, J Yergey, and RJ Cotter, Anal. Chem. 55, 1310, 1983.
3. TM Ryan, RJ Day, and RG Cooks, Anal. Chem. 52, 2054, 1980
4. TA Dang, RJ Day, and DM Hercules, Anal. Chem 56, 866, 1984.
5. KL Laali, G Maas, JE Hunt, A wagner, and RP Lattimer, Tetrahedron Lett., 29, 3463, 1988.
6. GJ Kunkel, KL Busch, R Dunphy, DJ Burinsky, R Barak, P Bel, G Amitai, and A Vincze, J. Mass Spectrom , 30, 282, 1995

Impulsive Excitation of Ions During Surface-Induced Dissociation

John A. Burroughs, Samuel B. Wainhaus, and Luke Hanley
University of Illinois at Chicago
Department of Chemistry, m/c 111
Chicago, IL 60607-7061

While surface-induced dissociation (SID) has been demonstrated for a variety of ion-surface collision partners, little is known about its mechanism of excitation and fragmentation. The large assortment of ions which are amenable to fragmentation analysis via SID suggests that there exists a general mechanism which applies to the majority of ion-surface pairs. These experiments describe a three step model of SID which was previously applied to the dissociation of $Cr(CO)_6^+$ scattered off organic multilayers [1].

These experiments used a tandem mass spectrometer coupled to an ultrahigh vacuum surface analysis chamber [2]. The detecting quadrupole was used to measure the scattered ion kinetic energies.

These experiments scattered 20 to 90 eV $FeCp_2^+$ (Cp = cyclopentadiene) and $SiMe_3^+$ ions off multilayers of propylene (C_3H_6), hexafluoropropylene (C_3F_6), and tetrachloroethylene (C_2Cl_4) adsorbed on Ni(111). The ion internal energies following the surface collisions of the different multilayers were estimated from the relative fragment ion intensities and are shown in Figures 1 and 2 (discrete data points). The kinetic to internal energy transfer efficiencies varied as follows: C_2Cl_4 (~15%) ≥ C_3F_6 (~14%) > C_3H_6 (~10%). The scattered ion kinetic energies were less than 10% of the incident ion energy and did not depend upon the incident ion energy or angles, but did depend upon the chemical identity of the multilayer.

The experimental data was analyzed in terms of a three step model of SID consisting of impulsive excitation, inelastic scattering and unimolecular dissociation. The impulsive collision model predicts the average internal energy, <Q>, imparted to a polyatomic ion during a surface collision to be

$$\langle Q\rangle = E \cdot [2M_aM_s/(M_s + M_a)^2] \cdot [M_s(M_{ion}-M_a)/(M_{ion})^2]$$

where E is the ion kinetic energy, M_a is the mass of the atom/functional group in the ion impulsively excited during the collision (Me or Cp), M_s is the effective mass of the surface (one adsorbate molecule), and M_{ion} is the mass of the entire ion [1]. The predictions of the impulsive model for the internal energies imparted to each ion are shown in Figures 1 and 2 (solid lines). Impulsive excitation was estimated to occur within 10 - 35 fs of the ion impact.

Inelastic scattering and unimolecular dissociation were the latter steps of this model. Both $FeCp_2^+$ and $SiMe_3^+$ underwent inelastic scattering, with the surface dissipating ~70% of the incident ion kinetic energy. Unlike the unimolecular dissociation observed for $Cr(CO)_6^+$ scattering off organic monolayers [1], the inelastic scattering and dissociation were separate here. Both $FeCp_2^+$ and $SiMe_3^+$ must have dissociated at the surface within 3 ps of the initial impact since all fragments from a given parent had similar kinetic energies.

Acknowledgment is made to the National Science Foundation (CHE-9220393) for support of this research. L.H. is supported by a National Science Foundation Young Investigator Award (1994-99).

1) J.A. Burroughs, S.B. Wainhaus and L. Hanley, J. Phys. Chem. **98** (1994) 10913.
2) Q. Wu and L. Hanley, J. Phys. Chem. **97**, 2677 (1993).

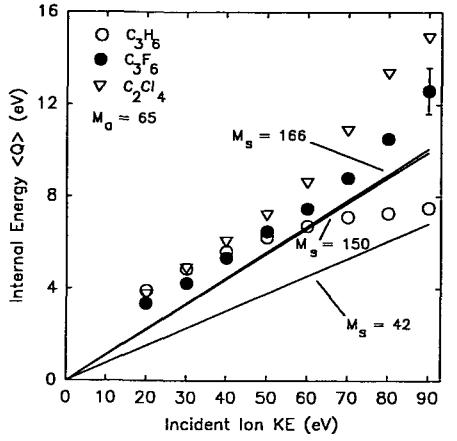

Figure 1: Kinetic to internal energy transfer efficiencies for $FeCp_2^+$ scattered off three separate organic multilayer covered Ni(111) surfaces: efficiency increased with surface mass. The solid lines are the prediction of the impulsive collision model (see text).

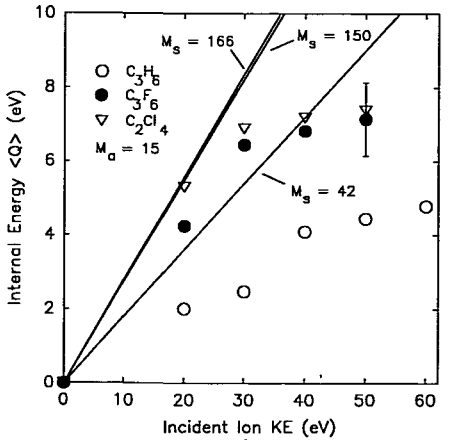

Figure 2: Kinetic to internal energy transfer efficiencies for $SiMe_3^+$ scattered off three separate organic multilayer covered Ni(111) surfaces: efficiency increased with surface mass. The solid lines are the prediction of the impulsive collision model (see text).

Electrospray Mass Spectra of Simple Aliphatic Diamines and Their Methosalts.

Xiaokui K. Zhang and Henry M. Fales

Laboratory of Biophysical Chemistry, National Heart, Lung, and Blood Institute, Bethesda, MD 20892-1676

For many years mass spectrometrists have been interested in charge repulsion in dicationized ions. Such ions, difficult to prepare in aliphatic systems using electron impact, are easily formed in electrospray mass spectrometry. Gross et al. (J. Phys. Chem. (1995) 99 4034) have recently reported the detection of doubly protonated α,ω-diamines $H_2N(CH_2)nNH_2$ when $n \geq 7$, and discussed their properties as studied by FTMS. Using a Finnigan TSQ-700 we have examined the corresponding permethylated diamines $(CH_3)_2N(CH_2)_nN(CH_3)_2$ where n=1-12 and their methiodides, also with a view toward examining the effects of charge repulsion on their subsequent decomposition by collisional processes.

In general, we find that the spectra of both the diamines and their methiodides are very dependent on the presence of auxiliary gas, concentration, and high tube (skimmer) voltage. All of these tend to reduce the intensity of the ions, especially those which are doubly charged (see Fig. 1). The free amines or their dihydrochlorides provide low intensity $(M+H)^+$ ions. When examined by MS/MS, these ions show as their main fragmentation pathway loss of dimethylamine, likely by a cyclic process involving participation by the uncharged amino group on the opposite end. Shorter chains, where $n \leq 4$ fail to show any doubly protonated ions. However, in contrast to the results of Gross et al. when $n \geq 5$ doubly protonated ions were indeed observed, probably due to their increased basicity due to methylation. These doubly charged ions also were examined by MS/MS and were found to cleave to singly charged ions by loss of dimethylammonium ion instead of dimethylamine. The very stable $(CH_3)_2N{=}CH_2^+$ and simple $C_nH_{2n-1}^+$ ions were also observed.

Spectra of the dimethiodides are considerably more complex. These show two series of ions. One is singly charged, deriving from adduction of an iodide ion and its relative intensity is augmented as expected by the addition of NH_4I. The other is the doubly charged ion itself and it is the base peak as long as auxiliary air is not used and the concentration kept low (Fig. 1). The iodide- adducted ion undergoes attack on either the methyl or methylene group adjacent to the positively charged nitrogen losing either methyl iodide or trimethylamine, respectively. The ion losing methyl iodide then undergoes loss of trimethylamine from the opposite end forming a cyclic ammonium salt. The other iodine-containing ion (resulting from attack on the methylene group) can split to form either a cyclic iodonium ion (if n=3 or 4) or undergo homolysis producing the radical cation of trimethylamine. The doubly charged diquaternary cation undergoes proton rearrangement losing trimethylammonium ion and $(CH_3)_2N{=}CH_2^+$ or simple homolysis to form the two radical cations m/z $59^{+\bullet}$ and $M\text{-}59^{+\bullet}$. Of considerable interest is the offset voltage applied to the collision cell that is required to cause this process to occur to the extent that these two ions are equal in intensity (Fig. 2). As can be seen, it is very nearly linear with respect to the chain length and does not reflect simple Coulombic repulsion.

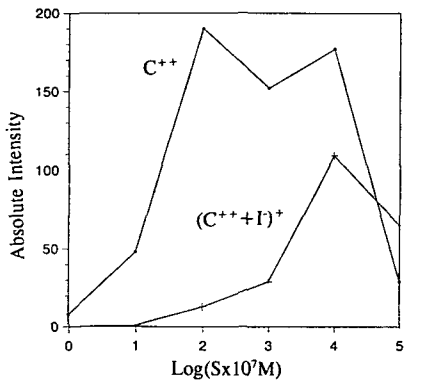

Fig.1 Effect of N,N,N',N'-tetramethyl nonanediamine 2MeI concentration (S) on the intensities of C^{++} $(C^{++}{:}(CH_3)_3N^+\text{-}(CH_2)_9\text{-}N^+(CH_3)_3$ and $(C^{++}+I^-)^+$.

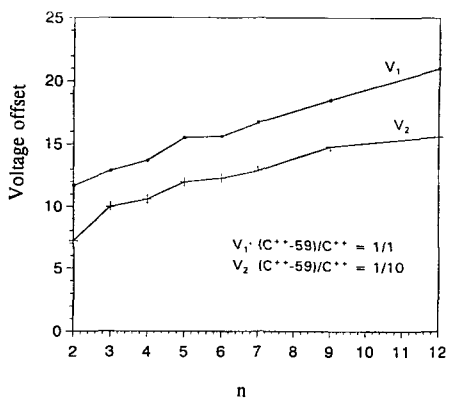

Fig.2 Variation of voltage offsets applied on collision cell for the cleavage of C^{++} to $[C^{++}\text{-}N^+(CH_3)_3]^+$ $(C^{++}\text{-}59)$ with n=1-7,9,12 for $(CH_3)_2N\text{-}(CH_2)_n\text{-}N(CH_3)_2$

Thermal radiative dissociation of covalent weakly-bound cations

Chuan-Yuan Lin and Robert C. Dunbar*
Chemistry Department, Case Western Reserve University, Cleveland, OH 44106
D. Scott Tonner and Terrance B. McMahon*
Chemistry Department, University of Waterloo, Waterloo, Ontario N2L 3G1, Canada

Radiatively activated thermal dissociation (ZTRID) has been demonstrated to be a promising technique to study weakly-bound ions, with dissociation energies in the range 0 5-1.0 eV Under extremely low pressure conditions, the dissociation can be activated radiatively by absorption of IR photons from surrounding A thermal dissociation theory has been described recently by Dunbar[1] which uses a steady-state truncated Boltzmann distribution and a simplified Tolman equation to extract the dissociation thermochemistry The main interest of the present work is carrying out the ZTRID experiment on some well behaved systems and extracting their thermochemical information using the thermal dissociation theory Here, the bond dissociation energies and corresponding thermochemical information of $Si(CH_3)_4^+$ (TMS) and $Si(C_2H_5)_4^+$ (TES) are reported.

Experiments were performed on an ion cyclotron (ICR) mass spectrometer The loss of the first ligand, L (L= CH_3^- or C_2H_5) from the parent ions gave the daughter ions, SiL_3^+ Both parent ions also react with a water molecule to give another product ions, $SiL_3(H_2O)^+$ The reaction scheme is:

$$SiL_4^+ \xrightarrow{k_r} SiL_3^+ + L \qquad (1)$$

$$SiL_4^+ + H_2O \xrightarrow{k_w} SiL_3(H_2O)^+ + L \qquad (2)$$

Fig 1 shows the time plots along with kinetic fits using this scheme. The nonzero intercept in the rate-pressure plots (Fig 2) indicates that the dissociation processes were activated radiatively. Using different buffer gases, CH_4 and C_4H_{10}, the y-intercept was the same (Fig. 2a) The activation energy (E_a) of eqn.1 can be derived from the Arrhenius plots (Fig. 3) which give 0 45 and 0 43eV for TMS and TES respectively To obtain the dissociation threshold energy, E_t, one can use either the Tolman equation or master equation modeling. From the result of the Tolman equation, E_t is estimated to be 0.56 and 0 70eV respectively. Master equation modeling gives E_t of 0.56 and 0.71eV respectively The dissociation threshold energies obtained from these two analyses are surprisingly consistent The heats of formation of the ion species, SiL_3^+, were derived from the E_t values and are shown in Table 1 As seen in the Table 1, the heat of formation of $Si(CH_3)_3^+$ is in excellent agreement with Baer's results The discrepancy of previous literature values of $\Delta H_f^0(Si(C_2H_5)_3^+)$ makes it difficult to compare the present value However, based on the sucess in estimating $\Delta H_f^0(Si(CH_3)_3^+)$ using ZTRID, the value of $\Delta H_f^0(Si(C_2H_5)_3^+)$ derived in this work is considered to be more reliable than the previous results From this quantitative study, it appears that ZTRID is a useful technique to measure the dissociation thermochemistry of weakly covalent bound ions

Table. 1 Heats of Formation

	$\Delta H_f^0{}_{298k}$(kcal mol^{-1})
$Si(CH_3)_4^+$	170[a]
$Si(C_2H_5)_4^+$	142[b]
$Si(CH_3)_3^+$	150.5±0.9[c]
	149.7±1[d]
$Si(C_2H_5)_3^+$	125[e]
	139[f]
	131.7±1[d]

[a]Ref 2 [b]Ref. 3 [c]Ref.4 [d]Present work [e]Ref 5 [f]Ref. 6.

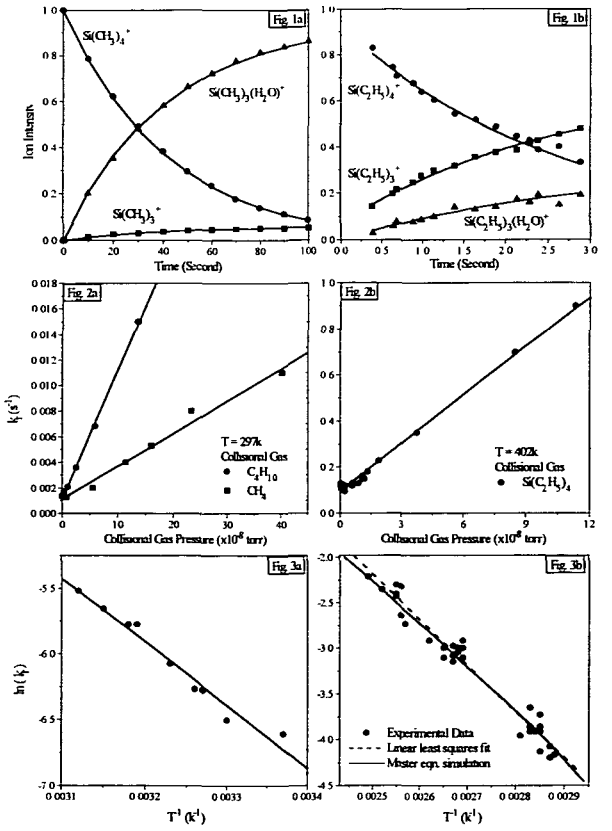

[1] Dunbar, R. C. *J. Phys Chem.* **1994**, 98, 8765.
[2] Steele, W V *J. Chem Thermodyn* **1983**, 15, 595
[3] Pedley, J. B ; Rylance, J. "Sussex-N P L Computer Analysed Thermochemical Data Organic and Organometallic Compounds", University of Sussex (1977)
[4] Szepes, L., Baer, T. *J Am Chem Soc.* **1984**, 106, 273.
[5] Ridder, J.J. de, Dijkstra, G. *Rec. Trav. Chim.*, **1967**, 86, 737.
[6] Potzinger, P., Ritter, A.; Krause, J *Z. Naturforsch. A* **1975**, 30, 347

Some more $C_3H_6O_2^{+\cdot}$ distonic ions

Yan An & John L. Holmes
University of Ottawa, Ottawa, Ontario

The experimental results presented here describe the direct production and characterization of the distonic radical cations $\dot{C}H_2CH_2{-}O{-}\overset{+}{C}HOH$ and $\dot{C}H_2CH_2\overset{+}{C}(OH)_2$.

Formation of $\dot{C}H_2CH_2O\overset{+}{C}HOH$ and $\dot{C}H_2CH_2\overset{+}{C}(OH)_2$

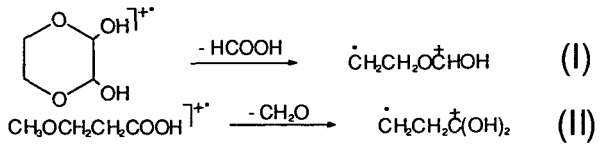

Characterization of $\dot{C}H_2CH_2O\overset{+}{C}HOH$ (I)

The MI mass spectrum of ion **I** (Table 1) shows that this distonic ion is distinguishable from its conventional isomer $[HCOOCH_2CH_3]^{+\cdot}$ by the intense fragment $C_2H_4^{+\cdot}$ and minor presence of $C_2H_5O^+$.

The doubly charged ion peak in the CID mass spectrum of **I** (Table 2) further confirms that this ion is more stable than $[HCOOCH_2CH_3]^{+\cdot}$. Indeed the $\Delta_f H^\circ$ value of **I** has been determined by an appearance energy measurement to be 137 ± 4 kcalmol^{-1}, which is 16 kcalmol^{-1} lower in energy than $HCOOCH_2CH_3^{+\cdot}$.

Characterization of $\dot{C}H_2CH_2\overset{+}{C}(OH)_2$ (II)

The MI mass spectrum of ion **II** is identical to that of $[CH_3CH_2COOH]^{+\cdot}$ (Table 1), however, the distonic structure of ion **II** is confirmed by $:CH_2$ loss in its CID mass spectrum (Table 2).

$$\dot{C}H_2CH_2\overset{+}{C}(OH)_2\ (II) \rightarrow CH_2C(OH)_2^{+\cdot} + :CH_2$$

Table 1. *MI mass spectra of $C_3H_6O_2^{+\cdot}$ isomers*[1]

Fragments	I	EF	II	PA
$CH_2CHC^+(OH)_2+H^\cdot$	100	100	100	100
$^\cdot CH_2CH_2CO^+ + H_2O$	100	98	-	-
$CH_3CHCO^{+\cdot}+H_2O$	-	-	33	35
$C_2H_5O^+ + HCO^\cdot$	3	-	-	-
$C_2H_6^{+\cdot}+CO_2$	16	17	6	5
$C_2H_4^{+\cdot}+HCOOH$	55	6	-	-

1. Relative intensities (%).

I: $^\cdot CH_2CH_2OC^+HOH$; **EF:** $HCOOCH_2CH_3^{+\cdot}$
II: $^\cdot CH_2CH_2C^+(OH)_2$ **PA:** $CH_3CH_2COOH^{+\cdot}$

Table 2. **CID mass spectra of $C_3H_6O_2^{+\cdot}$ isomers**[1]

Fragments	I	EF	II	PA
$C_3H_5O_2^+ + H^\cdot$	16	100	100	100
$C_2H_4O_2^{+\cdot}+CH_2$	-	-	3	-
$C_3H_4O^{+\cdot}+H_2O$	16	100	51	47
$CH_2O_2^+$, $C_2H_6O^{+\cdot}$	3	6	17	14
CHO_2^+, $C_2H_5O^+$	8	10	60	44
$C_3H_6O_2^{2+}$	1	-	3	3
$C_2H_6^{+\cdot}+CO_2$	5	18	28	22
$C_2H_4^{+\cdot}+HCOOH$	100	99	41	38

1. Relative intensities (%).

I: $^\cdot CH_2CH_2OC^+HOH$ **EF:** $HCOOCH_2CH_3^{+\cdot}$
II: $^\cdot CH_2CH_2C^+(OH)_2$ **PA:** $CH_3CH_2COOH^{+\cdot}$

I dissociates to $C_2H_4^{+\cdot}$ by HCOOH loss. The process is a direct bond cleavage, and thus sensitive towards collisional activation. In contrast, the H_2O loss, which is dominant in the MI dissociation of **I**, is inactive towards collisional activation. Therefore, the process involves other intermediate(s).

Since the daughter ion has been identified as $[CH_2CH_2CO]^{+\cdot}$, the dissociation process involves an O—C bond cleavage and a C—C bond formation. This is proposed to be a concerted process, and a possible intermediate is:

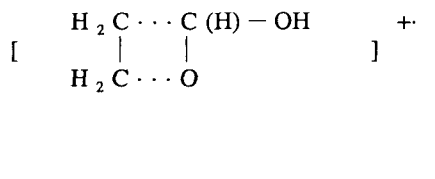

The Fragmentation of Geometric Isomers, Ionized Maleic and Fumaric Acids

Hongwen Chen and J.L. Holmes, University of Ottawa, Canada

The earliest example of geometrical isomerism dates back to the very beginning of three-dimensional chemistry, namely the Z,E isomerism of ethene-1,2-dicarboxylic acid (maleic and fumaric acids) first discussed by Van't Hoff in 1871 The influence of stereochemistry on the mass spectrometry of chemical compounds has long been recognized and the accumulated knowledge in this area has proved worthy of a recent monograph

The mass spectra of maleic and fumaric acids were first described in detail some twenty five years ago In brief, the EI mass spectra of the isomers differ significantly in that ionized maleic acid loses $^{\bullet}OH$, H_2O, CO and CO_2 while its E-isomer loses only $^{\bullet}OH$, H_2O and CO. The loss of CO_2 was proposed to be related to carboxyl-carboxyl interaction and furthermore it was argued that ionized fumaric acid was unable to undergo rotation about the formal C-C double bond - otherwise it too should lose CO_2.

In the present study the full range of tandem mass spectrometry experiments together with Ionization Energy (I.E.) and Appearance Energy (A.E) measurements have been used to extend our understanding of this pair of simple geometric isomers and to correct or modify the earlier speculative proposals.

Typically, geometric isomers have closely similar IEs, this is illustrated in Table 1. However, where the two carboxyl groups are rigidly held in the Z- configuration, o-benzene dicarboxylic acid and maleic acid, the ionization energies are conspicuously lower than those of their isomers This effect must result from carboxyl-carboxyl interaction.

Table 1 Thermochemical data. The experimental results from this work are in bold characters

molecule	IE (eV)	$\Delta_f H^\circ$ neutral (kJ mol^{-1})	$\Delta_f H^\circ$ ion (kJ mol^{-1})
Z-2-butenoic acid	10 08	(- 346)	627
E-2-butenoic acid	9 9	(- 350)	606
m-benzene dicarboxylic acid	9 98	- 696 ± 2	267
p-benzene dicarboxylic acid	9 86	- 718 ± 3	233
o-benzene dicarboxylic acid	**9.4 ± 0.1**	- 675 ± 1	**240 ± 10**
maleic acid (Z)	**10.0 ± 0.1**	- 679 ± 3	**287 ± 13**
fumaric acid (E)	10 7 **10.6 ± 0.1**	- 676 ± 6 (- 704)	355 (319)

In the metastable time frame, the molecular ions of maleic and fumaric acids display two common fragmentation channels, i.e H_2O and CO losses, note that the relative intensities of the MI peaks as well as their kinetic energy releases ($T_{0.5}$ values, in meV) are the same, shown in Table 2 below. Deuterium labelling experiments showed that H atoms did not completely lose their positional identity prior to loss of H_2O.

Molecular Ion	Fragment Ion, m/z						
	100 ($T_{0.5}$)	**99** ($T_{0.5}$)	**98** ($T_{0.5}$)	**90** ($T_{0.5}$)	**88** ($T_{0.5}$)	**74** ($T_{0.5}$)	**72** ($T_{0.5}$)
maleic acid	-	-	**22** (24)	-	**100** (164)	-	**200** (85)
maleic acid-2,3-d_2	**31** (24)	**38** (25)	-	**100** (173)	-	**108** (88)	-
maleic acid carboxyl-d_2	-	**28** (26)	**8** (24)	**100** (156)	-	**35** (88)	-
fumaric acid	-	-	**25** (27)	-	**100** (162)	-	-
fumaric acid-2,3-d_2	**36** (20)	**43** (20)	-	**100** (185)	-	-	-
fumaric acid-carboxyl-d_2	-	**30** (22)	**8** (20)	**100** (157)	-	-	-

43rd ASMS Conference on Mass Spectrometry and Allied Topics

These fragment ions along with those generated in the ion source were examined by CID. It was found that the characteristics of the corresponding ions from both acids are the same. The following reaction schemes, different from the original, are proposed. The structures of fragment ions were confirmed by independently generateing them for comparison with those from maleic and fumaric acids.

Maleic acid (M) has a unique reaction channel:

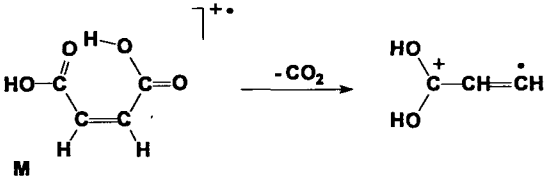

Both maleic (**M**) and fumaric acid (**F1**) rearranged to a common intermediate, **F2**, prior to dissociation.

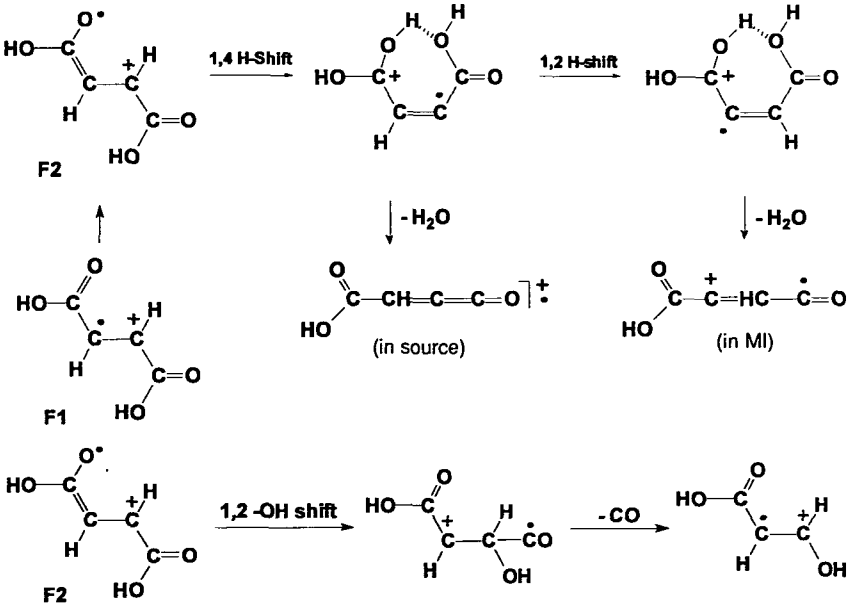

Reference: F. Benoit, J.L. Holmes and N.S. Isaacs, *Org. Mass Spectrom.* 2, 591 (1969).

CHARACTERIZATION OF SMALL HIGHLY OXYGENATED IONS.

C. Aubry and J.L. Holmes,
Chemistry Department, University of Ottawa, Canada.

Producing gas phase ions which have a high oxygen content is not always straightforward due to the tendency of the larger ionized precursor molecules to easily dissociate by losses of H_2O, CO and/or CO_2, thus eliminating some oxygen atoms. Examples of highly oxygenated species are $C_2O_2^+$, $C_3O_2^+$ (1) and $C_3HO_2^+$(2).

The mass spectrometry of different ions of general formula $C_3H_nO_3$ (n = 3 and 4), generated by electron impact of larger precursor molecules is presented here and structural information concerning these ions is described below. The precursor molecules were tartaric 1 and diglycolic 2 acids as well as propylene carbonate 3.

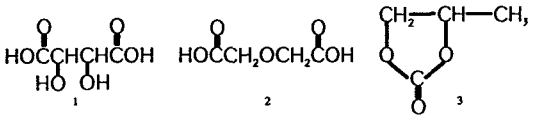

$C_3H_4O_3^{+\cdot}$ ions, m/z 88

Maleic, fumaric(3) and tartaric acids all show in their normal mass spectra the presence of a m/z 88 ion. MI and CA characteristics of these ions are identical. The proposed structure (3) for this ion is:

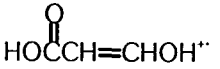

A distinct isomer can be produced by the unimolecular dissociation of diglycolic acid:

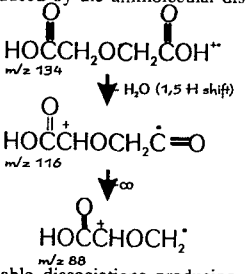

This ion shows three metastable dissociations producing ions at m/z 60 (loss of CO, $T_{0.5}$ = 41meV), m/z 58 (loss of H_2CO, $T_{0.5}$ = 22meV) and m/z 42 (loss of H_2CO_2, $T_{0.5}$ = 13meV). The H_2CO loss being the favoured dissociation channel. The identities of the m/z 60 and m/z 42 are not, as yet, firmly established. Preliminary results on source generated ions suggest that m/z 42 is not ketene, hydroxyacetylene or oxirene. As for the m/z 58 ion, the following distonic ion is in keeping with the CA results:

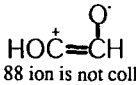

The dissociation of metastable m/z 88 ion is not collision sensitive and no NRMS recovery signal

is obtained when Xe and O_2 are used as neutralization and reionization gases respectively This may indicate that m/z 88 is not a covalently bonded ion, but better represented by an electrostatically bound complex of possible structure $[H_2CO...HCO_2H]^{+\cdot}$.

$C_3H_3O_3^+$ ions, m/z 87

Two distinct $C_3H_3O_3^+$ isomers have been produced from the unimolecular dissociations of tartaric acid and propylene carbonate.

The m/z 87 from tartaric acid shows three metastable process leading to the formation of m/z 69 (loss of H_2O), m/z 59 (loss of CO) and m/z 43 (loss of CO_2), m/z 69 being the predominant one. Three possible structures may be presented for this m/z 87 ion:

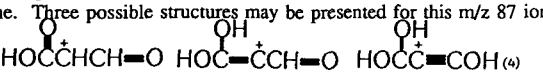

Daughter ion characteristics are needed in order to determine the correct structure for the m/z 87 ion. Dissociation characteristics of source generated m/z 43 indicates that it is not acetyl but most likely CH_2C^+OH ion. The kinetic energy released by this dissociation (114meV) suggests the presence of a large reverse activation barrier which could be associated with a major rearrangement of the precursor species before fragmentation. The CA characteristics of metastably generated m/z 69 from m/z 87 indicates that it is most likely to be $OCCHCO^+$ (2) ion.

The available data indicate that isomers a and b are satisfactory representations of the m/z 87 ion, but more information is needed to decide which particular structure is involved.

The m/z 87 ion from propylene carbonate shows two metastable dissociation processes producing m/z 59 (loss of CO) and m/z 43 (loss of CO_2) daughter ions, the latter being most intense. Characterization of the metastably generated m/z 43 indicates that it is the acetyl cation. Due to the small kinetic energy released by the dissociation of m/z 87 ion into the acetyl cation (1.7meV), the involvement of an ion-neutral complex, $[CH_3CO^+ ..CO_2]$, cannot be neglected That the CA mass spectrum does not indicate that new dissociation channels are opened and that no NRMS recovery signal is observed support proposal.

It has been shown that tartaric and diglycolic acids as well as propylene carbonate could be used as precursor molecules for generating highly oxygenated ions. These ions have structure dependent dissociations. As is often the case, the involvement of electrostatically bound complexes seem to the part of their dissociation.

It is evident that more work is needed to confirm the structures proposed. This will involve labelling compounds with deuterium atoms to provide the mechanistic and structural information needed.

References

(1) H. Chen and J.L. Holmes, *Int. J. Mass Spectrom. Ion Processes*, 133, 111 (1994).
(2) J. Tortajada, G. Provot, J.-F. Gal, P.-C. Maria, R. Flammang, Y, Govaert, *Int. J. Mass Spectrom. Ion Processes*, 141, 241 (1995).
(3) H. Chen and J.L. Holmes, in press, *J. Mass Spectrom.*
(4) M.H. Lien and A.-C. Hopkinson, *J. Mol. Struct. (THEOCHEM)*, 165, 37 (1988).

THE IDENTIFICATION OF $C_3H_6O^+$ FROM 2-METHOXYETHANOL

Michael J. Polce and Chrys Wesdemiotis

Chemistry Department, The University of Akron, Akron, OH 44325

The product formed upon water elimination from ionized 2-methoxyethanol was originally classified, more than 20 years ago, as a mixture of ionized oxetane and methyl vinyl ether.[1] More recently, the C_3H_6O ion produced by H_2O loss from 2-methoxyethanol ions was shown to be a mixture of ionized oxetane and methyloxirane,[2] or oxetane radical cation,[3] or oxetane molecular ion and/or eventually its ring-opened isomer $CH_2CH_2OCH_2^{+\cdot}$.[4] This study[5] presents results which identify the m/z 58 $C_3H_6O^+$ obtained from 2-methoxyethanol and resolve the question outlined in Scheme I.

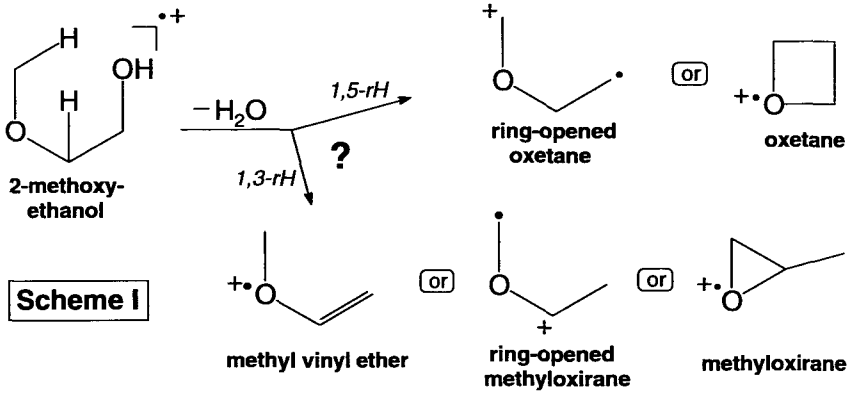

Scheme I

All experiments were performed with a modified VG Autospec instrument of E_1BE_2 geometry.[6] *The structure of source generated or metastably formed $C_3H_6O^+$ product from 2-*methoxyethanol was determined by comparison of its collisionally activated dissociation (CAD) and neutralization-reionization (NR) spectra with reference spectra produced from the above ions listed in Scheme I. Electron ionization of oxetane, methyl vinyl ether, and methyloxirane were used to provide their corresponding molecular ions, while dissociative EI of 1,4-dioxane and 2-methyl-1,3-dioxolane furnished ring-opened oxetane and ring-opened methyloxirane ions, respectively.

The CAD spectrum of m/z 58 from 2-methoxyethanol most closely resembles that of ring-opened oxetane. Both of these spectra include formation of $C_3H_6O^{++}$ dications (m/z 29), indicative of distonic ions; a prominent product of m/z 44 (CH_2 elimination), which is diagnostic for the $CH_2CH_2OCH_2^+$ connectivity;[7] m/z 57 as the most abundant CAD fragment; and a similar m/z 56:55 ratio. In sharp contrast, the oxetane ion shows an increased amount of $C_3H_{0-3}^+$ (m/z 36-39), characteristic of a structure with three carbons in a row; an absence of 58^{++}; and a sizeable m/z 55 fragment. The CAD spectra of the $C_3H_6O^+$ from 2-methoxyethanol and that of ring-opened oxetane are not identical. For example, the former contains more abundant m/z 15 and 42-43 peaks, suggesting that 2-methoxyethanol must coproduce other $C_3H_6O^+$ isomer(s). CAD of reference ions of methyl vinyl ether, ring-opened methyloxirane, and methyloxirane yield substantially more m/z 15 and 42-43. Based on the m/z 42:43 ratio observed for the 58^+ from 2-methoxyethanol, methyl vinyl ether is the best match.

The NR Xe/O_2 spectrum of $C_3H_6O^{+\cdot}$ from 2-methoxyethanol is most like that of ring-opened oxetane with a striking similarity of peak shapes and relative abundances observed for m/z 24-30. Neutralization of ring-opened oxetane ions yield the weakly-bound diradical $CH_2CH_2OCH_2$ that decomposes extensively and with large kinetic energy release to $CH_2{=}CH_2$ (28 u) and $O{=}CH_2$ (30 u).[7] As a result, substantial peak broadening is observed after reionization for m/z 24-30. Only a small fraction of the diradical survives intact based on the intensity of the survivor ion (m/z 58). Compared to ring-opened oxetane, the NR spectrum of m/z 58 from 2-methoxyethanol contains more abundant fragments above m/z 30 and a larger survivor ion. Evidence that at least one more $C_3H_6O^+$ isomer is formed. Based on NR survivor ion yields,[8] the m/z 58:57 ratio, and the relative abundances of m/z 42-43 vs. 58; only methyl vinyl ether can account for the additional component (<14% based upon survivor ion yields).

Metastable 2-methoxyethanol ions, which possess lower internal energies than 2-methoxyethanol ions dissociating in the source, produce a different $C_3H_6O^+$ mixture. The C_3H_6O ions formed in the metastable window yield less m/z 42-43 upon CAD and less ions above m/z 30 upon NR. Hence, 2-methoxyethanol ions of low internal excitation generate a larger proportion of $CH_2CH_2OCH_2^+$ and a smaller amount of methyl vinyl ether. Specifically, based on the absolute intensity of the survivor ion (m/z 58) in the NR spectrum of metastably generated 2-methoxyethanol, <2% of methyl vinyl ether ions are coproduced.

In summary, MS/MS experiments conclusively identify the m/z 58 C_3H_6O ions obtained from 2-methoxyethanol as a mixture chiefly comprised of the distonic radical cation $CH_2CH_2OCH_2^+$ (ionized ring-opened oxetane). These results also strongly indicate that the other minor component is ionized methyl vinyl ether. Methyl vinyl ether ions are thermodynamically more stable but their formation must require a higher critical energy since they are produced with a lower yield from metastable 2-methoxyethanol ions. We find no evidence for the generation of ionized oxetane, methyloxirane, or ring-opened methyloxirane.

REFERENCES

1 Van de Sande, C. C.; McLafferty, F. W. *J. Am. Chem. Soc.* **1975**, 97,4617-4620.
2 Cao, J. R.; George, M.; Holmes, J. L.; Sirois, M.; Terlouw, J. K.; Burgers, P. C. *J. Am. Chem. Soc.* **1992**, 114, 2017-2020.
3 Audier, H. E.; Milliet, A.; Leblanc, D.; Morton, T. H. *J. Am. Chem. Soc.* **1992**, 114, 2020-2027.
4 Milliet, A.; Sozzi, G.; Audier, H. E. *Org. Mass Spectrom.* **1992**, 27, 787-794.
5 Polce, M. J.; Wesdemiotis, C. *J. Am. Soc. Mass Spectrom.* **1995**, submitted April 1995.
6 Polce, M. J.; Cordero, M. M.; Wesdemiotis, C.; Bott, P. A. *Int. J. Mass Spectrom. Ion Processes* **1992**,113, 35-58.
7 Polce, M. J.; Wesdemiotis, C. *J. Am. Chem. Soc.* **1993**, 115, 10849-10856.
8 NR survivor ion yields: (2.2×10^{-6}, ring-opened oxetane); (2.3×10^{-5}, ring-opened methyloxirane); (3.8×10^{-5}, methyloxirane); (4.5×10^{-5}, $C_3H_6O^{+\cdot}$ from 2-methoxyethanol); (1.2×10^{-4}, oxetane); (3.0×10^{-4}, methyl vinyl ether).

Oxygen Rearrangement in N-Substituted Benzizothiazolinones on Electron Impact

József Langó
Department of Structure Research
Institute for Drug Research Ltd.
P.O. Box 82, Budapest, Hungary, H-1325

During the mass spectral studies on N-substituted benzizothiazolinone-1,1-dioxides and N-substituted benzizothiazolinones an oxygen atom rearrangement from the carbonyl group to the sulfur atom leading to loss of SO_3 and SO has been observed. A similar observation of an SO_3 loss has been reported earlier, but it was not confirmed [1].

EXPERIMENTAL

Materials: compounds studied were prepared in the **Institute for Drug Research** by known methods[2].
Mass spectrometric conditions: EI low resolution and MS/MS spectra were taken with a **VG Quattro** tandem mass spectrometer, electron energy of 70eV, trap current 200 μA, source temperature of 150 °C. CID MS/MS conditions: *collision* gas N_2, pressure: 1-6x10^{-4} torr, energy: 120-180 eV, scanning speed: 0.1 sec/decade. The peak intensities reported are the averages from 20-60 consecutive spectra. The HR measurements were made by peak matching method relative to PFK on an **Finnigan MAT 8430** double focusing mass spectrometer. HR conditions: electron energy: 70 eV, trap current: 500 μA, acceleration voltage: 3 kV, source temperature: 250 °C, resolution: 12500 (10 % valley definition).

RESULTS AND DISCUSSION

Fig.(I) contains the compounds studied. Fig.(II) shows (from up to down) the straight *EI⁺ spectrum* of **Ia**, the *product spectrum* of $M^{+\bullet}$ of **Ia** (*m/z*259, $C_{13}H_9NO_3S$, Δ=3.3 ppm) the *precursor spectrum* of ion *a* (*m/z*195, $C_{13}H_9NO$, Δ=2.7 ppm) and ion *b* (*m/z*179, $C_{13}H_9N$, Δ=0.6 ppm). Most of the ions that appear in the EI^+ spectrum of **Ia** are easy to explain by direct decompositions except for the relatively abundant ion *b*. The *product spectrum* of molecular ion of **Ia** is very similar to the EI^+ spectrum the differences are in the ion intensities only. *Precursor spectrum* of ion *a* and ion *b* show that the loss of SO_2 and SO_3 are **one-step processes**, *i.e.* there is an experimantal evidence that ion *b* results from a real rearrangement. Fig.(III) shows the most probable transition structure capable of SO_3 loss, where bonds of the 5-membered ring have been *rearranged*. Driving force of this process may be an interaction of the oxygen lone pair with the low energy unoccupied ***d*** orbitals of sulfur. Similar processes have been observed in the case of the compounds **Ib-c**. Data in Tab.(I) show the intensities of product ions of interest. Comparing these data of **I** type compounds the changes in the column can be explained by the increasing electronaffinities of substituents of **R**. Fig.(IV) shows (from up to down) the EI^+*spectrum* of compound **IIa**, the *product spectrum* of $M^{+\bullet}$ (m/z227, $C_{13}H_9NOS$, Δ=1.5 ppm), the *precursor spectrum* of ion *a* (m/z195, $C_{13}H_9NO$, Δ=1.7 ppm) and ion *b* (m/z 179, $C_{13}H_9N$ Δ=2.4 ppm). The *b* type of ion *has appeared* too, but with low intensity. The transition structure capable of an SO loss, similar to that for **I** type compounds. Same ions have also been observed in the case of **IIb-f**. Comparing the data in Tab.(I) a significant decrease in the intensities of ion *a* and *b* can be observed in the case of **II** type compounds. The difference is due to that in the-*heats of formation of neutral fragments* (SO_2 *v.* S, SO_3 *v.* SO) because of the ionic fragments are the same.

CONCLUSION

Experimental evidences show that loss of SO_3 and SO are one step decompositions of the title compounds. They assume bond rearrangement of the 5-membered ring probably promoted by the ***d*** orbitals of sulfur.

References

[1] Bentley, T. W., and Johnstone, R. A. W. in "Advances in Physical Organic Chemistry", (ed. by Gold, V.), vol. 8., p. 151-269, Academic Press, London and New York (1970)

[2] Grivas, J. C., J. Org. Chem., 40, 2029-2032 (1975)

43rd ASMS Conference on Mass Spectrometry and Allied Topics

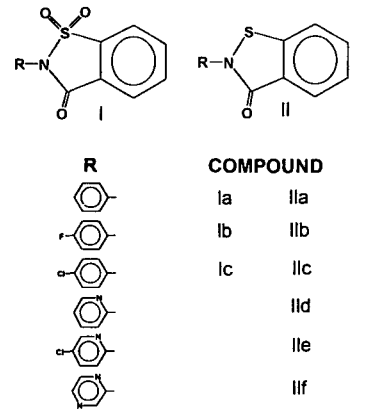

Figure (I): Structure of the compounds studied

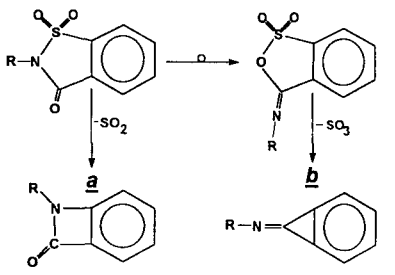

Figure (III): Probable transition structure of loss of SO_3

Comp./Ion Int (%)	$M^{+\bullet}$	*a* $(M-SO_2)^{+\bullet}$	*b* $(M-SO_3)^{+\bullet}$
Ia	100	45	47
Ib	100	18	28
Ic	100	8	14
	$M^{+\bullet}$	*a* $(M-S)^{+\bullet}$	*b* $(M-SO)^{+\bullet}$
IIa	100	13	2
IIb	100	6	2
IIc	100	4	1
IId	100	7	6
IIe	100	9	7
IIf	100	3	4

Table (I): Ion intensities of interest

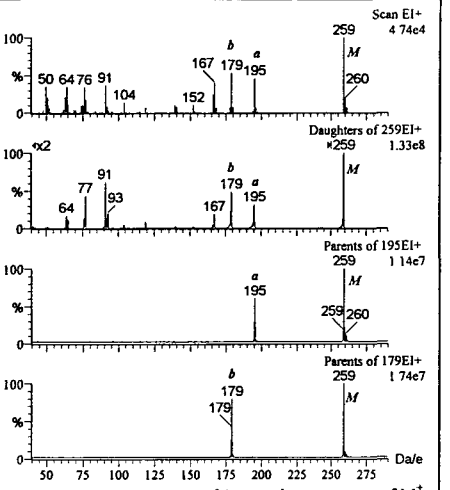

Figure (II): EI spectrum of Ia, *product* spectrum of M^+ ion of Ia, *precursor* spectra of m/z195,179 ions of Ia

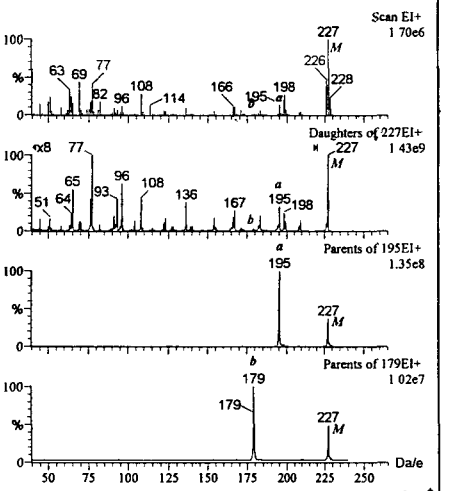

Figure (IV): EI spectrum of Ia, *product* spectrum of M^+ ion of Ia, *precursor* spectra of m/z195,179 ions of Ia

The Unimolecular Dissociation of Acetophenone Ions by Thermal Radiation

Marcelo Sena and José M. Riveros
Institute of Chemistry, University of São Paulo, Caixa Postal 26077, São Paulo, Brazil, CEP 05599-970

Weakly bound ions have been reported to undergo slow unimolecular dissociation in ICR cells through processes which exhibit weak pressure dependence.[1] Molecular ions with low energy fragmentation pathways (~ 10 kcal/mol) have also been shown to undergo such dissociation.[2] The case of acetophenone is particularly attractive case since its has been extensively characterized by mass spectrometry.

$$C_6H_5COCH_3^{+\cdot} \rightarrow C_6H_5CO^+ + \cdot CH_3 \quad \Delta E_{298K} = 8.2 \text{ kcal/mol}$$

A typical graph of the kinetics of dissociation observed for the molecular ion of acetophenone, $C_6H_5COCH_3^+$ in the cubic cell of our FT-ICR spectrometer is shown in Figure 1. The data were obtained at a nominal electron energy 9.5 eV, an acetophenone pressure of 4.9 x 10^{-8} Torr and cell temperature of 357 K. At this ionizing energy, the relative intensity of the unresolved *m/z* 121 ion, a mixture of $(C_6H_5COCH_3)H^+$ and $^{13}CC_7H_8O^+$, remains essentially constant indicating the ion/molecule reaction leading to protonated acetophenone is slow compared to the dissociation of the molecular ion. The kinetics of dissociation of molecular ions isolated 500 ms after ion formation yield the same rate constant within experimental error. A similar behavior is observed when the molecular ion is formed via a charge exchange reaction.

The analysis of the pressure and temperature dependence of the dissociation observed in these experiments yields a valuable clue as to the mechanism responsible for the dissociation. Rate constants for the dissociation of $C_6H_5COCH_3^{+\cdot}$ are shown in Figure 2 as a function of acetophenone pressure at different temperatures controlled essentially by the filament current. There is a very mild increase of the rate constant with pressure but a dramatic temperature effect. In all cases, extrapolation to zero pressure reveals that *the most significant contribution to the dissociation rate of the molecular ion of acetophenone is of a non-collisional nature*. A similar behavior was observed with SF_6 as a static bath gas, up to pressures of 6x10^{-6} Torr, or by raising the pressure progressively with longer gas pulses from the pulsed valve.

Similar experiments with $C_6H_5COCD_3^+$ yield the same behavior but the extrapolated zero pressure dissociation rates are 40 to 80% *slower* than for the normal acetophenone ion depending on the temperature.

The data on the collisionless dissociation of these molecular ions is consistent with the view that these processes are driven by the thermal radiation of the surroundings.[3] A model has been deveoped to simulate this phenomenon based on the assumption that the initial internal energy of the ions can be represented by a vibrational Boltzmann distribution truncated near the dissociation limit. A random walk in energy was then simulated by considering absorption of blackbody radiation, spontaneous and induced emission and dissociation when the interanl energy exceeds the critical energy for dissociation. The dissociation rate was determined by doing a large number of ion energy random walks simulations (~ 3000) from which the dissociation time of each ion can be obtained. The actual calculation involves the following steps: a) The initial internal energy and vibrational configuration were chosen using the truncated Boltzmann distribution as a weight function; b) Each harmonic oscilator can increase, decrease or not change its occuptation level. The probability of these events is related to the Einstein coefficients which were derived from the vibrational intensities obtained from an AM1 calculation on $C_6H_5COCH_3^{+\cdot}$ and $C_6H_5COCD_3^+$. Vibrational frequencies were also obtained from these calculations; c) If the total vibrational energy after each step exceeds the dissociation threshold, the elapsed time was recorded and a new simulation begins. Otherwise, the internal energy is redistributed (IVR) and a new step simulation is made.

The energy random walk simulation reveals a single exponential decay in time. The dissociation rate constant for $C_6H_5COCH_3^+$ is calculated to be 0.29 s^{-1} compared with the experimental value of 0.5 s^{-1}. The simulation and the semi-emprical calculation on the molecular ions also agree with the experimental finding that $C_6H_5COCD_3^+$ dissociates at a slower rate than $C_6H_5COCH_3^+$.

Figure 1

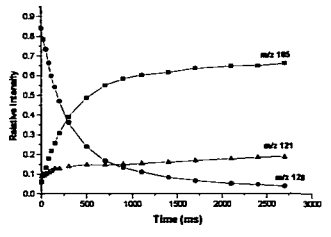

Figure 2

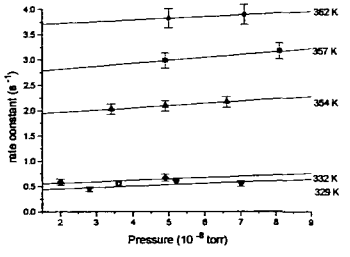

The authors thank the São Paulo Science Foundation (FAPESP) and the Brazilian Research Council (CNPq) for continuous support.

[1] (a) D.Thölmann, D. S. Tonner, T. B McMahon, *J. Phys Chem.* **98**, 2002 (1994); (b) H. V. Linnert, J M. Riveros, *Int. J. Mass Spectrom. Ion Processes* **140**, 163 (1994).
[2] M. Sena, J M. Riveros, *Rapid Commun. Mass Spectrom.* **8**, 1031 (1995).
[3] R. C. Dunbar, *J. Phys. Chem.* **98**, 8705 (1994).

HYPERTHERMAL SURFACE IONIZATION OF ORGANIC MOLECULES : ALKYL ALCOHOLS

HIROSHI KISHI (OYAMA NATIONAL COLLEGE OF TECH. ; OYAMA, TOCHIGI, JAPAN)
TOSHIHIRO FUJII (NATIONAL INSTITUTE FOR ENVIRONMENTAL STUDIES ; TSUKUBA, IBARAKI, JAPAN)

INTRODUCTION

Hyperthermal Surface Ionization Mass Spectra (HSIMS) for alkyl alcohols ($C_1 \sim C_5$) were obtained using ReO_2 as solid surface, and were compared with 70 eV EIMS. HSIMS exhibited completely different pattern from those of EIMS. Important ions observed in HSIMS were even electron ions(EE^+), such as $(M-H)^+$, $(M-3H)^+$, $(M-R)^+$, $(M-OH)^+$, $(M-H-H_2O)^+$, R^+, whereas characteristic odd electron ions ($OE^{+\cdot}$) are observed generally in EIMS. In addition to these abundant even electron ions, radical cations $(M-2H)^{+\cdot}$ were observed for some cases. Fragmentation patterns in HSIMS were strongly dependent on the kinetic energies of the molecules, whereas the surface temperature did not affect the patterns so much.

EXPERIMENTAL

The experimental setup for HSIMS has been reported in detail elsewhere[1]. The supersonic nozzle used was made of alumina with a pinhole of 100 μ m-ϕ, and was heated electrically to $\sim$ 1000 ℃ at its end of 1.5 cm by an external winding of tungsten wire, and its temperature T_N was measured by a Chromel-Alumel thermocouple. The dead volume of its heated part is 3×10^{-3} cm^3, flow rate of carrier gas $\sim$ 2 cm^3 /sec, and the residence time of the gas is few msec, therefore thermal dissociation of the organic molecules behind the nozzle is negligible.

RESULTS AND DISCUSSIONS

MASS SPECTRA HSIMS of methanol and *n*-propanol are shown in Fig. 1. The parent is missing and $(M-H)^+$, $(M-2H)^+$, $(M-3H)^+$, $(M-OH)^+$, $(M-H-H_2O)^+$, CH_3^+, H_2O^+ are observed These ions are produced on account of thermal dissociation in the surface collision The appearance of Na^+ and K^+ ions come from impurity atoms in the surface.
HSIMS for the other alkyl alcohol ($C_1 \sim C_4$) are tabulated in Table 1, as m/z (% Intensity).

EFFECT OF KINETIC ENERGY The ion yield of m/z 29, 30, 31, and m/z 23 for methanol is shown in Fig 2, as a function of incidint kinetic energy (E_K) at surface temperature of 600 ℃. At lower E_K, SI yields are enhanced with increase in E_K, the slope for m/z 31 the steepest
At higher E_K, the intensity of m/z 31 goes down, while those of the other ions increase steeper. In ethanol, similar kinetic energy dependence was observed for $(M-H)^+$, $(M-2H)^+$, $(M-3H)^+$, and alkali ion. These behaviors might be the consequence of some competitive surface reactions, including the energy transfer of molecular kinetic energy to the solid surface.

EVEN ELECTRON IONS HSIMS and 70 eV EIMS of 1-pentanol are shown in Table 2 Characteristic odd electron ions are observed in EIMS at m/z 70 $(M-H_2O)^{+\cdot}$ (37%) and m/z 42 $(M-H_2O-C_2H_2)^{+\cdot}$ (100%, McLafferty peak), whereas no $OE^{+\cdot}$ ion is observed for HSIMS at any combination of (E_K,T_S), and the m/z 69 peak constitutes the base peak. This suggests that radical species are first generated on the surface, followed by ionization of these species.

MASS SPECTRA OF ISOMERS No similarity exists between EI spectra of 1- and 2-propanol, and they exhibit low intensity for parent and quasi molecular $(M-H)^+$ ions In HSIMS, quasi molecular ions are abundant and some other signals can be reasonably assigned as $C_3H_7^+$ (43), $C_3H_5^+$ (41), CH_2OH^+ (31), $C_2H_5^+$ (29). HSIMS of butanol show each characteristic peaks for 4 isomers. 1-butanol : m/z43($C_3H_7^+$), 2-butanol m/z73$(M-H)^+$, iso-butanol : m/z58$(M-CH3)^+$, tert-butanol : m/z57$(M-OH)^+$. In this respect, the HSIMS contain structural information, hence the HSI results are very useful for diagonostic analysis.

Fig 1 HSI Mass of Alkyl Alcohol

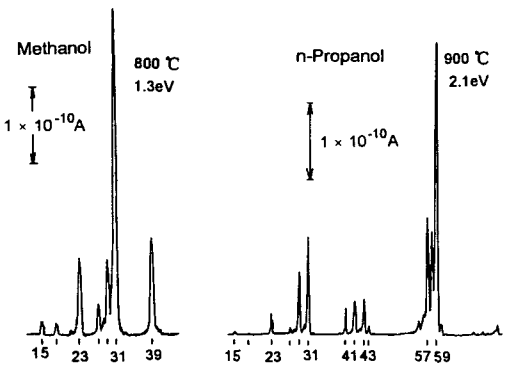

Fig 2 Kinetic Energy Dependence of m/z 31, 30, 29, 23 in methanol

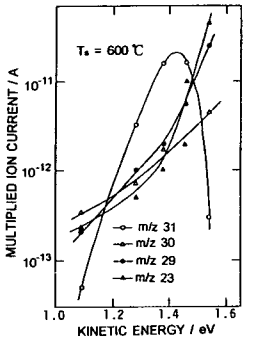

Table 1 HSI and EI Mass Spectra of Alkyl Alcohol ($C_1 \sim C_4$)

Compounds	T_S/ ℃ E_K/eV	m/z (% Intensity) HSI:Upper Column, EI:Lower Column
Methanol	600	31(100), 29(42), 18(10), 15(9), 28(4), 32(2)
CH_3OH	1.5	31(100), 32(74), 29(31), 15(13), 30(6), 28(4), 18(4), 14(2)
Ethanol	1070	45(100), 44(30), 43(12), 29(9), 41(8), 46(6), 30(6), 42(4), 27(4), 18(4)
C_2H_5OH	2.4	31(100), 45(39), 29(24), 27(24), 46(17), 26(9), 15(9), 30(6)
1-Propanol	850	59(100), 31(24), 41(9), 43(8), 60(3), 57(3), 29(3)
1-C_3H_7OH	2 1	31(100), 27(14), 29(13), 59(9), 42(8), 60(5), 41(5), 28(5),
2-Propanol	860	59(100), 43(38), 41(10), 31(6)
2-C_3H_7OH	2.6	45(100), 43(17), 27(16), 29(10), 41(7), 31(6), 39(5), 42(4), 60(0.34)
1-Butanol	846	55(100), 43(62), 71(19), 41(17), 73(16), 29(10), 31(10), 57(9), 56(9), 72(7)
1-C_4H_9OH	2 6	31(100), 56(86), 41(63), 43(60), 27(56), 29(34), 42(32), 39(19), 74(1.00)
2-Butanol	846	73(100), 57(23), 55(14), 41(12), 29(11), 43(5), 56(2), 31(2)
2-C_4H_9OH	2 6	45(100), 59(22), 41(18), 43(18), 31(15), 29(10), 27(10), 44(9), 74(0.41)
iso-Butanol	525	55(100), 58(60), 57(52), 73(49), 43(34), 41(30),29(21),56(18),31(13),72(12)
iso-C_4H_9OH	2 9	43(100), 31(67), 42(57), 41(55), 33(51), 27(44), 29(24), 39(21), 74(8.94)
t-Butanol	600	57(100), 56(68), 41(43), 55(35), 29(24), 43(16), 40(12), 70, 59, 58, 27(5)
t-C_4H_9OH	2.9	59(100), 41(50), 31(27), 56(20), 39(17), 43(11), 29(10), 27(9), 74(0.00)

Table 2 HSI and EI Mass Spectra of *n*-Pentanol

m/z	Possible Assignment	EI	HSI 950 ℃ 3.5eV	HSI 600 ℃ 2.5eV	HSI 950 ℃ 2 5eV	HSI 600 ℃ 3 5eV	$OE^{+\cdot}$ EE^+
88	$M^{+\cdot}$	0 00	—	—	—	—	OE^+
87	$(M-H)^+$	—	2	29	21	3	EE^+
70	$(M-H_2O)^{+\cdot}$	37.0	—	—	—	—	$OE^{+\cdot}$
69	$(M-H-H_2O)^+$	—	100	100	100	100	EE^+
57	$C_4H_9^+$	22	11	2	2	4	EE^+
55	$C_4H_7^+$	10	6	—	2	—	EE^+
45	$C_2H_5O^+$	—	9	4	4	8	EE^+
43	$C_3H_7^+$	28	18	5	9	10	EE^+
42	$C_3H_6^{+\cdot}$	100	—	—	—	—	$OE^{+\cdot}$
41	$C_3H_5^+$	60	48	4	6	24	EE^+
31	CH_2OH^+	68	10	—	—	4	EE^+
29	CHO^+	65	4	—	—	—	EE^+

[1]Hiroshi Kishi and Toshihiro Fujii, J. Phys. Chem ; Submitted.

Unimolecular Decomposition of Energy Selected 2,5-Dihydrofuran

Bibi Teklehaimanot, Gang Ma, and Gerry G. Meisels
Department of Chemistry, University of South Florida
Tampa, FL 33620

The unimolecular dissociation of energy selected 2,5-dihydrofuran ions has been studied using threshold photoelectron photoion coincidence (TPEPICO) time of flight (TOF) mass spectrometry The ion chemistry of the molecule is elucidated from measurements of breakdown curves, appearance energies (AP) and kinetic energy releases (KER). A detailed breakdown graph (BDG) obtained in the energy range 9.20 - 14.52 eV is shown in Fig. 1. The breakdown curve of m/z 69 shows considerable variation with two maxima at photon energies of 11.64 and 12.74 eV, corresponding to the third and fourth photoelectron bands respectively in the He-I PES of 2,5-dihydrofuran. This is contrary to what can be expected on the basis of simple statistical theories where fragmentation directly from a parent ion is predicted to result in a monotonic and smooth change of breakdown curves unless a new dissociation channel begins to open. Therefore the variation in the breakdown curve suggests that the process leading to m/z 69 involves more than one state or isomers at photon energies above 11 60 eV.

The average KER accompanying the formation of m/z 42 directly from the parent ion is found to be consistent with that computed on the basis of RRKM-QET (Fig. 2). However in the case of m/z 41 the experimental and theoretical average KERs agree only up to 11 5 eV.(Fig 3) The slope of experimental KER implies that there is an almost zero kinetic energy release at the threshold. This result suggests that the observed KER arises mainly from the excess internal energy of the activated complex and that there is negligible reverse activation energy.

Table 1. AEs and heat of formation of product ions form 2,5-dihydrofuran

Product Ion	[a]AE, eV	ΔH_f Kcal mol^{-1} This work	Literature[b]
$[C_4H_6O]^+$	9.10 ± 0.01	194 ± 1	195
$[C_4H_5O]^+$	10.15 ± 0.01	166 ± 1	165[c]
$[C_4H_4O]^+$	9 16 ± 0 01	195 ± 1	195[c]
$[C_2H_3O]^+$	10.25 ± 0.09	157 ± 3	157 ± 3.6[d]
$[C_3H_6]^+$	10.11 ± 0.10	243 ± 3	240
$[C_3H_5]^+$	10.94 ± 0.10	226 ± 3	226
$[C_3H_4]^+$	12.08 ± 0.13	289	289
$[HCOH]^+$	13.59 ± 0.07	230	231

ΔH_f values are determined from AEs and neutral ΔH_f values taken from the literature (1) All values are T=300 K.
[a]Determined by taking the mid point of first absent and last present.
[b]Unless other wise specified, values listed here are from reference 1
[c]From reference 2
[d]From reference 3

References

1. R. Levin and S G. Lias, "Ionization Potential and Appearance Potential Measurements, 1971-1981," Nat. Stand. Ref. Data Ser., Nat. Bur. Stand. (U.S.) 71, (1982).
2. J. K. Terlouw, P. C. Burgers and J. L. Holmes, J. Am. Chem. Soc. **101**, 225 (1979).
3. J.C. Trager, R.G. McLouglin and A.J C. Nicholson, J. Am. Chem. Soc. **104**, 5318 (1982).

43rd ASMS Conference on Mass Spectrometry and Allied Topics

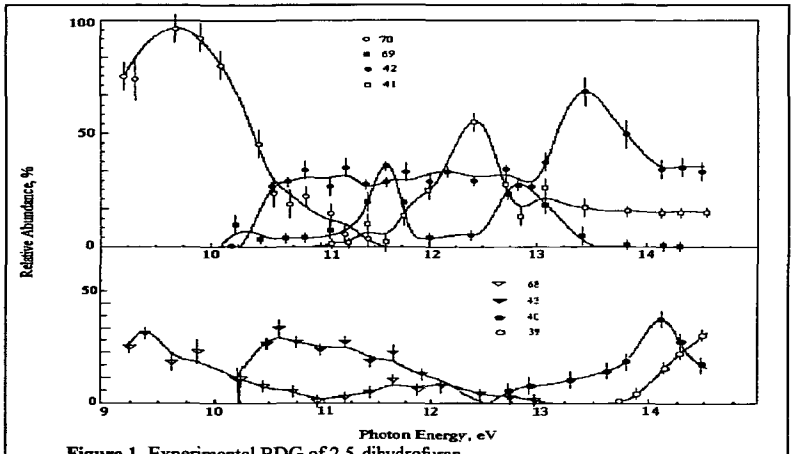

Figure 1. Experimental BDG of 2,5-dihydrofuran

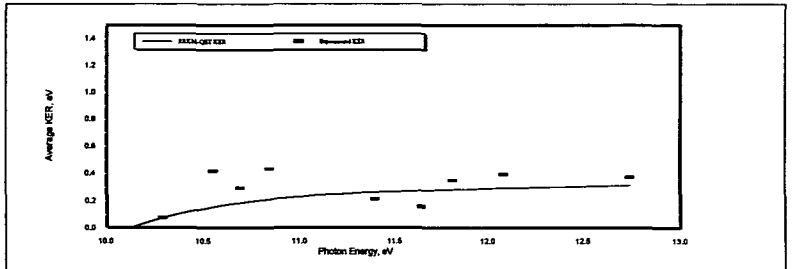

Figure 2 KER accompanying the formaion of m/z 42 directly from the parent ion.

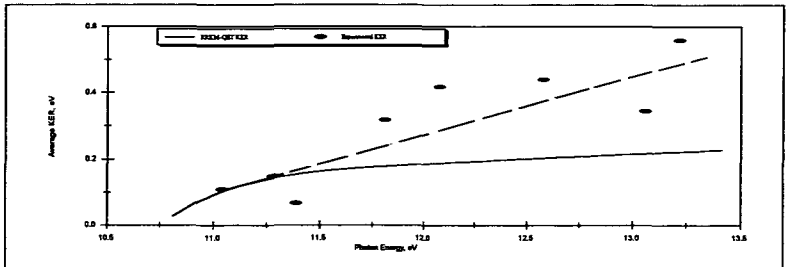

Figure 3 KER accompanying the formaion of m/z 41 directly from the parent ion.

Influence of Substituents on Propene Loss from n-Propyl Aryl Ether Ions

Henri E.K. Matimba, Steen Ingemann and Nico M.M. Nibbering
Institute of Mass Spectrometry, University of Amsterdam, Nieuwe Achtergracht 129, 1018 WS Amsterdam, The Netherlands

The loss of a propene molecule is the main unimolecular reaction of a series of ionized 3- and 4-substituted aryl n-propyl ethers ($YC_6H_4OCH_2CH_2CH_3$, Y = CH_3, CF_3, NO_2, OCH_3 and SCH_3) in the ion source as well as in the field free regions of a double-focussing quadrupole hybrid mass spectrometer. This reaction can proceed through two distinct pathways: i) a 1,5-H shift from the β-position of the propyl group to the ortho position of the ring (Eq. 1) and ii) intermediate formation of an ion-neutral complex consisting of a $YC_6H_4O^{\cdot}$ radical and a $^{+}CH(CH_3)_2$ cation (Eq. 2). The latter complex reacts further by proton transfer prior to dissociation.

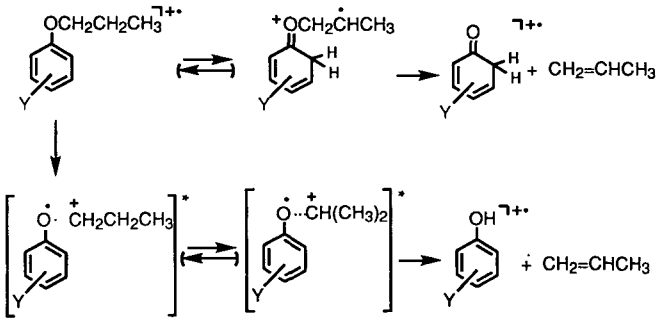

The occurrence of these pathways becomes visible by deuterium labelling of the propyl group at the β-position. If the 1,5-H shift initiated loss of propene is the only process occurring, C_3H_5D will be lost exclusively. By contrast, the process involving an ion-neutral complex is predicted to lead to a ratio of 5 to 1 between the losses of $C_3H_4D_2$ and C_3H_5D provided that only one deuteride shift occurs prior to the proton/deuteron transfer (isotope effect neglected). If all the hydrogen and deuterium atoms become equivalent through rapid hydride/deuteride shifts in the propyl carbenium ion this ratio is estimated to become 5 : 2.

Table. Relative importance of H- and D-transfer in the propene loss from the molecular ions of the labelled n-propyl aryl ethers, $ArOCH_2CD_2CH_3$.

Substituent	H-transfer : D-transfer		
	Ion-source react.ions		Metastable Ions
	70 eV	10 eV	
H	81:19	82:18	84:16
4-NO_2	85:15	85:15	84:16
4-CF_3	85:15	86:14	88:12
4-CH_3	80:20	83:17	81:19
4-CH_3O	76:24	76:24	74:26
4-CH_3S	75:25	76:24	72:28
3-NO_2	84:16	84:16	85:15
3-CF_3	74:26	84:16	88:12
3-CH_3	81:19	81:19	72:28
3-CH_3O	70:30	38:62	10:90
3-CH_3S	76:24	-	36:64

The experimentally obtained ratio's for the abundances of the products of $C_3H_4D_2$ and C_3H_5D loss are for most of the ethers close to that anticipated for both the ion-neutral complex mediated processes, as can be seen from the results in the Table. An exceptional result is obtained for the molecular ions with a CH_3O-group substituted at the 3-position (Table). For these molecular ions propene loss proceeds with a marked preference for transfer of a hydrogen atom from the β-position of the propyl group. This preference is even more pronounced for the metastable ions, which eliminate propene by a nearly selective β-hydrogen atom transfer. Furthermore, the initial 1,5-H shift for these ions is a reversible process, resulting in the retention of both deuterium atoms in a small fraction of the product ions. In addition, tandem mass spectrometric experiments support the inferred formation of substituted cyclohexadienone ions by the 1,5-H shift, whereas phenolic ions are formed by the pathway involving an ion-neutral complex.

Competing Kinematic Models for Describing Energy Transfer in Low-Energy CID of CS_2^+

Ronald E. Tosh, Anil K. Shukla and Jean H. Futrell
Department of Chemistry and Biochemistry
University of Delaware, Newark, DE 19716

Collision-induced dissociation (CID) of CS_2^+ ions to form CS^+ or S^+ has attracted attention in recent years because several earlier experiments suggested that excited electronic surfaces participate in the reaction dynamics. Small polyatomic ions like this are intermediate between diatomics, which typically either dissociate from repulsive curves in a single vibration or rapidly predissociate, and more complex polyatomics, in which dissociation occurs after electronic energy is redistributed among internal modes. Accordingly, a precise specification of the role of electronic excitation in the present system is expected to be helpful in developing a model for CID of small polyatomics that interpolates between exact quantum dynamics and quasi-equilibrium theory (QET). Moreover, the relative simplicity of this system makes it a good candidate for testing theoretical models of translational-electronic energy transfer in low- to intermediate-energy collisions, which has been found to be of some importance in CID of more complex cations.[1,2]

We report here the results of recent crossed-beam experiments on both the non-dissociative scattering and CID of CS_2^+ (to form S^+ or CS^+) in collisions with Ar atoms at 17.8 eV (CM). The crossed-beam technique, which permits simultaneous angle and energy measurements of reactants and products, is well suited to resolving state-to-state electronic excitation when the energy levels of the parent molecule are well-separated, as is the case with CS_2^+. All of our measurements clearly show that translational-electronic energy transfer is involved in distinct ways in each of the three processes, and the angular scattering patterns reveal that this is related to the existence of distinct underlying mechanisms for momentum transfer: one involving a simple two-body collision between the target neutral and parent ion, while the other involves an impulsive scattering event in which only part of the parent ion participates in the collision (the other part is a spectator).

The simple two-body scattering mechanism is clearly evident in the recoil spectra for $CS_2^{+(*)}$ that result from collisions with Ar at 8.9 and 17.8 eV (CM). In the latter case, the velocity contour plot shows that purely elastic scattering dominates at all scattering angles and that the relative probability for vibrational or electronic excitation appears to be negligible. The contour plot for 8.9 eV collisions is similar; however, in this case we carried out a more thorough search for backward scattered CS_2^+. As a result, we found peaks at recoil velocities consistent with simple two-body inelastic scattering that results in electronic excitation of CS_2^+ to the *A* and *B* states. This is a few percent of the corresponding forward-scattered signal at the same laboratory angle and may have been overlooked in the run at 17.8 eV. This will be reinvestigated in the future after some improvements are made to the energy analyzer.

Our initial measurements of the recoil spectra for the fragment ions S^+ and CS^+, performed on the Delaware "tandem" instrument, did not reveal any deviations from the two-body kinematic scheme that characterizes the non-dissociative scattering described above. Consequently, we used the conventional excitation/delayed-dissociation model to interpret the measured velocity contour plots in our recent publication.[3] However, more recent studies done with the Delaware "crossed-beam" instrument have shown scattering of both fragment ions outside of the elastic circle with a discernible symmetry about a point other than the reactant CM: for the S^+ data this point is the Ar/S CM; it is the Ar/CS CM for the CS^+ data. Such scattering is indicative of an impulsive mechanism like that described above (the neutral CID fragment in each case comprises the collision spectator) followed by a prompt dissociation, and thus constitutes a departure from the two-step model that is commonly used for interpreting CID data.

The "knock-out" model for CID presented here was recently developed to explain the angular scattering of S^+ resulting from CS_2^++Ar collisions at 17.8 eV (CM).[4] The model enables us to calculate the reaction Q (inelasticity) from the S^+ recoil circle, and the result we obtain, 4.5±0.8 eV, is very close to the minimum 4.8 eV necessary to break the S^+--CS bond. A slightly better fit to the scattering data results if the model is modified to allow for electronic excitation of the molecule by the amount Q as the reactants approach. The modification also presents us with a very satisfactory explanation for how the collision between Ar and S^+ can occur without momentum transfer to CS, since excitation of CS_2^+ by about 4.5 eV is sufficient to populate a non-bonding state for S^+ and CS.

Similar symmetry in part of the velocity contour plot for CS^+ implies that a complementary pathway exists for this reaction. The reaction Q determined from the velocity contour plot is 6.3±.8 eV , which is just above the minimum 5.7 eV necessary to break the CS^+--S bond. As with S^+, refinements of the model permit a slightly better fit to the data, suggesting that an electronic transition within the CS_2^+ ion occurs before the CS^+ moiety is knocked out. This explanation pertains to the ridge in the contour plot that is most discernible at large scattering angles; however, the large, highly inelastic peak in the forward direction extends over a large range of scattering angles but exhibits no symmetry about either the Ar/CS CM or the reactant CM. We are currently evaluating other kinematical models in an effort to understand it.

References

1 K. Qian, A. Shukla and J. Futrell, J. Chem. Phys., **92**, (1990) 5988.
2 K. Qian, A. Shukla and J. Futrell, J. Am. Chem. Soc., **113**, (1991) 7121.
3 A. K. Shukla, R. E. Tosh, Y. B. Chen and J. H. Futrell, Int. J. Mass Spectrom. Ion Proc., in press 1995.
4 Ronald E. Tosh, Anil K. Shukla and Jean H. Futrell, J. Phys. Chem., submitted 1995.

Acknowledgements

We gratefully acknowledge the financial support of this research by the National Science Foundation, Grant No. CHE-9021014.

Tandem Crosed-Beam Collision-Induced Dissociation of CO_2^+

Rahul Chawla, M. Krishnamurthy, A. K. Shukla and J. H. Futrell
Department of Chemistry and Biochemistry, University of Delaware, Newark, DE 19716

Angle and energy resolved CID provides valuable information about energy transfer, reaction mechanisms and role of excited states in activation and dissociation steps. Recent studies from our laboratory have demonstrated that electronic excitation is a prominent mechanism in low and moderate collision energy CID of certain molecules (acetone, nitromethane) but others (enol acetone, methane, propane, methyl nitrite) dissociate predominantly on the ground state hypersurface.

A current focus of our research is angle and energy resoved CID studies of triatomic cations whose potential surfaces are relatively well described. They are a logical bridge between diatomics (which dissociate in a single vibration) and more complex polyatomics (which generally follow RRKM/QET delayed dissociation mechanisms). In the accompanying poster we develop a prompt dissociation kinematics model and demonstrate that CID of CS_2^+ is well described by this model. Although the structure and energetics of CO_2^+ are similar to CS_2^+, we find rather different dissociation dynamics for the analogous O^+ and CO^+ products.

The hybrid tandem mass spectrometer used by us in these studies has several features which make it ideal for studying angle-and-energy-resolved CID of ions:

1. A series of tube and rectangular lenses capable of slowing a beam of several kV energy to a variable range between 1 eV to a few hundred eV while maintaining a well defined ion beam, monoatomic to within +/- 1 eV.

2. A supersonic neutral beam which overlaps the slit image of the ion beam. This provides us with higher gas densities and narrower velocity distribution than collision chamber experiments.

3. A hemispherical energy analyzer to provide high energy resolution and high ion transmission.

4. A rotating detector assembly consisting of hemispherical energy analyzer, quadrupole mass filter and detector.

CID of CO_2^+ with Ar to give CO^+ at 47.6 eV CM collision energy (Figure 1) shows that intensity maxima of CID peaks at different angles are all confined within the ESC and follow a circle whose center corresponds to Ar/CO_2^+ center-of-mass. It is a forward scattered peak with an endothermic energy transfer of 7 eV. At 8.7 eV with He , the peak is side scattered, again with an energy transfer of 7 eV. The threshold for this process is 5.7 eV, however, dissociation of CO_2^+ to CO^+ from C state takes place

through the $a^4\Pi_u$ state. Therefore, for the dissociation to take place, excess energy is transferred into CO_2^+ ions.

CID of CO_2^+ to form O^+ at 49 eV CM energy (Figure 2) shows a forward scattered peak just outside the elastic scattering circle. This suggests that O^+ is formed from a long lived excited state present in the reactant ion beam. Profile of distribution traces along the O^+/Ar scattering circle. At 15.2 eV CM and 8.6 eV CM collision energies, the peak maximum is clearly outside the ESC. The profile of the peak intensity as a function of scattering angle also circumscribes the O^+/Ar center of mass.

This demonstrates that the ions are already activated prior to collision, no energy transfer into internal modes for this dissociation process is observed even though this process is endothermic by at least 5.3 eV. Further, The contours have a ridge of intensity that is outside the ESC and follows a circle corresponding to the recoil velocity of O^+ from O^+/Ar collisions instead of CO_2^+/Ar CM. This is very similar to CID of CS_2^+ to S^+ ions except that the S^+ ions were inside the ESC at smaller scattering angles. The data are consistent with the hypothesis that our CO_2^+ beam includes a population of vibrationally excited $C_2\Sigma_g^+$ which require only a small perturbation to break the O-CO bond.

1. CID of CO_2^+ to give CO^+ and O^+ follow different kinematics. CO^+ ions are scattered within the elastic circle described by CO_2^+/Neutral and closely follows the traditional two-step kinematic model conventionally used to describe CID with this result. O^+ follows a spectator knockout model in which O^+ is scattered along the O^+/Neutral scattering circle.

2. The CO_2^+ ion beam formed by 70 eV electron impact consists of both ground state CO_2^+ ions which after collision preferentially give CO^+, and a smaller population of excited CO_2^+ ions which preferentially dissociate to O^+ ions.

Figure 1

CO_2^+ + Ar –> CO^+ + O + Ar at 47.6 eV CM energy

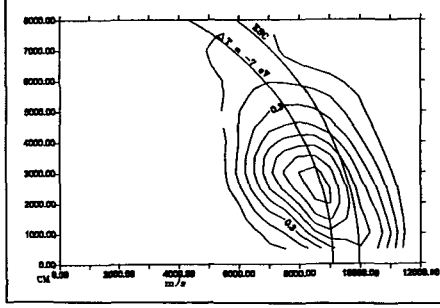

Figure 2

CO_2^+ + Ar –> O^+ + CO + Ar at 49 eV CM energy

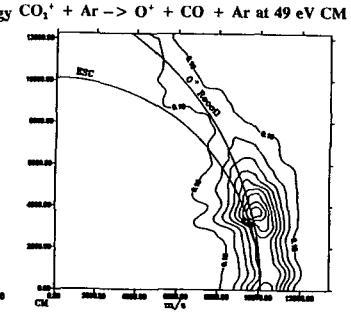

Investigation of *Trans* Influence in the Fragmentation of Dinuclear Platinum Complexes by Electrospray Ionization Surface-Induced Dissociation Tandem Mass Spectrometry

Thomas G. Schaaff, Yun Qu, Nicholas Farrell, Vicki H. Wysocki
Department of Chemistry, Virginia Commonwealth University
Richmond, Virginia, 23284, USA

Dinuclear platinum complexes of formula $[\{Pt(NH_3)_2Cl\}_2\mu\text{-}NH_2(CH_2)_nNH_2]^{2+}$ are novel antitumor agents of clinical interest.[1,2] In contrast to the pair of mononuclear cis/trans-$[Pt(NH_3)_2Cl_2]$ isomers, both cis and trans isomers in this dinuclear series display antitumor activity, but with different abilities to overcome cellular resistance to the "parent" cis-$[Pt(NH_3)_2Cl_2]$. [*Cis*-$\{Pt(NH_3)_2Cl\}_2(NH_2(CH_2)_nNH_2)](NO_3)_2$ (1,1/c,c) and [*trans*-$\{Pt(NH_3)_2Cl\}_2(NH_2(CH_2)_nNH_2)](NO_3)_2$ (1,1/t,t), where the diamine was 1,4-butanediamine (n=4) and 1,6-hexanediamine (n=6), were studied using electrospray ionization surface-induced dissociation[3] (ESI/SID) tandem mass spectrometry. The same fragment ions were observed for both the *cis* and *trans* isomers of a given diamine length, but the relative intensities were dependent on the isomer studied (Figure 1a and 1b). Capillary/skimmer CID, combined with SID, allowed for the determination of the two step fragmentation processes. The dinuclear complex was fragmented by increasing the potential difference between the capillary and skimmer in the source, then the fragment ions of interest were selected and fragmented by SID. For all of the complexes studied the first step in the fragmentation pathway was the dissociation of one of the Pt-N(diamine) bonds, forming the $[Pt(NH_3)_2(diamine)Cl]^+$ ion (m/z 380). The difference in the isomers was found in the second step. In the second step, two pathways were possible for the complexes: (i) dissociation of the other Pt-N(diamine) bonds in a two step process, producing the $[Pt(NH_3)_2Cl]^+$ (m/z 264) and the free diamine (m/z 117) fragment ions, and (ii) retention of the other Pt-N(diamine) bond. The first and second pathways produced principally the $[Pt(NH_3)_2Cl]^+$ (pathway i) and $[Pt(diamine\text{-}H^+)]^+$ (pathway ii) fragment ions; both ions fragmented further. It is proposed that in the second pathway the diamine binds to the platinum through the other NH_2, after the initial fragmenting collision. The ESI/SID data and energy resolved mass spectra (Figure 2a-2d) show that the position of the chloride plays a significant role in the fragmentation of these ions. The 1,1/t,t isomers fragmented to yield a larger abundance of $[Pt(NH_3)_2Cl]^+$, which corresponds to pathway (i) (i.e. cleaving the bonds *trans* to the chloride). In contrast, the 1,1/c,c complexes fragmented (at lower collision energies) to yield a larger abundance of $[Pt(diamine - H)]^+$; pathway (ii). A critical energy was reached for both the 1,1/c,c n=4 and n=6 complexes, at which the abundant fragment ion produced changed to the $[Pt(NH_3)_2Cl]^+$ ion.

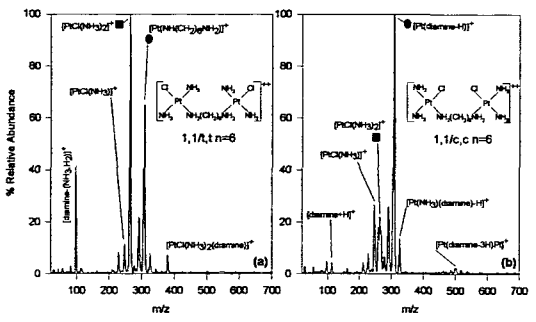

Figure 1:

50 eV ESI/SID spectrum for the 1,1/t,t n=6 (a) and 1,1/c,c n=6(b) complexes Note the difference in the ions corresponding to the two mechanisms, (i, ■) and (ii; ●)

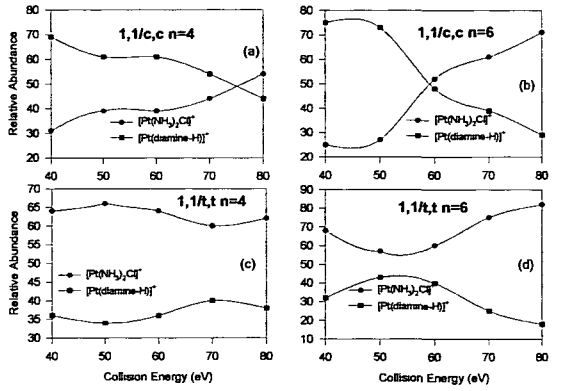

Figure 2:

Energy resolved mass spectra for the 1,1/c,c n=4,6 (a and b) and 1,1/t,t n=4,6 (c and d)

In solution phase, the trans influence allows for the prediction of reaction pathways of transition metal complexes. The thermodynamic property of the trans influence in platinum complexes holds that a Pt-N bond trans to a chloride donor is more labile than a corresponding Pt-N bond trans to a nitrogen donor. The differences in the ESI/SID spectra between the *cis* and *trans* isomers can be explained by the *trans* influence. By fragmenting the platinum complexes at varying collision energies, it was determined that the trans influence can be applied to the fragmentation pathways of platinum complexes in the gas phase. The cleavage of the Pt-N bond *trans* to chloride was the most favorable pathway for both isomers of the complexes in the ion-surface collision at lower collision energies. At higher collision energies, the steric effects of the molecule outweigh the thermodynamic stabilization due to the trans influence.

References:

1 Farrell, N. *Comments in Inorganic Chemistry*, **1995**, *16*, 373
2 Farrell, N. *Advances in DNA Sequence Specific Agents.* Vol 2. Hurley, L H, Chaires, J B, Eds, JAI Press Inc. In Press.
3 Cooks, R. G.; Ast. T; Mabud, MD A. *Int. J. Mass Spectrom. Ion Process.* **1990**, *100*, 309.

NI FAB and DCI-MS of Sulfonylurea Herbicides: CAD Spectra of $(M-H)^-$ Ions

Witold Winnik,*♥ Leon Betowski, William Brumley
United States Environmental Protection Agency, National Exposure Research Laboratory, Characterization Research Division, Las Vegas, Nevada 89193
♥ National Research Council Associate at the U.S. EPA, Las Vegas, Nevada.

A major goal of the analytical chemistry research program at the U. S. Environmental Protection Agency (Las Vegas) is to ensure that advances in mass spectrometry become incorporated into the tools available for routine environmental monitoring. Soft ionization techniques, such as fast atom bombardment (FAB), and selective ionization techniques, such as electron capture negative-ion mass spetrometry (ECNI MS) and proton-abstraction negative ion chemical ionization mass spectrometry, are underutilized in environmental analysis. An example of the application of these techniques to sulfonylurea herbicides is presented.

Negative-ion desorption mass spectra (DCI-MS) of sulfonylureas were obtained using a Finnigan-MAT TSQ 700 mass spectrometer employing methane, ammonia, deuterium oxide vapor, or a mixture of approximately 10% nitrous oxide in methane. A Finnigan direct exposure probe (DEP) was used as a desorption probe. Sulfonylurea herbicide standards were obtained from ChemService. Typically 100-1000 ng of solid was deposited on the tungsten wire of the DEP probe. NI/FAB/MS and NI/FAB linked-scan B/E experiments (Xe gas, 1mA, 8kV) were performed using a VG 7070EQ mass spectrometer. Glycerol, triethylenetetraamine (TETA), and 3-nitrobenzyl alcohol (NBA) were investigated as FAB matrices.

Background-subtracted negative ion FAB-MS spectra of the herbicides exhibit $[M-1]^-$ peaks and their fragmentation products. Of the three matrices used, TETA and NBA gave best results. Generally, enhanced fragmentation was observed with the TETA matrix. In contrast, in the NBA FAB spectra, high-abundance $[M-1]^-$ peaks and fewer fragment peaks were typically noted.

A similar fragmentation pattern of the precursor $[M-1]^-$ ions was observed in the DCI-MS/MS (TSQ-700) and FAB-B/E linked-scan (VG) experiments. The DCI-MS/MS experiments, however, demonstrated better sensitivity than the FAB-B/E experiments. The fragmentation pattern was supported by the MS/MS spectra of the *in situ* deuterated sulfonylureas and also by the spectra of the independently acquired compounds. For example, identity of the m/z 182 ion that was present in the MS and MS/MS spectra of several compounds (Fig. 1) was confirmed by the CAD experiments involving the ion obtained independently by deprotonation of saccharin. Similarly, the CAD spectrum of the sulfometuron methyl $[M-1]^-$ product ion (m/z 214) matched the spectrum of the ion derived from methyl-2-(aminosulfonyl)benzoate (Fig. 1).

Early in the desorption profile of the DCI-MS experiments, rather weak ions corresponding to M^- and $[M-H]^-$ were observed as well as some fragment ions. Spectra obtained in the later stages of desorption exhibited abundant peaks corresponding to thermal decomposition products.

Notice: The U.S. Environmental Protection Agency (EPA), through its Office of Research and Development (ORD), prepared this abstract for a poster presentation. It does not necessarily reflect the views of the EPA or ORD.

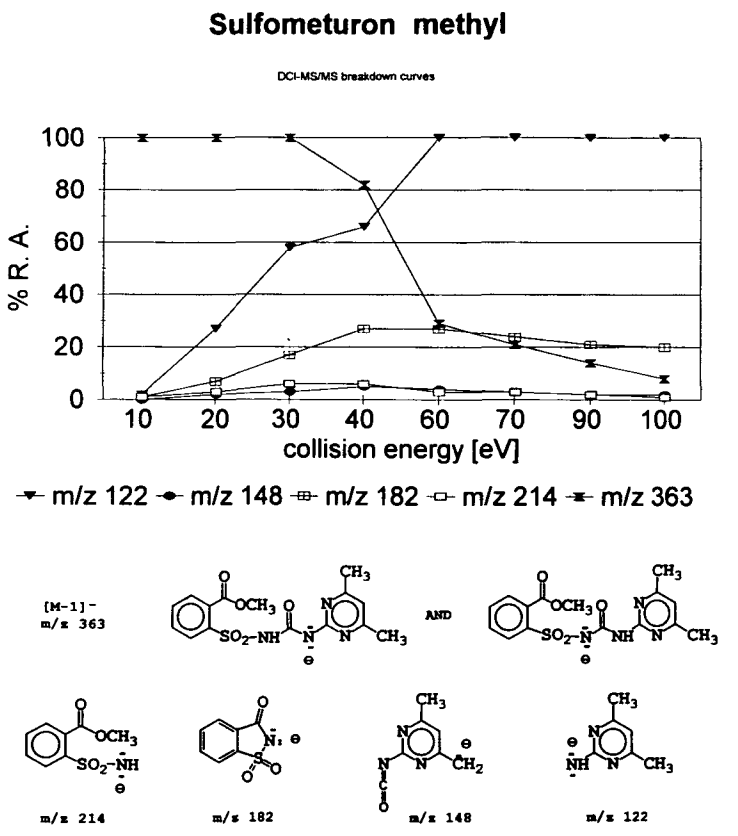

Figure 1. Breakdown curves and fragmentation pattern of sulfometuron methyl $[M-1]^-$ ion.

DEP/CI-MS/MS Characterization of Sulfonylurea Herbicides

Jodie V. Johnson and Richard A. Yost.
Chemistry Department, P.O. Box 117200, University of Florida, Gainesville, FL 32611-7200

Introduction. Sulfonylurea herbicides (SUs) are very potent herbicides, which have relatively short half-lives once applied in the field due to their thermal lability and ease with which they undergo chemical hydrolysis, as well as biological degradation[1]. This susceptibility to rapid degradation also contributes to the difficulty in analyzing these compounds. Although GC/MS has been used to characterize SUs via their stable derivatives or their thermal degradation products, more commonly they are analyzed via LC/MS[2,3] or LC/MS/MS[4] using one of the amenable ionization techniques. In this work, sulfonylurea herbicides are characterized by direct exposure probe/chemical ionization/tandem mass spectrometry (DEP/CI-MS/MS) utilizing methane and ammonia as reagent gases.

Experimental. All data were acquired on a Finnigan MAT (San Jose, CA) TSQ45 triple quadrupole tandem mass spectrometer operated in the CI mode with an ionization energy of 100 eV and an ion source temperature of 150 °C. The reagent gas pressures were adjusted to yield maximum intensity of the reagent ions: CH_5^+ and H_3O^+ for methane at 0.12 torr (indicated) and NH_4^+ for ammonia at 0.2 torr (indicated). Normal mass spectra were taken in the Q1MS mode with ion lense tuning performed to optimize transmission of m/z 414 of FC43 under CH_4 CI conditions. MS/MS daughter spectra were acquired with a collision energy of 20 eV and collision gas pressure of approximately 1.6-1.9 mtorr argon (ion lenses were tuned to yield maximum conversion of m/z 414 to m/z 69 of FC43). SUs were obtained from Chem Service (West Chester, PA) with certified purities > 98%. Approximately 1-2 μL of an SU solution (1-5 mg SU/mL CH_2Cl_2) were placed on the DEP filament, allowed to air dry, and then introduced into the ion source. Vaporization of the SU occurred via resistively heating the DEP filament from ambient to approximately 450 °C @ 5 °C/s.

Normal Mass Spectrometry. With the introduction/vaporization of SUs via a conventional out-of-source solids probe, thermal degradation predominated over vaporization with little or no evidence of molecular-type ions. However, with the introduction/vaporization of SUs via an in-source direct exposure probe, $(M+H)^+$ and $(M-H)^-$ ions were readily observable. The major PCI- and NCI-MS ions were due to cleavages along the sulfonylurea bridge with and without hydrogen rearrangement and were very indicative of the SU structure[2,3]. NH_3 PCI-MS resulted in reduced fragmentation compared to CH_4 PCI due to the higher proton affinity of NH_3 resulting in less internal energy in the formed $(M+H)^+$ ion. NH_3 NCI-MS resulted in increased numbers and intensities of fragment ions. This was due to the abundant NH_2^- reagent ions generated by NH_3 in contrast to the relatively low abundance of OH^- ions generated in CH_4 NCI. NH_3 adduct ions (e.g. m/z 123) were observed in the NH_3 NCI; no adduct ions were readily observed with CH_4 NCI.

Tandem Mass Spectrometry. The (M+H)+ and (M-H)- ions underwent collision-induced dissociation (CID) very easily and with high efficiency under relatively mild CID conditions (20 eV, 1 mtorr argon). The resulting daughter ions were indicative of the two portions of the SU (i.e. the sulfonamide and the heterocycle) and thus were highly characteristic of the individual SUs (Figures 1 and 2). The daughter spectra of the $(M+H)^+$ ions matched well with those obtained under CE/ESI-MS/MS conditions[4]. The daughter spectra of the $(M+H)^+$ and $(M-H)^-$ ions were essentially identical regardless of whether the parent ion was produced under CH_4 or NH_3 CI. The daughter spectra of common sulfonamide and heterocycle structural ions were identical. For example, Thifensulfuron (Harmony), Metsulfuron Methyl (Ally), and Chlorsulfuron (Glean) all contain the same heterocycle; CAD of its protonated ion (m/z 141) yielded the same spectra for all three SUs. Thus, it should be possible to utilize CI-MS/MS of the molecular-type ions and fragment ions of unknown SUs or SU degradation products to elucidate their structure.

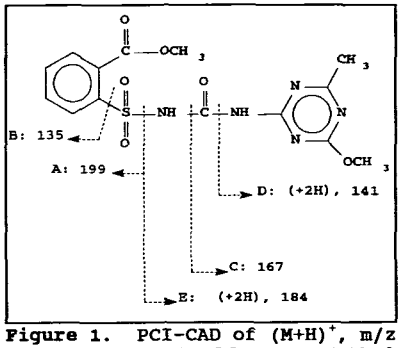

Figure 1. PCI-CAD of $(M+H)^+$, m/z 382, of Metsulfuron Methyl (Ally).

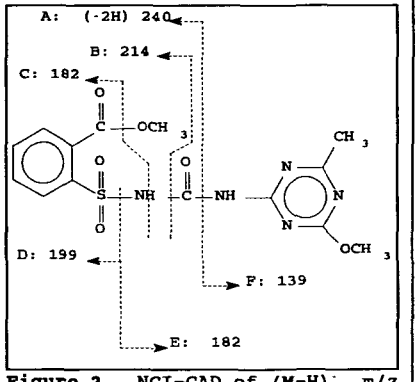

Figure 2. NCI-CAD of $(M-H)^-$, m/z 380, of Metsulfuron Methyl (Ally).

References

1. Beyer, E.M.; Duffy, M.J.; Hay, J.V.; Schleuter, D.D. "Sulfonylurea Herbicides" in *Herbicides: Chemistry, Degradation, and Mode of Action*, Vol. 3, Marcel Dekker: New York, 1987, Chapter 3, pp 117-189.
2. Reiser, R.W.; Barefoot, A.C.; Dietrich, R.F.; Fogiel, A.J.; Johnson, W.R.; Scott, M.T. *J. Chromatogr.* 1991, **554**, 91-101.
3. Shalaby, Lamaat M.; Bramble, Jr., F.Q.; Lee, P.W. *J. Agric. Food Chem.*, 1992, **40**, 513-517.
4. Garcia, F.; Henion, J. *J. Chromatogr.* 1992, **606**, 237-247.

DETERMINATION OF PROTON AFFINITIES OF PHOSPHONATES BY USING THE KINETIC APPROACH

A. Leroy[1], F.Fournier[1], J.C. Tabet[1]*, J. Dissard[2], I. Daoust-Maleval[2], and A. Tambuté[2].

[1]*Laboratoire Chimie Organique Structurale, EP 103, UPMC, Paris cédex 05, FRANCE,* [2]*Laboratoire Chimie Recherche Analyse, Centre d'études du BOUCHET, B.P. 3, 91710 Vert-le-Petit, FRANCE*

Organophosphorus compounds are widely used as pesticides, fertilisers or detergents in different fields like industry and agriculture They can be very efficient and are generally not persistent However, some of these compounds (or their corresponding degradation products) can be highly toxic and can affect irreversibly the environment[1]. Consequently, trace detections and identifications of such compounds required the use of an efficient analytical method such as mass spectrometry Moreover, tandem mass spectrometer coupled to gas chromatography can yield enhancement of the selectivity and specificity allowing to reach more structural informations[3], which is the case from decompositions of the selected $M^{+\circ}$ ions The studied $(RO)(R'O)P(CH_3)=O$ compounds are ·

1a R=R'=CH_3, 1b R = CH3, R'=C2H5 , 1d R=R'=C_2H_5, 1e R=CH_3, R'=iC_3H_7, 1g R=R'=nC_3H_7, 1f R=C_2H_5, R'=iC_3H_7, 1m R=R'=nC_4H_9, 1i R=CH_3, R'=C_6H_{11}, 1p R=R'=$CH(CH_3)C(CH_3)_3$, 1j R=CH_3 R'=$CH(CH_3)C(CH_3)_3$, 1r. R=R'=iC_4H_9, 1k R'=C_2H_5, R'=C_6H_{11} 1n R=C_2H_5, R'= $CH(CH_3)C(CH_3)_3$

Unfortunately, in EI, these compounds yield extensively fragment ions without detection of $M^{+\circ}$ Actually, formation of MH^+ ions is favored even at low pressure source Recently, mechanism of the MH^+ preparation has been investigated in ion trap instrument, and has been shown to proceed according to an ion-molecule reaction induced by the phosphonate $M^{+\circ}$ ion after ion isomerisation (Equation 1a) into an enolic form Alternatively, under CI-NH_3 conditions, they give rise to formation, as expected, of MH^+ and MNH_4^+ (in weak abundances) This trend reflects that proton transfer from NH_4^+ is exothermic meaning that PAs of phosphonates (noted as $PA_{(Pi)}$) are larger than $PA_{(NH_3)}$. In the present study, in order to obtain more informations on the phosphonate basicity, proton affinities of more than ten organophosphonate compounds have been estimated by using gas chromatography tandem triple quadrupole mass spectrometer according to the kinetic method developped some years ago by Cooks and col[3] from competitive decompositions of proton bounded mixted dimers according to the following relations obtained from RRKM theory

$$\mathbf{Ln\ k_1/k_2 = Ln(Q^*_1/Q^*_2)-[AP_2-AP_1]/RT \quad and \quad Ln\ k_1/k_2 \# -[AP_2-AP_1]/RT}$$

From trimethyl and triethylphosphate esters used as reference, metastable decompositions of the protonated phosphate/phosphonate dimers provide the first PA scale of phosphonates By using different measurements allowing the AP overlap, it appears that the obtained PA scale was self consistent over ± 2 (or less) kJ/mol in spite of the use of two references only In order to appreciate of the PA order of phosphonates as well as their corresponding values through the PA scale, a second approach based upon an indirect determination of $PA_{(Pi)}$ by using the PA scale (reported by Lias and modified by Harrison) of amines accurately known has been applied according to the modified kinetic treatment proposed by Fenselau *et al*[4] · $\mathbf{Ln\ k_{RNH2}/k_{Pi}=[Ln(Q^*_{RNH2}/Q^*_{Pi})-PA_{Pi}]+(AP_{RNH2}/RT)}$ in which each organo-

phosphorus can be compared to those of the appropriate amine serie Studied of the heterogeneous chemical mixed dimer provided a phosphonate PA scale very close to that obtained from TMP and TEP and furthermore PA_{TEP} determined by this latter was yield comparable results as proposed from Lias scale The choice of the proton affinity scales as reference (Lias or Harisson) does not modified strongly the relative PA values determined from both scales

Table 1. Comparison of the proton affinities of phosphonates determined by using PAs values of TMP and TEP, and the published values from the PA scales of Lias[8] and Harrison.

Organo-phosphorus	PA (kJ/mol) (*)	PA (kJ/mol) *Lias scale*	PA (kJ/mol) *Revised scale*
TEP	(907 1)&	908 5 ± 0 8	907 4
MiPrMP	903 2	905 3 ± 1.0	904 6
DEMP	904 6	904 2 ± 1 5	902 9
MCMP	910.2	908 9 ± 1 2	907.7
MPiMP	910 8	911 0 ± 0 6	908 9
DnPMP	911 3	913 2 ± 1 0	910 6
EiPrMP	911 4	911 3 ± 2 1	910 0
DBMP	911 5	910 5 ± 0 8	908 8
ECMP	917 9	916 1 ± 1 1	914 7
EPiMP	$	917 2 ± 1.0	916 9
DiPrMP	$	918 7 ± 0 8	916 2
DPiMP	919 4	918 3 ± 1 0	916 6

Ester substituants influence significantly the PA values Indeed, the change of CH_3OP into C_2H_5OP leads to a strong PA variation by 20 $kJ.mol^{-1}$, for relatively small phosphonate esters, and by 9 $kJ\ mol^{-1}$ for larger esters A ramification of the side chain ester leads to a slight increase of basicity by about 1kJ mol^{-1} The last point in the PA rises with increasing of the alkyl chain length which is due to a coiling effect providing a charge stabilization (i e polarisability effect). Both PA method of determinations seem to be consistent since similar PA values are obtained Furthermore, the PA scale from the second method seems to be less extended than the first one wich is shifted towards higher PA values by 10 kJ mol^{-1} Note that the PA value obtained for TEP from the second method is very close to that which was reported in litterature[4]. VERY LIKELY, AMINES ARE SUITABLE REFERENCES TO STUDY BASICITY OF PHOSPHATES AND PHOSPHONATE ESTERS Alternatively, these results indicate that the protonated dimers generated from phosphonate and phosphate esters as well as phosphonates and amines are characterized by a common structure very likely as proton bounded dimers rather than formation of covalent bounded complex

1 P A D'Agostino and L R Provost , Biomed and Environ Mass Spectrom., 13 231 (1986)
2 S A Mc Luckey, D Cameron and R G Cooks , J Am Chem Soc 103 (6), 1313 (1981)
3 X Cheng, Z. Wu and C Fenselau ; J Am Chem. Soc 115, 4844 (1993)
4 S G Lias, J.E Bartmess, J.F Liebman, J L Holmes, R D. Levin and W G Mallard , J Phys and Chem , Ref Data, 17, sup n°1 (1988)
5 Li and A G Harrison , Org Mass Spectrom , 28, 366 (1993).

CID STUDIES OF INORGANIC SPECIES RELEASED DURING BIOMASS COMBUSTION

David C. Dayton and Dingneng Wang
National Renewable Energy Laboratory
1617 Cole Boulevard
Golden, CO 80401-3393 USA

A limiting factor in using solid biomass fuels for electricity production is the accelerated fouling and slagging caused by alkali metal released during biomass combustion. A detailed understanding of alkali release mechanisms during biomass combustion as well as identification of these alkali metal species will provide insights as to how these vapors enhance deposit formation in power generating facilities A molecular beam sampling triple quadrupole mass spectrometer (MBMS) system, in conjunction with a variable-temperature quartz tube reactor, was used to directly sample the hot gases liberated from the combustion of small (20-60-mg) biomass samples The MBMS system is a three stage differentially pumped vacuum system. High temperature, ambient pressure gases underwent a freejet expansion as they were introduced into stage one through a 200μm diameter sampling orifice The expanded gases were skimmed at the entrance of stage two with a conical skimmer to form a molecular beam which was directed into the ionization region of the triple quadrupole mass spectrometer[1] in stage three.

Direct, real-time measurements of sampled gases during combustion of selected feedstocks have been used to identify gas phase alkali metal containing species as a function of feedstock composition[2,3] During these investigations, species with m/z = 81 and m/z = 120 were detected during combustion of alfalfa stems and almond hulls. Collision induced dissociation (CID) experiments were initiated to unambiguously identify these species released during the combustion of these high potassium and nitrogen containing feedstocks Both parent and daughter ion experiments were performed during the combustion of alfalfa stems and almond hulls at 1100°C in 20% O_2 in helium

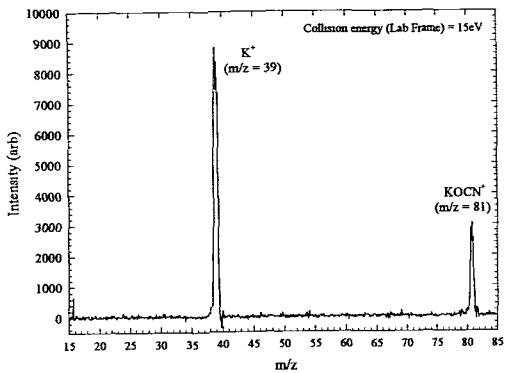

FIGURE 1: CID daughter spectrum of m/z = 81 recorded during the combustion of alfalfa stems at 1100°C in 20% O_2 in helium.

The only fragment daughter ion detected during the CID experiments on m/z = 81 measured during alfalfa stems combustion was K^+ at m/z = 39 as shown in Figure 1 This confirmed that the species with m/z = 81 released during combustion of alfalfa stems contained a potassium atom. Daughter ion spectra of m/z = 81 were also recorded during almond hulls combustion with identical results. Because this species definitely contains a potassium atom, the other fragment must have a mass of 42 amu. The only combination of atoms that is reasonable for this fragment is NCO and the identity of the species with m/z = 81 is $KOCN^+$ This signifies a new mechanism for alkali metal released during the combustion of high potassium and nitrogen containing feedstocks, like alfalfa stems and almond hulls, based on the vaporization of potassium cyanate.

After identifying the species with m/z = 81 as $KOCN^+$, the species with m/z = 120 could be identified as K_2OCN^+, the fragment ion of KOCN dimer OCN behaves like a pseudo-halogen based on the fragmentation characteristics and dimer formation of KOCN. This assignment was confirmed by recording CID daughter spectra of m/z = 120 during alfalfa stems combustion at 1100°C in 20% O_2 in helium where the only daughter fragment ion observed was K^+ at m/z = 39

During the combustion of high alkali containing feedstocks, most of the parent potassium containing species could be identified from the parent ions in the mass spectra. These species, however, undergo substantial fragmentation in the ionizer yielding an intense peak at m/z = 39, the K^+ fragment. Parent ion spectra of m/z = 39 were recorded during alfalfa stems and almond hulls combustion at 1100°C in 20% O_2 in helium to confirm the identity of all the parent potassium containing species which fragment to produce K^+

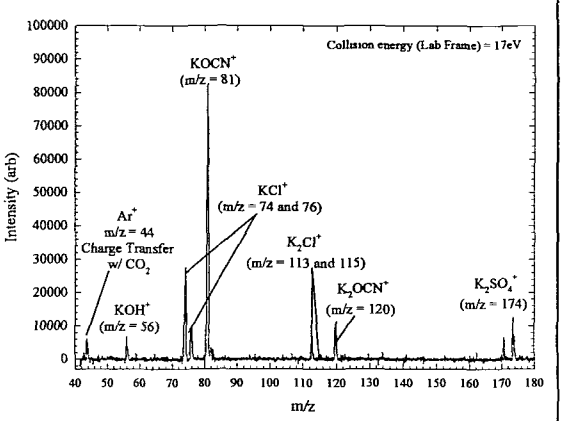

FIGURE 2: CID parent spectrum of m/z = 39 recorded during alfalfa stems combustion at 1100°C in 20% O_2 in helium

Peaks at m/z = 56 (KOH^+), m/z = 74(KCl^+), m/z = 76 (KCl^+), m/z = 81 ($KOCN^+$), m/z = 113 (K_2Cl^+), m/z = 115 (K_2Cl^+), m/z = 120 (K_2OCN^+), and m/z = 174 ($K_2SO_4^+$) were identified in the CID parent spectra of m/z = 39 recorded during alfalfa stems combustion as shown in Figure 2 Most of these parent ions were observed in the standard spectra recorded during alfalfa stems combustion, with the exception of the potassium sulfate parent ion. Similar spectra were recorded during almond hulls combustion Potassium hydroxide, potassium cyanate, and potassium sulfate are observed in the CID parent spectra of m/z = 39 recorded during almond hulls combustion. These experiments suggest that there are four different pathways for potassium release to the gas phase during alfalfa stems combustion: 1) via potassium hydroxide, 2) via potassium chloride, 3) via potassium cyanate, and 4) via potassium sulfate

[1]Extrel Corporation, 575 Epsilon Drive, Pittsburgh, PA 15238

[2]D C Dayton, R.J French, and T.A. Milne, "The Direct Observation of Alkali Vapor Release During Biomass Combustion and Gasification. I The Application of Molecular Beam/Mass Spectrometry to Switchgrass Combustion," submitted for publication in *Energy & Fuels*.

[3]R.J French, D C. Dayton, and T.A Milne (1994). The Direct Observation of Alkali Vapor Species in Biomass Combustion and Gasification, NREL Technical Report (NREL/TP-430-5597). January 1994

Photodissociation of Electrosprayed Ions in the Quadrupole Ion Trap

*Stephen M. Boue', James L. Stephenson, and Richard A. Yost

Traditionally, collision-induced dissociation (CID) has been the method of choice for the activation of polyatomic ions in quadrupole ion trap tandem (MS/MS) experiments. More recently, however, photo-induced dissociation (PID) has developed into an important alternative to CID for the structural elucidation of biologically important molecules. Recently, our group has constructed an electrospray-ion trap instrument utilizing a multi-pass optical arrangement for PID studies.[1] An RF-only octopole ion guide efficiently transmits ions from the high pressure source region to the lower pressure region of the analyzer. In this presentation we report the development of the ESI/QITMS system and the first results on the photodissociation of four classes of biologically important molecules (oligosaccharides, antibiotics, peptides, and oligonucleotides).

The ESI/QITMS instrument used in our experiments was designed and built at the University of Florida. A simplified schematic drawing of the instrument including the ESI source, differentially pumped vacuum chamber, RF-only octopole, and ion trap analyzer is seen in **Figure 1**. The RF-only octopole was constructed from 2.0 mm diameter, 30 cm long, stainless steel rods. The ratio of the rod diameter to the field radius was 0.33 and the optimum RF frequency was 1.659 MHz.[2]

For ion injection, two of the more important instrument parameters of our system were the electrospray gate lens and the octopole offset voltage. As shown in **Figure 2** for the electrospray gate lens, the maximum peak intensity for the individual charge states of the peptide Ubiquitin varied over a 20V range. The trend observed showed lower charge states (higher m/z values) required higher gate lens voltages for optimal transmission to the octopole. This mass dependency can also be seen when varying the octopole offset voltage. Although this mass discrimination can be problematic, when compared to traditional DC lens systems for ion injection, the amount of mass discrimination observed was significantly reduced

PID is an excellent tool for obtaining oligosaccharide sequencing information due to the ease in cleaving the **C-O-C** ether (glycosidic) linkage. The PID spectra of the ammonium adduct of stachyose (m/z 684) is shown in **Figure 3**. Complete fragmentation of the tetrasaccharide was obtained with two laser pulses. The peaks observed included $(M+NH_4-179)^+$ at m/z 505, $(M+NH_4-NH_3-179)^+$ at m/z 488, $(M+NH_4-NH_3-179-162)^+$ at 326, and $(M+NH_4-NH_3-179-162-162)^+$ at m/z 164. The loss of 179 corresponds to the loss of either the non-reducing or reducing end of the molecule, while the loss of 162 occurs due to internal cleavages. In addition to the complete fragmentation of oligosaccharides, PID is also useful for cleaving sugar moieties from the aglycone unit of antibiotics. Currently, work is being done with the antibiotics vancomycin and erythromycin.

The ability to cleave amide linkages has enabled PID to be useful in peptide (and protein) sequencing. **Figure 4** shows the PID spectrum of the $(M+3H)^{+3}$ ion of Angiotensin I using a cw IR laser. Typical fragments observed were mid-range singly charged b ions (b_5, b_6, and b_9) derived from β-cleavage and charge migration along the peptide backbone. Also observed were the y ions (y_2, and y_4, y_8^{+2}) originating from hydrogen ion migration(s) from the amino end of the peptide. Also, current experiments with oligonucleotides are being conducted to examine the utility of PID for DNA/RNA sequencing.

For the structural elucidation of biomolecules, photo-induced dissociation is an effective alternative to collision-induced dissociation of electrosprayed ions inside the quadrupole ion trap. In this study, four classes of biologically important molecules were examined. These compounds were chosen to demonstrate the capabilities of a new ESI/ion trap instrument designed and recently constructed for PID studies at the University of Florida. Currently, more complex biomolecules, including larger DNA

fragments and glycopeptides, are being characterized in our laboratory. The high level of control over energy added and higher fragmentation efficiency of PID enable this technique to provide invaluable structural information to the analytical biochemist.

1. Stephenson Jr, J.L.; Booth, M.M.; Shalosky, J.A.; Eyler, J.R., Yost, R.A. *J. Am. Soc. Mass Spectrom* **1994**, 5, 886-893.
2. Schwartz, J.C.; Syka, J.E.P., Bier, M., Finnigan MAT, San Jose, CA, Personal Communication

Figure 1
Electrospray/Ion Trap Instrumentation for Photo-Induced Dissociation

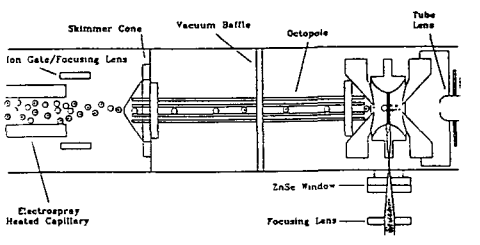

Figure 3
Photodissociation Spectra of the Ammonium Adduct $(M+NH_4)^+$ of Stachyose

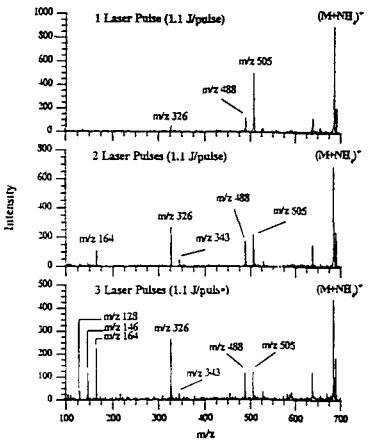

Figure 2
Mass Dependency of the Electrospray Gate Lens for the +12, +10, +8, and +6 Charge States of Ubiquitin

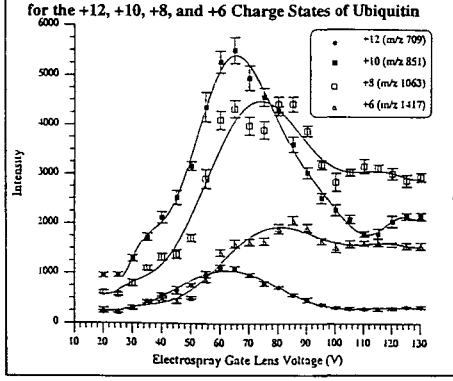

Figure 4
Photodissociation Spectrum of the $(M+3H)^{+3}$ Ion of Angiotensin I

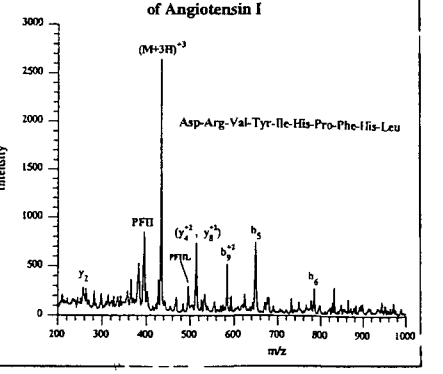

PULSED PRESSURE QUADRUPOLE ION TRAP FOR TANDEM MS OF PEPTIDES

Vladimir M. Doroshenko and Robert J. Cotter
The Johns Hopkins University School of Medicine, Baltimore, MD 21205

Collision-induced dissociation technique is widely used in tandem mass spectrometers including quadrupole ion traps (QIT). The main feature of QIT is the presence of helium buffer gas at relatively high pressure of ~ 1 mTorr. Collisions with helium atoms are commonly used also for fragmentation after additional excitation of parent ions. One of the problems which is specific for QIT, on the way of practical use of CID technique for elucidation of peptide in QIT is due to its ability to trap ions within limited range of m/z. Energy deposition in CID process is also limited due to the large mass difference between colliding partners. The effect of adding of heavy target gases on the CID efficiency and overall performance of QIT was extensively investigated. Higher activation energy reactions were observed in collisions with heavy gases. However, the trapping efficiency for introduced ions dropped with increase of content of heavy gas in buffer gas mixture. The buffer gas pressure also effects on the fragmentation pattern. In this work a pulse gas valve technique was used for studying the influence of heavy gases at separate experimental stages of QIT operation.

Experiments were carried out on a modified Finnigan MAT ion trap detector. These modifications include additional hardware for interfacing of ITD with laser and external control of the instrument, and developed in-house *TrapWare* software (see *Rapid Commun. Mass Spectrom.* **1994**, *8*, 766). A Quatech (Akron, OH) WSB-100/WSB-A12M waveform

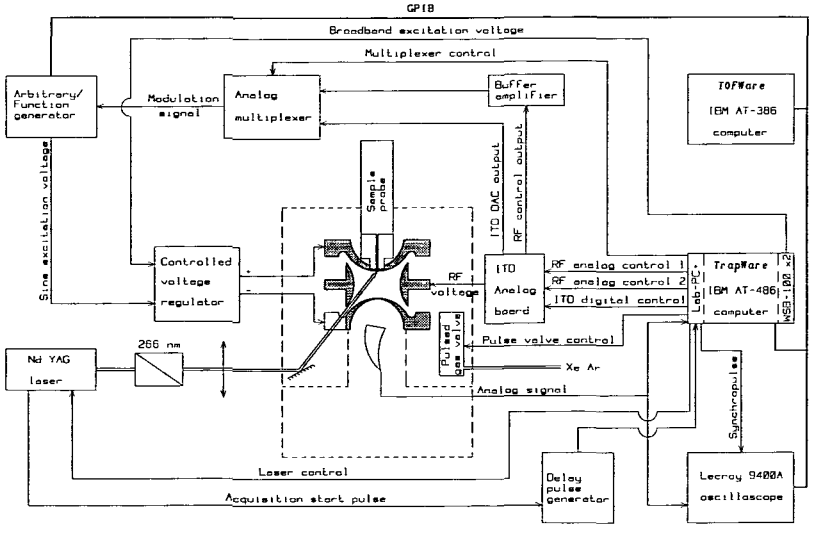

Fig. 1. Block diagram of the modified ITD instrument.

synthesizer plug-in board connected to an IBM computer was used for SWIFT waveform generation (see ASMS'95 poster ThPC 083 for details). The instrument scan functions and SWIFT pulses were designed by TrapWare software. For the pulsed gas introduction experiments the ion trap assembly was mounted on a new holder inside a two-section coffin vacuum chamber. The characteristic pumping time of the ion trap section was ~7.6 ms that allowed us to limit the influence of injected gas on a chosen stage only. A General Valve (Fairfield, NJ) Series 9 pulse valve with a bullet style body and 0.1 mm diameter exit orifice was placed inside vacuum chamber near the ion trap assembly.

The introduction of different gases was studied at different stages of ion trap operation. A significant improvement in QIT operation was observed only during the injection of heavy gases at the CID stage while the gas introduction during the ion trapping, ion isolation and analytical scan stages had negative effect. The effect of the sort of injected gases on the CID process at different q_z was studied using the protonated α-Casein Fragment 90-96 ions as a sample molecule. The CID efficiency was smaller for smaller q_z values and increased with the increase of the mass of collisional counterpartner which changed from 4 for He to 131 Da for Xe. No difference was observed for CID fragmentation pattern for partners without and with internal structure (such as NH_3 and air). In the case of ammonium this means that no chemically reactive collisions were observed. The most probable explanation is that in the case of α-Casein Fragment 90-96 the protonation does not occur at the amide bond. The increase of pressure of the injected gas in the limits studied in this work (up to 5 mTorr) resulted in the improvement of fragmentation. The exemplary CID mass spectrum of α-Casein is shown in Fig. 2. CID was performed using xenon as collision gas at q_z= 0.05 which allows the trapping of low mass product ions. The mass spectrum in Fig.2 contains long a and b fragment ion series that allows full recovering of amino acid sequence.

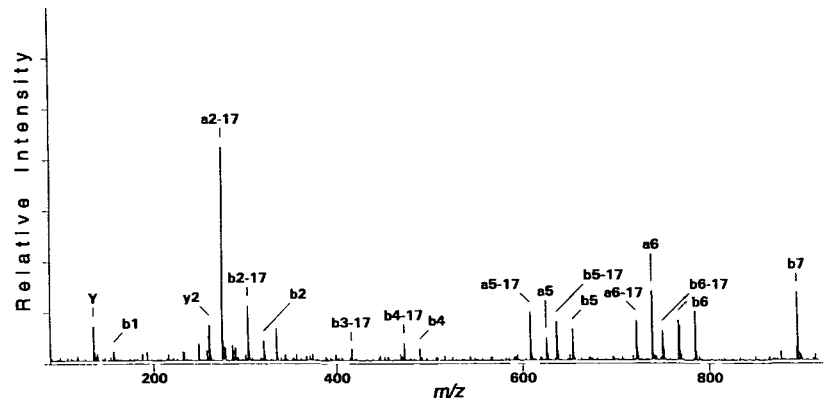

Fig.2. Monoisotopic tandem mass spectrum of protonated ions of α-Casein Fragment 90-96 (MW=913 Da) obtained with the use of a pulsed introduction of xenon at the pressure of ~2.5 mTorr for CID at q_z= 0.05.

Thermal Activation of Stored Ions in a Quadrupole Ion Trap

William J. Herron, Douglas E. Goeringer, and Scott A. McLuckey
Oak Ridge National Laboratory

Trapped ion techniques offer a unique opportunity to probe the nature of isolated ions in the gas phase. We have expanded our experimental capabilities by adapting an electrospray/atmospheric glow discharge quadrupole ion trap combination to allow for a heated vacuum system. (1) By increasing the temperature and the average collisional energy, we are studying changes in the dissociation behavior and the ion-molecule reactivity of ions as a function of temperature. The temperature plays a role in both the activation of unimolecular fragmentation and desolvation phenomena. This set-up has allowed us to acquire ESI mass spectra of multiply-charged Horse Heart Myoglobin and to explore its dissociation behavior as a function of bath gas temperature. Thermal activation which raises the internal energy of the ion, also affects intermolecular interactions such as the solvation of a multiply-charged ion by a large number of neutral species. Raising the temperature of multiply-charged species will "heat" them above the binding energy of the weakly bound neutral species, thus desolvating the ion. We have observed this process during the the thermal activation of multiply-charged Horse Heart Myoglobin.

We are particularly interested in relating collisional activation data acquired at room temperature with data acquired from thermal activation. Quantifying the effects of thermal activation on ion internal temperature requires an ion whose thermochemistry is well defined. We have resorted to the use of heavily-studied "thermometer" ions such n-butylbenzene to model ion activation. The basic assumption of thermal activation is that ions are in thermal equilibrium with the bath gas. This assumption is compromised by the ion isolation technique used to remove all other ions except the ions of interest in the quadrupole ion trap. The ion isolation is accomplished by ramping the primary RF trapping voltage amplitude applied to the ring electrode, while applying a small amplitude axial modulation frequency to the endcaps. This isolation step will kinetically heat the parent ions. To compensate, a cooling phase is added to the scan function which allows the parent ion populations to be collisionally cooled back to the ambient helium bath gas temperature (Figure 1). The extent of ion heating during the isolation step is inversely proportionally to the amount of helium, while the time required to regain equilibrium is proportional to the amount of helium. By judiciously selecting an excessive cooling period (20 ms, 1 mtorr He) the thermal activation of well characterized ions can be monitored. Within the temperature range accessible to our experimental set-up (25-100 °C), we did not observe the dissociation of the n-butylbenzene radical cation by thermal activation alone. However, we were able to increase the extent of collision induced dissociation by thermal activation (Figure 2).

Figure 1. The effect of the addition of a cooling phase after the isolation step. The isolated n-butylbenzene radical cation is (a) stored and kinetically excited by a small axial modulation amplitude for 25 ms, and (b) is collisionally cooled by the helium bath gas for 20 ms before being kinetically excited by a small axial modulation amplitude for 25 ms.

Figure 2. The effect of thermal activation of stored ions. The isolated n-butylbenzene radical cation is stored, collisionally cooled, (20 ms, 1 mtorr He) and kinetically excited by a small axial modulation amplitude for 25 ms (a) at 26 °C, and (b) and at 90 °C.

Reference:
(1) Herron, W. J.; Goeringer, D.E.; McLuckey, S.A. Proceedings of the 42nd ASMS Conference on Mass Spectrometry and Allied Topics, Chicago, Illinois, May 29-June 3, 1994.

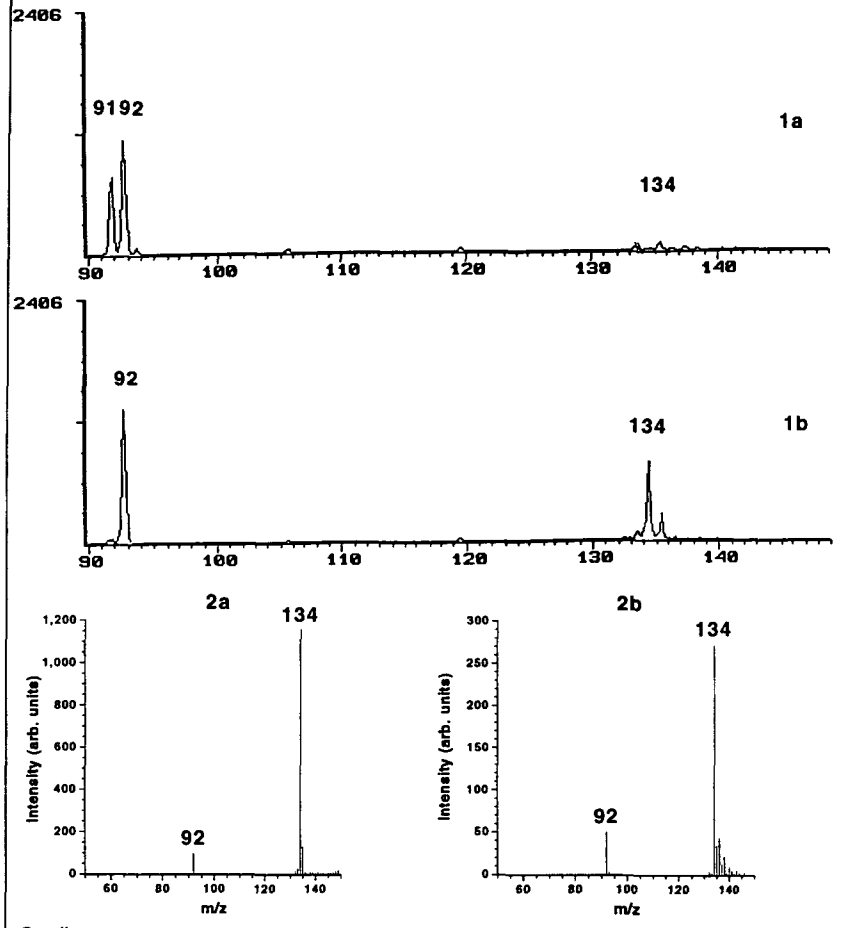

Credit:
Research sponsored by the U.S. Department of Energy, Office of Basic Sciences, under Grant DE-AC05-84OR21400 with Martin Marietta Energy Systems, Inc.

The Analytical Utility of Photodissociation in Tandem Mass Spectrometry

D. J. BEUSSMAN[1,2], T. A. ERICKSON[1], C. G. ENKE[1,2]
[1]Department of Chemistry, University of New Mexico, Albuquerque, NM 87131
[2]Department of Chemistry, Michigan State University, East Lansing, MI 48824

Photodissociation (PID) is an established method of fragmenting ions. Fundamental studies have been performed on a few select chemical systems, but no broad study has been undertaken to demonstrate the analytical utility of PID in mass spectrometry relative to the widely accepted approach of collisional-induced dissociation (CID).

CID is a well-established method of creating product ions in tandem mass spectrometers. CID is a nearly universal fragmentation method, at least for ions below a few thousand mass units, which contributes to its usefulness. However, CID does suffer from two drawbacks. As the molecular weight of a precursor increases, the energy imparted to it decreases, making CID less attractive as a fragmentation method for high-mass ions. Also, in time-of-flight applications, the product-ion spectrum generation rate is limited by the duration of the CID gas pulse and the time required to pump the gas away. For tandem mass spectrometry on the GC time scale this spectral generation rate is too slow.

The energy imparted to an ion with PID is not dependent on the molecular weight of the ion, but only on the wavelength of the light used. The spectral generation rate utilizing PID as the fragmentation method is limited to the repetition rate of the laser used. Laser repetition rates greater than 200 Hz are possible, which would allow multiple product spectra to be obtained during the elution time of a GC peak. For these reasons, PID appears to be an attractive alternative to CID for product ion creation.

The PID product spectra for a broad range of compounds with various functional groups, have been determined. Using 193 nm photons, all organic ions studied have been fragmented, including alkanes. Table 1 shows the % depletion for several ions using a laser pulse energy of 200 mJ. The effect of laser pulse energy on the PID process has been studied and the results used to calculate the PID cross-sections. For the ions studied at 193 nm, there is less than an order of magnitude difference in PID cross-sections, indicating that all ions are efficiently fragmented and that varying the functional groups does not significantly change the PID process at 193 nm. The linear relationship between the depletion of the precursor ion and the laser pulse energy indicates that all processes studied are single photon events.

In order to establish the general analytical utility of PID as a fragmentation method, the resulting product spectra have been compared to those obtained with CID on a triple quadrupole mass spectrometer. This indicates whether PID and CID provide comparable structural information. For all ions studied so far, the major product ions are the same for both CID and PID. PID does, however, yield fragment ions that are not present in the low-energy CID product spectrum. The results of these studies indicate that PID spectra for 193 nm photons may more closely resemble the high-energy CID product spectra.

Since all ions studied have been efficiently fragmented, including alkanes (Figure 1), PID using 193 nm photons appears to be a general fragmentation method for organic ions,

regardless of the functional groups present in the ions. Also, the high efficiency demonstrates that analytically useful product spectra can be obtained with every laser shot.

Molecule	Ion *m/z*	% Depletion (at 225 mJ)	PID Cross-Section (cm^2)
Toluene	39	9.2	2.9E-19
	65	16.6	5.2E-19
	91	21.0	6.6E-19
	92	12.7	4.0E-19
Bromobenzene	77	25.5	8.0E-19
	156	35.1	1.1E-18
n-Heptane	43	23.6	7.4E-19
n-Hexane	57	22.9	7.2E-19
2-Hexene	55	25.8	8.1E-19
2-Hexyne	53	44.6	1.4E-18
	67	20.7	6.5E-19
	82	30.3	9.5E-19
Triethylamine	86	18.8	5.9E-19

Table 1. % Depletion and 193 nm PID cross-sections for various ions.

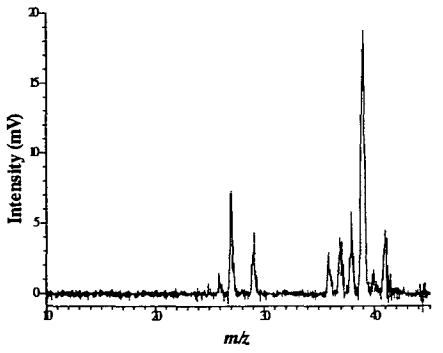

Figure 1. Product spectrum from PID of m/z 57 from hexane. Laser pulse energy of 200 mJ, 500 transients summed.

SMIKES: A New Scan to Determine Artefact Peaks in MIKE Spectra.

Yves Mouget and M.J. Bertrand,
Regional Center for Mass Spectrometry, Dept. of Chemistry,
University of Montreal, Montreal, Canada, H3C 3J7.

A common origin for artefacts in Mass Analyzed Kinetic Energy Spectra (MIKES) performed with instrument of reverse configuration is the decomposition of higher mass ions in the field free region before the magnet, such that the apparent mass ($m^*=m_2^2/m_1$) of the fragment corresponds to the mass selected during the scan. When MIKE scans are performed using EBE geometry instruments, artefacts are not necessarily eliminated but their intensity can be substantially reduced [1]. However, instruments of this latter geometry offer a scanning method that allows these artefacts to be identified. By linking and scanning the 1st and 2nd ESAs such that $E_1=E_2$, with the magnet set to the mass of interest, the spectrum shows only peaks that correspond to artefacts. This scan is labelled a Selected Mass analyzed Ion Kinetic Energy (SMIKE) scan. Experiments were performed with an EBEqQ geometry instrument, featuring an "experiment design" function, which allows analyzers to be linked and scanned by means of user-specified mathematical relationships. The SMIKE scan could also be performed by hard-wiring the two ESAs together.

Several artefacts appear in the MIKE spectrum of the protonated dimer of the dipeptide Lys-Lys, $[(Lys\text{-}Lys)_2H]^+$, of m/z 549.4 [2]. Intense peaks are observed at relative energies of 0.942, 0.939, and 0.936. They were found to result from the loss of an HCl entity from the higher mass ions $[(Lys\text{-}Lys)_2(HCl)_2H]^+$, at m/z 623, before the magnet. Using a recently proposed graphical method [1], the previous rationalization describing the presence of an artefact is represented in Figure 1. This approach uses a cube to reflect the effect of the three analyzers in an E_1BE_2 geometry instrument ($\rho1$ for E_1, $\rho2$ for E_2, and B for the magnetic sector). The decomposition of higher mass ions would be represented by a diagonal line (a-b) drawn from the mass of the precursor (m/z 623) on the B axis (at $\rho1=1$ and $\rho2=1$) to the origin. Artefacts in MIKE scans obtained using instruments of E_1BE_2 geometry correspond to fragmentations occurring between the first ESA and the magnet. This is reflected in Figure 1, where the diagonal line representing fragmentations of the precursor at m/z 623.4 has been projected on the (B, $\rho2$) plane at $\rho1=1$, and now intersects the MIKE scan line (c-d), which is also projected onto the (B, $\rho2$) plane. The intercept coordinates of the diagonal with the scan line correspond to the energy at which the fragment will be transmitted, and appear as an artefact in the MIKE spectrum.

Alternatively, if a line were drawn through the cube at a constant value of B, such that it reflects a variation in both E_1 and E_2 such that $E_1=E_2$, this line would intersect all the diagonal lines describing the decomposition of higher mass precursor ions. This line can be related to a real scan, a scan of the two ESAs, which will result in a spectrum containing only the artefact peaks that can be present in a MIKE spectrum. Such a scan is represented by the line d-e in Figure 1. It samples fragments formed in FF1, with ions reaching the detector only if their apparent mass of m* corresponds to the magnet mass. Figure 2 is a spectrum resulting from this SMIKE scan at $E_1=E_2$, with B set to 549.5. The result is two clusters of peaks, at relative energies of ~0.939 and ~0.998. The precursor and fragment ions determined for the resulting mass losses, by taking into account the energy at which each peak is transmitted with respect to the energy of the main beam, correspond to those previously suggested for the artefacts. For example, the peak which appears at 7508 Volts is the result of $[(Lys\text{-}Lys)_2(H^{35}Cl)(H^{37}Cl)H]^+$, of m/z 623.4, losing $[H^{37}Cl]$ to form the fragment $[(Lys\text{-}Lys)_2(H^{35}Cl)H]^+$ of m/z 585.4. The masses for the different fragment ions were confirmed by scanning the quadrupole located after E_2.

Vitamin K is another compound that may produce artefacts in a MIKE spectrum. When a MIKE scan of the fragment ion of m/z 198 is performed on an EBE geometry instrument, two narrow peaks at m/z 185 and m/z 186 are visible (Figure 3), corresponding to relative energies of 0.9342 and 0.9389, respectively. When the SMIKE scan of the fragment ion of mass 198 is performed, two peaks appear among several others at 0.9384 and 0.9340 of E_0, which is close to the energy at which the peaks appeared in the MIKE spectrum (Figure 4). It would therefore seem that these peaks could indeed be artefact peaks, corresponding to the decomposition of m/z 225-->211, and m/z 227-->212. When considering the structure of the two fragment ions of mass 225, the first loss could more easily occur from the $C_{16}H_{33}$ fragment ion, than from the $C_{15}O_2H_{13}$ fragment ion, both of which have a mass of 225. Such structure elucidation represents another advantage of this scan. The SMIKE scan is an example of an MS/MS scan developed by picturing the desired scan within the 3D visualization approach, and then defining the corresponding scan equation by means of an interpretation program. The resulting spectrum shows peaks that would correspond to artefact peaks in a MIKES, and the structural information obtained should therefore be considered complimentary to that obtained from the MIKE scan.

References:

1) Y. Mouget and M. J. Bertrand, *R. Com. Mass Spectrom.* **9**, 387 (1995).
2) A J. Alexander, P. Thibault, R. Guevremont, and R.K. Boyd, *R. Com. Mass Spectrom.* **2**, 79 (1988)

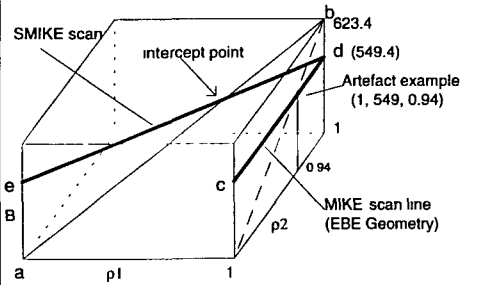

Fig. 1: Diagram of MIKE and SMIKE scans; B=549.

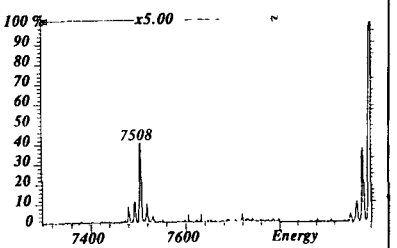

Fig. 2: SMIKE scan of Lys-Lys; B=549.4

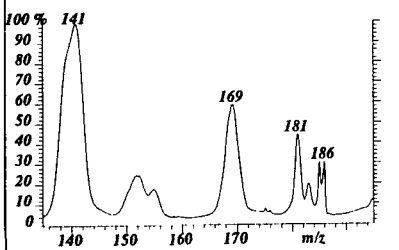

Figure 3: MIKE scan of m/z 198 (Vit. K).

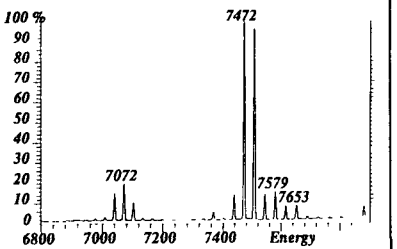

Figure 4: SMIKE scan of Vit. K; B=198.

Mapping Metastable Decays in a Time-of-Flight Mass Spectrometer with a Single-stage Ion Mirror

G. Brinkmalm, P. Håkansson, B.U.R. Sundqvist and D F. Barofsky[†]
Division of Ion Physics, Department of Radiation Sciences, Uppsala University, Box 535, S-751 21 Uppsala, Sweden
[†]*Department of Agricultural Chemistry, Oregon State University, ALS 1007, OR 97331-7301, USA*

We have developed a procedure to map unimolecular metastable decompositions in a time-of-flight mass spectrometer with a single-stage ion mirror. The procedure includes correlation of fragment ions to their precursor as well as extraction of the fragment masses.

Correlation is possible since the instrument is equipped with two stop detectors, a 0°-detector situated at the rear end of the mirror and a 180°-detector for the reflected ions. By comparing a normal 0°-mode spectrum (recorded with the mirror inactive) to a 180°-mode spectrum (with the mirror active and the instrument tuned for optimal resolution) the metastable ion peaks can be located. Reversed correlation on each metastable peak of interest (in the 180°-mode spectrum) is performed in order to determine the precursor ion undergoing decomposition. Normal correlation on each precursor of interest is performed, revealing any multiple decay paths.

Unimolecular metastable decompositions have been mapped for different precursor ions originating from thin film samples of valine, behenic acid and tri-alanine bombarded by 72 MeV $^{127}I^{13+}$ ions and 20 keV $^{69}Ga^{+}$ ions.

The masses of the fragment ions corresponding to these peaks can be approximately estimated using a simple relationship [1] between masses and true flight times in the 180°-mode spectrum

$$m_{fragment} = m_{precursor}\left(2\frac{t_{fragment}}{t_{precursor}} - 1\right). \quad (1)$$

Two ways to obtain more accurate mass assignment were investigated. One is to establish a correction curve to Eq. (1). The correction curve is established by plotting the deviation of $m_{fragment}/m_{precursor}$ from its theoretical value, $\Delta(m_{fragment}/m_{precursor})$, versus $m_{fragment}/m_{precursor}$ (see Fig. 1). Both linear and quadratic fits were attempted and the improvements are substantial in both cases.

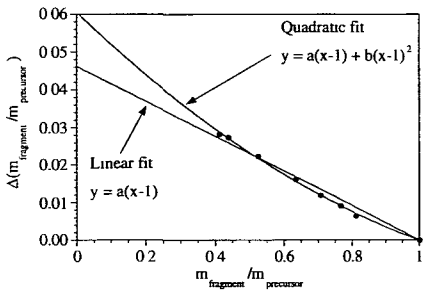

Figure 1. Generation of correction curves for more accurate mass assignment.

43rd ASMS Conference on Mass Spectrometry and Allied Topics

Another way is to match a fragment ion's flight time with that of its precursor [2]. This is accomplished by lowering the mirror voltage so that the fragment ion's flight time will be identical to the precursor's in the normal 180°-mode. When this condition is met, the ratio of the mirror voltages is exactly equal to the ratio of the masses of the respective precursor and fragment ions, and thus the fragment ion's mass can be accurately determined. The ultimate accuracy of this method is only limited by the mean and the degree to which the flight time can be matched.

The two methods are compared in Fig. 2 for the case of 72 MeV $^{127}I^{13+}$ primary ions. With our present apparatus, the quadratic correction and the path matching method yield comparable mass accuracy: better than 0.6% for keV primaries and better than 0.2% for MeV primaries (0.2% and 0.1% on average for the respective cases). With the path matching method, it is in principle possible to determine a fragment ion's mass to within an accuracy of 0.01% (the mass accuracy the instrument has for stable ions). This requires voltage supplies and meters with an accuracy better than 0.005% under operating conditions.

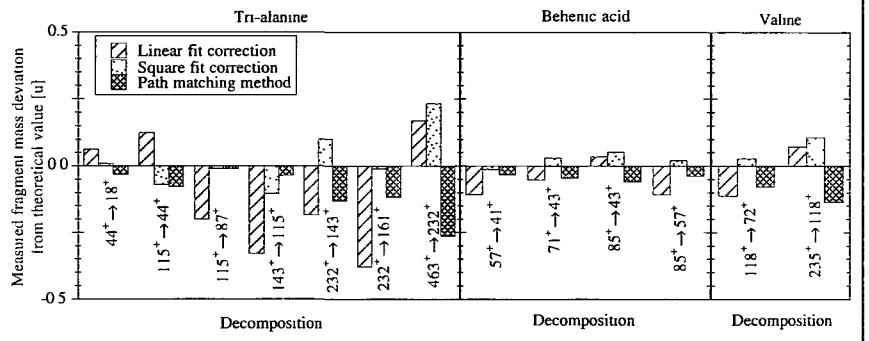

Figure 2. Comparison of the mass accuracy for the correction curve method and the path matching method for the case of 72 MeV $^{127}I^{13+}$ ions.

References

1 S. Della-Negra and Y. Le Beyec, *Int. J. Mass Spectrom. Ion Proc.*, **61** (1984) 21.
2. D F. Barofsky, G. Brinkmalm, P. Håkansson and B.U.R. Sundqvist, *Int. J. Mass Spectrom. Ion Proc.*, **131** (1994) 283.

Acknowledgment

This work was supported by the Swedish Natural Sciences Research Council (NFR), the Wallenberg Foundation, and the US National Institute of Environmental Health Science (NIEHS) Grant ES00210.

TANDEM MASS SPECTROMETRY UTILIZING THE ADVANTAGES OF BOTH MALDI AND FTMS

John A. Castoro*, Sanford Shew, Howard Stout, Brian Winger and Joseph Campana
Extrel FTMS, Inc., 6416 Schroeder Rd., Madison WI, 53711-2424

Matrix-assisted laser desorption/ionization (MALDI) is known to have several advantages over other ionization methods. For example, very large molecules (>200,000 Da) can be effectively ionized, and suppression effects from the presence of salts are less than other ionization techniques. MALDI is generally accepted as a "soft" ionization technique resulting in little or no fragmentation. However, metastable decay resulting in extensive fragmentation can be observed with sufficient laser power density and by increasing the time after desorption prior to detection. This decay process has been reported to take place with a half-life of several milliseconds[1] to approximately 10 ms for bovine insulin and melittin.[2] These results are consistent with RRKM theory, which generally predicts lower rates of unimolecular decomposition as the size and the number of degrees of freedom of a molecule increases.

Here we show how the variable ion trapping duration, tandem MS, high-resolution and accurate mass measurement capabilities of Fourier transform mass spectrometry (FT/MS), have been used to obtain sequence-specific information resulting from the metastable decay of MALDI-generated peptide ions. A standard Extrel FTMS Model 2001 mass spectrometer equipped with and a nitrogen laser (337 nm) was used for these studies.

The laser power density is a factor that can affect the extent of fragmentation. By maintaining the laser output energy, and varying the spot size, the extent of fragmentation as a function of power density was measured. In agreement with published literature, we have observed that the extent of fragmentation is directly proportional to the laser power density. Previously published data have indicated that the type of matrix or co-matrix used is another parameter that can effect the extent of fragmentation.

As an example of the amount of sequence information that can be obtained, MALDI activation was applied to the peptide bradykinin. A total of 270 femtomoles of the peptide was loaded onto a sample disk with an excess of 2,5-dihydroxybenzoic acid matrix. By increasing the time delay after ion trapping and prior to excitation and detection from 1 ms to 1000 ms, the extent of fragmentation with respect to time is observed. After a one second delay, the extent of fragmentation is such that the molecular ion is no longer the base peak, and nearly the entire sequence of the peptide is obtained. The y- and b- series ions are observed, which is in agreement with ion-trap/reflectron time-of-flight mass spectrometer measurements.[3] The average measured mass error for the 8 fragments detected (y_1'', b_2, y_2'', y_3'', y_4, b_5, b_7 and b_8) is less than 5 ppm for the all ^{12}C isotopes. These high mass accuracy results were obtained in the source cell of a dual cell system by using an external calibrant.

Structural information is typically obtained by tandem mass spectrometry performed by collision-induced dissociation (CID) of an isolated parent ion with a neutral inert collision gas. The efficiency and resulting fragmentation of on-resonance excitation, sustained off-resonance irradiation (SORI) and multiple excitation collisional activation (MECA) were compared by dissociating the $[M+H]^+$ species of the decapeptide pGlu-Leu-Trp-Pro-Arg-Pro-Gln-Ile-Pro-Pro, *m/z* 1214.67. The extent of fragmentation and efficiency of SORI (1 second, 500 Hz lower frequency) and MECA (1 ms excite, 50 ms collision delay, repeated 20 times) were similar, for a range of translational energies, with up to 70% fragmentation efficiency at 20 eV (using peak areas, and a 15% standard deviation of the control measurement). As expected, higher translational energies were required to obtain similar fragmentation for the on-resonance excitation measurements (1 ms excite, 1 second collisional delay) with less efficiency, up to 15%. Argon was used as a collision gas in all measurements (pulsed to ~10^{-6} torr)

The fragments produced by MALDI activation can be used for a second stage of mass spectrometry.

The MALDI-generated sequence ions b_8 and y_1'' of the peptide bradykinin, were isolated by stored waveform inverse Fourier transformation (SWIFT) for SORI-CID (Figure 1). The tandem mass spectrum of the y_1'' ion produced predominately y_3'' and y_4 ions while fragmentation of the b_8 ion produced b_5 and b_7 ions, in addition to the b_6 ion, which was not detected in the metastable decay measurement. The fragments detected from the tandem MS measurement, in addition to the metastable decay measurement produced complete sequence information.

As the size of the molecular ion increases, it becomes increasingly difficult to deposit sufficient energy into the ion to promote fragmentation by using standard tandem mass spectrometry. Depending on the MALDI conditions, the extent of metastable decomposition can be somewhat controlled and used as a method of obtaining analytically useful sequence information for peptides. The ion storage capabilities of a FT/MS ion trap can be used to perform a tandem MS measurement of the MALDI activated fragments produced for additional structural information.

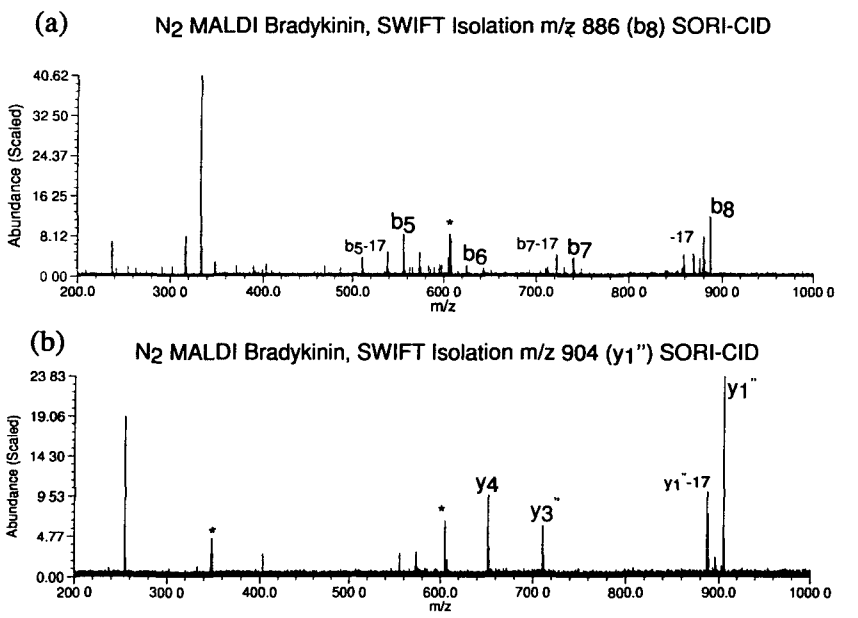

Figure 1: MALDI-FT mass spectrum of 270 femtomoles of bradykinin deposited onto a sample disk with a 1 second delay after desorption, SWIFT isolation for SORI-CID of MALDI-generated fragment (a) b_8 (15 eV, 25 laser shots) and (b) y_1'' (10 eV, 20 laser shots). * indicates a noise peak.

1. Fountain, S. T., Lee, H. and Lubman, D. M., *Rapid Commun. Mass Spectrom.*, **1994**, 8, 407-416.
2. Castoro, J. A. and Wilkins, C. L., *Anal. Chem.*, **1993**, 65, 2621-2627.
3. Qian, M. G. and Lubman, D. M., *Anal. Chem.*, **1995**, 67, 234A-242A.

MSMS STUDIES USING A HYBRID MAGNETIC SECTOR-ORTHOGONAL ACCELERATION TIME-OF-FLIGHT MASS SPECTROMETER; Thomas Keough, Martin P. Lacey, Mark D. Bauer and Yiping Sun; The Procter and Gamble Company, Miami Valley Laboratories, P.O. Box 398707, Cincinnati, OH 45239-8707.

A hybrid magnetic sector oaTOF mass spectrometer was recently developed for high sensitivity MSMS studies (1,2). It offers high resolution precursor ion selection, unit product ion selection and both low- and high-energy collisionally activated dissociation (CAD). The purpose of this study was to characterize the performance of this new instrument. Two configurations were evaluated: A = a 2 cm collision cell and a 4 in diffusion pump on the oaTOF housing; B = a 5 cm cell and 6 in diffusion pump. We assessed ion transmission into the oaTOF as a function of deceleration energy, CAD efficiencies and ion losses as a function of collision gas pressure, and the internal energy content of the fragmenting parent ions. The performance of the system was illustrated with both continuous (EI, static FAB and electrospray (see abstract by Yiping Sun and coworkers)) and pulsed (MALDI) ionization techniques.

Ion transmission losses occur in the deceleration region as mass selected precursor ions are decelerated from their initial energies of 8000 V to 800 V or less. This deceleration step is needed to improve oaTOF sampling, and it occurs prior to collisional activation. The MSMS experiments that we are concerned with here involve collisions of 800 V (or less) parent ions with neutral collision gases like He or Xe. Parent ion transmission varies from 45% (800 V precursors) to about 4% (50 V). Transmission losses were identical, within experimental error, for both configurations, and the losses appeared to be mass independent.

We've studied in detail the MSMS spectra obtained from a CsI cluster ion (m/z 1691.7) as a function of collision gas pressure (all experiments at 800 V collision energy). Both Xe and He were used in these experiments. With Xe as the collision gas using configuration A, the observed efficiency for fragment ion production (CAD efficiency) was 24%, and 45% of the non-attenuated parent ion beam was "lost" due to scattering and ion neutralization. CAD efficiency increased to 33%, and losses were reduced to 39%, with configuration B. With He, losses accounted for only 22%, and CAD efficiency was over 50% using configuration A. CAD efficiency increased to 94%, and losses were eliminated using configuration B. We believe that scattering of low mass fragment ions out of the acceptance angle of the oaTOF accounts for much of the observed ion loss. Therefore, we compared the transmission/detection of two low mass fragment ions (m/z 133 from the CsI cluster ion at m/z 1691.7 and m/z 70 from the bradykinin molecular ion) with previously published results from four sector MSMS instruments. The oaTOF equipment appears to perform as well as four sector instruments in this regard.

The fragmentation of the molecular ion of n-butylbenzene, a well-known "thermometer" molecule (3), was studied as a function of collision energy at a fixed pressure (He and Xe). The maximum average precursor ion internal energies sampled in these experiments, 7.0 eV (He) and 4.6 eV (Xe), were obtained with the 5 cm collision cell. MSMS of tungsten hexacarbonyl (4) was also carried out to assess the internal energy distributions of the fragmenting precursor ions. The distribution calculated from the MSMS spectrum obtained following 800 V collisions (He) shows an average energy of about 6 eV and a high energy "tail" that extends beyond 12 eV. This internal energy distribution is very similar to those previously reported from higher energy collision experiments (4). With 50 V collisions, the internal energy distribution shifts to much lower values. The observed average energy is 2.6 eV (He) and the high energy tail does not extend beyond 6 eV. These results confirm that MSMS spectra from the oaTOF instrument should be "tunable" over a wide range of precursor ion internal energies and that there is

sufficient energy to produce high-energy fragments like side-chain cleavage in peptides (2) or remote-site fragmentation for various classes of ionic surfactants (sulfonates, sulfates, quaternary ammonium salts).

The operation of the oaTOF instrument was evaluated for both continuous and pulsed ion sources. Excellent quality static FAB MSMS spectra of small peptides are typically obtained with 100 pmole of material. Usable quality FAB MSMS spectra of substance P have been obtained after loading as little as 3.8 pmoles of material onto the probe. The MSMS spectrum of the C16-trimethylammonium cation, generated by MALDI, is shown in the Figure. A total of 12.5 pmoles

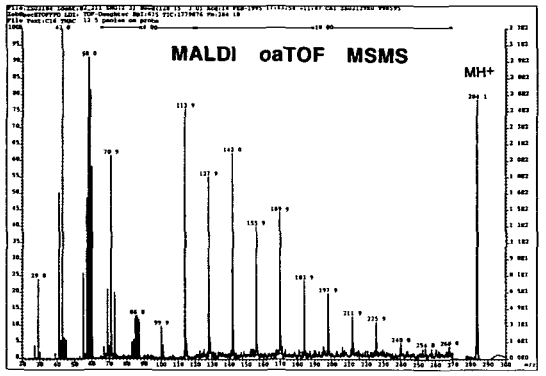

of material were loaded onto the solids probe for this experiment (in alpha-cyano-4-hydroxycinnamic acid matrix). Only about 20% of the sample was actually interrogated with the N_2 laser beam. MSMS spectra of singly, doubly and triply charged precursor ions have been successfully obtained with the oaTOF (electrospray ionization). The fragment ion mass range is up to 6000 Da, and fragment ion mass resolution is typically 1500 (FWHM), except at low mass. Product ion mass measurement accuracy of ±0.3 Da is routine. Collision energies spanning the range of 800 to 50V have been used, and the resulting spectra confirm that there is enough energy to produce both low- and various high-energy products.

Acknowledgments - We gratefully acknowledge the many contributions that R.H. Bateman, M.R. Green and R.G. Vickers (VG Fisons) made to this work. They designed, built and installed the oaTOF mass analyzer and the time-delay circuitry needed to perform the MALDI MSMS measurements. They offered many helpful suggestions on data acquisition. We also thank Kenny Morand (Procter & Gamble) for helpful discussions concerning the ion internal energy distribution measurements.

References - 1. E. Clayton and R.H. Bateman, **Rapid Commun. Mass Spectrom. 6**, (1992) 719. 2. R.H. Bateman, M.R. Green and G. Scott, Proceedings of the 42nd ASMS Conference on Mass Spectrometry and Allied Topics, Chicago, IL, May 29 - June 3, 1994. 3. T. Baer, O. Dutuit, H. Mestdagh and C. Rolando, **J. Phys. Chem. 92**, (1988) 5674. 4. V.H. Wysocki, H.I. Kenttamaa and R.G. Cooks, **Int. J. Mass Spectrom. Ion Processes 75**, (1987) 181.

Surface Induced Dissociation of Biomolecules by MALDI-FTMS

Salvador J. Pastor, Jie Yao, and Charles L. Wilkins
Department of Chemistry, University of California, Riverside, CA 92521

Introduction:

Surface-induced dissociation (SID) continues to be a viable alternative to the more popular techniques of collision-induced dissociation (CID) and photodissociation (PD). SID has several significant advantages over the other two techniques. SID is a universal ion activation technique because it is better candidate for high mass analysis as compared with CID, does not require a chromophore (necessary for photodissociation), and is better suited for the low-pressure conditions of an FTMS experiment. Some criticisms stem from the fact that dissociation efficiencies tend to be low, and, in the case of a trapped ion cell, frequent neutralization of the ion species occurs when an electrode is contacted. Despite these drawbacks, significant results have been achieved in a Fourier transform mass spectrometer[1,2] and, recently, by the McLafferty group using multiply charged ions introduced through an electrospray interface where they reported efficiencies up to 36%, and the high mass dissociation of carbonic anhydrase (29 kDa).[3]

This paper describes the analysis of singly charged biomolecules generated by MALDI undergoing surface induced dissociation in a standard cubic trap FTMS. The method is similar to the grazing incidence angle experiment demonstrated by Ijames and Wilkins.[4] Here we apply quadrupolar excitation in the presence of argon collision gas to effect a broadband axialization of the off-axis fragment ions to improve the trapping efficiency

Method:

All MALDI experiments were performed using an Extrel FTMS-2000 Fourier Transform Mass Spectrometer operating at 6 tesla and equipped with a differentially pumped dual cell and automatic solids probe. Samples were prepared by dissolving 0.5 mg of sample with 2,5-dihydroxybenzoic acid and d-fructose in the molar ratio 1:4000:2000 into 5 ml of methanol. Approximately 0.5 ml was aerosprayed onto a rotating stainless steel probe tip to create a uniform sample surface Ionization occurred via an excimer laser operating at 308 nm. Laser energies varied from 12 mJ/pulse - 28 mJ/pulse (power density of ~10^7 W/cm^2) and were measured at the laser.

The experiment described here is designed for a single cell experiment. Following MALDI, ions were trapped using a gated deceleration protocol. After a short delay, a SWIFT ejection was used to remove ions of lower mass [5] The parent ion was given an on-resonance 1 cm SWIFT excitation to raise its internal energy and place it off axis for the SID event. A carefully timed push potential from a prototype extended trapping module (Waters-Extrel, Madison, WI) was applied to the source trapping plate to accelerate the selected ion into the solid stainless steel conductance limit that was biased at a negative potential in a "quench-like" fashion Broadband quadrupolar excitation was applied to the cell through the use of a switching box to configure the cell for either a dipolar or a quadrupolar excitation. Argon collision gas was controlled by a combination electropneumatic gate valve/leak valve assembly. For bradykinin, broadband axialization of the SID product ions was demonstrated using a 1.75 volt SWIFT file from 450-1050 m/z and lasted approx. 5 msec. A delay of equal duration (5 msec) was added, and the broadband sequence was repeated for 500 cycles at a pressure of 5 x 10^{-6} torr to give an overall axialization time period of 5 seconds. Following the broadband axialization of the product ions, the cell was switched back to dipolar mode, and a 5 second delay was imposed to allow the background pressure to reach 5 x 10^{-8} torr before detection. A general excitation was applied from 50 - 200 kHz All detection was done in direct mode using a bandwidth of 400 kHz and 16k data points. Poly(ethylene glycol) 1000 served as the external calibrant, and standard Odyssey 3 0 calibration software was used (Waters-Extrel, Madison, WI).

Discussion:

Bradykinin was used as a test model for MALDI analysis. The objective was to apply quadrupolar axialization to the off-axis fragment ions to improve collection efficiency. This would afford a great reduction in the number of scans required to produce adequate S/N ratios. The figure is the spectrum resulting from an optimized SID/axialization experiment showing the co-addition of only 9 spectra. Fragment ions include sequential loss of amino acids from both terminal ends of the peptide. As with CID, major fragments are the m/z 886 and m/z and m/z 887 peaks which correspond to loss of -OH from the C-terminus and loss of arginine from either end. The peaks at m/z 1000 and m/z 983 (loss of 17) are due to impurities from the acetate salt buffer.

By applying the broadband axialization to the fragment species, the experimental dissociation and collection efficiency was increased to 39.0%. This is compared against an optimized SID experiment without axialization, which gave a dissociation efficiency of 7.0%, typical of previous efforts by many groups. These calculations were based on a more strict definition that uses the sum of the product ion abundances divided by the starting ion abundance of the molecular ion following an ejection event of the lower mass species. A spectrum of the same experimental sequence with the SID push event turned into a time delay showed no significant fragmentation or decay caused by *post-SID collisional activation. When the product ion abundances are referenced against each other,* the efficiency jumps to 95.5%! This seems to indicate that SID can be a very efficient process, and better collection schemes such as floating the cell[3] should show great improvements.

It appears that electrospray ionization might have a slight advantage for SID analysis due to the multiple charging, which promotes coulomb repulsion, lowers the m/z range, and increases an ion's chances of not being effectively neutralized. Both MALDI and ESI-FTMS have shown that in a trapped ion cell, it is essential to have timing such that the ions are allowed only one encounter with the dissociating surface. Last, it will be particularly interesting to see if the many motional modes of high masses can be overcome to produce desired fragmentation patterns for singly charged MALDI generated species.

References:

1. Williams, E.R., Henry, K.D , McLafferty, F W , Shabanowitz, J , Hunt, D F *J Am Soc Mass Spectrom* 1990, 1, 413-416.
2. Castoro, J.A.; Nuwaysir, L.M.; Ijames, C.F , Wilkins, C.L *Anal. Chem.* 1992, 64, 2238-2243.
3. Chorush, R.A., Little, D P., Beu, S.C ; Wood, T.D.; McLafferty, F W *Anal. Chem* 1995, 67, 1042-1046
4. Ijames, C.F ; Wilkins, C.L. *Anal Chem.* 1990, 62, 1295-1299.
5. Chen, L.; Wang, T -C ; Ricca, T L.; Marshall, A.G. *Anal Chem.* 1987, 59, 449-454

Bradykinin - SID with Axialization (9 Shots)

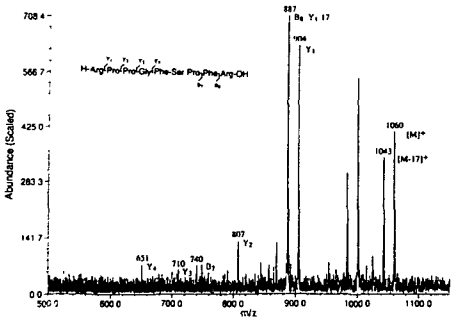

Identifying Possible Sources of Ion Neutralization During Low Energy Collisions at Self-Assembled Monolayer Surfaces

*Vince Angelico, Tom Kane, Hair Nair, Arpod Somogy, Vicki H. Wysocki
Department of Chemistry, Virginia Commonwealth University
Richmond, Virginia, 23284, USA

Low energy collisions (>100 eV) of polyatomic ions with a surface promote extensive, structurally characteristic fragmentation of the selected ion in an experiment referred to as surface-induced dissociation (SID)[1,2] Neutralization of the projectile ion at the surface is a major contributor to the loss of ion signal in the instrument. Alkanethiolates $^{-}S(CH_2)_nH$ (n=18,12,8,4)and $^{-}S(CH_2)_2(CF_2)_8F$ chemisorbed on gold substrates have been shown to act as electron transfer inhibitors when used as collisional targets, thereby reducing the amount of ion neutralization observed compared to bare metal surfaces [2]. Of particular interest here is to identify the possible mechanisms responsible for the amount of ion neutralization observed with SAM surfaces Because the ion neutralization process involves the transfer of electrons, a prediction would be that the measured scattered ion efficiency would increase with decreased I.E. of the incident ion, as well as the increased I.E. of the surface material (Table 1).

Table 1.

Monolayer		Film Thickness (Å) [a]	I.E.
Au-$S(CH_2)_{18}H$	(C18)	22.0	~9.5[b]
Au-$S(CH_2)_{12}H$	(C12)	15.3	~9.5[b]
Au-$S(CH_2)_8H$	(C8)	10.8	~9.5[b]
Au-$S(CH_2)_4H$	(C4)	6 38	9.14[3]
Au-$S(CH_2)_2(CF_2)_8F$	(PF)	14.4	~11.5[b]

a. calculated from atomic radii
b. extrapolated from experimental I.E. data of C_nX_{2n+2} X = H,F

Benzene and three benzene derivatives with varying ionization energies are employed as probes to investigate neutralization processes.
The amount of ion neutralization at the surface is measured using two separate methods [2].
Method I: A finite efficiency value is calculated for each monolayer surface from the ratio of the total ion current of a collision spectrum to the total ion current of the transmission spectrum (0 eV, no collision) at the same multiplier setting (Table 2).

Table 2. % Efficiency at 30eV collision energy (I_{col}/I_0 X 100)

Ion	I.E. (eV) [4]	%E (C18)	%E (PF)
Nitrobenzene	10.4	0.328	53.5
Benzene	9.25	13.2	62.6
$Cr(CO)_6$	8.24	14.9	66.4
NNDMA	7.12	37.4	75.6

Method II: The relative surface efficiencies are presented as a total ion current (TIC) plot measured at the detector with units of signal versus time. A multiple surface holder allows several monolayer surfaces to be present in the instrument at a given time. While the signal intensity/spectral data is continually obtained for a given energy ion collision, each surface is positioned in the ion optical path for a period of time. This method guarantees the same instrument tuning parameters and similar environment (e g , chamber pressure, temperature, etc.) for all of the surfaces investigated. Gold surfaces modified with n-alkanethiolates contain a small percentage of defect sites and regions of incomplete monolayer formation. In order to ascertain

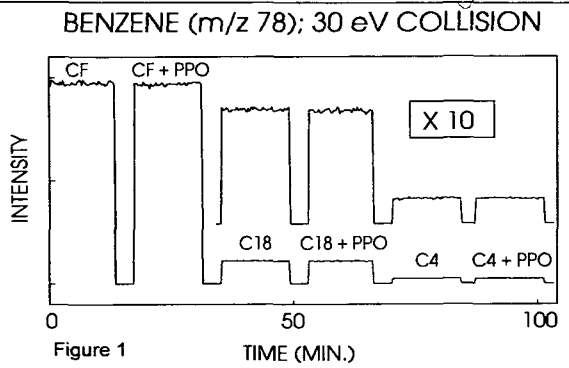

Figure 1

whether the ion neutralization is favored at the monolayer pinholes, a series of monolayer films are electrochemically passivated according to the procedure described by Finklea et al.[4], and the scattered ion efficiency is compared to that obtained with unpassivated monolayers. Any change in the scattered ion efficiency between surfaces of the same chain length will be associated with the presence of the pinholes in the monolayer films (Figure 1). Using data obtained from both methods the following conclusions were formulated.

- The efficiency of the hydrocarbon monolayer series indicates a decrease in ion neutralization with increasing alkanethiolate chain length (Figure 1).
- The fluorinated monolayer surface consistently yields the greatest scattered ion signal and the least amount of ion neutralization for all of the ion probes employed (Figure 1, Table 2).
- For these surfaces, the amount of ion neutralization increases with increasing ionization energy of the (neutral) projectile ion, and decreasing monolayer ionization energy (Table 2).
- The absence of any appreciable change in the TIC intensities between the electrochemically passivated and unpassivated monolayer surfaces suggests the pinholes present within the monolayer surface have a negligible role in the ion neutralization process (Figure 1).

Two separate but related electron transfer processes are supported by the data presented. The decrease in ion neutralization with increasing monolayer chain length, while maintaining similar chemical properties of the monolayer surface (e.g., surface I E , chemical composition, etc) suggests a remote transfer process from the underlying gold substrate to the incident ion (electron tunneling) [5]. In this mechanism, the monolayer acts merely as an insulating partition between the active donor-acceptor pair. Observing that the tunneling-monolayer thickness argument is not supported when comparing the highest % efficiency measured for the fluorinated surface for each incident ion. The thickness of the fluorinated surface is calculated to be 14.4Å, however greater neutralization is observed for the longer C18 surface (22 Å) The data in Table 2 indicates a correlation to the energy difference between the I.E. of the incident ion (neutral) and the surface. This suggests a second electron transfer mechanism where the electron originates from the monolayer material itself. Both processes are believed to occur simultaneously, however the differences in the % efficiencies of the C4 and C18 monolayer surface (representing the extreme short and long hydrocarbon chains) is considerably smaller in magnitude as compared to the fluorinated surface. This suggests the monolayer ionization mechanism is the dominant process

REFERENCES

1 Cooks, R.G , Ast, T.; Mabud, Md. A. *Int. J Mass Spectrom. Ion Processes* **1990**, *100*, 209.
2. Somogyi, A', Kane, T E., Ding, J -M., Wysocki, V H. *J. Am Chem. Soc.* **1993**, *115*, 5275
3. Lias, S G , Liebman, J.F., Levin, R.D., Kafafi, S.A. NIST Standard Reference Database 19A Positive Ion Energetics, V 2.0, **1993**
4. Finklea, H.O ; Snider, D.A., Fedyk, J *Langmuir*, **1990**, *6*, 371
5. Freeman, G.R., ed. Kinetics of Nonhomogeneous Processes John Wiley and Sons, New York, **1987** p 542.

HYDROGEN-ADDITION REACTIVITY OF IONS ON ODD VS. EVEN CHAIN ALKANETHIOLATE SELF-ASSEMBLED MONOLAYER FILMS

Rebecca L. Franklin, Wenqing Zhong, Árpád Somogyi, and Vicki H. Wysocki
Department of Chemistry, Virginia Commonwealth University
Richmond, Virginia 23284

Several methods such as wettability, ellipsometry, IR, Raman spectroscopy, electrochemistry and XPS have been used to describe the surface characteristics of various alkanethiolate self-assembled monolayer films (SAMs).[1] Studies by several groups indicate that the orientation of the terminal groups in an alkanethiolate SAM is different if the chain length of the thiolate is odd or even.[2] On gold, when the chain length is even, the terminal methyl group is oriented so that all of the hydrogens are equivalently exposed. For an odd chain length on gold, the terminal methyl group is oriented parallel to the surface so that one of the hydrogens is pointing out of the monolayer. This orientation is reversed when the assembly is on silver because the bond angle between the metal-S-C changes from roughly parallel (Au) to roughly perpendicular (Ag).[2a]

Recently, SAMs have been used extensively in surface-induced dissociation (SID) studies.[3-6] Correlations were found between the hydrogen-addition reactivity of alkanethiolate films toward simple organic projectile ions such as benzene and DMSO-d_6 and the chain length and chemical composition of the films.[4-6] It has been shown that peaks corresponding to the hydrogen-addition for low energy collisions (20-30eV) of various projectile ions on SAMs exhibit a drastic decrease for alkanethiolate chain lengths greater than 8 carbon units long.[7]

Experimental The instrument used consists of two Extrel quadrupoles positioned at 90° whose ion optical path is bisected by a metal surface.[8] Self-assembled monolayers were prepared by spontaneous assembly of thiols on vapor deposited gold or silver foil surfaces. The gold surfaces are first UV cleaned (Ag surfaces are mechanically polished with various mesh sizes of Al_2O_3) and placed in a solution of thiol in ethanol prior to use. Mixed monolayer SAMs were prepared so as to give a 1:1 ratio of each thiol on the surface after 12 hours.[9] Alkanethiolate SAMs ($n \geq 9$) on Au and Ag were prepared from 1 mM solutions of thiol in ethanol and were in solution for 75 (for $n \leq 8$, solutions were prepared in hexanes and were in solution for 1 hour) hours prior to use. The SAMs used in this study include $CH_3(CH_2)_{n-1}SH$ (n=2-18,22) and $HO(CH_2)_{11}SH$.

Results and Conclusions - Alkanethiolates on Au and Ag

The hydrogen-addition reactivity of benzene and DMSO-d_6 as low energy projectiles on alkanethiolate surfaces is enhanced for odd chain lengths (i.e. n=11,15,17) for monolayers prepared on gold surfaces. For monolayers prepared on silver foil the even chain lengths showed enhanced reactivity (see Figure 1).

Results and Conclusions - Mixed monolayers

Mixed monolayers prepared from a hydroxy-terminated alkanethiolate and alkanethiolates (n=22) showed hydrogen-addition reactivity intermediate to that of pure hydroxy and pure alkanethiolate surfaces. SAMs prepared from hydroxyl-terminated alkanethiolates are more reactive than alkanethiolate surfaces (see Figure 2).

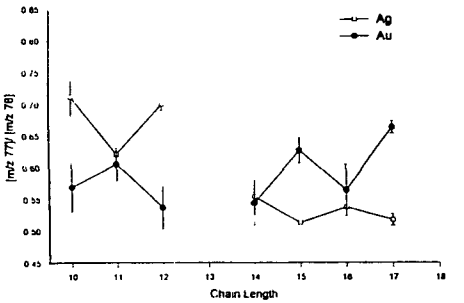

Figure 1 H-addition of benzene on Au and Ag surfaces

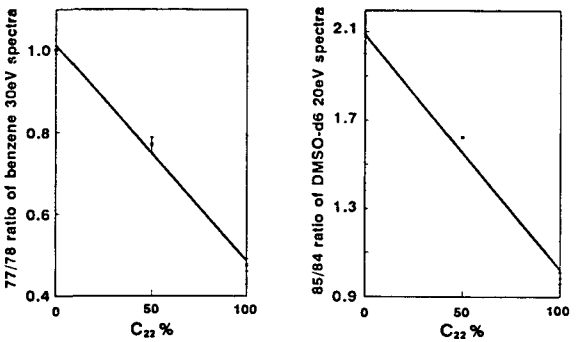

Figure 2. Mixed monolayer of C_{22} and $C_{11}OH$

1. (a) Porter, M.D.; Bright, T.B.; Allara, D.L.; Chidsey, C.E.D. *J. Am. Chem. Soc.* **1987**, *109*, 3559. (b) Bain, C.D.; Troughton, E.B.; Tao, Y. -T.; Evall, J.; Whitesides, G.M.; Nuzzo R.G. *J. Am. Chem. Soc.* **1989**, *111*, 321.
2. (a) Bryant, M.A.; Pemberton, J.A. *J. Am. Chem. Soc.* **1991**, *113*, 8284. (b) Nuzzo, R.G.; Dubois, L.H.; Allara, D.L. *J. Am. Chem. Soc.* **1990**, *112*, 558.
3. Cooks, R.G.; Ast, T.; Mabud, Md. A. *Int. J. Mass Spectrom. Ion Processes* **1990**, *100*, 209.
4. Somogyi, Á.; Kane, T.E.; Ding, J. -M.; Wysocki, V. H. *J. Am. Chem. Soc.* **1993**, *115*, 5275.
5. Kane, T.E.; Somogyi, Á.; Wysocki, V.H. *Org. Mass Spectrom.* **1993**, *28*, 1665.
6. Morris, M.; Riederer, D.E., Jr.; Winger, B.E.; Cooks, R.G.; Ast, T.; Chidsey, C.E.D. *Int. J. Mass Spectrom. Ion processes* **1992**, *122*, 181.
7. Franklin, R.L.; Angelico, V.A.; Kane, T.E.; Somogyi, Á.; Wysocki, V.H. *Proc. of the 42nd ASMS Conference*, Chicago, IL, **1994**, p 456.
8. Wysocki, V.H.; Ding, J.-M.; Jones, J.L.; Callagan, J.H.; King, F.L. *J. Am. Chem. Soc. Mass Spectrom.* **1992**, *3*, 27.
9. Bain, C. D.; Whitesides, G.M. *J. Am. Chem. Soc.* **1988**, *110*, 3665.

DERIVATIZATION REACTIONS FOR FAB, LSIMS AND ELECTROSPRAY IONIZATION

Richard E. Carlson and Kenneth L. Busch
School of Chemistry and Biochemistry
Georgia Institute of Technology, Atlanta GA 30332-0400

Derivatization reactions in mass spectrometry represent several creative examples of problem solving. Many of the same derivatization reactions developed for FAB and LSIMS can be used in electrospray ionization mass spectrometry. In FAB and LSIMS, these reactions were developed to increase the sensitivity of the analysis, or to provide a mass shift characteristic in the mass spectrum for easy recognition. Although the issue of sensitivity enhancement is unclear in electrospray, the characteristic mass shifts can be useful in interpretation of the ES mass spectrum and determination of the charge state of the ions. Most reactions target hydroxy, carboxylic, or amine functionalities in the analyte molecule. Some examples of the types of derivatization reactions for mass spectrometry are shown below. For FAB/LSIMS, the reaction of 2-dodecen-1-yl succinic anhydride with primary and secondary amines, as reported by Ligon and Dorn[1]. This derivatization scheme results in the formation of an amic acid (see below), which is easily desorbed and detected.

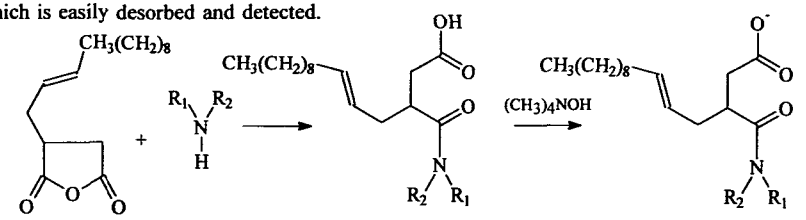

Griffiths and co-workers have reported the use of 4-aminobenzensulphonic acid[2a] to incorporate a stable charged end group on fatty acids as shown in the reaction below. Following CID, these derivatization products undergo charge-remote fragmentation. Aminoethanesulphonic acid derivatized bile acids have been reported[2b] to fragment similarly.

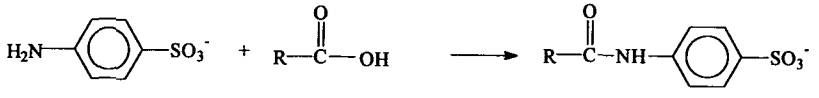

Bartlett and Busch[3a], and Cohen and Chait[3b] have both reported the use of 2-iminothiolane to derivatize the N-terminal amine group of small peptides.

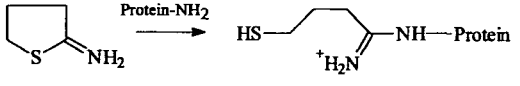

Charge-transfer reactions, which have proven to be valuable derivatization methods in FAB/LSMIS and SIMS for several years[4a], have also found application in ESI[4b,c]. These reactions are based on electron donor/acceptor chemistry and several derivatization analytes are available.

$$\text{DONOR} + \text{ACCEPTOR} \rightleftharpoons (\text{DA}) \longrightarrow D^{+\cdot} + A^{-\cdot}$$

Girard's P and T reagents have proven useful for the derivatization of carbonyl groups, as reported by Ross *et al.*[5]. These reactions result in the formation of a precharged cation, which is readily detected following desorption ionization techniques. A general reaction scheme for Girard's P is shown below:

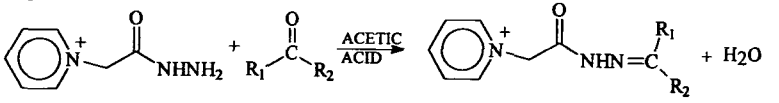

Interestingly, Laude and co-workers[6] have reported essentially the reverse of the above reaction, using acetone to derivatize N-terminal amines and amines on lysine residues in proteins. The authors report the utility of acetone derivatization to determine the charge state of the ions in low resolution ESI experiments. P represents a protein in the following scheme.

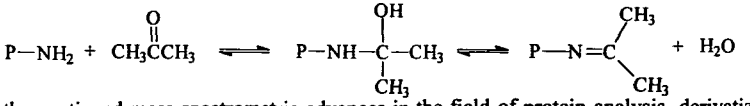

With the continued mass spectrometric advances in the field of protein analysis, derivatization chemistry may prove to be an invaluable link in providing additional mass spectrometric information.

References:

1. W.V. Ligon, Jr. and S.B. Dorn, *Anal. Chem.*, **58**, 1889-1892 (1986).

2. (a) Y. Yang, W.J. Griffiths, J.A. Lindgren, and J. Sjovall, *Rapid Commun. Mass Spectrom.*, **9**, 289-299 (1995). (b) W.J. Griffiths, J. Zhang, and J. Sjovall, *Rapid Commun. Mass Spectrom.*, **8**, 227-236 (1994).

3. (a) M.G. Bartlett and K.L. Busch, *Biol. Mass Spectrom.*, **23**(6), 353-356 (1994). (b) S.L. Cohen and B.T. Chait, *Proceedings of the 41st ASMS Conference on Mass Spectrometry and Allied Topics*, San Francisco, p.414a (1993).

4. (a) E. De Pauw, *Anal. Chem.*, **55**, 2195-2196 (1983). (b) G.J. Van Berkel and K.G. Asano, *Anal. Chem.*, **66**, 2096-2102 (1994). (b) J.M.E. Quirke, C.L. Adams, and G.J. Van Berkel, *Anal. Chem.*, **66**, 1302-1315 (1994).

5. M.M. Ross, D.A. Kidwell, and J.E. Campana, *Anal. Chem.*, **56**, 2142-2145 (1984).

6. Z. Guan, V.L. Campbell and D.A. Laude, Jr., *J. Mass Spectrom.*, **30**(1), 119-123 (1995).

EFFECT OF A MATRIX ON LIQUID-SIMS-INDUCED FRAGMENTATION OF THE PHOSPHATE ESTER BOND

CHHABIL DASS
THE UNIVERSITY OF MEMPHIS, DEPARTMENT OF CHEMISTRY, MEMPHIS, TN 38152, USA

INTRODUCTION: Liquid-SIMS has become a standard analytical technique for the analysis of biomolecules such as peptides. The success of liquid-SIMS, however, depends upon the use of a proper liquid matrix. The use of the matrix has the advantage that it acts as a medium to dissolve the sample molecules, facilitates the formation of the protonated and deprotonated molecule ions, and helps in maintaining persistent emission of the analyte ion current. Although a number of matrices are available for liquid-SIMS analysis, a careful selection of the matrix is needed to optimize the spectral appearance and the solute ion current. Glycerol, α-thioglycerol, a cocktail of dithiothreitol and dithioerythritol (5:1), and 3-nitrobenzyl alcohol are the common matrices used for the analysis of peptides. A unique advantage of a liquid matrix is that it can absorb the impact of the bombarding beam. In spite of this feature, analyte molecules are formed with excess energy over their ground state, resulting in the formation of compound-specific fragment ions. It was reported by us earlier (1) that the extent of fragmentation of peptides is dependent upon the type of matrix used, with glycerol leading to extensive fragmentation and α-thioglycerol and dithiothreitol producing least fragmentation. The spectra of other classes of compounds also differed from matrix to matrix.

OBJECTIVE: The loss of the phospho group (80 Da) is frequently observed from the protonated molecule of phosphopeptides, resulting in an ion that corresponds to the mass of the protonated molecule of the unmodified analogs. This aspect may render simultaneously detection of the phospho and nonphospho forms of a peptide difficult when they are present together. Therefore, it is important to search for a matrix that leads to the least amount of the loss of 80 Da. In this preliminary report, we discuss the effect of a few common liquid matrices (glycerol, α-thioglycerol, and dithiothreitol) on the loss of the phosphate moieties from the protonated molecules of phospho amino acids and peptides.

EXPERIMENTAL: All data were acquired by using VG AutoSpecQ mass spectrometer outfitted with the Digital VAX station-based Opus software. Ionization used a beam of 30 keV Cs^+ ions. A fixed amount of phosphopeptides (3.8 nmol) and amino acids (25 nmol) was dissolved in 1.40 μmol of the matrix and the spectra were obtained in the narrow mass range to encompass the molecular ion and the ions formed by the loss of the phosphate moieties and at a scan speed of 10 s/decade. All spectra are the sum of 10 (amino acids) or 20 (phosphopeptides) scans, all acquired within 40s of introducing the probe in the source. This way, the loss of matrices due to their differential evaporation rates was held to a bare minimum.

DISCUSSION: The phospho-Tyr usually exhibit the loss of HPO_3 and HPO_4 moieties, whereas, the phospho-Thr and -Ser residues undergo primarily the loss of H_3PO_4 molecule (2). The preliminary data presented here show that the extent of the loss of phosphate moieties from phospho-compounds when bombarded with Cs^+ ion beam is influenced by the liquid matrix used. Although no clear trend is observed, the data is consistent with our earlier observation (1). It is noted that the loss of HPO_3 from phospho-Tyr and H_3PO_4 from phospho-Thr is more pronounced when dithiothreitol is used as the matrix. On the other hand, the loss of HPO_3 and HPO_4 is greater from phospho-enkephalins dissolved in glycerol. It is evident that the $[M + H]^+$ ions are formed with different amount of internal energy. The sputtered $[M + H]^+$ ions are usually associated with the matrix molecule, the desolvation of which produces the $[M + H]^+$ ions with different amount of internal energy. It is obvious that the number of the solvent molecules associated with the ion-molecule complex and the strength of the solute-solvent and solvent-solvent bonds will have strong bearing upon the internal energy of the $[M + H]^+$ ions.

THE LOSS OF THE PHOSPHATE MOIETIES FROM PHOSPHO-AMINO ACIDS

peptide	group lost	glycerol	thioglycerol	dithiothreitol
Phospho-tyrosine	HPO_3	11 5	6.3	40 2
	HPO_4	6 7	3.3	6.9
Phospho-threonine	H_3PO_4	26.2	103.0	143.0

Values given are relative to the $[M + H]^+$ as the base peak

THE LOSS OF THE PHOSPHATE MOIETIES FROM PHOSPHOPEPTIDES

peptide	group lost	glycerol	thioglycerol	dithiothreitol
Phospho-leucine enkephalin	HPO_3	12.8	10.3	8 3
	HPO_4	6.9	3.5	2 9
Phospho-methionine enkephalin	HPO_3	11.7	10.3	10.6
	HPO_4	8.2	5.5	5 4

Values given are relative to the $[M + H]^+$ as the base peak

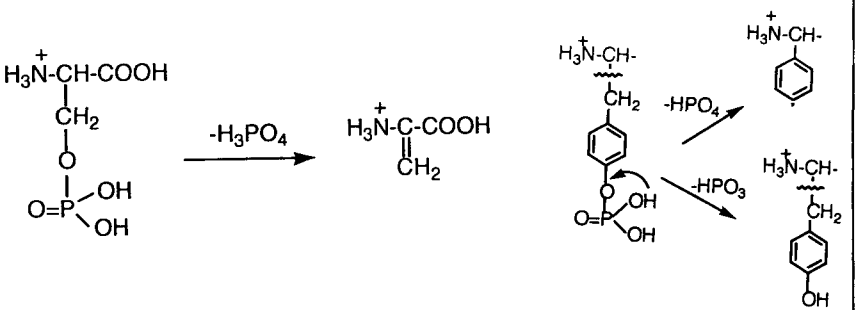

(1) C. Dass, Proceedings of the 39th ASMS Conference on Mass Spectrometry and Allied Topics, p.909 (1991).
(2) C. Dass, Rapid Commun. Mass Spectrom., **3**, 264 (1989).

Acknowledgment: The financial support was provided by the NIH (grant NS 28025).

PARENT RESOLUTION IN FFR1 MS/MS: REVELATIONS FROM ION INTENSITY PLOTS

Kevin D. Ballard, Richard W. Vachet[1], Ralph S. Orkiszewski, Gary L. Glish[1], J. James Vrbanac[2], and Simon J. Gaskell[3]. Center For Experimental Therapeutics, Baylor College of Medicine, Houston, TX 77030; [1]Department of Chemistry, University of North Carolina, Chapel Hill, NC 27599; [2]The Upjohn Company, Drug Metabolism Research, Kalamazoo, MI 49001; [3]Centre for Mass Spectrometry, UMIST, Manchester, M60 1QD, U.K.

Product ion scanning and constant neutral loss scanning experiments on double focusing instruments are frequently employed for studying parent-product ion relationships for first field-free region (FFR1) decompositions Previous studies from these laboratories have shown that the effective resolution of the parent ion varies during the course of such scans, and that the poor parent resolution and the variation therein are attributable to the occurrence of kinetic energy release during fragmentation. Lacey-Macdonald ion intensity diagrams[1] accurately reflect the decomposition events occurring in various regions of sector mass spectrometers. The application of such diagrams to the parent ion resolution issue has led to new means of defining and calculating the effective parent resolution for both product ion scans and constant neutral loss scans on double focusing instruments. The new approach incorporates the effects of kinetic energy release and fully accounts for the observed variation in parent resolution during the course of the scans.

Results. In ion intensity diagrams, fragmentation reactions can be plotted as elliptical regions of ion intensity, using the coordinate system $\rho=M_d/M_p$, $M^*=M_d^2/M_p$, where M_p and M_d are the masses of the parent and product, respectively. The size of the ellipses depends primarily upon the kinetic energy release involved in the fragmentations. Various scan functions, such as for product ions of a particular parent, are readily incorporated into these diagrams. Such plots reveal that, at higher proportional product ion mass, product ion ellipses derived from a given parent are relatively well resolved from neighboring scan functions, and thus the effective parent resolution is comparatively high. At progressively lower proportional product mass, however, neighboring scan functions begin to cross the elliptical regions, leading to progressively poorer effective parent resolution as proportional product mass decreases. Based on these diagrams, the scan function from a neighboring parent can be considered just resolved if it passes through one of the end-points of the major axis of a given ellipse. Parent resolution for product ion scans calculated in this fashion generates curves such as those shown in Figure 1 (where T=kinetic energy release). The curves in Figure 1 demonstrate that even a small amount of kinetic energy release exerts a profoundly detrimental effect on parent resolution. A method has been devised for predicting the relative contributions of interfering peaks in FFR1 product ion scans. The method assumes that the relative abundances of the parent species and the kinetic energy releases involved in the fragmentations are known. The method takes into account the gaussian, three-dimensional nature of the ion intensity regions, and involves integration over the area transected as the product ion scan function passes through the elliptical ion intensity region. This method has been applied to a few examples, and the predicted values are within ~10 % of the experimental observations. Constant neutral loss scans involving isotopomers on two-sector instruments can be especially deceptive regarding the effective resolution of the parents, because signals due to interfering parent-product relationships can precisely overlap with the intended signal. Rubidium bromide gives rise to isotopomeric clusters such as $[Rb_3Br_2]^+$ due to natural abundance ^{85}Rb, ^{87}Rb, ^{79}Br, and ^{81}Br. Various members of the isotopomeric cluster can lose either 165.8 or 167.8, but none can lose 169.8 as a neutral fragment. Nevertheless, when rubidium bromide is analyzed by constant neutral loss scanning with the neutral loss mass set to 169.8, four signals corresponding to members of the isotopomeric $[Rb_3Br_2]^+$ cluster are detected (Figure 2). This can again be explained through kinetic energy release considerations and ion intensity diagrams. The relative intensities of these peaks can again be predicted mathematically, with excellent agreement between theoretical and experimental results.

Reference [1] Lacey, M.J.; Macdonald, C.G ; Donchi, K.F.; Derrick, P.J. *Org. Mass Spectrom.* 1981, *16*, 351.

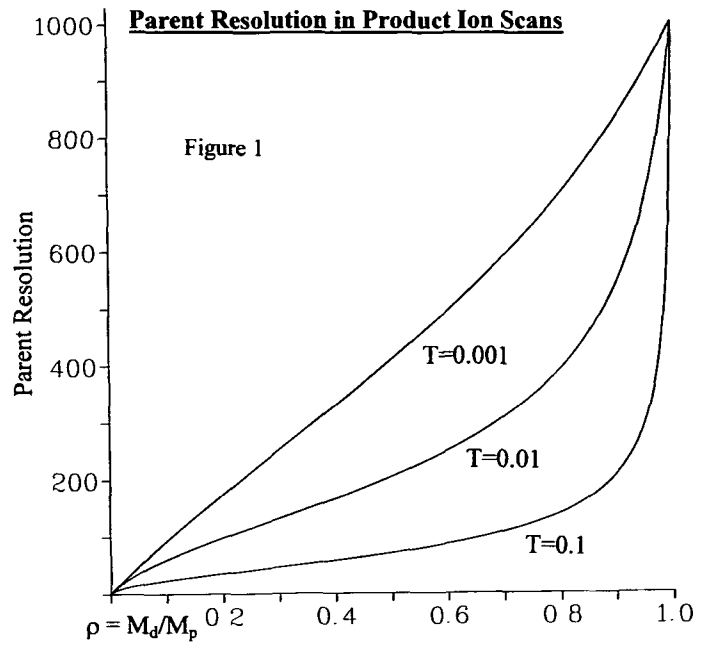

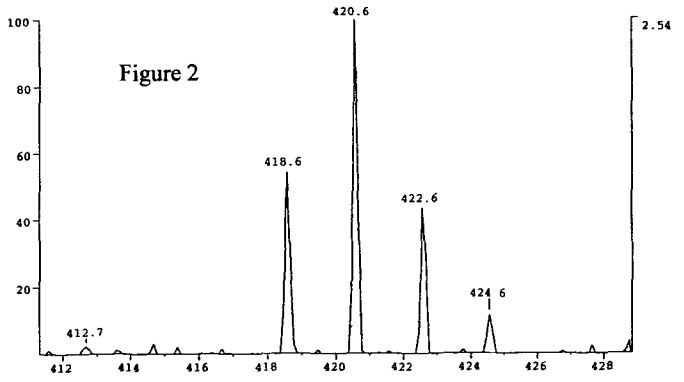

Identification of fullerenes in natural flames by APCI/LCMS

Koli Taghizadeh, William J. Grieco, Arthur L. Lafleur, and Jack B Howard
Center for Environmental Health Sciences and Department of Chemical Engineering
Massachusetts Institute of Technology,
77 Massachusetts Avenue, Cambridge , MA 02139

The recent discovery of fullerenes in mineral deposits [1] strongly suggests a natural means of fullerene formation Previous work in our laboratories showed that fullerenes were relatively abundant in benzene/oxygen flames [2] but not at ambient conditions Reports of the detection of fullerenes in soots from free-burning toluene and common candle flames under ambient conditions [3] led us to explore fullerene formation in natural flames.

In this paper we are reporting the detection of fullerenes from six soot samples collected from laboratory small open-flames The first four soot samples in Table 1 were collected from common candle flames and pine wood flames with and without an argon jet penetrating the flames. The soots were deposited in a water-cooled copper cup. Deposits were removed either by washing the collector with toluene or scraping off the soot and extracting with toluene. The last two wood soots were collected from burning pine woods diluted with nitrogen gas A water-cooled copper probe was inserted directly into the diffusion flame, and airflow through the probe was provided by a vacuum cleaner, an in-line glass wool plug was inserted between the probe and vacuum to trap solid materials The sample was collected by retaining the glass wool in toluene and cleaning the inside of the copper probe with toluene-soaked paper wipes Both the glass wool and wipes were sonicated, filtered and concentrated in a rotary evaporator.

In order to detect the small amount of fullerenes in these samples, preparative HPLC was necessary to remove polycyclic aromatic hydrocarbons (PAH) The majority of the PAHs were separated from fullerenes using a Beckman prep HPLC system with a two-wavelength detector and a 500 ul injection loop. Two Jordi Gel DVB (Divinyl Benzene) columns were used, each 500 mm in length, with IDs of 10 mm, packed with 5u particle size, and a 500 A pore size. The mobile phase was dichloromethane with a flow rate of 1.5 ml/min. Fractions of fullerenes were collected between 62 to 80 min. Depending upon the sample size, this step required two to four injections. The fractions from each sample were collected in a vial and concentrated almost to dryness, then re-dissolved in 50 to 100 ul of toluene of which a 20 ul solution was injected into APCI/LCMS system. The Beckman HPLC system consisted of dual pumps, a diode array detector, and a small Jordi Gel column (100 mm x 10 mm) Dichloromethane.benzene (98·2) was used as a mobile phase with a flow rate of 500 ul/min. This HPLC system was interfaced through a heated pneumatic nebulizer to PE/SCIEX APCI/MS. The conditions of the heated nebulizer and APCI/MS were as follows: nebulizer gas (air zero 1 0) 80 psi, auxiliary gas (air zero 1.0) 1 l/min, with the nebulizer temp set at 550 C, the curtain gas (nitrogen 5.0) at .8 l/min, the orifice at 35 volts, and an interface temp of 60 C. The mass spectrometer was scanned from 716 to 725 u , with steps of 0 1u, and a dwell time of 10 msec. for C60 for 0-25 min., and then from 836 to 845 u for C70 for 25.1-33.0 min.

The results of this study are summarized in Table 1. The total ion chromatogram of pine dowel and the extracted ion chromatograms for C60 and C70 are shown in Figure 1 The mass spectra for C60 and C70 are shown in Figure 2.

All six samples revealed the presence of C60 and the candle soots and last two wood samples showed the presence of C70, confirming other reports of fullerenes in common flames . In conclusion, these results suggest that wildfires could be a natural source of fullerenes.

Acknowledgment. This investigation was supported by the Division of Chemical Sciences, Office of Basic Energy Sciences, Office of Energy Research, US Dept. of Energy, Grant # DE-FG02-84ER13282 We thank David Nauman, Rose Marino, and Susan Weakland for assisting in the collection and analysis of the samples.

References. 1 L. Becker, J. L Bada, R. E Winans, J E Hunt, T E. Bunch, B.M French, Science , **265**, 642, 1994.
2 J.B. Howard, J T McKinnon, Y Makarovsky, A. L. Lafleur , M.E. Johnson , Nature , **352**, 139 (1991)
3. D.Heymann, L.P. F. Chibante, R. R. Brooks, W. S Wolbach, R. E. Smalley. Science **265**, 645, 1994

Table 1.

	C60	C70
Candle soot with argon	present	present
Candle soot without argon	present	present
Pine wood with argon	present	n/d
Pine wood without argon	present	n/d
Pine Dowel	20ppb*	0 74 ppb*
Loblolly Pine Sapwood	5 6ppb*	0 77ppb*

* based on wood weight

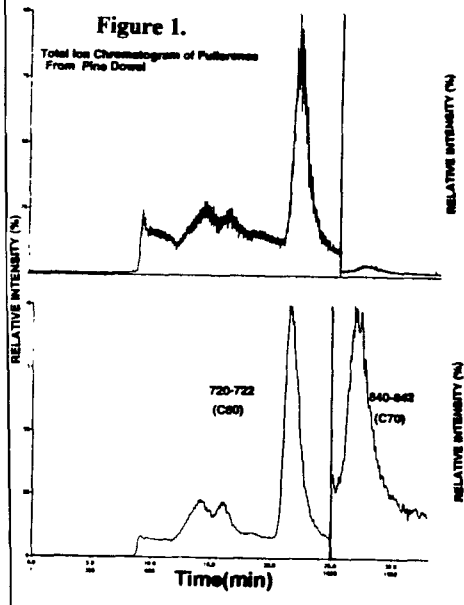

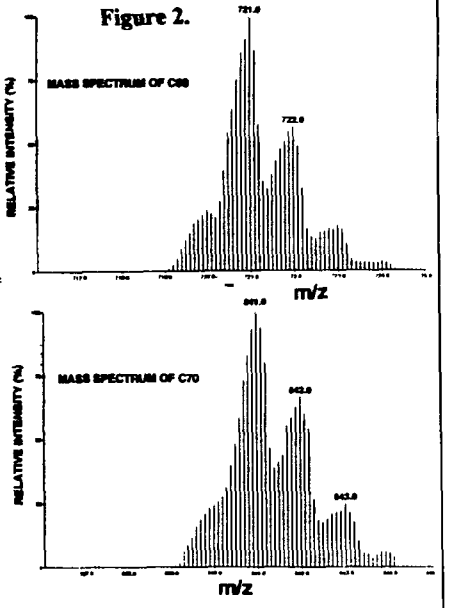

Effect of Mobile Phase Buffer Components on Sensitivity in Negative Atmospheric Pressure Chemical Ionization LC/MS

William H. Schaefer and Frank Dixon Jr., Drug Analysis Department, Drug Metabolism and Pharmacokinetics, SmithKline Beecham Pharmaceuticals, King of Prussia, PA 19406

Atmospheric pressure chemical ionization (APCI) is used routinely for high throughput and high sensitivity quantitative LC/MS assays. Negative ion APCI is particularly useful for analytes which contain acidic protons. Ionization by APCI is dependent on proton affinity of the chemical ionization reagent(s) relative to that of the analyte of interest. This consideration becomes very important since most reverse phase HPLC is done at pH <7 using mobile phases that contain acidic components. These acidic buffer components can inhibit the ionization of analytes which have a higher proton affinity. We have investigated the effect of several common buffers on the ionization of a series of model compounds which are amenable to negative APCI to determine the extent of ionization quenching which can occur. In addition, we have compared the sensitivity using these standard mobile phases to a mobile phase which does not contain an acidic buffer component, but rather a base (N-methyl morpholine). A better understanding of the interaction of solvent components with ionization of analytes should facilitate more rational development of chromatography conditions which are amenable to highly sensitive analyses.

Compound selection strategy Compounds were selected which contained functional groups commonly encountered in pharmaceuticals, including carboxylic acids, phenols, and hydroxamic acids, which could be analyzed in negative ion mode. The carboxylic and hydroxamic acids which were selected ranged from aliphatic to aromatic in order to cover a range of acidic strengths. One group of compounds was selected which contained only one protic functional group in order to avoid any additive or interfering effects of additional protic functional gorups. Additional compounds were analyzed which had multiple functional groups in order to compare their response relative to those with only one acidic functional group.

Solvent selection strategy The mobile phases buffers used to test ionization efficiency (or signal intensity) included 10 mM and 100 mM ammonium acetate (natural pH) which were selected to investigate the effect of acetic acid at low and high concentrations. Formic acid (10 mM) was used to test the effect of a stronger acid in negative APCI. An N-methylmorpholine mobile phase, which lacked an acidic modifier, was also used. N-methylmorpholine was a volatile, non-nucleophilic base which also provided good column retention perhaps by ion pairing with acidic analytes.

Instrument Optimization Instrument parameters including orifice potential, heated nebulizer temperature, and gas flows were optimized for each analyte in each mobile phase. Only orifice potential varied dramatically between compounds. Analytes which contained a phenylacetic acid moiety tended to eliminate CO_2 readily even at moderate orifice potentials (>60-70 V).

Sample Introduction and Mass Spectrometry In order to evaluate ionization efficiency, analytes were loop injected into the APCI source at a flow of 1 ml/min and the $[M-H]^-$ was detected using single ion monitoring (Q1 SIM). A mobile phase composed of acetonitrile/aqueous buffer (1:1) was used and analytes were dissolved in the appropriate mobile phase prior to analysis. Six sequential injections of 2 pmol/5 ul/injection were made for each analyte (as well as blank injections) in each mobile phase. The area of each peak (above background noise) was determined using the Sciex MacQuan software.

Chromatography The chromatographic behavior of several compounds was demonstrated under gradient conditions using a 10 mM N-methylmorpholine:acetonitrile mobile phase with a 4.6 x 150 mm EM Science Aluspher C8 column. N-methylmorpholine provided better retention of acidic analytes than either triethylamine or ammonium hydroxide, perhaps through better ion pairing. The stability of the analytes under basic these conditions must be evaluated when considering the use of these alkaline mobile phases.

A portion of the results are summarized in Table 1.

Table 1. Comparison of the Ionization of Model Compounds by Negative APCI in the Presence of Various Buffers (Mixed with Acetonitrile 1:1)

- Peak area values are expressed as a percent ratio relative to areas observed using N-methylmorpholine. The actual peak area values are shown in parentheses (area).

Carboxylic Acid Compounds	$[M-H]^-$	N-Methyl morpholine 10 mM	Ammonium acetate 10 mM	Ammonium acetate 100 mM	Formic Acid 10 mM
2-Norbornane acetic acid	153	100% (586550)	14% (84884)	2% (9574)	3% (15442)
3-(4-Methoxyphenyl) propionic acid	179	100% (425758)	47% (198069)	5% (22821)	2% (6434)
Ibuprofen	205	100% (339635)	96% (325740)	10% (32747)	3% (9661)
Acetylsalicylic acid	179	100% (268290)	28% (76061)	42% (113220)	14% (37641)

Phenolic Compounds	$[M-H]^-$	N-Methyl morpholine 10 mM	Ammonium acetate 10 mM	Ammonium acetate 100 mM	Formic Acid 10 mM
β-Estradiol	271	100% (97551)	6% (5787)	1% (1203)	1% (912)
Isoeugenol	163	100% (155067)	8% (11734)	3% (4974)	<1%

The N-methylmorpholine mobile phase, which lacked acidic components, generally provided the highest sensitivity for acidic compounds in negative APCI. For analytes possessing a single protic functional group, those which were stronger acids (in solution) were less severely effected by the more acidic buffer components. Formic acid, which was the most acidic modifier tested, tended to show the most pronounced inhibition of ionization. For analytes which were more weakly acidic, the 100 mM ammonium acetate showed more inhibition of ionization than the 10 mM ammonium acetate. Interestingly, ionization of some compounds which contained multiple functional groups was quite good in all of the mobile phases tested.

Conclusions

- Moderate orifice potentials can induce significant elimination of CO_2 from some carboxylic acids in negative APCI.
- The buffer components used in the HPLC mobile phase can have a dramatic effect on sensitivity using negative APCI and can even quench ionization completely.
- Formic acid (relatively strong acid) can be very detrimental to formation of negative ions.
- The mobile phase which contained an amine modifier (N-methylmorpholine), and lacked acidic components, generally provided the highest sensitivity for acidic compounds in negative APCI.
- For analytes which ionize poorly by positive APCI or electrospray (as a protonated or ammoniated adduct) or negative electrospray, the use of a volatile amine mobile phase (such as N-methylmorpholine) and an HPLC column which is stable at pH >9 may provide a useful analytical system.

ANALYSIS OF SELECTED PHARMACEUTICALS USING LIQUID CHROMATOGRAPHY COUPLED TO DIFFERENT ATMOSPHERIC PRESSURE IONIZATION MASS SPECTROMETRY TECHNIQUES

Paul C. Goodley and Steven Fischer, Bay Analytical Operations,
Hewlett-Packard Co., 1601 California Ave., Palo Alto, CA 94304

Liquid chromatography combined with mass spectrometry (LC/MS) has become one of the most powerful analytical techniques for specific identification of nearly all types of organic compounds. Atmospheric pressure ionization techniques such as atmospheric pressure chemical ionization(APCI and atmospheric pressure electrospray ionization (API-ES) provide a rapid and simple way to generate ions from compounds which were here-to-fore difficult or impossible to obtain for MS analysis. As a result of these ionization techniques, analytical chemical analysis of pharmaceuticals and most drugs can be analyzed with a high level of confidence and certainty. **Figures 1** and **2** provides a technical diagrams of the Hewlett-Packard APCI and the API-ES respectively.

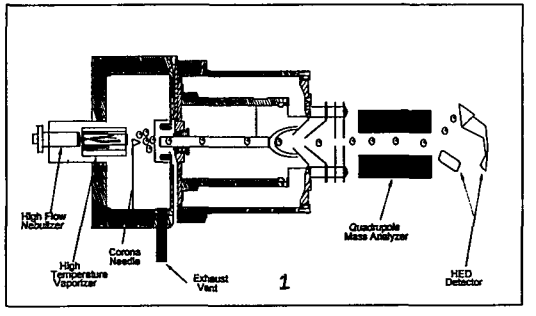

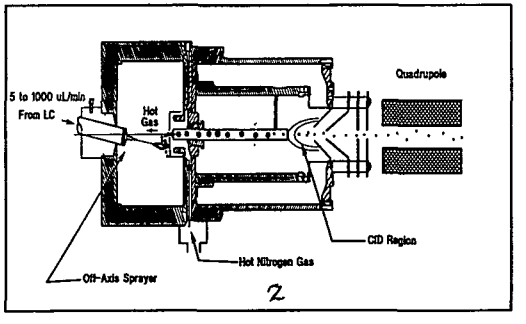

Figures 1 and 2. APCI and API-ES ion sources

Additional results using the APCI ion source is shown in Figures 3 and 4. Figure 3 shows the signal-to-noise measurement of 50 picograms of reserpine injected in the flow injection mode (FIA) while monitoring ion m/z=609.3. Figure 4 shows the signal-to-noise measurement of 20 nanograms injected using FIA while scanning the mass range, 100-650 using the APCI ion source. The peal-to-peak measurements were at 52 for the SIM measurement and 720 for the scan measurement of S/N respectively. The API techniques are indeed very powerful and sensitive with good linear response for reserpine, cortisol, and many other pharmaceuticals.

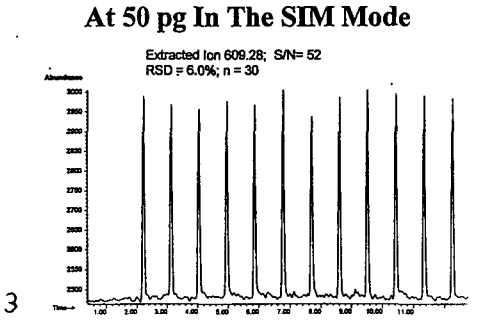

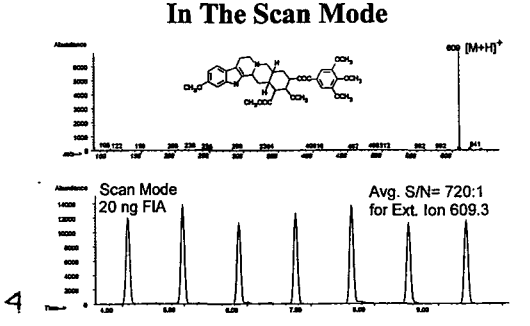

Figures 3 and 4. APCI of Reserpine In The SIM and Scan Mode

Oscillating Capillary Nebulizer Interfacing with Mass Spectrometers

Z Stacy Ho, Barry Drew and Richard F. Browner
School of Chemistry and Biochemistry
Georgia Institute of Technology, Atlanta, GA 30332-0400

Aerosol introduction is an important stage in the coupling of liquid chromatography with mass spectrometry and the performance of the nebulizer is a major determining factor in the quantity of the analysis. The ideal nebulizer should be simple and robust, and the performance of the nebulizer should be independent of the flow rate and mobile phase. A new nebulizer, the oscillating capillary nebulizer (OCN) shows great promise as a very versatile sample introduction system.

The OCN nebulizer consists of two concentric capillary fused silica tubes. Liquid flows through the inner capillary, while gas passes though the annular gap between the two concentric capillaries. Characteristics of the OCN include a smaller mean drop size and narrower drop size distribution than nebulizers available currently The OCN has been developed exclusively for inorganic analysis using an ICP LC/MS system The OCN can handle a wide liquid flow range and solutions containing a high salt content

Experiments have shown that the OCN can be coupled with a Hewlett-Packard particle beam interface, an Extrel ThermaBeam interface, and a Perkin-Elmer Sciex atmospheric pressure chemical ionization interface

Optimization and characterization of the OCN was carried out on a Hewlett-Packard particle beam interface. The relative positions of inner and outer capillary tubes are important to signal optimization A plot of signal vs the relative position of the capillaries shows there are multiple maxima and minima Plots of signal vs relative position of the capillaries and vs the flow rate show that at the optima, the slopes of the signal changes are very sharp However, at other

capillary positions, the performance of the OCN may be almost independent of tube position Best general operating conditions are with the liquid capillary tube sightly inside the outer capillary, and with a helium flow rate between 1.5 L/min and 2 5 L/min.

Measuring the OCN signal vs flow rate in the particle beam interface shows that best signal response is at a flow rate of about 10 ul/min. At flow rates between 0 05 ml/min and 0 2 ml/min, the signal becomes largely independent of the flow rate for both water and methanol as mobile phase. At above 0.2 ml/min, the signal degrades quickly

The performance of the OCN is quite stable Flow injection of caffeine with water as mobile phase shows a standard deviation of about 12% over a period of one hour At flow rates as high as 0.2 ml/min with 100% water as mobile phase, no water deposit is detected in the momentum separator after more than one hour of continuous pumping.

It has proved possible to interface the OCN at different water flow rates with both Hewlett-Packard and Extrel quadrupole instruments, and with a Perkin-Elmer Sciex triple quadrupole instrument

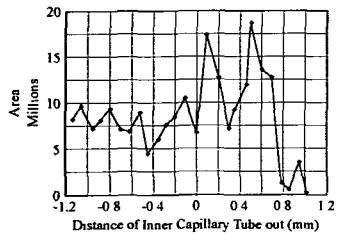

Fig. 1 OCN signals vs two capillary tubes relative positions. The experiments were done using caffeine as sample with methanol as mobile phase at flow rate of 0 2 ml/min.

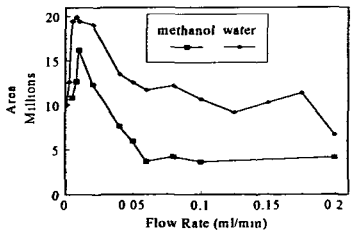

Fig. 2 OCN signals vs liquid flow rates with methanol or water as mobile phase The sample is caffeine

Evaluation and Application of Negative Ion Attachment LC/MS

Daniel L. Norwood, Dixie L. Fisher, and James O. Mullis
Glaxo Research Institute, 5 Moore Drive, Research Triangle Park, NC 27709

Introduction

Negative ion attachment LC/MS was evaluated as a technique for on-line molecular weight recognition, either as a complement to positive ion techniques or when applied to molecules that perform poorly as positive ions. Thermospray (TSP), electrospray (ESI), and atmospheric pressure chemical ionization (APCI) LC/MS interface/ionization processes were investigated. Initial evaluations were accomplished with a series of model compounds derived from pharmaceutical applications, including substituted phenylboronic acids, quaternary ammonium compounds, and phosphorus compounds. The phenylboronic acids, many of which produce poor positive ion spectra, were examined by ESI to study substituent effects on negative ion attachment. Trifluoroacetic acid (TFAA), a typical mobile phase modifier, was studied with all model compounds and LC/MS techniques Other potential attaching species (acetate, *p*-toluenesulfonic acid, chloride, bromide) were also investigated using ESI and APCI. Additional experiments included sensitivity assessment, optimization of source potentials (ESI and APCI), and optimization of probe temperature (APCI).

Experimental

TSP experiments were accomplished on a VG Trio-II quadrupole mass spectrometer, with ESI and APCI experiments accomplished on a VG Quattro triple quadrupole instrument. The HPLC mobile phase was typically acetonitrile/water at various ratios, with 0.05-0.1% modifier (TFAA, acetate, *p*-toluenesulfonic acid, chloroacetonitrile, bromoacetonitrile). Flows were 1 mL/min for TSP and APCI and 10 µL/min for ESI.

Discussion

Molecular specific confirmation using negative ion attachment was demonstrated with all model compounds and LC/MS techniques. As examples, Figures 1 and 2 show respectively the TSP- TFAA attachment spectrum of 3-nitrophenylboronic acid and the APCI- TFAA attachment for methylbenzethonium chloride. The technique was demonstrated to have good sensitivity when compared to detection of the [M-H]- ion from *p*-toluenesulfonic acid (Figure 3, a good negative ion performer). Instrument parameters (ESI and APCI) were shown to affect the attachment spectra in a compound dependent manner. ESI- TFAA attachment experiments with a series of variously phenyl substituted boronic acids clearly indicated that attachment was related to the net positive charge on the boron (a nucleophilic attachment process). An APCI- LC/MS experiment with 4 pairs of quaternary ammonium compounds and matched neutral controls (M_Q^+ and [M+H]+ isobaric) clearly demonstrated that quaternary ammonium compounds could be

unambiguously distinguished with a combination of positive ion and negative ion TFAA attachment experiments.

Figure 1

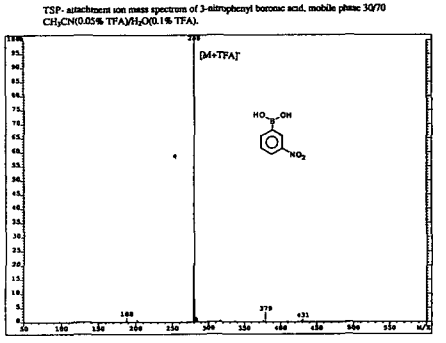

Figure 2

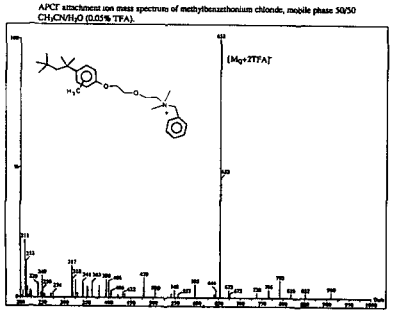

Figure 3

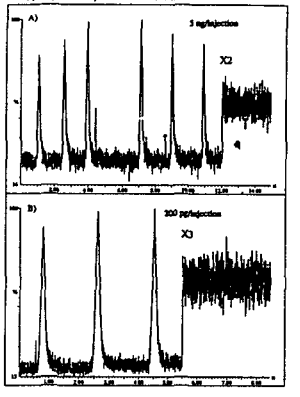

Analysis of Ceftiofur in Milk by LC/API-MS

Jeffrey Keever[1] Robert D. Voyksner[1] and Krystyna L. Tyczkowska[2]

[1] Analytical and Chemical Sciences, Research Triangle Institute, P. O. Box 12194, Research Triangle Park, North Carolina 27709
[2] Dept. of Anatomy, Physiology Sciences and Radiology, College of Veterinary Medicine, North Carolina State University, 4700 Hillsborough St., Raleigh, NC 27606

Introduction

A number of veterinary drugs which are frequently used to prevent infections, can contaminate meat and milk products destined for human consumption. Ceftiofur is a cephalosporin β-lactam antibiotic which is finding widely increased use to treat bacterial infections. While residues of ceftiofur and its metabolites have been reported in bovine milk and serum MS methodology has not been developed for the confirmation of this antibiotic. This paper presents the research into developing a screening procedure at the tolerance level of 50 ppb and developing a quantitative confirmation methodology based on liquid chromatography/electrospray-mass spectrometry (LC/ES-MS).

Results and Discussion

The development of the method took into account the need to handle large numbers of samples. For this reason the simple and rapid procedure of ultrafiltration using a 10 K molecular weight cutoff filter was chosen for sample cleanup. A 100 µL aliquot of the filtrate was concentrated on column (C_{18} 4.6 x 75 mm) followed by a gradient elution (5-60% acetonitrile in water containing 25 mM heptafluorobutyric acid (HFBA) in nine minutes, with a hold at initial conditions for 0.5 min at a flow rate of 1 mL/min. A 8:1 post column split and the post column addition of 75:25 propionic acid:isopropanol at 75 µL/min was used to achieve optimal electrospray operation, overcoming problems from suppression from the HFBA or 1 mL/min flow rate. Using the conditions ceftiofur eluted at a retention time of 8.6 min and the internal standard (cephapirin) at 6.3 min.

Furthermore, the use of an Rf ion guide (Analytica of Branford) on the electrospray interface improved the S/N ratio by 7.5 for the $[M+H]^+$ ion at m/z 524 for ceftiofur compared to the conventional lens stack. The ion guide also resulted in slightly better precision with a 7% RSD (n=5) compared to a 12% RSD (n=5) for the conventional lens stack. The sensitivity gains from on-column concentration, addition of propionic acid post column and the Rf ion guide permitted the detection of ultrafiltrate samples down to about 10 ppb for ceftiofur. A five point calibration curve from 0-200 ppb for the $[M+H]^+$ of ceftiofur (m/z 524) (using cephapirin $[M+H]^+$ at m/z 424 as an internal standard spiked into each sample at 100 ppb) was linear with a correlative coefficient of 0.993 (n=19). The ion chromatograms for the $[M+H]^+$ ion of ceftiofur at the 50 ppb level (ceftiofur tolerance in milk) and blank are shown in Figure 1A and 1B. The method was tested on milk samples collected from bovine milk following dosage with ceftiofur. The ion

chromatogram for ceftiofur determination in one of these samples is shown in Figure 1C and was measured to be present at 71 ppb. The other milk samples were measured to contain 27, 54, 66, 24 and 31 ppb.

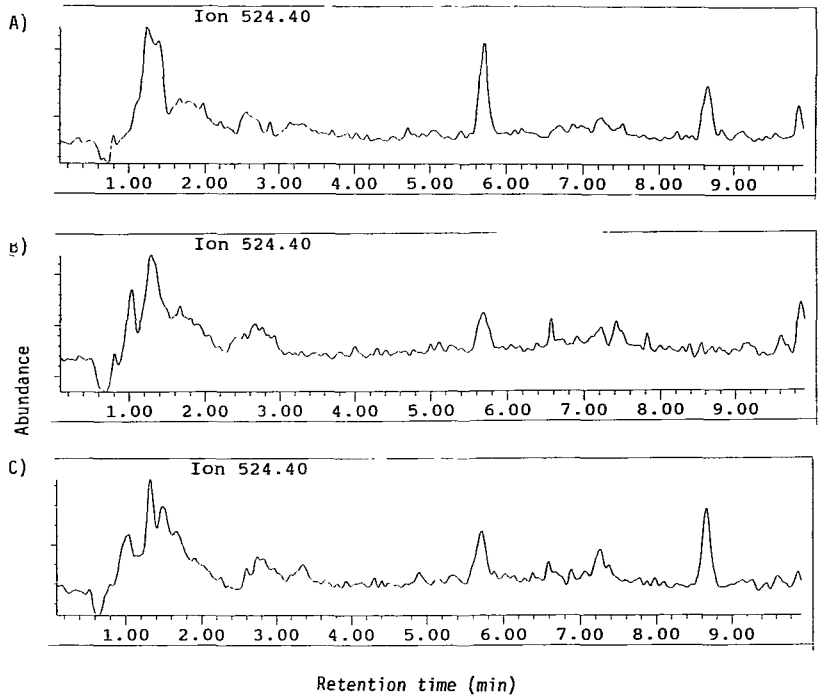

Figure 1. Ion chromatogram for the $[M+H]^+$ ion of ceftiofur (m/z 524), at a retention time of 8.6 minutes, from the LC/electrospray-MS determination for (A) 50 ppb of ceftiofur spiked into milk, (B) Blank milk and (C) milk sample which was above the 50 ppb tolerance for ceftiofur (measured level of ceftiofur was 71 ppb).

Acknowledgements

This work was supported by the Food and Drug Administration under Cooperative Agreement Number FD-U-000589. Also, the authors thank both Hewlett Packard and Analytica of Branford for technical assistance and instrumentation used in this work.

Electrospray Liquid Chromatography/Mass Spectrometry of Ginsenosides

Richard B. van Breemen, Chao-Ran Huang, Zhi-Zhen Lu, Agnes Rimando, Harry H. S. Fong, and John F. Fitzloff
Department of Medicinal Chemistry and Pharmacognosy, University of Illinois at Chicago (m/c 781), 833 South Wood Street, Chicago, IL 60612-7231

This investigation reports the first LC/MS analysis of ginsenosides and ginseng extracts. This study is also the first application of electrospray to ionize this class of compounds. In addition, unusual ginsenoside adduct ions, $[M+138]^+$, are described for the first time, and their origin as artifacts arising from the aminopropyl silica HPLC stationary phase is described.

EXPERIMENTAL SECTION

Panax quinquefolius and *Panax ginseng* are commonly known as "American ginseng" and "Korean ginseng", respectively. Ginseng (American or Korean) root powder was extracted with 80% methanol. An Extrelut QE extraction column (EM Industries, Inc.) was used for partial purification of the ginsenosides.

Electrospray mass spectra were obtained using a Hewlett-Packard (Palo Alto, CA) 5989B MS Engine quadrupole mass spectrometer coupled to a Hewlett-Packard 1090L gradient HPLC system by a pneumatic nebulizer-assisted electrospray LC/MS interface. HPLC separations were carried out using a Waters Associates (Milford, MA) Carbohydrate Analysis column (10 μm aminopropyl silica; 125Å pore size, 3.9 x 300 mm) at a flow rate of 1.0 ml/min. The mobile phase consisted of isocratic water/acetonitrile (17:83; v/v) for 8 min followed by a linear gradient from 17:83 (v/v) to 30:70 (v/v) over the next 22 min. During LC/MS, the flow was split 1:50 so that 21 μl/min entered the electrospray ionization source of the mass spectrometer. Ginsenoside standards (approximately 100 ng/μl in water/methanol/acetic acid, 50.50 0.05, v/v/v) were infused into the electrospray ionization source at 10 μl/min using a Harvard Apparatus (South Natick, MA) Model 22 syringe pump.

RESULTS AND DISCUSSION

Ginsenoside standards were analyzed by infusing solutions directly into the electrospray ion source. Positive ion electrospray produced abundant cationized ginsenoside ions, $[M+Na]^+$, but no protonated molecules. For example, an $[M+Na]^+$ ion of ginsenoside R_e (M. W. = 947) was detected at m/z 970 with no detectable fragmentation (Figure 1A) However, addition of sodium to the mobile phase (100 μM NaCl) did not significantly enhance the abundance of $[M+Na]^+$ ions. Initial experiments using negative ion electrospray mass spectrometry produced no sample ions. Acidification of the carrier solution with acetic acid was investigated as a means to enhance the formation of protonated molecules, but still no $[M+H]^+$ ions were observed. Therefore, post-column addition of acid was determined to be unnecessary.

Next, ginsenoside standards were injected onto an aminopropylsilica HPLC column and then detected upon elution using a photodiode array absorbance detector followed on-line by positive ion electrospray mass spectrometry. The positive ion electrospray mass spectrum of ginsenoside R_e, which eluted from the HPLC column at 11.6 min, is shown in Figure 1B. In addition to the expected sodium adduct detected at m/z 970, an unexpected adduct ion, $[M+138]^+$, was detected at m/z 1085, and an ion corresponding to loss of water from this unusual adduct was detected at m/z 1067. During LC/MS analysis of an extract of American Ginseng, ginsenoside R_e was detected with a retention time of 11.6 min as the adduct, $[M+138]^+$, m/z 1085, but no sodium adduct was observed (See mass spectrum in Figure 1C). Ions corresponding to the loss of one or two molecules of water from the ion of m/z 1085 were detected at m/z 1067 and 1049, respectively. Although sodium adducts and $[M+138]^+$ ions were observed together in the

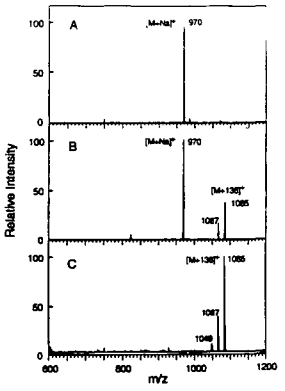

Figure 1

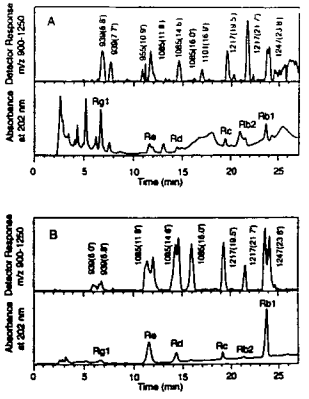

Figure 2

electrospray mass spectra of all ginsenoside standards obtained during LC/MS analysis, ginsenosides contained in ginseng extracts were detected only as $[M+138]^+$ ions, probably because the standards contained more sodium cations than did the ginseng extracts.

Positive ion electrospray LC/MS analyses of Korean and American ginseng extracts are shown in Figure 2. Ginsenosides were identified based on comparison to standards with respect to retention times, and m/z values (detected as $[M+138]^+$ ions). In all cases, ginsenosides eluted from the aminopropyl silica column in order of increasing molecular weight Although most ginsenosides were identified in both extracts, the relative proportions of each were different.

Because adducts ions, $[M+138]^+$, were only observed during LC/MS and not during infusion of standards, the origin of this unusual set of ions was determined to be the stationary phase. 3-Aminopropyltrialkoxysilanes may be used in the synthesis of 3-aminopropyl stationary phases and for end-capping active sites in HPLC columns. Consequently, 3-aminopropyltrihydroxysilane (molecular weight 137) would be a hydrolysis product that might strongly adsorb to the column and bleed off over a long period of time The column manufacturer confirms that this molecule might be present on the aminopropylsilica column used in this investigation. An alternative source of 3-aminopropyltrihydroxysilane might be degradation of the aminopropylsilica stationary phase. Therefore, the most likely identity of the cation weighting 138 is protonated 3-aminopropyltrihydroxysilane, $^+NH_3(CH_2)_3Si(OH)_3$. In support of the identification of the unusual cation as protonated 3-aminopropyltrihydroxysilane, ions were observed at m/z 138 in all the positive ion electrospray LC/MS spectra obtained using aminopropylsilica columns, and $[M+138]^+$ ions were more abundant than $[M+Na]^+$ adducts in LC/MS spectra of ginsenoside standards when a new aminopropylsilica column was used. Because elimination of a neutral molecule of water from ginsenoside adducts, $[M+138]^+$, was much more abundant than loss of water from $[M+Na]^+$ ions, the probable source of the eliminated water molecule was the less stable silanol moiety instead of a ginsenoside hydroxyl group.

ACKNOWLEDGEMENT

Use of the electrospray mass spectrometer was generously provided by the Hewlett-Packard Company. Support from the American Botanical Council (Austin, TX) is gratefully acknowledged.

ELECTROSPRAY LIQUID CHROMATOGRAPHY/MASS SPECTROMETRY OF CAROTENOIDS

Richard B. van Breemen, Department of Medicinal Chemistry & Pharmacognosy, College of Pharmacy, University of Illinois at Chicago, 833 S. Wood Street, Chicago, IL 60612-7231

More than 600 carotenoids have been isolated and identified from natural sources. Carotenoids in the human diet function as metabolic precursors to vitamin A, antioxidants, immunoenhancers, and potential cancer chemopreventative agents. High performance liquid chromatography (HPLC) with photodiode array absorbance detection is the preferred method for the separation, identification and quantitation of carotenoids from biological tissues.[1] However, in addition to HPLC uv/vis detection, mass spectrometric and tandem mass spectrometric analyses[2], which provide molecular weight and characteristic fragmentation patterns, may then provide final confirmation of individual carotenoid identities.

Previous reports exploring the application of LC/MS to carotenoid analysis used 1) a heated moving belt interface with EI ionization,[1] 2) particle beam interface with negative ion CI and a heated ion source,[3] or 3) continuous-flow FAB.[4] Among these methods, only continuous-flow FAB does not require the use of gas-phase ionization or a heated ion source, which might lead to carotenoid pyrolysis. However, the flow rate of continuous-flow FAB is limited to <10 µl/min. In the present investigation, the development of an electrospray LC/MS method is reported that is compatible with analytical scale HPLC column flow rates of 1.0 ml/min. This new electrospray LC/MS method will be demonstrated to be compatible with the C_{30} reversed-phase HPLC stationary phase recently engineered by Sander, *et al.*,[5] for the separation of carotenoids and their *cis/trans* isomers.

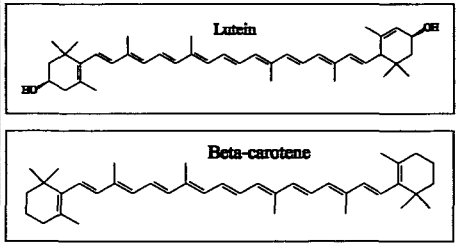

Figure 1.

METHODS

Mass spectra were obtained using a Hewlett-Packard (Palo Alto, CA) 5989B MS engine quadrupole mass spectrometry equipped with a pneumatic nebulizer-assisted electrospray LC/MS interface, and 1090L gradient HPLC system equipped with a photodiode array UV/vis absorbance detector. Unit resolution was used for all measurements; the quadrupole analyzer was maintained at 120°C; nitrogen pressure at 80 psi was used for nebulization; and the nitrogen bath gas was 350°C at a flow rate of 50 ml/min. The electrospray needle was maintained at ground potential, while the counter-electrode was at -5100 V. The range m/z 200-610 was scanned over approximately 2 s during LC/MS.

HPLC separations were carried out using a reversed-phase column, 4.6 x 125 mm, containing a C_{30} silica stationary phase.[5] The solvent system consisted of a 60 min gradient from 85:15 to 10:90 methanol/methyl-*t*-butyl ether containing 1.0 mM ammonium acetate at a flow rate of 1.0 ml/min Absorbance spectra were recorded from 250-600 nm using a photodiode array detector located in-line between the HPLC column and electrospray LC/MS interface. Based on the method of Van Berkel and Zhou,[6] carotenoids were oxidized in solution by postcolumn addition of a halogenated oxidant (i.e., 2% v/v 2,2,3,3,4,4,4-heptafluoro-1-butanol) at a flow rate of 50 µl/min. Optimization experiments were carried out in which different halogenated compounds at various concentrations were evaluated.

43rd ASMS Conference on Mass Spectrometry and Allied Topics

RESULTS

Positive ion electrospray mass spectrometry produced molecular ions, $M^{+\cdot}$, without any fragmentation for both polar xanthophylls (i.e., lutein) and nonpolar carotenes (i.e., β-carotene). A comparison of different halogenated solvents for solution-phase oxidation including heptafluorobutanol, hexafluoropropanol, heptafluorobutanoic acid, trifluoroacetic acid, and chloroform showed that postcolumn addition of heptafluorobutanol and hexafluoropropanol produced the most abundant molecular ions. The limits of detection of lutein and β-carotene were determined to be approximately 1-2 pmol during flow-injection analysis. Unlike the results of Van Berkel and Zhou,[6] who detected doubly-charged molecular ions and deprotonated, singly-charged ions for β-carotene during electrospray mass spectrometry with solution-phase oxidation, only singly-charged molecular ions were observed.

Electrospray LC/MS analysis of a mixture of α- and β-carotene is shown in Figure 2. Both *cis*- and *trans* isomers were separated by the C_{30} column and then detected by electrospray mass spectrometry. Because of the its lower sensitivity, only the more abundant *all trans*-carotenoids were detected by the UV/vis photodiode array detector (Figure 2B).

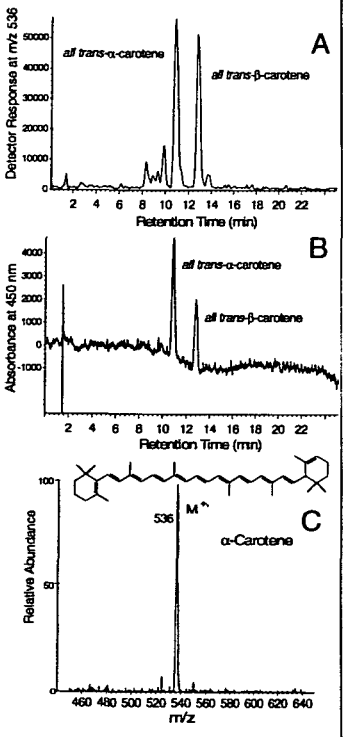

Figure 2. Positive ion electrospray LC/MS analysis of a mixture of α-carotene and β-carotene (20 ng each) using a C_{30} reversed phase HPLC column with postcolumn addition of heptafluorobutanol as oxidant. (A) reconstructed mass chromatogram of the molecular ions of m/z 536. (B) Absorbance chromatogram at 450 nm recorded on-line. (C) Electrospray mass spectrum of α-carotene at a retention time of 10.8 min.

ACKNOWLEDGEMENTS

Alexander Schilling and Steven Fischer provided fruitful discussions and technical assistance with mass spectrometry. Use of the electrospray mass spectrometer was generously provided by the Hewlett-Packard Co. The C_{30} HPLC column was a gift from Lane Sander of the NIST.

REFERENCES

1. Taylor, R. F.; Farrow, P. E.; Yelle, L. M.; Harris, J. C.; Marenchic, I. G. In *Carotenoids. Chemistry and Biology*; Krinsky, N. I., *et al.*, Eds.; Plenum Press: New York, 1990; pp 105-123.
2. van Breemen, R. B.; Schmitz, H. H.; Schwartz, S. J. *Agric. Food Chem.* **1995**, *43*, 384-389.
3. Khachik, F.; Beecher, G.R.; Goli, M.B.; Lusby, W.R.; Smith, J.C., Jr. *Anal. Chem.* **1992**, *64*, 2111-2122
4. van Breemen, R. B.; Schmitz, H. H.; Schwartz, S. J. *Anal. Chem.* **1993**, *65*, 965-969.
5. Sander, L. C.; Sharpless, K. E.; Craft, N. E.; Wise, S. A. *Anal. Chem.* **1994**, *66*, 1667-1674.
6. Van Berkel, G. J.; Zhou, G. *Anal. Chem.* **1994**, *66*, 3408-3415.

Multi-Residue Method for ß-Agonists By Immunoaffinity Extraction-LC/LC/MS/MS

Jianyi Cai and Jack Henion
Analytical Toxicology, Diagnostic Laboratory, Cornell University, 927 Warren Dr., Ithaca, NY 14850

Introduction

ß-agonists have been used as bronchodilators in human and veterinary medicine as therapeutic drugs for the treatment of pulmonary diseases. Recently, there has been evidence that the illegal and potentially poisonous drug, clenbuterol, is being used on calves as a growth-promoting agent within Europe and the United States. The widespread use of clenbuterol in European veal production has claimed at least five deaths. In addition to the most frequently used ß-agonist, clenbuterol, several other analogs have emerged over the past few years and have been found to be illegally used for improving meat production efficiency in livestock.

Since the use of such drugs has great risk to consumers of food products from treated animals, a good analytical method, preferably a multi-residue method, is essential. On-line immunoaffinity extraction (IAE) and coupled-column liquid chromatography-tandem mass spectrometry using an automated column-switching system and electrospray mass spectrometry has recently been evaluated in our laboratory. This presentation describes the implementation of this system for multi-residue analysis of several ß-agonists in spiked bovine urine without conventional sample pretreatment.

Experimental

The mass spectrometer used was a Sciex API-300 triple quadrupole mass spectrometer (Thornhill, Ontario). An automated column-switching system (INTEGRAL micro analytical workstation, PerSeptive Biosystems) was used for on-line sample clean-up and enrichment. Three columns were involved including a protein G immunoaffinity column (2.1 x 3.3 mm, 30 µm, ChromatoChem, Missoula, MT), a trapping column (C-18 packed-capillary column, 0.5 x 15 mm, 5 µm, LC Packings, Amsterdam, the Netherlands), and an analytical column (C-18 packed-capillary column, 0.3 x 150 mm, 3 µm particles, LC Packings).

The automated column-switching system was programmed to perform the complete process of on-line sample pretreatment, which includes priming the protein G antibody column, loading PBS-diluted urine sample onto the antibody column washing with PBS, desorbing bound analytes from the antibody column and trapping onto trapping column, and finally eluting the trapped analytes from the trapping column into the analytical column and to mass spectrometer for separation and identification.

Results and Discussion

To evaluate the performance of the automated on-line immunoaffinity extraction coupled column capillary HPLC and tandem mass spectrometry system, a synthetic mixture of five ß-agonists including clenbuterol, bitolterol, mabuterol, methyl-clenbuterol, and tulobuterol was prepared and analyzed using an antibody specific to clenbuterol. Figure 1 shows the results obtained with the synthetic mixture of ß-agonists. The system was also used for the analysis of bovine urine spiked with the ß-agonists. Figure 2 shows the SRM ion current chromatogram obtained with a 1 part per billion (ppb) levels of ß-agonists in spiked bovine urine by SRM/IAE/LC/LC/MS using the automated system.

Acknowledgments

Partial financial support from Advanced Bioanalytical Services, Inc. is greatly appreciated. We acknowledge PE Sciex for the loan of the API-300 triple quadrupole mass spectrometer, and PerSeptive Biosystems for the loan of the INTEGRAL micro analytical workstation. We thank LC Packings for the packed capillary columns, ChromatoChem for the protein G column, Dr. M.-P. Montrade of Ministere de l-Agriculture, France and Dr. L. Leyssens of Dr. L. Willems-Instituue, Belgium for supplying several ß-agonist standards. Special thanks also goes to Dr. T. Wachs for his technical support.

Figure 1

SRM/IAE/LC/LC/MS Analysis of ß-Agonist Synthetic Mixture

100 pg each injected on column

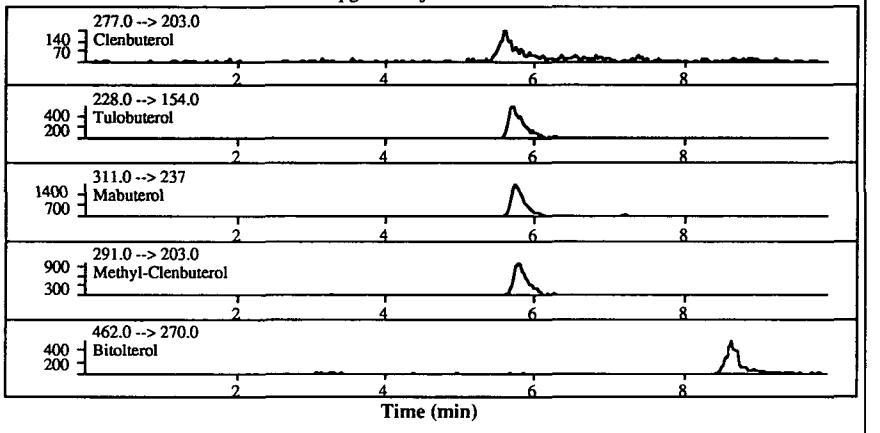

Figure 2

SRM/IAE/LC/LC/MS of Bovine Urine Spiked with ß-Agonists at 1 ppb Levels

50 mL of 20% bovine urine (diluted with PBS) injected on column

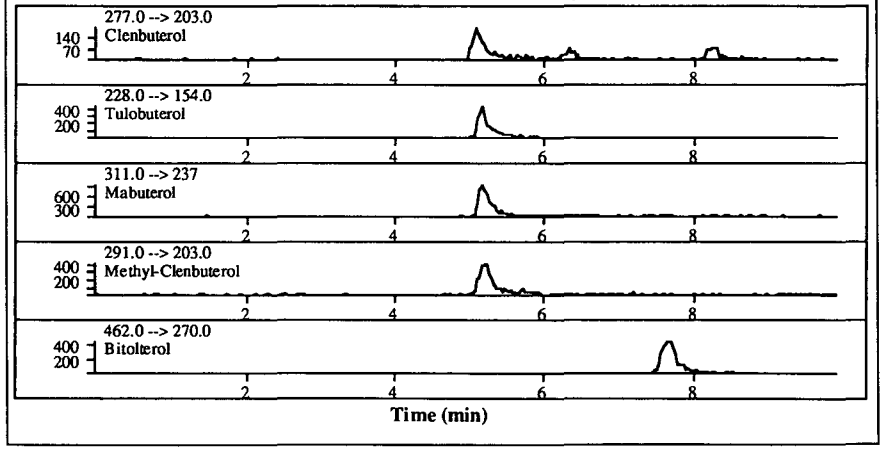

AN LC/MS METHOD FOR USING NON-VOLATILE MOBILE PHASE ADDITIVES WITH IONSPRAY MASS SPECTROMETRY

Larry M. Mallis and John R. B. Slayback

Bristol-Myers Squibb Pharmaceutical Research Institute
1 Squibb Dr., Building 90, New Brunswick, NJ 08903

To obtain satisfactory HPLC behavior during the analysis of multi-functional acidic compounds, it is often necessary to keep the charge sites protonated rendering the compound neutral. For this reason, the HPLC methods that are developed for purity assessment of in-process reactions typically employ a potassium phosphate buffered mobile phase adjusted to pH 3.0 using phosphoric acid. In addition, ion-pairing reagents such as hexanesulfonic acid are often used when analyzing basic compounds.

For impurity profiling applications using mass spectrometry (MS), an ammonium acetate buffered HPLC method is preferred since it is compatible with LC/ionspray mass spectrometry (LC/ISP-MS). Chromatographic resolution and peak shape considerations often prohibit the use of this volatile mobile phase buffer. Therefore, a modified LC/ISP-MS method was developed which uses a post-column HPLC pump for dilution (using acetonitrile/water as diluent) of the non-volatile mobile phase additive (e.g., potassium phosphate, hexanesulfonic acid, etc.). A schematic diagram depicting the LC/MS method is presented in Figure 1.

In the gas phase using ISP/MS, acidic compounds are preferentially ionized and detected in the negative ion mode as the $[M-H]^-$ specie. However, at a mobile phase pH of 3.0 most acidic compounds exist primarily in a non-charged state. The method presented herein also allows for post-column adjustment of the mobile phase pH. The higher pH and greater flow rate of the post-column diluent (acetonitrile/water) acts to raise the mobile phase pH, to approximately 4.2, above the first pKa of the acid. This enables the $[M-H]^-$ ion to be formed in high abundance for improved detection and sensitivity when analyzing in the negative ion mode.

Figure 2 shows the total ion chromatograms for the analyses (positive and negative ion modes) of several key intermediates in the formation of a triacid compound currently under development. Although a dilution of 4:1 occurs during the analysis, little or no loss of resolution or sensitivity is observed. In addition, this method has been used for as much as seven days running 10 hours per day. A wash of acetonitrile:water:methanol is used to flush the system of potassium phosphate. In an attempt to extend the utility of this new method, other non-volatile mobile phase buffers (i.e., sodium acetate, sodium phosphate, etc.) have been used.

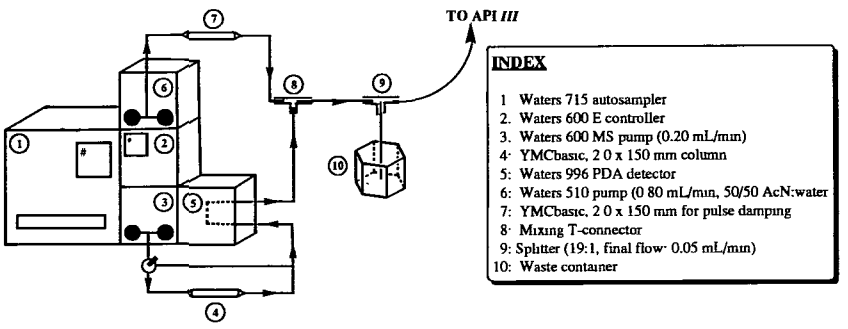

Figure 1. Schematic diagram of the instrumental setup used for post-column modification of the potassium phosphate pH 3 HPLC mobile phase and mass spectrometry detection.

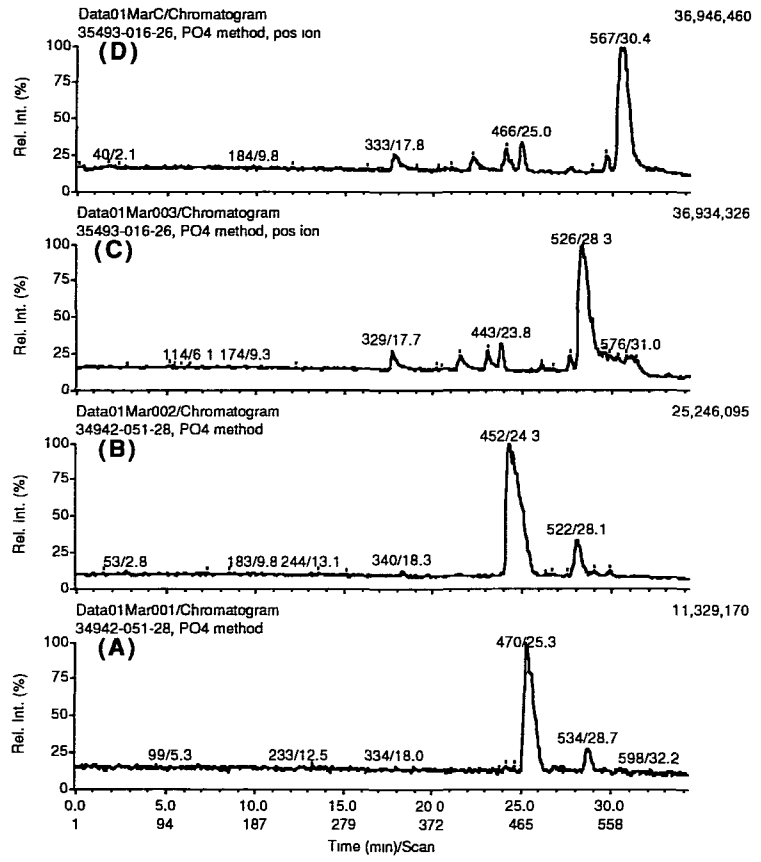

Figure 2. These four total ion chromatograms were acquired successively over a time span of 5 hours. Note that the overall sensitivity of the mass spectrometer has not degraded even though potassium phosphate is used in the HPLC mobile phase. Chromatograms A and B were acquired in the negative ion mode (A: 10 µL injection; B: 25 µL injection, respectively of BMS-188494) while chromatograms C and D were acquired in the positive ion mode (10 µL injection of BMS-192683.

A Rapid Universal LC/ESI-MS Method for Profiling Drug Metabolites

Susan C. Taylor, Anne M. Starrett, Gerald C. DiDonato, Mike S. Lee, Bristol-Myers Squibb Pharmaceutical Research Institute, Princeton, NJ 08543-4000

Increasing demands on the pharmaceutical industry to quickly market drug candidates have challenged scientists to expedite the drug discovery process. In response, our laboratory sought a rapid and efficient LC/ESI-MS method that would profile the majority of drug metabolism samples that we receive. Presently, a liquid chromatographic method is developed for each metabolism sample prior to LC/ESI-MS analysis. These methods, whether isocratic or gradient, frequently extend to one hour and require the availability of a variety of columns. Automated analysis is difficult when manual column or solvent switching is required for each run. The development of a universal method for analyzing metabolites from both *in vitro* and *in vivo* sources eliminates the need for lengthy method development time and hardware conversion and reduces overall analysis time.

A Perkin Elmer Series 4 Chromatograph equipped with an Applied Biosystems 783A Variable Wavelength UV detector set at 210 nm was used for all preliminary LC/UV method development. Subsequent LC/MS experiments were performed on a Waters 600MS HPLC system equipped with a Waters 717 autosampler, directly interfaced with a Finnigan Electrospray TSQ 700 mass spectrometer.

Most separations were performed on a YMC-ODS AQ, 3 micron, 150 x 4.6 mm, HPLC column. One additional column, a Waters Symmetry C_{18}, 5 micron, 150 x 4.6 mm, column was investigated. Mobile phases consisted of either 0.05 % trifluoroacetic acid or 50 mM ammonium acetate (pH 5), for the separation of acidic or basic compounds, respectively. Acetonitrile was used as an organic modifier to which 0.05% TFA was added when acid mobile phase was used. Linear gradients were run from 5/95 organic/aqueous to 95/5 organic/aqueous in 15 minutes. Flow rate of 1 mL/min was used to eliminate the need for a split.

The application of this universal system is shown below(Fig.1) in the LC/UV and LC/MS profiles of metabolites from microsomal incubations of BMS-180291, a thromboxane receptor antagonist. Hydroxylated and dihydroxylated metabolites were separated with very good efficiency. This method has also been applied to metabolites derived from basic compounds with similar results. This method has been proven as a useful tool in the rapid identification of biotransformation products.

43rd ASMS Conference on Mass Spectrometry and Allied Topics

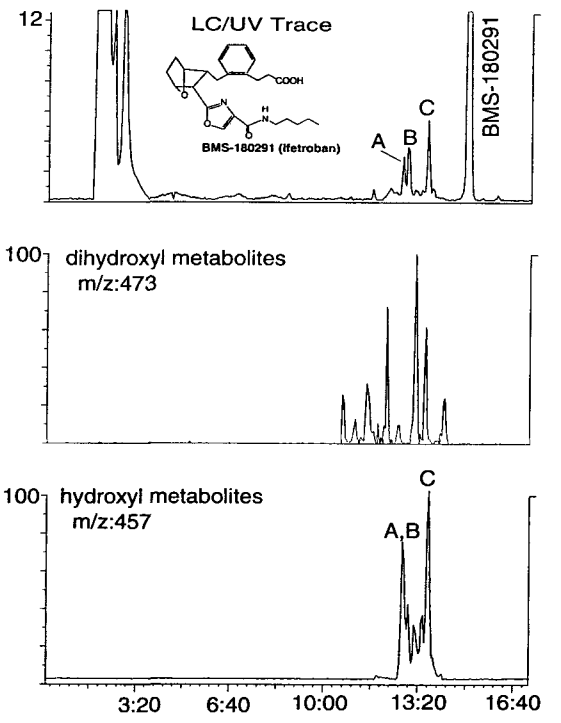

Figure 1. The separation of metabolites following incubation of BMS-180291 with rat liver microsomes using a rapid LC/MS profiling method.

Electrospray LC/MS Profiling in Evolving Drug Development Paradigms

Edward H. Kerns[1], Kevin J. Volk[1], Steven E. Klohr[1], Robyn Rourick[1], William L. Thompson[3], Jeffrey L. Whitney[1], and Mike S. Lee[2]
Bristol-Myers Squibb Pharmaceutical Research Institute,
[1]Wallingford, CT 06492, [2]Princeton, NJ 08543-4000, [3]New Brunswick, NJ 08903-0191

The intensity of pharmaceutical research activities are expanding as a result of emerging technologies, economic forces, and competition. As a result, pharmaceutical scientists are forced to respond to the growing number of samples with new strategies for analysis. One strategy which we have found successful is the expanded role of LC/MS. Despite growing awareness of the technique, application of LC/MS is often reserved for "special" studies using unique methods developed for each project. This is due, in part, to the highly regulated nature of the pharmaceutical industry and common use of traditional experimental paradigms. The expanded role of LC/MS has been examined, as part of a "front-line" analytical methodology to accelerate drug development experimental paradigms.

This has been accomplished through the development of a standard protocol for profiling front-line research samples using electrospray LC/MS, which may be applied to a majority of pharmaceutical research and development projects. This standard protocol approach provides rapid "front-line" profiling of components in mixtures from sample types commonly encountered throughout pharmaceutical research and development. This standard profiling approach takes advantage of electrospray characteristics (i.e., high sensitivity, reliable molecular ion formation, amenability to LC/MS, front end for MS/MS) to accelerate the analysis of many samples from various areas of pharmaceutical research for which "traditional" experimental paradigms involving scale-up, isolation, and individual spectroscopic analysis are used. Our approach is useful for profiling impurities, metabolites, degradants, natural products, and synthetic products.

Our standard LC/MS profile protocol utilizes a tandem quadrupole mass spectrometer (PE-SCIEX API III), gradient HPLC with diode array UV detector (HP1090), and a C_{18} HPLC column (Zorbax, 2 mmX150 mmX 5 µM) gradient programmed from 10% ACN/90% Buffer (2 mM NH_4OAc) to 90% ACN/10% Buffer in 30 min. at 200 µL/min). This integrated on-line system provides the following analytical data:

1) LC/UV provides t_R and UV spectrum of components to construct a library of components and permit matching to a library of previously elucidated analogs
2) LC/MS provides MW of components and further library comparisons or cataloging
3) LC/MS/MS provides substructural detail for structure elucidation of novel compounds.

Traditional drug development experimental paradigms for metabolites, impurities, degradants and natural products can be very expensive for an organization and delay progress on projects. A generalized scheme for the elucidation of structures in these areas involves many of the following stages: synthesis of radiolabeled drug, sample acquisition (biological fluid/bulk drug/active culture), HPLC/UV profile, extraction, fraction collection, scintillation detection, scale up batch size, fractionation, and spectroscopic analysis of each component. In contrast, front line LC/MS profiling involves only: use of small quantities of standard drug or sample

from biological fluid/bulk drug/active culture, LC/UV/MS, and LC/MS/MS. The advantages of this streamlined scheme can be illustrated by the following resource comparison:

	Traditional	LC/MS Profiling
Radiolabeled Drug	[1 month]	–
Biological Dosing	[4 hr]	[4 hr]
HPLC/UV Profile	[2 hr]	–
Extract/Prepare	[2 hr]	[0-2 hr]
Fraction Collection	[4 hr]	–
Scintillation Detection	[4 hr]	–
Scale Up	[24-40 hr]	–
Fractionate	[24 hr]	–
Analyze Each Compound	[6-24 hr]	[4-10 hr]
TOTAL TIME	[40-280 hr]	[8-14 hr]
COST	[$6,000-$35,000]	[$2,000]

The type of information obtained from this standard LC/MS protocol approach is illustrated in the results, in which impurities of paclitaxel (the active in TAXOL®) were rapidly profiled.

TAXOL® PROCESS SAMPLE

LC/MS PROFILE

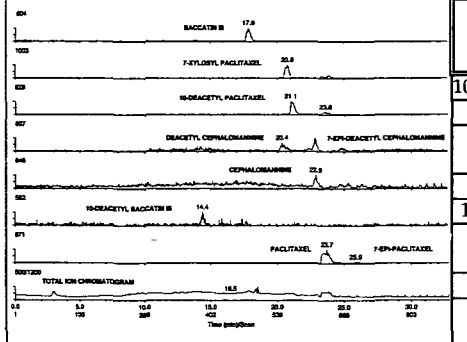

PROFILE LIBRARY OF TAXOL® SAMPLE

Proposed Structure	Relative Retention Time	Molecular Weight
10-Deacetyl Baccatin III	0.61	544
Baccatin III	0.76	586
10-Deacetyl Cephalomannine	0.86	789
7-Xylosyl Paclitaxel	0.88	985
10-Deacetyl Paclitaxel	0.89	811
7-Epi-10-Deacetyl Cephalomannine	0.96	789
Cephalomannine	0.97	831
7-Epi-10-Deacetyl Paclitaxel	0.99	811
7-Epi-Xylosyl Paclitaxel	1.0	985
Paclitaxel	1.0	853
7-Epi-Paclitaxel	1.09	853

Standard LC/MS profiling can be used as a front-line method for a variety of samples. The LC/MS profiling paradigm saves 50% to 90% of cost and wait for analyses. A "library" of components is created and includes: hplc t_R, UV spectrum, molecular weight, substructures, and proposed structures of components. This "library" is transferable throughout drug development stages of discovery, development, and manufacturing. This method, cost/time savings, and transferable libraries provide support for the accelerated rate of drug development.

TITLE: EXAMINATION OF CHIRAL PURITY BY HPLC-MS

D. S. Richards, S. M. Davidson, R. M. Holt, F. S. Pullen
Pfizer Central Research, Sandwich, Kent, UK.

An increasing number of compounds of therapeutic interest are being developed as single enantiomers. Therefore the need to determine chiral purity is becoming more important within the pharmaceutical industry.

Confirmation of chiral purity is usually carried out via HPLC separation. However, the mobile phases required to effect good separation, using polar organic phase chromatography on cyclodextrin columns, present the chromatographer with a number of problems. The major problem is the HPLC detection of compounds which have UV chromophores absorbing below the UV cut-off wavelength of the mobile phase(~240nm). The use of refractive index detectors is possible, but they often lack the necessary sensitivity and specificity. We have investigated the use of LC-MS techniques to overcome this problem.

The mobile phase composition is a critical factor in maintaining the enantiomeric selectivity of cyclodextrin columns in the polar organic mode and cannot be compromised to suit the mass spectrometry; consequently, our options were somewhat restricted. However after exploring a number of different approaches, a robust and reliable, analytical, chiral LC-MS system has been developed.

Coumachlor (p-chlorowarfarin) has no known pharmaceutical value but is used as an internal standard in the analysis of the rodenticide warfarin, and it serves as a good example of the method described.

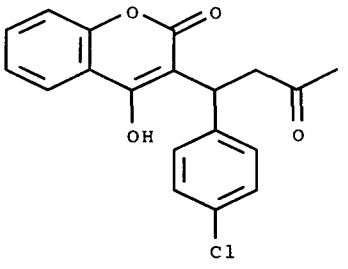

Coumachlor (p-chlorowarfarin)

The mobile phase required for separation (ref 1) is acetonitrile, acetic acid, triethylamine (998.25 : 1 : 0.75), which effectively prevents UV detection below 240nm. Unfortunately the λmax for Coumachlor is 207nm. However, this compound has a relative molecular mass (RMM) of 342 Da. and a distinctive isotope pattern.

In the presence of large quantities of triethylamine and acetic acid, particle-beam is an ineffective inlet system and soft ionisation techniques such as thermospray proved to be inefficient. It was found that plasmaspray mass spectrometry (PSP-MS), often considered as a fragmentation device for thermospray, is able to provide both the sensitivity and selectivity required for this work. Chromatograms for mass and UV detection are shown in figure 1

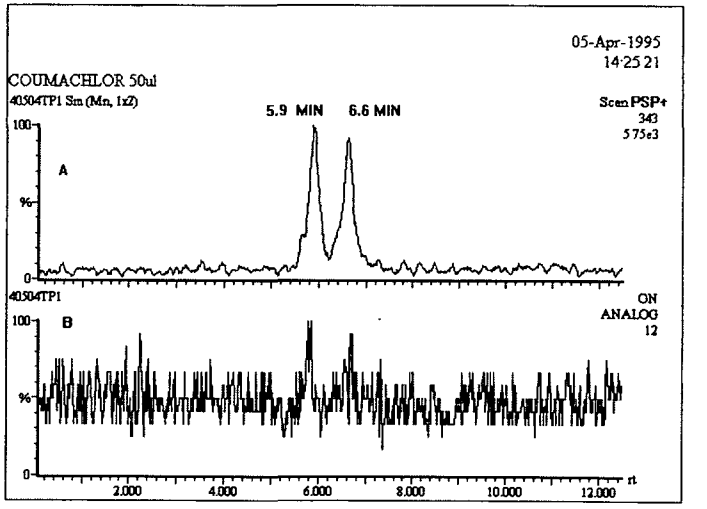

Figure 1: Chromatograms for A the $(M+H)^+$ ion at m/z = 343 and B the UV trace at 207nm.

The mass chromatogram above clearly shows a superiority in signal to noise ratio with respect to the UV chromatogram at the λmax for Coumachlor. Although setting up the system requires considerable expertise the method itself proved sufficiently robust that we were able to carry out the analyses and obtain the data presented using our 'open-access' LC-MS system (ref 2).

References

(1)Technicol Ltd., Cyclobond Chiral HPLC Seminar Workshop, 1993.
(2) F.S.Pullen & D.S.Richards. Rapid Communications in Mass Spectrometry, **9**, p188-90, 1995.

TP063

Quantitative Aspects of LC Peak Purity by Electrospray Ionisation/Mass Spectrometry (ESI/MS)

Duncan K. Bryant
SmithKline Beecham Pharmaceuticals, Old Powder Mills, Tonbridge, Kent TN11 9AN, United Kingdom.

When validating chromatographic methods and determining analyte purity, it is essential that the purity of the main chromatographic peak is established, particularly within the pharmaceutical environment. HPLC peak homogeneity can be determined by using multiple wavelength UV detection in conjunction with a number of chemometric manipulations such as principle component analysis (PCA) and factor analysis (FA). However, these methods require UV spectral differences between the main component and the coeluting impurity, a condition frequently not met for impurities closely related to the main component.

Mass spectrometry has been used to establish chromatographic peak homogeneity (1-3) and we have found IonSpray (nebulizer assisted electrospray) mass spectrometry to be particularly effective for analysis of HPLC peaks. Using our method, coeluting impurities can be observed down to a level of 0.01%. Clearly, it would be of great interest to be able to quantitate coeluting impurities observed by LC/MS. The objective of this study is therefore to see whether this can be achieved by comparing the responses for the coeluting impurity and the main component.

Mass spectrometry was performed on a Sciex API-III (Sciex, Toronto, Canada) triple quadrupole mass spectrometer using nebuliser assisted electrospray (IonSpray) as the ionisation technique. The structures of the two compounds used in this study are shown in the Scheme. The LC method was developed so that known impurites in ropinirole would coelute with ropinerole itself. The levels of SKF-96266-A in ropinirole were measured by comparing the mass spectral peak abundances for the two protonated molecules. The mass spectrometer was set up so that the low orifice voltage used (+50V) caused very little fragmentation to occur in the source and virtually all of the analyte ions that were detected were protonated molecules (3). A typical spectrum is shown in Figure 1 and was obtained by summing the spectra acquired across the main LC peak. The experiment was performed on solutions of 10^{-4}M ropinirole which contained SKF-96266-A at levels of 0.01, 0.02, 0.05, 0.1, 0.2, 0.5, and 1.0% w/w. The batch of ropinirole used was known to contain 0.01% w/w (by HPLC assay) of SKF-96266-A prior to spiking. Were the coeluting impurity to have an unknown structure it would be assumed that the relative response factor for the impurity is the same as the main component. A relative response factor of 1.0 has been used in this study for SKF-96266-A and ropinirole, and indeed the electrospray responses for ropinirole and SKF-96266-A are very similar. It is reasonable to assume that most impurities likely to coelute with the drug substance would have similar structures to the main component and that their mass spectral response would also be similar.

In order to observe the protonated molecule of the coeluting impurity at low levels, the protonated molecule of the main component had to be overloaded, thus preventing direct comparison of their responses. In many cases the carbon 13 peak of the major component was also overloaded to some degree, mainly due to the small dynamic range of the detector on the API-III. To overcome this, the reponses for the protonated molecule of the impurity and the $[M+3+H]^+$ ion (molecules containing three carbon 13 atoms) of the main component were compared in order to determine the levels of the impurity (Figure 1). It was assumed that the relative abundance of the $[M+3+H]^+$ peak of rropinirole was 0.133% that of the carbon 12 peak ($[M+H]^+$. Using this method, the responses for the protonated molecules of ropinirole and SKF-96266-A are shown graphically in Figure 2. It can be seen that a linear response is obtained with moderate precision (r^2=0.993) and good accuracy.

References

1. Roach,L.; Guilhaus,M. *Org Mass Spectrom.*, **1992**, *27*, 1071-1076.
2. Lincoln,D.; Fell,A.F.; Anderson,N.H.; England,D. *J. Pharmaceut. Biomed. Anal.*, **1992**, *10*, 837-844.
3. Bryant,D.K.; Kingswood,M.D.; Belenguer,A. *Proceedings of the 42nd ASMS Conference on Mass Spectrometry and Allied Topics*, Chicago, Illinois, p. 607, **1994**.

Scheme. Compounds Used in This Study.

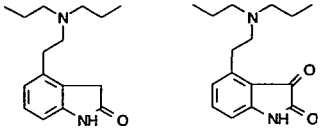

SKF-101468 Ropinirole SKF-96266

Figure 1. LC/MS Spectrum of SKF-101468-A Spiked with 0.2% w/w SKF-96266-A.

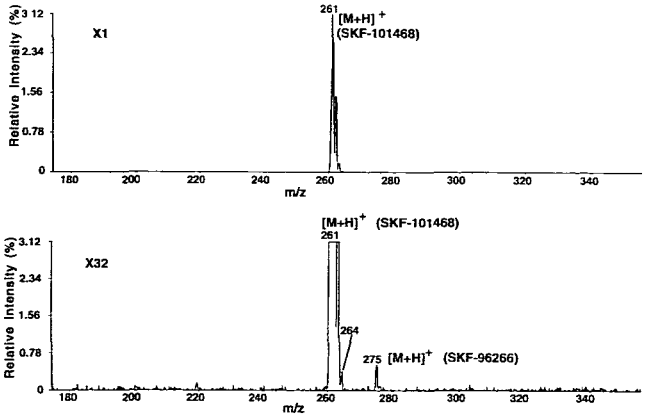

Figure 2. LC/ESI/MS Response for Coeluting Impurity, SKF-96266-A, in Ropinirole (SKF-101468-A).

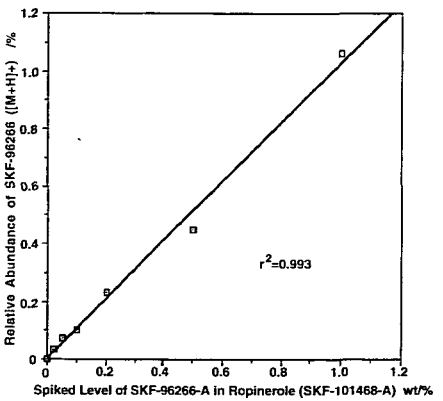

Data Dependent Automated MS/MS Switching Methods for Routine LC/MS/MS.

Iain Mylchreest, Clay Campbell, Kevin Wheeler and Michael Wakefield.
Finnigan MAT, 355 River Oaks Parkway, San Jose, CA 95134

Data dependent automated LC/MS/MS is a powerful analytical tool for the analysis of protein digests and other complex biological mixtures, providing amino acid sequences and other structural information with minimal analyst interaction with the experimental procedures. Data dependency can also be applied for the rapid screening of complex mixtures for target compound analysis using precursor and neutral loss scan modes.

Three methods to automatically switch between MS and MS/MS modes during a chromatographic run, and scan to scan are described. First, simple retention time windows can be used and multiple experiments can be performed across the eluting chromatographic peaks. For useful MS/MS spectra of peptides the optimal collision energy is not often known, therefore in a qualitative method the energy can be varied from scan to scan through three or more energies. The resultant spectrum gives an average energy fragmentation pattern which usually gives a more complete sequence than selecting a single energy across the whole peak. In the second method the mass spectrometer's data system can make decisions independent of retention times, based upon the appearance of an ion that meets a predefined intensity, signal to noise or peakwidth, comparing it with a list of ions that the analyst wishes to perform MS/MS experiments on. The instrument then decides which ion to perform the experiment on, turns on the CID gas and sets up the experiment based upon the data it has just acquired. The flow of this 'Data dependent method' is shown in figure 1. Figure 2 shows the RIC of a separation of five angiotensins in a data dependent MS/MS experiment The resultant individual collision energy CID spectra from -15, -20 and -25 eV for product ions of m/z 442 are shown in figure 3. The inverse of this experiment can also be performed, where MS/MS is carried out on all ions not in the main predefined list.

In the third method, described as 'monitor all ions', the data system can switch between scan modes based on the increase in ion signal when a peak elutes, checking for variables such as signal to noise in real time. This method requires no information about mass or retention time, but indiscriminately performs MS/MS on the base peak in a spectrum. An example of this is shown in Figure 4 for a tryptic digest of myoglobin. Each peak in the trace is a data dependent MS/MS experiment, demonstrating the potential for unattended peptide sequencing, and automated protein database searching.

The technique can also be used to screen for target compound classes and automatically collect full scan product ion spectra, when a predefined precursor ion is detected. This can be applied to the analysis of drug metabolites or post translational modifications, such as glycosylations. This method has been successfully applied to a neutral loss experiments, when screening for phosphorylations on peptides and drug metabolite functionality's in complex synthetic and natural product mixtures.

43rd ASMS Conference on Mass Spectrometry and Allied Topics

Figure 1: Automated MS/MS Switching by the Data-Dependent method

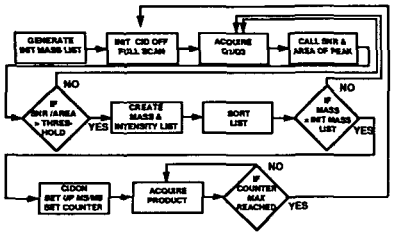

Figure 2: Automated LC/MS/MS analysis of a mixture of angiotensins using the "Data Dependent" method

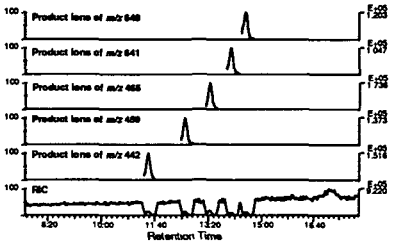

Figure 3: Effect of variable/rotating collision energy on the product ion spectra of $[M+2H]^{2+}$ at *m/z* 442 for angiotensin peak #1 (RVYVHPI)

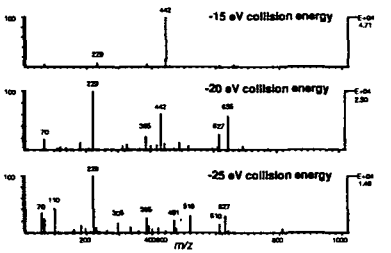

Figure 4: Auto CID of a Myoglobin digest using 'Monitor all ions' method with reference UV chromatogram for correlation

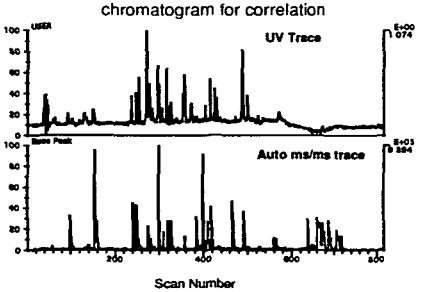

Comparison of Electrospray and Thermospray LC/MS for Analysis of Small, Chemical-Weapons-Related Molecules

William R. Creasy
EAI Corporation/AMC Treaty Laboratory Division
1308 Continental Drive, Suite J
Abingdon, MD 21009

The Chemical Weapons Convention, the treaty to ban chemical weapons, requires the detection of degradation products of chemical weapons agents in environmental samples for its verification. As part of the development of methods for this purpose, a comparison was done between electrospray and thermospray ionization for LC/MS analysis of some typical compounds in aqueous samples. The compounds include thiodiglycol (TDG) and thiodiglycol sulfoxide (TDGO), degradation products of mustard gas, and O-pinacolyl methylphosphonic acid (PMPA) and diisopropyl methylphosphonate (DIMP), related to nerve agents. These compounds have been found to be easily detected with thermospray ionization.

The thermospray equipment was the standard Hewlett-Packard system for the HP 5989A MS Engine. The electrospray system was sold by HP but manufactured by Analytica of Branford, Inc. The source was designed for high flow applications by using a nozzle that incorporated a drying gas flow coaxial to the liquid capillary, which assisted in the liquid nebulization. A 50 ppm PPG solution in 0.1 M ammonium acetate and 75/25 water/methanol was used for calibration and tuning of both sources The analyses were done on two separate MS Engines in the same lab

LC was done using a C_{18} (ODS Hypersil) column. The mobile phase was 100% 0.1 M ammonium acetate in water for TDG and TDGO. It was 60/40 water/methanol, 0.06 M ammonium acetate, for DIMP and PMPA. Flow rates were 0.2 ml/min with a 2.1 mm I.D. column for electrospray, and 1.0 ml/min with a 4.6 mm I.D. column for thermospray. The lower flow rates were used for electrospray to improve the performance, but no attempt was made to use smaller (1 mm or less) columns. No post-column addition of solvents was used.

The LC and MS source conditions were chosen to be appropriate for routine, general analysis of samples containing unknown compounds. As a result, the tuning of the source with a standard solution of the particular compounds of interest was not done. Instead, tuning was done using the PPG solution. This solution is recommended by Hewlett-Packard for tuning the thermospray source, and an autotune program is available for this purpose. It was also found to give good ion signal with electrospray. Since all PPG ions are singly charged, it is likely that the electrospray tuning conditions for PPG are more representative of the analytes of interest than a multiply-charged protein would be. Only the positive ion mode was used.

Results indicate that for these analytes and these conditions, thermospray is more sensitive, more stable, and has less compound-dependent sensitivity variation than electrospray. With thermospray, all four compounds could be detected at the 1 to 5 ppm level with the mass spectrometer in scan mode, and at sub-ppm levels in SIM mode. Sensitivity to TDG and TDGO was particularly good, with sensitivity in SIM mode to 50 ppb (S/N=10:1).

For electrospray, in contrast, sensitivity was adequate for 1-10 ppm detection levels only for DIMP. A comparison of the extracted ion LC chromatograms is shown in Figure 1. The mass spectrum base peak for thermospray ionization is m/z 181, but for electrospray it is the protonated dimer at m/z 361. PMPA had detection limits at the 10-100 ppm level in the scan

mode. The sensitivity to TDG and TDGO was even worse, since there was unacceptable signal to noise for even 100 ppm solutions. It is interesting that the least polar, least water-soluble compound, DIMP, provided the greatest sensitivity. This observation suggests that the factor that limits ionization in these cases is likely to be the solubility of the analyte in the sprayed droplets, rather than its affinity for charge.

Further improvements in the operating conditions or in the electrospray source design may improve the performance. Work is planned to compare the Analytica source to a Finnegan electrospray source.

This work was performed at and funded by the AMC Treaty Laboratory, ERDEC, Aberdeen Proving Ground, Edgewood Area, MD.

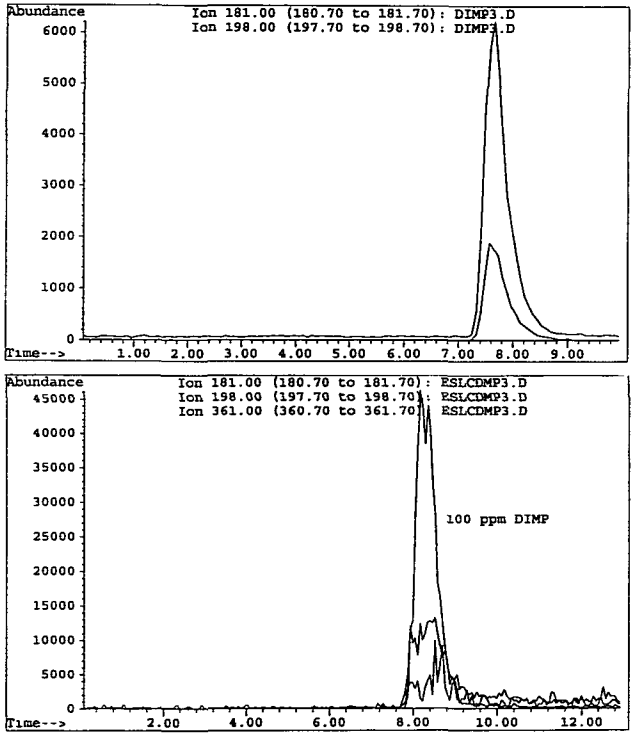

Fig. 1: Extracted ion chromatograms of DIMP with thermospray (top) and electrospray (bottom).

Enhanced Sensitivity LC/MS Using Low Resolution Quadrupole Mass Analysis

Dodsworth, D. W., Alexander, A. J., and Blackledge, J. A.
Bristol-Myers Squibb Co., Inc.
Pharmaceutical Research Institute
P.O. Box 4755
Syracuse, NY 13221-4755

LC/MS, using a quadrupole mass analyzer, is a well established technique in which the quadrupole mass analyzer is typically run at a resolution that maximizes sensitivity, yet provides adequate resolution of the isotope ions. This is in contrast to the low Q1 resolution used in the triple quadrupole experiment, where good parent ion sensitivity is essential. LC/MS analysis and identification of impurities and degradation products at less than 0.2% by area is frequently required for pharmaceutical products, and is a challenging analytical problem. Frequently, due to low ion intensities, only molecular weight information is obtained.

Using a Fisions Instruments VG Quattro triple stage quadrupole mass spectrometer, electrospray (ESI) LC/MS experiments were performed using Q1 resolutions of ca. 0.6 ("Unit Mass") to 5.0 ("Open") Da. half height peak width and data were acquired in continuum mode, thus allowing spectral averaging. The "Open" resolution condition resulted in ion signals that were minimally ca. 15 fold higher than those obtained by operation under "unit mass" resolution (Figure 1). This increase in ion abundance also resulted in qualitatively better spectra for the low level analytes, particularly when data was acquired using ESI in-source fragmentation. Mass accuracy problems (nominal mass rounding errors) are not evident until the mass of the analyte exceeded 1200 Da. or the elemental composition of the analyte differed greatly from that of the polyethylene glycol reference compound used for calibration (ie. In the case of CI containing compounds).

Figure 2 illustrates the theoretical peak shape change of an analyte ion as compared to a calibrant ion. The decrease in resolution results in a shift of the unresolved peak top to higher mass. The value of this positive mass shift is very similar for both the sample and calibrant. That is, any shift in the peak top of the analyte ion arising from the isotope contribution will be compensated by a corresponding shift in the calibration ion. This trend is also observed in analytes that contain one or two chlorine atoms. In this case, the shift to higher mass is greater, however if all mass defect values of 0.8 Da. or less are rounded down to nominal unit mass values, the mass assignment of the ion remains correct.

Figure 1: Comparison of "Open" vs. "Unit Mass" Resolution TIC's showing sensitivity enhancement.

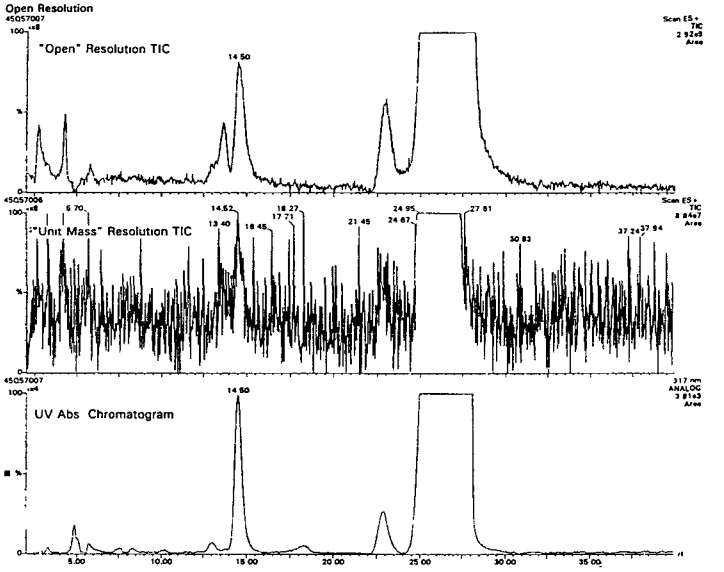

Figure 2: Effect of opening resolution on peak top assignment.

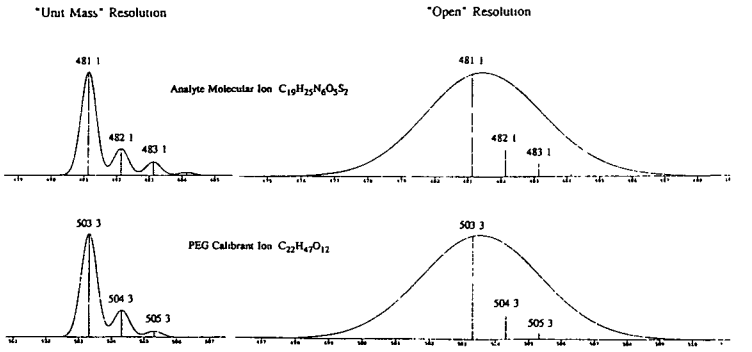

Electrospray Interface for Submicroliter LC/MS Analyses

Michael T. Davis, Douglas C. Stahl and Terry D. Lee
Beckman Research Institute of the City of Hope, Duarte, CA 91010

An ultra-low flow microcapillary HPLC system designed for the gradient elution of peptide and protein samples at nanoliter/minute flowrates has been coupled to a Finnigan TSQ 700 mass spectrometer via a simple sheathless electrospray interface. The coupled capillary HPLC - Microspray interface was optimized for column flowrates as low as 100 to 200 nanoliters/minute and UV detection of the column effluent was retained without loss of resolution in the mass spectrometer. True high performance LC was achieved using a packed 100 µm reverse-phase column coupled to a 100 µm on-column flowcell. Peak resolution was maintained throughout the system using 20 µm ID transfer lines from the column to the detector and from the detector to the microspray interface.

The microspray needle assembly utilized a flame drawn 150 µm ID x 350 µm OD FSC approximately 5 cm in length. Capillary drawing was performed manually using a vertically suspended section of FSC to which a small weight (HPLC Tee, ca 30g) had been attached. The capillary was slowly heated to melting using the smallest "blue" flame attainable from a Micronox torch (Alltech Associates, Deerfield, IL), which was then quickly withdrawn once the capillary began to draw. All tips were drawn to separation. Tip patency was confirmed by immersion of the tip into a vial of methanol followed by visual inspection for drawn solvent using a 8x ocular loop. A discontinuous 150 µm OD x 25 µm ID capillary was placed within the 150 µm ID needle to both minimize the deadvolume and retain a hydrophilic PVDF membrane filter. The final assembly was easiest to perform under a dissecting microscope. The needle was connected to the LC transfer line via a 1/32" stainless steel capillary union which served as a liquid-metal interface for application of the necessary potential (0.5 to 1 Kv) to the sample stream. The precise positioning of the microspray needle relative to the sampling capillary of the mass spectrometer was controlled using a XYZ multi-axis positioner and observed in real time using a micro borescope/video imaging system.

Ultra low flow LC/ESI/MS analyses of a standard peptide map were performed using a City of Hope built microscale HPLC system which is distinguished by its use of a preformed gradient for column development (1). A full presentation of the design and operational characteristics of the LC system is scheduled for publication in the June issue of JASMS . The general construction and packing of the microcolumn and the fabrication of the on-column flowcell was as previously described (2).

Mass spectral analyses were performed on a Finnigan TSQ 700 quadrupole mass spectrometer equipped with a Finnigan electrospray source with the voltage interlock locked in the closed position for use with the microspray interface. Automatic MS/MS analyses were performed using real time automated analysis programs developed in our laboratory (refer to poster WPB 026 for details).

Analyses performed at the sub ten femtomole level suggest limits of detection for proteins and peptide digest mixtures within the attomole range. The reduced spectral background facilitated the acquisition of MS/MS sequence information using automated real time analysis procedures. The benefits of on-line capillary LC - Microspray analysis over the conventional electrospray methodology is evident in reduced spectral background, decreased sample consumption and enhanced sensitivity.

References

1. Stahl, D. C., Davis, M. T. and Lee, T. D. Proceedings of the 42nd ASMS Conference on Mass Spectrometry and Allied Topics, Chicago, Illinois, May 29 - June 3, 1994

2. Davis, M. T. and Lee, T. D. Protein Science 1992, 1, 935-944

43rd ASMS Conference on Mass Spectrometry and Allied Topics

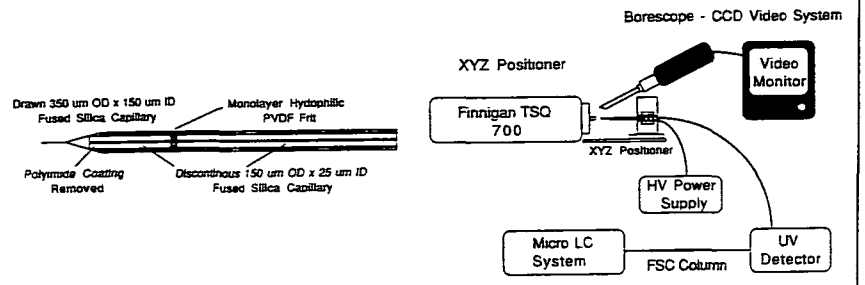

Two Femtomoles Cytochrome C Standard Digest Sheathless Microspray

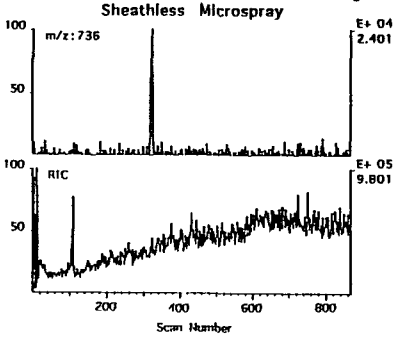

One Picomole Cytochrome C Standard Digest MS/MS Analysis - Sheathless Microspray

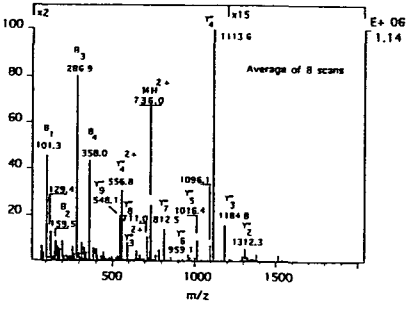

Two Femtomoles Cytochrome C Standard Digest Sheathless Microspray

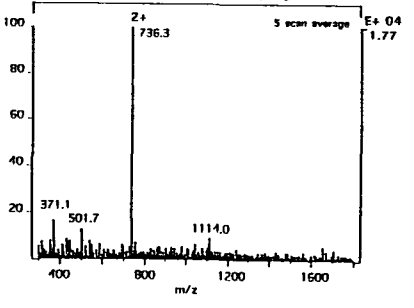

100 Femtomoles Cytochrome C Standard Digest MS/MS Analysis - Sheathless Microspray

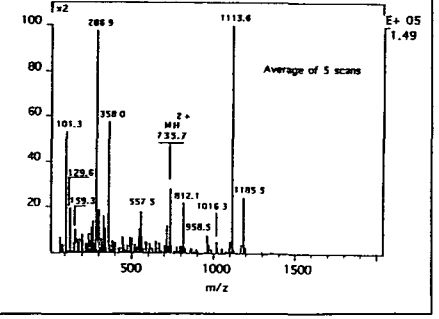

Separation and Analysis of Human Lens α-Crystallins by LC-ESIMS

Peiping Lin, Jean B. Smith and David L. Smith
Department of Chemistry, University of Nebraska - Lincoln, Lincoln, NE 68588

Crystallins are the structural proteins in the eye lens. Post-translatonal modification of crystallins may disrupt the order of crystallin packing and/or lead to protein aggregation resulting in opacification of the lens. This condition is commonly known as cataract. A series of separation methods have been developed and applied to isolate the crystallins according to differences in size (size exclusive chromatogaphy), hydrophobicity (reversed phase HPLC) and charge state (ion exchange and 2D-PAGE). In this study, post-translationally modified human α-crystallins were isolated and identified by combining these separation techniques with HPLC-ESIMS and other mass spectrometry methods shown in Fig. 1.

Two different HPLC-ESIMS systems were used to meet the requirements of 1) multi-step and 2) high sensitivity experiments. System 1 consists of a microbore reversed phase column and a post-column splitter which diverts 10% of the effluent to the ESIMS for molecular weight determination, and the other 90% to a UV detector and fraction collector Collected fractions were stored for use in subsequent experiments. System 2 consists of a capillary column directly-coupled to the ESIMS, permitting analysis of samples with higher sensitivity. After determining the molecular weight of modified protein, we identified the modification site of protein and confirmed the structure of modification by enzymatic digestion (peptide mapping example shown in Fig. 2), exact mass measurement and MS/MS.

The lens was homogenized in buffer consisting of 0.5M NaCl, 0.05M Tris, 0.001M EDTA, pH 7.4 and centrifuged at 15,000 *g* for 1h The supernantant was fractionated by Sephadex G-200 size exclusive chromatography (SEC). The α-crystallins from SEC were fractionated into αA and αB by reversed phase HPLC (RPHPLC). Isolated proteins were further fractionated by anion exchange (IEX) on a Mono Q column using 6M urea, 0.01M Bis-tris, pH 6.2 for αA, and 6M urea, 0.01M Tris, pH 7.5 for αB as buffers A, respectively. The proteins were eluted with a linear gradient to 50% of buffer B (buffer A + 0.2M NaCl).

The HPLC-ESIMS analysis of desalted proteins was performed on a VG Fisons Platform quadropole MS. The HPLC system consisted of Gilson pumps, an Upchurch low volumn mixing tee and a Rheodyne 8125 injector. Microbore separations were achieved using a 50x1mm C8 column, 50μl/min flow rate, and a post-column flow splitter with ratio of 1 (MS) to 9 (UV detector). Capillary separations were accomplished using a 50x0.3mm C8 column at a flow rate of 5μl/min. A splitter located before the injector was used to split the flow rate of 50μl/min from pumps by clamp pressure on the waste side outlet. Exact mass and MS/MS analyses of the enzymatic fragments were performed using a VG Fisons Autospec high resolution mass spectrometer equipped with an orthogonal acceleration TOF mass analyzer.

HPLC-ESIMS offers a fast and sensitive method in microanalysis of minor components present in the lens crystallins. In addition, it also minimizes the sample loss and contamination by reducing the sample handling steps. The combination of a variety of chromatographic separation techniques, including SEC, RPHPLC, IEX and 2D-PAGE, together with MS techniques, involving HPLC-ESIMS, peptide mapping, exact mass and MS/MS, proves to be useful in the determination of the post-translational modifications in human lens proteins.

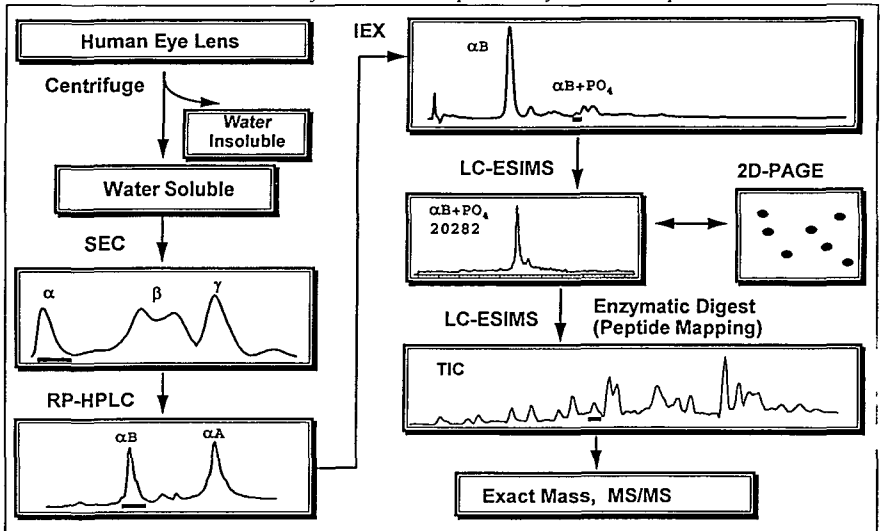

Fig. 1 Steps for purification and analysis of water soluble crystallins of human lens.

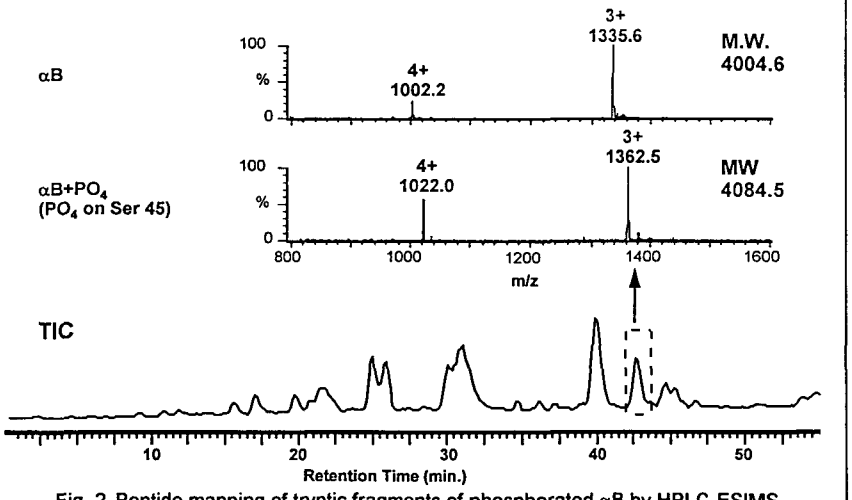

Fig. 2 Peptide mapping of tryptic fragments of phosphorated αB by HPLC-ESIMS.

Preparative Applications of Microcapillary HPLC for Mass Spectrometry

*Murray Hackett[1], Ronald C. Hendrickson[1], Rocco Falchetto[1], Carthene B. Walker[1], Jeffrey Shabanowitz[1], Donald F. Hunt[1,2]

Departments of Chemistry[1] and Pathology[2], University of Virginia, Charlottesville, VA 22901

Methods for collecting 50 to 500 nanoliter volumes during preparative microcapillary HPLC fractionation of complex peptide mixtures are described, with reference to further analysis by mass spectrometry. For MALDI-TOF analysis, fractions were collected directly into unmodified disposable 1 μL polyethylene micropipet tips (Fisher Cat. Num. 21-199-9). For triple quadrupole electrospray ionization microcapillary LC/MS/MS, fractions were collected in short (less than 3 cm) lengths of teflon tubing with the i.d. (typically 180 μm) matched to the o.d. of the microcapillary column used on-line with the mass spectrometer. The fractions were loaded into the reversed-phase analytical capillary column using N_2 pressure. The point of the exercise was to scale down the multiple stages of HPLC such that the total sample consumed was less than 5 pmol. These methods were applied to the study of bacterial exotoxins, insect neuropeptides, alcohol dehydrogenase N-termini and other projects which required multi-stage separations with minimal sample consumption. This approach allows the scaling down and application of HPLC methods which may not be easily compatible with LC/MS, but which offer chromatographic selectivity and (or) enhanced resolution not found using our standard reversed-phase microcapillary HPLC conditions. *Preliminary results with known standards of angiotension 1 and acylated peptides derived* from adenylate cyclase toxin suggest that two stages of microcapillary HPLC can be performed on 100 fmol of peptide before S/N becomes too low to acquire an interpretable CAD spectrum, using the TSQ mass spectrometer.

At right: an off-line microcapillary HPLC fraction, about 100 nL, was collected in a 180 μm i.d. X 2 cm teflon capillary tube, and the sample loaded roughly 50 nL at a time directly on the analytical capillary column, using a bomb under N_2 pressure. This approach was used to generate the second dimension HPLC trace and main beam ESI mass spectrum (A), and the free acid CAD spectrum (B) of the doubly charged ion at *m/z* 614, confirming the sequence shown in panel B. Leu was distinguished from Ile based on the gene sequence, P. Glaser *et al., Mol. Microbio.* 1988, *2*, 19-30. LC/MS conditions used with the upgraded Finnigan TSQ 70 (Finnigan API-ESI interface) were routine reversed-phase binary gradient elution, using a packed column length of 12 cm (PLRP-S 4000, Polymer Labs, Amherst, MA), 190 μm o.d., 75 μm i.d., 12 min gradient from 0-80% B, solvent A, 1% acetic acid, solvent B, neat acetonitrile, 400:1 precolumn split (solvent only). The flow rate measured at the capillary column at 0% B was 0.5 μL/min.

43rd ASMS Conference on Mass Spectrometry and Allied Topics

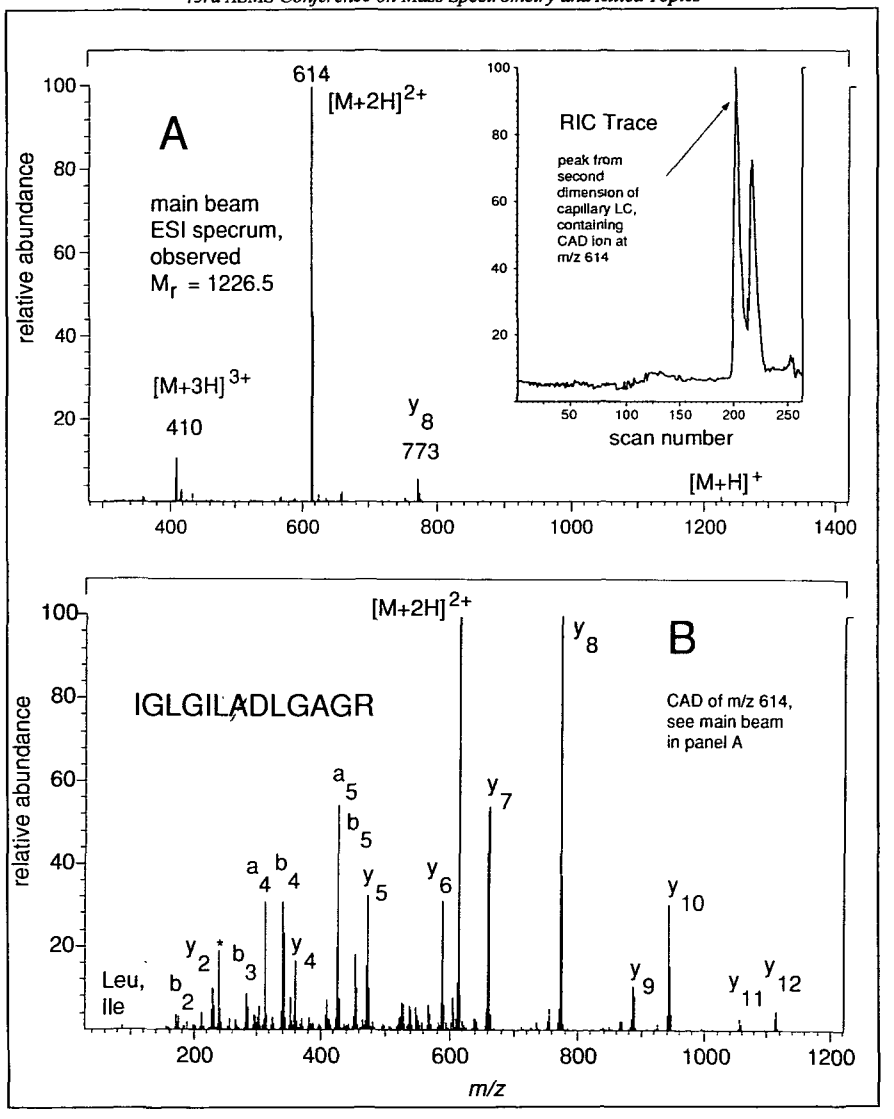

Integrated Multidimensional LC-MS and LC-MS/MS Analysis for Protein Sequencing and Mapping

Frank Hsieh, HongQi Wang, Chris Elicone, George Tarr, Fred Regnier, and Stephen Martin
PerSeptive Biosystems Inc., 500 Old Connecticut Path, Framingham, MA 01701

Multiple manual manipulations of small amounts of samples characteristically give poor sample recovery, increase the probability of contamination, and make it more difficult to analyze large numbers of samples. In this study, manual transfers were eliminated; i.e. once the sample was introduced into the multi-dimensional LC-MS system it would be automatically carried through all steps of the analysis to identification. This approach shows a wide ranged applications in pharmaceutical and biotechnological industry.

A novel integrated tandem chromatography-tandem mass spectrometry system (5 LC -MS, Figure 1) is used for protein sequencing and mapping. The antigen protein (normal or sickle-cell hemoglobin) is sequentially i) purified from the human serum by immunoaffinity perfusion chromatography using the immobilized anti-hemoglobin antibody (ImmunoDetection Cartridge, PerSeptive Biosystems) , ii) Hemoglobins were eluted with 12 mM HCl and neutralized with 10mM NH_4OAc (pH 7.5) in the buffer exchange column, i.e., the mixed-bed perfusion anion and cation exchange column (PerSeptive), iii) antigens are flow through an immobilized trypsin bed column (Porozyme, PerSeptive) in 5 minutes, iv) captured and rapidly desalted in a dilute capture column (PerSeptive), v) the trypsin digest fractionated by reversed phase chromatography, and vi) the separated peptides are identified and sequenced by ion spray mass spectrometry and MS/MS.

Tandem chromatography using on-line immunoaffinity, ion exchange, immobilized enzyme, dilute capture, and reversed-phase columns were explored with mass spectrometry (LC/LC/LC/LC/LC-MS). The results show the 5 LC-MS of total ions between *m/z* 400 - 1500 of both Hb A0 and Hb S, respectively. The total ion chromatograms (TIC) of 5 LC-MS mapped well with the sequence of Hb A0 (Figure 2) and Hb S (Figure 3). In the comparison of the novel tandem LC-MS TIC, only one peak pair differs. The different tryptic peptides can be further sequenced by 5 LC-MS/MS. The tandem LC-tandem MS spectra between *m/z* 50 - 1000 show the peptide sequences are VHLTPEEK and VHLTPVEK for normal-cell Hb and sickle-cell Hb, respectively. The coupling of tandem chromatography and the tandem mass spectrometry has been shown to be a powerful combination technique to determine protein sequence rapidly, automatically, and accurately. This modern analytical technique will provide a unique and excellent tool for biochemical and biomedical studies.

The multi-dimensional LC-MS may be formatted into a capillary size resulting in significant enhancement in sensitivity with much less sample required. The results from capillary multi-dimensional LC-MS (proteins are flowed through capillary trypsin column in 2 minutes, eluted into the capillary RP column, and then identified by MS, m/z 500-1500) using gradient elution (100% 0.1% TFA to 50% 0.1% TFA+80% ACN) at 2 µL/min show the detection may down to 5 pMole hemoglobin.

The integration of multi-dimensional LC with the orthogonal electrospray time-of-flight MS (LC-ESI TOF MS) may be an alternative bioanalytical technique for biological study (Figure 4). ESI-TOF MS provides very fast data acquisition and good resolution simultaneously compared to a quadrupole MS which requires compromises between scan step size, dwell time, and mass range to be made.

5 LC - MS/MS Robotic Analysis

Immunoaffinity Column -> Buffer Exchange Column -> Enzyme Column -> Dilute Capture -> RP Column -> Mass Spectrometry

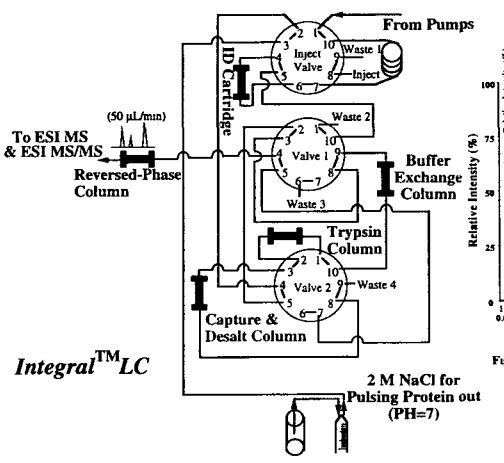

Figure 1 Automatic 5 LC-MS (ImmunoAffinity -> Buffer Exchange -> Enzyme -> Dilute Capture -> Reversed-Phase Column)

LC/LC/LC/LC/LC-MS (Normal Cell Hemoglobin)

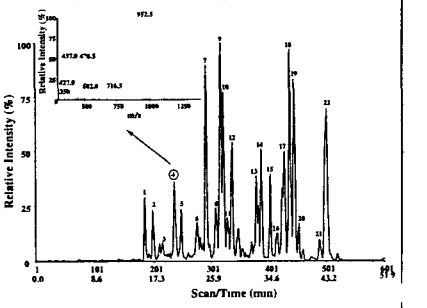

Figure 1 TIC of the 5 LC-MS for normal cell hemoglobin (Hb A0)

LC/LC/LC/LC/LC-MS (Sickle Cell Hemoglobin)

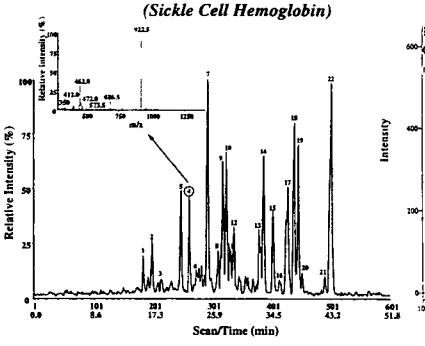

Figure 3 TIC of the 5 LC-MS for sickle cell hemoglobin (Hb S)

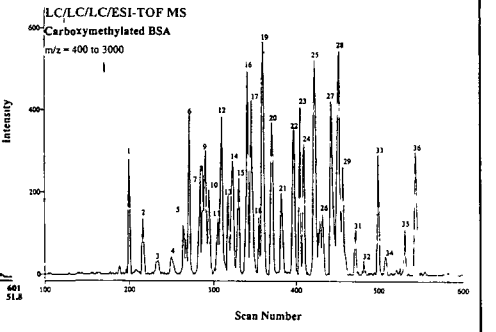

Figure 4: TIC of the 3 LC-ESI TOF MS for carbomethylated BSA.

The Effect of Column Diameter on Sensitivity for the Analysis of Peptide Mixtures by LC-ESI/MS

B. L. Ackermann, S. M. Fields, B. T. Regg, and T. A. Dourdeville*
Marion Merrell Dow Research Institute, Cincinnati, OH 45215
*Waters Chromatography, Milford, MA 01757

The concentration dependence of ESI has several implications for LC/MS operation. Of primary importance is the increase in sensitivity gained through the use of smaller bore columns, which due to operation at reduced flow rates, present more concentrated bands to the mass spectrometer for ESI/MS analysis. In this study, the sensitivity of four C18 columns was compared for the analysis of peptide mixtures in both the MS and MS/MS modes of operation. The four columns types examined were analytical bore (4.6 mm), narrow bore (2.1 mm), microbore (1.0 mm) and packed capillary (0.32 mm). Because concentration enrichment varies as the inverse of the square of the column diameter, the relative response for the four columns should be 1 : 5 : 21 : 207, respectively. In practice, the observed ESI signal intensity reflects several factors including the efficiency of the particular ESI interface used. As one would not expect the efficiency to remain constant over a wide range of flow rate (i.e., 1 to 1000 µL/min), an investigation of sensitivity vs. column diameter allows for a practical understanding of the performance for a given ESI interface. This work represents a study undertaken to evaluate an ESI interface based on a "heated capillary" design employing nebulization assistance.

The instrument used in this study was a Finnigan MAT TSQ 700 triple quadrupole equipped with a Finnigan ESI interface. Two peptide mixtures were examined: a test mixture of 7 synthetic peptides and the tryptic digest of horse apomyoglobin. Except for the packed capillary column, gradients were formed using a Waters 625 LC system. A Waters R&D prototype µLC system, operated at 5 µL/min, was used for packed capillary work.

Figure 1 compares the observed vs. predicted sensitivity enhancement obtained for the synthetic peptide mix at the 250 pmol level. For each column the data are expressed as a ratio relative to the performance of the analytical bore column operated at 1 mL/min. In each case, the overall enhancement factor represents an average of the individual factors determined for the 7 peptides. The trend displayed in Figure 1 was corroborated by a similar comparison of the 4 columns using 100 pmol of the tryptic digest of horse apomyoglobin. In this investigation, 5 representative tryptic fragments were considered and the results obtained were almost identical to the data in Figure 1 (results not shown). Although superior sensitivity was obtained by the use of smaller bore columns, the data in Figures 1 reveal that, the full measure of enhancement was not realized for the microbore (1.0 mm) or the packed capillary column (0.32 mm). A probable explanation for this outcome is the expected variation in interface performance at the different chromatographic flow rates used. To investigate this phenomenon, a post-column flow splitting experiment was performed to vary the flow introduced to the ESI interface while keeping the concentration fixed. The data from this experiment are plotted in Figure 2. Essentially, no change in performance was observed up to a split ratio of 5:1; however, as the flow to the MS was lowered to 50 µL/min or less, a significant degradation in response was observed. The observation that response at 10

µL/min could be improved through the co-introduction of 2-methoxyethanol suggests that the spray conditions at low flow rates are less than optimal.

These and other data acquired in this study enable recommendations to be made concerning column selection for the analysis of peptide mixtures: (1) analytical bore columns should only be used when high capacity needed, (2) for the interface used, a post-column effluent split of up to 5:1 can be implemented without a decrease in sensitivity (allows majority of sample to be recovered), (3) packed capillary LC is recommended for all sample limited situations (< 100 pmol), (4) microbore LC (1.0 mm) is not recommended since the gain in sensitivity does not offset the need to use a modified HPLC system, (5) a liquid sheath is advised when performing packed capillary LC with the interface used in this study.

Figure 1

Average Sensitivity Enhancement for 7 Peptides (relative to analytical bore, 4.6 mm I.D.)

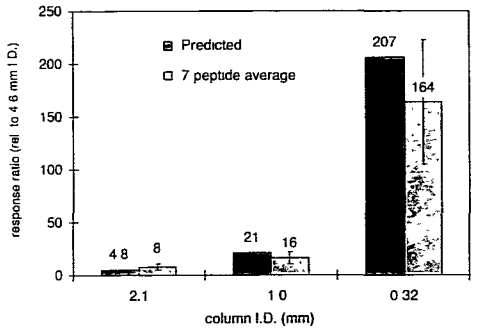

Figure 2

Effect of Post-Column Split on ESI/MS Signal

(250 pmol peptide test mixture injected onto 4.6 mm I.D. column)

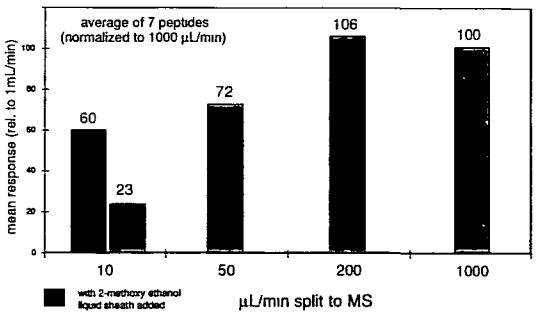

Enhancing API-MS Performance through Chromatography: Determination of Growth Hormone in Milk

Robert D. Voyksner* and Jeffrey Keever, Analytical and Chemical Sciences, Research Triangle Institute, P. O. Box 12194, Research Triangle Park, North Carolina 27709.

Introduction

Bioengineered human or bovine growth hormone (hGH or bGH) is now available from several sources. hGH has been approved by FDA for the treatment of hypopituitary dwarfism while bGH has been approved to increase milk production for cows. To better understand GH excretion and residue from metabolism as well as cases related to GH abuse or GH product labeling for food stuffs; fast, sensitive, and specific analytical methodology must be in place, namely LC/MS. Electrospray or Ion Spray MS [1-3] has been demonstrated to detect intact GH (molecule weight ~22,000) as well as various hydrolysis products at the sub-pmole level. In an effort to increase the resolution of the separation and decrease analysis time (often 30-60 minutes for LC) we propose to evaluate capillary perfusion LC/electrospray-MS for the determination of GH.

Results and Discussion

The development of an extraction and analysis method for hGH took into account the potential need for numerous analyses. Therefore, the simplicity and analysis time were parameters that required careful consideration, resulting in the proposed methodology of ultrafiltration clean-up and perfusion LC/electrospray-MS. The ultrafiltration approach employing a single stage filter provided >80% yield of hGH in milk. The addition of acetonitrile (1:1) to the sample was necessary to achieve these high yields. The evaluation of a 30K and 100K MWCO filter showed that hGH was partially retained on the 30K filter (18% yield) while the 100K filter resulted in a 89% yield. The separation of hGH on a perfusion column was developed using a gradient of 10-100% acetonitrile in water containing 0.1% TFA in 7 min., which resulted in a retention time of hGH of about 6.4 min. The electrospray mass spectrum of hGH peak exhibited a multiple ion cluster ranged from 13 to 20 charges on the protein. Deconvolution of this multiple charged cluster resulted in a measured molecular weight of 22,126.4, less than 0.006% error from the literature value of 22125.

To achieve the best sensitivity both selected ion monitoring for the MS and on-column concentrations were employed. The MS was set to monitor the three most intense ions for GH (+18, +17, +16 ions), each for 100 ms. Secondly due to the hydrophobic nature of GH, injection of 50-100 µL could be made on the 0.32 mm i.d. perfusion column in the initial mobile phase of the gradient (90% water), without significant peak broadening. Using these approaches the linearity and detection limits of GH spiked in milk was evaluated. The linear correlation coefficient for the six point GH calibration ranging from 0.1 -100 pmoles/mL was 0.9987. The detection limits for the LC/MS method is presented in Figure 1 for GH in milk. A 0.05 pmole/mL sample (55 µL injected) could be detected, with no interferences from the milk matrix.

This methodology is capable of detecting ppb levels of hGH in milk, demonstrating the potential of performing LC/electrospray-MS for monitoring food products employing GH or for monitoring hGH levels. The speed, sensitivity, and specificity of the method is well suited for the potential numerous determinations at trace levels in a matrix.

Acknowledgements

The author would like to thank both Hewlett Packard and LC Packings for technical assistance and instrumentation to perform this work.

Literature Cited

1. C.M. Whitehouse, R.N. Dreyer, M. Yamashita and J.B. Fenn. Anal. Chem., 57 (1985) 675-679.
2. E.C. Huang, T. Wachs, J.J. Conboy, and J.D. Henion. Anal. Chem., 62(13) (1990) 713-725.
3. R.D. Smith, J.A. Loo, C. G. Edmonds, C.J. Barinaga and H.R. Udseth. Anal. Chem., 62 (1990) 882-899.

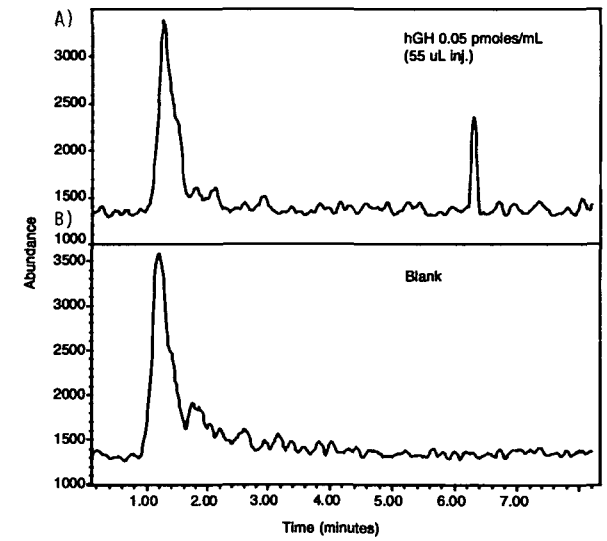

Figure 1. Perfusion LC/Electrospray-MS determination of hGH in milk using LC condition described for Figure 1. (A) Analysis of 0.05 pmoles/mL of hGH in milk (55 µL injected). (B) Blank milk 55 µL injected.

Effect of Salts and Trifluoroacetic Acid on Aerosol MALDI Ion Signal

Michelle D. Beeson, Xiaona Wei, and David H. Russell,

Laboratory for Biological Mass Spectrometry, Department of Chemistry

Texas A&M University, College Station, TX 77843

There is much interest in combining mass spectrometry with liquid separation techniques such as liquid chromatography and capillary electrophoresis. These techniques routinely use mobile phase modifiers, such as salts and acids, to yield a more efficient separation of analytes. Thus coupling the effluent of liquid chromatography or capillary electrophoresis with mass spectrometry brings these salts and acids into the mass spectrometer. Salts and acids in the chromatographic effluent interfere in the FAB and ESI ionization of analyte.[1] Alternatively, MALDI is reportedly tolerant of contaminants, including salts.[2] However, the typical MALDI experiment can not be easily coupled with liquid separation techniques for on-line analysis. We have developed an aerosol liquid introduction system combined with MALDI ionization[3] and have demonstrated its use in combination with HPLC.[4]

Using the aerosol MALDI technique, the matrix solution is delivered using a syringe pump to a mixing tee where it is mixed with the HPLC effluent and sprayed into the mass spectrometer as an aerosol. The aerosol first passes through a heated drying tube at 500 C to remove solvent and then ionization is performed at 355 nm using a frequency tripled Nd:YAG pulsed laser. The ions are orthogonally accelerated at 10 kV, mass separated in a 1.1 m flight tube, and are detected with a microchannel plate particle multiplier. Each laser pulse generates a mass spectrum of the HPLC effluent. The mass spectra are collected by a digital oscilloscope and downloaded to a microcomputer for analysis.[3,4]

The size of the aerosol particles created by aerosol MALDI is influenced by the solvent surface tension, viscosity, and density. Small aerosol particles are formed from solvents with low surface tension, low viscosity, and high density. These parameters also promote particle break-up: the same characteristics that yield small aerosol particles also promote particle break-up. During aerosol particle break-up, smaller particles are formed from the surface and large particles are formed from the interior of the initial aerosol particle. Because of hydrophobic interactions with the air, the hydrophobic species in the aerosol particles reside along the surface and the hydrophilic species remain in the interior of the aerosol particles. Thus the smaller particles are enriched in the *more* hydrophobic species and the larger particles contain the *less* hydrophobic species. If the solvent hydrophobicity is much less than that of the matrix and analyte, *or* if the matrix and analyte hydrophobicities are similar, the matrix and analyte are both forced to the surface of the aerosol particle. Matrix/analyte interactions can also be influenced by other species in the solution. For example, when trifluoroacetic acid (TFA) is present, the matrix/analyte interactions are increased, either by the TFA providing a hydrogen-bonding bridge between the matrix and analyte or through hydrophobic interactions[5] between the TFA/matrix/analyte, forcing the matrix and analyte to the surface of the aerosol particle. As a result, the small aerosol particles formed during break-up contain matrix and analyte, and yield increased ion signal. A decrease in ion signal is observed when the matrix and analyte are separated as a result of dissimilar hydrophobicities or because of an interference in matrix/analyte interactions. Decreased aerosol MALDI ion signal is observed at ammonium acetate,

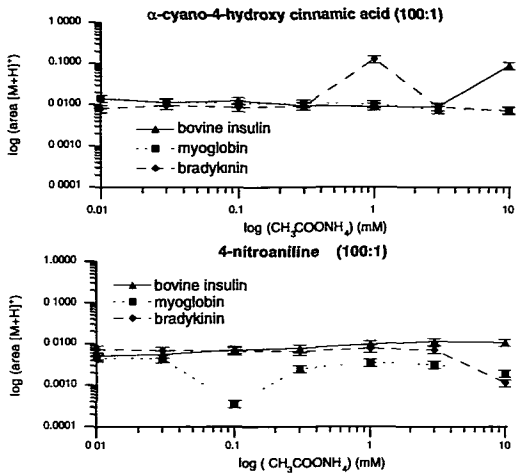

Figure 1. Log/log plots of the area of the $[M+H]^+$ ion signal as a function of the ammonium acetate concentration using the matrices a) α-cyano-4-hydroxy cinnamic acid and b) 4-nitroaniline. The laser energy was 13 mJ/pulse (160 MW/cm^2).

potassium dihydrogen phosphate, and sodium bicarbonate concentrations above 3 mM. Because solvent evaporation from the aerosol particles occurs rapidly,[3] the salt is forced into contact with either the matrix or analyte, separating the matrix and analyte. As more salt is added, more crystals of salt with matrix or analyte forms, further decreasing the ion signal. At concentrations below 3 mM, salts do not significantly affect the formation, redistribution, evaporation, or break-up of the aerosol particles.

The above model suggests that the salts typically used in chromatographic and electrophoretic separations do not interfere with aerosol MALDI ion formation at concentrations below 3 mM. This may be a result of the hydrophobicities of the analyte and matrix being different from that of salts, promoting the segregation of salt from the matrix and analyte. Using TFA in chromatographic and electrophoretic separations will promote the aerosol MALDI ion signal. Further work determining the effect of other organic acids is underway.

References:

1. a) M. A. Moseley, J. W. Jorgenson, J. Shabanowitz, D. F. Hunt, K. B. Tomer, *J. Am. Soc. Mass. Spectrom.*, **3**, 289 (1992). b) M. A. Moseley, L. J. Deterding, K. B. Tomer, J. W. Jorgenson, *J. Chromatogr.*, **516**, 167 (1990).
2. K. Strupat, M. Karas, F. Hillenkamp, *Int. J. Mass Spectrom. Ion Proc.*, **111**, 89 (1991).
3. K. K. Murray, D. H. Russell, *J. Am. Soc. Mass Spectrom.*, **5**, 1 (1994).
4. K. K. Murray, T. M. Lewis, M. D. Beeson, D. H. Russell, *Anal. Chem.*, **66**, 1601 (1994).
5. R. C. Beavis, J. N. Bridson, *J. Phys. D.*, **26**, 442 (1993).

Application of LC/IT/reTOF MS to Peptide Mapping and Drug Analysis

Mark G Qian, Li Liang, Ling He, and David M. Lubman

Department of Chemistry, The University of Michigan
Ann Arbor, MI 48109-1055

Introduction. The combination of liquid chromatography with mass spectrometry as a hyphenated technique (LC/MS) provides the possibility of taking advantage of both chromatography as a separation method and mass spectrometry as a highly selective and universal identification method In this presentation, the application of a new LC/MS system based upon an ion trap/reflectron time-of-flight mass spectrometer (IT/reTOF) is reported for fast peptide mapping and drug analysis. A unique data presentation method, which is based upon a 3-D topographic mapping of the mass spectra versus the chromatographic elution time, was successfully employed to exhibit the advantages of using the IT/reTOF mass spectrometer combined with liquid chromatography for both peptide mapping and for the analysis of small-molecular-weight drugs

Methods. A Star 9012 solvent delivery system (Varian Associates, Inc) was operated at a fixed flow rate of 200 µL/min for microbore HPLC separations. A prime/purge valve located immediately before the injection valve was used to split the mobile phase flow with a ratio of 3.1 Microbore separations were accomplished with a 1.0 mm x 15 mm C_{18} column (5 µm, 300 Å) at a flow rate of 50 µL/min Effluents exiting the columns were monitored by a Star 9050 (Varian Associates Inc.) variable wavelength UV detector at 214 nm. All separations were carried out with 0 1% TFA in water as solvent A and 0 09% TFA in 90/10 acetonitrile/water as solvent B A linear gradient was employed for the LC/MS separations beginning with 100% of A followed by ramping the B content to 80% in a period of 60 minutes The flow exiting the UV detector entered the ion spray source through a 50 cm length of 75 µm i d. x 175 µm o.d. fused silica capillary.

The quadrupole ion trap storage device used in this experiment was operated at a preset rf voltage and ions whose mass-to-charge ratios exceed a minimum cutoff value are trapped. The extraction of ions from the ion trap for TOF analysis is performed by turning off the rf voltage and applying a dc pulse on the exit endcap. This dc pulse is phase synchronized with the rf source The TOF of the extracted ion packets was measured on a high-speed transient recorder (Model 9845, Precision Instruments Inc) embedded in a Pentium PC compatible computer A user-written driving program was used to control the board and data processing. All the measurements were performed at a repetition rate of 2 Hz with a sampling time window width of 150 µs, which corresponds to a mass range from 0 to ~1500 amu. Each spectrum is an average of 4 transients and thus results in a sampling rate of 2 s/acquisition.

Results. Figure 1 shows the application of the IT/reTOF mass spectrometer for peptide mapping of 20 pmol β-lactoglobulin B tryptic digest In Figure 1a and b are shown the UV trace at 214 nm and the total ion chromatogram, respectively The full chromatographic separation can be displayed as a 3-D topographic map, in which each mass spectrum was plotted versus the chromatographic elution time where the difference of the intensity of mass peaks was indicated by different shades of color

Because of the extended trapping period, the solvent cluster ions are significantly reduced, which results in significant enhancement of sensitivity. In addition, the IT/reTOF is also useful for the detection of small-molecular-weight substances, like drugs Figure 2 shows the separation and sensitive detection of a mixture of 2 ng each of four quaternary ammonium drugs. Since the UV detection of such compounds may be not sensitive, the mass detector is better suited in this case Figure 2 is the total ion chromatogram of the separation which shows four peaks and which could be identified by their SICs. As shown in Figure 2b, the peak eluted at ~17 min and has a mass of 284, which is related to one of the mixture components, ipratropium bromide. Its mass spectrum is given in Figure 2c

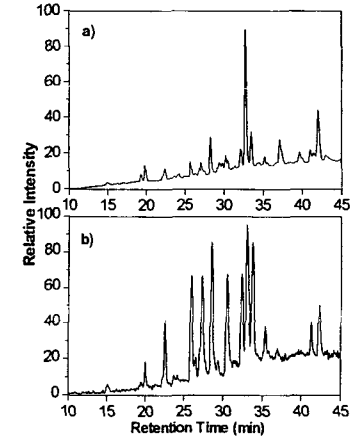

Figure 1

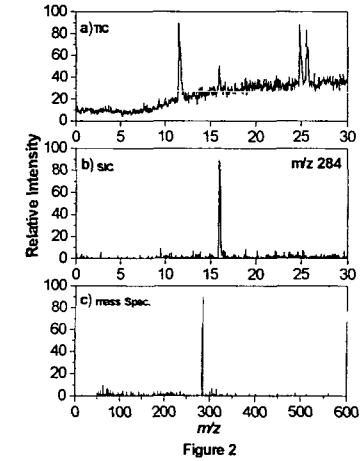

Figure 2

Conclusions. The ion trap storage/time-of-flight mass spectrometer serves as a rapid method of detecting the eluent of a liquid chromatographic separation over a broad mass range with a high duty cycle The SIC mode provides further enhancement of the S/N ratio, so that subpicomole detection can be obtained for each component. Using this methodology, peptide mapping and drug separation and detection could be carried out with excellent sensitivity in a relatively simple and inexpensive device

Acknowledgment. The work described herein received support under several sources which we wish to gratefully acknowledge including the National Science Foundation, Biological Instrumentation and Instrumental Develop program under grant #BIR-9223677, and Varian Associates, Inc , Ginzton Research Center.

Continuous Flow MALDI MS in an Ion Trap/reTOF Mass Spectrometer

Li Liang, Ling He, Benjamin Chien and David Lubman
Department of Chemistry
The University of Michigan
Ann Arbor, MI 48109

A LC/MS interface for the analysis of peptides and proteins has been developed by coupling a continuous flow probe with an ion trap/reflectron time-of-flight (IT/reTOF) mass spectrometer. The sample probe was directly inserted into the ion trap, and matrix-assisted laser desorption ionization (MALDI) method was used to ionize the peptides and proteins. The advantages of the ion trap include the ability to operate efficiently at the elevated pressure which is required for direct liquid introduction into the trap. Resonance ejection method can be used with the ion trap to selectively eject unwanted solvent and matrix ions from the ion trap by applying low voltage auxiliary field to the endcaps of the ion trap, providing enhanced signal to noise ratio and improved resolution for target peptide ions. It is demonstrated that picomole level sensitivity was routinely achieved by using this methodology. The upper detectable mass range for this system is greater than 12,327 Da. Absolute quantitative measurements using MALDI are difficult since the signal level is strongly dependent on laser fluence, laser beam homogeneity, sample homogeneity and probe surface conditions. Internal calibration with molecules having similar chemical properties was used in this work to obtain quantitative measurements. The response was shown to be linear for 3 orders of magnitude.

An important factor involved in obtaining reproducible continuous flow MALDI results is achieving stable operation of the continuous flow probe. The stable operation of the probe can be achieved when the rate of evaporation of the solvent from the probe surface and the pumping speed of the mass spectrometer are in balance. The evaporation rate can be adjusted by changing either the flow rate of liquid to the probe tip or the

amount of heat applied to the tip. Insufficient heat leads to freezing within the capillary tip and results in unsteady ion signals. When too much heat is applied to the probe tip, ion signals disappear due to the rapid evaporation of the matrix (3-NBA). A flow rate that is too high results in arcing inside the ion trap and space charge problems. The optimum temperature for the system was around 60°C. The optimum flow rate was 1.0-5.0 μl/min.

Structures of Biopolymers; A Combined MALDI - Ion Chromatography Approach

Thomas Wyttenbach, Gert von Helden, Seonghoon Lee and Michael T. Bowers
Department of Chemistry, University of California, Santa Barbara, CA 93106

The application of mass spectrometry to the analysis of large molecules has undergone explosive growth in the past decade. For the most part, this work has been carried out simply for mass determination and sample identification. In this paper we will present results of conformational studies applying a new method, which has recently been described.[1] An essential feature of this method is a new instrument that couples a MALDI source with our previously developed ion chromatography (IC) device. Another aspect is the significant amount of theoretical analysis that we apply in an effort to identify the conformation of the species in question. Here we will focus on Bradykinin (Bk).[2]

Experiment. The experimental setup has previously been described.[1] Briefly, ions are formed in a MALDI source using a pulsed N_2-laser. The ion pulse thus obtained is mass selected in a double focusing, reverse geometry, mass spectrometer and injected into the ion chromatography cell, which is filled with ~3 torr of He. The ion packet drifts through the cell under the influence of a weak electric field. Ions exiting the cell are collected on a multi channel scaler with 2 μs time resolution yielding an ion arrival time distribution. The drift time, and hence the mobility, of an ion depends strongly on its geometric shape, its conformation. While the mobility cannot directly yield the structure of the ion, theoretically determined structures can be converted to mobilities for comparison with experiment.

Calculations. For the calculation of structures we chose molecular dynamics methods. Since the site of protonation in Bk [2] is not *a priori* obvious, three isomers have been assembled.[3] For each of them 100 low energy conformations were located using a combination of 100 sequential molecular dynamics and energy minimization runs with the AMBER suite of programs. One cycle consists of a 30 ps dynamics simulation at 800 K to move across conformational space, a 10 ps dynamics run while temperature is dropped from 800 K to 200 K and finally an energy minimization to obtain the 0 K structure. Nine of the lowest energy conformations have been selected as input structures for semi-empirical calculations to obtain heats of formation. For all these structures orientation-averaged cross sections, or mobilities, are calculated using the Monte Carlo algorithm described previously.[4]

Results and discussion. The arrival time distribution of protonated Bk [2] shows only the presence of one single narrow peak, which agrees perfectly with a theoretical transport model fit of a single species. We can therefore conclude that either only one isomer in one conformation is present or, if there are multiple isomers and conformations, they have essentially identical collision cross sections of 242±5 Å^2 at 300 K, or the change from one conformation to another is fast on an experimental time scale. The value of 242 Å^2 is slightly higher than the cross sections determined for conformations of the AMBER calculations. It is interesting that all of the AMBER structures have common features. The protonated site is solvated by several groups with excess electron density, such as the neutral guanidine in arginine, the back bone acyl (>C=O) groups and the phenyl rings of the phenylalanines. This multiple coordination gives the ions fairly spherical shapes. Fig. *1a* shows cross section distributions of two 1 ns AMBER dynamic runs at

300 K, one for Bk protonated at the C-terminus arginine and one for the zwitter ionic structure.[3] The mean values of 232 and 225 Å^2 are indicated by vertical lines. Nine representatives of the 0 K AMBER structures, shown in fig. *1b* as a function of relative energy, have been used as input structures for semi-empirical AM1 (fig. *1c*) and PM3 (fig. *1d*) calculations. It can be seen that the semi-empirical structures thus obtained have larger cross sections than those predicted by AMBER and agree better with experiment. On the vertical axis of fig. *1c* and *1d* the heat of formation of the corresponding structure is given. It can be seen that all three isomers [3] have similar heats of formation. The AM1 calculations seem to indicate that the zwitter ionic isomer is the most stable one. PM3 calculations are known to underestimate the proton affinity of arginine by more than 10 kcal/mol.[5] Therefore the PM3 heats of formation for zwitter ionic Bk conformations might be underestimated by the same amount.

It is not *a priori* clear whether purely empirical (AMBER) or semi-empirical (AM1, PM3) methods are more accurate for calculating conformations of large molecules such as Bk. Both methods have advantages and drawbacks. The AMBER force field is highly optimized for peptides and this appears to be appropriate for our applications. However, AMBER has never been optimized for gas phase studies and thus may not be suitable in its present form. Semi-empirical methods, on the other hand, are pushed to the limit when applied to systems with 150 atoms. Furthermore, parametrisation was optimized for neutral molecules. However, we can conclude that structures obtained by semi-empirical methods yield cross sections which agree better with experiment than structures obtained by AMBER.

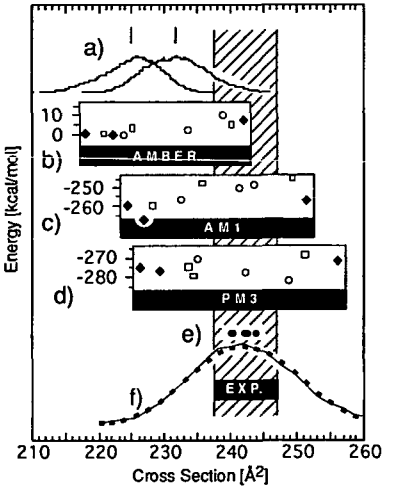

Fig. 1: He collision cross sections of Bk.[2] ○ Isomer *I*, □ isomer *II*, ◆ isomer *III*, see [3]. (a) AMBER dynamics. (b) AMBER, (c) AM1, (d) PM3 energy minimized structures. (e) Experimental values determined from (f) arrival time distributions (solid line) which agrees with theory including one single species (dotted line).

Comments and References

[1] G.v. Helden, T. Wyttenbach and M.T. Bowers, *Science* **267**, 1483 (1995); *Int. J. Mass Spectrom. Ion Proc.* (in press)
[2] Bradykinin (Bk): Peptide, composed of NH_2–Arg–Pro–Pro–Gly–Phe–Ser–Pro–Phe–Arg–OH.
[3] Isomer *I* is a Bk molecule protonated on the basic guanidine group of the N-terminus arginine, isomer *II* is protonated on the C-terminus arginine. Isomer *III* finally is a Bk molecule, which is protonated on both arginines and deprotonated on the only acidic site, the C-terminus carboxyl group (zwitter ionic structure). Note, that the doubly protonated Bk is experimentally not observed.
[4] G.v. Helden, M.T. Hsu, N.G. Gotts and M.T. Bowers, *J. Phys. Chem.* **97**, 8182 (1993).
[5] T. Wyttenbach and M.T. Bowers, unpublished results; J.L. Beauchamp, private communication.

CITP ESI-FTICR for the Study of X-Irradiation Damaged Tetranucleotides

*Steven A. Hofstadler[1], Zhongxi (Zack) Zhao[1], Richard D. Smith[1], Ed Budzinski[2], Jean Dawidski[2], Jason Gobey[2], and Harold Box[2]

[1]Pacific Northwest Laboratory, Richland WA 99352
[2]Roswell Park Cancer Institute, Buffalo, NY 14263-0001

A unique advantage of capillary isotachophoresis (CITP) is the ability to pre-concentrate low-level analytes and subsequently perform high resolution separations starting with relatively large (and dilute) sample volumes. The inherent isoelectric focusing and purification common to CITP make it well suited for trace analysis. The coupling of this technique to a high performance mass spectrometric detection scheme provides an unprecedented opportunity to obtain molecular weight and structural information from analytes which are present in a concentration limited regime. We have recently combined CITP with electrospray ionization (ESI) Fourier transform ion cyclotron resonance (FTICR) mass spectrometry in order to analyze and identify low level DNA damage products which result from the X-irradiation of oligomeric DNA in N_2-saturated aqueous solutions.

Damage to DNA is a critical event in mutagenesis, as well as for the initiation and possibly the promotion of carcinogenesis. The necessity of degrading polymeric DNA to the monomer level in order to carry out analyses has invariably complicated the study of DNA damage. Using short oligodeoxynucleotides of specific length and sequence, it is possible to isolate modified oligomers bearing specific lesions and to carry out analysis on the intact modified oligomers.

In this study, we are undertaking the analysis of radiation damage in the tetranucleotide triphosphate d(CpGpTpA). This oligomer provides a unique opportunity to study the relative susceptibility of the primary purine and pyrimidine DNA bases toward radiation damage. An N_2-saturated aqueous solution of d(CpGpTpA) was X-irradiated at a dose of 240 Gy. The resulting damaged (and undamaged) tetranucleotides were separated by HPLC (using an Ultremex 3 µm C_{18} 25 cm x 10 mm column; (Phenomenex)) and a 2 hour elution with a 0-10% acetonitrile gradient in 0.1 M ammonium acetate. A representative HPLC chromatogram is shown in a). Fractions were collected and further separated/concentrated using on-line reversed anionic capillary isotachophoresis utilizing a 50 µm uncoated capillary with 7 mM HCl/13 mM β alanine as the leading buffer and 10 mM caprioic acid as the trailing buffer. A series of FTICR spectra acquired at ≈3 second intervals is shown in b).

The FTICR detection scheme provides high resolution (i.e. > 25,000 FWHM) mass spectra with low ppm measurement error. Additionally, the application of MS/MS methods including collisional induced dissociation (CID) and thermal dissociation in the ESI source provide insight into the location and type of trace level nucleotide damage. The CID spectrum shown in figure c) (acquired on a triple quadrupole instrument) demonstrates fragmentation consistent with the conversion of thymine to hydroxyhydrothymine.

We are presently applying tandem FTICR mass spectrometry techniques, utilizing both sustained off-resonance irradiation and quadrupolar axialization, to probe the structure of several unidentified damage products.

Pacific Northwest Laboratory is operated by Battelle Memorial Institute for the U.S. Department of Energy, through contract DE-AC06-76-RLO 1830.

43rd ASMS Conference on Mass Spectrometry and Allied Topics

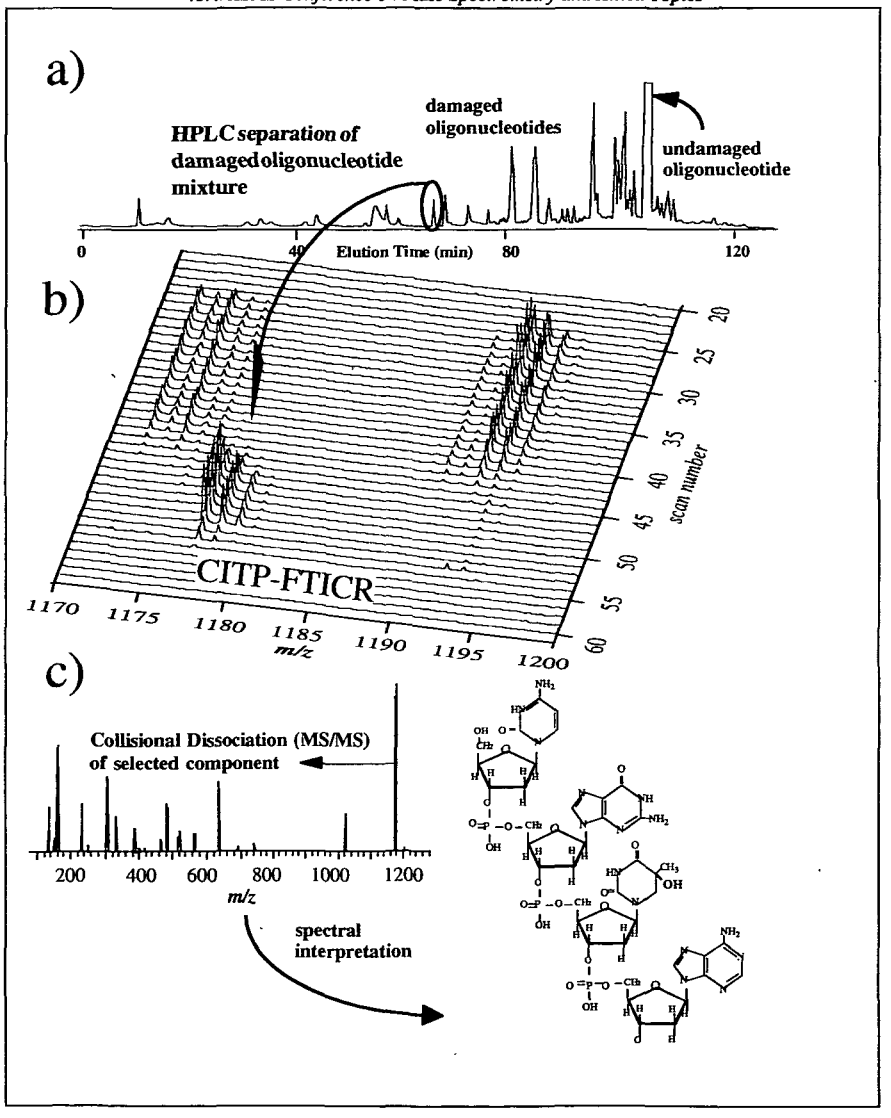

Complex Mixture Analysis by using Liquid Chromatography Coupled with Fourier Transform Mass Spectrometry

Brian E. Winger and John A. Castoro, Extrel FTMS, Waters, 6416 Schroeder Rd., Madison, WI 53711-2424.

High performance liquid chromatography (HPLC) in combination with electrospray ionization Fourier transform mass spectrometry (ESI-FT/MS) was used for the analysis of a drug mixture. By using stored waveform inverse Fourier transform, or SWIFT, to continuously eject the protonated drug molecule during the LC-MS analysis, trace impurities that co-eluted with the major component during the chromatographic separation, were detected. Additionally, other trace impurities that eluted after the main drug component were easily detected. Figure 1 shows a comparison of the TIC data obtained a) without the use of SWIFT and b) with continuous SWIFT ejection of the protonated drug molecule. The TIC data in Figure 1a shows only one peak, while the TIC data corresponding to SWIFT ejection of the protonated drug molecule shows several other components. The mass spectrum shown in Figure 2a corresponds to the TIC peak in Figure 1a. Along with the protonated drug molecule, only the proton-bound dimer of the drug and low-abundance fragment ions were observed. By using SWIFT to eject the protonated drug molecule, in addition to the two major fragment ions, peaks were observed between *m/z* 200 and 350 (Figure 2b) for the TIC peak #4. The chemical nature of these components have yet to be identified.

Figure 3 shows the LC-ESI-FT/MS spectra for two of the trace constituents detected by using SWIFT ejection during the analysis (Figure 1b). Figure 3a shows the mass spectrum for TIC peak #6 while the mass spectrum corresponding to peak #8 is illustrated in Figure 3b. Comparing the measured mass of the component in Figure 3a to the calculated mass resulted in a mass error of 0.5 ppm while the mass accuracy for the component in Figure 3b was 2.6 ppm. These data demonstrate that accurate mass analysis can be obtained for trace components in a mixture by using LC-ESI-FT/MS.

An alternative approach to analyzing complex mixtures by LC-MS is direct-infusion ESI-FT/MS in combination with SWIFT ejection of the most abundant species. Figure 4 shows the direct-infusion ESI-FT/MS spectrum acquired with SWIFT ejection of all species below *m/z* 275. The peaks designated with an asterisk (*) indicate trace components expected to be in the mixture. These were the same components that were detected by using LC-ESI-FT/MS. This data indicates that direct-infusion ESI-FT/MS in combination with SWIFT ejection is a viable methodology for the direct analysis of complex mixtures.

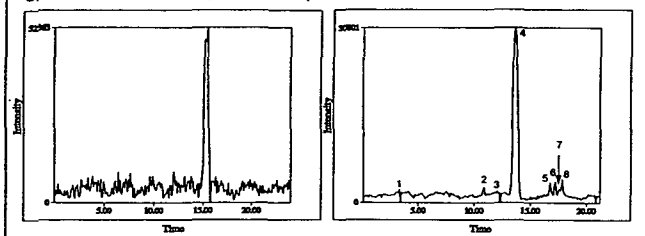

No SWIFT Ejection SWIFT Ejection of *m/z* 253

Figure 1

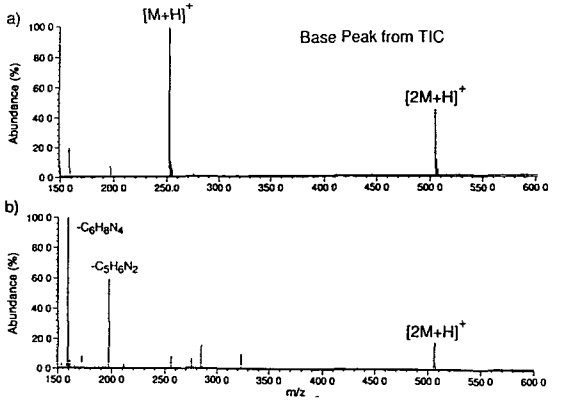

Figure 2

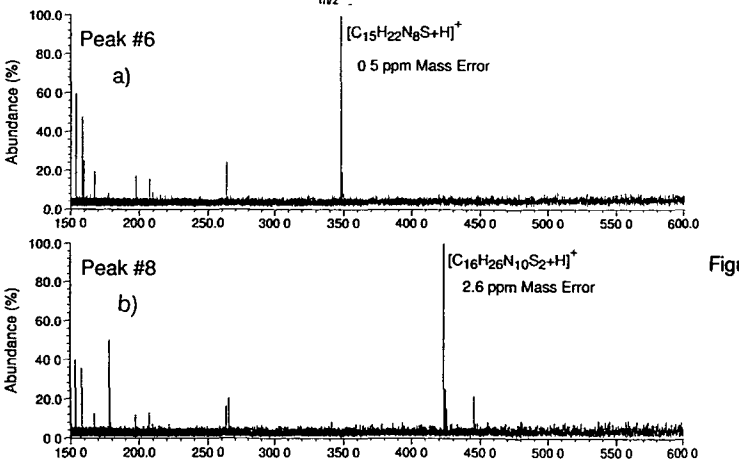

Figure 3

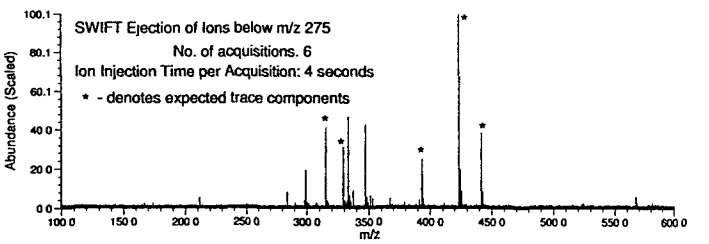

Figure 4

MALDI- TOF -MS of Organometallic Species: Comparison to FAB and ESI

Deborah A. Grimm[1], Aaron I. Baba[2], Liang Yongwu[2], Jerald Simon[2], and Russell H. Schmehl[2]
[1]Coordinated Instrumentation Facility and [2]Department of Chemistry
Tulane University, New Orleans, LA 70118

The purpose of this study is to qualitatively compare the MALDI, FAB and ESI spectra of a series of Ru-, Re- and dimetallic compounds. Organometallic species are often characterized by FAB-MS. The FAB technique is hindered by secondary processes and becomes less effective with higher mass and higher charge state. In recent years, ESI-MS has been used to analyze organometallic species. Such compounds have also been analyzed by laser desorption (LD) techniques. The recent development of MALDI-TOF-MS has found most of its application in the biochemical arena, we have had success analyzing organometallic species with this technique.

Organometallic species were synthesized. Their structures are outlined in Table 1. MALDI-TOF-MS were collected on a Finnigan LaserMat 2000. Analytes were mixed in 80% ACN at 1mg/100-500uL. Matrix was a-cyano-3-hydroxy cinnamic acid. About 0.5uL each of analyte, matrix and Sub P (as internal mass calibrant) were co-deposited on the target. 5-20 laser shots were averaged. FAB-MS and ESI-MS were reported at ASMS 1993.

——For comparison, Figs. 1 and 2 show FAB, ESI and MALDI for **I**. **A** has a +1 charge state and shows $(M\text{-}PF_6)^+$ by all techniques. The +2 compounds, **D**,**E**,**I** and **K**, also show $(M\text{-}PF_6)^+$ by all techniques. By FAB and to a greater extent by MALDI, they show loss of $2PF_6^-$'s with reduction. This reduction is not observed in ESI. The corresponding doubly charged ions are observed in FAB and to a greater extent by ESI. The +3 compounds, **B**,**C**, and **F**, show $(M\text{-}PF_6)^+$ by all techniques. The base peaks in both MALDI and FAB correspond to loss of $2PF_6^-$'s with reduction. The doubly charged ions are observed by FAB. ESI on these compounds does not show any reduction, only loss of successive PF_6^-'s. The +4 compounds, **H** and **J**, do not really give any information by FAB or MALDI. ESI appears to be more successful, but some reduction is observed with loss of 3-4 PF_6^-'s. A +8 compound, **L**, was attempted by FAB and MALDI, but no structural information was obtained. Fragmentation is observed in both MALDI and FAB. For example, **I** shows loss of the bpy ligand. (Figs. 1-2)

CONCLUSIONS

1. All techniques give information on organometallic species.
2. Based on the relative intensities of $-2PF_6^+/-2PF_6^{2+}$ the extent of reduction is: MALDI > FAB >> ESI.
3. Both FAB and MALDI appear to lose their effectiveness at higher mass and higher charge state.
4. ESI is much less hindered by higher mass and charge.
5. Both FAB and MALDI produce informative fragmentation.
6. ESI does not produce informative fragmentation.
7. MALDI-TOF-MS spectra are more difficult to interpret because of the lower mass resolution.

43rd ASMS Conference on Mass Spectrometry and Allied Topics

Table 1. Compounds Studied

SMP	STRUCTURE*
A	$[(CO)_3ClRe(b\text{-}b)Ru(tpy)Cl](PF_6)$
B	$[(dmb)_2Ru(b\text{-}b)Ru(tpy)CN](PF_6)_3$
C	$[(dmb)_2Ru(b\text{-}b)Ru(tpy)Cl](PF_6)_3$
D	$[Ru(dmb)_2bbdb](PF_6)_2$
E	$[Ru(dmb)_2bphb](PF_6)_2$
F	$[(dmb)_2Ru(bphb)Ru(tpy)Cl](PF_6)_3$
G	$[Ru(dmb)_2(b\text{-}b)](PF_6)_2$
H	$\{[Ru(dmb)_2]_2bphb\}(PF_6)_4$
I	$[Ru(bpy)_3](PF_6)_2$
J	$\{[Ru(dmb)_2]_2bbdb\}(PF_6)_4$
K	$[Ru(dmb)_3](PF_6)_2$
L	$\{[(dmb)_2Ru(b\text{-}b)]Ru\}(PF_6)_8$

*Ligand Structures

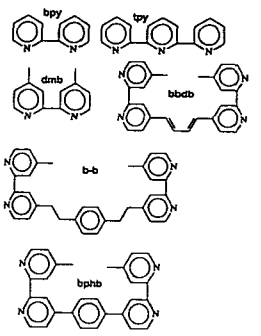

Figure 1. FAB-MS and ESI-MS of Compound I.

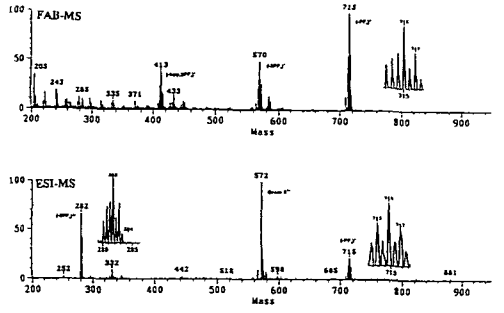

Figure 2. MALDI-TOF-MS of Compound I.

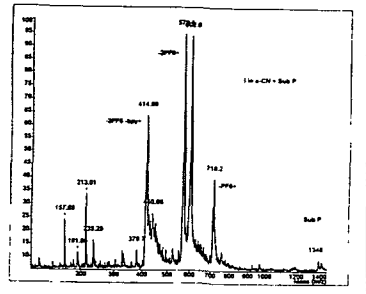

ACKNOWLEDGEMENTS

D. Grimm acknowledges the Coordinated Instrumentation Facility for financial support.
A. Baba, L. Yongwu, J. Simon and R. Schmehl acknowledge the Petroleum Research Fund and Tulane's CBR for support of the inorganic synthesis.

ATMOSPHERIC PRESSURE CHEMICAL IONIZATION FOR CE/MS

Yasuaki Takada, Minoru Sakairi and Hideaki Koizumi

(Central Research Laboratory, Hitachi Ltd., Kokubunji, Tokyo 185, Japan)

Capillary electrophoresis/mass spectrometry (CE/MS) is a promising technique for analyzing mixtures. Two types of interfaces, electrospray and fast atom bombardment, are currently used for CE/MS. However, present ionization techniques can not ionize all of the samples separated by the CE, and the buffer compositions that are available for electrospray are so limited that the extraordinary separation potential of CE has not been sufficiently utilized for CE/MS analysis. Therefore, new CE/MS interfaces based on different ionization methods are required for a wide range of applications.

We previously developed an atmospheric pressure chemical ionization (APCI) interface for CE/MS.[1] The on-line combination of micellar electrokinetic chromatography (MEKC) and MS has been examined using this APCI interface.[2]

The APCI interface consists of an electrospray-type nebulizer,[3] a vaporizer, and an APCI ion source (Fig. 1). We call this interface an "ES-CI interface".[2] One end of the capillary column (50-μm i.d., 150-μm o.d., and 50-cm long) was inserted into the electrospray probe (0.25-mm i.d. and 0.40-mm o.d. stainless steel). The probe was maintained at 3 kV. The sheath flow was pure methanol and the flow rate was 5 μL/min. The vaporizer consists of a stainless steel block, with a 5-mm i d., 60-mm long opening, that was uniformly heated to about 350°C by cartridge heaters. A 3 kV was applied to the needle electrode located between the vaporizer and a first aperture to produce a corona discharge. The vaporized samples and solvent molecules were ionized by the corona discharge, resulting in ion/molecule reactions. The separation mediums used were 25-mM phosphate buffers (pH 6.6) with and without 50-mM sodium dodecyl sulfate (SDS). A net voltage of 5 kV was applied to the capillary. The sample concentration was 1 mg/mL for each component.

When the CE buffers include high concentrations of nonvolatile salts, the APCI method is expected to be more useful than the conventional electrospray method because the APCI process is not heavily affected by these salts.[1] By using the ES-CI interface, we were able to conduct MEKC/MS analysis. Figure 2 show the ion electropherograms of alkaloids obtained by (a) ordinary CE/MS analysis and (b) MEKC/MS analysis. The alkaloids could not be separated by the CE mode, but were separated by the MEKC mode due to the interaction between the sample molecules and the SDS micelles, although the protonated molecular ions of the samples were clearly observed for each mode.

In conclusion, this CE/APCI-MS is a very promising technique because the APCI process is not heavily affected by the salts in CE buffers, allowing the use of a variety of CE buffers that include high concentrations of nonvolatile salts for CE/MS analysis.

Acknowledgment We are grateful to Professor Shigeru Terabe of the Himeji Institute of Technology and Mr. Hiroto Ozaki of Kaneka Techno Research Co. Ltd. for their helpful discussions about the MEKC separation.

1) Y. Takada, M. Sakairi and H. Koizumi, *Anal. Chem.*, **67**, 1474 (1995).
2) Y. Takada, M. Sakairi and H. Koizumi, *Rapid Commun. Mass Spectrom.*, in press.
3) R. D. Smith, C. J. Barinaga and H. R. Udseth, *Anal. Chem.*, **60**, 1948 (1988).

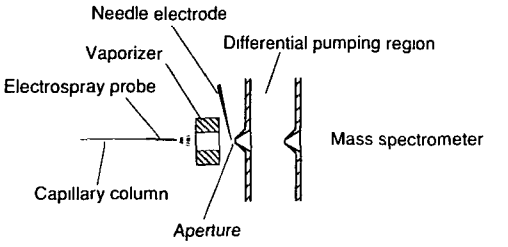

Figure 1. Schematic diagram of APCI interface.

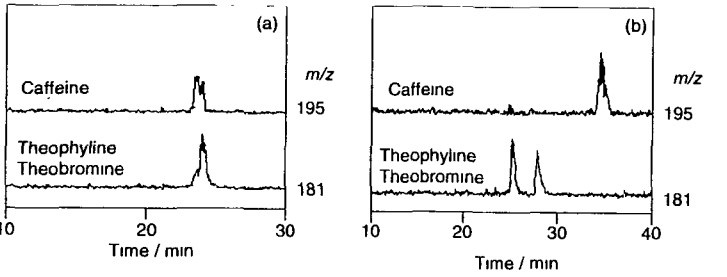

Figure 2. Selected ion electropherograms of alkaloids obtained by (a) ordinary CE/MS analysis and (b) MEKC/MS analysis. Buffers used were (a) a 25-mM phosphate buffer and (b) a 25-mM phosphate buffer with 50-mM SDS.

Determination of Amino Acids by On-line Capillary Electrophoresis-Electrospray Ionization Mass Spectrometry

Wenzhe Lu, George Yang, and Richard B. Cole*
Department of Chemistry, University of New Orleans
Lakefront Campus, New Orleans, LA 70148 (USA)

Amino acids and peptides are the basic building blocks of proteins and they are important in many scientific and medical areas. The main difficulty to be solved in the CE analysis of amino acids is the problem of detection. Since the majority of natural amino acids exhibit low absorbance characteristics in the UV-visible wavelength range, direct UV detection is rarely used for amino acid analysis. Alternative means of detection include chemical derivatization fluorescence, electrochemical detection, and indirect modes.

Compared to the optical methods of CE detection, mass spectrometry (MS) provides some unique advantages. In particular, much additional structural information can be obtained regarding ionic forms of the molecules separated by CE. The identities of unknown analytes can be deduced from mass spectral information in combination with migration times of the analytes, rather than solely from the migration times. This is particularly important for CE analyses since the reproducibility of migration times in CE is not always easy to control.

In this report, on-line capillary electrophoresis-electrospray ionization mass spectrometry (CE-ESMS) has been used for the separation and detection of amino acid and peptide mixtures. Four natural amino acids, histidine, tryptophan, phenylalanine, aspartic acid, and a tripeptide, glutathione, were separated and determined. Acetic acid electrolyte solutions have been used to separate and detect the amino acid mixtures using CE-ESMS. Elevated buffer concentrations which may offer improved CE separation are often incompatible with ESMS due to high conductance in the CE capillary. A high conductance may impede the ability to maintain a constant voltage, hence, a stable electrospray at the ES needle. Furthermore, high levels of background electrolyte can severely suppress analyte signals in ESMS. Many natural amino acids and peptides have relatively low pI values, hence, these compounds require low pH environments to become positively charged. In this study, relatively high concentrations of acetic acid (operating electrolyte) were used to provide environments sufficiently low in pH to enable protonation of analyte amino acids.

Parameters which have been examined and optimized include capillary diameter (50 to 100 μm internal diameter), applied separation voltage (20 to 30 kV), and electrolyte concentration (10% to 60% acetic acid). Stable working conditions were maintained when the CE currents were less than 18 μA. Protonated molecules were detected in the CE-ESMS mode with detection limits of about one pmol. Because background electrolytes are known to suppress analyte signals, the use of electrolyte solutions such as those described in this report instead of true buffers should offer advantages of reduced signal suppression, as well as increased signal stability.

43rd ASMS Conference on Mass Spectrometry and Allied Topics

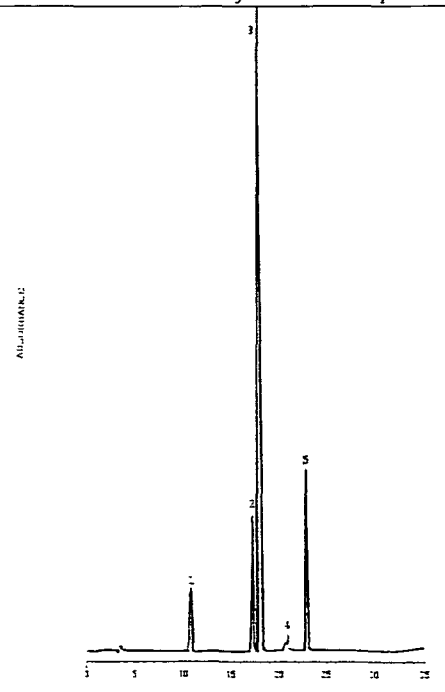

Figure 1 CE-UV trace showing the separation of 4 amino acids and a tripeptide, which are (1) histidine, (2) tryptophan, (3) phenylalanine, (4) aspartic acid, and (5) glutathione Experimental conditions sample concentration each component 500 ng/μL, CE voltage 30 kV over 50 μm x 100 cm capillary; electrolyte. 10% acetic acid (pH 3 1), electrokinetic injection· 25 kV for 10 s, detection wavelength. 195 nm

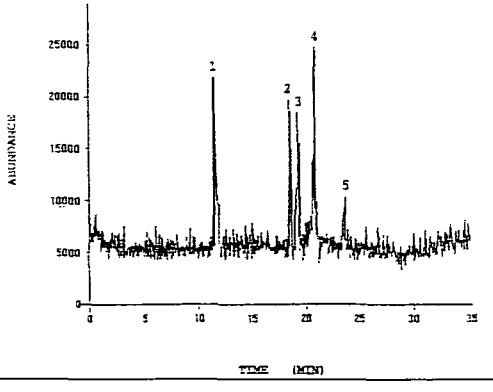

Figure 2. Selected-ion electropherogram showing raw data from on-line CE-ESMS analysis of the same five components shown in Fig. 1. Experimental conditions: sample concentration: each component 500 ng/μL; CE voltage: 30 kV over 50 μm x 100 cm capillary; electrolyte: 10% acetic acid (pH 3.1); electrokinetic injection: 25 kV for 10 s; ES voltage: 2.5 kV; MS scan rate: 3 s/scan.

Capillary Electrophoresis-Ionspray/MS Analyses of Protein Digests Using A Benchtop Single Quadrupole MS

Joseph F. Anacleto, Mark Allen and **Ron Bonner**, SCIEX, 71 Four Valley Drive, Concord, Ontario, Canada, L4K 4V8

Mass spectrometric detection of proteins and peptides separated by capillary electrophoresis offers several advantages over other detection systems. Analytes can be differentiated not only by their migration times but also by their molecular weights and characteristic fragmentation patterns. Mass spectrometry is anticipated to become one of the most powerful and popular detection methods for CE because of its universality, sensitivity, selectivity and structural elucidation capability.

This study illustrates the use of a novel benchtop single quadrupole mass spectrometer (the PE SCIEX API 100) as the detector for CE separations of protein tryptic digests. The API 100 system offers the ability to run a variety of scan modes simultaneously (called mixed-mode experiments). These types of experiments can be used to identify the sites of glycosylation and phosphorylation in glycoproteins and phosphoproteins, respectively, or determine the entire protein sequence in a single analysis by using collisionally induced dissociation (CID) and data base searching.

Glycosylation of proteins is an important feature of protein structure and function. The site of glycosylation and structure of the glycan are currently the focus of much investigation especially for glycoproteins used as therapeutics in humans. Methods have been developed to facilitate the location of glycopeptides in the LC-MS (1) and CE-MS (2) analysis of tryptic digests of glycoproteins by monitoring glycan marker ions at m/z 204 ($HexNAc^+$) and m/z 366 ($Hex\text{-}HexNAc^+$) produced by high energy CID reactions in the ion sampling region of the MS. This technique was used for the CE-MS analysis of a fetuin digest but with a mixed-mode acquisition of both full scan data (at a normal declustering potential in the orifice-skimmer region of the MS) and single ion monitoring (SIM) data of the fragment ion at m/z 204 (at a high declustering potential) in a single analysis. The full scan data provides molecular weight information while the SIM data indicates where the glycopeptides migrate.

Similar methods have been developed to identify phosphopeptides in the LC-MS analysis of tryptic digests of phosphoproteins by monitoring the PO_3^- (m/z 79) fragment ion produced by high energy CID reactions in negative ion mode (3). This technique was also used for the CE-MS analysis of ß-casein and α-casein (Figure 1) tryptic digests with a mixed-mode acquisition of both full scan data (at a normal declustering potential in positive ion mode) and single ion monitoring data of the fragment ion at m/z 79 (at a high declustering potential in negative ion mode) in single analyses. The polarity switching is important in these analyses since peptide molecular ions are usually much more abundant in positive ion mode while the marker ion can only be observed in negative ion mode.

Protein digests were also analyzed by CE-MS using a mixed-mode experiment where full scan data under both low and high energy CID conditions was acquired. The low energy spectra exhibit primarily molecular ions ($[M+2H]^{2+}$ and $[M+H]^+$) while the high energy spectra show prominent fragment ions above the mass of the doubly charged ion (the Y″ ion series). Examining the mass differences between prominent Y″ ions can reveal amino acid sequence information which can be used as a "sequence tag" (4). When the weight of the tryptic peptide along with the sequence tag are entered into the PE SCIEX PeptideScan™ protein database search routine, a list of known proteins containing the peptide is produced.

1) Carr, S.A.; Huddleston, M.J.; Bean, M.F. *Protein Science* **1993**, *2*, 183-196.
2) Kelly, J.F.; Locke, S.J.; Thibault, P. *J. Chromatogr.* in press.
3) Huddleston, M.; Annan, R.; Bean, M.F.; Carr, S. *J. Am. Soc. Mass Spectrom.* **1993**, *4*, 710.
4) Mann, M.; Wilm, M. *Anal. Chem.* **1994**, *66*, 4390-4399.

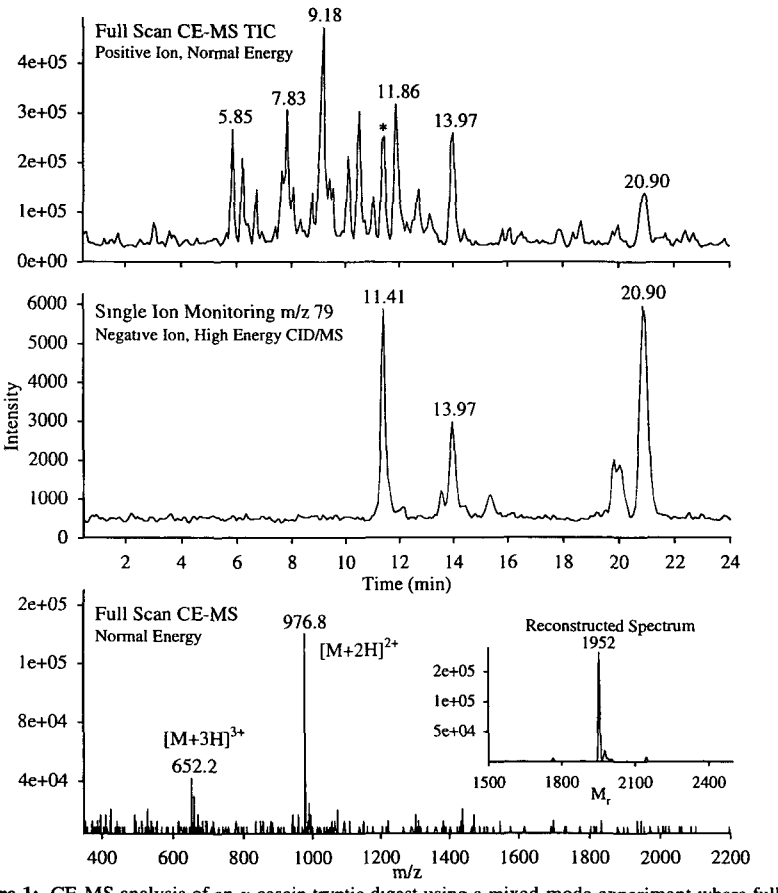

Figure 1: CE-MS analysis of an α-casein tryptic digest using a mixed-mode experiment where full scan data (at a normal declustering potential, 40 V, in positive ion mode) and single ion monitoring data (at a high declustering potential, -200 V, in negative ion mode) are acquired in a single analysis. The CE separation was performed with untreated fused silica (50 µm ID x 180 µm OD x 90 cm) and a 10 mM ammonium acetate, 1% formic acid, pH 2.4 buffer.

CE/ES/MS OF PEPTIDES AND PROTEINS USING A NEW SHEATH-FLOW PROBE

J. Fred Banks and Craig M. Whitehouse
Analytica of Branford, Inc. 29 Business Park Drive., Branford, CT 06405

While ES/MS has rapidly matured into a useful detector for LC, the practical application of CE with ES/MS has lagged behind. This is largely due to the additional challenges associated with CE operation and can be summarized here: (1) CE buffers generally contain no organic phase and therefore cannot be elctrosprayed (2) CE buffers are high in conductivity due to the presence of salts and therefore cannot be electrosprayed (3) CE flow rates are usually well below 1 µl/min and therefore cannot be electrosprayed (4) the CE column body is itself non-conductive so the CE buffer solution must be grounded at the column outlet while it is being electrosprayed.

To overcome these difficulties, we have designed a CE probe based on the sheath-flow concept developed by Smith et al. This arrangement allows for the use of many column chemistries and diameters without further modification and is thus convenient. Various critical parameters including sheath-flow flow rate and composition have been examined to determine optimum performance.

Figure 1 shows the effect that methanol added to the CE buffer phase (0.10 M acetic acid in water) has on the TIC of a separation of peptides (peaks: 1=Arg-Gly-Asp, 2=morphiceptin, 3=Val-Pro-Leu, 4=leucine enkephalin, 5=methionine enkephalin. In general, this shows a trend of increasing peak width and migration time of the analytes. The separation is adversely effected.

Figure 2 shows the effect of sheath flow rate (pure methanol) on the signal of leucine enkephalin analyses. Although the signal decreases, it only does so by about a factor of two over this range.

Figure 3 shows the linear dynamic range and detection limit for leucine enkephalin analyses in SIM and full scan (100-1000 m/z) modes. The detection limits here are 1.5 and 100 fmol, respectively.

Figure 4 shows the average of scans under one the leucine enkephalin peaks as in Figure 1.

43rd ASMS Conference on Mass Spectrometry and Allied Topics

Figure 1

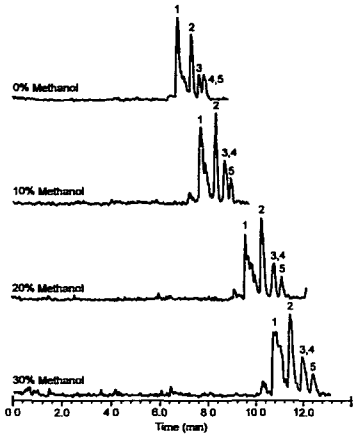

Figure 2

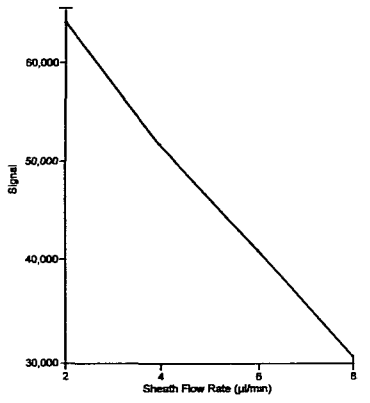

Figure 3

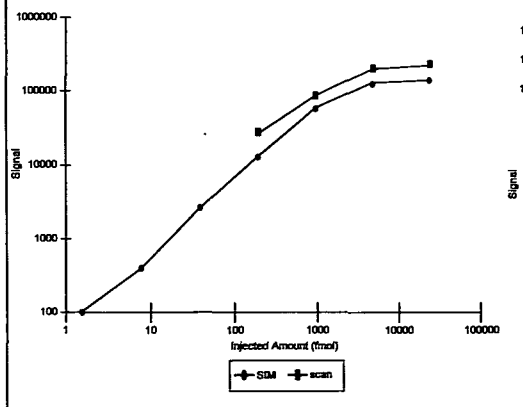

Figure 4

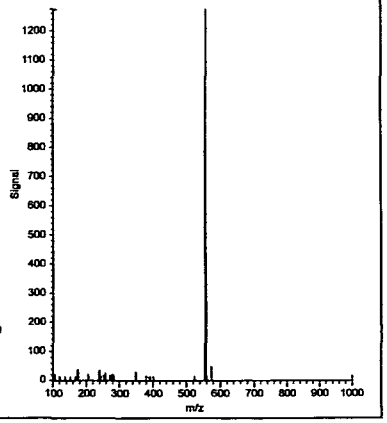

Analysis of Peptides and Proteins Using CE/ESI/MS

Mehdi Moini, Ping Cao, Kenneth L. Ray, Anthony W. Holbert

Department of Chemistry and Biochemistry, University of Texas at Austin, TX 78712

Electrospray is a soft ionization technique for analyzing nonvolatile and thermally labile compounds. This ionization technique is especially useful for mass analysis of high molecular weight biopolymers such as proteins and oligonucleotides. Capillary electrophoresis (CE) allows separation of large biomolecules under conditions that favor retention of biological activity. CE/MS is thus a technique of great interest and promise in the field of analytical biochemistry.

Our CE/ESI/MS interface consists of a P/ACE 2100 capillary electrophoresis instrument (Beckman Instruments), CE/ESI interface, and ESI/MS interface. The P/ACE 2100 CE is modified for CE/ESI/MS. In addition, the CE cartridge holder is modified to permit easy exchange between different CE cartridges. The end of the CE capillary is inserted inside a double layer coaxial tubing for sheath liquid and scavenger gas introduction. The ions formed in the electrospray are introduced into the mass spectrometer via an in-house-fabricated ESI interface [1] which consists of a heated capillary tube and then two stages of mechanical pumping in addition to the pumping capability of the Finnigan-MAT TSQ 70 mass spectrometer and the VG TS 250E MS.

Capillary Tip

Several kinds of capillary tips have been examined· HF etched with no gold coating; HF etched and chromium/gold coated; sanded tip; and treated gold coated tip. The latter two capillaries showed similar sensitivity and both showed higher sensitivity than the non-gold coated capillaries; however, the sanded-treated gold capillary was more durable than the HF-etched gold coated tip. Minimum peak width was observed when the gold coated capillary was used.

Capillary Position in the CE/ESI interface

The position of the CE capillary inside the sheath flow tubing plays an important role in peak shape of CE/MS electropherograms. Minimum peak tailing was observed when the end of the CE capillary was approximately 0.3 to 0.7 mm outside the sheath liquid capillary. This is shown in Figure 1. Strong peak tailing for gramicidin S was observed when the CE column was between 0.1 to 1 mm inside the sheath flow capillary, as shown in Figure 1b. In addition, lower sensitivity was observed when the CE capillary was inside the sheath flow capillary. However, the electrospray was more stable than when the CE capillary was outside.

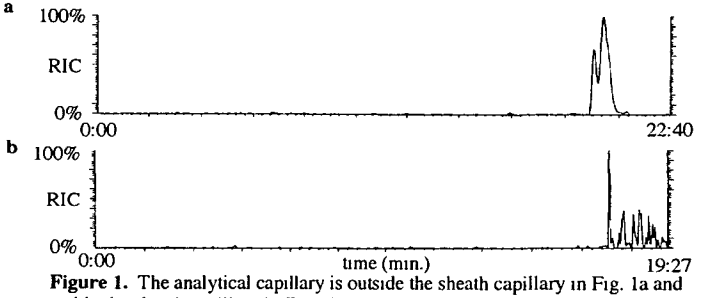

Figure 1. The analytical capillary is outside the sheath capillary in Fig. 1a and inside the sheath capillary in Fig. 1b.

Ethylchloroformate as a New Derivatizing Reagent for CE Capillaries

Successful separation of proteins by CE involves efficient suppression of adsorption to the fused silica wall. Basically there are two approaches to prevent protein adsorption: modifying the fused silica surface by dynamic or static coating or performing the analysis under the conditions that minimize adsorption. The most popular derivatization technique that has been used for CE/ESI/MS is that described by Bruin et al. [2] in which 3-aminopropyltrimethoxysilane (APTMS) is used as derivatizing agent. While this derivatization method has been successfully applied to analysis of proteins and peptides, this derivatization technique tends to clog the CE column. We have used ethylchloroformate (ECF) as a new derivatizing agent for CE capillaries. The ECF does not clog the column and gives separations similar to those of APTMS.

Figure 2 compares CE/ESI/MS of derivatized vs. non-derivatized column for a mixture of lysozyme, cytochrome C, and gramicidin S. As is shown, lysozyme is barely visible in the electropherogram of the non-derivatized column, and the peak for cytochrome c is very wide. With the derivatized CE column, however, peaks are only approximately 4 seconds wide. In addition, the reproducibility of the derivatized column is superior with respect to the non-derivatized column.

Conclusion

Coating the tips of the capillaries with gold increases the sensitivity of the CE/MS apparatus by preventing the dilution of the sample by the sheath flow of liquid. However, the capillary has a greater tendency to plug due to the absence of the cooling effects of the sheath flow liquid. Additionally, the gold coating can be vaporized by both heating due to the capillary current and electrical discharge between the CE and the MS. Further research on techniques to ameliorate these problems is in progress

Derivatization of the CE capillary with ECF decreases the adsorption of proteins on the CE column, enhancing the resolution and, therefore, the sensitivity of detection.

1. S. Jackett and M. Moini, Rev. of Sci. Instrum. 1994, 65, 591-596.
2. G.L.M. Bruin,R. Huisden, J.C. Kraak, and H. Poppe , J. Chromatogr. 1989, 480, 339-349.

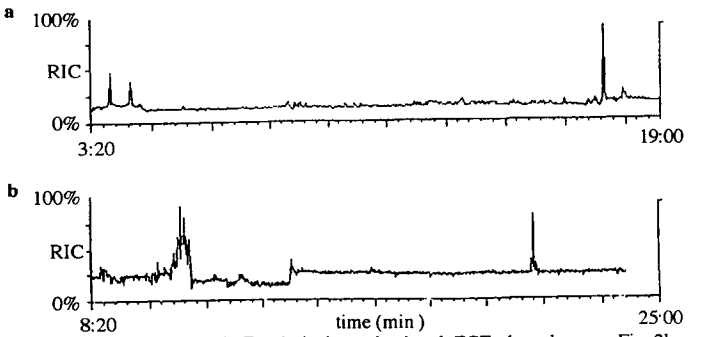

Figure 2. The column in Fig. 2a is derivatized with ECF; the column in Fig. 2b is not. Peaks from the left are lysozyme, cytochrome c, and gramicidin S.

On-line Characterization of Peroxidation Intermediates of NAD+ by CE-ESI-MS

Zhongxi (Zack) Zhao, Harold R. Udseth and Richard D. Smith
Chemical Methods and Separations Group, Chemical Sciences Department,
Pacific Northwest Laboratory, Richland, WA 99352, USA

Equine liver alcohol dehydrogenase (LADH) is one of the NAD-dependent enzymes with various physiological functions. LADH also exhibits several alternative catalytic activities. Among them, the most unusual one is the LADH-catalyzed degradation of NAD^+ in the presence of hydrogen peroxide (H_2O_2). A two-step reaction mechanism has been proposed for this enzymatic peroxidation. In the first (fast) step, NAD^+ catalyzed by LADH is converted to a (so far) unidentified intermediate: "compound I". The following slower step is enzyme independent and consists of at least two distinct processes; one of them leads to another unknown substance: "compound Y" which is the product of further reaction of "compound I" with excess H_2O_2; another process converts "compound I" to adenosine(5')-diphospho(5)-ß-D-ribose-NHCH=C(CHO)$CONH_2$ (NADX) if catalase is added to destroy excess H_2O_2 soon after the end of the faster enzymatic step.

One of the advantages of capillary electrophoresis (CE) is its fast operation cycle, which could be utilized to monitor relatively slow reaction processes. Capillary electrophoresis-mass spectrometry (CE-MS) has the capability of high resolution separations coupled with highly sensitive and selective detection providing crucial molecular weight and structural information.

In this presentation, reversed anionic capillary isotachophoresis (CITP)-electrospray ionization mass spectrometry (ESI-MS) has been demonstrated to separate the reaction mixture and to monitor the reaction process. Also, real-time CITP-tandem MS was utilized to provide both molecular weight and structural information of the interaction intermediates. For reversed anionic CITP, 7 mM HCl/13 mM ß-alanine was used as the leading electrolyte and 10 mM caproic acid as the trailing electrolyte.[1,2] A coaxial sheath liquid interface was used. The sheath liquid was composed of 0.1% formic acid, 24.9% water, and 75% methanol. The mass spectra of the reaction intermediates provided support for the reaction mechanism previously proposed. The results also indicate that a different reaction intermediate ("compound II") could possibly be involved in the interaction, which may provide a clue to further define the reaction mechanism. Figure 1 shows the proposed structural information and CITP-tandem mass spectrum of "compound I".

1. Z. Zhao, J. H Wahl, A. F. Fuciarelli, D. C. Gale, H. R. Udseth, R. D. Smith, *Proc. of 42nd ASMS Conf. on Mass Spec. and Allied Topics* Chicago, IL, 113(1994).
2. Z. Zhao, J. H. Wahl, H. R. Udseth, S. A. Hofstadler, A. F. Fuciarelli, R. D. Smith, *Electrophoresis* **16**, 389-395(1995).

Pacific Northwest Laboratory is operated by Battelle Memorial Institute for the U.S. Department of Energy, through contract DE-AC06-76-RLO 1830.

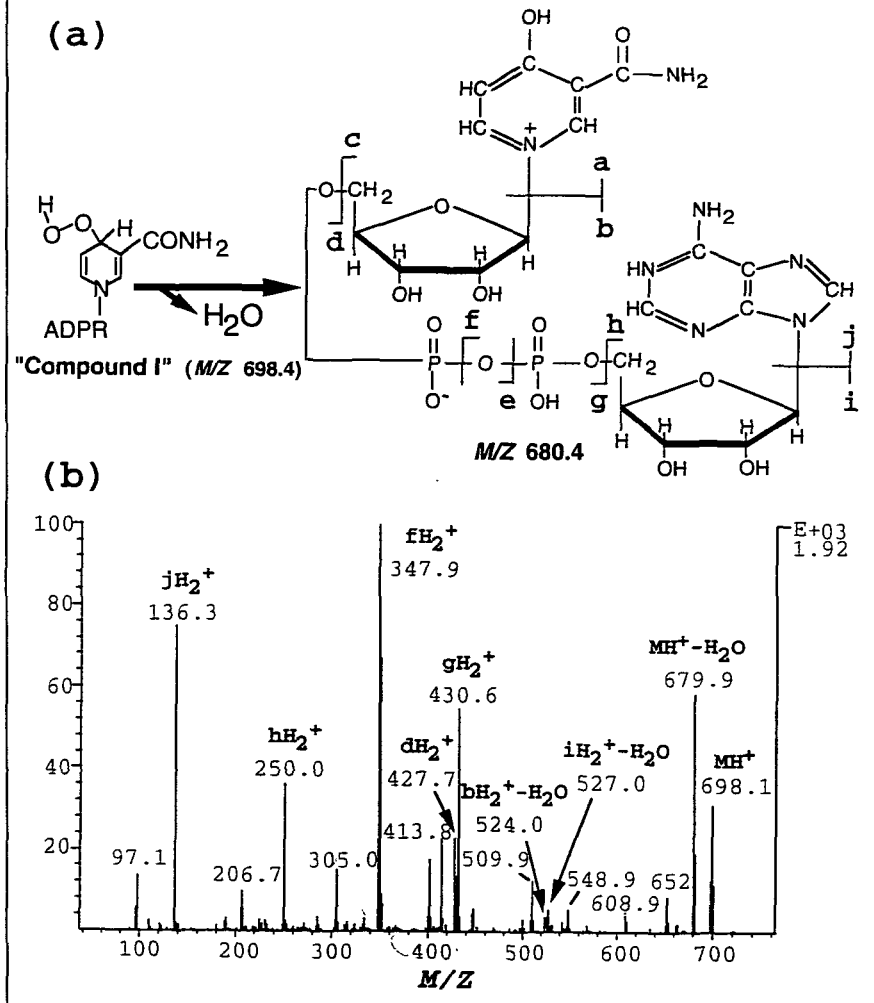

Figure 1. Proposed molecular structure (a) and CITP-tandem mass spectrum of "compound I" (b).

Electrospray LC/MS With An Ion Trap Mass Spectrometer

Catherine Stacey, Annette Hauser Fang, Frank Laukien, Bruker Instruments, Inc, Billerica, MA
Michael Schubert, Bruker Franzen Analytik, GMBH, Bremen

A new commercial mass spectrometer, the ESQUIRE, has been developed. The instrument uses QUISTOR technology and is supplied with an external ionization source for electrospray, MALDI or LSIMS. MS/MS and MS/MS/MS experiments are easy to perform on a QUISTOR. Collisionally induced dissociation of an isolated ion is easy to perform. Product ions are retained with high efficiency in the trap, to produce high sensitivity CID spectra. Resolution at a standard scan rate of 2000 a.m.u./s is 0.4u at any mass. Thus, resolution sufficient to resolve the charge state of most peptides is possible from on-line separation techniques. A slower scan rate is also available for higher resolution of up to 0.1u.

Further sensitivity enhancements are possible by switching from standard electrospray to low-flow electrospray methods as described below.The use of a new small-scale "micro electrospray" or "NanoSPRAY" needle[1] with a standard electrospray source allows for analysis of 1 µl or less of solution at a flow rate of 25nl/min.The long running time from this low flow rate allows for the analysis of complex mixtures, including the isolation and MS/MS of individual components on less than 5 pmol of sample An added advantage is that the "micro electrospray" is a much more efficient ion source. Concentration sensitivity is improved by the production of smaller droplets which leads to more efficient ion evaporation. The high field strength at the small needle tip allows for onset of the electrospray at low voltages so that aqueous, organic or high salt solutions can be sprayed without arcing.

Examples of proteins using the NanoSPRAY needles show good sensitivity in the low femtomole range Total sample applied to the needles was in the low picomoles and most of the sample could be recovered for other analyses. Analysis of a crude protein digest is possible directly with the NanoSPRAY needles. Since this method is tolerant of a wide range of solvent compositions and buffer and salt concentrations, no sample clean up is needed prior to analysis. Only 1-2µl of sample is used, most of which can be recovered for other techniques.The electrospray spectrum of a tryptic digest of myoglobin shows several prominent ions. Peptide masses were calculated assuming doubly charged ions in each case, and all masses were entered in the search.The search results are shown below. Only equine myoglobin matched to four of the peptides.

An ion from a Lys-C cytochrome c digest was isolated and fragmented by CID in the ion trap. The ion at *m/z* 780 produced an MS/MS spectrum from which the sequences [312]AFIM and [519]IK could be assumed. Searching for the first resulted in matches to cytochrome c in 36 species, all contained the sequence MIFAGIK, the second in 38 matches, including 2 non-cytochromes. A second peptide was isolated for MS/MS. The ion at *m/z* 647 was a double charged ion (M = 1292). Fragmentation produced a series of singly charged fragment ions from which the sequences GFIGHI and IHGIFG could be deduced (The assumption was made that this was the same internal sequence running from C- and N- terminal directions). This peptide was confirmed as TGPNLHGLFGRK, a peptide present in the cytochrome c of 37 species.

Total sample consumption for the series of MS and MS/MS spectra, which were generated in about 10 mins, was 600fmol. More sample remained in the needle should further experiments be required. No sample preparation was involved, and most of the available sample was left for LC/MS methods.

[1] M.Wilm and M.Mann, 42nd ASMS Conference on Mass Spectrometry, Chicago IL, June 1994.

The ESQUIRE™ is an ideal instrument for on-line detection of time-resolved components. Ion accumulation time in the trap can be set so that good sensitivity is possible without compromising the efficient duty cycle of the instrument. A fixed scan rate of 2000 a.m.u./s is available. Most synthetic or enzymatic peptides have an *m/z* range from 300-1000. For tryptic peptides, where cleavage is adjacent to a basic amino acid, fragments will have at least 2 basic sites, the N-terminus and the basic side chain. Thus 2+ions (or 3+ ions if the peptide contains His) are the most prevalent. The separation of a tryptic digest of myoglobin was carried out at a 50pmol, 5pmol and 1pmol level. Previous experiments showed that all significant ions had an *m/z* value > 500u. Each LC/MS run shows a number of peaks from which expected peptides can be confirmed.

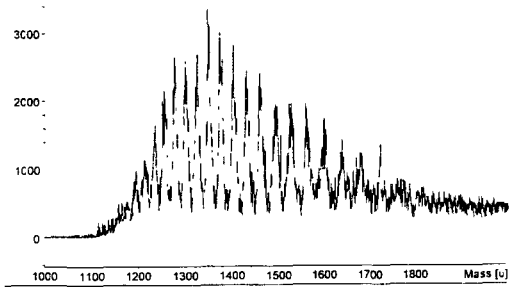

bovine serum albumin, 200fmol consumed

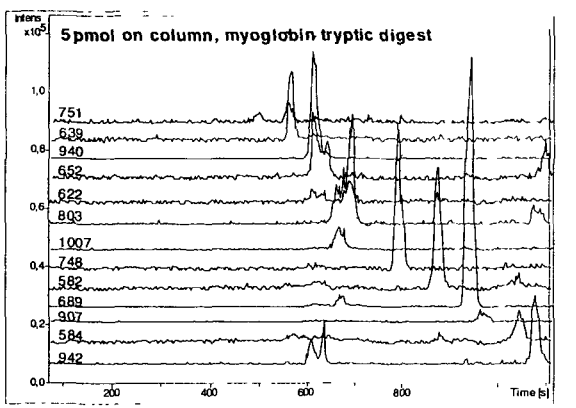

Extracted Ion Currents for Different *m/z* Values From an LC/MS Analysis of 5pmol of Myoglobin Tryptic Digest

Direct Analysis of Cellular Proteins by Capillary Electrophoresis FTICR MS

*Steven A. Hofstadler[1], Frank D. Swanek[2], Joanne Severs[1], David C. Gale[1], Zhongxi (Zack) Zhao[1], James E. Bruce[1], Andrew G. Ewing[2], and Richard D Smith[1]

[1]Chemical Sciences Department, Pacific Northwest Laboratory Richland, WA 99352
[2]Dept. of Chemistry, The Pennsylvania State University, University Park, PA 16802

Direct chemical analysis of living cells has received considerable attention in recent years; the single cell approach provides a major step towards answering important questions in the field of cellular biochemistry. In this work we present preliminary results which demonstrate the feasibility of using the CE-ESI-FTICR combination as a high performance detection scheme for the analysis of cellular proteins acquired directly from small populations of intact living cells. The human erythrocyte (red blood cell) was chosen as a model system owing to its availability, relatively homogeneous composition, and thorough documentation of contents by previous researchers. The contents of the erythrocyte are unusually homogeneous; nearly the entire volume of the cell is filled with hemoglobin, approximately 450 amol per cell, a challenging but attainable level for mass spectrometric detection with current instrumentation. In this work we demonstrate the on-line acquisition of high resolution mass spectra (average resolution ≥ 45,000 FWHM) of the α and β hemoglobin chains acquired from the injection of as few as 10 human erythrocytes† (this corresponds to ≈ 4.5 fmol of hemoglobin). Additionally, when used in conjunction with quadrupolar axialization and sustained off-resonance irradiation, it is possible to directly obtain partial sequence information of selected cellular components obviating the need for additional isolation/purification steps. Given the extremely small volume of the human erythrocyte (typically ≈ 87 fL/cell), we are optimistic that the techniques implemented here will be adaptable to the study of many larger mammalian cell systems.

Shown in Figure (a) is a total ion current (TIC) trace from the injection of 20 erythrocytes derived from the detection of the electrospray ion current signal from the ion beam impinging on the front shutter of the FTICR instrument. The initial peak observed in the TIC trace is attributed to buffer ions from the cell injection procedure. Approximately one minute after the buffer peak elutes, a broad peak due to the major cell contents is observed from which mass spectra of the α and/or β chains of hemoglobin are acquired. The noncovalent tetrameric hemoglobin complex consisting of two α chains and two β chains ($\alpha_2\beta_2$) is dissociated due to the low pH of the 10 mM HOAc CE running buffer. In general, the eluting peaks are broad and poorly resolved due to variations in cell lysing and injection times. The initial spatial distribution of the cell population combined with variable cell lysing times adversely affects the resolution of the separation. These effects are substantially reduced when fewer cells are injected.

The mass spectrum of the α chain in (b) was acquired from the injection of only 10 erythrocytes and demonstrates a nearly complete separation of the α and β chains. The MS/MS spectrum in (c) was acquired from the selective ion accumulation (using single frequency quadrupolar axialization) of the 18+ charge state of the α chain (≈ 75 erythrocytes) followed by sustained off-resonance irradiation (SORI) at -1000 Hz relative to the 18+ α chain. Extensive dissociation producing predominantly y and b fragments is observed.

Efforts are presently underway to improve sensitivity in order to facilitate the analysis of single cells. We believe there are still orders of magnitude improvement in sensitivity to be achieved with the incorporation of more efficient ion generation and ion accumulation methods.

†Hofstadler, S.A.; Swanek, F.D.; Gale, D.C.; Ewing, A.G. and Smith, R.D. *Anal. Chem.*, 67, (1995), 1477-1480

Pacific Northwest Laboratory is operated by Battelle Memorial Institute for the U.S. Department of Energy, through contract DE-AC06-76-RLO 1830.

43rd ASMS Conference on Mass Spectrometry and Allied Topics

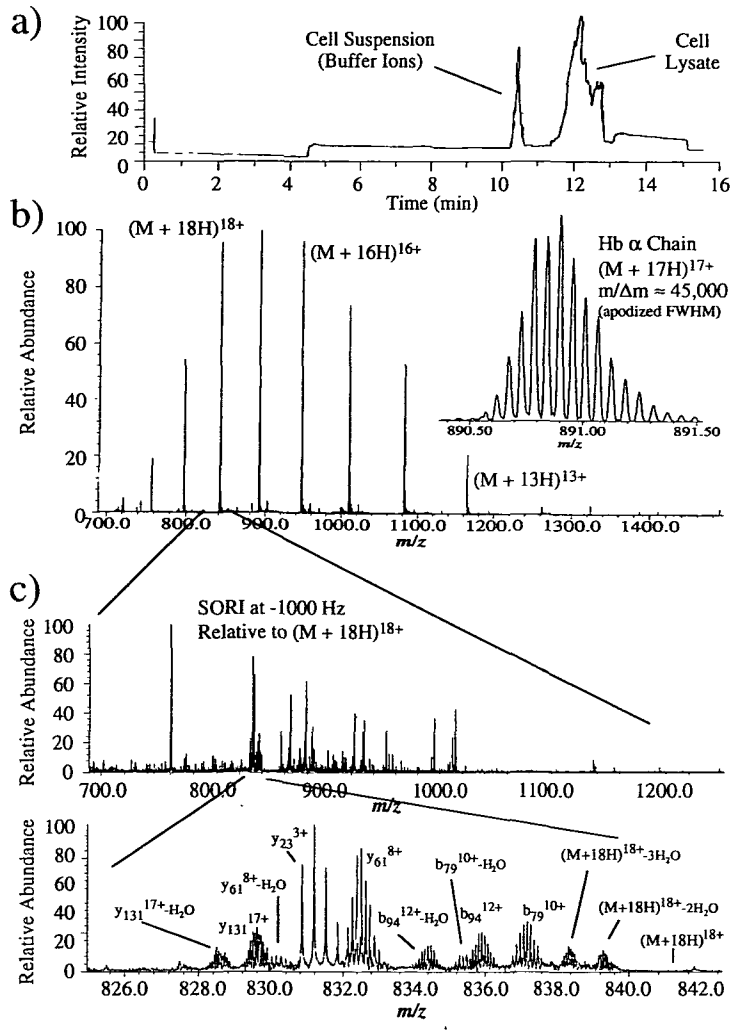

Capillary Electrophoresis/Ion Trap Mass Spectrometry: Achieving Ultra-low Detection Limits

R S Ramsey, D.E. Goeringer, G.J. Van Berkel, and S.A. McLuckey
Chemical and Analytical Sciences Division
Oak Ridge National Laboratory
Oak Ridge, TN 37831-6365

Sensitivity remains an important issue in the on-line coupling of CE with MS. The small sample volumes typically analyzed by CE (less than 1-2% of the total column volume) result in high concentration detection limits and the various approaches, including assorted on-line preconcentration strategies, that have been taken to improve LODs often compromise either separation or MS performance. We have interfaced CE with a quadrupole ion trap to exploit its inherent advantages in duty cycle and MS/MS efficiency for high sensitivity analysis. Our previous investigations using a conventional sheath flow electrospray source and 50 µm i.d. columns showed that full scan detection limits for peptides were at the 10 fmole level (1). In view of the advantages that have been cited for small diameter columns in on-line analysis (2,3), we have evaluated sheathless electrospray sources using small diameter gold-tipped capillaries. By optimizing ionization efficiency and enhancing trapping efficiency significant improvements in sensitivity have been obtained.

All analyses were conducted on a Finnigan MAT ITMS (San Jose, CA) modified for ESI. The trap was operated using up to 4 mtorr of helium pressure where an approximate 3 to 8 fold improvement in signal levels for various molecular ions was obtained relative to operation at 1mtorr pressure. The CE columns were tapered at the cathode end to ca. 40 µm o d and 3-5 µm i d. using a laser-based micropipette puller. Sheathless ES interfaces were prepared by coating these tips with a thin film of chromium followed by a 250 nm layer of gold using a magnetron sputtering system. Some continuous infusion experiments to compare capillaries of different i.d. were also performed using gold coated emitters prepared as previously described (4). CE analyses were typically conducted at 20 kV using acetic acid buffers and samples were injected electrokinetically.

Figure 1 shows the sensitivity which has been obtained on-line for our sheathless electrospray CE interface/ITMS combination using columns of moderate i.d. (20µm). A S/N ratio of 6:1 for the lowest injection level of leucine enkephalin indicates that midattomole detection limits in total ion electropherograms may be obtained. MS/MS data could also be acquired on-line from low femtomole injections as shown in Figure 2. In comparing different sources, the sheathless interface was found to provide only modest improvements in signal (factors of 3 to 4) relative to coaxial liquid sources using capillaries of the same diameter. The greatest gains in sensitivity were derived from the use of small diameter columns at low flow rates (e.g., a factor of 60 observed for a 100 vs. 25 µm i.d. emitter). The sheathless interface, however, eliminates solvent effects which may confound detection if the sheath solvent induces changes in charge state distribution which the analyzer is not "tuned" to detect.

1. R.S. Ramsey, D.E. Goeringer, and S.A. McLuckey, Anal. Chem. 65, 3521 (1993).
2. J.H. Wahl, D.R. Goodlett, H.R. Udseth, and R.D. Smith, Electrophoresis, 14, 448 (1993).
3. J.H. Wahl, D.R. Goodlett, H.R. Udseth, and R.D. Smith, Anal. Chem. 64, 3192 (1992).
4. M.K. Kriger, K.D. Cook, and R.S. Ramsey, Anal. Chem. 67, 385 (1995).

43rd ASMS Conference on Mass Spectrometry and Allied Topics

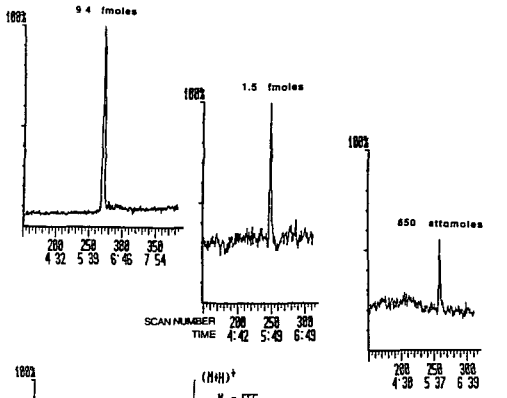

Fig. 1. TIEs from 3 electrokinetic injections of leucine enkephalin on a 20 µm i.d. gold-tipped column. Analysis using 50 mM acetic acid buffer at 20 kV (100 ms ion accumulation time/scan). Mass spectrum (below) obtained from the 650 attomole injection (16 scans averaged).

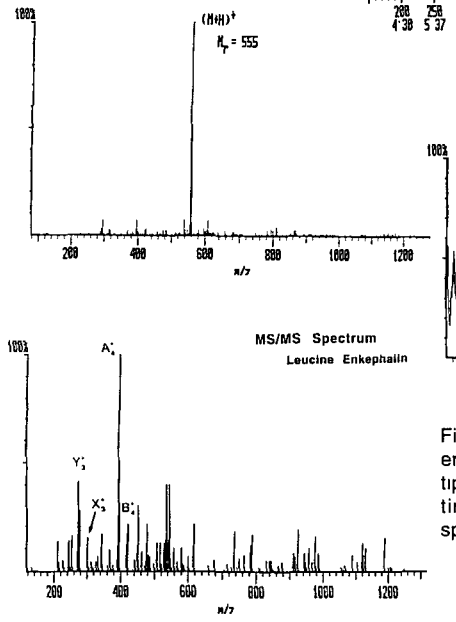

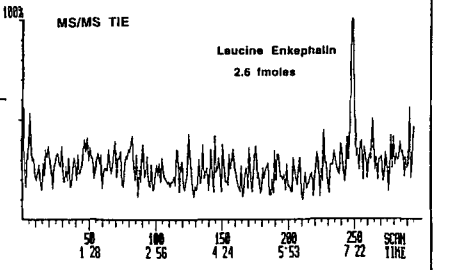

Fig. 2. MS/MS TIE for 2.6 fmoles of leucine enkephalin injected on 20 µm i.d. gold-tipped column (300 ms ion accumulation time/scan) (above) and the MS/MS spectrum (18 scans averaged).

Research supported by the National Institutes of Health under Grant No. R01GM45372 under Martin Marietta Energy Systems, Inc. Contract DE-AC05-84OR21400 with the Department of Energy.

A New Setup For On-Line CE-MS

Michael X. Li, Jingtao Wu, Hongwei Li, David M. Lubman
Department of Chemistry, The University of Michigan
Ann Arbor, MI 48109

The combination of capillary electrophoresis(CE) with electrospray ionization mass spectrometry(ESI/MS) has become a powerful analytical tool in biological field. In particular, the high separation efficiency and resolution of CE, combined with the abundant information acquired in the MS in terms of the molecular weight and structure, has made the on-line CE-MS a promising technique in various areas. However, scanning speed and detection mass range are often comprised to obtain sufficient MS signal-to-noise ratio from high efficiency separations. In other words, the sensitivity, scanning speed, and instrument duty cycle would sometimes be critical issues for the identification and characterization of unusually narrow peaks that result from the CE separation.

In this work, the capillary zone electrophoresis(CZE) system has been coupled to an electrospray interface with a quadrupole ion trap (IT)/ reflectron time-of-flight (reTOF) mass spectrometer Since TOF is a nonscanning mass analyzer possessing extremely high sensitivity, the duty cycle can be enhanced enormously, which is essential when it is employed with a CZE system The ion trap acts as a unique tool for the storage of ions over a wide mass range with excellent detection limits and removing unwanted background ions. After a period of storage, the ions are ejected into the TOF tube for mass analysis by applying a DC voltage to the ion trap end cap. Through this storage, both of the resolution and sensitivity were improved greatly

The coupling between the CZE and the electrospray interface utilized a common coaxial sheath flow, where the capillary cathodic end was directly inserted into the electrospray needle and the added sheath liquid flows through the space between them. The flow rate was around 5-10 μm/min, in order to meet the optimum condition for electrospray. The sample was directed into the capillary by electrokinetic method from the ~10^{-4}M sample solution. Separation and detection of peptide mixtures and biological samples have been performed so as to demonstrate the capability of applying this CZE-ESI-IT/re TOF setup in different situations.

Figure 1 shows the total ion electropherogram of three peptide mixture: Angiotensin I, Angiotensin II, and Angiotensin III The injection sample amounts were around high femtomoles. As noticed, when either the sample loading time or the applied injection voltage was increased, the electropherogram peaks became broader and more tailed. Figure 2 shows the separation and identification of two peptides: Substance P and Neurotensin, with FWMH around 20s. The sample consumption of Substance P was at low femtomole range. Figure 3 is the separation of two small peptide mixture· Leu-Gly, Met-Enke-Arg, and TBAH. It was observed that the signal can be optimized by appropriate tuning of the storage time, buffer gas pressure, and the RF voltage applied to the IT ring electrode. While both sample and buffer compositions are possible reasons for

the peak broadening, another important point is the fact that the fused silica capillaries were employed without any coating.

These preliminary results show the promising future of this combination to achieve the success in maintaining the CE resolution and catching up the concentration detection limits, given the potential of Ion Trap and TOF would be fully developed and tuned up in the coupling. As sensitivity around femtomole for most sample components was often achievable and the reconstructed total ion electropherograms with peak widths between 10 to 20s were routinely obtained, it is quite clear that the advantages of the combination that couples the CZE and the IT/reTOF could be really applied to many different application arenas. Nevertheless, in order to utilize this design more broadly, it is necessary to further narrow down the electropherogram peaks, and improve its detection limit so that it can be employed to the extremely diluted mixtures. To do this, several methods are available, e.g. optimize the CZE operating condition and coat the fused silica capillaries.

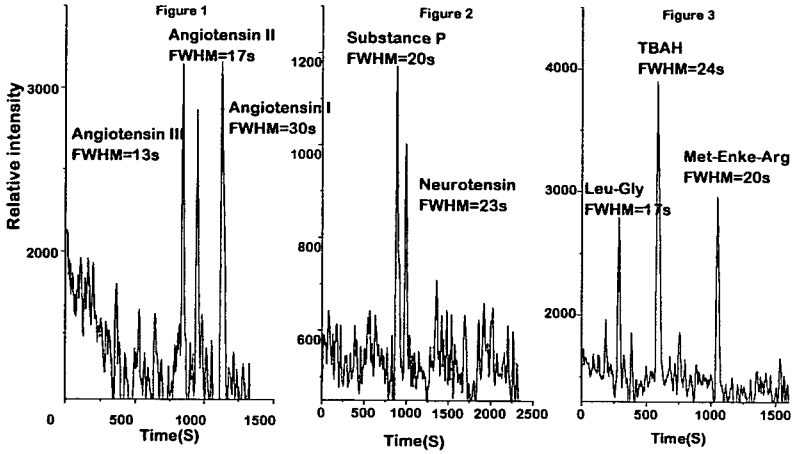

Figure 1. Separation of three peptide mixture: Angiotensin I, II, III
Figure 2. Separation of Substance P and Neurotensin
Figure 3. Separation of mixture of Leu-Gly, Met-Enke-Arg, and TBAH

References
1. Richard D. Smith, Jon H. Wahl, David R. Goodlet, Steven A. Hofstadler *Anal. Chem.* 1993, 65, 574A-584A.
2. W M. A. Niessen, U R. Tjaden, J. van der Greef *J. Chromatogr.* 1993, 636, 3-19

Acknowledgment· This work is partially supported by the National Science Foundation and Varian Associates, Inc., Ginzton Research Center.

OFF-LINE COUPLING OF CAPILLARY ELECTROPHORESIS AND MALDI-TOF MS

Kathleen L. Walker,* Rick W. Chiu, Curtis A. Monnig and Charles L. Wilkins,
Department of Chemistry, University of California, Riverside, CA 92521-0403

Capillary electrophoresis (CE) is an efficient tool for the separation of mixtures of ionized molecules. When compared with liquid chromatography, CE usually requires similar analyte concentrations (nanomolar and above) but smaller sample volumes (nanoliters). As a consequence, the quantity of analyte available for detection is extremely limited. The characterization of unknown molecules isolated by CE requires a sensitive detector which can provide detailed chemical information about the analyte. MALDI mass spectrometry is an analytical technique capable of providing the requisite sensitivity and chemical information, but it does not routinely lend itself to the analysis of complex mixtures. However, when mass spectrometry is coupled with CE the resulting instrument provides a very effective means for characterizing difficult samples.

The utility of capillary electrophoresis with mass spectrometric detection has long been recognized, but is difficult to implement. Most often these instruments have been coupled through on-line electrospray ionization sources. While electrospray MS is capable of monitoring a diverse range of chemical species, it can be adversely effected by ionic species such as buffer salts commonly used in CE separation buffers (NaH_2PO_4, NaH_2BO_3, etc). Previous efforts have been made to off-line couple CE and MALDI MS, however most did not demostrate tolerance of diverse CE analysis conditions.[1-4] A more useful coupling of these instruments would tolerate non-volatile and ionic electrolytes, and so not require that the separations be tailored to the shortcomings of the mass spectrometry.

The interface used in these studies contains an on-column ultraviolet absorbance detector to allow isolated zones to be observed prior to passing from the capillary A computer monitors the absorbance signal in real time and positions a laser-target probe tip under the capillary outlet so that zone is collected individually. A conductive polymer coated capillary or a co-axial flow capillary configuration allows electrical contact to be maintained during sample deposition and can allow simultaneous deposition of the sample and the matrix on the probe surface. After the samples have dried, the probes are manually transferred to a MALDI time-of-flight mass spectrometer for subsequent analysis.

The off-line interface is successfully applied to couple CE and MALDI TOF under a variety of separation conditions which are realistic for separation of biological macromolecules. Bonded coatings (Ucon, APTES) and chemisorbed (polyarginine) capillary coatings are used in conjunction with a variety of buffers ranging from 30 mM amine-acetate to high ionic strength (100 mM) sodium phosphate. Samples are collected directly on the laser target probe. The practicality of this instrument for complex mixture analysis is demonstrated by separation and analysis of peptides from a tryptic digest of cytochrome *c* and of synthetic mixtures of proteins. By decreasing the pH of the MALDI matrix solutions, spectral resolution and signal to noise are enhanced through the formation of increased amounts of protonated molecular ions in the presence of the buffer salts.

Sample quantities as large as a few picomoles can be separated and analyzed, however the separation quality is less than optimal under these conditions. Miniaturization of the interface and use of a capillary coated with a conducting polymer allow acquisition of high quality MALDI spectra from sample quantities as low as 150 fmol. Under these conditions the efficiency of capillary electrophoresis is optimal and separation of more complex mixtures is realistic.

Mass data from synthetic protein mixture separated by CE and analyzed by MALDI MS, 150 fmol of each analyte

PROTEIN	EXPECTED MASS#	MEASURED MASS	MASS ACCURACY, ppm	RESOLUTION
Myoglobin	16,951.7	16,949.7	118	142
Ribonuclease A	13,683	13,683.5	37	131
Cytochrome *c*	12,361.5	12,363.1	129	180
Lysosyme	14,307	14,306.7	21	157

#Average masses, $(M+H)^+$ ion

43rd ASMS Conference on Mass Spectrometry and Allied Topics

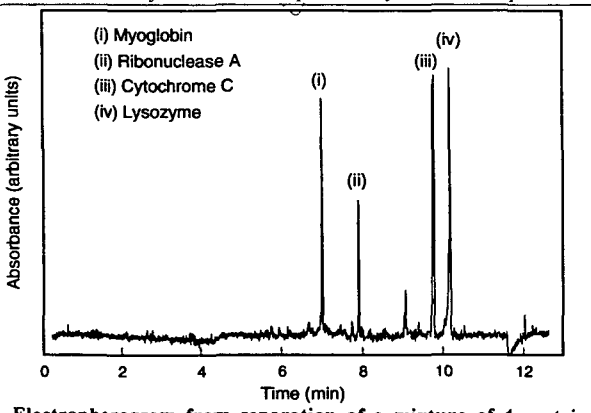

Electropherogram from separation of a mixture of 4 proteins. 25 fmol of each protein was injected. The capillary is coated with polyarginine and filled with 20 mM sodium acetate. The separation efficiency is 500,000 to 1,100,000 theoretical plates.

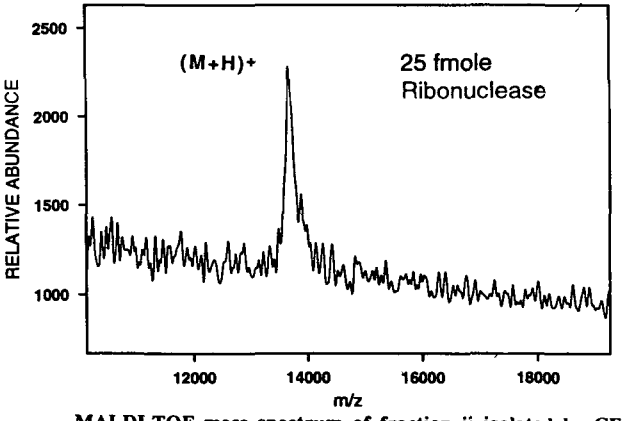

MALDI-TOF mass spectrum of fraction ii isolated by CE.

REFERENCES

1. Keough, T.; Takigiku, R.; Lacey, M. P.; Purdon, M. *Anal Chem*. 1992, *64*, 1594.
2. Castoro, J. A.; Chiu, R. W.; Monnig, C. A.; Wilkins, C. L. *J. Am Chem. Soc*., 1992, *114*, 7581.
3. van Veelin, P. A.; Tjaden, U. R.; van der Greef, J.; Ingendoh, A., Hillenkamp, F. *J Chromatogr*. 1993, *647*, 367.
4. Weinmann, W.; Parker, C. E.; Deterring, L. J.; Papac, D. I.; Hoyes,J.;Przybylski, M., Tomer, K. B. *J. Chromatogr. A*, 1994, *680*, 353.

Influence of the Source Geometry on Ion Formation in LC/Thermospray-MS.

M. Honing[1a], D. Barceló[1a], J. Abian[1b], E. Gelpí[1b], D. Volmer[2], K. Levsen [2], B.L.M. van Baar[3] and U.A.Th. Brinkman[3].

Departments of 1a) Environmental and 1b) Neurochemistry, CID/CSIC, Barcelona, Spain. 2) Department of Analytical Chemistry, Fraunhofer Institute, Hannover, Germany 3) Department of Analytical Chemistry, Free University, Amsterdam, The Netherlands.

LC/Thermospray-mass spectrometry has been extensively applied for the identification and determination of carbamate pesticides in various environmental samples, in our laboratories [1-3]. In these studies the influences of many parameters were investigated and optimized. For some carbamates significant differences between their mass spectra were observed, when using various interface types. Although it has never systematically been investigated, we thought that the ion source geometry might play a role in the ion formation of various types of compounds. In this presentation the results of a comparison study among three thermospray interfaces and their standard ion source (a Hewlett Packard 5988A, and a Finnigan MAT TSQ 700 with their respective standard TSP interfaces and a Vestec 700 TSP interface on a Finnigan SSQ 4600) are presented using 16 carbamate pesticides (*N*-methylcarbamates, *N*-phenylcarbamates, Methyl ester substituted carbamic acid and a *N*-dimethylcarbamate) [4].

Table 1. The main ions formed, and their relative abundances, of sixteen carbamates with a Vestec (A), a HP (B) and a Finnigan (C) type of thermospray interface, using filament assisted ionization with an 50:50 mixture of methanol-water and 100 mM ammonium acetate adjusted at pH 6.

	Compound	200 °C			250 °C			300°C		
m/z	ion structure	A	B	C	A	B	C	A	B	C
	Aldicarb									
249	$[M+59]^+$	3	8	10	2	11	14	1	7	16
222	$[M+32]^+$	23	13	2	20	13	5	21	29	17
208	$[M+NH_4]^+$	100	100	100	100	100	100	100	100	45
191	$[M+H]^+$	7	7	5	8	12	14	10	15	15
148	$[M+H-MeNHCOOH+MeOH]^+$	7	6	15	14	24	59	30	60	100
	Carbofuran									
280	$[M+59]^+$	3	11	9	2	10	4	1	3	2
239	$[M+NH_4]^+$	100	100	26	63	71	5	30	10	
222	$[M+H]^+$	72	30	100	100	100	100	100	100	100
	Promecarb									
266	$[M+59]^+$	2	12		1	7	2	1	8	2
225	$[M+NH_4]^+$	100	100	100	100	100	100	100	100	22
208	$[M+H]^+$	15	10	10	20	17	53	40	75	100

In Table 1 the results are listed for some representative carbamates. For 12 of the 16 investigated carbamates nearly identical results are obtained if the different thermospray interfaces are operated under comparable conditions and at an ion source temperature of 200 °C. The differences in the mass spectra of the other four compounds are related either to their thermal instability (asulam, thiodicarb and thiofanox) or to a strong heat and pressure dependence of the equilibrium between the protonated molecule and the ammonium adduct ion (carbofuran). Increasing the ion source temperature to 250 and 300 °C diminishes the formation of ammonium adduct ions and promotes fragmentation. This source temperature effect is largest for the Finnigan interface and consequently causes a divergence in the thermospray mass spectra obtained with the various TSP interfaces. It was found that an ion source temperature of 250-260°C results in the highest signal to noise ratio for all compounds and interfaces (Figure 1). Furthermore, for some carbamates at all ion source temperatures a [M+32]+ ion was observed, which is probably due to thermally-assisted hydrolysis of the carbamate group in the vaporizer probe prior to ionization.

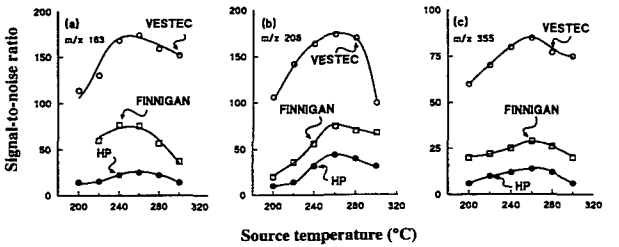

Figure 1. The signal-to-noise (S/N) ratios for the protonated molecules, $[M+H]^+$, of methomyl (A), promecarb (B), and thiodicarb (C), at m/z 163, 208 and 355, respectively, as a function of the ion source temperature

Acknowledgment

Miss R. Alonso is thanked for her assistance in performing the experimental work. This research was supported by the Environmental Programme of the Commission of the European Communities (Contract No. EV5V-T92-0061) and CICYT (Contract No. AMB93-1427-CE).

References

1) M. Honing, D. Barceló, B.L.M van Baar, U.A.Th Brinkman, *J Am. Soc. Mass Spectrom.*, 5 (1994) 913-927

2). D. Volmer, A. Preiß, K. Levsen and G. Wünsch., *J Chromatogr.*, 647 (1993) 235.

3). D. Volmer, K. Levsen, *J. Am. Soc. Mass Spectrom.*, 5 (1994) 655-676.

4) D. Volmer, K. Levsen, M. Honing, D. Barceló, J. Abían, E Gelpí, B L.M. van Baar and U.A Th. Brinkman, *J Am. Soc Mass Spectrom.*, in press.

Determination of Anabolic Steroids by HPLC UV-VIS/Particle Beam Mass Spectrometry

Mantai Z. Mesmer and R. Duane Satzger, USFDA, Forensic Chemistry Center,
1141 Central Parkway Cincinnati, OH 45202

In February of 1991 Congress designated 27 steroids and their esters, salts and isomers as Schedule III Controlled Substances. This action expanded the analyses of steroids from toxicological to forensic areas (seized exhibits). Commercially available anabolic steroids are synthetic derivatives of testosterone and include many closely related ring structures as well as their esters. Products seen in the illegal market are mostly oil based injectables, water suspensions, dietary supplements and herbal drugs marketed as capsules or tablets, which often do not contain the ingredients declared on the label.

The analysis of steroids is complicated by the sheer number of known steroids (over 7000), the close structural similarities common to the entire class, their poor volatility, thermal lability and low UV extinction coefficients. We have developed a general screening method for the determination of anabolic steroids in oil based injectables and other pharmaceutical preparations. The compounds are extracted into methanol and separated on a reversed phase column with an acetonitrile/water gradient and detected by using a uv-vis detector and mass spectrometer sequentially. Identification is based on retention time, uv spectra and mass spectra. Mass spectral confirmation is accomplished by matching with a standard when available, and/or by comparison with in-house generated or commercially available library of EI mass spectra

The mass spectrometer used is a Hewlett-Packard 5989A equipped with a particle beam interface. Mass spec parameters were set as follows: ion source temperature: 250° C, quadrupole at 100° C, EM voltage 2072V, mass range monitored 56-460. The HPLC is a Hewlett-Packard model 1090L equipped with a photodiode detector.

The EI mass spectra of 36 steroid standards were generated by FI introduction of 200-1000ng amounts into the mass spectrometer and stored in a unique library. This library is used frequently in our laboratory for confirmation of the presence of anabolic steroids in forensic samples. We have found acetonitrile to be a better mobile phase than methanol because, as the percent methanol goes above 90 there is a drastic increase in the baseline of the total ion chromatogram, while increasing percentage of acetonitrile has little effect on the baseline. In addition, acetonitrile shows less overall background and a lower UV cutoff. There is no significant difference in sensitivity when using either solvent.

Under the gradient conditions used (from 60% acetonitrile to 90% acetonitrile in 20 minutes) one can separate at least 21 of the anabolic steroids used in this study. The tandem nature of the analysis provides quantitative as well as qualitative information in a single experiment. Figure 1 is the total ion chromatogram of a herbal medicine claimed to cure a host of ailments. Only methyltestosterone and sugars were detected in the sample. Figure 2 is a total ion chromatogram of a veterinary drug sample suspected of containing four steroids in cottonseed oil. All four steroids were confirmed in the sample using the in-house generated library of EI spectra. The percent recovery for three representative steroids spiked in sesame oil is better than 96%. We have applied this method in the analysis of oil based steroid containing vet drugs, food supplements and herbal drugs.

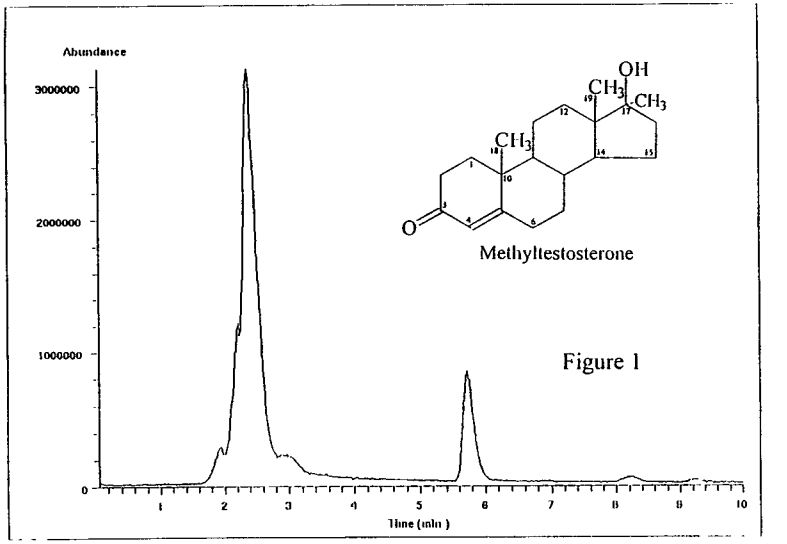

Figure 1

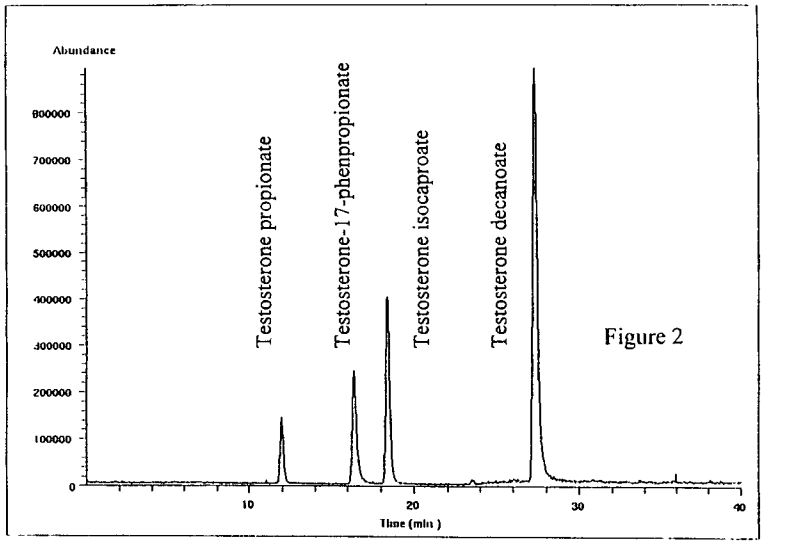

Figure 2

LC Particle Beam MS with Massive Cluster Impact

T.-C.L. Wang, L.J. Cornio and S.P. Markey
Section on Analytical Biochemistry, National Institute of Mental Health, Bethesda, MD 20892

Introduction

Massive cluster impact (MCI) uses very large, highly charged clusters of glycerol as a primary desorption beam. The primary beam is formed by electrohydrodynamic emission of an electrolyte-glycerol solution in a vacuum(1). One advantage of this technique compared to FAB/SIMS is the formation of singly and multiply charged molecular ions similar to electrospray ionization(2). Secondly, liquid matrices are not required for the successful desorption of biomolecules by MCI ionization. MCI produces spectra from dissolved samples in commonly used FAB/SIMS liquid matrices and from dry solid samples(3).

Particle beam LC/MS with FAB has been reported(4). Interfacing particle beam LC with MCI mass spectrometry allows transport of desolvated molecules to the probe target and desorption and ionization of the solid samples. The feasibility of LC particle beam with MCI was demonstrated by repetitive flow injections of acetylcholine and gramicidin S.

Experimental

All the experiments were performed on Finnigan-Mat TSQ-70 mass spectrometer equipped with a Phrasor Scientific (Duarte, CA) MCI ion gun. The MCI gun was positioned on a 0.5" thick Lucite window in line with the EI electron entrance hole. The solution used for cluster generation was 1.5 M ammonium acetate in glycerol. The flight tube for the cluster beam was approximately 1.5" away from the probe. Typical MCI gun operating voltages were 17 kV on the emitter, 15 kV on the focus element, and 2 to 5 kV on the extractor. The optimal signal stability was obtained when cluster current monitor indicated between 4 to 10 μA.

A Hewlett-Packard (HP) particle beam interface delivered essentially solvent-free analyte molecules through a side port directly into an EI ion source at room temperature (Figure 1). The EI ion source was inverted from its normal orientation and the filament block was removed. The LC (HP-1050) flow rate was 0.4 mL/min and the solvent was 1:1 water and methanol. For gramicidin S experiments, 0, 15, or 50 ppm of glycerol was added to the water.

A 45° polished copper probe tip similar to the Finnigan standard FAB/SIMS copper tip but four times larger surface area was positioned ~45° to the incidence of the cluster primary beam and ~45° to the incoming particle beam.

Results and Discussion

The feasibility of LC particle beam with MCI was first demonstrated by repetitive injections of 20, 50, 100 and 200 ng of acetylcholine. The ion chromatogram contains peaks 30sec wide with consistent height as detected by selected ion monitoring (SIM). This result indicates that dried molecules were transported by the particle beam and desorbed completely from the target surface by the massive cluster beam in a relatively short period of time. The background was monitored by characteristic debris ions from MCI (e.g., m/z 110, 202, etc.). They remain constant. LC particle beam MS with MCI was further tested with a larger molecule, gramicidin S. Full scan spectra of gramicidin with 10 to 1 S/N can be obtained by repetitive injections of 440 picomoles of gramicidin S. Clearly, molecules as large as gramicidin S were able to be transported by the particle beam, desorbed, and mass analyzed. It was found that mixing glycerol in the mobile phase improved the stability and sensitivity of detection. The sensitivity of the present instrument configuration was shown by repetitive injections of 44 picomoles of gramicidin S detected by SIM of the +2 charge state, $[M+2H]^{2+}$, of the molecule (m/z 571, Figure 2). In this experiment 25 ppm of glycerol was added to the mobile phase.

From our initial results, the LC particle beam MS with MCI shows great applicability and sensitivity for polar organic compounds and has potential of becoming a routine LC/MS device.

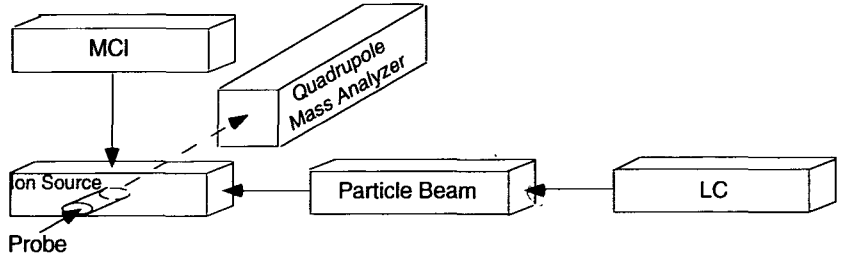

Figure 1. Block diagram of LC particle beam with MCI.

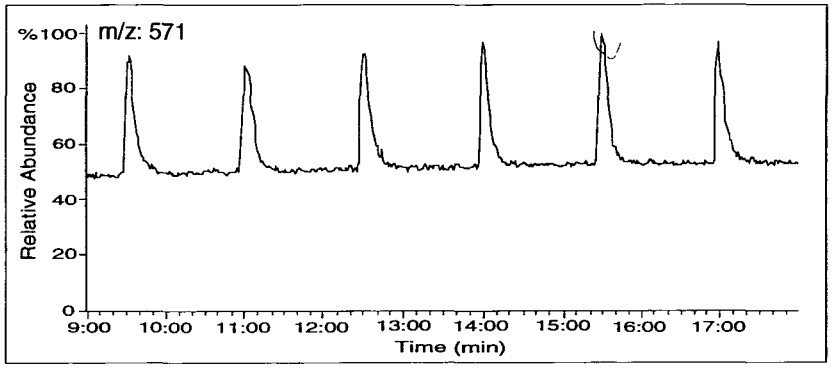

Figure 2. Flow injections of 44 picomoles of gramicidin S. Data were acquired in the SIM mode of the +2 charge state of gramicidin S.

References
(1) J. F. Mahoney, J. Perel, S. A. Ruatta, P. A. Martino, S. Husain and T. D. Lee, Rapid Commun. Mass Spectrom. 5, 441 (1991).
(2) D. S. Cornett, T. D. Lee and J. F. Mahoney, the 42nd Annual ASMS conference on Mass Spectrometry and Allied Topics, Chicago, IL., May 1994, p781.
(3) D. S. Cornett, T. D. Lee and J. F. Mahoney, Rapid Commun. Mass Spectrom. 8, 996 (1994).
(4) J.D. Kirk and R.F. Browner, Biomed. Environ. Mass Spectrom., 18, 355 (1989).

Particle Beam LC/MS using a Glow Discharge Ionization Source

Patrick A. DePalma, Jr., Jianzhang You, and R. Kenneth Marcus

Clemson University, Department of Chemistry, Howard L. Hunter Laboratories, Clemson, SC 29634-1905

Ross C. Willoughby and Edward W. Sheehan

Chem-Space Associates, 75 Chapel Ridge Place, Pittsburgh, PA 15238

The coupling of liquid chromatography with mass spectrometry has proven to be a powerful tool for the analysis of involatile organic compounds which heretofore have required substantial chemical processing for GC/MS analysis. Less common has been the use of LC separation of elemental (inorganic) species prior to mass spectrometric analysis. Unfortunately, ion sources which are applicable to one type of analysis (organic/inorganic) are not applicable for the other. For example, chemical ionization is not a viable option for elemental analysis. A "universal" ion source which could be applied to both sample types could be very valuable. The glow discharge is one such device.

For this presentation, we describe the interfacing of liquid chromatography to a hollow cathode ion source via a particle beam interface. Specifically, a hollow cathode discharge has been adapted to a particle beam LC/MS instrument (benchmark™, Extrel). The combination of a thermoconcentric nebulizer, particle beam interface, and the hollow cathode discharge allows the efficient introduction of low volatility mobile phases (e.g., water) at flow rates of up to 1.5 mL/min. Data will be presented illustrating the utility of this combination of sample introduction and ionization in the analysis of organic, organometallic, and elemental species. The role of discharge conditions on the fragmentation of organic species and intensities of atomic ions will be presented as a point of comparison to existing methodologies. Figure 1 contains the stacked electron impact (EI), chemical ionization (CI), and representative glow discharge (GD) spectra of brucine.

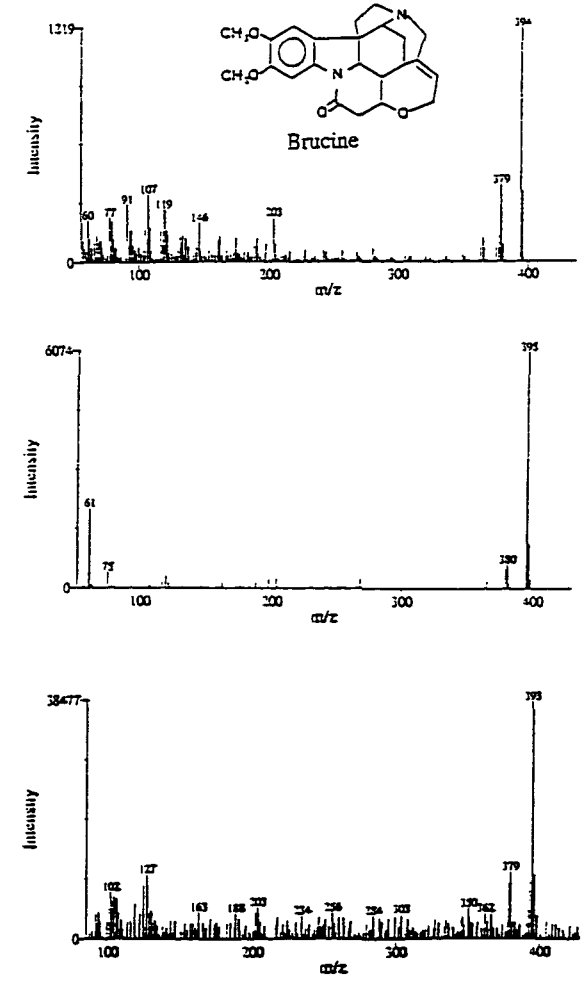

Figure 1. Electron impact (EI), chemical ionization (CI), and glow discharge (GD) mass spectra of brucine, respectively.

Application of LC/Particle Beam/MS for the Identification of N-Nitrosamines in Cosmetic Skin Products and Their Raw Materials

Stanley M. Billedeau, Jon G. Wilkes, David L. Vollmer, and Harold C. Thompson, Jr. FDA, NCTR, Jefferson, AR 72079

INTRODUCTION: For many years the occurence of volatile N-nitrosamines, known carcinogens (e.g.: R_2N-N=O), in various consumer products (bacon, latex rubber infant pacifiers, beer, and nitrite preserved hams packaged in latex rubber netting) has been monitored and regulated.To reduce or eliminate these hazardous contaminants and hence, lower the risk of cancer posed by human consumption or use of such products. Recently, a reversed phase LC/particle beam (PB) interfaced to a TEA or LC/PB/TEA method[1] for detection of low volatility N-nitrosamine contamination in cosmetic skin creams has been introduced using a parallel confirmation by LC/PB/MS employing EI/MS and (+) ion, methane CI/MS[2]. N-Nitrosodiethanolamine (NDELA) and N-nitrosomethyl-p-amino-2-ethylhexylbenzoate (NMPABAO) are two low volatility nitrosamines reported as contaminants in skin care cosmetic products.[1,3] In this study, a forced nitrosation reaction (1 M $NaNO_2$ at pH 2.5 and/or Bronopol addition) was performed on several cosmetic raw materials used in formulations of skin creams or moisturizers. The objective was to determine the possibility of formation of N-nitrosamines in the raw materials under similar conditions present in off-the-shelf cosmetic products.

EXPERIMENTAL INSTRUMENTATION: The LC/PB/TEA consisted of a Spectra Physics 8800 LC pump with a Universal Interface UIB (Vestec, Houston, TX) with a single stage momentum separator for particle beam and a TEA model 502 (Thermo Electron, Waltham, MA). The PB/MS used a UIB with a dual stage momentum separator interfaced to a Vestec LC/MS model 201 (Vestec, Houston, TX). The LC/Electrospray was performed on a Finnigan MAT TSQ7000 (San Jose, CA). The LC column used for LC/PB/TEA and EI/MS was a MetaChem C-8, 250 x 4.6 mm, pumped isocratically at 1 ml/min of 80:20 ACN/water (0.025 M NH_4 Acetate). The ESI/MS was performed on a Microbondapak C-18, 300 x 3.9 mm column at 1 ml/min of 85:15 ACN/water using a 1:4.5 split (or 222 μl/min into the MS).

NITROSATION PROCEDURE : A 20-50 mg sample of the raw material was weighed into a 10 ml tube. A 1 ml aliquot of $NaNO_2$ (1 M in 2.5 pH glacial acetic acid) solution was added to the tube and vortexed for 1 min to mix. The reaction was carried out for 1 hr at room temperature in the dark. The nitrosation is stopped by addition of 2 ml of sat. Na_2CO_3 (pH=10). The resulting solution is extracted with 5 ml of hexane (3 + 2 ml). The combined organic (top) phase was evaporated to dryness (in low light conditions). The raw material extract is made up in exactly 2 ml ACN. Ten microliter aliquots of the final 2 ml extract was analyzed by LC/PB/TEA and EI/MS and 20 ul of a 1:10 dilution was analyzed by LC/ESI/MS. The same extraction procedure was used on the non-nitrosated raw materials (with no $NaNO_2$ present) and a blank (1 ml of pH 2.5 glacial acetic).

RESULTS AND DISCUSSION:

LC/PB/TEA The TEA analysis of the nitrosated Padimate O recorded peaks at 6.3, 7.0, 7.7 and 8.5 min. The 7.0 min peak was the N-nitroso Padimate O (NMPABAO) which has also been confirmed by particle beam EI and (+) methane CI/MS in a cosmetic cream formulation.[2] The NMPABAO peak was an order of magnitude greater than in the parent material due to the forced nitrosation. Both allantoin and imidazolidinyl urea were subjected to the nitrosation procedure. No other TEA response was shown past the 2.3 min peak near the void volume (i.e. indicates no nitrosation occurred and little chance of problems from nitrosamine contamination in skin cream products).

LC/PB/EIMS Although the retention times were slightly shorter, the LC/PB/MS chromatogram (Fig. 1) indicated that following nitrosation of the Padimate O, the parent material is the major peak at 7.3 min exhibiting a strong EI spectrum with 277, 278, and 165 ions (M, M+1, and 100% peak, resp.) and four other peaks at 5.2, 5.5, 6.1, and 6.5 min. The 5.5 and 6.1 min peaks are the free amine, MPABAO, a very minor peak, and the N-nitrosamine of MPABAO (NMPABAO), respectively. These two peaks were previously identified by EI and (+) methane CI/MS in a nitrosated cosmetic sample containing Padimate O.

LC/ESI/MS To obtain molecular weight data, the nitrosated Padimate O extract was subjected to electrospray ionization (ESI). The RIC and several ion chromatograms are shown in Figure 2. Although retention times were not comparable with EI/MS chromatograms, the 6.1 min major peak was confirmed to be the parent material exhibiting M+H and M+H+ACN (or M+41 m/z) ions at 278 and 319 m/z. Although an NMPABAO peak was not detected, a 5.1 min peak with ions at 305 and 346 m/z was indicated which was also detected by EI/MS.

CONCLUSIONS: Two of the three raw materials, allantoin and imidazolidinyl urea, indicated no sign of N-nitrosamine formation following nitrosation. However, as in similar experiments on a cosmetic cream containing Padimate O, the nitrosation of the raw material produced the N-nitrosamine, NMPABAO, and several other possible compounds which need to be identified. The use of UV degradation studies using LC/PB/TEA and EI/MS may be useful in helping to identify the unknown peaks as UV labile N-nitroso compounds. Also, experiments using UV photolysis prior to ESI/MS will be used to further examine the nitrosated raw material as well. We feel that the combination of LC/PB/TEA, LC/PB/EIMS and LC/ESI/MS will be a powerful tool for helping to answer some if not all of the questions presented by environmental nitrosation of amine raw materials in cosmetic skin products. Although there are hundreds of primary, secondary, and tertiary amine raw materials used in formulating skin care cosmetic products, it is possible that utilizing analytical techniques such as these will make the job of determining which raw materials do not undergo nitrosation in real world cosmetic formulations a little easier for the FDA chemist.

REFERENCES:

1. Billedeau, S.M., Heinze, T.M., Wilkes, J.G., and Thompson, H.C.,Jr. J. Chromatog. A, 688 (1994) 55-65.
2. Wilkes, J.G., Heinze, T.M., Freeman, J.P., and Billedeau, S.M. Proceed. of the 42nd ASMS Conf. on MS and Allied Topics, May 29-June 3, 1994, 175.
3. Meyer, T.A. and Powell, J.B. JAOAC, 74 (1991) 766-771.

Figure 1.

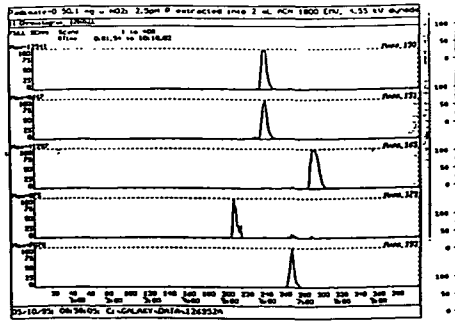

Figure 2.

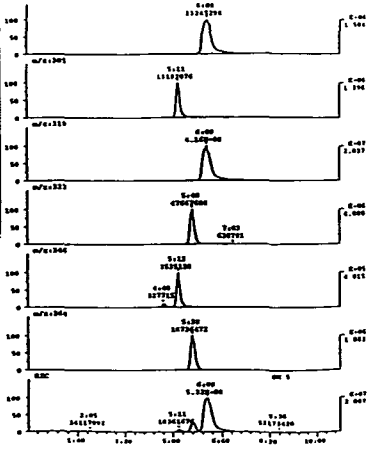

SFC/MS: DEVELOPMENT AND PROBLEM SOLVING

J. David Pinkston, Rosemary T. Hentschel, Claudia A. Smith, Timothy R. Baker, and Donald J. Bowling, The Procter & Gamble Company, Miami Valley Laboratories, P.O. Box 538707, Cincinnati, Ohio 45253-8707 U.S.A.

This presentation (1) illustrates the power of supercritical fluid chromatography/mass spectrometry (SFC/MS) for solving industrial problems with representative examples, and (2) describes the design of and early results from a modified electrospray ionization (ESI) interface for open-tubular SFC/MS. SFC/MS is a powerful technique for solving problems in a variety of industrial areas. The utility of SFC/MS is ultimately drawn from the unique combination of properties inherent in a supercritical fluid mobile phase: as compared to a liquid, supercritical fluids offer greater efficiency and/or greater speed of analysis; as compared to a gas, supercritical fluids provide greater molecular weight range. In addition, SFC/MS with a traditional ion source allows full access to electron and chemical ionization techniques for nonvolatile analytes. These ionization methods can be powerful tools in solving problems, and are not always available with modern liquid chromatography/MS methods. Applications of SFC/MS involve mixtures which range from nonpolar (polysiloxanes), to moderately polar (surfactants), to ionic (polyacrylates). Low molecular weight polysiloxanes and polysiloxane-containing polymers are important components in many industrial and consumer products. The detection and identification of low levels of polysiloxanes, especially functionalized polysiloxanes, can provide valuable clues in deciphering the structure of a polymer. Figure 1 shows an example of this type of work. The left trace shows the reconstructed-ion-current chromatogram of a functionalized polysiloxane. The NH_3 CI spectrum of one of the components, the oligomer containing 16 dimethylsiloxane units, is shown on the right. We postulate that this oligomer is capped with a phenyl group on one end, and an alkyl chain bearing a hydroxyl group on the other. Other examples of mixtures which we have characterized using SFC/MS include surfactants and emulsifiers, "active" (i.e., tend to adsorb on components of a chromatographic system) pharmaceutical agents, and polyacrylates.

Most open-tubular SFC/MS is performed with pure CO_2 as mobile phase, pressure/density programming, a fixed flow restrictor, and the direct-fluid-introduction interface coupled to an EI/CI ion source. The flow of CO_2 from the column to the ion source thus increases over the course of a separation. This usually has little effect, but can cause a change in the ionization mechanism and/or the ion transmission efficiency under some conditions. Atmospheric pressure ionization should avoid this potential source of problems. The groups of Henion (1) and Markides (2) have used the "heated nebulizer" and atmospheric pressure chemical ionization. Sadoun et al. have used ESI for SFC/MS (3). However, adding an organic modifier to the mobile phase was required for ionization. We've designed a "sheath-flow" interface for SFC/ESI-MS. Addition of modifier to the mobile phase prior to the separation is not required. Figure 2, an example of our early results, shows the SFC/ESI-MS chromatogram and spectrum for didodecylamine. As expected, the spectrum is dominated by the ammonium adduct ion. The [M+44+1] is an adduct with CO_2 which may be formed in the ion source or in the chromatographic column.

(1) Huang, E., Henion, J., and Covey, T.R., J. Chromatogr. 511:367-370, 1990.; (2) Tyrefors, L.N., Moulder, R.X., and Markides, K.E., Anal. Chem. 65:2835-2840, 1993.; (3) Sadoun, F., Virelizier, H., and Arpino, P.J., J. Chromatogr. 647:351-359 1993.

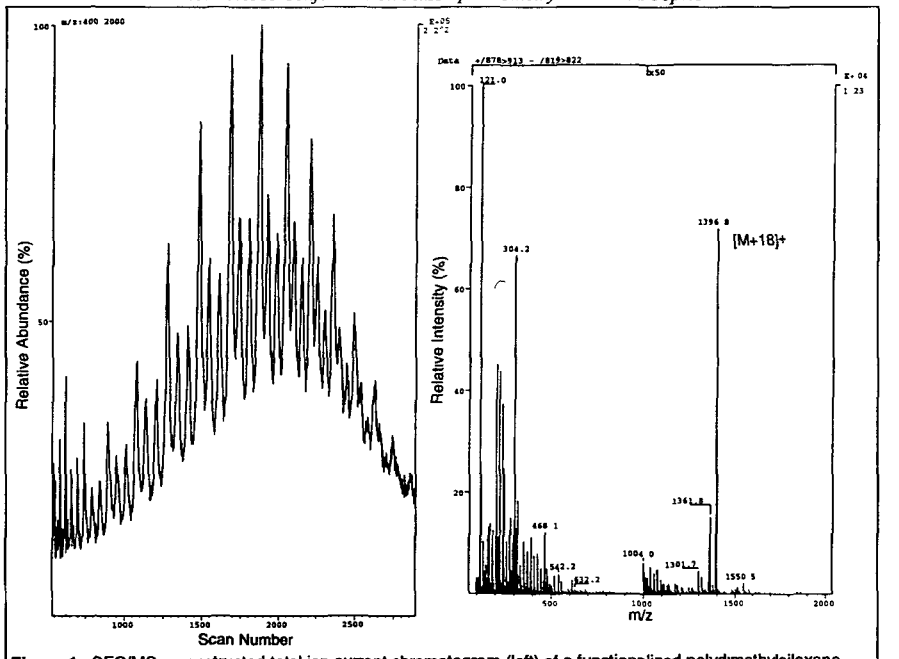

Figure 1. SFC/MS reconstructed-total-ion-current chromatogram (left) of a functionalized polydimethylsiloxane. These types of mixtures are important components of, or building blocks for polymers in, many consumer products. The NH_3 CI spectrum (right) is of the oligomer containing 16 dimethylsiloxane units.

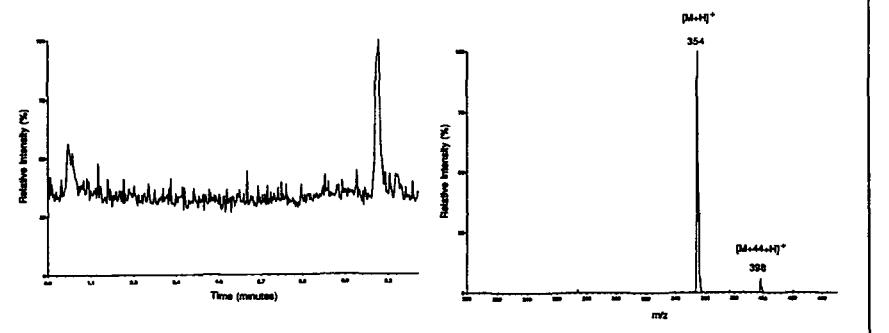

Figure 2. SFC/ESI-MS reconstructed-total-ion-current chromatogram (left) and spectrum (right) for didodecylamine

Separation and Identification of *meso* substituted tetraphenylphorphyrins

M. R.Marques Domingues, M. A. Faustino, M. G. O. Santana Marques, and A. J. Ferrer Correia

Department of Chemistry - Mass Spec. Lab., University of Aveiro - Portugal

Porphyrins and related tetrapyrrolic analogues are a large and important group of natural and synthetic compounds. They play a significant role in life biochemistry, chemistry, chemical industry, geology and medicine Some of their more recent applications are as oxidising catalysts, in the conversion of light energy in chemical energy, as diagnosis agents and in photodynamic therapy[1]. Mass spectrometry has been widely used for the characterisation of this compounds specially after the development of desorption ionisation methods.

In this work HPLC with Vis and MS detection was used to analyse a synthetic mixture of *meso*-substituted tetraphenylporphyrins that were not amenable to separation. The mixture was obtained by condensation of pyrrole with 4-methoxybenzaldehyde and 4-nitrobenzaldehyde by using a published method[2]. The presence of a mixture sample was confirmed by FAB-MS although it was not possible to identify, positively, all the constituent porphyrins. The porphyrins that we expected to be in the mixture are shown in Figure 1.

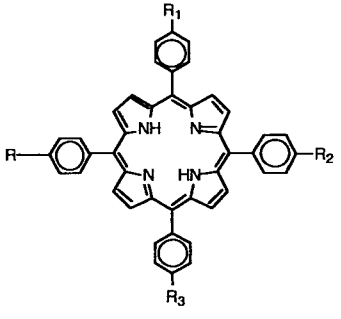

Porphyrins	
1	R=R1=R2=R3=OCH3
2	R=R1=R2=OCH3 ; R3=NO2
3	R=R1=OCH3 ; R2 =R3=NO2
4	R=R2=OCH ; R 1=R3=NO2
5	R=OCH3 , R1=R2=R3=NO2
6	R=R1=R2=R3=NO2

Figure 1

We were unable to separate this porphyrins by the usual methods, although several attempts were made using normal phase and reverse phase HPLC. Only when carbonated methanol was used as eluent in reverse phase HPLC the separation was possible.

HPLC separations were carried out using a reverse phase HPLC system (307 Gilson) and Vis absorbance detector (SFA 103, Kratos, Schoeffel Instruments) monitored at 410 nm. The eluent consisted of carbonated methanol prepared by addition of 1.4% ammonium carbonate to methanol HPLC grade. The flow rate was 0.5 ml/min. Samples were injected in the column (5μl) in chloroform solution.

FAB and Coaxial Continuous Flow-FAB mass spectra were obtained using a VG Autospec EBE-Q mass spectrometer equipped with a OPUS2.1c data system. A focused Cs ion gun with a primary ion of 20 keV energy and ion current about 3 μA was used. For FAB -MS 3-nitrobenzylalcohol was used as FAB matrix and for Coaxial Continuous Flow / FAB the matrix solution was methanol / 3-NBA / TFA 3% (87/10/3).

In the HPLC analysis of the mixture six peaks were separated. The FAB mass spectra of the mixture show some major peaks that we can identify as the $[M+H]^+$ ions of the porphyrins which were expected to be in the mixture. The correspondent molecular ion $M^{+\cdot}$ are also present but with less abundances, in agreement with other published FAB - MS studies of porphyrins[3]. The same HPLC system was also directly interfaced with a Coaxial Continuous Flow / FAB probe. The Selected $[M+H]^+$ Ions Chromatograms of porphyrin 1 and porphyrin 2 are shown in figure 2. The five porphyrins were identified by their $[M+H]^+$ ions.

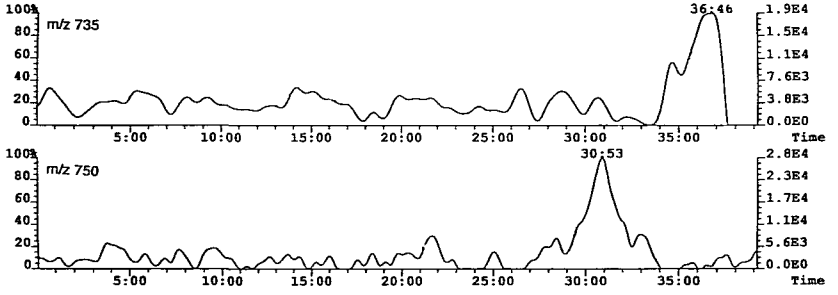

Figure 2-Selected $[M+H]^+$ Ions Chromatograms of porphyrin 1 (m/z 735) and porphyrin 2 (m/z 750)

The presence of six compounds is confirmed by HPLC and five of them are identified as the *meso*-substituted tetraphenylporphyrins 1-5, by HPLC/MS from their $[M+H]^+$ ions.

HPLC directly interfaced with a Coaxial CF-FAB is an important and rapid method for the analysis of mixtures such as the porphyrin mixtures obtained either during the process of organic synthesis or in the extraction from natural compounds.

---

1 - T. J. Dougherty, *Photochem. Photobiol*, **1987**, 45, 879

2 - M. d'A. Rocha Gonsalves, J. M. T. B. Varejão and M. M. Pereira, *J. Heterocyclic Chem. Commun.*,**1991**, 28, 635

3 - B. Musselman, D. Kessel and C. K. Chang, *Biomed Environ. Mass Spectrom.*, **1988**, 15, 257-263

Quantitative Analysis of Abscisic Acid in Plant Embryogenic Tissue Using Liquid Chromatography/Continuous Flow Secondary-ion Mass Spectrometry with Reaction Monitoring: a Comparision with the ELISA Assay

L.R. Hogge, S.R. Abrams, G.D. Abrams, C.A. Bock, D.I. Dunstan , D.J. Olson and A.C. Shaw

Plant Biotechnology Research Institute, National Research Council of Canada
110 Gymnasium Place, Saskatoon, Saskatchewan, S7N 0W9, CANADA

Introduction:

The plant hormone (+)-abscisic acid (ABA) is known to regulate many processes in higher plants. We are interested in how (+) and (-) ABA stimulate spruce somatic embryo maturation, in order to develop procedures that will be applicable to a broad range of genotypes. As part of this approach it was necessary to determine the uptake and fate of exogenous ABA by the plant tissue during the maturation process. An ABA-enzyme-linked immunosorbent assay (ELISA) system provides a relatively accessible and sensitive method for quantifying natural ABA. In addition to the ELISA system, we have used packed capillary liquid chromatography /liquid secondary ion tandem mass spectrometry (LC/LSIMS/MS) to achieve two objectives: a) to develop methodology for quantifying ABA extracted from spruce embryogenic tissue, and b) to discriminate between ABA of exogenous and endogenous origins. This report describes the MS methodology developed as well as the results obtained from the analysis of Picea glauca x engelmannii somatic embryogenic tissue extracts.

Experimental:

ABA extraction from tissues:

Internal standards [8',8',8',9',9',9'] (+) d_6 ABA and [7',8',9'] (±) $^{13}C_3$ ABA were synthesized at this institute using a procedure that will be published elsewhere. Two hundred ng of the d_6 ABA was added to 10 mg of lyophilized plant tissue and the mixture extracted with .05% acetic acid in MeOH overnight. The samples were centrifuged, filtered using 2 µm filters and evaporated using a SpeedVac. The extracts were re-dissolved in MeOH and eluted through an acidified LC-SCX column, the filter washed with MeOH and the eluates evaporated to dryness. The extracts were re-dissolved in 50% MeOH:water, filtered through a Centricon-3 filter using a centrifuge, divided into two aliquots (one for ELISA and one for LC/MS/MS) and evaporated to dryness. Finally the aliquots for LC/MS were dissolved in 25% acetonitrile in water at a concentration of 10 ng/ul of the d_6 ABA internal standard (calculated from the original amount of standard added).

ELISA:

An indirect ELISA for (+)-ABA was used, following the method of Walker-Simmons, 1987.

LC/MS and LC/MS/MS analyses:

All analyses were done using an Applied Biosystems Model 140A Solvent Delivery Syringe Pump System. Samples were injected through a Rheodyne Model 7520 injector (1 µL loop) on to a Spherisorb 3 micron C18 ODS2 (0.32 mm ID by 200 mm) packed capillary column prepared in this laboratory.

The mobile phase used for the LC analyses consisted of the following: solvent A, 0.1 % TFA and 2% glycerol in 95 % acetonitrile; solvent B, 0.1% TFA in 2 % glycerol. The gradient elution program was as follows: 90% solvent B to 30 % in 10 min, held for 2 min, then to 0% in 3 min and then held for 10 min.

The LC system was interfaced to a VG Analytical 70-250 SEQ hybrid mass spectrometer equipped for continuous flow SIMS analysis. Reaction monitoring experiments were carried out by monitoring the loss of water from the protonated molecular ions for d_6 ABA (m/z 271.1 to 253), $^{13}C_3$ ABA (m/z 268.1 to 250 .1) and ABA (m/z 265.1 to 247.1).

Results and Discussion:

The spruce cultures were grown on medium containing 40 µM (±) ABA. The ABA taken up by the cultures was measured using LC/MS/MS and the ELISA system.The LC/MS/MS results and a comparision of these data with the ELISA data are shown here.

It is important to note that in order to obtain useful LC/MS data with the packed fused silica columns, it was necessary to elute the extracts through a high molecular weight filter and an LC-SCX ion exchange column prior to analysis. Without these additional cleanup steps, we have observed a serious degradation in both the chromatographic separation and the intensity of the ion current.

The two internal standards, d_6 ABA and $^{13}C_3$ ABA were used for reaction monitoring (loss of water transition) MS quantitative analyses with several calibration curves generated. This was done by analysing a known amount of the d_6 and $^{13}C_3$ standards relative to varying amounts of natural ABA respectively as well as a known amount of d_6 relative to varying amounts of $^{13}C_3$ ABA. **Figure 1** shows the plot of the natural ABA ion count/ d_6 ABA ion count ratio against the amount of ABA injected. The plot is linear over at least the range of 500 pg to 13 ng of ABA injected.

For the MS analysis, the known amount of d_6 ABA was added to the lyophilized tissue before extraction in order to ensure accurate quantitative data. Using this method, an extract of tissue that had been fed racemic ABA and harvested after Day 1, was found to have taken up 615 ng ABA

Endogenous ABA can be distinguished from exogenous by feeding $^{13}C_3$ ABA and using d_6 ABA as the internal standard as described above. *Results from an experiment where* $^{13}C_3$ ABA had been added to the medium used to grow spruce embryogenic tissue showed that the tissue incorporated a significant amount of the labeled ABA. **Figure 2** shows a plot of comparison of the amount of $^{13}C_3$ ABA incorporated in the tissue over the time course (42 days) of the experiment determined by LC/MS/MS and the ELISA system. As an example, an extract obtained from 21-day-old tissue was found to contain 677 ng of $^{13}C_3$ ABA by MS and 358 ng of ABA using the ELISA.

The ELISA assay is specific for (+)-ABA, the naturally-occurring enantiomer, and will not detect (-)-ABA or either enantiomer of 2-trans ABA. In contrast, under the conditions reported here, the mass spectrometer detects both enantiomers of ABA as well as any 2-trans ABA that may be present.

No endogenous ABA was found in any of the tissue extracts harvested during the time course of this experiment. As the detection level for ABA using this method is about 250 pg, it can be calculated that if there is endogenous ABA produced under these conditions, the level is less than 450 pg per mg of tissue.

Figure 1

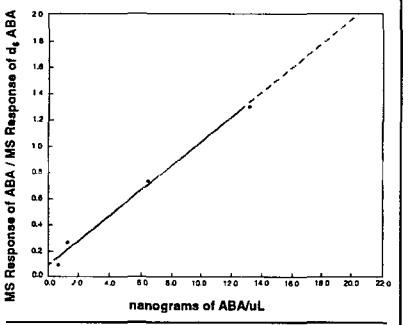

Figure 2

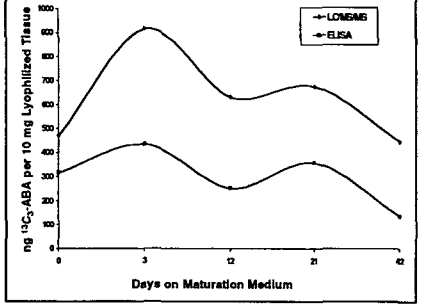

Evaluation of GCMS and FABMS for Analysis of Fungicidal DTTT Degradation

Lynn Teesch[†], Peter. S. Thorne and P. Subramanian[*]. Department of Preventive Medicine and Environmental Health and [†]High Resolution Mass Spectrometry Facility, University of Iowa, Iowa City, IA 52242

Introduction: DTTT (3,5-dimethyl-tetrahydro-2H-1,3,5-thiadiazine-2-thione) is a dithiocarbamic acid incorporated heterocyclic compound It is used as an agricultural fungicide, nematocide and herbicide and an industrial slimicide Hydrolysis of DTTT to the formation of primary intermediate (MeNH-C(=S)-S-CH_2-NHMe) has been hypothesized previously[1]. This intermediate is suggested to undergo further decomposition to formaldehyde and methylisothiocyanate (MeNCS) in aqueous media Decomposition of DTTT and the mechanistic pathways against the solution pH is not well understood[2] We have followed the degradation kinetics of DTTT in aqueous solutions and monitored the formation of intermediates and final products using UV-VIS and HPLC. We have carried out time-dependent FABMS analysis for the identification of primary intermediates from the hydrolysis reactions in FAB matrix from the partially hydrolyzed and aged DTTT solutions. We have also analyzed the hydrolytic degradation products of DTTT by GCMS and chemical derivatization methodologies. These techniques allowed the identification of several degradation products. Mass spectrometric results from these studies are discussed in this extended abstract.

Experimental: The sample preparation for GCMS analysis is as described· The product mixture resulted from the hydrolysis of DTTT in water ($5\ 0 \times 10^{-4}$ M or $1\ 0 \times 10^{-2}$ M) was freeze dried and extracted with 10mL CH_2Cl_2 and dried over anhydrous Na_2SO_4 Trimethylsilyl (TMS) derivatives were prepared by placing the freeze dried product mixture in reactivials with CH_3CN (200µL) and BSTFA (200µL) and stirring overnight or 7 days, at room temperature. 1µL of the extracts or their TMS derivatives in CH_3CN/ CH_2Cl_2 were injected for GCMS analysis GCMS analyses were carried out on a VG Trio-1 GCMS using DB-1 (DB-1, 15m; 0 32mm i d ; film thickness, 1µm) FABMS and collision induced decomposition (CID) experiments were performed on a VG ZAB-HF reverse geometry mass spectrometer The FAB matrices were thioglycerol, magic bullet, m-nitrobenzyl alcohol or triethanolamine Samples were bombarded with 8-keV Xe atoms and gun current of 1.5mA. Helium was used as the collision gas at analyzer pressures of 2×10^{-7} torr, as measured by the ion gauge in the second field-free region. Fragment ions formed by the unimolecular decomposition or by CID in the second field-free region were observed via MIKES The MIKES spectra are the results of averaging 8 to 10 scans

Results and Discussion: GCMS analysis allowed tentative identification of intermediates and products: 1,3-dimethyl-2-thiourea (**1**), N-methyl-dithiocarbamic-methyl ester (**2**), 2-methyl-5-dihydro-3H-4-thia-1,2-isooxazolidine-3-thione (**3**), 1,3,5-trimethyl-hexahydro-2H-1,3,5-triazine-2-thione (**4**), 4-methyl-5-methylimino-1,2,4-dithiazolidine-3-thione (**5**), 2,4-dimethyl-1,2,4-thiadiazolidine-3,5-dithione (**6**) Chemical derivatization with BSTFA allowed the characterization of -NH, -OH or -SH protons. Compound **4** (see below) had been previously synthesized[3] starting from methylamine, dimethylthiourea and formaldehyde. FABMS studies also allowed the identification of **4** and the structural confirmation was made by HR-FABMS and MIKES studies.

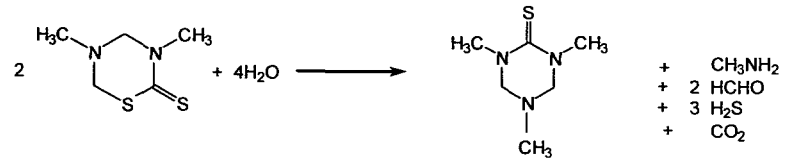

DTTT **4**

We have also analyzed CH_2Cl_2-extracts of MeNCS solutions by GCMS studies. Compounds **5** and **6** were observed as common products from MeNCS and DTTT solutions, with the same molecular formula and similar ions fragmentation pattern, but different GC retention times (t_r = 13.63min **5** 14 35min **6**) and relative abundance for m/z 105 and 137a.m.u. (Figure 1). Thorn had synthesized **5** and **6** by the oxidation of N,N'-dimethyldithiram disulfide[4]. N,N'-dimethyldithiram disulfide was synthesized by the mild oxidation of N-alkyldithiocarbamate. The CH_2Cl_2-extract containing products **1**, **4**, **5** and **6** were stable at 4°C for a period greater than 18 months.

43rd ASMS Conference on Mass Spectrometry and Allied Topics

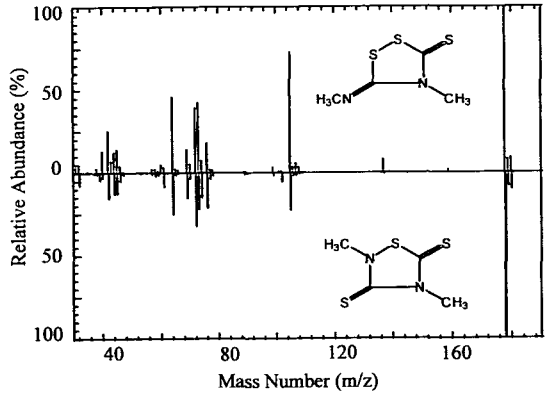

Figure 1 Mass spectra (EI) of products **5** and **6**

We were not successful in characterizing the putative intermediate(s) from the DTTT solution undergoing degradation in water or water-methanol solution. However, in strongly acidic solution (trifluoroacetic acid pH <2 0) and glycerol as the FAB matrix, mass ion having m/z 136a.m.u was observed When thioglycerol or magic bullet instead of glycerol was used as the FAB matrix, a new ion with m/z 140a.m u. was observed. We interpret that the compound having molecular weight 137 a.m.u undergoes a two electron reduction in thiol matrices as below

$$C_3H_7NOS_2 + 2RSH + H^+ \longrightarrow [C_3H_9NOS_2]H^+ + RSSR$$

Dithiocarbamates are also known to undergo easy oxidation and hence the formation of $[M-H]^+$ ion in glycerol matrix We tentatively assign the primary intermediate as N-methyl-N-hydroxymethyl-dithiocarbamic acid (**7**).

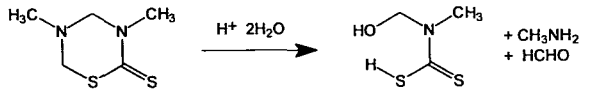

7

Time-dependent studies of DTTT decomposition using FABMS and GCMS techniques, GCMS provided most valuable information for the analysis and the identification of final products. Even though DTTT undergoes continuous decomposition in aqueous environment, GCMS is most useful technique for tracing the usage of DTTT by monitoring the most persistent triazine **4** which is efficiently extracted into CH_2Cl_2 We were unable to discern the ions corresponding to an intermediate following the addition of one mole equivalent water, possibly due to higher matrice background Currently, we are investigating HPLC-MS studies for the characterization of most polar intermediates and products from DTTT decomposition

Acknowledgement: The authors wish to acknowledge support from the University of Iowa Environmental Health Sciences Research Center, NIEHS (NIH/NIEHS P305605).

References

1 Goksöyr J. Acta Chem. Scand 1964, **18**, 1341-1352.
2. Morrell JJ, Lebow S. Wood and Fiber Sci 1988, **20**, 422-30.
3. Drescher N, Otto S. Residue Review. 1968, **23**, 49-54.
4 Thorn GD. Can. J Chem. 1960, **38**, 2349-58

Pentafluorobenzyl Chloroformate as a Derivatization Reagent for NCI/MS

J.T. Simpson, D.S. Torok and S.P. Markey
Section on Analytical Biochemistry, National Institute of Mental Health, Bethesda, MD 20892

Introduction

There have been several reports in the recent literature concerning the use of chloroformates for aqueous, rapid, room temperature one-step derivatization of amino acids (AA's) with analysis by GC or GC/MS [1,2].

We have investigated the use of pentafluorobenzyl chloroformate (PFBCF) as a reagent for this derivatization with analysis by GC/MS in negative chemical ionization mode [3]. In addition, PFBCF was used for the anhydrous derivatization of alcohols.

AA's were derivatized in aqueous solution, plasma and whole blood at room temperature. Phenethyl alcohol was derivatized under anhydrous conditions at 70°C.

Experimental

Preparation of pentafluorobenzyl chloroformate: The method of Lee and Norton [4] was used without significant modification. Briefly, PFBCF was formed by reaction of pentafluorobenzyl alcohol and phosgene, in the presence of dimethyl aniline. PFBCF was purified by distillation under vacuum (bp 116-117 °C, 20 mm). The chloroformate is stable when kept cold (-20°C), however, no special precautions were necessary for use at room temperature for derivatizations.

Standards: AA standards (AA-S-18 and individual) were obtained from Sigma Chemical Co. ^{13}C-ring labeled phenylalanine was obtained from Cambridge Isotopes. Phenethyl alcohol, dimethylaminopyridine (DMAP) and pentafluorobenzoyl chloride (PFBzCl) were obtained from Aldrich. All solvents were of HPLC grade.

Whole Blood and AA Standards Derivatization: Briefly, a 10 µL aliquot of an AA solution in 0.1M HCl, or 10 µL whole blood (with 10 µL 0 1M HCl added), was added to 100 µL of H_2O / ethanol / pyridine, 60/30/10, v/v/v, and vortexed. PFBCF (10 µL, neat) was then added and the solution vortexed for 30 sec. The reaction mixture was then extracted with 100 µL of toluene, frozen in dry ice, and an aliquot of the upper liquid phase transferred to an autosampler vial for GC/MS analysis. No prior extraction of the blood sample was performed.

Plasma: Samples of plasma (0.5 mL) from 4 human controls (3 male, 1 female) were purified by cation exchange chromatography as previously described [5]. The lyophilized residue was diluted to 1 mL with 0.1M HCl and 10 µL treated as described above.

Protein Hydrolysate: A sample (25.8 µg) of human apo A-I was subjected to HCl hydrolysis for 23 hrs at 105°C. A portion (6.4 µg) was dried and derivatized as described above.

Quantification of Phenylalanine in Human Plasma: A standard curve was constructed by PFBCF derivatization of duplicate samples of phenylalanine at 0 pg, 500 pg, 750 pg, 10 ng, 100 ng, 200 ng, 300 ng, 400 ng and 500 ng per tube. ^{13}C-ring-labeled phenylalanine (100 ng per tube) was used as the internal standard. Internal standard (100 ng) was added to duplicate 10 µL aliquots of the plasma and the samples derivatized.

Alcohol Derivatization: Phenethyl alcohol (PEA) was derivatized by adding 10 µL of PFBCF and 50 µL 1% pyridine (in CH_3CN) to 50 µL of a 26 ng/µL CH_3CN solution of PEA. The reaction mixture was heated at 70°C for 1 hr and analyzed by GC/MS. A duplicate sample of PEA was derivatized with 10 µL PFBzCl (1% in CH_2Cl_2) and 50 µL 1% pyridine (in CH_3CN). The solution was heated at 70°C for 1 hr and analyzed by GC/MS.

GC/MS Conditions: All data were collected on a HP-5989 mass spectrometer interfaced with a HP-5890 GC. The ion source temperature was 250°C and the transfer line 300°C. Full scan data was recorded from m/z 100 to 750. Methane was used as reagent gas for all chemical ionization experiments.

GC separations were performed on a DB-17, 15 m x 0.25 mm, 0.25 µm film thickness or a HP Ultra 2 (5% phenyl methyl silicone), 25 m x 0.2 mm capillary column, 0.33 µm film thickness. A typical oven ramp profile was 70°C to 150°C at 30°/min, 150°C to 250°C at 10°/min and 250°C to 300°C at 30°/min with a 3 min hold at 300°C. Injection was splitless at 300°C. All injections were 1 µL.

Results and Discussion

The N-pentafluorobenzyloxycarbonyl amino acid ethyl esters (*fø*-AA-OEt) formed readily at room temperature in seconds under aqueous conditions. The derivatives exhibited excellent GC properties and their NCI mass spectra were dominated by $[M-181]^-$. PFBCF derivatization was applied to AA's in protein hydrolysates, plasma and whole blood with no prior sample clean up necessary. Sensitivity and quantitative analysis were demonstrated by the analysis of phenylalanine in human plasma. Four subjects gave Phe concentrations ranging from 48-60 µmol/L. The yield for the reaction of PFBCF with phenylalanine was determined to be 97%.

The *fø*-AA-OEt derivatives have been stable over a period of months when kept at -20°C. Of the AA's tested, only arginine failed to elute from the GC column. Histidine and tyrosine gave two derivative peaks, as did tryptophan. *fø*-Ser-OEt had low sensitivity.

Phenethyl alcohol (PEA) was also derivatized with PFBCF. Alcohol derivatization required anhydrous conditions and heating at 70°C for 1 hr. Yields were 90%. The *fø*-PEA carbonate NCI mass spectrum was also dominated by the $[M-181]^-$ ion. Of technical note, an Alltech "CapSaver" GC injection port liner was used for splitless injection and gave dramatically better results than other liners used.

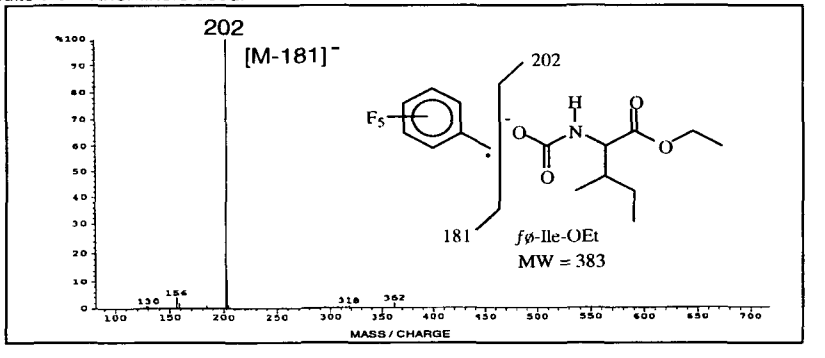

Figure 1: NCI mass spectrum of *fø*-Ile-OEt

References

1) Husek, P. *J. Chromatogr.* **1991**, *552*, 289.
2) Wang, J.; Huang, Z. H.; Gage, D. A ; Watson, J. T. *J. Chromatogr. A* **1994**, *663*, 71-78.
3) Simpson, J.T.; Torok, D.T.; Markey, S.P. *J. Am. Soc. Mass Spectrom.*, in press.
4) Lee, J. M.; Norton, S. J. *J. Agric. Food Chem.* **1990**, *38*, 273-278.
5) Schaefer, J.R.; Rader, D.J.; Ikewaki, K.; Fairwell, T.; Zech, L.A.; Kindt, M.R.; Davignon, J.; Gregg, R.E.; Brewer Jr., H.B. *Arteriosclerosis and Thrombosis* **1992**, *12*, 843-848.

THERMAL STUDY OF GLYCYRRHIZIC ACID BY ON-LINE THERMOGRAVIMETRY/ GAS CHROMATOGRAPHY/MASS SPECTROMETRY

Henry L. Chung*, John C. Aldridge, Gary M. Dull, and Chi-Kuen Shu

R. J. Reynolds Tobacco Company, Bowman Gray Technical Center, Winston-Salem, NC 27102

Thermal analysis has become an important analytical technique with the introduction of modern thermal analytical instruments. An on-line thermogravimetry/gas chromatography/mass spectrometry (TG/GC/MS) system (1) was used to study the stability, weight loss, and thermal degradation products of glycyrrhizic acid. The on-line TG/GC/MS system employed a Du Pont 951 thermogravimetric analyzer equipped with a 9000 thermal analysis system interfaced to a Hewlett-Packard 5890 GC/5970 MSD system. The TG/GC interface consisted of a heated transfer line, an adsorbent trap packed with Tenax and a six-way valve. Glycyrrhizic acid was heated and purged with air at a flow rate of 30 ml/min during the heating and purging process. The TG temperature was programed from 22°C to 900°C at 20°C/min. The volatile compounds generated in the TG were swept into an adsorbent trap. The purge gas, after passing through the trap, was vented to the atmosphere. After the heating and purging process, the trap was rapidly heated to 250°C and the volatile compounds in the trap were swept into the GC/MS system by helium at a flow rate of 35 ml/min. The volatile compounds were separated by GC. A 60 m X 0.25 mm ID DB-1701 (0.25 μ film thickness) fused silica capillary column was used for compound separation. The GC injection temperature was 250°C. The column head pressure was 25 psi. The column temperature was held at 35°C for 10 minutes, programmed to 220°C at 3°C/min and held for 48 minutes. An open-split GC/MS interface was used and the temperature was at 275°C. The mass spectrometer was operated at 70 eV in the EI mode. The ion source of the mass spectrometer was maintained at 250°C. The mass range scanned was from 29-500 amu. The volatile compounds were identified by mass spectra. The on-line

43rd ASMS Conference on Mass Spectrometry and Allied Topics

TG/GC/MS system permits evolution of thermal degradation products of glycyrrhizic acid by TG, separation of the volatile thermal degradation products by GC, and identification by MS. The thermogram of glycyrrhizic acid revealed that decomposition occurred in four steps. The first decomposition occurred over a temperature range of 39-131°C with a weight loss of 7%. The second decomposition was between 183-262°C with 14% weight loss. The third decomposition occurred over a temperature range of 262-350°C with 47% weight loss. The fourth decomposition was between 350-668°C, and involved a further 31% weight loss. Thus, a temperature and weight loss profile of glycyrrhizic acid was obtained. The total ion chromatogram showed that a number of thermally degraded compounds were generated from glycyrrihizic acid under the conditions studied. The volatile compounds were identified by mass spectra. The volatile degradation products were identified as ketones, esters, carboxylic acids, aldehydes, alcohols and hydrocarbons.

(1) H. L. Chung and J. C. Aldridge, "On-Line Thermogravimetry/Gas Chromatography/Mass Spectrometry", Analytical Instrumentation, 20, 123-135 (1992).

CHARACTERIZATION OF AROMATIZED BIOMARKERS BY GC/MS/MS WITH CHEMICAL IONIZATION

C. S. Hsu and G. J. Dechert
Exxon Research and Engineering Co., Annandale, NJ 08801
M. E. Schaps and G. B. Hieshima
Exxon Production Research Co., Houston, TX

Although present in trace amounts, biomarkers are extensively studied by geochemists to understand paleotransformation processes that convert ancient living organisms into petroleum components and to assess age, maturity and source input of the petroleum Most studied are saturated biomarkers that yield both molecular and characteristic fragment ions under high voltage (50-70 V) electron-impact ionization (HV/EI) conditions. Linking these molecular and fragment ions derived from saturated hydrocarbon compounds using GC/MS/MS resolves coeluting components and provides less ambiguous geochemical information than GC/MS.(1)

The same GC/MS/MS techniques cannot be applied to aromatized biomarkers because they yield trace or no molecular ions under HV/EI conditions. To overcome these difficulties, chemical ionization (CI) has been studied for producing ionic species more representative of molecules. Among the reagent gases evaluated isobutane yields predominantly protonated molecular ions while methane and ammonia yield more than one type of pseudomolecular ions. Thus, isobutane is the gas of choice for the aromatic biomarkers using GC/MS/MS with CI. This analytical technique is particularly useful for resolving overlapping monoaromatic steranes (MAS). Characterization of aromatic biomarkers more accurately would help us to understand better the maturation mechanism of petroleum molecules under thermal stress.

Reference:

(1) C. S. Hsu, G. J. Dechert, S. C. Blum and A. G. Requejo, *Proc. 39th ASMS Conf Mass Spectrom. Allied Top.*, Nashville, TN, May 19-24, 1991; pp. 1271-1272.

STERANE AROMATIZATION

Beginning during diagenesis and continuing throughout catagenesis, hydrogen is progressively removed from the steroidal hydrocarbon skeleton, resulting in increasing aromatization.

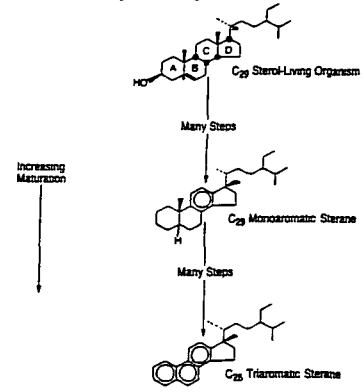

The degree of sterane aromatization can be used as an indicator of maturity in oils and source rocks.

COELUTION OF C_{28} AND C_{29} MONOAROM. STERANES CAN BE READILY DETECTED BY GC/MS/MS WITH CI

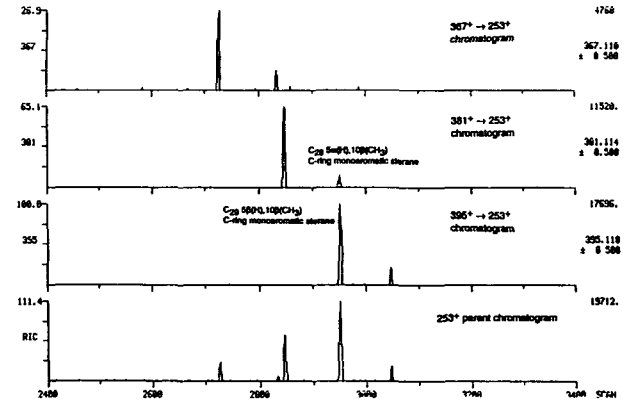

Structure Elucidation of Trace Components in Pharmaceuticals Using GC/MS^n

Steve Schachterle, Varian Chromatography Systems, Walnut Creek, CA

Introduction

Tandem mass spectrometry (MS/MS) is widely used to provide structural information for the identification of compounds in pharmaceutical products. Coupling gas chromatography to product ion MS/MS and MS/MS/MS (MS^3) can provide sufficient information to deduce the structure of minor components in the presence of the active compound and tablet compounding agents. An over-the-counter antihistamine tablet was analyzed using GC/MS/MS and GC/MS^3 and the fragmentation pathway and a possible structure were proposed for an impurity.

Experimental

A Saturn GC/MS with 4D MS/MS was used for all experiments.
The Toolkit® was used to build Ion Preparation Methods to perform MS^3 and automated methods development (AMD) MS/MS. Ions were produced from the sample by either EI, or by CI using the vapor from liquid acetonitrile as the CI reagent.

	Active Ingredient				Impurity			
Ion	P_1	V_{CID}	P_2	V_{CID}	P_1	V_{CID}	P_2	V_{CID}
$[M+H]^+$	275^+	42 V	230^+	72 V	241^+	42 V	196^+	72 V
$[(M+H)-45]^+$	230^+	72 V	167^+	92 V	196^+	72 V	167^+	92 V

Where P_1 = First Generation Parent Ion
P_2 = Second Generation Parent Ion

Sample: Generic chlorpheniramine maleate antihistamine tablets, purchased at local drug stores.
Sample preparation: Crush a tablet. Place 5-10 mg into a 2 ml vial. Add 0.9 ml water. Adjust to pH11 using 1.0*N* NaOH. Shake well. Add 1 ml methylene chloride. Shake again. Remove the methylene chloride layer. Inject 1µl

Results and Discussion

The structure of the active ingredient is shown in figure 3. Several common spectral features can be seen between the active ingredient and the impurity:

Analysis Type	Spectral Features
EIMS	Both spectra show 58^+, 72^+ ions. Neither spectrum shows M^+
CIMS	Both spectra show $[M+H]^+$ and $[(M+H)-45]^+$, with a difference of 34 between $[M+H]^+$ for the active ingredient and for the impurity.
CIMS/MS	Both spectra show $[(M+H)-45]^+$ as the major ion.
CIMS^3 of $[M+H]^+$	Both spectra show 167^+ as a major ion after MS^3.
CIMS^3 of $[(M+H)-45]^+$	The product ion spectra are virtually identical, implying that any difference in structure has been lost by this point.

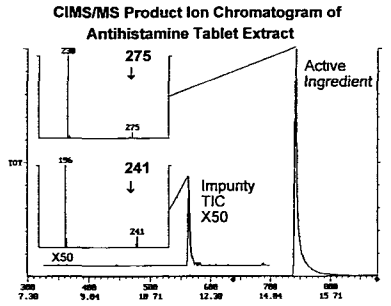

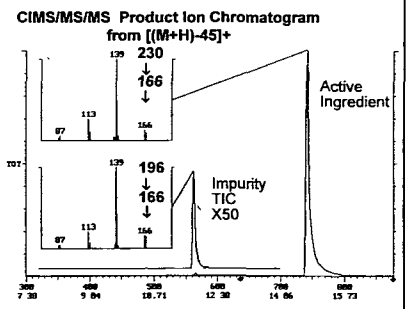

Mapping these features onto the structure of chlorpheniramine leads to the conclusion that the compounds are the same except for a chlorine atom which has been replaced by a hydrogen atom on the impurity. This compound, pheniramine, is also used as an antihistamine.

Chlorpheniramine, MW 274

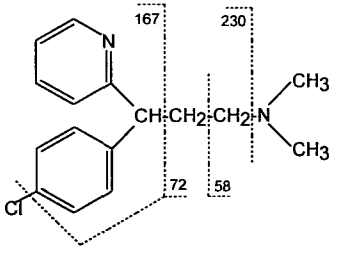

Pheniramine, MW 240

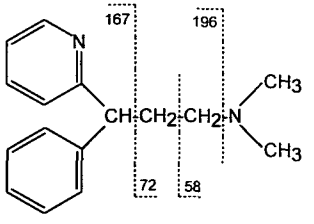

Conclusions

MS/MS allows the CID energy to be tuned to explore different fragmentation patterns. MS^3 provides an easy way to determine fragmentation pathways through a selected ion. In this example, an impurity was identified in an over-the-counter antihistamine tablet. Common ions in the various mass spectrometric modes were interpreted as common structure between the active ingredient and an impurity and allowed a structure for the impurity to be proposed.

Isotopically Labeled Internal Standards Analysis Using Ion Trap GC/MS/MS

Barbara A. Bolton, Steve Schachterle and Greg Wells

Varian Chromatography Systems
2700 Mitchell Drive
Walnut Creek, CA 94598

The ability to sequentially change ion trap scan functions from scan to scan allowed trap parameters to be varied numerous times during the elution of a sample peak from a gas chromatograph. The chromatogram could be divided into as many as 200 time segments; one for each compound. In each segment 10 different scan groups could be sequentially acquired. Each scan group could isolate and dissociate a different parent ion. The scan groups are sequentially repeated throughout the particular time segment, producing a spectrum for each group. In this work scan Group 0 was used to produce product ion spectra from phencyclidine (PCP) and scan Group 1 was used to produce product ion spectra from deuterated phencyclidine (D-5 PCP) as shown in Figure 1

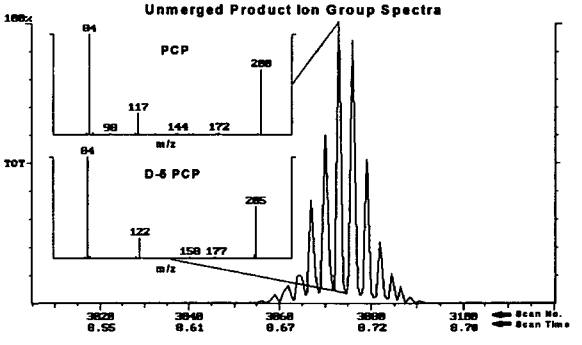

Figure 1

The set of individual group spectra could be directly merged to form a composite spectra (Figure 2); or specific ions could be extracted from the individual group spectra first and then merged to form the composite spectrum (Figure 3).

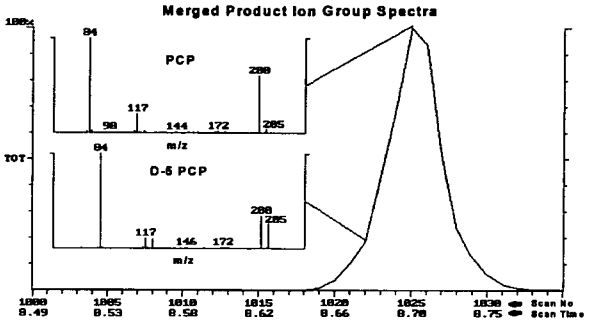

Figure 2

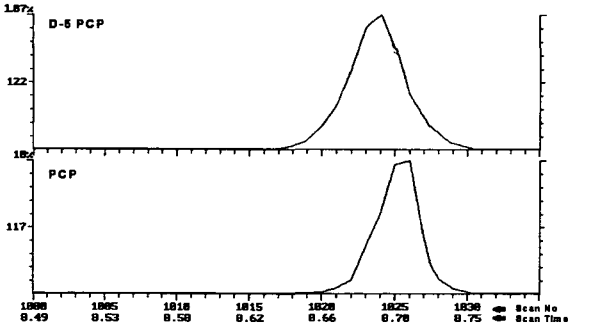

Figure 3

Reproducibility Study of GC/MS/MS with Ion Trap Mass Spectrometer

Barbara A. Bolton and Steve Schachterle
Varian Chromatography Systems ,Walnut Creek, CA, USA

Introduction

The utility of MS/MS for quantitative analysis depends explicitly on the *reproducibility* of the parent ion isolation and CID process for product ion formation The MS/MS experiment should produce an identical fragmentation pattern each time the same sample is analyzed Comparison of current MS/MS spectral data to MS/MS spectral data stored in a library maybe used for routine identification or confirmation of target compounds Any uncharacterized or uncontrolled changes in MS/MS spectral patterns compromise the integrity of that comparison

Recently, new methods of parent ion isolation and collision-induced dissociation (CID) have provided a reliable method for routine GC/MS/MS analysis with an ion trap (1-2). This method has the option of using either a non-resonant or resonant technique for the CID process. Using a standard mixture of semiviolatile organics, MS/MS method reliability was evaluated in terms of long-term reproducibility of sample response, linearity and relative ion ratios.

Methods

This study used a **Varian Saturn 4D** ion trap mass spectrometer. The four compounds, 2-methylnapthalene, acenaphthene, chlorpyrifos and chlordane, were dissolved in hexane to give six concentrations between 10 pg/µL and 1900 pg/µL Table 1 shows the EI/MS/MS method used for each compound A multisegment MS acquisition method was created to apply the appropriate MS/MS method to each analyte as it eluted from the GC column. The method was not altered over the course of this three month study Weekly routine checks of electron multiplier voltage, mass calibration and trap function calibration were the only potential causes of instrument paramter changes.

Results and Discussion

Ion Ratio Comparison

The relative abundance of ions in a mass spectrum or MS/MS spectrum are often used as a basis to distinguish isomeric compounds Relative product ion abundances have also been used as a measure of internal energy of the parent ions(3) Three scan average spectra (apex + adjacent scans) were analyzed for reproducibility of product ion intensity relative to base peak. The variation of the relative intensities are reported as %RSD in Table 2 Variation of product ion ratio data was greatest at the lowest concentration (~10 pg). The %RSD for relative ion abundance was much lower at concentrations of > 50 pg.

Library Search Comparison

MS/MS spectral interpretation relies on a comparison of current data with that obtained from previous samples or standards Saturn software provides for the generation of a MS/MS library based on mass spectra generated by the user, and uses the same search routines as used for the regular mass spectral library The Library search algorithm is sensitive to matches by mass and intensity The **Purity Search** measures the similarity between the sample mass spectrum and the library mass spectrum. A purity of 1000 implies that the library and sample mass spectra are identical with respect to both the presence and intensities of mass peaks. A Purity Search analysis of the compounds at the beginning, mid point and last week of the study is shown in Table 3.

Quantitation

External standard calibration curves generated for the four compounds for the first and last week of this study. The response was either linear or quadratic with excellent correlation coefficients The %RSD results for sample response (sample area/sample conc.) are shown in Table 4. Generally, the greatest variation in sample response was observed at the ~ 10 pg concentration level

43rd ASMS Conference on Mass Spectrometry and Allied Topics

Conclusions

- o A new method of isolation and excitation has provided a GC-MS/MS method that is reliable and reproducible Four compounds were examined for reproducibility of relative ion abundances, quantitation and library identification The MS/MS spectra gave good linearity with correlation coefficients > 998, and high fit when library searched
- o The CID method has provided controlled energy desposition and uniform fragmentation. Spectral integrity (relative ion ratios) was maintained over the concentration range (10 to 2000 pg) and was stable for several months The high reproducibility of ion ratios is comparable to that obtained with the electron ionization mode of analysis
- o Reproducibility of product ion spectra over time and concentration suggests that a useful data library for a wide range of compounds is feasible Preliminary examination of product spectra from different instruments using the same MS/MS method showed that small changes (several volts for non-resonant) in the excitation voltage may be required to obtain similar product ion spectra

References

1 B Bolton, G Wells and M Wang, Proc of the 41st Conf. on Mass Spectrom. and Allied Topics, San Francisco, CA 1993, p474a

2 M Wang and G Wells, Proc of the 41st Conf on Mass Spectrom and Allied Topics, San Francisco, CA 1993, p463a

3 Kenneth L Busch, Gary L. Glish and Scott A. McLuckey, *Mass Spectrometry/Mass Spectrometry: Techniques and Applications of Tandem Mass Specrometry,* VCH Publishers, Inc New York, New York, 1988

Table 1

MS/MS Isolation and Dissociation Parameters

COMPOUND	Chlordane	Acenaphthene	Chlorpyrifos	2 Methylnaphthalene
Parent Ion Mass	375 m/z	154 m/z	316 m/z	142 m/z
Mass Isolation Window	10 m/z	4 m/z	10 m/z	4 m/z
CID Mode	Non-Resonant	Non-Resonant	Non-Resonant	Non-Resonant
CID Time (mSec)	20 mSec	20 mSec	20 mSec	20 mSec
CID Amplitude	50 Volts	85 Volts	33 Volts	83 Volts
Excitation Storage Level	75 m/z	71.4 m/z	63.5 m/z	64.8 m/z

Table 2

Relative Ion Abundance Comparison

COMPOUND	Product Ions	%RSD[1] 7 replicates @ 6 conc.	%RSD[2] Conc. Range	%RSD (Avg[3]) 3 months
Chlordane	266	0 - 4.6%	0.2 - 2.1 %	0.70%
11 pg to 1400 pg	201	0 - 10.5%	2.0 - 4.7 %	1.10%
	237	1.4 - 13.0 %	1.1 - 7.8 %	2.80%
Acenaphthalene	93	0.8 - 5.5 %	1.7 - 3.2 %	0.80%
10 pg to 1240 pg	122	0%[4]	0%	0%
Chlorpyrifos	258	0 - 12.8 %	0 - 1.8 %	0.50%
14 pg to 1700 pg	265	1.2 - 28.0 %	2.8 - 10.8 %	2.00%
2-Methylnaphthalene	89	0.8 - 8.0 %	2.2 - 5.7 %	3.20%
15 pg to 1840 pg	115	0 - 1.7 %	0 - 1.9 %	0.30%

1. Range of %RSD for the ion intensity relative to base peak of 7 replicates at each concentration
2. Range of %RSD for the ion intensity relative to base peak for entire concentration range for a given week
3. Average %RSD for the ion intensity relative to base peak for entire concentration range for three months
4. Product ion 122 m/z was consistently the base peak

Table 3

Library Purity Search Comparison

COMPOUND	%RSD[1] 7 replicates @ 6 conc.	%RSD[2] Conc. Range	Avg Purity[3] 3 months (3 pts)
Chlordane	.2% 2.0 %	.8% 1.8 %	952
11 pg to 1400 pg			
Acenaphthalene	.7% 1.4 %	2.8% 2.0 %	878
10 pg to 1240 pg			
Chlorpyrifos	.3% 3.3%	1.0% 4.5%	850
14 pg to 1700 pg			
2-Methylnaphthalene	.7% 1.7 %	.2% .8%	951
15 pg to 1840 pg			

1. Range of %RSD for Purity Fit for 7 replicates at each concentration
2. Range of %RSD for Purity Fit for entire concentration range for a given week
3. Average Purity Fit of first week, mid point and last week of study.

Table 4

Quantitation

COMPOUND	Quantitation Ions	%RSD[1] 7 replicates @ 6 conc.	%RSD[2] Conc. Range	Correlation Coeff 3 months
Chlordane	266 + 201 + 237	1.1 - 5.2%	5.2 - 10.0 %	> .999
11 pg to 1400 pg				
Acenaphthalene	89 + 122	0.9 - 4.9%	2.7 - 8.4 %	> .998
10 pg to 1240 pg				
Chlorpyrifos	258 + 265	1.0 - 11.1 %	13.40%[3]	> .999
14 pg to 1700 pg				
2-Methylnaphthalene	89 + 115	0.8 - 8.4 %	3.7 - 10.4 %	> .993
15 pg to 1840 pg				

1. Range of %RSD for the sample response (sample area/sample concentration) of 7 replicates at each concentration
2. Range of %RSD for the sample response (sample area/sample concentration) of entire concentration range for a given week (linear curves only
3. Only one curve had a linear fit

High Speed Method Optimization For Routine GC/MS/MS In An Ion Trap

Greg Wells and Chuck Huston

Varian Chromatography Systems
2700 Mitchell Drive
Walnut Creek, CA 94598

The ability to sequentially change ion trap scan functions from scan to scan allows trap parameters to be varied numerous times during the elution of a sample peak from a gas chromatograph. The chromatogram can be divided into as many as 200 time segments; one for each compound. In each segment 10 different scan groups can be sequentially acquired. Each scan group can have a different value of a selected parameter (such as CAD voltage). The scan groups are sequentially repeated throughout the particular chromatographic time segment, producing a spectrum for each group An MS/MS method of five pesticides (Figures 1 and 2) was optimized and calibrated with only three sample injections.

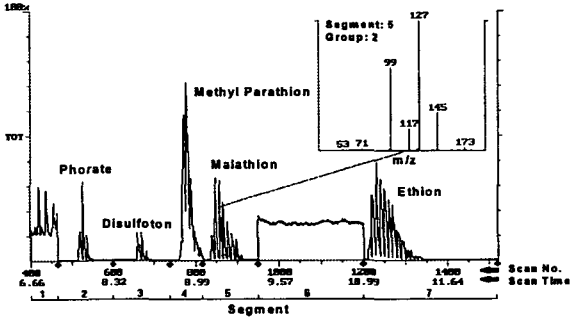

Figure 1

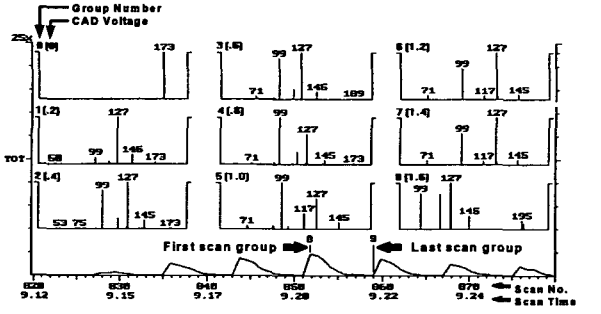

Figure 2

The spectra that resulted were inspected and the optimum CAD spectra were selected for each compound based on the operator's criteria. The value of the parameter associated with the scan group for each selected spectra was then entered into the final MS/MS method (Figure 3).

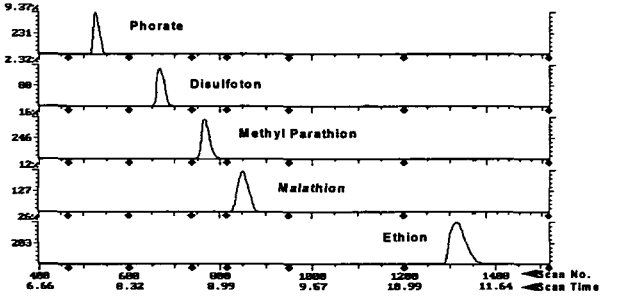

Figure 3

Dual Oven Multidimensional Fast Gas Chromatography with Spectral Detection

Tania A. Sasaki and Charles L. Wilkins
Department of Chemistry, University of California–Riverside, Riverside, CA 92521–0403

Multidimensional gas chromatography (MDGC) with spectral detection has been well established as a powerful tool for analysis of complex mixtures. The ability to acquire both mass and infrared spectra is desired because the complementary information that can be obtained leads to a more accurate identification of unknown components. In our research, a fast secondary separation is used to reduce the analysis time of this stage by at least an order of magnitude. We have also implemented a dual oven configuration so that heartcuts can be trapped and reinjected onto the fast column "on the fly." This configuration further reduces analysis time by allowing analysis of more than one heartcut per injection, which is analogous to using parallel traps. Although we succeeded in decreasing the analysis time, the fast separation creates some challenges for most spectral detectors. Because of the small retention time differences between compounds and the low column capacities of the fast columns, detection limits and chromatographic resolution become concerns when coupling fast GC to spectral detectors.

We have previously demonstrated the feasibility of fast GC with off–line matrix isolation FTIR detection. By using a programmable speed rotating cryogenic disk to trap the GC effluent, the chromatographic resolution is maintained by increasing the rotation rate. Signal averaging is used to improve the detection limits.

Although detection limits are not a problem for mass spectrometers, as they are inherently quite sensitive, maintaining the chromatographic resolution can be very difficult. This is especially true for scanning instruments such as the quadrupole mass spectrometer. In order to maintain good chromatographic resolution, the mass range scanned must be quite small. Most fast GC peaks are on the order of 250-350 ms (FWHH) so the scan rate must be at least 20 scans/second. Although the reduced mass range makes unambiguous identification using mass spectral information difficult at best, it can be used for target analysis of various compounds. This aspect of the fast MDGC/FTIR/MS system is be the focus of this paper.

The fast MDGC/FTIR/MS system utilized in this study consists of two gas chromatographs connected by a cryogenic trap housed in an external oven. For evaluation, a standard polynuclear aromatic hydrocarbon (PAH) sample was injected onto the pre-column and then directed to either a vent line or the cryogenic trap. Using rapid resistive heating, the sample was reinjected from the trap onto the fast column. Detection from the fast column utilized a flame ionization detector (FID), matrix isolation FTIR spectrometer, and quadrupole mass spectrometer. To obtain a selected ion chromatogram (SIC) and mass spectra of the target analytes, the mass range of the quadrupole was set to scan from 150 to 160 amu. The target analytes were acenaphthylene and acenaphthene, which correspond to peaks 2 and 3 in **Figure 1**, which shows the total ion chromatogram (TIC) of the sample. **Figures 2a** and **2b** show the SIC and FID chromatogram of the fast separation. The mass spectrum of peak 2 is shown in **Figure 3a**. **Figure 3b** shows the corresponding portion of the spectrum of peak 3 of Figure 1. The agreement between the two spectra demonstrate the feasibility of this method for the identification of target analytes. Infrared spectra, which were obtained in conjunction with the mass spectra, can be used to confirm the identification.

43rd ASMS Conference on Mass Spectrometry and Allied Topics

Compound	Figure 1 Peak No.	Figure 2a Peak No.	Figure 2b Peak No.
Naphthalene	1		2
Acenaphthylene	2	1	3
Acenaphthene	3	2	4
Fluorene	4		5
Phenanthrene	5		6
Anthracene	6	3	7
Fluoranthene	7		8
Pyrene	8		9
1,2–Benzanthracene	9		10
Chrysene	10		11
Benzo(b)fluoranthene	11		12
Benzo(k)fluoranthene	12		13
Water/CO_2			1
Polysiloxane			*

Table 1: Identifications of PAH standard mixture components

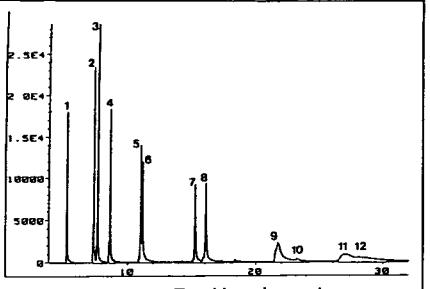

Figure 1: Total ion chromatogram of PAH standard separated on a DB–5 column.

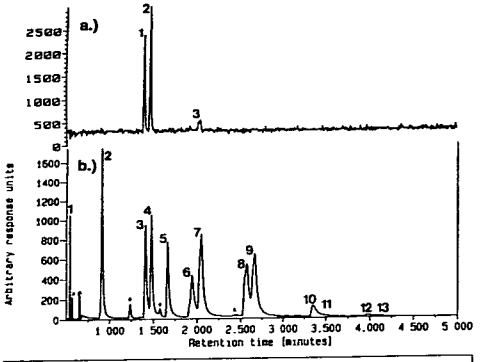

Figure 2: Chromatogram of fast separation of PAH standard, a.) selected ion chromatogram (SIC) and b.) FID chromatogram.

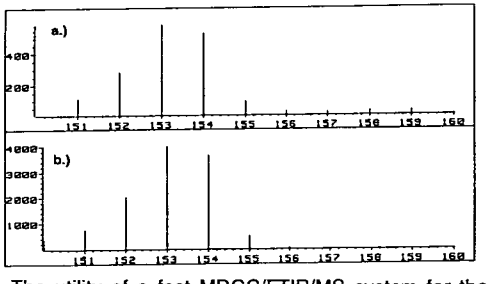

Figure 3: Mass spectrum of acenaphthene. a.) Selected ion mass spectrum of peak 2 in Figure 2a; b.) 150-160 amu section of spectrum from peak 3 in Figure 1.

The utility of a fast MDGC/FTIR/MS system for the target analysis of mixtures has been demonstrated. By selecting an appropriate, small mass range for the compounds of interest, the quadrupole mass spectrometer was able to both maintain the chromatographic resolution of the fast GC separation and collect spectra of the analytes of interest. The IR spectra which were simultaneously obtained were used for a more positive identification of the compound.

High-Speed GC/MS Using a Quadrupole Mass Filter

Casey C. Grimm & Steven W. Lloyd
USDA, Agricultural Research Service, SRRC
New Orleans, LA 70122

Linda Muchausen
Deptarment of Chemistry and Physics, Southeastern Louisiana University
Hammond, LA 70402

Gas chromatographic separations utilizing short narrow bore capillary columns (I.D. < 0.1 mm), can be performed with run times ranging from a few minutes down to a few seconds. The short columns and the high flow rates enable separations to be performed at lower oven temperatures. Sample capacities are limited to a few nanograms of each analyte, but the narrow peak widths result in an increase in the signal to noise ratio. GC peak-widths are on the order of 0.1 s and require high data acquisition rates which are problematic for scanning mass spectrometers.

Quadrupole mass spectrometers have proven to be relatively inexpensive, reliable and rugged. The major limitation to scanning a quadrupole mass filter is in the flight time required for a given molecule to pass through the filter. The flight time is determined by the quadrupole length, mass, and potential difference between the source and the quadrupole which is normally around 5 V. Table 1 shows the intensity of the m/z 69 ion from PFTBA as a function of source potential and sampling time after stepping the mass filter across 1 amu. The signal is at a maximum at 15 µs.

Intensity for m/z 69 as a Function of Sampling Time and Acclerating Potential

m/z 69	5 us	15 us	25 us	35 us	45 us	55 us	65 us	75 us
0 V	22	110	112	91	116	102	104	101
5 V	39	3380	2656	1645	878	845	796	814
10 V	135	3395	2238	1577	1018	1043	1080	1072
15 V	486	3395	2062	1592	1184	1130	1216	1196
20 V	1017	3473	2006	1514	1284	1237	1301	1298
25 V	1598	3724	2020	1663	1541	1364	1458	1436
30 V	1907	3564	2092	1602	1533	1357	1430	1404

A data acquisition and control program has been developed to exceed the physical limitations of a quadrupole mass spectrometer. By reducing the scan range, increasing the acceleration voltage, and reducing total sampling, scan rates exceeding 250 Hz over a 100 amu range have been achieved, resulting in scan speeds in excess of 25,000 amu/sec. The mass spectra are sufficient to identify the compounds. This system can be used for rapid analysis or on-line quality control. Figure 1 shows a total ion chromatogram produced by injecting 1µl of headspace above a mixture of pentane, hexane, heptane and octane. The GC head pressure was at 40 psi of H_2, and the capillary column was 1 m with a DB-5 stationary phase and a 50 µm I.D. A split injection of approximately 10:1 was used. The quadrupole mass spectrometer was scanned from 40 to 140 amu at 257 scans/S. The fast scan resulted in an increased M+1 peak due to the decreased mass resolution. However, the mass spectra were sufficient for unambiguous identification. Quantitation was not possible, partly due to the injection techniques and partly due to the accelerated scan rates.

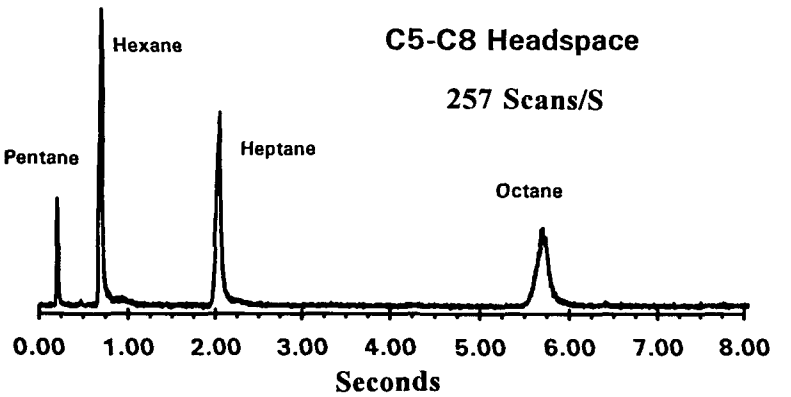

HIGH-SPEED GC/MS WITH A FAST DOUBLE-FOCUSSING MASS SPECTROMETER

Peter G. Van Ysacker, Jeff Brown*, Andy Phillips*, Hans-Gerd Janssen and Piet A. Leclercq
Laboratory of Instrumental Analysis, Department of Chemical Engineering
Eindhoven University of Technology, P.O. Box 513, 5600 MB, Eindhoven, The Netherlands
**VG Analytical, Floats Rd., Wythenshawe, Manchester M23 9LE, England*

Modern magnetic sector mass spectrometers have several advantages over quadrupole instruments and appear highly promising for on-line coupling to high-speed narrow-bore GC columns. Double-focussing instruments are capable of better sensitivity, higher resolution and selectivity than quadrupoles. In magnetic instruments ions of higher energy are used, and hence higher scan speeds than with quadrupoles can theoretically be obtained. With conventional sector instruments scan speeds are limited in practice to a few spectra per second. The state-of-the-art VG MassSpec, however, allows higher scan speeds because this EBE instrument has a small, fast, fully laminated low inductance magnet.

The performance of the MasSpec in combination with narrow-bore (50 μm I.D.) GC columns has been evaluated. The detection limits in the full scan mode are in the low pg range. In the SIM mode, detection limits as low as five to 50 fg are observed, depending on the resolving power of the mass spectrometer and on sample complexity. With complex mixtures, detection limits for a given compound are limited by interferences from other compounds. By increasing the mass spectral resolution in the SIM mode, interferences from ions of the same nominal m/z value are significantly reduced, thus enhancing the signal-to-noise ratio. Furthermore it was found that the mass spectrometer exhibits perfectly linear behavior over the entire dynamic range from the detection limits up to a few ng where overloading of the GC column starts to occur.

The maximum achievable scan speed in the full magnetic scan mode varied from three to ten scans over one decade per second, again depending on the spectral resolving power (2000 and 300, respectively). Over a smaller mass range (40 to 200 Dalton), up to 20 scans/s could be acquired at a mass resolution of 300. Scanning the electrostatic analyzer is not useful because the applicable mass range in this mode is too small to preserve good sensitvity.

In the SIM mode, more than 50 m/z values could be monitored per second when the electrostatic analyzer was used. However, the abundance of only 25 different ions per second could be obtained by changing the magmetic field strength.

The overall performance of this high-speed GC/MS system is illustrated by analyses of samples from industrial and environmental origin. An example is given in Figure 1.

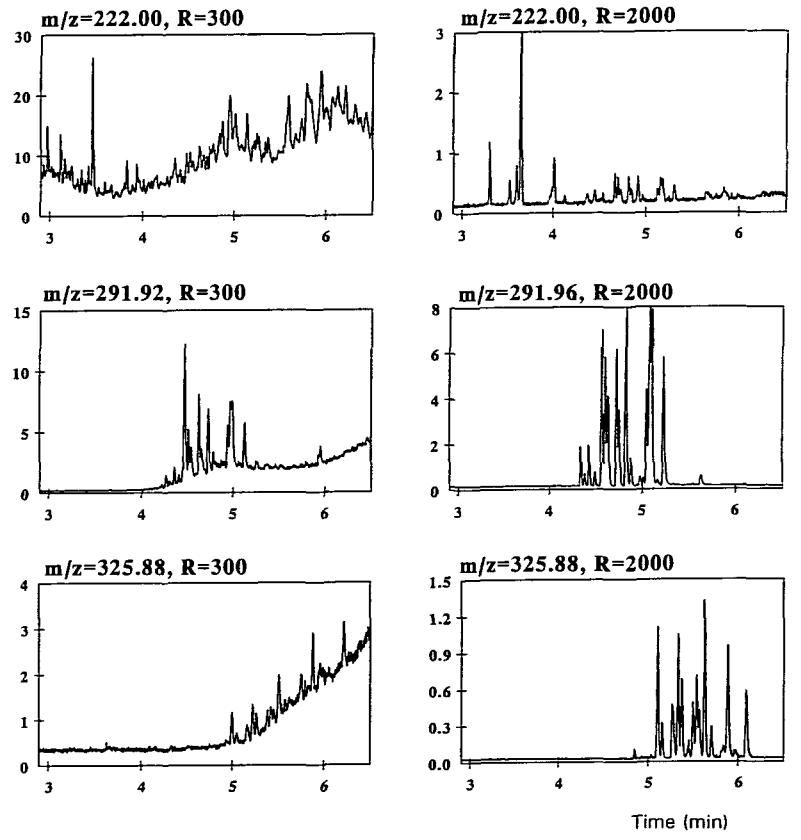

Figure 1. Fast separation of a waste oil spiked with PCB's (arochlor 1242). Ion current profiles of m/z 222.00, 291.92 and 325.88 are shown at mass resolving power of 300 (left) and 2000 (right). GC conditions: 5 m x 50 μm I.D. DB-1 column (0.17 μm film thickness), ballistically heated from 50°C to 280°C; helium inlet pressure 11 bar.

FAST, VERY FAST AND ULTRA FAST GC-MS IN SUPERSONIC MOLECULAR BEAMS

Aviv Amirav and Shai Dagan
School of Chemistry, Tel Aviv University, Tel Aviv 69978, Israel, Fax: 972-6409293

Supersonic molecular beams (SMB) are characterized by several unique features that make SMB an ideal sample introduction method, enable a unique fast GC inlet, and result in important implications to ionization processes.

A 50 cm long capillary column that connects the atmospheric pressure open inlet to a supersonic nozzle, serves as an ultra fast GC short column. Alternatively, a coupled conventional GC can serve as a fast or a very fast GC, with no restrictions on the column diameter, length or flow rate. With this GC, the two columns are simultaneously connected for increased flexibility.

GC-MS in SMB provides improved solutions to all the fast GC-MS requirements. A broad range of molecules, including relatively thermolabile and nonvolatile, are amenable for fast GC-MS. The directional kinetic energy is used to filter out vacuum background ions, thus tail free chromatograms are obtained, regardless of the molecular volatility. These chromatograms are combined with the electron impact mass spectra of the vibrationally cold supersonic beam molecules, that exhibit enhanced molecular weight peak and controlled degree of ion dissociation. Sufficient overall GC-MS resolving power is achieved by the use of Hyperthermal Surface Ionization (HSI) as a tunable selective ion source, and due to the enhancement of M^+ peak in electron impact. On the other hand, the fast GC peak widths usually exceed 0.5 seconds, being compatible with conventional quadrupole MS. These peak widths are achieved through the use of a high flow rate short megabore columns. The extreme sensitivity of HSI (400 attograms MDA), simplifies sample preparation requirements. Fast splitless injections are achieved through the very high gas flow rate prevailing, that further contributes to lower minimum detected concentration.

The GC-MS analysis time is defined in terms of speed enhancement factor (SEF), which is the multiplicity of the column length reduction by the gas linear velocity increase, in comparison with a conventional 30 meter long narrow bore capillary column, having 1 ml/min flow rate. Fast, very fast and ultra fast GC-MS have an SEF of 5-30, 30-400, 400-4000, respectively. The use of SMB enables a free choice of SEF with the trade off of handling thermally labile compounds, GC resolution, sensitivity and analysis time.

In figure 1 we show fast, very fast and ultra fast GC-MS analysis of different mixtures of

underivatized steroids that demonstrate this trade off between the SEF and the degree of decomposition observed. Note that corticosterone is effectively analyzed with very fast GC-MS, while with ultra fast GC-MS, even cortisone that is our most thermally labile compound, is analyzed. In figure 2 we demonstrate the application of fast GC-SMB-MS for the screening of drugs in urine. 0.3 mL of untreated urine were injected and the clean RSIM traces demonstrate low ppb range minimum detected concentration.

Recommended References on GC-SMB-MS:

1. A. Amirav., Org. Mass Spectrom. 26, 1-17 (1991),
2. S. Dagan and A. Amirav., Int. J. Mass. Spectrom. & Ion. Proc., 133, 187-210 (1994).
3. S. Dagan and A. Amirav., J. Am. Soc. Mass. Spectrom. 6, 120-131 (1995).
4. S. Dagan and A. Amirav, "Fast, Very Fast and Ultra Fast GC-MS of Thermally Labile Steroids, Carbamates and Drugs in Supersonic Molecular Beams, Sub. to Anal. Chem.

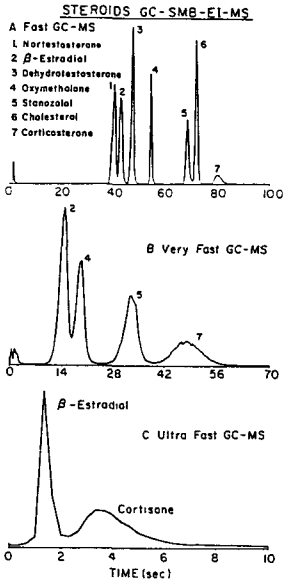

Fig.1 - Fast, very fast and ultra fast GC-MS of underivatized steroids

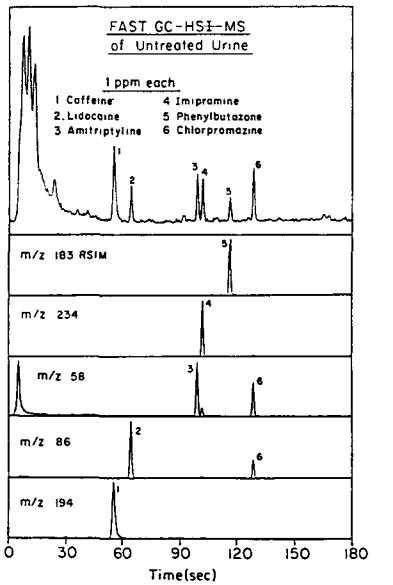

Fig.2 - Fast GC-MS of drugs in untreated urine

Non-Peptide Libraries: Structure Determination by LC/MS/MS.

Issakova, Olga; Ma, Nina; Kocis, Petr; Sepetov, Nikolai.
Selectide Corporation, 1580 E. Hanley Blvd, Tucson, Az 85737.

Synthetic combinatorial libraries are becoming an important tool of the pharmaceutical industry for the discovery of new drug candidates. Structure determination of hits, found after screening a large number of compounds (library) against a biological target, is a key element of the application of library technology for drug discovery. The sequencing of compounds from peptide libraries is well developed and can be done by either classical Edman degradation, ladder sequencing, or, because fragmentation characteristics of peptides are well known, by tandem mass spectrometry (MS/MS). However, direct structure determination of compounds from non-peptide libraries is analytically challenging.

Here we describe an example of direct structure identification by LS/MS/MS of compounds from a non-peptide library based on Kemp's triacid scaffold (Fig.1). The library was synthesized on solid phase in accordance with standard split-and-combine technology [1]. Synthesis was initiated with the coupling of Gly to the resin (TG-OH, 130 µm beads) via an ester bond, followed with the sequential coupling of β-Ala, Gly and β-Ala, forming a linker between the resin and first position for randomization. Thirty amino acids were used in the first randomization. Two of the three carboxyls of the Kemp's triacid were modified by ethylenediamine and served as two other positions for randomization (identical sets of fifty carboxylic acids were used for randomization at these positions). Thus, the library contained 75,000 different compounds. Compounds found as a result of screening against different biological targets, using on-bead binding procedures [1], were cleaved from the resin by alkaline hydrolysis. Releasates were analyzed by LC/MS/MS, using a micro HPLC (Michrom, BioResources Inc.) coupled on line with an API III triple qudrupole mass spectrometer (Perkin Elmer, Sciex Instruments, Thornill, Canada) equipped with a low energy collision cell. The analysis of a large variety of compounds showed that they fragmented at amide bonds, and that most of the daughter ions observed could be formally explained by cleavage of two or more amide bonds. Fig.2 presents a hypothesis for a fragmentation mechanism which we suppose is responsible for most of the observed fragmentation patterns. The proposed mechanism involves cleavage of an amide bond adjacent to the cyclic moiety with subsequent formation of a cyclic imide product (Fig.2a,b) and cleavage of another amide bond (Fig.2c). For example, in the daughter spectrum of a positive bead found after library screening (Fig.3, upper trace), all ions we were able to assign are marked with an *, and those whose origin we explain by the mechanism of cyclic imide intermediate formation, are marked with a circled *. Using the fragmentation patterns found, we developed computer software for automatic structure determination of compounds from this library, and used this software for structure identification of hits found after screening the library against biological targets. The accuracy of the analysis was confirmed by resynthesis.

In conclusion, this work demonstrates the successful practical

utilization of mass spectroscopy for direct structure elucidation of hits from non-peptide non-coded libraries.

1. M.Lebl, et al. Biopolymers vol.37, 1995.

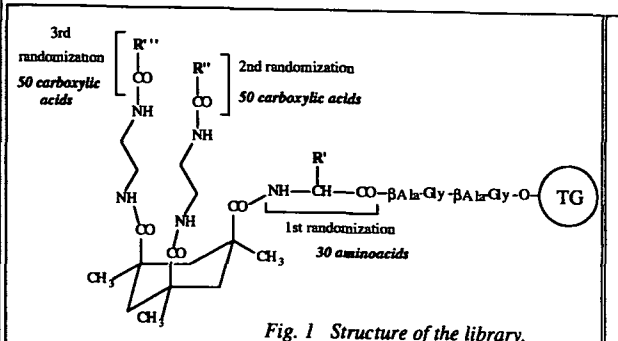

Fig. 1 Structure of the library.

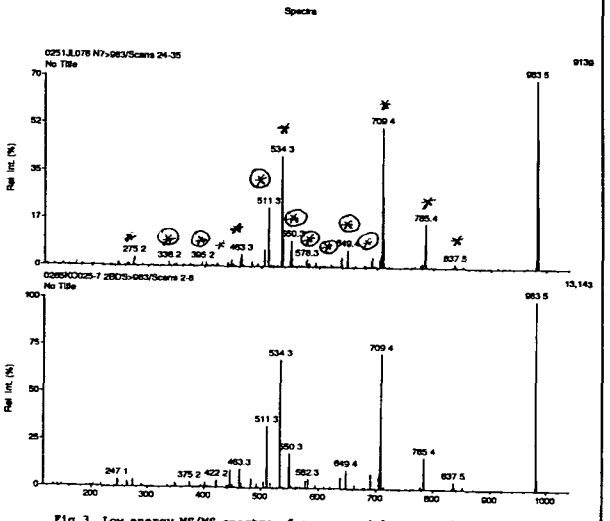

Fig.3. Low energy MS/MS spectra of a compound from a positive bead after screening (upper trace), and the daughter spectrum of the resynthesized compound (lower trace).

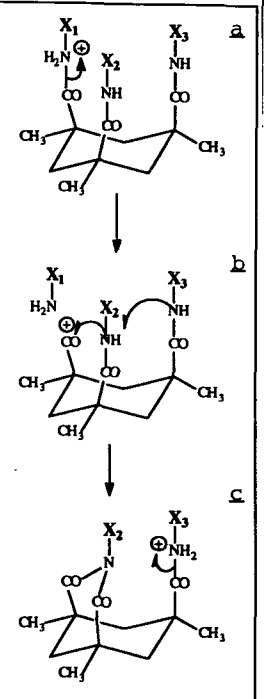

Fig. 2 Proposed mechanism of fragmentation.

X_1, X_2 and X_3 can be one of the following:

NH—CO—R'', or

NH—CO—R''', or

CH(R')—CO—(βAlaGly)$_2$—OH

OPTIMIZATION OF MALDI SEQUENCING OF SUPPORT-BOUND COMBINATORIAL LIBRARIES; R. Scott Youngquist, Gary R. Fuentes, Cathy M. Miller, Gregg M. Ridder, Martin P. Lacey and Thomas Keough; The Procter and Gamble Co., Miami Valley Laboratories, PO Box 538707, Cincinnati, OH 45253-8707.

Combinatorial libraries are a new approach to lead compound identification. Large mixtures of compounds are synthesized, and a selection strategy is applied to isolate the few compounds having the desired activity from the many compounds that don't. This approach has three main advantages relative to the classical method of screening extracts from bacteria, fungi or plants: First, all compounds are present at approximately equimolar concentration, which eliminates concentration effects in testing. Second, a chemist controls the synthesis, so it can be tailored for the required application. Third, isolation and screening of active compounds is fast and straightforward.

In this study we've optimized our previously reported (1,2) method for MALDI sequencing of biologically active molecules isolated from support-bound libraries. We optimized the synthesis and sample handling to facilitate the use of small resin beads (17 μm). We've automated the screening and sorting processes with flow cytometry, and extended the method to non-peptide chemistries including linear and cyclic carbamates (in collaboration with Dr. Charles Cho and Prof. Peter Schultz, UC Berkeley).

Initially, library screening and sorting was done manually, but there were several problems associated with that approach: First, the enzymes used for staining require specific conditions (pH = 9) that are different from our screening conditions, and this could affect target protein binding. Second, it is difficult to distinguish varying levels of staining. Third, manual isolation of the positive beads is slow and tedious.

To avoid these problems, we automated the screening and sorting process with flow cytometry. As an initial test, a small library containing multiple copies of only 128 distinct sequences (members) was analyzed to see if flow cytometry could successfully isolate the known high affinity ligand (Ac-HPQFx) to streptavidin. The flow cytometry screening and sorting results are given in the Figure, and several peaks (B,C,D and E) having varying Quantum Red fluorescence intensity are seen in the positive region. The beads associated with the highest fluorescence intensity, peak E, contained the expected recognition sequence. All 10 of the beads that were sequenced from peak E contained Ac-HPQFF. This sequence was not detected in any of the other peaks. The large peak associated with inactive peptides, peak A, showed random sequences having no homology. The observed intensity of peak E, 0.7%, agreed well with the calculated relative abundance of Ac-HPQFF in the small library (0.8%).

Larger libraries consisting of more than a few thousand members will have an extremely low percentage of actives. With these libraries, it is necessary to perform a two-pass sort. The first pass sort enriches the sample in positive beads while eliminating negatives. The sorted beads from each library are then run back through the flow cytometer and sorted a second time. The highest fluorescence beads from the target library sorts are then collected for subsequent sequencing with MALDI. With this approach, a library containing over 60,000 members was successfully screened against an anti-gp120 antibody, and the correct high affinity ligands were isolated. We are currently extending automated flow cytometry screening and sorting to libraries containing more than one million members.

43rd ASMS Conference on Mass Spectrometry and Allied Topics

Termination synthesis with MALDI sequencing is a very general method. Since it is not degradative, it is compatible with libraries of any compounds that can be prepared in a stepwise synthesis. For instance, it can be used with libraries of poly-N-substituted glycines, oligocarbamates, or nucleic acid analogs as well as libraries that combine several different monomers. Even monomers of identical mass, such as geometric or stereoisomers, can be easily distinguished (2). An example of non-peptide sequencing with termination synthesis/MALDI can be found in our previous study of methylphosphonate oligonucleotides (3). We are currently applying termination synthesis/MALDI sequencing to libraries of both linear and cyclic oligocarbamates. Synthetic procedures have been optimized, and excellent quality MALDI spectra have been obtained from the carbamate products isolated from single resin beads.

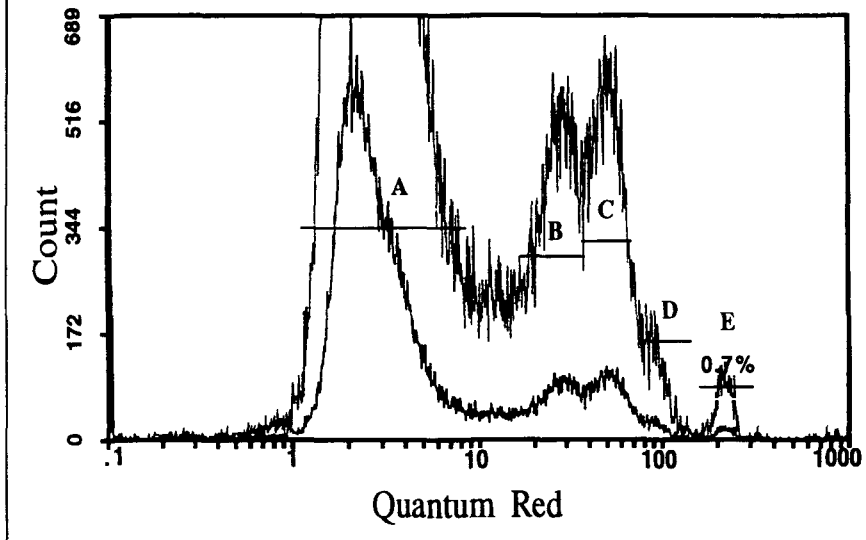

Acknowledgments: We gratefully acknowledge Dr. Charles Cho and Professor Peter Schultz (University of California at Berkeley), who synthesized all of the oligocarbamates sequenced in this study.

References: 1. R.S. Youngquist, G.R. Fuentes, M.P. Lacey and T. Keough, **Rapid Commun. Mass Spectrom. 8**, (1994) 77. 2. R. S. Youngquist, G.R. Fuentes, M.P. Lacey and T. Keough, **J. Am. Chem. Soc. 117**, (1995) 3900. 3. T. Keough, T.R. Baker, R.L.M. Dobson, M.P. Lacey, T.A. Riley, J.A. Hasselfield and P.E. Hesselberth, **Rapid Commun. Mass Spectrom. 7**, (1993) 195.

CHARACTERIZATION OF SMALL MOLECULES BY ESI AND APCI

Richard G. McKay, Charles N. McEwen, and Barbara S. Larsen
The DuPont Company, Central Research & Development
P.O. Box 80228, Wilmington, DE 19880-0228

Combinatorial libraries should prove useful in the discovery and optimization of new crop protection chemicals for the agricultural industry. A key advantage of the library approach is the rapid assembly of diverse, novel compounds by combining automation with synthesis on solid supports. Using a matrix synthesis approach, a chemist can quickly vary the type and nature of functional groups attached to selected organic scaffolds. One-hundred fold productivity increases the number of novel compounds synthesized for biological testing by these methods.

Rapid analytical support is critical for the chemist to develop the optimal synthetic processes and monitor the quantity of products produced. We report here our approach to rapidly analyze these samples by applying APCI.

We have upgraded our VG TRIO-2000 with APCI. The choice of APCI as an ionization technique is sound because it is robust, can be automated, and generates molecular ions for approximately 95% of the molecules synthesized. Shown in Figures 1 and 2 are a comparison of an electrospray and APCI spectra from a study, noting the observed fragmentation from the APCI spectrum. The system is configured using an HP1090 liquid chromatograph for direct injection of 10 µL of a 1.0 µg/µL solution. The diode array detector is used to check for the presence of the synthesized product monitoring an appropriate wavelength. The 1090 HPLC communicates to the MassLynx software allowing for a sample to be analyzed every 1.5 minutes (Figure 3). With this approach, 40 samples per hour can be analyzed with an averaged spectrum generated for each injection.

The volume of data from the mass spectrometer needs to be effectively managed. When a chemist begins with a new organic scaffold, we will work closely with them to assist in identifying the best conditions for library synthesis such as evaluating reactant and solvent concentrations. The mass spectrometer shows the chemist any side reactions or incomplete reactions. Once the synthetic route has been optimized, we provide only an excel spread sheet with an indication of whether the molecular ion was observed and the presence of other significant peaks. All spectra have been archived using a CD rom. Once a hit has been made using a whole plant screening approach all analytical data for that molecule can be retrieved.

43rd ASMS Conference on Mass Spectrometry and Allied Topics

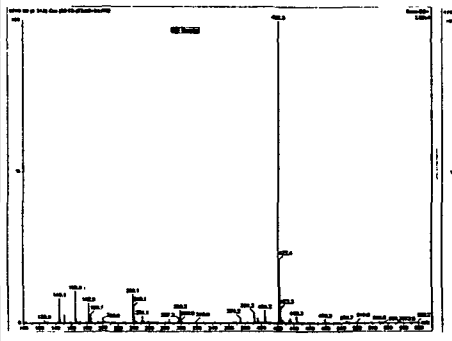

FIGURE 1

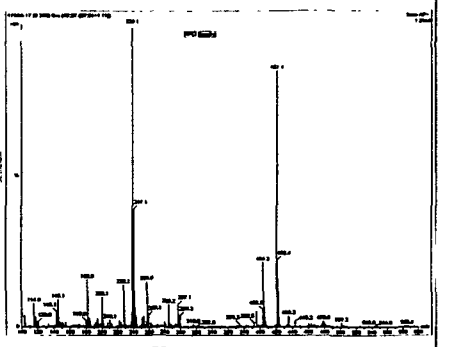

FIGURE 2

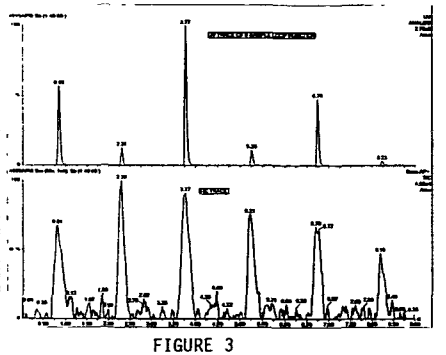

FIGURE 3

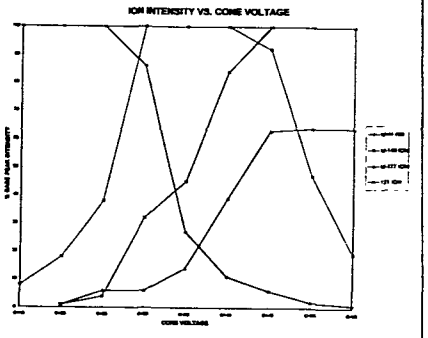

MS/MS of Thiazolidinones: Applications of MS in Combinatorial Chemistry

William L. Fitch, Nikhil Shah, Christopher P. Holmes and Gary C. Look
Affymax Research Institute, 3410 Central Expressway, Santa Clara, CA 95051.

Medicinal chemists are increasingly relying on robotic synthesis and solid phase combinatorial chemistry (SPCC) to leverage their drug discovery efforts. Affymax has been pioneering SPCC and we have been applying mass spectrometry to these efforts. In the rehearsal phase of SPCC, compounds are synthesized one at a time and their structures confirmed conventionally. In the library production phase of SPCC, using the "split and pool" method, compounds are made in mixture, one compound per bead. Mass spectrometry is the key method for quality control of these libraries. The pooled libraries can be bioassayed in the solid phase or after cleavage into microtiter plates. In either case, a decoding or deconvolution step is required to ascertain the structure of the active ligand. The MS behavior learned in the rehearsal phase is critical to the success of this sample limited step.

We illustrate these steps with pure compounds and libraries of thiazolidinones prepared by solution or solid phase condensation of amino acids, aldehydes and thioacetic acids. Mass spectra were recorded on a Finnigan TSQ7000 using ESI or APCI. APCI is more sensitive for these neutral molecules. Below is a typical MS/MS spectrum.

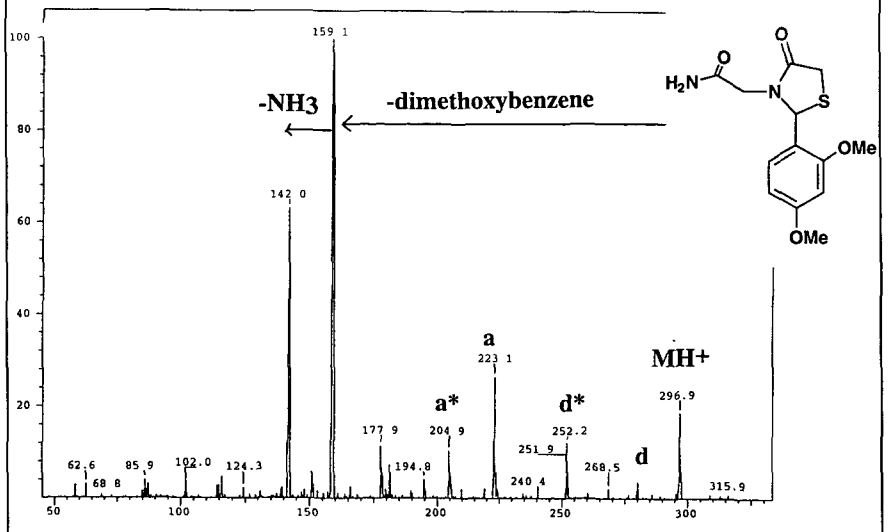

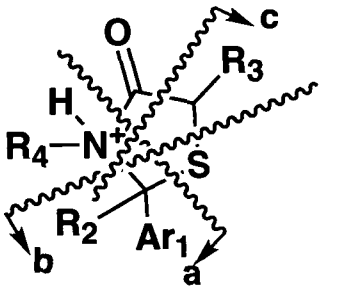

All of the compounds showed the a fragmentation pathway. Other dissociations were very dependent on the aromatic substituents and on the loss of neutrals from the R_2, R_3 and R_4 sidechains. The d and d* fragments in the opposing spectrum are due to loss of NH_3 and CO from the parent ion. The a* is due to loss of H_2O from a.

A 125 member library of thiazolidinones was prepared by SPCC and submitted blind to the MS lab. The APCIMS and APCIMS/MS of this compound are shown below. Of the 125 possible structures 5 had molecular weight 432. So the MS/MS experiment was necessary to complete the structure proof. All of the candidates had $CONH_2$ groups; the primary loses of NH_3 and CO were uninformative. But only the correct structure with an R_3=methyl would be expected to give the ion at m/z 300 due to a cleavage followed by loss of NH_3 and CO.

Thiazolidinone library 2, APCIMS of bioactive component, nominal 40 pmol, 40% of 1 bead photocleavage product

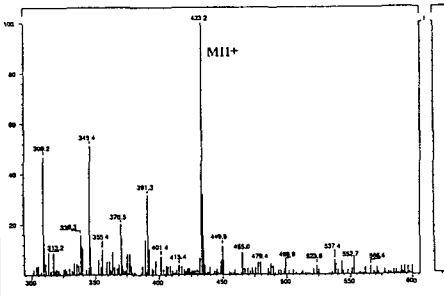

Thiazolidinone library 2, APCI/MS/MS, nominal 200 pmol, 2 bead equivalents

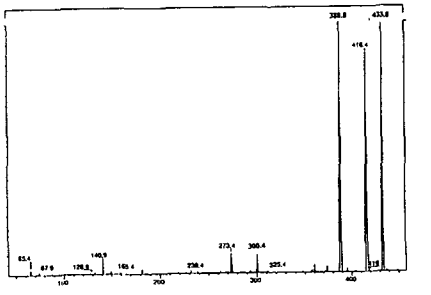

References:
1. E. M. Gordon et al, J. Med. Chem. 37, 1385(1994)
2. C. P. Holmes, submitted to J. Org. Chem.
3. W.L. Fitch et al, J. Org. Chem. 59, 7955 (1994)

Characterization of Complex Chemical Libraries Using LC/MS/MS

Kerry Nugent and Sam Baldwin,Michrom BioResources, Auburn, CA
Adrian Land, Mark Bier, and Kevin Wheeler, Finnigan, San Jose, CA
Kerry Spear, Gianine Figliozzi and Ron Zuckerman,Chiron, Emeryville,CA

The synthesis of combinatorial libraries of chemical compounds is a powerful tool for screening vast numbers of diverse molecules for biological activity. These techniques were first used with synthetic peptides, but are now being used with peptoids (oligo N-substituted glycines) and other small molecules to produce libraries with dozens to thousands of components. These libraries can then be screened for components with desirable biological characteristics in a wide range of bioassays.

For this study, a 272 component proprietary synthetic peptoid mixture, produced by split resin methodologies was used as a model system for analytical characterization. Although only a few components of any mixture may be of biological interest, it is often important to fully characterize the entire combinatorial library to validate that the multiple synthesis reactions are producing the expected results, and to verify the exact makeup of the library in the event that it has to be produced more than once.

With very complex samples, it is generally advantageous to provide some degree of separation prior to mass spectral analysis to aid in the data interpretation. An initial 30 minute LC/ESI/MS run showed that all of the components in the mixture had masses between 300 - 700, and several components had the exact same mass. Although most of the components in this mixture could be identified using multiple short LC/MS/MS runs, it was found that by running a high resolution, 120 minute LC/MS/MS analysis, the entire mixture could be characterized in a few runs.

Figure 1

20 Picomoles
272 Peptoid Mix

1x150 3u 100A RC18
5-65% ACN / 120 min

1-3 Peptoids / Peak

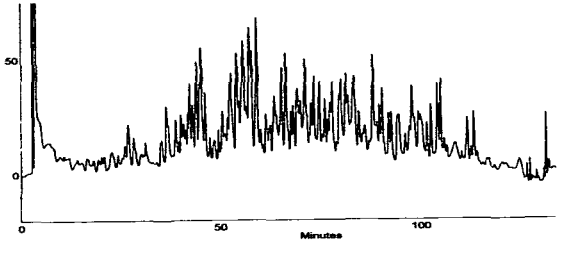

A Michrom UMA microbore HPLC was coupled to either a Finnigan TSQ 7000 Triple Quad MS/MS or a Finnigan LCQ Benchtop MS/MS to screen the sample for parent ions. The initial LC/MS runs employed a rapid 20 minute gradient from 5 - 65% B, to screen a 20 picomole aliquot of the 272 component peptoid sample, giving a total analysis time of 30 minutes. Over 90 parent ions were easily identified during this rapid screening run, and an automated MS/MS experiment was then set up to fragment and help identify these specific compounds.

Figure 2 shows a portion of the output of the automated LC/MS/MS experiment run on the Finnigan LCQ Benchtop MS/MS, with each spike representing an individual MS/MS experiment. The upper trace shows the results of monitoring one specific MH+ ion (419.1), while the lower trace shows the base peak output. Two major components (Peak A and Peak B) were found at different elution times, but had the exact same molecular weight (419.1).

From the MS/MS Spectra in Figures 3 and 4, it is clear that these two isobaric components are indeed different molecules. The automated MS/MS experiments produced useful spectra for most of the other target ions identified in the fast LC/MS runs. Using the proprietary information about the starting materials, all of sample components were easily identified from their MS/MS spectra.

Figure 2

Automated 30 Min LC/MS/MS Run
For 20 Picomoles of 272 Peptoid Mix

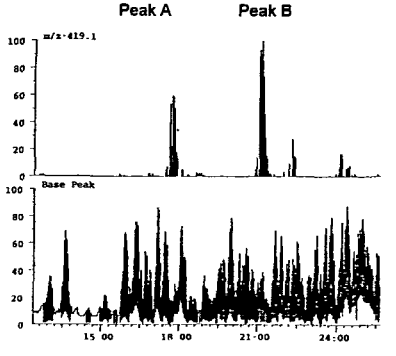

Figure 3 - MS/MS of Peak A

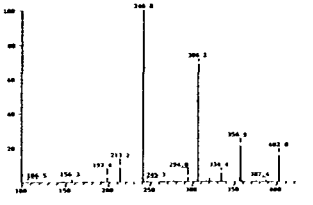

Figure 4 - MS/MS of Peak B

A Single Bead Decode Strategy using Electrospray Ionization Mass Spectrometry and a New Photolabile Linker: 3-Amino-3-(2-Nitrophenyl)Propionic Acid

*David S. Wagner, Bradley B. Brown, and H. Mario Geysen
Glaxo Research Institute, Diversity Sciences Department,

The advent of high throughput screens have increased the number of compounds screened per drug target, and augmented the need for large numbers of novel compounds. Combinatorial chemistry is a synthetic strategy that generates a huge number of chemical compounds and is designed to replace the expensive and time consuming process for individual synthesis. We are investigating procedures that allow for the partial cleavage of support-bound oligomers thereby extending the screening and analytical techniques available to identify active ligands.

A new polymer support that employs a photolabile 3-amino-3-(2nitrophenyl) propionyl functionality (ANP resin) has been developed.

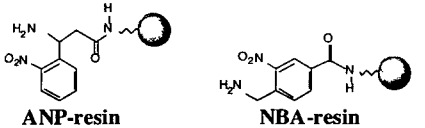

ANP-resin **NBA-resin**

Photolabile resins offer some advantages over traditional resins including the ability to promote partial cleavage [assay versatility], stability in acidic and basic reaction conditions, and reduction of the number of side products from cleavage. Rich and Gurwara[1] showed that polystyrene based *o*-nitrobenzylamide resins (**NBA-resin**) can be cleaved to carboxamides but often suffer from difficult preparation procedures, extended $t_{1/2}$ times, and low photocleavage yields. To determine if the ANP group provides an effective solution to many of the problems commonly encountered by the NBA resins, the utility of the ANP-resin was investigated (analysis by ESI-MS, LDI-MS).

A diverse set of 20 amino acids were individually coupled to ANP-resin and photolyzed for 2 hours (hand held Mineralight 720 uW/cm^2). The MH^+ ions were observed by ESI-MS(Sciex API-III) for all compounds and all protecting groups survived these photolytic conditions. After 16 hours, 3 of the protecting groups were either oxidized or reduced. A pool containing equal amounts of the 20 amino acids was photolyzed for 12 hours. Seventeen of the twenty amino acids were observed as MH^+ ions, figure 1, (3 samples not observed were the unstable protecting groups).

We prepared Fmoc-Arg(Tos)-**NBA** for comparison to the ANP analog. The intensity of the MH^+ (by ESI) was correlated with irradiation time. A standard solution of Fmoc-Arg(Tos)-NH_2 was used to normalize the intensity of the MH^+ signals and determine percent cleavage from resin. The overall yield from the ANP-resin > NBA-resin. The faster ANP$t_{1/2}$ is beneficial considering analytical and assay needs.

A single bead of Fmoc-Asp-Arg(Tos)-Val-NH2 in 5 ul of H_2O was partially cleaved by irradiating for 1 hour. The 5 ul was removed and diluted to a final volume of 25 ul. ESI-MS of 5 ul showed and intense MH+ ion at 764.2 Da, in complete agreement with the calculated value. MS/MS was performed on the remaining 20 ul and allowed for full mass spectral characterization of the tripeptide, figure 2. The same bead was then re-suspended and

irradiated for 16 hours. As before, ESI-MS detected a strong MH^+ ion, and MS/MS allowed for complete sequencing. Verifying structure elucidation utilizing partial cleavage (controlled release) on a single bead and without encoding methods.

Laser desorption (VG TofSpec SE) was employed to determine the feasibility of direct desorption from the solid resin (Figure 3). Several dry beads of the Fmoc-Arg(Tos)-NH2 were loaded on the sample probe. LD produced a weak but distinct MH^+ signal. Matrix (α-cyano) was added on top of the beads, MALDI produced a stronger MH+ signal. The 20 carboxamides were analyzed. Matrix enhanced the signal from the beads. Most samples produced a characteristic signal in the mass spectrum. Approximately 30% of the carboxamides produced distinguishable MH+ ions.

The ANP-resin proved to be a versatile solid support for the synthesis of C-terminal carboxamides. The cleavage rate of ANP > then the commonly employed NBA-resin. The synthesis and controlled release of tripeptide from a single bead validates the ESI-MS strategy for decoding resin-bound peptide libraries. LDI has shown promise for direct cleavage form the ANP-resin. Currently, modified ANP-resins and alternative analytical techniques are being evaluated for their application with solid phase small-molecule libraries.

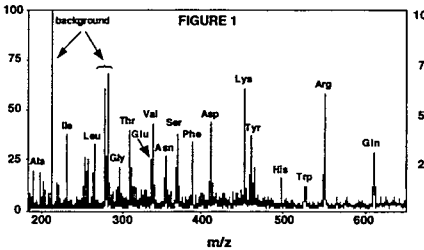

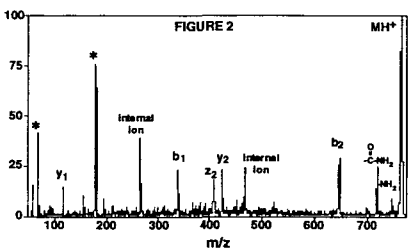

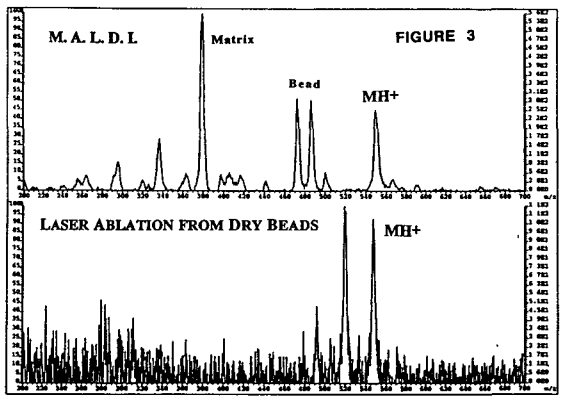

Rich, D.H. and Gurwara, S.K., *Tetrahedran Lett.*, **1975**, 301.

LC/MS Strategy for the Rapid Profiling of Solid Phase Synthetic Products

Robyn A. Rounck[1], Jeffrey L. Whitney[1], Steven E Klohr[1], Kevin J. Volk[1], Edward H Kerns[1] and Mike S. Lee[2], Bristol-Myers Squibb Company, [1]Wallingford, CT 06492, [2]Princeton, NJ 08543

Traditional synthetic chemistry methodologies used for the production of therapeutically relevant compounds often emphasize the "hand-crafting" of a single compound in milligram or greater amounts by a single chemist. Activity is assessed on each final product and is often used to determine the next relevant structural change to be made. A single chemist using the traditional approach produces, on average, less than 100 final compounds per year. Combinatorial chemistry methodologies facilitate the rapid systematic synthesis of molecularly diverse libraries using predetermined sequence variations on solid-phase supports[1-4]. These resulting libraries contain hundreds or even thousands of structurally similar compounds in sub-milligram amounts. The library or "matrix" of compounds produced can be tested for activity using high throughput screening techniques. Relevant targets often include membrane bound receptors, enzymes and metabolic intermediates. Many more compounds can be produced and tested with combinatorial techniques compared to traditional methods.

Libraries of compounds in solution or on solid support present numerous challenges when traditional proof of structure approaches are applied. Some analytical techniques, such as NMR, elemental analysis and infrared spectroscopy do not lend themselves to direct and rapid analysis of synthetic analogs at sub-microgram levels. The analytical methodologies we have developed over the past five years based on LC/MS and LC/MS/MS techniques have provided detailed structural information on trace impurities and degradants, metabolites from biological fluids, natural product extracts and crude reaction products[5,6].

Coupling solid phase synthesis with our profiling methodologies provides a rapid on-line approach for the identification of synthetic reaction products. Analytical strategies were developed utilizing solid phase chemistry and electrospray mass spectrometry for the rapid synthesis and profiling of reaction products. For this study, captopril (SQ 14,225) was the model compound chosen for the application of solid phase synthesis. Library design centered around the combination of five amino acid monomers and six acid R-groups; one combination producing Captopril. Standard peptide synthesis conditions were used involving a Wang-based resin, FMOC deprotection with piperidine, PyBOP coupling conditions, and resin release with TFA. Substructure screening methodologies were developed using LC/MS and LC/MS/MS techniques. Structurally related compounds were identified by screening for monomers contained in the compound matrix.

The released resin-bound compounds were initially characterized by flow injection analysis on an ESI equipped tandem mass spectrometer. The presence of Captoril was confirmed by observing the molecular ion and expected substructures. The negative product ion spectrum of m/z 217 indicated a major fragment at m/z 114, corresponding to the proline substructure. The negative precursor ion spectrum of m/z 114 indicated an ion at m/z 217, corresponding to the molecular ion of Captopril (fig. 1). The characterization and identification of compounds in the library mixture were performed using standard LC/MS and LC/MS/MS methodologies[5,6]. LC/UV data obtained on the mixture indicate the separation of several components with diverse retention times. Substructural screening methodologies were illustrated by the identification of three major components containing the proline substructure, using negative precursor LC/MS/MS on m/z 114 (fig 2). These components correspond to the addition of heptanoic, methyl valeric, and ethyl butyric R-group moieties.

3 Furka, A., Sebestyen, F., Asgedom, M., and Dibo, G , Int. J. Peptide Protein Res., **3 7**, 487-493 (1991).
4. Pavia, M.R., Sawyer, T.K., and Moos, W.H., Bioorganic & Medicinal Chemistry Letters, **3**, 3, 387-396 (1993)
5. M.S Lee, D.S. Hook, E.H Kerns, K.J. Volk and E.I Rosenberg, Biol. Mass Spectrom., **2 2**, 84 (1993)
6. E.H Kerns, K.J. Volk and S.E. Hill, J. Nat. Prod., **5 7**, 10, 1391-1403 (1994)

FIGURE: 1

IDENTIFICATION OF CAPTOPRIL PRODUCT

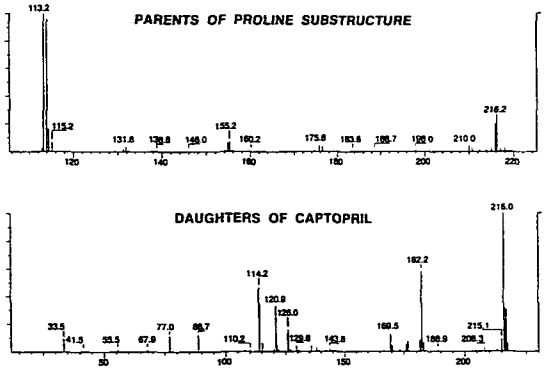

FIGURE: 2

LC/MS/MS SCREEN OF PROLINE SUBSTRUCTURE

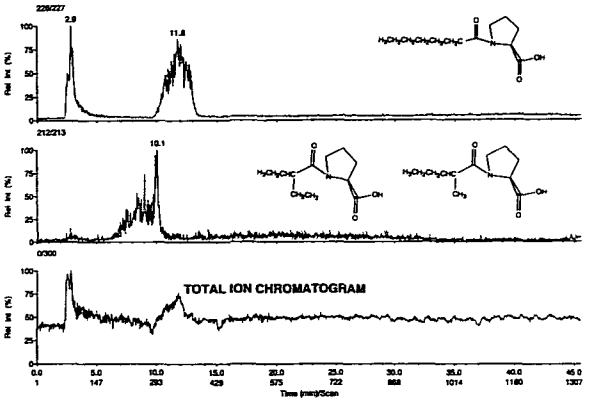

MALDI-TOF-PSD-MS of Peptides off of Single Polymeric Beads

Patrick R. Griffin and Zenon D. Konteatis
Merck Research Laboratories, Rahway, NJ 07065

Previously, we have shown that structural information of a peptide/peptoid can be obtained from analysis of a single bead by MALDI-TOF-MS (1). Here we present a strategy for direct structural characterization of peptide and/or non-peptide combinatorial libraries utilizing MALDI-TOF-PSD-MS and Sequest© (2). The strategy involves the use of differential cleavage linkers, three cleavage strategies, and direct structural identification of active compounds by MALDI-TOF-PSD. Differential cleavage was used to allow multiple biological assays in solution and /or direct assaying of the solid support (3). Advantages of the proposed strategy are as follows: First, it is fast, sensitive, flexible and easy to perform. Second, the strategy should be compatible with various types of chemistries, peptide and non-peptide. Lastly, the method does not rely on encoding or capping strategies. Both the encoding and capping strategies may limit compatibility with various chemistries or types of subunits used. In addition, additional ligands that would be present in both strategies may interfere with the biological assay in which the libraries are used.

The steps involved in identifying active structures were as follows: First, differential release of peptide/non-peptide from resin was performed either by exposing resin to acetic acid or TFA. Second, biological assays performed in solution. Third, treatment of active beads with cyanogen bromide (CNBr). Lastly, released peptide/non-peptide was analyzed using a Finnigan MAT Vision 2000 reflectron MALDI-TOF mass spectrometer in two modes. In the first mode, the normal reflectron mode of the instrument, the molecular mass of the compound was determined. Figure 1 shows a normal reflectron spectrum obtained from analyzing peptide, Phe-Ile-Phe-hSer(lactone), [M+H]+ = 509.6, released from a singly polymeric bead that was treated with CNBr. Next, the precursor mass was selected and analyzed in the PSD mode of the instrument. The PSD mode permits the analysis of metastable fragment ions of a pre-selected precursor ion that are formed in the first field-free region. These fragments are structurally informative and can be used to identify the structure of compounds from combinatorial libraries. Figure 2 displays a MALDI-TOF-MS-PSD spectrum obtained from analyzing the peptide described above. The insert on Figure 2 highlights the sequence ions observed in the spectrum.

To aid in the interpretation of PSD spectra, the database matching program Sequest©, developed by John R. Yates, III and Jimmy K. Eng of the University of Washington, was used.

1) Zambias, R.A.; Boulton, D.A., Grifin, P.R.; *Tetrahedron Letters*, **1994**, 35, 4283-4286.
2) Eng, J.K.; McCormack, A.L.; Yates, J.R.,III; *J. Am. Soc. Mass Spectrom.*, **1994**, 5, 976-989.
3) Lebl, M.; et. al. ; *Peptide Science*, **1995**, 37, 177-198.

43rd ASMS Conference on Mass Spectrometry and Allied Topics

Figure 1.

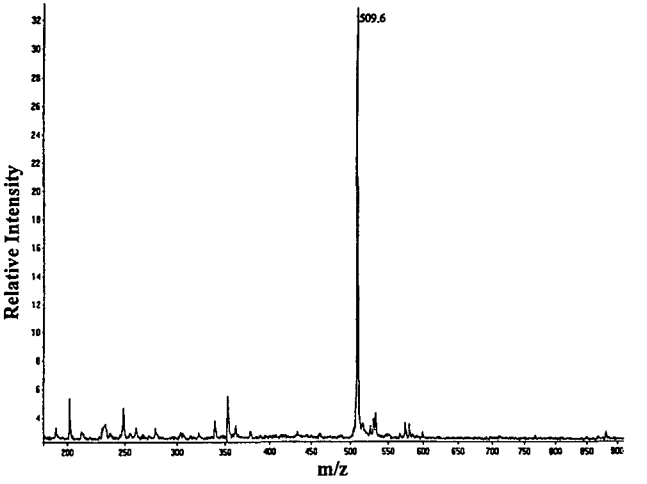

Figure 2.

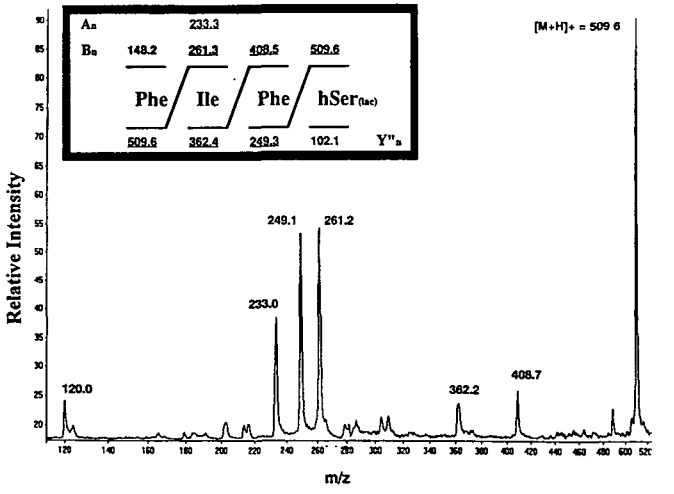

CHARACTERIZATION OF BENZODIAZEPINE COMBINATORIAL CHEMICAL LIBRARIES BY IAE/LC/LC/MS/MS

Michael Nedved, Bruce Ganem,* and Jack Henion
Cornell University, Analytical Toxicology, 927 Warren Dr., Ithaca, NY 14850
*Cornell University, Department of Chemistry, Ithaca, NY 14853

Recently developed combinatorial chemistry techniques allow the generation of large chemical libraries of potential drugs which must then be screened for pharmacological activity (1). Although individual components of combinatorial libraries have been characterized by the use of chemical or fluorescent tags (2), mass spectrometry provides a means for direct and more specific characterization. This has already been demonstrated using a MALDI-TOF mass spectrometer (3). We have demonstrated that a combination of immuno-affinity extraction (IAE) and reversed-phase chromatography followed by on-line, ion-spray mass spectrometry can be used to select and detect components of small benzodiazepine combinatorial chemical libraries using an antibody specific for benzodiazepines. From full-scan IAE/LC/LC/MS/MS data, it is shown that selected components can be characterized by their MS/MS spectra.

EXPERIMENTAL

Automated, on-line column switching was done using a PerSeptive Biosystem's Integral™ Micro-analytical Workstation. IAE was performed by loading a benzodiazepine monoclonal antibody onto a Protein G column (4.6 x 50 mm) which binds the antibody non-covalently. A buffer containing 10 mM NaH_2PO_4 pH 7.4, 0.15 M NaCl was used as the mobile phase at a flow rate of 1 mL/min. A mixture of benzodiazepines in this buffer was subsequently loaded onto the column with unbound components flushed to waste. Antibody and bound analytes were desorbed onto an SPS, C-18, internal-surface, reversed-phase column (0.3 x 10 mm) using 2% (v/v) acetic acid thereby separating the analyte from antibody which was flushed to waste. The trapped analytes were backflushed onto a third column (reversed-phase, C8 Betasil, 2 x 100 mm) at 200 µL/min using a mobile phase containing 40/60 CH_3CN/H_2O, 5 mM NH_4HCOO pH 3.5. Between runs, residual antibody was stripped from the Protein G column with 20% acetic acid (v/v). Full-scan, postive ion mass spectra were recorded using a Perkin-Elmer-Sciex API 300 tandem mass spectrometer by directing the effluent from the C8 column without splitting through an ion-spray interface at 4.1 kV. Full-scan MS/MS spectra were acquired using Argon as the collision gas. A known chemical library of 19 commercially available benzodiazepines, and an unknown, 20-component benzodiazepine chemical library were analyzed.

RESULTS

Figure 1 shows the full-scan LC/MS (A) and IAE/LC/LC/MS (B) chromatograms for a known, 19-component benzodiazepine chemical library. The monoclonal antibody is specific for benzodiazepines and thus does not display great selectivity towards any one component. One component, diazepam, was chosen, and in a subsequent experiment, a full-scan IAE/LC/LC/MS/MS chromatogram was acquired (Figure 2A). The MS/MS spectrum shown in Figure 2B is the average of 15 scans over the peak eluting at 11.44 minutes, and the fragment ions are characteristic of diazepam when compared to the MS/MS spectrum of a standard solution. The same approach is being used to characterize the unknown, 20-component benzodiazepine chemical library.

1. Baum, R. M., *Chemical and Engineering News*, Feb. 7, 1994, p. 20-26.
2. Borchardt, A.; Still, W. C. *J. Am. Chem. Soc.* 1994, **116**, 373-374.
3. Youngquist, R. S.; Fuentes, G. R.; Lacey, M. P.; Keough, T. *Rapid Comm. Mass Spectrom.* 1994, **8**, 77-81.

ACKNOWLEDGMENTS

This research was funded by the National Institutes of Health (GM47931). The unknown benzodiazepine chemical library was generously provided by Dr. Tai-Nang Huang of Hoffman-La Roche, Nutley, NJ. We thank PerSeptive Biosystems, Inc. for the loan of the INTEGRAL™ Micro-Analytical Workstation and Perkin-Elmer-Sciex for the loan of the API 300 mass spectrometer.

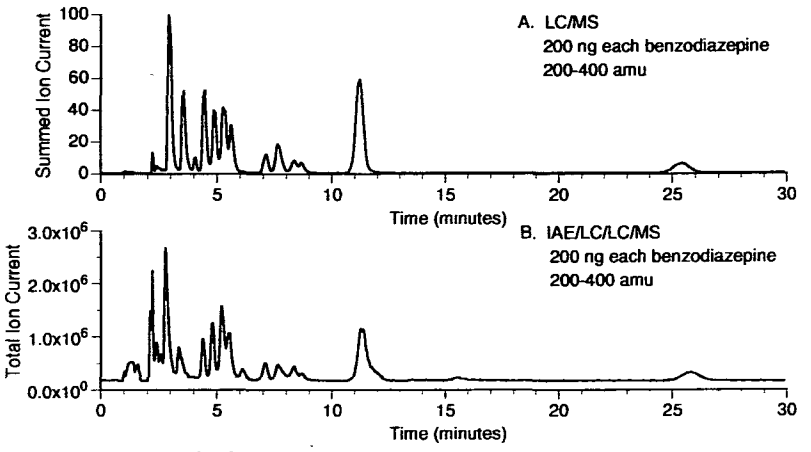

Figure 1. Full scan LC/MS (A) and IAE/LC/LC/MS (B) chromatograms of a known, 19-component benzodiazepine chemical library. The data in A represent the summed ion current (normalized) for all 19 components.

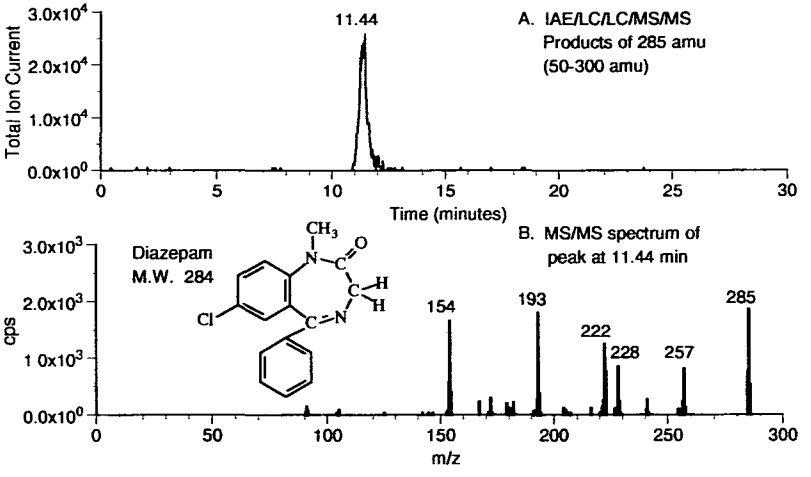

Figure 2. Full scan IAE/LC/LC/MS/MS chromatogram (A) using one component of the known, 19-component benzodiazepine chemical library. The MS/MS spectrum of the peak eluting at 11.44 min (diazepam) is the average of 15 scans.

ANALYSIS OF AN ACTIVE BEAD-BOUND ANGIOTENSIN II RECEPTOR ANTAGONIST BY MASS SPECTROMETRY

Mark E. Hemling, Dimitri E. Gaitanopoulos, Robert P. Hertzberg, Walter P. Johnson, Mary Mentzer, Gerald D. Roberts, Paul Taylor, Joseph Weinstock, & Steven A. Carr

Physical and Structural Chemistry, Medicinal Chemistry, and Biomolecular Discovery
SmithKline Beecham Pharmaceuticals, King of Prussia, PA 19406

INTRODUCTION The developing importance of parallel synthesis of large numbers of compounds either as combinatorial libraries (e.g., via the split synthesis method) or as discretely synthesized compounds on pins, on surfaces, or in 96-well plates puts increasing demands on the development of methods to identify the compounds synthesized. At certain stages during the development of a synthetic strategy, it may be important to analyze a number of the components of the library to verify that the synthesis is producing the desired compounds. However, analysis of every compound in a library that may contain over 10^6 compounds would be an onerous, if not impossible, task. Therefore, a reasonable strategy would be to provide a means to determine the structure of those compounds that are found to be active in biological assay systems. One approach is tagging, the encoding of the beads at each step of the synthesis with information about the chemical reaction at that step. The tag is then released from the bead and "read" using an high sensitivity analytical method appropriate to the tags employed. Tagging carries with it the burden of additional chemical reactions for each step of the combinatorial synthesis with the requirement that the tagging chemistry and the combinatorial chemistry be mutually compatible; also, the release chemistry for the tags and the library compounds must be mutually exclusive. Alternatively, direct mass spectral analysis of the active library compounds is an option. Such a strategy should include the ability to obtain both molecular weight information as well as fragmentation from the amount of compound that would remain on a bead after several rounds of partial compound release and biological assay. Good mass accuracy can help to reduce the MW redundancy that is typically observed in combinatorial mixtures, and reducing such redundancy may obviate the need for tags. Likewise, fragmentation can be used to further narrow the list of possible structures. Ideally, these methods should be amenable to high throughput modes of operation in order to efficiently deal with the large number of beads/compounds that would be generated through massive screenings of combinatorial libraries for biological activity.

RESULTS

- All three methods produce analytically useful results from ≤ 100 pmol of material – both molecular ions and interpretable fragmentation.
- Fragmentation efficiency is comparable for all 3 techniques. However, PSD efficiency in MALDI appears to be matrix-dependent.
- Reduction processes for susceptible compounds in MALDI may reduce utility of isotope ratios for identification of halogenated compounds.
- Mass accuracy is in the order: MALDI-ToF < ESI-Q^3 << MALDI-FTMS

for fragment ions	MALDI-ToF	ESI-Q^3	MALDI-FTMS
avg. std. dev.	0.026	0.012	na
avg. error (Da)	0.039	0.013	0.001
avg. error (ppm)	161	85 (27)[a]	4.4

[a] Without outliers at m/z 97 (412 ppm) and m/z 107 (395 ppm).

- Sensitivity appears to be sufficient to allow identification of compounds after several sequential releases of material for bioassay. However, it is obvious that cleavage conditions need to be well-characterized in order to provide a reasonable amount of material (e.g., ca. 100 pmol) after the after n rounds of bioassay to allow for complete mass spectral analysis.

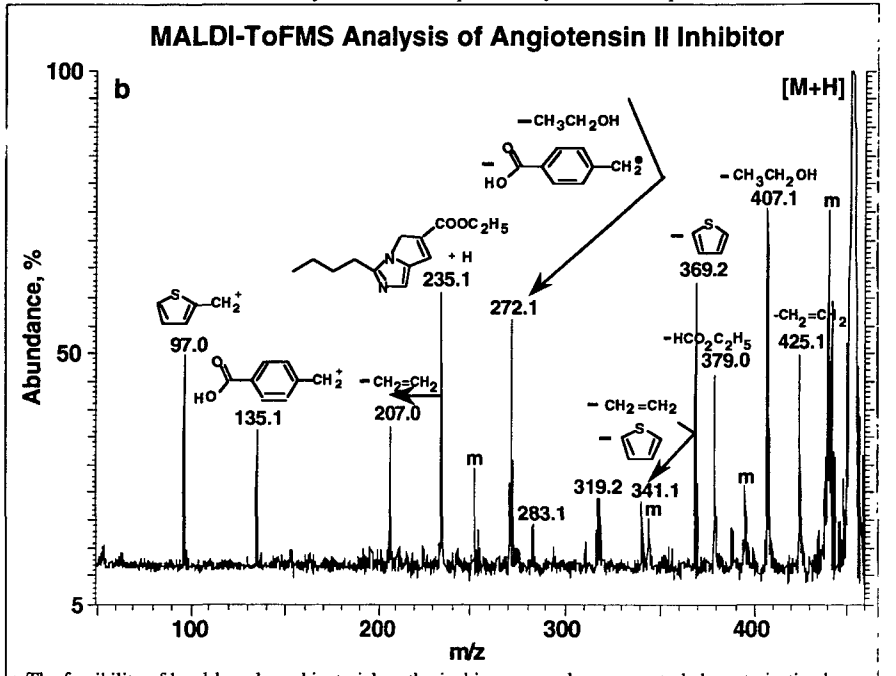

- The feasibility of bead-based combinatorial synthesis, bioassay, and mass spectral characterization has been demonstrated.

CONCLUSIONS We have found several methods that appear to be capable of producing the desired information at the desired sensitivity. We have demonstrated that both MALDI on a ToFMS (or FTMS) and ESI on a quadrupole mass analyzer are capable of providing MW information on the compound from a single bead with relatively high mass accuracy (<75 ppm); MALDI-FTMS provides ≤5 ppm mass accuracy. ESIMS/MS is capable of providing a useful fragment ion spectrum on another aliquot of material from the same bead. Taking advantage of post-source decay fragmentation in MALDI, we have been able to generate a comparable fragment ion spectrum. Taking advantage of the SORI technique in FTMS, we have been able to generate a comparable fragment ion spectrum with very good mass accuracy (≤10 ppm). We have also demonstrated the ability to analyze the compound remaining on a single bead after multiple successive cleavages and also from a single bead that was determined to be active in a angiotensin II receptor antagonist biological assay system tested with both active and inactive beads. This project demonstrates the feasibility of analysis of bead-bound combinatorial libraries by mass spectrometry and that, with libraries carefully designed to reduce mass redundancy, the need for a complete, systematic tagging scheme is obviated.

ACKNOWLEDGMENTS Special thanks to John Hoyes (VG Analytical) for obtaining preliminary MALDI-PSD data and to John Castoro (Extrel FTMS) for providing the MALDI-FTMS data.

DETERMINATION of the DIVERSITY of SMALL-MOLECULE LIBRARIES by CZE-ESI-MS

Yuriy M. Dunayevskiy[1], Paul Vouros[1], Thomas Carell[2], Edward A. Wintner[2], Julius Jr. Rebek[2]
1 Department of Chemistry and the Barnett Institute, Northeastern University, Boston, MA
2. Department of Chemistry, Massachusetts Institute of Technology, Cambridge, MA

Combinatorial chemistry is considered a powerful tool for the development of new therapeutic agents[1,2]. Instead of synthesizing individual compounds and evaluating their biological activity, promising lead candidates are efficiently selected from the vast mixtures through application of modern screening and isolation techniques. Nowadays the main interest lies in synthesizing the libraries in solution where a wide variety of efficient solution phase syntheses can be employed. However, chemistry in solution offers less control on the final mixture composition compared to synthesis on a solid support. Therefore, it is important to determine if all of the anticipated compounds are produced and if there are any side products that potentially can be responsible for the biological activity of the library We utilized electrospray mass spectrometry, both alone and coupled to capillary zone electrophoresis (CZE-MS), to evaluate the diversity of small-molecule libraries. Our approach allowed to investigate the "population density" of the "molecular landscape" generated by the compound variety

The synthetic procedure for the preparation of the molecular libraries is presented schematically in Figure 1 and has been described previously[3]. The libraries consisted of more than 65,000 compounds with different functional groups (19 amino acids) about a rigid xanthene core 1, which determined the overall shape of the molecules. The combinatorial libraries were subjected to a screening procedure to identify the bioactive component(s) to trypsin[3]. All experiments were performed on triple quadrupole mass spectrometers VG Quattro and TSQ-700.

In the view of the fact that complete characterization of the 65,341 component mixture was unrealistic, small representative sublibraries were synthesized based on the core molecule 2 which contained only two acid chloride groups in the position four and five. Molecule 2 provides a realistic test for the determination of building block combination not favored in the synthesis as positions two and five have the highest susceptibility to steric crowding Libraries containing theoretically 36, 45, 55, 78 and 120 compounds were obtained through reaction of 2 with mixtures of 8, 9, 10, 12 and 15 amino acids, respectively. First, we analyzed several single xanthene diamino acids and their simple mixtures in order to investigate the effect of different building blocks on the ionization efficiency of the molecules. The positive ion ESI mass spectra exhibited mainly the protonated molecules without fragmentation in the mass range of interest (m/z:500-900) under the experimental conditions employed. As expected, the derivatives of amino acids with positively charged side chain gave $(M+H)^+$ ions of higher intensity than the derivatives of non-charged and especially of negatively charged amino acids. However, the differences in response signals were not drastic, and there was no ion signal suppression. As the complexity of a mixture increases, one might observe a peak at virtually every nominal mass in the ESI spectrum Therefore, we examined mixtures with different relative concentrations of the components in order to determine when the molecules of lower ionization efficiency still constitute a signal distinguished from the background. As a result of these experiments the threshold of 10:1 S/N was set as a minimum acceptable signal for confirmation of the presence of any given compound in the mixture within the relative concentration range of ten. However, for the derivatives exhibiting peaks of a S/N ratio close to the threshold, additional evidence was deemed necessary to prove a "hit". For these purposes we used negative ion detection mode, which yielded well defined molecular ion data represented by the $(M-H)^-$ ion peaks and offered less background noise This complimentary information helped to verify the presence of the compounds obscured by basic analytes in positive ion mass spectra.

Even though we constructed the libraries to avoid the presence of isobaric compounds, some of the mixture components had the same molecular weights. MS/MS experiments were used as a third confirmatory step and revealed the occurrence of two major fragmentation pathways. The first one led to the formation of the fragment consistent with the core molecule and another one was determined by the structure of the attached amino acid. The CID results allowed us to detect and establish the structure of some side products with the related xanthene rigid core and differentiate between isobaric compounds. Thus, model libraries containing up to 55 components were analyzed and characterized by positive ion, negative ion and MS/MS detection modes. In order to reduce the number of

sub-libraries the analysis of larger mixtures was desirable. However, the increased number of compounds reduces peak capacity, since ions could be observed at every mass within the limited mass range. Accordingly, we explored the use of CZE-MS in order to introduce a fast and efficient further dimension to the analysis Electrophoretic conditions were chosen such that the complex mixture could be separated into several groups of compounds. Within each of the group only several peaks had the same masses and were distinguished by daughter ion spectra analysis An example of separation of isobaric compounds in a library of 120 entities (15 building blocks) is shown in Figure2, where asterisk represents an isotopic peak from Pro/X/Glu derivative (m/z 637) The investigation of the model sub-libraries revealed that most of the anticipated compounds were formed (approximately 85%) Only molecules containing one or more Trp^{Me} or multiple Gly^{Me} and Tyr^{Me} building blocks could be absent in the library based on core molecule 1

The combination of different mass spectrometric approaches allows the analysis of complex mixtures with closely related structure and determination of their composition and purity. The further introduction of a on-line separation method gives an opportunity to examine larger mixtures and, therefore, to reduce the number of tedious synthesis of representative sub-libraries. This provides for rapid screening of combinatorial libraries for their expected complexity and allow the optimization of the synthetic methodology in order to maximize the yield of library compounds.

[1] Gallop, M.A.; Barrett, R.W.; Dower, W.J., Fodor, S.P.A.; Gordon, E.M. *J.Med. Chem* 1994, *37*, 1233-1251
[2] Gordon, E.M.; Barrett, R.W., Dower, W.J., Fodor, S.P.A.; Gallop, M.A *J. Med Chem.* 1994, *37*, 1385-1401.
[3] Carell, T; Wintner, E.A., Sutherland, A.J., Rebek, J., Jr.; Dunayevskiy, Y.M., Vouros, P *Chem. Biol.*, 1995, *3*, 171-183.

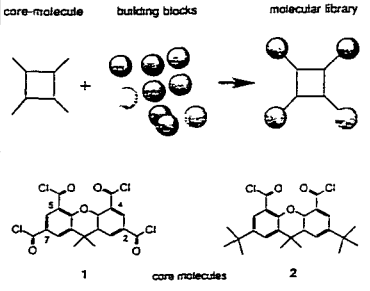

Figure 1. Schematic representation of the synthetic procedure for generation of small-molecule libraries.

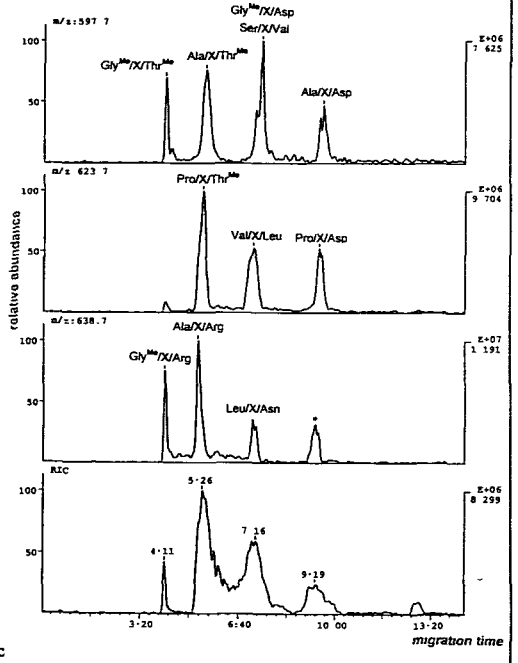

Figure 2. Selected ion chromatograms of isobaric compounds, separated in CZE run.

Mapping Chemical-Space: Application and Prediction within LC/MS

Samuel Mitrovich, Jr.* and Ross C. Willoughby
Waters Corporation, Extrel Mass Spectrometry 575 Epsilon Drive, Pittsburgh, PA 15238

We have developed chemical mapping techniques that allow the visualization of the domain of organic compounds using only the empirical formula and basic physical properties. These Chemical-Space maps can be used to establish a relationship between an analyte, or analyte class, relative to other compounds within the domain of organic compounds. We have constructed 3-D maps of Chemical-Space by plotting molecular weight, frequency of occurrence and specific refractivity using the Wiley data base of mass spectral compounds. The surface created is a graphic representation of the domain of organic compounds. Since the position of any single compound in this domain is a function of its intermolecular interaction and intramolecular properties, the relative position of any analyte on the map is used to predict the applicability of a specific analytical technique. We have also constructed 2-D maps of randomly selected compounds from the Merck Index by plotting molecular weight against a calculated quantitative polarity index (QPI). The QPI includes a factor for the dielectric constant. By including the dielectric constant the maps reflect the boundaries of the strongest intermolecular interactions.

Specific Refractivity

Specific refractivity is derived from the equation for polarizability also known as the Lorentz-Lorenz relation.

$$\alpha = \frac{3}{4\pi N}\left(\frac{n^2-1}{n^2+2}\right)\frac{M}{\rho}$$

(N is Avogadro's number, n is the refractive index, M is the molar mass and r is the density.)

Polarizability is related to the ease with which an electric field can distort the molecule, size of charge fluctuations, melting and boiling points, volume of the molecule as well as London dispersion forces. Unfortunately it is difficult to calculate. Therefore, another version of the Lorentz-Lorenz relation called molar refractivity is used; it is given by the equation:

$$R_M = \left(\frac{n^2-1}{n^2+2}\right)\frac{M}{\rho} = \frac{4}{3}N_A\pi\alpha$$

Molar refractivity can be calculated from the values of the bond refractions that make up a molecule. These values are known and are additive(1). It is only necessary to know the molecular formula to do the calculation. From those values the specific refractivity is calculated. Specific refractivity is the molar refractivity divided by the molecular weight:

$$R_S = \frac{\left(\frac{n^2-1}{n^2+2}\right)\frac{M}{\rho}}{M}$$

Quantitative Polarity Index

The QPI was calculated using the equation for estimated dielectric constant:

$$\varepsilon_{est} = (\alpha_1\varepsilon_1+\alpha_2\varepsilon_2+...)\frac{\rho}{M}$$

The equation assumes that each atom and group make a specific contribution to the dielectric constant. The information needed to do the calculations is similar to that needed

for calculating molar refractivity. To avoid the need for density values, the partial dielectric constant (ε_p) was calculated:

$$\varepsilon_p = \frac{(\alpha_1\varepsilon_1+\alpha_2\varepsilon_2+...)}{M}$$

The ε_p represents the relative contribution of each constituent atom to the total dielectric constant. QPI is calculated as the product of molar refractivity and the partial dielectric constant:

$$QPI = R_M\varepsilon_p = \frac{1}{\rho}\left(\frac{n^2-1}{n^2+2}\right)(\alpha_1\varepsilon_1+\alpha_2\varepsilon_2+...)$$

The equation contains aspects of intramolecular structure and intermolecular interaction. $R_M\varepsilon_p$ is equivalent to the specific refractivity (R_S) times the specific contribution of each atom or functional group to the dielectric constant.

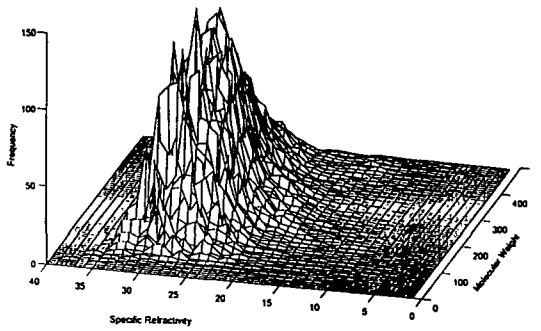

Figure 1: 3-D map of compounds from the Wiley data base.

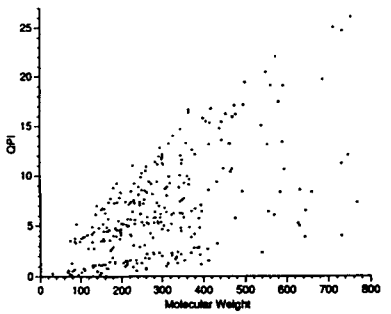

Figure 2: QPI vs. MW of compounds from the Merck Index.

(1) Vogel, J. of Chem. Science, 1948.

Alkylation of *E. coli* Thioredoxin by S-(2-chloroethyl)glutathione

John C. Erve[†‡], Elisabeth Barofsky[†], Douglas Barofsky[†], Max Deinzer[†], Don Reed[‡]
[†]Department of Agricultural Chemistry and [‡]Department of Biochemistry/Biophysics, Oregon State University, Corvallis OR, 97331

Introduction:

The tripeptide glutathione (GSH) is an important component of the cells defense mechanism due to its ability to combine with reactive electrophiles that can cause damage to biologically important macromolecules. It is now realized, however, that GSH conjugation may also lead to toxification reactions, such as occurs for the dihaloalkanes. 1,2-Dichloroethane (DCE) is a major organic chemical produced in the U.S. for use as a starting material for vinyl chloride synthesis. Following exposure to DCE, GSH conjugation can result in formation of S-(2-chloroethyl)glutathione (CEG). By a process of intramolecular cyclization, CEG can form a potent alkylating agent that can alkylate nucleophilic sites in DNA, such as the N^7 position of guanine. The focus of our research has been to better understand the protein alkylating ability of CEG, in order to elucidate the possible component of protein covalent binding in the mechanism of toxicity of DCE.

Materials and Methods:

E. coli thioredoxin was used as a model protein due to the presence of a reactive sulfhydryl group present at the active site of the enzyme. CEG, synthesized by the method of Reed and Foureman, was added in 5, 10 and 25 fold molar excess over reduced thioredoxin and allowed to react in an ammonium bicarbonate buffer at pH 7.4. Separation of the adducts utilized RP-HPLC with a C4 column. MALDI-MS was accomplished with a custom built TOF instrument and tandem mass spectrometry was accomplished with a Sciex III plus triple quadrupole.

Results:

The major thioredoxin alkylation product was a mono-adduct, which after collection off the HPLC column was pure, as judged by MALDI-MS (Figure 1). This adduct was digested with trypsin and analyzed by MALDI-MS. An alkylated tryptic peptide at *m/z* 2,370 corresponds to the tryptic peptide containing the two active site cysteines at positions 32 and 35 (Figure 2). This peptide was collected following separation of the tryptic digest peptides on a C18 column and analyzed by ionspray MS (Figure 3A). The doubly charged ion was fragmented to produce the product ion spectrum in Figure 3B. Ion y_5, seen at *m/z* 897, fragments to lose a glutamic acid residue to produce the peak observed at *m/z* 768. Examination of the fragment ions produced led to the conclusion that only one of the active site cysteines was alkylated by the episulfonium ion of CEG. The work presented here shows the power of mass spectrometry in identifying particular alkylation sites in proteins and should be useful in elucidating the role of protein covalent binding in the toxicity of certain toxic chemicals.

References:

Erve, J. C. L., Deinzer, M. L., and Reed, D. J. "Alkylation of oxytocin by S-(2-chloroethyl)glutathione and characterization of adducts by tandem mass spectrometry and Edman degradation." *Chem. Res. Toxicol.* **8** (1995):414-421.

Meyer, M., Jensen, O. N., Barofsky, E., Barofsky, D. F., and Reed, D. J. "Thioredoxin alkylation by a dihaloethane-glutathione conjugate." *Chem. Res. Toxicol* 7 (1994): 659-655.

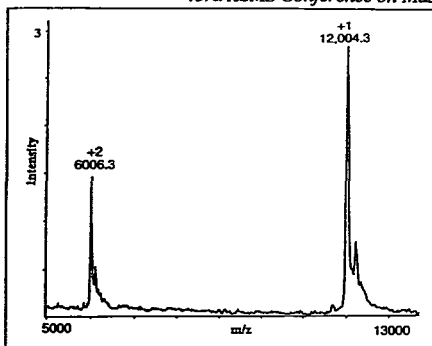

Figure 1. MALDI-MS spectrum of the mono-alkylated *E. coli* thioredoxin showing singly and doubly charged ions.

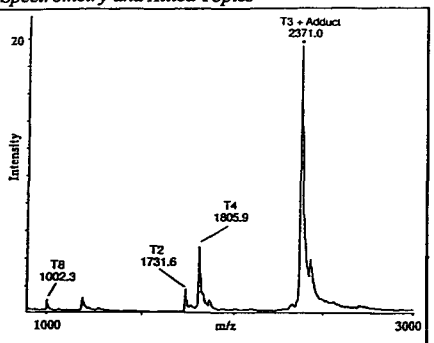

Figure 2. MALDI-MS spectrum of a tryptic digest of the mono-alkylated *E. coli* thioredoxin shown in Figure 1.

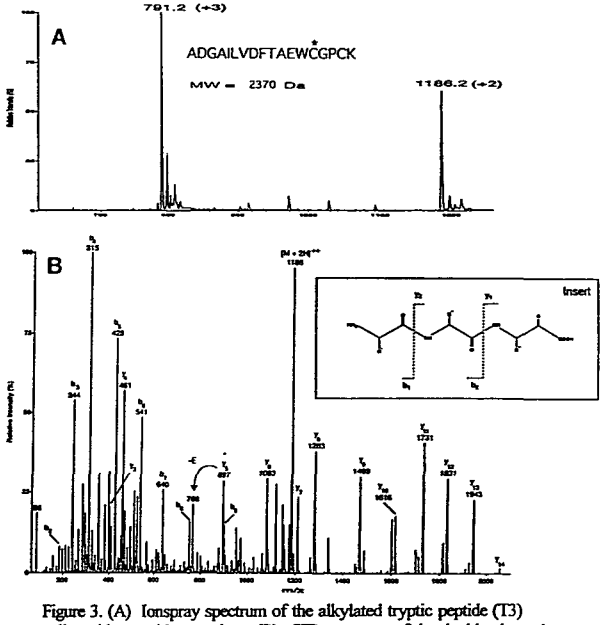

Figure 3. (A) Ionspray spectrum of the alkylated tryptic peptide (T3) collected by peptide mapping. (B) CID spectrum of the doubly charged ion. The fragment ion y_5 undergoes additional fragmentation to lose a glutamic acid residue from the adduct derived from CEG.

OPTIMIZATION OF EXPERIMENTAL PARAMETERS USED IN HRMS OF DNA ADDUCTS

Asoka Ranasinghe, Nova Scheller, Kuen Y. Wu, James A. Swenberg
Department of Environmental Sciences and Engineering, University of North Carolina, Chapel Hill, NC 27599-7400

The pursuit of more sensitive and specific methods for the detection and quantitation of DNA adducts has led to the application of high resolution mass spectrometry (HRMS), in combination with gas chromatography-electron capture negative chemical ionization (GC-ECNCI)[1]. In this work, we have investigated the effect of several experimental parameters, including mass resolving power, sample introduction and derivatizing reagent on the quantitation of N^2,3-ethenoguanine (EG), *a promutagenic adduct, using isotopic dilution mass spectrometry.*

The samples were analyzed using HP 5890 GC interfaced to a VG70-250SEQ mass spectrometer. Both on-column and direct injections were made on to a DB-5 fused silica capillary column (30m X 0.32 mm) with a He head pressure of 10 psi. Two reagents, pentafluorobenzyl bromide (PFBB) and 4-trifluoromethyl-2,3,4,5-tetrafluorobenzyl bromide (TTBB), were used for derivatization. ECNCI selected ion monitoring experiments were performed by monitoring the fragment ions, $(M\text{-}PFB)^-$ [m/z 354.0413, 358.0549 ($^{13}C_4$-labelled int. std.)] for PFB_2-EG and the ions, $(M\text{-}HFB)^-$ [m/z 404.0381, 408.0517 (IS)], for *diheptafluorobenzyl bromide*, HFB_2-EG. Perfluorokerosine (PFK) was used for tuning and for lock masses (m/z 354.9792 and 404.9760) during HRMS, and the dwell time was 50 ms per ion. The ion source temperature and the methane pressure were 250°C and $3X10^{-5}$ mbar respectively. The DNA assays were carried out according to previously published work.[2]

Although increased resolving power (RP) causes a decrease in intensity of the analyte signal, better detection limits than low resolution MS (LRMS) can still be obtained for biological samples because of the reduction in chemical noise obtained in the narrower mass window used at RP 10,000. For example, HRMS of a synthesized standard PFB_2-EG (190 amol) gives similar detection limits (S/N 9; Figure 1) to the reported[2] LRMS experiment. However, analyses of endogenous EG in human liver samples indicate S/N improvement when changing the RP from 1000 (Fig. 2a; S/N 44) to 10,000 (Fig. 2b; S/N 80). Derivatization using TTBB also seems to increase the method detection limit, perhaps due to greater electron affinity of HFB_2-EG (14 F atoms compared to 10 in PFB_2-EG). Electrophore-labelled biological samples are complex mixtures which can quickly degrade capillary columns when injected using on-column mode. Guard columns can extend the life of the analyte column but disrupt the system due to constant clipping at the injection port, and are prone to leaks each time they are handled. Direct injection (Fig. 2b; S/N 80) using a press-fit liner (uniliner #20355, Restek) has given better detection limits than on-column injection (Fig. 2c; S/N 45). These reusable liners allow as many as forty to fifty continuous injections with no increase of signal background and no need for column clipping.

Method calibration for ultra trace amounts of analyte (spiked EG)(Fig. 3) can only be done using HRMS because of the lower detection limit obtained. The HRMS for the lowest calibration point (25 fmol spiked; Figure 4) shows an excellent agreement with the expected RF (0.26 obs.; 0 18 calc.) while LRMS shows a much larger deviation (0.99 obs.). The method limit of detection for EG is 25 fmol/μmol G at a S/N of 5 inspite of limited sample recovery (12%) and injection of only 1 μl (500 amol) out of 50 μl final solution. These results demonstrate the strength of HRMS in the analysis of endogenous DNA adducts.

This work has been supported in part by a grant from the National Institute of Health (P42 ES05948).

REFERENCES:

1. A. Ranasinghe, N.A. Scheller, K.L. Mitro, P.B. Upton, J.A. Swenberg, *42nd ASMS Conf. Mass Spectrom. and Allied Topics*, Chicago, IL., p 868 (1994).
2. N.Fedtke, J.A.Boucheron, M.J.Turner Jr, J.A.Swenberg, *Carcinogenesis*, 11, 1279 (1990).

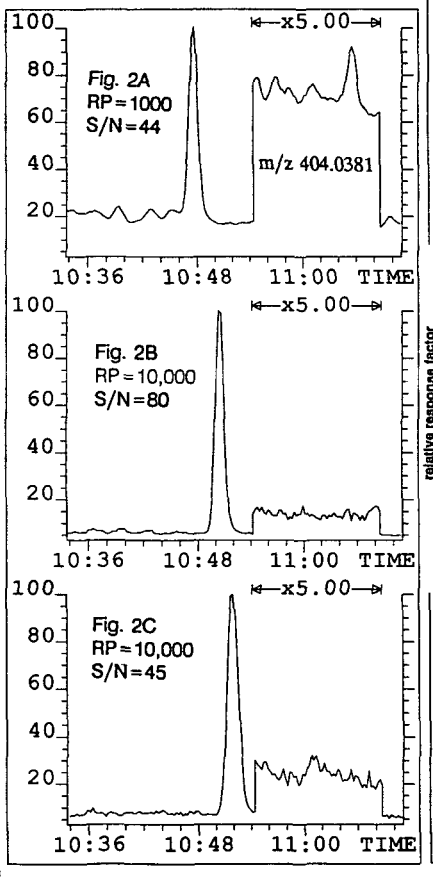

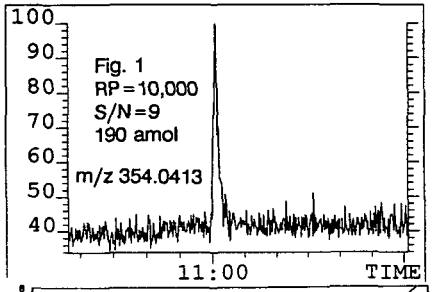

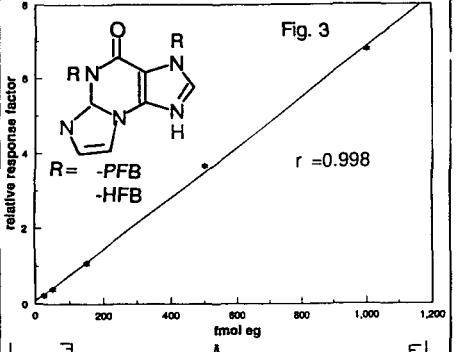

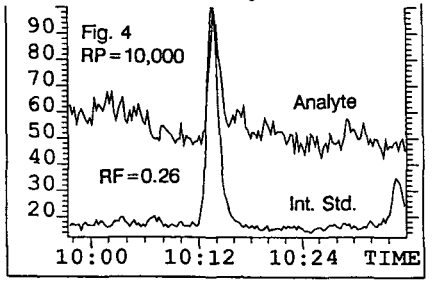

Quantitative Analysis of DNA Adducts by Using HPLC/ESI-MS

Ten-Yang Yen, Nadia I. Christova-Gueorguieva, Nova Scheller, James A. Swenberg and M. Judith Charles
Department of Environmental Sciences and Engineering, University of North Carolina
Chapel Hill, NC 27599-7400

Introduction: The analytical methods needed for the determination of DNA adducts in human or laboratory animals must have the capability to detect 1 adduct in 10^6-10^{10} parent bases with a high degree of specificity. Recently, gas chromatography-electron capture negative chemical ionization-mass spectrometry (GC-ECNCI-MS) has provided the sensitivity and selectivity needed for the analysis of DNA adducts *in vivo*[1]. This method normally requires sample extraction and chemical derivatization followed by clean-up prior to analysis by GC-MS. Due to low yields or analytical interferences arising in the derivatization procedure, sample quantitation can be ambiguous. DNA adducts can be analyzed by high performance liquid chromatography-electrospray ionization mass spectrometry (HPLC-ESI-MS) without derivatization. In this study, we selected the DNA adduct, N^2,3-ethenoguanine (EG, biomarker of vinyl chloride exposure), to develop and optimize a quantitative HPLC-ESI-MS method.

Experimental: The ESI-MS mass spectra were acquired on a Finnigan 4000 quadrupole mass spectrometer retrofitted with a Analytica of Brandford, Inc. pneumatic electrospray source and a Teknivent Vector 2 data system. The HPLC was performed with a LC Packings LC-18 300 μm i.d. x 150 mm column. The mobile phase was delivered through the column at a flow rate of 4μL/min with a linear gradient of 100% water to 20% water/80% methanol in 18 minutes. *In vitro* samples were prepared from 25 mg (2.5 mg/mL) calf thymus DNA (CTDNA) incubated with 210 μmol chloroethylene oxide (CEO) for 20 minutes at 25 °C[2]. A series of samples containing 18-54 μg CEO-CTDNA were prepared for analysis. After spiking each sample with an isotopically labelled internal standard, $^{13}C_4$-EG, EG was isolated[1] and dissolved in 30 μL water, of which 0.5 μL was injected and analyzed by HPLC-ESI-MS. Using selected ion monitoring (SIM), EG was quantified by determining the ratio of the chromatographic areas of EG (m/z:176) to $^{13}C_4$-EG (m/z:180).

Results and Discussion: The HPLC-ESI-MS has provided the sensitivity required for quantifying the DNA adducts. The full scan (m/z: 20-400) mass spectrum obtained from 3.8 pmol of EG is shown in Figure 1. We found that the injection volume on the capillary LC column was optimized at ≤ 0.5 μL for obtaining the lowest detection limit. We were able to detect 5 fmol of EG on column at a S:N = 2:1 by SIM. A linear dynamic range from 25 fmol to 500 fmol of EG (Figure 2) demonstrates the capability

of HPLC-ESI-MS for quantitative analysis of purified DNA adducts.

Figure 1

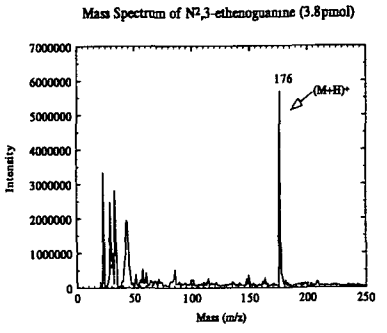

Figure 2

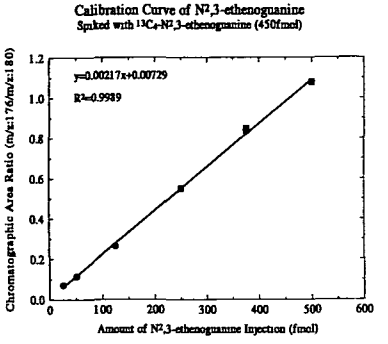

We were able to quantitate EG in 18-54 μg of CEO-CTDNA containing 45.7±5.0 pmol EG/μmol guanine from a set of 6 samples. We also tested the accuracy of the method by adding EG (4 pmol/sample) to the samples. Results of our analyses (2 samples before acid hydrolysis, and 2 samples after acid hydrolysis) showed a recovery of 3.33±0.21 pmol EG at an accuracy of 83.2±5.3 %. These data demonstrated that we can employ the HPLC-ESI-MS method to quantitate N^2,3-ethenoguanine in CEO treated CTDNA with a detection limit of 20 fmol/injection at a S:N = 5:1 (Figure 3).

Figure 3

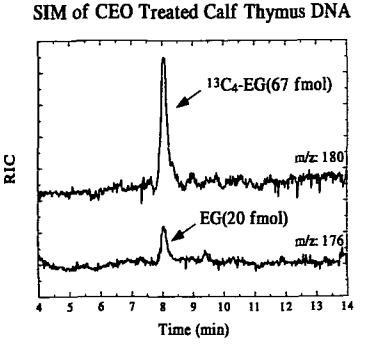

Reference: 1) N. Fedtke, J.A. Boucheron, M.J. Turner Jr and J.A. Swenberg; **Carcinogenesis**, 1990, **11**, 1279-1285.
2) F. P. Guengerich; **Chem. Res. Toxicol.**, 1992, **5**, 2-5.

Acknowledgements: This research was supported in part by a grant from NIEHS P42 ES05948.

Fragmentation of Thioether Conjugates using Electrospray Ionization and Low-Energy Collision Induced Dissociation

C.H. Oberth and A.D. Jones, Facility for Advanced Instrumentation, University of California, Davis, California, 95616

Thioether conjugation of reactive electrophiles is important as a biological mechanism of detoxification, but reactions with protein sulfhydryls have been shown to inactivate critical enzymes and are implicated in mechanisms of toxicity. Characterization of thioether conjugates of peptides and proteins is important for developing an improved understanding of the molecular basis of species- and tissue selective toxicity.

Many xenobiotic substances such as the alpha,beta-unsaturated aldehydes react with sulfhydryls via Michael addition, and our earlier work has shown that retro-Michael fragmentation complicates structural characterization of thioether conjugates of acrolein because the acrolein moiety is lost as a neutral fragment and CID spectra often contain little information about the site of modification.

The aim of this study has been to probe the mechanism of retro-Michael fragmentation by using a series of structurally related peptides that vary in the number of their basic functional groups.

N-Acetylcysteine-, glutathione-, and N-acetylglutathione-acrolein thioether conjugates and corresponding reduced S-(3-hydroxypropyl)- analogs, were used in this study. All of the mass spectrometry was performed on a Fisons/VGQuattro-BQ triple quadrupole mass spectrometer in positive ion mode.

The dynamics of competing fragmentation processes have been investigated by performing Energy Resolved Mass Spectrometry (ERMS) by varying the collision cell potential over the range of 0-50 V.

ERMS data from S-(3-oxopropyl)-N-acetyl-L-cysteine show that retro-Michael fragmentation predominates in spectra obtained at low collision cell potentials. Spectrum 1 shows the CID mass spectrum obtained at a collision cell potential of 0 V and these results suggest that retro-Michael fragmentation is a process with a low energy-of-activation barrier and that sulfur is the site of protonation (low-energy CID cleavages are principally charge-directed). The fragmentation process yielding the retro-Michael product is facilitated by the acrolein moiety undergoing a proposed keto-enol tautomerization.

Figure 1 is a plot of relative abundance's of five daughter ions as a function of increasing collision cell potential observed in ERMS spectra of S-(3-oxopropyl)-N-acetyl-L-cysteine. This plot shows the prevalence of retro-Michael fragmentation at low collision cell potentials but as higher potentials are reached, other higher energy fragmentation processes become accessible.

Reduction of the acrolein moiety is an effective measure to prevent this fragmentation process from occurring. In larger peptides the peptide backbone is more basic and sulfur no longer is a site of protonation. Therefore, retro-Michael fragmentation is not significant.

43rd ASMS Conference on Mass Spectrometry and Allied Topics

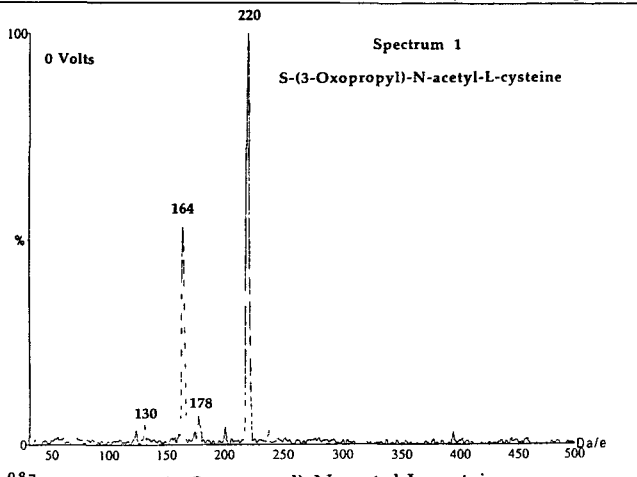

Figure 1: S-(3-Oxopropyl)-N-acetyl-L-cysteine Fragment Ion Intensity vs. Collision Cell Potential

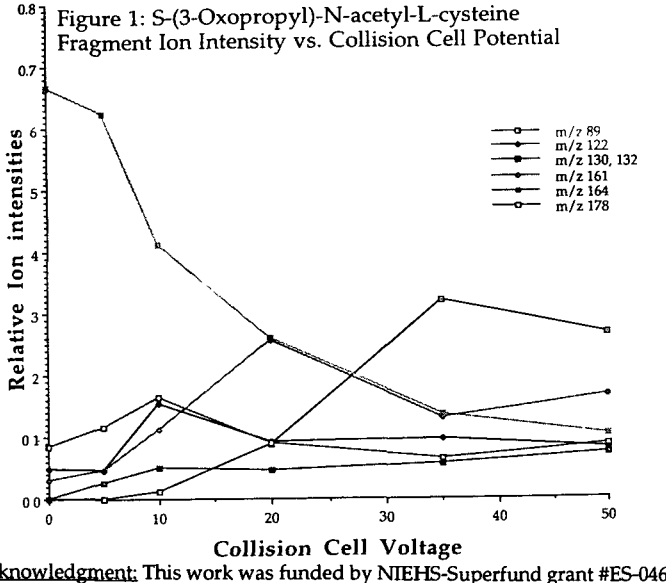

Acknowledgment: This work was funded by NIEHS-Superfund grant #ES-04699. The Quattro-BQ triple quadrupole was purchased by funding from NIEHS-Superfund grant #ES-04699 and NIEHS Center grant #ES-05707.

ESI-LC-MS ANALYSIS OF HETEROCYCLIC AROMATIC AMINES AND THEIR PHASE II CONJUGATES

W.G. Stillwell, J.S. Wishnok, L.R. Kidd, S.R. Tannenbaum, and R.J. Turesky[a]
Massachusetts Institute of Technology, Cambridge, MA 02139 and
[a]Nestle Research Centre, Nestec Ltd., Lausanne 26, Switzerland

The heterocyclic aromatic amines formed in cooked meat represent an important class of mutagenic/carcinogenic compounds with wide dietary impact. MeIQx (2-amino-3,8-dimethylimidazo[4,5-f]quinoxaline), PhIP (2-amino-1-methyl-6-phenylimidazo[4,5-b]pyridine), and related food-borne compounds are biotransformed in animals to give a variety of metabolic products including amine-and ring-hydroxylated metabolites, as well as sulfamate, sulfate and glucuronide conjugates. Because of their polarity and thermal instability many of these compounds cannot be analyzed by conventional mass spectrometric techniques. In the current study we have analyzed urine of MeIQx-treated rats for the presence of polar conjugates and are carrying out analytical studies for the determination of these metabolites in human urine. In previous work it was shown that humans excrete nanogram amounts of phase II metabolites of MeIQx in urine after ingestion of cooked meats (1). These studies employed acid hydrolysis of urine samples and negative ion chemical ionization GC-MS methods for measurement of derivatized MeIQx. These procedures were used to measure MeIQx in human urine in a multi-ethnic study of population groups in Los Angeles County (2). In the present study PhIP analysis in human urine is being carried out by ESI-LC-MS.

A Hewlett-Packard model 5989B mass spectrometer equipped with an electrospray ionization source was used to obtain mass spectral data. The standard amine conjugates of MeIQx and urine from MeIQx-treated rats were analyzed using Vydac reverse-phase narrowbore HPLC columns with a flow rate of 200 ul/min. A gradient buffer composed of 40 uM aqueous ammonium acetate (pH 4.0) and methanol was employed for the HPLC separation. For the analysis of PhIP a reverse-phase microbore column was used with a flow rate of 50 ul/min. The mobile phase was the same as above.

The glucuronide and sulfamate conjugates of MeIQx in positive ion mode showed protonated molecular ions in high abundance (figure 1). Analysis of the amine conjugates by selected-ion monitoring procedures gave good sensitivity. 250 Picograms of the *N*1-glucuronide injected on-column were detected with a signal-to-noise ratio of 60. Similar results were obtained with the N^2-hydroxy-N^2-glucuronide conjugate. ESI-LC-MS of an aliquot of urine from MeIQx-treated rats confirmed the presence of polar phase II conjugates (figure 2).

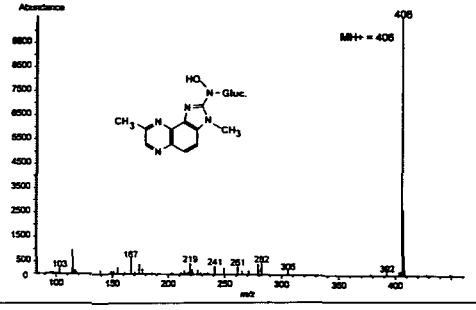

FIGURE 1

ESI mass spectrum of the N^2-hydroxy-N^2-glucuronide conjugate of MeIQx

43rd ASMS Conference on Mass Spectrometry and Allied Topics

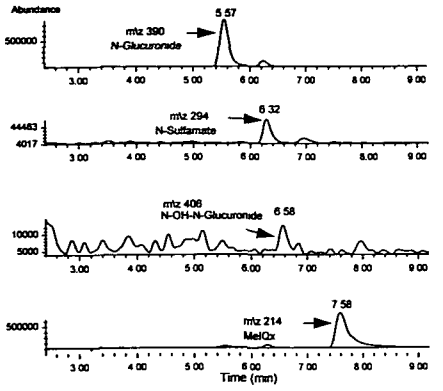

FIGURE 2

ESI-LC-MS analysis of urine from MeIQx-treated rat. A narrowbore column was used with a flow rate of 200 ul/min. The peaks identified by selected ion monitoring of the protonated molecular ions are the N^2-glucuronide (upper trace), the sulfamate conjugate (second trace), the N^2-hydroxy-N^2-glucuronide conjugate (third trace), and MeIQx (lower trace).

In our study of PhIP excretion, urine samples are hydrolyzed in 1 N HCl to cleave the *N*3-glucuronide conjugate of PhIP and liberate the parent amine. After extraction and purification by immunoaffinity chromatography the samples are run in positive ion mode and analyzed by selected ion monitoring of the protonated molecular ions of the amine and its deuterated (d_5-phenyl) internal standard. Good sensitivity has been obtained for the standard compound. 35 Picograms injected on column gave a signal-to-noise ratio of 26. The limit of detection for PhIP in urine is of the order of 10 pg/ml. Figure 3 shows a representative analysis of an extract from human urine.

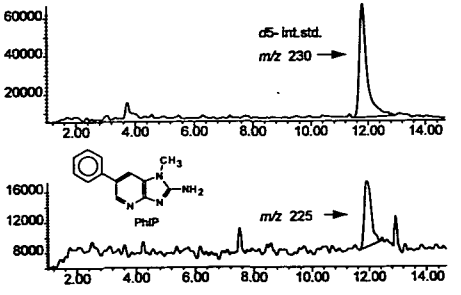

FIGURE 3

ESI-LC-MS analysis of PhIP in human urine. The selected ion chromatograms are of the d_5-deuterated internal standard (upper trace) and PhIP (lower trace). The concentration of PhIP in this urine sample was 29 pg/ml.

These results demonstrate that ESI-LC-MS can be utilized for the analysis of heterocyclic aromatic amines and their phase II conjugates in biological samples. The combination of immunoaffinity chromatography and microbore HPLC column separation provide sufficient specificity and sensitivity for the analysis of PhIP in human urine samples. Further work in sample clean-up and extraction is required for the direct analysis of MeIQx conjugates in human urine.

1. W.G. Stillwell, R.J. Turesky, et al., Cancer Epidemiol, Biomarkers & Prev., 3:399-405, 1994.
2. H. Ji, M.C. Yu, et al., Cancer Epidemiol., Biomarkers & Prev., 3:407-411, 1994.
Acknowledgements: This work was supported in part by NIEHS Grant ES05622.

Characterization of Heterocyclic Amine Metabolites by Electrospray Mass Spectrometry

Donald M. Eades[1], Michael A. Malfatti[2], and James S. Felton[2]

[1]Chemistry and Materials Science, [2]Biology and Biotechnology
Lawrence Livermore National Laboratory, Livermore, CA 94551

Heterocyclic aromatic amines (HAA) are found in cooked meat products and are potential dietary health hazards [1]. HAAs, formed as pyrolysis products during high temperature cooking, have been found to be potent mutagens in the Ames/Salmonella assay as well as carcinogens in animal models [2]. Of the known HAAs, 2-amino-1-methyl-6-phenylimidazo[4,5,-b]pyridine (**PhIP**) exhibits moderate mutagenic activity, but often is present in very high amounts compared to the other HAAs.

Once in the body, PhIP undergoes two metabolic routes, bio-activation and detoxification, both of which are initiated primarily by the P450 microsomal mono oxygenases (e.g. P4501A2). The bio-activation route forms intermediates by hydroxylation, acetylation, and sulfonation at the N_2 position while the detoxification route forms hydroxylation, sulfonation, and glucuronidation at the 4' position as well as glucuronidation at the N_2 position. Here we report a µLC-ESI/MS method for the identification of urinary metabolic intermediates of the food mutagen, PhIP.

All experiments were performed on either a Finnigan MAT TSQ 700 or SSQ 7000. Both instruments were coupled to a Finnigan electrospray ionization (ESI) source operated with the capillary at 250° C and 45V. The needle was at 4500V, octopole at -3V, and the N_2 pressure set at 50 psi. All CID spectra were obtained via "source-CID" by increasing the ESI octopole offset voltage to ~25 eV. The ESI interface was coupled to a Michrom BioResources micro-LC system (µLC). The LC method employed a Reliasil C-18 BDS column (1 mm diam. X 15 cm), a flow rate of 50 µLs/min, a linear gradient from 10%B-90%B in 15 min (solvent A: 2% Acetonitrile/0.1% TFA; solvent B: 95% Acetonitrile, 0.1% TFA), and on-line UV detection at 315 nm.

The µLC-ESI/MS method was used to analyze a mixture of PhIP metabolites present in the urine of animal models. Full scan spectra were collected during the 15 minute LC analysis of ~75 pmoles of each metabolite (i.e. PhIP, 4'-OH PhIP, 4'-SO_4 PhIP, and N_2-OH PhIP glucuronide). "Source CID" spectra were acquired by flow injection analysis of the individual metabolites. The full scan spectra exhibited the expected $(M+H)^+$ ion for each metabolite and, except for 4'-SO_4 PhIP, all exhibited efficient ion production in the positive ESI mode. The CID spectra exhibited characteristic fragmentation via the direct loss of the metabolic substituent or from cleavage of the lone methyl group on the parent PhIP compound. Shown in **Figure 1** are the CID spectra of a) PhIP, b) N_2-OH PhIP glucuronide, c) 4'-OH PhIP, and d) the bio-activated metabolic intermediate, N_2-OH PhIP. Note that the two hydroxyl isomers can be differentiated with the CID spectra. The N_2-OH isomer (Fig 1d) exhibited cleavage of the hydroxyl group (i.e. [M+H-OH]+, m/z 224), while the 4'-OH isomer (Fig 1c) exhibited a loss corresponding to the cleavage of the lone methyl group (i.e. [M+H-CH3]+, m/z 226). The loss of the methyl group from the 4'-OH isomer is similar to that exhibited by the parent PhIP molecule. These characteristic fragments can be used to confirm the presence of specific metabolites found in the urine.

Shown in **Figure 2** are the mass chromatograms from the µLC-ESI/MS SIM analysis of a 20 µL injection of a 75 fmole/µL metabolic mixture (a total of 1.5 pmoles of each metabolite loaded on the column). With the exception of 4'-SO_4 PhIP, each metabolite demonstrated a signal-to-ratio above 10. With further method optimization and MS-MS techniques, the detection limit is expected to be in the mid to low fmole range. Additionally, selective extraction protocols currently under investigation also are expected to improve the detection limits. Our aim is to quantify the individual urinary metabolites in animal models, and apply the technique towards the identification and quantitation of urinary metabolites in humans. Based on previous studies [3], human exposure to PhIP in cooked meat generates parent compound urinary concentrations in the low fmole/µL range. Further optimization of this method should allow metabolic studies of humans following normal dietary exposure to HAAs.

The authors wish to thank the following people for their assistance. Matt Sweeney, Finnigan MAT, Kerry Nugent, Michrom BioResources, David Chambers, Forensic Science Center, LLNL. This work was performed under the auspices of the U.S. DOE by LLNL under contract # W-7405-Eng-48 and supported by the NCI grant CA55861.

References:
1. D.W. Layton, K.T. Bogen, M.G. Knize, F.T. Hatch, V.M. Johnson, J.S. Felton, *Carcinog.*, **1995**, 16, 39-52.
2. R.H. Adamson, V.P. Thorgeirsson, E.G. Snyderwine, S.S. Thorgeirsson, J. Reeves, D.W. Dalgard, S. Takayama, T. Sugimura, *Japn. J. Cancer Res. (Gann)*, **1990**, 81, 10-14.
3. A.M. Lynch, M.G Knize, A.R. Boobis, N.J. Gooderham, D.S. Davies, S. Murray, *Cancer Rese.*, **1992**, 52, 6216-6223

Figure 1

"Source-CID" Spectra of PhIP Metabolites

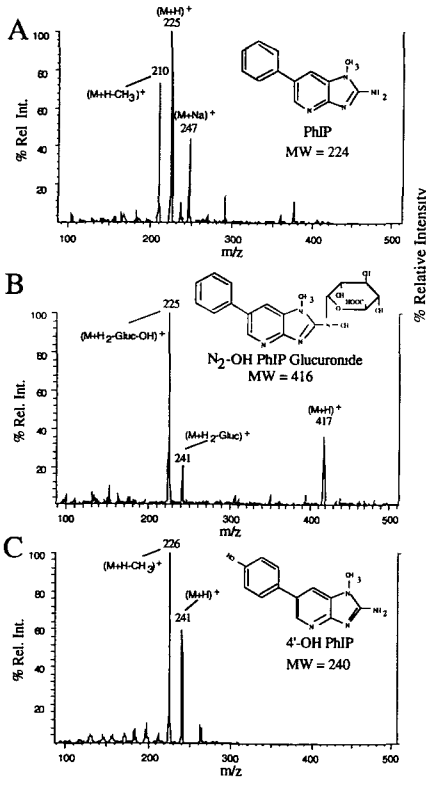

Figure 2

µLC-ESI/MS of PhIP Metabolites
(75 fmoles/µL, 20 µL injection, SIM Mode)

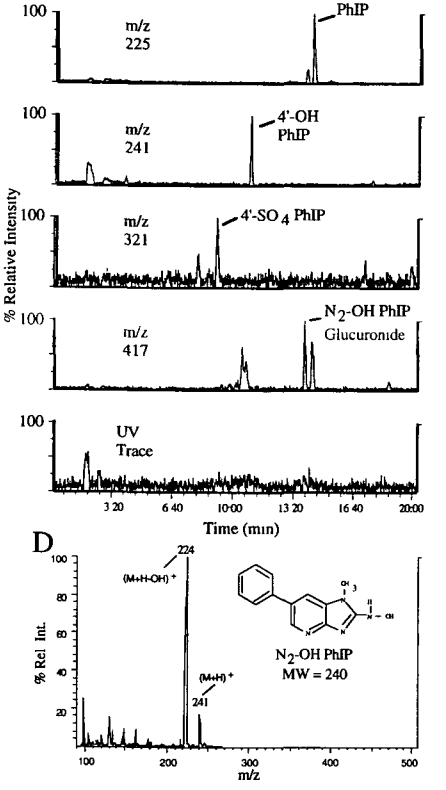

Determination of Nitrosamines by ESI with On-line Photochemical Enhancement David Vollmer*, S. M. Billedeau, and J. O. Lay, USFDA, National Center for Toxicological Research, Jefferson, AR 72079

Introduction N-nitroso compounds have been found in a wide variety of foods and consumer products such as meat, beer, cosmetics, infant pacifiers, and drug formulations. The occurrence of N-nitroso compounds in these constituents is of great concern owing to the carcinogenic properties that many of them exhibit.

Goal The goal of this study is to utilize an on-line photolysis reactor in the LC-MS experiment (LC-uv-MS) as a means for detection and confirmation of N-nitrosodialkylamines. Parameters such as irradiation wavelength, irradiation time, mobile-phase pH, and different organic-acid modifiers are investigated to evaluate the potential of the LC-uv-MS system.

Results and Discussion In consecutive experiments, the wavelength of the irradiation source is changed, whereupon the relative abundance of protonated N-nitrosodimethylamine (NDMA) or protonated N-nitrosomorpholine (NMOR) decreases from no irradiation, to 366-nm irradiation, to 254-nm irradiation, in which no protonated species is detected. Conversely, the relative abundance of the dissociative photolysis products increases from no irradiation, to 366-nm irradiation, to 254-nm irradiation. These results can be directly correlated to the molar absorptivity (a_m) for N-nitrosodialkylamines at lower-wavelength irradiation (254 nm; $a_m \sim 5500$ for NDMA) compared to those at higher-wavelength irradiation (366 nm, $a_m \sim 110$ for NDMA. That is, a larger molar absorptivity yields a greater relative abundance of dissociative photolysis products.

To determine the optimum signals for the molecular ion and the photolysis products, the flowrate through the on-line photolysis reactor is varied, which correspondingly changes the irradiation residence time. Although the flowrate is restrictive owing to the chromatographic separation of the N-nitrosodialkylamines and the electrospray response, the length of the reactor can be changed to yield the optimum irradiation time for a given flowrate. Upon 366-nm irradiation, the relative abundance of the molecular ions of NDMA and NMOR decreases exponentially with time, while the dissociative photolysis products increase. A log plot of the data is linear (NDMA, 0.98; NMOR, 0.99) and is consistent with previous reports indicating that photolysis of nitrosamines follows first-order kinetics. The relative rate of the dissociative photolysis, however, is greater for NDMA (relative rate of dissociative photolysis, $k_{dp} \sim 89$) than for NMOR ($k_{dp} \sim 71$), and can be attributed NDMA's larger molar absorptivity at 366 nm.

N-nitrosodialkylamines readily undergo photolysis in the presence of acid solutions. In consecutive experiments, the relative abundance of both protonated NDMA or NMOR decreases as the pH increases (2.5 to 3.0). Conversely, the relative abundance of the dissociation products increases as a function of pH. Similar trends are observed when comparing acetic acid ($pK_a = 4.75$), formic acid ($pK_a = 3.75$), and trifluoroacetic acid ($pK_a = 0.2$). That is, the rate of photolysis decreases as the strength of the acid increases.

The overall effectiveness of on-line photolysis is estimated by comparing, in consecutive experiments, the type of information obtained from dissociative-photolysis processes to that of in-source collision-induced dissociation (CID). Both techniques offer a means for producing structurally significant ions. For on-line photolysis, the dissociative photolysis process is class-specific; that is, the primary mode of dissociation for N-nitrosodialkylamines is formation of alkylidenealkylamine and parent amines. For in-source CID, the fragmentation patterns are more complicated and they are not class-specific. For example, the CID spectra for NDMA gives three main peaks whereas the CID spectra for NMOR gives 4 main peaks. These differences can be attributed to a greater number of fragmentation possibilities for NMOR compared to those of NDMA. Moreover, the structure of the fragment ions is not always obvious. NDMA dissociates to produce an ion at *m/z* 43, which can correspond to $[CHNO]^+$ or $[C_2H_5N]^+$. NMOR fragments to give an ion at *m/z* 57, which can be $[CHN_2O]^+$ or $[C_3H_7N]^+$.

There are also distinct differences between on-line photolysis and in-source CID with respect to absolute abundance. To produce CID spectra needed for structure confirmation, the potential difference is increased to amounts where there is a 20-60 % loss in ion signal for NDMA, and a 10-70 % loss in ion signal for NMOR. For on-line photolysis, a 10-15 % loss in ion signal is observed for NDMA, whereas a 20-30% *gain* in ion signal is seen with NMOR. Presumably, the signal enhancement for irradiated NMOR is related to the greater ability of its photolysis products to form ions in solution.

To validate the LC-uv-MS method, the linearity and detection limits are measured for NDMA, N-nitrosdiethylamine (NDEA), N-nitrosoethylbutylamine (NEBA), NMOR, N-nitrosopiperdine (NPIP), and N-nitrospyrrolidine (NPYR). External standard calibration curves are determined by summation of the peak areas for the two primary dissociative photolysis products and the molecular ion from a full scan spectrum (from *m/z* 10-250). The calibration curves for the six N-nitrosodialkylamines are linear from approximately 5 ng to 800 ng. The signal-to-noise ratios at the lowest concentrations on the calibration curve are at least 3-to-1 for all the compounds. The full-scan limits of detection, as estimated by a signal-to-noise ratio of 3-to-1, are ~ 2-6 ng for the N-nitrosodialkylamines. The limit of detection for NDMA can be decreased to 100 pg by using selected-ion monitoring (SIM). These limits of detection compare favorably with LC-TEA which were estimated to be approximately 500 pg.

Experimental The eluents used in the chromatographic separation were delivered by a HPLC pump at a flow rate of 1 mL/min. For separation of the N-nitrosodialkylamine standards, a 3.9 mm x 300 mm μ-Bondapak C-18 with 5-μm particles was used. The acetonitrile:water eluent composition was linearly programmed from a 5:95 ratio held for 5 minutes to a 95:5 ratio over 10 minutes and then held for an additional 10 minutes at a 95:5 ratio. The column was connected directly to an injection valve equipped with a 10- or 20-μL loop. A 15-m knitted-open tubular reactor (Aura Industries, Staten Island, N. Y.) was connected after the column and was followed by a 1:4.5 split. Approximately 220 μL/min of sample and eluent were admitted into the electrospray source of a triple-quadrupole mass spectrometer. Typical operating conditions were as follows: capillary temperature, 240 °C; electrospray voltage, 4.5 kV; and sheath gas pressure, 3100 Torr.

Conclusion Although the ability to detect N-nitrosodialkylamines by LC-MS at the low-ng level is significant, the additional capacity to confirm their presence by utilizing an on-line photolysis reactor is also of importance. For the N-nitrosodialkylamines, the LC-uv-MS system produces three primary ions: protonated nitrosamine, protonated alkylidenealkylamines and protonated parent amines. The optimized parameters for separation, irradiation, and detection of N-nitrosodialkylamines are as follows: irradiation wavelength, 366 nm; irradiation time, 45-75 seconds and mobile-phase organic acid modifier, formic acid at pH 2.75. Under these conditions, the linearity and detection limits compare favorably with conventional HPLC techniques for detecting N-nitrosodialkylamines.

MS/MS Criteria for a Confirmatory Method - Sarafloxacin in Catfish Tissue

Steven Cepa, Stanley Menacherry and Lalit Bavda
Abbott Laboratories, Dept. 418, Bldg. R-13, North Chicago, IL 60064

A common screening technique used for drug residue analysis of food products intended for human consumption is liquid chromatography with UV detection. However this technique is not specific for a particular residue, and should the screening indicate some level of the residue, other techniques may be needed as a confirmation.

Mass spectrometry is frequently used as a confirmatory technique, especially in regulated applications[1,2]. To date, most of those methods have used GC/MS with electron impact ionization or chemical ionization. Some have been developed using LC/MS with a thermospray or particle beam interfaces and normal scanning experiments[3].

Here we describe a confirmatory method for the animal antibacterial drug, sarafloxacin (Figure 1), using an LC/MS/MS product ion scan. Attempts to analyze the drug by thermospray, particle beam with CI, and electrospray all exhibited good molecular ion information, but no significant fragmentation. Confirmatory methods should exhibit at least three, and possibly four, structurally significant ions in order to be rigorous[1,2]. In addition, the relative abundances of these ions should be within a specified tolerance of the same ions in the reference standard. In this case, we were required to have the relative abundances of each ion within an absolute +/- 10% of the standard's product ion spectrum[4].

Experimental

Samples were prepared by homogenization, extraction and isolation of the residue with an SPE column. The mass spectrometer was a Sciex API-III operated with an Ion-Spray™ interface. The data system was operated in MRM mode, monitoring each channel (ion) for 100 msec at unit resolution (see Figure 2 and Results below). A reverse phase LC system was employed at a column flow rate of 1 mL/min and split 50:1 into the mass spectrometer.

Results

Figure 2 is an example of the MRM chromatographic trace. The retention time was sufficient enough to allow chromatographic separation of sample-preparation salts and buffers from small organic compounds. One of the confirmation criterion was that the retention time be within +/- 20 seconds of the standard's retention time. The specificity of the product ion scan would allow sarafloxacin to be distinguished from any coeluting compounds. However, analysis of control tissue with no added sarafloxacin, indicated that the sample clean-up had eliminated any coeluting components.

Table 1 lists the ions monitored and statistical results from analysis of 5 controls (tissue blanks), 10 spiked tissue extracts (0.65 ppm and 1.3 ppm), plus 10 biologically incurred tissue extracts. Four ions were monitored and all were within the requisite +/- 10% relative ion abundance compared to the first standard run of the day.

Key factors in obtaining these results were the sample preparation and SPE step to remove interfering components, especially salts which inhibited the mass spectrometric signal; the use of MRM mode to maximize signal; and the need for a strong signal to achieve adequate ion statistics. During method development, it was observed that at sarafloxacin levels below 0.5 ppm we could not achieve the necessary +/- 10% window for relative ion abundances, even though the signal strength made the drug easily detectable.

Table 1: Product Ion Summary

Ion (m/z)	Mean (%)	Standard Deviation	Range (%)
386	54.44	2.7	48.00-59.32
368	100.0	n.a.	base ion
342	16.50	1 0	14.71-17.90
299	26.65	1.7	24.41-30.49

Figure 1: Sarafloxacin and proposed mass spectral fragmentation

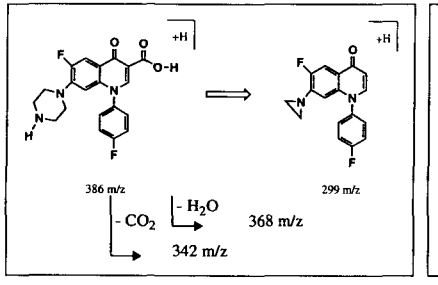

Figure 2: MRM chromatogram

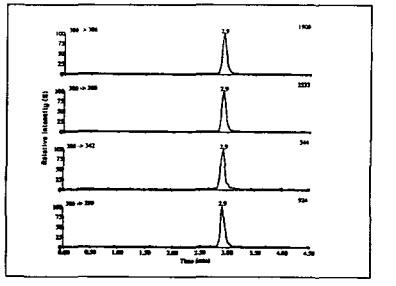

References

1. *Federal Register* **40**, 136 (1984).
2. Commission Decision 93/256/EEC of 14 April 1993, *Off. J. Eur. Communities L*: **118**, 64-79.
3. Delepine, B., Hurtaud, D. & Sanders, P. *Analyst* **119**, 2717 (1994) Identification of Tylosin in Bovine Muscle.
4. Requested by the U. S. Food and Drug Administration.

ANALYSIS OF BREVETOXINS IN "RED TIDE" ALGAE BY HIGH PERFORMANCE LIQUID CHROMATOGRAPHY WITH ON-LINE ELECTROSPRAY IONIZATION MASS SPECTROMETRY DETECTION

Yousheng Hua[1], Wenzhe Lu[1], Michael S. Henry[2], Richard H. Pierce[2], and Richard B. Cole[1*]

1. Department of Chemistry, University of New Orleans, Lakefront, New Orleans, LA 70148 USA
2. Mote Marine Laboratory, 1600 Thompson Pkwy, Sarasota, FL 34236 USA

Brevetoxins are a class of marine toxins found in "red tide" algae blooms. They are responsible for massive fish kills and they pose certain health risks to humans. So far, ten brevetoxins produced by the dinoflagellate *Gymnodinium breve* have been structurally characterized in red tide algae. We are reporting the development of an on-line high performance liquid chromatography-electrospray mass spectrometry (HPLC-ESMS) method which has been successfully applied to the separation and identification of brevetoxins in red tide algal extracts.

The HPLC-ESMS method employs reversed-phase microbore HPLC on a C-18 column with a mobile phase consisting of 85:15 (methanol : water), a flow rate of 8 µl/min, and a post-column split ratio of 1:3 (mass spectrometer : UV absorbance detector). Three known brevetoxins PbTx-1, PbTx-2, and PbTx-9 were tested as standards (separately and as a mixture) to examine the capability of this on-line LC-ESMS system for brevetoxin determinations. The mass spectra for each of these three brevetoxins show four related ions with overlapping elution profiles, corresponding to MH^+ (low abundance), $[M+Na]^+$ (base peak), $[3M+2Na]^{2+}$, and $[2M+Na]^+$. The brevetoxin molecules exhibited a high tendency to bind to alkali cations in positive ion ESMS. Detection limits and linear dynamic ranges were determined with the mass spectrometer scanning from m/z 850-950 to detect $[M+Na]^+$ forms of the various brevetoxins. The detection limits for PbTx-9, PbTx-2 and PbTx-1 were less than 600 fmol, 1 pmol, and 50 fmol, respectively (S/N = 3). Correlation coefficients of the signal response vs. concentration curves showed good linearity with r=0.989 (n=4), 0.988 (n=4), and 0.995 (n=6) for PbTx-9, PbTx-2, and PbTx-1, respectively. Linearity was maintained until the concentrations exceeded 20 µg/ml, where the column became overloaded.

A brevetoxin culture sample was found to contain at least six components (Figure 1) including two well-separated fractions of the brevetoxins PbTx-1 (sodium adduct, m/z 890) and PbTx-2 (sodium adduct, m/z 918), as well as four fractions of unknown components with molecular masses of 657, 959, 963, and 899 Da (sodium adduct ions appear at m/z 680, 982, 986, and 922, respectively). An unknown "U_a" with molecular mass of 899 Da has the same molecular mass as PbTx-9, although the two were well-separated on the column, suggesting that "U_a" is an isomer of PbTx-9. The unknown "U_d" with molecular mass of 657 is postulated to be a product of brevetoxin decomposition whose formation occurred in solution.

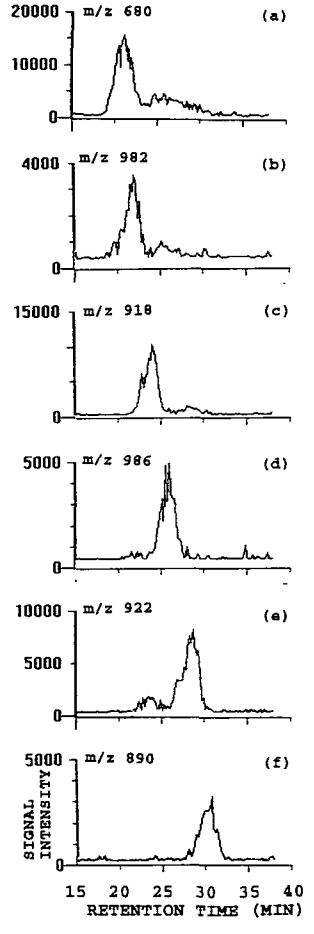

Figure 1. Reconstructed ion chromatograms for on-line HPLC-ESMS of a red tide extract "B" containing brevetoxins. Conditions: 100mm × 1mm ID C_{18} column, methanol:water (85:15,v/v) as mobile phase at 8 µl/min; post-column split to 2 µl/min into the mass spectrometer; injection volume 1 µl.

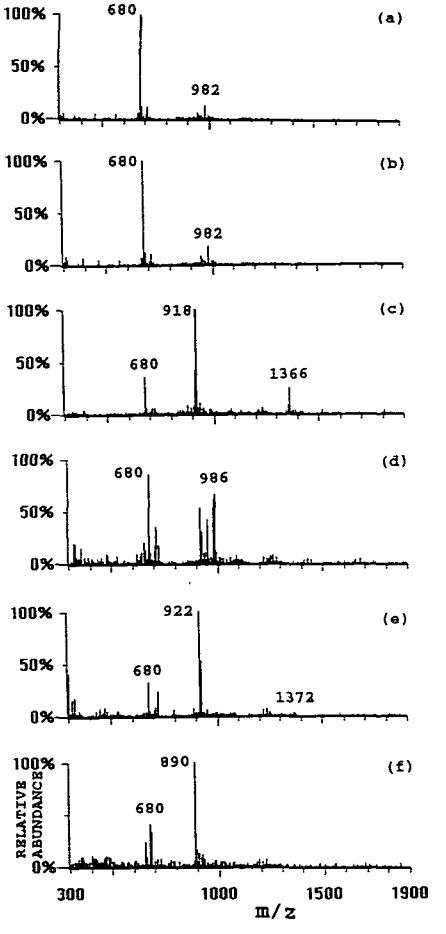

Figure 2. Electrospray ionization mass spectra obtained as an average of three scans at peak maximum from corresponding selected ion chromatograms (Figure 1) found immediately to the left of each spectrum.

DIFFERENTIATION OF PACIFIC AND CARIBBEAN CIGUATOXINS BY APCI/LC/MS

Steven M. Musser[1], H. Ray Granade[2] and Robert W. Dickey[2]

[1]Center for Food Safety and Applied Nutrition, Food and Drug Administration, Washington, DC 20204 and [2]Gulf Coast Seafood Laboratory,Food and Drug Administration, Dauphin Island, AL 36528

Introduction. Ciguatoxins are large cyclic polyether toxins produced by marine dinoflagellates and accumulated in the flesh of tropical reef dwelling fish. Human consumption of fish contaminated with small quantities (0.1 - 1 ng/g) of ciguatoxin results in unpleasant neurological and gastrointestinal symptoms (1). The presence of ciguatoxins in fish is usually verified by mouse bioassay. Although this method has sufficient sensitivity and is useful for screening purposes, it lacks accuracy and specificity. Because the structure of ciguatoxin varies according to its source (Caribbean or Pacific), a more definitive analytical method is needed to provide information regarding both the type and amount of toxin present in fish when cases of human poisoning have occurred. Electrospray (ES)/LC/MS has been used successfully to obtain the molecular weight of Pacific ciguatoxin (P-CTX1), as well as other toxins of similar structure (2). Consequently, we have evaluated ES and APCI as ionization methods, which combined with LC could be used to differentiate and quantitate cigautoxins in fish tissue.

Experimental. Approximately 50 grams of fish tissue known to cause human poisoning was first homogenized and extracted with acetone. The acetone extract was chilled to -20°C overnight. The chilled extract was filtered and evaporated, leaving an aqueous suspension. Methanol was added to completely dissolve the suspension. The resulting solution was defatted by extraction with hexane. The methanol/water fraction was then evaporated to an aqueous suspension. The aqueous suspension was extracted with chloroform and the aqueous fraction was disguarded. The chloroform fraction was applied to a Varian Mega Bond Elut silica column which was first washed with chloroform, followed by elution of the ciguatoxin fraction with 9:1 chloroform:methanol. The eluate was evaporated under nitrogen to yield a dry film of 5-10 mg.

A Hewlett-Packard (Palo Alto, CA) Model 1050 HPLC pump was used to provide linear gradients and a constant flow rate of 200 ul/min. All chromatography was performed on a YMC Inc. C-8 Basic HPLC column (2 x 250 mm). Chromatography conditions started with 50 % ACN followed by a linear gradient to 90 % ACN in 30 minutes. Formic acid, at a concentration of 0.1 %, was used to maintain a mobile phase pH of 3. A Finnigan Model TSQ-7000 triple-quadrupole mass spectrometer with the standard Finnigan ES or APCI ion source was used. Nitrogen was used as a nebulizing gas and the capillary temperature was 250°C for ESP and 150 °C for APCI. A vaporizer temperature of 450 °C was used for APCI experiments. The instrument was scanned over the range of 700-1300 amu at 1.5 sec/scan.

Results and Discussion. Electrospray LC/MS analysis of toxin contaminated fish extracts produced an [MH]+ ion for Caribbean ciguatoxin with little or no fragmentation. Although electrospray provided sufficient sensitivity at physiologically relevant levels, the lack of fragmentation diminished its usefulness as a regulatory technique. Attempts to increase the fragmentation by using CID in the high pressure region of the ion source resulted in increased noise levels and higher detection limits. Analysis of fish extracts (figure 1) for ciguatoxin using APCI yielded a 5-fold increase in sensitivity over that obtained with electrospray, in addition to producing structurally significant fragmentation

without increasing the overall noise level. Fragmentation of both Caribbean and Pacific ciguatoxins using APCI was limited to 3-4 consecutive losses of water from the molecular ion species. The ratio of the fragment ions to the parent ion, in addition to differences in parent ion mass (P-CTX1 = 1111.6, C-CTX1 = 1123.6) and LC retention time, allowed unambiguous identification of the geographical origin of the ciguatoxin.

1. Swift, A.E.B. and Swift, T.R., *Clin. Toxicol.*, **31**, 1 (1993).
2. Lewis, R.J., Holmes, M.J., Alewood, P.F. and Jones, A., *Nat. Tox.*, **2**, 56 (1994).

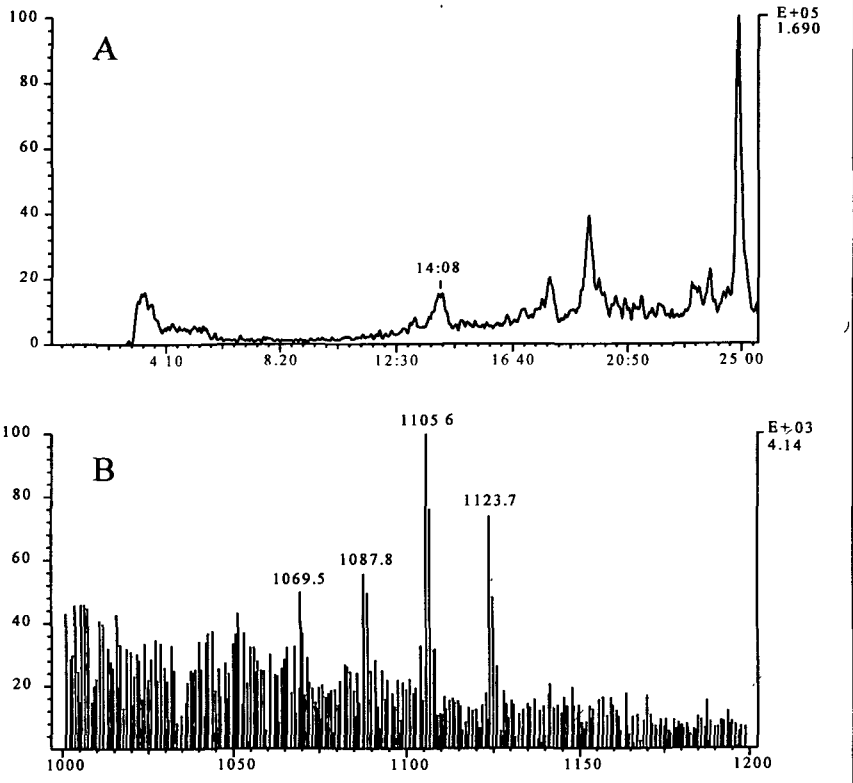

Figure 1. A) Summed ion chromatogram (m/z 1123>1124 + 1105>1106 +1087>1088) of extract obtained from Caribbean fish. B) Unsubtracted APCI mass spectrum of peak at 14:08 minutes.

Characterization of 3,4-Dichloro-1-butene Rat Metabolism by LC-MS-MS

Frank Brach, Zamas Lam, Steve Carpenter, and Doulgas Keller
The DuPont Company, Haskell Laboratory for Toxiciology and Industrial Medicine, P.O. Box 50, Elkton Rd, Newark, DE 19714

3,4-Dichloro-1-butene (3,4-DCB) is an intermediate in the manufacture of elastomers. 3,4-DCB is known to be a poor alkylator but is mutagenic in bacterial systems with activation. A study was undertaken to investigate the metabolism of 3,4-DCB as a key to understanding the lack of reactivity. The 3,4-dichloro- moiety of 3,4-DCB is a potential site for conjugation with glutathione (GSH). It is known that GSH conjugation at vicinal dichlorides can give rise to reactive episulfonium ions. The research described in this presentation was conducted to investigate the pathways of metabolism of 3,4-DCB.

RESULTS and DISCUSSIONS

In vitro experiments

No reaction of 3,4-DCB with GSH was detected, with or without added glutathione-*S*-transferase.

No reaction of 3,4-DCB with 4-nitrobenzylpyridine (4-NBP) was detected. By contrast, other DCB isomers and butadiene diepoxide reacted readily with 4-NBP.

In vivo experiments

HPLC analysis of bile from rats treated with 3,4-DCB revealed several peaks that were not present in control bile (m/z 412/414, m/z 414/416, m/z 283/285, m/z 285,287, and m/z 226/228). These peaks generally increased in size from 2 to 4 hrs post dosing, then declined in size over the next 20 hr. The urine of treated rats contained one major peak (m/z 268) that was not present in control urine.

MS analysis of the bile peaks showed that the peak eluting at approximately 22 min. contained one Cl as well as the addition of an O atom and GSH (m/z 412/414) . The peak eluting at approximately 18 min. contained the ring-open (hydroxylated) metabolite of the epoxide metabolite at retention time 22 min (m/z 414/416). The daughter ion (m/z 412) spectrum of the 22 min. peak revealed the structure of this species to be the GSH conjugate of an epoxide metabolite of 3,4-DCB, in which the epoxide has migrated from the 1,2 position to the 2,3 position, releasing one Cl.

The downstream conjugates of the parent conjugate, with the *glu* and *gly* residues removed, were detected with retention times of 18 and 15 min., with protonated molecular ion at m/z 283/285 and m/z 226/228, respectively. These structures were also confimed by MS/MS.

The Cl-containing peak detected in the urine was identified as the mercapturic acid of the bile conjugate with with protonated molecular ion at m/z 268.

CONCLUSIONS

* The major pathway of metabolism of 3,4-DCB determined from our experiments is shown in below. Metabolites derived from the primary pathway expected prior to the experiments, conjugation with GSH at a chlorine, were not detected in bile or urine. The mass of a GSH conjugate directly displacing a Cl would be 396, which was not detected.
* The primary pathway of metabolism of 3,4-DCB in the rat appears to be *via* epoxidation of the double bond, followed by GSH conjugation with the epoxide, with migration of the epoxide to the 2,3 position releasing Cl. The pathway leading to the highly reactive episulfonium ion was not detected.
* Epoxidation of 3,4-DCB as the initial step in metabolism may explain the lack of direct alkylation activity and the mutagenicity of 3,4-DCB after activation.

Postulated Pathway of 3,4-DCB metabolism in Rats.

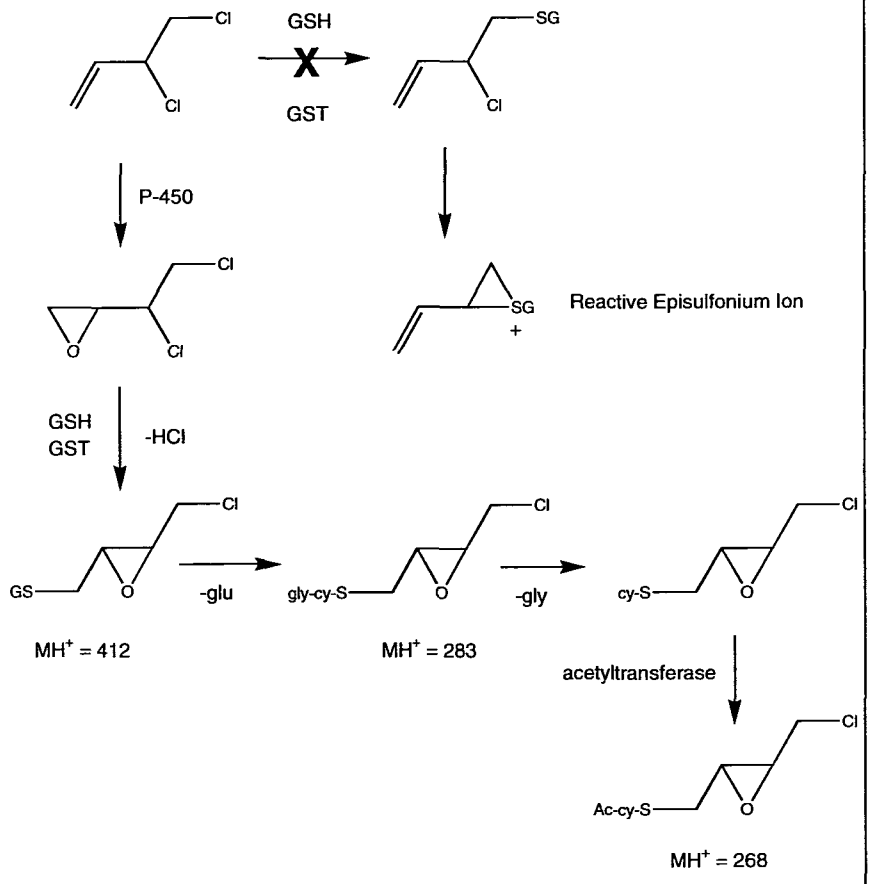

Preliminary Screen for the Biodegradation of Xenobiotics

Sean E Ottinger, M. Neal Guentzel, & Stephan B. H Bach
Division of Life Sciences & Division of Earth and Physical Sciences
The University of Texas at San Antonio, San Antonio, Texas 78249-0662

Introduction: Currently there a myriad of sites contaminated with an infinite number of combinations of chemicals or xenobiotics. Bioremediation is one method which poses strong potential for cost effective remediation of contaminated sites. However, the expediency and effectiveness by which biological organisms can remediate a site posses some problems. Inherent in bioremediation is the somewhat unpredictable nature of the microorganisms and their performance at a given site. By customizing the microbes used to afford the best match for a contaminated site both in terms of microbe survive-ability and efficacy, the unpredictability in performance can be elevated. Determining the efficacy a microbe will have for various contaminants can be done by GC/MS. Through the use of a preliminary screen coupled with GC/MS confirmation and quantitation, it is possible to determine the potential of a microorganism's ability to remediate the contaminants at a site in a quick and cost effective method.

The preliminary screen used is a mineral salts broth, metabolic indicator, and a xenobiotic as the sole carbon/energy source.[1] If the enzyme's produced by the microbe are able to utilize the chemical as an energy source then the breakdown products will react with the indicator and produce a color change. Confirmation of the microbial degradation is then done by GC/MS. In addition, GC/MS allows for identification of the metabolites produced. It is important to make sure that any metabolites generated were not more hazardous than the original starting product. However, if such a case were to arise it would still be possible to utilize another microbe to get degrade the toxic metabolite which was generated.

Methods: *Materials & Preparation:*

- VWR disposable culture tubes (16 X 125mm) were rinsed with 5mL of methanol
- Tubes were then baked for at least 12 hours in a hot air oven @ 180°C to both sterilize and remove any remaining methanol
- After the tubes cooled, the caps were then tightened completely down
- The mineral salts broth solution was then prepared and heated
- The mineral salts solution was then autoclaved for 21 minutes @ 250°C and 25psi
- The indicator was then dissolved in dH_2O to a concentration of .0005g/mL and filter-sterilized using a .22μm membrane filter
- Once the salt solution had cooled the indicator solution was added at a conc. of .001g/Liter of mineral salts broth
- 10mL of the salts solution was then asceptically dispensed into the sterilized tubes using a pre-sterilized Cornwall pipette
- 10μL of the xenobiotic was then added to the tube
- The pure microbial isolate was next added to a saline solution until a visual density equivalent to a Macfarland 1 was reached (roughly 10^8 CFU/mL)
- The microbial solution was then diluted to about 10^4 CFU/mL
- One drop of the diluted microbial solution was added to the tube
- For each tube of microbe and chemical tube there are two corresponding control tubes of chemical only and microbe only

Analyses.

- Microbial testing was done by removing 10μL of the test solution and using a four quadrant streak method to estimate the microorganisms or Colony Forming Units (CFU)/mL
- Tubes not containing microbes were sampled randomly to insure no microbial contamination occurred
- The pH of the solution was checked using test strips to simply estimate; pH testing was done the same time microbial analysis was done
- The chemical analysis was done by removing 25μL of the test solution and placing it into an autosampler vial containing 1475μL of methanol
- The GC/MS was tuned according to EPA method 624/8260[2]; *This was done both to quantitate the amount of chemical present and to allow for utilization of EPA MS library to identify the metabolites produced*
- The tune was then verified by injection of BFB
- Quantitation was done as specified by EPA method 624/8260[2], using a single characteristic ion

Results: In all cases the xenobiotics dissipated within several days. However, microbial counts revealed no substantial increase which would be associated with microbial enzymatic degradation. In addition, there was no drop or change in pH. A drop in pH and a color change in the solution would both occur if the microbes were utilizing the chemicals as carbon/energy sources. Neither pH nor the color changed. All microbes tested in all the repetitions produced almost identical results with complete dissipation of the chemical over a three week period.

Conclusions: Although the xenobiotics dissipated over time, we can not say that the microbes were the causative agent of the dissipation for two reasons. One, the volatilization controls also had dissipation occur at an identical rate. Two, no metabolites were detectable in any of the incubations containing microbe and chemical together. The results are primarily due to error in that the caps on the all the tubes were left loose instead of sealed The chemical concentration of .1% may have also lead to the rapid volatilization. Increasing the amount of chemical used would also be helpful, but it would be important that the concentration is not enough to become toxic to the microbes. In previous tests where caps were tightened down, there was some degradation and metabolite formation. In the past study using only TCE (plus an inducer) and different organisms, there was a small amount of degradation, but the metabolites formed were in such small concentration as to be extremely uncertain in regards to a possible identification of the metabolites In subsequent studies, it would be more advantageous to utilize a purge and trap as opposed to an autosampler. The inherent concentration of a purge and trap will allow for greater sensitivity in detection of any metabolites produced. Unfortunately from this study it can not be ascertained whether the mineral salts broth would be useful in a rapid cost-effective prescreen of a microorganism's degradative potential. However, coupling the mineral salts screen with GC/MS should provide a good piece of the puzzle in selecting which microbes to use on a given contaminated site and thus make bioremediation a much more viable choice in the removal of organic wastes from contaminated sites.

References: [1]M. Neal Guentzel; Proprietary screen; University of Texas at San Antonio, Division of Life Sciences, San Antonio, TX 78249-0662
[2]The Environmental Protection Acency, revision November 1990

Acknowledgments:
We would like to thank Catherine Check, Earle Stone, and Harlan McLaughlin their assistance and support.

Identification of Tamoxifen Metabolites in Patients on Long-term Therapy for Breast Cancer

G.K. Poon[1], P.E. Lønning[2], D.H. Phillips[1] and M. Jarman[1]
[1]*CRC Centre for Cancer Therapeutics, Institute of Cancer Research, Surrey, UK.*
[2]*Department of Oncology, University Hospital of Bergen, Haukeland Hospital, Bergen, Norway.*

Introduction

Tamoxifen is an antiestrogen widely and chronically used for the treatment of hormone-dependent breast cancer in postmenopausal women. Recently, it has also been a controversial antiestrogen drug undergoing clinical trial as a prophylactic for women who have a high risk of breast cancer [1]. This is because tamoxifen has been shown to be hepatocarcinogenic to female rats and human MCL-5 cells by forming DNA adducts [2,3]. The precise mechanism of formation of these DNA adducts has not been established. It has been proposed that tamoxifen give rise to DNA adducts in the livers of rats through metabolic activation involving α-hydroxylation of the ethyl group [4].

Previous studies of the metabolism and pharmacokinetics of tamoxifen in patients and animals have shown that the drug is extensively metabolized after oral administration. In human, the major metabolite is *N*-desmethyltamoxifen (metabolite **I**), whereas 4-hydroxytamoxifen (metabolite **II**) and tamoxifen *N*-oxide (metabolite **III**) are present in minor concentrations. Metabolite **II** and 4-hydroxy *N*-desmethyltamoxifen (metabolite **IV**) have been isolated as their glucuronides in human bile. This report demonstrates the utilization of liquid chromatography - electrospray ionization - mass spectrometry (LC-ESI-MS) methodology, it is possible to determine the minor and /or polar metabolites of tamoxifen.

Conclusion

In addition to several established human metabolites of tamoxifen modified by *N*-demethylation, 4-hydroxylation or *N*-oxidation, we have for the first time detected α-hydroxy (**VI** and **VII**) and monohydroxy-*N*-oxide (**X**) metabolites in plasma samples of patients receiving tamoxifen treatment as summarized in Figure 1. This result is an important finding, given the supposition that α-hydroxylation can lead to formation of DNA adducts and possible carcinogenicity. Whether these metabolites have any significance to formation of the DNA adducts is currently being investigated. When Phillips et al. [5] examined the genotoxicity of tamoxifen-d_5 in rat and human cells, they noticed a 2- to 3- fold decrease of DNA adduct formation compared with tamoxifen as a substrate. Oxidation at the ethyl side chain was at a slower rate due to an isotope effect. Thus, α-hydroxylation is a possible metabolic pathway for DNA adducts formation.

References

1. M. Morrow and V.C. Jordan: *Cancer Surv.*, **18**, 211-229 (1993).
2. G.M. williams, M.J. Iatropoulos *et al.*, *Carcinogenesis*, **14**, 315-317 (1993).
3. J.A. Styles, A. Davies *et al.*, *Carcinogenesis*, **15**, 5-9 (1994).
4. G.A. Potter, R. McCague and M. Jarman: *Carcinogenesis*, **15**, 439-442 (1994).
5. D.H. Phillips, G.A. Potter, M. Horton *et al.*, *Carcinogenesis*, **15**, 1487-1492 (1994).

Acknowledgment: This work is supported by the Cancer Research Campaign, U.K.

43rd ASMS Conference on Mass Spectrometry and Allied Topics

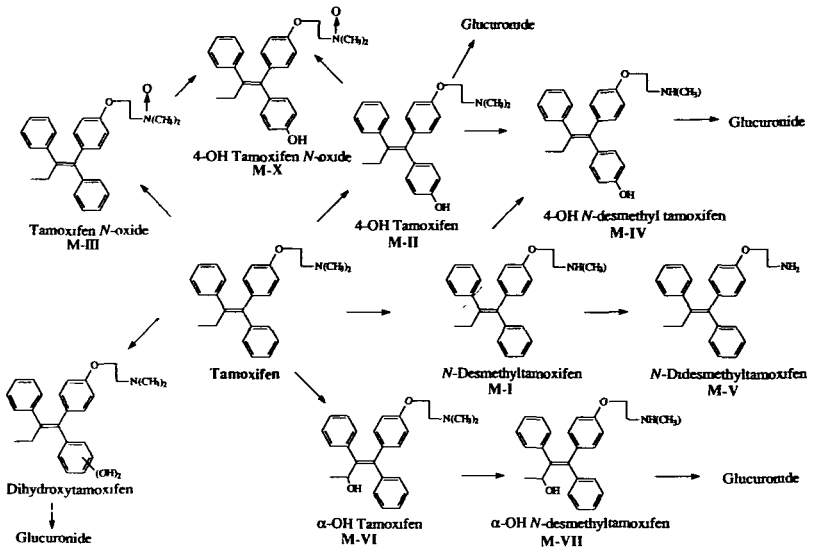

Fig 1 Metabolic Pathway of Tamoxifen after oral administration in human

In Vitro Metabolic Transformations of 2,4-Dipyrrolidinylpyrimidine: A Chemical Probe for P-450 Mediated Oxidation of Tirilazad Mesylate. Robert T. Streeper[§†], Paul G. Pearson[§], Zhiyang Zhao[§], Stephen A. Mizsak[#] and J. James Vrbanac[§*] — [§]Drug Metabolism Research and [#]Physical and Analytical Chemistry, The Upjohn Company, Kalamazoo, MI 49001.

Tirilazad (**T**, FREEDOX®), which is currently under clinical development for the treatment for subarachnoid hemorrhage and head injury, contains as part of its structure a 2,4-di(pyrrolidin-1-yl)pyrimidine (**2,4-DPP**) moiety. The identification of the oxidized metabolites of **T** is of considerable interest as this provides insights into the mechanisms of action and metabolic clearance of **T**. In the present investigation, we have employed **2,4-DPP** as a chemical probe to further characterize P-450 mediated oxidation of the heterocyclic domain of **T**. In pursuit of this objective, deuterium labelled analogs of **2,4-DPP** have been prepared and employed as metabolic probes (**1**, **2**, and **3**; below) in conjunction with LC-MS techniques to characterize *in vitro* biological transformations of **2,4-DPP** in male rat liver microsomes. We have determined that **2,4-DPP** undergoes three characteristic hydroxylations *in vitro*. We determined that the oxidations occurring in male rat liver microsomes were not aryl hydroxylations or formations of *N*-oxides by observing that all three observed metabolites had lost one deuterium when **3** was used as substrate. When **1** was incubated in male rat liver microsomes, **M1** and **M2** had not lost deuterium and **M3** had lost deuterium. When **2** was incubated with rat liver microsomes **M1** and **M2** were observed to have lost one deuterium while **M3** did not. Synthetically prepared 4-(3-hydroxypyrrolidinyl)-2-pyrrolidinylpyrimidine was observed to elute at the same time as **M1**, Tr = 20.0 minutes. Synthetically prepared 2-(3-hydroxypyrrolidinyl)-4-pyrrolidinylpyrimidine did not elute at the same time as any of the three hydroxylated metabolites. These data, obtained by particle beam-liquid chromatography-mass spectrometry, have characterize the three metabolites as: 4-(3-hydroxypyrrolidinyl)-2-pyrrolidinylpyrimidine (**M1**), 4-(2-hydroxypyrrolidinyl)-2-pyrrolidinylpyrimidine (**M2**) and 2-(2-hydroxypyrrolidinyl)-4-pyrrolidinylpyrimidine (**M3**).

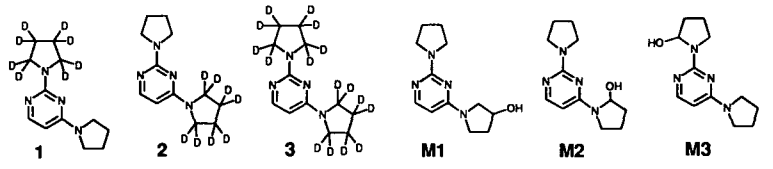

Manipulations which did not influence the formation of metabolites or result in the formation of other oxidation products included addition of 3% hydrogen peroxide, addition of superoxide dismutase and catalase individually and together and heating the microsomes to 55 °C for 90 seconds prior to incubation. Manipulations which decreased or eliminated the formation of the metabolites included addition of 1-aminobenzotriazole, carbon monoxide, *N*-octylamine and absence of microsomal protein, or a viable NADPH generating system. Collectively, these findings indicate an exclusive role for cytochrome

43rd ASMS Conference on Mass Spectrometry and Allied Topics

P-450 in the oxidation of **2,4-DPP** to **M1**, **M2** and **M3**. We observed that in microsomal incubations carried out in the presence of cyanide, a single 2-pyrrolidinyl cyanide adduct is formed implicating an iminium ion intermediate in the oxidation of the 2-pyrrolidine ring. **1**, **2**, and **3** were used to characterize the adduct.

As an initial experiment to elucidate the mechanisms of hydroxylation of **2,4-DPP** by cytochrome P450's, we performed an intermolecular deuterium isotope effect experiment by co-incubating **2,4-DPP** and [$^{16}H_2$]**2,4-DPP** (**3**) in equimolar concentrations. The observed isotope effects reported as the mean of five measurements for the three metabolites are: **M1**, $k_H/k_D = 14.55 \pm 0.54$; **M2**, $k_H/k_D = 6.01, \pm 0.65$; **M3**, $k_H/k_D = 5.35 \pm 1.18$. We interpret these data as suggesting that **M2** and **M3** are formed by the same mechanism, probably including the formation of an iminium ion, and that **M1** is formed by direct hydrogen abstraction.

We propose that the hydroxylation of the 2-position of the 2-pyrrolidine ring of **2,4-DPP** proceeds *via* a pathway(s) that includes formation of an iminium ion, evidence provided from studies with selectively deuterated analogs and cyanide trapping. Our observation of the large intermolecular isotope effect in the formation of **M1** seems to preclude a mechanism involving initial *N* electron abstraction with subsequent iminium ion formation in the formation of **M1**. Besides the large isotope effect, the loss of only one deuterium precludes the formation of **M1** ***via*** the mechanism detailed on the right below.

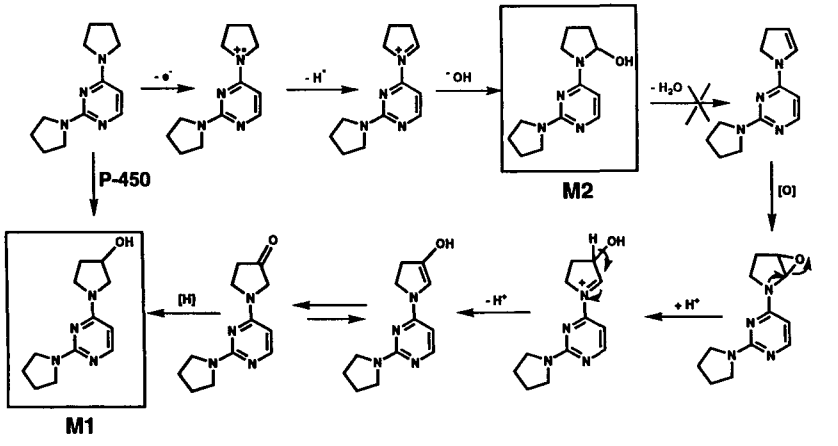

ANALYSIS OF PAHS IN HUMAN SERUM USING CLOUD POINT EXTRACTION AND LC/MS

Sarath R. Sirimanne, Li. Ma, Cheryl McClure, John Barr and Donald G. Patterson. Jr.
Centers for Disease Control and Prevention, National Center for Health, Environmental Health and Laboratory Sciences. Atlanta, GA 30341-3724.

Polycyclic aromatic hydrocarbons which are known to be mutagenic, carcinogenic and toxic to humans even at trace levels, are ubiquitous environmental pollutants resulting from emissions from sources such as automobile exhaust and industrial combustion of fossil fuels. Methods for quantifying these mixtures at trace levels generally involve solvent extraction and extensive sample cleanup procedure prior to the analysis. The extent of a cleanup depends on the complexity of the sample matrix. These solvent extraction methods utilize a considerable amount of organic solvents during sample cleanup generating a large quantities of solvent waste.

Aqueous solutions of many nonionic surfactants above their critical micellar concentration form turbids above a certain temperature also known as cloud point temperature. During the cloud point precipitation process, these micellar vesicles aggregate into a surfactant rich phase and any bound nonpolar species concentrate in the surfactant-rich phase. The analyte/surfactant-rich phase also permits analysis and quantification of the analytes by techniques such as reversed-phase HPLC without further sample cleanup.

In the recent past, cloud point extraction (CPE) attracted analytical chemists because of
(a) the ability to concentrate a variety of analytes with high concentration factors;
(b) safety and cost benefits. (It is an excellent alternative to conventional sample concentration methods which use large amounts of toxic and flammable organic solvents);
(c) easy disposal of the surfactant;
(d) the enhancement of the detection due to concentration;
(e) the compatibility of the surfactant rich phase with liquid chromatographic techniques;
(f) the preclusion of analyte losses during the evaporation of solvents used in traditional liquid-liquid extraction techniques;
(g) the inhibition of adsorption of nonpolar analytes to glass surfaces by the surfactants used.

In our laboratories, we assess human exposure to environmental toxicants by quantifying the levels of target toxicants in serum of exposed individuals. The levels of our target analytes are often in trace levels and hence preconcentration and cleanup are prerequisites to the analysis of these trace toxicants. We have identified cloud point extraction as an impressive alternative to conventional solvent extraction due its beneficial properties and the greater extraction efficiencies. We report for the first time, extraction of PAHs from human serum using cloud point technology and analysis by HPLC.

The quantification of PAHs in serum normally requires a series of steps consisting of extraction, concentration, and removal of detrimental impurities from the final analytical samples. In the recent past, there have been a number of applications of cloud point extraction to analytical sample preparation implicating its potential use as an alternative to solvent extractions. Since micellar serum samples failed to undergo CPE similar to water samples, we utilized sodium chloride to induce phase separation. Serum samples ranging from 0.5-5 mL can be easily worked up by the cloud point extraction. The initial analyses were carried out using HPLC/UV detection. The analysis of cloud point extracts using LC/Electrospray MS is also being explored. The optimum recoveries of individual PAHs were found to be quantitative at 8% Triton X-100, 5 M NaCl and at 60 °C and are summarized in the Table.

When extractions were performed at 60 °C, average recovery from the extractions of PAHs reaches a 100% maximum at 5.0 M NaCl and 8% Triton X-100 concentration. When the incubation

temperature was increased from 25°C to 50°C, the average recoveries tripled and the extraction recoveries were not significantly improved at temperatures above 60°C. The recovery of PAHs also increases as the sodium chloride concentration increases between 3.0 - 5.5 M. The concentrations above 5.5 M, NaCl remains undissolved indicating the serum/surfactant solution is saturated. The concentration of Triton X-100 has the greatest effect on the recovery of PAHs from serum. The recovery of PAHs increased from 50-100% as the Triton X-100 concentration was increased from 0.5-8% w/v.

The results presented in this paper indicate that the proper combination of temperature, salt concentration, and surfactant concentration can effect extraction PAHs from human serum with excellent recoveries. The simplicity and the advantages of the cloud point methodology prove that it is an excellent sample preparation technique for complex aqueous matrices such as serum.

Triton X-100 % (v/v)	0.5	2.0	4.0	6.0	8.0
Naphthalene	27	56	50	93	100
Fluorene & Acenaphthene	18	48	63	46	100
Phenanthrene	42	73	85	93	100
Anthracene	46	77	87	93	100
Fluoranthene	52	81	91	100	100
Pyrene	50	81	83	94	100
Benzo(a)anthracene	56	85	97	100	100
Chrysene	56	86	100	100	100
Benzo(b)fluoranthene	59	85	98	100	100
Benzo(k)fluoranthene	56	86	96	100	100
Benzo(a)pyrene	59	88	95	100	100
Dibenzo(a,h)anthracene	65	87	100	100	100
Benzo(g,h,i)perylene	59	84	100	—	100
Indeno(1,2,3,cd)pyrene	55	82	98	100	100
Average Recovery	**50**	**79**	**89**	**94**	**100**

Table: The effect of X-100 concentration on the recoveries of cloud point extraction of PAHs from Human serum. The NaCl concentration, extraction temperature, PAH level in serum are 5.0 M, 60 °C, 250 – 550 ppb respectively.

LC-APCI-MS/MS for the Analysis of PAP Biotransformation Products

L.M. Benson[1], A.N. Mayeno[2], G.J. Gleich[2], S. Naylor[1]
[1]Biomedical Mass Spectrometry Facility and Department of Biochemistry and Molecular Biology,
[2] Department of Immunology; Mayo Clinic, Rochester, MN. 55905, USA

During late 1989, the eosinophilia-myalgia syndrome (EMS) developed as an epidemic in the United States, with numerous additional cases reported in several other countries worldwide. Eight years earlier, a closely-related disease, the toxic oil syndrome (TOS) occurred in Spain as a massive foodborne epidemic. Although EMS was linked to the ingestion of tainted L-tryptophan, and TOS to aniline-denatured rapeseed oil, the etiologic agent(s) responsible for both diseases remains undetermined. Contaminants in these foodstuffs are believed to have triggered the diseases. Aniline contaminants, including 3-phenylamino-1,2-propanediol (PAP), have been reported in oil used by patients who developed TOS. A related aniline derivative, 3-(phenylamino)-L-alanine (PAA), was recently isolated from L-tryptophan associated with the onset of EMS. The presence of these two structurally similar aniline derivatives, PAP and PAA, suggests a possible related etiology. To investigate possible links between TOS and EMS, the biotransformation of PAP has been studied in rat hepatocytes and human liver tissue. On-line LC-APCI-MS/MS was used to identify and structurally characterize the resulting products. The initial studies to investigate the possible metabolic interconversion of PAP into PAA *in vitro* were accomplished using [^{14}C] PAP incubated with isolated rat hepatocytes or human liver tissue. The supernatants were analyzed by HPLC using on-line UV and ^{14}C-radioisotope detectors. One of these ^{14}C-labelled metabolites eluted with the same retention time as synthetic PAA and displayed an identical UV spectrum suggesting the conversion of PAP to PAA.

To unequivocally confirm the formation of PAA from PAP, LC-MS and LC-MS/MS analyses were performed on the incubation mixtures. HPLC was performed on an Ultrafast Microprotein Analyzer System using a Phenomenex Primesphere C18 column (3.2 x 250 mm) at a flow rate of 400 ul/min. A slow gradient of NH_4OAc and MeOH was used to separate the different components of the mixtures. MS and MS/MS analyses were performed on a Finnigan MAT 95Q mass spectrometer of BEQ_1Q_2 configuration. A Finnigan MAT APCI source was used in positive mode throughout with capillary and vaporizer temperatures at 200°C and 475°C, respectively, and the corona spray needle energy at 2.5 kV. Protonated molecular weight ions (MH^+) were subjected to collision-induced dissociation in the octapole collision cell utilizing an argon gas pressure of ~6 x 10^{-5} mbar with collision energies of 20-30 eV. The product ions were analyzed in Q_2 with spectra collected over a mass range of 40-200 with 10 to 20 scans acquired and averaged to afford a composite product ion spectrum.

LC-MS analysis of rat and human incubations are found in Figures 1 and 2, respectively. The extracted total ion chromatograms (m/z 104-300) demonstrate numerous peaks present in the mixtures. The extracted ion chromatograms at m/z 181 demonstrate a peak with the same retention time as standard PAA. For more conclusive evidence, LC-MS/MS analysis was done to obtain structural information. LC-MS/MS spectra of m/z 181 ions from the rat and human incubates (Figure 4A and 4B) proved to be identical to the standard PAA product ion spectrum (Figure 3).

In this study, we have demonstrated the *in vitro* biotransformation of PAP to PAA, linking related diseases TOS and EMS to a common chemical substance. PAA represents the first and only reported direct chemical link between TOS and EMS. The identification and characterization of PAA could readily be confirmed using LC-APCI-MS and LC-APCI-MS/MS. These powerful techniques continue to play an increasing role in the study and diagnosis of disease states.

43rd ASMS Conference on Mass Spectrometry and Allied Topics

Figure 1 LC-MS of Rat Hepatocyte Incubation

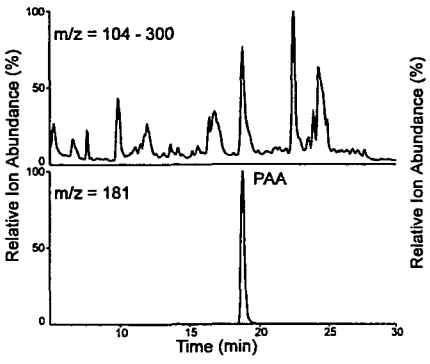

Figure 2 LC-MS of Human Tissue Incubation

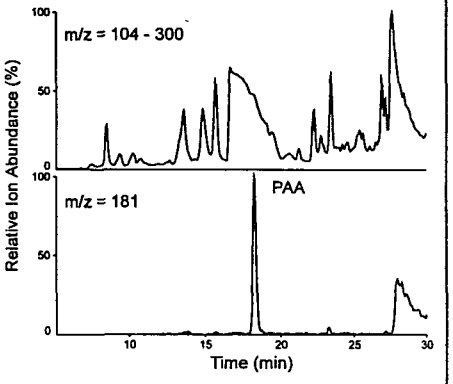

Figure 3 LC-MS/MS Analysis of Standard PAA

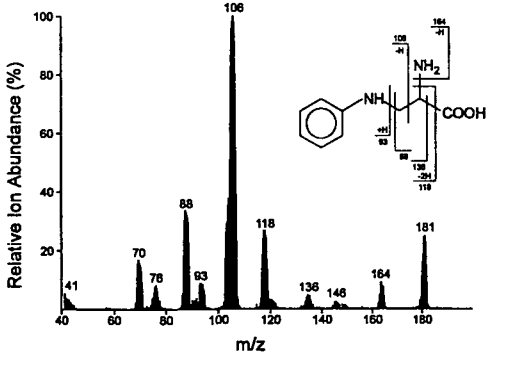

Figure 4 LC-MS/MS Analysis of *in vitro* PAA

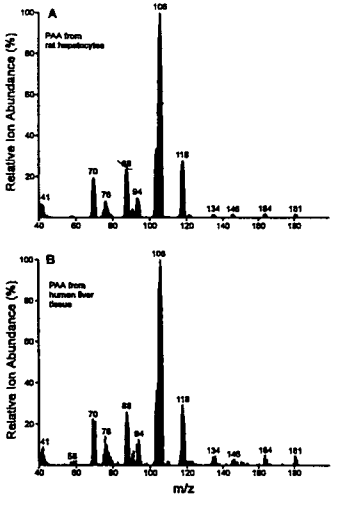

GC-MS Analysis of Hydroxytestosterones to Measure Cytochrome P-450 Activity

M.P. Purdon, L.D. Lehman-McKeeman, and D. Caudill
Procter & Gamble Company, Miami Valley Laboratories
P.O. Box 538707, Cincinnati OH, 45253

Introduction

Steroid hormones are natural substrates for microsomal cytochrome P-450 enzyme systems. Specific P-450 isozymes catalyze the regio- and stereospecific hydroxylation of the steroid ring structure. Given this, hydroxylation of testosterone has historically been used to profile specific P-450 activity.

Current HPLC-UV Method

Currently RP-HPLC with UV detection is used to identify hydroxytestosterones (HT) via chromatographic retention (Arch. Biochem. Biophys. 255:27 1987).This is a challenging separation involving the resolution of 17 isomers and 7 epimer pairs. The separation is further complicated because the testosterone can be oxidized to androstenedione, which then also generates hydroxy metabolites that elute along with the HT. As a result, the samples may need to be run under differing chromatographic conditions to identify the peaks with certainty. These technical challenges, along with the expense and lack of availability of the standards, limits general application of this potentially powerful technique.

Proposed GC-MS Method

Here a gas chromatographic separation is presented which can easily separate the testosterone metabolites as their TMS derivatives. In addition, by coupling with mass spectrometry the isomers can be identified by their EI-MS spectra. The separation was performed on a Hewlett Packard 5890 GC and 5971A MS (EI mode) using a J&W DB1701 column (25m x 0.25mm). The temperature program was 220°C to 300°C at 2°C/min. Full scan EI spectra could easily be generated injecting 2ng of each component (the same amount needed for the HPLC procedure). The derivatization must be done under gentle conditions so that the enol form of the 3-keto group is not silylated. Reaction with Sigma SIL A at room temperature for 1hr was found to derivatize all but the partially hindered 11β without significant enol silylation. The 11β was typically used as the internal standard for the HPLC procedure because it is not formed in this system. 19 hydroxytestosterone can be substituted as the internal standard for the GC procedure.

Advantages

The GC-MS procedure gives a more robust separation of the hydroxytestosterones and does not depend on retention to identify the specific metabolites. Quantification can be performed by splitting the column effluent to both an FID and MS. Since unity response should be expected for all isomers (by FID) the need for the expensive and rare standards is virtually eliminated.

43rd ASMS Conference on Mass Spectrometry and Allied Topics

P-450	Major	Minor
1A1	6β	2β
1A2		6β
2A1	7α, 6α	
2A2	15α, 18, 6β, 7α	A, 15β
2B1	16α, 16β, A	
2B2	A	16α, 16β
2C6		
2C7		16α
2C11	2α, 16α, A	6β
2C12		1α, 15α
2C13	6β	15α,16α
2E1		
3A1	2β, 6β, 15β	18, 1β, 16β, A
3A2	2β, 6β	2α, 16β, A

Testosterone Structure

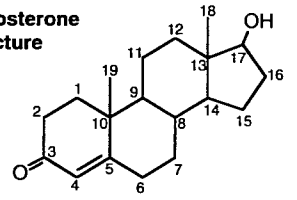

Hydroxylation by Cytochrome P450 3A1

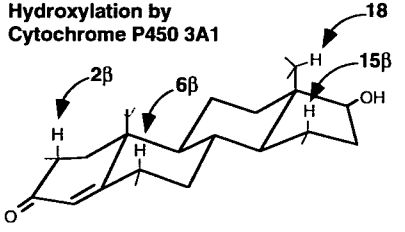

6β - Hydroxytestosterone (TMS)

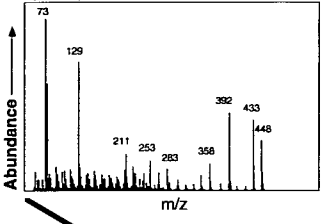

16α - Hydroxytestosterone (TMS)

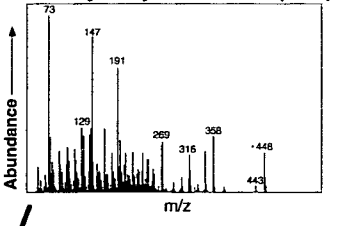

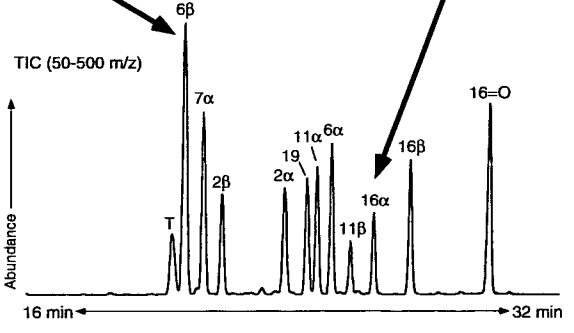

GC-MS Conditions

HP 5890 - HP 5971A MSD
DB1701 25m x 0.25mm
220°C - 300°C at 2°C/min
1mL/min constant flow

EI Scan 50-500m/z

DETERMINATION OF CLENBUTEROL IN RETINAL TISSUE BY ELECTROSPRAY LC/MS/MS

John A. Tomlinson, Rick A. Flurer and R. Duane Satzger
Forensic Chemistry Center, U.S. Food and Drug Administration
1141 Central Parkway Cincinnati, OH 45202

Introduction

Clenbuterol is an illegal veterinary drug. The FDA is particularly concerned about its use in food producing animals such as cattle, lamb and swine. Clenbuterol is considered a toxic substance. Some deaths caused by clenbuterol tainted bovine liver have been reported in Europe.

The FCC has received numerous samples of ocular tissue suspected of containing clenbuterol. Because of the large sample load, there was a need to develop a method that would permit handle a high sample throughput. The approach currently used by many laboratories is GC/MS with a methaneboronic acid derivitization.[1] Although the GC/MS method is adequate, sample preparation requires time to derivatize and the detection limit of approximately 4 ng/g is not always sufficient. The approach that was selected for development was LC/ESI/MS/MS. This technique was chosen for the selectivity, the sensitivity and the ability to obtain a high sample throughput.

The electrospray method allows for direct comparison of the concentration of clenbuterol in a sample to a clenbuterol standard. The percent recoveries of published methods for the determination of clenbuterol in retinal tissue are usually corrected with an internal standard carried through the method. The absolute recovery of clenbuterol through the sample preparation method is not addressed. In this work, methods are presented and evaluated on the basis of absolute percent recovery of a clenbuterol standard added to retinal tissue prior to sample workup. The goal is to develop a selective, sensitive and legally defensible method which permits quantitation of clenbuterol residues in retinal tissue.

Experimental

Two methods were developed for the determination of clenbuterol in retinal tissue:

Method #1:

Place a weighed amount of minced retinal tissue into a 20 mL glass vial and then add 5 mL of 0.1 M KH_2PO_4/ 0.1 M NaH_2PO_4 buffer solution. Sonicate preparation for 15 minutes, then centrifuge for 10 minutes at 5000 rpm. After centrifugation, decant the supernatant into a separate 20 mL glass vial. Add 2 mL of 2 M Na_2CO_3 to the supernatant to make the solution basic (pH ~ 12). Mix the Na_2CO_3 with the supernatant. Add 5 mL of ethyl acetate to the basic solution and then shake gently for 5 minutes. Centrifuge for 10 minutes at 5000 rpm. Decant upper ethyl acetate layer into a 4 mL vial and then reduce ethyl acetate to dryness at 80° C under nitrogen. Add an additional 5 mL of ethyl acetate to the aqueous layer and shake gently for 5 minutes. Centrifuge for 10 minutes at 5000 rpm and then decant upper ethyl acetate layer into the 4 mL vial which contains the first extraction residue. Dry the ethyl acetate as before. After residue has been completely dried reconstitute with 0.5 mL of 1% formic acid in H_2O.

Method #2:

Weigh out an amount of minced retinal tissue and place into a 20 mL glass vial. Add 5 mL of tris buffer (0.2 M tris HCl containing 0.1 M $CaCl_2 \cdot H_2O$ pH to 8 with 0.1 M HCl) and 5 mL of H_2O. Add 150,000 units of hyaluronidase to the buffered solution and heat vial at 37° C for 45 hours. At the end of the 45 hours add 250 µL of a 200 mg/mL solution of pronase E to the vial. Heat vial again at 37° C for 3 hours. At the end of the three hours quantitatively transfer the contents of the glass vial to a plastic vial and then centrifuge the vial at 7500 rpm for 10 minutes. Decant the supernatant to another plastic vial and then add 120 µL of 10 M NaOH(pH ~ 12). Shake vial for 10 seconds then add 5 mL of ethyl ether to the basic solution and shake for 5 minutes. After shaking, centrifuge the vial at 7500 rpm for 5 minutes and decant the ether layer into a 4 mL glass vial and reduce the ether to dryness at 80° C under nitrogen. Add another 5 mL of ethyl ether to the aqueous layer and again shake for 5 minutes, centrifuge for 5 minutes and decant the ether layer combining the residue and the ether layer. Reduce the ether to dryness at 80° C under nitrogen. Reconstitute the combined residues with 0.5 mL of 1 % formic acid in H_2O.

Results

Method #1 did confirm all positive and negative results of the immunoassay method, however the recovery of clenbuterol was 25% to 35%. The clenbuterol limit of detection for Method #1 is approximately 1 pg/µL with a signal to noise ratio of 3:1. No quantitation of clenbuterol was performed using this method because of the low recoveries; only an estimate of concentration could be given.

After exhausting all efforts to increase the recovery of Method #1, it was believed that the clenbuterol was being bound in the retinal tissue. References indicate that clenbuterol is also retained in synovial fluid for long periods of time after the cessation of administration. The mechanism for the binding of clenbuterol in the synovial fluid is electrostatic binding to acid mucopolysaccharides.[2] One of the polysaccharides that binds clenbuterol is hyaluronic acid. Hyaluronic acid is found in the vitreous humor and in the first few layers of the retina. From this information Method #2 was developed using two enzymatic digestions. The first digestion involves hyaluronidase to cleave the bond between clenbuterol and the hyaluronic acid. This digestion requires approximately 150,000 units of hyaluronidase and 45 hours digestion time at 37° C. The second enzymatic digestion employs pronase E to destroy the protein in the retinal tissue solution so the clenbuterol does not bind to the protein after it is cleaved from the hyaluronic acid. The protease digestion requires three hours at 37° C.

Method #2 was developed in the attempt to increase the percent recovery of clenbuterol from retinal tissue. The recovery of a clenbuterol spike increased significantly with the use of Method #2. The mean recovery was 101 7%*. Recoveries have been determined using retinal preparations spiked at 25 ng/g clenbuterol. Based on the response for the 25 ng/g clenbuterol spike it is estimated that detection of clenbuterol could be accomplished at a level of 500 pg/g in the retina. Although this method has not been optimized, results to date are promising and further experiments will be performed to determine this method's ruggedness and reproducibility.

* n=7 RSD=30%

References

1. EU Reference Laboratory for residues of veterinary drugs
2. Brambilla, G.; Agrimi, U.; *The Veterinary Record*, **1993**, 132, 64.

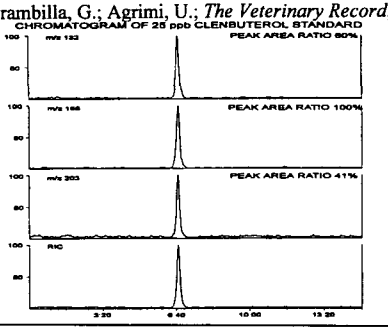

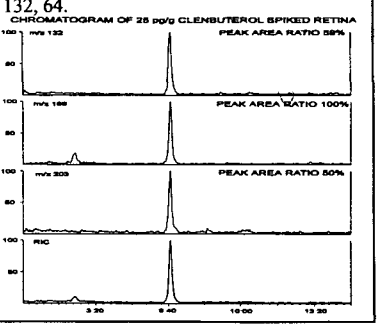

High Energy CID Spectra of Chlorambucil- or Melphalan-modified Peptides

Joseph Zaia and Catherine Fenselau, University of Maryland Baltimore County
5401 Wilkens Ave., Baltimore, MD 21228

Introduction. Metallothionein is a metal binding protein whose function has been linked to cancer drug resistance[1,2]. CID MS studies have determined the covalent binding sites for the nitrogen mustard drugs chlorambucil (CLB)[3] and melphalan (MEL)[4] on metallothionein. This work was made challenging by the unusually high cysteine content of MT, *i.e.* 20 of its 61 residues are cysteine. Specifically, MT proteolytic peptides ionize very poorly by FAB, and fragment poorly during CID. The fragmentation effect is compounded when either a CLB or a MEL molecule is attached to the MT peptide *via* a cysteine side chain.

The purpose of this work is to improve the CID fragmentation pattern produced from drug-modified MT peptides.

Methods. The dimethyloctylammoniumacetyl (DMOAA) derivatives were prepared using a published method[5]. CLB-modified MT peptides were isolated as has been described[3]. All CID spectra were acquired using 6 keV collision energy with a JEOL Ltd. (Akeshima, Japan) HX110/HX110 tandem mass spectrometer operating in the FAB ionization mode.

Results. Peptides modified at cysteine by CLB are characterized by abundant ions produced from fragmentation of the drug moiety and by peptide sequence fragment ions in low abundance. Scheme 1 describes the fragmentation that is specific to the modifying group. The second mustard group on the CLB moiety has been observed to undergo a variety of reactions involving substitution or elimination of the mustard chlorine atom. Therefore, the *m/z* of the ions produced will vary according to the reaction that has taken place. In all cases, an abundant ion is produced at low mass (*m/z* 254.6 for the ion with an intact second mustard group). Ions at high mass are also observed, and these result from loss of part or all of the CLB moiety as a neutral fragment. Generally, the ions noted as 2*, 4*, and 5* are observed for peptides that have at least one basic group. The 1* and 3* ions are produced only for those peptides containing multiple cysteines.

Model peptides, modified at cysteine with CLB, were used to study several means of affecting the appearance of CID spectra. Decreasing the collision energy from 6 keV to 0.5 keV reduced the relative abundances of peptide sequence fragment ions. N-acetylation increased the abundances of a few peptide sequence fragment ions, but the overall pattern was not conducive to interpretation. Substitution of the CLB chlorine atom with trimethylamine produced a fixed charge ion, the CID spectrum of which was also not readily interpretable for an unknown peptide. Attachment of a fixed positive charge to the N-terminus of the modified peptide was the only measure found to produce a spectrum coherent enough to render it interpretable in a reasonably straight-forward manner. The same conclusion was reached using MEL-modified peptides.

In order that both the fragmentation pattern and the ionization efficiency be improved, the DMOAA derivative was used for MT-peptides. An example spectrum is shown in Figure 1. The fragmentation pattern is consistent with MT 45-52 (CAQGCICK), modified at Cys-49 with a CLB group. The ions denoted $a_n+1\text{-}CH_3$ and $a_6+1\text{-CLB}$ are produced from loss of the CH_3 or CLB from the corresponding a_n+1 ion, respectively[6]. The *m/z* values of the ions produced from fragmentation of the drug moiety are consistent with substitution of an OH group for the mustard chlorine (see Scheme 1). The spectrum represents a significant improvement over that acquired without a charged derivative.

Conclusions. Attachment of a charged derivative to the N-terminus of a CLB-modified peptide was the most potent of the means investigated for producing an interpretable CID spectrum. The same conclusion has been reached for MEL-modified peptides, although space does not allow these spectra to be shown.

Acknowledgements. This work was supported by a grant from the National Institutes for Health. The prior work of Licong Jiang and Xiaolan Yu are acknowledged. The efforts of Daniele Fabris toward maintaining the instrument are greatly appreciated.

References.

1. Kelley, S.L. Basu, A Teicher, B.A. Hacker, M.P., Hamer, D.H. and Lazo, J.S. *Science* **1988**, *241*, 1813-1815.
2. Lazo, J.S. and Basu, A. *Cancer Biol.* **1991**, *2*, 267-271.
3. Jiang, L. and Fenselau, C. *Proc. 42nd ASMS Conf. Mass Spectrom. Allied Topics* **1994**, 65.
4. Yu, X., Wu, Z. and Fenselau, C. *Biochemistry*, **1995**, in press.
5. Stults, J.T., Lai, J., McClune, S., Wetzel, R. *Anal. Chem.* **1993**, *65*, 1703-1708.
6. Downard, K.M. and Biemann, K. *J. Mass Spectrom.* **1995**, *30*, 25-32.

Scheme 1.

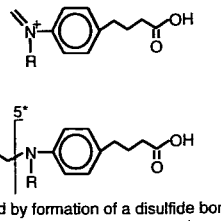

The 3* ion is produced by formation of a disulfide bond with loss of the drug moiety and a methyl group[4].

Low m/z Ion

R = CH_2CH_2Cl	CH_2CH_2OH
* m/z = 254.6	236.2

Mass lost from the precursor ion

R = CH_2CH_2Cl	CH_2CH_2OH
1* 315.8	297.3
2* 301.7	283.3
3* 283.7	265.2
4* 268.7	250.2
5* 241.6	223.2

Figure 1.

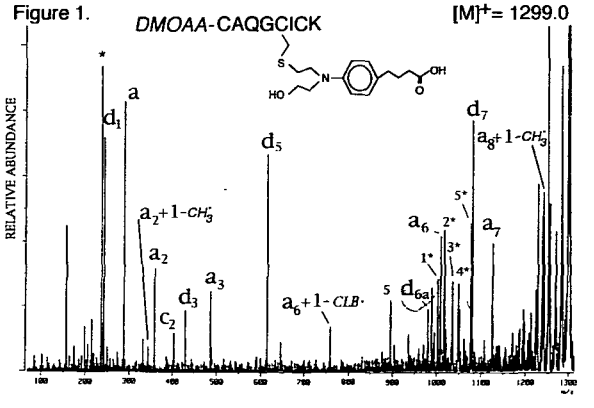

FAB-MS AND MS-MS STUDIES OF EXTRACTS FROM *PINUS PONDEROSA*

Lynn M. Teesch†, Diane J. Lamb†, John P. N. Rosazza, and Mohsen S. Al-Mahmoud
Division of Medicinal and Natural Products Chemistry, College of Pharmacy, and †High Resolution Mass Spectrometry Facility, The University of Iowa, Iowa City, IA 52242

Needles from the *Pinus ponderosa*, or western yellow pine, cause abortions in cattle if they are consumed late in gestation. Components in the pine needles are thought to cause premature parturition by decreasing uterine blood flow to the fetus. Numerous natural products have been isolated from the pine needles such as various types of terpenes and wax alcohols and acids. Several have been implicated as the causative agent, but no definite biological association has been determined, yet. The focus of this study is the characterization of components from the needle's cuticular membrane. The cuticular membrane is composed of cutin which is a complex mixture of lipids.

Pine needles are first subjected to soxhlet extract with diethyl ether, methylene chloride, and finally, methanol. Each extract was then tested for biological activity via a placentome bioassay (1). The methylene chloride extract, **F7**, showed the most activity. Further purification of **F7** by flash column chromatography resulted in four fractions. The first fraction, **M1**, gave very good results in placentome bioassays and was analyzed via NMR, IR, and GC-MS. Fast atom bombardment mass spectrometry (FAB-MS) was used to determine the mass of the isolated compound in **M1**. The sample was mixed with 3-nitrobenzyl alcohol on the probe. **M1** is in fact a mixture of four components that are separated by 28 u or 2 methylene groups. The $(M + H)^+$ ions in the FAB mass spectrum include *m/z* 568, 596, 624, and 652. All the data so far suggests that the isolated material in **M1** consists of ω-hydroxy-fatty acids, fatty acids, alkanols, and alkandiols esterified to produce diesters. This is similar to structures proposed for cutin waxes, but the intact molecules have never been identified (2).

There are structurally important low mass fragment ions in the FAB mass spectrum of **M1** Because the isolated material is a mixture, we are unable to assign the low mass ions to a particular precursor ion. By using tandem mass spectrometry (MS-MS), the fragmentation pattern of each $(M + H)^+$ can be obtained. Several synthetic standards, such as 1,14-tetradecanedioyl-dilaurate (12:14:12) or 1,12-dodecanedioyl-1-laurate-12-myristate (12:12:14), are also available for MS-MS analysis (3). Thus, by comparing the **M1** results with that of the standards, we can identify possible structures.

MIKES experiments are used to acquire the metastable ion spectra of the four components in **M1** and standards. The $(M + H)^+$ ions are allowed to unimolecularly decompose in the second field free region of a VG ZAB-HF reversed geometry mass spectrometer. The observed fragmentations involve cleavages at the ester linkages, Scheme 1. Two of the metastable ion decompositions involve a hydrogen

Scheme 1
(x and z can be either10 or 12; y can be either 12 or 14)

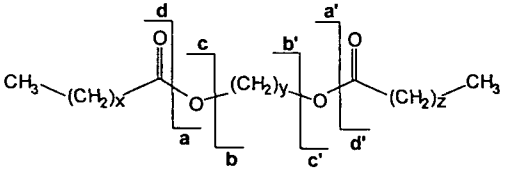

rearrangement to produce an ω-hydroxy-fatty acid ester (**a** and **a'**) which can then lose H_2O (**b** and **b'**). The another set of decompositions involve cleavage to yield fatty acids (**c** and **c'**), which can also then lose H_2O (**d** and **d'**).

Figure 1 includes the metastable ion spectra of the $(M + H)^+$ ions of two components in **M1** and their corresponding standards. The standard compounds include 12:12:14 and 12:14:12 for the ion of *m/z* 596 (Figure 2A and 2B), and 14:14:12 and 14:12:14 for the ion of *m/z* 624 (Figure 2D and 2E). The fragmentation pattern of the unknown ion of *m/z* 596 (Figure 2C) and 624 (Figure 2F) correspond to 12:14:12 and 14:14:12, respectively. The most likely structure for the lowest mass $(M + H)^+$ ions (*m/z* 568) is 12:12:12. The identification of the highest mass ion of *m/z* 652 is more difficult, because its metastable ion spectra is more complex. However, after comparing the theoretically calculated fragmentations for 12:14:16, 12:16:14, and 14:12:16, the unimolecular decompositions of 14:14:14 and the unknown, the ion of *m/z* 652 is probably a mixture of 14:14:14, 12:14:16 and 12:16:14.

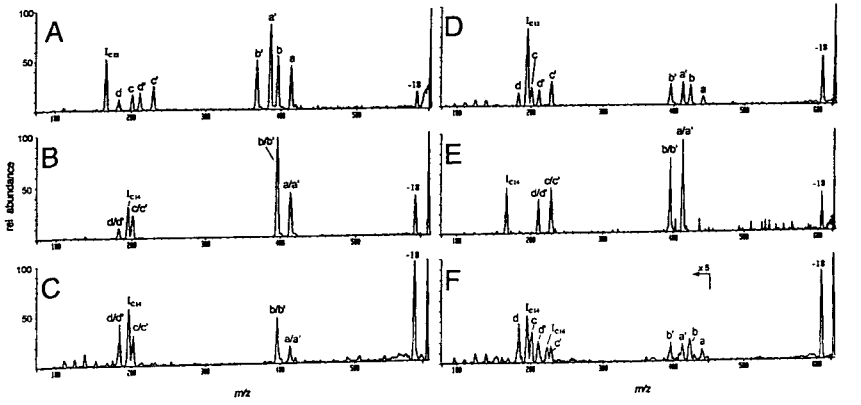

Figure 1. Metastable Ion Spectra of $(M + H)^+$ ions of *m/z* 596 standards, 12 12 14 (A) and 12:14:12 (B), and **M1** (C), and of *m/z* 624 standards, 14:14:12 (D) and 14:12:14 (E), and **M1** (F).

Collision-induced decompositions (CID) of $(M + Li)^+$ ions are also structurally informative and include charge-remote fragmentations analogous to those previosly observed for $(M + Li)^+$ions of fatty acid methyl esters.[4] We studied these complexes, because the dramatic effect these compounds have on the potassium sensitive channels during the placentome bioassays.

References:

1. Conley, A. J.; Ford, S P. *J. Anim. Sci.* **1987**, *65*, 500.
2. a) Zinkel, D. F. *Applied Polymer Symposium* **1975**, *28*, 309-27. b) Robinson, T. *The Organic Constituents of Higher Plants*; Cordus Press: Amherst, MA, **1991**, p 91.
3. Al-Mahmoud, M. S., Ford, S. P. Short, R. E., Farley, D. B., Rosazza, J P. N *J. Agric. Food Chem.* submitted 1995.
4 Contado, M. J.; Adams, J. *Anal. Chim. Acta* **1991**, *246*, 187.

A Multi-Dimensional Approach to the Characterization of Environmental Contaminants: Yeast, DNA and Liquid Chromatography-Mass Spectrometry (LC/MS).

JOSE SERRANO and DOUGLAS KUEHL
U.S. Environmental Protection Agency
Environmental Research Laboratory-Duluth
Duluth, MN 55804 (218)720-5559

Mutagenicity assays using budding yeast *Saccharomyces cerevisiae* are important tools for the detection of genetically active chemicals, especially when combined with complementary microbial screening techniques such as the Ames test. We have developed a new analytical, multi-endpoint approach for the assessment of the mutagenic potential of environmental chemical contaminants, including those in complex mixtures. The method integrates for the first time, the principles of yeast genetics and LC/MS. The objective of the yeast assay is to measure the mutation frequency of a yeast/*E. coli* shuttle plasmid DNA (pDNA) that has been previously modified *in vitro* with selected contaminants (with or without fish liver microsomes). A portion of the pDNA is analyzed by LC/MS and LC/MS/MS to characterize the type (reaction sites) and amount (frequency of alkylation) of adducts formed, as well as the electrophilic characteristics of the toxicant (N vs O bonding). The *in vivo* bioassay of a second portion of the sample included the fast transformation of pDNA into various yeast strains (mutant and wild type cells) via electroporation, and the cloning of chemically-induced mutant plasmids (at the URA3 gene) by selection for 5-fluoroorotic acid (5-FOA) resistance. Mutation frequency is defined as mutants/transformants/µg pDNA. A series of allylhalides with different chemical reactivity (chloride, bromide, isothiocyanate) and benzo[a]pyrene (B[a]P), were used as model compounds for direct-acting toxicants and those requiring metabolic activation, respectively. A mixture of PAHs (B[a]P, pyrene and benzo[e]pyrene), was used to test the effectiveness of the method to estimate the mutagenic potential of model complex mixtures. It was demonstrated that a linear dose-response ocurred between mutation frequency and the toxicant dose measured by LC/MS for low doses of allylbromide and B[a]P (Figures 1 and 2). Mutation frequency was also found to be proportional to the relative reactivity of the allylhalides (Figure 3). Further, B[a]P/DNA adduct formation as well as mutation frequency were altered by the PAH co-contaminants present in the model complex mixture (Table 1). LC/MS results correlated well with those previously observed for the *in vitro* reactions of calf thymus and fish liver DNA with the same contaminants.

References

1. Kuehl, D. and Serrano J., *J. Chromatogr. A* , 684 (1994) 113.
2. von Borstel, F., *Mol. Gen. Genet.*, 214 (1988) 396.
3. Serrano, J. and Kuehl, D., *J. Chromatogr. B* , 615 (1993) 203.
4. Liu, H., *Genetics*, 132 (1992) 665.

43rd ASMS Conference on Mass Spectrometry and Allied Topics

Figure 1.
Mutation frequency versus dose of allylbromide for two yeast strains

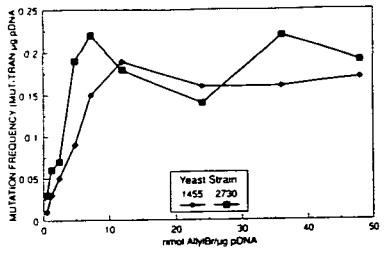

Figure 2.
Mutation frequency versus dose of B[a]P for two strains of yeast

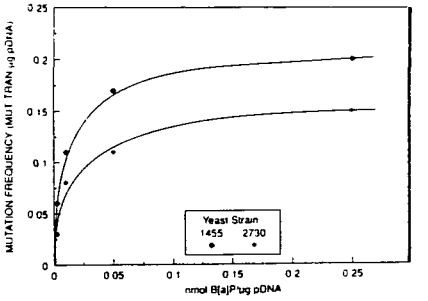

Table 1
LC/MS response and mutation frequency for DNA arylated with B[a]P in presence of other PAH contaminants.

Dose nmoleTOX/µgDNA	LC/TSP/MS (C. thymus DNA) m/z 453/dGuo (%)	PAH Used	Dose nmoleTOX/µgDNA	MUT/TRAN/µgDNA S2730	MUT/TRAN/µgDNA S1455
0.5	0.23	B[a]P	0.30	0.09	0.19
0.5/0.5	0.44	B[a]P + Pyr	0.30/0.30	0.19	0.28
0.5/0.5	0.47	B[a]P + B[e]P	0.30/0.30	0.14	0.20
0.5/0.5/0.5	0.25	B[a]P + Pyr + B[e]P	0.30/0.30/0.30	0.06	0.17

Figure 3.
Mutation frequency of a wild type yeast strain is proportional to the relative reactivity of a series of allylhalides.

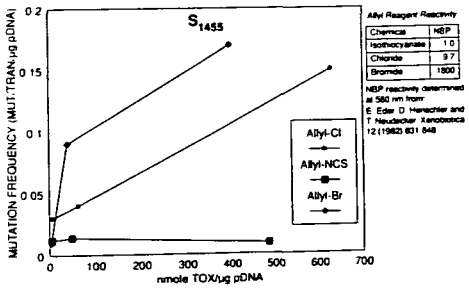

MONITORING ACID- AND BASE-INDUCED 'LIPID A' DEGRADATION BY ELECTROSPRAY IONIZATION MASS SPECTROMETRY

Richard B. Cole* and Yan Wang

Department of Chemistry, University of New Orleans, Lakefront, New Orleans, LA 70148

Lipopolysaccharides (LPS) are endotoxins produced by all gram-negative bacteria. They elicit a variety of biological, medical and immunological activities such as induction of fever, change in the white blood cell count, diarrhea, or even shock and lethal toxicity [1,2]. Because of these important properties, the study of the relationship between LPS structure and its toxicity has been an area of intensive investigation. Contained within lipopolysaccharides is a "lipid A" portion which constitutes the outer cell wall of gram-negative bacteria. Lipid A often takes the form of a β-1,6 linked D-glucosamine disaccharide; it is believed to be responsible for the toxicity exhibited by lipopolysaccharides. Approaches to detoxification of lipopolysaccharides include chemical degradation via acid and base hydrolysis.

A particular LPS that we have been investigating [3,4] is that produced by *Enterobacter agglomerans*, a gram-negative bacterium commonly found in field cotton. LPS in cotton dust has been found to be the cause of respiratory diseases such as byssinosis. Negative ion electrospray mass spectrometry was used to characterize structural changes to lipid A from *Enterobacter agglomerans* incurred after acid and base treatment. Shown in Figure 1 (a-d) are the negative ion electrospray mass spectra of lipid A from *Enterobacter agglomerans* obtained after 0, 30, 60, and 120 min of acid treatment (1% acetic acid, 100 °C). These mass spectra provide direct evidence of the substantial degree of hydrolysis of ester-linked fatty acyl chains resulting from acid treatment. The acid hydrolysis process with the fastest rate constant corresponded to removal of the palmitoyl group from the hepta-acyl form of lipid A. In the presence of excess acid, this reaction conformed to pseudo-first order kinetics with a rate constant of 3.3×10^{-3} min^{-1}. An approximate order of lability of acyl side chains on the lipid A molecule to acid hydrolysis was also deduced: R'_4 (palmitoyl) > R'_1 (myristoyl or hydroxymyristoyl) > R_3 (hydroxymyristoyl at position 3) > R_1 (oxymyristoyl group at position 3') > R'_2 (lauroyl). The negative ion electrospray mass spectra of the products of 0, 15, 30, and 60 min base treatment (0.05 N NaOH in 95% EtOH, 65 °C) are shown in Figures 2a, b, c, and d, respectively. Base hydrolysis under the employed conditions was observed to be even more effective than acid treatment at hydrolyzing ester-linked fatty acyl chains. Both approaches have been shown to be effective at lowering the endotoxin level as measured by the *Limulus* amebocyte lysate (LAL) assay. Mass spectral evidence also suggested that breakage of the glucosidic linkage may be occurring during base hydrolysis. The latter process could be responsible for the toxicity reduction known to accompany base treatment.

1. Galanos, C.; Roppel, J.; Weckesser, J.; Rietschel, E.; Mayer, H. *Infect. Immunity*, 1977, 16, 407-412.
2. Rietschel, E.T.; Brade, H. *Scientific American*, 1992, Aug., pp. 54-61.
3. Cole, R.B., Domelsmith, L.N., David, C.M., Laine, R.A., Delucca, A.J., (1992) *Rapid Commun. Mass Spectrom.*, 6, 616-622.
4. Cole, R.B.; Harrata, A.K.; (1993) *J. Am. Soc. Mass Spectrom.*, 4, 546-556.

43rd ASMS Conference on Mass Spectrometry and Allied Topics

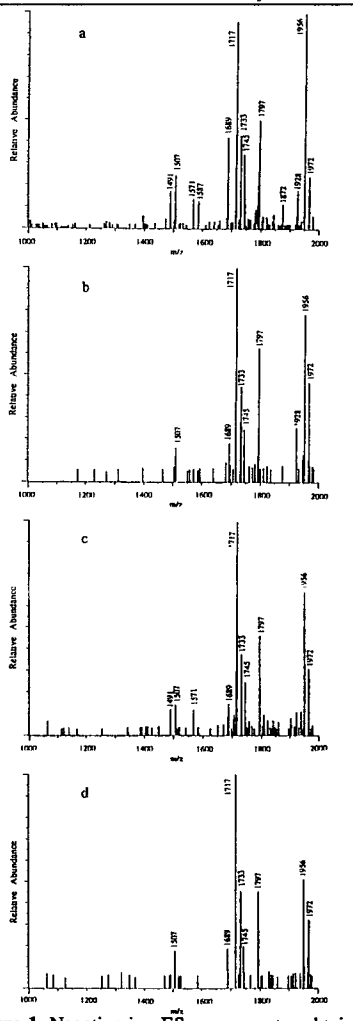

Figure 1. Negative ion ES mass spectra obtained from *Enterobacter agglomerans* lipid A subjected to mild acid treatment (1% acetic acid, 100 °C) for: (a) 0 min; (b) 30 min; (c) 60 min; and (d) 120 min.

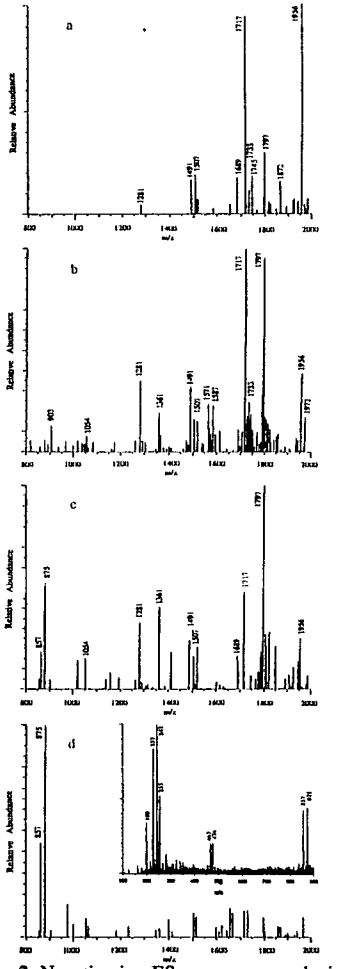

Figure 2. Negative ion ES mass spectra obtained from *Enterobacter agglomerans* lipid A subjected to base treatment (0.05 N NaOH in 95% ethanol, 65 °C) for: (a) 0 min; (b) 15 min; (c) 30 min; and (d) 60 min. Inset in (d) is lower mass portion (m/z 100-900) after 60 min base treatment.

HPLC/IonSpray/MS/MS Analysis of Common and Illicit Drugs in Case Samples

Pierre Picotte, Direction des expertises judiciaires, Ministére de la Sécurité publiquè, Gourverment du Québec, Montréal, P. Q. H2L 4K6; Gabriel Sanchez, Bori Shushan and Takeo Sakuma*, PE-SCIEX Instruments, Concord, Ont. L4K 4V8

Among standard techniques utilized in forensic toxicology, immunoassays, GC/FID/ECD/NPD and GC/MS/MS are considered suitable. However, certain compounds are thermally labile or too polar to be GC-compatible without appropriate sample derivatization. These current methods lack sensitivity for some important drugs, and it is a limiting factor in pursuing forensic analyses. The IonSpray technique does not involve heat and offers gentle ionization of polar and thermally labile compounds. This method has been in use for the analysis of polar and thermally labile compounds for the last few years. In order to evaluate various aspects of HPLC/IonSpray/MS/MS techniques, standards and case extracts were prepared and analyzed for the presence of tetrahydrocannabinol(THC), Δ^9 - THC-OH, Δ^9 - THC-COOH, clonazepam, lorazepam, nitrazepam, procyclidine, salbutamol, temazepam, heroin, morphine, 6-acetylmorphine, cocaine and benzoylecgoine.

A 5-mL urine specimen for cocaine, morphine and 6-actylmorphine was added to a Cleanscreen solid phase extraction cartridge. A 0.1 M phosphate buffer (2 mL) was added to this cartridge. The eluent was centrifuged and filtered with a 20 µm frit. The cartridge was conditioned successively with 3 mL methanol, 3 mL water and 1 mL phosphate buffer (0.1M, pH 6). The filtered sample was passed at a rate of 1 - 2 mL/min through the conditioned cartridge under reduced pressure. This cartridge was washed with 2 mL water, 2 mL acetate buffer(0.1 M, pH 4.5) and 3 mL methanol. The cartridge was dried for 10 min. at 254 mm Hg. The analytes were eluted from the cartridge with 3 x 1 mL of a freshly prepared mixture of 70% methylene chloride, 20% isopropanol, 2% ammonia and 18% water. The combined eluent was evaporated with a nitrogen jet, and reconstituted with ethanol.

A blood specimen (5 mL) for clonazepam was mixed with 20 mL saturated saline solution, vortexed and centrifuged. The supernatant was filtered with a 20 µm frit. A Waters C18 solid extraction cartridge was conditioned with 5 mL methanol followed by 5 mL saline solution. The filtered sample was passed thorough the cartridge under reduced pressure. The cartridge was washed with 2 x 5 mL saline and 2 x 5 mL pentane, and dried under vacuum for 15 min. The analyte was eluted with 4 x 1 mL of a mixture of 50% methanol and 50% chloroform. The combined eluents were evaporated with a nitrogen jet, and reconstituted with ethanol.

A 5-mL urine sample for THC carboxylic acid was hydrolyzed with 500 µL of a 60% KOH solution for 30 min. at 60°C. The mixture was allowed to cool down, and its pH was adjusted to 1 - 2 with 500 µL of a 12 N HCl solution. The mixture was transferred to a 50 mL separatory funnel. To this a 25-mL mixture of 65% hexane and 35% ethyl acetate was added, and mixed well. After settling, the organic layer was filtered over a Whatman No. 1 filter paper. The filtrate was evaporated with a nitrogen jet, and reconstituted in ethanol.

HPLC separation was made using base-deactivated 100 x 1 mm or 150(or 100) x 2.1 mm Hypersil BDS C18 or NovaPak C18 columns. Acetonitrile, water and 0.1% formic acid were used either under isocratic or linear gradient conditions to give 2-5 minute elution time.

A PE-SCIEX API III plus LC/MS/MS system equipped with a TurboIonSpray inlet was used for the acquisition of basic data for commonly encountered drugs of abuse and their metabolites by flow injection analysis. The predominant ions were either MH^+ for basic compounds or $[M - H]^-$ for acidic compounds without any obvious fragmentation. Unique product ions were selected for rapid screening (2 - 6 elution time) of blood and urine extracts in the multiple reaction monitoring mode with a detection limit of 0.1 - 0.5 ng/mL. Calibration curves were prepared in the concentration range of 0.2 ng/mL to 2 µg/mL using a 1 x 100 mm or 2.1 x 100(or 150)mm base deactivated column. Excellent linearities (r2 ≥ 0.99) were obtained. The confirmation of these substances was done by LC-Product Ion spectral acquisition. The product ion spectra obtained from several case samples were almost identical to those obtained from chemical standards. The following compares product ion spectra obtained from morphine standard, urine and plasma extracts obtained from the same subject.

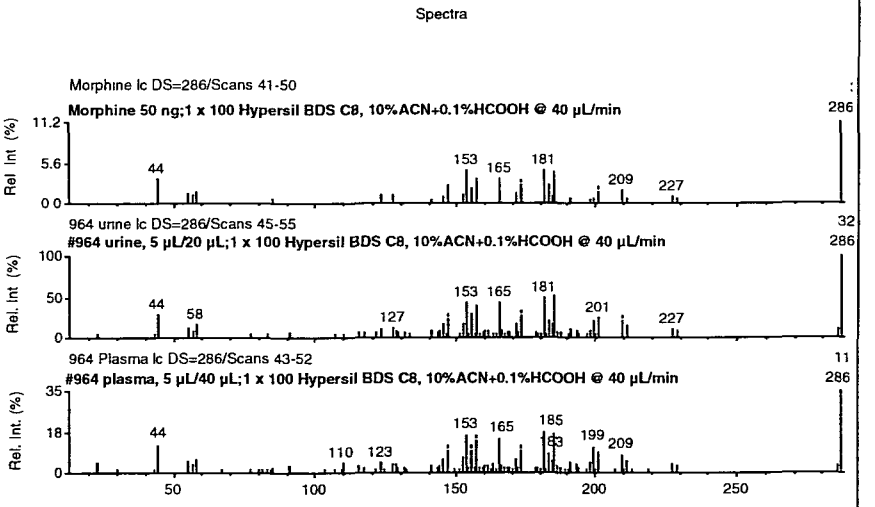

It has been shown that the use of fast chromatography combined with excellent specificity of the tandem quadrupole mass spectrometer and high sensitivity of the IonSpray technique to polar and thermally labile substances greatly improve the accuracy and speed of processing case samples for forensic chemists.

The authors wish to thank Ms. Carole Péclet and Ginette Rosato, toxicologists from the Direction des Expertises Judiciaires for their assistance in case selection and sample preparation.

IN VIVO METABOLISM OF PEPTIDE E, A LEU- AND MET-ENKEPHALIN PEPTIDE PRECURSOR, IN RAT BRAIN STUDIED BY MICRODIALYSIS/MICRO-ELECTROSPRAY MASS SPECTROMETRY

Per E. Andrén, Mark R. Emmett and Richard M. Caprioli
Analytical Chemistry Center and Dept. of Biochemistry and Molecular Biology, University of Texas Medical School, 6431 Fannin, Houston TX 77030

INTRODUCTION

Peptide E (YGGFMRRVGRPEWWMDYQKRYGGFL) is a mu-selective opioid peptide derived from proenkephalin A (263 amino acids). Peptide E and its known metabolites have been identified in brain and gastrointestinal tissue. Peptide E is unusual in that it contains two biological active peptides that could contribute to opioid actions, i.e. the [Met]^5-enkephalin sequence at the amino-terminus and [Leu]^5-enkephalin sequence at the carboxyl-terminus. In the present work we have studied the *in vivo* metabolism of peptide E in rat brain by using microdialysis/micro-electrospray mass spectrometry (micro-ES/MS).

In addition, we have utilized the highly sensitive micro-ES/MS-technique in order to detect endogenuous [Met]^5-enkephalin at attomole levels from brain microdialysis perfusates of freely-moving rats.

MATERIALS AND METHODS

In Vivo Metabolism of Peptide E

The microdialysis probe (CMA/10, 4 mm) was implanted in the striatum (AP+2.4, ML±3.0, DV-6.8) or the globus pallidus/ventral pallidum (GP/vP) (AP+1.0, ML±2.8, DV-4.3) of anesthetized rats. Peptide E was dissolved in artificial CSF (10 pmol/µL) and perfused at a flow-rate of 300 nL/min through the microdialysis probe. The probe was used to both deliver the peptide into the brain and to collect the degradation products. Samples were taken every 30 min.

Endogenous release of [Met]^5-enkephalin

A microdialysis guide cannula (CMA/10 Microdialysis AB, Sweden) was stereotaxically implanted under pentobarbital anesthesia (45 mg/kg) such that the microdialysis probe (CMA/10, 4 mm) would fully extend from the bottom of the cannulae and be positioned in the GP/vP. Three to five days after the surgery the microdialysis probe was inserted into the GP/vP through the guide cannula of the freely moving animal. The microdialysis probe was perfused with artificial CSF (5 mM KCl, 120 mM NaCl, 1.2 mM $MgCl_2$, 1.8 mM $CaCl_2$, 0.15% phosphate buffer pH 7.4) at a flow rate of 436 nL/min.

Capillary-liquid chromatography/micro-electrospray mass spectrometry

Mass spectra were obtained with a TSQ70 triplequadrupole mass spectrometer (Finnigan MAT, San Jose, CA) equipped with a micro-ES source. A capillary-LC/C18-packed column (50 µm i.d., 40 nL bed volume) was used for the concentration and desalting of the neuropeptides. The peptide samples were loaded with 2% MeOH/ 0.25% acetic acid on to a 10 µL loop on a 10-port valve (Valco Corp., Houston TX). The needle voltage was set to 3.5 kV, nozzle voltage 250 V, and repeller voltage to 10 V. Samples were eluted with 50% MeOH/0.25% acetic acid.

CONCLUSIONS

The present results showed that peptide E was metabolized *in vivo* to [Met]^5-enkephalin and [Leu]^5-enkephalin in the rat GP/vP. Larger fragments found were both N-terminal and C-terminal fragments, as well as internal fragments.

The structure-specific molecular detection of the endogenous neuropeptide [Met]^5-enkephalin released *in vivo* in rat brain has been accomplished using microdialysis and tandem mass spectrometry. The sensitivity of the technique for [Met]^5-enkephalin was in the attomole/µL range.

Measurements of the amounts of [Met]^5-enkephalin in the microdialysates obtained from studies of stimulated release showed that [Met]^5-enkephalin was present at a level of approx. 4-6 femtomoles per 10 µL dialysate, and that the baseline level was at approx. 1 femtomole per 10 µL dialysate.

The present study indicate that the methods and instrumentation described are suitable for detailed studies of neuropeptides in living animals, and this technique can be extended to studies of neuropeptide formation from precursors and their subsequent metabolism.

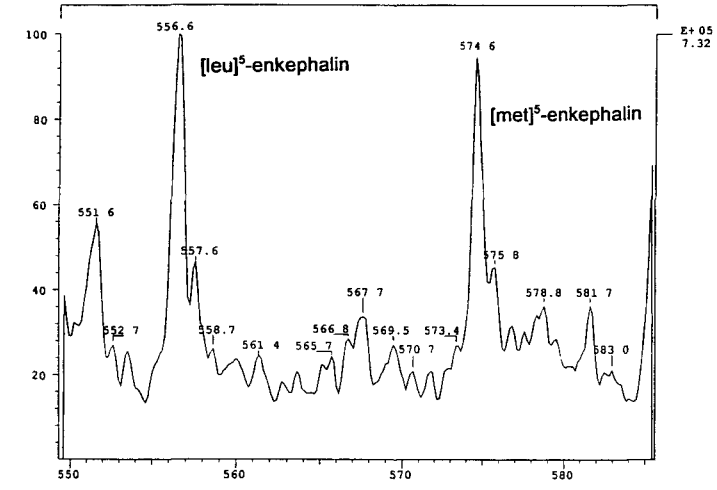

A microdialysis probe was used to both introduce peptide E into the brain and to collect metabolic products. Peptide E was metabolized to [Leu]^5-enkephalin (m/z 556.6), the C-terminus of peptide E, and [Met]^5-enkephalin (m/z 574.6), the N-terminus of peptide E, *in vivo* in the rat brain (GP/vP).

Characterization of Metabolites of a CCK Ligand on a LC/ESI/(MS)^n Ion Trap Mass Spectrometer, Arthur Moseley*[1], Tim Tippin[1], John Walsh[1], Jae Schwartz[2], Adrian Land[2], and Ian Jardine[2], [1]Department of Drug Metabolism, Glaxo Wellcome Research Institute, RTP, NC, [2]Finnigan MAT, San Jose, CA

GG772 is a novel 1,5-benzodiazepine derivative under study as a ligand of cholecystokinin (CCK). Biliary excretion in the guinea pig after iv administration of GG772 has been studied by LC/fluorescence and LC/MS. Prior to LC/MS, the bile sample was concentrated and cleaned up using a solid phase extraction procedure. The concentrated sample and corresponding predose bile were analyzed using microbore LC/ESI/(MS)^n on a Finnigan LCQ ion trap.

Prior to the analysis of the bile sample, reference (MS)^n spectra were acquired using a constant infusion of GG772. Each (MS)^n reference spectrum was obtained from approximately 6 ng of GG772. Reference spectra with high signal-to-noise ratios were acquired from n=1 (MS) to n=5 (MS/MS/MS/MS/MS). It was found that (MS)^3 was sufficient for the qualitative identification of the expected metabolites.

In order to evaluate the on-column levels of GG772 required to give useful LC/ESI/(MS)^3 spectra, an injection of 5 µL of 78 pg/µL of GG772 was made onto a 1 x 50 mm Hypersil BDS-C18 LC column. From this one injection of 390 picograms, LC/MS, LC/(MS)^2 and LC/(MS)^3 reference spectra were acquired.

A 2µL aliquot of the bile sample was analyzed using gradient elution from a 1 x 250 mm YMC AQ-C18 LC column. The gradient was 50% to 80% (10 minutes) of acetonitrile/2mM ammonium acetate (pH 4.5), with a mobile phase flow rate of 50 µL/minute. This analysis revealed a demethylated metabolite, a demethylated + sulfate metabolite, two major and three minor monooxidated metabolites, as well as parent GG772. The LCQ ion trap was able to acquire LC/MS, LC/(MS)^2, LC/(MS)^3, and LC/(MS)^4 spectra from the demethylated+sulfate metabolite, and LC/MS, LC/(MS)^2, and LC/(MS)^3 spectra from the demethylated metabolite, the two major monooxidated metabolites, and parent GG772. These spectra gave abundant structural information about these metabolites. For example, Figure 1 compares the LC/ESI/(MS)^3 spectrum obtained from 390 pg of GG772 with the LC/ESI/(MS)^3 spectrum of one of the monooxidated metabolites, indicated that the oxygen was located on the F2 portion of the molecule.

The ion trap's low full scan detection limits, coupled with its ability to perform LC/(MS)^n data acquisition, cause it to be very useful for the qualitative identification of drug metabolites from a "real world" samples.

Microbore LC / ESI / Ion Trap Mass Spectrometry

1 x 50 mm Hypersil BDS-C18 LC column, 3 µm particles
60% MeCN / 2mM ammonium acetate (pH 4.5), 80 µL / minute
5 µL injection, 78 pg / µL, 390 pg injected on-column
NOTE: LC/MS, LC/MS/MS, AND LC/MS/MS/MS FROM SAME INJECTION

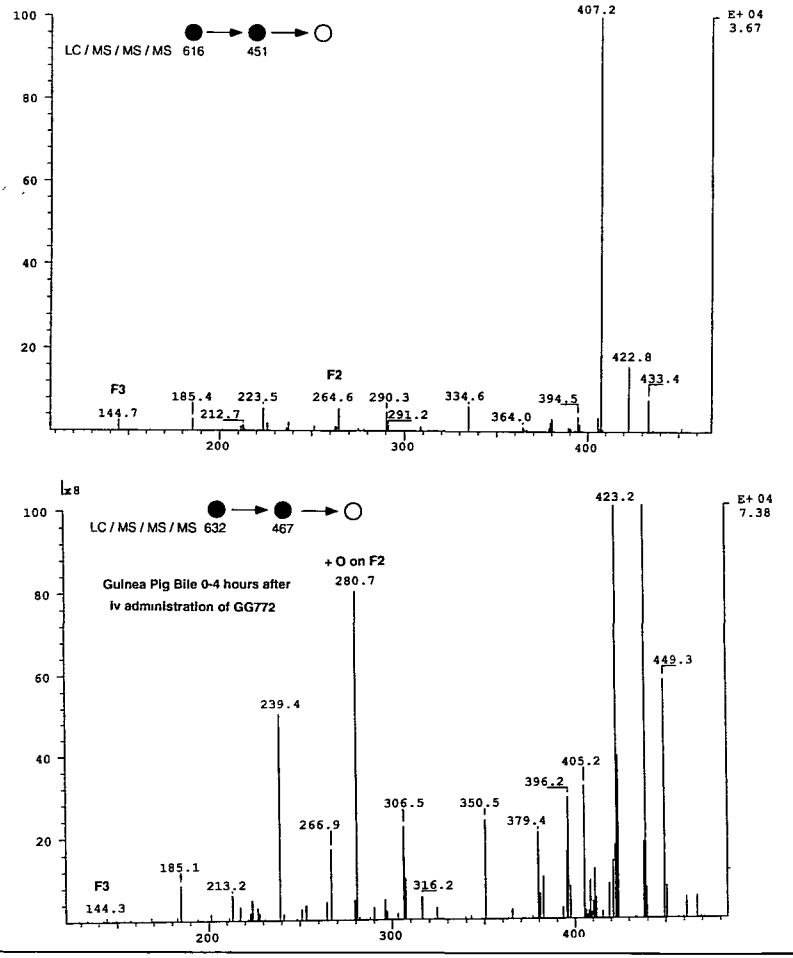

Investigation of the Interactions Between Bicyclomycin and Rho Protein

[1] K.A. Cox, [1]S.J. Gaskell, [2]H.-S. Moon, [2]H.-G. Park, [2]W.R. Widger, [2]H. Kohn
[1] The Michael Barber Centre for Mass Spectrometry; UMIST; Manchester M60 1QD, U.K.
[2] Department of Chemistry; University of Houston, Houston, TX 77004

Bicyclomycin (MW 302) is a structurally unique antibiotic which possesses a broad spectrum of antimicrobial activity against a variety of Gram-negative bacteria (1). Its broad utility combined with a novel method of activation and bonding to nucleophiles at near neutral pH values (2) make it particularly interesting in the development of new antibiotics. In *E.coli,* the primary site for drug binding is rho transcription termination factor (3), a cellular protein necessary for antibacterial growth. This protein is comprised of six identical 47 kDa subunits which recognize and bind to discrete regions within the newly synthesized RNA chains. Rho then extends its interaction toward the 3' end of the RNA polymerase elongation process, destabilizing the complex and releasing RNA from the transcription bubble (4). Bicyclomycin (BCM) binds to rho protein, affecting bacterial protein synthesis. The interaction of bicyclomycin with rho protein is not yet fully understood, but model studies suggest bonding of the protein by Michael addition to the exocyclic methylene group of bicyclomycin (2). The aim of the work shown here was to use electrospray ionization mass spectrometry to investigate the nature of BCM bonding to rho protein under a variety of incubation conditions. The reaction of BCM with several model peptides was also studied using tandem mass spectrometry.

BCM Incubated with Rho Protein

The m/z spectrum of native rho protein is shown in Figure 1a. Rho protein has an expected molecular mass of 47,006 Da. The mass spectrum of rho protein (Figure 1b) was processed by MaxEnt, an iterative algorithm which uses the method of maximum entropy to produce a mass spectrum from a multiply charged electrospray spectrum. When rho protein was incubated with BCM for only 30 minutes, apparent incorporation of one molar equivalent of BCM was observed (Figure 2). However, the mass spectrum gave no indication of the site of BCM incorporation. When rho protein was incubated with BCM for 8 hours, a prominent cleavage product was observed at 14,378 Da. No unmodified rho was detected, and although the large number of peaks observed in the m/z spectrum suggested a mixture of a number of products, no series could be identified. Partial proteolysis studies have indicated that rho contains a trypsin sensitive site at or near residue 130 (4). Cleavage at the arginine residue (128) would result in a fragment with a mass of 14,374 Da. Further studes indicated the presence of a proteolytic contaminant in the BCM preparation obtained from the supplier.

BCM Incubated with Model Peptides

In an effort to understand further the interaction of BCM with proteins, BCM was incubated with a series of model peptides of the form Ac-YGFXGF-NH_2, where X= Lys, Arg, His and Cys. In the case of the basic residues, Lys and Arg, complete cleavage was observed, as would be seen upon incubation with trypsin. When BCM was incubated with the His and Cys-containing peptides, clear signs of adduction were observed.

Ac-YGFHGF-NH_2 + BCM: The HPLC fraction of this incubation revealed a peak at m/z 1070, as expected for the addition of BCM to the peptide, and a peak at m/z 1071 of a relative abundance greater than that expected from isotopic contributions, suggesting the presence of two species. This could also be due to conversion of the C-terminal amide to a carboxylic acid independent of BCM adduction. In addition, a peak at m/z 687.6 was observed, corresponding to the addition of 2 BCM moieties to this peptide. Product ion spectra of these species clearly identified the histidine residue as the site of BCM adduction.

Ac-YGFCGF-NH_2 + BCM: HPLC purification of this incubation mixture revealed two fractions, producing virtually identical mass spectra. The mass spectra showed a series of peaks from m/z 1036 to 1039; the expected mass for the proposed adduct is 1036 Da. Another species was observed at m/z 1019, corresponding in mass to the addition of BCM to the peptide with loss of 17 Da. Previous studies examining the incubation of BCM with cysteine derivatives gave a piperidinedione product (R+BCM-NH_3) at neutral pH and two structurally distinct (R+BCM) products at higher pH (5). The CID spectra of m/z 1036 and m/z 1019 show cysteine as the site of BCM modification. The CID spectra of the m/z 1019 species show the same fragments as in the dissociation of m/z 1036, with corresponding NH_3 losses observed only from the fragment ions which incorporate the BCM moiety, consistent with the existence of the piperidinedione structure. However, no ions were observed corresponding to cleavage of the BCM moiety, precluding further conclusions about its structure.

1) Abuzar, S.; Kohn, H. *J. Am Chem. Soc.*, **1988**, *110*, 4089-4090.
2) Kohn, H.; Abuzar, S. *J. Org Chem.*, **1988**, *53*, 2769-2773.
3) Zwiefka, A.; Kohn, H.; Widger, W.R. *Biochemistry*, **1993**, *32*, 3564-3570.
4) Richardson, J.P. *Biochim. Biophys Acta*, **1990**, *1048*, 127-138.
5) (a) Abuzar S.; Kohn, H. *J. Am. Chem. Soc.*, **1990**, *112*, 3114-3121; (b) Kohn, H.; Abuzar, S. *J. Org. Chem* , **1989**, *54*, 4000-4003.

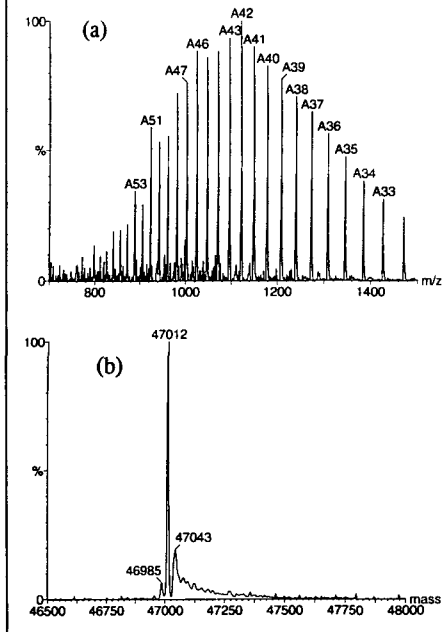

Figure 1

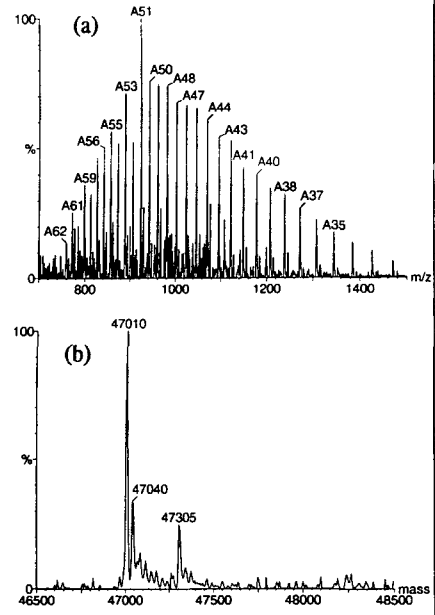

Figure 2

Characterization of Limonene Metabolites in Patients with Advanced Cancer

G.K. Poon*[1], D. Vigushin[2], R.C. Coombes[2] and M. Jarman[1]
[1]*CRC Centre for Cancer Therapeutics, Institute of Cancer Research, Surrey, U.K.*
[2]*Dept. of Medical Oncology, Charing Cross Hospital, London, U.K.*

Introduction

d-Limonene (*p*-metha-1,8-diene) is a monoterpene with broad cellular anitproliferative activity and potent chemopreventive/chemotherapeutic activity in carcinogen-induced animal tumor models. Transforming activity of $p21^{Ras}$ and related 21-26 kDa GTP-binding proteins is dependent on post-translational isoprenylation but constitutively mutated, oncogenic forms of *ras* proteins have been associated with a broad spectrum of human malignancies including 90% of pancreatic and 50% of colorectal adenocarcinomas [1]. Farnesyl-protein transferase (FPTase) is the enzyme that catalyzes protein prenylation, and inhibitors of this enzyme may be potential antitumor agents. Limonene inhibits the post translational isoprenylation of $p21^{ras}$ and other small G proteins and has been demonstrated to have antitumor activity against *N*-methyl-*N*-nitrosourea (NMU) and 7,12-dimethyl benz-(a)anthracene (DMBA) induced tumors in the rat. It is the first FPTase currently undergoing phase I clinical trial in patients with advanced cancer.

Limonene is extensively metabolized *in vivo* to active metabolites and the parent compound is only a minor component. Quantitation and characterization of these metabolites are critical because they have greater pharmacological potency than limonene in the inhibition of small G protein isoprenylation. This report describes the direct analyses of limonene and its metabolites presence in the plasma and urine samples of patients by liquid chromatography - mass spectrometry, utilizing the atmospheric pressure chemical ionization (APCI) for the phase I metabolites and the electrospray ionization (ESI) interface for the phase II metabolites.

Conclusion

Four major metabolites were observed in the plasma samples, namely perillic acid, dihydroperillic acid, limonene-1,2-diol and limonene-8,9-diol. Together with limonene-10-ol, all these metabolites were also present in the urine samples as their corresponding glucuronides. All of these compounds are 5-10 times more potent than limonene *in vitro* in the inhibition of protein isoprenylation and cellular proliferation [2]. The rapid biotransformatin of limonene to these metabolites constituting the predominant terpene component in plasma, each substantially more potent than the parent compound strongly suggests that the biological activity of limonene is mediated by these plasma metabolites.

1. J.B. Gibbs, A. Oliff and N.E. Kohl, *Cell*, **77** 175 (1994).
2. P.L. Crowell, Z. Ren *et al.*, *Biochem. Pharmacol.*, **47**, 2405 (1994).

Acknowledgment: This work is supported by the Cancer Research Campaign, U.K.

43rd ASMS Conference on Mass Spectrometry and Allied Topics

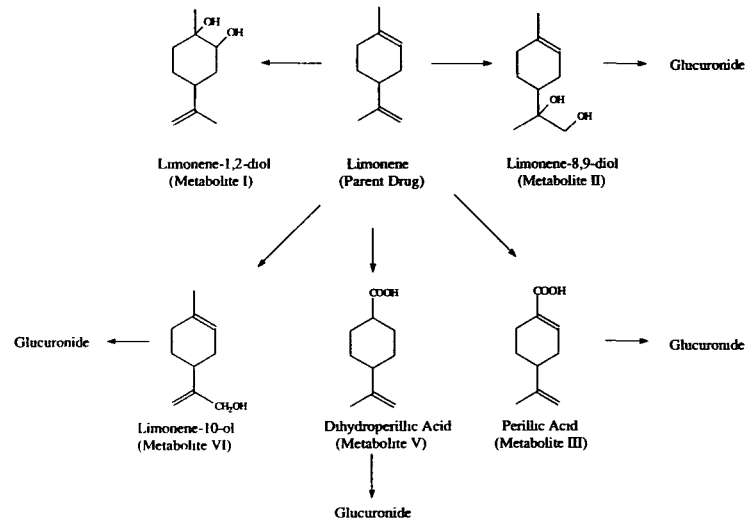

Metabolic Pathway of limonene after oral administration in human

An Electrospray Mass Spectrometric Study of the Gold Drug Myochrysine.

Richard W Smith, Daren J LeBlanc, Colin J.L. Lock and Helen E.Howard-Lock
Department of Chemistry, McMaster University, 1280 Main St W, Hamilton, ON, L8S 4M1, CANADA.

Although the gold (I) drug myochrysine (sodium gold-thiomalate) has been used for the treatment of rheumatoid arthritis for more than 60 years, its characterization by conventional methods such as NMR, X-ray crystallography and mass spectrometry has proven unsuccessful (1)

This drug, marketed as a mixture of several components (including excess di-Na thiomalate, glycerol and ethanol) has a number of toxic side-effects, some of which may be related to one or more of the Au containing minor components The characterization of the Au species may lead to improvements in the synthesis and purification of the unidentified active compound which is thought to be a Au(I)/thiomalic acid (L= $HO_2CCH_2CH(SH)CO_2H$) oligomer for which open and closed chain structures including pentamers, hexamers, and octamers have been postulated (1,2,3). Two classes of L Au complexes are thought to exist (1) in these samples, (i) closed ring oligomers with bridging S between two Au atoms with a L:Au ratio of 1·1, considered to be neutral apart from the ionizable carboxyl groups and (ii) open chain oligomers with both bridging and terminal S atoms, with a higher than 1.1 L:Au ratio (eg. the 2 1 and 3·2) and, in addition to the ionizable carboxyl groups, an overall negative charge due to the terminal thiol group(s)

Pneumatically assisted electrospray experiments were performed with 50/50 CH_3CN/H_2O as the mobile phase at a flow rate of 15µl/min employing a Brownlee Microgradient syringe pump Samples were introduced by flow injection at a concentration of 0.01M + 0.001M of NH_4OH for both the +ESI and -ESI experiments Full scan ESI experiments were performed with a Fisons Platform quadrupole instrument and the MS/MS data were generated with a Fisons Quattro II triple quadrupole instrument. Collisional activation (CA) MS/MS was performed with Ar as the collision gas at a main beam attenuation of 25% and a collision energy of 35eV All data was acquired in MCA mode (10 scans) A cone voltage (CV) of 35V was employed in all ESI experiments (unless otherwise stated) All samples employed in this study were used as supplied by the manufacturer or synthesized by conventional methods.

Analysis of the sodium and ammonium salts of gold-thiomalate by electrospray mass spectrometry indicated that the primary species is a molecular weight 1384 tetramer (Au_4L_4). In the case of the Na salt, the +ESI and -ESI mass spectra were very complex due to extensive Na^+/H^+ exchange, however, the ions corresponding to those observed from the NH_4^+ salt were present. Consequently, discussion of the results will be restricted to the NH_4^+ salt of myochrysine. In the negative ion mode, the ammonium salt exhibited intense singly, doubly and triply charged ions at m/z 1383, 691 and 460 respectively whereas in the positive ion mode the protonated and ammoniated ions dominated at m/z 1385 and 1402 (Figure 1) In addition, ions were observed at m/z 1267, 1151, 633 and 575 in -ESI which may correspond to the singly and doubly charged ions originating from species such as Au_4L_3SH and $Au_4L_2(SH)_2$ as well as an ion at m/z 495 which may correspond to the Au_1L_2 species Ions corresponding to the $Au_4L_{y=4-2}(SH)_{z=0-2}$ species were not observed in +ESI perhaps indicating that the -ESI species were fragment ions originating from the $[M-H]^-$ / $[M-2H]^{2-}$ ions In order to further clarify these observations CA MS/MS was performed. The $[M-2H]^{2-}$ ion yielded the same singly and doubly charged ions observed from myochrysine that is, the $Au_4L_{y=4-2}(SH)_{z=0-2}$ species The facile cleavage of the C-S bonds in the -Au-S-C- system has been reported previously (4) consequently, the observation of these fragment ions might be expected However, if the $Au_4L_{y=4-2}(SH)_{z=0-2}$ species are formed by "in source" fragmentation of the Au_4L_4 tetramer, then varying the cone voltage may further elucidate whether the ions observed are in fact derived from components of myochrysine

In +ESI (CV=25V) only the $[M+NH_4]^+$ and $[M+H]^+$ ions were observed while at a CV of 55V, the consecutive loss of 4 H_2O molecules was seen. In addition, the ion corresponding to the protonated Au_4L_3SH

species was observed at a CV of 80V In -ESI (CV=20-50V), the ions corresponding to the $Au_4L_{y=4-2}(SH)_{z=0-2}$ and Au_1L_2 species were observed Higher CV's (>60V) caused extensive dissociation of the Au_4L_4 species which produced intense ions such as m/z 495 (Au_1L_2) These results indicate that the Au_4L_4 tetramer is the major component of myochrysine. However, the presence of $Au_4L_{y=4-2}(SH)_{z=0-2}$ and Au_1L_2 in myochrysine still has to be determined due to the ambiguous nature of the results described here.

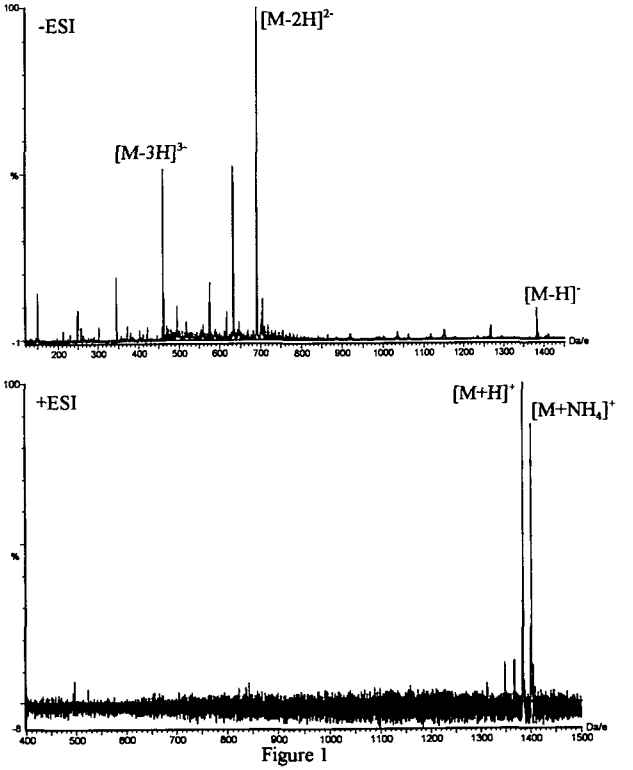

Figure 1

References·
(1) Parish R V , Interdisciplinary Sci. Rev. 17(3), 221 (1992)
(2) Al-Sa'ady A.K H , Moss K., McAuliffe C A and Parish R V. JCS Dalton Trans:1609 (1984).
(3) Sadler P J Struct Bonding; 29:171 (1976)
(4) Dilworth J R and Hu J Adv Inorg Chem; 40:411 (1993)

Acknowledgements: The authors wish to express thanks to Dr. C.A. Kingsmill and the Ontario Ministry of Agriculture and Food for the use of their Fisons Quattro II instrument for the MS/MS experiments

Identification of Diphenhydramine Metabolites Using Deuterated Ammonia DCI MS

T.M. Heinze, E.B. Hansen, Jr., J. Deck and C.E. Cerniglia
Food and Drug Administration, NCTR, Jefferson, AR 72079

INTRODUCTION The aim of this investigation was to isolate diphenhydramine metabolites formed from the fungal metabolism of diphenhydramine (DPH) and to identify them by using mass spectrometry and proton nuclear magnetic resonance spectroscopy. Deuterated ammonia (ND_3) desorption chemical ionization (DCI) mass spectrometry (MS) was used for the differentiation between possible isobaric diphenhydramine metabolites and for probing the mechanisms of ion formation under ammonia (NH_3) DCI conditions.

METHODS *Biotransformation and Semi-Prep HPLC Isolation of Metabolites:* DPH was metabolized by *C.elegans* in suspension culture for 168 hours. A methylene chloride extract of culture supernatant pooled with aqueous and methanolic cell washes was evaporated in vacuo. The residue was dissolved in HPLC mobile phase, 60% buffer (10 mM PO_4, 20 mM TMA, pH 7 with KOH) / 40% ACN. The metabolite isolation was on semi-prep HPLC columns (10 mm X 250 mm 5 μ, Cyano-propyl and SCD-100) at 5 ml/min. Peaks 1A, 1B, 2, 3, and 4 were isolated. *Proton Nuclear Magnetic Resonance (^{1}H-NMR):* Identities were confirmed by ^{1}H-NMR spectroscopy at 500MHz (Bruker Instruments) in methylene chloride-d_2. *Mass Spectrometry:* Experiments were performed by using a single quadrupole mass spectrometer (Finnigan MAT) model 4023 with PPINICI that was upgraded to a 4500. Sample introduction was via a direct exposure probe (DEP) with a rhenium wire and DEP programmer (Finnigan MAT) ramped at 5 mA /sec from 0 to 0.65 A. NH_3 DCI MS: positive ion, 50 to 650 daltons/1sec cycle, ionizer temp set at 120 and electron energy at 120 V. Reagent gas was a mixture of 10% NH_3 / 90% N_2 which was introduced until the analyzer pressure was 3.5 X 10^{-5} Torr with the probe inserted. Similar reagent gas mixture and conditions were used for ND_3 DCI MS.

RESULTS HPLC Peaks 1B, 2, 3 and 4 were identified as N-acetyl-DPH, DPH-N-oxide, N-desmethyl-DPH and recovered DPH, respectively. DEI MS, NH_3 DCI MS and ^{1}H-NMR spectroscopy confirmed the assignments. DEI and NH_3 DCI mass spectra indicated Peak 1A could be one of two isobaric metabolites, N-formyl-DPH or N-acetyl-N-desmethyl-DPH. The mass spectra of peak 1A were very similar to those of N-formyl-DPH standard, formylated Peak 3. ND_3 DCI mass

spectral analysis of peak 1A (Figure1a) solved the problem. Peak 1A had to be N-acetyl-N-desmethyl-DPH based on an extra exchangeable proton.

Acquisition of ND_3 DCI mass spectra for HPLC peaks 1B, 2, 3 and 4 completed the data set. The ion at *m/z* 167 common to all NH_3 and ND_3 DCI mass spectra of DPH and its metabolites was probably related to the ion at *m/z* 182 in the FAB mass spectra of doxylamine and its metabolites (1). Reaction of DPH-N-oxide with ammonia could yield the parent DPH and N-desmethyl-DPH resulting in a ND_3 DCI mass spectrum (Figure 1b) that looked like a composite of $[M+D]^+$ for the DPH-N-oxide and ions from N-desmethyl-DPH and DPH.

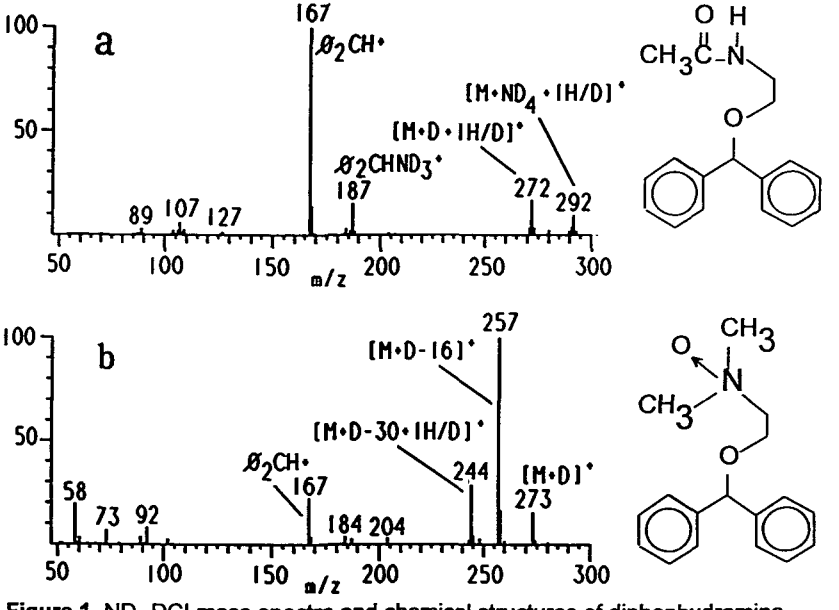

Figure 1. ND_3 DCI mass spectra and chemical structures of diphenhydramine metabolites found in Peak 1A (a) N-acetyl-N-desmethyl-DPH and Peak 2 (b) DPH-N-oxide.

REFERENCE

1. Lay, J.O.,Jr., et al. *Biomed Environ. Mass Spectrom.* **18**, 157-167, 1989.

LC/MS/MS Detection of the GSH-glucuronide Conjugate of (E)-2,4-Diene VPA in Rats

Wei Tang and Frank S. Abbott
Division of Pharmaceutical Chemistry, Faculty of Pharmaceutical Sciences,
University of British Columbia, Vancouver, BC, CANADA, V6T 1Z3

The hepatotoxicity of the anticonvulsant drug valproic acid (VPA) is thought to be related to the formation of toxic metabolites, namely 4-ene VPA and (E)-2,4-diene VPA (1,2). Previous work in this laboratory has shown that (E)-2,4-diene VPA, a product of 4-ene VPA metabolism in mitochondria, could react with the residing GSH and therefore deplete the mitochondrial GSH pool (2). In our continuing effort to explore the mechanism of VPA-associated hepatotoxicity, we report herein a LC/MS/MS characterization of new GSH-related conjugates of (E)-2,4-diene VPA. Bile samples collected from male Sprague-Dawley rats dosed i.p. with (E)-2,4-diene VPA (100 mg/kg) were injected onto a HP Hypersil ODS column (100 x 2.1 mm, 5 μm) interfaced to a Fisons VG Quattro LC/MS/MS instrument using electrospray ionization. Collision-induced dissociation (CID) involved argon as the target gas at a pressure of 3.0 x 10^{-4} mbar. The core voltage was 29 V with skimmer offset by 5 V, collision energy 50 eV and source temperature 80°C. LC mobile phase consisted of methanol/water (0.05% TFA) at a flow rate of 50 μL/min: 75% water for 2 min, a decrease to 50% water during 2-5 min, a hold at 50% water to 12 min, a decrease to 15% water during 12-16 min, a hold at 15% water to 30 min. Initial Q1 parent ion scanning indicated that the daughter ion *m/z* 162, a major fragment associated with the GSH conjugate of (E)-2,4-diene VPA, could also be derived from the ion at *m/z* 624. Subsequent MS/MS CID on the parent ion at *m/z* 624 revealed a neutral loss of 176 Da which is characteristic of glucuronides (Fig. 1). A similar neutral loss of 176 Da was observed in the daughter ion spectrum of a biliary metabolite arising from [$^2H_7$]-4-ene VPA dosed i.p. to rats, where the ion fragments containing the VPA portion were 7 amu higher than that seen in the bile of rats treated with unlabelled drug (Fig. 1). The daughter ion spectrum of the peak of interest also gave ion fragments characteristic for GSH conjugates, such as the loss of glycine (MH^+ - 176 - 75) and glutamate (MH^+ - 176 - 129) moieties (Fig. 1). Taken together, the evidence indicated the presence of a di-conjugated metabolite which was assigned initially as 5-GS-3-ene VPA-glucuronide by comparing its mass spectrum with the corresponding mono-GSH conjugate formed from (E)-2,4-diene VPA (3). Further proof of structural identity was obtained from ^1H NMR of the HPLC purified metabolite. The *N*-acetylcysteine-glucuronide di-conjugate of (E)-2,4-diene VPA was similarly characterized by LC/MS/MS as a biliary and urinary metabolite in rats treated with (E)-2,4-diene VPA. Because extensive glucuronidation of (E)-2,4-diene VPA occurs in rats, the GSH-glucuronide di-conjugate is most likely formed through the reaction of GSH with (E)-2,4-diene VPA-glucuronide. In support of this hypothesis, 2,4-diene VPA-glucuronide isolated from rat bile was incubated with GSH in the presence or absence of GST enzyme and the resultant 5-GS-3-ene VPA-glucuronide was readily detected by LC/MS/MS (Fig. 2). To our knowledge, this is the first recorded instance in which a drug is activated by glucuronidation to further conjugate with GSH *via* a Michael addition reaction.

Reference

1. Kassahun, K., Farrell, K. and Abbott, F. (1991) *Drug Metab. Dispos.* **19**, 525-535.
2. Tang, W., Borel, A.G., Fujimiya, T. and Abbott, F.S. (1995) *Chem. Res. Toxicol.* (in press).
3. Kassahun, K., Hu, P., Grillo, M.P., Davis, M.R., Jin, L. and Baillie, T.A. (1994) *Chem. Biol. Interact.* **90**, 253-275.

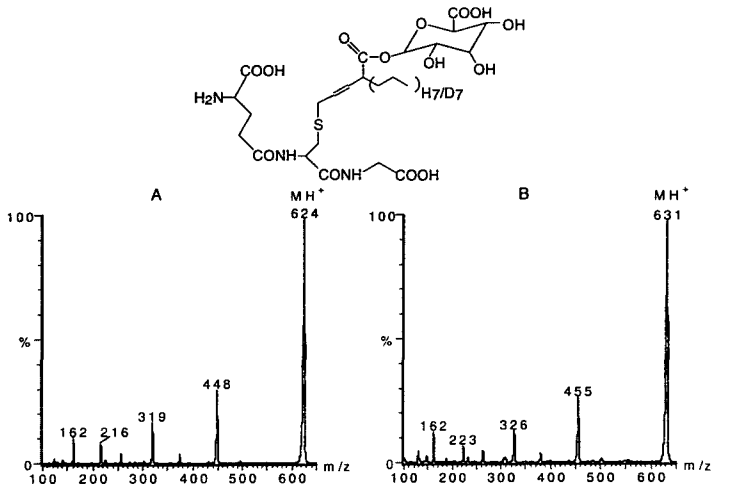

Fig. 1. MS/MS mass spectra of 5-GS-3-ene VPA-glucuronide obtained as (A) the biliary metabolite in rats treated with (E)-2,4-diene VPA and (B) the biliary metabolite in a rat dosed with [$^2H_7$]-4-ene VPA.

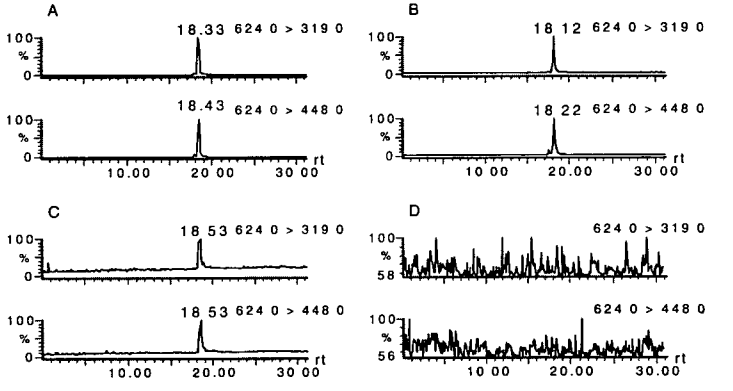

Fig. 2. On-line LC/MS/MS detection of 5-GS-3-ene VPA-glucuronide (*m/z* 624 → 319 and *m/z* 624 → 448) in (A) the aqueous solution spiked with the purified metabolites; (B) the incubation involving 2,4-diene VPA-glucuronide, GSH and GST enzyme; (C) the incubation involving 2,4-diene VPA-glucuronide and GSH; (D) the incubation containing 2,4-diene VPA-glucuronide only.

Characterization of a Novel Metabolic Reaction Observed in the Metabolism of LY315535

Todd A. Gillespie, R. Mike Goodwin, John T. Catlow, and Steve P. Swanson
Department of Drug Metabolism and Disposition, Lilly Research Laboratories, Indianapolis, IN 46285

LY315535 (Figure 1), 1,2,3,4-tetrahydro-8-(5-isoxazolyl)-N,N-dipropyl-2-naphthalenamine, is a potent serotonin (5HT-1a) agonist with muscarinic antagonist activity and is under development for the treatment of irritable bowel syndrome (IBS). The objectives of these studies were to characterize the major and minor metabolites of LY315535 by on-line LC/ES/MS/MS to subsequently determine the preliminary metabolic profile in rats, dogs, and monkeys (*in vivo*). In addition, to determine the *in vitro* metabolism using microsomal incubates to help in the selection of an appropriate species for toxicological studies.

Sample Preparation: Rats were administered an oral dose of either 25 mg/kg/day over 5 days or 75 mg/kg of LY315535 (free base) for urine collection and plasma collection at 1 hr, respectively. Dogs and Monkeys were both administered an oral dose of 10 mg/kg of LY315535 for plasma collection at 1 hr. The urine was diluted 2:1 with 50 mM NH_4OAc (200 µL/100 µL) and plasma was diluted 1:1 with ACN (500 µL/500 µL). In addition, microsomal incubates were prepared appropriately and diluted with (50/50) ACN/50 mM NH_4OAc.

LC/ES/MS/MS: Samples were injected (50 µL or 100 µL) onto an Inertsil C8 (15cm x 3.0mm) column. Potential metabolites were then separated with a gradient consisting of 80% 50 mM NH_4OAc/20% ACN linearly ramped to 100% ACN over 20 minutes at a flow rate of 0.7 mL/min. Mass spectrometry analysis was performed on a Finnigan MAT TSQ700 equipped with a Finnigan API source and electrospray interface. Positive ion detection was achieved with a spray voltage of +4500 V, capillary heater temperature of 275°C, sheath gas of 70 psi (N_2), and an auxiliary gas flow of 20 mL/min (N_2). The CAD analysis utilized a collision offset energy of -30 eV and a collision gas pressure of 1.5 mTorr (argon).

Results and Discussion: A number of LY315535 metabolites have been identified both *in vitro* and *in vivo* by LC/ES/MS/MS. The main sites of metabolism appear to be the isoxazole ring and the propyl moieties. Comparison of the major metabolites observed between species showed no significant differences. However, differences were observed in the minor metabolites within the various species. The despropyl metabolite has been identified as a major metabolite in all analyzed species. In addition, oxidation (hydroxyl) on the propyl function has been observed as a minor metabolite in all of these except for the cynomolgus monkey. Interestingly, a novel metabolic reaction involving the opening of the isoxazole ring and subsequent loss of CN to yield the methyl ketone metabolites has been identified. Additionally, both despropyl and hydroxyl metabolites of the methyl ketone have been observed. Further experiments have identified both the carboxylic acid (Figure 2) and cyano (Figure 3) metabolites to be present. Consequently, the carboxylic acid has been postulated as a precursor to the formation of the more prominent methyl ketone metabolites. In addition, the cyano metabolite has been observed *in vitro* in all analyzed species.

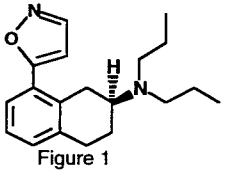

Figure 1

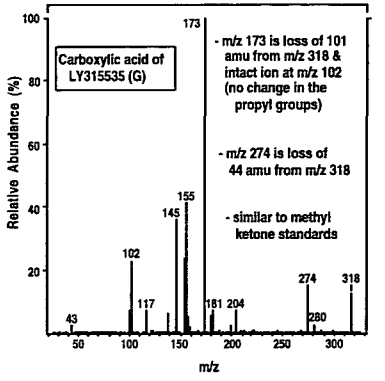

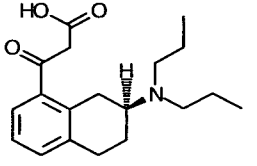

Figure 2

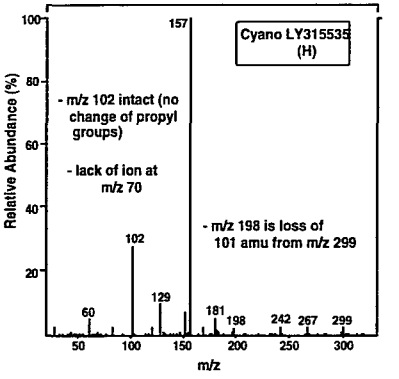

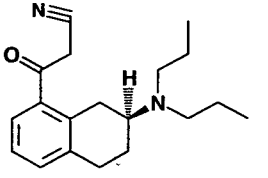

Figure 3

Summary of Microsomal Incubates

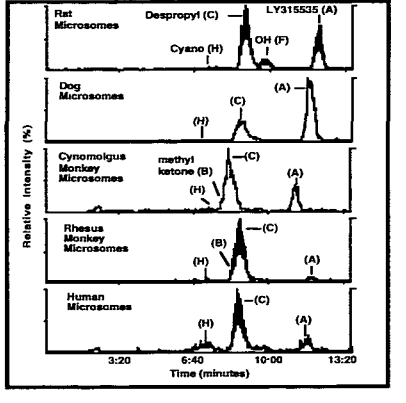

Summary of LY315535 Metabolite Identification

Species	Major	Minor	Trace
Rat Unne	des>MK	par,OH-par	acid
Rat Pls	des	CN,par	MK
Rat Micro	des>par	OH-par	CN
Dog Pls	par=des	OH-par	MK
Dog Micro	par>des	OH-par	CN
Cyno Pls	des>par	MK,des-MK	-
Cyno Micro	des>par	-	CN,OH-par
Rhes Micro	des>par	CN,OH-par	-
Hum Micro	des>par=CN	OH-par	-

API III-MS of Natural Products: Structural Elucidation of Bisbenzylisoquinoline Alkaloids by Ionspray-MS and MS/MS

*Wu-Nan Wu and Michael D. Moyer, Department of Drug Metabolism, The R. W. Johnson Pharmaceutical Research Institute, Spring House, Pa 19477, U.S.A.

INTRODUCTION

Natural products are an important source of novel therapeutic agents in a drug discovery program. For example, bisbenzylisoquinoline alkaloids exert hypotensive, antimicrobial, analgesic, muscle relaxant and antitumor activities (1-8). Previously, structural characterization of these natural products have relied mainly on EI-MS, CI-MS and FABMS; however, these techniques need >10 ug of material (1-8). Early EI-MS and CI-MS studies displayed low abundance molecular/adduct molecular ions and fragment ions (3-8). The objective of this study is to elucidate the structures of bisbenzylisoquinoline alkaloids isolated and identified previously from *Thalictrum* sp. (*Ranunculacea*) (3-8) using Ionspray-MS and Tandem mass spectrometric techniques.

METHODS

- 20 Bisbenzylisoquinoline alkaloids (17 diether, 3 monoether linkages, Fig&Tab) (2-8) were prepared at 20-50 ng/uL in acetonitrile/water (50/50, v/v) with 5 mM ammonium acetate (pH 4).
- Alkaloids were analyzed using PE/Sciex API-III, a triple quadrupole mass spectrometer interfaced to a Hitachi solvent delivery system (L-6200 A Intelligent Pump) via an Ionsprayer/Heated Nebulizer.
- Solvent system - methanol/water (1:1, v/v) at 100 uL/min (Ionsprayer) or 1 mL/min (Heated Nebulizer) flow rate into a 20 uL injection loop.

RESULTS AND CONCLUSIONS

- 20 Bisbenzylisoquinoline alkaloids were analyzed using PE/Sciex API-III-MS and MS/MS.
- Structures, summarized MS and MS/MS data for each alkaloid, and representative mass spectra (Q1 Scan, MS/MS) for 9 alkaloids are presented.
- Ionspray-MS exhibited intense protonated molecular/molecular ions for the alkaloids and intense doubly charged ions for the diether-linkage alkaloids.
- MS/MS analysis of the protonated molecular/molecular ion for each alkaloid revealed an apparent parent ion along with prominent as well as diagnostic daughter ions for the important isoquinoline moities which provided structural information for the alkaloid.
- Ionsprayer and Heated Nebulizer - similar MS data.
- Detection of protonated molecular ions - ng quantities.

REFERENCES

1. P.L. Schiff, Jr., J. Nat. Prod., **46**, 1 (1983).
2. G.C. Caldwell, J.A. Masucci and W.N. Wu, Org. Mass Spectrum, **29**, 220 (1994).
3. L.A. Mitscher, W.N. Wu, R.W. Doskotch and J.L. Beal, Chem. Comm. (J. C. S.), 589 (1971).
4. W.N. Wu, J.L. Beal and R.W. Doskotch, Tetrahedron Lett., **41**, 3687 (1976).
5. W.N. Wu, J.L. Beal, R.P. Leu and R.W. Doskotch, J. Nat. Prod., **40**, 281 (1977).
6. W.N. Wu, J.L. Beal, R.P. Leu and R.W. Doskotch, J. Nat. Prod., **40**, 384 (1977).
7. W.N. Wu, J.L. Beal, E.H. Fairchild and R.W. Doskotch, J. Org. Chem., **43**, 580 (1978).
8. W.N. Wu, J.L. Beal and R.W. Doskotch, J. Nat. Prod., **43**, 372 (1980).

Summary of Ionspray-MS and MS/MS Data

No.	Alkaloid Name	MW	Ionspray-MS m/z (% relative abundance) $[M+H]^+$	Ionspray-MS m/z (% relative abundance) $[M+2H]^{++}$, $[M+H]^{++}$	Ionspray-MS/MS m/z (% relative abundance) Daughter ions of $[M+H]^+$ and M^+
1.	Obamegine	594	595(17)	298(100)	579(2), 564(9), 552(8), 532(18), 382(4), 367(92), 351(5), 339(3), 266(4), 227(5), 213(5), 192(100), 176(24), 148(9), 146(10).
2	Thalrugosine	608	609(44)	305(100)	594(3), 578(16), 566(18), 546(21), 532(4), 472(3), 382(10), 381(9), 367(100), 351(7), 336(4), 280(5), 227(6), 192(49), 177(7), 176(23), 174(24), 146(13).
3	Isotetrandrine	622	623(31)	312(100)	607(7), 592(6), 576(9), 560(9), 400(3), 396(2), 395(2), 381(51), 363(8), 353(3), 335(9), 294(11), 227(11), 206(8), 204(14), 190(31), 174(100), 162(35), 146(38).
4.	Homoaromoline	608	609(39)	305(100)	593(5), 578(34), 566(35), 535(20), 520(14), 416(12), 400(18), 385(15), 382(9), 381(8), 367(100), 358(22), 350(14), 340(12), 266(27), 239(24), 227(43), 213(38), 192(8), 190(64), 176(78), 146(24).
5.	Oxyacanthine	608	609(43)	305(100)	593(5), 578(36), 566(35), 535(20), 396(7), 395(6), 387(18), 381(100), 367(58), 213(42), 206(41), 192(61), 176(92), 146(23).
6.	Obaberine	622	623(24)	312(100)	607(4), 592(17), 580(18), 400(17), 396(5), 395(3), 381(100), 365(12), 354(8), 280(12), 227(27), 206(25), 192(10), 190(26), 176(49), 174(57), 146(11).
7.	Thalicberine	608	609(100)	305(36)	592(2), 578(29), 566(44), 396(12), 367(29), 381(24), 367(11), 280(13), 222(24), 213(14), 206(28), 192(100), 176(65), 174(44), 159(39), 146(7).
11	Thalidasine	652	653(29)	327(100)	637(4), 622(15), 607(33), 590(28), 578(37), 560(25), 426(3), 425(4), 411(93), 395(20), 379(34), 365(47), 227(24), 206(100), 204(87), 192(32), 190(73), 174(52), 162(17), 159(22).

No. 2 Thalrugosine

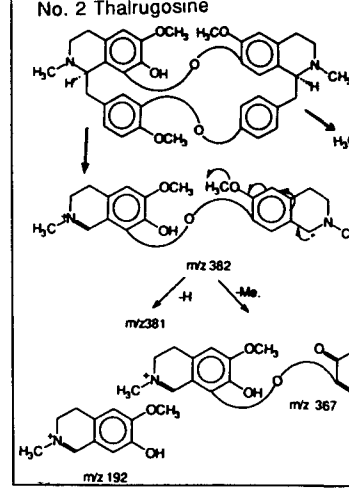

No. 11 Thalidasine

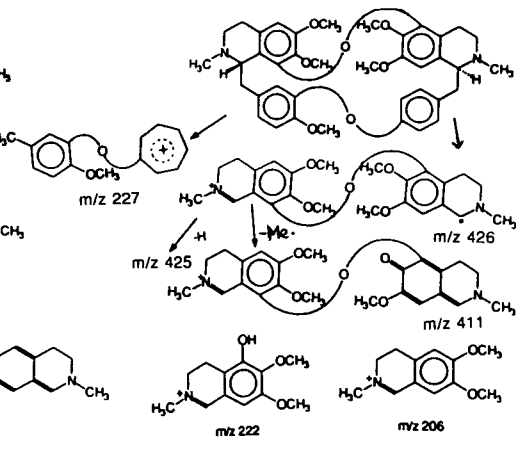

Metabolism of the Antipsychotic Agent, Mazapertine Succinate: Structural Elucidation of Human Urinary Metabolites of Mazapertine Using LC/Ionspray-MS and MS/MS

*Wu-Nan Wu, Lee G. Gisclon and Linda A. McKown, Department of Drug Metabolism, The R. W. Johnson Pharmaceutical Research Institute, Spring House, PA 19477, U.S.A.

INTRODUCTION

Mazapertine (RWJ-37796) succinate, 1-[3-[[4-[2(1-methylethoxy)phenyl]-1-piperazinyl]methyl]benzoyl]piperidine succinate, is a new antipsychotic agent. The metabolism of mazapertine in dogs and rats (1, 2) and the effect of food on the bioavailability of mazapertine in humans (3) were reported recently. The objectives of this study were to investigate the metabolism of mazapertine and to characterize and elucidate the structures of mazapertine metabolites in humans using LC/Ionspray-MS and MS/MS techniques

METHODS

- 2 Healthy male volunteers.
- Mazapertine succinate (40 mg/kg as free base, oral).
- Urine collection - 0-48 h after dosing.
- Urine sample pooled (0-24 h) - Amberlite XAD-2 adsorption and methanol extraction for untreated and Glusulase-treated urine pools, and HPLC (C8) separation.
- Unchanged mazapertine and its metabolites were characterized and identified using PE/Sciex API-III Ionspray-MS and MS/MS, and by comparison to synthetic samples (mazapertine, M1, M2, M4, M6, M7, M8, M10).

RESULTS AND CONCLUSIONS

- Unchanged mazapertine plus 10 metabolites (M1-M10) were characterized, and tentatively identified from the urine samples.
- Structures, representative mass spectra for unchanged mazapertine and metabolites are presented.
- Ionspray-MS and tandem mass spectrometric analyses of mazapertine and the metabolites revealed apparent protonated parent ions and informative as well as prominent daughter ions for the structural elucidation of metabolites.
- Sites for the formation of mazapertine metabolites and the proposed metabolic pathways for mazapertine in humans are presented.

REFERENCES

1. W.N. Wu, L.A. McKown, W.J. Jones, A.R. Takacs, A.R. Reitz and M.E. McDonnell, Presentation at the 42nd ASMS Conference on Mass Spectrometry and Allied Topics, Proceedings, Abstract p 344 (1994).
2. W.N. Wu, L.A. McKown, A.D. Gauthier, W.J. Jones and A.R. Takacs, Presentation at the 9th AAPS Annual Meeting, Pharm. Res. 11(10) Abstract S-344 (1994).
3. L.G. Gisclon and C.R. Curtin, Presentation at the 8th AAPS Annual Meeting, Pharm. Res. 10(10) Abstract S-398 (1993).

Metabolism of Mazapertine (RWJ-37796) in Humans :

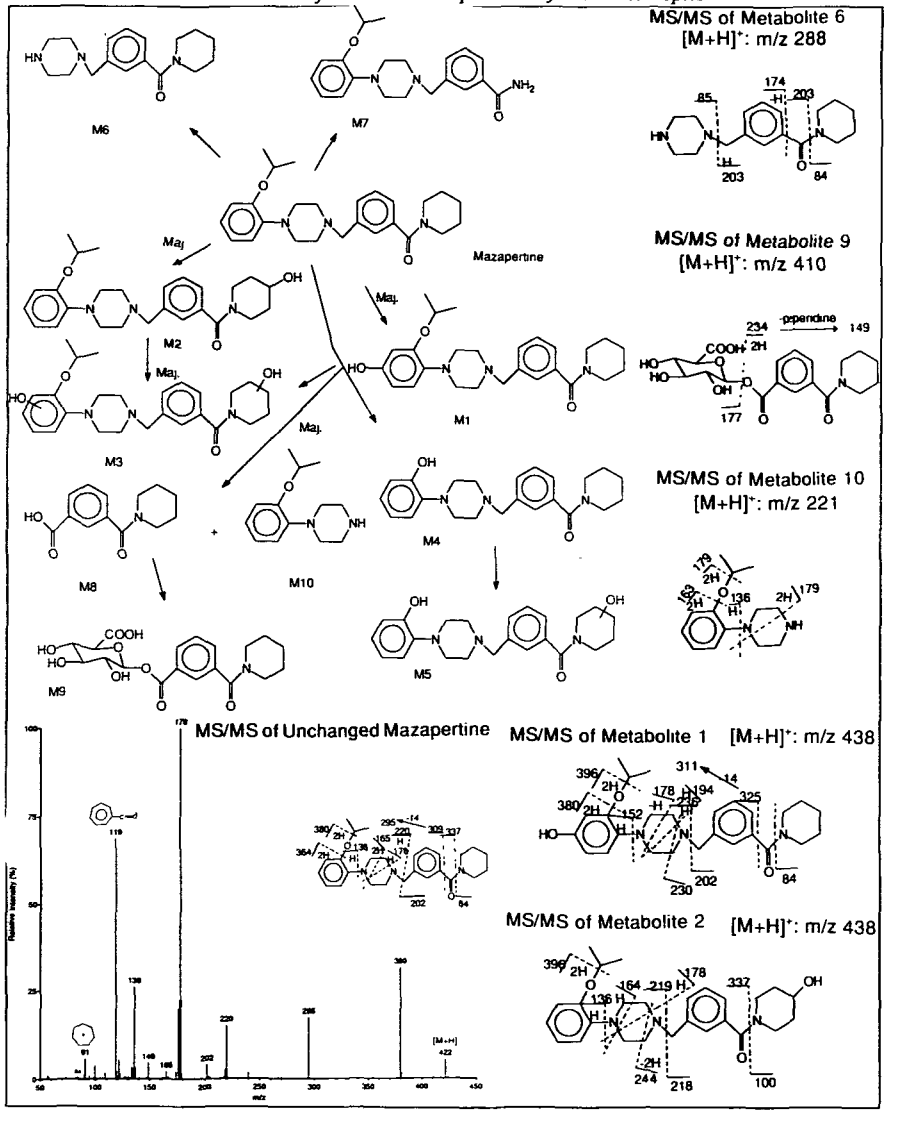

Analysis of Tamoxifen and Its Metabolites by On-line Capillary Electrophoresis-Electrospray Ionization Mass Spectrometry Employing Nonaqueous Solvent

Wenzhe Lu[1], Grace K. Poon[2], and Richard B. Cole[1*]

1. Department of Chemistry, University of New Orleans, New Orleans, LA 70148, USA
2. CRC Center for Cancer Therapeutics, The Institute of Cancer Research, Surrey, UK

Tamoxifen [trans-1-[4-(2-dimethylamino)ethoxy]phenyl-1,2-diphenylbut-1-ene] is an antiestrogen drug that is routinely used for the treatment of breast cancer [1]. Tamoxifen is thought to act mainly by blocking the estrogen receptor in tumor tissue, thus inhibiting tumor growth. Alternative mechanisms of action have also been suggested. Isolation and structural characterization of the products of tamoxifen metabolites are necessary steps to understanding the mechanism responsible for drug activity.

HPLC-MS has been applied to the determination of tamoxifen metabolites in breast cancer patients [2]. Compared to HPLC separation methods, capillary electrophoresis (CE) offers the potential for higher resolution and faster analysis of many pharmaceutical compounds. Another advantage for sample limited studies is that very small sample quantities (e.g., fmol) can be analyzed.

We report the analysis of tamoxifen and its metabolites using on-line capillary electrophoresis-electrospray ionization mass spectrometry (CE-ESMS). Tamoxifen and its analogs, *N*-desmethyltamoxifen, 4-hydroxytamoxifen, 4-hydroxy-*N*-desmethyltamoxifen, tamoxifen-*N*-oxide, 4-hydroxytamoxifen-*N*-oxide, and tamoxifen epoxide, were separated and determined using nonaqueous solvent (methanol) as the CE electrolyte. This CE medium provided better resolution and detection sensitivity compared to aqueous systems or highly aqueous water/methanol electrolyte mixtures. Improved stability of electrospray ionization conditions are achievable when methanol electrolyte is employed as compared to highly aqueous systems because the lower surface tension permits droplet breakup at lower applied voltages while decreasing the tendency to produce unwanted electric discharges. The relative ease of methanol solvent evaporation may contribute to an improved yield of protonated analytes as compared to highly aqueous solutions. The enhanced CE resolution can be at least partially attributed to the better solubility of analytes in this solvent. Higher solubility implies less aggregation of hydrophobic analytes and thus improved homogeneity in solution.

Surfactants have been employed as buffer additives in CE-ESMS although their presence may cause severe suppression of analyte ion signals in ESMS [3]. The effect of sodium dodecyl sulfate (SDS) on ESMS sensitivity was examined, and the detection limit for *N*-desmethyltamoxifen was determined to be about 7 ug/mL when the SDS concentration was 7 mM. When this rather low concentration (below CMC) of surfactant SDS was added to the methanol electrolyte, the resolution was augmented relative to the unadulterated methanol electrolyte. The metabolites α-hydroxytamoxifen and 4-hydroxytamoxifen, which could not be resolved in methanol electrolyte, were completely separated upon addition of 7 mM SDS. The methanol-surfactant electrolyte system has been successfully used to determine tamoxifen and its metabolites formed after incubation of tamoxifen with mouse hepatocytes.

[1] V.C. Jordan, *Br. J. Pharmacol.*, 110 (1993) 507.
[2] G.K. Poon, Y.C. Chui, R. McCague, P.E. Lonning, R. Feng, M.G. Rowlands, and M. Jarman, *Drug Metab. Dispos.*, 21 (1993) 1119
[3] J. Varghese, and R.B. Cole, *J. Chromatogr. A*, 652 (1993) 369

43rd ASMS Conference on Mass Spectrometry and Allied Topics

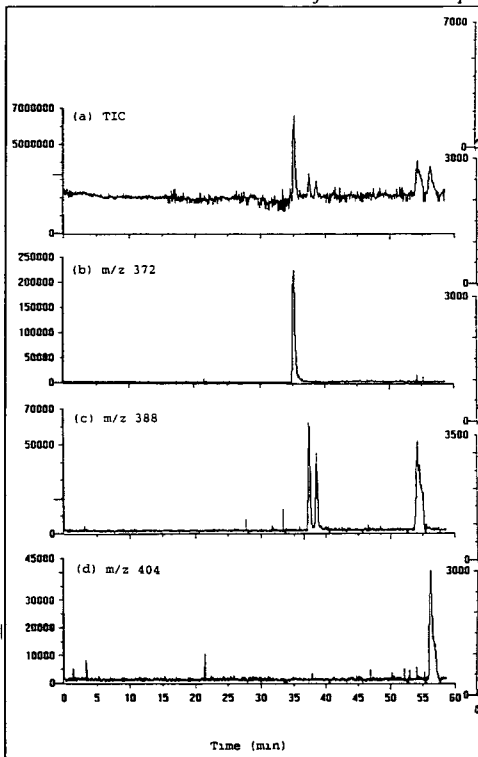

Figure 1. Selected-ion electropherogram showing raw data from on-line CE-ESMS analysis of tamoxifen and 4 analog standards, (a) total ion current of 5 components (b) tamoxifen (MH^+, m/z 372), (c) isomers: α-hydroxytamoxifen and 4-hydroxytamoxifen, and tamoxifen-*N*-oxide (in elution order, MH^+, m/z 388), and (e) 4-hydroxytamoxifen-*N*-oxide (MH^+, m/z 404). Experimental conditions: sample concentration: each component 300 ng/μL, CE voltage: 25 kV; capillary: 100 μm x 100 cm; electrolyte: 7 mM SDS, 2.5 mM NH_4OAc and 50 mM acetic acid in methanol; gravity injection: 15 cm for 2 s; ES voltage: 2.48 kV; MS scan rate: 3 s/scan.

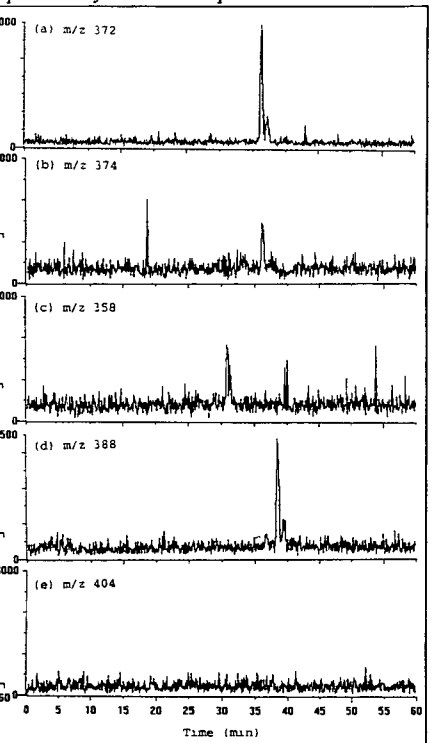

Figure 2. Selected-ion electropherograms from on-line CE-ESMS analysis of an extract from incubation of tamoxifen with mouse hepatocytes, (a) tamoxifen (MH^+, m/z 372), (b) 4-hydroxy-*N*-desmethyltamoxifen (MH^+, m/z 374) (c) *N*-desmethyltamoxifen (MH^+, m/z 358), , and (d) an unknown, α-hydroxytamoxifen and 4-hydroxytamoxifen (MH^+, m/z 388) (e) 4-hydroxytamoxifen-*N*-oxide (MH^+, m/z 404). Experimental conditions are same as Figure 1.

IDENTIFICATION OF LORATADINE METABOLITES FROM HUMAN LIVER MICROSOMES.

T.D. Cyr, B. Dawson, J. Ethier, M Jurima-Romet, A. Menzies and L. Whitehouse. Bureau of Drug Research, Drugs Directorate, Health Canada, Banting Research Centre, 2201A, Ottawa, K1A OL2, Canada

INTRODUCTION Loratadine, Claritin®, is a widely used, non-prescription, non-sedating antihistamine. The main metabolite is descarboethoxy-loratadine (Roman et al, Clin. Rev. Allergy, **11** 89-110, 1993) ; additional metabolites were detected as part of an ongoing study of drug-drug interactions. We have undertaken the structure determination of these metabolites by HPLC purification followed by electrospray/MS, GC/MS and NMR spectroscopy.

The human liver tissue was obtained from the Human Liver Bank, Dept. of Pharmacol., University of Toronto. Loratadine and descarboethoxy-loratadine were obtained from the Schering-Plough Research Institute, Lafayette, NJ.

Sample Preparation: The metabolites were produced by incubation of loratadine with human liver microsomes, at 37°C, with NADPH in phosphate buffer (2 mL incubation volume). The reaction was stopped by adding methanol (2 mL) or by adding methanol and HCl (0.1 mL). The samples were centrifuged, basified with 4 mL of 0.5 M Na_2HPO_4, loaded onto a 3 mL C-18 solid phase extraction column (conditioned with acetate buffer at pH 4). The column was washed with water, then the compounds of interest were eluted with methanol. The mixtures were chromatographed on an Inertsil ODS-2 HPLC column using an CH_3CN versus 0.1% $(ET)_3N$/ NH_4PO_4 buffer gradient.

RESULTS HPLC Analysis: Figure 1. shows the distribution of loratadine and its metabolites from human liver microsomes. In general, the main metabolite is descarboethoxyloratadine and the effects on the metabolite distribution of adding HCl/methanol versus methanol alone to stop the system. The products labelled 62 B, 61 A, 63 B, Fraction 9, and Fraction 10 were collected by preparative HPLC then analyzed by ES/MS, GC/MS, and NMR.

Mass Spectral Analysis: {ES/MS}: EI/MS: Unless indicated otherwise, all peaks have a Cl^{37} isotope peak.

Loratadine, m/z: {445 (adduct?, 405(adduct?),383(M^+), 337, 295, 282, 268}; 382 (100%), 292, 280 (no Cl), 266, 244 (no Cl)

Descarboethoxyloratadine, m/z: 310 (83%), 280 (no Cl), 266, 244 (no Cl), 216

62 -B, mixture, m/z.{ 460 (adduct?),399(M^+), 381, 335, 293, 281, 265} ; 398 (100%), 381, 308, 296 (no Cl), 282, 278

61 A, mixture, m/z {397(M^+), 381, 367, 293}, 396 (100), 395, 367, 323, 295, 242, 154 (no Cl)

63 B, single compound: m/z:{461, 399 (M^+); 398, 369 (100), 282 (no Cl), 268, 260 (no Cl), 254

Fraction 9, mixture of 3 (isomers?), m/z:{443 (adduct?),381(M^+), 353, 335, 310, 293, 281, 258, 246, 244, 228}; 380 (100%), 379 (85), 351, 307, 279 (no Cl)

Fraction 10, single compound, m/z {443 (adduct?), 389, 387, 371, 293, 281, 267, 258, 246, 228}, 380 (93%), 379 (69), 351, 307, 279 (100, no Cl)

ES/MS: Figure 2 shows the effect of varying the cone voltage on the degree of fragmentation as well as agglomeration for the parent drug, loratadine In general, data were collected for a few scans at a cone voltage of 55% to obtain good molecular ion information, then cone voltage was increased to 85% to obtain fragmentation information.

IDENTIFICATION The distribution of metabolites is sensitive to the pH of the workup medium. The new metabolites are hydroxylated on the aromatic and on the aliphatic rings, and there is indirect evidence for an N-oxide. We did not find major amounts of the metabolites of descarboethoxyloratadine.

43rd ASMS Conference on Mass Spectrometry and Allied Topics

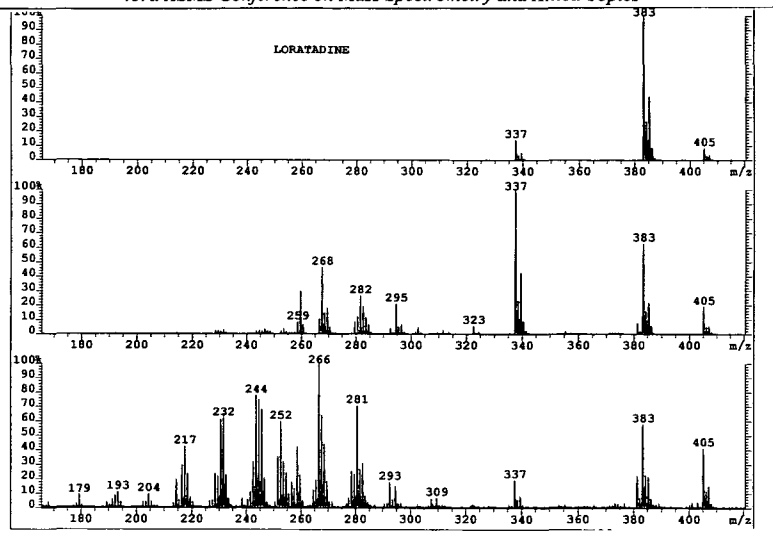

FIGURE 1. ES/MS of Loratadine: effect of sampling cone voltage: top = 33, middle = 55 and bottom =85%.

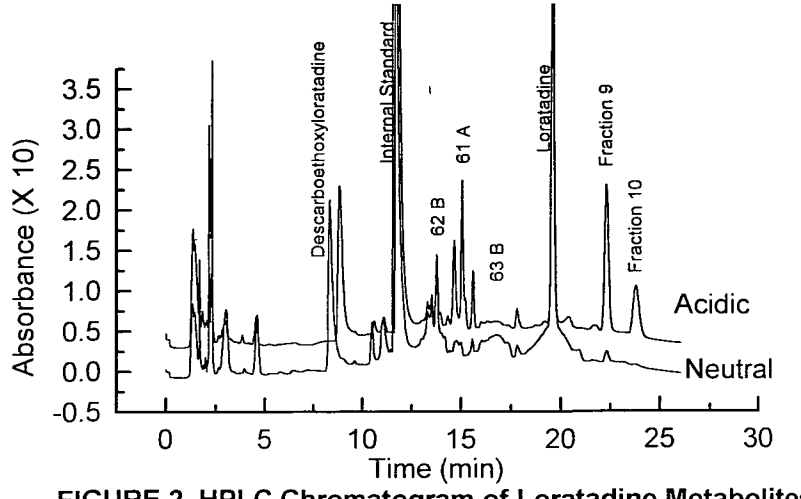

FIGURE 2. HPLC Chromatogram of Loratadine Metabolites.

BIOMARKERS OF OH RADICAL FORMATION IN RAT BRAIN BY MICRODIALYSIS WITH MPP^+.

L. Ste-Marie, L. Vachon, D. Boismenu and J. Montgomery. Research Centre, Notre-Dame Hospital, Montréal, Québec, Canada.

In rat striatum, the neurotoxin, 1-methyl-4-phenylpyridinium ion (MPP^+), elicits dopamine (DA) release with a concomitant increase in hydroxyl radical ($^{\bullet}OH$) formation. We investigated $^{\bullet}OH$ formation by administering MPP^+ to the anterodorsal striatum. $^{\bullet}OH$ radicals were trapped with either 2-hydroxybenzoate (2HBZ) or 4-hydroxybenzoate (4HBZ) which are converted to 2,3- and 2,5-dihydroxybenzoate and 3,4-dihydroxybenzoate (34DHBZ) respectively. In our study, microdialysis probes were implanted bilaterally in the striatum and infused with artificial CSF (1μl/min). After 75 min equilibration, 4HBZ (300 mg/kg) was injected intraperitoneally (IP). At 90 min, MPP^+ was infused unilaterally (5 mM; 20 min), followed by a 90 min period where MPP^+ was replaced by CSF. A second series of microdialyses was performed to determine the effect of a monoamine oxidase B inhibitor, deprenyl, on $^{\bullet}OH$ production. The rats were injected IP with deprenyl just prior to starting the experiment. Microdialysate samples were analysed for DA, dihydroxyphenylacetate, norepinephrine and homovanillate by HPLC with electrochemical detection (EC) and 34DHBZ (formed by 4HBZ hydroxylation) was assayed by HPLC-EC or by GC-MS. Microdialysis samples plus [α,α-$^2H_2$]-phenylacetic acid added as internal standard were extracted and the residues were converted to TBDMS derivatives which were analyzed under electron impact conditions using a Varian Saturn II ion trap GC-MS.

Results show that MPP^+infusion alone did not augment the production of 34DHBZ compared to controls (Figure 1, Group 1). However, 34DHBZ normalized to 4HBZ release to account for individual regional differences in 4HBZ cerebral concentration, indicated that the MPP^+ side had a higher ratio of 34DHBZ/4HBZ (Figure 2, Group 1). Deprenyl caused a decrease in 34DHBZ production both with and without MPP^+ but its effect was more pronounced without MPP^+ (Figure 1, Group 2). Again, the ratio 34DHBZ/4HBZ indicated a greater proportion of 34DHBZ with MPP^+ treatment (Figure 2, Group 2). However, deprenyl treatment resulted in a lower ratio, 1/10th that observed in the series of microdialyses without deprenyl. Our results confirm that MPP^+ exerts some of its neurotoxic effect via a free radical mechanism.

In preliminary experiments using a microdialysis protocol where the HBZ trapping agent was infused via the microdialysis probe, we were hampered by an apparent "contaminant" in analyzing DHBZs by HPLC-EC. Using GC-MS and HPLC-EC we demonstrated the non-tissue derived production of $^{\bullet}OH$ radicals induced by contact with metal surfaces. When HBZ added to artificial CSF was infused through a microdialysis system (without a rat), we measured unacceptably high non-specific production of $^{\bullet}OH$ radicals. In addition, the effect of re-using a microdialysis probe in a subsequent experiment was demonstrated using a dual probe protocol, where one probe had been used before and the other was new. No MPP^+ was infused and the artificial CSF contained 4HBZ (1 mM). Microdialysis of rat striatum resulted in increasing production of 34DHBZ with time in both probes, with the used probe producing up to 9 pmol/15 min and the new probe less than 2 pmol/15 min.

Considerable technical difficulties were encountered due to the non-tissue derived production of $^{\bullet}OH$ radicals as measured by 34DHBZ production from 4HBZ. The combined use of GC-MS and HPLC-EC allowed positive identification of these products. This difficulty of non-specific $^{\bullet}OH$ radical production was circumvented by constructing an infusion system that minimizes contact with metal surfaces (1). Using this system in the experiments described above, we demonstrated 34DHBZ production comparable to that reported for DHBZ production from salicylate in a similar system (2).

(Financial support from the Medical Research Council and Heart and Stroke Foundation of Canada.)

References:

1. Montgomery, J.A., Ste-Marie, L., Boismenu, D. and Vachon, L., *Free Rad. Biol. Med.*, revised manuscript submitted, May 1995.
2. Obata, T. and Chiueh, C.C., *J. Neural Trans.*, **89**: 139 (1992).

43rd ASMS Conference on Mass Spectrometry and Allied Topics

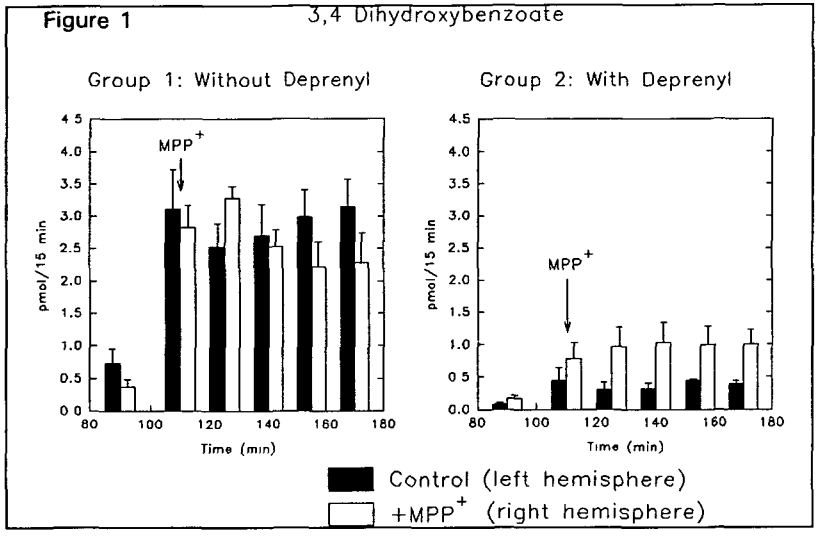

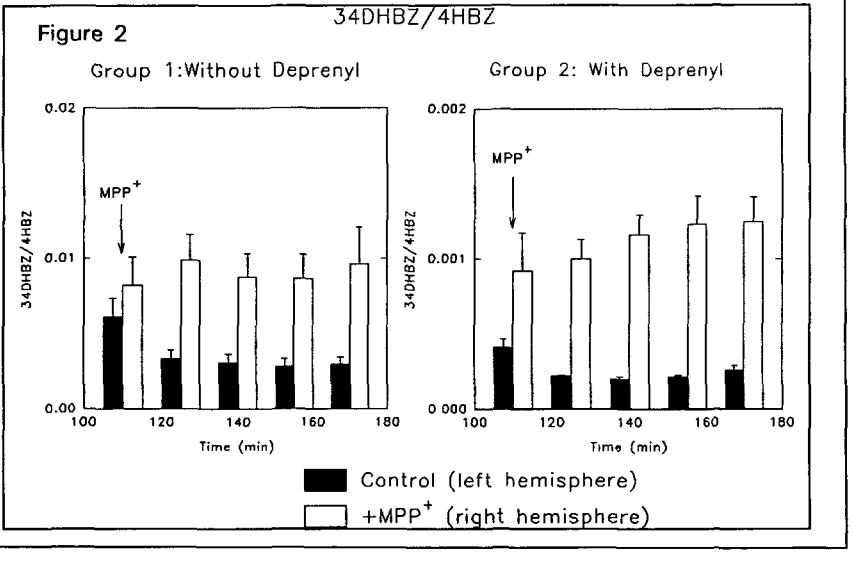

2K3MVA IS NOT AN OBLIGATE INTERMEDIATE BETWEEN ISOLEUCINE & ALLOISOLEUCINE

O.A. Mamer, MS Unit, McGill University, 1130 Pine W, Montréal Qué Canada H3A1A3
F.L. Lépine, Institut Armand-Frappier, 531 boul des Prairies Laval Qué Canada H7N 4Z3

Introduction

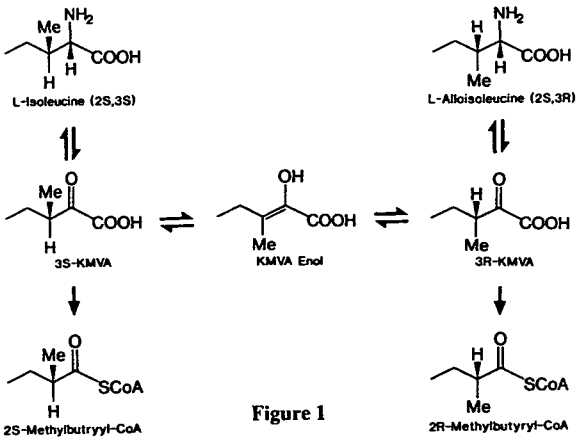

Figure 1

L-Isoleucine and L-allo-isoleucine have long been known to be interconvertible *in vivo*, and for the last half-century, the intermediate has been thought (without firm proof) to be an enol of the corresponding keto acid, 2-keto-3-methyl-valeric acid (KMVA), Figure 1. Here we present experiments that show that alloisoleucine is made from isoleucine *with retention* of the amino nitrogen, denying the possibility of the intermediacy of KMVA, and confirming an earlier proposal (1).

Experimental

Two rats (200 g) were given oral 20 mg loads of unlabelled and $^{15}N,^{13}C_6$-L-isoleucine. Urine samples were collected for 6 h following the loads and their amino acids were isolated and analyzed as their TBDMS derivatives in EI by SIM - GC/MS (HP-5988). Ions monitored were the $[M - t\text{-butyl}]^+$ and $[M - COOTBDMS]^+$ ions (m/z 302 and 200 respectively for the unlabelled derivatives of isoleucine and alloisoleucine).

Results

Figure 2 shows the SIM chromatograms for the urine collected following the loading with labelled isoleucine. The major peaks appearing in the unlabelled m/z 200 and 302 chromatograms are leucine (before 7.2 min RT), and alloisoleucine and isoleucine (in that order, after 7.2 min RT). It is clear that the majority of the alloisoleucine excreted is labelled with ^{15}N (m/z 206 and 309). The much smaller response at m/z 205 for alloisoleucine is due mostly to isotopic impurity (both ^{15}N and ^{13}C) in the original labelled isoleucine (determined by similar analysis). These observations are inconsistent with KMVA as the intermediate between the amino acids but support the mechanism of Figure 3 (PE = pyridoxal phosphate - transaminase complex) which represents a modification of the mechanism for the transamination of alanine proposed by Babu and Johnston (2). The existence of an enamine intermediate in that mechanism analogous to D was proven by NMR techniques (3). Isoleucine (**A**) and alloisoleucine (**A'**) form Schiff base aldimines (**B** and **B'**) with the pyridoxal aldehyde group which enzymatically isomerize to ketimines **C** and **C'**. The latter are much more enolizable than the keto acids **E** and **E'** (the imino N is more easily protonated than the keto O), and form the enol-like enamine **D**, thereby racemizing the chiral 3-carbon.

A large fraction of the excreted isoleucine derived from the load had lost its ^{15}N label (m/z 205 and 308), presumably by reverse reamination of $^{13}C_6$-KMVA, **E**. Part of the exchanged $^{14}N,^{13}C_6$-alloisoleucine could have been formed through **D** from the large amount of $^{14}N,^{13}C_6$-isoleucine produced by reamination of **E**. The formation of alloisoleucine is then an unavoidable consequence of the catabolism of isoleucine. It would appear from the relative amounts of N-exchanged isoleucine and fully labelled alloisoleucine that enolization of **C** to form **D** is much slower than the equilibration of **C** with **E** or **B**. The effects produced by this relationship have been well known from studies of metabolic errors affecting subsequent KMVA catabolism, even though the underlying mechanism was not known.

43rd ASMS Conference on Mass Spectrometry and Allied Topics

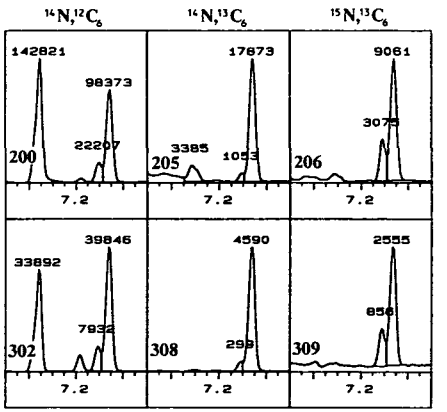

Figure 2

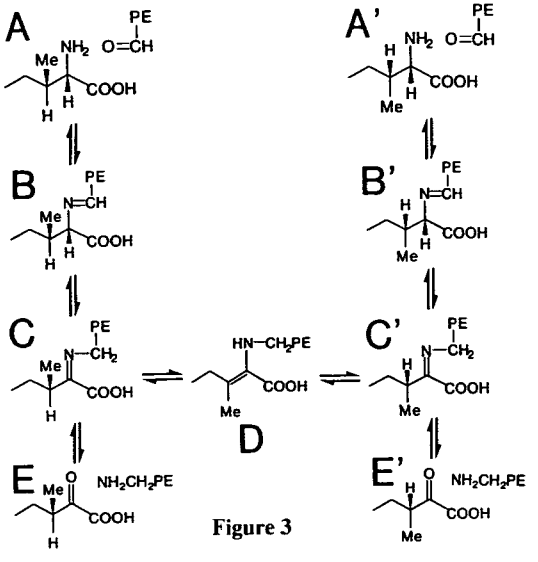

Figure 3

1. Mamer, O.A., and Reimer, M.L.J. (1992) *J. Biol. Chem.*, **267**, 22141
2. Babu, U.M., and Johnston, R.B. (1974) *Biochem. Biophys. Res. Commun.* **58**, 460
3. Golichowski, A., Harruff, R.C., and Jenkins, W.T. (1977) *Arch. Biochem. Biophys.* **178**, 459

Characterization of reactive drug intermediates by ESI mass spectrometry

H.K. Lim, J.H. Bhasav, K. Chan and S. Sisenwine
Wyeth-Ayerst Research, Princeton Corporation Plaza
9 Deer Park Drive, Suite 100, Building 3, Monmouth Junction, NJ 08852

The cytochrome P-450 family of enzymes is considered to be responsible for the oxidation of a variety of drugs with diverse structures to reactive electrophiles. An equally important family of enzymes known to catalyze both one and two-electron oxidation of drugs to reactive intermediates is the peroxidases such as prostaglandin synthase and human leucocyte peroxidase (also known as myeloperoxidase). In peroxidase-rich organs such as kidney, bone marrow, etc., this family of enzymes plays an important role in the organ-specific toxicity of drugs. The direct detection of reactive intermediates presents a challenge because of their extremely short half-lives. Fortunately, a defense mechanism based on conjugation with nucleophilic glutathione exists for neutralizing these reactive electrophiles and the more stable glutathione conjugates can be used to characterize these intermediates. The recent reports on the high accuracy (<0.01%) of molecular weight determination of proteins (< 133,000 Da) by electrospray mass spectrometry provides a new way for rapid determination of covalently bound proteins with reactive intermediates. Proteins often contain a variety of nucleophilic sites that can undergo reactions with electrophiles, and they are not subjected to repair like DNA. Therefore, protein adducts are excellent surrogates for detection of genotoxic reactive intermediates.

The current work focused on the characterization of reactive intermediates as glutathione conjugates and covalently modified hemoglobin by electrospray LC/MS. The drug used in the study is an antimalarial drug, amodiaquine, a known myelotoxin and hepatotoxin in man. This drug has been of clinical concern recently because of its association with ocassionally fatal agranulocytosis (1) and liver damage ranging from mild hepatitis (2) to sub-massive necrosis (1). The objective is to investigate the mechanism of myelotoxicity of amodiaquine.

Initial efforts were directed to establish whether amodiaquine can be metabolized by myeloperoxidase to reactive intermediates. Total ion chromatogram (top panel) shows that amodiaquine was metabolized by myeloperoxidase via one and two-electron oxidation to semiquinone imine and quinone imine as suggested by the detection of mono and di-glutathione conjugates of amodiaquine. In addition, a tri-glutathione conjugate of an amodiaquine metabolite was also formed. All of these conjugates were formed in larger quantities by horseradish peroxidase catalyzed oxidation of amodiaquine (data not shown) and consequently, this enzymatic system was used to generate the glutathione conjugates for characterization by ESI LC/MS and LC/MS/MS. In addition to reaction with glutathione, these reactive intermediates also reacted with α and β-chains of human hemoglobin as indicated by their corresponding mass shift from native α and β-chains. This is illustrated by a mass spectrum showing covalent binding of amodiaquine to α-chain of hemoglobin (bottom panel). Interestingly, there were 3 partially resolved chromatographic peaks that show covalent binding of amodiaquine to α-chain. This observation suggested that in addition to covalent binding to the sulphydryl group of the only cysteine residue in the α-chain, oxidative intermediates of amodiaquine also bound to 2 other distinct nucleophilic sites.

The detection of several glutathione conjugates of amodiaquine and the covalently bound amodiaquine to relevant biomacromolecules like hemoglobin is suggestive that reactive intermediates may play a role in the myelotoxicity of amodiaquine.

References
1. K.A. Neftel, W. Woodtly, M. Schmid, P.G. Frick and J. Fehr, *Br. Med. J.* **292**, 721 (1986)
2. D. Larrey, A. Castot, D. Pessayre, P. Merigot, J.-P. Machayekhy, G. Feldmann, A. Lenoir, B. Rueff and J.-P. Benhamou, *Ann. Int. Med.* **104**, 801 (1986).

Top Panel

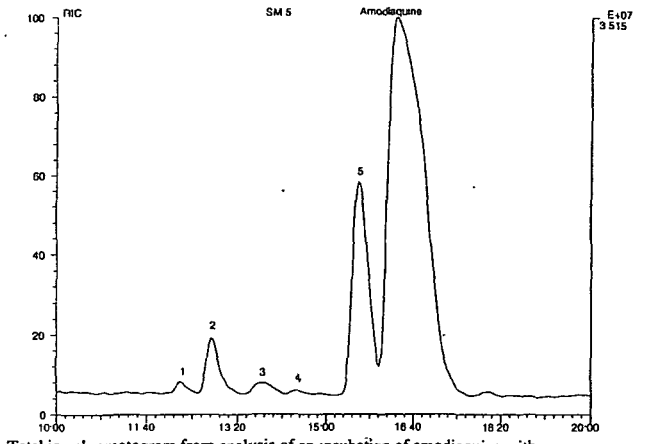

Total ion chromatogram from analysis of an incubation of amodiaquine with myeloperoxidase, hydrogen peroxide and glutathione. 1: tri-glutathione conjugate of amodiaquine metabolite; 2: di-glutathione conjugate of amodiaquine; 3,4 and 5: regioisomers of mono-glutathione conjugate of amodiaquine.

Bottom Panel

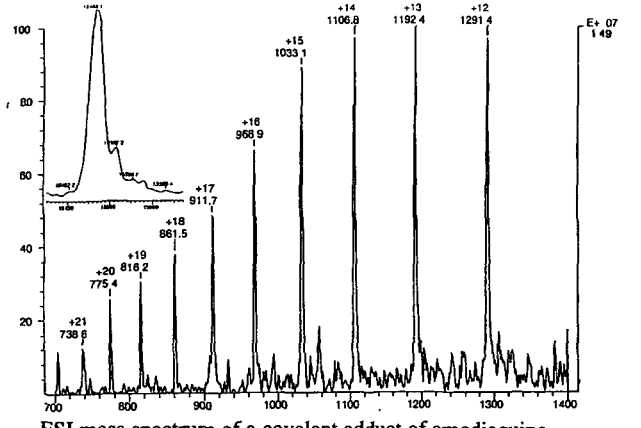

ESI mass spectrum of a covalent adduct of amodiaquine with α-chain of hemoglobin: Determined MW = 15,482.1 and calculated MW = 15,480.2.

CAPILLARY HPLC / CF-LSIMS CHARACTERIZATION OF LTD$_4$ ANTAGONIST METABOLITES, *J. A. Yergey, D. Nicoll-Griffith, N. Chauret, L. Trimble, Merck Frosst Centre for Therapeutic Research, P. O. Box 1005, Pointe Claire - Dorval, Quebec, Canada H9R 4P8

INTRODUCTION: Peptidoleukotrienes are postulated to play a critical role in the pathophysiology of human asthma. Antagonists directed against the leukotriene-D$_4$ (LTD$_4$) receptor, which is believed to be particularly important in mediating the asthmatic response, have, therefore, become key therapeutic targets. MK-0476 is currently in clinical trials as a treatment for asthma.

Studying the metabolic fate of compounds early in the discovery process has allowed for more immediate and meaningful feedback to the medicinal chemistry efforts. In particular, *in vitro* incubation of compounds with liver microsomes and hepatocytes has provided a straightforward means of generating relatively clean mixtures of metabolites. The *in vitro* metabolic profiles of MK-0476 and related analogs would be expected to include several metabolites analogous to those previously described for verlukast (MK-0679), including sulfoxidation, quinoline epoxidation under certain conditions, and acid glucuronidation.

Although isolation of individual metabolites remains necessary for NMR characterization and definitive identification of sites of metabolism, capillary HPLC with continuous-flow liquid secondary ion mass spectrometric detection (HPLC / CF-LSIMS) has provided a powerful means to examine the incubation mixtures directly. This poster details the oxidative biotransformations of MK-0476, with emphasis on the effective utilization of CF-LSIMS as a characterization tool.

EXPERIMENTAL: Liver Microsome Incubations: Incubations of 200 µM MK-0476 in 0.5 mL were made with 1 mg microsomal protein (species include rat, ß-naphthaflavone treated rat, ßNF-mouse, Rhesus monkey and human). Oxidation co-factors included 2 mM $MgCl_2$, 2 mM NADP, 20 mM glucose-6-phosphate, in a 100 mM PO_4 buffer, pH 7.4 plus 2 units of glucose-6-phosphate dehydrogenase. One hour reactions at 37°C were quenched with 0.5 mL of CH_3CN.

Capillary HPLC / CF-LSIMS Conditions: A Waters 600MS HPLC pump supplied 1 mL/min of mobile phase consisting of CH_3OH:20 mM NH_4OAc, pH 5 (1.5 % glycerol in each). The main flow was split prior to the injection valve using ~ 5 cm of 50 µm fused silica on a Valco ZDV tee. The split flow of 3 µL/min passed through a 10 µL injection loop on 6-port electrically actuated Valco valve, then through the KAPPA BDS-Hypersil ODS-2 0.3 x 100 mm capillary column (Keystone Scientific) and into the JEOL HX-110A CF-LSIMS mass spectrometer ion source. Injections were of 10 µL of a 10-fold dilution of incubation mixture. CF-LSIMS spectra were acquired from 0-1000 Da every 4 sec.

SUMMARY OF RESULTS: While capillary HPLC / CF-LSIMS total-ion chromatograms, which include glycerol adduct ions, often contain little chromatographic information regarding minor metabolites, reconstructed-ion chromatograms corresponding to likely metabolites or mass ranges, which exclude glycerol oligomers, provide noise-free and sentive information (Figure 1). Full-scan CF-LSI mass spectra contain extensive but useful fragmentation as well as pseudo-molecular ions (Figure 2,3). Glycerol background is substantially less than for probe samples, and can be effectively subtracted. Fragmentation in the primary mass spectrum usually allows the metabolized substructure to be pinpointed (Figure 3), although NMR is still required for precise positional information. Furthermore, full-scan CF-LSI mass spectra, including useful fragmentation, can be readily obtained at levels of 1-5 pmol. The capability of CF-LSIMS to provide both excellent sensitivity and structural information in the primary LC/MS mass spectrum make it an ideal tool for rapid characterization of metabolic profiles of drug candidates, as summarized below for MK-0476.

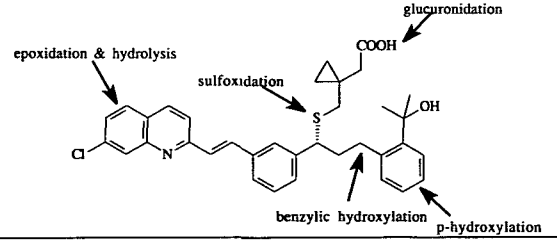

43rd ASMS Conference on Mass Spectrometry and Allied Topics

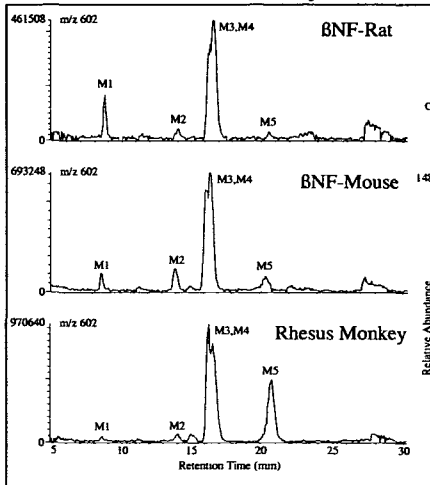

Figure 1: RIC corresponding to likely metabolites (MK-0476 MH+ + O = m/z 602) Liver microsome incubations were diluted and 100 pmol injected. Capillary HPLC gradient used was 68 32 to 78 22 CH_3OH:20mM NH_4OAc in 30 min.

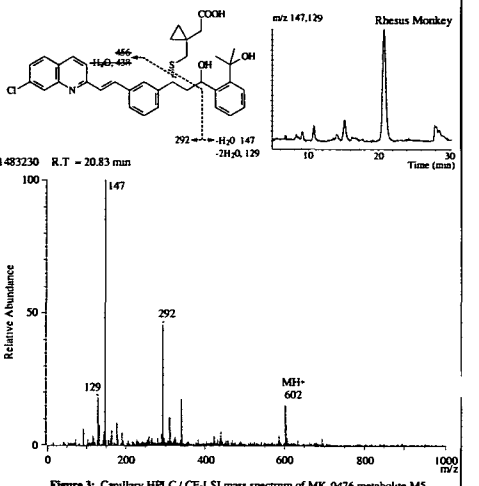

Figure 3: Capillary HPLC / CF-LSI mass spectrum of MK-0476 metabolite M5 Inset. RIC for ions specific to this metabolite (m/z 129,147), indicating substructure where metabolism occured.

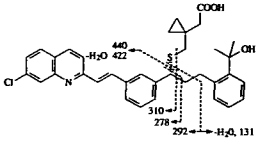

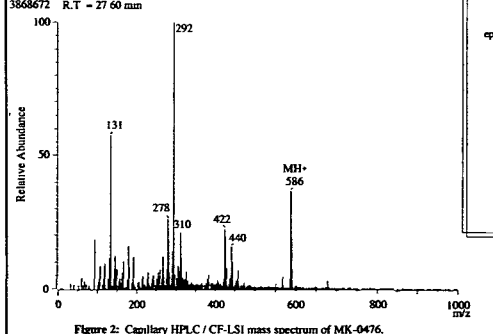

Figure 2: Capillary HPLC / CF-LSI mass spectrum of MK-0476. Fragmentation in the primary MS is extensive, but very informative.

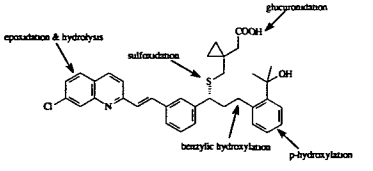

Figure 4: Summary of metabolites of MK-0476 characterized from liver microsome incubations using capillary HPLC / CF-LSIMS.

TP 168. CE-ES-MS ANALYSIS OF DRUG METABOLITES IN URINE.

Alison E. Ashcroft[1], Hilary J. Major[1], Stephen Lowes[1], Ian D. Wilson[2],
1. Fisons Instruments VG Organic, Altrincham, Cheshire, WA14 5RZ, UK.
2. Zeneca Pharmaceuticals, Alderley Park, Macclesfield, Cheshire, SK10 4TG, UK.

Introduction.

CE-ES has emerged as a viable on-line technique. The aim of these studies was to couple the sensitivity and specificity of ES-MS with the high resolution of CE to produce a practical method of analyzing and identifying small quantities of drug metabolites in urine while minimizing work-up procedures.

The drugs chosen were ibuprofen, flurbiprofen, aspirin and paracetamol, all of which produce metabolites of particularly high polarity. The results from ibuprofen are discussed in this abstract

Method.

Urine work-up After a therapeutic oral dose of one of the drugs, human urine from a healthy male volunteer (2mL) was passed through a solid phase extraction cartridge, evaporated to dryness and reconstituted in methanol (200µL).

CE-ES-MS CE was performed using a Beckman P/ACE system 2000 (Beckman Instruments Inc., Palo Alto, CA) with in-line UV (λ 200nm) detection. A 10 second pressure injection (30nL injection) was followed by a 20kV, 20mM aq ammonium acetate pH 9 buffer separation using a 100 cm capillary column

The CE capillary was interfaced directly through a CE-ES probe to a VG Quattro II (Fisons Instruments VG Organic, Altrincham, Cheshire, UK) tandem quadrupole mass spectrometer A make-up flow of 80:20 (v/v) water:propan-2-ol (8µL/minute) was teed co-axially into the probe.

Standard negative ionization ES conditions were set with the probe tip held at 4kV. To obtain molecular mass information i e. to optimize the $(M-H)^-$ ions, a low cone voltage was set For cone voltage fragmentation (CVF) this value was raised.

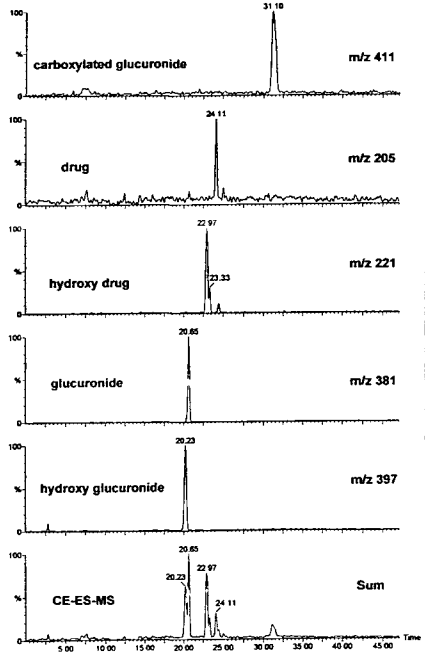

Figure 1. CE-ES-MS of Ibuprofen.

MS-MS fragmentation was achieved by introducing argon collision gas into the collision cell between the first and second analyzers.

Ibuprofen.

CE-ES-MS with a low cone voltage provided the molecular masses of several of the components including ibuprofen, hydroxylated ibuprofen, the glucuronide metabolites of both of these, and the carboxylated glucuronide metabolite, (Figure 1).

The experiment was repeated using CVF and also by MS-MS monitoring the product ions from the major components. The CVF spectra and product ion spectra show similarities indicating the potential of CVF on a single quadrupole mass spectrometer in producing interpretable fragmentation. All three of the glucuronide metabolites gave rise to a common fragment ion at m/z 175, representing the sugar moiety, and a complementary loss of 176 amu from the $(M-H)^-$ to leave the $(M-H)^-$ of the aglycones i e. m/z 205, 221, and 235.

A further MS-MS experiment monitoring the precursor ions of m/z 175 (Figure 2) readily highlighted the major glucuronides of ibuprofen.

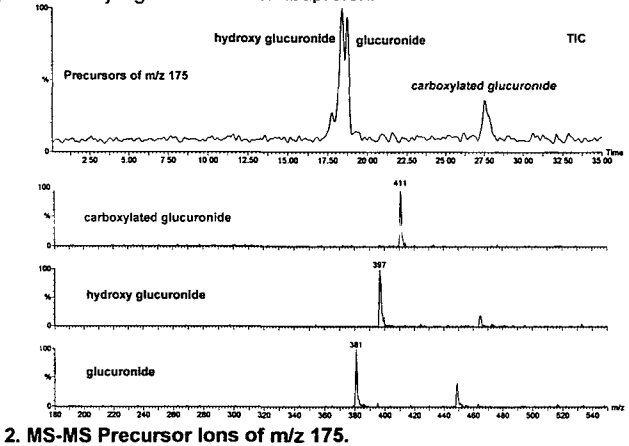

Figure 2. MS-MS Precursor Ions of m/z 175.

Summary.

Capillary electrophoresis has been coupled to negative ion ES-MS for the analysis of drug metabolites in human urine. Molecular masses were generated and in addition structurally useful fragmentation was produced by in-source CVF and also by low energy MS-MS. Selective screening for the presence of glucuronide metabolites was readily achieved by on-line CE-ES-MS-MS recording the precursor ions of the characteristic dehydrated glucuronic acid unit

The system used is robust and was operated for several days without any maintenance due to the fact that CE requires only minimum amounts of dirty matrices to be injected An environmental advantage of this technique over LC-MS methods is that solvent consumption is minimized

Analysis of β-Agonists Using Solid Phase Extraction and LC/APcI/MS/MS

Steve Preece[1] and Géry van Vyncht[2]
[1]VG Organic, Tudor Road, Altrincham, Cheshire, UK, WA14 5RZ and [2]University of Liège, Mass Spectrometry Center, B6, Sart Tilman, 4000 Liège, Belgium

β-Agonists are used in human medicine and veterinary science for the treatment of pulmonary disorders. When the dosage is increased to levels greater than ten times those used for therapeutic purposes, these compounds have a secondary effect of repartitioning metabolism to encourage the accretion of muscle tissue at the expense of fat deposition [1] This has led to the illegal use of β-agonists in cattle farming where, by increasing the ratio of muscle tissue (meat) to fat, the value of an animal is increased. At the higher levels used to produce repartitioning, there are concerns about the harmful effects to humans through eating contaminated meat and in 1990 there were recorded cases of food poisoning in Europe from the consumption of clenbuterol contaminated liver from veal calves[2] Thus the use of β-agonists for this purpose is prohibited in both the European Community and North America and screening is undertaken. This paper looks at the analysis of β-agonists in bovine urine and liver Urine analysis is necessary to allow the monitoring of cattle on farms for β-agonist abuse and liver analysis is necessary to monitor meat for human consumption In addition, as the liver is the centre of metabolic activity in the body, it often contains higher levels of residues Due to the high potency of β-agonists and the subsequently low dosages and because of the complexity of the matrices which are analysed, the analytical method for these compounds is required to be both sensitive and specific The use of LC/MS with atmospheric pressure chemical ionisation (APcI) as the ionisation method is already documented [3] Using APcI/MS provides the sensitivity and specificity required for the analysis and the use of liquid chromatography allows the analysis of β-agonists without the need for a derivatisation step which is required prior to analysis by gas chromatography. Thus the time required for analysis is reduced An improved method of solid phase extraction has been developed which, when coupled with analysis by LC/APcI/MS, allows the detection of five selected β-agonists down to and below the UK regulatory level of 0.5ppb in urine and liver

Experimental

Solid Phase Extraction - For urine analysis, 5mL were centrifuged prior to extraction. For liver analysis, 5g were homogenised and hydrolysis of any β-agonist conjugates was carried out by the use of β-glucoronidase prior to extraction. The extraction of the β-agonists was accomplished using a SCX solid phase (Varian) This phase contains benzene sulphonic acid groups allowing the extraction of β-agonists by ion exchange The eluted volume containing the β-agonists was evaporated to dryness and redissolved in 1mL of methanol.

Liquid Chromatography - The chromatography was carried out using a HP1050 quaternary solvent delivery system and a 3 x 250 mm (5μm) α-Chrom column (Upchurch) with the following conditions: injection volume : 50 μL, flow rate 0 5 mL/min. Mobile phase : A- 77% acetonitrile, 12% 10mM NH_4OAc (pH 7 0), 11% water and B- 65% acetonitrile, 35% 25mM NH_4OAc (pH 3.5) with a gradient of 0 - 5 5min - 100% A stepped to 100% B for 5 6 - 15min

Mass Spectrometry - A VG Quattro II tandem quadrupole mass spectrometer was used for detection. The instrument was equipped with an atmospheric pressure ionisation source operating in positive ion mode with a nebuliser temperature of 550°C and a cone voltage of 20 or 25V. Data was acquired in MS/MS mode using multiple reaction monitoring (MRM) with a collision cell argon pressure of $2x10^{-3}$ mbar and a collision energy of 15eV. In each case the selected parent ion was the protonated molecule and the most intense product ion was chosen for detection Terbutaline 226 → 152, Cimaterol 220 → 160, Salbutamol 240 → 148, Clenbuterol 277 → 203 and Mabuterol 311 → 237

Samples - Urine samples were spiked with the 5 ß-agonists in the range 0.5 to 25 ppb prior to extraction Liver samples were spiked in the range 2.5 to 25 ppb. Samples taken from animals treated with clenbuterol and salbutamol were also analysed These were spiked with d_6-clenbuterol as an internal standard prior to extraction

Results

The five β-agonists selected for this study were cimaterol, terbutaline, salbutamol, clenbuterol and mabuterol. These were chosen as they are commonly used, with clenbuterol and salbutamol known to be most frequently abused due to their high potency Extraction recoveries for clenbuterol and salbutamol were determined by using tritiated standards and radio-immunoassay. For clenbuterol the recoveries were 82% in urine and 45% in liver and for salbutamol, 60% in urine and 55% in liver. For the urine analyses, all five compounds could easily be detected down to the required level of 0 5ppb with signal to noise ratios for the MRM chromatograms in the region of 20 1. It was recognised that by dissolving the residues obtained from the SPE step in a smaller volume, there was a potential to reduce the detection levels further. Redissolving the residues in 100μL of methanol (instead of 1mL) resulted in improved detection of all of the compounds except for terbutaline where the chromatographic resolution was impaired, probably due to the effect of increased matrix concentration For the liver analyses the results are similar to those found for urine, except for terbutaline which has poor chromatographic peak shape This is likely to be due to effects from the more complex liver matrix It may be possible to improve the chromatography of terbutaline by redissolving the liver extract in a solvent other than methanol, but this has not been tested Analysis of the samples taken from animals treated with clenbuterol and salbutamol (with d_6-clenbuterol internal standard) showed that the method is suitable for detecting these compounds when they have been administered in a real life situation.

Conclusions

The combination of an improved solid phase extraction method and LC/APcI/MS/MS has been shown to provide a system suitable for the analysis of β-agonists. The efficiency of extraction and the sensitivity and selectivity of APcI/MS/MS allow the detection of these compounds down to, and below, the UK regulatory level of 0.5ppb The use of LC also negates the need for the derivatisation of β-agonists which is required prior to GC/MS analysis

References

1. M.F Miller et al, J. Animal Sci , 66, (1988), 12
2 J.F Martinez, Lancet, 336, (1990), 1311
3. D.R. Doerge, S. Bajic, L R. Blankenship, S W Preece and M.I Churchwell, Determination of β-agonist Residues in Human Plasma Using LC-APcI/MS, accepted for publication in J Mass Spec 1995

Analysis of Cytochrome P-450 Metabolites of Arachidonic Acid using LC MS/MS.

*Carlos O. Garner[1], Frank J. Belas[2], and Ian A. Blair[1,2]. Department of Chemistry[1], Vanderbilt University and Department of Pharmacology[2], Vanderbilt University School of Medicine, Nashville, TN 37232.

The cytochrome P-450 (CYP-450) metabolism of arachidonic acid (AA) produces a number of structurally distinct eicosanoids with overlapping biological activities. It is becoming increasingly evident that this activity can be mediated by other enzymes involved in eicosanoid metabolism such as cyclooxygenase (COX) and lipoxygenase (LOX). Biotransformation of cyclooxygenase and lipoxygenase metabolites of arachidonic acid by CYP-450 has long been recognized. However, it is has been only recently that attention has become focused on the possible bioactivation of CYP-450 metabolites by COX and LOX. There is compelling evidence that COX plays a key role in the biological activity of several of the CYP-450 metabolites, including the four regioisomers of epoxyeicosatrienoic acid (EET). The physiological roles of these metabolites are only partially understood. Nonetheless, in studies to examine the effects of 8,9-EET on human platelet aggregation extensive COX metabolism of the EET was observed.[1] These metabolic products were identified as 11-and 15-hydroxy-EET (HEET). We propose that the formation of these HEETs is due to transcellular metabolism of CYP-450 AA metabolites by COX and that this process is important in determining the observed biological activities of these eicosanoids. In order to fully understand the suggested transcellular mechanism of CYP-450 metabolites to COX derived HEETs, it is necessary to have a convenient method of analysis for both of these metabolites. This method describes the development of a LC MS/MS assay for the quantitative determination of these metabolites.

Racemic EETs were purified and separated from the internal standard, 14,15-epoxyeicosaenoic acid, by reverse phase chromatography prior to ESI MS/MS analysis. Liquid Chromatography was conducted using a Hewlett-Packard 1090 series II liquid chromatograph equipped with a Zorbax Rx C-8 column (2.1 mm x 150 mm, 5 µm). A 0.2 µm pre-column filter was also used to prolong column life. Solvent A was 5 mM aqueous ammonium acetate and solvent B was 5 mM ammonium acetate in methanol:water (9:1). The flow rate was 200 µL/min. A linear gradient was employed over the first 2 minutes after injection at which the initial solvent composition was 20% A : 80% B, and the final composition was 10% A : 90% B. This solvent composition was maintained for the next 11 minutes, after which the solvent composition was returned to the initial conditions during a 2 minute period. A 5 minute post time was employed to allow the column to equilibrate at these conditions. EETs and HEETs were dissolved in a 1:1 mixture of methanol:water and injected onto the HPLC column.

Mass spectrometry studies were conducted using a Finnigan TSQ 7000 triple quadrapole mass spectrometer equipped with an electrospray (ES) ion source operating in the negative ion mode with a needle voltage of 4.5 kV. Nitrogen was used as the sheath gas (70 psi) and the auxiliary gas (25 psi) to assist with nebulization. The capillary was heated to 200 °C to provide optimal desolvation, and the electrospray interface and mass spectrometer parameters were optimized to obtain maximum sensitivity without sacrificing unit resolution. Flow injections of each EET isomer and HEET were conducted to determine the isomer-specific fragmentation of precursor ions (Figure 1). Selected reaction monitoring (SRM) experiments were then conducted with each regioisomer and internal standard to observe its characteristic transition. For each EET and EEA, the M-1 precursor ion was chosen and inherent transitions were monitored. For 8,9-EET the *m/z* 319→156 transition was monitored. Similarly, for 14,15-EEA the *m/z* 323.5→305.5 transition was monitored (Figure 2). Likewise, MS/MS experiments will be carried out to characterize and monitor a non-specific transition for the COX I

43rd ASMS Conference on Mass Spectrometry and Allied Topics

metabolites of 8,9-EET, 11- and 15-HEET.

Once methodology for the analysis of CYP-450 metabolites of AA and their subsequent COX derived metabolites is well defined, studies to elucidate the pathophysiological roles of these compounds will be undertaken. This research will not only expand our understanding of the physiological conditions associated with these eicosanoids but will also provide new methodologies for the study of a wide range of metabolic processes.

Supported by NIH grant DK38226

References

1. Zhang, J Y., et.al. Biochem. Biophys. Res. Commun. 183, 138-143, 1992.

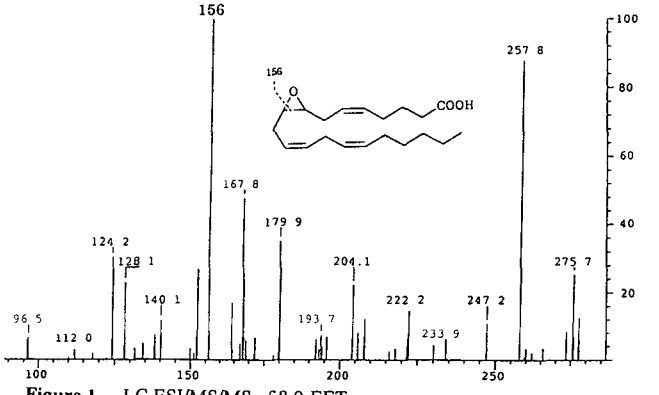

Figure 1 LC ESI/MS/MS of 8,9-EET

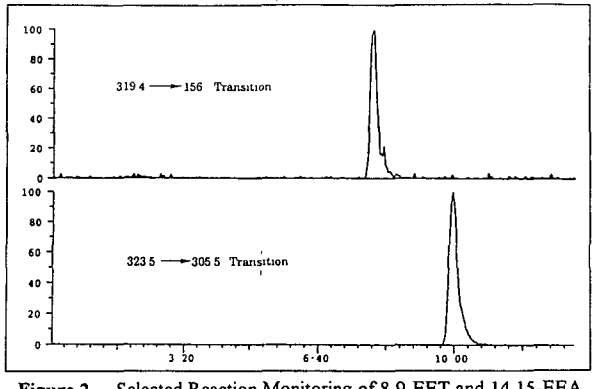

Figure 2 Selected Reaction Monitoring of 8,9-EET and 14,15-EEA

GC/MS/MS Characterization of Acylcarnitines

Shannan M. Carlson, Ulrich R. Bernier, Jodie V. Johnson, Peggy R. Borum† and Richard A. Yost
Departments of Chemistry and Food Science† University of Florida, Gainesville, FL 32611

Carnitine, an important metabolite, transports fatty acyl groups across mitochondrial membranes. Regular monitoring of carnitine concentrations is of clinical importance in the care of preterm infants and dialysis patients. Inherited disorders of metabolism (e.g. organic acidurias and Reye's Syndrome) are often associated with abnormally high ratios of acyl to free carnitine in the blood and urine.[1]

The standard method for the determination of carnitine concentrations is by radioenzymatic assay; however, only free and total carnitine can be determined using this method. Differentiation among the various acylcarnitines is necessary to determine the mechanism of carnitine metabolism and to assess the potential therapeutic role of carnitine supplementation. A number of methods for the determination of specific acylcarnitines have been developed, with mass spectrometric methods showing the most promise. While a continuous flow FAB/MS/MS procedure is the most complete method reported to date,[2] it has limited utility for unknown acylcarnitines or mixtures. Although HPLC methods also exist, the analyses are not specific and are labor-intensive. Recently, Gage and co-workers used a two-step derivatization to form N-demethylated propyl esters of free carnitine and acylcarnitines (**FIGURE 1**) followed by GC/MS on a double-focusing mass spectrometer.[3] Utilizing the Gage derivatization procedure to form N-demethylcarnitine t-butyldimethylsilyl esters, this work focuses on the use of several modes of GC/MS/MS on a triple quadrupole mass spectrometer. MS/MS analyses provide increased selectivity over single stage analyses.

All experiments were performed on a Finnigan MAT TSQ70 triple quadrupole mass spectrometer equipped with an octopolar collision cell in place of the second quadrupole. Sample introduction was from a Varian 3400 gas chromatograph (GC). The column employed for this study was a 30m, 0.25 mm i.d. open tubular DB5-MS temperature programmed from 140C (one minute hold time) to 290C at 20C/min. Unless otherwise noted, MS/MS experiments were performed with 1.0-1.2 mTorr argon at a collision energy of 10 eV The mass spectrometer was calibrated using perfluorotributylamine (PFTBA).

All samples were prepared by the Department of Food Science at the University of Florida. Standard acylcarnitine stock solutions (3 mM) were prepared in 1:1 methanol/chloroform. Red blood cells were hypotonically lysed prior to extraction. Plasma and red blood cell samples were extracted with methanol and chloroform, then filtered through a 0.2 µm nylon membrane via centrifugation to remove proteins. A 100 µL aliquot of the supernatant was allowed to evaporate to dryness overnight. Aliquots of standard acylcarnitines were dried in an analogous fashion. The dried samples were derivatized by silylation with MTBSTFA, DMP, TMP, and TMIS in methylene chloride. Samples were stored at -20C until the time of analysis.

Ten acylcarnitine standards were analyzed by GC/MS using methane chemical ionization (CI) to determine retention times and identify the $[M+H]^+$ ion characteristic to each. GC/MS/MS daughter spectra of the $[M+H]^+$ ion of the individual standards (**FIGURE 2**) were acquired to provide the basis for the identification of metabolites. The remarkable similarity of the daughter spectra of the $[M+H]^+$ ions of the different acylcarnitines provided an excellent foundation for monitoring carnitine concentrations. Identification of unknown acylcarnitines was possible using parent spectra of the common daughter ion at m/z 244. At a collision energy of 10 eV, the base peak was the $[M+H]^+$ parent ion with characteristic daughter ions observed at m/z 262, 244, 202, 199, 115, 112, 84, and 73 for all of the acylcarnitines. Parent and daughter spectra were taken of all characteristic ions to determine the fragmentation pattern.

After characterization of the fragmentation patterns of the acylcarnitines, standard mixtures were analyzed by GC/MS/MS. To maximize selectivity, selected reaction monitoring (SRM) was employed for the analysis of standard mixtures, plasma and red blood cell extracts. An instrument control language (ICL) routine was written to vary the selected parent ion during the GC run. External standard calibration curves were linear for eight different acylcarnitine standards over the 1-40 ng range with a coefficient of determination (r^2) of 0.98 or better.

While the radioenzymatic assay is used to indicate the ratio of free to total carnitine, the GC/SRM method allowed the elucidation of acylcarnitine profiles (e.g. identification of individual acylcarnitines) in plasma and red blood cells (**FIGURE 3**). The plasma data were in agreement with the radioenzymatic assay which generally indicates approximately 85-90 percent of carnitine in the plasma of healthy individuals is free carnitine. Comparison of plasma and red blood cell acylcarnitine profiles showed a variation in partitioning of acylcarnitines between the plasma and red blood cell compartments Free carnitine was observed as the most abundant of the carnitines detected in the plasma sample, while the red blood cell profile showed decreased free carnitine and increased acylcarnitines (**FIGURE 4**). Since this is one of the first reported comparisons of acylcarnitine profiles of plasma and red blood cells, the dramatic difference between the two metabolic compartments reveals many opportunities for enhancing the understanding of carnitine metabolism. Although red blood cell carnitine concentrations have not been studied extensively, the red blood cell compartment is a significant contributor in carnitine metabolism. Whole blood analyses may limit the diagnostic capabilities due to the variations between plasma and red blood cell carnitine concentrations. The full impact of these data is yet to be realized. Improvement in the quantitation of this method will be achieved when an appropriate internal standard is obtained.

1. Liberato, D.; Millington, D.; Yergey, A. *Mass Spectrometry in the Health and Life Sciences*, **1995**, 333-345.
2. Millington, D.; Norwood, D.; Kodo, N.; Roe, C , Inoue, F. *Analytical Biochemistry*, **1989**, *180*, 331-339.
3. Huang, Z.; Gage, D.; Bieber, L.; Sweeley, C.; *Analytical Biochemistry*, **1991**, *199*, 98-105.

Figure 1
Carnitine and Carnitine Derivatives Studied

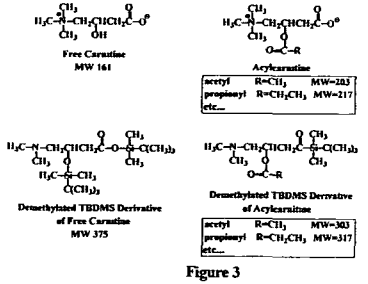

Figure 2
GC/MS/MS Daughter Spectrum of the $[M+H]^+$ ion of the TBDMS Derivatized Demethylated Isobutyrylcarnitine

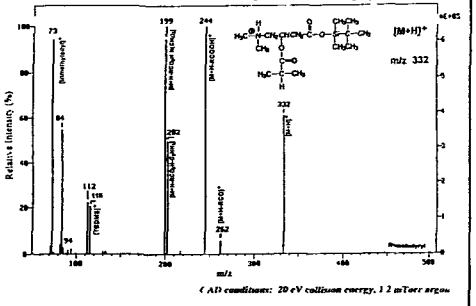

Figure 3
GC/SRM Chromatograms of Acylcarnitines

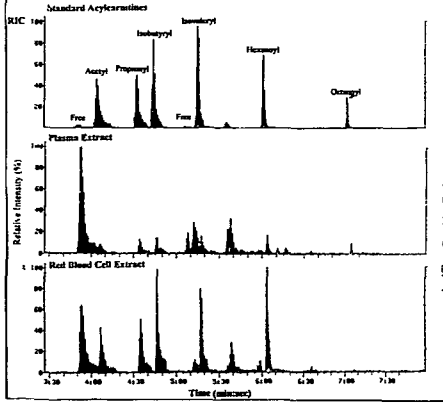

Figure 4
Comparison of Acylcarnitine Profiles of Plasma and Red Blood Cells

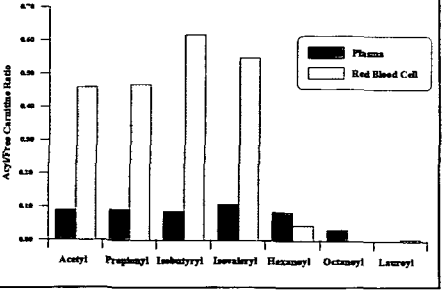

Identification of in-vitro and in-vivo metabolites of Bosentan by LC-MS/MS

G. Hopfgartner, B. Lausecker, M. Zell, C. Husser, A. Viger-Chougnet and R. Haas
F. Hoffmann-La Roche, Pharma Division, Department of Drug Metabolism & Kinetics, CH-4002 Basel

Introduction

Endothelin is a bicyclic-21-amino acid peptide and a very potent long lasting vasoconstrictor. It is also a growth factor for vascular smooth muscle, mesangial and cancer cells and a potent bronchoconstrictor. Bosentan® (Ro 47-0203) an endothelin receptor antagonist is potentially useful in the treatment of diseases associated with abnormal vasoconstriction, such as subarachnoid hemorrhage (SAH), Raynaud's syndrome, migraine, NSAID-induced gastric ulcers and hypertension.

In a first step, the metabolism of the endothelin receptor antagonist has been studied in vitro using different liver preparations (liver homogenate S9 supernatant, microsomes, hepatocytes) of different species. The structures of the metabolites of the radio-labeled parent drug were characterised by liquid chromatography - ion spray tandem mass spectrometry in positive and in negative mode and NMR for the main metabolite.

In a further step the metabolites were analysed in biological fluids such as rat and dog bile. A semi-quantitative screening of the metabolites identified from in vitro experiments was performed in human plasma and urine using LC-MS/MS and LC-UV detection.

Experimental

MS detection was performed on an API III and an API III^{plus} (PE Sciex, Thornhill) with the ion spray interface in positive (4-6 kV) and in negative mode (3-4 kV) and no post-column splitting.
The declustering potential (OR) was in the range of ± 50-70 eV.
For tandem MS experiments (SRM, Neutral Loss, Precursor Ion Scan or Product Ion Scan) argon, was used as collision gas. An UV detector (equipped with a micro cell 2.4 µl, 8 mm length) was placed in serial prior MS detection. A Merck Hitachi L-6200A pump was used, equipped with a low pressure gradient module.

1) Kromasil 100, C18, 5 µm, 125 x 2 mm, Solvent A: MeOH / 5 mM CH_3COONH_4 30 / 70 (v/v), Solvent B: MeOH / 5 mM CH_3COONH_4 80 / 20 (v/v), Flow Rate = 200 µl/ml ; Gradient T_1 = 0 min 90 % A, T_2 = 10 min 10 % A, T_3 = 16 min 10% A.
2) Superspher RP-18, 5 µm, 125 x 2 mm, Solvent A: CH_3CN/ 2 mM CH_3COONH_4 with 1% HCOOH,30 / 70 (v/v), Solvent B: CH_3CN/ 2 mM CH_3COONH_4 with 1% HCOOH, 80 / 20 (v/v), Flow Rate : 200 µl/min, Gradient T_1 = 0 min 100 % A, T_2 = 10 min 20 % A, T_3 = 20 min 20% A.

The metabolism has been studied in vitro using different liver preparations (liver homogenate S9 supernatant, microsomes, hepatocytes) of different species (rat, dog, rabbit, marmoset, man).

0.5 ml of the urine or plasma samples were extracted with chloroform/isopropanol (4:1) at pH 8. The aqueous phase was removed and the sample was evaporated to

dryness under nitrogen. Prior injection the reconstitued sample was filtered over a 0.45 µm filter.

Results

In all conditions studied in vitro, the formation of the same major metabolite (M1) was observed corresponding to an hydroxylation of the parent drug occurring at the tert-butyl moiety. This was confirmed later on by synthesis and NMR. Other less important metabolites were also characterised by LC-MS/MS, which correspond to demethylation (M2) and and hydroxylation (M3) processes.

During the metabolic investigations the fragmentation process of Bosentan was extensively studied with a series of analogs and resulted in the observation of an unexpected case of a radical fragmentation of an even-electron-ion.

Using LC-MS/MS, it was possible to confirm the presence of the main metabolite (M1) in rat and dog bile by direct injection without prior purification.

Tandem LC-MS in combination with UV detection allowed the screening and the semi-quantitative determination of the major metabolites present in human plasma and urine without radio-labeled parent drug.

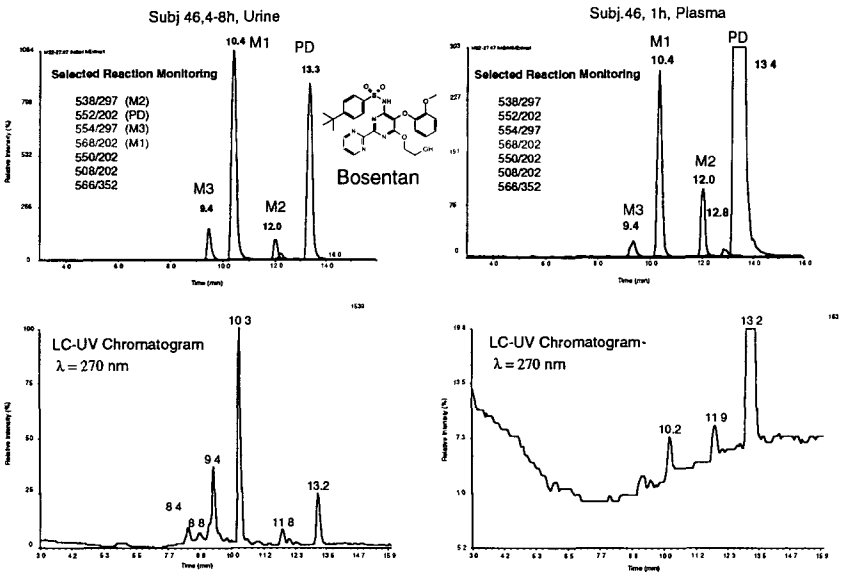

Mechanisms of Leukotriene B_4 Metabolism: Negative ion ESI MS/MS analysis

Pat Wheelan and Robert C. Murphy
National Jewish Center for Immunology and Respiratory Medicine,Denver, CO

Leukotriene B_4 (LTB_4) is a potent chemotactic lipid produced by activated cells involved in the immune response and is rapidly inactivated by numerous cell types. Extraction from biological samples and purification by HPLC followed by derivatization and GC/MS analysis has resulted in the identification of over 25 metabolites of LTB_4. In the present work, fragment ions observed in the negative ion electrospray ionization MS/MS spectra of LTB_4 metabolites were shown to arise principally *via* mechanisms previously described for the low energy decompositions of monohydroxy unsaturated fatty acids (**Figure 1**).[1]

Figure 1

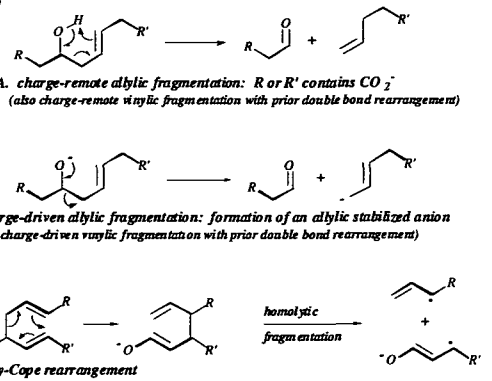

The presence of the conjugated triene system in LTB_4 and in many of its metabolites requires a double bond rearrangement not previously observed in simple monohydroxy compounds. This rearrangement likely involves formation of a cyclohexadiene structure and results in prominent ions at m/z 195 and m/z 129 in the MS/MS spectra of LTB_4 (**Figures 2 and 3**). Deuterium exchange of labile protons and ^{18}O exchange of carboxylate oxygens were used to verify ion structures.

Metabolites were analyzed by negative ion electrospray ionization MS using a Sciex API III+ mass spectrometer with flow injection (1-5 ng of metabolite in methanol:water) using methanol:water (1:1) as the mobile phase at a flow rate of 20 µL/min. CID of the carboxylate anions were obtained using a collisional offset energy of 20 eV and a pressure of argon that resulted in a 40-80% reduction in the carboxylate anion. Deuterium exchange of labile protons was accomplished by dissolving the sample in MeOD followed by evaporation (X2) and reconstituting the sample in MeOD:D_2O (1:1) for negative ion ESI analysis using MeOD:D_2O (1:1) as the mobile phase. Exchange of carboxylate oxygens with ^{18}O was accomplished using porcine liver esterase in $^{18}OH_2$ as previously described.[2]

References

1) Wheelan, P., Zirrolli, J. A., and Murphy, R. C. (**1993**) *Biol. Mass Spectrom.* 22, 465.
2) Westcott, J. Y., Clay, K. L., and Murphy, R. C. (**1985**) *Biomed. Mass Spectrom.* 12, 714.

Acknowledgment: This work was supported in part by a grant from the National Institutes of Health HL25785.

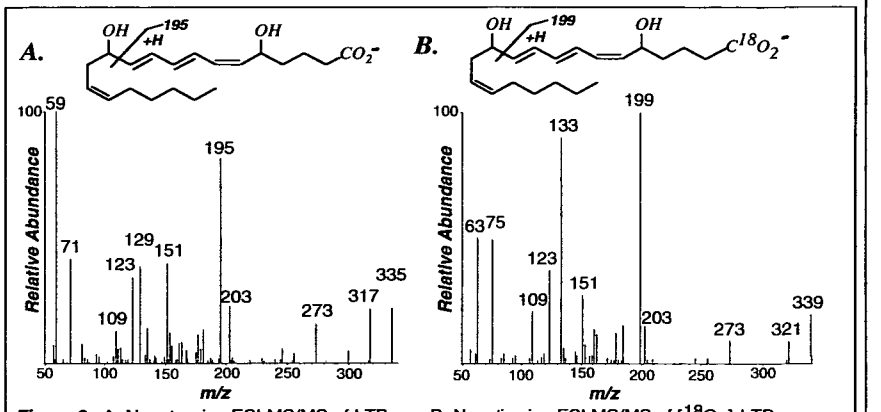

Figure 2. A. Negative ion ESI MS/MS of LTB_4. B. Negative ion ESI MS/MS of [$^{18}O_2$]-LTB_4.

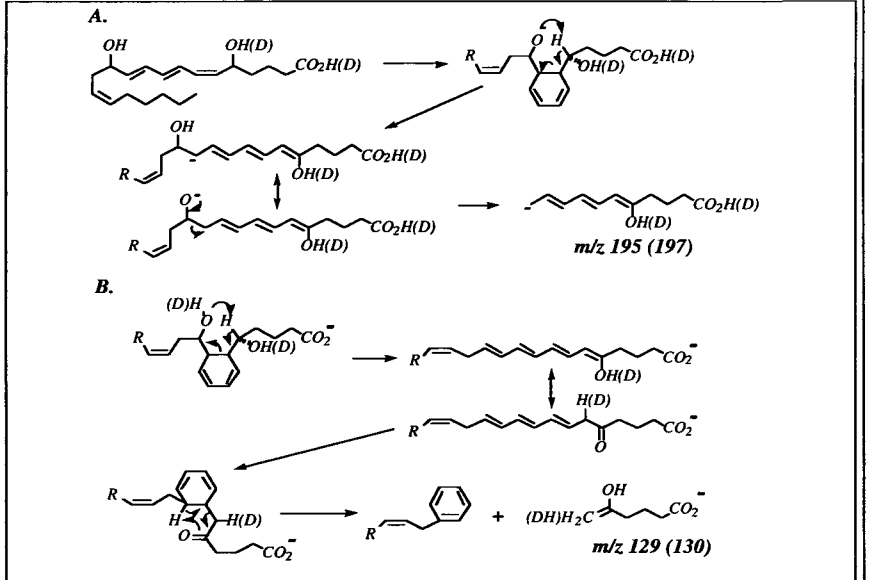

Figure 3. A. Formation of m/z 195 in CID of LTB_4. B. Formation of m/z 129 in CID of LTB_4.

CHARACTERIZATION OF ACIDIC TRITERPENES BY HPLC/ESI/MS

Susan T. Weintraub, Robert T. Streeper, Neera Satsangi and William B. Stavinoha
Departments of Biochemistry and Pharmacology
The University of Texas Health Science Center at San Antonio

G. lucidum and its preparations have a long history of use throughout the East as traditional medicines in the treatment of a broad range of disorders. More recently it has been found that this mushroom contains a number of pharmacologically active molecules. Amelioration of the pain and inflammation associated with arthritis has historically been attributed to preparations of *G. lucidum* . We have determined that extracts rich in ganoderic and lucidenic acids prepared from various portions of the mushroom possess potent systemic and topical anti-inflammatory properties. The general structure for a ganoderic acid is shown below. Since the treatment of arthritis by chronic use of aspirin and other non-steroidal anti-inflammatory drugs (NSAIDs) is complicated by serious side effects, the identification of an agent that has potent anti-inflammatory properties but lacks the negative side effects of NSAIDs is of considerable importance. In this report, we present some of our initial observations on the biological activity of *Ganoderma lucidum* extracts as well as the results of preliminary chromatographic and mass spectrometric analyses of several of the ganoderic acids.

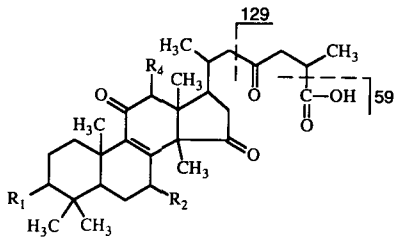

In view of the tremendous structural heterogeneity of the acidic triterpenes produced by *G. lucidum* and the effort required to separate sufficient quantities of pure ganoderic acids for controlled testing of *in vivo* activity, for our preliminary investigation we assessed the anti-inflammatory efficacy of crude water and ethyl acetate extracts of the mushroom. For our *in vivo* assay, mice were treated both orally and topically with water and ethyl acetate extracts of *G. lucidum*. The ability of these extracts to alleviate the swelling produced by the irritant croton oil was compared to the efficacy of one of the most commonly used topical anti-inflammatory drugs available, hydrocortisone. We found that topical application of the ethyl acetate extract of *G. lucidum* results in significant anti-inflammatory activity that compares favorably with the activity of hydrocortisone. The water extract, on the other hand, has little or no topical effect. After oral administration of the extracts, both the ethyl acetate and the water extracts have significant anti-inflammatory activity that extends for a longer time than hydrocortisone.

Mass Spectrometry - In preparation for structural elucidation of the acidic triterpenes in *G. lucidum*, we analyzed three reference ganoderic acids by ESI-MS and EI-MS. The ESI mass spectra obtained by infusion of ganoderic acids B, C2 and H in 70% aqueous acetonitrile/0.5% acetic acid solution at a flow rate of 1 µl/min were characterized by $[MH]^+$ of modest intensity. Although we could not quantitatively assess the relative proportions of the components on the basis of the ESI-MS data alone, it was immediately apparent that the ganoderic acid B and C2 samples were not pure. Moreover, ganoderic acid B appears to show a propensity to lose water under our analysis conditions while C2 and H do not.

Analysis of methylated ganoderic acids B, C2 and H by EI-MS reveals that a number of characteristic fragments are generated along with several obvious differences. In agreement with the ESI-MS data, there are additional components in the ganoderic acid B and C2 samples whereas H appears to be significantly more pure. The molecular ions for methylated B and C2 are substantially more intense than for methylated H while the cross-ring cleavage indicative of hydroxylation pattern (producing the ions at m/z 304 and m/z 306) is greater in H than in B and C2. Many of the differences in the fragmentation patterns are due to the presence of the C-12 acetate on ganoderic acid H.

HPLC Fractionation - Analysis of the ganoderic acids of *G. lucidum* is complicated by the exceedingly large number of ganoderic and lucidenic acids produced by the mushroom. Standard separation techniques relying on C18 reversed-phase fractionation are not equal to the task of resolving the hundreds of structural variants that are present. However, if semi-preparative C18 chromatography is followed by sub-fractionation using Supelco's new mixed function ABZ+ column, it is possible to separate, to a significant degree, a large number of the ganoderic acids. For example, when the 37-min fraction from semi-preparative C18 HPLC of the ethyl acetate extract of *G. lucidum* was analyzed by ESI-MS, it was clear that multiple species were present. When this fraction was treated with ethereal diazomethane and the product analyzed by EI-MS, the presence of intense ions at m/z 129 and m/z 59 indicate the predominance of ganoderic acids in the sample. Moreover, the observation of both m/z 304 and m/z 306 indicate that at least two different patterns of hydroxylation are present in these molecules. Evidence for a mixture of species is further borne out by the diversity of ions in the mass range anticipated for molecular ions of methylated ganoderic acids.

After methylation of the combined 31- and 32-min fractions from the ABZ+ column, the EI mass spectrum was in agreement with the results obtained by ESI-MS, showing that this fraction appears to be highly enriched in a single species. Although the mass spectrum is nearly the same as that of ganoderic acid H, the retention times of these substances are not identical on the ABZ+ column. Since we are not able to determine the isomeric variations in these compounds from the EI mass spectra, it will be necessary to utilize NMR to obtain more definitive structural information.

In conclusion, our data show that extracts of *G. lucidum* possess significant anti-inflammatory activity. While it is premature in this investigation to assign a rank order of potency to all of the members of this complex mixture of ganoderic and lucidenic acids, our preliminary studies have suggested that relatively minor structural differences among the components leads to measurable differences in anti-inflammatory potency. As we improve our abilities to isolate and characterize individual ganoderic acids, we expect to be able to deduce comprehensive structure-activity relationships for these molecules. This effort will be important not only for elucidating the mechanism of action of these molecules but also for future analog drug development.

Acknowledgements - The authors wish to convey their appreciation to Lone Star Growers (San Antonio, Texas) for providing the mushrooms used in this work and to the Il Yang Pharm. Co., Ltd. (Seoul, Korea) for their support of the *in vivo* work. We are also grateful to Tracy Ascah and Supelco Incorporated for generously donating one of their new Supelcosil ABZ+ HPLC columns, which has been of considerable help in resolving the tremendously complex mixtures of ganoderic acids.

Microbore HPLC/MS/MS of CP-166,572 Metabolites in the Rat

M. Avery, W. Ballinger, W. Zembrowski, P. Inskeep, L. Mylari and H. Fouda. Central Research Division, Pfizer INC Groton CT, 06340

CP-166,572 is a sorbitol dehydrogenase inhibitor with potential utility for the management of diabetic complications. , Following oral administration. CP-166,572 is extensively metabolized in the rat. Urinary metabolites were identified by on line HPLC/tandem atmospheric pressure ionization mass spectrometry.

An atmospheric pressure SCIEX API III triple quadrupole mass spectrometer was used. Sample introduction was via HPLC using a 1.0 X 250mm BDS-Hypersil C18 column (Keystone Scientific, Bellefonte, PA). A dual piston syringe pump (Applied Biosystems model 140B, Foster City, CA) delivered the mobile phase to the column at the rate of 40 µL/min. A binary gradient of acetonitrile and water, each containing 0.1% trifluoroacetic acid (TFA) was used.

Five µL aliquots of urine were injected onto the HPLC column. The effluent from the column was connected to a UV detector set at 251 nm . The outlet of the UV detector was connected to the ionspray interface of the mass spectrometer with fused silica tubing. The interface was operated in the positive ion mode with a nebulizer gas setting of 60 psi and a sprayer voltage of 5200V. Collision induced dissociation (CID) studies were performed using argon gas at a collision gas thickness of 3.3 $x10^{14}$ atoms/cm^2 and a collision energy of 30 eV.

Under positive ion APIMS conditions, CP-166,572 forms MH^+ at m/z 302. If m/z 302 is subjected to collision induced dissociation, the product spectrum shown in Figure 1 is obtained.

Analysis of MS data obtained from a rat urine sample suggested thirteen possible metabolites. Prominent HPLC peaks were observed for parent drug at m/z 302 as well as responses for 478 (drug + 176 daltons), 316 (drug + 14 daltons), four components at 318 (drug +16 daltons), 288 (drug -14 daltons) and 274 (drug -28 daltons). CID data was obtained for each of these possible metabolites.

The rat urine sample was then run by HPLC/UV/MS/MS and full product spectra obtained on each possible metabolite.

Since both HPLC/UV and HPLC/MS/MS MRM data are acquired simultaneously, the relative abundance's of each metabolite can be determined from the UV responses. A summary of the identified metabolites is given in Table 1.

Table 1. Relative abundances of drug related material in urine of rat dosed with CP-166,572.

Met. #	Structure	% Abundance
7	N-Desmethyl	40
3	Pyrimidine hydroxyl	34
5	Pyrimidine hydroxyl	13
9	N-Desmethyl, piperazine hydroxyl	10
8	N,N-Didesmethyl	5
2	Carboxylic acid	3
1,4	Unchanged drug	3
6	O-Glucuronide+N-methyl hydroxyl	1
10	Piperazine hydroxylation	1
11	N-Desmethyl-O-glucuronide	1
12	N-Desmethyl- N-methyl hydroxyl	1
13	N-Desmethyl-N-methyl hydroxyl	1
14	N-Desmethyl-piperazine hydroxyl	1
	N-Desmethyl-pyimidine hydroxyl	1

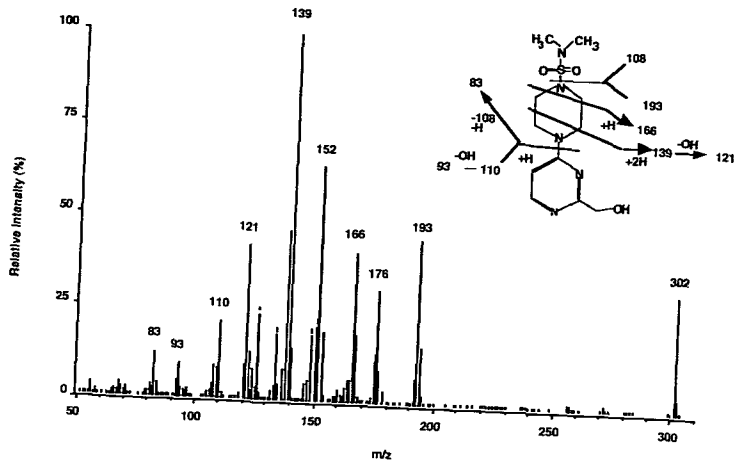

Figure 1. CID Product Ion Spectrum of m/z 302 from CP-166,572.

High Pressure Liquid Chromatography/Ionspray MS/MS for the Identification of *In Vitro* Metabolites of CP-118,954

Donghui Cui and Chandra Prakash
Department of Drug Metabolism, Central Research Division, Pfizer Inc., Groton, CT 06340

Introduction:

CP-118,954, 5,7-dihydro-3-[2-1-(phenylmethyl)ethyl]-6H-pyrrolo[4,5-f]1,2-benz-isoxazol-6-one, is a potent and selective antagonist of acetylcholinesterase (AChE) with low affinity for butyrylcholinesterase (BuChE), a property which accounts for potent central effects without confounding peripheral activity. The compound is being developed for the palliative treatment of the cognitive decline in Alzheimer's disease. Preliminary studies using hepatic microsomes indicate that CP-118,954 is extensively metabolized to several metabolites. The microsomal data exhibit species differences in the metabolism of CP-118,954. The objective of present study was to characterize the *in vitro* metabolites of CP-118,954 using hepatic microsomal preparation from rat, dog, monkey and human liver microsomes in order to predict the *in vivo* metabolism. Metabolite identification was carried out by ion spray LC/MS using a combination of parent, daughter, and multiple ion reaction monitoring techniques.

Experimental procedures:

The microsomal incubation of [^{14}C]-CP-118,954-11 (labeled at C-3 position of the benzisoxazole moiety) with rat, dog, monkey, and human liver microsomes were carried out in potassium phosphate buffer with a NADPH regenerating system. The mixture was incubated at 37 °C for an hour. The reaction was terminated by addition of 1 ml methanol and was evaporated to dryness on a Speed-Vac evaporator. The residue was reconstituted in 1 ml of HPLC mobile phase, sonicated, and centrifuged. The supernatant was separated and an aliquot (60 ul) was analyzed by HPLC. Chromatography was carried out on a YMC basic HPLC column (4.6 mm x 250 mm, 5 µm: YMC) with a binary mixture of methanol and ammonium acetate (pH 5.0). The separation of metabolites of CP-118,954 was obtained by using a gradient system. The flow rate was 1 ml/min and the eluate was monitored with a β-RAM using Ecolite(+) scintillation fluid at 4 ml/min.

The analysis of the metabolites was performed on a SCIEX API III HPLC/MS/MS system (Toronto, Canada) using ion spray. The effluent from the HPLC column was split and about 50 ul/min was introduced into the atmospheric ionization source via an ion spray interface. The remaining effluent was directed into the flow cell of the β-ram. The ion spray interface was operated at 5000 V and the mass spectrometer was operated in the positive mode. Collision activated dissociation (CAD) studies were performed using argon gas at an orifice voltage of 65 eV and a collision gas thickness of 2.5 x 10^{14} molecules/cm^2.

Results:

A total of ten radioactive metabolites were identified from the incubations with rat, dog, monkey, and human microsomes. The identified metabolites in each spieces accounted for more than 90% of the total radioactivity detected by β-ram. The CAD

product ion spectrum of the parent drug is shown in Figure 1. The proposed major metabolic routes of CP-118,954 in liver microsomes are summarized in Figure 2.

Conclusions:

- CP-118,954 was extensively metabolized by PB induced rat and monkey liver microsomes.
- The metabolism of CP-118,954 in monkey was similar to that of human.
- The major metabolite was the N-debenzylated CP-118,954 in all species.
- No qualitative differences were found in the metabolism of CP-118,954 among rat, dog, monkey, and human liver microsomes.
- Structural characterization of the metabolites revealed that the metabolism of CP-118,954 occurred by three pathways: 1) oxidative N-dealkylation of the benzyl side chain attached to the piperidine nitrogen, 2) scission of the isoxazole in the benzisoxazole ring system and 3) oxidative cleavage of piperidine ring.

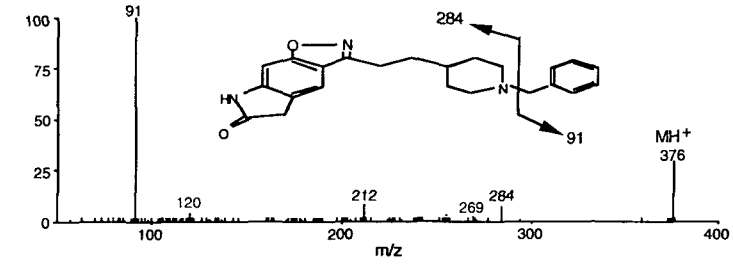

Figure 1. CAD daughter spectrum of CP118,954.

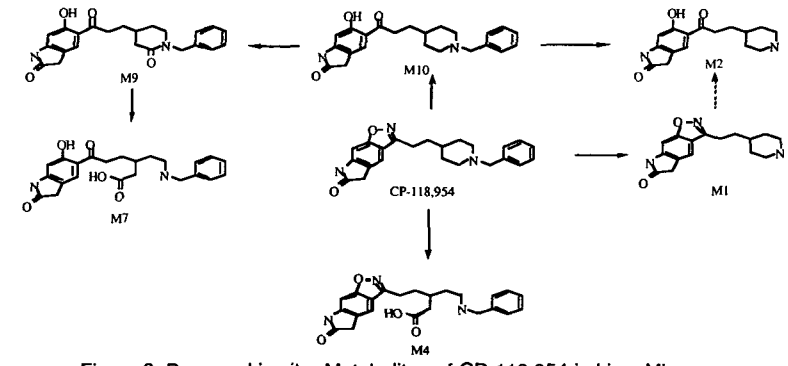

Figure 2. Proposed in vitro Metabolites of CP-118,954 in Liver Microsomes.

INHIBITION OF ALDEHYDE DEHYDROGENASE BY DISULFIRAM AND METABOLITES

K. A. Veverka[1,2], K. L. Johnson[1,3], D. C. Mays [2,5], J. J. Lipsky[2,4,5], and S. Naylor[1,2,3,5]
[1]Biomedical Mass Spectrometry Facility, [2]Department of Pharmacology, [3]Department of Biochemistry and Molecular Biology, [4]Department of Internal Medicine, [5]Clinical Pharmacology Unit, Gugg C009B, Mayo Clinic, Rochester MN 55905

Introduction: Disulfiram (DSF, trade name Antabuse, Fig. 1) is used clinically in the aversion therapy of recovering alcoholics. DSF acts by inhibiting the hepatic enzyme aldehyde dehydrogenase (ALDH) which leads to an accumulation of acetaldehyde in the blood upon subsequent ingestion of ethanol. DSF alone can inhibit ALDH *in vitro*, however, a variety of biotranformation products are thought more likely to be physiologically important, and many have greater inhibitory capacity than DSF itself. Two such compounds are methyldiethylthiocarbamoyl-sulfoxide and methyldiethylthiocarbamoyl-sulfone (MeDTC-SO and MeDTC-SO_2, respectively, Fig. 1). We report a systematic approach to study the mechanism of ALDH inhibition by DSF and metabolites which combines the direct analysis of protein and protein-drug interactions with bioassay.

Results: Yeast ALDH (yALDH), containing an ~ equimolar mix of the mitochondrial and cytoplasmic isozyme was used as a model, and the ESI-MS of the native enzymes is shown in Figure 2A (M_r=53962±5amu and 54099±5amu, respectively). Samples of purified yALDH protein were reacted with drug *in vitro* and the NAD activity of ALDH was assayed spectrophotometrically. Other samples of yALDH were treated with dithiothreitol to monitor the effects of a reductant on ALDH activity (both with and without inhibitor). After sample clean-up the reacted yALDH samples were further subjected to ESI-MS analysis.

ESI-MS analysis alone of DSF-treated yALDH establishes no recognizable difference in mass from native yALDH (Table 1). Bioassay provides the additional information that although no observed shift in mass is associated with DSF treatment of yALDH, activity is abolished. Moreover, if DTT is added to the sample as a reductant, activity is restored even though the mass remains unchanged.

yALDH that is likewise treated with MeDTC-SO or MeDTC-SO_2 affords a ~100 amu adduct or ~100 and ~200 amu adduct, respectively (Table 1). ESI-MS analysis of the intact protein reacted with MeDTC-SO is shown in Figure 2B. ALDH activity is inhibited in these samples and correlates with the observed protein adduct. If DTT is added to MeDTC-SO-inhibited yALDH as a reducing agent at pH 7.3, activity remains inhbitied (Table 1) and the protein remains adducted. This suggests that in the range of physiological pH the adduct is stable. High pH alone has no effect on destabilizing the sulfoxide-derived adduct, however, upon adding 1 mM DTT at increased pH (~pH 9), activity is fully restored (Table 1) and the mass of yALDH is lowered by ~100 amu (not shown).

Conclusions: Based on these results at least two mechanisms of inhibition of yALDH by DSF and related biotransformation products are now apparent. It seems conceivable that *in vitro* DSF acts directly on yALDH to oxidize proximal cysteines thought to occupy the active site, and thereby inhibits enzymic activity by forming an internal disulfide bond (not shown). Furthermore, our *in vitro* data supports the hypothesis that a nucleophile, perhaps cysteine 302 of the ALDH active site, attacks the electrophilic center of MeDTC-SO and/or MeDTC-SO_2 which forms a covalent adduct with the enzyme (Figure 3). The overall importance of this mechanism is that the covalent modification inactivates the ability of ALDH to metabolize acetaldehyde. Neither reduction or base hydrolysis is able to release the adduct and recover yALDH activity. Rather, DTT has sufficient nucleophilic character at high pH to attack the electrophilic center of the proposed thiocarbamoyl adduct and releases the adduct with a concomitant regaining of enzyme activity.

43rd ASMS Conference on Mass Spectrometry and Allied Topics

FIGURE 1. Pathway of DSF Biotransformation

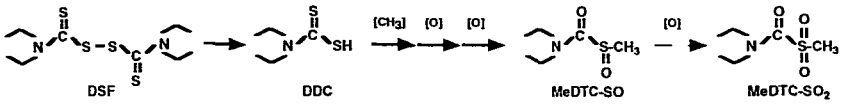

FIGURE 2. Deconvoluted ESI-MS Spectra of yALDH and MeDTC-SO-treated yALDH

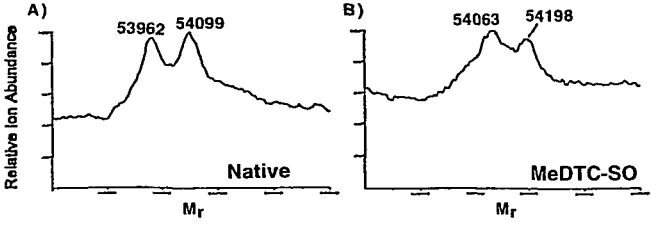

TABLE 1. Summary of yALDH Inhibition Studies in Conjunction with ESI-MS

Added Inhibitor	NAD Activity	Mass Difference by ESI-MS	Addition of DTT Regain of Activity	Addition of DTT (pH 9.1) Regain of Activity
Native	Yes	–	Yes	Yes
MeDDC	Yes	0	Yes	Yes
DSF	No	0	Yes	Yes
MeDTC-SO	No	~+100	No	Yes
MeDTC-SO_2	No	~+100, +200	No	Partial

FIGURE 3. Proposed Mechanism of Inhibition of yALDH by MeDTC-SO

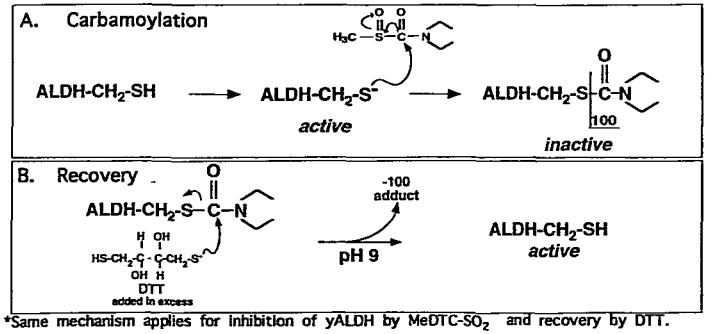

*Same mechanism applies for inhibition of yALDH by MeDTC-SO_2 and recovery by DTT.

A Study of the Structures of Metabolites of Rifabutin by Electrospray Mass Spectrometry and Tandem Mass Spectrometry

Toni J.Thompson[1];Tanya Koudriakova[2]; Ilya Utkin[2]; Nicholas Gerber[2]; Paul Vouros[1];

1 Department of Chemistry, Northeastern University, Boston, MA

2. Ohio State University, Columbus, OH

Rifabutin, a drug used as a prophylactic in treating patients with immun deficiencies for *Mycobacterium avium* complex (MAC) hasshown in vitro activity against *M. tuberculosis.* Most studies to date have been aimed at enhancement rifabutin's effectiveness by concurrently injecting metabolism inducing drugs. One of the metabolites, 25-O-deacetyl-rifabutin, is known to exhibit activity equal to rifabutin against MAC and is itself responsible for 10% of the overall drug activity. This activity exhibited by metabolite suggests that some of the other metabolites may also exhibit activity against MAC and *M. tuberculosis.* One author suggests that more than 20 metabolites my exist. Only six metabolites have been isolated and their structures identified. The major metabolic pathways appear to be oxidation of a methyl group or of the 6' N (forming an N-oxide), deacetylation and demethylation.

In our work, the origins of the various fragment ions were determined based on the mass value shifts observed in the spectra of the reference anaolgs This information assisted in ,the development of a library of pertinent fragment ion structures.

The metabolites were obtained from two sources—urine collected from rats injected with rifabutin, and liver microsome extracts. The microsomes were obtained by homogenizing excised livers and centrifuging the homogenate. Rifabutin and co-factor cytochrome P450 were then added and the metabolites extracted using a mixture of butyl chloride and sodium phosphate, pH 7 The metabolites were extracted from the urine with the same method The metabolites were then separated on a conventional HPLC column (C-18, 4.6 mm id, 15 cm long) with UV detection at 275 nm The buffers were B=acetonitrile and A=3%TEA, 0.3%TFA, H_3PO_4 to pH 2 in aqueous solution. The gradient was 27-45% B over 60 minutes. The fractions were collected and further purified by HPLC using the same buffers but substituting 1%TFA or 1% heptafluoro butyric acid for the 0 3%TFA. These purified fractions were analyzsed by electrospray ionization mass spectrometry to obtain molecular weight information. The samples were then analyzed by CID with collision gas (argon) at ~2mtorr and collision energy at -51eV All sample were infused into the mass spectrometer at 5μL/minute. The mass spectrometer was a Finnigan TSQ700 equipped with a Finnigan electrospray source.

The structures and CID spectra of three new metabolites, 27-O-deacetyl rifabutin and 31-OH-32-OH, are reproduced on the next page were shown. Several other metabolites have been analyzed by ESI/MS/MS and structures have tentatively been assigned to them. Several fragment ions are significan when analyzing these spectra. CID of rifabutin produces ions at *m/z* 112, 423, 545, 573, 632 When rifabutin is oxidized with two oxygens, some of these ions shift by 16u as dictated by the position of oxidation (i.e. *m/z* 112,423,561, 664). In the case of N-oxidation, the ion shifts are *m/z* 128, 439, 561, 589, 648

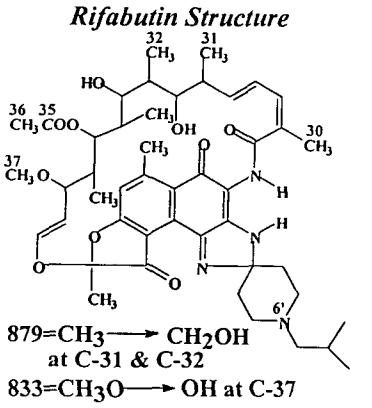

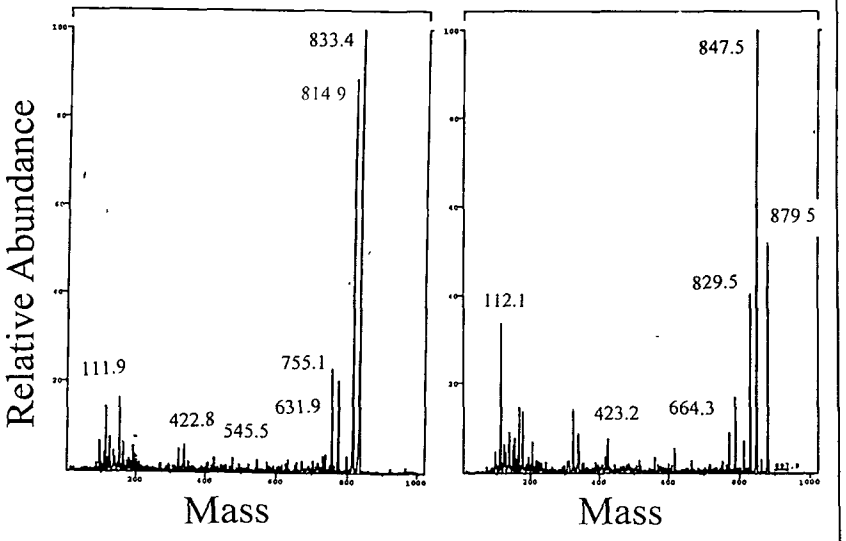

LC/IonSpray/MS/MS Analysis of Bile Acids

Guy LePage and Ibrahim Yousef, Hôpital Ste-Justine, Unversité de Montreal, 3175, Côte Ste-Catherine, Montréal(Québec) H3T 1C5, Canada; and Gabriel Sanchez, Bori Shushan and Takeo Sakuma, PE-SCIEX, 71 Four Valley Dr., Concord, Ontario L4K 4V8, Canada

There are 2 million Canadians suffering from hepatic disease. It is the 4th most common cause of death among Canadians between 35 and 55 years of age.

Accurate analysis of bile acids(BA) is essential in the bile research, as BA undergo complex biotransformation in both healthy and sick people. Mass Spectrometry(MS) has opened up the field of inborn errors of BA metabolism and greatly increased the understanding of the metabolism and biosynthesis of BA. The coupling of GC to MS is useful for the separation and identification of free BA. However, BA conjugates with taurine, glycine and ornithine must undergo time-consuming and labor intensive sample preparation procedures, i. e., extraction, hydrolysis, a second extraction, purification and derivatization prior to GC/MS analysis. B. M. Warrack and G.C. DiDonato(1) applied the microbore HPLC/IonSpray/MS technique to the analysis of bile acid components of monkey bile in the 40 - 100 fmole range using the selected ion monitoring mode.

In this paper we examined 17 BA standards, lithocholic acid(LC), glycolithocholic (GLC), taurolithocholic (TLC), beta-lithocholic (ß-LC), deoxycholic (DC), glycodeoxycholic (GDC), tauro-deoxycholic(TDC), chenodeoxycholic (CDC), glycochenodeoxycholic (GCDC), taurochenodeoxy-cholic (TCDC), cholic (C). glycocholic (GC), taurocholic (TC), ursodeoxycholic (UDC), glycourso-deoxycholic (GUDC), tauroursodeoxycholic (TUDC) and hyodeoxycholic acid (HDC).
Single MS mode spectra were obtained from these BA standards in the positive and negative ion modes. In the positive ion mode most BA produced strong MH^+ ions except for LC, ß-LC, UDC and HDC that underwent dehydration to give $[M-H_2O]H^+$ as base peak. As our LC method used trifluoroacetic acid, subsequent work was done in the positive ion mode.

Product ion spectra were obtained from these BA. Common fragments observed were 323, 341 from LC, GLC, TLC and ß-LC; 321, 339 from DC, GDC, TDC, CDC, GCDC, TCDC, UDC, GUDC, TUDC and HDC; 319 and 337 from C, GC and TC.

We also discovered that N-(carboxymethyl)-amide containing "glyco-" BA produce strong 76 fragment ions, whereas N-(2-sulfoethyl)-amide containing "tauro-" BA form intense 126 product ions. These features were also observed from 2 crude human bile samples under the precursor ion and product ion scan modes. These spectra exhibited different fragmentation patterns and gave sufficient information for identification with the detection limits in the low picogram range.

The formation of Fragments 76 and 126 was also achieved by applying a high orifice potential of 100 - 150 V in the single MS mode followed by scanning from 340 - 600 amu using 60 V potential for the detection of parent ions. Figure 1 compares extracted ion chromatograms of 76, 126 and 340 - 600 amu. The top chromatogram shows "glyco-" BA, the middle chromatogram "tauro-" BA and the bottom the TIC.

1) B. M. Warrack and G. C. DiDonato, Biological Mass Spectrometry, 22, 101-111(1993)

Fig. 1 Extracted Ion Chromatograms from the LC/MS of Crude Bile Sample

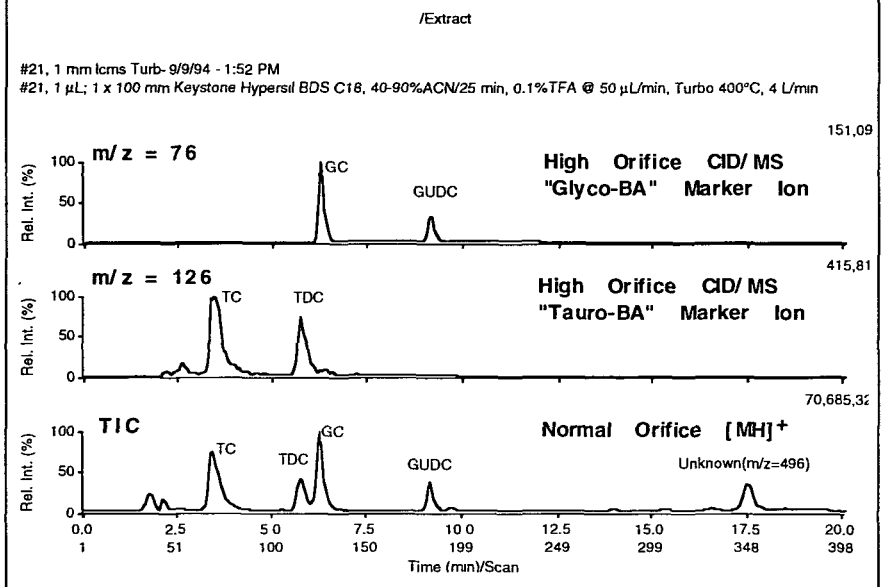

Our results have proven that LC/MS/MS is the tool needed for research in the fate of BA in humans. Without MS/MS analysis of BA standards it would have been very difficult to discover the various marker ions indicative of certain BA compound classes. Subsequent analysis by LC/MS, under simultaneous high and low energy conditions, enables the acquisition of all the analytical information on the BA profiles including conjugate distribution and the characterization of unknown metabolites without any preparation of the biological samples.

Detection of Trypanothione Conjugates in Cell Cultures by ESI Tandem MS

Mark S. Bolgar and Simon J. Gaskell
The Michael Barber Centre for Mass Spectrometry, UMIST, Manchester, M60 1QD, U.K.

Kenneth T. Douglas, Amanda N. Wilton
Department of Pharmacy, University of Manchester, Manchester M13 9PL, U.K.

Trypanosomes are a group of flagellated protozoa responsible for African sleeping sickness and Chagas' disease. Trypanosomes differ from other organisms in their use of primarily trypanothione [N1, N8- bis (glutathionyl)spermidine] rather than glutathione to provide an intracellular reducing environment to protect against oxidative damage. By analogy with glutathione (GSH), it is anticipated that conjugation with trypanothione [$T(SH)_2$] may represent an important mechanism for the scavenging of xenobiotic-derived electrophilic compounds in these organisms. Since this pathway has not been definitively established we have investigated mass spectrometric procedures for the screening and identification of $T(SH)_2$ and GSH related conjugates from cell lysates. As a model system, the $T(SH)_2$ and GSH conjugates of 1-chloro-2,4-dinitrobenzene (CDNB) were prepared and examined by ESI MS and product ion scanning to determine common fragmentation pathways on which to base tandem-MS screening procedures. The GSH conjugate fragmented via loss of a neutral fragment 129 Da corresponding to the γ-glutamyl moiety. Scanning for a constant neutral loss of 129 Da has been previously demonstrated to be an effective method for the detection GSH conjugates (1-3). In addition to loss of a neutral γ-glutamyl moiety, its corresponding acylium ion was observed at m/z 130. The fragmentation pathways observed in the product ion spectra of the doubly protonated $T(SH)_2$ conjugate were similar to those of the GSH conjugate despite the difference in charge state of the precursor ions. The $T(SH)_2$ conjugate, like the GSH conjugate, fragmented by loss of a neutral γ-glutamyl moiety, but since the precursor ion had a charge state of 2^+, a neutral loss of 64.5 Da (129/2) was observed. Fragmentation via the consecutive losses of trypanothione's two γ-glutamyl residues resulted in a neutral loss of 129 Da. The γ-glutamyl moieties were also cleaved to form an acylium ion at m/z 130. Based on the observed fragmentation pathways, scanning for precursors of m/z 130 should detect GSH or $T(SH)_2$ conjugates regardless of their charge state. Scanning for a constant neutral loss of 129 Da should allow detection of singly charged GSH conjugates or doubly charged $T(SH)_2$ conjugates, while scanning for a neutral loss of 64.5 Da will be specific for doubly charged $T(SH)_2$ conjugates. The suitability of these tandem MS methods for the detection of conjugates in biological matrices was evaluated by analyzing 50 µL of a *Trypanosoma brucei brucei* lysate spiked with 25 pmol of the $T(SH)_2$ and GSH CDNB conjugates. After desalting, the lysate was analyzed by ESI MS and by precursor and neutral loss scanning (Fig 1) with 4 pmol of analyte consumed per experiment. Analysis of the spiked lysate by full scan ESI MS (Fig 1, top) did not allow reliable detection of the spiked conjugates due to chemical interference. Scanning for precursors of m/z 130 (Fig 4, upper middle) resulted in a large reduction in background interference and allowed detection of both the $T(SH)_2$ and GSH conjugates regardless of the charge state of the precursor ion. Scanning for a constant neutral loss of 64.5 Da (Fig 4 lower middle) resulted in the detection of only the doubly charged species of the $T(SH)_2$ conjugate, as expected since this loss corresponds to cleavage of a neutral γ-Glu residue from a doubly charged precursor. Scanning for a constant neutral loss of 129 Da (Fig 4 bottom) resulted in detection of primarily the GSH conjugate although the doubly protonated species from the $T(SH)_2$ conjugate was also detected.

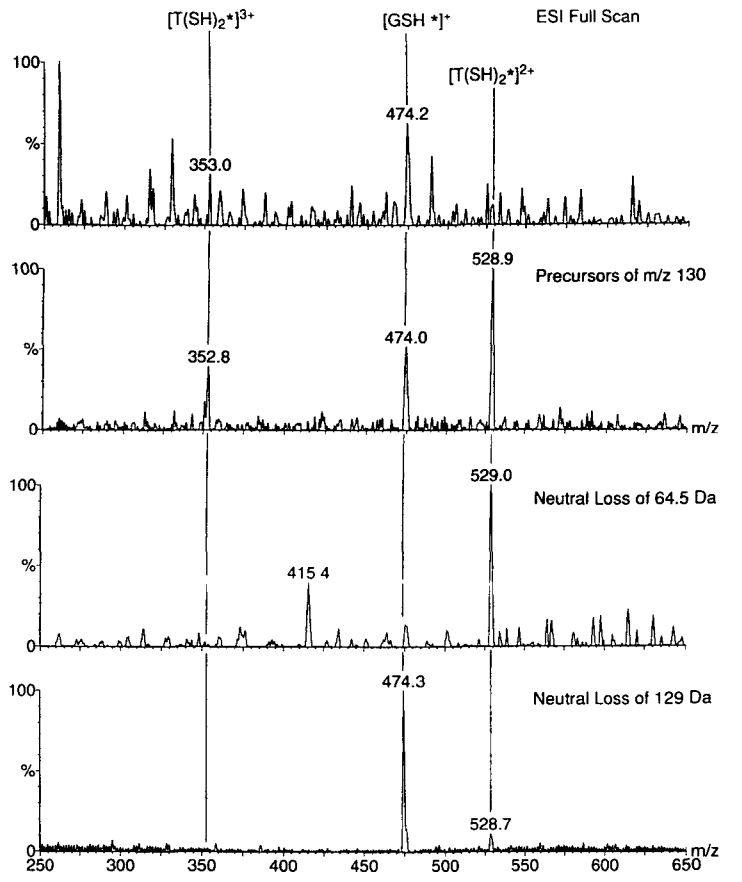

Figure 1. ESI MS and tandem-MS analyses of a *T. brucei brucei* lysate spiked with glutathione (GSH*) and trypanothione [$T(SH_2)$*] CDNB conjugates.

1) Ballard, K.D.; Raftery, M.J.; Jaeschke, H., Gaskell, S J.; J Am Soc. Mass Spectrom. 1991; 2. 55-68.
2) Haroldsen, P.E ; Reilly, M.H ; Hughes, H.; Gaskell, S.J ; Porter, C J., Biomed. Environ. Mass Spectrom. 1988; 15. 615-621.
3) Baillie, T.A., Davis, M.R.; Biol. Mass Spectrom. 1993; 22: 319-325.

Characterization of Hemiketals of MDL 101146 by Normal Phase LC/ESI/MS

Paul W. Brown, W. Bart Emary and Nisar Akbari
Marion Merrell Dow, Kansas City, MO 64134

INTRODUCTION

MDL 101,146 is an orally active inhibitor of the enzyme elastase and has been approved as a clinical candidate for the treatment of chronic obstructive pulmonary disease. An unknown was detected after MDL 101,146 was dissolved in mobile phase for approximately two hours. Utilizing LC/UV, it was shown that the amount of unknown increased with time when MDL 101,146 was dissolved in mobile phase. This indicated that the detection of this compound was time dependent, and this property is not consistent with an impurity. The goal was to identify the unknown. The structure of MDL 101,146 is shown below:

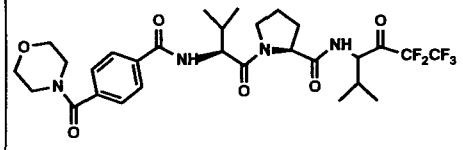

MDL 101,146

After analysis by LC/UV, the sample which had been prepared in mobile phase was analyzed by LC/MS with electrospray ionization. MDL 101,146 was reacted with various solvents and the products were analyzed by LC/MS with electrospray ionization (ESI). The temperature of the heated capillary in the ESI source had a dramatic effect on the fragmentation of the unknown molecule.

Fragmentation Pathway of MDL 101,146 Hemiketal

Shown in Figure 1 is a scheme of the proposed thermally induced fragmentation pathway of MDL 101,146 hemiketals. This fragmentation pathway is unique to the hemiketals and is not observed in the ESI mass spectrum of MDL 101,146. The extent of fragmentation was correlated with three different capillary temperatures: 1) at 200°C very little fragmentation is observed compared to the natriated adduct, 2) at 225°C both the fragment ion and the natriated adduct are detected, and 3) at 250°C primarily the fragment ion is detected with minor contribution due to the natriated adduct. Thus the fragment ion which is produced from the unique and characteristic loss of 120 daltons (CF_2HCF_3) from the natriated adduct of the hemiketal is more abundant with increasing temperature.

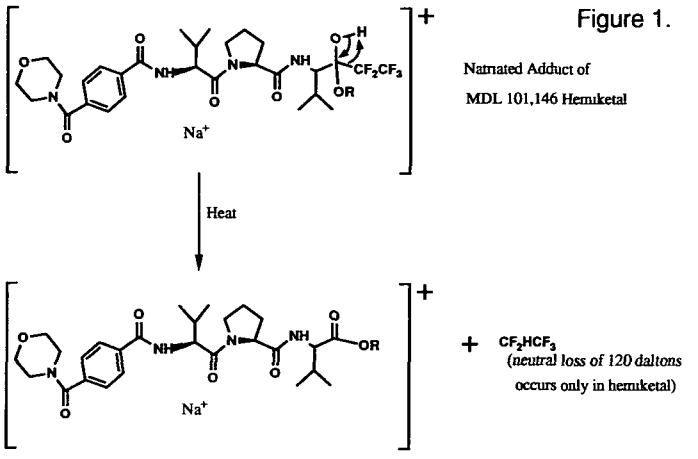

Figure 1.

Natriated Adduct of MDL 101,146 Hemiketal

where R=CH_3, CH_2CH_3 and $CH_2CH_2CH_3$

CONCLUSION

The unknown was determined to be MDL 101,146 methanol hemiketal.

The ketone moiety of MDL 101,146 also shows reactivity with water. When MDL 101,146 was dissolved in solution containing water, the hydrate (gem-diol) of MDL 101,146 was detected. The ketone moiety of MDL 101,146 will also undergo reversible nucleophillic addition reactions with water and straight chain aliphatic alcohols. Artifact (methanol hemiketal) formation can arise when compounds possessing a ketone moiety in close proximity of strong electronegative groups are prepared in solutions containing methanol, a common organic modifier. Hemiketals are thermally labile compounds which historically have been characterized by NMR and IR. Mass spectrometry has been used indirectly to characterize hemiketals because they can convert back to the ketone form upon volatilization in a GC inlet. Negligible molecular ion signal is usually observed because facile alpha cleavage results in a resonance stabilized ion (1).

REFERENCES

1. F.W. McLafferty, "Interpretation of Mass Spectra", 3rd ed., (1980), p.211.

Analysis of secondary plant metabolites in crude plant extracts by electrospray LC-MS

Jean-Luc Wolfender and Kurt Hostettmann, Institut de Pharmacognosie et Phytochimie, Université de Lausanne, BEP, CH-1015 Lausanne, Switzerland
Winfried Wagner-Redeker, Spectronex AG, Rotterdam-Strasse 21, CH-4002 Basle, Switzerland

The characterisation of natural products and their metabolites by mass spectrometry involves molecular weight determination as well as structural elucidation of a large variety of chemical compounds. As these substances are usually polar and thermally labile, often only soft ionisation methods are employed for their on-line LC-MS analysis. Much work has been done by thermospray (TSP) (1) and continuous flow FAB (CF-FAB), the former method giving molecular weight and structural information of small to medium sized metabolites (100 to 1000 u), while CF-FAB has been successfully applied for molecular weight determinations of metabolites ranging up to 3000 u. For rapid screening of plant extracts, routine coupling of mass spectrometry with liquid chromatography is of great importance; it permits, in conjunction with LC-UV, the early recognition of known constituents, thus avoiding their time-consuming isolation. In addition, an efficient localisation of interesting metabolites is possible (1).

Polyphenol and triterpene aglycones and glycosides have been studied by atmospheric pressure (API) LC-MS. The results were compared to previous TSP and CF-FAB measurements. API experiments were performed with a Finnigan MAT TSQ 700(0) and a prototype version of a Finnigan MAT LC-MS ion trap mass spectrometer. Electrospray (ES) and atmospheric pressure chemical ionisation (APCI) measurements were carried out in both positive and negative ion modes, with TFA and NH_4OAc buffer and with upfront CID on or off. The LC separation of the crude plant extracts was performed with a RP-18 column and H_2O/MeCN as gradient system.

For the LC-MS analyses of polyphenol aglycones and glycosides in crude plant extracts, TSP has been widely used (1). This technique however does not always give molecular weight information, especially for glycosides bearing more than 2 sugar units (2) or for compounds having a high degree of hydroxylation. In order to investigate the complementarity of different ionisation techniques, the crude MeOH extract of *Chironia krebsii*, a species of the Gentianaceae particularly rich in xanthones, has been analysed by ES, APCI, CF-FAB and TSP LC-MS. The TSP LC-MS (pos. ions) analysis of this extract showed a satisfactory response for all the peaks detected by UV at 254 nm. Generally $[M+H]^+$ ions were observed. In the case of glycosides, aglycone fragments $[A+H]^+$ were also formed. In ES and APCI, on the other hand, measurement with both ion polarities was necessary to give a general picture of the extract composition. Highly methoxylated xanthones or secoiridoids were only detected in the positive ion mode. Hydroxylated xanthones formed $[M-H]^-$ ions in the negative ion mode. The LC-MS spectra obtained for a xanthone monoglycoside clearly showed the dependence of ES on the solvent composition. In the negative ion mode with TFA or NH_4OAc, adducts of the respective anions $[M+TFAc]^-$ and $[M+Ac]^-$ were observed. The TFAc adducts were not fragmented by upfront CID while the Ac adducts

were easily cleaved, leading to $[M-H]^-$ ions and aglycone fragments $[A-H]^-$. ES and CF-FAB (pos. mode) only produced weak $[M+H]^+$ ions; TSP gave intense $[M+H]^+$ and $[A+H]^+$ ions.

In the case of triterpene glycosides (saponins), CF-FAB and TSP have already been used (3). Generally if more than 2 sugars were attached, TSP gave mainly aglycone information. CF-FAB, on the other hand, yielded both aglycone and sugar sequence information. ES was compared to these two latter techniques for the analysis of saponins bearing 2-5 sugars in the MeOH extract of *Swartzia madagascariensis* (Leguminosae) and *Phytolacca dodecandra* (Phytolaccaceae). By looking at the molecular weight ion traces of these different saponins, ES (neg. mode) was the method of choice (best sensitivity and peak shape). With NH_4OAc as buffer, some structural information was obtained by upfront CID, but the complete sugar sequence was not always observed. With TFA, only strong $[M+TFAc]^-$ were present and were not cleavable by upfront CID or MS/MS on the TSQ. In order to perform MS/MS on the strong TFA adducts produced in ES, a prototype of the new ion trap system LCQ from Finnigan MAT, equipped with an external API source, was used . CID of TFA adducts occurred at a very high yield in the ion trap. It was not possible to obtain all the sugar sequence information in one MS/MS measurement. Application of an MS^n experiment however yielded the complete sequence information. By adjusting the collision energy it was possible to cleave only one sugar at a time in a pentaglycosylated saponin, making the interpretation of the spectra very simple. The time requirement for switching between the different stages of the MS^n experiment was about 50 ms. Therefore three to four stages of the MS^n experiment could be readily performed during the time of a normal LC peak.

The comparison of techniques such as ES, APCI, TSP or CF-FAB has shown the complementarity of these various approaches. If API techniques are now easy to handle, they are also rather selective and are not always superior to the older techniques. Solution chemistry has always to be taken into account. Used in a suitable way, it provides an additional tool in LC-MS and can be used to increase sensitivity or to control the fragmentation of the ions formed. Looking at the different results makes it clear that ionisation of plant metabolites has to be investigated in more depth. There is still need to establish rules to predict the types of ions generated from the different classes of compounds in all these interfaces. For all techniques, MS/MS is an important additional feature. Comparison of MS/MS experiments of TSQ and ion trap shows that collision efficiencies are significantly higher in an ion trap than in the collision cell of a TSQ, probably due to the much higher residence time of ions in the trap. It has been shown that the MS^n experiments which can be carried out in ion traps represent a very powerful tool for on-line identification of plant metabolites.

1. Wolfender, J.-L., Maillard, M. P. and Hostettmann, K. (1994). *Phytochem. Anal.* **5**,153-182.
2. Wolfender, J.-L., Maillard, M. P. and Hostettmann, K. (1993). *J. Chromatogr.* **647**, 183-190.
3. Maillard, M. P. and Hostettmann, K. (1993). *J. Chromatogr.* **647**, 137-146.

Angiotensin II Receptor Antagonist Metabolite Identification by MS/MS

William DeMaio and George Morton
American Cyanamid Company*, Drug Metabolism Department
Pearl River, NY 10965
*** Current name is Wyeth-Ayerst Research**

CL 190,064 (cis-(+/-)-2-Butyl-6-(hexahydropyrrolo[1,2,-b]isoxazol-2-yl)-3-[[2'-(1H-tetrazol-5-yl)[1,1'-biphenyl]-4-yl]methyl]-4(3H)-quinazolinone) is an angiotensin II receptor antagonist with potential for use in the treatment of hypertension. The metabolism of CL 190,064 was investigated in rat liver preparations. Metabolites were purified from rat liver preparations prior to FAB-MS, MS/MS and NMR spectroscopic analyses. A Finnigan MAT TSQ 70 triple quadrupole mass spectrometer was used for FAB-MS and MS/MS analyses. Two metabolites of CL 190,064 isolated from rat liver preparations were analyzed to identify their structures. The Summary Figure contains the structures of CL 190,064 and two of its metabolites, A and B, which were identified as described below:

Comparison of the product ion mass spectra of CL 190,064 and its methyl substituted analog, CL 190,133 showed which product ions contained the "methyl label." CL 190,133 product ions 14 Da greater than corresponding CL 190,064 product ions indicated the presence of the carbon atom at position 5 of the isoxazole. Both CL 190,064 and CL 190,133 lose C_4H_6NO (85 Da) from the hexahydropyrrolo-isoxazole to give the *m/z* 463 and 477 product ions, respectively. For CL 190,064, the biphenyl-tetrazole system fragments from the quinazolinone to form the *m/z* 229 and 207 fragments. For CL 190,133 this process forms the *m/z* 243 and 207 fragments. The *m/z* 420 fragment of CL 190,064 and *m/z* 434 for CL 190,133 seemed to form directly from the molecular ion. The structure of these ions were assigned with less confidence than the other structures shown.

The molecular weight of A was 549, 2 Da higher than CL 190,064. The product ion spectrum of *m/z* 550 shows the same product ions as for CL 190,064. This means that the metabolism took place on the hexahydropyrrolo-isoxazole atoms which were lost to form the *m/z* 463 product ion. These data do not precisely indicate the specific site of metabolism to form A. For the NMR spectra of metabolite A vs. CL 190,064 in d6DMSO/TFA, H5' shifted upfield from 4.76δ to 3.0-3.7δ. H6' shifted upfield from 2.2-2.8δ to 1.8-2.4δ. H7' shifted upfield from 5.91δ to 4.93δ. The proposed structure for metabolite A was synthesized and found to have an HPLC retention time, molecular weight and product ion mass spectrum matching that for metabolite A.

Metabolite B is 16 Da larger than CL 190,064 and 14 Da larger than A and has a similar product ions spectrum as A. For the NMR spectra of metabolite B in CD_3OD and CL 190,064 in CD_3OD/NaOD, H2' was not present in metabolite B. H3' shifted from 1.78δ to 2.31δ. H6' shifted from 2.48δ to 1.95δ. H7' shifted from 5.25δ to ~4.9δ. Since H2' is missing and the mass spectrum indicates a net gain of 14 Da, the lactam structure is a good choice and this would be consistent with a conversion of metabolite A to metabolite B by addition of oxygen at C2'.From the exploratory metabolism study, we know that B most likely was formed from A. Therefore, B is formed by substitution of an oxygen atom for two hydrogen atoms of A.

Summary Figure

Partial Biotransformation Pathway of CL 190,064

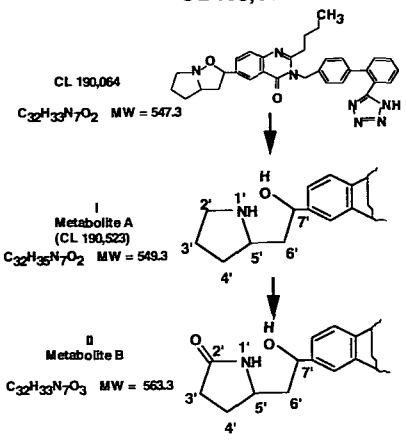

Structures of CL 190,064 and its Product Ions

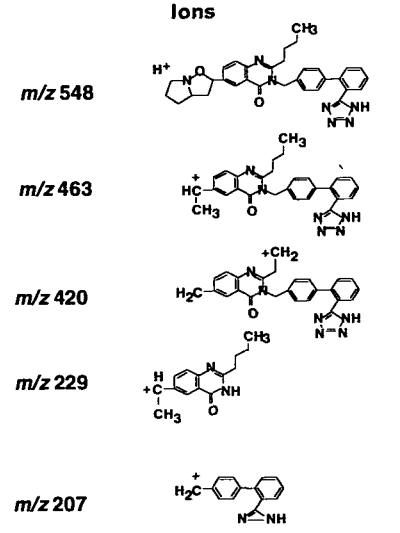

FAB Mass Spectrum of Metabolite A and Products of *m/z* 550

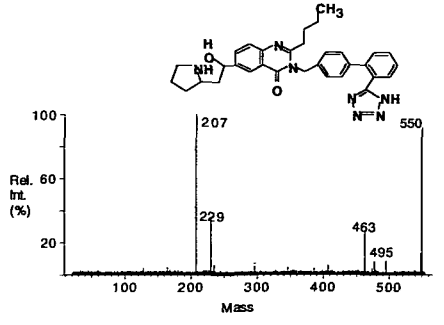

IN VITRO HEPATIC METABOLISM OF TACROLIMUS (FK506) USING SIMS and MALDI MASS SPECTROMETRY

Arkady I GUSEV[1]; David C. Muddiman[1,3]; Andrew Proctor[1]; David M.Hercules[1,4]; Prasad Tata[2]; Raman Venkataramanan[2].

[1] Department of Chemistry, University of Pittsburgh, Pittsburgh PA 15260; [2] School of Pharmacy, University of Pittsburgh, Pittsburgh PA 15261; [3] present address: Chemical Methods and Separation group, Chemical Sciences, Department, Pacific Northwest Laboratory, Richland WA 99352;[4] present address: Department of Chemistry, Vanderbilt University, Nashville, TN 37235.

Tacrolimus is a recently approved immunosuppressive agent efficient in preventing the rejection of transplanted organs. However the chemical nature of its metabolites and their pharmacological activity and toxicity is not completely understood. *In vitro* results reported by other groups indicate that de-methylation and hydroxylation are the major metabolic pathways [1,2]. The objective of this work was application of matrix assisted laser desorption ionization (MALDI) time-of-flight (TOF) mass spectrometry and TOF secondary ion mass spectrometry (SIMS) for qualitative and quantitative analysis of the *in-vitro* hepatic metabolism of Tacrolimus.

Baboon microsomal preparations (2mg/mL) were incubated up to 60 min at 37°C with Tacrolimus in the presence of 20mM NADPH. 100-200μL of these incubates were mixed with Rapamycin and then extracted with ethyl ether. Ether was evaporated under a stream of nitrogen [3]. The residues were reconstituted in 150 μL of ethanol - water (1:1) before analysis. The MALDI matrix used in this study [2,5-dihydroxybenzoic acid (DHB) (20 mg/mL):fucose (2 mg/mL) dissolved in 1:9 ethanol-water] was mixed with each sample in a volume ratio of 1:1 [4]. A 2-μL aliquot of this mixture was deposited on polished stainless steel substrates and dried in high purity N_2. Sample preparation for SIMS analysis involved deposition of 1-μL of aliquots on previously etched silver substrates [8].

Several matrices i.e. sinapinic acid, ferulic acid, etc, have been evaluated for analysis of Tacrolimus (TAC). The best matrices were found to be DHB and DHB/fucose. The major limiting factor was the relatively large contamination resulting from the simple ether extraction from microsomal incubates. However, DHB and DHB/fucose provided consistent results for both methanol and ether extracts. The major peaks in MALDI were due to Na and K-cationization which led to some peak overlaps. SIMS spectra had the major peaks due to silver ($Ag^{107/109}$) cationization, hence, provided complementary results for metabolite identification. The difference between the major metabolite peaks and parent drug peak was found to be 14 Da, which indicates that these are mono and double de-methylated species i.e., (TAC-CH_3+H+Na, 812.5Da) and (TAC-$2CH_3$+2H,+Na, 898.5Da). Figure 1 presents the time course of *in-vitro* hepatic metabolism of Tacrolimus. Based on MALDI and SIMS results, 7 metabolites have been identified.

Quantification of the Tacrolimus was carried out using the MALDI instrumental protocol which is described elsewhere [4]. TOF SIMS application for quantitative analysis of immunosuppressive drug cyclosporin A is also described elsewhere [5]. Rapamycin was used as the internal standard for both SIMS and MALDI analysis. The relative standard deviation of the slope was 1.3-2.5% and the correlation coefficient (r_o) was 0.9980-0.9998. Using a proof of equal instrumental sensitivity for Tacrolimus and its major metabolite, Tacrolimus and de-methylated and double de-methylated metabolites have been quantified, Figure 2. SIMS and MALDI produced similar results. Thus successful application of MALDI and TOF SIMS for

qualitative and quantitative analysis of Tacrolimus hepatic metabolism has been demonstrated.

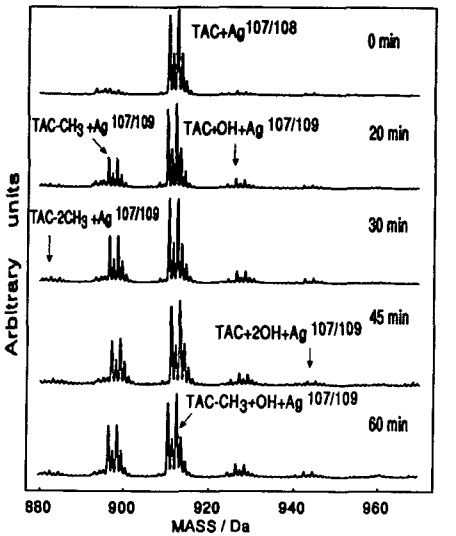

Figure 1. Mass spectra of Tacrolimus (TAC) hepatic metabolism for different incubation times using SIMS

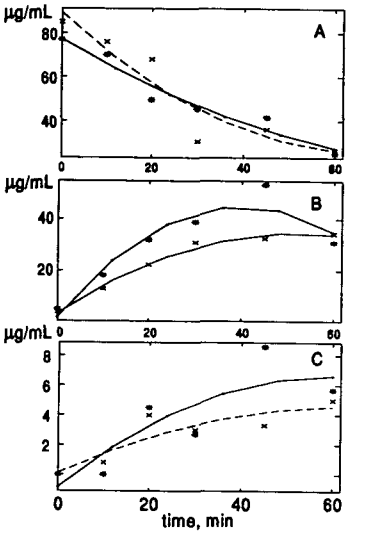

Figure 2. Concentration of Tacrolimus (A), mono (C) and double de-methylated (C) metabolites as a function of incubation times using: x — SIMS and • —MALDI.

This work was supported by U.S. EPA Grant R819809-01.

REFERENCES

1. Lhoëst, G., Maton, N., Laurent, A.,Verbeeck, R.K., *J. of Pharm. and Boimed. Analysis.*,**1994**, 12, 235.
2. Iwasaki, K., Shiraga, T., Nagase,K., Tozuka, Z., Noda, K., Sakuma, S., Fujitsu, T., Shimatami, K., Sato, A., Fujioka, M., *Drug Metabol.and Dispos.*, **1993**, 21, 971.
3.Stiff, D.D.,Venkataramanan, R., Prasad, T.N.V, *Research Comm. in Chem. Pathology and Pharm.* **1992**, 78, 121.
4. Gusev, A.I., Wilkinson, W.R., Proctor, A., Hercules D.M., Venkataramanan, R., Diven,W., *Anal.Chem.*,**1994**, 67, 1034.
5. Muddiman, D.C., Gusev, A.I., Proctor, A., Hercules D.M., Venkataramanan, R., Diven,W., *Anal.Chem.*,**1993** 66, 2362.

Identification of Levodopa and its Metabolites by HPLC-Ion Spray-MS

Mohammed R. Koupai-Abyazani, Barbara Esaw and Barbara Laviolette
Can Test Ltd., 1523 West 3rd Avenue, Vancouver, B.C., V6J 1J8, Canada

A combination of levodopa (*L*-3,4-dihydroxyphenylalanine) and a decarboxylase inhibitor such as carbidopa is used therapeutically in the treatment of Parkinson's disease. Levodopa is extensively metabolized in the human body mainly by decarboxylation to dopamine and also by methylation to 3-O-methyldopa. Other metabolites are 3,4-dihydroxyphenylacetic acid (DOPAC) and 3-methoxy-4-hydroxyphenylacetic acid (homovanillic acid, HVA).

HPLC with electrochemical detection is the most common technique used for the analysis of levodopa and its metabolites. This identification, however, is solely based on the comparison of the retention times of the compounds with those of the standard references. The application of a mass spectrometer as a detector for HPLC provides structural information which confirms the identification especially in complex matrices. This paper presents a liquid chromatographic-atmospheric pressure ionization mass spectrometric (API LC/MS) method for the analysis of levodopa and its metabolites in equine urine and serum. The method consisted of alumina extraction, isocratic separation of the compounds on a RP-18 column and detection using an API MS with ion spray interface.

Urine and serum samples (up to 24 h) collected from a standardbred mare after oral administration of 2 g levodopa and 500 mg carbidopa were analyzed. The HPLC analysis of levodopa and its metabolites requires the use of an ion-pair reagent such as 1-octanesulfonic acid in order to improve the retention and separation of these polar compounds on a reversed-phase column. The isocratic separation of these compounds demonstrated better reproducibility than the gradient elution.

The positive ion mass spectra of levodopa, its metabolites and carbidopa exhibited $[M+H]^+$ ion, with the exception of DOPAC and HVA which showed strong adduct ion $[M+NH_4]^+$ and weak $[M+H]^+$ ion. The $[M+H]^+$ ion was the base peak in the mass spectra of levodopa and 3-O-methyldopa while $[M+NH_4]^+$ ion was the base peak in the case of DOPAC. Other characteristic fragments in the mass spectra of some of the compounds were: $[M-NH_3+H]^+$ ion (M-16), $[M-COOH]^+$ ion (M-45) and $[M-HCCOOH]^+$ ion (M-58). The major ions observed in the positive mode mass spectra of these compounds are listed in Table 1. Figure 1 shows the positive ion mass spectrum of levodopa. The application of the method was demonstrated for the analysis of equine serum and urine.

Urine and serum samples were analyzed using the LC/MS method. The levodopa metabolites, dopamine, DOPAC and HVA were detected in all the administration urine samples collected. Figure 2 shows the extracted ion chromatograms of levodopa and its metabolites in a 12-14 h post-administration urine sample. The parent drug, however, was detected in the serum at the early collection times. Several administration samples were hydrolyzed in order to investigate the presence of conjugates of levodopa and its metabolites. The comparison of the chromatograms obtained for these samples before and after hydrolysis did not

exhibit the presence of any drug conjugates in the administration samples studied. The analysis of several pre-administration urine samples (blanks) did not show any naturally occurring levodopa and its metabolites under the conditions reported in this work.

Acknowledgments: This study was funded by the Canadian Pari-Mutuel Agency, a division of Agriculture Canada, as part of their Equine Drug Evaluation Program. The copyright is owned by Her Majesty the Queen in the Right of Canada represented by the Minister of Agriculture.

Table 1. Major ions and relative abundances in positive ion mass spectra of levodopa, its metabolites and carbidopa.

Compound	MWt	Major ions (relative abundance)
Levodopa	197	198(100), 181(20), 152(74), 139(28)
Dopamine	153	154(54), 137(100), 119(25), 91(22)
3-O-methyldopa	211	212(100), 195(35), 166(60), 153(44)
HVA	182	200(71), 183(5), 137(7), 18(100)
DOPAC	168	186(100), 169(2), 123(4), 18(94)
Carbidopa	226	227(95), 195(9), 181(100), 139(19), 123(15)

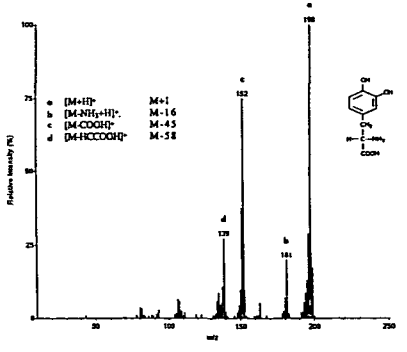

Figure 1. Positive ion mass spectrum of levodopa.

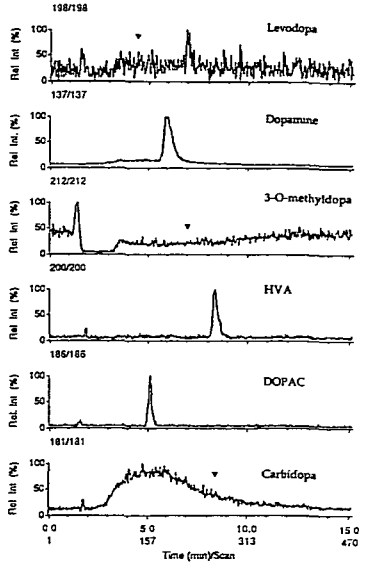

Figure 2. Extracted ion chromatograms of levodopa and its metabolites in a 12-14 h post-administration urine sample. The arrow shows the location of the peak in each chromatogram.

Identification of the urinary metabolites of Brivudin in the rat.

*A. Triolo[1], G. Agostara[2], F. Bonelli[2], A. Crea[2], H.-G. Freude[3], E. Monteagudo[2], A. Raffaelli[4].

*A. Menarini Firenze (Italy)[1], Menarini Ricerche Sud Pomezia (Italy)[2], Berlin-Chemie Berlin (Germany)[3], CNR Pisa (Italy)[4].

* Chemical Res. Dept., via Sette Santi 3, 50131 Firenze (Italy).

Brivudin (5-(2-Bromo-E-ethenyl)-2'-deoxyuridine, BVDU) is a modified deoxynucleoside characterized by potent anti-herpetic activity, expecially against herpes simplex virus type 1 (HSV-1) and varicella-zoster virus (VZV). Since its introduction in 1979, very few information about its biotransformation have been obtained. Early work by Y. Robinson et al., dated 1984, detected a prominent plasma metabolite in various animal species and in man, and identified it as the deglycosylated drug, that is 5-(2-bromo-E-ethenyl)uracil (BVU) [1]. Other in vivo and in vitro studies in the rat by C. Desgranges et al. [2] showed that BVU is not metabolized by the usual catabolic pathway of pyrimidines, and acts as an inhibitor of the metabolization of pyrimidines such as thymine and 5-fluorouracil. During the investigation of the metabolism of BVDU, two other metabolites besides BVU were detected by us after analysis by reverse-phase HPLC with radioactive detection in the urines of rats treated with the C2-radiolabeled compound. These metabolites, M1 and M2 respectively, were characterized by much higher polarity with respect to BVDU and BVU, as deduced by their HPLC retention times; their UV spectra, taken during an HPLC run by means of a diode-array UV detector, were different from that of the parent compound (showing two characteristic strong bands at 250 and 290 nm due to vinyl conjugation to the pyrimidine system), and quite similar to natural pyrimidine bases such as uracil (one band at about 260 nm).

Given the high polarity of M1 and M2, which caused their HPLC coelution with a great number of endogenous substances and rendered their detection by direct HPLC-MS urine analysis very troublesome, extraction and fractionation of pooled rat urine was undertaken: urine was extracted with ethyl acetate using an Extrelut® column, obtaining an extract containing M2, whereas M1 was eluted after washing with methanol. The extracts were furtherly purified by preparative HPLC

EI-MS and proton NMR analysis of the M2 fraction allowed easy identification of thymine, whereas M1 identification still could not be achieved, due to either difficulties in obtaining a satisfactorily pure fraction, or to difficulties in mass spectrometric investigation, which was performed unsuccessfully by a variety of ionization techniques (EI, DCI, FAB, Ion spray with

flow-injection analysis). Finally, a partially purified fraction of M1 was subjected to HPLC-tandem MS with Ion spray ionization, and the fragmentation pattern obtained from the collisionally-activated decomposition of the identified quasi-molecular ion (m/z 171), allowed identification of M1 as ((1H,3H)pyrimidine-2,4-dione-5-yl)acetic acid. The assignment was then confirmed by comparison with a sinthetic standard.

From the above data, the following metabolic scheme is proposed:

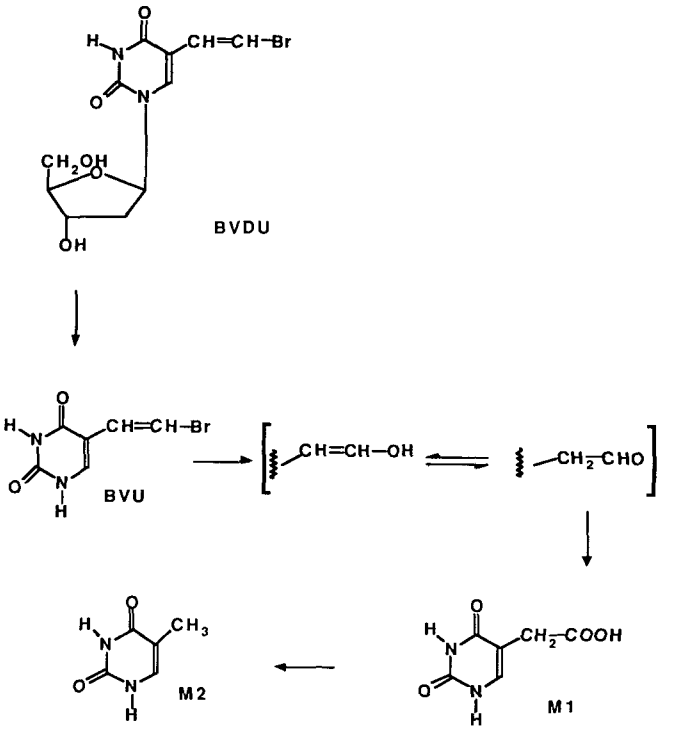

[1] Y. Robinson, N. Gerry, R. D. Brownsill, C. W. Vose, Biomed. Mass Spectrom. 11(4) 199 (1984).

[2] C. Desgranges, G. Razaka, H Bricaud, E. De Clercq, Biochem. Pharmacol. 34(3) 403 (1985)

METABOLISM OF THE NEUROMUSCULAR BLOCKER CISATRACURIUM (51W89) BY LC-MS WITH SIMULTANEOUS RADIOACTIVITY MONITORING (LC-RAM-MS).

G.J. DEAR, A.E. JONES AND S. PLEASANCE
GLAXO-WELLCOME, Group Development Operations, Department of Bioanalysis and Drug Metabolism, Langley Court, Beckenham, Kent, BR3 3BS, U.K.

Cisatracurium, (1*R*, 1'*R*, 2*R*, 2'*R*)-2,2-(3, 11-Dioxo-4, 10-dioxatridecamethylene) bis (1, 2, 3, 4-tetrahydro-6, 7-dimethoxy-2-methyl-1-veratrylisoquinolinium) dibenzenesulphonate (51W89, see Figure), is an intermediate-acting neuromuscular blocking agent. 51W89 is one of ten isomers contained in TRACRIUM® (atracurium besylate) and represents approximately 15 percent of the atracurium mixture. Clinical studies have indicated that 51W89 is more potent and is significantly weaker as a histamine releaser than atracurium. *In vitro* studies in human plasma have shown that, like atracurium, 51W89 spontaneously degrades at physiological pH by Hofmann elimination to form laudanosine (**II**) and the quaternary monoacrylate (**III**). Subsequent ester hydrolysis of the monoacrylate generates the monoquaternary alcohol (**IV**). In rat plasma, 51W89 is also metabolised by non-specific carboxylesterases to the monoquaternary alcohol and the monoquaternary acid (**V**), the former being rapidly hydrolysed further to the more stable acid. It has been reported that laudanosine can be further metabolised via *N*-demethylation to yield tetrahydropapaverine (**VII**). The rate limiting step in the degradation of 51W89 in human plasma is Hofmann elimination, whilst in rat plasma, the action of non-specific carboxylesterases is rate limiting.

The disposition of ^{14}C-51W89 following a single intravenous bolus dose has been studied in various animal species and humans, and in the present work we describe the identification of 51W89 metabolites in urine and bile samples from these studies by high performance liquid chromatography mass spectrometry with simultaneous detection by a radioactivity monitor (LC-RAM-MS). All experiments were conducted on a Hewlett Packard Model 1090 liquid chromatograph coupled in series to a Bertold LB 507B radioactivity monitor and a Finnigan-MAT TSQ-700 mass spectrometer. The effluent from the RAM (1 ml/min) was directed to an electrospray interface without splitting and the ^{14}C radioactivity signal was connected to the TSQ-700 data system. Separations were achieved on a 250 x 4.6 mm i.d. Zorbax Rx-C8 column (Dupont) operated at 40°C, using gradient elution and a mobile phase consisting of 25mM aqueous NH_4 formate (pH 3.5) and acetonitrile.

Under electrospray ionisation, 51W89 is observed as its doubly-charged molecular species, $[M]^{2+}$, at m/z 464, by virtue of its two quaternary nitrogens (see Figure). The metabolites are observed as either singly charged molecular species, $[M]^+$, (**III, IV** and **V**) or protonated molecules, $[M+H]^+$, (**II** and **VII**). The extracted-ion chromatograms for 51W89 and its metabolites, **II-V**, from a human urine sample (0-8hr post-dose) compare very favourably with the simultaneously acquired radioprofile (see Figure). The ability to obtain molecular weight information directly from radioactive peaks enabled not only the confirmation of expected metabolites but also the detection of a number of urinary and biliary conjugated metabolites which co-chromatographed with an early eluting 'unknown' peak in the radioprofile (see Figure). Using a combination of enzyme hydroysis and tandem mass spectrometry these were identified as *O*-glucuronic acid conjugates of monodesmethyl laudanosine and monodesmethyl tetrahydropapaverine. A sulphate conjugate of monodesmethyl laudanosine was also identified in cat bile.

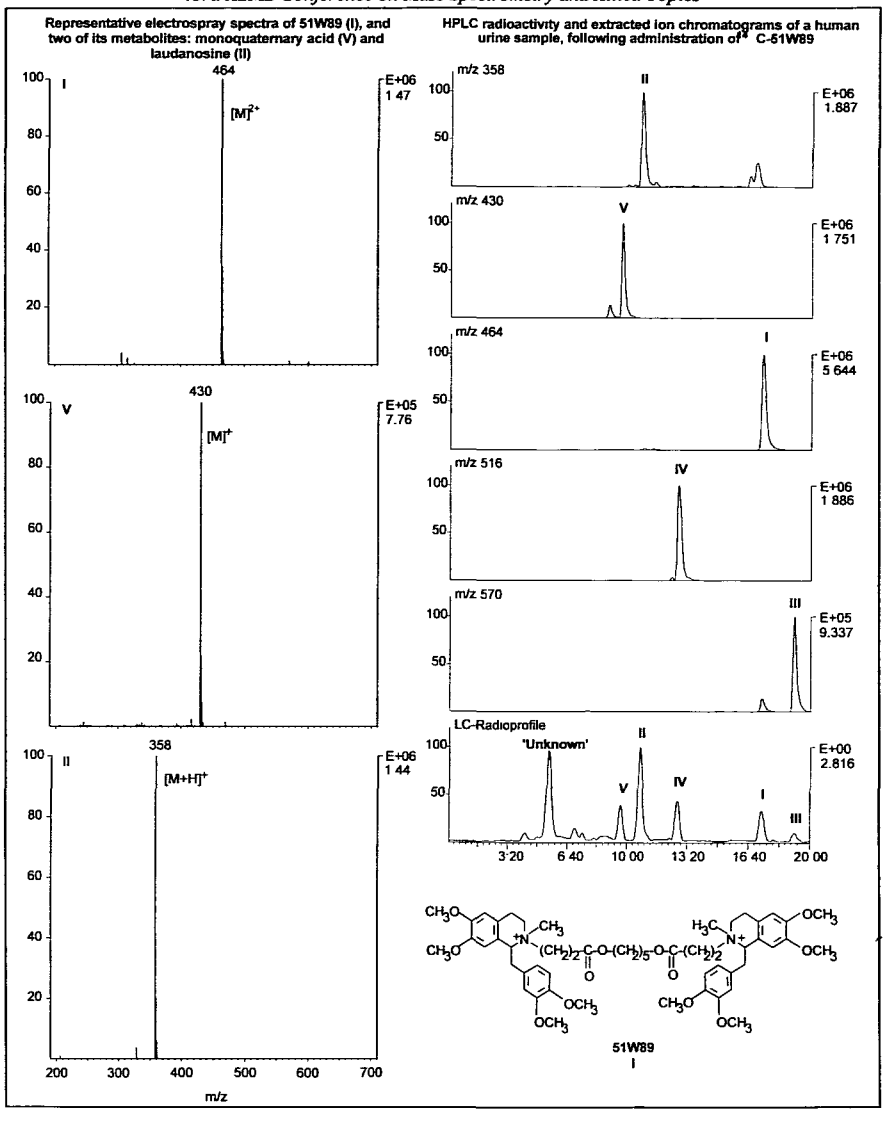

Development of A Sensitive LC/ESI/MS/MS Assay for the Antineoplastic Agents Cyclophosphamide and Ifosfamide. Charles A. Goldthwaite, Jr.[1], Frank J. Belas[1], Mark A. Phillips[1], Lowell Anthony[2], and Ian A. Blair[1,3]. Departments of [1]Pharmacology, [2]Oncology and [3]Chemistry, Vanderbilt University School of Medicine, Nashville, TN 37232.

Cyclophosphamide (2-bis(2-chloroethyl)amino tetrahydro-2H-1,3,2-oxazaphosphorine 2-oxide; CPA), a synthetic antineoplastic alkylating agent, is widely used in chemotherapy due to its capacity to undergo hepatic metabolic activation rather than alkylating cells directly. CPA is metabolized *in vivo* by cytochromes p450 into 4-hydroxy-CPA (4-OH-CPA) which exists in equilibrium with its acyclic tautomer, aldophosphamide (AP). AP spontaneously decomposes via a beta-elimination cleavage into stoichiometric amounts of the active cytotoxins acrolein and phosphoramide mustard (PM). Ifosfamide (3-(2-chloroethyl)-2-(2-chloroethylamino) tetrahydro-2H-1,3,2-oxazaphosphorine 2-oxide; IFOS) is a recently approved oxazaphosphorine alkylating agent used in cancer chemotherapy as an antitumor agent and immunosuppressant. A nitrogen mustard derivative and structural isomer of cyclophosphamide (CPA), IFOS has been successfully utilized in the treatment of non-Hodgkin lymphomas and solid malignomas such as bronchogenic carcinoma and certain sarcomas. Analogous to CPA, IFOS is a prodrug hepatically activated by a microsomal mixed-function oxygenase, although its metabolism may proceed through a different mechanism than CPA metabolism generating a different toxicity profile. Side-chain oxidation and subsequent liberation of the toxin chloroacetaldehyde comprises a competitive metabolic pathway to the ring oxidation at the C4 position (generating 4-OH-IFOS) observed with CPA. 4-OH-IFOS undergoes a subsequent spontaneous beta-cleavage to generate the active cytotoxins acrolein and IFOS-phosphoramide mustard (IFOS-PM). Consequently, serum concentrations of IFOS-PM are lower than those of the corresponding activated CPA mustard measured after administration of the same dose of parent compound, and IFOS is usually administered in greater dose than CPA.

Gas chromatography/mass spectrometry (GC/MS) and methodologies based upon high performance liquid chromatography (HPLC) with ultraviolet (UV), fluorescence and electrochemical detection have been developed to quantitate CPA and its metabolites in biological fluids. However, none of these techniques offers the sensitivity and rapid analysis time necessary for extensive clinical analyses. Consequently, we have developed an accurate, precise, rapid, and specific LC/MS assay for CPA and IFOS utilizing on-line coupling of an HP 1090 Series II LC with a Finnigan TSQ 7000 mass spectrometer. The chromatographic system consisted of a Zorbax C_8 reverse-phase column (2.1 x 150 mm; 5 μm) operated at 50 °C using a flow rate of 200 μL/min and a methanol/water solvent system containing 0.05% (v/v) acetic acid. Chromatographic conditions were as follows: A 65:35 H_2O:MeOH solution was held isocratically for thirteen min followed by a linear gradient to 80% MeOH in eight min. This condition was held isocratically for an additional five min prior to a ten min re-equilibration.

Mass spectrometric analysis was conducted using electrospray ionization (ESI) with a needle voltage of 4.5 kV. All operating parameters were optimized using CPA. Nitrogen was used as the sheath gas (65 psi) and the auxiliary gas (20 psi) to assist with nebulization. The capillary was heated to 200 °C to provide optimal desolvation, and the ES interface and mass spectrometer parameters were optimized to obtain maximum sensitivity without sacrificing unit resolution. Trofosfamide (N,N,3-Tris(2-chloroethyl)tetrahydro-2H-1,3,2-oxazaphosphorin-2-amine 2-oxide; TROFOS) was utilized as the internal standard, and selective reaction monitoring (SRM) experiments were conducted for each analyte. Figure 1 represents an LC/ES MS/MS analysis from an on-column injection of 800 pg each of CPA, IFOS and TROFOS displaying ion current chromatograms for *m/z* 323 → *m/z* 154 (TROFOS; top panel), *m/z* 261 → *m/z* 140 (CPA) and *m/z* 261 → *m/z* 154 (IFOS; middle panel) and the total ion current (bottom panel) for a gradient analysis. As seen in the Figure, IFOS and CPA were separated

to baseline resolution and eluted at 10.2 min and 11.4 min, respectively. TROFOS eluted at 24.1 min.

During SRM studies, a collision offset energy of -24.0 eV and a collision cell pressure of 2.48 mTorr were employed to induce fragmentation within the collision cell. Argon was used as the collision gas. The tube lens and the capillary were optimized for operation at 110.4 V and 20.0 V, respectively, and the electron multiplier was set at 1600 V. This technique allows for reproducible, specific, rapid and precise analysis of these compounds and will be validated for determination and quantitation of these antineoplastic agents in biological media.

This work was supported by NIH grant CA 68485-01.

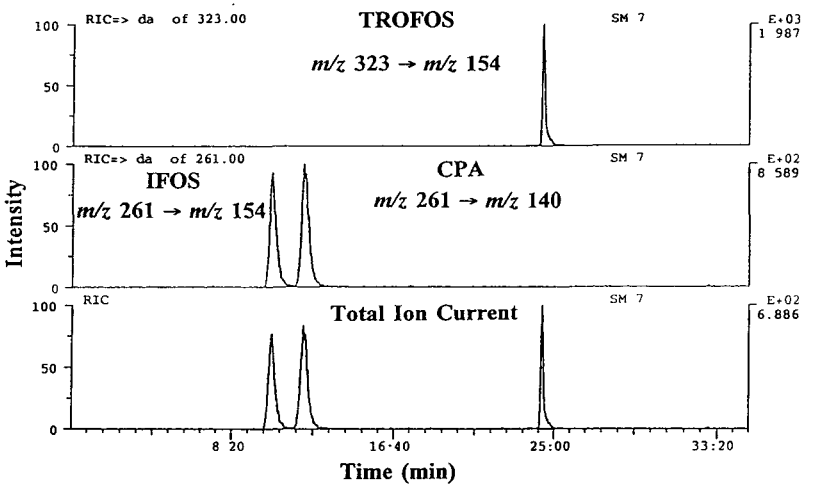

Figure 1. LC/ES MS/MS analysis from an on-column injection of 800 pg each of CPA, IFOS and TROFOS displaying ion current chromatograms for *m/z* 323 → *m/z* 154 (top panel), *m/z* 261 → *m/z* 140 and *m/z* 261 → *m/z* 154 (middle panel) and the total ion current (bottom panel) for a gradient analysis.

Determination of 2-Amino-5,6-dichloro-3,4-dihydroquinazoline, a Major Urinary Metabolite of Anagrelide, by Liquid Chromatography/Tandem Mass Spectrometry (LC/MS/MS)

Frank J. Belas[1], Suresh N. Yeola[1], Carlos O. Garner[3], Samir A. Saleh[1], Ajai K. Chaudhary[1,2], Bruce H. Migdalof[4], and Ian A. Blair[1,3]. Departments of Pharmacology[1], Biochemistry[2], and Chemistry[3], Vanderbilt University School of Medicine, Nashville, TN 37232 and Roberts Pharmaceutical Corporation[4], Meridian Center III, 6 Industrial Way West, Eatontown, New Jersey 07724

Anagrelide (6,7-dichloro-1H-2,3,4,5-tetrahydroimidazo-[2,1-b]-quinazolin-2-one monohydrochloride) is a potent inhibitor of agonist-induced platelet aggregation (Fleming and Buyniski, 1979), and its major urinary metabolite is 2-amino-5,6-dichloro-3,4 dihydroquinazoline (Figure 1). The present study was initiated in order to help delineate the fate of anagrelide after dosing human subjects. The assay is based upon liquid chromatography/tandem mass spectrometry (LC/MS/MS) using the monochloro-analog of anagrelide, 6-chloro-1,5-dihydroimidazo-[2,1-b]-quinazolin-2(3H)-one, as the internal standard (Figure 1).

Liquid chromatography was conducted using a Hewlett-Packard 1090 series II liquid chromatograph equipped with a Zorbax Rx C-8 column (2.1 mm x 150 mm, 5 μm) interfaced with a Finnigan TSQ 7000 triple quadrupole mass spectrometer operating with an electrospray ionization (ESI) source. Solvent A was 5 mM aqueous ammonium acetate containing 0.5 % (v/v) acetic acid and 0.02 % (v/v) trifluoroacetic acid, and solvent B was 5 mM ammonium acetate in acetonitrile:water (9:1) containing 0.5 % (v/v) acetic acid and 0.02 % (v/v) trifluoroacetic acid. The flow rate was 200 μL/min. The solvent composition was held at 85 % A:15 % B for 4 minutes after which a linear gradient to 20 % A:80 % B was employed over the following 8 minutes. The solvent composition was held at 20% A : 80% B for 1 minute and was then returned to the initial conditions during the next 3 minutes. Samples were dissolved in a total volume of 2 mL, and 50 μL of this solution was injected on column. The mean retention times for the metabolite and internal standard were 12.50 and 12.27 min, respectively.

Mass spectrometry studies were conducted using a Finnigan TSQ 7000 triple quadrupole mass spectrometer operating with an ESI needle voltage of 4.5 kV. Nitrogen was used as the sheath gas (70 psi) and the auxiliary gas (25 psi) to assist with nebulization. The capillary was heated to 240 °C to provide optimal desolvation, and the ESI interface and mass spectrometer parameters were optimized to obtain maximum sensitivity without sacrificing unit resolution. A selected reaction monitoring (SRM) experiment was conducted by monitoring the *m/z* 216 → *m/z* 199 transition of the metabolite. Similarly, for the internal standard, the *m/z* 222 → *m/z* 165 transition was monitored. An SRM ion current profile from urine (1 mL) containing metabolite (17.2 ng) and internal standard (20.0 ng) is shown as Figure 2. Calibration curves obtained by plotting the peak height ratio of metabolite to internal standard against the amount of metabolite added to the urine were linear in the range 1.7 ng/mL to 86.1 ng/mL using a weighted (1/concentration) least squares regression analysis. Correlation coefficients of 0.995 or better were obtained. The within-day precision of the method was determined from the relative standard deviation (RSD) of the mean for seven replicate analyses of the three control

pools on each of three days. The overall precision of the method was determined from the RSD of the mean of 21 analyses of the three control pools over 3 days. The within-day precision of the metabolite assay ranged from 3.7 % to 9.7 % RSD at the three control concentrations in human urine during the three days of the assay. The overall precision was 8.4 % for the lower quality control (LQC), 5.9 % for the middle quality control (MQC), and 6.5 % for the upper quality control (UQC), respectively. The accuracy of the urine metabolite assay was determined by comparing the means of the measured concentrations with the theoretical concentrations of metabolite in the urine controls. The overall mean values, at each level, did not exceed 8.8 % of their expected values. The lower limit of quantitation (LLQ) of the anagrelide urinary metabolite was 1.72 ng/mL. At this level, the RSD (n = 7) of the measured concentrations was 13.1 %. The deviation of the mean of the measured concentration from the theoretical concentration (DEV %) was -9.5 %.

The method presented for the determination of the urinary metabolite of anagrelide in human urine shows acceptable specificity, linearity, precision, and accuracy for the determination of metabolite concentration at a lower limit of quantitation of 1.7 ng/mL. The method is simple, robust, amenable to high sample throughput and further illustrates the utility of LC/MS/MS methodology for obtaining quantitative information from clinical studies.

References:

Fleming, J.S., and Buyniski, J.P. A potent new inhibitor of platelet aggregation and experimental thrombosis, anagrelide (BL-4162A). *Thrombosis Research*, **15**, 373-388, 1979.

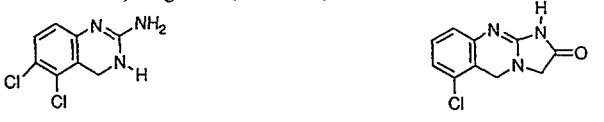

2- Amino-5,6-dichloro-3,4-dihydroquinazoline 6-Chloro-1,5-dihydroimidazo-[2,1b]-quinazolin-2-(3H)-one

Figure 1. Structures of the urinary metabolite of anagrelide (2-amino-5,6-dichloro-3,4 dihydroquinazoline) and the internal standard (6-chloro-1,5-dihydroimidazo-[2,1-b]-quinazolin-2(3H)-one).

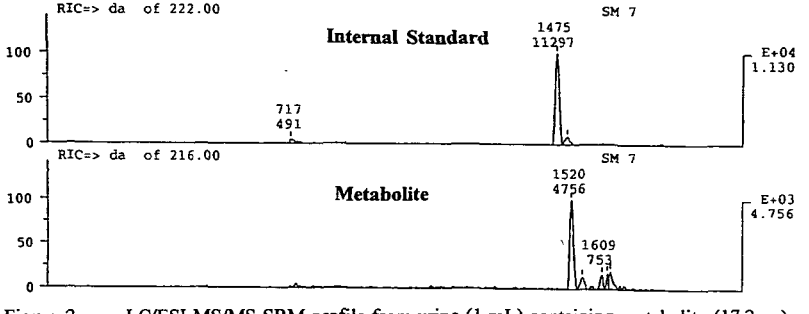

Figure 2. LC/ESI MS/MS SRM profile from urine (1 mL) containing metabolite (17.2 ng) and internal standard (20.0 ng).

STRATEGIES FOR THE QUANTITATIVE ANALYSIS OF OPIOID PEPTIDES IN PLASMA

Cristina Marquez and Philip C. Smith
The University of North Carolina at Chapel Hill

Robert T. Streeper and Susan T. Weintraub
The University of Texas Health Science Center at San Antonio

Structural elucidation and quantitative analysis of biologically active peptides are of considerable importance in understanding both the roles that these peptides play in normal and disease states as well as in the development of peptide-based pharmaceuticals. Neuroactive peptides are of particular interest due to the probability that disorders of neuropeptide processing are responsible for various pathological conditions. Essential to the study of neuropeptide pharmacology is the development of specific and sensitive analytical methods. Problems with many currently used assays for neuropeptides have led us to employ HPLC-ESI/MS/MS for the quantitative analysis of neuropeptides. The high degree of selectivity and sensitivity of this technique combined with the shortened analysis times and minimal requirements for sample preparation make LC-ESI/MS/MS ideal for analysis of samples of biological origin. This presentation describes the quantitative analysis of two opioid peptides, Met-enkephalin-Arg-Gly-Leu (Tyr-Gly-Gly-Phe-Met-Arg-Gly-Leu) and DSLET (Tyr-D-Ser-Gly-Phe-Leu-Thr) in plasma, using microbore-HPLC-ESI/MS/MS. Application of the analytical method to study the disposition of DSLET in rats is also described.

Peptide Stability - Stability studies were performed *in vitro* by incubation of each peptide at a concentration of 100 µg/ml in 25% plasma. Aliquots were removed at intervals between 0 and 30 min and the peptide quantified by HPLC with UV detection at 214 nm. The half-life of Met-enkephalin-Arg-Gly-Leu in 25% plasma was found to be 40 min while for DSLET $t_{1/2}$ was 480 min.

Sample Preparation - Standard samples were prepared by serial dilution and added to 0.5 ml of human plasma (0 - 1000 ng of peptide/ml of plasma). The corresponding deuterated internal standards were added to yield 50 ng/ml for Met-enkephalin-Arg-Leu-Gly-d_{10} (Tyr-Gly-Gly-Phe-Met-Arg-[$^2H_{10}$]Leu-Gly) and 10 ng/ml for DSLET-d_3 (Tyr-D-Ser-Gly-Phe-[$^2H_3$]Leu-Thr). The peptides were isolated from the plasma by solid-phase (C18) extraction. The peptide fractions were dried *in vacuo* and reconstituted in 25 µl of mobile phase prior to analysis by HPLC-ESI/MS/MS. Extraction recovery was assessed by radioactivity monitoring of [^{3}H]-DSLET and by HPLC with UV detection for Met-enkephalin-Arg-Gly-Leu and its deuterated analog. The overall recoveries were: Met-enkephalin-Arg-Gly-Leu, 65%; DSLET, 85%.

Mass Spectrometry - Electrospray ionization mass spectra were acquired on a Sciex API III mass spectrometer fitted with an ionspray interface. MS conditions were: ionspray voltage, 5500 V; orifice voltage, 60 V; collision gas, argon; collision energy, -20 V for Met-enkephalin-Arg-Gly-Leu and -25 V for DSLET; collision gas thickness, 131 for Met-enkephalin-Arg-Gly-Leu and 120 for DSLET. A polypropylene glycol mixture was utilized for instrument calibration.

HPLC - Chromatographic fractionation was accomplished by means of an Applied Biosystems model 140B solvent delivery system in conjunction with a Keystone Hypersil BDS C18 column (1.0 x 50 mm) fitted with a 20 mm guard column. The flow rate of the mobile phase was 50 µl/min. The binary solvent system consisted of: solvent A, 2 mM ammonium acetate, pH 4.4; solvent B, 60% aqueous acetonitrile. The gradient was produced by increasing the concentration of B from 20 to 80% over 10 min at which time the mobile phase was maintained at 80% B for an additional 2 min. A Valco switching valve that was connected to the mass spectrometer by a short length of fused silica capillary tubing was utilized to direct the effluent from the HPLC. The fractions eluting prior to 5 min were discarded. In order to ensure stability of the electrospray ion current, a 10-µl/min flow of 60% acetonitrile/2 mM ammonium acetate, pH 4.4 (1:1) was maintained through the interface during the initial 5-min period.

Quantitative Analysis - Quantification of peptides was accomplished by selected reaction monitoring of the following transitions: Met-enkephalin-Arg-Gly-Leu, m/z 450.5—>136.0 for d_0 and m/z 455.5—>136.0 for d_{10}; DSLET, m/z 687.0—>540.0 for d_0 and m/z 690.0—>543.0 for d_3. A representative selected ion retrieval chromatogram is shown below along with a typical standard curve for DSLET added to plasma. Linearity was routinely observed for both peptides over the range of 5 to 1000 ng/ml, with a limit of detection of 0.25 ng/ml for Met-enkephalin-Arg-Gly-Leu. A comparison of approaches to evaluate the standard curve data showed that a linear regression weighted by 1/x gave a better fit for the low mass range than when a non-weighted regression was employed.

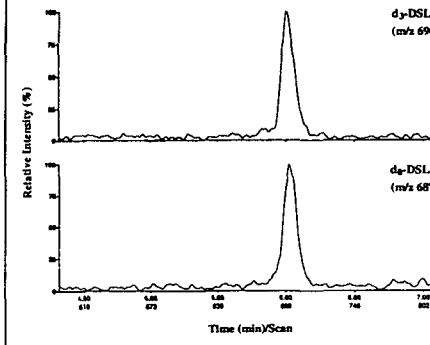

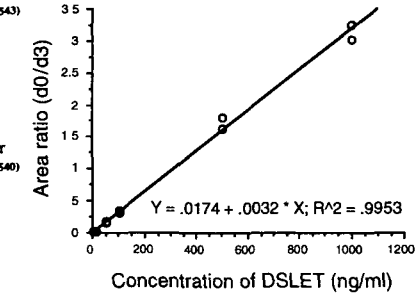

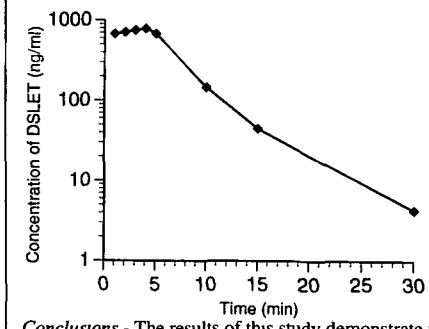

DSLET Disposition in Rats - The disposition of DSLET was examined in rats administered an intravenous dose of 10 mg/kg of the peptide. Arterial blood samples (0.25 ml) were collected at intervals between 0 and 30 min after injection. After addition of 10 ng/ml DSLET-d_3, the peptide fraction was isolated as described above. A representative concentration-time profile is shown to the left.

In agreement with the results obtained by other methods, quantitative analysis by HPLC-ESI/MS/MS showed that DSLET has a short half-life and high clearance value.

Conclusions - The results of this study demonstrate that HPLC-ESI/MS/MS can be utilized for quantitative analysis of Met-enkephalin-Arg-Gly-Leu and DSLET in plasma. A 5-fold lower detection limit was observed for Met-enkephalin-Arg-Gly-Leu as compared to DSLET. However, DSLET exhibited a broader range of linearity than Met-enkephalin-Arg-Gly-Leu. In most instances, the coefficient of variation for replicate samples was less than 15%, although occasional lack of reproducibility was observed. Further experiments must be conducted to determine if this variability is related to sample preparation or is of instrumental origin.

Acknowledgements - We are grateful to Glaxo Inc. for the use of the Sciex API III mass spectrometer and to Dr. Arthur Moseley, Dr. Steve Unger and Kathy Halm in the Department of Drug Metabolism for their assistance with this project. This work was supported by NIH grant number GM41828 and a Pharmaceutical Manufacturers Association Foundation Faculty Development Award to PCS.

Electrospray LC/MS and LC/MS/MS of Ecdysteroids

Russell P. Grant, Dai E. Games, M.S.R.U, Chemistry Department,
U.W. Swansea, Swansea, Wales, SA2 8PP
Ian D.Wilson, E. D. Morgan, Department of Chemistry,
Keele University, Keele, England, ST5 5BG

Introduction

Ecdysteroids are polyhydroxylated steroid compounds which participate in the regulation and development processes of invertebrates. Ecdysteroid concentrations in plant samples are very low, hence, highly sensitive and specific methods of analysis are required to identify them. Previous investigations have used GC, SFC, TLC and HPLC coupled with EI, CI, FAB and thermospray mass spectrometry. The requirement of pre-derivatization, however, precludes their use in trace analysis. The sensitivity potential of pneumatically assisted electrospray LC/MS combined with the specificity available via LC/MS/MS suggest that these techniques could be useful for the screening of plant samples.

Experimental

An HP1050 hplc system (Palo Alto, CA) with a C18 analytical column (200 x 4.6mm, 5 micron) (Shandon, Runcorn, UK) was employed using a flow rate of 1 ml/minute of Acetonitrile 23% : Water (TFA 0.1%) 77%. Mass spectrometry was performed using a Finnigan MAT TSQ 700 triple stage quadrupole via an electrospray interface (both Finnigan, MAT, San Jose, CA). Positive ions were detected in full scan mode (200-600 m/z, 2 seconds) with 200 ul/minute flow rate, 60 psi sheath N_2, 40 psi auxiliary N_2 and a capillary temperature of 240°C. A collision cell pressure of 1.5 mTorr of argon and a collision offset potential of -50eV were employed in the MS/MS studies.

Results and Discussion

The LC/MS analysis of a large number of ecdysteroids shows a variety of peaks corresponding to various ions being produced in the source. A typical spectrum is that shown for ecdysone (figure 1). The diagnostic spectra produced enable molecular mass elucidation, although with the number of analogs present within complex biological samples, these spectra cannot be considered specific. The detection limits for ecdysone and 20-hydroxyecdysone are 100ng and 50ng in full scan mode and 250pg and 150pg on-column in SIM respectively. These limits allow full scan screening of complex samples for ecdysteroids and a *Silene nutans* plant extract is shown (figure 2). The peaks were assigned using LC/MS/MS and a typical spectrum is shown (figure 3). The various ions seen originate from cleavages in the side chain (1-7) and also from losses of water molecules (8,9) from the parent ion (10) ($[M + H - H_2O]^+$, the base peak for ecdysone).

Conclusions

The use of LC/MS and LC/MS/MS via electrospray is shown to be very useful in the analysis of ecdysteroids. The detection limits available in full scan mode allow the screening of complex biological mixtures to be undertaken and the diagnostic LC/MS spectra combined with the highly specific LC/MS/MS spectra enable unambiguous assignment of ecdysteroid components.

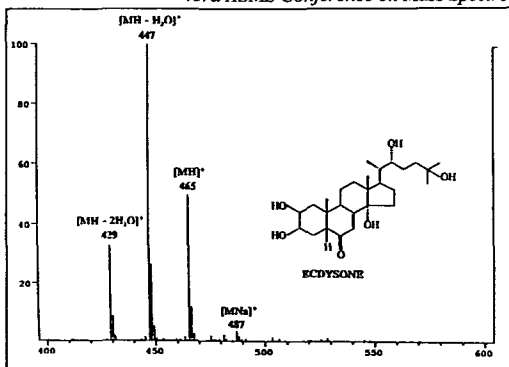

Figure 1 LC/ES/MS spectrum of Ecdysone

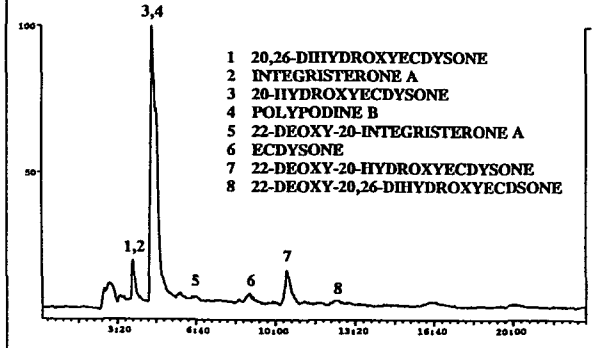

Figure 2 LC/ES/MS spectrum of a *Silene nutans* plant extract

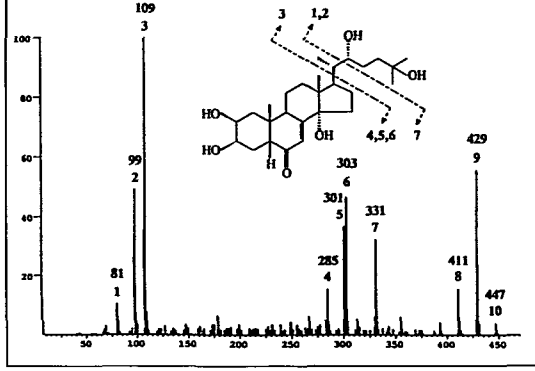

Figure 3 LC/ES/MS/MS spectrum of Ecdysone

High Performance Liquid Chromatography/Electrospray Ionization/Tandem Mass Spectrometry Studies on the Metabolic Fate of the Atherosclersis Combatant CP-230,821

E. W. Luther, M. J. Cole, S. Boyer

Drug Metabolism Department, Central Research Division, Pfizer Inc, Groton, CT 06340

CP-230,821 (Figure 1) is currently undergoing evaluation in our laboratories as a novel compound to combat atherosclerosis. Identification of metabolic pathways aids in the discovery and long-term development processes. HPLC with ESI and triple quadrupole mass spectrometry provide an effective means by which to elucidate these metabolic pathways.

Nine mono-oxidation products were identified in rat microsomal preparations. Individual HPLC precursor and CAD product ion scans were used to determine the presence and structures of the metabolites. The two major metabolites identified are hydroxylation on the 1,4 benzodioxane moiety, and represent oxidation of the cis and trans isomers of CP-230,821.

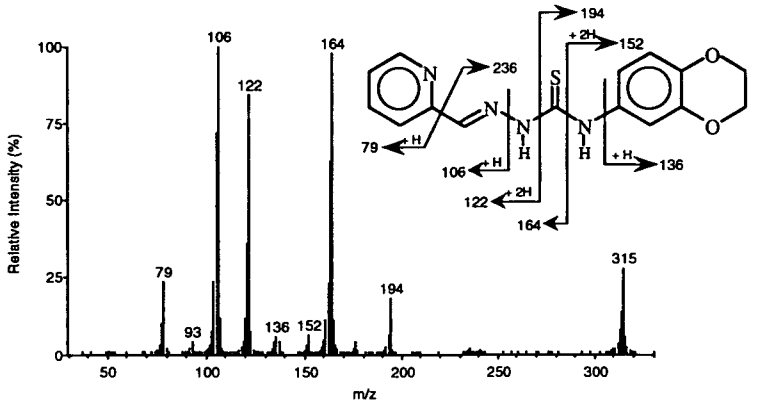

Figure 1. CID spectrum and proposed dissociation of CP-230,821.

Structures of CP-230,821 and Proposed Metabolites Found in Rat Microsomal Preparations

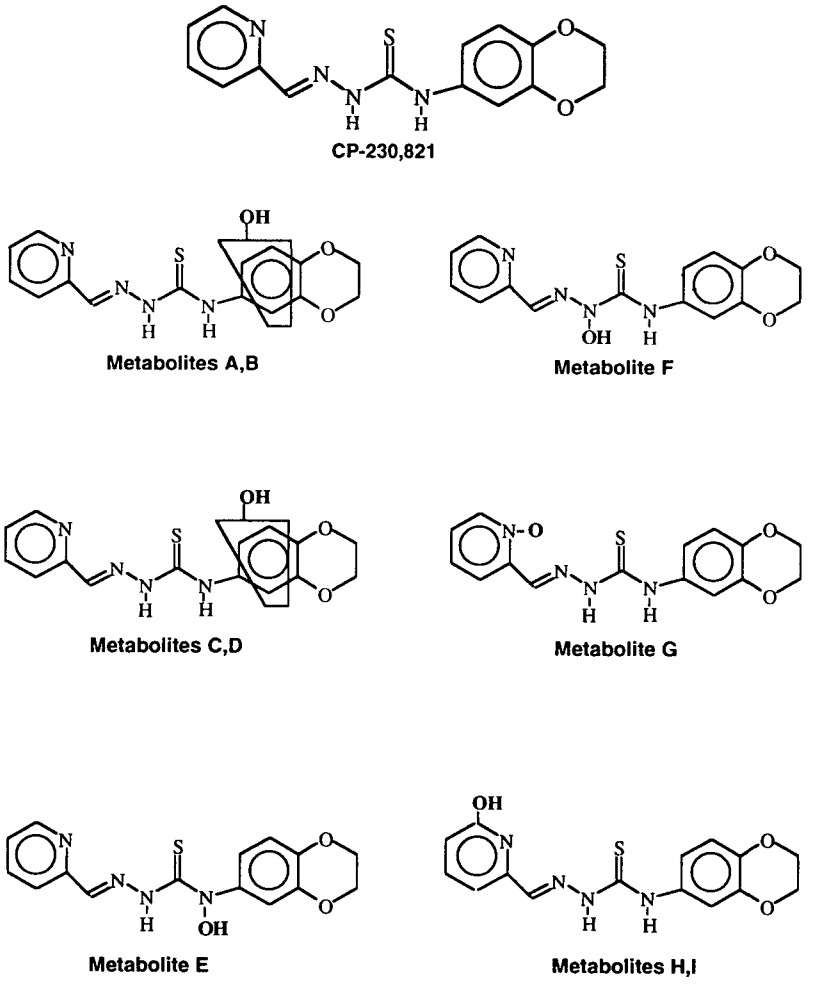

High-Performance Liquid Chromatography/Diode-Array Detection/ Electrospray Ionization/Tandem Mass Spectrometry Studies on the Metabolic Fate of the Novel PDE4 Inhibitor CP-80,633

J.W. Gauthier, M.J. Cole, E.L.Bachert, T.E. Liston

Drug Metabolism Dept.
Pfizer Inc, Central Research
Eastern Point Road
Groton, CT 06340

ABSTRACT:

CP-80,633 is a novel PDE4 inhibitor currently undergoing evaluation in our laboratories. Identification of metabolic pathways aids in the discovery and long-term devlopment processes. HPLC/on-line diode array detection combined with electrospray ionization and triple quadrupole mass spectrometry provide an effective means in which to elucidate these metabolic pathways.

Samples were analyzed from several different biological matrices, including rat plasma following I.V. and I.P. administration, human serum following oral administration, and rat urine following I.P. administration. Six drug-related compounds were identified in these matrices. A variety of mass spectrometric experiments, including precursor, neutral loss, full CID product ion, and conventional mass spectral scans provided a full metabolic profile. Metabolites identified were all Phase I-type species and included 2 species representing hydroxylation of the norbornyl moiety, 3 products corresponding to carbonyl formation on the norbornyl moiety, and one species representing O-demethylation. On-line diode array detection allowed relative quantitation of the metabolites. Norbornyl oxidation is the major route of metabolism for this molecule.

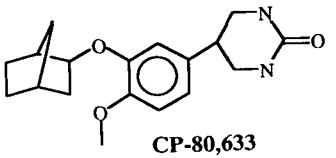

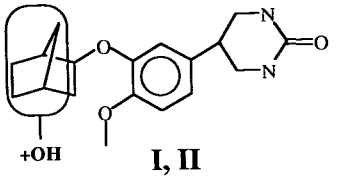

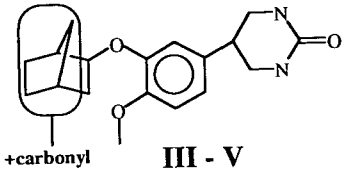

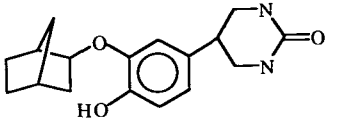

FIGURE 1: Structures of CP-80,633 and the proposed metabolites

HPLC/ESI/MS/MS Studies on the Metabolic Fate of the LTB4 Receptor Antagonist CP-105,696 and Evidence of Intramolecular Acyl Migration of an Ester Glucuronide Conjugate

Mark J. Cole, Jeffrey W. Gauthier, Elbridge W. Luther, Hassan G. Fouda, Rosalina Destito, Theodore E. Liston

Drug Metabolism Department, Central Research Division, Pfizer Inc, Groton, CT 06340.

Plasma and bile metabolite profiles of the LTB_4 receptor antagonist CP-105,696 were generated to investigate the degree of metabolism in rat, dog, and monkey. High performance liquid chromatography, in conjunction with electrospray ionization tandem mass spectrometry, was used to identify eleven metabolites. The determination of these metabolites was based on a scheme of precursor and CAD product ion scans that identify drug-related components and provide structurally significant data, respectively. The CAD spectrum and structure of CP-105,696 are shown in Figure 1.

Three of the eleven metabolites were the result of glucuronidations. The chromatogram obtained from CAD scans of the expected glucuronide ion contains an early eluting peak and two closely-spaced later eluting peaks. The early eluting peak was identified as glucuronidation of the 4-hydroxy-chroman-7-yl moiety. The later two peaks represent ester glucuronides; the first represents the conventional ester glucuronide and the second results from an intramolecular acyl migration[1]. The structures of these latter two glucuronide conjugates were determined from their CAD spectra, as shown in Figure 2. The numerous peaks between m/z 622 and 411 in the CAD spectrum of the migration product provide evidence for the structure as drawn. The resistance of the migration product to B-glucuronidase provided further evidence for this assignment. Acidification of the sample during collection assured that this product was not formed as a result of sample handling.

1. E. Faed, *Drug Metab. Rev.*, 1984, *15*, 1213-1249.

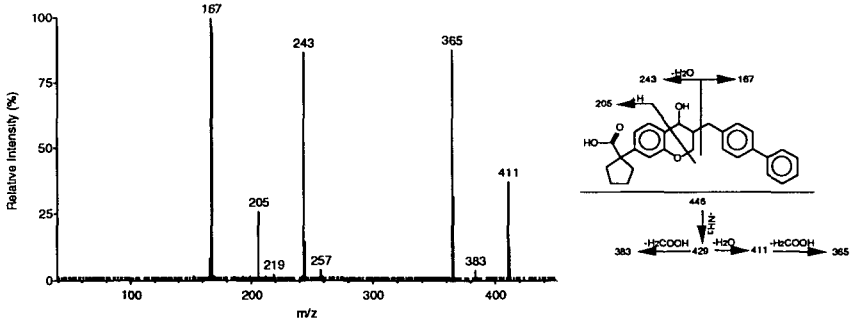

Figure 1. CAD Spectrum and Proposed Dissociation of CP-105,696

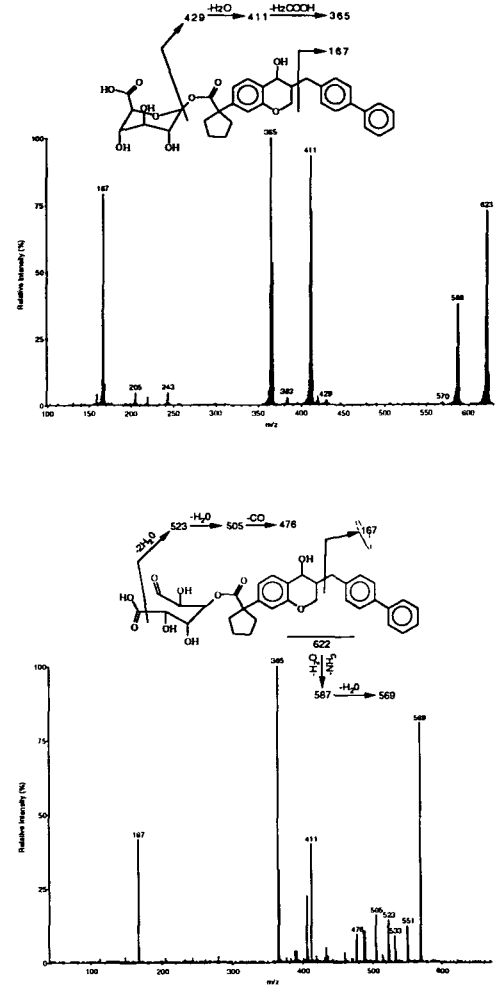

Figure 2. CAD spectra and proposed dissociations of a) acyl glucuronide and b) acyl migration product

HPLC/MS/MS Determination of CP-118,954 in Human Serum

M. Avery, S. Needham and H. Fouda
Central Research Division, Pfizer INC. Groton, CT 06340

CP-118,954 (Figure 1) is a cholinesterase inhibitor with utility for the management of Alzheimers disease. An analytical method for its determination in plasma was desired to support the investigation of its pharmacokinetics.

At clinically relevant doses, serum concentrations of 10 pg/mL were expected. GC/MS methods were not viable due to significant adsorption on capillary columns and attempts at derivatization failed. Standard HPLC methods were not successful due to insufficient sensitivity using UV detection. A successful assay was developed using a simple liquid-liquid extraction and detection by HPLC/APCIMS/MS. A stable isotope internal standard (I.S.) was used to correct for differences in extraction efficiency and to improve accuracy and precision.

The experimental procedure consisted of fortifying a 1 mL serum sample with the internal standard, adjusting the pH to 10 and extracting with 5 mL of n-butyl chloride. The organic layer was isolated after freezing the aqueous layer in dry ice/i-propanol and the solvent removed by evaporation. The reconstituted sample was chromatographed on a NovPak C18 column using a mobile phase of 72/25 MeOH/ 10 mM ammonium acetate. The entire HPLC column effluent was introduced into the APCI ion source of a SCIEX API III+ mass spectrometer where positive molecular ions were generated by a Corona discharge. MH^+ ions at m/z 376 were dissociated by collision with Argon and the major product ion at m/z 91 was monitored. This Multiple Reaction Monitoring (MRM) experiment produced high sensitivity and selectivity (Figure 2). Since the internal standard contained 5 deuterium's in the phenyl ring, the MRM reaction m/z 381->96 was used to measure the I.S. Typical responses for blank samples, LLOQ (10 pg/mL) and 0.1 ng/mL are shown in Figure 2.

The performance of the assay was characterized by assaying six replicates at serum concentrations of 0.01, 0.05, 1.0, 5.0, and 10 ng/mL. The results, shown in Table I, demonstrate that the assay has an accuracy and precision of 94% and 10% respectively.

Table 1. Analysis of human serum samples known amounts of CP-118,954: intra-assay parameters; 6 samples at each concentration.

Fortified Drug Conc. (pg/ml)	Mean Conc.found (pg/mL)	R.S.D. (%)	Mean Accuracy (%)
10	10.8	5.2%	108%
50	49.9	10%	99.8%
1000	1058	2.5%	106%
5000	5160	2.5%	103%
10,000	10,600	4.2%	106%

43rd ASMS Conference on Mass Spectrometry and Allied Topics

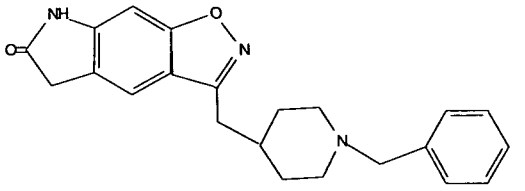

Figure 1. Structure of CP-118,954; molecular weight is 375 daltons.

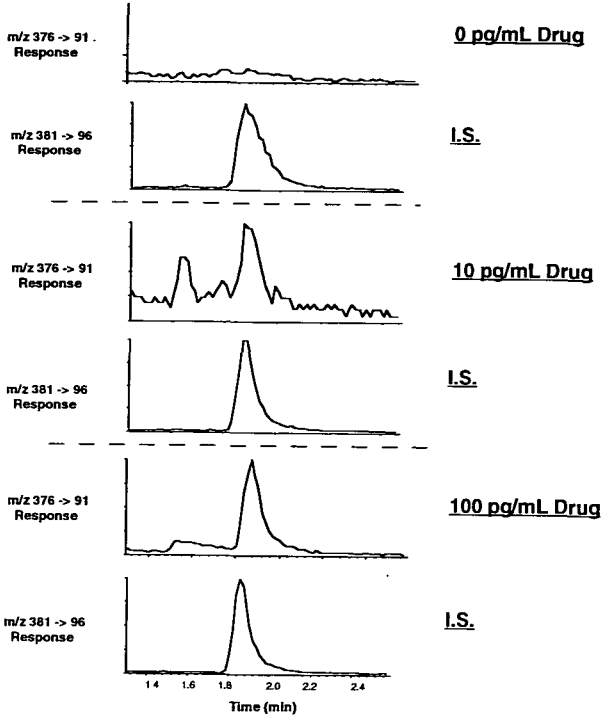

Figure 2. MRM responses for HPLC/APCIMS/MS analysis of extracts of human serum fortified with CP-118,954.

An HPLC/APCI-Tandem Mass Spectrometry Method for the Quantitative Analysis of the Cholesterol Absorption Inhibitor 11-ketotigogenin cellobioside (CP-148,623) and its metabolite 11-ketotigogenin (CP-154,528).

J.W. Gauthier,* P. Butala, E.W. Luther, M.J. Cole, and H.G. Fouda

Drug Metabolism Dept.
Pfizer Inc, Central Research
Eastern Point Road
Groton, CT 06340

ABSTRACT:

CP-148,623 is a promising cholesterol sequestering agent currently undergoing clinical evaluation. Serum levels are expected to be low, and therefore a sensitive and specific method was required to support pharmacokinetics studies. The assay utilizes HPLC and atmospheric pressure chemical ionization tandem mass spectrometry (APCI-MS). The drug and internal standard, penta-deuterated CP-148,623, are extracted from 1.0 ml of serum after protein precipitation with acetonitrile, and then derivatized with acetyl chloride, increasing the molecular weight of each by 294 daltons. The protonated molecule of both drug and internal standard undergo collisionally-activated dissociation (CID) to form a specific product ion. Concentrations of CP-148,623 in serum are determined by monitoring this reaction. The upper and lower levels of quantitation are 500 ng/ml and 10 ng/ml, respectively, for the high volume assay and 15 ug/ml and 0.1 ug/ml for the low volume assay. The assay is robust and analyses have been performed on several thousand toxicology and clinical samples. In addition, an assay for the putative metabolite of CP-148,623, CP-154,528, has been developed in a similar fashion.

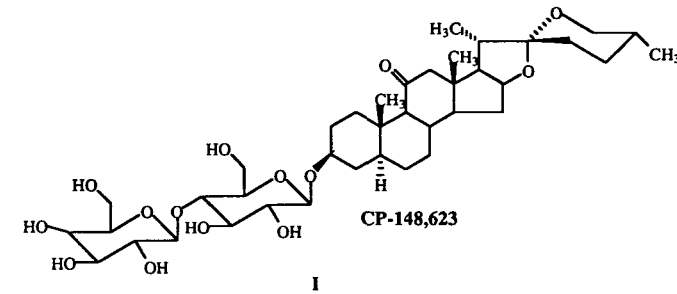

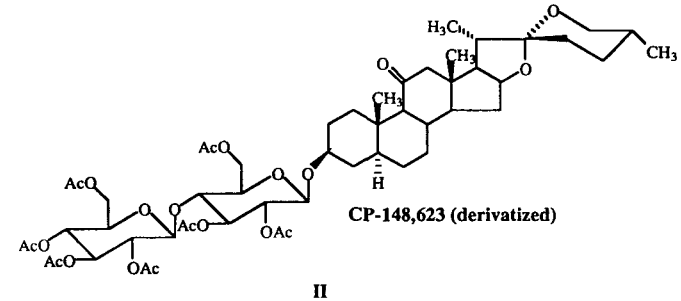

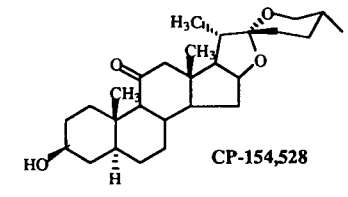

FIGURE 1: Structures of CP-148,623 and CP-154,528

Characterization of Metabolites of Ziprasidone in Human by LC-MS/MS

Chandra Prakash*, Amin Kamel, Wayne Anderson and Keith Wilner
Departments of Drug Metabolism and Clinical Research, Central Research Division, Pfizer Inc., Groton, CT 06340.

Introduction:

Ziprasidone, 5-[2-{4-(1,2-benzisothiazole-3-yl)-1-piperazinyl}ethyl]-6-chloro-1,3-dihydro-2H-indole-2-one hydrochloride hydrate, is a new neuroleptic agent undergoing investigation that displays a pharmacological profile indicative of atypical antipsychotic activity with little or no liability for motor side effects. It has extremely potent central serotonin 5-HT2 and potent dopamine D2 receptors antagonistic properties. Previous studies have shown that ziprasidone was extensively metabolized in laboratory animals, since < 2% of the administered dose was excreted in urine as an unchanged drug. This work was conducted to determine the metabolic pathways of ziprasidone in human subjects. HPLC, in conjunction with ionspray mass spectrometry and simultaneous monitoring the radioactivity, was used to detect and identify the metabolites.

Materials and Methods:

Four normal healthy male volunteers received a single oral 20 mg dose of a mixture of ziprasidone labeled with ^{14}C at the C-2 position of the ethyl group attached to the piperazinyl nitrogen and ^{3}H at the C-7 position of benzisothiazole (Figure 1). The use of two labels at these positions, not only facilitated the tracing of metabolites that were formed through cleavage of ziprasidone, but also aided in their identification. Blood, urine and feces were collected at various intervals for determination of total radioactivity and metabolite profiles in three matrices

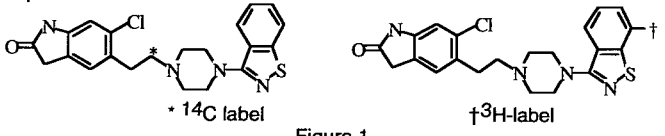

Figure 1

The analysis of the metabolites was performed on a SCIEX API III HPLC/MS/MS system using ion spray. HPLC was carried out on a YMC basic HPLC column (4.6 µm x 250 mm, 5 µm: YMC) with a binary mixture of 20 mM ammonium acetate (pH 5.0, solvent A) and methanol (solvent B). The mobile phase initially consisted of solvent A/solvent B (90:10) for 10 min. It was then linearly programmed to solvent A/solvent B (20:80) over 50 min. Chromatography was carried out under isocratic conditions for 7 min and then programmed back to the starting solvent mixture over 8 min. The effluent from the HPLC column was split and about 50 µl/min was introduced into the atmospheric ionization source via an ion spray interface. The remaining effluent was directed into the flow cell of β-RAM. The β-RAM response was recorded in real time by the mass spectrometer that provided simultaneous detection of radioactivity and mass spectrometry data. Collision associated dissociation (CAD) studies were performed using argon gas at a collision energy of 56 eV and a collision gas thickness of 6.5 x 10^{14} molecules/cm^2.

Results and Discussion:

A total of 8 radioactive peaks were detected in the chromatogram of a urine sample (0-24 h) from a male volunteer following oral administration of [^{3}H]- and [^{14}C]-labeled

ziprasidone. The metabolites were identified by ion spray LC/MS using a combination of parent, daughter, selected ion, and multiple ion reaction monitoring techniques. Ziprasidone and its metabolites gave the intense protonated molecular ions. CAD product ion spectra of protonated molecular ions provided a number of structurally informative fragment ions. CAD product ion spectra of monooxygenated isomeric metabolites (m/z 429) are shown in Figure 2. Based on the structures of the metabolites, four major routes of metabolism of ziprasidone were identified: 1) N-dealkylation of the ethyl side chain attached to the piperazinyl nitrogen; 2) oxidation at sulfur resulting in the formation of sulfoxide and sulfone; 3) oxidation on the benzisothiazole moiety (other than sulfur) and 4) hydroxylation on the 3-position and subsequent oxidation of the benzisothiazole moiety. The identified metabolites accounted for approximately 97, 64 and 98% of the total radioactivity extracted from urine, serum and feces, respectively.

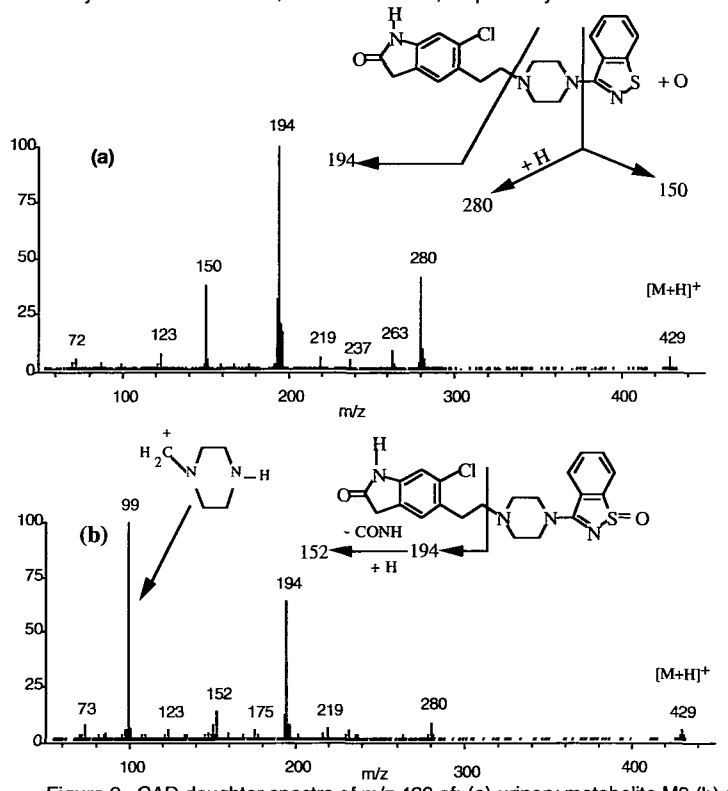

Figure 2. CAD daughter spectra of m/z 429 of: (a) urinary metabolite M9 (b) urinary metabolite M10.

PRECLINICAL DRUG SELECTION - APPLICATION OF IONSPRAY LC-MS AND LC-MS/MS.

*Michele A. Kelly, Guang Xiao, Gerald E. Greenberg, Sandra Kuzmich and Philmore Robertson. Ciba Geigy Corporation, Pharmaceuticals Division, 556 Morris Avenue, Summit, NJ 07901.

Information regarding the metabolism, cell penetration, bioactivation or other properties of compounds is frequently needed at an early stage in drug development in order to ensure optimal compound design and selection. The use of LC-MS and LC-MS/MS, coupled with a partial clean-up of the sample through extraction and/or rudimentary LC separation, can provide the needed information in a relevant time frame. Such timely feedback allows rational drug design to progress, accompanied by the vital information that can be obtained by coupling biological preparations with mass spectrometry. *In vitro* incubations with biological matrices are increasingly used in drug discovery in order to explain and/or predict results from *in vivo* models. The lack of availability of well-established analytical methods often preempts early compound evaluation, where information on stability and/or metabolism would be valuable for compound selection.

Due to the wide variety of cofactors, buffers, etc., required for *in vitro* incubations, sample clean-up or product ion monitoring are used in conjunction with LC-MS when interfering substances are evident. Three distinctly different examples are presented, which demonstrate the utility of LC-MS and LC-MS/MS to quickly deliver relevent information regarding drug candidates. These include the examination of the routes of bioactivation of prodrugs, identification of major routes of Phase I and Phase II metabolism of developmental compounds, and investigation and validation of a gut permeation model.

A PE Sciex API III instrument was utilized for all LC-MS analyses presented here. A Waters HPLC 625 LC system was interfaced on-line with the mass spectrometer. Gradient elutions were carried out using the mobile phases A:acetonitrile and B:10mM ammonium acetate, 0.1% formic acid (pH 3.5), typically from 20:80 to 90:10 (A:B). The HPLC flow rate of 1 mL/min was split in order to deliver approximately 40 µL/min to the ionspray interface. Typical ionspray MS conditions were as follows (positive ion mode): nebulizer flow = 40 psi, curtain gas flow = 1 L/min, interface temperature = 50 °C, ISV = 5 kV, OR = 70 V.

CGS 30440, a double prodrug of a dual inhibitor of angiotensin converting enzyme (ACE) and neutral endopeptidase (NEP), was examined in various *in vitro* incubation conditions in order to understand its routes of bioactivation *in vivo*. A comparison of product profiles from one hour incubations of CGS 30440 in rat and dog plasma shows that the high esterase activity in rat plasma resulted in the partial conversion of CGS 30440 to des-ethyl-CGS 30440, as well as to the intended, fully activated drug CGS 30008. A third product was identified as the disulfide dimer of CGS 30008. In dog plasma, CGS 30440 remained intact after the one hour incubation.

In vitro liver preparations examined at various time points were also utilized to probe the bioactivation of CGS 30440. Incubation in either rat liver homogenate or microsomes resulted in a more complex activation than that seen above in rat plasma. There were subtle differences in the two liver preparations, although they were qualitatively comparable. An additional product formed in rat liver, but not found in rat plasma, was identified as des-acetyl-CGS 30440. This product, containing a free thiol, also formed a disulfide dimer. In liver homogenate, the mono-des-ethyl disulfide was also detected. Des-ethyl-CGS 30440 was again present, and CGS 30008 was detected after an extended incubation period. Providing this information at an early stage in the development of CGS 30440 has aided in understanding the bioactivation process for this drug candidate.

A series of structurally related, arylamidine-containing compounds have been evaluated for efficacy as LTB_4 receptor antagonists. In support of preclinical evaluation of this series, the major routes of metabolism were determined *in vitro* for an N-hydroxy amidine-containing compound. Five metabolites of the N-hydroxy amidinewere present after incubation in rat liver microsomes. The compounds identified, in order of elution, were (A) oxidized and (B) hydroxylated parent drug, (C) amidine, (D) parent drug, (E) ketone, and (F) nitrile.

A characteristic fragment ion was observed for this class of compounds in the positive ion mode. This provided information on the site of metabolism using LC-MS only. The mass differences observed between the molecular ions and the fragment ions confirmed that the modifications shown for compounds C-F occurred on the amidine-containing portion of the molecule. The imino and keto metabolites

probably formed via N-reduction and oxidative transformation[1] pathways, respectively. The nitrile was an unusually lipophilic metabolite, eluting well after the parent compound. The N-hydroxy amidine was also investigated in a human Caco-2 cell line, where metabolism to its amidine was observed.

LC-MS/MS was utilized in the investigation of the metabolism of an early developmental drug. The unknown metabolites of this compound in certain *in vitro* situations were difficult to analyze using LC-MS, due to interfering components. A TIC of a full scan analysis of a Phase I/II incubation of parent drug in rabbit liver microsomes for four hours is shown in Figure 1. Interfering substances are evident, where detergent is masking out much of the baseline. Having analyzed pure parent drug by LC-MS/MS previously, a product ion of this drug was chosen for a precursor ion scan of related compounds. Figure 2 shows the increased selectivity obtained using this method upon injection of the same sample shown in the previous figure.

Using this precursor ion scan, the parent drug (P), Phase I metabolite (M), and their respective Phase II glucuronide conjugates were readily detected as major products. A constant neutral loss scan for 176 Da confirmed the presence of the two glucuronides. A subsequent one hour Phase II analysis of the parent compound in dog liver microsomes also produced a glucuronide conjugate.

The examples presented above represent the variety of pharmacological problems often encountered in early compound development. By exploiting the versatility of ionspray LC-MS and LC-MS/MS, information can now be obtained for use in drug selection, which was previously unattainable. Feedback regarding the bioactivation, metabolism or other properties of drug candidates aids in the drug selection process, where structurally similar compounds often require further means of differentiation beyond pharmacological activity. LC-MS in conjunction with *in vitro* biological preparations is a useful way in which to obtain timely information to facilitate drug discovery.

1 Bernd Blement and Frand Jung *Drug Metabolism and Disposition.* 22(3), 486-497. (1994)

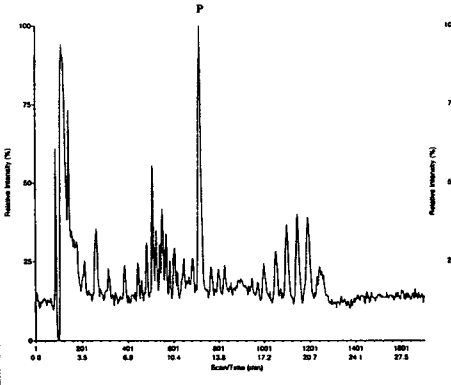

Figure 1: Full scan TIC of parent drug (P) incubated in rabbit liver microsomes

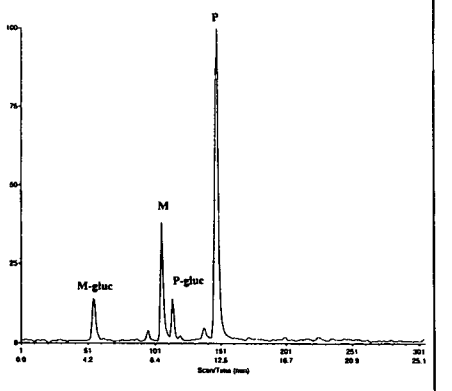

Figure 2: Phase I/II metabolites of parent drug (P) detected via precursor ion scan

Acknowledgments: We thank Dr. James Chovan, Mr James Cassidy and Mr. Roger Kramp for providing the sample in the Phase I/II experiment.

Monitoring the *In Vivo* and *In Vitro* Metabolism of Immunomodulators by Time-of-Flight Mass Spectrometry

David C. Muddiman[1,a], Arkady I. Gusev[1], Andrew Proctor[1], David M. Hercules[1,b]
Raman Venkataramanan[2,3], Prasad Tata[3] and Warren Diven[4]

Departments of: 1. Chemistry 2. Medicine 3. Pharmaceutical Sciences 4. Pathology
University of Pittsburgh, Pittsburgh, Pennsylvania 15260

Present Addresses:

a. Pacific Northwest Laboratories
Chemical Sciences Division
Battelle Blvd. P.O. Box 999
Richland, WA 99352

b. Department of Chemistry
Vanderbilt University
Box 1822 Station B
Nashville, TN 37235

Time-of-Flight Secondary-Ion (TOF-SIMS) and Matrix-Assisted Laser Desorption/Ionization (MALDI) Mass Spectrometry are emerging as useful methods for the investigation of drugs and metabolites in real biological systems [1,2]. Mass spectrometry is a powerful tool for the analysis of drugs and metabolites that may prove to be a viable alternative to high performance liquid chromatography (HPLC) and immunoassays (e.g. Fluorescence Polarization Immunoassay (FPIA)) in the clinical laboratory.

Cyclosporin A (CsA) is a well characterized and extensively used anti-rejection drug with newer agents, such as FK-506, undergoing clinical trials. The therapeutic index of these agents can be improved by understanding the nature of their metabolism and pharmacokinetics. This report expands upon the initial CsA study [1] by monitoring the *in vivo* metabolism of the drug and quantifying the major metabolite, AM1 (M17) in whole blood extracts. Initial MALDI results of the *in vitro* metabolism of FK-506 using a hepatic microsomal system are also presented. FK-506 metabolism was investigated using Baboon microsomes because FK-506 will be used in xenotransplantation; thus it is important to understand how the drug is metabolized by other species that may serve as donors.

Figure 1A shows the HPLC trace of a transplant sample. The HPLC data indicates extensive metabolism of CsA which is supported by the high CsA FPIA/HPLC concentration ratio of 3.2. Figure 1B shows the TOF-SIMS spectrum of the same sample. The spectrum contains several Ag-cationized peaks which are not present in standard blood extracts (data not shown). The MALDI spectrum (Fig. 1C) obtained from the same blood extract clearly indicates the presence of several CsA metabolites. Thus, both TOF-MS methods are accurately detecting CsA and its metabolites when compared to the standard method, HPLC.

Quantification of CsA and its major metabolite by both TOF-MS methods was carried out on 8 transplant samples. The correlation coefficients (r_0) were determined to be 0.988 and 0.986 for the TOF-SIMS and MALDI methods (compared to HPLC), respectively. The quantification of AM1 by both TOF-MS methods resulted in r_0 values of 0.997 and 0.991 for the TOF-SIMS and MALDI methods, respectively.

Figure 2 shows the MALDI spectra of ether extracts obtained at several different *in vitro* reaction times (0, 10, 20, 30, 45, and 60 minutes) with their corresponding peak assignments and the adduct in parenthesis. Note the relative decrease in the FK-506 parent drug intensity and the appearance of several new species with increasing reaction time. The major peaks identified in the data matrix presented in

Figure 2 indicate the major metabolites of FK-506 are de-methylated, doubly de-methylated and mono-hydroxylated. These results are consistent with previously reported studies. A normalized intensity vs. reaction time plot (data not shown) indicates that the desmethyl metabolite is rapidly formed while the didesmethyl and mono-hydroxylated metabolites are formed at lower rates. Collectively, these results illustrate that TOF-SIMS and MALDI-TOF can be applied to real biological systems providing superior detection limits, specificity and speed of analysis over HPLC and FPIA.

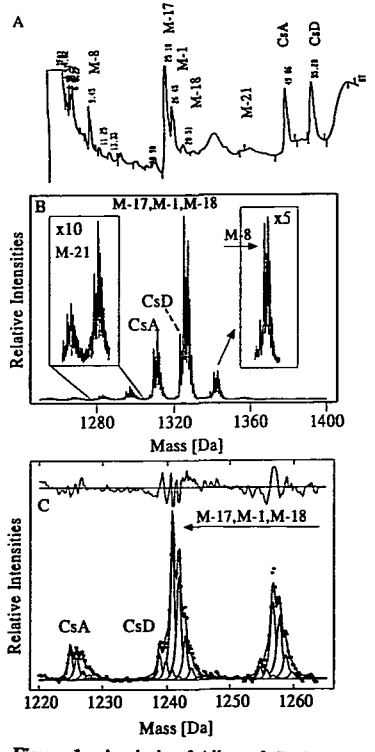

Figure 1: Analysis of Allograft Patient Sample under CsA Therapy by A) HPLC B) TOF-SIMS C) MALDI

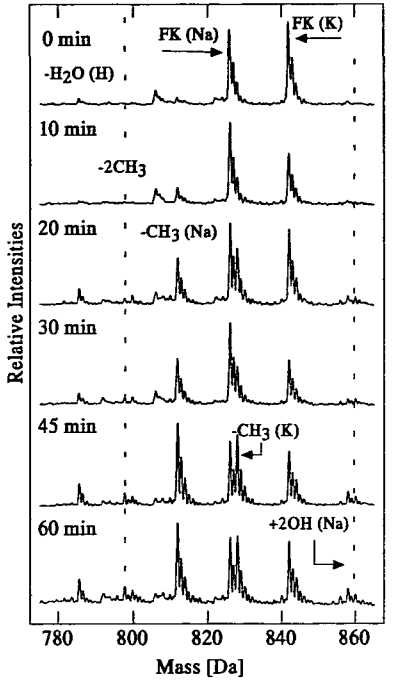

Figure 2: MALDI Analysis of FK-506 Hepatic Microsomal Incubates

References:

1. Muddiman, D.C.; Gusev, A.I.; Proctor, A.; Hercules, D.M.; Venkataramanan, R.; Diven, W.; *Anal. Chem.*, **1994**, 66, 14, 2362-2368.
2. S. Jespersen, W.M.A. Niessen, U.R. Tjaden, J. van der Greef, *J. Mass Spectrom.*, **1995**, 2, 357.

The Analysis of Stable Isotope-Labeled Drug Metabolites Using LC/CRI MS and LC/ESI MS/MS

*Feng-Yin Hsieh[2], Charles A. Goldthwaite, Jr.[2], Brian Nobes[2], Robert F. Mayol[3], Lewis J. Klunk[3], Ajai K. Chaudhary[2], and Ian A. Blair[1,2]. Department of [1]Chemistry and [2]Pharmacology, Vanderbilt University, Nashville, TN 37232; [3]Bristol-Myers Squibb Co., Pharmaceutical Research Institute, Wallingford, CT 06492.

The use of radioisotopes as tracers in drug metabolism studies has long been recognized as a simple, sensitive and selective method. However, for a variety of reasons, an alternative to the use of radiolabeled drugs for metabolism studies in human subjects would be welcomed. An attractive alternative technique that avoids the use of radioisotopes is the use of stable isotopes, such as ^{13}C and ^{15}N, as tracers in isotopic substitution experiments. Therefore, there is increasing interest in the development of instrumentation for the analysis of stable isotope-labeled drugs, metabolites and xenobiotics. The technique of chemical reaction interface mass spectrometry (CRI MS) is an elegant tool for selectively detecting stable isotopes. The basic concept of CRI MS is to completely atomize and then oxidize an analyte within a microwave induced plasma (MIP) oven with the addition of reactant gas (such as SO_2) in the MIP oven. This produces an array of low molecular weight gaseous species corresponding to stable isotope oxidation products (*m/z* 44 for $^{13}CO_2$, and *m/z* 31 for ^{15}NO) which are detected by a quadrupole or magnetic sector mass spectrometer using the selected ion monitoring (SIM) method. Therefore, quantitative analysis can be carried out regardless the original structure of the compound. However, the destructive nature of CRI MS provides no structural information for the unidentified metabolites. Therefore, electrospray ionization tandem mass spectrometry (ESI/MS/MS) was employed for structural characterization.

The CRI MS system has been coupled with high performace liquid chromatography (HPLC) via a particle beam interface. The [$^{15}N/^{14}C$]buspirone *in vivo* metabolites were chosen as a model system to demonstrate the application of the LC/CRI MS technique in drug metabolism studies. Rat bile and urine samples were collected after dosing the aminals with [$^{15}N/^{14}C$]buspirone. and were directly analyzed using the LC/CRI MS system without requiring any further sample clean-up procedure. ^{15}N labeled species were selectively detected in the *m/z* 31 channel. The bile and urine samples were also analyzed using LC/radiomatic detection. The accuracy of the LC/CRI MS method was evaluated by comparing the results from LC/CRI MS with the results from the radiomatic detection. The structures of the conjugated buspirone metabolites were characterized using LC/ESI MS/MS.

The LC/CRI MS chromatograms showing the ^{15}N enriched channel (*m/z* 31; ^{15}NO) and the non-labeled nitrogen channel (*m/z* 30, ^{14}NO) from the analysis of [$^{15}N/^{14}C$]buspirone metabolites in rat bile are shown in Figures 1a and 1b, respectively. The radiochromatogram from the analysis of the bile sample is shown in Figure 1c. Four major metabolites were detected (in Figure 1a and 1c, metabolites 14' and 15' co-eluted), and they were identified as the dihydroxylated monoglucuronide (9' and 11') and monohydroxlyated monoglucuronide (14' and 15') anaogs of buspirone. In urine, the N-dealkylation product 1-Pyrimidinylpiperazine (1-PP, lmetabolite 1 in Figure 2a and 2c) was the major metabolite, and no significant conjugated metabolites were detected. Figures 2a, 2b, and 2c shows the LC/CRI MS chromatograms of the ^{15}N enriched channel, the non-labeled nitrogen channel, and the ^{14}C radiochromatogram, respectively. The LC/CRI MS chromatograms of the ^{15}N enriched channel (Figures 1a and 2a) are almost identical to the radiochromatograms (Figures 1c and 2c) from the analyses of [$^{15}N/^{14}C$]buspirone metabolites in rat bile and urine. The resolution of the LC/CRI MS system is superior to that of the LC/radiomatic detection. The non-labeled interferences in the bile did not affect the detection of the isotope labeled metabolites in the ^{15}N enriched channel (*m/z* 31; ^{15}NO).

These results show that the LC/CRI MS technique is a stable isotope sensitive and compound-independent detection tool, which is especially suitable for drug metabolism studies. Excellent correlations between the CRI MS and radioactive methods were found. The combination of the LC/ESI MS/MS with LC/CRI MS provides a powerful technique for the complete identification and structural characterization of newly discovered metabolites. Supported by Bristol-Myers Squibb and NIH GM31304.

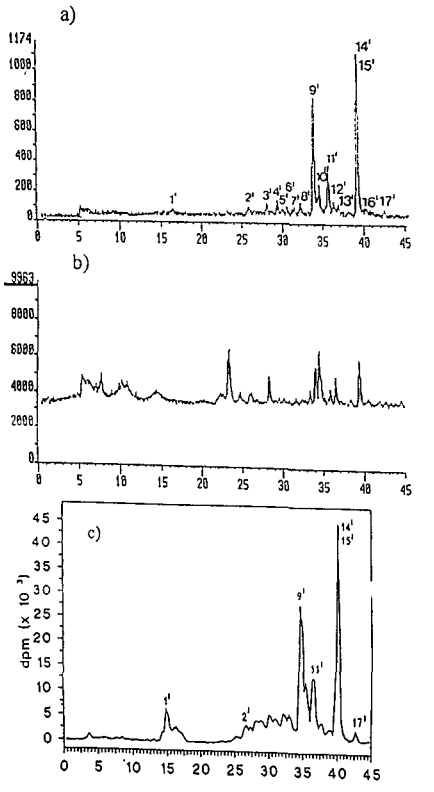

Figure 1. LC/CRI MS chromatograms of the a) ^{15}N enriched channel; b) non-labeled channel; and ^{14}C radiochromatogram of the [$^{15}N/^{14}C$] buspirone metabolites in rat bile.

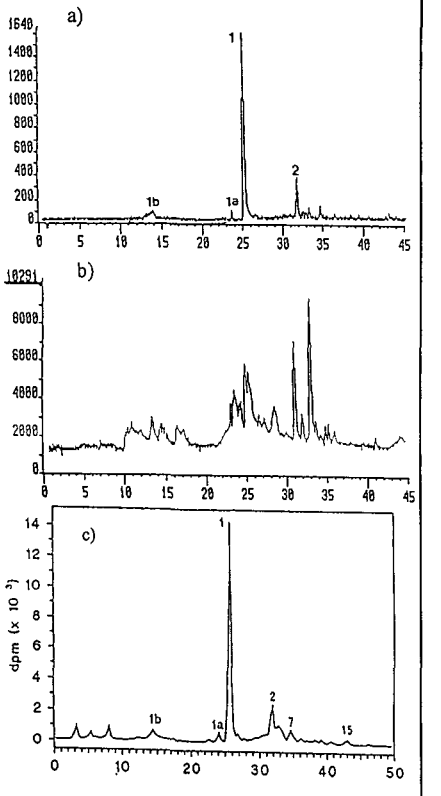

Figure 2. LC/CRI MS chromatograms of the a) ^{15} enriched channel; b) non-labeled channel; and ^{14}C radiochromatogram of the [$^{15}N/^{14}C$] buspirone metabolites in rat urine.

Analysis of levobunolol and timolol in ocular tissues: an observation of orifice voltage dependent oxidation of dihydrobunolol to levobunolol

W. Luo[1], A. Acheampong[1], S. Lam[1], D. Tang-Liu[1] and A. Breau[2]
[1]Department of Pharmacokinetics, Allergan Inc, Irvine, CA 92715
[2]The Perkin-Elmer Corporation, San Jose, CA 95131

Levobunolol and timolol, non selective beta-adrenergic blockers, are commonly used for the treatment of open-angle glaucoma. Both drugs reduce intraocular pressure by suppressing the rate of aqueous humor production from the secretory site, namely iris-ciliary body (1). Posterior sites of action have also been proposed for glaucoma drugs that may lead to undesirable effects on optic nerve head perfusion (2, 3). The study was designed to compare the concentrations of timolol and levobunolol in aqueous humor, iris-ciliary body, vitreous humor, choriod/retina and optic nerve. Following a single drop of 0.5% opthalmic solutions into albino rabbit eyes, those tissues were collected. An LC/MS/MS assay has been developed to analyze the concentrations of timolol, levobunolol and its equipotent metabolite dihydrobunolol.

Blank tissues were obtained from untreated rabbits. The solid tissues were weighed, except aqueous humor, which was measured by volume. Each point of standard curve was prepared by spiking a known amount or volume of tissue or fluid with varying concentrations of drug. Timolol was the internal standard for analysis of levobunolol and dihydrobunolol. Levobunolol was the internal standard for analysis of timolol.

Tissue samples were each extracted with 1 ml of acetonitrile and shaking for 10 min. The acetonitrile layer was transferred to clean silylated test tube and evaporated to dryness under nitrogen. The residue was reconstituted in 1 ml of double-distilled water and 30 µl of 3 N NaOH and 5 ml of ethyl ether. The organic layer and evaporate to dryness under nitrogen. Reconstitute in 100 µl of double-distilled water and inject onto LC/MS/MS.

Samples were injected onto a YMC basic (4.6 X 3 mm) 3 µm particle size column. The mobile phase used was 80% MeOH, 20% 20 mM NH_4OAc, 2 mM TEA at a flow rate of 1.5 ml/min. A Sciex API III+ triple quadruple mass spectrometer was operated in the positive ion detection mode with an APCI interface. The MRM modes were set at 292/235.5 for levobunolol, 294/237.5 for dihydrobunolol and 317/260.5 for timolol.

During the development process of analyzing levobunolol and its major metabolite dihydrobunolol, the conversion of the metabolites back to parent compound was observed. A careful analysis of the various ion source parameters revealed that the orifice potential accounted for the observed oxidation. As shown in Fig, 2 and Fig. 3, at orifice setting 60 V, ion 292/235.5 split into two peaks, one of which matches the retention time of dihydrobunolol which indicted that it was the oxidation product of dihydrobunolol. The magnitude of this oxidation was proportional to the magnitude of the orifice potential used in the study. In order to analyze both compounds, a low orifice potential was used. However, the utilization of this low orifice potential compromised the detection of levobunolol.

References:

1. L. M. Hurvitz, P. L. Kaufman, A. L. Robin, R. N. Weinreb, K. Crawford and B. Shaw. New developments in the drub treatment of glaucoma. Drugs 41: 514-532, 1991
2. A. Grajewski, G. Ferrari-Dileo, W. Feuer and D. Anderson. Beta-adrenergic responsiveness of choroidal vasculature. Ophthalmol. 98: 989-992, 1991
3. P. P. Elena, M. kosina-Boix, G. Moulin and P. Lapalus. Autoradiographic localization of beta-adrenergic receptors in rabbit eye. Invest. Ophthalmol. Vis. Sci. 28: 1436-1441, 1987.
4. A. Acheampong, A. Breau, M. Shackleton, W. Luo, S. Lam and D. Tang-Liu. J. of Ocular. Pharm. accepted.

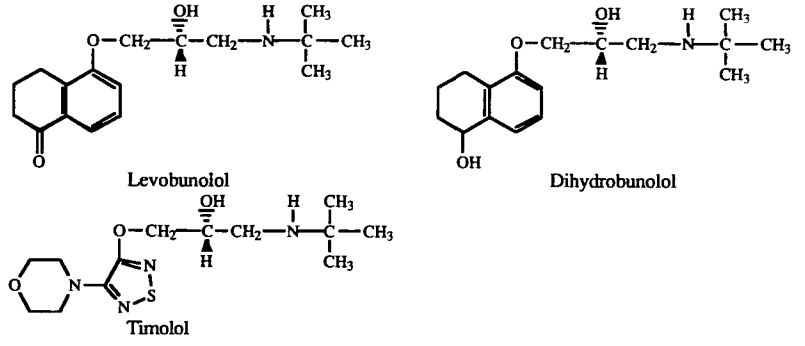

Fig. 1. Structures of levobunolol, dihydrobunolol and timolol.

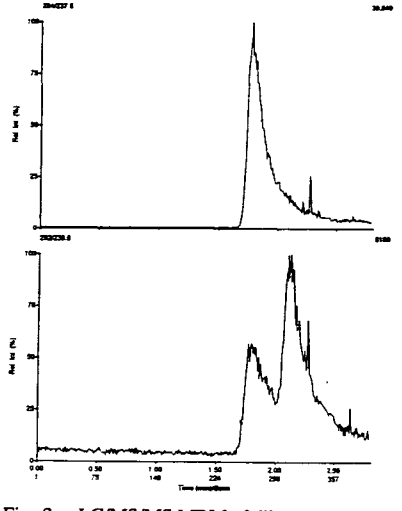

Fig. 2. LC/MS/MS MRM of dihydrobunolol (top) and levobunolol (bottom) at orifice setting 60 V. The first of the doublet peaks of ion 292/235.5 matches the retention time of dihydrobunolol, shows that the oxidation occurred at this orifice setting.

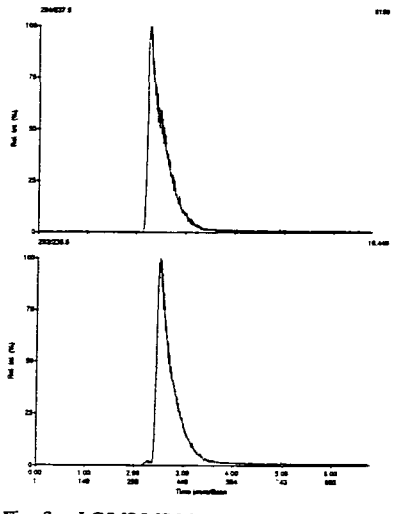

Fig. 3. LC/MS/MS MRM of dihydrobunolol (top) and levobunolol (bottom) at orifice setting 40 V. The doublet peaks of ion 292/235.5 disappeared at this condition indicates that the conversion dihydrobunolol to levobunolol did not occur at low orifice setting.

Metabolic Profiling using On-line Microdialysis Sampling with Tandem Quadrupole Mass Spectrometry

Robyn A. Rourick[1], Edward H. Kerns[1], Kevin J. Volk[1], Jeffrey L. Whitney[1], and Mike S. Lee[2], Bristol-Myers Squibb Company,
[1]Wallingford, CT 06492, [2]Princeton, NJ 08543

The rapid identification of drug metabolites is a vital component of the drug discovery process. To accelerate research, to reduce the use of living animal resources, and to minimize sample degradation it would be advantageous to analyze *in vitro* metabolic reactions on-line for drug metabolite profiling. Microdialysis sampling has demonstrated advantages for obtaining chemical information from biological systems. Originally developed for sampling neurotransmitters in the brains of living animals, it's use has been expanded into sampling of other tissues and physiological fluids in pharmaceutical research. Dialysate fluid provides a continuous sample of the drug and metabolites from the biochemical system sampled.

Here we describe a method for *in vitro* metabolic profiling using microdialysis sampling, tandem quadrupole mass spectrometry via an electrospray interface (1,2) and a systematic approach for metabolite identification. A metabolic profile was obtained for buspirone, an anxiolytic drug, in microsomal incubations using a model CMA/12 microdialysis probe and a CMA 100 syringe pump. Ammonium acetate (2mM) was used for dialysis fluid at a flowrate of 5 μL/min. Reactions were performed at 37 °C in a 1 mL Reacti-Vial equipped with a stir bar. The CMA 12 microdialysis probe was coupled directly to the electrospray interface of the Sciex API III tandem quadrupole mass spectrometer. Reactions were initiated by the addition of glucose-6-phosphate dehydrogenase in the buffered microsomal solution.

Prior to the initiation of microdialysis studies, a library of microsomal buspirone metabolites was generated using standard LC/MS and LC/MS/MS profiling methodologies (Figure 1). Full scan MS analysis during the LC/MS studies and microdialysis studies provided molecular weight information for the metabolites. Structural information was obtained for two compounds corresponding to the hydroxy and di-hydroxy metabolites via on-line microdialysis sampling. Comparison of the product ion spectrum of each metabolite to that of the parent drug provided information about the site of the metabolic transformation (Figures 2 - 3). The MS/MS fragmentation patterns indicated changes in specific substructures consistent with hydroxy buspirone and di-hydroxy buspirone.

In-vitro microdialysis sampling allowed real-time acquisition of metabolic information from microsomal incubations of buspirone. Furthermore MS/MS techniques on-line with microdialysis provided substructural insights about metabolic fate of buspirone.

References:

1. Lin, S. and Capriolli, R., Proceedings of the 36th ASMS Conference, 1000 (1988).
2. Kerns, E., Lee, M.S., and Rosenberg, I., Proceedings of the 39th ASMS Conference, 286 (1991).
3. Kerns, E., Combs, C., Knipe, J., Klunk, L.J., and Rosenberg, I., Proceedings of the 38thASMS Conference, 367 (1990).
4. Capriolli, R. and Fan, T., Anal. Biochem., 154, 596-603 (1986).
5. Jajoo, H., Mayol, R., LaBudde, J. and Blair, I., Drug Metab. Dispo., 17, 625 (1989).
6. Rodriques, D.A., et al, Drug Metab. Dispo., 22, 788 (1994).

FIGURE 1:

LC/MS METABOLITE PROFILE

RETENTION TIME (MIN)	MOLECULAR WEIGHT	PROPOSED STRUCTURE
9.6	417	DIHYDROXY
10.4	417	DIHYDROXY
11.4	417	DIHYDROXY
11.6	401	HYDROXY
12.6	401	HYDROXY
15.1	417	DIHYDROXY
15.2	401	HYDROXY
15.8	401	HYDROXY
19.1	401	HYDROXY
21.6	385	BUSPIRONE

FIGURE 2:

Product Ion Spectrum of Hydroxy Buspirone from Microdialysis Sampling of Microsomal Incubation at T = 65 Minutes

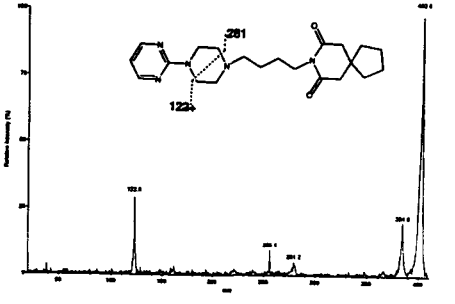

FIGURE 3:

Product Ion Spectrum of Buspirone from Microdialysis Sampling of Microsomal Incubation at T = 5 Minutes

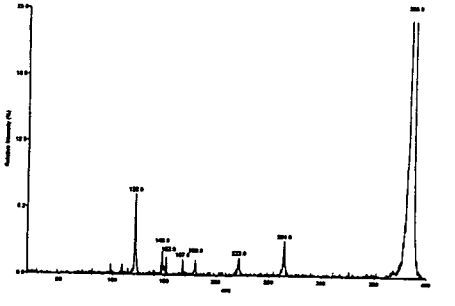

Automated HPLC/Tandem Mass Spectrometric Approaches for Rapid Identification of Metabolic Pathways

Mark J. Cole, Jeffrey W. Gauthier, Elbridge W. Luther, Hassan G. Fouda

Drug Metabolism Department, Central Research Division, Pfizer Inc, Groton, CT 06340.

The availability of biotransformation data very early in the drug discovery program allows the chemists to tailor synthetic efforts toward blocking metabolically labile sites, provides structural information on active or toxic metabolites, and can guide the selection of the most optimum drug candidate for further development. Other important discovery and development processes, such as the selection of *in vivo* animal efficacy and safety models and the interpretation of toxicology and clinical findings, can also benefit from the early availability of comparative metabolism information. Traditional approaches to metabolite identification are time consuming and the data are often generated too late to have an impact on the discovery process.

We are exploring ways not only to provide biotransformation data on numerous prototypes at a discovery pace, but to also integrate and standardize experimental approaches and methodologies within the discovery process. A standardized chromatography system consisting of a general-use gradient mobile phase and dual narrow-bore columns allows the analyses of most compounds without prior development of individual chromatography conditions. In addition to saving significant development time, this system is portable between mass spectrometry and other laboratories, all chromatography data are easily correlated regardless of which laboratory they were collected in, and metabolism rates can be studied in other laboratories without further mass spectrometric work. An on-line diode-array detector provides a better representation of the relative abundances of metabolites, helps to further confirm metabolite structures, and provides a common type of data between mass spectrometry and chromatography laboratories. The heart of the system is a triple-quadrupole mass spectrometer sophisticated enough to simultaneously collect multiple mass spectrometric experiments, automatically tune itself on each new compound, provide control over switching valves, HPLC systems, and diode-array data collection, and encompass all of this with a programming language and direct control over all instrument parameters. The simultaneous collection of data from multiple mass spectrometric experiments, and the ability to collect these data automatically, significantly decreases the operator involvement with, and time required for, data collection. As a result, data are collected, analyzed, and reported rapidly at the pace of the discovery program.

What is Rapid Automated Biotransformation Identification (RABID)?

RABID is an HPLC/DAD/MS/MS instrument bundled with a suite of software packages that allows a user to collect many Phase I/Phase II data automatically and unattended with no *a priori* knowledge of the metabolism, chemistry, or mass spectrometric dissociation of the compound. The user must know the molecular weight of the compound, but does not necessarily need to know how to run the instrument to collect the data. Data interpretation and the experimental decisions resulting from interpretation still require an expert.

Much of the Data Collection Can Be Automated

- Many of the experiments are "knowledge-based", lending themselves to automation (for example, CAD product ion scans of MH+16 will look for hydroxylations/oxides).
- The Finnigan TSQ-7000 provides a programming environment, true instrument control over every parameter and element of the instrument, and the ability to communicate with, and control, other instrumentation.
- A single gradient chromatography system can be developed that will be suitable for a wide range of pharmaceutical compounds.

RABID Features

- Modular system: user can easily install different gradients, autosampler programs, add additional or different experiments (different CAD experiments, PAR/NL, CAD/MS/MS, etc.) or delete unwanted experiments
- GUIDE Interface: leads user through all steps of sample entry, instrument preparation, control of the program, and data acquisition
- Samples can easily be entered/deleted/changed at any time during normal operation. Clicking the "START" button at the end of the day will begin automated operation.

Analysis of Diuretics in Urine by HPLC/APCI/MS and CE/UV

Yuan-Ping Yang and Jentaie Shiea*
Dept. of Chemistry, Natl Sun Yat-sen Univ., Kaohsiung, Taiwan 804

Diuretics have been banned at major sporting events since the 1988 Winter Olympic Games Although very low detection limit can be achieved by GC/MS analysis, finding an universal derivatizing reagent for various diuretics is very difficult. The development of new analytical procedures without derivatization will then be very helpful in rapidly screening and confirming the diuretics in urine. Here, we report two analytical processes which potentially can be used in rapidly examining the diuretics from urine:

1 The diuretics in spiked urine samples were separated by a C18 RP-HPLC column and the LC effluent was directed into APCI/MS system for compound identification. A PE Sciex API 1 LC/MS system equipped with an atmospheric pressure chemical ionization (APCI) source was used. Figure 1 shows the mass chromatograms of twelve diuretics by HPLC/APCI/MS. The mass of pseudomolecular ion (MH^+) of each diuretic was chosen to obtain the mass chromatogram. It can be seen that all of the diuretics were successfully protonated in the APCI source. Although the diuretics can be rapidly separated and identified by HPLC/APCI/MS, high concentration of the phosphate salt in the mobile phase causes problems in efficiently sampling ions into the mass analyzer especially in long term operation. To solve the problem, the mobile phase with low salt content has to be developed in the future

2. Owing to its extremely high resolution capability and very short time required, capillary electrophoresis (CE) is used for the analysis of diuretics in urine The CE/UV system is consisted with an Applied Biosystems 270 A-HT CE system equipped with a PE model 1022 personal integrator. Figure 2 shows CE electropherogram of the diuretics mixture. It can be seen that fourteen diuretics were separated and detected by CE/UV in less than thirteen minutes. Since the retention time of the analyte in CE is not so reproducible, we then developed an analytical procedures to solve the problem. Because the retention time of the analyte changes in the solutions which contains different amount of SDS (so called micellar electrokinetic capillary chromatography), a retention ratio can then be calculated. The definition of the retention ratio is as follow

$$\text{Retention Ratio} = \frac{RT_{CE,diuretic} - RT_{CE,standard}}{RT_{MECC,diuretic} - RT_{MECC,standard}}$$

It was found that the value of the retention ratio is different for each analyte. This value can then be used in identifying particular analyte eluted from CE. Figure 3 shows the electropherograms of furosemide in the solution contain (a) 0 mM SDS and (b) 10 mM SDS Ethacrynic acid was used as the internal standard. Table 1 shows relative retention times and retention ratios of fourteen diuretics. It can be seen that a quite wide range of retention ratio is obtained for 14 diuretics (from -2 to 3).

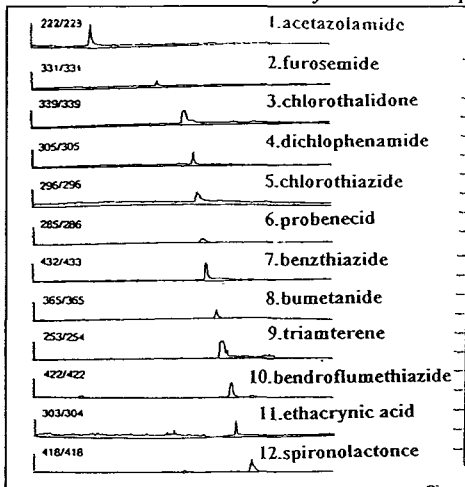

Figure 1. Mass chromatograms of 12 diuretics by HPLC/APCI/MS.

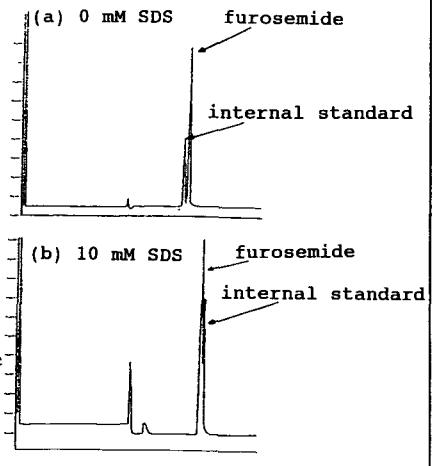

Figure3. CE electropherogram of bumetanide in (a)0 mM SDS, (b)10 mM SDS (internal standard : ethacrynic acid).

Table 1. Relative retention times and retention ratios of the diuretics in methanol solutilon (n=5).

diuretic	ΔT for CZE, RSD	ΔT for MECC, RSD	Ratio
acetazolamide	1.880 · 3.56%	1.260 · 3 43%	1.492
bendroflumethiazide	-0.588 · 3.04%	1.848 · 3.28%	-0.319
benzthiazide	1.352 · 1.09%	1.086 · 1.05%	1.245
bumetanide	0.206 · 15.19%	-0.102 · 22.35%	-2.019
chlorothalidone	-0 790 · 2.37%	-0 680 · 2.33%	1.162
chlorothiazide	5.512 · 2.83%	6.004 · 9.66%	0.918
dichlophenamide	3.600 · 3.73%	2.822 · 3.23%	1.276
ethacrynic acid	0.000	0.000	0.000
furosemide	0.594 · 2.76%	0.360 · 4.39%	1.650
hydrochlorothiazide	1.224 · 6.55%	0.960 · 8.04%	1.275
hydroflumethiazide	0.948 · 3.76%	0.710 · 11.52%	1.335
probenecid	-0.044 · 12.45%	-0.412 · 2.03%	0.107
spironolactonce	-2.156 · 1.02%	-2.842 · 0.46%	0.759
triamterene	-2.242 · 1.76%	-0.712 · 7.25%	3.149

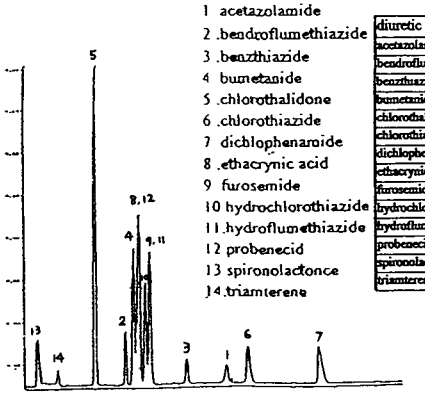

Figure 2 CE electropherogram of standard diuretics mixtures

THE DETECTION OF CONCEALED DRUGS BY FIELD PORTABLE IMS AND GC/MS

Dean D. Fetterolf[1], Brian Donnelly[2], Thomas Jourdan[2], Forensic Science Research Unit[1], Chemistry Toxicology Unit[2], FBI Laboratory, Washington, DC

Introduction: Over the last two decades illicit drug distribution has grown from simple "drug pushing" where drugs were distributed by poorly organized individuals to today's well organized and well financed drug cartels. While traditional methods continue, new highly sophisticated smuggling techniques have been discovered.

The national drug control strategy calls for the development of new technology and the innovative adaptation of existing technology for use in the war on drugs. In the past few years, the FBI Laboratory has introduced several new tools into the agents' technological arsenal for use in support of drug investigations. The most successful tools have been a field portable ion mobility spectrometer, and a transportable GC/MS.

The forensic identification of trace physical evidence from drugs on a suspect's clothing, possessions, and conveyances in the field can provide the investigator with time-sensitive lead value information or probable cause.

Methods: The Barringer IONSCAN (Barringer Instruments, New Providence, NJ) is shown in Figure 1. Samples are collected by a small handheld vacuum onto a small teflon filter and thermally desorbed into the IMS (Figure 2) or extracted for GC/MS analysis. Using Ni-63 ionization, the nicotinamide internal calibrant also acts as a reagent ion of moderate proton affinity, thus offering enhanced selectivity. In the drift region, the ions are separated based upon their mobility. Temperatures for the desorber, inlet and IMS cell are 280° C, 290° C and 235°C, respectively. Sample, drift, and exhaust flows are 200 cc/min, 300 cc/min, and 500 cc/min, respectively. The self-calibrating, 5-second analysis can detect 5 ngs of cocaine and 15 ngs of heroin. Other drugs of abuse such as THC, LSD and methamphetamine are detected at comparable levels. Peak detection and alarm conditions are determined by a series of algorithms which examine peak location, size, and shape.

The Viking SpectraTrak GC/MS (Viking Instruments, Herndon, VA) is a ruggedized full featured Hewlett Packard MSD offering versatile sample introduction such as purge and trap, desorption tubes, headspace and GC analysis capabilities in a transportable package. As a matter of practice all positive field samples are confirmed in the field by the GC/MS or in the laboratory by MS/MS using deuterated internal standards.

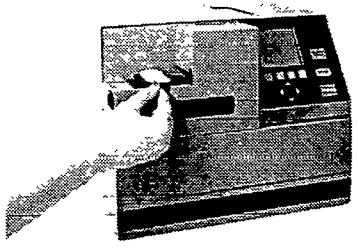

Figure 1. Field portable IMS

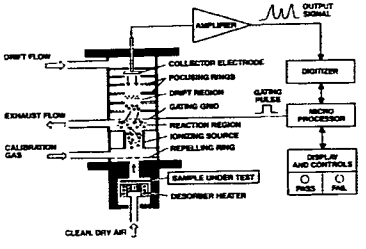

Figure 2. IMS Block diagram

Results: The IMS has proven successful on a routine basis in the field when operated by trained law enforcement investigators. To illustrate its' usefulness a few examples of real-world applications will be described. During the course of an investigation solvents and chemicals used for cocaine reprocessing and 355 pounds of injection molded polystyrene pipe fittings were recovered. Drug detection canines and cobalt thiocyanate field test kits proved negative. The plasmagram is shown in Figure 3. The plasmagram is plotted as intensity vs. drift time in milliseconds. The table on the left side is a list of common drugs, their mobility and drift times. The plastic pipe was determined to be 20-30% by weight cocaine. The portable GC/MS was used to confirm the IMS results and to identify the solvents.

In another investigation, a dog kennel (Figure 4) was intercepted upon entry into the United States. Mixed in the fiberglass matrix of the cage during manufacturing was over 3 Kg of cocaine which was undetected by drug canines and color test kits. Other unique concealments include cocaine hidden in railroad ties and hidden vehicle compartments.

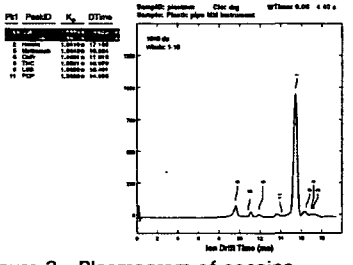

Figure 3. Plasmagram of cocaine.

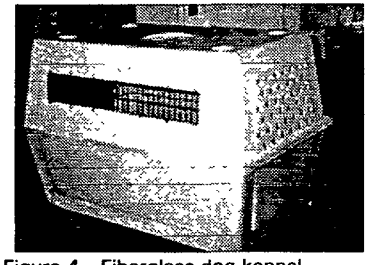

Figure 4. Fiberglass dog kennel

The forensic document examiner can often identify the type and amount of drug activity from seized clandestine drug records. Their interpretation is further enhanced by the use of the ISM to detect the presence of trace drug evidence.

A wide variety of other forensic and criminal justice applications of ion mobility spectrometry have been explored. They include probable cause, search and seizure, asset forfeiture, unusual concealments, probation and parole, correctional facilities, clandestine drug laboratory safety, fit for duty issues, and explosives detection.

Law enforcement agencies also become hazardous waste producers when they seize chemicals associated with the clandestine drug manufacturing. The transportable GC/MS permits the identification of the drugs and solvents without the need for shipping hazardous materials to the laboratory.

Conclusions: On-site crime scene analysis for trace physical evidence of drugs can provide the law enforcement investigators with time sensitive and important lead information. The IMS offers a rapid, sensitive, court proven screening method. From a procedural standpoint all positive field samples should be confirmed. Nationwide numerous arrests, prosecutions, and convictions can be directly attributed to the results of field analysis using portable mass spectrometers.

ANALYSIS OF "ECSTASY" AND OTHER DESIGNER DRUGS USING HPLC/APCI/MS

E.B. Hansen, Jr., M.I. Churchwell, C.R. Clark[1], J. DeRuiter[1], F.T. Noggle, Jr.[2], and D.R. Doerge, FDA, NCTR, Jefferson, AR 72079, [1]Dept. of Pharm. Sci., Auburn University, Auburn, AL 36849, [2]Alabama Dept. of Forensic Sciences, Auburn, AL 36830.

INTRODUCTION

"Ecstasy" is a street name for 3,4-methylenedioxymethamphetamine (MDMA). Monitoring abuse of MDMA and "designer drug" analogues of the parent drug, MDA, requires sensitive and selective analytical methods for their detection and confirmation in biological samples. Reported here is an HPLC method using electrochemical (ECD) and APCI-MS detection for the analysis of five MDA-derivatives, including Ecstasy, in human urine at levels as low as 5 ng/ml.

EXPERIMENTAL

HPLC

The HPLC system included a 7125 injector (20 μl loop, Rheodyne), a 600E system controller and pump (1 ml/min, Waters), a 250 X 4.6 mm I.D., 5 μ SCD-100 column (Synchrom, Inc.), and a mobile phase of 87% 0.1% formic acid/acetonitrile.

Electrochemical Detection (ECD)

ECD was performed using a 5100A Coulochem detector (ESA). The 5020 guard cell, set at +1.2 V, was placed between the column and a 5010 detector cell set at -0.1 V. Electrode 1 of the 5010 cell was monitored using Millennium Chromatography Manager software and a SAT/IN module (Waters). The guard cell was modified by replacing the steel tubing at the inlet and outlet of the cell with .005 mm I.D. Peek tubing.

Mass Spectrometry (MS)

MS was performed using a VG Platform benchtop single quadrupole mass spectrometer (Fisons Instruments/VG BioTech) equipped with an APCI interface. The HPLC effluent was introduced directly into the API source via a heated nebulizer probe using nitrogen as the nebulizing and carrier gas. Mass spectra were obtained in the positive ion mode, using full scans (m/z 100-400, cycle time 1 s) or selected ion monitoring (SIM, dwell time 0.2 s, span 0.02 m/z). To obtain mass spectra with fragment ions the cone voltage was varied between 10 and 40 V. The APCI source and probe temperatures 120°C and 400°C, respectively.

Sample Preparation

Urine (20 ml) was pH adjusted to 8.4 with phosphate buffer and passed through a strong cation exchange cartridge (PRS, Varian). The cartridge was washed twice with water and eluted with 1 ml of 1 M ammonium formate/acetonitrile (2:1) and analyzed by HPLC.

43rd ASMS Conference on Mass Spectrometry and Allied Topics

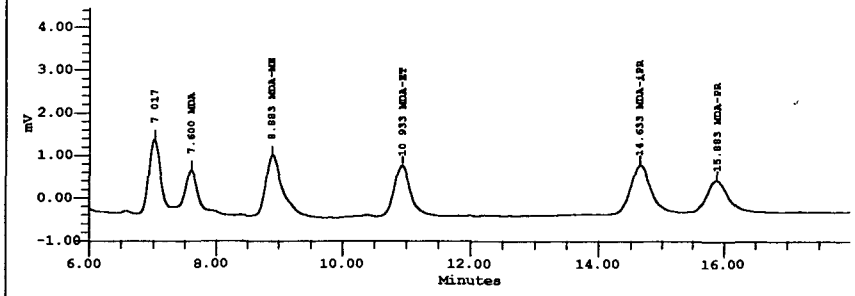

Figure 1. HPLC-ECD chromatogram from analysis of a 10 ppb spiked urine.

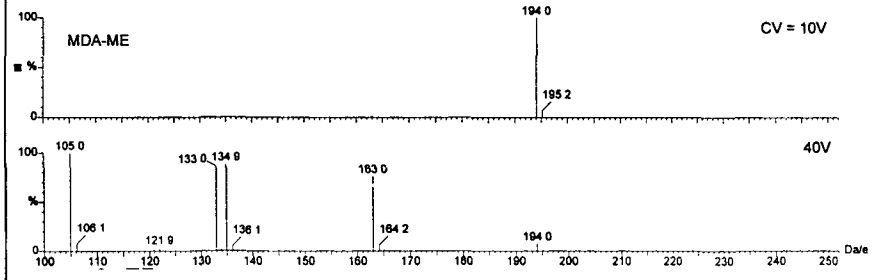

Figure 2. Cone-voltage-dependent fragmentation of MDMA.

RESULTS AND DISCUSSION

HPLC-APCI-MS and HPLC-ECD were successfully utilized to determine MDA and four "designer drug" analogs in human urine. The analysis provided baseline separation with a total run time under 18 min (Fig 1). The ECD in the configuration described appears very selective for compounds containing a methylenedioxy-moiety. The minimum detectable amount of these drugs using ECD was about 1 ng on-column. Using APCI-MS detection, $[M+H]^+$ions were obtained as the base peak with no significant fragment ions when the sampling cone voltage was set at 10 V. Analysis using varying cone voltages up to 40 V provided spectra containing diagnostic fragment ions (m/z 164,135,133,and 105) common for this class of drugs (Figure 2). The minimum detectable amount of these drugs by HPLC-APCI-MS analysis using selected-ion monitoring of the ions listed above is about 200 pg injected on-column.

These preliminary results indicate a level of quantitation for these drugs in urine as low as 5 ng/ml. With future modifications a minimum level of quantitation of 1 ng/ml or less is expected.

Immunoaffinity Extraction-LC/LC/MS/MS for the Determination of LSD Analogs in Urine

Jianyi Cai, Jack Henion
Analytical Toxicology, Diagnostic Laboratory, Cornell University, 927 Warren Dr., Ithaca, NY 14850

Remco van Soest
LC Packings, Baarsjesweg 154, 1057 HM Amsterdam, The Netherlands

Introduction

The determination of trace levels of analytes from complex matrices requires highly selective sample pretreatment techniques. Immunoaffinity extraction techniques are powerful tools in this field owing to their high specificity for targeted analytes which can also provide considerable sample enrichment. On-line trace enrichment eliminates tedious and time-consuming sample pretreatment associated with most LC/MS applications. The objective of this study is to evaluate the feasibility of coupling an immunoaffinity extraction system on-line with packed-capillary HPLC and tandem mass spectrometry (MS/MS). The system combines automated sample throughput with improved detection sensitivity. Tandem mass spectrometric detection offers additional selectivity and confirmatory information.

Due to its low dose and extensive metabolism, the determination of LSD and its metabolites in body fluids is a challenging task. Considerable effort has been directed towards the development of more sensitive and selective analytical methods. In this study, the direct analysis of trace levels of LSD, its analogs, and metabolites in human urine is demonstrated using an on-line immunoaffinity extraction-coupled column capillary HPLC-tandem mass spectrometry system.

Experimental

The mass spectrometer used was a PE Sciex TAGA 6000E API triple quadrupole mass spectrometer (Thornhill, Ontario) updated to an API-III. A column-switching system was developed, which involves three columns including an immunoaffinity column, a trapping column, and an analytical column. A protein G column with noncovalently-bound antibodies against LSD was used as the immunoaffinity column (2.1 x 3.3 mm, 30 µm, ChromatoChem, Missoula, MT). Both the trapping column (C-18, 0.5x15 mm, 5 µm, LC Packings, Amsterdam, The Netherlands) and the analytical column (C-18, 0.3x150 mm, 3 µm particles, LC Packings) were packed capillary columns. The use of packed capillary HPLC columns has several advantages over conventional HPLC columns, including improved detection sensitivity, and easy coupling to electrospray mass spectrometry.

On-line sample pretreatment involves several steps. The antibody column was primed by injecting antibody against LSD. PBS-diluted urine sample was then loaded onto the antibody column. After washing the antibody column with PBS, the bound analytes were desorbed from the antibody column and trapped onto trapping column. The trapped analytes were finally eluted from the trapping column to the analytical column and mass spectrometer for separation and characterization.

Results and Discussion

On-line immunoaffinity extraction coupled with capillary liquid chromatography-mass spectrometry (IAE/LC/LC/MS and IAE/LC/LC/MS/MS) were investigated and evaluated for the determination of LSD and its analogs in spiked human urine. LSD-positive human urine specimens were also analyzed using the described system. The two mass spectrometric operational modes (see Figure 1 and 2), selected ion monitoring (SIM) and selected reaction monitoring (SRM), as well as on-line UV detection were compared for the analysis of human urine spiked with LSD and it analogs at the 10 part per trillium (ppt) levels. Using SRM/IAE/LC/LC/MS, 2.5 ppt levels of LSD and several analogs in spiked human urine were detected. This is 20-fold below our previous limit of detection using solid phase extraction and SRM/LC/MS method.

Acknowledgments

We acknowledge Drs. R. Foltz and C. Nelson of Northwest Toxicology, Salt Lake City, UT, for providing us with several analytical standards and LSD-positive human urine specimens, Dr. R. Hammen of ChromatoChem for providing us with the protein G columns, and Dr. S. Salomone of Roche Diagnostic Systems for supplying several antibodies against LSD. Technical support from Dr. T. Wachs is greatly appreciated.

Figure 1

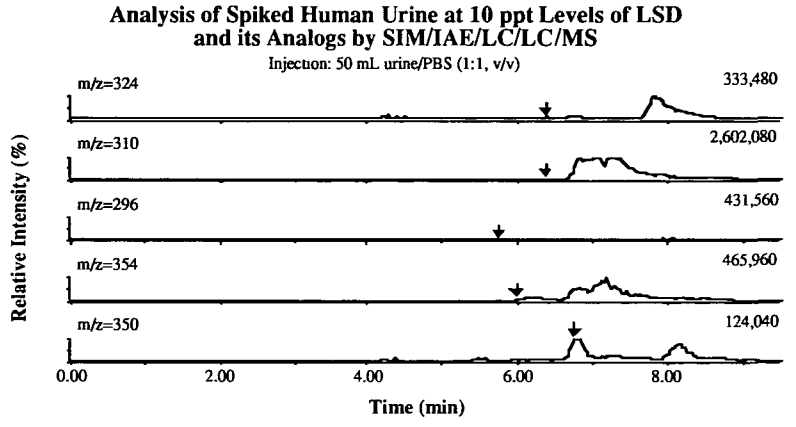

Figure 2

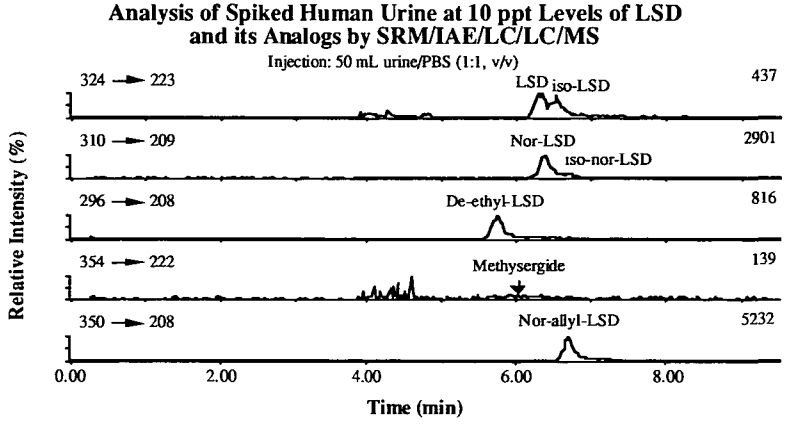

Identification of Previously Unreported Metabolites of LSD in Human Urine

Chad C. Nelson,[1] Matt H. Slawson,[1] Scott A. Reuschel,[1] Rudolf Brenneisen,[2] Rodger L. Foltz[1]
1 Northwest Bioanalytical, Salt Lake City, Utah 84124.
2 University of Berne, Berne, Switzerland.

LSD is a well known potent hallucinogen which was popular in the 1960's, and continues to be a significant drug of abuse today. LSD undergoes rapid and extensive metabolism such that only about 1% of ingested LSD is excreted unchanged in human urine.[1] Although the metabolism of LSD has been studied extensively, only a few minor metabolites have been identified in human urine[1] and human liver microsomes.[2] The major metabolic products have not been previously determined in human plasma or urine. 2-oxo-LSD has been reported to be a metabolite of LSD in laboratory animals and has been suspected to be a human metabolite.[3] However, 2-oxo-LSD, decomposes relatively rapidly in solution and has been difficult to identify in humans. In the present study, MS/MS was used as a means to identify new metabolites of LSD and products derived from the putative 2-oxo-LSD compound. A new major metabolite of LSD (2-oxo-3-OH-LSD) in human urine and plasma has been identified and is presumably derived from 2-oxo-LSD. The 2-oxo-3-OH-LSD structure was confirmed by comparison of CID spectra and GC retention time with authentic standard. Several other new metabolites have also been tentatively assigned. CID spectra and product-ion dissociation pathways of LSD, Nor-LSD, and 2-oxo-LSD models were initially studied.[4] Based on these model compounds, precursor and neutral-loss experiments were used to determine chemical degradation products of the 2-oxo-LSD standard. For instance, protonated molecules at *m/z* 328, 336, 338, and 356, were characterized as degradation products of 2-oxo-LSD and assigned as an amino ketone derivative of 2-oxo-LSD, unsaturated forms of 2-oxo-LSD (*m/z* 336 and 338), and 2-oxo-3-OH-LSD, respectively. GC/MS/MS and DCI/MS/MS was used to "screen" specifically for these products in urine extracts of participants in a LSD clinical study. Neutral-loss scans for elimination of the diethylamide moiety of the LSD molecule (NL 101) identified those metabolites or decomposition products which had undergone modifications in the ring system of the LSD molecule. Hydroxylated metabolites showed a characteristic neutral mass loss of 191u, corresponding to loss of diethylamide (101u) and TMSOH for TMS derivatives. Figure 1 shows an example of the mass chromatograms from selected-reaction monitoring of the 2-oxo-3-OH-LSD metabolite and the parent LSD drug in urine extracts. By comparison at this collection time, the intensity of the 2-oxo-3-OH-LSD metabolite is approximately 50 times greater than the intensity of LSD. Pharmacokinetic data for LSD and the 2-oxo-3-OH-LSD metabolite in human plasma is shown in Figure 2. The plasma profile of the 2-oxo-3-OH-LSD metabolite indicates that the metabolite can be detected in plasma for a significantly longer period of time compared with LSD.

References

1. Foltz, R. L., Foltz, R. B. in Advances in Anal. Toxicol., Baselt, R. C., Ed., Yearbook Medical Publishers, Inc.: Chicago, IL, (1989), 140-158.
2. Cai, J., Hennion, J. Proc. 42nd ASMS Conf. Mass Spectrom. Allied Topics (1994).
3. Stead, A. H., Watton, J., et al *Forensic Sci. International* (1986), 32, 49-60.
4. Nelson, C. C., Foltz, R. L. *Anal. Chem.* (1992) 64, 1578-1585.

Acknowledgement

Research at Northwest Bioanalytical was funded by the Naval Research Laboratory, Contract No. N00014-93-C-2040. The authors thank David Nichols for the 2-oxo-3-OH-LSD standard.

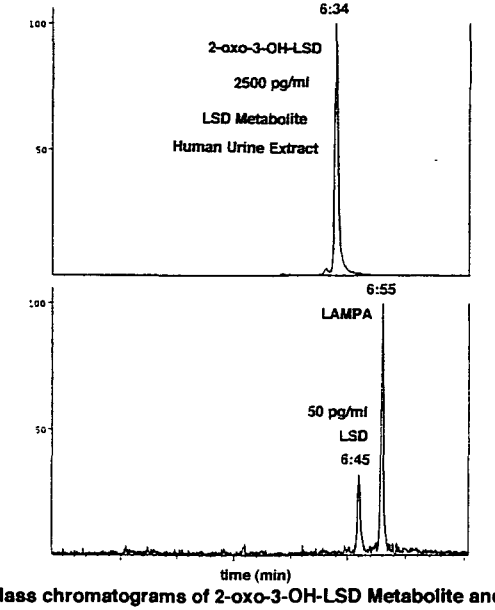

Figure 1. Mass chromatograms of 2-oxo-3-OH-LSD Metabolite and LSD. Human urine collected 2-3 hours following ingestion.

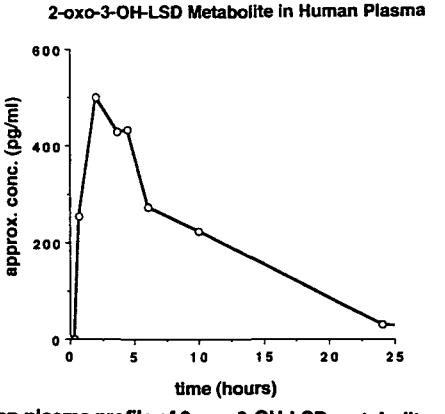

Figure 2. Human plasma profile of 2-oxo-3-OH-LSD metabolite.

Development of Methodology for Detection of Fluoxymesterone and Metabolites in Urine by GC/ECNI

Naxing Xu and J. Throck Watson, Department of Chemistry, Michigan State University
East Lansing, MI 48824

Fluoxymesterone, an anabolic steroid, was banned by the International Olympic Committee because of its abuse in sports. Fluoxymesterone is metabolized in man primarily by 6-hydroxylation, 3-keto-reduction, and via other pathways. Usually GC/EI/SIM is used to detect urinary anabolic steroids after TMS derivatization. More selective and sensitive quantitative methodology is proposed for urinary fluoxymesterone and metabolites based on ECNI with sample introduction by GC. The analytes are transformed to electrophilic species via an oxidation reaction. Preliminary results show remarkable discrimination against background in the detection of fluoxymesterone in the urinary matrix.

In this methodology, 6-methylprednisolone, a structurally similar compound, is added to the urine sample as an internal standard. The urine sample is extracted on a Sep-Park C-18 cartridge. The conjugated steroids are hydrolyzed by *Helix pomatia* obtained from Sigma. Fluoxymesterone and its metabolites are extracted with diethyl ether and evaporated to dryness under vacuum.

The dry extract is dissolved in 1ml CH_2Cl_2. 10 mg of anhydrous sodium acetate are used to buffer the acid liberated during the oxidation. An excess of the PCC(pyridine chlorochromate)/celite(1:2) is added to the vial. The reaction mixture is stirred and heated at 60°C for 5hr. The oxidized sample is cleaned up by 200 mg silica SPE column. The oxidized fluoxymesterone and its metabolites are eluted with 15% acetone in CH_2Cl_2. After evaporation, the sample is reconstituted in 100µl ethyl acetate.

A Finnigan 4600 GC/MS system was used for both EI and ECNI operation. Methane was used as buffer gas. The relative response of oxidized products under ECNI conditions are listed below:

steroid	characteristic ions of the oxidation product under ECNI	relative ECNI response
testosterone	286	1
6-methylprednisolone	312	350
fluoxymesterone	314, 334	500
6-OH-fluoxymesterone	350, 330	700
9-fluoro-17-methylandrost-4-ene-3,6,11,17-tetrol	350, 330	700
9-fluoro-18-nor-17,17-dimethylandrost-4,13-diene-11-ol-3-one	316	400

Fig. 1 illustrates the sensitivity and selectivity gained by using oxidation and ECNI. Shown in Fig. 1(a) is the total ion current chromatogram produced from an oxidized urine extract during GC/MS with EI ionization. EI is a non-selective mode of ionization which makes evident the large number of components

in the urine matrix. The selectivity of ECNI for electrophilic compounds is illustrated by comparison of Fig. 1(a) and 1(b). Only a few peaks are contained in the ECNI total ion current chromatogram of the same oxidized urine sample(Fig. 1b). The enhancement in sensitivity afforded by ECNI is also apparent by comparison of the integrated peak areas for oxidized fluoxymesterone and its main metabolites. This methodology shows great potential for the quantitative determination of fluoxymesterone and its metabolites in urine.

Fig. 1(a) Sample: 5 ml positive urine collected 24 hours after administration(from Aegis Lab, TN); 200 ng 6-methylprednisolone added as internal standard
Instrument mode: EI, full scan m/z 50-450

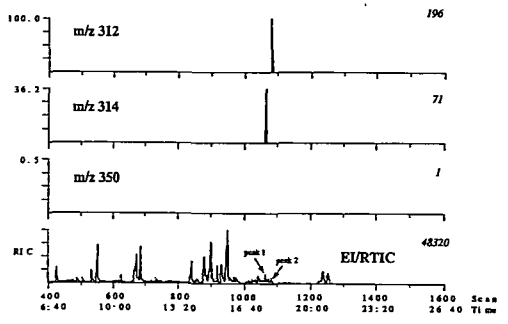

* The number shown on the top right of RTIC or mass chromatogram represents ion current counts
* Peak 1 observed at RT 17.47 min corresponds to oxidized fluoxymesterone
* Peak 2 observed at RT 17.59 min corresponds to oxidized 6-methylprednisolone

Fig. 1(b) Sample: 5 ml positive urine collected 24 hours after administration(from Aegis Lab, TN); 200 ng 6-methylprednisolone added as internal standard
Instrument mode: ECNI, full scan m/z 50-450

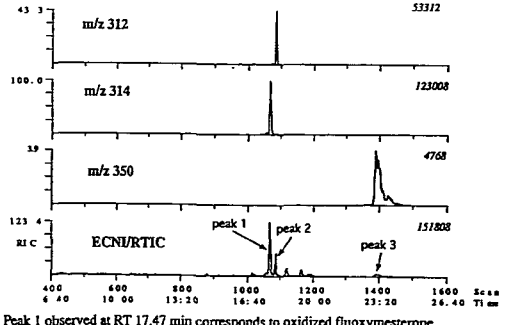

* Peak 1 observed at RT 17.47 min corresponds to oxidized fluoxymesterone
* Peak 2 observed at RT 17.59 min corresponds to oxidized 6-methylprednisolone
* Peak 3 observed at RT 23.01 min corresponds to oxidized 6-OH-fluoxymesterone

Ion Trap GC/MS and GC/MS/MS Measurement of Cocaine and Its Metabolites

Larry D. Bowers and Kelly Fregien
Department of Pathology and Laboratory Medicine
Indiana University Medical Center
Indianapolis, IN 46202-5120

Recent developments in quadrupole ion trap technology have demonstrated the versatility of this approach to mass analysis. By applying various wave forms to the end caps and ring electrode of the trap, ions can be selectively stored, caused to undergo collision induced dissociation (CID), and ejected. As a result, GC/MS/MS can be relatively easily performed. In theory, the ion trap approach should provide improved detection limits. We report here on our studies of detection of small amounts of cocaine (C), cocaethylene (CE), benzoylecgonine (BE), ecgonine methyl ester (EME), norcocaine (NC0), and norcocaethylene (NCE). Our interest is to develop an analysis that will allow determination of cocaethylene pharmacokinetic profiles in single animal models. All studies were performed on a Varian (Walnut Creek, CA) Saturn III GC/MS system.

Two approaches to GC/MS/MS analysis were taken: electronic ionization (EI) MS/MS and selected ejection chemical ionization (SECI) MS/MS with acetonitrile as the reagent gas. The collision process was carried out in the non-resonant mode. In the EI case, the t-butyl-dimethylsilyl-derivatives of BE, EME, NC, and NCE were separated on a DB-5ms capillary column (J&W, Folsum, CA). For these derivatives, the (M-57)+ ion was isolated, collisionally dissociated, and the product ions scanned. For C and CE, the m 182 and 196 ions were used as parent ions. Each of the compounds required different collision energy for optimum product ion formation. The amplitude of the energy was programmed for change during each segment of the run to allow sensitive detection of all of the species.

Acetonitrile (MeCN) can be used as a reagent gas for SECI due to the low gas concentration required for CI in the ion trap. MeCN provided gentle ionization of these compounds resulting in predominantly protonated molecular ions (e.g.,m/z 304 (100); 182(10); 82(15) for C). For SECI/MS/MS, (M+H)+ was used as the parent ion and the most abundant product ion was monitored for quantitation (e.g., m/z 304→182 for C). Again, kinetic energy requirements for the various compounds differed, and thus the acquisition conditions were varied during the run to optimize detection.

Either technique provided increased sensitivity for the detection of C and its metabolites relative to GC/MS. A typical chromatogram is shown below illustrating the signals observed with 100 pg of a standard preparation. Detection limits on the order of 50 pg on-column were observed for the various cocaine metabolites using CI/MS/MS.

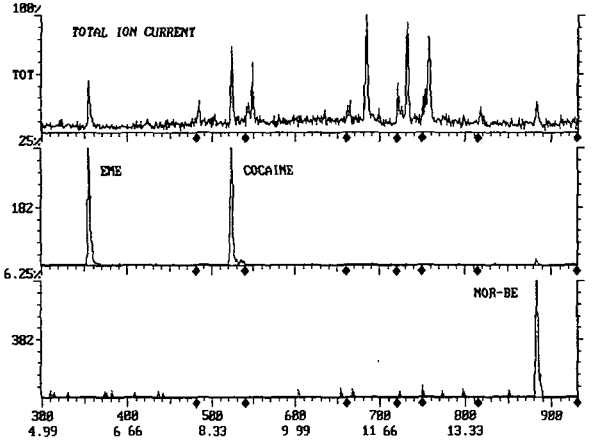

Selected Ion Storage and Tandem Mass Spectrometry of Anabolic Steroids

Larry D. Bowers
Department of Pathology and Laboratory Medicine
Indiana University Medical Center
Indianapolis, IN 46202-5120

The use of anabolic steroids (AS) continues to be problematic in sports. Improved limits of detection of AS and their metabolites are desirable. Traditionally, the trimethylsilyl-derivatives of AS are analyzed by selected ion monitoring (SIM) GC/MS to achieve sufficient limits of detection. This has required the simultaneous acquisition of numerous ions and the programming of multiple groups of ion collections. The operation of the quadrupole mass filter requires compromises between detectability and the number of ions that can be acquired. Quadrupole ion trap technology does not have this limitation, since ranges of ions ban be stored in (or specifically ejected from) the trap. The advantage of selected ion storage (SIS) is that only the ions of interest are stored, eliminating previously reported "space charging" effects. We report here on our study of SIS for the screening of AS. We have also studied GC/MS/MS as a means to improve limits of detection for confirmation analyses. All studies were performed on a Varian Saturn III GC/MS system (Walnut Creek, CA).

Several groups of trimethylsilyl-derivatives of AS were separated on a DB-5ms capillary GC column (0.25 mmx30 m; J&W, Folsum, CA). The 35 steroids were endogenous and potential exogenous AS or their metabolites. The SIS program was configured such that a range of ions (e.g., m/z 405-445) or a single ion of structural significance (e.g., m/z 143) was stored in the trap. Using the programmable acquisition tune events function, several such ranges could be programmed into the acquisition run as a function of time. Thus limited scan ranges could be adjusted to observe the ions of interest in the GC trace. This approach was significantly more sensitive than 20 ion SIM groups on an HP 5970. It was particularly used for compounds such as chlorodehydrotestosterone in which the specific isotopic pattern is useful for confirming the identity of the steroid. Unfortunately, a number of steroids whose derivatives are isobaric do not separate well by capillary GC (e.g., androstandione and epitestosterone). For this reason, MS/MS would be helpful in identifying the structure.

We investigated both non-resonant and RF resonant collision induced dissociation (CID). With appropriate adjustment of the energy, non-resonant excitation gave spectra which contained ions arising from the steroid nucleus (e.g., m/z 432→209 for testosterone-di-TMS) as well as characteristic TMS fragmentation (e.g., m/z 432→342).

Modulated RF resonant excitation specifically depleted the parent ion from the spectra. As shown in the Figure below, modulated RF resonance excitation gives rise to most of the ions observed in the non-resonant spectra. Detection limits for testosterone-di-TMS were 20 pg on-column.

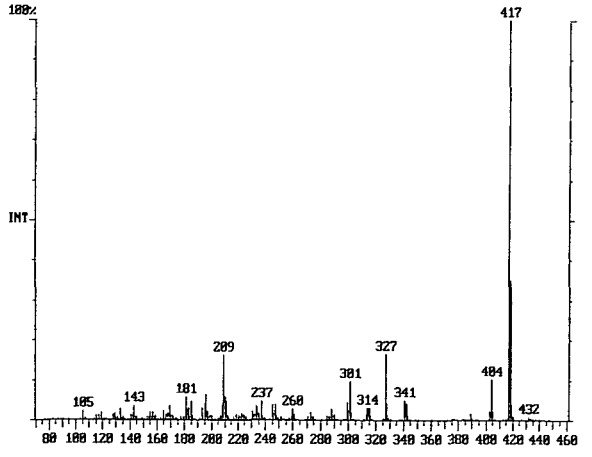

Quantitative determination of the phosophodiesterase inhibitor CP-80,633 in human serum by HPLC/MS/MS

A. Kamel*, R. Schneider, K. Navetta, E. Luther and H. G. Fouda
Central Research Division, Pfizer Inc, Groton, CT 06340

CP-80,633 is a potent and highly selective inhibitor of phosphodiesterase type 4 (PDE4) which is implicated in the release of pro-inflammtory mediators. As such, it useful for the treatment of atopic dermatitis. Clinical evaluation of CP-80,633 required an analytical method for its quantitative determination in human serum. This presentation describes an assay which utilizes on-line HPLC and atmospheric pressure chemical ionization (HPLC-APCI) tandem mass spectrometry (MS / MS). A structural analog served as the internal standard for the assay. The drug and the internal standard are extracted from human serum and aliquots are injected onto a standard reverse phase HPLC column. The effluent from the HPLC column at 1ml/min is introduced into the atmospheric pressure source of a SCIEX API III mass spectrometer. The protonated molecular ion, generated by corona discharge chemical ionization, is subjected to collision induced dissociation to a specific product ion. CP-80,633 concentrations in serum are determined by the selected monitoring of the product ion from the drug and the internal standard.

The assay concentration range extends from 0.2 ng/ml to 50 ng/ml, and its precision and accuracy over that range are within 8%.

TABLE 1. ANALYSIS OF SERUM SAMPLES CONTAINING KNOWN AMOUNTS OF CP-80,633: INTRA-ASSAY PARAMETERS; 6 SAMPLES AT EACH CONCENTRATION.

Fortified drug conc (ng/ml)	Mean conc found (ng/ml)	%RSD	%mean accuracey
0.2*	0.21	7.41	107
0.5	0.55	6.25	110
1*	1.08	2.96	108
2	2.10	1.10	105
5	5.26	3.29	105
10	10.15	2.57	102
20	19.75	2.76	99
30	28.19	3.28	94
40	36.83	3.38	92
50	46.38	3.24	93

* n=5

Positive ion CID product ion spectrum of m/z 317 from CP-80,633

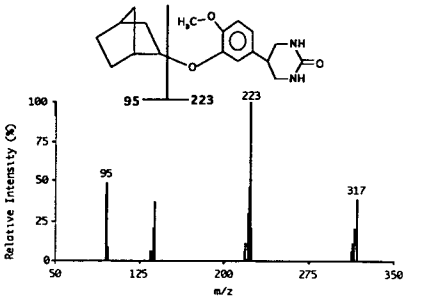

HPLC/API/MS/MS Chromatograms of Serum Extracts

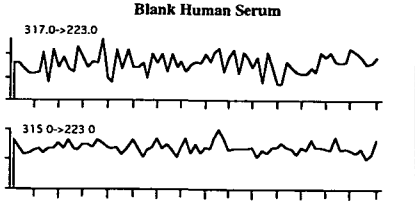

Human Serum Fortified with 0.2 ng/ml of CP-80,633

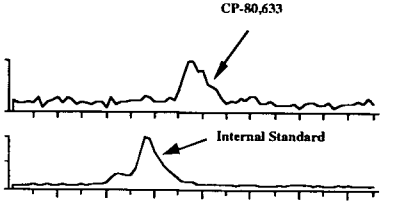

Positive ion CID product ion spectrum of m/z 315 from the internal standard CP-102,699

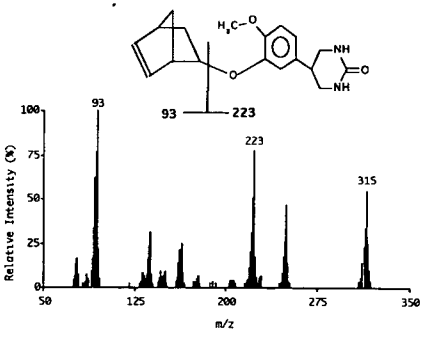

Human Serum Fortified with 5ng/ml of CP-80,633

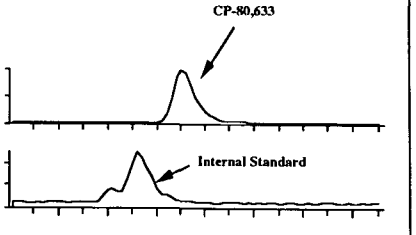

Protocols for DNA Mapping and Screening by MALDI MS by Jian Bai, Yan-Hui Liu, Xiaoli Liang, Mark G. Qian, and David M. Lubman, Department of Chemistry, The University of Michigan, Ann Arbor, MI 48109-1055

INTRODUCTION Tremendous effort and progresses have been made in adopting MALDI MS as an alternative to elctrophoresis for DNA mapping, screening, and sequencing, which can be attributed to the developments of novel matrices, improved instrumentation, and sample preparation techniques, as well as the fundamental understanding of MALDI MS of DNA, among others. The presence of impurities in the samples can generally complicate the MALDI sample preparation process and cause degradation of the MALDI MS spectrum, further limiting the size of the DNA molecules that can be analyzed. This work intends to address some technical and experimental aspects of DNA mapping and screening using MALDI MS on a Nafion film substrate, including mass calibration, mixture analysis, as well as application of MALDI MS for the detection of genetic variations based on PCR amplification of DNA collected from buccal cells, blood cells, and other sources, particularly for the typing of DNA polymorphisms associated with genetic disorders

EXPERIMENTAL A linear TOF mass spectrometer was used for detection and 355 nm laser radiation for LD/I. PCR amplification was conducted using generic protocols using template DNA obtained from buccal cells collected from voluntary individuals, and blood cells. Digestion of PCR product was performed by adding enzyme directly in the cycled reactions. A commercial PCR purification kit was used for the purification of both PCR products and the digests.

RESULTS AND DISCUSSION

Mixture Analysis The ability of MALDI MS to analyze DNA mixture is limited by the fact that as the size of DNA increases the MALDI MS sensitivity drops rapidly. We believe that the formations of multiple adduct ions between Na^+/K^+ and DNA is one of the major factor accounting for these phenomena. All fragments in the *Msp* I digest of the pBR322 DNA ranging from 9 bp to 622 bp can be detected using the Nafion film substrate (Fig. 1), even though the identification of larger fragments is still not unambiguous. There also seems to be a clear drop of sensitivity at above 250 bp. This was later identified as due to the acidity of the Nafion film, which may render the DNA molecule unstable during MALDI, generating spurious peaks and degrading the sensitivity for larger fragments. This is confirmed by using neutralized Nafion film substrate with ammonia, with which much better signals for both small and larger fragments were obtained (Fig. 2).

Mass calibration The low resolution and that only ss-DNA were observed even for ds-DNA in MALDI is limiting the general applicability of the MALDI MS. It is impossible to resolve the signals from the two strands with different but complementary sequences. However the peak originated from a ds-DNA may represent the average of the two complementary ss-DNA. On the basis of this assumption, the average MW of any two ds-DNA stands will be n(k±0.25), by a mass deviation of only ± 0 25n, or 0 08% where n is the DNA size in bp, and k the average mass of the four nucleotide units. Liner regressions performed by taking the bp and TOF squared, and residue and statistical analyses indicate that the precision using these methods can be within 2 bp in the range of 9 - 622 bp, and within 1 bp (usually < 0.5 bp) in the range of 9 - 250 bp. The poorer precision in the broader range is caused by the increasing difficulty to determine the peak centroid of the larger fragments.

DNA Screening and Detection of Genetic Variations Several PCR products derived from human genomes ranging from 86 to 426 bp were analyzed and expected signals were detected by MALDI MS on the Nafion film substrate (Fig. 3). The 212 and 426 bp fragments were CA II and CFTR genes

amplified from buccal cell DNA. Detection of larger fragments was facilitated by using the neutralized Nafion film substrates. Typing of the RFLP were also performed on several genes including the carbonic anhydrase (CA) II and III genes, and cystic fibrosis transmemebranes regulator (CFTR) genes, by direct digestion of the PCR products amplified from bucall cells using restriction enzymes. Figure 4 show the spectra obtained with the CA II genes from two selected homozygous individuals.

CONCLUSION The results reported here using active substrate, such as Nafion, demonstrate that DNA mapping and screening with MALDI MS is becoming a reality, where large DNA fragments in complex mixtures can be detected, and DNA amplified from various DNA sources using different PCR procedures can be analyzed. The mass calibration scheme established is sufficient to determine the size of the DNA fragments of < 622 bp within 2 bp. DNA samples obtained from typical biochemical procedures and settings can be routinely analyzed with minimal processing. The method reported here can be a valuable alternative to electrophoresis for the detection of genetic variations based on PCR amplification for molecular pathology and linkage studies.

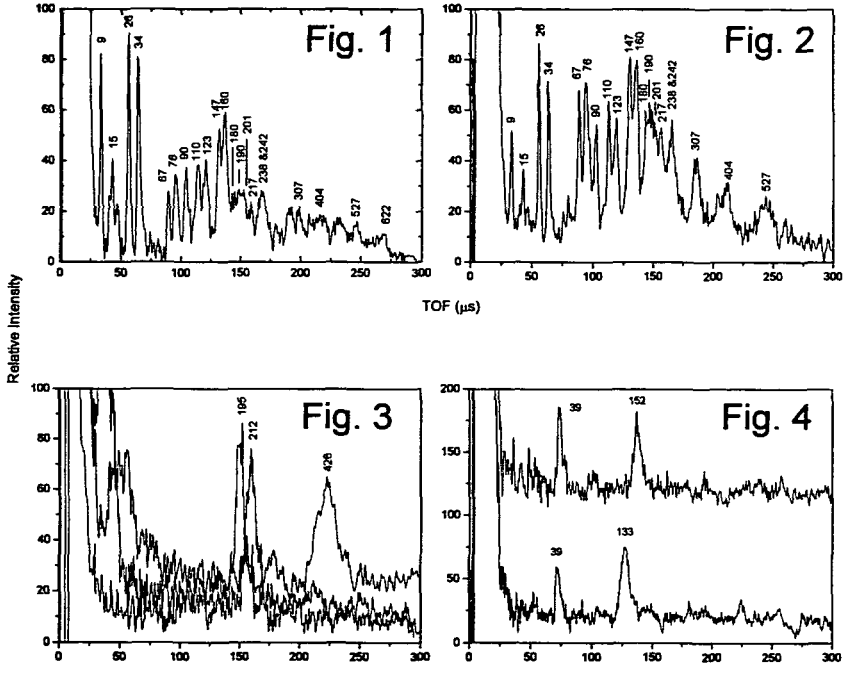

MALDI OF SYNTHETIC OLIGONUCLEOTIDES

Catherine Bentzley,[1] Murray Johnston,[1] and Barbara Lasrsen[2]
[1]Department of Chemistry, University of Delaware, Newark, DE 19716
[2]The DuPont Company, Science & Engineering Labs
P.O. Box 80228, Wilmington, DE 19880-0228

Introduction

MALDI-TOF is a valuable technique for the study of oligonucleotides. Synthetic oligonucleotides are important to the fields of molecular biology and medicine. The synthetic oligomers are used as probes in cDNA hybridization studies, primers in DNA sequencing and PCR amplification, as well as specific gene expression. Frequently, the synthetic oligonucleotides are used with no verification of the correct sequence or purity.

In this report, we analyzed numerous synthetic oligonucleotides to measure their molecular weight to initially verify their composition. We can consistently obtain the molecular ion for oligomers containing as many as 60 bases. The protocol we applied used 3-hydroxypicolinic acid (HPA) as the matrix (saturated solution) with 50-100 pmol/µl of sample which was treated with 0.5M ammonium citrate. Mass accuracy is <0.07% for all measurements which is sufficient to verify the base composition of the sample.

Providing composition verification of the oligonucleotides does not ensure that the sequence is correct. We have been developing enzymatic procedures to obtain sequence information. Shown in Table 1 and Figure1 is the digestion od a mixed base 24mer reacted for 9 minutes with Calf Spleen Phosphodiesteraseto obtain the 5' sequence os the bases. By digesting the oligomers with Calf Spleen Phosphodiesterase we were able to obtain the 5' sequence of the bases. Similar digests have been performed on larger oligonucleotides with moderate success It appears that the enzyme has a preference for particular base sequences especially thymine.

Conclusions

These values were acquired with <0.07% mass accuracy. The advantages of the techniques used here would allow for the routinue analysis of oligonucleotides using a UV laser.

Several oligonucleotides were digested to determine their base composition and sequence A procedure was developed to analyze the digestion of oligomers even for samples of mixed base compositions The same mass accuracy was expected for the digested units as was obtained for the molecular ion.

Table 1

Time Elapsed	M/Z Theoretical	Peak Experiment	Sequence	Number of Remaining Units
0 minutes	7323	7323	—	24mer
4 minutes	7323	7323	—	24mer
	6994	6993	G	23mer
	6705	6704	C	22mer
9 minutes	7323	7323	—	24mer
	6994	6993	G	23mer
	6705	6704	C	22mer
	6416	6414	C	21mer
	6127	6123	A	20mer
	5814	5812	A	19mer
	5510	5514	T	18mer
	5181	5171	G	17mer
45 minutes	6127	6125	—	20mer
	5814	5815	A	19mer
	5510	5511	T	18mer
	5181	5181	G	17mer
	4852	4849	C	16mer
	4563	4562	G	15mer
	4274	4274	C	14mer
	3970	3966	T	13mer
	3641	3639	G	12mer
	3352	3350	C	11mer
	3023	3024	G	10mer
	2734	2738	C	9mer
	2445	2438	T	8mer
	2141	2140	G	7mer

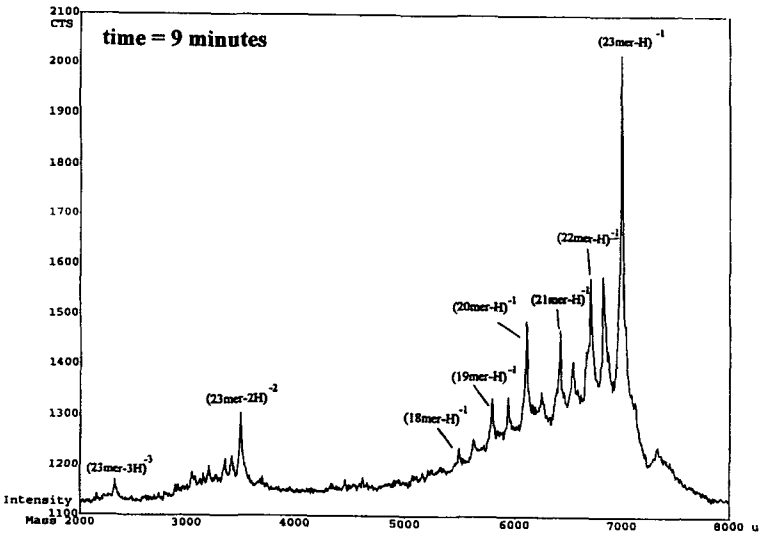

Figure 1

Reflectron MALDI-TOF Spectrum of Digested

5'-GCC AAT GCG CTG CGC TGT CAA TGC -3'

Improving Mass Resolution in MALDI-TOF Analysis of DNA

Kai Tang, Sequenom Inc , 101 Arch Street, Boston, MA 02110, USA
Timothy A. Worrall, and Robert J Cotter, Middle Atlantic Mass Spectrometry Laboratory, The Johns Hopkins University, School of Medicine, 725 N. Wolfe Street, Baltimore, MD 21205, USA
Hubert Köster, Faculty of Chemistry, Department of Biochemistry and Molecular Biology, University of Hamburg, Martin-Luther-King-Platz 6, 20146 Hamburg, Germany

While the mass range for detection of oligonucleotides by MALDI-TOF has been extended significantly (1), mass resolution in the high mass range remains poor. The major problems appear to be low desorption/ionization effiency and instability of molecular ions formed in the MALDI process, leading to losses of G, A and C bases through cleavage of the N-glycosidic bond. When such fragmentation is metastable and occurs in the acceleration region, considerable peak broadening results, which cannot be corrected or compensated by ion optical means. Therefore, our goal is to eliminate or at least minimize fragmentation during acceleration.

In our recent study, we observed that small DNA ions (up to 25-mer) are stable if an appropiate matrix (3-HPA + 10% ammonium citrate, dibasic) is used. We analyzed in a curved field reflectron TOF (2) a mixture of 12-mer, 16-mer and 20-mer with mass resolution of 1000 Neither prompt nor metastable fragments were present (figure 1). A 25-mer was also observed in a separate test under similar conditions with mass resolution of 900.

For longer DNA oligomers, metastable fragmentation was generally observed with a reflectron TOF (Vision 2000, Finnigan MAT). The most notable metastable ions resulted from the loss of a guanine base. For oligomers shorter than 60-mer, mass resolution in the reflectron was still high enough to routinely distinguish the molecular ions and the depurinated metastable ions. However, considerable broadening of the molecular ion peak was observed and probably resulted from the loss of much smaller metastable fragments which could not be resolved by the reflectron, or metastable decay in the ion source. For comparison, the metastable fragments were not observed when a linear TOF mass spectrometer (Kompact MALDI III, in linear mode, Shimadzu) was used

With the reflectron instrument, a degraded 60-mer was analyzed (figure 2) Fragments from the cleavage of the phosphodiester bond were correctly assigned from the 4-mer to 55-mer. This result demonstrates the feasibility to measure complex DNA mixtures by MALDI-TOFMS and is encouraging for applying the technique to DNA sequencing. Further, a mixture of synthetic ss-DNAs up to 50 bases long that mimic the sequencing ladder produced by ddTTP was analyzed, and detection sensitivity was determined at about 50 fmol for each ladder component (figure 3).

References

1. Tang, K., Taranenko, N. I., Allman, S. L., Chang, L. Y and Chen, C. H. (1994) *Rapid Comm. Mass Spectrom.* **8**, 727-730.
2. Cornish T, J , and Cotter, R. J. (1994) *Rapid Comm. Mass Spectrom.* **8**, 781-785.

43rd ASMS Conference on Mass Spectrometry and Allied Topics

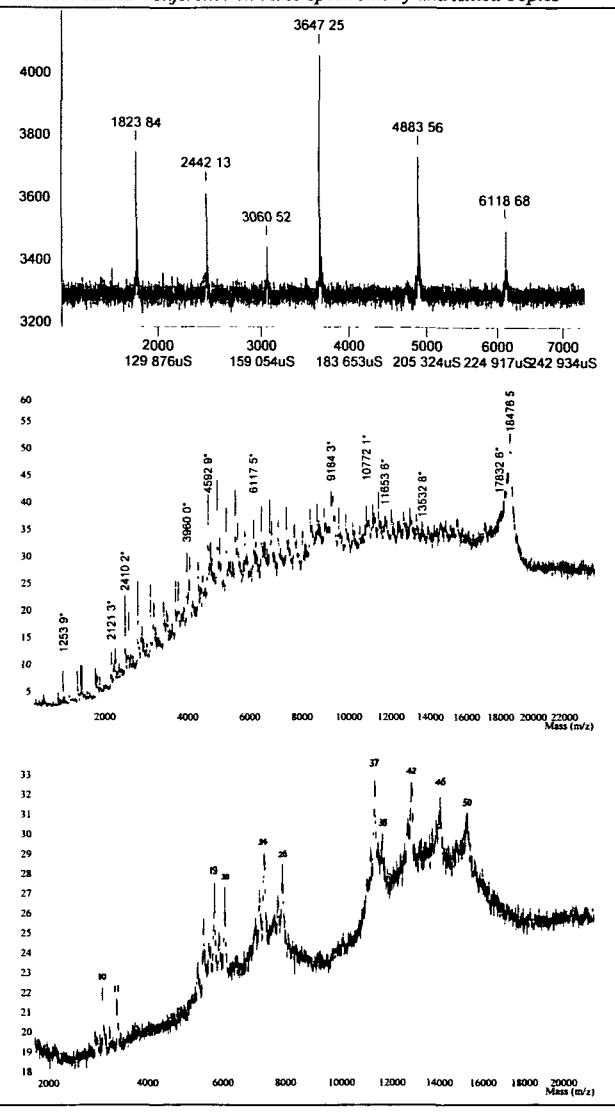

Probing the Stability of Phosphorothioate Oligodeoxynucleotides Using Matrix-assisted Laser Desorption Ionization Time-of-Flight Mass Spectrometry

Bing H. Wang *, Andre J. Bourque, Alexi B. Belenky, and Aharon S. Cohen
Hybridon, Inc., Milford, MA 01757

Introduction

Due to their nuclease resistance and the ability to promote Rnase H activity, phosphorothioate oligodeoxynucleotides (sODNs) are a group of promising antisense agents for the sequence-specific inhibition of gene expression. *In vitro* studies have shown the activity of sODNs against human immunodeficiency virus (HIV) and other viral targets. The inhibitory activity of sODNs against HIV *in vivo* is currently under clinical trials For therapeutic applications, the stability of sODNs has to be evaluated and the degradation products have to be identified, since they may lead to toxic side effects.

Although techniques such as anion-exchange high performance liquid chromatography (AE-HPLC) and capillary gel electrophoresis (CGE) are powerful techniques for separating mixtures of sODNs and their derivatives, it is tedious to ascertain the identity of individual components in a mixture using these techniques Matrix-assisted laser desorption ionization time-of-flight mass spectrometry (MALDI-TOFMS) has recently been applied to the analysis of sODNs (1) The much higher specificity of molecular weight information over that of migration time coupled with the knowledge of a sODN sequence prior to its degradation allows a rapid identification of the degradation products.

Experimental

A phosphorothioate 25-mer (GEM91) was synthesized in house. To obtain its thermal degradation products, an aqueous solution of the 25-mer was stored at 60°C for 2 months. Light-induced degradation products were obtained by storing a solid sample of the 25-mer in a light chamber of 1000 foot candles at 30°C for 2 months. In the *in vitro* enzymatic digestion experiment, the 25-mer was incubated with snake venom phosphodiesterase I (SVP I) at 55°C for 2 hours Samples from above sources were analyzed without further purification In the experiment involving *in vivo* enzymatic digestion of the 25-mer, the metabolites were obtained from the plasma of a Rhesus monkey collected 8 hours after subcutaneous injection of the precursor compound sODN products were extracted from the plasma by anion-exchange solid phase extraction followed by reverse-phase solid phase desalting.

A mixture of 3-hydroxypicolinic acid and N-(3-indolylacetyl)-l-leucine was used as the matrix (2) To reduce the formation of sodium and potassium adducts, the matrix solution was heated to 50°C for 15 min in the presence of cation-exchange resin in NH_4^+ form (200- 400 mesh) Negative ion mass spectra were acquired with a Bruker Reflex MALDI-TOF mass spectrometer in the linear mode All spectra were the summed results of 20 -30 laser shots

Results

Thermal degradation. Extensive sequence fragments were generated by prolonged heating (Figure 1) Cleavage invariably occurred on those glycosidic bonds that were attached to the ribose which had lost the base. Not surprisingly, purine bases are the favored sites of cleavage In contrast to pyrimydine bases, cleavage at purine base can produce a 5'-end fragment with the ribose residue attached, in addtion to the 3'-end and 5'-end fragment pair. This mechanism accounts for the production of peaks at *m/z* 1654, *m/z* 2304, and *m/z* 3553

Light-induced degradation. In contrast to thermal degradation, only small fragments (smaller than 12 bases) were observed from light irradiated samples The mechanism of the fragmentation is currently under investigation.

Enzymatic digestion. The mass spectrum of the metabolites collected from the monkey plasma 8 hours after the injection of the 25-mer consists of mostly peaks from a sequence ladder, which was generated by the successive removal of 3'-end phosphorothioate deoxynucleotides (Figure 2) The spectrum resembles closely that of the products produced by *in vitro* digestion of the 25-mer by SVP I. However, MALDI-TOFMS analysis of metabolites collected after 8 weeks of daily injection and 24 hours after the last injection showed that products from 5'-end digestion are also present. Significantly, oxygenated products were present among the metabolites.

Conclusion

The generation of degradation products or metabolites of GEM91 are environment dependent While degradation at 60 °C gives prominent depurination products, light-induced degradation tends to produce fragments smaller than 12-bases In a Rhesus monkey, 3'-exonucleases exhibited much higher activity than 5'-exonucleases. The last finding suggests that efforts should be directed towards the modification of the 3'-end of an antisense agent to increase its nuclease resistance

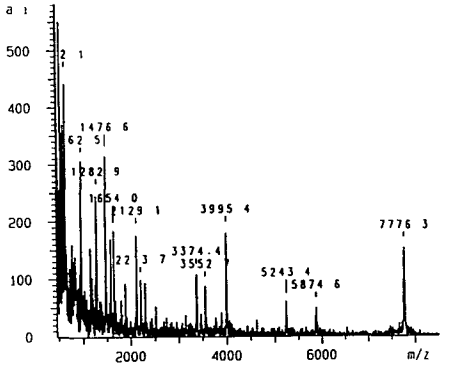

Figure1 MALDI-TOF mass spectrum of GEM91 after the aqueous solution had been stored at 60°C for 2 months

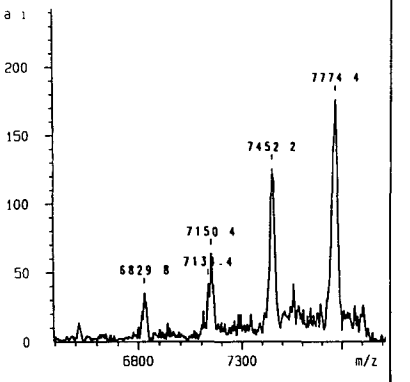

Figure 2 MALDI-TOF mass spectrum of GEM91 and its metabolites extracted from the plasma of a Rhesus monkey 8 hours after subcutaneous injection of GEM91

Reference

(1) Wang, B H , Belenky, A , Cohen, A S *Proceedings of the 42nd ASMS Conference on Mass Spectrometry and Allied Topics*, Chicago, 1994, p145
(2) Walker, K L , Wilkins, C L *Proceedings of the 42nd ASMS Conference on Mass Spectrometry and Allied Topics*, Chicago, 1994, p146

6-AZA-2-THIOTHYMINE: A GOOD MATRIX FOR THE ANALYSIS OF OLIGONUCLEOTIDES

P. Lecchi, H. M.T. Le, and L.K. Pannell, Lab. Analytical Chemistry, NIDDK, NIH, Bethesda, MD (USA)

The analysis of oligonucleotides has become important to this laboratory. In our research into the existing experimental protocols and matrices for MALDI, we found that it was hard to obtain satisfactory results. We decided to develop a MALDI method that would give consistent results with oligonucleotide samples. The use of 6-aza-2-thiothymine (ATT) as a matrix for MALDI has been reported (1), but not with oligonucleotide samples. Since ATT has a molecular structure closely related to that of purines, and has an UV absorption at the wavelength commonly used for MALDI (337 nm), it seemed a reasonable candidate to be tested.

All spectra were acquired on a KRATOS MALDI III (Shimadzu, Columbia, MD). After desorption and ionization, negative ions were accelerated at 22 KeV, in linear mode. Approximately 50 shots of the laser across the sample surface were averaged to produce the spectra shown .

Experimental protocols described for 2',4',6'-trihydroxy acetophenone (THA) (2), 3-hydroxy picolinic acid (3-HPA) (3) and ATT (4) were compared using a 16-mer oligonucleotide (TTTAGAGTCTGCTCCC). In all the three experimental protocols 1 µl of matrix solution was mixed on the sample probe with 0.8 µl of analyte solution. As internal standards, bovine insulin β chain and bovine insulin (peaks at m/z 3494.3 and 5732.0) were used. The MALDI spectra clearly show ed that ATT gave better resolution. To further compare the three matrices, the 16-mer oligonucleotide was run with ATT, THA or 3-HPA, 30 times for each matrix, in three different experiments. Statistical analysis shows that ATT gives the best resolution and reproducibility (Fig. 1).

With a mixture of oligonucleotides a clean spectrum is obtained at 10 pmoles/each. With as low as 0.1 pmoles, a spectrum that shows all of the analytes in the mixture is still seen. The longest nucleotides tested so far with ATT are 33 and 45 nucleotides in lenght, and molecular ion peaks were obtained. A crude deprotected 23-mer oligonucleotide (trytil-OFF) was analyzed with ATT, and the impurities and by-products of synthesis could be clearly seen.

A 12/16 nucleotide long, double-stranded (ds) DNA EcoRI adaptor was analyzed using ATT or THA as a matrix. No peak at the MW expected for the DNA duplex was seen with THA. With ATT, the intact ds-DNA peak is clearly seen, as well as those of the two dissociated single strands. The single-strand (ss) DNA specific enzyme Nuclease S1 was used to digest the ss-DNA present in the sample prior to ionization. The spectrum shows a significant reduction of the peaks corresponding to the dissociated ss-DNA, thus implying that dissociation of the DNA duplex did not occur during the desorption process.

In conclusion: a) ATT is an optimal matrix for the analysis of oligonucleotides; b) ATT gives better resolution, accuracy and reproducibility than THA and 3-HPA; c) ATT gives high sensitivity, tolerance to contaminants and good upper mass limit; d) Double-stranded DNA can be detected as an intact duplex when ATT (but not THA) is used as a matrix.

REFERENCES:

1. Juhasz,P.; Costello,C.E.;Biemann,K. (1993) J. Am. Mass Spectrom. 4, 399.
2. Piels,U.; Zurcher,W.; Schar,M.; Moser,H.E. (1993) Nucleic Acids Res. 21, 3191.
3. Wu,K.J.; Shaler,T.A.; Becker,C.H. (1994) Anal. Chem. 66, 1637.
4. Lecchi,P.; Lee,H.M.T.; Pannell,L.K. (1995) Nucleic Acids Res. 23, 1276.

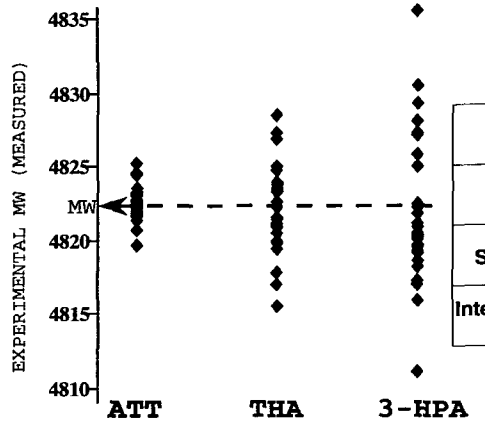

	ATT	THA	3-HPA
Resolution	480	240	280
Mean (n=30)	4822.3	4821.6	4822.5
Std. Deviation	1.04	4.38	5.01
Interassay var. %	±0.006	±0.057	±0.045

Fig.1 Comparison between ATT, THA and 3-HPA

MALDI-MS AS A NEW TOOL TO MONITOR THE ACTIVITY OF NUCLEIC ACID MODIFYING ENZYMES

E. Nordhoff, F. Kirpekar, K. Kristiansen, P. Roepstorff, S. Hahner[1], F. Hillenkamp[1], R. Cramer[2], and R. F. Haglund[2]

Department of Molecular Biology, University of Odense, Denmark, [1]Institute for Medical Physics and Biophysics, University of Münster, Germany, and [2]Department of Physics and Astronomy, University of Vanderbilt, Nashville, USA.

UV-MALDI-MS analysis of DNA and RNA using 3-hydroxypicolinic acid as matrix has been applied for the study of the activity and specificity of different nucleic acid modifying enzymes[1,2]. Alkaline phosphatase catalyzes the removal of 5'-terminal monophosphate groups of DNA and RNA and of 5'-di- and 5'-triphosphate groups of RNA leading to reduction in molecular mass of 80 Da for each released phosphate group. Polynucleotide kinase catalyzes the transfer of the terminal phosphate group of ATP to the 5'-hydroxylated termini of DNA and RNA resulting in increase of molecular mass by 80 Da. T4-RNA ligase catalyzes the formation of an internucleotide phosphodiester bond between a 5'-terminal phosphate and a 3'-terminal hydroxyl group of linear oligo- or polyribonucleotides by the use of ATP. Depending on the reaction conditions, especially on the concentration of the educt species, and sequence length of the educts this reaction can generate either circular RNA or intermolecular ligation products. Circularization leads to a mass loss of 18 Da corresponding to the phosphodiester bond formed in addition (elimination of one water molecule). With UV-MALDI RTOF-MS using 3-hydroxypicolinic acid as matrix this mass difference has been resolved, e.g., for a RNA 20-mer. Ligation of two species of type M lead to a ligation product of molecular mass of 2M-18 Da.

Terminal transferase catalyzes a template independent addition of deoxyribonucleotides to the 3'-termini of single- or double-stranded DNA. The stepwise addition and the resulting size distribution after a chosen reaction time can be visualized by mass spectra. An example is given on the right side: mass spectra of the elongation of an octathymidylic acid after 3 min incubation with terminal transferase in the presence of (a) adenosine triphosphate and (b) 7-deaza-adenosine triphosphate are shown[3]. Specific exonucleases degrade stepwise oligonucleotides (DNA and RNA) either from the 3'- or the 5'-terminus. A time course of this activity by MS allows one to determine the sequence of oligonucleotides in a very elegant way[4,5].

T3- as well as T7 RNA polymerase transcribe DNA into RNA. If applied to a restriction-enzyme linearized DNA template exhibiting the corresponding promotor region large quantities of in-vitro RNA transcripts can be obtained and the sequence length of those can be determined by the specificity of the used restriction enzyme. However, the transcription of such templates does always lead to RNA products exhibiting a strong 3-heterogeneity. Premature termination of the transcription as well as unspecific elongation of the full length transcript, both highly depending on the template and used enzyme, were observed[6]. The complexity and kind of heterogeneity were characterized by MALDI-MS.

43rd ASMS Conference on Mass Spectrometry and Allied Topics

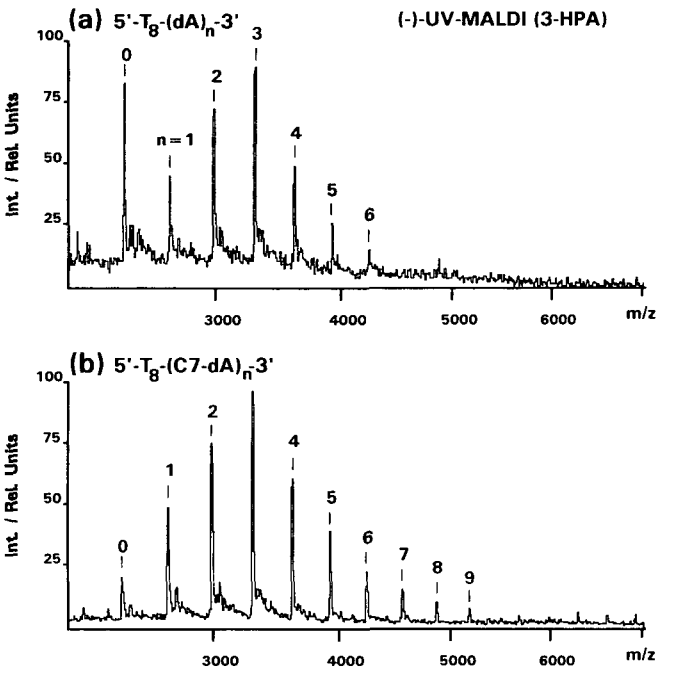

References

1 **K. J. Wu, A. Stedding and C. H. Becker**, *Rapid Commun. Mass Spectrom.*, 7, (1993) 142.

2. **Nordhoff, E., F. Kirpekar, M. Karas, R. Cramer, S. Hahner, F. Hillenkamp, K. Kristiansen, P. Roepstorff, and A. Lezius**, *Nucleic Acids. Res.*, 22 (1994) 2460.

3. **Kirpekar, F., E. Nordhoff, K. Kristiansen, P. Roepstorff, S. Hahner, and F. Hillenkamp**, *Rapid Commun. Mass Spectrom.*, accepted March 1995.

4. **Pieles, U., W. Zürcher, M. Schär, and H.E. Moser**, *Nucleic Acids Res.*, 21 (1993) 3191

5. **Nordhoff, E., S. Hahner, M. Karas, F. Hillenkamp, F. Kirpekar, K. Kristiansen, and P. Roepstorff**, *Proceedings of the 13th International Mass Spectrometry Conference, Budapest, August 29th - September 2nd*, (1994) 218.

6. **Kirpekar, F., E. Nordhoff, K. Kristiansen, P. Roepstorff, M. Karas, S. Hahner, A. Lezius, and F. Hillenkamp**, *Nucleic Acids. Res.*, 22 (1994) 3866.

Acknowledgment. Part of this work was done in partial fulfillment of the requirement for the pH. D. degree of S. Hahner at the University of Münster. Financial support of this work by the Commission of the European Communities (grant No.: GENO-CT93-0082 (SSMA)) is greatly appreciated.

Study of PAH-DNA adducts by CF-FABMS

Sylvie Plante and M.J. Bertrand
Regional Center for Mass Spectrometry, Dept. of Chemistry,
University of Montreal, Montreal, Canada, H3C 3J7

Polycyclic aromatic hydrocarbons (PAH) are pollutants whose toxicity to several species has been proven. The formation of adducts between the DNA and PAHs is believed to induce processes such as mutagenesis, teratogenesis and cancerogenesis. This study examines the adducts formed betwen deoxyguanosine (dG) and Benzo[a]pyrene (BaP) (Figure 1). These adducts were synthesized electrochemically in this laboratory [1,2]. Subsequently, CF-FAB-MS and capillary LC/FAB-MS, under both positive and negative ionization modes, were used to analyse these compounds. As well, the conditions of the mobile phases were optimised with respect to the pH level and glycerol content. Since two different adducts are obtained (C8dG and C8Gua) and recovered during the synthesis, a chromatographic separation was undertaken. In LC/MS the intensity of the molecular ion was found to vary with the pH of the matrix. In the positive ion mode, an optimal signal is observed for a pH adjusted to a value of 2.0 using trifluoroacetic acid (TFA). When less acidic mobile phases are used, the signal weakens. For the negative ions, a better signal for both adducts is observed when the mobile phase pH is adjusted to a value 9.5 using sodium hydroxyde (NaOH). It is possible to vary the concentration of the FAB matrix (Glycerol) in the mobile phase in order to optimize the sensitivity of the signal. A mobile phase with 2% of glycerol was used for both ion modes. Similar results are obtained using mobile phases of 2% Gly, 60% EtOH, 38% H_2O, or 2% Gly, 60% ACN, 38% H_2O. The same pH values obtained under the CF-FAB conditions was used for the LC/MS experiments. The optimal flow rate used to separate both adducts was 2.0 uL/min. Figure 2 illustrates the mass chromatograms obtained under positive ionization. Chromatogram A corresponds to m/z 402, and chromatogram B to m/z 518. C8Gua has a m/z of 402 and, therefore, corresponds to one of the two peaks in chromatogram A. However, the mass spectrum of the peak in chromatogram B shows the molecular ion of C8dG, as well as a fragment at m/z 402 (Figure 3). This peak elutes in coincidence with one of the peaks in chromatogram A of Figure 2, which suggests that the other peak in the chromatogram corresponds to the C8Gua adduct. The mass spectrum of this peak confirmed an ion of m/z 402, however, no characteristic fragmentation is observed for this molecule under these experimental conditions. The parent-molecular ion of C8dG, at m/z 518, appears less intense than the fragment at m/z 402. The difference in mass between the both ion is that of a sugar ($C_5H_9O_3$). These results suggest that the two adducts are indeed separated and present in the mass chromatograms of Figure 2. The mass chromatograms obtained in the negative ion mode were very similar to those obtained for positive ions. This confirms that the pH of the eluent does not dramatically change the chromatographic conditions. A mass chromatogram of m/z 400 again shows two peaks, of which the second belongs to the C8Gua parent-molecular ion. Here again no characteristic fragmentation is observed in the mass spectrum for this adduct under these conditions. The mass spectrum (Figure 4) of the peak in the mass chromatogram of m/z 516, shows a peak at mass 400. Again, loss of a sugar molecule is deemed responsible for the ion of m/z 400. The intensity of this fragment is less than that of the molecular ion. In order to achieve the separation of the adducts, while also providing suitable FAB ionization conditions, the optimisation of certain parameters, such as the content of glycerol and the pH of the mobile phase was required. The best results were obtained using 2% of glycerol in the mobile phase, in both

positive and negative ion modes. The pH study demontrates that an acidic pH of 2.0 provides a better signal of adduct molecular ions under positive ionization, while a pH of 9.5 is favorable for negative ionization. The mass spectra of C8dG indicates the loss of a sugar entity from the molecular ion, under both positive and negative ionization modes, while no intense fragments were observed in the spectra of C8Gua.

REFERENCES:

1) E.G. Rogan et al., J. Am. Chem. Soc. 110, 4023 (1988)
2) N.V.S. RamaKrishna et al., Chem. Res. Toxicol., 5, 293, (1992)

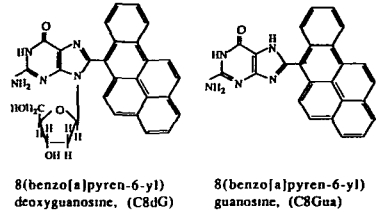

Figure 1. Electrochemical reaction of the adducts.

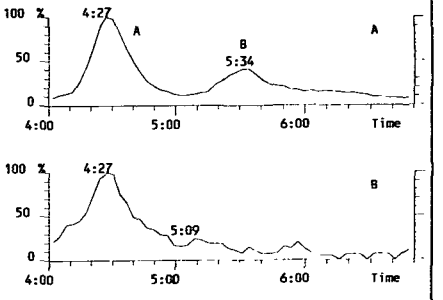

Figure 2. Mass chromatogram of A) m/z 402, B) m/z 518 in positive ionization.

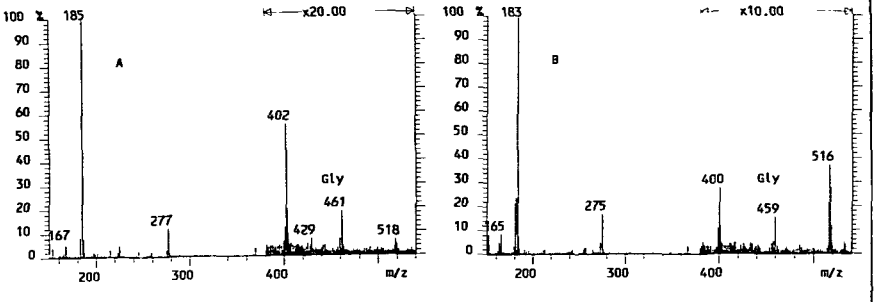

Figure 3. Mass Spectrum for the C8dG A) in positive ionization, B) in negative ionization.

MALDI-TOF Analysis of Steriod/PAH-modified DNA Adducts at the femtomole Level

J. K. Gooden,[1] M. L. Gross,[1] D. Stack,[2] P. Mulder,[2] K. Li,[2] E. Cavalieri[2]

[1]Dept. of Chemistry, Washington University, 1 Brookings Drive, St. Louis, MO 63130
[2]Eppley Institute, University of Nebraska Medical Center, Omaha, NE 68198

Covalent binding of polycyclic aromatic hydrocarbons (PAH's) and steroids to DNA to form adducts is one of the first events in the process of tumor initiation in carcinogenesis. Structure elucidation and characterization of these adducts provide important information that leads to further understanding of their biological metabolic pathways. In in vivo and in vitro steroid/PAH-DNA binding studies, the reaction products (adducts) are often of low amount (low picomole to femtomole).

Previous results from our laboratory have shown that the sensitivity of MALDI-TOF can be improved by proper matrix selection.[1] An increase in sensitivity can also be obtained with the use of *d*-fucose as a co-matrix.

In this study 4-phenyl-α-cyanocinnamic acid, **PCC**, 4-benzyloxy-α-cyanocinnamic acid, **BCC**, ferulic acid, **FA**, α-cyano-4-hydroxycinnamic acid, **4HCCA**, and 3-(2-naphthyl)-2-cyanoacrylic acid, **NCA,** were used in the determination of the limit of detection for two different DNA adducts dibenzocarbazole-5-*N*7Ade, and 4-hydroxyestrone-*N*7Gua. Matrices were used as saturated solutions of 1% TFA in 50% acetonitrile/water except for ferulic acid, which was used as a 0.14 M solution. Solutions of matrices utilizing *d*-fucose as a co-matrix were prepared as 0.5 M solutions in the same solvent for all matrices. Standard solutions of DBC-5-*N*7Ade , and 4-OH-estrone-*N*7Gau were prepared in methanol at 4 pmol/μL concentrations. Analyte and matrix were premixed before application to the sample plate.

Experiments were carried out on a PerSeptive Biosystems Voyager RP MALDI-TOF Mass Spectrometer equipped with a nitrogen laser. Ions were detected in positive ion mode at an accelerating voltage of 25 kV. PSD spectra were obtained under the same conditions. The limit of detection was determined by the lowest amount of analyte that would produce a signal to noise of 3 to 1 or better in three separate trials. The result of forty to sixty laser shots were averaged for each spectrum.

Increased sensitivity can be achieved when the matrix compound and the analyte are structurally similar. The limits of detection for DBC-5-*N*7Ade using **BCC**, **NCA**, and **PCC** is 125 fmol/μL or lower (Table 1). When these matrices are combined with *d*-fucose as a co-matrix, the limit of detection becomes 50 fmol/μL or lower. The lowest limit of detection was acquired with **BCC**/fucose at 17 fmol/μL. The DNA adduct 4-OH-estrone-*N*7Gua is composed of a polar purine base and a polar steroid. The limit of detection for this adduct using **4HCCA** and **FA**, both of which have polar groups separated by an aromatic ring, is 267 and 520 fmol/μL respectfully (Table 1). Using *d*-fucose as a co-matrix affords detection limits of 167 fmol/μL for **4HCCA**/fucose and 25 fmol/μL for **FA**/fucose.

Structural information from DNA adducts can also be obtained from Post Source Decay (PSD) analysis. An example of this analysis is the PSD of DBC-5-N7Ade, which is compared with the CAD spectrum of the same adduct, obtained on a four-sector tandem instrument. (Fig 1).

1. George, M.;Wellemans, J. M. Y.; Cerny, R. L.; Gross, M. L.; Li, K.; Cavalieri, E. L. *J. Am. Soc. Mass Spectrom.* **1994**, 5, 1021-1025

Matrix	DBC-5-*N*7Ade	4-OH-estrone-*N*7Gua
4HCCA	*	267
BCC	63	425
PCC	125	550
FA	333	520
NCA	41	1,300
4HCCA/fucose	*	167
BCC/fucose	17	200
PCC/fucose	50	333
FA/fucose	250	25
NCA/fucose	30	500

Table 1. Detection limits (in femtomoles/microliter) for DNA adducts
* Determination of detection limit precluded because matrix ions interfered

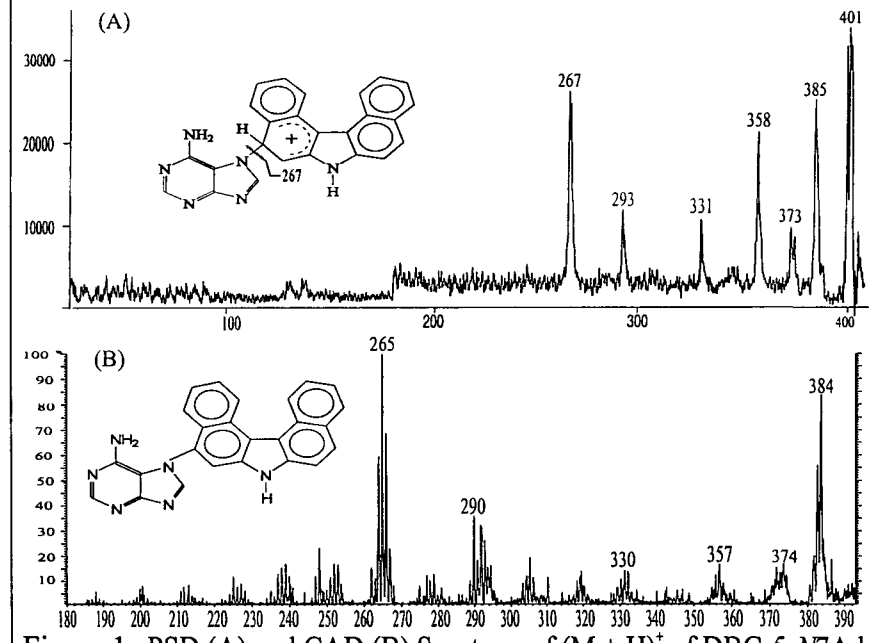

Figure 1. PSD (A) and CAD (B) Spectrum of $(M + H)^+$ of DBC-5-*N*7Ade

Tandem MS/MS for Determining Structural Isomers of PAH-DNA Adducts

J. Byun[1], I. Vidavsky[1], M. L. Gross[1], P. Mulder, K. Li[2] and E. Cavalieri[2] (1) Department of Chemistry, Washington University, One Brookings Drive, St. Louis, MO 63130, (2) Eppley Institute for Research in Cancer, University of Nebraska Medical Center, 600 South 42nd Street, Omaha, NE 68688-0362

Polycyclic aromatic hydrocarbons (PAHs) such as methylcholanthrene (MC), dibenzo[*a,l*]pyrene (DBP), and dimethylbenz[*a*]anthracene (DMBA) are carcinogenic because they give rise to PAH-DNA adduct formation. Our laboratory has demonstrated that tandem mass spectrometry is effective for distinguishing and characterizing these isomers.

The main goal of this study is to investigate the structural isomers isolated from reactions of DBP, 1,2,3,4-tetrahydro-7,12-dimethylbenanthracene (THDMBA), and MC radical cations with DNA, to identify the structure of fragment ions produced by CAD, and to understand fragmentation processes of modified DNA adducts.

The tandem CAD mass spectra were acquired by using a VG ZAB-T, a four-sector tandem mass spectrometer of BEBE design. A Cs^+ ion gun operated at 30 kV was used to desorb the ions from the probe. CAD spectra were obtained after precursor ion activation in the third field-free region (between MS 1 and MS 2) by addition of helium to attenuate the ion beam by 50 %.

DBP-Ade Adducts

Upon collisional activation (CA), the $[M + H]^+$ ions of *m/z* 436 from DBP-Ade adducts decompose to generate major fragment ions of *m/z* 419 $(M + H - NH_3)^+$, *m/z* 327 $(C_{24}H_{13}NC)^+$, *m/z* 314 $(C_{24}H_{12}N)^+$, *m/z* 302 $(C_{24}H_{14})^+$, *m/z* 300 $(C_{24}H_{12})^+$, *m/z* 287 $(C_{23}H_{11})^+$, *and m/z* 274 $(C_{22}H_{10})^+$. The most abundant fragment ion is of *m/z* 300 $(C_{24}H_{12})^+$, Fig. 1. The ions of *m/z* 302 and *m/z* 419 are of particular interest for distinguishing the different structural isomers.

As shown in Scheme 1, the generation of the *m/z* 302 ion from the parent ion of *N7*- and *N9*-adducts occurs by the cleavage of PAH-DNA bond. For *N7*Ade adduct, the formation of the *m/z* 302 and 419 ions is now more competitive because a six-membered ring intermediate is stabilized by hydrogen bonding. However, the relative abundance of the *m/z* 302 ion in *N9*Ade is larger compared to that of *N7*Ade because the proton attached at C_{10} position may not interact with other basic groups, leading to the greatest weakening of the C-N bond in this set of isomers. The relative abundances of the fragment ions $(C_{24}H_{14})^+$ at *m/z* 302 and $(M + H - NH_3)^+$ at *m/z* 419 are inversely related and serve as "finger-prints" of the various isomers to give information about the site of attachment of the DBP on the base.

THDMBA-7CH$_2$- and 12CH$_2$-N7Ade and Gua Adducts

The CAD mass spectra of the $[M + H]^+$ ions for the modified Ade (Fig. 2) and Gua adducts show several important fragment ions giving structural information. The prominent ion of *m/z* 259 fragments in a distinctive way, identifying the position of pyridine attachment to 1,2,3,4-TH-7,12-DMBA. When the attachment is at C_{12}, the fragment *m/z* 244 is more abundant, whereas for attachment at C_7, the fragment *m/z* 243 is more abundant (Scheme 2).

Methylcholanthrene(MC)-Base and Nucleoside Adducts

During CAD, the $[M + H]^+$ ion of MC related compounds decompose to generate several ions that are diagnostic of the adduct. All adducts give as the most abundant product ion of *m/z* 267. Unfortunately this fragmentation is so facile that different sites of attached of MC to the base cannot not be distinguished.

In conclusion, FAB MS/MS can be used to distinguish structural and/or positional isomers on the basis of the relative peak intensities and fragment ions. Our ongoing efforts include determination of these adducts formed *in vivo* studies by MS/MS, using continuous-flow and co-axial flow FAB as well as ESI to overcome some drawbacks generated in FAB MS/MS.

43rd ASMS Conference on Mass Spectrometry and Allied Topics

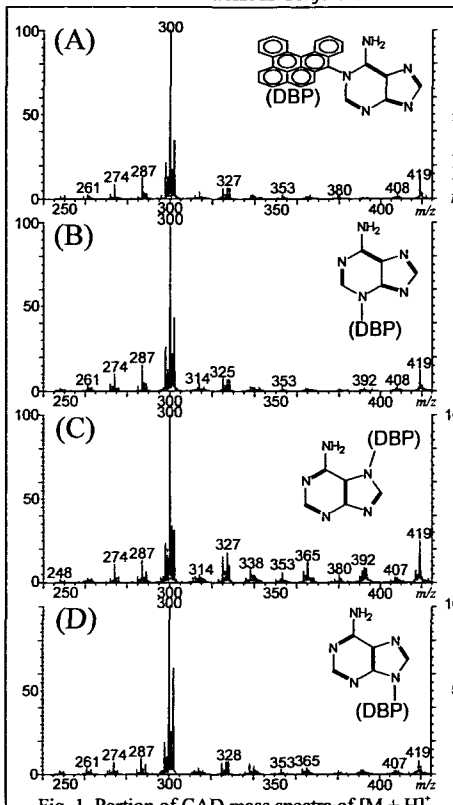

Fig. 1 Portion of CAD mass spectra of $[M + H]^+$ of *m/z* 436 from DBP-Ade adducts.

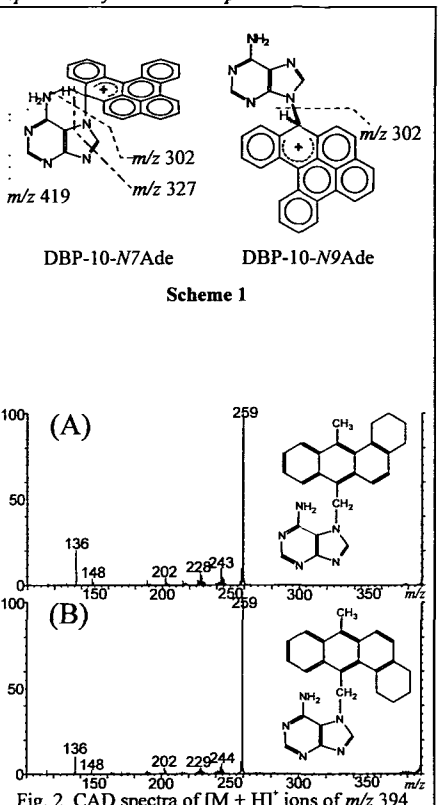

Scheme 1

Fig. 2 CAD spectra of $[M + H]^+$ ions of *m/z* 394 from THDMBA-Ade adducts.

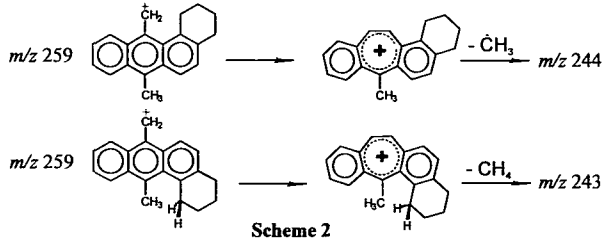

Scheme 2

A GENERAL METHOD FOR DETERMINING ETHYLENE OXIDE AND RELATED N7-GUANINE DNA ADDUCTS BY GC-EC-MS.

Amir Abushamaa, Xiaoning Wang, Veeravagu Murugaiah, Abdul Naim, Manasi Saha, and Roger Giese. Department of Pharmaceutical Sciences in the Bouvé College of Pharmacy and Health Sciences, and Barnett Institute, Northeastern University, 360 Huntington Avenue, Boston, MA 02115.

INTRODUCTION:

The N7 position of guanine is a prominent site of attack on DNA both in vitro and in vivo by a variety of alkylating agents. Humans are exposed occupationally, chemotherapeutically or otherwise (e.g. smokers) to alkylating agents. For example, approximately 2.5 x 10^6 tons of ethylene oxide are produced annually in the United States, where 150,000 workers deal with it daily in various industrial processes [1986 figures]. Ethylene oxide is considered a probable carcinogen in humans. N7-G adducts potentially are a favorable class of DNA adducts for measurement since heating the DNA in water releases such adducts as free nucleobases. We are developing a general method for the detection of "small" N7-G DNA adducts by GC-EC-MS (Hewlett Packard 5988A).

RESULTS AND DISCUSSION:

Our scheme for detecting N7-G ethylene oxide and related adducts is shown in Figure 1. Starting with a 100 µg amount of DNA spiked with 100 pg of this analyte and a corresponding stable isotope internal standard, we obtained the mass chromatograms shown in Fig. 2 A, B. The triplicate analysis gave absolute yields of 9.7 ± 3.0% and 9.7 ± 3 3% (x ± SD) of final products, respectively, for the analyte and internal standard. Fig. 2C shows the corresponding analysis of a sample containing no DNA. The variation in peak symmetry is due to variation in column age and plotted peak height (see inset in Fig. 2C). The generality of the method was demonstrated by applying it successfully to 50 ng amounts of analogous methyl, benzene and styrene N7-G adducts. During this study a new mechanism (masking by contaminants) was discovered for evaporative loss of a trace analyte, especially after solid phase extraction. Using the scheme shown in Figure 3, the data shown in Tables 1 and 2 were obtained, which showed that such contaminants not only exist in the purest water routinely available, but are enhanced and vary significantly after solid phase extraction using different commercial packings.

CONCLUSION:

Previously we obtained a 17% overall yield preparatively when 20 mg of a pure sample of the N7-G ethylene oxide adduct was converted to the final derivative shown in Figure 1. Now, starting with about 10^8 less analyte and spiked into DNA, our absolute analytical yield is 9.7%. This method has been transferred to another laboratory where it is being used successfully to measure this adduct and animal and human samples. During the course of the work, it was learned that an evaporation can risk loss of a trace analyte from masking by packing-derived solvent contaminants. This tends to counteract the common strategy of redissolving a trace analyte by using a good solvent for it. This work was funded by a Grant from NIOSH (Centers for Disease Control and Robert A. Taft Labs).

43rd ASMS Conference on Mass Spectrometry and Allied Topics

Figure 1

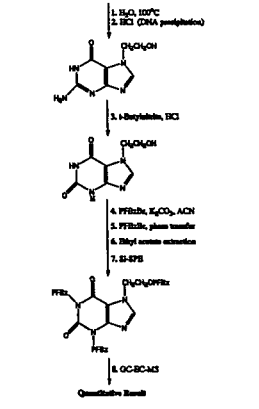

Figure 2

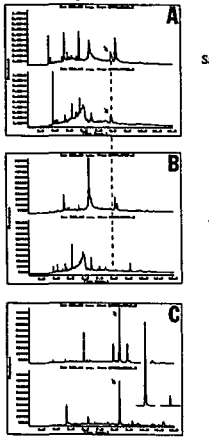

Fig. 3 Scheme for testing alkyl-bonded silica packings in a solid phase extraction procedure.

Sample: 50 µl ACN + 2.0 ml H_2O + X.
(X = nothing, KCl, or K_2CO_3; 6 mg)
(ACN = acetonitrile)

1. Load onto a prewashed (acetonitrile, water) solid phase extraction column containing C18-Si
2. Wash: 10ml H_2O and 2 ml 10% aq. ACN
3. Elute: 1 ml ACN
4. Evaporate

Visible white residue

Table I. Residues derived from evaporation of water (on Saran Wrap in a microwave oven), or from the acetonitrile eluent (evaporation in a vial placed in a 105° C oven) described in Fig. 3

Experiment	Residue: visible intensity	Residue: weight (µg) (± SD)	Residue: totally soluble in water?
Evaporate 1 ml of Ultrex II water	+	a	yes
Evaporate 1 ml of HPLC-grade water	++	a	yes
Fig. 3			
X = nothing	+++	7 ± 2	no
" = KCl	+++	8 ± 0	no
" = K_2CO_3	++++	16 ± 2c	no

a The weight is below the range of our microbalance
b 200 mg of Octadecyl-Silica obtained from J.T. Baker was packed in-house in a Supelclean cartridge.
c Corresponding data from an equivalent experiment, except that a cartridge was obtained pre-packed from J T Baker, is shown in Table II.

Table II. Residues derived from the acetonitrile eluent of a solid phase extraction column (see Fig. 3) after applying an aqueous/acetonitrile K_2CO_3 sample to a solid phase extraction column (plastic tube and frit)

Supplier and Packing	Packing Characteristics: monomeric (m) or polymeric (p)	Packing Characteristics: end capped	Amount of Packing (mg)	Weight of Residue (µg): observed (± SD)	Weight of Residue (µg): normalized (to 200mg)
J.T. Baker					
Octadecyl	p	yes	500	73 ± 8	29
Light Load Octadecyl	p	no	500	84 ± 19	34
Octyl	p	yes	500	165 ± 23	66
E.M. Separations					
RP-18	m	no	200	62 ± 5	62
RP-18a	m	no	200	7.3 ± 0.6	7
RP-18e	m	yes	200	40 ± 8	40
RP-18ea	m	yes	200	8 ± 3	8
RP-Select B	m	no	200	106 ± 9	106
Waters Chromatography					
C18 plus	m	yes	360	236 ± 13	131
t C18 plus	m	yes	400	32 ± 3	16
C8 125Å plus	m	yes	400	42 ± 4	21
Supelco					
LC-18	m	yes	500	180 ± 6	72
ENVI-18	p	yes	500	40 ± 2	16
LC-8	m	yes	500	179 ± 26	72
Varian					
BONDESIL-C18a	p	yes	200	89 ± 8	89
ENVIRELUT	p	yes	200	41 ± 7	41
BOND ELUT-C18c	p	yes	200	132 ± 40	132

a Packed in-house, all other packings came pre-packed from the manufacturers
b This is a C8-Si packing.
c BOND ELUT-C18 is a pre-packed form of BONDESIL-C18

LC/ESI/MS/MS Analysis of Hydroxyl Radical Modification of DNA

Eileen M. Kowalski,[1] Ajai K. Chaudhary,[2,3] and Ian A. Blair,[1,3] Departments of Chemistry,[1] Biochemistry,[2] and Pharmacology,[3] Vanderbilt University, Nashville, TN 37232-6602

The role of exogenous substances such as pollution, tobacco, and industrial chemicals in causing DNA modifications is well-studied. However, less emphasis has been placed on studying the effects of substances which occur naturally in the body. Endogenous oxygen free radicals induce a variety of adducts, many of which are not well characterized. Our laboratory is studying these adducts to determine their structures and their biological implications.[1,2] Recent studies in our laboratory have centered on developing LC/ESI/MS/MS methods to analyze DNA modified by hydroxyl radicals. The initial system for study involves ferrous ion and hydrogen peroxide, collectively known as Fenton's reagent. Calf thymus DNA (0.5 mg/ml) was incubated with 600μM $FeSO_4$, 600μM EDTA, and 3mM H_2O_2 at 37 °C for one hour to effect DNA modification. DNA was precipitated with ethanol and subsequently redissolved and enzymatically hydrolyzed using micrococcal nuclease, alkaline phosphatase, and phosphodiesterase I. After filtration to remove the enzymes, samples were analyzed by LC/ESI/MS/MS.

A Finnigan TSQ 7000 mass spectrometer equipped with an electrospray source was used for MS analysis. Tandem mass spectrometry was performed in constant neutral loss (CNL) mode with an offset of 116 mass units between the first and third quadrupoles in order to detect the loss of the deoxyribose moiety from the

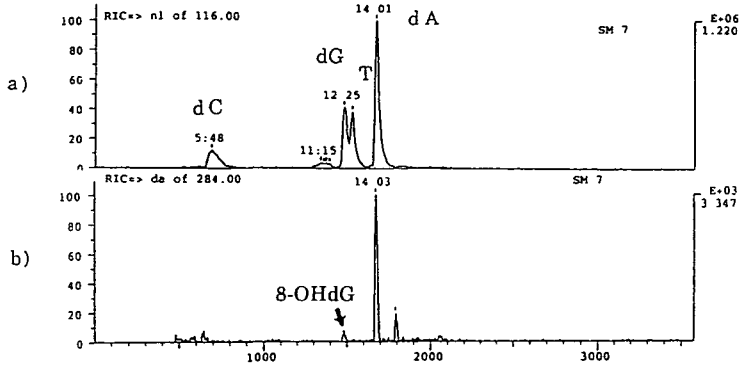

Fig. 1. Reconstructed ion chromatograms of LC/ESI/MS/MS analysis of Fenton-EDTA treated DNA. a.) CNL mass chromatogram of DNA hydrolysate. b.) Mass chromatogram of product ions of m/z 284.

analytes. Further information about modified DNA was obtained by product ion scans. An HP 1090 Series II LC system was employed for solvent delivery. Samples were analyzed using a Zorbax C-8 column (2.1 mm ID x 15 cm) with a two-component gradient. Component A was 5mM ammonium acetate and 0.04% acetic acid in water, and component B was 5mM ammonium acetate and 0.04% acetic acid in methanol. Analyses were performed using the following gradient: 0-5 min, 100% A; 10 min, 30% A; 12 min, 5% A; 25 min, 5% A; 30 min, 100% A. The flow rate was 0.2 ml/min. Under these conditions, all deoxynucleosides and adducts eluted within 15 minutes.

Results obtained from DNA treated and analyzed as above are shown in Figure 1. CNL analyses show the presence of the four normal deoxynucleosides. However, LC/MS/MS analysis of m/z 284 (MH^+ of 8-OHdG) revealed that the hydrolysate contained 7,8-dihydro-8-oxo-2'-deoxyguanosine (8-OHdG), a common product of hydroxyl radical modification, which coeluted with thymidine and therefore could not be detected in CNL scans. This adduct generated *in vitro* had the same retention time and fragmentation pattern (Figure 2) as an 8-OHdG standard.

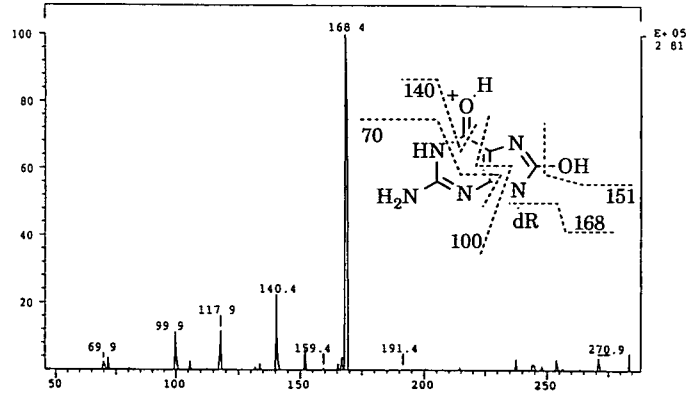

Fig. 2. LC/ESI/MS/MS analysis of 8-OHdG. Product ion spectrum of m/z 284.

The Fenton system will be used to develop LC/ESI/MS/MS methodology to detect and quantify DNA adducts. Since this method simplifies sample preparation, LC/ESI/MS/MS would facilitate analysis of a large number of samples.

Supported by NIH grants ES00267 and GM08320-06.

1. Chaudhary, A.K.; Nokubo, M.; L.J.Marnett; and Blair, I.A. *Biol. Mass Spectrom.*, **23**, 457-464, 1994.
2. Chaudhary, A.K.; Nokubo, M.; Reddy, G.R.; Yeola, S.N.; Morrow, J.D.; Blair, I.A.; and Marnett, L.J. *Science*, **265**, 1580-1582, 1994.

The Application of CE/ESI/MS/MS for Detection of IQ Adducts of DNA

Diane Rindgen[1], Robert J. Turesky[2], and Paul Vouros[1]
[1]Department of Chemistry and the Barnett Institute, Northeastern University, Boston, MA 02115
[2]Nestle Ltd. Research Center, Lausanne, Switzerland

Heterocyclic aromatic amines are formed in protein-containing foods such as meat and fish during normal cooking processes (1). 2-Amino-3-methylimidazo[4,5-*f*]quinoline (IQ) is a structurally representative member of this class of xenobiotics and has been shown to be a liver carcinogen in monkeys (2). Following metabolic activation, IQ covalently binds to deoxyguanosine forming a major adduct identified as N-(deoxyguanosin-8-yl)-IQ (dG-C8-IQ) and a minor adduct, 5-(deoxyguanosin-N^2-yl)-IQ (dG-N^2-IQ) (3, 4) We have evaluated the use of capillary electrophoresis/electrospray ionization/tandem mass spectrometry for detection of IQ adducts of deoxyguanosine-3'-monophosphate and present results obtained from the analysis of a synthetic sample containing both the C8 and N^2-adducts along with the examination of adducts formed *in vitro* with calf thymus DNA.

The results presented were obtained on a VG Quattro (Fisons Instruments, VG Biotech, Altrincham, UK) triple quadrupole mass spectrometer equipped with a VG electrospray source and capillary electrophoresis probe The probe was designed to allow for both a coaxial flow of sheath liquid and nebulizing gas (N_2). All analyses were performed in the negative ion mode using isopropyl alcohol as the sheath liquid at a flow rate of 3 μL/min. The coaxial and bath gas (N_2) flow rates were optimized at the start of each set of experiments CID and MRM were performed using argon as the collision gas. The CE high voltage was provided by a Spellman CZE1000R (Spellman High Voltage Electronic Corp , Plainview, NY) reversible high voltage power supply Capillary electrophoresis was performed in uncoated fused silica capillaries (*ca* 40 cm contained in the CE probe) using 10 mM ammonium acetate, pH 10 2 - 10.4 (adjusted with ammonium hydroxide), as the running buffer. Analyte injections were made hydrodynamically or by using the on-column sample preconcentration technique known as sample stacking (5, 6) The dG-C8/N^2-IQ-3'PO_4 standards and the IQ-modified calf thymus DNA were prepared as described in reference 4 and reconstituted in Milli-Q water (Millipore, Milford, MA) prior to mass spectrometric analysis. The *in vitro* adduct estimates were as follows: C8 - 45.6 ng, N^2 - 6.5 ng

The negative ion ESI normal scan mass spectrum of the synthetic adduct sample presented the expected MH^- ion at *m/z* 542.5 CID of *m/z* 542 produced two product ions at *m/z* 346 and *m/z* 195 (deoxyribose-3'PO_4) The ion at *m/z* 346 corresponds in mass to both the aglycone ion (A^-) formed by cleavage of the glycosidic bond and the MH^- ion of deoxyguanosine-3'PO_4 resulting from loss of the IQ moiety The CID spectrum of *m/z* 346 (Figure 1) was significantly different from the negative ion CID spectrum of unadducted deoxyguanosine-3'PO_4 which exhibited product ions at *m/z* 79 (PO_3^-), *m/z* 97 ($H_2PO_4^-$), m/z 150 (guanine) and *m/z* 195 (deoxyribose-monophosphate). Low pg level detection was possible for the targeted dG-C8-IQ-3'PO_4 adduct by monitoring the transition *m/z* 542 → *m/z* 346. The results of the MRM analysis of the dG-C8/N^2-IQ-3'PO_4 synthetic mixture are shown in Figure 2. A response for the C8-adduct was observed at 8 min however, it is unclear which additional signal corresponds to the N^2-adduct. Considering the isomeric relationship of the two adducts, it seems reasonable to speculate that the peak at 7.7 min, immediately preceding the C8-adduct response, is due to the N^2-adduct. The ratio of peak areas is consistent with the estimated quantities of each adduct. However, the area ratio of the 6.5 and 8 min peaks also agrees with the relative amounts of C8/N^2 adduct present in the sample. The behavior of the minor adduct under the conditions employed for these analyses could not be determined due to the lack of sufficient quantities of pure dG-N^2-IQ-3'PO_4 standard.

The mass electropherogram of *m/z* 542 obtained during a normal scan acquisition of the IQ-modified calf thymus DNA sample exhibited a peak at 7.4 min the spectrum of which showed *m/z* 542.5 and 346.5. CID of *m/z* 542 produced two product ions, *m/z* 195 and 346, which were also observed in the CID spectrum of the dG-C8-IQ-3'PO_4 standard. A single response was observed in the MRM scan of *m/z* 542 → *m/z* 346 which appeared at a migration time generally characteristic of dG-C8-IQ-3'PO_4. The mass spectrometric results obtained with a control DNA sample (no IQ modification) showed no interferences in the region of migration of the IQ adduct.

In conclusion, 2-amino-3-methylimidazo[4,5-*f*]quinoline (IQ) adducts of deoxyguanosine-3'PO_4 are amenable to analysis by on-line capillary electrophoresis/mass spectrometry using electrospray ionization in the negative ion mode. Low pg level detection was achieved by monitoring the transition *m/z* 542 → *m/z* 346. Although unambiguous detection of the dG-N^2-IQ-3'PO_4 adduct in the synthetic mixture was not achieved, the combined CE/MS data identified the dG-C8-IQ-3'PO_4 adduct and confirmed its presence in the *in vitro* IQ-modified calf thymus DNA sample

1. Felton, J. S., Knize, M. G., Shen, N. H., Andresen, B. D., Bjeldanes, L. F , Hatch, F. T , *Environ. Health Perspect* , **67**, 17 (1986).
2. Adamson, R. H., Thorgeirsson, U. P., Snyderwine, E. G., Reeves, J., Dalgard, D W , Takayama, S., Sugimura, T , *Jpn. J. Cancer Res.*, **81**, 10 (1990).
3 Turesky, R J , Rossi, S C , Welti, D H , Lay, J O , Jr , Kadlubar, F F , *Chem Res Toxicol.*, **5**, 479 (1992).
4. Turesky, R J , Markovic, J , *Chem. Res. Toxicol.*, **7**, 752 (1994).
5 Chien, R. L., Burgi, D. S , *Anal. Chem.*, **64**, 489A (1992).
6. Wolf, S M., Vouros, P., *Anal. Chem.*, **67**, 891 (1995).

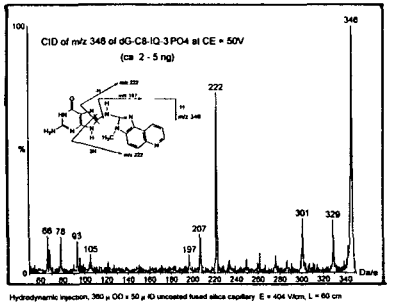

Figure 1

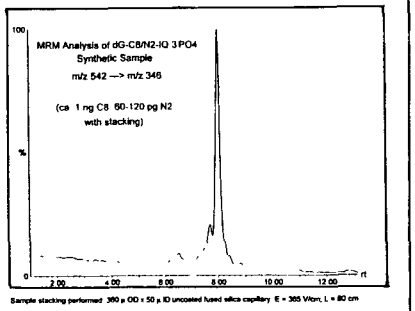

Figure 2

GC/MS Quantitation of DNA Oxidation Products

Chang-Hwan Oh and Charles R Iden

Department of Pharmacological Sciences, Health Sciences Center,
SUNY-Stony Brook, Stony Brook, NY 11794-3400

DNA oxidation is a natural, ongoing process which takes place in both nuclear and mitochondrial DNA. Chemical modification to deoxynucleotides occurs through interaction with oxygen free radicals or other activated oxygen species produced either chemically within the cell or by ionizing or non-ionizing radiation. A large number of oxidized purines and pyrimidines have been isolated and characterized, some of which have been shown to be potential mutagens. In its own defense, the cell maintains a family of repair enzymes which continually monitor the fidelity of the DNA sequence and repair errors such as oxidized nucleotides that are located Among these enzymes are the gene products of MutM, MutY, and MutT whose mechanisms of repair are under investigation. Of particular interest is the FPG protein which acts as a glycosylase and releases 8-oxoguanine (8-oxoGua), 8-oxoadenine (8-oxoAde), 2,6-diamino-4-oxo-5-formamidopyrimidine (Fapy-Gua), and 2,6-diamino-5-formamidopyrimidine (Fapy-Ade) from damaged DNA We have developed a GC/MS assay for selected oxidation products essential for this research and tested the protocols on known amounts of a synthetic oligomer containing a single 8-oxo-2′-deoxyguanine within the sequence The assay includes 2,6-diamino-8-purinol as an internal standard. We have carefully examined established procedures for release of the oxidation products (formic acid hydrolysis) and trimethylsilyl-derivatization of the nucleobases that are released

Standards 8-oxoGua, 2,6-diamino-8-purinol, and normal nucleobases were obtained from Aldrich. Fapy-Ade was purchased from Sigma Chemical Company, and Fapy-Gua and 8-oxoAde were synthesized using literature procedures Formic acid (Janssen Chimica) was diluted to 88% with Millipore water. All silylation reagents and solvents were purchased from Pierce Chemical Company. Stock solutions of the standards were prepared in 0.04 mM ammonium hydroxide and stored at -4 °C. A Hewlett Packard 5970 MSD GC/MS was used in the selected ion monitoring mode to quantify the selected oxidation products. The instrument is equipped with a Hewlett Packard 5890A gas chromatograph, and separations were obtained on a DB-5ms (30 m × 0.2 mm I.D., 0.33 μm film thickness) column using splitless injection (240 °C) and helium carrier gas (15 psig, 0 75 ml/min) The MSD was operated at 70 eV ionization energy, and *m/z* 354 (Fapy-Ade), 352 (8-oxoAde), 442 (Fapy-Gua), 440 (8-oxoGua), and 454 (internal standard) were monitored in the SIM mode.

Reaction conditions for the formation of volatile derivatives of the selected oxidation compounds using three different reagents for trimethylsilylation and one reagent for trifluoroacetylation were examined carefully. Many reaction conditions produced multiple TMS species for the standard compounds and were not appropriate for quantitative analysis. Final reaction conditions were selected such that only the fully trimethylsilylated compounds were produced for each standard. These were 5 ng each standard, 50 μl acetonitrile with 2% pyridine, 50μl BSTFA with 1% TMCS, 100 °C for 30 min. Product formation did not increase with increased reaction time or increased reaction temperature Sensitivity for each of the derivatized compounds is approximately one picogram injected onto the column. Stability of the internal standard has been established in both the hydrolysis and derivatization procedures.

43rd ASMS Conference on Mass Spectrometry and Allied Topics

The full analysis was verified for 8-oxoGua by taking known quantities of a synthetic oligodeoxynucleotide containing a single 8-oxo-2′-deoxyguanosine residue and performing the complete analysis for 8-oxoGua. The sequence of the oligomer was 5′-GTTCA(8-oxo-dG)GTTGC-3′, and this material was purified in a double pass HPLC procedure prior to use. The internal standard (5 ng) was added to a measured quantity of oligomer, and nucleobases were released by 88% formic acid at 150°C for 1 h. The results for the analysis of five different quantities of oligodeoxynucleotide are shown in Figure 1. For quantities of oligomer greater than 1 μg the measured amount of 8-oxoGua corresponds very closely to the calculated amount of 8-oxoGua derived from the oligomer For small quantities of the oligomer, there appears to be losses in the procedure which lead to unusually low measured values of the nucleobase. In Figure 2 the amount of normal guanine released from the oligomer is compared to the amount of 8-oxoGua which is released. The curve is linear with a good correlation coefficient, indicating that as more of the oligomer is used in the analysis, the quantities of Gua and 8-oxoGua increase in a linear fashion, as expected.

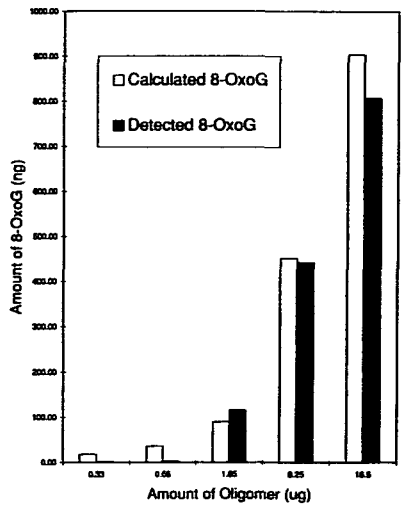

Fig. 1. Measured vs. calculated 8-oxoGua found in a synthetic oligodeoxynucleotide containing an 8-oxo-2′-deoxyguanosine residue.

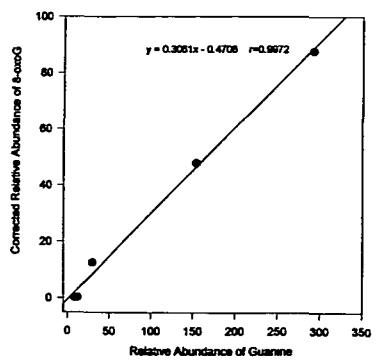

Fig. 2. Linear regression of the measured quantity of Gua and 8-oxoGua obtained from the synthetic oligomer. The oligomer contains two Gua and only one 8-oxoGua.

Capillary Isotachophoresis-Mass Spectrometric Determination of DNA Damage

Zhongxi (Zack) Zhao*, Amy C. Harms, Harold R. Udseth,
Alfred F. Fuciarelli, and Richard D. Smith
Chemical Sciences Department,
Pacific Northwest Laboratory, P.O. Box 999, Richland, WA 99352

Analysis of DNA damage as indicators of human exposure to radiation levels represents a challenge for trace analyses to analytical chemists. Mutagenesis is one possible outcome of DNA base modification arising from such damage. These modifications may lead to DNA misreplication which can initiate and promote carcinogenesis. Electrospray ionization mass spectrometry (ESI-MS) with high ionization efficiency and gentle nature can be used to identify and quantify these modifications and opens the opportunity to study structurally related factors in the damage to DNA. The radiation-damaged products are generally present in very low abundance, which requires a highly efficient and/or concentrating separation technique prior to mass spectrometric detection. High performance capillary isotachophoresis (CITP), with its zone self-sharping and concentrating capacities, can be utilized to distinguish the small amount damaged from the large excesses native free bases, nucleosides, and nucleotides. In combination with electrospray ionization, the potential exits to obtain extraordinary sensitivity.

In this presentation, the on-line coupling of reversed anionic capillary isotachophoresis to electrospray ionization mass spectrometry will be reported. Separation and identification of radiation damaged tetranucleotide using CITP-MS will be described. The tetranucleotide d(CGTA) was first X-irradiated in N_2-saturated aqueous solution. Then, the damaged products were fractionated by semi-preparative HPLC. Finally, on-line CITP-ESI-MS and tandem MS were used to provide the positional and structural information of the damaged products. In reversed anionic CITP, leading electrolyte was 7 mM HCl/13 mM ß-alanine and trailing electrolyte was 10 mM caprioic acid.[1,2] A coaxial sheath liquid interface was used. The sheath liquid was composed of 0.1% formic acid, 24.9% water, and 75% methanol. Single and double base damages were determined. The results indicate that cytocine was modified to uracil, hydroxyuracil and hydroxyhydrouracil; Guanine was modified to cyclo-guanosine. Thymine was changed to dihydrothymine and hydroxyhydrothymine. Figure 1 shows typical CITP-ESI-MS results for an LC fraction. CITP-tandem mass spectra of LC fraction #14 are listed in Figure 2. We are now applying this approach to study the radiation chemistry of large oligonucleotides and DNA.

1. Z. Zhao, J. H Wahl, A. F. Fuciarelli, D. C. Gale, H. R. Udseth, R. D. Smith, *Proc. of 42nd ASMS Conf. on Mass Spec. and Allied Topics* Chicago, IL, Abs. 113,1994.
2. Z. Zhao, J. H. Wahl, H. R. Udseth, S. A. Hofstadler, A. F. Fuciarelli, R. D. Smith, *Electrophoresis* **16**, 389-395(1995).

The authors would like to thank Dr. H. C. Box from the Rosewell Park Cancer Institute for the preparation of X-irradiated sample and for semi-preparative HPLC fractionation. Pacific Northwest Laboratory is operated by Battelle Memorial Institute for the U.S. Department of Energy, through contract DE-AC06-76-RLO 1830.

43rd ASMS Conference on Mass Spectrometry and Allied Topics

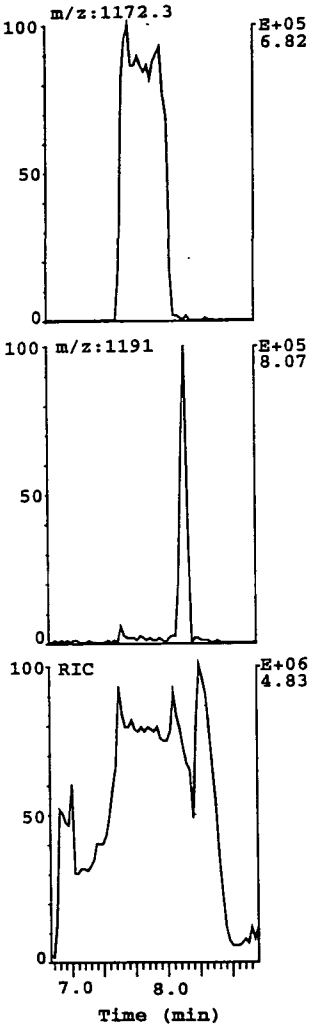

Fig. 1. CITP-ESIMS of LC fraction #14

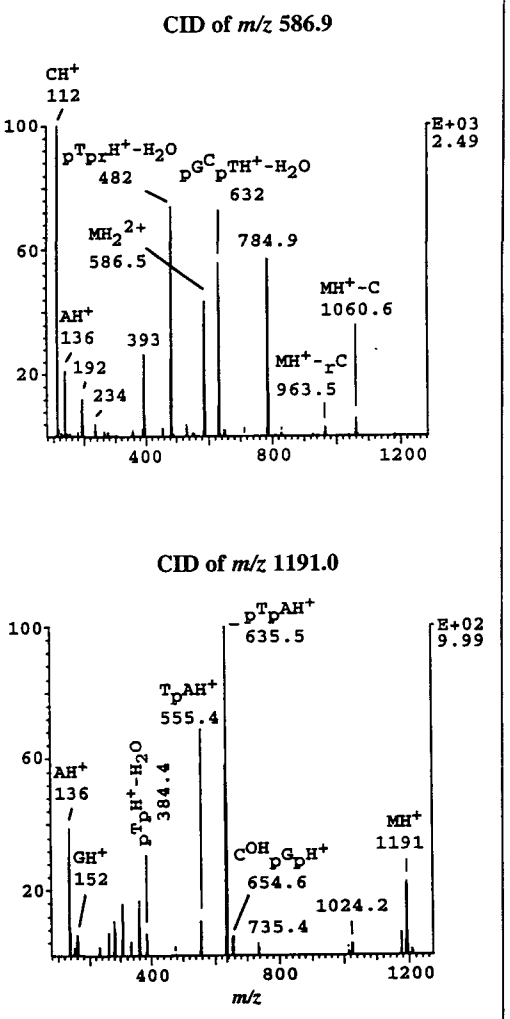

Fig. 2. CITP-MS/MS of LC fraction #14

Analysis of DNA base modifications in oligonucleotides using LC/ES MS.

A. K. Chaudhary[1,2,3], G. R. Reddy[2,3], J. L. Compton[1], L. J. Marnett[2,3], and I. A. Blair[1].
Departments of Pharmacology[1] and Biochemistry[2] and A. B. Hancock Jr. Memorial Laboratory for Cancer Research[3], Vanderbilt University School of Medicine, Nashville, TN 37232.

The involvement of exogenous carcinogens in effecting DNA modifications is well documented. However, DNA adducts produced from endogenous chemicals arising from normal metabolism, oxidative stress, and chronic inflammation are equally critical in carcinogenesis. Malondialdehyde (MDA), an endogenous product of lipid peroxidation, induces frameshift mutations and G to T transversions. The major MDA-DNA adduct at physiological pH is pyrimido- [1,2-a]-purine-10(3H)-one (M_1-dG). The tetrahydro analog of M_1dG is Propanodeoxyguanosine (P-dG). We have developed methods to quantitate and characterize this adduct in rodent (1) and human tissues (2) using GC/ECNCI MS. The complete characterization of this adduct in human liver using LC/ES MS/MS was also achieved.(3) Our laboratory is involved in construction of viral genomes containing M_1G and PdG to study the mutagenic potential of this adduct. Oligonucleotides, 5'-CGCXCGGCATG-3' (I) and 5-CGTXTCCG-3' represent mutation hotspots in *Salmonella typhimurium* hisD3052 gene. These oligonucleotides and a number of other modified and unmodified oligonucleotides have been synthesized. We report the use of electrospray (ES) ionization for the analysis of oligonucleotides. ES typically produced an envelope of charged states which allowed accurate determination of molecular weights. Salts of oligonucleotides formed a series of multiply charged anions under negative ES conditions. The molecular weight of oligonucleotides could then be calculated by transforming the charged envelope. PC-based software was developed for the characterization of these oligonucleotides from the observed multiply-charged peaks. LC/ES analysis was performed on a Finnigan TSQ-7000 mass spectrometer equipped with an electrospray source. The sample was introduced to the mass spectrometer through an injector positioned between the HP 1090 HPLC system and the source. The solvent composition was acetonitrile/water (50/50 v/v) containing 0.1% acetic acid at a flow rate of 50 microliter/min. The presence of acid in the mobile phase effectively leads to the shifting of the multiply charged envelope towards smaller charged states. ES source parameters were optimized to provide maximum ionization of a 7-mer oligonucleotide (5'-CGGCATG-3'). Multiply charged ions for 5'-CGCGCGGCATG-3' (Figure 1a) were observed at *m/z* 1118 (3-), 838 (4-), and 671 (5-) [observed MW = 3358, calculated MW = 3358)]. Similar ions were observed at *m/z* 1130, 847, and 678 for the modified 11-mer 5'-CGC-M_1dG-CGGCATG-3' (Figure 1b) [observed FW = 3394, calculated FW = 3394]. Modified and unmodified oligonucleotides ranging from 3-mer to 20-mer were analyzed. A series 11-mer oligonucleotides is shown in Table 1. The observed molecular weights for these modified and unmodified oligonucleotides were found to be within 0.02% of the calculated value. HPLC/MS was configured to provide on-line desalting of these samples. A PRP-1 column (2.1 mm i.d. x 150 mm) was used with mobile phase consisting of 15 mM ammonium formate/acetonitrile (80/20) at a flow rate of 200 µL/min. The column effluent was diverted away from mass spectrometer for first 7 min by an automated switching valve.

Supported by NIH grant CA47479 & ES00267

1. A. K. Chaudhary *et al.*, *Biol. Mass Spectromet.*, 23, 457-464 (1994).
2. A. K. Chaudhary *et al.*, *Science*, *265*,1580-1582 (1994).
3. A. K. Chaudhary *et al.*, *J. Mass Spectromet*, In press (1995).

Oligonucleotides	Calculated MW	Observed MW	%Deviation
CGCGCGGTCAG	3358.21	3358.16	0.001
CGC-PdG-CGGTCAG	3398.21	3397.67	0.016
CGC-M_1dG-CGGTCAG	3394.19	3393.93	0.008
CAC-PdG-ACCTGCC	3302.16	3301.27	0.027
GCGCAGGTGGTG	3453.27	3453.63	0.011
CGGACAAGAAG	3399.28	3399.00	0.008

Table: **LC/ES MS analysis of 11-mer oligonucleotides.**

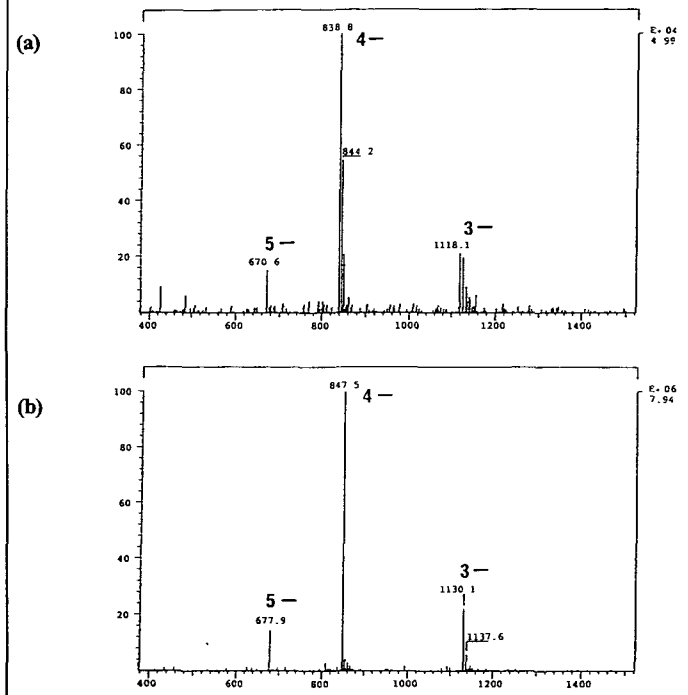

Figure 1: **LC/ES mass spectrum of 11-mer CGC-X-CGGCTAG. (a) X = G. (b) X = M_1dG**

Micro electrospray MS/MS for the analysis of modified oligoribonucleotides

M. A. Wolter[1], M. S. Wilm[2], M. Mann[2], J. W. Engels[1]
[1]*Institute for Organic Chemistry, Johann Wolfgang Goethe-University, 60054 Frankfurt, Germany*
[2]*European Molecular Biology Laboratory, Meyerhofstr. 1, 69117 Heidelberg, Germany*

Mass Spectrometry especially tandem mass spectrometry techniques offer a fast and sensitive method to study the primary structure of oligonucleotides. It is applicable to all kinds of modified oligonucleotides once the principle fragmentation pathways are described. These pathways were studied for oligodeoxynucleotides (DNAs) by ion trap (1, 2, 3) and FTMS (4). This is of interest for the antisense (5, 6) and ribozyme (7) approach where modified oligonucleotides are used as highly effective drugs. The traditional methods for the sequence determination of oligonucleotides [Sanger, Maxam and Gilbert] are limited in accuracy and do not allow the analysis of modified oligomers. Specifically, 2'-O-methyl modified oligoribonucleotides (RNAs), which are used within the ribozyme as well as antisense approach, were chosen to test the performance of tandem mass spectrometry within these fields. Up to now, RNAs are only targets of very few MS/MS investigations. Di- (8, 9) and trimers (10, 11) were invested by FAB. Decamers were studied by ESI (12).

Measurements were done on a triple quadrupole (Sciex API III) equipped with an updated collision cell. The standard ESI source was replaced by a micro ESI source (13). The collision energy was optimized for each sample so that the high mass fragments exceeding *m/z* 1000 were produced with maximal intensity. This optimization procedure gave relatively low E_{LAB} settings. The dry samples were dissolved in water and 1 µl of the solution added to 2 µl of a 1/1 conc. NH_3 (aq.)/MeOH mixture. 1 µl of this final solution were sufficient for 45 minutes working time. The used fragment ion nomenclature is due to McLuckey et al. (1).

MS/MS CID spectra of the $[M\text{-}4H^+]^{4-}$ ions derived from 5'-r(AGUAGUCCCA)-3' and 5'-r(AmGUAmGUmCCCA)-3' can give extensive information on the sequence, types of the modifications and their locations. The mass differences between the depicted ions, allow to localize the modification sites. This information is present in multiple ions, to simplify matters some of these have been selected. The w-series are dominant and allow to determine the sequences and reading frames. For the same chain length w_i-fragments dominate d_i-fragments (14) and y_i-fragments dominate b_i-fragments. x_i, z_i and c_i fragments were not observed. These rules hold for all the RNAs we studied.

Collision induced fragmentation of multiply charged oligonucleotides can be used to identify type and location of modifications. The proper tuning of the collision energy is important to avoid extensive fragmentation but to produce still complete ion series.

This work was supported (M.A.W.) by a grant of the European Community (ERB4001GT942747).

1. S. A. McLuckey, G. J. V. Berkel, G. L. Glish, *J. Am. Soc. Mass Spectrom.*, **3**, 60 (1992).
2. S. A. McLuckey, S. Habibi-Goudarzi, *J. Am. Chem. Soc.*, **115**, 12085 (1993).
3. S. A. McLuckey, S. Habibi-Goudarzi, *J. Am. Soc Mass Spectrom*, **5**, 740 (1994).
4. D. P. Little, R. A. Chorush, J. P. Speir, M. W. Senko, N. L. Kelleher, F. W. McLafferty, *J. Am. Chem. Soc.*, **116**, 4893 (1994).
5. P. C. Zamecnik, M. L. Stehpenson, *Proc. Nat. Acad. Sci. USA*, **75**, 280 (1978).
6. M. L. Stephenson, P. C. Zamecnik, *Proc. Nat. Acad. Sci. USA*, **75**, 285 (1978).
7. J. A. McSwiggen, T. R. Cech, *Science (Washington, D. C., 1883-)*, **244**, 679 (1989).
8. F. W. Crow, K. B. Tomer, M. L. Gross, J. A. McCloskey, D. E. Bergstrom, *Anal. Biochem.*, **139**, 243 (1984).
9. R. L. Cerny, M. L. Gross, L. Grotjahn, *Anal. Biochem.*, **156**, 424 (1986).
10. R. L. Cerny, K. B. Tomer, M. L. Gross, L. Grotjahn, *Anal. Biochem.*, **165**, 175 (1987).

11. M. A. Wolter, J. W. Engels, L. Montanarella, R. Tilho, S. Facchetti, *J. Mass Spectrom.*, **30**, 485 (1995).
12. M. S. Wilm, M. A. Wolter, L. Montanarella, S. Facchetti, M. Mann, MO D17, *13th IMSC*, Budapest (1994).
13. M. S. Wilm, M. Mann, *Int. J. Mass Spectrom. Ion Processes*, **136**, 167 (1994).
14. M. T. Rodgers, S. Campbell, E. M. Marzluff, J. L. Beauchamp, *Int. J. Mass Spectrom. Ion Processes*, **137**, 121 (1994).

MS/MS CID spectra comparison of $[M\text{-}4H^+]^{4-}$ derived from 5'-r(AGUAGUCCCA)-3' [c=20 pmol/µl, 9 scans, E_{LAB}=90 eV, argon pressure 241 x 10^{13} atoms/cm^3] and 5'-r(AmGUAmGUmCCCA)-3' [c=50 pmol/µl, 20 scans, E_{LAB}=92 eV, argon pressure 270 x 10^{13} atoms/cm^3].

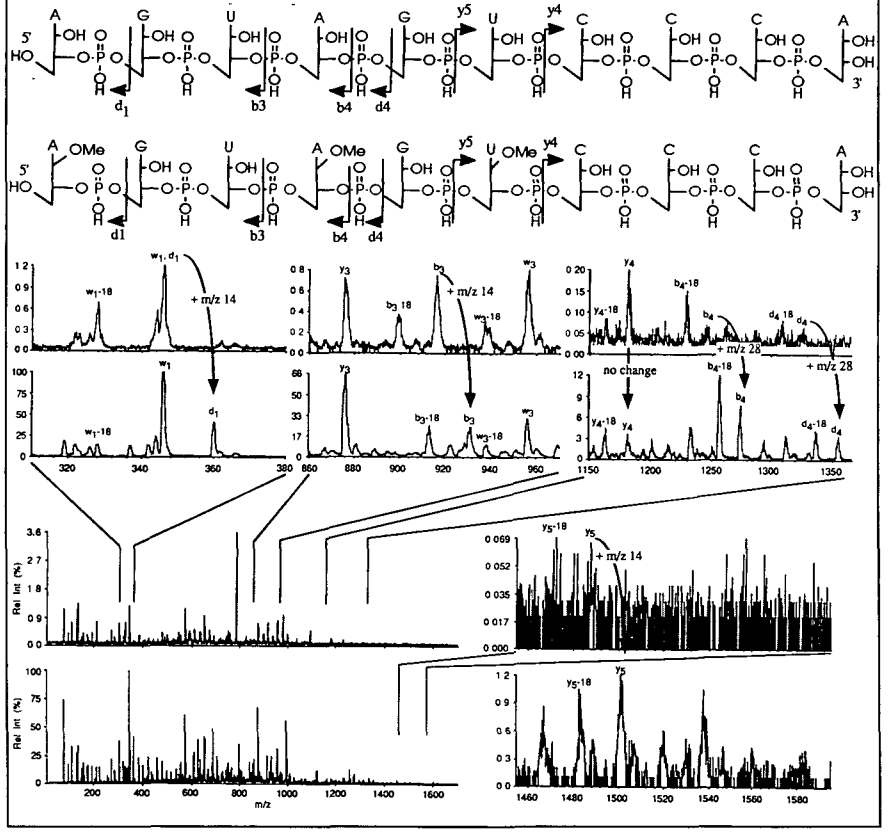

ESI-MS of synthetic oligonucleotides and non covalent interactions studies

N. Potier and A. Van Dorsselaer
Laboratoire de Spectrometrie de Masse Bio-Organique, URA31-CNRS, Université Louis Pasteur, 67000 Strasbourg, France.

INTRODUCTION: Nucleic acids are highly charged polyanionic structures that are known to interact with a broad range of molecules like metals, drugs, proteins...These non covalent interactions play a crutial role in their structure and function in the cell. While X-ray cristallography or NMR are often difficult on such macromolecules complexes, we investigated the conditions for studying interactions between oligonucleotides and polycationic species by ESI-MS which is known to preserve non covalent associations[1].

A prerequirement to characterize non covalent complexes is to determine conditions allowing mass analyses of both polycationic species and oligonucleotides separately. Mass measurements of oligonucleotides larger than 10 kDa are quite difficult because of the formation of oligonucleotide-sodium or -potassium adducts which persist after ionization and desolvation. The presence of sodium adducts becomes a major problem in the case of large oligonucleotides where the resolution of the generally employed quadrupole analyzers is insufficient to resolve the different sodium adducts peaks leading to erroneous average mass measurements. Reduction of the amount of sodium adducts is thus crutial to obtain high quality spectra.

EXPERIMENTAL: A VG Bio-Q triple quadrupole mass spectrometer with a mass range of 4000m/z units was used to carry out negative electrospray ionization mass spectra. A probe equipped with a peak capillary was required to evoid residual salts contamination or acidity coming from classical fused silica capillaries. A potential of 2.2 to 2.8 kV was applied to the needle and the cone voltage value was typically set to 50V. The source was maintained at 50°C and nitrogen was used as nebulizing and drying gaz. The solutions were directly infused into the source at a final concentration of 20µM and at a flow rate of 2µl/min. For oligonucleotide/peptides interactions, oligonucleotides were dissolved in deionized water at a final concentration of 25µM, mixed with 0.2 mM polylysine peptide and infused into the source at a flow rate of 2µl/min. The optimization of the drying gaz rate is required to aid electrospray droplet desolvation.

RESULTS:

Mass measurements of synthetic oligonucleotides: After an intensive removal of salt ions[2], negative ion mass spectra were obtained on synthetic oligonucleotides up to 40 kDa (132-nucleotides)[3] with an accuracy of 0.01%. For large oligonucleotides (>50-mer), this desalting procedure can be repeated several times in order to enhance the displacement of sodium ions.

The high accuracy of mass measurements allowed also the characterization of oligonucleotides analogues such as phosphorothioate designed for antisense applications.

Oligonucleotide/peptide non covalent interactions: Recently, non covalent complexes between oligonucleotides and basic peptides have been observed by MALDI-TOF showing the utility of this complexes formation for the mass determination of acidic compounds[4]. Within the context of specific non covalent interactions studies between oligonucleotides and proteins, ESI-MS appears as a more appropriate technique.

Figure 1 displays the obtained mass spectra for ionic non covalent complexes between a 40-mer (MW=12292.4 Da) dessalted as previously described[3] and various polylysine peptides.

They reveals the very high affinity of polyamines for oligonucleotides insofar as they were able to displace the tighly bound sodium ions on the phosphate groups of the oligonucleotides and to form non covalent complexes which have persisted after ionization and desolvation. The complexes formation occurs through electrostatic interactions resulting from ionic bounds between positively charged protein side chains and the polyphosphate oligonucleotide backbone. The abundance and the number of the complexes ions increase with the number of lysine residues and the presence of organic solvent such as acetonitrile.

CONCLUSION: ESI-MS can be used routinely for the evaluation of oligonucleotide/peptide interactions when the interactions are known as ionic bounds. These ionic interactions are quite strong since neither the temperature (untill 70°C) nor the cone voltage value (untill 70V) were very critical.

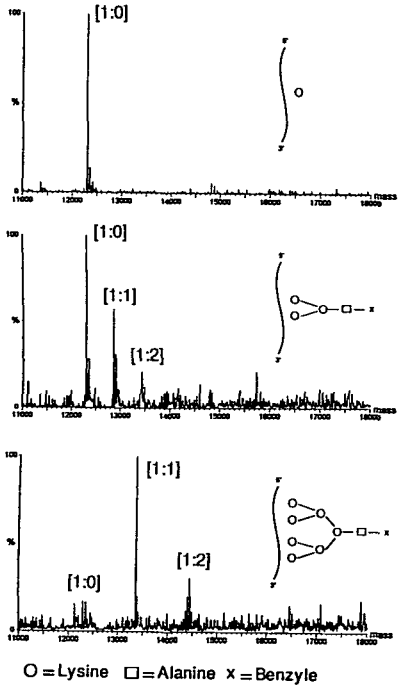

Figure 1: Transformed mass spectra of non covalent complexes between a 40-mer and various polylysine peptides

[A:B]: [oligonucleotide:peptide]

Molecular masses: [1:0]: 12293.8 Da

[1:0]: 12291.5 Da
[1:1]: 12853.1 Da
[1:2]: 13417.7 Da

[1:0]: 12290.2 Da
[1:1]: 13367.6 Da
[1:2]: 14443.8 Da

REFERENCES:

1: Smith, R.D. and Light-Wahl, K.J., *Biol. Mass Spectrom.*, 1993, **22**, 493-501
2: Stults, J.T. and Marsters, J.C., *Rapid Commun. Mass Spectrom.*, 1991, **5**, 359-363
3: Potier, N. and Van Dorsselaer, A., *Nucleic Acids Res.*, 1994, **22**, 3895-3903
4: Juhasz, P and Biemann, K., *Proc. Natl. Acad. Sci.*, 1994, **91**, 4333-4337

Non-Covalent Associations of Metal Complexes with DNA Duplexes by ESI-MS

Amy C. Harms and Richard D. Smith
Pacific Northwest Laboratory, Richland, WA 99352
and
Yonchu Jenkins and Jacqueline K. Barton
Division of Chemistry and Chemical Engineering, California Institute of Technology, Pasadena, CA 91125

Transition metal complexes are being used as probes to determine the conformational structure of oligonucleotides, to recognize specific binding sites, and to probe the capability for electron transfer reactions in DNA strands. Non-covalent interactions, such as intercalation and hydrophobic groove binding of the metal complexes with oligonucleotide duplexes, provide the basis for probing DNA sequence and structure.

Electrospray ionization mass spectrometry (ESI-MS) has been used for the analysis of a wide variety of biomolecules, including oligonucleotides. Recently this technique has been utilized in the characterization of non-covalent associations. In this work we report the use of ESI-MS for the detection of non-covalent associations of several metal complexes with two oligonucleotide duplexes and compare these results with observations from solution.

Previous work has characterized the binding of several complexes to DNA in solution. $Ru(bpy)_3^{2+}$ has a negligible binding to DNA. $Ru(phen)_3^{2+}$ is an intercalator with a binding strength of $K=6.2\times10^3\ M^{-1}$ whereas $Ru(phen)_2dppz^{2+}$ binds more strongly with $K>10^7\ M^{-1}$. These complexes are seen to bind non-cooperatively with a four base pair site. Each of the metal complexes were added to the 12-mer duplex solution with a ratio of 1:1 duplex : metal The mass spectra showed a series of peaks corresponding to the bare single DNA strands, the bare DNA duplex, the single strands with one or more complexes, and the duplex with one or more metal complexes. Figure 1 shows the 12-mer combined with the complex with the lowest binding constant, $Ru(bpy)_3$. The spectrum shows that very little of the metal complex is bound to the DNA. In comparison, when $Ru(phen)_3$ or $Ru(phen)_2dppz$ was added the majority of the peaks contained these compounds, as is shown in Figure 2. When an excess of $Ru(phen)_2dppz$ is added, the reaction can be driven to produce primarily the [duplex + three metal] complex.

The same metal complexes were also studied with a longer DNA strand. The same series of peaks that were observed with the 12-mer were also seen with the 15-mer. As before, when $Ru(bpy)_3$ was added, there is more bare DNA than DNA-$Ru(bpy)_3$ complex. When $Ru(phen)_3$ was added, most of the DNA was observed to be associated with the metal. Figure 3 shows four $Ru(phen)_3$ complexes can bind to a 15 base pair duplex instead of the three complexes that were seen to bind to the 12-mer. This indicates that another binding site is available in the 15-mer.

Under appropriate ESI interface conditions, the mass spectra reflect the solution behavior of DNA-metal complexes in their binding strength and exclusion site size, verifying the specificity of the associations.

Pacific Northwest Laboratory is operated for the U.S. Department of Energy by Battelle Memorial institute under Contract DE-AC06-76RLO 1830.

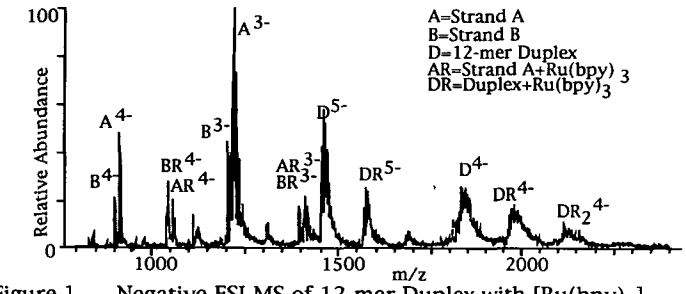

Figure 1. Negative ESI-MS of 12-mer Duplex with $[Ru(bpy)_3]$

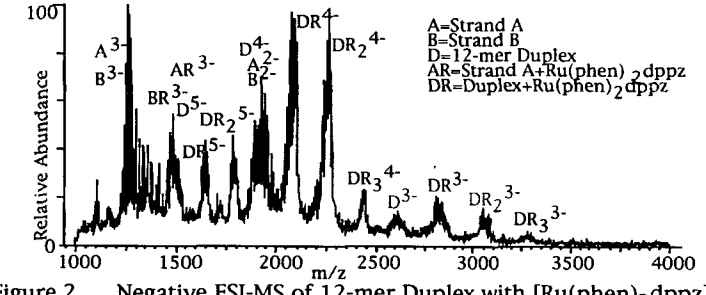

Figure 2. Negative ESI-MS of 12-mer Duplex with $[Ru(phen)_2dppz]$

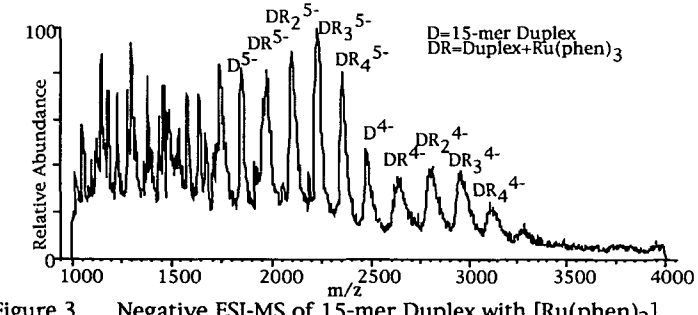

Figure 3. Negative ESI-MS of 15-mer Duplex with $[Ru(phen)_3]$

Correlation Between ESI-MS, CID, and DNA Duplex Melting Temperature

David C. Gale, A. Kirk Morris, Ellen C. Sisk, Al F. Fusciarelli, Brenda L. Schwartz, Amy C. Harms, David G. Camp II, and Richard D. Smith.
Chemical Sciences Department, Pacific Northwest Laboratory, Richland WA, 99352

Electrospray ionization mass spectrometry (ESI-MS) has become an important analytical method for characterizing proteins, peptides, and small biologically active molecules. One particular class of molecules that are amenable to analysis by ESI-MS are oligonucleotides. Oligonucleotide duplex and small molecule/oligonucleotide duplex noncovalent complexes have recently been studied by ESI-MS.[1-3] If ESI-MS is to become a useful technique in the analysis and characterization of small molecule/oligonucleotide duplex noncovalent complexes, a comprehensive understanding of the oligonucleotide duplex must be performed by ESI-MS . The goal of this research was to investigate the relationship between the melting temperature (ΔT) of an oligonucleotide duplex, ESI-mass spectra, and collision induced dissociation (CID).

A large number of small molecule/oligonucleotide duplex studies have been performed utilizing 12-base pair oligonucleotides. Our initial success in observing noncovalent complexes formed between known DNA binding small molecules and oligonucleotide duplexes of this size by ESI-MS,[3] led us to use 12-base pair oligonucleotides as models for the present studies. Several sequence specific and self-complementary 12-base pair oligonucleotide duplexes were designed, purified, and analyzed. Oligonucleotide duplex melting temperature measurements were obtained using UV/Vis spectrophotometry from solutions containing the buffer used in the ESI-MS experiments (30 mM ammonium acetate). Initial results indicate that the melting temperature of the duplex, a measure of stability in solution, is reflected in ESI mass spectra. Peaks corresponding to the noncovalent complex of the low ΔT duplex, were observed in low relative abundance, compared to the high ΔT duplex.

Similar results were observed for the collision induced dissociation (CID) of low and high melting temperature oligonucleotide duplexes. This data was acquired with a Finnigan TSQ 7000 instrument using Ar as the collision gas. For both oligonucleotides duplexes, the 5- charge state was mass selected for analysis. The CID results are shown in Figures 1 and 2. The low ΔT duplex is observed to dissociate into single stranded oligonucleotides much more readily than the high ΔT duplex. These results indicate that oligonucleotide duplexes with high melting temperatures are more stable than low melting temperature oligonucleotide duplexes in CID experiments, reflecting their greater stability in solution. These results suggest that ESI-MS experiments (ESI-MS and CID) may be useful in providing rapid, qualitative data on the stability of oligonucleotide duplex noncovalent complexes.

1. Light-Wahl, K. J.; Springer, D. L.; Winger, B. E.; Edmonds, C. G.; Camp, D. G., II; Thrall, B. D.; Smith, R. D. *J. Am. Chem. Soc.* **1993**, 115, 803-804.
2. Ganem, B.; Li, Y.-T.; Henion, J. D. *Tetrahedron Lett.* **1993**, 34,1445-1448.
3. Gale, D. C.; Goodlett, D. R.; Light-Wahl, K. J.; Smith, R. D. *J. Am. Chem. Soc.* **1994**, 116, 6027-6028.

CID of Sequence Specific Oligonucleotide Duplex
5'-dTCTTATCTTTCT-3' (L1) / 5'-dAGAAAGATAAGA-3' (L2)(ΔT=26 °C)

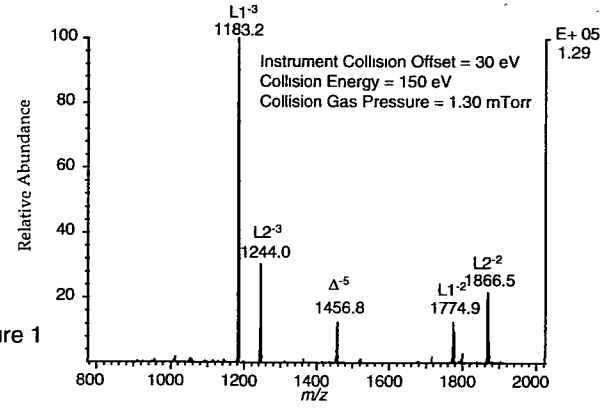

Figure 1

CID of Sequence Specific Oligonucleotide Duplex
5'-dCGCCTCGTCCGC-3' (T1) / 5'-dGCGGACGAGGCG-3' (T2) (ΔT=57 °C)

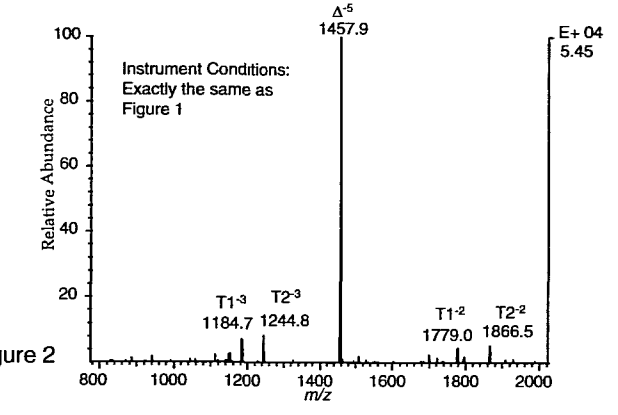

Figure 2

Pacific Northwest Laboratory is operated for the U.S. Department of Energy by Battelle Memonal Institute under contract DE-AC06-76RLO 1830

Characterization of oligonucleotide-peptide hybrids by MALDI and ESI MS

Marek Sochacki, Frank Bergmann, Steve Tam, and Hanspeter Michel
Hoffmann - La Roche Inc., Nutley, New Jersey, 07110-1199

INTRODUCTION

Hybrid compounds consisting of oligonucleotide and peptide components are currently *under investigation for their effectiveness in antisense therapy.*
Mass spectrometry is essential for the structural characterization of such compounds. Molecular weight determination of oligonucleotide-peptide hybrids was achieved from negative ion mass spectra with matrix assisted laser desorption ionization time-of-flight mass spectrometry (MALDI TOF MS). Structural characterization had to be done in multiple steps because of the simultaneous presence of both highly negative charged oligonucleotide and neutral or positively charged peptide components.

EXPERIMENTAL

Enzymatic digestion

Enzymatic digestion was performed by continuous introduction of substrate to the appropriate amount of enzyme during 10 minutes. For the digestion from 3'- and 5'-ends phosphodiesterase I (EC 3.1.4.1) from Crotalus adamanteus and phosphodiesterase II (EC 3.1.16.1) from calf spleen were used respectively.

MALDI and ESI mass spectra

Negative ion MALDI mass spectra were recorded on the BRUKER (REFLEX) TOF instrument in 2,4,6-trihydroxyacetophenone matrix.[1,2] Positive ion ESI mass spectra were recorded on the Finnigan MAT TSQ-700 instrument. Samples were introduced via a 6 cm x 0.1 mm ID capillary column filled with the C-18 reverse phase packing.[3]

RESULTS

Figure 1. shows the structure of the oligonucleotide-peptide hybrid compound which was chosen to verify the sequence of oligonucleotide as well as peptide parts.

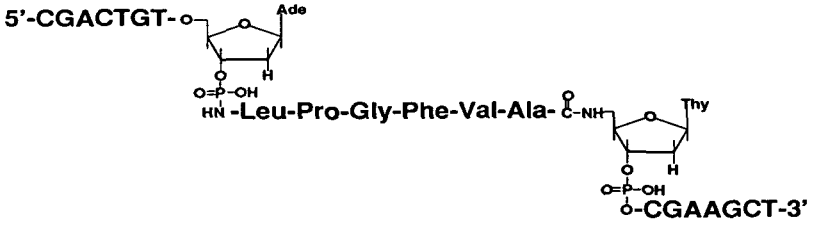

Fig. 1. Structure of the oligonucleotide-peptide hybrid compounds.

Appropriate digestion with phosphodiesterase I or II followed by MALDI TOF mass spectrometry gave the sequence confirmation from 3'- and 5'-ends of the oligonucleotide part.

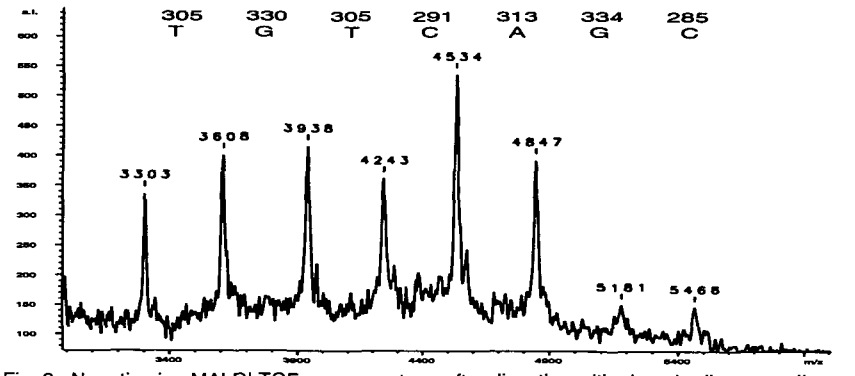

Fig. 2. Negative ion MALDI TOF mass spectrum after digestion with phosphodiesterase II.

Separation of the peptide part by LC allowed its characterization by ESI MS.

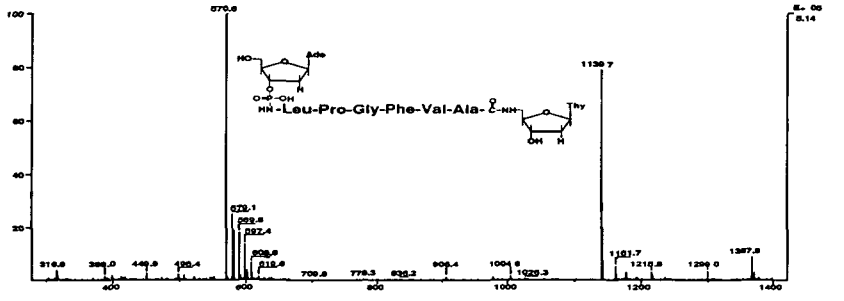

Fig. 3. ESI mass spectrum of the peptide part of the oligonucleotide-peptide hybrid compound.

Fragmentation induced by collisions with an inert gas gave the possibility to sequence the peptide part of the hybrid compound.

REFERENCES

1. Hillenkamp, F.; Karas, M. Methods Enzymol., **1990**, 193, 280-295
2. Pieles, U.; Zurcher, W.; Schar, M.; Moser, H.Z. Nucl. Acids Res., **1993**, 21, 3191-3196
3. Hunt, D.F.; Alexander, J.E.; McCormack, A.L.; Martino, P.A.; Michel, H.; Shabanowitz, J.; Sherman, N.; Moseley, M.A.; Jorgenson, J.W.; Tomer, K.B. In *Techniques in Protein Chemistry II*; Villafranza, J.J. Ed.; Academic Press, New York, **1991**, 441-454.

ROUTINE FAB MASS SPECTRA OF OLIGONUCLEOTIDES; ENHANCEMENT BY CROWN ETHERS

Han Le, Paolo Lecchi, Jane Sayer, Donald Jerina and Lewis Pannell
Laboratories of Analytical Chemistry and Bioorganic Chemistry
NIDDK, NIH, Bethesda MD 20892-0805

Introduction:

Over the past few years, there has been a significant increase in oligonucleotide research at NIH and requests for the analysis of synthetic oligomers has become a common occurrence. We had little success in running these samples by FAB, even when they had been ion exchanged into the ammonium form Residual alkali salts (esp. sodium) from the glassware, etc, caused sensitivity a large loss in sensitivity and often nothing was seen at all. Having used crown ethers in other applications, we decided to investigate the combination of crown ethers with common FAB matrices as a way to enhance the spectra

Method

Spectra were acquired on a JEOL SX102 mass spectrometer using 6keV xenon atoms Data was acquired in profile mode using electric field scans The results are the sum of approximately 14 scans spread over 0.6 minutes. The matrices used were glycerol, 3-nitrobenzyl alcohol (noba), "magic-bullet" (m-b) and thioglycerol.

The matrix (0 5μl) was applied to the probe, the sample (1μl) added, and then the crown ether (1μl) solution placed on top. A standard solution of both 15C5 and 18C6 crown ethers (10mg/ml) was prepared and then 10, 100, 1000 fold dilutions made of each

For a 9-mer oligonucleotide (GGTCACGAG, 1 8mg/ml, M-H 2762 5) which had not been well desalted, spectra were not obtained in any of the plain matrices employed although there was a very small response with noba. However, using glycerol matrix in the presence of crown ethers, good spectra could be obtained Increasing amounts of crown ether helped the spectra and reduced the amount of sodium adducts 18C6 was better at doing this than the 15C5 and the highest concentration used (10mg/ml) was best

With an ammonium exchanged oligonucleotide (CCTCGTGACCG, 2.4mg/ml) very weak spectra were obtained without the addition of crown ethers(see spectra on next page) However, in the presence of 18C6 or 15C5, noba, m-b and glycerol matrices all gave good spectra Increasing levels of sodium adducts were detected as the amount of crown ether was reduced. The limit of sensitivity was reached when the sample was diluted to 0 12mg/ml.

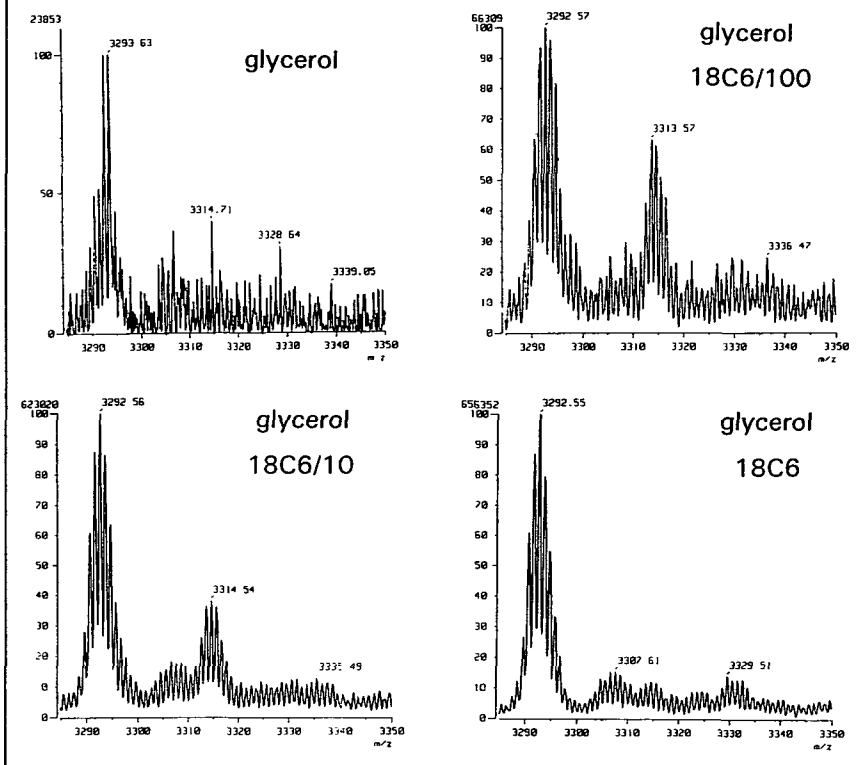

The limit of mass analysis was reached with a 16-mer oligonucleotide of m/z 4820 (TTTAGAGTCTGCTCCC, 0 9mg/ml) which gave the best results in noba and m-b without the addition of either crown ether Although the presence of the sodium adducts is obvious, crown ethers caused a loss of sensitivity rather than improving the result.

Conclusion:

Crown ethers can significantly enhance the spectra of oligonucleotides run under FAB The smaller oligomers give better spectra in glycerol but as the length increases, 3-nitrobenzyl alcohol and magic-bullet give better results.

Fragmentation of Multiply-Charged Oligonucleotides in Triple Quadrupoles

Steven C Pomerantz and James A. McCloskey
Department of Medicinal Chemistry, University of Utah, Salt Lake City, UT 84112

Introduction

The dissociation pathways of larger, multiply-charged oligonucleotides are complex [1], reflecting the conformational flexibility of the nucleotide chain, and the large number of proton-donating and -accepting functionalities that can interact with anionic phosphate groups, but on the other hand they contain all of the elements required for sequence determination (for leading references see ref. 2). To date, a sufficiently good understanding of the chemistry of dissociation of oligonucleotides is in hand [2] that putative sequences can generally be verified, but has not reached the stage that sequences of oligonucleotides of completely unknown structure can be routinely established [3]. Toward this latter goal, an understanding of the fragmentation behavior of oligonucleotides in the rf-only quadrupole collision cell has been sought. The goal of the present work is to gather evidence to allow for a comparison of the dissociation behavior of multiply-charged oligonucleotides in triple quadrupoles, quadrupole ion traps [2], FT-ICR [4,5] and, by extension, singly-charged oligonucleotides in MALDI-TOF [6] This research is compelled by the need to discern if the dissociation mechanisms in each of these instruments is different.

Collision Efficiency of Triple Quadrupoles

We have selected d(CGAGCTCG) for study, to compare mass spectra from CID in a triple quadrupole instrument with those acquired from a sequence isomer [d(GGACGTCC)] using an ion trap mass analyzer [1], and from the same compound using FT-ICR [4]. The present data shows that the extent of fragmentation induced by low energy collision, and thus the amount of structural information, appears to be greatest in triple quadrupoles. In contrast, FT-ICR mass spectra of this same 8-mer exhibit incomplete sequence ions from each terminus but with some overlap in the middle [4]. The a–Base b, d, y, and w ion series can be read completely from one terminus to the other, in apparent disregard of the reported propensity of base loss (A>T>G,C), which according to the proposed mechanisms from ion trap studies, is a necessary condition for the subsequent formation of b and d series ions (from a–B) and y series ions (from w) [2]. Regardless of the mechanisms of dissociation, sufficient fragmentation is obtainable to completely establish the sequence independently through several ion series. This information is straightforward to obtain using a triple quadrupole, by activation of essentially any abundant molecular ion.

Loss of Base is not a Prerequisite for Backbone Cleavage

In order to test the proposed hypothesis that loss of a base is a prerequisite first step in dissociation [2], the oligonucleotide tetra-pseudouridine-3'-phosphate (Ψ_4p) and the control sequences U_4p and dU_4p were synthesized. A consequence of the symmetry of the molecules is that the d and y ion series are isobaric, and in the case of dU_4p, the w and a-Base series are indistinguishable. Nevertheless, the sequence of all 3 oligomers can be completely established through the b, d/y, and w series ions. The notable result of these experiments is that the spectrum of Ψ_4p is completely devoid of any ions resulting from loss of the base moiety, including the 'pseudouracil' anion and ions corresponding to z-Base (the 3' counterpart to a-Base) which were observed in the spectrum of AAΨA (data not presented). It is not yet clear whether these data are indicative of thermodynamic, kinetic, or conformational effects.

Monomeric Units

The identities and structures of some of the ions observed in the mass range corresponding to nucleotide mono- and diphosphates were ascertained by isotopically labelling the phosphate backbone of d(CGAGCTCG). The labels were incorporated at either every position, or alternating positions. Little has observed [4] via FT-ICR that the ions that are assignable as pNp are actually a doublet of peaks consisting of both pNp and Npf where f is a furan arising from loss of substituents from the deoxyribose ring. In order to determine whether in fact both of these ions are produced, and if so their relative abundances, the per-^{18}O labelled octadeoxynucleotide was synthesized. Ions which bear 2 phosphate groups (pNp) would thus shift 4 Da, while ions which bear only one phosphate group (Npf) would only shift 2 Da toward higher mass. The data clearly shows that both ions are in fact produced, with a general trend being observed that pNp ions are generally favored over Npf ions. Delineation of the location of the phosphate group in nucleotide monophosphates was accomplished by synthesizing the same oligonucleotide with alternating labelled phosphates. In this construct, C and A residues are labelled on the 3' side, while G and T residues are labelled on the 5' side. The spectrum dramatically demonstrates that the ions are almost exclusively 5' phosphates.

Conclusions

- Triple quadrupole mass spectrometers are apparently more efficient at generating sequence-specific cleavages than trapped ion instruments. Oligonucleotides up to 8 bases in length can routinely be sequenced completely through via multiple ion series with a single stage of collisional activation.
- The loss of the base has been demonstrated to not be prerequisite for backbone cleavage of an oligonucleotide. It is not yet known whether this is a kinetic or thermodynamic effect, or even potentially a conformational effect. Further experiments and theoretical calculations are in progress in order to further elucidate these findings.
- Monomeric ions of the type Npf and pNp are both produced, with pNp apparently being favored Additional experiments will be required to determine whether this is a consequence of ion production or ion stability, or even whether some sort of sequence context affects the relative proportions of these ions.
- Monomeric ions which bear a single phosphate are almost exclusively pN and not Np. However, further experiments are warranted to ensure that some sequence effects have not biased this admittedly limited sample set

Acknowledgement

The authors gratefully acknowledge Dr. D. R. Davis, Department of Medicinal Chemistry, University of Utah for the kind donation of the pseudouridine phosphoramidite, and Dr. R. W. Schackman, DNA/Protein Synthesis Facility, University of Utah for technical support. This work was supported NIGMS grant GM21584, and by NIH grant CA42014 to the Huntsman Cancer Institute

References

1 S A. McLuckey, G. J. Van Berkel, and G. L. Glish, *J. Am. Soc. Mass Spectrom.* **1992**, *3*, 60-70.
2. S. A. McLuckey and S Habibi-Goudarzi, *J Am Chem. Soc.* **1993**, *115*, 12085-12095.
3. P. A. Limbach, P. F. Crain, and J. A. McCloskey, *Current Opinion Biotechnol.* **1995**, *6*, 96-102.
4. D P. Little, R. A. Chorush, J. P. Speir, M W. Senko, N L. Kelleher, and F. W. McLafferty, *J. Am. Chem Soc.* **1994**, *116*, 4893-4897.
5. M. T. Rodgers, S. Campbell, E. M. Marzluff, and J. L. Beauchamp, *Int. J. Mass Spectrom. and Ion Processes* **1994**, *137* 121-149.
6. E. Nordhoff *et al.*, *J. Mass Spectrom.*, **1995**, *30*, 99-112.

A New Approach for DNA Sequencing and Mutation Detection with ESI-MS

Hideya Terunuma[b], Yasuhiro Naito[a], Toshihiro Tsuneyoshi[a], Ryuichi Arakawa[d], Keiichiro Ishikawa[e], Yoshinori Koga[e] and Darwin J Prockop[d]

[b]Dept. Surgery, Suruganishi Hospital; [a]Dept. Biochem,Hamamatsu Univ. School of Med.; [e]Dept. Material Sci.,Shizuoka Inst. of Sci. and Tech; [d]Dept. Applied Chem.,Faculty of Engineering, Osaka Univ.; [e]Dept. Analytical Chem., Natl. Inst. Materials and Chem. Res., Japan; [d]Dept. Biochem. and Mol. Biol., Thomas Jefferson Univ., U.S.A.

Principles

Sequencing

The single strand DNA (ssDNA) are synthesized from deoxy nucleotides triphosphate(dNTP) of 4 types, dATP, dCTP, dGTP and dTTP. Each unit has unique M.W., 313.2, 289.2, 328.2 and 304.2 corresponding to the base, A, C, G and T, respectively. We assume that ssDNA of unknown sequence is digested from 3' end with the enzyme like Exonuclease III and form ssDNA mixture of various length fragments. Those fragments are applied to mass spectrometer (MS). If we calculate the molecular weight (M.W.) difference between nearest neighbor values, we can determine nucleotide sequence.

Mutation detection

Two ssDNAs, which are different from each other in only one nucleotide, are applied to MS for the M.W. analysis. Mass spectrum of them show two groups of ion fragment peaks which correspond to the two ssDNAs, demonstrating the detection of mutant DNA from wild type DNA by MS.

Materials and methods

Totally seven kinds of oligonucleotides were synthesized(shown in table 1). Sample solutions dissolved in 1% triethylamine and 80% acetonitrile were applied to MS, JMS-HX110(Nihon denshi co. Tokyo, Japan). For the demonstration of sequencing by MS, ssDNA mixture of two to five bases (HT1, HT2, HT4 and HT6), whose sequences are identical to the COL1A2 gene sequence around the mutation site of real osteogenesis imperfecta patient, were applied to MS for the determination of M.W. of each ssDNA.

For demonstrating the model experiment of mutation detection, a mixture of two ssDNAs, HT6(ACCCT) and HT7 (ACGCT), whose five bases (reverse complementary)sequences are wild type(HT6) and mutant type(HT7) of the COL1A2 gene, were also applied to MS for the determination of M.W. of each ssDNA.

Table 1 Specifications of synthesized ssDNAs. PM depicts each ssDNA, M.W. molecular weight, Seq sequence of ssDNA, mM concentration of the solution applied to MS in millimole/liter, and Qty total amount applied to MS in millimole, respectively.

PM	M.W.	Seq	mM	Qty (mmole)
HT1	541.4	AC	0.346	0.356
HT2	830.6	ACC	0.114	0.114
HT3	869.6	ACG	0.291	0.291
HT4	1119.8	ACCC	0.246	0.246
HT5	1158.8	ACGC	0.332	0.332
HT6	1424.0	ACCCT	0.337	0.337
HT7	1463.0	ACGCT	0.334	0.334

Results

For the model experiment of sequencing, mass spectrum of the mixture of four kinds of ssDNAs(shown in Fig.1 and Table 2) enabled us to determine the base type of 3' end nucleotide of each ssDNA. Mass spectrum of two ssDNAs mixture of wild and mutant type sequence showed clear two peaks(shown in Fig.2), indicating the detection of different DNA types.

Table 2 Subtraction of negative ion peaks of MS in Fig.1.

peak subtraction	corresponding base
1422.6 - 1117.5 = 305.1	Thymine; T
1117.5 - 828.4 = 289.1	Cytosine; C
828.4 - 539.3 = 289.1	Cytosine: C

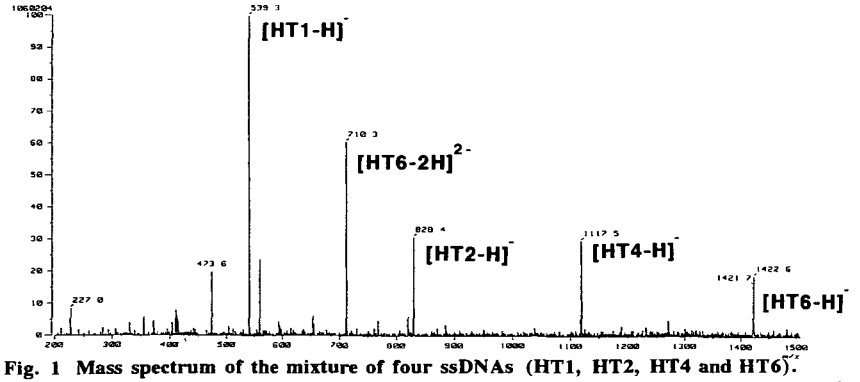

Fig. 1 Mass spectrum of the mixture of four ssDNAs (HT1, HT2, HT4 and HT6). The 1422.6 peak corresponded to M.W. of HT 6. The 1117.5 peak was consistent with HT4. The 828.4 and 539.3 peaks also agreed with HT2 and HT1, respectively.

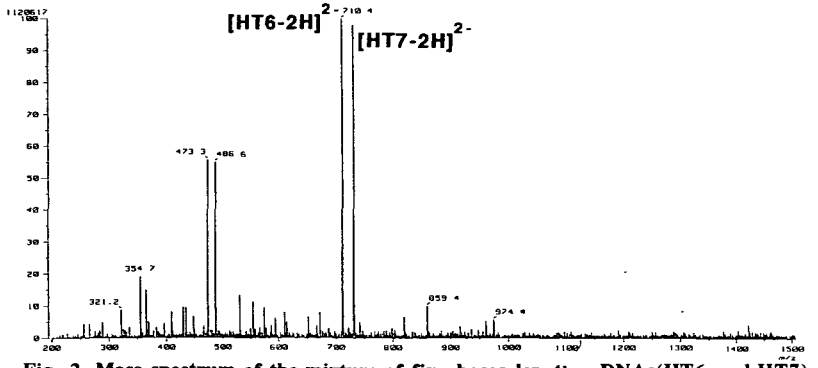

Fig. 2 Mass spectrum of the mixture of five bases length ssDNAs(HT6 and HT7). The 730.4 peak agreed with $[HT7 - 2H^+]^{-2}$ and the 710.4 peak also agreed with $[HT6 - 2H^+]^{2}$.

Electrospray mass spectrometry on a sector instrument for the analysis of small oligoribonucleotides

M. A. Wolter[1,2], J. W. Engels[2], L. Montanarella[1], S. Facchetti[1]
[1]Commission of the European Communities, Joint Research Center, TP290, 21020 Ispra, Italy
[2]Institute for Organic Chemistry, Johann Wolfgang Goethe-University, 60054 Frankfurt, Germany

For the antisense [1, 2] and ribozyme [3] approach the sensitive analysis of small modified oligonucleotides is needed. The 2'-O-methyl [4, 5] is one of the favored modifications within the ribozyme approach to stabilize the oligoribonucleotides (RNAs) against nuclease activity.

The traditional methods for the sequence determination of oligonucleotides (Sanger], Maxam and Gilbert) are limited in accuracy and do not allow the analysis of modified oligomers. In contrast, mass spectrometry can in principle detect any modification in the primary structure of oligonucleotides. While the molecular weight may confirm the presence of a modification, reproducible fragmentation schemes are needed to identify the modification side.

Electrospray has been fitted on sector instruments in 1989 [6]. Encouraged by the performance of this combination, we studied electrospray nozzle-skimmer fragmentation [7, 8] on a VG 70-SEQ hybrid mass spectrometer with EBqQ geometry and commercial ESI interface [9] (Fisons) for the fragmentation scheme of small RNAs. Unmodified and 2'-O-methyl modified RNA decamers were chosen to test the performance of the method.

For small DNAs in Fourier transform mass spectrometry, the spectra of nozzle-skimmer fragmentation are closely similar to the CID MS/MS spectra [10].

The nomenclature of McLuckey et al. [11] is used for the observed fragment ions. With flow rates of 0.5-5 µl/min the direct lens gives a two fold better response than the chicane lens. Thus, we were able to perform analysis in the picomol range. The voltage setting in an electrospray source for sector instruments can be rather critical [12]. However, in the mass range we studied, we do not observe any mass discriminatory effects due to the interface settings. The published settings are based on different interface geometries and therefore hardly comparable.

The difference in the molecular weight allows to distinguish a modified and unmodified RNA decamer. However, the kind and location of the modifications remain unclear. Multiple fragmentation series are generated when the potential during the expansion into the vacuum is increased. In analogy to the DNA fragmentation pattern [10], the w-series is dominant. However, represented by strong water- and base-loss signals the series do not cover the whole sequence. The modified and unmodified RNA decamers show significant differences in their fragmentation behavior. Because both give equal 5'-sequence ions until n=4, the 3'-terminus must be the same. In contrast, the fragmentation in the 5'-terminus, where the modifications are located, is completely different.

Electrospray nozzle-skimmer fragmentation can generate sequence specific fragments, representing not the whole sequence but additional certainty towards the modification site. Accuracy and resolution of the sector instrument in combination with the moderate charge states of the precursors allow a definitive fragment assignment. However, there is no complete and dominant fragment series which would allow the sequence determination of unknown RNAs, as it was the case for MS/MS experiments done on a triple quadrupole instrument [13].

Work was supported (M.A.W.) by a grant of the European Community (ERB4001GT942747).

1. P. C. Zamecnik, M. L. Stehpenson, *Proc. Nat. Acad. Sci. USA*, **75**, 280 (1978).
2. M. L. Stephenson, P. C. Zamecnik, *Proc. Nat. Acad. Sci. USA*, **75**, 285 (1978).
3. J. A. McSwiggen, T. R. Cech, *Science (Washington, D. C., 1883-)*, **244**, 679 (1989).

4. G. Paolella, B. S. Sproat, A. I. Lamond, *J. Eur. Mol. Biol. Org.*, **11**, 1913 (1992).
5. C. Boiziau, B. Larrouy, B. S. Sproat, J.-J. Toulmé, *Nucleic Acids Res.*, **23**, 64 (1995).
6. M. H. Allen, I. A. S. Lewis, *Rapid Commun. Mass Spectrom.*, **3**, 255 (1989).
7. J. A. Loo, H. R. Udseth, R. D. Smith, *Rapid Commun. Mass Spectrom.*, **2**, 207 (1988).
8. A. M. Starrett, G. C. DiDonato, *Rapid Commun. Mass Spectrom.*, **7**, 12 (1993).
9. A. R. Woolfitt, P. Jonathon, P. A. Bott, *ASMS Conf. Mass Spectrom.*,, 759 (1994).
10. D. P. Little, R. A. Chorush, J. P. Speir, M. W. Senko, N. L. Kelleher, F. W. McLafferty, *J. Am. Chem. Soc.*, **116**, 4893 (1994).
11. S. A. McLuckey, G. J. V. Berkel, G. L. Glish, *J. Am. Soc. Mass Spectrom.*, **3**, 60 (1992).
12. H. Murata, T. Takao, Y. Shimonishi, *Rapid Commun. Mass Spectrom.*, **8**, 205 (1994).
13. M. A. Wolter, M. S. Wilm, M. Mann, J. W. Engels, *ASMS Conf. Mass Spectrom.*, TP 231 (1995).

Figure:
Electrospray nozzle-skimmer fragmentation spectra of an unmodified and modified ribonucleotide decamer: 5'-r(AGUAGUCCCA)-3' (c=338 pmol/µl, MW 3144.0) and 5'-r(AmeGUAmeGUmeCCCA)-3' (c=386 pmol/µl, MW 3186.0).

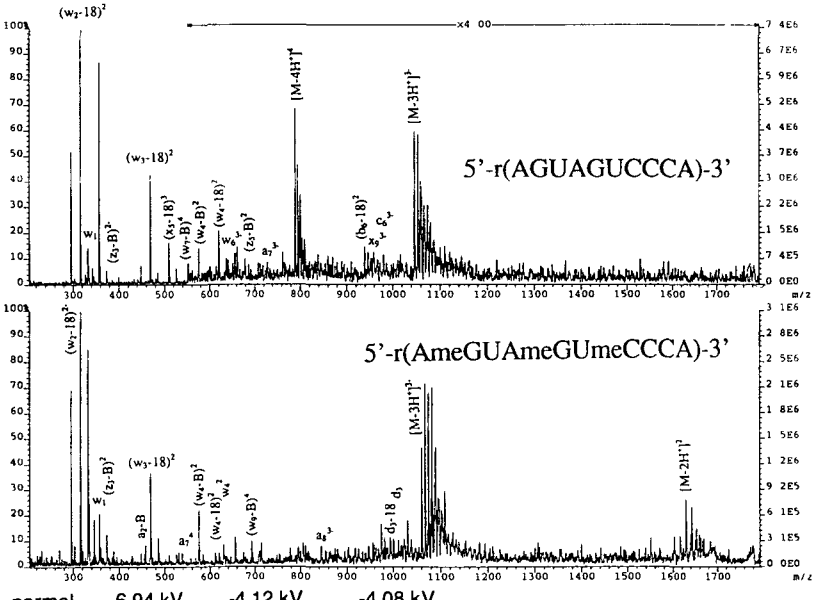

	needle	counter electrode	cone	skimmer	hexapole	ring electrode
normal	-6.94 kV	-4.12 kV	-4.08 kV			
collision	-7.41 kV	-4.60 kV	-4.15 kV	-4.04 kV	-4.03 kV	-4.02 kV

FAB/MS Confirmation of Modified Deoxynucleotides in Small Oligomers

Robert A. Rieger and Charles R. Iden

Department of Pharmacological Sciences, Health Sciences Center,
SUNY-Stony Brook, Stony Brook, NY 11794-3400

The ability to incorporate a modified deoxynucleoside at any position in the sequence of a synthetic oligodeoxynucleotide is a powerful tool which can be used to examine the effects of novel structures in DNA. Oligomers may be used directly, annealed to a complementary strand, or placed in plasmids to study the reaction of polymerases, DNA repair enzymes, or other cell enzyme systems to this abnormal structure. Automated synthesis of oligomers with modified deoxynucleosides typically employs a 5'-dimethoxytrityl (5'-DMT)-protected nucleoside phosphoramidite which must be synthesized and characterized independently. Incorporation into an oligomer is successful when the modified deoxynucleotide is stable to the conditions of DNA synthesis. One method to verify deoxynucleoside stability is to expose the modified, 5'-DMT-protected monomer to each of the reagents from the solid phase synthesizer for a predetermined time interval and reanalyze the material by HPLC to see if degradation has occurred. This procedure works well in many cases, but with some substances analysis may become tedious and require further manipulation. To simplify this procedure, we have designed a short, test oligomer, 5'-TTXTT-3', which is used routinely to examine the stability of the modified deoxynucleoside. Their are several advantages in using this oligomer. Thymidine has no functional moieties that require protection, so final cleavage of the product from the resin should generate a pure oligomer which is uncomplicated by partial deprotection. Multiple products can only occur from a partially deprotected X moiety, if, indeed, it has a protecting group. Also, negative ion FAB/MS of small oligomers is uncomplicated and produces structurally significant fragment ions. Due to the palindromic nature of this sequence, masses of the 3'- and 5'-phosphate series are the same, and a simplified FAB mass spectrum is observed.

Oligodeoxynucleotides were synthesized on a Dupont Coder 300 DNA synthesizer. Commercial phosphoramidites and DNA reagents were purchased from Applied Biosystems Inc. (Foster City, CA). Modified phosphoramidites were synthesized using literature protocols. After completion of a synthesis, oligomers were cleaved from the resin in 28% NH4OH. Crude 5'-DMT-protected DNA was HPLC purified on a Waters 990 photodiode array HPLC system. Collected fractions were dried *in vacuo*, deprotected at the 5'-position, and analyzed on a Kratos MS890 mass spectrometer system. An Ion Tech saddle field fast atom bombardment (FAB) source provided 7 Kv xenon atoms for sample ionization. The mass scale was calibrated in the negative ion mode with cesium iodide (130-2000 amu) at a scan rate of 10sec/dec. Samples were dissolved in a glycerin matrix and scanned for approximately 3 minutes.

Recently, we have developed a series of modified 8-oxo-2'-deoxyguanosines for incorporation into oligomers for the study of DNA repair. One of these compounds, O^6-methyl-8-oxo-2'-deoxyguanosine, was placed in the X position of the test oligomer and the HPLC chromatogram of the 5'-DMT-protected product is shown in Fig 1. The chromatogram is dominated by failure sequences appearing near the void volume for this column. However, two significant peaks appear in the DMT region of the chromatogram at 35 and 40 min. These peaks were collected as fractions and analyzed by FAB/MS. The calculated molecular weight for the test oligomer, 5'-TTXTT-3' where X is O^6-methyl-8-oxo-2'-deoxyguanosine, is 1513. In the negative ion FAB mass spectrum for Peak A (Fig. 2a), an intense ion at *m/z* 1512 appears to be the negatively

charged molecular ion formed by loss of a proton. Sequence ions derived from cleavage of the 3'-carbon oxygen bonds (w series) and 5'-carbon oxygen bonds (d series) are present Ions at *m/z* 321 and 625 are monomers and dimers formed from the first two thymidine residues The ion at *m/z* 984 is a trimer and corresponds to an addition of 325 d to the dimer mass, exactly the mass of the O^6-methyl-8-oxo-2'-deoxyguanosine monophosphate. Two final thymidine residues are added to yield ions for the tetramer and pentamer at *m/z* 1288 and 1512 respectively. Thus, the desired oligomer was identified as Peak A, the modified base has been identified as the central base in the sequence, and the mass of the oligomer and the modified deoxynucleotide have been confirmed.

The negative ion FAB mass spectrum of the second fraction (Peak B) is shown in Fig 2b The apparent mass of this substance is 1647, derived from an apparent molecular ion at *m/z* 1646. This molecular mass is 134 d greater than that determined in the previous fraction. Since the phenoxyacetyl (PAC) group is used to protect the 2-amino group during synthesis and adds 134 mass units to the monomer, it must be suspected as the candidate to explain this apparent shift in mass. If true, the sequence ions that contain the modified base should also contain the additional PAC group and, therefore, exhibit the same shift in mass. Sequence ions at *m/z* 321 and 625 are the monomers and dimers, and appear unchanged from the previous mass spectrum. The ion at *m/z* 1118 representing the trimer is shifted by 134 d. from the mass of the trimer in the previous spectrum, and the modified deoxynucleoside containing the PAC protecting group appears responsible Addition of T to form the tetramer (*m/z* 1422) and pentamer (*m/z* 1646) behave normally. Thus, our conclusions are that the deprotection step in this case is not complete and must be reexamined and that FAB/MS analysis of short, test oligomers is an effective means to examine problems in DNA synthesis

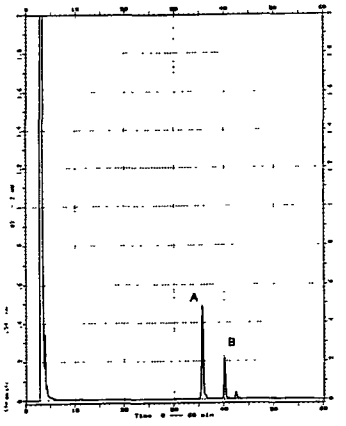

Fig. 1. HPLC chromatogram of 5'-DMT-protected test oligomer, TTXTT, where X is O^6-methyl-8-oxo-2'-deoxyguanosine.

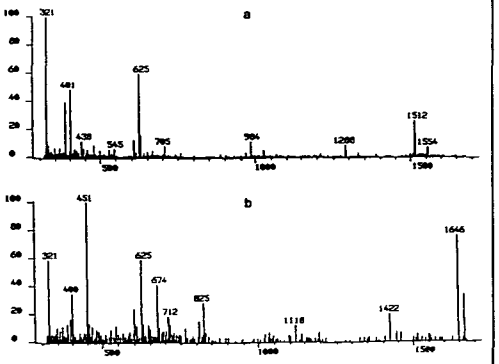

Fig. 2. Negative ion FAB mass spectrum of a) Peak A and b). Peak B in Figure 1.

Mass Selection and Post-Experimental Viability of Gas Phase Viruses

Gary Siuzdak, Brian Bothner, Mark Yeager, Christophe Brugidou,
Claude M. Fauquet, Kenway Hoey, and Cheng-Ming Chang

The Scripps Research Institute
and
R. W. Johnson Pharmaceutical Research Institute
La Jolla, CA, 92037

Most macromolecular complexes studied by mass spectrometry are relatively small, on the order 10^3-10^4 Daltons. These studies rely on indirect evidence such as isotope exchange, charge state distribution, and changes in molecular weight to infer that native structure is retained in the gas phase. The question remains whether native conformations are preserved during the ionization/vaporization process and the vacuum of the mass spectrometer. A second issue, a vestige of the Manhattan Project where Calutron mass spectrometers were employed to separate uranium isotopes, is whether this technology can be used as a separation and collection device for biomolecules. Our work addresses these issues with the first direct observation of a supramolecular (4×10^7 Da) complex in which biological activity is preserved.

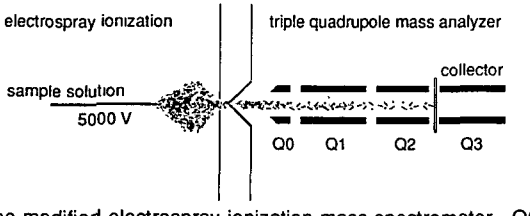

Figure 1. The modified electrospray ionization mass spectrometer. Q0, Q1, Q2, and Q3 represent four different sets of quadrupoles in the mass analyzer allowing for ion focusing and mass selection. The instrument was modified by placing an ion collector in the flight path of the ions between Q2 and Q3. The instrument was a Perkin Elmer SCIEX API-3 triple quadrupole mass spectrometer.

In order to detect large ions (>1,000,000 Da) which do not produce significant secondary electron emission, we have applied a concept analogous to that of the photographic plates originally used for ion detection. Instead of detecting secondary electrons or incident light from a phosphorous screen, the actual ions are physically collected whereby the isolated specimen can be directly examined by electron microscopy. Fig. 1 illustrates the basic design of the mass analysis instrumentation employed.

Figure 2. Two viruses were analyzed, tobacco mosaic virus (TMV) and rice yellow mottle virus (RYMV). TMV's rod-like structure has a diameter of 17.5 nm, a length of 300 nm, and a molecular weight of 40.5×10^6 Daltons. RYMV is 28.8 nm in diameter with a molecular weight of 1.5×10^6 Daltons. Post-analysis samples were found intact when viewed with an electron microscope.

To demonstrate mass selection for the viral studies, we utilized the radio frequency (RF-only) mode for Q0, Q1, and Q2 in the triple quadrupole mass analyzer. By lowering the accelerating voltage between Q0 and Q1, low mass ions drifted out of the analyzer before reaching the detector, while high mass ions retained sufficient momentum to reach the detector.

In the mass analysis process the virus particles were exposed to a number of conditions that could potentially damage tertiary or quaternary protein structure or the nucleic acid structure, resulting in a non-viable specimen. Since electron microscopy is limited in its ability to determine whether this damage had occurred, specimen viability after electrospray mass analysis was tested. The production of characteristic local lesions on the leaves of tobacco cultivar Xanthi NN plants inoculated with post-analysis TMV demonstrates that the virus retained infectivity.

This work has addressed two aspects of electrospray mass spectrometry. Retention of virus ultrastructure and infectivity provide direct evidence that native structure is conserved into the gas phase, producing results on ions forty times larger than any previously reported biomolecule and over a hundred times larger than any biomolecular complex. Secondly, higher accuracy for molecular weight determination and the ability to separate biomolecular complexes, while retaining viability, suggest that electrospray may be developed for *preparative mass spectrometry.* Recent improvements in sensitivity by micro electrospray further support the feasibility of using mass spectrometry for biomolecular purification.

References:
1) B. Ganem, Y.T. Li, J D Henion, *J. Amer. Chem Soc.* **113**, 6294 (1991).
2) V Katta, B.T Chait ,*J. Amer. Chem. Soc.* **113**, 8534 (1991).
3) L.P. Smith, W E Parkins, A.T.Forrester, *Phys. Rev.* **72**, 989 (1947).

Acknowledge Jennifer Boydston, Drs. George Scott, Stephen B. H. Kent, Richard A. Lerner, Mark W. Duncan, and Michael Fitzgerald. This work was supported by The Lucille P Markey Charitable Trust and NIH #1 S10 RR07273-01.

Analysis of Oligonucleotides and their Analogues by Electrospray Mass Spectrometry

*Ling Chen, Lydia M Nuwaysir and Karen Fearon**
*Perkin Elmer, Applied Biosystems Division, Foster City, *LYNX Therapeutics, Inc., Hayward, CA*

INTRODUCTION The routine analysis of oligonuceotides by electrospray ionization (ESI) mass spectrometry provides a powerful and sensitive tool for quality control of the synthetic DNA's. A method is described for rapid on-line desalting and preconcentration of the oligonucleotides prior to ESI mass analysis. General application of ESI mass spectrometry in assaying oligonucleotide synthesis and QC/QA of oligonucleotide therapeutic products are discussed.

EXPERIMENTAL A PE SCIEX API 100 benchtop single-quadrupole mass spectrometer was used for this study and operated in the IonSpray negative-ion MS mode. The sample preparation method for oligonucleotides is ethanol precipitation from ammonium acetate as described in Ref. 1. This method, however, requires sample amount in the nanomole range to be handled easily. For desalting and preconcentration of dilute samples, we adapted the on-line approach previously used for protein/peptide samples (Ref. 2) for desalting of oligonucleotides.

Protocol Put the trap cartridge (LC packing pre-column) in place of the injector loop on a injector (Reodyne 7125). The oligonucleotide was desalted by washing the precolumn with 200 ul of 20mM ammonium acetate in water. The sample was then eluted for mass analysis by directing the LC effluent (10 mM ammonium acetate, 50% acetonitrile 50% water) through the precolumn by switching the injector valve. The results of the loop-wash protocol are shown below. ESI Spectrum of a 41 mer desalted by ethanol precipitation and analyzed by infusion is shown in Figure 1a and 1b. Large amount of sodium adducts reduced the sensitivity, mass accuracy and could overshadow the minor components of interest. The spectral quality was greatly improved by the on-line desalting protocol as shown in Figure 1c and 1d. No sodium adducts were observed.

ES Analysis of Oligonuleotide Analogues in Pharmaceutical Application For pharmaceutical applications, as well as in studies aimed at refining synthesis of oligonucleotide (ODN) and their analogues, it is necessary to address issues of product identification and purity, characterization of impurities and reproducibility of synthesis and purification methods. The routine analysis of oligonuceotides by electrospray ionization (ESI) mass spectrometry provides a rapid and sensitive tool for structure confirmation and quality control of the synthetic ODN's. The following ODN phosphodiester is designed for treatment of chronic myelogeneous leukemia. Various chemically modified compounds were synthesized to help prevent 3'-exonuclease degradation and to facilitate transport across membranes (cellular uptake). Correct synthesis of the desired modification were readily confirmed by ESI mass spectrometry (Fig.2a and 2b). Attention has focused on using phosphorothioate ODN's as "antisense" agents because the S-ODN's are resistant to degradation by nucleases, form stable duplexes and are now readily synthesized. The following S-ODN is designed for treatment of acute myelogeneous leukemia. 5'-
d(CpsCpsCpsTpsGpsCpsTpsCpsCpsCpsCpsCpsCpsTpsGpsGpsCpsTpsCpsC)
ESI mass spectrum is shown in Fig 2c. The families of much lower intensity ions seen in Fig. 2c are due to minor impurities. The peaks found at MW 6190 and 6174 Da correspond to the synthesis defects where either one or two phosphodiester (PO) linkages were formed instead of phosphorothioate (PS) linkages. The PO defects can be attributed to the incomplete stepwise sulfurization with S-Tetra in the solid-phase phosphoramidite method. Based on independent quantitation method (IEC data not shown), we believed that, in general, impurities in the S-ODN products are detectable in the ESI-MS if they are at least 1 mol-% of the material analyzed.

REFERENCES

1. J. T. Stults and J. C. Marsters, Rapid Com. in Mass Spec., Vol 5, 359-363 (1991).
2. M. E. Hail, B. M. Warrack, G. C. DiDonato, and M. S. Lee, Presented at 3rd International Symp. on Mass Spec. in the Health and Life Sciences, San Francisco, September 13-18, Poster No.1156.

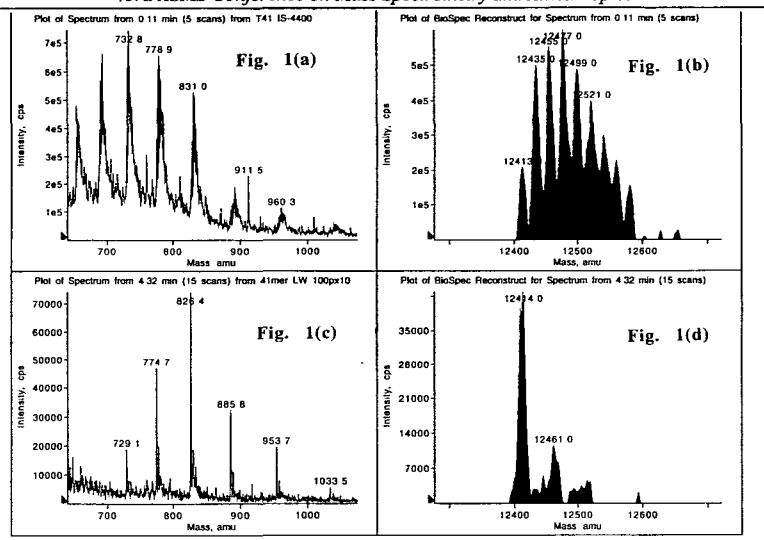

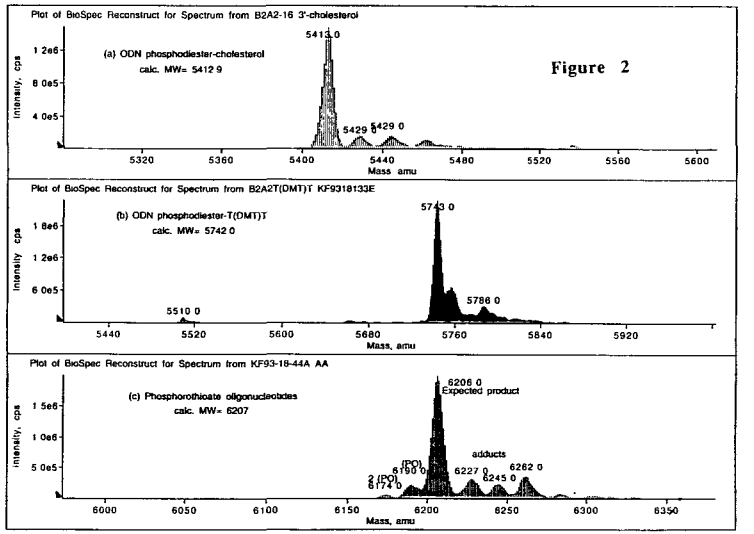

Detection of Imidazoleacetic Acid Riboside by FAB/MS and ESI/MS

Robert A. Rieger[1], D Meghanath Reddy[1], Boban Thomas[2], George D Prelli[2], and Charles R. Iden[1]

[1]Department of Pharmacological Sciences, Health Sciences Center, SUNY-Stony Brook, Stony Brook, NY 1179-3400

[2]Department of Pharmacology, School of Medicine, Mt. Sinai Medical Center, New York, NY 10029-6574

Imidazoleacetic acid is a potent agonist in biological systems and exerts numerous biological effects including analgesia, sedation, and reduction of blood pressure, body temperature, and motor activity. It is a normal constituent of plasma and urine and may exist as the free compound or in conjugated form where it is bound to a ribosyl moiety. Two isomers are possible depending on whether the acetic acid moiety is bound to the C4- (tele isomer) or the C5-position (pros isomer) of the imidazole ring. GC/MS methods for analysis of the two isomers have been developed and require trimethylsilyl-derivatization in order to increase volatility and decrease retention on GC columns. These methods have employed both EI and CI techniques and have achieved excellent sensitivity for biological samples

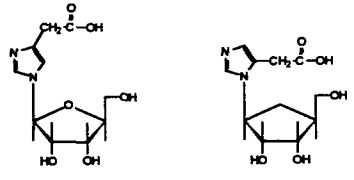

We have developed methods for the detection of imidazoleacetic acid riboside and ribotide in biological samples using FAB and ESI techniques. Both methods do not require sample derivatization; thus, the analysis can be simplified when compared to that for the GC/MS technique. FAB mass spectra were produced on a Kratos MS-890 mass spectrometer equipped with a DS-90 data system. Fast xenon atoms (7 kV) were generated in a Ion Tech saddle field source and were permitted to impact the sample dissolved in a 1:1 glycerine/thioglycerine or nitrobenzyl alcohol matrix. Mass spectra were acquired in the positive ion mode while the instrument was scanned repetitively over the range *m/z* 1500-130 at 10 sec/dec. Electrospray mass spectra were acquired in both the positive and negative ion mode on a Fisons Instruments Trio-2000 GC/MS instrument equipped with an electrospray ion source. Samples (10 μl) were introduce by loop injection into a solvent stream of methanol/water/ammonium hydroxide (90:9:1) flowing at 6μl/min. The instrument was operated in the multichannel analyzer mode with a scan time of 8 sec over the range *m/z* 80-600. Spectra are an average of 10-15 scans.

Perfused rat brains were collected and homogenized in 0.4 N perchloric acid and centrifuged at 50,000 g for 45 min. The total supernatant was made basic with 10 N KOH and centrifuged again at 50,000 g for 45 min. The supernatant was placed on a Waters C_{18} solid phase extraction column, drawn through with mild suction, and applied to a phenylboronate (PBA) extraction column. The column was washed with triethylamine and eluted with 3 ml 6 N formic acid. Samples were brought to pH 10 with NH_4OH and applied to columns containing conditioned AG-1-X8 resin in acetate form. Columns were washed with water

and eluted with 10 ml 10 N formic acid This eluate was desalted on a column of mixed anion-cation exchange resin (BioRad MSD 501) and dried on a vacuum centrifuge.

Positive ion FAB/MS analysis of the imidazoleacetic acid riboside and ribotide standards in a glycerin/thioglycerine matrix generate excellent mass spectra (Fig. 1). $(M+H)^+$ and $(2M+H)^+$ dominate the spectrum, and fragmentation is not abundant. BH^+ and BH_2^+ are not evident since they appear (*m/z* 126, 127) below the limit of the mass calibration. As expected, the tele- and pros-isomers cannot be distinguished by FAB/MS. When extracts from rat brain samples were analyzed under similar conditions, no peaks corresponding to the molecular ions of the riboside and ribotide were found. Even when a standard was added directly to the sample on the FAB probe, molecular ions still were not apparent in the mass spectrum. However, when the sample was trimethylsilylated (TMS) and the hydroxy groups were protected, peaks corresponding to the *tris*-TMS-derivative and the *tetrakis*-TMS derivative of imidazoleacetic acid riboside were present in the FAB mass spectrum Positive ion ESI/MS confirmed the presence of imidazoleacetic acid riboside in rat brain. Figure 2 shows the ESI spectra of a standard of the riboside, showing an intense molecular ion at *m/z* 258 and a sample generated from rat brain, also with a strong peak at *m/z* 258 and several background peaks nearby. Thus, this preliminary data indicates the presence of imidazoleacetic acid riboside in rat brain at detectable levels, while no evidence for the ribotide was found by these methods

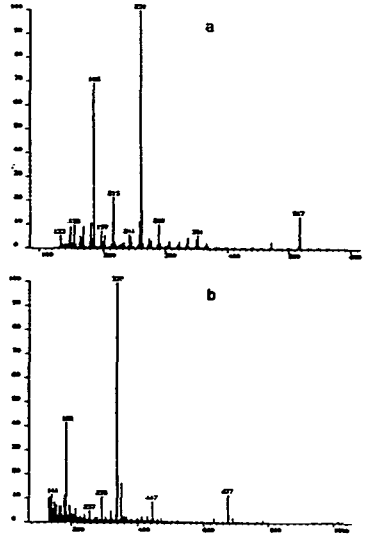

Fig. 1. Positive ion FAB mass spectra of standards of a). imidazoleacetic acid riboside and b). imidazoleacetic acid ribotide. Matrix ions are not background subtracted

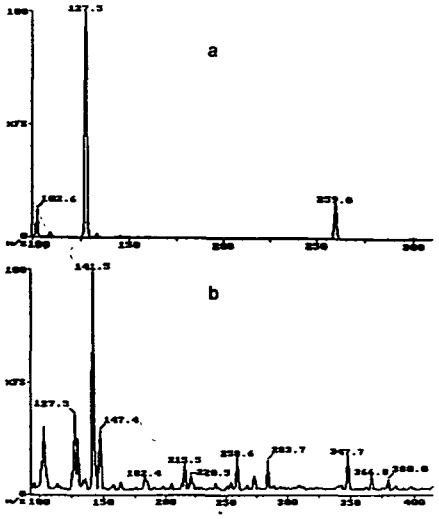

Fig. 2. Positive ion electrospray mass spectra of a). imidazoleacetic acid riboside standard and b). a sample extracted from rat brain.

Liquid Chromatography/Electrospray Ionization Tandem Mass Spectroscopy (LC/ESI MS/MS) Analysis of 1,2-epoxybutene Adducts of Purine Deoxynucleosides.

Sara J. Kambouris [1,2], Ajai K. Chaudhary [2,3,4], Ian A. Blair [1,2,4]

Department of Chemistry [1], Vanderbilt University, Departments of Pharmacology [2] and Biochemistry [3], A. B. Hancock Jr. Memorial Laboratory for Cancer Research [4], Vanderbilt University School of Medicine, Nashville, TN, 37232, USA.

Incomplete fuel combustion from mobile exhausts results in a major contribution of 1,3-butadiene (BD) to the environment. Stationary sources and tobacco smoke also contribute significantly to environmental BD. Formaldehyde and acrolein are the major products from the atmospheric breakdown of BD. BD causes tumors in mice and rats and has been classified as a probable human carcinogen by the U.S. Environmental Protection Agency (EPA) and the International Agency for the Research on Cancer (IARC). A major route of BD metabolism involves conversion of BD to 1,2-epoxybutene (BDO) and 1,2,3,4-diepoxybutane (BDO_2) primarily by cytochrome P450 2E1. BDO and BDO_2 are both genotoxic and carcinogenic. Studies on the characterization of DNA modification by BD and its metabolites are very limited. Two DNA adducts, 7-(2-hydroxy-3-buten-1-yl)guanine and 7-(1-hydroxy-3-buten-2-yl)guanine, have been identified after reacting BDO *in vitro* with guanosine.[1] 7-(2-hydroxy-3-buten-1-yl)guanine and 7-(2,3,4-trihydroxy-butan-1-yl)guanine have been detected in livers of B6C3F1 mice exposed to ^{14}C-BD.[2] To date, BDO_2-DNA adducts have not been characterized.

Methodology has been developed for the analysis of BDO adducts of purine 2' deoxynucleosides.[3,4] BDO was reacted with guanine (G) or adenine (A) at room temperature for 15 min in 0.1 M KOH solution. Unreacted BDO was removed by extraction with diethyl ether, and the resulting adducts were analyzed using LC/ESI MS/MS. Calf thymus DNA was reacted with BDO in phosphate buffered saline at 37 °C for 12 h. The DNA was then ethanol precipitated and hydrolyzed with 1 M HCl to release DNA bases.

LC/ESI MS/MS studies were conducted using a Finnigan TSQ-7000 interfaced with an HP series II liquid chromatograph. LC was conducted using a C8 column (4.6 mm x 250 mm; 5 um) maintained at room temperature with a flow rate of 500 uL/min. Solvent A was 5 mM aqueous ammonium acetate containing 0.01 % trifluoroacetic acid and solvent B was 5 mM ammonium acetate in methanol:water (9:1) containing 0.01 % trifluoroacetic acid. A linear gradient run as follows: 0 min, 5 % B; 2 min, 5 % B; 5 min, 15 % B; 20 min, 17 % B; 25 min, 50 % B; 30 min, 80 % B; 35 min, 90 % B; 40 min, 5 % B. Nitrogen was used as the sheath (70 psi) and auxiliary (20 psi) gas to assist with nebulization. A potential of 4.5 kV was applied to the ESI needle and the capillary was maintained at 240 °C in order to provide optimal desolvation of the ions generated by ESI. Mass spectrometer parameters were optimized, to obtain maximum sensitivity, without sacrificing unit resolution. MS/MS scanning was performed by setting the parameters in quadrupole 1 (Q1) to allow the parent ions (MH^+ ion of mono adducts of BDO, *m/z* 206 for A-BDO and *m/z* 222 for G-BDO) to traverse to quadrupole 2 (Q2). Collision induced dissociation (CID) was performed using argon, as the collision gas, at a pressure of 2.25×10^{-3} Torr in Q2. Quadrupole 3 (Q3) was scanned from 50 to 250 Da for the product ions generated from CID. Reaction of BDO with A resulted in seven A-BDO adducts with MH^+ ion *m/z* 206. CID was performed for ions with *m/z* 206 and product ion spectra recorded in Q3. A characteristic fragment ion with *m/z* 136, corresponding to the loss of BDO, was observed (Figure 1). LC/ESI MS/MS chromatogram of the ethanol supernatant, from calf thymus DNA incubated with BDO, showed two distinct peaks (Figure 2) corresponding to peaks 3 and 4. The preliminary evidence suggests that these adducts correspond to regioisomeric N-7 adducts for deoxyadenosine (dA) which can be spontaneously depurinated and released from the DNA backbone. These results are very encouraging and may help in the development of BD exposure biomarkers. LC/ESI MS/MS analysis of DNA hydrolyzate showed four distinct A-BDO adducts (Figure 3) which correspond to peaks 1, 2, 6 and 7. The absence of adducts 3 and 4, from DNA hydrolyzate, also strengthens the argument concerning spontaneous depurination of these adducts. We also have evidence for the formation of formamidopyrimidine (FAPY) adducts of A-BDO with MH^+ ions at *m/z* 224. Similar experiments were carried out with G. Eight G-BDO adducts were found by monitoring *m/z* 222. Two of these adducts were present in the ethanol supernatant of calf thymus DNA-BDO, and at least four adducts were present in the DNA hydrolyzate. In addition to these data, we also have some preliminary data suggesting the presence of cytosine-BDO and thymidine-BDO adducts in BDO treated calf thymus DNA.

Supported by Health Effects Institute 93-1.

43rd ASMS Conference on Mass Spectrometry and Allied Topics

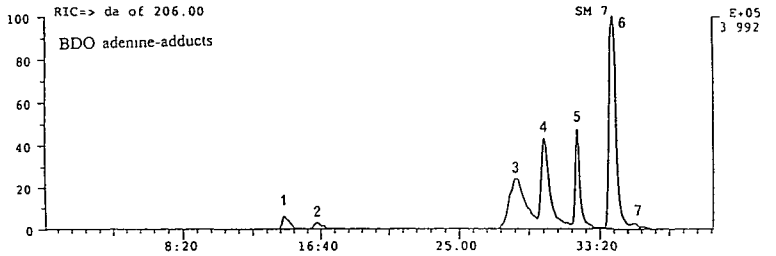

Figure 1: LC/ES/MS/MS chromatogram of reaction mixture of adenine with BDO. Product ions for *m/z* 206 (BDO-A adducts) were monitored.

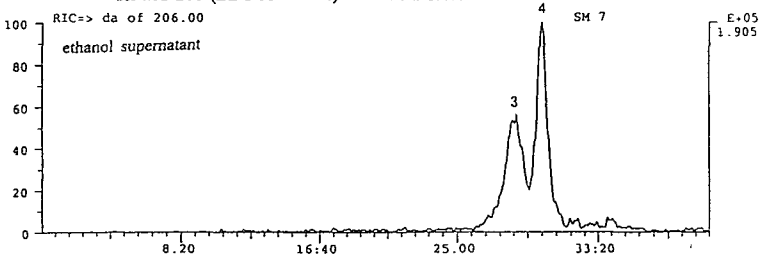

Figure 2: LC/ESI/MS/MS chromatogram of ethanol supernatant obtained after modification of calf thymus DNA with BDO followed by ethanol precipitation. Product ions for *m/z* 206 (BDO-A adducts) were monitored.

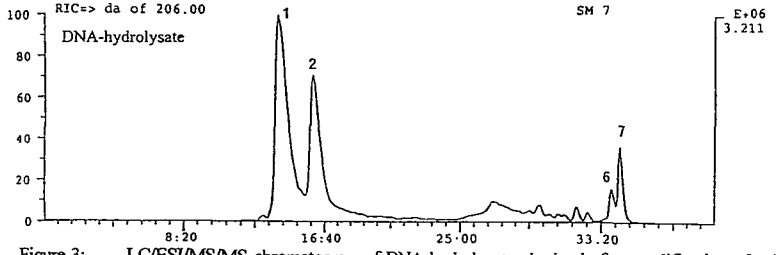

Figure 3: LC/ESI/MS/MS chromatogram of DNA hydrolyzate obtained after modification of calf thymus DNA with BDO followed acid hydrolysis. Product ions for *m/z* 206 (BDO-A adducts) were monitored.

1. Citti, L *et al*, *Carcinogenesis*, 5, (1984), 47-52.
2. Jehtto, B *et al*, *Biol Monitoring Arch Tox Suppl 13*, (1989) 246-249.
3. Chaudhary, A. K. *et al*, *J. Mass Spectrom*, In press, (1995).
4. Kambouris, S. J. *et al*, Eleventh Annual HEI Conference, April 30 - May 2, 1995.

A Study of Metal Ion Interactions with Nucleosides by LSIMS

G.J.C. Paul[1], T. Theophanides[1], J. Anastassopoulou[1], I. Marcotte[2], M.J. Bertrand[2], [1]National Technical University of Athens, Zografou 15780, Athens, Greece, [2]Department of Chemistry, University of Montreal, Montreal, Canada, H3C 3J7.

Metal ions have been implicated in vital biological processes involving DNA and its component parts such as DNA replication/transcription processes and metabolic reactions. As well as providing information on intrinsic cation binding tendencies, the characterization of metal ion interactions with nucleic acid components such as nucleosides may be useful when considering more complex real situations. In this study, the interactions of metal ions with cytidine and guanosine are probed by liquid secondary ion mass spectrometry (LSIMS) with glycerol/DMSO as the liquid matrix. Complementary gas phase collision-activated dissociation (CAD) was also performed using helium as the collision gas.

Considering the alkali metals (X = Li^+, Na^+, K^+, Rb^+, Cs^+), a typical LSIMS mass spectrum for cytidine/NaCl is shown in Figure 1. In the molecular ion region, the ions MH^+, MX^+ and $(M-H+X)X^+$ are observed. The presence of BHX^+ indicates that metal bonding takes place on the base and CAD with MX^+ as the precursor supports this. Likewise, CAD of $(M-H+X)X^+$, as shown in Figure 2, yields BX_2^+ which suggests that both proton substitution by an alkali metal and metal ion attachment occur at the base. For guanosine, it is thought substitution takes place at the most acidic N1 site, with binding of the alkali metal shared between O6 and N7. For cytidine, however, proton substitution by the metal is expected on the sugar portion and attachment at the N3 position. Gas phase rearrangement of $(M-H+X)X^+$ upon CAD with subsequent alkali metal attachment to N1 may explain the formation of BX_2^+ for cytidine systems (Figure 2).

A characteristic LSIMS mass spectrum for the alkali earth metals (Y = Mg^{2+}, Ca^{2+}, Ba^{2+}) and nucleosides is shown in Figure 3. The major ions incorporating both metal and nucleoside are $G(M-H+Y)^+$ and $MG(YZ)^+$ where Z = Cl^- or NO_3^-. The enhancement of these species over $(M-H+Y)^+$ and $M(YZ)^+$ in LSIMS shows the co-ordination of the metal provided by two molecules is favored over single nucleoside binding. CAD of $G(M-H+Y)^+$ yields BY^+ as the major product ion. Similar to the alkali metals, it is believed that substitution occurs at N1 for guanosine, while gas phase rearrangement occurs for cytidine complex where the metal ion migrates on the sugar to the N1 position of the base. LSIMS data involving D-ribose shows proton substitution from the sugar by an alkali earth metal can indeed take place. The CAD spectrum of $MG(YZ)^+$ reveals that the monovalent $(YZ)^+$ species attaches itself to the base since $BH(YZ)^+$ is observed. Interestingly, a small peak corresponding to $G(M-H+Y)^+$ is also present which shows gas phase decomposition can contribute to the formation of this species in LSIMS.

Unlike the alkali and alkali earth metals, the trends observed in LSIMS for the transition metals are found to be metal ion-dependent. For Fe^{2+}/nucleoside systems, the mass spectral features mirror those of the alkali earth metals where complexation involving $(FeZ)^+$ and $(M-H+Fe)^+$ occurs. The LSIMS mass spectrum for Co^{2+}/guanosine is shown in Figure 4. In addition to the typical complexes formed when the metal is in the divalent state,

43rd ASMS Conference on Mass Spectrometry and Allied Topics

ionic species which contain Co^+ (M_nCo^+, n=1,2) are also observed. It is supposed that Co^+ formation in LSIMS is a consequence of beam-induced reduction in solution and that the resultant metal ions bind to the nucleosides in a similar manner to the alkali metals, although $(M-H+Co)Co^+$ is not observed. Analogous behavior is observed in the LSIMS for the Ni^{2+}/nucleosides systems. For Cu^{2+}/nucleosides, bare copper ions in the monovalent state predominantly complex the nucleosides. Cu^{2+} is known to have a high reduction potential which may explain the preferential formation of monovalent metal ion complexes for this metal relative to the other transition metals. Interestingly, $(CuNO_3)^+$ complexes are also observed in the mass spectrum where copper is present in the divalent state. The CAD data obtained for the ionic transition metal/nucleoside species are consistent with that for the alkali and alkali earth metals.

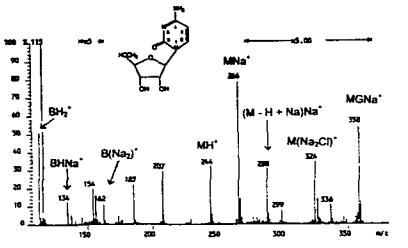

FIGURE 1

LSIMS MASS SPECTRUM OF CYTIDINE/NaCl

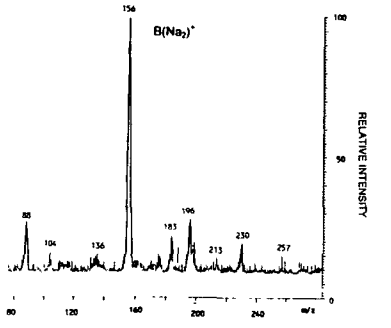

FIGURE 2:

CAD SPECTRUM OF (M-H+Na)+ WHERE M = CYTIDINE

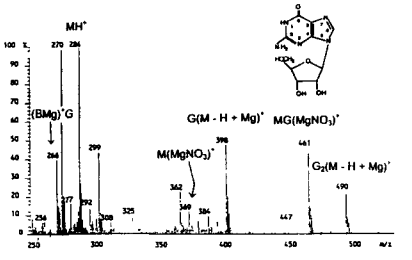

FIGURE 3:

LSIMS MASS SPECTRUM OF GUANOSINE/Mg(NO3)2

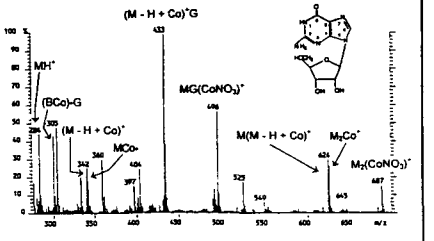

FIGURE 4:

LSIMS MASS SPECTRUM OF GUANOSINE/Co(NO3)2

GAS-PHASE CHEMISTRY OF COMPLEXES BETWEEN TRANSITION METAL(II) IONS AND NUCLEOSIDE MONOPHOSPHATES

Jill H. Hamilton and Jeanette Adams, Department of Chemistry and the Emory University Mass Spectrometry Center, Emory University, Atlanta, GA 30322

Experiments were conducted to determine: (1) the gas-phase structures of complexes between transition metal(II) ions and ribonucleoside monophosphates; (2) whether monophosphate Me^{2+} complexes, in which $Me^{2+} = Mn^{2+}$, Co^{2+}, and Ni^{2+}, reflect solution or gas-phase structures and chemistry. MS^2 and MS^3 experiments were performed using a JEOL JMS-SX102/102A/E five-sector tandem mass spectrometer.

Metastable ion decomposition experiments show that the lowest energy decomposition pathway is expulsion of the sugar. This fragmentation results in ions that contain the base (B), the metal ion (Me^{2+}), and the phosphate group (H_2PO_4) $(B + Me^{2+} + H_2PO_4)^+$ ions. CID results in ions containing the metal ion coordinated to either the base $(B + Me^{2+} - H)^+$ or to the phosphate group $(Me^{2+}H_2PO_4)^+$. MS^3 spectra of the first-generation $(B + Me^{2+} + H_2PO_4)^+$ ions show that the $(B + Me^{2+} - H)^+$ and $(Me^{2+}H_2PO_4)^+$ ions are formed by decompositions of $(B + Me^{2+} + H_2PO_4)^+$ ions.

CID experiments performed at different amounts of main beam reduction show that the rate of formation of $(B + Me^{2+} - H)^+$ ions ($Me^{2+} = Co^{2+}$ and Ni^{2+}) out-competes the rate of formation of $(Me^{2+}H_2PO_4)^+$ ions for GMP and CMP at all energies. The opposite is true for UMP.

The gas-phase data show that transition metal(II) ions form chelates with ribonucleoside monophosphates. Evidence for chelate formation is established from the formation of $(B + Me^{2+} + H_2PO_4)^+$ product ions. The population of precursors from which $(B + Me^{2+} + H_2PO_4)^+$ ions arise must contain the metal ion coordinated to the base and phosphate group (Structure 1a-b). Both Structures 1a and 1b can give rise to the $(B + Me^{2+} + H_2PO_4)^+$. It is unlikely, however, that the $(B + Me^{2+} - H)^+$ ions arise from Structure 1a. The $(B + Me^{2+} - H)^+$ ions can, however, arise from Structure 1b, in which the base has been deprotonated, and bound to the metal ion.

In solution, transition metal(II) ions bind to both the base, at (N7), and to the phosphate group of purine ribonucleoside monophosphates [1]. Three metal-ion coordinating modes have been observed: (1) one in which the metal ion is directly coordinated to (N7) of the base and indirectly (via molecules of water) to the phosphate group (Structure 2); (2) one in which the metal ion is indirectly coordinated to the base and indirectly to the phosphate; (3) one in which the metal ion is directly coordinated to the base and phosphate group [2]. In pyrimidine monophosphates, however, metal ions are only directly or indirectly coordinated to the phosphate group and do not interact with the base [2]. These solution structures are not observed in the gas phase.

These results show that the gas-phase structures of complexes between ribonucleoside monophosphates and transition metal(II) ions are not the same as in solution. Solvent effects mask the intrinsic binding chemistry between the metal(II) ion and ribonucleoside monophosphates, chemistry that involves expulsion of the sugar. Solvent molecules reduce the strain energy that would accompany chelate formation by forming water bridges and by filling the remaining coordination sphere of the metal(II) ion.

References

1. *Metal Ions in Genetic Information Transfer*; Eichhorn, G. L.; Marzilli, L. G. (Ed.). Elsevier North-Holland: New York 1981.
2. Sigel, H.; Massoud, S. S. *Inorg. Chem.* **1988**, *27*, 1447-1453.

43rd ASMS Conference on Mass Spectrometry and Allied Topics

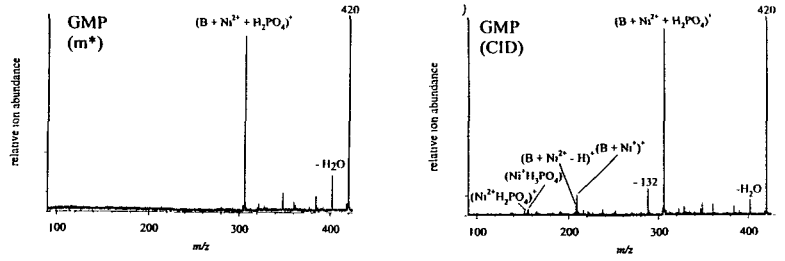

Figure 1. Metastable ion (m*) and CID spectra of $(M + Ni^{2+} - H)^+$ complexes of GMP.

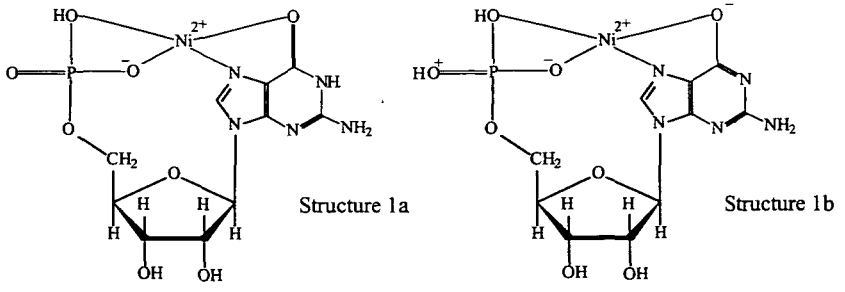

GMP

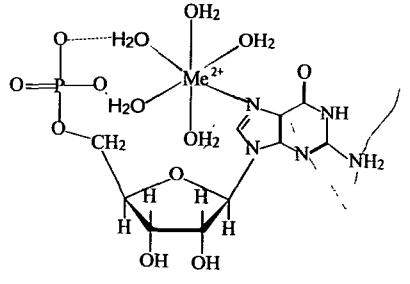

Structure 2

In situ digestion procedures and analysis of the digest by capillary HPLC/ESI/MS

R. Falchetto, J. Shabanowitz, J. Lamer, and D. F. Hunt
Departments of Chemistry, Pathology and Pharmacology, University of Virginia, Charlottesville, VA 22901

Introduction

One of the most common and powerful resolving techniques in biochemistry is SDS-polyacrylamide gel electrophoresis (SDS-PAGE). Handling of very small amounts of protein, which are resolved according to their molecular weights, is very convenient with SDS-PAGE and identification is possible by using easy staining procedures. Beside being a useful analytical tool, electrophoresis is also a powerful preparative technique. Proteins have been isolated from gels, digested by chemical or enzymatic methods, and the resulting peptides then fractionated and sequenced by Edman degradation. The method of choice has been to transfer the protein from the gel onto a solid support (1). We have combined these classical biochemical techniques with HPLC/ESI/MS analysis (2) of various proteins identified and isolated by SDS-PAGE, such as a drug-binding protein (3), transcription factors, tumor-specific proteins, and several others. To standardize our *in situ* proteolysis procedure, we have compared different kinds of digestion approaches and different types of membranes.

Methods and Results

Three types of transfer membrane were compared: PVDF, Nitrocellulose and Immobilon-CD (a PVDF-based membrane with a cationic surface). 140pmol of bovine ß-lactoglobulin were separated and transferred onto the membranes, cleaved *in situ* with 0.1µg trypsin, and aliquots of the digests analyzed by HPLC/ESI/MS. Protein immobilized on CD membranes was digested following the procedure described by Hess et al. (4) while protein immobilized on regular PVDF membranes was digested as described in (1) and (5). The amounts of peptide recovered from both membranes were approximately the same. However, the staining procedure for CD membranes was more cumbersome and less reliable than that used on PVDF membranes and, thus, CD membranes were not investigated any further. Next, two digestion procedures were compared on PVDF membranes: To prevent sequestering of the protease on "free" sites on the membrane the latter have to be blocked either by an inert polymer (PVP-40)(1,5) or by a detergent. We have chosen the hydrophilic detergent n-octylglucoside which is added to the digestion buffer at a 1% concentration. A small amount of this solution was added to the protein band for cleavage. Analysis of the digest by HPLC/ESI/MS, however, was severely hampered by the high amounts of detergent which eluted through the early part of the HPLC gradient and no reasonable comparison with the other digestion procedure could be done. Finally, digests of lactoglobulin on PVDF and nitrocellulose were compared using the procedure described in (1) and (5). The amounts of peptide recovered from the digests were plotted against those recovered in a solution digest of the same amount of lactoglobulin. Tryptic fragments were detected corresponding to 72% of the entire protein sequence.

The figure shows that PVDF gives better recovery than nitrocellulose (36% vs. 23%). Moreover, blank digests of membrane regions containing no protein showed a higher background generated by nitrocellulose membranes.

Data collected on 2.8pmol bovine lactoglobulin digested with trypsin (total initial amount 140 pmol)

Fragment #	Most abund. ion	CountsX10^6 Solution	CountsX10^6 PVDF	%	CountsX10^6 NC	%
1	467	38	7	18	4.3	11
				24{		12{
1(ox)	476	3.7	3.2	86	0.6	16
3	1355	8.3	0.7	8	0.18 2	
				11{		3{
3(ox)	1362	0.5	0.3	60	0.1	20
4	772	36	12	33	5.7	16
5,6	597	-	-	-	-	-
8,9	452	7	2 6	37	1.8	26
9	337	3.4	2.4	70	2	59
11,12	597	3.3	3	*90	1.9	*57
14,15	546	49	20	41	3	6
17	419	11	3.5	32	2	18
				34{		23{
17(ox)	427	0.17	0.27	160	0.6	353
18 + acrylam.	866	-	20		3	
Average % (*not included)		100		36		23

This technique has been useful in identifying the phosphorylation sites on pyruvate dehydrogenase isolated by SDS-PAGE and digested *in situ*, and helped determine which of these sites has physiological relevance in the inactivation of the enzyme (6).

(1) Aebersold, R. H., Leavitt, J., Saavedra, R. A., Hood, L. E., and Kent, S. B. H. (1987) Proc. Natl. Acad. Sci. USA 84, 6970-6974
(2) Hunt et al. (1992) Science 255, 1261-1263
(3) Hamlin et al. (1995) manuscript in preparation
(4) Hess et al. (1993) Prot. Sci. 2, 1342-1351
(5) Falchetto et al. (1994) Proceedings of the 42nd ASMS Conference on Mass Spectrometry and Allied Topics, Chicago, IL, May 29-June 3, 1994
(6) Abe et al. (1995) manuscript in preparation

ENZYMATIC FRAGMENTATION WITH IMMOBILIZED ENZYMES AND LC/MS ANALYSIS

Manfred Raida, Wolf-Georg Forssmann

Lower-Saxony Institute for Peptide Research (IPF)

Feodor-Lynen-Strasse 31, D - 30 625 Hannover, Germany

The LC / MS analysis of peptide fragments obtained by specific enzymatic or chemical cleavage, peptide mapping, is an indispensable tool for solving many analytical problems Amongst these are the identification of peptides or proteins by their typical fragment pattern, localization and characterization of posttranslational modifications, selection and characterization of fragments for overlapping sequence analysis, identification of genomic variants, analysis of synthetic peptides or recombinant proteins, and the assignment of disulfide bridges.

The fragments are usually obtained by cleavage in solution and then either applied directly to reversed-phase chromatography or freeze-dried to reduce the volume prior to separation These techniques have important limitations Large volumes of directly applied solutions have to be injected onto columns running at the low flow rates used in LC/MS analysis. Fragments may get lost due to adsorption on plastics. Autoproteolytic fragments of enzymes may result Nonspecific cleavage due to long incubation times may lead to errors in sequence analysis or in the interpretation of LC/MS analysis With unknown amounts of protein it is difficult to calculate an optimal enzyme : substrate ratio Particularly in the case of LC/MS analysis of low amounts of protein fragments these limitations lead to difficulties in the interpretation of results

The use of immobilized enzymes or enzyme microreactors helps to overcome the majority of these limitations In the recent years several attempts have been made to use immobilized enzymes in protein and peptide analysis. In many cases agarose or acrylamide based gels were used which are not compatible with high flow rates or increased pressure. The use of enzymes bound to wide-pore materials opens up new paths in the use of immobilized enzymes and the analysis of minor amounts of proteins and peptides.

In the experiments described here, synthetic large-pore materials with immobilized trypsin (POROSzyme, Perseptive Biotechnologies, USA) was used. The column used for the experiments is a 2.1 x 10 mm pressure stable column which allows high flow rates. Standard HPLC equipment with a minimal flow rate of 25 µl / min is used to transfer the peptides through the trypsin microreactor to the consecutive separation on 1 x 250 mm C-18 column The chromatographic separation was carried out using a double syringe pump with a flow rate of 20 µl / min, and a standard water / TFA and acetonitrile / TFA gradient system with an increase of 1 % per min. The column outlet was directly connected through a UV detector equipped with a capillary Z-cell to the electrospray interface of a triple-stage quadrupole mass spectrometer (API III, SCIEX, Toronto, Canada).

Horse hemoglobin or horse heart cytochrome C were chosen as test proteins for the experiments presented here. Concentrations of 1 µg / µl to 0 01 µg / µl were used in the experiments, the digestion buffers and transfer buffers were 50 mM / l ammonium acetate or ammonium formiate with 5 % methanol and a pH of 8.1 or 7 0. The trypsin microreactor was kept at 37° C throughout the experiment The eluate

from the trypsin microreactor was either collected and lyophilized for further separation or transferred on-line onto the C-18 separation column with a flow rate of 25 µl / min. After the total transfer of the protein, the separation column was equilibrated with 0 06 % TFA in 10 % acetonitrile and then connected with the separation HPLC and the electrospray interface.

The total digest of the protein was achieved within 30 minutes at a flow rate of 25 µl / min and a concentration of 0 1 µg / µl. Both increased flow rates or increased concentrations led to incomplete cleavage. Nevertheless all expected fragments could be observed even at high concentrations and flow rates alongside the intact protein. In on-line experiments the fragments of 20 pM cytochrome C could be identifed clearly by LC / MS using 1 mm ID columns.

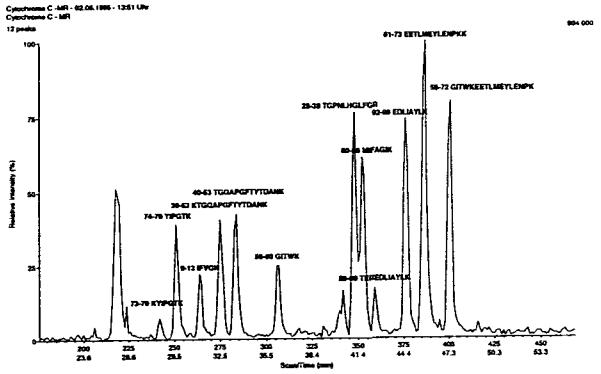

Figure: Total ion chromatogram of the tryptic fragments of 20 pM cytochrome C. The intact protein was transferred at a flow rate of 25 µl / min through the trypsin microreactor onto the 1 x 250 mm C-18 separation column and the fragments eluted by a linear water/TFA to acetonitrile/TFA gradient at 20 µl / min.

In the example shown here, all expected tryptic fragments from cytochrome C above four amino acids could be detected in the LC / MS analysis. The experiments were performed within 2 hours

The experiments show that enzymatic microreactors help to overcome the limitations of enzymatic digestion in solution and to increase sensitivity in the detection. In the experiments presented here the tryptic digest of cytochrome C was obtained within 30 minutes, nonspecific cleavage or autoproteolytic fragments were not observed.

Separation and Manipulation of Proteins using Polymeric μ-HPLC Columns On-line with Electrospray Ionization/Mass Spectrometry

Mark E. Hail[1], Bethanne M. Warrack[1], Susan C. Taylor[1], Sam Baldwin[2], Ken Stoney[2], and Mike S. Lee[1]

[1]Bristol-Myers Squibb Pharmaceutical Research Institute, P.O. Box 4000, Princeton, NJ 08543
[2]Michrom BioResources, Inc., 1945 Industrial Drive, Auburn, CA 95603

In the pharmaceutical industry, there has been expanding interest in the structural characterization of proteins, since proteins are most often the targets of new therapeutic drugs. Electrospray ionization mass spectrometry (ESI/MS) is unique when compared to other structurally informative methods (e.g. NMR or X-ray crystallography) in that information can be obtained rapidly on small quantities of sample. Unfortunately, the luxury rarely exists that the sample is highly pure or is dissolved in a solvent that is optimal for ESI/MS. For example, highly aqueous solutions or those containing high concentrations of involatile salts or detergents, often lead to poor signal-to-noise if direct sample infusion is attempted. In addition, protein mixtures often result in uninterpretable ESI/MS data due to overlap of the multiply charged ion envelopes.

For these reasons, we have developed methods using on-line ESI/LC/MS for protein/peptide characterization. Our strategy has focused on the use of 300-4000 Å polymeric (polystyrene divinylbenzene) microbore HPLC columns for separation and short polymeric protein/peptide "trap cartridges" for rapid desalting or preconcentration of biomolecules. It was found that utilization of these polymeric HPLC columns resulted in improved signal-to-noise and mass accuracy relative to infusion analysis, particularly for samples containing salts or protein mixtures. The polymeric packings are exceedingly rugged and are not harmed by injections of 70% formic acid, which is used after each analysis to wash remaining adsorbed protein from the columns and traps, preventing sample carryover.

Examples of the applicability of these methods to large hydrophobic proteins include cytosolic phospholipase A_2 ($cPLA_2$) and the microsomal triglyceride transport protein (MTP). $cPLA_2$ is an 85 kDa phosphorylated protein which is involved in the production of prostaglandins, and is thus the target of new anti-inflammatory drugs. ESI/LC/MS analysis of $cPLA_2$ revealed the existence of five peaks separated by 80 Da at the expected MW of this protein which indicates the presence of at least four possible phosphorylated residues. MTP is a noncovalently-bound heterodimer consisting of 55 kDa protein disulfide isomerase and a larger subunit with a MW of 97 kDa. Using polymeric μ-HPLC combined with ESI/MS we were able to separate these two subunits and deduce the origin of modification in this protein, which was yielding two slightly different active forms when purified from bovine liver. The two forms of the protein were found to be different on the large subunit due to C-terminal processing of the last two residues.

For situations when sample quantity is very limited, we have begun to evaluate a new enzymatic digestion method for peptide mapping experiments, whereby a protein can be injected and preconcentrated on a polymeric "trap cartridge" followed by digestion *in situ*. This work is similar to a previous study by Burkhart et al., who investigated digestion of proteins from enzymes immobilized on Poros™ columns (1). We have expanded these studies to investigate the more convenient "trap cartridges", which allow rapid buffer exchange and/or sample manipulation requiring only a syringe. The goal is to take advantage of the sample preconcentration ability of these "traps" and to eliminate the sample losses that occur during the many manipulation and transfer steps that are required for typical solution digestion procedures (e.g. buffer exchange, reduction, alkylation, etc.). Our early results indicated that *in situ* digestion with Lys-C protease yielded results comparable to those obtained from solution digests, with the *in situ* method resulting in the production of more partially digested fragments. However, as shown in Figures 1 and 2, the *in situ* digest is more complete and results in higher recovery of peptides when small quantities of

protein are used in the digestions. This is probably due to the avoidance of sample loss with the *in situ* method. In a separate experiment depicted in Figure 3, a complete peptide map of lysozyme was obtained after *in situ* reduction of its four disulfide bonds and subsequent digestion of the protein with Lys-C. Interestingly, when trypsin was used no digestion was observed for a number of test proteins under a variety of conditions. This suggests that results from digestions *in situ* will be dependent on how the protease is adsorbed to the packing (e.g. accessibility of enzyme active site).

In summary, the small polymeric "trap cartridges" and columns are a convenient means of preconcentrating, separating, and manipulating proteins for analysis by ESI/MS. The packings are exceedingly rugged and are ideally suited for high throughput analyses. It is also anticipated that these trap/alkylate/digest/elute *in situ* methods will allow future implementation of automation.

Reference:

(1) Burkhart, W., (1993) *In* "Techniques in Protein Chemistry IV" (Angelletti, R. ed.) 399-406.

Figure 1. *ESI/LC/MS base peak chromatogram of in situ 50 pmole Lys-C digest of cytochrome C.*

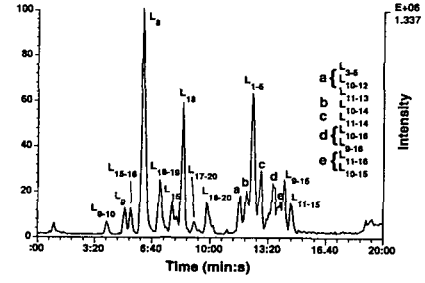

Figure 2. *ESI/LC/MS base peak chromatogram of solution Lys-C digest of cytochrome C performed with 50 pmoles total protein.*

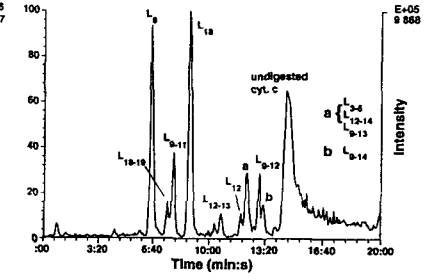

Figure 3. ESI/LC/MS base peak chromatogram of 50 pmole analysis of lysozyme which was reduced and digested with Lys-C *in situ*.

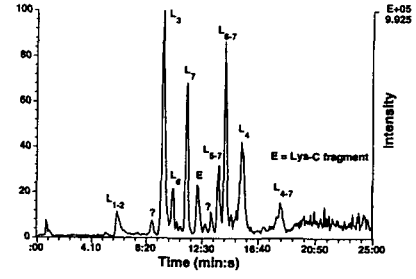

Comparison of a Quadrupole MS to a Reflectron TOF MS with Electrospray Ionization

Anatoli Verentchikov*, Frank Hsieh, Michael Tomany,
Stephen Gabeler, Marvin Vestal, Stephen Martin
PerSeptive Biosystems, Inc., 500 Old Connecticut Path, Framingham, MA 01701

The identification and characterization of novel factors of biological significance require the isolation, purification, and enzymatic digestion of smaller and smaller amounts of material. Integral strategies are being developed to reduce the sample quantity and volume, including immobilized reagents and capillary columns. These strategies require that the specifications of the mass analyzer include simultaneous sensitivity, resolution, mass range, scan speed, and mass accuracy.

A comparison was made between a quadrupole mass spectrometer and an orthogonal deflection - reflectron time of flight mass spectrometer [1] for these specifications when used in the analysis of peptides and proteins using electrospray ionization. The comparison was made using constant infusion, direct injection, and on-line LC methods.

Figure 1 shows the simultaneous sensitivity and resolution of the time of flight instrument with 5 femtomole of neurotensin (1673 amu) consumed. Figure 2 shows good sensitivity with a quadrupole at low resolution (below isotopic) and figure 3 shows marginal sensitivity when the quadrupole is tuned to resolve the isotopes. In both Figures 2 and 3, the mass range of the quadrupole instrument was reduced to 500 amu to achieve these results. The mass range of the time of flight analyzer shown in Figure 4 is well beyond the capabilities of the quadrupole tested (2400 amu). This spectrum repeats the work of reference [2]. Figures 5 and 6 compares the ultimate resolution achievable on both instruments for the +4 charge state of Melitin (2844.6 amu). Time of flight resolution was greater than 5000. Figure 7 is the TIC chromatogram of an immobilized enzyme digestion of Myoglobin followed by reverse phase LC separation at 1 second per full mass range scan [1]. The chromatographic separation produced 13 second peaks which are well sampled at 1 second per scan. The time of flight analyzer is well suited for LC/LC/MS experiments by providing this rapid scanning, full mass range detection, and isotopic resolution of the multiply charged proteolytic peptides. To obtain the same resolution and mass range using the quadrupole analyzer, the scan time required for high resolution became incompatible with the time scale of the reverse phase separation. Mass accuracy's were evaluated by measuring the standard deviation of mass determinations from each charge state of a multiply charged protein. Using 3 sigma for a 99% confidence, the quadrupole showed about 450 ppm (0.045%) and the time of flight showed about 50 ppm (0.005%). The accuracy and resolution of the time of flight instrument made molecular weight determinations much easier and reliable. Being able to resolve the isotopic distributions and their spacings makes the determination of charge state simple and direct as well as giving confirmation based on the isotope distribution pattern.

[1] A. Verentchikov et.al. Proceedings of the 42nd ASMS conference on Mass Spectrometry and Allied Topics, May 29 - June 3, 1994, Chicago IL, p. 773
[2] Xue-Jun Tang et.al. Rapid Communications in Mass Spectrometry, Vol. 8, 750-754 (1994)

5 femtomol of neurotensin consumed

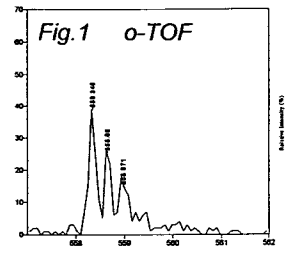

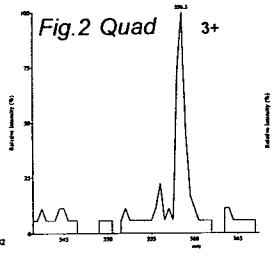

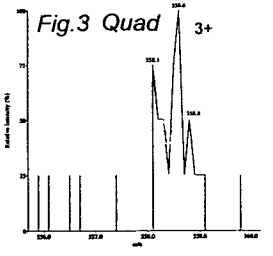

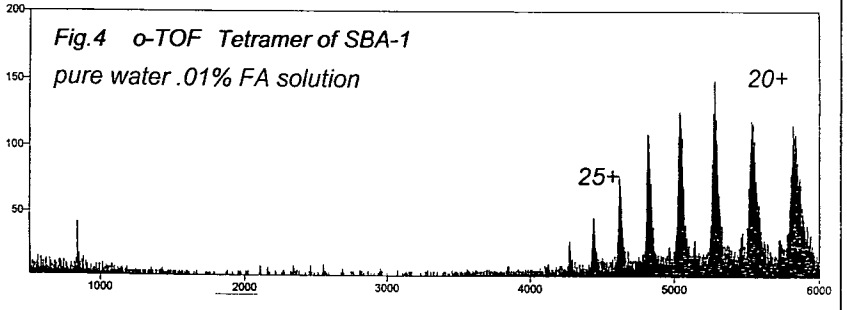

Ultimate resolution. Melittin 4+

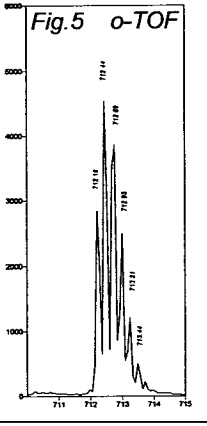

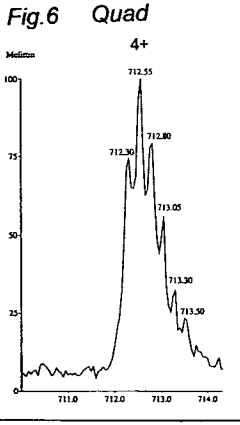

Fig.7 o-TOF On line Digest /LC/MS

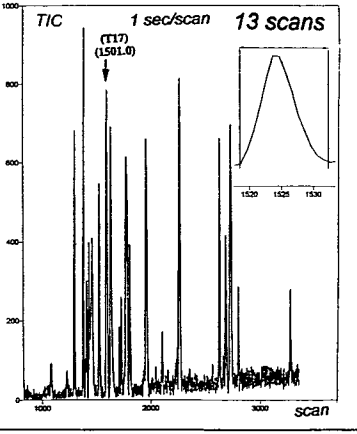

Peptide Mapping on a Nitrocellulose Membrane with Analysis by Matrix-Assisted Laser Desorption/Ionization Mass Spectrometry by Jian Bai, Mark G. Qian, Yanhui Liu, Xiaoli Liang and David M. Lubman, Department of Chemistry, The University of Michigan, Ann Arbor, MI 48109

Introduction It has been shown that proteins bound to membranes are amenable to chemical/enzymatic digestion followed by MALDI MS analysis for the identification of proteins, peptide mapping, and localization of modifications **(1-3)**. In the present work, we examine the use of nitrocellulose (NC) membrane for the mapping of CNBr peptides by MALDI/MS and compare nitrocellulose with Immobilon-N and Immobilon-CD membranes. NC is found to be versatile in such analyses due to its excellent retention of both small and large fragments during digestion and washing.

Experimental 1-D SDS-PAGE, electroblotting, and staining were performed under standard conditions. The thoroughly destained protein bands were cut into small pieces and washed before digestion in 10 µl of CNBr (0.5 M in 0.1 N HCl). The CNBr fragments still on the membrane were washed thoroughly, then extracted from the membranes with 10 µl of CHCA in water/acetonitrile (up to 2:3) with TFA (1.25 %). 2.5 µl of the extracts was applied and dried on the probe tip before MALDI MS analysis. An improved recovery procedure of CNBr peptides **(4)** from NC membrane using a dissolution method was also reported here In this method, CHCA prepared in acetone (1% TFA) was used to dissolve the NC for peptides recovering.

Results and discussion The NC membrane has better retention properties for both large and smaller CNBr fragments generated from the above procedures, and were not affected by additional reaction steps such as reduction/alkylation and additional washings. There is a loss of smaller CNBr fragments, and selective loss of larger CNBr fragments with Immobilon-CD and Immobilon-N membranes (Figure 1a & b) Direct extraction of the CNBr fragments from membranes without washing the membrane improved the recovery of smaller fragments; spurious and uninterpretable peaks arise in the MALDI/MS spectrum for β-casein in the case of using Immobilon-CD. Washing the membranes after digestion significantly improves the quality of the MALDI MS signal, particularly when low level proteins are digested on the membrane

CNBr digestion on the NC membrane can provide a better and direct means for further characterization of electroblotted proteins using MALDI MS. The extraction efficiency of the CNBr peptides from NC with the above described matrix/solvent system is still low This is demonstrated by comparing the result from the dissolution method (Figure 2a & b), where dramatically improved extraction efficiency was achieved. This method has been proven to be very effective for recovering proteins and their digests for MALDI MS analysis **(4)**

Conclusion MALDI/MS can provide a general means for the characterization of electroblotted proteins on membranes by incorporating chemical digestion methods directly on the membrane A nitrocellulose membrane with moderate binding capacity and excellent retention for both small and large fragments, is advantageous in cases where multiple reaction and washing steps are used. It effectively eliminates possible cross contamination between reactions and contamination at the final stage before MALDI/MS analysis. The incorporation of MALDI/MS with the membrane immobilization technique has provided a fast and effective means of peptide mapping based on chemical digestion without the use of conventional separation or fractionation methods.

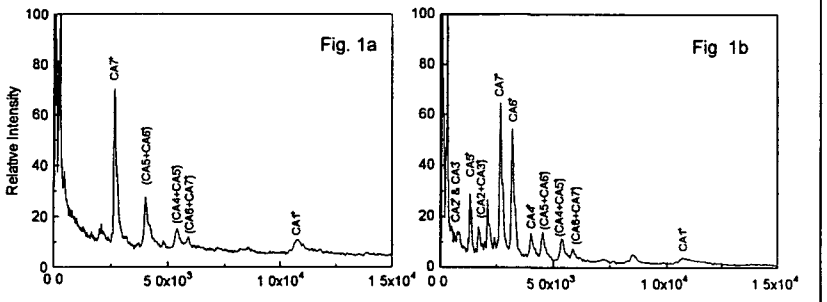

Figure 1. MALDI MS spectra of the CNBr peptides of β-casein on (a) Immobilon-CD and (b) nitrocellulose membranes

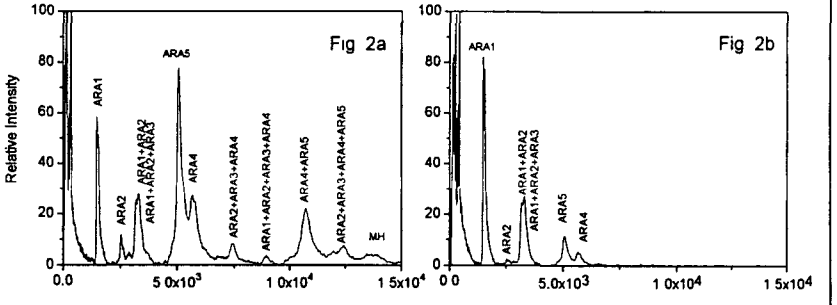

Figure 2. MALDI MS spectra of the CNBr peptides of alkylated ribonuclease A on nitrocellulose with (a) the dissolution and (b) the extraction methods

References:

(1). Zhang, W.; Czernik, A. J., Yungwirth, T.; Aebersold, R., Chait, B. T., *Protein Sci* **1994**, *3*, 677-686.

(2). Henzel, W. J ; Billeci, T. M.; Stults, J. T.; Wong, S. C., Grimley, C.; Watanabe, C.; *Proc. Natl. Acad. Sci. USA*. **1993**, *90*, 5011-5015.

(3). Klarskov, K.; Roepstorff, P ; *Biol. Mass Spectrom.* **1993**, *22*, 433-440.

(4). Xiaoli Liang, Jian Bai, Yan-Hui Liu, and David M. Lubman, Manuscript in preparation.

Rapid Identification of Variant Enzymes from Commercial Detergent Products

M P Lacey, T Keough, Y Sun, M D Bauer, R A Grant, C.B. Bennett and A M Fieno
The Procter and Gamble Company, Miami Valley Laboratories
P O. Box 538707, Cincinnati, OH 45253-8707

Commercial laundry products are complex mixtures of cleaning agents. These mixtures typically consist of surfactants, builders, soil release agents, bleaches and enzymes. The most common enzymes used in these mixtures are a group of alkaline proteases known as subtilisins[1] Subtilisins have been extensively engineered to make them more suitable for laundry applications. The characterization of these enzymes can be accomplished with a variety of techniques. In the following two examples, various mass spectrometry methods (MALDI, PDMS, ESI, FAB, oa-TOF) are used in conjunction with chemical and enzymatic digestions to quickly identify specific mutations found in enzymes from commercial products.

Enzyme A

Enzyme A was isolated from a laundry detergent purchased in Japan. After purifying the enzyme with HPLC, a portion of the enzyme was sequenced to determine the N-terminal amino acids. The first 28 cycles were identical to Savinase®, a common detergent protease Ionspray analysis of the intact enzyme gave a molecular mass of 26,724.5, quite different from that expected for Savinase (26,699 6). The intact enzyme was digested with cyanogen bromide in 0 1N HCl for 2 hours at 37°C in the dark. Subsequent ionspray analyses of the purified fragments are shown in the table below

Residues	Enzyme A	Savinase	Δ
1-117	11,405 3	11,406.6	+1 3
118-169	5,013 4	5,013.5	+0 1
170-216	4,705 3	4,706 0	+0 7
217-269	5,512.8	5,488 2	+24 6

The isolate containing residues 217-269 was sub-digested with trypsin (1μg, 0.1M NH_4Ac, pH=8 2, 37°C, 30 minutes) The resulting mixture was analyzed by PDMS and the table below summarizes the results

Residues	Enzyme A	Savinase	Δ
217-229	1234 4	1206.4	+28 9
230-241	1458 3	1457 6	+0 7
242-245	511 7	511 6	+0 1
246-269	2367 4	2369 6	-2.2

The mass difference of +28 in residues 217-229 could be a result of several single site mutations: A→V, Q→R, K→R, S→D, C→M and T→E. Several of these could be ruled out immediately due to lack of C, S and Q in the original sequence of this fragment However, a double mutation was also a possibility. Residues 246-269 also had a mass difference of -2 2. Although this is within the mass error of the instrument, we routinely get accuracies of ±1 Da in this mass range Therefore, we submitted both fractions for Edman sequencing The Edman sequencing results confirmed a single mutation in residues 217-229 and a double mutation in residues 246-269

217-229 ATPHVAGVAALVK
246-269 NTATGLGNTNLYGSGLVNAEAATR

Therefore, the enzyme in this product was identified as a triple mutant of Savinase: A224V, S250G and S253N

Enzyme B

Enzyme B was isolated from a European laundry detergent. The intact molecular weight was found to be 26,824.8. Subsequent CNBr digestion and analysis of the isolated fragments gave peptides with the following molecular weights: 11,501 3, 5487 5, 5,043.7 and 4,707.1 These values were entered into MassMap®, a program from Finnigan MAT Ltd. used to search databases of digestion products that had been calculated according to specific cleavage rules[2] The results of the search gave three possible subtilisins as candidates. Of the three, only Subtilisin BL Alkaline Protease, or BLAP[3], had a molecular weight consistent with our measured value.

To confirm this identification, we digested the intact enzyme with a new immobilized trypsin column from PerSeptive Biosystems (Cambridge, MA). Intact enzyme B was passed through the Poroszyme® trypsin column in a buffer of 0.1 M ammonium acetate, pH = 8 2 at 50 μl/min. The resulting mixture was analyzed by PDMS . Using these measured masses, the MassMap search of the tryptic peptides also identified the enzyme as the BLAP protease. Merging the results of the CNBr and tryptic digests gave only three possibilities, all subtilisins, with the highest score given to BLAP. The results of the tryptic digest of enzyme B are summarized below·

Fragment	Residues	Enzyme B	BLAP
T1	1-10	1,102 0	1,101 3
T2	11-19	965.3	964.1
T3	20-27	719 0	718.8
T4	28-44	1,823 1	1,822.1
T5	45-92	4,591 1	4,591 1
T6	93-99	688 8	687 8
T7	100-143	4,355.0	4,353.8
T8	144-164	1,965 5	1,964.2
T9	165-180	1,713 4	1,710 8
T10	181-229	4,798 3	4,800 4
T11	230-231	n d.	275.3
T11 & T12	230-241	1,458 6	1,457 6
T12	232-241	1,202.7	1,201.3
T13	242-245	n.d.	511 6
T14	245-269	2,370 6	2,369 6

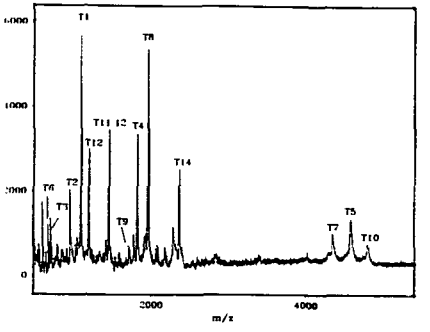

PD mass spectrum of tryptic digest of enzyme B

Conclusions

We have used several mass spectrometry methods along with enzymatic and chemical digestions to identify the enzymes present in commercial detergent products. Enzyme A was identified as a triple mutant of Savinase· A224V, S250G and S253N. We identified enzyme B as the BLAP protease, an enzyme identical to Savinase, but with five mutations: S97D, S99R, S101A, V102I and G157S. We have successfully applied these methods to many other products from all global regions, and have identified both wild-type enzymes and enzymes that contained only single-site mutations.

References

1. Wells, J.A. and Estell, D.A., **Trends Biochem. Sci. 13**, 291-297 (1988).
2. Pappin, D.J C., Højrup, P. and Bleasby, A.J., **Current Biology, 3**, 327-332 (1993)
3. Goddette, D.W., Paech, C., Yang, S.S., Mielenz, J.R., Bystroff, C., Wilke, M.E. and Fletterick, R.J., **J. Mol.Biol. 228**, 580-595 (1992).

HPLC-ESI Ion Trap MS/MS Analysis of Proteins separated by 2D-PAGE

Michiko Kanai[1], Kazuo Seta[1),2], Hiroshi Nakayama[2], Toshiaki Isobe[2], Tsuneo Okuyama[2], Adrian Land[3] and Mark Bier[3]
1) Finnigan MAT Instruments, Inc 2-5-8 Hatsudai, Shibuya-ku, Tokyo 151, Japan
2) Tokyo Metropolitan University, Hachioji-shi, Tokyo 192-03, Japan
3) Finnigan MAT, 355 River Oaks Parkway, San Jose, CA 95134-1991

Introduction

Two dimensional polyacrylamide gel electrophoresis (2D-PAGE) is widely used for the high resolution analysis of complex protein mixtures. It is also used for preparative purposes, for instance, to obtain gene probe sequence. We previously developed a sensitive two step method for the structural analysis of proteins. The first step is 2D-PAGE separation followed by extraction of a stained protein spot from the gel The second step is the analysis digest of the protein using a capillary HPLC-ESIMS and MS/MS. We have utilized a newly developed bench top HPLC-Ion Trap MS^n system with this methodology for the identification of proteins in rat cerebellar extracts.

Experimental

Mass spectrometer: A Finngan MAT LCQ system equipped with an ESI source was used

Sample preparation: (1) A protein mixture extracted from rat cellebella was subjected to a 2D-PAGE (10 cm x 14 cm) separation. (2) Copper staining had to be used to visualize protein spots on the slab gel, since the recovery was higher than other staining methods (3) A spot was cut out from the slab gel and transfered into a polypropylene tube (4) The copper was removed from the gel piece with 0.025 M Tris-Gly buffer (pH 8.3) (5) The protein was extracted from the gel piece by shaking for 10 hours with 0 1 M Tris-Gly buffer (pH 8 8) containing 0 1 % SDS and EDTA. (6) An extract was subjected to a reversed-phase HPLC purification with a small column in order to remove contaminants from the slab gel and the reagents (7) A protein fraction was collected and the mobile phase was evaporated. (8) The protein was digested using Lys-C endoproteinase and then subjected to HPLC-ESI MS^n analyses.

HPLC conditions: A 1 mm x 150 mm ODS column was used. A 35 minute linear gradient elution from 100 %A (A 0 1 % TFA in water) to 70 %B (B 0.09 % TFA in water/acetonitrile = 1/9) was performed. The flow rate was 40 µl/min and the effluent was introduced directly into the ESI source

ESI conditions: The spray voltage was 4 5 kV.; N_2 was used for both the sheath gas (60 psi) and the auxiliary gas (5 unit) , A heated capillary was operated at a temperature of 200°C

Ion trap conditions: Ion injection time was 50 msec , Scan range was 300 - 1700 amu with 5µscans

Results and Discussion

The spot #246 in a brain protein map had previously been determined to be stathmin using HPLC-ESIMS/MS with the triple quadrupole mass spectrometer, an amino acid sequencer and a data base search Figure 1 shows HPLC-ESIMS chromatograms of Lys-C digests derived from the spot #246 (stathmin) and the spot #247 (unknown) The molecular weights of the two peaks indicated by ↓ differed by 80 Da, but the molecular weights of all other peaks were identical Since the spot #247 was observed to be more acidic than the spot #246 (stathmin) on the 2D-PAGE separation, it suggests that the spot #247 is phosphorylated stathmin. The two peptides indicated by ↓ correspond to Lys-C fragment 4 (29-40, ESVPEFPLSPPK) Figure 2 shows the MS/MS spectrum of Lys-C fragment 4 from the spot #247. This spectrum shows that the 37th Ser is phosphorylated This spectrum was obtained using a data dependent

experiment, which automatically performed zoom scans, MS/MS and MS/MS/MS of base peaks whose intensities were above threshold. As sufficient structural information could be obtained from this experiment, it is possible to eliminate peptide mapping using a normal MS scan, and hence reduce sample consumption. Enough material for structural analyses of proteins by HPLC-ESI MS^n with an ion trap mass spectrometer could be obtained from only one or two pieces of slab gel

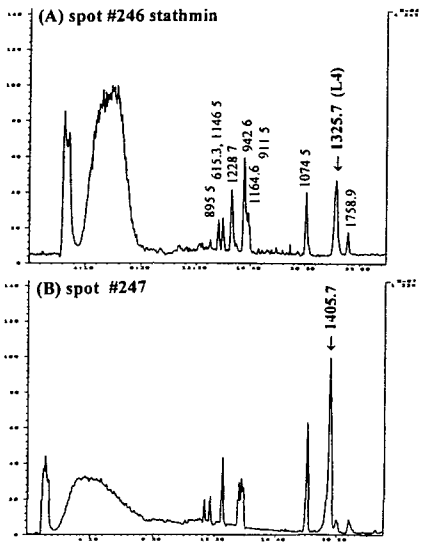

Figure 1
HPLC-ESIMS chromatograms of Lys-C digests of (A) spot #246 and (B) spot #247

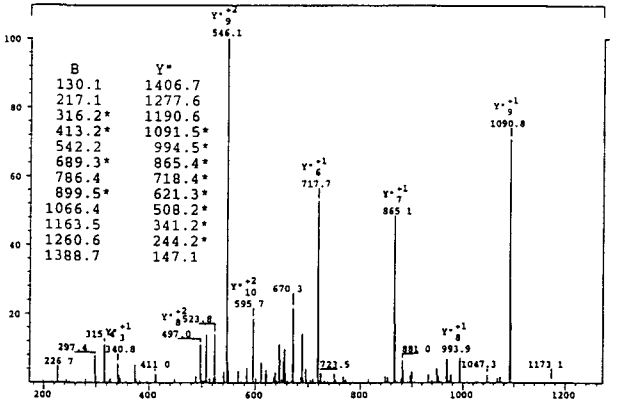

Figure 2. MS/MS spectrum of $(M+2H)^{2+}$ of L4 from the spot #247.

Strategies for Identification of 2D Gel Proteins by Mass Spectrometry

Karl R. Clauser and Alma L. Burlingame
Department of Pharmaceutical Chemistry, Box 0446
University of California
San Francisco, CA 94143-0446

2D PAGE allows simultaneous separation and visualization of the myriad proteins present in a whole cell lysate, but requires protein identification to decipher the gel's information content. 2D PAGE difference mapping, i.e. comparing the lysates from: a) drug-treated cells vs. untreated cells, or b) diseased vs. healthy cells, is particularly useful when there are many differences in the proteins expressed and/or there is no way of isolating particular proteins in a more specific manner.

Peptide-mass "fingerprints" obtained by using MALDI to measure the peptide masses present in the enzymatic digest of a protein have been shown to be frequently capable of predicting the identities of proteins whose sequence already exists in a database (1-4). If a protein is truly an unknown, its sequence will not be in a database. Characterization of such a protein can then be done by obtaining peptide sequence, and cloning the gene. However, the growth of sequence databases fueled by the Human Genome Project will increasingly reduce the chances of discovering unknown proteins, and the ability to unambiguosly identify a protein through a database search will require data of increasing discriminating power. While peptide sequence data can establish protein identity with a high degree of certainty, peptide-mass data alone can predict protein identity with some ambiguity and / or uncertainty (5).

What remains to be seen is: can mass spectrometric approaches produce "fingerprint" data that yield information somewhere between the levels of complete peptide sequences and peptide masses alone which continue to give enough database discrimination power to routinely produce high-certainty protein identifications? Toward that end, we have sought to use MALDI in a reflectron instrument, VG TofSpec SE, to obtain peptide sequences from post-source decay (PSD) spectra. The unseparated peptides recovered from in-gel digestion of a 2D PAGE spot were applied to a MALDI target, selected parent ions were transmitted into the reflectron using an ion-gate, and PSD spectra of the products were obtained.

(1) Henzel, W. J.; Billeci, T. M.; Stults, J. T.; Wong, S. C.; Grimley, C.; & Watanabe, C. (1993) *Proc. Natl. Acad. Sci. USA* **90**, 5011-5015.
(2) Mann, M.; Hojrup, P.; & Roepstorff, P. (1993) *Biol. Mass Spectrom.* **22**, 338-345.
(3) Pappin, D.J.; Hojrup, P.; & Bleasby, A.J. (1993) *Curr. Biol.* **3**, 327-332.
(4) Yates, J.R.; Speicher, S.; Griffin, P.R.; & Hunkapiller, T. *Anal. Biochem.*, **1993** (214) 397-408.
(5) Clauser, K.R.; Hall, S.C.; Smith, D.M.; Webb, J.W.; Andrews, L.E.; Tran, H.M.; Epstein, L.E.; & Burlingame, A.L. (1995) *Proc. Natl. Acad. Sci. USA* **92**, 5072-5076.

Financial support for this work was provided by NIH NCRR (Grant RR01614), the NSF Biological Instrumentation Program (Grant 8700766), the NIEHS Superfund Program (Grant E504705), UC TRDRP (Grant 2RT0089), NIH Grant CA 27903, and a UC Systemwide Biotechnology Grant.

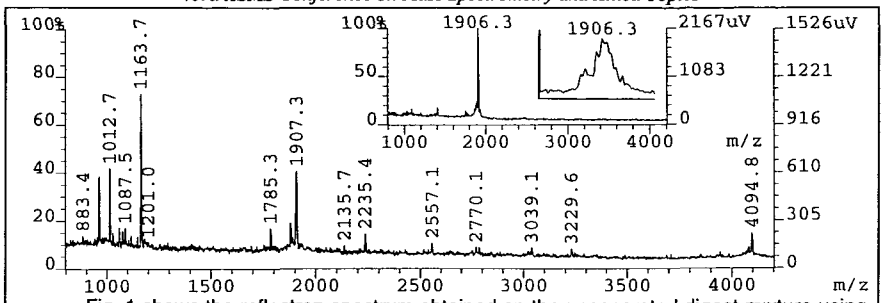

Fig. 1 shows the reflectron spectrum obtained on the unseparated digest mixture using an α-cyano-4-hydoxycinnamic acid matrix. By setting the ion-gate to 1907 Da, a ~15 Da mass window is selectively transmitted to the reflectron (Fig. 1 inset). Expansion of the region around the selected parent ion, reveals that two species (1906 Da and 1903 Da) are actually passed through the gate. The data obtained from the unseparated digest, were used as a peptide-mass fingerprint to search the Swiss-Prot database using PeptideScan (2). The highest scoring protein from this search, Heat -shock Protein 27 (HSP-27), contains a tryptic peptide of MH^+ = 1906.0, LATQSNEITIPVTFESR (□) and one of MH^+ = 1902.9, GPSWDPFRDWYPHSR (Δ).

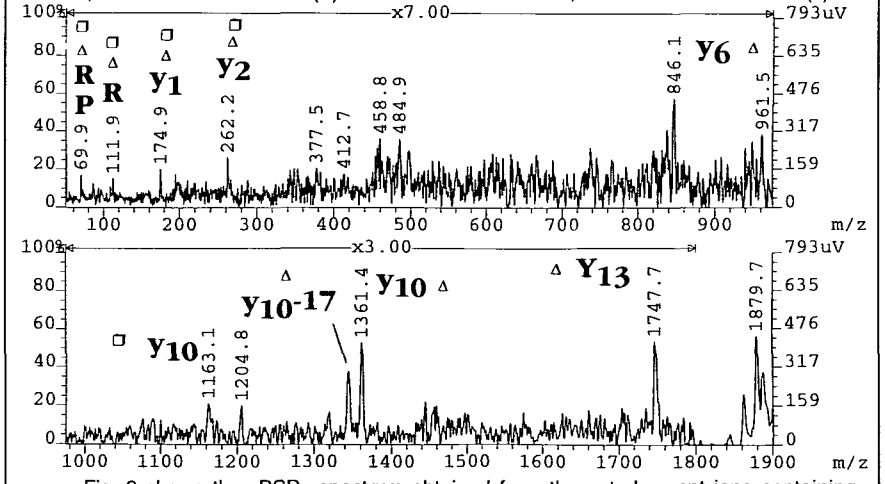

Fig. 2 shows the PSD spectrum obtained from the gated parent ions containing fragment ions consistent with both peptides. Note that relative intensities of the parent ions in Fig. 1 does not correlate with intensity of fragment ions observed in Fig. 7B). The spectrum is smoothed so that partially resolved isotope peaks appear as single "average-mass" peaks. In this case, only partial sequence information is present. While the peptide sequence of an unknown could not be derived, strong support is provided to the prediction of Heat-shock Protein 27 by peptide-mass database searching.

Mass Spectrometry of Proteins Directly Isolated from SDS Gels

Martina Schuhmacher, Markus Wunderlin and Michael Przybylski
University of Konstanz, Faculty of Chemistry, P.O. Box 5560 M732, 78434 Konstanz, Germany

Sodium dodecyl sulfate-polyacrylamide gel electrophoresis (SDS-PAGE) is the most frequently used technique in analytical biochemistry and molecular biology for the separation and characterization of proteins. However, a considerable disadvantage of SDS-PAGE is the lack of efficient isolation and purification methods, suitable for subsequent structural characterization. One method to recover the separated proteins is electro-elution, in which sodium dodecyl sulfate (SDS) is usually present in large excess in the elution buffer. SDS complexes the proteins and highly disturbs mass spectrometric characterization. Electrospray mass spectrometric studies of protein-SDS-mixtures showed protein-SDS-adducts, so that exact molecular weight determinations of eluted proteins were only possible after removal of SDS. Proteins can be purified from SDS excess by ion pair extraction according to Konigsberg [1] which, however, has been found to be laborious, difficult to reproduce, and not suitable for subsequent mass spectrometric analysis.

We have developed a new method for the isolation of proteins separated by SDS-PAGE using electro-elution with a modified buffer system, suitable for direct mass spectrometric characterization An additional purification step is no longer necessary. After separation with SDS-PAGE (non-reducing-conditions) the proteins were stained with Coomassie Blue, the protein bands were cut out and proteins isolated by electro-elution using SDS-free ammonium acetate solutions (pH 8.0 and 2.5) as elution buffers. Depending on the net-charge of the proteins at the applied pH, they either move to the anode or to the cathode, and protein-SDS-complexes are dissociated during the elution. The isolated proteins were analyzed without further purification by ^{252}Cf plasma desorption (PD), electrospray (ES) and matrix assisted laser desorption / ionisation (MALDI) mass spectrometry. In the spectra obtained no SDS-adducts to the proteins were observed and the spectra were comparable to those of the native proteins.

43rd ASMS Conference on Mass Spectrometry and Allied Topics

For standard isolation of proteins an ammonium acetate elution buffer with pH 2.5 was employed At this pH-value most proteins have positive charges, so that the polarity of the electro-elution system was reversed. The efficiency of this method was first demonstrated by ESMS and PDMS of model proteins (insulin, hen eggwhite lysozyme and serum albumin) and mixtures of myoglobins and lysozymes. For these proteins recovery rates ranged from 25 % to 58 % as was determined densitometrically after re-electrophoresis of the isolated proteins.

In first applications the effects of the reducing agents such as β-mercaptoethanol or dithiothreitol (DTT) during electrophoresis were studied with lysozyme ESMS of the isolated proteins showed the formation of mixed disulfides between protein and reducing agent. In the case of DTT the relative amounts of mixed disulfides were much lower than with β-mercaptoethanol. Furthermore, ubiquitin was cross-linked by carbodiimide leading to ubiquitin oligomers. After their separation by SDS-PAGE the oligomers were electro-eluted and characterized by MALDI-MS. In addition to the ubiquitin oligomers, side products were observed consisting of covalent carbodiimide adducts to the protein.

In a first bioanalytical application, hemofiltrate proteins were separated by SDS-PAGE and the proteins of the two most intensive bands were isolated. ESMS characterization of the protein isolated from the gel band between 10 kD and 14 kD yielded a molecular weight of 11.733 D The second gel band between 14 kD and 16 kD consisted of two different proteins that could not be separated by SDS-PAGE. The molecular weights of these proteins were 13 418 D and 14.725 D.

[1] L.E Henderson, S. Oroszlan, W. Konigsberg, Anal Biochem. 93, 153-157 (1979)

Sequencing peptides: post-source decay MS without scanning the reflectron.

Cordero M.M.; Cornish, T.J.; Cotter, R.J.
The Johns Hopkins University School of Medicine, Baltimore, MD 21205

This paper evaluates the sequencing capabilities of a recently developed MALDI-TOF curved field reflectron mass spectrometer.[1] (Fig.1) Its major advantage over other reflectron instruments used for post-source decay sequencing is that *complete* sequence information is obtained all at the same time, *without* scanning the reflectron or stepping the voltage.

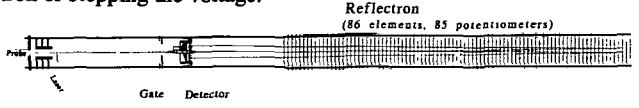

Figure 1 Coaxial Curved Field Reflectron TOF-MS

PSD products calibration is accomplished using the program TOFWARE (Ilys Software, Pittsburgh, PA). The calibration curve was generated from data points from the PSD MS of (Pro)14-Arg. This calibration curve is very close to the arc of a circular function and requires only the precursor ion mass to assign simultaneously all the product ion masses.

To obtain the PSD spectra shown in Figs. 1-3 typically 1-5 pmol of peptide were loaded on the probe after pre-mixing with a-cyano-4-hydroxycinnamic acid. Detection of fully developed PSD spectra in the low fmolar region was achieved for many of these peptides. A nitrogen laser was used for ionization, with 500 shots averaged per spectrum. For angiotensin II, precursor resolution is 2840 in a normal MS. In the PSD spectrum the precursor has a resolution of 1000 and the product ions have resolutions between 500 to 200 (lower resolution for lower masses).

In summary, high speed and high sensitivity sequencing of peptides can be achieved with the MALDI-TOF coaxial curved-field reflectron mass spectrometer. The curved field reflectron permits *multichannel* analysis of PSD products without the need for voltage stepping or reflectron scanning. The mass spectra can be easily calibrated by assigning the precursor ion mass. This is the first pass of the calibration and we are in the process of refining it.

(1) Cornish, T.J.; Cotter, R.J. *Rapid Commun. Mass Spectrom.* 1994, 8, 781-785

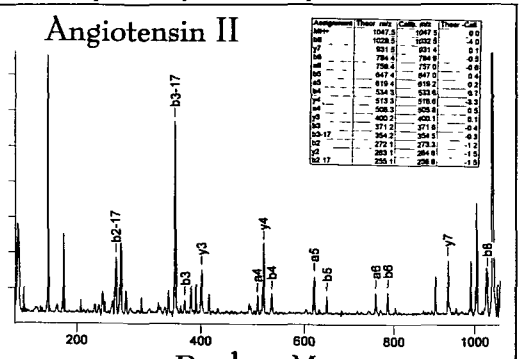

Figure 1
PSD mass spectrum
of angiotensin II

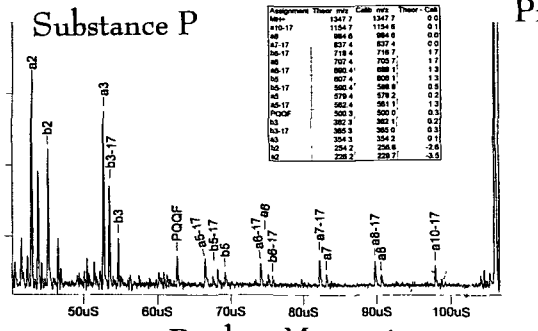

Figure 2
PSD mass spectrum
of substance P

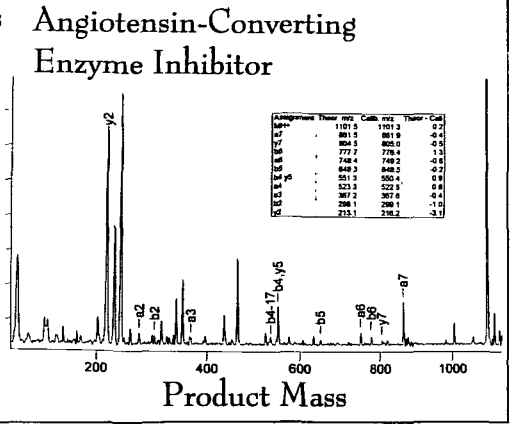

Figure 3
PSD mass spectrum
of angiotensin-converting
enzyme inhibitor

EVALUATION OF PSD-MALDI AND CID-MALDI FOR STRUCTURAL ANALYSIS

Steven A. Carr, Gerald Roberts, Roland S. Annan, Mark E. Hemling, John Hoyes (1)
SmithKline Beecham Pharmaceuticals, King of Prussia, PA 19406 and (1) VG Analytical, UK

Post source decay (PSD) of MALDI-generated ions is a new and potentially useful method for producing structurally-informative fragmentation of biopolymers. We are using a new, high resolution, single-stage reflecting MALDI-TOF instrument (TofSpec -SE, Fisons-VG) equipped with a collision gas cell to investigate the PSD-MALDI and CID-MALDI behavior of a variety of biological molecules. This instrument has a 3.4 m effective path length and incorporates a three stage ion source and a Bradbury-Nielson ion gate for parent ion selection (see also MPB 076, J. Hoyes, et al.). A resolution of > 2000 (FWHM) has been achieved for mass-selected product ions produced by PSD-MALDI. This resolution is sufficient to determine monoisotopic mass up to at least m/z 1800 in the product-ion analysis mode, and it greatly reduces uncertainty in the mass assignment and structural interpretation of fragment peaks.
All product ion spectra were recorded using eight or fewer segments (25% reduction in energy with each step) and between 25 and 50 shots per segment. For CID, sufficient air was admitted to the collision cell to increase the source pressure from 2×10^{-7} mbar to 7×10^{-7} mbar (parent ion intensity decreased to ca. 1/3 of that without the gas). Calibration and segment stitching were performed automatically by the VG-Opus data system. The results obtained using a designed series of peptides, commercially available peptides, and isolated peptides, phosphopeptides and glycopeptides are summarized below.

FRAGMENTATION PROCESSES OBSERVED IN PSD:

- High quality PSD and PSD-CID spectra are obtained using 0.1 to 5 picomoles of peptide or glycopeptide.
- Normal PSD spectra are very similar to low energy CID spectra of singly-charged M+H ions. Abundant $\mathbf{a_n}$, $\mathbf{b_n}$ or $\mathbf{y_n}$ ions as well as internal acyl and immonium ions are observed.
- Strong $\mathbf{y_n}$, $\mathbf{b_n}$ and usually weaker $\mathbf{z_n}$ ions are observed in peptides which possess a basic residue (Arg or Lys) at or near the C-terminus (e.g. tryptic peptides).
- Cleavage C-terminal to acidic residues, especially Asp to form $\mathbf{y_n}$ ions is favored (as first noted by S. Martin et al.), while cleavage C-terminal to Pro to form $\mathbf{y_n}$ ions is not.
- Significant $\mathbf{a_n}$, $\mathbf{a_n+1}$, $\mathbf{b_n}$, and, if Arg is present, strong $\mathbf{a_n\text{-}NH_3}$ and $\mathbf{b_n\text{-}NH_3}$ ions are observed in peptides with basic residues at or near the N-terminus.
- The PSD mass spectra of peptides containing phospho-Tyr provide the sequence of the peptide including the location of the phosphorylated residue. An intense peak corresponding to the loss of HPO_3 is always present, as is a satellite 18 Da lower in mass due to loss of water.
- In the PSD spectra of glycopeptides, facile cleavage of the GN-GN bond of the inner core with charge retained on the shortened glycopeptide is observed. We also observe a novel through-ring cleavage of the linker HexNAc sugar (0-1 and 2-3 bonds cleaved) with the peptide portion again retaining the charge. The precise structure of this fragment is under study.

ADDITIONAL FRAGMENTATION PROCESSES OBSERVED IN PSD-CID SPECTRA:

- Abundant side-chain fragment ions of the $\mathbf{w_n}$, $\mathbf{v_n}$ and $\mathbf{d_n}$ type may be produced by CID in a collision cell in the instrument. These fragment ions are common to high energy CID spectra, but are generally absent in low energy CID spectra. For tryptic peptides ending in Arg the spectra represent a nearly ideal mix of simple to interpret sequence ions and side-chain cleavage ions. The $\mathbf{w_n}$- and $\mathbf{d_n}$-type ions are particularly important because they permit Ile to be distinguished from Leu.
- Obtaining PSD and CID spectra is very simple, only involving toggling on the collision gas. Both PSD and PSD-CID spectra are routinely obtained on the same spot of material.
- PSD is a dominant process which is very difficult to shut down completely. The matrix plays a critical role in determining the initial internal energy of the ions formed, and the use of "cooler" matrices such as sDHB (versus a-cyano) can reduce the amount of PSD observed in the PSD-CID spectra.
- It is likely that highly basic or fixed charge derivatives used previously in high energy CID-FAB to direct fragmentation will also be of value in enabling the observation of side-chain cleavages in the PSD-CID spectra of otherwise refractory peptides.

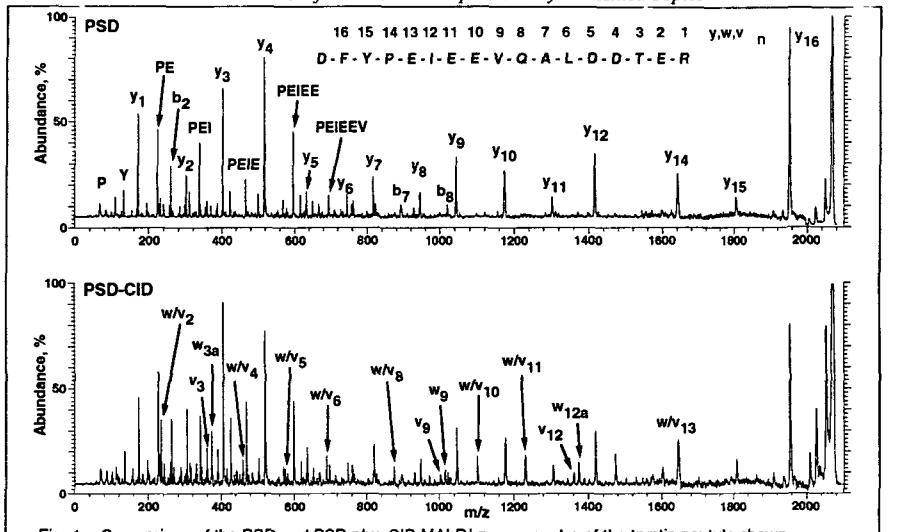

Fig. 1. Comparison of the PSD and PSD plus CID MALDI mass spectra of the tryptic peptide shown

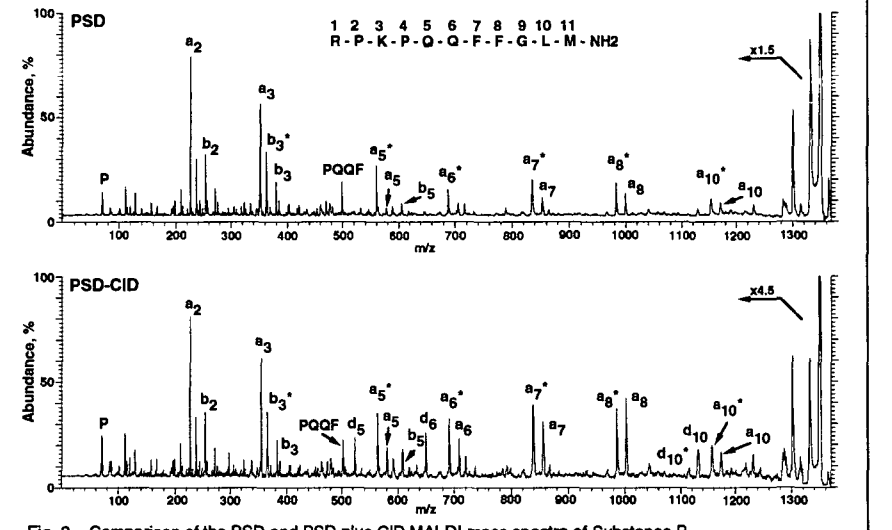

Fig. 2. Comparison of the PSD and PSD plus CID MALDI mass spectra of Substance P.

Peptide Sequencing: MALDI-TOF vs. ESI-3Q

W. A. Jeffery, M. Bartlet-Jones, and D. J. C. Pappin, Imperial Cancer Research Fund, London WC2A 3PX, UK. A. Keane, M. Harrison, and J. S. Cottrell, Finnigan MAT Ltd., Paradise, Hemel Hempstead, Herts HP2 4TG, UK

Introduction: The aim of this poster is to provide a back-to-back comparison between MS-MS spectra obtained by two different techniques: Post Source Decay (Spengler, B. et. al., Rapid Commun. Mass Spectrom., 6, 105-8 (1992)) and Collision Induced Dissociation. Three peptides were analysed: (i) Native Glu-fibrinopeptide B, (ii) Glu-fibrinopeptide B modified to enhance CID fragmentation, (iii) Glu-fibrinopeptide B modified to enhance PSD fragmentation.

Experimental: PSD data were obtained using a Finnigan MAT Vision 2000 (matrix assisted laser desorption ionisation source + reflectron time-of-flight analyser). The matrix was DHB. Approximately 5 pmol of peptide was loaded onto the target, although only a small fraction of this was consumed. The mass scale was calibrated using Substance P as an external standard. The spectra shown here were acquired by stepping the reflector voltages down in 10 increments of 25%. The ion beam energy was 10keV.

CID data came from a Finnigan MAT TSQ7000 (electrospray source + triple quadrupole analyser). Samples were infused at concentrations between 0.1 and 2 pmol per µl. The collision gas was xenon.

Peptide Derivatisation: Peptides were modified to enhance the formation of A and B fragments by substitution of the amino terminus and basic residue side chains (Arg and Lys). For PSD, the N-terminus was a given a quaternary ammonium group carrying a fixed charge.

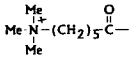

For CID, the N-terminal group was 3-pyridylacetyl, chosen to provide a mobile proton. Further details of this modification can be found in poster TPG265 (N. E. Sherman *et. al.*). In both cases, the derivatisation procedure results in loss of the N-terminal residue, (Glu). Thus, for an unknown, the first residue must be identified from the molecular weight shift between the native and modified peptides. Derivatisation also makes the peptide more hydrophobic.

Results

Native Glu-fibrinopeptide B:

- The two MS-MS spectra are surprisingly similar. Both show a strong series of 11 Y ions accompanied by weaker Z ions. The A and B series cover the residues which are missing from the C-terminal fragments, together with extensive overlap. Thus, both spectra provide coverage of the full sequence with extensive redundancy.

- The CID data were obtained from a very low concentration sample, 0.1 pmol per µl, so that the signal to noise ratio is lower than usual. The signal to noise in the PSD spectrum is good, considering that even lower levels of sample have been consumed, but the mass resolution is inferior, leading to less precise mass values.

Modified Glu-fibrinopeptide B:

- In the CID spectrum, the intensity of the Y ions is greatly diminished, and the B series now dominates. However, there are still a number of strong C-terminal fragment peaks present, particularly Y_1 to Y_4.
- The N-terminal fixed charge has completely eliminated C-terminal fragments from the PSD spectrum. Unfortunately, the A and B series are slightly patchy, and there are a number of peaks which have not yet been assigned.
- In both cases, the known mass of the N-terminal group makes it easy to identify the start of the A and B series. Given a reasonably complete series of sequence ions, this makes it much simpler to "read off" the sequence.

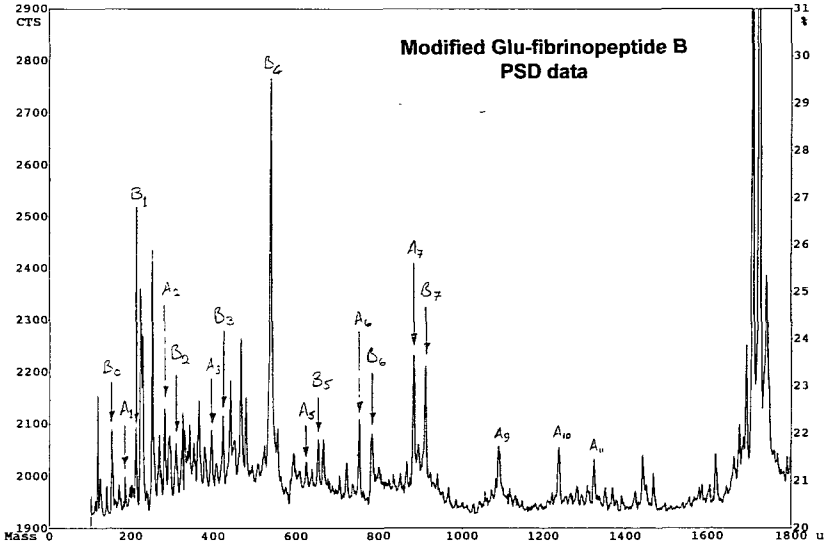

DEUTERATED TERMINATING AGENTS FOR LADDER SEQUENCE ANALYSIS BY LSIMS AND MALDI-TOF MS

Ricky D. Holland[1], M. Paul Chiarelli[3], David Vollmer[1], Martha Gay[2], James Sphon[2], and Jackson O. Lay, Jr.[1], Food and Drug Administration, (1) National Center for Toxicological Research, Jefferson, AR, (2) Center for Food Safety and Applied Nutrition, Washington, DC. and (3) Loyola University, Chicago, IL.

Introduction

A long standing approach to peptide sequence analysis is the Edman degradation method (1). A recently introduced variation for sequence determination by mass spectrometry involves the addition of a terminating agent to irreversibly block a portion of the peptide during each cycle. This method, referred to as "protein-ladder sequencing" (2), usually involves the use of MALDI-TOF MS to analyze a pool of chemically modified peptide fragments. This pool consists of peptide fragments, which differ only by the sequential removal of individual amino acids from the N-terminus. Sequence information is preserved in a representative portion of each cleavage-product based on blocking of some of the remaining peptide at each cycle using a terminating reagent, phenylisocyanate (PIC). Thus, the differences between fragment masses allow N-terminal peptide-sequence determination. The presence of one interfering peak using this method could result in mis-identifying two amino acids. A larger number of non-sequence related ions would likely make sequence determination for an unknown peptide impossible. The sequence terminating reagent provides an opportunity to incorporate a fingerprint for sequence related ions into each step of the peptide-ladder sequence approach. In this work we report the use of a mixture of PIC and d_5-PIC to incorporate such a fingerprint into the mass spectrum.

Experimental

Pyridine and Phenyisothiocyanate (PITC) were purchased from Pierce (Rockford, IL). PIC, α-cyano-4-hydroxycinnamic acid (matrix), all peptides, 1,1,1,3,3,3-hexafluoro- 2-propanol (HFIP) and glycerol were purchased from Sigma (St. Louis, MO). Trifluoroacetic acid (TFA) and trimethylamine (TMA) were purchased from Fluka (Ronkonkoma, NY). Acetonitrile was purchased from Baker (Phillipsburg, NJ). Ethyl acetate was purchased from Aldrich (Milwaukee, WI) and heptane from Fisher (Fair Lawn, NJ). Deuterated phenylisocyanate (d_5-PIC) was purchased from Bionetics Corporation (Jefferson, AR), an on-site synthesis contractor at NCTR.

The procedures for the peptide-ladder sequence method summarized below did not differ significantly from those published in reference 1 except for the use of both PIC and d_5-PIC. The coupling/ terminating step was carried out by adding 20 μL of PITC:d_5PIC:PIC:Pyridine: HFIP (30:0.5:0.5:76:4 v/v) and reacting for 3 minutes at 50°C, rather than using the reagents described in reference 2. The reacted peptide was dissolved in 20 μL of 0.1%TFA. One μL of peptide solution was mixed with 9 μL of a saturated matrix solution The matrix, α-cyano-4-hydroxy -cinnamic acid, was dissolved in a 2:1 mixture of acetonitrile:water with 0.1%TFA. One μL was placed on the sample pin and allowed to air dry. Spectra were obtained using a Vestec Lasertec (Houston TX) MALDI TOF MS in the positive ion mode using an acceleration voltage of 20 kV. From the same solution used to produce the MALDI TOF mass spectrum, 1 μL was removed and mixed on a stainless steel target with about the same amount of glycerol. LSIMS spectra (25 kV Cs ions) were obtained using a VG Autospec Q (Manchester, UK), magnetic sector-quadrupole hybrid operated as a magnetic sector instrument.

Results and Discussion

A modification of Chait's (1) peptide ladder sequence approach was used to provide a distinguishing "fingerprint" for sequence-related ions in the mass spectrum. Isotopic peaks were incorporated into sequence related ions based on deuterium in the blocking reagent. Each cycle of the peptide-ladder sequence produced two blocked products, one having 5 deuterium atoms, the other having none. With MALDI-TOF MS two partially resolved peaks differing by 5 amu were usually observed, corresponding to the average molecular weight (plus a proton) for the deuterated and non-deuterated sequence ions For ions greater than about 1400 amu, however, resolution was not adequate to separate both the d_0 and d_5 products. Because this mass difference was generated by reaction with the terminating reagent and was not observed in non-sequence related background ions, it provided a useful means for confirmation of the peptide sequence.

With LSIMS the spectra were more complicated because carbon isotopes were also resolved. Thus, the sequence ions typically showed prominent signals for the $^{12}C/d_0$, $^{13}C/d_0$, $^{12}C/d_5$, and $^{13}C/d_5$ products. Because of this higher mass resolution, isotope peaks were resolved even at the highest masses used in this study (about m/z 1700). This combined use of deuterated and non-deuterated terminating agents provides a fingerprint to aid in the identification of sequence ions from small peptides using the ladder sequencing method and mass spectrometry.

References

(1) Edman, P., *Acta Chem. Scand.*, **1950**, **4**, 283.
(2) Chait, B. T.; Wang, R.; Beavis, R. C.; Kent, S. B. H., *Science* **1993**, **262**, 89.

Characterizing Chemically- Generated Peptide Sequencing Ladders by ESI

Sanat K. Saha, James A. Carroll & Ronald C. Beavis
Skirball Institute for Biomolecular Medicine
Department of Pharmacology
New York University Medical Center
550 1st Avenue
New York, NY 10016

A new method for determining the primary structure of proteins and peptides was described recently that utilized the Edman degradation reaction to convert a single peptide into a collection of truncated peptides that all had the same C-terminus but were of different lengths[1] This peptide mixture was then analyzed using a mass spectrometer, allowing peptide sequence determinationby measuring the molecular mass differences between peptides that differed only by the N-terminal residue. Assigning a peptide sequence by measuring mass differences between adjacent peaks in a single operation was called "protein ladder sequencing".

The collection of peptides for ladder sequencing was originally generated by carrying out the Edman degradation reaction, using a mixture of phenylisothiocyanate (PITC) and phenylisocyanate (PIC) (95.5) as the Edman reagent. After one cycle, 5% of the original peptide was irreversibly protected with the PIC, leaving 95% of the peptide one residue shorter, ready for the next cycle. The reaction conditions used multiple step extraction process requiring considerable care.

Bartlet-Jones *et al.* have reported a novel volatile Edman degradation reagent, trifluoroethylisothiocyanate (TFEITC)[2] This reagent was synthesized specifically for use in the generation of a protein ladder sequencing mixture. Volatile trifluoroethylisothiocyanate can be removed by vacuum evaporation, eliminating the potential for sample loss involved in the original extraction procedure.

This paper describes research into the development new Edman reagents, that have the desirable volatility of TFEITC, and a reduced reaction rate at lysine side chain amino groups. A number of candidate isothiocyanate compounds were tested and evaluated using a standard set of reaction conditions. The best of these new candidate reagents, N-hexylisothiocyanate, was then used to evaluate the usefulness of electrospray ionization as an ion source for "reading" the sequencing ladders generated. Sequencing ladders generated with a peptide synthesizer were also examined to explore the general usefulness of electrospray ionization in analyzing peptide mixtures.

A survey of commercially available isothiocyanate derivatives revealed that isothiocyanates attached to aromatic groups reacted at a similar rate to PITC. Aliphatic isothiocyanates react at a slower rate than the aromatic derivatives. N-

hexylisothiocyanate had the best combination of reaction rate, volatility and ease of extraction. Aliphatic groups shorter than hexyl were too volatile, making them very dangerous reagents to work with in the laboratory. HITC had the additional property of reacting slowly with the e-amino group of lysine, resulting in simple ladder sequencing mass spectrum for lysine-containing peptides.

Isothiocyanate Derivative	Comments
Phenyl ITC	High Rection rate with N-terminal and lysine amino groups (involatile)
n-Hexyl ITC	Slowere reaction rate with N-terminal amino groups and much slower with lysine amino groups (volatile)
Cyclohexyl ITC	Similar to n-hexyl ITC (volatile)
2-Phenyl-ethyl ITC	Slower reaction rate than PITC (involatile)
3-Chloro-4-fluoro ITC	Low reaction rate (involatile)
Propyl ITC	Similar to n-hexyl ITC (volatile)
Pyridine ITC	Incompatible with reaction conditions used

Table 1 A comparison of the properties of several commercially available isothiocyanate derivatives for generating peptide ladders by the Edman reaction.

The electrospray spectra obtained using peptide ladders generated using n-hexylisothiocyanate as the Edman reagent showed that electrospray ionization coupled with a quadrupole mass spectrometer (Sciex API-1) could effectively read the sequencing ladders. Complicated ladders generated from peptide libraries could be read with little difficulty.

1 B.T. Chait, R. Wang, R.C. Beavis and S.B.H. Kent, *Science* 262,89 (1993).
2. M. Barlett-Jones, W.A. Jeffery, H F. Hansen and D.J.C. Pappin, *Rapid Commun. Mass Spectrom.* 8, 737 (1994).

Sequence Analysis of C- and N-Terminal Blocked Peptides by PSD-MALDI

A. Ingendoh, H. Ikezawa, K. Seta, M. Kanai, Y Yamakawa*, T. Omori-Satoh*, T. Isobe# and T Okuyama#
Finnigan MAT Instruments Inc., 2-5-8 Hatsudai, Shibuya-ku, Tokyo 151, Japan
*Japanese National Institute of Health, Shinjuku-ku, Tokyo 162, Japan
#Tokyo Metropolitain University, Dept. of Biochemistry, Hachioji-shi, Tokyo 192-03, Japan

Introduction

Since its introduction in 1992 by Spengler and Kaufmann, Post Source Decay Matrix-assisted Laser Desorption/ Ionization (PSD-MALDI) has gained main interest as a very promising tool for sequencing peptides Conventionally, sequence analysis of peptides is done by Edman degradation, which is based on the analysis of PTH amino acids produced by the reaction between N-terminal amino acids with a free amino group and a derivatizing agent for those groups. Therefore, this degradation cannot be used for N-terminal blocked peptides C-terminal sequencing is nowadays a very challenging area for the identification of the amino acid sequence. However, as well as for N-terminal sequencing it requires a free carboxylic acid in the C-terminus So, particularly for N- and C-terminal blocked peptides PSD-MALDI could be a very valuable alternative to these conventional methods Here, we present results of PSD-MALDI on peptides that are blocked on both termini.

Methods

Sample Preparation: Matrix (2,5-dihydroxybenzoic acid) and samples (three biochemically active peptides· Luteinizing hormone releasing hormone, Levitide, Bombesin) were dissolved in 9 1 0 1% aeqeous TFA / acetonitrile Concentrations in solution were 10 g/l (matrix) and $5 \cdot 10^{-5}$ M (peptides) The sample amount loaded on target was ca 20 pmol

Experimental Setup. The MALDI-TOF instrument was a VISION 2000, Finnigan MAT It is operated under fully computer control and equipped with a PSD-software that allows semi-automatical processing of generating fragment spectra When starting a new experiment, the only information needed is the mother ion mass, the wanted reflectron drop and the lowest fragment mass expected The software calculates and sets all voltages, generates the different fragment windows and calibrates and puts them together automatically to a complete fragmentation spectrum Thus, results on the sequence of peptides can be obtained within about 20 min.

Results

Ion signals of the intact peptides could be obtained with a mass resolution of 3000-3500 and a mass accuracy of about 0.5 Da (fig.1) In the PSD mode, the entire sequences of all peptides could be verified by comparing the PSD-MALDI spectra and theoretical fragmentation patterns Mostly N-terminal fragments (A/*, B/* type) are observed (fig.2). The averaged mass accuracy of the fragment determination was better than 0.5 Da in all examined cases (table1) Also, the even more important value of the accuracy for the determination of the different amino acids in the sequence was calculated. It is derived by substracting the molecular weights from neighboring groups of fragments. As result, the masses of the different amino acids could be verified with an averaged deviation from the theoretical values of below 0 2 Da So, the determination of mass differences in those PSD-MALDI spectra is even more accurate than that of the absolute molecular weights The capability of sequencing N-and C-terminal blocked peptides by PSD-MALDI has clearly been demonstrated

BOMBESIN: pGlu-Gln-Arg-Leu-Gly-Asn-Gln-Trp-Ala-Val-Gly-His-Leu-Met-NH_2

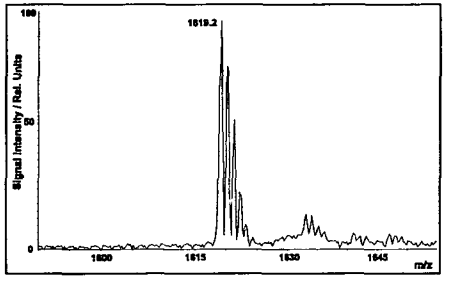

Fig. 1: Monomer signal peak in the MALDI spectrum of Bombesin (Theor. MW avrgd 1619 87 Da, monoiso 1618 81 Da). Sum of 10 laser shots The measured monoisotopic molecular weight is assigned. Mass accuracy 0 61 Da.

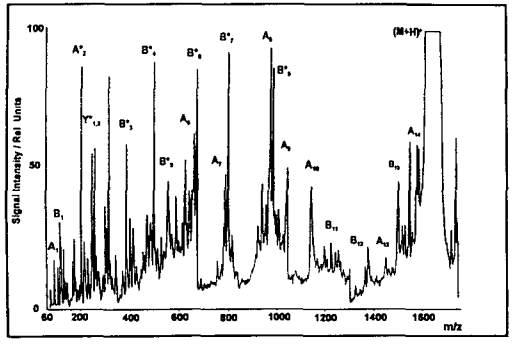

Fig. 2: Complete PSD-MALDI spectrum of Bombesin. Sum of 50 laser shots for each fragment window. Molecular weights for the different fragments are summarized in table 1

Table 1: Comparison of observed and theoretical molecular weights of the different fragments of Bombesin. The averaged mass accuracies for all fragments δm and for the determination of the different amino acids δm_{aa} is calculated

Fragment Description	A1	B1	A*2	B2	B*3	B*4	B*5	A6	B*6
Theo. MW / Da	84.1	112.1	195 2	240.2	379 4	492.6	549.6	652.7	663 7
Obs MW / Da	84 9	111.8	194 1	239.1	377 8	491 4	548 7	652 2	662.8

Fragment Description	B*7	A8	B*8	A9	A10	B11	B12	A13	A14
Theo MW / Da	791.8	967 1	978.1	1038 2	1137.3	1222 4	1359.5	1444 6	1575 8
Obs MW / Da	791 6	967.1	978 2	1038.1	1137.1	1222 4	1361 6	1445.9	1574.4

Averaged mass accuracy for all fragments:

$$\delta m = \frac{\sum_{1}^{n}(m_i^{theo} - m_i^{obs})}{n} = 0\ 47\ \text{Da}$$

Standard deviation of the averaged value $\sigma = \pm 0.87$ Da

Averaged mass accuracy for the determination of the different amino acids:

$$\delta m_{aa} = \frac{\sum_{1}^{n}[(m_{i+1}^{theo} - m_i^{theo}) - (m_{i+1}^{obs} - m_i^{obs})]}{n} = 0\ 1\ \text{Da}$$

Standard deviation of the averaged value: $\sigma = \pm 0\ 95$ Da

An Evaluation of Peptide Fragmentation by MALDI-TOF PSD and MALDI CID MS/MS

Gregory W Adams, Katalin F. Medzihradszky, David A. Maltby, Steven C. Hall,
Alma L. Burlingame. Mass Spectrometry Facility, University of California,
San Francisco, CA 94143.
Robert H. Bateman, Martin R. Green, Anne Maisey. VG Organic, Manchester, M23 9LE, UK

Ample evidence has accumulated which supports the hypothesis that the efficiency of ionization of peptides and proteins by MALDI provides inherently higher sensitivity than other ionization techniques at present. In MALDI a large fraction of the analyte ions undergo post-source decay (PSD) in the field free drift path, and fragment ion spectra can be recorded using a reflectron time-of-flight instrument (VG TofSpec SE). Such PSD spectra allow for peptide sequence analysis in a similar manner to well documented collision-induced dissociation mass spectra recorded using tandem mass spectrometry. Using a combined hybrid magnetic sector and orthogonal acceleration TOF instrument (VG AutoSpec SE oa-TOF), CID spectra can be obtained from MALDI generated monoisotopic precursor ions. We have evaluated the relative behavior of a variety of peptides in both the MALDI-TOF PSD and MALDI CID mode using collisional activation at 800eV with Xenon.

Figures 1 and 2 illustrate the MALDI-PSD and MALDI-CID mass spectra of a synthetic peptide.

Observed Characteristics of MALDI-PSD spectra are:

- Similar to low energy CID fragmentation
- No side chain fragments (i.e. **d**, **v** and **w** ion formation)
- Basic amino acids control the fragmentation: preferential charge retention on the basic residue
- Unusually abundant **y** ions formed by cleavages at the N-terminus of Asn or at the C-terminus of Asp residues
- When Arg is present, significant fragmentation due to sequential neutral losses from **a**, **b** and **y** ions is observed, the neutral loss fragments can be categorized as:
  a) loss of NH_3 (17 Da), H_2O (18 Da) and NH=C=NH (42 Da) from **a** or **b** ions.
  b) **y** ions predominantly show loss of NH_3 (17Da), the ion formed this way is isobaric with a **z** ion.
  c) internal ions exhibit similar losses.
  In most cases, sequential neutral losses are observed.

Observed Characteristics of MALDI-CID spectra are:

- Mixed high energy and PSD-like fragmentation:
- Abundant immonium and related ions: amino acid composition of the peptides.
- However, CID spectra do not show side-chain losses from the molecular ion
- Side-chain fragment ions **d**, **v** and **w** are observed, depending on sequence position of the basic amino acid.
- However, when the basic amino acid is His or Lys, the relative abundance of these side-chain fragments is relatively low in comparison to the CID spectra acquired in LSIMS-CID experiments
- Abundant ions due to neutral losses. Unusually abundant **y**-17 ions for C-terminal ions formed by peptide bond cleavage at a Pro residue (These **y** ions cannot yield **z** ions).
- Unusually abundant **y** ions formed by cleavages at the N-terminus of Asn or at the C-terminus of Asp residues.

Interpretation of MALDI-PSD spectra generally yield partial sequences. When PSD sequence data is combined with observed molecular masses , protein database searching will lead to a more unambiguous protein identification. The advantages of MALDI-CID over MALDI-PSD include the ability to select a monoisotopic precursor ion, the CID spectra generally provide comprehensive sequence content and the high energy fragmentations can differentiate between the isomeric amino acids Ile/Leu.

This work was supported by NIH National Center for Research Resources grant RR01614 (to ALB) and NIEHS Superund Grant ES04705 (to ALB).

43rd ASMS Conference on Mass Spectrometry and Allied Topics

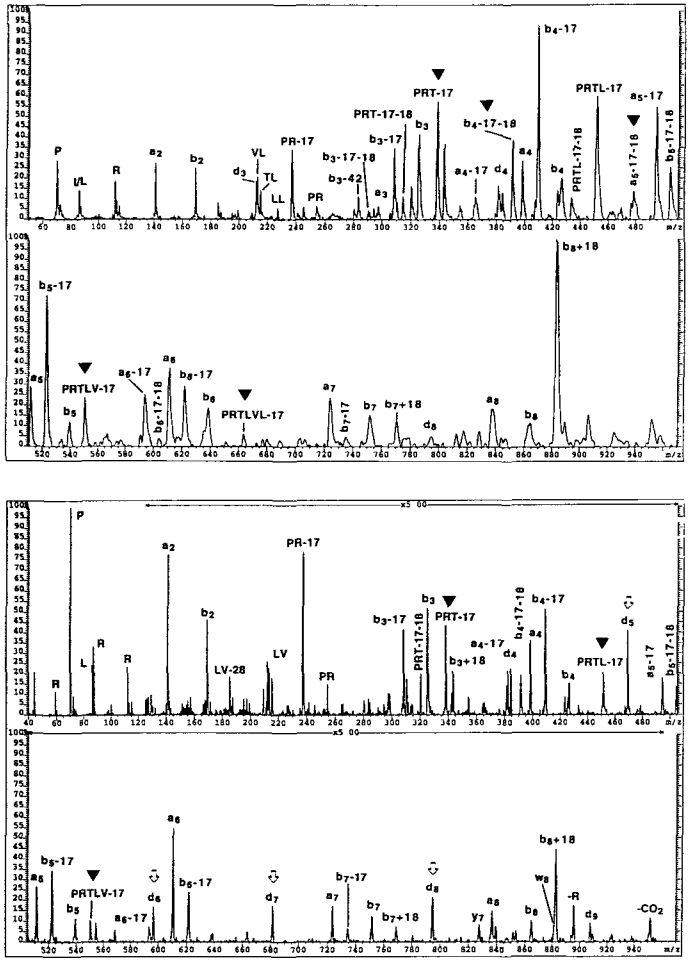

Figure 1. MALDI-PSD spectrum of a synthetic peptide APRTLVLLL (MH^+ = 995.6). Some of the characteristic PSD fragments e.g. abundant sequential neutral losses from **a** and **b** and internal ions are labelled with the symbol ▼ Figure 2. MALDI-CID spectrum of a synthetic peptide APRTLVLLL. Some of the characteristic high energy fragments e g. side chain fragments are labelled with the symbol ⇩ PSD *like fragments e.g abundant sequential neutral losses from* **a** *and* **b** *and internal ions are labelled with the symbol* ▼.

A Novel N-Terminal Derivative Designed to Simplify Peptide Fragmentation

Nicholas E. Sherman*, Nathan A. Yates*, Jeffrey Shabanowitz, Donald F. Hunt
Department of Chemistry, University of Virginia, Charlottesville, Virginia, USA

William Jeffery, Mike Bartlet-Jones, Darryl J. C Pappin
Protein Sequencing Laboratory, Imperial Cancer Research Fund, London, UK

Peptide sequencing techniques, specifically micro-capillary HPLC combined with electrospray-ionization tandem mass spectrometry, are receiving considerable attention in the field of biochemistry due to their unique ability to analyze complex biological mixtures at or below femtomole levels. However, the successful interpretation or deduction of a peptide sequence from a collision activated dissociation (CAD) spectra can be a complex and time-consuming task

Proton mobility is generally accepted as the key requirement for obtaining structurally diagnostic CAD spectra Collisional activation of protonated peptides can lead to intramolecular proton exchange. This results in an equilibrium population of ions, which only differ in the protonation site. Peptide fragmentation occurs at these protonation sites, producing a variety of sequence fragments, usually dominated by y_n, b_n, and a_n ions. Competing processes, such as side chain rearrangements and cyclization reactions, produce additional ion fragments that often complicate the CAD spectra

Here, we describe the application of a new pyridine based derivative designed to enhance sequence ion intensity, reduce rearrangement products, and maintain ESI sensitivity. This unique N-terminal derivative directs fragmentation by supplying a mobile proton to the peptide backbone. Unambiguous identification of the first and second N-terminal amino acids is possible with the use of this pyridyl reagent because it allows for easy identification of b_1 ions In addition, the derivative further simplifies CAD spectra by blocking rearrangements that involve the N-terminus The water soluble, hydophylic, pyridine based reagent is used to acylate peptides at extremely low levels On-column derivatization can be performed with as little as 20 femtomoles of peptide Excess reagent and reaction by-products are easily removed by washing before commencing gradient elution.

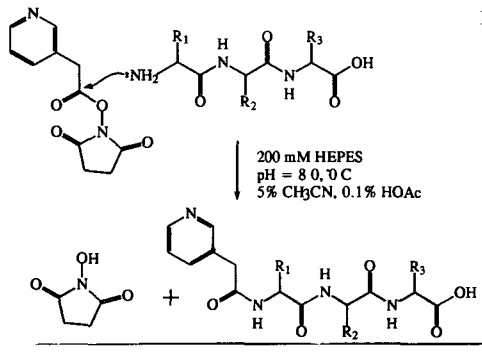

Figure 1 N-terminal peptide derivatization reaction for 2-(3-pyridyl) acetic acid N-hydroxysuccinimide ester and three amino acid residue peptide

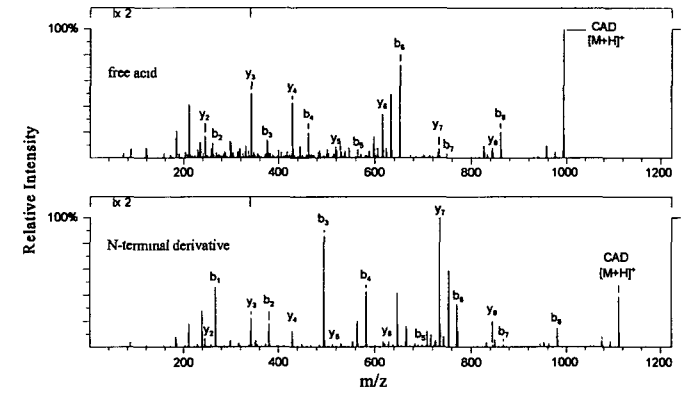

Figure 2 Product ion spectra for the protonated peptide FLDSTSPLL Acquired for the free acid and N-terminal derivative using a triple quadrupole mass spectrometer with a collision offset of -34 eV Note that the b_1 can easily be identified with the use of the N-terminal derivative.

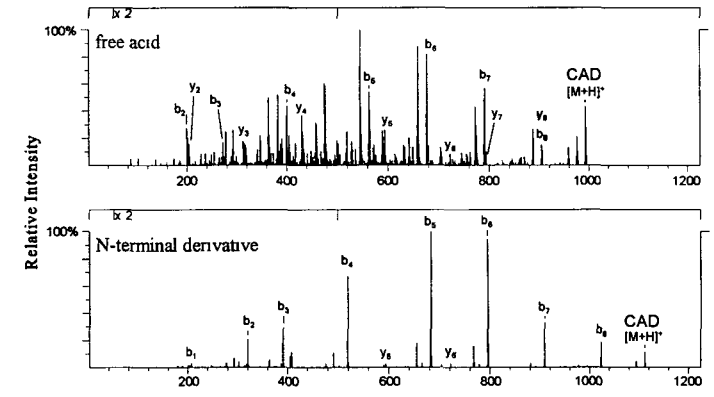

Figure 3. Product ion spectra for the protonated peptide SLAQYINA Acquired for the free acid and N-terminal derivative using a triple quadrupole mass spectrometer with a collision offset of -39 eV. Note the reduction in rearrangement products with the use of the N-terminal derivative.

Unusual Fragment Ions in the High Energy CID Spectra of Peptides Containing S-Alkyl Cysteine

Susan M. Wolf and Klaus Biemann, Department of Chemistry, MIT, Cambridge, MA, 02139

A review of the high energy CID spectra of a number of S-alkyl cysteine-containing peptides revealed the presence of many unknown peaks, the further investigation of which resulted in the characterization of a set of previously undocumented fragmentations which share as a common feature the scission of alkylcysteine thioether C-S bonds. It is expected that the information regarding sequence requirements for the formation of these ions will be useful for the optimization of computer-based algorithms employed for the automated sequencing of peptides from MS/MS data.

Experimental. The peptides used in this study were obtained from the proteinase K digestion of human serum albumin, trypsin digestion of RNase A, commercial vendors or synthetic preparation at the M.I.T. Biopolymers Laboratory. Proteins and peptides dissolved in 6M guanHCl 0.05M tris pH 8.0 were typically reduced with triethylphosphine or dithiothreitol and alkylated using a 5-10X molar excess of alkylating agent (4-vinylpyridine, iodoacetamide, iodoacetic acid, or 2-vinylquinoline) over thiols prior to clean-up via reversed phase HPLC. Proteins were then enzymatically digested and the resultant peptides isolated by reversed phase HPLC. High energy CID product ion spectra were obtained for FAB ionized precursors using an HX110/HX110 tandem four sector ($E_1B_1E_2B_2$) mass spectrometer at a collision energy of 7 kV using a collision cell floated at 3 kV and employing He collision gas to attenuate precursor intensities to 30%. Precursor ion scanning was accomplished by linked scanning of MS1 to detect 10 kV CID products formed in the first FFR.

Results. A number of MS/MS spectra of peptides containing pyridylethylcysteine (peC) show peaks which can be assigned as $[x_n$ - vinylpyridine$]^+$ where the nth amino acid is peC. For instance, the MS/MS spectrum of the pyridylethyl derivative of LNCR, a short peptide synthesized for the further investigation of these ions, demonstrates a prominent signal corresponding to the x_2-105 fragment at m/z 304 (Figure 1). A precursor spectrum for this ion indicated x_2 (or x_2+1) as the likely precursor. MS/MS spectra of source-derived x_2 and x_2+1 indicated that each of these ions was able to fragment to form the observed product at m/z 304. Presuming that the initial structure of x_n+1 is as depicted in Scheme 1, the formation of $[x_n$ - vinylpyridine$]^+$ from x_n+1 is easily rationalized mechanistically. Any formation of this ion from an x_n intermediate presumably involves rearrangement to give a similarly stabilized product, perhaps through an initial formation of a cyclic sulfonium ion prior to vinylpyridine loss. As further evidence for the identity of this fragment, the exact mass of the MS1 $[x_2$ - 105$]^+$ ion was determined to be 304.1086 which agrees well with the mass calculated for an $[x_2$ - vinylpyridine$]^+$ ion at m/z 304.1080. A review of the spectra of peC-containing peptides from a number of other sources showed that these fragments were observed in all peptides in which pyridylethylcysteine was situated N-terminal to a basic amino acid (e.g. lysine or arginine) but which did not itself constitute the N-terminal amino acid. Peptides containing cysteine modified with other common alkylating reagents were found to undergo an analogous fragmentation.

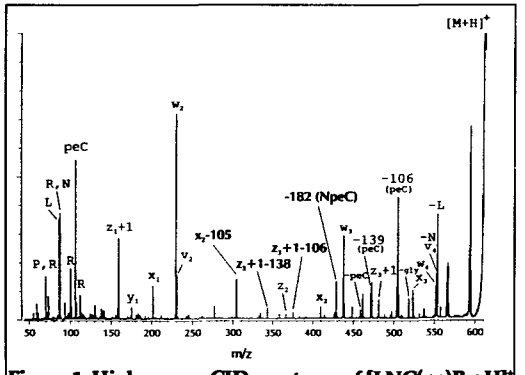

Figure 1. High energy CID spectrum of [LNC(pe)R +H]+

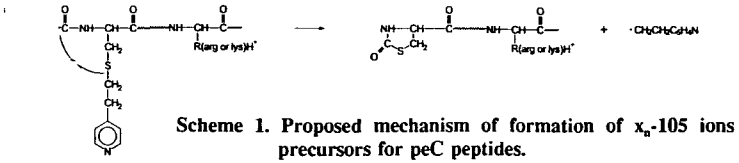

Scheme 1. Proposed mechanism of formation of x_n-105 ions from x_n+1 precursors for peC peptides.

In addition, it has been found that for peptides in which an S-alkyl cysteine is located directly adjacent to asparagine, aspartic acid or leucine, ions are observed which correspond to the combined losses of RS· with ·C(O)NH_2, ·C(O)OH, and ·CH$(CH_3)_2$, respectively. The structures of the combined side chain loss ions presumably represent stabilized 6-membered ring products as shown in Scheme 2. Aside from the circumstantial evidence linking certain sequences with the presence of these ions, other data support these assignments. For instance, the MS/MS spectrum of [LNC(pe)R + H]+ shows a peak at m/z 428 assignable as an -NC- combined side chain loss ion. The precursor spectrum of m/z 428 which contains two peaks, corresponding to $[M + H - pyrCH_2CH_2S\cdot]^+$ and $[M + H - 44]^+$, supports this conclusion. Also, peaks representing combined side chain losses of -LC- (711) and -CN- (710) appear at the same mass for all of the S-alkyl cysteine derivatives of LCNFYK and LCNFYR, indicating that the alkyl group, at least, is not present in these fragment ions.

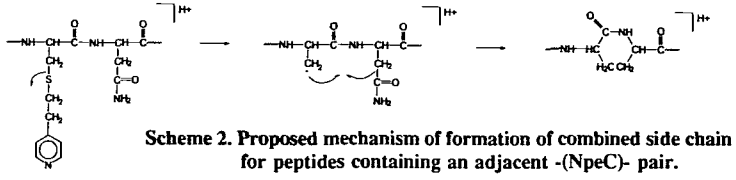

Scheme 2. Proposed mechanism of formation of combined side chain loss ions for peptides containing an adjacent -(NpeC)- pair.

Not unexpectedly, fragmentations analogous to those recently described for methionine- and methylcysteine-containing peptides[1] have been observed. For instance, $[z_{n+1}$ +1 - $pyrCH_2CH_2S\cdot]^+$ ions (where pyridylethylcysteine is the nth residue) have been noted in the MS/MS spectra of C(pe)YFQNC(pe)PR, STMSITDC(pe)R, SITDC(pe)R and LNC(pe)R. In this case, such ions constitute a subset of a class of previously described ions in which w-type side chain losses occur from z_n+1 ions where the nth residue is positioned one amino acid to the N-terminal side of the fragmenting side chain[2]. In addition to these ions, the similar $[z_{n+1}$ +1 - $pyrCH_2CH_2\cdot]^+$ ions have been observed, the formation of which is easily rationalized as resulting in the formation of a stabilized closed shell 6-membered ring product. Also, as would be expected, the corresponding a_{n+1}+1-derived ions are observed in the MS/MS spectra of peptides containing basic sites N-terminal to the alkylcysteine position. Such fragments are also observed for peptides containing other S-alkyl cysteines. In most spectra in which these ions were observed at all (especially in the case of z_{n+1}+1-derived ions), this set of fragments tended to demonstrate a rather low relative intensity.

(1) Downard, K.M., Biemann, K. *J. Mass Spectrom.* **30** (1995) 25-32.
(2) Johnson, R.S., Martin, S.A., Biemann, K. *Int. J. Mass Spectrom. Ion Proc.* **86** (1988) 137-154.

Surface-Induced Dissociation of Cyclic Peptides.

Ashok R. Dongré, Mark J. Hayward and Vicki H. Wysocki

Department of Chemistry, Virginia Commonwealth University, Richmond, VA 23284-2006
Agricultural Research Division, American Cyanamid Company, Princeton, NJ 08543- 0400

Cyclic peptides constitute a very important subgroup of biologically active compounds. The cyclic backbone fixes these peptides in a particular conformation which may lead to fixed secondary structure. These structures may exhibit specific properties that can lead to such applications as antibiotics or immunosuppresants. Classical sequencing techniques such as Edman degradation cannot be utilized for cyclic peptides due to lack of a free N-terminus. Therefore, with the advent of soft ionization techniques there has been increased interest in analyzing cyclic peptides by mass spectrometry.

Collision-induced dissociation (CID), both high and low energy, has been applied to sequence various biologically active cyclic peptides.[1,2] However, to obtain fragment ions from cyclic peptides at least two covalent bonds need to be cleaved which can require high energy deposition. In order to sequence cyclic peptides, it is neccessary to obtain a self consistent set of fragment ions. Surface-induced dissociation (SID) has been successful in sequencing linear peptides;[3] the advantages offered by SID such as high internal energy deposition, narrow energy distribution and its easy variability can be exploited to study fragmentation of cyclic peptides The current investigation deals with fragmentation of biologically active cyclic peptides related to Bacitracin and Telomycin complexes. Figure 1 represents an SID spectrum of Bacitracin A on a fluorinated alkanethiolate monolayer surface. The bacitracin A structure has a linear and cyclic portion making it more difficult to sequence and obtain a consistent set of fragment ions. Siegel and coworkers have performed a detailed investigation to elucidate the structure for Bacitracin A by CID.[2] In order to obtain complete sequence information they performed MS/MS/MS (nozzle-skimmer CID to elucidate the sequence of the linear portion followed by CID/MS on the cyclic portion to obtain its sequence). A single SID spectrum yields sequence ions both from the linear and the cyclic portion of the peptide without the need for the additional Cap-Skimmer fragmentation. The same ions as those observed by CID were obtained by SID. Figure 2 represents an SID spectrum of Telomycin on a octadecanethiolate monolayer surface. The proline and hydroxy-proline in the cyclic portion of the peptide render two amide bonds more facile which helps yield a consistent set of fragment ions making it easier to obtain the sequence of the cyclic portion.

The above results demonstrate the utility of SID to obtain structural information for cyclic peptides.

43rd ASMS Conference on Mass Spectrometry and Allied Topics

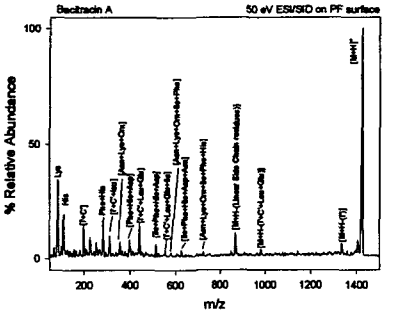

Figure 1

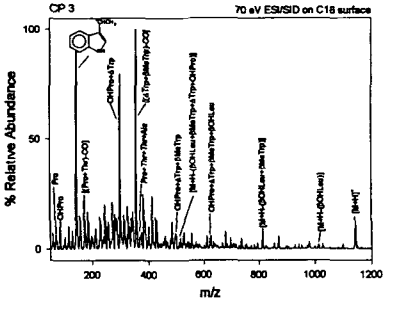

Figure 2

References:

(1) Eckart, K.; *Mass Spec Reviews*, **1994**, *13*, 23-55.
(2) Siegel, M. M.; Huang, J.; Lin, B.; Tsao, R.; and Edmonds, C. G.; *Bio. Mass Spectrom.* **1994**, *23*, 186-204.
(3) McCormack, A. L.; Somogyi, Á.; Dongré, A. R.; Wysocki, V. H., *Anal. Chem.* **1993**, *65*, 2859-2872.

Peptide Sequencing at the Low Femtomole Level Using On-Line Membrane Preconcentration-Capillary Electrophoresis-Tandem Mass Spectrometry (mPC-CE-MS/MS)

Andy J. Tomlinson, Kenneth L. Johnson, and Stephen Naylor
Biomedical Mass Spectrometry Facility and Department of Biochemistry and Molecular Biology Mayo Clinic, Rochester, MN 55905, USA

Peptide sequence determination by mass spectrometry is a well-established technique. However, biologically active peptides that are currently presented for sequencing by MS techniques yield two major challenges. First, these analytes are usually components of complex mixtures and are not easily isolated by standard procedures. Second, such peptides are invariably present in extremely low concentrations (typically attomoles per microliter).

Initially, we developed CE-MS/MS conditions for this application. However, while such methods yield high analyte resolution, the concentration limits of detection of all CE-MS techniques were inadequate for detection of biologically derived peptides. These limitations motivated us to develop on-line membrane preconcentration CE-MS/MS (mPC-CE-MS/MS). This technique utilizes a hydrophobic membrane at the inlet of the CE capillary and enables the analysis of large sample volumes (tens of µL) without compromising analyte resolution or CE separation efficiency. Therefore, mPC-CE-MS/MS affords a very appropriate method for sequencing low concentrations of biologically active peptides.

From preliminary mPC-CE-MS/MS studies we found that the influence of subtle changes of CID conditions upon MS/MS data was greater when analyzing low fmol amounts of peptide than is often observed at higher (pmol) levels. Therefore, we systematically investigated the effects of CID parameters on the appearance of peptide MS/MS spectra.

Initially we evaluated the use of argon or xenon in the collision cell of our hybrid MS by analysis of ~70 fmol of the synthetic peptide SIINFEKLT (Figure 1). As expected, at the same collision energy (22 eV), xenon increased the attenuation of the doubly charged precursor ion. This tended to improve product ion yield and the overall appearance of the MS/MS spectrum of this peptide (Figure 1B).

We have also evaluated the effect of collision energy on peptide MS/MS (Figure 2). These MS/MS data were obtained using a xenon pressure of 1.5 x 10^{-5} mbar and a collision energy either of 18-22 eV or 26 eV. Clearly each spectrum yields partial sequence of the synthetic peptide SIINFEKL. However, since the quality of such data is dependent on peptide chemical nature, it is difficult to predict the optimal collision energy to sequence low levels of an unknown peptide. From these studies, we concluded that a collision energy ramp with scan is potentially most appropriate for this application.

Other factors that improve mPC-CE-MS/MS sensitivity include reducing the internal diameter of the PC-CE capillary. Smaller i.d. capillaries increase ESI performance. This greatly enhances the signal:noise of MS/MS spectra obtained by mPC-CE-MS/MS of low fmol amounts of peptide (Figure 3). Furthermore, esterification of acidic residues improves the efficiency of peptide ionization by ESI and MS/MS fragmentation processes which leads to more complete sequence upon analysis of ~40 fmol of peptide (Figure 4).

This work was funded in part by NIH Contract Grant #N01-AI-45197 and Mayo Foundation. We also acknowledge the support of Finnigan MAT.

Figure 1 mPC-CE-MS/MS Analysis of ~70 fmol of SIINFEKLT Collision Energy 22eV, Collision Gas A = Ar @ 2x10^{-5} mbar, B = Xe @ 1.2x10^{-5} mbar

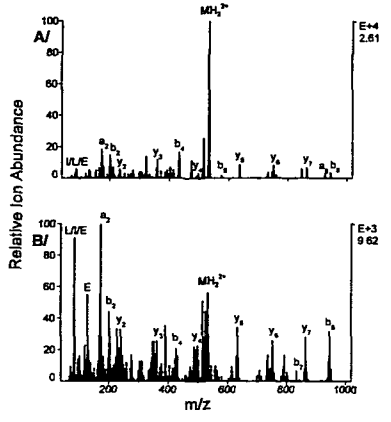

Figure 2 Effects of Collision Energy on the MS/MS Spectrum of ~70 fmol of SIINFEKL Collision Gas Xe @ 1.2x10^{-5} mbar

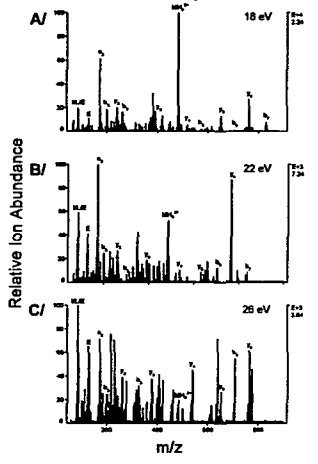

Figure 3 mPC-CE-MS/MS Analysis of ~70 fmol of SIINFEKL Collision Energy 22eV, Collision Gas Ar @ 2x10^{-5} mbar, A = 50 µm id mPC-CE capillary B = 25 µm id mPC-CE capillary

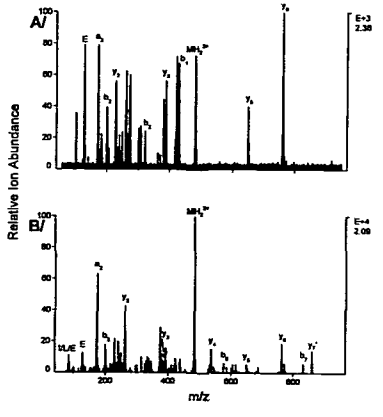

Figure 4 mPC-CE-MS/MS Analysis of SIINFEKL Collision Energy 22eV, Collision Gas Ar @ 2x10^{-5} mbar, A = ~80 fmol Native Peptide B = ~40 fmol Methylated Peptide

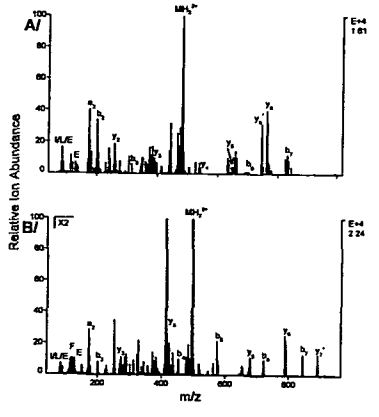

CONTROLLED FRAGMENTATION OF DERIVATIZED PEPTIDES

Ingemar Lindh, William Griffiths, Tomas Bergman and Jan Sjövall
Department of Medical Biochemistry and Biophysics, Karolinska Institutet
171 77 Stockholm, Sweden

Introduction

In an earlier study with fast atom bombardment (FAB) ionization (Lindh *et al.*, Rapid Commun. Mass Spectrom., **8**, 797-803 (1994)) it was shown that the C-terminal derivatization of peptides with 4-aminonaphthalenesulphonic acid created a specific charge site on the peptide. Upon high-energy collision-induced dissociation (CID) the derivatized peptides fragmented only into C-terminal ions. Derivatization of the peptides combined with acetylation increased the sensitivity of detection by between one and two orders of magnitude. However, still a considerable amount of material (1-2 nmol) was needed to obtain CID spectra from which the amino acid sequence could be deduced. In the present study, we have determined the sensitivity of detection and fragmentation behaviour of the peptide derivatives by ES mass spectrometry.

Mass spectrometry

Negative-ion ES mass spectra were recorded on a VG AutoSpec-OA-TOF-FPD mass spectrometer. ES/CID linked scan (constant B/E) spectra were generated using helium as the collision gas in the first field free region gas cell at a pressure sufficient to give a 50% reduction of the parent ion-beam intensity (50% att.). CID spectra were also recorded using the orthogonal acceleration time-of-flight (OA-TOF) analyzer using xenon as collision gas at 50% att. The samples were introduced in a $MeOH/H_2O$ solution with continuous infusion.

Results

All the derivatized peptides could be detected on the hundred attomol-level using negative-ion electrospray ionization and focal plane array detection. During high-energy collision-induced dissociation, the peptide derivatives fragmented solely into C-terminal ions which greatly facilitates the interpretation of the spectra. The benefit of the derivatization procedure is shown for the peptide Glu-Leu-Gly-Gly-Gly (C-1). Figs. 1 and 2 show ES/CID spectra of naphthalenesulphonated C-1, recorded at the focal plane array detector and at the OA-TOF analyzer, respectively. The two ES/CID and earlier recorded FAB/CID fragmentation patterns are similar but have differences, partly due to the different collision energies used in the experiments. Almost a complete set of sequence ions "X, Y, 'Z, 'V and 'W are formed. The sensitivity of detection is much higher using ES/CID than FAB/CID. Sequence information can be obtained from as little as 50 fmol of material consumed.

43rd ASMS Conference on Mass Spectrometry and Allied Topics

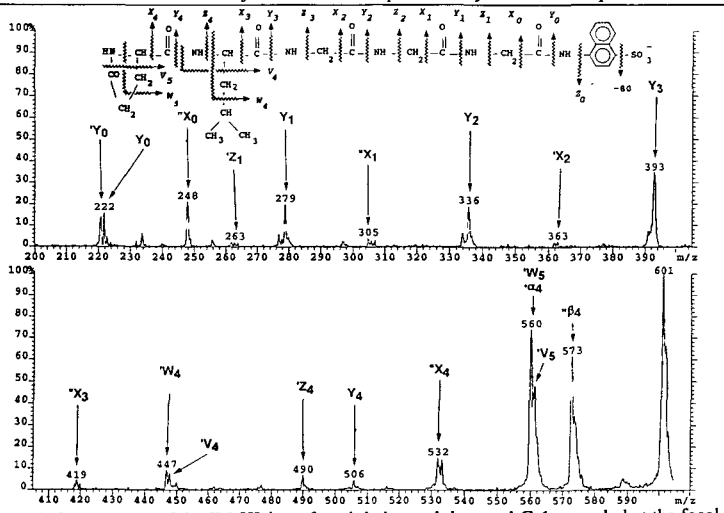

Fig. 1. ES/CID spectra of the $[M-H]^-$ ion of naphthalenesulphonated C-1 recorded at the focal plane array detector, m/z = 617, 50 pmol consumed, flow 1 μl/min., 50 pmol/μl.

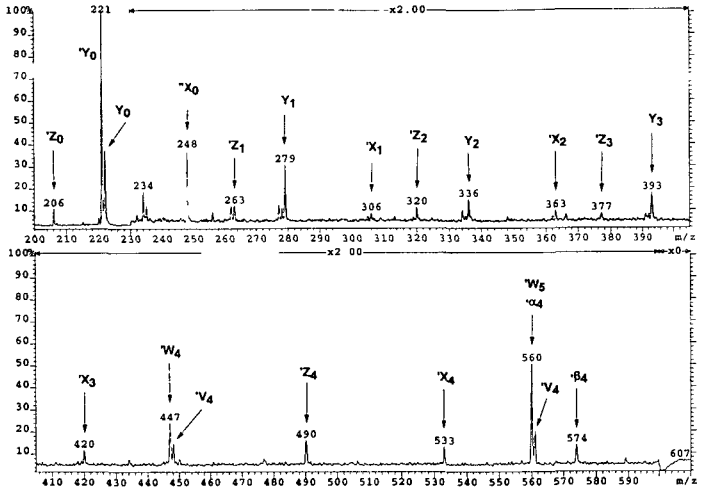

Fig. 2. ES/CID spectra of the $[M-H]^-$ ion of naphthalenesulphonated C-1 recorded with the OA-TOF analyzer, m/z = 617, 50 pmol consumed, flow 2 μl/min., 200 pmol/μl

Fragmentation Study of Small Non-Polar Peptides Containing NMeAla And Pro.

*Tomas Vaisar, * and Jan Urban*

Molecumetics Ltd., 2023 120th Ave NE, Bellevue, WA 98005, USA

Collision induced dissociation (CID) spectra of protonated peptides generally show main fragments of *a*, *b* and *y* type spread along the entire peptide chain. However, it was found that proline has a pronounced effect on the fragmentation pattern of protonated peptides opening low-energy fragmentation channel leading to *y* fragment ion with N-terminal proline.[3] This 'proline effect' was used to support a newly proposed fragmentation mechanism via an oxazolone-like intermediate.[4] The formation of *y* ions requires a transfer to the forming ion of the proton originating from a nitrogen of amide bond adjacent towards the N-terminus of the bond cleaved.[5,6]

We report on the fragmentation of a series of peptides with N-alkylated residues of the general structure H-Ala-Val-X-Leu-Gly-OH,with the following substitutions at the three position; Ala, NMeAla, Pro, L-pipecolinic acid (Pip) and D-Pip. The Pro residue was found to induce almost exclusively formation of a *y*-type ion with Pro at the N-terminus in peptides H-AVXLG-OH (X=P). Surprisingly, other N-alkylated amino acid residues (NMeAla and L-Pip) induce almost exclusively formation of *b*-type ion with N-alkyl residue at the C-terminus(Table 1). We suggest that this large difference in fragmentation should be attributed to the rigid five-membered Pro ring, a structure which disables transfer of proton to its C-terminal amide bond. We further suggest that N-alkylation on the more flexible systems, like NMeAla or L-Pip containing peptides, enhances transfer of proton from the N-alkylated amide bond's oxygen to the amide bond on the C-teminus of this residue either to N (conforming to 'classical' mechanism) or to O (according to mechanism via cyclic oxazolone-like intermediate proposed by Hunt). The striking difference in fragmentation pattern of peptides with L- and D- Pip implies the importance of an energetically accesible conformation of protonated peptide which facilitates the transfer of proton to certain amide bond.

Y_{n-1} ions were found in the spectra of compounds when there is no N-bound proton available for transfer to the forming ion (Fig.1). Deuterium labeling at the acetyl group revealed transfer from the acetyl methyl group. The ionizing proton also is retained by the *y* ion. When the deuteron is transferred to the tertiary nitrogen of Pro, there is clean incorporation of one deuteron observed, while for the transfer to the secondary nitrogen of Val the the ratio H : D approx. 1:1 is observed. When the N- bound proton is present

(AcAla at the N-terminus) there is no deuterium incorporation observed proving that this is a primary source of transferred proton in standard peptides.

References:

1. J. Urban, T. Vaisar, R. Shen, and M.S. Lee, manuscript in preparation.
2. M. Przybylsky, I. Dietrich, I. Manz, and H. Bruckner, *Biomed. Mass Spectrom.* **11**, 1984, 569-582.
3. B.L. Schwartz, M.M. Bursey, *Biol. Mass Spectrom* **21**, 92-96 (1992)
4. D. Arnott, D. Kottmeier, N. Yates, J. Shabanowitz, D.F. Hunt, *42nd ASMS Conference on Mass Spectrometry*, Chicago 1994, p. 470.
5. D.R. Mueller, M. Eckersley, W.J. Richter, *Org. Mass Spectrom.* **23**, 217-222 (1988).
6. T.M. Kenney, K. Nomoto, R. Orlando, *Rapid Commun. Mass Spectrom* **6**, 95-97 (1992).

Table 1. CID spectra of H-Ala-Val-X-Leu-Gly-OH peptides, ES+, Ar, E_{LAB} = 10 eV (relative abundances, % TIC).

	$[M+H]^+$	b_2	b_3	b_4	y_3
H-Ala-Val-**Pro**-Leu-Gly-OH	62.9	1.2	1.2	1.2	33.6
H-Ala-Val-**NMeAla**-Leu-Gly-OH	41.7	0.3	54	1.7	2.3
H-Ala-Val-**L-Pip**-Leu-Gly-OH	37.6	0	51.9	0.3	10.2
H-Ala-Val-**D-Pip**-Leu-Gly-OH	58	0.4	17.1	3.2	21.4

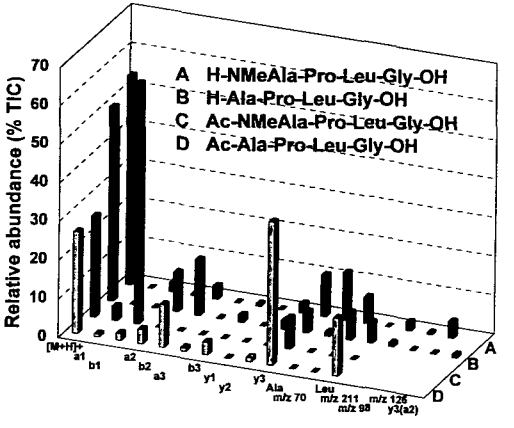

Fig. 1, CID of peptides with N-terminal NMeAla residue, ES+, Elab = 30 eV

DETECTION OF MODIFIED PEPTIDES IN ENZYMATIC DIGESTS BY μLC-APICID-MS AND DOUBLE-POLARITY HYBRID-SCANNING TECHNIQUE

Paul Jedrzejewski, Martina Schnölzer*, Wolf D. Lehmann
Central Spectroscopy Department and *Department of Cell Biology
German Cancer Research Center, Im Neuenheimer Feld 280, 69120 HEIDELBERG, Germany

Characterization of protein modifications is an important aspect in the analysis of protein structure and function. Post-translational modifications such as phosphorylation, sulfation, glycosylation, and N-terminal blocking are a means of cellular regulation of protein function. Non-biological modifications such as deamination, formylation, oxidation or coupling with acrylamide may also arise during sample preparation. The acrylamide modification may occur during polyacrylamide gel electrophoresis, where cysteine residues may be covalently modified, resulting in a mass increment of 72 da per cysteine residue.[1,2] Conventional protein sequencing methods are not suitable for detection of these protein modifications.

The use of APICID to generate specific marker ions for the detection of phosphorylation, sulfation and glycosylation was introduced by Carr and Huddleston.[3,4] In their investigations modified peptides were identified by employing a single-polarity hybrid-scanning technique for the detection of fragments and molecular mass of a single type of modification. Extending these studies, we have developed a new double-polarity acquisition scheme which allows for simultaneous determination of peptide mass and the presence of various peptide modifications. The technique utilizes APICID electrospray-MS to generate specific marker ions indicative of phosphorylation (-79, PO_3^-), sulfation (-80, SO_3^-), and acrylamide modification (+104, $[S\text{-}CH_2\text{-}CH_2\text{-}CONH_2]^+$). The scanning technique presented here uses polarity switching during a hybrid scan to detect various marker ions irrespective of their optimum polarity.

Fragmentation is controlled by modifying the APICID offset voltage. Optimum APICID conditions for each modification were determined by investigation of model compounds. During a hybrid scan, fragmentation is maximized at low m/z values by selecting marker ion-specific APICID offsets, whereas molecular mass information is obtained with the APICID offset turned off at high m/z values

In order to evaluate the on-line capabilities of this new double-polarity hybrid-scanning technique a tryptic digest of 100 pmol β-casein was spiked with cholecystokinin (sulfo-tyrosine) peptide and with a synthetic acrylamide-modified peptide. The resulting total ion chromatogram and the modification-specific single ion chromatograms at m/z -79, -80, and +104 are given in Figure 1. Each single ion chromatogram indicates the precise retention time for a specificly modified peptide, and the simultaneously obtained molecular mass information provides positive identification. In the double-polarity hybrid mass spectrum of the phosphorylated T6 fragment of β-casein (Figure 2), which was recorded in the LC-APICID-MS run shown in Figure 1, both the $[PO_3]^-$ -ion, specific for phosphate esters, and the $[M+H]^+$ of the intact phosphorylated T6 peptide can be recognized.

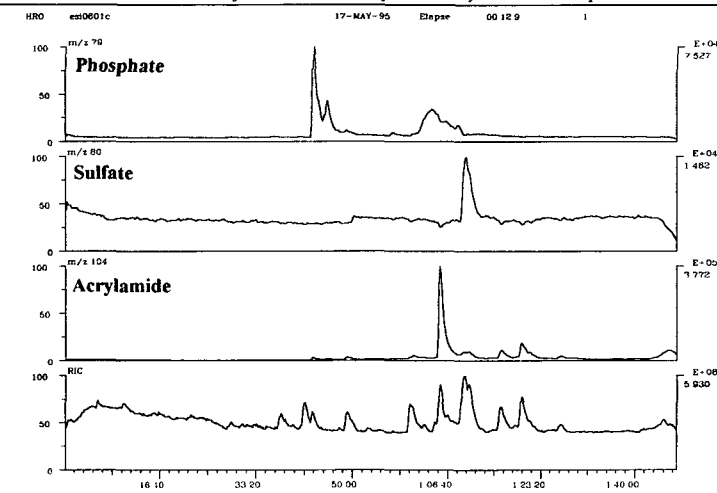

Figure 1: LC-APICID-ESI analysis of a tryptic digest of β-casein spiked with a cholecystokinin (sulfo-tyrosine) peptide and with an acrylamide-modified peptide; double-polarity hybrid-scanning was used for specific detection of modified peptides.

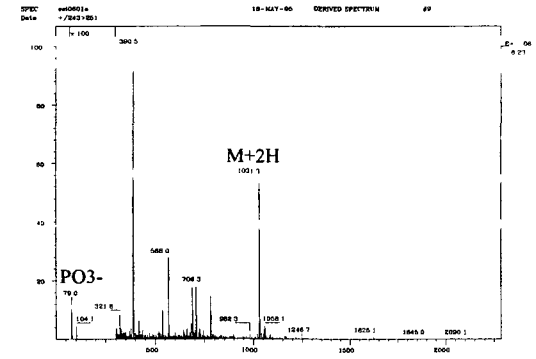

Figure 2:
ESI (double-polarity hybrid scan) mass spectrum of the phosphorylated T6 fragment of β-casein detected in the LC-MS run displayed in Figure 1.

References
1. Hall, S. C. *et al.* (1993) *Proc. Natl. Acad. Sci. USA* **90**, 1927-1931.
2. Bonaventura, C. (1994) *Anal. Biochem.* **222**, 44-48.
3. Carr, S. A.; Huddleston, M. J.; Bean, M. F. (1993) *Protein Sci.* **2**, 183-196.
4. Huddleston, M. J. et al. *J. Am. Soc. Mass Spectrom.* **4**,710-717.

Enzymatic Reactions on Membranes for the MALDI Analysis of Phosphoproteins

Pao-Chi Liao[1,2], Douglas A. Gage[2], and John Allison[1], Department of Chemistry[1] and Biochemistry[2], Michigan State University, East Lansing, MI 48824

We have previously reported a method to locate phosphorylation sites in a phosphoprotein with known primary sequence, using peptide mass mapping by combining specific enzymatic degradation with matrix-assisted laser desorption/ionization mass spectrometry (MALDI-MS) [1]. There are three steps to locate phosphorylation sites in a phosphoprotein: 1. degradation of the phosphoprotein into peptides by specific enzymatic or chemical reactions; 2. identification of the phosphopeptides by -80 (or multiples of -80) Da mass shifts in the mass spectra after dephosphorylation with alkaline phosphatase; 3. location of the phosphorylation sites by peptide mass-mapping. The second step, using the enzymatic dephosphorylation reaction, is a critical step in the analysis. The dephosphorylation reaction allows a phosphopeptide to be identified by mass shifts using simple mass measurements of the peptide before and after the dephosphorylation reaction. The procedure does not require an MS/MS technique. The enzymatic reaction is highly selective and sensitive. A further refinement of the experimental procedures for the enzymatic dephosphorylation reaction is discussed here. The goal is to minimize sample loss from manipulations and facilitate simple, rapid analyses. This is especially important when only picomolar amount of samples are available. Our procedure also provides a sensitive means to remove the impurities which may interfere with the enzymatic dephosphorylation reaction and/or the MALDI mass spectral analysis.

A protocol has been developed to immobilize low picomolar phosphopeptides on a supporting material, wash the sample when necessary, conduct enzymatic dephosphorylation, remove reaction buffers, then add matrix compound and analyze the final reaction products by MALDI *in situ*. The immobilization material must meet both requirements for efficient separations and be an effective interface to a MALDI mass spectrometer. Nylon-based membranes exhibit these properties [2]. The use of Zetabind (Cuno Laboratory Products), a positive charge-modified nylon membrane, is described here. 10 pmol of a phosphopeptide, KRP(pS)QRHGSKY-amide, was immobilized by air-drying the peptide solution on a piece of membrane fixed on a stainless steel probe with double-sided tape. The sample probe was washed with 0.5 mL 0.1% trifluoroacetic acid (TFA) solution twice to remove any water-soluble contamination. 2 μl of 50 mM NH_4HCO_3 buffer solution (pH 8.0) containing about 3 units of calf intestine alkaline phosphatase was applied to the sample probe. An incubation assembly was designed to prevent the reaction mixture from evaporation and used for the dephosphorylation reaction in a water bath at 37°C. After 4 hours of reaction time, the sample probe was washed with 0.5 mL 0.1% TFA solution twice to remove reaction buffers. Then, 1 μl of 20 mM α-cyano-4-hydroxycinnamic acid matrix solution (in a 1:1 solution of 0.1% TFA : acetonitrile) was added to the sample probe. When the peptide/matrix mixture was dried and cocrystallized on the membrane, the sample was subjected to analysis by MALDI. All MALDI data were obtained in linear mode on a ResearchTec time-of-flight (TOF) mass spectrometer (Vestec Corp., Houston, TX). The Figure below shows the expected -80 Daltons mass shifts in the MALDI mass spectra due to the loss of phosphate moieties after using this protocol.

This design is especially important when the peptide sample contains chemical substances which interfere with the subsequent dephosphorylation reaction and only a limited amount of sample is available. We have found that phosphopeptides purified from metal ion affinity columns may contain iron impurities which interfere with the dephosphorylation reaction. The problem can be avoided by this sample immobilization and washing protocol. A putative phosphopeptide, obtained from the tryptic proteolysis of sucrose-phosphate synthase (SPS), has been purified by Fe^{3+}-IDA affinity chromatography. The attempt of direct dephosphorylation reaction (without the immobilization on the membrane and subsequent washing procedure) failed to show a -80 Da mass shift by mass spectrometry. It was suspected that there are impurities in the sample that may interfere with the enzymatic activity of phosphatase. A "spike" experiment was carried on a pure phosphopeptide, KRP(pS)QRHGSKY-amide, and the expected -80 Da mass shift was not observed. Our protocol described here was used to remove the contaminations and overcome the interference problem. The protocol eliminates substantial sample clean-up procedure (e.g., dialysis, which may introduce sample loss), prior to MALDI-MS analysis.

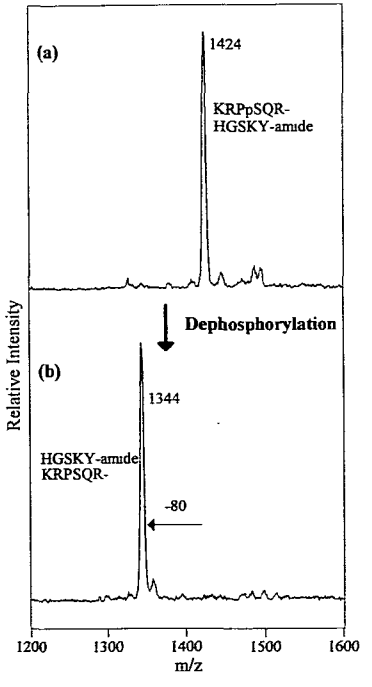

[1]. Liao, P.-C., Leykam, J., Andrews, P. C., Gage, D. A., and Allison, J., *Anal. Biochem.* **219**, 9-20 (1994).
[2]. E. J. Zaluzec, D. A. Gage, J. Allison, and J. T. Watson, *J. Am. Soc. Mass Spectrom.* **5**, 230 (1994).

Improved Low Energy CID Spectra of Peptide Ions Using Stepped Collision Potentials.

R.S. Annan and S.A. Carr
SmithKline Beecham Pharmaceuticals
King of Prussia PA 19406

The overall appearance of low energy CID spectra of peptide ions is largely dependent upon three factors: the peptide sequence, the collision energy, and the collision gas pressure. For a given peptide sequence, changes in the collision energy can dramatically alter the relative abundance of the product ions. Because of the multiple collision regime under which low energy CID operates, a product ion may decompose to a lower m/z fragment upon undergoing secondary collisions. Low m/z fragment ions, such as internal sequences and immonium ions have found new importance due to the recently introduced technique of searching peptide MWs against protein sequence databases. A short partial sequence of even two amino acids, or the presence of some of the less common amino acids identified via an immonium ion, together with the peptide molecular weight can either uniquely identify the peptide, or greatly reduce the number of peptide matches.

Unfortunately abundant immonium ions and low m/z internal sequences are frequently produced at the expense of high m/z sequence ions, giving rise to spectra which show a rapid fall off of fragment ions above the multiply charged precursor. This type of spectrum is of little use if coverage of the entire sequence is necessary, for instance to identify the site of phosphorylation in a peptide. We have found that ions higher in m/z than the doubly charged precursor are generally the most useful for sequencing purposes (for one, there is no charge state ambiguity), and therefore, we make every effort to maximize them. However, we do not want to give up an abundant yield of immonium ions. We have found that by recording the CID spectrum at two different collision energies a more even distribution of product ions results, with abundant immonium and high m/z sequence ions.

All CID spectra were recorded on a Perkin Elmer Sciex API III triple quadrupole mass spectrometer using either the standard articulated ionspray interface, or a custom built nanoliter flow ionspray interface (M. Mann EMBL). Peptide samples were reconstituted in methanol:water:formic acid (50:50:0.2) and infused into the MS using either a Harvard syringe pump operated at 2 μL/min, or the nanospray device where typical flow rates are on the order of 25–40 nanoliters per minute (1). The collision energy (E_{coll}) on the Sciex API III is determined by the difference in voltages (R0 and R2, respectively) applied to Q0 (RF only focusing rods prior to Q1) and Q2 (RF only collision cell) such that $E_{coll} = z(R0-R2)$, where z is the charge on the precursor. Thus recording a spectrum using different collision energies is accomplished by stepping the voltage on Q2 to a higher or lower value as Q3 is scanned from low to high m/z. All collision energies are reported as collision potentials, ie. the voltage difference between R0 and R2.

Figure 1 demonstrates that a more even distribution of fragment ions can be generated following CID if the spectrum is acquired using two collision potentials. Even under experimental conditions where one has the time to carefully optimize the parameters affecting CID (such as when using a nanospray interface), it is still generally beneficial to perform a two step CID experiment. Unfortunately, under the current software limitations, only one voltage can be changed with mass during a scan. Therefore, these experiments can only be done under conditions where the fragment ion spectrum is acquired at less than unit resolution, because operating in the higher resolution mode requires changing more than one voltage simultaneously. For normal ionspray operation, this is not a drawback, since this mode of operation provides the highest sensitivity. However, with the advent of nanoliter flow ES interfaces and the ability to

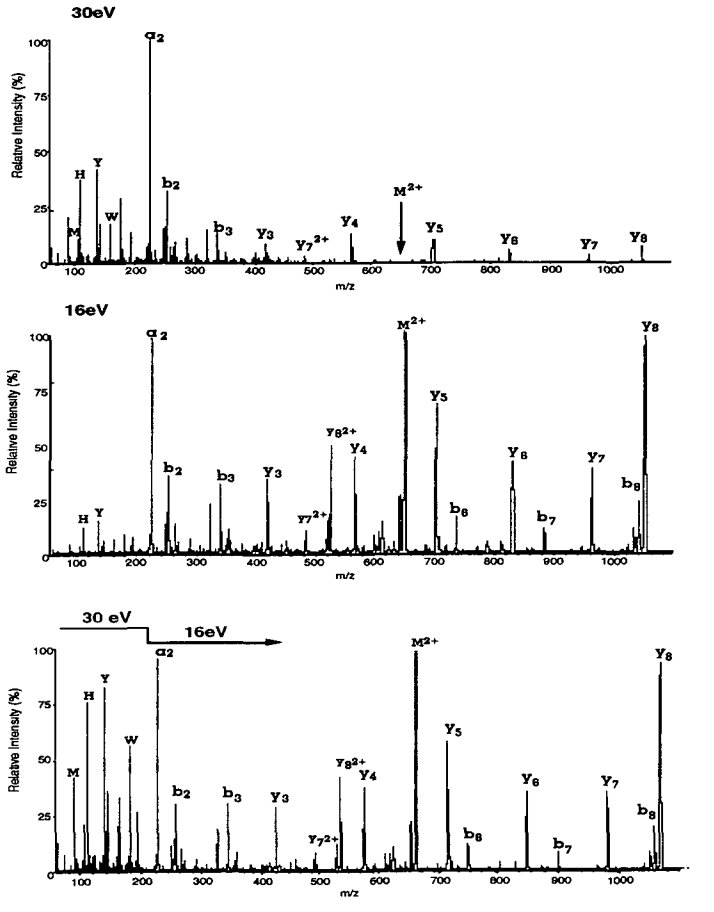

.Figure 1

signal average for long periods of time, with a small amount of sample, the acquisition of isotopically resolved fragment ions become realistic and, therefore, desirable.

The authors are grateful to Michael Huddleston for help with the nanoliter flow interface

(1) M. Wilm and M. Mann, Int. J. Mass Spectrom. Ion Proc. (1994), 136, 167.

Location of peptide phosphorylation sites by use of (+) and (−)ESI-MS/MS. M. Busman, K.L. Schey, D.R. Knapp, Department of Pharmacology, Medical University of South Carolina, Charleston, SC

Introduction Recently, rhodopsin and rhodopsin kinase phosphorylations have been studied by ESI-MS/MS and FAB-MS/MS.[1,2] In our studies of rhodopsin phosphorylation we have synthesized a series of reference phosphopeptides, corresponding to the peptides from the C-terminal region that could be isolated after enzymatic digestion of rhodopsin. A complete set of mono- and di-phosphorylated analogs of the fragment peptides ASTTVSKTE and TSQVAPA was synthesized.[3] Here we report the results of the analysis of these synthetic peptides by ESI-MS/MS and, in particular, the complementary use of experiments utilizing positive and negative ions, as well as different charge number ions, as precursor ions for CID.

Experimental. The preparation of the synthetic phosphorylated peptides has been previously described.[3] Peptides were analyzed by ESI-MS on a SCIEX API III triple quadrupole mass spectrometer. Solutions of the peptides were prepared at a concentration of ~1 x 10^{-4}M in 47.5/47.5/5 (v/v/v) methanol-water-acetic acid for positive mode (+)ESI-MS and 47.5/47.5/5 (v/v/v) methanol-water-piperidine for negative mode (−)ESI-MS. CID was carried out in the rf-only quadrupole region, Q2, to generate product ions from peptide precursor ions.

Results-Discussion The product ion spectrum for the $[M+H]^{+1}$ ion of T(p)SQVAPA is shown in Figure 1(a). Sufficient fragmentation information is not provided from the product ion spectra of the $[M+H]^{+1}$ ions alone to unequivocally assign location of the sites of phosphorylation on each peptide. The product ion spectrum for the $[M-H]^{-1}$ ion of T(p)SQVAPA is shown in Figure 1(b). While the product ion spectra from the $[M-H]^{-1}$ ions alone do not provide sufficient information to deduce the complete sequence of the peptides, it is apparent that the CID experiments on $[M+H]^{+1}$ and $[M-H]^{-1}$ ions provide complementary information, allowing assignment of the sequence, including site of phosphorylation.

The product ion spectra for the $[M+H]^{+1}$ and $[M+2H]^{+2}$ ions of AS(p)TTVSKTE are shown in Figure 2. Losses of H_3PO_4, indicated by a loss of 98 Th (or in the case of the doubly charged species, −49 Th) from the $[M+H]^{+1}$, $[M+2H]^{+2}$ and, where appropriate, the y- and b-type product ions are seen. The results of the CID experiments on the two charge states provide complementary information, allowing unequivocal assignment of the location of all sites of phosphorylation. Similar results were obtained from singly and doubly charged ions from the di-phosphorylated analogs of ASTTVSKTE, allowing location of both sites of phosphorylation in most of the peptides.

Figure 3 shows the CA(−)ESI-MS spectrum for angiotensin I. Based upon y-type fragment information in the spectrum, the complete sequence for the molecule can be assigned. Figure 4 shows the (−)ESI-MS/MS spectrum for leucine enkephalin. Notable in this spectrum is the presence of c-type fragment ions. The detection of c-type fragments in low energy tandem mass spectrometry experiments of ions produced by (−)ESI has been previously noted by Loo *et al.*[4] Sufficient information is available from the spectrum to assign the sequence of the molecule. The results of these experiments demonstrate the ability of the ESI-MS/MS technique to provide sequence information for small peptides. Such observations are contrary to previous observations of the apparent lack of backbone fragmentations upon CID of FAB generated negatively charged ions.[5,6]

43rd ASMS Conference on Mass Spectrometry and Allied Topics

Conclusions The complementary use of different forms of the ESI-MS/MS experiment has been utilized to determine sites of phosphorylation in synthetic phosphopeptides based on sequences from the C-terminal region of rhodopsin accessible by enzymatic digestion. Sites of phosphorylation for most of the phosphopeptides could be determined. In the data presented here, many of the peptides yielded complete sequence information by the (−)ESI-MS/MS technique. The majority of the fragment ions detected could be rationalized in terms of cleavages of the peptide backbone. Only in a few cases were ions resulting from side chain cleavages a major contribution to the MS/MS spectrum.

Acknowledgement We thank Dr. Peter Moeller at the National Marine Fisheries Service, Southeastern Laboratory, Charleston, SC for use of the SCIEX API III. This work was supported in part by NIH Grants EY 08239 and HL 07260 (postdoctoral fellowship for MB).

References

1. Ohguro, H.; Palczewski, K.; Ericsson, L.H.; Walsh, K.A.; Johnson, R.S. *Biochemistry* 1993, *32*, 5718-5724.
2. Papac, D.I.; Oatis, J.E.; Crouch, R.K.; Knapp, D.R. *Biochemistry* 1993, *32*, 5930-5934.
3. Knapp, D.R.; Oatis, J.E.; Papac, D.I. *Int. J. Peptide Protein Res.* 1993, *42*, 259-263.
4. Loo, J.A.; Ogorzalek Loo, R.R.; Light, K.J.; Edmonds, C.G.; Smith, R.D. *Anal. Chem.* 1992, *64*, 81-88.
5. Waugh, R.J.; Bowie, J.H.; Gross, M.L.; Vollmer, D. *Int. J. Mass Spectrom. Ion Process.* 1994, *133*, 165-174.
6. Marzluff, E.M.; Campbell, S.; Rodgers, M.T.; Beauchamp, J.L. *J. Am. Chem. Soc.*, 1994, *116*, 7787-7796.

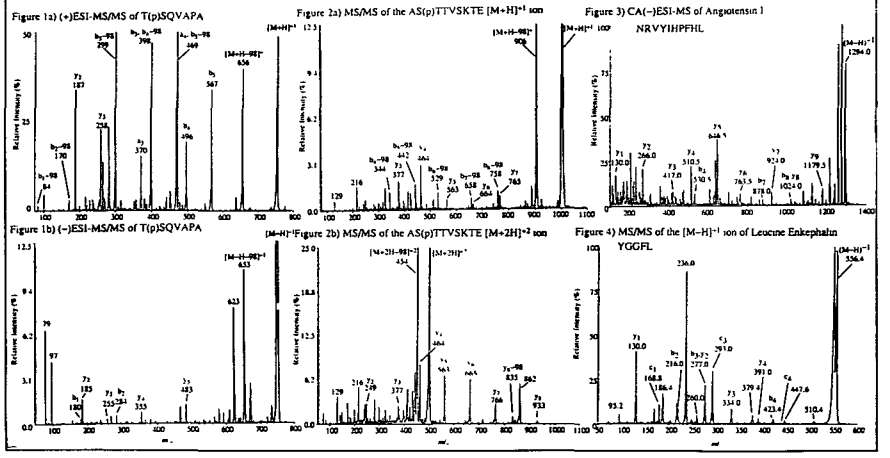

Phosphorylation and N-terminal Acetylation of Phosrestin I in Fly Eyes

Tomoya Kinumi[1,2], Kenneth W. Jackson[1], Masayuki Kubota[2], Mamoru Ohashi[2] and Hiroyuki Matsumoto[1]
[1] The Univ. of Oklahoma, Health Sciences Center, Oklahoma City, Oklahoma.
[2] The Univ. of Electro-Communications, Tokyo, Japan.

INTRODUCTION Protein phosphorylation cascade plays important roles in cell signaling. In the photoreceptor cells of the fruitfly, *Drosophila melanogaster*, two-dimensional (2-D) gel analysis reveals at least three classes of phosphoproteins which undergo light-induced reversible phosphorylation. Two of these are named phosrestin I (PRI) and phosrestin II (PRII). PRI and PRII are homologous to mammalian arrestins which are known to inactivate G-protein-linked receptors such as rhodopsin and β-adrenergic receptor. Previously, the phosphorylation site of PRI had been determined to be Ser_{366} *in vitro*. In order to confirm that Ser_{366} is also the phosphorylation site *in vivo* and to study other post-translational modifications of PRI, we have developed a protein micro analysis technique using LC/MS after in-gel digestion of 2-D gel purified protein (1).

METHODS The phosphorylated form of PRI was isolated on 2-D gels from light-adapted *Drosophila* eye homogenates prepared from 3,000 flies. The PRI spots were visualized by a brief staining with Coomassie blue. The in-gel digestion was performed according to Rosenfeld *et al.* (2). The spots were cut out and incubated with water overnight and washed three times with 60% MeCN/H_2O. After washing, the gel spots were slightly dried, then 2 μl of TPCK-trypsin solution was applied (0.2 mg of TPCK-trypsin in 1 ml of 200 mM ammonium bicarbonate pH 7.8) for each gel spot. The spots were incubated in 0.2 ml of 200 mM ammonium bicarbonate at 27°C for 24 hrs. The resulting peptide fragments were extracted with 60% MeCN/0.1% TFA/H_2O and applied to a microbore C18 HPLC column (1 mm i.d. ×150 mm) The HPLC was directly interfaced with an electrospray ionization mass spectrometer (PE-Sciex Model API-III).

1) **Determination of the *in vivo* phosphorylation site.** We searched for the PRI tryptic fragment containing Ser_{366} (phospho-$PRI_{364-371}$: MKS(P)IEQHR, MH^+=1108.5) by single ion monitoring (SIM). For the authentic phospho-$PRI_{364-371}$, we synthesized the peptide MKSIEQHR and phosphorylated it to obtain MKS(P)IEQHR by using PRI kinase extracted from fly heads. The retention time of the putative phospho-$PRI_{364-371}$ was compared with that of the synthetic MKS(P)IEQHR by SIM.

2) **N-terminal modification of PRI.** We searched for the possible N-terminal tryptic fragment(s) using SIM. One of the N-terminal fragments was sequenced by CID. For CID analysis, the in-gel digested peptide fragments were partially purified by reversed phase HPLC. The purified fragments were applied to MS.

RESULTS 1) From the stored data of the PRI tryptic digests scanned from m/z=350 to 1200 on LC/MS, a single peak was extracted between m/z=1108 to 1109 (Peak A in Fig 1). [MKS(P)IEQHR, MH^+ = 1108.5]. The mass spectrum of the Peak A is shown in Fig 2. Peak A exhibited the same retention time as that of the authentic phosphopeptide MKS(P)IEQHR. Furthermore, co-injection of the PRI tryptic digests and the synthetic MKS(P)IEQHR resulted in a single peak. In the simulated tryptic digests of PRI, another peptide fragment, whose MH^+ is close to 1108.5, was expected. *i.e.*, PRI_{74-82}, FSKELILCR, MH^+ =1108.6. In order to eliminate the possibility that the Peak A represents PRI_{74-82}, we synthesized the authentic peptide, FSKELILCR, and measured its retention time. This peptide eluted 5 minutes later than the Peak A under the

conditions used. This result is consistent with our conclusion that the Peak A represents phospho-$PRI_{364-371}$, MKS(P)IEQHR.

2) The expected N-terminal tryptic fragment of PRI is MVVSVK. However, we failed to observe MVVSVK in the digests. Instead, we observed two related peaks, VVSVK and acetyl-MVVSVK in SIM (Fig 3). The peptide sequence of one of these SIM peaks, VVSVK, was confirmed by CID (Fig 4).

CONCLUSION 1) PRI is phosphorylated at Ser_{366} *in vivo* as predicted from the experiments which had been conducted *in vitro*. 2) There are two chemical species of PRI N-termini, one in which the initiation Met has been removed and the other in which the Met remains, but is acetylated. However, we observed no N-terminal fragment of PRI which remains intact.

This study demonstrates that combination of 2-D gel electrophoresis, in-gel digestion and LC/MS is a powerful tool to elucidate *in vivo* protein modification.

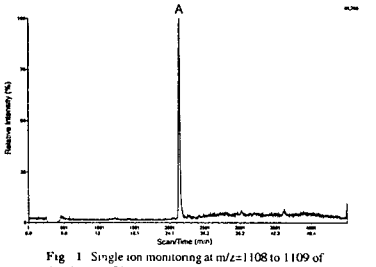

Fig 1 Single ion monitoring at m/z=1108 to 1109 of the phospho PRI tryptic fragments after in gel digestion

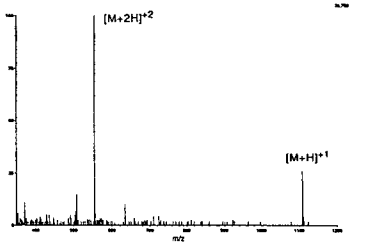

Fig. 2 Mass spectrum of peak A in Fig 1, the molecular weight is 1107 5

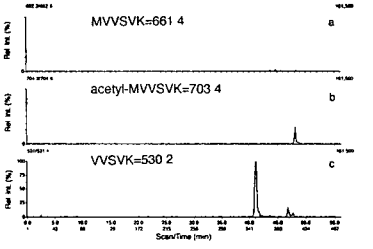

Fig. 3 Single ion monitoring of PRI N-terminal tryptic fragments, monitored $[M+H]^{+1}$ ions at m/z= a) 662 2 to 662 6, b) 704 2 to 704 6, c) 531 0 to 531 4

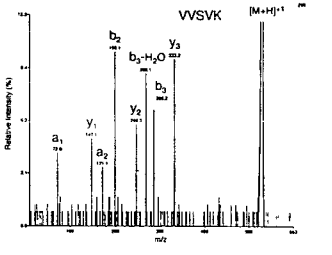

Fig. 4 CID spectrum of the $[M+H]^{+1}$ of m/z=531, VVSVK

REFERENCES

[1] H. Matsumoto *et al.*, *Neuron* (1994) **12**, 997-1010.
[2] J. Rosenfeld *et al.*, *Anal. Biochem.* (1992) **203**, 173-179.

ACKNOWLEDGEMENTS Supported by grants from the National Institutes of Health (EY06595) to HM and the Grant-in-Aid from the Japanese Ministry of Education to MO.

Electrospray FTICR Mass Spectrometry of Modified Peptides and Proteins

Joseph P. Nawrocki, Clifford H Watson and John R. Eyler
Department of Chemistry, University of Florida, Gainesville, Florida 32611

ABSTRACT

We have been investigating novel blocked and modified proteins using electrospray FTICR-MS. Modified peptides and proteins are readily analyzed via ESI and readily undergo CAD to provide structurally useful product ions. High resolution detection of the parent and product ions allows for the unambiguous identification of the amino acid residues and the identity of the modification This proves very useful for synthetic proteins as well as for novel proteins that may have been post-translationally modified Phosphorylation, one such modification, holds much interest in biochemistry Methods to easily study these proteins using positive ion ESI/FTICR-MS are currently being developed in our lab.

INTRODUCTION

ESI mass spectrometry has quickly become an important tool for the analysis of many biological samples Accurate mass determination has proven useful for synthetic peptides and proteins and for novel uncharacterized proteins The technique of CAD can yield much information about the parent ion, but can sometimes be ambiguous due to mass similarities between attached moieties including those from post-translational modifications, blocking groups and amino acids The combination of ESI with FTICR-MS allows for the differentiation between groups of similar nominal masses due to the high resolution of the instrument

Phospho-peptides/proteins hold much interest for study, but cannot usually be studied in positive ion mode Terminal phosphates, with pKa values of 1.0 and 6 5, are negatively charged under typical electrospray conditions Negative ion electrospray has only recently been achieved on our commercial FTICR mass spectrometer and conditions are not yet well characterized It has been shown that phosphate groups bind appreciably to certain M^{3+} and M^{4+} ions. [1,2] Such metals include Fe^{3+}, Sc^{3+}, Th^{4+} and Lu^{3+}. However, various other metals show no affinity for these proteins These metals should neutralize the negative charge or convert it to a net positive charge depending on the binding mechanism, provided these metals bind in the gas phase. Various conditions of concentration and pH are being examined to determine ideal binding conditions.

EXPERIMENTAL

Ions were produced via an electrospray source (Analytica of Branford, Branford, CT) mounted in the external source housing of a 7-tesla FTICR mass spectrometer. Ions were then transported via a series of electrostatic lenses. Samples were run at concentrations of about 5 x 10^{-5} M in water/methanol/acetic acid 49/49/2 CAD was accomplished by increasing the potential difference between the capillary exit and the first skimmer Running conditions included. capillary potential=-4 0kV, cylinder potential=-3.0kV and needle at ground potential Needle capillary distance usually varied between 10-15mm Calibration was done in heterodyne mode using fragment ions produced by ESI/CAD of bradykinin.

RESULTS

ESI/FTICR mass spectrometry has proven to be a very useful tool for the unambiguous determination of modifications on peptides and will be used to study larger modified proteins Figures 1 and 2 illustrate the determination of a blocking group on a synthetic pentapeptide A loss of 56 107 amu is indicative of tert-butyl blocking group which was used during synthesis This type of unambiguous mass determination will prove very useful for post-transnational modifications of larger proteins.

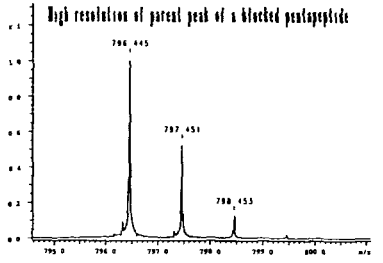

Figure 1. Blocked pentapeptide before CAD retaining all tert-butyl groups

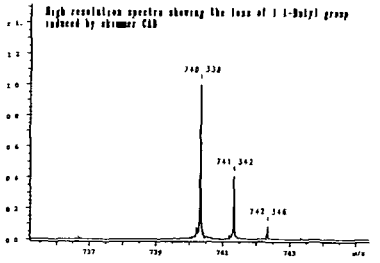

Figure 2. Blocked pentapetide after CAD showing the loss of one tert-butyl group

REFERENCES

1) Anderson, L, Porath, J , *Analytical Biochemistry*, 1986, **154**, 250-254

2) Arendt, A.; Palczewski, K ; Moore, W ; Caprioli, R., McDowell, H , Hargrave, P., *Int. J. Peptide and Protein Res.*, 1989, **33**, 468-476

MASS SPECTROMETRIC PROTEIN IDENTIFICATION IN COMPLETELY SEQUENCED GENOMES

Matthias Mann, Ole N. Jensen, Ole Vorm, Peter Mortensen, Andrej Shevchenko, Tony Houthaeve, and Matthias Wilm
European Molecular Biology Laboratory
Meyerhofstr. 1, D-69012 Heidelberg, Germany

Introduction

The completion of many genome sequencing projects will change the focus of protein analysis in the near future. Since comprehensive DNA sequence information will be available for many species the major objective will be to identify a gene product and thereby the gene (open reading frame) associated with a given biological activity or function. Peptide mapping and peptide sequencing by mass spectrometric methods have potential for rapid identification of proteins by means of "peptide mass fingerprints" and "peptide sequence tags" combined with computerized searches in DNA and protein sequence databases. Completely sequenced genomes are ideal for mass spectrometric protein identification because the chances of assigning a "false positive" due to the absence of the correct protein sequence in the database are extremely low: There will always be at least one correct match.
To ascertain the applicability of current mass spectrometric techniques to protein identification in completely sequenced genomes we have investigated the requirements for unambiguous identification of proteins encoded in the genomes of vaccinia virus (200 open reading frames) and yeast (*Saccharomyces cerevisiae*, ~7000 open reading frames).

Experimental

Peptide mass mapping was performed using a Bruker Reflex reflector TOF mass spectrometer capable of post-source-decay (PSD) analysis. The instrument control and data acquisition software (LaserOne for Macintosh) was developed in-house. Matrix surfaces were prepared by the fast evaporation method using 4HCCA as the matrix compound (1). ES MS/MS was performed using the NanoES source (2) on a Sciex API III triple quadrupole mass spectrometer. Prior to NanoES MS/MS analysis peptide samples were desalted using custom made reversed-phase columns (Wilm *et al*, submitted). Database searches using peptide mass data and peptide sequence tags (3) were performed by PeptideSearch, a Macintosh application developed by us. Vaccinia-only, yeast-only, GenPept, and SwissProt databases were used. The software allows database searches to be performed using a variety of parameters, including peptide sequence tags. A "second pass" search feature allows rapid evaluation of high-scoring protein sequences.

Results

The fast evaporation method for sample preparation and an automated internal mass calibration procedure for MALDI reflector TOF mass spectrometry allow us to routinely obtain (monoisotopic) mass accuracies of 0.01% or better in the useful tryptic peptide mass range from m/z 600 to 2500. This improved mass accuracy puts a strong constraint on the subsequent database searches and greatly reduces the likelihood of detecting false positives.
We have also tested MALDI PSD reTOF for the generation of peptide sequence tags. Using a single PSD peptide sequence tag in combination with an accurately determined precursor ion mass uniquely identify the 14 kDa fusion protein in the vaccinia virus sequence database (Figure 1). Although further improvements are necessary, this technique has the potential to rapidly generate peptide sequence tags. NanoES MS/MS is another powerful method for producing several peptide sequence tags from a peptide mixture because it allows 30-45 minutes of MS/MS analysis time on a small volume (1 µL) of sample. We routinely use this method to identify proteins from yeast and other species.

Conclusion

MALDI reflector TOF MS and NanoES MS/MS can produce data that, in combination with database searching, unambiguously identify proteins in well-characterized genomes, such as those of vaccinia virus and yeast. The combination of MALDI MS for producing peptide maps and NanoES MS/MS for generating peptide sequence tags provides 1) good coverage of the protein sequence; and 2) protein specific sequence information.
In our experience, the requirements for unambiguous identification of a protein in sequence databases by mass spectrometric data are one or more of the following:

- More than 10 peptide masses determined with a mass accuracy of better than 0.01% of which 5 or more produce the same protein match and cover more than 10% of the protein sequence.
- Two or more peptide sequence tags producing the same protein match
- A combination of the above methods, i e. a peptide mass map (0.01% accuracy) and several peptide sequence tags.

Using these requirements we have to date identified more than 50 proteins from a variety of sources. We have not found the use of "limited" databases, *i.e.* species-specific databases to improve the search results significantly using the described mass spectrometric techniques. We recommend that searches be performed in an all-inclusive protein database because contaminating proteins such as human keratin (often found in protein preparations) also will be identified.
Having the above mentioned mass spectrometry and software tools available we now pursue developments to increase sample throughput and to investigate defined subcellular compartments and specific multiprotein complexes. The experience gained to date make us believe that mass spectrometry will revolutionize protein analysis in completely sequenced genomes.

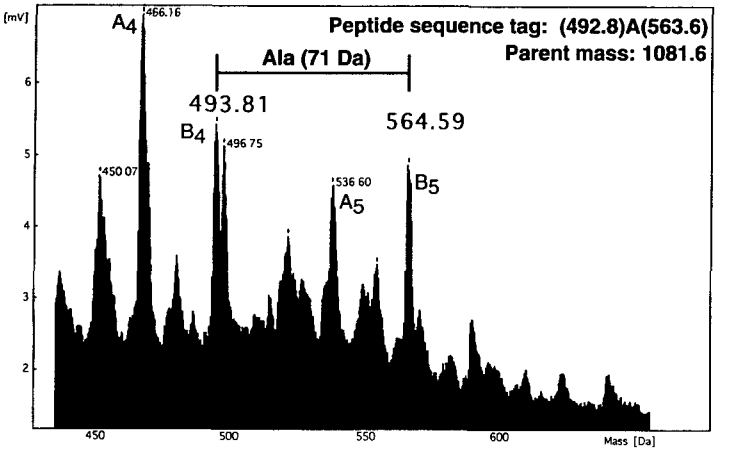

Figure 1. MALDI post-source-decay mass spectrum of a m/z 1082 peptide present in a peptide mixture. Pulsed deflection plates were used to remove ion signals outside a mass-window of approximately 50 Da centered around the m/z 1082.6 ion signal. The A/B ion seried were detected by noticing the characteristic 28 Da mass difference. The generated peptide sequence tag (492.8)A(563.6) in combination with the precursor peptide mass (1081.6 ± 0.1 Da) uniquely identifies the 14 kDa fusion protein in the vaccinia protein database.

1. Vorm, O., Roepstorff, P., and Mann, M. (1994) *Anal. Chem.* **66,** 3281-3287.
2. Wilm, M. S., and Mann, M. (1994) *Int. J. Mass Spectrom. Ion. Proc.* **136,** 167-180.
3. Mann, M., and Wilm, M. S. (1994) *Anal. Chem.* **66,** 4390-4399.

E-mail: mann@embl-heidelberg.de
URL: http://mac-mann6.embl-heidelberg.de/

USEFUL TABLES OF POSSIBLE AND PROBABLE PEPTIDE MASSES

M. Mann, European Molecular Biology Laboratory (EMBL)
Postfach 10.2209, D-69012 Heidelberg, Germany

Peptide masses are often calculated as "nominal" or integer masses obtained by setting the peptide masses equal to the added mass of the integer number of atomic constituents. However, it is well known that peptide masses are not arbitrarily distributed but exhibit a certain "mass offset" from the nominal mass. This mass offset depends on the mass considered and increases with increasing mass (Fractional Mass Values). Here the phenomenon is quantified by calculating all possible peptide masses in the range of 0 to 2000 Da and tabulating all actual peptide masses from sequence databases and practical uses of these mass distributions are suggested.
All calculations were done with the program "CompFinder" which runs on the Macintosh series of computers. CompFinder is normally used to calculate compositions corresponding tc measured masses or mass differences (see fig. 1). Calculations were done with 32 bit double values for amino acid molecular weights and performed for monoisotopic and average masses. Glutamyl and Lysyl residues were considered different but Isoleucyl and Leucyl were not counted separately. Computing times to find a 50 Da wide mass distribution ranged from less than a second below mass 600 to 18 hours at mass 2000 on a PowerPC Macintosh Fig 1 shows mass distributions obtained by calculating all possible peptide compositions around mass 500. The centroids of the distributions give the average mass offset at each mass. It is apparent from the figure that - particularly at small masses - the distribution of masses is quite narrow. For example, at mass 510 the width is only 0.25 Da, that is, all peptides with nominal mass 510 must be within 0.13 Da of the average mass offset. The area between the peaks is a "forbidden zone" where no peptide mass is possible.
The distributions were also tabulated for sequence databases like SWISS-PROT with identical results.

The data in the mass distributions can be summarized in the following formulas:
(1) $\Delta m = 0.00048 * m$ (monoisotopic)
(2) $\Delta m = 0.00115 * m$ (average mass)
(3) $Wm = 0.19\ Da + 0.0001 * m$

with Δm the mass offset in Da, m the mass in Da, and Wm the width of the mass distribution encompassing 95% of all amino acid compositions.

A computer program can mark unlikely mass values in the following way (monoisotopic case):

```
if (Abs((m-[m])-(m * 0.00048)) < (0.095 + 5*10-5 *m)) {
 //do nothing
}
else {
 MarkPeakInRed(m);
}
```

where Abs is the absolute value; m is the molecular weight in Da; [m] is the lower interger value of m and hence m-[m] is the mass offset (this works until mass 2000); MarkPeakInRead is a subroutine to display a peak value in red

Some possible applications include:
- Check peptide masses for outliers. For example, tryptic peptide masses which are more than 0.3 Da in error can be flagged as such.
- Check stability of mass calibration. If several peptide masses are in forbidden zones or unlikely zones the mass calibration has shifted.
- Find "non-typical" peptides, i.e. peptides with a substantial glyco part, peptides which contain two sulfur atoms such as peptides containing a disulfide bridge (personal communication A. Tolmachev, Moskow) and peaks which are not peptides at all (noise peaks or background).
- Estimate error from the peptide masses in a peptide map. It is possible to estimate the mass error without any other information than a table of measured masses.
- Improve calibration by eliminating linear mass errors.
- Avoid embarrasment; i.e. you can't measure mass 1000.0 ± 0.01 % Da (mono). :-)

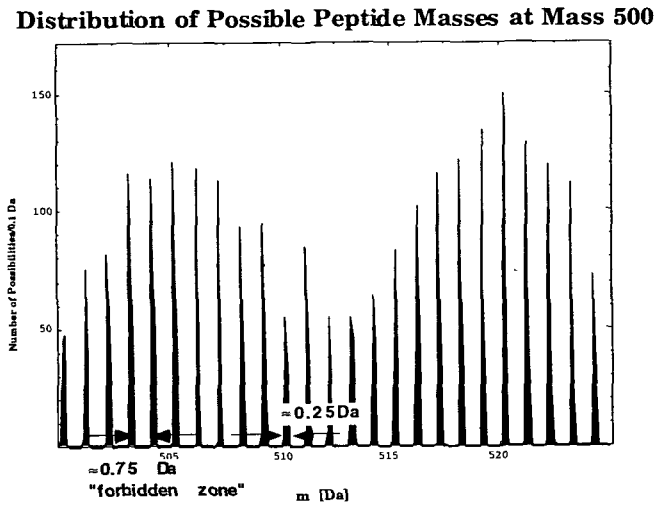

Figure 1
Mass distributions around mass 500 dalton showing the area in which peptide masses must lie and where they can't lie ("forbidden zones").

Analysis of Immuno-affinity Purified Proteins by Tandem Mass Spectrometry

David M. Schieltz, Jimmy K. Eng, and John R. Yates III
Department of Molecular Biotechnology, University of Washington, Seattle WA 98195

Traditionally, proteins have been identified through biochemical assays, immunoblotting or chemical sequencing. These methods can be time consuming and laborious. Our laboratory has developed methods for identifying proteins using MS/MS analysis of peptides generated by enzymatic cleavage of the protein. Using the SEQUEST program developed by Eng and coworkers(1), peptide tandem mass spectra are searched against possible sequences of amino acids in the protein databases. This allows for a rapid identification of proteins.

To demonstrate this approach, the antibody reactive against a conserved region of the v-H-ras protein was used to probe a whole cell S. cerevisiae lysate. Approximately 10 mg of the lysate was incubated at 4°C for 2 hours with the antibody-agarose conjugate. The antibody-agarose was washed with lysis buffer followed by an elution buffer consisting of 1 M acetic acid. The pH was adjusted to 8.5 with ammonium bicarbonate prior to digestion with trypsin.

Three microliters of the digest was loaded onto a 100 µm i.d micro-capillary column packed with Perseptive Biosystems POROS 10 R2. The fritted end of the column was inserted into the needle of the electrospray ion source on a Finnigan TSQ-700. The HPLC pump was programmed to ramp the organic phase gradient from 0 to 80% B in 30 minutes. Automated tandem mass spectra were acquired using a program written with the Finnigan Instrument Control Language (ICL). The program selects precursor ions from the MS scan when the intensity and signal to noise ratio exceeds specified values. Doubly charged species were assumed, therefore the collision offset and the mass range could be calculated for the product ions. The acquired tandem mass spectra were searched using the program of Eng and coworkers(1) against the OWL database v25.2 (100909 entries) which is a nonredundant database containing sequences from Genbank (NCBI), Protein Information Resource (NBRF) and NRL (Brookhaven National Laboratory).

Figure 1. shows the result of the search from the OWL database identifying the $(M+2H)^{2+}$ ion at m/z 813.9 as a peptide belonging to the ras2 protein. One other tandem mass spectrum was matched to a sequence from the ras2 protein and several other masses that were not selected for product ion scans fit the predicted masses of the tryptic fragments. Co-eluting peaks were present in the ion chromatogram that did not belong to the ras protein. The database search identified a yeast ribosomal protein from a doubly charged peak

43rd ASMS Conference on Mass Spectrometry and Allied Topics

at m/z 656. This methodology illustrates one of the consequences of the analysis of protein purification from cell lysates. Other proteins may bind non-specifically to the antibody or the agarose leading to multiple proteins being isolated. The presence of ras was substantiated even in the presence of a mixture of proteins. Approximately 6 kDa of the ras2 sequence was found in analysis of the MS/MS data and cursory inspection of the MS data.

The objective of this experiment was to demonstrate a new approach for the analysis and identification of immuno-purified proteins. To demonstrate this approach the ras gene product was used as the target for immuno-affinity purification from a whole cell lysate. The enzymatically digested proteins were analyzed by tandem mass spectrometry followed by database searching and protein identification with the MS/MS data.

(1) J.K. Eng, A.L. McCormack and J.R. Yates III, *J. Am. Soc. Mass Spectrom.* **5**, 976 (1994).

```
ds0514rs1.0652 0654 out
SEQUEST v.B15, Copyright 1993-95
Molecular Biotechnology, Univ of Washington, J.Eng/J.Yates
05/15/95, 12:54 PM, 1 min 42 sec. on nootka
mass = 1626.3(+2), fragment tol = 1 00, mass tol = 3 00, AVG
# amino acids = 31147930, # proteins = 100909, # matched peptides = 1587459
immonium (HFYWM) = (00000), total inten = 8906 1, lowest Sp = 576 7
rho = 0 200, beta = 0 375, top 7, /usr/users/massspec/OWL/owl v25 2

 #   Rank/Sp  (M+H)+    Cn     deltCn  C*10^4   Sp      Ions  Access#       Peptide
---  -------  ------  ------  ------  ------  ----    ----  -------       -------
 1    1 /  1  1625 8  1 0000  0 0000  4 2305  1779 8  21/26  RAS2_YEAS+1   QAINVEEAFYTLAR
 2.   2 / 26  1624.7  0 7315  0 2685  3 0946   998 2  16/26  Y085_CAEE     SHSPVFDSELTYLE
 3    3 /152  1626 0  0 7283  0 2717  3 0811   718 8  16/28  PANB_ECOL+1   AQLLVLECVPVELAK
 4    4 /  2  1624.1  0 7120  0 2880  3 0121  1742 2  20/26  S30030        LMIVAKLSMLPLFF
 5.   5 / 22  1625.8  0.6883  0 3117  2 9118  1033 0  18/26  AROA_ARAT+1   VVDNLLNSDDINYM
 6    6 /  4  1624 9  0 6879  0 3121  2 9100  1378 0  19/26  S41158        SLNINLNSDKLVFF
 7    7 /  3  1626 9  0.6860  0 3140  2 9022  1401 5  19/26  MGU01698      TVLTIKMAENLTEY

 1   RAS2_YEAST RAS-LIKE PROTEIN 2  - SACCHAROMYCES CEREVISIAE (BAKER'S YEAST)
 2.  Y085_CAEEL HYPOTHETICAL 35 7 KD PROTEIN ZK1236.5 IN CHROMOSOME III. - CAENORHABDITIS
     ELEGANS.
 3   PANB_ECOLI 3-METHYL-2-OXOBUTANOATE HYDROXYMETHYLTRANSFERASE (EC 2 1 2 11) (KETOPANTO
     ATE HYDROXYMETHYLTRANSFERASE)  - ESCHERICHIA COLI
```

Fig. 1. Search results from the OWL database v 25.2 of the product ion scan of $(M+2H)^{2+}$ of m/z 813.9. Top score is the sequence QAINVEEAFYTLAR from the ras2 protein.

Protein Database Searching with Ion Trap MS^n data

by Jimmy K. Eng, John R. Yates III, and David M. Schieltz

INTRODUCTION

Recent developments in the analysis of mass spectrometry data using protein databases has provided a powerful new tool for protein identification. Expansion of the databases as a result of the various genome projects will provide an important set of tools for the analysis of data from biological experiments. The ability to directly correlate fragmentation patterns from mass spectrometers to sequences in protein databases without extensive data evaluation will speed the interpretation of results and aid biological studies.

Application of the database searching program SEQUEST for protein identification and peptide sequencing utilizing spectra generated from MS^3 and MS^4 experiments conducted on an atmospheric pressure ionization quadrupole ion trap mass spectrometer is demonstrated. Such instruments are capable of multiple stages of mass spectrometry and can generate fragment ions that cover a significant portion of the sequence of a polypeptide or protein. This approach allows for the identification of polypeptides which are too large or highly charged to fragment in tandem mass spectrometry experiments.

EXPERIMENTAL

Spectra were acquired on a Finnigan MAT LC/Q ion trap mass spectrometer (San Jose, CA). Peptides were infused directly into the electrospray ionization source at a concentration of 2.5 pmol/mL in 1:1 0.5% acetic acid:methanol. Precursor ions were isolated in the ion trap and resonantly excited. A fragment ion was then chosen for further fragmentation.

RESULTS

MS^4 Example 1. An MS^4 experiment was conducted on an $[M+4H]^{+4}$ ion at m/z 872. The molecular weight of the peptide was 3482.8 u. Initially, an MS/MS spectrum was acquired for a precursor ion at m/z 872. From the MS/MS spectrum of m/z 872, a fragment ion at m/z 842 was selected for a subsequent stage of MS/MS analysis. A third MS/MS spectrum was generated by selecting an ion at m/z 1450 which was a fragment ion of m/z 1085 which in turn was a fragment ion of the original m/z 872 precursor ion. The three spectra were combined by summation and used to search the OWL composite protein database (version 25.2). Out of the 100,909 sequences in the OWL database, 503,043 peptides matched the input $[M+H]^+$ mass of 3483.8 within the specified ±1 u mass tolerance. The correct sequence HSQGTFTSDYSKYLDSRRAQDFVQWLMNT from glucagon was ranked in the top position. The (abbreviated) SEQUEST search results are displayed in Figure 1.

MS^3 Example 2. An MS^3 experiment was conducted on an $[M+3H]^{+3}$ ion at m/z 822. The molecular weight of the peptide was 2465.7 u. An MS/MS spectrum was generated from the precursor ion at m/z 822. The resulting fragment ions at m/z 768 and 505 were then selected independently for subsequent stages of MS/MS analysis. The combined spectrum, generated by summing the three spectra, was used to search the OWL database with the search results shown in Figure 2. Of the 100,909 sequence entries in the database, 518,504 peptides matched the input mass of 2466.7 within the specified mass tolerance of ±1 u. The correct peptide RPVKVYPNGAEDESAEAFPLEF from Corticotropin/ACTH was ranked in the 2nd position of the output list. Figure 3 shows the search results from SEQUEST when searching with the spectrum from a just the single stage of MS/MS on the precursor ion at m/z 822. For this case, the correct peptide was identified as the top ranked sequence.

CONCLUSION

The current results indicate that SEQUEST in conjunction with MS^n experiments can be an effective means of analyzing peptides that are not well suited for tandem mass spectrometry experiments. Particularly encouraging is the positive result achieved when searching with only the single stage of MS/MS of the ACTH precursor ion. Given that SEQUEST was able to correctly identify the peptide with the limited fragment ions from only one MS/MS stage, improvements in acquiring the MS^3 and MS^4 spectra and exploring better methods of combining the multiple spectra into one spectrum should make this method even more promising for protein sequencing. Additionally, tailoring the search algorithm to specifically consider the fragmentation patterns associated with MS^n spectra will also improve results.

ACKNOWLEDGMENT

Special thanks to Nathan A. Yates at the Department of Chemistry, University of Virginia, for supplying the ion trap data.

REFERENCES

Eng, J. K.; McCormack, A. L.; Yates, J. R. III, *J. Am. Soc. Mass Spectrometry*, 1994, *5*, 976-989.

Output 1. Glucagon search result, MS^4 analysis

```
SEQUEST v.B16, Copyright 1993-95, Molecular Biotechnology, UW, J.Eng/J.Yates
mass = 3483.8(+3), fragment tol. = 1.00, mass tol. = 1.00, AVG
# amino acids = 31147930, # proteins = 100909, # matched peptides = 503043

Rank/Sp  (M+H)+  C*10^4  Sp     Ions   Access#   Peptide
-------  ------  ------  ----   ----   -------   -------
 1 /424  3483.8  3.5364  401.9 26/112  GLUC_BOVI  HSQGTFTSDYSKYLDSRRAQDFVQWLMNT
 2 /  4  3484.7  3.0601  702.9 36/148  VASA_DROM  VGGSGGEGGGYQGGNRDVFGRIGGGRGGGAGGYRGGNR
 3 /167  3484.8  2.9858  445.2 25/116  CID_DROME  SETIASNHYREQSNIYYTNKQILTPPSNVD
```

Output 2. ACTH search result, MS^3 analysis

```
SEQUEST v.B16, Copyright 1993-95, Molecular Biotechnology, UW, J.Eng/J.Yates
mass = 2466.7(+3), fragment tol. = 1.00, mass tol. = 1.00, AVG
# amino acids = 31147930, # proteins = 100909, # matched peptides = 518504

Rank/Sp  (M+H)+  C*10^4  Sp     Ions   Access#   Peptide
-------  ------  ------  ----   ----   -------   -------
 1 / 10  2466.9  2.8019  653.6  23/80  A44396     YNNISEHIKINYPLLFEALAC
 2 /273  2466.7  2.7784  441.9  21/84  COLI_BALP  RPVKVYPNGAEDESAEAFPLEF
 3 /342  2466.8  2.7733  427.1  21/84  CBP1_CANA  YMSGIYAADCILENIFRNDVTG
```

Output 3. ACTH search result of precursor spectrum only

```
SEQUEST v.B16, Copyright 1993-95, Molecular Biotechnology, UW, J.Eng/J.Yates
mass = 2466.7(+3), fragment tol. = 1.00, mass tol. = 1.00, AVG
# amino acids = 31147930, # proteins = 100909, # matched peptides = 518504

Rank/Sp  (M+H)+  C*10^4  Sp     Ions   Access#   Peptide
-------  ------  ------  ----   ----   -------   -------
 1 /  1  2466.7  3.3006  1248.7 36/84  COLI_BALP  RPVKVYPNGAEDESAEAFPLEF
 2 /  2  2465.7  3.0633  1109.0 34/84  COLI_BOVI  RPVKVYPNGAEDESAQAFPLEF
 3 / 37  2466.9  2.2196   508.0 23/80  A44396     YNNISEHIKINYPLLFEALAC
```

Mass Accuracy Requirements to Map Proteolytic Peptides from a Protein

Pao-Chi Liao[1,2], Holly Rockensuess[2], John Allison[1], and Douglas A. Gage[2]
Department of Chemistry[1] and Biochemistry[2]
Michigan State University, East Lansing, MI 48824

Mass spectrometry has been an important tool for the identification of the proteolytic peptide fragments derived from enzymatic or chemical cleavages of a protein. If the amino acid sequence of a protein is known and the protein is cleaved by a protease or reagent with known specificity, then a set of possible proteolytic peptide fragments can be calculated, and the mass measurements of proteolytic peptides derived from this protein can be compared to the set of postulated peptide fragments. This analysis, "peptide mass mapping", allows rapid characterization of the amino acid sequences of proteolytic peptides by the use of mass spectrometric methods. This information can be used to confirm cDNA-derived protein sequences, and to locate the site(s) of post-translational and/or other chemical modification(s) of a protein (e.g., phosphorylation [1]). A computer program, "MSU MassMap", was written using Microsoft® Visual Basic™ for Windows™ to calculate the average masses of possible proteolytic peptide fragments from a protein, and the average m/z value of the mass spectral peak for the corresponding $[M+H]^+$ ion. The program computes masses for peptides from not only complete, but also partial digestion.

A procedure has been established to evaluate the likelihood of ambiguity in sequence assignments which may arise in peptide mass mapping analysis. All of the possible proteolytic peptides from a protein were calculated and sorted according to their mass values. Each adjacent pair of peptides were used to calculated the difference in mass values relative to their mass average, Δ_i/m, where Δ_i = (mass value of $peptide_{i+1}$ - mass value of $peptide_i$), m = (mass value of $peptide_{i+1}$ + mass value of $peptide_i$)/2, and $peptide_i$ is the ith peptide in the list. Each Δ_i/m for adjacent peptide fragment pairs was compared to the given mass accuracy of the mass spectrometer to determine if there is a potential ambiguity in sequence assignments. For example, given the mass accuracy of ±0.1% (1 ppt) of an instrument, if $\Delta_i/m < 0.2\%$ (2 ppt), then there is a potential ambiguity in sequence assignments for these two peptides. All the Δ_i/m were calculated and categorized into five subcategories: I. $\Delta_i/m =< 2$ ppm, II. 2 ppm < $\Delta_i/m =< 20$ ppm, III. 20 ppm < $\Delta_i/m =< 200$ ppm, IV. 200 ppm < $\Delta_i/m =< 0.2\%$ (2 ppt), and V. 0.2% (2 ppt) < Δ_i/m. Each category corresponds to a different mass accuracy requirement. The distribution of Δ_i/m in five categories was used to predict the likelihood of ambiguity in sequence assignments in the peptide mass mapping analysis of a protein.

It is expected that a large protein will generally have a larger number of possible proteolytic peptides than a smaller one. Since more peptides are likely to be found within a particular mass range, this might require increased mass accuracy for peptide

mass mapping. To evaluate how protein size affects the mass accuracy requirement, 200 protein sequences were obtained from the "Entrez" database and analyzed to evaluate the likelihood of ambiguity in sequence assignments. The molecular weights (MW) of the proteins range from 3-140 kDa. The protease used was trypsin and only proteolytic peptides within the mass range 500-5000 Da was considered. The calculation includes incomplete digestion products. The 200 proteins are grouped by their sizes (MW). The result shows that 0.1% (1 ppt) mass accuracy is generally suitable to perform peptide mass mapping for proteins with MW's in the range of 3-20 kDa. For 20-70 kDa proteins, a mass accuracy of 100 ppm may be necessary. For 70-140 kDa proteins, 10 ppm mass accuracy may be required.

If the proteolysis reaction is complete (all the cleavable sites are cleaved by the protease or chemical reagent), then the number of possible proteolytic peptides is greatly reduced. When the mass range of 500-5000 Da and trypsin are considered, our calculations show that 0.1% (1 ppt) mass accuracy is suitable to perform mass mapping for proteins with MW's ranging from 3-70 kDa in most of the cases, provided the proteolysis reactions are complete. For 70-140 kDa proteins, a mass accuracy of 100 ppm may be necessary in some cases. Incomplete proteolysis (i.e., some cleavable sites are not cleaved) is not uncommon. It would be advantageous in peptide mass mapping that a method is developed to ensure complete digestion. The absence of partial proteolytic fragments will allow mass spectrometers with modest (0.1%) mass accuracy to be employed for unambiguous peptide mass mapping of larger proteins. Some proteases may not be very specific in certain cases. Others, such as pepsin, have inherently less specificity. An extreme case, totally non-specific proteolysis, was considered. That is, the hydrolysis can take place at amide bonds between any two adjacent amino acid residues. When the mass range 500-5000 Da is considered, our calculation shows that none of the mass accuracies considered (from 1 ppt to 1 ppm) provides unambiguous peptide mass mapping for proteins in most of the cases (except for 3-10 kDa proteins) when the proteolysis reaction is totally non-specific.

Among the mass spectrometers available, the mass accuracy of different instruments varies. MALDI-TOF is reported to have at least 0.1% mass accuracy. A 10 ppm mass accuracy for peptides and proteins up to 5700 Dalton has been reported by MALDI-FTMS instruments [2]. From our analyses, one can predict the mass accuracy required to perform unambiguous peptide mass mapping in different situations. When dealing with a specific protein, one can use the computer program developed to evaluate the required mass accuracy for peptide mass mapping.

[1]. Liao, P.-C., Leykam, J., Andrews, P. C., Gage, D. A., and Allison, J., *Anal. Biochem.* **219**, 9-20 (1994).
[2]. Li, Y., McIver, R. T., Jr, and Hunter, R. L., *Anal. Chem.* **66**, 2077-83 (1994).

Protein Identification by Database Searching: A Bayesian Algorithm

Wenzhu Zhang and Brian T. Chait

The Rockefeller University, 1230 York Ave., New York, NY10021

The identification of isolated proteins is an important requirement for many biological investigations. Database searching using mass spectrometric peptide mapping has proved to be a sensitive and facile method for protein identification [1,2,3,4,5]. The method involves comparison of masses obtained in peptide mapping experiment with the masses calculated by applying the appropriate cleavage rule to each protein in a protein sequence database. The objective of this work is to use a Bayesian algorithm to rank the candidate proteins with probability.

Application of Bayes' Theorem: $P(k|DI)=\frac{P(K|I)P(D|KI)}{P(D|I)}$, where k is the hypothesis that the sample protein is protein k (protein k is an entry in the protein sequence database), D is data from a mass spectrometric peptide mapping experiment, I is background information (including all assumptions and prior information), $P(k|DI)$ is posterior probability for the hypothesis k in view of data D and background information I, $P(k|I)$ is prior probability for the hypothesis k given background information I only, $P(D|kI)$ is likelihood probability for data D given the hypothesis k and background information I, and $P(D|I)$ is a normalization constant.

Database of peptide fragments of proteins: The peptide database is derived from the OWL protein sequence database (> 80,000 proteins). For each protein k in the protein database, both complete and partial proteolysis digestion products are included in the peptide database. The partial peptide fragments contain up to 5 contiguous complete fragments. We found that extended partials are present in many digestions and the presence of the partials can provide useful information for the protein identification.

Probability calculation: Posterior probability for the sample protein to be protein k given data D and background information I has been derived by logical inference [6], and is given by

$$P(k|DI) \propto P(k|I)\frac{(N-r)!}{N!}\prod_{i=1}^{r} g_i\left(\frac{m_{max}-m_{min}}{2\sigma}\right)^r \exp\left[\frac{r}{2}-\frac{\sum_{i=1}^{r}(m_i-m_{i0})^2}{2\sigma^2}\right]$$

with normalization condition of $\sum_{k}^{database} P(k|DI)=1$, where the assumption is made that the sample protein exists in the protein database. In the above formula, N is the number of peptides generated in computer-simulated fragmentation of protein k, r is the number of hits (matches between the measured and calculated peptide masses), g_i is the multiplicity of the ith hit, $(m_{min}-m_{max})$ is the range of mass measurement, σ is the standard deviation of the mass measurement, m_i is the measured mass of the ith hit, and m_{i0} is the calculated mass of the ith hit.

The ranking of the candidate proteins is based the values determined for their posterior probability $P(k|DI)$.

Discussion: *Using data from multiple digestions:* When existing data are not sufficient to identify a sample protein, a different enzyme/chemical can be used to generate more data. The Bayesian algorithm naturally incorporates the new data into the inference for protein identity. In this situation, the prior probability before evaluating new data is the posterior probability for the old data. *Identification of components of a protein mixture:* The algorithm also allows identification of individual proteins in mixture of proteins. For this purpose, the protein sequence database is expanded to include entries that are combinations of single protein sequences.

References

[1]Henzel W.J., Billeci J.T., Stults J.T., Wong S.C., Grimley C. and Watanable C. 1993. *Proc. Natl. Acad. Sci.* USA *90:* 5011-5015.

[2]Mann M., Hojrup P. and Roepstorff P. 1993. *Biol. Mass Spectrom. 22.* 338-345.

[3]James P., Quadroni M., Carafoli E. and Gonnet G. 1993. *Biochem. Biophys. Res. Commun. 195:*58-64.

[4]Pappin D.J., Hojrup P. and Bleasby A.J. 1993. *Curr. Biol. 3:*327-332.

[5]Yates J.R.III, Speicher S. Griffin P.R. and Hunkapiller T. 1993. *Anal. Biochem. 214:*397-408.

[6]Bretthorst L. 1994. In *Maximum Entropy and Bayesian Methods.* Heidbreder G. *Eds.*, Kluwer Academic Publishers, Dordrecht the Netherlands.

Applications of a New Algorithm for Deconvolving Multiply Charged Spectra

V. J. Barclay, R. F. Bonner, *PE SCIEX, 71 Four Valley Drive, Concord, Ont. Canada, L4K 4V8*

L. K. DeNoyer, J. G. Dodd, *Spectrum Square Associates, 755 Snyder Hill, Ithaca, N.Y. 14850*

and D. N. Nguyen *Eli Lilly & Company, Lilly Corporate Center, Indianapolis, IN 46285*

Samples ionized by Electrospray Ionization (ESI) and IonSpray™ produce ions in a variety of charge states. For small molecules (< 3000 amu) only a few charge states are generated and the spectra can be interpreted with ease, but for large molecules (>10,000 amu) many charge states are generated and the resulting spectra can be difficult to interpret. This is especially true if the sample is a mixture or the spectrum is noisy.

Assuming Bayesian statistics and a Poisson noise process, we have developed a new algorithm, BioSpec Reconstruct, that uses maximum likelihood techniques to reconstruct the most probable zero-charge spectrum from multiply charged ion spectra.

In this report we briefly describe the new algorithm and the user interface and show that optimizing the weighting factor for the charge states can allow small signals to be accurately deconvolved even in the presence of larger signals. We show applications of the algorithm in a variety of areas of biological importance, such as: the determination of trace impurities in recombinant proteins, C-terminal protein sequencing, determination of glycoform heterogeneity, and the analysis of complex protein mixtures.

The algorithm is fast and effective even with low signal/noise data and with spectra from complex mixtures. The algorithm has been incorporated into our new data processing program so that the user is able to invoke the deconvolution algorithm directly and then manipulate the resulting zero-charge spectrum using standard tools such as thresholding, smoothing and centroiding.

Prior to maximum likelihood processing, the program automatically generates a charge distribution envelope (CDE) from the data; the user can modify this if required to optimize the processing. The CDE, which is shown as the dashed line superimposed on spectrum (a), acts as a weighting factor in the algorithm.

BioSpec Reconstruct is based on Bayesian statistics, which relates the conditional probability of two events.[1] In the case of a real-life spectrum, Bayesian statistics assumes that both the "ideal" or true unknown spectrum **u** and the equally unknown image noise **n** are *jointly most probable*. A Bayesian treatment of the zero-charge spectrum problem seeks both the true spectrum and the image noise spectrum which will maximize the joint probability P(**u**|**n**). The use of the standard multinomial probability law for obtaining the *a priori* probability of the object means that the entropy of the system is taken into consideration. The inclusion of further *a priori* knowledge about typical ESI spectra leads to "cross entropy;" and the method used is a Maximum Cross-Entropy method (MCE).

To give a context to the use of maximum cross entropy theory in spectral analysis, consider the basic relationship of the true or underlying spectrum **u** to its noisy recorded spectrum **y**:

$$y_m = \sum_k s_{mk} u_k + n_m = a_m + n_m. \qquad [1]$$

Here, s_{mk} is a point-spread function positioned around point k, n_m is the noise associated with each point m, and a_m is the noise-free signal image.

Let P(**u**|**y**) represent the probability of the set of **u**, given the set **y**. From a Bayesian perspective, the underlying "true" spectrum is an hypothesis whose probability, P(**u**|**y**), given the observed spectrum {**y**}, is equal to the ratio of the true and observed spectra, P(**u**) and P(**y**), and the probability (or likelihood) of data **y**, given the hypothesis **u**, P(**y**|**u**):

$$P(\mathbf{u}|\mathbf{y}) = P(\mathbf{y}|\mathbf{u})\,\frac{P(\mathbf{u})}{P(\mathbf{y})} \qquad [2]$$

Standard methods set P(y) = 1, and take the logarithm of equation [2]:

$$\ln P(\mathbf{u}|\mathbf{y}) = \ln P(\mathbf{u}) + \ln P(\mathbf{y}|\mathbf{u}). \qquad [3]$$

For the terms on the RH side of this equation, we assume multinomial statistics and Poisson noise characteristics; the latter substituted into Eq.[3] gives the maximum entropy[2] component. When the *a priori* estimate of the true spectrum **u** is not uniform, but instead is {Q_m}, then the term ln(P(**u**)) in Equation [3] should be replaced with the cross entropy function.

The algorithm assumes an initial uniform guess for the true spectrum, $u_m = Q$. An estimated image is created through the relation $y_m = \sum_k s_{mk} u_k$, the estimated image is compared with the data, and then our guess for u_m is updated.

Many different algorithms are used in image processing for updating u_m. Finding an efficient algorithm is the art of the method. The difficulties of this image restoration problem are all buried in the definition of the point-spread function s_{mk}. Our point-spread function is simply a classical multiple-image transformation. Classical imaging, without distortion, is either an enlargement, or a reduction, and can be described by the affine class of transformations.[3]

The most challenging ESI spectra to deconvolve are those which have several components present in small amounts such as in Figure (a), the spectrum of myoglobin which was partially digested using a carboxypeptidase mixture.[4] Figure (b) shows its deconvolution; note the small peaks are real. The mass differences between successive peaks can be attributed to the loss of the amino acid residues as noted. By comparison, the zero-charge spectrum found using an additive reconstruction technique would have too many spurious peaks which, due to the presence of other trace constituents, cannot be properly filtered.

Since the carboxypeptidases remove residues one by one from the C-terminus, we read backwards from the main peak in the figure to see that the sequence is ...LGFQG. This sequence fragment can then be used as input to a protein database searching algorithm. Even the small portion "LGFQG" is enough, in this case, to effect a rapid identification of myoglobin, the protein being digested.

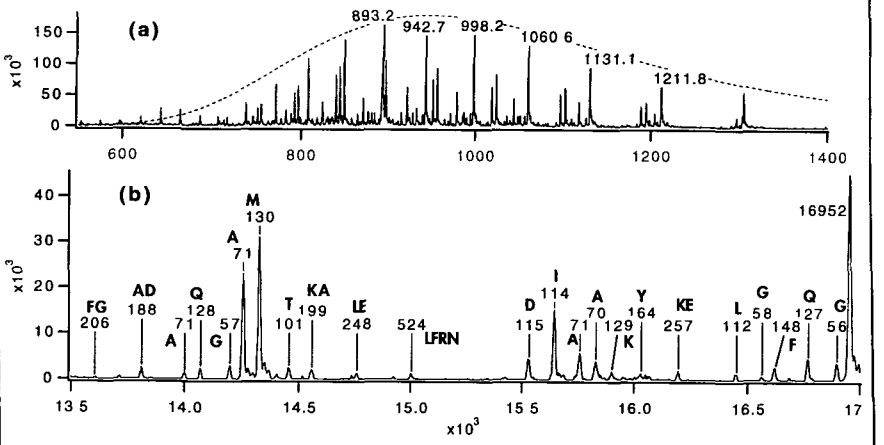

[1] C R. Smith and W. T. Grandy, Jr, ed. *Maximum-Entropy and Bayesian Methods in Inverse Problems* Dordrecht: Reidel (1985)

[2] So named because of its functional similarity to the Boltzmann definition of entropy

[3] A. J. McConnell *Applications of Tensor Analysis* Dover New York (1957).

[4] D. N. Nguyen, G. W Becker, and R. M Riggin, submitted.

MassBank - a Protein Mass Spectrum Database

David Fenyő [†], Ron C. Beavis[‡], and Brian T. Chait[†]
[†]The Rockefeller University, New York, NY 10021
[‡]Skirball Institute, New York University Medical Center, New York, NY 10016

Introduction

"...our methods of transmitting and reviewing the results of research are generations old and by now totally inadequate for their purpose."
V. Bush, The Atlantic 176 (1) (1945) 101.

Fifty years has passed since this was written and not much has changed in the way scientists obtain information. However, presently there are tools available to completely change the way scientific results are disseminated and make it easier to obtain information. For example, experiments are being made with electronic journals and the amount of information available from a wide variety of databases over the Internet is growing fast. The success of making a global scientific library easily available from anywhere is dependent upon the development of databases for the different types of scientific data as well as on the interconnection of all databases. Our contribution to this development is MassBank - a database for mass spectra of proteins.

Previously, no public database existed for mass spectra of proteins. However, there exists a large body of mass spectrometric data on proteins, including molecular masses, peptide maps generated by enzymatic digestion of proteins, as well as mass spectrometric fragmentation patterns of component peptides. A major proportion of the existing mass spectral data is never published and therefore inaccessible to the public, even though these mass spectra contain valuable information. Therefore, we have developed a prototype for a publicly accessible database where both published and unpublished mass spectra can be submitted and where the information can be accessed through a Word Wide Web server.

Description of the Database

A prototype has been developed of a database for mass spectra of proteins, enzymatic digests of proteins, and mass spectrometric fragmentation patterns of peptides. This database includes the mass spectra of proteins purified from natural sources (with the primary structure fully known, partially known, or unknown) and also mass spectra of recombinant proteins.

Tools are provided to search and analyze the mass spectra in the database on-line or to download the data and analyze it on the user's computer.

To enhance the utility of the database, a wide range of information about proteins from other databases are being made easily available during the process of examination of the mass spectral data. This information includes amino acid sequences, post-translational modifications, three dimensional structures, literature references, and positions on two dimensional gels. Tools are also provided to the primary structure of proteins with reference to the mass spectra in the database. These tools allow for the analysis of enzyme digests, amino acid compositions, hydrophobicities, post-translational modifications and mass spectrometric fragmentation.

The database is publicly accessible through a Word Wide Web server (URL http://chait-sgi.rockefeller.edu/). All submissions, searches and analysis of the mass spectra and protein sequences are done by filling out hypertext markup language (HTML) forms or through clickable maps. Figure 1 shows the interface for spectrum analysis. Simple operations on the mass spectra as zooming and "clicking" on peaks to obtain their mass are supported.

Conclusions

It is anticipated that within a few years the DNA sequence of the human genome will be known and this will leave a vast amount of protein chemistry to investigate. Mass spectrometry has the possibility to play an important role in the charcterization of proteins and therefore it is important to collect and organize the mass spectrometric knowledge. Therefore, we have developed a prototype for a database for protein mass spectra.

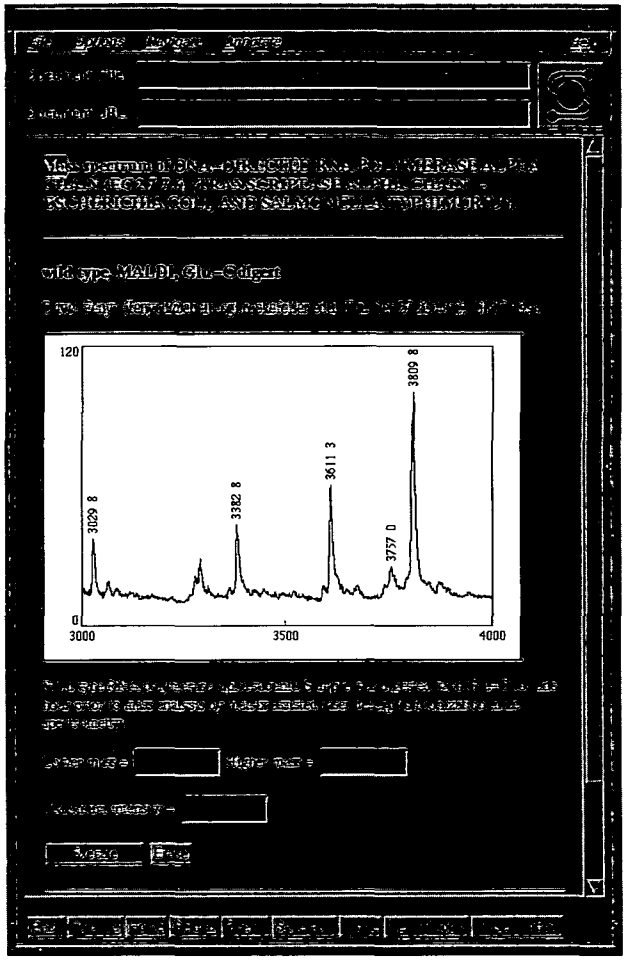

Figure 1. The interface for spectrum analysis as seen with NCSA Mosaic.

CHARACTERIZATION OF PROTEIN DIGESTS USING NOVEL SCANNING (FUNKY RAMPS)

Mark Allen, Joe Anacleto, Ron Bonner, Lydia Nuwaysir* and Bori Shushan.
Perkin Elmer SCIEX, 71 Four Valley Drive, Concord, ON, Canada.
* Perkin Elmer, Applied Biosystems Division, 850 Lincoln Centre, Foster City, CA.

Introduction

This study involves the use of a single quadrupole, benchtop LC/MS system (Perkin Elmer - SCIEX API 100) for the characterization of protein tryptic digests. Three LC/CID/MS examples are presented demonstrating:

- The identification of sites of glycosylation in fetuin
- The identification of sites of phosphorylation in ß-casein and
- Protein characterization using rapid high/low orifice scanning and a sophisticated, automated data base searching routine.

These analyses involve the LC/MS of protein tryptic digests while simultaneously combining different polarity, scan and ion source conditions in a continuous loop. We call such experiments 'funky ramps' or mixed-mode experiments. This new functionality enables the sensitive, discrete and simultaneous determination of marker ions indicating sites of glycosylation or phosphorylation, the peptide molecular weight and the partial amino acid sequence, in a **SINGLE** LC/CID/MS analysis.

Experimental Conditions

For all analyses an ABD 140B syringe pump delivered a gradient from 0 to 40 % B in 30 minutes (A= 100% aqueous, 0.1% TFA; B= 100% ACN, 0.1% TFA) at 40 µL/min into the IonSpray source. An Aquapore ODS300 1 x 100 mm LC column was used. Low energy (normal declustering) CID/MS experiments were performed with an orifice-to-skimmer potential difference of 40 V, while high energy CID/MS experiments were performed with an orifice-to-skimmer potential difference of 90 V for positive ion mode and -200 V for negative ion mode.

Identification of Sites of Glycosylation - Fetuin

Methods have been developed to facilitate the location of glycopeptides in the LC/MS of tryptic digests of glycoproteins involving the observation of glycan marker fragment ions at m/z 204+ (HexNAc+) and m/z 366+ (Hex-HexNAc+)[1]. For the data described here these two fragment ions are produced by CID of glycopeptide molecular ions between the orifice and skimmer lenses. The present example involves the LC/CID/MS of a Fetuin digest while undertaking two experiments in a SINGLE LC/MS analysis: 1) full scan 400 - 3000 u under normal ion source conditions and; 2) **TRUE** SIM of the 204+ and 366+ glycopeptide marker ions under high energy ion source conditions. The former provides molecular weight information and the latter identifies where the glycopeptides elute. The two TIC's are shown in Figure 1 with the bottom trace indicating three major glycopeptides eluting at 21:52, 29:30 and 31:00 min respectively.

43rd ASMS Conference on Mass Spectrometry and Allied Topics

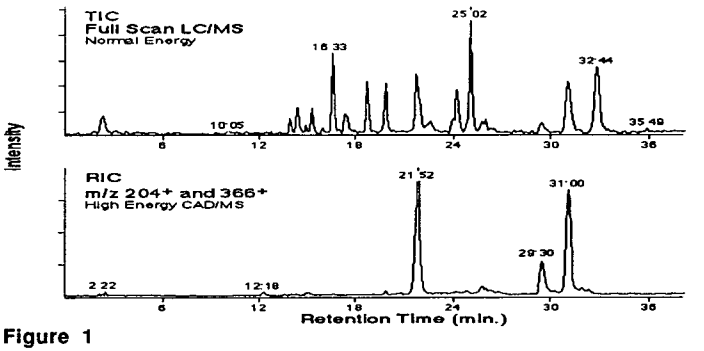

Figure 1

Identification of Sites of Phosphorylation — ß-Casein

Similar results were obtained for phosphorylated proteins when a digest of ß-Casein was analyzed by a SINGLE LC/MS analysis while two MS experiments were run in a consecutive loop. The two experiments were: 1) full scan 400 - 3000 u in the positive ion mode under normal ion source energies providing molecular weight information and; 2) SIM of m/z 79 (the PO_3^- marker ion indicating sites of phosphorylation)[2] in the negative ion mode, under high ion source energy conditions. This LC/MS run required a polarity reversal between each experiment which was performed because peptide molecular ions are usually more abundant in the positive ion mode while the marker ions are only observed in negative ion.

Protein Characterization Using Rapid High/Low Orifice Scanning – Cytochrome C

The analysis of proteolytic digests by LC/CID/MS is an important method for characterizing proteins. Once again, the ion source energy (ion-sampling orifice potential) is varied between high and low energy conditions with alternating scans; for both experiments full scan (300 - 3000 u) data is acquired. The two experiments (high and low energy) show almost identical TIC traces, as one would expect.
A plot of the IonSpray/MS spectra shows that the low energy (normal orifice potential) spectrum exhibits primarily molecular ions and the high energy experiment shows prominent fragment ions, as well as unfragmented precursors.
When the molecular weight of a tryptic peptide from the low energy conditions along with the *sequence tag*[3] from the high energy, fragmenatation conditions are entered (automatically using scripting) into the PeptideScan protein database search routine a list of known proteins containing the peptide and sequence tag is produced. For this analysis the sequence of 6 Cytochrome C variants were identified by searching the Swiss Prot. data base.

References:

1. S.A. Carr, M.J. Huddleston, M.F. Bean, Protein Science (1993) 2, 183-196.
2. M.J. Huddleston, R.S. Annan, M.F. Bean and S.A. Carr, J. Am. Soc. Mass Spectrom. (1993) 4, 710-717.
3. M. Mann and M. Wilm, Anal. Chem. (1994) 66, 4390-4399

Interpretation of Peptide CID Spectra using Artificial Neural Networks

R. E. Scarberry, Z. Zhang, and D. R. Knapp
Medical University of South Carolina, Charleston, SC 29425

One of the major advantages in the use of high energy collision-induced dissociation (CID) tandem mass spectrometry for the determination of peptide sequence over the more traditional method of Edman degradation is the very short data generation time, which is typically only a few minutes. However, without some automated means for evaluating the data sets collected, the time saving is of little consequence since subsequent manual interpretation of the data can require hours to days of an experienced expert's time. The development of a reliable computerized system for rapid interpretation of CID spectra is, therefore, essential to exploiting the time saving advantage of the mass spectrometric approach to peptide sequencing.

The most extensively used program described to date[1] generates sequences in a stepwise fashion using a rule base of fragmentation knowledge for the evaluation of candidate sequences. A recently reported method[2] relies on classifying peaks using a pattern-based scoring function. The latter algorithm, by mathematically converting the classified ions to corresponding y ions, generates an idealized spectrum of only y type ions, which it then interprets in a conventional manner. Our program combines elements of both approaches with the use of artificial neural networks to classify ions. Two backpropagation networks are utilized: the first classifies peaks as being, or not being, one of the common ion types (a, b, c, d, v, w, x, y, z+1), while the second network assigns peaks to specific types. The classified peaks are then used to generate a transformed spectrum of y ions from which sequences are derived and evaluated iteratively using a fragmentation rule base.

The prototype algorithm has been tested on a set of CID spectra of forty-three reference peptides (containing approximately 2750 peaks). For twenty-six (60%) of the spectra, the correct sequence received the top ranking each time they were tested, while thirty-five (81%) ranked in the top five sequences each time they were tested. The program also successfully differentiated between the isomers isoleucine and leucine 64% of the time based on the observed masses of d and w ions. Work is underway to further explore this approach by training the neural networks on much larger data sets and by refining the rule base. This method offers the potential for an effective new approach to peptide CID spectra interpretation which could facilitate peptide sequencing by tandem mass spectrometry[3].

Overall Program Structure

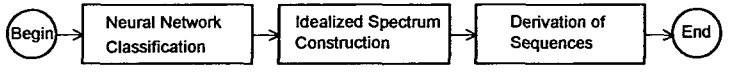

1 R.S. Johnson, K. Biemann. Biomed. Environ. Mass Spectrom.18: 945-957, 1989.
2 W. M. Hines et al. J. Am. Soc. Mass Spectrom. 3: 326-336, 1992.
3 For a more complete description of this work see R. E. Scarberry, Z. Zhang, and D. R. Knapp, J. Am. Soc. Mass Spectrom., in press.

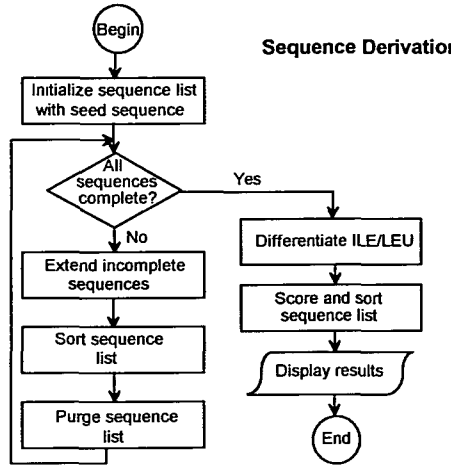

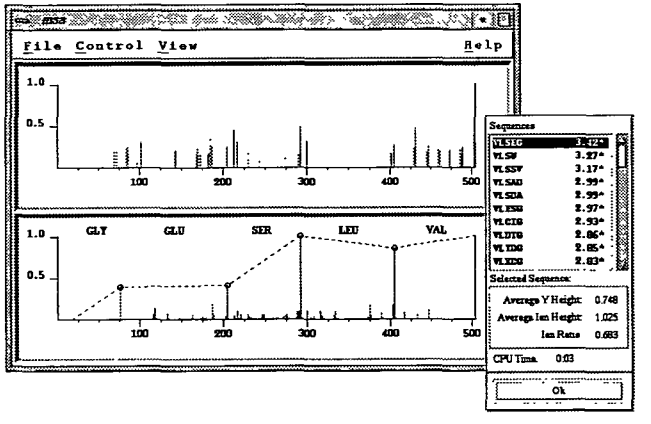

The sequencing program display as it appears in the X/Motif environment. In the actual screen display, the peaks in the upper spectrum are color coded to indicate the ion type as determined by the neural network module.

Peak Matching Techniques for Characterizing Protein Heterogeneity

Kenneth L. Johnson[1,2], Melissa R. Snyder[2], Andy J. Tomlinson[1,2]
Franklyn G. Prendergast[2,3], Stephen Naylor[1,2,3,4].

[1]Biomedical Mass Spectrometry Facility, [2]Department of Biochemistry and Molecular Biology, [3]Department of Pharmacology, [4]Clinical Pharmacology Unit, Mayo Clinic, Rochester, MN 55905

The analysis of proteins by electrospray mass spectrometry often reveals mixtures of related species. The mass differences between species can often be linked to post-translational events such as phosphorylation, glycosylation, etc. While the mass shifts caused by these processes are well defined, ambiguity in the assignment of a mass difference between species can leave some question of what modification is being observed.

Sector and FT-ICR instruments have been used to mass measure individual isotopes of proteins as a means of more accurately measuring the protein's molecular weight[1-4]. Until recently this approach carried an increasing degree of uncertainty in assigning the all ^{12}C isotope as the molecular weight of the protein increased[4]. An alternative to isotopically resolving the protein is to centroid the isotopic envelope of one of the charge states.

We have adapted peak matching software from our Finnigan MAT 900 sector instrument to more accurately measure the mass differences between protein species. This approach centroids the isotopic envelopes of two species at a medium resolution (typically 2000-5000). A reference M_r value is assigned to one of the species which is used to calculate the M_r of the other specie. The peak match method requires 3 parameters: **1)** the m/z of the ion being measured as an unknown, **2)** the m/z of the ion to be used as the reference, and **3)** a M_r value (either experimental or reference) to be associated with the reference ion Initially a full scan spectrum is acquired to select these parameters before performing the following peak match steps:

- Sum and store 5 scans of the reference ion in Peak Match Register 2.
- Sum and store 5 scans of the unknown ion in Peak Match Register 1.
- Calculate the theoretical m/z value for the reference ion using the assigned M_r value.
- Calculate the unknown ion and convert it's m/z to an M_r value using the reference ion.
- Calculate the mass difference between the two M_r values.

These steps are repeated to calculate a mean and std. dev. for replicate measurements.

Figure 1 and Table 1 show results from this method using Ribonuclease B as a model. Experimental results were within +/- 0.2 mass units of published values with one exception

The method was applied to the analysis of a glycosylated protein, EDN, which is isolated from human eosinophils. Figure 2 and Table 2 show the spectrum and peak match results for this sample. Components of the sample differed by masses corresponding to known carbohydrate moieties.

This technique, which has been successfully demonstrated on proteins with well characterized classes of heterogeneity, is expected to be a valuable aid in characterizing the nature of less predictable systems such as adduction of xenobiotics to proteins.

43rd ASMS Conference on Mass Spectrometry and Allied Topics

Figure 1 Mass Spectrum of Ribonuclease B Used for Peak Matching Measurements

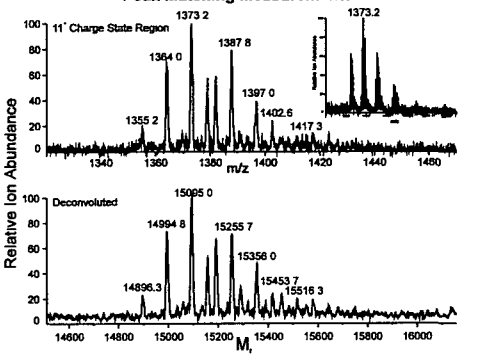

Table 1 Peak Match Results for Ribonuclease B

M_r (Measured)	M_r (Published)	ΔM_r (ppm)
14996.71	14996.69	0.02 (1.3)
15094.78	15094.67	0.11 (7.3)
15094.87	15094.67	0.20 (13.2)
15094.84	15094.67	0.17 (11.3)
15094.86	15094.67	0.19 (12.6)
15158.85	15158.74	0.11 (7.3)
15193.04	15192.65	0.39 (25.7)
15256.91	15256.72	0.19 (12.5)
15354.89	15354.89	0.00 (<1)

Figure 2 Mass Spectrum of the Glycosylated Protein EDN

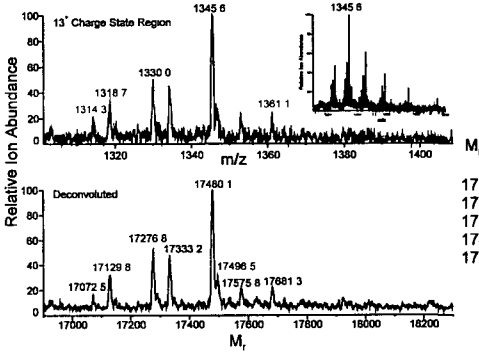

Table 2 Peak Match Measurements of Glycoforms of the Protein EDN

$M_{r(Expt)}$	$\Delta Mr_{(Expt)}$	$\Delta M_{r(Calc.)}$	Glycosylation moiety
17131.1	-349.2	-349.1	-Deoxyhexose+HexNAc
17277.4	-202.9	-203.1	-HexNAc
17334.0	-146.3	-146.1	-Deoxyhexose
17496.5	+16.2	+16.0	Oxidation of Methionine
17683.3	+203.1	+203.1	+HexNAc

References
1. Dobberstein, P.; Schroeder, E.; Rapid Commun. Mass Spectom. 1993, 7, 861-864.
2. Cody, R.B; Tamura,J.; Musselman, B.D.; Anal.Chem. 1992, 64, 1561-1570.
3. Senko, M.W.; Beu, S.C.; McLafferty, F.W.; JASMS. 1995, 6, 229-233.
4. Winger, B.E. et al.; JASMS 1993, 4, 566-577.

IDENTIFICATION OF PROTEINS USING LC/MS/MS ON AN ION TRAP MASS SPECTROMETER

William S. Lane, Adrian P. Land*, Ian Jardine*, Mark E. Bier*
Microchemistry Facility, Harvard University, Cambridge MA 02138
*Finnigan MAT, San Jose, CA 95134

A principal function of a Protein Core Facility is to provide primary peptide and protein sequence information in a timely and an accurate manner, often when the sample is available only in very low amounts. It has been our experience that the majority of protein samples sent to the facility for sequence analysis are expected to be novel by the submitting investigator. In contrast to as recent as two years ago, more than 50% currently are found to have sequences already recorded in the protein databases. As the content of the databases continues to increase at a high rate, the proportion of samples containing novel sequence can be expected to decrease significantly.

Experiments were carried out on a new LC/MS/MS ion trap mass spectrometer (*LCQ*, Finnigan MAT, San Jose, CA) to determine its suitability for the rapid screening of samples for known sequence. For pure samples, peptide molecular weight (M.W.) information from a handful of peaks in a map can be sufficient to identify a protein (e.g., Pappin et al. '93). However, for mixtures of proteins, the sequence-specific information generated by MS/MS is required to identify each component within the mix (Yates et al. '94).

The ion trap is used as an intelligent on-line detector for peptide mapping experiments. The instrument was programmed for a three stage data dependent acquisition. Full scan MS data (unit resolution) are collected until the base peak ion exceeds an intensity threshold; this triggers acquisition of a ZoomScan (resolution sufficient to resolve isotope peaks for up to +4 ions), and then, a full scan MS/MS spectrum. (unit resolution), Figs. 2(a-c). Thus, for each chromatographic peak, the detector automatically determines the charge-state of the ion, and hence an accurate M.W., and then generates an MS/MS spectrum. The data can then be analyzed using database search algorithms, allowing identification of all major, known proteins present in the sample. M.W. information was analyzed using *MassMap* software (Finnigan MAT, Hemel Hempstead, UK) with a database built from the Swiss-Prot library. MS/MS spectra were searched against an 83,556 entry protein database (NCBI) using PepSearch (Finnigan MAT, San Jose, CA).

Enzymatic digests for several samples were analyzed using HPLC/MS/MS. Tryptic equine myoglobin was used as a reference standard, 10pmol of sample yielding 16 molecular weights and 13 MS/MS spectra during a 20 minute separation. The ensemble of molecular weight information correctly identified the protein. Nine of the MS/MS spectra yielded positive database identifications, with the remaining four spectra giving null results, no false negatives were obtained.

A user unknown sample submitted to the facility was digested with trypsin and analyzed using traditional off-line HPLC/fraction collection/Edman sequencing techniques. 10pmol of this digest was then analyzed directly using LC/MS/MS on the LCQ. M.W. data and MS/MS spectra were acquired for 10 components in a 30 minute separation. Of these, 8 spectra gave positive identifications as "26kDa Protein", more commonly known as interleukin-6 , in agreement with the more laboriously obtained off-line results. For this case also, *MassMap* was able to confirm independently the identification of the protein.

In order to mimic the challenging, but by no means rare, case, of a protein of interest buried under an excess of contaminant, a mixture of 2pmol myoglobin in 50pmol bovine serum albumin was analyzed. The base peak chromatogram for this separation is shown in Fig. 1, with an example of each scan in Figs. 2 (a,b,c). Database search results for this spectrum are shown in the table opposite. MS/MS spectra that yielded positive database identifications for myoglobin were obtained for 4 components of the mixture.

The sensitivity and specificity of this new LC/MS/MS technology will contribute greatly to the ever increasing demands made of Protein Core Facilities. Using automated technology, turnaround times for analyses of these samples can be reduced to several hours, with a corresponding reduction in the average cost per analysis.

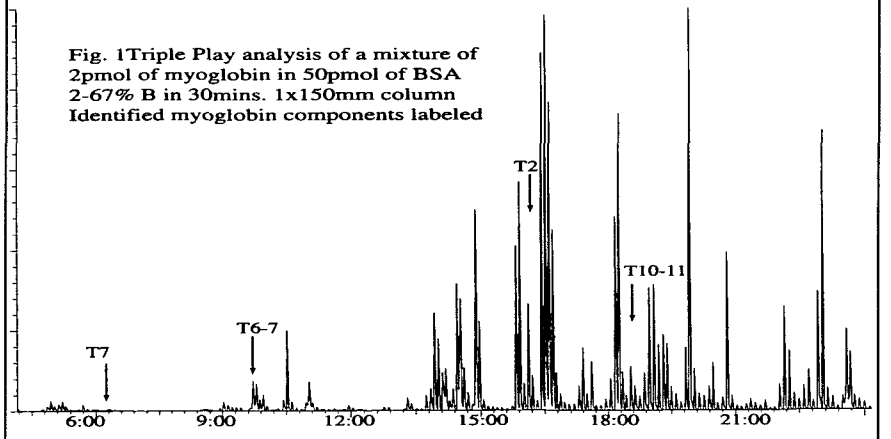

Fig. 1Triple Play analysis of a mixture of 2pmol of myoglobin in 50pmol of BSA 2-67% B in 30mins. 1x150mm column Identified myoglobin components labeled

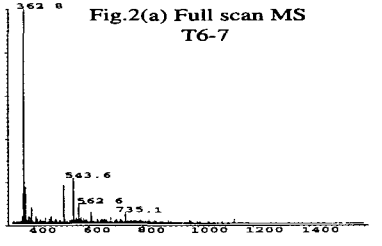

Fig.2(a) Full scan MS T6-7

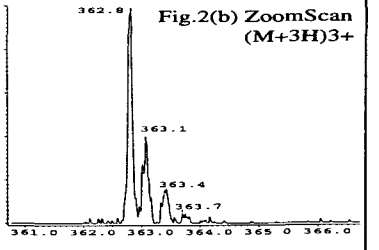

Fig.2(b) ZoomScan (M+3H)3+

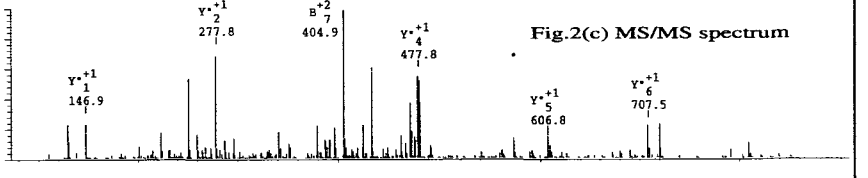

Fig.2(c) MS/MS spectrum

Score	Descriptor	Mult.	NCBI	Sequence
1.000	MYOGLOBIN	+2	127638	HLKTEAEMK
0.807	angigenin [swine,blood serum,Peptide,123 aa]	+2	298570	GRYCESIMK
0.734	cin1p	+1	563615	ENLHLTTMK
0.717	helicase II		606833	HLKTKTCKK
0.703	alpha-actin (AA-1-377)	+44	28330	ETTYNSIMK

D.J.C. Pappin, P. Hojrup and A.J. Bleasby, Current Biology (3), 1993
J.K. Eng, A.L. McCormack and J.R. Yates III, J. Am. Soc. Mass Spec. (5), 1994

High Sensitivity Protein Sequencing with ESI-FTMS

Ziqiang Guan, David J.Aaserud, Gary A. Valaskovic, Neil L.Kelleher, Peter B. O'Connor, Daniel P. Little and Fred W. McLafferty, Department of Chemistry, Cornell University, Ithaca, NY 14853

Low sample consumption, effective ion dissociation, and a comprehensive interpretation strategy are critical for making electrospray ionization/Fourier transform mass spectrometry (ESI/FTMS) a versatile, routine technique for protein analysis. For this, we describe advancements in: a)Achieving different and complementary fragmentation pathways using ultraviolet photodissociation for tandem mass spectrometry; b)Distinguishing b-type from y-type ions by their stabilities for more straightforward sequencing; c)A micro-ESI source with picomole volume, nL/min flow rate, and attomole detection limit.

Ultraviolet photodissociation (UVPD) is an attractive alternative for obtaining more sequence information, because infrared (IRMPD) and collisional activated dissociation (CAD) (nozzle-skimmer, SORI, SID) [1-3] produce similar sequence (b- and y- type) fragments, and leave sequence gaps. UVPD could proceed through the excitation of electronic states, while in IRMPD only vibrational excitations are involved. Fragment spectra by UVPD (193nm) of melittin and ubiquitin (8.6 kDa) show dramatic differenences from those by IRMPD and CAD. In the spectrum (Figure 1) shown here, c- and z- type ions are dominant, in contrast to b- and y- type ions by IRMPD and CAD. UVPD produces more than 12 new sequence informative fragments .

Identifying complementary pairs of fragment ions (mass sums equal to the MW value) is a key first step in sequencing; next each fragment is identified as b-type (N-terminal) or y-type (C-terminal). The IRMPD of ubiquitin [3] indicated that b-type ions are generally less stable than y-type ions. The generality of this rule for sequencing has been studied using larger proteins, such as carbonic anhydrase (29 kDa). IRMPD studies of three separate swift isolated molecular ion charge states of carbonic anhydrase, as well as IRMPD of all of the charge states of at once (Figure 2), show b-type ions from complementary pairs decomposing at shorter irradiation times. Nozzle/skimmer dissociation of carbonic anhydrase also shows b-type ions less stable than y-type. Extension of this method to identifying complementary pairs from fragments by MS^n should lead to even more sequence information.

A new approach to micro-ESI [4] combines the ease of use of the fused silica-capillary method [5] with the low flow rate (25 nl/min) of the glass capillary micro-tip approach [6]. Small inside diameter fused silica tubing (5-20 µm ID) is pulled to submicrometer dimensions (100 nm ID) using a micropipette puller with a CO_2 laser heat source, tip ID's are then increased to 1-5 µm with HF etching. These tips have a minimum volume < 200 pL and an ultra-low minimum flow rate, <0.25 nL/min. Figure 3 shows mass spectra of equine cytochrome c (12.4 kDa) in 2% acetic acid acquired with 2 µm ID tips made from 5 µm ID tubing. The top spectrum (S/N=400:1) shows isotopic resolution of the 16+ charge state for an 860 pL load of 10 µM (8.6 fmol) for a 3 s acquisition (150 amol consumed) delivered at 0.3 nL/min. The bottom spectra (S/N=60:1) shows the same charge state for a 216 pL load of 1 µM (216 fmol) for a 3 s acquisition (10 amol consumed) delivered at 0.23 nL/min. The detection limit with S/N of 3:1 is 10 amol loaded, 0.5 amol consumed.

Reference:

1. M. W. Senko, J. P. Speir and F. W. McLafferty, Anal. Chem. 1994, 66, 2801-2808.
2. R. A. Chorush, D. P. Little, S. C. Beu, T. D. Wood and F. W. McLafferty, Anal. Chem. 1995, 67, 1042-1046.
3. D. P. Little, J. P. Speir, M. W. Senko, P. B. O'Connor and F. W. McLafferty, Anal. Chem. 1994, 66, 2809-2815.
4. G. A. Valaskovic, N. L. Kelleher, D. P. Little, D. J. Aaserud, F. W. Mclafferty, Anal. Chem. submitted for publication.
5. M. S. Wilm, M. Mann, Int. J. Mass Spectrom. Ion Process. 1994, 136, 167-180.
6. M. R. Emmett, R. M. Caprioli, J. Am. Soc. Mass Spectrom. 1994, 5, 605-613.

43rd ASMS Conference on Mass Spectrometry and Allied Topics

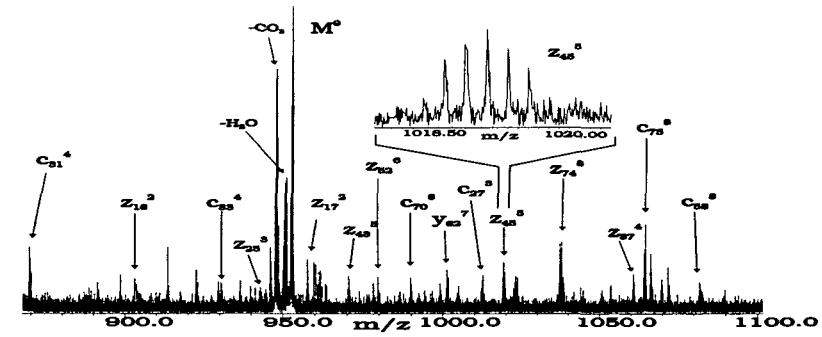

Figure 1. UV(193 nm) photodissociation of ubiquitin (+10)

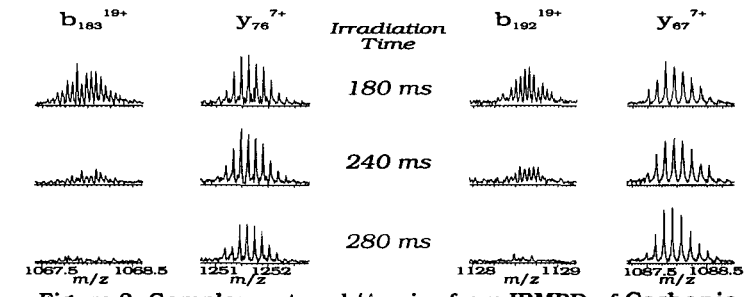

Figure 2. Complementary b/ẏ pairs from IRMPD of Carbonic Anhydrase, showing b-type ions less stable than y-type

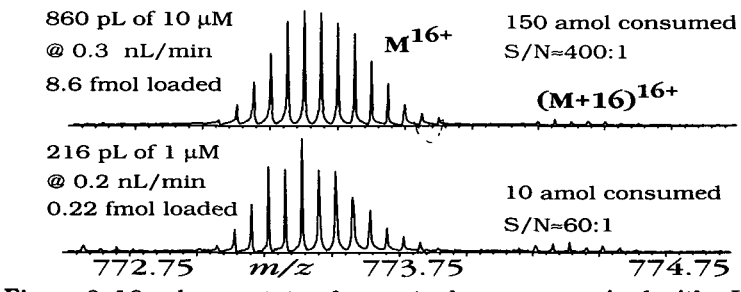

Figure 3. 16+ charge state of eq. cytochrome c acquired with pL volume µESI. Detection limit=10 amol loaded.

Creatine Kinase (43 kDa) and Thiaminase I (42 kDa): Heterogeneity, Sequence and Active Site Location with ESI/FTMS

Troy D Wood, Neil L Kelleher, Daniel P Little, Einar K Fridriksson, Lorenzo H. Chen, Montie Borders, George L. Kenyon, Tadhg P Begley and Fred W McLafferty
Cornell University, Dept. of Chemistry, Ithaca, NY 14853-1301

Electrospray ionization/Fourier Transform mass spectrometry (ESI/FTMS) has emerged as a powerful method for structural analysis of proteins above 10 kDa[1]. It is applied here to enzymes larger than 40 kDa, including creatine kinase (ck) and thiaminase I.

Heterogeneity Rabbit muscle ck, which catalyzes transfer of phosphate from phosphocreatine to ADP, shows 3-band heterogeneity in isoelectric focusing gels[2] However, ESI-FTMS shows isotopic clusters in the molecular ion region (**Figure 1**, resolving power (RP) 110,000) that have isotopic peak abundances resembling those of a single component with three isozymes whose MW values differ by only 1 or 2 Da (e g., deamidations, NH_2 --> OH). ESI/FTMS of thiaminase, (**Figure 2a**; RP 70,000) which catalyzes the degradation of vitamin B_1, reveals heterogeneity invisible by SDS-PAGE Three species were observed at isotopic resolution [MW reported as $^{13}C_{26}$; 42,127.2, 42,198 1 (+ Ala), and 42,254 9 (+ GlyAla)] due to nonspecific cleavage of the first 28 N-terminal residues at three adjacent backbone sites during post-translational processing.

Sequence Nozzle-skimmer (NS) dissociation of ck molecular ions (**Figure 3**) produces many fragment ions readily predictable from the DNA-derived amino acid sequence. For thiaminase I, heterogeneous b ions were observed (**Figure 4**) and a sequence error was localized to 50 C-terminal residues out of 379 which prompted DNA resequencing Subsequent refinement yields a sequence consistent with 61 fragment ions observed with ~ 2 - 15 ppm mass accuracy

Active Site Such fragment ion data is particularly useful to identify enzyme active sites by comparison of fragmentation data sets between wild-type enzyme, and enzyme with its active site tagged by a reactive substrate mimic Fragments that shift in mass contain the tagged residue Phenylglyoxal covalently modifies an essential Arg residue of ck in the putative nucleotide binding site, and a chloropyrimidine acts as a mechanism-based inhibitor by irreversibly binding the active site nucleophile of thiaminase I (**Figure 2b**). ESI/FTMS shows molecular ions for underivatized, singly-, and doubly-derivatized ck (1.3 1), based on NS fragmentation data, the essential Arg is between residues 122-212 (380 total) Fragmentation of inactivated thiaminase I resulted in localization of the active site nucleophile to a 99 aa region (Pro^{79}-Thr^{177}) Additional efforts using tandem mass spectrometry are in progress to further define the positions of the essential Arg and the nucleophilic residue of thiaminase I

References

1 McLafferty, F. W. *Acc. Chem. Res.* **1994**, *27*, 379.
2 Chen, L. H ; Babbitt, P C., Vasquez, J. R., West, B L., Kenyon, G. L *J. Biol. Chem.* **1991**, *266*, 12053.

43rd ASMS Conference on Mass Spectrometry and Allied Topics

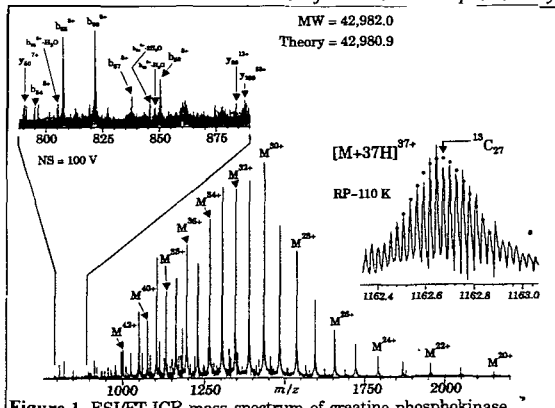

Figure 1 ESI/FT-ICR mass spectrum of creatine phosphokinase

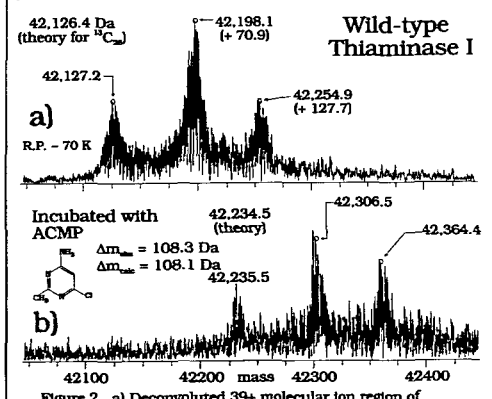

Figure 2. a) Deconvoluted 39+ molecular ion region of wild-type thiaminase, 25 scans. b) Deconvoluted 38+ region of covalently modified thiaminase, 20 scans.

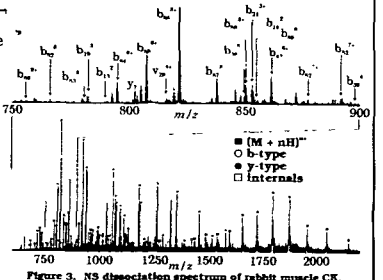

Figure 3. NS dissociation spectrum of rabbit muscle CK, NS 200 V, sum of 25 scans.

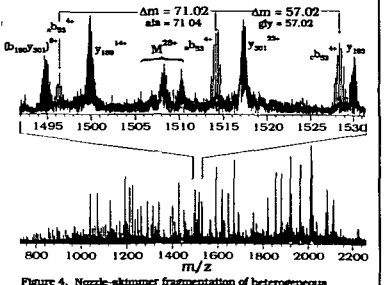

Figure 4. Nozzle-skimmer fragmentation of heterogeneous thiaminase I yields heterogeneous b ions, indicating a "ragged" N-terminus Correlation of y ions with the original DNA-derived sequence localized an error to 50 C-terminal residues.

Peptide Mapping by LC/MS/MS Using a Triple Quad or Ion Trap Spectrometer

Samuel W. Baldwin[1], Ken Stoney[1], Adrian P. Land[2], Mark E. Bier[2], and Kevin Wheeler[2]
Michrom BioResources[1], Inc, 1945 Industrial Dr., Auburn, Ca 95603, and Finnigan[2] MAT, 355 River Oaks Parkway, San Jose, Ca 95134

Mass spectrometry is one of many tools for the biochemist, if properly used, it should provide more than one piece of structural information. Four common proteins (B-lactoglobin, cytochrome c, carbonic anhydrase, and myoglobin) were digested by various proteases (trypsin, endo lys-C, and endo glu-C) and used as test material for LC/MS and LC/MS/MS analysis. Common proteolytic digestion conditions resulted in partial or no digestion of some of the test proteins. RP-HPLC of proteins prior to digestion, addition of denaturants, and on-column digestion resulted in the ability to proteolyze the protein standards that were resistant to the digestion conditions.

MS and MS/MS analysis using a triple quadrupole and a LCQ benchtop MS/MS instrument provided more information than UV analysis and demonstrated the efficiency of proteolytic digestion. LC/MS analysis was used to map cytochrome C after proteolytic digestion. Automated MS/MS analysis from selected ions rapidly provided sequence information to confirm the cysteine containing peptide. A summary of MS analysis using the triple quadrupole and the LCQ benchtop ESI/MS/MS mass spectrometer is presented.

RP-HPLC of tryptic peptides of Cytochrome C in 0 1 M Tris, pH 8 1, 10% ACN UV detection at 214 nm.

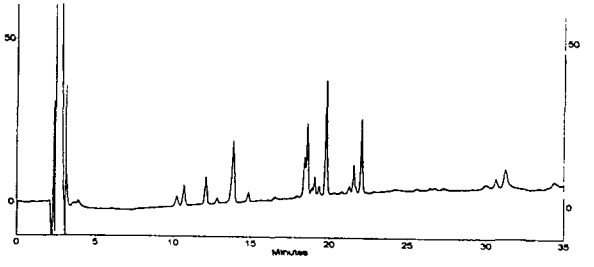

Cytochrome c was digested by trypsin or endo lys-C and the peptides were separated by RP-HPLC. One-two ugs of protein were subjected to LC/ESI/MS analysis. MS analysis of the endo lys-C peptide map using the LCQ MS/MS instrument resulted in identification of all cytochrome c peptides except the N-terminal residues 1-7. MS/MS analysis of scan 502 identified the cys containing peptide (9-22). There were many incomplete digestion products. Analysis of a single MS/MS scan (479) of M/Z 804 using the LCQ pepmatch data system identified the sequence as residues 88-100. The additional lysine was located on the C-terminus of the peptide.

Multiple peptides under a single UV peak were observed in MS analysis for both endo lys-C and trypsin peptide maps of cytochrome c. Trypsin peptides were separated and analyzed using the TSQ 7000. The cysteine containing peptide 9-22 was observed prior to treatment with 4VP. After alkylation there was an absence of the 9-22 peptide with UV and base peak analysis A definitive peptide containing 1 or 2 pyridylethyl-cysteine derivatives was not observed and is under further investigation.

LC/MS of endo lys-C peptides of cytochrome C. Inset: LC/MS/MS of scan 502. (808.3 and 744.2 are B^{+2} fragments)

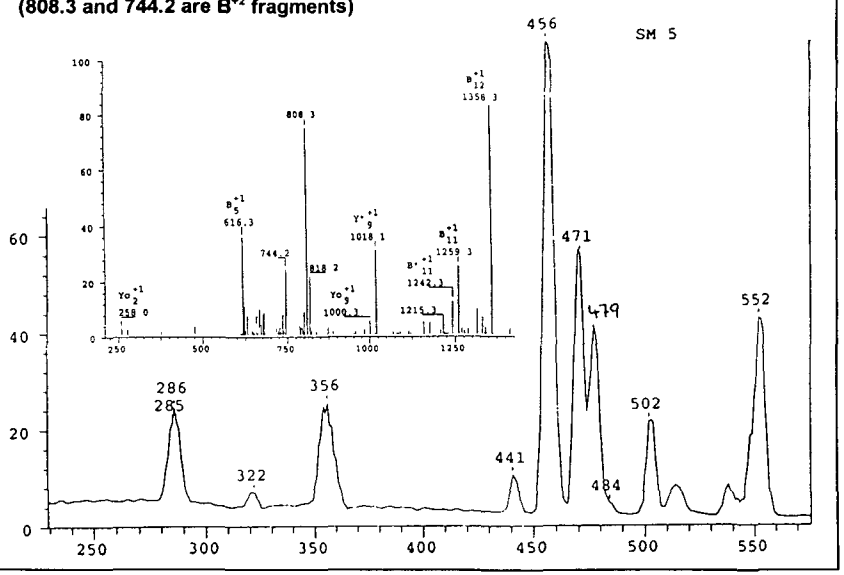

PROTEIN MOLECULAR WEIGHT DETERMINATION ON QUADRAPOLE AND ION TRAP SYSTEMS

Adrian P. Land, Kevin P. Wheeler, Iain C. Mylchreest, Mark Sanders, Ian Jardine
Finnigan MAT, San Jose, CA 95134

Protein molecular weight measurements were performed using quadrapole and ion trap mass spectrometers, where the ESI source on each analyzer was functionally equivalent. Relative sensitivity, mass range, mass resolution and mass accuracy (and precision) were measured. The quadrupole system used was the Finnigan MAT TSQ 7000 triple quadrupole, while the ion trap was the *LCQ* system.

In general, the results from both of these high performance systems for the analysis of proteins were similar. That is, protein molecular weights could be determined on either system at equivalent sensitivity with low pmol/uL protein sample concentrations, presented to the system by infusion or from an HPLC.At this sample level, both instruments were routinely able to determine molecular weights with both accuracies and precisions of better than 0.015%.

The 4,000 m/z mass range of the TSQ 7000 system is an advantage for the analysis of very large proteins, such as monoclonal antibodies, because the multiply charged envelope of these proteins often extend beyond m/z 2000 as shown in Figure1.

On the other hand, the ion trap has a unique higher resolution scan capability (ZoomScan) which allows increased resolution to be obtained over narrow mass ranges. An example of the separation of the alpha and beta chains of bovine and porcine hemoglobin using this ZoomScan technique is shown in Figure 2.

We have found that it is always advantageous to prepurify proteins before ESI/MS analysis to remove salts and reduce the complexity of protein mixtures. This can be conveniently carried out using reversed-phase HPLC with polymeric (PLRP-S, Michrom BioResources, Auburn, CA) columns. Following injection, the sample is washed free of salts (3mins at 2%B), followed by a rapid elution (2-95%B in 15 mins). An example of this technique is shown in the separation and molecular weight analysis of the alpha and beta subunits of bovine and porcine hemoglobin on the LCQ ion trap (Figure 3).

Both the quadrupole system and the ion trap system allow analysis of non-covalently bound complexes, as shown in Figure 4 for the analysis of the porcins heme complexes with the alpha and beta chains on the TSQ 7000 quadrupole system.

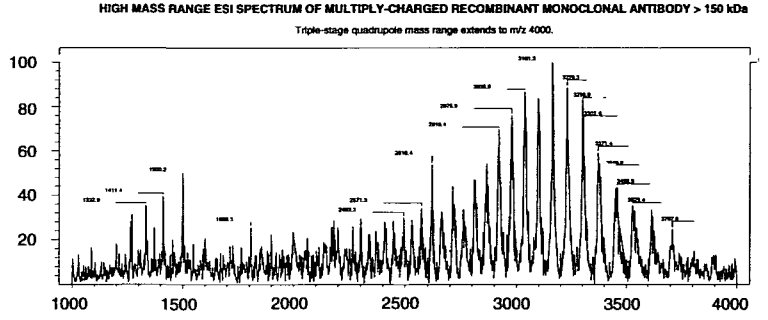

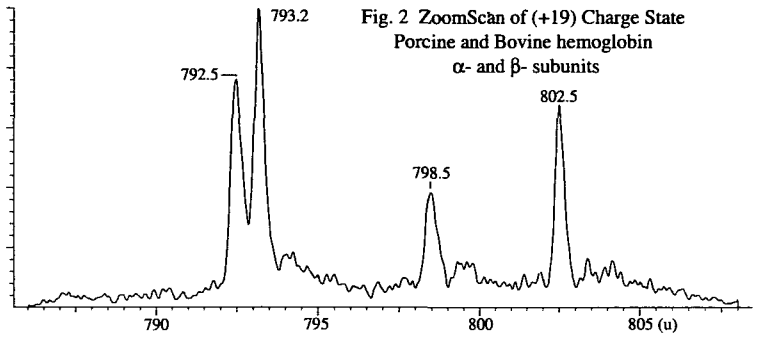

Fig. 2 ZoomScan of (+19) Charge State Porcine and Bovine hemoglobin α- and β- subunits

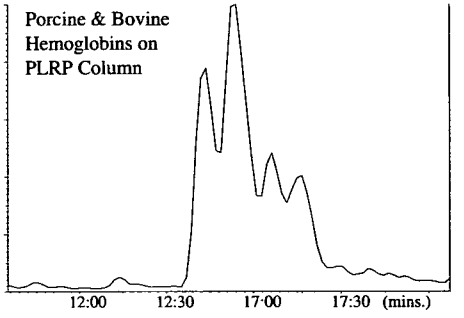

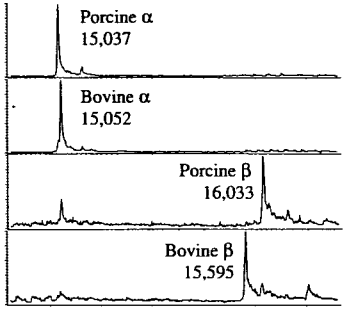

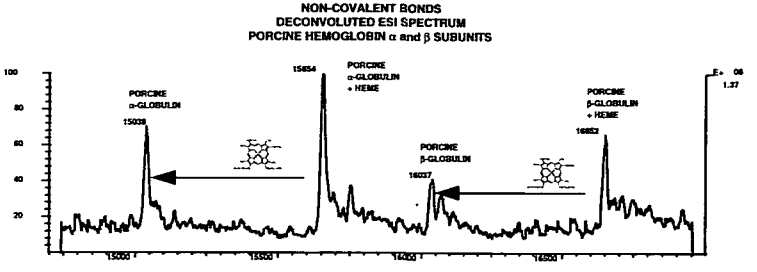

MS/MS in an Ion Trap/reflectron Time-of-flight Mass Spectrometer

Mark G. Qian, Yu Zhang, Jian Bai, and David M. Lubman

Department of Chemistry, The University of Michigan
Ann Arbor, MI 48109-1055

Introduction. There is currently a great deal of interest in the development of time-of-flight mass spectrometry (TOFMS) for the analysis of biologically important drugs, peptides, and proteins However, present limitations of this method include the lack of ion storage and MS/MS capabilities. Alternatively, the ion trap has become popular for such analysis using the electrospray ion source due to its relatively wide mass range, high duty cycle, and its ion storage and integration capabilities, which are important for sensitive detection. In addition, the trap operates at an elevated pressure (10^{-2}-10^{-4} torr), which can be conveniently used as an ion activation device to perform tandem mass spectrometry (MS/MS) through multiple collisions of the trapped ions with the buffer gas in the trap. However, there have been few reports to deal with the application of this method for peptide sequencing The main problems seem to be associated with the difficulties and complexities in terms of controlling the activation parameters and scanning high mass (m/z > 600) out of the trap without using an auxiliary radio frequency voltage, which may result in a deterioration of the mass accuracy, resolution and scan speed. In this work, we report the use of the ion trap/reflectron time-of-flight mass spectrometer (IT/reTOFMS) as a tandem mass spectrometer for accumulating, isolating, and activating multiply-charged peptide ions Single-frequency collisional activation of multiply-charged peptide ions has been studied for several characteristic peptides with m/z ranging from 700 to 1700

Methods. The electrospray-produced ions were injected and accumulated for a period of 500 ms and parent ions of interest were isolated by applying a multi-frequency AC voltage with amplitudes of 1.5-2 5 V_{pp} on the entrance endcap to eject unwanted ions. Isolated parent ions then underwent single-frequency collisional activation. The four time events, i.e., ion isolation, collisional cooling, ion activation, and collisional cooling, were controlled by a multi-step delayer/trigger which triggered a custom-built multichannel waveform generator For a typical MS/MS experiment, the four durations were typically at 20-30, 5, 20-30, and 20 ms, respectively. The first channel of the generator/combiner consists of five voltage-controlled oscillators (VCOs), while the second channel worked as a combiner to couple the single-frequency for activating isolated target ions. Since the MS/MS experiments described herein were carried out under the condition of q_z < 0.4, the corresponding β_z values of analyte ions were calculated using the approximated equation $\beta_z = [a_z + (q_z^2/2)]^{1/2}$[1] and the secular frequencies of analyte ions under a given q_z were therefore calculated from the equation $f_z = \beta_z\Omega/2\pi$.

Results. The electrospray spectrum of bradykinin, as shown in Figure 1a, is dominated by the doubly-charged peaks and a very weak singly-charged peak where the intensity is only ~10% of the former. The main reasons for this may include the intrinsic Coloumbic repulsion of the N-terminal site from the adjacent Arg[1] side chain or the relatively high pH in a 2% acetic acid solution. The lack of peaks from unwanted ions may ease the ion isolation process as evidenced in Figure 1b, which shows the spectrum of the same peptide after ejecting the singly-charged ions during the ion isolation process The CID fragmentation spectrum of bradykinin is shown in Figure 2. A low fragment ion peak intensity of

molecules with basic residues is a characteristic of low-energy CID spectra However, the CID spectrum shown in Figure 2 contains relatively complete complementary b and y pairs The lack of the doubly-charge product ions implies that one of the external protons must have been mobilized along the peptide backbone following collisional activation, even under the strong charge localization influence of the two Arg side chain amino groups. This CID spectrum shows similarity with the low-energy CID (70-250 eV) spectrum obtained on a triple-quadrupole tandem device using a moderate collisional energy[2].

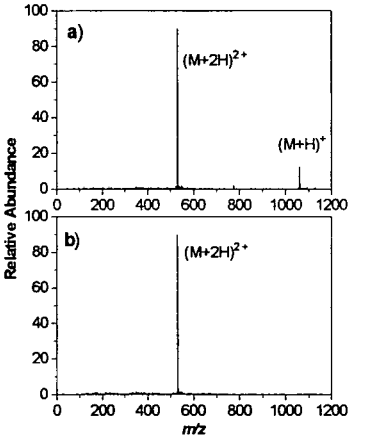

Figure 1

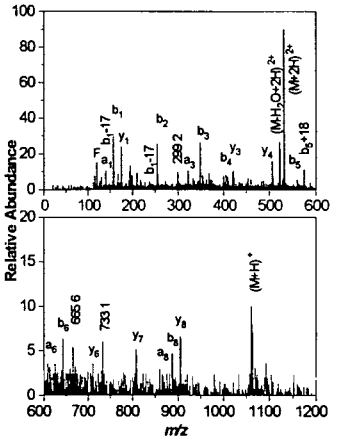

Figure 2

Conclusions. The results show that meaningful sequence information is available from this simple and relatively inexpensive tandem instrument with a sensitivity in the low picomole level Further, excellent resolution in the range of ~1,500 can be obtained for the fragment products due to the cooling effects of the buffer gas in the trap before analysis by the reTOF.

References.

[1] March, R., Hughes, R. *Quadrupole Storage Mass Spectrometry*, Wiley New York, **1989**
[2] Tang, X. J.; Thibault, P ; Boyd, R. K. *Anal. Chem.* **1993**, *65*, 2824-2834

Acknowledgment. The work described herein received support under several sources which we wish to gratefully acknowledge including the National Science Foundation, Biological Instrumentation and Instrumental Develop Program under grant #BIR-9223677 and Varian Associates, Inc., Ginzton Research Center.

MS/MS of Alkali Cationized Peptides Using a Quadrupole Ion Trap

Tong Lin and Gary L. Glish
Department of Chemistry, University of North Carolina, Chapel Hill, NC 27599-3290

INTRODUCTION

It has been previously demonstrated by a number of groups that alkali cationized peptides dissociate by -OH transfer from the C-terminus to the adjacent residue with subsequent loss of the C-terminal residue. The ion that is generated, $(b_{n-m} + Cat + OH)^+$, may well have the structure of the peptide ion one residue shorter than the initial peptide ion. This reaction is often the dominant process for metastable ions, which suggests that the reaction is a low energy process. The quadrupole ion trap, due to the energetics and time frame of CID, often has high specificity and sensitivity for low energy processes. The purpose of this work is to investigate the potential of using the above reaction and MS^n with a quadrupole ion trap as a new approach to sequence peptides.

EXPERIMENTAL

A modified Finnigan ion trap and regular Finnigan Rev.B ITMS and ICMS-FL[1] software were used for the experiments. Peptides were dissolved in 20/75/5 H_2O/MeOH/acetic acid solution and were used at about 250 μM. Alkali cationized peptides were made by mixing ~1:5 molar ratio of peptides with sodium chloride or lithium chloride. Ions were generated by electrospray ionization. All the lenses voltages were optimized and the liquid flow rate was set at 1-2 μl/min. Helium was used as bath gas and to effect collision-induced dissociation at a typical pressure of 7×10^{-4} torr.

Leucine enkephalin was used as obtained from Sigma. Leucine enkephalin analogues: YGLFL, YGSFL, YGPFL, YGWFL, and YGRFL were synthesized in the protein synthesis lab in our department.

RESULTS AND DISCUSSION

Experiments using lithium and sodium cationized peptides on a quadrupole ion trap have demonstrated similar reactions to those observed previously on sector instruments. The major exception is that only the C-terminal residue and associated peptide linkages are involved in dissociations in any individual stage of MS/MS. It has been observed that the dissociation of $(M+Cat)^+$ ions can proceed almost exclusively by -OH transfer and loss of the C-terminal residue and only C-terminal dissociation is observed. High CID efficiency combined with the MS^n capabilities of the ion trap allow further stages of dissociation to be performed. This series of fragmentations is analogous to Edman degradation except that the cleavage occurs from the C-terminus instead of N-terminus. Figures 1 and 2 show two examples of this dissociation process. However, our preliminary results show that glycine complicates spectra by yielding many product ions when it becomes the C-terminal residue of the parent ion. This is not explained by any of the previously postulated mechanisms. It seems likely that the side chain has some kind of stabilizing effect on the -OH transfer and thus for glycine, without this stabilizing effect, other C-terminal dissociation process are more competitive.

Previously in the literature, two mechanisms have been proposed for the formation of $(b_{n-m} +Cat+OH)^+$ ions, Gross'[2] and Adams'[3]. Overall, our data including all the **a** and **b** types of ions fit Gross' mechanism more closely than Adams'. The dissociation pathway that loses the C-terminal residue is very general, and the product ions are consistent with Gross proposed mechanisms. We do not observe the loss of 88 u that was seen by Adams et al. when leucine is the C-terminal residue. That was a main piece of evidence used to support their mechanism. However, our experiments were performed with a quadrupole ion trap, in which the MS/MS conditions are substantially different from

sector instruments. Additionally, the ionization technique we used generates ions with less internal energy than the ionization technique used in previous studies. Thus it is not at all unlikely that we are sampling a different population of ions in our experiments.

This presentation shows the potential capability of using the quadrupole ion trap to sequence peptides. However, more research needs to be carried out. A broader study needs to be performed to investigate other combinations of amino acids to determine the general applicability of this approach along with its limitations.

Acknowledgement
This work was supported by NIH (GM 49852)

References

1. ICMS-FL software, provided by R.A. Yost and N.A. Yates at Univ. of Florida
2. R.P. Grese, R.L. Cerny, and M.L. Gross, *J. Am. Chem. Soc.*, 1989, 111, 2835-2842
3. L.M. Teesch, R C Orlando, and J. Adams, *J. Am. Chem. Soc.*, 1991, 113, 3668-3675

Figure 1.

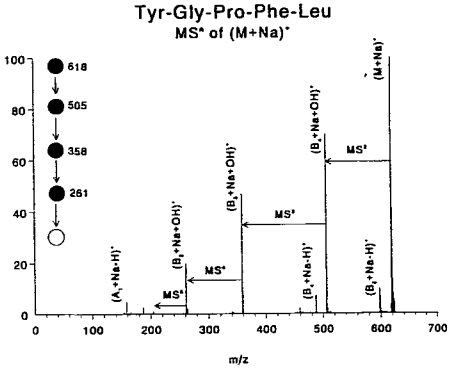

Figure 2.

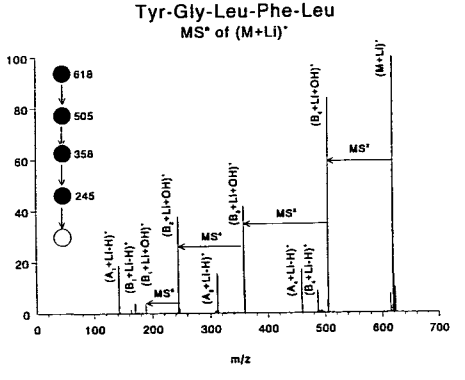

Tertiary Structure of Protein Ions in the Gas-Phase

Clifton K. Fagerquist, Paul D. Schnier, Deborah S. Gross, Sandra E. Rodriguez-Cruz and Evan R. Williams
Department of Chemistry, University of California, Berkeley
Berkeley, California 94720

Electrostatic interactions are long-range forces that play a key role in the function and conformation of biomolecules. We have recently developed a method[1-3] to quantitatively measure Coulomb energy through comparison of experimentally measured apparent gas-phase basicities (GB^{app}) to those calculated using a relatively simple model[2] in which charges are assigned to specific locations in the ion based on the combined effect of intrinsic basicity of protonation sites and total Coulomb energy in the ion. The magnitude of the electrostatic energy in an ion depends on ion conformation; for a given charge state, a fully denatured protein ion has less Coulomb energy than a tightly folded compact form. We present here, experimental results for lysozyme that indicate that both tightly packed and fully denatured conformations of proteins exist in the gas-phase.

Multiply protonated protein ions produced by electrospray ionization are introduced and collisionally trapped in a FTMS cell. Individual charge states of the protein are isolated with SWIFT and then reacted for increasing reaction delays. Rate constants are determined from the kinetic data for deprotonation of isolated charge states of the protein. We observe double exponentials for some charge states of the protein. For example, Figure 1 shows the decline in the 9+ charge state of lysozyme when reacted with the triethylamine (GB = 227.5 kcal/mol). These data require two rate constants for an accurate fit and suggests the presence of two stuctural isomers. From these rate constants, we assign values GB^{app} for each of the individual charge states.

Figure 2 shows the measured GB^{app} of lysozyme ions in its "native" (disulfide intact) and disulfide reduced form. Figure 2 also shows GB^{app} calculated using the "native" crystal structure and the linear conformation of lysozyme. Significant differences in the measured basicity between the "native" and reduced forms are observed for some charge states. For example, we measure a 17 kcal/mol difference in the GB^{app} of the "native" and reduced form of the 9+ charge state. Our electrostatic model indicates that this difference is consistent with calculated values for ions in a crystal structure and completely denatured conformation, respectively. In contrast, lower charge state ions formed from both these solutions have indistinguishable reactivities, indicating isomerization to a common structure which appears to be partially folded.

S-carboxymethylation of the cysteine residues in the disulfide-reduced lysozyme is used to confirm that all disulfide linkages are broken by the reducing agent dithiothreitol (DTT). The decline in the 9+ charge state of S-carboxymethylated has a rate of 1.6×10^{-11} cm^3/mol·sec and DTT-reduced lysozyme has a rate of 2.6×10^{-11} cm^3/mol·sec when reacted with triethylamine *simultaneously* in the ICR cell. Simultaneous reactions insures that both protein ions are exposed to identical base pressure. The S-carboxymethylated lysozyme appears to deprotonate somewhat slower than the DTT-reduced lysozyme which may be due to an inductive effect of the carboxymethyl group.

We are currently extending these measurements to probe the conformation of ribonuclease A, which also has four disulfide bonds, as well as proteins which do not have disulfide bonds but which have significant non-covalent hydrophobic interactions to determine if these ions have a folded conformation in the gas-phase.

43rd ASMS Conference on Mass Spectrometry and Allied Topics

1. Gross, D.S.; Williams, E.R. *J. Am. Chem. Soc.*, 883, *117* (1995).
2. Schnier, P.D.; Gross, D.S.; Williams, E.R. *J. Am. Chem. Soc., accepted.*
3. Gross, D.S.; Rodriguez-Cruz, S.E.; Bock, S.; Williams, E.R. *J. Phys. Chem.*, 4034, *99*, (1995).

Figure 1

Kinetics of Deprotonation of the 9+ Charge State of Lysozyme by Reaction with Triethylamine (GB = 227.5 kcal/mol)

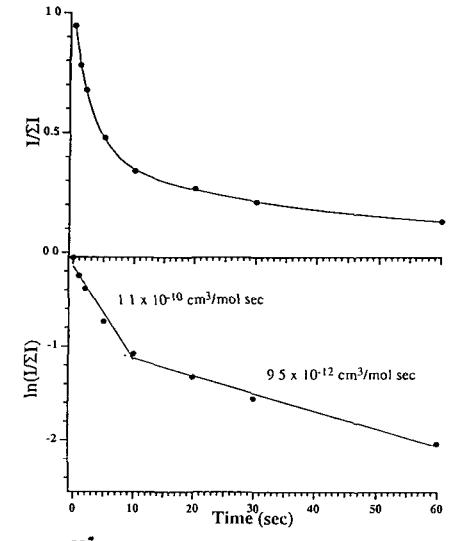

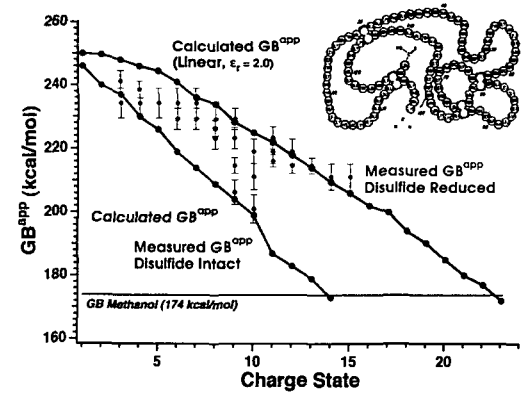

Figure 2

STRATEGIES FOR ACCURATE MASS API LC-MS ANALYSIS OF COMPLEX MIXTURES

D. J. Pugh, A. R. Woolfitt and R. H. Bateman,
VG ORGANIC, Floats Road, Wythenshawe, Manchester M23 9LZ, U.K.

In most reports to date, high resolution magnetic sector electrospray and APCI LC-MS analyses have employed a continuous post - column infusion of a standard reference compound, such as PEG or PPG This approach is satisfactory for the accurate mass analysis of simple mixtures, but is less useful in the case of complex mixtures, which often contain unknown or unexpected components at low levels.

An alternative strategy is presented here, in which discrete post - column injections of the mass reference compound are made at approximately 10 minute intervals throughout the gradient LC-MS wide scan analyses of several tryptic digests of proteins, using the setup shown in Figure 1 All analyses were carried out using a VG AutoSpec hexapole API interface, and the instrument was scanned from m/z 1100 to 500 at 10 cycles per minute at a resolution of 5000 (10% valley). The reference material, a mixture of 0.1% (v/v) PPG 725 and PPG 1000, was injected using the complete loop filling method. Although some MS data were lost during the reference injections, the UV trace was not affected.

A horse cytochrome C tryptic digest was used to evaluate the method, and the mass accuracies obtained for the identified peptides are given in Figure 2 The tryptic peptides were mostly within 10 ppm of their expected values, confirming that the mass accuracy was satisfactory. Similar results for the cytochromes from rabbit and yeast, and for horse myoglobin, were obtained.

It has previously been suggested that the heme moiety in cytochromes exists as a radical cation under electrospray conditions, based on high resolution studies of the intact proteins, and a low resolution (1500 RP) analysis of a horse tryptic digest The 5000 RP accurate mass analyses of the horse, rabbit and yeast heme - containing peptides, figure 3, all support the earlier findings. All three ions are observed at 1 Da (~600 ppm) below the expected values based on the usually assumed $[M+2H]^{2+}$ composition, and all three are within 10 ppm of the $[M+H]^{2+}$ theoretical compositions.

More importantly, a number of subtle discrepancies that would easily go unnoticed at low resolution were also apparent in these accurate mass analyses For instance, an intense singly charged ion of mass 718 in the horse digest was of particular interest, because based on its nominal mass it would have seemed reasonable to attribute it to one of two peptides produced by one nonspecific cleavage and one tryptic cleavage. However, since its measured mass differed by 60 and 90 ppm from the two candidates, it was clearly neither of these. The ability to distiguish these relatively small discrepancies between the observed peptides and any theoretical sequences has important implications for correct sequence assignments.

By using a strategy of discrete injection of the reference material, as opposed to continuous infusion, the lower intensity components can be located easily, with significantly less chance of interference. Although part of the LC-MS run is lost, it is possible to repeat the analysis with reference injections made at different times if necessary

43rd ASMS Conference on Mass Spectrometry and Allied Topics

Schematic of gradient LC system used for accurate mass LC-MS analysis.

Figure 1.

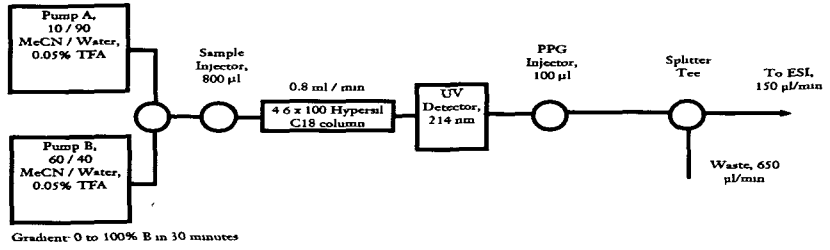

Horse Cytochrome C accurate mass tryptic digest

Figure 2.

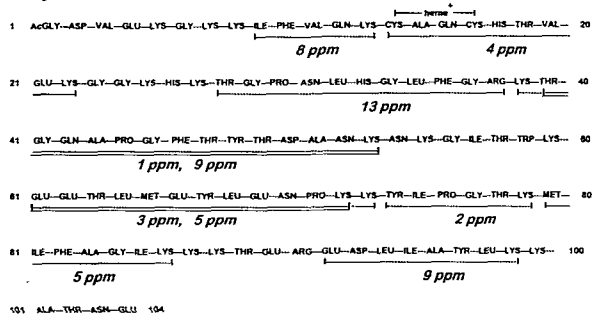

Heme - containing Tryptic Peptides from various Cytochrome C's

Figure 3.

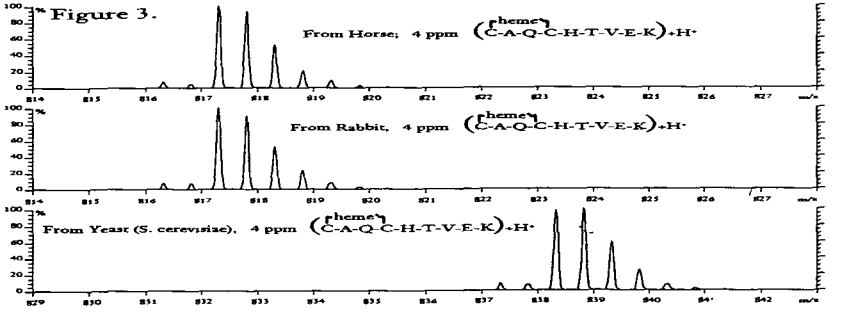

Quantitative Electrospray Mass Spectrometry of Oligonucleotides

Michael Greig*, Patrick Klopchin, Michael Winniman, Henri Sasmor, and Rich Griffey

Isis Pharmaceuticals
2280 Faraday Avenue
Carlsbad, CA 92008

Several types of synthetic failures or side reactions may occur during the synthesis of oligonucleotides. These products need to be identified and quantitated; in the case of GMP preparation for complete characterization of clinical samples or during synthesis of novel oligomers to research unexpected problems. The oligonucleotide's polyanionic backbone make these molecules perfect for ES-MS analysis but also results in a molecule with a strong propensity for multiple cation complexes The adduction of these cations not only reduces sensitivity, but creates multiple signals for each charge state, making it difficult or impossible to detect minor contaminants. Multiple cationic interactions have been dealt with by various means such as HPLC, dialysis, cation exchange or chemical additives. Instead of using sample and labor intensive techniques, we found the addition of a strong base can be used to suppress a majority of the salt adducts however this occasionally results in the reduction of detectable ion abundance Our solution to this loss of peak intensity is the co-addition of a second, weaker base. With both bases added, up to a ten-fold increase in peak intensity and almost complete suppression of salt adducts is observed. This allows for detection and quantitation of minor products whose composition is less than 1.5% of the total analyte.

The quantitation of oligonucleotide synthesis products including failure sequences and incompletely deprotected oligomers is presented ES-MS analysis of the various synthesis products is compared to analytical methods such as NMR, cation-exchange and reverse-phase HPLC, and capillary gel electrophoresis. Problems in the use of electrospray for quantitation of oligonucleotides are identified. These include CID loss of adenosine and pH dependent ionization differences of thymine containing oligomers

The use of chemical additives in ES-MS provides a method for characterizing and quantitating a variety of oligonucleotide synthesis products and side reactions. This method is rapid, requires minimal sample and sample preparation, and in a single assay gives results that presently require several analytical methods.

43rd ASMS Conference on Mass Spectrometry and Allied Topics

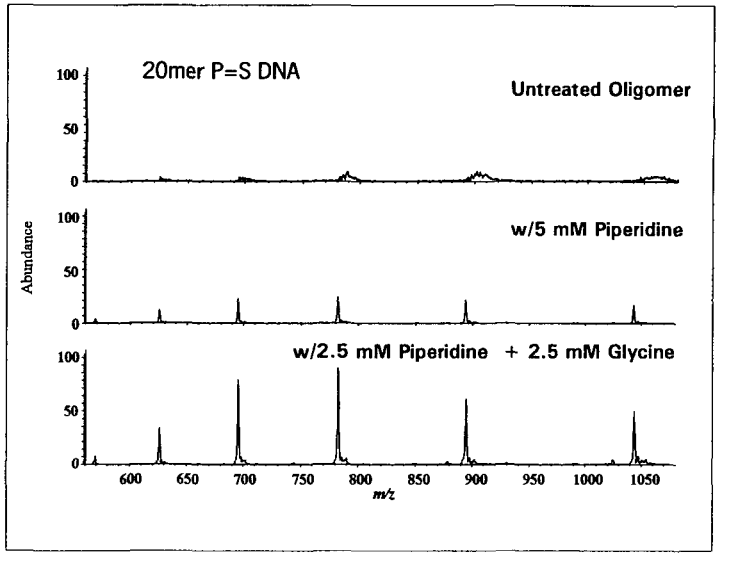

RAPID QUANTITATION OF EICOSANOIDS IN INFLAMMATION MODELS BY ES/MS/MS

Kevin L. Duffin, Alon Margalit, and Peter C. Isakson, Monsanto/Searle Research and Development, Monsanto Company, St. Louis, MO 63198

Assessment of eicosanoid levels in biological systems is important for understanding their role in cell function and pathophysiological events. Current methods of eicosanoid quantitation are limited by sensitivity, scope, or throughput. The development of a new method for eicosanoid assessment in biological samples by electrospray and tandem mass spectrometry in the multiple reaction monitoring (MRM) mode is described here. In this study, 14 biologically-significant eicosanoids and arachidonic acid (AA) were quantitated in a single sample. Complete sample analysis required two repeated injections of 5 µl with an analysis time of 1.5 min/injection. Limits of detection ranged from 0.5 pg for thromboxane B_2 (TxB_2) to 10 pg for 6-keto prostaglandin $F_{1\alpha}$ (6-keto $PGF_{1\alpha}$). The MS/MS method was used to explore eicosanoid production in 2 inflammation models: lipopolysaccharide(LPS)-stimulated human whole blood and carrageenan-challenged rat air-pouch. The most abundant metabolites in LPS-stimulated whole blood were prostaglandin E_2 (PGE_2), TxB_2 and 6-keto $PGF_{1\alpha}$; prostaglandins E_1, D_2, and $F_{2\alpha}$, and leukotrienes B_4 and C_4 were detected in lower amounts. Levels of TxB_2 and PGE_2 determined by MS/MS were similar to those obtained by immunoassay. The most abundant metabolites detected in carrageenan-challenged rat air pouch were PGE_2, 6-keto $PGF_{1\alpha}$, and TxB_2; substantial amounts of AA were also observed. The method described in this work is accurate and rapid and should greatly aid in evaluating the role of multiple eicosanoids in future biological studies.

Solid-Phase Extraction of Biological Samples. One ng of PGE_2-d_4 was spiked into each sample of 0.5 ml of the biological preparation, and solid-phase extraction was performed. The C18 cartridges (Bond Elute C18, Analytichem Int., Harbor City, CA) were pre-conditioned with 2 ml of methanol and 2 ml of H_2O. After the samples were applied, the cartridges were successively washed with 2 ml H_2O and 2 ml petroleum ether. The eicosanoids were eluted in 1 ml methyl formate. The methyl formate residue was evaporated under a dry N_2 stream and the samples were resuspended in 50 µl ethanol. The samples then were transferred to autosampler vials and stored under nitrogen at -80° C until analysis.

Mass Spectrometry. A Sciex API III triple-quadrupole mass spectrometer equipped with an atmospheric pressure ion source was used to sample negative ions produced from a pneumatically-assisted electrospray (ionspray) interface (Sciex Inc., Thornhill, Ontario). Eicosanoid standards that were dissolved in ethanol (1 µg/ml) were introduced continuously through the ionspray interface at a rate of 4 µL/min. The ionspray interface

was maintained at -4.5 kV with respect to the ion entrance of the mass spectrometer. As deprotonated eicosanoids entered the mass spectrometer, they were accelerated through a potential difference of 40 volts. Product ion MS/MS spectra of the deprotonated eicosanoid standards were acquired from 15 amu up to and including the mass of the parent ion. The argon target gas thickness was maintained at 2.3×10^{14} atoms/cm^2 and collision energies were adjusted to 30 eV with respect to the laboratory reference for this study.

Eicosanoids were quantified by delivering duplicate 5 µl injections of the samples through a 75 µm i.d. x 75 cm capillary to the mass spectrometer. A Hewlett Packard 1090 autoinjector (Hewlett Packard,Palo Alto, CA) was used to inject the samples into a 50 ul/min stream of ethanol. Injections were made every 1.5 min. The mass spectrometer was operated in the 'multiple reaction monitoring' (MRM) mode. In this mode experiments were performed using the same instrument conditions as used for the product ion MS/MS experiments. MRM experiments were performed by setting the first quadrupole to pass the $(M-H)^-$ of a selected eicosanoid while simultaneously setting the third quadrupole to pass a selected fragment ion of that eicosanoid. Up to 8 different eicosanoids were quantified in one experiment by adjusting the first and third quadrupoles to the selected masses in 0.3 sec increments/eicosanoid. The following masses were used to quantify the different eicosanoids:

Eicosanoid	Parent Ion	Fragment Ion (rel. abund.)
Arachidonic acid	303 (100)	**59(13)**
PGE_2	351 (7)	**175(10)**
D_4-PGE_2	355 (4)	**275(100)**
PGD_2	351 (3)	**233(11)**
PGF_{2a}	353 (92)	**193(45)**
PGE_1	353 (6)	**317(100),**
6-Keto PGF_{1a}	369 (100)	**163(40)**
TxB_2	369 (2)	**169(100)**
HxA_3	335 (35)	**127(100)**
12-HPETE	335 (15)	**153(100),**
12-HETrE	321 (57)	**181(100)**
12-HETE	319 (32)	**179(100)**
15-HETE	319 (35)	**219(36)**
LTB_4	335 (100)	**203(23)**
LTC_4	624 (100)	**272(36)**

Serum Albumin Determination using LC/MS with Affinity Chromatography

David M. Bunk and Michael J. Welch
National Institute of Standards and Technology
Gaithersburg, MD 20899 USA

With a goal of developing methods to produce clinical reference materials of serum proteins, we have been investigating the quantitative aspects of electrospray ionization mass spectrometry (ESI-MS) for protein analysis. Previously (1), we have demonstrated that for pure proteins (in the absence of a complex sample matrix) ESI-MS can yield excellent quantitative results, providing calibration curves linear over three orders of magnitude of analyte concentration with a precision of less than 5%.

These promising results from our model study have led us to the next stage of this project: the analysis of a protein in a complex matrix. For this stage, we chose human serum albumin (HSA) as our analyte. To introduce the serum samples into our Finnigan TSQ-700 triple quadrupole mass spectrometer equipped with an Analytica electrospray source, we used capillary reverse-phase LC/MS. LC/MS analysis of a reconstituted freeze-dried serum sample (produced by the College of American Pathologists) yielded an albumin electrospray mass spectrum distinctly different from that of a pure albumin standard (**Figure 1**). The molecular weight of the albumin from freeze-dried serum is higher and is distributed more heterogeneously than that of the albumin standard. Initially, we believed that this heterogeneous molecular weight distribution was the result of the non-covalent binding of small hydrophobic molecules to the surface of the albumin. But after exhaustive attempts to delipidate the freeze-dried serum, we were not able to "clean up" the observed molecular weight profile. We began to suspect that this distribution resulted from covalent adducts to the protein that occurred during freeze-drying This suspicion was confirmed when we analyzed a sample of fresh-frozen serum and obtained a molecular weight profile essentially identical to that of the albumin standard shown in Figure 1.

One of the important lessons that was learned from our model studies was that an internal standard was essential for good quantitation. Because our experimental plan included the use of antibody affinity chromatography to isolate the albumin from the serum matrix (to determine the effects of the matrix on quantitation), the affinity chromatography necessitated the use of a modified human albumin as an internal standard because any other protein would not bind to an anti-HSA monoclonal antibody. To prepare the internal standard, we biotinylated the one free thiol group of HSA, found on cys-34. Fortunately, because of the singularity of the reaction site, biotinylation of HSA did not alter the binding to the anti-HSA antibody and also served as an affinity tag for its facile purification using avidin/biotin on a monomeric avidin stationary phase.

Using the biotinylated HSA (bHSA) internal standard, we performed a quantitative determination of the albumin in fresh-frozen serum using LC/MS. The calibration curve obtained from this determination is shown in **Figure 2**. From this calibration curve, the concentration of albumin in the fresh-frozen serum sample was determined to be 3700±200 mg/dL. This concentration is within the

1. Bunk, D.M.; Welch, M.J. *Proceedings of the 42nd ASMS Conference on Mass Spectrometry and Allied Topics*, 1994, 1005.

expected range of normal serum albumin concentrations (3500-5000 mg/dL) but lower than the value of 4700±400 mg/dL that we obtained for the same serum sample using the conventional dye-binding assay (with bromocresol green). Additional work is planned to determine why LC/MS produces results different from the dye-binding assay and to characterize the covalent modification of HSA in freeze-dried serum.

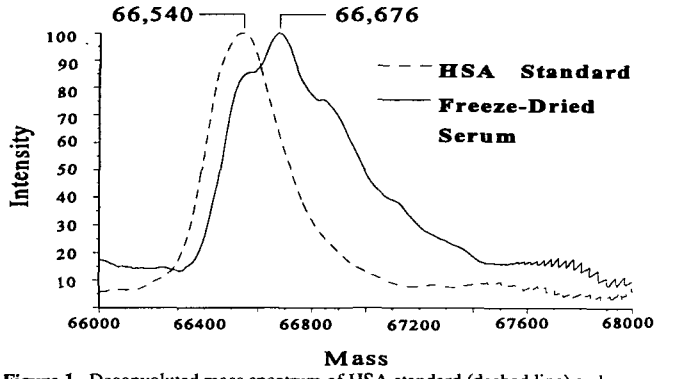

Figure 1. Deconvoluted mass spectrum of HSA standard (dashed line) and albumin from freeze-dried human serum (solid line)

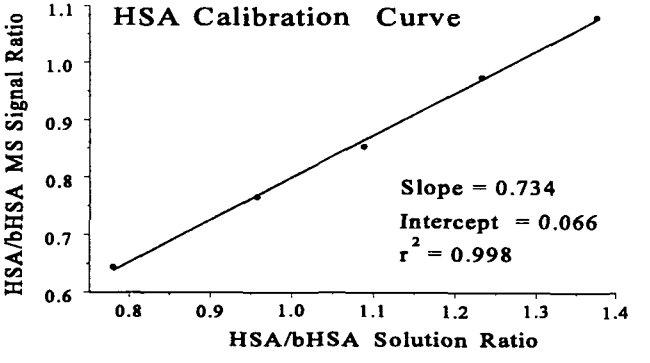

Figure 2. Calibration curve for the determination of HSA in fresh-frozen serum using biotinylated albumin (bHSA) as internal standard

Quantification of Pranlukast and SB 218663 in Plasma Samples Using LC/MS/MS

H.Bi, D. Lundberg, J. Pirhalla, C. McHugh and A. Marchese

SmithKline Beecham Pharmaceuticals, King of Prussia, PA 19406

INTRODUCTION

Pranlukast (SB 205312, 4-oxo-8-[4-(4-phenylbutoxy)benzoylamino]-2-(tetrazol-5-yl)-4H-1-benzopyran, Figure 1a) is a potent and selective peptidoleukotriene receptor antagonist which is currently under development as a potential therapy for asthma at SmithKline Beecham Pharmaceuticals. A very simple, robust and high speed analytical method has been developed to quantify Pranlukast simultaneously with its inactive hydroxy metabolite, SB 218663 (Figure 1b) in plasma by ionspray LC/MS/MS. This new method has a very short run time of 0.6 min, which enables a single analyst to process two to three hundred clinical samples per day. This represents a major advance in terms of productivity and efficiency in quantitative bioanalysis.

EXPERIMENTAL

Sample preparation was accomplished by simple protein precipitation with acetontrile. Plasma samples (100 uL) were treated with an equal volume of acetonitrile containing SB 218658 (internal standard, Figure 1c). No evaporation process was involved. Following centrifugation (12,000 g) the supernatant was mixed with 50 uL of 10 mM ammonium acetate and 5 uL of the mixture were directly injected for LC/MS/MS analysis. Hitachi L-6000 and L-6200A HPLC pumps were used to deliver the mobile phase (10 mM NH_4OAc : acetonitrile, 25/75) to a Keystone BDS Hypersil C_{18}, 20 x 2 mm i.d. guard cartridge column at a flow rate of 250 uL/min. Column effluent was split approximately 1:4 before reaching the ionspray interface. A SCIEX API III Plus mass spectrometer was operated in negative ion and MS/MS mode. Collision energy of 30 eV and collision gas (argon) thickness of 300 $x10^{12}$ atoms cm^{-2} were employed. Data acquisition was performed using multiple reaction monitoring (MRM) in count-by-10 mode. The following precursor-to-product ion reactions, m/z 484 to 424 (Pranlukast), m/z 496 to 172 (SB 218663) and m/z 494 to 438 (internal standard), were monitored with 200 ms dwell time for each reaction.

RESULTS AND DISCUSSION

This rapid LC/MS/MS method was developed and validated to quantify Pranlukast and SB 218663 in plasma from five different species including man. The lower limit of quantification (LLQ) was 10 ng/mL for both Pranlukast and SB 218663 using a 100 uL aliquot of sample. The specificity of the assay was demonstrated by analyzing drug-free plasma samples (n>6 for each species). No endogenous interferences were found at the retention time of either of the analytes or the internal standard. The intra- and inter-assay precisions were better than 15% at all concentrations in plasma from all the species studied. Similarly, the intra- and inter-assay accuracies were within 15% of all the nominal concentrations. The recovery from plasma sample of different species was always better than 87%. This new method has been proven to be robust, sensitive, specific, accurate and reproducible. Due to the combination of a simple extraction method with a very short HPLC run time (0.6 min), the sample throughput has been significantly increased when compared with previous conventional HPLC/UV methods.

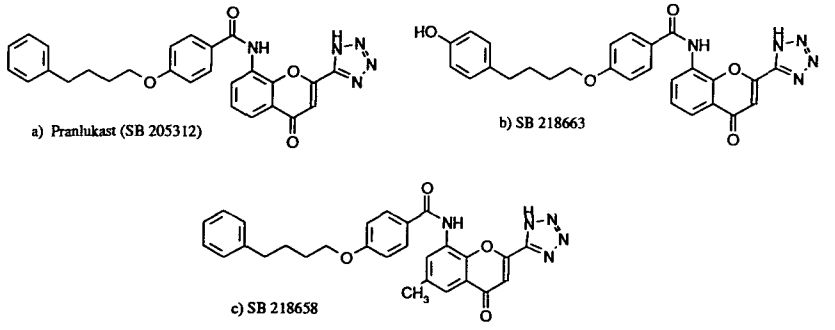

Figure 1. Chemical structures of Pranlukast, SB 218663 and SB 218658 (internal standard).

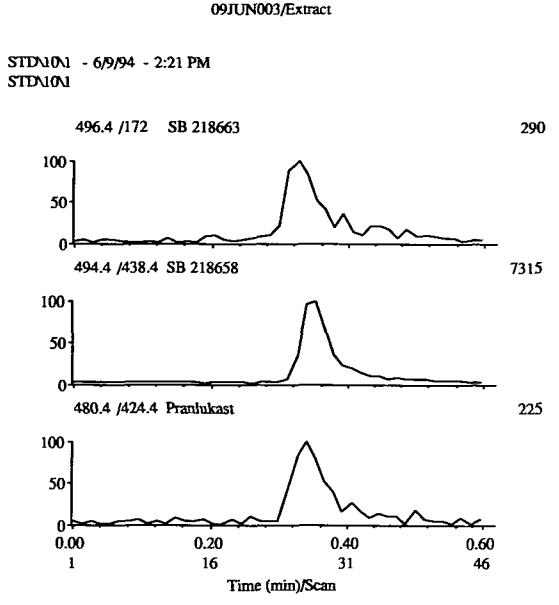

Figure 2. Typical chromatogram of human plasma containing 10 ng/mL of Pranlukast and SB 218663.

Application of Ionspray MS/MS Quantification of Beclomethasone Dipropionate

Karl S. Schorno and L. D. Winslow, Kansas City Analytical Services, 12700 Johnson Drive, Shawnee, Kansas 66216

Old analytical procedures for common drugs such as Beclomethasone Dipropionate (BDP), an antiallergic and aniti-inflammatory drug, are continually being upgraded to meet lower limits of detection necessary for todays assays. The quantitative analysis of BDP to 1 ng/mL has been reported by Girault, et. Al. (1991) using a liquid/liquid extraction and HPLC particle beam methane collision induced dissociation (CID) mass spectral analysis. We would like to report the development of a solid phase extraction HPLC API Ionspray Argon CID Mass Spectral analysis. The mass spectral analyses is fast and sensitive to less than 100 pg/mL using the ratio of analyte to internal standard. The instrument used for his assay is a PE/SCIEX API *III* + tandem mass spectrometer. The assay includes BDP, Beclomethasone 17-propionate (BMP-17) and 21-propionate (BMP-21), Beclomethasone (BOH), and Dexamethasone (internal standard). The HPLC-mass spectral analysis is carried out in less than 5 minutes per sample.

The presentation will cover only the development of the mass spectral method of the assay. Because all of the analytes are similar and give similar precursor and product ions in the ionspray analysis, only BDP will be treated in this presentation. A C18 SPE similar to that reported by Plezia (1985) was used for the isolation of the analytes from plasma.

The development of the mass spectral and HPLC conditions for the assay consists of the following:

1. Determination of Precursor Ions by Q1 Scan (full scan) infusion ionspray Mass Spectrometry
2. Determination of the Product Ions for multiple reaction monitoring (MRM) by Precursor to Product Ion infusion ionspray Argon CID Mass Spectrometry (Figure 1)
3. Determination of lower limit of quantitation (LLOQ) by HPLC-tandem mass spectrometry
4. Development a fast HPLC separation (less than 5 minutes per sample) that does not degrade the integrity of the mass spectral analysis
5. Establish linearity over the analytical range of interest (Figure 2).

A schematic of a portion of the CID fragmentation is given in Figure 3. The major product ions that are used in the MRM analysis are 521=>503 Daltons (BDP), 464=>447 Daltons (BMP-17 and -21), 408=>391 (BOH), and 392=>355 Daltons (Dexamethasone). With the exception of Dexamethasone each analyte loses water first. As noted in Figure 3, each analyte follows the same degradation path as BDP.

Linearity over the analytical range of interest is determined by a six point (in duplicate) calibration curve from the LLOQ to the highest concentration level analyzed. The calibration curve is linear for all analytes. The correlation coefficient is greater than 0.998 for each analyte quantitated.

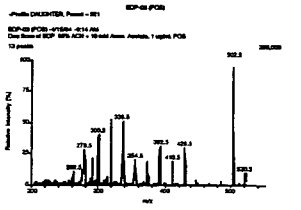

Figure 1. Precursor to Product Ion Mass Spectrum of BDP

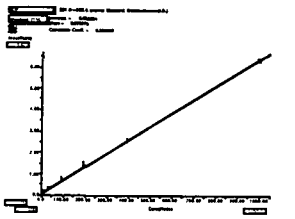

Figure 2. Linearity Curve for BDP.

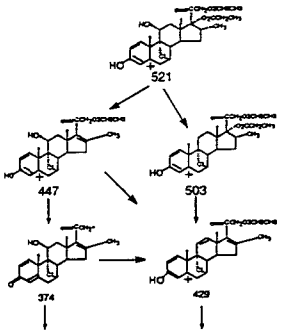

Figure 3. Schematic of the Fragmentation of BDP

REFERENCES.

Girault, J. et al., J. Chrom., 564, 43-53 (1991).

Plezia, P. et al., Clinical Chemistry 31(11), 1870-1872 (1985).

Quantitative Analysis of Low Molecular Weight Biomolecules by MALDI-tof

M. W. Duncan and R. O. Lidgard, Biomedical Mass Spectrometry Unit, University of New South Wales, Sydney, 2052, Australia.

Introduction

Matrix-assisted laser desorption ionization (MALDI) mass spectrometry has proved to be an important tool in synthetic- and bio- polymer characterization, but applications for low molecular weight analytes i.e., less than 1000 Da have been restricted. Following investigations which demonstrated the general utility of MALDI (1) and our earlier work on quantitative applications (2), we have moved on to quantify low mass analytes in biological matrices.

Quantitation

MALDI has several significant limitations that become evident in quantitative applications. Variability in peak height or area, both shot-to-shot and sample-to-sample, is significant. This means that duplicate samples give widely disparate peak heights or areas, even for the same analyte loading. We have therefore employed stable isotope internal standards to 'correct' for this irreproducibity. The limited resolution available on our linear tof instrument (Finnigan Lasermat 2000) means that a minimum of three labelled atoms must be incorporated for the analogue to be a practical standard.

Results

We initiated our quantitative studies by attempting to determine the epinephrine (adrenaline; figure 1) content of a sample of phaeochromocytoma tumour tissue (a catecholamine secreting tissue). Using [$^2H_3$]-epinephrine as the internal standard (fixed concentration), a standard curve was obtained over the concentration range 2 - 1,500 pmol ($r^2 > 0.995$). A sample of tumor tissue was then ultrasonically disrupted in dilute acid containing the internal standard, and an aliquot was then examined by MALDI (figure 2). The epinephrine content of the tissue was calculated by reference to the standard curve and was found to be 26.70 ± 4.80 mg/g (c.f. the reported range of 0.08 - 50 mg/g.)

To further investigate the general applicability of the technique we have attempted to quantify some analytes in urine samples. Our preliminary results indicate that direct quantitation of abundant analytes such as creatinine and urea is possible, and that simple acid extraction of urine allows metabolites such as hippuric and α-amino-hippuric acids to be quantified. Less abundant urine components were not evident because of ion suppression as a consequence of the large excess of Na^+ and K^+ in the sample. Furthermore, we have found that some analytes are simply not amenable to MALDI analysis (as indicated by our attempts to analyse pure standards), and in our hands several relatively abundant urinary components could not be quantified. We suggest that sample clean-up/extraction, e.g., by HPLC or solid phase techniques, is a prerequisite for the quantification of most urinary metabolites, and we are exploring this avenue in more detail.

Conclusion

MALDI is a versatile ionization technique applicable to a wide range of analytes. In particular we have demonstrated that low mass analytes are generally amenable to this method, and the use of stable isotope labelled internal standards allows acceptable quantitation in some instances. Abundant urine, tissue or plasma analytes can be monitored and quantified directly (i.e.,without clean-up), but selective extraction and or work-up is required in most instances.

References

1. Lidgard, R. & Duncan, M.W., Rapid Commun. Mass Spectrom., (1995), 9, 128-132.
2. Duncan, M.W. Matanovic, G. & Cerpa-Poljak, A. *ibid.*, (1993),7,1090-1094.

43rd ASMS Conference on Mass Spectrometry and Allied Topics

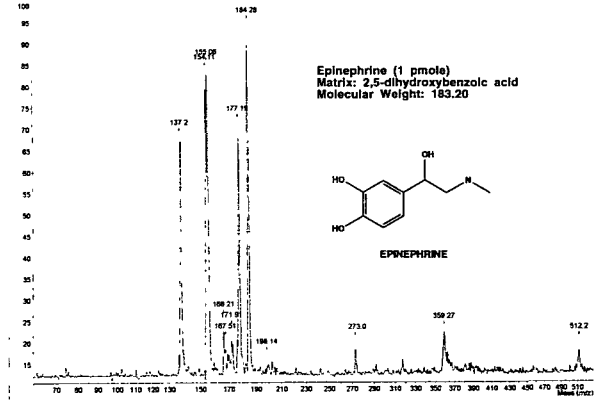

Figure 1. MALDI mass spectrum of epinephrine. Note protonated molecule at *m/z* 184

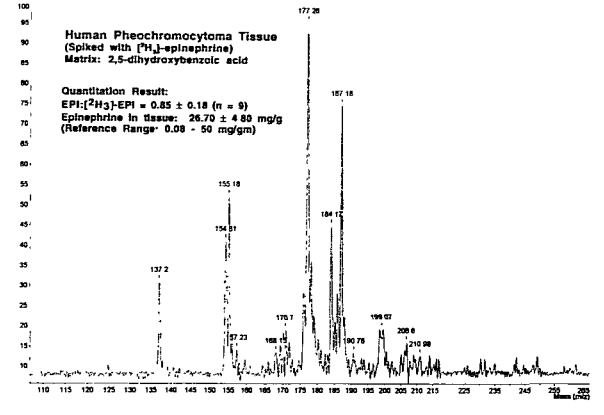

Figure 2. MALDI mass spectrum of an extract of human pheochromocytoma tissue spiked with stable isotope labelled epinephrine. Note *m/z* 184.2 & 187.2.

Quantitative Analysis of Angiotensin II by Matrix-Assisted Laser Desorption/Ionization Mass Spectrometry

Anthony J. Nicola[1], Arkady I. Gusev[1], Andrew Proctor[1], David M. Hercules[1a], and Edwin K. Jackson[2]

Departments of: 1. Chemistry 2. Clinical Pharmacology
University of Pittsburgh, Pittsburgh, Pennsylvania 15260

a. Present address: Department of Chemistry, Vanderbilt University
Box 1822 Station B, Nashville, Tennessee 37235

Although Matrix-Assisted Laser Desorption/Ionization Mass Spectrometry (MALDI) has been successfully applied for quantitative analysis of biomolecules[1-3], there are several problems still associated with this technique. These include sample heterogeneity, signal degradation, and insufficient linearity of the instrumental acquisition system. There are two major ways of compensating for these problems: use of an internal standard, and development of a sample preparation protocol which addresses improvement of absolute signal reproducibility. The present work focusses on sample homogeneity by application of a modified "fast-evaporation" sample preparation method[4], employing an internal standard, for quantitative analysis of Angiotensin II. The results will be compared to those obtained using the established method of sample preparation (using a multicomponent matrix[5]).

For the multicomponent matrix investigation, a mixture of 2,5-dihydroxybenzoic acid (DHB, 20 mg/mL) and 5-methoxysalicylic acid (MSA, 1 mg/mL) was used as the matrix. The matrix and analyte/internal standard (Angiotensin II: 90-6000 nM/ 1-SAR-8-Ile Angiotensin II: 660 nM) were premixed and deposited onto stainless steel substrates in volumes of 2-5 μL. For the fast evaporation technique, α-cyano-4-hydroxycinnamic acid (15 mg/mL in acetone) was deposited onto stainless steel substrates to make the matrix layer over the whole substrate surface. A mixture of matrix (α-CHCA, 10 mg/mL in 1:1 MeOH:H_2O) and analyte/internal standard (Ang. 2: 45-3000 nM/ 1-SAR-8-Ile Ang. 2: 330 nM) was then deposited onto the matrix layer.

An instrumental protocol to determine the optimum laser energy and to address the problem of signal degradation was established for the fast-evaporation method. Discarding the first ten laser shots and collecting the next forty laser single-shot mass spectra enhanced absolute signal reproducibility by 20-30%. Quantitative analysis of Angiotensin II using the fast-evaporation technique showed improved results over using a multicomponent matrix in several areas. Comparative results are presented in Table 1, and calibration curves are shown in Figures 1A and 1B. The relative standard deviations (RSD) of the analyte/internal standard intensity ratios (point RSD) were improved by a factor of three for the fast evaporation technique over the multicomponent matrix method. The RSD of the standard curve slope (slope RSD) was improved by a factor of two over use of a multicomponent matrix. Furthermore, the detection limit was lowered by a factor of two for the fast-evaporation technique. The precision of a single determination of concentration from the standard curve was improved by a factor of two in comparison to the multicomponent matrix method. We confirmed that mass resolution was

enhanced[4] by nearly a factor of two using the fast-evaporation method ($m/\Delta m$ = 2000), compared to using a multicomponent matrix ($m/\Delta m$ = 1150). The fast-evaporation method of sample preparation has thus proven itself to be a successful method for quantitative analysis by MALDI.

Table 1: Comparison of fast-evaporation and multicomponent techniques

Technique	Point RSD (%)	Slope RSD (%)	Corr. coeff.	Detection Limit (nM)	Precision[1]	Quant. Range (nM)
Fast evap. Ang. II	2-7%	2.2%	0.996	5.5	7% (1400 nM)[2]	45-3000
Multicomp. matrices Ang. II	10-20%	4.5%	0.976	11	16% (2740 nM)[2]	90-6000

Internal Standard = 1-SAR-8-Ile Angiotensin II
[1] -- Precision at 95% confidence level
[2] -- Concentration for which precision was calculated

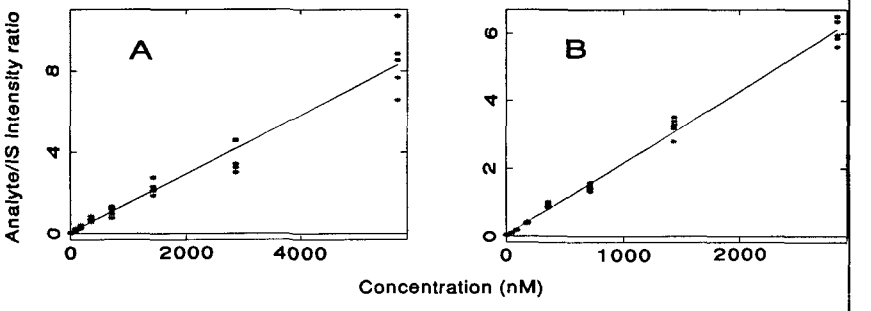

Figure 1: Standard curves of Angiotensin II with the internal standard 1-SAR-8-Ile Angiotensin II.
A: Multicomponent Matrix (IS: 660 nM); B: Fast-Evaporation (IS: 330 nM)

1. D.C. Muddiman, A.I. Gusev, A. Proctor, D.M. Hercules, R. Venkataramanan, W. Diven, *Anal. Chem.* **66**, 2362 (1994).
2. D.J. Harvey, *Rap. Comm. Mass Spectrom.* **7**, 614 (1993).
3. R.W. Nelson, M.A. McLean, T.W. Hutchens, *Anal. Chem.* **66**, 1408 (1994).
4. O. Vorm, P. Roepstorff, M. Mann, *Anal. Chem.* **66**, 3281 (1994).
5. A.I. Gusev, W.R. Wilkinson, A. Proctor, D.M. Hercules, *Anal. Chem.* **67**, 1034 (1995).

Selection of an Internal Standard for Quantitative Analysis by Matrix Assisted Laser Desorption/Ionization Time of Flight Mass Spectrometry (MALDI-TOF MS)

William R. Wilkinson[1]; Arkady I. Gusev[1]; Andrew Proctor[1]; Marwan Houalla[1] and David M. Hercules[1-2]

[1]*Department of Chemistry, University of Pittsburgh, Pittsburgh, PA 15260*
[2]*Department of Chemisry, Vanderbilt University, Nashville, TN 37235*

Introduction

In quantification of macromolecules by MALDI-TOF, the use of an internal standard is critical. Determination of what constitutes a good internal standard is addressed in this report using bovine insulin as a model analyte. The means of measurement of the signal intenisty is also discussed, including the use of direct peak integration and non-linear least squares curve fitting (NLLSCF).

Experimental

A previously described [1] analytical protocol was used in the collection of spectra. Samples were prepared in a matrix consisting of 2,5-Dihydroxybenzoic acid (20 mg/mL), 5-Methoxysailcylic acid (2 mg/mL) and fucose (5 mg/mL) in a solvent of 9:1 water:ethanol (v/v). The matrix was mixed with the analyte solution in a 1:1 volumetric ratio deposited on a stainless steel substrate. Samples were visually monitored to determine good matrix crystals for analysis. Fifteen to twenty laser shots were discarded because of wild variations in the analyte to internal standard peak height ratio. The next 25 laser shots were collected and averaged before the selection of a new crystal and repetition of the process. This process was repeated to provide averaged spectra consisting of 200 averaged single-shot spectra.

Spectra were collected for bovine insulin with the following internal standards: bovine insulin chain B, horse heart cytochrome C, des-pentapeptide human insulin human arg-insulin and des-octapeptide porcine insulin.

Results and Discussion

Intensity measurement was accomplished by both direct integration of the analyte peaks following subtraction of a linear background and non-linear least squares curve fitting (NLLSCF) which is more completely described in reference [2]. Peaks used in the NLLSCF include $M+H^+$, $M+H-H_2O^+$, $M+Na^+$, $M+K^+$ and a broad peak corresponding to metastable decay products. A sample curve fitted insulin spectrum is shown in Figure 1.

Evaluation of the relative standard deviation of the slope of the standard curves shows very little difference between methods of intensity measurement. This was confirmed when the squares of the standard deviations of the slopes were compared with an F test, which revealed no difference between methods.

The standard curve statistics using the different internal standards are compared in Table 1. Des-pentapeptide human insulin was the most desirable internal standard, judged by comparison of the relative standard deviation of the slopes, and the simplicity of the intensity measurement. Of the remaining standards, bovine insulin chain B is formed in the fragmentation of the insulin molecule, thereby causing the apparent concentration of chain B to vary with laser intensity. Des-octapeptide insulin and horse heart cytochrome C yielded similar results, possibly as a result of imperfect inclusion of the peptides into the matrix, and

these results were shown by an F test to be significantly poorer than those seen for des-pentapeptide insulin. Arg-insulin, although providing good accuracy, was not completely resolved, thereby complicating the data analysis.

Thus, a recommended means of selection of an internal standard for quantitative MALDI includes the use of a molecule which has a sufficiently different mass that baseline resolution may be achieved between molecules.

[1] Gusev, A.I.; Wilkinson, W.R.; Proctor, A.; Hercules, D.M. *Anal. Chem.* **1995**, *67*, 1334
[2] Hercules, D.M.; Houalla, M.; Proctor, A.; Fiedor, J.N. *Anal. Chim. Acta.* **1993**, *283*, 42

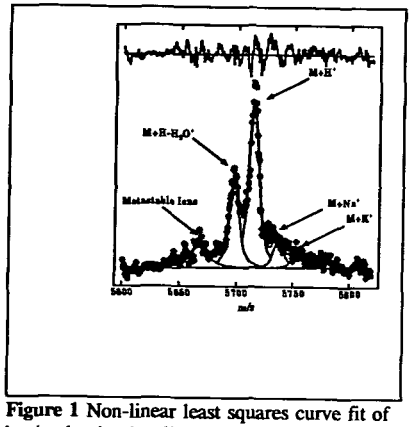

Figure 1 Non-linear least squares curve fit of bovine bovine insulin using $M+H^+$, $M+H-H_2O^+$, $M+Na^+$, $M+K^+$ and metastable decay products.

Table 1: Comparison of Internal Standards in the Quantitative Analysis of Bovine Insulin by MALDI

Standard	Correlation Coefficient	RSD Slope (%)	Quantitative Range (μM)
Chain B	0.930	9.81	1–30
Des-Octapeptide Insulin	0.975	6.30	1–20
Des-Pentapeptide Insulin	0.988	2.99	0.5–40
Cytochrome C	0.977	6.54	1–30
Arg-Insulin*	0.990–0.997	1.4	0.25–50

* Previously Published Data

"Use of Isotopic Surrogates in the Quantitation of Endogenous Analytes" Alexander M, Abolin C, Coopersmith B, and Zhang J. Sandoz Research Institute, East Hanover NJ 07936

ABSTRACT

As indicators of health status or therapeutic response to new treatments, the concentration of endogenous compounds is of interest to clinicians and drug development scientists. A major difficulty in developing quantitative methods for endogenous compounds is instrument calibration; specifically, how can an internal standard calibration curve for the endogenous analyte be constructed in the presence of high concentrations of the analyte itself?

Conventional clinical chemistry approaches have drawbacks. To obtain an analyte-free matrix for construction of a calibration curve, some investigators attempt to remove the endogenous analyte, use synthetic biologic matrixes or use external standardization in a solvent matrix. With these approaches, no assurance exists that either the recovery or the background obtained from such altered matrices will accurately mimic the unaltered matrix Chemical homologs of the endogenous analyte have also been used; however, there can be no assurance that the recovery or instrument response of the homolog surrogate analyte would be identical to the analyte itself.

The proposed solution takes advantage of mass selective detection by using a ^{13}C-labelled isotopic surrogate analyte of the compound of interest. The use of a ^{13}C-labelled isotopic surrogate with a sufficiently different nominal mass assures the same chemistry, hence the same recovery, chromatography and instrument response as the endogenous analyte. In addition, by using liquid chromatography with atmospheric pressure chemical ionization (APCI) instead of gas chromatography, sample preparation can be simplified by avoiding a derivitization step. Finally, this LC/APCI/MS approach can provide high sensitivity, wide dynamic range, ruggedness and automation.

As an example of the stable isotopic surrogate approach, an assay was developed for free (non esterified) palmitic acid in human plasma. Palmitic acid is the major endogenous free fatty acid in human plasma and its endogenous concentrations have been used as indicators of fatty acid metabolism

For this palmitic acid assay, $^{13}C_4$-palmitic acid was used as the isotopic surrogate analyte. The $^{13}C_4$-palmitic acid isotopomer was chosen because of its low natural abundance (<0.1%) and minimal isotope effects. Sample preparation for the standard curve was straightforward. After adding the perdeuterated internal standard ($^2H_{31}$-palmitic acid) and $^{13}C_4$-palmitic acid to 200 µL of an untreated sample, plasma proteins were precipitated with 400 µL methanol and filtered to remove solids. Lastly, 40 µL of the filtrate was injected onto the LC column. A binary mobile phase system was used for LC: Mobile Phase A was an aqueous solution of 2mM ammonium acetate with 0.2% added triethylamine, with pH adjusted to 7.8 with acetic acid; Mobile Phase B was 95% methanol / 5% acetonitrile (v/v). The LC conditions were: a Keystone BDS Hypersil 2 x 150 mm 3µ ODS column held @30°C was operated isocratically (80% B) at 0.35 mL/min. Palmitic acid and its isotopomers typically eluted in < 7 minutes. The APCI interface was operated at a vaporizer temperature of 400°C and a capillary temperature of 150°C, with a N_2 sheath gas pressure of 30 psi, no auxiliary gas, and a corona current of 6 microamperes.

Figure 1 shows a selected mass chromatogram of unadulterated human plasma. No signal was observed in either the M+4 or M+31 channels, demonstrating that neither the isotopic surrogate analyte nor the isotopic internal standard are affected by interferences from either endogenous palmitic acid or other matrix substances. Figure 2 shows a mass selected chromatogram of a human plasma sample spiked with $^{13}C_4$-PMA and $^2H_{31}$-PMA. The assay was validated to cover a concentration range of 124 to 282,000 ng/mL, as shown in Figure 3 Figure 4 presents endogenous palmitic acid levels found for 8 diabetic patients. The average value of ~30,000 ng/mL agrees with reported HPLC/UV determinations [1].

In summary, stable isotopic surrogate analysis is a novel approach for the determination of endogenous analytes, permitting calibration by internal standardization in unaltered biological fluids. Use of LC/APCI/MS permits analysis of underivitized analytes using simple sample preparation. This type of assay could be highly advantageous in a high volume clinical laboratory setting.

[1] Baty, J.D. Pazouki, S. Dolphin, J; Journal of Chromatography 395, 403-411 (1987).

Figure 1
Mass Selected Chromatograms from an Extracted Sample of Human Plasma
(no $^{13}C_4$-PMA or $^2H_{31}$-PMA added)

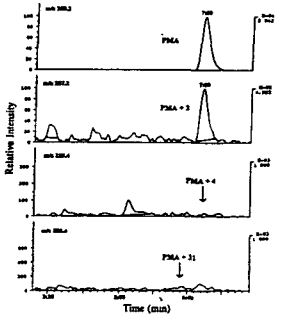

Figure 2
Mass Selected Chromatograms for an Extracted Sample of Human Plasma
Spiked with $^{13}C_4$-PMA (18100 ng/mL) and $^2H_{31}$-PMA

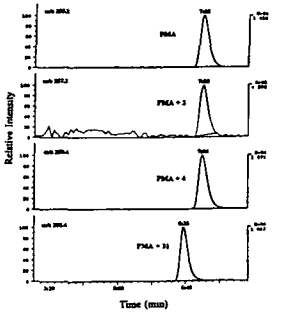

Figure 3
Standard Curve Using $^{13}C_4$-PMA

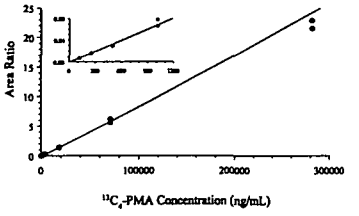

Figure 4
Endogenous PMA by LC/APCI/MS
Stable Isotope Surrogate Method

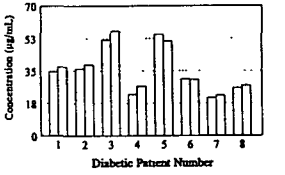

Electrochemical Aspects of Electrospray

Feimeng Zhou and Gary J. Van Berkel
Chemical and Analytical Sciences Division, Oak Ridge National Laboratory
Oak Ridge, Tennessee 37831-6365

Electrospray mass spectrometry (ES-MS) has proven especially useful in the molecular weight determination and structural analysis of involatile, polar and thermally labile compounds. However, the mechanism(s) involved in the generation of gas-phase ions from species in solution during the ES process is not well understood. In this study, attention is given to the electrochemical processes that occur at the metal/solution interface in the ES capillary. Kebarle and co-workers postulated that the mechanism responsible for charge balance in the ES capillary was electrochemical in nature and that the ES source was in fact "an electrolytic cell of a somewhat special kind."[1] We demonstrated that the radical cations observed in the ES mass spectra of some easily oxidized organic compounds were formed via electrochemical oxidation in the ES capillary[2]. Recently, similar data from an ES-MS study of various metallocenes was also presented.[3] A better understanding about the electrochemical processes in ES is desirable because it might lead to means for improving ES-MS performance (e.g., improving dynamic range and detection limits), means to expand the range of analytes amenable to analysis and possibly the means to control or alter the ionic species observed in the gas-phase.

Comparison of a Controlled Current Electrolytic Cell and an Electrospray Ionization Source. A comparison of a controlled-current electrolytic (CCE) cell and an ES ionization source reveals that these two devices are analogous in terms of their configuration and operation. Examination of the parameters that govern the magnitude of the ES current (Hendricks' equation), i_{ES}, and those that govern the faradaic current (i_F) in a CCE cell are those relevant to the transport of charge between the two electrodes by the electrolyte in solution, viz, solution conductivity, electrical field at the ES capillary tip, and flow rate.

Novel ES Ionization Source Combined On-line with UV/visible Spectroscopy. Shown in Figure 1 is a schematic representation of the ES ionization source used in this work to acquire UV/visible spectra of the solution exiting the ES capillary. The photo diode array detector monitors products that are generated in the ES capillary from the model compounds prior to the spraying process By doing so, possible complications arising from gas-phase reactions are avoided.

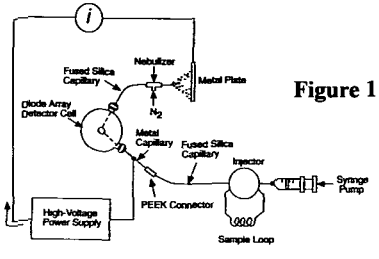

Figure 1

Experimental Verification of the Operation of an ES Ionization Source as a CCE Cell. (I) Effect of Varying the Solution Conductivity on the Extent of Analyte Oxidation. The effect of varying the ES solution conductivity on the magnitude of i_{ES} and on the extent of oxidation of nickel(II) octaethylporphyrin ($Ni^{II}OEP$) to its radical cation was determined

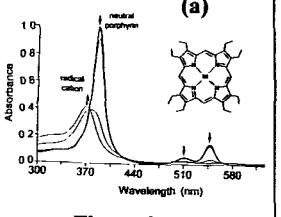

Figure 2

on the basis of five separate flow injection experiments in which the voltage applied to the ES capillary, the solution flow rate, and the concentration of $Ni^{II}OEP$ in the injected samples were kept constant, but the concentration of an added electrolyte (C_E), lithium trifluorosulfonate, was increased. The five UV/visible spectra of $Ni^{II}OEP$ shown in Figure 2a that were obtained during these experiments demonstrate that as C_E increased, i_{ES} increased, the amount of porphyrin oxidized also increased. The spectrum recorded when no electrolyte was added to the system is that of the neutral porphyrin (λ_{max} = 386, 510, and 548 nm), while that recorded when the electrolyte concentration was 9.0 mM is that of the porphrin radical cation (λ_{max} = 370 nm). This observation is in accordance with what is expected from a controlled-current electrolysis. It is worth noting that the data in Figure 2a represent the first direct proof that electrolysis of solution species can occur in the ES capillary *(ii) Effect of Varying the Voltage Applied to the ES Capillary on the Extent of Analyte Oxidation.*

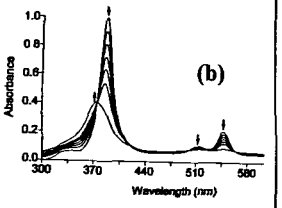

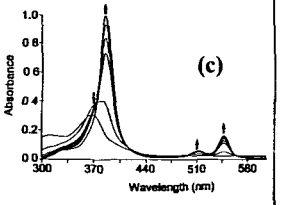

The effect of varying the magnitude of the voltage on the magnitude of i_{ES}, and on the extent of oxidation of $Ni^{II}OEP$, was determined in an experiment in which a 5.0 μM solution of $Ni^{II}OEP$ containing 1.0 mM of electrolyte was continuously infused through the ES capillary and the voltage was varied from 0.0 to 5.0 kV As the magnitude of voltage increased, the magnitude of i_{ES} increased as expected from Hendricks' equation. The seven UV/visible spectra of $Ni^{II}OEP$ shown in Figure 2b demonstrate that as i_{ES} increased, in response to an increase of the ES voltage, the amount of porphyrin oxidized increased.

(iii) Effect of Solution Flow Rate on the Extent of Analyte Oxidation. With a relatively high electrolyte concentration (a few mM), the magnitude of i_{ES} is affected little by changes in the flow rate. This is analogous to the situation in a CCE cell. The effect of varying flow rate on the extent of $Ni^{II}OEP$ was determined in an experiment in which a 5.0 μM solution of $Ni^{II}OEP$ containing 1.0 mM of electrolyte was continuously infused through the system at values of flow rates, from 10 to 80 μL/min. The UV/visible spectra of $Ni^{II}OEP$ shown in Figure2c demonstrate that although the magnitude of i_{ES} changed little with flow rate, the fraction of porphyrin oxidized changed dramatically from essentially 100 percent at 10 μL/min to near zero at 80 μL/min Such a change in the proportion of porphyrin oxidized with changing flow rates indicates that the oxidation reaction is controlled by the rate of porphyrin mass-transfer to the metal/solution interface in the ES capillary, a phenomena expected from any types of electrolysis experiments.

Armed with the knowledge that the ES source operates as CCE cell, the means to maximize the efficiency of the electrolysis process for ionization of neutral analytes are at hand. Three requirements are key to utilizing the effect for this purpose: (1) the magnitude of the ES current must be sufficient to oxidize/reduce the molar equivalent of the analyte exiting the ES capillary, plus the molar equivalent of all other species present in the ES capillary, (2) the flow rate of the solution must be sufficiently slow to allow adequate time for the analyte to be transported to the metal/solution interface within the capillary where the redox reactions takes place, and (3) the steps taken to ensure the first two requirements must not inhibit the formation of gas-phase ions from the ions generated electrochemically in solution.

(1) Blades, A. T., Ikonomou, M. G.; Kebarle, P Anal Chem. 1991, 63, 2109-2114. (2) Van Berkel, G J, McLuckey, S. A., Glish, G L Anal Chem 1992, 64, 1586-1593. (3) Xu, X., Nolan, S.P., Cole, R.B. Anal Chem. 1994, 66, 119-125.

Research sponsored by the United States Department of Energy, Office of Basic Energy Sciences under contract DE-AC05-84OR21400 with Martin Marietta Energy Systems, Inc.

High-Frequency Synchronization of an Electrospray Current using a Pulsed Voltage

Charbonnier, F.; Rolando, C.; Sablier, M.; Saru, F.; Simonneau, G. *Ecole Normale Supérieure, Département de Chimie, URA 1679 du CNRS, 24 rue Lhomond 75005 Paris, FRANCE.* Hapiot, P.; Pinson, J. *Laboratoire d'Electrochimie Moléculaire de l'Université Paris 7, URA 438 du CNRS, 2 place Jussieu, 75005 Paris, FRANCE.* Beaugrand, C. *AIRND, 78230 Le Pecq, FRANCE*

In electrospray ionization, gaseous ions are directly obtained by solvent evaporation in charged droplets, formed from a liquid flowing through a capillary submitted to an electric field. At the capillary tip, connected to a high voltage supply, the emission of current (droplets) is actually a discontinuous phenomenon, the frequency of which can be observed by measuring current intensity. We recently described(1) an experimental device allowing studies of fast processes up to 1 MHz, for investigating the time-dependent behavior of the electrospray current. Various electrolytes and solvents were used and, in every case, a discontinuous and roughly periodic intensity was observed for the current at the needle. Instantaneous current amplitudes remain roughly constant. Averaged spray intensities are in the commonly described range (0,1 to 1 μA). They grow with increasing applied high voltage, due to the increase in frequency of current (droplet) emission.

We were able to show the existence of three main functioning modes, corresponding to three frequency ranges of applied voltage: 10 Hz to 1 kHz, 1 to 10 kHz and 100 to 500 kHz. These modes might be correlated with the « Cone Jet », « Multi Cone Jet » (2) and « Rim Jet » modes of droplet emission during the electrospraying of a liquid, so called commonly after the shape of the flowing liquid at the capillary tip.

These earlier experiments allowed us to define the high voltage ranges that produce a stable spray and, for each range, the spraying frequencies. Though it was possible to choose selected conditions to optimize the stability of the spray in such a « free » version, the DC voltage conditions were difficult to reproduce. By applying an alternating voltage superimposed on the DC electrospray voltage (figure 1), we have

been able to synchronize the electrospray emission mode near its own natural frequency. By this means, the high frequency emission process could be observed precisely and the spraying process could be maintained during several hours in a given mode with a complete stability). This synchronization can be made efficient even in the highest frequency range (100 to 500 kHz: Figure 2). The experimental observations reported here may be related to the increase and stabilization of electrospray emission current obtained when the needle is vibrated by using a piezo electric transducer at subsonic frequency (3).

Figure 1: Experimental setup for the synchronization of Cone Jet or Multi Cone Jet mode

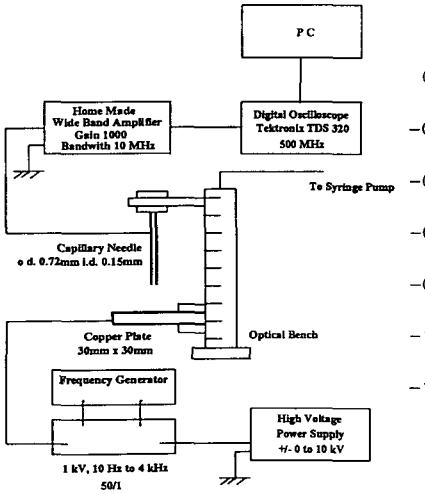

Figure 2: Current intensity (mA) versus time for synchronized Rim Jet mode

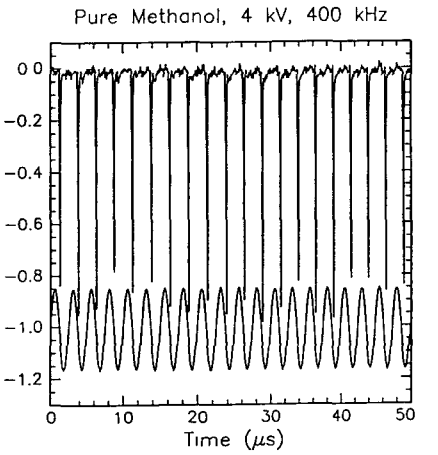

1) Charbonnier, F.; Rolando, C.; Saru, F. and Hapiot, P.; Pinson, J. *Rapid Commun. Mass Spectrom.* **1993**, *7*, 707-710. (2) Cloupeau, M. *J. Aerosol Sci.* **1994**, *25*, 1143-1157. (3) Banks, J.F.Jr.; Shen, S.; Whitehouse, C.M.; Fenn, J.B. *Anal. Chem.* **1994**, *66*, 406-414.

Characterization and Implementation of Micro-Flow Electrospray Nebulizers

Thomas Covey PE/Sciex Concord, Ontario Canada

Purpose of this work was to examine the electrospray process in the sub-μL/min range. Particular attention was paid to determining the parameters most important for maximizing the efficiency of ion desorption and ion transmission steps. Operating the system at the very low flow proved to be revealing regarding the nature of the ionization process unmasking certain characteristics not observed at the more commonly used flows > 1μL/min.

Electrospray needles with inside diameters varying from 100μ to 3μ ID. were created from gold plated fused silica according to the method of Kriger & Cook (1). The addition of a gentle sheath gas was used to aid in the collimation and desolvation of the charged droplets. The width of the Taylor cone at the base where it contacts the fused silica was measured as a function of flow rate at successively increasing distances from the center ID bore of the capillary. With an infusion pump the flow was gradually increased and the ion current was monitored. Stable signal indicated electrical contact with the base of the Taylor cone was achieved. The base of the Taylor cone where electrical contact is made cannot be visualized microscopically because the film can be very thin where contact occurs.

Two distinct modes of low flow operation were identified with respect to the geometry of the Taylor cone produced at the tip. When the Taylor cone just bridged the inside diameter of the capillary ("bridge flow") the maximum ionization/ion transfer efficiency achievable for that particular capillary ID was attained. This occurred at the indicated flows for the following tubing ID's. For a 100μ capillary ≈600nL/min, for 50μ ≈300nL, for 20 μ capillary ≈100nL/min, for 10μ ≈ 60nL, for 5μ ≈ 40nL, and for 2μ ≈ 30nL. This last observation (2μ at ≈ 30μ) approximates the flows achieved by Mann & Wilm (2) with similar diameter drawn borosilicate capillaries flowing by virtue of their own electrostatic force. When the flow was reduced below these values the cone retracted within the capillary and produced extremely unstable ion current traces. When the flow was increased above these values the Taylor cone spread across the face of the capillary and eventually down along the outside sheath of the capillary for a distance of several millimeters. Under these "over-flow conditions" (base of cone > I.D. of capillary) ionization/ion transfer efficiency varies with flow as a result of the changing diameter of the charged droplet emitting from the cone, as predicted by Wilm & Mann(2). The efficiency is always sub-optimal but the signal remains constant as the mass flux compensates for the decreasing ionization/ion transfer efficiency giving the appearance of a concentration sensitive response. Under "bridge flow " conditions very small changes in flow result in proportional changes in ion current revealing the true nature mass of the ion evaporation process as a mass sensitive one. Apparently the inner edges of the capillary stabilize the size of the Taylor cone over a very narrow flow range preventing a change in the diameter of the ion emitting droplet with a change in flow. The ionization efficiency thus remains constant and variations in mass flux are reflected in changing ion current levels.

1. Kriger, S.; Cook, K. Anal. Chem., 1995, 67, 385-389.
2. Wilm,M.; Mann,M. Int'l Journ. Mass Spectrom. Ion Physics, 1994, 136, 167.

43rd ASMS Conference on Mass Spectrometry and Allied Topics

HOW ARE ELECTROSPRAY IONS BORN FREE? - DOLE VS. IRIBARNE REVISITED.

John B. Fenn and Joan Rosell
Virginia Commonwealth University, Richmond VA 23284-2006

Solute ions from charged droplets have been widely used as grist for the mills of mass analysis for almost 20 years. During that time most attempts to explain the ion formation have been based on one of two mechanisms: The Charged Residue Model (CRM) originated by Malcolm Dole, and the Ion Evaporation Model (IEM) later proposed by Iribarne and Thomson. The CRM holds that solvent evaporation and consequent Coulomb explosions ultimately produce droplets so small that each one contains a only a single analyte molecule that retains some of the droplet charge to become an ion when the last of the solvent leaves. The IEM assumes that before CRM's ultimate droplet stage is reached the droplet surface field becomes strong enough to lift an ion into the ambient gas. In a recent review Kebarle and Tang concluded that uncertainty remained but that they favored the CRM [1]. Here we examine *representative experimental observations that the CRM seems unable* to explain and conclude that in most cases the IEM probably applies.

First we note that the CRM requires formation of at least one separate droplet for each ion produced. We then conclude that if an ES spectrum shows that any of the following conditions are met, the CRM cannot account for its ions: (A) The number of charges on an ion is less than both the number the parent molecule can hold and the probable number on the droplet from which the ion came; (B) The relative abundance of observed ions varies greatly with small changes in structure or composition of either its parent molecule or the droplet solvent; (C) There are no ions present from molecules abundant enough in the sample to be detected if they were the only solute species.

Figure 1 shows relative abundances for 10 tetra alkyl ammonium ions from 10 uM solutions of their bromides in 50-50 methanol water infused at 3 uL/min. A change of one carbon atom in the side chain changes abundance by a factor of up to forty! The sharp drop above 7 carbon atoms, due to "precipitation" of analyte as solvent evaporates, disappears (dashed curve) when analyte solubility is increased by a change of solvent to 50-25-25 n-propanol-methanol-water. these variations meet Condition B so the CRM cannot account for the ions.

Figure 2 shows the dependence of relative abundance for ES ions of Cu+ on the water content of dilute solutions of copper sulfate in acetonitrile. It's hard to understand how such small increases in water content can decrease the number of ultimate droplets by enough to account for the decrease in ion abundance. Once again condition B is met so that the CRM does not apply.

The two spectra in Fig. 3 show the coherent sequences of peaks characteristic of ES spectra for large molecules. To avoid rejection of the CRM by condition A above, the ions of each peak in Fig. 3 can have come only from droplets having the same number of charges as are on the ions of that peak. Thus, droplets must have been produced with charge states in the same relative abundances shown by the ions of the spectra. Those charge states go from 10 to 13 for ions of lysozyme in Fig. 3B and from 35 to 62 for alpha analyse in Fig. 3C. How can initially formed droplets possibly anticipate how many droplets

in each charge state they will have to produce for the particular analyte species they happen to contain. Even if they "know" a priori, *how can they control the evaporation-explosion sequence to produce* the droplet distributions required to avoid condition A?

Figure 4 shows the result of an experiment previously described in detail [2]. In brief, the increase in countercurrent gas flow rate (circle points) increases the droplet evaporation rate which increases the number of charges on the most abundant ion (ordinate values). With increasing flow rate of concurrent gas (triangles) the droplet evaporation rate and thus the number of charges on the most abundant oligomer both decrease. The CRM cannot reasonably account for this result but the IDM can, as shown in Ref. [1]

In sum, for these cases, and for many others, the ES spectral features can be more readily explained by the IDM than by the CRM.

[1] P. Kebarle, L. Tang, Anal. Chem. 65, 973A (1993)

[2] Fenn, J.B., JASMS 4, 524 (1993)

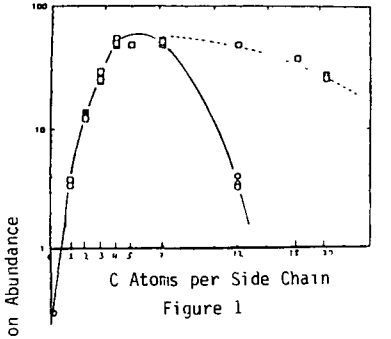

Figure 1

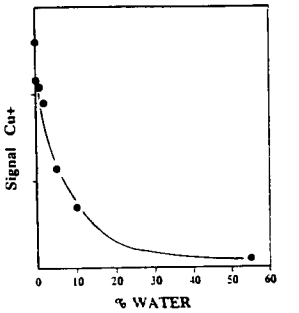

Figure 2

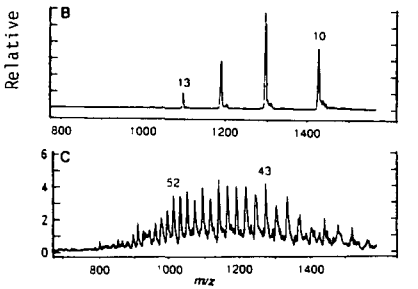

Figure 3

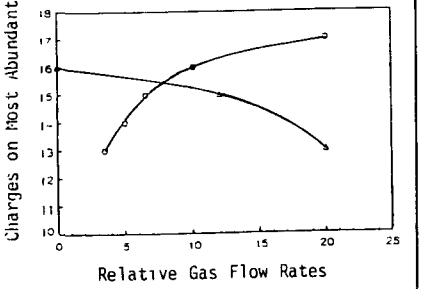

Figure 4

Is Electrospray Ion Production Concentration Dependent?

Brad I. Coopersmith, Brenda H. Hamilton, Craig R. Abolin
Sandoz Phamaceuticals, 59 Route 10, East Hanover, NJ 07936

Liquid chromatography/electrospray ionization/tandem mass spectrometry (LC/ESI/MS/MS) at high liquid flowrates (>50 uL/min) shows much promise for high throughput quantitative analysis of many drugs and their metabolites. Upon cursory examination, LC/ESI/MS/MS calibration curves, such as that shown in Figure 1, produce a linear dynamic range of 2 to 4-orders of magnitude. While the coefficient of determination suggests a linear response ($r^2 > 0.99$), closer examination reveals significant deviation from the curve-fitted weighted regression line at both the high and the low ends of the calibration curve.

The relative response factor (RRF), defined as the standard concentration divided by the peak area ratio, is a more sensitive measure of the detector linearity than the coefficient of determination because it provides point estimates of the inverse slope of the calibration curve. The RRF should remain constant for an ideal linear calibration curve The RRFs from the data shown in Figure 1 is plotted in Figure 2. This response is typical of most LC/ESI/MS/MS calibration curves, the RRF was found to increase with increasing concentrations of analyte, thus establishing nonlinearity.

Any concentration dependency that is observed should be a direct result of the energetics of the ESI process Of the three stages of ESI (droplet formation, droplet desolvation, and gas-phase ion formation), only the droplet formation stage has been shown to be concentration independent [1]. Our studies focussed on the last stage, gas-phase ion formation, since this stage should possess the highest activation energy and therefore be the easiest to measure In order to quantitate the activation energies, three assumptions were made (1) gas-phase ion formation must be both energetically and kinetically favorable, thus transition state theory can be used to describe the rate of gas-phase ion formation; (2) from the design of the Finnigan MAT ESI interface used, any ions which are detected must be formed before exiting the heated capillary; and (3) the surface temperature of the droplet inside the heated capillary is proportional to the heated capillary temperature. These assumptions led to the following equation to estimate the activation energy required for gas-phase ion formation:

$$\text{Ln [Ion Signal]} = -\frac{\Delta G^{\ddagger}}{kT} + \text{Ln}\left[\frac{kT}{h}\right] \qquad (1)$$

Figure 3 displays the plot obtained from the above equation for 19 5 ng of sample (17 ng of analyte and 2.5 ng of internal standard) on-column The trend obtained from the slopes of plots of equation (1) as a function of analyte concentration is shown in Figure 4. While the absolute values of the slopes changed upon repetition of the experiment, the trend did not which suggests a distinct concentration dependency in the gas-phase ion formation stage.

Of the proposed mechanisms for this stage, only the Ion Evaporation Model [2] is supported by these data. According to that mechanism, the final droplet will partially desolvate and then expel an ion near the droplet surface into the gas phase due to the high electric field at that point Colligative effects (boiling point elevation) due to the high mole fraction of analyte molecules in the final droplet will affect the activation energy of this stage As the analyte concentration increases, the mole fraction of the analyte in the final droplets will increase, thus increasing the energy needed to desolvate the droplet to the point where gas-phase ion formation occurs.

REFERENCES

1. Fernandez de la Mora, J , Loscertales, I.G *J. Fluid Mech.* **(1994)**, *260*, 155-184
2. Iribarne, J V , Thomson, B A. *J. Chem. Phys.* **(1976)**, *64*, 2287-2294.

Figure 1

LC/ESI/MS/MS Calibration Curve for SDZ CPI 975

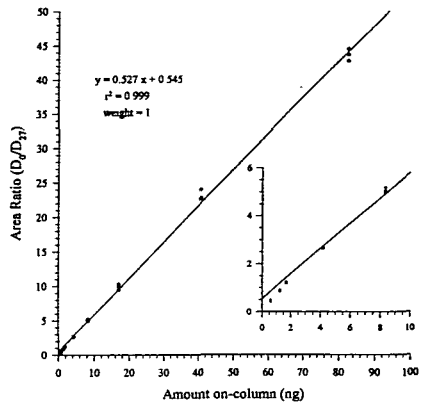

Figure 2

Relative Response Factors Obtained from the LC/ESI/MS/MS Analysis of SDZ CPI 975

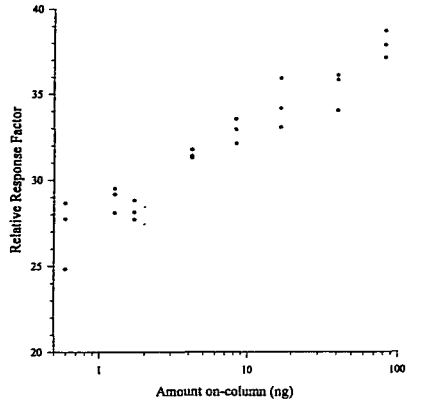

Figure 3

Ln [Area Sum] versus 1/Temperature (0.5 mL/min; coeluting peaks; 4.5kV needle)

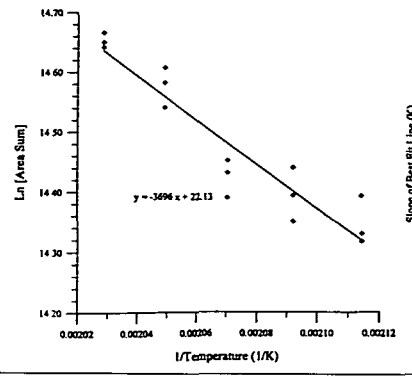

Figure 4

Slope of Best Fit Line for Ln[Area Sum] vs 1/T as a Function of Total Amount of Sample On-Column

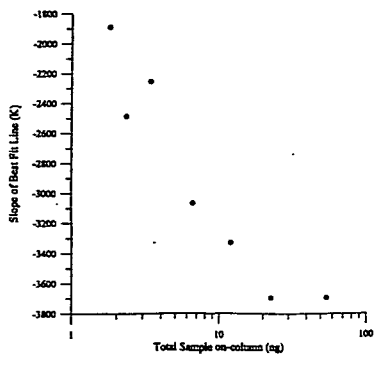

Dependence of Charge State Distributions on Analyte Concentrations in Electrospray Ionization Mass Spectrometry

Guangdi Wang and Richard B. Cole*
Department of Chemistry, University of New Orleans
Lakefront, New Orleans, LA 70148

Earlier investigations [1,2] into the behavior of liquids under electrospray conditions showed that the total ion current follows a weak dependence on the conductivity of the sprayed liquid, given as: $I \approx H\sigma^n$, where H and n ($0.2 < n < 0.4$) are constants, and σ is the liquid conductivity. Solution conductivity can be enhanced either by addition of external electrolytes, or by increasing the concentration of a dissociating analyte in solution. In both cases the total ES ion current increases as a result, although the magnitude of the current increase is considerably less than the magnitude of the rise in concentration. We have shown [3] that upon addition of external electrolyte (not participating in charge attachment to/removal from the analyte), the charge state distributions of analytes do not change significantly despite a dramatic reduction in overall analyte signal response in the presence of increasing electrolyte signal intensity. Increasing the concentration of the analyte itself, present in salt form, represents a different means of influencing solution conductivity which merits a separate treatment.

The effect of analyte concentration upon charge state distributions in electrospray ionization mass spectrometry (ESMS) was investigated using four compounds which showed doubly charged and singly charged positive ions (gramicidin S, 4,4'-bipiperidine), multiply charged negative ions (Trypan Blue), or doubly charged and singly charged negative ions (eosin Y) in ES mass spectra. For each of the above compounds, the charge associated with analyte molecules was calculated to increase in solution with increasing concentration, yet the analyte charge state distributions in ES mass spectra were observed to monotonically shift toward lower values. In order to rationalize these observations, we introduce N/N_o, the ratio of the number of excess charges on all droplets produced by electrospray (N) to the total number of analyte molecules in all droplets (N_o). The N/N_o value decreases with increasing analyte concentration, indicative of an increasing number of ion-paired analyte molecules in the droplets. The lower N/N_o value is proposed to be an underlying factor critical to explaining the desorption of a higher proportion of gas-phase ions of lower charge state at elevated analyte concentrations. Furthermore, in comparing N/N_o values and observed analyte charge state distributions as functions of increasing analyte concentration, the decreasing ratio of N/N_o predicts a much greater extent of shifting of analyte charge states toward lower values than was observed. This implies that the actual degree of ion-pairing in droplets was considerably alleviated as compared to that indicated by the calculated N/N_o values. This finding conforms to a description of the ES process wherein uneven fission of droplets occurs at the Rayleigh limit, thereby generating offspring droplets of enhanced charge to mass ratio, hence an augmented N/N_o value.

References:

1. Pfeifer, R. J; Hendricks, C. D. *AIAA J.* **1968**, 6, 496-502.
2. Smith, D. P. H. *IEEE Trans. Ind. Appl.* **1986**, IA-22, 527-535.
3. Wang, G.; Cole, R. B. *Anal. Chem.* **1994**, 66, 3702-3708.

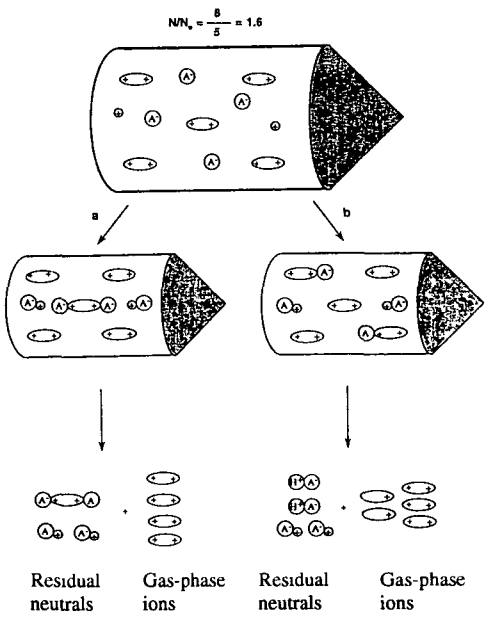

Figure 1. Schematic diagram of a portion of a charged droplet containing an excess of positive charges in the form of doubly protonated analyte (doubly charged ellipse) initially introduced in the neutral salt form with two anions attached. Droplet charging occurred by electrophoretic removal of anions (A^-) and by electrochemical production of cations (smallest circles). The droplet becomes smaller as solvent evaporates such that ions of opposite charge move closer together to eventually form contact ion pairs. The diagram depicts the relation between N/N_o (top) and the charge states of ES generated gas-phase ions (bottom). Pathway b corresponds more closely to experimental observations. Ellipses are horizontally oriented for visual clarity.

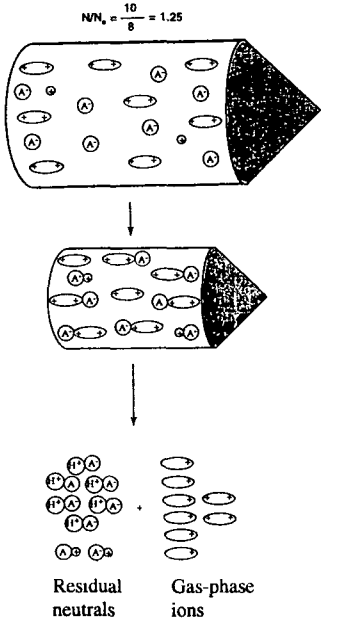

Figure 2. Schematic diagram of a portion of a charged droplet containing a higher concentration (relative to Figure 1) of the neutral salt form of the same dibasic analyte. The observed increase in the proportion of singly charged ES generated ions at higher concentration is attributed largely to the reduced N/N_o value.

Physical Processes of Electrospray

Willoughby, Ross; Sheehan, Edward; Mitrovich, Samuel
Chem-Space Associates. 75 Chapel Ridge Place, Pittsburgh, PA 15238

The current studies are an attempt to rationalize the physical processes associated with droplet formation and ion production in electrospray using thermodynamic models Previously we have evaluated the behavior of the electrospray needle cone-jets using the laws of conservation of energy, mass and charge to characterize the process of conversion of high electrostatic potential energy into high kinetic and surface energy in the primary droplet formation process of electrospray [1] This model treats the transition of effluent flowing from the high voltage needle into an aerosol, and ultimately into gas-phase ions as a thermodynamic change in state. Each step in this transition may be evaluated separately for boundary conditions, thresholds, and driving forces.

It has been well established that the deformation of the liquid surfaces in electrospray is attributable to "Rayleigh instabilities"[2], however, no comprehensive model has been put forth to explain the system behavior once the Rayleigh limit has been reached; particularly for isolated droplets.

The present studies attempt to tie the processes occurring in the aerosol to the processes occurring on the needle. One important question to be addressed in the our evaluation is the scaleability of processes occurring in electrospray Are the forces resulting in the formation and continuation electrospray cone-jets from needles the same as those from droplets? What are the similarities? What are the differences?

Evaluation of the Rayleigh theory for charge saturation of a liquid surface results in several interesting observations The saturation charge of a spherical (q_s) surface per unit mass is calculated to be less than the saturation charge of a cylinder (q_c) of equal mass The ratio of q_s:q_c is 0 94:1. This relationship accounts for the natural transition from the spherical to cylindrical geometry when a given system reaches the limit of charging. The observed conical liquid geometries on both needle tips and on isolated droplets in electrospray is physical evidence that charge saturated systems move from surface tension dominated geometries below charge saturation to electrostatic stress dominated geometries above the charge saturation limit.

Figure 1 shows the relationship between charge on a liquid surface and radius resulting from the application of high potential to an electrospray needle. The initial geometry is spherical; above the limit of charging the surface deforms in the "deformation region" to produce a cone. When the kinetic energy flow is equal to the surface energy flow in the highest field region of the cone, a cylindrical liquid jet emerges. The liquid jet subsequently relaxes back to spherical geometries in the lower field regions and primary droplets are formed.

Figure 2 shows the relationship between charge on a droplet surface and radius resulting from evaporation of an electrospray produced droplet. The initial geometry may be spherical; however as the droplet evaporates and the potential of the droplet increases, conical deformations result similar to needle cones.

Our experimental results and modeling studies indicate that the processes governing needle cone-jet formation are scaleable to the submicron droplet dimension.

Figure 1

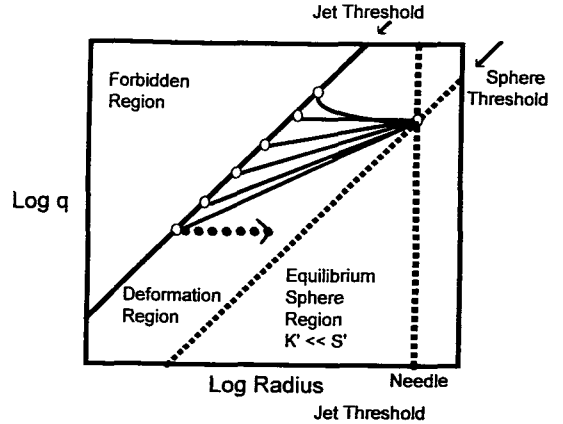

Figure 2.

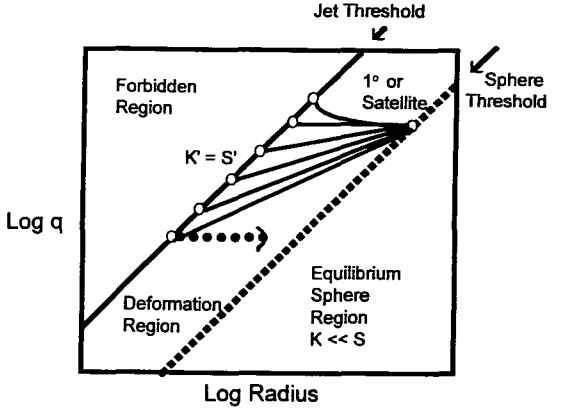

1) Willoughby, R.C.; Sheehan, E.W ; Jarrell, A.; Pedder, R,; Marecic, T.; Penn, S; Studies of the physical processes of electrospray; Proceedings of the 41st ASMS Conference on Mass Spectrometry and Allied Topics, San Francisco, CA, May 30 - June 4, 1993.

2) Bailey, A.G. Electrostatic Spraying of Liquids John Wiley & Sons, 1988.

Acknowledgments: The authors wish to thank Waters Corp. for technical and financial support.

ION MOBILITY SPECTROMETRIC / MASS SPECTROMETRIC INVESTIGATION OF ELECTROSPRAY IONS

R. Guevremont, K.W.M. Siu, and J.Wang, Institute for Environmental Research and Technology, National Research Council of Canada, Ottawa, Ontario, Canada K1A 0R6

Ion mobility spectrometry is ideally suited to the investigation of the nature of electrospray ions; the separation of ions occurs at atmospheric pressure and detection of ions is a simple measurement of electrical current. Although the ion mobility spectrometer lacks resolution, it has the capability of separating and detecting ions over very wide range of size. A commercially available instrument (PCP Inc., West Palm Beach Fla.) was interfaced to an electrospray chamber via a 15 cm length tube 1/8 in. od. The tube ended within the 'reaction zone' of the IMS instrument and therefore was held at approximately +2000V in order to match the voltage level within the instrument. The electrospray chamber was flushed by 3L/min N_2 which entered the chamber concentrically to the exit tube leading to the IMS. Of this gas 1.5L/min carried the electrospray ions into the IMS, and 1.5L/min exited directly from the cell. This countercurrent of gas minimized the entrance of neutrals and large droplets into the IMS instrument. Because of the low mobility of electrospray ions of interest, the gating function was extended from the usual 1ms up to 8ms (note wide peaks in Figures 1 to 4). This permitted good sensitivity detection of ions with mobility as low as 0.2 cm^2/V-s. IMS/MS was performed on a different instrument (PCP Inc., West Palm Beach Fla.) which had an IMS cell with two gates 5cm apart, and a quadrupole mass spectrometer with range to m/z1200. The interface between the IMS and MS was an orifice approximately 25um in diameter. The mobility cell in the IMS/MS instrument was run at 200C.

Figure 1 illustrates IMS spectra of several tetraalkylammonium ions. The spectra are all characterized by ions of mobilities ranging from over 1.5 cm^2/V-s to as low as 0.2 cm^2/V-s. The ions of high mobility in electrospray of tetraalkylammonium salts are the tetraalkylammonium ion and an adduct between this ion and another tetraalkylammonium bromide. Figure 2 illustrates IMS (upper trace) and the IMS/MS with single ion monitoring of these ions from electrospray of tetraoctylammonium bromide. Unexpectedly, a considerable fraction of the adduct ion appears to be converted back into a simple tetraoctylammonium ion in the MS interface. Figure 3 illustrates the IMS spectra of tetraoctylammonium bromide as a function of concentration. At concentrations above 0.1mM (in which the adduct is detected in IMS), a conventional electrospray-MS measurement does not reflect the actual relative abundance of the tetraalkylammonium ion and its adduct. IMS spectra of several tetrabutylammonium salts including dihydrogenphosphate, hydroxide and acetate were acquired. In these experiments only the halide anion formed an adduct sufficiently stable to be detected.

Figure 3 illustrates the limitation in dynamic range usually observed in electrospray ionization. At low concentration the IMS spectrum is dominated by the tetraalkylammonium ion. The ion current detected for this ion ceased to increase once the lower mobility ions appear in the spectra. All of the traces in Figure 3 have equal scaling of the signals. Figure 4 illustrates the temperature-induced changes in the mobility of ions originating in the electrospray of 1.5 mM of tetraoctylammonium bromide solution. The ES cell is at room temperature, whereas the IMS spectrometer temperature is increased. The mobility of the large ion appears to <u>decrease</u> as the temperature of the IMS spectrometer is increased.

43rd ASMS Conference on Mass Spectrometry and Allied Topics

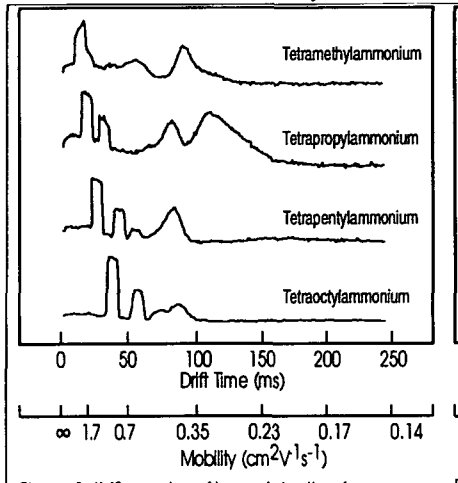

Figure 1. IMS spectra of ions originating from electrospray of tetraalkylammonium salts (1.2 mM)

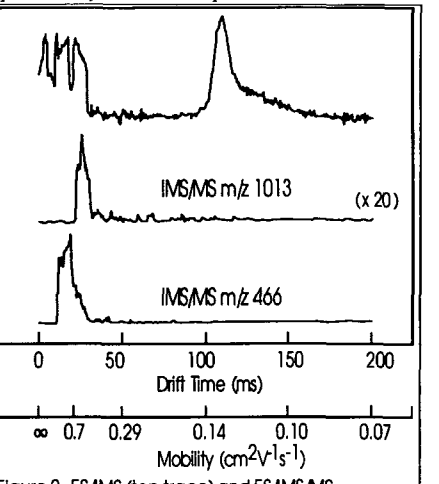

Figure 2. ES/IMS (top trace) and ES/IMS/MS single ion monitoring, tetraoctylammonium bromide (2.8mM)

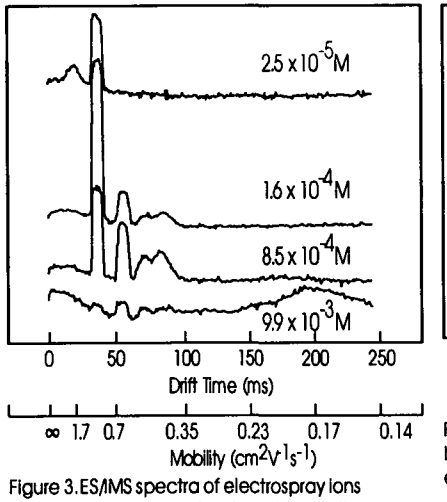

Figure 3. ES/IMS spectra of electrospray ions from tetraoctylammonium bromide solutions.

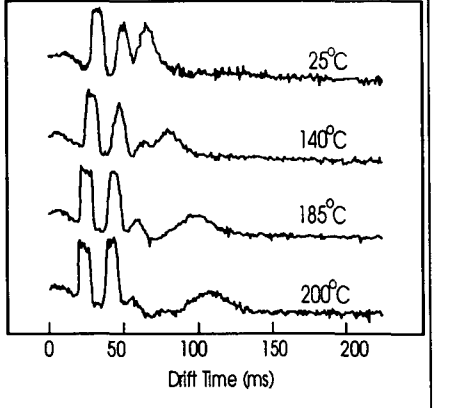

Figure 4. ES/IMS spectra of tetraoctylammonium bromide: ES room temperature, IMS cell at elevated temperatures.

Principles and Design of Ion Traps for FT-ICR Mass Spectrometry

Alan G. Marshall* and Shenheng Guan*

Center for Interdisciplinary Magnetic Resonance, National High Magnetic Field Laboratory, Florida State University, 1800 E. Paul Dirac Dr., Tallahassee, FL 32310

* Member of the Department of Chemistry, Florida State University

Virtually all Fourier transform ion cyclotron resonance (FT-ICR) mass spectrometry experiments are based on ion confinement in a Penning trap: namely, a spatially homogeneous static magnetic field, B, and a 3-dimensional axial (along B) quadrupolar electrostatic trapping potential, $\Phi(x,y,z) = \Phi(0,0,0) + \text{constant}\cdot(2z^2 - (x^2 + y^2)$. The 3-dimensional axial quadrupolar electrostatic potential has the desirable property that the ion equations of motion separate into independent cyclotron rotation, magnetron rotation, and axial oscillation, and the frequency of each motion is independent of ion position in the trap. Of the many possible excitation and detection modes,[1] the most common is one-dimensional dipolar excitation, produced by a time-varying electric field, $\Phi(x) \propto x(t)$, with Fourier spectral amplitude at each ion cyclotron frequency of interest, followed by dipolar image current detection with the same electrode arrangement. Finally, ion magnetron-to-cyclotron conversion requires a two-dimensional rf potential of the form, $\Phi(x,y) \propto (x^2 - y^2)$.

Each of these three potentials may be generated by infinitely extended electrode arrangements, as shown in Figure 1.

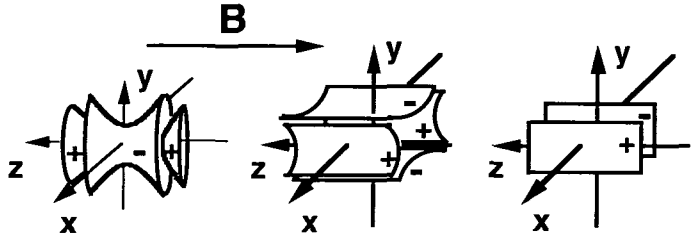

Figure 1. Electric potentials for: (left) ion trapping (three-dimensional axial quadrupolar); (middle) magnetron-to-cyclotron interconversion for ion axialization and cooling (two-dimensional azimuthal quadrupolar); and (right) excitation and detection (one-dimensional dipolar). The applied magnetic field, **B**, points in the negative z-direction.

The potentials actually produced by any of various (finite-size) ICR ion trap geometrical configurations (see Fig. 2) generally approximate one (but never all three) of the above potential fields.[2] For example, the "compensated" traps (Fig. 1f,g) apply different static potentials to concentric segments of the trap end cap electrodes to produce a more nearly 3D-quadrupolar electrostatic trapping potential. The "open" trap (Fig. 2n) is designed to open the end cap aperture to facilitate injection of

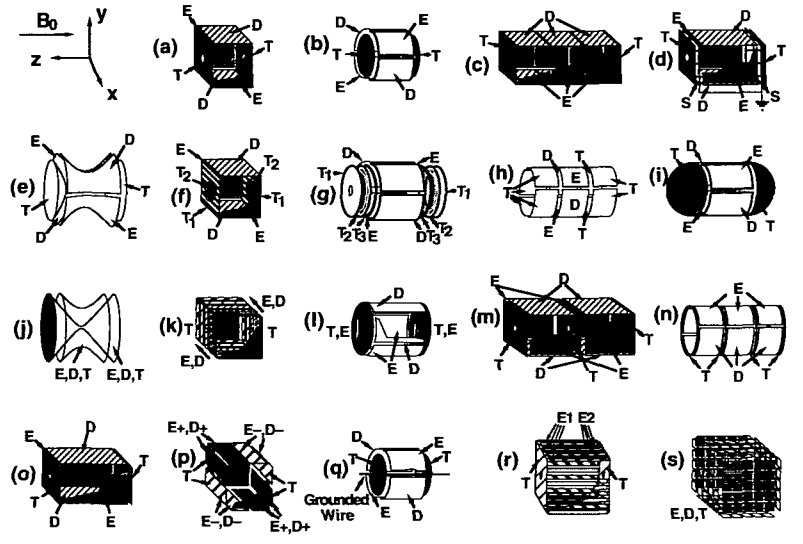

Figure 1. ICR ion trap configurations. E = Excitation; D = Detection; T = End Cap ("Trapping"); S = Screen. (a) cubic; (b) cylindrical; (c) three-section; (d) screened; (e) hyperboloidal electrodes; (f) and (g) end caps segmented to "compensate" electrostatic trapping potential; (h) open-ended; (i) hemispherical end caps; (j) two-electrode; (k) linearized for azimuthal dipolar excitation/detection; (l) infinity; (m) dual; (n) open; (o) elongated; (p) segmented for xz-excitation; (q) central wire; (r) filar electrodes;(s) "universal".

externally formed ions, while maintaining the electrostatic trapping potential (by applying the same d.c. voltage to end of the outer rings, which serve as "end caps", and by capacitively coupling all three segments together to produce a more spatially homogeneous rf dipolar excitation potential. The "screen" trap differs from the rest in that it is designed to produce a "particle-in-a-box" (rather than 3D quadrupolar) electrostatic trapping potential, so as to allow ions to spread out axially for increased dynamic range and reduced frequency shift due to the trapping potential. The most general design (also the newest) is the "universal" trap (Fig. 2s) described elsewhere in these Proceedings.[3] This work was supported by NSF (CHE-93-22824), NIH (GM-31683), and the National High Magnetic Field Laboratory at Florida State University.

1. L. Schweikhard and A. G. Marshall, *J. Amer. Soc. Mass Spectrom.* **1993**, *4*, 433-452.
2. S. G. Guan and A. G. Marshall, *Int. J. Mass Spectrom. Ion Proc.*, **1995**, *000*, 00-00.
3. G. S. Jackson, S. Guan, and A. G. Marshall, this volume, paper ThP 077.

ADVANTAGES OF HIGH MASS ACCURACY MALDI-FTMS FOR TRYPTIC MAPPING OF RECOMBINANT PROTEINS

John T. Stults
Protein Chemistry Department, Genentech, Inc., South San Francisco, CA 94080

Yunzhi Li and Robert T. McIver, Jr.
Chemistry Department, University of California, Irvine, CA 92717

The ultra-high mass resolution achievable by FTMS has been one of the primary and most recognized characteristics of the technique. The resolution achieved with MALDI-FTMS is no less impressive (1-3). High mass accuracy, in the absence of internal mass standards, is a feature of MALDI-FTMS that is routinely of far greater utility. Internal mass standards are required to achieve good mass accuracy (±0.01% = 100 ppm) with linear time-of-flight (TOF) mass spectrometry; however, the mass standard(s) must produce a signal of similar intensity to the analyte, which can require multiple cycles of sample preparation/measurement to achieve. Furthermore, for low analyte quantities, addition of a standard may suppress what little analyte signal was present initially. Thus high mass accuracy without an internal standard is a much more efficient means of analysis. An accuracy of 0.01% can be achieved routinely with reflector TOF instruments with external calibration. Much higher accuracy (<10 ppm) can be achieved with MALDI-FTMS with external calibration. Although most MALDI instruments to date are based on TOF analyzers, MALDI-FTMS is shown here to yield results for individual peptides with similar subpicomole detection limits, but with substantially greater mass accuracy.

Tryptic mapping is one of the primary methods for the detailed molecular analysis of proteins. Tryptic peptides are most easily identified by their mass, based on the known sequence of the protein from which they were derived (4). The accuracy of MALDI-FTMS yields much greater specificity in peptide identification than techniques with lower mass accuracy. The identification of amino acid modifications is also improved, and may include determination of the elemental formula of the modification. These same features permit the verification of correct peptide synthesis with equally high specificity. The ability to generate ions for multiple experiments from a single sample by MALDI-FTMS allows detailed questions to be answered for multiple peptides in a mixture. For example, narrowband excitation may be used when ultra-high resolution ($m/\Delta m$ >100,000) is needed. Fragment ion spectra may also be generated by collision-induced dissociation.

The data in this study were acquired with an IonSpec HiResMALDI FTMS instrument. Ions were produced in an external source (N_2 laser, DHB:fucose 1:1 matrix) and transported via a quadrupole ion guide to an elongated cell in a 4.7 T magnet. Argon was admitted to the cell by a pulsed valve immediately before ion injection in order to collisionally cool the ions. The mass axis was calibrated with a mixture of vasopressin, renin substrate, and insulin B-chain.

Replicate measurements of a series of synthetic peptides showed that mass accuracy with external calibration was ≤5 ppm with excellent reproducibility. Figure 1 shows the molecular ion region for 100 fmol of a synthetic peptide acquired with (a) 32K data points and (b) with 512K points (5 scans averaged for each). The resolution had little effect on the mass accuracy. The lower resolution observed for a 32K acquisition (~6000, FWHH) was more than adequate for isotope separation; the shorter transient required shorter data acquisition and Fourier transformation times, and required significantly less data storage than a longer transient. High resolution is also accompanied by a higher signal-to-noise ratio, another unique feature of FTMS, because the signal frequencies are essentially averaged for a greater length of time.

Table 1 lists the peptides observed and their masses for the tryptic digest of human growth hormone. Due to the mass dependence of the trapping delay time and the quadrupole rf voltage, the data were acquired in four segments. The T6-T16 peptide, m/z 3762, could only be observed with fucose present in the matrix to reduce fragmentation, and with a short acquisition time. Its higher mass error is due to its wider peak width and mass that lies above the highest mass standard used.

In conclusion, these preliminary experiments demonstrate that MALDI-FTMS routinely provides improved mass accuracy for peptides, including tryptic digests of proteins, in the absence of internal mass standards, yet with subpicomole detection limits.

Figure 1. Molecular ion regions of the MALDI-FTMS spectra of a synthetic peptide (Ac-IWRYGYI-NH_2, 100 fmol loaded in DHB, calculated $M+H^+$=1011.542).

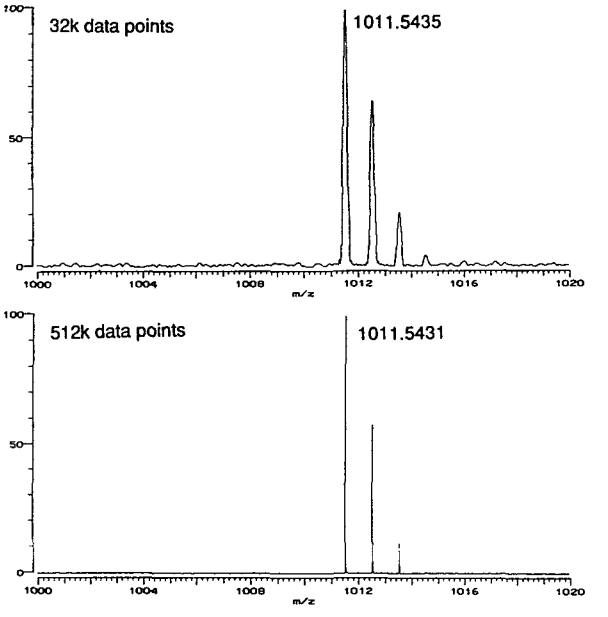

TABLE 1 - Peptides observed for the tryptic digest of human growth hormone

peptide	sequence	observed m/z	theoret. m/z	error
T8	SNLELLR	844.4894	844.489	1 ppm
T1	FPTIPLSR	930.5447	930.541	4
T2	LFDNAMLR	979.5046	979.503	2
T18+19	DMDKVETFLR	1253.6184	1253.620	1
T11	DLEEGIQTLMGR	1361.6697	1361.675	4
T17+18+19	KDMDKVETFLR	1381.7085	1381.715	5
T20-T21	IVQCR/SVEGSCGF	1400.6332	1400.630	2
T9	ISLLLIQSWLEPVQFLR	2055.1990	2055.201	1
T4	LHQLAFDTYQEFEEAYIPK	2342.1240	2342.123	1
T6-T16	YSFLQNPQTSLCFSESIPTPSNR/NYGLLRCFR	3761.8271	3761.773	14

(1) R.T. McIver, Jr., Y. Li, and R.L. Hunter, *Proc. Natl. Acad. Sci. USA* **1994**, *91*, 4801-4805.
(2) R.T. McIver, Jr., and Y. Li, *Rapid Commun. Mass Spectrom.* **1994**, *8*, 743-749.
(3) Y. Li, R.T. McIver, Jr., and R.L. Hunter, *Anal. Chem.* **1994**, *66*, 2077-2083.
(4) T.M. Billeci and J.T. Stults, *Anal. Chem.* **1993**, *65*, 1709-1716.

EVALUATION OF DISSOCIATION TECHNIQUES FOR MALDI-FTMS OF OLIGONUCLEOTIDES*

Robert L Hettich[1] and Elizabeth A. Stemmler[2]

[1] Oak Ridge National Laboratory, Oak Ridge, TN 37831-6120
[2] Dept. of Chemistry, Bowdoin College, Brunswick, ME 04011

The development of MALDI-FTMS has provided a convenient method of generating and trapping molecular ions for large biomolecules. We have optimized MALDI-FTMS for the generation of molecular ions for modified oligonucleotides up to 11-mers. In order to exploit the capabilities of FTMS for structural investigations, it is necessary to design and evaluate methods to examine these MALDI-produced ions in detail The focus of this presentation is to examine three methods of monitoring oligonucleotide fragmentation with MALDI-FTMS: 1) variation of the laser matrix compound, 2) variation of the time delay time between ion formation and detection, and 3) comparison of off-resonance dissociation methods (SORI) with on-resonance collision-induced dissociation All experiments were conducted with an Extrel FTMS-2000 instrument (3T magnet) equipped with a Nd:YAG pulsed laser (355 nm). MALDI experiments were conducted by mixing a few pmol of analyte with an excess of 2,5-dihydroxybenzoic acid (DHBA) or 3-hydroxpicolinic acid (HPA).

The extent of analyte fragmentation observed in MALDI-FTMS is dependent on the matrix compound used, and can be varied to provide either molecular weight or sequence information. This was demonstrated for a series of modified oligonucleotide 8-mers, obtained through collaborations with Drs Thomas and Connie Harris, Dept. of Chemistry, Vanderbilt University, Nashville, TN. MALDI-FTMS of d(AGGCGCCT) with DHBA did not yield molecular weight information, but rather generated primarily low mass fragment ions (m/z < 1000), providing sequence information about the first few nucleotides in this oligomer. In contrast, MALDI-FTMS with HPA generated an abundant molecular $(M-H)^-$ ion at m/z 2408, and lower abundances of sequence-specific Y-type ions, shown in Figure 1 These Y-ions were sufficient to verify the complete sequence of the 8-mer. Two other 8-mers with the same sequence, but with adducts on the third guanine from the 5' end, were also examined with DHBA and HPA MALDI-FTMS (HPA) was sufficient to identify the molecular weights, sequences, and adduct locations of these normal and modified 8-mers.

The amount of analyte fragmentation in MALDI-FTMS can also be controlled to some extent by the addition of a delay time between laser ionization and ion detection For example, the use of a 3 ms delay in the MALDI-FTMS (HPA) of d(A^{BPI}CGAGG), where A^{BPI} = benzo(a)pyrene diol epoxide adduct of deoxy-adenosine, yields primarily a molecular $(M-H)^-$ ion at m/z 2139. In contrast, the use of a 100 ms delay with the same experimental conditions yielded not only the molecular ion, but also a variety of abundant Y-type ions which were sufficient to resolve almost all of the oligomer sequence While the use of delay times provided extensive fragmentation information in some cases (such as modified hexamers), this technique was limited in utility for determining the complete sequences of larger oligomers (such as 11-mers).

Collisional dissociation experiments have proven to be very useful for probing the fragmentation of a variety of ions. However, some of the fragment ions observed in a MALDI-FT mass spectrum are difficult to dissociate with conventional CAD conditions. For example, MALDI-FTMS of pd(AGCT) generates a molecular $(M-H)^-$ ion at m/z 1252, and abundant fragment ions at m/z 939 (Y3) and 610 (Y2) While the m/z 939 is easy to collisionally dissociate with conventional CAD conditions, the m/z 610 ion, which corresponds to pd(CT), is difficult to dissociate in a similar fashion, as shown in Figure 2a The use of sustained off-resonance irradiation (SORI) experiments was examined as a method to improve the dissociation efficiency of these ions SORI of m/z 610 (pd(CT)) was found to be efficient for producing informative fragment ions for this Y2 ion, as shown in Figure 2b Based on these results, SORI was applied to a variety of other difficult-

to-fragment Y2 ions, and was found to be successful for the interrogation of these ions as well. The fragmentation information obtained in this way was used to determine that the Y2 ions fragment not only by elimination of a nucleic base and simple cleavage of the phosphate linkage, but also by complex rearrangement processes, including migration of a phosphate moiety to generate a (Y1 + HPO_3) fragment ion.

* Research sponsored jointly by the National Cancer Institute (Interagency Agreements DOE 0485-F053-A1 and NCIY01-CP-20512-13) and the Office of Health and Environmental Research, U S Department of Energy (contract DE-AC05-84OR21400 with Martin Marietta Energy Systems, Inc) EAS would also like to acknowledge support from the DOE Faculty Research Participation Program under contract DE-AC05-76OR00033 between the U.S. Department of Energy and Oak Ridge Institute for Science and Education.

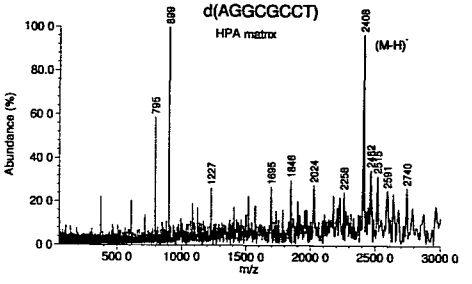

Figure 1

Figure 2a

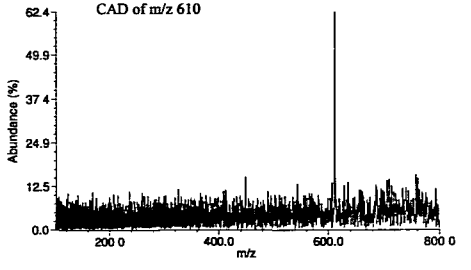

Figure 2b

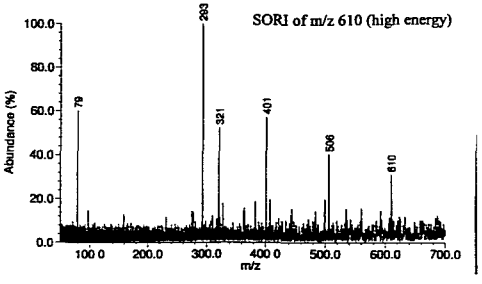

"The submitted manuscript has been authored by a contractor of the U.S. Government under contract No. DE-AC05-84OR21400 Accordingly, the U.S. Government retains a nonexclusive, royalty-free license to publish or reproduce the published form of this contribution, or allow others to do so for U.S. Government purposes."

A Dual Chamber FT-MS Instrument with Electrospray, MALDI, Liquid SIMS Capability

Eric Gard, kirk Green, Sharron Penn, Steven Fannin, Elvira Camara, James Carroll, Jane Wu, and Carlito Lebrilla
Chemistry Department, Unversity of California at Davis, Davis CA 95616

The wide range of compounds analyzed by Mass Spectrometry today requires a variety of different ionization sources. This is because the various ionization techniques have different sensitivities for different classes of compounds. As a mass analysis technique FT-MS presents advantages like ultra-high resolution and high sensitivity irrespective of the ionization technique. One draw back of FT-MS, however, has been the inability to switch between the available ionization techniques. The dual chamber system, shown in Figure 1, offers nearly simultaneous ionization techniques, minimizes down time, and facilitates instrumental development. In addition, this FT-MS system utilizing a single superconducting magnet and one data acquisition system which represents a significant saving over two separate instruments. Each of the chambers rolls freely in and out of the magnet while under vacuum. This allows us to move the functional instrument into the magnet while the other is pulled out of the magnet for testing or alteration This is ideal for allowing instrumental modifications, source changes (FAB, MALDI, EI, ESI), and regular maintenance to take place on one instrument while the other is producing data.

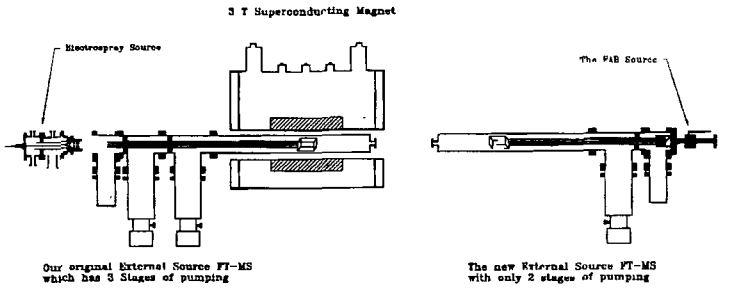

Figure 1: The dual chamber FTMS system.

Results for biomolecules ranging from Gramicidin S to Serum Albumin (~66,000 Daltons) obtained using the ESI source coupled with one chamber which utilizes five stages of differential pumping are presented in Figure 2 below. An example of the results for a obtained using the MALDI source coupled to the second chamber, which uses only two stages of differential pumping, are shown in Figure 3 below.

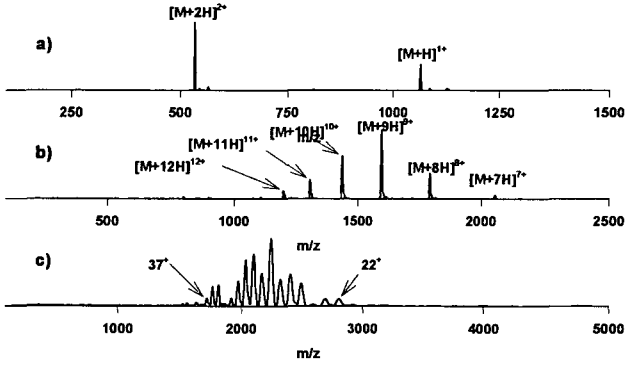

Figure 2: ESI/FTMS results, a) Bradykinin mw = 1060, b) Lysozyme mw = 14,313, c) Bovine Serum Albumin mw = 66,000.

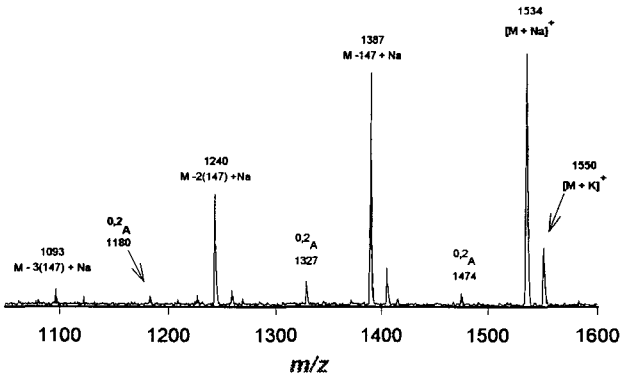

Figure 3: MALDI results; Trifucosyllacto-N-hexaose from human milk.

FT-ICR Mass Spectrometry of Very-Highly-Charged Atomic Ions

L. Schweikhard[1], B. Beck[2], St. Becker[3], P. Beiersdorfer[2], and S. R. Elliott[2]

[1]Johannes Gutenberg-Universität, Institut für Physik, D-55099 Mainz, Germany
[2]Lawrence Livermore National Laboratory, Livermore, CA 94551, U.S.A.
[3]Gesellschaft fur Schwerionenforschung, D-64220 Darmstadt, Germany

The electron beam ion trap (EBIT) at Livermore produces very highly charged atomic ions by successive ionization in collisions with an intense (up to 120 mA, 4000 A/cm^2), energetic (up to 200 keV) electron beam [1] The ions are trapped radially in the electrostatic field of the electron beam While it is on, and with the beam off by a 3-T magnetic field produced by a pair of superconducting Helmholtz coils. Axially, the ions are trapped by a bias potential on the top and bottom electrodes (see Fig. 1). The central electrode is 4.2 cm long and has a diameter of 1 cm EBIT was originally designed as an x-ray source [2], and six slots allow direct line-of-sight radial access to the trapping region for x-ray measurements.

For the present measurement, we made use of the access provided by the radial x-ray slots (see Fig. 2). We constructed two probes that could be inserted into the 2-mm wide slots. The probes each subtend only 25° and face each other 180° apart [3] For most measurements we used only one probe for excitation and the other for detection A typical transformed spectrum of highly charged 84Kr ions obtained with this arrangement is shown in Fig. 3. The spectrum was obtained by exciting with a 300-us sweep from 17.5 MHz to 19.5 MHz. The resonance peaks of $^{84}Kr^{34+}$, $^{84}Kr^{35+}$, and $^{84}Kr^{36+}$ are clearly seen

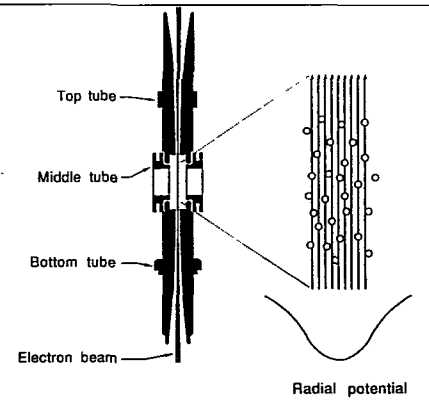

Figure 1. Schematic of the trap region (vertical cut). In the presence of the electron beam, ions are trapped in the space charge of the electron beam. In its absence, they are trapped axially by the potential applied to the top and bottom drift tubes and radially by the axial magnetic field.

Because the electrostatic field of the electron beam dominates the ion motion, it must be turned off during the ion cyclotron resonance measurement, i.e. during excitation and detection. We found that turning the electron beam off does not compromise the ion confinement needed for a successful measurement. Trapping times exceeding 1 s were found in the absence of the electron beam. We also found a decay time of 10 ms for the coherent ion motion after excitation. We estimate that there were as much as 10^5 Kr ions in the trap; in addition, there were at least as many ions from low-Z background gases such as hydrogen, carbon, nitrogen, and oxygen, as well as argon. The mass resolving power achieved (m/Dm(FWHM) ≈ 5 000) was limited by the number of digitization points of the Fourier transform (50,000 as determined by the LeCroy 9314L digitizing scope used for the measurements) and possibly by magnetic field inhomogeneities and/or by the large number of ions in the trap.

The use of the FT-ICR on an EBIT device holds several promises for future applications· First, as demonstrated, we can detect and measure different charge states and isotopes simultaneously. Second, using segmented trap electrodes for excitation and detection we will be able to determine the number of ions. Third, it should be possible to detect a single highly charged atomic ion. Finally, many measurements can be performed more quickly with the FT-ICR technique than with conventional diagnostics For example, we have been able to measure the relative abundance ratio of adjacent ionization stages twenty times faster with the ICR technique than by conventional x-ray methods. The FT-ICR method thus is becoming one of the most important tools for studying highly charged atomic ions in an EBIT device.

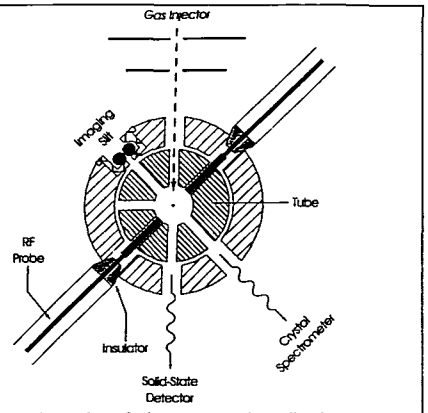

Figure 2 Schematic of the trap region (horizontal cut) showing the location of the two ICR probes as well as different x-ray instrumentation.

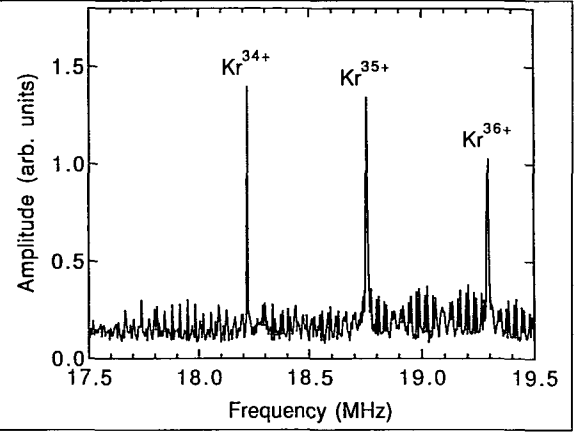

Figure 3. FT-ICR spectrum of highly charged krypton ions.

This work was supported in part by NATO Collaborative Reserach Grant CRG-930125 and performed by Lawrence Livermore National Laboratory under the auspices of the U S. Department of Energy under contract W-7405-ENG-48

[1] D A. Knapp, R.E Marrs, S R. Elliott, E.W. Magee, R. Zasadzinski, Nucl. Instrum Meth. A 334 (1993) 305.
[2] M A. Levine, R.E Marrs, J.R. Henderson, D.A Knapp, M B Schneider, Physica Scripta T22 (1988) 157
[3] P. Beiersdorfer, B. Beck, S. Elliott, R. Marrs, L. Schweikhard, Rapid Comm Mass Spectrom 8 (1994) 141.

ESI/FTMS Instrumentation for Tandem Mass Spectrometry

Peter B. O'Connor, David J. Aaserud, Ziqiang Guan, Daniel P. Little, Gary A. Valaskovic, Troy D. Wood, Fred. W. McLafferty
Baker Chemistry Laboratory, Cornell University, Ithaca, NY, 14853

Classical methods for the structural characterization of large proteins and other biomolecules utilize condensed phase degradation reactions (difficult for subpicomole samples) and microseparations for limited resolving power (RP) and mass accuracy. Gas phase MW determination and sequencing is especially promising with ESI/FTMS (RP $>10^5$) using sequential ion separations and dissociations (MS^n), with femtomole samples analyzed despite poor efficiencies in MS^n and ESI. Improvements reported here include quadrupolar excitation (QE) for axialization of large protein ions, a capacitively coupled cell selecting single isotope peaks (RP = $3x10^4$) for MS/MS, micro-ESI, and 193 nm ion photodissociation for high efficiency production of complementary fragment ions.

The cylindrical open trapped ion cell exhibits coupling of axial and radial motions during irradiation due to excitation field inhomogeneities which causes ions be ejected from the cell during QE.[1] As shown earlier,[2] capacitively coupling the excitation field onto the trapping electrodes solves this problem, effectively achieving the ideal infinitely extended excitation electrodes. QE with this cell has allowed axialization of protein ions up to protein A (45 kDa). The capacitively coupled cell also makes possible high resolution SWIFT[3] isolation of single isotopic peaks up to 29 kDa.[4] This capability is very useful for isolation of single components of overlapping isotopic distributions for further study; however, single isotope peak isolation and fragmentation can also be used to determine the number of ^{13}C's in an isotopic peak for increased mass accuracy through resolution of the uncertainty in isotopic assignment associated with statistical samples of large proteins. For example, in Figure 1, fragmentation of the $^{13}C_3$ and $^{13}C_5$ isotopes of ubiquitin yields fragment isotopic distributions easily distinguished from the model distributions from fragmentation of the precursor isotopic peaks with +/- 1 heavy isotope.

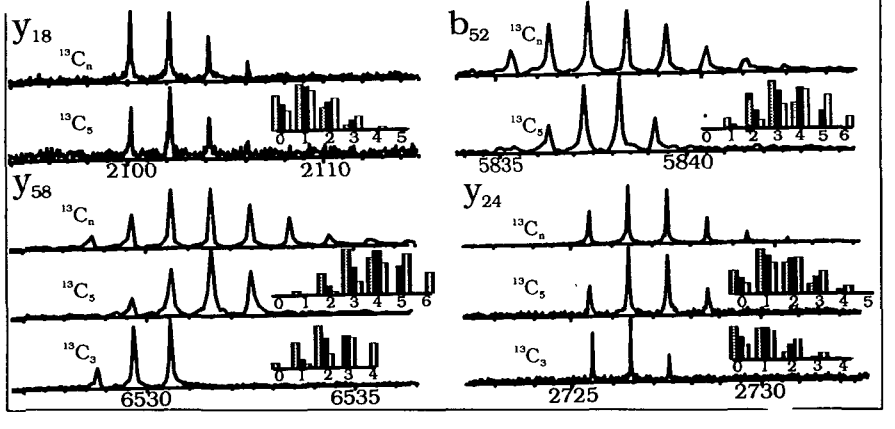

Recent results by Ron Orlando et al[5] showed the power of doing both low and high energy dissociations for elucidation of large peptide structure. Analogously, we have implemented both IRMPD (low energy, 10.6 μm)[6] and UV (high energy, 193 nm)[7] photodissociation on our instrument and generated UV photofragmentation data for ubiquitin (Figure 1, 8.6 kDa), as well as melittin (2.8 kDa) and carbonic anhydrase (29 kDa). UV dissociation generates primarily C and X ions as opposed to the lowest energy B and Y ions typically formed. Ideally, we will use IRMPD for selective generation of small fragments, isolate them and then dissociate these small fragments with high energy UV photodissociation for generation of full sequence information.

Implementation of micro-ESI[8] using pulled silica capillary coated with a gold film allows routine spectral acquisition on femptomole quantities of material. 15 fmols loaded into the electrospray source allowed acquisition of both a molecular ion and a nozzle skimmer spectrum of Ubiquitin, while 0.22 fmols loaded yields signal/noise of 60:1 for Cytochrome C. This is by no means the lower limit on sensitivity.

(1) Guan, S.; Kim, H. S.; Marshall, A. G.; Wahl, M. C.; Wood, T. D.; Xiang, X. *Chem. Rev.* **1994**, *94*, 2161-2182.
(2) Beu, S. C.; Laude, D. A., Jr. *Anal. Chem.* **1992**, *64*, 177-180.
(3) Chen, L.; Wang, T. C. L.; Ricca, T. L.; Marshall, A. G. *Anal. Chem.* **1987**, *59*, 449-454.
(4) O'Connor, P. B.; McLafferty, F. W. *J. Am. Soc. Mass Spectrom.* Submitted.
(5) Kumar Kolli V. S.; Orlando, R. *J. Am. Soc. Mass Spectrom.* **1995**, *6*, 234-241.
(6) Little, D.P.; Speir, J. P.; Senko, M.W.; O'Connor, P.B.; McLafferty, F. W. *Anal. Chem.* **1994**, *66*, 2809-2815.
(7) Beu, S. C.; Senko, M. W.; Quinn, J. P.; Wampler, F. M.; McLafferty, F. W. *J. Am. Soc. Mass Spectrom.* **1993**, *4*, 557-565.
(8) Valaskovic, G. A.; Kelleher, N. L.; Little, D. P.; Aaserud, D. J.; McLafferty, F. W.; *Anal. Chem.* submitted.

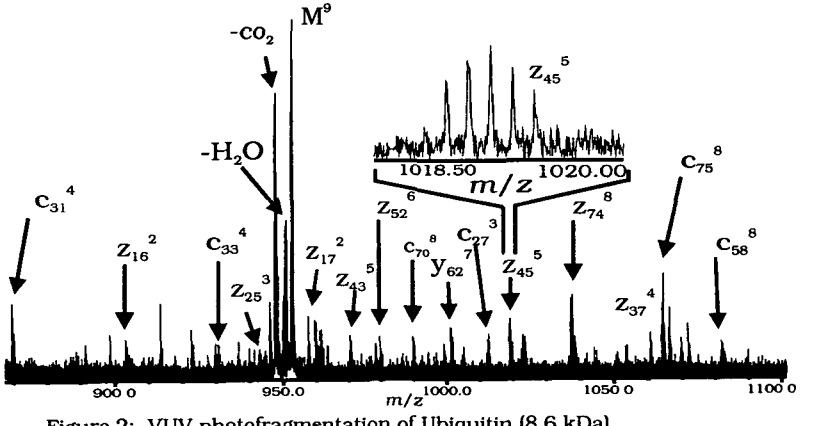

Figure 2: VUV photofragmentation of Ubiquitin (8.6 kDa)

Fragmentation of Labelled lysozymes and derivatives by FT MS

Carol V Robinson, Andrew Miranker,
Gary Kruppa and Christopher M. Dobson.

Oxford Centre for Molecular Sciences,
South Parks Road, Oxford, OX1 3QT, UK.

Introduction

Recently we have shown the power of ESI MS and hydrogen deuterium exchange labelling in the characterisation of protein folding intermediates[1,2]. Whilst it is possible to monitor populations of intermediates, and their evolution with folding time, it has not been possible to assign deuterated fragments within the protein sequence without the aid of enzymatic digestion and separation of the resulting fragments by HPLC[3] This method suffers from the inherent disadvantage that hydrogen exchange rates for peptides are considerably faster than for proteins since the overall tertiary structure of the protein affords considerable protection from exchange In this study we demonstrate the use of FT MS for the fragmentation and assignment of protein fragments within the protein sequence using a range of isotopically labelled proteins and solutions in which the tertiary structure of the protein is modified.

Results and Discussion

A comparison of the +11 charge state for the globular protein hen egg white lysozyme is shown in figure 1. The isotopic resolution available with this technique not only enables accurate determination of the mass of the fragment ion but also allows ready assignment of the charge of the fragment since the isotopic spacing is related to the charge state of the ion

(a) (b)

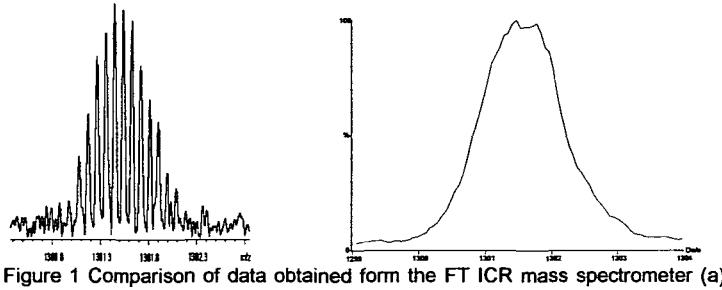

Figure 1 Comparison of data obtained form the FT ICR mass spectrometer (a) with data obtained on a quadrupole mass spectrometer (b).

Source to skimmer fragmentation of lysozyme yields some 51 fragments of which only 2 are triply charged, 15 are doubly charged and the remaining 34 are singly charged The presence of predominantly low charge state ions may reflect the relatively mild acidic conditions used to preserve the native state of this protein or the restrictions imposed on the conformation of the protein in the gas phase by the presence of the four disulphide bonds In order to investigate these effects lysozyme was introduced under a variety of different solvents known to produce dramatic changes in the tertiary structure of the protein, however, very little effect was seen on the fragmentation pattern of the protein. Greater effects on the fragmentation pattern were observed upon reduction and carboxymethylation of one of the critical disulphide bonds.

In order to utilise information obtained from fragment ion spectra it is necessary to assign the ions to specific regions of the protein A program was written to compute all possible fragments from this 129 residue protein and considers all a,b,c and x,y,z fragments and traces fragments through disulphide links and optionally allows disulphide cleavage. Such a program yields a total of 10^5 possibilities and despite the high mass accuracy afforded by FT MS a number of ambiguities remain In order to delineate these possibilities spectra were obtained from ^{13}C and ^{15}N labelled protein These isotopically labelled proteins allow unambiguous assignment of the protein since they enable the number of carbon and nitrogen atoms present in each fragment to be determined. Similarly, protein samples in which deuterium is incorporated show mass increases in fragments and allow the assignment of deuterium labelled regions of the protein during protein folding pathways

Conclusions

The results from this study suggest that the overall folding of the protein has little effect on the number and size of fragments seen but preliminary results have shown that for proteins in which disulphides have been reduced the fragmentation pathway is changed dramatically. The use of istopically labelled proteins reduces ambiguity in the assignment of proteins and thus allows individual regions of the protein to be monitored during protein folding pathways.

References

1.Miranker, A.; Robinson, C.V.; Radford, S.E.; Aplin, R T., & Dobson, C M. *Science* **1993**, *262*, 896.

2.Hooke, S D ; Eyles, S.J , Miranker, A.; Radford, S.E., Robinson, C.V.; & Dobson, C.M. *J. Amer. Chem. Soc* **1995**, in press.

3.Zhang, Z.; Smith, D.L. *Protein Science* **1993**, *2*, 522-531

ESI-FTICR METHODS FOR BIOAFFINITY CHARACTERIZATION MASS SPECTROMETRY

James E. Bruce, G.A. Anderson, R. Chen, X. Cheng, D. C. Gale,
S. A. Hofstadler, B. L. Schwartz and R. D Smith
Pacific Northwest Laboratory, Richland, Washington 99352

The characterization of biomolecular associations for the determination binding and binding sites and elucidation of potential drug leads is a difficult problem spanning a diverse field of analytical methods. Current techniques that are based upon the formation of noncovalent associations generally require the removal of noncovalent complexes from solution and thus limit the applicability of these approaches. A technique that would allow the investigation of these complexes directly from solution and promote rapid screening of combinatorial libraries by direct observation of the complex(es) is attractive. Technical details of the new method called bio-affinity mass spectrometry (BACMS) which promises to promote a more practical approach than current techniques employed in combinatorial chemistry and affinity chromatography are presented.

The BACMS approach is based on Fourier transform ion cyclotron resonance (FTICR) mass spectrometry which, when coupled to electrospray ionization (ESI), allows the investigation of specific noncovalent complexes formed in solution. The unique attributes of ESI-FTICR, such as the well established high resolution, accurate mass analysis and MS^n capabilities with more recently developed techniques involving quadrupolar excitation (QE) and selected-ion accumulation (SIA)[1], permit the investigation of noncovalent interactions directly from solution, even at very low relative concentrations. ESI-FTICR mass spectra of bovine ubiquitin (M_r=8565) were acquired from direct infusion of a 1 1x10^{-9}M solution with broadband SIA over the *m/z* range of 1200 to 1740. This required the injection of 300 attomoles of ubiquitin, and similar results were obtained with the peptide, bradykinin. Much lower limits of detection are predicted based on the implementation of the low nL/min flow rate "microspray" ESI source of Mann et al [2] and the use of the quadrupole excitation-based remeasurement technique from Amster's group[3]. More importantly, however, this demonstrates the successful application of ESI-FTICR methods to the analysis of very low concentration solutions, such as will be encountered in the BACMS studies.

An important test for the new facilities involves the detection of low concentration species in the direct analysis of complex mixtures with widely varying concentrations since the noncovalent associations that can provide information on new drug leads may be formed only at very low relative concentrations. This can present difficulties for FTICR analysis given the inherent dynamic range limitations brought about by the maximum ion population that can be effectively addressed. The results of our new approach involving SIA to reduce this effect by sequentially removing species from our filtered or "colored" noise accumulation "mask" is shown in Figure 1 with a mixture of the proteins bovine insulin, bovine ubiquitin, and bovine cytochrome *c*, in concentrations of 9 x 10^{-5}M, 9 x 10^{-7}M, and 1 x 10^{-8}M, respectively. Figure 1(a) shows the mass spectrum obtained with SIA using broadband QE from *m/z* 1000 to 2000. Modification of the QE waveform to remove those frequencies corresponding to the 4+ and 5+ charge states of insulin produced the "accumulation mask" shown in Figure 1(b) and, with a 5 second accumulation, the mass spectrum shown in 1(c) This spectrum shows the 7+ charge state of ubiquitin as the largest peak. Removing the frequencies corresponding to the ubiquitin ions produced the mask shown in Figure 1(d). A 20 s accumulation with this mask produced the mass spectrum shown in 1(e), in which the largest peaks are now insulin-related impurities (even these species appear more concentrated than the cyctochrome *c*). However, the 11+ charge state of cytochrome *c* is detected with unit mass resolution as is

illustrated in the inset of this figure. These results demonstrate the successful application of SIA and BBQE to produce a significant extension of the dynamic range with FTICR. Importantly, these extensions can be made with any continuous source of ions and without any prior knowledge of the injected ion identities (other than an approximate *m/z* range), as is dictated by the BACMS technique.

References·

1) Bruce, J. E.; Anderson, G.. A.; Hofstadler, S. A.; Van Orden, S. L.; Rockwood, A. L.; Sherman, M. S.; Smith, R. D., *Rapid Comm. Mass Spectrom.* **1993**, *7*, 914.
2) Wilm, M.; Mann, M. *13th International Mass Spectrometry Conference*; Budapest, Hungary, September, 1994.
3) Speir, J. P.; Gorman, G. S.; Pitzenberger, C. C.; Turner, C. A.; Wang, P. P.; Amster, I. J. *Anal. Chem.* **1993**, *53*, 1746.

Figure 1

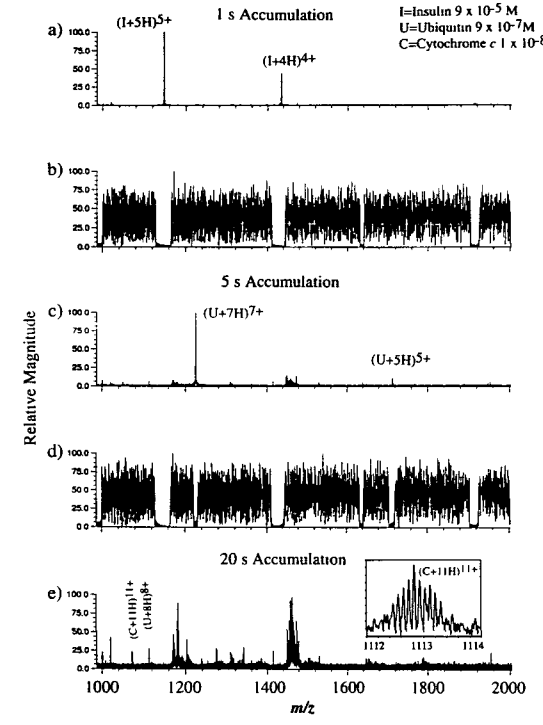

We thank the U.S. Department of Energy for support of this research through internal PNL Exploratory Research under contract DE-AC06-76RLO 1830.

Fast Metastable Ion Fragmentation In MALDI

Duane Reiber, John J. Lennon and *Robert S. Brown, Department of Chemistry and Biochemistry, Utah State University, Logan, UT 84322-0300

Until recently, matrix-assisted laser desorption/ionization (MALDI) has generally been considered a very gentle ionization method, producing predominantly intact protonated molecular ion species. This early view of MALDI has evolved into the understanding that a significant degree of metastable ion decay occurs with MALDI generated ions. This metastable ion decay is generally believed to result from both bimolecular collision processes and unimolecular ion decay. This delayed, post source decay (PSD) of MALDI generated ions has been exploited on the tens of microsecond time scale in reflecting time-of-flight (TOF) mass spectrometers to provide significant structural information for moderate sized peptides. In the conventional PSD experiment, it is not possible to distinguish between bimolecular and unimolecular decay processes. If the dense plume model for MALDI is correct, it is likely that significant activation of the MALDI generated ions occur due to energetic collisions between analyte ions and neutrals in the expanding plume of matrix molecules when continuous ion extraction is employed. This is supported by the similarity of PSD spectra obtained with reflecting TOF mass spectrometers and low energy collisional activation spectra. PSD spectra of peptides reported in the literature exhibit a, a-17, b and b-17 fragment ions.

One approach to studying the unimolecular decay process in MALDI is to utilize a delay between ion formation and ion extraction. This allows the initially dense matrix plume to expand sufficiently to reduce the collisional rates for the desorbed analytes. When this is implemented on a linear TOF mass spectrometer (337 nm), a small but significant degree of metastable ion decay is observed that is structurally different from what is observed with PSD spectra. With delayed pulsed ion extraction, amide bond cleavages leading to c, y and z type ions are observed. This fragmentation also occurs on a very fast time frame. Fragmentation appears to be complete by no later than 300 ns (current minimum pulse delay) after the laser event. No generation of PSD type metastable ions are observed with delays out to 2 µs. This is consistent with the suggestion that much of the PSD metastable ion decay is due to collisional processes. As with continuous ion extraction in a linear TOF mass spectrometer, any collisional metastable ions would not be observed with the delayed pulsed ion extraction experiment if the activation is associated with the ion acceleration process.

Substantial fast metastable ion decay has been observed for a variety of small to medium sized peptides including substance P, neurotensin and melittin. All peptides studied to date produce similar fragmentation results. Even cross-linked peptides such as (porcine) insulin can produce a limited amount of fast metastable ion fragmentation. For insulin, fragmentation occurs from the terminal ends and proceeds until a disulfide bridge is reached. The fast metastable ion decay spectrum of insulin is complicated by the two cross linked chains which each have two terminal ends from which fragmentation occurs. These fast metastable ion decay spectra can be easily mass calibrated (internally or externally) to produce mass accuracies of typically ±0.3 Da for peptides as large as insulin. Selected larger proteins have also been observed to exhibit fast metastable ion decay (cytochrome C and myoglobin).

This fast metastable ion decay appears to result from unimolecular ion decay processes associated with the ionization step in MALDI. One plausible mechanism that has been suggested in the literature is a very fast exothermic proton transfer reaction, presumably to an amide nitrogen. Rapid localized bond cleavage than occurs (randomly along the peptide backbone) prior to internal energy conversion within the molecule. This model is supported by the fact that the most significant differences are observed in the metastable ion decay species when chemically different matrices are employed. This difference in fragmentation can be observed in the fast metastable ion decay spectra obtained when ferulic acid and 7-hydroxy coumarin are employed as the MALDI matrix for the B chain of bovine insulin (Figures 1 and 2).

Finally, preliminary studies with a quadrupled Nd:YAG laser (266 nm) have shown similar fragmentation ions as that observed at 337 nm. Some overall increase in the absolute intensity of the metastable decay ions with the shorter wavelength laser has been observed in addition to an increase in the intensity for some smaller fragment ions. Studies are underway to acess the effects of both laser wavelength and pulse width on the fast metastable ion decay process.

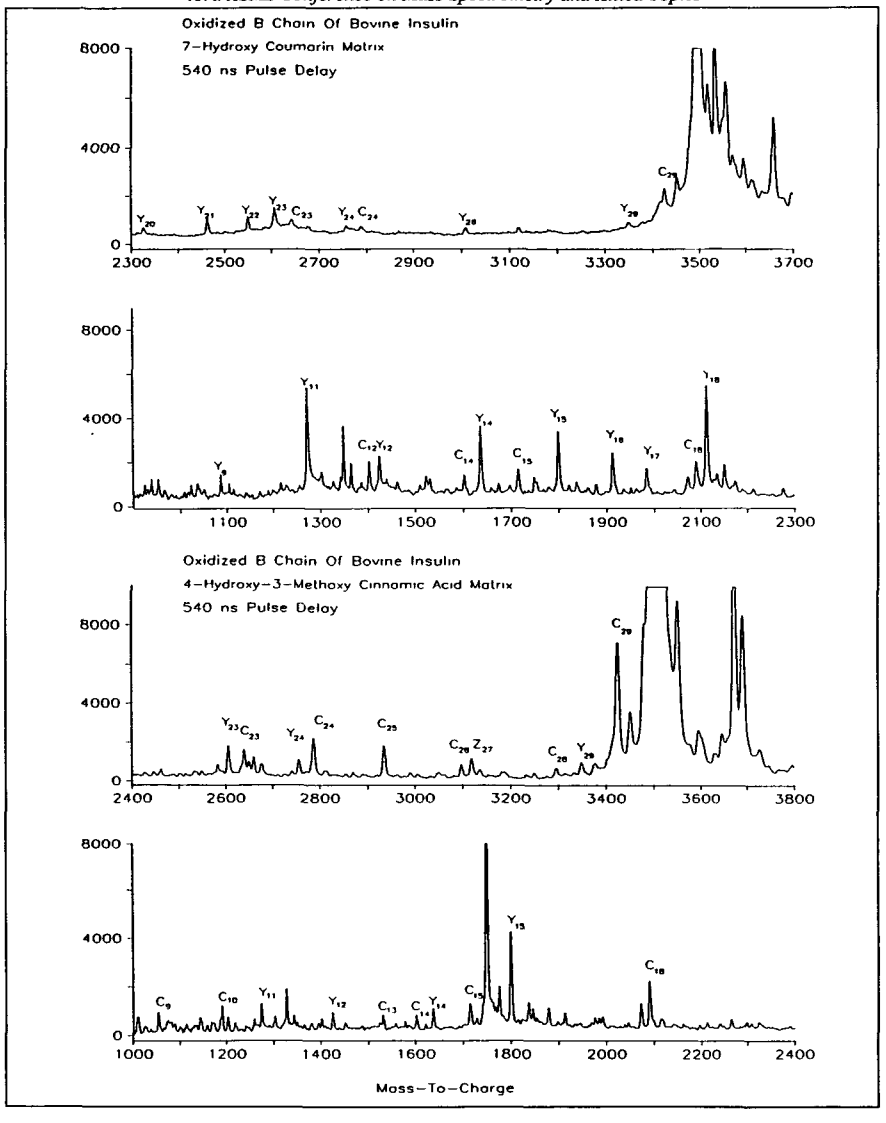

Delayed Extraction in Matrix-Assisted Laser Desorption

W. Ens, R. G. Dworschak, V Spicer, K.G. Standing
Department of Physics, University of Manitoba, Winnipeg, Canada R3T 2N2

In general, time-of-flight mass spectra obtained by matrix-assisted laser desorption/ionization (MALDI) in a linear time-of flight TOF spectrometer are characterized by modest mass resolution and almost no structurally significant information. The resolution is usually limited by the initial energy spread and by metastable decay in the field-free flight tube, both of which are strongly influenced by the high dc extraction field strength normally used to acquire MALDI spectra [1,2]. Recently two groups have shown considerable improvement in resolution by using delayed extraction [3,4]. This decouples the ion desorption process from the extraction process, reducing metastable decay caused by collisions in the plume, and allows time-lag energy focussing as described by Wiley and McLaren [5]. We have obtained similar results using a delayed extraction pulse (1 - 4 kV) applied to the target which along with the first grid is at a potential up to 25 kV. A second grid is held at ground potential. The geometry is illustrated in Fig. 1 (d1 = 6 mm, d2 = 1.0 cm and L = 1.3 m). The length of the delay is typically between 1 and 3 µs.

Fig. 2 shows the molecular ion regions for horse and sheep myoglobin obtained with pulsed extraction in the linear mode. The molecular weights for these compounds differ by 28 Da; the resolution is approximately 1200 The doubly charged molecular ion of carbonic anhydrase (29 157 Da) is shown in Fig. 3 with dc extraction and with pulsed extraction. If the shoulder on the low time side of the delayed extraction peak represents a fragment, then it appears that the instrumental resolution is about 1200 for this peak as well.

The use of pulsed extraction with a reflecting TOF instrument is also expected to give improved performance, especially for larger proteins. While good resolution for peptides is possible with dc extraction, tails caused by metastable decay limit resolution for larger species Simply lowering the extraction fields reduces the metastable decay [2] but this introduces an increased time spread in the extraction region. Such a time spread can be avoided for a given mass by using pulsed extraction to focus the ions at some intermediate plane before entering the mirror. For optimum use of the mirror, this plane should be near the source, and this requires that the field is approximately the same in both regions. With our present geometry, only low extraction fields can satisfy this condition so we have not yet demonstrated high resolution in this mode. However, we have demonstrated that ions injected with a delayed pulse are much more stable than ions injected by a dc extraction field. Since the ions have time to decay to stable fragments *before* they are accelerated, rather than in free flight, the fragments appear in the ordinary TOF spectrum at their apparent mass. Fig. 4 shows the full spectrum of melittin and a small portion expanded to indicate the fragmentation. Similar sharp peaks corresponding to prompt structural fragments appear throughout the spectrum, but the two broad peaks are the only evidence for metastable decay. For higher molecular weight species like cytochrome C, as much as 95% of the signal disappears when dc extraction is used instead of delayed extraction. With a redesigned source geometry, we hope to exploit this improved transmission to obtain improved resolution for high molecular weight species.

1. J. Zhou, W. Ens, K.G. Standing and A. Verentchikov, *Rapid Commun. Mass Spectrom*, 6 (1992) 671.
2. W Ens, R. Dworschak, V. Spicer, and K. G. Standing, ASMS 1994, p.3.
3. J. J. Lennon and R. S. Brown, ASMS 1994, p. 502.
4. W. C. Wiley and I H McLaren, *Rev. Sci. Instrumen. 26* (1955) 1150.

43rd ASMS Conference on Mass Spectrometry and Allied Topics

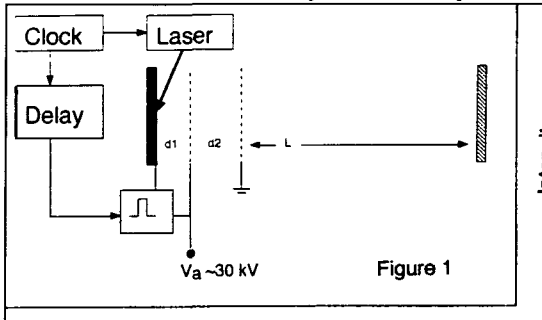

Figure 1

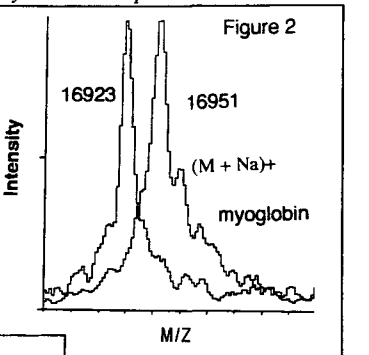

Figure 2

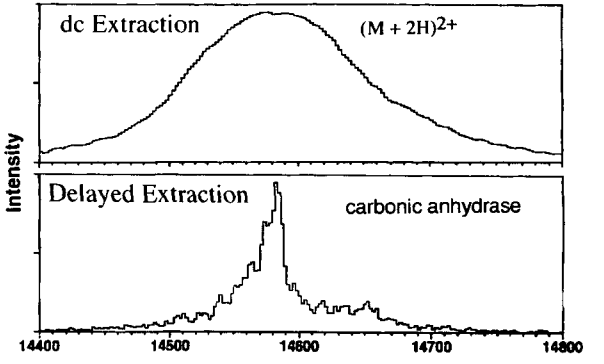

Figure 3

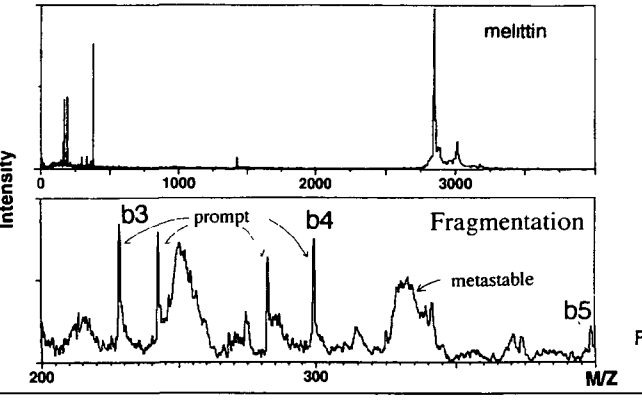

Figure 4

Investigation of Selective Detection of Peptide Mixture by MALDI Mass Spectrometry

Wen Yu, James E. Vath, Bruce S. Tangarone and Hubert A. Scoble
Structural Biochemistry, Genetics Institute, One Burtt Road, Andover, MA 01810

The ability to detect femto-mole quantities of peptides from a complex mixture in the presence of common digest buffers is a distinct advantage of MALDI mass spectrometry comparing to other ionization modes. Many important applications, including protein identification by mass profiling [1], have been built upon such promise. In practice, the sequence coverage from the analysis of digest mixture often varies widely and seemingly mysteriously from case to case, though the relative abundance of the peptides seems to be reproducible once the MALDI conditions are held constant. Understanding this phenomena, termed "peptide detectability", is becoming more critical as MALDI mass spectrometry is being widely applied to the field of protein characterization and identification.

We have examined peptide detectability using a known mixture derived from the Lys-C digest of a recombinant glycoprotein. The matrix, α-cyano-4-hydroxycinnamic acid, was chosen as it is the most common matrix used for mass profiling in our experience. For each MALDI mass spectrum acquired from the peptide mixture at various dilution, the relative abundance of the peaks were transformed into a user defined peak intensity index ranging from 0 to 5. The indexes are then ploted against the hydrophobicity indexes of the corresponding peptides calculated from their amino acid composition and hydrophobicity established from the 3-D structure of the proteins [2]. The results for the dataset at the matrix/analyte (M/A) ratio of 10000 in Figure 1(A) suggest that the detectability of the peptide in the mixture is hydrophobicity dependent as more hydrophilic peptides are detected at higher abundance while the peptides absent from the MALDI mass spectrum tend to cluster around the hydrophobic region. The favoritism for the hydrophilic peptides seems to diminish for the data at lower M/A ratio as shown in Figure 1(B) since the peak intensity indexes of the detected peptides do not follow any pattern. This would point to the additional dependence of peptide detectability in the mixture on M/A ratio.

The peptides in the mixture can be categorized into those able to gain (Figure 1C) or lose (Figure 1D) preference for detection and others that are not effected. To understand the behavior of peptides at the point of M/A ratio = 420 (highlighted by the thick vertical lines), we looked at the recovery of peptides being included or excluded by the matrix on an individual basis as shown in Figure 2. This experiment clearly demonstrates that at a M/A ratio of 420, the hydrophobic peptides eluting later in the chromatogram were preferentially included into the matrix while the hydrophilic peptides at the earlier part of the chromatogram were nearly totally excluded. This is consistent with the trends observed in Figure 1C and 1D. We proposed that the selective incorporation of the peptide is the determining factor at low M/A ratio while the dissociation of peptide from the matrix molecules in the gas phase, which favors the hydrophilic peptide because of weaker interaction, plays a more important role at higher M/A ratio.

The same methodology was applied to the dataset collected from 5 mass profiling experiments. The probability that a given peptide in the digest mixture may or may not be detected by MALDI MS was found to be dependent on its calculated hydrophobicity and hydrogen binding tendency [3]. The estimated probability of detectibility can be included into the calculation of matching probability and likelihood ratio for better evaluation of the matching patterns during the mass profiling experiments.

43rd ASMS Conference on Mass Spectrometry and Allied Topics

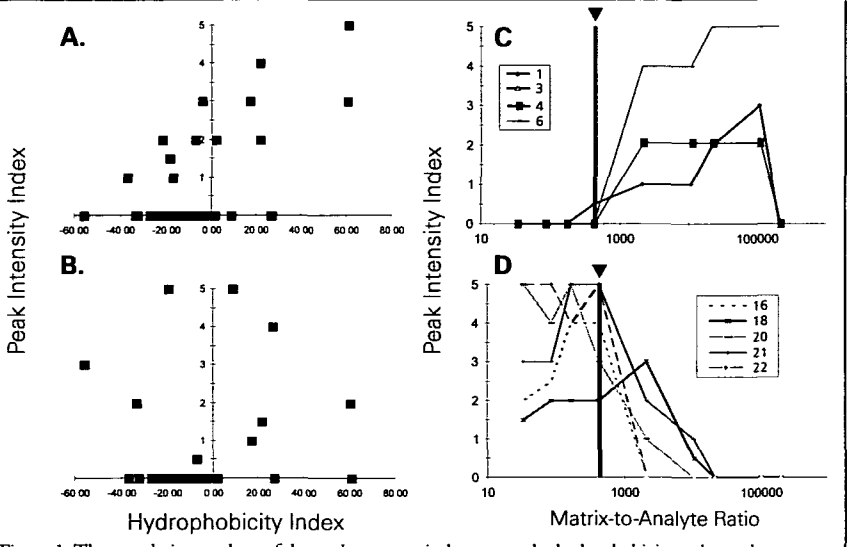

Figure 1. The correlation analysis of the peak intensity index versus the hydrophobicity index and matrix/analyte (M/A) ratio. The peptide mixture derived from the Lys-C digest of the recombinant glycoprotein was diluted with saturated solution of 4HCCA before analyzed by MALDI TOF MS in linear mode. A) M/A ratio = 10000 with 40 fmol per peptide, B) M/A ratio = 420 with 2 pmol per peptide, C) trends for peptide 1,3,4,6, D) trends for peptide 16,18,20,21,22 (same numbering as used below).

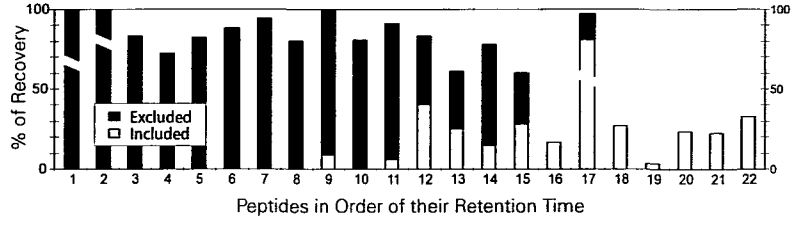

Figure 2. The partitioning of peptides within and outside the matrix crystals. The matrix particles prepared from the starting mixture at M/A ratio of 420 was washed with cold water over a 30 kD cutoff memberane several times before redessolving in 70% ACN. The washed and redessolved matrix were then seperated on RP-HPLC using establish conditions. The percent recoveries were calculated from the HPLC area compared to that of the starting material.

1. Cottrell, J.S.; Peptide Research, 1994, 7(3), 115-124
2. Holbrook, S.R.; Muskal, S.M.; Kim, S -H.; *Protein* Engineering, 1990, 3(8), 659-665
3. Stickle, D.F.; Presta, L.G.; Dill, K.A.; Rose, G.D.; J. Mol. Biol., 1992, 226, 1143-1159

Examining MALDI Ion Formation at Various Laser Fluences

Ricky D. Edmondson, Karen K. Campo, and David H. Russell
Laboratory for Biological Mass Spectrometry
Department of Chemistry, Texas A&M University
College Station, TX 77843

We have observed that two thresholds exist for ion formation in MALDI. At low laser fluences(2mJ/cm^2) ions are only produced from the first laser shot on each spot. In order to generate more ions from this spot, fluences must be increased three to four times. Ions are then produced for many consecutive shots from that sample spot. The instrument used in this study was a PerSeptive Voyager Elite TOFMS. Spectra were acquired in the linear mode(2m drift tube) with an acceleration voltage of 30kV. Spectra of Mellitin and Vitamin B_{12} were each taken with alpha-cyano-4-hydroxycinnamic(ac4h) acid at both the high and low ionization thresholds. Each spectrum is the average of 25 shots. For the low fluence spectrum(fig 1,3) one shot is taken on 25 new sample spots and averaged, whereas in the high fluence spectrum(fig 2,4), 25 shots were averaged from one spot The enhancement in analyte/matrix signal and increased resolution is seen in the low fluence spectrum of Mellitin in figure 1. Vitamin B_{12} can provide some information on the energetics of ion formation. The high fluence threshold spectrum of B_{12} shows no intact molecular ion(figure 4), only the prompt fragment of the loss of the labile cyano ligand. However, the $M+H^+$ is a prominent peak in the low fluence spectrum(figure3).

These high resolution spectra obtained in the linear mode suggest that the ions formed at the low laser fluence threshold have narrow energy distributions. The B_{12} results support an argument that these ions are formed with lower internal energies.

We propose a model that the lower ionization threshold is a surface component and the higher threshold is a component of the bulk material.

43rd ASMS Conference on Mass Spectrometry and Allied Topics

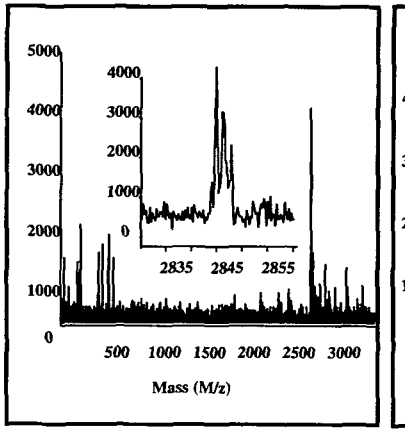

Figure1.
Mellitin at the low fluence(2mJ/cm^2) threshold

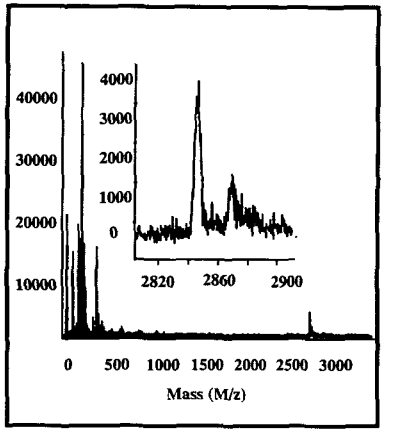

Figure2.
Mellitin at the high fluence(6mJ/cm^2) threshold

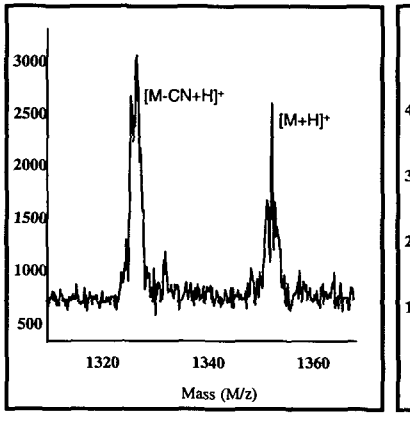

Figure3
Vitamin B_{12} at the low fluence(2mJ/cm^2)threshold

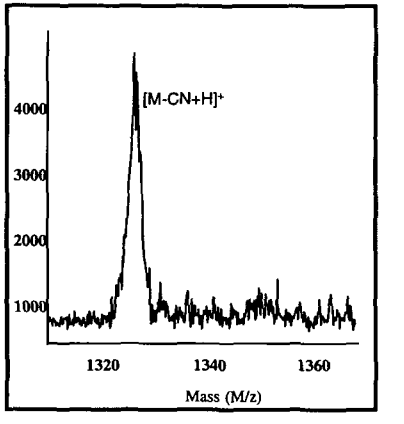

Figure4
Vitamin B_{12} at the high fluence(6mJ/cm^2) threshold

Continuous Flow MALDI in an Ion Trap-Reflectron TOF Mss Spectrometer

Ling he, Li Liang, Xuhui Li, David M. Lubman
Chemistry Dept, The University of Michigan, Ann Arbor,MI 48109-1055

MALDI as an ionization method has been extensively studied in the static mode with solid matrices. Only a few research work has been done to explore the MALDI in the liquid and continuous mode. The possibility to combine the advantages of MALDI with the on-line separation techniques is the major driving force for this project

An novel ion trap/ReTOF mass spectrometer is used as the interface to perform MALDI in the continuous mode The instrument configuration is depicted in Figure 1. Samples are injected using a 4-port Reodyne injection valve with 5μl internal loop. Matrix solution (3-NBA:H20· acetonitrile Ethylene glycol = 8 40:50:40·2 v/v, containing 0 1% TFA) and the carrier solvent (H2O acetonitrile = 1:1 v/v, containing 0.1%TFA) are mixed through a mixing tee and the flow rate after splitting is typically below 3μl/min.. The flow probe transmits the sample/matrix mixture into a hole on the ring electrode of the ion trap The laser (266nm) comes from the counter position and ionizes the sample exited from the flow probe tip. After ions from several laser shots are stored and accumulated in the ion trap for a certain time, a DC pulse is applied to the end cap to extract all the ions out of the ion trap and into the ReTOF mass analyzer to measure the m/z It is demonstrated that this configuration can provide a resolution of more than 300 (FWHM) for neurotensin(Mw. 1672.9) and Gramicidin (Mw. 1140). Figure 2 shows the spectrum of neurotensin in the continuous mode. The detection limit is in the low picomole range for peptides with molecular weight up to 8500D. Signal of Cytochrome C is observed in the continuous mode. An analogue frequency scanning is applied to the entrance end cap to kick out the low mass ions before the stored ions are pulsed out of the ion trap. The background noise is reduced in htis way. Both the resolution and S/N ratio are improved by reducing the space charge effect. The pressure inside the ion trap is found to be the most important factor that influences both the resolution and the sensitivity. A whole spectrum can be obtained in one extraction pulse Quantitative analysis of neurotensin using gramicidin as the internal standard in the continuous mode shows there is a nice linear relation between log(Sn/Sg) and log(Cn/Cg) within a range of two orders of magnitude Single matrix and mixture matrix were both tried and there were not significant differences

In conclusion, a continuous flow MALDI system is built successfully by the hyphenation of an ion trap and a ReTOF mass analyzer. This system is ready for coupling with LC separation techniques such as capillary HPLC Also it is possible to couple this system to CE due to its low solvent flow rate required and high sensitivity obtained

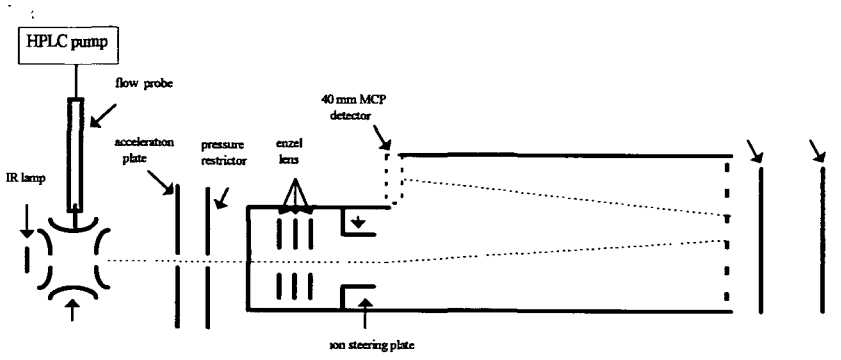

Figure 1 Instrument configuation of the continuous flow MALDI in an IT/ReTOF system

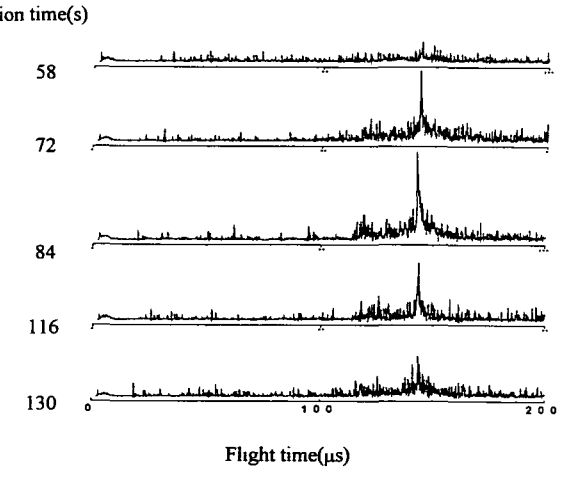

Figure 2 Mass spectra of neurotensin in the continuous mode

LANTHANIDE OXIDE CLUSTER IONS PRODUCED BY LASER ABLATION*

John K. Gibson, Chemical and Analytical Sciences Division
Oak Ridge National Laboratory, Oak Ridge, TN 37831-6375

Positive ions produced by XeCl excimer laser ablation of inorganic solids were studied by reflectron time-of-flight mass spectrometry to elucidate chemical speciation and the physical processes comprising ablation. The results are relevant to developing enhanced techniques for pulsed laser deposition of thin films and laser ablation sampling for materials analyses.

The initial emphasis has been on studying simple gas-phase inorganic clusters, which often exhibit novel chemistries and/or structures and provide a discernible bridge between the molecular and condensed states of matter. We have developed vacuum ablation of lanthanide oxalates (LnOX) as a source of lanthanide oxide cluster ions, representable as $Ln_mO_n^+$ ($m \leq 64$; $n \approx [3/2]m$). The LnOX mass spectra (shown for YbOX in Fig. 1) exhibit two primary cluster series, in both of which the Ln^{+3} oxidation state is predominant: $\{Ln^{3+}{}_mO^{2-}{}_{1/2(3m-1)}\}^+$ with m = 3, 5, 7, etc., and $\{Ln^{2+}Ln^{3+}{}_{m-1}O^{2-}{}_{1/2(3m-2)}\}^+$ with m = 4, 6, 8, etc. In addition to the Ln^{2+} sites in the latter series, other (minor) clusters exhibited compositions indicative of less-common lanthanide valence states, including those specified in Table I. The assignment here of discrete localized oxidation states assumes ionic cluster bonding, consistent with conventional lanthanide oxide chemistry. Alternatively, average lanthanide valences may be considered, as in Figure 2 in which are evident the singular tendencies of Tb to form the +4 oxidation state and Gd to form exceptionally metal-rich (low-valent) clusters which presumably comprise metallic Gd_p^o subclusters The genre of lanthanide oxide clusters being discussed apparently provides unique local atomic environments in which subtle distinctions between lanthanide electronic structures, including 4f occupancy, are clearly manifested. Solids which preserve distinctive cluster properties could offer routes to novel lanthanide nanomaterials, such as enhanced catalysts, with atypical chemical/valence states

Experiments are being performed to clarify the mechanism of ablation production of lanthanide oxide clusters, specifically whether formation is by intact ejection from the solid target or by aggregation of small species in the plume. The dramatic enhancement in cluster formation induced by the gaseous oxalate decomposition products (CO, CO_2 and H_2O) suggests a gas-phase aggregation mechanism. Accordingly, it was shown that the concentration of clusters relative to small ions is enhanced in the (cooler) tail of the plume. As additional evidence for gas-phase aggregation, we have prepared mixed lanthanide oxide clusters, such as $La_4Ho_3O_{10}^+$, by ablating physical mixtures of oxalates; the most plausible explanation for atomistic mixing from physically blended solids is by aggregation in the plume

Given its exceptional sensitivity and sample utilization efficiency, pulsed laser ablation mass spectrometry is ideally suited to studying scarce and/or radioactive materials such as transuranium actinides. The demonstration in the present work of clear manifestations in oxide cluster chemistry of subtle distinctions between lanthanide electronic structures particularly suggests this approach for micro-scale investigation of otherwise inaccessible actinide chemistry.

Table I - Representative oxidation states / cluster ions (minor states in parentheses)

Sm ▸ +3 / $Sm_9O_{13}^+$	**Gd** ▸ +3 / $Gd_3O_4^+$; (+2 / $Gd_6O_8^+$)	**Eu** ▸ +2 / $Eu_4O_4^+$, +3 / $Eu_{10}O_{13}^+$
Tb ▸ +3 / $Tb_7O_{10}^+$; (+2 / $Tb_8O_{11}^+$; +4 / $Tb_8O_{12}^+$)		**Yb** ▸ +3 / $Yb_{13}O_{19}^+$; (+2 / $Yb_{12}O_{17}^+$).

43rd ASMS Conference on Mass Spectrometry and Allied Topics

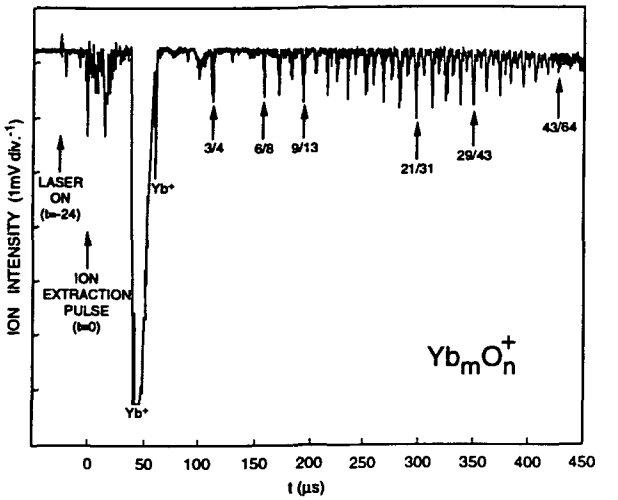

Figure 1 - TOF laser ablation mass spectrum for YbOX.

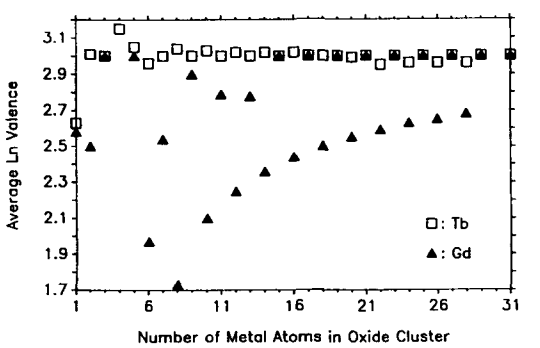

Figure 2 - Average Ln valences in $Tb_mO_n^+$ and $Gd_mO_n^+$

* Research sponsored by the Division of Chemical Sciences, Office of Basic Energy Sciences, U. S. Department of Energy under Contract DE-AC0584OR21400 with Martin Marietta Energy Systems, Inc.

The Role of Solubility in the Preparation of Synthetic Polymer Samples for Analysis by Matrix-Assisted Laser Desorption/Ionization Time-of-Flight Mass Spectrometry

Richard C. King, Robert Goldschmidt, Yansan Xiong and Kevin G. Owens*, Department of Chemistry, Drexel University, Philadelphia, PA 19104
Scott D. Hanton, Air Products & Chemicals, Inc., Allentown, PA 18195

Sample preparation is considered to be an art in matrix-assisted laser desorption/ionization (MALD/I). The analysis of synthetic polymers, which possess a wide range of chemical properties, presents significant issues in the development of sample preparation methods. While discussed peripherally by numerous groups, the issue of solubility is one that must be addressed in order to successfully analyze a wider range of samples. It will be demonstrated here that solubility is the key to solid-state (crystal) sample preparation.

Three solubility issues must be considered: the solubility of the analyte in the solvent, the solubility of the matrix in the solvent, and the solubility of the analyte in the solid matrix crystal. Changes in synthetic polymer solution solubility as a function of the molecular weight in different solvents is well-known[1]. Solvent fractionation, accomplished by slowly adding a non-solvent to a polymer solution, is used to separate polymer samples into fractions of different molecular weight. Anything that affects solubility: temperature, solvent composition, ionic strength, polarity, acid or base character, the presence of other sample constituents, will affect the incorporation of the sample into the matrix crystal and therefore the success of the MALD/I experiment.

A number of different solubility metrics are in use in various disciplines[2]. Many of these are calculated from readily measured molecular properties. One of the earliest is the Hildebrand[3,4] solubility parameter (δ), which was developed to quantify "polarity" and to predict interactions between non-polar materials. Due to the strict limitations of the applicability of Hildebrand parameters to non-polar solvents, they have been augmented with a three-tier delineation in terms of the hydrogen bonding capability (poor, medium or strong) of the solvent. In practice, the Hildebrand parameter of solvents within each class are compared to predict solute/solvent interactions. Later Hansen[2] proposed an additional solubility metric that attempts to quantify the dispersion (δ_d), polarity (δ_p), and hydrogen bonding (δ_h) characteristics of each solvent independently. Hansen parameters are tabulated for a large variety of solvents as well as polymer systems, and are widely used as a guide to polymer solvent selection.

In separations science, Rohrschneider[5]/McReynolds[6] constants are widely used to classify gas chromatographic stationary phases. A series of test compounds is used to quantify the various types of molecular interactions between analyte and stationary phase. Tables of McReynolds constants exist, allowing for an informed choice of stationary phase for the desired separation. In a similar fashion, Snyder's polarity index[7] (developed using three test solvents) is widely used to select the appropriate liquid chromatography mobile phase. Although there is currently some discussion about the correctness of some of these metrics[8], the presence of some kind of solubility standard greatly simplifies the practice of these techniques.

In this presentation we present an empirical classification of several popular MALD/I matrices (see below) based upon our results with a number of different synthetic polymer chemistries. Several points are clear from this work. First, there is a large gap in matrix "solubility parameter" between trans-3-indoleacrylic acid (IAA) and 5-chlorosalicylic acid (CSA). Second, there is a need for a matrix more polar than 2,5-dihydroxybenzoic acid (DHB).

In this work two techniques were employed independently to study the analyte-matrix solvent system. Fluorescence microscopy was used to demonstrate the incorporation of the analyte in

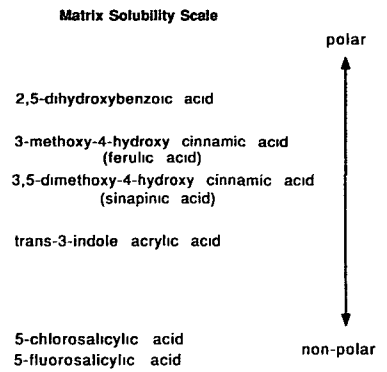

the matrix crystal. Ultraviolet MALD/I experiments were used to confirm the success of the sample preparation method. Polymers investigated include polyethylene glycol (PEG), polytetramethyleneglycol (PTMEG), polydimethylsiloxane (PDMS), polymethylmethacrylate (PMMA), polyethyleneterphthalate (PET) and polystyrene (PS). A wide range of solvents of varying polarity (solubility parameter) has been studied with several matrices, including DHB, IAA, 5-fluorosalicylic acid, CSA, and 2,4,6-trinitrophenol. The discussion in this presentation will focus on two key areas: solubility of the analyte in the solvent and solubility of the analyte in the matrix crystal.

Samples are normally prepared as dilute solutions. Note, however, that the solubility characteristics of the solution may change dramatically as the sample crystallizes. Factors that change the sample drying rate, including choice of solvent, heating, or pressure (e.g., drying under vacuum), will affect the incorporation of the analyte in the matrix crystals. As crystallization is a physical separations method, those things that affect the sample drying rate will obviously have an impact on the results. Additionally, sample preparation steps such as ion exchange, solution buffering, complexation using metal salts or binding proteins, or the addition of matrix additives are discussed as having a direct effect on the incorporation of the analyte by changing the solubility characteristics of the sample solution.

Solubility is demonstrated to be key to the analysis of synthetic polymer systems. Although most proteins can be analyzed using well-known sample preparation methodologies, it is likely that methods developed here for the analysis of synthetic polymers will be useful for the analysis of strongly hydrophilic or hydrophobic biological materials.

References

[1] A.F.M. Barton, CRC Handbook of Solubility Parameters and Other Cohesion Parameters, Boca Raton, FL: CRC Press, Inc., 1991.

[2] J.H. Hildebrand, R.L. Scott, The Solubility of Non-Electrolytes, New York: Reinhold Publishing Co., 1950.

[3] J.H. Hildebrand, J.M. Prausnitz, R.L. Scott, Regular and Related Solutions, New York: Van Nostrand Reinhold, Co., 1970.

[4] L. Rohrschneider, "Solvent Characterization by Gas-Liquid Partition Coefficients of Selected Solutes", Anal. Chem., 45(7), 1241-7, 1973.

[5] W. O. McReynolds, "Characterization of some Liquid Phases", J. Chromatogr. Sci., 8, 685-91, 1970.

[6] L.R. Snyder, "Classification of the Solvent Properties of Common Liquids", J. Chromatogr. Sci., 16, 223-34, 1978.

[7] C.F. Poole, S.K. Poole, "Characterization of Solvent Properties of Gas Chromatographic Liquid Phases", Chem. Rev., 89, 377-95, 1989.

MECHANISTIC IMPLICATIONS OF MALDI ION SIGNAL PROFILES

Gary R. Kinsel
The University of Texas at Arlington, Department of Chemistry, Arlington, TX 76019

Ricky D. Edmondson and David H. Russell
Texas A&M University, Department of Chemistry, College Station, TX 77843

Profile analysis of bovine insulin cluster ion signals produced by MALDI in a TOFMS are found to consist of two distinct Gaussian profiles. For all cluster ion signals the two component fits consist of a broad profile which contributes to the poorly resolved base of the ion signal and a sharp profile which contributes to the improved resolution of the ion signal half-width. Calibration of the mass spectrum from the masses of the cluster ion signals and the flight times of the sharp component of the two component Gaussian fit using the TOFMS calibration equation ($TOF = k(m/z)^{1/2} + b$) yields significant improvements in the linearity of the calibration plot over calibration attempts using the flight times of the maximum cluster ion signal intensities. In addition, calibration using the sharp component of the two component profiles returns an average instrumental offset parameter, b, of 1.0±15 ns. This value reflects complete agreement with the expected line delays between firing of the desorbing laser and triggering of data collection. The overall error in flight time assignment (and mass assignment), determined by back calculation of the cluster ion flight times using the calibration parameters determined from linear regression, is significantly improved (see figure 1)

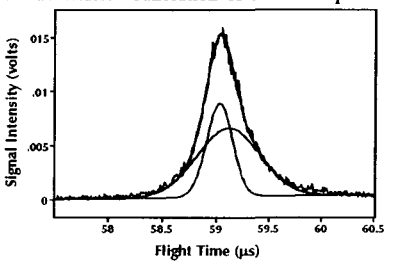

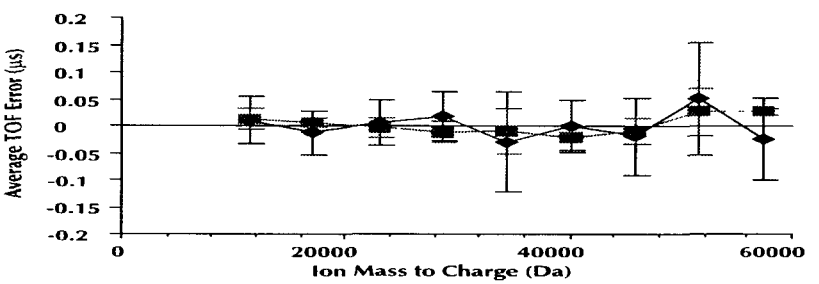

Figure 1 Errors in calculated ion flight times from spectrum calibration using (♦) flight times of maximum cluster ion signal intensity and (■) flight times of sharp component of two component Gaussian fits Average % error of flight times calculation for six spectra over entire mass range is 0.02% and average error in mass assignment is 0 04% for calibration using the sharp component

Two important insights are drawn from calibration using the sharp component of the ion signal profiles and the resulting calibration parameters. First, **NO** significant systematic mass dependent ion energy is associated with the desorption of the ions which make up the sharp component of the ion signal. A mass dependent ion energy would result in both curvature of the TOF vs. $(m/z)^{1/2}$ calibration plot and a

value for the instrumental offset parameter inconsistent with the experimental approach. Second, ion formation must be prompt *i.e.* within ten to fifteen nanoseconds of the desorbing laser pulse. Otherwise, delayed ionization would result in an inappropriately large offset parameter. From these results we conclude that the mechanism of formation of the ions contributing to the sharp component must involve prompt, laser induced surface ionization of the analyte followed by emission of the analyte ions with a constant (not necessarily thermal), mass independent initial kinetic energy.

Interpretation of the dynamics of ion formation for the ions which make up the broad component of the asymmetric ion signals is more complex. It is found that the flight time of the centroid of the broad component gradually shifts from longer flight times relative to the sharp component at low mass (< 20 kDa) to shorter flight times relative to the sharp component at high mass. Although mechanisms such as adduct formation or metastable decay could explain one observation or the other, neither process can independently explain the entire trend observed. Instead, we interpret the dynamics of formation of the ions making up the broad component in terms of neutral material accelerated to a constant entrainment velocity followed by delayed gas phase ionization of this material. This combination of dynamic processes yields ions with total energies, $E = E(acc) + 0.5(m/z)^{1/2}v(ent)^2 - FP(gpi)$, where E(acc) is the total acceleration voltage, v(ent) is the entrainment velocity, F is the source region electric field and P(gpi) is the point in the source region where gas phase ionization occurs. Using an iterative regression approach values of v(ent) and P(gpi) were varied to arrive at values which yielded calculated flight times for the broad component in agreement with experimentally observed flight times (see figure 2)

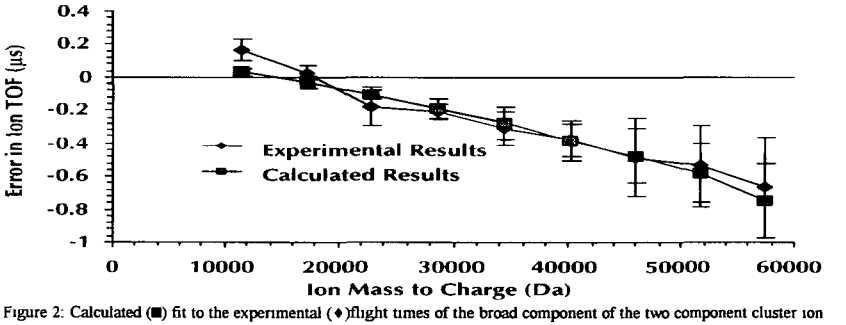

Figure 2: Calculated (■) fit to the experimental (♦)flight times of the broad component of the two component cluster ion signals by allowing the ionization to occur from entrained neutral material in the gas phase above the probe surface. Best fit for experimental flight times recorded in 6 mass spectra over the entire mass range yields v(ent) = 830±130 m/s and P(gpi) = 30±10 µm with an overall average % error in flight time agreement of 0 1%

Although these results reflect studies of bovine insulin cluster ion signals, the proposed two component mechanism of ion formation applies in general to MALDI analyte ion formation. Evidence for the two component mechanism of ion formation has been obtained for non-clustered ions from expected shifts in relative flight times of the broad and sharp components as a function of source region electric field, changes in the yield of high energy ions as a function of source region electric field and shifts in flight times of broad and sharp components as a function of flight tube length. Furthermore, the two component mechanism proposed for ion formation in MALDI is supported by previous studies of the kinetic energies of MALDI ions by electrostatic analyzer TOFMS.

DISSECTING MALDI-TOF MASS SPECTRA

John Allison, Pao-Chi Liao, Gary Lavine & Joseph Hiller
MSU/NIH Mass Spectrometry Facility
Michigan State University, East Lansing, MI

Hundreds of MALDI mass spectra have appeared in the literature, documenting unprecedented detection and analyte mass limits. Most of these spectra either represent single transients, resulting from single laser shots, or are the sum/average of 20-200 transients. The implication in presenting either is that they represent *the* results of the MALDI experiment - while absolute intensities vary with each laser shot, the spectra are essentially the same. We have found that this is not necessarily the case. Relative intensities change with time, and it is appropriate to consider a collection of spectra, rather than a single spectrum, as best representing the MALDI experiment. With multiple spectra, a variety of correlations of peak intensities with each other, and in time, can be made - not unlike what is done in other MS experiments that yield time-dependent spectra such as GC/MS.

In many MALDI MS experiments, when multiple transients are summed, conditions are changed during the acquisition process to maximize the signal in each transient. The approaches used include moving the laser beam across the target surface as transients are being acquired, and/or changing laser power. One reason why such approaches may be required is that a focused laser spot is traditionally used, and a small fraction of target crystals are irradiated. The small laser spot also contributes to problems in reproducibility in the MALDI experiment, since mass spectrometrists are always searching for "hot spots" on the target that yield intense ion currents.
The first change we have made is to increase the spot size. When a larger area is irradiated, more reproducible results are obtained between samples. Also, many spectra can be generated without having to either move the laser or change the power. We call this "Big Spot MALDI". The second change we have made is to accumulate a series of "component spectra" in an experiment. Each component spectrum represents the sum of 10 successive transients. With this approach to the accumulation of data, we have begun to analyze a number of features of the experiment, in an attempt to better define MALDI.

One feature that is of particular interest is the power/resolution relationship. To date we have explored this in the context of the linear MALDI TOF experiment. It is "common knowledge" in the MALDI MS community that the best resolution can be obtained under low laser power conditions. Higher powers yield lower resolution. However, higher powers are necessary in some cases, especially when mixtures involving analytes over a wide MW range are being analyzed. Higher MW analytes require higher powers for the desorption/ionization process to occur. When many

spectra are obtained, using a variety of powers above threshold, one always observed signal decay as a function of time. As peak intensities decrease, resolution increases. Thus, if high powers are used, peaks are initially intense and exhibit low resolution. In subsequent spectra, intensities drop and resolution increases. Thus, it is possible to obtain "low power" resolution in "high power" experiments. Such observations suggest new possibilities for mixture analysis in MALDI, in which many spectra are accumulated, and each component need not be evaluated (mass most accurately determined) in the same spectrum.

Another experiment that we have evaluated is referred to here as a "Power Titration". In this experiment, one begins at the lowest power at which any ions are formed, usually only matrix ions. Ten transients are summed into a single component spectrum (again using Big Spot MALDI). The power is then stepped to a higher value, and a second component spectrum is obtained. Many component spectra, representing a range of laser powers, are collected. This is a complex experiment when a single large spot is used - at a fixed power, the total ion current for successive component spectra would decrease. However, increasing power tends to yield *more* intense signals. The result is a series of spectra that are very sensitive to matrix, analytes, and target preparation procedures. It represents yet another trajectory through the power/time/spectra surface on which we work in MALDI.

We are not suggesting here that MALDI results need be obtained in a time-dependent way. For many applications, single spectra suffice for providing the chemical information required. However, if the identification of minor components in a mixture is a problem, if a wide range of MW's in a single mixture are encountered, and/or if the resolution and mass accuracy obtained is insufficient, such approaches may lead to improved results.

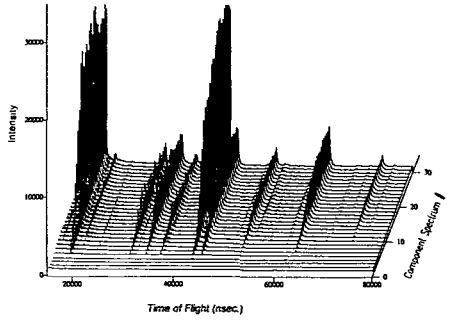

Power titration results for a multicomponent peptide mixture containing the following components (in order of increasing MW): bradykinin, angeotensin, melitin, insulin b chain, insulin, cytochrome C and myoglobin. In some cases, both the singly and doubly charged peptides are observed. The portions of the spectra representing low mass matrix peaks are not shown.

MALDI Sample Preparation Techniques by X-ray Photoelectron Spectroscopy

DS Jones, KS Robinson, SP Thompson & P Humphrey

Kratos Analytical, Barton Dock Road, Manchester, M41 7LD, UK.

Sample preparation techniques for Matrix Assisted Laser Desorption Ionisation (MALDI) are being investigated by a number of groups[1,2,3] in order to improve the uniformity of coverage, reproducibility and ease of application of sample & matrix. This paper reports the investigation of the surface chemistry of MALDI samples which have been prepared by a number of different methods as described in the literature. Analysis of the surface was carried out by X-ray photoelectron spectroscopy (XPS) in order to confirm coverage and investigate the surface concentration of proteins.

Samples were prepared from specific proteins (BSA and β-casein) and sinapinic acid was used as the matrix. They were analysed in a Kratos Kompact MALDI III.

The comparison in figure 1 shows the sample preparation method as proposed by Xiang & Beavis has several advantages in terms of both absolute signal level and relative stability.

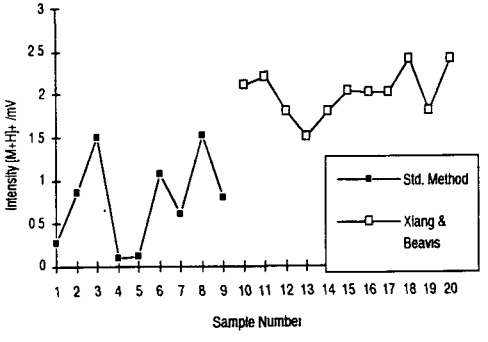

Figure 1 - Comparison of sample preparation methods for MALDI of BSA with sinapinic acid

It was decided to investigate this sample method by XPS. The MALDI sample was prepared as above and analysed in a Kratos Axis HSi Electron Spectrometer. The spectra of the protein and the matrix were each measured by themselves to obtain characteristic spectra. The sinapinic acid, being free of nitrogen, simplified the elemental analysis as the N1s could be used as a direct marker for the protein.

The three spectra are shown in figures 2-4. The β-casein spectrum clearly shows a significant nitrogen peak which is virtually absent from the sinapinic acid spectrum alone. The protein also contains small amounts of sulphur which are visible in the spectrum. More subtle

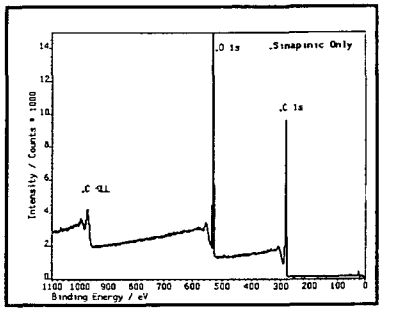

Figure 2 - XPS spectrum of sinapinic acid

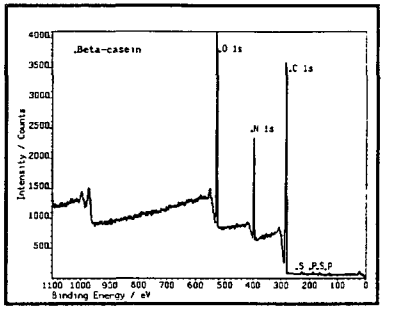

Figure 3 - XPS spectrum of β-casein

differences were also seen in the high resolution scans of the C1s orbital which could be correlated to the different forms of carbon present in the two molecules. It can be seen immediately that despite the sinapinic been present in vast molar excess the spectrum of the prepared MALDI sample is virtually identical to the spectrum of β-casein alone.

The level of β-casein as determined from quantitiation of the N1s signal indicates that there is a significant enhancement of the surface concentration of sample protein when compared with the bulk concentration suggesting segregation of the sample to the surface during crystallisation.

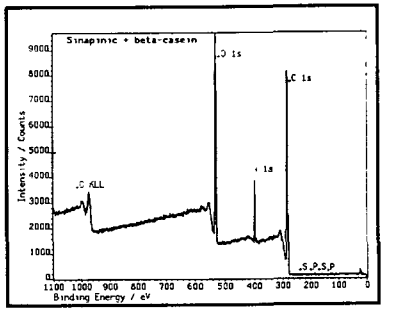

Figure 4 - XPS spectrum of MALDI slide of β-casein with sinapinic acid

References

1 RC Beavis & JN Bridson; J. Phys. D. Appl. Phys., **26**, 442, (1993).

2 F Xiang & RC Beavis; Proceedings of 42nd ASMS Conf. on MS & Allied Topics, p 974, (1994).

3 B Spengler, M Hubert & R Kaufmann, 13th IMSC Budapest, (1994).

SIFT STUDIES OF THE REACTIONS OF H_3O^+ AND $H_3O^+ \bullet H_2O$ WITH A SERIES OF SULFIDES AND THIOLS

Ted L. WILLIAMS, Lucia M. BABCOCK, Nigel G ADAMS, and Brian K. DECKER, Chemistry Department, University of Georgia, Athens, GA 30602.

H_3O^+ is an important ion in the molecular synthesis in interstellar clouds, being one of the nine ions detected. H_3O^+ and $H_3O^+ \bullet H_2O$ are dominant ionic constituents of the D-region of the terrestrial ionosphere and of importance in the earth's stratosphere. Sulfur is the ninth most cosmically abundant element after H, He, O, N, Ne, Si, Mg. Sulfur containing compounds comprise 13% of the species detected in the interstellar medium. The oxygen containing analogs have also been detected as have larger oxygen containing compounds. Thus, it seems reasonable that larger sulfur containing compounds will be present also. Many sulfur compounds are anthropogenic pollutants in the terrestrial atmosphere. For example, the paper and pulp industry emits H_2S, CH_3SH, C_2H_5SH, n-C_3H_7SH, iso-C_3H_7SH, $(CH_3)_2S$, $CH_3SC_2H_5$, and C_4H_4S.

The reactions of these last mentioned sulfur compounds with H_3O^+ and $H_3O^+ \bullet H_2O$ were studied using a selected ion flow tube (SIFT). The reactant ions were produced in a high pressure microwave discharge in H_2O and separately injected into the flow tube A sufficient pressure of H_2O was used to quench any excitation in the ions. Low injection energies were used to minimize fragmentation of $H_3O^+ \bullet H_2O$. Reactant sulfur compounds were then introduced into the flow and the parent and product ions detected by a downstream mass spectrometer. Rate coefficients and product ion distributions (%) were obtained in the usual manner (Smith and Adams, 1988). Rate coefficients are considered to be accurate to within ± 25% and product distributions to within ± 5 %.

Rate Coefficients, k, ($cm^3\ s^{-1}$) for H_3O^+ and $H_3O^+ \bullet H_2O$ Reactions with Sulfur Compounds

	H_3O^+	$H_3O^+ \bullet H_2O$	
Reactant Neutral	k	k	Ion Product Distribution (%)
Thiols			
CH_3SH	1.8(-9)	1.7(-9)	100% $CH_3SH_2^+ \bullet H_2O$
C_2H_5SH	2.0(-9)	1.9(-9)	100 % $C_2H_5SH_2^+ \bullet H_2O$
n-C_3H_7SH	2.3(-9)	2.0(-9)	70 % $C_3H_7SH_2^+ \bullet H_2O$ 30% $C_3H_7SH_2^+$
iso-C_3H_7SH	2.3(-9)	2.1(-9)	5 % $C_3H_7SH_2^+ \bullet H_2O$ 95% $C_3H_7SH_2^+$
Sulfides			
H_2S	1.4(-9)	1.3(-12)	---------
$(CH_3)_2S$	1.7(-9)	1.7(-9)	100% $((CH_3)_2S)H^+$
$CH_3SC_2H_5$	2.4(-9)	2.2(-9)	100 % $(CH_3SC_2H_5)H^+$
C_4H_4S	1.8(-9)	1.4(-9)	100 % $(C_4H_4S)H^+$

All of the H_3O^+ reactions proceed by proton transfer, consistent with the reaction energetics. The rate coefficients that were obtained are typical of proton transfer reactions, i.e., collisional or close to the collisional rate. With the exception of the H_2S reaction, the $H_3O^+ \bullet H_2O$ rate coefficients were consistently slightly smaller than the H_3O^+ rate coefficients which is consistent with the larger reduced mass of $H_3O^+ \bullet H_2O$ system than that of H_3O^+ system. This trend is in agreement with the previous studies of Fehsenfeld et al. (1978) and Bohme et al. (1979) of H_3O^+ and $H_3O^+ \bullet H_2O$ with oxygen containing compounds. Though direct proton transfer was seen for the H_3O^+ reactions, only half of the $H_3O^+ \bullet H_2O$ reactions proceed by direct proton transfer. This occurs when the proton transfer reaction is exothermic, the energy available in the reaction being smaller than the equivalent H_3O^+ reaction by the cluster ion dissociation energy. When proton transfer is endothermic as in the case of CH_3SH and C_2H_5SH, the primary product is of the form $(RSH)(H_2O)H^+$, with the secondary product being $(RSH)_2H^+$. The second product confirms that the proton is most likely contained within the sulfur component, i.e., $RSH_2^+ \bullet H_2O$, as expected. For the cases where the proton transfer reactions are thermoneutral or close to thermoneutral, a combination of the above two processes is seen:

$$H_3O^+ \bullet H_2O + RSH \rightarrow RSH_2^+ + H_2O$$
$$\rightarrow RSH_2^+ \bullet H_2O + 2H_2O$$
$$RSH_2^+ + RSH \rightarrow (RSH)_2H^+$$

This behavior is observed for both of the propanethiols. Such ligand switching/rearrangement was previously seen in two $H_3O^+ \bullet H_2O$ reactions with CH_2O, CH_3OH by Fehsenfeld et al. (1978) and one with dimethyl methylphosphonate by Passarella et al. (1987).

Using laser induced fluorescence, we have also shown, consistent with previous data, that OH reactions with sulfur containing compounds, i.e., H_2S, n-C_3H_7SH, and iso-C_3H_7SH, are fairly rapid. Therefore, these compounds will be mainly destroyed before they reach the stratosphere and D-region where most of the H_3O^+ and $H_3O^+ \bullet H_2O$ exist. Thus, reaction with these ions would have to occur in the troposphere. In regions where $H_3O^+ \bullet H_2O$ coexist with sulfur containing compounds, the water clusters would catalyze the formation of sulfur clusters for those species for which proton transfer with $H_3O^+ \bullet H_2O$ is thermoneutral or endothermic. Any detection of these clusters would thus be evidence for the existence of the related neutral sulfur compound. From this information, trace neutral compositions could be measured as has been done previously for other species (Viggiano 1993).

In the interstellar medium, recombination of H_3O^+ with electrons forms OH (65 %), H (100 %) and presumably some H_2O (Adams et al. 1991.), serving as a loss process for H_2O. However, in the presence of sulfur containing compounds, H_3O^+ can react by proton transfer to produce H_2O. Therefore, depending on the fractional abundance of the sulfur containing compounds and the competition between H_3O^+ recombination and proton transfer, the H_2O to OH ratio would be enhanced.

Adams et al. *J. Chem. Phys.* **1991**, 94, 4852.
Bohme et al. *J. Amer. Chem. Soc.* **1979**, 101, 3724.
Fehsenfeld et al. *J. Geophys. Res.* **1978**, 83, 1333.
Passarella et al. *Int. J. Mass Spectrom. Ion Phys.* **1987**, 81, 227.
Viggiano et al. *Mass Spectrom. Rev.* **1993**, 12, 115.
Smith and Adams. In *Advances in Atomic and Molecular Physics*; Bates, D. R. and Bederson, B, Eds. ; Academic: Orlando, **1988**, 24, 1.

Unimolecular Kinetics of $CHClF^{\bullet}$ by Variable-Time Neutralization-Reionization Mass Spectrometry

Martin Sadílek and František Tureček
Department of Chemistry, Box 351700,
University of Washington,
Seattle, WA 98175-1700

Hydrochlorofluorocarbons (HCFC), which are currently being introduced to replace chlorofluorocarbons (CFC), undergo oxidative degradation in the troposphere that lowers the amount of HCFC reaching the stratospheric ozone layer. However, an unknown fraction of surviving HCFC molecules is lifted to the stratosphere, where they undergo photolysis by UV solar radiation to form chlorine atoms. The complementary HCFC radicals retain part of the excitation energy and may further fragment to generate $Cl^{\bullet}$, HCl, $F^{\bullet}$ or HF. These secondary dissociations of excited HCFC radicals have not been studied so far. We report the results of a mass spectrometric study that addresses unimolecular dissociations of $CHClF^{\bullet}$ radicals prepared by fast collisional neutralization of $CHClF^{+}$ cations utilizing the new method of variable-time neutralization-reionization mass spectrometry abbreviated here as VT-NRMS *(1,2)*.

Dissociations of $CHClF^{\bullet}$ and $CHClF^{+}$ were studied with a tandem quadrupole mass spectrometer described previously *(3)* and modified for kinetic studies *(1,2)*. Radicals are generated from precursor ionization energies. In one series of experiments the radicals were allowed to drift for a fixed period of time (4.1 μs), and the neutral species were reionized to cations, mass-analyzed, and detected. In variable-time measurements, the neutral and ion lifetimes were varied between 0.41 and 2.59 μs by carrying out reionization in a segmented drift region (conduit) whose parts were floated at appropriate potentials *(1,2)*. Phenomenological rate constants were obtained by fitting equations for unimolecular kinetics to match the experimental ion relative intensities.

An overall NR spectrum of $CHClF^{+}$, obtained with C_6H_5Cl/O_2 at 70% ion beam transmittance (**Figure 1a**), shows abundant survivor $CHClF^{+}$ ion of 20% relative abundance, indicating that the $CHClF^{\bullet}$ radical is stable on the time scale of our observations (4.1 us). The most intense peaks correspond to CF^{+} at *m/z* 31, $CHF^{+\bullet}$ at *m/z* 32 and Cl^{+} at *m/z* 35. Weaker peaks of $HCl^{+\bullet}$, CCl^{+}, $CHCl^{\bullet+}$, and $CClF^{+\bullet}$ appear at *m/z* 36, 47, 48 and 62, respectively, while very weak peaks of $C^{+\bullet}$, CH^{+}, and F^{+} are found at *m/z* 12, 13, and 19, respectively. There is no peak of $HF^{+\bullet}$ at *m/z* 20. Hence the $CHClF^{\bullet} \rightarrow HF + CCl^{\bullet}$ fragmentation does not occur significantly although it has the lowest reaction enthalpy. This indicates a presence of a barrier for the reaction.

NR spectra of $CHClF^{+}$ ($IE_v(CHClF^{\bullet}) = 9.16$ eV) were obtained by neutralization with di-n-butyl ether, chlorobenzene, di-n-butylamine, aniline, and N,N-dimethylaniline of vertical ionization energies decreasing in the range of 9.45, 9.10, 8.45, 8.0 and 7.45 eV. The overall NR spectra show only little dependence on the neutralization gas ionization energy with the exception of di-n-butylamine which induces slightly increased fragmentation.

More dramatic effects are observed in the C_6H_5Cl/O_2-NR spectra of $CHClF^{+}$ generated by charge-transfer ionization with $N_2^{+\bullet}$ in a high-pressure ion source (**Figure 1b**). The latter spectrum shows a substantial increase of the survivor ion intensity and much lower relative intensities of CF^{+}, $CHF^{+\bullet}$, and Cl^{+}. This is attributed to thermalization of the $CHClF^{+}$ precursor ion, which is estimated to have on average <20 kJ mol^{-1} internal energy.

By contrast, ion relative intensities are not effected much by different exoergicities of

neutralization.

VT-NRMS measurements allow us to distinguish between the fragmentation of the neutral radical (k_N) and the reionized cation (k_i) as shown in **Table 1** for neutralizations with di-n-butyl ether and N,N-dimethylaniline. The rate parameters indicate similar contributions from neutral and ion decompositions in the formation of Cl^{+} and CHF^{+} fragments due to simple bond cleavage. $CHCl^{+\bullet}$, CCl^{+} and HCl^{+} are formed mainly by ion dissociations, in agreement with the respective reaction endothermicities and considering energy barriers for the eliminations of hydrogen chloride and hydrogen fluoride. The CF^{+} fragment may be formed by a consecutive dissociation from reionized $CClF^{\bullet}$. The increased exoergicity in the neutralization step does not change the rate parameters significantly.

Figure 1: C_6H_5Cl/O_2 (70% transmittance) $^{+}NR^{+}$ mass spectra of
(a) $CHClF^{+}$ from 70-eV EI of $CHClF_2$ at 10^{-5} Torr.
(b) $CHClF^{+}$ from $N_2^{+\bullet}$ charge-transfer ionization of $CHClF_2$ at 0.2 Torr N_2.

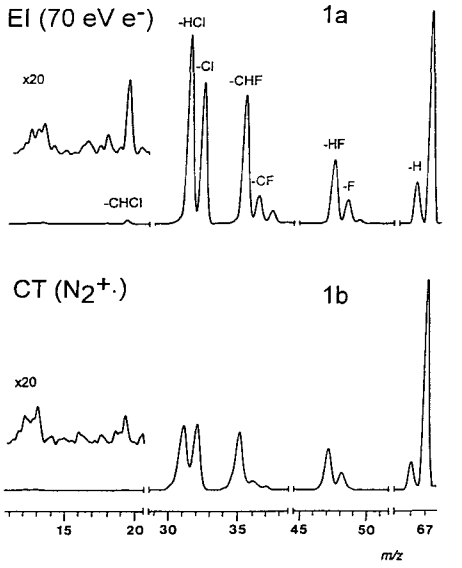

Table 1: Rate parameters (10^6 s^{-1})

	di-n-butylether		dimethylaniline	
	k_N	k_i	k_N	k_i
CHCl	0.03	0.08	0.00	0.04
CCl	0.09	0.16	0.01	0.66
HCl	0.04	0.20	0.03	0.04
Cl	0.29	0.65	0.35	0.58
CHF	0.32	0.30	0.41	0.28
CF	0.42	0.65	0.63	0.41

(1) D. W. Kuhns, T. B. Tran, S. A. Shaffer, and F. Tureček, *J. Phys. Chem.* **1994**, *98*, 4845.
(2) D. W. Kuhns and F. Tureček, *Org. Mass Spectrom.* **1994**, *29*, 463.
(3) F. Tureček, M. Gu, and S. A. Shaffer, *J. Am. Soc. Mass Spectrom.* **1992**, *3*, 493.

Astrophysical Thermochemistry: The Heats of Formation of C_3H_2 Isomers.

Leonard J. Chyall and Robert R. Squires

Department of Chemistry, Purdue University, West Lafayette, IN 47907-1393

Astronomers have been interested in the C_3H_2 potential energy ever since cyclopropenylidene (**1**) was detected in interstellar space.[1] Spectroscopic evidence for the presence of the isomeric species propadienylidene (**2**) has also been reported.[2] However, the other linear isomer propargylene (**3**) has thus far eluded detection.

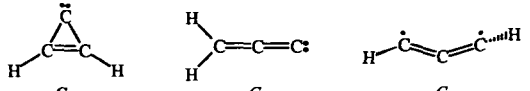

C_{2v} C_{2v} C_2

1 2 3

Molecular orbital theory predicts cyclopropenylidene to be the global minimum on the C_3H_2 potential energy surface, while the other two stable isomers are higher in energy. For example, calculations at the G2 level of theory suggest that the $^1A_1$ ground state of propadienylidene and the $^3A''$ ground state of propargylene are 13.5 and 16.4 kcal mol^{-1} higher in energy than **1**, respectively.[3] Because of the widespread interest in these molecules, and the need for experimental verification of the theoretically predicted stability ordering, we have undertaken gas-phase thermochemical investigations of the C_3H_2 isomers.

The proton affinity and absolute heat of formation of cyclopropenylidene (c-C3H2) have been derived from the translational energy threshold for endothermic proton transfer from c-$C_3H_3^+$ to ammonia in a flowing afterglow triple-quadrupole instrument.

$$c\text{-}C_3H_3^+ + NH_3 \longrightarrow c\text{-}C_3H_2 + NH_4^+$$

The cyclopropenium cation $C_3H_3^+$ was prepared in a helium flow reactor at room temperature by the reaction of ionized ethylene with acetylene, and from dissociative electron ionization of bromocyclopropane. The kinetic energy dependence of the cross sections for proton transfer from this ion to ammonia and other neutral amines was characterized in a triple quadrupole mass analyzer (Figure 1). The threshold energy for the reaction with ammonia was determined to be 23.3 ± 1.8 kcal mol^{-1}. Combining this with the known proton affinity (PA) of ammonia (204.0 ± 1.0 kcal mol^{-1}) gives a value for PA(c-C_3H_2) of 227.3 ± 2.1 kcal mol^{-1}. From the measured proton affinity and the known heats of formation of c-$C_3H_3^+$ and the proton, the 298 K heat of formation of cyclopropenylidene is determined to be 119.5 ± 2.2 kcal mol^{-1}. This value is slightly higher than a previous experimental estimate[4], but is in good agreement with the 298 K heat of formation predicted by high-level molecular orbital calculations.

Reaction of 1-d_1-propargyl chloride with hydroxide produces ions of *m/z* 73 and *m/z* 74 in approximately a 1:1 ratio.

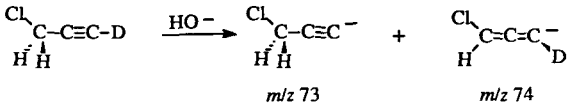

m/z 73 *m/z* 74

The ion of *m/z* 73 (presumably the 3-chloroacetylide ion) was collisionally activated with argon and the appearance energy for chloride ion was measured (Figure 2).

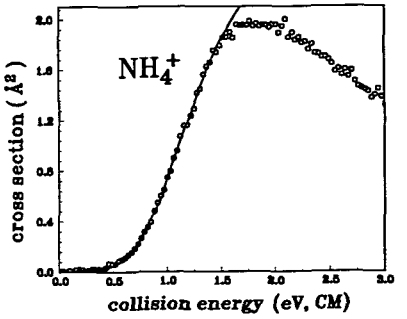

Figure 1

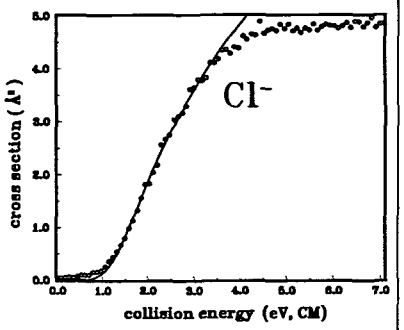

Figure 2

The enthalpy change of 29.0 ± 2.0 kcal mol^{-1} for this process was used as part of a thermochemical cycle to determine a value of 124.0 ± 3.5 kcal mol^{-1} for the heat of formation of propadienylidene. The measured heat of formation of propadienylidene is 4.5 kcal mol^{-1} higher than that obtained for cyclopropenylidene. This difference in heats of formation of the two isomers is much lower than the 13.5 kcal mol^{-1} difference that is predicted by G2 molecular orbital theory.

References

1. A. Dalgarno, J. Chem. Soc. Faraday Trans., 89 (1993) 2111.
2. J. Cernicharo, C. A. Gottlieb, M. Guelin, T. C. Killian, G. Paubert, P. Thaddeus, and J. M. Vrtilek, Astrophys. J., 368 (1991) L39.
3. M.W. Wong and L. Radom, J. Am. Chem. Soc., 115, (1993) 1057.
4. H. Clauberg, D.W. Minsek and P. Chen, J. Am. Chem. Soc., 114 (1992) 99.

Oxidation Reactions of Cationic Vanadium Clusters Studied Using Guided Ion Beam Mass Spectrometry.

M. T Rodgers, J. B Griffin and P. B. Armentrout, Department of Chemistry,
University of Utah, Salt Lake City, UT 84112

The kinetic energy dependence of reactions of V_n^+ with O_2 was studied using a guided ion beam mass spectrometer that has been described in detail elsewhere.[1] Thermochemical analysis of the observed product cross sections is treated as discussed previously.[2,3] The chemistry observed for reactions of V_n^+ with O_2 is quite complex. The reactions are facile and have large cross sections (in excess of 100 $Å^2$ at low energies) which drop off with increasing collision energy. Product cross sections are often multi-featured indicating that the corresponding product ions are formed by more than one reaction pathway. Monoxides dominate the chemistry of the smallest clusters as can be seen for the reaction of V_4^+ with O_2 shown in Figure 1. The chemistry observed in the larger clusters, those containing five or more atoms, is remarkably similar and quite complicated as a result of an increased number of possible products. However, the observed chemistry is dominated by dioxide formation. The major product channels observed for the reaction of V_8^+ with O_2 are shown in Figure 2 Lifetime effects begin to play a role in clusters containing as few as seven atoms, but significantly alter the observed product yields for clusters containing ten or more atoms. The number of bare metal cluster fragments observed and the cross sections for their production decrease with increasing cluster size.

One of many minor reaction pathways observed for all clusters is production of the parent monoxide. Assuming that there is no barrier to reaction (no evidence exists for one in cluster systems), bond energies of vanadium monoxide cluster ions, $D(V_n^+\text{-}O)$ can be determined from measurements of the corresponding reaction thresholds by making use of the following thermodynamic cycle.

$$\begin{array}{ll} V_nO^+ + O \rightarrow V_n^+ + O_2 & -E_0 \\ \underline{O_2 \rightarrow O + O} & \underline{D(O-O) = 5\ 12eV} \\ V_nO^+ \rightarrow V_n^+ + O & D(V_n^+ - O) \end{array}$$

Formation of V_nO^+ is thermoneutral or exothermic for $n \leq 4$, therefore $D(V_n^+\text{-}O) \geq 5.12$ eV and cannot be determined explicitly. In the larger clusters, where $n \geq 5$, formation of V_nO^+ is endothermic making direct determination of $D(V_n^+\text{-}O)$ possible. Threshold energies and bond dissociation energies for the vanadium monoxide clusters are summarized in Table 1.

In all but the smallest clusters, $n \geq 5$, the primary reaction process at low energies is exothermic loss of two vanadium atoms from the oxygen adduct (i.e., formation of $V_{n-2}O_2^+$). As the collision energy is increased, competitive dissociation of this product results in further loss of either a vanadium atom or of vanadium oxide to produce $V_{n-3}O_2^+$ and $V_{n-3}O^+$, respectively. In all cases,

[1] S. K. Loh, D. A. Hales, L. Lian and P B. Armentrout, *J. Phys. Chem.* **90**, 5466 (1989).
[2] R. H. Schultz, K. C. Crellin and P. B. Armentrout, *J. Am. Chem. Soc.* **113**, 8590 (1991).
[3] T. Beyer and D. F. Swinehart, *Comments Assoc. Comput. Machines* **16**, 379 (1973).; S. E. Stein and B. S Rabinovitch, *J. Chem. Phys.* **58**, 2438, (1973), *Chem. Phys. Lett.* **49**, 183 (1977).; R. G. Gilbert and S. C. Smith, *Theory of Unimolecular Recombination Reactions* (Blackwell Scientific, Oxford, 1990).

vanadium atom loss is the preferred reaction pathway. Estimates of bond energies of vanadium dioxide cluster ions, $D(V_n^+\text{-}O_2)$ have been obtained by comparison to CID data for the bare metal cluster cations and are summarized in Table 2. Direct determination of the dioxide bond energies is not possible for clusters where $n < 10$ because the di-oxygenated parent ion is not observed until n=10. This is the result of lifetime effects associated with the unimolecular dissociation of these species. The values obtained for the dioxide bond energies indicate that O_2 dissociatively binds to the metal cluster. The large difference in the monoxide and dioxide bond energies may be the result of suppression of the V_nO^+ product channel resulting in an increased apparent threshold and a decreased apparent bond energy. Therefore, the monoxide bond energies may represent lower limits rather than actual bond energies.

Table 1. Vanadium Monoxide Cluster Bond Energies in (eV).

n	$E_0(V_nO^+ + O)$	$D(V_n^+\text{-}O)$
1	-	6 00[5]
2	< 0	> 5.12
3	< 0	> 5.12
4	< 0	> 5.12
5	0.25	4.87
6	0.60	4.52
7	0.75	4.35
8	0.77	4 34
9	0.81	4.31
10	0 78	4 33

Table 2. Vanadium Dioxide Cluster Bond Energies in (eV).

n	Lower limit from CID (eV)[4]	Upper limit from CID (eV)[4]
2	10.92	14.16
3	11.89	16.02
4	12 49	16.35
5	13.11	17.10
6	12.97	16.64
7	12.78	16.74
8	12 75	16.71
9	13.04	17.17
10	13 21	17 86

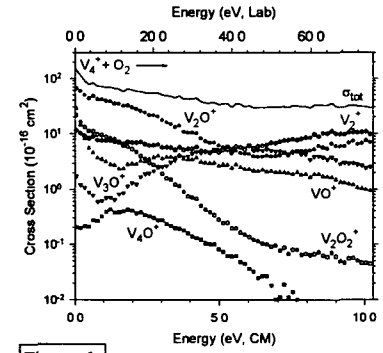

Figure 1

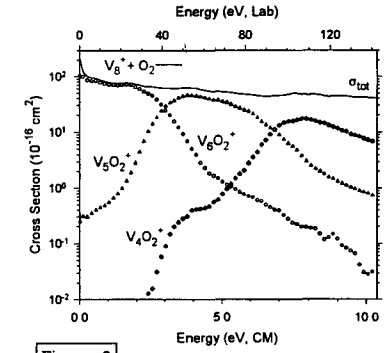

Figure 2

[4] C.-X. Su, D. A. Hales and P. B. Armentrout, *J Chem Phys* **99**, 6613 (1993).
[5] N. Aristov and P. B. Armentrout, *J. Chem Phys.* **90**, 5135 (1986)

Chemisorption of Hydrogen Molecules on Vanadium Cluster Cations

G. Dietrich[1], K Dasgupta[3], H -J. Kluge[4], M. Lindinger[2], K. Lützenkirchen[1], L. Schweikhard[2], and J. Ziegler[2]

[1]Johannes Gutenberg-Universität, Institut für Kernchemie, D-55099 Mainz, Germany
[2]Johannes Gutenberg-Universität, Institut für Physik, D-55099 Mainz, Germany
[3]Bhabha Atomic Research Center, Bombay 400085, India
[4]Gesellschaft für Schwerionenforschung, D-64220 Darmstadt, Germany

Due to the simple structure of the hydrogen molecule studies of its adsorption on cluster surfaces are particularly attractive for an understanding of the interaction on a microscopic level. Several publications dealing with transition metal clusters and their reactivity with hydrogen or deuterium are found [1].

In this contribution we report on the reaction between vanadium cluster ions V_n^+ and hydrogen. Clusters are produced by laser vaporization, injected into a Penning trap and stored for variable reaction duration. For identification, product ions are ejected out of the trap and detected by time-of-flight mass spectrometry. For a detailed description of the experimental setup see ref. [2].

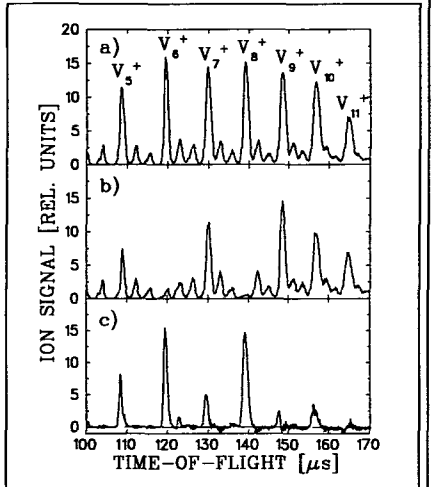

Fig. 1: Mass spectra with (b) and without (a) RF-excitation of the vanadium clusters (n = 5-11) at a hydrogen pressure of 8×10^{-6} mbar and a storage period of 360 ms. The peaks in the difference spectrum (c) represents the intenisties of the naked cluster ions V_n^+.

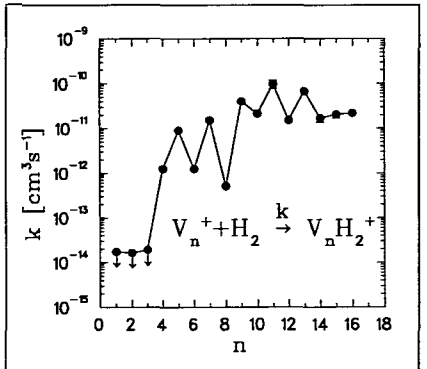

Fig. 2: Absolute rate constants k for the reaction of hydrogen and vanadium cluster ions (n = 1-16). For n = 1-3 only an upper limit could be measured.

The reaction rate constants for n = 1-16 were determined at a hydrogen pressure of 8×10^{-6} mbar. Difference spectra are obtained by substracting two spectra, one with and one without radial ejection of the bare vanadium clusters (fig. 1). The normalized intensities in the difference spectra represent those clusters which did not react with hydrogen during the storage period. Thus the absolute rate constants for the first reaction step are achieved (fig. 2) and an obvious odd-even effect can be recognized for n = 4-14. For the smaller clusters an upper limit is given.

Another item of interest is the maximum number of adsorbed hydrogen molecules m as a function of cluster size n. Saturation is achieved at a hydrogen pressure of 1.6×10^{-5} mbar and a storage period of 760 ms. In figure 3 the average number $\langle m\rangle$ is shown for n = 4-17. A linear increase can be seen for the system $V_nH_m^+$, $n \geq 10$. The slope represents the ratio $\langle m\rangle/n = 3/2$. The lower region shows an evident odd-even effect towards the takeup of H_2.

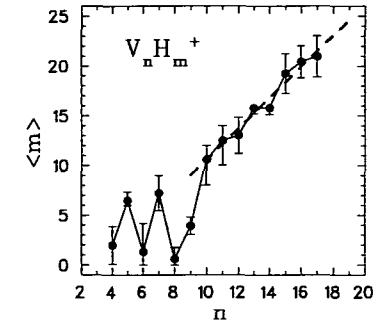

Fig. 3: Average number of adsorbed hydrogen atoms on vanadium clusters under saturation conditions (storage period of 760 ms, $p = 1.6\times10^{-5}$ mbar). The dashed line with the slope $\Delta\langle m\rangle/\Delta n$ = 1.5 has been fitted to the data with n = 10-17

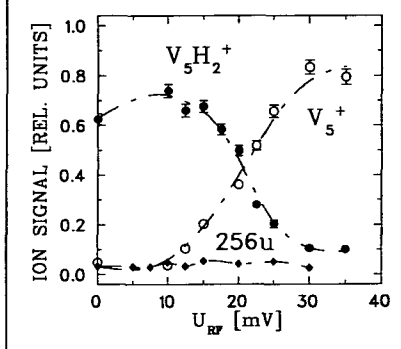

Fig. 4: Collision induced dissociation of $V_5H_2^+$ on argon ($p = 1.4\times10^{-6}$ mbar). The data shows the relative ion signal for $V_5H_2^+$ (●), V_5^+ (○) and "256 u" (= $V_5H_1^+$, ♦). with increasing excitation voltage U_{RF}. The dashed lines are to guide the eye.

The question of molecular versus dissociative chemisorption of the hydrogen molecules is addressed, as an example, for the adsorption of a single hydrogen molecule on a vanadium pentamer. Dissociation of the selected species $V_5H_2^+$ is induced by acceleration with a rf-field and collisions with argon atoms (fig. 4). The only products observed are the selected ions and the naked pentamers. No vanadium pentamer ion with one hydrogen atom attached is detected. (A trace amount at 256 u, which is independent of the collision energy, is fully explained by the isotopic distribution of vanadium.) By comparing the threshold energies of $V_5H_2^+$ with the known one of V_5^+ [3] the relative separation energy can be calculated as 1.9±0.3 eV. This result is in agreement with the calculated V-H binding energy [4] and leads to the assumption that the hydrogen molecule is adsorbed dissociatively

This work was supported by the Deutsche Forschungsgemeinschaft and the Materialwissenschaftliches Forschungszentrum Mainz.

[1] J.A. Martinho Simões et al., Chem. Rev. **90** (1990) 629; E.K. Parks et al., J. Chem. Phys. **88** (1988) 1622, M.R. Zakin et al , J. Chem. Phys. **88** (1988) 6605; M.E. Geusic et al., J. Chem. Phys **81** (1985) 590; S.C. Richtsmeier et al., J. Chem. Phys. **82** (1985) 3659
[2] St. Becker et al., submitted to Rev. Sci. Instrum.
[3] C.-X. Su, D.A. Hales, P.B. Armentrout, J. Chem. Phys. **99** (1993) 6613
[4] J.K. Nørskov, Rep. Prog. Phys. **53** (1990) 1253

Metal Ion/Molecule Chemistry Using a Radio Frequency Glow Discharge Source

Ritchie C. Eanes, Steven J. Christopher, and R. Kenneth Marcus

Department of Chemistry
Howard L. Hunter Laboratory
Clemson University
Clemson, SC 29634-1905

Radio frequency glow discharge mass spectrometry (rf-GDMS) has been used as a reliable technique for the direct elemental analysis of a variety of solid samples ranging from metals to glasses. The glow discharge is a reduced pressure plasma which relies on cathodic sputtering to generate gas-phase atoms from a solid sample target, which subsequently undergo a separate ionization step. The glow discharge may be a promising source for analyte specific ion-molecule chemistry where the plasma's unique ability to generate predominantly ground state metal ions holds an advantage over other more traditional sources employed in ion-molecule chemistry. Of the more traditional sources for metal ion formation, electron impact suffers from the fact that a suitable volatile complex, usually involving a metal carbonyl, must be used. Surface ionization from a heated filament also involves the use of a volatile metal salt and is limited to some of the less exotic metals in the periodic table. Laser ionization methods are prone to a more violent type of ionization event as compared to the glow discharge. This, in combination with the fact that laser ionization usually involves the formation of multiply charged species, may complicate or inhibit desired ion molecule chemistry.

The importance of ion-molecule chemistry to the analytical community has grown steadily in recent years. Freiser has used metal ion chemical ionization reagents to determine isotopolog and isotopomer distributions for perdeuterated napthalene [1], a problem that might be difficult to solve with high resolution NMR spectroscopy. Amster and co-workers have used sequential laser ablation steps to produce Fe ions that react efficiently with volatilized peptides [2].

Preliminary studies have shown that Fe ions emanating from the glow discharge react with cyclohexane in the collision chamber of a double quadrupole MS facilitating the formation of various Fe-alkene complexes as described by Eller and Schwarz [3]. Figure 1 shows a high sensitivity background scan for Fe prior to the

introduction of cyclohexane reactant gas. Figure 2 displays the spectrum obtained after cyclohexane was introduced into the collision cell of our double quadrupole MS system. The peak at m/z 128 is indicative of an Fe-pentene complex [3]. Also seen is a stable Fe-butene complex (m/z 112). The structure displayed in figure 2 resembles one of two stable bis(olefin) complexes formed after collisionally activated dissociation of an $FeC_6H_{12}^+$ ion [4].

High Sensitivity Background Scan Prior to Introduction of Cyclohexane

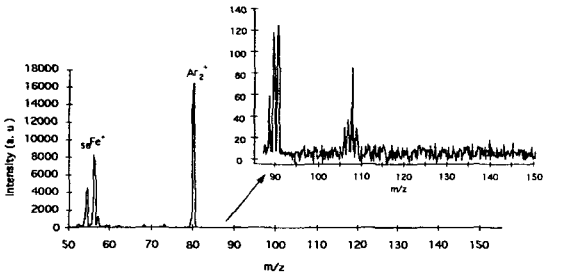

Figure 2 Fe Cyclohexane Background Scan

Fe/Cyclohexane Ion-Molecule Reaction

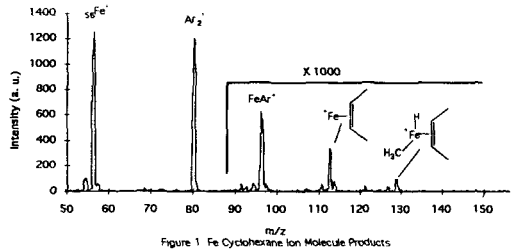

Figure 1 Fe Cyclohexane Ion Molecule Products

References

[1] Freiser, B. S.; Huang, Y.H.; Profilet, R.D.; Ng, J.H.; Ranasinghe, Y.A.; Rothwell, I.P. *Anal. Chem.* **1994**, 66, 1050-1055.
[2] Amster, I.J.; Speir, J.P.; Gorman, G.S.; *J Am Soc Mass Spectrom* **1993**, 4, 106-110.
[3] Eller, K.; Schwarz, H.; *Chem. Rev.* **1991**, 91,1121-1177.
[4] Ridge, D.P.; Gross, M.L.; Peake, D.A., *J. Am Chem Soc.* **1984**, 106, 4307-4315.

Generation and Characterization of Silacyclopentadienyl Complexes of Iron

D. J. Kardash*, S. Kloos, P. Boudjouk, and D. B. Jacobson
Center for Main Group Chemistry, Department of Chemistry
North Dakota State University, Fargo, North Dakota 58105-5516

There is considerable interest in generating metallocenes with a heavier group 14 element (Si, Ge, Sn) incorporated in the ring since these complexes may exhibit unique redox chemistry. Coordinated group 14 metallacyclopentadiene complexes have been investigated in great detail because they are reasonable precursors to group 14 η^5-metallacyclopentadienyl species. However, this approach proven to be unsuccessful. Tilley and co-workers recently reported the synthesis and characterization of the first stable η^5-metallacyclopentadienyl complexes with germanium $[(\eta^5\text{-}C_5Me_5)Ru\{\eta^5\text{-}C_4Me_4GeSi(SiMe_3)_3\}]$ (**1**) and silicon $[(\eta^5\text{-}C_5Me_5)Ru\{\eta^5\text{-}C_4Me_4GeSi(SiMe_3)_3\}]$ (**2**) incorporated in the ring.

Although it is very difficult to synthesize coordinated silacyclopentadienyl compounds in solution, they may be readily generated in the gas phase by reaction of transition metal ion complexes with silacyclopentanes. However, reactions of Fe^+ with simple silanes are complex where $Si(Me)_2H_2$ undergoes exclusive 1,1-dehydrogenation from the Si atom and silacyclobutane yields exclusive ring cleavage. However, reactions with unsaturated silacycloolefins may be much simpler with initial coordination to the site of unsaturation that would direct subsequent dehydrogenations to yield diene and dienyl complexes. In accord with this hypothesis, silacyclopent-3-ene yields exclusive dehydrogenations with $FeC_5H_6^+$ and $FeC_5H_5^{+\cdot}$, reactions 1 and 2.

$$FeC_5H_6^+ + H_2SiC_4H_6 \longrightarrow (C_5H_5)Fe(SiC_4H_5)^+ + 2H_2 \qquad 1$$

$$FeC_5H_5^+ + H_2SiC_4H_6 \xrightarrow{0.60} [(C_5H_5)Fe(SiC_4H_5)]H^+ + H_2 \qquad 2a$$

$$FeC_5H_5^+ + H_2SiC_4H_6 \xrightarrow{0.40} (C_5H_5)FeSiC_4H_4^+ + 2H_2 \qquad 2b$$

A proposed general mechanism for reaction 1 is presented below and predicts formation of a metallocene ion $(C_5H_5)Fe((SiC_4H_5)^+$ (**3**). The structure of **3** may consist of either the η^5-silacyclopentadienyl complex **3a** or an η^4-diene structure **3b**. A cationic germacyclopentadienyl

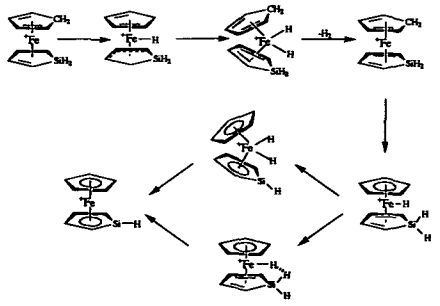

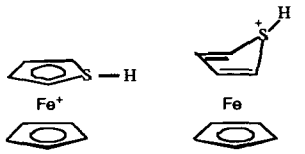

3a **3b**

complex, (germacyclopentadieneyl)$Fe(CO)_3^+$, has been isolated and spectroscopic studies suggest that it has an η^4-diene structure. $Fe(C_5H_5)_2^+$ yield characteristically simple CAD and photodissociation spectra with sequential loss of the C_5H_5 units. In contrast, **3** yields complex CAD spectra with H_2, SiC_2H_2, (H_2 + FeH), and FeC_4H_5 losses observed. This complexity in fragmentation suggests that coupling between the two groups occurs upon collisional activation.

The above dehydrogenation mechanism predicts that $FeC_5H_5^+$ should yield the protonated metallocene $[(C_5H_5)Fe(SiC_4H_5)]H^+$ (**4**) As with **3** the CAD spectra of **4** are complex with H_2, (FeH_2), (H_2 + FeH), and SiC_4H_5 losses dominant. The most likely structure for **4** is with protonation on the Si atom. Tilley and coworkers determined the X-ray structure of the protonated metallocene, $[(\eta^5\text{-}C_5Me_5)Ru\{\eta^5\text{-}C_4Me_4GeSi(SiMe_3)_3\}]H^+$. They found that it has the general structure of a protonated metallocene with protonation on the ring-silicon atom and with significant interaction with the metal (agostic M-H-Si bonding). The five membered C_4Si ring of the silacyclopentadienyl ligand is planar and the Si ring atom appears to have considerable sp^2 character. Therefore, **4** may consist of either **4a** or **4b** or a structure intermediate between these to extremes.

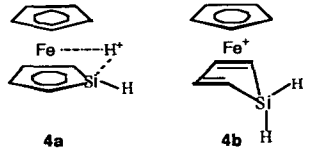

4a **4b**

The proton affinity (PA) of the corresponding neutral metallocene, $(C_5H_5)Fe(SiC_4H_5)$ (**5**), was probed by proton abstraction by reference bases. **4** does not undergo proton transfer to bases with PA'S less than that of $N(CH_3)_3$ (PA = 225.1 kcal/mol), however, facile proton transfer occurs with $N(CH_3)_2C_2H_5$ (PA = 227.5 kcal/mol) and stronger bases. This allows the PA of **5** to be bracketed between 225.1 and 227.5 kcal/mol with a value of 227 ± 3 kcal/mol assigned. This value is considerably larger than that for the PA of $Fe(C_5H_5)_2$ (207 kcal/mol).

To our knowledge, **5** has by far the highest reported PA of any organotransition metal complex. The high PA of this complex relative to $Fe(C_5H_5)_2$ (ca. 20 kcal/mol difference) may be reflective of silicon's propensity for sp^3 hybridization. The π-bond energy for C=Si species (35.6 kcal/mol) is significantly less than that for the corresponding C=C species (65.4 kcal/mol). This supports a structure for **4** consisting of silicon protonation with little agostic bonding (i.e., **4b**). However, the results of Tilley and co-workers support a structure with significant agostic bonding.

Structure and reactivity of $Fe(CN)(C_3H_5Cl)^+$ complexes

Capron, L.; Mestdagh, H.; Rolando, C.; Sablier, M.
Ecole Normale Supérieure, Processus d'Activation Moléculaire U.R.A. 1679
24, rue Lhomond - 75231 Paris cédex 05 (France)

The reactivity of transition metal complexes in the gas phase is very dependent on the nature and number of ligands. Study of the reactivity of $Fe(CO)_n^+$ ions with allyl chloride has shown the occurrence of ligand coupling (for a number of CO ligands n = 4,5) in the resulting metal complex $FeC_6H_{10}Cl_2^+$ (1). In the course of our investigations dealing with ion-organic radical reactions, we have been able to generate a new kind of metal-carbon bond leading to $M(CN)^+$ complexes by reaction of bare metal cations of the first row with cyanogen iodide and bromide (2). In a similar way, the iron carbonyl cations $Fe(CO)_n^+$ have shown a similar reactivity towards cyanogen iodide, affording iron cyanogen complexes $Fe(CN)^+$ and additionally have led to the formation of $Fe(I_xC_yN_y)(CO)_n^+$ complexes (x=1-2, y=1-3, n=0-3).

We report here the reactivity of these $Fe(I_xC_yN_y)(CO)_n^+$ complexes with allyl chloride C_3H_5Cl which results in a different type of gas-phase coupling involving the (CN) ligand.

$Fe(I_xC_yN_y)(CO)_n^+$ complexes were generated in the EI/CI source of a multiquadrupole MS/MS/MS mass spectrometer by electron impact on a mixture of the corresponding molecular species ($Fe(CO)_5$ and ICN). The resulting cations $Fe(I_xC_yN_y)(CO)_n^+$ were then mass selected in the first analyzer and guided to the first collision cell where they were allowed to react with allyl chloride. Either another reaction or collisionally activated dissociation with argon were carried out in the second collision cell after selection of product ions in the second analyzer. The final products were then detected by scanning the third analyzer. The pressure in each of the collision cells could be varied in the mTorr range.

The following reaction scheme was established for the $Fe(CN)(ICN)^+$ complex

$$Fe(ICN)CN^+ + C_3H_5Cl \rightarrow \underset{158^+-160^+}{FeCNC_3H_5Cl^+} + ICN$$

$$FeCNC_3H_5Cl^+ + C_3H_5Cl \rightarrow \underset{108^+}{C_7H_{10}N^+} + FeCl_2$$

The reaction of $Fe(CN)(ICN)_2^+$ or $Fe(ICN)_2^+$ complexes with allyl chloride afforded the same successive product ions $FeCNC_3H_5Cl^+$ and $C_7H_{10}N^+$.

The final product $C_7H_{10}N^+$ was shown to be identical with a C_3H_5-C=N+-C_3H_5 structure resulting from the reaction of $C_3H_5^+$ ion with allyl cyanide. Therefore its formation requires the formation of two new bonds, one C-C bond and one N-C bond.

In order to establish the structure of the intermediate $FeCNC_3H_5Cl^+$, its reactivity and CAD spectra were compared to those of isobaric complexes generated by reaction of iron precursor cations with allyl cyanide, propenyl cyanide (leading respectively to two isomeric cyanide complexes $(C_3H_5CN)FeCl^+$) or allyl isocyanide (leading to an isocyanide $(C_3H_5NC)FeCl^+$ complex). Of these three isomeric ions only the isocyanide complex gave the $C_7H_{10}N^+$ ion when reacted with allyl chloride. In addition, its CAD spectrum was identical with that of our intermediate, whereas those of the two cyanide complexes were different (also distinct from each other). Therefore we concluded that the $FeCNC_3H_5Cl^+$ intermediate is the isocyanide complex $(CH_2{=}CH{-}CH_2{-}N{=}C){-}Fe{-}Cl^+$.

The following scheme is proposed for the formation of the $C_7H_{10}N^+$ cation :

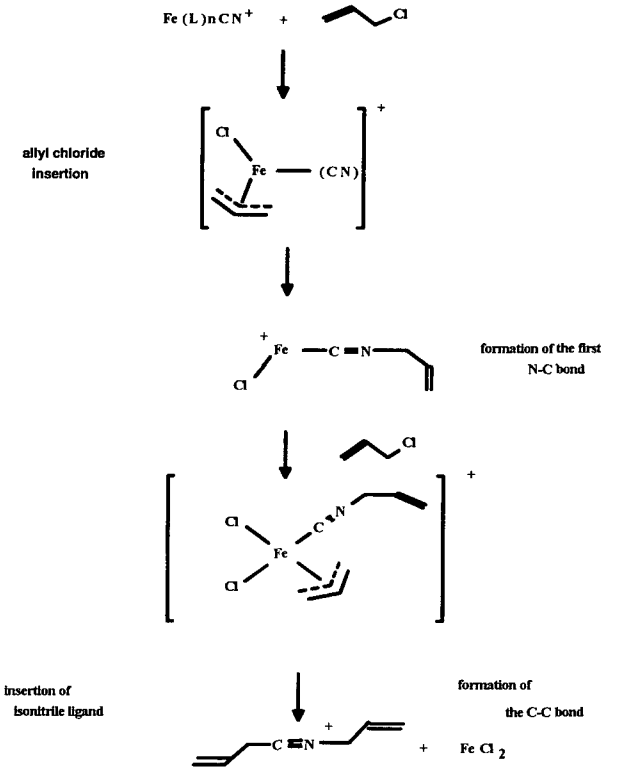

These successive gas phase N-C and C-C bond formations are very close to well-known organometallic reactions in solution which lead to alkyl isocyanide complex formation through cyanide complex alkylation and insertion of isocyanide ligand into a metal-carbon bond (3).

1 - H. Mestdagh and C. Rolando, *J. Am. Chem. Soc.* **1989**, *111*, 3476.
2 - M Sablier, L. Capron, H. Mestdagh and C. Rolando, *Tetrahedron Lett.* **1994**, *35*, 2895.
3 - Collman, J. P.; Hegedus, L. S., Norton, J. R.; Finke, R.G. in "Principles and Applications of Organotransition Metal Chemistry", University Science Books, Mill Valley, **1987**, p148

Ethylene Insertion and Hydrogenolysis Rates of $[(C_5Me_4)SiMe_2(N\text{-}t\text{-}Bu)ZrMe^+$

*Hayes, T W., Alameddin, N. G ; Richardson, D E , Eyler, J. R , Watson, C H.
Department of Chemistry, University of Florida
Gainesville, Fl 32611-7200

The chemistry of various Ziegler-Natta zirconocene complexes have been extensively studied in solution to determine the effects of ancillary ligands upon their ability to polymerize olefins. The study of the gas phase reactions allows mechanistic information to be obtained concerning the metal-olefin interaction in the absence of secondary effects due to solvation and ion pairing with the counterion.[1]

In an ongoing investigation of the gas phase reactions and kinetics of metallocene complexes,[2] the reactions of $[(C_5Me_4)SiMe_2(N\text{-}t\text{-}Bu)ZrMe^+$ (Fig 1) with ethylene have been studied with Fourier transform ion cyclotron resonance mass spectrometry (FTICR-MS) It was expected that the open metal coordination center resulting from the silicon bridging and amide coordinating ligand would lead to enhanced reactivity over related complexes

In a typical experiment the air sensitive catalyst was loaded into a glass capillary tube through the use of a glove box and affixed to the end of a solids probe. The probe was then inserted into the main vacuum chamber until the catalyst was about 20 cm from the ICR cell. A catalyst pressure of 3 0-4 0×10^{-8} torr was set by heating the probe Ethylene was leaked into the vacuum chamber by a precision leak valve to give a total pressure of 2.0-5 0×10^{-7} torr. The cationic metallocene complex was generated by electron impact in the ICR cell and after a thermalization period all unwanted ions were ejected, thereby isolating the isotopic distribution corresponding to the metallocene Following a variable reaction period all ions were excited and detected An IonSpec Omega data system was used to collect and store the data

Ideally, for a given reaction, a set of spectra taken at varying reaction times are generated and by following the ion abundances with time, a pseudo-first order rated constant can by extracted In reality, complex dimerization reactions occur which complicate the analysis Through the use of double resonance techniques partial assignment of the reaction scheme (Fig 2) was possible although constraints were required on rate constants k_5-k_7 to keep them consistent with previously studied zirconocene insertion reactions. The experimental data were fit from kinetic models based on the experimentally determined reaction pathways. The equations are solved analytically and a nonlinear least squares fit was used to extract the pseudo-first order rate constants The rate constants, combined with the pressure of the neutral reactant, give the second-order rate constants

A typical data fit (Fig 3) and the rate constants determined (Table 1) are shown It is apparent from the decay of the catalyst that both a reactive and unreactive species are present in a ratio of 3.1 The rate constant of the insertion of ethylene (k_1) is consistent with that of a previously studied zirconocene catalyst $Cp_2SiZrMe^+$ and 40 to 240 times more reactive than non-bridged species (see Table 2) The enhanced reactivity of the silicon bridged species is consistent with the idea that the silicon acts to "tie-back" the cyclopentadienyl and N-t-butyl ligands, thereby reducing the steric hindrance encountered by the ethylene molecule upon insertion The "tie-back" effect should be even more pronounced in insertion reactions involving bulkier olefins such as isobutylene.

Further study of the insertion of olefins and their deutero analogs into $[(C_5Me_4)SiMe_2(N\text{-}t\text{-}Bu)ZrMe^+$ is underway to determine kinetic and mechanistic insights.

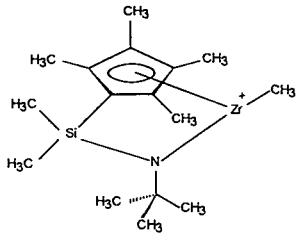

Figure 1

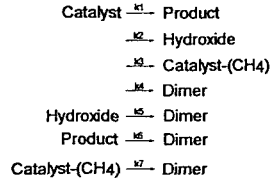

Figure 2

Table 1: Rate Constants for the reaction of $[(C_5Me_4)SiMe_2(N\text{-}t\text{-}Bu)]ZrMe^+$ with Ethylene

	Rate constant (M^{-1} S^{-1})
k1	$(8.0 \pm 1.5) \times 10^{10}$
k2	$(4.9 \pm 1.1) \times 10^{12}$
k3	$(7.7 \pm 3.1) \times 10^{11}$
k4	$(1.7 \pm 2.2) \times 10^{11}$
k5	$(1.4 \pm .63) \times 10^{11}$
k6	$(1.4 \pm .60) \times 10^{11}$
k7	$(4.1 \pm 1.4) \times 10^{11}$

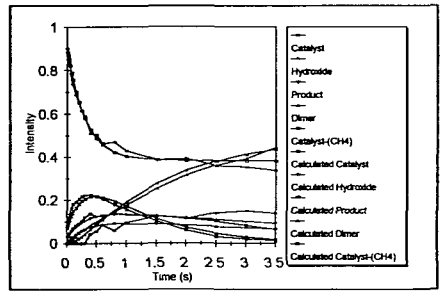

Figure 3

Table 2: Second Order Rate Constants for the Insertion of Ethylene into Zirconocene Catalysts:

Compound	Rate constant (M^{-1} S^{-1})	Reference
$Me_2SiCp_2ZrMe^+$	$(9.6 \pm 1\ 8) \times 10^{10}$	2
$[(C_5Me_4)SiMe_2(N\text{-}t\text{-}Bu)]ZrMe^+$	$(8.0 \pm 1\ 5) \times 10^{10}$	This Work
Cp_2ZrMe^+	$(3.4 \pm 0\ 9) \times 10^{10}$	2
$IndCpZr^+$	$(2.1 \pm 1\ 4) \times 10^{9}$	2
Ind_2ZrMe^+	$(3.5 \pm 0\ 4) \times 10^{8}$	2

1 Christ, Jr , C S.; Eyler, J. R , and Richardson, D. E , *J. Am Chem Soc.* **1990**, 112(2),596
2 Alammeddin, N. G.; Ryan, M F., Eyler, J. R.; Siedle, A R.; and Richardson, D E., submitted to Organometallics

Gas Phase Reactions of +1 and +2 Chlorotitanium Ions With Isobutene

Kurt Kneen, George E. Leroi, and John Allison

Department of Chemistry, Michigan State University, East Lansing, Michigan 48824

When $TiCl_4$ is subjected to 70 eV electron impact ionization, the full series of $[Ti(Cl)_n]^+$ ions (n=0-4) and $[Ti(Cl)_n]^{+2}$ ions (n=0-3) are formed. The chemistry of the singly charged ions, with a variety of organic compounds, changes dramatically as a function of n [1,2]. For example, when n=4, the ion reacts with oxygen containing organic compounds predominantly by ligand substitution, with the organic molecule displacing a weakly bound Cl atom. With olefins, the ion was found to be unreactive. When n=2,3, the ions react with olefins by elimination HCl, and cleavage of skeletal bonds. $TiCl^+$ ions react by eliminating H_2. Using an ion beam mass spectrometer, we have been able to observe additional chemistry. By studying the chemistry between the singly charged chlorotitanium ions and isobutene, we have been able to observe additional chemistry and have found the ions to more reactive than previously thought. $TiCl_4^+$ reacts with isobutene by ligand substitution, displacing a Cl atom, with the elimination of HCl. $TiCl_3^+$ reacts by eliminating not only a single HCl molecule but 2 HCl molecules. $TiCl_2^+$ reacts by forming a charged complex with the olefin, eliminating HCl, and undergoing charge transfer to generate $C_4H_7^+$. $TiCl^+$ reacts by eliminating H_2, CH_4, C_2H_5, and HCl & H_2.

We have also performed collision-induced dissociation experiments on the $TiCl_n^+$ ions to determine bond dissociation energies (BDE's). We have compared our results (BDE's of $TiCl_n^+$ ions generated by 70 eV EI) to BDE values of ground-state $TiCl_n^+$ ions. The differences are shown in the following figure.

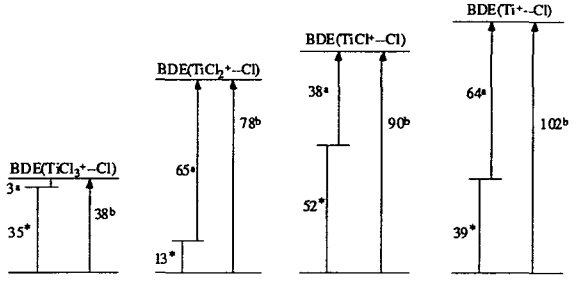

a) BDE's determined during this study (70 eV EI), b) BDE's determined by Kiser et. al. (ground state values)[3], *difference in BDE's and represents the approximate internal energy of the ion.

This allows us to estimate the internal energy of the ions as a result of the ionization process. With these approximations, as well as the additional chemistry that was observed, we have been able to modify some conclusions drawn from earlier work. For example, based on the earlier work, the BDE($TiCl^+$--C_4H_6) would have a lower limit of 42.8 kcal/mole. With our results we have been able to assign a lower limit of 95.6 kcal/mole. We have also been able to assign lower limits to BDE's of addtional complexes such as $TiClC_4H_7^+$, $TiCl_2C_4H_7^+$, and $TiClC_2H_3^+$.

Using the saddle-field source, we were able to generate doubly-charged chlorotitanium ions in unusually high abundances. This allowed us to study the chemistry between these +2 ions and isobutene. Our study has found that dissociative charge transfer dominates the chemistry between isobutene and each +2 chlorotitanium ion resulting in the generation of $C_4H_7^+$ (losing a H atom), $C_3H_5^+$ (with the loss of CH_3), and/or $C_3H_4^+$ (representing the loss of CH_4). Because the generation of a small potential gradient through the octopole was necessary to detect the organic ions, reliable measurements of the translational energy were not possible.

1. J. Allison and D.P. Ridge, *J. Am. Chem. Soc.*, **100**, 163 (1977).
2. J. Allison and D.P. Ridge, *J. Am. Chem. Soc.*, **99**, 35 (1977).
3. R.W. Kiser, J.G. Dillard, and D.R. Dugger, "Mass Spectrometry in Inorganic Chemistry", Adv. Chem. Ser., **No. 72**, 153 (1968).

ELECTROSPRAY MASS SPECTROMETRY (ESI-MS) OF METAL CHELATES

Andrew R.S. Ross+, Michael G Ikonomou* and Kristin J. Orians+
+ Department of Chemistry, University of British Columbia, Vancouver BC, Canada
* Contaminants Science Section, Institute of Ocean Sciences, Sidney BC, Canada

Metal chelates play an important rôle in regulating the free ion concentration and bioavailability of certain metals (e.g. Fe, Ni and Cu) in natural waters. The study of such complexes as they exist in solution requires *in situ* methods of analysis. The ionisation properties of electrospray (ESI) preserve solution conditions and permit the analysis of dissolved ionic species by mass spectrometry. ESI-MS of dissolved metal chelates can provide structural information which may assist in interpreting data obtained using other techniques. The aim of this study was to evaluate ESI-MS as a method for detecting metal chelates in solution under natural conditions. Experiments were performed using a VG Quattro tandem mass spectrometer.

Changes in ion yield as a function of ESI-MS interface conditions were first studied using 8-hydroxyquinoline (Hox) complexes of Cu^{2+} and Fe^{3+}. Positive ion electrospray (ESI+) mass spectra of 50/50 2mM NH_4OAc/MeCN solutions (pH 6.7) containing 100 µM ligand and 50 mg/L metal included peaks corresponding to $[M(ox)_n + H]^+$ and $[M(ox)_{n-1}]^+$ ions (Fig. 1a). To establish whether or not the ligand-loss reaction.

$$[M(ox)_n + H]^+ \rightarrow [M(ox)_{n-1}]^+ + Hox \qquad (1)$$

was due to collision induced dissociation (CID) in the ESI source, the focus lens potential was varied between 10 and 60 volts and the intensities of the peaks due to $[M(ox)_n + H]^+$ and $[M(ox)_{n-1}]^+$ ions recorded (Fig 2). Results show that the relative intensities of these ions are highly dependant on focus potential, and imply that $[M(ox)_{n-1}]^+$ ions are formed by fragmentation in the ESI-MS interface rather than as a result of solution equilibria. MS/MS experiments (Fig. 1b) confirmed that fragmentation of the protonated ligand ion (Eq. (1)) and reduction of the metal cation[1] (e.g. $[Fe^{III}(ox)_2]^+ \rightarrow [Fe^{II}(ox)]^+$) can both result from CID. Mild ESI-MS interface conditions (focus potential = 20 V) were subsequently used during the analysis of similar solutions containing model ligands and selected metals (Table 1).

In many instances ions corresponding to identifiable metal chelates were not observed, possibly as a result of the instability of the complexes at neutral pH, or inability to acquire charge in solution (a prerequisite for ESI-MS detection). For the metal chelates detected, however, ESI-MS determined the molecular weight and metal:ligand ratio of the complex, confirming the oxidation state and coordination number of the metal cation. Replacing MeCN with MeOH improved resolution towards Cu chelates (especially for binuclear complexes and weaker ligands) by reducing competition from solvent molecules. Cu and Fe complexes with Hox were successfully detected in 50/50 seawater/MeCN (pH 8) through the formation of Na^+ rather than H^+ adducts.

These results demonstrate the ability of ESI-MS to detect metal chelates in a variety of aqueous media. The combination of ESI-MS detection with HPLC separation techniques for the study of interactions between natural ligands and metal cations in environmental samples is currently under investigation

43rd ASMS Conference on Mass Spectrometry and Allied Topics

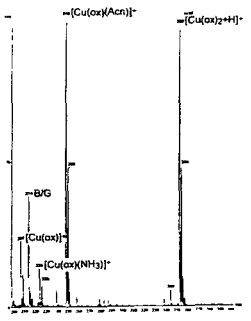

Figure 1a :

(ESI+) Mass Spectrum of Cu^{2+} and Hox in 50/50 2mM NH_4OAc/Acn

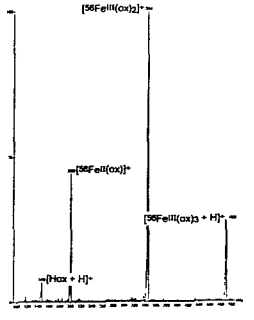

Figure 1b :

(ESI+) MS/MS CID Mass Spectrum of the Chelate Ion $[^{56}Fe^{III}(ox)_3 + H]^+$

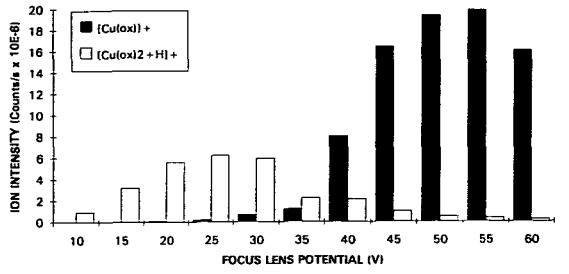

Figure 2 : Dependance of Cu:ox Ratio on Focus Potential

LIGAND (L)	METAL ION (M)				
	Ni^{2+}	Cu^{2+}	Fe^{3+}	Al^{3+}	Pb^{2+}
8-hydroxy-quinoline (HOX)	[L + H]+ [2L - H + M]+ [L - H +Acn + M]+	[L + H]+ [2L - H + M]+ [L - H +Acn + M]+ [3L - 3H + 2M]+	[L + H]+ [2L - 2H + M]+ [3L - 2H + M]+	[L + H]+ [2L - 2H + M]+ [3L - 2H + M]+	[L + H]+
diethyldithio-carbamate (HDDC)	[2(L - H) + H]+ [2L - H + M]+ [3L - 3H + M]+	[2(L - H) + H]+ [2L - H + M]+ [L - H +Acn + M]+ [3L - H + 2M]+	[2(L - H) + H]+	[2(L - H) + H]+	[2(L - H) + H]+ [L - H + M]+ [3L - 3H + M]+
dithizone (DZ)	[L + H]+ [2L + H]+	[L + H]+ [2L + H]+ [L + M]+ [2L + M]+ [L +Acn + M]+	[L + H]+ [2L + H]+	[L + H]+ [2L + H]+	[L + H]+ [2L + H]+ [2L + H + M]+ [3L + H + M]+ [3L + M]2+ [4L + M]2+
dimethyl-glyoxime (DMG)	[L + H]+ [2L - H + M]+	[L + H]+ [2L - H + M]+ [3L - 3H + 2M]+	[L + H]+	[L + H]+	[L + H]+

Table 1 : ESI-MS Analysis of Model Chelates in 50/50 2mM NH_4OAc/Acn (pH 6.7)

Blades A.T., Jayaweera P., Ikonomou M.G., Kebarle P.; *J. Chem. Phys.* **92** 5900 (1990)

Gas-Phase Actinide Ion Chemistry: Reactions of Th^+ and U^+ with CH_4 and C_2H_6

Joaquim Marçalo, João Paulo Leal, and António Pires de Matos

Departamento de Química, Instituto Tecnológico e Nuclear
P-2686 Sacavém Codex, Portugal

The gas-phase reactivity of the actinide series ions Th^+ and U^+ with methane and ethane were studied by Fourier transform ion cyclotron resonance mass spectrometry (FTICR/MS), using an Extrel (Waters) FTMS 2001-DT spectrometer. The metal ions were produced by laser desorption/ionization of pure metal pieces and the reagents were admitted to the instrument through a leak valve; argon, introduced through pulsed valves, was used for collisional cooling of the metal ions.

Th^+ ions dehydrogenated methane with a rather low efficiency (k/k_L = 0.014) to form $ThCH_2^+$, implying that $D(Th^+–CH_2) \geq 460$ kJ/mol With ethane, single and double dehydrogenations were observed, producing $ThC_2H_4^+$ and $ThC_2H_2^+$ (relative intensity ca 1 1) with a moderate efficiency (k/k_L = 0 124), indicating that $D(Th^+–C_2H_4) \geq 136$ kJ/mol and $D(Th^+–C_2H_2) \geq 312$ kJ/mol. In the absence of collisional cooling, minor products like ThH^+, ThH_2^+, $ThCH_2^+$, and $ThCH_3^+$, either endothermic or corresponding to processes with high kinetic barriers, were also observed in the ethane reaction The facile oxidation of the products of both reactions by residual water and oxygen dominated the secondary steps, indicating that the primary products of the methane and ethane reactions are unreactive with these gases.

U^+ ions were found to be essentially unreactive with methane and ethane The formation of oxygenated products from background water and oxygen was the main process observed either in the presence or absence of thermalization, although in this last case inefficient formation of dehydrogenation products was also observed with both reagents

The results obtained in the reactions of Th^+ and U^+ with methane and ethane, as well as those previously obtained with benzene and other arenes [1], not unexpectedly show similarities to the reactivity of the early *d* transition metal cations [2,3] and the lanthanide cations La^+, Ce^+, and Gd^+ [1,4,5] However, the differences in reactivity between Th^+ and U^+ reported herein, appear to indicate that simple electronic arguments (ground state configuration of Th^+ - $5f^06d^27s^1$, ground state configuration of U^+ - $5f^36d^07s^2$, low-lying

configurations at 0.04 eV - $5f^36d^17s^1$ and 0.57 eV - $5f^36d^27s^0$) may not be sufficient to explain the reactivities of actinide ions with hydrocarbons, and significant electronic effects in the reactivity along the actinide series can be anticipated.

Acknowledgement

The authors thank JNICT (PBIC/C/CEN/1193) for financial support.

References

1. Leal, J.P.; Marçalo, J.; Pires de Matos, A., Marshall, A.G ; Yin, W.W.; Spirlet, J.C. *Proceedings of the 2nd European FTMS Workshop, Antwerp 1993*, Van Vaeck, L., Ed.; University of Antwerp (UIA), 1994; p. 312
2. Eller, K.; Schwarz, H. *Chem. Rev.* **1991**, *91*, 1121.
3. Irikura, K.K.; Beauchamp, J L. *J. Phys. Chem* **1991**, *95*, 8344.
4. Heinemann, C.; Schroder, D.; Schwarz, H. *Chem. Ber.* **1994**, *127*, 1807 Cornehl, H.H , Heinemann, C.; Schröder, D.; Schwarz, H. *Organometallics* **1995**, *14*, 992.
5. Yin, W W.; Marshall, A.G., Marçalo, J ; Pires de Matos, A *J Am Chem. Soc.* **1994**, *116*, 8666.

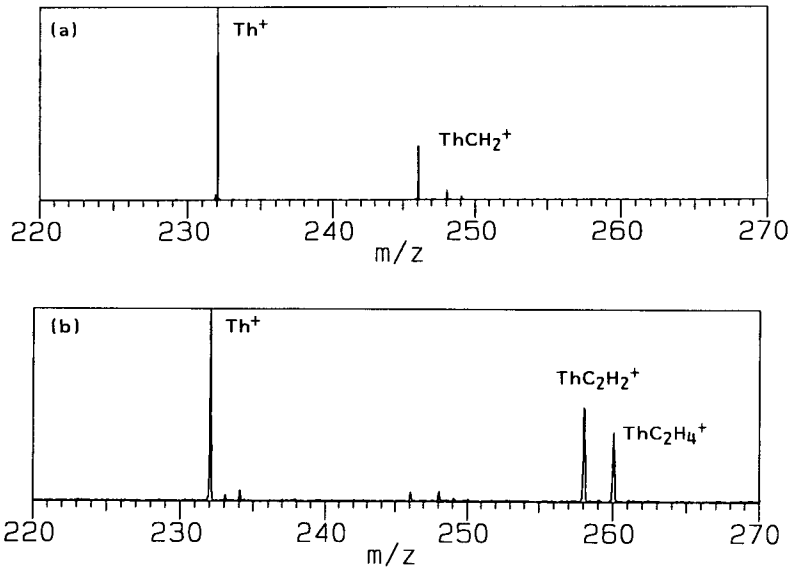

Figure 1. FTICR mass spectra of the Th^+ reactions with (a) methane (0 2 s, 4.7 x 10^{-7} Torr) and (b) ethane (0.1 s, 7 0 x 10^{-7} Torr)

Gas-Phase Reactivity of Transition Metal Cations with Atomic Species

Angeli, C.; Leymarie, N.; Mestdagh, H.; Rolando, C.; Sablier, M.
Ecole Normale Supérieure, Processus d'Activation Moléculaire U.R.A. 1679
24, rue Lhomond - 75231 Paris cédex 05 (France)

Whereas a large number of ion-molecule reactions, as well as various atom-molecule reactions, have been studied in the gas phase, there is a scarcity of experimental data concerning the reactivity of ions, particularly metal or metal-containing ions, with free atoms such as hydrogen and nitrogen or with radical species (1).

Interest in the knowledge of such processes is two-fold : (i) Astrophysical : free atoms, the most abundant of which being H·, are important components of the interstellar medium, and electropositive elements such as transition metals are likely efficiently photoionized to positive ions; therefore metal ions might react with free atoms or radicals under interstellar conditions and perhaps play the role of catalysts (2). (ii) Chemical : reactions of free atoms with metal-containing ions may lead to new organometallic species or provide useful thermochemical data.

The reactivity of iron pentacarbonyl cations $Fe(CO)_n^+$ (where n is the number of CO ligands, n=0-5) with molecular and atomic hydrogen/nitrogen have shown that $Fe(CO)_n^+$ cations do not react with molecular gases. With the discharge on, a product appeared due to replacement of a CO ligand by a H or a N atom (3). The present communication reports further information on the reactivity of metal carbonyl ions with atomic hydrogen.

Investigation of the reactivity of various transition metal carbonyl ions (chromium, molybdenum, tungsten, manganese, ruthenium) showed that most of them react more or less efficiently according to the same scheme as iron :

$$M(CO)_n^+ + H^\cdot \rightarrow M(CO)H_{n-1}^+ + CO$$

None of the bare metal ions (n = 0) reacted with either molecular or atomic hydrogen. The reaction efficiencies for MCO^+ cations follow the order Fe >> W > Cr ≥ Mo ≥ Ru. $MnCO_n^+$ ions are completely unreactive. For the first row transition metals Cr and Fe, the maximum reaction efficiency was found for MCO^+ ions (n = 1) and decreased steadily with increasing n; $Fe(CO)_5^+$ and $Cr(CO)_n^+$ (n = 3-6) gave no detectable product. On the contrary, in the case of heavier metals, the maximum reaction efficiency corresponded to n = 2 (W, Ru) or 3 (Mo).

In the course of our investigations, we have recently been able to increase the dissociation efficiency by more than one order of magnitude, using an improved fitting device. With our enhanced means of producing $H^\cdot$ concentrations with good reproducibility, it is now possible to measure relative rate constants.

Results for the reaction of iron monocarbonyl cations $FeCO^+$ and chromium monocarbonyl cations $CrCO^+$ with atomic hydrogen are presented below (see figure). The rate of formation of the major reaction product FeH^+ or CrH^+ is proportional to H_2 pressure in both cases. The ratio of the corresponding apparent rate constants is $k_{Fe}/k_{Cr} = 21 \pm 6$

Assuming a residence time of approximately 0.7 ms (corresponding to thermal velocity along the cell axis) for ions in the cell, the apparent first-order rate constant versus H_2 pressure is $3.95 \pm 0.4 \times 10^{-12}$ $cm^3.molecule^{-1}.s^{-1}$ for the reaction of $FeCO^+$ ions with atomic hydrogen. According to the classical Langevin capture collision cross section model, the maximum rate constant value for this reaction was calculated to be 2.1×10^{-9} $cm^3.molecule^{-1}.s^{-1}$ versus $H^\cdot$ pressure. The ratio of these two values is of the order of magnitude of the estimated average $[H^\cdot]/[H_2]$ ratio in the cell : ca. 0.2%, considering that the "useful" zone corresponding to the beam coming from the discharge (a few percent dissociation ratio) is about 1/20 of the cell length.

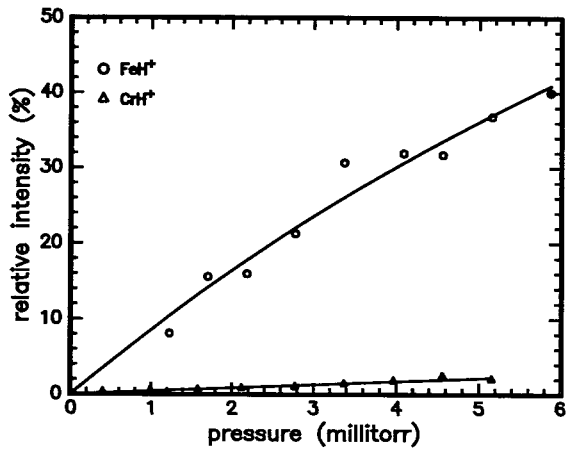

Therefore, the rate constant for the reaction of $FeCO^+$ ions with $H^\cdot$ is likely close to the Langevin value. This reaction is actually the fastest that we have observed among the reactions of various organic cations with $H^\cdot$.

The question remains, whether the lower reactivity observed for chromium and other metals is due to slow reaction of MCO^+ in its fundamental state, or to rapid reaction of a slightly populated metastable excited state.

In order to study which electronic structure of the metal carbonyl cation is involved from a theoretical point of view, calculations on the adiabatic energy curves of Fe(CO)+ corresponding to the states ^6D, ^4F, ^4D of Fe^+ and $^1\Sigma^+$ of CO have been performed using Multireference Quasi Degenerate Perturbation Theory (CIPSI algorithm) to take into account the electronic correlation. Equilibrium geometry (R_e) and bond energy (D_e) for the ground state ($^4\Sigma^-$ correlating to ^4F excited state of Fe^+) are in good agreement with those of experimental determinations (4) (for which only D_e is actually available) and theoretical calculations (5). Spin orbit interaction and dynamics of dissociation are under study to determine the possibility of transition between states with different spins during the dissociation.

1 - Rolando, C.; Sablier, M. *Mass Spectrom. Rev.* **1994**, *12*, 285.
2 - Inkura, K.K.; Goddard, W.A III; Beauchamp, J.L. *Int. J. Mass Spectrom. Ion Processes* **1990**, *99*, 213.
3 - Mestdagh, H.; Rolando, C.; Sablier, M.; Billy, N.; Gouédard, G.; Vigué, J. *J. Am. Chem. Soc.* **1992**, *114*, 771.
4 - Shultz, R.H ; Crellin, K.C.; Armentrout, P.B. J. Am Chem. Soc. 1991, 8590.
5 - (a) Barnes, L.A.; Rosi, M.; Bauschlicher, C.W. *J. Chem. Phys.* **1990**, *93*, 609
(b) Berthier, G.; Cimiraglia, R.; Daoudi, A.; Mestdagh, H.; Rolando, C.; Suard, M. *J. Mol. Struct. (Theochem)* **1992**, *43*, 254.

An Experimental and Theoretical Study on the Organometallic Distonic Ion: Fe(*p*-benzyne)$^{+\cdot}$

Young C. Xu, Samuel A. Lee, Steven Z. Kan, Sara K. Poehlein, and Ben S. Freiser*
H. C. Brown Laboratory Of Chemistry, Purdue University, West Lafayette, IN 47907
Charles W. Bauschlicher, Jr.*
NASA Ames Research Center, Moffett Field, CA 94035

Prompted by the synthesis of $^{+}P(OCH_3)_3C_6H_4^{\cdot}$ and related distonic ions by Smith and Kenttämaa[1] and by the study of the metal ion complexes Fe(phenyl)$^{+}$ and Fe(o-benzyne)$^{+}$ in our laboratory,[2,3] we have recently generated a metal-containing radical cation, $^{+}FeC_6H_4^{\cdot}$, using FT-ICR-MS. Laser desorbed Fe^{+} reacts with 1,4-diiodobenzene to form 1-Fe-4-iodobenzene ($FeC_6H_4I^{+}$), which is then subjected to sustained off-resonance irradiation (SORI). Loss of $I^{\cdot}$ from $FeC_6H_4I^{+}$ then yields Fe(p-benzyne)$^{+\cdot}$, i.e., $^{+}FeC_6H_4^{\cdot}$. In order to identify and distinguish Fe(p-benzyne)$^{+\cdot}$ from its isomer Fe(o-benzyne)$^{+}$ and Fe(3-ene-1,5-hexadiyne)$^{+}$, collision-induced dissociation and selected ion-molecule reactions of Fe(p-benzyne)$^{+\cdot}$ were studied and compared with those of Fe(o-benzyne)$^{+}$ and Fe(3-ene-1,5-hexadiyne)$^{+}$. Generations of Fe(*o*-benzyne)$^{+}$ have been reported previously. Fe(ene-hexadiyne)$^{+}$ was produced by the reaction of Fe(1,5-hexadiyne)$^{+}$ via dehydrogenation. Both experiment and theory strongly support the view that this new radical cation is an organometallic distonic ion, $^{+}FeC_6H_4^{\cdot}$.

The experiments were performed on a prototype Nicolet FTMS-1000 Fourier transform mass spectrometer, equipped with a 5.2 cm cubic trapping cell and a Varian 1 Tesla electromagnet. Fe^{+} was generated by laser desorption-ionization of the pure metal target using a Nd:YAG laser. 1,4-diiodobenzene, a solid sample, was introduced into the cell at a pressure of ~0.8-1x10^{-7} Torr through a Varian leak valve accompanied by heating the sample and inlet system to ~ 70-100 °C. Other Neutral reagents were pulsed into the cell through General Valve Corporation Series 9 solenoid pulsed valves. Background argon, kept at ~2.0 x 10^{-5} Torr, served as the collision gas for thermalization and for collision-induced dissociation (CID) or SORI excitation.

Collision-induced dissociation experiments gave Fe^{+} as the only fragment for all three isomers, however, yielded three different energy profile, revealing their unique structures and indicating that D°(Fe^{+}- o-benzyne) > D°(Fe^{+}- p-benzyne) > D°(Fe^{+}- ene-hexadiyne).

The neutral reagents used for the ion-molecule reaction studies include some alkenes and halogenated compounds, which have been used for the study of Fe(o-benzyne)$^{+}$, as well as methyl disulfide and methyl diselenide, which have been shown to be good indicators of distonic ions, transferring $\cdot SCH_3$ or $\cdot SeCH_3$, respectively, to the radical site of many organic distonic ions. The distonic ion is observed to exhibit different reactivity from that of its isomeric structure Fe(o-benzyne)$^{+}$ and Fe(ene-hexadiyne)$^{+}$. Although methyl disulfide is observed to react with Fe(p-benzyne)$^{+\cdot}$ exclusively by charge exchange, the characteristic transfer of $\cdot SeCH_3$ from methyl diselenide to this distonic cation is observed. These two reactions, however, were not observed for the other two isomers. Another interesting reaction is with allyl iodide, given that allyl iodide has a low homolytic C-I bond dissociation energy (40.7 kcal/mol) and iodine atom abstraction is commonly observed for other radicals upon reaction with allyl iodide. The distonic ion is observed to abstract $I^{\cdot}$ from allyl iodide and so is Fe(ene-hexadiyne)$^{+}$, while Fe(o-benzyne)$^{+}$ is not. However, SORI excitation on the iodine abstraction product $FeC_6H_4I^{+}$ of Fe(p-benzyne)$^{+\cdot}$ yields loss of $I^{\cdot}$ to reform the distonic ion and a minor product FeI^{+}, while that of Fe(ene-hexadiyne)$^{+}$ only yields FeI^{+}. These facts indicate that $I^{\cdot}$ abstraction for Fe(p-benzyne)$^{+\cdot}$ takes place at the radical site and not at the metal center, while on the contrary, the iodine abstraction is at the metal center for Fe(ene-hexadiyne)$^{+}$.

D°(Fe^{+}- p-benzyne) is estimated to be 66±10, 71±10, and 80±10 kcal/mol from different experiments and relevant information. Density functional theory calculations further support the experiment results. The calculated D°(Fe^{+}- p-benzyne)=73.3 kcal/mol, in line with the estimated value.

This is the first example of what we expect will be a new class of organometallic distonic ions. This preliminary study reveals a whole new area of organometallic ion chemistry. In addition to the usual metal-center initiated reactions, the radical site may operate either separately or in concert with the metal center to open new reaction pathways.

---

(1) Smith, R. L.; Kenttämaa, H. I. *J. Am. Chem. Soc.* **1995**, 117, 1393.
(2) Xu, Y.; Garcia, E.; Freiser, B. S. *J. Am. Chem. Soc.* in preparation.
(3) (a)Huang, Y.; Freiser, B. S. *J. Am. Chem. Soc.* **1989**, 111, 2387. (b)Huang, Y.; Freiser, B. S. *J. Am. Chem. Soc.* **1990**, 112, 1682. (c)Garcia, E.; Huang, Y.; Freiser, B. S. *Inorg. Chem.* **1993**, 32, 3595.

Gas-Phase Isomeric Differentiation Study of $FeC_7H_7^+$

Young C. Xu, Edna Garcia, and Ben S. Freiser*
H. C. Brown Laboratory of Chemistry, Purdue University, West Lafayette, In 47907
Charles W. Bauschlicher, Jr.*
NASA Ames Research Center, Moffett Field, CA 94035

Three isomeric structures of $Fe(C_7H_7)^+$, i.e., Fe(tropylium)$^+$, Fe(benzyl)$^+$, and Fe(tolyl)$^+$, formed from different neutral precursors are studied with the FT-ICR-MS and by the theoretical calculations. Of particular interest is the role of the metal in stabilizing the tolyl ligand, given that the unmetallated tolyl ion, $C_6H_4CH_3^+$, rearranges to benzyl ion on the time scale of the FT-ICR-MS experiments.[1]

All experiments were performed on a prototype Nicolet FTMS-1000 Fourier transform mass spectrometer, equipped with a 5.2 cm cubic trapping cell and a Varian 1 Tesla electromagnet. Laser desorption-ionization was used to generate the metal ion Fe^+. Neutral reagents were obtained commercially in high purity and were introduced into the cell either through General Valve Corporation Series 9 pulsed solenoid valves or Varian leak valves. The isolation of the desired ions were accomplished by using swept double resonance ejection pulses.

Ions with the empirical formula $Fe(C_7H_7)^+$ were generated by three synthetic routes: (1)reaction of bare metal Fe^+ with cycloheptatriene; (2)reaction of Fe^+ with iodobenzene to form Fe(phenyl)$^+$, which then reacts with toluene; and (3)reaction of Fe^+ with chlorobenzene to form Fe(benzyne)$^+$,[2] which then reacts with methyl iodide.[3] The hypothesis is that these three reactions result in the formation of Fe(tropylium)$^+$, Fe(benzyl)$^+$, and Fe(tolyl)$^+$, respectively.

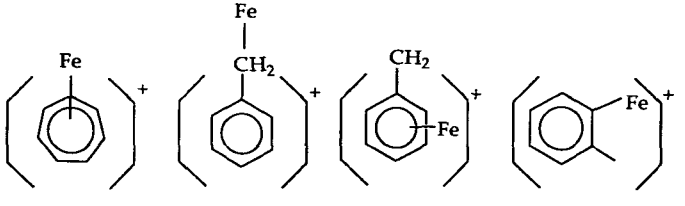

Fe(tropylium)$^+$ I | Fe(σ-benzyl)$^+$ IIA | Fe(π-benzyl)$^+$ IIB | Fe(tolyl)$^+$ III

43rd ASMS Conference on Mass Spectrometry and Allied Topics

Energy resolved collision-induced dissociation and photodissociation experiments unequivocally distinguish Fe(tropylium)$^+$ from Fe(benzyl)$^+$ and Fe(tolyl)$^+$, clearly showing that the Fe(tropylium)$^+$ has the highest stability and strongest Fe^+- C_7H_7 bond energy among the three. Both experiments fail to clearly differentiate Fe(benzyl)$^+$ and Fe(tolyl)$^+$, which might indicate the rearrangement of Fe(tolyl)$^+$ to Fe(benzyl)$^+$ prior to dissociation. However, the three isomers, especially Fe(benzyl)$^+$ and Fe(tolyl)$^+$, can be distinguished by their ion-molecule reactions with p-xylene and methyl iodide and by the subsequent CID on their product ions. Scheme I and II illustrate the ion-molecule reactions of Fe(benzyl)$^+$ and Fe(tolyl)$^+$ and the CID fragmentation results on reaction product ions.

Additionally, the Fe^+- C_7H_7 bond energies are bracketed as 73 kcal/mol < $D°(Fe^+$- tropylium) ≤ 129±5 kcal/mol, 71±5 kcal/mol ≤ $D°(Fe^+$- tolyl) < 111 kcal/mol, and 55±5 kcal/mol < $D°(Fe^+$- benzyl) ≤ 63±5 kcal/mol. *Ab initio* calculations yield $D°(Fe^+$- tropylium) = 86.8 kcal/mol, $D°(Fe^+$- tolyl) = 84.4 kcal/mol, and $D°(Fe^+$- benzyl) = 69.4 kcal/mol, which support the experimental results.

In summary, our results show that Fe enhances the stability of tolyl ion. Thus, metallated tolyl ion can be retained for at least seconds, while, for comparison, tolyl ion itself rearranges to the more stable benzyl structure in under 1 ms on the time scale of FT-ICR-MS. Upon activation, however, Fe(tolyl)$^+$ rearranges to Fe(benzyl)$^+$ prior to dissociation.

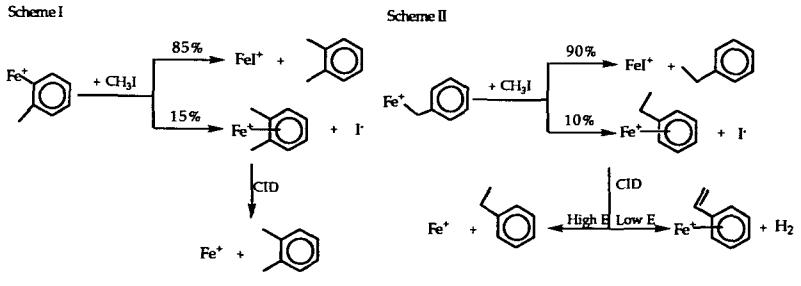

(1) For a review, see Lifshitz, C. *Acc. Chem. Res.* **1994**, 27, 138.
(2) Dietz, T. G.; Chatellier, D. S.; Ridge, D. P. *J. Am. Chem. Soc.* **1978**, 100, 4905.
(3) Garcia, E.; Huang, Y.; Freiser, B. S. *Inorg. Chem.* **1993**, 32, 3595.

Experimental and Theoretical Studies of $Nb_6C_7^{0/+}$

Samuel A. Lee, Steven Z. Kan, Young Hie Kim, Ben Freiser*
Marina Miletic, Richard E. Bleil and Sabre Kais*

H. C. Brown Laboratories of Chemistry
FTMS Cluster Research Group
Purdue University
West Lafayette, IN 47907

The chemistry of $Nb_6C_7^+$ with various reagents, including H_2O, CH_3CN, CH_3OH, and C_6H_6, is studied using a FTICR mass spectrometer coupled to a supersonic expansion source. For reaction with H_2O, sequential attachments up to 4 water molecules occur. The 5th and 6th water molecule attachments were observed but they do not grow to be base peaks. (Fig. 1) For reactions with CH_3CN, CH_3OH, and C_6H_6, intense 4 attachments are observed. Rate constants for the reactions with H_2O, CH_3CN, CH_3OH, and C_6H_6 are determined to be 5.15×10^{-10}, 3.66×10^{-11}, 1.5×10^{-10}, 2.39×10^{-11} cm^3 $molecules^{-1}$ s^{-1}, respectively using pseudo-first-order kinetic plots. Multiple excitation collisional activation (MECA) on $Nb_6C_7^+$ resulted in loss of Nb-C and Nb-C_2 units.

Ab initio calculations of Nb_6C_7 support the hypothesis that Nb_6C_7 has four active sites and 2 less active sites. A proposed structure of Nb_6C_7 consists of two cubes with one carbon at the exact inversion center of the D_{2h} symmetry (Fig. 2). Four of the six niobium atoms are equivalent but different from the remaining two. Furthermore, these four equivalent niobiums have bonds with only three surrounding carbons, while both of the remaining niobium atoms bond with five nearby carbons. The Mulliken charge distribution shows that four of the niobium atoms have a calculated partial charge of +0.055880, and the remaining two niobium has a charge of +.243986.

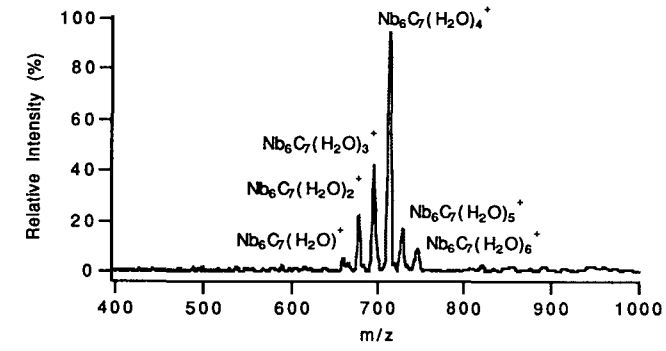

Figure 1. Reaction of $Nb_6C_7^+$ with water

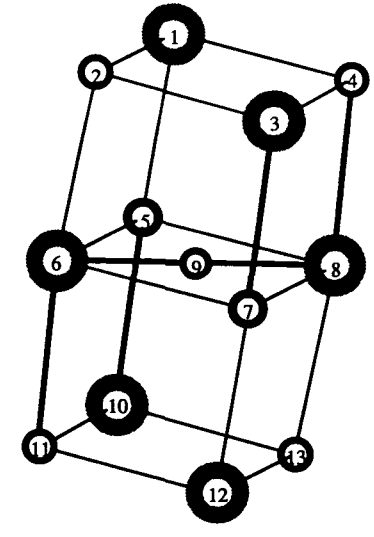

Figure 2. Calculated structure of Nb_6C_7 with a D_{2h} symmetry from Hartree-Fock calcualtions. A small and solid circle represents a carbon atom and and a gray circle a niobium atom, respectively.

GENERATION AND REACTIVITY OF YTTRIUM-CARBON CLUSTER IONS

Steven Z. Kan, Samuel A. Lee, and Ben S. Freiser
Department of Chemistry, Purdue University, West Lafayette, IN 47907 USA

In 1992, Castleman and co-workers reported the production of the ionic transition metal-carbon clusters, $M_8C_{12}^+$ (M = Ti, V, Zr and Hf).[1-4] Like the observations of pure carbon clusters such as C_{60} and C_{70}, these metal-carbon clusters were observed as "magic" peaks in the mass spectra obtained from a supersonic expansion ion source.[5] These intense peaks are indicative of the high stability of these clusters which are proposed to have symmetrical, cagelike structures with the geometry of a pentagonal dodecahedron. $M_8C_{12}^+$ species are thus termed metallo-carbohedrenes, or met-cars for short. Like fullerenes, met-cars are of both fundamental interest and hold promise as a new class of important materials and, hence, have become the focus of both theoretical and experimental investigations. Along with these species, metal-carbon clusters of other stoichiometries such as $Ti_8C_{11}^+$, $Ti_8C_{13}^+$, $Ti_7C_{12}^+$, $V_{14}C_{13}^+$, $V_{14}C_{12}^+$, and $Nb_4C_4^+$ have also been examined.[6,7] Here we report on the yttrium-carbon system in which a broad range of metal-carbon cluster ions are observed.

All of the experiments were performed on an Extrel FTMS-2000 Fourier transform ion cyclotron resonance (FT-ICR) mass spectrometer equipped with a 3 Tesla superconducting magnet. A Smalley compact supersonic expansion ion source equipped with a Jordan PSV fast pulsed valve and a Balzers 300 l/s turbopump was used to generate metal-carbon cluster ions. **Figure 1** shows a schematic set-up of the instrument. A Nd:YAG laser (Quanta Ray DCR - 2), frequency doubled to produce 532 nm light and set to have a 10 ns pulse width and ~30 mJ/pulse power, is used for desorbing a pure yttrium target to generate metal plasma. The disk target is driven by two stepping motors such that a spiral path is followed in order to expose a fresh metal surface for laser desorption at the beginning of each FT-ICR event sequence. In the mean time, helium seeded with 2% methane at a backing pressure of ~200 psi is introduced from the fast pulsed valve. The time between the laser pulse and the gas pulse is controlled so that a high-pressure burst of the gas mixture arrives at the metal target region right after the laser is fired. The metal plasma generated by laser desorption is cooled by the helium/methane gas mixture and complete dehydrogenation occurs in this process to produce metal-carbon cluster ions. The potential on the front trapping plate of the ICR cell is dropped from 9.8 V to 4.5 V to allow the decelerated ions to enter the trapping cell and then raised back to 9.8 V to trap and detect the metal-carbon cluster ions.

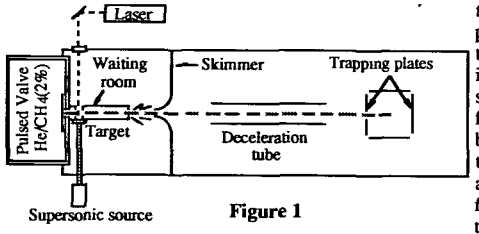

Figure 1

Figure 2 illustrates the yttrium-carbon cluster ions formed by varying the timing between the laser pulse and the gas pulse. The neighboring ion peaks are 12 mass units (carbon) apart. Yttrium-carbon clusters containing up to eleven metal atoms could be generated. Unlike the vanadium/carbon and the titanium/carbon systems that have been examined previously, the number of carbon atoms corresponding to a particular size metal atom cluster also varies over a greater range. $Y_4C_7^+$ is one of the local maximum peaks for the yttrium-carbon clusters containing 4 metal atoms. Its high intensity is indicative of its higher stability relative to its neighboring clusters in the same group (4 metals).

Collision-induced dissociation (CID) on $Y_4C_{7,8}^+$ and $Y_3C_{7,8}^+$ yields loss of Y and YC_2 group. Both $Y_4C_7^+$ and $Y_4C_8^+$ abstract a bromide from CH_3Br, reaction 1. The $Y_4C_{7,8}Br^+$ formed do not react with CH_3Br further and yield $Y_4C_{7,8}^+$ upon CID. $Y_4C_7^+$ and $Y_4C_8^+$ have 39 and 43 valence electrons, respectively. It is possible that the unpaired electron in each of the ions pairs with a bromide to form a σ bond and the reaction is terminated since all the other electrons become paired. Supporting this are the

reactions of $Y_3C_{7,8}^+$ (36 and 40 valence electrons, reaction 2) where bromide abstraction does not occur.

$$Y_4C_{7,8}^+ + CH_3Br \rightarrow Y_4C_{7,8}Br^+ + CH_3 \quad (1)$$
$$Y_3C_{7,8}^+ + CH_3Br \rightarrow Y_3C_{6,7}(H)Br^+ + C_2H_2 \quad (2)$$

Interestingly, while $Y_4C_{7,8}^+$ dehydrogenate water, reactions 3, $Y_3C_{7,8}^+$ undergo sequential reactions with water to form yttrium-oxygen cluster ions and acetylene molecules, reactions 4 to 7 for $Y_3C_8^+$. *Ab initio* calculations are underway to test the stabilities and the structures of the Y-C clusters and to explain why these clusters are in general different from other transition metal carbon cluster ions.

$$Y_4C_7^+ + H_2O \rightarrow Y_4C_{7,8}O^+ + H_2 \quad (3)$$
$$Y_3C_8^+ + H_2O \rightarrow Y_3C_6O^+ + C_2H_2 \quad (4)$$
$$Y_3C_6O^+ + H_2O \rightarrow Y_3C_4O_2^+ + C_2H_2 \quad (5)$$
$$Y_3C_4O_2^+ + H_2O \rightarrow Y_3C_2O_3^+ + C_2H_2 \quad (6)$$
$$Y_3C_2O_3^+ + H_2O \rightarrow Y_3O_4^+ + C_2H_2 \quad (7)$$

(1) Guo, B. C.; Kerns, K. P.; Castleman, A. W. *Science* **1992**, *255*, 1411.
(2) Guo, B. C.; Wei, S.; Purnell, J.; Buzza, S.; Castleman, A. W. *Science* **1992**, *256*, 515.
(3) Wei, S.; Guo, B. C.; Purnell, J.; Buzza, S.; Castleman, A. W. *Science* **1992**, *256*, 818.
(4) Yeh, C. S.; Afzaal, S.; Lee, S. A.; Byun, Y. G. *J. Am. Chem. Soc.* **1994**, *116*, 8806.
(5) Maruyama, S.; Anderson, L. R.; Smalley, R. E. *Rev. Sci. Instrum.* **1990**, *61*, 3686.
(6) Yeh, C. S.; Byun, Y. G.; Afzaal, S.; Kan, S. Z.; Lee, S. A.; Freiser, B. S.; Hay, P. J. *J. Am. Chem. Soc.* **1994**, 4042.
(7) Lee, S.; Gotts, N. G.; Helden, G. V.; Bowers, M. T. *Science* **1995**, *267*, 999.

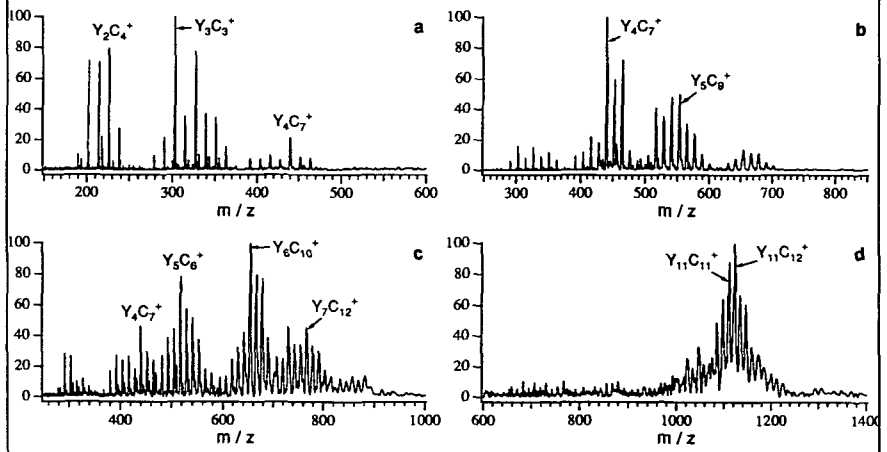

Figure 2. Mass spectra of yttrium-carbon cluster ions acquired under otherwise identical conditions, except that the timing of the laser pulse is decreased with respect to the firing of the pulsed valve of the supersonic expansion source by 2 microseconds in each subsequent spectrum (**a** to **d**).

FT-ICR Studies of the Structures and Reactivities of Metal-Carbon Clusters

Y. G. Byun, C. S. Yeh, S. Afzaal, S. A. Lee, S. Z. Kan, and Ben S. Freiser
H. C. Brown Laboratory of Chemistry, Purdue University, West Lafayette, Indiana 47907

Castleman and co-workers were the first to report the growth of the unusual met-car clusters. A new class of transition metal-carbon clusters with the stoichiometry M_8C_{12} (M=Ti, V, Zr, Hf, Cr, Fe, Mo, and Nb), Nb_4C_4 and $M_{14}C_{13}$ (M=Ti, V) has become a focus of intense research area.

Th, D_{2d}, and T_d structural isomers of M_8C_{12} were proposed. In order to study the coordination chemistry of $V_8C_{12}^+$, water, acetonitrile, and benzene were chosen to be reacted. Surprisingly, $V_8C_{12}(H_2O)^+$ reacted with water through dehydrogenation to form $V_8C_{12}(OH)_2^+$. $V_8C_{12}(H_2O)(OH)_2^+$ and $V_8C_{12}(H_2O)_2(OH)_2^+$ were also formed at longer reaction times, with water truncation occurring at four attachments, $V_8C_{12}(H_2O)_2(OH)_2^+$. Acetonitrile and benzene underwent sequential association reactions, yielding mass spectra that truncated sharply at $V_8C_{12}L_4^+$ (L=CH_3CN, C_6H_6). Thus, these results obtained under low pressure conditions were consistent with either the D_{2d} or T_d structural isomer.

$Nb_4C_4^+$ is one of the smallest cubic crystallite structures (2x2x2) in the transition metal-carbon cluster family. This $Nb_4C_4^+$ reacted with both water and methanol through two competitive pathways . These two pathways depended on the cooling gas, argon. In the absence of a cooling gas, $Nb_4C_4^+$ was observed to attach a maximum of four solvent molecules, $Nb_4C_4(OH)(H_2O)_3^+$ and $Nb_4C_4(OCH_3)(CH_3OH)_3^+$ at longer reaction times. With a cooling gas, $Nb_4C_4(OH)_2(H_2O)_2^+$ and $Nb_4C_4(OCH_3)_2(CH_3OH)_2^+$ at longer reaction times were produced. Ab initio calculations indicated that Nb_4C_4 has a slightly distorted cubic structure.

$V_{14}C_{13}^+$ and $V_{14}C_{12}^+$ were found to react with water, undergoing both the elimination of H_2 molecules and association reaction mechanisms to yield $V_{14}C_{13}(OH)_2(H_2O)_6^+$ and $V_{14}C_{12}(OH)_2(H_2O)_6^+$. However, loss of $2H_2$ was also observed to form $V_{14}C_{13}(OH)_4^+$ for $V_{14}C_{13}^+$. $V_{14}C_{13}(OH)_4^+$ then reacted with water through association reactions to yield $V_{14}C_{13}(OH)_4(H_2O)_4^+$. In contrast to the water reactions, $V_{14}C_{13}^+$ and $V_{14}C_{12}^+$ reacted

with acetonitrile through addition reactions. Also seen were the combination reaction products, $V_{14}C_{13}(CH_3CN)_7(H_2O)^+$ and $V_{14}C_{12}(CH_3CN)_7(H_2O)^+$ which were formed by reactions with background water. In both water and acetonitrile cases, mass spectra showed that truncation occurred at all eight ligands attached to the $V_{14}C_{13}^+$ and $V_{14}C_{12}^+$. The reaction products observed here support the fcc unit cell structure.

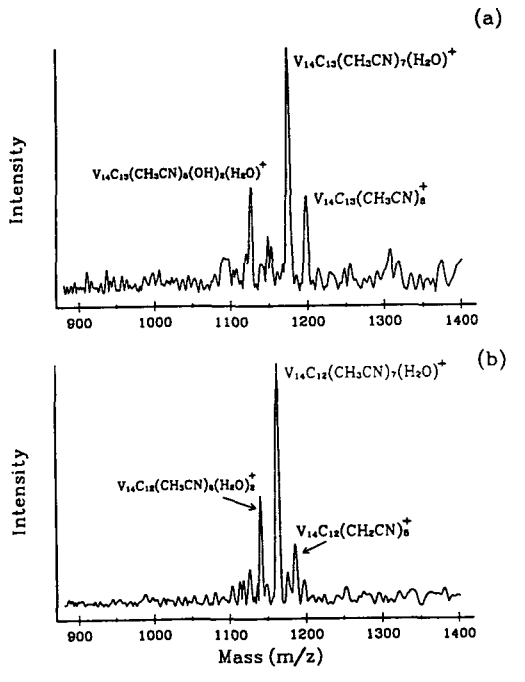

Figure. (a) Reactions of $V_{14}C_{13}^+$ with CH_3CN (~ 1.6 x 10^{-6} torr) for 6 seconds; (b) Reactions of $V_{14}C_{12}^+$ with CH_3CN (~ 1.9 x 10^{-6} torr) for 7 seconds

Gas-Phase Ion-Molecule Reactions of Lanthanides with Crown Ethers

Forest M. White, Tianpei Xin#, and Alan G. Marshall*

Center for Interdisciplinary Magnetic Resonance, National High Magnetic Field Laboratory, Florida State University, 1800 E. Paul Dirac Dr., Tallahassee, FL 32310

*Member of the Department of Chemistry, Florida State University
#Department of Chemistry, Berea College, Berea, KY

We report gas-phase ion-molecule reactions of lanthanide ions, M^+ (e.g La, Ho, Pr, Sm, and Gd) with neutral 18-crown-6 ether. Previously, the lanthanide ion electronic configuration was found to control the reaction pathways and distribution of the product ions for reactions of lanthanide ions with tri-*t*-butylbenzene.[1] Here, FT-ICR mass spectra were acquired in the source compartment of a dual-trap 3.0 tesla Extrel FTMS-2000 (Extrel FTMS/Waters, Madison, WI) equipped with an automatic solids insertion probe. Metal ions were generated by laser desorption with a Nd:YAG laser (Surelite II, Continuum Inc., Santa Clara, CA) operating at 1064 nm with a pulse width of 7 ns. A constant pressure of crown ether in the source-side ion trap was generated by dissolving the 18-crown-6 in acetone and applying it to the back side of a standard Extrel probe tip. After allowing the acetone to evaporate, praseodymium metal was applied to the front of the probe tip with double-sided adhesive tape. This configuration gave a fairly constant pressure of ~5 $\times 10^{-8}$ torr (background pressure ~2 $\times 10^{-8}$ torr) for ~1 h. After desorption of the metal ions, a variable length time delay allowed for reactions of the metal ion with crown ether neutrals. Following formation of metal:crown ether fragment complexes, collision-activiated dissociation yielded metal oxide ions which could subsequently be isolated and allowed to react again with crown ether neutrals. In this way, "hot" (reactions within several milliseconds after desorption) metal oxide ions with crown ether neutrals and "cold" (reaction at least 5 seconds after desorption) metal oxide ions reactions with crown ether neutrals could be compared.

Figure 1 shows the results of PrO^+ ions reacting with 18-crown-6 neutrals. Praseodymium ions are representative of the lanthanide ion series as a whole—each of five different lanthanide ions followed the same reaction pathway. The first mass spectrum (after only 10 ms reaction period) shows only Pr^+ and PrO^+ ions, whereas the middle spectrum (500 ms reaction period) demonstrates the first step in the reaction pathway, namely fragmentation of crown ether neutrals on formation of an adduct with PrO^+ ions. Ions corresponding to $PrO(C_2H_4O)_n^+$ (n = 0-5) were observed. The bottom spectrum demonstrates a second reaction pathway, namely addition of an intact neutral crown ether to the metal:crown ether fragment complex, giving ions corresponding to $PrO(C_2H_4O)_n^+$ (n = 7-11).

This work was supported by NSF (CHE-93-22824) and the National High Magnetic Field Laboratory at Florida State University.

1. W. W. Yin, A. G. Marshall, J. Marcalo, and A. Pires de Matos, *J. Amer. Chem. Soc.* **1994**, *116*, 8666-8672.

43rd ASMS Conference on Mass Spectrometry and Allied Topics

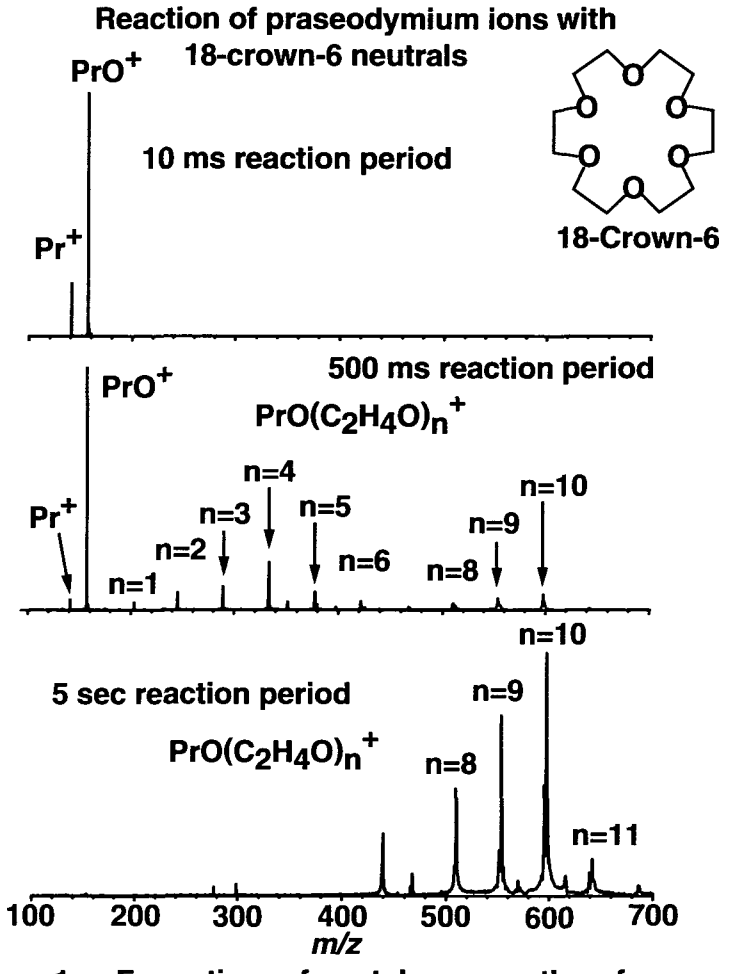

Figure 1. Formation of metal:crown ether fragment complexes (middle) is followed by attachment of an intact crown ether molecule (bottom).

Gas Phase Reactions of Pt^+, Au^+, and Hg^+ with Small Hydrocarbons

W.S. Taylor* and A.S. Campbell, University of Central Arkansas, Conway, AR 72035
L.M. Babcock and Christopher Linder, University of Georgia, Athens, GA 30602

Introduction

The chemistry of the third-row metal ions has received growing interest over the last several years. It has been shown by us[1] and others[2-4] that these ions display considerably greater reactivity than their first- and second-row homologues. In a previous study focusing on the chemistry of the group 11 ions with C_2H_6, C_3H_8, and n-C_4H_{10}, we observed that Au^+ exhibits bimolecular chemistry not seen with either Cu^+ or Ag^+.[ref] The key feature of these reactions is that when thermochemically favorable, hydride abstraction occurs exclusive of all other product channels This indicates that there is little or no kinetic barrier to hydride abstraction, and that the thermochemistry of this product channel indirectly governs access to other product channels. In order to test this behavior with other systems we have examined several systems which are exoergic (or nearly so) with respect to hydride abstraction: Au^+ + i-C_4H_{10}, and Pt^++ C_2H_6, C_3H_8, n-C_4H_{10} and i-C_4H_{10} In addition, several reactions which are endoergic with respect to hydride abstraction were examined: Hg^+ + C_2H_6, C_3H_8, n-C_4H_{10}, and i-C_4H_{10}

Experimental

The reactions in question were examined using a drift cell reactor and a flowtube equipped with a flowing afterglow (FA) source and a SIFT source. These instruments represent thermal (near-thermal in the case of the drift cell) environments For the flowtube work, metal ions were either injected directly into the flowtube or were mass selected in the SIFT source and then injected into the flowtube. Reactant ions are carried through the flowtube by a He flow of approximately 10 slm pumped by a Roots Blower The total pressure in the reactor is approximately 0.5 torr Neutral reactants are injected downstream and the reaction is monitored with a quadrupole mass filter In the drift cell studies, ions are transported via ion optics to the cell which contains 1 torr of a He/hydrocarbon mixture in a ratio of 10^4/1. Ions are drawn through the gas mixture by an electric field established by a set of guard rings. Reactant and product ions exiting the drift cell are monitored with a quadrupole mass filter. Effective temperatures in the drift cell are manipulated by altering the drift voltage. In all experiments, metal ions were produced by a dc glow discharge Au^+ and Pt^+ ions were formed by a sputter-bombardment process in which the metal to be studied serves as the cathode in the discharge. Hg^+ ions were produced by venting Hg vapor directly into the discharge plasma

Results and Discussion

A summary of the reactions carried out in this work is given in Table 1. Note that several of the Au^+ reactions examined previously with the FA were examined again using the drift cell and the SIFT In all cases, the observed products are consistent with our earlier work. The reaction of Au^+ with i-C_4H_{10} carried out in the drift cell indicates that hydride abstraction is the dominant product channel Also, the reactions of Hg^+ with C_2H_6 and n-C_4H_{10} exhibit no evidence of hydride abstraction. Indeed, Hg^+ does not appear to react with C_2H_6 under these conditions Hg^+ is depleted by n-C_4H_{10}, but no mercury-containing products are observed. Hydride abstraction does not appear to be significant in the Pt^+ reactions regardless of exoergicity Instead, H_2 elimination dominates product formation. All of the Pt^+ reactions exhibit initial formation of a Pt^+·alkene species which is itself depleted in a secondary H_2 elimination. Similar behavior was observed with both the drift cell and in the SIFT

Table 1: Summary of Reactions

Reaction	Products	Method	Temperature (K)*
Au^+ + C_2H_6	$Au^+{\cdot}C_2H_6^+$ $Au^+{\cdot}C_2H_4^+$	FA	300
Au^+ + C_3H_8	$C_3H_7^+$	FA	300
		SIFT	300
		Drift Cell	310
Au^+ + n-C_4H_{10}	$C_4H_9^+$	FA	300
		SIFT	300
		Drift Cell	320
Au^+ + i-C_4H_{10}	$C_4H_9^+$	Drift Cell	320
Pt^+ + C_2H_6	$Pt^+{\cdot}C_2H_4$ $Pt^+{\cdot}(C_2H_4)_2$	Drift Cell	310
Pt^+ + C_3H_8	$Pt^+{\cdot}C_3H_6$ $Pt^+{\cdot}C_3H_4$ $Pt^+{\cdot}(C_3H_6)_2$	Drift Cell SIFT	310, 340 300
Pt^+ + n-C_4H_{10}	$Pt^+{\cdot}C_4H_6$ $Pt^+{\cdot}C_4H_6{\cdot}C_4H_8$ $Pt^+{\cdot}C_4H_6{\cdot}C_4H_{10}$	Drift Cell SIFT	320, 820 300
Pt^+ + i-C_4H_{10}	$Pt^+{\cdot}C_4H_6$ $Pt^+{\cdot}C_4H_8$ $Pt^+{\cdot}C_4H_6{\cdot}C_4H_8$ $Pt^+{\cdot}(C_4H_8)_2$	Drift Cell	380, 420, 820
Hg^+ + C_2H_6	none observed incorporating Hg	Drift Cell	300
Hg^+ + n-C_4H_{10}	none observed incorporating Hg	Drift Cell	320

* effective temperatures reported for drift cell reactions

The specific H_2 elimination chemistry exhibited by each system is unique While the Pt^+/C_2H_6 system displays simple sequential H_2 elimination resulting ultimately in the formation of $Pt^+{\cdot}(C_2H_4)_2$, the reactions with C_3H_8, n-C_4H_{10}, and i-C_4H_{10} are more complex This is illustrated by the formation of $Pt^+{\cdot}C_3H_4$ from the reaction of Pt^+ with propane. Possible structures for this species include a Pt^+·allene complex or a hydrido-platinum cyclopropenyl structure. Also notable is the formation of the Pt^+·butadiene complex This species is not only observed in the Pt^+/n-C_4H_{10} system, but in the Pt^+/i-C_4H_{10} system as well, where it likely results from a metal-induced isomerization

References

1. Ward, E E, Taylor, W.S. Babcock, L.M.; McNeal, T L, *Proceedings of the 41st ASMS Conference on Mass Spectrometry and Allied Topics*, San Francisco, CA, May 30-June 1, **1993**, 169.
2. Weil, D A, Wilkins, C.L. *J Am Chem Soc* **1985**, *107*, 7316.
3. Irikura, K K., Beauchamp, J.L *J Phys. Chem.* **1991**, *95*, 8344
4. Chowdhury, A.K.; Wilkins, C.L. *J. Am. Chem. Soc.* **1987**, *109*, 5336

GLOW DISCHARGE/SIFT STUDIES OF GAS PHASE METAL IONS: REACTIONS OF MG^+

Christopher B. Linder, A. Leigh Dalton, and Lucia M. Babcock, Department of Chemistry, University of Georgia, Athens, GA 30602
William S. Taylor, Department of Chemistry, University of Central Arkansas, Conway, AR 73027

Gas phase reactions of Mg^+ with several (26) small neutral molecules have been examined using the newly developed glow discharge (GDIS)/SIFT apparatus which provides a clean source of Mg^+. It has been shown that Mg^+ reactions with small hydrocarbons, H_2O, and other small neutrals are crucial to understanding lower ionospheres of the giant planets.[1] While MgNC has been observed in circumstellar shells, pathways to its production are not known. Theory[2] and spectroscopic studies[3] have determined bond dissociation energies (BDE's) and structures for several Mg^+-L complexes, but no kinetic studies have been done. Moreover, BDE's for several ligands lie within experimental or calculational error of each other, and the exact ordering is not known We present a survey of reactions of 26 ligands with Mg^+ and detailed kinetic studies for four of these. Ligand switching reactions have been carried out *for several pairs of ligands to determine relative ordering of Mg^+-L bond strengths*

The only products observed for any reactions between Mg^+ and the ligands, L, are cluster ions $Mg^+(L)_n$ with varying degrees of clustering. Of the 26 ligands examined, 16 cluster with Mg^+: C_2H_2, C_2H_4, C_2H_6, C_3H_4, C_3H_6, c-C_3H_6, C_3H_8, C_4H_{10}, CO_2, H_2S, CH_3SH, CH_3OH, $(CH_3)_2O$, CH_3CN, C_6H_6, and $(CH_3)_2CO$. Reactions which proceed more efficiently are reflected in formation of higher clusters. Kinetics of clustering support this observation. Ten of the ligands examined (SO_2, H_2O, NH_3, H_2, N_2, NO, N_2O, NO_2, CH_4, CO) were found not to cluster directly with Mg^+ under our experimental conditions, and upper limits on rate coefficients have been determined.

For clustering reactions proceeding via collisional stabilization, the observed bimolecular rate coefficient is a function of pressure We have measured rates of reaction for Mg^+/L reactions as a function of (He) for L = CH_3OH, C_3H_6, C_3H_8, H_2S, and CH_3CN Apparent bimolecular rate coefficients are a function of (He) and are well below the collision rates, showing that these reactions are not saturated

In virtually all mass spectra of Mg^+/hydrocarbon reactions, a peak corresponding to $Mg^+(H_2O)$ was observed. However, our kinetic studies indicate that H_2O does not cluster directly to Mg^+. Therefore the cluster must be formed in a switching reaction; for example:

$$Mg^+(C_3H_8) + H_2O \longrightarrow Mg^+(H_2O) + C_3H_8$$

We formed $Mg^+(C_3H_8)$ upstream and added H_2O downstream confirming the switching reaction. The rate coefficient obtained is $k \geq 1.7 \times 10^{-9}$ cm^3 $molec^{-1}$ s^{-1}. A limit of $k \geq 1.4 \times 10^{-9}$ cm^3 $molec^{-1}$ s^{-1} for the switching reaction

$$Mg^+(C_3H_6) + H_2O \longrightarrow Mg^+(H_2O) + C_3H_6$$

has also been determined. Lower limits for are reported for k since formation of the Mg^+/hydrocarbon complex may not be complete prior to addition of H_2O. However, the rate coefficients are significant fractions of the theoretical rate, k_{ADO} (1.9×10^{-9} cm^3 $molec^{-1}$ s^{-1} for both), indicating that switching most likely occurs at the collision rate.

We are in the process of continuing our ligand switching studies, including more detailed quantitative studies, but the general Mg^+-L bond ordering obtained thus far is as follows:

$$\text{hydrocarbons} < H_2O < CH_3OH < NH_3$$
$$H_2O < C_6H_6 < NH_3$$
$$H_2O < (CH_3)_2CO < NH_3$$

We have employed the newly developed GDIS/SIFT to examine reactions of 26 ligands with Mg^+. Our results support the picture of weakly bound $(Mg^+\text{-}L)_n$ complexes of ground state Mg^+ obtained from theoretical[1] and spectroscopic[2] studies. Rate coefficients as well as the extent to which clusters form parallel the magnitude of the electrostatic Mg^+-L interaction as indicated by the ion-induced dipole (Langevin) or ion-dipole (ADO) capture rates as well as by bond dissociation energies (where available). The notable exception is H_2O for which we *observe no cluster formation despite a strong electrostatic interaction and the fact that* $Mg^+(H_2O)$ forms readily in switching reactions. This same behavior is noted for NH_3 which does not cluster to Mg^+ directly, but is more strongly bound than acetone, methanol, and water according to our switching studies. We also observe only small amounts of the n=1 cluster for CO_2 despite its BDE of 14.7 kcal mol^{-1}, and H_2S associates with Mg^+ only very slowly despite strong electrostatic interactions. Because these anomalies are observed for small ligands (H_2O, H_2S, CO_2, and NH_3) with fairly large BDE's, it is likely that k_d for $(Mg^+\text{-}L)^*$ is large, and collisional stabilization cannot compete under our experimental conditions. Castleman[4] observes formation of water clusters of Mg^+ up to n=5 and of $MgOH^+(H_2O)_5$ in his flow tube; this is attributed to direct clustering via the Lindemann mechanism. We see no evidence at all for direct formation of any water clusters by association reactions under similar flow tube conditions (i.e. P_{He}, T, and P_{water}) In Castleman's experiments, Mg^+ is produced by laser vaporization of solid Mg in the flow tube itself. In our work, Mg^+ is produced under the much less energetic conditions of the glow discharge source, and then selectively injected into the flow tube via the SIFT No undesired ions or neutrals enter the reaction region. Furthermore, energetic species such as Ar metastables and electrons do not exit the source/SIFT region to enter the reaction zone.

1. J.R. Lyons, Science **1995**, *267*, 645.
2. H Partridge and C.W Bauschlicher, Jr., J. Phys. Chem. **1992** *96*, 8827.
3. C.S. Yeh, J.S. Pilgrim, K.F Willey, D L Robbins, and M.A. Duncan, Int. Rev in Phys. Chem., **1994**, *13*, 231; and references therein
4. A.C. Harms, S N. Khanna, B. Chen, and A.W. Castleman, Jr J. Phys Chem **1994**, *110*, 3540

REACTIONS OF SINGLY-CHARGED METAL IONS WITH CYCLOPENTENE

Jinsong Ni[1] and Alex. G. Harrison
Department of Chemistry
University of Toronto
Toronto, Canada

The development of a tandem mass spectrometric method, involving reactive collisions in a quadrupole collision cell, to study the reactions of metal ions with organic substrates is reported. This approach has been evaluated by studying the reactions of singly-charged trasnsition metal ions with cyclopentene.

The transition metal ions Sc^+ through Cu^+ were produced by fast atom bombardment (7-8 keV Ar^o) of the appropriate solid metal chloride depositied on the FAB probe. Although all metal salts were found to give singly-charged metal ions, the chlorides gave the best yields. After mass-selection of the metal ions by the double-focussing (BE) stage of a hybrid BEqQ mass spectrometer,[2] the metal ions were decelerated and introduced into the r.f.-only quadrupole collision cell at low ion injection energy where they underwent reaction with cyclopentene. The ionic reaction products were mass analyzed by the final quadrupole Q.

Table 1 summarizes the spectra observed for an incident ion energy of 3 eV (lab scale) and an indicated pressure of $3x10^{-5}$ torr cyclopentene. The Mn^+ ion is largely unreactive with cyclopentene. The major primary product for Sc^+, Ti^+, V^+, Fe^+, Co^+ and Ni^+ is $M^+(C_5H_6)$ involving reductive H_2 elimination from the $M^+(c\text{-}C_5H_6)$ complex. Cr^+ and Cu^+ show only clustering to form $M^+(C_5H_8)$. The $M^+(C_5H_6)$ product reacts further to produce $M^+(C_5H_5)_2$, presumably the ionized metallocene, except for $Co^+(C_5H_6)$ which also produces $Co^+(C_5H_6)_2$ and $Ni^+(C_5H_6)$ which clusters to produce $Ni^+(C_5H_6)(C_5H_8)$. Where comparison is possible these results are in good agreement with earlier results obtained by ICR techniques,[3,4] indicating that the present tandem MS method is a viable method for studying metal ion reactions.

The mechanism of formation of $M^+(C_5H_6)$ is illustrated schematically in Scheme 1. Thermochemical arguments indicate that the failure of Cr^+ and Cu^+ to dehydrogenate cyclopentene results from the fact that insertion of the metal ion into the C-H bond is endothermic in these two cases, presumably as a result of the d^5 and d^{10} configuration of Cr^+ and Cu^+, respectively.

This work will appear in Int. J. Mass Spectrom. Ion Processes.

1. Present address: Department of Medicinal Chemistry, University of Utah, Salt Lake City, Utah
2. A.G. Harrison, R.S. Mercer, E.J. Reiner, A.B. Young, R.K. Boyd, R.E. March and C.J. Porter, *Int. J. Mass Spectrom. Ion Processes*, 74, 13 (1986).
3. D.B. Jacobson and B.S. Freiser, *J. Am. Chem. Soc.*, 105, 7492 (1983).
4. L.M. Lech and B.S. Freiser, *Organomet.*, 7, 1948 (1988).

Products from M^+/Cyclopentene Reaction

% of Base Peak

Product	Sc	Ti	V	Cr	Mn	Fe	Co	Ni	Cu
M^+	26	73	40	64	100	29	9	4	23
$M^+(C_5H_5)$		10	10		1	2			
$M^+(C_5H_6)$	8	12	5			4	7	4	6
$M^+(C_5H_8)$				12	6				16
$M^+(C_5H_5)_2$	100	100	100			100	73		
$M^+(C_5H_5)(C_5H_6)$		16	37			7			
$M^+(C_5H_6)_2$							100		
$M^+(C_5H_5)(C_5H_8)$					5				
$M^+(C_5H_6)(C_5H_8)$								100	8
$M^+(C_5H_8)_2$				100	20				100

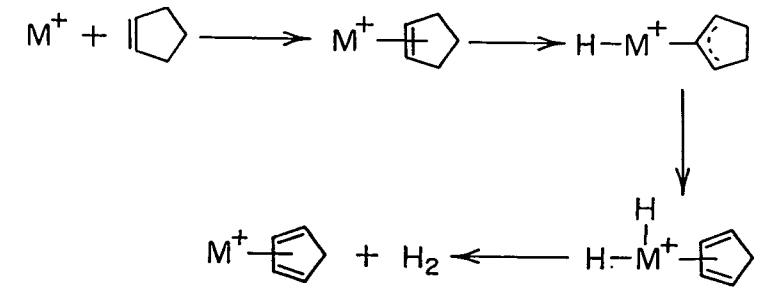

C_5H_8 ISOMER DISTINCTION BY METAL ION REACTIONS

Jinsong Ni[1] and Alex. G. Harrison
Department of Chemistry
University of Toronto
Toronto, Canada

It is well-established that the positive ion electron ionization (EI) mass spectra of unsaturated hydrocarbons provide little isomer distinction because of rapid rearrangements in the molecular ions.[2-4] Since transition metal ions frequently show distinctive reactions with organic molecules,[5] we have undertaken a study of the reactions of singly-charged transition metal ions with the C_5H_8 isomers cyclopentene, 1-pentyne, 2-pentyne, 1,3-pentadiene, 1,4-pentadiene, 2-methyl-1,3-butadiene and 3-methyl-1,2-butadiene to evaluate the potential of metal ion reactions to characterize the hydrocarbon isomers.

The transition metal ions Sc^+ through Cu^+ were prepared by fast atom bombardment (7-8 keV Ar^o) of the appropriate solid metal chloride deposited on the FAB probe. After mass-selection of the metal ion by the double-focussing (BE) stage of a hybrid BEqQ mass spectrometer[6], the metal ions were decelerated and introduced into the r.f.-only quadrupole collision cell at low ion injection energies where they underwent reaction with the C_5H_8 neutral. The ionic reaction products were analyzed by the final quadrupole Q.

The reactions of the transition metal ions with cyclopentene have been described in the previous paper (WPA 021). With the remaining C_5H_8 isomers Cr^+, Mn^+, Ni^+ and Cu^+ reacted mainly by clutering to form $M^+(C_5H_8)$ and $M^+(C_5H_8)_2$. Fe^+ and Co^+ showed a variety of products resulting from C-H and C-C bond insertion followed by fragmentation as well as simple clustering. The greatest isomer distinction was obtained for the reactions of Sc^+, Ti^+ and V^+. The two figures summarize the results obtained at 3 eV incident ion energy and a nominal C_5H_8 pressure of $3x10^{-5}$ torr for the reactions of Sc^+ and Ti^+ with six C_5H_8 isomers. A complex distribution of products is observed under these conditions which can be rationalized qualitatively in terms of C-H and C-C bond insertion followed by fragmentation. However, the distribution of products is quite strongly dependent on the isomer indicating that the reactions of the early singly-charged transition metal ions show considerable potential in characterizing unsaturated hydrocarbon isomers.

1. Present address: Department of Medicinal Chemistry, University of Utah, Salt Lake City, Utah.
2. J.T. Bursey, M.M. Bursey and D.G.I. Kingston, *Chem. Rev.*, **73**, 191 (1973).
3. K. Levsen, *Fundamental Aspects of Mass Spectrometry*, Verlag Chimie, Weinheim, 1978.
4. F.W. McLafferty and F. Turecek, *Interpretation of Mass Spectra*, 4th Edition, University Science Books, Mill Valley, 1993.
5. For a review see K. Eller and H. Schwarz, *Chem. Rev.*, **91**, 1121 (1991).
6. A.G. Harrison, R.S. Mercer, E.J. Reiner, A.B. Young, R.K. Boyd, R.E. March and C.J. Porter, *Int. J. Mass Spectrom. Ion Processes*, **74**, 13 (1986).

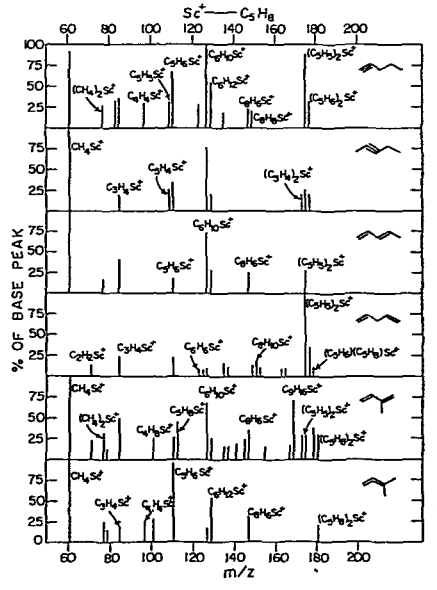

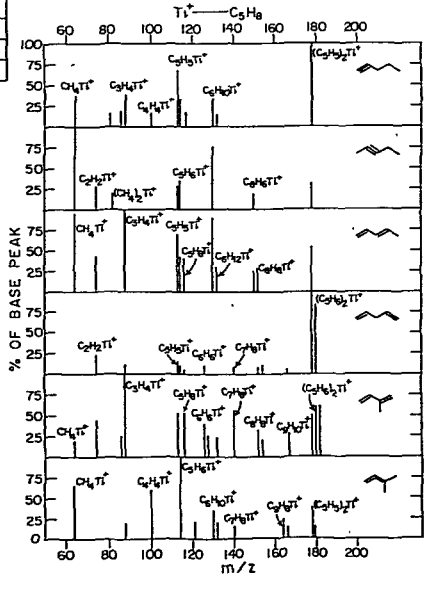

Radiative Association Rate and Bond Strength of Metal Ion-Neutral Complexes

Yen-Peng Ho and Robert C.Dunbar*
Chemistry Department, Case Western Reserve University, Cleveland, OH 44106

Introduction

Gas-phase reaction of transition metal ions with hydro-carbons has been an active area for decades. *Several techniques have been applied to measure metal-ligand bond energies. This includes collision-induced* dissociation, ligand exchange reactions, and photodissociation methods. Here we propose another approach to obtain metal-ligand binding energies by using a metal-ligand association technique. In the low pressure region where collisional stabilization of the association complex is not important, the reaction efficiency is normally determined by the competition between infrared radiative stabilization and back dissociation of the activated complex. Since the redissociation rate is a strong function of binding energy of the complex, measuring the low-pressure association rate gives an accurate method to evaluate the binding energy.

Methods

The association experiments were carried out in the Fourier-transform ion cyclotron resonance mass spectro-meter, using an IonSpec data system. The ions were trapped in a one inch cubical cell with a magnetic field of approximately 1.4 Tesla. The metal ions were produced by focusing the 532 nm light pulse (generated by a Nd.YAG laser) onto a metal plate attached to a sample holder near the cell. Neutral molecules were introduced through a leak valve For the reaction of Cd^+ and benzene, only the $Cd(C_6H_6)^+$ product was observed. For the association of Ag^+ with C_6H_6, both $Ag(C_6H_6)^+$ and $Ag(C_6H_6)_2^+$ were formed. This is also true for the association of Ag^+ with isoprene and 2-pentene The intensities of metal ion and ion complex were monitored as a function of reaction time to derive the association rate constant The time-plot for the association of Cd^+ with benzene at 300 K and 4.0×10^{-8} torr is shown in Fig. 1. The curves are fits of data to a pseudo first-order rate law. The apparent rate constant is 5.02×10^{-12}cc molecule^{-1} s^{-1}. The time-plot for the association of Ag^+ with benzene at 300 K and 2.0×10^{-8} torr is shown in Fig 2. Consecutive reaction kinetics was applied to the three Ag+ complexes to get the calculated curves. As shown in Fig. 2, the fit gives an apparent association rate constant of 2.46×10^{-11} cc molecule^{-1} s^{-1} for $Ag(C_6H_6)^+$ formation

The apparent bimolecular rate constant K_2 is defined as the rate $d[M^+]/dt$ divided by the neutral density. A linear pressure-dependent equation for k_2 can be derived as shown in the eq. (1)

$$k_2 = k_{ra} + k_3[N] \qquad (1)$$

k_3 is the termolecular rate constant k_{ra} is called the *radiative association rate constant* and is independent of neutral density. This rate constant was obtained by measuring the pressure-dependent k_2 and extrapolating to zero pressure, or measuring the apparent rate in the low pressure region (~2×10^{-8} torr) where the collisional stabilization is negligible. For example, the k_2 vs pressure plot shown in Fig. 3 gives an intercept of 2.41×10^{-11} cc molecule^{-1} s^{-1} which corresponds to the radiative association rate constant (k_{ra}) of $Ag(C_6H_6)^+$.

Results

To obtain the complex binding energy a thermal phase space model was used[1]. When the association efficiency is low enough, kra as given in eq (2) can be calculated in terms of densities of states for the complex and for the reactants. Since the density of states for the complex is a function of dissociation energy, a fit of calculated association rate constant kra to experimental results gives the dissociation energy of the complex ion. The calculations were performed using Klippenstein's phase space program[1].

The association reaction of Cd^+ with benzene and the association reactions of Ag^+ with benzene, isoprene and 2-pentene were studied. The k_r's and corresponding binding energies (E_o) are listed in Table 1 The binding energy of $Cd(C_6H_6)^+$ is lower than those of silver ion complexes The similar binding energies for the three Ag^+ complexes might suggest the electronic effects are not important in those systems. To check the validity of our method, the binding energies for $Ag(C_6H_6)^+$ from several studies are given in Table 2 for comparison. The value (1.31 eV) derived from charge transfer experiments is somewhat too low and the value (2.39 eV) from photodissociation seems too high. All the other values including ours are similar and fall into the range between 1.5 and 1.75 eV.

Conclusions

The binding energy for $Ag(C_6H_6)^+$ obtained in this work (1 74 eV) is a reasonable number compared to the previous studies. This gives us confidence in the E_o assignments for $Cd(C_6H_6)^+$, $Ag(isoprene)^+$ and $Ag(2\text{-pentene})^+$ *which are 1.55, 1.73 and 1.61 eV respectively. Furthermore, the sensitive dependence of radiative association rate* on the binding energy offers another approach to determining metal ion-ligand bond strengths.

43rd ASMS Conference on Mass Spectrometry and Allied Topics

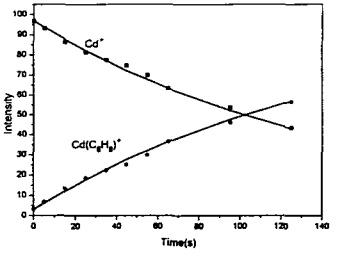

Fig. 1. Association reaction of Cd^+ with benzene at 300 K and at a pressure of 4×10^{-8} torr

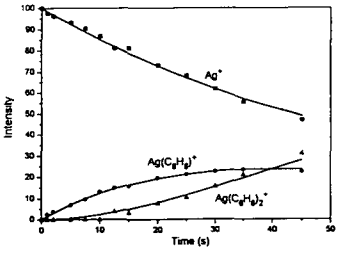

Fig. 2. Association reaction of Ag^+ with benzene at 300 K and at a pressure of 2×10^{-8} torr .

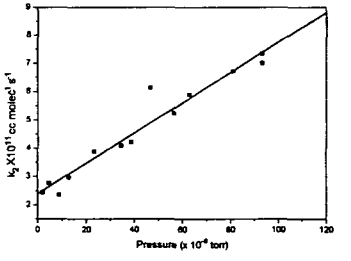

Fig. 3 Apparent bimolecular association rate constants (k_{ra}) for the formation of $Ag(C_6H_6)^+$ complex, as a function of pressure

Table 1 Radiative association rate constants and binding energies

Complex	Radiative association rate constant (kr) (cc molecule^{-1} s^{-1})	Binding energy (Eo) (eV)
Cd(C6H6)+	3.90×10^{-11}	1.55±0.1
Ag(C6H6)+	2.41×10^{-11}	1.74±0.1
Ag(isoprene)+	3.79×10^{-11}	1.73±0.1
Ag(2-pentene)+	3.84×10^{-11}	1.61±0.1

Table 2 Binding energies for Ag(C6H6)+

Eo (eV)	Method	Reference
1.58	theory	2
1.31	charge transfer	3
<1.52	high-pressure MS	4
1.62±0.07	ion beam	5
<2.39±0.22	photodissociation	6
1.74±0.1	present work	

References

1. Dunbar, R. C.; Klippenstein, S. J.; Hrusak, J , Schwarz, H. "The binding energy of Al^+(C6H6) from radiative association kinetics", manuscript in preparation.
2. Bauschlicher Jr., C W ; Partridge, H , Langhoff, S R. *J. Phys Chem.* 1992, 96, 3273
3. Wiley, K F , Cheng, P. Y ; Bishop, M. B.; Duncan, M. A *J. Am Chem Soc* 1991, 113, 4721
4. Freiser, B S , private communication, cited in ref. 2.
5. Chen, Y. M., Armentrout, P B. *Chem. Phys. Letters* 1993, **210**, 123.
6. Afzaal, S.; Freiser, B. S. *Chem. Phys Letters* 1994, **218**, 254.

SIMION 3D Version 6.0

David A. Dahl
Idaho National Engineering Laboratory
PO. Box 1625, Idaho Falls, ID 83415

Introduction: SIMION 3D Version 6.0 is the latest version of the SIMION PC ion optics simulation program developed by the author for use on IBM compatible personal computers. Its new features and capabilities significantly broaden its applicability to ion optics and related experimental problems. Complete instruments can now be simulated. The new 3D capability allows simulation of quadrupoles including end regions, 3D ICR cells, and 3D source and detector geometry. Enhancements in user programming allow simulations involving viscous or collisional cooling for ion mobility simulations. A new charge repulsion capability allows detection of the onset of charge repulsion problems as well simulating things like combined repulsion and cooling effects in ion traps.

Discussion: The new version of SIMION has been rewritten in C. It is a 32 bit virtual DOS program that can run as a DOS application in DOS, Windows (3.xx, 95, or NT), and OS/2 (2.x or Warp). The program is based on a 32 bit GUI developed by the author for in-house data system development. Unlike previous FORTRAN versions of SIMION, this version is complete. It and its GUI, device drivers and DOS extender are all bound together into a single .EXE file.

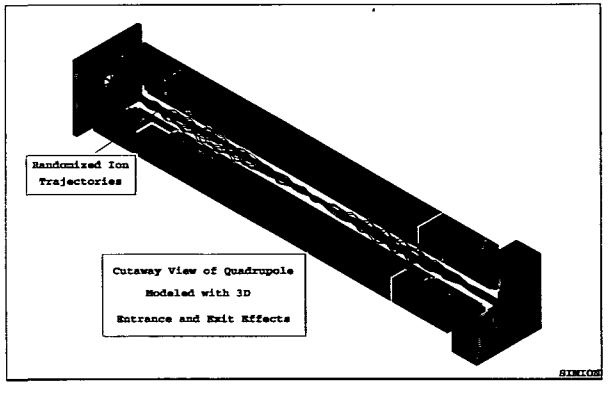

The program makes use of potential arrays to simulate the electrode and/or pole geometry of electrostatic and/or magnetic simulation problems. These arrays can be either 2D (planar or cylindrical) or 3D planar asymmetrical. Individual arrays can contain up to 10 million points. A new geometry language (with compiler) supplements the interactive Modify function for defining complex electrode/pole geometry.

Fields are calculated (refined) via finite difference techniques. A new skipped point refining method developed by the author provides refine times that are proportional to n (Where n is the number of points in the potential array). This significantly reduces large potential array refine times over traditional n^2 finite difference methods.

Instances (3D images) of these potential arrays are projected into a ion optics workbench volume of up to eight cubic kilometers. As many as 25 potential array instances can be defined within an ion optics workbench volume. Potential array instances can be arbitrarily scaled, positioned, and oriented within the workbench volume. This allows complete instruments to be modeled.

All potential array instances are viewed as 3D objects within the workbench. SIMION has quick 3D visualization capabilities that allow the user to switch views, cut into instances to see inside, and more. Ions can be flown separately or in groups and viewed as rays or moving dots as appropriate. The user environment is highly interactive, allowing the user to switch views, adjust voltages, move instances, and etc. while ions are flying.

User programming has been enhanced with an expanded language, compiler and built in development system. The new user programming model allows user programs to read and change potentials, gradients, accelerations, and ion state parameters. This allows effects like viscous drag to be modeled with facility. Potential energy surfaces can now be updated via user program control. This allows observation of ion motions while the potential energy surface undulates (e.g. in an ion trap).

Initial Results: Various beta versions of SIMION 3D have been in use within the community for about six months. SIMION 3D has simulated the Phi-Evans TOF instrument using voltages that are within a few percent of the as-built instrument. It has been successfully used in the design of new commercial ion sources and detectors. The formation of cooled ion crystal structures in ion traps have be simulated with crystal structure and size in good agreement with experimental observations (illustrated below). Our group's personal experience with this new version has been positive. It appears to simulate our ion optics problems with voltages that are within few percent of the as built.

Acknowledgements: This work was supported by the Division of Chemical Sciences, Basic Energy Sciences, Office of Energy Research, Department of Energy under contract 3ED102.

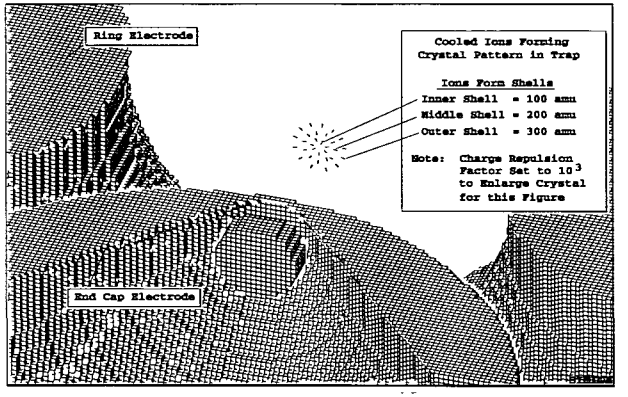

MacSimion Past, Present and Future

D. C. McGilvery and R. J. S. Morrison
Department of Chemistry, Monash University, Clayton, Victoria, Australia 3168

Ion trajectory simulation programs such as MacSimion are useful tools for understanding existing ion-optical designs and evaluating new ones. Although MacSimion operates in just two dimensions, it suffices for problems with planar or cylindrical symmetry, such as an ion source with tall narrow slits, a set of quadrupole rods, or an aperture lens system. Many real systems possess no simple symmetry or have overlapping regions with different symmetries. The interface region between an ion source and a quadrupole mass analyzer, or that between the latter and an AC-only quadrupole (as in a triple quadrupole instrument) are examples which require a full three dimensional treatment.

Small 2D calculations use arrays of perhaps 100 by 200 points to represent a single plane of a problem This often only provides a minimal rendering of the electrode geometries but is adequate to produce semi-quantitative results. One expects the same minimal calculation in 3D to require tens of megabytes of memory, with refine times running into many hours. High performance computers using RISC processors would appear to be attractive platforms on which to tackle such simulations.

A native code version of MacSimion for the PowerMac was evaluated for numerical simulations by building an energy-compensating electrostatic mirror Ion trajectories in the mirror are shown in Fig 1 Ion flight times in the mirror have been incorporated into analytical calculations in Mathematica to simulate a reflectron time-of-flight mass spectrometer [1,2] The RISC platform was found to out-perform earlier CISC processors by as much as a factor of five in the MacSimion phase of these calculations.

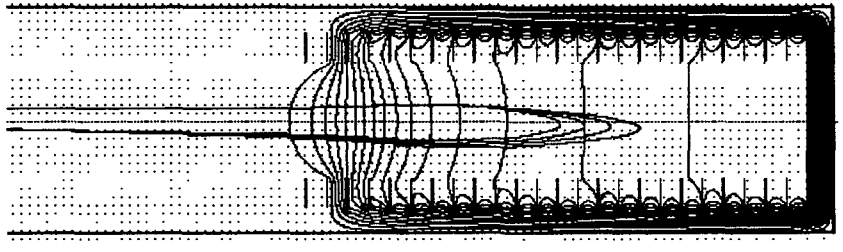

Fig. 1 Electrostatic mirror for energy compensation in a reflectron TOF mass spectrometer

MacSimion 3D is a new program we have developed, allowing a system of electrodes to be set up in 3D The memory requirements for a simulation are (4n+2) xyz bytes, where x, y and z are the dimensions and n is one greater than the number of time-dependent waveforms in the problem Laplace's equation is solved iteratively on the three-dimensional grid by a relaxation process (refining) until satisfactory convergence is reached. To improve execution speed the procedure initially operates on a coarse grid and progresses to maximum resolution near the end of the refining operation, which typically takes about one hour for an array containing 10^6 grid points. The resulting potential distributions can be exported into, and examined using the 3D visualization package, Dicer.

During ion trajectory calculations we compute a 64 term interpolating polynomial for the potential which has the form $V = \sum_{i,j,k} c_{ijk} x^i y^j z^k$,$(i,j,k \le 3)$ A new set of coefficients c_{ijk} are required each time the ion moves into a new cell (defined by the 8 grid points immediately surrounding the ion). Standard Runge-Kutta integration routines are used to compute the trajectory.

To illustrate the capabilities of MacSimion 3D, numerical simulations of ion motion in selected regions of a triple quadrupole instrument [3] have been undertaken. The complete instrument is far too complex to handle as a single entity, and must be decomposed into smaller, more manageable problems. Fig. 2 shows an ion trajectory in the region between a source and a mass analyzer. The system was represented using two 91x91x100 arrays to store the electrodes in a grid with a spacing of 0.2 mm. In the first array the rods were held at ground potential, while in the second array the source electrodes were grounded. Potentials were computed using the additive property of solutions to Laplace's equation and a modulation function to apply the appropriate ratio of DC and RF potentials to the rods.

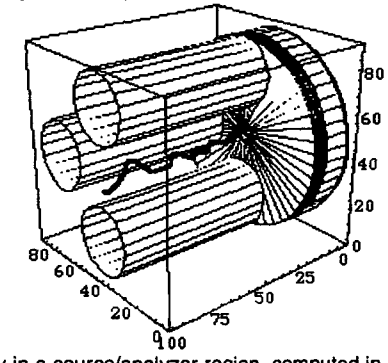

Fig.2 Ion trajectory in a source/analyzer region, computed in MacSimion 3D

We have also modelled the interface region between the first analyzer and the collision cell in a triple quad, which needs three arrays. Memory and time constraints currently restrict the physical volume of regions which can be studied in MacSimion 3D to about 10 cm^3 We are currently exploring the use of phase space methods [4] to compute ion trajectories near the center of the mass analyzing quadrupoles. We anticipate that future work will focus on a hybrid approach combining numerical calculations with these phase space methods, thereby greatly enhancing the usefulness of such 3D simulations

References

1. W. Gohl, R. Kutscher, H. J. Laue and H. Wollnik, Int. J. Mass Spectrom. Ion Phys., 48 (1983) 411.
2. H J. Neusser, U. Boesl, R. Weinkauf and E W. Schlag, Int. J. Mass Spectrom. Ion Processes, 60 (1984) 147.
3. R. A. Yost, C. G. Enke and J. D. Morrison, U.S. Patent No. 4,234,791 (1980).
4. M Baril, R. Le and P. Marchand, Int. J Mass Spectrom. Ion Processes, 98 (1990) 87.

The Practical Application of Data Controlled Mass Spectral Analysis

Douglas C. Stahl, Kristine M. Swiderek, Michael T. Davis & Terry D. Lee
Beckman Research Institute of the City of Hope, Duarte, CA 91010

Introduction

Compounds of interest often occur in minute quantities and as components of complex mixtures. For this reason, a primary focus of chemistry research has been directed toward increasing the sensitivity of mass spectrometry, HPLC, and sequence analysis. The physical connection of multiple isolation and analysis steps has reduced sample losses and has greatly increased the quantity and quality of structural information that can be obtained from a single sample. However, the volume and complexity of data generated by these improved analytical techniques currently limits its effective and efficient use toward the solution of problems. After completion of an analysis, an interpretation of collected data is usually necessary to determine how to proceed with the next analysis. A post-analysis evaluation of data often reveals information that could have been used to optimize analyses in real time. There is no established technique for using previously collected data to control subsequent data acquisition. In addition, there is no established technique for targeting a specific subset of information in a complex mixture, or for selectively discriminating against subsets of information that are known or not of interest. The loss of information between tandem analyses has been minimized through the development of a logical interface between physically connected analytical methods. A mass spectrometer data system was used to continuously evaluate incoming spectral data against a variety of user definable variables. The resulting conclusions were used to modify analyses at subsequent steps. Using computer programs developed in our laboratory, we have prepared examples of "data controlled" experiments that exploit the existing capabilities of a mass spectrometer data system to increase the effectiveness and efficiency of tandem analyses.

Materials and Methods

Ultra low flow LC/ESI/MS and LC/ESI/MS/MS analyses were performed using a microscale HPLC system built by the authors (1, 2, 3). On column UV detection was performed at 200 nm using an ABI 759A UV/VIS spectrophotometer (Applied Biosystems, Inc. Foster City, CA) equipped with a capillary flowcell holder. All mass spectrometry was performed on a Finnigan TSQ700 triple sector quadrupole mass spectrometer using the ICIS data system version 7.2. Programs for data acquisition and data system control were developed using Finnigan Instrument Control Language (ICL) version 7.27 (4).

Results and Discussion

Example 1

Various amounts of a standard mixture were loaded onto the micro flow LC/MS system to determine how much structural information can be obtained in an automated mode during a single analysis and to evaluate the sensitivity limitations of data controlled analyses. Data controlled LC/MS/MS analyses on all ions above a user-defined signal to noise threshold were performed. At 1 pmol and 500 fmol eight of nine ions were selected by the computer and resulted in interpretable MS/MS spectra. One ion was not selected because its low signal to noise ratio. Loading 200 fmol, six of nine ions were selected by the computer and yielded interpretable spectra and at 100 fmol four of nine ions were selected. Three of those four ions yielded partial sequence information. The fourth ion yielded a complete sequence. Using signal to noise ratio as the criteria for ion selection, the practical limitation of data controlled MS/MS studies is defined by the sensitivity of the instrument. Partial protein sequence information can be obtained automatically with as little as 100 fmol of sample and more structural information can be obtained by performing repeated analyses with progressively lower signal to noise threshold values.

43rd ASMS Conference on Mass Spectrometry and Allied Topics

Example 2

LCMS analysis of a synthesized peptide showed its mass to be 64 amu higher than expected (expected mass = 10,342). A tryptic digestion was performed to check for a mass difference on the peptide level. Under the assumption that the mass difference is caused by a single amino acid exchange, a list with all expected masses was preloaded and MS/MS was automatically performed on all ions that differed by the observed 64 amu shift. The doubly charged ion of only one peptide was automatically selected for MS/MS. The resulting MS/MS spectra indicated a valine/tyrosine exchange in position 87 of the polypeptide corresponding to a mass shift of 64 amu. By continuously evaluating incoming data against a list of expected masses, it is possible to isolate discrepancies, minimize analysis time, and reduce the volume of data. This could be used to easily confirm and localize site directed mutagenesis or posttranslational modifications of a protein.

Assuming the mass difference is caused by multiple sequence errors, a list with all expected masses was preloaded and MS/MS spectra on all masses that differ from the expected values were automatically acquired. Seven masses were selected by the program for MS/MS. Six of the seven were identified as either unspecific cleavage products of the polypeptide, or were associated with minor contaminants. The MS/MS data for mass 1242 indicated a valine/tyrosine substitution. Unexpected masses can be automatically isolated and selected for MS/MS in real time and the structural analysis of an unknown component in a sample contaminated with a known component can be performed.

Example 3

Structural analysis was requested on a minute quantity of unknown protein that had been separated and digested in SDS gel in the presence of detergent. A single LC/MS analysis was performed to generate a list of candidate masses. These potential peptide masses were preloaded into a list and a data controlled MS/MS analysis that searches each spectrum for masses contained in the list was performed. The list was loaded with 26 candidate masses. 11 masses were automatically selected for MS/MS analysis. Three of the 11 masses were derived from the detergent. One peptide MS/MS spectrum could not be interpreted. The remaining five peptide MS/MS spectra yielded interpretable data. A database search using the resulting sequence resulted in a match with the known protein transferrin. 13 of the 26 masses originally entered into the list matched masses associated with transferrin. Without additional data analysis, MS/MS was performed on detergent peaks as well as peptide peaks. All time spent on the analysis of detergent peaks minimized the change of obtaining structural information on peptides.

The MS/MS analysis of detergent peaks seen in the analysis described above, helped to establish a "fingerprint" MS/MS spectrum for that detergent. An additional ICL program was written to detect the fingerprint spectrum when it occurs. When the MS/MS fingerprint was detected, the mass spectrometer immediately returned to normal scan mode. Otherwise, MS/MS spectra was collected on the mass for as long as possible. LC/MS/MS was performed on all signals above the signal to noise threshold. The MS/MS analysis of detergent peaks was terminated after one scan, and the detergent masses were recorded so that they will be rejected in all following scans. Approximately 84 detergent peaks were detected and eliminated from further consideration. 17 peptide MS/MS spectra were obtained. Four of those spectra were uninterpretable, Of the remaining 13, four corresponded to transferrin. The remaining nine could not be matched with a known protein. Data controlled LC/MS/MS analysis of all masses above a threshold signal to noise value will yield the maximum amount of data when combined with the automatic detection and elimination of data related to contaminants. Lists of contaminants can be created once and used for the analysis of many samples. This method could be used to discriminate against detergents and contaminants associated with in-gel digestions, digestions of proteins on membranes, and preparation of cell lysates.

References

1. M. T. Davis, D. C. Stahl, and T. D. Lee, J. Amer. Soc. Mass Spectrom., 1995, in press
2. Stahl, D. C., Davis, M. T., and Lee, T. D., Proceedings of the 42nd ASMS Conference on Mass Spectrometry and Allied Topics, Chicago, IL, May 29-June 3, 1994
3. Davis, M. T.,and Lee, T. D., Protein Science 1992, 1, 935-944
4. Stahl, D. C., Martino, P. A., Swiderek, K. M., Davis, 5. M. T., and Lee, T. D., Proceedings of the 40th ASMS Conference on Mass Spectrometry and Allied Topics, Washington, DC, May 31-June 5, 1992

Possible Use of a Time Domain Signal Inverse Algorithm in FTICR-MS

Michael V. Gorshkov* and Richard T. Kouzes

Environmental Molecular Sciences Laboratory
Pacific Northwest Laboratory, Richland, WA 99352

*Member of the Institute of Energy Problems of Chemical Physics, Russian Academy of Sciences, Moscow, Russia 117829

The most widely used numerical method for spectral enhancement is the Fourier transform (FT) [1]. There are several algorithms that have been developed to improve FT spectra [2]. We developed a time-inverse algorithm (TIA) for rapid signal prediction into negative time. The resulting time-domain signal then consists of two juxtaposed parts: the original signal and the time-inverted one. In FTICR, the post-excitation phases of different ions are the same and equal to the phase of the excitation field. The assumption is made that the ion motion will be the same for $t < 0$ as it is for $t > 0$ (Fig.1). From these assumptions, we may elongate the real time-domain signal f(t) to obtain: $f_{Inv}(t) = f(t)$ when $t > 0$ and $f_{Inv}(t) = f(-t)$ when $t < 0$. The TIA frequency spectrum $F_{Inv}(\omega)$ is the convolution of frequency spectra from cosinusoid $S_{Inv}(t)$, boxcar $\Pi_{Inv}(t)$, and exponential $E_{Inv}(t)$ functions, respectively: $F_{Inv}(\omega)=S_{Inv}(\omega)*\Pi_{Inv}(\omega)*E_{Inv}(\omega)$. It was found from analysis of the shape of $E_{Inv}(\omega)$ function that the spectral amplitude of the TIA signal will be doubled, the peakwidth will be narrower by factor of $\sqrt{3}$, and the noise level will be a factor $\sqrt{2}$ higher. Thus, resolution and signal-to-noise level will be higher. Fig.2 shows an example of an unresolved doublet, and the same doublet after applying the TIA method. In Fig.3 the mass spectrum from bovine insulin $[M+4H]^{4+}$ protonated molecular ion is shown. Ions were formed by ESI (7T FTICR at Pacific Northwest Laboratory [3]). It was also found that the TIA method may be used for the case of quadrature detection as well. In practice, the phases of ion motions may not be the same when detection is started. For the TIA method, the initial phase is crucial to the correct juxtaposition of the original and predicted signals. Related artifacts can be eliminated by phase correction in the complex FT spectrum of the original signal. For the original signal each individual phase ϕ_i may be rotated in the corresponding FT spectrum $F_i(\omega)=Re_i(\omega)+i\,Im_i(\omega)$ to obtain pure absorption $A_i(\omega)$ and dispersion $D_i(\omega)$ spectra that correspond to $\phi_i=0$. The phase rotation procedure is described by the following expressions [1]: $A_i(\omega)=Re_i(\omega)\cos\phi_i - Im_i(\omega)\sin\phi_i$; $D_i(\omega)=Re_i(\omega)\sin\phi_i+Im_i(\omega)\cos\phi_i$. We found the following advantages of the method: (1) increase in resolution and signal-to-noise ratio; (2) simplicity of the algorithm. The TIA method may be helpful for analysis of low resolution and unresolved spectra especially in low field FTICR.

This work was supported by Associated Western Universities under the Grant DE-FG06-89ER-75522 with the Department of Energy and by Pacific Northwest Laboratory.

(1) Marshall, A.G.; Verdun, F.R. *Fourier Transforms in NMR, Optical, and Mass Spectrometry: A User's Handbook*; Elsevier: Amsterdam, **1990**, 460 pp.
(2) Balcou, Y. *Rapid Comm.Mass Spec.* **1994**,*8*,942; Kim, H.S., Marshall, A.G. *Private Comm.in ICR/Ion Trap Newslett.* **1995**, *37*; Dromey,R.G., Morrison,J.D., Peel, .B. *Chem. Phys. Lett.* **1973**,23,30; Brenton, A.G., Lock,C.M. *Rapid Comm. Mass Spec.* **1995**,*9*, 143.
(3) Winger, B.E., Hofstadler, S.A., Bruce, J.E., Udseth, H.R., Smith, R.D. *J. Amer. Soc. Mass Spectrom.* **1993**, *4*, 566-577.

43rd ASMS Conference on Mass Spectrometry and Allied Topics

FIGURE 1

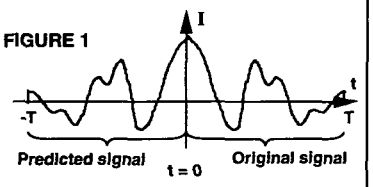

FIGURE 2

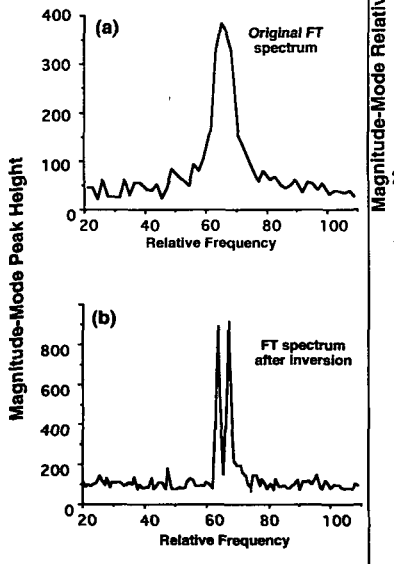

FIGURE 3

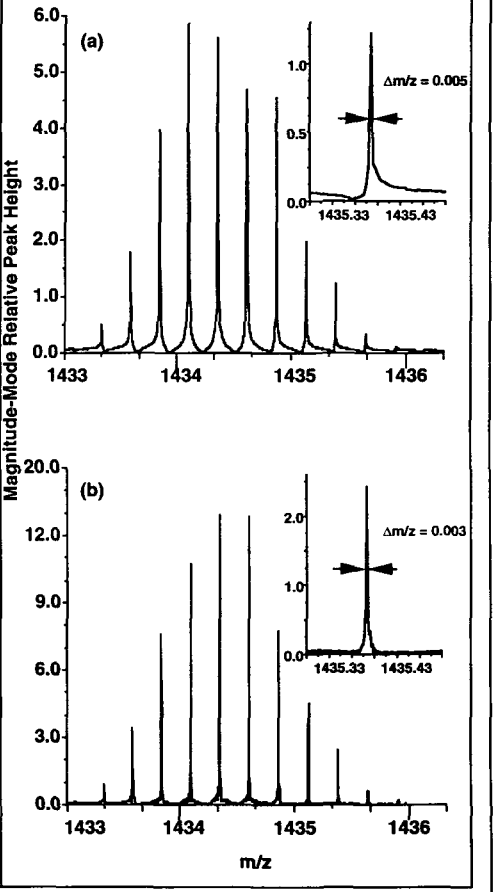

HOMOLOGOUS SERIES PLOTS: A NEW SLICE THROUGH THE GC/MS DATA SET

Gregory G. Dolnikowski, and Brian Smith,
Jean Mayer USDA-HNRCA at Tufts University, Boston MA 02111 and
Spectros Associates, Mendon MA 01756

We have developed a computer program that takes a new slice through the GC/MS data set. The new slice is called a homologous series plot because it passes through all the ion current maxima that are caused by a homologous series of compounds eluting from the GC while they are being detected by a scanning MS.

The program for extracting homologous series plots from GC/MS data is written in Array BASIC and runs under GRAMS/386, which is a general-purpose data system for lab instruments sold by Galactic Industries. The user first finds two peaks which may be part of an homologous series using the total ion chromatogram and mass spectra. The user then enters into the program the scan number and m/z value for each peak. The program determines the equation of the homologous series slice based on the scan numbers and on the natural log of the m/z values. The program then extracts the correct m/z values from each mass scan in the data file according to the equation of the slice, assembles the m/z values into a single file, and stores the new file. Finally the program draws a homologous series plot of ion abundance versus m/z on the computer screen.

Data for this presentation were collected using a HP 5980 Series II GC/HP 5988A MS. The fused silica capillary column in the GC was 30 m long, 0.25 mm i.d., and coated with DB-5 stationary phase. The oven was programmed from 75°C to 325°C at 10°C per minute. The MS was scanned from 250-650u repetitively, and methane positive ion chemical ionization (PCI) was employed for detecting the sample.

Figure A shows the total ion chromatogram (TIC) of an extract of lipids from a marine organism. The lipids have been saponified, reduced, and derivatized to fatty acid methyl esters and fatty alcohol acetates. Under methane PCI, fatty alcohol acetates form $(MH - CH_3COOH)^+$ ions as the base peak of their mass spectra. A homologous series plot (Figure B) of the $(MH - CH_3COOH)^+$ ions indicates that there is a seven member homologous series of fatty alcohol acetates from C_{20}-C_{32} present in the sample. A similar homologous series plot of the $(MH)^+$ ion of the fatty acid methyl esters reveals a homologous series with eight members ranging with some gaps from C_{15}-C_{24}.

The homologous series plot is useful for visualizing an entire homologous series of compounds in complex chromatograms that may contain unresolved peaks or other homologous series. In chemically noisy chromatograms, the homologous series plot can often detect peaks that can not be distinguished using the TIC.

43rd ASMS Conference on Mass Spectrometry and Allied Topics

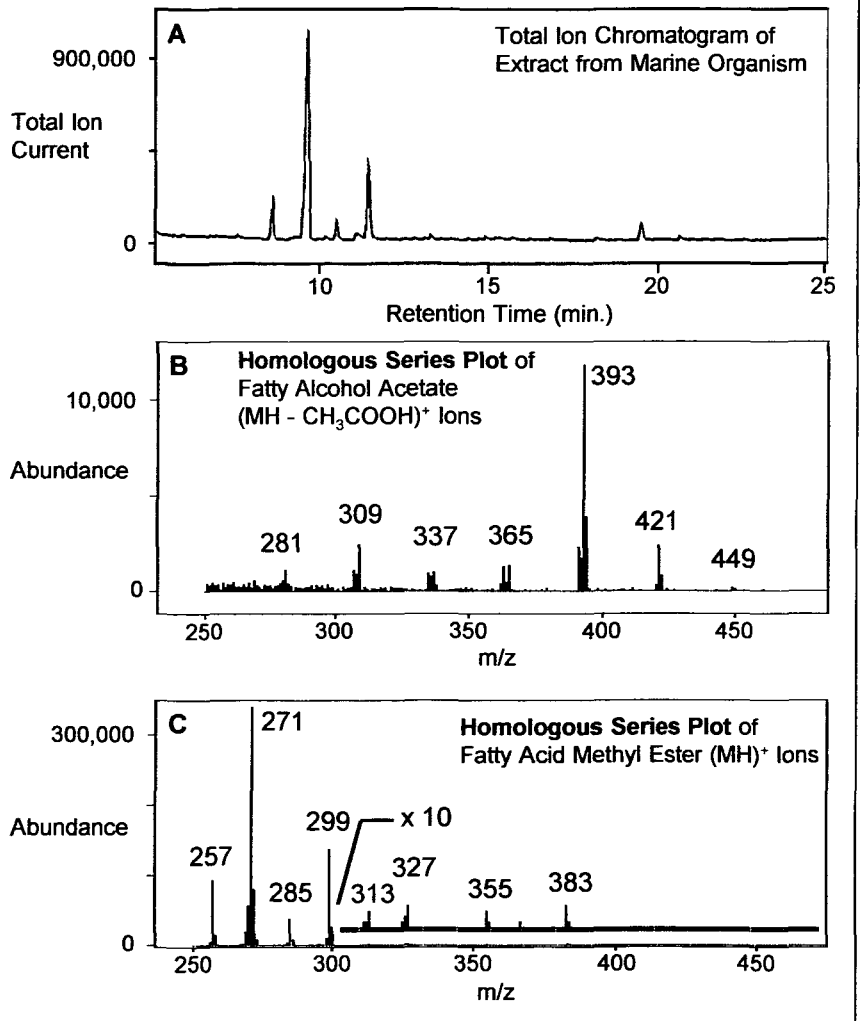

THE DETERMINATION OF ELEMENTAL COMPOSITION BY LOW RESOLUTION MS/MS.

Jia-shen Wang
Clairol Inc., Stamford, CT 06922

In theory, elemental compositions can be derived by MS based on the isotopic patterns of molecular ion clusters[1]. In a routine application, this technique is very useful for elements such as Cl and Br and to some degree for elements such as S and Si. An accurate determination of the carbon content of a compound, however, is a challenge. The method described here is an approach which determines the carbon content of a compound based on the known neutral loss peaks of the $[m+1]^+$ daughter spectra.

THEORY

The M+1 peak in a molecular ion cluster contains one heavier (by 1u) isotope for those elements which have heavier (by 1u) isotopes. The peaks of the daughter ions of these M+1 ions, therefore, appear as pairs (different by one mass unit), because the heavier isotope will be present either in the ion or neutral fragments. A peak intensity ratio (I_H/I_L) of the high (I_H) and low (I_L) mass peaks is

$$(I_H/I_L) = \sum m_i X_i / \sum n'_i X_i \qquad \text{..... (1)}$$

where X_i is the relative abundance of the heavier isotope of element X and m_i and n'_i are the numbers of element X in the ion and neutral fragments, respectively. This equation is derived based on an assumption that there are no isotopic effects in the formation of these ions. The elemental composition of a compound will be obtained, once all m_i's are solved, *since the sum of m_i and n'_i is the content of the respective element in a compound.* All m_i's in Equation (1), however, can not be solved, simultaneously. Fortunately, an approximation can be made since the terms related to carbon in Equation (1) are by far much larger than the terms of all the others. Thus equation 1 is reduced to the form:

$$(I_H/I_L) = m_c/n'_c \qquad \text{..... (2)}$$

The carbon content of a compound, therefore, can be determined by using Equation (2), since the value of n'_c is known. This is because the respective neutral loss is known. Subsequently, the possible compositions of a compound can be limited to a very small number, and evaluated with other information.

EXPERIMENTAL & PROCEDURE

The mass spectrometer used here is a Finnigan TSQ-7000 MS/MS system. The sample is introduced by a direct insertion probe (solid probe). The calculations are done by computer using standard spreadsheet softwares. The procedure of the analysis is summarized in three steps: (1.) Use $[m]^+$ ion to adjust the experimental conditions, (2.) Measure the intensities of the peaks (pair) of $[m+1]^+$ daughter spectra where the neutral losses are known, and (3) derive the possible compositions and use equation (1) to evaluate the answers.

RESULTS & DISCUSSION

Figure 1a.

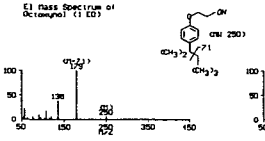

Figure 1b.

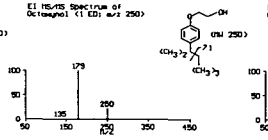

Figure 1c.

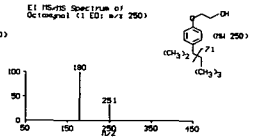

Figure 2a.

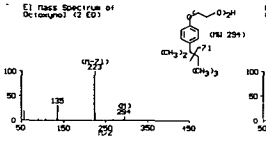

Figure 2b.

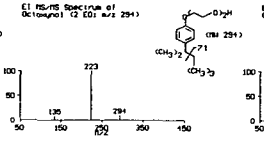

Figure 2c.

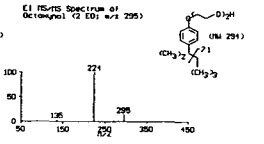

Two compounds with similar structures were selected to test the method. The EI mass spectra are shown in Figures 1a and 2a. The neutral loss (C_5H_{11}) of the base peaks is common for these compounds. The daughter spectra of $[m]^+$ of the respective compounds are shown in Figures 1b and 2b. The spectra indicate that, under the selected experimental conditions, the interfering ions are negligible. The daughter spectra of $[m+1]^+$ are shown in Figures 3a and 3b. The carbon contents are calculated to be 16.03 and 18.14 by equation 2 with the respective peak ratios. The experimental errors (0.03 and 0.14) are from two sources. One is due to the approximations of equation 2. This one can be solved by trial-and-error with equation 1 for possible compositions. The reduction of equation 1 to equation 2 causes negligible errors in most cases for hydrogen and oxygen. The other is just experimental error. This error is minimized by data averaging. With the current example, a 10% error in peak intensity measurement will cause an error of one carbon. This issue does not appear to be a problem with the results obtained here.

SUMMARY

The method shown here to determine the carbon content of a compound is based on the capabilities of an MS/MS system and the knowledge of many common neutral losses which have been established. While the example shown here is a simple C-H-O compound, the method can be applied to much more complex compounds which can also include other elements.

1. (a) McLafferty, F.W., "*Interpretation of Mass Spectra*", 2nd ed., W.A. Benjamin Inc., Reading, MA 1973. (b) Silverstein, R.M., et. al., "*Spectrometric Identification of Organic Compounds*" 4th ed., John Wiley & Sons, NY 1981.

THE USE OF PM3 MOPAC SEMIEMPIRICAL CALCULATIONS TO PREDICT PHOTOINDUCED PROTON-TRANSFER IN H-BONDED CLUSTERS

Mary Gimon Kinsel, Yong Huang, Damon C. Barbacci and David H. Russell
Laboratory for Biological Mass Spectrometry, Department of Chemistry, Texas A&M University, College Station, Texas 77843

Photoionization of substituted aromatic acids in amine clusters $M(NR_3)_n$, where R = H, CH_3 or C_2H_5, generated using a supersonic nozzle yields both protonated amine clusters $H(NR_3)_m^+$ (m<n) and radical cation species $M^+(NR_3)_n$. We have studied the proton-transfer from several aromatic acids including the MALDI matrices 4-hydroxy-3-methoxycinnamic acid (ferulic acid) and α-cyano-4-hydroxycinnamic acid. We are interested in the value of semiempirical calculations as interpretive tools in the study of photoinduced chemistry in hydrogen-bonded clusters. In this poster we present preliminary calculations (PM3-type) on hydrogen-bonding of the solvent molecules to the aromatic acid and the effects of solvation on the thermodynamic properties of the cluster.

Semiempirical Calculations

The semiempirical calculations were performed using MOPAC version 6.0 (CaChe Worksystem) running on a MacIntosh Quadra 900. The starting geometries of the substituted aromatic acids were obtained using the Molecular Editor Program. One, two, and three solvent molecules were allowed to approach the polar substituents along the reaction coordinant defined by hydrogen-bonding donor and hydrogen-bonding accepter moities of the aromatic acid and solvent molecules. The thermodynamic properties of the system were calculated as a function of the distance between these two groups.

Results and Discussion

Figure 1 shows a slice of the resulting potential energy surface obtained when an ammonia molecule approaches the phenolic hydrogen of ferulic acid that is already hydrogen bonded by two additional ammonia molecules. The potential energy surface has a minimum at a distance of 1.8A which corresponds to the most stable hydrogen-bond formed. The hydrogen bonding of three ammonia molecules at the polar substituents of ferulic acid results in a net lowering of the ionization potential by approximately -0.5eV. The solvent identity was changed to methylamine and analogous calculations were performed. In this case the ionization potential was lowered by approximately -1eV. We are currently

investigating the effects of solvation at alternative sites on the aromatic acid including the π-clouds of the aromatic rings.

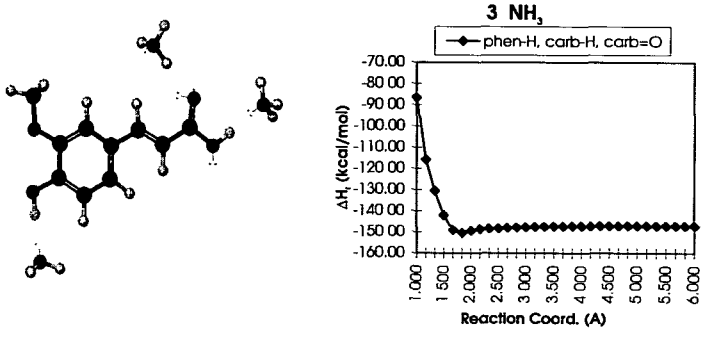

Figure 1: Ferulic acid solvated by three ammonia molecules. The graph depicts the energy of the system as one ammoniz molecule approaches the phenolic hydrogen of ferulic acid.

Future Studies

Experimental results show that as the basicity of the solvent molecule increases, there is a decrease in the abundance of the solvated radical cation and a corresponding increase in the abundance of protonated solvent ion signal in the TOF mass spectrum. We are investigating this observation in detail by calculating the heats of formation of the solvated aromatic acid radical cations as well as that of the solvated proton. Our ultimate goal is to apply this type of experiment combined with the results of semiempirical calculations to explore the mechanism of matrix assisted laser desorption/ionization as a proton transfer process within a cluster environment.

Application of a Fuzzy Logic Peak-finding Algorithm for GC/MS Analysis

Peter Sander, Bruker-Franzen Analytik GmbH,
Postfach 33 01 26, 28331 Bremen, Germany

In order to speed up the evaluation of GC/MS analysis and to also improve common GC/MS evaluation techniques a fuzzy logic-based peak-finding algorithm has been developed. Advances are given in a wide range of GC/MS analysis[1]:

First, GC/MS analysis according to standard procedures (e.g., EPA VOAs) requires positive identification of the target compound spectra and "up to 10 organic compounds of greatest apparent concentration". Here, interference of overlapping substance peaks, especially of those not listed in the target compound list, increases the time to complete the evaluation significantly. Second, "field" applications of GC/MS (e.g., task force for chemical spills, accident or fire on chemical plants or other hazardous material sites, ...) have to account for complex mixtures of numerous substances and also require a fast and reliable analysis to ensure fastest possible response. In these cases the novel *Dissect* algorithm is indispensable to perform quickly and reliably the complete GC/MS evaluation.

Methods:

The fuzzy logic based algorithm, named *Dissect*, is using the maximum amount of information available from the GC/MS measurement to separate mass spectra of overlapping compound peaks without any user-interaction.[1] Fuzzy logic permits to implement the decision-making process of interpreting and evaluating mass spectra into a reliable, automatic algorithm. The result of this algorithm is a list of all substance peaks along with a short chromatographic track of each individual substance, its mass spectrum, and its integrated area. The resulting mass spectra are background-subtracted and without contributions of neighboring, overlapping substances, thus enabling an unambiguous and accelerated identification in a mass spectral library.

Results:

The novel *Dissect* algorithm can be included in an evaluation procedure to determine the amounts of calibrated substances as well as the intensity of all other containing compounds. Fig. 1 shows the result of a combined evaluation procedure. The sample has been taken at an inspection well of a waste disposal site for hazardous materials. The evaluation procedure performed here evaluates calibrated VOA compounds by their (single-ion) target ions and all other compounds by *Dissect*. The result of the evaluation procedure is listed in Tab. 1. VOA compounds evaluated by their target ions are listed here with a 'Peak Name' (e.g., *Toluene* (peak# 21), *Ethene, chloro-* (peak# 2), ...). All other compounds in this list were previously not known. These compounds have been evaluated by *Dissect* and identified by library search in the mass spectral library of the *National Institute of Standards and Technology*. Note, that among others the two major components of this sample (*Disulfide, dimethyl* (peak# 19) and *1,3-Butadiene, 1,1,2,3,4,4-hexachloro-* (peak# 52)) are compounds not listed in the EPA's list of VOAs. A standard evaluation procedure relaying on the evaluation of VOAs only will not list these hazardous compounds. The *Dissect* algorithm performed this evaluation automatically, reliable, fast, without user-interaction, and, as already pointed out, without previous knowledge about what compounds to expect.

Conclusion:

The *Dissect* algorithm is a valuable addition to standard GC/MS analysis by delivering previously not known compounds instantly. The qualities of this algorithm also allow to use shorter GC columns and/or faster temperature ramps, reducing the total time for a complete GC/MS analysis even more. For "task force" applications of GC/MS – facing the challenge of identifying numerous compounds as fast as possible to ensure fastest possible response – the *Dissect* algorithm is irreplaceable by performing the task of evaluation fully automatically and delivering the complete list of compound spectra for an unambiguous identification in a mass spectral library.

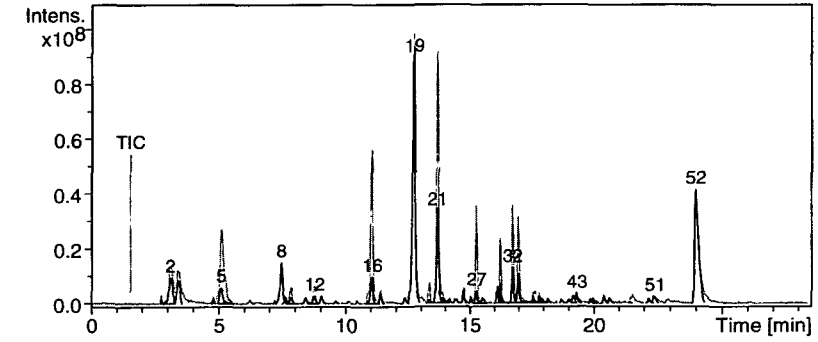

Fig 1 On-site GC/MS analysis with Bruker EM 640. Evaluation of VOAs and all other compounds by *Dissect*.

Peak #	Area [%]	Peak Name	Substance Name from NIST Library Search
19	33.4		Disulfide, dimethyl
52	16.1		1,3-Butadiene, 1,1,2,3,4,4-hexachloro-
21	9.5	Toluene	Toluene
2	4 5	Ethene, chloro-	Ethene, chloro-
3	3.4		Methanethiol
16	3.0	Trichloroethylene	Trichloroethylene
32	3.0	Ethylbenzene	Ethylbenzene
33	2.7	Xylene	Benzene, 1,3-dimethyl-
5	2.1	Ethene, 1,1-dichloro-	Ethene, 1,1-dichloro-
31	1.6	Benzene, chloro-	Benzene, chloro-
8	1.3	Ethene, 1,2-dichloro- (total)	Ethene, 1,2-dichloro-, (Z)-
29	1.2		2-Butene, 1,4-dichloro-
25	1.1		2-Butene, 1,4-dichloro-, (E)-
27	1.0	Tetrachloroethylene	Tetrachloroethylene
17	0.9		Heptane
12	0.8	Ethane, 1,2-dichloro-	Ethane, 1,2-dichloro-
10	0.7	Chloroform	Chloroform
11	0 7		1-Propene, 3-chloro-2-methyl-
51	0.7		1,3-Butadiene, pentachloro-

Tab. 1 Evaluation report of the GC/MS analysis in Fig. 1 (excerpt only; sorted by rel. intensity).

[1] P. Sander, *Enhanced Separation of Overlapping GC/MS Peaks by Fuzzy Logic*, Proceedings 42nd ASMS Conference on Mass Spectrometry, **1994**, 491

Software Tools for the Analysis of High Resolution Mass Spectra

Price, John M., Myers, James D., Rockwood, Alan W.,
Van Orden, Steven, Williams, Ernest L.

Environmental Molecular Sciences Laboratory,
Pacific Northwest Laboratory,
Richland, Washington.

We present a suite of software tools for the analysis of the high resolution mass spectra of large molecular weight species. This program, called MERCURY, includes tools for:

- the prediction of isotope distribution patterns for arbitrary molecular formulas, including fragment ions
- a prototype automated wavelet transform algorithm for assigning the charge states of spectral features
- a "protein editor" to conveniently generate molecular formulas for biopolymers and biopolymer fragment ions from sequence information
- the assignment of protein sequences by computer assisted interpretation of ladder sequences from collisionally activated dissociation (CAD) data.
-

MERCURY uses new high speed methods for the calculation of the isotope distributions of fragments of arbitrary molecular formula and charge.[1] The algorithm uses Fourier transform methods to generate the transformed mass (or mu-domain) representation for the input molecule, which may be used to calculate theoretical isotope distributions. This tool swiftly calculates the distributions in high resolution mode, giving the distribution over all the isotopic peaks of a molecule or fragment at speeds considerably faster than existing algorithms. The speed arises from two factors. The isotope distribution of a compound can be thought of as the convolution of the distributions of all the elements in the compound. Since convolutions done in the mu domain reduce to a multiplication of vectors, it is much quicker to calculate them there. Similarly, for a compound containing n atoms of a given element, the isotope distribution would be an nth order complex convolution, which reduces to computing the nth power of the mu domain spectrum, which, if done in polar coordinates, reduces further to computing a scalar power of the magnitude, and a rotation of the polar angle. Performing these calculations in the mu domain and then transforming to the m/z domain greatly reduces the computational effort required. Ultrahigh resolution (a mass defect spectrum of a single isotopic peak) calculations are also implemented. This calculation requires a further digital filtering step. The program shown incorporates the above methods into an efficient algorithm coded in C. Under the Windows operating system, the code can be used as a dynamic link library and called from other languages. We have developed a graphical front end using Visual Basic that allows manipulation of fragment formula and charge, the line widths, and the choice of gaussian or lorentzian line shapes. The code also allows for specification of the

43rd ASMS Conference on Mass Spectrometry and Allied Topics

center mass and mass range of the calculated spectrum, allowing easy comparison with experimental spectra. The program uses a modifiable database of isotopic abundances, allowing calculation of isotope distributions for labeled compounds.

A prototype tool automatically assigns charge states from isotopically resolved and partially resolved mass features. This tool makes use of wavelet packet transforms to find the characteristic spacing of isotope structure within a peak cluster. Because of the localization of the wavelet basis functions, this method offers advantages over methods that rely on Fourier transforms. We have investigated the use of several wavelet bases, including the Daubechies series, as well as local trigonometric transforms. In both cases, as the spatial resolution of the transform nears the width of isotope distributions in a CAD spectrum, the isotope peak frequency can be discerned. The fundamental frequency is then interpreted as the fragment's charge. Our algorithm uses an initial guess, f, of the fundamental isotope frequency to make initial charge state assignments across the spectrum. Peaks above a threshold (typically 60-80% of the maximum peak) are identified in the frequency spectrum of each spatial bin. Peaks within f/2 of each other are considered to be part of the same band. Once the frequency bands are identified, the centroid of the band is determined. Charge states are defined as the nearest integer to the sum(Cj/j). The initial guess is then refined using the centroids of the fundamentals and overtones and the charge assignments, using f=Sum(WiSum(Cj/Nj)) where f is the new frequency, Wi is the total signal in the ith spatial bin, Cj is the centroid of the jth overtone band, and Nj is the charge assignment*overtone number (fundamental=1, seconds harmonic=2,...). The assignment process is then iterated to improve the assignment. Initial guesses of the single charge isotope frequency within 25% of actual converge well for spectra with S/N >50.

Using the protein sequencing functions, the user may interactively construct amino acid chains and specify cleavage mechanisms. The program then generates theoretical ladder sequences based on a user selected peak., identifies probable matches in the experimental data, and labels the matches graphically. The user specifies the m/z tolerance defining a match and can graphically compare the calculated mass of these fragments to experimental results. The program also has a user modifiable database of fragment masses and identities which can be used by the built in search algorithm to automatically assign ladder sequences of amino acid fragments from a given spectral feature. The current algorithm searches for all matches that could arise from one or two database fragment chains.

1 A.L. Rockwood, S.L. VanOrden and R.D. Smith, ASMS conference, 1994.

Processing MALDI time-of-flight data : A Maximum Entropy Approach.

David J.Reynolds, Elaine Scrivener, Peter J.Derrick and Richard T.Gallagher.
The Institute of Mass Spectrometry, University of Warwick, Coventry, CV4 7AL, UK.

Introduction. Matrix assisted laser desorption ionisation (MALDI) is a powerful technique for the analysis of intact molecular ions of high mass species such as proteins. In this technique a small amount of analyte is mixed with a large molecular excess of matrix compound. A laser pulse is then applied to the sample which causes the desorption of intact analyte-matrix ions (1,2). The pulsed nature of this technique has made it ideal for time-of-flight (TOF) instruments.

The method of maximum entropy (MEM) (3) reduces a raw data set to one which contains the least amount of information consistent with the original, subject to certain constraints. Unlike other techniques, such as Fourier transform, MEM iteratively approaches the solution by predicting the original data on the basis of its solution and subsequently modifying this guess until agreement is reached. The MEM process has been successfully applied to electrospray data and has been shown to provide significant spectral enhancement (4,5). In contrast to electrospray MALDI does not give rise to a series of multiply charged peaks (although some clustering can occur) and therefore does not possess the inherent reproduction of data of the former technique. The method of data collection does, however, contain many independent data sets that are normally summed together to produce an averaged spectrum. These may be used to improve the performance of the *Maximum Entropy Method* (MEM)(1).

Maximum Entropy Method (MEM) The Maximum Entropy Method determines the most likely underlying spectrum by eliminating inconsistent data by an iterative process. The resultant spectrum will have the maximum configurational entropy consistent with the original data set. A Gaussian blurring function was used with the full width at half maximum (FWHM) being approximately determined by the isotopic envelope. As with electrospray data processing, the programme provides routines for the emulation and subsequent elimination of instrumental and isotopic broadening. An example of the iterative process is shown in figure 1.

Experimental. A Kratos Kompact MALDI III time-of-flight mass spectrometer was used in reflectron mode at +20kV accelerating potential to analyse a mixture of Pig Cytochrome C (12231Da) and Chicken Cytochrome C (12238 Da) mixed at a ratio of 1:1. For each sample Bovine Insulin was used as a calibrant and sinapinic acid used as the matrix. Sample conc. was 10^{-5} molar, and the matrix was 0.1 molar. Samples were collected over 100 laser shots.

Results and Discussion. The data obtained from each acquisition was processed using a Maximum Entropy software routine developed in-house and run on a Sun SPARC station IPC computer. The software processes a window of 3000 data points around the selected area of interest. An applications

of this software on the chosen sample mixture is shown in figure 6 and 7 which show the difference between the original data obtained at a resolution of 1500 to the processed data at up to 7000 (FWHM).

Conclusions We can report the development of a MEM programme for the time-of-flight mass spectrometer which utilises the independent data sets and its application to data produced by MALDI-TOF. Significant resolution enhancement has been obtained allowing the deconvolution of a mixture of pig and chicken cytochrome C, which differ by only 7 Daltons, to be fully resolved.

References. [1] T.W.D.Chan, A.W.Colburn and P.J.Derrick. Org. Mass Spectrom. 27, 53-56 (1992).
[2] M.Karas, D.Buchmann, U.Bahr and F.Hillenkamp, Int. J. Mass Spectrom., 4,228 (1990).
[3] J. Skilling (Ed) 'Maximum Entropy and Bayesian Methods', Kluwer, 45 (1989).
[4] A.Ferrige et al., Rapid Commun. Mass Spectrom, 6,11,707-711 (1992).
[5] D.J.Reynolds, P.J.Derrick, J.R.Chapman and G.J.Daniell, 19th meeting of the British Mass Spectrom. Society, University of St.Andrews, Scotland. Sept, (1992)

Figure 1. Example of Iterative MEM process on Bovine Insulin data.

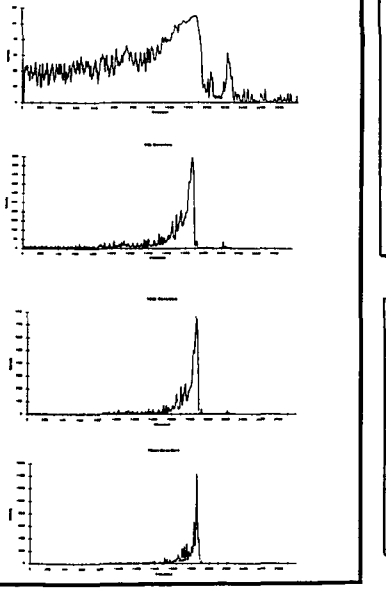

Figure 6. Reflectron MALDI-TOF-MS of Pig and Chicken Cytochrome C Mixture.

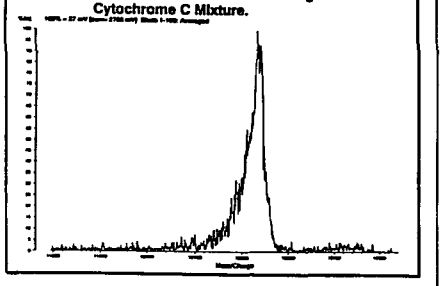

Figure 7. MEM processed Cytochrome C mixture.

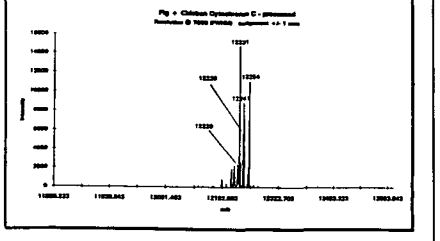

Hybrid Neural Network for Mycobacterial Detection and Speciation by GC-MS

Christopher D. Herold, Robert L. Fitzgerald and David A. Herold, VAMC, San Diego, CA 92161
and Department of Pathology, U.C.S.D., La Jolla, CA 92093
Taiwei Lu, Sean Zhao, and Jeremy Lerner, Physical Optics Corporation, Torrance, CA 90501-1821

Introduction

Current artificial neural networks do not perform all of the same functions as their biological counterparts. They are, based on similar concepts in the hope that some of the flexibility and power of the human brain would be reproduced. The basic building block of the neural network is the artificial neuron or node. Each neuron performs a summing, thresholding, mapping or nonlinear transformation function on an input data set. Neurons are organized into layers; input, hidden and output, with connections between layers. Each connection has a weighted strength, much like a valve or programmable circuit array that attenuates or magnifies transferred signals. The weights can be changed by a set of learning rules that modifies the weights in response to the input signals and the value supplied by the transfer function. Learning rules allow the neuron's response to change with time, depending upon the nature of the input signals. This is the means by which the network adapts itself to the data and so organizes information within itself. In short, this is the human brain counterpart of learning. The essence of neural networks is to embed learning and processing algorithms into parallel interconnected architectures. As a result, a neural net computations are faster and more robust compared to serial computers. The back-propagation method determines the interconnections between layers in a multilayer neural network where only the input and output neurons and layers are known. This model is applied to determine the interconnections for the hidden layer. The input is propagated through the network and the output is computed. The output is then compared with the known output and an error valued is determined. The error value is then propagated back through the network passing through each layer and appropriate weight changes are made. A multilayer neural network can be trained to perform non-linear transformations which are very difficult to model by conventional algorithms. We can train a neural network to perform these complex operations by presenting input and output pairs. The neural network gradually learns the input/output relationship by converging its internal energy states into a minimum.

Methods

Inoculation and Growth of Mycobacterial Cultures: Mycobacterial was inoculated into 5 mL of BBL 7H9 broth with glycerol. The liquid cultures were allowed to grow for 21 days at 37 C with a 8% carbon dioxide atmosphere. They were then autoclaved at 121 C and 16 psig for 1 hour to kill the mycobacteria.

Cell Separation from Broth: Autoclaved culture tubes were centrifuged at 3000 rpm for 15 min to pellet mycobacteria after which ~90% of the 7H9 broth was aspirated, avoiding aspiration of mycobacteria clumped at the bottom the tube. Four mL of deionized (DI) water was added to the culture tube to "washed" the specimen three more times to eliminate approximately 99% of the broth. With a mix of ~0.5 mL of DI water and cells remaining in the tube, 10 uL of 10 ng/uL octadecanol-d_{37} was added as internal standard.

Extraction of Alcohols from Mycobacteria: The washed mycobacteria were lysed with 2 mL of 5% sodium hydroxide (in DI water/ methanol, 1:1) for 30 minutes at 70 C. The lysate with 3 mL of hexane. The hexane layer was collected and evaporated to dryness under nitrogen.

Derivitization of Alcohols: Anhydrous pyridine (50 uL) and 10% pentaflurobenzoylchloride (PFBO) (50 uL) in acetonitrile were added to each dried tube followed by vortex mixing. The reaction was allowed to proceed at room temperature for 30 minutes after which 1.5 mL of DI water and 1.5 mL of hexane were added to the reaction mixture to separate the fatty alcohols from excess derivatizing reagent. The mixture was vortexed vigorously for 5 minutes and the hexane layer containing the fatty alcohols was collected and evaporated to dryness under nitrogen. The residues were reconstituted with 100 uL of acetonitrile.

GC/MS Conditions: Data was collected on a Finnigan 4500 GC/MS (Finnigan MAT, San Jose, CA) equipped with negative ion detection capabilities.The GC column was a 15 m x 0.32 mm i.d. crosslinked dimethylpolysiloxane with a 0.25 µm film thickness. The mass spectrometer was operated in the negative chemical ionization mode with methane (Matheson 99.99%) as the reagent gas at an ionizer pressure of 0.95 torr which corresponded to an analyzer pressure of 1.1×10^{-5} torr. Prior to analysis each mycobacteria is studied to determine what fatty alcohols are characteristic of the species. Using the Selected Ion Monitoring mode, 15 different preselected m/z outputs are obtained from the GC-MS analytical run. Prior to the hybrid neural net analysis no software signal processing was done on the mass spectral data.

Neural Network Data Acquisition: The study was run on a PC 486 computer (50 MHZ clock speed). The detected spectral signals were digitized and sent to a personal computer for training or analysis. A customized neural network software package (Physical Optical Corporation, Torrance, CA) was used to recognized the GC/MS spectra. The neural network first preprocesses the input spectrum, performs a nonlinear transformation to extract the chromatographic features and then classifies the results. The neural network software was written in C language and occupies less than 100 kbytes of memory. A backpropagation model is used to train the neural net for recognition of the species of mycobacteria tested. The training time is less than 15 minutes. The fast convergence of the training is mainly due to the optimum preprocessing algorithm and the proper selection of the hidden layer neurons in the hybrid neural network. After training the hybrid neural net is ready for operation. Seven output neurons represent the seven different species of mycobacteria evaluated. Each output neuron gives an output value normalized between 0 to 100 that indicates the confidence of the classification result. (See Table). By testing the neural net with a set of known data, proper calibration and threshold values can be set. The neural net can then be challenged with blinded specimens.

Results: The hybrid neural net was trained and applied to 11 unknown test data. Challenge test results are shown in the Table. The results demonstrate that using the hybrid neural network for data processing results in the correct assignment of all 11 specimens. Assignments are made in less than a second.

Conclusion: We utilized a hybrid neural network for detecting and species identification of mycobacteria by gas chromatography-mass spectrometry. This optimized hybrid neural network consists of a windowed cross-correlation algorithm that extracts the signal peaks in the chromatogram and a multi-layer feedforward neural net for feature recognition. We trained and tested the hybrid neural net for classifying mycobacteria into 7 species. The results demonstrate that the hybrid neural net, by careful design of both preprocessing algorithm and the neural network architecture, is capable of correctly identifying the specimen.

Neural Network Output for Mycobacteria Analysis

Challenge Specimen	Avium	Fortuitum	Gordonae	Intracellulare	Kansasii	Tuberculosis	Xenopi
Tuberculosis	0	0	1	0	0	**97**	1
Fortuitum	0	**97**	0	0	0	0	0
Avium	**89**	1	19	38	0	0	0
Gordonae	1	0	**97**	0	1	1	0
Intracellualare	0	0	0	**98**	0	0	0
Kansasii	0	1	1	1	**98**	1	0
Xenopi	0	49	0	0	0	4	**62**
Tuberculosis	0	0	0	0	0	**97**	1
Intracellualare	0	0	0	**97**	0	0	0
Tuberculosis	0	0	1	0	0	**98**	0
Kansasii	0	1	1	1	**98**	1	0

Evaluating EI Mass Spectral Library Search Results

O. David Sparkman
O. David Sparkman & Associates, 4045 Eagle Ridge Drive, Antioch CA 94509

As the size of various collections of electron ionization mass spectra increases, there is a continuing and increasing propensity to rely on the results of computerized library searches. The results of these computerized searches do not necessarily account for a spectrum that is the result of two or more different compounds. Examination of the Reconstructed Chromatographic Peak will not always be an indicator that more than one compound is present. The reliability of the numerical confidence factors placed on the search results by the computer, no matter how high, should be questioned with respect to an actual visual evaluation of the mass spectrum.

A good example of how a "good search result" can lead to an incorrect conclusion is shown in the following example of the analysis of a mixture of volatile organic compounds by GC/MS. While the library search results were well within the positive match criteria set by the description of the program, the identification was incorrect.

A GC/MS analysis was performed on a mixture of volatile organic compounds using the purge and trap method described in US EPA Method 524.2 for the analysis of drinking water. Figure 1 shows a portion of the Reconstructed Total Ion Current Chromatogram (RTICC) indicating the presence of at least eight different compounds. It is clear from an examination of the shape of Peak 1 that it represents at least two different compounds There is nothing about the shape of any of the other remaining six peaks that indicates the presence of more than one compound. An identification was attempted of the spectrum that represented the apex of Peak 3 in the RTICC (Figure 2). This spectrum was a good candidate for analysis by library search because of the apparent lack of a molecular ion peak.

The spectrum was compared against the NIST/EPA/NIH Mass Spectral Library. This library is composed of 74,827 spectra of 62,235 compounds All are 70 eV spectra collected on a variety of different types of mass spectrometers.

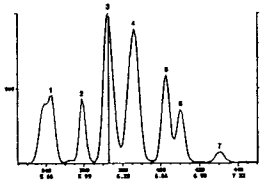

Figure 1

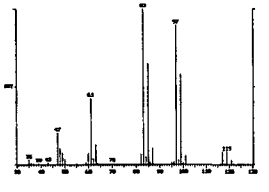

Figure 2

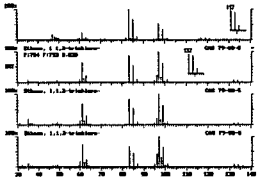

Figure 3

Figure 3 shows the unknown spectrum at the top and the spectra of the first three matches. The first three matches from a comparison with 74,827 spectra are all of the same compound as indicated by the Chemical Abstracts Service (CAS) Registry Number in the upper right corner of each spectrum.

The confidence levels for these particular library search results are very high. The manual accompanying the software states that values of 800 to 900 for all three indicators give a high probability that the spectrum of the unknown and the library spectrum are the same compound. The three values in the upper left of the best match, along with the first three matches all being

the same compound, indicate a high probability that the unknown spectrum is that of 1,1,2-trichloroethane.

However, a closer examination of the unknown spectrum and the best match indicated something much different. Besides differences in the intensity of major peak clusters, the unknown spectrum has a cluster of peaks with a nominal m/z value of 117. This cluster does not appear in any of the spectra of the first three matches. The appearance of this cluster indicates that it represents an ion that contains three atoms of chlorine. All of the spectra of the first three best matches have a cluster of peaks with an identical pattern and intensity to that of the unknown's cluster at m/z 117 with a nominal m/z value of 132 (the molecular weight of 1,1,2-trichloroethane). It is obvious that the three best matches are of the same compound; but, it is not so obvious that the unknown spectrum is of that same compound.

The RTICC Peak was re-examined. This time, a scan near the base on each side of the peak was examined. As seen in Fig. 4, Peak 3 appears to consist of at least two different compounds

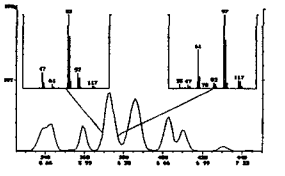

Figure 4

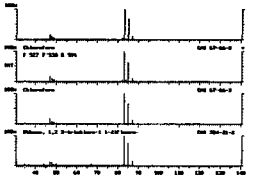

Figure 5

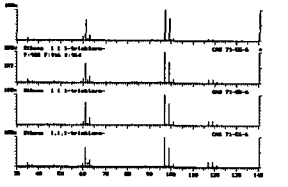

Figure 6

Figures 5 and 6 show the result of selective background subtraction followed by library searching. Both the examination of the unknown spectrum as compared to the library search spectra and the numeric confidence levels provide the closest to an unambiguous identification of the two compounds in this mixture without doing a direct comparison of the two unknown spectra with spectra obtained on putative samples of the identified compounds.

Similarly, you can have a low set of numeric indicators as to the correctness of the search; and, the result is an identification of your unknown

A computerized library search will generally yield an answer. Do not be too quick to accept the answer as an unambiguous identification of the analyte or reject it as not being possible due to low numeric indicators of correctness.

The quality of the results from a computerized library search is dependent on:

* the quality of the spectra in the library;
* whether the spectra in the library are searched as complete or condensed spectra;
* the search algorithms; and
* the quality of the submitted spectrum.

Weakness in any of these areas must be compensated for by careful examination of both the submitted and library spectra. Additional information about the sample's origin and characteristics of the identified compound can be used to increase the confidence of, or even confirm, any identification based on mass spectral data alone.

Substructure Identification by Library Searching

Stephen E. Stein, Dmitrii V. Tchekhovskoi
NIST Mass Spectrometry Data Center, Gaithersburg, MD 20899.

A new computer method for identifying structural features of a compound from its electron-ionization mass spectrum has been developed. Like other "nearest neighbor" (KNN) [1] methods, it extracts structural information from compounds in a reference library whose spectra are most similar to a submitted spectrum It uses algorithms similar to those used for compound identification [2] and is therefore relatively easy to implement and relies on match factors already familiar to many users It generates readily understood substructure present and absent probabilities for a wide range of structural features.

Some significant differences between the present system and two well-developed interpretive search systems, SISCOM [3] and STIRS [4], are:

1) Match Factor Computation: A single match factor measures the similarity of the unknown and a library spectrum: $MF = 1000\left(\sum A_U^{1/2} A_L^{1/2}\right)^2 \Big/ \left(\sum A_U \sum A_L\right)$ (sums are over all peaks, A_U and A_L are abundances for unknown spectra and library spectra, respectively).

2) Match Factor Weighting. Contributions of retrievals are weighted by their relative 'distance' from the submitted spectrum [5]. The weight of the retrieval of rank **r** (**r**-th member of a hit list) is $w_r = 2^{\frac{MF(r)-MF(1)}{75}} \Big/ N$; normalization factor N is such that $\sum w_r = 1$. (75 is empirical constant to optimize the substructure identification). The overall weight W_S of substructure S is the sum of weights of retrievals that contain the substructure.

3) Absolute Probabilies. These were derived using a large test set comprised of one spectrum of each of the 7891 compounds in the NIST Selected Replicates Library. Probabilities of the substructure occurrence were derived from W_S values derived from searches of the 1992 version of the NIST/EPA/NIH reference library (61,500 compounds).

4) Screening: An efficient means of rapidly locating similar spectra reduced search times to levels comparable to those typical of traditional library-search identification methods.

5) Substructure Absent Probability: These are determined in the same manner as substructure-present probabilities.

If the molecular weight of the unknown compound is supplied, identification of certain substructures can be improved by including 'neutral loss' peaks. Slight modifications of the present method permits the identification of chemical formula, molecular weight and number of rings + double bonds.

Two sets of substructures were used for testing. One contained the most common structural groups employed in earlier studies. Results of test studies are discussed below. A second group of substructures was comprised of most common sets of up to 10 connected atoms found in NIST/EPA/NIH library. This allows the extraction of a large fraction of all structural information contained in hit lists.

Comparisons of the present method with earlier STIRS and KNN results [1] are shown in the Table. Separate studies [5b] show that that a principal reason for the superior performance of the present system is simply due to the use of a larger library. For **KNN** about half of the improvement is due to the use of optimized algorithms.

Table

Substructure	*Num. in test set*	*% in lib*	*RC**	*STIRS %C***	*Present %C***	*RC**	*KNN %C***	*Present %C***
C=O	3111	47	31	100	99	51	71	96
OH	1558	23	42	78	95	45	71	86
-O-	2348	37	40	98	98	54	74	96
OCH_2OCH_3	1806	29	49	81	95	36	66	97
OC=O	1435	22	55	87	94	29	61	97
Phenyl(any)	2421	33	75	86	96	71	70	97
$-NH_2$	396	5.3	44	69	87	17	62	92
>NH	430	11	19	58	94	25	41	75
-N<	875	18	30	89	97	51	72	87
-S	653	11	35	86	100	32	60	100
-F	274	6.1	61	84	100	18	40	100
-Cl	834	8.8	74	96	100	54	89	100
Alkyl ≥ C_3	1612	19	56	70	85	54	68	86
Alkyl ≥ C_2	1554	19	19	78	95	32	49	85
C=C	1202	18	38	88	85	42	68	83
-CH<	2917	45	44	63	92	49	58	91
>C<	1464	27	20	85	99	41	57	96
C-ring	1090	15	20	83	98	54	70	96
Het-ring	1895	46	31	95	98	57	71	92
Average			42.8	82.8	95.1	42.7	64.1	92.2

* percent of test compounds containing substructure which have been identified as such (recall)
** percent of correct identifications for given recall (RC) value.
Both STIRS and comparative studies used neutral losses.

References

1. Lowry, S.R.; Isenhour, T.L.; Justice, Jr., J.B.; McLafferty, F.W.; Dayringer, H.E.; Venkataraghavan, R.J. *Anal. Chem.* **1977** *49*, 1720-2.
2. Stein, S.E.; Scott, D.R., *J. Am. Soc. Mass Spectrom.*, **1994**, *5*, 869-66.
3. Domokos, L.; Hennenberg, D.; Weimann, B. *Anal. Chim. Acta* **1984**, *165*, 61-74.
4 Haraki, K.S.; Venkataraghavan, R.; McLafferty, F.W. *Anal. Chem.* **1981**, *53*, 386-392.
5. a) Stein, S.E. *J. Am. Soc. Mass Spectrom.*, **1994**, *5*, 316-323; b) *ibid.*, **1995**, in press.

Sharing Corporate Mass Spectral Data Bases

J. L. Little, W. M. McSpadden,
Eastman Chemical Company
Kingsport, TN, 37662-5150
Tel. No. 615-229-8685

Goal/Current Status. Our corporate mass spectral database is composed of 29,500 spectra and 15,500 structures. Our goal is to share this database between all of our mass spectrometers (35 instruments, 60 users) within Eastman Chemical Company. Our corporate and various commercial databases are used extensively in our research, development, industrial hygiene, and environmental work. The instruments, located in Tennessee, Texas, and Arkansas, are connected by an ethernet network. Our instruments employ data systems from a variety of manufacturers including Finnigan (PDP-11, UNIX), Hewlett Packard (DOS, UNIX), and VG (VAX workstations).

We have two approaches for reaching our goal. One involves the transfer of data to a host computer for processing and the other employs local processing of the data.

Approach #1: Processing Data on Host Computer. Data files are transferred to a host computer in Tennessee for processing and the results are displayed on the user's local computer (see References 1-3). The VG OPUS software is employed for data processing and a "user-friendly" VAX DCL interface is employed for file transfer/conversion. This is the preferred approach and is employed by users whose primary responsibility is mass spectrometry. This approach allows searching of databases by substructure, advanced data processing capabilities, and the automatic addition of user spectra to the corporate database

There are several disadvantages to this approach. The user must have a network connection and must learn an additional software package. Also, the files must be transferred/converted which requires 1-30 minutes depending on file format and file length.

Approach #2: Processing Data Locally. The second approach (see References 4) is to process the data locally on a PC (DOS/Windows) employing standard software from Hewlett Packard (HP). Our corporate database and structures were transferred to the HP format. This approach only displays structures with library results and does not allow searches of the databases by structure. The advantages of this approach are that most of the targeted users already employ the HP data system for their mass spectrometry analyses and no file transfer/conversion is required.

There are several disadvantages to this approach. The HP software will search multiple libraries, but only the results from one library at a time are displayed. The PBM search algorithm is used for the searches and gives poor results in many cases for the electron impact spectra of "low-level" ("noisy") components. The structures displayed do not show hydrogens attached to nitrogen, oxygen, sulfur, etc. This is a limitation of the HP software and not the MOL files created by the Exographic's software from the SMILES files.

Creation of HP Electron Impact Mass Spectral Data Base for DOS and UNIX computers. Our corporate library is maintained on our VAX mainframe in the VG OPUS format. Entries added to individual's OPUS libraries are automatically added to the corporate library daily. This process is described in Reference 4.

A variety of programs were used to transfer our VG OPUS corporate library to the HP UNIX and DOS formats. The programs include the VG OPUS Specbase utility, VAX DCL macros, user-written C programs, Palisade MASSTransit, and HP Windows utilities. The process employed is described in Reference 2.

The data base files are identical for the HP UNIX and DOS computers. The HP binary data base was created on the UNIX computer because the conversion time was significantly smaller. The HP UNIX software required approximately 33 hours to convert 29,500 entries and could create the data base in two steps. The total process was estimated to take 30 to 60 days of computer time on the HP DOS/Windows computer and 30 step! Our corporate data base can be searched on the HP UNIX computer system. However, no attempt was made to create a UNIX structural data base.

Creation of HP Structural Data Base for DOS and UNIX computers. Structures are added to all our VG OPUS corporate data base entries when the electron impact mass spectrum is entered (see References 1-3) The structures are drawn with a drawing package that is part of the VG OPUS software. The structures are saved in SMILES format.

The HP software requires structures be in a MOL format. A variety of programs were used to transfer structures in SMILES format in our corporate library to the MOL format. The process for this conversion is detailed in Reference 4 The programs include the VG OPUS Specbase utility, VAX DCL macros, user-written C programs, Palisade MASSTransit, MDL ISIS Draw, Exographic's Consystant, HP Windows utilities, and a user-written HP macro.

The HP DOS/Windows software uses the CAS number in the electron impact data base to cross-reference to the CAS number and structure in the structural data base. If the CAS number of the library result is found in the structural data base, the library entry is displayed with structure. None of our entries are assigned CAS numbers. Our entries were assigned "pseudo-CAS" numbers of between 1 and 49-99-9. The first real CAS number is 50-00-0 for formaldehyde. The last digit in the CAS number is a "parity" check, but we do not employ a parity check in our numbering system which gives us a factor of 10 more "pseudo-CAS" numbers.

References

1. J. L. Little, Handout at Poster Session of 1994 Chicago ASMS Meeting, "Network Processing of Mass Spectral Data."
2. J. L. Little, Proceedings of the 42nd ASMS Conference on MS and Allied Topics, Chicago, Illinois, pp 479-480, " Network Processing of Mass Spectral Data," 1994
3. J. L. Little, Handout at Poster Session of 1994 Chicago ASMS Meeting, OPUS user's manual, "Getting Started in OPUS (Edition 1.9)."
4. J. L. Little, Handout at Poster Session of 1995 Atlanta ASMS Meeting, "Creation of Data Base for HP Mass Spec Data Systems."

ARTIFICIAL NEURAL NETWORKS FOR IDENTIFYING COMPONENTS IN MIXTURES BY MASS SPECTROMETRY

Jackson O. Lay, Jr. and Jerry A. Darsey
FDA, NCTR, Jefferson, AR; University of Arkansas at Little Rock, Little Rock, AR

INTRODUCTION

Spectral libraries are used as a rapid means of identifying unknowns (1). Identification is based on a comparison between the unknown spectrum and spectra in the library. Algorithms used range from simple geometric techniques to probability-based matching methods that incorporate known relationships (2,3). Strategies that rely on comparisons between unknown and reference spectra are based on the assumption that the unknown spectrum represents a single component. Because a skilled interpreter may recognize components in a mixture-spectrum by inspection, a computational system designed to mimic human thought might have distinct advantages, especially if it was "self-training". An artificial neural network (ANN) is such a computational system. It has been defined as "a computing system made up of a number of simple, highly interconnected processing elements, which process information by its dynamic state response to inputs" (4). ANNs do not store information in separate memory arrays; rather they "learn" by taking weighted sums of inputs and comparing their results to known outputs after application of an appropriate transfer function. The result of this process is that information is stored in a weighed distribution of connections between the same set of inputs and outputs (4-6). Although "self-training" requires minimal intervention or knowledge of computational methods, this initial step involves many calculations. The weighted distribution of connections generated in the training, however, can be transported between computers and used to identify inputs (e.g. unknown mass spectra in this instance) in a few seconds. In a related study, an ANN was used for the interpretation of infrared spectra (7). In that study the emphasis was on the identification of functional groups. We report the use of ANNs to identify individual mass spectra from mixtures after training the ANN using spectra from pure compounds. The ANN output values were compared to Similarity Index values.

EXPERIMENTAL METHODS

Spectra of 6 compounds were obtained from the PC version (4.0) of the NIST/EPA/NIH MS data base. The ANN was trained using metolachlor (I), metribuzin (II), methyl parathion (III), alachlor (IV), and 2,6-dichloro-N,N-dimethyl-benzamide (V). Di(2-ethylhexyl)-phthalate (VI), was included in some mixture-spectra but was not used to train the ANN. Mixture-spectra were obtained by summing the intensity values at each mass from each component. The mixtures included two binary mixture-spectra for compounds I+II, and III+IV, and two ternary mixtures, I+II+III, and I+II+VI. The spectra of selected components were multiplied by weighing factors to produce unequal mixtures. These mixtures included spectra corresponding to the following compositions: III(60%)+IV(40%), I(90%)+II(10%), and III(90%)+IV(10%).

The ANN software was NNETS (VAX version) written at NASA. The architecture was as follows: (1) Input: 300 nodes (m/z 1 to m/z 300); (2) Output: 5 nodes for compounds I-V; and (3) One hidden layer with 15 nodes that connect all input and output nodes and "learns" the values needed to identify I-V. The ANN was programmed by entering the intensity of each mass, from 1 to 300 daltons, in the corresponding numbered node. For training, output nodes were assigned a magnitude of 0.9 (compound present) to the output mode corresponding to the correct compound and 0.1 (compound absent) to the remaining nodes. The mixture-spectra were evaluated using the ANN and the Extensive Search algorithm from the NIST/EPA/NIH MS database.

RESULTS AND DISCUSSION

For spectra corresponding to similar contributions from each component, both the ANN and the NIST/EPA/NIH "Extensive Search" method provided evidence regarding the presence of individual compounds in the mixtures. The finding of a high Similarity Index value by the NIST/EPA/NIH search program, but no positive response by the ANN for one of the training compounds not present in a test mixture-spectrum, suggests that the ANN has a different and complementary selectivity for discriminating against false positive responses. Both the difference in selectivity and the near instantaneous response to input (spectra) after training suggest that neural network computing may be a useful complement to existing methods for the interpretation of spectra from mixtures.

REFERENCES

(1) Ramos, L.S.; Bebee, K.R.; Carey, W.P.; Sanchez, E.M.; Erickwon, B.C.; Wilson, B.E.; Wangen, L.E.; and Kowalski, B.R; *Anal. Chem.* **1986**, *58*, 294R.
(2) Varmuza, K.; *Pattern Recognition in Chemistry*, Springer, Berlin, **1980**.
(3) Peysna, G.M.; Venkataraghaven, R.; Dayringer, H.E.; and McLafferty, F.W.; *Anal. Chem.*, ***1976***, *48*, 1362-1368.
(4) Caudill, M.; *AI Expert*, **1987**, *12*, 46-52.
(5) Caudill, M.; *AI Expert*, **1988**, *2*, 55-61.
(6) Lippmann, R.P.; *IEEE ASSP Magazine*, **1987**, *4*, 4-23.
(7) Robb, E.W.; and Munk, M.E.; *Mikrochim. Acta [Wien]* **1990**, *1*, 131-155.

DESIGN OF A COMPUTER-CONTROLLED MAGNETIC SECTOR MASS SPECTROMETER

[1]Robert B. Cody, [2]S. Makino, [2]T. Asada, [2]K. Yoshidome
[1]JEOL USA, Inc., 11 Dearborn Rd., Peabody, MA 01960
[2]JEOL Ltd., Musashino 3-1-2, Akishima, Tokyo, Japan

Introduction. Effective computer control of a high resolution mass spectrometer can be complex. Support of both research and routine analysis requires both interactive and automated tuning and data acquisition. The computer must control the ion source, the magnetic and electric sectors, focusing lenses, slits, gas supplies, probe, inlet and detector conditions.

We have developed a fully automated mass spectrometer with a user interface that makes extensive use of graphical instrument diagrams. Tuning is facilitated by ion optics which use quadrupole lenses to maximize ion transmission and minimize the number of control parameters. A deterministic approach to auto-tuning mirrors the procedure followed by a human operator.

Methods. The mass spectrometer ion optics are based upon a QQBQE design that makes use of DC-quadrupole lenses to control beam shape and maximize ion transmission. This design minimizes the number of elements that need to be controlled to achieve high-resolution mass spectra. The procedure for tuning the mass spectrometer is very systematic and reproducible and therefore easy to program.

The auto-tuning times were determined for standard reference compounds for several ionization modes at both low and high resolution conditions (resolution = 1000 and resolution = 10,000, respectively). The reported times correspond to full tune-up from a completely untuned starting condition ("full tuning") and partial tune-up starting from a previously stored parameter set ("quick tuning").

User Interface For Instrument Control. The user interface is mouse- and window-driven and based upon extensive graphical instrument diagrams. Parameters are grouped according to functionality. Parameter groups are reached through a central window (called the "Mode Controller") that represents the overall instrument configuration and status. Windows that control parameter groups can be accessed through any of three redundant means. These consist of (1) menu choices, (2) icons and (3) pushbuttons next to a symbolic representation on the "Mode Controller". This redundancy avoids the common problem of having only one way to get to a particular display. The user interface operates as a X-Windows / Motif application to permit operation of the mass spectrometer over a network.

Auto-Tuning Scripts. Auto-tuning is based upon a grid-search procedure defined by the operator in a script file. The script defines (1) which parameters are tuned, (2) the order in which the parameters are tuned, (3) the range over which a parameter is swept, and (4) whether or not pairs of parameters are to be optimized simultaneously. This "simultaneous"

tuning is useful for optimizing the three ion source lens pairs: left and right focus 1, left and right focus 2, and upper and lower deflector.

Once a valid set of instrument parameters has been determined, these parameters can be loaded and used as a starting point for "quick tuning" a few selected parameters. The remaining parameters are stable over long periods of time and do not need frequent re-adjustment.

AUTO-TUNING TIMES

Ionization Mode	Full Tuning	Low Resolution Quick Tuning
EI	1 min. 5 s.	14 s.
CI	1 min.	15 s.
FAB	1 min. 27 s.	23 s.
FAB (FD source)	1 min. 41 s.	22 s.
FD	50 s.	15 s.

Ionization Mode	Full Tuning	High Resolution Quick Tuning
EI	2 min. 26 s.	17 s.
CI	2 min. 27 s.	17 s.
FAB	3 min. 14 s.	22 s.
FAB (FD source)	2 min. 50 s.	27 s.

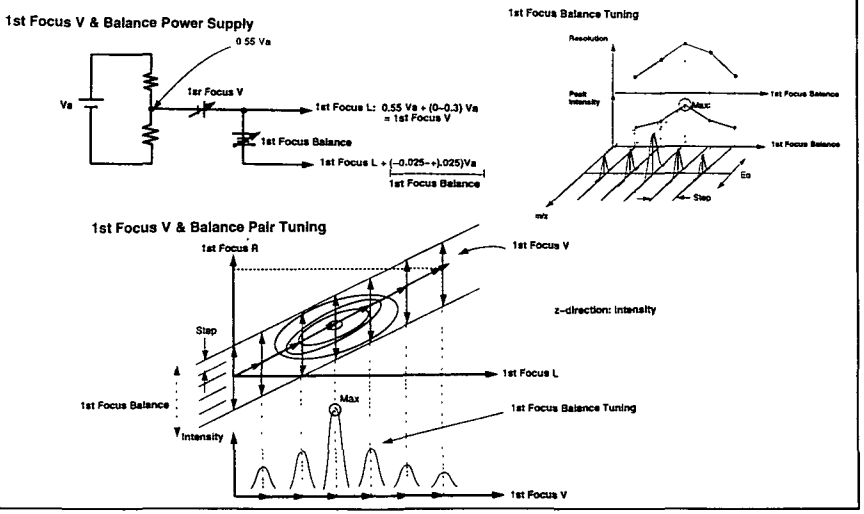

A High-Performance FT-ICR Mass Spectrometer Data System

Michael W. Senko, Jesse D. Canterbury, Shengheng Guan,* and Alan G. Marshall*

Center for Interdisciplinary Magnetic Resonance, National High Magnetic Field Laboratory, Florida State U., 1800 E. Paul Dirac Dr., Tallahassee, FL 32310

* Department of Chemistry, Florida State University

A flexible high-performance FT-ICR data system (**M**agnet laboratory **I**on cyclotron resonance **D**ata **A**cquisition and analysis **S**ystem, **MIDAS**) has been designed and constructed with VXI architecture and a personal computer running Microsoft Windows. Emphasis is on flexible hardware and software for generating complex event sequences while maintaining ease of use.

Timing is controlled by an Interface Technologies 96-channel digital pattern generator with 40 ns time resolution and 8,192 distinct events. Events are linked in tables which may be looped and nested to produce sophisticated experimental sequences. An in-house instrument controller converts the digital output of the pattern generator into four 12-bit voltages, four 8-bit voltages, eight TTL triggers, and eight pulsed-valve current sources. Frequency-sweep ("chirp") and SWIFT ion excitation waveforms are created by a Hewlett-Packard arbitrary waveform generator with 256K 13-bit words. The time-domain signal is acquired with a Hewlett-Packard 10 megasample/second digitizer with 4M 16-bit words, and on-board digital heterodyning capability. All processing is performed on the host computer (90 MHz Pentium®), which executes a fast Fourier transform in less than 5 seconds for 256K data .

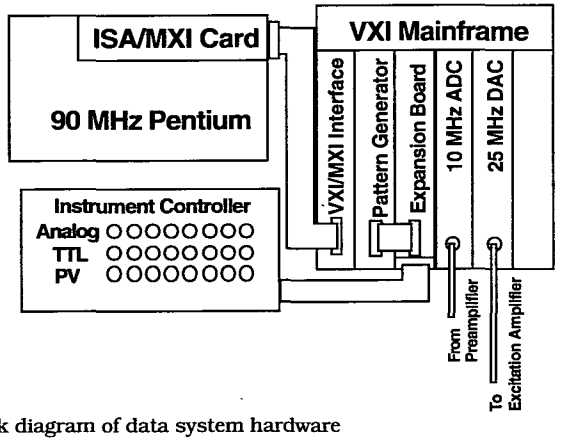

Figure 1. Block diagram of data system hardware

Individual programs for acquisition, analysis and wave form generation have been created by use of National Instruments Lab Windows/CVI, which produces stand-alone Windows executables. The acquisition program allows for simple creation and editing of experimental sequences by use of an intuitive graphical interface designed to minimize user input. Data files are stored in a custom format that uses ASCII text for all experimental parameters to simplify data access, and standard binary format for data to minimize storage requirements.

The analysis program allows for simultaneous viewing of multiple data files in resizable windows. Standard Windows drawing programs may be used for publication quality output: spectra are copied to the clipboard in vector format by use of an external module created with Borland Delphi and Pinnacle Publishing Graphic Server SDK. Customized analysis routines can be written in any language that supports dynamic data exchange (DDE) for communication with the DDE server in the analysis program.

Future work will focus on improvements to the acquisition module for the support of more complex experimental sequences, optimization of the analysis program to reduce memory requirements and expanding the functionality of the DDE server. This work was supported by the National Science Foundation (CHE-94-13008), NIH (GM-31683), and the National High Magnetic Field Laboratory at Florida State University.

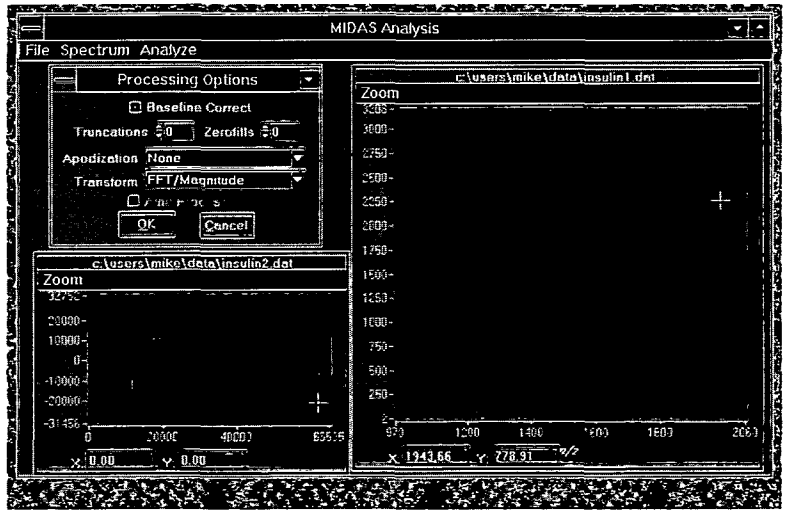

Figure 2. View of data analysis program

High Performance Data System for Ion Trap Mass Spectrometry

Gregor Overney and Christie G. Enke
Department of Chemistry, University of New Mexico, Albuquerque, New Mexico 87131-1096

Kevin Hart and Marc B. Wise
Organic Chemistry Section, Chemical & Analytical Sciences Division, Oak Ridge National Laboratory, Oak Ridge, Tennessee 37831

We have developed a universal, high performance data system for an ion trap mass spectrometer to support advanced ion trap experiments such as fast scan rates (> typical 5000 *u/s*), large mass ranges (> typical 650 *u*), high mass resolution (> typical 1 *u* resolution), custom waveform applications, coordination with direct sampling interfaces, and exploration of new scan modes in a customizable software and hardware environment.

All software components of the data system are programmed using LabVIEW® version 3 [2] extended by modules written in WATCOM's 32 bit C compiler version 10 to increase performance. LabVIEW was selected because it is an icon based programming environment with a wide range of pre-programmed data acquisition drivers. The main menu structure consists of five points: calibration of system, definition of experiment, running of experiment, data displaying and analysis, and utilities During the definition of the experiment, a scan function editor (SFE) is used to multiplex several experiments (e.g., alternating EI/CI scans). The SFE is programmed with LabVIEW® using an array with dynamic memory allocation to store a large number of single scan tables. An important feature during the running of the experiment is the fast mass peak finder (MPF) program. The MPF is entirely written in ANSI C and appended to the LabVIEW main program using the concept of code interface nodes (CINs). CIN modules allow fast program execution of time critical jobs such as mass peak finding. In addition, an optional Savitzky-Golay (S-G) smoothing [3] can be used to improve the reliability of the MPF. Especially very small peaks, hardly distinguishable from the back ground noise, can easily be made accessible to MPF after S-G smoothing.

The dynamic experimental control has been possible through a real time buffer access. Each of the VXI [1] hardware components for data acquisition has its own high speed memory buffer. The hardware modules are interconnected via the VXI bus and are the C-size format. The VXI bus is often encountered in industrial measurement and test applications such as auto emissions monitoring and chemical process control. We are using an embedded 486 VXI host controller from National Instruments, a 16 bit, 500 kSamples/sec ADC/DAC from Kinetic Systems (two

boards), a Tektronix 25 MSamples/sec Arbitrary Waveform Generator (AWG), and a 48 channel Digital I/O module from Tektronix. The ADC board V207 from Kinetic Systems is used for synchronized data acquisition of microscans using internal VXI TTL trigger lines. Three additional channels of the V207 board are available for digitizing other experimental parameters. The DAC board V285 from Kinetic Systems is generating the signals for the primary RF generator (mass selection). Filament gating (monitored by internal VXI TTL trigger lines), multiplier on/off, calibration gas on/off, filament on/off, and valve control of CI-gas are controlled by the Digital I/O board VX4801 from Tektronix. The AWG board VX4790A from Tektronix generates signals for the end-cap waveform amplifier responsible for MS/MS features.

This data system also integrates the direct sampling interfaces developed at ORNL for environmental monitoring of volatile organic contamination of air, water and soil. It can also be extended for acquisition of MS/MS and MS^n spectra. An option for remote control of the instrument using TCP/IP will be implemented using LabVIEW's network protocol library.

We thank all members of the research group of Prof. Enke for their suggestions and interest in this project. This project is part of a subcontract between The University of New Mexico and Martin Marietta Energy Systems, Inc. as specified in proposal SS259. This work was supported by the Offices of Technology Development and Arms Control, U.S Department of Energy, under contract DE-AC05-85OR21400 with Martin Marietta Energy Systems.

[1] VME extension for instrumentation. Recognized standard for card-modular automated instrumentation since 1987.
[2] National Instruments Corporation, 6504 Bridge Point Parkway, Austin, TX 78730-5039.
[3] A. Savitzky and M.J.E. Golay, *Anal. Chem.* **36**, 1627 (1964).

Programming the Teledyne Filtered Noise Field System

N.J. Clarke, D. Hoekman* and J.F.J. Todd
The Chemical Laboratory, University of Kent, Canterbury, Kent, CT2 7NH, Uk
**Teledyne ET, 274 Terra Bella Ave, Mountain View, CA 94043, USA*

I. Introduction

The Teledyne Filtered Noise Field(FNF) unit allows a supplementary AC field to be applied to the end caps of a quadrupole ion trap mass spectrometer. This field can be customised by the operator and allows the user to retain specific ions of interest whilst ejecting all other ions from the trap simultaneously. This is achieved by applying a broad range of radio frequencies in a single waveform. These frequencies come into resonance with the secular frequencies of the trapped ions and cause their trajectories to become unstable by imparting energy. The ions are then lost either through holes in the end cap electrodes of the ion trap or by colliding with the trap walls. The waveform can be customised so that "notches" or areas of zero amplitude can be created within the waveform. These notches correspond to mass/charge values for the ions of interest, and when the waveform is applied it ejects all ions which come into resonance but leaves any others untouched.

The controlling software for the Teledyne is written in FORTH and a program has been developed allowing the user to automate the use of the system as well as control parameters which are normally fixed.

II. Experimental

II.1 General Information

The software was written using the version of FORTH supplied by Laboratory Microsystems Incorporated (LMI). The original code for the Teledyne control software written by Teledyne ET and permission to use or alter it was obtained.

The aim of the project was to reduce the amount of user input required to set up the system and to automate the calibration and recording of the data. Further it was hoped to develop a program which would be able to intelligently produce a customised waveform from a series of *m/z* values provided by the user. This would lead to the possibility of automated tandem MS using the Teledyne unit to isolate and dissociate the ions of choice. The *m/z* values are passed to the computer via a text file set up by the operator beforehand.

II.2 Description of Program

The system starts by loading in the *default* waveform for the program. This waveform has a known number of *components*, all of which are set to a standard amplitude of 100 percent. The overall gain of the system is set to a predetermined value, normally 2000, and the system then automatically calibrates the waveform. This calibration uses two frequency and mass values to carry out a standard calibration of the waveform, determining a *m/z* value equivalent to each frequency present.

Once this is complete the system opens the file containing the *m/z* data. The filename is provided by the user, either directly within the program code, or interactively on running the

program. If this file does not exist the program displays an error and terminates. Once the file is open the first data item is read onto the stack. The format of this file is specific; the first entry within the file is the number of masses that are to be isolated: on each succeeding line the *m/z* value to be isolated is placed by itself and the line delimited by a carriage return.

For each *m/z* value read in turn the following procedure is applied: the system calculates the mass for each subsequent frequency within the waveform and compares this to the *m/z* value read from the file under examination. The program then scans the *m/z* value list which has been set up during calibration and checks for the closest match. This is classed as the centrum of the window and set to zero amplitude. The frequencies above and below are then converted to *m/z* values and if they lie within a user defined range surrounding the centrum they are also set to zero. The way the calibration is carried out means that at the high mass end of the scale the mass gap between frequencies components is quite large, often over 20 mass units. At the lower end of the range however each *m/z* value will be represented by several frequency components as the resolution of the system increases. This weighting of the frequencies means that the *window* notched into the waveform at the lower end of the mass range will cover more components of the waveform but actually covers a smaller mass range than the same sized window at a higher mass range. The program realises this and uses a weighting principle to reduce the size of the frequency window applied at the higher end of the mass range. Once the window of frequencies has been notched out of the waveform the program repeats the entire procedure for the next *m/z* value in the file. As the end-of-file marker is read the waveform is updated and ready to be applied to the system. The usual triggering system of two pulses supplied from the ion trap is used to implement the waveform.

III. Results

The system has been tested and encouraging results have been obtained. The program produces identical results to those obtained by human operators in most cases. Further work is underway to couple the ITMS system directly with the Teledyne to allow a feedback loop to be exploited. This would enable the Teledyne to "fine tune" the waveform for optimum isolation and peak intensity.

IV. Acknowledgements

NJC thanks the University of Kent and Pfizer Central Research Ltd for financial support.

A High Speed Data Acquisition System for Fast GC-MS

A Gilbert[1], P Atherton[1], S Hanson[1], L Lu[1], S Smith[1], A Preston[2]
[1]Fisons Instruments V.G.Organic, Manchester, U.K.
[2]University of Manchester, Manchester, U.K.

Fast Gas Chromatography can produce peak widths of substantially less than one second for individual components. The use of a scanning mass spectrometer as a detector in these circumstances requires that the spectrometer and its associated data acquisition system be sufficiently fast to faithfully capture the peak profile, and avoid distortion of the spectra when the intensity is changing rapidly. 10 spectra per peak is generally considered sufficient.

Time of Flight (TOF) mass spectrometry has the ability to produce thousands of spectra per second, and has been available for many years, however its use as a chromatographic detector has been limited, until recently, by the availability of electronics systems able to digitise TOF data, and the prohibitive size and cost of computers with sufficient power to process the data in real time. Relatively few references to fast GC-MS can be found in literature

A system (fig 1) has been constructed capable of acquiring, processing, and storing up to 100 scans per second. These data can then be manipulated using a standard MS data system (V.G. MassLynx).

Data are digitised using a 200 MHz 8 bit analog to digital converter. Successive flights are averaged to provide the required number of spectra per second. A DEC Alpha processor detects and assigns masses to peaks, which are stored to a local disc controlled by a transputer subsystem.

The system is housed in an industry standard P.C. which provides networked access for users. This effectively decouples the acquisition data storage from any user activity.

43rd ASMS Conference on Mass Spectrometry and Allied Topics

Results show GC-MS of a solvent mixture with all components eluting in under 1 minute with specta acquired at 35 per second.

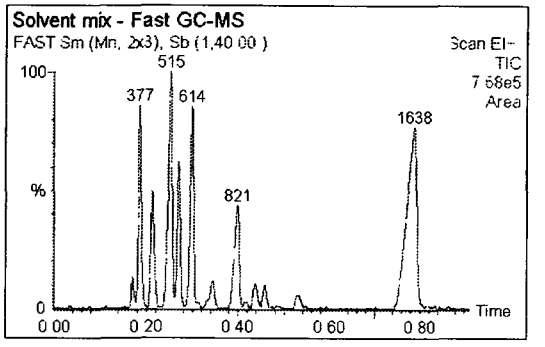

References

1 R D McLane, J Allison, C G Enke, G E Yefchak, R Grix, J.T Watson, J.F.Holland, 39th ASMS 1991
2. A.Amirav, S.Dagan, 41st ASMS 1993
3. P.G.Van Ysacker, H.G.Janssen, H.M.J.Snijders, P.A.Leclerq, C.A.Cramers, H.Wollnik, 16th International Symposium on Capillary Chromatography 1994

Display and Manipulation of Three-Dimensional Plots of Ion Trap Data

Li, Rebecca; Hoekman, Don; Wilson, Ray; McHugh, Sean; Karr, Dane
Teledyne Electronic Technologies, Scientific Instruments, Mt. View, CA 94043

The development of graphics-oriented data systems and high resolution video displays and printers allows mass spectrometry data to be displayed in a variety of new and interesting formats. By combining these features with a research-grade ion trap data system, capable of acquiring and storing full-scan profile data, we may display true three-dimensional plots representing both ion trap peak intensity and peak shape.

In addition to conventional plots representing mass, intensity, and time, ion trap experiments may generate three-dimensional data plots representing peak shape, intensity, and virtually any ion trap parameter, adding an extra dimension of information to the displayed data plots.

Data may be displayed using the following rendering methods, in order of complexity:

Wireframe
- Simple and fast - no hidden surface removal or shading.

Painted
- Fast - flat shading and depth sorted.

Partial Hidden Surfaces
- Fast - wireframe rendering with primitive hidden surface removal.

Flat Z Buffer
- Fast - flat shading with more accurate hidden surface removal.

Full Z Buffer
- Slow - phong shading algorithm with accurate hidden surface removal.

The display of true three-dimensional plots, representing raw mass spectrometry data, allows us to peer one level deeper into the nature of the ion trap.

Just as a finished quantitation report, containing compound names and amounts is derived from a series of individual mass chromatograms, the mass chromatogram is derived from a series of spectra, the spectrum is derived from a series of mass peaks, and each mass peak is derived from a collection of individual ions. It is at this most fundamental level that we have explored, where characteristics of the ion trap mass spectrometer may be displayed in a manner both educational and entertaining.

43rd ASMS Conference on Mass Spectrometry and Allied Topics

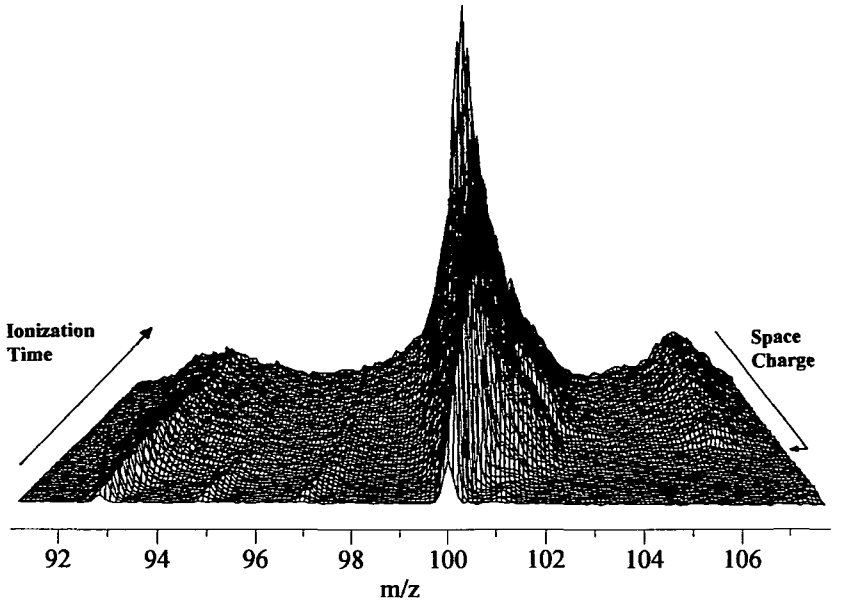

Three Dimensional Plot of Profile Data of m/z 91 to 108 as a Function of Ionization Time

Notice the intense broadening of the m/z 100 peak, and its shift to the higher mass range of the plot, as it passes into the space charge region. Also note the disappearance of the smaller peaks upon passing the space charge threshold, and the appearance of peak data at the m/z 106 position that only emerges upon passing the space charge threshold.

Interactive Setup and Control of Ion Trap Mass Spectrometry Experiments

Wilson, Ray; Hoekman, Don; McHugh, Sean; Li, Rebecca
Teledyne Electronic Technologies, Scientific Instruments, Mt. View, CA 94043

Experiments with research-grade ion trap mass spectrometers have typically involved the manual adjustment of one or more parameters in an ion trap scanning function, followed by the manual interpretation and display of the results.

We have developed a graphics-oriented experiment program designed to simplify the construction, execution, and data reporting operations involved in typical ion trap mass spectrometry experiments, providing a simple method to investigate and plot various functions of an ion trap. The experiments may vary from such things as a plot of multiplier linearity, to the conversion efficiency of an MS/MS/MS experiment as a function of CID tickle time.

To use the experiment editor from the 3DQ *Discovery* software, the operator first selects the parameter to be investigated, followed by its initial, final, and incremental value. The experimental parameter may either be pre-defined, or selected from any table in any scan function. Therefore, any of the following parameters may serve as the basis for an automated ion trap experiment:

Ionization time	Pump oscillator frequency
Ionization trapping level	Pump oscillator phase
Emission current	Pump oscillator offset
Multiplier voltage	Pump oscillator slope
Microscans	Prime oscillator frequency
Scan rate	Prime oscillator phase
Scan range	Prime oscillator offset
FNF waveform amplitude	Prime oscillator slope
FNF waveform time	MS/MS tickle time
Post-ion FNF time	MS/MS tickle amplitude
RF level for any table	Time for any table
FNF amplitude for any table	FNF time for any table

Due to the software intensive nature of the ion trap scanning function, the number of possible mass spectrometry experiments that may be performed is virtually unlimited. Therefore, the experiment program has proven itself to be a very convenient tool for investigating and plotting various characteristics of ion traps. This improved capacity to quickly generate experimental data has given us a better insight into the performance of the ion trap, while freeing us from the burden of manually deciphering an often overwhelming collection of data.

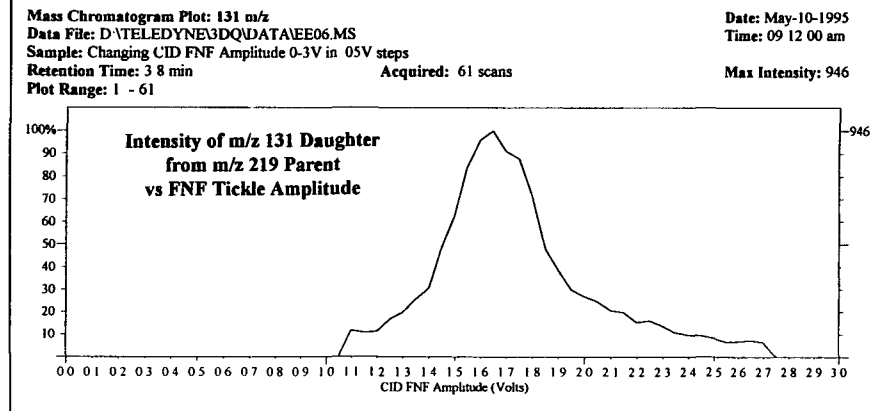

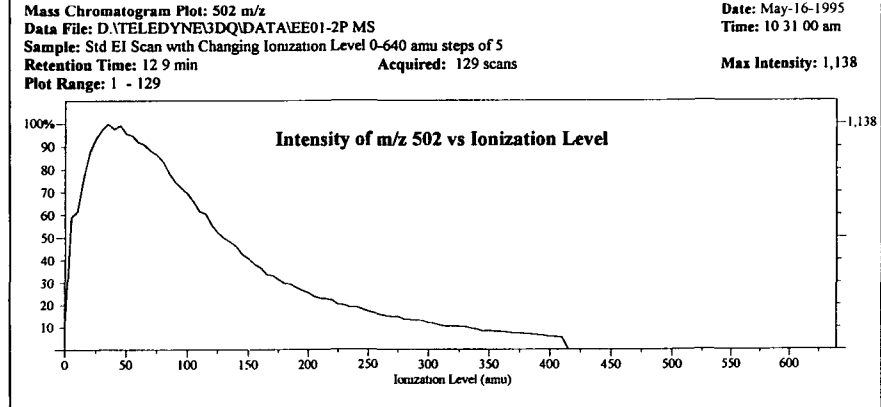

Automating Mass Spectrometry with AppleScript (WPB 046)

Ron Bonner[1], Lyle Burton[1], Matthias Mann[2] and Matthias Wilm[2]
[1]PE-SCIEX, 71 Four Valley Drive, Concord, ON, Canada L4K 4V8
[2]EMBL, Heidelberg, Germany

Over the last few years Apple Computer® have been developing a system of sending messages between application programs known as Apple Events®. Programs can generate Apple Events to be sent to themselves or to other programs or they can be generated by a high-level scripting language called AppleScript. Appropriately written programs can support AppleScript at several levels:

- Scriptable. Scriptable programs can be controlled directly from a user-written script; they contain a "dictionary" which describes the available Apple Events and parameters. This dictionary can be opened by Apple's Script Editor which is also used to write scripts.

- Recordable. If a program is recordable then the recording feature of the Script Editor can be used to automatically generate a script from operations performed by the user. This facility is very useful when a series of operations are to be repeated several times since a simple script can be generated quickly. It is especially useful when learning the scripting language.

AppleScript is very powerful, straightforward to use and learn, and is able to control multiple applications. Our new data processing program described here, MultiView, is both scriptable and recordable.

Programs that are not scriptable can still be controlled from an AppleScript—to a certain extent—by using a program such as PreFab Player™. This program essentially records user operations in terms of mouse clicks and key presses that can later be "played back" under script control.

This presentation gives four main examples of the use of AppleScript to process data. The first, "Find Metabolites", automates an operation that is common in the identification of metabolites, namely plotting the XICs of expected masses based on the mass of the parent drug and the mass offsets of likely metabolites. The second, "Start PeptideScan with Tags", illustrates the ability to control several programs from a single script. It transfers mass values from the MultiView program to the PeptideScan program which searches a database for the peptide sequence.

The third example, "Auto MS/MS", shows the use of PreFab Player to control the data acquisition software, which is not properly scriptable, in the analysis of peptide mixtures using the MicroSpray ion source. This device allows 1µL of a sample to be sprayed for upwards of thirty minutes giving enough time to perform many experiments. The device can, however, demonstrate high chemical background signals that make location of the molecular ions difficult, but if the peptide mixture is derived from the tryptic digestion of a protein, the y_1 ions should be at either m/z 147 (C-terminal Lys) or 175 amu (C-terminal Arg). A precursor scan for these species will often reveal the molecular ions of the peptides; these can be used as the precursor ions in product ions scans. The script demonstrates the automation of this procedure.

The final example exploits an important feature of AppleScript applications—the ability to periodically perform some action, in this case examining the contents of a folder to determine if there have been any new items added. Once again different applications and

now two separate AppleScripts are involved. These scripts implement a "Walk-up" API machine, *i.e.* routine users enter sample information at any time and the samples are run when the machine is free.

The package consists of three components:

- A user interface module (shown below) that allows the user to specify that a number of samples have been added to the autosampler, to name the samples, to specify the final destination folder (which could be on another computer), and to select the acquisition and post-processing methods. This application builds a text file which can be loaded into the acquisition program. While this module could have been implemented using a program such as "FaceSpan" which supplies a user-interface to scripts, it was decided to implement this as an application written in C.

- A "Sample File Watcher" script which checks for a new batch text file every ten seconds. If a new file exists (and the instrument is free), PreFab Player is used to load the batch and start the acquisition.

- A "Data File Watcher" script which checks for a new data file every ten seconds. If one is found it is moved to the final destination folder and processed with the selected script.

In operation, an experienced user builds the acquisition methods and the data processing scripts, places them in specific folders and starts the "WalkUp" application. This in turn starts the two watcher scripts. A routine user adds one or more samples to the autosampler, fills in the information in the "WalkUp" program and clicks the "Add" button.

This package can be used with any PE Sciex API instrument and allows great flexibility because of the ability to choose the acquisition and processing methods from a simple user interface.

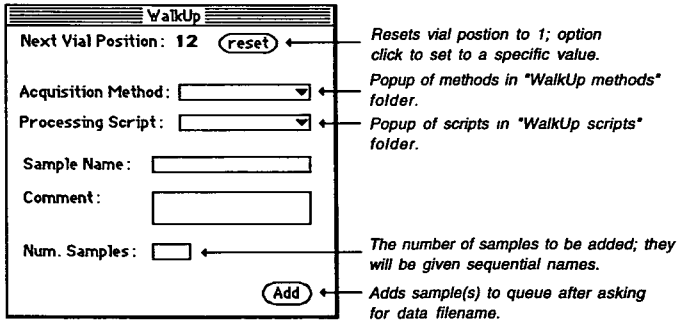

A New Mass Spectrometry Data Processing Program

R. F. Bonner and L. L. Burton

PE Sciex Instruments, 71 Four Valley Drive, Concord, Ontario, L4K 4V8, CANADA

We describe the development of a new data processing program that has been designed with several objectives:

- Ease of use: it is important that the user interface be intuitive and that it does not intrude between the analyst and the operations being performed. The system should be responsive and minimize the amount of typing that is required.
- Flexible: it should be possible to view data in different ways so that the various features can be emphasized as needed. The user should be able to 'browse' the data while searching for the important details.
- Comparison: since much data processing involves comparing data sets, these operations should be as direct as possible.
- Visualization of linkages: when data is derived from other data, the linkages should be emphasized so the user remains aware of the source of any particular data set.
- Interpretive tools: the user should be assisted in the interpretation of the data. It should also be possible to confirm the interpretation.
- Automation: there should be a straightforward mechanism for automating operations. Ideally the user should be able to record operations and play them back later (recordable) as well as being able to write scripts directly.

The program provides users with a variety of ways to examine complex data sets obtained from LC/MS analyses, in either general or specific ways. The User Interface is built around the concept that a window can be divided into separate regions (called 'panes') each of which contain data—either different data that is to be compared, or the same data treated differently. Panes can display data from the same file or different files and are created whenever new data is opened or generated. The panes are initially placed in default positions, but can be rearranged by the user as desired.

Virtually all of the common data processing operations are available with mouse clicks, either on icons that are in each pane or on a tool palette; pane icons deal with operations that involve two panes (such as subtraction that requires a source and a target pane), while the tool palette contains single pane operations. The latter include zooming a pane to the full size of the window, hiding, deleting and copying. In order to ease data comparison, panes can be locked together so that any zoom or scroll operation on one is repeated for all the others. Panes also contain a pop-up menu of commands that are specific to that pane; this again eases the process of manipulating data and allows easy access to common commands.

There are a variety of ways to 'browse' the data: spectra are generated from chromatograms and a marker shows the origin of the spectrum—if the marker is moved the spectrum will be updated. Similarly SICs are generated from spectra and can be changed by moving the highlight. These operations can also be performed from contour displays. Browsing is illustrated in the figure which also shows the tool palette and the pane icons.

All operations can be automated and results obtained can be transferred to other programs via scripts which are written using AppleScript®, an object-oriented, high-level language developed by Apple®. Scripts can be generated by writing them directly with a script editor, but can also be produced by recording operations. Since scripts can control multiple application programs, very powerful automatic processing can be implemented (see also WPB047).

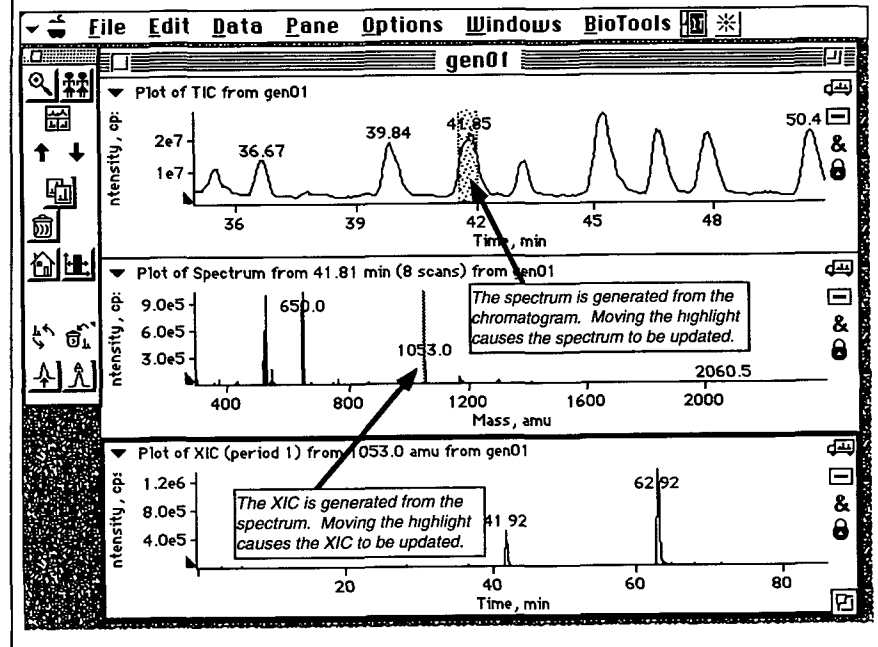

In addition to the traditional tools for displaying and processing data, the program contains a variety of new features that are designed to allow the analyst to more rapidly focus on the areas of interest and interpret the data:

- Contour displays that allow instantaneous color control so that an entire data set can be 'visually thresholded' and small peaks or noise immediately ignored. Contours can be linked to spectra and SICs allowing the user to interactively examine the data.
- Cluster analysis. The user can specify isotope patterns that are of interest and filter the data to obtain a subset containing ions that match the given pattern. This is especially powerful when used with the contour displays and is of importance in drug metabolism studies, environmental analysis, etc. The algorithm can be configured to perform a 'software neutral loss experiment' by looking for mass differences that may or may not be within the same scan, i.e. related components can be found even if they are separated by the chromatography.
- Interpretive tools. The program contains tools to interpret data, especially product ion spectra obtained from peptides, and includes the ability to visualize the interpretation. This is achieved by linking different views of the same data so that predictions made by one algorithm can be visually confirmed by another. The result is a powerful system for exploring the mass spectrometry of proteins, peptides, drug metabolites, etc.

These new capabilities provide users with powerful but simple ways to process data from many sources, such as drug metabolism, peptide sequencing and peptide mapping.

Automating Pharmaceutical API/LC/MS/MS Quantitation

Michael Wakefield, Klaus Weissenberg, Finnigan MAT, San Jose, CA

Introduction

Expanding FDA regulations and the trend towards lower dosage drugs has increased the demands on the analytical departments of every Pharmaceutical company. API/LC/MS/MS has become the analytical technique of choice for quantitative analysis of a product progressing through clinical trials. The demand to analyze hundreds of samples per week requires the entire quantitative process to be automated if meaningful results are to be delivered in a reasonable time frame. We have developed a new, intuitive and "easy to use" user interface for automating the entire quantitative process, called QuanGuide. The flow of the quantitation process using QuanGuide will be described and an example of a typical pharmaceutical assay will be presented.

Quantitation Process Flow

Processing quantitation data post acquisition involves three major steps:

1. Create a "Master Quan File" for processing standards, QC's and unknowns.
2. Create a calibration curve manually or automatically.
3. Process QC's and unknown samples manually or automatically.

QuanGuide is a shell that operates on top of the ICIS Quan environment. It is a software program Tcl/Tk developed at the University of California, Berkeley. It's designed to allow quicker creation of user interfaces in the UNIX programming environment. We have implemented Tcl/Tk to create a "user friendly" interface for ICIS Quan that will guide novice and experienced users through the entire quantitation process.

Generating Summary Quantitation Reports

The AutoQuan menu of QuanGuide includes the capability to create a single summary quantitation report from multiple quantitation files generated from an assay. The analyst simply creates a namelist of the quantitation files to be summarized, presses the QuanSummary report button and a summary quantitation report is generated. This report is saved as a quantitation file and as a tab delimited text file in a separate directory. This file can then be easily transferred to a networked computers spreadsheet or LIMS database for further manipulation.

Conclusions

Automating the entire quantitation process has been simplified with the development of QuanGuide. It has streamlined the setup, use and automation of the ICIS Quantitation package. Coupled with the Finnigan MAT TSQ 7000 and the API source, excellent accuracy and precision are attainable for any LC/MS assay.

43rd ASMS Conference on Mass Spectrometry and Allied Topics

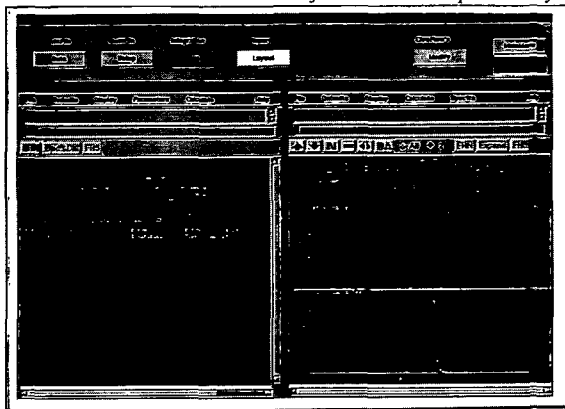

QuanGuide

QuanFile Entry

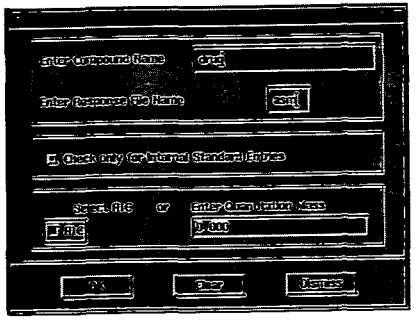

Quantitation Summary Report

Data File	Compound Name	Area	Area(x)/ Area(std	Area Int std	Specified Amount	Calculated Amount	Percent Difference	
curve1_1	drug	11508	0.014	850705	0.010	0.010	-3 00	
curve1_2	drug	16158	0.020	798627	0.016	0.016	-0.15	
curve1_3	drug	31375	0.038	826967	0.034	0.031	-8.23	
curve1_4	drug	59070	0.074	800008	0.063	0.063	0 40	
curve1_5	drug	107564	0 159	676416	0 126	0 138	10 17	
curve1_6	drug	202230	0.307	658268	0.251	0.269	7.24	
curve1_7	drug	364584	0.581	627213	0.503	0.512	1.82	
curve1_8	drug	493386	1.111	443994	1.005	0.980	-2.46	
qc05_1_1	drug	42474	0.061	694171	0.050	0.052	3.76	Low QC
qc05_1_2	drug	42798	0.058	731798	0 050	0 049	-1.01	
qc05_1_3	drug	44497	0.059	749859	0 050	0.050	0.50	
qc05_1_4	drug	45990	0.059	775272	0.050	0.050	0 46	Mean
qc05_1_5	drug	47314	0.062	768459	0.050	0.052	4.12	0.052
qc05_2_1	drug	46479	0.063	741002	0.050	0 053	6.18	Std Dev
qc05_2_2	drug	43956	0.061	722239	0.050	0 051	2.86	0.002
qc05_2_3	drug	45226	0.062	725302	0 050	0 053	5.52	
qc05_2_4	drug	47146	0.066	714478	0.050	0.056	11.99	%RSD
qc05_2_5	drug	44609	0.062	723457	0.050	0.052	4.28	3.84

A New Multi-Vendor "CLP-Like" Report Generator for GC/MS Data

Adam Patkin, The Perkin-Elmer Corporation
761 Main Avenue, Norwalk, CT 06859-0257

INTRODUCTION

In the late 1970's the US EPA promulgated a GC/MS reporting format for its Contract Laboratory Program (CLP). While having no legal status beyond that specific program, in which only a relatively small number of laboratories participated, these formats have become the *de-facto* standard for reporting environmental data.

The GC/MS CLP reports consist of a set of tabular "Forms" and supporting graphical chromatographic and spectroscopic data. Official CLP laboratory analysis must perform the CLP protocol exactly. "Industrial CLP", or "CLP-like" analyses are very similar, but can differ slightly in calculation details and deliverables. Software programs for the latter are somewhat simpler and less expensive.

This paper will discuss Aquarius 2000™, a new Microsoft Windows™ based program designed to produce these "CLP-like" reports quickly and easily.

Aquarius 2000 is based upon the widely used Aquarius™, which ran on HP RTE operating system mini-computers. Aquarius was written by ETC, Corp., a large environmental laboratory, and introduced in 1983. Aquarius 2000 was also written by ETC (now Astrix Software Technology, Inc.) and developed in conjunction with Perkin-Elmer.

OVERVIEW

- Based upon the industry-standard Aquarius Software
- US EPA environmental reports
- Industrial CLP ("CLP-like") deliverables for GC/MS
- High productivity, high throughput
- Single-user, single GC/MS
- Multi-user, multi-GC/MS networked GC/MS laboratory
- Microsoft Windows
- IBM PC-compatible computers

FEATURES

- Fast and flexible report production
- High-speed processing
- Automated Tentatively Identified Compound (TIC) Searching
- High-speed calibration and quantitation
- Powerful data review
- Distributed Parallel Processing
- Security, aids GLP and GALP compliance
- Automatic data archiving to removable media
- Supports the Perkin-Elmer Q-Mass 910 GC/MS
  - also HP ChemStation™
  - many other GC/MS systems with optional software

DISCUSSION

The software emphasizes high productivity and ease-of-use. Productivity is enhanced by *Distributed Parallel Processing*, a software approach that enables various processing tasks to execute on remote computers for enhanced system performance. The Windows interface facilitates simple processing of Sample Delivery Groups (SDG's). A "copy and paste" approach to target compound lists expedites and simplifies construction of customized "Industrial CLP" reports within the software, rather than requiring customized macros

Aquarius 2000 has been designed for the high-volume laboratory. Related tasks are placed in close proximity. Large push-buttons have been emphasized to simplify operation and avoid "hiding" features under multiple menus. Special care has been taken to minimize the number of keystrokes required for common tasks.

Automated Matrix Assisted Laser Desorption as a Tool for QC Applications

Paul Humphrey & David C Dingley
Kratos Analytical, Barton Dock Road, Urmston, Manchester, M41 7LD, UK.

Matrix assisted laser desorption ionisation (MALDI) is now becoming established as an immensely powerful analytical tool for peptides and proteins and its uses encompass reaction monitoring, product confirmation and routine quality control. This has resulted in the need for a cost effective solution for the modern laboratory combining a high-performance, laboratory-priced package offering a high degree of automation.

(i) Fully-automated "Sweet-spot" location

One of the apparent weaknesses of MALDI to a new user is the variable shot-to-shot reproducibility. This is partly due to the fact that the matrices crystallise unevenly with varying degrees of sample inclusion. The MALDI process itself can be used to find the sweet-spot. This slide is scanned beneath the laser while the data system monitors the secondary ion signal of the mass range of interest. Typically 20 - 50 laser shots are taken across the sample and the intensity of the analyte ion signal is plotted against laser shot.

The spectrum is then collected from the maximum in the analyte ion chromatogram. The selection of the sweet-spot from the chromatogram can be manual or left entirely to the data system. The procedure is shown schematically in figure 1.

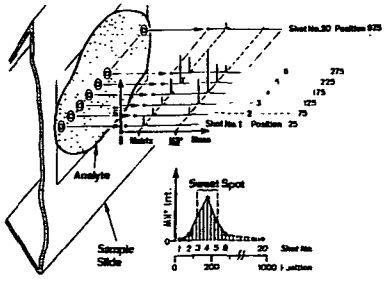

Figure 1 - Schematic of "Sweet-spot" locating

(ii) Fully-automated laser power threshold tuning

With the exception of sample preparation, which is external to the instrument, the most important parameter in the MALDI experiment is the laser power.

The threshold behaviour of the MALDI process is well known. If the laser power is too low there will be no ion emission and minimal damage to the sample by the laser irradiation. As the laser flux is increased, ion emission occurs and a spectrum begins

to appear. Increasing the flux further will result in further ion emission and a more intense spectrum is obtained. The excess energy will result in a broadening of the analyte ion peak thus reducing the practically obtainable mass resolution. Adduct formation is also more likely. As the laser flux is increased again the signal rises but at the expense of resolution. At extreme powers the peaks are very broad and the signal may actually fall due to either the detector signal saturating and subsequent instability or by actual depletion of the $[M+H]^+$ channel by increasing ion fragmentation. A high baseline is usually also seen due to the time-unresolved fragment ions. The laser threshold behaviour is shown schematically in figure 2 with insets of MALDI spectra of substance P acquired at the positions indicated.

The ideal power is then just above threshold which can be selected automatically by a method similar to that described above. This time the laser power is ramped while the data system again monitors the secondary ion signal. The analyte ion chromatogram will then show a threshold curve and the appropriate position on the curve can then be selected manually or automatically. This procedure can be performed separately or in conjunction with the procedure described in section (i) and typically thirty samples can be analysed in less than 20 minutes with no manual intervention being necessary.

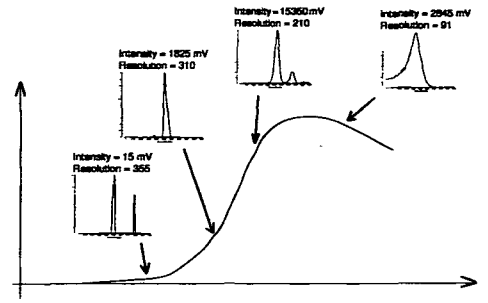

Figure 2- Laser threshold behaviour

(iii) On-line peptide digest database searching

One approach to protein analysis is to perform a protein digest (which can be carried out on the sample slide) and acquire a MALDI spectrum of the digest fragments. The masses of these can then be selected from the spectrum and used as the search elements for a search of a protein database. Using predictive software, which theoretically digests sequences withh a defined protease, all protein sequences in a database are theoretically digested using the appropriate enzyme and matches are sought between the resulting fragments and those observed in the MALDI spectrum. Searching can be performed locally or at a remote location using internet connections. The software then reports a list of possible fits ranked with a 'goodness of fit' actor. The tolerance of the search matching can be adjusted and variations such as missed cleavages can be taken into account.

Evaluation of TICfilt as a Software used in LC/MS analysis.

A. Carrier, D. Zidarov and M.J. Bertrand, Regional Center for Mass Spectrometry, Department of Chemistry, University of Montreal, Montreal, Canada, H3C 3J7.

A significant challenge facing LC/MS techniques is making reliable compound identification at low level or in complex samples, where the background signal generated by the mobile phase can lead to misinterpretation. Indeed, the solvents and buffers present in the mobile phase produce a substantial background signal that can cause problems in locating weak elution peaks of unknown compounds in the TIC. A background treatment algorithm, TICfilt, was recently developed to detect weak eluting peaks in the TIC and to facilitate the identification of unknown analytes (1). In order to broaden the scope of application of TICfilt, data generated by different ionization processes commonly used in LC/MS analysis were treated. Experiments were conducted with various mobile phase compositions to study the influence of the background generated and the effect of the algorithm on the quantification was also studied. In order to illustrate the ability of TICfilt to extract peaks from the background and to enhance the quality of the mass spectra the algorithm has been applied to different LC/MS data sets generated under different ionization conditions such as IonSpray™, APCI, CF-FAB and DLI using an in-source μ-TSP interfaces (2). The treated data obtained demonstrate how the algorithm eliminates the effect of heavy background and permits the extraction of compounds from the background signal. The results from these experiments clearly indicate that regardless of the ionization technique employed for the LC/MS analysis, TICfilt can successfully extract significant ions from the overall signal. For example, the use of a liquid matrix associated with fast atom bombardment ionization produces important background ions that can lead to problems in interpreting the mass spectra of unknowns. The algorithm was used to treat CF-FAB data and the results obtained for a deoxyadenosine sample are shown in Figure 1. The elution peak for deoxyadenosine was found to be clearly distinguished from the background signal of glycerol that corresponds to the major ions of the raw mass spectrum (Figure 1a). The treated spectrum (Figure 1b) shows a base peak at m/z 252 that corresponds to the parent ion of deoxyadenosine. Experiments were conducted with various mobile phase compositions to study the influence of the background signal generated. The results obtained with different compositions (0,25,50,75,100%) in two chromatographic systems, acetonitrile/water and hexane/ethyl acetate, indicate that the performance of TICfilt is independent of the signal generated by the mobile phase. The elution peak corresponding in the treated data to the analyte injected was found to be clearly distinguished from background signal. The influence of TICfilt on the quantification was studied by injecting various quantities of chloroaniline

(normal phase) and phenylhexane (reversed phase) ranging from 10 to 1000 ng in the scanning mode. Figure 2 A) (chloroaniline) and B) (phenylhexane) represent the calibration curves for the elution peak before and after treatment of the TIC. The results indicate that the linearity of the calibration curves for both compounds is preserved and that TICfilt is independent of the concentration of the analyte injected. The subtraction process minimizes the effect of solvent noise and interferences in the data and maximizes spectral quality both in the total ion chromatogram and in the mass spectra. TICfilt is in all aspects equivalent to single ion chromatograms without requiring any information on the nature of the eluting compound.

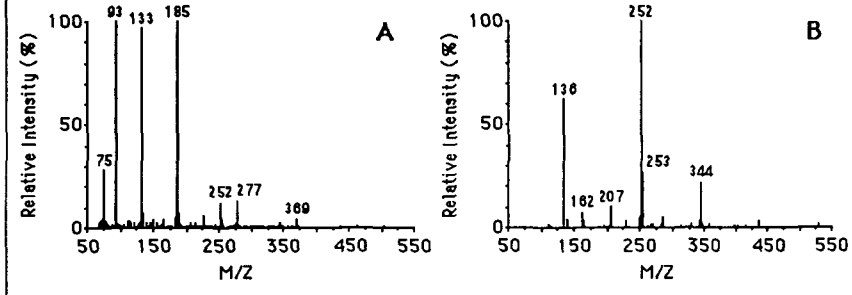

Figure 1. Mass spectrum for a 300 ng injection of deoxyguanosine obtained by CF-FAB. A) original TIC, B) TIC treated by TICfilt.

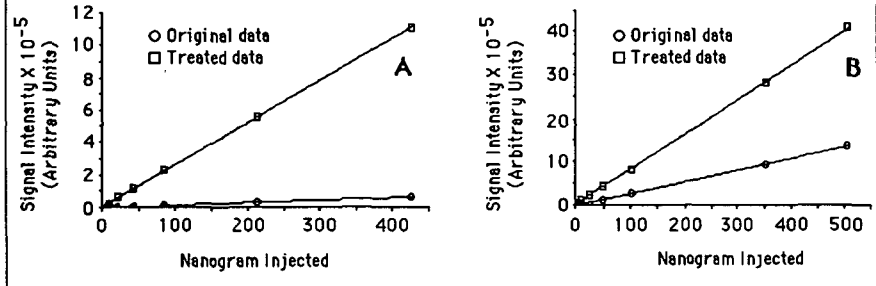

Figure 2. Calibration curves before and after treatment for a) chloroaniline and b) phenylhexane

REFERENCES:

1) A. Carrier, D. Zidarov and M.J. Bertrand, Proceedings of the 42 nd ASMS Conference on Mass Spectrometry and Allied Topics, Chicago, Il, 1993, 490.

2) A. Carrier and M. J. Bertrand, J. Chromatogr., (1995) in press.

Direct Temperature resolved Mass Spectrometry (DTMS) as a Tool to Study Painted Art: a case study of "De Eendenfamilie" by W.Maris, a 19th century Dutch impressionist painter.

Jaap J.Boon[1], K-J. van den Berg[1], J. Pureveen[1], G. van der Doelen[1], Karin Groen[2], J. van Och[3] and A. van Grevenstein[3]. MOLART-project for Painted Art, FOM Institute for Atomic and Molecular Physics, Kruislaan 407, 1098 SJ Amsterdam, NL. fax. 31-20-6684106 (2) Centraal Laboratorium voor de Studie van Voorwerpen van Kunst en Wetenschap, Amsterdam, NL. (3) Stichting Restauratie Atelier Limburg, Maastricht, NL.

Mass spectrometry can play a unique role in the definition of the current condition of art objects because of its low sample requirement and its sensitivity for a wide range of chemical compounds. Questions to be addressed are not only the chemical composition of the original materials used by the artist but also the molecular changes that are taking place after completion of the art work due to ageing, environmental effects and restoration. DTMS (Direct -i.e. in source- Temperature resolved Mass Spectrometric analysis [1]) using a resistively heated platinum/rhodium filament probe is presently the most versatile technique used to profile the chemistry of minute paint samples [2,3] because it gives information about the chemical composition as well as about the ways in which the compounds are chemically bound. The temperature resolution allows the separation into mobile "free" fractions and chemically bound fractions, which require a higher appearance temperature. Mass spectrometric analysis of the different layers (varnish, paint layers, ground, canvas and lining materials) obtained by dissection under a microscope visualises the molecular "cross-talk" between the layers.

DTMS was applied to samples taken from De Eendenfamilie (Family of Ducks, Van Abbe Museum, Eindhoven, inv. nr. 83) by W.Maris (1844-1910), a typical representative of the Dutch Impressionist "Haagse School" (The Hague School). The painting has been made in high impasto with paints which are presently unusually soft. This makes restoration and varnish removal with solvents a hazardous operation. The painting has not been wax or glue lined and has kept its original canvas support. Paint and varnish samples were analysed by DTMS (using a Jeol SX102A B/E-MS) and PYGCMS (using a FOM4LX-Curie point pyrolysis unit mounted on a Carlo Erba 8565 HRGC coupled to a Jeol DX303 E/B-MS). A cross section of a paint chip was investigated by reflected light microscopy and SEM-EDAX for elemental analysis.

The painting was found to be covered with a yellowed varnish with an unusual DTMS spectrum indicative a possibly aged synthetic methylcyclohexanone resin [5] (DTMS points to homologous ion series with an mass increment of about 110 Da) and a small amount of residual highly oxidised natural Dammar resins, most likely an earlier varnish. Paints investigated were a chocolate brown paint (8 µm) with vermilion (HgS) and Prussian blue (ferriferrocyanate), on top of an olive green paint (40 µm) with Naples yellow (lead antimonate), lead chromate, Prussian blue and zink white. The organic fraction of these paints contains beeswax and is depleted in binding oil derived components because the concentration of C16FA, C18FA and azelaic acid is very low. The paint layers are isolated from a chalk priming ground by a thin partly cracked layer of lead white (15 µm). The ground layer (100 µm) was very much enriched with fatty acids possibly originating from drying oil absorbed from the poorly drying upper layers. SEM and DTMS shows that no "drying" transition metals are present in the ground. Figure 1 shows the DTMS spectra from a paint sample in the lower right hand corner of the painting which could be separated with a dissecting microscope into sample A (top layer), B (olive green paint and attached lead white layer) and C (chalk ground).

Varnish removal test. A[1] presents the DTMS after superfast varnish removal (isooctane/ethanol (1/1); exposure time 2 seconds) using a home made solvent suction device. The DTMS shows that with this approach not only the aged synthetic varnish but also fatty acids from the paints (note m/z 256 and 284) are selectively removed, whereas the beeswax additive consisting of odd long chain hydrocarbons and wax esters remains. The loss of fatty acids from the painting is undesirable. Changing the polarity of the cleaning solvent to a lower polarity (less ethanol) could leave the fatty acids but may lead to selective extraction of the waxes. Since the paint is presently coated with a synthetic varnish, it is likely that it has been "cleaned" earlier most likely involving loss of paint constituents in the process.

Softness of the paint. Beeswax is mostly found in paintings which have been lined with a new canvas support. In this case the wax is impregnated in existing well cured oil paint layers. In the 19th century painters have added waxes and other additives to their paint in order to improve the brushability or to obtain certain topographical effects (impasto)[4]. Maris must have modified his paints for that reason by addition of wax. Beeswax is a polymerisation inhibitor of the binding oil and may lead to long drying times. The high amount of fatty acids in the ground layer points to absorption of the binding oil from the paint layers which must have happened at an early stage of the production of the painting. Undersaturation of the paint layers with binding oil relative to "drying" agents such as the lead antimonate pigment in combination with the added beeswax is thought to be the main reason for the unusual softness of the paint which never dried properly. This scenario is confirmed by the composition of a brown well dried hard paint clot on top of the frame which is devoid of bees wax. Further tests with PyGCMS in the presence of tetramethylammoniumhydroxide for direct transalkylation of fatty acids and diacids shows that the soft paint layers have unusually low azelaic acid concentrations, a C9 diacid formed by oxidation from the polyunsaturated fatty acids in drying oil [5], compared to the hard paint.

References:

1 J.J Boon (1992) International Journal of Mass spectrometry and Ion processes, 118/119, 755-787.
2 J. J.Boon, J. Pureveen, D Rainford and J H Townsend (1995) The Opening of Wallhalla, 1842: Studies on the Molecular Signature of J.M.W Turner's Paint by Direct Temperature resolved Mass Spectrometry (DTMS). In: Turner's Painting Technique in Context. UKIC. London. In press.
3 J.J. Boon, J.Pureveen, D.Rainford and K.Groen. (1995). Direct temperature resolved mass spectrometry of the mobile and chemically bound organic constituents in Rembrandt's Jewish Bride. Restauratie Jaarboek Volume 1. De Acht Rembrandts. Rijksmusem, Amsterdam, in press
4. L.Carlyle and A Southall (1993). No mechanic road to fame. the implications of certain artists' materials for the durability of British painting: 1770-1840. In Robert Vernon's gift, (Ed. R.Hamlyn), Tate Gallery.
5. J.S Mills and R. White (1994).The Organic Chemistry of Museum Objects Butterworth-Heinemann. London.

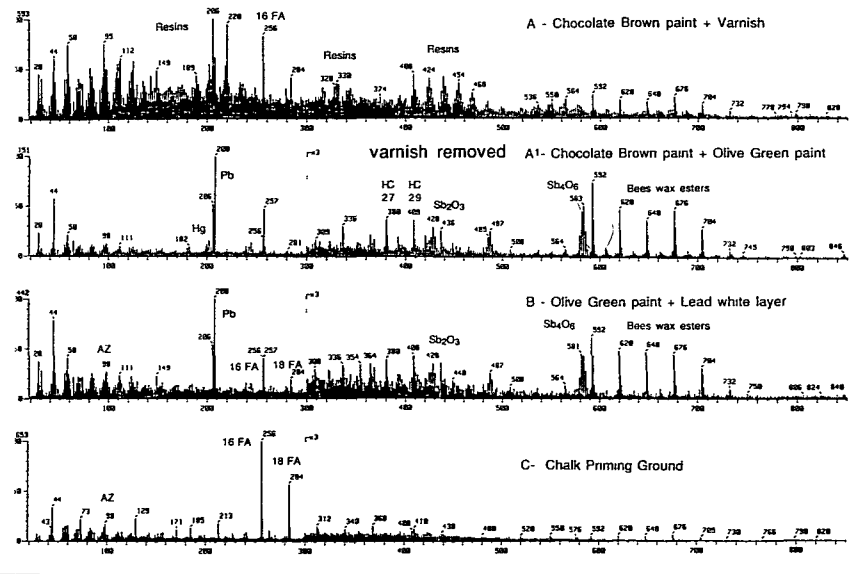

HPLC-FAB-MS and GCMS study of aromatic components of "gum benzoin" resins.

I.Pastorova, C.G. de Koster aand J.J. Boon
FOM-Amolf, Kruislaan 407, 1098 SJ Amsterdam, The Netherlands

" Gum benzoin" resins originating from North Sumatra were studied by modern analytical techniques because of their commercial value for the local population. It is known, that these resins contain some valuable aromatic esters, but until now, studies of these type of compounds involved an alkaline hydrolysis step, concentrating therefore on the free acid and alcohol content.
We omitted the hydrolysis step and analysed the resins both with and without a derivatisation step.
For GC/MS measurements, the resins were silylated with BSTFA and dissolved in DCM prior to on-column injection. The following compounds were identified:

benzyl alcohol	benzoic acid	p-hydroxybenzaldehyde
vanillin	cinnamic acid	p-coumaryl alcohol
coniferyl alcohol	cinnamylbenzoate	benzylcinnamate
cinnamylcinnamate	p-coumarylbenzoate	4-hydroxy-3-methoxybenzoic acid
coniferylbenzoate	p-coumarylcinnamate	coniferylcinnamate
pinoresinol	triterpenoic acids	

The identification is based purely on comparison of mass spectra of the silylated compounds with reference data from libraries. P-coumaryl and coniferyl esters of benzoic and cinnamic acids are unique to these resins, therefore no reference spectra of their TMS derivatives are available. Identification was based on interpretation of mass spectra, structure of the abundant fragment ions and mechanisms of their formation were proposed [1].

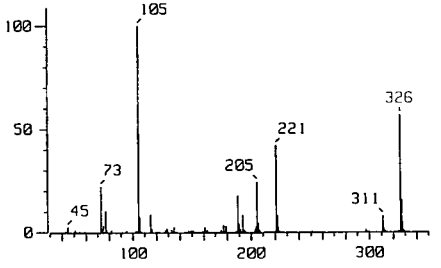

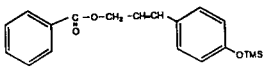

p-Coumarylbenzoate

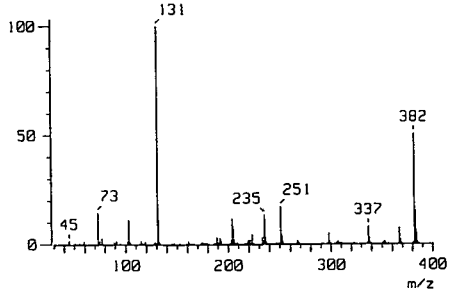

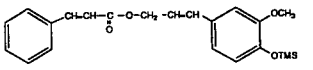

Coniferylcinnamate

To confirm the structure of these unique esters, the underivatised resins were dissolved in acetonitrile and injected on a RP-C18 column and HPLC-frit-FAB+ MS was performed. Glycerol was used as the matrix, acetonitrile and water as eluents. We focused our attention primarily on the detection of the cinnamic and benzoic esters.

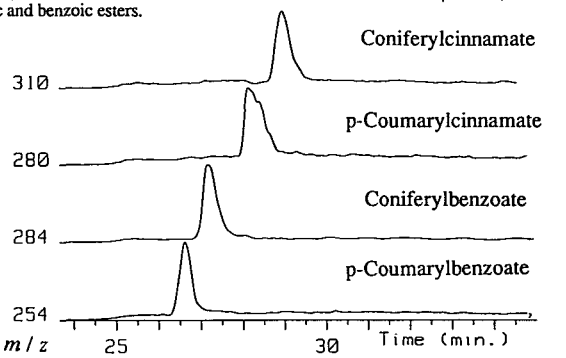

In the mass spectra we can observe a relatively strong molecular radical cation, a phenomenon observed in positive FAB spectra of different organic molecules [2,3].
The fragments in the mass spectra are typical for p-coumaryl (m/z 133) and coniferyl (m/z 163) alcohols [4].

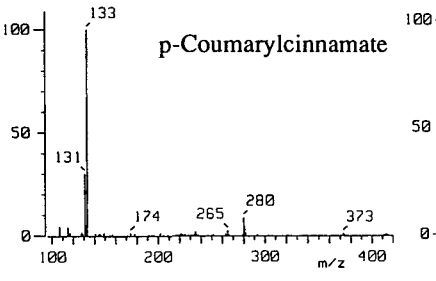

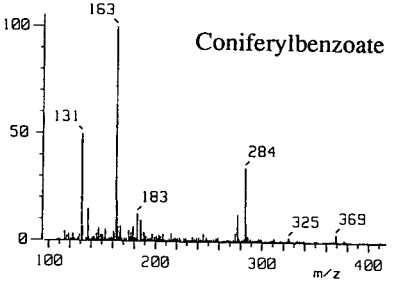

Conclusions

1) GC/MS of TMS derivatives of "gum benzoin" proved to be a powerful tool for analysis of these type of samples. Many unique aromatic components were identified, based on the fragmentation patterns in their mass spectra.

2) HPLC-FAB-MS results confirmed the proposed structure of the aromatic esters.

3) The formation of the abundant molecular ion (radical cation) will be studied further with model compounds.

References:

1.) I. Pastorova, M. Bobeldijk, C. de Koster and J.J. Boon, will be submitted to Phytochem. Anal.
2.) M. Takayama, J.Am.Soc.Mass Spectrom. 6 (1995) 114-119
3.) M. Takayama, M. Iwamura and S. Fuchibe, Org.Mass Spectrom. 29 (1994) 601-606
4.) E.R.E. van der Hage, Ph.D. thesis, Univ. of Amsterdam/Fom-Amolf, 1995

DEVELOPMENT OF A REFERENCE CORPUS FOR GC/MS ANALYSIS OF VEGETABLE ADHESIVES FROM ARCHAEOLOGICAL ORIGIN

REGERT M.*, DELACOTTE J.-M.#, ROLANDO C.#
Ecole Normale Supérieure, Département de chimie, URA 1679
24, rue Lhomond, 75005 Paris
* Musée du Louvre, Laboratoire de recherche des musées de France, EP97
16, rue des Pyramides
75041 Paris cedex 01

INTRODUCTION

Black and amorphous organic residues have been discovered for many years in archaeological prehistoric sites. Some of them were used as adhesives either to repair ceramic potteries or to secure a spearhead on a shaft of wood for example, during the paleolithic and the neolithic periods. Our purpose is to identify the natural origin of these adhesives in order to infer the technology of prehistoric people.

The organic residues consist of complex molecular mixtures of biopolymers and volatile compounds. The only biomarkers, *i.e.* characteristic molecules for a species, a genus or a family, can give us some information about the natural origin of the material. However, a set of biomarkers is necessary to find the natural origin of the investigated archaeological samples. Moreover, these markers must be quite stable in time

Some biomarkers are more or less distributed in nature. For example, the triterpenoid betulin is often thought to be characteristic of birch bark ; but a publication shows that a lot of species contain this molecule[1]. In order to find criteria to understand the natural origin of archaeological samples, we have analysed actual products which probably were used by neolithic people as glue.

We present here a comparison of results from MS and GC/MS analysis of different natural samples (resins, oils, beeswax) after derivatization. Beeswax and oils are not really adhesive but they could have been mixed with resins or tars to improve their properties such as plasticity or stickiness.

METHODS

Reference samples : the samples (about 5 mg) were ground in an agate mortar, then extracted with 1 ml of dichloromethane. In all cases, the samples were entirely soluble.
MS analysis : sample analysis was performed with R10-10 Nermag.
GC/MS analysis : sample analysis was performed after diazomethane methylation with GC/MS instrument (Finnigan 46 ; GC Varian 9611) equipped with a (25m X 0.25mm) CP Sil 5CB (25µm) column from Chrompack using EI+ ionization.
Temperature programs :
Beeswax, fir and pistachio resins : 1mn : 60°C ; 20°C/mn : 60 to 150°C ; 4°C/mn : 150 to 310°C ; 310°C during 30mn.
Pine resin : 1mn : 80°C ; 4°C/mn : 80 to 200°C ; 2°C/mn : 200 to 250°C ; 4°C/mn : 250 to 310°C.
Linseed oil : 1mn : 60°C ; 4°C/mn : 60 to 280°C ; 280°C during 10mn.

RESULTS

- *Resins* : in all the studied resins, we identified either diterpenoids (pine and fir) or triterpenoids (pistachio). But in some cases, these terpenoids are common to different species. In particular, almost all the biomarkers usually considered as characteristic of the pine resin also pertain to the fir resin. However, the fir resin contains some higher molecular weight markers which could be used to distinguish the two genuses
- *Beeswax* : beeswax doesn't really contain biomarkers but a set of hydrocarbons, fatty acids and esters. It has been shown that the hydrocarbons were damaged with time whereas esters seem to be quite stable[2]. Even if esters can't be considered as biomarkers, their distribution can indicate to us the presence of beeswax in the sample. We can only see one ester on our chromatogram because of the limitation in temperature of the column but the mass spectrum of beeswax shows the presence of the other esters.
- *Oils* : all the oils (lin, poppy, olive) contain the same fatty acids and fatty acids are important in nature. So, fatty acids can't really be used to identify the natural origin of archaeological samples. The oils also contain sterols which are good biomarkers , but they are present in small quantities in the oils. So we can imagine that they could be difficult to find in old samples except in well preserved samples.

CONCLUSION

Based on the analysis of reference natural products probably used by prehistoric people to make glues, we can propose methods of study and interpretation of archaeological adhesives.

Concerning an unknown sample, we can first study the mass spectrum of the sample in order to make a first hypothesis. The preliminary results from mass spectrometry permit us to distinguish triterpenoid from diterpenoid samples and those containing beeswax or oil. After derivatization choice (in some cases, trimethylsilylation is necessary, for birch bark tar, for example), GC/MS permits us to identify the biomarkers and the other constituents. It is important to note the necessity to develop a wide reference corpus since many markers are present in different species (pine and fir resin, for example). In absence of biomarkers (beeswax), it is necessary to work on very stable compounds in order to obtain characteristic chromatographic profiles. These first results obtained on reference products should permit us to find the nature of archaeological adhesives in order to understand the management of these products by prehistoric people

REFERENCES

1- Hayek E., Jordis U., Moche W. and Sauter F., *Phytochem.*, 1989, **28**, 2229.
2- Evans K. and Heron C., *Chem. & Ind.*, 1993, **446**.
3- Audier H.E., Bory S., Fétizon M. and Anh N.T., *Bull. Soc. Chim France*, 1966, **12**, 4002.

Terminal Group Effects on the TOF-SIMS Spectra of Polydimethylsiloxanes

Xia Dong and David M. Hercules[1]
Department of Chemistry, University of Pittsburgh, Pittsburgh, PA 15260
[1]: Present address: Department of Chemistry, Stevenson Center, Box 1822, Station B, Vanderbilt University, Nashville, TN 37235

Introduction:

The degradation mechanism of polydimethylsiloxanes (PDMS) has been studied by electron impact[1] and pyrolysis mass spectrometry[2]. These studies, however, have focused on the low mass range. Time-of-flight second-ion mass spectrometry (TOF-SIMS) offers the advantage of high resolution and high sensitivity in the high mass range. We have previously examined the effect of molecular weight on the fragmentation of PDMS by TOF-SIMS[3]. The purpose of the present research is to investigate the effect of terminal groups on PDMS fragmentation by TOF-SIMS.

Experimental:

PDMS spectra were obtained using time-of-flight secondary-ion mass spectrometer, TOF-SIMS III (Ion-Tof GmbH, Münster, Germany). The samples were prepared by casting thin films on etched silver. The targets were bombarded by 10keV Ar^+ beam with the pulsed primary ion current varying from 0.3-0.5 pA. The total collection time was 300 s.

Results and Discussions:

PDMS terminated by trimethylsilyl, silanol, aminopropyl and amidepropyl groups were investigated. The low mass range spectra of PDMS were very similar. The characteristic peaks of end groups were observed in the spectra of PDMS terminated by trimethylsilyl, aminopropyl and amidepropyl groups. The PDMS silanol spectrum did not show the peak characteristic of hydroxyl group.

A major difference in the spectra is observed in the mass range from 600 -1000 Da. Spectra of PDMS in this mass range are shown in Figure 1. The spectrum of trimethylsilyl terminated PDMS has been discussed in detail before[3]. The major series detected in the spectra of PDMS terminated by silanol groups are linear oligomer and cyclic fragment cationized by silver. Two intense clusters are observed in the spectrum of aminopropyl-terminated PDMS. One corresponds to the intact linear oligomer cationized by silver, the other to a linear fragment formed by loss of the aminopropyl group from oligomer but not cationized by Ag ($[nR+116]^+$). Similarly, the spectrum of PDMS amidepropyl contains two intense clusters, an intact linear oligomer cationized by silver and a linear fragment with intrinsic charge formed by the loss of the amidepropyl group from the oligomer ($[nR+158]^+$).

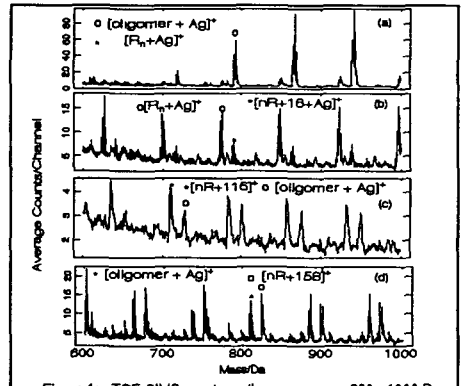

Figure 1: TOF-SIMS spectra in the mass range 600 - 1000 Da for PDMS with different terminal groups
(a):silanol-terminated (b): trimethylsilyl-terminated
(c): aminopropyl-terminated (d): amidepropyl-terminated

The linear fragments observed in the spectra of PDMS aminopropyl and amidepropyl have structures containing an intrinsic positive charge instead of being neutral fragments cationized by Ag^+. Large fragments with intrinsic charge are rarely observed in the TOF-SIMS spectra. Both the amino and amide groups contain one nitrogen atom. This indicates that the presence of nitrogen in the end group has some effect on the fragmentation of PDMS. One interesting phenomenon is that the intensity of a linear fragment with intrinsic charge decreases with increasing mass range. In the mass range above 1200 Da, the dominant fragment peaks are silver cationized cyclic fragments which are also the major fragments in the spectra of PDMS trimethylsilyl and PDMS silanol.

Figure 2 shows detailed patterns of PDMS terminated with aminopropyl and trimethylsilyl groups in the mass range above 1200 Da. The intensity of the cyclic fragments compared to the oligomer peaks in the spectra of aminopropyl-terminated PDMS is higher than for PDMS with a trimethylsilyl group. This indicates that desorption of intact oligomer is more difficult for aminopropyl- terminated PDMS. The factors controlling desorption of intact oligomer are not well understood, and may be related to the conformation of the polymer chain on the substrate. Since the amine group contains a nitrogen atom with a lone pair of electrons, which tends to form a complex with silver, PDMS aminopropyl may interact more strongly with the silver target, thus making the desorption of the intact oligomer more difficult.

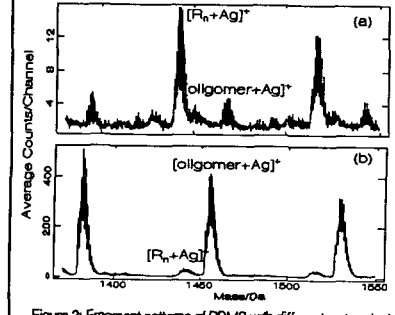

Figure 2: Fragment patterns of PDMS with different terminal groups in the mass region above 1200 Da
(a): aminopropyl-terminated M_n=1900 Da
(b): trimethylsilyl-terminated M_n=2000 Da

Conclusions:

Effects of end groups on the fragmentation of PDMS have been observed. In the spectra of aminopropyl and amidepropyl-terminated PDMS, large linear fragments with intrinsic positive charge which do not appear in the spectra of trimethylsilyl and silanol-terminated PDMS are observed. The relative intensity of the cyclic fragment of aminopropyl terminated PDMS is higher than that of PDMS trimethylsilyl with similar molecular weight. This may be caused by the strong interaction between amine group and silver substrate.

References:

1. G. P. Pickering; C. J. Oliff; K. J. Rutt *Org. Mass Spectrum.* **10**, 1035 (1975)
2. S. Fijimoto; H. Ohtani; S. Tsuge *Fresenius Anal. Chem.* **331**, 342 (1988)
3. X. Dong; D. M. Hercules presented at the *42nd ASMS Conference on Mass Spectrometry and Allied Topics*, Chicago, IL, 1994

Application of ESI MS for the Analysis of Polysulfide Polymers

Armelle Buzy, Andrea Mahon, Terry J. Kemp and Keith R. Jennings
Department of Chemistry, University of Warwick, Coventry, CV4 7AL, U. K.

Few previous studies have been reported of the analysis of polymers by electrospray ionisation mass spectrometry (ESI MS) [1]. In this work, ESI MS is used to characterise liquid polysulfide polymers (LPs) that are widely used as high performance sealants in industry. Their characterisation is of considerable importance in identifying the photochemical processes that they undergo and which can result in the failure of the seal. Chemically, LPs are polymers of bis-(ethylene oxy) methane containing disulfide linkages of the general structure: $H(SC_2H_4OCH_2OC_2H_4S)_nH$.

Ten individual LPs, with a nominal molecular weight (nMW) ranging from 1000 to 8000 Da and differing in the percentage of branching agent, have been studied in this project. No apparent major differences between the various grades were detected by ^1H, ^{13}C NMR and IR spectrometry and, to date, no data have been obtained by means of Matrix-Assisted Laser Desorption Ionisation (MALDI). These LPs, however, form singly-charged species by ESI MS, when dissolved in 0.5 % NH_4Cl THF/MeOH. The ESI spectrum obtained for one LP of nMW 1000 Da (LP-1400C) is shown in Figure 1. In addition to the series corresponding to the expected structure (labelled A in Fig. 1) up to 7 other series were also observed (labelled B to H), each series yielding peaks at mass intervals of the monomer unit (166 Da). Similar types of complex distributions were observed in the ESI spectra given by all LPs studied. These series were tentatively assigned to compounds that are based on 'anomalous' repeat units containing either fewer or additional S atoms, oxymethylene and oxyethylene unit. This is not unexpected in view of the method of preparation of LPs [2]. The CID spectra of selected ions of each series were recorded in order to confirm these assignments. They are reported in Figure 2 for Series A (expected series) and B (one fewer S-atom). Additional fragments observed in the CID spectra for Series B to H compared to Series A allowed one to confirm the composition of the individual ions. Characterisation of higher nMW (> 4000 Da) polymers was prevented by the absence of peaks due to multiply-charged ions. Furthermore, no difference in MW distribution was observed for LPs with nMW of 1000, 2600 and 4000. Although this could suggest that ESI discriminates against ions at higher m/z values, it is also possible that the higher mass components are less soluble and so may not have been present in the sample that was ionised.

In summary, ESI MS has been shown to be a very useful technique for revealing and identifying the compounds of closely-related structures that are present in each sample of low nMW LPs polymers and should be suitable for monitoring their photodegradation.

[1] Campana, J. E., Sheng, L. -S., Shew, S. L. and Winger, B. E., *Trends in Analytical Chemistry*, 1994, 13, 239-247.
[2] Lucke, H. ALIPS-Aliphatic Polysulfides, Hüthig and Wepf, Basel, 1994, 191 pp.

43rd ASMS Conference on Mass Spectrometry and Allied Topics

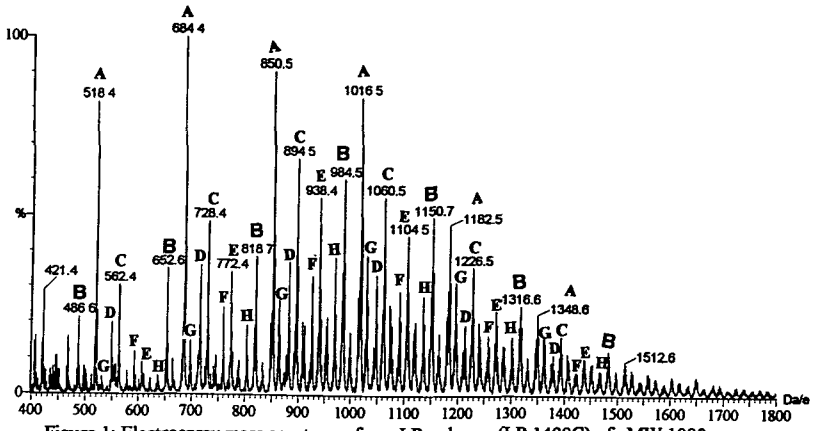

Figure 1: Electrospray mass spectrum of one LP polymer (LP 1400C) of nMW 1000. Labels indicate the different identified series.

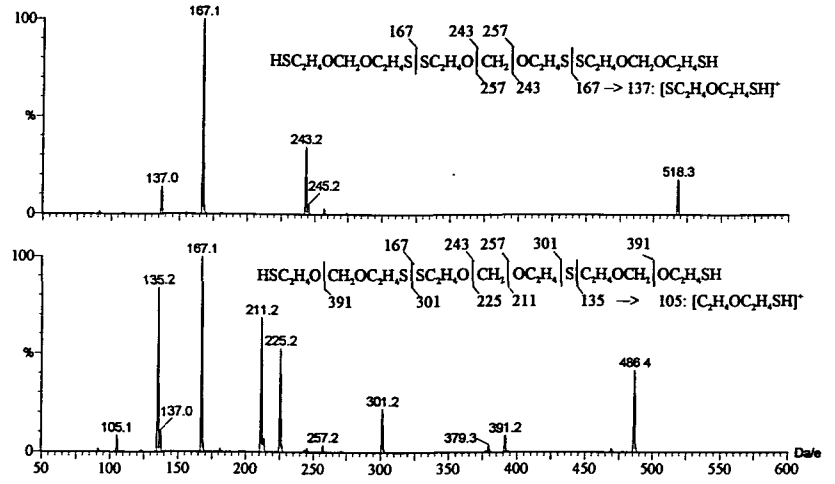

Figure 2: Collision-induced dissociation spectra of ions selected from the electrospray mass spectrum of LP-1400C (Figure 1). Collision gas-argon (pressure 3.8 x 10^{-3} mbar), collision energy 20 eV. Upper: ion at m/z 518.3 from Series A; lower: ion at m/z 486.4 from Series B.

The Analysis of Polymer Additives by Means of Tandem Mass Spectrometry.

Tony T. Jackson[1], Armelle Buzy[1], Jim H. Scrivens[2] and Keith R. Jennings[1].
[1]Department of Chemistry, University of Warwick, Coventry, CV4 7AL, U.K.
[2]ICI Materials, PO Box 90, Wilton Centre, Middlesbrough, TS90 8JE.

A 5-component mixture of four antioxidants (Irganox 1076, Irganox 3114, Hostanox 03 and Irganox 1010) and a UV absorber (Tinuvin 327) of RMM 300-1200 daltons has been analysed by mass spectrometry and a comparison made of results obtained using various ionisation techniques. The ionisation techniques used were electron impact (EI), chemical ionisation (CI), liquid secondary ion mass spectrometry (LSIMS), field desorption (FD), electrospray (ESI) and matrix assisted laser desorption/ionisation (MALDI). Collision-induced dissociation (CID) spectra of molecular ions generated by EI, CI, LSIMS and FD were then obtained by means of tandem mass spectrometry (MS/MS). The internal energy effects of the precursor ions formed by these techniques are compared. ESI-MS/MS spectra are also presented.

The FD-MS spectrum of an equimolar mixture of polymer additives is shown in Figure 1. The ideal technique for the quantitative mass spectrometric analysis of a mixture of polymer additives is FD-MS. Matrix effects make LSIMS and UV-MALDI unsuitable as ionisation techniques for these analyses.

The high energy FD-MS/MS spectrum of Irganox 1010 (RMM 1177) is shown in Figure 2. The fragment ions at m/z 219 and 203 are characteristic of Irganox compounds with a 4-alkyl-2,6-tertiary-butylphenol structure. The proposed mechanism of generation of m/z 203 from m/z 219 is shown in Scheme 1. The characteristic fragment ions in the high energy MS/MS spectra of the antioxidants studied (Irganox compounds and Hostanox 03) aid structural elucidation. Other mechanisms are proposed and are consistent with results from precursor ion scanning experiments.

Precursor ions generated by different ionisation techniques generate high energy MS/MS spectra that differ quantitatively. The spectra indicate that the structures of precursor ions generated by EI, CI, LSIMS and FD are the same. Precursor ions with higher internal energy before collision give rise to a MS/MS spectrum with more intense lower mass fragments.

The fragment ions in low energy ESI-MS/MS spectra are not as characteristic of the class of additives. For example, the ions at m/z 219 and 203 are often not prominent at these collision energies. Probing the mechanisms of formation of fragment ions in low energy MS/MS spectra is aided by the ease of performing precursor ion scanning experiments on the triple quadrupole instrument.

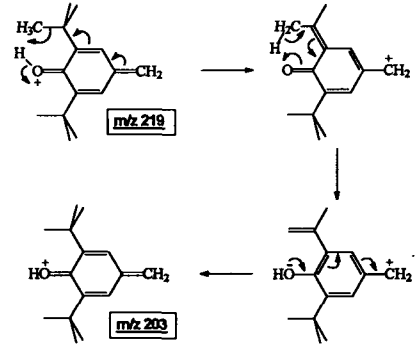

Scheme 1: Generation of m/z 203 for Irganox Compounds.

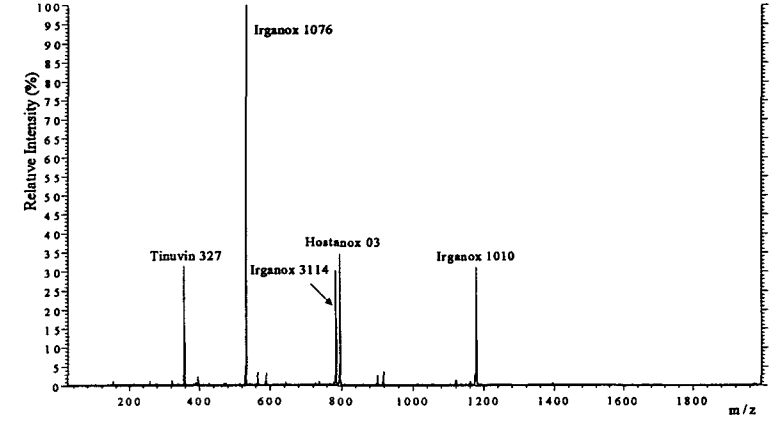

Figure 1: FD-MS Spectrum of an Equimolar Mixture of Five Polymer Additives.

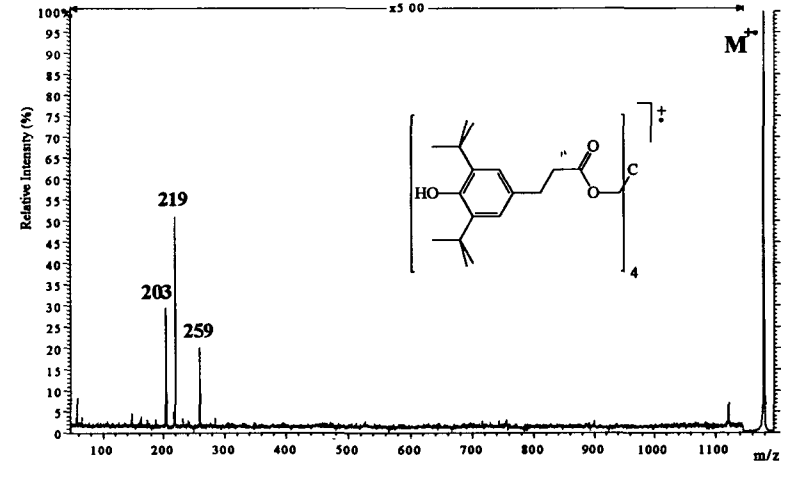

Figure 2: FD-MS/MS Spectrum of Irganox 1010 ($M^{+\cdot}$ 1177 daltons).

Average Mass and End Group Information on Polymers By Means of LSIMS and MS/MS.

Tony T. Jackson[1], Jim H. Scrivens[2] and Keith R. Jennings[1].
[1]Department of Chemistry, University of Warwick, Coventry, CV4 7AL, U.K.
[2]ICI Materials, PO Box 90, Wilton Centre, Middlesbrough, TS90 8JE.

The introduction of soft ionisation techniques such as matrix-assisted laser desorption ionisation (MALDI) and developments in instrumentation has increased the interest in the analysis of polymers by means of mass spectrometry. Mass spectra of ions produced by means of MALDI give mean mass values and mass envelopes that correlate well with other techniques of analysis such as gel permeation chromatography. Currently, very few laboratories are able to undertake tandem mass spectrometry experiments with ions generated by MALDI and it is therefore difficult to obtain end group information. The combination of accurate average mass measurements, mass envelopes and end group information can, however, be achieved by carrying out two experiments. First, the mass values are obtained with MALDI spectra. Ions of the same mass as those present in MALDI spectra are then generated by liquid secondary ion mass spectrometry (LSIMS) or field desorption (FD) in a sector instrument and collision induced dissociation (CID) experiments performed yielding fragment ions in the CID spectra that can give end group information.

The classes of synthetic polymers studied include polymethyl methacrylates (PMMA) and polystyrenes (PS). UV-MALDI spectra were obtained by means of a TOFSPEC time-of-flight mass spectrometer (VG Organic) and LSIMS and FD spectra were acquired by means of a ZAB-T four-sector mass spectrometer (VG Organic). The calibration for MALDI experiments was obtained from a mixture of polystyrenes covering the mass range of interest.

Figure 1 is the UV-MALDI-MS spectrum of PMMA 2010 in linear mode. The ions generated are $[M+Na]^+$ and $[M+K]^+$ adducts. A similar distribution is observed in reflectron mode, with improved resolution. The LSIMS-MS/MS spectrum from $[M+Na]^+$ for the n=20 oligomer, m/z 2025.8, is shown in Figure 2. The fragment ions aid end group characterisation, as demonstrated by the scheme in Figure 2. A mechanism for the loss of methanol and carbon monoxide from m/z 224, generating the m/z 164 fragment ion, is shown in Scheme 1. MALDI-MS spectra of PMMA samples with different end groups was also presented.

The ions in MALDI-MS spectra of polystyrene samples were all assigned as adducts with silver, $[M+Ag]^+$. End group information was obtained from the FD-MS/MS spectrum of polystyrene 1700. The low ion currents generated by FD makes MS/MS spectra difficult to obtain.

MALDI-MS spectra of polystyrene 7600 and 95,000 obtained in linear mode were also presented.

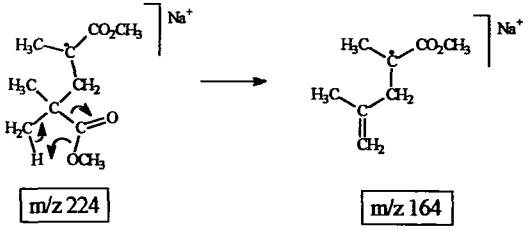

Scheme 1: Mechanism for Generation of m/z 164 for PMMA 2010.

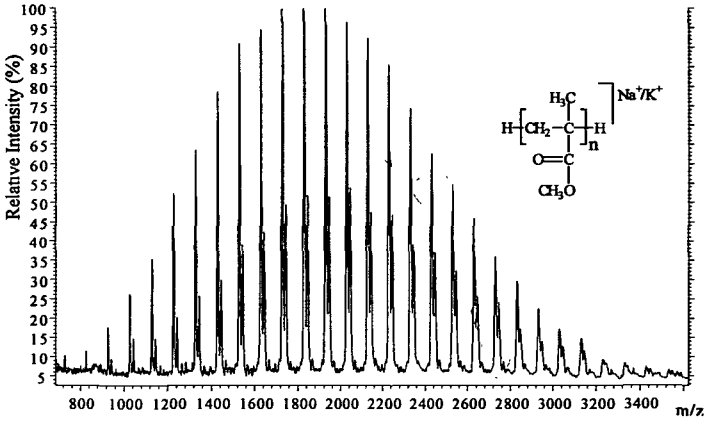

Figure 1: MALDI-MS Spectrum of PMMA 2010 in Linear Mode.

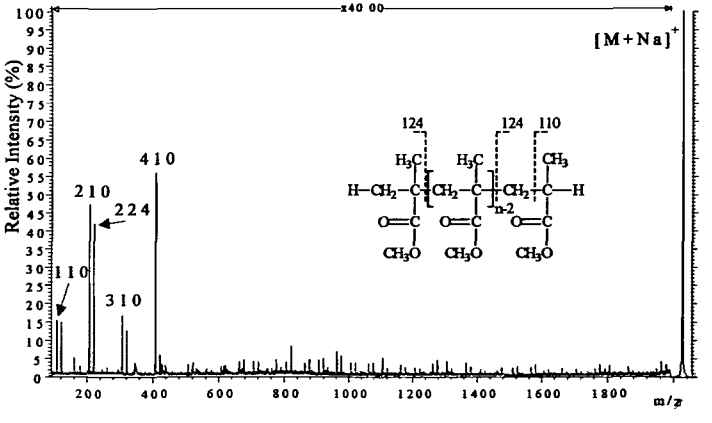

Figure 2: LSIMS-MS/MS Spectrum of PMMA 2010 ([M+Na]+, m/z 2025.8).

MASS SPECTROMETRIC ANALYSIS OF ALKYLATED BENZOTHIOPHENES BY NEGATIVE CHEMICAL IONIZATION WITH OXGEN

Herbert Budzikiewicz and Georg Drabner

Institut für Organische Chemie der Universität zu Köln
Greinstraße 4, D-50939 Cologne, Germany

Crude oil contains besides alkyl thiophenes also benzo- and dibenzothiophenes substituted with methyl and/or ethyl groups. These compounds are indicators for the origin, age and the prevailing geological conditions during the genesis. Alkyl thiophenes can readily be analyzed by EI mass spectrometry: The ratio of the benzylic cleavages of the side chain without and with back-transfer of one hydrogen atom allows to differentiates between substitution in 2- and 3-position. In cases where the result is not clearcut due to secondary effects (e.g., additional substituents) transformation into the corresponding sulfones in most cases will give a definite answer: 3- but not 2-alkyl thiophenes show benzylic cleavage with back-transfer of two hydrogen atoms. From thiophenes with annelated benzene rings only molecular masses, but no structural information can be obtained by EI mass spectrometry. We searched, therefore, for an alternative method.

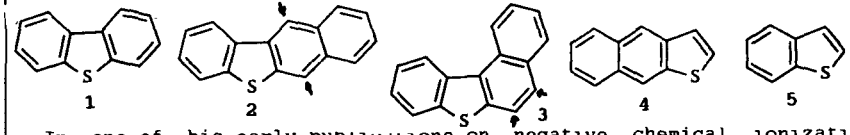

In one of his early publications on negative chemical ionization (NCI) Hunt *et al.* reported that dibenzothiophene (**1**) yielded $[M + 32]^-$-ions most likely due to the formation of a sulfone in addition to M^- and some species of lower mass which must have benn formed by degradation of the ring system. Reinvestigation of the NCI(O_2) spectrum of **1**, its d_8-analog and of a series of oxidation products lead to the following conclusions: The bulk of the ions observed does not stem from gas phase reactions of **1**; they are rather the result of a series os surface catalyzed oxidation and oxidative degradation reactions the products of which are then ionized. *Inter alia*, the ion *m/z* 184 is not M^- of **1** but of *o*-sulfobenzoic acid anhydride (**c**) (cf. Scheme 1, where the major processes are depicted).

As can be seen from Scheme 1 one of the benzene rings is degraded yielding the ions **a**, **b** and **c**. Unsymmetrically substituted derivatives of **1** will give two series of ions which allow to recognize which groups are located in which benzene ring. For benzo[*b*]naphtho[*d*]thiophenes there is a competition between the formation of the sulfone ($[M + 2\ O]^-$) and oxidation of the central benzene ring resulting in a quinone ($[M + 2\ O - 2\ H]^-$; see arrows in **2** and **3**). A *p*-quinone ion is more, an *o*-quinone ion is less abundant than the sulfone ion.

Naphthothiophenes (e. g. **4**) are isomers of **1**. Having a central benzene ring they also can form quinones (*p* prferred over *o*). Sulfone formation is only of secondary importance which seems to be typical for compounds with a terminal thiophene ring. $[M - O - H]^-$ (phenolate) ions which can be found occasionally in the spectra of the compounds discussed before compete especially with the formation of *o*-quinones.

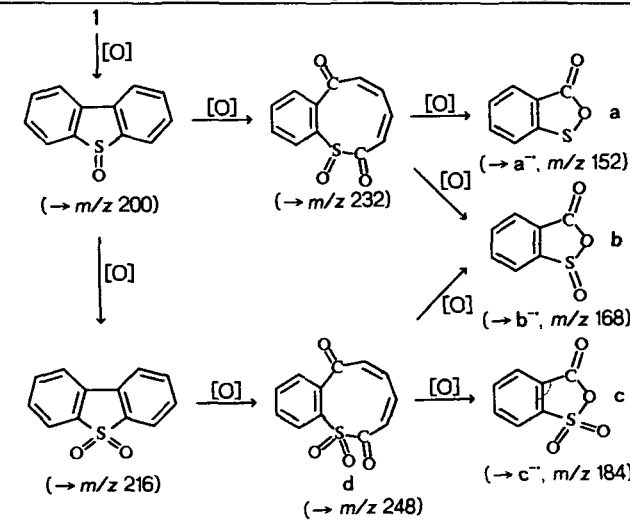

Scheme 1.

Degradation of the thiophene ring leads to ions in the lower mass range. Benzo[*b*]thiophene (**5**) and it s alkyl derivatives show pronounced $[M + O - H]^-$ formation and degradation of the thiophene ring which allows to distinguish betwee n substituents in 2- and 3-position. Alkyl thiophenes do not give any useful NCI(O_2) spectra as only uncharacteristic degradation products can be seen.

In summary, as depending on the structure different oxidation products (sulfone, quinone, phenolate) are responsible for the most abundant ion in the upper mass range NCI(O_2) should be used only in combination with another ionization method which yields M^- or M^+ (EI, CI). Structural information may then be obtained by this method.

References.

Hunt, D. F.; Stafford Jr., G. C.; Crow, F. W.; Russel, J. W. "Pulsed positive negative ion chemical ionization mass spectrometry," *Anal. Chem.* 1976, **48**, 2098-2105

Lange, D.; Budzikiewicz, H." Side chain effects on the fragmentation behaviour of alkylthiophenes," *Org. Mass Spectrom.* 1994, **29**, 432-438

Budzikiewicz, H.; Lange, D. "Fragmentation behaviour of alkylated thiophene-1,1-dioxides," *Org. Mass Spectrom.* 1992, **27**, 489-494

Drabner, G.; Budzikiewicz, H. "Oxidation reactions of dibenzothiophene subjected to negative chemical ionization with oxygen," *J. Am. Soc. Mass Spectrom.* 1993, **4**, 949-954

Drabner, G.; Budzikiewicz, H. "The analysis of benzannelated thiophene derivatives with negative chemical ionization using O_2 as a reagent gas," *J. Mass Spectrom.* 1995, **1**, in press.

Characterisation of Cyclic PET Oligomers by LC-MS

Hilary Yates, Jim Scrivens, Julie Hedley, Mike Taylor
ICI Wilton Research Centre, PO Box No 90, Wilton, Cleveland, England

INTRODUCTION

The combination of chromatographic separation techniques with a mass spectrometer as a detector provides a specific, sensitive and quantitative approach to mixture characterisation. Atmospheric Pressure Ionisation (API) has emerged recently as providing the most universally applicable solution in situations where thermal labilities or involatilities would rule out GC-MS. A recent application of API LC-MS has involved a mixture of cyclic poly ethylene terepthalate (PET) oligomers. Cyclic PET has been the focus of effort in the polymer films industry as an alternative to the traditional linear polymer , due to the variation in processing requirements and product properties potentially offered. LC-MS characterisation supports and enhances field desorption results of cyclic PET oligomers.

EXPERIMENTAL

A spherisorb S50DS2, 250x4.6mm column has been used for introduction of the oligomers to the mass spectrometer at a flow rate of 1ml / minute in acetonitrile / water mobile phase (gradient). A Finnigan MAT TSQ 7000 triple quadrupole mass spectrometer has been employed in APCI mode of positive polarity. 25eV and 35eV ion source voltages were used for 'soft' and 'hard' ionisation respectively. Collision energies of 30eV argon were used for MS-MS experiments. Field desorption data was obtained on a VG Organic ZAB2 SE double focussing mass spectrometer.

RESULTS

Figure 1 displays the mass chromatograms of eluting oligomers ionised by APCI in positive polarity in the presence of traces of ammonium salt. All have been ionised as $M + NH_4^+$. Collision induced dissociation under conditions *described has resulted in MS-MS of each cyclic oligomer, illustrated by the* case of pentamer in Figure 2 . A major loss of 576 Da is observed, indicative of a cyclic trimer neutral. A cyclic trimer loss has been observed consistently for all cyclic PET structures studied where n > 3. This mechanism for dissociation, ie. ejection of a cyclic neutral by a cyclic oligomer of PET has not been previously reported.

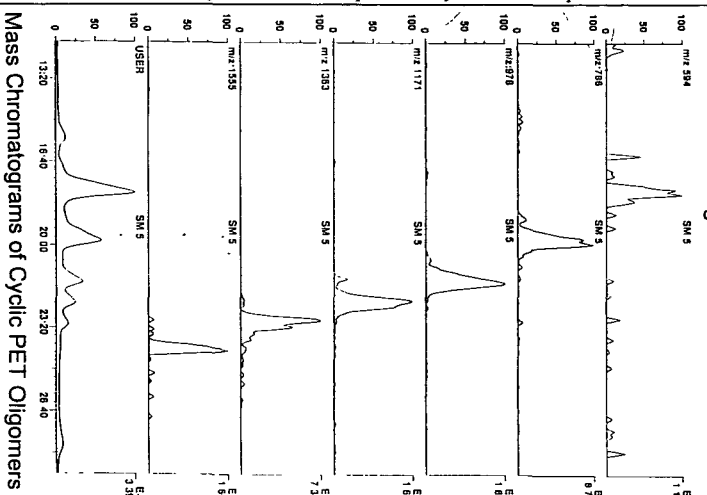

Figure 1

Mass Chromatograms of Cyclic PET Oligomers

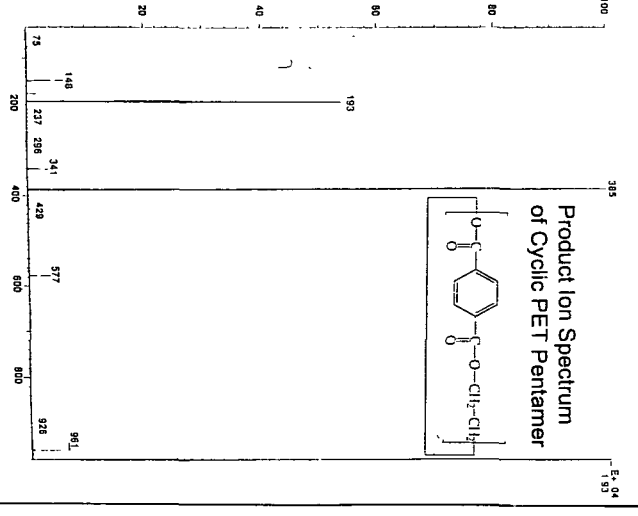

Figure 2

Product Ion Spectrum of Cyclic PET Pentamer

LC-MS Characterisation of a Surfactant Complex Mixture

Hilary Yates, Jim Scrivens, Julie Hedley
ICI Wilton Research Centre, PO Box No 90, Wilton, Cleveland, England

INTRODUCTION

Atmospheric Pressure Ionisation has recently emerged as a widely applicable mass spectrometric interface to liquid chromatography. The combination of the LC separation with the specificity and sensitivity of mass spectrometry has proven an invaluble tool in the analysis of industrial complex mixtures. One successful illustration has involved the analysis of Alkyl Polyglycosides (APG) which are a range of surfactants derived from sugar and natural alcohol which are currently being investigated as a 'green' alternative to the traditional non-renewable resource formulations. The exact composition of the final APG product is dependent on alcohol type, feedstock ratios and exact processing conditions, with the resulting product in all cases being extremely complex.

EXPERIMENTAL

A Spherisorb S50DS2, 250x4.6mm column has been used for introduction of the mixture to the mass spectrometer at a flow rate of 1ml / minute in acetonitrile / water mobile phase (gradient). A VG Organic Quattro triple quadrupole has been employed in negative ESI mode. Comparitive results have been obtained by positive APCI in the presence of traces of ammonia 30 and 50eV ion source voltages were used for 'soft' ionisation and source induced fragmentation respectively. Collision energies of 30eV argon were used for MS-MS experiments. Off-line LC detection employed a Varex 11a light scattering detector.

RESULTS

By negative ESI, ionisation was found to occur by loss of hydrogen, ie $(M-H)^-$ with subsequent loss of water. This water loss was not however observed under 'soft' conditions in the case of the mono glycoside. The equivalent observation was made when ionisation was carried out under positive APCI mode with ammonium salt added to encourage cation attachment. Increased sensitivity was also observed in the presence of ammonium. The mass chromatograms obtained under the latter conditions for the alkylated components are displayed in Figure 1. The deconvolution of oligomers and isomers for both the alkylated and saccharide product has revealed previously undetected coelutions which have been critical to quantitative specification of final products.

43rd ASMS Conference on Mass Spectrometry and Allied Topics

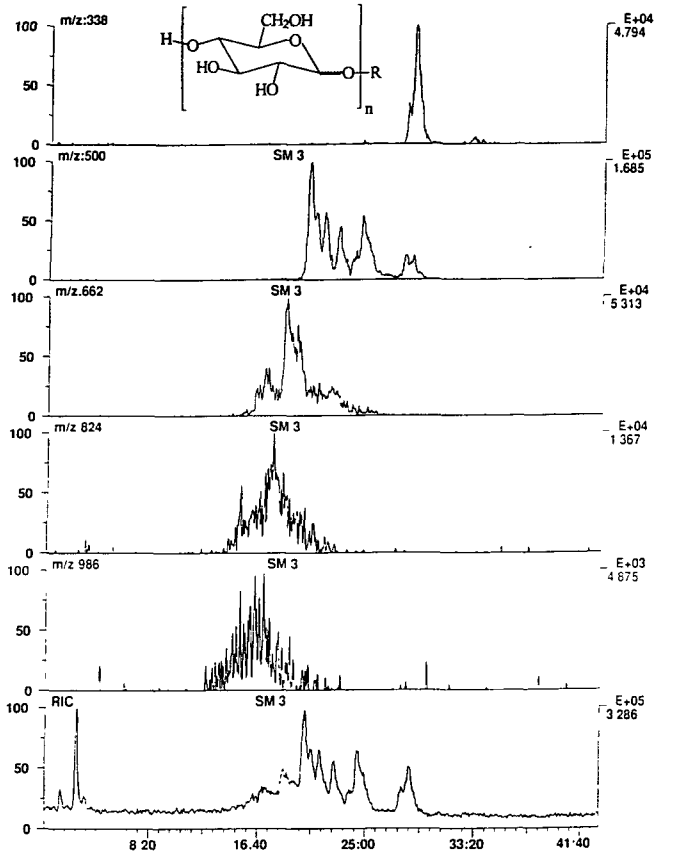

Figure 1 Mass Chromatograms of Mono to Penta glycoside

MASS SPECTROMETRY OF POLYOXYALKYLENE BLOCK COPOLYMER SURFACTANTS

H.T. Kalinoski*[1], L.O. Hargiss[1], B.J. Shay[1] and P.J.W. Schuyl[2]
[1]Unilever Research US 45 River Road Edgewater NJ 07020 USA
[2]Unilever Research Laboratory Vlaardingen The Netherlands

Block copolymers of ethylene oxide (EO) and propylene oxide (PO) possess properties of both polymers and surfactants. Through modification of molecular weight, block size and EO/PO ratio, the physical and surfactant properties of mixtures can be tailored to meet a range of requirements. This has led to a great variety of applications and commercial products containing these materials. Complete characterization of surfactant mixtures requires detailed information on chemical and molecular structure of components. A number of analytical and spectroscopic techniques are applied in the characterization of EO/PO block copolymers (1), but the use of mass spectrometry has been limited by the average molecular weights (up to 15,000 Daltons) and low volatility of these surfactants. The development of electrospray ionization (ESI)(2) and MALDI-TOF (3) mass spectrometry present new opportunities for surfactant characterization.

Size exclusion chromatography (SEC) provides a powerful approach for the determination of average molecular weights and molecular weight distributions of polymer mixtures (1). Unfortunately SEC determinations generally utilize standards of known molecular weight and composition (as similar to the analyte mixture as possible) for molecular weight and composition assignments. Such standard materials are uncommon for copolymers such as the EO/PO surfactants. As separation in SEC is determined by molecular size in solution, the technique is more reliable for larger, higher molecular weight materials. EO/PO block copolymers are small by conventional SEC standards. The situation for EO/PO copolymers is further complicated by the fact that they are surfactants, with hydrophilic and hydrophobic portions on the same molecule. This can lead to aggregation and micelle formation, increasing apparent size in solution and confounding efforts to produce meaningful SEC data.

For these reasons, mass spectral techniques based on ESI and MALDI were examined to augment the amount and type of information available from more traditional polymer characterization techniques. The techniques both offer the possibility of coupling to SEC (4,5) either on- or off-line. The conditions required to obtain useful information from a series of representative EO/PO copolymer surfactants were evaluated. The parameters influencing each technique were probed and the appearance of the resulting mass spectra examined. Directions for future work with these techniques for such complex mixtures are suggested.

Both ESI and MALDI-TOF are directly applicable to the mixture and structural characterization of EO/PO block copolymer surfactants. In both cases, cationization with sodium is the primary source of ions present in mass spectra. Mixtures of different composition and molecular structure can be distinguished from one another using either technique. Due to spectral complexity at higher sample average molecular weights, MALDI-TOF may be more applicable to the characterization of higher molecular weight (over 3000 Daltons) mixtures. Calculations of mixture average molecular weights can be made from mass and intensity data produced in electrospray mass spectrometry, with good agreement to expected values. Both singly- and doubly-charged ions can be used in these calculations. It may be that higher molecular weight EO/PO copolymers are more likely to attach two sodium ions, yielding more representative mass spectra and better determinations of average molecular weights. This is similar to results found in work on homopolymers (6). Conditions used for ESI should be applicable to coupling with SEC, to increase the amount of information available from both techniques for EO/PO copolymer surfactants. Lower sample concentrations should be used to obtain best size exclusion. Sample preparation has a profound effect on the appearance of MALDI-TOF mass spectra of EO/PO surfactants. Further work is planned to examine the causes and implications of sample preparation.

REFERENCES

(1) H.T. Kalinoski, "Chemical Analysis of Polyoxyalkylene Block Copolymers" in POLYOXYALKYLENE BLOCK COPOLYMER NONIONIC SURFACTANTS (V. Mark Nace, ed.), Marcel Dekker, New York, (1995)
(2) M. Yamashita and J.B. Fenn, *J. Phys. Chem. 88*, 4451 (1984)
(3) M. Karas and F. Hillenkamp, *Anal. Chem. 60*, 2299 (1988)
(4) L. Prokai and W.J Simonsick, Jr., *Rapid Commun. in Mass Spectrom. 7*, 853 (1993)
(5) W.J. Simonsick, Jr. and L. Prokai, *Proceedings of the 42nd ASMS Conference*, Chicago, p. 318 (1994)
(6) C.N. McEwen, B.S. Larsen and W.J. Simonsick, Jr., *Proceedings of the 42nd ASMS Conference*, Chicago, p. 317 (1994)

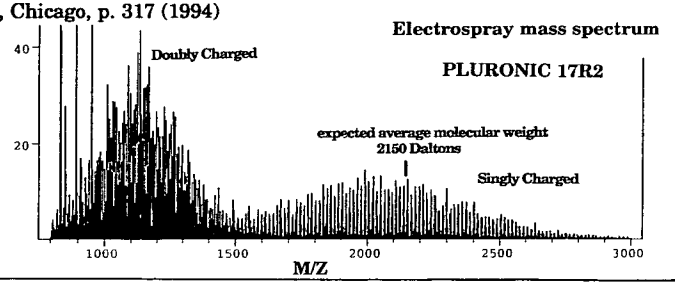

DIFFUSION OF ARGON IN POLYIMIDE AND ITS CARBON FIBER LAMINATES *

Michael A. Grayson, McDonnell Douglas Corporation, St Louis MO 63166

The diffusion of argon in neat and carbon fiber laminates of a thermoplastic polyimide was determined by precision abrasion mass spectrometry (PAMS) (Ref 1). In this method, samples that have been exposed to the diffusing species in a controlled environment are periodically removed and loaded into the PAMS apparatus mounted on the ion source housing of a time-of-flight mass spectrometer. The measurement is accomplished by drilling a hole through the sample with an end mill while continuously recording an ion characteristic of the diffusing species and the position of the tool in the sample. The distribution profiles thus obtained can be mathematically fitted with a solution to Fick's law, thereby permitting determination of diffusion coefficients. Sample coupons approximately 3 by 12 by 25 mm were cut from panels of the neat resin, $[90°]_{8S}$ uniaxial, $[+15°/-15°]_{4S}$ cross-ply, and $[+45°/0°/-45°/90°]_{2S}$ quasi-isotropic laminates and dried to constant weight. The samples were placed in special vessels that could be evacuated and back-filled with argon. The vessels were placed in ovens at four different temperatures in the range of 45 to 120°C. At selected times, a coupon was removed from the argon atmosphere and the distribution profile of argon through the thickness of the sample was measured by PAMS. Several measurements were made in each sample and the results deconvoluted, averaged together, and folded about the midpoint. It should be noted that this method of determining the diffusion coefficient does not need to be corrected for edge effects. This is because the holes are drilled in the samples at a sufficiently large distance from the edge that edgewise diffusion of argon cannot affect the distribution profile at the point of measurement. The diffusion coefficient was calculated by using a least-squares fit of a series solution of Fick's law to the measured distribution profile. The value of diffusion coefficient that gives the best fit to the experimental data is taken as the diffusion coefficient for the sample under those conditions of temperature, exposure time, and sample thickness. In theory, for a given exposure temperature, the value of the diffusion coefficient should be invariant with exposure time. Therefore, the various experimentally determined values at different times at one temperature can be averaged together to obtain the diffusion coefficient. A typical distribution profile of argon in the $[+45°/0°/-45°/90°]_{2S}$ carbon fiber polyimide laminate after it was exposed to one atmosphere of argon for 70 hours at 120°C is shown in Figure 1. It is a composite of three separate holes that have been averaged together and folded about the mid-point. Note that the measured concentration is not shown near the surface of the laminate. As soon as the laminate is removed from the argon atmosphere, desorption of argon commences. In the time it takes to remove the sample from the argon atmosphere, load it into the mass spectrometer, evacuate the instrument, and stabilize the operation of the mass spectrometer; the initial 0.25 mm of the surface of the laminate has developed a concentration profile that reflects desorption of argon. These experiments were performed on a variety of material forms to compare experimental results with previous theoretical calculations of the diffusion coefficient in materials with and without reinforcing carbon fibers (Ref 2). In addition, this approach will serve to reveal any anomalous behavior of diffusion in the laminates. According to Shen and Springer, (Ref 2) the diffusion coefficient of a laminate can be calculated based on knowledge of the diffusion coefficient in the neat resin and the volume fraction of carbon fibers according to the relation:

$$D_n = \left(1 - 2\sqrt{V_f / \pi}\right) D_r \,. \qquad \text{Eqn. 1}$$

Where: D_n is the diffusion coefficient normal to the plane of the fibers in a laminate;
D_r is the diffusion coefficient in neat resin;
V_f is the volume fraction of fibers in the laminate.

One can see that as the volume fraction of fibers increases from 0 to 1, the value of D_n will decrease from D_r to a small number. Typically, laminates of the type in this study have fiber volume fractions on the order of a half. According to Eqn 1, the diffusion coefficient normal to the plane of the fibers should be approximately 20% of the diffusion coefficient in the neat resin for all laminates irrespective of layup. The results of the diffusion coefficient measurements are shown in the Arrhenius plot in Figure 2. Note that all of the material forms have about the same activation energy for diffusion of argon, 43kJ/mol, as evidenced by the nearly constant slopes of the lines fit to the data. However, the laminates have lower diffusion coefficients compared to the neat resin. In theory, all of the laminates have the same volume fraction of fiber, so the rate lines for the diffusion coefficient should be shifted down by the same amount. Shen and Springer's prediction based on a volume fraction of fiber of 0.5 is shown as the bold line close to the experimental data for the quasi-isotropic laminate. There is enough data from these measurements to indicate that there is a statistically significant difference in the diffusion of argon in the quasi-isotropic laminate compared to the uniaxial and +/-15° layups. Precision abrasion mass spectrometry was used to measure the diffusion coefficient of argon in neat polyimide and several of its laminates of different layups. The values of diffusion coefficient are in the range normally expected for gas diffusion in polymers. The shift to lower values of diffusion coefficients in the laminate forms follows Shen and Springer's theoretical prediction. There is an anomaly in the behavior of the quasi-isotropic laminate compared to the other laminates which warrants further study.

Ref. 1) M. A. Grayson, E. A. Theby and K. O. Lippold, Rev. Sci. Instrum., (1981), **52(10)**, 1521.
Ref. 2) C-H. Shen and G. S. Springer, J. Compos. Mater., (1976), **10**, 2.

* Work performed under NASA Contract NAS1-18862

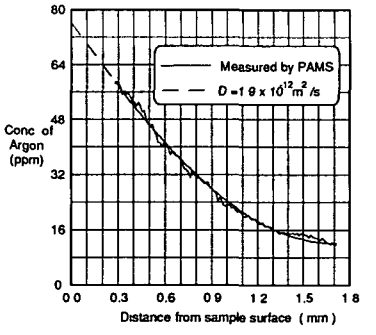

Figure 1. Measured and least squares fitted argon distribution profiles in quasi-isotropic laminate after 70 hours exposure to argon at 120°C

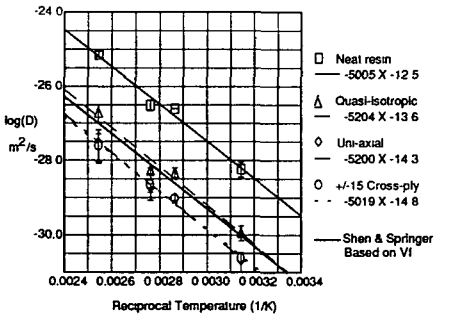

Figure 2. Arrhenius plot of diffusion coefficient data from argon transport study.

THE CHARACTERISATION OF COMMERCIAL LUBRICANT FORMULATIONS

Jim Scrivens, Hilary Yates, Alan Bunn, Paul Tayler, Malcolm Beckett, Mike Taylor, Richard Jennings

ICI Wilton Research Centre, PO Box 90, Wilton, Cleveland, England, TS90 8JE

INTRODUCTION

Modern lubricant formulations are complex mixtures of base esters, antiwear additives, corrosion inhibitors and other modifiers. Their characterisation poses a difficult analytical challenge. A major market for these products is in the replacement of traditional CFC based refrigerants by modern alternatives. Conventional lubricants such as mineral oil are incompatible with the new refrigerants.
Soft ionisation mass spectrometry (CI,LSIMS and FD), coupled with tandem mass spectrometry where required, has been used in conjunction with GC-MS and NMR in order to characterise these formulations. Statistical analysis of the soft ionisation data has provided further information regarding the detailed composition of the complex esters. This combination of experimental approaches provides a powerful method for the characterisation of these materials. A number of different types of polyol are used in the manufacture of the base esters with tetra and hexa esters the most common. The acids used, in general, vary in carbon number and in isomeric distribution and this leads to considerable complexity in the product.

EXPERIMENTAL

Proton and ^{13}C NMR spectra were obtained on JEOL GSX 400 and GX 400 spectrometers. GC-MS results on a VG Organic Trio-1 quadrupole mass spectrometer. The CI, LSIMS and FD soft ionisation spectra were collected using a VG Organic ZAB-T four sector mass spectrometer of BEBE geometry (in two sector mode). The CI spectra were obtained by introducing the sample via a heated probe, programming the temperature, and averaging the resulting spectra. FD spectra were obtained using 13 m activated carbon emitters supplied by Linden ChroMasSpec (Bremen). The emitters were programmed from 0-40 mA, or until the signal disappeared. Product ion mass spectra were also obtained on the ZAB-T using 4000 eV collision energy with argon as collision gas and using an array detector.

RESULTS

Figure 1 shows FD and NH_3 CI spectra for a tetra acid formed from pentaerythritol and a mixture of C8, C9, C10 and C11 aliphatic acids. The agreement between the two methods is very good with the CI data giving the most reproducible results. The FD data however shows fragment peaks at lower mass corresponding to $[RCO]^+$ which makes qualitative identification of the acids present easier. Table 1 shows the results of a statistical analysis of this data which gives a result of 66.9%C8, 17.6% C9, 12.8% C10 and 2.7% C11.

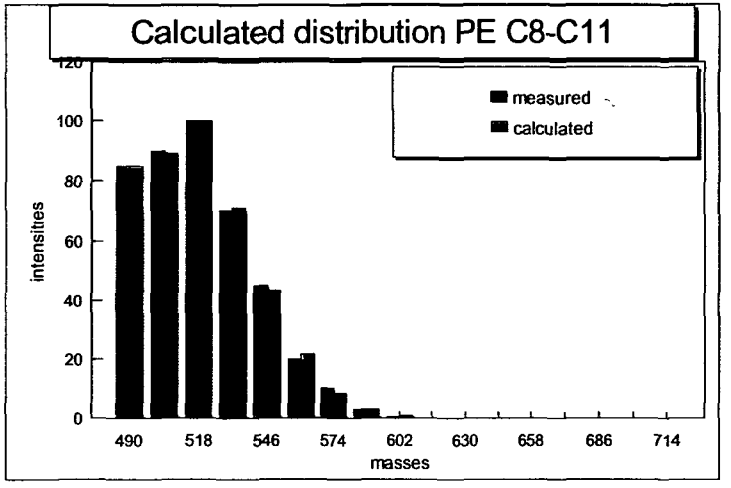

Table 1

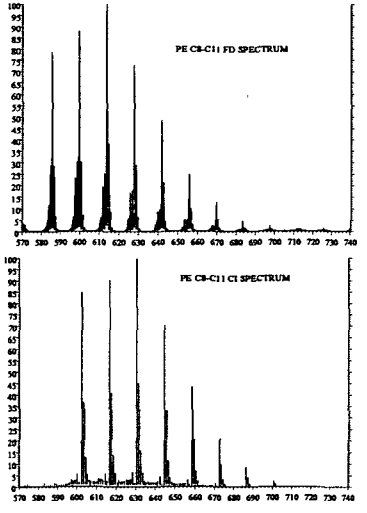

Figure 1

CONCLUSIONS

A combined NMR and MS approach has been used successfully to characterise a series of lubricant formulations. NMR is extremely useful in isomeric differentiation and in identifying polyol and acid type. Both CI and FD ionisation methods give similar results with CI having the edge in reproducibility. Product ion spectra have been used where neccessary to aid interpretation. A statistical approach to the calculation of expected mass spectrometric intensities has been found to give useful results for both tetra and hexa ester systems. Quantitative information regarding carbon number of acid used has been derived. A comparasion of data obtained from tetra and hexa ester can indicate whether a common acid feedstock was used in their manufacture.

IMPACT OF CONVERSION LEVEL ON HYDROCARBON TRANSFORMATION IN FLUID CATALYTIC CRACKING PROCESSES STUDIED BY COMBINED CHROMATOGRAPHY AND MASS SPECTROMETRY

Kuangnan Qian, Robert H. Harding and Xinjin Zhao
W.R. Grace Co.-Conn., Washington Research Center, Columbia, MD 21044

INTRODUCTION

A fundamental understanding of the impact of feedstock properties on catalyst performance and on the molecular transformation in the fluid catalytic cracking (FCC) process has been of great interest to both petroleum and catalyst manufacturers. For the latter, this understanding provides an important guide toward the design and improvement of catalyst structure and formulation to achieve desired product performance. The level of conversion (conversion wt%) is an important measurement of optimized catalyst performance. Combined chromatography separation and mass spectrometry provides an effective tool to study the impact of conversion level on hydrocarbon transformation and to identify the nature of hard-to-crack molecules and their contributions to the bottoms yield.

EXPERIMENTAL

The feed selected for this study is a low sulfur (0.3%) petroleum fraction (450°F+). The feedstock was cracked by an FCC catalyst in a Riser unit at two different conversion levels (73.6% (Run A) and 67.1% (Run B), respectively). The heavy cycle oil (HCO or bottoms) and the light cycle oil (LCO) from the two different conversions, together with the feed, were characterized by combined clay-gel elution chromatography (ASTM D2007) and mass spectrometry. The oil samples were separated by clay-gel into saturates, aromatics, polars and asphaltenes. The saturate and aromatic fractions were analyzed on a Finnigan TSQ 700 mass spectrometer equipped with a Varian 3400 GC. The mass spectrometric data of the two fractions were processed using group-type methods as described in ASTM D2786 and D3289. The polar fraction was analyzed by low voltage (12 eV) probe mass spectrometry.

RESULTS AND DISCUSSION

Analyses of the LCO products from the two different conversions showed that alkyl naphthalenes are the most abundant species in the LCOs, followed by paraffins, alkyl benzenes and 1-4 ring naphthenes. The increase in conversion results in significant reduction of paraffins, particularly the iso-paraffins, but has no impact on the concentration of aromatic molecules. The results indicate that the LCO yield is strongly affected by the total concentration of di-aromatics in the feed.

Analyses of the bottoms from the two different conversions showed that tri- and tetra-aromatics are the major hydrocarbon types in the bottoms (Figure 1). The higher conversion increases the concentration of heptane-insolubles by 38%, suggesting the formation of highly condensed hydrocarbon structures by the FCC process. The increase in conversion has the most impact on saturate hydrocarbons (more than 50% reduction). Compared to the feed, significant reductions of mono- and di-aromatics were observed, mostly due to the cleavage of the long chain aromatics into short chain benzenes (gasoline) and naphthalenes (LCO). It is interesting to note that the concentrations of 3+ ring aromatics in the bottoms are as high as that in the feed, suggesting that the bottoms yield is closely related to the total concentration of 3+ ring aromatics in the feed.

The impact of conversion level can be measured by the relative change (RC%) in concentration of a chemical component at the two conversions: RC% = (Run B -Run A)/Run A × 100. As shown in Figure 2, the impact of conversion level decreases sharply as the aromatic type changes from mono-aromatics to tri-aromatics and changes very slowly afterwards. Note that the higher conversion actually

increases the concentrations of the "core" aromatics (phenanthrenes, pyrenes, benzopyrenes, etc.) in the bottoms. The aromatics in the bottoms are found primarily to be methyl/ethyl substituted species.

The analyses also show that the conversion level has little impact on the aromatic sulfurs.

Benzocarbazoles were found to be the predominant nitrogen compounds in the bottoms. Overall, the catalytic cracking reduces all nitrogen compound types in the bottoms, particularly the carbazoles. The fact that we did not detect a significant amount of carbazoles in the LCO fractions suggests that most of the short-chain carbazoles have been absorbed by the catalyst and are converted into part of the coke.

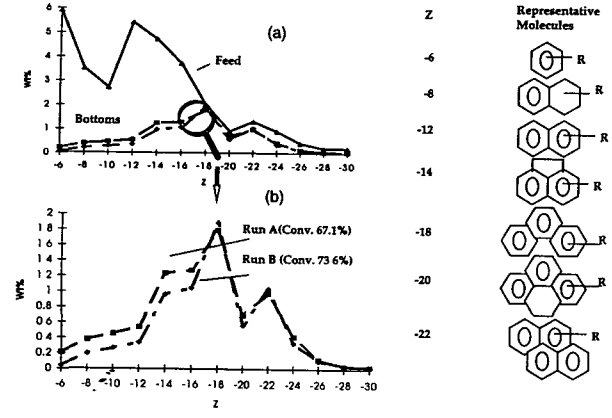

Figure 1. Aromatic hydrocarbon type distribution in the feed and the bottoms

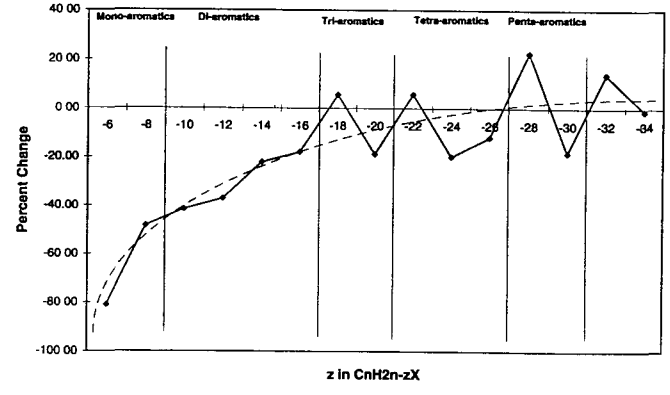

Figure 2. Relative change (in wt%) of aromatic types as conversion is increased from 67.1 to 73.6%

Quantitative Analysis of Reformulated Gasoline by Mass Spectrometry

D. Drinkwater and V. Nero
Texaco Research and Development
P.O. Box 509
Beacon, NY 12508

Reformulated gasoline (RFG) is a new product offered in the United States since January 1, 1995 in an effort by the EPA to meet the Clean Air Act. RFG is a highly-designed product with tight specifications for aromatics, benzene, oxygenate content, distillation properties, sulfur content, toxics content, and vapor pressure. Because of all the new regulatory requirements on this product, a number of new analytical techniques have been specified for its analysis, including GC/MS for total aromatics,. Data from the EPA and proposed ASTM methods for RFG analysis are presented, along with data suggesting a number of extensions and improvements on these methods. The accuracy and precision of these methods are evaluated

The use of micro-bore and mini-bore capillary GC columns for quantitative analysis provides a number of advantages over conventional capillary columns In addition to the decreased elution time provided by the more efficient separation, the decreased capacity of these columns may be used to increase the dynamic range of the mass spectrometer, thus improving calibration linearity and accuracy The smaller inside surface area and shorter length of these columns leads to a much reduced phase bleed level in the ion source, lengthening the time between ion source cleanings and, therefore, instrument recalibration. The decreased gas flow through the narrow-bore columns greatly improves the gas load into the ion source, as well as simplifying the running of these columns at high split ratios for neat samples such as gasolines.

The extension of the GC/MS method for total aromatics to report other RFG regulated parameters such as benzene and oxygenate concentrations is particularly important for refinery laboratories with limited space, manpower, and time resources Data is presented comparing GC/MS results on benzene and oxygenates with the mandated analysis techniques, both measured in a refinery setting by refinery personnel. The high precision and accuracy of the mass spectrometry data suggests that the mandated GC/MS method can replace both the benzene and oxygenate analyses which are currently mandated by GC methods, thus replacing three instruments and analyses with one

Figure I. shows a partial reconstructed m/z 120 ion chromatogram of the C9H12 isomers using the fast chromatography method (20m x 0 10mm ID x 0 4 um DB1 column, 0.1 second scans m/z 70-170). Figure II. shows the agreement between benzene concentration in gasolines by Method D3606 and GC/MS measured at four different laboratories (including refinery data measured by newly trained personnel).

43rd ASMS Conference on Mass Spectrometry and Allied Topics

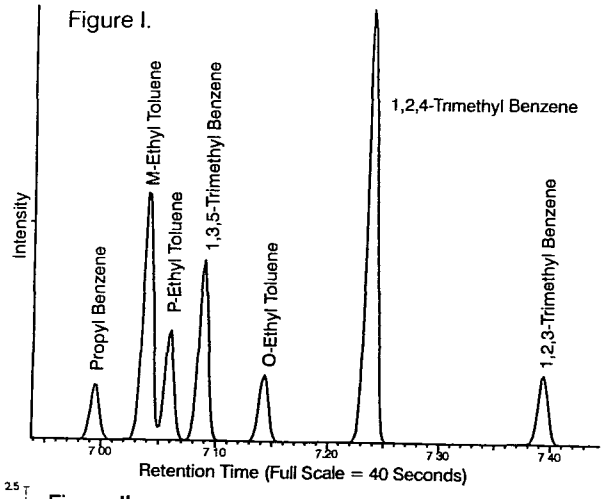

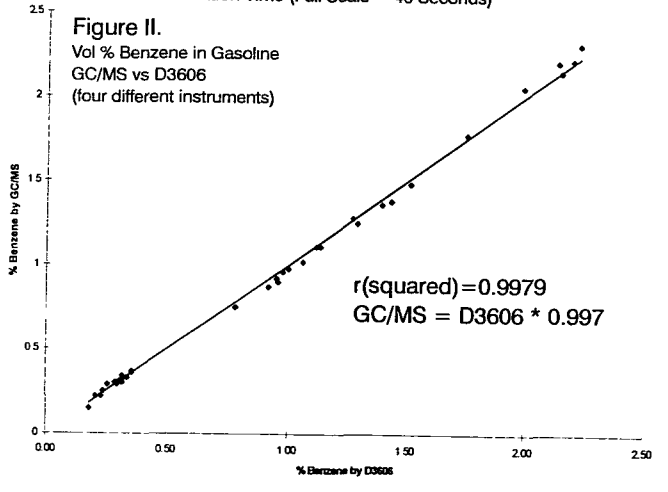

Characterization of Acidic Components in Midway Sunset Crude Oil

George W. Haas, Leroy Ellis, Jerry E. Hunt, and Randall E. Winans

Chemistry Division, Argonne National Laboratory, Argonne, IL 60439

The crude oil from the Midway Sunset Field in California contains 70% non-distillable constituents called resid. Analysis of Midway Sunset crude components using standard analytical techniques such as GC and GC-MS is difficult due to the complex and intractable nature of the resid. Acidic components in crudes are of importance because the presence of these compounds results in problems related to pipe corrosion and waste-water contamination. Detailed characterization of the acidic components of Midway Sunset crude using high-resolution electron impact (HREI) and chemical ionization (HRCI) mass spectrometry have been undertaken.

Experimental

The Midway Sunset crude was subjected to an analytical separation involving six steps. 1). Extraction of the acidic components with sodium hydroxide/methanol. 2). Back extraction of nonacidic components with *n*-hexane. 3). The base extract was then filtered and centrifuged to remove precipitated asphaltenes. 4). The acid extract (3.5% w/w) was chilled for 24 hours at ≈-20 °C, resulting in precipitation of some species. 5). The acid extract, referred to as Fraction A, was decanted from the precipitate. 6). Acidic Fraction A was then methylated using diazomethane in methylene chloride before analysis.

The GC-MS run was acquired with a Hewlett Packard 5970 MSD fitted to a 5890 Series II GC. A fused silica capillary column (DB-5 MS) of 60 m in length with an ID of 0.25 mm was employed with oven conditions of 50 to 300 °C at 4 °C/min.

The full-scan HREIMS and HRCIMS data were acquired with a Kratos MS50TC triple analyzer mass spectrometer of EBE design. The results for all of these experiments were obtained at ≈12k dynamic resolution at a scan rate of 10 s/decade. The ionization energy for the HREI experiments was ≈70 eV using high-boiling perflurokerosene (PFK) as the internal calibrant. The reagent gas used for the HRCI experiments was isobutane with poly-(dimethylsiloxane)-methyl terminated (MW 770) as the internal calibrant. A direct-insertion probe was used to vaporize the samples into the gas phase with a maximum temperature of ≈400 °C and a source temperature of ≈200 °C.

Results and Conclusions

A GC chromatogram (see **Figure 1**) of the methylated acidic Fraction A shows a broad, unresolved hump. This unresolved complex mixture indicates the presence of a large number of components in the final methylated acidic Fraction A.

The HREI and HRCI mass spectra display a distribution of ions ranging from 100 to ≈500 u (see **Figures 2** and **3**), which is very similar to the GC-MS run. The most striking distinction between the spectra is the distribution of more abundant higher-mass ions in the HRCI mass spectrum as compared to the HREI mass spectrum. This is attributed to the softer CI process. The higher mass components which are observed in the 400 to ≈500 u range for the HREI data, are not seen in the HRCI data. Bar graphs of the mol % vs rings + double bonds calculated from the HREI and HRCI data, indicate less hydrocarbon (HC) content from the HRCI result in comparison to the HREI result (attributed to the softer CI process). A homologous series containing mono-, di-, and trioxygenated compounds are observed by both ionization techniques, which are suggested to represent methylated phenolic and carboxylic acid constituents. Also identified are sulfur and sulfur-oxygenated containing species along with other

heteroatom constituents. The sulfur-oxygenated series are tentatively identified as thioacid esters. HREIMS and HRCIMS data have been used to provide detailed information on compound classes and carbon numbers.

Figure 1

GC-MS Chromatogram of Midway Sunset 'Acidic' Fraction A (Methylated)

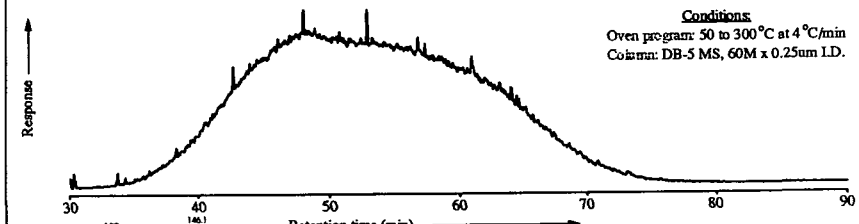

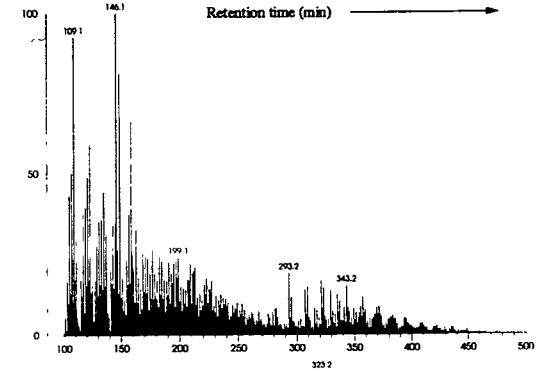

Figure 2
HREIMS

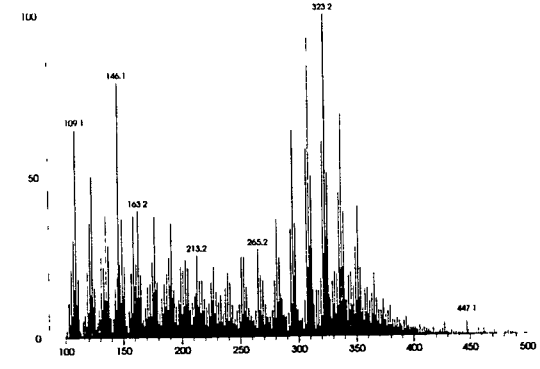

Figure 3
HRCIMS

PYROLYSIS-PHOTOIONIZATION MASS SPECTROMETRY

C.W. Bookwalter, D.L. Zoller and M.V. Johnston
Department of Chemistry and Biochemistry
University of Delaware, Newark DE 19716

Pyrolysis mass spectrometry has been performed by photoionization with coherent vacuum ultraviolet (VUV) radiation. Pyrolysis mass spectra are often difficult to interpret owing to the complex distribution of ions formed Much of this complexity can be ascribed to the heterogeneity of samples typically analyzed or to the numerous reaction pathways accompanying pyrolysis. Indeed, information of this type is often the goal of a pyrolysis experiment. However, fragmentation induced by the ionization process can also be extensive and often obscures useful information. VUV photoionization with 9.6 to 10.5 eV radiation minimizes fragmentation by photoionizing just above the ionization threshold.

The pyrolysis-photoionization technique was used to obtain spectra for n-tetracontane and cholesterol. In a typical 70 eV EI spectrum, n-tetracontane and cholesterol show extensive fragmentation. Figure 1 shows the 10 5 eV photoionization mass spectrum of n-tetracontane with a probe temperature of 375°C. Relatively little fragmentation and an intense molecular ion peak is observed. Cholesterol has a narrow temperature range within which it is stable as a gaseous molecule. However, similar to the n-tetracontane spectrum, little fragmentation and an intense molecular ion peak is observed for cholesterol at 150°C.

The pyrolysis-photoionization technique was then extended to polymer samples. Figure 2 shows the 10.5 eV photoionization mass spectra of a polybutadiene sample (Mw = 450,000) at two different temperatures. With probe temperatures between 325-400°C, the relative intensities of peaks attributed to β(C-C) bond cleavage are more intense than those arising from other pathways. With probe temperatures above 400°C, higher energy process occur and the preference for β-cleavage disappears. Pyrolysis products from a polystyrene oligomer (M_W = 45,000) were also identified using this technique. Polystyrene showed three series of peaks corresponding to different fragmentation pathways for each oligomer.

Different classes of coal have different levels of sulfur and aromatic hydrocarbons. Both Wyodak and Illinois #6 coal samples were analyzed using pyrolysis-photoionization mass spectrometry. A temperature ramp from 100-860°C at 20°C/min in conjunction with 10.5 eV photoionization was used for these experiments. Wyodak is classified as a subituminous coal while Illinois #6 is classified as a highly volatile, class C coal. Wyodak is a younger coal containing more aliphatic chains than Illinois #6. In addition, Wyodak is known to contain less sulfur (<1%) than Illinois #6 (>3%). Both of these differences were reflected in the mass spectra. Wyodak gives peaks in the high m/z range (396, 424, 452...) separated by 28 Da which are not observed in the Illinois #6. This suggests the presence of compounds containing a series of only odd or only even length aliphatic chains. In addition, Illinois #6 contains peaks at m/z 34 (H_2S), 48 (CH_3SH) and 64 (S_2). Wyodak contains some of these peaks (m/z 34 and 48) but with much less overall intensity.

43rd ASMS Conference on Mass Spectrometry and Allied Topics

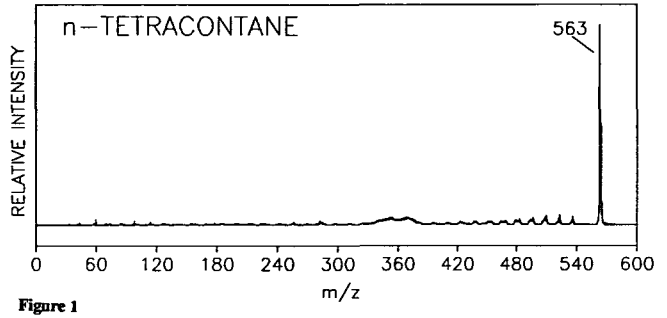

Figure 1

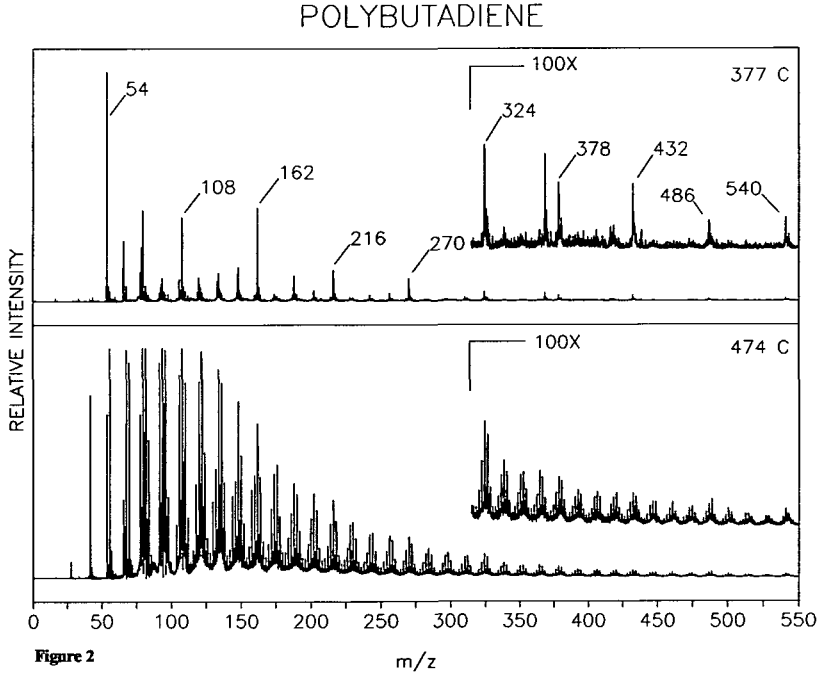

Figure 2

THE ACCURACY OF CHEMICAL TYPE ANALYSIS USING A DYNAMIC BATCH INLET SYSTEM

S. G. Roussis and A. S. Cameron
Imperial Oil, Sarnia Research Centre, Sarnia, Canada, N7T 7M1

Hydrocarbon chemical type analysis by mass spectrometry is a very useful analytical technique that provides information about the chemical composition of petroleum samples. Important industrial processes are based on the results obtained from standard ASTM (American Society for Testing and Materials) mass spectrometric tests. These tests are based on standard 70 eV Electron Ionization experiments that produce highly repeatable and reproducible results. The sample is typically introduced into the mass spectrometer via an inlet system that does not permit any compositional change, partial loss or contamination of the sample in the introduction step. The industry's standard sample introduction system is a large, all-glass heated system that allows the continuous flow of the sample from a large expansion volume (~1L - 2L) to the mass spectrometer via a heated capillary transfer line. Sample introduction is achieved with high temperature glass valves that control the flow of the sample to the mass spectrometer.

A simplified introduction system that allows the dynamic introduction of hydrocarbon samples to a mass spectrometer, consists of a small expansion unit that can be easily installed in the oven of most commercial gas chromatographs. The expansion unit is interfaced to the injection port and to the mass spectrometer via deactivated fused silica tubing. The advantages of the simplified batch system are: (i) transportability, (ii) simplicity, (iii) suitability for automation, (iv) low cost, (v) ease of operation and maintenance. The historical data obtained with the standard ASTM test methods are important, therefore, a critical aspect, prior to the acceptance of the dynamic batch inlet system as the standard sample introduction system, is the accuracy of the results compared to the existing static batch inlet. The present study examines the results obtained with the dynamic batch inlet system compared to the accepted results obtained with the static batch inlet system.

A heated (300°c) large expansion unit (1L) from Brunfeldt Co. (Bartlesville, OK) was used for the static analyses. The samples were introduced into the expansion unit using an ampoule or gallium frit inlet. A schematic of the dynamic inlet is shown in Figure 1. A small expansion unit (2 cc) was installed in the GC oven of an HP GC/MS instrument. All temperatures in the systems were kept at 300 °C. Each sample inlet system was coupled with a 5970 HP MSD mass spectrometer. The 10-800 m/z range was scanned at a rate of 0.5 scans/sec.

Typical standard and in-house modified ASTM test methods were used for the evaluation: ASTM-D2786 (Saturates), ASTM-D3239 (Aromatics), ASTM-D2789 (Naphthas), Middle Distillate and Total Oil Analysis. An example of the repeatability and reproducibility of the new bulb system compared to the static inlet is shown in Table 1, for methods D2786 and D3239. Equivalent repeatability is demonstrated by both systems. No significant difference was observed between the two methods. The reproducibility of the results obtained by the static and dynamic inlets in our lab, is equivalent or better than that of the reference ASTM methods. That is, the results obtained by either inlet system are within the same margins of error as the results obtained by the static system in different labs. Similar results are obtained for the other test methods.

The average absolute difference between the results obtained with the dynamic and static sample introduction methods was less than 1.5% (Fig. 2). An example of the difference of the mean values for ASTM-D3239 is shown in Fig. 3. Comparison of the MS results (D2786, Middle Distillate, Total Oil

tests) and the results obtained by SFC and HPLC methods, showed an average absolute difference of less than 1.5% This demonstrates a very good agreement between the MS and the chromatographic techniques. For such comparisons, the ASTM guidelines should be followed in selecting the proper MS test based on the nature of the sample.

FIGURE 1. DYNAMIC BATCH TYPE ANALYSIS SYSTEM

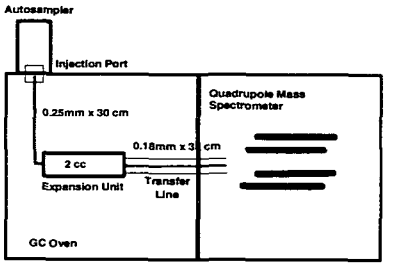

TABLE 1. REPRODUCIBILITY: LAB VS. ASTM (MANUAL INJECTION)

SATURATE-D2786	LAB 'R' *		ASTM 'R' **	
CHEMICAL TYPES	MEAN	STD DEV.	MEAN	STD DEV
0-RING ISOPARAFFINS	28.7	1.38	10.5	1.60
1-RING CYCLOPARAFFINS	19.4	0.74	17.3	1.50
2-RING CYCLOPARAFFINS	17.3	1.56	15.8	1.50
3-RING CYCLOPARAFFINS	16.2	0.51	16.7	1.00
4-RING CYCLOPARAFFINS	8.9	1.10	30.1	3.40
5-RING CYCLOPARAFFINS	4.4	1.16	6.8	1.30
6-RING CYCLOPARAFFINS	1.8	0.66	2.8	1.10

AROMATIC-D3239	LAB 'R' *		ASTM 'R' **	
CHEMICAL TYPES	MEAN	STD DEV.	MEAN	STD DEV
ALKYLBENZENES	27.1	1.15	13.7	1.00
NAPHTHENE BENZENES	15.7	0.53	13.3	1.10
DINAPHTHENE BENZENES	11.9	0.65	13.7	0.40
NAPHTHALENES	2.3	0.31	6.7	0.80
ACENAPHTHENES	5.4	0.67	9.0	0.20
FLUORENES	5.2	0.64	10.7	0.20
PHENANTHRENES	2.5	0.66	8.6	0.30
NAPHTHENEPHENANTHRENES	2.8	0.47	4.5	0.40
PYRENES	1.4	0.25	5.7	0.50
CHRYSENES	1.1	0.43	2.8	0.40
PERYLENES	0.8	0.15	1.7	0.20
DIBENZANTHRACENES	0.4	0.06	0.4	0.10
BENZOTHIOPHENES	5.5	0.59	1.0	0.40
DIBENZOTHIOPHENES	2.9	0.25	1.5	0.30
NAPHTHOBENZOTHIOPHENES	0.7	0.12	0.5	0.30

*LAB 'R' generated from both static and dynamic inlets
** ASTM results are from different sample

FIGURE 2. AVERAGE ABSOLUTE DIFFERENCE BETWEEN STATIC AND DYNAMIC METHODS

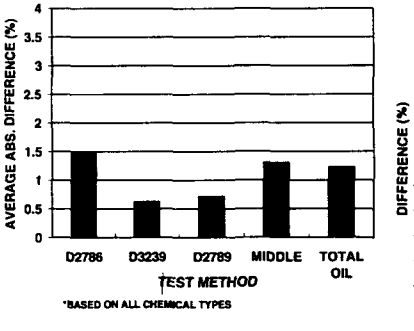

*BASED ON ALL CHEMICAL TYPES

FIGURE 3. DYNAMIC VS. STATIC SAMPLE INTRODUCTION: AROMATIC-D3239

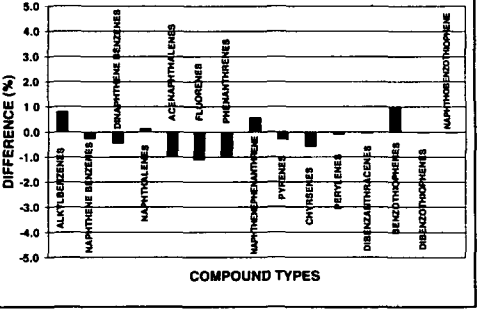

IMPROVING THE REPRODUCIBILITY OF PYROLYSIS MS TECHNIQUES

S. G. Roussis and J. W. Fedora
Imperial Oil, Sarnia Research Center, Sarnia, Canada, N7T 7M1

The analysis of the majority of volatile samples is primarily accomplished with established techniques (EI, CI). These techniques are based on the direct vapourization of the sample, upon heating, in the ionization source of a mass spectrometer. Typical analytical techniques, able to analyze non-volatile samples are those that allow the desorption of components from the solid or liquid phase directly to the gas phase. Field Desorption (FD) and Desorption Chemical Ionization (DCI) are two of these techniques. Fast Atom Bombardment (FAB) has been more successful in analyzing polar samples than non-volatile hydrocarbon samples. Limited information is available for the capabilities of the newer ionization techniques (Electrospray Ionization, ESI; Matrix Assisted Laser Desorption Ionization, MALDI) to characterize the non-volatile hydrocarbon samples. ESI of mixtures of compounds produces complex mass spectra, consisting of multiply charged ion species, that may be difficult to interpret. MALDI has the potential for ionization of non-volatile hydrocarbon samples, but extensive research is required to determine the appropriate matrix compounds that will permit the unbiased desorption of all sample components. An important requirement in the characterization of the non-volatile samples using direct desorption techniques without prior chromatographic separation, is the use of ultra high resolution (>50,000), for the separation of high molecular weight isobaric peaks.

In the past, pyrolysis techniques have been used for the analysis of non-volatile samples. Pyrolysis techniques supply enough thermal energy to cause bond rupture. Hydrocarbon macromolecules with very high molecular weights are thus broken into smaller parts that are volatile enough to be analyzed by standard 70 eV Electron Ionization. This approach is very useful when *molecular weight distribution information is not required. The major problem with pyrolysis techniques* is the difficulty in generating reproducible results. In the present work, the experimental parameters affecting reproducibility have been studied, and optimum conditions have been determined that permit reproducible analysis.

A pyrolysis unit (Thermex, Ruska, Houston TX) coupled, via a heated transfer line, to a Hewlett Packard 5971 GC/MS system, was used for the experiments. The sample was weighed into a fritted quartz ampoule and was placed into a temperature programmable pyrocell. The vapourized material was swept through the heated transfer line to the head of the GC column, where it was cold trapped. The pyrolysis step was followed by conventional 70 eV EI GC/MS analysis. The GC/MS parameters remained fixed throughout the series of experiments. A schematic diagram of the Ruska pyrocell used for these experiments is shown in Figure 1. The effect of several pyrolysis parameters on the reproducibility of pyrolysis was studied using model polymers (i.e. cis-polybutadiene, polyethylene, etc.). The pyrolysis parameters were: (i) pyrolysis temperature, (ii) heating rate, (iii) final pyrolysis time, (iv) interface temperature, (v) purge pressure, and (vi) sample preparation.

The interface temperature, purge pressure, final time and the method of sample preparation affected the total ion current of the mass chromatograms. The percent yield of the monomer was affected by the heating rate and the final pyrolysis time. These two parameters appear to have the most significant effect on the pyrolysis products, for a given pyrolysis temperature. A higher percentage of monomer is produced at faster heating rates and at longer final pyrolysis times. The optimum experimental conditions obtained are presented in Table 1.

The results obtained in this study demonstrate that furnace-pyrolysis GC/MS can be used reproducibly for the analysis of polymers. Repeat analyses of cis-polybutadiene performed on different

dates are shown in Fig. 2. Optimum furnace-pyrolysis conditions were determined that are independent of the sample preparation method (Table 2). The % standard deviation of the method, at optimum conditions was found to be less than 8%.

FIGURE 1: DIAGRAM OF THE PYROCELL IN THE PYROLYSIS UNIT.

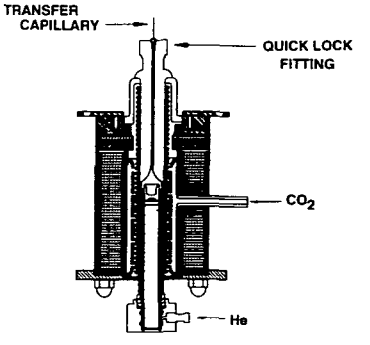

TABLE 1
OPTIMUM EXPERIMENTAL CONDITIONS

SAMPLE PREPARATION	FROZEN, SLICED
SAMPLE WEIGHT	1.0 mg
INITIAL TEMPERATURE	50°C
INITIAL TIME	0 min.
HEATING RATE	19°C/min.
PYROLYSIS TEMPERATURE	600°C
FINAL TIME (Time @ Py. Temp.)	2.0 min.
PURGE/CARRIER GAS	He
PURGE PRESSURE	18 psig
INTERFACE TEMPERATURE	290°C
TRANSFER LINE TEMPERATURE	290°C
TRAPPING TEMPERATURE	10°C

FIGURE 2: REPRODUCIBILITY OF PY-GC/MS; (A) MASS CHROMATOGRM OF CIS-POLYBUTADIENE AND (B) REPEAT AT A LATER DATE.

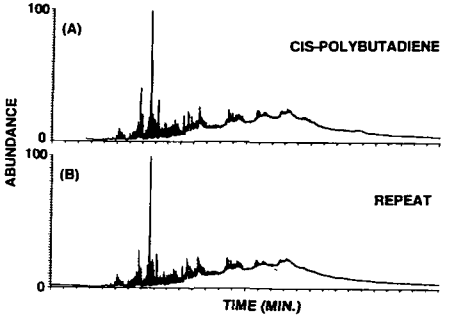

TABLE 2
FURNACE-PYROLYSIS REPRODUCIBILITY AT OPTIMUM EXPERIMENTAL CONDITIONS

SAMPLE PREPARATION METHOD	RUN NUMBER	SAMPLE WT. (mg.)	AREA (E+9)	% STD. DEV.
FROZEN, SLICED	1	1.04	1.9	
	2	1.07	2.2	7.6
	3	1.02	2.3	
5% IN THF	1	1.02	1.8	
	2	1.02	1.5	8.0
	3	1.02	1.9	
CYCLOHEXANE WASHED	1	1.08	19.3	
	2	1.04	19.6	5.9
	3	1.04	17.1	

Analysis of Pyrolysis Residues from Poly(vinyl alcohol)

R. T. Pogue, K. L. Ackley and V. Majidi
University of Kentucky, Department of Chemistry,
Lexington, KY, USA 40506

INTRODUCTION

Homes, automobiles, clothes and other necessities are all made up, in some part, from polymeric compounds. One problem with this widespread polymer use is that most polymers are flammable. Because of this, polymeric materials can accelerate flame propagation. The result of this accelerated propagation is that the amount of time it takes for flames to consume a structure may be drastically reduced. Non-flammable polymers can provide solutions in many of these cases, however, many of these polymers generate toxic gases at high temperatures. Therefore, personal injury may be caused by inhalation of harmful fumes rather than by the flames. For these reasons, it is important to gain a better understanding of the thermal processes which occur in polymers so that safe materials can be designed and produced.

Most studies investigating the pyrolysis characteristics of polymers focus on the gases evolved from the polymer as temperature is increased. Hyphenated techniques such as thermogravimetric analysis-mass spectrometry (TGA-MS) and thermogravimetric analysis-infra-red spectroscopy (TGA-IR) are used to add qualitative information to the quantitative traces obtained during normal TGA. The intent of our research is to study the residue (or char) which is left after a polymer has been heated. To characterize these chars, we are using laser desorption mass spectrometry (LD-MS). In addition to LD-MS, we have found that collection of the semi-volatile materials evolved from the polymer, and subsequent GC-MS analysis, help to give a more complete explanation of the processes which are taking place. We have chosen a series of poly(vinyl alcohols) (PVA) as the subject of our study because of the widespread use of these compounds and their derivatives.

DISCUSSION

Prior to beginning the bulk of our work, it was determined that TGA and TGA-MS of several PVA's should be conducted to determine if it was appropriate to use a model molecular weight or if full investigation of all molecular weights was necessary. Upon completion of these studies, it was determined that the 78 % hydrolyzed poly(vinyl alcohol), with average MW = 2000 Da, would be a suitable model. Subsequent experiments were carried out using this material.

The TGA traces discussed above were used to determine the appropriate temperatures for charring. Chars were produced by preheating the ceramic furnace and placing a known amount of PVA inside. The polymer was heated for several hours isothermally in order to allow the entire sample to pyrolyze. Laser desorption mass spectrometry of chars created at different furnace temperatures did not produce ions from unmodified PVA.

The literature reports that several low molecular weight compounds have been isolated during the pyrolysis of poly(vinyl alcohol) (1). We have found, however, that GC-MS analysis of the semi-volatile materials collected at different charring temperatures indicates the presence hydrocarbons containing greater than 20 carbon atoms. Results also indicate that the composition of the semi-volatile mixture varies greatly depending upon the temperature at which the char is made.

REFERENCES

(1) Conley, R. T.; Malloy R. "Vinyl and Vinylidene Polymers" in Thermal Stability of Polymers, Conley, R. T. Ed., Marcel Dekker Inc., New York, NY, 1970, Chapter 8

TPD MS OF CHEMICALLY MODIFIED ULTRAFINE OXIDES

Professor **Valeriy A. Pokrovskiy**
Institute for Surface Chemistry, National Academy of Sciences,
Pr. Nauki 31, 52022 Kiev, UKRAINE

The abilities of modern methods for the study of surface phenomena are strongly limited in the case of dispersed oxide systems. The limitations are caused by the large surface area and by the variety and lability of active sites on the surfaces, i.e. just by those properties which make oxides diverse and promising matrices for technical applications. Very few mass spectrometry studies of molecules bound by the active sites and of reactions in adsorption layer of ultrafine oxides are availiable in the literature [1]. Study of decomposition of different groups bound to ultrafine oxide surfaces caused by heating or by their interaction with particular environment is of interest as such materials are widely used in chemical industry and their stability has a great importance for many applications in material science, medicine biotechnology and agriculture.

EXPERIMENTAL. TPD MS technique has been developed, for the purposes of surface chemistry studies on pyrogenic oxides by analogy with previous works [2,3]. The samples were placed in a quartz-molybdenum tube and evacuated then attached to the ion source of a mass spectrometer MI-1201 (Sumy, Ukraine).

A computer-aided system was used for the automation of experiment and treatment of mass spectrometric data. During the experiments the continuous record was made of selected components of mass spectra simultaneously with the temperature increase controlled by a computer program. The TPDMS information was represented either as a set of mass spectra, or as a set of temperature dependences of mass spectrometric components.

DESORPTION MODELS. For the interpretation of thermograms we assume that desorption equation is as usual

$$d\Theta/dt = -k\Theta^n \qquad [1]$$

where Θ is the surface coverage, n is the reaction order (assumed to be known from experimental data) and the desorption rate is

$$k = k_o \exp(-E_d/k_b T) \qquad [2]$$

where E_d is the activation energy of desorption, and k_o the pre-exponential factor (both parameters considered to be known from experiments). At the initial condition $\Theta_{t=0} = 1$ we have the solutions of Eq [1]

$$\Theta(t) = \exp(-\Phi(t)) \quad \text{for } n = 1$$
$$\Theta(t) = 1/(1+\Phi(t)) \quad \text{for } n = 2 \qquad [3]$$
$$\Theta(t) = 1/(1+2\Phi(t))^{1/2} \quad \text{for } n = 3$$

where

$$\Phi(t) = \int_0^t k\,dt \qquad [4]$$

The desorption rate (which is directly proportional to ion current) from Eqs [3] can be obtained as

$$d\Theta(t)/dt = -k\exp(-\Phi(t)) \quad \text{for } n = 1$$
$$d\Theta(t)/dt = -k/(1+\Phi(t))^2 \quad \text{for } n = 2 \qquad [5]$$
$$d\Theta(t)/dt = -k/(1+2\Phi(t))^{3/2} \quad \text{for } n = 3$$

The Eqs [5] show the typical temperature dependences of ion current, the second-order desorption curve being nearly symmetrical, the first-order curve decreasing faster in the high-temperature side, the converse being true for the third-order process.

DISCUSSION. The main features of samples studied in our experiments are large surface area (hundreds of square meters), amorphous structure and non-porosity of pyrogenic oxide surfaces. The adsorption capacity provides desorption of up to 1% weight the sample. The result is a gain in sensitivity about million in comparison with bulk samples. All the experimental scheme of temperature programmed desorption for ultrafine samples becomes similar to a thermal analysis experiment with mass spectrometry of volatile products of decomposition. This similarity has a fundamental base because surface processes are involved in most of the topochemical reaction models in thermal analysis [4]; on the other hand, typical pictures of thermal decomposition accompanied by multi-channel chemical reactions in adsorption layers were repeatedly observed in our TPD experiments.

Ultraffine oxides show interesting and unexpected effects in thermal desorption and decomposition of surface complexes including phase transitions in adsorption layer. Application of various known multi-parameter models [5] to systems of such a kind has the implicit danger that they provide adjustment to experimental data and foster an illusion of understanding, irrespective of the adequacy of the model [6].

The advantage of our simple approach is that results are obtained in analytical form which facilitates the computer treatment of experimental thermograms.

1. P.Basu, J.R.Yates, Jr. *Surf. Sci.* **177**, 291 (1986).

2. Pokrovskiy, V. A., Bratushko, Yu. I., Yatzimirskiy, K. B. et al., *Teor. Exp. Khim.*, **14**, 754 (1978).

3. Pokrovskiy, V. A., Yatzimirskiy, K. B., Nazarenko, V. A. et al., *Teor. Eksp. Khim.*, 23, 377 (1987).

4. Zhdanov, V.P., *Elementary Physicochemical Processes at Surface*, Nauka, Novosibirsk, 1988.

5. Logvinenko, V. A., *Thermal analysis of coordination compounds and clatrates*, Nauka, Novosibirsk, 1982.

6. Menzel, D., *Chemistry and physics of Solid Surfaces IV*, Springer-Ferlag, Berlin, 389, 1982.

Thermogravimetric Analysis-MS with Data Logging on a Teknivent Data System

Fred D. Hileman, Deborah A. Johnson, John J. Tria
Monsanto Corporate Research, 800 N. Lindbergh Blvd. St. Louis Missouri 63167

William A Grote
ITC, Inc. 125 Peeke Ave Kirkwood, Missouri 63122

Peter D. Norberg
Peter Norberg, Consulting, Inc. P.O. Box 9141, Richmond Heights, Missouri 63117

Thermogravimetric analysis is important to the chemical industry in understanding the weight loss that occurs when a material is heating to a specific temperature under a given environment. However, there is always a missing piece of information in this analysis and that is the composition of the compound involved in the weight loss. To address this problem a Mettler Model TA-1 Thermogravimetric Analyzer (TGA) has been interfaced to a Hewlett-Packard 5970 mass spectrometer (Figure 1). The mass spectrometer (MS) is connected to a Swagelok tee via a 23 cm length of .075 mm ID fused silica capillary tubing which serves as a leak into the MS A 75 cm length of 0.5 mm ID fused silica capillary encased in a resistively heated stainless steel tube serves as a transfer line from the TGA and is also connected to the tee butting against the MS leak capillary. The final leg of the tee is connected to a vacuum pump which is outfitted with a throttle valve which can be used to control the gas flow from the TGA and the gas flow into the MS. The MS is controlled by a Teknivent Vector II data system which runs on a 486 computer operating under an OS-2 based operating system. This Vector II data system has the capability of recording up to 16 analog channels and this feature is used to monitor the temperature (T), weight loss (TG) and differential thermal analysis (DTA) data from the TGA. Having the Vector II data system collecting data from both the MS and the TGA makes it particularly convenient in displaying the data since all the information can be manipulated and displayed with the same data system. In most TGA systems it is common to plot the measured parameters (i.e. weight loss, DTA) versus temperature rather than time as is common in most MS data systems. The conversion of the X-axis from time to temperature in the MS data system was accommodated by the development of a subsystem (PRMTTIME) that reads the temperature channel from the TGA and then uses this information to convert the time axis to a temperature axis. This allows the plotting of the TGA data as well as the MS data versus temperature.

This system has been applied to variety of projects. The most common application is the plotting of weight loss and DTA curves versus various m/z values characteristic of anticipated decomposition products (water, carbon dioxide, carbon monoxide, etc.) as shown in Figure 2 for calcium oxalate. Another application is the identification of unknown compounds evolved during a given temperature regime. The library search feature of the Vector II data system aids in the identification of these compounds A particularly nice feature of coupling the TGA to a data system designed for GC/MS applications is that many of the features for processing chromatography data are applicable to TGA and MS data. As a case in point, the capability to integrate ion current peak areas was used to assess the amount of water retained by a certain polymer system. The Mettler TA-1 accommodated this analysis by being able to handle gram quantities of polymer allowing low levels of absorbed water to be determined. In conclusion, a state of the art data system has been used to combine two pieces of good, but somewhat dated, equipment and has rendered them very useful in resolving a variety of problems confronting the chemical industry.

Figure 1. Thermogravimetric Analysis - Mass Spectrometer

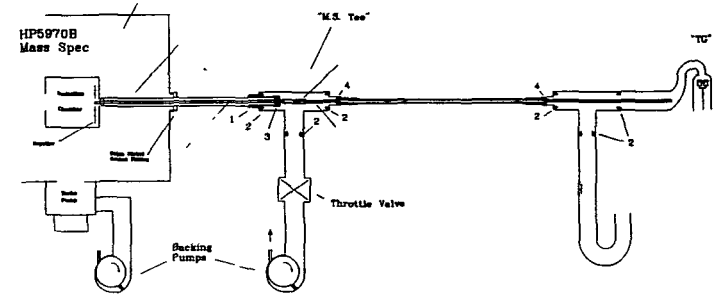

Figure 2. TGA-MS Analysis of Calcium Oxalate

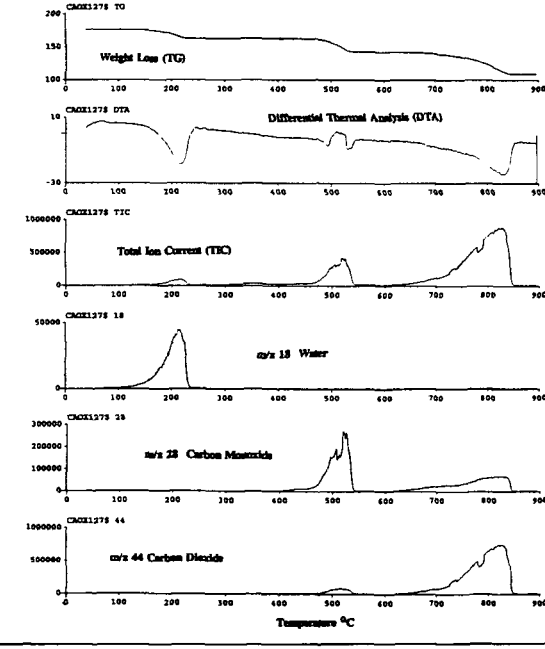

Improved Performance of a Quadrupole Based Glow Discharge Mass Spectrometer

Robert E. Valiga, Douglas C. Duckworth, David H. Smith
Oak Ridge National Laboratory, Oak Ridge, TN 37831-6375

Introduction

Glow discharge mass spectrometry (GDMS) has experienced most of its commercial success in trace multi-element analysis using sector-based mass spectrometry. In most cases, the mass resolution available with these instruments allows elements of interest to be analyzed, even in the presence of polyatomic interferences (e.g., ArC+, ArN+, ArO+). Because quadrupole mass filters have little more than unit resolution, background equivalent concentrations (BEC's) for many elements can be quite high (1-100 ppm). Because of this, many have discounted quadrupole GDMS as a useful trace analysis technique. In this work, we have explored methods of reducing the polyatomic interferences.

Experimental

A Fisons Gloquad mass spectrometer was used with an argon or a neon discharge gas. The sample used in the experiments was a NIST high purity gold standard.

Results

Initially, analysis of the gold standard was done using argon as the discharge gas. High polyatomic interference peaks were encountered. Evacuation and bake out of the discharge gas delivery system gave only a limited reduction of the interferences. We investigated using background subtraction but discovered that the interferences varied unacceptably over a 5 hour period. We decided to use neon as the discharge gas to see how the interferences generated by it would differ from those of argon. Perhaps some method could be developed to negate interferences by using two discharge gases. The figure and table on the next page show the results of this study. As is evident, the Gloquad was capable of sub-ppm analysis. Following conversations with the getter manufacturer, it was concluded that the most probable cause of improved performance with neon was due to a higher getter temperature, which removed contaminants more efficiently. The higher temperature was the result of neon's higher thermal conductivity. The effects of contaminants in the discharge gas have been studied by others. However, the high purity (sub-ppb to low ppb) discharge gas required to effectively eliminate the interferences has not been previously achieved. We have designed and ordered a high purity discharge gas delivery system for use on the Gloquad.

Conclusions

High purity discharge gas is required to significantly reduce polyatomic interferences in GDMS. It is anticipated that we will be able to demonstrate sub-ppm quantification capabilities in quadrupole GDMS with the new high purity discharge gas system.

TYPICAL DATA USING NEON DISCHARGE GAS

SAMPLE: NIST SRM 685-W HIGH PURITY GOLD

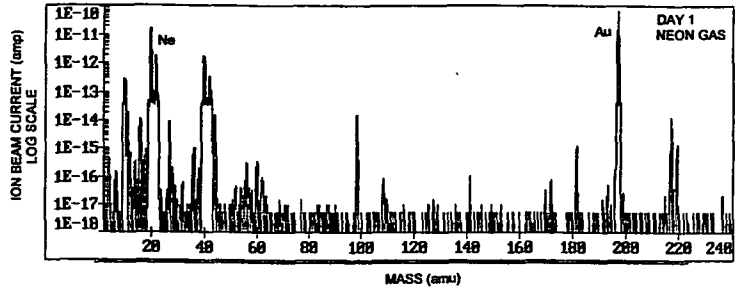

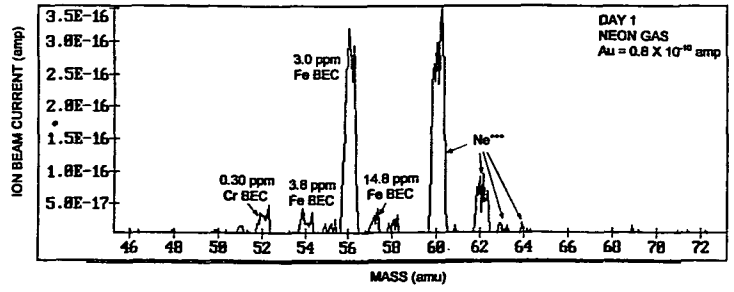

CONCENTRATION DATA USING NEON GAS
HIGH PURITY GOLD NIST SRM 685-W

ELEMENT	NIST VALUE (ppm)	GLOQUAD VALUE (ppm)*
Fe	0.3	0.370
In	0.007	ND
Al	< 0.3	0.080
Cl	< 0.1	0.041
Cr	< 0.05	0.078
Mg	< 0.2	0.020
Mn	< 0.01	0.048
Ni	< 0.05	0.037
Sc	< 0.01	0.009
Si	< 0.3	0.951
Sr	< 0.03	ND
V	< 0.05	0.035

* RSF VALUES PROVIDED BY FISONS.
ND - not detected

ELEMENTAL QUANTIFICATION BASED ON SECONDARY SPECIES IN THE GLOW DISCHARGE

Goodner, Kevin L.; Eyler, John R.; University of Florida, Gainesville, FL 32611-7200
Barshick, C. M.; Smith, David H.; Oak Ridge National Laboratory, Oak Ridge, TN 37831-6375

Introduction. A barrier to absolute quantification in glow discharge MS, as in other types of inorganic MS, is the presence of polyatomic interferences. While it is possible to suppress, eliminate, or discriminate against these interferences, we took a different route. Instead of trying to correct for these interferences, we used the "interferences" to quantify the metal concentration. By quantifying the argides (MAr^+), dimers (M_2^+), and doubly charged species (M^{+2}) of our analyte (which were not interfered with), we were able to achieve equal or better accuracy and precision than when we use the M^+ [1].

Experimental. A VG-9000 reverse geometry Nier-Johnson double focusing glow discharge mass spectrometer was used in these experiments. For optimization of the method, NIST aluminum SRMs 601, 602, 603, and 604 were used. For testing of the method on an unknown, NIST SRMs 644 and 1190 were used as standard and unknown, respectively.

Results. Before performing any experiments, we characterized the possible test species at constant pressure and power. All of these species behave in a similar manner, increasing with increasing power, at constant pressure. Since the concentrations of these ions ultimately depend on the corresponding metal atom density, these results can be attributed to the increase in sputter atomization that accompanies either the increased current (incident number of ions) or increased voltage (incident ion energy), or both. Magnesium oxide, aluminum oxide, and copper oxide all mirror the oxygen ion signal, but titanium oxide behaves differently. Since titanium is among the more aggressive oxygen getters, it competes more favorably for the relatively scarce oxygen atoms than the other metals; hence the TiO signal is correspondingly higher. As the power increases, the other metals can compete more favorably for the oxygen. At constant power, two different trends are observed, that of the singly-charged metal ions and that of the other test species. It has been shown by Hess et al. that metal ions mirror the argon metastable population, increasing to a maximum and then decreasing with increasing pressure. This is the trend seen for the M^+, but not the other species. As pressure increases the voltage decreases and with it the atom density.

As seen in Table 1, the M^+ species gave excellent accuracy (<5% relative error), due to lack of interferences and high concentrations of the analyte. The average errors found using MAr^+ and M^{+2} were around 15%, except for Cu^{+2}, where the error is much higher (due to its higher second ionization potential). The errors associated with the dimers averaged ca. 40% relative error, due to species interfering with the dimers. However, this will not always be the case. Table 2 shows molybdenum concentrations obtained using species containing $^{95}Mo^+$ and $^{96}Mo^+$. Using these doubly-charged and molecular species, a 15% relative error was found, compared to the 24% relative error found when $^{95}Mo^+$ and $^{96}Mo^+$ were used. This confirms the usefulness of this approach. The error associated with using all the molybdenum isotopes versus the ^{95}Mo and ^{96}Mo (52% versus 24%) suggests that these two isotopes were interfered to a lesser extent than the others.

Conclusions. Metal argides, metal dimers, and doubly-charged metal ions have been shown to be useful for quantification when the singly-charged analyte is obscured by interference peaks. This technique gives reasonable accuracy (ca. 15% relative error) for elemental compositions approximately 0.1% or greater of the sample. While this technique should be used with caution, we have demonstrated that it gives the analyst a viable alternative in those cases where it is impossible to address interferences in other ways.

References [1] Goodner, Kevin L.; Eyler, John R.; Barshick, C. M.; Smith, David H.; Int. J. of Mass Spectrom. Ion Proscesses, in print.

Table 1. Concentrations of several elements in an NIST aluminum standard determined from the secondary species studied.

		NIST Value	M^+	M^{+2}	MAr^+	M_2^+
Magnesium	Concentration %	1.49	1.45	1.44	1.59	1.03
	Relative Error %	—	2.7	3.5	6.7	31
Silicon	Concentration %	0.13	0.13	0.16	0.14	0.09
	Relative Error %	—	0	2.3	7.7	31
Iron	Concentration %	0.28	0.28	—	0.22	0.13
	Relative Error %	—	0	—	21	55
Manganese	Concentration %	0 63	0.6	0.67	—	0.22
	Relative Error %	—	4.8	6.3	—	65
Copper	Concentration %	4.44	4.34	2.46	3 49	3.15
	Relative Error %	—	2.3	45	21	29

Table 2. Molybdenum isotopic concentrations determined for an NIST 1190 reference material using various species.

		^{95}Mo	^{96}Mo
Cerified Isotopic Concentration (%)	NIST 644	0.53	0.6
	NIST 1190	0.56	0.63
M^+	Value	0.70	0.78
	Relative Error	25.0	23.8
M^{+2}	Value	0 46	—
	Relative Error	17.9	—
MAr^+	Value	0.46	0.51
	Relative Error	17.9	19.0
M_2^+	Value	0.55	0.52
	Relative Error	1.78	17.4

Reduced Mass Range Ion Trap Mass Spectrometry for Atomic Ions

C.J. Barinaga, G.C. Eiden, D.W. Koppenaal
Pacific Northwest Laboratory*
Richland, Washington 99352

P.H. Hemberger
Los Alamos National Laboratory
Los Alamos, New Mexico 87545

In an attempt to apply some of the real and perceived advantages of quadrupole ion trap mass spectrometry to elemental/isotopic mass analysis a prototype Inductively Coupled Plasma-Ion Trap Mass Spectrometer (ICP-ITMS) has been built with a linear quadrupole between the vacuum interface and the ion trap. Initial results (1,2) show some promise for ICP-ITMS to be a useful technique. However two limitations are the charge capacity and dynamic range of the standard Finnigan ITMS.

The mass range for the standard ITMS is approximately 640 m/z which exceeds the range needed to cover the atomic ions of elemental and isotopic analysis. If one keeps the RF voltage, RF frequency, and the q_{eject} the same then the controlling equation

$$m/z = 4\,V \,/\, q_{eject}\, r_o^2\, w^2$$

indicates that decreasing the mass range to one half (~315 m/z, covering the entire elemental range) would require a trap of radius r_o=1.44. The larger trap should be able to accomodate a greater number of ions before experiencing significant space charge effects. Given the same number of acquisition channels and scan rate (channels/sec) the reduced mass range should also enable greater mass scale resolution.

A 1.44 r_o trap was designed and machined at LANL for PNL based on the Finnigan ITD trap electrodes. Utilizing the standard ITMS ceramic spacer/insulators, l = 0.180", an "unstretched" trap is produced. One of these traps has recently been installed in PNL's ICP-Q_L-Q_T (ICP-ITMS).

This first report of a larger than standard trap applied to atomic ions will show some very preliminary data based on brief operational experience. Initial indications are that the characteristics of the ICP-ITMS with standard trap apply to the large trap also. These include a significantly attenuated argon ion beam and an absence of plasma and sample matrix polyatomic ions. Reasonable initial mass spectra were obtained with the 1.44 r_o trap (see Figure 1). It appears that more ions (and 44% bigger ions!) can be injected before noticable space charge effects (i.e., peak degradation) occur. Although ions appear at approximately twice their m/z, consistent with the above equation and the data system, the resolution to date appears no better than the standard trap.

Future work will be directed to more completely characterize this enlarged trap for elemental/isotopic applications in regard to space charge limits and effects, ion injection efficiency, mass resolution, and analytical utility.

43rd ASMS Conference on Mass Spectrometry and Allied Topics

References

1) CJ Barinaga and DW Koppenaal, *Rapid Comm. Mass Spectrom.*, 1994, **8**, 71.
2) DW Koppenaal, CJ Barinaga, and MR Smith, *J. of Anal. Atomic Spectrom.*, 1994, **9**, 1053.

* PNL is operated for the U.S. Dept. of Energy by Battelle Memorial Institute under contract DE-AC06-76RLO 1830

Figure 1. A multi-element solution. Note the approximately 2X indicated m/z for the various isotopes.

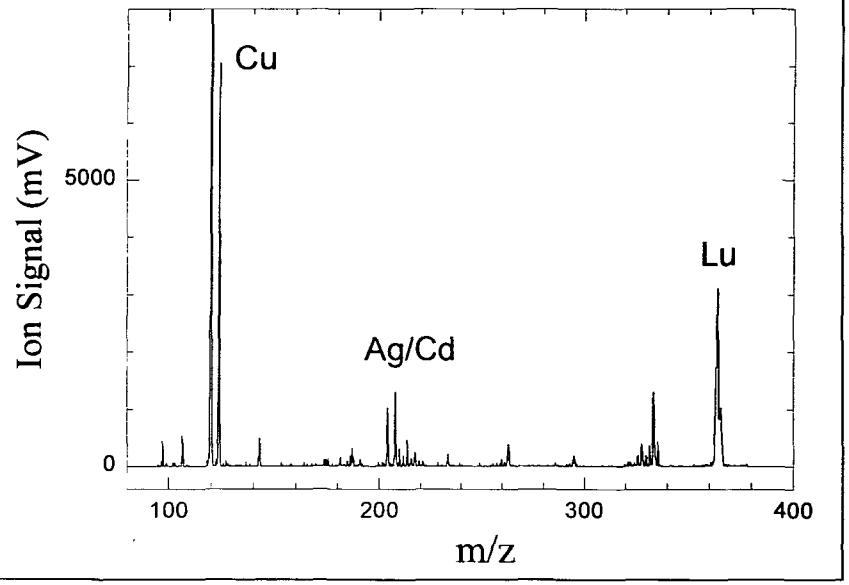

Reducing Energy Dispersion in Plasma-Source Sector-Field Mass Spectrometry

Thomas W. Burgoyne, Gary M. Hieftje, and Ronald A. Hites
Department of Chemistry and School of Public and Environmental Affairs,
Indiana University, Bloomington, IN 47405

Introduction

Energy dispersion is a critical component of focusing in sector-field mass spectrometry. One method of accelerating the ion beam in plasma-source, sector-field mass spectrometry is to float the source and to set the desired accelerating potential on the sampling plate. Although studies have been conducted with the interface floated at a few tens of volts, little is known about the beam energy and beam-energy dispersion when the sampler is set at higher potentials. Beam-energy measurements were made on a sector-field plasma-source interface of an inductively coupled plasma that will soon be used with a Mattauch-Herzog mass spectrograph.

Methods

Ions are accelerated by setting the first vacuum stage to the accelerating potential. To eliminate unwanted discharge, the first-stage roughing pump operates at the first stage potential and a capacitor couples the sampling plate to the torch housing (this capacitor is not needed when a "torch shield" is used).

An energy-analyzing Faraday cup measures the beam energy roughly 20 cm down from the third-stage orifice. A voltage (which we will call the stopping potential) on a grid in front of the Faraday cup was ramped and the ion signal was measured as a function of the stopping potential. The average beam energy and energy dispersion (measured at FWHM) were calculated from the derivative of the signal versus grid stopping potential curve.

During all of the ion beam energy measurements, the forward RF power was maintained at 1.35 kW, with the reflected power less than 5 W. The outer, intermediate, and central-channel argon flow rates were 14, 1.06, and 1.00 L/min, respectively. The first, second, and third stage vacuum regions were 0.8, 1×10^{-4}, and 1×10^{-6} torr, respectively. An average scan length was 70 sec. Deionized water was introduced at 1 mL/min and ion optics were grounded unless needed to boost signal levels.

The beam energy was measured under four different instrument configurations: 1) Measurements were first performed with the initial instrumental design. 2) A grid was placed behind the skimmer (roughly 1 cm from the third-stage orifice). This grid was hypothesized to provide a shorter and more uniform accelerating region in the second stage. 3) A torch shield was installed to eliminate an orifice-linked discharge. The grid behind the skimmer was in place during this experiment. 4) A new ion-optic configuration was designed which consists of a third-stage orifice roughly 2 cm from the skimmer orifice followed by a linear acceleration region. The ion lenses consist of an einzel lens followed by a quadrupole doublet.

Results

The results are best represented as plots of the relative energy spread versus the interface potential (see graphs below). The initial interface arrangement (Graph 1) resulted in a 23 ± 5% energy spread. Adding a screen behind the skimmer (Graph 2) reduced the energy spread dramatically to 6.2 ± 0.63%. Unfortunately, this reduced the signal level as well. Ion simulations demonstrate that fewer ions enter the third stage orifice with the grid in place. Adding a torch shield (grid installed, Graph 3) additionally reduced the energy spread to 5.2 ± 0.78%. The Student's t-test indicated that addition of a torch shield made a statistically significant difference. The new ion optic design reduced the energy spread without sacrificing signal level (Graph 4). More importantly, the energy spread with this new ion optic arrangement is a function of the interface potential. A mass spectral comparison with the initial and new ion optic design also displays the reduced energy dispersion.

Conclusions

The above experiments demonstrate that energy dispersion can be a serious problem in the sector-field mass spectrometer interface. Because the energy spread was independent of the interface potential with the initial design, we assume that the energy dispersion originated from the interface - most probably in the second stage. A likely scenario is that the beam extracted from the second stage has both plasma and ion beam characteristics. Accelerating the "plasma-beam" unevenly over a 5-cm distance (as in the original design) resulted in a very large energy spread. Accelerating more evenly and over a shorter distance (with the grid installed) dramatically reduced the energy spread and the signal level. The addition of a torch shield also helped to reduce the energy spread. Because the torch shield eliminates the orifice-linked discharge, the plasma extracted into the second stage is less dense, and the beam energy is affected accordingly. The newly designed ion optics took into consideration the above experiments. The distance between the second and third stage apertures was decreased (to roughly 2 cm) and the ion beam acceleration takes place in the third vacuum stage over a 5 mm distance. This ion optic arrangement reduced the beam energy spread which, importantly, is now a function of the interface potential.

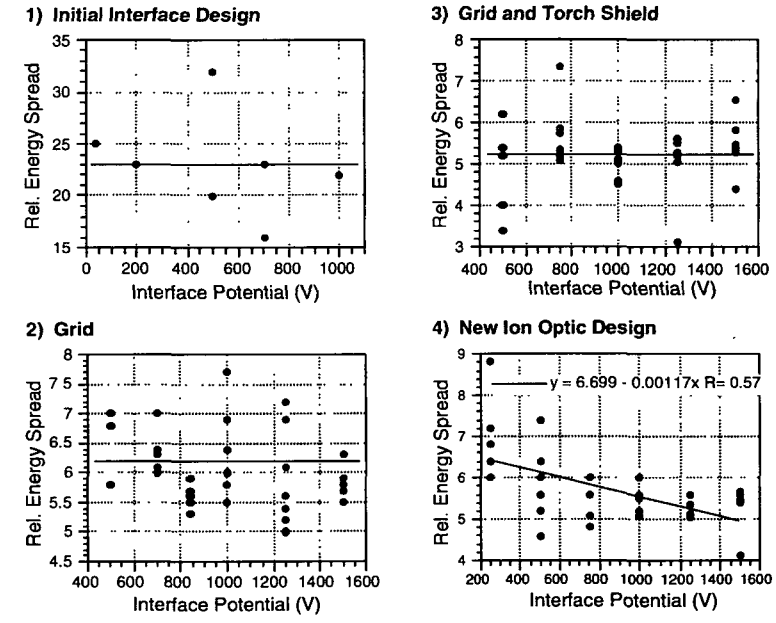

Insulator Surface Potential Measured by TOF-SIMS

X. Q. Guo and R. T. Short
Oak Ridge National Laboratory, MS6365, Oak Ridge, TN 37831

A technique has been developed to determine the electrostatic surface potential of insulating samples which are subject to analysis by secondary ion mass spectrometry (SIMS). A special three-stage reflectron time-of-flight (TOF) mass spectrometer was used to simultaneously obtain mass spectra and to measure the shifts of TOF peaks resulting from changes in the sample surface potential. The measured shifts were then used to determine the surface potential of insulators and the effectiveness of charge compensation to a precision of a few volts.

Besides the nominal acceleration potential, secondary ions can gain excess energy from surface charging (for insulators) as well as from sputtering processes (initial ion kinetic energy). If the extraction region is small, it is impossible to distinguish whether the excess energy is obtained from the sputtering process or sample charging; once ions enter the flight tube, it is only the total energy of ions which affects the flight time. However, the flight time of ions through the extraction region does depend on where the excess energy comes from, since sputtering is related to initial ion velocities, and sample charging to the acceleration of ions in the extraction region. In "conventional" TOF mass spectrometers used in SIMS, a small extraction region is normally used (typically a few mm), and the kinetic energy distribution of ions can be compensated by use of a reflectron. Thus the shifts of peaks in the spectra when surface potential varies by a few volts are generally negligible. For this reason, in the present experiment the extraction distance was chosen to be large, about 25 mm.

Shifts of flight time due to initial ion energy are of the same order as those due to surface charging. Thus, a method must be used to compensate for initial ion kinetic energy effects while retaining the shifts due to charging. This excludes the use of linear TOF mass spectrometer for such studies. It has been proven both theoretically and experimentally that a three-stage ion mirror with the right ratio of electric field strengths for the second and third stages ($E_3/E_2 = 0.895$ for our apparatus) can compensate flight times of ions with different energies in both the extraction and field-free regions [1]. In Fig. 1. the calculated flight time of ions differs by less than 10 ns for an energy spread of 50 eV, showing good energy compensation. Shifts of peaks due to charging greatly surpass this distribution of flight times. Therefore, the present technique (three-stage ion mirror with large extraction distance) allows us to separate sputtering processes from surface charging, and shifts of TOF peaks can then be related directly to surface charging.

In this experiment, TOF spectra were obtained using various sample potentials by biasing a conducting sample. TOF peak positions and shapes were calculated by folding in secondary ion kinetic energy distributions. Good agreement was achieved between the calculations and the experimental data (see Fig. 2). Next, spectra from insulating samples, such as Teflon and mica, were obtained, using low energy electrons (30 eV) for charge compensation. By varying the electron current, the extent of surface charging was changed, resulting in various shifts of the TOF peak positions. In Fig. 3a, the K ion peak positions as a function of electron current (voltage dial setting) are plotted. By comparing these shifts to those at known sample potentials, the surface potentials were determined as a function of electron current (see Fig. 3b). These results demonstrate that surface potentials can be measured to within a few volts using this technique.

References

1. R. T. Short and P. J. Todd, *J. Am. Soc. Mass Spectrom.* 1994, 5, 779.

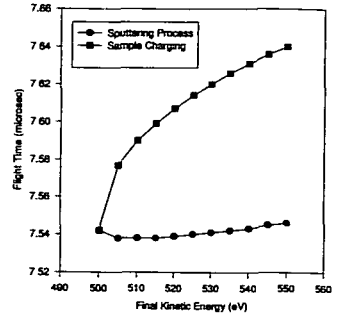

Figure 1. Calculation of Lithium ion flight time in 3-stage reflectron TOF spectrometer.

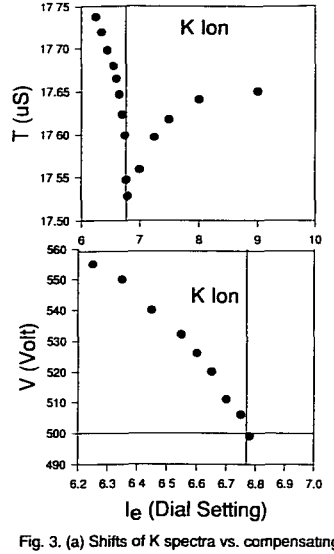

Fig. 3. (a) Shifts of K spectra vs. compensating electron current. (b). Deduced surface potentials

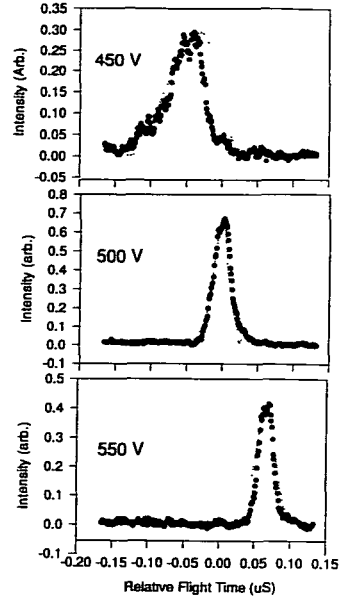

Fig. 2. Shifts of Li spectra vs. the sample bias. Calculations shown in dots.

"The submitted manuscript has been authored by a contractor of the U.S. Government under contract No. DE-AC05-84OR21400. Accordingly, the U.S. Government retains a nonexclusive royalty-free license to publish or reproduce the published form of this contribution, or allow others to do so, for U.S. Government purposes."

RESONANT LASER ABLATION - THIN FILM AND MULTILAYER ANALYSIS

T.M. Allen[1], P.B. Kelly[1], C.G. Gill[2], J.E. Anderson[2], and N.S. Nogar[2]
1. Department of Chemistry, University of California, Davis
2. Chemical Science and Technology Division, Los Alamos National Laboratory

While most laser ablation mass spectrometry has been performed with fixed frequency lasers operated at high fluxes, there has been recent interest in the use of tunable lasers to enhance the ionization yield of selected components in an analytical sample. Resonant laser ablation (RLA) uses a single tuned to a one- or two-photon resonant transition in the analyte of interest, and performs simultaneous ablation and ionization with modest intensity laser pulses for monitoring specific elements of interest. Recently, Ledingham's group [1-3] and our own [4-5] have begun systematic study of the RLA process on a variety of materials. Advantages of RLA, in addition to the use of a single laser, include: (1) simplification of mass spectra by enhancement of the signal of the analyte of interest, (2) improvement in the absolute detection limits resulting from the enhanced ionization efficiency over non-resonant ionization and (3) improvement in the relative sensitivity as a result of the decrease in the ion signal obtained from other components with the sample.

Depth-resolved information concerning the composition of layered and multilayered structures is important in semiconductor and optical applications. In some instances, dopant and impurity distributions at the ppm and ppb levels may be important for performance. We demonstrate that RLA has potential use in the profiling of thin layer and multilayer structures.

In order to generate tunable light, a XeCl (308 nm) excimer laser was used to pump a dye laser (Coumarin 460). The dye laser produced pulses at 10 Hz which exhibited a 12 nsec pulse duration, pulse energies of 1-5 mJ and a 0 35 cm^{-1} bandwidth (FWHM) The dye laser pulse energies were attenuated to 5-25 μJ/pulse. The samples used were silicon (110) wafers coated with either 20 Å ± 10 Å or 100 Å ± 10 Å of high purity copper (99.9995%).

Constant dye laser irradiation on the sample results first in a rise in the RLA copper signal, followed by a decline, as shown in the Top Figure for 100 Å Cu film on Si (110). The fall in the copper RLA signal is believed to be due to removal of the copper thin film within the region of laser irradiation. For a 20 Å Cu film on Si (110), about 5 times fewer shots on average were observed for exhaustion of the RLA copper signal Ion signals were typically obtained at low laser pulse energy, and material removal rates of the copper were found to increase monotonically with increasing laser fluence (Bottom Figure). For a given laser fluence, the time required to exhaust the signal from a thin film is directly related to the film thickness.

References
1. Ledingham, K.W.D., Borthwick, J.S. & Singhal, R.P., Surf. Interface Anal. 18, 576-8 (1992).
2. Wang, L., Ledingham, K.W.D., McLean, C.J. & Singhal, R.P., Appl. Phys. B54 71-75 (1992).
3. Borthwick, J.S., Ledingham, K.W.D. & Singhal, R.P., SAB 47B, 1259-65 (1992).
4. Eiden, G.C. & Nogar, N.S., Chem Phys. Lett. 226, 509 (1994).
5. Eiden, G.C., Anderson, J.E. & Nogar, N.S., The Microchemical Journal 50, 289-300 (1994).

43rd ASMS Conference on Mass Spectrometry and Allied Topics

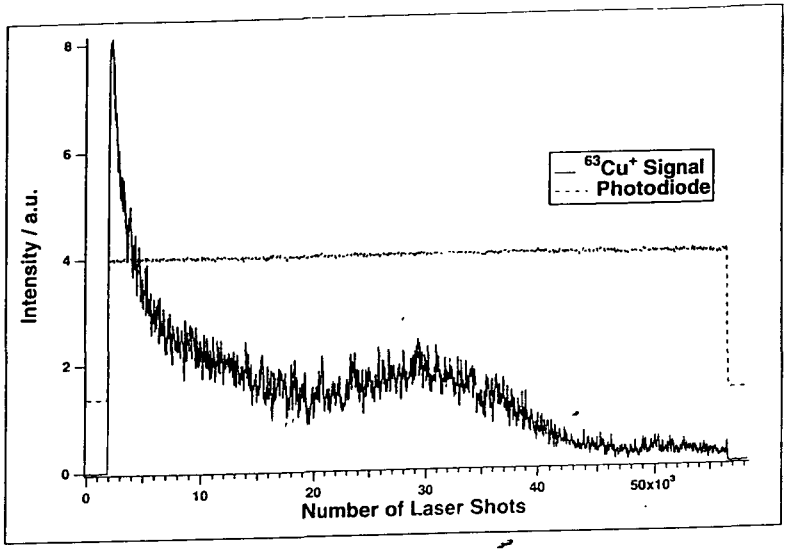

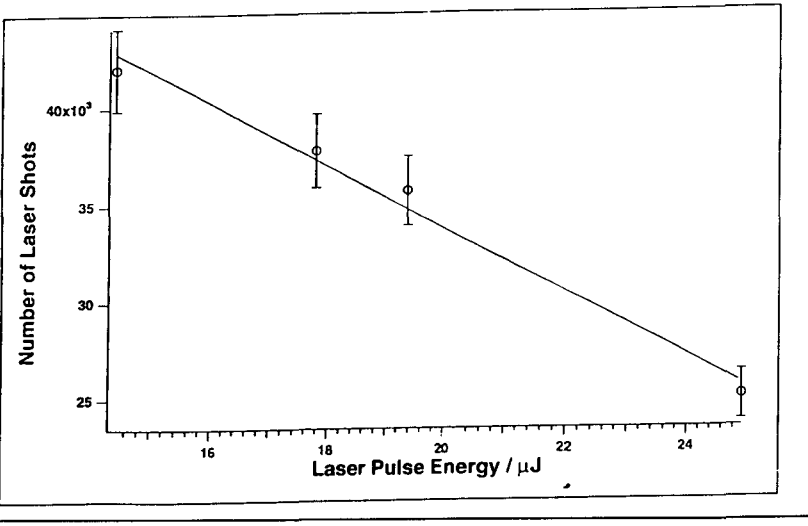

Submicrogram Sensitivity LC-Combustion-IRMS Based On A Moving Belt

Richard J. Caimi and J. Thomas Brenna
Division of Nutritional Sciences
Cornell University
Ithaca, New York

Application of Gas Chromatography-Combustion-IRMS to most biological molecules is difficult due to thermal instability and low volatility. In order to extend CSIA to these molecules, Caimi and Brenna (1993, 1995) developed an interface that coupled liquid sources with high precision combustion IRMS instrumentation. The primary limitation of this interface design was poor sensitivity due at least in part to the inability of the wire transport to capture more than 1% - 3% of the total analyte supplied. In an attempt to improve the sensitivity of the moving transport interface the authors have constructed an interface employing a continuous nichrome belt.

The prototype moving belt interface was constructed using a variable speed DC powered drive motor with a 95:1 gear ratio (Dayton , Chicago USA) operated at 5.75 cm sec^{-1} . A continuous nichrome belt (1.5 mm x 0.08 mm x 115 cm) was used as the transport. This belt first passes through a cleaner furnace (900°C) purged with a parallel flow of O_2 (15 ml min^{-1}) then loops around a pulley and enters an enclosed coating block. In the block, solution containing the analyte of interest is converted into a heated (150°C) pneumatic spray directed at the belt at a 45° angle. Solvent remaining after the coating process is subsequently evaporated as the belt passes through a 12 cm drying oven (200°C) that is purged with He gas (100 ml min^{-1}). Analyte molecules deposited on the belt are then combusted into CO_2 and H_2O in a CuO charged furnace maintained at 850°C. This furnace consists of a quartz tube (~2 mm i.d. x 20 cm) that has two He purge inlets (leading and lagging flows) that are maintained at approximately 30 ml min^{-1}. A third port is used to sample the products of combustion and transfer them to a 10 cm long Nafion™ based water trap. The dried CO_2 remaining is then transferred via a 2 m long x 0.1 mm i.d. fused silica capillary to the ion source of a Finnigan MAT 252 GIRMS instrument operated with a source pressure of 1 x 10^{-6} Torr and an accelerating potential of 8 kV.

An SSI (State College, PA, USA) HPLC pump equipped with a 10 ul injection loop was used as the liquid source. All analyses were performed in the flow injection mode using Optima hexane (Fisher, Pittsburgh, PA, USA) as the carrier solvent at a flow rate of 0.5 ml min^{-1} . Linoleic acid analytical standards of graded isotope ratio were isotopically calibrated prior to LCC-IRMS flow injection analysis by loading 2 mg of standard into 6 mm Vicor tubes containing 200 mg of CuO and 25 mg of Ag flake, evacuating, and baking at 850°C for 3 hours. Standard tubes were then analyzed by conventional dual inlet analysis. Signals for m/z 44, 45, 46 were processed by vendor-supplied software.

Flow injection analysis was used to assess the accuracy and precision of the isotope ratio measurements, the linearity of the isotope ratio versus quantity of analyte, and the linearity of signal area versus quantity of analyte. The accuracy and precision of the isotope ratio measurements were assessed using replicate injections of isotopically calibrated linoleic acid (2.5 ug) standards with graded $^{13}C/^{12}C$ ratios. The linearity of isotope ratio and signal area versus the

quantity of analyte loaded was evaluated using multiple injections of standards containing between 250 ng and 5 ug of natural abundance linoleic acid. All isotope analyses were calibrated versus an internal standard using both the Finnigan ISODAT data system and a commercially available non-linear regression program (Jandel) previously used by Goodman and Brenna to recover isotope ratios in the presence of low signal or poor chromatographic resolution.

The average peak area for the belt interface is 114.5 V s (2.5 ug load) while the previous interface designs yielded peak areas of 2.6 V s, 14.5 V s, and 58.4 V s (50 ug loads). This represents ~ a 40 fold increase in sensitivity attributed to the ability of the belt to capture a larger proportion of the total analyte.

Signal linearity was assessed for analyte loads ranging from 25 ng to 5 ug. At loads significantly higher than 5 ug the m/z 46 Faraday cup saturated. Although injections of as little as 25 ng of analyte yielded signals clearly discernible from baseline noise, peaks could not be accurately detected until the 250 ng level. However, the sensitivity of the interface was shown to be linear (R^2 = 0.9932) over the range of 250 ng to 5 ug.

In previous designs it had been observed that the precision of isotope analyses degraded, and apparent isotope ratio increased below analyte loads of 1ug. Analysis of varying analyte loads in the present system resulted in similar trends. In an attempt to improve the accuracy and precision of the isotopic measurements curve-fit analysis was employed. Attempts to fit peaks with a single peak function yielded poor fits while simultaneously using two peak functions to fit a single peak improved the R^2 values. The best fits (i.e. best R^2) were obtained by fitting each peak with a combination of two Non-linear Chromatography peaks, however data processing with this function is extremely slow. Therefore a combination of two Exponentially Modified Gaussian (EMG) peaks was used. On average Peakfit analysis improved the precision of SD (δ 45) by an average of 0.42 ‰ . The accuracy of the isotope ratios was improved on average 0.5 ‰ by Peakfit analysis, however the accuracy still deviated systematically from the true isotope ratio for both the vendor and Peakfit analyses. Due to the systematic nature of this deviation, simple linear calibration should restore the isotope ratio to the correct value.

Finally, the accuracy and precision of the interface over the natural abundance range was examined . No significant difference was found in the average precision of SD (δ 45) for data analyzed by Peakfit analysis (SD (δ 45) = 0.479) and the vendor supplied software (SD (δ 45) = 0.481). The average accuracy as compared to dual inlet analysis was however improved significantly using Peakfit analysis. The vendor supplied software on average overestimated the δ 45 by 1.624 ‰ while Peakfit analysis on average overestimated the δ 45 by only 1.244 ‰. As observed in the assessment of linearity with varying analyte loads, the isotope ratio varied systematically with varying isotope ratio and therefore simple linear calibration should help restore isotope ratios to the true value.

LC Combustion Interface for High Precision Isotope Ratio Mass Spectrometry

***P. Dobberstein** and W. Brand*, Finnigan MAT, 28197 Bremen, Germany

Since its introduction [1] and commercial realisation [2], GC Combustion Isotope Ratio MS (GCC-IRMS) has generated increasing interest of scientist from different disciplines as for instance organic geochemistry and metabolism research and meanwhile has become a well established technique. The limitation of gas chromatography to less polar, volatile and relatively low molecular weight components is a restriction, which can be overcome by applying a LC combustion technique in place of GC combustion.
Quantitative removal of the solvents, especially in case of organic solvents, prior to the combustion is a prerequisite for obtaining high precision, therefore the moving wire principle [3] is the method of choice.

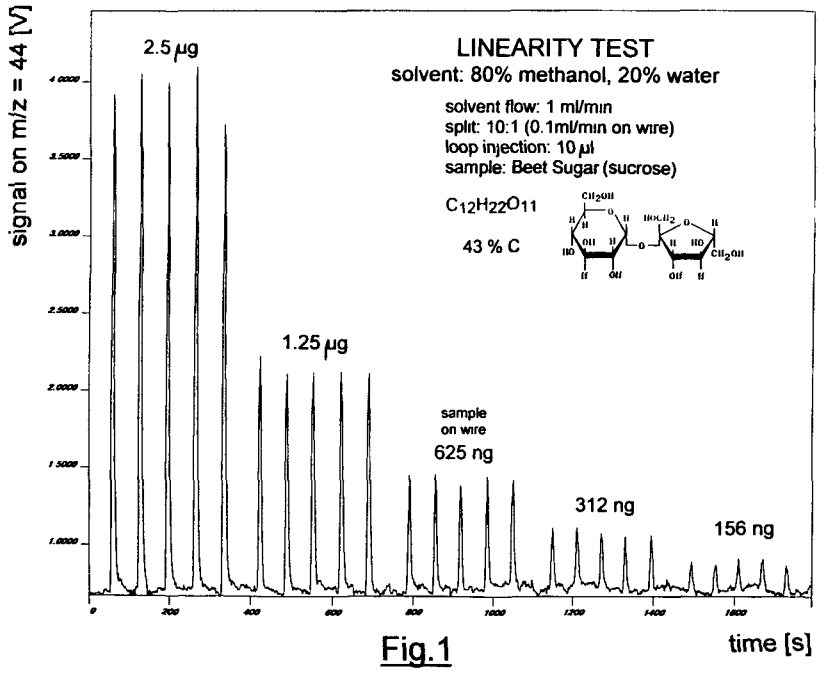

Fig.1

43rd ASMS Conference on Mass Spectrometry and Allied Topics

The HPLC eluent is splitted 10:1 and the remaining flow of typically 0.1 ml/min is contineously deposited on a moving wire (0.25 mm diameter Ni), which then passes a drying stage for solvent removal. The wire afterwards moves into and a combustion oven, where the carbon atoms of the sample deposit are quantitatively converted into CO_2. A He gas stream, passing the combustion oven, carries the CO_2 via a Nafion water trap to an open split interface, where typically 10% of the CO_2 is sniffed via a fused silica capillary into a Delta C isotope ratio ms.
First measurements have been performed by flow injection of 10 µl of sample solution (**Adenosin** in water or **Beet Sugar** in methanol/water) into the liquid flow of 1 ml/min 100% water or methanol/water prior to the eluent split at sample concentrations between 2.5 µg/µl and 156 ng/µl. In both solvent systems the moving wire interface showed a linear response between signal output at m/z = 44 and sample input (**Fig.1**)
For 2.5 µg **Beet Sugar** deposited on the wire an output signal of 25.7 Vs was obtained; taking into account the sensitivity of the Delta C (1 ion per 2000 molecules) and a split ratio of 10 to 1 at the open split, this corresponds to an overall yield of 20%, which means that 80% of the sample is lost during sample deposition, drying and combustion.

In order to test the capability of the moving wire interface for isotope ratio measurements, we made subsequent loop injections of **Beet** and **Cane Sugar,** both at 2.5 ug/ul in water with the following sequence: 5x Beet, 5x Cane, 5x Beet, 5x Cane.

Calculations of the delta 13-C vs PDB values from this measurement are shown on **Fig.1**. The delta value of Beet Sugar, known from sealed tube combustion to be -26.2‰ was used to calibrate the first data-point; the other values were measured relativ to this value. This result opens the perspective, to distinguisch between natural occuring variations of isotope ratios by LC Combustion IRMS.

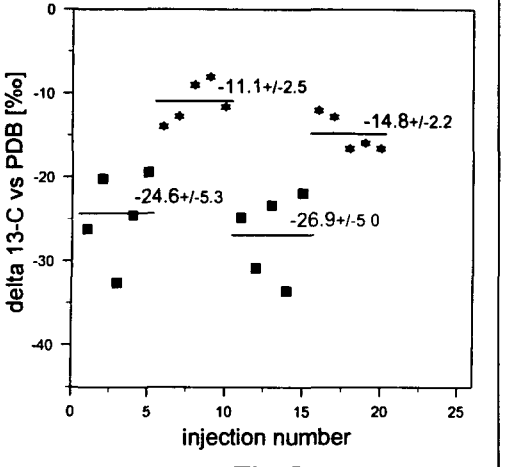

Fig.2

[1] D.E. Mathews and J.M. Hayes, *Anal. Chem.* 1978, **50**, 1465
[2] W. Brand, M. Ricci and K. Habfast, *11th Intl. MS Conf., Bordeaux, France,* 29.8.-2.9. 1988, paper FRM OR
[3] R.J. Caimi and J.T. Brenna, *J. Mass Spectrom.* 1995, **30**, 466

OPTICAL SPECTROSCOPY VERSUS MASS SPECTROMETRY: THE RACE FOR FIELDABLE ISOTOPIC ANALYSIS

C.M. Barshick, J.P. Young, R.W. Shaw, D.H. Smith, and J.M. Ramsey
Chemical and Analytical Sciences Division
Oak Ridge National Laboratory
Oak Ridge, TN 37831-6375

Several techniques have been developed to provide on-site isotopic analyses, including decay-counting and mass spectrometry, as well as methods that rely on the accessibility of optical transitions for isotopic selectivity (e.g., laser-induced fluorescence and optogalvanic spectroscopy). We have been investigating both mass spectrometry and optogalvanic spectroscopy for several years. Although others have considered these techniques for isotopic analysis, we have focussed on the use of a dc glow discharge for atomization and ionization, and a demountable discharge cell for rapid sample exchange. Our goal is a fieldable instrument that provides useful uranium isotope ratio information.

Diode Laser Excited Optogalvanic Spectroscopy

Precision and accuracy have been evaluated for several optical transitions. Samples that were enriched, natural, or depleted in ^{235}U were easily distinguishable from one another (see Table 1). Using a 150 mW diode laser at 832 nm, the measured $^{235}U/(^{235}U + ^{238}U)$ ratio for a depleted uranium oxide sample was improved to 0.0026 from 0.0035 (the value obtained with a 30 mW diode laser at 776 nm); this value is within 3.7% of the thermal ionization mass analysis value. The run-to-run reproducibility was ± 7.8%, an improvement of a factor of two over the 776 nm result. These results are sufficient for many applications where information about the isotopic composition of a sample provides the basis for further investigations. The success of this study has given us the incentive to begin construction of an instrument suitable for field analyses that will incorporate a high power 832 nm diode laser.

Ion Trap Mass Spectrometry

Because the ion trap laboratory was not designed to handle radiological samples, copper was used as a surrogate. Fifty runs of 10 μScans each were averaged to evaluate the precision; five of those trials are shown in Table 2. Although the run-to-run repeatability is better than 5%, there is some concern because the numbers are all biased low. Previous work on a magnetic sector mass spectrometer indicated that there should be no bias associated with the glow discharge, and it therefore may be related to the mass analyzer. Although only presently in the design stages, it is clear that the ion trap will be a powerful field tool because it provides simultaneous isotope ratio and elemental composition information.

Table 1. Optogalvanic data recorded using a 30 mW diode laser at 776 nm

Sample	Optogalvanic Values $^{235}U/(^{235}U + ^{238}U)$	Measurement Precision (percent)	Thermal Ionization Values $^{235}U/(^{235}U + ^{238}U)$
depleted UF_4	0.0034	± 11.6	0.00490 ± 0.00003
natural uranium metal powder	0.0090	± 14.4	0.00716 ± 0.00005
enriched uranium metal	0.10	± 3.14	0.101 ± 0.002
enriched U_3O_8 NIST SRM U-200	0.20	± 1.84	0.201 ± 0.002

Table 2. Ion trap data recorded using a Teledyne 3DQ mass spectrometer

Sample	ITMS Values $^{63}Cu/^{65}Cu$	Measurement Precision (percent)	Natural Abundance $^{63}Cu/^{65}Cu$
machined brass rod	2.119	± 3.17	2.235
	2.159	± 2.69	
	2.126	± 3.34	
	2.143	± 3.30	
	2.159	± 3.46	

Research was sponsored by the U.S. Department of Energy, Office of Research and Development. Oak Ridge National Laboratory is managed by Martin Marietta Energy Systems, Inc. for DOE under Contract DE-AC05-84OR21400.

Alumatrane Revisited: Distribution of Oligomeric Ions in EI, CI, and LSIMS

Michael G. Bartlett, Scot A. Burns, David A. Bruce, and Kenneth L. Busch
School of Chemistry and Biochemistry, Georgia Institute of Technology, Atlanta, GA 30332-0400

The EI mass spectrum agrees with the earlier mass spectrum reported by Lacey and Macdonald with the exception of ions observed in our spectrum at *m/z* 389, 489 and 562. The conclusions of Lacey and Macdonald, *viz.* that this compound is dimeric in the gas phase, is immediately called into question by observation of these higher mass ions. Recently, Pinkas and Verkade reinvestigated the mass spectral behavior of alumatrane, and also report the ion at *m/z* 562 in their EI spectra, although they do not identify it. They do conclude that this ion indicates the presence of the tetrameric form of alumatrane in the gas phase. This conclusion is at variance with our identification of the *m/z* 562 ion as the product of addition of AlO^+ to the trimer. Pinkas and Verkade did not report higher mass ions in their EI mass spectrum, and we do not observe higher mass ions either. The EI mass spectrum of alumatrane does not contain a signal corresponding to the monomer (*m/z* 173) of alumatrane, and only a very weak signal corresponding to the dimer ion (*m/z* 346). The most abundant ions in the mass spectrum correspond to the loss of CH_3COH (*m/z* 302) and loss of CH_2O (*m/z* 315) from the dimer ion. Positive ion chemical ionization mass spectra of alumatrane reveal the presence of the gas-phase dimer ion as $[2M+H]^+$, and additionally as $[2M+NH_4]^+$ with ammonia reagent gas. In the methane and ammonia positive ion CI mass spectra, an ion at $[2M-H]^+$ is observed, representing dehydrogenation of the protonated dimer ion. Such ions are not unknown in positive ion CI, but are relatively uncommon. Their presence here (and in the LSIMS mass spectra to be discussed shortly) indicates that there may be a special stability for such ions. The structure of this ion remains to be established; loss of two hydrogens may occur from methylene groups within a single linkage, or a new bond may be formed between carbons in adjacent linkages. The added proton is conveniently considered to reside on the nitrogen to create a quaternary nitrogen charge localization. Despite evidence in the EI mass spectra for the trimeric form of alumatrane, the positive ion CI mass spectra contain ions only for the dimeric form.

The methane negative ion CI mass spectrum of alumatrane contains both $[2M-H]^-$ and $[2M+H]^-$ ions. Proton addition to form $[2M+H]^+$ in the positive ion mass spectrum is mirrored by hydride addition to form $[2M+H]^-$. There is a small signal for $[4M-H]^-$ in the methane NCI mass spectrum, but no analogous signal for $[4M+H]^-$. The ammonia NCI mass spectrum of alumatrane, in contrast, provides stronger support for the existence of higher order oligomeric ions. The mass spectrum contains abundant signals for the dimeric ion $[2M-H]^-$ at *m/z* 345 and the tetrameric ion $[4M-H]^-$ at *m/z* 691. There are also ammonia adducts associated with both the dimer $[2M+NH_3]^-$ and the tetramer $[4M+NH_3]^-$. This mass spectrum is similar to the ammonia NCI spectrum reported by Pinkas and Verkade with the exception of a higher relative intensity for the peak at *m/z* 389, identified here as $[2M+AlO]^-$ with a relative intensity of 70%. The same peak is present with only a 5% intensity by Pinkas and Verkade, and is not identified in their paper.

The negative ions $[2M+H]^-$, $[2M+NH_3]^-$, and $[4M+NH_3]^-$ are unusual. The $[2M+H]^-$ ion may represent an adduct of two negatively charged molecular ions with a single proton. Support for this formulation is found in the observation of the analogous $[2M+AlO]^-$, in which the AlO^+ replaces the proton. Ions $[2M+NH_3]^-$ and $[4M+NH_3]^-$ are not accompanied by $[3M+NH_3]^-$, although trimeric forms of alumatrane are seen in the electron ionization mass spectrum. The structures of these ions, and the processes through which they are formed, are under study.

Desorption chemical ionization (DCI) differs from chemical ionization in that the sample is placed on a heated filament placed directly in the ion source. The mass spectrum contains ions corresponding to the protonated dimer through the hexamer, appearing as ion pairs $[nM+H]^+$ and $[nM-H]^+$, as in the CI mass spectrum. In addition, the trimer and the pentamer (but not the dimer or the tetramer) produce an ion by addition of AlO. The AlO^+ can formally be considered as a replacement for the proton that would form $[nM+H]^+$, although the lack of reactivity for the dimer and tetramer suggest a different structural end result. Overall, although higher mass ions can be seen in the DCI mass spectrum, the intensities of these ions are low, and no special ion stabilities are evident.

The first unique feature of the LSIMS spectrum is the presence of the ion at *m/z* 174, corresponding to the protonated monomer. An ion for the monomer is not observed in mass spectra generated by any other ionization technique. A series of ions is observed at $[M_n+42]^+$ and $[M_n+102]^+$ in the LSIMS mass spectrum of alumatrane. This series begins with the dimer and is repeated in the trimer and tetramer clusters. Exact mass measurements show that these ions are additions of AlO and Al_2O_3 to the alumatrane oligomers 2M, 3M, and 4M. Oligomers consisting of 6 and 7 alumatrane molecules are contained within a more complex distribution of ions formulated as $[M_n+(AlO)_a+(Al_2O_3)_b]^+$. An addition of Al_3O_4 is separable into $(AlO+Al_2O_3)$. Similarly, Al_5O_7 is $[AlO+2(Al_2O_3)]$, Al_6O_8 is $[2(AlO)+2(Al_2O_3)]$, and Al_8O_{11} is $[2(AlO)+3(Al_2O_3)]$. The AlO group carries a charge, and Al_2O_3 can be considered as a neutral molecule. When more than one AlO^+ is added to the oligomer, a proton loss must occur to preserve the single positive charge, as in the ions at *m/z* 1112, *m/z* 1285, and 1345.

The product ion MS/MS spectrum of the ion at *m/z* 562 ($[3M+AlO]^+$) contains 3 fragment ions at *m/z* 519 (35 relative intensity), *m/z* 449 (20), and *m/z* 389 (100), representing the loss of AlO, $C_6H_{11}ON$, and an intact alumatrane molecule (M), respectively. As listed, the most intense fragment ion represents loss of alumatrane to form $[2M+AlO]^+$, The converse loss of AlO to generate $3M^+$ is observed with a lower relative intensity. The fragment ion at *m/z* 449 is formed in a dissociation of the parent ion in which we speculate that each of the three alumatrane molecules loses some portion of its organic linkage, and then regroups around a central Al_2O_3. The energy-minimized structure shows an ion in which the added AlO becomes a central, integral part of the ion, with reorganization of the bonding in each of the original alumatrane molecules The predominant loss of a single alumatrane molecule to form $[2M+AlO]^+$ is easily accommodated by cleavage and a slight rearrangement to form a bond between an aluminum and an oxygen that are in close proximity in this ion. The reluctance of such a structure to dissociate to $3M^+$ is also evident.

The energy-minimized structure for the ion at *m/z* 837, formulated as $[4M+Al_3O_4]^+$ shows a high degree of symmetry, with four alumatrane molecules converging in a central core in which all seven aluminum atoms are fully coordinated. The stability of such as ion must be the driving force behind the considerable rearrangements that would be required for its formation.

The LSIMS mass spectrum of the boron analog of alumatrane, borotrane, contains a sequence of ions that correspond to $[M_n+H]^+$ where n=1-6. However, there are no additions of oxygen, boron, or boron oxide molecules. Boron prefers to be coordinated by either three or four atoms instead of six like the aluminum atoms in alumatrane. The central boron molecule is already bound to the three oxygen atoms and to the nitrogen atom, its valency requirements are fulfilled without the formation of adduct ions.

Characterization of Supported and Unsupported Transistion Metal Complexes

M.G. Bartlett, D.A. Bruce, S.M. Thomas, M.G. White, J.A. Bertrand and K.L. Busch
School of Chemistry and Biochemistry, Georgia Institute of Technology, Atlanta, GA 30332-0400

Metal acetylacetonates (acac) can be analyzed using a number of ionization techniques including electron ionization (EI) and secondary ion mass spectrometry (SIMS). When using LSIMS for the analysis of metal acacs m-nitrobenzyl alcohol (m-NBA) was found to be the optimum matrix. m-Nitrophenyloctylether also worked well for these compounds but did not provide the same level of signal-to-noise, the exception being $Fe(acac)_3$, where the intensity of the molecular ion was improved by a factor of five versus m-NBA.

All of the compounds analyzed show the loss of an acac ligand as the most abundant fragment ion. The LSIMS mass spectra of these compounds all contain additions of metal atoms and additional acac ligands. However, there are several additional peaks in the LSIMS mass spectra of the acac's that are interesting to note. An earlier study of the LSIMS mass spectra cobalt(III) acac, states that there are no peaks in the spectrum that are associated with the matrix or are there any matrix adducts present. We find that the three samples where the metal atom has an oxidation state of +3 have no peaks that are composed only of matrix molecules, but adducts of the metal acac's with m-NBA exist as significant signals in the spectra. The mass spectra of the other acac's have considerable background ions that result from the matrix, as well as, adducts with m-NBA molecules. The matrix-sample adducts consist of between one and four m-NBA molecules. For adducts that contain more than one metal atom there appears to be a hydride abstraction for every m-NBA molecule that is added to the complex. The reason behind this is not clear, but the addition of these m-NBA molecules could follow the loss of the hydrogen on the alcohol group of the m-NBA molecule. Since, it appears that it is necessary to have two metal centers before the addition of a deprotonated m-NBA molecule is observed, it is likely that the m-NBA molecules are bridging between two metal centers, as is shown in Figure 1. The only example of an ion consisting of a single metal atom and m-NBA molecules is observed in the spectrum of copper (II) acac. In this case the neutral m-NBA molecules are observed to be added to the metal atom instead of deprotonated m-NBA molecules. In this case, it is likely that the copper ion interacts only with the nitro-group of the m-NBA molecule instead of interacting with both the nitro- and alcoxy-functional groups.

Three additional transition metal complexes were analyzed using LSIMS, copper (II) diethanolamine $[Cu(deta)_2ClO_4]$, copper (II) ethylenediamine $[Cu(en)_2(ClO_4)_2]$, and tris-cobalt (III) ethanolamine $[Co_3(eta)_6(ClO_4)_3]$. The copper complexes were determined to give the optimum response when analyzed using a 1:1 (v/v) mixture of glycerol/thiodiethanol as the LSIMS matrix. The cobalt complex provided the optimum response when analyzed using sulfolane as the matrix.

In order to determine the composition of the transition metal complexes on the support surface we first attempted to analyze the sample directly. A few micrograms of the supported sample was placed directly on the direct insertion probe. The mass spectra of these supported samples, without the use of LSIMS matrices, only yields signals that correspond to the metal ions. Mixing the supported sample with a LSIMS matrix prior to analysis does not yield any ions that are associated with the transition metal complexes. However, we observed that sonicating the sample with a moderately polar organic solvent such as, methanol or acetonitrile remove neutral transition metal complexes (metal acetylacetonates) from the support surfaces. The organic solvent can then be placed on the LSIMS probe and evaporated prior to addition of the matrix. Although, the use of organic solvents can remove these neutral transition metal complexes, this method was not found to be effective for the removal of any of the transition metal salts. In addition, it was observed that the transition metal complexes could also be

removed simply by sonication with the LSIMS matrix prior to analysis. Since, this method was found to be as effective as the use of organic solvents, and far less time consuming, all data was acquired using this method.

In order to analyze the supported transition metal salts, sodium chloride was added to the LSIMS matrix and the supported sample prior to sonication. The sodium ions act as an ion exchange agent displacing the sample from the surface. The mass spectrum of $Cu(deta)_2^+$ is shown in Figure 2. Instead of the protonated molecular ion the sodiated molecular ion is observed at *m/z* 295. The identification of this ion is facilitated by the presence of the copper isotope pattern which is clearly observed in the ratio of the ions at *m/z* 295 and 297. Although sodium chloride was useful in removing $Cu(deta)_2^+$ from the silica surface it was not possible to remove any of the other transition metal salts from their supports using this method. This is due to other salts having a higher charge and consequently being more difficult to displace from the support.

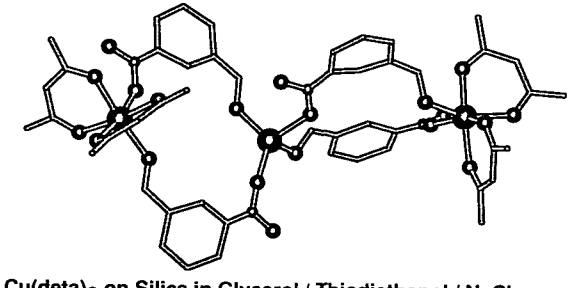

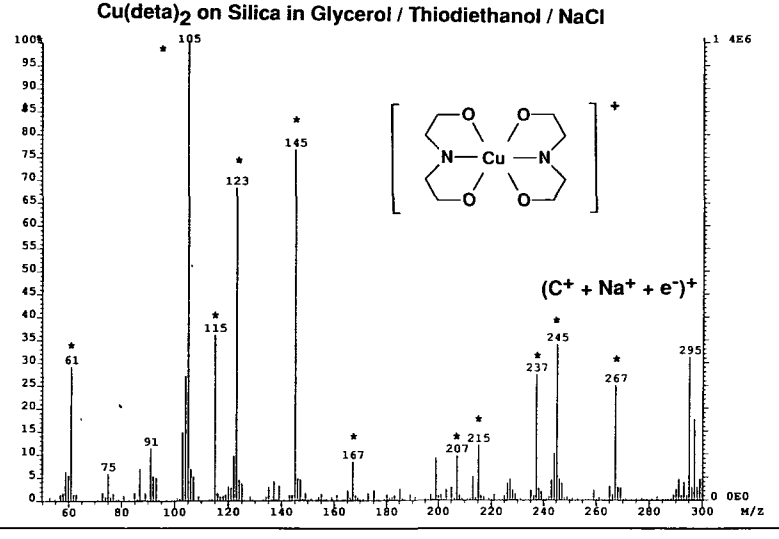

A STUDY OF THE CLUSTER ION DISTRIBUTION FROM METAL NITRATES USING PDMS

W. R. Ferrell, M. J. Van Stipdonk and E. A. Schweikert

Center for Chemical Characterization and Analysis, Department of Chemistry
Texas A&M University
College Station , TX 77843-3144, USA
Fax. (409) 845-1655
E-Mail EASGROUP @ CHEMVX.TAMU.EDU

The impact of MeV ions on solid surfaces causes the emission of atomic, polyatomic, cluster and molecular species whose mass, yield, radial velocity and angular distribution can be used to elucidate the mechanism of secondary ion (SI) formation Radial velocity and angular distribution measurements have contributed greatly to improvements in the understanding of the molecular ion formation process from organic insulators under MeV bombardment. However SI, in particular cluster ion, emission from non-molecular solids and the underlying chemical changes often induced within the fission track, are not well understood. Cluster ions (atom aggregates made up of smaller units) are of interest as they may contain chemical and structural information. A PDMS study of the composition, distribution and stability of cluster ions from metal nitrates was undertaken to probe the chemistry and physics underlying cluster ion formation from inorganics. A study of cluster ions from the ternary nitrates should provide additional information to that obtained from binary and mono-elemental systems. Moreover, nitrates are disposed to track formation and ion emission in PDMS because of their excellent insulating properties. A reflection geometry, plasma desorption mass spectrometer was used for these studies. Computer evaluations of cluster ion peak areas in total ion counts were made and the log of these areas were plotted against the cluster number n.

Two predominant positive cluster series were identified: the protonated metal-oxide based cluster series, $(MO)_nH^+$, and the metal excess cluster series, $(MO)_nM^+$

(M=metal atom). Cluster ion formation and growth is apparently initiated by the preferential formation of metal-oxide (MO) monomers at high temperatures and pressures ($\approx$ 4300k and 10^4 atm) within the infratrack plasma created by the fission fragment The formation of oxides is facilitated by their low (negative) heats of formation and high lattice energies relative to other possible reaction products. Generally, the intensities of the predominant clusters follow a roughly decreasing exponential function of cluster size with discontinuities or enhanced abundances at certain "magic-numbers" of n. For example, magic numbers for the $(MO)_nH^+$ clusters of the Group IIA nitrates, generally occur at n=2, 4, 6, 9, and 12 while those for the $(MO)_nM^+$ clusters are identical, except lowered by one unit. Also, for Co and Cd, the $(MO)_3^+$ ion is exceptionally stable. Since emitted clusters are accelerated to their full energies within a relatively short time ($\leq 0.01\mu s$ acceleration region), the intensity anomalies arise prior to emission and probably during the actual cluster ion *production process* within the fission track. Similar patterns in abundance maxima have been reported for $(CaO)_n^+$, $(MgO)_n^+$ $(CaO)_nCa^+$ and $(MgO)_nMg^+$ clusters generated in a gas aggregation source [1,2]. For the Group IIA nitrates, the abundance or stability patterns correlate with the energetically favored, *cubic-like* sub-units of the fcc bulk structure of the metal-oxide. In addition, the relative stabilites of the $(MO)_nH^+$ clusters from the various nitrates seem to be influenced by the ionicity and strength of the M-O bond.

REFERENCES

[1] P. J. Ziemann and A. W. Castleman, Jr., J. Chem. Phys., 94 (1991) 718.

[2] P. J. Ziemann and A. W. Castleman, Jr., J. Phys. Chem., 96 (1992) 4271.

Electrospray Ionisation of Polyoxoanions of W, Mo and Si in Aqueous Solution.

Scott G. Summerfield, Oliver W. Howarth and Keith R. Jennings.
Department of Chemistry, University of Warwick, Coventry, CV4 7AL.

Aqueous oxoanions of tungsten and molybdenum are of importance in a number of areas of chemistry including oxidation catalysis, paper production, solar energy conversion and as antiviral agents. On addition of hydrogen peroxide, the partial replacement of O^{2-} by O_2^{2-} occurs to yield peroxometalates. It is thought that the peroxo species play an active role during the catalysis process and currently, these metalates offer an environmentally superior method for the manufacture of paper from wood pulp. In many cases, the lifetimes of such species are pH and time dependent, ranging from hours to days, and their characterisation is difficult since a variety of species coexist in solution. The application of NMR to this area is restricted because of the insensitivity in detecting metals such as ^{95}Mo and ^{183}W coupled with the problem of working with long acquisition times for species having only a limited lifetime. However, many species have been identified by the careful use of these methods and ^{17}O studies [1].

Because electrospray ionisation (ESI) generates ions directly from solution, it may provide a rapid method for investigating the species present in these solutions. The results described show the electrospray ionisation of aqueous solutions of oxometalates performed in a VG Quattro II instrument.

The concentration of many peroxometalate species is usually too low to allow detection by means of NMR or other methods. In the case of electrospray ionisation, these ions are readily observed at low concentrations and may be identified by the shift in mass of the anion due the replacement of O^{2-} by O_2^{2-}. This has been used to investigate the reaction of aqueous hydrogen peroxide with powdered tungsten, the products of which have not been characterised previously. As shown in Figure 1, the reaction generates the $[W_6O_{19}]^{2-}$ anion. Adjacent peaks demonstrate up to 4 successive replacements of O^{2-} by O_2^{2-}. No previous studies have observed the $[W_6O_{19}]^{2-}$ anion in aqueous solution although this may have been due to the low sensitivity of other detection methods. Other species such as $[HWO_4]^-$ and $[HW_2O_7]^-$ are produced in large abundance and peroxidation of these species is also evident as shown in Table 1.

Electrospray ionisation provides a rapid method for characterising the aqueous solutions of metalates and peroxometalates. This technique offers many advantages including the possibility of identifying components present in low concentrations and the analysis of aqueous solutions before significant degradations can occur. The use of electrospray alongside NMR methods may provide a more powerful approach to understanding the chemistry of these complex systems.

References.

1. O. W. Howarth, J. J. Hastings, *J. Chem. Soc. Dalton Trans.*, 209 (1992).

Nomenclature.

mo	monotungstate	di	ditungstate
tri	tritungstate	tet	tetratungstate
hex	hexatungstate	dec	decatungstate

Peroxidation:

$$hex^{2-} = [W_6O_{19}]^{2-},\ hexO^{2-} = [W_6O_{18}(O_2)]^{2-},\ hexO_n^{2-} = [W_6O_{(19-n)}(O_2)_n]^{2-}$$

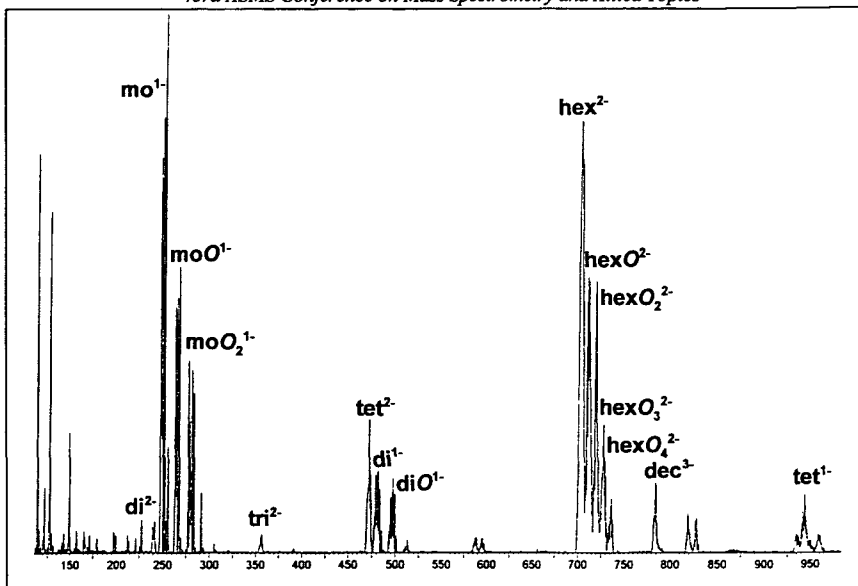

Species	$[HW_{10}O_{32}]^{3-}$	$[H_2W_{10}O_{32}]^{2-}$	$[W_6O_{19}]^{2-}$
m/z	784	1,177	704
Max. Peroxo.	0	0	4
label	dec^{3-}	dec^{2-}	hex^{2-}
Species	$[HW_6O_{19}]^-$	$[W_5O_{16}]^{2-}$	$[W_4O_{13}]^{2-}$
m/z	1,409	588	472
Max. Peroxo.	4	2	overlapped
label	hex^{1-}		tet^{2-}
Species	$[HW_4O_{13}]^-$	$[W_3O_{10}]^{2-}$	$[W_2O_7]^{2-}$
m/z	945	356	240
Max. Peroxo.	1	1	2
label	tet^{1-}	tri^{2-}	di^{2-}
Species	$[HW_2O_7]^{2-}$	$[HWO_4]^-$	
m/z	481	249	
Max. Peroxo.	overlapped	2	
label	di^{2-}	mo^{1-}	

Table 1: Tungsten oxoanions observed under ESI conditions and the number of successive peroxidised complexes observed.

STUDY OF THE STABILITY OF METAL ION - MACROCYCLE COMPLEXES BY ESI-MS/CID/MS

Calin G. Znamirovschi[a,b], Dinorah Frutos[b], and Christie G. Enke[a,b]

[a] *Department of Chemistry, Michigan State University, East Lansing, Michigan 48824-1322, USA*
[b] *Department of Chemistry, University of New Mexico, Albuquerque, New Mexico 87131-1096, USA*

Electrospray ionization mass spectrometry (ESI-MS) has lately emerged as an increasingly popular analytical method for inorganic and organometallic analysis [1,2]. The ability of ESI to convert solvated ions and ionic associations into gas phase ions with minimum or no fragmentation makes the method amenable to studying the interactions between metal ions and organic ligands in the gas phase.

We chose for this study two metal ions that exhibit contrasting behavior, K^+ and Ag^+, a "hard" and a "soft" cation, respectively Three analog macrocyclic ligands, 18-crown-6 (**L**), 1-aza-18-crown-6 (**L'**), and 1,10-diaza-18-crown-6 (**L"**) were chosen for their particular complexing trends toward K^+ and Ag^+.

In the ESI-MS experiments on the K^+ interaction with **L**, **L'**, and **L"** the predominant species present in the spectrum were the bare metal ion and the 1:1 complex ion. With an increase in the number of "soft" donors (i.e., nitrogen atoms) in the ligand, an increasing abundance of protonated uncomplexed ligands was found (Figure 1). This follows the decreasing trend of complex stability in solution (Table 1).

The study of Ag^+ interaction with the same series of macrocyclic ligands however, shows that Ag^+ is absent in the spectrum, the predominant ion being the 1:1 complex in the case of all three ligands considered. The larger abundance and a wider structural variety of protonated uncomplexed ligands are due to the increased proton affinity of nitrogen-containing ligands **L'**, and **L"**, respectively

Collision-induced dissociation (CID) studies provide additional information about the behavior of potassium and silver complexes in the gas phase. A unique dissociation pattern, with the bare metal ion retaining the charge, is noticed for K^+ complexes with all three ligands considered. There are no other charged or protonated fragments in the spectra Silver complexes however, undergo ligand-specific dissociation. Ag^+ is present in the CID spectrum of $(AgL)^+$ only. In the nitrogen-containing silver complexes, (i.e., $(AgL')^+$, $(AgL'')^+$) the high proton affinity of nitrogen atoms explains the absence of any silver-containing ionic fragment, except the dehydrogenated complex ions. Also, because the nitrogen-containing fragments are more likely to retain the charge, silver preferentially forms neutral **AgH**, and is therefore not part of any charged or protonated fragment in the spectra (Figure 2).

43rd ASMS Conference on Mass Spectrometry and Allied Topics

Cation/Ligand	L	L'	L"
Potassium	6.10	3.90	2.04
Silver	1.60	3.30	7.80

Table 1 - Stability constants (log K_s) of K and Ag complexes with L, L', and L" in methanol solution (9:1 CH_3OH : H_2O) [3]

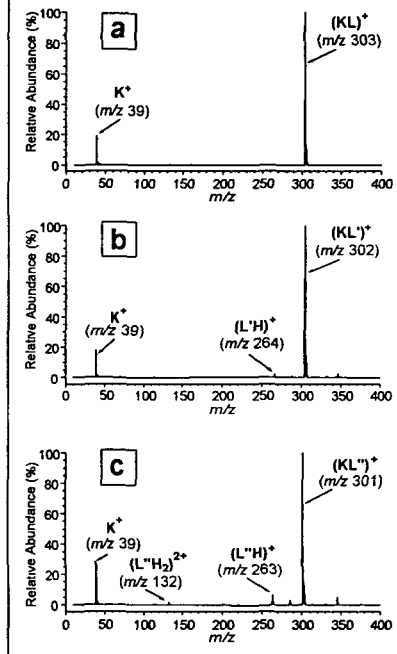

Figure 1 - ESI spectra of (a)$(KL)^+$, (b) $(KL')^+$, and (c) $(KL'')^+$

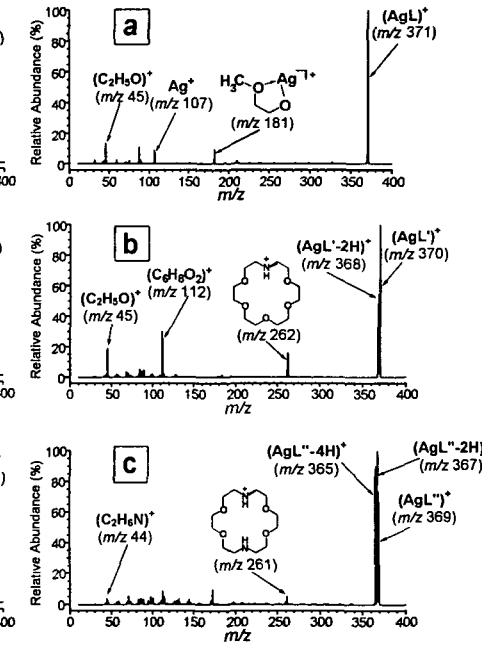

Figure 2 - CID product spectra of (a) $(AgL)^+$, (b) $(AgL')^+$, and (c) $(AgL'')^+$

References:
[1] G.J.Van Berkel, S.A.McLuckey, G.J Glish - The 39th Conference on Mass Spectrometry and Allied Topics, Nashville, TN, May 1991
[2] G.J.Van Berkel, S.A.McLuckey, G.J Glish - Anal Chem **1991**, *63*, 1098
[3] F.Vögtle, E.Weber in *Crown Ethers and Analogs* , John Wiley and Sons: New York, **1989**, Ch.4

Atmospheric Pressure Chemical Ionization of Novel Heterocyclic Bismuth Compounds

G.B. Yhard[1], L. Agocs[1], N. Burford[1] and J.M. Curtis[2]
1. Department of Chemistry, Dalhousie University, Halifax, Nova Scotia, Canada, B3H 2J3
2. National Research Council, 1411 Oxford Street, Halifax, Nova Scotia, Canada, B3H 3Z1

Introduction: A number of bismuth containing compounds, eg. bismuth subcitrate, are known for their anti-*Helicobacter pylori (Hp)* activity and are used in the treatment of peptic ulcers [1,2]. However, the currently used preparations involve an uncharacterized, complex mixture of bismuth compounds [2]. We are currently investigating structurally simple, low coordinate bismuth compounds as part of a search for alternative treatments (Figure 1).

Figure 1-Compounds Examined

R = $(CH_2)_2$ (1), $(CH_2)_3$ (2), $(CH_2)_2S(CH_2)_2$ (3), $(CH_2)_2O(CH_2)_2$ (4)

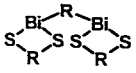

R = $(CH_2)_2$ (5), $(CH_2)_3$ (6), $(CH_2)_4$ (7), $(CH_2)_2S(CH_2)_2$ (8), $(CH_2)_2O(CH_2)_2$ (9)

The low solubility of many bismuth compounds makes recrystallization extremely difficult; often a crystal structure cannot be obtained. NMR data is usually of little value because bismuth has a quadrupolar nucleus, resulting in very broad absorption peaks. Atmospheric pressure chemical ionization (APCI) is an effective technique enabling the mass spectral characterization of these compounds.

Structural information obtained from conventional and tandem mass spectrometry provide definitive evidence supporting structures **2** and **6-9** which have not yet been demonstrated by other techniques. Previously the known structures **1** and **3-5**, determined by crystallography, were used to infer the structures of **2** and **6-9**, prepared via a similar synthetic procedure.

Experimental: APCI spectra were obtained using a PE/SCIEX API-III$^+$ triple quadrupole mass spectrometer (PE/SCIEX, Thornhill, Ontario, Canada), equipped with a standard heated nebulizer interface. The mobile phase for flow injection analysis was 1:1 water:acetonitrile (MeCN) introduced at 200 µL/min. Fragment ion spectra used argon as collision gas.

Results: The major ions in the positive ion APCI spectra of **1**, **2** (Figure 2), **3** and **4** dissolved in DMSO or MeCN are $[M-Cl]^+$, $[M-Cl+A]^+$, and $[M-Cl+2A]^+$ (A=solvent). The relative abundance of the uncomplexed versus the solvated cations was found to be dependent on the orifice voltage. Fragment ion spectra (not shown) of the precursors $[M-Cl+A]^+$, and $[M-Cl+2A]^+$ show sequential loss of the solvent adducts. Bi^+ and BiS^+ ions are formed with increasing argon gas pressure.

The APCI spectra of the bridged compounds **5** (figure 3) or **9** dissolved in acetonitrile with 1% HCl show $[M+H]^+$ ions. Fragment ions formed from **5** include $BiS_2C_2H_4^+$ (and its MeCN adduct), $Bi_2S_3C_4H_9^+$ and $BiS_3C_4H_7^+$. The fragment ions $BiS_2C_2H_4O^+$, (and its MeCN adduct), Bi^+, and $BiS(CH_2)_2O^+$ are present in the spectrum of **9**. The fragment ion spectrum of the protonated molecular ion supports the proposed structure.

Conclusions: We have observed the first example of moisture stable bismuthenium cations using APCI mass spectrometry. This technique allows the analysis of low solubility bismuth compounds and often provides the only definitive evidence of their structure. Compounds **1-4** were found to form $M-Cl^+$ cations in solution. Protonated molecular ions for **5** and **9** were observed in their APCI spectra together with several fragment ions. Compounds **6-8** appear to be unstable in solution, forming a single ring fragment of the parent compound.

Several bismuthenium species form solvent adducts, which can be observed in their APCI mass spectrum. Future work will include determination of the relative strength of the solvent adduct - cation bond for various bismuthenium complexes by varying the orifice voltage. In addition, an LC/MS method to separate bismuth compounds is currently being developed.

Figure 2 APCI Mass Spectrum of 2 in MeCN

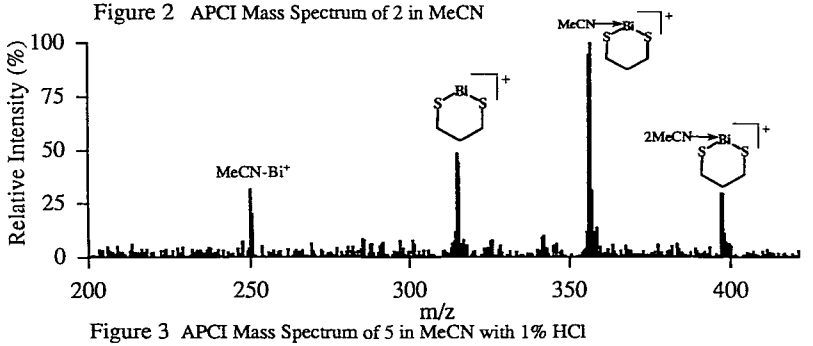

Figure 3 APCI Mass Spectrum of 5 in MeCN with 1% HCl

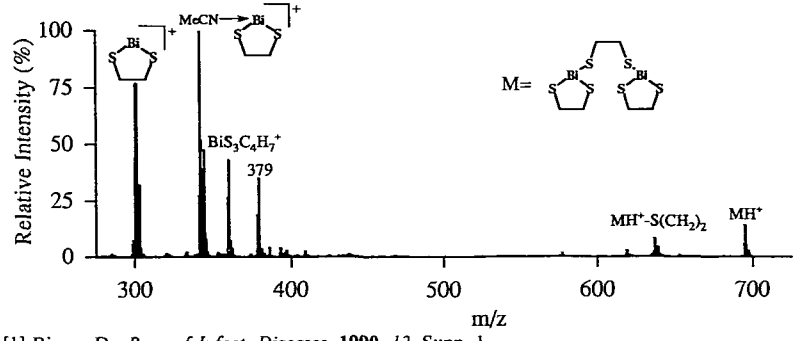

[1] Bierer, D.; *Rev. of Infect. Diseases*, **1990**, *12*, Supp. 1.
[2] Asato, E. et al; *Inorg. Chem.*, **1993**, *32*, 5322.

Comparison of ICR cells with open geometry

F. Kuhnen, I. Spiess, K.P. Wanczek
Institut für Anorganische und Physikalische Chemie,
Universität Bremen

The use of open endcap ICR cells became more pronounced the last years. In physical aplications the open endcap ion trap was implemented mainly because of its accessibility towards particle beams or lasers. Open endcap ion traps are interesting for all techniques where ions are injected into the trap. Closed and open cylindrical ICR cells are similar but also have some characteristic differences. The analytical expressions for the trapping potential of a closed cylindrical ICR cell and for the trapping potential of a cylindrical ICR cell with open endcaps are of the same form if certain boundary conditions are assumed. For closed cylindrical ICR cells the endcaps are set to a trapping voltage of V_t, while the cylindrical surface is set to zero. With these boundary conditions the trapping potential is found to be [1.]

$$V(\rho, z) = V_t \cdot \left(1 - \sum_{k=1}^{\infty} \frac{4 \sin(k\frac{\pi}{2})}{\pi k \, I_0(\gamma_k r_0)} \cos(\gamma_k z) \; I_0(\gamma_k \rho)\right) \qquad (1)$$

$$\gamma_k = k\frac{\pi}{L}$$

where L and r_0 denote the length and the radius of the cell. Open cylindrical ICR cells consist of a central excitation and detection ring of zero voltage, while the trapping rings at both sides are set to a trapping voltage V_t. This configuration is assumed to be periodic with a period of 2L. These boundary conditions lead to the trapping potential

$$V(\rho, z) = V_t \cdot \left(\frac{L - z_0}{L} - \sum_{k=1}^{\infty} \frac{4 \sin(\gamma_k z_0)}{\pi k \, I_0(\gamma_k r_0)} \cos(\gamma_k z) \; I_0(\gamma_k \rho)\right) \qquad (2)$$

where L and z_0 denote the half total length and the half length of the trapping ring of the ICR cell. Fig. 1 shows the potential well depth in dependence of the aspect ratio $2z_0 / r_0$ for various 21 mm radius open ICR cells of different ratio of $2L / r_0$.

The trapping potential can be expanded into polynomials of the form

$$V = V_t \sum_{k_{even}=0}^{\infty} C_k \left(\frac{r}{r_0}\right)^k P_k(\cos(\theta)) \qquad (3)$$

When (z_0 / L) equals 1/2 then an open ICR cell has the same representation in polynomials as a closed ICR cell. By appropriate choice of the trap dimensions, the potential can be shaped to achieve certain variations in the polynomial representation of the potential.
Open ICR cells are an extension of analytical applications in FT-ICR, since they allow the trapping potential to be taylored for certain purposes with the variation of the relative center electrode to trapping ring size. As the polynomial approximations of the trapping potential are valid only in the center of the cell, the full performance of these cells can only be used with some sort of ion cooling, especially the z motion has to be cooled, since a wide distribution of amplitudes of the z motion means also a wide distribution of radial electrical field. The excitation behaviour is sensitive towards the proportion of the inner excitation and detection ring so that an elongated arrangement shows less coupling of radial to axial excitation.

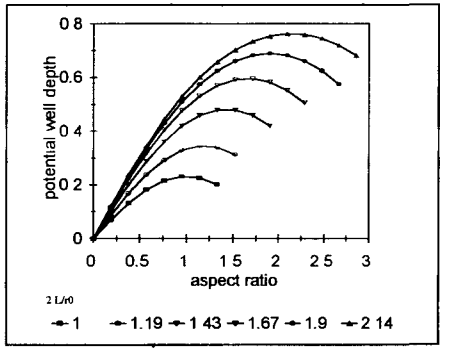

Fig. 3 potential well depth of a cylindrical open ICR cell vs $2z_0 / r$ for different ratio L / r_0 .

References

[1.] P. Kofel, Externe Ionisierung in der Ionen-Cyclotron-Resonanz-Spektrometrie, Dissertation, Bremen, 1987.

A comparison of fundamental principles and properties of ion traps

Peter Engelmohr and Karl Peter Wanczek
Institute of Inorganic and Physical Chemistry, University of Bremen
PO Box 330440, D-28334 Bremen, Germany

Magnetic traps

In magnetic traps ions are trapped by static magnetic (**B**) and electric fields (**E**) An ion moving with the velocity v in the presence of this fields **E** and **B** is subjected to the Lorentz force given by

$$F = m \cdot \frac{dv}{dt} = q \cdot \mathbf{E} + q \cdot v \times \mathbf{B} \qquad (1) \qquad\qquad \omega_c = q \cdot \mathbf{B}/m \qquad (2)$$

In a strong homogeneous magnetic field, ion motion in the x-y-plane assumes circular orbits with cyclotron frequency (ω_c) Equation 2 describes the fundamental relationship in ICR mass analysis.
Ion motion in the z-direction along the magnetic field lines is restricted by applying a continuous potential to trapping electrodes positioned at right angles to the magnetic field Ions oscillate in the potential with the trapping frequency (ω_t)

$$\omega_t = \sqrt{\frac{k \cdot q}{m}} \qquad \omega_{eff} = (\omega_c^2 + \omega_t^2)^{1/2} \qquad \omega_L = \omega_{eff} + \omega_m$$

Observed is an effective frequency ω_{eff} which is a superimposition of the frequencies ω_c and ω_t. One important consequence of the applied trapping field is the generation of a second form of radial motion in the cell, the magnetron motion (ω_m). The magnetron motion leads to new frequencies ω_L The cyclotron motion of the ion ensemble has a random phase With resonant energy absorption from an applied field to the side plates, the ions get into phase coherent cyclotron motion This motion induces an image current in the detection plates. This detected current is amplified, digitized and stored for data processing. Fourier transformation of the acquired signal yields a frequency spectrum in which the frequency of the peak is indicative of ion mass

Electric traps

A standard quadrupole ion trap consists of three hyperbolic isopotential surfaces The geometry of the device is described by the relationship $r_0^2 = 2 \cdot z_0^2$. In a normal mode of use an rf oscillating potential is applied to the ring electrode and zero to the end cape electrodes to generate a three-dimensional rotationally symmetric quadrupolar electric field.
For this field the motion of the ion can be expressed by Mathieu's second-order differential equation.

$$\frac{d^2u}{d\xi^2} + (a_u - 2q_u \cos 2\xi)\, u = 0$$

U represents the radial and axial coordinate axes, r and z respectively and ξ is a dimensionless quantity equal to $\Omega t/2$, Ω being the radial frequency of the alternating potential. The dimensionless parameters a and q are given by

$$a_z = -2a_r = \frac{-8eU}{mr_0^2\Omega^2} \qquad\qquad q_z = -2q_r = \frac{-4eV}{mr_0^2\Omega^2}$$

where V is the zero-to-peak amplitude of the rf-potential and U is the d.c potential. For a trapped ion, its trajectory must be stable both radially and axially. The stability of a trajectory can be portraited by a stability diagram. The values of β_r and β_z at any point in the stability diagram determine the frequency spectrum of stable ion trajectories, where β_u is a function of the parameters a_u and q_u The frequency

spectrum is given by

$$\omega_{u,n} = (n + \beta_u/2) \cdot \Omega \qquad n = -\infty, \ldots, -1, 0, 1, \ldots, \infty \qquad \omega_{u,0} = \beta_u \Omega/2$$

ω is defined as a secular frequency of nth order, for n = 0, the fundamental frequency is given by $\omega_{u,0}$
The form of the ion trajectory in the r,z plane has the general appearance of a Lissajous curve, with a superimposed micromotion of frequency $\Omega/2\pi$ (Hz)

Comparison:

	magnetic traps	**electric traps**	**combined traps**	**FT electric traps**
trapping field	static magnetic and static electric	r.f. oscillating electric	static magnetic and r f oscillating electric	r f. oscillating electric
excitation field	homogeneous, not coupled to trapping field	non-homogeneous, coupled to trapping field	non-homogeneous, coupled to trapping field	homogeneous, not coupled to trapping field
mass analysis	FT of image current transient	charge detection after ejection	charge ejection after ejection	FT of image current transient
mass range	1-10 MD with high resolution	100 kD with low resolution		1-10 MD with high resolution expected
resolution	up to 10^9	up to 10^6	up to 10^6	up to 10^9 expected
accuracy	1-10 ppm	1000 ppm		
sensitivity	10 ions with FT	1 ion with charge detection	1 ion with charge detection	10 ions with FT expected
scan time / amu	1 ms to 10 s	1 ms		
dynamic range	low	low	medium	low
ion detection	non destructive	destructive	destructive	non destructive
pressure range	very low pressure $<10^{-6}$ mbar	medium pressure $<10^{-3}$ mbar	medium pressure $<10^{-3}$ mbar	very low pressure $<10^{-6}$ mbar
damping gas	no with FT	yes	yes	no with FT
applied frequency range	1 kHz to 100 MHz for ion detection	1 MHz for ion trapping	1 MHz for ion trapping	100 Hz to 10 kHz for ion detection

A new structure for a FT Ion Trap used in electrical and combined mode

Peter Engelmohr and Karl Peter Wanczek
Institute of Inorganic and Physical Chemistry, University of Bremen
PO Box 330440, D-28334 Bremen, Germany

A ion trap with a **new electrode structure** for the generation of an exact three dimensional quadrupolar electric field will be presented In normal ion traps with hyperbolic electrodes it is not possible to generate an exact three-dimensional quadrupole electric field, because of the finite size of practical electrodes. Y Wang and K P. Wanczek (1) have shown that there exists other possibilities to generate such a field It can be generated by closed boundaries with continuously varied potential, in the ideal case by simple cone-shaped boundaries with linearly variable potential. Equation (1) is the general solution of an arbitrary curve of a three dimensional quadrupole field

$$\left[\frac{(dz/dr)r^2+2zr}{2r-4z(dz/dr)}\right]^2+\frac{1}{4}r^2-\frac{1}{\left[(r_0^2/\phi_{q0})b\right]^2}r^2(r^2+4z^2)=0 \qquad (1)$$

In the simplest case, with b=0, it follows that ϕ_q=const and from eq (1) hyperbolic isopotential surfaces are obtained (eq 2) This describes the classical Paul trap The second most important case is given by equation 3

$$r^2-2z^2=const \qquad (2) \qquad\qquad b=const=\frac{d\phi_q}{ds} \qquad \phi_q=bs \qquad (3)$$

Eq (3) corresponds to the potential values which vary linearly along the plane curves The plane curves are rotationally symmetric about the z axis and there exists a simple rhombic closed plane curve to generate a quadrupole field.

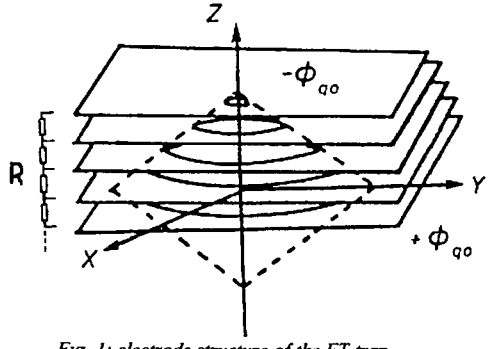

Fig. 1: electrode structure of the FT-trap

43rd ASMS Conference on Mass Spectrometry and Allied Topics

To build the cone-shape closed boundary with linearly variable potential, we constructed the new electrode structure for the generation of an exact three dimensional quadrupolar electric field To realize this, we use 13 metallic sheets of 0 5mm thickness with circular holes to form the inner surface of a cone To get exact circular holes in the electrodes they are burned with a laser into the metallic sheets The biggest hole in the middle has a radius of r_0 = 15 mm and the distance between the electrodes is 1 2mm

In a normal mode of use an rf oscillating potential is applied to the first, middle and last electrode to generate a three-dimensional rotationally symmetric quadrupolar electric field. Because of the symmetry of the device there are two electrodes with a zero potential, these can easily be used for detection. Within the cone shaped boundaries, an ideal homogeneous field in the direction of the symmetry axis can be generated and superimposed without interaction with the quadrupole field. This field can be used for excitation of the kinetic energy of the stored ions and this gives way to a detecting method which can be compared with FT-ICR mass spectrometers.

The motion of the ion ensemble has a random phase With resonant energy absorption from an applied field to the excitation plates (first and last electrode in fig.1 with 180^0 phase shift) the ions get into phase coherent ion motion. This motion induces an image current in the detection plates and the difference of the signals is formed for the transient This detected current is amplified, digitized and stored for data processing. Fourier transformation of the acquired signal yields a frequency spectrum with very high resolution in which the frequency of the peak is indicative of ion mass The great advantage of the recording of the transient is this non-destructive simultaneous detection procedure. Experimental studies with this new electrical FT trap are prepared

Results

In the first Experimental studies with this new electrical FT trap we used the trap as a normal ICR-cell to check the detection behavior of the new electrode structure

The first and last plates are used as trapping plates with 5 Volts and all the others are used for detection (to get a larger detection surface). The constant voltage traps the ions along the z-axes, and in the xy-direction the ions are trapped by the magnetic field of 7 02 T. With this geometry it is only possible to get a signal of the trapping motion v_z along the z-coordinate axis of the ions

It is not possible to detect the cyclotron motion because of the right angle between the motion of the ions and the detection plates. But we have done the experiment only to show that it is possible to store ions in this new trap. The trapping frequency of H_3O^+ ions with a frequency of 82 kHz has been measured. The total observation time of the transient is several milliseconds with the pressure of $1*10^{-8}$ mbar. The ions are created by electron impact ionization in the trap For the excitation a frequency sweep from 20 to 300 kHz within 1ms is used

The first experiment shows that it is possible to store and detect ions in this device The next steps will be to store the ions only with the quadrupolar electrical field and to use only two detection plates as it is described in this poster.

Another subject that need to be studied is the behavior of the new quadrupole FT-trap as a combined trap. This kind of a trap has large stability regions for positive and negative ions with large mass differences and also a trap with the advantage of non destructive ion detection with high mass resolution

Reference:

(1) Y Wang, K.-P. Wanczek, J Chem. Phys. 98 (1993) 2647

Characterisation of a Multi Purpose Open Endcap ICR Cell

I. Spiess, F. Kuhnen, K.P. Wanczek.
Institut für Anorganische und Physikalische Chemie,
Universität Bremen

Two different concepts of ICR cells with open endcaps are introduced. The ICR cells consist of a central trapping ring, two adjacent correction rings and two outstanding trapping rings. The "cubic" arrangement is compared with an elongated arrangement. In the "cubic" arrangement the length of the inner trapping ring and the correction ring equals the trap diameter (fig. 1). For the elongated arrangement the ratio of length of inner trapping ring and correction rings to the trap diameter is 4:3 (fig. 1).The centerline potentials of both cells are shown in fig. 2.
When the potential is expanded into polynomials of the form

$$V_t(\rho, z) = V_0 \sum_{k=0}^{\infty} C_k \left(\frac{\rho}{r_0}\right)^k P_k\left(\frac{z}{\sqrt{z^2+\rho^2}}\right) \qquad (1)$$

C_2 is the quadrupolar part of the trap potential which is a good aproximation of the trapping potential in the center of the trap. C_2 corresponds to the frequency shift of the trap like

$$\alpha = -\frac{C_2}{\pi r_0^2 B} \qquad (2)$$

where α is the frequency shift in Hz V^{-1}.
In a 7 Tesla magnet, transients of the ^{132}Xe Isotope are aquired. These are processed with Fourier transformation and magnitude calculation for different applied trapping voltages to analyse the slope of the reduced cyclotron frequency with respect to the applied trapping voltage. Relation 2 is then applied to calculate the experimental factor C_2 of the cell (Table 1). For the elongated arrangement, 3 different C_2 coefficients can be measured. The trapping can be achieved with the trapping rings set to V_t and the rest to 0 Volts, with trapping- and correctionrings set to V_t and the rest to 0 Volts and the correction rings alone set to V_t and the rest of the cell to 0 Volts.
The elongated arrangement is usefull for the simultaneous trapping of positive and negative ions, if a negative voltage is applied on the correction rings, while the trapping ring is held on a positive voltage.
It is obvious, that the theoretical and experimental C_2 values are different with a factor of approximately 2.5. This can be

explained with the flat part of the potential in the area of the trapping rings. In that region, there is a very low radial electrical field, so there is a contribution to C_2 of zero. Therefore the averaged experimental C_2 is smaller than the theoretical factor. To obtain the optimum performance, the z motion of the ions has to be cooled, to restrict the ion motion to that area of the cell, where the quadrupolar approximation of the trapping potential is valid.
An interesting feature is the simultaneous trapping of positive and negative ions, where the ion capacities of the potential wells can be tuned to match the intensities of positive and negative ions.

type of cell	frequency shift Hz V^{-1}	C_2 experimental	C_2 theoretical
cubic arrangement	-21.26	0.20677	0.3588
elongated arrange-ment	-16.56	0.0581, 0.1313*, 0.0559†	0.1767, 0.3151, 0.1384

Table 1 collects the frequency shifts, therefrom the experimental C_2 and the theoretical C_2. trapping via trapping rings and correction rings, † trapping via correction electrodes.*

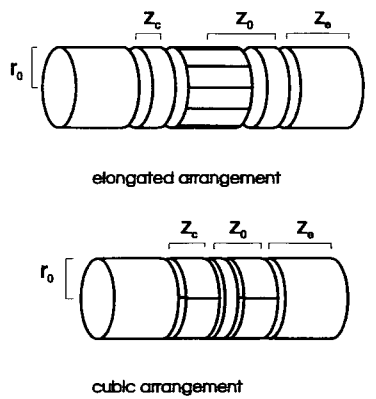

Fig.1 Trap layout and dimensions

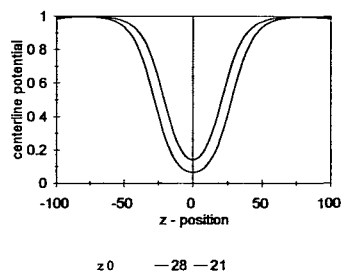

Fig. 2 Centerline potentials of the two open ICR cells.

Examples in Hierarchies of Optimally Triple Frequency Focused FTMS Cubic Traps

D. L. Rempel and M. L. Gross, Department of Chemistry, Washington University,
1 Brookings Drive, St. Louis, MO, 63130-4899

In the trap of a Fourier transform mass spectrometer (FTMS), unavoidable variations in cyclotron, magnetron and z-mode amplitudes are mapped to detected frequencies via an excitation event. In the normal cubic trap, this map is not constant resulting in degraded peak shapes which can be improved through compensation schemes in which the trapping electrodes are segmented with selected voltages applied to the segments. A theoretically determined first order triple frequency focusing scheme in which each trapping electrode has four segments has been shown [1].

First order triple frequency focusing is defined as follows. The Hamiltonian for a single ion was simplified by using a canonical transform computed by the Deprit perturbation series while in action-angle coordinates. The mode frequencies were obtained as a function of the action coordinates. The cyclotron frequency derivatives with respect to the cyclotron, magnetron and z-mode actions were computed at a fixed nonzero cyclotron-mode amplitude (in this case, 30% of maximum) while the magnetron and z-mode amplitudes are at zero. If the three derivatives are zero then we say that we have first order triple frequency focusing.

The first order triple focusing scheme that was shown in [1] is not unique. The three segment-separating radii in the example are free variables so that there is a solution for each reasonable combination of radii. Some solutions are clearly better than others. If one uses as a criterion of goodness the volume of mode amplitudes for which the frequencies do not deviate by more than, say for example, +/- 12.5 ppm then one can ask if there is an optimal combination of radii that maximizes the volume. Larger volumes are desirable to accommodate broader distributions of mode amplitudes. This is particularly important for the magnetron-mode amplitude distributions which become large at high mass.

The first order triple focusing schemes are also mass dependent. In the solutions computed so far, solutions computed at high mass show excellent behavior when evaluated at lower masses while the reverse is not always true.

A combination of radii that maximizes the mode-amplitude volume has been found at 10% of the critical mass. This solution is significant in that the linear size of the volume at 10% critical mass is about the same as the linear size of the volume at 1% critical mass for the first reported first order triple focusing scheme. The solution together with a frequency surface evaluated at 10% of the critical mass is shown in Fig. 1.

Other criterion may include the smallness of the magnitudes of higher derivatives of the cyclotron frequency with respect to the mode actions. One might consider the three second derivatives obtained from the three already used first derivatives differentiated with respect to the z-mode action as a predictor of good peak shape, for example, as an alternative to the volume criterion. The solution together with a frequency surface evaluated at 10% of the critical mass is shown in Fig. 2. A better peak shape is expected from the simpler surface and the solution is more practical because the electrode voltage ratios are lower. Also the solution was constrained so that the difference in consecutive radii was more than 2% of the trap size. Notice that the IZN, IMN, ICN sizes are almost as large as those acheived in Fig. 1.

Naturally, one is lead to seek the solution for which all six of the significant second derivatives are zero. This would be an example of a second order triple focused trap. One has been found for the case when the trapping plates have ten segments each. This solution is not unique because the nine segment-separating radii are free variables. If one considers additional criterion, an optimal second-order solution can be found...

Thus, by considering different combinations of criteria, hierarchies of optimal solutions are established.

43rd ASMS Conference on Mass Spectrometry and Allied Topics

[1] D. L. Rempel, C. L. Holliman and M. L. Gross, Proceedings of the 42nd ASMS Conference on Mass Spectrometry and Allied Topics, Chicago, IL, 1994, p 727.

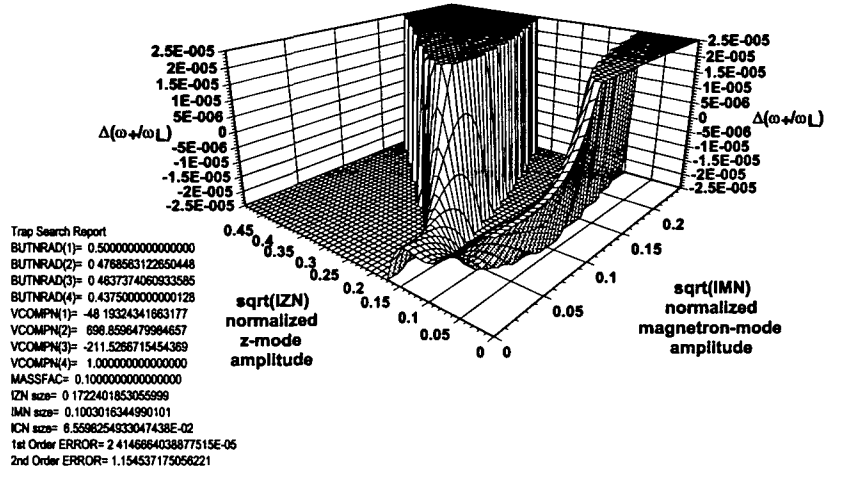

Fig. 1.

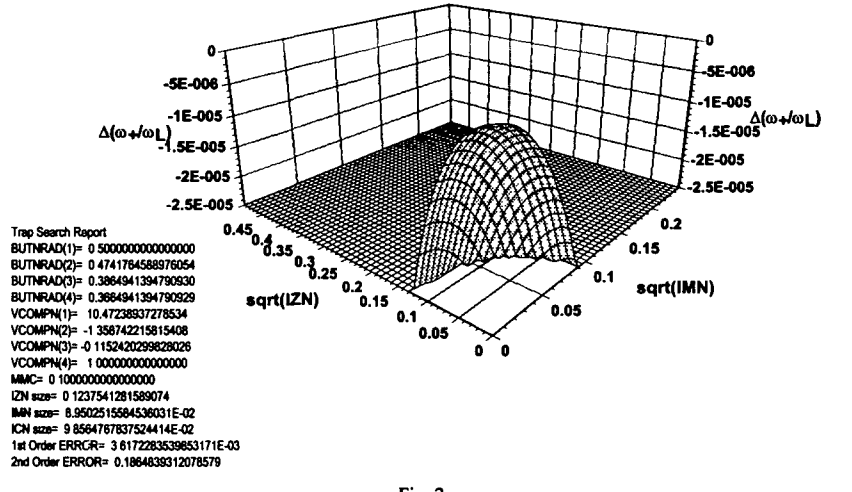

Fig. 2.

SHORT-BORE CONCENTRIC TUBE SOURCE FOR COUPLING HPLC TO ESI/FTICR

C.J. Harper*, J.J. Drader, V.L. Campbell, L. Stevenson, D.A. Laude
Dept. of Chemistry and Biochemistry, University of Texas at Austin, Austin, TX 78712

INTRODUCTION

Although there are several instrument designs in the literature for coupling liquid chromatography/electrospray ionization sources (LC/ESI) to quadrupole mass analyzers, there are few demonstrated for Fourier transform ion cyclotron resonance mass spectrometers (FTICR). The main obstacle to introducing any external ion source to an FTICR system is transportation of ions into the strong magnetic field while achieving low pressures in the detection cell for optimal FTICR performance. In overcoming this obstacle, many research groups have utilized a series of differentially-pumped vacuum stages that are separated by conductance limits. However, each stage of pumping adds more length to the source inlet, causing the ionization region to be positioned outside of the magnetic field. As a result, complicated ion focusing optics are needed to transfer the ions across the magnetic field gradient into the trapped ion cell. In order to overcome this problem, a concentric tube vacuum chamber has been developed which positions the ionization source within the magnetic field. This technique takes advantage of the magnetic field as a force to confine the radial motion of the ions making their transfer through the conductance limits more efficient. Further improvements have been made to this design by the addition of a mechanical shutter. The shutter, which covers a 5 mm conductance limit, is rotated away from the orifice during ion injection and then rotated over the orifice to block the flow of ions and neutrals to the detection region. Pressures for detection with the shutter closed are in the 10^{-9} Torr range, constituting a two order of magnitude drop in pressure.

The addition of the shutter has greatly enhanced the performance of our FTICR instrument. For example, the spectrum in Figure 1 shows the high resolution capabilities of the new shutter instrument. This spectrum is of the +14 charge state of horse heart myoglobin (MW = 16951 Da) and has a mass resolution of ~300,000 at 1233 m/z. Before installation of the shutter, mass resolution was limited to ~100 at 1233 m/z due to the high pressures in the analyzer cell. Furthermore, because a much larger conductance orifice can be used in the shuttered region, the sensitivity of this instrument has been enhanced by more than 40-fold. For example, spectra with a S/N of approximately 9 can be achieved with only 22 attomoles of bovine insulin and only 88 attomoles of horse heart myoglobin.

DEVELOPMENT OF SHORT-BORE ESI FOR CHROMATOGRAPHY

Because the concentric tube/shutter design offered higher sensitivity and better resolution than previous instruments, we decided to develop this instrument for use with on-line separation techniques. However, the long length of the electrospray probe needed to position the source within the magnetic field makes coupling this source to chromatography impractical. In particular, the probe length in the concentric tube design is 72 inches and an additional 36 inches of Teflon tubing is needed to connect the probe to the syringe pump for sample delivery. Therefore, the sample must pass through 9 feet of tubing before reaching the electrospray needle which results in greatly deteriorated chromatographic resolution. Consequently, a "short-bore" ESI source was designed and built as pictured in Figure 2. As shown, the probe length has been shortened to 12 inches. This was achieved by removing one stage of differential pumping and by shortening the length of the remaining stages to their practical limit. Nevertheless, when the shutter is closed, pressures in the detection region reached the mid-10^{-8} Torr. In addition to the shortened length, the design also includes a larger diameter probe. This was done so that, as shown in Figure 3, the separation column

could be easily placed within the probe thus further shrinking the distance from column to electrospray needle to less than 2 inches.

In order to evaluate the new short-bore instrument, flow injection experiments were first conducted to optimize shutter manipulation, data acquisition, and other factors. The data presented in Figure 4 represent a 1μL injection of 10 μM bradykinin, for which the +2 charge state was monitored, at a flow rate of 5 μL/min. Sample was delivered from the injector to the spray cavity by 10 feet of 0.007" I.D. polyether ether ketone (PEEK) tubing. This experiment emphasizes the loss of chromatographic resolution that results from passage through lengthy amounts of tubing. For example, the elution profile of this analysis is approximately 4 minutes long which corresponds to an elution volume of 20 μL; however, the injection volume was only 1 μL. Based on estimates of the area under the elution profile and calculations made from injection time, it can be shown that the spectrum in Figure 4a taken at time 13:64, the most intense part of the profile, consumed approximately 40 femtomoles of sample. By extrapolation, the amount of sample consumed in Figure 4b for time 15:52 (at the trailing edge of the profile) was only 7 femtomoles with a signal-to-noise ratio of 5. Because these spectra were not acquired under ideal conditions, it is expected that additional improvements to the instrument will increase the sensitivity making detection of attomole quantities routine. This preliminary data obtained from flow injection experiments shows that the short-bore design presented here is capable of achieving chromatographic analysis. However, further improvements to the current instrument should result in enhanced performance. For example, the installation of a cryopump in the analyzer region will reduce the pressures below 10^{-8} Torr for better mass resolution capabilities and a faster duty cycle. In addition, optimization of the instrument for compatibility with faster HPLC flow rates will be necessary.

Figure 1

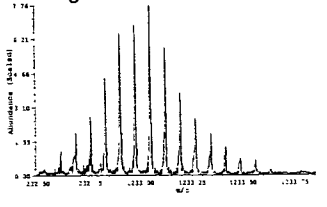

Figure 2

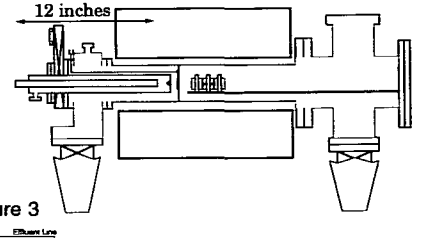

Figure 3

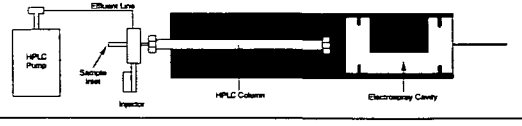

Figure 4

a)

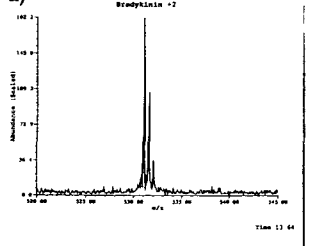

b)

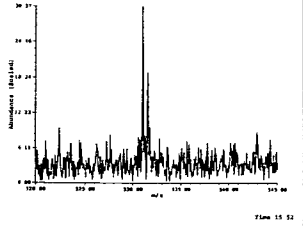

Observation of Collective Oscillation and Motional Averaging for Control of Magnetron Motion in FT-ICR V. H. Vartanian and D. A. Laude, The University of Texas at Austin, Austin, Texas 78712-1167

Collective oscillation and motional averaging of ions is observed in an open cell by virtue of the axially dependent radial electric field which reverses orientation The magnitude of the inward-directed radial electric field increases with axial displacement and acts concertedly with the Lorentz magnetic field. As ions are radially focused to the center of the cell during oscillation in the well, magnetron motion is reduced and cyclotron frequency increases. In experiments in which the ion axial amplitude increases, cyclotron frequency increases from the reduced to nearly the unperturbed frequency without peak broadening, indicative of coulombically-coupled axial motion. Modulation between the reduced and unperturbed frequencies is controlled by an axial cooling delay. A suspended trapping event maximizes the ion z-amplitude, increasing cyclotron frequency. Axial excitation is also used to promote coherent axial motion in the single-trap electrode open cell, and cyclotron frequency dependence on axial displacement is observed. Cyclotron frequency is observed up to 300 Hz above the unperturbed frequency in a nested trap. The magnitude of the frequency shift increases with ion number as space charge increases the axial extent of the ion cloud, allowing ions to spend more time in the inward-directed radial field.

A collection of trapped ions with a distribution of axial positions or amplitudes would be expected to encounter different average radial electric fields. During the detection process the ion ensemble would then exhibit cyclotron frequency peak broadening as a result of oscillation within the potential well. However, peak broadening does not occur as a result of z-axis oscillation since the trapping frequency is usually much greater than the magnetron frequency. Rather, motional averaging of the radial electric field during ion z-axis oscillation yields an average radial electric field that, while reducing cyclotron frequency, does not generate peak broadening [1-3]. If the ion z-amplitude or the radial displacement changes due to collisional damping of the axial motion or growth in the magnetron radius during the detection process, peak broadening results. Yet, even under experimental conditions likely to produce broadening, no variation in cyclotron frequency is observed. When detection immediately follows electron ionization at low pressure, ions are formed with a uniform distribution of z-axis amplitudes. Consequently, ions experience different radial electric fields in the trapping well, yet no peak broadening results.

The absence of peak broadening under typical experimental conditions can be attributed to the effect of coulombic-induced coupling between ions. Coupling has been observed in Paul traps for different ions in which the collective rather than the independent axial motions results in a single frequency resonance at intermediate position between two individual frequencies [4]. The strength of the coupling is a function of the number of ions and their difference in frequency. Coupling occurs even more strongly for ions of like mass. Coulombic-coupled cyclotron motion has also been observed in an FT-ICR cell [5].

Experiments were performed using a single-trap electrode and an open nested trapped-ion cell having four collinear trap electrodes, within a 3.00686 Tesla, 150 mm warm-bore superconducting magnet. Either benzene or dichloromethane were introduced through a precision leak valve and ionized with a 60 eV, 5 uA electron beam for 5 ms. Ions produced along the centerline of the cell experienced various radial electric field environments during axial oscillation in the cell. Cyclotron frequency was measured as a function of delay time to evaluate the effect of the radial electric field.

Cells with closed endcaps produce a radial electric field that is outward-directed at every position along the z-axis and is responsible for the destabilizing magnetron motion that results in eventual ion loss. However, in open cells, reversal of the radial electric field occurs at increased z-axis displacement. The radial electric field for the single-trap also exhibits a similar shift in orientation at increased z-amplitude. Ions with significant z-amplitude exhibit cyclotron frequency approaching the unperturbed frequency.

Presented in Figure 1 are a series of frequency shift profiles for ions formed in an open cell and allowed to cool to the center of the cell. For each of three trap potentials (3, 5, and 8 V), a 100 µs suspended trapping event is applied in which the trap electrodes are grounded during which time the z-amplitude of the ions increases. Trap potentials are then reinstated and the effective cyclotron frequency detected as a function of cooling delay. In this plot, ions having greater axial amplitudes are shaded increasingly darker. As ions undergo large z-amplitudes, a cyclotron frequency (591.607 kHz) close to the unperturbed cyclotron frequency (591.618 kHz) is detected, but as collisional cooling increases, ions collisionally relax to the center of the cell where cyclotron frequency decreases. The rate of cyclotron frequency decrease is a function of trap potential, as ions collapse more rapidly to the center of the cell.

In a more stringent test to verify that the observed shift in peak frequency is a function of axial position, peak position was measured as a function of axial cooling delays (D1-D3) at constant trap potential following consecutive suspended trapping events (S1-S3) for the same ion population. Presented in Figure 2 are frequency shift plots for three consecutive 100 µs suspended trapping events followed by 5 second cooling delays. Each suspended trapping event increases the reduced cyclotron frequency close to unperturbed frequency as the ion population undergoes a significant radial stabilizing force from the applied trapping field. Furthermore, the peaks do not exhibit broadening, indicating coulombic-coupling. Resonant excitation at the trapping frequency may also be used to axially expand the ion cloud, increasing cyclotron frequency (Figure 3). After the ion cloud is cooled to the center of the cell, excitation various excitation levels allows ions to penetrate the regions of radial stability at increased z-axis displacement.

An open cell can be constructed in which ions spend a greater time in the regions of the cell where the radial electric field works in concert with the Lorentz magnetic force. The potential well and radial electric field profile for a nested trap shown with outer trap electrodes biased to -6 V and inner trap electrodes biased to +3.5 V is shown in Figure 4, producing a shallow potential well. The shallow well increases the time positive ions spend in the inward-directed radial electric field at the well extremes at the expense of time spent in the center of the cell. The radial electric field at increased z-axis amplitude becomes increasingly inward-directed because of the effect of the negative bias on the outer trap electrodes. Negative ions or electrons trapped in the outer trapping wells also increase the cyclotron frequency of positive ions, as the negative ion space charge acts concertedly with the Lorentz magnetic force. In conventional closed cells, increasing ion number results in a linear reduction in cyclotron frequency. Cyclotron frequencies have been observed in the nested trap that surpass the unperturbed cyclotron frequency by up to 300 Hz, with the magnitude of the shift a function of ion number (Figure 5).

References:

1. Wang, T.-C. L.; Marshall, A G. *Int. J. Mass Spectrom. Ion Processes* **1986**, *68*, 287-301.
2. Chen, S.-P.; Comisarow, M. B. *Rapid Comm. Mass Spectrom.* **1991**, *5*, 450-455.
3. Chen, S.-P.; Comisarow, M. B. *Rapid Comm. Mass Spectrom.* **1992**, *6*, 1-3.
4. Jungmann, K.; Hoffnagle, J.; DeVoe, R. G.; Brewer, R. G. *Phys. Rev. Lett.* **1987**, *36*, 3451-3454.
5. Huang, J.; Tiedemann, P. W.; Land, D. P.; McIver, R. T.; Hemminger, J C. *Int. J. Mass Spectrom. Ion Processes* **1994**, *134*, 11-21.

Figure 1

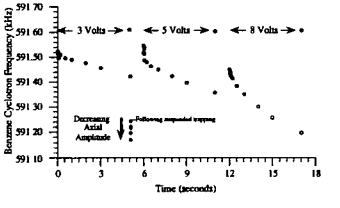

Figure 2

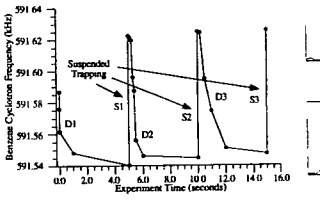

Figure 3

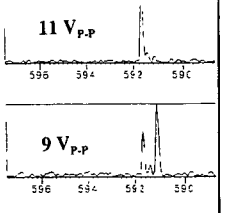

Figure 4

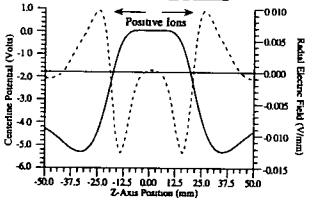

Figure 5

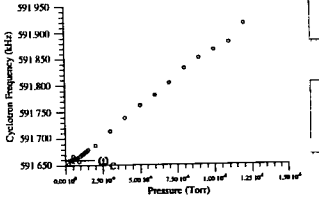

Investigations of Gas Phase Ion-Ion Reactions in an FTICR Trapped Ion Cell

*T.A. Torres, E. Stevenson and D.A. Laude
Department of Chemistry, The University of Texas at Austin, Austin, Texas 78741

The gas phase study of ion-ion reactions are investigated using Fourier transform ion cyclotron resonance (FTICR) mass spectrometry in a novel trapped ion cell that simultaneously confines both positive and negative ions (1). An open-ended cell geometry with twin, oppositely biased trapping electrode rings creates overlapping potential depressions to house both types of ions. In contrast with previous cell designs that were impractical for ion-ion studies, this cell does not promote ion quenching at the boundaries (2) and has a broad mass range for trapping. These attributes allow the low pressure reaction chemistry of positive and negative ions to be monitored over periods of several seconds. The study of reactions between ions of dissimilar charge magnitude are presented here. Specifically of interest are the reactions of multiply protonated electrospray ions with anions.

The open cell presented in Figure 1 is a variation of a shimmed cell design with two trapping electrode rings on either end of the interior excitation and detection electrodes (3). The cell was constructed of 0.030 in. thick x 2 in. i.d. OFHC copper tubing sectioned and mounted with aluminum cylinders. The total length of the cell was 75 mm with the excitation/detection electrodes 25 mm long, the inner set of traps 5 mm long, and the outer set of traps 16 mm long. All electrodes were separated by 2 mm air gaps.

An FTICR/ESI/LD/EI system used to perform all experiments. Briefly, the multi-electrode cell was mounted into a 3.0 T superconducting magnet controlled by an Odyssey based data station. A concentric tube network was used to interface the electrospray ion source to the spectrometer. A Nd:YAG laser operating at 1064 nm was used to generate laser desorbed ions at 1×10^{8} W cm^{-2} power densities. Electron ionization (EI) mass spectra were performed at 5×10^{-7} Torr and samples introduced to the system were ionized by a 3μA, -60 eV beam of 10 ms durations.

A potential well diagram using SIMION is shown in Figure 2. Here the potential depressions are produced by applying -5V to the outer traps and +5V to the inner traps. Two separate potential wells for positive and negative ions are formed. Nested within the negative depression is a central positive well formed by the application of the positive voltage to the inner pair of electrodes. The two small potential lobes form two regions into which negative ions are trapped. Variations in the potential well depth can be achieved by altering the applied potentials. The positive, negative, and combined EI mass spectra of chloroform are presented in Figure 3. These spectra indicate that the trap provides a stable environment for each type of ion.

The type of ion-ion reactions of interest are those that generate charged product ions rather than a neutralized product. Specifically, the reaction of the multiply charged protein, melittin, generated by electrospray ionization with laser desorbed metallic gold ions was studied. The melittin ions were sprayed into the laser desorbed plasma of negative gold ions. The inner trap plates were set at potentials of -0.15V and the outer traps to +4.0V. More definitive information can be drawn about charged product formation by examining relative abundances of the bare ions and product ions as the reaction time is raised. The decreasing

abundances of both the melittin (4+) and the gold (1-) ions after 1 and 20 second reaction delays indicate a loss of reactant ions. Additionally, the formation of a charged product of increasing abundance at 263 m/z seems to indicate that melittin (4+) ions have undergone reaction with gold ions.

A more extensive study of the ion-ion chemistry of proteins with metals is planned. In addition, the reactions of organic anions with proteins can be investigated with the incorporation of quadrupolar excitation (QE). QE has proven to be an effective means of axializing an ion of specific m/z. This will enable us to selectively isolate reactant ions for enhanced control of product formation.

References

(1) V.A. Vartanian and D.A. Laude, *Org. Mass Spectrom.* **29**, 692-4 (1994).
(2) Y. Wang and K.P. Wanczek, *Rev. Sci. Instr.* 64, 883 (1993).
(3) G. Gabrielse, S.L. Rolston, L. Haarsma, W. Kells, *Phys. Lett. A* **129**, 38 (1988).

Figure 1

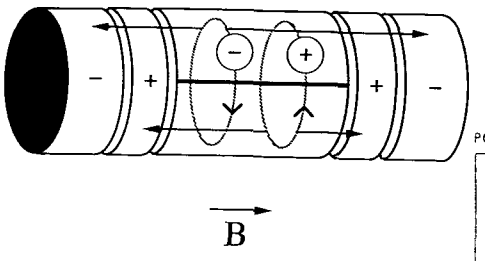

Figure 2

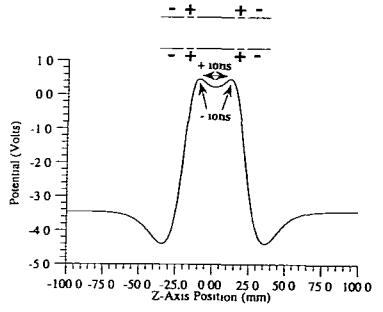

Figure 3

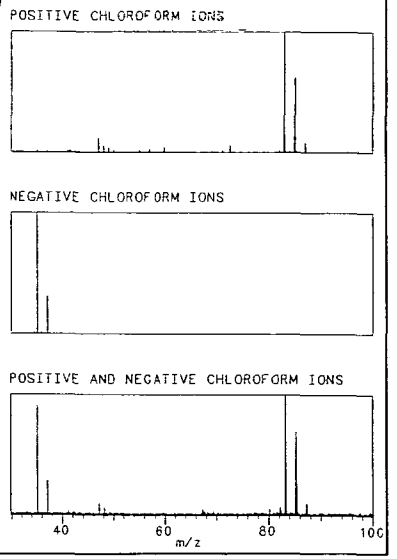

FTICR/TOF for Measuring Large Ion Populations in Penning Traps

E.G. Schmidt and D.A. Laude
The University of Texas at Austin, Austin, Texas 78712-1167

The ability to evaluate the evolution of an ion cloud stored in the trapped ion cell over the course of an FTICR experiment is important when developing new analytical instrumentation and methodologies. Especially when evaluating ion populations formed under high space charge conditions or in non-ideal regions of the trapped ion cell, FTICR detection itself provides limited or suspect information because of dynamic range constraints or inappropriate parameter selection.

To be presented are results from the construction of an FTICR with time-of-flight detection that permits a more detailed evaluation of spatial and kinetic energy distributions for ions formed under non-ideal conditions. As a first example, laser desorbed metals formed under plasma ignition conditions and allowed to cool in the trapped ion cell are evaluated. The ability of quadrupolar excitation (QE) to assist in shaping the ion cloud for detection is considered.

Experimental

A 4.7 Tesla vertical bore superconducting magnet with 98 mm originally employed for NMR was reconfigured to accommodate an FTICR vacuum chamber. Laser desorption was used to create the desired ion populations. A 1.4 m time-of-flight path to an electron multiplier (ETP, Auburn, MA) supported above the superconducting magnet was created. This added flight length was necessary in order to operate the detector. Time-of-Flight spectra were collected using a digital oscilloscope. Quadrupolar excitation (QE) was accomplished using an external relay circuit to rapidly switch between quadrupolar and dipolar excitation.[1]

Conventional FTICR data was acquired using broadband swept excitation following ionization and a cooling delay. During this delay, a pulsed valve could be opened to introduce buffer gas to 1×10^{-5} Torr to perform quadrupolar excitation (QE). A potential of up to 70 V could be applied to the rear of the cell to direct ions to the detector

For all laser desorption measurements, indium foil was used as the sample. 1064 nm light for a Nd:YAG laser was introduced through a fiber optic and was incident on the sample with a laser fluence of 1×10^{8} W/cm^2, sufficient to promote plasma ignition conditions. All of the TOF profiles were generated as a summed average of 10 laser shots.

TOF OF TRAPPED LASER DESORBED IONS

The profiles in Figures 1 and 2 are for time-of-flight of In^+ trapped in the ICR cell for 10 ms and 10 s cooling times, respectively, with a 2 V trapping potential. In Figure 1a, ions trapped in the cell for 10 ms arrive at the detector in 700 µs, which corresponds to a kinetic energy of 2.4 eV. In Figure 2a, even after a 10 s cooling delay, a bimodal distribution is still observed even though the 1.7 ms flight time indicates ions have been cooled to 0.41 eV. Figures 1b and 2b include a +70 V pulse applied to the rear trap electrode to direct the ions to the detector. Similar profiles in both cases indicate that ions are retained in the trap and can be detected by TOF even when ion energies in the cell are insufficient to direct ions to the detector.

QE OF TRAPPED LASER DESORBED IONS

Presented in Figures 3 - 4 are TOF profiles for laser desorbed In^+ initially trapped in the ICR cell and subjected to various cooling delays. The profiles are for cooling delays of 100 ms and 1 s, respectively, in a 70 V trapping well. The signal is substantially degraded, likely due to an increase in the radial extent of the ion cloud due to magnetron effects. Figures 3b and 4b are

for conditions identical to those shown in Figures 3a and 4a, with the exception that a QE cooling delay replaces the simple cooling delay event. As the profiles indicate, QE serves two functions, both in reducing the axial extent of the ion cloud resulting in a narrower TOF profile in Figure 3b, and dramatically reducing the radial ion distribution, thus significantly increasing the intensity of the TOF profile in Figure 4b.

CONCLUSION

Although FTICR instruments have the ability to trap large ion populations, the resulting signal is not linear under high space charge conditions even at small trapping potentials. The use of FTICR/TOF alleviates this problem by detecting the ion signal on an external electron multiplier which has a large linear dynamic range thus allowing for the evaluation of different ion trapping techniques. It has been shown in these studies that quadrupolar excitation is a successful method for cooling of externally injected ions to the center of the trapped ion cell

In the future, an electron ionization (EI) source will be added which will provide more control over initial ion formation as well as allowing more quantitative measurements to be made.

1. Speir, Paul J., Gorman, Greg S., Pitsenberger, Cynthia C., Turner, Cheryl A., Wang, Ping R., Amster, Jonathan I., Anal. Chem. 1993, 65, 1746

Figure 1

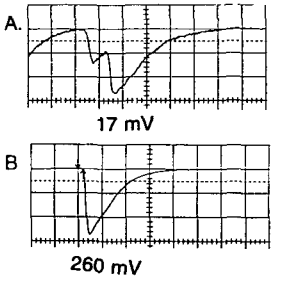

Figure 2

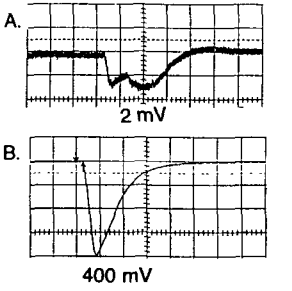

Figure 3

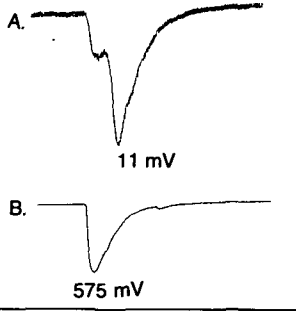

Figure 4

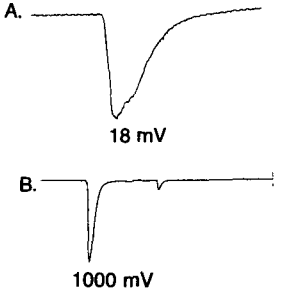

Improved Ion Injection in a Single-Trap Electrode Cell for FTICR

J. S. Anderson*, T. A. Torres, V. H. Vartanian, Department of Chemistry and Biochemistry, University of Texas at Austin, Austin, Texas 78712

A distinct advantage of the open geometry trapped-ion cell is the relative ease of external ion injection without complications arising from electrode charging and ion trajectory perturbations characteristic of the closed-cell geometry. Coupling this advantage with the inherent flexibility of open geometry construction leads to a unique trapped ion cell with a single trapping electrode at the cell center. Absent in this cell design is the presence of an electrostatic barrier predominant in both conventional closed and open cells. Instead, a potential depression is formed into which ions of any initial kinetic energy may descend and potentially be trapped. Previously employed for FTICR feasibility studies with electron ionization and low molecular weight compounds[1], the single trap electrode cell is used here to probe trapping mechanisms for externally generated laser-desorbed ions and contrast the results with similar experiments in conventional geometry cells.

Experiments were performed in a 3.0 Tesla superconducting magnet with a modified Extrel-FTMS dual cell assembly. This particular arrangement consisted of a 5.0 cm closed cubic cell and the single-trap electrode cell. Laser desorption experiments included MALDI of small proteins and IRLD to allow cation-attachment of similarly sized molecules. For the MALDI process, laser light from a nitrogen laser at 337 nm (Laser Science, Inc., Cambridge, MA) is focused into a 200 μm. all-silica fiber optic (General Fiber Optics, Inc., Fairfield, NJ) and directed onto a probe tip with matrix (2,5 Dihydroxybenzoic acid) and analyte. Laser experiments conducted with IR light employed a Nd:YAG Surelite 1 laser (Continuum, Santa Clara, CA) operating at 1064 nm.

The methodology of trapping externally generated ions is fundamentally different in the single-trap electrode cell from all conventional FTICR cells. As shown in Figure 1a, efficient introduction of ions in a two-trap electrode cell using accumulated trapping requires the ion to have translational kinetic energies sufficient to overcome the potential barrier projected at the front trap electrode. The distinction from conventional cells with terminal trap electrodes is that both gated and accumulated trapping mechanisms are represented simultaneously in the single-trap electrode cell. All ions, regardless of their kinetic energies, will be able to penetrate the trapping volume in the single-trap electrode cell. The same ion in Figure 1a will readily penetrate the negatively biased potential depression shown in Figure 1b, and potentially be trapped.

One theory behind cation-attachment of neutral molecules is that precursors, such as K_2Br^+, attach to neutral molecules, M, to form $(M+K)^+$. Overall, the trapping process is dependent on ion kinetic energy and the applied trap potential, with only certain ions being able to enter conventional cells at a fixed trap potential. In contrast, the single-trap electrode cell provides a different set of conditions for trapping $(M+K)^+$ ions. The combined nature of accumulated and gated trapping allows $(M+K)^+$ ions of low kinetic energies to enter the cell and be trapped. Consequently, as a first order approximation, this trapping process is integral in that all ions may enter the cell and be trapped without exclusion of lower kinetic energy ions.

Experimental results for trapping $(M+K)^+$ gramicidin S ions are shown in Figure 2. As discussed above, the single-trap electrode cell is shown to be efficient at trapping low energy ions with negligible ion loss. Demonstrated for the cubic cell is the derivative trapping characteristic of all conventional FTICR cells.

The conventional method for trapping MALDI/FTICR ions is gated trapping with a decelerating potential applied to the rear electrode[2]. Precise timing of the gated trapping event is required to prevent repulsion of ions by the applied decelerating potential. Trapping mechanisms in the single-trap electrode cell are inherently different from its conventional two-trap electrode counterpart. First, the possibility of accumulated trapping exists because of the absence of a potential barrier at the cell entrance. In addition, the injection period of MALDI ions is not limited by the presence of any decelerating potential as with conventional cells. Shown in Figure 3 is a comparison of injection profiles for both cubic and single-trap electrode cells where accumulated trapping occurs in the single-trap electrode cell. Alternative gated trapping schemes may also be employed in the single-trap electrode cell for MALDI generated ions. Shown in Figure 4a-d are three types of gated trapping along with accumulated trapping for external ions.

The integrative trapping, characteristic of combined accumulated and gated trapping, within the single-trap electrode cell exhibits novel trapping of externally generated laser desorbed ions. Low energy thermally desorbed ions, which experience kinetic energy discrimination in conventional two-trap electrode FTICR cells, can penetrate the potential depression formed by the single-trap electrode cell without energy discrimination. In addition, MALDI ions injected into the single-trap electrode cell do not experience the same electrostatic repulsion that occurs during conventional MALDI gated trapping. As a result, ions experience a longer injection duty cycle in the single-trap electrode cell. Lastly, unit mass resolution has been achieved in the single-trap electrode cell with small proteins such as gramicidin S.

1 Vartanian, V. H., Laude, D. A., accepted for publication, JASMS, (1995).
2 Castoro, J. A., and Wilkins, C. L., Anal. Chem. 65, (1993) 2621-2627.

FIGURE 2

1a Conventional Open Cell

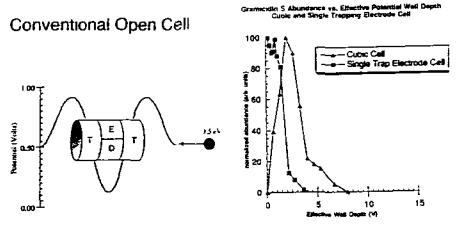

FIGURE 3

1b Single Trap Electrode Cell

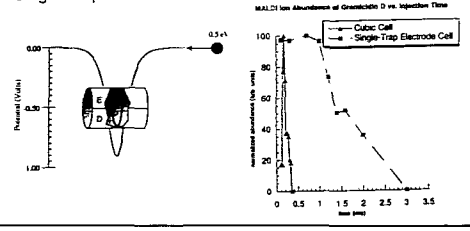

FIGURE 4

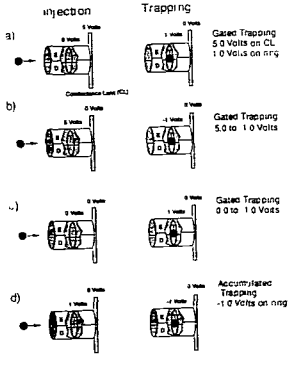

Quadrupolar Excitation Efficiency in Non-Ideal FTICR Trapped Ion Cells

J.J. Drader, C.L. Hendrickson, J.M. Robinson and D.A. Laude, Jr.; Department of Chemistry and Biochemistry, University of Texas at Austin, Austin, TX 78712

Quadrupolar excitation is being used increasingly in FTICR-MS as a technique for improving the quality of the ion population stored in a trapped ion cell. As the name of the technique implies, the axialization of the ion cloud is optimally achieved in regions of the cell subject to a pure quadrupolar potential. Thus a potential problem with the technique is that in cells without hyperbolic geometry, the QE process will not be effective in cooling the ion cloud. Fortunately, the potential at the center of all trapped ion cells is to some degree quadrupolar.

The purpose of this poster is to determine to what extent QE and related procedures will work under non-ideal conditions. The premise will be that rather than construct a cell geometry that is optimized for QE at the expense of analytical utility, the applied fields can be modified. To perform the work, an elongated open cell which is ideally suited for external ion injection, but not optimized for QE, will be employed. A collection of cooling experiments will be investigated to determine the conditions under which axialization of the ion cloud is feasible.

The experiments were performed on a 3 Tesla concentric tube electrospray equipped with a 2.5 inch diameter open elongated cylindrical cell. Concentric tube pumping combined with a mechanical shutter reduced the pressures in the analyzer region to 1 x 10^{-9} Torr. Argon gas was pulsed in the cell at a pressure of 5 x 10^{-5} Torr during axialization. A switching circuit was employed to convert between dipolar and quadrupolar excitation modes. The data was collected and processed with use of an Odessey data station, however, it was necessary to employ a PC based data station to continuously output waveforms for broadband quadrupolar excitation.

Quadrupolar excitation is conventionally applied to two pair of opposed electrodes, however, it has been shown [1] that QE can be simplified by applying the excitation to only one pair of opposed electrodes. All of the following data has been collected with the two plate configuration.

One of the advantages of coupling electrospray ionization with FTICR is the ability to obtain isotopic resolution on large proteins. A difficulty that arises when collecting high resolution data is overcoming space charge effects associated with a large population of ions spread over a range of charge states. Following an initial excitation/detection of horse heart myoglobin (MW = 16,951 Da), QE was used to axialize the +14 charge state. A 40 second pump down delay allowed system pressures to reach 2 x 10^{-9} Torr. A high resolution spectrum was obtained by applying a second excitation followed by high resolution detection. The resulting charge state was isotopically resolved with a resolution of 300,000.

Typically, a perfect quadrupolar field is desired to facilitate ion axialization. However, in an actual ion trap the field deviates from a pure quadrupolar potential. Bollen et. al. [2] have shown that there can be a significant quadrupolar component associated with dipolar excitation. Following an initial scan of horse heart myoglobin, dipolar excitation was applied to selectively cool a charge state . The excitation profiles in Figure 1 illustrate the quadrupolar component of the dipolar field diminishes as the ions approach the cell center.

Bollen et. al. also predict that axialization should be facilitated by application of an octupolar field (twice the cyclotron frequency). Such a field should be present as a non-ideal component of the azimuthal quadrupolar field. This was confirmed by isolating one charge

state of horse heart myoglobin after applying such a frequency. The excitation profile in Figure 2 confirms that the octupolar component only exists significantly at the cell perimeter.

The ability to cool over an arbitrary mass range is essential in realizing the full analytical utility of axialization. The coupling of quadrupolar axialization with SWIFT excitation has been shown to be ideal in achieving this result [3]. As an example, Figure 3 shows a remeasurement of horse heart myoglobin after applying a 4 second SWIFT quadrupolar excitation. This remeasurment yielded a larger abundance than the original scan. It should be noted that remeasurement in the absence of axialization was unsuccessful at the large excitation radius used.

The selectivity afforded by the SWIFT technique is demonstrated by the spectra in Figure 4 which shows selective axialization. An overlay of the SWIFT waveform used for axialization shows the requested quadrupolar excitation amplitude.

Trapped ion cells typically used in FTICR experiments are incapable of producing perfect excitation fields and instead produce fields which are composed of a linear combination of higher order components. In this work these multipole components are evaluated in an open cylindrical cell. These results indicate that a pure azimuthal quadrupolar field is unnecessary for performing efficient ion axialization and that the higher order fields can also be used to cool ions to the cell center.

References

1. C. L. Hendrickson, J. J. Drader, and D. A. Laude, Jr., J. Am Soc. Mass Spectrum. In press.
2. G. Bollen, R. B. Moore, G. Savard, and H. Stolzenberg, J. Appl. Phys., 68 (1990) 4355.
3. S. Guan, A. G. Marshall, and M. Wahl, Anal. Chem., 66 (1994) 1363.

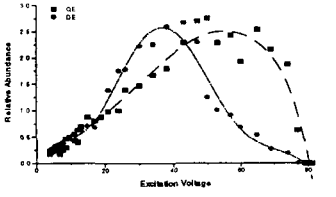

Figure 1

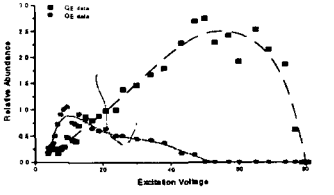

Figure 2

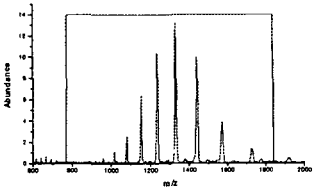

Figure 3

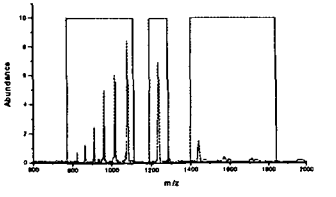

Figure 4

MALDI/FTICR Using Quadrupolar Excitation in a Single Trapped Ion Cell

J. S. Anderson*, and D. A. Laude, Department of Chemistry and Biochemistry, University of Texas at Austin, Austin, Texas 78712

In recent years, MALDI ionization coupled with FTICR detection has demonstrated continued progress and versatility for many different experiments[1-3]. The recent development of quadrupolar excitation[4] (QE) for motional conversion and ion cooling has lead to still improved ion trapping and detection efficiency of MALDI generated ions. Many of these applications employ very homogeneous (100 ppm over the cell volume) high magnetic fields with dual cell arrangements or electrostatic ion guides for efficient ion transfer and optimum performance. In work presented here, we employ QE to facilitate high performance FTICR with a single trapped ion cell in a low homogeneity 7.2 Tesla magnet. Theoretical discussions are made concerning the deleterious effects of gradient (ΔB) magnetic fields on premature ion loss from the trapped ion cell. In addition, our results indicate that the analytical utility of a low homogeneity magnet relies on the use of quadrupolar excitation to help localize and entrain ions inside the cell.

Laser light employed for MALDI ionization is transferred by fiber optic through a probe interface to the matrix/analyte sample. A nitrogen laser using light of 337 nm (Laser Science, Inc., Cambridge, MA) transmits energy of 40-50 µJ through the fiber onto the sample surface. Various proteins are mixed with an abundance (1000-5000/1 molar ratio) of 2,5 dihydroxybenzoic acid for the final sample composition.
All MALDI experiments were controlled by Odyssey V3.1 (Extrel-FTMS, Madison, WI) software. Following the pulse gas and laser event, application of QE for a variable time period is followed by a cooling delay and subsequent dipolar excitation and detection. All experiments were done in a 1.00" closed cylindrical OFHC copper trapped-ion cell.

A major point of experimental concern is the effect of axial magnetic inhomogeneity on overall FTICR performance. In our particular magnet, the field homogeneity is 1 ppThousand over 1 cm DSV with 7.2 Tesla at the cell center and approximately 7.16 Tesla at the trap electrodes. Prior studies of magnetic field inhomogeneities have focused on cyclotron frequency shifts[5] and low energy ion injection[6] in regions of magnetic field gradient. In these studies, ions experience a much greater axial magnetic field inhomogeneity within the cell volume than previously used for high performance FTICR studies. These field gradients are detrimental for achieving high sensitivity and high mass resolution.
In a constant magnetic field, ions oscillate along the z-axis centerline with constant radius and velocity and cyclotron frequency are position invariant. In the curved magnetic field representation, the first order approximation of ion motion can be understood as follows[7]. Ion radius along the z-axis will change with axial position and radial velocity and cyclotron frequency are position dependent. Such inhomogeneity causes ion loss and deterioration in resolution.
In a homogeneous magnetic field, externally generated ions spiral around magnetic field lines and are focused directly along the z-axis centerline into the trapped-ion cell. This spatially defined packet of ions typically encounters negligible ΔB gradients in an FTICR cell. Ion loss usually occurs due to effects of electric field perturbations. In our case, MALDI ions injected through the initial mesh trap electrode are not confined radially along the z-axis and as a result are not adequately defined energetically or spatially. Such ions experience greater electric field inhomogeneities at the cell boundaries, greater ExB forces, and are prematurely lost from the cell.

Plots of normalized bovine insulin b chain ion abundance versus delay time between laser firing and quadrupolar excitation application are shown in Figure 1. In plot a) it is readily observed that ion signal decreases rapidly in the 7.2 Tesla magnet without immediate QE. The plot in b) represents an identical experiment in a homogeneous 3.0 Tesla system. Here, ΔB gradients are not a factor and retention of ions is not immediately dependent on QE application.

In prior experiments without application of QE, MALDI ions up to the mass of bovine insulin could be effectively trapped. However trapping times and ultimate mass resolution were severely limited ($m/\Delta m$=3000-4000 at m/z 1600). Employing QE, increased trapping time, a 75-100 fold increase in signal-to-noise, and mass resolution far above unit mass resolution for proteins up to bovine insulin b chain have been achieved. In Figure 2, the duration of QE application is shown to be important for resolving the sodium and potassium attached adducts of gramicidin D. In our experiments, application of QE for more than 3-4 seconds is needed for optimum resolution. In Figure 3, the QE selectivity is shown as the QE is adjusted to give both different isotopes and adducts of gramicidin D. In many cases, single isotopes can be selected for subsequent excitation/detection. Mass resolution for each of these spectra is approximately 15,000 for all isotopes and adducts. Maximum mass resolution to date for single isotopes is 30,000 for gramicidin D and 7,000 for bovine insulin b chain.

1. J. A. Castoro and C. L. Wilkins, Anal. Chem., 65, (1993), 2621-2627.
2. J. A. Marto, S. Guan, and A. G. Marshall, Rapid. Comm. in Mass Spec., 8, (1994), 615-620.
3. R. T. McIver, Jr., Y. Li, and R. L. Hunter, Rapid. Comm. in Mass Spec., 8, (1994), 237-241.
4. L. Schweikhard, S. Guan, and A. G. Marshall, Int. J. Mass Spectrom. Ion Processes, 120, (1992), 71-83.
5. D. W. Mitchell, A. L. Rockwood, and R. D. Smith, Int. J. Mass Spectrom., 141, (1995), 101-116.
6. E. L. Kerley, C. D. Hanson, M. E. Castro, and D. H. Russell, Anal. Chem., 61, (1989), 2528-2534.
7. J. D. Jackson. "Classical Electrodynamics", 2nd. ed., (1975),

FIGURE 1

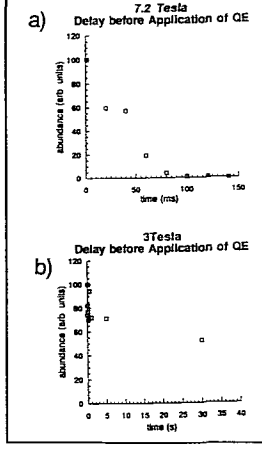

FIGURE 2

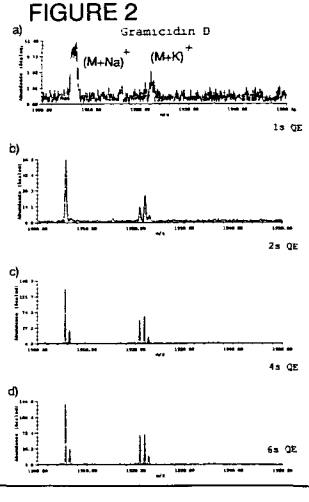

FIGURE 3

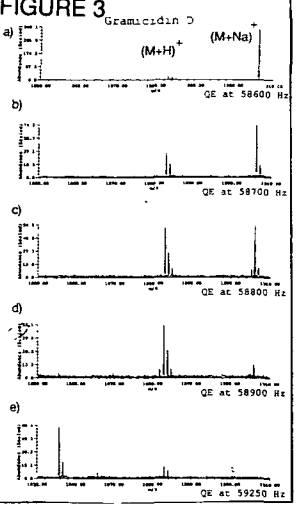

ESI/SORI/FTICR Analysis of Protein Dissociation Pathways and Reactivity to Probe Structure

V. L. Campbell*, B. J. Bolanos, and D. A. Laude
Department of Chemistry and Biochemistry,
The University of Texas at Austin, Austin, TX, 78712

INTRODUCTION

Electrospray mass spectrometry (ESI/MS) is a fast, efficient and versatile method of obtaining information that the biochemist seeks: primary amino acid sequence and protein conformation, as well as determining the location of reactive sites along the peptide backbone. Structural characterization of proteins by mass spectrometry is often carried out using fragmentation processes, such as sustained off-resonance irradiation (SORI), collision cell or nozzle-skimmer dissociation. The purpose of this work is to evaluate how these techniques may be exploited further to provide conformational data, as well as identify and locate reactive amino acid residues along the peptide backbone.

Several approaches are explored. Energy-dependent fragmentation pathways are evaluated for the SORI fragmentation process. Fragmentation pattern is studied as a function of charge state as a means of evaluating protein conformation. Proteins are treated with site-specific reagents to produce covalently-bonded adducts, which are then fragmented to locate the site of reaction.

INSTRUMENTATION

All spectra were obtained with a 3.0T FTICR mass spectrometer with four differentially-pumped concentric vacuum chambers coupled to a Chait-type electrospray ionization source. The spectrometer included a 6" diameter bore magnet into which the vacuum chamber was inserted. Two-plate quadrupolar excitation (QE) was applied during the accumulated trapping event to exclusively trap ions at the m/z value of interest for further study. Once such ions had been isolated, a single frequency excite was applied 1500 Hz off-resonance for a period of 1.5 seconds. Peak-to-peak voltage was increased until sufficient energy was deposited to surpass the fragmentation threshold. Argon was pulsed into the cell at a pressure of 2 x 10-5 torr during the QE and SORI events.

ENERGY-DEPENDENT FRAGMENTATION PATHWAYS

Nozzle-skimmer dissociation has been used extensively to fragment biomolecules prior to mass analysis. It is well documented that proline residues are the predominant site of fragmentation due to their inherent rigidity. The proline bond strain results in direct cleavage when the molecule encounters the high-energy collisions of the nozzle-skimmer region. However, SORI provides a mechanism that favors low-energy dissociation pathways.

Yeast ubiquitin was fragmented using SORI to determine if proline residues would be the predominant site of fragmentation as in the case of nozzle-skimmer dissociation. Surprisingly, only one, low-abundance proline (Pro) cleavage was observed, whereas aspartates (Asp) and glutamates (Glu) appeared to be the dominant fragmentation sites. The dominance of acidic residue rearrangement over proline cleavage can be explained by evaluating the fragmentation pathway as a function of energy deposition. At lower energies the rearrangement process occurs but the cleavage does not. However, once the energy threshold for cleavage is achieved, the cleavage mechanism occurs at a faster rate than the rearrangement process. Angiotension II was chosen as a model compound because it has one aspartic acid and one proline residue. Figure 1 demonstrates the energy-dependence upon site of fragmentation. At low energies, no fragmentation occurs. In contrast, just above the fragmentation threshold, aspartic acid fragmentation is more abundant than proline cleavage. As the energy increases, the proline cleavage becomes more favorable until it becomes the dominant fragmentation pathway.

FRAGMENTATION PATTERN AS A FUNCTION OF CHARGE STATE

If all charge states fragmented alike, this would suggest that either all the charge states had an identical conformation or that the internal energy from SORI disrupts conformational interactions as well as peptide bonds. However, the spectra of melittin in Figure 2 indicate that charge states exhibit different fragmentation patterns. This change in location and abundance of fragmentation for different charge states may be due to coulombic repulsion effects or the dissociation of different gas-phase conformations. If Coulombic repulsion is the cause, then more fragmentation should occur as the number of charges on the molecule increases. However, this is not true for melittin; fragmentation decreases as charge state increases. Therefore, variations of gas-phase conformation with charge state may be responsible for the different fragmentation patterns.

EVALUATION OF SITE REACTIVITY AND LOCATION

The basic goal of protein chemistry is to relate specific structural features of biomolecules to their physical, chemical, and biological properties. Recently, "active-site-directed" reagents have been designed to react preferentially with only those parts of protein molecules that are physically in the vicinity of particular biochemically active sites. ESI/SORI/FTICR analysis of these chemically modified proteins would provide a quick and efficient method of determining the location of reactive residues along the peptide backbone.

To provide a simple demonstration of this technique, acetone was added to an aqueous solution of yeast ubiquitin, later followed by the addition of methanol and acetic acid. Reaction between the free amine sites of the protein and the carbonyl carbon of acetone produces a Schiff-base. The -C=N- bond formed is sufficiently strong to survive the ion dissociation process and each Schiff-base increases the molecular weight by 40.06 Da. Figure 3 presents the SORI analysis of the modified ubiquitin protein. Modified protein ions were selectively trapped using QE accumulated trapping. Figures 3a and 3b demonstrate how the relative abundance of modified to unmodified fragments can be used to elucidate site reactivity and location.

Figure 1

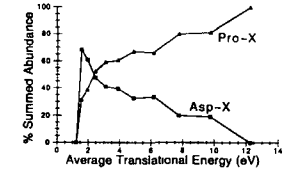

Figure 2

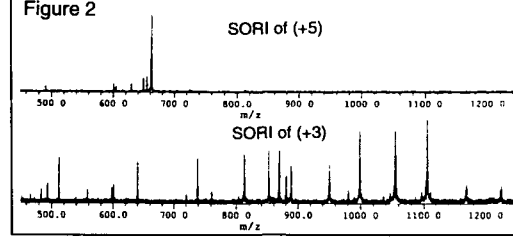

Figure 3

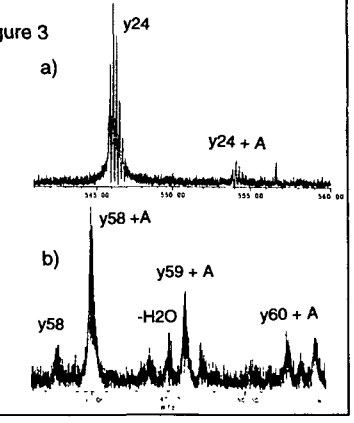

Three-Dimensional Collisionally Stabilized Motion in an Open Cell Applied to Remeasurement in FT-ICR

V. H. Vartanian and D. A. Laude, The University of Texas at Austin, Austin, Texas 78712-1167

Introduction: The first demonstration of dynamic motional stability of high amplitude trajectories of small organic ions in an open cell [1] using only a d. c. trapping field is applied to the FT-ICR remeasurement experiment [2]. Remeasurement efficiencies of more than 99.62% have been observed over 300 cycles for benzene using helium as the buffer gas. In the open cell, ions can penetrate axially past the physical boundaries of the trap electrodes into regions where the radial electric field actually becomes inward-directed. Since the radial electric field reverses orientation at increased axial displacement, it is possible to refocus ions back to the z-axis of the cell to reduce magnetron motion. The ability to maintain a constant magnetron radius even in the presence of a high pressure buffer gas can be immediately applied to the remeasurement experiment. The open cell axial position dependent radial electric field passively stabilizes collisionally destabilized ions. Ions are maintained in stable trajectories as long as they penetrate sufficiently far into the potential well where the radial electric field orientation shift occurs. A static pressure of a low mass buffer gas can be used to increase the ion axial amplitude similar to the mechanism observed for collision-induced axial excitation in the CID experiment [3].

Theory: The principal limitation in remeasurement is the inability to retain ions long enough to perform a sufficient number of remeasurements. Consecutive excitation events are performed in an outward-directed radial electric field which causes radial drift of the ion cloud, preventing the relaxation of the ion cloud to the original radius. The result is ion loss, and the limitation of remeasurement efficiency. Although the addition of a high-pressure buffer gas damps the cyclotron motion for subsequent reexcitation, the high collisional rate further destabilizes the magnetron motion and accelerates off-axis drift. As the ion mass decreases with respect to the buffer gas, the radial scattering angle increases. Remeasurement experiments without quadrupolar excitation (QE) have relied on minimizing the radial electric field in the cell.

Represented in Figure 1a is a SIMION plot of the radial electric field for the closed elongated cell as a function of z-axis position. An ion sustaining a collision with a neutral molecule anywhere in the cell would experience magnetron destabilization. However, the open cell intrinsically produces the required radial stability for ion reaxialization. In the open cell illustrated in Figure 1b, the radial electric field is outward-directed near the center of the cell, but becomes increasingly inward-directed (negative) at increased axial displacement. An ion of low oscillation amplitude that sustains a collision experiences magnetron destabilization while an ion of large axial amplitude experiences radial stabilization in the inward-directed radial electric field. The reaxialization ions experience is a function of time spent in the stabilizing regions of the cell and ions undergoing large-amplitude oscillations experience greater stability. The dynamic effect of radial electric field focusing on radial ion trajectory in closed and open cells is shown in Figure 2a where a 0.02 eV ion in a closed elongated cell indicates that after only 220 us, the ion has collided with a cell electrode. In actuality, ion motion is radially stabilized by the Lorentz magnetic force. In contrast, Figure 2b indicates that a 0.73 eV ion in an open cell may remain trapped indefinitely.

If the ion trajectory following a collision results in increased axial amplitude allowing ions to experience the inward-directed radial electric field, then the radial expansion of the ion cloud can in principle be offset. In CID, high buffer gas pressure is used to affect fragmentation as ions are accelerated to several keV. As target neutral pressure and excitation power increase, axial ejection increases as the ion cloud expands axially. As the ion-to-neutral mass ratio decreases, axial ejection increases due to greater z-amplitude scattering. Ion loss decreases as trapping potential increases, in contrast to what is observed for radial ion diffusion. The same tendencies have been observed in the open cell remeasurement experiment.

Experimental: Remeasurement was performed in an open cell appended to the analyzer side of a dual cell assembly in a 3.0 Tesla magnet. Helium buffer gas was maintained at 2×10^{-4} Torr. Neutral benzene was maintained at a pressure of 6×10^{-6} Torr in the source side where it diffused through the conductance limit to a pressure of 1×10^{-8} Torr in the analyzer side. A remeasurement pulse sequence was used with the form $I\text{–}D_z\text{–}[Ex\text{–}A\text{–}D_{xy}]_n\text{–}Q$. The ionization event, I, using a 5μA, 5 msec, and -15 eV electron beam generated ions. A 1 second axialization delay, D_z, permitted collisional cooling of axial motion prior to excitation. Multiple applications (n) of the three event cycle $[Ex\text{–}A\text{–}D_{xy}]$ resulted in ion excitation (Ex) with a 100-μsec pulse. A pressure-dependent collisional cooling delay (D_{xy}) of varied duration facilitated

relaxation of the cyclotron motion prior to the next measurement. Parameters effecting remeasurement efficiency were altered including excitation power, relaxation time, and trap voltage.

Results and Discussion: Figure 3a depicts a plot of signal intensity as a function of excitation power, indicating that during eight remeasurements, maximum signal intensity occurs at 3.48 $V_{P\text{-}P}$, or at a radius at 13% of the cell radius. At greater excitation levels, ions encounter regions of the cell where relaxation is not as efficient or energies associated with increasing excitation radius may promote axial or radial ion scattering. In Figure 3b, a plot of abundance versus relaxation delay between successive excitation events involving eight excite-τ-excite cycles followed by detection indicates that maximum signal intensity occurs with a 500 ms relaxation delay. The effect of trap voltage on remeasurement as a function of excitation energy is shown in Figure 3c where increasing trap voltage increases radial drift, reducing signal.

Figure 4a is a plot of the summed signal intensity for benzene versus the number of remeasurement cycles. The top plot represents the theoretical performance expected for 100% remeasurement efficiency while the bottom plot represents the experimental 99.62% remeasurement efficiency. Because the chief motivation of remeasurement is S/N enhancement, Figure 4b illustrates S/N ratio of benzene versus number of measurements. The top plot represents the S/N enhancement for theoretical 100.0% efficiency where the signal should increase as the square root of n measurements (in this case there is no ion loss). The bottom plot represents experimental 99.62% remeasurement efficiency following 300 measurements.

1. Beu, S. C.; Laude, Jr., D. A. *Int. J. Mass Spectrom. Ion Processes* **1992**, *112*, 215-230.
2. Williams, E. R.; Henry, K. D.; McLafferty, F. W. *J. Am. Chem. Soc.* **1990**, *112*, 6157-6162.
3. Riegner, D. E.; Laude, Jr. D. A. *Int. J. Mass Spectrom. Ion Processes* **1992**, *120*, 103-116.

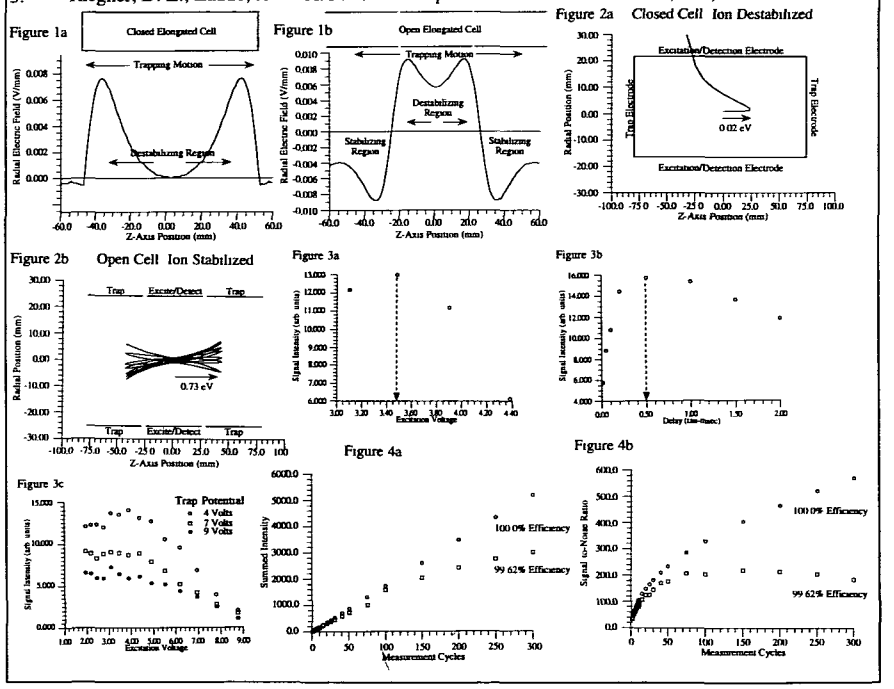

Facile Implementation of Quadrupolar Axialization in FTMS

C. F. Ijames
Section on Analytical Biochemistry, National Institute of Mental Health, Bethesda, MD 20892

Quadrupolar excitation coupled with collisional damping of the resultant cyclotron motion is an important new tool in FTMS. As originally described, two waveforms, differing in phase by 180°, are applied to the plates parallel to the magnetic field of the trapped ion cell. Each waveform is applied to a parallel pair of plates. Irradiation at the cyclotron frequency effects periodic interconversion of magnetron and cyclotron motion, and by matching the interconversion rate to the collisional damping rate, ions can be spiraled back to the center of the cell. This reverses the natural growth of the magnetron radius with collisions, the primary limitation on ion storage time, and provides a much more localized ion packet for subsequent manipulations such as transfer to another cell or excitation and detection.[1]

Several limitations exist with this scheme, however. If the cell is also to be used for detection, then the cell plates must be disconnected from the excite amplifier and reconnected to the preamp inputs during the experiment sequence. This is very difficult to do with adequate shielding and without adding additional capacitance, both of which reduces the signal-to-noise ratio. Also, a popular high voltage excite amplifier used in commercial FTMS systems has severe constraints on the capacitive loading of its outputs, such that it is impossible to merely connect two cell leads directly to the amplifier output without causing oscillation and damage. While fast (millisecond) relays certainly can be used to switch the amplifier outputs, they require some care in use in the strong fringing field of typical superconducting magnets, and require the appropriate control and driving electronics.

Here we describe the implementation of quadrupolar excitation using an unbalanced mode, where only one waveform is applied to a parallel pair of cell plates, while the other pair is left grounded (or connected to the preamp inputs) This reduces the electric field by half, requiring twice the applied voltage or twice the interconversion time, but eliminates the problems of switching the preamp inputs. It also causes a modulation of the trap potential, but so long as the resonance at twice the trap frequency is avoided, causes no ill effects. Further, the high voltage excite amplifier is actually a dual amplifier, providing two independent differential outputs with well matched gain characteristics. By using the in-phase outputs of both channels and applying each channel to only one cell plate, the capacitive loading problems are eliminated. Finally, the dipolar excitation can be performed in an unbalanced mode as well. While this is less ideal than balanced dipolar excitation, increasing the susceptibility to space charge effects, reducing the observed signal slightly, and reducing the ultimate resolution by perhaps half, it does allow quadrupolar axialization to be implemented merely by interchanging two cables connecting the dual cells of a FTMS 2000 (Extrel FTMS, Madison, WI) to the high voltage excite amplifier. This permits both dipolar and quadrupolar excitation to be applied in the unbalanced mode to both cells, without disturbing the preamp inputs and without using relays to switch the amplifier-cell connections.

Also presented are four cell connection schemes of various complexity (numbers of relays required) to allow quadrupolar and dipolar excitation to be applied in the balanced and unbalanced modes (see Table 1). Scheme 1 is the most complete implementation, providing balanced quadrupolar excitation in cell 1 and balanced dipolar excitation in both cells, but requires five relays and switches the inputs of both preamps. If there is only one cell a dummy load must be connected to S+ and S- during non-quadrupolar excitation events. Scheme 2 is a simplified version of scheme 1, requiring only 2 relays, which

provides balanced quadrupolar excitation in cell 1 and balanced dipolar excitation in cell 2 but does not allow dipolar excitation/detection in cell 1. This is equivalent to the experimental arrangement utilized in previous dual-cell quadrupolar excitation reports, and does not switch the preamp inputs.[1] Rather than leave unused cell plates floating, a 1 megohm resistor can be connected between each plate and ground. Scheme 3 is the most efficient. It provides unbalanced quadrupolar excitation in both cells, balanced dipolar excitation in both cells, does not switch the preamp inputs, and requires only 2 relays. Scheme 4 provides unbalanced quadrupolar excitation and unbalanced dipolar excitation in both cells, and does not require any switching during an experiment, making it the simplest to implement.

Table 1. Possible Dual-Cell Connection Schemes for Extrel High-Power Excite Amplifier

		Quadrupolar Excitation									Dipolar Excitation/Detection								
			Cell 1[d]				Cell 2					Cell 1				Cell 2			
N[a]	Rel[b]	Sym[c]	T1	T2	R1	R2	T1	T2	R1	R2	Sym	T1	T2	R1	R2	T1	T2	R1	R2
1	5	B	A+	S+	A-	S-	1 M	1 M	SP+	SP-	B	A+	A-	P+	P-	S+, 1 M	S-, 1 M	SP+	SP-
2	2	B	A+	S+, 1 M	A-	S-, 1 M	1 M	1 M	SP+	SP-	B	A+	1 M	A-	1 M	S+, 1 M	S-, 1 M	SP+	SP-
3	2	U	A+	S+	P+	P-	A-	S-	SP+	SP-	B	A+	A-	P+	P-	S+	S-	SP+	SP-
4	0	U	A+	S+	P+	P-	A-	S-	SP+	SP-	U	A+	S+	P+	P-	A-	S-	SP+	SP-

a. Connection scheme number
b. Number of DPDT relays necessary
c. Symmetry: B, balanced; U, unbalanced
d. Wiring connections: T1, T2, transmitter plates; R1, R2, receiver plates; A+, A-, analyzer excite amp outputs; S+, S-, source excite amp outputs; P+, P-, analyzer preamp inputs; SP+, SP-, source preamp inputs; 1 M, 1 megohm resistor to ground

1. Schweikhard, L.; Guan, S.; Marshall, A. G.; *Int. J. Mass Spectrom. Ion Proc.* **1992,** *120,* 71-83.

Electron Beam Enhancement of Laser Desorbed Ion Signals in FT-ICR

Easterling, Michael L.; Amster, I. Jonathan

Department of Chemistry, University of Georgia, Athens, GA 30602-2556

Laser desorption and matrix assisted laser desorption ionization are among the most powerful methods of generating ions of non volatile molecules. These modes are adept at ionization of large molecules and especially well suited for FT-ICR mass spectrometry. The major weakness in laser desorption for our experiments is the often oscillation of the ion signal intensity seen in successive shots on a given region of the sample. Also, the desorption parameters of laser irradiance and sample preparation must be meticulously adjusted to produce desired ions

In our lab, we have observed the application of a low energy electron beam applied along the magnetic axis of an FT-ICR mass spectrometer can significantly enhance the amplitude of the observed ion signal.. Experimentally, we use a 1 Tesla electromagnet with a cubic ICR cell. A filament placed just outside of a trapping plate provides the electron beam that propagates along the magnetic axis. An **IonSpec™** digital-analog controller modifies the potential of the filament, and can be programmed for microsecond resolution throughout the trapping sequence The laser beam path to the sample probe lies perpendicular to the magnetic axis.

Unlike normal modes of electron beam operation that use acceleration voltages of 60-70 eV, ion signal enhancement appears to be most efficient when the filament potential is near ground. The electrons are drawn out into the cell by the 3 V trapping potential used in this experiment. The beam is normally pulsed for 2-3 repetitions of 10-20 ms for a 2 second trapping sequence. As the acceleration voltage is low, ionization effects from the electron beam are not observed.

The ion signal enhancement varied as a function of filament current and was observed to have an optimal range of around 1.9 - 2.1 A. This corresponded to a measured emission current of 4-10 uA. Signal improvement was nominally 2-40 times that of the background signal In many cases, signals could be obtained from a sample that produced only noise under normal conditions. Also, low intensity ions that were not normally identifiable were detected with the electron beam enhancement.

Although a combination of sequences were used for the electron beam event, it was observed that the beam must not be active during the detect phase. Although transient signals last much longer in the presence of the electron beam, a current dependant mass shift will result. In extreme cases, this mass shift approached 10-12 m/z units If the electron beam is quenched prior to detection, mass shifting and resolution degredation is not observed.

43rd ASMS Conference on Mass Spectrometry and Allied Topics

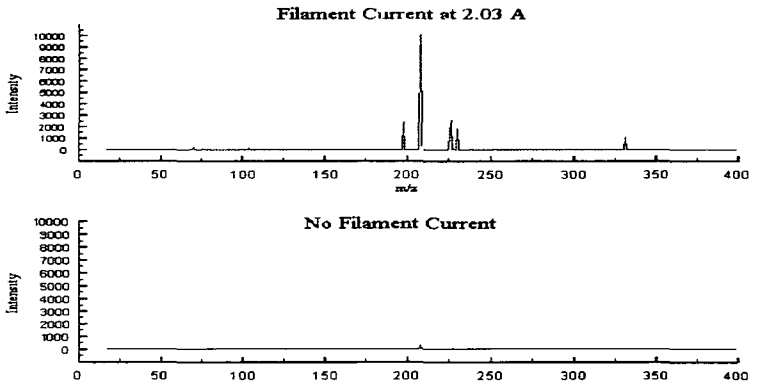

Figure 1: Figure showing the effect of a 2 03 ampere filamnet current on a MALDI spectrum of val-pro-leu in sinapinic acid

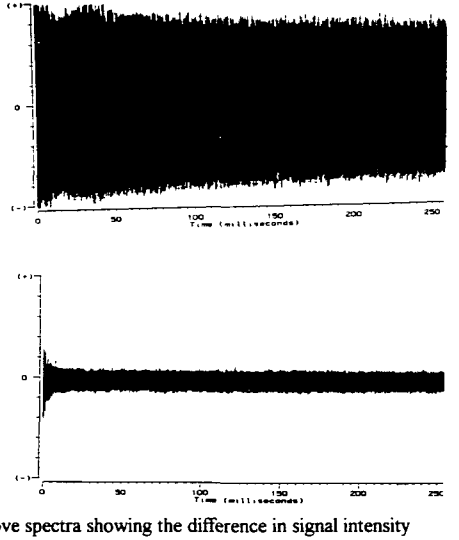

Figure 2 Transients of above spectra showing the difference in signal intensity

EXPERIMENTAL STUDIES OF BROADBAND QUADRUPOLAR EXCITATION IN FT-ICR

C. C. Pitsenberger*, I. J Amster
Department of Chemistry, University of Georgia, Athens, Georgia 30602

Since its debut, quadrupolar excitation (QE) has attracted considerable attention for the enhancement it provides to FT-ICR performance [1-4] When combined with collisional damping, QE leads to axialization of ions. QE has been shown to provide unique capabilities for permitting ion remeasurement leading to high mass resolution and sensitivity Most published work has focused on single frequency excitation Axialization over a mass range has been reported,[4-6] in particular using SWIFT QE for transferring ions from source to analyzer in a dual cell ICR systems. Yet, the utility of this technique has not been fully developed for MS/MS studies or for ICR systems lacking SWIFT capabilities. For some time now, our group has been working on extending the capabilities of single frequency QE (in a single cubic cell) to a broadband axialization (in a single cubic cell). One of our principle goals for this research is to develop well characterized MS/MS experiments Our single analyzer cell and pulsed gas flexibilities will allow us multiple MS/MS with high resolution capabilities when used in conjunction with QE Here we describe some of the different methods used in pursuit of this goal, including repetitive chirp excitation and filtered noise excitation. The efficiency and applicability of broadband repetitive chirp excitation is presented and we introduce, specifically for the first time, the method feasibility and signal enhancement gained when using filtered white noise QE

Two plate quadrupolar excitation[7] was used in these experiments Both broadband repetitive chirp and filtered noise QE experiments were similar in sequence A 1-T electromagnet and 337 nm output of an excimer laser were used for laser desorption of the peptide (Val-Pro-Leu) studied. Both white noise and continuous frequency chirps originated from a Stanford Research Systems frequency synthesizer. White noise was passed through an active filter before amplified and applied to the cell plates. The bandpass could be adjusted to select the desired frequency range for excitation.

Both broadband repetitive chirp and filtered white noise quadrupolar excitation efficiently axialize ions in our instrument. Figure 1a illustrates MALDI of VPL in the absence of QE. Figure 1b Illustrates axialization of VPL ions in the presence of filtered noise QE This demonstrates the phase independence of QE.[5] Efficiencies are in excess of 98% for repetitive chirp excitation and greater than 99.5% for single frequency quadrupolar excitation (See Figure 2). Remeasurement efficiencies for filtered white noise QE were found to be much lower (80%), but this is in part attributed to the initial selection of the active filter. The active filter will next be modified to yield a flatter bandpass and sharper cutoffs. It is demonstrated that both repetitive chirp and filtered noise QE have potential to enable high resolution analysis. The duration of the transient signal increases by more that three orders of magnitude when either broadband QE method (chirp or noise) is used to axialize ions before the detection event. Remeasurement efficiencies and high resolution experiments should be more efficient using QE at higher magnetic field strength. The

ability to efficiently remeasure ions is obvious for MS/MS analysis of biopolymers and we have presented two techniques that hold great potential for this application

REFERENCES:

1 Speir, J P.; Gorman, G G.; Pitsenberger, C. C , Turner, C. A., Wang, P. P ; Amster, I. J *Anal Chem* **1993**, *65*, 1746
2. Guan, S H.; Wahl, M. C.; Wood, T. D.; Marshall, A. G. *Anal Chem.* **1993**, *65*, 1753.
3. Wood, T. D., Ross, C W.; Marshall, A. G. *J. Am. Soc. Mass Spectrom* **1994** *5*, 900.
4 Guan, S. H , Wahl, M. C ; Marshall, A G. *J. Chem. Phys.* **1994**, *100*, 6137.
5. Schweikhard, L.; Guan, S H.; Marshall, A. G. *Int. J. Mass Spectrom. Ion Processes*, **1992**, *120*, 71
6. Marto, J. A.; Guan, S. H., Marshall, A. G.; *RCMS*, **1994**, *8*, 615.
7 Hendrickson, C. L , Drader, J. J ; Laude, D A. *J Am. Soc Mass Spectrom* **1995**, *6*, 448.

Figure 1.

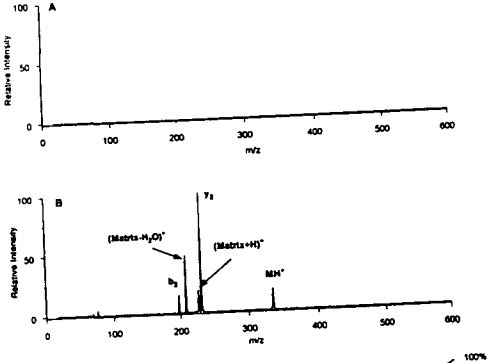

Figure 2

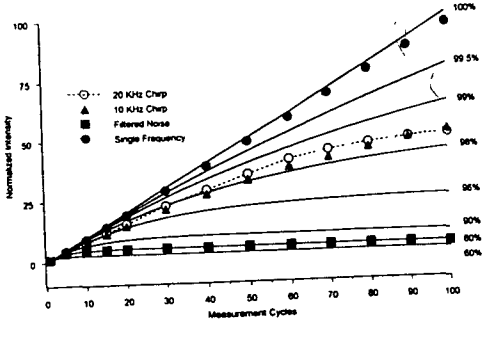

Quadrupole Excitation Trapping during Electron Beam Events in ICR Spectrometry

Joey Hatcher, John Bartmess*, Department of Chemistry, University of Tennessee, Knoxville TN 37996-1600

The generation of cations by electron ionization is straightforward above the ionization energy, all compounds form some cations, with only ca. two orders of magnitude variation in the ionization cross-section.

Formation of anions, however, is much more variable The cross-section varies over more than seven orders of magnitude, and in a non-monotonic fashion with electron energy. Few compounds fall in the high-cross-section end of the range. Relatively high pressures for many of the neutral precursors are thus required to yield reasonable signal intensities in negative ion EIMS.

For example, in ICR spectrometry, Cl^- from CCl_4 yields an intense signal with a partial pressure of CCl_4 at $1x10^{-8}$ torr, with a 10 msec, 1 microamp electron beam. In contrast, to produce a comparable amount of hydroxide from water at the appropriate E_{max} requires an H_2O pressure of ca. $5x10^{-6}$ torr.

Such high pressures result in signal broadening in ICR spectrometry, and leave little "pressure range" above that for other reactant gases. Although external ion sources can inject any ion into a low pressure reactive gas environment in ICR spectrometry, we seek a lower cost method.

Experiments were carried out on a home-built ICR mass spectrometer. Pumping was via a 100-l/s turbomolecular pump. This is normally throttled down considerably for the constant pressure experiments, to minimize pressure gradients. Quadrupole excitation was implemented essentially as described in the literature.[1] A General Products pulsed valve was overdriven at ca 70 V in a 1 msec pulse, to raise the pressure of the anion precursor to the 10^{-5} torr range. Backing pressure was the vapor pressure of water at 25^0C, 25 torr.

Typical optimized values for parameters include an quad rf level of ca. 150 mV (about 5 times theoretical value)[1] and a frequency several percent higher than theoretical ideal (at δ_c) The latter may be in part due to the electron beam being present in the cell, at the location to which the ions relax.

For development, benzene was used as the pulsed gas, with no constant pressure gas. The benzene radical cation was detected, when the electron beam event commenced at the start of the gas pulse. The gas pulse peaked at approximately mid 10^{-5} torr, and was below 10^{-6} torr at ca 700 msec Quadrupole excitation trapping was carried out from the start of the electron beam event, for 700 msec, then detection was performed staring at 900 msec.

In negative ion mode, water gave abundant HO^- under comparable conditions. With ethylbenzene present at $1x10^{-6}$ torr, it required quadrupole trapping at both 105^- and 17^- to obtain the 105^- signal

This is intriguing, in that the full chemical sequence is:

$H_2O + e^- \rightarrow H^- + HO^\cdot$

$H^- + H_2O \rightarrow HO^- + H_2$

$HO^- + PhCH_2CH_3 \rightarrow H_2O + PhCHCH_3$ (105^-)

and m/z 1, the primary ion, was not trapped via QE The second reaction must be far more rapid than ion loss.

At this point the pulsed valve developed an air leak, as evidenced by the 32^- signal becoming the base peak when trapping 17^-. Interestingly, we were not irradiating at the 32^- frequency; this may be due to exothermic electron transfer from HO^- to O_2 in the lower pressure latter stages of the experiment.

1. Guan, S H ; Kim, H.S., Marshall, A.G , Wahl, M C., Wood, T.D., Xiang, X.Z *Chem. Rev.* **1994** *94*, 2161.

43rd ASMS Conference on Mass Spectrometry and Allied Topics

Studies of Individual Large Molecules by ESI-FTICR Mass Spectrometry

Ruidan Chen, James E. Bruce, Xueheng Cheng, Dale W. Mitchell, Steven A. Hofstadler, Gordon A. Anderson, and Richard D. Smith
Pacific Northwest Laboratory, Richland, Washington 99352

We have developed methods for molecular weight (MW) determination of megadalton molecules based on the measurements of individual ions by FTICR-MS. Stepwise charge state shifts of individual ions in reaction with selected reagents produce multiple peaks from the same ion, from which charge states and MW can be calculated.[1,2] Alternatively, the number of charges can be measured simultaneously with the mass-to-charge ratio to obtain the molecular weight of an individual ion, although with precision currently limited to 5 ~ 10%. For the case of very large molecules (>10 MDa), only the latter approach has been effective thus far.[3,4]

To extend the study of such large molecules, two efforts have been carried out. First, theoretical explanation of the mass-discrimination in FTMS during excitation for large ions was explored. We have previously observed that, for ions having similar m/z values but different masses, lighter ions are excited to larger radii than heavier ions. Several mechanisms may be involved, such as collisional damping that expands lighter ion's magnetron radius more rapidly than heavier ion's. The Coulombic interactions between large (heavier and more charge) and small (lighter and fewer charge) ions may constrain small ions move around the large ones which makes the smaller ones being ejected earlier. The so-called "centrifugal separation"[5] of different ionic species may also involved in such a process. Second, we studied theoretically the damping (or expansion) rate for large ions and our results showed that large ions (MW > 1,000,000 Da) have much slower damping (and magnetron expansion) rates, consistent with our previous observations. Furthermore, we acquired several long transients from Coliphage T4 DNA ions. Figure 1 shows a 1040 second transient (limited by the Odyssey Data system used in our experiments), much longer transients could be acquired when appropriate hardware and software were available.

Pacific Northwest Laboratory is operated by Battelle Memorial Institute for the U.S. Department of Energy under Contract DE-AC06-76RLO 1830.

1. Smith, R. D., Cheng, X., Bruce, J. B., Hofstadler, S. A. and Anderson, G. A., *Nature*, **1994**, *369*, 137-139
2. Bruce, J. E., Cheng, X., Bakhtiar, R., Wu, Q., Van Orden, S., Anderson, G. A. and Smith, R. D., *J. Amer. Chem. Soc.*, **1994**, *116*, 7839-7847
3. Chen, R., Wu, Q., Mitchell, D. W., Hofstadler, S. A. and Smith, R. D., *Anal. Chem.*, **1994**, *66*, 3964-3969
4. Chen, R., Cheng, X., Mitchell, D. W., Hofstadler, S. A., Wu, Q., Rockwood, A. L., Sherman, M. G. and Smith, R. D., *Anal. Chem.*, **1995**, *67*, 1159-1163
5. O'Neil, T. M., *Phys. Fluids*, **1981**, *24*, 1447-1451

Figure 1. Spectra from Coliphage T4 DNA (MW= 110,000,000 Da). a) Time-domain signal from a few of T4 DNA ions (at ~ 1×10^{-9} Torr); b) Fourier transform of the time-domain signal of 0 - 9 seconds; c) Fourier transform of the time-domain signal of 987 - 996 seconds. The signal loss is likely due to ion-ion interactions and charge shifting due to ion-molecule reactions.

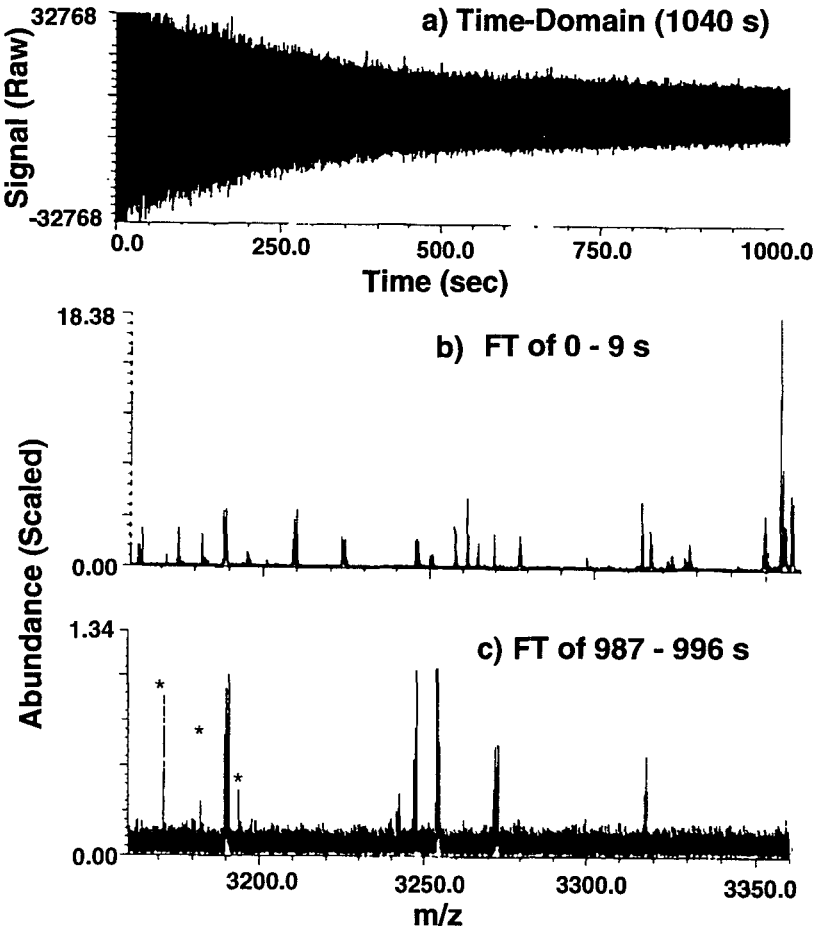

A New Dual Cell Trap for Selective Ion Accumulation and Separation in ESI-FTICR Mass Spectrometry

Ruidan Chen, James E. Bruce, Xueheng Cheng, Steven A. Hofstadler, Gordon A. Anderson, Alan L. Rockwood, Harold R. Udseth, and Richard D. Smith
Pacific Northwest Laboratory, Richland, Washington 99352

The selective accumulation from externally generated low ion currents in an FTICR mass spectrometer can be effectively accomplished.[1] The selective ion accumulation process can facilitate many types of studies, and is particularly effective in conjunction with continuous injection from an electrospray source. However, this technique also requires relative high background gas pressure ($\geq 10^{-5}$ Torr), which can limit the optimal performance for subsequent FTICR measurements at pressure of $\sim 10^{-8}$ Torr and below. To resolve these conflicting demands, we have designed a new dual cell-type of ion trap. The first cell is sealed in a box which is slightly larger than the cell itself. A gas inlet line is connected to the box, and collision gases are introduced directly into the first cell (see Figure 1). This reduces the gas load upon the vacuum chamber during selective ion accumulation by as many as 4 orders of magnitude. This feature allows greatly extended selective ion accumulation. After the selective ion accumulation, the accumulated ions can be transferred through a conductance limit into the second cell for further manipulation and detection, where pressure is $\sim 10^{-9}$ Torr. To increase the obtainable pressure difference beyond the two orders of magnitude typically achieved in dual cell designs, a "shutter" over the conductance limit has been incorporated, and which is only open during transport of ions between the cells. Thus, this new cell allows the combination of the continuous ion injection and selective accumulation in the first cell, the periodic sampling from the first cell, and high performance analysis by the second cell. In a control experiment, buffer gas is continuously leaked into the first cell by a leak valve for ion accumulation, while the selected ions are transferred to the second cell for detection.

To utilize this dual cell trap for the analysis of large complex biosystems, e.g., a mixture of a biotarget and a large inhibitor library, two more experiments are carried out: 1) Selectively accumulated ions can be transferred to the analyzer cell in a multistage transfer sequence (see Figure 2). The ion intensity (Ubiquitin, 1 mg/ml in 10 mM acetic acid) detected in the analyzer cell increases linearly with the number of ion transfers until the space charge limit is reached where frequency shift and/or peak distortion occur. 2) Accumulated ions can also be selectively transferred to the analyzer cell by using magnetron excitation and single frequency quadrupolar cooling. A dipolar magnetron excitation waveform can also be used to enlarge the ion magnetron radius in the first cell. Only those ions which are "cooled" by a quadrupolar cooling waveform can be transferred to the analyzer cell through the conductance limits (see Figure 3).

Pacific Northwest Laboratory is operated by Battelle Memorial Institute for the U.S. Department of Energy under Contract DE-AC06-76RLO 1830.

1. J. E. Bruce, G. A. Anderson, S. A. Hofstadler, S. L. Van Orden, M. G. Sherman, A. L. Rockwood and R. D. Smith, *Rapid Commun. Mass Spectrom.* 7, 914 (1993)

43rd ASMS Conference on Mass Spectrometry and Allied Topics

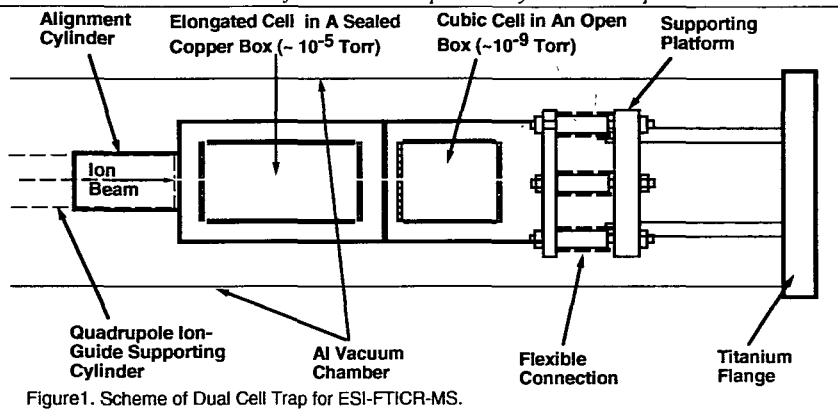

Figure1. Scheme of Dual Cell Trap for ESI-FTICR-MS.

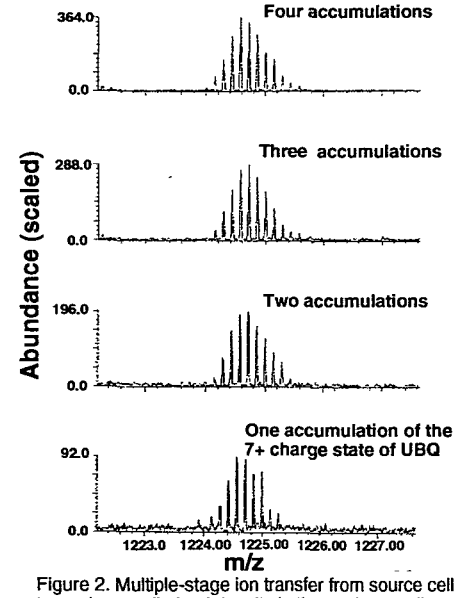

Figure 2. Multiple-stage ion transfer from source cell to analyzer cell. Ion intensity in the analyzer cell increases linearly with the number of transfers until the space charge limitations apply.

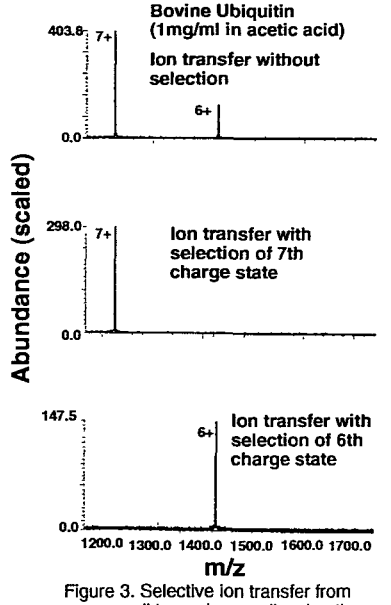

Figure 3. Selective ion transfer from source cell to analyzer cell, using the combination of magnetron excitation and quadrupolar cooling.

ENHANCED SELECTIVE ION ACCUMULATION WITH DIPOLAR MAGNETRON EXCITATION

James E. Bruce, G.A. Anderson, R. Chen, X. Cheng, D. C. Gale,
S. A. Hofstadler, B. L. Schwartz and R. D Smith
Pacific Northwest Laboratory, Richland, Washington 99352

Fourier transform ion cyclotron resonance (FTICR) mass spectrometry is becoming a powerful technique for the investigation of large biomolecules. This evolution has been made possible with the advent of new ionization techniques, such as matrix assisted laser desorption-ionization (MALDI) and electrospray ionization (ESI). However, with this introduction of new methods of ionization has arisen a broad range of new challenges for detection. For example, the high ionization efficiency of ESI provides a basis for considerably surpassing the sensitivity and dynamic range of FTICR, and in fact, most mass spectrometers. The development of methods for the generation of large libraries of biomolecules, such as those employed in combinatorial studies, and the desire to apply ESI to the analysis of these types of mixtures further enhances the motivation for even greater sensitivity and dynamic range. We have developed the technique of selective-ion accumulation (SIA)[1] for the purposes of increasing both the sensitivity and dynamic range of FTICR mass spectrometers with the application of quadrupole excitation during the ion accumulation period. This process has been shown to provide many advantages, two of which are the accumulation over relatively long time periods and *m/z* selectivity of the accumulation process. These features both arise from the continuous reduction of magnetron orbits which would otherwise lead to ion loss. For example, the effective analysis of low concentration solutions is increased three orders of magnitude since the accumulation period can become arbitrarily long (at least as long as pumping allows), with the reduction of ion loss through magnetron motion that normally occurs due to the extended high pressure.[2] The dynamic range is enhanced by the removal of more intense species, simultaneous with the accumulation process, thus allowing longer accumulation events focused on the detection of less abundant ions. A possible limitation of this dynamic range expansion arises from the speed with which non-selected ions can be forced off axis by increased magnetron motion. The magnetron motion of these species has normally been increased through collisions with neutral buffer gas molecules. Under our normal operating conditions, non-selected ions can still be detected (although with reduced peak intensities and resolution) after several seconds of high pressure. In a continuation of our development of the SIA process, we report here the application of a dipolar excitation waveform simultaneous with the SIA event, similar to those previously reported for purposes of collisional activation during quadrupole excitation[3]. Here, however, dipolar excitation is applied at the magnetron frequency to *actively* increase the magnetron orbits of all ions and thus, provide faster separation of selected from non-selected ions

Figure 1 illustrates the application of magnetron excitation concurrent with the selected ion accumulation process. Figure 1 (a) shows the normal accumulation spectrum of bovine ubiquitin without the use of selected-ion accumulation or magnetron excitation. The largest peaks here are those of the 6+ charge state. Figure 1 (b) shows a spectrum acquired with a 1 second selected-ion accumulation of the 7+ charge state (and various adducts) followed by a 1 second continuation of the high pressure and quadrupole excitation to further move non-selected ions off axis. The largest peaks are those due to the 7+ charge state; however, those due to the 6+ charge state are still evident and will require at least an additional 4 seconds of extended high pressure to be completely removed from the spectrum under these conditions. Figure 1(c) illustrates the results obtained under the same experimental conditions as applied to produce the spectrum in 1(b) except this time with the application of magnetron excitation of 300 mV at 18 Hz. These data illustrate the increased removal of unwanted ions from the FTICR cell with SIA and

the use of magnetron excitation to provide increased speed of ion removal during selected-ion accumulation (by a factor of about 5). Greater magnetron excitation voltage levels can provide an even faster magnetron ejection and accumulation, but may also produce higher levels of collisionally activated dissociation since the selected ions can achieve greater magnetron orbits prior to interconversion.

In summary, active magnetron excitation has been shown to provide faster removal of the undesired ions for more efficient selected-ion accumulation. Modest gains in efficiency are reported and further gains are predicted, but require careful tuning of quadrupole and magnetron excitation amplitudes to balance CAD, magnetron expansion and cyclotron damping rates.

References:

1) Bruce, J. E.; Anderson, G.. A.; Hofstadler, S. A.; Van Orden, S. L.; Rockwood, A. L.; Sherman, M. S.; Smith, R. D., *Rapid Comm. Mass Spectrom.* **1993**, *7*, 914.
2) Bruce, J. E., Anderson, G. A. Chen R., Cheng, X., Gale, D. C., Hofstadler, S. A., Schwartz, B. L., Smith, R. D., *Rapid Comm. Mass Spectrom.* **1995**, submitted.
3) Guan S., Marshall, A. G., Wahl, M. C., *Anal. Chem.* **1994**, *66*, 1363.

Figure 1

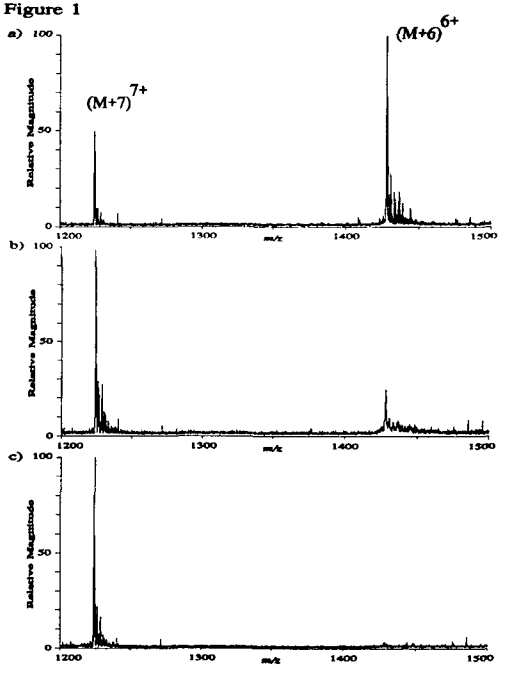

We thank the U.S. Department of Energy for support of this research through internal PNL Exploratory Research under contract DE-AC06-76RLO 1830.

Selective Ion Excitation and Isolation in Trapped-Ion Mass Spectrometry

Shenheng Guan* and Alan G. Marshall*

Center for Interdisciplinary Magnetic Resonance, National High Magnetic Field Laboratory, Florida State University, 1800 E. Paul Dirac Dr., Tallahassee, FL 32310

* Department of Chemistry, Florida State University

Stored Waveform Inverse Fourier transform (SWIFT) excitation, introduced in FT-ICR nearly ten years ago,[1] is the method of choice for selective ion excitation and isolation over an arbitrarily wide range in mass-to-charge ratio. Originally developed for dipolar radial excitation of ion cyclotron motion, the SWIFT technique may also be applied to broadband azimuthal quadrupolar excitation for axialization in FT-ICR MS.[2] The advantages of SWIFT excitation for one-dimensional experiments also carry over to new two-dimensional FT-ICR MS experiments.[3a] A SWIFT-based method can even excite relativistic ions whose cyclotron frequency changes during the excitation process.[3b] Finally, the SWIFT method has been adapted for selective ion axial dipolar excitation and ejection in a quadrupole ion trap.[4]

Full realization of SWIFT's advantages depends on optimal phase-encodement of a given frequency-domain excitation magnitude profile. Fig. 1 compares several phase modulation methods, where all of the waveforms are obtained from a smoothed square magnitude spectrum.[5] For linear phase encodement, the time-domain waveform has a very high peak amplitude due to the superposition of all the sinusoids at a particular instant. Pseudo-random phase encodement yields a waveform with very low peak amplitude, but with very non-uniform time-domain excitation magnitude. A "minimum" phase may be obtained by Hilbert transform of the magnitude spectrum to give a time-domain waveform with minimum group delay, but without much amplitude reduction. Optimal peak amplitude reduction is achieved by use of optimized phase[7] which distributes excitation power over a specified time segment.

Ion motion *along* the magnetic field in an ICR trap may also be selectively excited. Isolation of ions according to their linear axial motional frequencies is especially attractive for low-mass ions whose cyclotron frequencies may be too high for commonly available ICR electronics. Fig. 2 shows selective axial ejection of ions from a crude oil sample. Another advantage of ion axial ejection is its low kinetic energy requirement: ions need be excited to only a few eV axial kinetic energy for axial ejection whereas cyclotron (radial) ejection requires a few hundreds of eV. Work supported by NSF (CHE-94-13008), NIH (GM-31683), and the National High Magnetic Field Laboratory at Florida State University.

1. A. G. Marshall, T. C. L. Wang, and T. L. Ricca; *JACS* **1985**, *107*, 7893-7897.
2. S. Guan, M. C. Wahl, and A. G. Marshall, *J. Chem. Phys.* **1994**, *100*, 6137-6140.
3. (a) C. W. Ross, III, S. Guan, P. B. Grosshans, T. L. Ricca, and A. G. Marshall; *J. Am. Chem. Soc. 1993*, 115, 7854-7861; (b) S. Guan, M. V. Gorshkov, G. M. Alber, and A. G. Marshall; *Phys. Rev. A* **1993**, *47*, 2730-2737.
4. S. Guan and A. G. Marshall, *Anal. Chem.* **1993**, *65*, 1288-1294.
5. S. Guan, *J. Chem. Phys.* **1990**, *93*, 8442-8445.
6. S. Guan and R.T. McIver, Jr., *J. Chem. Phys.* **1990**, *92*, 5841-5846.

43rd ASMS Conference on Mass Spectrometry and Allied Topics

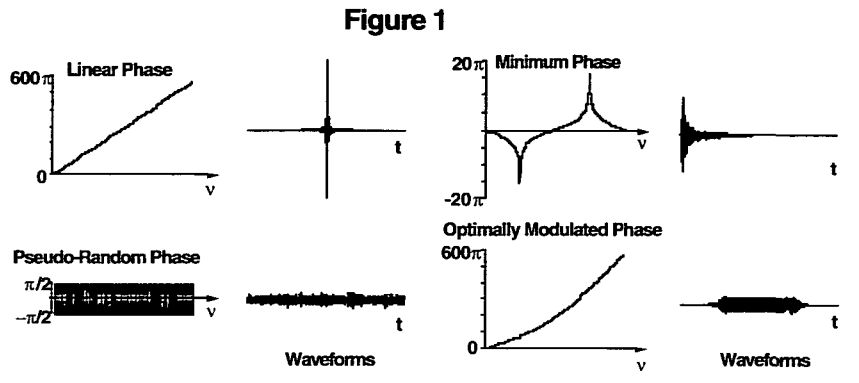

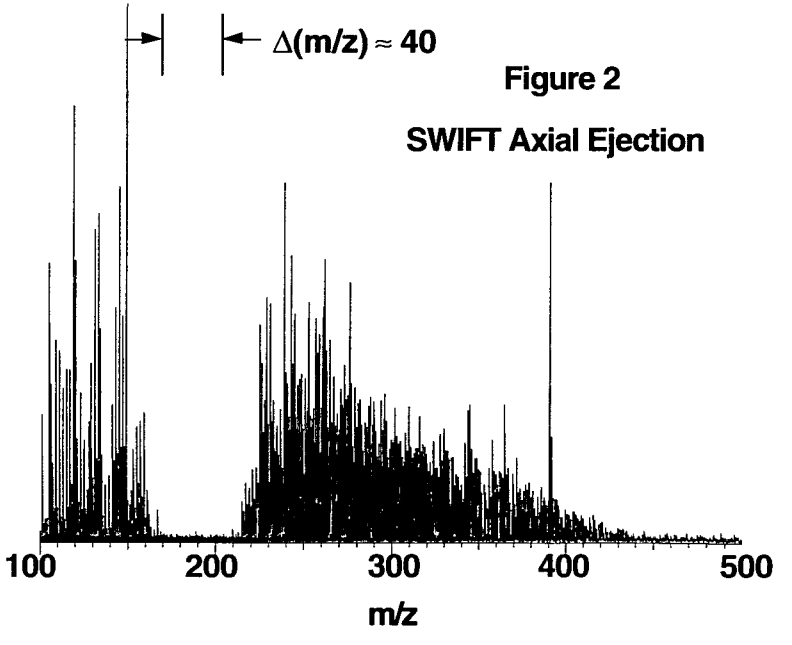

A Unified Description of Space Charge Effects in FT-ICR Mass Spectrometry

Dale W. Mitchell and Richard D. Smith
Pacific Northwest Laboratory, Richland, WA 99352

A deeper understanding of space charge effects is required in order to make further improvements in the FT-ICR method. Due to the Coulombic interaction between different m/Z ion clouds, the cyclotron trajectories of the ions are perturbed from circular orbits moving with the cyclotron frequency, resulting in a sometimes dramatic variation from the behavior predicted for a single ion. Phenomena arising from the Coulombic interaction due to interactions between different m/Z ion clouds, same m/Z ions, or image charge induced on the trap electrodes, are generically referred to as space charge effects Trap geometry as well as the shape of the ion cloud determine the maximum number of ions which can be confined in a Penning-like ion trap. We consider the two important cases of either spherically or cylindrically shaped ion clouds (i.e coherently moving ion ensembles with different m/Z). These models exhibit the most important space charge effects in Fourier transform ion cyclotron resonance mass spectrometry including frequency shifts, amplitude and phase modulation and phase-locking. Both positive and negative frequency shifts are possible for spherical ion clouds when their cyclotron radii differ Due to the Coulombic interaction between ion clouds, cyclotron radius and phase modulation occurs. This modulation increases inversely to the cyclotron frequency difference. Cyclotron phase-locking results when two ion clouds have similar mass to charge ratios and a sufficiently large ion population, at which point a mass spectrum shows only a single peak. Spherical ion clouds are usually more likely to phase-lock than cylindrically shaped clouds. The phase-locking threshold sets new limits to the maximum resolution, mass accuracy and dynamic range achievable by mass spectrometry. Numerical and analytical methods are applied to two related problems of immense importance to FT-ICR mass spectrometry [1]. The first studies the dynamics of an individual ion cloud in the presence of external perturbing forces which act to destroy cloud coherence. The second problem involves the dynamics of Coulombically interacting ion clouds

I. Stability of Individual Ion Clouds

When many ions are simultaneously confined within the trap, the single ion description breaks down due to Coulomb interactions and one is confronted with a complicated many body problem A mean field approach is employed to study the stability of coherent cyclotron and magnetron motion. That is we investigate the stability of a test ion located initially on the edge of the ion cloud which interacts with the space charge electric field arising from the ion cloud The total charge within the ion cloud is assumed to be much greater than the charge of the test ion, therefore, while the test ion is perturbed by the ion cloud, the ion cloud is assumed unaffected by the presence of the test ion. The space charge electric field arising from the ion cloud introduces a fourth fundamental ion motion in addition to the $\omega_{\pm}$ and ω_z harmonic oscillations; the spin rotation of the ion cloud about its own symmetry axis in the x-y plane at a frequency ω_r [2] The ion cloud spin originates form the **E x B** drift where **E** is due to the ion cloud's own space charge electric field. Therefore, if the ion cloud is moved off of the trap z-axis (e.g. given a coherent non-zero magnetron or cyclotron radius), the ion cloud still has spin at frequency ω_r about the cloud symmetry axis with coherent magnetron or cyclotron motion superimposed. The theory is applied to force gradients arising from trap imperfections, magnetic bottle and image charge.

II. The Cyclotron Motion of Coulombically Interacting Ion Clouds.

Coulomb induced frequency shifts, amplitude and phase modulation, and phase-locking are the most important space charge effects in FT-ICR. The Coulomb interaction between two different m/Z ion clouds excited to some cyclotron radius (not necessarily the same radius) modifies the radial electric field experienced by the ion clouds. The cyclotron frequencies are shifted from their unperturbed values as a result of this space charge induced radial electric field Since the distance between the ion clouds changes with periodicity $\approx \Delta\omega_c^{-1}$, where $\Delta\omega_c$ is the cyclotron frequency difference, the cyclotron phases are modulated. The cyclotron radii are modulated as well since the mutual **E x B** drift between the two ion clouds, where **E** is the space charge induced electric field, causes a variation in radius with time However, if $\Delta\omega_c$ is small compared to the **E x B** drift frequency, the two ion clouds may phase-lock, whereby both clouds revolve around one another as well as the trap center During phase-locking, a mass spectrum shows only a single peak, and not two peaks. Theoretical relations are derived for the phase-locking threshold [1]. Good agreement is found between our predictions, results of numerical simulations on two ion clouds, and previously published experimental data [3] Our theory differs quantitatively from a recent investigation [4]. We have also carried out numerical simulations on cyclotron phase-locking involving more than two ion clouds

III. Space Charge Limits in FT-ICR

i z-confinement: Space charge potential cannot exceed trapping well depth This sets a maximum total charge which can be contained in the trap

ii. radial-confinement: Force balance between the radial space charge electric field, Lorenz magnetic force and coriolis force sets a maximum number density called the Brillioun limit which can be achieved.

iii cloud stabilization: The **E x B** drift rotation due to the ion cloud's own space charge electric field acts to maintain coherence for sufficiently dense ion clouds The ion cloud is destroyed if force gradients across the cloud diameter exceed a critical value.

iv. phase-locking: Related to cloud stabilization Consider two different m/Z ion clouds. If the **E x B** space charge cloud dynamics dominates the relative cyclotron motion then the ion clouds likely phase-lock, i.e. have identical detected cyclotron frequencies. Excited pure magnetron modes are almost always phase-locked due to the near m/Z independence of the unperturbed magnetron frequencies.

This work is supported by the U.S. Department of Energy. Pacific Northwest Laboratory is operated by Battelle Memorial Institute through contract DE-AC06-76RLO 1830

[1] D.W Mitchell and R.D. Smith, manuscripts in preparation
[2] A.J Peurrung and R.T. Kouzes, Phys Rev. E **49**, 4362 (1994)
[3] J Huang, P.W.Tiedemann, D.P.Land, R.T.McIver, J.C.Hemminger, IJMSIP **134**, 11 (1994)
[4] Y. Naito and M. Inuoue, J. Mass Spectrom. Soc. Japn **42**, 1 (1994).

Minimization of Frequency Shifts for Improved Mass Accuracy in FT-ICR MS

Kent Gillig, Brian Bluhm, David H. Russell
Laboratory for Biological Mass Spectrometry
Department of Chemistry, Texas A&M University
College Station, TX 77843

Matrix Assisted Laser Desorption Ionization (MALDI) is an excellent method for ionizing a wide variety of large biomolecules. Thus, there has been considerable interest in combining the high resolution and accurate mass measurement capabilities of FT-ICR mass spectrometry with MALDI. In this study, the performance of several ICR cell geometries are compared (cubic, field corrected, elongated cylindrical, wire ion guide[1]) in terms of trapping efficiency and observed trapping voltage frequency shifts. The most accurate mass measurements are obtained using a wire ion guide cell, which produced trapping frequency shifts of ~1.6 Hz/Volt. Results from SIMION suggest that the improved performance of the wire ion guide cell is due to a more homogeneous trapping potential inside the cell. Figure 1 contains a internally calibrated broadband spectra of bovine albumin. Using a linear calibration curve the experimental mass of Bovine Serum Albumin was less than 1% different from the actual value (using 3 point calibration with Gramicidin S, Melittin, Bovine Insulin) as shown in Figure 2. Using conventional ion cells we were unable to detect ions for each component of the mixture; however, using the WIG cell, the abundance of each component is comparable. This WIG cell has been coupled with high trapping voltages to investigate their combined effects on trapping efficiency. An increase in trapping efficiency has been noticed along with a decrease in observed frequency shifts. To further improve trapping efficiency the ion cell geometry has been modified to emulate an electrostatic Kingdon Trap[2]. By applying DC voltages to all six plates and the wire of the WIG cell a Modified Kingdon Trap has been integrated into a conventional FTICR experiment. This has been accomplished by the addition of a relay system to switch from DC trapping to rf excitation in a one section cell. Figure 3 contains a diagram of a standard electrostatic Kingdon Trap and a diagram of a Modified Kingdon Trap used in FTICR experiments. Simulations of ion trajectories in the x-y plane of a Modified Kingdon Trap and a Modified Kingdon Trap in a 7-tesla magnetic field are shown in figure 4 and figure 5, respectively.

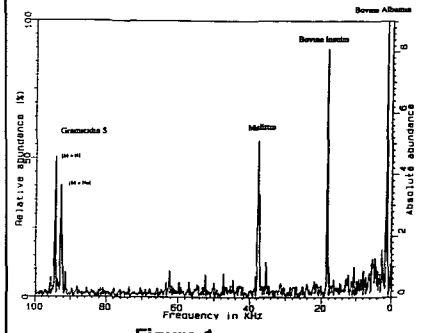

Figure 1

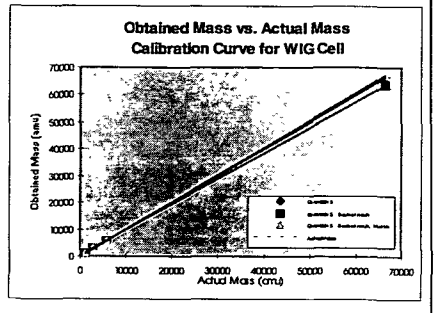

Figure 2

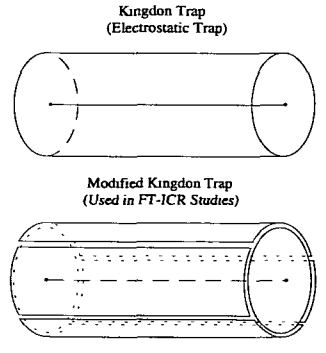

Figure 3

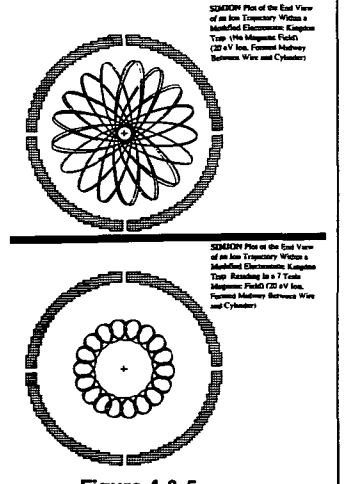

Figure 4 & 5

References

1. Solouki, T.; Gillig, K. J.; Russell, D. H. *Anal. Chem.*, **1994**, *66*, 1583.
2. Kingdon, K. H. *Phys. Rev.*, **1923**, *21*, 408.

FT and non-FT Spectral Analysis of Unevenly Sampled Biomolecule ICR Time-Domain Data

Michael W. Senko, Shenheng Guan, Yulin Huang, Alan G. Marshall*, and Fred W. McLafferty**

Center for Interdisciplinary Magnetic Resonance, National High Magnetic Field Laboratory, Florida State University, 1800 E. Paul Dirac Dr., Tallahassee, FL 32310

* Department of Chemistry, Florida State University
** Department of Chemistry, Cornell University, Ithaca, NY 14853

The coupling of electrospray ionization (ESI) with FT-ICR MS provides unrivaled sensitivity, mass accuracy, and resolving power for large biological molecules. By use of SWIFT isolation of individual charge states and infrared multiphoton dissociation for gas-phase ion desolvation, unit mass resolution FT-ICR mass spectra of molecules as large as bovine serum albumin (66 kDA) may be obtained,[1] although a single-scan spectrum may have poor signal-to-noise ratio. Here, we demonstrate dramatic improvement in signal-to-noise ratio, without the loss of mass resolving power, by use of enhanced analysis routines which have been incorporated into a new high performance data system built at the National High Magnetic Field Laboratory.

Time-domain ICR data for ions generated by ESI from large biological molecules typically consist of narrow "beats", which are widely spaced due to the numerous isotopic peaks which are almost equally spaced in frequency.[2] The intervals between beats consist primarily of noise, so that FFT magnitude mode spectra (which are obtained from equally-spaced samples thorughout the time-domain data) are quite noisy (Figure 1, top). A (non-FFT) analysis that selectively extracts the signal from the beats while ignoring the noise between them, should thus produce dramatically improved signal-to-noise ratio.

One simple FT-based method for enhancing spectral quality is to set all data between the beats to zero-amplitude, thereby suppressing the low-signal data while preserving the "beats" which contain most of the signal. FFT of such a partly-zeroed data set remains computationally simple and produces modest improvement (Figure 1, center).

A standard algorithm for non-linearly sampled data[3] produces a dramatically enhanced spectrum (Figure 1, bottom), at the cost of significantly higher computational effort. This work was supported by NSF (CHE-93-22824), NIH (GM-31683), and the National High Magnetic Field Laboratory at Florida State University.

References:

1. J. P. Speir, M. W. Senko, D. A. Little, J. A. Loo, and F. W. McLafferty, *J. Mass Spectrom.* **1995**, *30*, 39-42.
2. S. A. Hofstatler, J. E. Bruce, A. L. Rockwood, G. A. Anderson, B. E. Winger, and R. D. Smith, *Int. J. Mass Spectrom. Ion Processes* **1994**, *132*, 109-27.
3. N. P. Lomb, *Astrophys. Space Sci.* **1976**, *39*, 447-62.

43rd ASMS Conference on Mass Spectrometry and Allied Topics

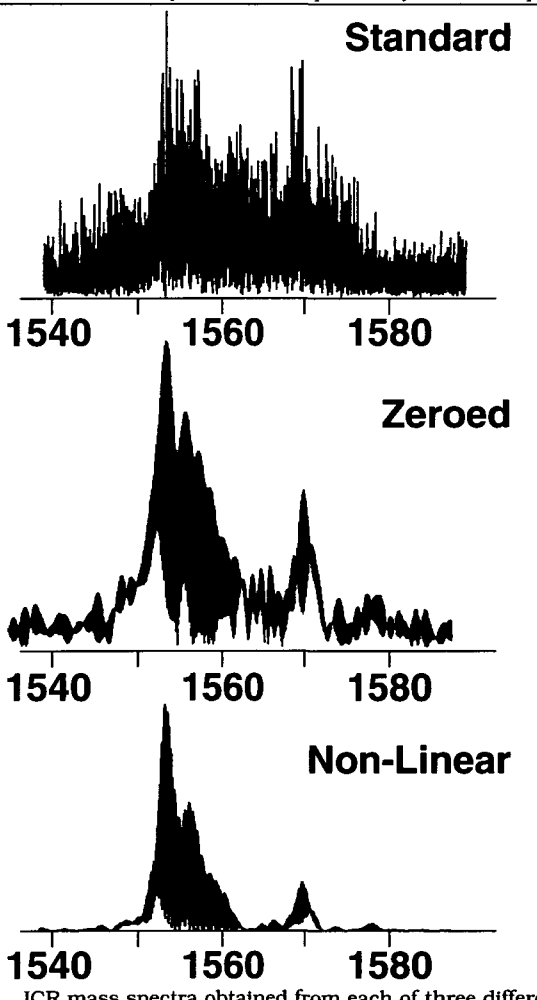

Figure 1. ICR mass spectra obtained from each of three different time-domain ICR data processing methods for the 43+ charge state of porcine albumin (67 kDa). Top: FFT of raw data. Middle: FFT of data which has been zeroed between time-domain "beats". Bottom: non-FT data reduction based on data taken only from the "beats".

Optically Detected Electron Spin Resonance of Trapped, Mass Selected Gas Phase Molecular Ions

Guo-Zhong Li, Shenheng Guan,*
Nar S. Dalal,# and Alan G. Marshall*

Center for Interdisciplinary Magnetic Resonance, National High Magnetic Field Laboratory, Florida State University, 1800 E. Paul Dirac Drive, Tallahassee, FL 32310

#Department of Chemistry, West Virginia University, Morgantown, WV 26506

* Department of Chemistry, Florida State University

We are developing the first experimental attempt at optical detection of electron spin resonance (ESR) spectroscopy of gas-phase molecular ions which have been mass-selected by ion cyclotron resonance. The generally accepted detection limit for conventional power absorption-based ESR detection is ~10^9 spins for a single one-second scan at room temperature of a 1 cm^3 sample of 1 Gauss linewidth at 3 tesla (84 GHz electron Larmor frequency).[1]

Optically detected magnetic resonance (ODMR) on phosphorescent neutral (singlet ground-state) molecules in solids dates back to 1967.[2] Use of optical rather than microwave photons for the detection of magnetic resonance offers vastly improved sensitivity compared to microwave detected ESR, leading to the recent ODMR detection of magnetic resonance of a single molecule.[3] In a cubic ICR ion trap at 3.0 tesla, only ~10,000,000 mass-selected organic ions are easily confined, so that ODMR methods are needed. Although ODMR of atomic ions has been observed by several groups,[4] ODMR of organic ions is much more difficult due to additional relaxation mechanisms (leading to much shorter electron spin-lattice relaxation time, T_1, and thus higher required microwave power to saturate the ESR transitions).

The experimental apparatus is shown in Figure 1. We use an open-ended multi-section cylindrical Penning ion trap to collect electron-ionized organic molecular cations in the presence of continuous azimuthal quadrupolar excitation to cool, axialize, and mass-select the ions as they fill the trap.[5] We propose to start with simple molecular ions like hexafluorobenzene. which should form abundant doublet ground state molecular radical cations. We shall monitor visible fluorescent emission while scanning the microwave irradiation frequency until the microwave frequency matches the Zeeman splitting; electron spin resonance is then inferred from a change in the fluorescent emission intensity. Automated and calibrated control of the experiment will be provided by a PC running under LabWindows and interfaced to a Hewlett-Packard VXI bus, GPIB and R232.

This work was supported by the National Science Foundation (CHE-93-22824) and the National High Magnetic Field Laboratory at Florida State University.

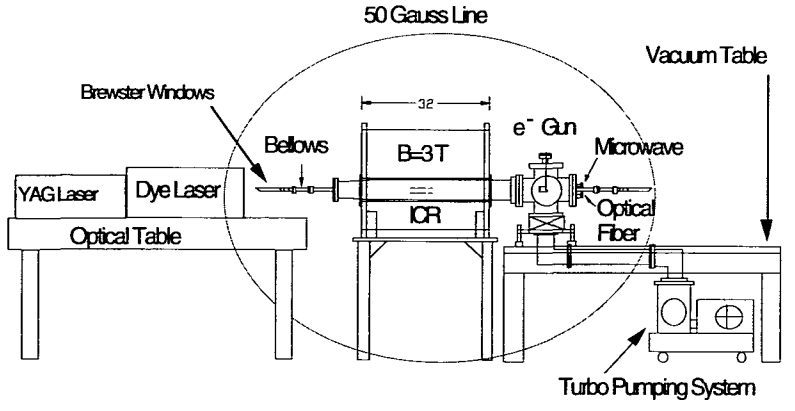

Figure 1. Apparatus for optically detected electron spin resonance of trapped, mass-selected molecular ions. The vacuum chamber is pumped to 10^{-9} torr by a turbomolecular pump (550 L/s). The solenoidal superconducting magnet is 3 tesla (Oxford Instruments) with 150 mm diameter bore for trapping ions. Two Brewster windows reduce the scattered light from the laser.

References

1. Y. S. Lebedev, in *Modern Pulsed and Continuous-Wave Electron Spin Resonance*, Ed.: L. Kevan and M. K. Bowman (Wiley, NY, 1990), Chapter 8, pp. 365-404.
2. M. Sharnoff, J. Chem. Phys.1967, 46, 3262-3264; A. L. Kwiram, *Chem. Phys. Lett.* **1967**, *1*, 272-275; J. Schmidt and J. H. van der Waals, *Chem. Phys. Lett.* **1968**, *2*, 640 - 642.
3. J. Köhler, J. A. J. M. Disselhorst, M. C. J. M. Donckers, E. J. J. Groenen, J. Schmidt, and W. E. Moerner, *Nature* **1993**, *363*, 242-244; R. Brown, J. Wrachtrup, M. Orrit, J. Bernard, and C. von Borczyskowski, *J. Chem. Phys.* **1994**, *100*, 7182-7191.
4. W. M. Itano, J. C. Bergquist, and D. J. Wineland, *J. Opt. Soc. Am.* **1985**, *B2*, 1392-1394; H. Knab, K. H. Knöll, F. Scheerer, G. Werth, *Z. Phys.* **1993**, *D25*, 205-208.
5. S. Guan, H.S. Kim, A. G. Marshall, M. C. Wahl, T. D. Wood, and X. Xiang, *Chem. Rev.* **1994**, *94*, 2161-2182

A Three-Section Quadrupole Ion Trap for FT-ICR Mass Spectrometry

Yulin Huang, Guozhong Li, Shenheng Guan*, and Alan G. Marshall*

Center for Interdisciplinary Magnetic Resonance, National High Magnetic Field Laboratory, Florida State University, 1800 E. Paul Dirac Dr., Tallahassee, FL 32310

* Department of Chemistry, Florida State University

We propose a novel three-section ion cyclotron resonance ion trap capable of high-pressure operation (Figure 1). Each section of the trap consists of four parallel circular cross-section rods. The middle section of four rods is held at ground potential. Axial confinement of ions along or opposed to the magnetic field direction is provided by applying the same d.c. potential to each set of "end cap" rods. Ions are trapped in the radial direction by the combination of a spatially homogeneous static magnetic field, B_0, and an azimuthal rf-inhomogeneous field produced by applying differential rf voltages to four rod electrodes parallel to the magnetic field axis. The overall effect is much like that of a quadrupole mass filter. When the rf frequency is high enough (several MHz), the azimuthal rf-inhomogeneous electric potential field forms an "effective" electrostatic potential (or "pseudopotential") well with a minimum at the center of the trap. Ion cyclotron frequency increases with the strength of the applied rf trapping field. Ion trajectories are stable even in the presence of ion-neutral collisions. Upper mass detection limit is dramatically increased by the addition of an rf electric potential. The trapping properties are revealed by construction of a "stability diagram".

Possible applications of this trap are as follows. First, for a given mass-to-charge ratio, m/q, we may adjust the rf amplitude to make the effective rf electric field, E_{rf}, equal in magnitude and opposite in direction to the regular dc trapping field, E_{dc}. In that limit, there is no magnetron motion (the magnetron frequency, ω_-, is zero); the "reduced" (observed) ICR frequency, ω_+, is unshifted by the electric field in the trap (for simplified mass calibration);

$$\omega_+ = \frac{qB_0}{m} = \omega_c$$

$$\omega_- = 0$$

and there is no upper mass instability limit. Second, the detectable upper mass limit may thus be extended to the theoretical limit for thermal motion, by setting the rf voltage amplitude, V_0 (see Fig. 1), such that $E_{rf} > E_{dc}$. For example, for V_{dc} = 1 V.

m/z	V_0(V)
1	2.2
10^3	69
10^5	690

Third, for all ions with mass less than the upper mass limit, ion motion is stable (i.e., the ion remains within the trap) even in the presence of collisions. Fourth, the effective magnetic field increases slightly on application of V_0.

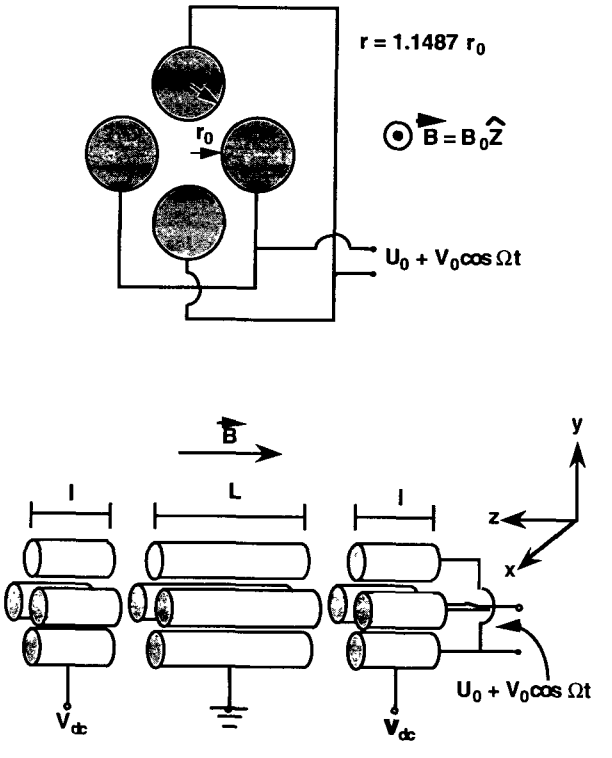

U_0: dc voltage amplitude
V_0: rf voltage amplitude
V_{dc}: dc voltage in z-direction;
Ω: rf frequency;

Figure 1. Proposed configuration of linear quadrupolar ion trap.

This work was supported by NSF (CHE-93-22824) and the National High Magnetic Field Laboratory at Florida State University.

Delayed Photofragmentation of Size Selected Gold and Silver Cluster Ions

M. Lindinger[1], K Dasgupta[2], G. Dietrich[3], H.-J. Kluge[4], S. Krückeberg[1], K. Lutzenkirchen[3], B Obst[1], L. Schweikhard[1], C Walther[1], and J. Ziegler[1]

[1]Inst. f Physik, Johannes Gutenberg-Universität, D-55099 Mainz, Germany
[2]Bhabha Atomic Research Center, Bombay 400085, India
[3]Inst f. Kernchemie, Johannes Gutenberg-Universität, D-55099 Mainz, Germany
[4]Gesellschaft fur Schwerionenforschung, D-64220 Darmstadt, Germany

The evaporation of neutrals is one possible decay channel of excited metal clusters. The time scale on which this process takes place is mainly determined by the statistical distribution of the excitation energy over the internal degrees of freedom of the cluster and the probability to locate a sufficient amount of energy on one degree suitable for dissociation [1] Investigations of the dynamics of the cluster fragmentation via beam experiments allows the observation of the decay only during short time windows determined by the length of the drift section of the apparatus, typically several hundred microseconds [2] The use of an ion trap for the storage of cluster ions extends the observation of the dynamics of fragmentation processes from microseconds to several seconds The experiments we report have been performed on gold and silver cluster ions of size n = 9 and 21 The clusters were excited via photons in the energy range between 3.7 eV and 4.4 eV

The cluster ions are produced by laser evaporation/ionization of a metal wire into a helium gas pulse which is expanded adiabatically into the vacuum [3]. They are transferred and injected into a Penning trap where they are stored in a 5T magnetic field. Specific cluster sizes are selected by resonant ejection of all unwanted ions. The mass selected cluster ions are centered by a combination of buffer gas cooling and quadrupolar rf excitation in the middle of the trap to obtain an optimal geometric overlap between clusters and laser beam. The beam of a Nd·YAG pumped Dye laser, whose output is frequency doubled (covering the wavelength range from 840 nm to 210 nm), is focused along the flight path of the ions into the center of the trap After the interaction the reaction products are identified via mass analysis using a two-stage time-of-flight mass spectrometer

Varying the delay between laser pulse and detection of the reaction products over a range of a few microseconds to hundreds of milliseconds the temporal development of the fragment pattern is observed Figure 1 shows on the upper part the signals of the precursor Ag_{21}^+ and its fragments at several times after the selected cluster Ag_{21}^+ has been excited. While the intensities of the precursor and all clusters with n≤18 stay constant, the Ag_{20}^+ ions decay to Ag_{19}^+ in the time range of about 2 ms The fragmentation behavior can be understood by considering the number of photons absorbed by the selected Ag_{21}^+ cluster Some will not absorb any photon and do not fragment Others absorb more than one photon and therefore decay fast to small cluster sizes n ≤ 18 Finally, the precursors Ag_{21}^+ that absorb just one photon decay to the next smaller cluster size "spontaneously", i.e in a period short compared to the duration of extraction from the Penning trap (about 20 μs). These primary fragment products, Ag_{20}^+, continue to decay to Ag_{19}^+ The time constant of this decay is a function of the photon energy and varies from 1 ms to 20 μs for photon energies from 3.7 eV to 4 4 eV

43rd ASMS Conference on Mass Spectrometry and Allied Topics

Analogous studies on Au_{21}^+ show a different behavior. The creation of the fragment Au_{20}^+ and Au_{19}^+ is observed on different time scales Au_{19}^+ is created spontaneously, while the time constants for the appearance of the fragment Au_{20}^+ (fig. 1 lower part) at photon energies from 3.8 eV to 4 4 eV vary from 1,3 ms to 50 μs.

In this case similar conclusions can be drawn about the absorption of photons as above for the fragmentation of Ag_{21}^+. The slow development of the fragment Au_{20}^+ is due to the absorption of one photon by the precursor. The fragments n≤19 appear quasi-spontaneously and are the result of the absorption of at least two photons by Au_{21}^+. This explanation is also supported by the photon flux dependence at long (40ms) and short (12μs) decay times of the decay of Au_{21}^+ One finds a linear slope for the former case whereas the latter shows quadratic behavior and a lower fragment abundance (see also the contribution of C Walther et al.). The data are currently further evaluated and binding energies of the cluster ions will be extracted by use of RRK - models

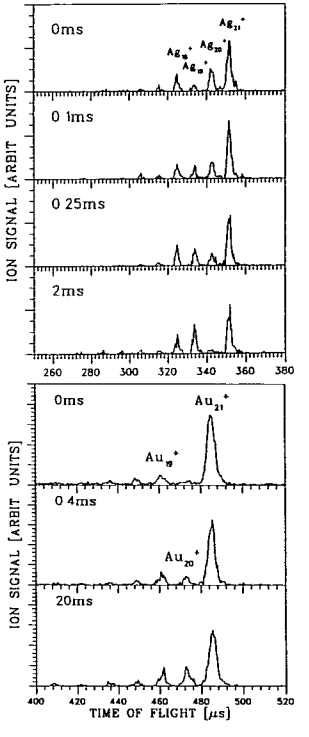

Figure 1. Time-of-flight mass spectra after photoexcitation of size-selected gold and silver clusters (delay periods between excitation and detection as indicated) Top· Ag_{21}^+ at a photon energy of 3.8 eV (time constant for the decay of Ag_{20}^+ and the appearance of Ag_{19}^+ 460 μs) Bottom Au_{21}^+ at a photon energy of 3.9 eV (time constant for the decay of Au_{21}^+ and the appearance of Au_{20}^+: 860 μs)

This work was supported by the Deutsche Forschungsgemeinschaft and the Materialwissenschaftliches Forschungszentrum Mainz

[1] M. F. Jarrold, Springer Series in Chemical Physics 52 (1994) 163
[2] C Brechignac et al., J. Chem Phys. 93 (1990) 7449
[3] H. Weidele et al., Z. Phys. D 20 (1991) 411

Instabilities of Ion Motions in Ion Cyclotron Resonance Traps

L. Schweikhard[1], J. Ziegler[1], H. Bopp[1], and K Lützenkirchen[2]

[1]Inst. f. Physik, Johannes Gutenberg-Universität, D-55099 Mainz, Germany
[2]Inst. f. Kernchemie, Johannes Gutenberg-Universität, D-55099 Mainz, Germany

Ion cyclotron resonance (ICR) traps (as used e.g. for Fourier Transform-ICR) store charged particles via a superposition of static magnetic and electric fields. In dependence of these fields ions of a very broad range up to a maximum mass-over-charge ratio $(m/q)_{crit}$ (the so-called critical mass) can be trapped. This theoretical mass limit for an ideal ICR trap (Penning trap) has been compared with experimental results

The measurements were performed by use of gold cluster ions and a Penning trap at a magnetic field of $B = 5\ T$ After production in an external source and transfer to the trap the ions were captured and size-selected at a low trapping voltage The trapping voltage was then varied to probe the maximum value possible, the critical trapping voltage U_{crit} (in analogy to $(m/q)_{crit}$ to which it can easily be transformed). Ion detection was achieved by axial ejection into a time-of-flight section. The setup has been constructed for the study of the properties of metal cluster ions by various mass spectrometical and laser spectroscopical methods as described in a recent review [1].

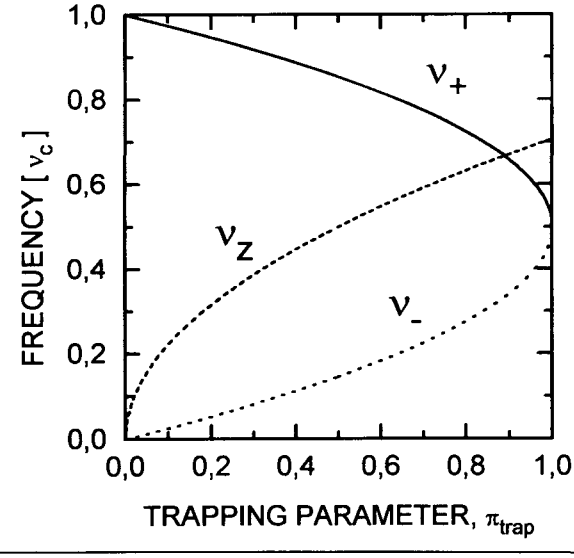

Figure 1. Eigenfrequencies of ion motion ω_+, ω_z, and ω_- (normalized to the cyclotron frequency) as a function of the trapping parameter π_{trap}.

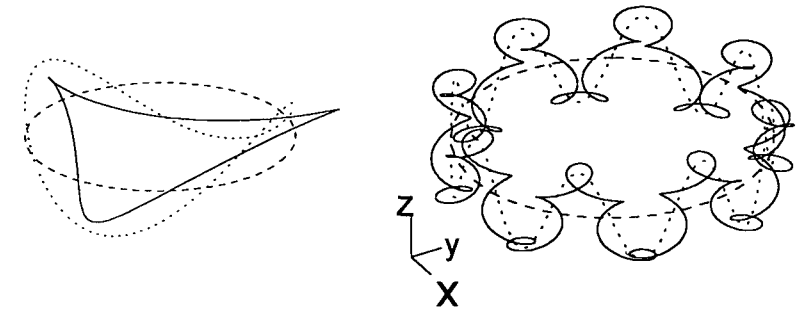

Figure 2. Ion motion in a Penning trap Dashed line. magnetron motion only, dotted line· combined magnetron and trapping motion; solid line full ion motion, i e combined magnetron, cyclotron, and trapping motion Left: $\omega_+ = \omega_z = 2\omega_-$. Right $\omega_+ = 4\omega_z$, $\omega_z = 8\omega_-$

In order to describe the trapping conditions with respect to the critical mass a generalized trapping parameter can be introduced [2]·

$$\pi_{trap} = 2\frac{\omega_z^2}{\omega_c^2} = \frac{U}{U_{crit}} = \frac{m/q}{(m/q)_{crit}} = \frac{2U}{d^2B^2}\frac{m}{q} \qquad (1)$$

$\pi_{trap} = 1$ corresponds to the critical condition ω_z and ω_c denote the trapping and cyclotron (in the absence of the electric field) frequency, respectively and d gives the dimension of the trap electrodes By use of the single parameter π_{trap} all ratios of the eigenfrequencies of the ion motion (ω_z, as well as the reduced cyclotron frequency, ω_z, and the magnetron frequency, ω_-), and their relation to ω_c (Figure 1) may be described simultaneously

The prediction of eq. 1 is in good agreement with the experimental results [2]. In addition to the well-known motional instability of ions exceeding the critical mass a new instability has been found at trap parameters that have so far not been considered to be 'critical' It appears at $\pi_{trap} = 8/9$. This means that the ratio of eigenfrequencies is $\omega_+ = \omega_z = 2\omega_-$. The ions' motion is a simple closed loop (Fig. 2 left) as compared to motions where the ions sample a larger part of the trap (Fig 2 right) Therefore the reduction in trapping efficiency may be understood by considering the repeated influence of perturbations of the ion motion from deviations of the actual trapping fields with respect to those of a perfect Penning trap [2].

Supported by the Deutsche Forschungsgemeinschaft and the Materialwissenschaftliches Forschungszentrum Mainz.

[1] L. Schweikhard et al, Physica Scripta, in print
[2] L. Schweikhard et al, Int J Mass Spectrom. Ion Processes, 141 (1995) 77

Single - and Two - Photon - Fragmentation of Stored Gold Cluster Ions

C. Walther[1], G Dietrich[2], H.-J. Kluge[3], M. Lindinger[1],
K. Lützenkirchen[2], L Schweikhard[1], and J. Ziegler[1]

[1]Inst. f. Physik, Johannes Gutenberg-Universität, D-55099 Mainz, Germany
[2]Inst. f Kernchemie, Johannes Gutenberg-Universität, D-55099 Mainz, Germany
[3]GSI, D-64220 Darmstadt, Germany

Gold cluster ions (containing n = 3 to 23 atoms) are produced by laserevaporation of a metal wire into a helium gas pulse which is expanded adiabatically into the vacuum [1]. They are transferred and injected into a Penning trap where they are stored in a 5T magnetic field Specific cluster sizes are selected by resonant ejection of all unwanted ions. The mass selected cluster ions are centered in the middle of the trap by a combination of buffer gas cooling and quadrupolar rf excitation.

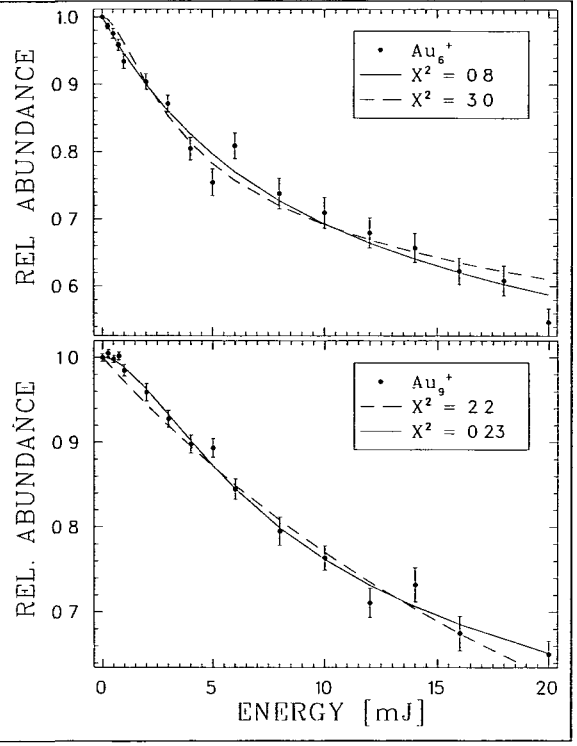

Figure 1. Photofragmentation of Au_n^+ using the second harmonic of a Nd:YAG laser (2 3eV). Top. Fragmentation of Au_6^+ The flux dependence shows a linear slope at low intensities indicating a one-photon process.
Bottom· Fragmentation of Au_9^+. A quadratic behavior is observed corresponding to a two-photon transition.

The second, third, and fourth harmonic of a Nd:YAG laser (wavelengths of λ = 532 nm, 355 nm, and 266 nm, respectively) is focused axially into the trap. In addition the output of a Nd YAG pumped dye-laser can be frequency doubled covering the wavelength range from 840 nm to 210 nm. The selected clusters and their reaction products are identified by mass analysis using a two-stage time-of-flight mass spectrometer. The experiments are an extension of previous work where the stored clusters have been collided with a buffer gas to induce dissociation [2].

The observed fragmentation patterns show a preferred production of odd cluster sizes, indicating that those clusters (containing an even number of atomic valence electrons) are more stable than even ones Clusters with an even number of atoms always evaporate monomers. For low laser intensities at 532 nm and 355 nm we found small odd clusters to prefer the evaporation of neutral dimers whereas at 266 nm the emission of single atoms was as likely This can be understood as follows: For photon energies near the fragmentation threshold only the energetically most favorable channel is populated. At photon energies considerably above the monomer evaporation becomes equally probable.

Using one fixed photon energy (2 3 eV) a cluster may need one or two photons to fragment, depending on its binding energy. In the former case one observes a linear increase of fragments with rising photon flux density as shown in the top of Fig 1. The latter results in a quadratic slope for low laser pulse energies (see bottom of Fig. 1). By use of the χ^2-values of the corresponding fits one can distinguish the two possibilities very well. (However, it is nontrivial to deduce the binding energies from these data.

For a given cluster size a transition from one to two photon fragmentation is achieved when the photon energy is lowered stepwise. Again, the transition energy is not identical with the fragmentation threshold but significantly higher. In the case of Au_{21}^+ the binding energy was found to be 2.0 (1) eV although for energies up to 4.0 eV (311 nm) 2-photon fragmentation is observed This difference increases, the more atoms the cluster consists of.

The fragmentation is understood as a statistical process. The excitation energy absorbed by the electrons of the cluster is transferred very rapidly into vibrations of the ionic core. Because of the finite temperature of the cluster before excitation, thermal energy (corresponding to room temperature in our case) has to be added. For an evaporation to take place it is necessary to accumulate an amount of energy exceeding the binding energy into one degree of freedom Especially if the excitation energy exceeds the binding energy only by a small amount this can take times up to tens of milliseconds. In contrast to beam experiments trapping the ions enables us to measure decay constants in this time domain. Being limited to short time scales may lead to an incomplete observation of fragments as the following example may illustrate· For Au_{21}^+ and a photon energy of 4 3 eV the time constant of the monomer evaporation (i.e. buildup of Au_{20}^+) is 50 (10) µs. But a certain amount of Au_{20}^+ appears quasi-spontaneous on the time scales accessible with our apparatus (faster than 10µs) Investigating the photon flux dependence at long (40 ms) and short (12 µs) delay times yields a linear slope for the former case whereas the latter shows quadratic behavior and a lower fragment abundance. This indicates the absorption of two photons and thus a higher excitation energy. Binding energies may be extracted by use of a RRK - model (see also M. Lindinger et al.).

This work was supported by the Deutsche Forschungsgemeinschaft and the Materialwissenschaftliches Forschungszentrum Mainz.

[1] H. Weidele et al., Z. Phys. D **20**, 411 (1991)
[2] St Becker et al., Z. Phys. D **30**, 341 (1994)

Analysis of the substituent distribution in *O*-methyl celluloses by MALDI-FT-ICR-MS

C.G. de Koster, M.C. Duursma, P.W. Arisz, R.M.A. Heeren and J.J. Boon

FOM institute for Atomic and Molecular Physics, Kruislaan 407, 1098 SJ Amsterdam, The Netherlands

Methyl celluloses are heterogeneous mixtures of cellulose *O*-methyl ethers with a variable degree of substitution at different sites of the constituing monomers. Both the degree of substitution and the substituent distribution along the backbone determine the thermogelation temperature of the compounds. The *O*-Me substituent distribution along the cellulose backbone has been investigated by GC of their monomers and by FAB-MS with a sector instrument of perdeuteromethylated oligomers prepared by partial hydrolysis of the samples [1]. The distribution of the methyl groups in the perdeuteromethyl-*O*-methyl-cellotriose is derived from the peak intensities of the sodiated molecules in the FAB-MS spectrum. FAB-MS analysis of larger oligomers is hampered, due to the upper limit of mass resolution of the sector instrument, by the interference of fragment ions originating from sodiated oligomers with a higher degree of polymerization. Another complication in this context is the presence of FAB matrix cluster and fragment ions as a chemical background in the mass spectra.

FT-ICR-MS analysis of MALDI ionized perdeuteromethylated partial hydrolysates of methyl celluloses is a potentially highly advantageous method for the determination of the *O*-methyl substituent distribution in oligomers with a higher degree of polymerization than that of cellotriose. The external ion source FT-ICR-MS used in this work was a modified Bruker Spectrospin APEX 70e, 7T FT-ICR-MS with a home built ion source. MALDI of derivatized partial hydrolysates mixed with 2,5-dihydroxybenzoic acid (DHB) in a 1 : 1000 analyte / matrix molar ratio (sample size: a few ng on the target) produces sodium cationized molecules with a sufficient yield to detect the ions in the ICR cell. In a typical broad band experiment resolutions of 12,000 $(m/dm)_{50\%}$ were obtained with a S/N ratio of 30 at m/z 906 (tetramers). The perdeuteromethyl-*O*-methyl-cellotriose, -cellotetrose and -cellopentose pseudomolecular ion distributions were determined in heterodyne mode.

The MALDI-FT-ICR mass spectrum (heterodyne mode) of the perdeuteromethylated pentasaccharide obtained from a methyl cellulose hydrolysate is shown as a typical example in Fig. 1. The mass spectrum covers the entire methyl substituent distribution of perdeuteromethylated/methylated compounds CD_3O-(nCH_3O / (15-n)CD_3O-cellopentose)-CD_3 beginning with [CD_3O-(15CH_3O-cellopentose)-CD_3 + Na]$^+$ at m/z 1095.57 unto the CD_3O-(15CD_3O-cellopentose)-CD_3 + Na]$^+$ cations at m/z 1140.85. MALDI ionization of the derivatized cellopentose produces predominantly sodiated molecules giving peaks at equidistant intervals of 3 Dalton. No signals from potassiated or protonated species are observed. The resolution $(m/dm)_{50\%}$ is approximately 55,300 with a signal to noise ratio of 210 at m/z 1110.67 [CD_3O-(10CH_3 / 5CD_3O-cellopentose)-CD_3 + Na]$^+$ for a sample amount of a few ng on the target. Two ion series coincide with the mass range of the perdeutero/methyl cellopentoses. The series of peaks at the low mass end of the spectrum differs 17 Dalton with the corresponding [M+Na]$^+$ ions from the cellopentoses. These lower mass ions originate most likely from glycosidic

bond fragmentations of higher oligomers with charge retention on the reducing end [2]. The resolving power which is required to separate these fragment ions from the sodiated perdeuteromethyl/methyl cellopentose molecules is 30,000. The origin of the series of peaks at the high mass end of the spectrum is less obvious. However, both series of peaks do not interfer with the pseudomolecular ion distribution of the perdeutero/methyl cellopentose molecules. Therefore, the resolution of 55,000 $(m/dm)_{50\%}$ in heterodyne mode is sufficient to mass resolve interfering fragment ions and pseudomolecular ions, enabling the estimation of the O-methyl distribution along the backbone of methyl cellopentose.

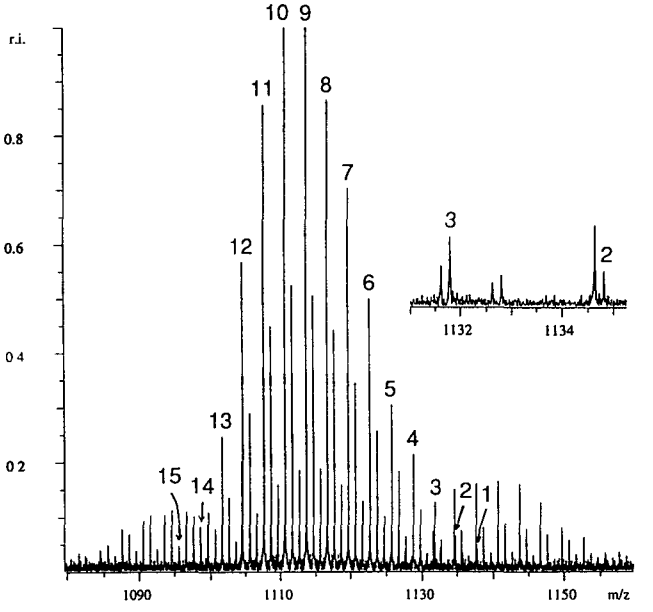

Fig.1 MALDI-FT-ICR mass spectrum of the cellopentose fraction in a perdeuteriomethylated partial hydrolysate of methyl cellulose. The peaks are labelled by the number of CH_3 groups (n) in the CD_3O-(nCH_3O / (15-n)CD_3O-cellopentose)-CD_3 compounds.

[1] P.W. Arisz, H.J.J. Kauw and J.J. Boon, *Carbohydr. Res.*, in press.
[2] B. Domon and C.E. Costello, *Glycoconjugate J.*, 5, 397 (1988).

Characterisation of Electrosprayed polymers with MALDI-FT-ICR-MS

Ron M.A. Heeren, G.J. van Rooij, Marc C. Duursma, Chris G. de Koster and Jaap J. Boon.
FOM-Institute for Atomic and Molecular Physics,
Kruislaan 407, 1098 SJ Amsterdam, The Netherlands.

The combination of an ionisation technique like Matrix Assisted Laser Desorption Ionisation (MALDI) with mass spectrometry has already proven to be a valuable technique to characterise the molecular weight distribution and the dispersity of synthetic polymers. In this paper we have used the unequivocally high resolution of Fourier Transform Ion Cyclotron Mass Spectrometry (FT-ICR-MS) to additionally identify the elemental composition of the monomer and endgroup of several (homo)polymers. The information thus obtained provides insight in both initiation and termination of the polymerisation reaction cycle, as parts of the reactants are found back as structural components in the end-groups. In all experiments, MALDI performed in a homebuild external ion source [1] was used as ionisation technique. Sample preparation turned out to be critical for the succes of this method. In the following sections we will discuss a new sample preparation method which we found to yield very strong and reproducable MALDI-FT-ICR-MS signals of polymeric compounds.

All experiments in this paper were performed on a Bruker-Spectrospin APEX 70e, 7T FT-ICR-MS equipped with an in house designed MALDI ion source. The instrument is equipped with a Bruker Infinity™Cell for improved sensitivity. A differential pressure of 5 orders of magnitude between the ICR-cell region and the source can be maintained, with a three stage differential pumping scheme, without using cryopumps. The vacuum system used was described in previous publications [1,2] and enabled us to perform helium collisional cooling experiments when required. The source was interfaced with a nitrogen gas discharge laser (Photon Technology International, Model PL2300), which delivered a 600 ps, 0.5 mJ pulse of 337 nm to the target probe inside the ion source. By means of a simple telescope the beam was transported from the laser to the ion source, and focussed through a quartz window to a 1.5x3 mm spot size. The ions formed in the source are transported by means of an electrostatic ion guide to the ICR cell, where they are subsequently analysed.

In the course of our MALDI experiments, we evaluated two sample deposition methods, a dried droplet method and a new, electrospray sample deposition method. In the second method, the analyte-matrix solution was nebulised in a 4 kV/cm electric field. The stainless steel sample probe was the ground electrode in this homebuild electrospray set-up, and was positioned approximately 1 cm away from the tip of a 180 um i.d steel capillary. We found that this method yields superior shot-to-shot reproducebility and signal-to-noise ratio. We attribute this improvement to the quick formation of small crystals over a large surface area. This method gives us excellent control over deposition area, deposition speed and sample thickness. The method also eliminates the time consuming search for a good crystal on the probe, and the ability to use thick sample layers ensures a long lasting signal from one particular probe position. Typically we obtain 1000 reproducible shots from one position in a PEG1000-2,5-DHB mixture. NaI, LiI and KI were added to the analyte-matrix solution to promote sodium cationisation.

The broadband MALDI-FTMS mass spectrum of native PEG1000 is shown in figure 1. Note that the front and back trap electrode of our ICR cell were biased at 2.5 and 3.5 V respectively during this experiment.

This uncommonly low trapping voltage could be used by the virtue of the external ion source. Also no pulsed gas was applied to the cell to enhance the trapping efficency. The cell pressure during these experiments was $1.3*10^{-10}$ mbar. This resulted in a broadband resolution of 30000 $(m/dm)_{50\%}$ with a S/N of 100 at m/z 965 for the $[M_{21} + Na]^+$ monoisotopic peak. This resoltution enables us to perform linear regression analysis on the measured masses for each monoisotopic peak as a function of the corresponding degree of polymerisation. An example of such a plot is given in figure 2, were the measured masses of both native and per-deutero methylated PEG1000 with different cation adducts has been plotted versus their degree of polymerisation. The intercept of the fitted line yields the residual endgroup mass of the polymer. Its slope yields the mass of the repeating unit in the polymer. This value can also be deduced from the equidistant (m/z 44) peaks in the molecular weigth distribution, and subsequently be used as fixed coefficient for the linear regression analysis. This will result in a slightly more accurate endgroup mass.

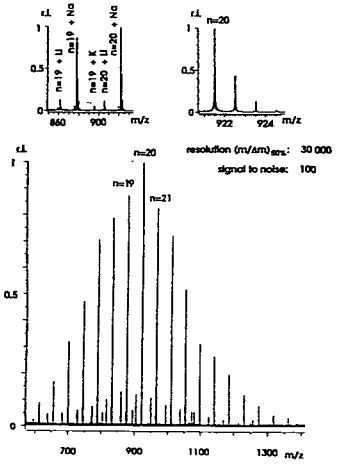

Figure 1 A broadband MALDI-FT-ICR-MS spectrum of a native PEG1000.

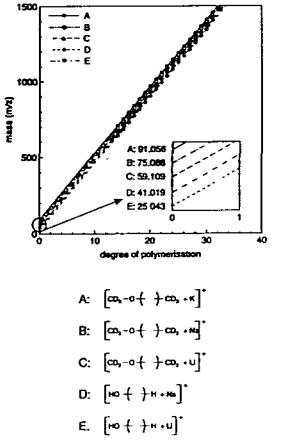

Figure 2. Linear regression analysis of native and per-deutero methylated PEG1000 with different cation adducts.

Similar experiments were perfomed on a PEG4000, where the error in endgroup analysis was appr. two orders of magnitude larger due to the larger extrapolation error. However, the accuracy was still more than sufficient to positively identify the distal part of the polymer. Using isotopically resolved peaks containing 2 ^{13}C isotopes, we were able to distinguish a PEG4000 with a di-propyl end group from a PEG4000 with a di-acetyl endgroup, both having nominally identical masses.

[1] R M.A Heeren, J.J. Boon and P. Caravatti, *Proceedings of the 42nd ASMS conference on Mass Spectrometry and Allied Topics*, Chicago, 1994, pp 231-232
[2] R.M.A. Heeren, C.G. de Koster and J.J Boon, Submitted to Anal. Chem.

FT/MS Analysis of Block and Random Polyester-Urethane Polymers

Paul Souchek, James DeFelippis, Yvonne Berry-Walker and *Robert Ludicky, Morton International, 1275 Lake Avenue, Woodstock IL 60098

Introduction

Polyester-urethanes are utilized in a wide range of adhesives and coatings. These polymers can be either mixes or blocks of polymers tied together. Block copolymerization allows the synthesis of copolymers which can be tailored for a wide variety of physical properties. This tailoring process, however, also means that the final performance of the copolymer will depend on both monomer composition and exactly how the polymer is assembled. Traditional polymer analysis, by techniques such as pyrolysis, hydrolysis and NMR can easily determine a polymer's composition. These same techniques, however, are very weak at determining whether the composition of a polyester-urethane is random or block. In this day of specialized step polymerized polymers, monomer composition is no longer sufficient for block copolymer characterization.

Experimental

Two different sets of block and random polyester-urethanes were analyzed by negative ion carbon dioxide laser desorption FT/MS. Each set consists of a random and block polyester-urethane of identical monomeric composition. The only differences between members of a set relates to the number of polyesters utilized to produce each member. The compositions of the four polyester-urethanes are given below:

Polyester-Urethane 1		Polyester-Urethane 2	
Prepared from DEG-NPG-AA +MDI		Prepared from DEG-AA, NPG-AA +MDI	
MDI	11.07 %	MDI	11.44 %
DEG	24.58 %	DEG	24.60 %
NPG	23.37 %	NPG	23.35 %
AA	40.96 %	AA	40.60 %

Polyester-Urethane 3		Polyester-Urethane 4	
Prepared from DEG-NPG-IPA-AA +MDI		Prepared from DEG-IPA-AA, NPG-IPA-AA +MDI	
MDI	9.15 %	MDI	11.44 %
DEG	25.30 %	DEG	23.96 %
NPG	22.57 %	NPG	23.57 %
IPA	21.48 %	IPA	20.65 %
AA	21.48 %	AA	20.65 %

All the percentages given in the preceding table are mole percents. The following abbreviations were utilized to name the polyester-urethane components: Methylene Diisocyanate (MDI), Diethylene Glycol (DEG), Neopentyl Glycol (NPG), Adipic Acid (AA) and Isophthalic Acid (IPA).

Discussion

The negative ion laser desorption spectra of the random and block polyester-urethanes of nearly identical monomeric composition, urethanes 1 and 2 and urethanes 3 and 4, were quite different from one another. The block copolymers, urethanes 2 and 4, gave two repeating ion series. The random polyester-urethanes 1 and 3 gave only one set of ions apiece. The differences in the number of sets of ions appears to be directly related to the number of polyesters utilized to produce a particular urethane. The mass spectra of all four urethanes were very similar to those obtained from their base polyesters. For the block copolymers, the mass spectra of urethanes 2 and 4 appear as if the two polyesters utilized to produce these urethanes were mixed without MDI. This fact makes identification of the base polyesters relatively easy. This fact, however, also raises a question about how the polyester-urethanes can be ionized and fragmented without showing the presence of MDI.

There appears to be two possible explanations for the unusual mass spectral behavior discussed above: Massive fragmentation which results in selective ionization of polyester fragments or laser desorption of residual polyesters. The NMR spectra of the polyester-urethanes does not show any detectable hydroxyl functionality but does show free isocyanate groups. FT/MS experiments carried out with short time delays also are shifted to higher mass. These two pieces of data tend to support the massive fragmentation hypothesis and oppose the residual polyester hypothesis. Regardless of the mechanism, it appears that FT/MS can quickly and easily distinguish between random and block polyester-urethanes of very similar monomeric composition. In this day of tailored polymers, where monomer analysis by itself if often not sufficient, this type of information may be crucial to understanding how a polymer performs.

Analysis of Urban Air Particulates, SRM 1649, by Negative Ion FT-ICR MS and GC/NCI MS

Ming Xu, Hyun Sik Kim,* Shenheng Guan,* Alan G. Marshall,* Ralph C. Dougherty

Department of Chemistry, Florida State University, Tallahassee, FL 32306-3006

*Center for Interdisciplinary Magnetic Resonance, National High Magnetic Field Laboratory, Florida State University, 1800 E. Paul Dirac Dr., Tallahassee, FL 32310

Urban air particulates are composed mostly of inorganic components, e.g. ammonium sulfate. A large number of organic chemicals are adsorbed on the inorganic matrix at ultra-trace to ppm levels. The organic chemicals come from surface sources and are often modified in the atmosphere.[1] Some of the chemicals are mutagens and/or carcinogens.[2] High electron affinity, in the gas-phase or in solution, correlates with mutagenicity,[3] suggesting that negative ion screening might be a productive approach to evaluation of hazards in air particulates. We have applied this approach to ambient urban air particulates, National Institute of Standards and Technology Standard Reference Material (SRM) 1649 by use of negative ion laser desorption/ionization FT-ICR MS and GC/NCI MS.

Dichlorophene, an artifact from the SRM collection, dominated the negative ion spectra of extract SRM 1649.[4] This compound produced peaks corresponding to $(M+O-2H)^-$ and $(M-4H)^-$, in addition to the $(M-H)^-$ anion when it was subjected to laser desorption/ionization. The product ions correspond to dichloro-dihydroxybenzophenone ($C_{13}H_8O_3Cl_2$) and dichloroxanthone ($C_{13}H_6O_2Cl_2$), respectively. The relative signal magnitude increased after axialization of the ions in the ICR ion trap. The reactions that lead to dichlorodihydroxybenzophenone from dichlorophene are similar to the formation of $(M+14)^-$ reported by Buchanan *et al.*[5] Dichloroxanthone arises from dehydration of dichlorodihydroxybenzophenone.

Product ions from dichlorophene corresponding to the dimer anion, $C_{14}H_{10}O_2{}^{35}Cl_2$ (m/z 280) of 4-chloro-1,2-quinomethane ($C_7H_5O^{35}Cl$, m/z 140) were observed by use of 7 eV ionization, and detection at 10^{-9} torr in the analyzer of a dual cubic trap. An anion at m/z 407 ($C_{20}H_{14}O_3{}^{35}Cl_3$) that corresponds to an adduct of the deprotonated molecule and the 4-chloro-1,2-quinomethane was also prominent in the spectrum. Positive electron ionization (EI, 70 eV) of dichlorophene resulted in product ions corresponding to protonated 4-chloro-1,2-quinomethane ($C_7H_6O^{35}Cl$, m/z 141) and 4-chlorophenol ($C_6H_5O^{35}Cl$, m/z 128) in addition to the molecule ion ($C_{13}H_{10}O_2Cl_2$, m/z 268). Dichlorodihydroxybenzophenone was confirmed by GC/NCI MS of a standard sample of dichlorophene.

A small sample (0.1 g) of SRM1649 was Soxhlet-extracted with methylene chloride. The extract was partitioned by 10% aqueous sodium hydroxide into acidic and neutral fractions. The basic solution was neutralized (HCl) and the organic components were back-extracted with methylene chloride. Solvent was removed using a Kuderna-Danish followed by a stream of high purity nitrogen.

43rd ASMS Conference on Mass Spectrometry and Allied Topics

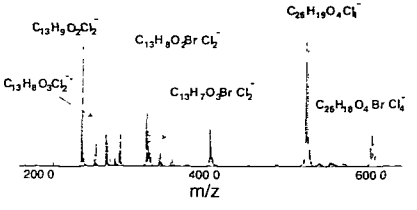

Figure 1. Gold film-assisted laser desorption/ionization negative ion FT-ICR mass spectrum of the neutral fraction of SRM 1649 extract.

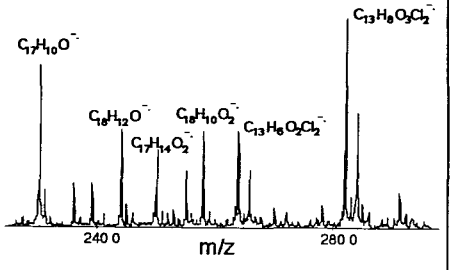

Figure 2. Gold film-assisted laser desorption/ionization negative ion FT-ICR mass spectrum of the neutral fraction of SRM 1649 extract.

Figure 1 illustrates the negative ion spectrum of the acid fraction obtained by gold film assisted laser desorption/ionization. Components that apparently arose from addition of dichlorophene to the collection filter included dichlorodihydroxy-benzophenone (m/z 281.9791), dichlorophene (m/z 267.0015), and monobrominated dichlorophene ($C_{13}H_9O_2BrCl_2$, m/z 346.9274). The presence of all of these components in the sample was confirmed by GC/NCI MS.

The negative ion spectrum of the neutral fraction obtained by gold film assisted laser desorption and ionization is shown in Figure 2. Dichloroxanthone ($C_{13}H_6O_2{}^{35}Cl_2$, m/z 263.9824) and dichlorodihydroxy- benzophenone (m/z 281.9832) were present in this fraction with relatively high abundance. Of oxy-polynuclear aromatic hydrocarbons, the spectrum shows the molecule anions for benzanthrone isomers ($C_{17}H_{10}O$, m/z 230.0715), benzanthracene-dione isomers ($C_{18}H_{10}O_2$, m/z 258.0677), hydroxybenzanthracene/methyl benzanthrone isomers ($C_{18}H_{12}O$, m/z 244.0854) and a C_3-alkyl anthroquinone isomer ($C_{17}H_{14}O_2$, m/z 250.0983). With the exception of the hydroxybenzanthracene/methyl benzanthrone isomers the existence of these components in the mixture was confirmed by GC/NCI MS.

The correlation between mutagenicity and electron affinity[3] suggests that the new components of atmospheric air particulates that were revealed by this LD FT-ICR screening procedure should be examined toxicologically. Work supported by N.S.F. (CHE-94-13008) and the National High Magnetic Field Lab at Florida State Univ.

1. T. E. Graedel, D. T. Hawkins, and L. D. Claxton, *Atmospheric Chemical Compounds, Sources, Occurrence and Bioassay*, 1986.
2. J. Lewtas, *Pharmacology & Toxicology* **1993**, *72* (supplement I), s55-s66
3. G. Bakale and R. D. McCreary, *Carcinogensis* **1987**, *8*, 253-264; *ibid.*, **1990**, 10, 1811-1818
4. H. S. Kim, M. Xu, S. Guan, A. G. Marshall, and R. C. Dougherty, *Proc. 42nd ASMS Conf. on Mass Spectrometry and Allied Topics*, Chicago, IL, **1994** p 261.
5. M. V. Buchanan, I. B. Rubin, M. B. Wise, and G. L. Glish, *Biomed. Environ. Mass Spectrom.* **1987**, *14*, 395-399

A New Approach for the Analysis of Volatiles in Complex Matrices

S.A Barshick, M V Buchanan, and M.R. Guerin
Oak Ridge National Laboratory, Oak Ridge, TN 37831-6120

Introduction: Analytical methods for the analysis of volatile organic compounds (VOCs) in water are well established in EPA methods. These methods, however, typically have limited applicability to the direct analysis of solid samples or complex media, falling short in the sample preparation and sampling areas. A novel off-line blender-purge and trap sampling device was developed to overcome some of the problems encountered in the analysis of VOCs in solids and/or complex matrices (1). The blender-purge and trap sampling device was designed to allow simultaneous or sequential homogenization and sampling of solids or complex media to be conducted in a closed system thereby minimizing loss of volatile analytes during the sample preparation steps This device offers several unique advantages for analyzing complex matrices including the ability to customize the homogenization and purge processes to accommodate sampling of any solid or liquid matrix and the ability to be used in a purge and trap mode (purge outlet is connected to a sorbent trap for GC/MS analysis) or in a direct sampling mode (purge outlet is connected directly to an ion trap MS)

Experimental: In this design, a commercial 1L stainless steel Waring blender with a 7 speed motor was modified. The original 1L blender container was replaced with a 50-250 mL capacity stainless steel mini-container. To obtain a closed system, a stainless steel lid was made and mounted to the blender container by welding a half inch wide rim to the top of the container and placing a neoprene gasket between the container and lid The lid was designed with 3 cajon fittings: a 1/16" fitting provided connection for the purge inlet line, a 1/4" fitting was used to connect to the purge outlet line, and a second 1/16" fitting served as an injection port through which water or internal standards could be added to the sample. An additional modification was the replacement of the original blending assembly with a special bearing cap and replaceable pressure seal that allowed the sample to be blended and purged without leaking.

Results and Discussion: The blender-purge & trap sampling device was developed as part of a GC/MS method for the quantitative determination of benzene in foods. To evaluate the blender-purge and trap method versus a more conventional purge and trap method, a series of studies were conducted to establish the detection limits, accuracy, and reproducibility of the two approaches. The results for the analysis of target foods were compared to a standard purge & trap GC/MS method based on EPA Method 624. Results are shown for the mean concentration of benzene found (ppb) ± 95% confidence interval as determined from linear regression analysis of standard addition data for triplicate analyses. Concentrations given in ( ) indicate that the quantitative results were not statistically different from zero. The results, shown in Tables 1 & 2, demonstrate several advantages of blender-purge & trap sampling over the conventional approach including: improved reproducibility (lower confidence intervals), the ability to quantitate both liquid and solid samples equally well with respect to accuracy and reproducibility, low ppb to ppt detection capabilities in complex matrices, and accuracy well within EPA QA acceptance criteria.

The ability to alter the types of volatile compounds sampled using the blender-purge & trap device also was investigated for qualitative GC/MS analysis In preliminary studies, the effects of various sampling treatments on the production of volatiles from reference cigarettes were investigated. The treatments included heat, aqueous extraction, and change in pH. Several observations can be made from these results, including: an increase abundance of hydrocarbons in the dry heated samples, the appearance of chlorinated hydrocarbons in the aqueous extracted samples, and a change in sensitivity for certain compounds (e.g. tetrahydrofuran & acetic acid ethyl ester) as a function of sample pH. These pilot studies demonstrated the ability to alter selectively the types of volatile compounds that can be observed by changing sample conditions.

Table 1: Comparison of Methods for the Determination of Benzene in Foods

Sample	Conventional Purge & Trap GC/MS	Blender-Purge & Trap GC/MS
Coffee	(0.07 ± 0.99)	0.10 ± 0.09
Tea	(0 16 ± 0.35)	0.11 ± 0.07
Cranberry juice	0 69 ± 0 66	0 55 ± 0.19
2% Milk	(0.00 ± 0.59)	(0.02 ± 0.05)
Orange juice	(0.00 ± 1.01)	(0.04 ± 0 05)
Raw Chicken	2 44 ± 0 87	(0.06 ± 0.12)
Cooked Chicken	(2.04 ± 2.83)	0.11 ± 0.02
Scrambled Eggs	(0 20 ± 0.50)	0.10 ± 0.07
Instant Oatmeal	(0 31 ± 3 80)	0.07 ± 0 05
Tomatoes	(0.36 ± 1 08)	(0.02 ± 0.02)

Table 2: Determination of Benzene in QA/QC Fortified Food Samples

Sample	Reported Conc. ± 95% C.L.	QA/QC Fortified Conc.	% Error
Chicken	0 47 ± 0.28	0 51	8%
2% milk	0 36 ± 0 16	0 31	16%
Tomato	0.22 ± 0.06	0.24	8%

Conclusions: A method for the analysis of volatiles in complex matrices was developed using a novel blender-purge & trap sampling device. Several significant advantages of this device compared to conventional methods for the analysis of VOCs were demonstrated including the ability to sample and analyze both liquid and solid samples with minimal loss of analyte, accuracy well within EPA QA acceptance criteria (for benzene: 37-151%), and low ppb to ppt detection limits in complex matrices, such as foods. Additionally, the use of this sampling device for qualitative & quantitative GC/MS analysis was demonstrated. Future work will involve the development of this device in conjunction with Direct Sampling Ion Trap Mass Spectrometry (DSITMS) as a screening method for VOCs in a variety of complex matrices.

(1) Barshick, S A., Smith, S M., Buchanan, M.V , and Guerin, M. R. "Determination of Benzene Content in Food Using a Novel Blender-Purge & Trap GC/MS Method", *Journal of Food Composition & Analysis*, in press.

Research sponsored by the National Cancer Institute under Interagency Agreement 0485-F053-AL with the U S Department of Energy under contract No. DE-AC05-84OR21400 with Martin Marietta Energy Systems, Inc

EPA Method 8270 (Semivolatiles) using a GC/Ion Trap Spectrometer

S.A Barshick, S. Worthy, and W H. Griest
Oak Ridge National Laboratory, Oak Ridge, TN 37831-6120

Introduction· EPA method 8270 describes the analysis of over 70 semivolatile organic compounds (SVOCs) in groundwater, soils, and solid and mixed wastes. Estimated quantitation limits for this method using a quadrupole mass spectrometer are in the µg/L or µg/kg range. To achieve these concentrations levels, liter volumes of water or tens of grams of solid waste must be extracted and concentrated to 1-2 mL prior to GC/MS analysis. The inherent sensitivity of the ion trap mass spectrometer (ITS) and its compatibility with GC introduction makes GC/ITS ideal for use in EPA methods The goal of this work was to demonstrate the improvements possible in EPA protocols using an ion trap mass spectrometer. Method 8270 was chosen for this evaluation.

Experimental· Sample extracts were prepared and analyzed according to Method 8270 using both a quadrupole GC/MS and an ion trap GC/MS. The quadrupole GC/MS system used was a Hewlett Packard Mass Selective Detector (GC/MSD) GC/MSD analysis was performed by a certified laboratory (Analytical Services Organization, ORNL) following the standard EPA method 8270 conditions and procedures The ion trap GC/MS system used was a Finnigan MAT Magnum Ion Trap mass Spectrometer (GC/ITS) GC/ITS analysis was performed using EPA method 8270 as a guideline and the conditions shown in Table 1

Table 1. GC/MS Operating Parameters

Mass Range.	45 - 500 amu
Scan Rate:	1 sec/scan
Automatic Gain Control:	on
Filament Delay:	300 sec
Source Temperature:	220°C
Emission Current	50 µA
Transfer Line Temperature	290°C
Initial Column Temperature	40°C hold 4 minutes
Temperature Program	40-280°C @ 8°C/min
Injection mode·	on-column
Injection port temperature:	35 °C hold 0.1 min
Temperature program:	35-280°C @ 180°C
Column head pressure:	16 psi
Carrier gas:	helium @ 50 cm/s (@ 40°C)

Results and Discussion: Using the GC/ITS, quantitation limits in the ng/L range were possible compared to the µg/L quantitation limits listed in Method 8270 Initial calibrations were performed according to SW-846 Method 8270, however, the quantitation criteria required by the method could not be met using the GC/ITS and the splitless injection technique. All quantitation criteria, however, could be met using a programmable on-column injection system

Use of the temperature programmable injection method also resulted in improved resolution and increased sensitivity for the late eluting compounds compared to the splitless injection To validate the GC/ITS method, performance evaluation samples were analyzed by both instruments. Two one liter water samples (low and high level) were extracted and concentrated to a final volume of 1 mL. Half of the resulting extract was analyzed directly using the GC/MSD. The other half of the extract was used to prepare 1/1000 and 1/100 dilutions in methylene chloride. These dilutions were then analyzed using the GC/ITS Results for the low (10 to 50 µg/L) level sample compared well for the two instruments as shown in Table 2 To complete the method evaluation, both instruments were used to analyze several real sample extracts from various sources Results from those analyses demonstrated the ability of the GC/ITS to detect surrogates and analytes in samples with large hydrocarbon (oil) backgrounds, while the GC/MSD was unable to detect either

Table 2. Method Validation Results: APG Level 1

Compound Name	Reported GC/MSD	Reported GC/ITS 1/1000	1/100	All labs Mean	Acceptance Range
bis(2-chloroethyl)ether	54 8	49 8	62.8	74 1	39 0 - 109 2
hexachloroethane	13 9	16 5	17.7	18 8	5.6 - 32 0
2,4-dimethylphenol	13 5	**1.1**	7.2	14 6	3.2 - 26 0
2,4-dichlorophenol	22 8	**5.6**	21 8	32.2	13 6 - 50 8
naphthalene	23 9	22 4	25 8	32.8	15 8 - 49 8
hexachlorobutadiene	22.3	21.7	24.4	27.1	17 0 - 37 2
4-chloro-3-methylphenol	20 0	**10.2**	16 9	24.9	12.0 - 37 8
2,4,6-trichlorophenol	11 2	7.2	9.2	14.5	6.2 - 22.8
2,6-dinitrotoluene	16.2	13.4	19.6	19 7	10.7 - 28.7
acenaphthene	23.4	21.0	24.9	27.7	17.9 - 37.5
2,4-dinitrophenol	32 8	0 5	12.8	40 1	0 0 - 85 3
4-nitrophenol	37.0	1 7	22.6	31 5	0 0 - 72 0
2,4-dinitrotoluene	28 1	**8.5**	23 6	32.4	17 4 - 47 4
diethylphthalate	58 9	43 4	61 2	57.1	14 0 - 100.2
di-n-butyl phthalate	37 4	20.3	32.0	42.4	15.8 - 69 0
fluoranthene	20 6	15.9	22.1	23.5	12.4 - 34 6
bis(2-ethylhexyl) phthalat	24 8	**9.4**	13.7	23.6	10.4 - 36.8

Conclusions With the high sensitivity and dynamic range of the GC/ITS, regulatory limits for each analyte were met and exceeded The results for the method validation studies demonstrated the ability to accurately quantitate target compounds even in solutions that were 100 times or greater more dilute than those analyzed by the GC/MSD. This improvement in sensitivity equates to the ability to use smaller sample sizes and decrease solvent waste, to dilute out interferences or co-extracted radioactivity, and to increase sample throughput

Research sponsored by the Office of Technology Development, U S. Department of Energy, under contract No DE-AC05-84OR21400 with Martin Marietta Energy Systems, Inc.

FACTORS AFFECTING MEMBRANE INTRODUCTION MASS SPECTROMETRY

Susan Ohorodnik, John Callahan, Mark Anderson, and Steve McElvany
Naval Research Laboratory, Chemistry Division, Code 6113, Washington, DC 20375-5342

Membrane introduction mass spectrometry (MIMS) has been increasing in popularity as an environmental analysis technique for volatile organic compounds (VOCs) due to its ease of use and low detection limits. This research is concerned with developing a real-time, on-site MIMS analysis method for a wide range of volatile and semi-volatile organic compounds. Of particular interest is the modification and development of pervaporation membranes and mass spectrometer instrumentation to increase the selectivity and sensitivity of MIMS. The effects of membrane-mass spectrometer interface, selected ion storage techniques, and membrane composition on MIMS analysis for VOCs in aqueous solutions were reported.

Two membrane interfaces were investigated: a direct insertion probe inlet (MIMS Technology, Inc.) and a membrane/jet separator assembly. Both the DIP and membrane/jet separator inlets were configured to accept only membrane sheets. Detection limits for the DIP and membrane/jet separator systems were in the ppb and sub-ppb ranges, respectively. Lower detection limits were obtained with the membrane/jet separator system due to the removal of water from the system by the jet separator. The identification and quantification of VOCs in real environmental samples can be rather difficult requiring additional techniques such as MS/MS, selected ion storage methods, and ion-molecule reactions for accurate analyses.

In order to improve sensitivity by removal of unwanted background species and improve selectively for possible ion/molecule reactions, two ion monitoring methods were investigated: a user implemented SWIFT (stored waveform inverse Fourier transform) and (2) the commercially available selected ion storage (SIS) software package (Varian, Walnut Creek, CA). Dramatic improvement in S/N was observed when these methods were used for the isolation of 91 Da for p-xylene (Figure 1). SIS showed increased sensitivity, while SWIFT had detection limits similar to using no isolation. SIS outperformed SWIFT because it was capable of operating at longer ionization times. When SIS is operated at a fixed ionization time of 2.5 ms, the results were comparable to SWIFT results. Little improvement in sensitivity was observed when either SWIFT or SIS was employed with the jet separator assembly. Since the jet separator already efficiently lowers the water background, further improvements in sensitivity will require longer ionization times. Overall SIS and SWIFT are capable of giving comparable performance. SWIFT does have the advantage of allowing unlimited mass isolation ranges at varying isolation voltages while SIS currently only allows 5 mass ranges at a single isolation voltage.

Separation in MIMS is dependent on the differences in membrane permeability between the analyte compounds and feed solution. Silicone rubber (polydimethylsiloxane) has proven to be a very effective MIMS membrane. It is hydrophobic with high nonpolar organic permeability. However, its sensitivity tends to decrease and elution times increase for polar and semi-VOCS. Therefore, it is necessary to investigate or develop new membranes for selectivity and/or sensitivity toward these more difficult VOCs. The following membranes have been initially screened for MIMS analysis: cellulose ester, asymmetric polyvinylidene fluoride (PVDF), symmetric PVDF, styrene/butadiene copolymer, and acrylonitrile/butadiene copolymer. The copolymers appear to be the most promising once difficulties in casting the membranes are overcome.

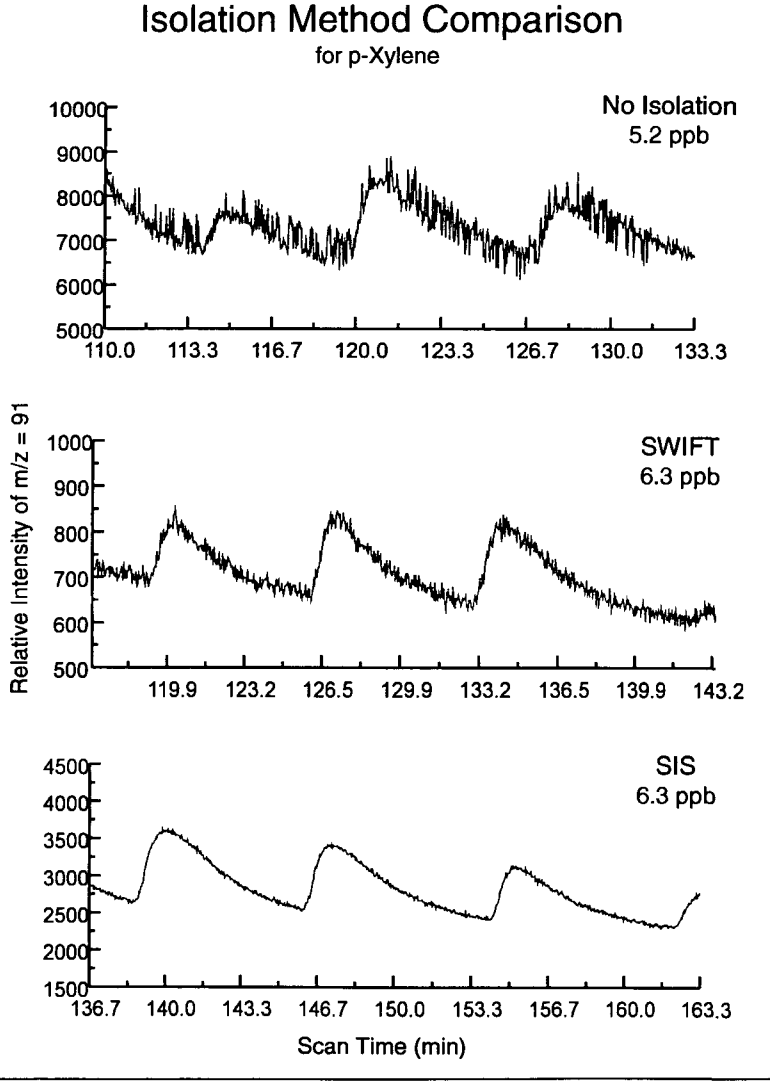

DIRECT SAMPLING ION TRAP MASS SPECTROMETRY vs. GC/MS FOR MONITORING VOCs IN GROUNDWATER

Marcus B. Wise, Roosevelt Merriweather, Michael R. Guerin
Chemical and Analytical Sciences Division, Oak Ridge National Laboratory
Oak Ridge, Tennessee 37831-6120

Direct Sampling Ion Trap Mass Spectrometry (DSITMS) has been under refinement and demonstration by our laboratory for several years. The general technology is applicable to a wide range of problems which would benefit from high sample throughput, fast availability of results, and relatively low cost per sample analysis when compared with conventional analytical methods. At the present time, DSITMS can be used to determine targeted analytes in air, water, soil, and other media. This is accomplished by equipping an ion trap with a direct inlet system which consists of a splitter, capillary restrictor, and a set of sample inlet modules. The capillary restrictor provides the interface between atmosphere and the vacuum in the ion trap while the splitter enables sampling modules which require high gas flow rates to be used with the system. The sampling modules consist of a purge module for analyzing VOCs in water or soil, a direct air sampling module, and a thermal desorber. These modules are designed to be easily interchanged by means of quick connect fittings and a single electrical cable. In general, the DSITMS sample inlet system works equally well on all of the commercially available ion traps with which it has been tested including the Finnigan MAT ITMS, Finnigan MAT Magnum, Varian Saturn, and the Teledyne 3D-Q. Both the Magnum and 3D-Q instruments have been utilized for field applications as well as laboratory analysis.

The work presented here represents continued efforts to generate data necessary to gain acceptance of the DSITMS technology by regulatory agencies for routine use in environmental applications. Much of this effort is being devoted to the generation of comparative data between DSITMS and accepted standard methods in order to demonstrate equivalency with respect to data quality. This particular study is a comparison of DSITMS with a purge and trap GC/MS for compliance monitoring of VOCs in groundwater. The DSITMS method involves the direct purge of VOCs from water into the ion trap using helium as the purge gas at a flow rate of 100 mL/min. No sample preparation is required other than adding difluorobenzene to the sample as an internal standard. The ion trap is operated in a mode which provides alternating electron ionization and chemical ionization using water as the CI reagent. The EI mode provides spectra which are useful for the determination of halogenated hydrocarbons and alkanes. The CI mode provides enhanced sensitivity for aldehydes, ketones, and other water soluble compounds. Chemical ionization also produces pseudo-molecular ions for alkyl aromatics which are commonly found in the environment from fuel spills. Detection limits for most VOCs are in the range of 500 pptr to 5 ppb depending on the analyte. Additional sensitivity can be achieved by use of selective ion storage such as Filtered Noise Fie ld as with the Teledyne 3D-Q.

In this study, samples from over 100 groundwater wells were analyzed by DSITMS and by a certified laboratory using an approved Contract Laboratory GC/MS method. The primary contaminants which were found in the samples included dichloroethenes, chloroform, carbon tetrachloride, trichloroethylene, perchloroethylene, benzene, and gasoline constituents. Overall, nearly 70% of the samples analyzed were found to be blank by both methods. Those samples which were found to be contaminated had constituents which ranged in concentration from 1 ppb to 5 ppm. Quantitative agreement between the DSITMS results and the GC/MS results were generally very good. The DSITMS samples were typically analyzed in triplicate with the precision being less than 10% in most cases. In terms of cost per sample ($25-$50) and availability of results to the customer (same day), DSITMS has a significant advantage over GC/MS.

DIRECT PURGE APPARATUS

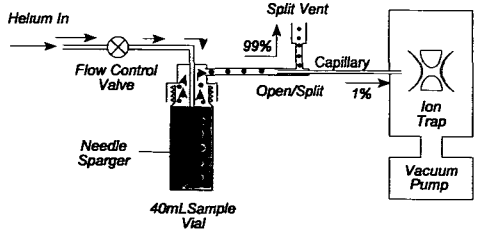

Comparison of DSITMS and GC/MS Results

Trichloroethylene in Groundwater

Well Number	DSITMS	GC/MS
1	3 ppb	3 ppb
2	89 ppb	81 ppb
3	5 ppb	3 ppb
4	1 ppb	0 ppb
5	3 ppb	0 ppb
6	11 ppb	8 ppb
7	28 ppb	19 ppb
8	90 ppb	56 ppb
9	72 ppb	76 ppb
10	5 ppb	2 ppb
11	7 ppb	7 ppb
12	1 ppb	1 ppb
13	61 ppb	53 ppb
14	4 ppb	4 ppb
15	40 ppb	49 ppb

*Research Sponsored by the U.S. Department of Energy, under contract DE-AC05-84OR21400 with Lockheed-Martin Energy Systems, Inc.

"The submitted manuscript has been authored by a contractor of the U.S. Government under contract No. DE-AC05-84OR21400. Accordingly, the U.S. Government retains a nonexclusive, royalty-free license to publish or reproduce the published form of this contribution, or allow others to do so, for U.S. Government purposes."

Rapid Sampling for Rapid Analysis: A New Method for VOCs in Drinking Water

Ben D. Gardner[1], Jennifer A. Johnson[1], Viatcheslav B. Artaev[3]
O. David Sparkman[4], John F. Holland[2]
Departments of Chemistry[1] and Biochemistry[2], Michigan State University, East Lansing, MI 48824
Meridian Analytical Systems, Inc.[3], 2310 Science Parkway, Okemos, MI 48864
O.David Sparkman & Associates[4], 4045 Eagle Ridge Dr., Antioch, CA 94509

Until recently, there has been only moderate emphasis placed on the time consumption of the sampling process in many gas chromatography/mass spectrometry (GC/MS) analyses. Historically, the total analysis time has been primarily dependent upon the chromatographic separation and detection steps, and significant decreases in sample preparation time have had little impact on overall sample throughput. The recent maturation of gas chromatography/time-of-flight mass spectrometry (GC/TOFMS) using time array detection has decreased chromatographic separation and mass spectrometric detection times by factors of 10 or more, leaving the sampling process as a significant and often limiting factor in the total analysis time

Current methods for the analysis of volatile organic compounds (VOCs) in drinking water utilize headspace or purge and trap techniques requiring 20-30 minute sampling times to extract these compounds for analysis by GC/MS Solid-phase microextraction (SPME) has recently been presented as a viable alternative to the above methods. Sampling and desorption times of less than 10 minutes have been reported for part-per-billion levels of volatile organics in aqueous solution [1] These rapid times suggest a potential for combining SPME and GC/TOFMS technologies to create a methodology for high sample throughput.

We have modified a GC/TOFMS system (Hewlett Packard 5890/Meridian Analytical Systems FCD-650) to accommodate external SPME sampling and cryotrapping as shown in Figure 1 The external cryotrap design allows simultaneous cryotrapping and chromatographic separation of alternate SPME samples Temperature and gas flow through the split/splitless injection port is controlled by the GC, with a 4-m 0.10-mm i.d. Rtx-5 capillary column used for chromatographic separation with a 9-cm loop at the beginning of the column placed in liquid nitrogen to accomplish cryotrapping. A heated transfer line into the GC minimizes the occurrence of cold spots.

Figure 1

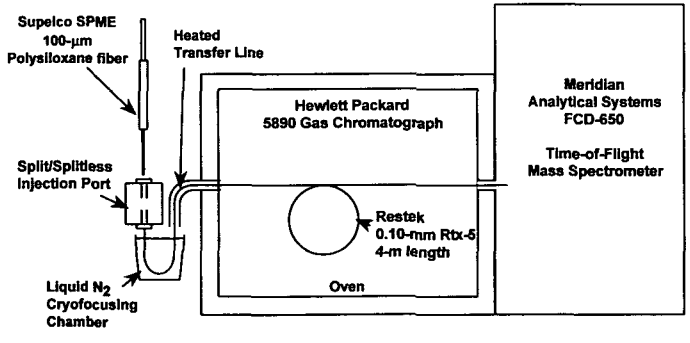

To demonstrate this system, 50- and 200-ppb mixtures of aqueous VOC samples were prepared from a commercially available stock solution (Ultra Scientific) The headspace above 1-mL aliquots of these solutions in sealed vials was sampled for 5 minutes using a 100-µm polydimethylsiloxane fiber SPME device and constant stirring The SPME fiber was then transferred to a 260° injection port in splitless mode and desorbed for 3 minutes The desorbed analytes were cryotrapped on column using a removable container of liquid nitrogen Chromatographic separation was initiated by rapidly heating the cryofocus region of the column using a convective heat source The oven temperature was then ramped from 40°C to 140°C at 50°/minute. Mass spectral detection was performed over a range of *m/z* 40–290 at an acquisition rate of 50 spectra/second Desorption and cryotrapping of subsequent samples occurred during chromatographic separation of the previous sample. Using this system in multiplexed mode as illustrated in Figure 2, a steady state analysis rate of 5 minutes/sample was achieved

Figure 2

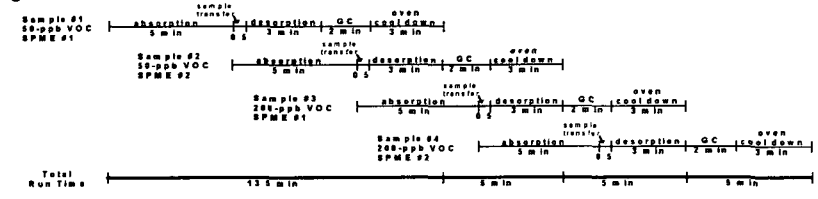

This combination of utilities illustrates the rapid analysis rates achievable when an appropriate sample introduction system is interfaced with GC/TOFMS for separation and detection. The utilization of *time compressed chromatography* where, using standard gas chromatographic equipment, gas flow rates and temperature ramps are maximized and column length is minimized, enables analyses to be performed in only a few minutes The use of high spectral acquisition rates and mass spectral deconvolution minimizes the chromatographic separation required for complete information recovery. A typical result is shown in Figure 3 illustrating the complexity of the sample and the time frame of the chromatographic analysis Library matchable spectra were obtained for each component of the mixture, deconvoluting where necessary

Figure 3

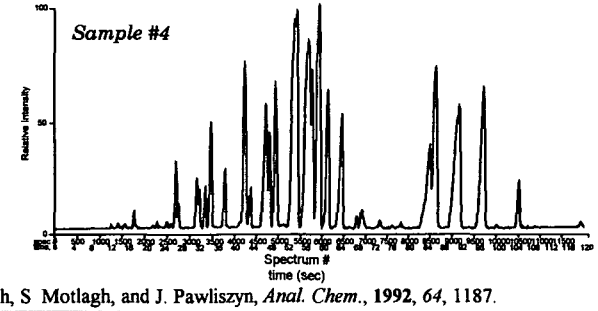

[1] D Louch, S Motlagh, and J. Pawliszyn, *Anal. Chem.*, **1992**, *64*, 1187.

Monthly Variations of Haloacetic Acids in Drinking Water by GC/MS

Frank M. Benoit, David T Williams and Guy L. LeBel
Health Canada, Environmental Health Directorate, Tunney's Pasture, Ottawa, ON

Introduction. In a national survey of 53 drinking water plants in Canada, haloacetic acids (HAA) were identified as major disinfection by-products (DBPs) and were found in all the chlorinated drinking water supplies examined. The HAA levels were observed to vary with season (summer and winter), water treatment practice (chlorination, chloramination and ozonation) and distance from the treatment plant. In an effort to understand better the dynamics of HAA formation, three drinking water plants that used different disinfectant combinations (chlorine - chlorine, chlorine chloramine and ozone - chlorine) were studied each month (over a period of 1 year, 1994) at five locations within each supply system. Three HAA (mono- (MCAA), di- (DCAA) and tri-(TCAA) chloroacetic acids) were monitored in the present study, however, MCAA were consistently found at lower levels than DCAA and TCAA; only the DCAA and TCAA results are presented here.

Methods. Duplicate water samples (30 mL) were collected at the treatment plant (raw (R) and treated (T)) and at 3 locations within the distribution system at increasing distance (D1 3-4 km, D2 6-13 km and D3 15-20 km) from the treatment plant. The samples were extracted with diethyl ether and derivatized with diazomethane. The HAAs were analyzed as the methyl esters by selected ion monitoring of the [M - 59] ions. Response factors for the individual acids were obtained from the periodic analysis (replicate) of clean water samples that had been spiked with a suite of HAA standards of known concentration. 1- Bromo-4-chloro benzene was used as quantitation standard and 2-bromo-n-butyric acid was used as recovery standard. The accuracy of the method (ca 20 %) was estimated from the periodic analysis of water samples spiked with known levels of analyte. The minimum quantitation level was 0.01 μg/L.

Results. For chlorine - chlorine treated water (fig. 1), both DCAA and TCAA levels peak during the summer months. The DCAA annual variation (mean max/min = 3 ± 1) was less than the TCAA (mean max/min = 9 ± 5) annual variation. The DCAA levels ranged from 3 to 26 μg/L throughout the year (all samples) and TCAA levels range from 2 to 37 μg/L throughout the year (all samples). DCAA levels generally maximized at locations (T or DI) closer to the treatment plant than TCAA levels (D2). Both DCAA and TCAA are reduced at the furthest location (D3) from the treatment plant.

For chlorine - chloramine treated water (fig. 2), the chloramine residuals are known to mitigate the formation of organochlorines within the distribution system. DCAA (mean max/min 2 ± 0.4) and TCAA (mean max/min 5 ± 2) levels peaked twice but at different times during the year at most locations. D2 was located downstream from a reservoir; the low DCAA levels observed at D2 (fig 2) in the summer was attributed to the release of higher volumes of mature water from the reservoir into the distribution line as a result of high consumer demand. DCAA levels ranged from 2 to 25 μg/L (all samples) and TCAA levels ranged from 2 to 15 μg/L (all samples).

For ozone - chlorine treated water (fig 3), ozone treatment mitigates most organochlorine formation. DCAA peaked in the summer at T and in the fall at DI, D2, and D3. TCAA peaked in the summer at T, DI and D2 and in the fall at D3. In order to control algae which clog the filter media, an additional chlorine treatment is applied prior to ozonation; this resulted in elevated HAA levels in the summer and early fall. DCAA levels ranged from 3 to 13 μg/L (winter/spring) and from 3 to 53 μg/L (summer/fall). TCAA levels ranged from 1 to 13 μg/L (winter/spring) and from 2 to 22 μg/L (summer/fall).

Fig.1 Seasonal HAA Levels (μg/L) Chlorine-Chlorine Treated Water

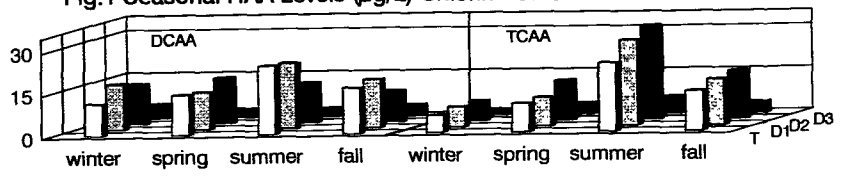

Fig.2 Seasonal HAA Levels (μg/L) Chlorine-Chloramine Treated Water

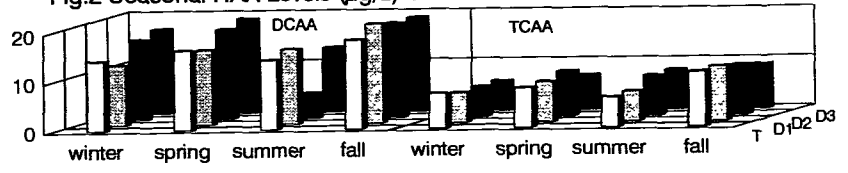

Fig.3 Seasonal HAA Levels (μg/L) Ozone-Chlorine Treated Water

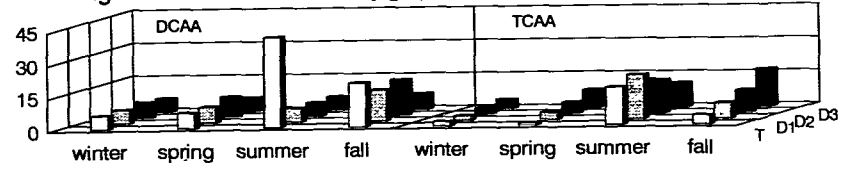

Conclusions. DCAA and TCAA were found in all treated water samples analyzed in the present study. The DCAA and TCAA showed significant variations as a function of month, location and treatment as illustrated in figs 1, 2 and 3. The HAA profiles for the three treatment processes are strikingly different. Of particular importance - no single sampling point gave simultaneous maximum concentrations for both HAAS. DCAA levels were similar for chlorine - chlorine and chlorine - chloramine treatments and slightly lower for ozone - chlorine treatment (except location T where the DCAA levels were considerably higher in the summer). TCAA levels were higher for chlorine -chlorine treatment than chlorine - chloramine and ozone - chlorine treatment (in summer and early fall TCAA levels were slightly higher at some locations). TCAA (and to a lesser extent, DCAA) levels minimized during the summer for chlorine-chloramine treatment whereas TCAA levels maximized during the same time period for chlorine - chlorine and ozone - chlorine treatments. The likely reason for this contrary behaviour is kinetic - HAAs are intermediate products and the measured values are dependent on the stage of the reaction for each individual HAA. In mature water, where the reaction time is sufficient to achieve completion, and in warm water, where the reaction is accelerated, the HAA levels will tend to be reduced.

Determination of Haloacetic Acids in Drinking Water by Electrospray LC/MS

David D. Kryak and Thomas D. Behymer
U.S. Environmental Protection Agency
Office of Research and Development
National Exposure Research Laboratory
26 W. Martin Luther King Drive, Cincinnati OH 45268

A number of studies have shown that haloacetic acids (HAAs), by-products of drinking water disinfection, are of concern to human health. Five compounds of this group, monochloro- (MCAA), monobromo- (MBAA), dichloro- (DCAA), dibromo- (DBAA) and trichloroacetic acid (TCAA), are proposed for regulation by the USEPA at a total maximum contamination level (MCL) of 60 μg/L in drinking water. Current methodology, such as EPA methods 552 and 552.1, utilizes gas chromatographic separation with electron capture detection (ECD). While these methods are capable of meeting this proposed MCL for haloacetic acids, they are complicated by the need for extraction and derivatization. In addition, identification of eluting analytes is dependent on retention times which may lead to misidentification when in the presence of coeluting ECD active compounds. Information obtained from mass spectrometry (MS) is generally more indicative of the eluting component(s) and is better suited for analysis of unknowns. With the development of electrospray ionization (ESI) techniques, a new approach has emerged for the analysis of small, nonvolatile, environmentally significant compounds without the need for derivatization.

ESI/MS and ESI/MS/MS was used with anion exchange high pressure liquid chromatography (LC) to identify and quantify the five HAAs proposed for regulation and bromochloroacetic acid (BCAA) after 20 fold concentration of fortified reagent water samples by lyophilization.

Chromatography was achieved using a Hewlett-Packard 1090 LC with solvents: A = 1 mM NH_4OH, B = acetonitrile, and C = 200 mM NH_4OH. Separation of 100 μL injections of an HAA mixture was achieved with a Dionex PAX 500 ion exchange column (4 x 50 mm) and a 0.5 ml/min flow rate with the following gradient: 81%A:19%B:0%C at 0 min,48%A:37%B:25%C at 15 min.

ESI/LC/MS measurements were achieved with a Finnigan MAT TSQ 700 triple quadrupole mass spectrometer equipped with a Finnigan ESI source. The ESI source conditions were: negative ion mode, 5 kV spray voltage, 200°C capillary temperature, 70 psi sheath gas (N_2) and rotameter setting of 30 for auxiliary gas (N_2). The mass spectrometer was scanned 90-300 amu in 1 s for full scan experiments. For all HAAs, $(M-H)^-$ was the base peak ion under negative ion conditions. For SRM experiments, the collision gas (Ar) was set at 2.5 mTorr and the collision offset was set at 15 v for all the HAAs except for TCAA which was set at 10 v. The most abundant daughter ion resulting from the collisionally induced dissociation of the $(M-H)^-$ was used as the quantitation ion. In the cases of the mono-halide compounds, the halide was the predominant daughter ion, while $(M-H-CO_2)^-$ was the predominant daughter ion in the cases of di- and tri-halide compounds.

Full scan and SRM instrument detection limits were determined at a signal to noise ratio of 3:1 as shown in Table 1. The instrument detection limit (IDL) by SRM was more than one hundred times lower than the IDLs by full scan for all HAAs studied here, except MCAA which was 25 times more sensitive by SRM.

Table 1. Estimated Instrument Detection Limits

Target Analyte	Full Scan ng	SRM ng
MCAA	1	0.040
MBAA	1	0.010
DCAA	1	0.010
BCAA	0.6	0.005
DBAA	5	0.010
TCAA	20	0.120

Quantitation was achieved using internal standard calibration. Bromopropionic acid which has similar chemical properties to the HAAs was chosen as the internal standard. Internal standard calibration plots showed good linearity from 0.1 to 25 ng. Daily instrument stability was determined by ESI/LC/MS analysis of 8 replicate analyses of 10 ng of each HAA. Relative standard deviations (RSDs) of less than 10% were obtained for all compounds.

Method detection limits (MDLs) were obtained by analyzing 7 replicate injections of 1 μg/L fortified reagent water which had been concentrated 20 fold by lyophilization. As shown in Table 2, recoveries were 86 to 135% with RSDs ranging from 8.6 to 16.9%. MDLs for all compounds are below 1 μg/L which exceeds the proposed MCL for the regulated HAAs.

Table 2. MDL data at 1 μg/L by ESI/LC/MS/MS using internal standard calibration

Analyte	Average Recovery %	RSD %	MDL μg/L
MCAA	113	8.6	0.31
MBAA	96	10.3	0.31
DCAA	86	14.0	0.38
BCAA	100	16.9	0.53
DBAA	100	10.7	0.33
TCAA	135	14.3	0.60

MDL = $t_{(n-1,1-alpha=0.99)}$ * Std. Dev., n = 7 replicates

Direct Analysis of Volatile Organic Compounds in Water at the Parts-per-Quadrillion (PPQ) Level using Membrane Introduction Mass Spectrometry (MIMS)

Scott Bauer, Jan Bauer, MIMS Technology Inc.

1900 S. Harbor City Blvd. Suite 115

Melbourne, FL 32901

Ion trap mass spectrometers have been used in membrane introduction mass spectrometry (MIMS) applications for years. The ion traps are very sensitive and perform exceptionally well in MIMS mode Typical detection limits for most volatile organic compounds in water are in the low parts-per-trillion range in ion traps. As sensitive as these ion traps are, the parts per quadrillion direct organic analysis barrier had never been crossed. The presentation describes experiments in population augmentation in the ion trap using stored waveform inverse fourier transform (SWIFT) to allow the direct analysis of organic compounds in water at the sub-parts-per-trillion level

A Finnigan Magnum ion trap configured for MIMS use was further modified through the addition of an analog switch, amplifier, balun, arbitrary waveform generator, and scan editing software to allow selected ion trapping in the spectrometer A scan function was produced with a 150 msec ionization time during which SWIFT pulses were applied to the end cap electrodes to destabilize all mass except m/z 96, the molecular ion for 1,2-dichloroethene. The long ionization time allowed the population of m/z 96 to grow large enough to detect the compound at sub parts-per-trillion levels while the SWIFT pulses removed enough of the unwanted ions to eliminate space charging conditions. Post acquisition data smoothing to enhance detection limits even further was also demonstrated. The 1,2-dichloroethene was detected at the parts-per-quadrillion level while in solution with other volatile organic compounds at much higher concentrations. The accompanying figure shows the mixture mass spectrum with the swift pulse on and off.

43rd ASMS Conference on Mass Spectrometry and Allied Topics

Mass Spectrum of Analyte Mixture Without SWIFT

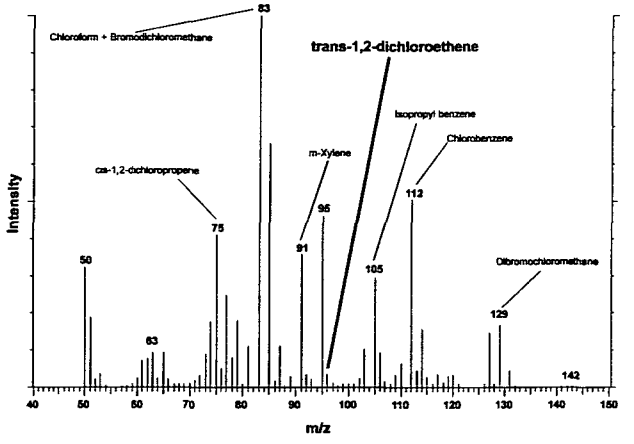

EI Mass Spectrum of Analyte Mixture Containing 100 PPtr 1,2-Dichloroethene using SWIFT Isolation

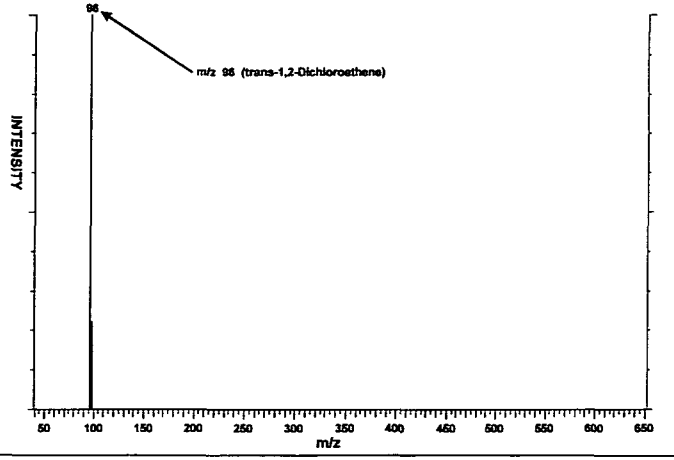

Analysis of Pesticide Residues in Drinking Water Using Megaflow ESI

*J. Rontree, *S.Lowes, *J.Claereboudt, **P. Ackermans and **F. van Hoof
* Fisons Instruments VG Organic, Tudor Road, Altrincham, WA14 5RZ, UK
** Laboratorium Antwerpse Waterwerken, 2018 Antwerpen, Belgium.

Introduction

European community directives dictate that the levels of pesticides in drinking waters should not exceed 100ng/l of each pesticide and 500ng/l total amount of pesticides. In order to comply with these regulations analysts require instrumentation which can achieve low levels of detection with high specificity and good linearity of response.

Several GC/MS and LC/MS methods have been developed for pesticide analysis. However, GC based methods are limited because of the thermal lability of many of these compounds and LC/MS methods have mainly used thermospray ionization which has suffered from poor reproducibility and fluctuating ion signals.

More recently, atmospheric pressure ionization techniques have been used for environmental monitoring with most methods employing atmospheric pressure chemical ionization (APCI) In view of the popularity of electrospray ionization for other LC/MS applications, we investigated the use of this technique for the analysis of phenyl urea and triazine herbicides in drinking water and field run off surface water samples

Results

The initial experiments concerned separating a mixture of 16 standard herbicides Full scan LC/MS gave excellent TIC signals and spectra at the 10ng level. Spectra for all of the 16 herbicides studied were dominated by protonated molecular ions [M+H]+. The 10ng level represents the detection limit quoted for thermospray techniques, however, this application of electrospray allowed full scan detection to at least 200pg on column for each of the standard herbicides (Fig 1)

At this stage, identification of the herbicides in solid phase extracted (SPE) surface water samples proved difficult due to the complex nature of the concentrated water matrix. As an alternative to more extensive sample clean-up, LC/MS/MS was employed for all further analyses of the herbicides in the environmental matrices (i.e surface water and the drinking water samples)

In order to investigate the potential for pesticide screening, an MS/MS library was created from the product ion spectra of 40 different pesticide standards The library was constructed from the collision induced dissociations (CID) of each pesticides' protonated molecular ion Fixed CID conditions of 20eV collision energy and an argon gas pressure of $2x10^{-3}$ mbar were maintained for each of the standard samples

Each product ion spectra from an LC/MS/MS analysis of the 16 herbicide mixture, at the level of 50pg per component, was then screened against the created library. All the standards were

correctly identified in the library as first hits From the studies conducted, 50pg on column was regarded as the limit of detection across the range of pesticides investigated These limits are of course restricted because of the need to maintain constant MS/MS conditions in order to screen unknown samples Using the same screening technique, 8 common herbicides were identified in each of the concentrated environmental samples. The product ion chromatograms for the drinking water sample is shown in Fig. 2

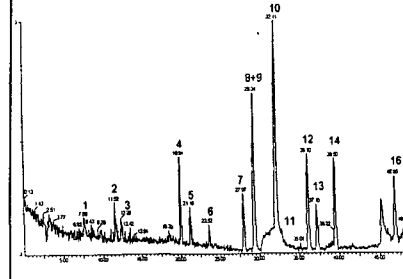

Fig. 1

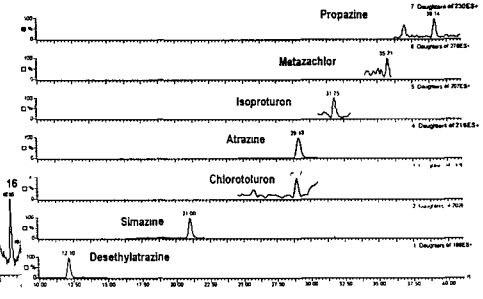

Fig. 2

Four of the most offending pesticides were quantitatively analysed in the three environmental samples using MRM scanning. The pesticides studied were simazine, atrazine, isoproturon and diuron. Calibration curves were constructed from concentrated standard solutions using a rapid LC separation. Linearity of response was observed from 10ng/l to 1µg/l, encompassing the European Community directive levels of 100ng/l for individual pesticides

(Values are in ng/l)	*Simazine*	*Atrazine*	*Isoproturon*	*Diuron*
Drinking water	138	249	16	146
Surface water 050	30	72	18	33
Surface water 110	167	134	16	99

The experiments confirmed some seasonal herbicide crop applications and the presence of 3 herbicides in the drinking water sample above the European Community regulatory levels. The higher concentration levels in the drinking water could be explained on the basis of the sample collection period All samples were collected in September, a period when herbicide application is low and hence the relatively low levels in the field run off samples It takes at least 8 weeks for the water from the fields to reach the reservoir for use as drinking water Therefore, the drinking water represents that which is derived from the summer season when herbicide application is high. This highlighted the need to recycle this drinking water before human consumption.

FORMATION OF ORGANOCHLORINE COMPOUNDS DURING WATER CHLORINATION

Lebedev A.T., Moshkarina N.A., Brodsky E.S., Klujev N.A., Petrosyan V.S.

Moscow State M.V.Lomonosov University, Organic Chemistry Department
119899 Moscow Russia

Chlorination has been used in water desinfection since the beginning of the 20th century. Being a very effective desinfectant chlorine is relatively inexpensive and stable enough to remain in water distribution systems for a long time. However, in the early 70th it was found that chlorination of drinking water led to the generation of undesirable organochlorine and other compounds which have been shown to be a serious chemical contamination of drinking water. A number of studies have confirmed that water chlorination was directly responsible for the formation of mutagenic chemicals in drinking water.

Until recently the attention was focused mainly on trihalomethanes $CHHal_3$, while natural humic material was shown to be the precursor of these compounds in drinking water. However, values for total organic halogenated compoundsformed in water exposed to chlorination were greater than could be accounted for by the amount of trihalomethanes formed. As a result a number of publications dealing with the identification of individual organochlorine compounds formed during water chlorination from humic material appeared.

Due to the complexity and variability of the composition and structures of natural humic substances it is extremely difficult to stady the detailed mechanism of their reactions with formation of organochlorine products, or to derive the pathways of their formation. This fact led to the wide use of simple model compounds comprising structural fragments of humic material in chlorination studies. A number of structural fragments of humic material were studied earlier, while this work deals with the water chlorination of diphenyl, dibenzofuran and dibenzodioxin.

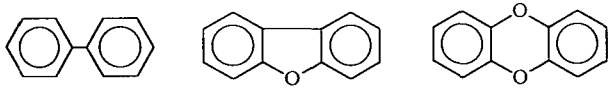

These compounds may present individually in natural water or be structural fragments of humic or fulvic acids. The main interest to these particular compounds involves the fact that the organochlorine derivatives of these substrates are known to be extremely toxic pollutants while their presence in drinking water should be completely avoided.

The chlorination of the selected compounds was conducted in the dark at 20 C in 0.2M phosphate buffer solutions prepared from reagent grade potassium phosphate monobasic, sodium phosphate dibasic and distilled water (pH=7.2). Chlorine was used in water solution prepared by passing of gaseous chlorine through the distilled water at the Rublovo Water Treatment Station. Chlorine content was determined by iodometric

titration just before every chlorination procedure. In all the reactions substrate concentrations were 10^{-3} M while these of Cl_2 varied from 3.7 mg/l to 3.5g/l. Reaction time was 24 hrs.

Each sample was analysed with Varian-MAT 44S and Finnigan ITD 700 GC-MS systems using SE-54 (30m) and SPB-1 (30m) fused silica capillary columns. Interpretation of the qualitative and quantitative results (chromatograms and mass spectra) was performed manually using retention time information obtained by using model mixtures of chlorinated standards.

The most general equation for the reaction rate of the chlorination of an organic substrate may be presented as follows:

$$V = [S]^x \cdot [Cl_2]^y$$

Since chlorine concentration was up to 1000 times higher, while that of substrates at least 10^6 higher (comparing to the conditions of industrial water chlorination used) the rate of chlorination in laboratory was at least 10^9 times higher (x=y=1).

The most stable among the studied compounds surprisingly appeared to be dibenzodioxin, which even in the most strict conditions ($[S]/[Cl_2]$=1:50) gives only the traces of the monosubstituted product.

Diphenyl reacted with chlorine giving mostly two isomers of monochlorinated diphenyl and three isomers of dichlorodiphenyl. Therefore diphenyl underwent electrophilic substitution, although the reaction rates were not high. The products of the chlorination were identified as 2-chlorodiphenyl,4-chlorodiphenyl; 3,4-dichlorodiphenyl, 4,4'-dichlorodiphenyl and 2,4'-dichlorodiphenyl. No products of ring fission were observed.

Chlorination of dibenzofuran brought only to monochlorosubstituted derivatives while $[S]/[Cl_2]$ ratio was in the range from 1:1 to 1:10. However the subsequent increase of chlorine quantity ($[S]/[Cl_2]$=1:50) led to a sharp increase of the chlorination products. 3 Isomeric monochlorodibenzofurans 13 isomeric dichloro-, 27 isomeric trichloro- and 27 isomeric tetrachlorodibenzofurans were detected.The most toxic 2,3,7,8-TCDF may be among the reaction products, while the degree of conversion of the precursor dibenzofuran into this toxicant was about 10^{-3}%.

Therefore it is possible to carry on the following conclusions:

1. Only mono- and dichlorosubstituted diphenyls are recorded even under the most severe experimental conditions. The most toxic tetra-, penta- or hexachloro- congeners are not obtained at all. Thus there are no chance to get toxic polychlorinated diphenyls during industrial chlorination of natural water.
2. Only monochlorodibenzodioxins are recorded even under the most severe experimental conditions. The most toxic congeners are not obtained at all. Thus there are no chance to get toxic polychlorinated dibenzodioxins during industrial chlorination of natural water.
3. 2,3,7,8-Tetrachlorodibenzofuran was recorded among the other products of aqueous chlorination of dibenzofuran (degree of conversion 2 10^{-3}%). However due to the fact that the reaction rate in the experiment was at least 10^9 times higher than in real conditions it is possible to conclude that it is hardly possible to get this compound or its toxic congeners during industrial water chlorination.

Multispectral Identification of Ozonation By-products in Drinking Water

*Susan D. Richardson, Alfred D. Thruston, Jr., Timothy W. Collette,
U.S. Environmental Protection Agency, Athens, GA 30605.

Kathleen S. Patterson and Benjamin W. Lykins, Jr.,
U.S. Environmental Protection Agency, Cincinnati, OH 45268.

Because of concern over the presence of trihalomethanes (THMs) and other chlorinated by-products in chlorinated drinking water, alternative disinfection methods are being explored. One of the most popular alternative disinfectants is ozone. Ozone is more effective than chlorine for killing harmful microorganisms in drinking water and does not produce the high levels of THMs that chlorine does. It is also effective for taste and odor control. Although ozone has been used for more than 80 years to treat drinking water, very little is known about the identity of organic disinfection by-products (DBPs) that are produced.

Using multispectral identification techniques--gas chromatography coupled with low and high resolution GC/EI-MS, low resolution GC/CI-MS, and Fourier transform infrared spectroscopy (GC/FT-IR), we identified many ozonation by-products formed at a pilot drinking water plant in Jefferson Parish, LA. Rather than attempting to identify a few target by-products that are regulated for drinking water, our objective was to identify every compound that was detected in the sample extracts.

Experimental

Multispectral identification techniques included gas chromatography coupled with low and high resolution electron-impact mass spectrometry (GC/EI-MS), low resolution chemical ionization mass spectrometry (GC/CI-MS), and Fourier transform infrared spectroscopy (GC/FT-IR). CI-MS experiments utilized methane and 2% ammonia in methane gases. GC/MS analyses were performed on either a VG 70-SEQ high resolution hybrid mass spectrometer or a Finnigan 4500 quadrupole mass spectrometer. GC/FT-IR experiments were performed on a Hewlett Packard Model 5965B IRD.

For this study, Mississippi River (Jefferson Parish, LA) raw water was treated at a pilot plant that uses ozone. Because ozone does not persist in water, an additional residual disinfectant, such as chlorine or chloramine, is required to maintain disinfection in the distribution system and to the home tap. As a result, the effect of residual chlorine and chloramine was also studied. All of these samples were concentrated onto XAD resins, eluted with ethyl acetate, and rotoevaporated to 1 ml. Half of the ethyl acetate eluents were reserved for diazomethane methylation reactions.

Results and Discussion

Numerous by-products were identified, many of which were not present in any spectral database and have never been identified before in drinking water. Many times, molecular ions were not present, necessitating the use of CI. High resolution data was essential for determining unknown structures, and GC/FT-IR was very useful for a few compounds where there was a choice of structures (based on mass spectral information). IR was definitive on the choice of functional group.

Ozone, by itself, produced a surprisingly small number of by-products, none of which

was chlorinated. The major DBPs produced were a series of aldehydes and carboxylic acids. The most concentrated by-product was heptanal, which was present at approximately 50 ppt (ng/L). Special derivatizations to extract highly polar aldehydes (e.g., glyoxal, methyl glyoxal) were not performed, so these previously observed aldehydes were not detected. However, because 1-chlorodimethyl glyoxal was detected in the ozonated water treated with residual chlorine, the presence of these aldehydes is suggested. 1-Chlorodimethyl glyoxal is likely a reaction product of chlorine and the ozonation by-product, dimethyl glyoxal. The levels of DBPs produced using ozone alone were much lower than what is typically found for chlorine. However, when residual chlorine was used, numerous chlorinated by-products were produced, among them some potentially hazardous halomethanes and haloacetic acids. The concentrations of these by-products ranged from approximately 5 to 300 ppt (ng/L). However, because volatile analyses were not done, it is likely that concentrations of the halomethanes were much higher than we observed. We used a semi-volatile method; volatiles would be lost in the concentration step. When chloramine was used as the residual disinfectant, fewer chlorinated by-products were produced (relative to chlorine), and no halomethanes were produced. One of the more interesting compounds identified was 1,2-dichloroethanol acetate, which was produced in both the residual chlorine and chloramine samples. Mass spectral and infrared data is shown below.

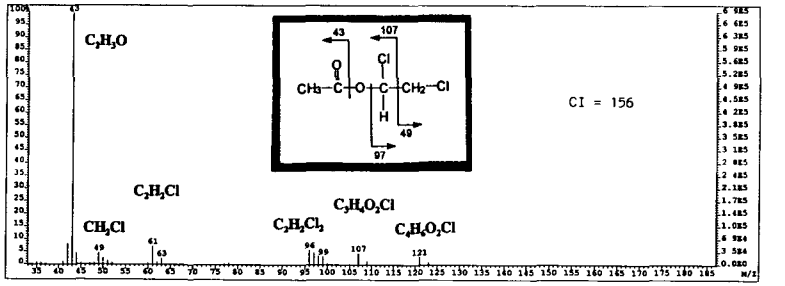

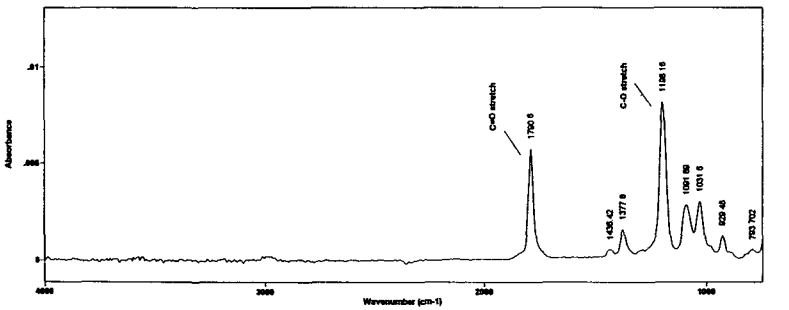

Identification of Brominated Organics in Ozonated Drinking Water

Alfred D. Thruston, Jr., Susan D. Richardson, and Timothy W. Collette
U.S. Environmental Protection Agency, Athens, GA 30605

Kathleen S. Patterson and Benjamin W. Lykins, Jr.
U.S. Environmental Protection Agency, Cincinnati, OH 45268

INTRODUCTION

The use of ozone for disinfection of drinking water is increasing as public utilities search for alternatives to the chlorination disinfection process, which produces trihalomethanes (THMs) as by-products. In drinking water treatment with ozone, the water is further treated with small amounts of chlorine or chloramine to maintain residual disinfection since ozone does not persist in water. However, little is known about the identity of the disinfection by-products (DBPs) that are formed in this treatment.

If bromide is present, as it would be in many coastal water supplies, it may be oxidized to hypobromous acid. This acid reacts with natural organic matter and residual chlorine or chloramine, producing brominated organic compounds.

We have identified a series of brominated compounds found in extracts of drinking water samples spiked with sodium bromide from a pilot drinking water treatment plant that uses ozone

EXPERIMENTAL

Identification techniques included gas chromatography coupled with low high resolution electron-impact mass spectrometry (GC/EI-MS), methane chemical ionization MS, and Fourier transform infrared spectroscopy (GC/FT-IR).

GC/MS were performed on a VG 70-SEQ high resolution hybrid mass spectrometer and a Finnigan 4500 Quadrupole mass spectrometer. GC/FT-IR analyses were performed on a Hewlett Packard Model 5965B IRD.

At the Jefferson Parish, LA, Pilot Treatment Plant, raw water from the Mississippi River was clarified by addition of coagulants and sand filtration. The water was spiked with 1ppm NaBr, a portion retained for background, and the rest was treated with ozone. The water disinfected with ozone was split, and one portion post-disinfected with chlorine (Cl_2) and the other with chloramine (NH_2Cl). All of these samples were concentrated onto XAD resins, eluted with ethyl acetate, and rotoevaporated to 1 ml.

Among the compounds found were bromohydrins, bromoalkanes, bromoacetonitriles, bromonitroalkanes, bromo acids, and bromophenols.

Multispectral techniques were used to identify most of the compounds. An unique example is the identification of **nitrodibromomethane**. The spectrum was not in MS spectral databases. Little structural information, other than the presence of bromine, could be gleaned from LR/EI/MS alone. Methane CI/MS showed no molecular ion. However, HR/EI/MS showed the m/z 43 to be $[CHNO]^+$, m/z 46 to be $[NO_2]^+$, and m/z 122 to be $[CHNOBr]^+$.

The IR spectrum is consistant with this structure. The O=N=O group gives 2 highly unique peaks, the antisymmetric and the symmetric stretching peaks at 1596 and 1326 cm-1, respectively. The C-Br stretching peak is observed at 794 cm-1. No features are present in this spectrum that are not consistant with this structure.

SUMMARY

The halogenated disinfection by-products (DBPs) detected in the Br - spiked water concentrates, were mostly brominated and mixed bromochloro compounds.

A comparatively large amount of 2-bromoethanol (1ppb) was only found in the ozonated sample post-disinfected with NH_2Cl.

A comparatively large amount of bromoform (3 ppb) was found in the ozonated sample post-disinfected with Cl_2.

It is apparent that when Br - is present in raw water, ozone can oxidize Br - to produce HOBr, which, in turn combined with chlorine, or chloramine, reacts with naturally occurring organic matter to produce numerous brominated DBPs.

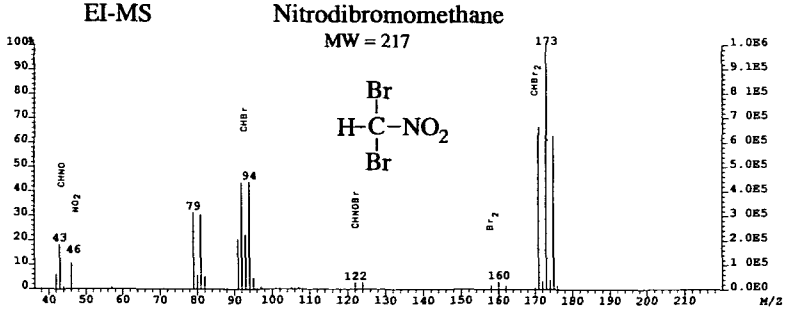

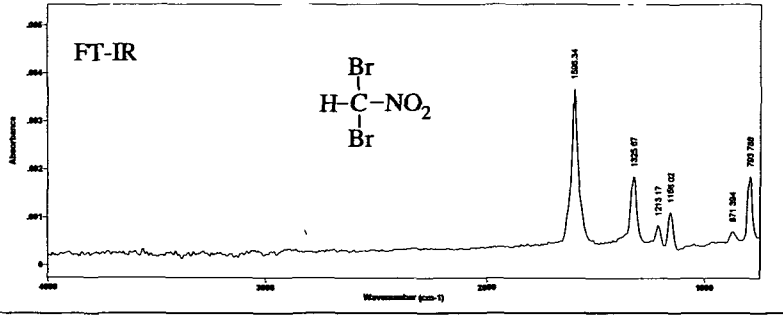

Isotope Ratio Monitoring for Stable Isotope Analysis on CH_4 and N_2O in Air

Brand, Willi A. and Seedorf, Ronald,
Finnigan MAT, Barkhausenstr.2, 28197 Bremen, Germany

It is a prominent disadvantage for isotopic monitoring of atmospheric trace gases that the required sample size using the traditional techniques is high. For CH_4-work for instance, typically more than 50 liters of air per sample are necessary (1). The idea to use the irm-GCMS (2-4) technique for high precision isotope analysis on trace gases like CH_4, CO or N_2O is obvious and suggests itself. For this purpose we have developed an automated pre-GC concentration device ("PreCon"). Its principle is outlined in **figure 1**:

For N_2O work, air samples of 100 ml size containing 1.4 nmol of analyte gas are driven through a H_2O and CO_2 scrubber tube using a Helium flow of ≈25 ml/min ("He-piston" technique). The CO_2 is withheld in the ascarite trap with an efficiency >0.999. A small amount of CO_2, all of the N_2O and most of the other air constituents escape the scrubber tube. The manual trap 1 downstream is not active, the combustion furnace is kept at ≈200°C, not being functional either. In trap 2 the condensibles are removed from the gas stream at -196°C. Trap 2 is made of a stainless steel tube (1 mm i.d.) filled with Ni wires for quantitative trapping. The automated trap is moving in and out of a LN_2 filled Dewar by means of an air actuated piston. It forms the loop of a 6-port valve (VALCO).
After sampling for 15-30 min the 6-port valve is rotated thus making the loop part of the injection system into the GC. Because of the size of the loop, the analyte components are transferred to a small diameter trap (0.5 mm i.d.) from where the GC analysis is started by removing the trap from the LN_2 container. Excellent GC resolution is mandatory for high precision results in N_2O isotope analysis.

For CH_4 work, the manual trap 1 is immersed in liquid nitrogen. Only compounds volatile at this temperature (N_2, O_2, Ar, CH_4, CO) pass the trap and enter the μ-combustion furnace at 1000°C. The latter is a vitreous alumina tube of 0.8 mm i.d., filled with 3 Ni wires (0.13mm). Before analysis the furnace was conditioned over night using clean O_2 (≈ 1ml/min) to burn off residual carbon or carbon containing compounds. The reaction products from CH_4 oxidation are frozen and transferred to the GC for further separation/purification in the same manner as described for N_2O.

Results:
The precision obtained for the trace gases in ambient air were:

N_2O: $\delta^{15}N$ = 0.155 ‰ (1σ) $\delta^{18}O$ = 0.20 ‰ (1σ)
CH_4: $\delta^{13}C$ = 0.16 ‰ (1σ)

Figure 2 demonstrates the ability of the method to monitor the changes of the isotopic composition of N_2O in ambient air over a period of 7 hours.

43rd ASMS Conference on Mass Spectrometry and Allied Topics

[1] D. C. Lowe, C. A. M. Brenninkmeijer, S. C Tyler and E. J. Dlugokencky, J. Geophys. Res. 96, **1991**, 15455
[2] D.E. Matthews and J.M. Hayes, Anal. Chem 50, **1978**, 1465
[3] W.A.Brand, K.Habfast, M.Ricci, in: Adv.Mass.Spectrom. 11B, ed P.Longevialle, Heyden&Son, London **1989**, 1800
[4] D. A. Merritt, Ph.D. thesis, Bloomington, Indiana, **1993**

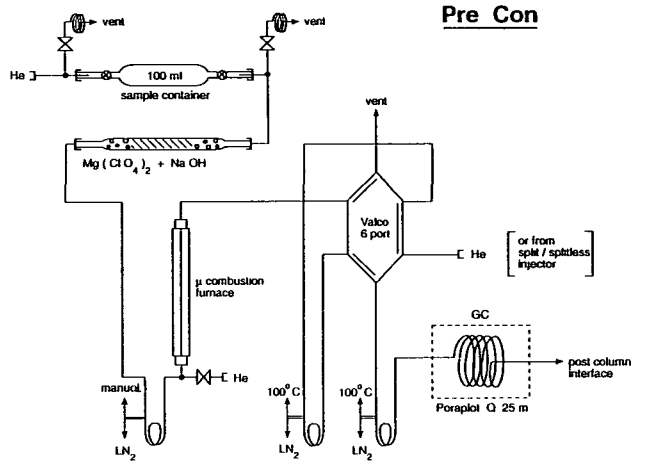

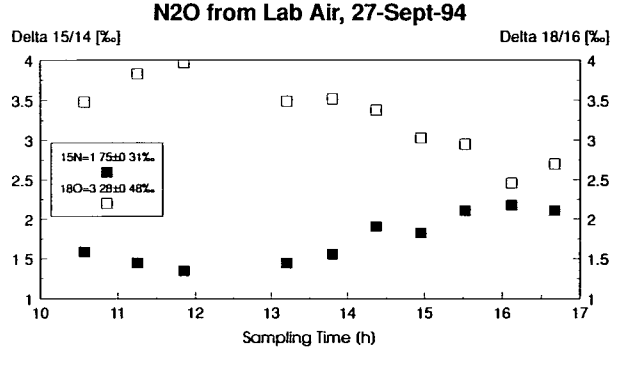

Evalution the Air Quality in Mass Spectrometry Laboratories by SPTD/GC/MS

Anren Hu and Jentaie Shiea*
Dept. of Chemistry, Natl Sun Yat-sen Univ., Kaohsiung, Taiwan 804

Mass spectrometer is one of the analytical instrument which need to be operated in the vacuum. If the mechanical pumps are set in the mass spectrometry laboratory, trace of volatile organic compound (VOC) originated from pump oil may leak to the air. Exposure in such contaminant environment for a long period of time will endanger workers' health especially in respiratory system. In this study, we examined the air quality of twelve mass spectrometry laboratories in Taiwan.

The air pollutant was adsorbed in Tenax-TA tube and a short path thermal desorption unit connecting to GC/MS was used for desorbing, separating and identifying the volatile pollutants. Figure 1 shows the result of analyzing 18 liters of indoor air sample from a mass spectrometry laboratory (#1) To ensure that the inside air not polluted by the exhaust from pump oil, the mechanical pumps are enclosed in a plastic box. The major component of the organic volatiles in the indoor air sample include a variety of aromatics such as toluene and xylenes and hydrocarbons characteristic of gasoline(Table1). The relative abundance of the aromatics with different molecular weight is as the following:

Toluene > Xylene > C3 benzene > Naphthalene.

By comparing the chromatogram of the outdoor air sample, it was found that the composition of pollutants in both air samples is nearly identical Obviously, the pollutants found in the mass spectrometry are originated from common air pollution especially from car engine exhaust. Except the difference in relative abundance, the type of volatile organics found inside the plastic box where the mechanical pumps are enclosed is nearly identical to those found outside the box and also outdoor (Figure 2). The order of the abundance of some aromatics is like:

Naphthalene > C3 benzene > Xylene > Toluene.

The most possible origin of the aromatics with higher molecular weight detected inside the box is from the pump oil. To testify such suggestion, a purge and trap sampling system equipped with a heater sleeves was used to collected the volatile organics from the pump oil. It was found that the volatile organics obtained from unheated pump oil is dominant with toluene and the GC chromatogram is nearly identical to those in Figure 1. However, once the pump oil is heated at 150°C, the volatile organics is dominant with xylene (Figure 3). Since the temperature of running mechanical pump itself is also extremely high at both inside and outside parts. This temperature effect will then make the evaporation of the aromatics with higher molecular weight become much easier and this is the reason why higher concentration of such compounds is detected

Figure 4 shows the GC chromatogram of one of the mass spectrometry laboratory (#2). As it can be seen, the concentration of xylene is greater than that of toluene After carefully examined the mass spectrometer, a series leakage at the joint of exhaust pipe to the body of the mechanical pump was found. According to the results shown here, the presence of unusually high concentration of xylene or C3 benzene in the air seems to be a good indication (marker) of air pollution by pump oil

Table 1. The identities of the volatiles in the air samples.

Peak	Compounds identified	Peak	Compounds identified	Peak	Compounds identified
1	Benzene	22	1,7,7-Trimethyl-bicyclo-2,2,1-hept-2-ene	43	2-Methyl-naphthalene
2	n-Heptane	23	Unknow	44	n-Tridecane
3	Toluene	24	1-Methyl-4(1-methylethyl)-benzene	45	1-Methyl-naphthalene
4	n-Octane	25	1-Ethyl-3,5-dimethyl-benzene	46	2,6-Dimethyl-naphthalene
5	Isobutyl acetate	26	1-Methyl-3-propyl-benzene	47	n-Tetradecane
6	Polysiloxane	27	1-Methyl-2-propyl-benzene	48	1,3-Dimethyl-naphthalene
7	Ethyl-benzene	28	1-Ethyl-2,4-dimethyl-benzene	49	1,6-Dimethyl-naphthalene
8	p & m-Xylene	29	4-Ethyl-1,2-dimethyl-benzene	50	2,3-Dimethyl-naphthalene
9	o-Xylene	30	2-Ethyl-1,4-dimethyl-benzene	51	2,5-Bis(1,1-dimethylethyl)-2,5-cyclohexadiene-1,4-diene
10	n-Nontane	31	2-Ethyl-1,3-dimethyl-benzene	52	Unknow
11	1,1,2,2-Tetrachloroethane	32	n-Undecane	53	n-Pentadecane
12	1-Methylethyl-benzene	33	Unknow(ketone)	54	Unknow
13	Propyl-benzene	34	1,2,4,5-Tetramethyl-benzene	55	n-Hexadecane
14	1-Ethyl-3-methyl-benzene	35	1,2,3,5-Tetramethyl-benzene	56	Unknow(acid)
15	1-Ethyl-4-methyl-benzene	36	C5-Benzene	57	Benzophenone
16	1,3,5-Trimethyl-benzene	37	C5-Benzene	58	n-Heptadecane
17	1-Ethyl-2-methyl-benzene	38	C5-Benzene	59	Unknow
18	1,2,4-Trimethyl-benzene	39	C5-Benzene	60	n-Octadecane
19	n-Decane	40	Naphthalene	61	n-Nonadecane
20	Polysiloxane	41	n-Dodecane	62	n-Eicosane
21	1,2,3-Trimethyl-benzene	42	Unknow(ketone)		

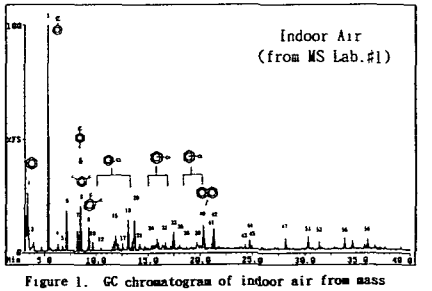

Figure 1. GC chromatogram of indoor air from mass spectrom. Lab.#1

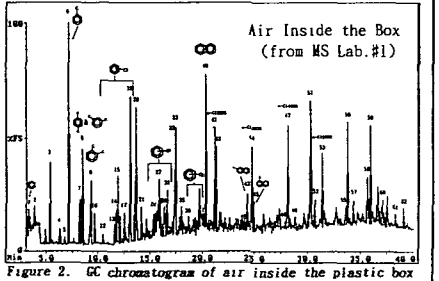

Figure 2. GC chromatogram of air inside the plastic box where two mechanical pumps are enclosure. (from mass spectrom. Lab.#1)

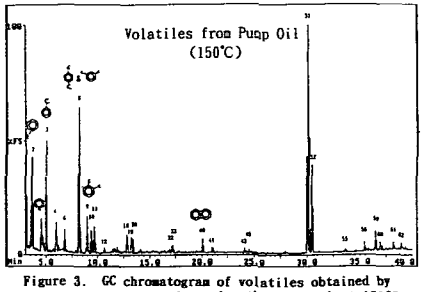

Figure 3. GC chromatogram of volatiles obtained by purging and traping the pump oil at 150°C

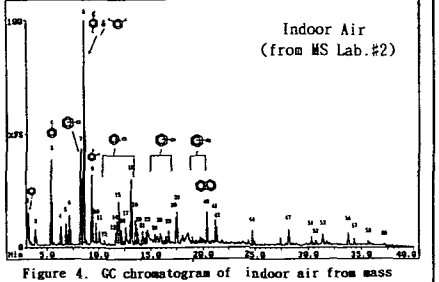

Figure 4. GC chromatogram of indoor air from mass spectrom. Lab.#2

Gas chromatography-tandem mass spectrometry a novel approach for monitoring the bacterial load in air.

M. KRAHMER*, K. FOX, and A. FOX. University of South Carolina, School of Medicine. Columbia, SC. 29208

Exposure to bacterial components can lead to pulmonary irritation and allergic reactions. Unfortunately, culture-based quantification of the bacteria present in airborne dust is inadequate for determination of the total bacterial load. The use of analytical microbiological techniques utilizing muramic acid (MA), as a marker for peptidoglycan allows comparisons of environments for overall contamination with culturable.

MA has been assayed in the past using a variety of methods. The earliest methods included spectrophotometry and later either gas or liquid chromatography. Recently mass spectrometry has increased selectivity while tandem mass spectrometry using multiple reaction monitoring has allowed dramatic improvements in specificity coupled with selectivity of detection.

METHODS AND MATERIALS

Culture:

Samples were collected in horse and hay barn using a single stage Anderson sampler with a flow rate of 18-20 liters per minute. Traditional colony counts were done for comparison to analytical methods to determine the percentage of nonculturable bacteria present in this specific environment. Profile evaluation of the culturable bacterial were determined using tryptic soy agar containing the fungal inhibitor cycloheximide TSA/H.

Sampling:

MA content present in dust samples was evaluated using teflon filters (air flows of 10-20 l/min) collected from the same environment over periods of 3-31 days.

Muramic acid analysis:

Samples were derivitized using the alditol acetate method. In brief, samples were sonicated, then hydrolyzed with 2N sulfuric acid for 3 h at 100°C Methylglucamine (2 µg) was added as an internal standard while rhamnose (1 mg) was added as a carrier to all samples Samples were neutralized with N,N-dioctylmethylamine:chloroform (50.50 vol/vol). The aqueous phase was passed through a C-18 column and reduced with 5 mg sodium borohydride. Methanol-acetic acid (200:1 vol/vol) evaporation was done under nitrogen to remove borate. The samples were dried and acetylated at 100°C overnight. Acetic anhydride was decomposed with water, then chloroform was added and the aqueous phase discarded. Ammonium hydroxide was added and the mixture passed through a Chem Elut column. The samples were evaporated to dryness and resuspended in 30 µl of chloroform.

The samples were analyzed using GC-MS-MS. The GC was a Fison:'s 8000 series equipped with an automatic sample injector (model A200S) and a SP-2330 fused-silica capillary column (Supelco, Bellefonte, PA). The MS-MS was a VG Quattro (Fisons, Boston, MA). Electron impact ionization and collision induced dissociation were performed.

43rd ASMS Conference on Mass Spectrometry and Allied Topics

RESULTS AND DISCUSSION

Colony forming units/m^3 air were determined using TSA/H for isolation of viable bacterial load. Distribution of colony forming units (cfu) was highly variable between replicates and sampling times. Gram positive organisms were always predominant with Actinomycete-like bacteria generally a principal colony type. The study covered 5 months with 3 different representative sampling times and colony counts ranging from 51 to 375 cfu.

Concentrations of dust collected from the air varied from 9.1 to 40.3 μg/m^3 air with a mean and standard deviation of 20.3 $\pm$ 7.8. The MA concentration in the air sampled varied between 0.65 to 3.0 ng/m^3 with a mean and standard deviation of 1.4 $\pm$ 0.66. The MA values in airborne dust varied from 25.9 to 120.6 ng/mg with a mean of 76.8 $\pm$ 31.5.

Total viable and nonculturable bacteria were calculated from muramic acid values using two different methods, one which calculates the MA values based on the calculated average of MA content for a Gram positive population and the other which uses a calculated average of MA content for a Gram negative population. In both methods the weight of each cell was calculated assuming the density of a bacterial cell was approximately 1.0 and the cell dimensions taken from Bergey's Manual of Systematic Bacteriology. Four different genus of Gram positive and seven different Gram negatives were used.

Using the average weight of muramic acid per cell for either Gram positive or Gram negative bacteria and the muramic acid concentration of air (as determined by GC-MS-MS) the total viable and nonculturable bacterial concentration was calculated. The average MA concentration of various bacteria were used to determine the percent MA in a model bacterium. The percent dry weight MA of four Gram positive bacteria and seven Gram negative bacteria were used to calculate an average bacteriums' dry weight. For example, from Sept. 1-7, 1994 (1.2 ng/m^3) muramic acid values translated to 70,600 bacteria/m^3 air and from Sept.7- Oct. 8, 1994 (1.3 ng/m^3)there were 76,500 bacteria/m^3 air using the average Gram positive MA dry weight. While using the average dry weight MA for Gram negative bacteria the MA concentrations obtained on September 1-7, 1994 , and September 7-October 8, 1994 , the total bacterial load was respectively 120,000 cfu/m^3 and 130,000 cfu/m^3. The viable bacteria in this period was 1200 cfu/m^3 air.

The calculated cfu/m^3 obtained from the MA data does not correlate to the actual data obtained on culture. It is well established that the nonculturable population of bacteria contributes significantly to the overall bacterial load in diverse environments . Currently, few techniques are available to evaluate for this segment of the bacterial community. Using the Gram positive model as an indicator of the nonculturable population the calculated cfu/m^3 were increased sixty fold. However, the cfu/m^3 obtained using a model bacterium showed an increase of 2 orders of magnitude over actual culture.

This is the first attempt to evaluate the total bacterial load in airborne dust. The use of MA for detection of total bacteriological load in airborne dust provides an independent means to determine bacterial contamination without culture. Muramic acid values (as a measure of PG contamination) have the potential to become one of a battery of standard tests to aid the determination of bacterial biopollution in indoor air.

Effects of Transfer Line on MS Sampling and Analysis of VOCs in Air

Cyril V. Thompson, Marcus B. Wise, and Michael R. Guerin
Instrumentation/Chemical & Analytical Sciences Division,
Oak Ridge National Laboratory

The growing development of field analytical techniques for use in characterization of remediation sites, continuous emission monitoring of chemical processes, and locating sources for fugitive emissions has produced a variety of new methods and instrumentation for determination of volatile organic compounds (VOCs) in air and soil gas samples. Transfer lines are often used to convey these samples from remote sites, subsurface environments, or chemical reactors. The objective of this study was to determine the suitability of Silcosteel™ tubing for such applications.

Six compounds were used in the experiments, h-hexane, benzene, chloroform, toluene, trichloroethylene (TCE), and perchloroethylene (PCE). The experimental apparatus was designed so that an in-line air monitor sampled VOC-laden gas from a manifold, which could be switched so that sample was drawn through either the transfer line or a by-pass. The transfer line was maintained at a temperature of 57° F in a refrigerator during the experiments, as were the gas samples, to simulate physical conditions in subsurface environments. Experiments were conducted in triplicate at concentrations of 0.01, 0.1, 1, 10, 100, 1000, and 10,000 ppm. Gas samples were prepared by injecting methanolic solutions of the individual VOCs into Tedlar bags containing air at 90% RH (57° F), allowing the solution to evaporate, and placing the bags into the refrigerator to equilibrate at 57° F before sampling. The high humidity used to prepare the gas samples is typical of subsurface conditions in both arid and humid climates. Further experiments were conducted in which the transfer line was held at 35° F to simulate above-ground sampling in cold weather. Benzene and TCE were analyzed at 0.1 and 100 ppm and n-hexane and PCE were analyzed at 10,000 ppm under these conditions to provide both medium VOC exposure levels and high and low volatilities at high concentrations. Finally, experiments were conducted to determine the adsorption/desorption characteristics and clearance rates of the individual compounds from the Silcosteel transfer line. In these experiments, the transfer line was exposed to 10,000 ppm concentrations of the individual VOCs for a period of 30 minutes. The response for the compound was monitored after cessation of the

43rd ASMS Conference on Mass Spectrometry and Allied Topics

exposure for periods of up to 530 minutes to determine elapsed times to either 0.01 ppm or lowest achievable response from the transfer line.

Under the standard conditions of 57° F and 90% RH, the Silcosteel™ transfer line had only a minimal (7 - 9%) retentive effect on chloroform, TCE, and PCE, and then only at the 10 ppb level. n-Hexane, benzene, and toluene were unaffected by the transfer line at all concentrations. In the cold transfer line experiment with PCE at 10,000 ppm, the PCE apparently condensed in the transfer line. The response through the transfer line rose to only 54 % of the response through the by-pass. Also, the response for PCE, which would typically decline to baseline 30 seconds after exposure end, continued at near maximum levels for over 10 minutes. In all other experiments with the transfer line at 35° F, there was no effect on the air samples.

In the adsorption/desorption experiments, the Silcosteel tubing typically required 3 minutes or less to reach 10 ppm in the effluent from the transfer line after exposure to 10,000 ppm of the VOC had ceased. Sub-ppm effluent levels were reached in less than one hour in all cases. These times are quite favorable when compared with the tens of hours or even days to clear other types of tubing. Clearance times were generally correlated with the relative volatilities of the compounds.

In conclusion, Silcosteel™ transfer lines appear to be particularly well-suited for air sampling of in air, as they are much less adsorptive than other materials such as tubing of Nylon™, polyethylene, or even Teflon™. Response for VOCs through Silcosteel tubing is rapid, and quantitation is accurate, due to the low adsorptive properties of the tubing. Silcosteel tubing can also be resistively heated, further reducing its adsorption of VOCs, while polymer transfer lines must be wrapped in a heat tape or some such device to accomplish the same effect.

"The submitted manuscript has been authored by a contractor of the U.S. Government under contract No. DE-AC05-84OR21400. Accordingly, the U.S. Government retains a nonexclusive, royalty-free license to publish or reproduce the published form of this contribution, or allow others to do so, for U.S. Government purposes."

MONITORING TRACE CONTAMINANTS IN AIR VIA ION TRAP MASS SPECTROMETRY

P.T. Palmer, Dept. of Chemistry, SF State University, SF, CA
D. Karr, Teledyne Electronic Technologies, Mountain View, CA
R. Pearson, G. Valero, and C.M. Wong, NASA Ames Research Center, Moffett Field, CA

The ever-growing number of applications requiring fast, accurate, and reliable monitoring of trace-level contaminants in air is a major factor driving the development of new instrument technologies for in-situ, real-time analysis. The quadrupole ion trap is particularly well-suited to these applications due to its small size, high sensitivity, and programmable selectivity available through tandem mass spectrometry. A number of ongoing NASA investigations stand to benefit from the use of ion trap mass spectrometry for analysis of the Earth's atmosphere. These include monitoring various chlorofluorocarbon (CFCs) species regulated by the Montreal Protocol, determining baseline levels and emission profiles of volatile organic compounds (VOCs), and performing atmospheric assessments in support of the High Speed Research Program (advanced aircraft development).

Ambient concentrations of specific contaminants depend on the location, time, and many other parameters. Typical values for selected species are given in the table below.

compound	mean global concentration	urban concentration
carbon dioxide	350 ppm	200-1000 ppm
methane	1.7 ppm	1-5 ppm
trichlorofluoromethane (CFC11)	260 ppt	100-7000 ppt
dichlorodifluoromethane (CFC12)	260 ppt	200-3000 ppt
carbon tetrachloride	100 ppt	-
benzene	10 ppt	2-40 ppb
toluene	5 ppt	3-60 ppb

The purpose of this study is to evaluate commercial ion trap instruments for monitoring CFCs and VOCs in air. Our primary interest is in developing the capability to monitor **ambient** concentrations of these species in the atmosphere, which are typically orders of magnitude lower than those found in urban air samples.

These experiments were performed on Teledyne 3DQ and Finnigan ITS40 instruments. CFC and VOC gas standards were obtained from commercial sources or generated via a Environics gas dilution system. Three different sampling methods, direct sampling, gas chromatography (GC), and cryotrapping were evaluated. The direct sampling mode utilized a Valco 10-port valve configured in the gas sampling mode. This valve was equipped with an appropriately size sample loop, enclosed in a small oven heated to 100^0C, and connected to the ion trap via a short length of 0.25 mm ID capillary transfer line. Helium was employed to flush the air sample through the loop and into the ion trap at a flow of about 1 mL/min. The GC mode added a column in between the valve and transfer line. The cryotrapping mode added Tekmar Aerocan and Aerotrap interfaces to concentrate VOCs from large sample volumes.

Direct monitoring represents the simplest configuration of the ion trap for air analysis. Its biggest drawback is the relatively poor sensitivity which results from attempting to detect trace species against a large background of air. Although radiofrequency (RF) levels can be set to prevent ionization of background ions and Filtered Noise Fields (FNF) used to exclude unwanted ions, mass resolution is severely degraded as the "air slug" is flushed into the ion trap. As the offending neutral gas molecules are pumped away, mass resolution quickly returns to nominal levels. The cycle times (defined here as the

time difference between sample injection and completion of data acquisition) are approximately 10 seconds. Detection limits are on the order of 1 ppm for a 0.25 mL sample loop. Note that a number of investigators have utilized different implementations of direct sampling for ion traps and achieved detection limits ranging from ppm to ppb levels (1-4).

GC provides a means for separating air from the components of interest, thus avoiding the concomitant reduction in resolution and signal degradation. A DB-5 column provides complete separation of air, CFC12, CFC11, and carbon tetrachloride. Cycle times are approximately 5 minutes for an isothermal analysis at ambient temperatures. Detection limits depend on sample loop size. Injection of larger sample volumes results in broader peaks and less efficient chromatography. Detection limits on the order of 100 ppb for a 10 uL loop and 1 ppb for a 1 mL loop are easily achieved. Several groups have demonstated the use of transfer line GC on the ion trap to provide even faster cycle times and ppb-level detection limits (5-7). It should also be noted that atmospheric sampling glow discharge ionization and membrane introduction have provided comparable detection limits (8,9). Further reductions in detection limits are necessary before these techniques can be used to reliably monitor CFCs in "clean air" samples at high precision.

Cryotrapping addresses a number of problems including both air and water removal and enhanced sensitivity. It presents the most stringent requirements in terms of space, complexity, and materials (LN2). Moreover, the various steps in the sample processing (i.e.; evacuating, flushing, sampling, cryotrapping, desorbing, etc.) result in cycle times on the order of 50 minutes. Detection limits on the order of 1 ppt are easily achieved for a 1 L sample volume. For the purposes of our work, only cryotrapping was found to provide the ppt-level detection limits required for monitoring ambient levels of VOCs.

A detailed and rigorous intercomparison between MS and MS/MS modes of operation on the two instruments was not within the scope of this study. Our results indicated comparable detection limits between the ITS40 and 3DQ via both MS and MS/MS. The use of FNF to isolate the ions of interest showed improved signal-to-noise ratios versus conventional scanning on the 3DQ instrument.

We have rack-mounted and flight-qualified a system which incorporates a 3DQ instrument, a cryotrapping unit, and an atmospheric sampling unit that supplies constant sample pressures regardless of altitude. This system is currently being evaluated in flight experiments on NASA's DC-8 aircraft and will undergo further testing and flight deployments this summer.

References:

1. Berberich, D.W. and Orth, R.G., Proc. 41st ASMS Conference, 1993, p. 1279.
2. Thompson,C.V., Wise, M.B., Blacock, A.V., and Hurst, G.B., Proc. 40th ASMS Conference, 1992, p. 653.
3. Wise, M.B., Hurst, G.B., Thompson, G.B., Theobold, D.L., and Geurin, M.R., Proc. 39th ASMS Conference, 1991, p. 1205.
4. Brink, C.A., Cisper, M.E., and Hemberger, P.H., Proc. 39th ASMS Conference, 1991, p. 1483.
5. Doherty, S., Proc. 42nd ASMS Conference, 1994, p. 251.
6. Arnold, N.S., McClennan, W.H., and Meuzelaar, H.L., Proc. 41st ASMS Conference, 1993, p. 21a.
7. Hail, M.E., and Yost, R.A., Anal. Chem., 1989, 61, p. 2410.
8. Gordon, S.M., Callahan, P.J., Kenny, D.V , and Pleil, J.D., International Symposium on Field Screening Methods for Hazardous Wastes and Toxic Chemicals, Feb. 1996, Las Vegas, NV.
9. Cisper, M.E., Gill, C.G., Townsend, L.E., and Hemberger, P.H., Anal. Chem., 1995, 67, p. 1413.

Air Analysis for VOCS: Tenax Collection vs. On-Line Membrane Sampling

M. E. Cisper, C.G. Gill, P.H. Hemberger, Los Alamos National Laboratory, Los Alamos, NM 87545
G.L. Kok, National Center for Atmospheric Research, Boulder, CO

We have investigated two sampling methodologies for the analysis of volatile organic compounds in air. Both techniques employ a secondary jet separator stage for sample enrichment and ion trap mass spectrometry for detection.

The first method utilizes dual Tenax traps for continuous off-line adsorption and preconcentration of contaminants from a flowing air stream. As one Tenax trap is sampling, desorbed contaminants from the second trap are injected into a cryo-cooled injection loop. Subsequently, helium carrier gas sweeps VOCs from the heated injection loop to the on-line jet separator.

The second air sampling technique employs a pneumatically-assisted silicone membrane interface for on-line air analysis.(1) VOCs in air permeate through the outside of the tubular membrane into a coaxial helium flow in the membrane interior, which carries contaminants into the jet separator. Calibration and air sampling are accomplished using the flow injection process.

VOC transport efficiency through the membrane was estimated by using a Tenax trap to sample the air stream both before and after the membrane. The Tenax trap was then desorbed onto a gas chromatographic column. For the chlorinated and aromatic compounds we sampled, membrane transport efficiency ranged from 10 to 25% for concentrations ranging from 0.5 to 400 ppb in air.

Memory effects and interferences were studied for the membrane sampling system. Membrane response to a low level contaminant in air (70 parts-per-trillion toluene) was investigated under varying conditions. Neither the presence of a co-contaminant at 100 times the toluene concentration nor high toluene exposure appeared to significantly affect the reproducibility of low-level toluene response.

Chemical ionization (CI) can be readily implemented with the membrane introduction ion trap mass spectrometer. During air sampling, sufficient oxygen crosses the membrane to act as a charge exchange reagent with VOCs in the ion trap. Response to methyl ethyl ketone in air with the membrane sampling ion trap was improved by over two orders of magnitude using this method. For particular organic compounds, CI operation may prove a much more efficient ionization technique than conventional electron impact.

Both sampling methodologies have been successfully used in various air monitoring applications. Outdoor air was sampled during an eight-hour period using the off-line Tenax sampling technique. The results from that experiment are displayed in Figure 1. Detection of toluene in outdoor air could be readily correlated with uncontrolled events in the vicinity. On-line process monitoring of an air stream was accomplished with the membrane interface instrument. In one experiment, the plasma discharge breakdown of trichloroethene in air was observed over a one-hour period. Figure 2 displays fluctuations in TCE response which are readily associated with discharge events.

The two sampling methods are compared in Table 1. While Tenax collection offers greater sensitivity due to a higher flow rate and a longer, discrete sampling period, membrane introduction permits continuous air monitoring. A short membrane fiber (9.5 cm) has been

used to minimize response time; 90% of maximum peak height is attained within 60 seconds or less. Contaminants in air at the 20 parts-per-trillion by volume level have been detected following reductions in the membrane sampling interface volume.

Membrane introduction mass spectrometry provides rapid, near real-time assessment of air quality. Sample archiving and later verification by GC-MS can be achieved by adding the option of off-line air sample collection. Newly-designed circuitry which triggers off-line collection of air samples once a user-defined threshold is exceeded can be used to automate VOC collection on Tenax.

Figure 1. Outdoor Air Monitoring by Off-Line Tenax Collection

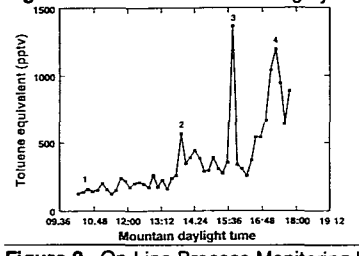

Outdoor air was sampled over an eight hour period. Events correspond to numbers as follows:
(1) Wind from south
(2) Delivery truck in parking lot; wind shifts to opposite direction
(3) Wind stagnant; response is spiked and erratic
(4) "Rush hour" starts

Figure 2. On-Line Process Monitoring by Membrane Introduction

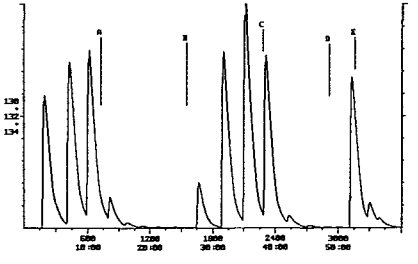

Scan 1	TCE flow on
Scan 680 (A)	Discharge on
Scan 1530 (B)	Discharge off
Scan 2300 (C)	Discharge on
Scan 2890 (D)	Discharge off
Scan 3160 (E)	TCE flow off

Table 1.
Comparison of Air Monitoring Methods

	Tenax collection	Membrane sampling
Flow Rate	1000 ml/min	200 ml/min
Sampling Period	10 min	continuous
Cycle Time	20 min	continuous
Response Time	seconds (following 10 min sampling period and start desorb cycle)	90% of peak height attained in 60 seconds

References
1 Cisper, M.E.; Gill, C.G.; Townsend, L.E.; Hemberger, P.H.; *Anal. Chem.* **1995**, 67, 1413.

CHARACTERIZATION OF VOLATILE ORGANIC COMPOUNDS BY THERMAL DESORPTION/GAS CHROMATOGRAPHY/MASS SPECTROMETRY

Cheng-Yu Ma, J. Todd Skeen, Amy B. Dindal, Cecil E. Higgins, and Roger A. Jenkins

Chemical and Analytical Sciences Division
Oak Ridge National Laboratory*

INTRODUCTION Carbonaceous triple sorbent traps (TSTs) have been widely used to collect and concentrate volatile organic compounds (VOCs) in vapor phase samples for subsequent GC/MS analysis. Recently, our laboratory has been involved in sampling and analyzing VOCs collected from various emission sources, including headspace samples from underground storage tanks at the Deparment of Energy's Hanford site, in Richland, Washington. In order to evaluate the sampling adequacy and to assess any health-related impact based on the analysis results, a validated method must be employed. Therefore, the main objective of this study was to develop a methology for thermal desorption/gas chromatography/mass spectrometry (TD/GC/MS) determination of VOCs in the vapor phase samples collected on Carbotrap C/Carbotrap/ Carbosieve S III triple sorbent traps. Techniques used in method validation included VOC standard generation, thermal desorption efficiency, reproducibility of spiking on and recovery from TST, use of internal standards, detection limits determination, linearity and reproducibility of calibration.

EXPERIMENTAL TD/GC/MS analysis was performed either on a Hewlett-Packard 5995 or 5972A GC/MS system. A modified injector port was installed to adopt an in-house manufactured short path desorber for transferring desorbate directly onto a cryofocusing loop in a splitless mode. A capillary fused silica column (Rtx-5, 0.32mm ID, 60m, 5u film thickness) was connected to a SS cryofocusing loop via a Valco 3-way ZDV switching valve. During the flash desorbing (400^0 C in 1.5 min) process, the carrier flow was increased to 50 ml/min by switching the valve to vent position.The oven temperature program (10^0 C for 10 min, 3^0 C/min to 230^0 C) was initiated immediately after the liquid nitrogen bath was removed from the cryofocusing bath. EI spectra were obtained with an electron energy of 70 eV. Mass spectral data were acquired with a scan rate of 1.2 scan/sec over a mass range of 29-300 amu. Positive CI mass spectra were obtained on a Hewlett-Packard 5985 GC/MS system using methane as reagent gas and the following instrument conditions: source temperature 200^0 C; electron energy 200 eV; emission current 300 uA; and source pressure 0.5 torr. VOC standards (target, internal, surrogate standards) used for method validation were generated using a method similar to the static dilution method described in EPA Methods TO-1. An aliquot of this standard was spiked onto TSTs with a gas tight syringe and 200 ml/min of helium purging through a preheated vapor injector.

RESULTS AND DISCUSSION The method delivered excellent results in terms of reproducibility, desorption effiency, stability of VOCs on TST, linearity, and method detection limit. The in-house manufactured short-path desorber and the cryofocusing system allowed us to perform flash thermal desorption in 5 minutes and to transfer desorbed VOCs directly and

quantitatively onto the GC column. Vapor phase standards generated from 4 internal standards, 3 surrogate standards and 23 target compounds (C_6 - C_{13} alkanes, alkyl alcohols, alkyl nitrile, alkyl ketones, and aromatic hydrocarbons) were used for method validation. A desorption efficiency of greater than 91% was obtained for all the standards studied, based on the ratio of MS response generated from TD/GC/MS to that generated from direct injection of the same standard followed by GC/MS analysis. In order to evaluate method reproducibility and to determine method detection limits for the entire procedure (including gas standard generation, spiking onto and desorbing from TSTs), triplicate TSTs spiked with gas standards at five concentration levels (5-200 ng/trap) were analyzed by TD/GC/MS in a random order over a two week period. The % RSD of the corrected area response (ratio of target compound response to internal standard response) was determined to be less than 10% for the TSTs spiked at 50 to 200 ng/trap level, and increased to less than 25% for the TSTs spiked at 5-10 ng/trap level. For twenty one target compounds, the method detection limit (MDL) was determined to be less than 10 ng. For the remaining two target compounds, the MDL was determined to be 15 and 20 ng. Thus, the higher level of %RSD were normally associated with TSTs spiked with gas standards at a level close to the MDL. Over a period of five months, four calibration curves were constructed at five concentration levels (20 to 700 ng/trap). The linear correlation coefficient (R^2) for all the target compounds falls in a range of 0.910 to 1.000. Additionally, the long-term reproducibility for selected target compounds has been evaluated by carrying out sixteen mid-level (180 ng/trap) calibrations on the same days when field samples were analyzed. In general, the response factor for the mid-level calibration deviated less than 16% from the average response factor generated from the five point calibration. The pre-analytical holding times or the practical reporting times (PRTs) for selected target compounds on TSTs were also determined as part of the QA/QC plans. Except for four target compounds (three alkanones and one alkanol), the PRTs are 30-84 days under refrigeration (2^0 C), as well as at ambient temperature (22^{0}C).

The validated method has been successfully applied to the characterization of VOCs collected from various emission sources in a diversified concentration range. For example, over an eighteen month period, about 150 headspace samples collected from 30 underground waste storage tanks at the DOE's Hanford site have been analyzed. The majority of VOCs were first tentatively identified based on their EI spectra, then were confirmed based on their chemical ionization mass spectra. In some cases, additional confirmation was carried out by GC retention time matching with authentic gas standards. The major VOCs present in those tanks are quite similar and represent a wide range of chemical classes and volatilities: alkanes, alkenes, alkylated cycloalkanes, alkyl nitriles, alkanones, alkanols, alkanoic acid esters, and alkyl phosphates and phosphonates. The recovery rates of three surrogate standards (spiked on TSTs prior to shipping to sampling sites and for process control) range from 87 to 98% with %RSD of 7 to 15%, indicating the spiking process as well as the analytical methodology are very reproducible, and the sample matrix has no or little effect on VOCs collected on TSTs. A relative standard deviation of less than 35% was generally obtained for the quantitation of target compounds. The higher %RSD for the entire process (sampling and analysis) presumably was due to the sampling process under less controllable conditions at the tank storage sites.

* Managed by Martin Marietta Energy Systems, Inc., under contract DE-AC05-84OR21400 with the U.S. Department of Energy.

Analysis of Air Samples from Two Polypropylene Film Plants using Thermal Desorption/GC-MSD

C.W. Chuang; E.J. Arnold; T.A. Roy
Stonybrook Laboratories Inc. P.O. Box 1029, Princeton, NJ 08543

INTRODUCTION

Title III of the Clean Air Act Amendments (CAAA) of 1990, which is Hazardous Air Pollutants (HAPs), mandates that the US EPA address emissions of HAPs from both area and point source. In order to comply with Title III, industry must know what kind of materials are being emitted from the facilities. The availability of the speciation and quantitation of point- and area- specific emission data along with the risk information enables the industry to respond correctly to the regulatory agencies.

Ambient and stack air samples collected from two polypropylene (PP) film plants were analyzed for non-polar volatile organic compounds (VOC) using a thermal desorption unit interfaced with a gas chromatograph-mass selective detector (TDU/GC-MSD). The purpose of the study was to examine the VOC profile of both ambient and stack air inside the PP film plants.

EXPERIMENTAL

Air samples were collected on 6 mm o.d. x 20 cm Pyrex tubes containing 200 mg of Carbopack B and 350 mg of Carbosieve S-III (both from Supleco, Bellfonton, PA). Each tube was refurbished by thermal desorption at this laboratory prior to transport to the sampling sites. Air samples were collected from four stacks on a PP processing line and two ambient locations inside plant A and from three stacks on three separate PP processing lines and two ambient locations inside plant B.

Thermal desorption unit (TDU)--The TDU used was a UNACON 810 (Envirochem, Inc., Kembleville, PA). The sample sorbent tube is thermally desorbed in the tube desorber. The analytes are transferred to trap#1(2 mm i.d. x 20 cm) and then to trap#2 (<1 mm i.d. x 20 cm) before being swept out of trap#2 and cryotrapped at the head of GC column. The GC run is started at the beginning of the trap#2 desorption. After 1.5 minutes of GC acquisition, a liquid nitrogen cryofocus vessel is removed, the GC oven fan turned on and the GC run continued.

GC-MSD--A Hewlett-Packard 5890 gas chromatograph interfaced with a HP 5970B mass selective detector (MSD) was used for the sample analysis. The GC-MSD data system used for analysis was the Hewlett-Packard RTE-6 (Rev. F). The GC column used was a 0.25 mm i.d., 30 meter, 1.4 µm film thickness J&W (Folsom, CA) DB-624 fused silica capillary. The front portion (about 55 cm) of the column was looped and immersed in liquid nitrogen for cryofocusing during analyte transfer from trap #2 to the head of GC column.

Analytes were tentatively identified based on the retention window of C_6-C_{19} n-alkanes and a manual comparison of their mass spectra with the computer based mass spectra library search. Quantitation of compounds was based on the response factor of benzene (i.e., 5000 area count/ng). The method detection limit (MDL) was approximately one-part-billion (ppb) or 3.2 µg/m³ of benzene.

RESULTS & DISCUSSION

Non-polar volatile organic compounds were collected and analyzed following the general procedures outlined in the EPA Compendium of Methods for the Determination of Toxic Organic Compounds in Ambient Air (June 1988), Methods TO-1 and TO-2 [1].

The total non-polar VOC concentrations of stack air samples from the PP film plant A ranged from 0.1 to 7 mg/m^3. The majority of the individual components were tentatively identified as C_9-C_{14} alkanes/alkenes. The thermal and thermooxidative degradation of PP has been studied by Frostling et. al. [2] both in the laboratory and industrial setting. The profile of PP-derived thermal/thermooxidative products observed at the PP film plant A was very similar to those observed by Frostling and this laboratory. Most of the non-PP derived components were believed to originate from the terpene resin. The literature [3-5] shows that the basic terpene ring structure can undergo heat and acid-induced rearrangement, oxidation and condensation reactions to from numerous structural isomers and bicyclics, vinyl and aromatic derivatives and dimers. Compounds tentatively identified as $C_{10}H_{14}$, $C_{10}H_{16}$, and $C_{10}H_{18}$ appear to arise from unimolecular rearrangement and/or oxidation of terpenes. Compounds tentatively identified as terpene dimers are believed to originate from bimolecular rearrangement of terpenes.

The total non-polar VOC concentrations of stack air samples from the PP film plant B ranged from 0.006 to 7 mg/m^3. The majority of the individual components were tentatively identified as C_9-C_{16} alkanes. The profile of PP-derived thermal/thermooxidative products observed at this PP film plant was similar to that observed by Frostling. Additionally, compounds tentatively identified as semi-volatile non-polar organics (i.e., $>C_{12}$), which were not measured by Frostling, contributed significantly to the overall VOC emissions in the plant.

CONCLUSION

The qualitative profile of vapor phase compounds found at both sampling sites is consistent with that reported in the literature for pyrolysis/thermooxidative degradation of PP and terpenes.

REFERENCES

1. "Compendium of Methods for the Determination Of Toxic Organic compounds in Ambient Air" *EPA 600/4-89/017* , June **1988.**

2. Frostling, H.; Hoff, A.; Jacobsson, S.; Pfaffi, P.; Vainiotalo, S.; and Zitting, A. "Analytical, Occupational and Toxicological Aspects of the Degradation Products of Polypropylene Plastics" *Scand. J. Work Enviro. Health*, **1984**, 10, 163-169.

3. Traynor, S.G.; Crowley, K.J.; Cocker, W. "The Pyrolsis of Limonene: A Reappraisal" *J. Chem. Research (S)*, **1981**,175.
4. Spraul, M.H.; Nitz, S.; Drawert, F. "Photochemical Reactions of *p*-mentha-1,3,8-triene and Structural Related *p*-menthadienes" *Tetrahedron*, **1991**, 47(18/19), 3037-3044.

5. Thomas, A.F.; Bessiere, Y. "Limonene" *National Products Reports*, **1989**, 291-309.

VOLATILE ORGANIC COMPOUND (VOC) ANALYSIS IN BLOOD USING SPRAY EXTRACTION

F. St-Germain[1], B. Vachon[1], J. Brunet[1], O. Mamer[2], C. Des Rosiers[1] and J. Montgomery[1], [1]Dept. of Nutrition, Université de Montréal and [2]McGill University Biomedical Mass Spectrometry Unit, Montréal Québec, Canada.

The quantitation of volatile organic compounds (VOC) in gaseous or liquid media has important ramifications for identifying environmental and medical risks. Due to the volatile nature of these compounds, they are difficult to measure accurately. We describe here a new device (1,2) which extracts volatile and semi-volatile compounds from aqueous samples and transfers them to an ion trap mass spectrometer (MS) for analysis. Our inertial spray extraction interface (ISEI) consists of a nebulizer coupled to a chamber which is at room temperature. The sample is sprayed into the chamber thus facilitating the evaporation of VOCs from the aqueous sample. A continuous flow of helium transports the VOCs to the MS (Varian Saturn II ion trap). Depending on the compound analyzed, the ion trap is operated either in electron impact or in positive chemical ionization mode using methane as a reagent gas. Following injection of a 1 ml sample, less than five seconds are required to return to baseline conditions. Figure 1 presents an example of an injection of an aliquot of an aqueous solution of halothane, a common volatile anesthetic. The intensity of the ions of interest is proportional to sample concentration when normalized with an added internal standard. Detection limits are less than 10 parts per billion for many compounds including chloroform, acetaldehyde, and toluene and in the parts per trillion for others, for example benzene.

We present examples of analytical applications using ISEI. Blood samples from a pig anesthetized with halothane were analyzed both before and after induction of anesthesia (Figure 2). The mass spectrum obtained from the sample after anesthesia is dominated by the ions characteristic of halothane (Figure 1). The halothane signal was proportional to the dose administered and decreased rapidly when the anesthetic was withdrawn. In another experiment, human blood samples spiked with toluene and xylene were analyzed by both conventional headspace gas chromatographic assay and by our ISEI system. In another experiment, rats were exposed to air spiked with known concentrations of toluene and xylene and blood samples were analyzed by both methods. In both of these experiments, excellent correlation coefficients were obtained between the two methods. Analysis of VOCs in blood is possible in volumes as low as 0.2 ml, thus permitting blood sampling by finger-prick rather than venipuncture. ISEI coupled directly to an ion trap MS provides a quick, clean and reproducible way to analyze VOCs in aqueous samples. Unlike membrane introduction mass spectrometry, spray extraction avoids discrimination effects due to analyte solubility in the membrane. The ISEI has immediate use in the field of occupational health and coupled with MS/MS for compound verification would be applicable to other medical diagnostic procedures. (Financial support from Theratechnologies, Inc. and the Medical Research Council of Canada).

References:

1. St-Germain, F., Mamer, O., Brunet, J., Vachon, B., Tardif, R., Abribat, T., Des Rosiers, C. and Montgomery, J., Volatile organic compound analysis by an inertial spray extraction interface coupled to an ion trap mass spectrometer, *Anal. Chem.*, submitted 1995.
2. Patent pending

43rd ASMS Conference on Mass Spectrometry and Allied Topics

Figure 1 TIC AND MASS SPECTRA OF PIG BLOOD BEFORE (A) AND AFTER (B) HALOTHANE EXPOSURE

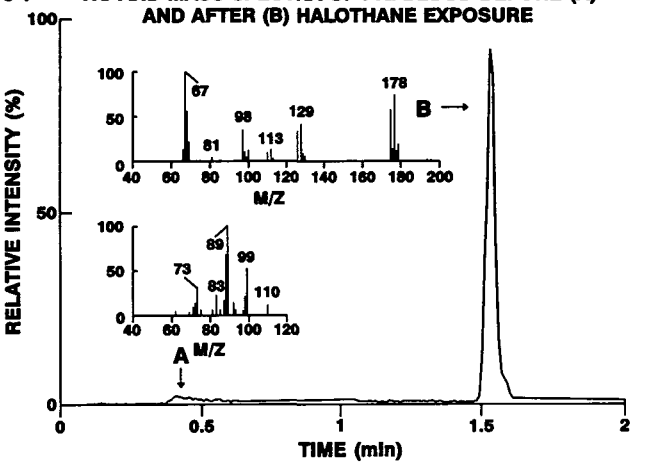

Figure 2

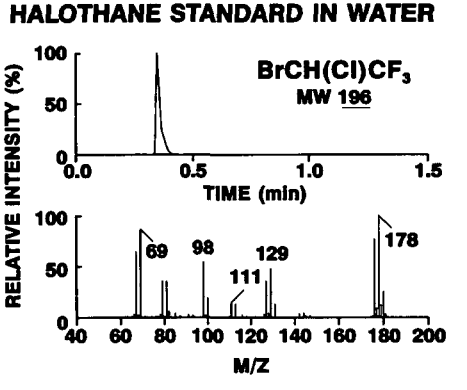

A Study of Semi-Volatile Organic Emissions of Polymer Combustion by GC/MS

J. Carlson[1], Y. Dunayevskiy[1], A. Atal[2], T. Panagiotou[2], P. Vouros[1], Y. Levendis[2]
[1]Department of Chemistry, Northeastern University, Boston, MA 02115
[2]Department of Mechanical Engineering, Northeastern University, Boston, MA 02115

The incineration of waste polymeric materials in air inevitably produces a large variety of hazardous organic emissions[1]. The organic emissions from the combustion of polystyrene, polyvinylchloride, polyethylene were evaluated by GC/MS. The evolved soot was retained on glass fiber filters and the semi-volatile organics were trapped on XAD-4 resin. The organics were removed with soxhlet extraction from both the glass fiber filters and XAD-4 with methylene chloride.

Methylene chloride was used to extract the organic compounds from both the filter paper and the XAD-4 resin. 100μg of d_8 naphthalene were added to the methylene chloride prior to soxhlet extraction and solvent reduction to provide a semi-quantitative indication of component amounts. 100μg of d_{10} anthracene was then added to the resulting 1ml of solution. The comparison of the peak areas of the deuterated naphthalene and anthracene in the total ion chromatogram (TIC) provided an indication of extraction efficiency. The combustion of the polymers was repeated if the TIC peak area for d_8 naphthalene was less than 40% of the peak area for d_{10} anthracene.

To account for the variablities in material handling, extraction efficiency, solvent concentration, and instrumental analysis, the data was normalized to the remaining d_8 naphthalene concentration. This procedure enables the relative comparison of semivolatile organic components generated in the combustion of polymers as a function of variations in combustion conditions, but does not provide an accurate quantitative analysis for the component concentration within a single sample analysis.

The filter paper that was placed over the XAD-4 resin physically trapped most of the soot that was generated during the combustion process. The comparative analysis of the soot/filter paper and the XAD-4 resin showed that all the semivolatile components observed on the filter paper extracts were also observed in the XAD-4 resin extracts. Despite some small differences in the ratios of some of the semivolatile components observed in the filter paper and the XAD-4, the data generated by the filter paper analysis provided no additional insight as to the identity and quantity of the semi-volatile components generated by the combustion process and therefore were not presented.

An empty combustion vessel was exposed to the combustion process to determine the identity and quantity of interferents resulting from the furnace, filter paper, XAD-4 resin, solvents and GC/MS instrument.

The GC/MS analysis of the semi-volatile organics emanating from the burning of polymeric wastes was conducted as a function of particle size, flame propagation, temperature, residence times and reaction rates. Organic emissions from horizontal furnaces at 900C typically produce high concentrations of polyaromatic hydrocarbons while polymers burned in laminar drop tube furnaces at 950-1250°C produce significantly reduced quantities of PAHs.

Polyvinylchloride (PVC). The largest number and quantities of polyaromatic hydrocarbons evolved from the combustion of PVC in a horizontal furnace. Similar levels of PAH's were observed when unsteady particle clouds (puffs) were combusted in the vertical furnace. No PAH's, with the possible exception of naphthalene, were observed in the vertical furnaces with

dilute particle aerosols at temperatures greater than 950°C. The largest component in the XAD-4 extracts resulted from the formation of benzoic acid.

Polystyrene (PS). Three major classes of combustion products were observed in the XAD-4 extracts in PS. Thermo-oxidative degradation of PS produced many low molecular weight oxygen containing species. The second class is low molecular weight polyaromatic hydrocarbons such as naphthalene, phenanthrene, anthracene, biphenyl and fluoranthene. The largest class consists of the compounds that are formed in "classical" type reactions of the styrene olefinic system, such as bibenzyl, stilbene, 1,4-diphenyl-1,3-butadiene.

Polyethylene (PE). The number of PAH's observed in the combustion of PE is remarkably reduced when compared to similar combustions of PS and PVC. The prevalent form of PAH were fused mulitple ring aromatics with the largest relative quantities of polyaromatic hydrocarbons for compounds with the chemical formulas $C_{12}H_8$, $C_{14}H_{10}$, $C_{16}H_{10}$, $C_{18}H_{10}$ and $C_{20}H_{12}$. A set of total ion chromatograms (TIC) are shown in Figure 1, with PAH's from the horizontal furnace (HF) shown in the back, while the temperature range of 950°C to 1250°C are shown for the vertical furnace (VF). PAHs were not observed with the higher temperature combustions. Peaks at about 10 minutes and 20 minutes represent d_8 napthalene and d_{10} anthracene respectively.

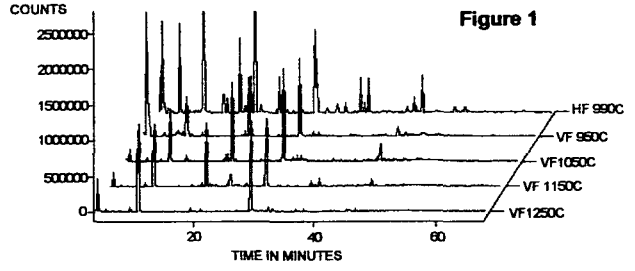

Figure 1

Reference

1. Panagiotou, T., Levendis, Y. A., *Combust. Flame*, **99**, 53-74, 1994.

STRATEGIES FOR IDENTIFICATION OF VOLATILE ORGANIC COMPOUNDS OFFGASSED FROM MATERIALS AND ASSEMBLED ARTICLES

L. Yang*, H. Leano, M. Martin, T. Limero, and J. James[1]
Biomedical Operations and Research Branch and KRUG Life Sciences, Inc.,
[1]NASA-Johnson Space Center, Houston, TX 77058

Trace amounts of volatile organic compounds (VOC) offgassed from on-board equipment can degrade the respirable air in the closed environment of a spacecraft. Exposures to these chemicals may affect the health and performance of crewmembers. Consequently, NASA requires that all non-metallic materials and assembled articles present in the habitable areas of a spacecraft be assessed to ensure that the offgassed products meet established toxicological safety criteria. The offgassing test (OGT) object is enclosed in a test chamber in a zero-air test atmosphere at 1 atm., then heated to 50°C and held at this temperature for 72 hours. After cooling, a gas sample from the chamber is analyzed for its constituents[1]. The capillary column GC/MS combined with cryogenic preconcentration is the primary method we use to analyze the complex mixtures of VOCs released from OGT objects. The goal of our present research is to develop strategies for accurate and fast interpretation of GC/MS chromatograms, resulting in accurate and expeditious identification of VOCs in offgassed product mixtures. Ultimately, the goal is to efficiently provide quality analytical results to support toxicological assessments.

Offgassed products released from non-metallic materials or assembled articles are complex gas-phase mixtures of volatile organic compounds. A total ion chromatogram obtained from a typical offgassed product mixture is shown in Figure 1. Identification of OGT compounds is normally accomplished by searching the spectrum of each total ion chromatogram peak against commercial mass spectral libraries. The library search identification is confirmed by matching the spectrum and the retention time of a standard to the best library identification. For those spectra that have no match, manual deconvolution is attempted to identify any superimposed spectra. The deconvolution results are further confirmed by the comparison with GC/MS analytical results of standards. Figure 2 shows a no-library-match unknown spectrum extracted from an OGT total ion chromatogram peak. By means of manual deconvolution and standard confirmation, two compounds, nitroethane and tetrahydrofuran, were identified from this mass spectrum. Identification of isomers, such as acetaldehyde and ethylene oxide, is achieved by separating the mixture on a non-polar stationary phase capillary column before MS detection. The most difficult unknowns generated in OGTs are those that present the same mass spectrum in two different stationary phase capillary column GC/MS analyses, and the spectrum does not match any spectrum in commercial mass spectral libraries. In this case, typical mass spectral interpretation techniques are used to identify unknowns. The mass spectrum shown in Figure 3 is an example. The peak of ion 74 in the spectrum would be a common fragment ion of aliphatic nitrite, $ONOCH_2CH_2^+$[2]. The peak of ion 30 suggests the presence of NO^+, and the peaks of ions 39 to 43 for $C_3H_7^+$. Because the candidate standard, propyl nitrite, was not available in our laboratory, the GC retention times of 16.6 min., 18.0 min., and 25.6 min. on the same non-polar stationary phase column for methyl nitrite, ethyl nitrite, and butyl nitrite, respectively, were used to support the mass spectral interpretation of the unknown spectrum at retention time of 20.0 min.

The capillary column GC/MS system, interfaced with a preconcentration inlet system, is a powerful tool for identifying and quantifying volatile organic compounds in offgassed product mixtures. More than 400 VOCs have been identified using the strategies described above. These compounds include some long-term "unknowns". Those compounds positively identified are collected into the OGT-VOC library along with their GC retention time windows, mass spectra, and chemical properties. With this database, VOCs released from additional offgassing test objects can be accurately and expeditiously identified on the basis of their retention time windows and three major characteristic fragment ions or abundant base ions. In general, an offgassed product mixture of 60 VOCs can be identified in less than 4 hours. Some "tough" unknowns still have yet to be positively identified by use of the GC/MS method. Strategies based on a GC/MS/MS method are currently under development in our lab to better support toxicological assessments.

ACKNOWLEDGEMENT: We are grateful for financial support from the NASA/JSC Center. We also thank Mr. John Boyd, Mr. Phil Covington, Dr. Marilyn Matney, and Dr. Jay Cross of KRUG Life Sciences,Inc. for their contributions to this research project.

REFERENCES: 1. NASA Document NHB 8060.1C.
2. F.W. McLafferty, Interpretation of Mass Spectra, 3rd. Edition.

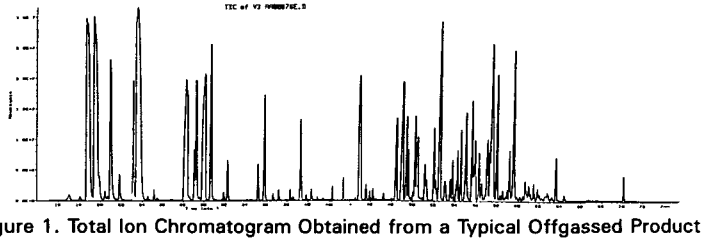

Figure 1. Total Ion Chromatogram Obtained from a Typical Offgassed Product Mixture.

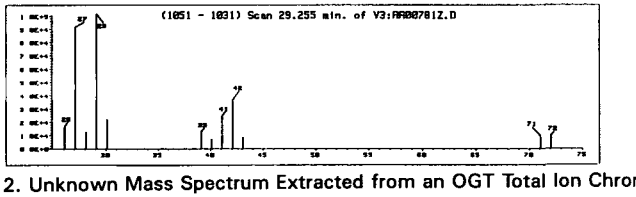

Figure 2. Unknown Mass Spectrum Extracted from an OGT Total Ion Chromatogram.

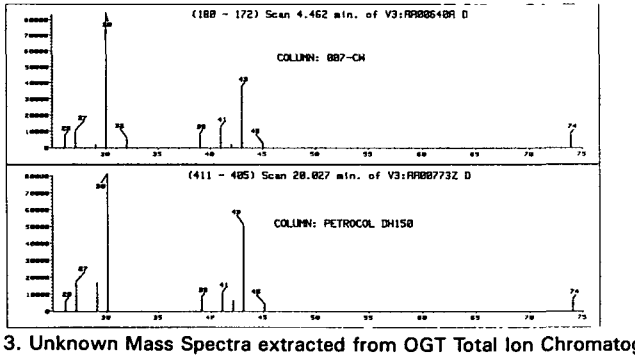

Figure 3. Unknown Mass Spectra extracted from OGT Total Ion Chromatograms.

Electrospray Ionization and Tandem Mass Spectrometry of Dyes

Jennifer B. Fencl, Gary L. Glish and Robert D. Voyksner*
Department of Chemistry, University of North Carolina, Chapel Hill
Research Triangle Institute, RTP, North Carolina

Introduction

The identification of dyes and their components is a critical aspect of screening industrial waste streams. Because of their deleterious effects, a sensitive technique is needed for rapid identification of potentially harmful compounds. Thermospray ionization on a triple quadrupole has been previously utilized for this purpose.

As an alternative approach, we have investigated the use of electrospray ionization (ES) on a quadrupole ion trap. ES was tested on various dye classes to demonstrate its viability as a method of ionization for dyes. MS/MS and MS^3 experiments were performed to elucidate structural information. These results were compared to the data acquired using thermospray ionization on a triple quadrupole.

Experimental

Dyes were obtained from the Environmental Protection Agency, or purchased from Sigma. Stock solutions were prepared in ACN:H_2O:HOAc (50:50:1%) or CH_2Cl_2:ACN:TFA (50:50:1%) in millimolar concentrations. Aliquots of these solutions were diluted 10 to 100-fold and analyzed by the mass spectrometer to determine optimum ssample concentration. Flow rates were adjusted between 1 and 2 µl/min.

Five classes of dyes were analyzed using a quadrupole ion trap with a home built ES ionization source as shown in figure 1. Dyes were observed in the positive ion mode at a helium pressure of 1.1×10^{-3} torr.

Results

An example of the dyes studied using MS/MS is illustrated in figures 2 ,3 and 4. Figure 2 data is from a triple quadrupole, and and figures 3 and 4 are spectra from a quadrupole ion trap. Similar product ions appear in both spectra, but the quadrupole ion trap provides more information about the structure. MS^3 was performed on the product ion with the greatest intensity to obtain further structural information.

Discussion

It has been determined that data from the quadrupole ion trap provides as much or more information about the structure of various dyes. This is a result of two general factors. First of all, a quadrupole ion trap has a longer time window for fragmentation that favors low energy processes and facilitates detection of more low energy fragments. In addition, higher energy processes are also able to be viewed using MS^n because enough energy has been imparted to the ion(s) of interest from successive isolations and resonance excitation voltages.

Acknowledgement

This work was funded in part by the Environmental Protection Agency through cooperative agreement number CR-819555

Conclusion

An electrospray ionization source coupled with a quadrupole ion trap is a viable method for detection of dye compounds. Results indicate that fragmentation is more extensive in MS/MS and MS^3 experiments, providing greater structural elucidation than on a triple quadrupole. Both methods provide a complementary approach for detection and characterization of various dye classes.

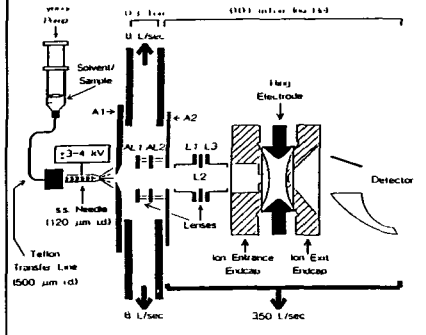

Figure 1 . Quadrupole ion trap with an electrospray ionization source

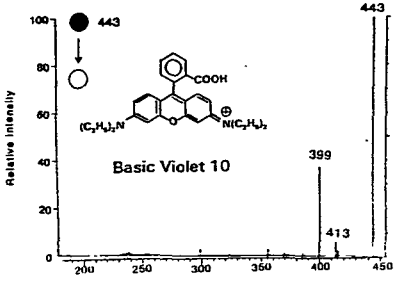

Figure 2. Triple quadrupole data* for Basic Violet 10

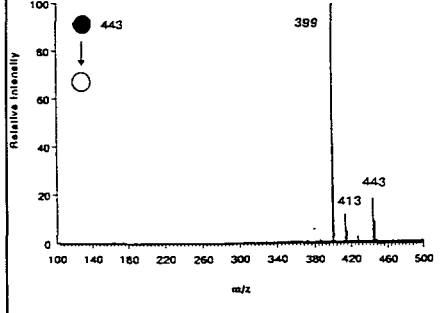

Figure 3. MS/MS data of Basic Violet 10 on a quadrupole ion trap

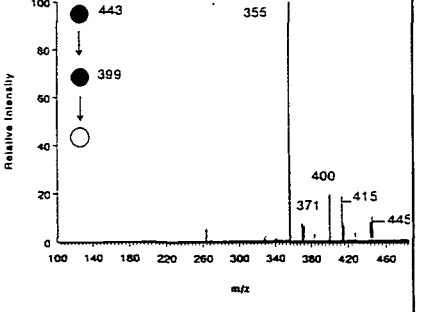

Figure 4. MS^3 data of Basic Violet 10 on a quadrupole ion trap

References

* Betowski *et al.* Environmental Protection Agency publication, 1984
Betowski *et al.* Organic Mass Spectrometry, **21** , 575, 1986
McLuckey *et al*, Analytical Chemistry, **62**, 1285,1990

ANALYSIS OF SURFACTANTS AND THEIR METABOLITES IN WASTEWATER BY HPLC-IS-MS AND MS-MS

by Andrea RAFFAELLI, Sergio PUCCI, Laura CAMPOLMI, Piero SALVADORI

Centro di Studio del CNR per le Macromolecole Stereordinate ed Otticamente Attive, Dipartimento di Chimica e Chimica Industriale, Università di Pisa, Via Risorgimento 35, 56126 PISA, Italy.

INTRODUCTION. The most common procedures for the analysis of cationic and anionic surfactants in wastewater are based on colorimetric methods. Although simple, these methods are neither very specific nor very sensitive. Moreover, they can completely fail on some metabolites, if the functional group responsible of the formation of the coloured adduct is not present anymore. Considering that sometimes the metabolites can be more toxic and stable with respect to the original surfactant molecule, this can be a real problem if a good control is required.
Mass spectrometry, owing to its high sensitivity and specificity, can be a very useful technique for the development of new analytical procedures, especially if hyphenated to suitable separation techniques. Due to the very low volatility of this class of analytes, liquid phase separation and ionization methods appear the right choice.
We present here a detailed study of different classes of detergent surfactants, as well as of opportune mixtures, by flow injection analysis (FIA) and high performance liquid chromatography (HPLC) coupled with Ionspray mass spectrometry and tandem mass spectrometry. Anionic, non ionic, cationic and anphoteric surfactants have been considered for this investigation. FIA-MS allowed to check the composition of different raw materials used for the preparation of final formulates. Reverse-phase HPLC has been used keeping in mind that the final target was the development of a universal analytical method for all different classes of tensides in water solutions. So we decided to look for a general gradient elution capable to separate at least the classes of compounds.
We are also studying some chemical degradation mixtures, obtained mainly by treating the above raw materials with oxidation agents. MS-MS will also be used in order to improve the method sensitivity and to elucidate the structure of unknown metabolites.

EXPERIMENTAL. A Perkin Elmer Sciex API-III Plus triple quadrupole mass spectrometer was used for Ionspray ionization MS and MS-MS measurements. A Harvard 22 syringe pump was used to provide a constant flow (infusion) of analyte at 5 µl/min into the source. FIA and HPLC were carried out using a Perkin Elmer Series 200 dual solvent delivery system, equipped with a loop-injector (20 ml). FIA eluent was a 10mM ammonium acetate water solution (50 µl/min). HPLC separations were performed on a Perkin Elmer C18 (3 µm particle size; 4.6 mm i.d. x 3 cm length) using ACN and FIA solvent in gradient elution (1 ml/min, split 1:40). Sample preparation involved diluting the raw materials in the FIA eluent.
Chemical degradation mixtures were obtained from Triton X-100 and sodium dodecylsulfate water solutions treated with H_2O_2 in presence of Fe^{2+} (Fenton's reagent). Order of addition and reagent ratios were varied in order to evaluate their relations with the nature of reaction products.

FIA-IS-MS RESULTS. We used ammonium acetate as an ionization aid in order to minimize the presence of alkali metal adducts that would decrease the sensitivity of the method by spreading the signal of each component into different ions of the spectrum. Moreover, alkali metal adducts are not

suitable to give significant product ion spectra in Tandem Mass Spectrometry.
Each surfactant raw material was analyzed both in the Positive (PI) and the Negative Ion mode (NI). Non ionic and cationic surfactants did not give relevant NI spectra. Different anionic oligomers of the same family showed very different response factors in PI with respect to NI.

HPLC-IS-MS RESULTS. The gradient elution method elaborated allows the elution of anionic and anphoteric surfactants first (8-13 min), whereas non ionic surfactants are more retained (25-40 min). We observed also a partial separation of ethoxylated oligomers. Cationic surfactants could not be eluted under these conditions. A sample chromatogram of a mixture of four different raw materials ir reported in the figure, showing the total ion current chromatogram (Top left and right traces) and the extracted ion current chromatogram for a single component of the four tensides (mid and bottom traces).

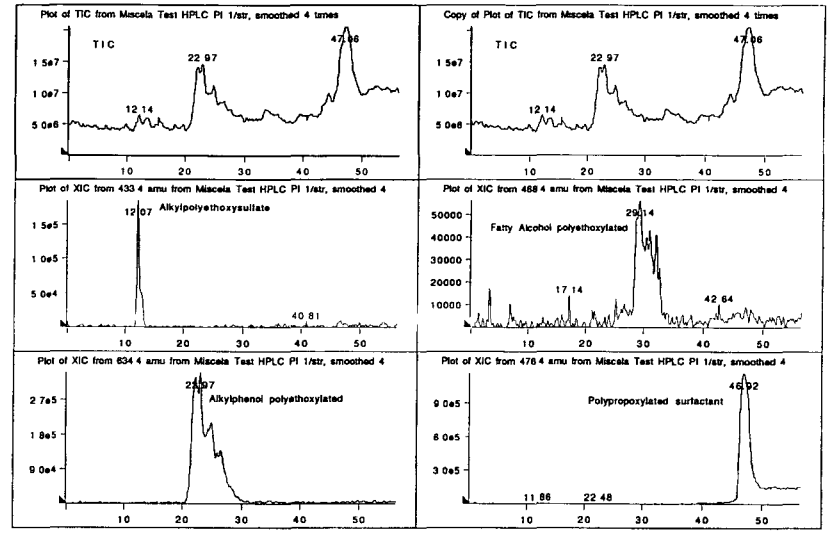

PRELIMINARY INVESTIGATION ON METABOLITES. Analysis by FIA-IS-MS of the oxidation reaction mixtures obtained by treating the surfactant of choice (Triton X-100 or sodium dodecyl sulfate in the experiments so far performed) with Fenton reagent showed the presence of higher as well as lower molecular weight products, in variable amounts depending on reaction conditions. The nature of the metabolites obtained in now under investigation. Separation by reverse phase HPLC was not achieved in the condition described above, as all components but the precursor eluted with the solvent, thus suggesting a very polar nature for these compounds.

The analysis of surfactants by lc and lc-ms.

SD Scullion, MR Clench and M Cooke

Division of Chemistry / Environmental Research Centre, School of Science, Sheffield Hallam University, Pond Street, Sheffield, UK. S1 1WB.

The determination of surfactants in drinking, surface and groundwater is currently a very "live" topic of analysis It is important to monitor the two most widely used forms of surfactant, i e. the non-ionic alkylphenol ethoxylates and the anionic alkylbenzene sulphonates. Recently it has been shown (1) that non-ionic surfactants of the alkylphenol ethoxylate type and their degradation products exhibit weak oestrogenic properties and may be implicated in the increase in male infertility in the western world.

The analysis of non-ionic surfactants of this type is made complex by the fact that they are formulated as a mixture of oligomers/homologues of a parent compound Non-ionic surfactants of the alkylphenol ethoxylate type are usually formulated so that the ethoxylate side chain varies from 1 to 30 units Analysis may be carried out by spectrophotometric or lc methods employing conventional detectors. However, neither of these techniques offers unambiguous identification of surfactant type and chain length Hence lc-ms has been investigated as a possible method of analysis

Particle beam lc-ms has been used in the determination of non-ionic surfactants in surface water(2) and drinking water(3) Clark et al(3) determined alkylphenol ethoxylates in drinking water after continuous liquid/liquid extraction of 500 litres of finished water The resulting extract was then analysed by pb-lc-ms (detection limits in the ng region were obtained) The method used by Clark(3) offers excellent sensitivity but is very time consuming. We have conducted experiments using lc-pb-ms and although reproducible TICs are readily obtainable poor sensitivity limits this method in terms of routine laboratory analysis Lc-APcI-ms offers robust and sensitivity means of analysis for the analysis of environmental samples containing surfactant mixtures.

We have investigated methods for the determination of surfactants by solid phase extraction C18 and SAX cartridges in series. Hplc separation of anionic and non-ionic surfactants on a C1(TMS) column has been achieved with detection via both fluorescence and liquid chromatography-mass spectrometry (atmospheric pressure chemical ionisation interface). Recoveries are approximately one hundred percent with detection limits of 50 ng on column for detection by fluorescence Alkylphenol ethoxylates have been detected in samples taken from the River Rother in South Yorkshire U.K at levels of 5.6 ppb

References :

(1) Jobling_ S and Sumpter_J P. Aquatic Toxicology, 27(1993)361-372,

(2) Bristow_A, Clench_MR, McDonnel_M, Smith_J and Willis_S , Proc. 19th Ann Meeting of British Mass Spectrometry Society, St. Andrews University 13th-16th Sept 1992 p 92-95.

(3) Clark_LB, Rose_RT, Hartmann_TG, Louis_JB, Suffet_IH, Lippincourt_RL and Rosen_JD, Intern. J Environ. Anal Chem., 47(1992)167-180

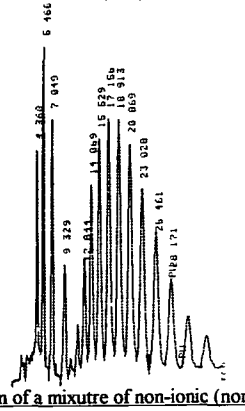

Figure 1 hplc chromatogram of a mixutre of non-ionic (nonylphenol ethoxylate)and anionic (linear alkylbenzene sulphonate) surfactants

Kinetics and Pathways of Biodegradation by ES/APCI/MS and ^{14}C Labeling

S. W. Morrall, D. L. Lawrence, T. W. Federle
Environmental Science Department, Procter & Gamble Co., Cincinnati OH 45217

The environmental fate and ultimate effect that a water soluble compound will have in the environment is highly dependent on the complex process of biodegradation. Conventional evaluation of "biodegradation" is limited to removal of soluble organic carbon (SOC) and CO_2 production as metrics. These data are useful in screening compounds and setting criteria for "biodegradability", but have little diagnostic capability. The application of ESI/APCI/MS/MS has greatly improved the range and depth of information available concerning the biodegradation process.

METHODS

I - Biodegradation Test System

Two types of testing are typically used to determine the "biodegradability" of compounds disposed into waste water. A semi-continuos activated sludge (SCAS) experiment measures removal of soluble organic carbon (SOC). The amount of SOC attributed to the test material is determined by difference between the test compound and a control, which gives background SOC. Acclimated sludge from the SCAS unit can be used to inoculate another vessel where CO_2 emission is monitored. The outcome of this "mineralization" test is expressed as a percent of theoretical CO_2 evolved (based on total carbon contained in dose of test material) relative to a "background CO_2" control.

In order to have sufficient signal (SOC or CO_2) above the natural background, unrealistically high doses of the test material (~20 ppm) must be used. These high doses do not usually affect the judgment of whether a material is "inherently" biodegradable, but often induce a delay in the onset and decrease the rate of biodegradation. These effects are often attributed to the toxicity of the high dose and/or the time required for sufficient biomass growth to handle the high carbon loading

II - Radio Isotope Label (^{14}C)

Selective labeling of the test material with ^{14}C enables the biodegradation tests to be conducted at realistic concentrations (10-80 ppb) and provides a direct link between measured SOC/CO_2 and parent compound. Rad-TLC analysis of the test matrices provides additional data concerning primary degradation (loss of parent) and the presence and disappearance of intermediates. A carbon mass balance can be obtained for the test system However, the chemical structures of the intermediates and the pathways of the biodegradation process cannot be directly determined from the radio analytical experiments.

III - ESI/APCI/MS/MS

MS analyses (VG Quattro) of the SOC in the SCAS/CO_2 test system provides information about intermediate structures, biodegradation pathways, and any functional groups or components in the test material that is resistant to biotransformation. Analyses of extracts from the Rad-TLC plates directly links the ^{14}C kinetic data with intermediate structures. A variety of MS experiments are

used, depending on test material and matrix. Aqueous samples from the SCAS/CO_2 test are preserved and pre concentrated by SPE. Positive and negative ion modes are used with MS/MS confirmation of structures identified by mass of the molecular ion. Samples from the simpler matrices are often introduced by flow injection, with HPLC separation being used for the more complex samples.

RESULTS

I - Linear Alkyl Benzene Sulfonates (LAS)

LAS is a mixture of homologs (C_{9-13}) and isomers (branching and substitution on alkyl chain). Branched isomers (ABS) resist biodegradation, but are difficult to differentiate from LAS in environmental samples. ABS can be quantified using MS/MS (MRM) with appropriate standards.

A major biodegradation pathway is oxidation of the alkyl chain to form sulfophenyl carboxylates (SPC's). The doubly charged anions are useful for identification and quantitation of SPC's in complex matrices.

A lag phase of up to 10 days is seen between the high dose SCAS/CO_2 test relative to the more realistic ^{14}C die-away test (75 ppb, label in benzyl ring). However, biodegradation is complete at both concentrations without any evidence of persistent intermediates.

II - Alkyl Ethoxylates (AE's)

AE's are complex mixtures of several homologs (C_{9-18} and EO_{0-20}). Biodegradation can occur via several pathways with external cleavage of the EO chain being dominant in the SCAS/CO_2 test systems. Short chain PEG (Mw <600) is the primary intermediate.

H+ adducts were the dominant ions produced in APCI if an amino precolumn were used to separate inorganic cations (Na+) prior to ionization. ESI tended to produce both Na+ and H+ adducts (as well as NH_4+ if added). Quantitation was made difficult by a change in the relative abundance of the adducts as a function of EO chain length. The distribution can be easily shifted to all sodium adducts. However, H+ and NH_4+ adducts are more amenable to MS/MS analyses.

III - Nonylphenol Ethoxylates (NPE's)

NPE's are a mixture of ethoxylated homologs. Parent NPE degrades slowly, primarily via oxidation and cleavage of EO portion with limited oxidation of the highly branched alkyl chain. This degradation of EO portion produces a long lived intermediate (nonylphenol), which is more toxic than parent NPE

The pitfalls of nonspecific analyses being used to evaluate biodegradation are illustrated by a "commercial" NPE evolving a high level of CO_2 in a screening test. HPLC/ESI/MS experiments showed that a PEG contaminant was degrading, but the parent NPE was being biotransformed into nonylphenol.

ACKNOWLEDGMENTS

The following scientists and associates in the Environmental Science Department of Procter & Gamble made significant contributions to the work presented in this poster ^{14}C analytical - Nina Itrich, Sampling / Preparation - Bill Begley, HPLC - Ron Herzog , SCAS / CO2 - Melanie Hansmann, Biodegradation Test Development - Beth Bookland and Robert Larson

Detection of Atmospheric Contaminants Adsorbed on Surfaces Using Static SIMS

Gary S. Groenewold, Evan M. Harrison, James E. Delmore, Jani C. Ingram, Anthony D. Appelhans, David A. Dahl, Idaho National Engineering Laboratory, Idaho Falls, ID 83415-2208

The sensitivity of static secondary ion mass spectrometry (SIMS) to the detection of adsorbed atmospheric contaminants has long been recognized, but not exploited. Early in the history of static SIMS, Benninghoven noted that many of the ions observed in static SIMS spectra originated from contaminants which were probably of atmospheric origin.[1] Cooks and coworkers had attributed much of the observed hydrocarbon-type ion signal to pump oil present in the vacuum housing of most organic SIMS spectrometers.[2] In research conducted in our laboratories, it was noted that many compounds (e.g., tri-*n*-butyl phosphate[3]) may adsorb to a variety of surfaces, and are readily detectable using SIMS.

Analysis of cyclohexylamine (CHA) on soil. A compound which displays a particularly pronounced tendency to adsorb to SIMS samples and form abundant secondary ions is CHA. CHA is added to the boiler system of the author's laboratory in order to prevent scale build-up and corrosion. The blow-down from the boiler is used to humidify the laboratory, and typical indoor atmospheric concentrations in the winter months are in the 300 ppb range. CHA used in this fashion has been recognized as a potential chemical health concern, because even though it is not an acute toxin, it can be a sensitizer.[4]

When soil samples (aluminosilicate minerals) were exposed to the laboratory air and analyzed using static SIMS, an abundant ion at *m/z* 100^+ is observed, which corresponds to $[CHA + H]^+$. Other abundant ions are also observed, but these could not be ascribed to CHA because of hydrocarbon background originating from other organic surface contaminants. However, when the soil was exposed to CHA-d_{11}, rich fragmentation chemistry could be observed.

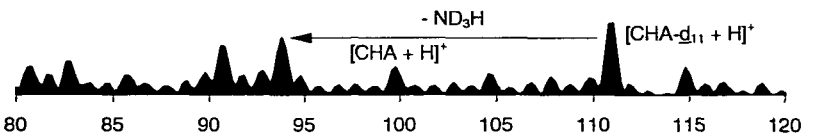

CHA-d_{11} was also used to estimate the amount of CHA on the soil surface. It was found that the exposure could be controlled by vaporizing a gravimetric quantity of CHA-d_{11} in a sealed glass jar containing the soil, and then allowing the jar to cool to room temperature. SIMS analysis of samples exposed in this manner showed that the abundance of the secondary ions was related to the level of exposure, expressed in monolayers. By comparing the abundance of $[CHA\text{-}d_{11} + H]^+$ to $[CHA + H]^+$, it was estimated that the concentration of adventitious CHA on a soil sample was approximately 0.3 monolayers. Sensitivity plots also show that CHA-d_{11} appears to facilitate the sputtering of CHA.

[1] Benninghoven, A.; *Surface Science*, **1973**, *35*, 427 - 457.
[2] Cooks, R. G.; Ast, T.; Mabud, MD. A., *Int. J. Mass Spectrom. Ion Proc.*, **1990**, *100*, 209-65.
[3] Groenewold, G. S., Ingram, J. C., Delmore, J. E., Appelhans, A. D., *J. Am. Soc. Mass Spectrom.*, **1995**, *6*, 165.
[4] Orlando, R. A.; Lao, Y. J. *J. Environ. Health*, **1993**, *56*, 6-9.

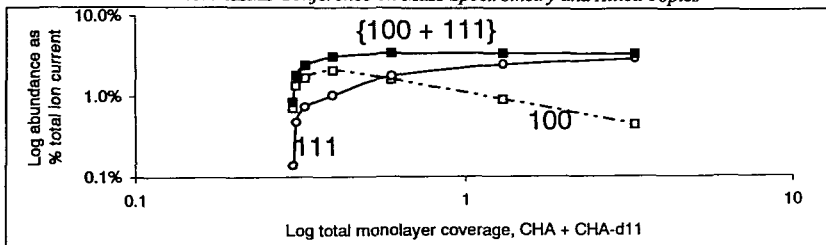

Analysis of small organic acids on basic surfaces. The observation of CHA on the soil samples led to experiments designed to see whether volatile acids would behave similarly. Samples in these experiments were exposed to gaseous acids by merely holding the sample proximate to the liquid acid for 20 sec. In fact, when soil samples were exposed to formic acid, low abundance ions corresponding to HCO_2^- were observed. The abundances of these (and related) ions were greatly enhanced when alkali metal (M) hydroxides were exposed to formic, acetic and propionic acids. The anion spectra showed ions corresponding to the conjugate base (CB^-), and the cluster ion $M(CB)_2^-$, and M_2CB^+ was observed in the cation spectra. An abundant ion corresponding to $M_3CO_3^+$ was also observed in all the spectra of the alkali metal hydroxides, which demonstrates the ability of these compounds to fix CO_2 from the atmosphere.

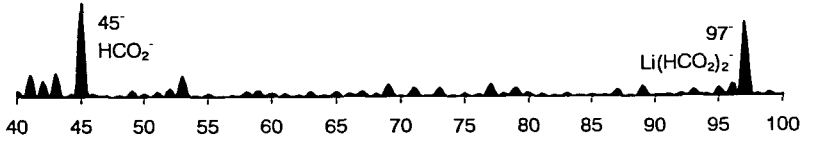

When the alkali metal hydroxides were compared, it was found that the abundances of the acid-derived ions were dependent on the cation M. Generally, the most abundant secondary ions were observed for Na^+ and K^+. This result is similar to the findings of Hand, et al. in working with perrhenate salts: K^+ resulted in the formation of the most abundant complex ions observable using ion bombardment.[5] A second interesting observation resulted when the acids were compared: the most abundant complexes involved formate, followed by acetate, and finally propionate.

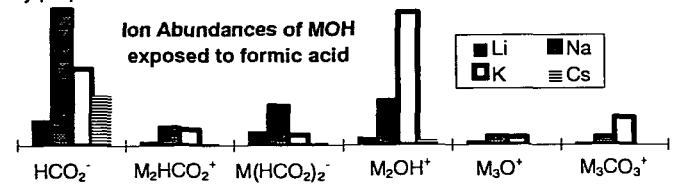

ACKNOWLEDGMENT: The support of the U. S. Department of Energy, Office of Health and Environmental Research is gratefully acknowledged.

[5] Hand, O. W.; Scheifers, S. M.; Cooks, R. G. *Int. J. Mass Spectrom. Ion Proc.*, **1987**, *78*, 131-146.

DETERMINATION OF RADIATION STABILITY OF CROWN ETHERS

J.A. CAMPBELL, D.W. WESTER, V.M. ABASHKIN, K.E. GRANT, AND P.F. JOHNSTON
PACIFIC NORTHWEST LABORATORY*
RICHLAND, WA 99352

INTRODUCTION

The 50th anniversary of the Hanford Site was celebrated in 1994. The Hanford reservation, a 560-square-mile site, is approximately 120 miles south of Spokane, Washington, and 220 miles southeast of Seattle, Washington. The Hanford Site was built by the Army Corps of Engineers and the Du Pont Corporation in 1943 to produce plutonium for nuclear weapons in support of the World War II effort. The facility was very successful; within two years after its formation, Hanford had supplied the plutonium (Pu) used for the bomb dropped on Nagasaki in World War II. As with all production operations, plutonium production created large quantities of (mixed) radioactive waste. Plutonium production continued after the war until January 1987 when the last production reactor ceased operation at the Hanford site. Reprocessing fuel from nine production reactors created a large quantity of radioactive mixed wastes, much of which was and continues to be stored in underground storage tanks. Three major reprocessing flowsheets (e.g., processes), the large scale recovery of enriched uranium (U), radioactive cesium (Cs) and strontium (Sr) recovery, and a variety of other waste management operations led to a variety of major chemical processing facilities and thus waste types. Both inorganic- and organic-containing waste was produced and is being stored at Hanford.

The wastes must be stabilized and isolated from the environment for thousands of years to ensure that radioactivity will decay to levels that pose no hazards to living organisms. The current treatment plan is to vitrify much of the waste, both low and high level, and send it to long term storage in a geological repository. The waste and by-products of nuclear production are primarily solid and aqueous solutions of ionic compounds in which acutely hazardous and/or radioactive compounds are present in relatively low concentrations. If advanced chemical separations could be implemented to remove the radionuclides without increasing the waste volume, treatment costs could be reduced significantly, and environmental acceptability would be improved. Materials derived from macrocyclic ligands such as crown ethers appear to be most promising, and their use in separations based on solvent extraction membranes are being investigated.

Crown ethers have attracted great attention primarily as specific ligands exhibiting high selectivity for nearly all kinds of cations. Unfortunately, the limited availability of crown ethers and especially a lack of experimental data for reprocessing of highly irradiated and concentrated aqueous solutions using crown ethers as extractants have somewhat inhibited the evaluation and recognition of crown ethers as new agents in the reprocessing of industrial nuclear fuel and radioactive waste. The most promising properties are related to dicyclohexano-18-crown-6 (DCH-6) and its derivatives. Mass spectrometry has been used to determine the relative radiation stability of the pure stereoisomers, cis-syn-cis-DCH-6 and cis-anti-cis-DCH-6.

EXPERIMENTAL

A Hewlett-Packard 5988A mass spectrometer was equipped with an HP 5980 gas chromatograph operated in the splittess mode. Separation was obtained with a DB-5 capillary column (30 m X 0.25 mm i.d., 0.25 µm-film thickness, J & W Scientific). The injector port was heated to 250°C, mass spectrometry interfaces 280°C, and source 200°C. The oven temperature was typically programmed in the following manner: 50°C for 1 min, 8°C/min to 300°C, and 300°C for 5 min. The mass spectrometer was scanned from 50 to 500 amu.

Fast atom bombardment experiments were performed with a JEOL SX-102/SX-102 double-focusing mass spectrometer equipped with a UNIX data system. The fast atom beam was generated from Xe ions, which were accelerated to 5 kV. The FAB gun emission current was 10 mA. The liquid matrix used was m-nitrobenzyl alcohol.

Pure samples of each DCH-6 isomer in glass vials were irradiated using a ^{60}Co gamma source. The dose rate was 3.0 Gy/s (1.08 x 10^6 R/h). The maximum total dose was 1.5 X 10^6 Gy (1.5 X 10^8 R).

RESULTS AND DISCUSSION

Figure 1 is a total ion chromatogram of non-irradiated DCH-6. Figure 2 is a total ion chromatogram of irradiated DCH-6.

The cis-syn-cis isomer of DCH-6 is more stable to gamma radiation than the cis-anti-cis isomer. The main components of radiation degradation products include monocyclohexyl polyethers (alcohols and aldehydes). Further studies are underway to examine the effect of radiation on the other isomers.

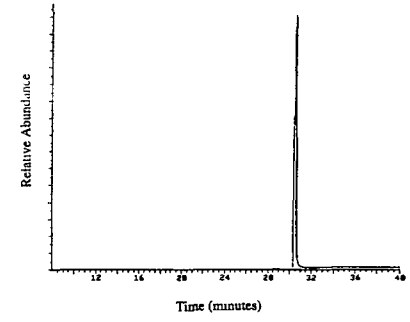

Fig. 1. Total Ion Chromatogram of Non-Irradiated DCH-6

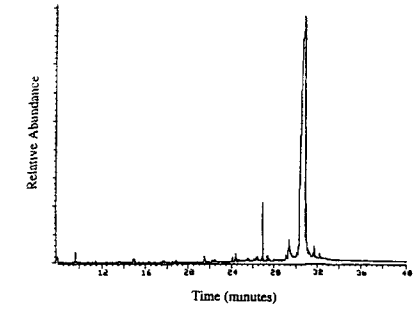

Fig. 2. Total Ion Chromatogram of Irradiated DCH-6

* This work was supported by the Department of Energy under contract DE-AC06-76RLO 1830. Pacific Northwest Laboratory is operated by Battelle Memorial Institute.

Vapor Characterization of Hanford Waste Tanks using SUMMA™ Canisters and GC/MS Analysis

R.B. Lucke, B.D. McVeety, G.S. Klinger, T.W. Clauss, J.S. Fruchter, and S.C. Goheen
Pacific Northwest Laboratory*
Richland, WA 99352

INTRODUCTION

The end of the plutonium-production mission at the Hanford site (southcentral Washington state) left a legacy of environmental problems. One of the most prominent environmental and safety issues facing Hanford cleanup efforts is the radioactive wastes stored in the underground tanks. About 60 million gallons of high-level waste and 260 million curies of radioactivity are stored in 177 tanks. The long-term strategy is to reduce the volume of tank wastes, remove organic constituents, and separate remaining wastes into low and high level components for permanent isolation.

One task associated with the cleanup efforts is characterizing the vapors in the headspaces of high-level waste storage tanks. This is needed for three reasons: 1) to provide information in regards to potential worker health and safety hazards associated with the toxicity of the vapors, 2) to provide information about the flammability of the vapors in the tank, and 3) to provide screening information in regards to the actual waste in the tanks.

METHOD

Hanford vapor samples were collected with evacuated pre-cleaned SUMMA™ canisters. The SUMMA™ canister samples were analyzed by a modified version of U.S. Environmental Protection Agency compendium Method TO-14. The method uses an EnTech cryoconcentration system interfaced with a Hewlett Packard 5972 gas chromatograph/mass spectrometer (GC/MS). The EnTech concentrator was used to pull a metered volume of sample air from the SUMMA™ canister, cryogenically concentrate the air volume, then transfer the volume to the GC/MS for analysis. During analysis, the SUMMA™ canisters were heated to 120°C in specially constructed heating mantles to ensure recovery of polar and semivolatile compounds. Since 100-mL vapor samples were injected, water management was required. This was accomplished on the principal of a microscale purge-and-trap system. Using a cryogenically cooled glass-bead trap, sequentially followed by a Tenax adsorbent trap, this technique successfully reduced the water concentration in the sample while allowing relatively polar compounds such as ketones, alcohols, aldehydes, nitriles, and nitrates to be concentrated from the air volume and subsequently analyzed.

RESULTS/CONCLUSIONS

The sampling and analysis method described was applied to 25 different waste tanks representing 4 different tank farms. Over 200 organic compounds and several permanent gases have been identified and quantified in the tank-headspace samples analyzed to date. The chemical composition of tank headspaces is directly related to both recent and historical usage. Tanks in a particular farm have similar histories and therefore often share similarities in the composition of stored wastes. This appears to be especially true in the cases where tanks are linked together through cascading overflows. Tank vapors are generally comprised of varying concentrations of a homologous series of alkanes, alkenes, alcohols, aldehydes, ketones, and alkynitriles. We have observe that these series often extend from C3 to C10. It is possible that other homologues are also present, but not observed under current procedures.

The concentration of many organic compounds, especially the n-alkanes, can range over 4 orders of magnitude when comparing one tank to another. This can be explained by differences in the degree of venting, the amount of radioactivity in tank wastes changing the rate of waste aging, and the presence or absence of floating organic liquid layers. The semivolatile normal paraffinic hydrocarbons (NPH), ranging from C11 to C15, are examples of common extraction-process materials. The NPHs were constituents of diluents used with tributyl phosphate (TBP) to extract plutonium from spent uranium fuel. In several tanks, NPH as well as decahydronaphthalene and their radiolytic decomposition products have been found. Butanol, the main volatile decomposition product of TBP under alkaline conditions, is usually also found at relatively high concentrations.

Table 1. Concentration ranges (ppmv) of 2/3rds of the 25 high-level waste tank headspace samples analyzed to date.

Compound Class	Concentration (ppmv)
C_3-C_{10} n-Alkanes	0.01 to 5
C_3-C_{10} n-Alkenes	0.01 to 5
C_6-C_{10} branched-Alkanes/Alkenes	0.01 to 5
C_{11}-C_{15} n-Alkanes	0.01 to 50
C_{11}-C15 branched-Alkanes/Alkenes	0.01 to 5
C_3-C_{10} Ketones	0.01 to 5
C_3-C_{10} Aldehydes	0.01 to 0.1
C_3-C_{10} Alcohols	0.01 to 5
C_3-C_{10} Nitrles	0.005 to 0.1
C_1-C_6 Nitrates	0.005 to 0.05
C_1-C_5 Decahydronaphthalene (Decalin™)	0.005 to 0.5
C_1-C_5 Cyclohexanes	0.005 to 0.5
Hydrogen	*100 to 1000*
Nitrous oxide	*100 to 800*
Carbon dioxide	*200 to 700*

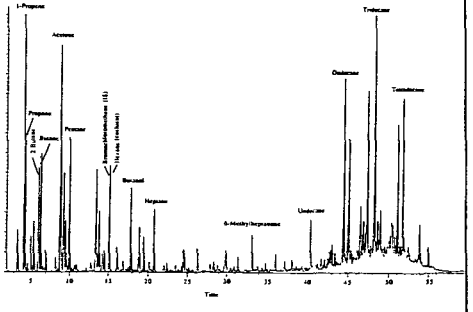

Figure 1. Selective GC/MS Chromatogram of Hanford Waste Tank BY-104 SUMMA™ Canister Tank Headspace Sample.

Our laboratory has successfully analyzed vapors from Hanford waste tanks; this has allowed flammability and toxicity issues to be resolved. The data from these analyses have also helped in classifying and evaluating the Hanford tanks, a small but significant step toward complete tank waste characterization.

* Pacific Northwest Laboratory is operated for the U.S. Department of Energy by Battelle Memorial Institute under Contract DE-AC06-76RLO 1830.

MASS SPECTROMETRY ANALYSIS OF TANK WASTES AT THE HANFORD SITE

J.A. CAMPBELL, G.M. MONG, S.A. CLAUSS, AND R.B. LUCKE
PACIFIC NORTHWEST LABORATORY*
RICHLAND, WA 99352

INTRODUCTION

The Hanford Site in southeastern Washington is a 560-square-mile reservation built by the U.S. Army Corps of Engineers and the Du Pont Corporation in 1943 to produce plutonium (Pu) for nuclear weapons in support of the World War II effort. Major chemical processing facilities were constructed to reprocess fuel from nine production reactors and recover enriched uranium (U), radioactive cesium (Cs), and strontium (Sr). Reprocessing and other waste-management operations created a quantity of radioactive mixed wastes, much of which is stored in underground tanks. Three major processes led to a variety of chemical processing facilities and waste types. Both inorganic- and organic-containing wastes were produced and are being stored at Hanford.

Twenty-five of the 177 high-level waste storage tanks at the Hanford Site in southeastern Washington are being watched closely because of the possibility that flammable gas mixtures may be produced from the mixed wastes contained in the storage tanks. One tank in particular, Tank 241-SY-101 (Tank 101-SY), has exhibited episodic releases of flammable gas mixtures since its final filling in the early 1980s. It has been postulated that the organic compounds present in the waste may be precursors to the production of hydrogen. Mass spectrometry has proven to be an invaluable tool for the identification of organic components in wastes from Tank 101-SY and C-103. A suite of physical and chemical analyses has been performed in support of activities directed toward the resolution of an Unresolved Safety Question concerning the potential for a floating organic layer in Hanford Waste Tank 241-C-103 to sustain a pool fire. The aqueous layer underlying the floating organic material was also analyzed for organic components.

EXPERIMENTAL

The waste samples represented several segments of actual waste obtained by core drilling the waste in Tank 101-SY. This material was radioactive and contained a high concentration of nitrate and nitrite; the OH^- concentration was 2 M. A 5-g aliquot of the waste sample was weighed and then stirred with 10 mL of doubly distilled water overnight. The aqueous phase was filtered through a 0.45-µm filter. The filtrate was then passed through a cation exchange column (10 g, AG50W-X8 resin, Na^+ form) and then rinsed using an additional 10 mL of water to quantitatively remove the organic material from the resin. The resulting sample volume was 20 mL. After surveying the samples for radioactivity levels, the aqueous solution containing the organics was removed from the hot cell facilities. Aliquots (2 mL) of the sample were transferred to Teflon®-sealed vials, evaporated to dryness using nitrogen blow-down techniques, and derivatized with 2 mL of BF_3/methanol to produce methyl esters. The sample was heated to 100°C for 1 h. The reaction mixture was then quenched with a KH_2PO_4 solution and extracted with chloroform. The chloroform extract was then analyzed by gas chromatography/mass spectrometry (GC/MS).

The HP 5988 mass spectrometer was equipped with an HP 5980 GC operated in the splitless mode. A fused silica column (DB-5, 30 m X 0.25 mm i.d., 0.25-µm film thickness, J & W Scientific) was used. The oven temperature was typically programmed in the following manner: 50°C for 1 min, 8°C/min to 300°C, and 300°C for 5 min. The mass spectrometer was tuned daily with perfluorotributylamine. In these studies, the mass spectrometer was scanned from 50 to 500 amu and operated in the electron impact mode (70 eV). The source temperature was 200°C, the injector port temperature was 250°C, and the interfaces were also at 250°C.

Accurate mass measurements were performed using a JEOL SX-102/SX-102 double-focusing mass spectrometer equipped with an HP 5980 GC. Separation was obtained with a DB-5 fused silica column. The temperature program was the same as listed above.

RESULTS AND DISCUSSION

Six samples of core segments from Tank 101-SY, obtained during the window E core sampling, have been analyzed for organic constituents using derivatization GC/MS, liquid chromatography (LC), and LC/MS. Four of the samples were from the upper region, or convective layer, of the tank and two were from the lower, nonconvective layer. The combined techniques of derivatization GC/MS and LC have accounted for approximately 73 to 93% of the total organic carbon, depending on the sample.

The elemental compositions of 25 components in the derivatization GC/MS total ion chromatogram (Figure 1) have been determined using high resolution mass spectrometry. Several nitroso compounds were also unambiguously identified; however, thermospray LC/MS indicated the nitroso compounds were formed during the derivatization procedure. Thermospray LC/MS has been used to identify many of the small organic acids, including citric, acetic, formic, and glycolic. The total ion LC/MS chromatogram is illustrated in Figure 2.

Composition information of the floating organic layer in Tank C-103 was required to enable calculations to be made to estimate the lower flammability limit. Both normal paraffin hydrocarbon and tributyl phosphate were found to be the principal constituents of the organic layer. In addition to these components, branched alkanes and dibutyl butylphosphonate were also found in lesser quantities.

Mass spectrometry has proven to be an invaluable analytical tool for the analysis of organics in tank waste.

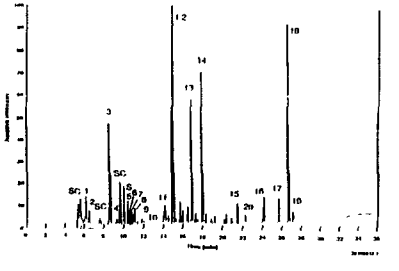

Fig. 1. GC/MS Total Ion Chromatogram of Derivatized Tank Waste

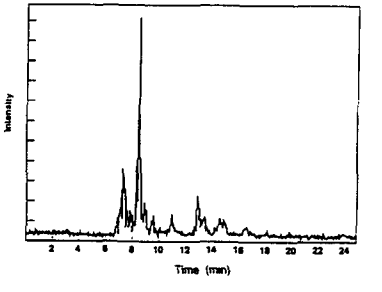

Fig. 2. Thermospray LC/MS Total Ion Chromatogram of Tank Waste

* This work was supported by the Department of Energy under contract DE-AC06-76RLO 1830. Pacific Northwest Laboratory is operated by Battelle Memorial Institute.

GC/MS METHOD DEVELOPMENT FOR THE CHEMICAL SPECIATION OF ARSENIC AND SELENIUM COMPOUNDS

Douglas Cameron, Tara Brozovich - Ford, Heath Watts, and Jin Wang
Chemistry and Geochemistry Dept., Montana Tech, Butte, Montana 59701-8997

INTRODUCTION Arsenic (As) and selenium (Se) are elements of economic value in a variety of industries. These elements are often naturally associated with minerals of economic value Consequently, these elements have multiple pathways into the environment As and Se can each exist in a number of inorganic and organic chemical forms The form of each element is dependent on its chemical, physical, and biological environment [1] The properties of these elements, such as mobility in the environment and toxicity to plants and animals, are dependent on the chemical form [2] Therefore, an understanding of the effects of Se or As in the environment requires a knowledge of both the chemical form and the concentration of the elements

A variety of chromatographic, spectroscopic, and hyphenated instrumental methods have been developed for the speciation of As and Se compounds [3,4] Hydride generation atomic absorption spectroscopy (HGAAS) is the most common method However, HGAAS does not determine most forms of As and Se directly, and the technique suffers from a variety of matrix effects. A technique, such as GC/MS, is needed that will determine all the chemical forms directly, at a reasonable cost, and at environmentally important concentrations

METHODS Aqueous solutions of the arsenic or selenium oxyanions were prepared using either the sodium salts or acid forms of the analytes For the liquid-liquid extraction experiments, optimal extraction efficiencies were obtained with an aqueous solution pH of 2 and cyclohexanone as the extraction solvent Extraction efficiencies were compared with and without the ion-pairing agent, tetrabutyl ammonium iodide Solid-phase extractions (SPE) were done using a variety of silica gel-based, bonded phase packings (Supelco). The extractions were vacuum assisted Cyclohexanone and N,N-dimethyl formamide were used as extraction solvents

HGAA was done using an Instrumentation Laboratory spectrophotometer with a homemade hydride generator Arsenate and selenate are reduced to arsenite and selenite for the analysis

GC/MS analyses were done using a Hewlett-Packard 5971 MSD A HP-5 30m column was used with a 0 25mm i.d and a 0 25 µm film thickness. An injection port temperature of 250°C and a detector temperature of 280°C were used Temperature programming from 50° to 300°C at 15 deg/min was used

RESULTS AND DISCUSSION We previously reported the results of our work on the GC/MS analysis of selenite, selenate and arsenate [5,6] After extraction into an organic solvent, these oxyanions are derivitized with N-(tert-butyldimethylsilyl)-N-(trifluoromethylacetamide). A t-butyl-dimethylsilyl group adds to each acidic oxygen. The mass spectra of these compounds matched those reported by Mawhinney[7] The mass spectra are characterized by no detectable molecular ion peak, a small peak for loss of CH_3 (M-15), an abundant peak for loss of the t-butyl group (M-57), and a variety of peaks for fragmentation of the remaining silyl groups However, we were not able to detect any derivatized arsenite (As^{3+}) as AsO^{3-} Since our initial report, we believe we have found arsenite in the meta form (AsO_2^-). The chromatogram of derivatized arsenite solution shows a peak not present in the blank (solvent and derivitizing agent) The peak is from a compound that elutes prior to derivitized arsenate, and the peak area is proportional to the amount of arsenite in the solution. Figure 1 is the EI mass spectrum of what **appears** to be the derivitized meta arsenite ($C_6H_{15}SiAsO_2$) The molecular weight of this compound is 222 The mass range about the molecular ion shows significant loss of multiple hydrogens. A disturbing feature is the over abundant peak at m/z 223. Approximately 20% of the 223 peak intensity is attributed to isotopic contributions from the 221 peak, Si (3 4%), O's (0.4%), and C's (0.2%) The peaks at m/z 206 and 164 represent losses of CH_3 and $C(CH_3)_3$ respectively from m/z 221 The low mass fragment peaks match those of derivatized arsenate

Quantitative analysis using our extraction and GC/MS method has proven difficult The oxidation or reduction of the analytes during extraction, storage, or derivitization has prevented quantitation The majority of selenate in a solution of N,N-dimethylformamide is reduced to selenite within 30 min This is contrary to the stability listed in the literature [7]

HGAAS has been used as our reference method for determining extraction efficiencies, however HGAAS is prone to matrix interference. Aqueous solutions of arsenic (as arsenite) at level of 8 49 µg/L range from 5-15 µg/L depending on what organic compound is added to the matrix The direction of these signal changes was always constant for a given matrix component but the magnitude of the change was not very reproducible Optimal liquid-liquid extraction efficiencies are approximated at 40-70% SPE efficiencies range from 0-100%, however elution efficiencies are currently unknown

CONCLUSION A GC/MS method using either liquid-liquid or solid-phase extraction has been demonstrated for the qualitative analysis of arsenite, arsenate, selenite, and selenate in aqueous solutions After extraction into an organic solvent and derivitization, arsenite appears to be in the meta form, AsO_2^- Several factors; including analyte stability, extraction and elution efficiencies, and arsenite composition, must be more thoroughly understood and controlled before the GC/MS method can be made quantitative Work must also be done on the methodology to analyze the environmentally important organic forms of arsenic and selenium

Acknowledgement This work was supported by research grants from the DOE/EPSCoR Graduate Assistance Program - Montana Organization for Research in Energy and the Mine Waste Technology Program - Activity IV, Project 2, IAD ID NO DW89935117-01-0 U S EPA & DOE Contract NO DE-AC22-881D12735

Figure 1. Electron Ionization Mass Spectrum of tert-Butyl Dimethyl Silyl Arsenite $C_6H_{15}SiAsO_2$

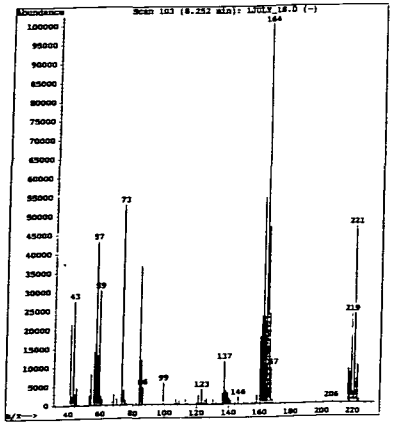

REFERENCES (1) *Biogeochemistry of Trace Metals*; Adriano, D C , Ed.; Lewis Publishers Boca Raton, 1993 (2) Masscheleyn, P.H.; Delaune, R.D ; Patrick, Jr , W H , *J. Environ. Qual.*, **1991**, 20, 522-527 (3) Quevauviller, P ;Donard, W F X.; Maier, E.A.; Griepink, B.; *Mikrochim. Acta*, **1992**, 109, 169-190 (4) Shum, S C K , Neddersen, R.; Houk, R.S ; *Analyst*, **1992**, 577- 582 (5) Brozovich, T , Cameron, D , *A Method for Speciation of Selenium Using Gas Chromatography/Mass Spectrometry* , 42nd ASMS Conference on Mass Spectrometry, Chicago, IL, May 1994, p270 (6) Watts, H.D ; Cameron, D , *A Method for Speciation of Arsenic Using Gas Chromatography/Mass Spectrometry*, 42nd ASMS Conference on Mass Spectrometry, Chicago, IL, May 1994, p271 (7) Mawhinney, T.P., *J. Chromatogr.*, **1983**, 257, 37-44

Organoarsenic and Organotin Speciation by Ionspray-MS-MS and LC-MS-MS

J.J. Corr[1] and K.W.M. Siu[2]
1: SCIEX, 71 Four Valley Drive, Concord, Ontario, L4K 4V8, Canada
2: National Research Council of Canada, Montreal Road, Ottawa, Ontario, Canada

The impact of trace metals on the environment has been the subject of extensive recent study by many groups. Since the toxicity and bioavailability of an element depends on its particular chemical form, it is no longer sufficient to employ total-element analysis. Hence the necessity for speciation anaylsis, which involves the determination of the exact chemical form of an element, whether it be an inorganic oxidation state or an organometallic compound.

In the present report ionspray (IS)-MS-MS has been employed to study synthetic and real samples containing arsenic and tin species. A selectable degree of declustering of solvent adducts or fragmentation of molecular ions in the differentially pumped interface (DPI) of the MS-MS system enabled the system to function as a molecular detector or as an elemental analyzer. In elemental analysis mode parameters were chosen such that maximum fragmentation of molecular species occurred, which promoted charge reduction and hence the observation of singly-charged bare elements.

Combining this declustering with an advanced collision cell allowed the detailed mapping of collision induced dissociation (CID) pathways for a number of organoarsenicals, including arsenobetaine (AsB) and arsenocholine (AsC). Both these species, and all others examined, were detected in fully intact molecular form at over 1e+6 cps per ppm, or could be fragmented in the DPI to bare As^+, or Sn^+, while retaining sensitivity. Two of the preferred CID pathways for these species were fragmentation to trimethylarsine for AsB or trimethylarsine + H for AsC, and loss of water. Another main CID channel for AsB was loss of CH_2CO, which resulted in a path through CH_3AsOH (m/z 107). Many of the CID channels involved the molecules CH_3AsCH (m/z 103) and CH_3AsH or AsO (m/z 91). For all organoarsenicals studied it was possible to observe bare As^+ through CID.

The liquid chromatographic retention of AsB was observed by combining this system with ion pairing LC. A C_{18} column with a mobile phase of 80:20 DIW-MeOH with 0.1 mM octanesulphonate and acetic acid, pH2.7-3.0, was employed to demonstrate the retention of AsB down to the level of 200 pg.

All the organotin species examined behaved somewhat similarly under DPI fragmentation and CID. For example, dissociation of the environmentally high profile species tributyltin (TBT) was primarily through loss of butyl groups. Since tin species do not readily form oxides in the ionization process, or in the interface, they are relatively easy to fragment in the DPI to bare Sn^+. The ease with which this system functioned in either analysis mode was indicated by flow injection analysis (FIA) of the NRC harbour sediment certified reference material PACS-1. Following extraction of TBT with 1-butanol and employing a carrier solution of methanol with 1 mM ammonium acetate, TBT was detected by single ion monitoring (SIM) of bare Sn^+ as

well as by selected reaction monitoring (SRM) of the dibutyltin product ion of tributyltin (see Figure 1).

The arsenic species examined in this work were arsenite, arsenate, monomethylarsonic acid (MMA), dimethylarsinic acid (DMA), tetramethylarsonium ion (TMA^+), AsB and AsC. TBT, triphenyltin (TPhT), tripropyltin (TProT), and dibutyltin (DBT) were the organotin species studied.

The dual mode capabilities of IS-MS-MS and the results of this study indicate that IS-MS-MS possesses great promise for speciation anaylsis.

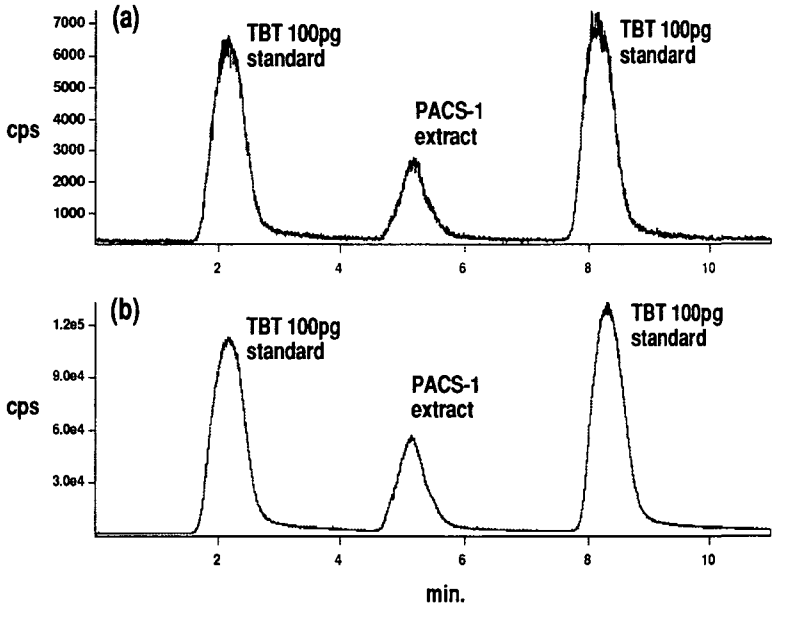

Figure 1. Flow injection analysis of an extract from PACS-1. Carrier solution: methanol with 1 mM ammonium acetate; 5 µL sample loop; 10 µL/min flow rate. Figure 1(a) displays molecular detection mode by SRM of m/z 291/235. Elemental analysis mode is indicated by SIM of bare Sn^+ (m/z 120) in Figure 1(b).

Quantitation of a CCK Ligand from Serum using LC / ESI / MS / MS on Ion Traps and Triple Quadrupoles,

Arthur Moseley*[1], Tim Tippin[1], Robert Hart[1], Tom Lloyd[1], Robert St. Claire III[1], Kathy Halm[1], Jae Schwartz[2], Adrian Land[2], and Ian Jardine[2],
[1]Department of Drug Metabolism, Glaxo Wellcome Research Institute, RTP, NC
[2]Finnigan MAT, San Jose, CA

The objective of this work was to evaluate the quantitative capabilities of the Finnigan LCQ ion trap mass spectrometer with both mobile phase standards and with "real world" rat serum samples from an in-vivo pharmacokinetic study. As a reference, the exact same samples were also analyzed on a triple quadrupole mass spectrometer using the same brand of autosampler. To permit high throughput sample analysis, we used a "fast" LC column (1x50 mm Hypersil BDS-C18 with 3 µm particles at 80µL/minute, retention time of 2.5 minutes, k' of 4) with selected reaction monitoring for detection of the analyte and internal standard. Prior to analysis the serum samples were cleaned up using an automated solid phase extraction procedure on a Zymark robot.

Mobile phase standards over the range of 1.22 to 5000 ng/mL were analyzed in triplicate, and spiked serum standards over the range of 1 to 7500 ng/mL were analyzed in duplicate (before and after the actual samples). Also note that in order to extend the dynamic range of the analysis the upper level standards were diluted.

A comparison of normal resolution (unit mass) and open resolution (4 m/z peak width at half height) conditions on the triple quadrupole showed a very significant increase in absolute signal, and a 4-fold improvement in the LOQ. Whenever possible, we use open resolution conditions for our LC/MS/MS quantitation on this triple quadrupole. Therefore, we used open resolution conditions to analyze the spiked serum samples on the triple quadrupole. Note that the use of open resolution conditions reduces the specificity of the analysis, so this approach must be used with caution. The ion trap was operated under unit mass resolution conditions at all times.

The triple quadrupole (under normal resolution conditions) and the ion trap gave an identical LOQ of 9.75 ng/mL (1/(x*x) weighting, r>0.990) with mobile phase standards (analyzed in triplicate). When open resolution conditions were used on the triple quadrupole, a four-fold lower LOQ was obtained. In contrast to the analysis of the mobile phase standards, the analysis of the spiked serum samples on the ion trap and on the triple quadrupole (under open resolution conditions) gave the same LOQ of 5 ng/mL (1/(x*x) weighting, r>0.990). Note that both data sets would meet GLP validation criteria.

43rd ASMS Conference on Mass Spectrometry and Allied Topics

GG772 LC / ESI / MS / MS Quantitation

Finnigan LCQ
Selected Reaction Monitoring m/z 616 to m/z 451
1 x 50 mm Hypersil BDS-C18 LC Column, 3 µm particles
60 % MeCN / 2mM NH_4Ac (pH 4.5), 80 µL/minute
LOQ - 9.75 ng/mL mobile phase standard (48.8 pg on-column)

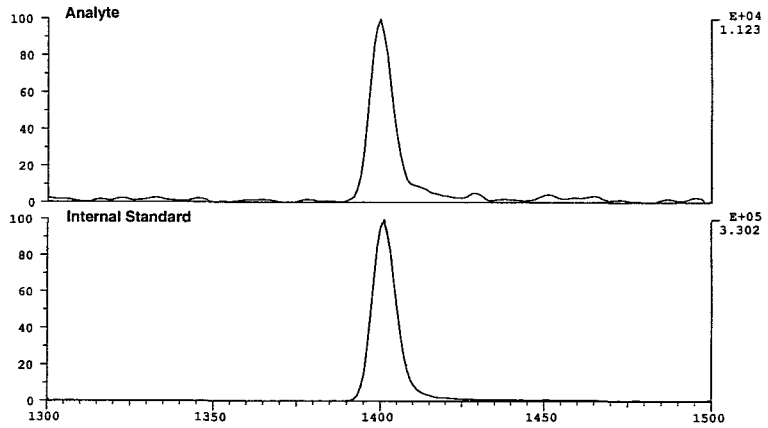

Mobile Phase Standards Analyzed in Triplicate
1st Order Polynomial Fit from 9.75 ng/mL to 5000 ng/mL, $1/(x^2)$ weighting, r = 0.996

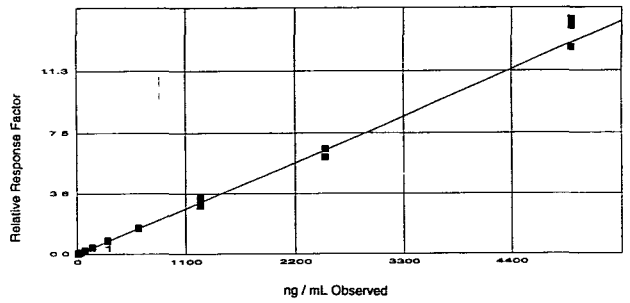

Development of an LC/MS/MS assay for the concomitant detection of AGN 190168 and its metabolites from human urine

W. Luo[1], R. Matsumoto[1], D. Tang-Liu[1] and A. Breau[2]

[1]Department of Pharmacokinetics, Allergan Inc, Irvine, CA 92715
[2]The Perkin-Elmer Corporation, San Jose, CA 95131

AGN 190168 (tazarotene) is a synthetic retinoid currently being investigated for the topical treatment of acne and psoriasis. The concomitant detection of AGN 190168 and its metabolites, AGN 190299, AGN 190832, AGN 190844 (Fig. 1) from human urine following topical dosing with AGN 190168 gel was accomplished by atmosperic pressure chemical ionization (APCI) and multiple ion monitoring (MRM) on a PE-Sciex API III$^+$ triple quadruple mass spectrometer. Following liquid-liquid extraction and sample concentration, a 1 ng/ml level of quantitation was achieved for all four analytes. The assay methodology illustrates the versatility of atmosperic pressure ionization / tandem mass spectrometry, in conjunction with HPLC, for the separation and quantitation of drugs and their metabolites in the nanogram per mililitre range with acceptable precision and accuracy.

To 2 ml of human urine, 20 ng of ($^2H_7$)AGN 190168 and ($^2H_7$)AGN 190299 were added and mixed briefly. 2 ml of double distilled water, 200 µl of 1 N HCl and 4 ml of ethyl acetate:hexane (70:30) were then added. After rotary mixing for 5 min, the test tubes were centrifuged for 5 min to get better phase separation. The organic layer was decanted into another tube. Extracts were evaporated to dryness in a Turbo-Vap under nitrogen at 35-45°C. The residue was reconstituted in 200 µl of mobile phase A and 100 µl were injected onto the LC/MS/MS system.

A Sciex API III$^+$ triple quadrupole mass spectrometer equipped with an APCI interface was used for sample analysis. Processed samples were injected onto a Keystone ODS Hypersil (4.6 X 50 mm, 3 µm particle size) column for chromatographic separation. Mobile Phase A consisting 20 mM NH_4OAc and 5% AcOH. Mobile phase B consisting 20 mM NH_4OAc and 5% AcOH in methanol. The starting conditions were 53% A and 47% B with a curve 3 gradient to 10% A and 90% B in 6.3 minutes. After holding at 10% A and 90% B for 1.7 minutes, the column was re-equalibrated at initial condition. The flow rate was 1 ml/min.

The positive ion mode was used to detect all the analytes. The multiple reaction monitoring (MRM) was used, with a dwell time of 200 msec/channel. The analysis was divided into two periods. Period 1 included 340 to 280 (AGN 190844) and 368 to 280 (AGN 190832). Period 2 included 324 to 294 (AGN 190299), 331 to 297 ($^2H_7$-AGN 190299), 352 to 324 (AGN 190168) and 359 to 331 ($^2H_7$-AGN 190168). (Fig. 2)

A Sciex software MacQuan was used to construct the calibration curves for all the analytes. The dynamic range of the assay was 1 ng/ml to 100 ng/ml for all the analytes except AGN 190844 which had a dynamic range of 1 ng/ml to 50 ng/ml (Fig 3). The precision and accuracy of the standard curve read-back concentrations for all four analytes were all within the acceptable limits (±20%).The precision and accuracy of the 2 ng/ml, 10 ng/ml and 50 ng/ml quality control samples for all four analytes were all within acceptable limits (±20%).

Urine samples collected from two clinical trails conducted in the Department of Dermatology at Tokyo Women's College in Tokyo, Japan, were assayed for AGN 190168, AGN 190299, AGN 190832 and AGN 190844 using this validated LC/MS/MS method. Approximately 280 clinical urine samples were analyzed. The only detected analyte was AGN 190844. The highest measured concentration of AGN 190844 in any of the samples was 23.5 ng/ml, however, the majority of the measurable AGN 190844 concentrations were in the 1-10 ng/ml range.

43rd ASMS Conference on Mass Spectrometry and Allied Topics

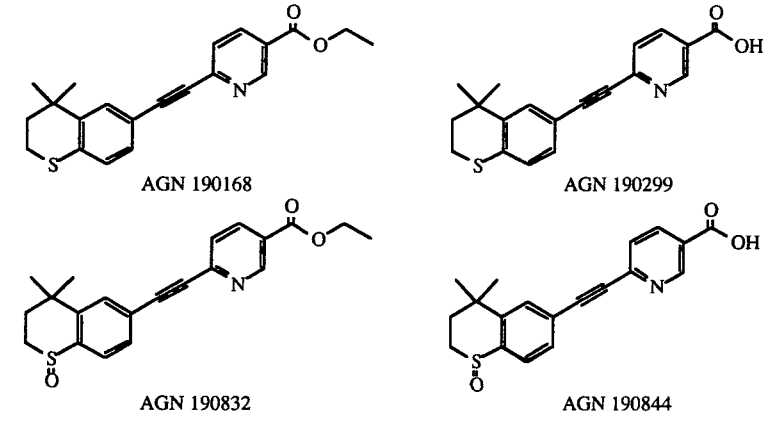

Fig1. Structures of AGN 190168 and its metabolites AGN 190299, AGN 190832 and AGN 190844.

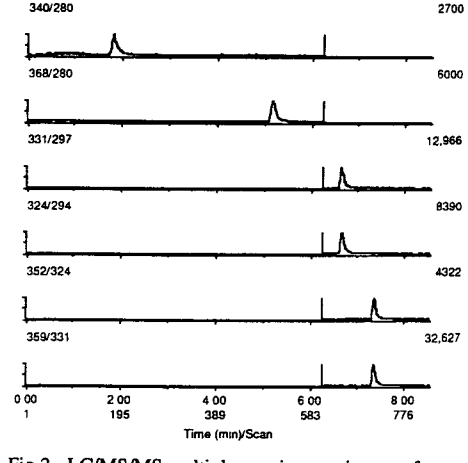

Fig 2. LC/MS/MS multiple reaction monitoring of a 1 ng/ml standard for AGN 190844 (top), AGN 190832 (2nd), $^2H_7$-AGN 190299 (3rd), AGN 190299 (4th), AGN 190168 and $^2H_7$-AGN 190168 (bottom) in human urine.

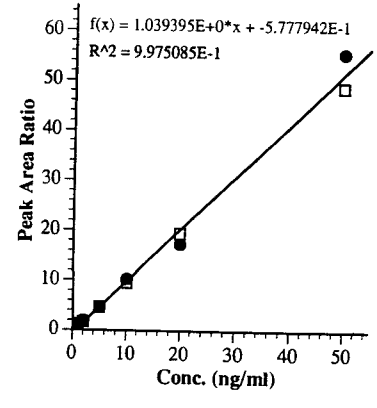

Fig 3. A representitive calibration curve of the major metabolite AGN 190844 in human urine.

Quantitative Analysis of Dofetilide and its N-desmethyl metabolite in Human Serum by Microbore High Performance Liquid Chromatography / Ionspray MS/MS.

R. P. Schneider and H. G. Fouda
Central Research Division, Pfizer Inc, Groton, CT 06340

Dofetilide is a selective and potent Potassium Channel Blocker useful for the treatment of re-entrant tachyarrhythmias. It acts by prolonging myocardial repolarizations with no effect on conduction parameters[1]. The pharmacokinetics and metabolism of dofetilide in animals and man have been described[2,3]. Following a single ^{14}C-dofetilide dose to human subjects, the parent drug was the main component in circulation. Only very low metabolite levels were detected in plasma [3].

Current assays for the determination of dofetilide concentrations in biological fluids include an HPLC/UV procedure with a lower limit of quantification of 2.5 ng/mL[4] and an RIA method with a lower limit of quantification of 0.05 ng/mL[5]. The development of an alternate specific method was desired. This report describes the development of a microbore HPLC / atmospheric pressure ionization MS/MS assay.

Control human serum was fortified with a structural analog internal standard and extracted with ethyl acetate under alkaline conditions. The organic layer was evaporated to dryness, and reconstituted in acetonitrile. Following a hexane wash, the acetonitrile was evaporated and the residues reconstituted in HPLC mobile phase. Samples were assayed by HPLC/MS/MS.

Validation parameters are shown in Tables 1 and 2. For dofetilide, intra-assay precision was better than 8.3% and the accuracy of the assay was within 2.6% of the nominal concentration. For the N-desmethyl metabolite, intra-assay precision was better than 9.6% and the accuracy of the assay was within 14.5% of the nominal concentration. The linear dynamic range of the assay was 0.05 to 3.0 ng/mL for dofetilide and 0.1 to 3.0 ng/mL for the N-desmethyl metabolite.

1 B. N. Singh, Arrhythmia control by prolonging repolarization: the concept and its potential therapeutic impact. *Europ. Heart Journal*, 14, 14-23, 1993.

2 H. S. Rasmussen, M. J. Allen, K. J. Blackburn, et al. Dofetilide, a novel class III antiarrhythmic agent. *J Cardiovasc. Pharmacol.* 20(2), 96-105, 1992.

3 D. A. Smith, H.S. Rasmussen, D. A. Stopher, et al. Pharmacokinetics and metabolism of dofetilide in mouse, rat, dog, and man. *Xenobiotica*, 22(6), 709-719, 1992.

4 D. K. Walker, D. A. Smith, D. A. Stopher. Liquid-liquid extraction and high performance liquid chromatography for the determination of a novel antidysrhythmic agent (UK-68,798) in human urine. *J Chromatog.* 568(2), 475-480, 1991

5 D. K. Walker, G. W. Aherne, J. E. Arrowsmith, et al. Measurement of the class III antidysrhythmic drug, UK-68,798, in plasma by radioimmunoassay. *J Pharm. Biomed. Anal.* 9(2), 141-149, 1991.

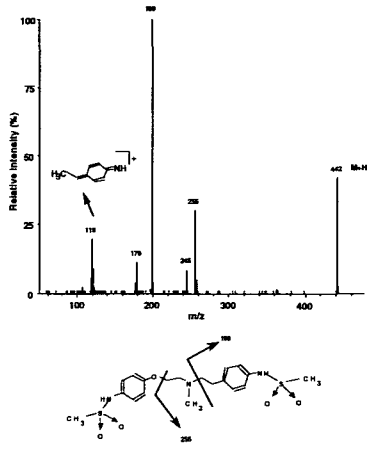

CID spectrum and proposed fragmentation of Dofetilide

Table 1
INTRA-ASSAY PRECISION AND ACCURACY DATA FOR DOFETILIDE

Analysis of human serum samples containing known amounts of drug
Summarized data are shown for n=6 samples at each fortified concentration

fort conc (ng/mL)	*mean conc found (ng/mL)*	*% RSD*	*mean accuracy*
0 05	0 051	8.3	101 9
0 10	0 10	8 0	102.2
0 50	0 49	3 4	98 6
1 0	1 03	4 0	102 6
3 0	3 02	2 1	100 6

Table 2
INTRA-ASSAY PRECISION AND ACCURACY DATA FOR N-DESMETHYL DOFETILIDE

Analysis of human serum samples containing known amounts of metabolite
Summarized data are shown for n=6 samples at each fortified concentration

fort conc (ng/mL)	*mean conc found (ng/mL)*	*% RSD*	*mean accuracy*
0 05**	0 039	7 5	77 2
0 10	0 09	9 6	85 5
0 50	0 48	5 1	96 1
1 0	0 94	3 1	94 2
3 0	2 83	3 5	94 3

**not considered as the LLOQ due to poor accuracy, data point excluded from dynamic range of the N-desmethyl metabolite

Measurement of CO_2 Exchange Rates in Transferrin by Mass Spectrometry

Todd Brown and Fred Hileman
Monsanto Corporate Research, 800 N. Lindbergh Blvd. St. Louis, MO 63167

Wes Harris
University of Missouri-St. Louis, Dept. of Chemistry, St. Louis, Mo 63121

There has been a long standing interest in the measurement of the exchange rate of carbonate with transferrin bound iron, especially in the presence of various anions. These measurements have typically been made with radiolabeled $^{14}CO_3^{2-}$ as a probe. This work involves the alternative use of $^{13}CO_3^{2-}$ as a probe combined with a purge and trap device and conventional mass spectrometry. Carbonate containing samples were placed in a specially designed purge and trap system (see Figure 1) in which acid was subsequently added to the sample to release the carbon dioxide. The evolved carbon dioxide was passed through a -20°C scrubber to remove the water and then cryogenically trapped on a short length of a Poraplot column maintained at -140°C. The trapped carbon dioxide was thermally desorbed into a conventional electron impact ionization mass spectrometer which used selective ion monitoring to quantitate both the native and labeled carbon dioxide.

Considerable care was taken to eliminate the background CO_2 in the system. Helium was used as the purge gas and it was necessary to remove any residual CO_2 from the helium prior to use. This was done by passing the helium through a liquid nitrogen trap and then through a molecular sieve 5A trap. Stainless tubing was used throughout the system to minimize the background.

To evaluate the system a standard curve was prepared. Solutions of 1 mM $NaHCO_3$ were made which contained 0, 25, 50, 75 and 100% $NaH^{13}CO_3$. All solutions were prepared in 50 mM HEPES buffer at pH 7.4. 100 uL aliquots of these solutions were introduced into the purge and trap device using the loop injector and were then acidified with 100 uL of 1N H_2SO_4 via a second loop injection. The released CO_2 was trapped and injected into the mass spectrometer where the $CO_2/^{13}CO_2$ ratio was determined. A plot of expected versus measured percent of CO_2 and $^{13}CO_2$ was then generated showing excellent linearity.

The experiments were carried out using 1 mM monoferric transferrin saturated with $^{13}CO_3^{2-}$ in 50 mM HEPES buffer at pH 7.4 containing 1 mM $NaHCO_3$. Perchlorate at various concentrations was introduced into the sample causing exchange of the carbonate between the protein and the buffer and the time course of this exchange was followed. Aliquots of the transferrin/carbonate/perchlorate solution were taken at specific time intervals. The supernatant of the aliquot was separated from protein via centrifugation through a membrane with a 10,000 dalton cutoff. A 100 uL sample of the supernatant was injected into the purge and trap system and the $CO_2/^{13}CO_2$ ratio was determined. The time course evaluation for a 100 mM perchlorate solution did not show any detectable exchange over a 4 hour period. When the experiment was repeated using 500 mM perchlorate the exchange shown in Figure 2 was observed. This illustrates the applicability of the technique and that it offers an alternative to the use of radioisotopes to follow this exchange.

Figure 1. Purge and Trap - Mass Spectrometry

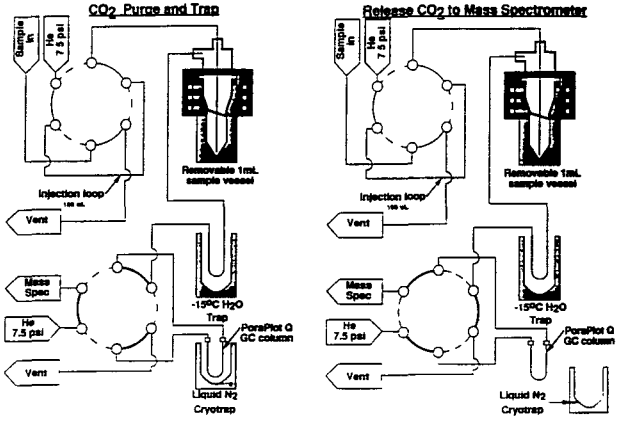

Figure 2. Exchange of carbonate in 1mM $^{13}CO_3^{2-}$ saturated monoferric transferrin with 1 mM $NaHCO_3$ in the presence of 500 mM $NaClO_4$

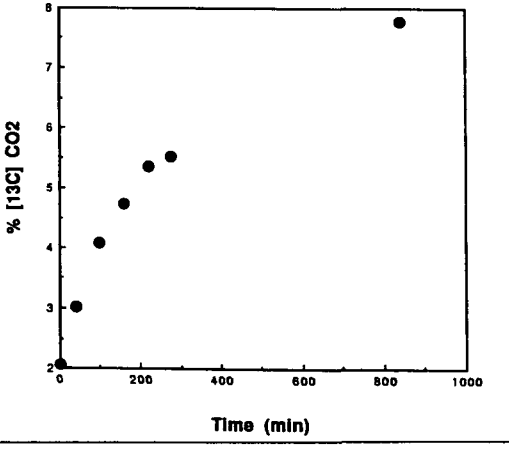

DETERMINATION OF 2-BUTOXYETHANOL AND METABOLITES IN HUMAN URINE USING GC/MS & ESI/MS

Dan A. Markham, M. J. Bartels and R. A. Corley, The Dow Chemical Company, Midland, MI 48674 & A. W. Rettenmeier, University of Tubingen, Germany

Industry and consumer cleaning product manufacturers use 2-butoxyethanol (BE) extensively due to it's versatile applications resulting from compatability in both hydrophilic and lipophilic systems [1]. The primarly metabolite of BE, butoxyacetic acid (BAA), has been shown to cause hemolysis in rats [2-4] and it's effect is being studied in humans. BAA is primarily eliminated via the urinary tract in humans [5], therefore an effective manner to calculate the exposure of BE is through monitoring the concentration of BAA in the urine. However, in a recent human exposure study, Rettenmeier, et al. [5], indicated that as much as 60% of BAA may be eliminated as the glutamine (primary) conjugate and to a lesser extent the glycine conjugate. To accurately determine the level of BE exposure both the unconjugated (free) and conjugated BAA must be determined. The accepted method to determine total (free + conjugated) BAA is to acid hydrolyze the urine samples prior to analysis [5,6]. This methodology will produce accurate total BAA determinations, however, due to possible BE exposure in everyday life it could be difficult to correlate the sources of BE exposure to the elimination of total BAA. This laboratory has observed background levels of BE ranging from 20 to 50 ppb in human urine. The stable isotope labelled analog ^{13}C-BE was therefore employed to distinguish between endogenous and dosed material and the related ^{13}C-metabolites. In addition, the possible elimination of BE metabolized as ethylene glycol (EG) was to be investigated.

A sensitive and selective chemical derivatization gas chromatography/methane negative chemical ionization/mass spectrometry (GC/NCI/MS) method has been developed to simultaneously quantitate 2-butoxyethanol (BE), 2-butoxyacetic acid (BAA see; Figure 1), and ethylene glycol (EG) in human urine. The BE and EG were derivatized using pentafluorobenzoyl chloride and the BAA using pentafluorobenzyl bromide. This method employs the use of both ^{13}C-labeled and deuterium-labeled analogs of each analyte as test materials and internal standards, respectively, to improve limits of quantitation and precision. The above method was also expanded to quantitate conjugated BE, BAA, and EG following acid hydrolysis of human urine. Calibration curves were generally linear over one order of magnitude, with limits of quantitation of 36 ng BE, 84 ng BAA, and 17 ng EG per gram of urine. In addition, a high performance liquid chromatography/ positive electrospray ionization/ mass spectrometry (HPLC/+ESI/MS) method was developed to confirm and quantitate N-butoxyacetylglutamine (NBGL see; Figure 2), the major urinary conjugate of BAA. Calibration curves were generally linear over one order of magnitude, with limits of quantitation of 204 ng NBGL per gram of urine. This poster will present the urinary results from a study in which six human male subjects were dermally exposed (single arm) to an atmosphere containing 50 ppm ^{13}C-BE to support the construction of a physiological based/ pharmacokinetic (PB/PK) model [7].

43rd ASMS Conference on Mass Spectrometry and Allied Topics

FIGURE 1 TYPICAL GC/NCI/MS ION CHROMATOGRAMS OF ACID HYDROLYZED HUMAN URINE SAMPLE

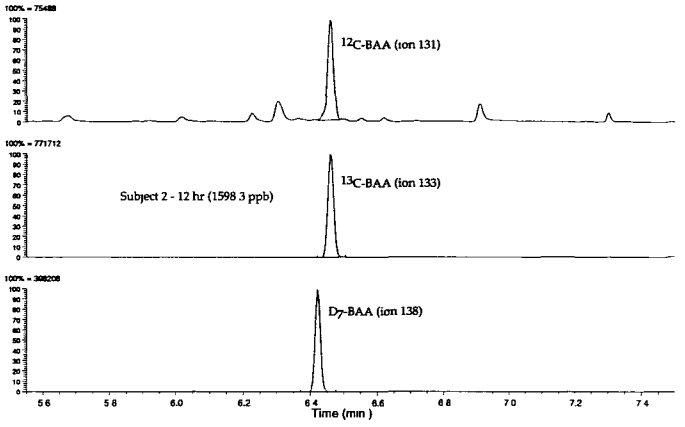

FIGURE 2. TYPICAL +ESI/MS ION CHROMATOGRAMS OF HUMAN URINE SAMPLE

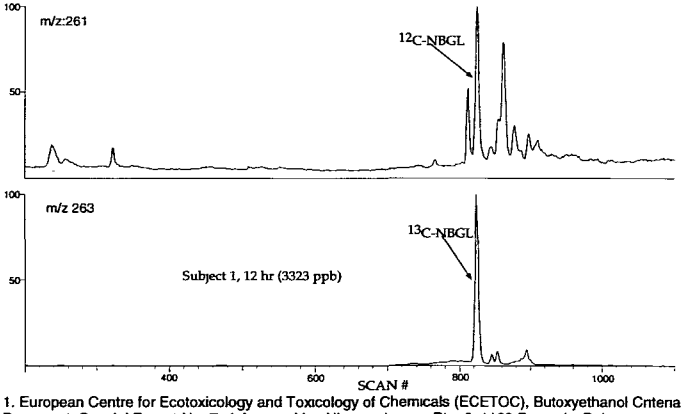

1. European Centre for Ecotoxicology and Toxicology of Chemicals (ECETOC), Butoxyethanol Criteria Document, Special Report No. 7, 4 Avenue Van Nieuwenhuyse, Bte. 6, 1160-Brussels, Belgium
2 B. I. Ghanayem, L T Burka, and H. B. Mathews, *J. Pharmacol. Exp. Therap*, 242 (1987), 222-31.
3 F G. Bartnik, A K. Reddy, G. Klecak, V. Zimmermann, J J Hoystnek, and K. Kunstler, *Fund Appl. Toxicol.*, 8 (1987), 59-70.
4 B. I Ghanayem, *Biochem. Pharmacol.*, 38 (1989), 1679-84.
5. A. W. Rettenmeier, R Hennigs, and R. Wodarz, *Int. Arch. Occup. Environ. Health*, 65 (1993), S151-S153.
6. T. Sakai, T. Takaharu, Y. Monta, and Y. Masuyama, *Int. Arch. Occup. Environ. Health*, 66 (1994), 249-254.
7. R. A. Corley, et al, *The Toxicologist*, 15, 1 (1995), #255, 47

Evaluation of Nalmefene Metabolism in Rats and Dogs Using Thermospray LC/MS

C. Mathur, S. Murthy, L T Kvalo and J.A. Wilhelm
Ohmeda Pharmaceutical Products Division Inc., Murray Hill, NJ 07974

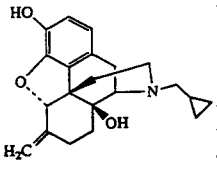

NALMEFENE

Nalmefene is a selective narcotic antagonist that is structurally similar to naloxone. Nalmefene's pharmacological activity is mediated via competitive inhibition of opioid receptor sites. It is indicated for the complete or partial reversal of opioid depression, including respiratory depression, and for the diagnosis and treatment of opioid overdose. For these indications, nalmefene will primarily be administered as an intravenous bolus

As part of a more comprehensive pre-clinical evaluation of nalmefene metabolism, *in vitro* and *in vivo* studies were performed in order to: 1)compare metabolite profiles generated from rat and dog liver microsome incubations to those obtained from rat and dog biological fluids (plasma, urine and feces), 2) positively identify the metabolites using co-chromatography of authentic standards and thermospray LC/MS, 3)further characterize the plasma concentration-time profile of nalmefene metabolites in the rat following intravenous bolus administration of nalmefene.

Metabolite Profiling and Identification: *In vitro* (rat and dog liver microsomal incubations) and *in vivo* (plasma, urine, feces samples from rats, n=3, and dog, n=1) metabolites were eluted with methanol from C-18 solid phase extraction (SPE) cartridges. Chromatographic separation was accomplished by HPLC using gradient elution (20-50% methanol in 0.05M ammonium acetate buffer, pH 4.5) with a flow rate of 1 ml/min and a Beckman C-18 Ultrasphere column (150 x 4.6 mm). *In vitro* studies indicated that the rat liver microsomes convert nalmefene to a phase I N-dealkylated metabolite, nornalmefene, while the dog liver microsomes did not produce nornalmefene to a significant extent. Comparative mass spectral profiles of urinary rat and dog nalmefene metabolites revealed the following metabolites: dog - nalmefene glucuronide and nalmefene diglucuronide; rat - nornalmefene, nalmefene glucuronide and nornalmefene glucuronide. Structural elucidation of the metabolites, based upon comparison of elution times and mass spectra, are provided.

Metabolite Pharmacokinetics: Rats (n=4) were surgically prepared and each rat received an iv bolus dose of 5 mg/kg nalmefene.HCl in saline. Metabolite plasma concentrations at 0, 5, 30, 60, 120, 180, 240 and 300 minutes were determined following SPE after the addition of the internal standard, naloxone. Mass spectral instrumentation conditions were: Finnigan MAT SSQ710 with thermospray interface, vaporizer temperature = 95°C, source temperature = 220°C, aerosol

temperature = 280 °C, electron multiplier =1500 volts, dynode = 15 Kvolts, discharge ionization = 0 volts and filament off. Plasma samples (0 2 ml) were assayed initially for free nalmefene and nornalmefene. Total nalmefene and nornalmefene (unconjugated and conjugated) were determined following overnight incubation with β-glucuronidase, SPE and LC/MS analysis. Chromatographic separation was achieved using a reversed phase system consisting of a Beckman C-18, Ultrasphere analytical column (150 x 4.6 mm) with isocratic mobile phase, methanol/ 0 05M ammonium acetate, pH 4.5 buffer, 30:70 (v v) at a flow of 1 ml/min. Detection and quantitation was accomplished in SIM mode. The data was processed and it generated plasma-concentration time profiles as shown above.

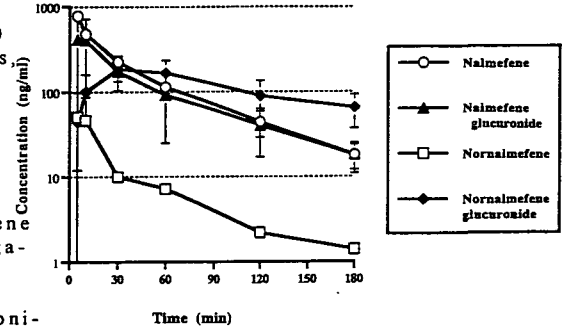

Plasma concentration-time curves of nalmefene and corresponding metabolites following an iv bolus dose of 5 mg/kg nalmefene. HCl

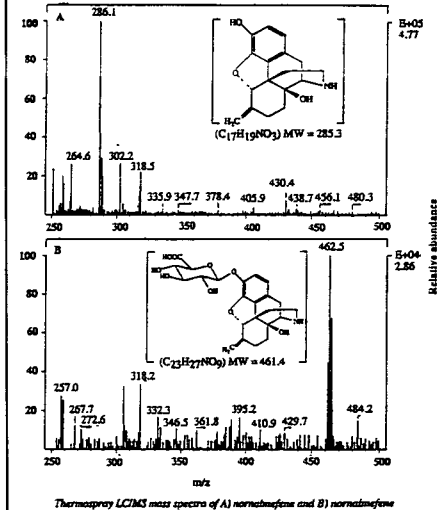

Thermospray LC/MS mass spectra of A) nornalmefene and B) nornalmefene glucuronide isolated from rat urine

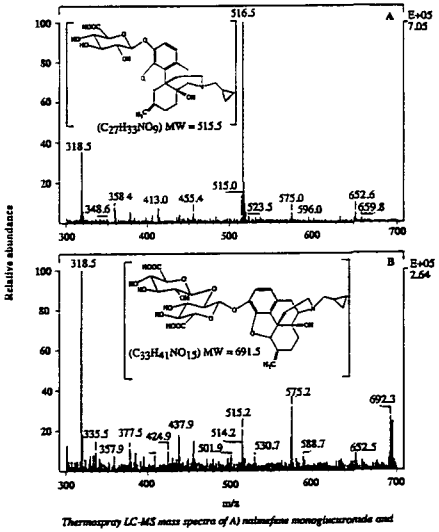

Thermospray LC-MS mass spectra of A) nalmefene monoglucuronide and and B) nalmefene diglucuronide isolated from dog urine.

QUANTITATION OF RITALIN & RITALINIC ACID IN HUMAN PLASMA BY API LC/MS/MS

* Luca C. Matassa, Ken C. Cassidy
NOVAMANN (Ontario) Inc.
5540 McAdam Road, Mississauga, ON L4Z 1P1 CANADA

Ritalin (methylphenidate), Figure 1 is generally considered to be the drug of choice for the treatment of children with hyperactivity (ADD, Attention Deficit Disorder). It has been reported that about 80 % of such hyperactive children respond favourably when treated with methylphenidate 1. In humans, methylphenidate is metabolized primarily by de-esterification to ritalinc acid (Figure 1) which is therapeutically inactive.

Many methods for the quantitation of methylphenidate and ritalinic acid in plasma or urine have been described (GC/MS, HPLC) 2,3,4. Most of these methods require extensive extraction procedures and/or derivatization and lack the sensitivity required to characterize the pharmacokinetics of methylphenidate after an oral dose. Also most of these methods cannot extract both analytes together from the same samples. This is important with limited sample volume available for sample assay. Our objective was to develop an HPLC/MS/MS method for the detection and quantitation of 1 and 2 in human plasma which was sufficiently sensitive for analysis of clinical bioequivalence samples.

A reverse phase HPLC/MS/MS (Sciex API III - Plus, MRM mode, positive ion, IonSpray interface) method developed and validated at NOVAMANN (Ontario) Inc. for the quantitation of methylphenidate and ritalinic acid in human plasma is described. The extraction procedure involves solid-phase (C18) isolation of the analytes and internal standard (phenylalanine ethyl ester) after buffering the sample. Sample evaporation temperature was critical for the success of the assay. Plasma calibration curves extracted over 4 separate assay batches were linear from 1.0 to 60.0 ng/mL for methylphenidate and 10.0 to 600 ng/mL for ritalinic acid. Intra-batch and inter-batch precision and inaccuracy for methylphenidate and ritalinic acid over the 4 days was less than 15 %. Typical MRM chromatograms for a blank plasma sample extract and a plasma sample spiked with the analytes and the internal standard are given in Figure 2. Calibration curves are given in Figure 3. This method has been used to assay clinical bioequivalence samples.

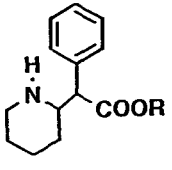

1 Methylpheindate R=Me
mw= 233
2 Ritalinic Acid R=H
mw= 219

Figure 1

43rd ASMS Conference on Mass Spectrometry and Allied Topics

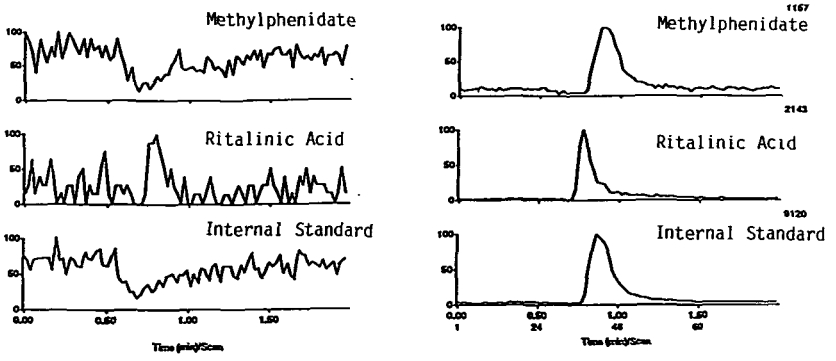

Plasma Blank

Plasma spike containing 1 ng/mL methylphenidate 10 ng/mL ritalinic acid and internal standard

Figure 2

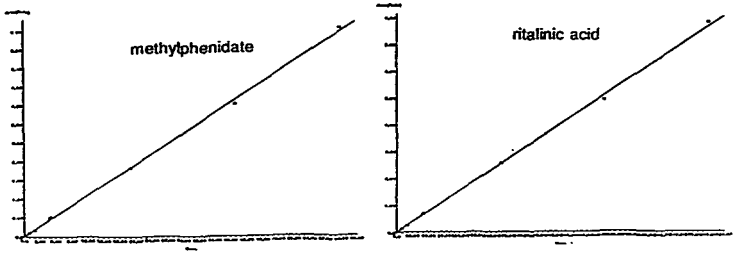

Calibration curves for methylphenidate and ritalinic acid in human plasma

Figure 3

Automated LC/ESI/MS/MS Quantitation of a Phospholipid Drug in Human Plasma

Brenda Hamilton, Elizabeth Graham, Craig Abolin*
Sandoz Pharmaceuticals
East Hanover, NJ 07936

*Robert White** and Thomas Oglesby*
Taylor Technology Inc.
107 College Road East
Princeton, NJ 08540

INTRODUCTION

An electrospray tandem mass spectrometry (LC/ESI/MS/MS) method was developed, validated and used for the quantitative analysis of Sandoz compound SDZ CPI 975 in hundreds of human plasma samples on a routine basis in support of clinical pharmacokinetic studies. This phospholipid compound is a potential drug for the treatment of non-insulin dependent diabetes mellitus (NIDDM). It is not easily detected in biological fluids using conventional physicochemical detection (UV, Fluorescence) because it has no chromophore. Additionally, the compound is thermally labile making it incompatible with gas chromatography or thermospray mass spectrometry analysis.

EXPERIMENTAL

A stable isotope labeled analog of SDZ CPI 975 with twenty seven deuterium atoms was used as the internal standard. The sample preparation entailed the addition of this D_{27}-CPI 975 internal standard to 200 µL plasma standards or unknowns followed by protein precipitation with 400 µL of methanol. After waiting 30 minutes, the samples were centrifuged for 10 minutes and the supernatant filtered through a 0.45 µm Gelman filter. Reverse phase chromatography of 50 µL of the filtrate was performed on a Hewlett Packard Series II 1090M liquid chromatograph using a YMC Basic®C-8 column (2.0 x 100 mm, 5 µm) at a flow rate of 0.5 mL/min. Elution of the analyte and internal standard was performed at a temperature of 40°C using a gradient starting at 50% methanol and ending at 100% methanol over three minutes. Both SDZ CPI 975 and D_{27}-CPI 975 coeluted with a typical retention time of 3.5 minutes. To minimize contamination of the electrospray source, a post column divert valve was used so that non-retained (<3.2 min.) and late eluting (>4.0 min.) materials were diverted to waste. The column effluent containing SDZ CPI 975 and its internal standard was introduced into the Finnigan electrospray source without splitting in positive ion mode. The parent ion of SDZ CPI 975 and its deuterated internal standard at m/z 438.3 and 465.3 respectively were collisionally fragmented resulting in the same product ion at m/z 144. (see Figure 1).

RESULTS

The LOQ of the assay was 24.5 ng per mL of SDZ CPI 975 in plasma using relative response factors (RRF=conc./area ratio). A typical plot of RRF's is shown in Figure 2. No interferences from endogenous materials were observed.

CONCLUSION

The simple and rapid procedure described in this paper provides a highly sensitive and accurate method for the quantitation of SDZ CPI 975 in plasma by electrospray LC/MS/MS.

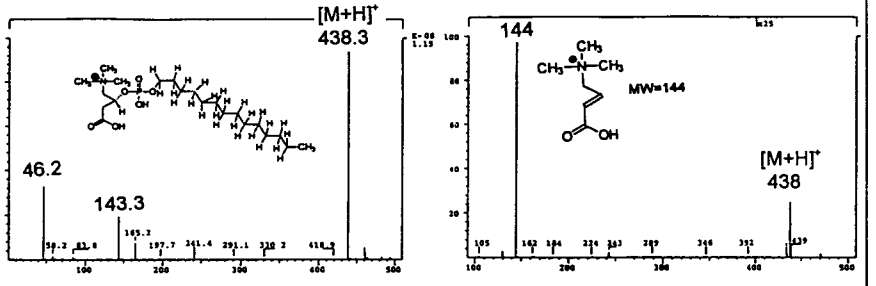

Figure 1 MS and MS/MS Spectra of SDZ CPI 975

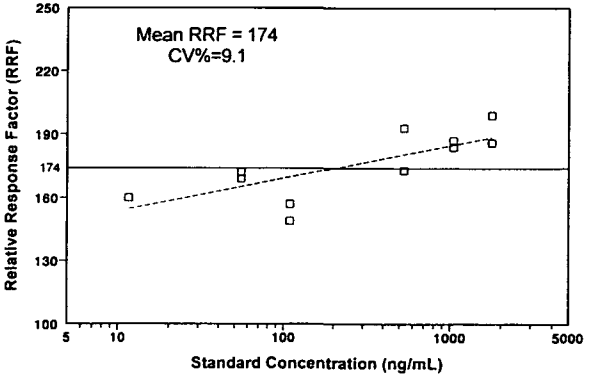

Figure 2 Plot of Relative Response Factors

Ultra-Trace LC/MS/MS Determination of Reserpine in Plasma

Melissa Anderson*, Tim Wachs, and Jack Henion

Cornell University, Analytical Toxicology, 927 Warren Drive, Ithaca, NY 14850

*Monsanto Corporate Research, 800 N. Lindbergh Blvd., St. Louis, MO 63167

Introduction

GC/MS is the most widely accepted technique for the identification of drug metabolites. However, it has been generally unsuccessful for the determination of low volatility and thermally labile compounds such as reserpine. This basic drug is an ideal candidate for ionization techniques such as ion spray that do not require analyte volatility. Additionally, HPLC, the method of choice for separation of polar, low volatility drugs, is an ideal separation technique for these compounds with detection by ion spray mass spectrometry.

Reserpine is used for the treatment of hypertension and psychoses in humans, and as a tranquilizer in horses. Few data are available on the pharmacokinetic properties of reserpine because of the lack of an assay capable of detecting low concentrations of the drug or its metabolites. For clinical analyses where a high-volume of samples may need to be analyzed, rapid methods for sample preparation and analysis are needed.

Experimental

The goal of rapid, high-throughput analyses can be met by coupling good sample preparation and clean up with fast liquid chromatography with MS/MS as the final "separation" step. Isocratic conditions using an eluent of 80:20 acetonitrile:water, 5 mM ammonium acetate allow for a short analysis time. The use of a 1 mm column (Keystone Scientific Betasil C18 100 mm) combined with MS/MS in the selected reaction monitoring (SRM) mode provided a retention time of approximately three minutes for reserpine and the internal standard, rescinnamine. The ion spray interface on a Sciex TAGA 6000E triple quadrupole upgraded to an API III (operated at 4.6 kV in positive ion mode) received 50 μL/min from the column effluent with no post-column split.

A three step liquid/liquid extraction (1) was used to isolate reserpine and the internal standard, rescinnamine, from equine plasma. This extraction technique provides clean extracts with good recovery (60%) at low picogram levels. However, this method is very tedious and time consuming. We are continuing to develop improved alternative sample preparation procedures.

Results and Discussion

Calibration standards were prepared in duplicate by adding aliquots of reserpine and the internal standard, rescinnamine, to 2 mL of control equine plasma. The concentrations of the standard in the calibration curve were 10, 25, 50, 500, 2000, and 5000 pg/mL. The concentration of the internal standard in each standard curve sample was 1800 pg/mL.

Using liquid/liquid extraction, the lower limit of quantitation (LOQ) of reserpine in equine plasma is 50 pg/mL with a linear response up to at least 5000 pg/mL. The limit of detection (LOD) of reserpine in equine plasma is 10 pg/mL based on 2 mL aliquots. The accuracy from quality control (QC) samples (20, 200, 3000 pg/mL) was <15% for each QC level except at the lower limit of quantitation.

(1) Suckow, R. F.; Cooper, T. B.; Asnis, G. M. *J. Liq. Chromatogr.* 1983, 6, 1111-1122.

43rd ASMS Conference on Mass Spectrometry and Allied Topics

Figure 1

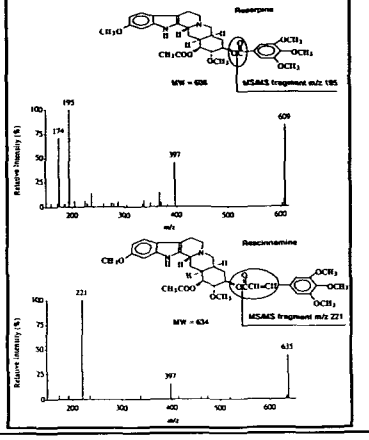

Figure 2

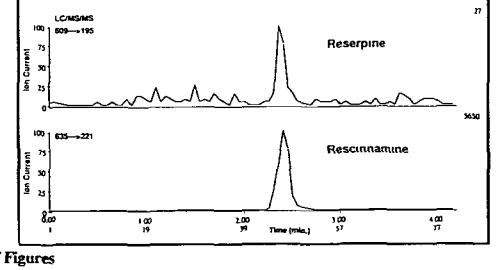

Legend of Figures

Figure 1. Structures and MS/MS Spectra of Reserpine and Internal Standard Rescinnamine.

Figure 2. SRM LC/MS Ion Current Profile from an Extract of 2 mL Equine Plasma: Reserpine 10 pg/mL, Rescinnamine 1800 pg/mL.

DETERMINATION OF LOVASTATIN AND HYDROXY-ACID LOVASTATIN IN DOG PLASMA VIA LC-APCI/MS/MS

Walter A. Korfmacher[1], Amelia P. Lapiguera[1], Chin-Chung Lin[1], Carolyn Langevin[2] and Thomas Oglesby[2]

[1]Department of Drug Metabolism and Pharmacokinetics
Schering-Plough Research Institute
2015 Galloping Hill Road
Kenilworth, NJ 07033-0539

[2]Taylor Technology, Inc.
350 Alexander Road
Princeton, NJ 08540

Lovastatin (LOV) (see figure 1) is a drug used for the treatment of high cholesterol. One of the metabolites of lovastatin, hydroxy-acid lovastatin (LOV-OH), is an active metabolite. Thus, a sensitive assay was needed for the determination of both lovastatin and LOV-OH in plasma.

The most sensitive assay that was found in the literature was a complicated multi-step GC-MS procedure. It was decided that the technique of HPLC combined with atmospheric pressure chemical ionization (APCI) tandem mass spectrometry (MS/MS) should provide the necessary sensitivity and selectivity to determine these two analytes at low levels.

Finnigan-MAT TSQ (7000 and 700) triple quadrupole mass spectrometers equipped with the Finnigan APCI source were used for the study. Dog plasma samples (1.0 ml) containing internal standards (simvastatin and simvastatin-OH) were subjected to solid-phase extraction. The dried extract was then resolvated and injected into the LC-APCI/MS/MS system. An HPLC system based on a reversed phase column (C-8) and a gradient elution provided a good chromatographic system for these compounds. The mobile phases (A & B) each contained 10 mM ammonium acetate. The MS analyses were performed using the selected reaction monitoring (SRM) technique. In each case, the $[M + NH_4]^+$ molecule was chosen as the precursor ion by MS1 (Q1) and a suitable product ion was selected for MS2 (Q3). Figure 2 shows a typical mass chromatogram for LOV spiked into dog plasma at 0.5 ng/ml, the limit of quantitation (LOQ) for this assay.

This assay has been validated and found to have an intra-day precision (%CV) of not more than 11% at the three quality control (QC) levels. The inter-day precision was not more than 13% at all three QC levels. In addition, LOV and LOV-OH were found to be stable in dog plasma stored at -70 °C for nine days or carried through three freeze-thaw cycles. The validated method was found to be linear over the range of 0.50 to 50 ng/ml plasma for lovastatin and 10 to 500 ng/ml for LOV-OH. The assay was found to be suitable for dogs dosed with lovastatin.

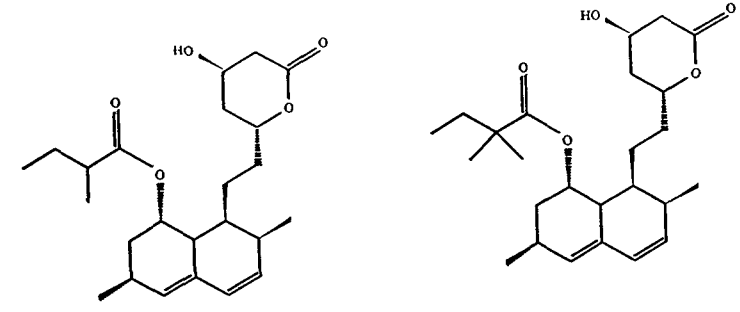

LOVASTATIN (LOV)

SIMVASTATIN (SIM)

Figure 1 Structures of LOV and SIM

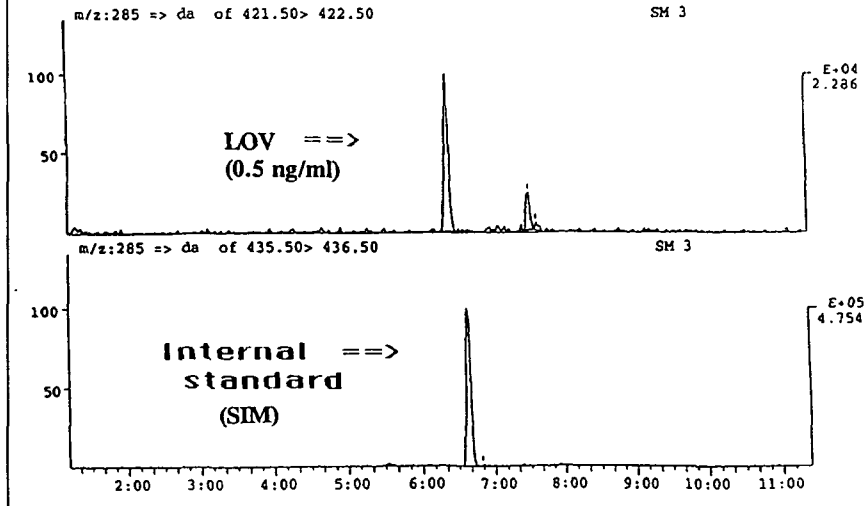

Figure 2 Typical mass chromatogram for LOV spiked into Dog Plasma

LC/MS/MS Quantitation of Lovastatin and Its Hydroxy Acid in Mouse and Rat Plasma

Henry Y. Wu[1], Jamie Zhao[1], Jack Henion[1], Walter A. Korfmacher[2] and C. C. Lin[2].
[1]Advanced BioAnalytical Services, Inc., 15 Catherwood Rd., Ithaca, NY 14850
[2]Schering-Plough Research Institute, 2015 Galloping Hill Rd., Kenilworth, NJ 07033

INTRODUCTION

The determination of Lovastatin (Lov) and its hydroxy acid (Lov-OH) metabolite in biological matrices has been reported using LC/UV[1] and GC/MS[2-4] techniques. Although the reported GC/MS methods showed good sensitivity for both compounds, time-consuming derivatization procedures were required for all analytes. In addition, the methods reported may not provide sufficient sensitivity for applications requiring plasma samples as small as 0.1 mL with trace level detection limits. We have developed an alternative method employing ion spray LC/MS/MS techniques that meets the needs of trace bioanalytical analysis.

A sensitive and novel analytical method was developed to simultaneously and directly quantitate Lovastatin and Lovastatin hydroxy acid in mouse and rat plasma without derivatization. This method employs a solid-phase extraction procedure to isolate Lovastatin and Lovastatin hydroxy acid from the biological matrix. Simvastatin (Sim) and Simvastatin hydroxy acid (Sim-OH) were used as internal standards for the respective compounds. Reconstituted extracts were analyzed by ion spray liquid chromatography/tandem mass spectrometry (LC/MS/MS).

EXPERIMENTAL

Bond Elut™ C8 SPE Cartridges were obtained from Varian/Sample Preparation Products, Harbor City, CA 90710. The liquid chromatography part of the system included a Hewlett-Packard Model 1090M pump, Hewlett-Packard, Avondale, PA 19311. Kromasil™ C18 columns, 2 x 50 mm, were obtained from Keystone Scientific, Inc., Bellefonte, PA 16823. The mass spectrometer was a PE-SCIEX API III+ from PE-SCIEX, Thornhill, Ontario. After solid-phase extraction, the reconstituted extracts were analyzed by ion spray LC/MS/MS. For each sample, the mass spectrometer was first operated in the negative ion mode for the detection of Lovastatin hydroxy acid, and then was switched to the positive ion mode for the detection of Lovastatin. The Kromasil™ C18 column was subjected to gradient elution with 1 mM ammonium acetate (pH 4.0) and acetonitrile.

RESULTS AND DISCUSSION

Figure 1 shows the full-scan product ion spectra of Lov and Lov-OH. The assay has a limit of quantitation (LOQ) of 500 pg/mL plasma for both Lov and Lov-OH based on 0.1 mL aliquots of mouse or rat plasma. Figure 2 presents the extracted ion current chromatograms of rat plasma extract at the LOQ level. The standard curves were linear from 0.5 ng/mL to 100 ng/mL for both Lov and Lov-OH. The intra- and inter-assay precision, calculated from QC samples, was less than 7% for Lov and less than 6% for Lov-OH in both matrices. The inter-assay accuracy as determined from QC samples was less than 6% for Lov and less than 8% for Lov-OH acid in both matrices. The overall recovery of Lov was 54% in mouse plasma and 55% in rat plasma, and the overall recovery of Lov-OH was 100% in mouse plasma and 67% in rat plasma. The recoveries of Lov and Lov-OH were not concentration dependent. Lov-OH was found to be stable in all experiments, while Lov was found to be unstable in plasma at ambient temperature for 4 hours and in the reconstitution buffer at ambient temperature for 24 hours. However, Lov did appear to be stable in the reconstitution buffer at 4 °C for 24 hours. Both analytes were also shown to be stable after three freeze(-70 °C)/thaw(4 °C) cycles in plasma and to be stable up to 4 days as dry extracts

43rd ASMS Conference on Mass Spectrometry and Allied Topics

at 4 °C. Since Lov is unstable in mouse and rat plasma at ambient temperature, sample preparation was carried out in an ice-water bath.

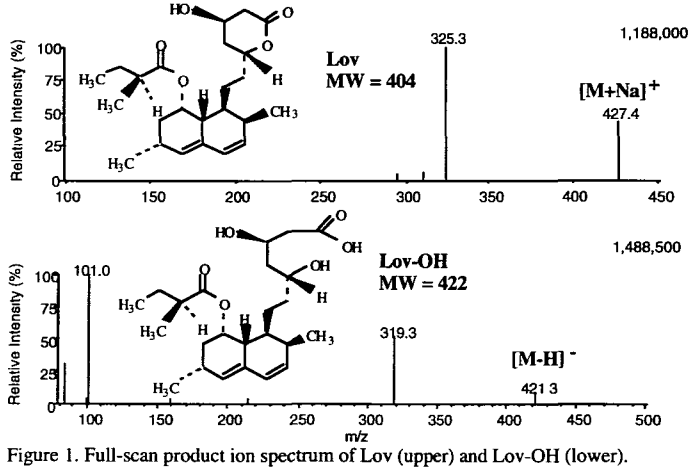

Figure 1. Full-scan product ion spectrum of Lov (upper) and Lov-OH (lower).

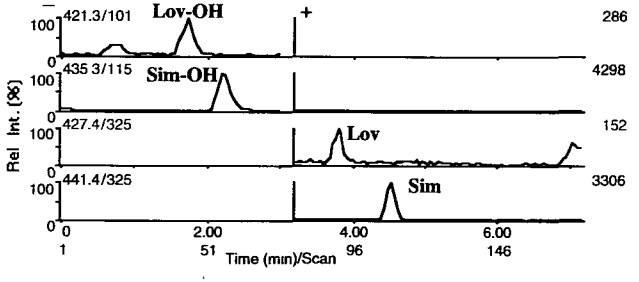

Figure 2. Selected reaction monitoring chromatogram of 500 pg/mL of Lov; 500 pg/mL of Lov-OH; 10 ng/mL of Sim; 10 ng/mL of Sim-OH from rat plasma extract.

REFERENCES

1. R. J. Stubbs, M. Schwartz, and W. F. Bayne, J. Chromatography, **1986**, *383* , 438-443.
2. T. Takano, S. Abe, and S. Tata, Biomed. Environ. Mass Spectrom., **1990**, *19*, 577-581.
3. D. Wang-Iverson, E. Ivashkiv, J. Jemal, and A. I. Cohen, Rapid Commun. Mass Spectrom., **1989**, *3*, 132-134.
4. M. J. Morris, J. D. Gilbert, J. Y.-K. Hsieh, B. K. Matuszewski, H. G. Ramjit, and W. F. Bayne, Biol. Mass Spectrom., **1993**, *22*, 1-8.

QUANTITATION OF LTE_4 IN HUMAN URINE BY ION SPRAY LC/MS/MS

Henry Y. Wu[1], Lily Y.-T. Li[1], Jack D. Henion[1] and George J. Krol[2].
[1]Advanced BioAnalytical Services, Inc., 15 Catherwood Rd., Ithaca, NY 14850;
[2] Bayer Corporation, 400 Morgan Lane, West Haven, CT 06516

INTRODUCTION

Leukotrienes (LTs) are biologically important compounds derived from arachidonic acid by the action of the enzyme 5-lipoxygenase. LTE_4 is a sulfidopeptide leukotriene that is difficult to quantitate because it is relatively unstable in the presence of metal ions and oxidants. Recently, the determination of LTE_4 in human and rabbit urine has been reported using solid-phase extraction (SPE)-HPLC-enzyme-immunoassay (EIA) and HPLC-UV, respectively.[1,2] However, the reported methods do not provide sufficient sensitivity for applications requiring trace level detection limits. A sufficiently sensitive but a rather complicated GC-MS procedure for the analysis of LTE_4 in urine has also been reported.[3]

We have developed a new sensitive and simple LC/MS/MS method to quantitate LTE_4 in human urine. This method employs a solid-phase extraction procedure using Empore™ extraction disks to isolate LTE_4 and the internal standard LTE_4-d_3 from the urine stabilized with 4-HO-TEMPO and EDTA.

EXPERIMENTAL

Empore™ C18 extraction disks were obtained from 3M Industrial and Consumer Sector, St. Paul, MN 55144. The liquid chromatography part of the system included a Hewlett-Packard Model 1090M pump, Hewlett-Packard, Avondale, PA 19311. Kromasil™ C8 columns, 2 x 50 mm, were from Keystone Scientific, Inc., Bellefonte, PA 16823. The mass spectrometer was a PE-SCIEX API III+ from PE-SCIEX, Thornhill, Ontario.

After solid-phase extraction, the reconstituted extracts were analyzed by liquid chromatography/tandem mass spectrometry (LC/MS/MS) operated in the negative ion mode using a TurboIonSpray™ interface. The Kromasil™ C8 column was eluted isocratically with methanol and aqueous ammonium acetate (pH 5.6) at a ratio of 70:30.

RESULTS AND DISCUSSION

The full-scan product ion spectrum of LTE_4 is shown in Figure 1. The assay has a lower limit of quantitation (LOQ) of 50 pg/mL of urine for LTE_4 based on 5 mL aliquots. The standard curves were linear from 0.05 ng/mL to 10 ng/mL by weighted (1/y) least squares regression of concentration versus peak area ratio of the analyte to the internal standard. Figure 2 presents the extracted ion current chromatograms for the control blank human urine extract and the urine extract at LOQ level. The intra- and inter-assay precision, calculated from QC samples, was less than 9% for LTE_4. The intra-assay precision was less than 11% for the LTE_4 standards. The intra and inter-assay accuracy was less than 14% and 8% for each QC level, respectively. The intra-assay accuracy was less than 14% for each standard level. LTE_4 was found to be stable in human urine (in the presence of 4-hydroxy TEMPO and EDTA) at -70 °C for at least 33 days, at ambient temperature up to 24 hours, and in the reconstitution buffer at 5 °C for 24 hours. LTE_4 was also shown to be stable after 3 freeze(-70 °C)/thaw cycles in human urine and to be stable for 2 days as dry extracts at -70 °C. The recovery of LTE_4 during solid-phase extraction was independent of LTE_4 concentration in human urine. The mean recovery of LTE_4 from human urine was found to be 72%. Several important parameters such as pH of the urine and pH of the wash solution need to be considered during the sample preparation.

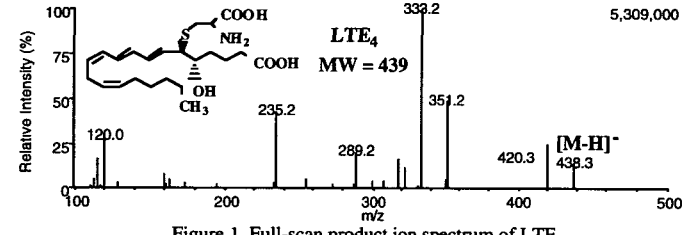

Figure 1. Full-scan product ion spectrum of LTE_4

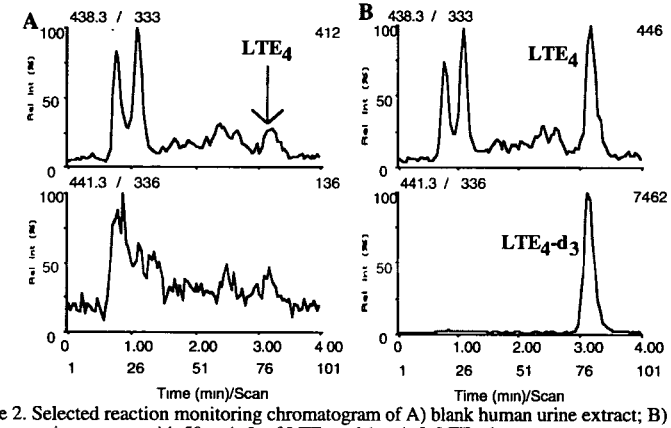

Figure 2. Selected reaction monitoring chromatogram of A) blank human urine extract; B) human urine extract with 50 pg/mL of LTE_4 and 1 ng/mL LTE_4-d_3

ACKNOWLEDGEMENT

We thank Dr. Robert Murphy of the National Jewish Center for Immunology & Respiratory Medicine for his helpful suggestions during the method development.

REFERENCES

1. A. Celardo, G. Dell'Elba, Z. M. Eltantawy, V. Evangelista, C. Cerletti, J. Chromatogr. B, **1994**, *658*, 261-269.
2. A. Sala, L. Armetti, A. Piva, and G. Folco, Prostaglandins, **1994**, *47*, 281-292.
3. D. Tsikas, J. Fauler, F. M. Gutzki, Th. Röder, H. J. Bestmann, J. C. Frölich, J. Chromatogr. B, **1993**, *622*, 1-7.

Automation of Rapid, High Sensitivity Pharmacokinetics Assays by LC/MS/MS

Ken Stoney and Kerry Nugent, Michrom BioResources, Auburn, CA
Adrian Land, Mark Bier, Jae Schwartz and Kevin Wheeler
Finnigan MAT, San Jose, CA

Trace level detection and quantitation of pharmaceutical compounds and their metabolites in biological samples can be a very challenging analytical problem. During the development of a new drug candidate, researchers may be required to analyze thousands of samples to fully characterize the metabolism of the compound of interest in the target organism. Current methodology often requires extensive manual cleanup, including protein precipitation, liquid-liquid partition and/or solid phase extraction prior to analysis by HPLC or LC/MS. These techniques are often time consuming, and can lead to errors in quantitation from manual sample handling.

An automated LC/LC/MS/MS system has been developed which allows on line removal of high molecular weight compounds from physiological fluid samples by Gel Filtration (GFC) prior to analysis by RP-HPLC/MS/MS. These high molecular weight compounds are often the major problem in LC/MS studies, since they can rapidly contaminate HPLC columns and MS inlet systems. This automated LC/LC/MS/MS system allows overnight unattended analysis of up to 96 physiological fluid samples for trace level drugs and metabolites. Samples are loaded onto a GFC column to remove all of the high MW impurities (>2kD), then the small molecules are trapped, concentrated and desalted online, prior to final analysis. In this study, two tripeptides (MW 341 and 425) were used to characterize this system, and final analysis was done by LC/UV, LC/ESI/MS and LC/ESI/MS/MS.

Figure 1

GFC of Plasma

500 ng Standard

100 ul Spike

100 ul Plasma

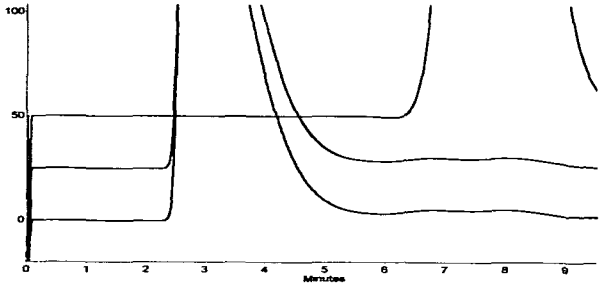

Although the automated GFC cleanup is not sufficient when using HPLC with UV detection, a mass spectrometer may be the ultimate detector for these rapid, automated pharmacokinetic assays. With a single quadrapole MS system, good sensitivity and selectivity can be obtained using the selected ion monitoring mode (SIM), where only the parent ions of the compounds of interest are monitored. With an instrument that has MS/MS capabilities (such as the TSQ 7000 Triple Quad and the LCQ Benchtop MS/MS systems used in this study), even greater sensitivity and selectivity can be achieved using the selected reaction monitoring mode (SRM).

Initial experiments run on the Michrom UMA Microbore HPLC / Finnigan TSQ 7000 Triple Quad MS/MS used a standard peptide column and mobile phase, but it was felt that the presence of TFA had an impact on the limit of detection. In the second set of runs using the Michrom UMA / Finnigan LCQ Benchtop MS/MS, a new column developed to allow good separation of peptides with acetic acid (HAc) in place of TFA was employed. Although the peptide peaks were slightly broader using HAc in place of TFA, the improvement in MS/MS sensitivity far outweighed the small loss of chromatographic resolution. The LCQ SRM runs allowed quantitation at the 0.5 ng/ml level, and the MS/MS spectra could be used at this level to positively identify the compounds of interest.

Figure 2 - LC/SRM of 100 ul Plasma Blank

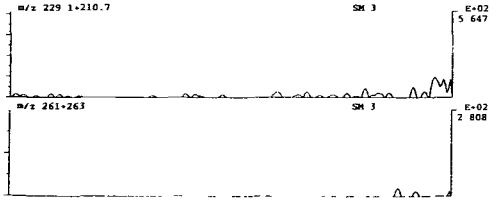

Figure 4 - MS/MS of P342

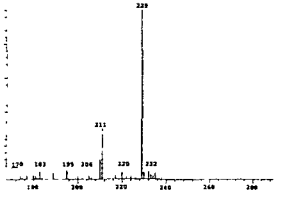

Figure 3 - LC/SRM of 100 ul Plasma + 50 pg Std

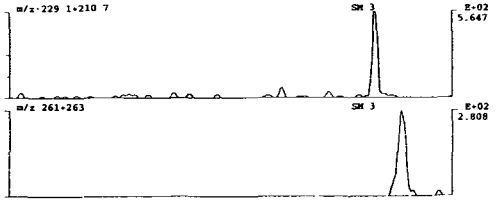

Figure 5 - MS/MS of P426

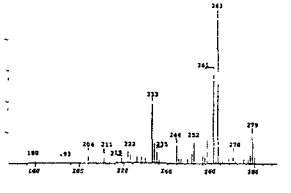

A Rapid Semi-automated Method for Quantitation of CGS 20286A in Rat Plasma Using Electrospray LC/MS/MS.

Michael J. Hayes, Jill C. Joshi, Steve F. Carlsen and Mark L. Powell, Ciba-Geigy Corp.,Pharmaceuticals Div., Research Dept., Summit NJ 07901

CGS 20286A ((+)-(5R)-4-(5,6,7,8-tetrahydroimidazo-(1,5-a) pyridin-5-yl) benzonitrile hydrochloride) is the (+) enantiomer of fadrozole. Fadrozole is a potent and highly selective non-steroidal aromatase inhibitor under investigation for treating estrogen-dependent diseases such as breast cancer, endometrial cancer, idiopathic oligospermia and endometriosis.
CGS 20286A is the pharmacologically inactive enantiomer of fadrozole and a method was needed to support a toxicokinetic study planned for the enantiomer in rats.

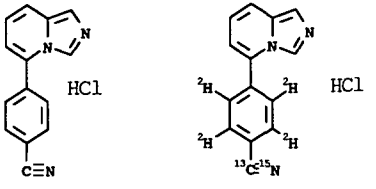

CGS 20286A **Internal standard**

Solid phase extraction was performed with a Gilson ASPEC XL sample processor The columns were 500 mg C8 extraction cartridges. One ml samples were applied to the columns, washed with 2 ml of 40% methanol in water and eluted with 2 ml of 80% methanol in water. A 10 ul aliquat of the eluent was taken for injection on the LC/MS/MS.

The instrumentation consisted of a Waters 590 pump with external mixing using a Lee TCMA 0120113 mixer. The column was an Inertsil 5 um ODS-2 column (150 x 2.0 mm). The mobile phase was 80% 0 05% acetic acid 20% acetonitrile at a flow rate of 0 25 ml/min. A CTC-200S Analytics autosampler with a 6-port Valco injection valve was used The mass spectrometer was a Finnigan TSQ 700, with the Finnigan electrospray source. Positive ion multiple reaction monitoring was utilized with argon collision gas at 2.5 mTorr and 35 eV energy. The parent ions were the $[M+H]^+$ ions at m/z 224 and 230 for the drug and internal standard respectively. Peak area measurement of both CGS 20286A and IS is done by monitoring the m/z 81 daughter ion. The scan time was 0.5 seconds and the capillary temperature was 200°C. The MS/MS fragmentation is shown in the diagram at right.

The calibration curve was from 5 to 10,000 ng/ml and the regression was log-log regression with y-correction ($Y = AX^B + C$) of peak area ratios. Standards were in duplicate at concentrations of 5, 10, 50, 200, 2000 and 10,000 ng/ml. Six replicate quality control samples were analyzed at concentrations of 5, 10, 200, and 10,000 ng/ml.

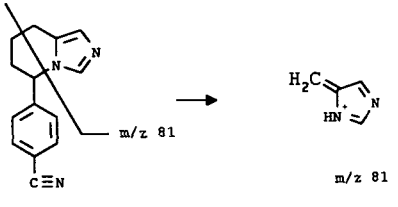

The method showed very high inherent sensitivity due to the high ionization efficiency of the compound. This is a result of the ease of protonating the imidazol nitrogen atoms and the resulting resonant stabilization of the daughter ion that is formed. The MS/MS spectrum is shown in Figure 2 The use of MS/MS provided very high selectivity eliminating interferences from the plasma matrix. Figure 2 shows a chromatogram of a 5 ng/ml rat plasma standard.

The method was applied to the analysis of rat plasma samples from a 13 week toxicokinetic study and provided rapid throughput with high accuracy and precision. The quality control samples showed a mean recovery of 95.2% with a CV of 8.5.

Figure 1

MS/MS Spectrum of CGS 20286A

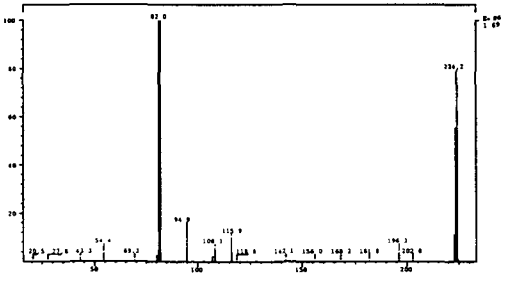

Figure 2

Chromatogram of 5 ng/ml Plasma Extract

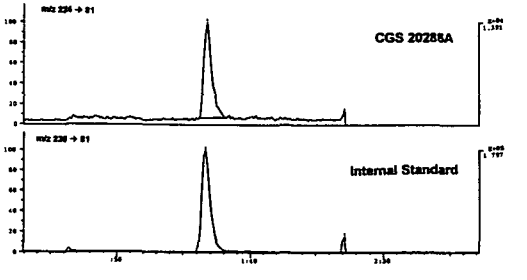

QUANTITATION OF CEFOXITIN IN TISSUES AND BIOLOGICAL FLUIDS BY NEGATIVE ION ELECTROSPRAY LC-MS

Jiri Zamecnik and Eugene Florio
Defence and Civil Institute of Environmental Medicine, North York, Ontario M3M 3B9, Canada

Sodium cefoxitin (3-[[(Amino carbonyl) oxy] methyl]-7-methoxy-8-oxo-7-[(2-thienylacetyl)amino]-5-thia-1-azabicyclo [4.2.0] oct-2-ene-2-carboxilic acid Sodium) is a semi-synthetic antibiotic from cephamycin C family, active against Gram-positive and Gram-negative bacteria. It is an important therapeutic agent because of its resistance to destruction by bacterial b-lactamase. It is commonly used for treatment of sepsis in Canadian Armed Forces. The high renal clearance limits the usefulness of this potent antibiotic. Our work involved studies of a liposome encapsulation of cefoxitin, to extend its 30-50 min. blood serum half life. For the study of pharmacokinetics and bioavailability we needed a sensitive and specific assay, which would allow us to look at the low concentration of this drug in small samples of various tissues, blood plasma and urine obtained from laboratory mice. The published methods deal with TLC, fluorometric assay and HPLC. None of these methods had the required sensitivity and specificity. We wish to report here a simple rugged quantitative assay of cefoxitin by HPLC with a mass spectral negative ion electrospray method of detection either using SIM or SRM. We have used cefuroxime as an internal standard. Cefoxitin and cefuroxime are structurally similar compounds.

Cefoxitin and cefuroxime were purchased from Sigma, St. Louis, MO. Fresh solutions were prepared from powdered drugs for every assay, since both antibiotics have a limited shelf life as aqueous solutions. Precautions were taken not to expose the solutions to strong light. Mouse blood plasma samples and aqueous tissue homogenates were extracted by a Bligh/Dyer method. Internal standard, cefuroxime (100 ng/10µL of saline) was added into 100 µL of plasma or tissue homogenates. Samples were then diluted with 210 µL of methanol, vortexed, 100 µL of chloroform was added, vortexed and spun for 5 min at 3000 rpm. Supernatant was diluted with 100 µL of chloroform, vortexed and again spun for 5 min. at 3000 rpm. The proportions of solvents is crucial for a proper phase separations. The organic layer was removed and water/methanol layer dried almost to completion under stream of N_2 at 40°C. Samples were dissolved in 100 µL of 1% formic acid, filtered using 4 mm, 0.47 mm Nylon syringe filters. Aliquots of the samples (10-20 µL) were injected onto LC-MS. The assay was done on Finnigan TSQ-700 equipped with Finnigan APCI/ESI LC-MS interface and Waters 600 HPLC with a WHISP autosampler. The HPLC conditions were as follows: 12.5 cm x 4.7 mm Whatman 5 mm PartiSphere C-18 reverse phase column fitted with a pre-column filter. Mobile phase methanol: 1% formic acid (40:60), flow rate 0.3 mL/min. The retention time of cefuroxime was 11 min. and cefoxitin 16 min. The mass spectrometer electrospray (ES) source spray set at 1500V gave a current around 1.5 mA. The capillary heater was set at 240°C, sheath gas N_2 pressure set at 40 psi. The skimmer pump pressure was 800 mtorr. The mass spectrometer was used in a negative ion mode, either :

- by scanning the first quadrupole sector from 422 amu to 427 amu in 5 sec. Areas under masses 423 m/z (cefuroxime) and 426 m/z (cefoxitin) were monitored.
- or by SRM, monitoring daughter ions 318 m/z and 336 m/z of cefuroxime parent 423 m/z and daughter 333 m/z of cefoxitin parent 426 m/z.

The manifold temperature was set to 80°C, the electron multiplier, equipped with 5 kV dynodes, was set at 1500V. The area ratios of cefoxitin / cefuroxime were plotted against a concentration of cefoxitin. The calibration curves were prepared by spiking 100 µL of blank mouse plasma with cefoxitin (0.01, 0.1, 1, 5, 10 µg/mL) and 100 ng of cefuroxime internal standard. The standards were processed identically to the samples. A least square fit was calculated using Excel spreadsheet resulting in a linear fit with a correlation coefficient greater than 0.999. Within assay coefficient of variation was <5% (n=10), between assay <10% (n=5).

Samples of mouse blood plasma, liver, spleen, kidney and lung were analyzed by this method. Positive ion electrospray yielded M^++1 ion and multiplicity of molecular ion+sodiums and molecular ion+potassiums adducts. The proportion of these adducts varied between assays and between samples within an assay. The attempts to stabilize these adducts were unsuccessful. The negative ion monitoring yielded mostly just ions of interest without any interference in SIM mode of operation. The selective ion monitoring (SRM) was not really necessary to obtain reliable results. The liposomal encapsulation of cefoxitin extended half-life of the drug several fold.

CEFOXITIN - daughters - Negative Ions

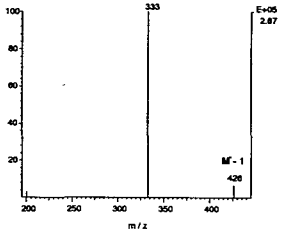

CEFUROXIME - daughters - Negative Ions

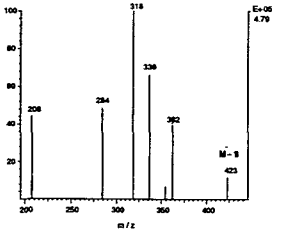

Cefoxitin - electrospray negative ion

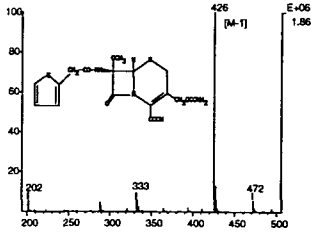

Cefuroxime - electrospray negative ion

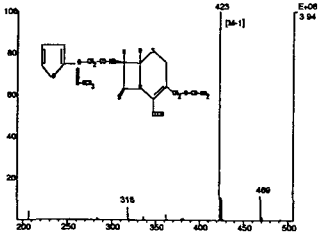

Detemination of Novel Thrombin Inhibitors in Animal Plasma by LC/API-MS.

Dineen J. White, John W. Russell and David Wang-Iverson
Bristol-Myers Squibb Pharmaceutical Research Institute
Princeton, New Jersey 08543-4500

The identification of a selective, orally active thrombin inhibitor with a long duration of activity has been an objective of the cardiovascular discovery program of the Bristol-Myers Squibb Pharmaceutical Research Institute. Preliminary pharmacokinetic data were required to evaluate first pass metabolism and oral absorption for a series of these compounds. The inhibitors in this series were administered to animals via three routes: oral, intravenous (iv) and intraportal (ipt, dogs only) or intraperitoneal (ip). Two of these inhibitors are presented in this work, BMS-184664, administered to rats, and BMS-185576, administered to dogs, rats and mice. Initial attempts to perform quantitative assays in plasma samples using HPLC with UV detection were unsuccessful due to insufficient sensitivity arising from the poor chromophore present in these analogs. LC/API-MS using pneumatically assisted electrospray as the interface was therefore selected for the analysis of these compounds. A sensitive, accurate and precise assay was developed for this series of thrombin inhibitors.

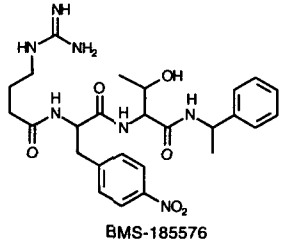

BMS-185576

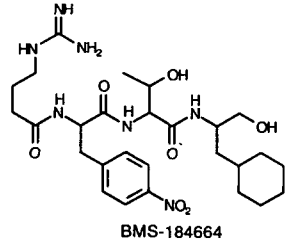

BMS-184664

METHOD

Plasma samples (0.1 mL) were de-proteinized with three volumes of acetonitrile containing internal standard. The sample was vortexed, centrifuged and the clear supernate transferred to glass vials and dried under N_2. The dried extracts were reconstituted in 50 µL of loading buffer. The injection volume was 10 µL. The LC/MS system consisted of a Hewlett Packard 1090 HPLC and a Sciex API I mass spectrometer. The HPLC column was a Keystone Hypersil ODS 2 mm x 50 mm, with 3 µM particles, maintained at 60°C and a flow rate of 0.3 mL/min. The flow was split 1/6 prior to the ionspray source. The mobile phase containing H_2O, MeOH and 10 mM NH_4OAc utilized a 4 minute linear gradient from 30% to 90% MeOH. $(M+H)^+$ ions for both compounds were monitored. The standard curve range was 7.8 to 1000 ng/ml. Quality control (QC) sample concentrations were 20, 400, 800, and 4000 ng/ml. The 4000 ng/mL QC was diluted 1/10 with blank matrix prior to extraction.

RESULTS

QC samples in rat, mouse and dog plasma, as appropriate, were assayed on each of three separate days (n=6 for each level, each day). Accuracy and precision data for both compounds showed total assay variabilities of less than 15% at all QC levels. Average

deviations from nominal concentrations were also less than 15%. Dose-normalized areas under the curve (AUC) of each drug after ip or ipt administration were compared to those after iv administration to obtain an estimate of the first pass elimination of the drug. In the case of BMS-185576 in dogs, the extent of first pass elimination was estimated to be 17%. Similarly, a comparison of the dose-normalized AUCs after oral administration to that after iv administration provided an estimate of the oral bioavailability. After oral administration, C_{max} (651 ng/ml) occurred by 1 hr and the oral bioavailability was estimated to be 6%. The ratio of oral bioavailability to the ip (or ipt) bioavailability yielded an estimate of the extent of absorption of the drug, which was determined to be 7% for BMS-185576. This assay proved applicable for bioanalysis of other analogs in the series. Such pharmacokinetic results provided information to the chemists, aiding their synthetic strategies, as to whether first pass elimination and/or incomplete gastrointestinal absorption was the reason for a drug's poor oral activity.

BMS-185576 Accuray and Precision in Dog Plasma

Concentration (ng/mL)	20.0	400	800	4000
grand mean (n=18)	16.9	392	788	3888
Δ%	-15.7	-2.12	-1.54	-2.80
interday %RSD	11 0	10.0	7.65	10.1
intraday %RSD	7.39	5 02	3.93	2.89
total %RSD	13.3	11.2	8.60	10.5

Plasma Concentration of BMS-185576 After Intravenous, Intraportal and Oral Administration to Beagle Dog

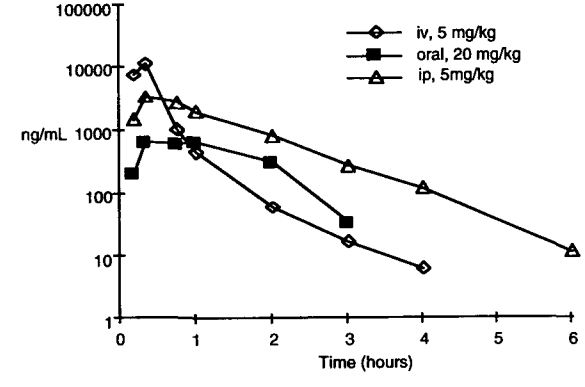

LC/MS/MS METHOD FOR THE DETERMINATION OF NICOTINE AND COTININE IN HUMAN PLASMA

Allan Xu*, Jim Havel, Mary Petersen, John Fiene, James Hulse
Harris Laboratories, Lincoln, NE 68501

Cigarette smoking is the leading cause of preventable disease and death in the United States today. Several nicotine containing products have been introduced for the facilitation of smoking cessation. The current methodology for monitoring nicotine and its metabolite, cotinine, concentrations in human plasmas includs EIA (Elisa test, RIA), HPLC, GC and GC/MS. The disadventages of the above methods are lack of specificity, long sample preparation time, interfences and relatively long retention time (low throughput).

The purpose of this study is to develop and validate an LC/MS/MS with high sensitivity, specificity and throughput to support the on going pharmacokinetics investigations.

An LC/MS/MS method was validated for the determination of nicotine and its metabolite, cotinine, in human plasma using nicotine-methyl-d3 and cotinine-methyl-d3 as internal standards. Compounds were extracted from alkalinized human heparinized plasma with methylene chloride. Dried extracts are reconstituted with a solution of ammonium acetate/ methanol/ acetaonitrile and analyzed on a Keystone BDS Hepersil C18 column with a PE Sciex API III Plus MS/MS detecter operatd with APCI interface.

Figure 1.
Full scan spectrum of nicotine (A) shows m/z 163.2 as protonated molecular ion (MH+). The product spectrum of nicotine (B) has a base peak at m/z 84. Q1 full scan spectrum of cotinine (C) shows m/z 177.2 as the base peak (MH+). The product ion spectrum of cotinine (D) has a base peak at m/z 98. The above prarmeters were used to establish multiple reaction monitoring (MRM) condition for quantitative analysis.

Figure 2.
a)Extracted blank plasma sample with ISTD. Notice trace amount of nicotine (100-200pg/mL) present in non-smoker.b)Extracted 1ng/mL nicotine standard. Limit of quantitation is 1ng/mL for this assay.c)Extracted subject sample, nicotine concentration is 10.2ng/mL.e)Extracted blank plasma sample with ISTD.e)Extracted 10ng/mL cotinine standard, limit of quantitation is 10ng/mL for this assay.f)Extracted subject sample, cotinine concentration is 113.4ng/mL.

An LC/MS/MS method with APCI interface was developed and validated for the quantitative determination nicotine and its metabolite, cotinine, in human plasma. This method was successfully applied to several pharmacokinetic studies with more than six thousand clinical samples. The instrument parameters were optimized to obtain 1.0 minute run time with baseline separation of nicotine from cotinine. The method was validated over a range 1ng/mL to 50ng/mL for nicotine and 10ng/mL to 500ng/mL for cotinine, using 1 mL of plasma. The between-run precision and accuracy of the calibration standards were 1.7 to 3.9% C.V and -4.6 to +4.0% ralative error (RE). The within-run precision and accuracy of QC's (2.5, 15, 37.5ng/mL) were 4.3 to 5.9% CV and -2.9 to +1.2% RE. Stability of nicotine and cotinine in human plasma and processed samples has been established. The method was found to be easy, rugged, and suitable for pharmacokinetic studies of nicotine formulations used to aid smoking cessation.

The major advantage of this method is very short run time compared to HPLC or GC methds. At 1 minute per sample, we were able to analyze 400 clinical samples within 8 hr. When operated continuosly, we were able analyze 1000 samples within 24 hr. With this rapid turn around time, the investigator will be able to make decisions much faster.

43rd ASMS Conference on Mass Spectrometry and Allied Topics

Fig.1.

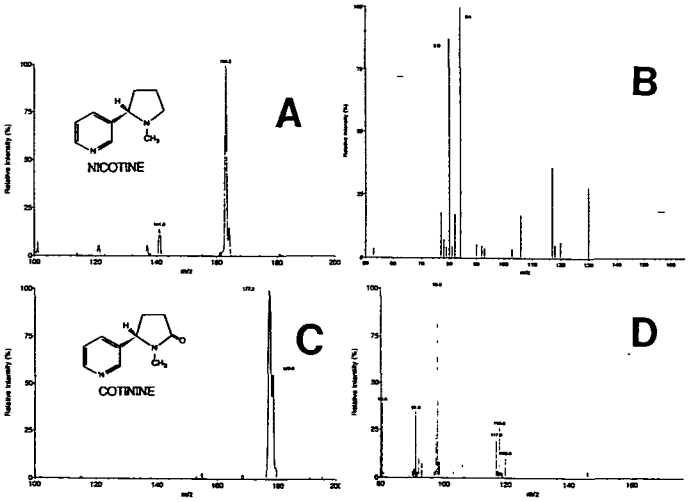

Fig.2.

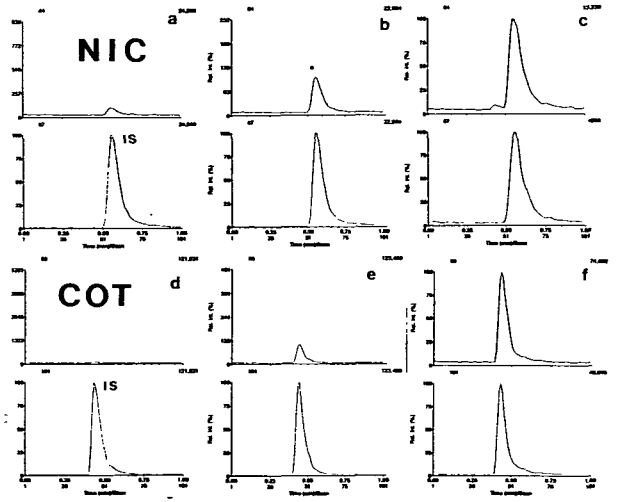

Tetracyclines in Honey and Animal Tissues by ESI MS and MS/MS

Neil S. Snider and Greg P. Malis
Agriculture and Agri-Food Canada
Laboratory Services Division, Central Experimental Farm
Ottawa, Ontario, K1A 0C6, Canada

Introduction

Tetracycline antibiotics such as tetracycline (TC), oxytetracycline (OTC) and chlortetracycline (CTC) are widely used in modern agriculture. Human health and food safety concerns dictate regulatory antibiotic residue analysis to a 0 1 ppm level These antibiotics are most commonly analyzed by HPLC with UV or fluorescence detection and have produced false positives[1] In comparison, LC/MS offers a significant advantage of a more specific determination. FAB/MS has been the only MS technique applied to samples for residue analysis. TLC and LC/FAB/MS have been used for animal tissues and honey at the 0.1 ppm level[2,3]. The goal of this work was to develop a selective and sensitive ESI MS method for the qualitative and quantitative determination of tetracyclines in honey and animal tissues.

Methods

ESI/MS was carried out on a Fisons VG Quattro triple quadrupole mass spectrometer equipped with an electrospray interface. The source was kept at a temperature of 125 C For MS/MS analysis a pressure of 2.2 X 10^{-4} torr and an energy of 20 eV was used in the collision cell.

HPLC was carried out using three Fisons Phoenix 20 syringe pumps. The HPLC column was a Phenomenex Prodigy C 8, 2.0 X 100 mm, with 5 micron particle size. Two solvent systems were investigated at flow rated ranging from 75 to 150 ul/min The first utilized 0.005 M trifluoroacetic acid (TFA), acetonitrile (ACN) and Methanol (MeOH) A gradient from 90 % 0 005 M TFA, 5 % ACN, 5 % MeOH to 20 % 0 005 M TFA, 40 % ACN, 40 % MeOH in 10 minutes eluted the tetracyclines in approximately 7 minutes. A second solvent system used 0 02 N oxalic acid (OX), ACN and MeOH The gradient holds 90 % 0.02 N OX, 5 % ACN, 5% MeOH for 5 minutes, changing to 20 % 0.02 N OX, 40 % ACN, 40 % MeOH by 15 minutes This elutes the tetracyclines in approximately 9 minutes.

Results and Discussion

Positive electrospray results in a strong M+H ion for each of the tetracyclines An increase in the focus voltage (F), the potential difference between the electrospray capilliary and the skimmer lens increased the fragmentation observed for each of the tetracyclines At a focus voltage of F=30 V virtually no fragmentation is observed, at a focus voltage of F=60 V the three tetracyclines exhibit similar fragmentation each showing $[M+H-NH_3]^+$ and $[M+H-NH_3-H_2O]^+$ Figure 1 shows the MS/MS spectrum of tetracycline.

The daughter ion spectra of the [M+H] parent ions exhibit the same fragmentation observed at the higher focus voltage. For MS/MS conditions were optimized to give approximately equal intensities of each daughter ion thus giving two confirmatory ions for tetracycline identification. To achieve maximum sensitivity only the transitions of interest were monitored through multiple reaction monitoring (MRM)

When monitoring spiked sample extracts of honey and beef muscle using just the [M+H] ions of each tetracycline it became evident that there were to many interferences for positive identification In contrast figure 2 shows an MS/MS analysis of a beef muscle extract spiked at 1.0 ppm with each of the tetracyclines Virtually all interferences are removed by monitoring the daughter ions

Figure 2 also shows the present limit of detection for this method at 1.0 ppm for beef samples (1 0 g/mL) and 0.2 ppm for honey samples (5 0 g/mL) The injection volume is only 5 ul corresponding to 5 ng of each tetracycline being injected.

Conclusion

By utilizing LC/ESI/MS a selective and sensitive method for the determination of tetracycline residues in honey and animal tissues has been established Limits of detection are 1 0 ppm in beef muscle and 0.2 ppm in honey.

Future

By experimenting with larger injection volumes and by concentrating the extracts it is hoped that the limit of detection can be lowered to 0.1 ppm in both honey and animal tissue matrices.

References

1 Oka H , Ikai Y , Hayakawa J , Harada K I , Masuda K., Suzuki M , Himei R , Horie M , Nakazawa H., Journal of the Food Hygenic Society of Japan, 34(6), 517-523, 1993
2 Oka H., Ikai Y , Hayakawa J , Harada K I., Masuda K , Suzuki M., Martz V , MacNeil J , Journal of Agriculture and Food Chemistry, 41(3), 410-415, 1993
3 Oka, H , Ikai Y., Hayakawa J., Harada, K.I., Asukabe H., Suzuki M., Himei R., Horie M., Nakazawa H , MacNeil J , Journal of Agriculture and Food Chemistry, 42(10), 2215-2219, 1994

Figure 1

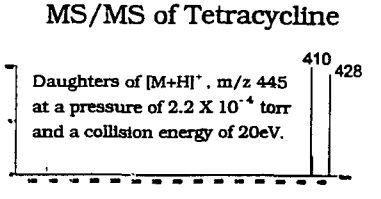

Figure 2

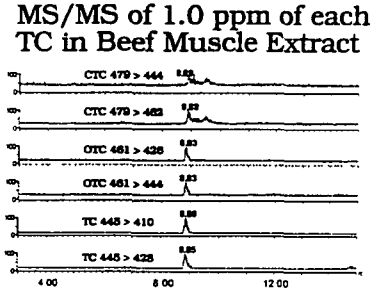

Determination of a 4-Azasteroid in Serum Using Negative Ion APCI LC/MS

Kathy A. Halm, Thomas L. Lloyd and M. Lee Moss, Drug Metabolism Department, Glaxo Wellcome, Inc., Five Moore Drive, Research Triangle Park, NC 27709

INTRODUCTION

We report a bioanalytical method for the determination of a GI198745, a 4-azasteroid in rat serum. GI198745 is among a class of 5-α reductase inhibitors under development for the treatment of benign prostatic hyperplasia (BPH). Inhibition of the 5-α reductase enzyme prevents the conversion of testosterone to dihydrotestosterone, thereby decreasing the growth of the prostate in the male. The HPLC/UV method did not provide adequate sensitivity for the low dose pre-clinical studies, and therefore a high sensitivity LC/MS method was developed on a Finnigan TSQ-700 mass spectrometer. The analytical range was validated from 0.5 to 500 ng/ml.

SAMPLE PREPARATION

The serum samples (200 microliters) were prepared using an automated method developed on a Zymark robot. The internal standard (GI200402, a structural analogue) was dissolved in acetonitrile and added to the samples for protein precipitation. The automated sample preparation time was 10 minutes per sample. Samples were reconstituted manually and transferred to microvial inserts for LC/MS analysis.

LC/MS ANALYSIS

The atmospheric pressure chemical ionization (APCI) source which accommodated conventional HPLC flow rates (1mL/minute) was used for the LC/MS analysis. Negative ion APCI MS provided high specificity and therefore selected ion monitoring (SIM), which showed greater sensitivity over selected reaction monitoring (SRM), could be used for detection. The mobile phase consisted of 40:60 (v/v) deionized water : acetonitrile. The separation was performed using a 4.6x50 mm BDS Hypersil C_{18} (3micron) column which reduced the analysis time while providing excellent resolution of GI198745 from the majority of endogenous serum components. Flow switching with a 6-port Valco switching valve minimized contamination of the APCI source. The retention times for GI198745 (m/z 527) and internal standard (m/z 543) were 2.9 and 4.7 minutes, respectively. The LC/MS analysis time was 6 minutes per sample.

RESULTS

Analytical method validation criteria were met for linearity, accuracy and precision. The intra-run precision of the quality control samples (1.5, 75, 360 ng/ml) ranged from 2.3 - 3.2% and accuracy was greater than 97%. The inter-run precision ranged from 3.0 - 6.8% and accuracy was greater than 98%. The extraction efficiency of the 4-azasteroid averaged 86.3% over the concentration range. The LC/MS method was cross-validated for serum from other species (mouse, dog, rabbit, marmoset and human).

SIM Chromatograms of GI198745 (LOQ, 0.5 ng/ml) and Internal Standard

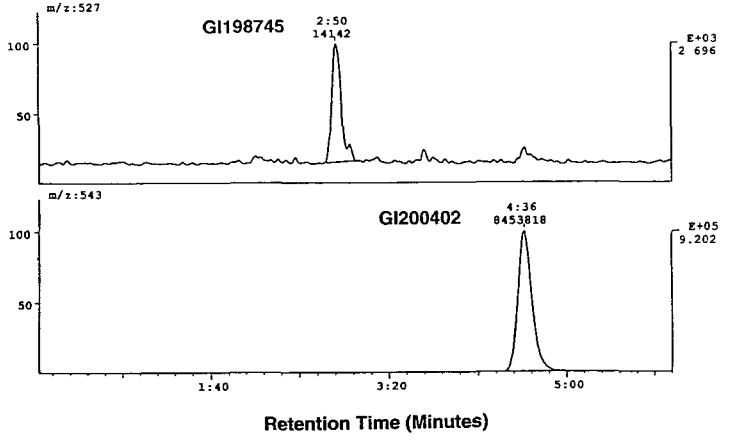

CONCLUSIONS

The LC/MS method provided sensitivity, specificity and rugged, high sample throughput in support of pre-clinical studies over the range of 0.5 to 500 ng/ml extracted from 200 microliters of serum. The maximum number of samples analyzed by the LC/MS method in a single run was 117 samples over a period of 14 hours.

DETERMINATION OF 311C90, A 5-HT RECEPTOR AGONIST FOR THE TREATMENT OF MIGRAINE, IN HUMAN PLASMA BY LC-MS-MS.

I. J. FRASER, A.E. JONES, J.A. ALLANSON and S. PLEASANCE
GLAXO-WELLCOME, Group Development Operations, Department of Bioanalysis and Drug Metabolism, Beckenham, Kent, BR3 3BS, U.K.

Migraine, characterized by a throbbing headache which is usually unilateral and often associated with nausea, vomiting, photophobia and phonophobia, is a debilitating and recurrent disease affecting approximately 9-16% of the western population.

The neurotransmitter and vasoactive monoamine, 5-hydroxytryptamine (5-HT), that is widely distributed within both the CNS and the periphery, has been identified as having a central role in the pathophysiology of migraine [1], although its precise pathogenic role remains undefined. The novel compound 311C90 [(S)-4-[(3-(2-dimethylaminoethyl)-1H- indol-5-yl) methyl]-2-oxazolidinone] is an analogue of 5-HT displaying potent, selective agonist actions at the 5-HT$_{1D}$ receptor subtypes. The combination of high potency and an ability to act at central as well as peripheral elements of the trigemino-vascular system may offer a superior anti-migraine profile.

An HPLC method has been developed for the determination of 311C90 and its metabolites in human plasma to support early clinical development. The method employs automated solid-phase extraction (ASPEC) of plasma followed by HPLC using a TMS column (250 x 4.6 mm, Zorbax) and fluorescence (FLD) detection with excitation and emission wavelengths at 290 and 350 nm, respectively. The HPLC-FLD method provides a lower limit of quantitiation (LLOQ) for 311C90 and its metabolites of 2 ng/ml, sufficient to provide plasma concentration profiles for oral doses of 311C90 of 5 mg. Recent clinical studies have employed doses below 5 mg and consequently a more sensitive liquid chromatography tandem mass spectrometry (LC-MS-MS) based method using atmospheric pressure ionisation has been developed.

Both 311C90 and its desmethyl metabolite generate abundant protonated molecules under positive ion atmospheric pressure chemical ionisation (APCI) which subsequently give intense product ions during tandem mass spectrometry (see Figure) suitable for selected reaction monitoring (SRM). The increased selectivity and sensitivity offered by LC-MS-MS enables higher sample throughput since both the sample preparation time and the run time can be significantly reduced. The solid-phase extraction procedure used in the HPLC-FLD method was modified and a portion of the extract (20µL) is injected directly onto an SCX column (30 x 4.6 mm). A mobile phase of 30% 25mM ammonium formate (pH 5) 70% acetonitrile (v/v) at 1 mL/min resulted in an analysis time of approximately 4 minutes. Using a deuterated internal standard the LC-MS-MS method provides a LLOQ of 200 pg/mL with excellent precision and accuracy. In order to cross validate the LC-MS-MS method against the HPLC-FLD, quality control samples and plasma samples from clinical studies were analysed by both methods. A comparison of the data (see Figure) revealed the two method provided equivalent results across the overlapping ranges of quantitation. More recently the increased selectivity of the LC-MS-MS method has been successfully employed to support clinical interaction studies.

[1] J.W. Lance, 5-Hydroxytryptamine and its role in migraine, *Eur. Neurol.* 31,279-281 (1991).

43rd ASMS Conference on Mass Spectrometry and Allied Topics

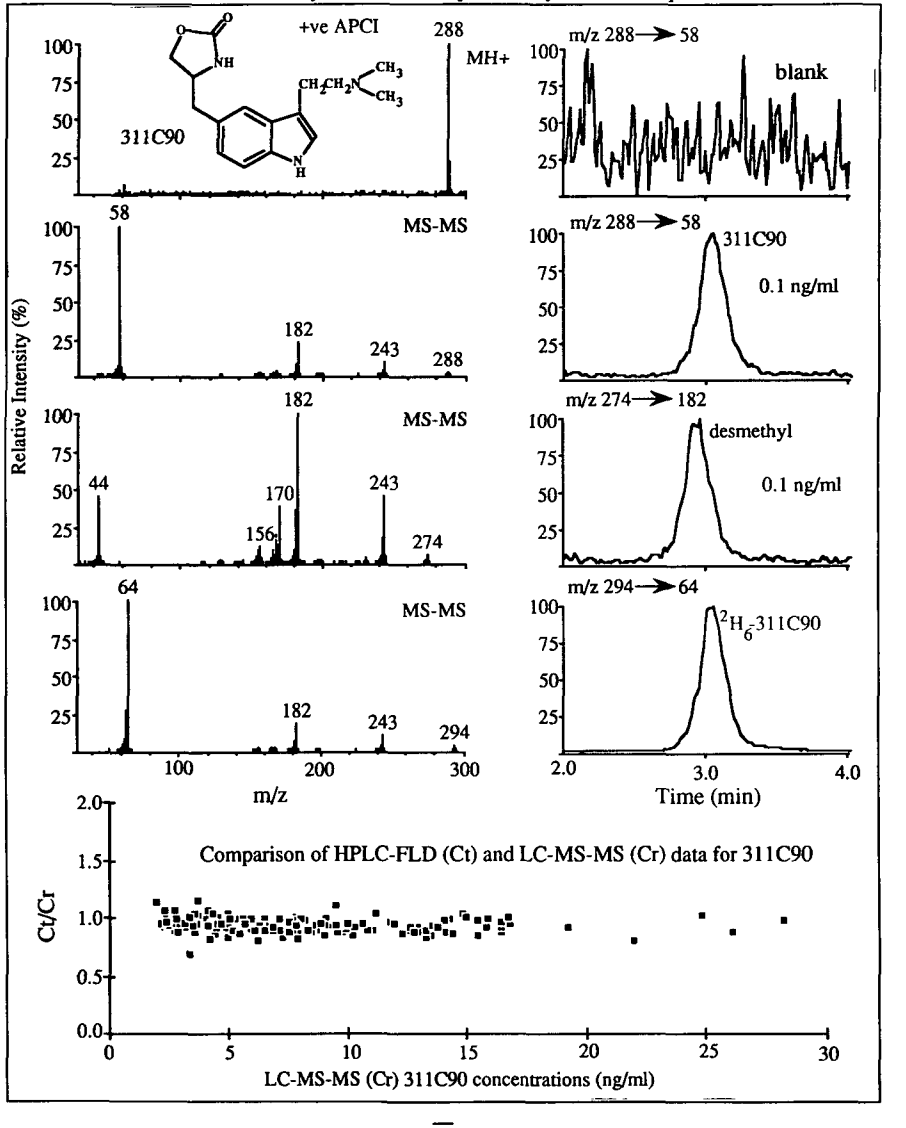

Quantitative Analysis of Tirilazad Mesylate (FREEDOX™) in Rat and Dog Plasma by Liquid Chromatography Atmospheric Pressure Chemical Ionization Tandem Mass Spectrometry.

Michael J. Hauer, Theresa A. Moore, Rick C. Steenwyk, Paul A. Bombardt, and Paul G Pearson.
Drug Metabolism Research, The Upjohn Company, Kalamazoo, Michigan

Tirilazad mesylate (FREEDOX™) is the first in a series of novel compounds that have been demonstrated to be potent inhibitors of membrane lipid peroxidation *in vitro*. Tirilazad has demonstrated efficacy in animal models for the prevention of neuronal damage due to head trauma, subarachnoid hemorrhage, spinal cord injury and ischemic stroke. As a consequence, tirilazad mesylate has the potential to improve the clinical prognosis in conditions where lipid peroxidation occurs secondary to traumatic tissue injury. A highly selective and sensitive atmospheric pressure chemical ionization tandem mass spectrometry (APCI-MS/MS) method for the quantitation of tirilazad in rat and dog plasma has been developed and validated. Mass spectrometric analysis was performed on a Finnigan-MAT TSQ 700 triple quadrupole mass spectrometer equipped with a Finnigan APCI source. The protonated molecular ion of tirilazad at m/z 625 underwent collisionally activated dissociation to afford a product ion at m/z 260 In a similar manner, the protonated molecular ion of [$^{13}C_3$,$^{15}N_2$]tirilazad (IS) at m/z 630 afforded a product ion at m/z 265. Selected reaction monitoring of the these transitions were used for quantitation. The method was refined to include an automated column switching device to eliminate carry-over of residual analyte following injection of high concentration samples Installation of a second HPLC pump and a custom valve switching device permitted the autosampler to be switched off-line during the analytical run. During this time, blank plasma samples were injected by the autosampler to facilitate elimination of residual analyte from the HPLC system; mobile phase flow to the analytical HPLC column was supplied by the second HPLC pump at the time of column bypass. Analytical separations were performed on a Kromasil 100-5C18 column (15 cm x 4 6 mm, 5 µm) using a mobile phase consisting of methanol:isopropanol:1 M ammonium acetate pH 4.5 (90:5.5) at a flow rate of 1 0 mL/min Under these conditions the retention time of the analyte and internal standard was 3.2 minutes. Aliquots (100 µl) of unknown plasma samples, standards of tirilazad in plasma (0.5 to 10000 ng/mL), and plasma controls (16 to 8000 ng/mL) were prepared for APCI-MS/MS analysis by precipitation of protein with acetonitrile containing IS. Unknown plasma samples were quantitated from the peak height ratio of the analyte to the internal standard using a weighted linear regression model. The limit of quantitation (LOQ) of tirilazad mesylate was approximately 0 5 ng/mL and the upper limit of quantitation (ULOQ) of tirilazad mesylate was approximately 10000 ng/mL

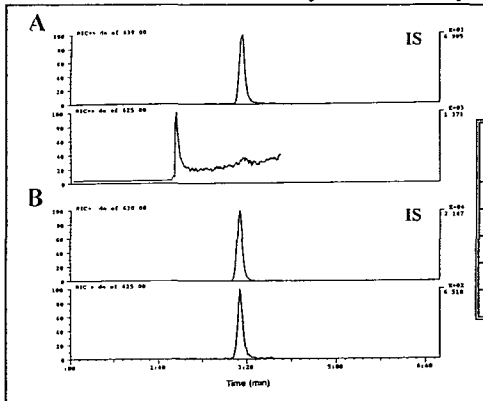

Figure 1
Representative chromatograms from multiple reaction monitoring of tirilazad mesylate and ^{13}C ^{15}N pyrimidine labelled tirilazad mesylate (IS), from dog plasma samples containing: (A) Blank plasma (B) 0.5 ng/mL standard (C). Tirilazad mesylate eluted at approximately 3.2 mins, allowing for analysis of over 100 samples in a single analytical run.

Table 1
Summary of Controls

Comparison Conc. (ng/mL)	N	Mean Conc. (ng/mL)	% Recovery
15.7	6	15.0	96
58.9	6	57.3	97.2
588.7	6	639	109
2356	6	2330	99
7849	6	8020	102.2

Assay Linearity and Dynamic Range

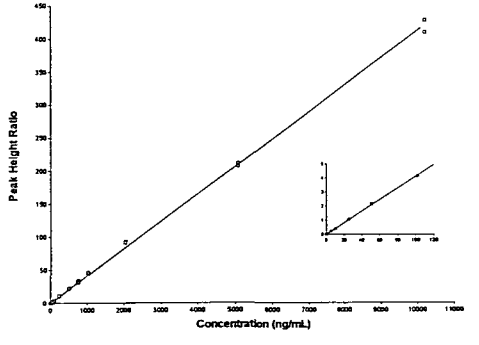

Table 2
Summary of Regression Parameters

Regression Parameter*	N	Mean	S.D.	C.V. (%)
Linear	4	1.104	0.006	0.6
Linear C.V.	4	0.74	0.8	
r	4	0.99928	0.0023	

*Model y=m(1/x) + B

GC/MS AND LC/MS CONFIRMATION OF MALACHITE GREEN IN CATFISH

Sherri B. Turnipseed, José E. Roybal, Jeffrey A. Hurlbut, Austin R. Long
Animal Drugs Research Center, FDA, P.O. Box 25087, Denver, CO 80225-0087

Malachite green (MG) is a triphenylmethane dye used in aquaculture as a topical antiseptic to prevent fungal infections. Studies have indicated that these compounds can be carcinogenic and teratogenic, which makes monitoring of dye residues in some food products crucial. Determinative methods have been developed to quantitate the amount of MG and leucomalachite green (LMG), a reduced metabolite of MG, residues in fish tissue [1]. For complete analytical detection, mass spectral confirmatory methods are critical for the unambiguous identification of suspect residues found in the sample.

Confirmation of dye residue can be accomplished using particle beam LC/MS or GC/MS methods. The EI spectrum for LMG, obtained with the particle beam interface is shown (Fig 1). The most abundant fragment ions consist of m/z 330$[M]^+$;329 $[M-H]^+$; 253 $[M-Ph]^+$;210 $[M-C_6H_4N(CH_3)_2H]^+$; 165 M^{++}. The mass spectrum of MG is very similar with reduction of the cationic dye in the mass spectrometer leading to a large abundance for the ion corresponding to MH^+. An advantage of the LC/MS method is that the chromic and reduced forms of the dye can be confirmed simultaneously. However, the detection limits for the drugs in tissue are 20 ppb or higher and the relative abundances of the ions in the chromic dye vary due to reactions occurring in the mass spectrometer source. For catfish fortified at the 20 ppb level and incurred tissues (live catfish exposed to bath containing 1.0 µg MG/g water for 1 hr) after 24 depuration time, the LMG ion abundances(m/z 330, 329, 253, 210) are within 10% of that observed in the standard. For MG, however, the abundances vary more, 10-15% as compared to a standard. The ion at m/z 165 was also monitored as additional evidence for the drugs, but the relative abundance of this ion was not consistent.

Using GC/MS only the leuco form can be confirmed. However, this appears to be the marker residue for malachite green in catfish. The GC/MS method has been determined to be very sensitive (5 ppb) selective and rugged. The extracts from the HPLC/VIS determinative method [1] can be used with additional cleanup to isolate the leuco metabolite. The criteria for confirmation as described by Sphon [2] is met for LMG in all fortified and incurred tissue analyzed by GC/MS. Specifically, the retention time for LMG does not vary by more than 0.02 min (<1%) from that of LMG standard chromatographed the same day. In addition, the relative abundance of the five ions monitored varies by less than ±10% as compared to the same ratios calculated for a standard extract. Ion chromatograms for LMG in incurred catfish tissue (catfish exposed to bath containing 20 ng MG/g water for 1 hr, 24 depuration time) are shown in Figure 2. Validation of the GC/MS method was performed using fortified tissue and with several sets of incurred tissue with LMG concentration ranging from approximately 8 to 80 ng/g tissue.

(1) J.E. Roybal, A.P. Pfenning, R.K.Munns, D.C. Holland, J.A. Hurlbut & A.R. Long, *J. AOAC Int.*, 78 (1995) 453.

(2) Sphon, J.A., *J. Assoc. Off. Anal. Chem.*, 61 (1978)1247.

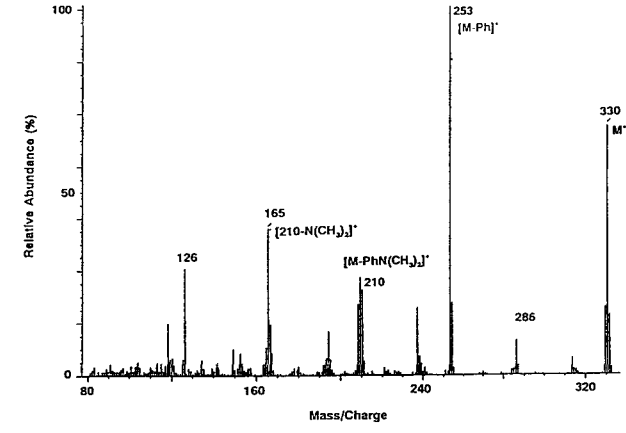

Figure (1). EI mass spectrum of LMG obtained by particle beam LC/MS.

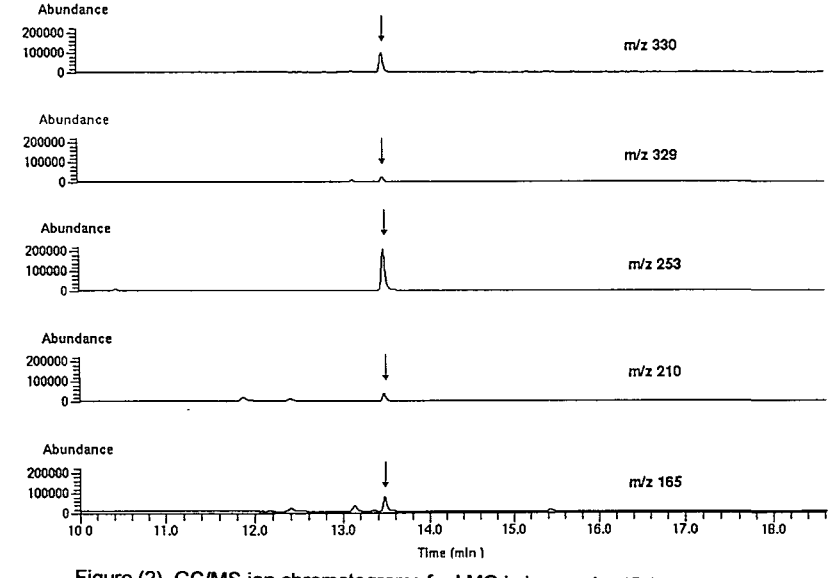

Figure (2). GC/MS ion chromatograms for LMG in incurred catfish tissue.

ESI-MS ANALYSIS OF BIOACTIVE ISOLEUKOTRIENES

Kathleen A. Harrison and Robert C. Murphy
National Jewish Center for Immunology and Respiratory Medicine
1400 Jackson Street
Denver, CO 80206

INTRODUCTION

Free radical oxidation of glycerophospholipids is now recognized to yield a series of complex products including isoprostanes which have biological activity when hydrolyzed to the free carboxylic acid (1,2). The mechanism of formation of these doubly oxygenated products of arachidonic acid would suggest that other complex structures could also result, including compounds isomeric to another class of arachidonic acid metabolite having biological activity, namely the leukotrienes. Leukotrienes are formed by enzymatic oxidation of arachidonic acid by 5-lipoxygenase leading to formation of conjugated trienes including the 5,12-dihydroxyeicosatetraenoic acids such as LTB_4 (3). We have investigated the free radical oxidation of 1-hexadecanoyl-2-arachidonoyl-glycerophosphocholine using Fenton reaction conditions (4) to generate hydroxyl radical.

RESULTS

Oxidation of the precursor glycerophosphocholine containing arachidonic acid at the *sn*-2 resulted in a complex mixture of products, some of which absorbed ultraviolet light characteristic of conjugated trienes. These were detected by HPLC separation of the reaction products as shown in Figure 1A. The UV spectrum of one component in this complex mixture is shown in Figure 1B suggesting the presence of a conjugated triene as a structural feature of this metabolite. Electrospray ionization mass spectrometry of this HPLC fraction as well as fractions 46 and 47 resulted in abundant ion at 798.6, which upon collisional activation yielded the carboxylate anions at *m/z* 255 (hexadecanoic acid) and *m/z* 335 (arachidonic acid) plus two oxygen atoms (data not shown).

Following saponification of these glycerophospholipid metabolites, UV absorbing components were isolated by reverse phase HPLC which had the characteristic UV absorption maximum at 270 nm. Furthermore, testing of this biological extract using human neutrophils loaded with the fluorescent dye Indo-1 revealed each component to cause an increase in intracellular free calcium. This increase was blocked by a receptor antagonist to leukotriene B_4 suggesting this biological activity was mediated through the LTB_4 receptor.

Structural identification of the conjugated triene metabolites was carried out using ESI/MS/MS of *m/z* 335. Figure 2 and 3 show the CID spectra of the major triene metabolites in HPLC fractions 46 and 47 revealing formation of *m/z* 195 from *m/z* 335 characteristic of 5,12-dihydroxyeicosatetraenoic acids (5). Electron ionization mass spectrometry of the catalytically reduced, trimethylsilylated PFB esters produced major ions corresponding to α-cleavage adjacent to the hydroxyl groups at m/z 555, 215, 369, and 401 revealed both of these reduced metabolites to be 5,12-dihydroxyeicosanoic acids. Since a conjugated triene could only exist between the 5 and 12 positions and the additional double bond has been assigned at the 14-15 position as in the original arachidonic acid, these metabolites were identified as 5,12-dihydroxy-6,8,10-eicosatetraenoic acids. These two metabolites (Figures 2 and 3) as well as several other metabolites were found to have biological activity. These molecules are formed as intact phospholipids and represent a novel class of free radical products of lipid peroxidation.

ACKNOWLEDGEMENT - This work was supported by a grant from the National Institutes of Health (HL34303).

REFERENCES

1. Morrow, J. D., Minton, T. A., Mukundan, C. R., Campbell, M. D., Zackert, W. E., Daniel, V. C., Badr, K. F., Blair, I. A., and Roberts, L. J., II (1994) *J. Biol. Chem.* **269**, 4317-4326.
2. Morrow, J. D., Minton, T. A., and Roberts, L. J.,II (1992) *Prostaglandins* **44**, 155-163.
3. Samuelsson, B. and Funk, C.D. (1989) *J. Biol. Chem.* **264**, 19469-19472.
4. Halliwell, B. and Gutteridge, J. M. (1984) *Biochem. J.* **219**, 1-14.
5. Wheelan, P. and Murphy, R. C. (1995) Proc. 43rd Ann. Conf. Mass Spectrom. This volume.

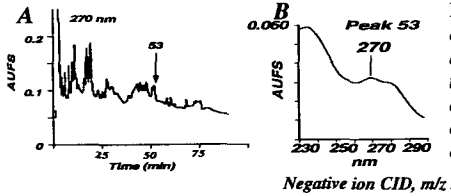

Figure 1 *(A) HPLC separation of free radical oxidation products of 1-hexadecanoyl-2-arachidonoyl-GPC. (B) Fractions eluting from the HPLC between 40-55 min had UV absorption spectra characteristic of a conjugated triene as seen for the components eluting at 53 min (Peak 53).*

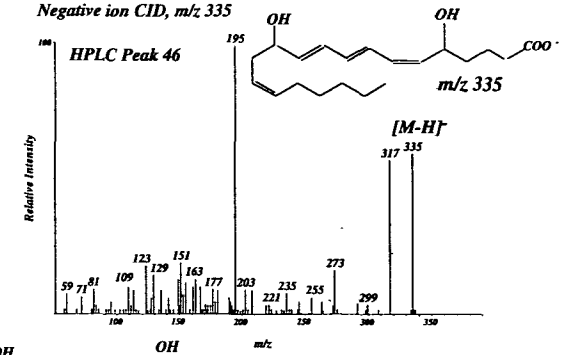

Figure 2 *ESI/MS/MS of m/z 335 from the major conjugated triene component isolated from HPLC fraction 46 following saponification.*

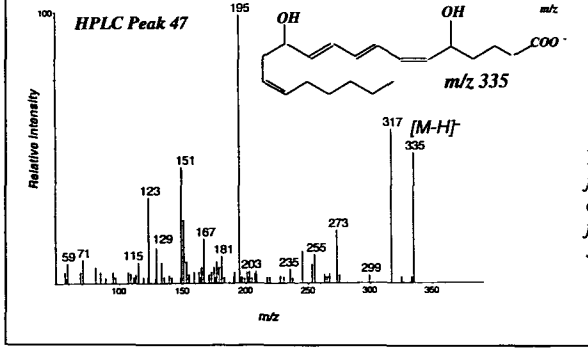

Figure 3 *ESI/MS/MS of m/z 335 from the major conjugated triene component isolated from HPLC fraction 47 following saponification.*

LC-ESI-MS/MS OF POLYAMINES AND BASIC AMINO ACIDS.

Gottfried J. Feistner
Beckman Research Institute of the City of Hope, Duarte, California 91010

Recently, my interest in the biosynthesis of proferrioxamines prompted me to develop a method for the comprehensive profiling of basic amino acids and polyamines in microbial culture supernatants [1]. The method takes advantage of the complementary characteristics of dansylation and capillary reversed-phase chromatography - electrospray mass spectrometry (cLC-ESI-MS), and is characterized by convenience (no sample work-up required), good sensitivity and chromatographic resolution, and low solvent consumption. However, closely eluting isobaric compounds needed to be distinguished by co-chromatography. It was thus of interest to explore whether the specificity of the method could be improved by extending it to cLC-ESI-MS/MS. Without derivatization, the target compounds give rise to characteristic product ion spectra but are not amenable to RP-LC [1]. Whether the dansyl derivatives would give useful MS/MS spectra, was far from clear, since under EI conditions, the dansyl derivatives of biogenic amines have been reported to predominantly, and sometimes exclusively, give rise to dansyl group-related fragment ions [2], which are useless for structural characterization. This study therefore was initiated to explore whether the targeted dansyl derivatives give useful product ion spectra under LC-ESI-MS/MS conditions, whether isobaric derivatives can be distinguished in this way, and whether general fragmentation mechanisms can be deduced that may allow identification of related compounds in the absence of authentic reference compounds.

Figs. 1-3 show the product ion spectra of three pairs of isobaric compounds, namely Dns_2-diaminobutyric acid and Dns_2-2-hydroxycadaverine, Dns-acetylputrescine and Dns-agmatine, and didansyl N^1- and N^8-acetylspermidine, respectively. Clearly, the product ion spectra of these dansyl derivatives are structurally informative and readily allow to distinguish isobaric compounds. For example, $[M+H-H_2O]^+$ ions, which reportedly can be abundant for free basic amino acids under CI conditions [3], are not seen under ESI-MS/MS conditions (compare Fig. 1a), but are quite abundant for hydroxy derivatives (see Fig. 1b) Likewise, $[M+H-NH_3]^+$ ions appear to be characteristic for those target compounds that contain guanidino or urea moieties, obviously due to the fact that these groups are not amenable to dansylation (compare Fig. 2b). The two acetylspermidines, which are very difficult to distinguish chromatographically, fortunately also give sets of characteristic fragment ions; most notably a strong *m/z* 100 ion for N^1-acetylspermidine, which in all likelihood arises from the acetylaminopropyl moiety.

Establishing the entire fragmentation pathways in an unambiguous manner requires accurate product ion mass measurements, multistage tandem mass spectrometric analyses, and/or appropriate isotope-labeling experiments. Such rigorous analyses in turn require sophisticated instrumentation, such as four-sector or FT-ICR mass spectrometers, and/or considerable synthetic efforts, and could not yet be performed. Nevertheless, low-resolution tandem mass spectrometric analyses of a larger number of homologous or otherwise related amino acids and polyamines allowed to deduce rational fragmentation pathways. This in turn led to the identification of three unknown compounds in microbial culture supernatants as citrulline, acetylpropane, and diacetylspermine [4]. The identifications are, in part, based on the facts that Dns-acetylpropane and Dn_2-diacetylspermine both give rise to the characteristic *m/z* 100 ion, and that citrulline looses NH_3 from the molecular ion. Also, the MS/MS spectrum of suspected citrulline closely matched that of authentic citrulline.

[1] Feistner GJ *Biol. Mass Spectrom.* **23**, 784 (1994); [2] Addeo F et al. *Anal. Biochem.* **64**, 98 (1975); Walther H et al. *Biomed. Environm. Mass Spectrom.* **14**, 229 (1987); [3] Leclerq PA & Desiderio DM *Org. Mass Spectrom.* **7**, 515 (1973); [4] Feistner GJ *Biol. Mass Spectrom.* **23**, 793 (1994).

43rd ASMS Conference on Mass Spectrometry and Allied Topics

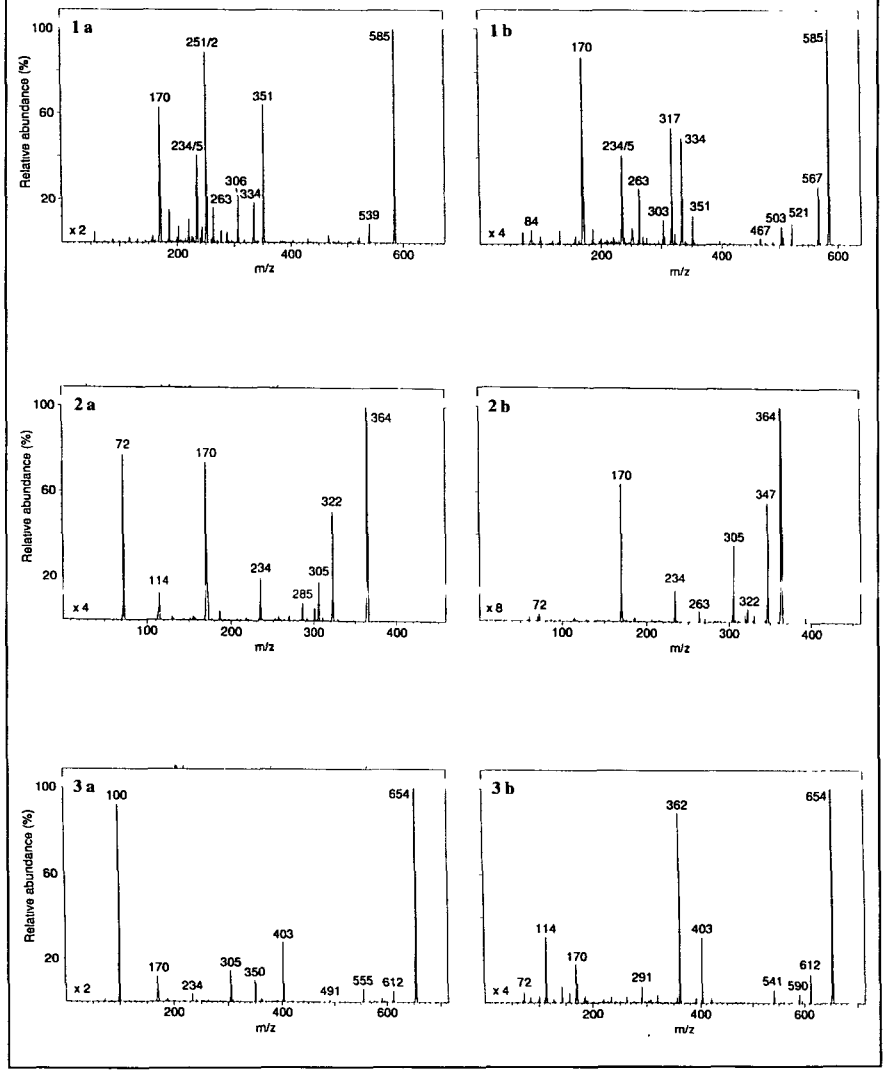

LC/LC/MS/MS ANALYSIS OF HUMAN PLASMA FOR A "STICKY" PEPTIDE

Lily Y.T. Li[1], Jamie Zhao[1], Jack Henion[1], and Mike Newman[2]
[1]Advanced BioAnalytical Services, Inc., 15 Catherwood Rd., Ithaca, NY 14850
[2]Cortech Inc., 6850 North Broadway, Denver, Colorado 80221

INTRODUCTION

CP-0127 is a new potential drug for treatment of traumatic shock. CP-0127 (MW = 2805 Da) is a dimeric peptide with 6 arginines. ^{13}C-CP-0127 is used as an internal standard by replacing the $^{12}C_6$ ring of L-Phe, the $^{12}C_1$ of Leu, and the $^{12}C_1$ of Gly with ^{13}C to give a 16 Da increase in molecular weight. HPLC-UV and SIM LC/MS techniques are not selective or sensitive enough for quantifying CP-0127 in human plasma. The "stickiness" of this peptide causes considerable problems (e.g., poor recovery from a solid-phase extraction and carryover from a previous injection). Using solid-phase extraction followed by LC/MS/MS, an LOQ of 10 ng/mL can be achieved. The technique of LC/LC/MS/MS improves sensitivity to give an LOQ of 2 ng/mL in plasma. A series of subsequent HPLC solvent rinsing methods following an analytical HPLC method solved the carryover problem.

EXPERIMENTAL

Sample preparation involves protein precipitation with acetonitrile/ethanol followed by centrifugation, concentration to dryness by freeze-drying, and reconstitution in 0.1% TFA. These samples are then analyzed by column switching techniques which use three different column technologies. The first column is a Michrom BioResources protein removal cartridge (3 x 10 mm), the second column is a PerSeptive ID AD Sensor cartridge (2.1 x 30 mm) and the third analytical column is a Keystone Asahipak ODP C18 (2 x 50 mm). The total effluent from this column is directed to an ion spray LC/MS interface with TurboIonSpray-assistance to improve spray solvent volatilization. The PE Sciex API III ^{plus} tandem triple quadrupole mass spectrometer was operated in the selected reaction monitoring (SRM) mode.

RESULTS AND DISCUSSION

The protonated triply charged CP-0127 and ^{13}C-CP-0127 were monitored as precursor ions while corresponding structurally informative product ions were also monitored. From our earlier solid-phase extraction (SPE)-LC/MS/MS results (Figure 1), a limit of quantitation was determined at the 10 ng/ml level due to its "stickiness" resulting in poor recovery by SPE. After acetonitrile/ethanol protein precipitation followed by LC/LC/MS/MS, sensitivity was increased five-fold (Figure 1). On-line sample preparation eliminates sample loss that appears to occur with the solid-phase extraction. The "sticky" nature of this peptide also causes an HPLC injector carryover problem. Following a series of subsequent HPLC solvent rinsing methods, carryover was effectively reduced to less than 1% (33 counts, Figure 2) after a 400 ng/mL plasma standard (upper limit of quantitation) was injected (6308 counts, Figure 2). The technique of LC/LC/MS/MS provides not only the required selectivity but also improved sensitivity over the SPE-LC/MS/MS method.

43rd ASMS Conference on Mass Spectrometry and Allied Topics

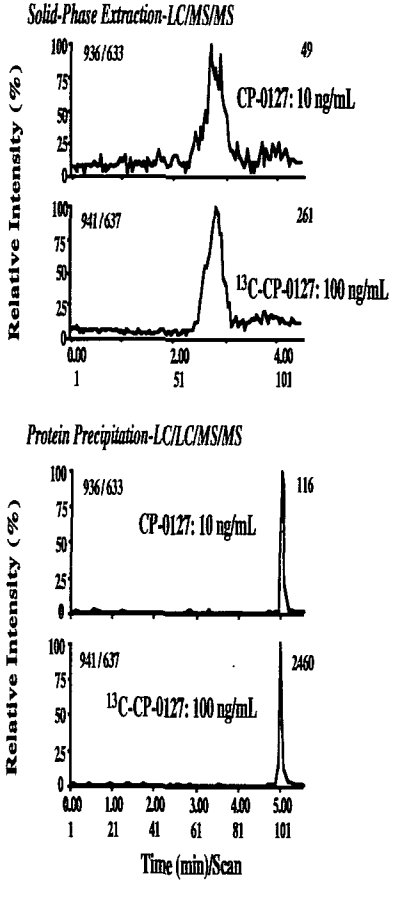

Figure 1. Comparison of Chromatograms Between LC/MS/MS and LC/LC/MS/MS

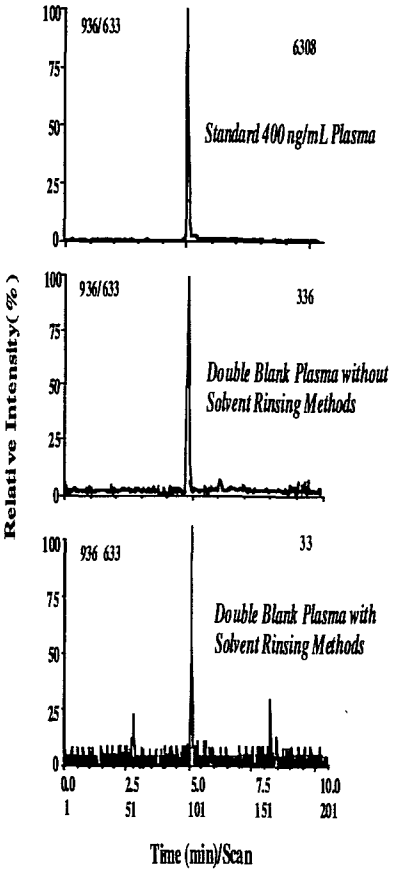

Figure 2. A Comparison of Carryover with and without Solvent Rinsing Methods

DETECTION OF ENDOGENOUS NITRIC OXIDE GAS FROM LIVING ANIMALS BY MASS SPECTROMETRY

DELACOTTE J.M., FAYE T., *REGERT M., ROLANDO C. and SABLIER M.

Ecole Normale Supérieure, Dpt Chimie, CNRS-URA 1679, 24 rue Lhomond, 75231 Paris, FRANCE

Nitric oxide (NO) is an important mammalian intercellular messenger [1]. At present, the determination of NO gas solubilized in the effluents from tissues of a living animal, collected with a microdialysis probe would be of great interest.

Thus, pharmacologists are waiting for new methods for measuring NO that have at least three essential properties :

-A great sensitivity (to detect quantities less than or equal to 10^{-13}M) ;

-A small sample-test volume (few microliters) ;

-A great specificity.

In a first approach, we have adapted and simplified the determination of NO, as proposed by GUTZKI and al. [2]. But this method has a major disadvantage : The best purified waters contain nitrates. So the preparation of low level standard solutions is uncertain.

In a second approach, we intend to use the reactivity of nitric oxide towards diradicals [3] : The 1,2-bis(exoisopropylidene)cyclohexa-3,5-diene II comes from the decarbonylation of 1,1,3,3-tetramethyl-2-indanone I under ultraviolet irradiation [4]. In the presence of NO, the biradical/triplet state of II can react with the solubilized gas to form the 1,1,3,3-tetramethylisoindolin-2-yloxyl III [5].

In a preliminary experiment, we bubbled nitric oxide in a 15.6 mM deoxygenated solution of I in cyclohexane. This saturated solution of nitric oxide was exposed to UV irradiation during 20 mn.

The chromatogram (figure 1) of the resulting solution shows two compounds · The unchanged indanone I (scan 1916) and its already known photoproduct IV [6] (scan 1665). The nitroxide III is also detected (scan 2012) ; Calculated on the basis of peak areas, the conversion yield was approximatly 2%. The identity of III was confirmed by comparison with an authentic sample of 1,1,3,3-tetramethylisoindolin-2-yloxyl III.

1-GALLA H.J., Ang Chem. Int. Engl, 1993, 32, 378.

43rd ASMS Conference on Mass Spectrometry and Allied Topics

2-GUTZKI F.M., TSIKAS D., ALHEID U. and FROLICH J.C., Ibidem, 1992, 21, 97.

3-MARUTHAMUTHU P. and SCAIANO J.C., J Phys.Chem., 1978, 82, 1588.

4-WINTGENS V., NETTO-FERREIRA J.C., CASAL H.L. and SCAIANO J C., J. Am. Chem. Soc , 1990, 112, 2363.

5-KORTH H.G., INGOLD K.U., SUSTMANN R., DE GROOT H. and SIES H., Angew. Chem. Int. Engl., 1992, 31, 891.

6-STARR J.E. and EASTMAN R.H., J. Org. Chem., 1966, 1393.

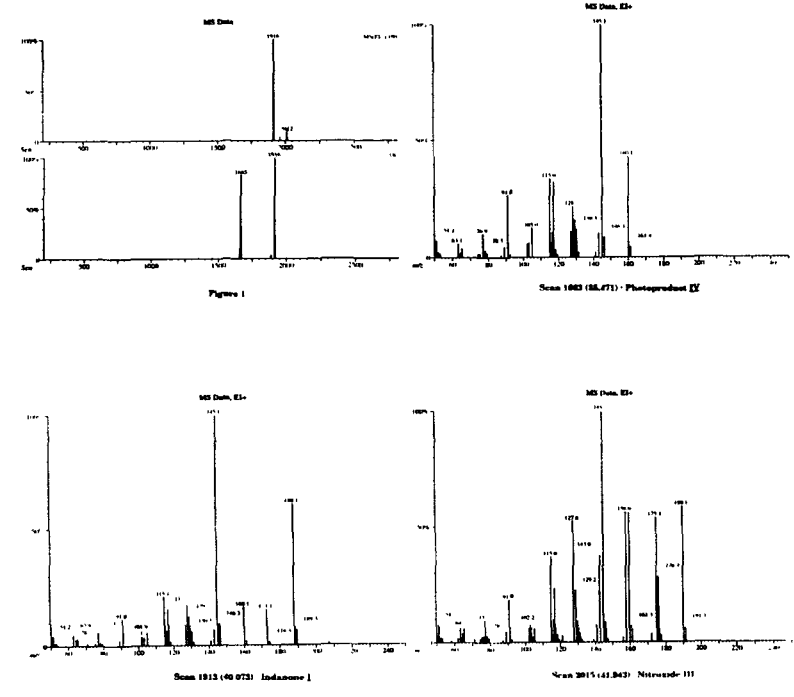

Figure 1

MACROMOLECULE ISOTOPE-RATIO MEASUREMENTS WITH HPLC/CRIMS

Blaire L. Osborn and Fred P. Abramson, Department of Pharmacology,
George Washington University, Washington, D.C. 20037

The increased use of proteins as therapeutic agents intensifies the need for methods to study pharmacokinetics and metabolism of these macromolecules. These drugs are frequently used to augment endogenous protein in the body. To accurately perform pharmacokinetic and metabolism studies of therapeutic proteins, it is necessary to be able to distinguish between endogenous and exogenously administered protein. This study uses HPLC/CRIMS to determine the amount of stable-isotope labeled protein that can be detected against a background of unlabeled material.

Chemical reaction interface mass spectrometry (CRIMS), when combined with high performance liquid chromatography (HPLC/CRIMS), permits the study of nonvolatile species, such as intact proteins. The fundamental process of CRIMS involves a reaction chamber in which a microwave-induced plasma is generated that decomposes each analyte to its component elements. These elements then react with atoms from a second, reactant, gas to produce stable product species that can be detected by a conventional mass spectrometer using selected-ion monitoring. Since the products of the reaction are predictable, there is no need for hypotheses about metabolic products in order to detect them.

In this feasibility study, we have tested whether HPLC/CRIMS can detect a labeled protein against a background of unlabeled material. We chose an easily isolated macromolecule, phycocyanin (**P**), a chlorophyll-associated protein which is heavily expressed in cyanobacteria. Lyophilized algae (*Spirulina platensis*) grown under $^{13}CO_2$ as well as under a normal atmosphere were purchased, and **P** was isolated using ammonium sulfate precipitation. The **P**-containing solution was passed through an anion-exchange column, the deepest blue fractions were combined, dialyzed, lyophilized and stored at -20°C until used.

The mass spectrometer was set to obtain a minimum of twenty samples across the peaks. The reactant gas was SO_2, which oxidizes the elements of the analytes. The carbon in the protein was measured as CO_2, with $^{13}C^{16}O_2$ detected at mass 45, and the unlabeled carbons detected at mass 44 ($^{12}C^{16}O_2$). By integrating any HPLC peaks of interest for these two mass channels, calculating their ratio, and comparing this ratio to that for the naturally abundant species, one determines the isotopic enrichment of the sample. Studies were analyzed using a weighted ($1/y^2$) linear regression.

The initial experiments to evaluate purity used a 300Å pore, 30 mm x 4.6 mm Brownlee C4 column. Solvent A was 95% water: 5% methanol, and solvent B was 95% methanol:5% water. Both solvents contained 0.1% trifluroacetic acid. **P** was eluted from the C4 column using a gradient of 70-90% B and a flow rate of 1 mL·minute^{-1} over 10 minutes (Fig. 1). For the isotope-dilution experiments, a 2.1 x 30 mm Poros R1 perfusion column (PerSeptive Biosystems) was used for better resolution, sensitivity, and speed. Solvent A was 95% water:5% acetonitrile, solvent B was 95% acetonitrile:5% water, and both solvents contained 0.1% TFA. **P** was eluted from the column with a 30-60% gradient of B run over 2 minutes at flow rate of 1 mL·minute^{-1}. For the isotope dilution studies, labeled and unlabeled **P** were reconstituted in water. ^{13}C-labeled **P** was added to samples of unlabeled **P** to produce enrichments of up to 10%. Samples containing approximately 28 pmol, 110 pmol and 1100 pmol of unlabeled protein spiked with varying amounts of ^{13}C-labeled **P** were injected into the HPLC system using a 20 μL injection loop and eluted as described.

P isolated from the labeled Spirulina was highly enriched with ^{13}C. As shown in Figure 1, the predominant form of CO_2 was seen at m/z 45. With the C4 column, ^{13}C-**P** is separated into various subcomponents. The two large peaks presumably represent the α and β subunits of **P**. The third small peak could be a second type of α subunit called α_2, which is present in some species of **P**. When the areas of the two mass chromatograms are compared, the isotopic enrichment of ^{13}C-**P** is calculated as

75%. Other labeled peaks were not seen in the chromatogram.

The isotope ratio of CO_2 from naturally-abundant **P** was 0.01300 ± 1.4x10^{-4} (mean ± SD, N = 4) as determined in the 1100 pmol experiment. The coefficient of variation was 1.1%. The isotope ratios obtained in the other two experiments were similar. The criterion for deciding whether enrichment was measurable was set to a value above the mean plus two standard deviations of the naturally-abundant protein. The dashed horizontal lines in Figures 2-4 represent this decision level.

As seen in Figure 2, using the largest amount of unlabeled protein, the lowest enrichment quantifiable at a background of 1100 pmol was 0.033 mole %, or about 330 femtomoles of ^{13}C-labeled protein. A similar level of detection was seen when starting with 110 pmol (Figure 3). Starting with 28 pmol of unlabeled **P**, a lower amount, 91 fmol, of ^{13}C-enriched protein was measured (Figure 4) but the limit of detectable enrichment was higher, 0.33 mole %. The limit of detection, as predicted from the intersection of the regression line and the dashed line, could be substantially lower (between 30 and 200 fmol) for all 3 experiments.

It is possible to detect femtomole amounts of labeled material against a 3000-fold background of unlabeled protein. When coupled with good HPLC separation, one should be able to obtain accurate information about labeled macromolecular species from biological matrices. These results support the hypothesis that HPLC/CRIMS will be a useful technique for obtaining pharmacokinetic and metabolic information on therapeutic proteins.

An additional experiment was conducted to estimate the ability of HPLC/CRIMS to perform material balance studies using stable isotopes. **P** was incubated with the enzyme Lys-C for several hours. At 0, 1, 2, and 4 hours 20 μL samples were injected into the HPLC/CRIMS system. The area under the multiple peaks produced by the degradation of the protein were 68-91% of the area of the single **P** peak at time 0. The addition of an internal standard should improve the accuracy of this study.

Figure 1. ^{13}C-**P** eluting from the C4 column. The amount of ^{13}C is enriched far above the natural abundance allowing the labeled protein to be detected at m/z 45 ($^{13}C^{16}O_2$) rather than at m/z 44 ($^{12}C^{16}O_2$).

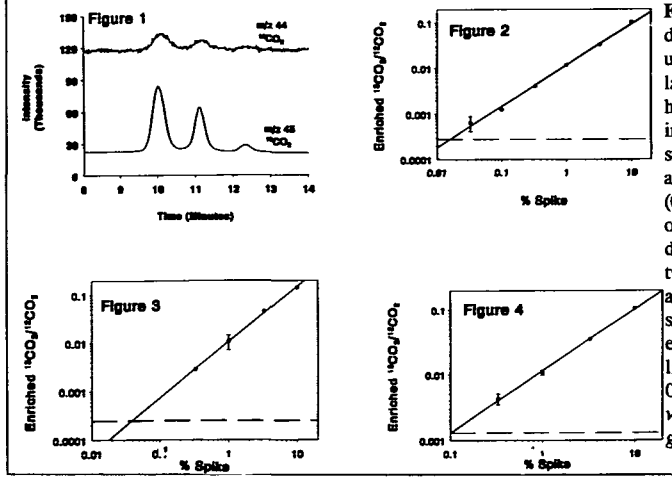

Figures 2-4. Isotope dilution studies using unlabeled and ^{13}C-labeled **P**. These data have been transformed into ^{13}C enrichment by subtracting the naturally-abundant isotope ratio (0% spike) from the observed data. The dashed line represents two standard deviations above the 0% spike sample. All three experiments were highly linear with r^2 values of 0.994-0.999. *This work was supported by NSF grant BIR-9216935.*

QUANTITATIVE ASPECTS OF MASS SPECTROMETRIC IMMUNOASSAY

Randall W. Nelson, Jennifer R. Krone, J. Kathleen Lewis, Peter Williams
Department of Chemistry and Biochemistry
Arizona State University
Tempe AZ 85287-1604

INTRODUCTION

We have recently developed a method for the rapid and sensitive determination of antigenic species present in biological fluids. The technique has been termed mass spectrometric immunoassay (MSIA) [Nelson, R.W. *et al. Anal. Chem.* **67**, 1153 (1995)]. Briefly, MSIA combines the ability of immunoaffinity chromatography to selectively concentrate antigens with matrix-assisted laser desorption/ionization (MALDI) mass spectrometric detection. The assays are performed, however, in a manner much different than conventional chromatography/mass spectrometric methods; that is, the assays are performed with nanoliter volumes of reagent in a pipettor tip, rather than in columns with microliter volumes. This enables the assays to be performed quite rapidly, requiring on average ~ 15 minutes/assay, and with high sensitivity (picomolar concentrations).

While the qualitative nature of the assay is obvious -- specific antigens are selectively retrieved from solution and identified in the mass spectrum at characteristic m/z values -- the quantitative nature of the assay is not. Considering that the criteria for successful quantitative MALDI analysis - the need to introduce an internal reference species (IRS) into the mass analysis in order to compensate for signal variations due to different laser irradiances and sample preparations [Nelson, R.W. *et al. Anal. Chem.* **66**, 1408 (1994)] - are further complicated by the sub-microliter volumes associated with the affinity isolation step, novel methods of IRS introduction are necessitated. These methods should be, within reason, fairly independent of both the volume of the analytical sample, and the volume of the affinity reagent. The most obvious approach is introduction in a manner analogous to that by which the analyte is retained, i.e., the internal reference species is introduced into solution to be retrieved by the affinity reagent. In this way, precise quantities of IRS can be delivered into the relatively large volumes of analytical sample (100's of microliters). Also, as long as the affinity reagent is not saturated by either the analyte or IRS, the approach becomes independent of the volume of affinity reagent used. Retrieval of the IRS can be accomplished by either; use of two antibody/antigen systems (the antigens being the analyte and the IRS), or, a single antibody/antigen system capable of retrieving the antigen and a modified variant of the antigen (used as an IRS). We have undertaken both approaches to quantitative MSIA and report here our findings on the latter; quantitative methods utilizing a single antibody system and modified variants of the antigen as IRSs.

RESULTS

Fig. 1 shows the results of a quantitative MSIA applied to the isolation of the toxin, myotoxin *a* (MTA, MW = 4,822), from human whole blood containing 0.002 mg/mL *C.v. viridis* venom. A version of the myotoxin *a* in which the lysines had been converted to homoarginine (H-MTA, MW = 5,242) was used as an internal reference species. Samples containing 10 - 100 nM of purified myotoxin *a* were used to generate a standard working curve **(overlay)** which was then used to quantify the toxin present in the venom-laced sample **(inset)**. A myotoxin *a* concentration of 25 nM was determined for the analytical sample. **Fig. 2** shows an alternate approach in which a series of modified variants of the antigen (MTA iodinated at the tyrosine residues) were introduced into the analytical sample to create an internal calibration "bargraph" for antigen quantification. Each species represents a particular concentration of the MTA **(inset)**. A myotoxin *a* concentration (for blood laced with 0.002 mg/mL venom) of between 20 and 30 nM is indicated.

CONCLUSION

Quantitative mass spectrometric immunoassays have been developed which use a single species of antibody covalently immobilized on a solid support to retrieve both the intrinsic antigen and modified variants of the antigen which have been introduced into the analytical system as internal reference species. A traditional working curve method has been employed and found to give reasonably accurate quantitative estimates (~ 10%) over at least an order of magnitude range of antigen concentration. Alternatively, the calibration scale can be built into the assay as a "bargraph" of multiple, mass-displaced variants of the antigen, each of an intensity indicative of a different antigen concentration. In this manner, antigen quantitation can be performed by simply equating antigen signals with those of the nearest concentration markers.

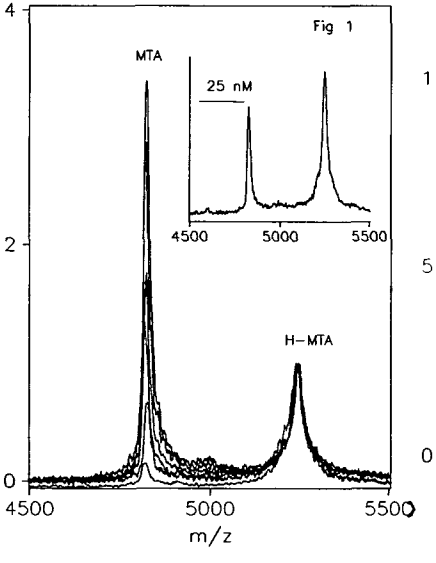

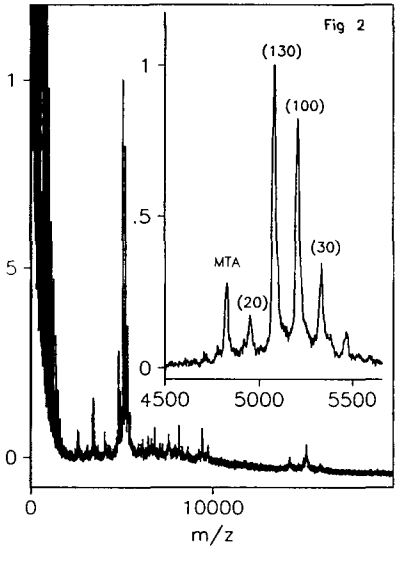

Fig. 1 Overlay of calibration spectra for MTA quantitative MSIA. The inset shows a MSIA spectrum of an analytical (blood) sample containing 0.002 mg/mL CVV venom.

Fig. 2 "Bargraph" method of quantitation in which the calibration curve is built into the MSIA spectrum. Iodinated MTA species were introduced into the analytical sample at levels to indicate 20, 130, 100, and 30 nM. The approximate concentration of MTA was then determined by equating the antigen signal with that of the nearest concentration markers. In this case, an antigen concentration of between 20 and 30 nM is indicated.

Analysis of Flunixin Residues in Animal Tissues by NICI-GC-MS

David Kwok, Pauline Chow, Larry Young and Brian Mori

Health Protection Branch, Health Canada
3155 Willingdon Green, Burnaby, B.C. Canada V6S 2J6

Introduction

Flunixin (Banamine®), 2-[[2-methyl-3(trifluoromethyl)phenyl]amino]-3-pyridinecarboxylic acid, (FLU) is a potent non-steroidal, anti-inflammatory and antipyretic veterinary drug which has been evaluated for the treatment of bovine respiratory disease and acute endotoxin-induced bovine mastitis in food-producing animals. FLU is currently not permitted for use in food-producing animals in Canada. Previous pharmacokinetic studies of the radiolabelled drug in cattle have suggested the persistence of tissue bound residues, creating concerns in the assessment of total residue depletion data.

To survey and determine the state of compliance of targeted food commodities with respect to veterinary drug residues, a SIM-NCI-GC/MS method has been developed for the confirmation and quantitation of FLU in pork and beef liver tissues with a limit of quantitation (LOQ) at 10 ppb.

Experimental

A HP Model 5988A mass spectrometer was interfaced to a Model 5890 GC under the control of a Model 59970C Pascal Chemstation for automated analysis. A DB-5ms, 30m x 0.25mm id x 0.25μm, capillary column was used with a temperature program and with helium as a carrier gas at a column head pressure of 12 psi (uncompensated). The injector and transfer line temperatures were at 250°C and 280°C, respectively. Mass spectral data were collected in the negative ion mode with a dwell time of 50 msec. Electron multiplier voltage was at 3000eV. Methane was used as a reagent gas with an ion source temperature and pressure at 180°C and 1.2 torr, respectively.

Beef and pork liver tissues were fortified with FLU. Niflumic acid (NFA) was used as an internal standard. An aliquot of 5.0±0.1g tissue was acidified with 2 ml of 6 M HCl followed by extraction with 100 ml of dichloromethane (DCM):acetone (1:1) by homogenization with a Polytron® in a 250 ml glass centrifuge bottle. The sample was centrifuged at 2000 xg and the solvent was decanted through a glasswool plug into a collection flask. The sample was likewise extracted with an additional 2 x 100 ml solvent. An aliquot of 75 ml of DCM was added to the pooled extract followed by passing the sample through a 100 g anhydrous sodium sulphate column. The solvent was removed by rotatory vacuum evaporation and the sample was reconstituted with 10 ml of DCM.

Sample purification was carried out using a 5g BondElut Florisil® solid-phase extraction cartridge, previously conditioned with 10 ml of DCM. Following sample loading, 10 ml of acetone was eluted through the cartridge and discarded. FLU was eluted by gravity with 50 ml of DCM:methanol (4:6). The solvent was removed by rotatory vacuum evaporation and the sample was reconstituted with 1 ml of acidified methanol. Methylation of FLU was carried out with 3 ml of freshly prepared ethereal diazomethane. The sample was subsequently evaporated to dryness under nitrogen in a 40°C block heater followed by reconstitution with 0.5 ml of iso-octane:acetone (9:1) for GC/MS analysis.

Results and Discussions:

Beef and pork liver samples were fortified with flunixin at 10, 50 and 100 ppb as quality control (QC) samples during method validation. Linear least square regression analysis was performed (without weighting) for the calibration samples on each analytical day. The calculated QC concentrations, expressed as percent deviation from the expected values (**Table 1**), were used to assess assay accuracy (% deviation), precision (%RSD) and overall assay bias.

Table 1. QC data for flunixin fortified in beef and pork liver at 10, 50 and 100 ppb.

	Beef			Pork		
ppb fortified	ppb calculated	% deviation from expected	%RSD	ppb calculated	% deviation from expected	%RSD
10	11.2	12.2		9.4	-5.8	
10	10.3	3.2		9.0	-10.1	
10	10.2	1.6		10.6	5.7	
10	10.6	5.9		10.0	0.4	
10	10.8	8.1		12.7	27.3	
10	10.3	3.0	3.6	11.3	13.2	12.9
50	48.9	-2.3		46.1	-7.8	
50	45.0	-10.0	5.9	48.4	-3.3	3.4
100	98.7	-1.3		100.9	0.9	
100	104	4.0	3.7	101.5	1.5	0.4
mean bias		2.4			2.2	

An assay LLOQ of 10 ppb was determined (n=6) with mean inter-day assay accuracy of 5.7% and 5.1% deviation from the expected concentration in beef and pork liver, respectively. An inter-day assay precision (%RSD) of 12.9 and 3.6 were obtained for beef and pork samples, respectively.

The mean (n=2 to 4) assay extraction recovery of FLU from beef liver fortified at 10, 50 and 100 ppb were found to be 70%, 69% and 98%, respectively. The mean (n=2 to 4) of FLU from pork liver over the same concentrations were determined to be 86%, 104% and 127%, respectively.

A representative selected-ion chromatogram and mass spectrum of FLU and NFA is shown in **Figure 1**. Mass spectral data acceptance criteria for the confirmation of FLU residues include i) GC chromatographic retention time established from the QC samples; ii) mass ion fragment ratio at m/z 310/280 and iii) isotope abundance ratio at m/z 310/311. This assay has been demonstrated to be a sensitive and reliable procedure for the routine confirmatory determination of FLU in beef and pork liver tissues.

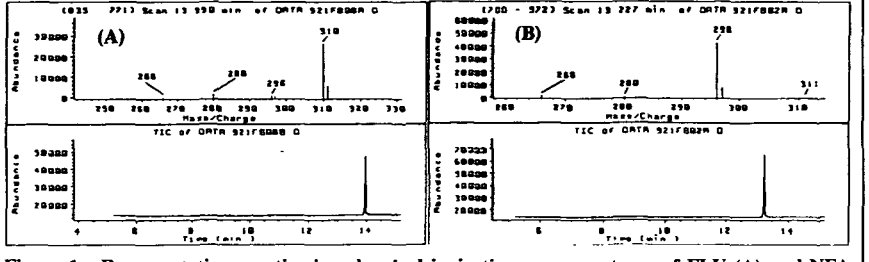

Figure 1. Representative negative ion chemical ionization mass spectrum of FLU (A) and NFA (B) as their methyl ester derivatives.

Metabolism of Perillyl Alcohol Following a Single Oral Dose in the Dog as Determined by Gas Chromatography/Mass Spectrometry

Lawrence R. Phillips, Jeffrey G. Supko and Louis Malspeis

Laboratory of Pharmaceutical Chemistry
Developmental Therapeutics Program
Division of Cancer Treatment
National Cancer Institute
Frederick, Maryland 21702-1201

Limonene, a monocyclic terpene that is a major component in many citrus essential oils, inhibits post-translational isoprenylation of 21-26 kDa cellular proteins implicated in cell proliferation [1]. Perillyl alcohol was found to be one of the most potent compounds among a group of 24 limonene-related monoterpenoids tested for antitumor activity *in vitro* [2]. Our efforts focussed on characterizing the disposition of perillyl alcohol and identifying its principal circulating metabolites.

Sample Preparation and Analysis. Briefly, plasma samples (50 μl) were mixed with 50 μl of an aqueous solution 0.2 M in phosphoric acid and 1 M in potassium chloride, and then 100 μl of *tert*-butyl methyl ether containing the internal standard (perillyl hexyl ether) was added. Following mixing and centrifugation, the upper organic phase was transferred to a silanized borosilicate vial and analyzed by GC/MS, which was performed using a 5890 Series II GC in combination with a 5971A mass selective detector controlled by a DOS series MS ChemStation (Hewlett-Packard). Detection (EI, 70 eV) was performed by selected ion monitoring, measuring ions at *m/z* 121 and *m/z* 122 sequentially, utilizing a 75 ms dwell time. Standard curves were constructed by plotting the peak area ratio of each analyte to the internal standard against the respective concentration of the analyte. Linear least squares regression was performed using a weighting factor of $1/Y_{obs}$, without inclusion of the origin. Analyte concentrations in unknown samples were calculated using results of the regression analysis. The lowest concentration of analyte quantified with acceptable reproducibility in 50 μl of plasma was 0.25 μg/ml. The GC/MS assay was linear over the range of 0.25 to 7.5 μg/ml. Coefficients of variation for the mean predicted analyte concentration of each of the seven plasma standards were less than 10% within this concentration range for 12 standard curves prepared independently and assayed over a 4 week period.

Results. Plasma samples acquired from a beagle dog following oral administration of 250 mg/kg perillyl alcohol were analyzed by GC/MS using mass scanning detection. Mass spectra (EI) and retention times of the chromatographic peaks observed in plasma samples were compared to authentic standards of the potential phase I metabolites. Results of these analyses indicated the presence of only perillic acid and dihydroperillic acid (as a *cis-trans* mixture), representing the major and minor metabolites, respectively. The isomers of dihydroperillic acid could be distinguished on the basis of their mass spectra.

The plasma concentration of perillyl alcohol remained below the limit of detection (about 1.5 μM by selected ion monitoring) at all times after dosing. Peak plasma concentrations of perillic acid and dihydroperillic acid were 0.90 and 0.036 mM, occurring at 2.5 and 5.0 hr, respectively. Plasma levels of perillic acid could be monitored for 24 hr after dosing, whereas dihydroperillic acid was only detectable for 12 hr. The area under the plasma concentration-time profile of perillic acid (14.23 mM·hr) was 21-times greater than for dihydroperillic acid (0.69 mM·hr).

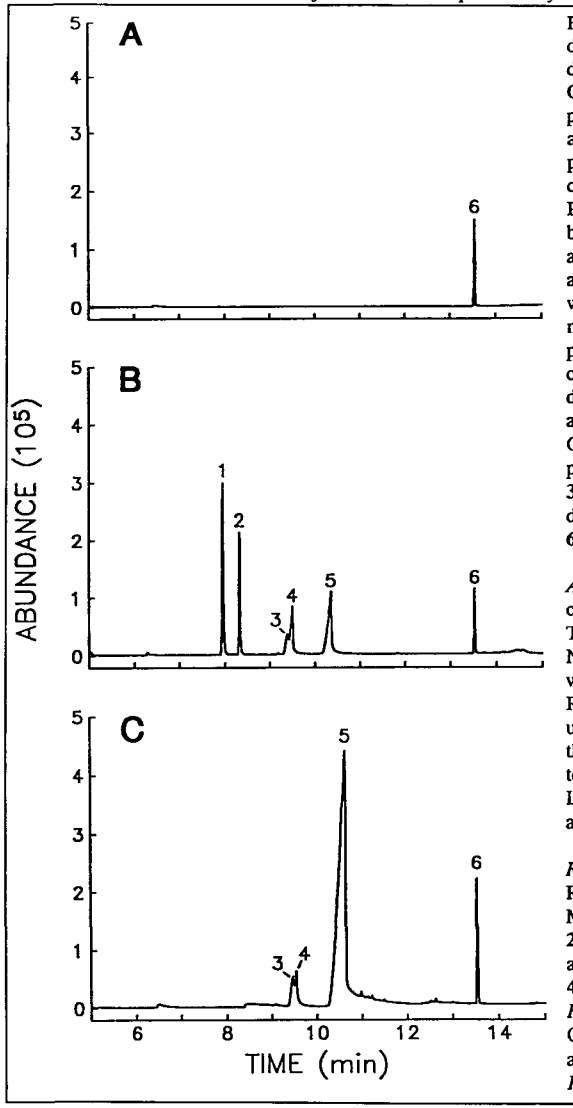

Figure 1. Gas chromatograms determined with mass selective detection at *m/z* 121 and 122. **A**, Chromatogram of drug-free dog plasma. **B**, Plasma to which perillyl alcohol and authentic samples of its potential metabolites were added at a concentration of 0.1 mM. **C**, Plasma acquired from a female beagle dog 8 hr after the administration of 250 mg/kg perillyl alcohol po. The sample was assayed without dilution, which resulted in minor distortion of the perillic acid peak due to column overloading, to clearly demonstrate the absence of drug-related peaks other than perillic acid and dihydroperillic acid. Chromatographic peaks: **1**, perillaldehyde; **2**, perillyl alcohol; **3**, *cis*-dihydroperillic acid; **4**, *trans*-dihydroperillic acid; **5**, perillic acid; **6**, IS (perillyl hexyl ether).

Acknowledgments. This study was conducted in cooperation with the Toxicology Branch, DTP, DCT, NCI. Dosing and sample collection were performed at the Midwest Research Institute (Kansas City, MO) under contract NO1-CM-37836 from the NCI (Bethesda, MD). We wish to thank Tyra L. House and Tracy L. Wolfe for their expert technical assistance in analyzing the samples.

References. 1. P. L. Crowell, R. R. Chang, Z. Ren, C. E. Elson, and M. N. Gould (1991) *J. Biol. Chem.* **266**, 17679-17685; J. L. Goldstein and M. S. Brown (1990) *Nature* **343**, 425-430; W. A. Maltese (1990) *FASEB J.* **4**, 3319-3328. 2. P. L. Crowell, Z. Ren, S. Lin, E. Vedejs, and M. N. Gould (1994) *Biochem. Pharmacol.* **47**, 1405-1415.

Positive chemical ionisation GC-MS analysis of nicotine and cotinine.

Dalene M.[2], Loftus, N J.[1], Skarping G.[2], Speakman A.[1]
[1]Fisons Instruments, VG Organic, Crewe Road, Wythenshawe, Manchester, UK.
[2]University Hospital, Lund, Sweden.

Introduction.
Tobacco is one of the most widely used stimulants with recognised adverse health effects. In spite of the recognised adverse health effects, the dependence upon nicotine is still high and the prevalence of smoking approaches almost a third of the western population.

The risk of developing chronic lung disease is not restricted to active smoking, environmental tobacco smoke [ETS] inhalation (often referred to as passive smoking) presents a health hazard to both adults and children It is quite possible that children may be at a greater risk given the incomplete development of the respiratory and immune systems. Risk assessment studies of ETS exposure with children has taken into account exposure measured by non-invasive techniques such as air sampling and biological monitoring. The latter approach can be used as a direct measure of nicotine intake, however to provide meaningful data there is a clear need for a sensitive and specific assay using an appropriate biomarker Measuring the major metabolite of nicotine, cotinine, has been shown to be the intake marker of choice. In this study urinary levels of both nicotine and cotinine were measured by GC-MS using positive chemical ionisation detection in assessing the extent of exposure to ETS in populations of children in Sweden aged between 7-9 years with smoking and non-smoking parents

Methods.
Nicotine and cotinine were extracted from urine [2mls] spiked with trideuterated internal standards into dichloromethane [3mls] following the addition of sodium hydroxide [0.5mls 5N NaOH]. The two phases were shaken for 20 minutes and the layers were separated after centrifugation at 1500g for 10 minutes Most of the aqueous layer was removed before being placed in a cooling solution of solid carbon dioxide and acetone to freeze the remaining portion of water. The solvent layer was then transferred to a clean new vial and blow to dryness under a gentle stream of nitrogen. For GC-MS analysis the sample was then reconstituted in toluene [1ml] and the components separated on a DB5-ms column [30m in length, 1 0μm film thickness, 0.22mm internal diameter] using a splitless injection.

The MD800 mass spectrometer (Fisons Instruments, VG Organic) was optimised for the positive chemical ionisation detection of nicotine and cotinine using a source temperature of 250°C, interface temperature 280°C, emission 300μA, and electron energy set to 70eV. Ammonia reagent gas pressure optimised for

the intensity of m/z 35 proved optimum for cotinine. Single ion recording acquisition monitoring ions for nicotine [m/z 163], cotinine [m/z 177]; together with the corresponding trideuterated internal standards monitored at m/z 166 and 180 respectively using a dwell time of 0.2 seconds, span 0 10 amu and an inter-scan delay of 0 02 seconds.

Results.

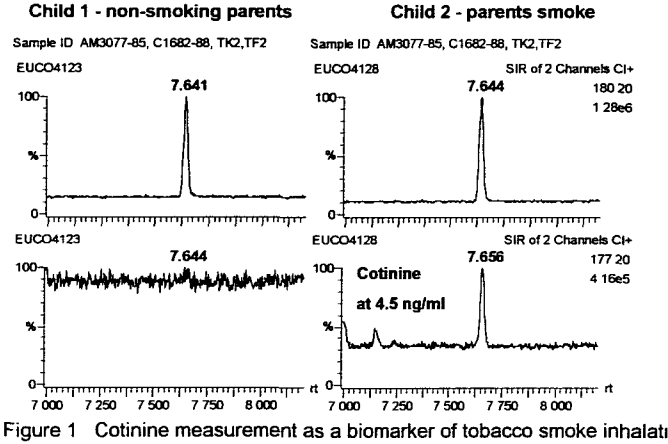

Figure 1 Cotinine measurement as a biomarker of tobacco smoke inhalation from passive smoking in children. The mass chromatograms of cotinine [m/z177] and the ($^2H_3$) internal standard [m/z180] in two urine samples

The results of the study show a clear relationship between tobacco smoke intake in children and parental smoking habits.

No. of children	130	12	23	21
Average	0.1	0.5	1.11	1.19
Minimum	0	0	0.2	0.1
Maximum	1 3	1.8	2 7	5 1
Median	0.04	0.24	0.81	0 88
	Neither	Father only	Mother only	Both

Conclusion.
Quantitative positive chemical ionisation has proved to be a precise and accurate means of measuring urinary levels of nicotine and cotinine [regression coefficients were typically r>0.9996; with a precision of 5.8% on absolute raw area, n=24 for the 20ng/ml standard, LOD at 0.1ng/ml]

Analysis of Anagrelide, in Human Plasma by GC / ECNCI MS.

Suresh N. Yeola[1], Sam A. Saleh[1], Stephanie C. Sanchez[1], Sara J. Kambouris[3], Ajai K. Chaudhary[1,2], Bruce H. Migdalof[4] and Ian A. Blair[1,3]

Department of Pharmacology[1], Biochemistry[2] and Chemistry[3], Vanderbilt University School of Medicine, Nashville, TN 37232
Roberts Pharmaceutical Corporation[4], Meridian Center III, 6 Industrial way west, Eatontown, NJ 07724

Anagrelide, (6,7-dichloro-1,5-dihydroimidazo-[2,1-b]-quinazolin-2(3H)-one monohydrochloride) is a potent inhibitor of agonist induced platelet aggregation. However, anagrelide was found to cause thrombocytopenia when given in high dosage to normal volunteers. This undesired side effect has been used to advantage for the treatment of myeloproliferative disorders such as thrombocythemia where there is increased platelet production. The present work represents a quantitative analysis of anagrelide (6,7-dichloro-1H-2,3,4,5-tetrahydroimidazo[2,1-b]quinazolin-2-one) in human plasma[1]. The assay is based on gas chromatography/electron capture negative chemical ionization mass spectrometry (GC/ECNCI MS). The internal standard used in the assay was a [^{13}C]labeled analog of anagrelide (2,3-[$^{13}C_2$]-6,7-dichloro-1H-2,3,4,5-tetrahydroimidazo[2,1-b]quinazolin-2-one). The synthesis[2] of an internal standard was performed as shown in Scheme 1. Separation of anagrelide and the internal standard from interfering substances was efficiently carried out by solvent extraction of the plasma. Anagrelide and the internal standard were then converted to their corresponding pentafluorobenzyl (PFB) derivatives for GC/ECNCI MS analysis. Full scan spectra typical of PFB derivatives were observed. The major negative ions for anagrelide corresponding to the molecular ions (M) - PFB appeared at *m/z* 254, *m/z* 256, and *m/z* 258 in the ratio of 9:6:1. These ions contained [$^{35}Cl_2$], [$^{35}Cl^{37}Cl$], and [$^{37}Cl_2$], respectively. Similarly, the [M-PFB]$^-$ ion for the internal standard appeared at *m/z* 256, *m/z* 258, and *m/z* 260 (Figure 1a, 1b).

The ions *m/z* 254 for anagrelide and *m/z* 258 for internal standard were monitored. Chromatography was carried out on a 30 m SPB-50 fused silica capillary column using a temperature programmed from 70 °C to 300 °C. The extraction procedure from plasma involved initial adjustment of the plasma to pH 9.2 and extraction into *tert*-butylmethyl ether (TBME)/ethyl acetate (4:1) with subsequent extraction from the organic solvent into dilute hydrochloric acid. This was followed by making the aqueous layer basic and back-extraction into TBME/ethyl acetate (9:1). Derivatization was carried out at room temperature by reaction with pentafluorobenzyl bromide dissolved in acetonitrile in the presence of diisopropylethylamine. Analyses were carried out using selected ion monitoring of *m/z* 254 (anagrelide) and *m/z* 258 (internal standard). Calibration curves obtained by plotting the peak height ratio of *m/z* 254 to *m/z* 258 against the amount added to the plasma, were non-linear (polynomial) in the range 0.083 ng to 8.248 ng using a weighted (1/concentration^2) non-linear regression analysis. Accuracy and precision studies were conducted and the method was found to be accurate and reproducible for anagrelide at the three concentrations that were tested. The lower limit of quantitation was 0.083 ng/mL.

References:

1. E. H. Kerns, J. W. Russell and D. G. Gallo, *J. Chromatogr.*, **416**, 357 (1987).
2. T. A. Jenks, W. N. Beverung Jr., R. A. Partyka, *U. S. Patent*, 4,146,718 (1979).

Acknowledgment:

This work was supported by Roberts Pharmaceutical Corporation, Eatontown, NJ.

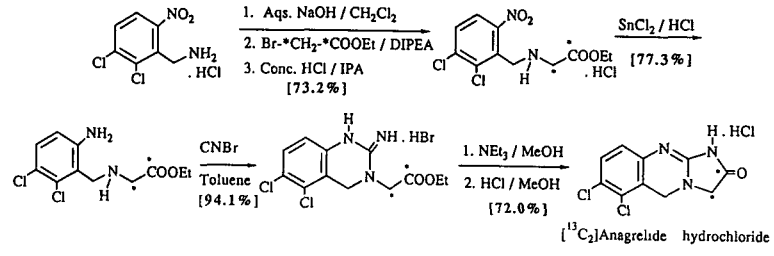

Scheme 1: Synthetic Scheme for the Preparation of [$^{13}C_2$]Anagrelide.

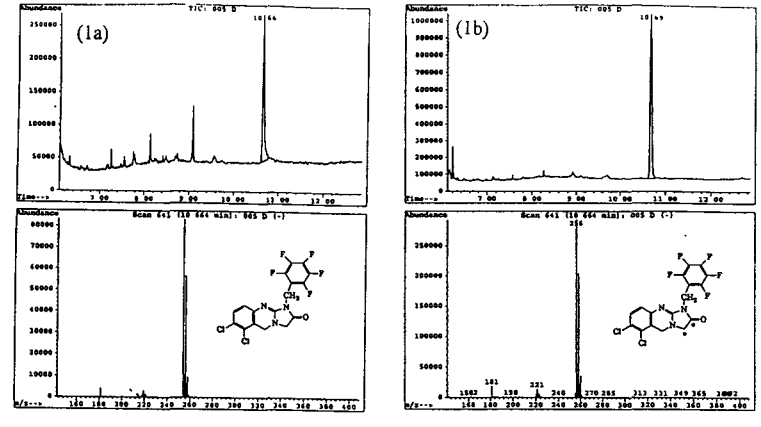

Figure 1: Total Ion Current Chromatograms and Electron Capture Negative Chemical Ionization Mass Spectra of Anagrelide (1a) and Internal Standard (1b).

A RAPID ANALYTICAL METHOD FOR THE QUANTITATIVE DETERMINATION OF ω-HYDROXY-TRIDECANOIC ACID DIMETHYLAMIDE IN HUMAN PLASMA

M. BRUDNY-KLOEPPEL, C. GUENTHER & C. WEISS
Institute of Pharmacokinetics
SCHERING AG, D-13342 Berlin, Germany

ω-Hydroxy-tridecanoic acid dimethylamide (ZK 118 372) is developed for the topical therapy of acne, because of its antimicrobial, comedolytic and anti-inflammatory properties. Prior to clinical studies, toxicological characterization was carried out with different animal species. In order to study the pharmacokinetics of the drug in man, ZK 118 372 was tested after intravenous and topical application. The evaluation of the experimental data required a sensitive and specific GC/MS method, which enables the quantification of the drug from the different biological matrices in a concentration range of 0.1 to 500 ng per ml serum or plasma.

The assay was developed and validated using rabbit serum as biological matrix. For the evaluation of clinical studies, the method was revalidated with human plasma. The drug and the internal standard ω-hydroxy-tridecanoic acid di-n-propylamide (ZK 135 704) were isolated from the biological matrix by a liquid-liquid-extraction using nanograde peroxide-free diethylether. The serum extracts were derivatized with 3,5-bis(trifluoromethyl) benzoyl chloride. For the separation a 30 m RTX®-5 Amine column with an internal diameter of 0.25 mm and a film thickness of 0.5 µm was used. The compounds were detected by means of NCI-GC/MS. The standard curve was linear in the range of 0.1 to 10 ng/ml and of 10 to 500 ng/ml (Fig. 1). The lower limit of quantification was 0.1 ng/ml with a precision of 14.2 %.

In order to assess the quality of the assay, six quality control samples with concentrations of 0.8, 8, 20, 80, 150 and 400 ng/ml plasma were included in the sample batch and were each analysed 5-fold. Nominal and measured concentrations (mean ± S.D.) as well as precisions (C.V.) and accuracies are presented in Tab. 1. During validation, revalidation and analysis of the clinical study, the intraassay precision of the lowest quality control sample was 5.3 %, 6.7 % and 3.7 %, respectively.

The method developed for the quantitative determination of ZK 118 372 from biological matrices is a rapid and precise analytical procedure. The assay is suitable for pharmacokinetic and bioavailability studies as well as for therapeutic drug monitoring.

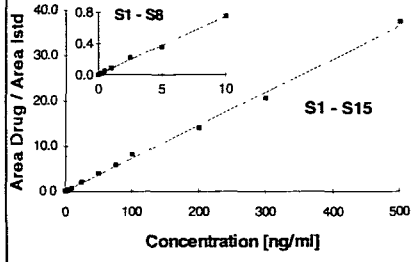

Fig. 1: Standard curve of ZK 118 372 in human plasma

Content [ng/ml]	Mean [ng/ml]	S.D. [ng/ml]	C.V. [%]	Accuracy [%]
0.8	0.77	0.03	3.7	96.3
8	7.68	0.20	2.6	96.0
20	18.8	1.1	5.9	93.8
80	78.6	2.5	3.1	98.2
150	153.3	3.4	2.2	102.2
400	417.6	23.7	5.7	104.4

Tab. 1: Quality criteria of the assay: nominal and measured concentration (mean ± S.D.), intraassay precision (C.V.) and accuracy

The plasma level-time course of ZK 118 372 was investigated in six healthy male volunteers over 50 years of age following intravenous and topical application. During intravenous infusion of 4.2 mg ZK 118 372, drug plasma levels increased rapidly to a maximum of 95 ng/ml at the end of the 10 min infusion period (Fig. 2). Postmaximum plasma levels decreased monoexponentially with a half life (t½) of ca. 2 min and were below the lower limit of quantitation (LLQ) of 0.1 ng/ml within 22 min after the end of infusion. The area under the plasma level-time curve (AUC) was 16 ng*h/ml. The clearance rate (Cl) was calculated to be 4.4 l/min, the apparent volume of distribution (Vc) was 11 l per individual.

After topical application of 50 mg ZK 118 372 as 10 % hydrogel to 100 cm² intact back skin (5 mg formulation per cm²), ZK 118 372 plasma levels did not exceed the LLQ of 0.1 ng/ml. After topical application of an identical dose to damaged skin, from which the stratum corneum was removed by multiple adhesive tape stripping, ZK 118 372 plasma levels exceeded the LLQ within 1 hour, and reached a maximum concentration of 3.1 ng/ml after 4 hours (Fig. 3). Postmaximum ZK 118 372 plasma levels decreased slowly reaching a concentration of 1.1 ng/ml after 24 hours. The $AUC_{(0\text{-}24h)}$-value after application to stripped skin was 44 ng*h/ml. The percutaneously absorbed dose (D) was 11.5 mg, corresponding to 23 % of the dose applied, resulting in a mean percutaneous flux of 4.8 $\mu g*cm^{-2}*h^{-1}$.

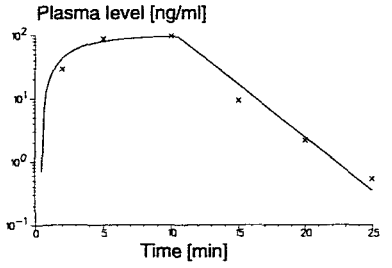

Fig. 2: Semilogarithmic plot of drug plasma level-time course after i.v. infusion

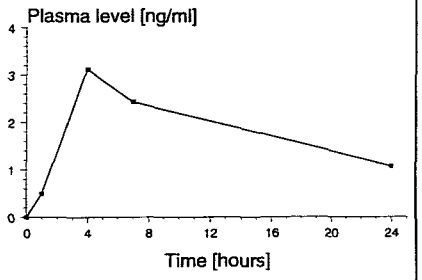

Fig. 3: Drug plasma level-time course after topical application to stripped skin

The basic pharmacokinetic properties of ZK 118 372 were determined after intravenous infusion. ZK 118 372 exhibited a limited distribution throughout the body and was very rapidly eliminated from the plasma. The drug was extensively metabolized as indicated by radio-HPLC[1] and the high clearance rate. The clearance rate exceeded distinctly the hepatic blood flow indicating additional extrahepatic metabolism. The very rapid elimination from plasma might be seen as an advantage for a topically applied drug, because the systemic drug load is reduced.

ZK 118 372 was released from the hydrogel formulation to the skin as was demonstrated following application to stripped skin. Only after adhesive tape stripping prior to the application, percutaneous absorption of ZK 118 372 was detectable. Thus, the stratum corneum has to be considered as the major skin diffusion barrier for ZK 118 372.

[1] Data on file, Schering AG.

Quantitation of Odd-Numbered Long Chain Fatty Acids in Red Cell Membranes

Giordano G.*, Burlina A.B., Magarotto M., Edini C., Zacchello F.
Department of Pediatrics, University of Padova, Padova, Italy

INTRODUCTION

Patients with propionate metabolism disorders as propionic acidemia (PA) and methylmalonic acidemia (MMA) accumulate propionyl-CoA in large amount. Odd carbon number fatty acids (OLCFA) are precursors of propionyl-CoA but this metabolite can replace acetyl-CoA as a "primer" for de novo long chain fatty acids synthesis, leading to the formation of odd-numbered fatty acid.

Recently Wendel et al. (1) reported that the relative abundance of OLCFA (C15 and C17) in red cell membranes are elevated in patients with MMA and PA under catabolic conditions.

In order to evaluate if the levels of C15 and C17 OLCFA may represent an early biochemical parameter that can be used for long term assessment of these disorders we studied, in red cell membranes of 10 subjects affected by MMA (n=7) and PA (n=3), the OLCFA with a new quantitative method GC/CIMS in the positive ion mode with isobutane as the reagent gas.

MATERIALS

Blood sample of seven patients with methylmalonic acidemia B_{12} unresponsiveness and three patients with propionic acidemia were studied. All the subjects were diagnosed on the basis of clinical presentation and urinary metabolite excretion patterns In every patient, after an initial phase of induction of anabolism and/or toxin removal, treatment was started which consisted of restriction of dietary protein intake, supplementation of the diet with essential amino acids free of valine, isoleucine, methionine, and threonine, as well as carnitine and metronidazole.

In particular, one patient with severe form of MMA difficult to manage was weekly monitored for 8 months to better define the relationship among OLCFA urinary organic acids and different diet prescriptions. A group of patients with low protein diet, including PKU and urea cycle disorders, were also studied. For each patients lactate and ammonemia were also measured

METHODS

Red blood cells were isolated from heparinized sample using 154 mM NaCl and 0.23 mM butylated hydroxy toluene and stored at -20° C until analysis (2). Lipids were extracted from 0.1 ml of packed red cells twice with 4ml of isopropanol and 2 ml of chloroform. The extract was evaporated to dryness using nitrogen. Methyl esters were prepared using methanolic HCl for 45 min at 100° C, then neutralized with potassium carbonate. The methyl esters were extracted with hexane and concentrated to a volume of 100 µl. Chromatographic separation was performed on 25 m 0.2 mm i.d. H.P. SE-52 capillary columns using helium as the carrier gas. Quantitation of the fatty acid methyl esters was carried out using GC/CIMS (MD800 Fisons) in the positive ion mode with isobutane as the reagent gas. The data system was programmed to acquire at 70 eV, 300 mA emission, 0.08s dwell time, 0.02s interscan delay and 0.3 span. The abundances of $[M+H]^+$ positive ions of C15:0(m/z 257), C17:1(m/z 283), C17:0(m/z 285) and the internal standard C15:1(m/z 255) were recorded using selected ion monitoring technique.

Concentrations of OLFCA were expressed as µg/mg of membrane protein. They were measured from the erythrocyte membranes by a modified Bradford assay after wash with PBS, lyse with a lysing buffer and a centrifugation at 29.000xg at 4°C for ten min.(3)

RESULTS

1.There were no differences between the group on low protein diets and the normal subjects.The concentrations of $C_{15:0}$, $C_{17:1}$ and $C_{17:0}$ were in the range of 1-5, 1-2,2-4µg/mg respectively. (Table 1)

2.Two patients who were monitored during the course of acute episodes of decompensation showed significant increase in the concentrations of OLFCA immediately before clinical symptoms became apparent (Table 1). In one patient with a severe form of MMA, C15 and C17 concentrations increased dramatically following the decompensation episode (Figure 1). After one month of treatment, including overnight infusion, the same metabolite returned to asymptomatic levels.

3.We propose that the monitoring of OLFCA levels could represent a valuable tool in the management and follow up of patients with propionic and methylmalonic acidemia.

REFERENCE

1.Wendel U., et al. Eur. J Pediatr (1993) 152:1021-1023
2.Morice D., et al. Chim. Clin. Acta, (1988) 171·11-18
3 Ramsay J., et al. Biochem. J. (1991) 275:685-688

Fig. 1) The graphic shows the significant increased of OLFCA before the onset of acute decompesation and the correlation with MMA concentration and the dramatic increase after the decompensation episode with the reduction of MMA concentration.

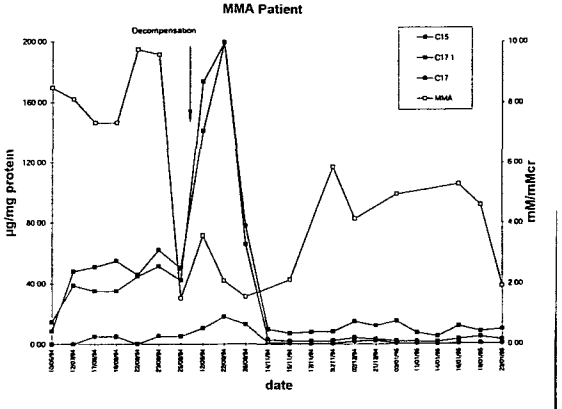

Table 1: Propionate Metabolism Disorders

µg/mg protein

	N	C15:0	C17:1	C17:0
Asymptomatic	10	4.7 ± 2.1	3.4 ± 2.3	5.3 ± 2.2
Acute episodes	2	75.1 ± 58.1	7.7 ± 4.9	74.7 ± 65.8
Low protein diet controls	8	1.8 ± 1.1	1.5 ± 0.7	2.2 ± 1.6
Normal controls	10	1.8 ± 1.1	1.6 ± 0.8	3.2 ± 2.6

Analysis of Fadrozole Pseudoracemic Mixture in Human Plasma Using a Novel Approach for the Analysis of Nitrile Containing Compounds By GC/MS

Iannucci, Robert, M., Linberg, Leonid, F. and Powell, Mark, L.

Ciba Pharmaceuticals, Research Dept., Summit, NJ 07901

Fadrozole is as an orally active, non-steroidal aromatase inhibitor under clinical development for the treatment of estrogen-dependent mammary tumors. Fadrozole is a racemate The (-)-(S)-enantiomer (i.e., CGS 20 287A, eutomer) is responsible in-vitro and in-vivo for the inhibition of the aromatase enzyme system, while the (+)-(R)-enantiomer (i.e., CGS 20286A, distomer) is much less active towards this enzyme system. Fadrozole contains a nitrile group which makes it difficult to analyze by gas chromatography/mass spectrometry (GC/MS) because of its polarity and low volatility. Fadrozole also has a molecular weight of 223 which is coincident with the bleed peaks common to polysiloxane-based GC capillary columns and as a consequence, there is difficulty in attaining very low sensitivity in the EI mode. A previous analytical method utilizing GC/MS in the electron impact (EI) mode was developed by Ackermann and Kaiser to quantitate underivatized fadrozole in human plasma and urine with a limit of quantitation (LOQ) of 1.1 ng/mL [Biomed. Environ Mass Spec., 18 538 (1989)]. A new approach has been developed which involves reduction of the nitrile to the amine by lithium aluminum hydride. This is followed by derivatization of the amine with pentaflouroproprionic anhydride This method allows the use of the more sensitive negative chemical ionization (NCI) mode and shifts the monitored ions into a higher mass range free of bleed peaks and chemical noise. The method was validated with a LOQ of 0.25 ng/mL for both unlabeled and $[D_4]$-fadrozole. An M+6 stable isotope of fadrozole ([M+6]-fadrozole) was used as the internal standard.

This analytical method was used to determine the pharmacokinetics of the fadrozole enantiomers after administration of an 8-mg fadrozole HCl pseudoracemate dose containing a 1:1 molar mixture of unlabeled CGS 20286A and $[D_4]$-CGS 20287A to patients.

Mass spectrometry demonstrated the $[M-HF]^-$ ion derived from the perfluoroacyl derivative of fadrozole to be the major ion suitable for quantitation. For single ion monitoring analysis, the $[M-HF]^-$ions monitored were m/z 499, 503 and 505 for the unlabeled fadrozole, $[D_4]$-fadrozole and the internal standard ([M+6]-fadrozole), respectively.

Average correlation coefficients (r) of 0.9932 and 0.9909 were obtained for unlabeled fadrozole and $[D_4]$-fadrozole, respectively, indicating a good fit to the weighted linear regression model used. The overall accuracy, as indicated by the mean relative recovery for quality control samples was 105.3% for unlabeled fadrozole and 107.2% for $[D_4]$-fadrozole. The LOQ was 0 25 ng/mL and was defined as the lowest drug concentration for both unlabeled fadrozole and $[D_4]$-fadrozole, where acceptable accuracy was within 100 ± 15% and precision (CV) ≤ 20%.

Figure 1 shows the differences in the mean plasma concentrations of CGS 20286A and $[D_4]$-CGS 20287A. The pharmacokinetic behavior of the two enantiomers was significantly different. The (+)-R-enantiomer (CGS 20286A) showed significantly higher mean plasma concentrations than the (-)-S-enantiomer (CGS 20287A). CGS 20286A and $[D_4]$-CGS 20287A demonstrated mean(± SD) C_{max} values of 22.5(4.7) and 4.7(2.3) ng/mL, respectively CGS 20286A and $[D_4]$-CGS 20287A also demonstrated significantly different AUC(0-72) and $T_{1/2}$ values i.e., mean(± SD) AUC(0-72) values of 316 2(87 1) and 15.8(9 5) ng·hr/mL and mean(± SD) $T_{1/2}$ values of 13.0(4.1) and 2.0(0.6) h, respectively. In addition, CGS 20286A and $[D_4]$-CGS 20287A showed mean(± SD) T_{max} values of 1.6(0.4) and 1.0(0.3) h, respectively

Figure 1

Mean plasma CGS 20286A and $[D_4]$-CGS 20287A concentrations in patients administered 8 mg fadrozole HCl pseudoracemate

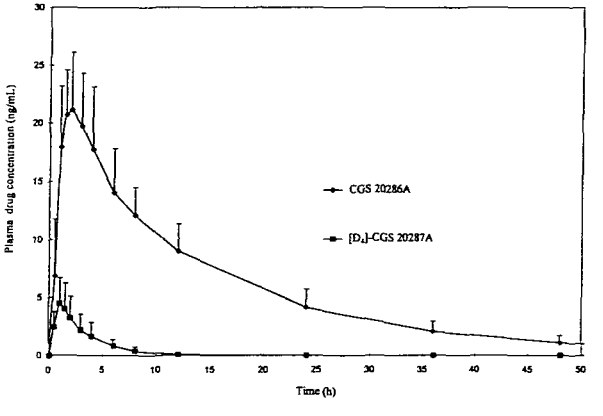

Sonic Spray Ionization for API Mass Spectrometry

A. Hirabayashi, M. Sakairi, Y. Takada and H. Koizumi
Central Research Laboratory, Hitachi, Ltd., Kokubunji, Tokyo 185, Japan

We have developed a sonic spray ionization method in which a solution is sprayed from a fused-silica capillary with gas flow coaxial to the capillary. Protonated molecules produced from 1-μM solutions of molecules, regarded as neurotransmitters such as catecholamine, by this ionization method were analyzed with a quadrupole mass spectrometer. The S/N ratios for the protonated molecules in the mass spectra were nearly equal. Furthermore, protonated dopamine molecules were detected in a 10-nM solution.

Introduction

In the past few years, the science of the brain has developed significantly owing to a breakthrough in the functional magnetic-resonance imaging method.[1] For the next step, an understanding of the functional chemistry of the brain is important. A combination of mass spectrometry with on-line liquid-phase separation methods, such as capillary electrophoresis and liquid chromatography, is one candidate for analyzing neurotransmitters, such as catecholamine. The sensitivity of this method is, however, rather low in comparison with that of the electrochemical detection method. This is mainly because the current interfaces used in spray ionization methods, such as the atmospheric pressure chemical ionization[2] and electrospray (or ion spray)[3] methods, have low ion-production efficiencies for these molecules.

We previously developed a spray ionization method for the interfaces used in capillary electrophoresis/mass spectrometry (CE/MS) and liquid chromatography/mass spectrometry (LC/MS). In this "sonic spray" ionization method,[4] a solution introduced through the capillary is sprayed with gas flow coaxial to the capillary, and the ions are produced at atmospheric pressure. The ion intensity strongly depends on the gas velocity and reaches a maximum at a Mach number of about one: the sonic velocity.

Experimental Setup

The details of our experimental setup were described elsewhere,[4] so a brief account is given here. A solution was pumped by a syringe pump into the fused-silica capillary of an ion source at a flow rate of typically 30 μl/min. The fused-silica capillary tip was inserted into an orifice. The potential of the ion source was set to the ground level. Nitrogen gas was passed through the orifice to the atmosphere. A spray was thus generated in which droplets and free ions were produced. A quadrupole mass spectrometer was used to analyze the ions; the scan period was 4 s for m/z = 0 to 1000.

43rd ASMS Conference on Mass Spectrometry and Allied Topics

Results and Discussion

Typical mass spectra obtained from epinephrine and norepinephrine solutions in 50:50 methanol-water at concentrations of 1 μM are shown in Fig. 1. Protonated epinephrine and norepinephrine molecules were clearly detected at m/z = 184 and 170, respectively. Furthermore, protonated molecules of methanol, hydrated methanol, and methanol dimer were detected at m/z = 33, 51, and 65, respectively. The ion at m/z = 18 is the ammonium ion.

Solutions of dopamine, serotonin, γ-amino-butyric acid (GABA), and dopa with solution concentrations of 1 μM were also analyzed. The S/N ratios for the protonated molecules in the mass spectra were nearly equal. We also analyzed the dopamine solution at a concentration of 10 nM. The S/N ratio for the protonated dopamine molecule was about 20. Since the S/N ratio of the protonated dopamine molecule produced by the current ion spray ionization method from a 1 μM solution is about 20, the ion production efficiency of the sonic spray is two orders of magnitude higher than that of the ion spray. Note that a concentration of 10 nM is at about the detection limit of the electrochemical detector, which is connected to the capillary zone electrophoresis for analyzing the catecholamine.[6] With respect to the S/N ratio, the sensitivity of sonic spray mass spectrometry is an order of magnitude higher than that of electrochemical detection.

References

1) Syllabus, *Functional MRI of the Brain*, the Society of Magnetic Resonance in Medicine and the Society for Magnetic Resonance Imaging, Virginia, 1993.
2) H. Kambara, Anal. Chem. *54*, 143, 1982.
3) M. Yamashita and J. B. Fenn, J. Phys. Chem. *88*, 4451, 1984; A. P. Bruins, T. R. Covey and J. D. Henion, Anal. Chem. *59*, 2642, 1984; R. D. Smith, C. J. Barinaga and H. R. Udseth, Anal. Chem. *60*, 1948, 1988.
4) A. Hirabayashi, M. Sakairi and H. Koizumi, Anal. Chem. *66*, 4557, 1994.
5) R. A. Wallingford and A. G. Ewing, Anal. Chem. *61*, 98, 1989.

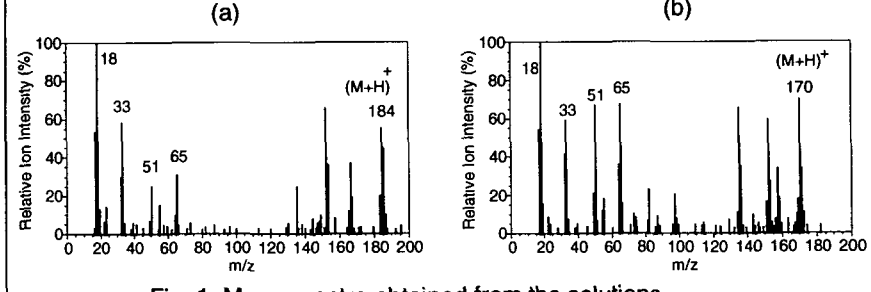

Fig. 1 Mass spectra obtained from the solutions of a) epinephrine and (b) norepinephrine.

Electrospray LC/MS With Ion Trap TOFMS

Randy W. Purves and Liang Li*
Department of Chemistry, University of Alberta
Edmonton, Alberta, Canada T6G 2G2

Electrospray ionization (ESI) has become an increasingly important technique for ion generation in mass spectrometry. ESI is particularly useful for the analysis of polar and ionic species, including peptides and proteins. Since the solutions used for liquid chromatography (LC) are compatible with the ionic solutions used in ESI, these two techniques can be readily combined for on-line chemical identification and structural analysis. Presently, a quadrupole mass spectrometer is most commonly used for this type of analysis. However, for rapidly eluting species from an LC column, a time-of-flight mass spectrometer (TOFMS) possesses some inherent advantages, such as allowing for a high data acquisition rate over the entire mass range, and having a high detection sensitivity. Coupling of an ESI source to a TOFMS has been previously achieved either with the source orthogonal to the flight tube, or in a parallel configuration with an ion trap [1].

Reported here is the development of a linear TOFMS for the mass analysis of ions generated by ESI. Although this instrument was designed to be used either orthogonally, or with the ion trap, the work presented here is obtained exclusively with the ion trap present. A schematic of the instrumentation used in this study is illustrated in Figure 1. The sensitivity and resolution of this instrument are explored. With this linear TOFMS system, mass resolution values in the range of 600 to 950 fwhm are routinely obtained. Figure 2 represents a mass spectrum of equine cytochrome C in which the major peak, 16^+, has a mass resolution of 920 fwhm. This represents a marked improvement over previously reported optimal resolution values for linear TOFMS instruments. Shown in Figure 3A is an ion profile of an injection of 75 fmol of bradykinin, or 0.5 μL of a 125 nM solution. The ion profile is obtained by integrating the area of the major bradykinin peak, which corresponds to the 2^+ charge state, as a function of time. Figure 3B represents the complete mass spectrum that was obtained from this injection. Work on actual separations of protein mixtures using a micro-column LC system has been recently initiated.

REFERENCE:

[1] Qian, M.G., and Lubman, D.M., *Anal. Chem.*, **1995**, 67, 234A-242A.

43rd ASMS Conference on Mass Spectrometry and Allied Topics

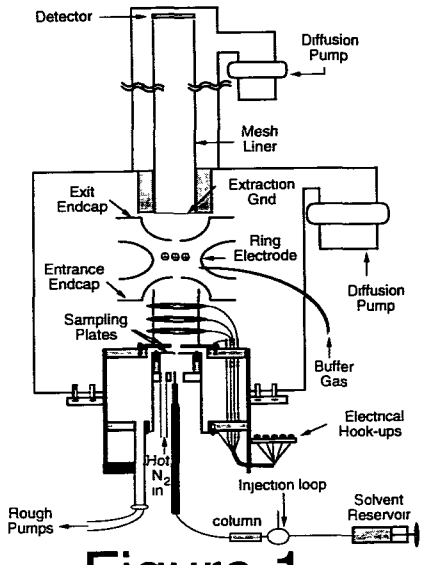

Figure 1

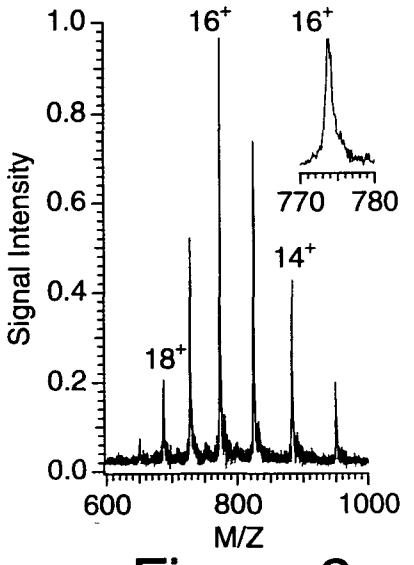

Figure 2

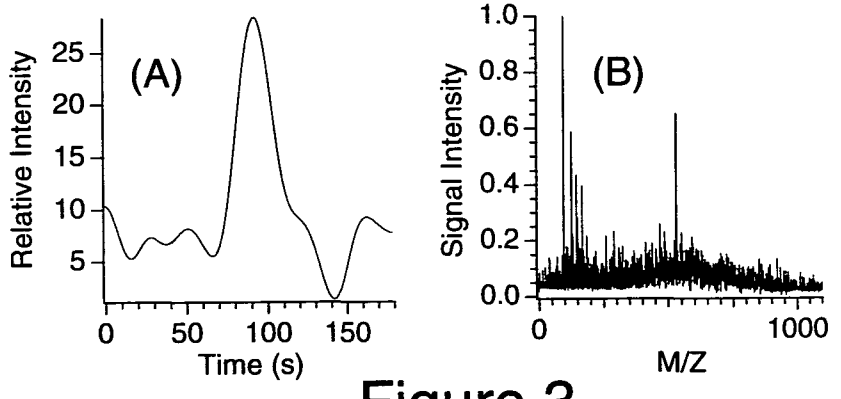

Figure 3

High Sensitivity Electrospray With A Fourier Transform Mass Spectrometer

Catherine Stacey, Gary Kruppa, J. Paul Spier, Matthias Wilm* and Matthias Mann*

Bruker Analytical Systems Inc., Billerica, MA

*European Molecular Biology Laboratories, Heidelberg, Germany

Current electrospray ion sources spray liquid from a needle at flow rates above 1µl/min. Optimization of conditions for high sensitivity MS/MS analysis may consume over 100 pmol of a sample. The use of a new small-scale "micro electrospray" or "NanoSPRAY" needle with an electrospray source permits the analysis of 1 µl or less of solution of low pmol/µl concentration at a flow rate of 25nl/min. Sensitivity enhancements result from more efficient ion evaporation from the smaller droplet and sampling a larger proportion of the ions produced by a combination of a smaller spray and a closer distance. Additionally, a wider variety of solvents, such as pure water or pure organics, can be sprayed without the use of sheath gas or nebulization since the effects of surface tension are less important with this design.

A sample of 2µl of myoglobin tryptic digest (40pmol) was applied to the NanoSPRAY needle. Identifiable peaks resulted from a single scan spectrum with a consumption of 4 fmol and an averaged spectrum using 65fmol is also shown (The presence of high levels of acids and salts in the digest sample results in lower sensitivity than expected from pure peptides in methanol/water/3% acid). The spectrum resulting from the analysis of the tryptic digest of myoglobin showed a number of ions. Charge state are easily determined from the isotopic spacing.

These masses were entered into PeptideSearch, allowing for only ppm errors in mass. Hits to myoglobins were found, with only horse myoglobin matching to 10 of the fragment masses

Using the same sample, one of the masses was isolated for SORI (Sustained Off-Resonance Irradiation) MS/MS. A partial sequence for the peptide resulted which can also be used for searching protein sequences. The CID spectrum was also obtained with fmol amounts of sample consumed. Two partial sequences could be determined from this spectrum as -HGAI/L- and -LV-. Without knowing if these ions are from b or y" series, the direction of the sequence is unknown

Searching for these patterns as either b or y" series also results in matches to myoglobin

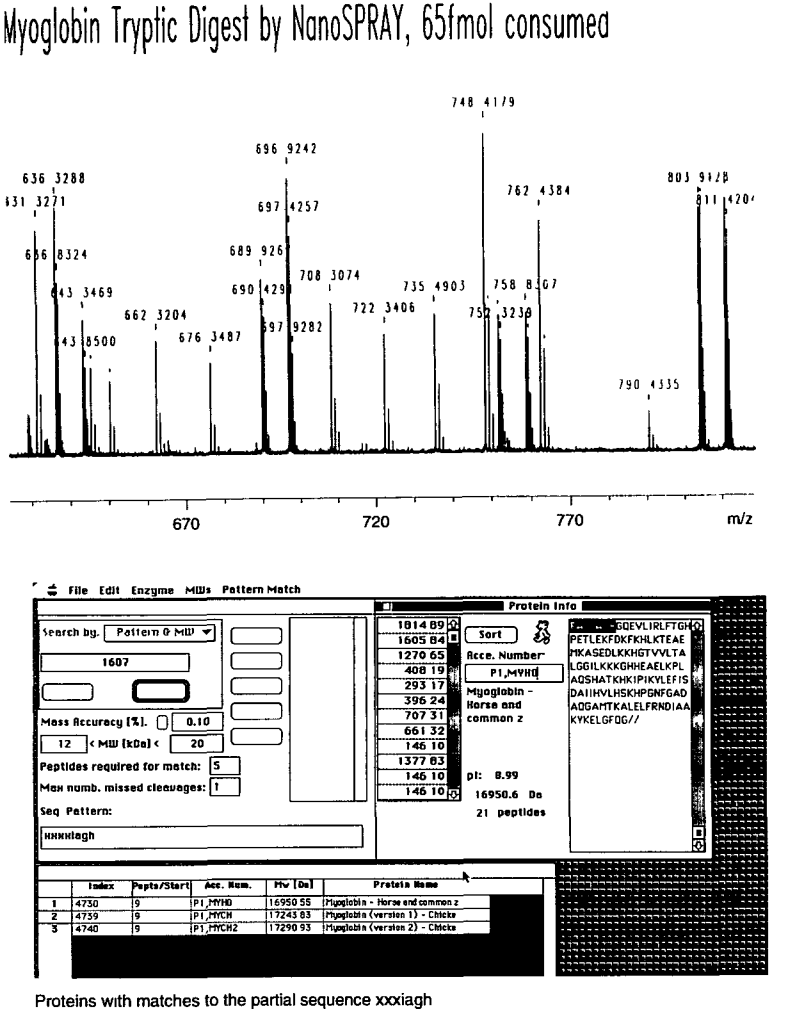

Proteins with matches to the partial sequence xxxiagh

Characterization of *in vitro* Metabolites of Ziprasidone by HPLC/RAM/ESI/MS/MS

Amin Kamel*, and Chandra Prakash
Pfizer Central Research, Department of Drug Metabolism Groton, CT 06340.

Ziprasidone, 5-[2-{4-(1,2-benzisothiazole-3-yl)-1-piperazinyl}ethyl]-6-chloro-1,3-dihydro-2H-indole-2-one hydrochloride hydrate, is a potent and highly selective inhibitor of dopamine D2 and serotonin 5-HT2 receptors Ziprasidone demonstrates clinical efficacy against positive and negative symptoms of schizophrenia with reduced extra pyramidal symptoms *In vitro* Metabolism of CP-88,059 labeled with [^{3}H]-and [^{14}C] was investigated to predict the *in vivo* metabolism using hepatic microsomal preparation from phenobarbital (PB) induced rat liver microsomes The metabolites were separated on reversed phase HPLC using an YMC basic column A total of 12 radioactive peaks were detected by HPLC-RAM. Comparison of *in vitro* metabolism of ziprasidone using rat, dog, monkey and human liver microsomes indicated similarities in the major metabolites in all species.

Chemical structures of the metabolites were proposed based on ion spray LC/MS using a combination of Q1 scan, parent ion and product ion monitoring techniques Atmospheric pressure ion mass spectra of ziprasidone and its metabolites gave intense protonated molecular ions. Collision activated dissociation (CAD) product ion scans of protonated molecular ions provided the structurally informative fragment ions. The structures of 7 metabolites were confirmed unambiguously by co-elution on HPLC with the synthetic standards Five major metabolites were identified as the sulfoxide and sulfone of ziprasidone, and benzisothiazole and its sulfoxide and sulfone. The other metabolites were due to N-dealkylation of the benzisothiazole moiety and degradation of the piperazine ring, resulting in the formation of oxindole ethyl piperazine and ethylenediamine analog, respectively A scheme for the metabolism of ziprasidone is proposed

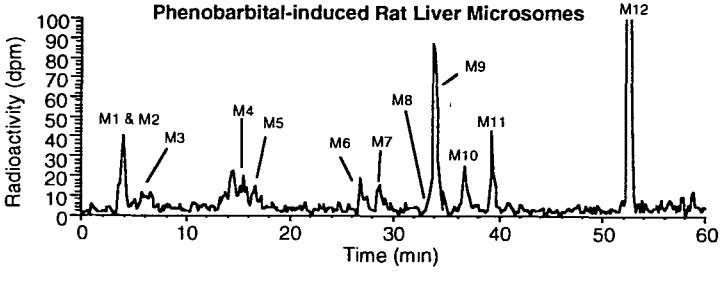

Figure 1. HPLC- Radiochromatograms of *in vitro* metabolites of ziprasidone

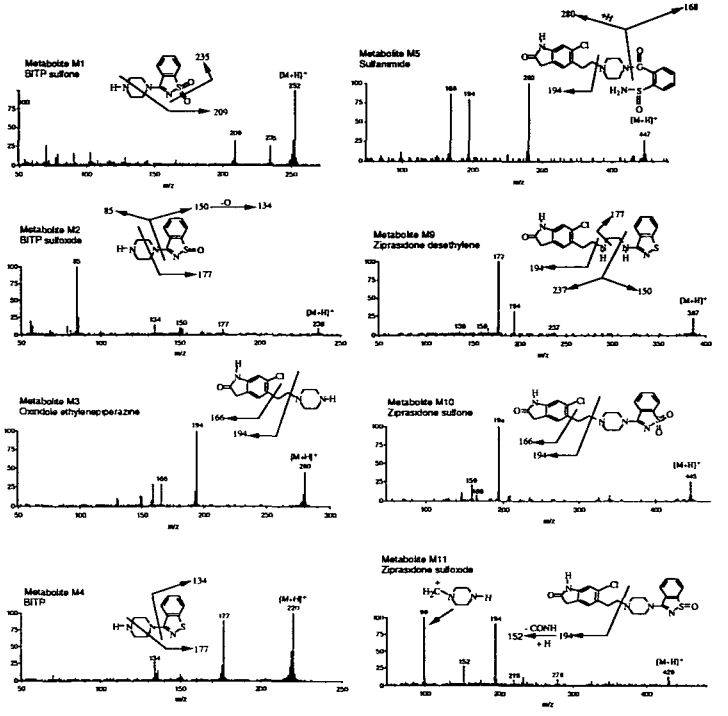

Figure 2. CAD product ion mass spectra of *in vitro* metabolites of ziprasidone

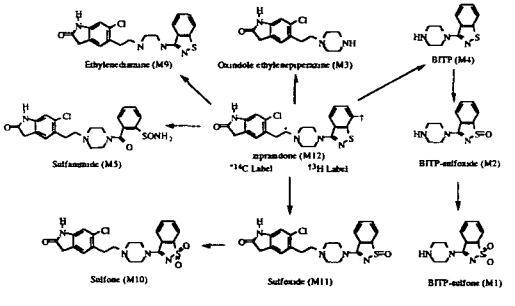

Figure 3. Proposed *in vitro* metabolites of ziprasidone

Reduction of Ambient Air Contaminants

Beat Aebi and Jack D. Henion
Analytical Toxicology, Diagnostic Laboratory, Cornell University,
927 Warren Drive, Ithaca, NY, 14850

To reduce the chemical noise on our Ion Spray - API Ion Trap mass spectrometer (ref 1-5), we have looked at the possible sources of contamination. The contaminants from the ambient air were found to be very important. As the heated shield uses heat for the desolvation of the analyte ions, plastic components were found to be gassing out elevated levels amounts of plasticizers and other substances. Ambient air penetrating the ionization region on this open interface appeared to produce a variety of background ions. Several experiments indicated that uncharged gaseous contaminants in the ionization region were ionized and entered the ion trap analyzer, producing different levels of chemical noise. We have modified the original, open heated shield interface to a plastic-free, closed type of interface with both bath and curtain gas to prevent any contaminants from entering the ionization region. Additionally, we have added a temperature controller to stabilize and hold the shield temperature at the desired level.
The closed shield interface was found to reduce chemical noise significantly and to produce a more stable ion current than the open shield interface. As a result, the scanned mass range could be expanded (from 100 or 200 Da to the full range of 10-650 Da) and the amount of substance detected in the extracted ion current could be lowered, yielding proper mass spectra without using signal averaging and backgound subtraction. The continuous removal of the ionization region atmosphere to allow new gas to enter and to purge solvent and contamination vapors could be the reason for the much better desolvation efficency and lower chemical noise.

The authors would like to thank the Eastman Kodak Company (Rochester, NY) and also the Varian Instrument Company for the generous support of this work . Special thanks go to Mr. Jerry Zweigenbaum from Eastman Kodak and Drs. B. Buttrill and B. Shaffer from Varian for invaluable assistance during this work.

Ref: 1.) A.V. Mordehai, G. Hopfgartner, T.G.Huggins, J.D. Henion, Rapid Comm. MS, 1992, 6, 508-516
2.) A.V. Mordehai, J.D. Henion, Rapid Comm. MS, 1993, 7, 205-209
3.) A.V. Mordehai, J.D. Henion, U.S. Patent 5,268,572
4.) J.D. Henion, A.V. Mordehai, J. Cai, Analyt. Chem., 1994, 66, 13, 2103-2109
5.) M.E. Emmett and R.M. Caprioli, JASMS 1994, 5, 605-13

API-MS Heated Liquid Shield Interface

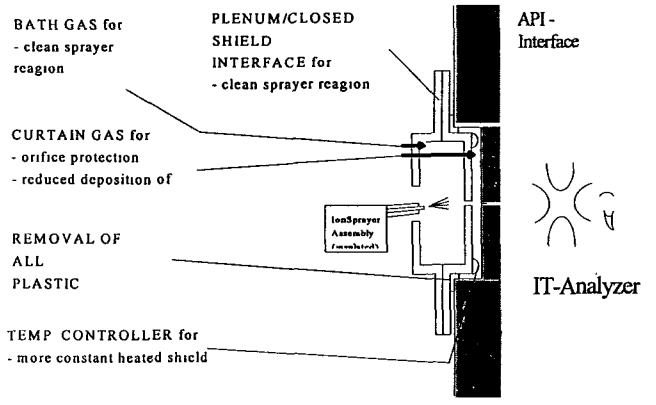

Ion Spray Mass Spectrum of Berberine (3.2pg)
New Type of Interface, Full Mass Range 10-650 amu
One Scan, no Signal Averadging or Background Subtraction

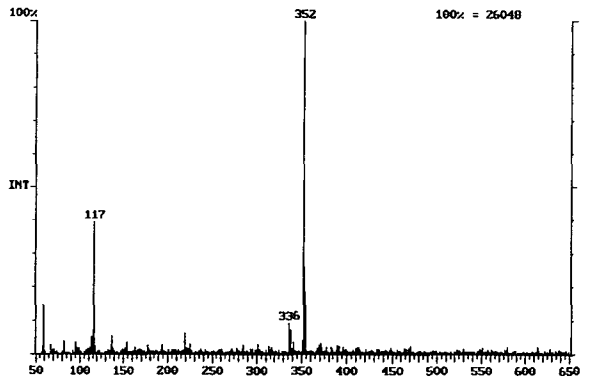

Pulsed Electrospray and Selected Ions from Electrospray Ion Source by Ion Mobility Spectrometry*

#Guo-Zhong Li, Weimin Wang, Tamen Kim, R. B. Moore

Foster Radiation Laboratory
Department of Physics, McGill University
Montreal, Quebec, Canada, H3A 2B1

Electrospray as an Atmospheric Pressure Ion (API) source has been widely used in mass spectrometry because of it being an ideal interface between liquid chromatography and mass spectrometry, and because it can produce highly charged bimolecular ions. Ion Mobility Spectrometry (IMS) has been widely used for the detection of chemical weapons, drugs and explosive materials etc. [1], and even as a detector for liquid chromatography [2,3].

In this work we have investigated the pulsing of an electrospray source. There are several possible applications for such a source. One is to use a pulsed electrospray to replace the Bradbury-Nielson shutter-grid gate usually used for IMS. The advantage of this is the large ion current that can be delivered. Another is to use pulsed electrospray together with the Bradbury-Nielson shutter to enhance the selectivity of the IMS system. A third possibility is to use pulsed electrospray to replace the usual DC electrospray source for mass spectrometry. The advantage of this is to improve the efficiency of transferring ions from atmosphere into a vacuum by focusing the ions onto the vacuum orifice.

A schematic of the instrumentation used for pulsed electrospray and IMS is shown in fig. 1. High voltage pulses for the electrospray and the shutter were created by a high-voltage transistor switch from Belke Electronic. The voltage on the needle required for electrospray was less than 8 kV. At these voltages there was no corona and no sparking, the ions coming exclusively from the electrospray process. Polypropylene glycol with a molecular weight of 2000 Daltons was used as a sample, at a flow rate of 0.33 microliters/min. The IMS cell was at room temperature and the nitrogen gas flow rate through it was 300 microliter/s.

Figure 2 gives an example of the ion mobility spectrum without the Bradbury-Nielson shutter. We believe this to be the first use of a pulsed electrospray. Ions could be produced by a HV pulse of only one microsecond. However, for ionization efficiency and stability the pulse width used for the data of fig. 2 was chosen to be 4 ms. The ions could also be further selected by choosing the duration of the electrospray pulse and the delay time between the source pulse and the opening of the shutter. Figure 3 shows the result of using this combination.

*Work supported by NSERC (Canada) strategic grant.
#present address: National High Magnetic Field Laboratory, Tallahassee, FL32306

(1) G. A. Eiceman and Z. Karpas, Ion Mobility Spectrometry, CRC press, Inc., **1994**;
(2) D. Jones and A. G. Brenton et al., Rapid Commun. in Mass Spectrometry, **7**,561-566 (**1993**);
(3) D. P. Wittmer, Y. H. Chen, B. K. Luckenbill, H. H. Hill, Jr. Anal. Chem. **66**, 2348-2355 (**1994**)

43rd ASMS Conference on Mass Spectrometry and Allied Topics

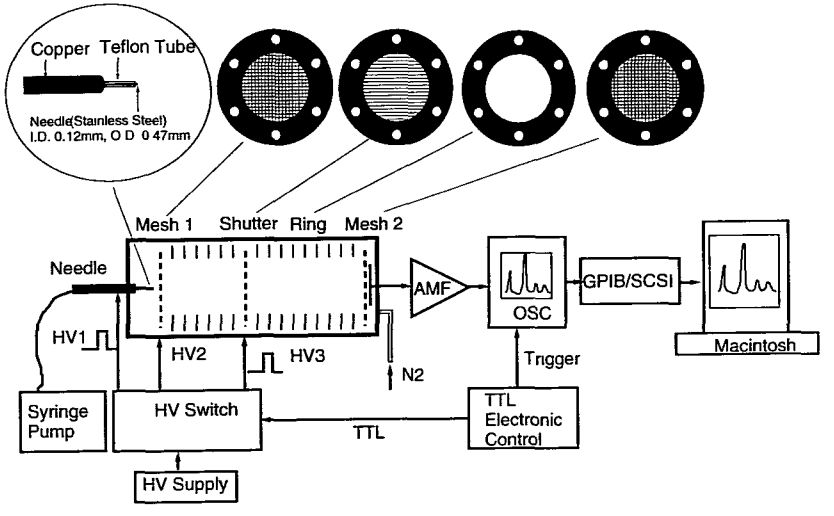

Fig. 1. Ion Mobility Spectrometry with pulsed electrospray

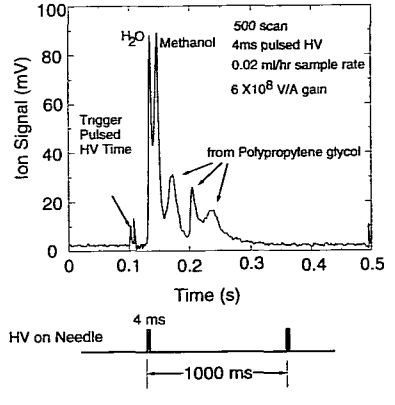

Fig. 2. Ion mobility spectrum of polypropylene glycol using pulsed electrospray.

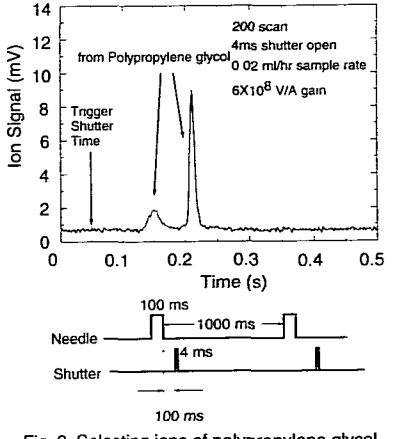

Fig. 3. Selecting ions of polypropylene glycol by Ion Mobility Spectrometry with pulsed electrospray combined with a Bradbury-Nielson shutter.

Achieving High Sensitivity LC/MS with an API-Ion Trap Mass Spectrometer

Sohrab Habibi-Goudarzi and **Jack Henion,** Analytical Toxicology, Cornell University, 927 Warren Drive, Ithaca, NY 14850
Kevin L. Duffin and **Fred D. Hileman**, Analytical Sciences Center, Monsanto Co., 800 N. Lindbergh Blvd., St. Louis, MO 63167

Introduction:

An EI/CI Finnigan ion trap mass spectrometer has been extensively modified and equipped with a heated capillary type (1) atmospheric pressure ionization source. Our goal is to build upon the pioneering work of McLuckey, et al. at Oak Ridge National Laboratories (2) and the experience present in the Cornell laboratory (3) and construct an API-ITMS that is rugged, simple, reliable and that can be used with a number of on-line separation techniques with target sensitivity in the sub-femtomole range. We have achieved low femtomole sensitivity by on-line CE/MS and low picomole sensitivity by LC/MS.

Experimental:

Prior to every on-line experiment, the trap conditions were optimized by continuous infusion of a standard solution of the analyte(s) of interest. The trap typically is filled with ultra-pure Helium to a partial pressure of about one mTorr. Typical ion accumulation times of about 0.1 to 0.3 seconds were used at rf trapping voltage range of 496 to 958 volts (0-p) which corresponds to m/z cut-off at m/z 43 to 83. The total data acquisition time was adjusted to be suited for the width of the eluting peak.

The ion trap was coupled with a Hewlett-Packard ^{3D}CE via a sheath-flow interface. CE/MS experiments were carried out to analyze a mixture of eight β-Agonists. The fused-silica capillary column used had a 50 μm i.d and was 90 cm long and was maintained at 30 kV. The buffer was composed of 10 mM ammonium acetate and 0.1% acetic acid.

A waters 616 HPLC system was also coupled with the ion trap via an ion-spray interface. A Keystone Betasil C_{18}, 1 mm i.d. x 100, 5 μm particle size, column was used to analyze Reserpine from equine plasma extracts (through a three step liquid/liquid extraction). The HPLC separations were carried out under isocratic conditions using 80:20 acetonitrile : water and 5 mM ammonium acetate at 50 μL/min.

Results and Discussion:

The data were collected using our first version of the API-ITMS system. Many hardware changes were made which have increased the sensitivity. The most significant improvement took place by applying an improved ion-gating conditions. We still need to better understand the source of the chemical noise and reduce or eliminate it. Our goal is to be able to detect the presence of an analyte in the total ion current of a full-scan mass spectrum which is essential when analyzing ultra-trace level unknowns. We can now routinely observe low to sub-picomole levels of analytes from both standards (Figure 1) and "real" samples, e.g. reserpine in plasma extracts (Figure 2) in the TIC. The heated capillary inlet seems to work very efficiently, i.e. declustering in the trap via delay time is not needed. The capillary temperature can be lowered if the formation of clusters is desirable (e.g. in noncovalent interaction studies). At this time, the API-ITMS system provides quality data and the results are encouraging. However, we still need to improve the on-line sensitivity of the system by 100-1000 fold.

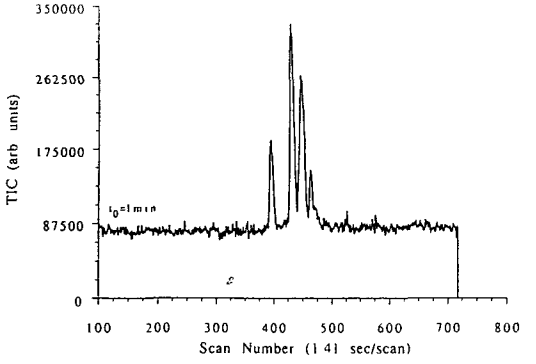

Figure 1: CE/MS of a mixture of eight β-Agonists. The amount of sample injected is one picomole. Scan range is m/z 40-640.

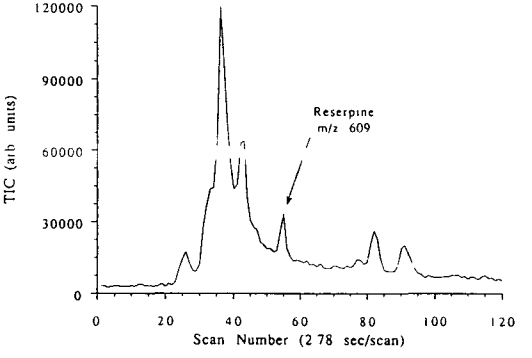

Figure 2: LC/MS determination of eight picomoles of Reserpine in an extract of spiked equine plasma. Scan range is m/z 80-640.

Acknowledgments:
SHG and JH would like to thank the Analytical Sciences Center of Monsanto Co. (St. Louis, MO) for supporting this work. The CE/MS experiments were carried out in collaboration with Robin Sheppard and the LC/MS experiments with Dr. Melissa Anderson Dr Tim Wachs, Karen Bean, Jianyi Cai, and Dr. Mike Nedved are appreciated for their assistance in a variety of tasks. Jerry Zweigenbaum of the Eastman Kodak, Co., is thanked for his assistance with the heated capillary modification.

References:

1) S.K. Chowdhury, V. Katta, and B.T. Chait, RCM 1990, 4, 81.
2) G.J. Van Berkel, G.L. Glish, and S.A. McLuckey, Anal. Chem., 1990, 62, 1286.
3) A.V. Mordehai, and J. Henion, RCM, 1993, 7, 205.

Capillary, multicapillaries or porous tube for electrospray ion source

Claude Beaugrand#, Florence Charbonnier*, Christian Rolando*, Michel Sablier* and Florence Saru*

(#) AIRND, 35 rue Victor Hugo, 78230 Le Pecq, France
(*) Ecole Normale Supérieure, Département de Chimie, URA 1679, Procesus d'Activation Moléculaire
24 rue Lhomond, 75231 Paris Cedex 05

A major problem in electrospray ion sources is the transfar of ions from atmospheric pressure to vacuum. Most of the actual designs use a heated capillary tube (1). Using the three stages design, whith an RF only transfer quadrupole, we described last year (2), we have investigated how to improve the transfer of ions.

Various capillary tubes from 0.25 to 1.5 mm diameter have been tested, keeping the same pressure in the expansion area. This led us to use pumping speeds up to 80 cubic meters per hour. In all cases, electrospray ions can be obtained. Surprisingly, with large capillary diameter, results are not the best: total intensity is not higher and clusters intensity rises.

Desolvatation problems are due to a high velocity sampling flow in the capillary, which depletes the electrospray Taylor cone, or/and to low heat transfer to the bulk flow. Our best compromise is a 0.5 mm diameter capillary (as in most instruments). The pressure distribution is then : P_1 ca 1 Torr, $P_2 = 8x10^{-2}$ Torr, $P_3 = 7x\ 10^{-5}$ Torr. One way to solve those problems is to increase the flow but whitout enlarging the flow speed. This can be done by using several capillaries of smaller diameter.

We made a tube composed of seven small tubes welded together (Figure 1). The external diameter of each tube is 0.8 mm and the external diameter of the bunch is 1/8 inch. By closing one or several tubes we can modify the collecting surface.

Another approach is to create a flow speed gradient inside the tube. This can be achieved by exchanging the capillary tube by a porous metal one, of the same length but pumped separately by a mechanical pump.

The spray current of a solution of 10^{-5} mol.l^{-1} of TDA recorded after mass selection is given in the table below:

Number of tubes	1	5	5**	7
Current*	1	1.75	1.5	3.5

* relative values ** whithout center tube

TDA: (tris[2-(2-methoxymethylethoxy)ethyl]amine

The current we can obtain in the mass analyzer is not proportional to the sampling surface of the capillary. The position of the sampling surface in front of the needle plays a role. There are other problems in the limitation of the useful spray current than the maximum flow admitted to the system.

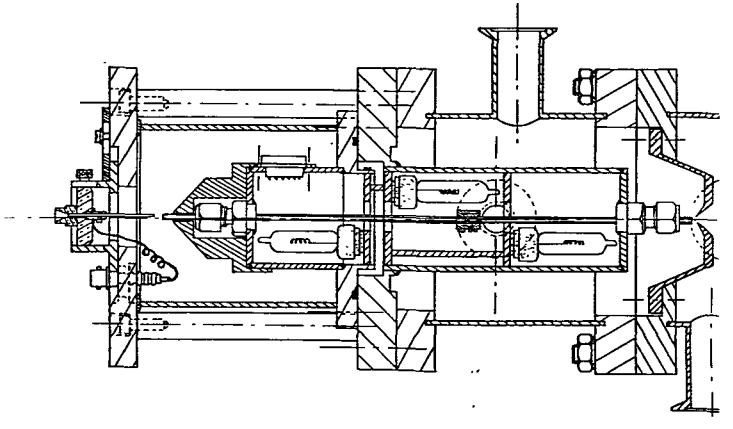

Figure 1: Three Pumping stages Electrospray Source with Multicapillaries tube

(1) Swappan K. C., Viswanatham K. and Chaitt B. T., Rapid Comm. Mass Spectrom , 4, 81 (1990)
(2) Rolando C. et al, 42nd ASMS Conference on Mass Spectrometry and Allied Topics, Chicago, p 761.

Transport of Electrospray Particles through the Interfaces

P.V. Bondarenko and R.D. Macfarlane
Department of Chemistry, Texas A&M University, College Station, Texas 77843

A stainless steel capillary, a teflon tube and a flat orifice were tested as atmospheric pressure/vacuum interfaces for electrospray particles. A solution of red Rhodamine B dye was employed to facilitate the quantitative measurements of transport efficiency using spectrophotometric analysis. The optimal transport efficiency was obtained where the 100 µm o.d. fused-silica electrospray capillary was positioned 1 mm from the 250 µm i.d. flat orifice. In that case, more than 99% of the electric current and dye component were transported into the vacuum.

The electrostatic deflection of the particles in vacuum allowed us to calculate an energy-to-charge ratio (E/z). The mean E/z ratio is 5000 eV/e. Assuming that the velocity of a typical particle is equal to the velocity of an air jet entering vacuum (velocity of sound), one can estimate the m/z ratio of the particles to be in the order of 10^7 u/e. From the electrospray flow rate of 0.5 µl/min and electrospray current of 40 nA used in our experiment, the m/z ratio of typical parent droplets was found to be equal to $2x10^7$ u/e. Those two m/z ratios are similar. Hence, the particles behind the orifice are predominantly parent charged droplets. The mass of those droplets is much larger than the mass of air molecules in the entering jet. Due to this fact, the charged droplets are directed strictly perpendicular to the orifice plane, with narrow angular distribution.

In the second stage of our investigation, the electrospray particles were introduced into a high vacuum chamber ($4x10^{-5}$ Torr) through the two additional pumped regions separated by two conical skimmers (Figure 1). The electrostatic deflection study showed that the particles keep their m/z ratio close to m/z ratio of the parent charged droplets. More than 30% of electrosprayed sample was transported into the vacuum through the orifice and the skimmers. Those droplets are requiring further evaporation to produce ions for mass spectrometry.

Evaporation in high vacuum is a difficult problem, because collisions with residual molecules of air are very rare. The charged droplets "freeze" in high vacuum and require an input of energy for evaporation and ion formation. At that point of our study, we introduced a Heated Electrostatic Particle Guide (HEPG) between the electrospray source and a mass analyzer (Figure 2).

The HEPG serves two purposes. First, it emits infrared and visible radiation. This radiation provides energy which is required for the evaporation and ion formation from the charged droplets (Figure 2). Second, as a component of the ion optics, it transports the droplets and ions through the vacuum chamber and focuses them onto the entrance of the mass analyzer. SIMION calculations (Figure 3) show that ions emitted from the droplets at the distance of a few millimeters from the wire will be captured by the field, transported along the rest of the guide and focused into the entrance of the mass analyzer. The HEPG-focusing electrode assembly was built according to the SIMION calculations and tested. It allowed us to focus the particles into a 7 mm dia. spot at the entrance plane of the mass analyzer.

Recently, we have built a time-of-flight mass analyzer which is the final step in the development of our mass spectrometer (Figure 1). With this analyzer, we plan to determine the m/z ratio of the final particles and observe the influence of the heating of the droplets on the ion formation and fragmentation.

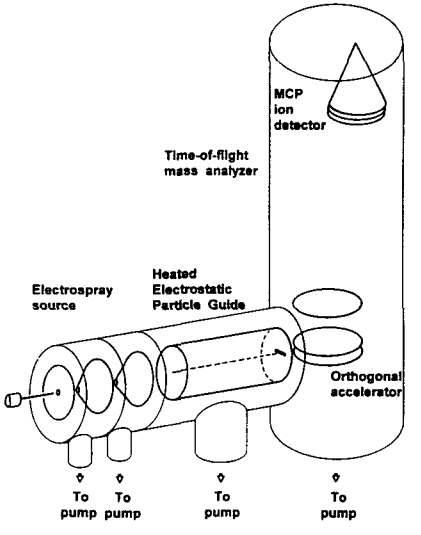

Figure 1. Schematic diagram of electrospray TOF-MS.

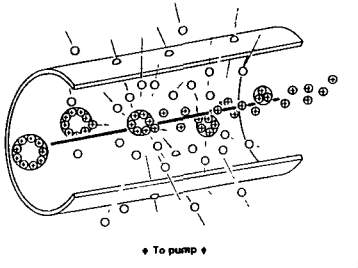

Figure 2. Schematic representation of processes in heated electrostatic particle guide (HEPG).

Trajectory Parameters:

O m/z of ions	1200	O Ion energy	5 eV
O Starting coords	Y=1.27 mm DX=1.27 mm	O Angle to X-axis	0 degrees
		O No. of trajectories	10

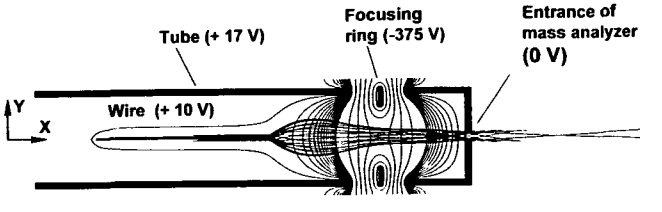

Figure 3. SIMION ion trajectory simulation in region of HEPG.

Electrospray Ion Distributions and Efficiency of Transferring Ions from Atmosphere into Vacuum*

#Guo-Zhong Li, Weimin Wang, Tamen Kim, R. B. Moore

Foster Radiation Laboratory
Department of Physics, McGill University
Montreal, Quebec, Canada, H3A 2B1

The mechanism of electrospray has been extensively studied during the past several years. In its application to high resolution mass spectrometry an important aspect of such a source is the efficient transport of its ions through an orifice into a vacuum. In this paper we present results of a study of the ion distribution near a vacuum orifice and the efficiency of transferring ions through the orifice. The motion of electrospray ions from a source into a vacuum is determined by four effects, the spatial distribution of the ionization, the electric field from the voltage on the needle, Coulomb interaction between the ions and the gas dynamics near the orifice. The ions are usually produced in a small volume near the needle and in their early motion follow the electric field lines from the needle according to their mobilities. However, as the field drops rapidly away from the needle the ion speed considerably diminishes and Coulomb interactions between the ions become important, pushing them away from the axis of the transport system. Finally, as the ions approach the orifice, the electric field becomes relatively unimportant and gas dynamics become the overriding consideration, causing the ions to speed up again as they pass through the orifice and exceed the speed of sound.

A schematic of the instrumentation to study this motion is shown in fig. 1. Two samples were used in the study; 2-Propanol and polypropylene glycol of molecular weight 2000 Daltons. The orifice flow was attained by a Roots blower (Alcatel model MIV 350) with 116L/s pumping speed. The vacuum interface was made of a printed circuit board with copper rings concentric to a 0.6 mm orifice. Currents on the rings and the detector were measured by current meters. The total electrical current to the needle was measured by a current to voltage amplifier specially made to be floated at high voltage.

When there was no pumping, the ion intensity distributions were as shown in fig. 2. At high voltages on the needle the distributions were seen to have a ring shape with a depression at the axis of the system. With pumping so that the pressure on the vacuum side of the orifice became 0.57 Torr the distribution was as shown in fig. 3. In this case the current through the orifice was found to be always proportional to the current on the inner ring and that the efficiency of transfer of the ions through the 0.6 mm orifice could be as large as 6%. This indicates that with such a relatively large orifice the transfer efficiency can be made to be largely determined by the gas dynamics at the orifice.

*Work supported by NSERC (Canada) strategic grant.
#present address: National High Magnetic Field Laboratory, Tallahassee, FL32306

43rd ASMS Conference on Mass Spectrometry and Allied Topics

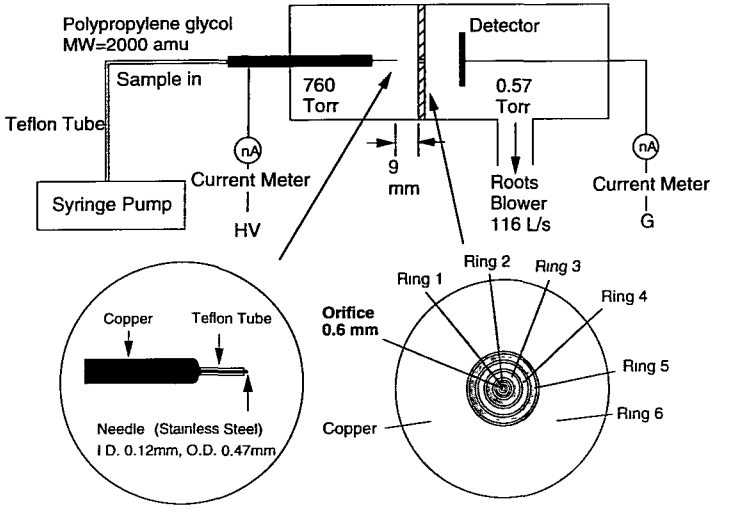

Fig. 1 Electrospry system for measuring the ion distributions at a vacuum interface.

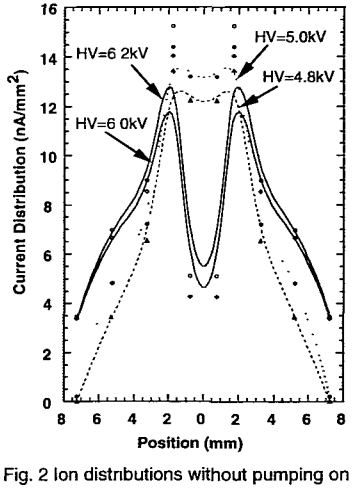

Fig. 2 Ion distributions without pumping on the orifice

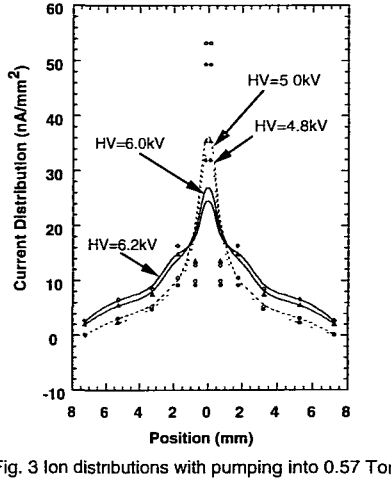

Fig. 3 Ion distributions with pumping into 0.57 Torr in the vacuum chamber

Stability Of A Liquid Jet Emerging From An Electrospray Cone-Jet

Edward W Sheehan and Ross C Willoughby
Chem-Space Associates, 75 Chapel Ridge Place, Pittsburgh, PA 15238

In a continuing effort to understand the underlying mechanism of electrospray we present here an argument for the formation of an electrospray cone-jet based on the Rayleigh limit. When a liquid flows through a cylindrical capillary at low flow rates, spherical droplets emerge from the tip and are held by surface tension until gravity overcomes the adhesive forces; then the drops detach. When an electrical potential is applied to the capillary, the liquid is electrified. As the liquid is charged to a higher potential, the spherical liquid surface at the tip of the capillary deforms into a conical surface and a liquid jet emits from the apex of the cone. This liquid jet breaks up into droplets which undergo further deformation producing smaller droplets or ion clusters which eventually lead to gas-phase ions. The objective of the following study was to compare the Rayleigh limit for spheres and cylinders and observe the effects of density, surface tension, and viscosity of various solvents on the stability of liquid jets.

What is the Rayleigh Limit? Lord Rayleigh[1] described the stability of liquid surfaces as the balance of two forces, an inward pressure due to surface tension and an outward pressure due to charge repulsion. He formulated this as follows:

$$p^2 = n(n-1)/\rho r_s^3 \{(n+2)\gamma - (q^2/8\pi r_s^3)\} \quad (1)$$

where $(n+2)\gamma$ represents the surface energy component and $q^2/8\pi r_s^3$ the electrostatic component. For a spherical droplet, if the surface energy is greater than the electrostatic component ($p^2 > 0$) the spherical form is stable for all deformations When the charge density (q/r_s) is great ($p^2 < 0$), electrostatic forces dominate and the spherical form becomes unstable. Under these conditions the liquid droplet deforms, a cone forms, and liquid is thrown out in a fine jet (a cylinder).

Charge Limit for a Sphere and a Cylinder. The maximal allowable charge on a spherical droplet is:

$$q_s = 8\pi\varepsilon_0^{1/2} \gamma^{1/2} r_s^{3/2} \quad (2)$$

while the maximum allowable charge on a cylinder is:

$$q_c = 6^{1/2} \pi\varepsilon_0^{1/2} \gamma^{1/2} l_c r_c^{1/2} \quad (3)$$

where γ = surface tension; ε_0=permittivity constant; r_s is the radius of a drop; and l_c and r_c are the length and radius of a cylinder, respectively.

Ratio of the Maximal Allowable Charge of a Sphere and a Cylinder. Comparing the charge limits of a sphere and a cylinder (q_s/q_c) results in:

$$q_s/q_c = 0.94 \quad (4)$$

The fact that the ratio is not 1 or greater implies (1) that cylinders can hold more charge than a sphere of the same mass; (2) the 6% excess charge on the jet surface at the charge limit must be dissipated in droplet, cluster or ion formation process(es); (3) as a sphere reaches its charge limit it can relieve the electrostatic forces on it by forming a jet to carry away the excess charge; and (4) the transformation from a sphere to a jet is a cone.

Current Onset for Various Solvents. The onset of a stable cone/jet was observed for various solvents, such as water, methanol, ethanol, isopropanol, acetonitrile, and hexane. Figure 1 shows the variation in current with applied voltage for water and isopropanol (IPA). Two things were noted (1) for water: there was no observed stable cone/jet and the collected current was due to the discharge of the air surrounding the needle; (2) for isopropanol (and the rest of the solvents, not shown): a stable cone/jet was observed but in addition, as the applied voltage was increased the jet for IPA narrowed and took on a cone-like appearance before the jet broke up. This narrowing of the jet was not observed for less viscous solvents, such as methanol, ethanol, acetonitrile, and hexane. From these observations it was concluded that (1) for liquids with high surface tension (such as water), the gases surrounding the needle will discharge before the charge density on the surface of the liquid is high enough to form a cone/jet; and (2) viscosity may play an important role in the stability of a jet. Viscosity was not considered in the original treatment of the stability of electrified liquids by Lord Rayleigh and therefore to gain a more complete understanding of jet stability and the eventual production of gas-phase ions, viscosity warrants further investigation and inclusion in any theoretical treatment of cone/jet electrospray.

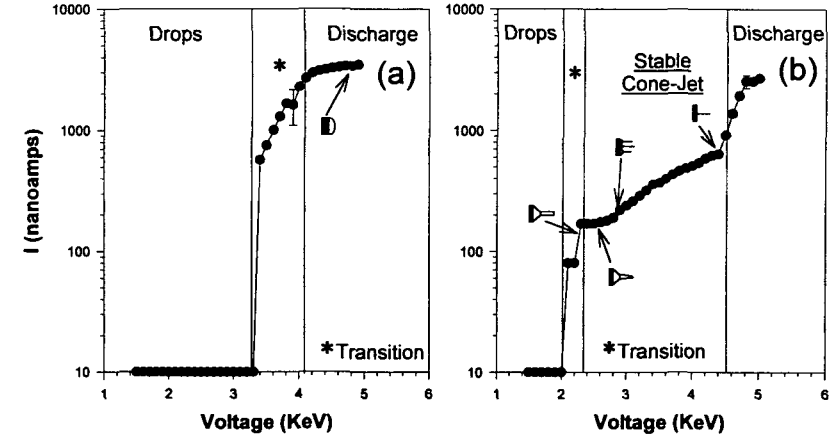

Figure 1. Variation of current with applied voltage by electrospraying water (a) and isopropanol (b) in air. The appearance of the cone/jet is also indicated on the figure. The distance between the needle tip and the grounded plate was ~ 2 cm. The current was determined by directing the droplets at the grounded plate and measuring the current between the plate and ground with a microampmeter. The needle, the electrospray cone, and liquid jet were observed through a microscope. Deionized water and pesticide grade isopropanol were used. Flow 1μL/min.

[1]Rayleigh, Lord *Proc. Phil. Mag. Series*, 1882, *5*, 184.

Secondary Droplet and Ion Formation in Electrospray: The Teardrop Model

Sheehan, Edward, and Willoughby, Ross
Chem-Space Associates, 75 Chapel Ridge Place, Pittsburgh, PA 15238

Experimental evidence has shown that at least one mechanism for secondary droplet and ion cluster formation in electrospray is through conical deformation of a charge saturated primary droplet. Photographic evidence has been produce from droplet electrospray[1], liquid droplets[2], and particle residues[3].

These results show that spherical droplets deform under the influence of high field. The high field is produced as a result of evaporation of droplets past there Rayleigh limit.[4] The deformation results in the observed "teardrop" geometry which can be evaluated for energy, charge, and mass balance as the deformation occurs. Any deformation of the droplet will result in a potential difference across the deformation and a net decrease in the potential of the droplet. If the system loses charge and moves matter, the potential energy of the system must be reduced.

Another important observation from the particle residue photographs was the consistency of the geometry in the particle. We conclude from these data that the teardrop process of secondary droplet and ion cluster ejection is a sustainable process; at least under conditions of high evaporation rate in these experiments. Few spherical geometries were observed.

The surface of a teardrop shaped droplet can be described by,

$$A_t = 2\pi r_s^2 (1 + \sin\theta + 0.5 (\cos\theta \cot\theta))$$

$$A_t = A_s (0.5 + 0.5 \sin\theta + 0.25 (\cos\theta \cot\theta))$$

where A_t = surface area of the teardrop, A_s = surface area of the sphere, r_s = radius of the sphere, and θ = angle of conical deformation.

The volume of a teardrop shaped droplet can be described by,

$$V_t = (4/3)\pi r_s^3 (0.25 \cos^2\theta - 0.25 \cos^2\theta \sin\theta - 0.75 \sin^2\theta + 0.25 \sin^3\theta))$$

$$V_t = V_s (0.25 \cos^2\theta - 0.25 \cos^2\theta \sin\theta - 0.75 \sin^2\theta + 0.25 \sin^3\theta))$$

where V_t = volume of the teardrop, V_s = volume of the sphere, r_s = radius of the sphere, and θ = angle of conical deformation.

The radius of a teardrop shaped droplet can be described by,

$$r_t = r_s (0.25 \cos^2\theta - 0.25 \cos^2\theta \sin\theta - 0.75 \sin^2\theta + 0.25 \sin^3\theta)^{1/3}$$

where r_t = radius of the teardrop and r_s = radius of an undeformed sphere.

The potential for a teardrop as a function of radius and angle of deformation can be described by,

$$V(r,\theta) = (1/4\pi\varepsilon_o)\ (q_s/r_t)$$

$$V(r,\theta) = (1/4\pi\varepsilon_o)\ (q_s/\ r_s\ (0.25 \cos^2\theta - 0.25 \cos^2\theta \sin\theta - 0.75 \sin^2\theta + 0.25 \sin^3\theta)^{-1/3})$$

Figure 1 is a graph of the potential of a droplet as a function of a teardrop deformation. This calculated decrease in potential may be used to evaluate the energy balance associated with the teardrop mechanism of secondary droplet and ion formation.

Future studies are intended to more fully characterize this model for the partitioning of energy in a similar manner to the needle cone-jet deformation process previously described.[5]

Figure 1.

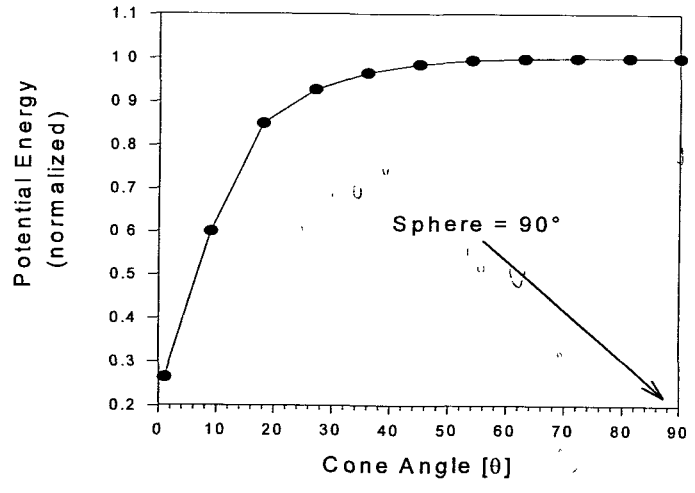

1) Hager, D.B. et al. Anal. Chem. 66,22, Nov. 15, 1994.
2) Gomaz, A. Phys. Fluids, 6 (1), 404, January 1994.
3) Sheehan, E.; and Willoughby, R Photographic Studies of Electrospray Aerosols, Proceedings of the 41st Conference on Mass Spectrometry and Allied Topics, San Francisco, CA, June 1993.
4) Rayleigh, Lord, Phil. Mag. 1882.
5) Willoughby, R. et al. Studies of the physical processes of electrospray; Proceedings of the 41st Conference on Mass Spectrometry and Allied Topics, San Francisco, CA, June 1993

Acknowledgments: The authors wish to thank Waters Corp. for technical and financial support

ROLE OF PEPTIDE STRUCTURE IN THE PRODUCTION OF IONS FROM CHARGED DROPLETS*

Kevin M. Downard and Klaus Biemann
Department of Chemistry, Massachusetts Institute of Technology
Cambridge, MA 02139-4307 U.S.A.

To date, there remains at a best a superficial understanding of the component mechanisms involved in the electrospray ionization process. This is due in large part to the complexity of the ionization event where analyte molecules dissolved in an electrostatically-sprayed solution are transferred to the gas-phase as a distribution of multiply-charged ions. The upper and lower charge state limits are influenced by a variety of experimental factors including the analyte's primary and higher order structure. Despite numerous investigations in several laboratories, the precise role an analyte's structure has on its charging behavior is poorly understood. Here we investigate the relationship between the structure of an analyte and the number and position of charge-carrying protons it supports by studying a series of specifically constructed arginine-rich peptides which differ in the length of the peptide chain and the number and proximity of the arginine residues.

The peptides studied are shown in Table 1 together with the maximum, and average (based on the ion intensities), charge state for each peptide. Note that although peptide $(RG)_3$ supports a maximum of three charge-carrying equal to the number of arginine residues it contains, this is not the case for the larger $(RG)_n$ peptides (n=6,10,15) where the extent of protonation of the arginine residues decreases with increasing n. The CID spectrum of the $[M + 3H]^{3+}$ ion of $(RG)_3$ (Figure 1) is consistent with protons localized on each arginine side chain in a high proportion of the precursors, commensurate with our previous observations that protons remain highly localized in singly and multiply-charged ions of basic peptides [1,2], even during their dissociation at high (keV) collision energies.

The reduced protonation of the larger peptides is not a consequence of a lack of charge-bearing protons available per analyte molecule, since identical results were obtained as the peptide concentration in solution was decreased by two orders of magnitude, and as the pH of the solution was lowered (to 2). Furthermore, conformational effects are unlikely to contribute substantially to their reduced protonation (relative the number of arginine residues) since a similar charging behavior is observed for isomeric peptides $(RG)_6$, $(RRGG)_3$ and (R_6G_6) (Table 1). This is also the case for peptide pairs $(RG)_n$ and $(R\bar{A})_{n-1}R$ (n=10,15) despite the fact that the peptide backbone has increased in length by almost 50%, and the arginine residues are further separated in peptides $(R\bar{A})_9R$ (where $\bar{A}$ = Ava = ε-amino valeric acid).

In the context of a reported mechanism for the electrospray ionization process [3], the results of this study suggest that the larger peptides leave the droplets as gas phase ions much sooner than peptide $(RG)_3$. This is the case irrespective of the conformation of peptides $(RG)_n$ and $(R\bar{A})_{n-1}R$ (n=10,15) since their size is sufficiently large that most (if not all) of the arginine side chains would be protonated if their ions were released at the same time as those of $(RG)_3$. If, as the model suggests, the charge-carrying species are equidistant at any time during the evaporation event [3], then the protons should be evenly distributed along the peptide backbone in the larger peptides provided they remain localized during ionization and dissociation. In accord, all of the major product ions of the CID spectrum of the $[M + 5H]^{5+}$ ions of $(RG)_{10}$ (shown partially in Figure 2) can be accounted for if their charges are well-separated and their dissociation reactions proceed through charge-remote fragmentation pathways.

Figure 1

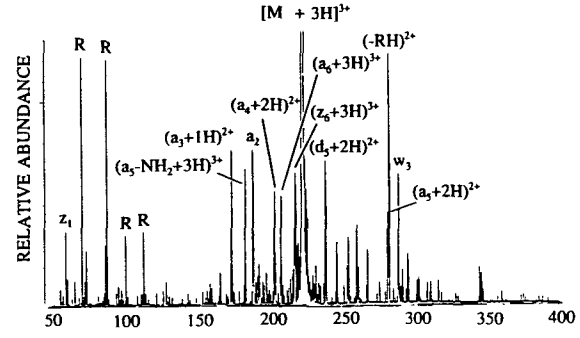

Table 1

Peptide	# backbone bonds	Max. z observed	Av. z observed	% R protonated
$(RG)_3$	20	3	2.8	95
$(RG)_6$	38	5	4.6	77
$(RRGG)_3$	38	5	4.0	67
(R_6G_6)	38	4	4.0	67
R_6	20	4	3.9	65
$(RG)_{10}$	62	5	4.0	40
$(R\bar{A})_9R$	86	6	4.7	47
$(RG)_{15}$	92	9	7.0	53
$(R\bar{A})_{14}R$	131	10	8.3	55

$\bar{A}$ = ε-aminovaleric acid

Figure 2

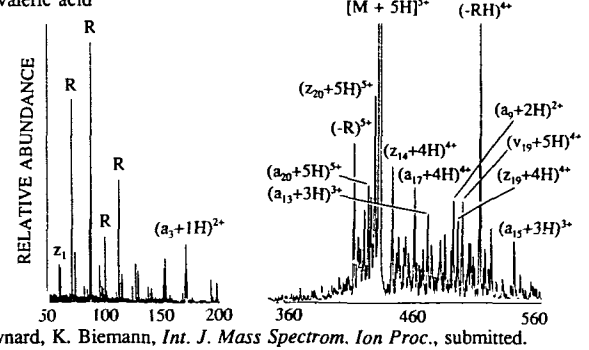

References

* K.M. Downard, K. Biemann, *Int. J. Mass Spectrom. Ion Proc.*, submitted.

(1) R.S. Johnson, S.A. Martin, K. Biemann, *Int. J. Mass Spectrom. Ion Proc.*, **1988**, *86*, 137.

(2) K.M. Downard, K. Biemann, *J. Am. Soc. Mass Spectrom.*, **1994**, *5*, 966.

(3) J.B. Fenn, *J. Am. Soc. Mass Spectrom.*, **1993**, *4*, 525.

Acknowledgments

We thank the National Institutes of Health (Grant # RR00317) for support of this work.

TUNING PARAMETERS: A CRITICAL DETERMINANT OF RELATIVE ION INTENSITIES IN ELECTROSRAY IONIZATION MASS SPECTROMETRY

John B. Cunniff and Paul Vouros. Barnett Institute and Chemistry Dept, Northeastern University, Boston, MA 02115

Ion intensities observed within the electrospray spectrum are a function of several parameters and may be expressed as:

$$I \sim N_o B_1 B_2 T_1 T_2 \qquad [1]$$

Whereby:

- I is the intensity of a specific ion peak [e.g.$(M+H)^+$,$(M+nH)^{n+}$,$(M-H)^-$,$(M-nH)^{n-}$]
- N_o is the number of sample molecules introduced into the ion source
- B_1 is the efficiency of producing the ion within the liquid phase
- B_2 is the efficiency of extracting the ion from the liquid phase into the gas phase
- T_1 is the transmission efficiency of the ions within the source
- T_2 is the transmission efficiency of the ions in the mass spectrometer

Much research has focused on the degree of contribution of the factors which influence ion intensity. Although the determination of I and N_o is rather straightforward, the quantitation of the remaining terms (B_1,B_2,T_1 and T_2) is not such a facile task.

Figure 1 illustrates that, for substance P, a large shift in relative ion intensities of the $[M+H]^+$ ion relative to the $[M+H]^{2+}$ is the direct result of changing a single lens voltage. Similarly, Tuning conditions were also shown to demonstrate a strong effect on the ion profile of an apo-myoglobin solution. Finally, by performing an "auto-tune on an m/z calculated to be a myoglobin/biotin complex (on a myoglobin/biotin solution for which no complex ion was initially detected), a new spectrum (Figure 2) was generated which indicates the presence of biotin complexes/adducts.

Small variations in lens voltages or tuning parameters have dramatic effects on relative ion intensities. The results indicate that relative ion intensities may be manipulated to an extreme degree by small tuning alterations. The results indicate that the typically observed ion profile is strongly a function of tuning parameters regardless of solution conditions. The results also indicate that nonspecific noncovalent complex ions can be detected with the simple manipulation of tuning parameters. Furthermore, because relative ion intensities are strongly a function of lens voltages, these nonspecific noncovalent complexes may be indistinguishable from any specific noncovalent complexes based on any given ion stoichiometry. Finally, the fact that different instruments and laboratories detect varying relative ion intensities may be attributed to the lack of any universal **intensity** calibrant for ESI mass spectrometers.

43rd ASMS Conference on Mass Spectrometry and Allied Topics

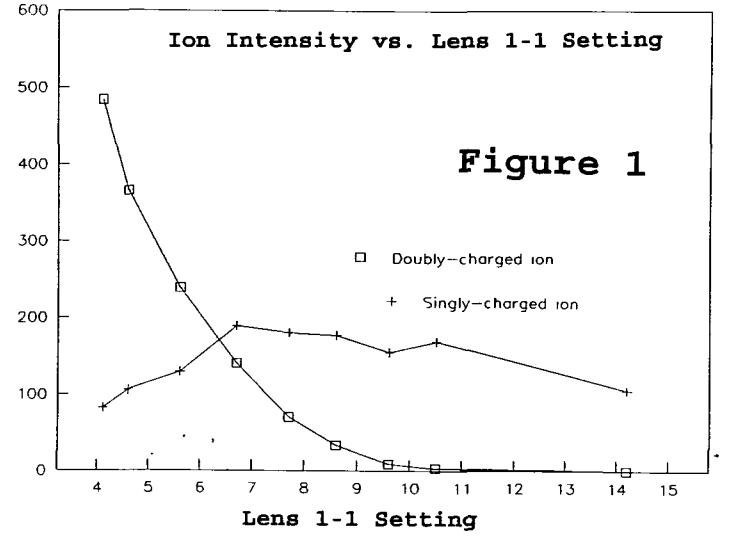

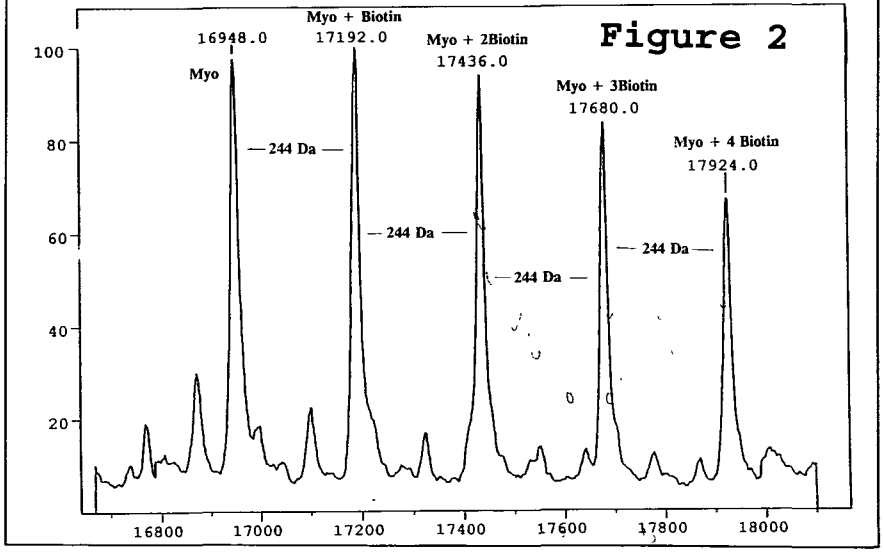

Characterization of m/z Deviates in Electrospray MS Data and Molecular Mass Measurement Uncertainty

Paul L. Juneau[1], Anne B. Giordani[2] and David A. Pyne[1]
Departments of Biometrics[1] and Chemistry[2]
Parke-Davis Pharmaceutical Research, Division of Warner-Lambert Company
2800 Plymouth Road, Ann Arbor MI 48105

A unique feature of electrospray (ES) mass spectra is that single spectra can provide multiple molecular mass estimates and hence the potential to estimate the mass measurement uncertainty without the burdensome task of conducting multiple determinations. Evaluation of the uncertainty of mass measurement by ES-MS is important to establish the quality of molecular mass determinations.

It is common practice to report the mean of the values calculated from each peak in the spectrum as an estimate of molecular mass. When a measure of the uncertainty is reported, the standard deviation of the molecular mass values calculated from each peak in the spectrum is typically used. The underlying assumption in using the standard deviation as a measure of the uncertainty in an ES mass spectrum is that each peak in an ES spectrum provides an independent measure of molecular mass.

In our poster from last year, we showed that the assumption that each peak in an ES spectrum provides an independent measure of molecular mass is not always valid because the m/z measurements may be autocorrelated[1]. If there is a positive autocorrelation and it is not addressed in molecular mass calculations, the derived uncertainty may underestimate the true uncertainty of the molecular mass measurement[2].

In terms of mathematical statistical theory, do other features of m/z measurements have the potential to affect molecular mass uncertainty estimates or even the molecular mass estimates themselves? Are these features consistent with the existence of autocorrelation in the m/z data? Do these properties vary with charge, and if so, does a simple model explain the relationship?

One property of ES m/z data is its *deviance*. The *deviance* of a measurement is the difference between its empirical value and the predicted value. For a known compound, m/z values can be predicted; thus, the measured m/z values can be compared to the predicted m/z values at every peak.

The arithmetic difference between an empirically derived (measured) m/z value and a predicted m/z value for a known compound may be viewed as a *deviate*. If there are at least three replicate determinations of a spectrum, the distribution of deviates can be constructed at each of the peaks. The deviates can be used to assess measurement bias. If the central tendency of the deviates between adjacent peaks is non-zero, a bias in the m/z measurement method may exist.

43rd ASMS Conference on Mass Spectrometry and Allied Topics

A second property of m/z data that can affect uncertainty measurements is its *dispersion* or the spread in measured values at each peak. Peaks which have similar dispersion are said to be *homoscedastic*; those with differing dispersion *heteroscedastic*. Both inaccurate molecular mass estimates and underestimation of the true uncertainty can result from data which are heteroscedastic.[3] The m/z data dispersion may be compared by an examination of the deviate distributions.

This poster examines the statistical properties of deviance and dispersion in ES-MS data.

Conclusions

- An evaluation of the deviance in ES m/z data revealed evidence of bias. The pattern is consistent with positively autocorrelated data, which can lead to underestimation of mass measurement uncertainty.

- An evaluation of the dispersion in ES m/z data revealed evidence of heteroscedasticity, which can lead to both poor molecular mass estimates and poor estimates of the molecular mass measurement uncertainty.

- The relationship between the mean m/z deviates and charge cannot be readily explained in terms of a simple linear model.

References

[1]Juneau, P., Giordani, A. and Pyne, D ; "Statistical Evaluation of the Uncertainty of Molecular Mass Measurement from Single Electrospray Mass Spectra;" Proceedings of the 42nd Conference on Mass Spectrometry and Applied Topics, Chicago, Illinois, May 29 - June 3, 1994.

[2]Neter, Wasserman, and Kutner, "Applied Linear Regression Models", Homewood: Irwin, pp. 446-447 (1983).

[3]Neter, Wasserman, and Kutner, "Applied Linear Regression Models", Homewood: Irwin, p. 170 (1983).

[4]Neter, Wasserman, and Kutner, "Applied Linear Regression Models", Homewood: Irwin, p. 446 (1983).

Chemical Redox Reactions in ES-MS: Study of Electrode Reactions

Feimeng Zhou and Gary J. Van Berkel
Chemical and Anlytical Sciences Division, Oak Ridge National Laboratory
Oak Ridge, Tennessee 37831-6365

We have previously demonstrated that chemical redox reactions can be used to ionize neutral compounds for electrospray mass spectrometric (ES-MS) detection[1]. The same approach can also be used, in conjunction with some electrochemical technique such as cyclic voltammetry(CV), to study electrode reactions. It has long been recognized that MS can be a powerful technique to provide molecular weight and structural information regarding the intermediate/products generated in electron-transfer reactions[2-3]. Although the principle behind using chemical redox reactions on-line with ES-MS for the study of electrode reactions is much the same as that behind using electrochemistry on-line with MS (EC/MS), a major advantage of the former approach is that the possible suppression of analyte signal by the added electrolyte used in excess in conventional electrochemical experiments is eliminated. This suppression effect and means to overcome it are discussed in greater detail in poster #222 which is related to the combination of electrochemistry on-line with ES-MS (EC/ES-MS).

Two different compounds, viz, $C_{60}F_{48}$ and β-carotene were used to demonstrate the utility of chemical redox reactions on-line with ES-MS for the elucidation of mechanisms of complicated electron-transfer reactions[4] and for the kinetic study of electrode reactions in which relatively short-lived intermediates are involved[5].

(1) Elucidation of Mechanisms of Complicated Electron-Transfer Processes:

Cyclic voltammetry reveals that $C_{60}F_{48}$ can be reduced in CH_2Cl_2 to its dianion which undergoes a fast follow-up chemical reaction (Figure 1a). A flow injection experiment employing a CH_2Cl_2 carrier solution containing ferrocene as the oxidant yielded a peak in the ES-mass spectrum (Figure 1b) whose *m/z* value corresponds to $C_{60}F_{47}^-$. Thus the chemical redox reaction between ferrocene and $C_{60}F_{48}$ suggests that the product from the follow-up reaction of $C_{60}F_{48}^{2-}$ should be $C_{60}F_{47}^-$. $C_{60}F_{47}^-$ can be further reduced to $C_{60}F_{47}^{3-}$ in the same solvent system and the CV (Figure 1c) indicates that $C_{60}F_{47}^{3-}$ also undergoes a fast chemical follow-up reaction. Another flow injection experiment is carried out with decamethylferrocene as the oxidant. The ES-mass spectrum, shown in Figure 2d, again provides information about the product of the follow-up reaction. Similar to $C_{60}F_{48}^{2-}$, $C_{60}F_{47}^{3-}$ also has a strong tendency to lose a F-.

On the basis of the CV behavior and the ES-MS mass spectra of $C_{60}F_{48}$ obtained using different chemical redox reagents, the following mechanism was proposed.

$C_{60}F_{48} + e^- \rightleftharpoons C_{60}F_{48}^{\cdot-}$	Electron-transfer, E
$C_{60}F_{48}^{\cdot-} + e^- \rightleftharpoons C_{60}F_{48}^{2-}$	Electron-transfer, E
$C_{60}F_{48}^{2-} \rightarrow C_{60}F_{47}^- + F^-$	Chemical Reaction, C
$C_{60}F_{47}^- + e^- \rightleftharpoons C_{60}F_{47}^{2-}$	Electron-transfer, E
$C_{60}F_{47}^{2-} + e^- \rightleftharpoons C_{60}F_{47}^{3-}$	Electron-transfer, E
$C_{60}F_{47}^{3-} \rightarrow C_{60}F_{48}^{2-} + F^-$	Chemical Reaction, C

(2) Kinetic Study of Electrode Reactions:

CV (solid curve in Figure 2a) and other electrochemical studies suggest the oxidation reaction of β-carotene in CH_2Cl_2 to be a simple two-electron transfer reaction forming the dication. The dication undergoes a follow-up reaction (EEC mechanism). A simulation based on the EEC mechanism using the same experimental parameters (dotted curve in Figure 2b) yields a rate constant for the first-order chemical reaction of 0.3 s^{-1}, or 2.7 s for the half-life of the dicationof β-carotene.

A flow-injection experiment using CH_2Cl_2/0.1% trifluoroacetic acid (v/v) as the carrier solution on-line with ES-MS shows two major peaks at *m/z* values expected for the dication of β-carotene, M^{2+},

43rd ASMS Conference on Mass Spectrometry and Allied Topics

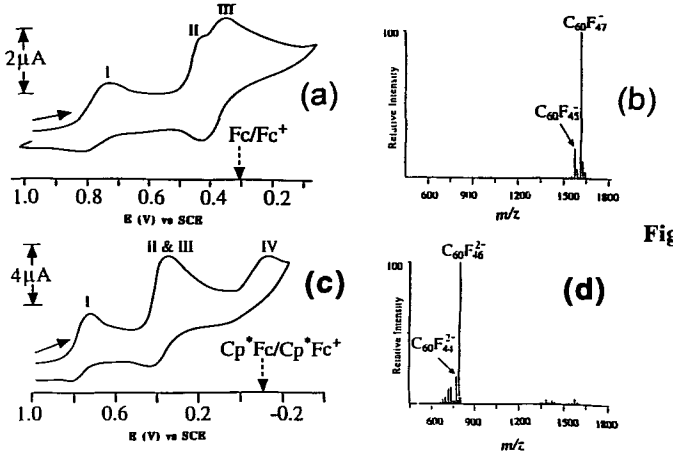

Figure 1

and at the *m/z* value corresponding in mass to $(M-1)^+$, respectively (Figure 2b). The peak at $(M-1)^+$ was assigned to the product of the follow-up reaction generated in the following reaction,

$$M^{2+} \rightarrow (M^{2+}-H^+)^+ + H^+$$

The relative abundances of the β-carotene dication and the species $(M^{2+}-H^+)^+$ were plotted as a function of flow rates. The linear plot yields a slope of 0.11 s^{-1} which is the rate constant of the above chemical reaction. Therefore, the solution lifetime of the β-carotene dication is determined to be 6.3 s by the flow injection experiment. This value is in good agreement with what is estimated from the simulation of β-carotene CV.

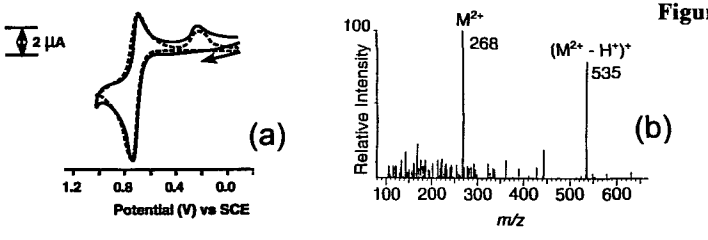

Figure 2

(1) Van Berkel, G. J.; McLuckey, S. A.; Glish, G.L. *Anal. Chem.* **1991**, 63, 1098-1109.
(2) Bruckenstein, S.; Gadde, R.R. *J. Am. Chem. Soc.* **1971**, 93, 793-794.
(3) Volk, K. J.; Yost, R. A.; Brajter-Toth, A. *Anal. Chem.* **1992**, 64, 21A-33A.
(4) Zhou, F.; Van Berkel, G. J.; Donovan, B. T. *J. Am. Chem. Soc.* **1994**, 116, 5485-5486.
(5) Van Berkel, G.J.; Zhou, F. *Anal. Chem.* **1994**, 66, 3408-3415.

Research sponsored by the United States Department of Energy, Office of Basic Energy Sciences under contract DE-AC05-84OR21400 with Martin Marietta Energy Systems, Inc.

ELECTROCHEMISTRY ON-LINE WITH ELECTROSPRAY MASS SPECTROMETRY

Gary J. Van Berkel and Feimeng Zhou
Chemical and Analytical Sciences Division, Oak Ridge National Laboratory
Oak Ridge, Tennessee 37831-6365

We have found electrospray (ES) to be a suitable interface for coupling electrochemistry (EC) on-line with mass spectrometry (MS) [1-4]. In contrast to many of the ionization methods/interfaces that have been used to couple EC and MS, ES involves no heating of the solvent systems, gas-phase reactions of the analyte/products are minimal, and a wide variety of solvent systems, ranging from water to nonpolar organic solvents like methylene chloride, can be used. Figure 1 is a *schematic representation of the electrochemical flow cells used on-line with ES-MS, viz., (a) thin-*layer, (b) dual-tube, and (c) coulometric. As shown in Figure 2, a decoupled mode (potentiostat control) (a) or a floated mode (b) (constant-current (c) or constant-potential (d) control) were used to connect the electrochemical flow cells on-line. In terms of carrying out on-line EC/ES-MS, selected applications showed that when either controlled-current electrolysis (CCE) or controlled-potential electrolysis (CPE) can be used, the CCE mode of operation offers several advantages. These advantages include, (1) the simple circuitry for CCE that can be easily floated at the high ES voltage, (2) the fact that CCE is easier to perform in resistive solutions than CPE (i.e., minimal electrolyte is needed which benefits ES-MS), (3) a reference electrode is not needed in CCE, and (4) the problem of potential drift that plagues two-electrode CPE is avoided in CCE. In terms of response time for gas-phase detection, the floated mode is most advantageous since a long transfer line from the cell to the ES source is avoided. The 50-100 mM concentration of nonvolatile electrolyte normally used in electrochemical experiments causes problems with plugging and degraded performance of the ES atmospheric sampling interface Even more significant is suppression of the analyte gas-phase ion signal that can result from this high electrolyte concentration. The most commonly used electrolytes (e.g., quaternary ammonium salts) have a very large propensity for gas-phase ion formation and concentrations even as low as ten to a few hundred micromolar can lead to significant signal suppression. Fortunately, less commonly used, but no less functional electrolytes, such as alkali metal salts, e.g., lithium triflate and lithium hexafluorophosphate, have a much lower suppression effect, which enabled their use in the present studies at concentrations as high as a few millimolar.

We carried out three selected applications which demonstrated the utility and versatility of the EC/ES-MS combination. These were the ionization of neutral analytes for detection by ES-MS, the study of the products of electrode reactions, including those or relatively short-lived species (i.e., half-life < 1.0 s) and the enhanced determination of metals achieved by coupling anodic stripping voltammetry [5] on-line with ES-MS. As an example, nickel(II) octaethylporphyrin ($Ni^{II}OEP$) was used to demonstrate the utility of EC/ES-MS for the detection of electrochemically generated species via stepwise electron-transfer reactions. $Ni^{II}OEP$ undergoes two reversible one-electron oxidation reactions (*E,E,* mechanism) in a variety of nonaqueous solvents. Because the products are stable, and therefore, do not require rapid detection, this work was carried out with the coulometric cell in the decoupled, three-electrode operational mode. The mass spectrometric hydrodynamic voltammograms in Figure 3 clearly indicate that the mono- and dication are formed at two different electrode potentials, the difference in these electrode "appearance potentials" being 0.50 V, which is in good agreement with the peak potential difference measured from the CV (i.e., 0.53 V).

43rd ASMS Conference on Mass Spectrometry and Allied Topics

FIGURE 1

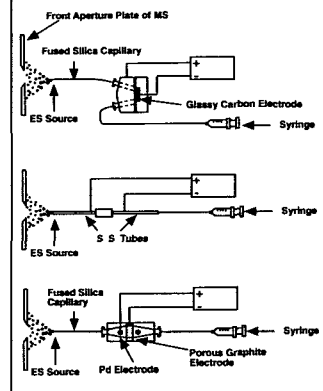

FIGURE 2

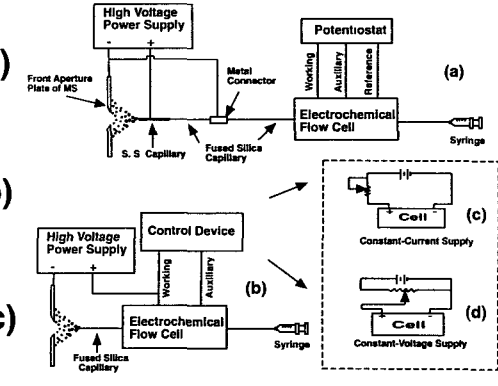

FIGURE 3

EC/ES-MS hydrodynamic voltammograms for the monocation (O) and the dication (●) of $Ni^{II}OEP$ obtained using the coulometric flow cell in the decoupled, three-electrode operational mode. The cyclic voltammogram (CV) of $Ni^{II}OEP$ obtained in a separate off-line experiment (dotted curve) is also shown.

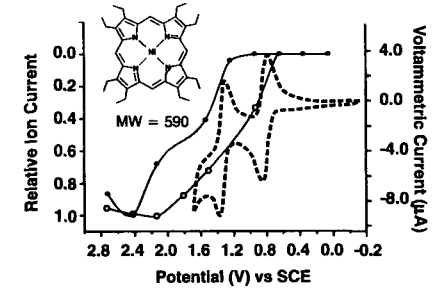

[1] Van Berkel, G J , McLuckey, S A., Glish, G L *Proceedings of the 39th ASMS Conference*, Nashville, TN, 1991, pp 1237-1238. [2] Asano, K. G , Van Berkel, G.J. *Proceedings of the 41st ASMS Conference*, San Francisco, CA, 1993, pp 1068a-1068b. [3] Zhou, F , Van Berkel, G J. *Proceedings of the 42nd ASMS Conference*, Chicago, IL, 1994, pp 1002 [4] Zhou, F , Van Berkel, G J. *Anal. Chem* , submitted [5] Wang, J Stripping Analysis Principles, Instrumentation and Applications; VCH Publishers· Deerfield Beach, FL, 1985

This research was sponsored by the United States Department of Energy, Office of Basic Energy Sciences under contract DE-AC05-84OR21400 with Martin Marietta Energy Systems, Inc.

Formation of Protonated Ions from Acidic Species at High pH in Electrospray.

Richard W Smith
Department of Chemistry, McMaster University, 1280 Main St W, Hamilton, ON, L8S 4M1, CANADA

Electrospray (ES) analysis of the anti-arthritic drug myochrysine in the negative ion mode abundantly yielded the $(M-H)^-$, $(M-2H)^{2-}$ and $(M-3H)^{3-}$ species when the sample was dissolved in CH_3CN/H_2O containing NH_4OH. In the positive ion mode, ions were observed which were identified as the $(M+NH_4)^+$ and $(M+H)^+$ species Remarkably, these positive ion species persisted even at pH 9.9 although at a much reduced intensity Considering that myochrysine contains eight carboxyl groups, this observation is difficult to explain in terms of acid/base equilibrium calculations in solution (1) To probe the mechanism of positive ion formation from myochrysine, we have studied the ESI and ammonia chemical ionization (NH_3 CI) characteristics of several model compounds including the three isomeric phthalic acids, maleic acid (cis) and fumaric acid (trans)

Pneumatically assisted electrospray ionization (ESI) was performed with 50/50 CH_3CN/H_2O as the mobile phase at a flow rate of 15µl/min employing a Brownlee Microgradient syringe pump Samples were introduced by flow injection at a concentration of 0 01M + 0 001M of base unless otherwise stated. The pH of these solutions ranged from 2.6 to 4.4 Full scan ESI experiments were performed with a Fisons Platform quadrupole instrument and the MS/MS data were generated with a Fisons Quattro II triple quadrupole instrument. All data was acquired in MCA mode (10 scans) A cone voltage of 35V was employed in all ESI experiments (unless otherwise stated) All NH_3 CI experiments were performed with a VG Analytical ZAB-E mass spectrometer The samples employed in this study were used as supplied by the manufacturer

The +ESI and NH_3 CI mass spectra of 1,2-phthalic acid (Figure 1) and maleic acid exhibit a number of intense ions characterised as $(M+NH_4)^+$, $(M+H)^+$ and $(MH-H_2O)^+$ In contrast, the corresponding ESI mass spectra of the 1,3- , 1,4- isomers and fumaric acid yield some of these ions at very low intensity (approximately a 50 fold decrease) This indicates that the facile formation of $(M+NH_4)^+$ adduct ions requires the presence of adjacent carboxyl groups. In ESI, the ratio of these ions is highly dependent on the cone voltage employed At low cone voltages (10V), 1,2-phthalic acid and maleic acid exhibit $(M+NH_4)^+$ and $(M+H)^+$ ions, which results in an ESI mass spectra very similar to the NH_3 CI mass spectrum shown in Figure 1 As the cone voltage is increased from 20V to 100V, the $(M+NH_4)^+$ and $(M+H)^+$ ions decrease in intensity and the $(MH-H_2O)^+$ species dominates This indicates a collisional activation component to the ESI mass spectra, which explains the significant intensity differences between the ions observed in the ESI and NH_3 CI mass spectra shown in Figure 1 Part of the $(M+NH_4)^+$ ions lose (i) NH_3 to yield the $(M+H)^+$, and (ii) NH_3 + H_2O, to yield the $(MH-H_2O)^+$ ion as established by MS/MS as well as D and $^{15}NH_4^+$ labelling

In an ESI study of 1,2-phthalic acid, where the pH was varied from 2 9 to 9 9 with conc NH_4OH, the intensity of the positive ions decreased by a factor of 20 however, the $(M+NH_4)^+$, $(M+H)^+$ and $(MH-H_2O)^+$ ions were always observed. At pH 9.9, 1,2-phthalic acid would be almost completely dissociated in solution (pKa = 5 51) yielding the $(M-H)^-$ and $(M-H-CO_2)^-$ species. The summed negative ion intensities were approximately 10 times greater than the positive ion yield across the same pH range, increasing to a maximum at the pKa of the first carboxyl group and then slowly decreasing. It is possible that the decrease in +ESI response may reflect the extent of dissociation in solution but may in part be due to ion suppression because of the high electrolyte concentration (2). However, positive ion formation must occur somewhat independent of solution pH indicating that gas-phase reactions may play an important role in the ESI generation of the $(M+NH_4)^+$ and $(M+H)^+$ ions

The observation of a +ESI mass spectrum from acidic species employing NH_4OH to effect ionization is interesting however, it is of little analytical use because a mobile phase containing 0.01% NH_4OH (pH > 9) would dissolve silica based HPLC columns A study was undertaken to discover whether other bases

(including NH_4OAc) cause ionization and if a correlation exists between the observed positive ion species and the proton affinities (PA) or the pKas of the bases The results indicate that there is little correlation with either PA or pKa For example, aniline and $(NH_2)_2(CH_2)_4$ with 1,2-phthalic acid The bases have very different PAs (209 5 and 237 6 respectively) and pKas (4 63 and 11.15/9 71 respectively) however, the resulting ESI mass spectra and relative responses (summed intensities for the ions observed) are very similar Indeed, all of the bases studied yielded similar ESI mass spectra although the relative responses vary by a factor of 3 The 1,3-, 1,4- phthalic acid isomers and fumaric acid yielded very low intensity +ESI mass spectra (if at all) although a good +ESI response was seen for 1,3-phthalic acid with $(NH_2)_2(CH_2)_2$ and $(NH_2)_2(CH_2)_4$ Consequently, it is proposed that two criteria must be satisfied in order that an intense +ESI response be observed from acidic species eluting in base Namely, (i) formation of a BH^+/sample complex (where B is the base used) and (ii) stabilization of this complex by dicarboxylic acids that contain adjacent, cis or interacting carboxylates

It has been reported that the favoured site for gas-phase protonation in carboxylic acids is the carbonyl oxygen (3) and that the loss of H_2O from protonated carboxylic acids with adjacent or cis carboxylates, such as 1,2-phthalic acid and maleic acid, is enhanced when compared to carboxylates that can not interact This behaviour is similar to the +ESI behaviour reported here The loss of H_2O from species such as protonated 1,3-, 1,4-phthalic acid and fumaric acid requires a 1,3- H shift which is symmetry forbidden and has a large energy barrier (4). This 1,3- H shift is obviated in species with a second interacting carboxyl group and the elimination of H_2O is favoured by the formation of the stable protonated anhydride, the m/z 149 ion in the +ESI mass spectra of 1,2-phthalic acid (Figure 1) Consequently, the formation of the $(M+NH_4)^+$, $(M+H)^+$ and $(MH-H_2O)^+$ ions in the ESI mass spectra of 1,2-phthalic acid, maleic acid and by analogy, myochrysine may involve reactions occurring in the gas-phase.

Figure 1: 1,2-PHTHALIC ACID

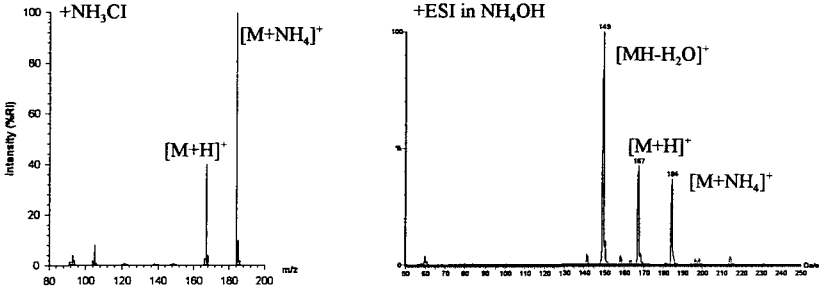

References
(1) J C Y LeBlanc et al Int J Mass Spectrom. Ion Proc 125, 145, (1993).
(2) G. Wang and R.B Cole Proceedings of the 42nd ASMS Conference p991 (1994)
(3). F.M Benoit and A.G Harrison J Am Chem. Soc , 99, 3980 (1977)
(4). N.E Middlemiss and A G Harrison Can. J. Chem., 57, 2827 (1979)

Acknowledgements: The author wishes to express thanks to Dr C A. Kingsmill and the Ontario Ministry of Agriculture and Food for the use of their Fisons Quattro II instrument for the MS/MS experiments

Modeling the Maximum Charge State and Proton Transfer Reactivity of Electrosprayed Ions

Paul D. Schnier, Deborah S. Gross, Evan R. Williams
Department of Chemistry, University of California, Berkeley, Ca, 94720

Electrospray ionization (ESI) mass spectrometry has become a powerful method for the analysis of large biomolecules. Multiply charged ions formed by electrospray are destabilized by electrostatic forces, resulting in greatly enhanced rates of reactivity and dissociation. We have recently developed a model which quantitatively accounts for the energetics of gas-phase proton transfer reactions. Here we describe the application of this model for calculating the maximum charge state of ions formed by ESI.

For a multiply protonated ion, the apparent gas-phase basicity (GB^{app}) can be calculated from estimates of the intrinsic proton transfer reactivity of the sites of protonation ($GB_{Intrinsic,\,t}$) and point charge Coulomb interactions experienced by the charge sites (equation 1)

$$GB^{app} = GB_{Intrinsic,t} - \sum_{i=1}^{n} \frac{q^2}{(4\pi\varepsilon_o)\varepsilon_r r_{i,t}} \qquad (1)$$

where ε_r is the effective shielding between charges in these ions. To calculate GB^{app} for a protein, the location of charges in the ion must be known. To determine the most energetically favorable location of charges for a given charge state, a pseudo random-walk algorithm is used.[1] This algorithm places charges at specific residues in a protein initially in a random configuration, and moves the protons such that equation 2 is minimized and the lowest energy charge configurations are found.

$$\sum_{\substack{i,j \\ i>j}}^{n} \frac{q^2}{(4\pi\varepsilon_o)\varepsilon_r r_{i,j}} - \sum_{i=1}^{n} GB_{Intrinsic,i} \qquad (2)$$

Typically, numerous charge configurations with a GB^{app} within 3 kcal/mol of the lowest energy structure are found. Some fraction of all of these configurations should be present near thermal conditions. We approximate this distribution by assigning the GB^{app} of the charge state as an average of all charge configurations within 3 kcal/mol of the lowest energy structure.

Peptides and proteins electrosprayed from denaturing solutions are modeled as elongated "strings" with residues separated by 3.8 Å. Proteins containing disulfide bonds, or electrosprayed from solutions in which they have a native conformation, are modeled using X-ray crystal coordinates. For proteins, $\varepsilon_r = 2.0$ is used in the calculations based on the experimentally determined effective ε_r of gas-phase cytochrome *c* ions.[2] The $GB_{Intrinsic}$ values are obtained from GB measurements of small peptides containing one basic residue.

Our calculated maximum charge state is obtained by comparing the calculated GB^{app} of a charge state to the GB of the solvent from which the ion is formed. The first charge state with GB^{app} < GB(solvent) is the predicted maximum charge state. Higher charge state ions should undergo proton transfer to gas-phase solvent molecules. The calculated GB^{app} as a function of charge for nine proteins is shown in Figure 1. The maximum experimental charge state reported in the literature for each molecule, electrosprayed from a methanol containing solution is circled. For these molecules, the calculated GB^{app} of the maximum charge states is close to the

1 Schnier, P D.; Gross, D S ; Williams E. R., submitted.
2 Schnier, P. D ; Gross, D. S , Williams E R., *J. Am. Chem Soc.*, in press

GB of methanol (GB = 174.1 kcal/mol). For 15 commonly electrosprayed proteins, our calculated maximum charge state is within 6% of the experimental value. For these same proteins, the sum of basic residues (Arg, Lys, His, and N-terminus) differs from the experimental value by an average of 20%. Thus, the maximum charge state of electrosprayed ions is determined by gas-phase proton transfer reactions. Similar results are obtained for peptides with many basic sites ($\varepsilon_r = 1.3$). In contrast, the maximum charge state of a peptide with few basic sites appears to correlate with the charge state in solution.

This model has been extended to explain the formation of specific fragment ions upon ion dissociation. For a given charge state of an ion, the Coulomb strain on each bond is calculated for all lowest energy ion configurations. Primary sites of fragmentation are predicted to occur in regions where Coulomb repulsion is greatest. Due to the large number of charge configurations that can occur for some charge states, the predicted fragmentation must occur in at least 25% of these structures. For example, we calculate the greatest Coulomb strain for the 9+ charge state of ubiquitin to be between residues 33-42, 42-48, 42-54, and 54-63. These calculations are consistent with the y_{18}, y_{24}, and y_{37} fragments observed experimentally from multiphoton dissociation data of McLafferty and co-workers.[3] Figure 2 shows the calculated frequency of protonating residues in denatured ubiquitin as a function of charge state. For the 9+ to 12+ charge states of ubiquitin, our calculations are consistent with 83% of the experimentally assigned fragments in the multiphoton dissociation data.[3]

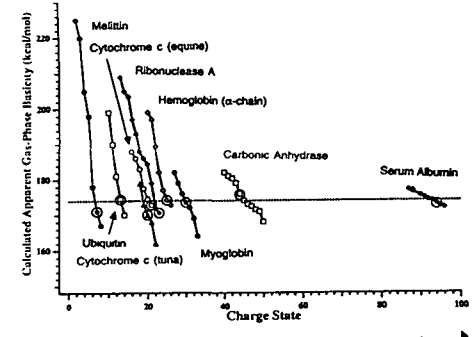

Figure 1

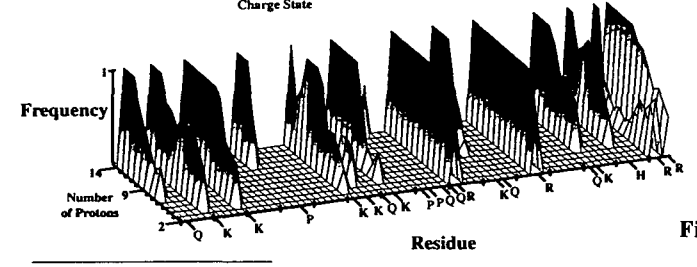

Figure 2

3 Little. D. P.; Speir, J. P.; Senko, M. W.; O'Connor, P. B., McLafferty, F. W. *Anal. Chem.* 1994, *66*, 2809-2815.

Protein Cations from Basic Solutions with an API III and an API 300

J.C.Yves Le Blanc(1), K.W.Michael Siu(2), Roger Guevremont(2) and Bori Shushan(1)
(1) Sciex, 71 Four Valley Drive, Concord (Ontario) Canada L4K 4V8; (2) National Research Council, IERT, Montreal Road, Ottawa (Ontario) Canada K1A 0R6.

In previous work, we proposed a model based on aqueous solution equilibrium to explain observed ion distributions of proteins in electrospray mass spectrometry (ES-MS)[1,2]. This model was successfully applied to both positive ions produced from acidic solutions[1] and negative ions electrosprayed from basic solutions[2]. One of the well accepted facts among users of ES-MS is that ions observed in the mass spectrum are pre-formed in solutions. The model we proposed also suggested that strong correlation between solution phase and the observed ion distribution. Kelly et al.[3] demonstrated that both positive and negative protein ions could be observed from acidic solutions (pH 3). Similarly, protein ions of both polarity could be observed from basic solutions (pH 10). Since proteins are "expected" to be anions in basic solutions and cation in acidic solutions, these observations were rather puzzling. Based on observations where gramicidin s was electrosprayed from nitrogen base solutions we concluded that the formation of doubly charged gramicidin ion at high pH involves two steps[4]. The first step is the formation [M+xB+nH]+2 ions in solution, where B represents the nitrogen base used to adjust the solution pH and M represents gramicidin s (x=0-2 and n=2). The second step involves the breakdown of the complex to form [M+nH+]+2 or [M+(n-1)H+]+ from collision induced dissociation processes that occur in the sampling orifice region of the mass spectrometer. In other words, the observation of multiply protonated species from high pH solution may only be rationalized by combining solution phase chemistry and gas phase chemistry phenomena. Since a gas phase processes appear to play a role in the observed ES ion distribution of multiply charged species, we investigated the formation of multiply charged protein cations from basic solutions on an API III and the new API 300 bench top mass spectrometer.

Instruments - Experiments were carried on three different systems: a TAGA 6000e, an API II and an API 300. Bot h the TAGA and the API II are equipped with cryogenic pumping and the analyzer region is separated from atmosphere by a nitrogen curtain gas. The API 300 is equipped with turbo-molecular pumps and the first analyzer is separated from atmosphere by both a nitrogen curtain gas and a differentially pumped region (Figure below). The API 300 interface offers a few advantages over that of the other two instruments. First, the differentially pumped region could be used to produce more energetic collisions when the ions are sampled for mass spectrometric analysis. Second, a larger orifice allows to introduce more analyte for better sensitivity. Third, the high pressure focusing quadrupole (Q0) serves to stabilize weak complexes before mass analysis.

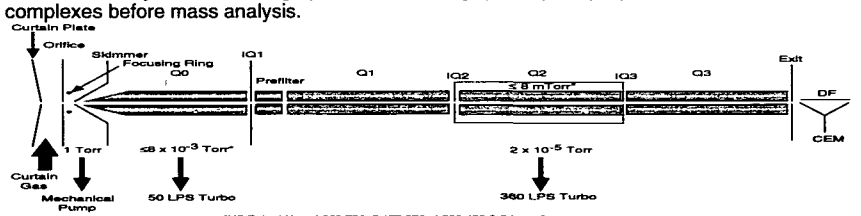

*US Patent Nos. 4,963,736 5,179 278, 4,328,420 & 5,248 875

Results - Myoglobin was electrosprayed from a water:methanol (25:75) with 0.1M NH4OH with the API III and API 300. In both cases, the spectrum shows the apparently protonated myoglobin ions and the ion distribution ranges from +6 to +19 protons. From sequence information, apomyoglobin has 21 acidic groups and 33 basic amino groups. Even if all the amino sites retained the proton from the hydrogen-bonded ammonium ion after the CID process, the protein would have a net charge of +12 if one assumes that all carboxylic groups are deprotonated in a pH 10.1 solution. However, protonated carboxylic groups can be created in the lens region if some of the carboxylate anions were complexed with ammonium ions in solution. The formation of carboxylate-ammonium ion pairs in solution could then yield cations having charges higher than +12 after the CID process in the lens region. It is important to note that even though ammonium ions and myoglobin ions are desorbed into the gas phase during electrospray, proton transfer from ammonium ion to carboxylate anion in the gas phase cannot occur because of the overall charge of the myoglobin ion is positive. Ammonium ion can only approach a myoglobin cation in a medium of high dielectric constant (i.e. a solution) where electrostatic shielding is effective.

Even though the API 300 interface may be used to produce more energetic CID processes in the interface region, it may also be used to observe protein-amine complexes by lowering the potential difference between the orifice and the skimmer and/or the skimmer and Q0. Figure 1 shows the effect of reducing the potential difference between the skimmer and Q0 when an insulin/butylamine solution is electrosprayed. Insulin-butylamine complexes can easily be observed under mild sampling condition. At higher potential skimmer-Q0 potential difference we observe only the protonated insulin species.

Conclusion - The results strongly suggest that positive protein ions emerging from basic solutions are actually sampled as a ions of the form (M+nH+xB)z+ , where M represents the protein, n the number of protons in excess, x the number of nitrogen base attached to the protein either by hydrogen-bonded complexes with amino basic sites or by ion pairing with carboxylate anion sites and z represents the net charge of the ion sampled in the early stage of the ES process. The values of n and x for the original ions will more likely depend on the type of base used as well as the structure of the protein in solution. The API 300 sampling interface certainly offers the ability to sample both protein-amine cations and protein cations provided that the potentials across the sampling orifice-skimmer-Q0 are carefully selected

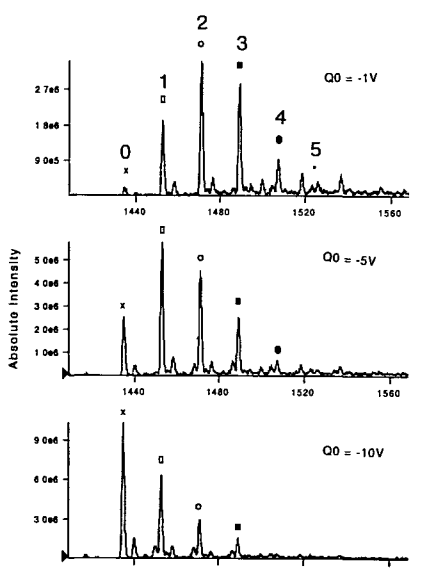

Figure 1: ES-MS of insulin in DDW:MeOH(25:75) 0.1M Butylamine. The values indicate the number of butylamine attached to the protein. All ions have 4 charges

Effect of Organic Solvents on Aerosol MALDI Ion Signal

Michelle D. Beeson, Xiaona Wei, and David H. Russell,

Laboratory for Biological Mass Spectrometry, Department of Chemistry

Texas A&M University, College Station, TX 77843

The effect of solvent on surface MALDI ion signal has been investigated by several groups.[1-7] Rapid evaporation of solvent produces a homogeneous sample surface consisting of small crystals. Surfaces composed of small crystals produce a more uniform ion signal over the sample surface as well as increased ion yield.[1] Improved sensitivity and mass resolution from surfaces composed of small crystals have also been reported.[2] Rapid solvent evaporation has also been achieved through the use of a flow of ambient or heated air,[3,4] dry nitrogen,[5] heat lamps,[6] or vacuum drying.[6] Other laboratories have prepared samples by spraying the solution of matrix and analyte onto the probe surface.[7] These sample spray methods promote solvent evaporation due to the large surface area to volume ratio of the aerosol particles of which the spray is composed.

In our previous work, we noted that solvent evaporation rates are important for aerosol MALDI: drier aerosol particles appear to produce larger ion signal.[8,9] In fact, aerosol MALDI ion signal was obtained with the present apparatus only after a 25 cm long heated drying tube was added between the nebulizer and TOF ion source region. Based on these observations, it seems reasonable to postulate that the more volatile solutions would yield drier aerosol particles resulting in improved MALDI ion signal.

Using the aerosol MALDI technique, the matrix and analyte-containing solution is delivered using a syringe pump to a pneumatic aerosol generator and sprayed into the mass spectrometer as an aerosol. The aerosol first passes through a heated drying tube at 500 C to remove solvent and then ionization is performed at 355 nm using a frequency tripled Nd:YAG pulsed laser. The ions are orthogonally accelerated at 10 kV, mass separated in a 1.1 m flight tube, and are detected with a microchannel plate particle multiplier. The mass spectra are collected by a digital oscilloscope and downloaded to a microcomputer for analysis.[8,9]

In addition to solvent volatility, matrix-analyte interactions are an important consideration in both solid and aerosol MALDI. For example, Beavis and Bridson proposed that hydrophobic interactions between the matrix and analyte lead to inclusion of the analyte into matrix crystals, thereby enhancing the ion yield.[10] Both hydrophobic and hydrophilic interactions between matrix and analyte molecules are undoubtedly affected by the solvent and the concentration of the matrix and analyte. It is probable the solvent can alter matrix-analyte interactions, and thus influence the aerosol MALDI ion signal. For example, we observed that optimum matrix to analyte ratios for aerosol MALDI are lower than for surface MALDI,[9] typically 10-100:1, as opposed to 100-1000:1 for surface MALDI.[1-7] We postulated that solvent/matrix/analyte interactions are responsible for this difference.

In previous work, we observed that drier aerosol particles produce larger aerosol MALDI ion signal.[8,9] Thus it might be expected that the most volatile solvent that dissolved the matrix and analyte would produce the largest aerosol MALDI ion signal. The volatility of the solvents used in this work is methanol > ethanol > isopropanol ≈ acetonitrile. The data presented in Figure

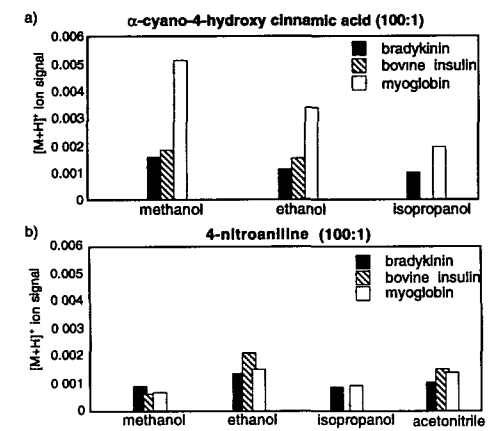

Figure 1. Bar graphs showing the aerosol MALDI ion signals in 100% organic solvents using the matrices **a)** α-cyano-4-hydroxycinnamic acid and **b)** 4-nitroaniline. The laser energy used was 13 mJ/pulse.

show that the aerosol MALDI ion signal is not directly related to solvent volatility For example, the ion signals obtained with 4-nitroaniline are nearly the same in all neat solvents, regardless of volatility. For more than 80 % of the analyte-matrix-solvent combinations examined the aerosol MALDI ion yield is greatest in organic/water mixtures even though the volatility of the organic/water mixtures is lower than that of the neat organic solvents. Thus the data indicate that aerosol MALDI ion yield is not strongly dependent on solvent volatility, but that the chemical interactions between the matrix and analyte are solvent dependent. Thus the choice of solvent in aerosol MALDI plays a key role in obtaining optimum ion signal.

References:

1. F. Xiang and R. C. Beavis, *Rapid Commun. Mass Spectrom.*, **8**, 199, (1994).
2. O. Vorm, P. Roepstorff and M. Mann, *Anal. Chem.*, **66**, 3281, (1994).
3. R. C. Beavis and B. T. Chait, *Rapid Commun. Mass Spectrom.*, **3**, 233, (1989).
4. K. Strupat, M. Karas and F. Hillenkamp, *Int. J. Mass Spectrom. Ion Proc.*, **111**, 89 (1991).
5. T. Chan, A. W. Colburn and P. J. Derrick, *Org. Mass Spectrom.*, **26**, 342 (1991).
6. S. R. Weinberger, K. O. Boernsen, J. W. Finchy, V. Robertson, B. D. Musselman, *Proc. ASMS Conf. Mass Spectrom. Allied Top.*, **41st**, 775 (1993).
7. J. A. Castoro and C. L. Wilkins, *Anal. Chem.*, **65**, 2621 (1993).
8. K. K. Murray and D. H. Russell, *J. Am. Soc. Mass Spectrom.*, **5**, 1, (1994).
9. M. D. Beeson, K. K. Murray, D. H. Russell, *Anal Chem.*, in press.
10. R. C. Beavis, J. N. Bridson, *J. Phys. D.*, **26**, 442 (1993).

"Analyzing Thermally Labile Compounds in Electrospray Sources using Heated Capillaries"

Brent L. Kleintop, H. K. Lim, Thomas D. Oglesby[1], Kelvin W. Chan, and Samuel F. Sisenwine
Wyeth-Ayerst Research, CN 8000, Princeton, NJ 08543-8000
[1]Taylor Technology, 107 College Rd. East, Princeton, NJ 08540

Introduction

The recent development of atmospheric pressure ionization (API) sources as LC/MS interfaces has led to the development of several different commercially available API sources. One design incorporates a metal-clad heated capillary to facilitate desolvation to allow the use of LC flow rates ranging from 1-1000 ml/min. A potential problem of this design is that some compounds may thermally decompose or form adducts while passing through the heated capillary. Although this is not always the case, we have seen examples of compounds decomposing in the ion source under "normal" operating conditions (*i.e.* higher capillary temperatures at higher flow rates). Intact molecular ions are essential in metabolite identification studies because thermal decomposition products or adducts may be incorrectly assigned as metabolites. Intact molecular ions are also important in quantitative analyses using stable isotope labeled internal standards. Thermal decomposition may result in the loss of the stable isotope label; the decomposition products for both the analyte and internal standard would be identical. This type of decomposition would require the use of a different stable isotope labelled compound. Finally, the heated capillary may affect the detection of non-covalently bound complexes, an exciting potential ESI/MS application.

This presentation addressed considerations for operating API sources with heated capillaries to minimize thermal decomposition to promote the formation of intact molecular ions. These effects were illustrated by the ESI spectra of some low molecular weight pharmaceutical compounds which readily decompose in the heated capillary under "normal" operating conditions. The mass spectra of a non-covalently bound complex obtained on two different source designs was also compared.

Experimental

Mass spectra were acquired using a Finnigan MAT TSQ-7000 and Finnigan API source. A schematic of the source is shown in Figure 1. Samples were infused at a flow rate of 5 ul/min into a 350 ml/min mobile phase flow resulting in a total flow rate of 355 ul/min into the ESI source. Mass spectra were acquired after performing signal averaging for 30 seconds. A Vancomycin-DALAA (non-covalent complex) mass spectrum was acquired by infusing the sample into the instrument at a flow rate of 5 ul/min and signal averaging for 30 seconds (10 scans). The mass spectrum of Vancomycin-DALAA was also acquired using a PE Sciex API III. The sample was infused into the instrument at a flow rate of 5 ul/min. The mass spectrum shown is the sum of 10 scans.

Results

The effect of capillary temperature and tube lens voltage on mass spectra of ACA-147 is illustrated in Figures 2a and 2b below. At the flow rate used for these experiments, we would normally use a capillary temperature of 225 C to produce efficient desolvation. However, at this temperature a significant amount of decomposition was observed (Figure 2a). Reducing the heated capillary temperature yielded poor desolvation which produced mass spectra which contained predominately solvent ion clusters. One method to overcome the loss of desolvating power at low capillary temperatures is by using in-source CAD to promote solvent declustering in the capillary/skimmer region of the interface. The higher voltages applied to the tube lens or capillary are more likely due to the need to decluster solvent ions rather than focus ions through the skimmmer. The mass spectra of Figures 2b demonstrate a significant increase in molecular ion production using lower capillary temperatures (125 C) with higher tube lens voltages (+190 V). At these conditions, stable molecular ion signal was observed for 10 minutes.

Another method to affect desolvation is the use of high flows of auxiliary gas. The effects of the auxiliary gas flow rate are illustrated in the mass spectra of ACA-147 shown in Figures 3a - 3b. These

mass spectra demonstrate that the use of higher flows of nitrogen auxillary gas helped to promote desolvation and greatly reduce the amount of methanol solvent clusters observed at temperatures. lower capillary temperatures.

The mass spectra of the non-covalently bound complex of Vancomycin and Diacetyl-Lys-Ala-Ala obtained using both an ESI source which incorporates a heated capillary and another design which doesn't incorporate heat were also compared. Both mass spectra showed detection of the Vancomycin-DALAA complex. However a much larger abundance of singly charged complex and free Vancomycin was observed in the heated capillary source. This may be a result of charge stripping caused by the heated capillary.

Conclusions

This presentation demonstrated that intact molecular ions of thermally labile compounds may be produced in ESI sources using heated capillaries at high flow rates (200-400 ul/min) and low capillary temperatures. The loss of desolvating power at low capillary temperatures may be overcome by using high tube lens voltages to promote solvent declustering via in-source CAD in the capillary/skimmer region of the interface. The use of higher flows of auxillary gas may also promote desolvation. Good molecular ion signal stability was observed when using low capillary temperatures at higher flow rates. Finally, non-covalently bound complexes can be detected using ESI sources of two different designs.

Figure 1

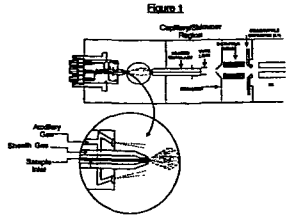

Figure 3a

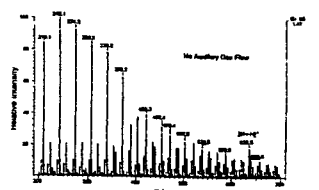

Figure 2a

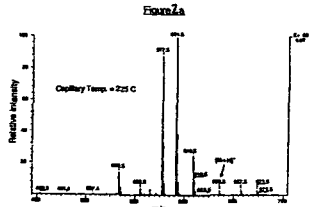

Figure 3b

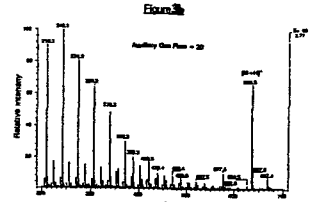

Figure 2b

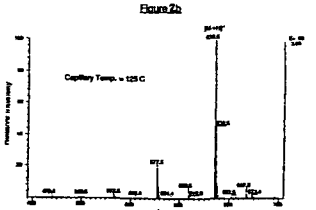

Figure 3c

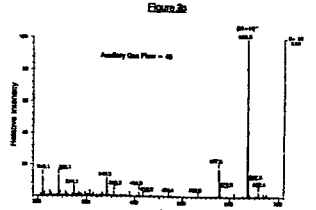

Peptide Mixture Analysis by Combining Electrospray-CID-MS and Chemometrics

William H. Cusworth, III and Frantisek Turecek
Dept. of Chemistry, BG-10, University of Washington, Seattle, WA 98195, USA

Introduction: Electrospray Ionization (ESI) has been shown to have wide applications in the analysis of peptides and other biomolecules. However, quantitative analysis of complex mixtures of peptides is often very difficult and usually requires a long separation step. Here a new analytical method for the analysis of peptide mixtures is evaluated. The method employs a novel second order mass spectral data collection scheme followed by second order chemometric analysis. The second order data is generated by collecting spectra produced under varying degrees of source-CID where fragmentation is induced in the interface region of the electrospray source. There are inherent advantages in second order data analysis. Unlike zero and first order methods, second order chemometric methods can offer a calibration that is not compromised by the introduction of unknown interferents such that calibration samples need only contain the target analytes (1).

Experimental: Two sets of experiments were conducted using mixtures of dipeptides as analytes to be quantitated and 100 μM solutions of the pure dipeptides as calibration standards. All samples used a solvent matrix of 80:20 MeOH:H_2O with 0.2% acetic acid.

The first set of experiments were carried out on a Hewlett-Packard 5971A bench top mass spectrometer which has been modified to support electrospray ionization using the transfer capillary design first published by Chait et. al. (2). Binary mixtures of the dipeptides Phe-Leu (FL) and Leu-Phe (LF) were chosen as a simple two-component model system for evaluation. FL and LF are isomers which give a parent ion at *m/z* 279. At higher collision energies, FL yields an *a*-type fragment ion at *m/z* 120 while LF yields an *a*-type fragment ion at *m/z* 86. The samples were injected using a simple FIA system at 5 μL/min. Ions exiting the transfer capillary are subject to CID by externally applying a voltage bias in the expansion region (1.2-1.4 torr) between the capillary and the skimmer. The quadrupole is scanned at low resolution in the selected ion monitoring mode (SIM) mode at 2 scans per minute for 30 preselected parent and fragment mass channels of importance. The voltage bias is applied in 25 V steps in one minute intervals to coincide with the scan of the quadrupole such that 9 discrete biases (18 scans) ranging from +125 V to +325 V are monitored. The data collected is combined into a 18 x 30 matrix. Figure 1(a) shows the second order spectra generated for the mixture of 80 μM FL and 40 μM LF.

The second set of experiments were carried out on a Finnigan TSQ 7000, a commercial tandem quadrupole mass spectrometer. Six-component mixtures of the dipeptides FL, LF, FG, GF, SL, and LS were made such that each component would have an *m/z* overlap of both its parent ion and the fragment ions. The components of these mixtures cannot be accurately quantitated by standard zero-order methods due to the absence of any unique peaks for calibration. Samples were infused from a syringe pump at 5 μL/min. Fragmentation was induced in the first octopole by ramping the voltage bias (software-controlled) in 1 V steps from +5 V to +34 V between the skimmer and analyzer assembly, which has the configuration: octopole-quadrupole-octopole-quadrupole. The first

quadrupole was operated in the RF-only mode while the second quadrupole was scanned from *m/z* 30 to 325 every 15 sec (1 scan for each voltage bias step). The resulting data matrix was reduced to a size of 30 x 50 by selecting 50 parent and fragment mass channels of importance. Figure 1(b) shows the second order spectra generated for the mixture of 40 μ M FL and 20 μM of the other 5 components.

Results: The second order data produced by the method described are non-bilinear in nature and were analyzed by Non-Bilinear Rank Annihilation (NBRA)(1), an extension of the Generalized Rank Annihilation Method (GRAM). Results of the NBRA (second-order) data analysis were compared to results of the standard zero-order method of predicting concentrations based on the ratio of the peak height of the parent or a fragment ion in the mixture to that in the standard. In the first set of experiments (binary mixtures on modified HP 5971A), it was found that the predictions using NBRA (using 1 principal component (PC) for FL, 2 PCs for LF) for most of the mixtures correlated well with predictions based on the ratio of unique fragment peak heights. As expected, predictions became worse as more mass channels containing primarily noise were included in the analysis. The six-component mixtures of dipeptides were unable to be analyzed due to the low signal of the in-house modified HP5971A, hence the use of the Finnigan TSQ 7000, which yields a greater than ten-fold better signal to noise ratio, in the second set of experiments. These experiments showed that concentration predictions based on peak heights of the parent ions were not in agreement with what one would expect based on the known isobaric overlaps. The signals for FL and LF appear to be enhanced in the mixtures while the other components are suppressed. The high total peptide concentrations ranging from 110 to 150 μM may account for the interaction between the analytes. The NBRA analysis (using 4 PCs) yielded predictions significantly closer to the actual values for FL, LF, and LS but not for FG and GF. Singular-Value Decomposition revealed that the matrices only had a rank of four, which means that at most four analytes can be quantitated successfully in this set of data.

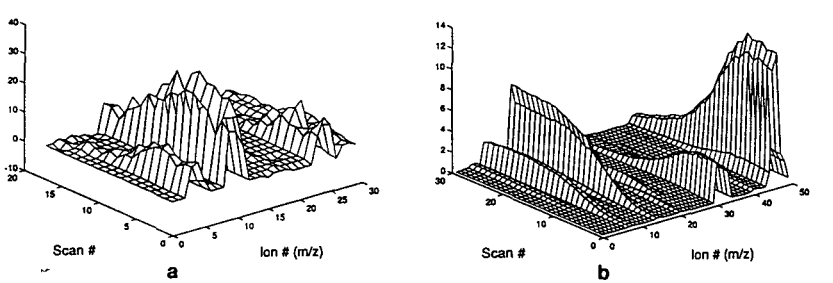

Figure 1. Second-Order Spectra of a) 80 μM FL & 40 μM LF on modified HP 5971A b) 40 μ M FL & 20 μM LF, FG, GF, SL, & LS on Finnigan TSQ 7000.

References:

1) Wang, Y., Borgen, O., Kowalski, B., Gu, M., Turecek, F., *J. Chemometrics* **1993**, *7*, 117.
2) Chowdhury, S.K., Katta, V., Chait, B.T., *Rapid Commun. Mass Spectrom.* **1990**, *4*, 81.

Ion Solvation in Electrospray Generated SDS Clusters

Q. Gao, A. C. Harms, J. Zhang, H. R. Udseth, A. L. Rockwood,
M. G. Sherman and R. D. Smith

Chemical Sciences Department
Pacific Northwest Laboratory, Richland, WA 99352

The investigation of ion solvation is important for understanding solution behavior. The extent of solvation of ions and molecules is not only a fundamental concern for elucidating reaction kinetics and thermodynamics, but also strongly influences molecular structure, stability and reactivity. In this research sodium ion solvation in the sodium dodecyl sulfate (SDS) surfactant clusters has been investigated using mass spectrometry.

Electrospray ionization was employed to generate gas phase ion clusters from SDS aqueous solutions. Gas phase sodium ions solvated by water were only observed for small singly charged clusters at low (100°C) capillary inlet temperatures (Fig. 1a). Larger size ion clusters $Na(SDS)_n^+$ ($n > 4$) preferentially associate SDS molecules (Fig. 1a). For multiply charged cation clusters (multiple sodium ion adduction) water solvation was not observed. This trend is opposite to that of metal halide salt clusters where greater solvation was reported for doubly charged ions than that for singly charged ions in a comparison experiment [1]. While the total number of associated water molecules with each sodium ion may depend on the kinetics of the desolvation process in the heated capillary, the preferential SDS attachment to large ions likely results from the higher thermodynamic stability for SDS association. This is confirmed from collision induced dissociation (CID) studies. The strength of association among SDS molecules is estimated to be a factor of 4 stronger than the association of water molecules to the SDS cation clusters. It is postulated, based on the CID results, that the SDS clusters are primarily bound by electrostatic forces rather than van der Waals forces.

For anion clusters (detachment of sodium ions), no solvation was observed at 100 °C capillary temperature (Fig. 1b), which may be attributed to the hydrophobicity of the hydrocarbon chain. Theoretical studies suggest that large halide anions would reside at the surface of water clusters, rather than being solvated internally by small water clusters [2]. This would lead to weaker water-anion interactions, hence, easier desolvation.

1. Z. L. Cheng, K. W. M. Siu, R. Guevremont, and S. S. Berman, J. Am. Soc. Mass Spectrom. 3 (1992) 281

2.(a) L. Perera and M. L. Berkowitz, J. Chem. Phys. 95 (1991)1954; (b)ibid 96 (1992) 8288; (c) ibid 100 (1994)3085; (d) J. W. Caldwell and P. A. Kollman, J. Phys. Chem. 96 (1992)8249

Pacific Northwest Laboratory is operated by Battelle Memorial Institute for the U.S. Department of Energy, through Contract No. DE-AC06-76RLO-1830

43rd ASMS Conference on Mass Spectrometry and Allied Topics

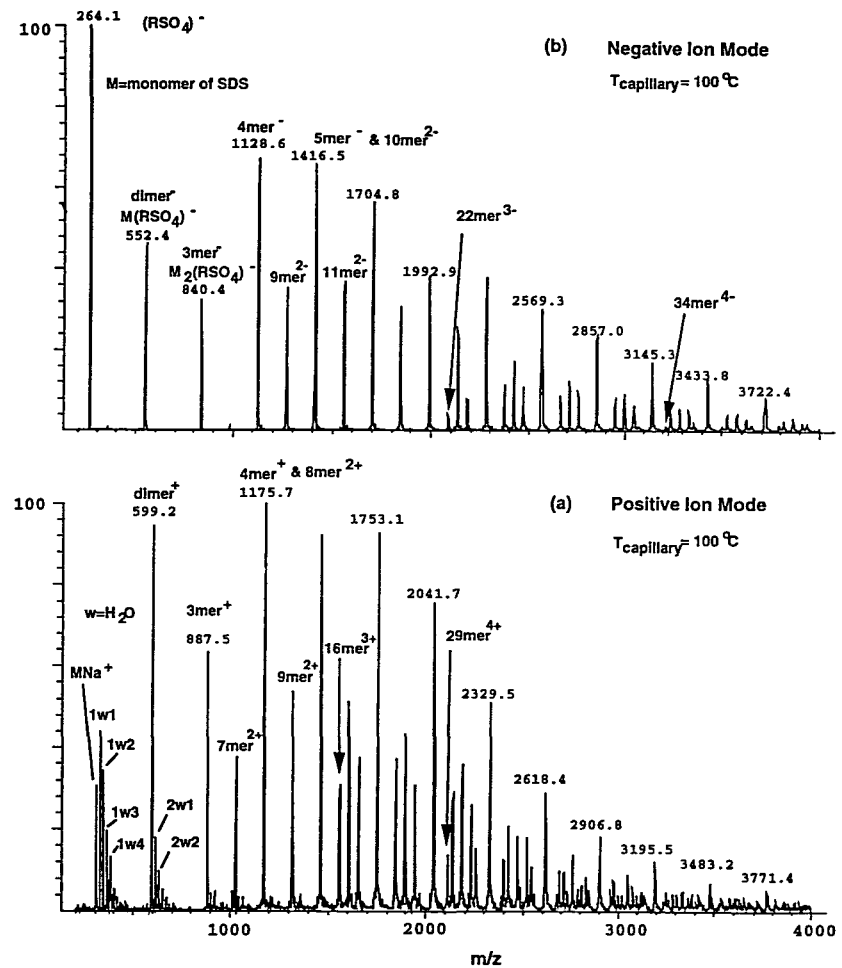

Fig. 1 Electrosprasy Ionization Mass Spectrum of SDS Aqueous Solution

RAPID MOLECULAR WEIGHT DETERMINATION USING ELECTROSPRAY IONIZATION MASS SPECTROMETRY

Rich Gedamke, Gerald C. DiDonato, Mark E. Hail, and Mike S. Lee
Bristol-Myers Squibb Pharmaceutical Research Institute, Princeton, NJ 08543

In the pharmaceutical industry, molecular weight characterization of synthetic organic compounds has been traditionally accomplished using probe techniques such as fast atom bombardment (FAB) and desorption chemical ionization (DCI). The choice of technique is usually determined by compound volatility and thermal stability, with DCI chosen for volatile compounds usually less than 700-800 Da. FAB is the technique of choice for peptides, salts, and intermediates with unstable protecting groups. Both techniques usually involve manual sample preparation and analysis.

The commercialization and availability of electrospray ionization (ESI) provides an additional method of sample characterization via mass spectrometry. ESI is capable of producing gas-phase ions from solution with little or no internal energy, resulting in simplified spectra often containing only a major ion associated with the molecular ion species. It would appear that ESI will have a significant role, complementary or perhaps exclusive, with respect to molecular weight characterization.

This poster describes our efforts to develop ESI conditions that would provide molecular weight information for the greatest percentage of all synthetically prepared samples submitted to our laboratory for molecular weight characterization. Amongst the parameters investigated were sample concentration, sample dissolution and preparation, LC eluent, pH, mobile phase flow rates, and instrument control.

EXPERIMENTAL

These studies were performed using a Finnigan TSQ700 mass spectrometer equipped with a Finnigan ESI source. The chromatographic system included a Waters Model 600MS LC and a Waters 717 autoinjector with 96 sample carousel under the control of the mass spectrometer data system.

RESULTS AND DISCUSSION

A small amount of sample is placed into a 1 mL autosampler vial. The sample amount is "eyeballed", but is generally in the range of a few hundred micrograms. In our initial studies samples were dissolved in the solvent indicated on the sample submission card as indicated by the submitting chemist. However, this procedure proved to be cumbersome and time consuming. In order to facilitate sample preparation, we sought the use of a single solvent system. A mixture of water, acetonitrile, methanol, and acetone was evaluated and is now routinely used since it can dissolve most of the compounds submitted for analysis. Typical exceptions to this are synthetic peptides which require dissolution in 0.1% TFA. Typically, 2 µL of this solution is injected, with the exception of peptides, in which 10 µL is injected. This results in injection quantities on the order of a few hundred nanograms.

Selection of an appropriate solvent system was central to the goal of developing automated flow injection ESI that could result in the successful analysis of the highest percentage of synthetic organic compounds. Our initial experiments with ESI involved the use of several

different mobile phase modifiers, including ammonium acetate, ammonium formate, formic acid, and TFA, in acetonitrile/water, in both positive and negative ion mode.

Both TFA and formic acid appeared to chemically cleave acid-sensitive protecting groups such as trityl and phenyl,di-tertiary butyl groups. Less degradation was noted when ammonium acetate or ammonium formate was used, however we were obtaining accurate molecular weight data on only 65% of submitted samples. Most successful analyses were those that yielded good positive ion data. We then evaluated several mobile phases in an effort to increase negative ion production and therefore increase the number of successful analyses. Several novel mobile phases were evaluated, including KOH in methanol, potassium-tert-butoxide in tertiary butanol, ethyl diisopropyl amine in methanol, and ammonium hydroxide. Both KOH/methanol and potassium-tert-butoxide/butanol were found to "salt out" of solution thus clogging the PEEK tubing and ESI manifold of the instrument. Ethyl diisopropyl amine in methanol was found to produce excellent negative ions for medium sized molecules with only one labile proton, including simple alcohols. Routine use of this solvent system was abandoned due to high background in positive ion mode. Ammonium hydroxide proved to be the most useful solvent for negative ion analysis across a wide range of structures. Further experimentation indicated that ammonium hydroxide could produce excellent positive ion data as well. Currently the method has been refined with a mobile phase consisting of 0.1% aqueous ammonium hydroxide/acetonitrile (50/50).

DATA REDUCTION AND INSTRUMENT CONTROL

Following the successful implementation of flow injection ESI it became apparent that the bottleneck in high-throughput automated analysis would be instrument control and data reduction. In order to facilitate these processes, an instrument control language (ICL) procedure, which we call pulsed positive ion negative ion electrospray ionization (PPINIESI), has been written which controls the Waters 600 MS HPLC and 717 autosampler and the TSQ700 mass spectrometer. Up to 96 samples can be loaded into the sample rack of the Waters autosampler. The operator simply appends the PPINIESI procedure with the list of compounds to be run. The instrument then acquires both positive and negative ion ESI data for each sample in the rack. Using a separate data system script, written in the UNIX C-shell environment, the raw data is automatically background subtracted and printed.

CONCLUSIONS

We have developed an automated flow injection ESI system capable of molecular weight characterization of over 85% of compounds received in our laboratory. Sample preparation is straightforward, requiring the use of a single dissolution solvent. Analysis of each sample in both positive and negative ion mode, using a single LC solvent, takes approximately 2 minutes per sample. Based upon our work it appears that ESI is a nearly all-encompassing molecular weight determination tool. ESI is very well suited to high-throughput molecular weight determinations. Future efforts with molecular weight characterization will almost certainly require the use of ESI sources on relatively simple quadrupole or ion trap mass spectrometers.

Adventures in the positive ion ESI/MS of acids and neutral molecules

Nikhil Shah and William L. Fitch
Affymax Research Institute, 3410 Central Expressway, Santa Clara, CA. 95051

Introduction

Electrospray ionization (ESI) has revolutionized the introduction of compounds for mass analysis. This simple technique can be used with ionics and non-ionics, with polar and reasonably non-polar compounds, with high and low molecular weights. As a general method for structure confirmation to a diverse population of small molecule and peptide chemists we utilize flow injection, positive ESI. Amines and quaternary ammonium compounds behave extremely well in ESI. Acidic and neutral compounds are not always so sweet.

Affymax is pioneering the automation of chemical synthesis and generating mixtures or "libraries" of compounds for drug discovery. One of our tasks is to develop MS methods for quality control of these mixtures. MS of a mixture is much more difficult when individual components of the mixture yield solvent adducts, oligomers, cation adducts or fragment ions.

Among the problems we are addressing:

Phthalate contamination, Solvent adducts and oligomers, Ion suppression by impurities and Artifacts from reactive solvents.

Conclusion

After one year of analyzing over 400 samples per month we are confident of our ability to obtain ESI molecular weights for 80-90% of the small molecules generated in a diversity chemistry lab.

Phthalates can arise from HPLC pump seals, impure water and impure acetic acid. We know how to avoid these problems.

Solvent adducts and oligomers arise from insufficient declustering in the heated capillary ESI interface. These artifacts can be lowered by adjusting ionization voltages and temperatures, by decreasing compound concentration and by doing low flow infusion instead of flow injection.

Suppression of ESI signal can occur when analyzing mixtures if different components have very different ionizabilities. LC/MS is the general solution to this phenomenon but not practical for routine analysis. We have shown that ion supression with the Dionex scrubber can be useful in some cases to remove the offending cations and allow the "hard to ionize neutral's" spectrum to come through. This phenomenon may be useful in mixture analysis.

43rd ASMS Conference on Mass Spectrometry and Allied Topics

ESI mass spectrum of FMOC-Val
10pmol/uL flow injection

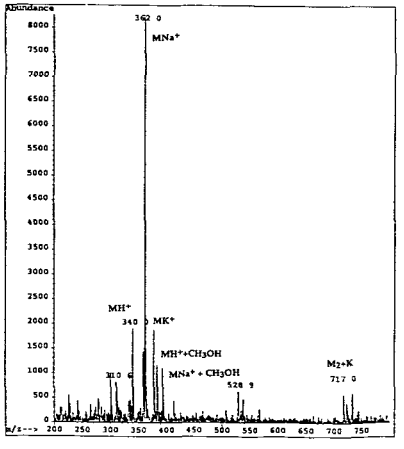

ESI mass spectrum of FMOC-Val
10pmol/ul infused

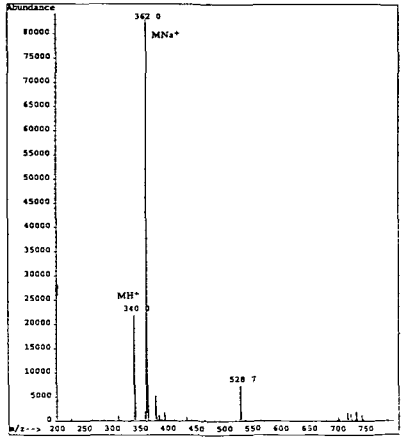

Ampicillin+Penicillin in ACN H2O
100pmol/uL flow injection

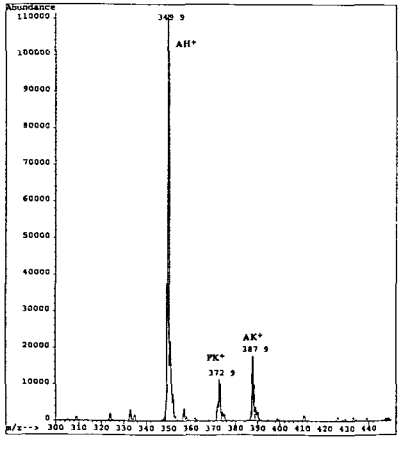

Ampicillin+Penicillin in ACN·H2O
100pmol/uL after dionex suppressor

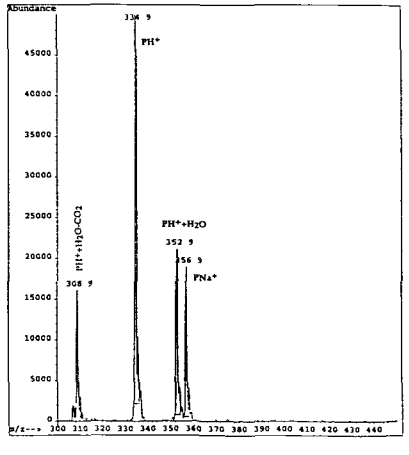

Electrospray Ionization of Neutral Complexes from Non-Polar Solvents

Xueheng Cheng[1], Quanyin Gao[1], Richard D. Smith[1], Eric E. Simanek[2], Mathai Mammen[2], George M. Whitesides[2]

[1] Chemical Sciences Department and Environmental Molecular Sciences Laboratory, Pacific Northwest Laboratory, Richland, WA 99352.

[2] Department of Chemistry, Harvard University, Cambridge, MA 02138

INTRODUCTION

The characterization of noncovalent complexes from solution using electrospray ionization (ESI) constitutes a new capability for mass spectrometry (MS). Observation of many types of charged complexes has been reported. However detection of neutral, noncovalent complexes becomes difficult using ESI-MS when the molecules (complexes) do not have ionizable groups or when they are insoluble/unstable in the more typically used solvents. We will show that the use of organic-soluble charge carriers such as tetraphenylphosphonium chloride (Ph_4PCl) or tetraphenylboron sodium (Ph_4BNa) presents a new strategy to facilitate ionization for these neutral noncovalent systems. A family of self-assembled aggregates have been designed based on the cyanuric acid•melamine (CA•M) hydrogen-bonded lattice (Figures 1 and 2). These noncovalent complexes have been characterized using a variety of techniques and the results indicated the formation of tight complexes in non-polar organic solvents with a range of stoichiometries. Studies by vapor pressure osmometry suggested, however, that the molecular weights were 50-80% higher than those expected for these stoichiometries.

EXPERIMENTAL

A Finnigan MAT TSQ 7000 triple-quadrupole mass spectrometer with a home-built microspray emitter optimized for very low sample infusion rate (0.2-0.5 ul/min) was used. A solution containing 1-5 mM Ph_4PCl or Ph_4BNa and 1-5 mM analyte was prepared for the electrospray ionization by mixing appropriate amounts of each component in a 10 mM stock solution with the non-polar organic solvent. The solution was directly infused into the ion source of the mass spectrometer. In the collision-induced dissociation (CID) experiment, the precursor ion was selected using the first quadrupole with a window of ±5 *m/z* units, accelerated and collided with added argon gas in the second (rf only) quadrupole (E_{lab} = 35 eV, P_{Ar} = 1.58 mTorr). The product ions were detected using the third quadrupole with unit *m/z* resolution. For thermo-dissociation experiments, the desolvation capillary temperature was varied systematically while all other instrumental parameters were kept constant.

RESULTS

Successfully detection of several intact hydrogen-bonded supramolecular complexes using ESI-MS was made possible in non-polar organic solvents by attachment of small organic-soluble ions using reagents such as Ph_4PCl. These complexes have been observed using mass spectrometry for the first time and the accurate molecular weight measurements confirmed the stoichiometries inferred in solution. Figures 1 and 2 show the ESI-MS spectra for complex **4** and **7** using Ph_4PCl as charge donor. The Cl^--attached complex ions with expected stoichiometries were observed as the predominant species in these spectra. Additional structural features and relative stabilities of these complexes were revealed by thermally (Figures 3 and 4) and collisionally induced dissociation techniques. Complex **7** was shown to be more stable than complex **4**, consistent with results of solution studies. The dissociation of complex **4** produced predominately the individual components, demonstrating the highly cooperative nature of the subunit binding while complex **7** gave substantial amount of 1:1 complex in addition to the individual components. Successful detection of these complexes were also made using other organic soluble salts (such as Ph_4BNa) and solvent systems (such as CH_2Cl_2).

Pacific Northwest Laboratory is operated by Battelle Memorial Institute for the U.S. Department of Energy, through Contract No. DE-AC06-76RLO 1830.

43rd ASMS Conference on Mass Spectrometry and Allied Topics

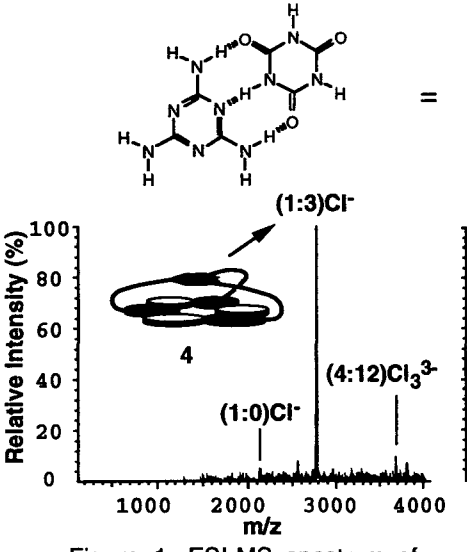

Figure 1. ESI-MS spectrum of complex **4** in $CHCl_3$ with Ph_4PCl.

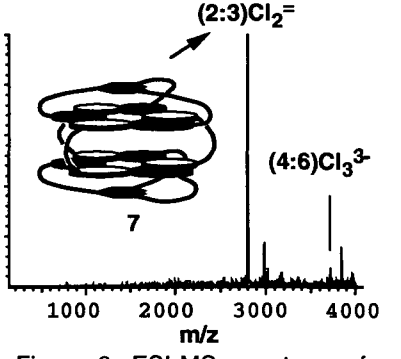

Figure 2. ESI-MS spectrum of complex **7** in $CHCl_3$ with Ph_4PCl.

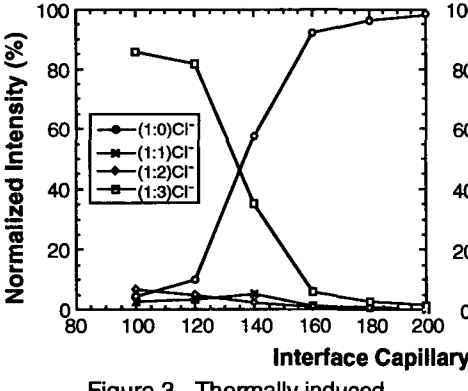

Figure 3. Thermally induced dissociation of complex **4**.

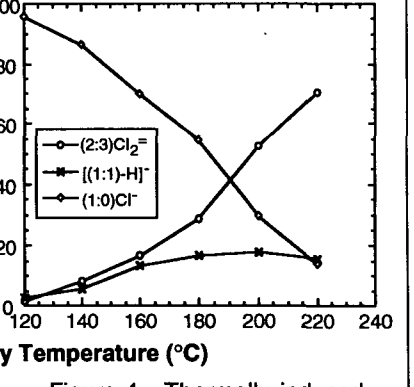

Figure 4. Thermally induced dissociation of complex **7**.

Electrospray Mass Spectra of Less Polar Compound Dissolved in n-Hexane

Wen-Shyang Wang, S-Wan Huang, and Jentaie Shiea*
Dept. of Chemistry, Natl Sun Yat-sen Univ., Kaohsiung, Taiwan 804

Electrospray ionization (ESI) has seldon been used in the anaslysis of less polar compound. This is because that the analyte has to be dissolved in nonpolar solvent and the electrospray of the nonpolar solvents has seldon been studied. In this study, it was found that good electrospray mass spectra of several less polar compounds such as long chain alcohols, acids, and esters dissolved in n-hexane were obtained. The ESI mass spectra were obtained by a PE Sciex API-1 mass spectrometer equipped with an ion spray source The sample solution was introduced by continuous infusion by a syringe pump at 5 ul/min through a fused-silica capillary column of 100 um i.d. The temperature of the electrospray interface chamber was held at 55 ± 1°C

Since the analyte such as long chain alcohols dissolved well both in n-hexane and methanol, the ESI mass spectra of the analyte obtained in both solvents were compared. Figure 1 and 2 show the ESI mass spectra of n-dodecanol ($C_{12}H_{25}OH$, 0.05 M) dissolved in mathanol and in n-hexane The required voltage for electrospray for n-dodecanol/methanol solution is 4200 V and the mass spectrum is dominant with sodium adduct ions such as MNa^+, M_2Na^+, M_3Na^+, and M_4Na^+ (Figure 1) The possible sources of the sodium ions are originated from trace impurities in the solvent or chemicals. The mass spectrum of n-dodecanol/n-hexane solution electrospraying at 5300 V is shown in Figure 2 The spectrum is dominant with the ions such as MH^+, $M(H_3O)^+$, M_2H^+, and M_3H^+ The results shown here indicate that the ions generated in n-hexane solution are dominant with protonated or hydronium-adduct ions which are different from those found in methanol.

Since very high voltage was applied during electrospray of n-hexane solution, it is possible that the moisture in the air will also be discharged. The formation of hydronium ions and the protonated water clusters by discharging become good sources to supply proton and hydronium ion to n-dodecanol. The protonated n-dodecanol can be formed by a series of ion-molecule reaction as those occurred in chemical ionization Since n-hexane is not involved in the process of ion formation, it is unnecessary for the mechanisms described above to be occurred only in n-hexane solution. At 5300 V, even in the methanol solution, the protonated (MH+) or hydronium adduct n-dodecanol ions ($M(H_2O)^+$) can be seen.

43rd ASMS Conference on Mass Spectrometry and Allied Topics

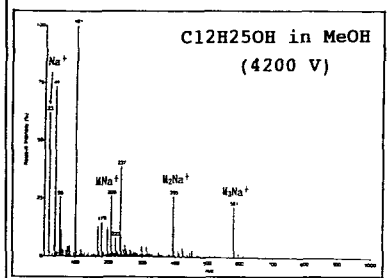

Figure 1. The ESI mass spectrum of 0.05M n-dodecanol in methanol (V 4200V)

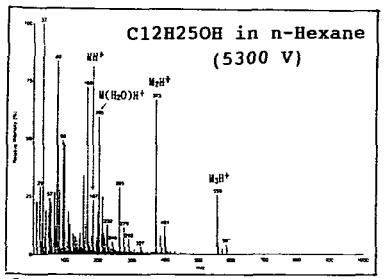

Figure 2 The ESI mass spectrum of 0 05M n-dodecanol in hexane (V :5300V)

Low Temperature Electrospray Ionization Mass Spectra of Thermally Unstable Compound

Wen-Shyang Wang, Chin-Hsiung Wang, and Jentaie Shiea*
Dept of Chemistry, Natl Sun Yat-sen Univ., Kaohsiung, Taiwan 804

2,5-Dimethyl-2,5-dihydrothiophene is not only a very volatile but also a very reactive compound The compound is synthesized by the flash vacuum pyrolysis (FVP) at 600 C and 0.01 torr Once generated, the compound was collected in CH_2Cl_2 and the solution was then caped and stored in CH_2Cl_2/dry ice. The structural characterization of such compounds can only be done by low temperature NMR. So far, good mass spectra of such compound have never been reported This is because that none of the ionization techniques used in mass spectrometry can efficiently operate and generate ions at such low temperature. Since the freezing points of CH_2Cl_2 is - 95℃, a very low temperature ESI mass spectrum of the analyte in such solvent can be obtained. Here, we report the ESI mass spectra of both compounds by a home-built low temperature ESI source at - 78℃ (Figure 1)

To prevent the occurrence of decomposition and polymerization of the sample molecule, the temperature of the source is maintain at - 78℃ by putting it into a plastic box which is covered with fine dry ice powder The outside part of the box was then surrounded with a thick layer of foam to isothermally isolate it from environment The sample solution was introduced by continuous infusion. Since the glass syringe leaks at - 78℃, a special sample injection and storage unit was built for the analysis. About 0 3 ml of cold solution was rapidly transferred into one arm of a three-way tee. This was simply done by injecting the solution through a teflon tube by a 5 ml gas-tight plastic syringe. One arm of the tee was connected to a 50 ml air-tight plastic syringe. The sample solution in the tees will be delivered to the electrospraying needle by compressing the air in the syringe by a syringe pump. No nebulizing gas is used in this design. The high voltage required for electrospray was added through the stainless steel tube. The ion generated by the low temperature electrospray source was detected by a PE Sciex API 1 mass spectrometer. The operating parameters of mass spectrometer for the low temperature solution were similar to that at room temperature The temperature of the electrospray interface chamber in the mass spectrometer was held at 55 ± 1℃

Figure 2 shows the ESI mass spectrum of DMDHT (in CH_2Cl_2) at room temperature The required on set voltage of electrospray from pure CH_2Cl_2 at room temperature is about 5300 V. It can be seen that the intensity of MH^+ is low. Since the compound is very volatile, we speculate that most of the sample molecules evaporated during sample handling processes. Figure 3 shows ESI mass spectrum of DMDHT at -78℃. The peak from pseudomolecular ion of DMDHT (m/z 111) is the prominent peak on the spectrum. It was also found that the electrospray at such low temperature is more stable than that at room temperature. The required on set voltage of electrospray is nearly the same as that required at room temperature (i.e. ca. 5300 V). This imply that surface tension of CH_2Cl_2 does not increase too much when temperature drop from 25℃ to -78℃ As described before, the compound is very reactive, therefore, it is usually stored at low concentration condition to prevent the occurrence of polymerization Even at -78℃, polymerization still occurs for the solution with high concentration of the sample (Figure 4).

43rd ASMS Conference on Mass Spectrometry and Allied Topics

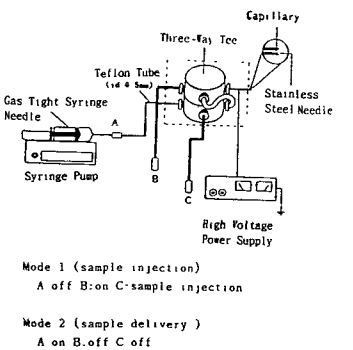

Figure 1. Sctematic diagram of low temperature ESI source

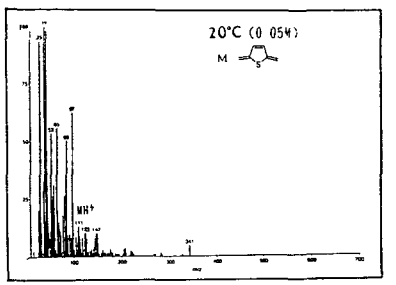

Figure 2. The ESI mass spectrum of 0 05M DMDHT in CH_2Cl_2,20℃

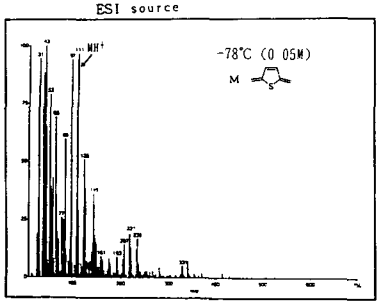

Figure 3. The ESI mass spectrum of 0.05M DMDHT in CH_2Cl_2,-78℃

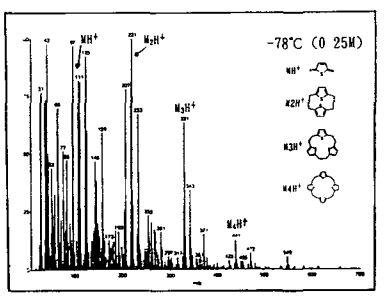

Figure 4.The ESI mass spectrum of 0 25M DMDHT in CH_2Cl_2,-78℃

Multiple Channels Electrospray Ionization Source for Directly Coupling to HPLC

Ching--hsiung Wang and Jentaie Shiea*
Dept. of Chemistry, Natl Sun Yat-sen Univ., Kaohsiung, Taiwan 804

The problem of directly connecting HPLC to electrospray ionization (ESI) source is that good electrospray can not be generated under high flow of the HPLC eluent One way to solve the problem is to use multi-sprayer to take the high flow from HPLC[1]. Here, we report that two multi-channel electrosprayers which contains sixteen and seven sprayers respectively were built for this study. Figure 1 and 2 show schematic diagrams of the multi-channel electrosprayers. The ESI mass spectra were obtained by a PE Sciex API-1 mass spectrometer equipped with an ion spray source.

The electrospray source with sixteen sprayers was built for the purpose of directly connecting HPLC eluent to ESI/MS. Each sprayer is made by inserting a capillary column through a teflon tube which is held on an acrylic plate. The distance between two capillary column is about 3 mm To prevent the vibration of the sprayers during electrospray, the teflon tubes are glued together with epoxy No nebulizing gas is used in this design The required high voltage for electrospray (ca. 6-10 kV) is introduced into the solution through a thin stainless steel electrode inserted at one arm of the three way tee. The solution is delivered by a HPLC pump at a flow rate of 0 3 ml/min. Since the C-18 stationary phase in HPLC packing can not efficiently separate the analytes, each sample is introduced into the system by flow injection at one minute interval. Figure 3 shows that good mass chromatograms of five biomolecules can be obtained at the LC flow up to 0.3 ml/min. For higher HPLC flow, a source with more sprayers is required.

With the help of electrospray, the study of the gas phase chemistry of macromolecule become possible In this study, it was found that the multi-sprayer can also be used in this kind of study. The electrospray source is comprised of two syringe pumps which are used to deliver the solution with different composition (see Figure 2). The solution which contain myoglobin dissolved in 1% acetic acid solution was passed through the one of the spraying channel located at central position of the source The solution flowing through the rest of six channels is comprised of diethanol amine. DEA is known for its high basicity in the gas phase and can grabe proton from the denatured myoglobin ion in the gas phase. Figure 4 shows the ESI mass spectra of deprotonated myoglobin by DEA in the gas phase. As the concentration of DEA increasing the effect of deprotonation becomes more clear and the number of the charge on the myoglobin shift to lower number.

REFERENCES

1 Kostiainen, R. and Bruins, A.P. (1993) Proceeding of the 41st ASMS Conference on Mass Spectrometry, San Francisco, California, USA, 744a.

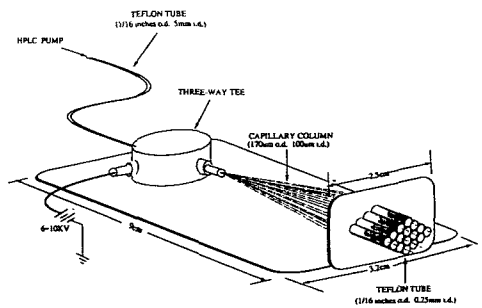

Figure 1. Schematic diagram of sixteen channel ESI source.

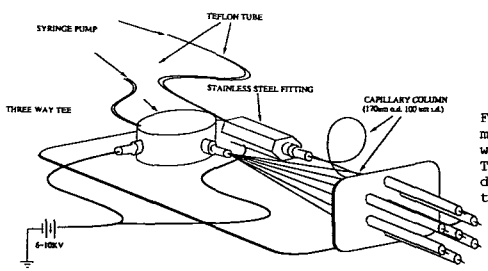

Figure 2. Seven channel ESI source. The myoglobin solution (in 1% acetic acid) was flowing through the central column. The reactant solution (0.5 M or 1 M diethanol amine in water) was flowing through the outside six columns.

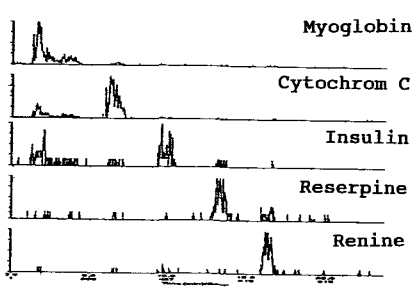

Figure 3. Mass chromatograms of five biomolecules eluted from HPLC (flow rate: 0.3 ml/min) and were detected by sixteen channels ESI/MS.

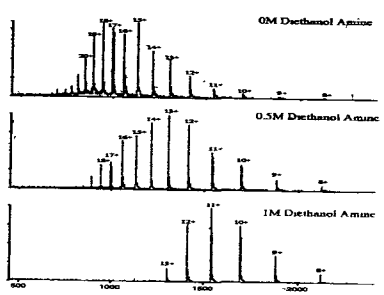

Figure 4. The ESI mass spectra of myoglobin obtained by (a) single channel ESI/MS; (b) seven channels ESI source, DEA:0.5 M; (c) seven channels ESI source, DEA:1 M.

Negative-Ion ESI/MS Mechanism of TFA/TFE Derivatives of Glyphosate and AMPA

Hideji Fujiwara, Rajendra K. Singh, Ronn G. Nadeau, Robert C. Chott

Monsanto Co, Life Sciences Research Center, 700 Chesterfield Parkway North, St. Louis, Missouri 63198

Glyphosate, N-(phosphonomethyl) glycine (Glyph) **1**, is a widely used herbicide effective on a very broad spectrum of plant species and is registered for agricultural as well as residential uses. The most common metabolite of glyphosate in plants, animals or soil environments is aminomethylphosphonic acid (AMPA) **2**. These compounds are very polar and nonvolatile.

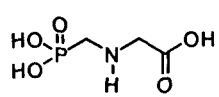

Glyphosate
1

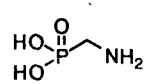

AMPA
2

We recently found that trifluoroacetyl/trifluoroethanol (TFAA/TFE) derivatives of Glyph and AMPA demonstrated dramatically improved sensitivity during negative-ion electrospray ionization / mass spectrometric (ESI/MS) analysis and gave rise to abundant molecular ions. ESI/MS analysis of TFAA/TFE derivatives made possible the detection of nonvolatile products.

The formation of the derivatives and their ionization mechanisms were also investigated by analyses of the derivatives of various deuterium labeled Glyph as well as non-deuterated AMPA analogs.

43rd ASMS Conference on Mass Spectrometry and Allied Topics

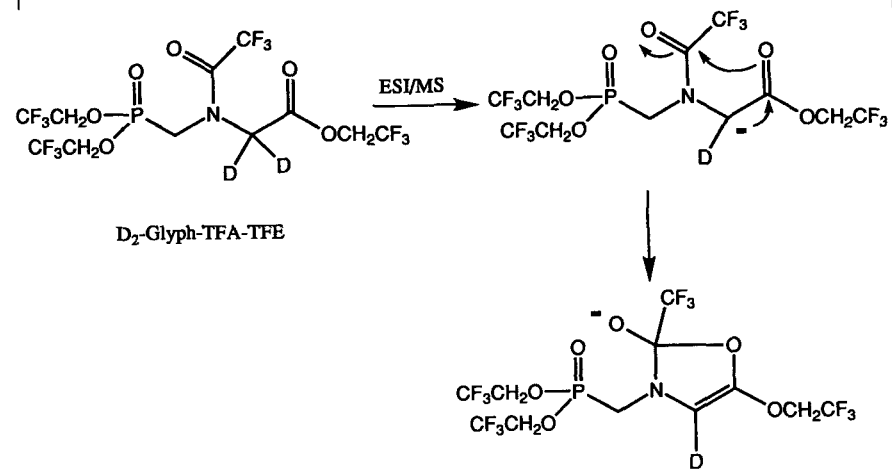

D_2-Glyph-TFA-TFE

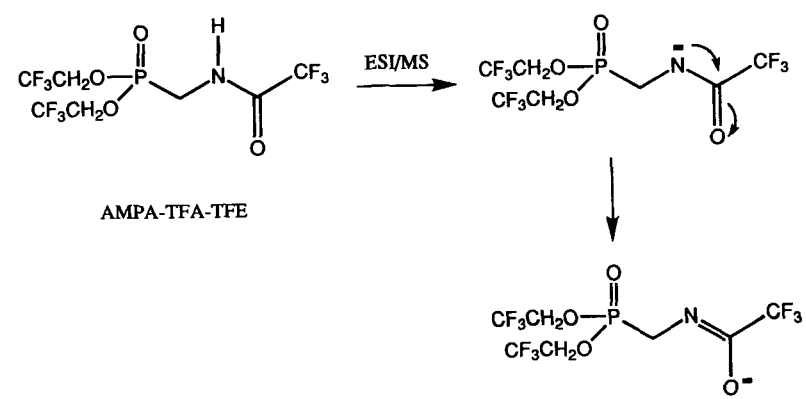

AMPA-TFA-TFE

MAtrix Assisted Laser Desorption/Ionization of Non-Covalently Bound Compounds.

A.S. Woods, J.C. Buchsbaum, J.M. Berg and R.J. Cotter. Johns Hopkins Medical School, Baltimore, MD 21205.

Proteins are biopolymers made of amino acid subunits joined head to tail by a peptide bond (a **Covalent** bond) between the carboxylic acid group of one amino acid and the amino group of the next. Although the amino acid sequence determines the information content of a protein, to use the information depends on much weaker **non-covalent** bonds. As the environment of a folded protein is altered by changing pH, temperature, or pressure, its physical properties do not change gradually. Instead it usually exhibit no change until a point is reached, at which there is sudden drastic change and a loss of biological function. This phenomenon is known as **denaturation**. Denaturation leads to disruption of non-covalent bonds, which lead to loss of tertiary structure and thus of protein function.

In matrix assisted laser desorption ionization (MALDI) mass spectrometric analysis, protein samples are usually dissolved in an aqueous solution of 0.1% TFA 20% or more CH_3CN, pH < 2.0. The matrix of choice is saturated 3,5-dimethoxy-4-hydroxy-cinnamic acid in 1:1 CH_3CN or C_2H_5OH:H_2O pH < 1.5. These highly acidic conditions are denaturing to proteins and peptides, thus making the study of non-covalently bound compounds impossible.

In this study we show that if the harsh acidic conditions present in MALDI MS are changed by using conditions that preserve the tertiary structure of the protein or peptide (pH 4 to 8), we can use this method to study: non-covalent complexes such as zinc finger peptides or enzyme substrate complexes. Mass spectra were obtained on a Kratos (Manchester, England) KOMPACT MALDI III.

a. Zinc Finger Peptides: Two zinc finger peptides were used CP MW 2962.2 PYKCPGCGKSFSGKSDLVKHNRTHTG and CP_{V22} which differs by substitution of a Val for an Arg at position 22. The matrix was a saturated solution of α-cyano-4-hydroxy-cinnamic acid in 1:1 1M NH_4HCO_3:C_2H_5OH. Solutions of CP and CP_{V22} (11pmoles/ul) with and without Zn or Co added were made using a 1M NH_4HCO_3 pH 8.5 buffer. In order to distinguish the different affinities of the Cys_2-His_2 motif for Zn and CO, we prepared a set of peptide samples with 0.5, 1, 5 and 100 equivalents of Zn or Co. All sample spotting on the sample slide were made in an anaerobic chamber. ZFP are small independently folded motifs, that model the multiple zing finger domains found in many DNA-binding proteins. The use of a 1M NH_4HCO_3 pH 8.5 buffer to prepare the peptide solution, as well as the matrix, resulted in a sample-matrix mixture with a pH of 7.2. The peptides used CP and CP_{V22} correspond to consensus sequences developed from earlier zinc finger data base. In this paper we show the first example of a coordinate-covalent metal complex using MALDI mass spectrometry. We also have on a crude scale distinguished between the affinities for binding of a zinc finger domain to two different metals, by "titrating" with equivalents of metal ions. We compared The spectrum of

CP+1.0 equivalent of Zn under anaerobic conditions, to the spectrum of the same sample after exposure to air and found a significant decrease in the MH^+ of ZFP+ Zn. ZFT are highly sensitive to oxydation and will oxidize on exposure to room air. The resulting disulfide bonds that are formed between the two cysteines, as well as other oxidative products involving cysteine preclude the formation of coordinate-covalent complexes between metal ions and Cys or His residues. Mass spectra of CP_{V22}+1.0 equivalent of Zn shows a more prominent $(M+Zn-H)^+$ than that of CP_{V22}+0.5 equivalent of Zn, while the $(M+Co-H)^+$ is barely visible when one equivalent of Co is added.

b. Enzyme-Substrate Complexes: Aminopeptidase I and growth hormone releasing factor (GH) MW 5107.8 were purchased from Sigma. GH solution was made in 1M ammonium citrate pH 6.0 (10pmoles/ul). The matrix was a saturated solution of 3,5-dimethoxy-4-hydroxy-cinnamic acid in 1:1 1M ammonium citrate:C_2H_5OH. Enzyme-substrate complexes have been extensively studied using a variety of methods. Most of these methods, however, require large quantities of enzymes which are not always available. MALDI MS could be an alternative method to the study of enzyme-substrate complexes. MALDI MS has the distinct advantage of requiring picomolar concentrations of protein to give the same information as more well-established methods.

We combined aminopeptidase I with the substrate (GH) and quenched the reaction by matrix addition. The mass spectrum of GH + aminopeptidase, shows MH^+ at 5108.8 amu (GH), 29970.9 amu (aminopeptidase I) and at 35117.5 amu (Enzyme-Substrate complex). The detected masses are well within the 0.1% margin of error typical of MALDI TOF spectra.

These results suggest that by avoiding denaturation of proteins and peptides MALDI TOF could be used as an effective tool to study various types of non-covalent bonding. Non-Covalent complexes have been more easily observed using ESI (1, 2 and 3). However the above results suggest that the effect of the matrix (which usually has an acidic pH) on the tertiary structure of proteins and peptides, rather than the laser desorption/ionization process itself, may limit the observation of non-covalent complexes. Thus, we expect that careful attention to the effect of the UV-absorbing matrices will improve the capabilities for observing the weaker interactions involved in non-covalent complexes.

1. Ganem, B., Li, Y. and Henion J. Am. Chem. Soc., 1991, 113, 6294-6296.

2. Ganem, B., Li, Y. and Henion J. Am. Chem. Soc., 1991, 113, 7818-7819.

3.Katta, V. and Chait, B.T. J. Am. Chem. Soc., 1991, 113, 8534-8535.

Primary Structures of Proteins Characterised by Proteinase K Digestion and MALDI Mass Spectrometrry

Houjun Yang, Matthias Amft, Johann M. Grundwürmer, Xiaoling Li
and Jürgen Grotemeyer*
Institute of Physical Chemistry, Wuerzburg University, 97070 Wuerzburg, Germany

The advents of matrix-assisted laser desorption/ionization mass spectrometry (MALDI-MS) have enabled the determination of biomacromolecular mass with high sensitivity and accuracy. The technique finds many applications in solving problems encountered in biochemical and molecular biological research. A shortage of the technique is the production of the quasi-molecular ion with the absence of fragmentations, this is mostly a disadvantage in structural elucidation of biopolymers such as proteins The shortage of fragmentation can principally be improved by combining with enzymatic hydrolysis. The enzymes typically employed to completely hydrolyze proteins with high specificity into several lower-weight fragments which can then be sequenced are endopeptidases like trypsin. The less specific hydrolytic enzymes such as proteinase K has seldom been used for protein structure determination in combination with mass spectrometry However, the low specificity of proteinase K could be employed to advantage in hydrolyzing the substrate, since it can produce a series of peptide fragments somewhat like the sequence ions generated in mass spectrometry. Because proteinase K can hydrolyse the peptide bond adjacent to aliphatic or aromatic residues, it may act on every one of these peptide bonds in a protein exposed to proteolysis yielding a variety of fragments with different lengths, thus providing information about the primary structure of the protein. This is important especially in studying large molecules We have already been successful in investigating polypeptides with the method described above[1], it will be interesting to examine whether the method works for proteins which have high molecular weights

Insulin B-chain was first studied as a model compound with low molecular weight by incubating with proteinase K and subsequently being analysed with MALDI mass spectrometry. A series of peptide fragments were observed in the mass spectrum with reasonable intensities, and a careful calibration of the mass scale allows to identify each of the fragments (Table 1), thus providing reliable sequence information about the protein

Hen-egg white lysozyme and horse heart cytochrome C are well folded into globular in

their native state where many of the possible cleavage points are burried into the inner part and resistant to proteolysis. After unfolding in 3M guanidine hydrochloride abundant fragments can be produced from proteinase K digestion of the proteins, from which the primary structure of the proteins can be checked (see Table 2 for cytochrome C).

Table 1. Peptide fragments liberated from proteinase K digestion of insulin B-chain (m/z).

Asn_3-Phe_{25} (2688)	Val_2-Gly_{23} (2491)
Asn_3-Gly_{23} (2392)	Val_{12}-Ala_{30} (2211)
Glu_{13}-Ala_{30} (2112)	Val_2-Leu_{17}, Asn_3-Val_{18} (1842)
Val_{12}-Phe_{25} (1651)	Tyr_{16}-Pro_{28}, Phe_1-Ala_{14} (1600)
Glu_{13}-Phe_{24} (1404)	Phe_1-Leu_{11} (1301)
Val_2-Leu_{11} (1154)	Asn_3-Val_{12} (1154)
Ser_9-Val_{18} (1142)	Tyr_{16}-Phe_{24} (1091)
Cys_7-Leu_{15} (975)	Glu_{13}-Gly_{20} (914)
Phe_{24}-Ala_{30} (874)	Cys_7-Ala_{14} (862)
Cys_{19}-Phe_{24} (716)	Phe_{24}-Pro_{28} (675)
Val_{18}-Gly_{23} (667)	Ser_9-Ala_{14} (654)
Tyr_{26}-Ala_{30} (578)	Asn_3-Leu_6 (654)
Ser_9-Val_{12} (454)	Val_{12}-Leu_{15} (430)
Tyr_{16}-Val_{18} (393)	Glu_{13}-Leu_{15} (331)

Table 2. Peptide fragments of horse heart cytochrome C unfolded in 3M GuHCl followed by proteinase K digestion (m/z).

several fragments produced in 2 min.	
Gln_{12}-Gly_{37} (3366)	AcetylGly$_1$-Gly_{41} (5051)
Asp_2-Ala_{51} (6004)	Pro_{44}-Glu_{104} (7096)
fragments produced in 120min	
Leu_{35}-Pro_{44} (1075)	Phe_{36}-Phe_{46} (1167)
Glu_{21}-Leu_{32} (1267)	His_{33}-Gly_{45} (1328)
Glu_{21}-Leu_{35} (1575)	Phe_{82}-Ile_{95} (1647)
Val_{11}-Val_{20} (1731)	Val_{11}-Val_{20} (1731)
Ala_{83}-Glu_{104} (2518)	Lys_{25}-Ala_{51} (2902)
Thr_{78}-Glu_{104} (3138)	Lys_{25}-Ile_{57} (3557)
Thr_{47}-Gly_{77} (3674)	Phe_{10}-Gly_{41} (4083)
AcetylGly$_1$-Gly_{34} (4290)	Val_{11}-Gly_{45} (4290)
Thr_{58}-Leu_{94} (4457)	

Reference

1. X. L. Li, H. J. Yang and J. Grotemeyer, Rapid Commun. Mass Spectrom. 8, 833-6 (1994).

MALDI/TOF/MS AND RECOMBINANT HIV PROTEIN EXPRESSION

Carol E. Parker, Damon I. Papac, Kenneth B. Tomer

Laboratory of Molecular Biophysics
National Institute of Environmental Health Sciences
PO Box 12233
Research Triangle Park, NC 27709

We have been involved in a project to determine the epitope on recombinant HIV p24 that interacts with commercial antibodies. The method selected for this determination is proteolytic protection assays combined with MALDI/TOF/MS. As part of this project, we have used MALDI/TOF for verification of commercially-available recombinant p24. Because of the poor quality of the commercially available p24, and the low quantity available of p24 with the correct sequence, we have had to turn to expressing recombinant p24 in our laboratory

One of the most common methodologies for producing large amounts of proteins is by protein expression in genetically altered bacteria or yeast. The specific end-use of the recombinant protein can influence the exact expression strategy employed for protein production. Structural studies, in which the natural configuration is retained, are the most stringent end-uses of recombinant proteins in terms of the requirements for expression and purification This usually requires that the protein be made in a soluble form that does not require a denaturation/renaturation step in its purification. The protein must also be expressed in a system that minimizes proteolytic degradation In addition, the cloned gene is often introduced into the cell in combination with a gene that codes for a highly expressed carrier protein i e , as a fusion protein If chosen properly, the carrier protein can be exploited in protein purification

One example of a carrier protein is glutathione-S-transferase (GST) The recombinant protein is expressed as a fusion protein with the GST The fusion protein can be purified by affinity chromatography with an immobilized glutathione-agarose column In general, fusion proteins containing GST are soluble and can be purified under non-denaturing conditions. An additional gene is often incorporated into the fusion protein that expresses an amino acid sequence between the desired protein and the GST that can be cleaved by a site-specific protease, such as blood coagulation factor Xa. After the fusion protein is bound to the glutathione-agarose column and impurities removed by washing, the recombinant p26 can be cleaved from the GST while it remains bound to the affinity column. The cleavage of the recombinant protein is typically followed by SDS-PAGE.

We have expressed recombinant p26 (which contains the p24 protein along with several residues from flanking proteins) in *E. Coli* provided by Dr. I M. Jones (NERC Inst. Virology, Oxford, UK). During this procedure, we have noted that the use of MALDI/TOF to follow the purification and cleavage of the fusion protein through direct analysis of affinity bound analytes [Papac et al , *Protein Sci* (**1994**) *3* 1485] is much more facile than is the use of SDS-PAGE. We have also incorporated the use of HIV protease instead of Factor Xa to cleave the recombinant protein This enzyme cleaves p26 at two positions to give p24

The first figure is a bar graph of the time course of a Factor Xa cleavage of the fusion protein affinity bound to the glutathione column. This graph shows the absolute areas of the peaks due to starting material and to the product demonstrating a nearly steady and quantitative increase in product ions over time The second figure shows one time point in the HIV protease cleavage of the affinity bound fusion protein The spectrum shows the relative abundances of the ions for the starting material, intermediate products and final products. This spectrum can be obtained in minutes and demonstrate the ease, resolution, and utility of MALDI/TOF over SDS-PAGE.

Figure 1.

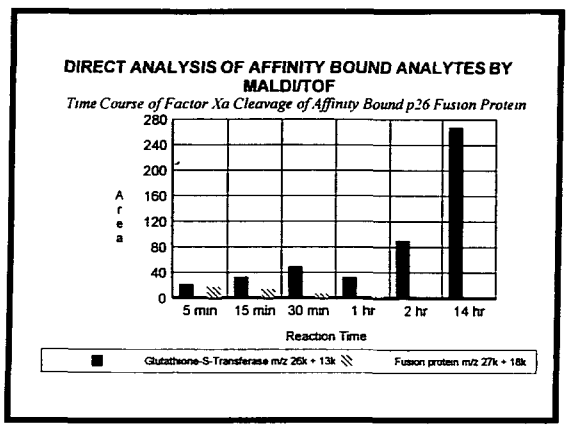

Figure 2.

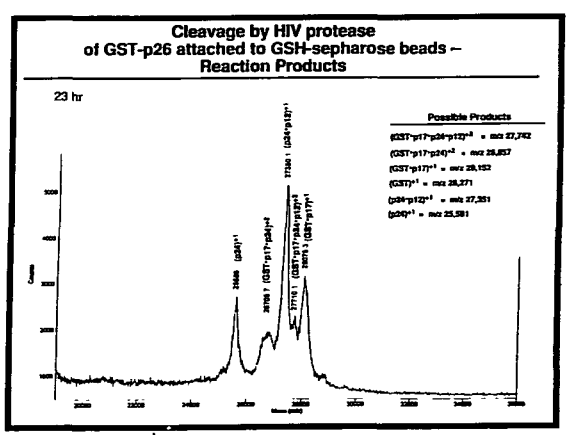

MALDI-TOF Analysis of Peptide Digestion Mixtures with Detergents

Farzin Gharahdaghi, Joseph Fernandez, and Sheenah M. Mische
The Rockefeller University Protein/DNA Technology Center 1230 York Ave., N.Y, N.Y. 10021

Matrix-assisted laser desorption/ionization time-of-flight (MALDI/TOF) mass spectrometry, in combination with enzymatic digestion of proteins and peptide-mass database screening, provides a rapid means for tentative identification of known proteins at the subpicomole level (1-3). In general, regardless of whether the protein is "on-membrane" or "in-gel", the ideal digestion method would : 1) produce peptides in high yield. 2) produce longer species for Edman sequencing (important for unknown proteins, as more contiguous sequence data allows for better DNA probe design for subsequent screening of libraries). 3) recover peptides in an extraction buffer compatible with other microanalytical methods (i.e., RP-HPLC and MALDI-TOF MS). The inclusion of nonionic detergents has been shown to be essential for obtaining peptides in high yield, especially hydrophobic species and longer length peptides (4). Digestion methods employed for peptide-mass screening have not used detergents due to signal suppression effects (5,6). As a result, peptides recovered using these methods tend to be short, relatively hydrophilic and of low yield, suitable for peptide-mass database screening, but not ideal for the subsequent HPLC purification and Edman sequence analysis required for proteins not present in databases. Here we describe a one-step peptide preparation method that fulfills all three criteria. Utilizing a modified matrix solution of α-cyano-4-hydroxycinnamic acid containing 50% organic solvent, direct analysis of detergent/peptide mixtures by MALDI-TOF MS, mass spectra was obtained using *hydrogenated Triton X-100 (RTX-100), Octylglucopyranoside (OGP) or Tween-20.* Peptide-mass database searches were performed with 1-2% of peptide-detergent mixtures using the molecular weight search **(MOWSE)** fragment database and associated search and scoring algorithms (1). The results from peptide-mass profile search for human transferrin are summarized in **Table 1.** Peptide-mass database analysis provided rapid tentative identification of proteins in the database, and those not identified were subsequently characterized as unknown proteins by Edman sequencing of purified peptide, illustrating the utility of this approach for rapid protein identification of both known and unknown proteins using a one-step method for protein digestion.

Sample transferrin	RTX-100 / Tris	RTX-100 / NH4HCO3	OGP / Tris	OGP / NH4HCO3	Tween-20 / Tris	Tween-20 / NH4HCO3
50pmole	correct	correct	correct	correct	correct	false
25pmole	correct	correct	correct	correct	correct	false
12.5pmole	false	false	false	correct	false	false

Table 1: Search results for tentative identification of PVDF-bound protein by using 50%CH3CN in matrix solution (Error =+/- 2 daltons; *"Correct" designation =identified with highest rank (1)).*

Summary

I.) 50% CH3CN saturated matrix solution produced mass spectra from all detergent / peptide mixtures *(RTX-100, Tween-20* or *OGP)* with either Tris or ammonium bicarbonate buffer **II.)** Ammonium bicarbonate buffer provided the most sensitive direct analysis in combination with any of the detergents tested for direct analysis of detergent / peptide mixtures by MALDI-TOF MS using 50% CH3CN saturated matrix solution. **III.)** *OGP* is the preferred nonionic detergent, as it does not form clusters with buffer ions. **IV.)** 50% CH3CN saturated matrix solution in combination with 1% OGP / 25 mM NH4HCO3 buffer provided the most accurate peptide-mass profiles obtained from MALDI-TOF MS analysis of peptide-detergent mixtures from PVDF-bound proteins.

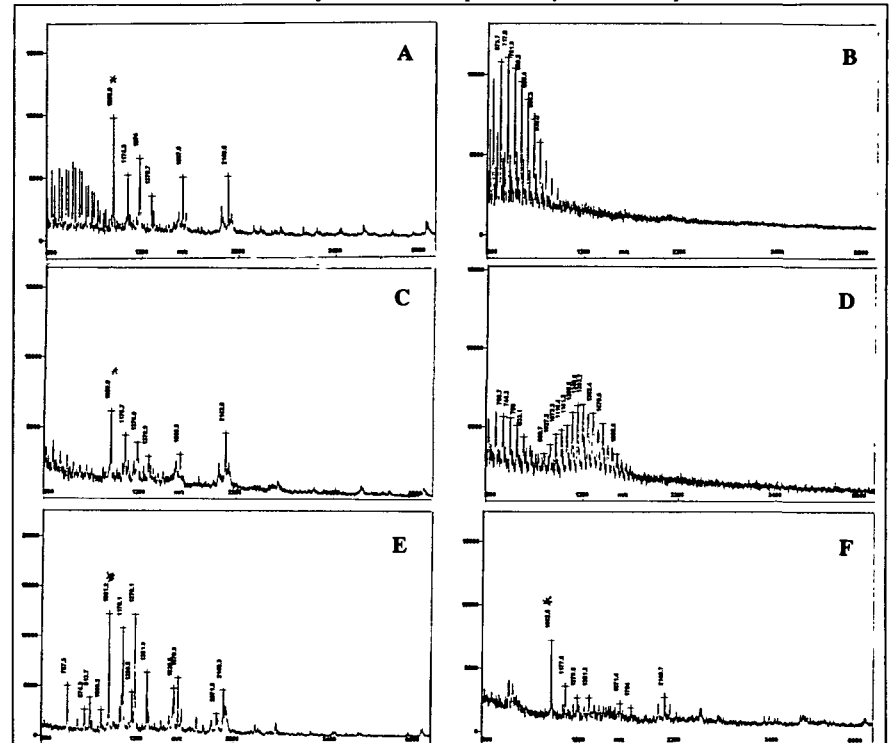

Figure 1 : PVDF-BOUND PROTEIN DIGESTED IN THE PRESENCE OF 1% OGP / 10% CH3CN/ 25 mM NH4HCO3 AND ANALYZED USING 50% CH3CN MATRIX SOLUTION IS THE PREFERRED METHOD FOR PEPTIDE-DETERGENT MALDI-TOF ANALYSIS. 50%CH3CN (A, C, E), or 30%CH3CN (B, D, F) matrix solutions were used for obtaining spectra from detergent/peptide mixtures performed with 25 mM NH4HCO3 . Digestion was performed in the presence of *RTX-100* (A, B), *Tween-20* (C, D) and *OGP* (E,F). Spectra represent 0.5% of the total digest mixture (125 fmol). Asterisks indicate internal standard (bradykinin).

References
1. Pappin, D.J.C, P. Hojrup, and A.J. Bleasby (1993) Current Biol. 3:327-332
2. James.P, M.Quadroni, E. Carafoli, and G. Gonnet (1993) BBRC, 195:58-64
3. Henzel.W.J, T.M. Billeci, J.T. Stults, S.C. Wong, C. Grimley and C. Watanabe (1993) Proc. Nat'l. Acad. Sci., U.S.A. 90:5011-5015
4. Fernandez, J., L. Andrews, and S.M. Mische (1994) Anal.Biochem. 218: 112-117
5. Fernandez., J., F. Gharahdaghi, and S.M. Mische (1995) Techniques in Protein Chemistry VI (J.W.Crabb, Ed.) Academic Press, San Diego, CA. pp. 135-142
6. Vorm, O., B.T. Chait, and P. Roepstorff (1993) Proc. 41st ASMS Conf. pp. 621a-622a

Sample Preparation for Protein Fingerprinting of Bacteria Using MALDI MS

Xiaoli Liang, Teresa C. Cain, Jian Bai, Yan-Hui Liu and David M. Lubman
Department of Chemistry, The University of Michigan, Ann Arbor, MI 48109-1055

Direct analysis of proteins from bacterial cell extracts has been proposed as a potential means for the identification of bacteria. This work demonstrates the differentiation of bacteria by mass spectrometry. Using MALDI TOF mass spectrometry, protein profiles of several bacterial species have been obtained (1). These profiles are distinctly different and allow differentiation of bacteria to the species level. The bacteria can be identified based on the presence of particular mass markers present in the protein profile. The identification of a mass marker(s) can be used to identify a single bacteria present in a mixture of bacteria. The protein profiles contain proteins in the mass range of 2,000 - 20,000 u.

The proteins were precipitated by the addition of water-miscible organic solvents, such as acetone and methanol. However, due to the complexity of the cell contents, extraction of proteins from the cell with organic solvents is selective, and often ineffective for removing the impurities from the crude extracts and for liberating the proteins from the cell membranes. Detergents are used most often for the extraction and purification of these membrane proteins. However, solubilized membrane proteins form mixed micelles with detergent such that the hydrophobic domain of the protein is shielded from contact with the aqueous buffer by detergent molecules. The use of SDS, in particular, can inhibit the precipitation with commonly used solvent systems The presence of impurities, particularly residual detergents can cause severe interferences with MALDI MS analysis, often resulting in the suppression of analyte signals, or reduced signal intensity.

Procedures involving the use of membranes and different organic solvent systems with the addition of detergents are evaluated for the extraction and purification of proteins from disrupted *E. coli* cells. The detergents used include sodium dodecylsulphate (SDS), Triton X-100, Tween 20, and Tween 80. The ether/ethanol system was used successfully for the precipitation of proteins from solutions containng nonionic detergents such as Triton X-100 and Tween 20 (Figure 1). Several poly(vinylidene

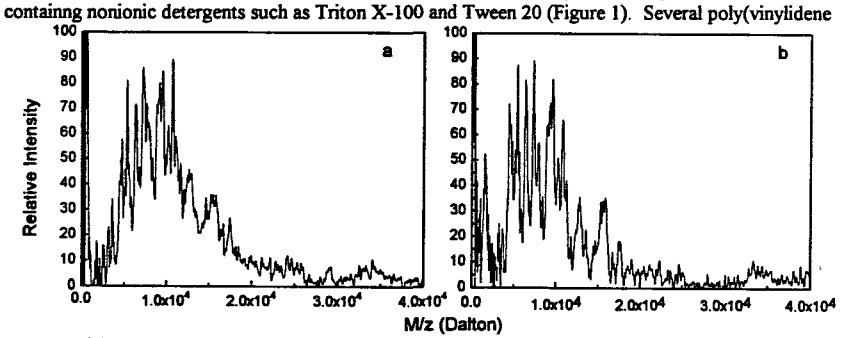

Figure 1. MALDI MS spectra of *E. coli* proteins precipitated by ether/ethanol (3:1) in the presence of (a) Triton X 100 and (b) Tween 20.

fluoride) (PVDF) based membranes are tested for the direct extraction of proteins from the bulk cell extract and for the removal of detergents (Figure 2). The results showed that the membranes can selectively absorb the proteins from complex mixtures. This may result from the competition between the protein/detergent and protein/membrane interactions. The membranes showed different selectivity toward the proteins. PVDF-CD was found to be the most useful one.

Another procedure tested was dot blotting, where the protein and detergent mixture was applied onto a NC membrane, and blotting was conducted in a semi-dry blotter. During the electroblotting, the proteins were transferred to the NC membrane, and were separated from the detergents. The NC membrane with the transferred proteins was washed to remove other unbound impurities, and the protein content was extracted from the NC for MALDI MS analysis (Figure 3).

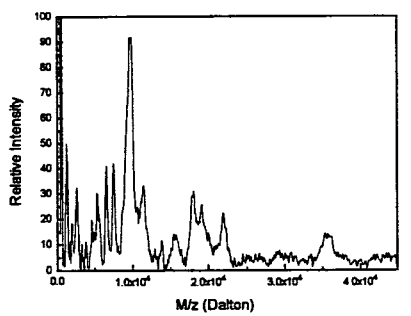

Figure 2. MALDI MS spectrum of *E. coli* proteins extracted by Immobilon-CD from a crude extract containing SDS.

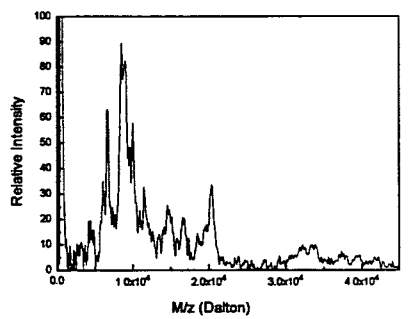

Figure 3. MALDI MS spectrum of *E. coli* proteins acquired by electroblotting from a SDS-containing mixture onto the NC and then extracted by the CHCA solution.

The use of membranes allows rapid extraction and purification of proteins in complex mixtures, particularly those that contain detergents. The purified proteins can be extracted and are found to be suitable for MALDI MS analysis for profiling purposes. Although the extraction and purification of proteins with membranes are used only for crude bacterial cell extracts, it may find potential applications in various biological systems.

References

(1) Cain, T. C.; Lubman, D. M.; Weber, W. J., Jr. *Rapid Commun. Mass Spectrom.* **1994**, *8*, 1026.

MALDI COMBINED WITH CHEMICAL REACTION METHODS FOR STUDYING PROTEIN FOLDING

Jian Zhang, Yajun Wang**, Rick Edmondson, Kent Gillig, Timothy Hayes***, and David H. Russell*
*Laboratory for Biological Mass Spectrometry, Department of Chemistry,
**Department of Chemical Engineering
***Department of Entomology
Texas A&M University, College Station, TX 77843

Disulfide bonding plays an important role in the folding and unfolding of many proteins. Creighton pioneered the use of reduction/alkylation reaction chemistry for trapping disulfide-bond intermediates with iodoacetic acid, Figure 1. This method can also be adapted to mass spectrometry analysis as demonstrated by Morris et al.[1]. The objective of the study is to evaluate the use of MALDI-MS for performing detailed studies of disulfide bond reduction. MALDI is useful for such studies because it is an ionization process that forms ions of the intact protein. The strategy we have developed involves three steps, Step 1: The molecular weight of the protein is determined by MALDI-MS. Step 2: The protein is partially reduced by reaction with dithiothreitol (DTT) and alkylated with iodoacetamide. Step 3: The number of disulfides reduced is determined by measuring the MW of the alkylated protein; each disulfide adds two CH_2CONH_2 units (2 x 58 = 116 mass unit shift in MALDI-Mass spectra), Figure 2.

To determine which disulfide units of a multiple disulfide containing protein was reduced the following strategies were developed. Step 1: The partially reduced/alkylated protein is digested with chymotrypsin, and the MALDI-Mass spectra of the digest shown in Figure 3 is compared with the structure of bovine insulin to assign the fragments. The peaks at m/z 1892, 1910, and 1927 were assigned as fragments containing disulfide-linkage Cys-A20-Cys-B19 and the peaks at m/z 2450 and 2469 were assigned as fragments containing disulfide-linkage Cys-A7-Cys-B7. Step 2: The peak assignments of the fragments containing disulfide-linkages was confirmed by post-source decay. Figure 4 contains the post-source decay spectra of the m/z 1888 and 1911 ions.

The combination of MALDI-MS and partial reduction/complete alkylation of proteins is a useful probe of protein folding/unfolding. This study demonstrates the utility of MALDI-MS for monitoring chemical reaction of complex biomolecules. This work shows the sensitivity and efficiency of MALDI-MS for examining protein folding/unfolding as well as the utility of post-source decay experiments for unambiguously assigning the sequence of protein fragments.

1. Howard R. Morris, Piero Pucci, Maria Panico and Gennaro Marino, *Biochem. J.*, 268, 803-806(1990)

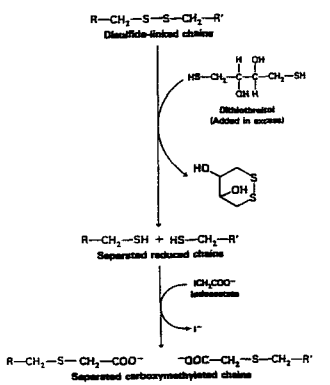

Figure 1 Polypeptides linked by disulfide bonds can be separated by reduction with dithiothreitol followed by alkylation

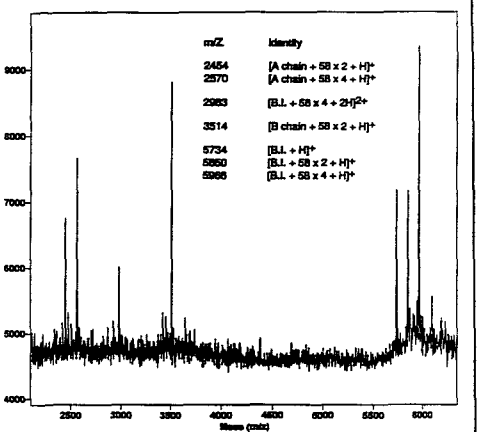

Figure 2. MALDI-MS spectrum of bovine insulin (20 nmoles) partially reduced with 5.0 mM dithiothreitol and completely alkylated with iodoacetamide.

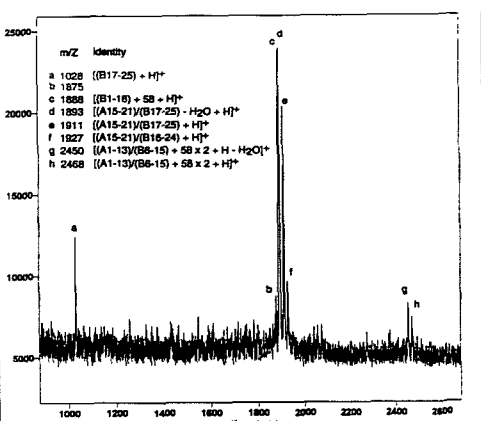

Figure 3. MALDI-MS spectrum of the chromatographically separated bovine insulin (20 nmoles) partially reduced with 5.0 mM dithiothreitol, alkylated at four positions with iodoacetamide, and digested with chymotrypsin.

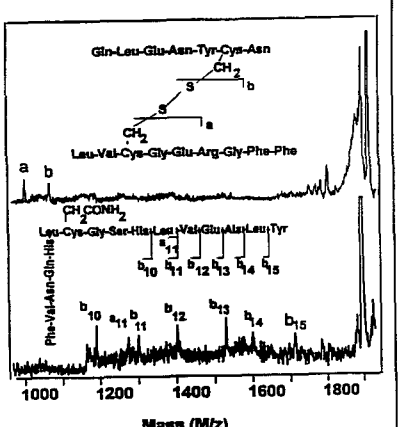

Figure 4. MALDI-MS post-source decay spectra of bovine insulin (20 nmoles) partially reduced with 5.0 mM dithiothreitol, alkylated with iodoacetamide digested with chymotrypsin, and using fragments m/z 1911 [(A15-21)/(B17-25) + H]+ (top) and m/z 1888 [(B1-16) + 58 + H]+ (bottom) as parent ions.

CARBOXYL-TERMINAL LADDER SEQUENCING OF PEPTIDES AND PROTEINS

Rong Wang and Brian T. Chait
The Rockefeller University, New York, NY 10021

Facile, effective methods for carboxyl-terminal amino acid sequence determination have long been sought. None of the approaches developed to date rivals the effectiveness of amino-terminal sequence determination techniques based on the Edman degradation. One promising approach involves the use of carboxypeptidases in conjunction with mass spectrometry. However, the different rates of cleavage of carboxypeptidases for the different amino acids leads to gaps in the measured sequence. Here, we explore a new approach to C-terminal sequencing that addresses this problem.

Attachment of quasi-terminating groups to the C-terminal of polypeptide chains during the hydrolysis of polypeptides by carboxypeptidases can yield a peptide ladder that is free of gaps. In this approach, hydrolysis and aminolysis are set up as competing reactions catalyzed by the same carboxypeptidase. Hydrolysis removes terminal amino acid residues, while aminolysis adds the quasi-terminating group to the newly formed termini. Aminolysis is brought about by adding a large molar excess of amino amide to the peptide/enzyme solution. Terminal amino amides are quasi-terminating because they have a much slower rate of hydrolysis than terminal amino acids (1,2).

Carboxypeptidase Y was used in this study. Peptides (10 - 100 pmol) were dissolved in 10 μL of pH 7.3 buffer which consists of 100 mM Hepes and 10 mM EDTA. An enzyme-to-substrate molar ratio of 1:60 was used in this experiment. Lysinamide was used as the nucleophile and added into the reaction with the final concentration of 1 M. Digestion was carry out at 37 °C for 10 to 30 minutes. The reaction was stopped by adding 1 ul of 10% TFA. The resulting ladder sequence was read-out by matrix-assisted laser desorption mass spectrometry.

Renin substrate tetradecapeptide has sequence of DRVYIHPFHLLVYS (with one letter code for amino acid residues) and molecular weight of 1759.0 Da (Figure 1). The competitive carboxypeptidase Y sequencing reaction was carried out in the presence of excess amount of lysinamide (1 M) and the resulted sequencing spectrum is shown in Figure 2. This spectrum yields the carboxyl terminal sequence of the polypeptide up to six amino acid residues in a single operation. The first carboxyl terminal amino acid residue was determined by adding 127.2 Da (L-Lysinamide residue mass) to the mass of the intact molecular ion (1759 Da), followed by subtraction of the highest mass of lysinamide modified peptide peak (1799.0 Da). This calculation gives a mass difference of 87.2 Da, which corresponds to a serine residue. The remaining carboxyl terminal sequence can be read out from the mass differences between adjacent peaks in the spectrum. The mass difference of 127.1 Da between the peaks at m/z 1423.5 and 1296.4 corresponds to the lysinamide. The peaks on the lower mass side of the lysinamide residue correspond to the unmodified peptides and the peaks on the higher mass side of lysinamide corresponds to the lysinamide modified peptides. For comparison, the sample peptide was digested with carboxypeptidase Y in the absence of lysinamide. Figure 3 shows the sequencing spectra resulted by using 5, 10, 20, 100 ng of carboxypeptidase Y after 10 minutes reaction at 37 °C. Comparison of Fig. 2 and Fig. 3, show that the fast hydrolysis reactions has been balanced by the aminolysis reactions. The sequence gaps in the normal carboxypeptidase Y digestion (Figure 3) can be filled up by the lysinamide modifications.

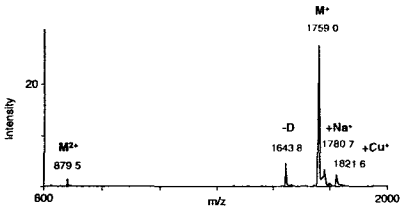

Figure 1 MALDI-MS spectrum of renin substrate decapeptide

Lysinamide functions as a nucleophilic reagent that competes with water for reaction with the newly generated peptide acyl-enzyme complex during the hydrolysis reaction. This competition results in the reduction of the overall hydrolysis reaction rate. The amide introduced by the lysinamide further slows down the hydrolysis of the modified peptide chain since the hydrolysis of the amino amide is far slower than that of the free C-terminal amino acid. These kinetic effects plus the positive effect of the lysinamide derivative on the mass spectrometric response make the application of carboxypeptidase for C-terminal sequencing much easier to control and read-out. This competitive reaction (or balanced reaction) strategy in C-terminal carboxypeptidases sequencing has the potential to be a easy and reliable method for protein and peptide C-terminal sequencing.

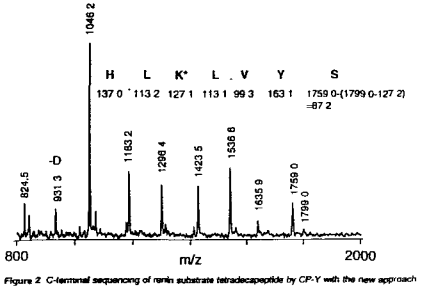

Figure 2 C-terminal sequencing of renin substrate tetradecapeptide by CP-Y with the new approach

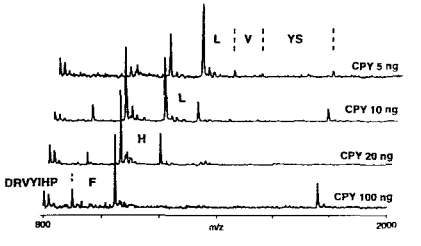

Figure 3 C-terminal sequencing of renin substrate tetradecapeptide by enzyme titration

REFERENCES

1) Raaschou-Nielsen, M.; Mortensen, U. H.; Olesen, K.; Breddam, K. *Peptide Research* **1994**, *7*, 132-135.
2) Mortensen, U. H.; Stennicke, H. R.; Raaschou-Nielsen, M.; Breddam, K. *J. Am. Chem. Soc.* **1994**, *116*, 34-41.

Protein Conformation, Hydrogen Bonding, and Energy Transfer in MALDI

Akos Bencsura[1] and Akos Vertes[2]
[1]Department of Chemistry, Catholic University of America, Washington, D.C. 20064
[2]Department of Chemistry, George Washington University, Washington, D.C. 20052

One of the critical steps in matrix-assisted laser desorption ionization (MALDI) mass spectrometry is sample preparation. The basis of the best established method is co-crystallization of matrix and analyte from their saturated solution [1]. A laser generated phase transition in the matrix crystals is believed to be at the core of the MALDI process [2].

Macromolecule folding in aqueous environment and macromolecule–water interactions are intensively studied and well described phenomena. Based on developments in molecular dynamics and semiempirical quantum chemical codes, conformation, hydrogen bonding, and phase transition characteristics can be calculated in relatively large protein–water systems.

Embedding of guest molecules into matrix crystals, and co-evaporation of matrix and guest molecules were studied using model systems. We wanted to explore peptide–matrix structures on the microscopic level and enhance our understanding of co-crystallization and co-evaporation in MALDI using molecular dynamics (MD) simulations.

Both the selected matrix (pyridine-3-carboxylic acid, nicotinic acid) and the analyte (leucine enkephalin, Tyr-Gly-Gly-Phe-Leu) were represented by their detailed molecular structure based on crystallographic data. The CHARMM (Chemistry at HARvard Molecular Mechanics) molecular dynamics code was used to model crystal dynamics upon laser excitation. Originally the program was developed to describe protein molecules in aqueous environment. An attractive feature of this code was that it accounted for the internal structure of molecules. The intermolecular potentials were calculated using *ab initio* (GAUSSIAN) and semi-empirical (AM1) quantum chemical codes.

In our simulation a ∅500 pm hemispherical volume of nicotinic acid molecules represented the matrix around a leucine enkephalin molecule. The validity of the model potentials was tested by comparing both the equilibrated nicotinic acid crystal structure to X-ray diffraction data, and the calculated heat of sublimation ($\Delta H_{calc.}$(sublimation)=101.5 kJ/mol) to the measured value (ΔH_{exp} (sublimation)=104.6 kJ/mol) for the matrix at 300 K. The peptide molecule showed hydrogen bonding to the matrix and preferential embedding along the layered structure of the host crystal [1].

Introduced by the laser pulse, an adiabatic temperature jump to 1500 K led to vigorous evaporation of the matrix molecules and to the desorption of the peptide. Detailed statistical analysis of the matrix structure showed dramatic changes in the pair distribution functions (PDF). At 300 K the N–O1 PDF between the pyridine N and the O in the carboxyl OH exhibited two sharp maxima at 300 pm and 410 pm, corresponding to the hydrogen bond and to the intramolecular correlation, respectively (Figure 1). At 1500 K a large part of the contribution from the hydrogen bond disappeared along with the long range order.

Due to the fast breakup of the crystal structure the energy corresponding to hydrogen bonds dropped, and in about 3 ps reached a new steady state value (Figure 2). It was interesting to note that a substantial part of the crystal did not evaporate and about half of the cohesive energy remained unchanged.

The fate of the peptide molecule was followed by recording the position of its center of mass relative to the matrix surface (Figure 3). Initially, the guest molecule was buried ~250 pm below the surface. In less than 1 ps the guest molecule emerged and lifted off the surface. The velocity of the neutral guest molecule showed exponential decay with a decay time of ~6 ps and a limiting value of ~155 m/s (Figure 4).

43rd ASMS Conference on Mass Spectrometry and Allied Topics

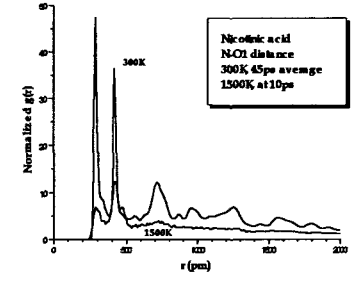

Figure 1. Normalized pair distribution functions between the pyridine N and the O in the carboxyl OH at 300 K and 1500 K.

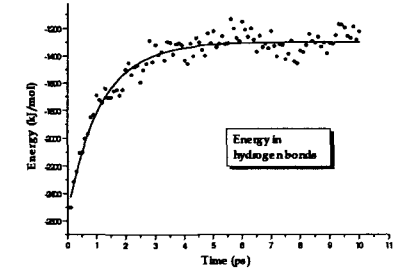

Figure 2. Time dependence of the energy stored in hydrogen bonds of the nicotinic acid crystal after an adiabatic temperature jump from 300 K to 1500 K.

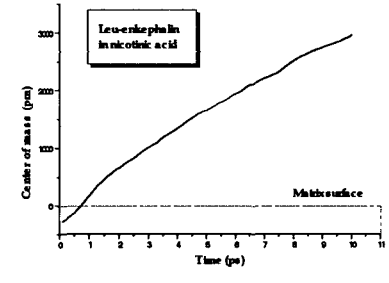

Figure 3. Position of the leucine enkephalin center of mass perpendicular to the matrix surface as a function of time after the excitation.

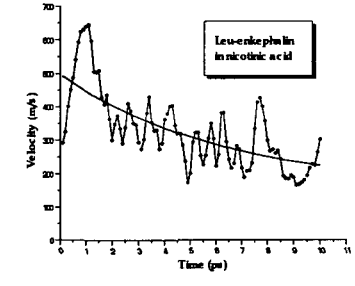

Figure 4. Center-of-mass velocity of the guest molecule after expulsion from the energized matrix.

References

[1] Beavis, R.C., Bridson, J.N. (1993). *J. Phys. D: Appl. Phys.* **26**, 442.
[2] Ens, W., Mao, Y., Mayer, F., Standing, K.G. (1991). *Rapid Commun. Mass Spectrom.* **5**, 117.

Mass Tracer Methods based on MALDI

Randy M. Whittal, David C. Schriemer, and Liang Li*
Department of Chemistry, University of Alberta
Edmonton, Alberta, Canada
T6G 2G2

The principle of mass tracing involves using the mass spectrometer to follow the fate of certain species carried through a particular process. As with any tracing method, it relies on the incorporation of a tag, however the tag does not have to provide the basis for detection, as this is supplied by the mass spectrometer. This principle has been applied previously to the MALDI experiment in the work of Hutchens and Yip [1].

Two other extensions of this principle to MALDI are currently being investigated in this laboratory. In one approach, the inherently low sensitivity of oligosaccharides can be improved with the incorporation of certain labels [2]. This allows for the detection of products of enzymes involved in oligosaccharide biosynthesis/degradation directly from crude serum. An illustration of this can be found in figure 1. The disaccharide αFuc(1→2)βGal-TMR$^+$, possessing the tetramethylrhodamine (TMR) label, receives a galactose residue from uridine diphosphogalactose (UDP-Gal) under the action of a blood group-B galactosyltransferase enzyme. The product of this reaction (B-TMR$^+$), though present in approximately 0.50 pmol/μL is easily detectable due to the sensitivity enhancement provided by the TMR label [3].

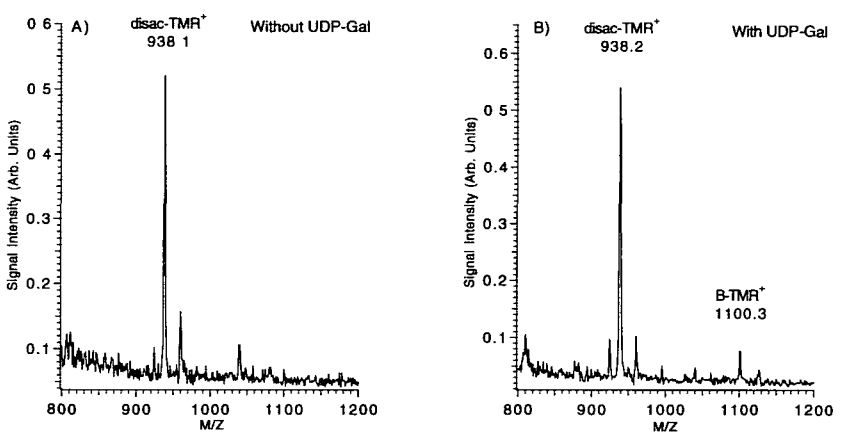

Figure 1

A second application is based on the selective binding of biotin by immobilized avidin, incorporated into a MALDI technique similar to the approach of Tomer et al [4]. A small quantity of immobilized avidin gel is added to a mixture containing a biotinylated compound. The gel is then washed to remove the unbound components of the mixture, whereupon the beads are directly analyzed by MALDI, for detection of the biotinylated compound. Sample preparation simply involves the deposition of a water slurry of the gel onto a thick layer of matrix. Figure 2 demonstrates this procedure on a synthetic mixture of the following species:

1. bradykinin
2. synthetic peptide
3. insulin chain B
4. insulin
5. insulin-biotin
6. insulin-(biotin)$_2$

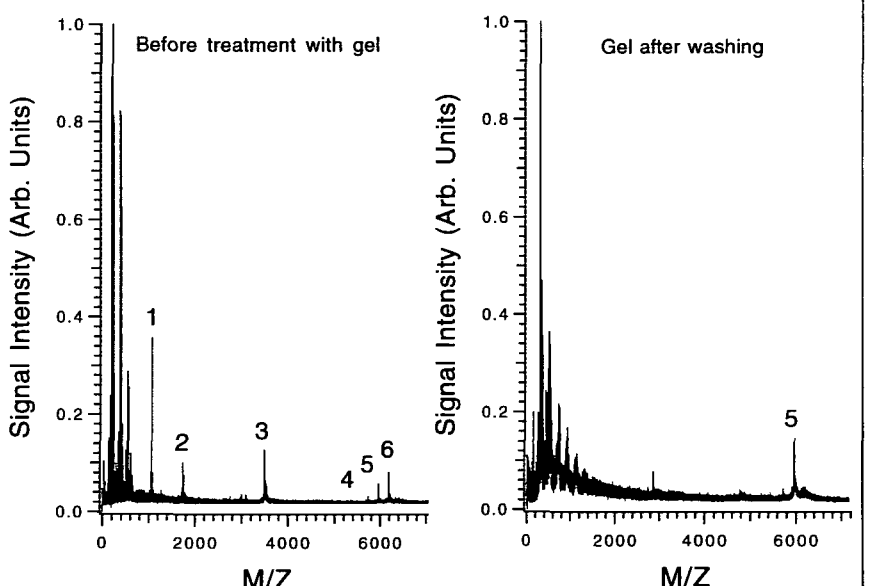

Figure 2

References

[1] Hutchens, T.W.; Yip, T.-T. *Rapid Commun. Mass Spectrom.* **1993**, 7, 576-580.
[2] Juhasz, P.; Costello, C.E. *J. Am. Soc. Mass Spectrom.* **1992**, 3, 785-786.
[3] Whittal, R.M.; Palcic, M.M.; Hindsgaul, O.; Li, L. Submitted to *Anal. Chem.*
[4] Papac, D.J.; Hoyes, J.; Tomer, K.B. *Anal. Chem.* **1994**, 66, 2609-2613.

MALDI-MS of Proteins Directly from Polyacrylamide Gels

R. R. Ogorzalek Loo†, T. I. Stevenson§, C. Mitchell†, J. A. Loo§, and P. C. Andrews†
†University of Michigan, Dept. of Biological Chemistry, 2560 MSRB II, Ann Arbor, MI 48109
§Parke-Davis Pharmaceutical Research, Division of Warner-Lambert Company, Ann Arbor, MI 48105

A method for the analysis of proteins has been developed which takes advantage of the high sensitivity and mass range of matrix assisted laser desorption/ionization time-of-flight (MALDI-TOF) mass spectrometry and the high resolution separations attainable by electrophoretic methods, particularly isoelectric focusing (IEF). Previous methods involving electroblotted proteins and MALDI have been hampered by low resolution, poor mass accuracy, low sensitivity, or have required infrared lasers not widely used. We have obviated these problems by using ultrathin polyacrylamide gels which dry to thicknesses of 10 µm or less. Thin layer electrophoresis has the additional advantages of rapid preparation and run times. Proteins may be desorbed directly from dried gels or passively transferred to membranes, avoiding electroblotting. Spectra obtained by this method appear similar to analyses directly off the sample probe, including high sensitivity (sub-picomole), resolution, and mass accuracy. This method works well with IEF, native, and sodium dodecyl sulfate (SDS) polyacrylamide gels. The good quality mass spectra obtained directly from gels also makes it possible to run virtual 2-D gels in which proteins are resolved in the first dimension on the basis of their charge (i.e., IEF gels) while the second dimension is MALDI-MS instead of SDS gels electrophoresis. Virtual 2-D gels reduce the ambiguity in protein identification inherent in true 2-D gels by accurately determining mass. This method has been applied to the two- and three-dimensional analysis of complex mixtures with identification of component proteins by their isoelectric points, intact mass, and their CNBr fragment masses. When applied to non-denaturing gels, the method represents a very useful way to probe noncovalent complexes between proteins and a variety of ligands.

Thin layer IEF, native, and SDS polyacrylamide gel electrophoresis were performed under standard conditions. In some experiments, passive elution of the macromolecules from the gel to an appropriate membrane with subsequent analysis of the membrane-bound macromolecules by MALDI-MS was tested. MALDI mass spectra were acquired on a PerSeptive-Vestec (Houston, TX) LaserTec ResearcH™ time-of-flight mass spectrometer operating in the linear mode, employing a nitrogen laser (337 nm) for desorption.

The thinness of the gels greatly enhance mass transport efficiencies relative to a conventional thicker gel, facilitating transfer and desorption. For SDS gels, the surfactant is present only in the buffer and the lower SDS concentrations can be reduced effectively by washing after electrophoresis. Spectra have been obtained for 60 pmole loadings of cytochrome *c* onto SDS gels. Spectra have also been obtained from IEF gels with 1 pmole myoglobin and 650 fmole hemoglobin loadings. Resolution is excellent for desorption from gels, we have achieved resolutions as high as 450 for myoglobin (17 kDa) desorbed from a native gel. Clearly, the sensitivity and mass resolution can be comparable to conventional desorption off the sample probe. By using calibration standards, good mass accuracy can be achieved. Solution containing internal standards can be applied directly to the band of interest or to the side of the band (0.1-0.2% accuracy). Standards should be spotted in several locations along a lane, because the calibration varies by 1-2% from top to bottom of a lane, if standards are not employed.

Although obtaining mass spectra directly off the gel has many advantages, the sensitivity, reproducibility, and mass accuracy for proteins larger than 20 kDa were found to be better in desorption from membranes. Protein bands were efficiently transferred from the gels to teflon or polyethylene membranes by diffusive transfer. Passive diffusion is most effective with ultrathin gels because transfer is simple and efficiency is quite good with relatively short transfer times. Spectra were obtained for bovine serum albumin (66 kDa) and bovine carbonic anhydrase (29 kDa) after passive diffusion from an IEF gel to which 11 and 14 pmol, respectively had been loaded.

Once the mass of an intact unknown protein is determined, additional structural information is required for identification. One method is to chemically or proteolytically digest the protein band (in-gel digest) and measure the masses of the resulting fragments (in-gel). This new information can then be used to mass search proteins in databases. The mass spectrum from an in-gel cyanogen bromide digest of horse heart myoglobin is shown in Figure 1. Approximately 60 pmol was loaded on the gel which was subsequently Coomassie blue-stained and CNBr digested. Coomassie blue adducts are apparent in the digest data obtained with sinapinic acid. All 3 complete cleavage products and one incomplete cleavage product were observed.

The combination of MALDI mass spectrometry and gel electrophoresis makes it possible to examine many noncovalently-bound systems because some gel electrophoresis methods can be run under non-denaturing conditions where many macromolecules maintain their native structures and thus their functions. Commonly used MALDI-MS methods destroy all evidence of noncovalent interactions. Avidin is a 64 kDa tetrameric glycoprotein with a high affinity for biotin and biotinylated-macromolecules. A gel loaded with 75 pmol biotinylated bovine albumin and 75 pmol of the avidin tetramer was run. The resulting bands were transferred by passive diffusion to a teflon membrane which was stained with sulforhodamine. The MALDI mass spectrum (Figure 2) shows molecular ions for both biotinylated-albumin (1+, 2+, and 3+ charges) and the avidin subunit (16 kDa), indicating that the avidin and biotinylated-albumin molecules migrated as a complex on the gel. Peaks are broad, indicating heterogeneous labeling with biotin and possible sulforhodamine adducts.

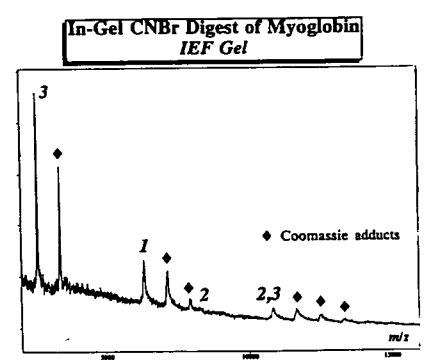

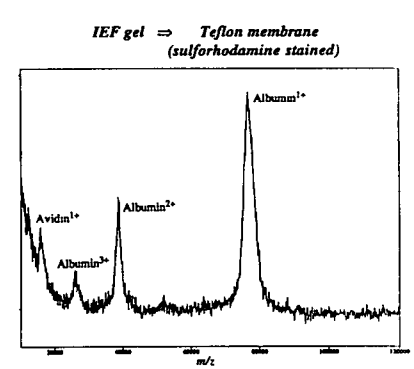

Evaluation of MALDI.MS For Agricultural Applications

L.M. Shalaby[1], N.L. Hubbard[1], B. Stahl [2], F. Hillenkamp[2], and J. Zeng[2]
[1]. DuPont Agricultural Products, Wilmington, Delaware
[2]. Department of Medical Physics and Biophysics, University of Munster, Munster, Germany

In search for an analytical technique to study the structure of Ag biomolecules such as starch and its functional characteristics. We conducted several studies for specific starch fractions and other glycans using MALDI.MS. In addition, we evaluated the applications of the technology to investigate specific molecules which can be of special value for supporting AG discovery, biotechnology and formulation science. Among those molecules were enzymes, antibodies, natural products and formulated sulfonylurea.

Experimental and Sample Preparation

All data were generated on two instruments, a reflectron-type time of flight mass spectrometer (Lamma 1000, Leybold Heraeus) and a Finnigan Model Vision 2000. The Lamma instrument is equipped with a nitrogen laser at 337 nm and the Vision system was equipped by a Nd:YAG laser. The samples were dissolved in ultra-pure water at concentration of 1µg/µL. A one µL is pipetted on the stainless steel target (~0.5 inch diameter width). The target can be used to deposit up to seven sample spots in a time. One of the spots was always a standard mixture of known proteins which is used to check mass calibration and optimize the instrument parameters (melitin, insulin, cytochrome C and myoglobin, mass range 2000 to 18000 amu). Four microliters of the dihydroxy benzoic acid matrix were added to the sample spot and dried by blowing stream of hot air to the sample target while rotating the target.

Results and Discussion

Starch

Starch is a large and complicated molecule whose structure has not been well characterized. It is a mixture of two molecular entities, a linear fraction, amylose (α,1,4), and its branched counterpart, amylopectin with a branch point at the 1, 6 position . The basic building block is α-D-Glucose. All debranched starch samples were successfully ionized by MALDI by MALDI. On the other hand, the non-debranched fractions could not be ionized and no mass spectra were generated by MALDI. This can be explained due to the high mass and the nature of the starch crystal structure and intermolecular bonding. A typical MALDI mass spectra for a debranched starch fraction indicate an envelope of molecular ions in the range of 1000 amu to ~5000 amu with 162 mass unit difference between each two adjacent mass ions. The difference accounts for one glucose unit which is the monomer unit of starch. All detected ions were in the form of a sodium adducts. The degree of polymerization was calculated for the polymeric fractions to be 10 -30 dp. The debranched, *waxy (wx)* soluble and insoluble starch fractions indicated similar envelope but the spectra for the soluble fraction (Figure 1) indicated a baseline hump more apparent than the insoluble fraction.

The MALDI mass spectra for the debranched high *amylose* starch indicated a merged molecular ion hump with 14 mass ion difference. The detection of the 14 mass unit difference (baseline hump) was due to methylation. There is a correlation between numbers of long chains (amylose type) and susceptibility of the starches to methylation. In order to see if all the starch had been debranched, a further digestion of the debranched starches was completed with the enzyme, pullulanase. MALDI analysis of starch fractions during the course of the reaction with pullulanase indicated build up of ion signals at the 10,000 Da to >150,000 Da mass range These results indicate that further debranching can be carried out by selective enzymes. A combination of selective enzyme debranching, derivatization and MALDI analysis are the keys to unravel the starch molecules and relate it to functional performance.

Antibodies and enzymes

The antibodies and the enzymes were successfully ionized by MALDI The molecular weight for the antimethomyl antibody was detected at 147,828 amu which is the expected molecular weight range. The four enzymes were selected as a model for low pI enzymes which are more difficult to

ionize with current techniques. The enzymes samples included carbonic anhydrase, glucose oxidase, ß lactoglobulin and trypsin inhibitor. The MALDI mass spectra for each indicates the molecular ion M+, 2M+ and M2+.

The protein pellet from Klee and Rottannen honey

The MALDI mass spectra for the protein pellet from Klee and Rottannen honey.indicated the same component mass spectra of MW 52,763 amu protein. The peak shape and chromatographic behavior of the molecule with gel electrophoresis could indicate that the molecule is conjugated somehow and may be a glycoprotein. The results indicated that its structure is not related to the botanical origin of the feed. The two unifloral honey, Klee and Rottannen contain the same high-mass trace compound.

Formulated Sulfonylurea

Figures 2 shows the MALDI mass spectra of Ally® herbicide formulation at the sample spot rim and center. An interesting result was the difference in the spectral pattern observed within the sample spot. At the rim, the spectrum indicated mainly the specific ions for the active ingredient, metsulfuron methyl while the mass spectrum from the center of the sample spot indicated mainly the water soluble components as sugar. An explanation for this results is that the more water soluble compounds migrate with the water to the center as the spot has been dried off. The fragmentation pattern of sulfonylurea were informative and similar to the electrospray ionization using the source collision dissociation to induce fragmentation. The spectrum indicated a strong molecular ion adducts MH and M+Na in addition to 5-7 fragment ions.

Conclusion

MALDI is applicable to all the biomolecules we have selected and to study sample mixtures. It is a qualitative technique which can detect a large scope of compounds which could not be detected by other mass spec techniques. It handles mixture and matrices better than other techniques. Currently it is not a quantitative technique but could be in the future.

Figure 1

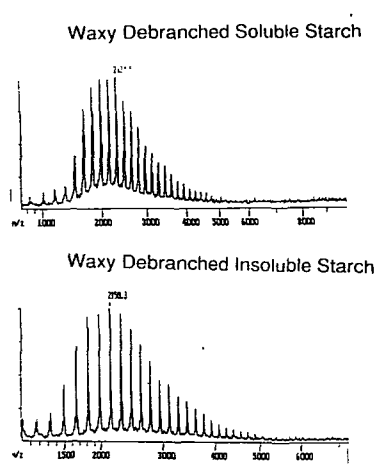

Figure 2

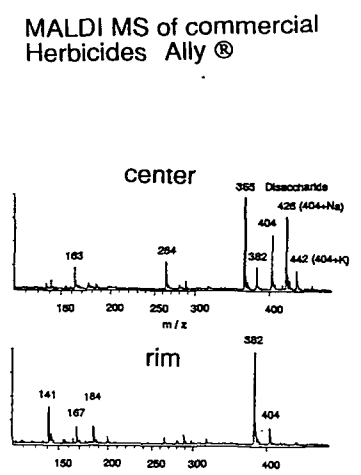

CID studies of MALDI generated peptide ions by RETOF MS

Holle, Armin, Köster, Claus
Bruker-Franzen Analytik GmbH, 28359 Bremen, Germany

Introduction

In recent years matrix-assisted laser desorption/ionization time-of-flight mass spectrometry (MALDI TOF MS) [1] has grown rapidly in its importance in the analysis of biomolecules. As an additional tool, post source decay (PSD) measurements with reflectron time-of-flight mass spectrometers (RETOF) has become an established technique for obtaining structural information from picomol amounts of small peptides [2].
PSD is a collisionally activated dissociation technique. The activation step in this case occurs as: (1) multiple early collisions between the analyte ions and (neutral) matrix molecules during the plume expansion and ion acceleration, (2) from collision events with gas molecules in the field free path.
While in many cases it is possible to obtain useful sequence information for the peptides being analysed, one might frequently obtain more information if the activation step were more controlled
The control of the pressure of gas molecules in the field free region represents a means to obtain greater control of the activation step and thus the extend of ion fragmentation. For this reason, we have prepared and installed a special "collision cell" in a MALDI TOF mass spectrometer

Methods

The measurements were performed on a BRUKER REFLEX instrument equipped with a special "collision cell" This cell consists of a pulsed gas valve mounted about 10 cm downstream from the ion source The 1 mm aperture of the valve is directed orthogonal to the ion beam axis at a distance of 4 mm The advantage of this arrangement is to provide a high gas density along the beam axis without significant changes in the instrument background pressure (2 10^{-7} mbar without gas, 5 10^{-7} mbar with gas at 10 Hz repetion rate).
10 pmol of analyte were mixed with α-cyano-4-hydroxy-cinnamic acid as matrix (analyte/matrix = 1/5000)
Data were acquired using a 125 MHz digitizing rate The detector response of low-mass matrix ions was minimized by the application of a deflection voltage pulse. The total PSD-spectra are pasted from a set of 21 PSD-spectra where each spectrum represents the sum of 100 consecutive laser shots.

Results

In figure 1 is shown a comparison of PSD and PSD-CID measurements of angiotensin II in a low mass range which represents the behaviour of other investigated peptides like substance P, ACTH 18-39, bovine insulin b-chain or ubiquitin In the PSD-CID study almost every mass below 200 amu is occupied The signal-to-noise of pure PSD spectra in this low mass range is significantly reduced compared to the PSD-CID spectra This is especially true for increasing parent ion mass

Conclusion

High energy PSD-CID measurements show, besides fragment ions due to pure PSD, intense fragmentation in the low mass region. The most intense mass peaks can be assigned to immonium ions $(H_2N{=}CHR)^+$ or I-type ions which indicate the cleavage of the entire peptide backbone structure

References

1. M Karas, F Hillenkamp; Anal. Chem. 60, 2299 (1988).
2. B Spengler, D. Kirsch, R Kaufmann, J Phys. Chem. 96, 9678 (1992)

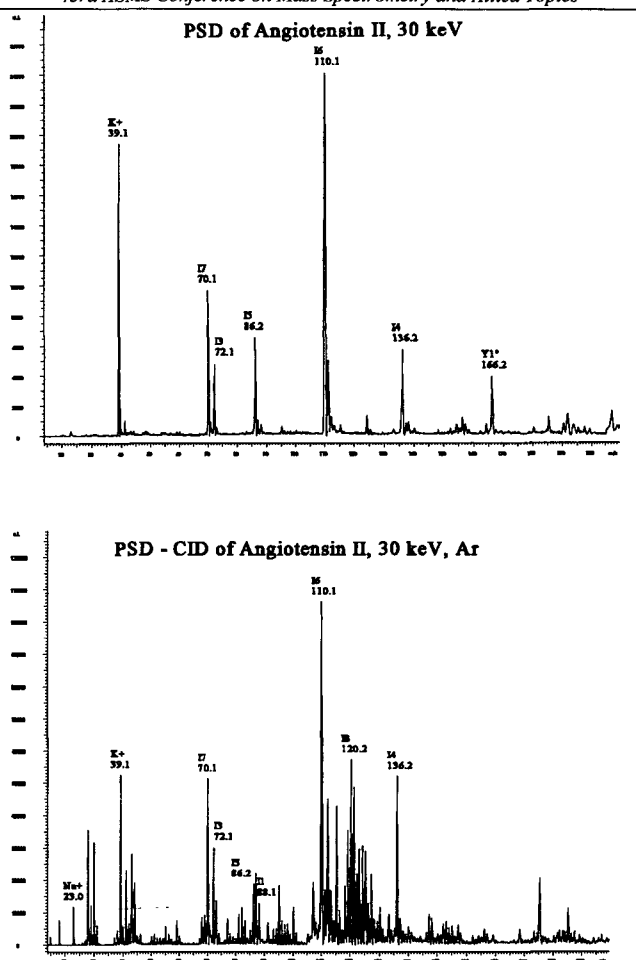

Figure 1: Comparison of a pure 30 keV PSD spectrum of angiotensin II and a 30 keV PSD-CID spectrum with argon as collision gas.

Effective Methods for Characterization of Membrane Proteins by MALDI-MS

Bao-Jen Shyong, Charles Mitchell, and Philip C. Andrews
Protein & Carbohydrate Structure Facility, University of Michigan, MSRBII, Room 2560, 1150 W. Medical Center Drive, Ann Arbor, MI 48109-0674

Introduction:

The application of peptide mapping using laser desorption mass spectrometry (MALDI-MS) in conjunction with chemical and enzymatic digestion provides a fast and sensitive method for protein characterization(1). However, membrane proteins present a number of problems in purification and structure analysis compared with glycoproteins and cytosolic proteins. This type of protein is generally quite hydrophobic and is often contaminated with interfering substances used in the purification process (e.g. detergents) which must be removed for accurate mass analysis. Hydrophobic proteins tend to aggregate or precipitate and as a result are difficult to purify by HPLC. SDS-PAGE is an alternate technique for analytical separation and characterization of complex protein mixtures which is more suitable for hydrophobic proteins. The goal of this study is to develop a systematic protocol to characterize interesting membrane proteins by incorporating MALDI-MS with other chemical and separation technologies. Bacteriorhodopsin, a membrane protein, was used as a model to evaluate the protocol.

Experimental And Instrument:

Bacteriorhodpsin and glycophorin were purchased from Sigma and G protein (β-subunit) of bovine brain is a gift from Dr. Neubig (University of Michigan). The primary separation is performed as one dimensional SDS-PAGE on a Phast-Gel electrophoresis system (Pharmacia). After the separation and purification, the protein band(s) were directly subjected to CNBr or/and Lys C digestion(2). Pure proteins without the purification treatment were used as a control to determine the yield and suitability of the protocol.

For LD-MS analysis, the Lys C digested mixtures were desalted by HPLC with an isocratic gradient on a C4 column. The dry mixtures generated by CNBr or Lys C digestion were re-dissolved into 100 µl 0.1% $TFA_{(aq)}$ or 100% formic acid. An aliquot of peptide mixture (1 µl) was mixed with or without 1 µl of insulin (@ 0.5 pmol) as an internal standard and 1 µl of matrix solution (α-cyano-4-hydroxycinnamic acid @ 100 mM), loaded on stainless steel dowel pin, then air dried for MALDI-MS analysis. The mass spectrometer used in this work was a Vestec-2000 (Houston, TX), which is a LaserTec ResearcH laser desorption linear time-of-flight mass spectrometer, equipped with a 1.2 m flight tube, operated at 23 KV ion accelerating voltage and 3.5 KV multiplier voltage, a 337 nm VSL-337 ND nitrogen laser (Laser Science, Inc.) with a 3-ns pulse width. Spectra were summed from 15 to 20 laser shots.

Results And Discusions:

1. The Phast-gel electrophesis system provides a higher recovery yield for extraction than mini or regular gel systems. The thickness of this gel (SDS-PAGE) is 0.45 mm and the proteins are applied to the surface of the gel.
2. In general, protein(s) subjected to CNBr or Lys C digestion could supply reasonable lengths of peptides to avoid the matrix interference (<500 a.m.u.) of MALDI-MS and for other analytical methods. For unknown sequences of protein, the CNBr digestion might be a good first choice due to easy handling without further purification.
3. The MALDI-MS spectra obtained from 1-D SDS-PAGE are similar to those of the control. The intensity and number of species appearing in the spectra may vary due to the concentration of the mixture, suppression of the mixture, the interaction among components of the mixture, presence of an internal standard, and the matrix employed (See Fig. 1, 2, 3, and 4). For unknown protein, further separtion is necessary to obtain the internal seqence.

4. The flow chart for the characterization of membane proteins is shown as Schedule 1.

Reference:

(1) Todd M. Billeci and John T. Stults (1993) Anal. Chem. **65**, 1709-1716.
(2) Jorge Rosenfeld, joel Capdevielle, Jean Claude Guillemot, and Pascual Ferrara (1991) Analy. Bicchem. **203**, p173-179.

Acknowledgments:

The authors wish to acknowledge Dr. Neubig for supplying the β-subunit G-protein of bovine brain, S. Williams for amino acid analyses, and J. Tropea for protein sequencing.

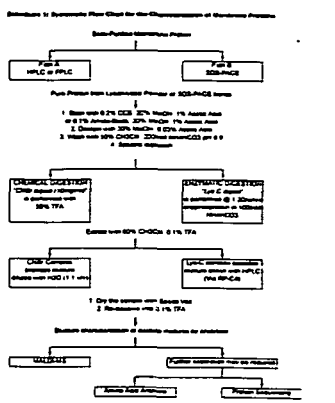

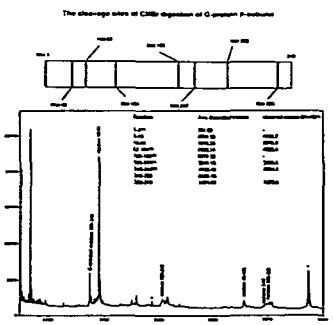

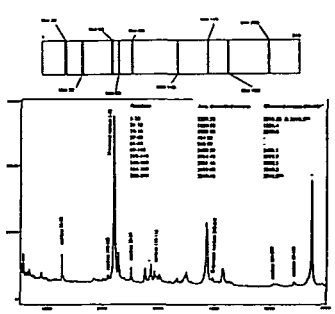

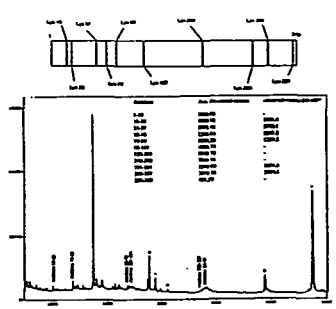

Assessment of Photoaffinity Crosslinking of Macromolecules by MALDI MS

Terry B. Farmer and Richard M. Caprioli
Department of Biochemistry and Molecular Biology and Analytical Chemistry Center, University of Texas-Houston Medical School, Houston, Tx 77225

Introduction

Chemical crosslinking reagents are dependent for their action on the groups available on the surface of the molecule for the crosslinking reaction to occur. Crosslinkers containing photoaffinity groups can be used to examine molecular interactions when reactive residues such as Lys are not available because the photoaffinity crosslinking reaction is nonspecific.

Experimental

Protein Crosslinking

Sulfosuccinimidyl-6-[4'-azido-2'-nitrophenylamino] hexanoate (sulfo-SANPAH), p-azidophenyl glyoxal (APG), and bis-[β(4-azidosalicylamido)ethyl] disulfide (BASED) (Pierce Chemical Co.) were used to examine crosslinking of equine alcohol dehydrogenase (eADH), lactate dehydrogenase (LDH), yeast alcohol dehydrogenase (yADH), glucose 6-phosphate dehydrogenase (G6PD) (Sigma Chemical Co.) and the chi and psi subunits of the DNA polymerase III holoenzyme (Dr. Charles McHenry). The crosslinkers **must** be handled in the dark until exposure to UV light for activation. APG and BASED, with limited solubility in aqueous solutions, are first dissolved in DMSO at a concentration of 200 μg/μl. BASED is then diluted to 6 μg/μl in DMSO and added to the buffered reaction solution so that the final reaction concentration is 1 mM in ≥ 10% DMSO. APG is first diluted to 6 μg/μl concentration in 50 mM ammonium bicarbonate (pH 8) when it precipitates out. To redissolve APG it is heated at < 100°C for less than 1 minute and added to the reaction for a final concentration of 5 mM. Sulfo-SANPAH is dissolved in 50 mM aqueous buffer with no primary amines (pH 8) at a concentration of 50 μg/μl and added to the reaction solution for a final concentration of 1 mM.

Protein concentrations were 10 pmol/μl. Protein solutions with added APG and sulfo-SANPAH were allowed to react in the dark for 45-60 minutes and then exposed to UV light at 365 nm (Spectroline E-Series, Spectronics Corp.) for 10 minutes on ice. BASED was added to the protein solution and after 5 minutes was exposed to UV light at 254 nm (Mineralight Lamp, UVP Inc.) for 10 minutes on ice. The reaction mixtures were then immediately washed with 6x volume of buffer using Ultrafree-MC 10,000 NMWL filtration units (Millipore).

MALDI TOF MS

Spectra were obtained using a PerSeptive Biosystems Voyager Elite MALDI TOF instrument with a N_2 laser and an acceleration voltage of 25 kV. Uncrosslinked and crosslinked proteins were analyzed with the same laser power and peak areas were determined using an integration algorithm in GRAMS386. Samples were prepared two ways: 1. Protein solution (0.5 μl) was added to 0.7 μl of saturated sinapinic (70% acetonitrile/30% 0.1% TFA) on the target. 2. Saturated sinapinic (2:1 water:acetonitrile) was pipetted onto the target and allowed to air dry. After drying, a glass slide was used to crush surface crystals and excess matrix was removed by gently brushing with a Kimwipe tissue. A 1:1 mixture of protein solution:saturated sinapinic (2:1 0.1% TFA:acetonitrile) was pipetted onto the first layer of matrix[1]. Both sample preparations were then allowed to air dry and were mass analyzed.

Results and Conclusions

In the present experiments the utility of photoaffinity crosslinkers was examined with proteins that have been analyzed both successfully and unsuccessfully by amine specific crosslinking reagents. Using glutaraldehyde, eADH, a dimer, showed addition to the monomer, but no multimer formation. However, using both APG and sulfo-SANPAH, an increase in the formation of dimer was seen from 4:1 monomer:dimer with no crosslinker to 1:1 monomer:dimer using these crosslinkers (Table 1). Gel filtration data indicates chi and psi subunits of the DNA polymerase III holoenzyme form a heterodimer[2]. Amine specific crosslinkers were ineffective for crosslinking because psi has one Lys residue. Crosslinking with APG and sulfo-SANPAH with subsequent mass analysis (Figure 1) showed formation of a heterodimer with some formation of higher oligomers. The results indicate that homo- and heterobifunctional photoaffinity crosslinkers can be used to examine intermolecular interactions. The efficiency of the crosslinkers (calculated by subtracting the % uncrosslinked multimer from the % crosslinked multimer) was 5-20% for APG, 0-10% for BASED, 10-40% for sulfo-SANPAH, while for an amine specific crosslinking reagent such as glutaraldehyde it was typically 50-80%. Low crosslinking yields for the photoaffinity crosslinking reagents may be due to limited aqueous solubility, especially in the case of APG and BASED. Work is currently in progress to analyze the chi and psi subunit interactions in the presence of the other gamma subunit components.

		Relative % Peak Area*			
Protein	Multi-mer	No Crosslinker	APG	Sulfo-SANPAH	BASED
eADH (Dimer)	1	54	41	44	None detected
	2	30	40	40	
	3	16	19	16	
G6PD (Dimer)	1	62	43	22	40
	2	29	46	36	38
	3	9	11	18	11
	4	-	-	24	1
LDH (Tetramer)	1	40	20	None detected	None detected
	2	29	26		
	3	16	21		
	4	15	33		
yADH (Tetramer)	1	50	26	17	33
	2	34	41	52	36
	3	11	18	31	16
	4	6	15	47	15
Chi and Psi	1(Psi)	39	9	24	None detected
	1(Chi)	39	27	37	
	Psi_2	6	-	-	
	Psi/Chi	9	26	27	
		7	-	-	
	Chi_2	-	14	12	
	3	-	24	-	
	4				

Table 1. Comparison of relative % peak area of proteins before and after crosslinking with photoaffinity reagents. (*Corrected for mass discrimination)

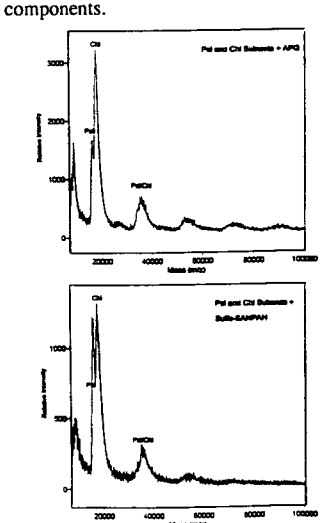

Figure 1. MALDI TOF spectra of the psi and chi subunits of DNA polymerase III holoenzyme crosslinked with either 5 mM APG or 1 mM sulfo-SANPAH.

References: 1. S. Patterson and V. Katta, Anal. Chem. **66**, pp. 3727-32 (1994).
2. H. Xiao, Z. Dong, and M. O'Donnell, JBC **268**, pp. 11779-84 (1993).

Acknowledgements: We would like to thank Dr. C. McHenry for the chi and psi subunits of DNA polymerase III holoenzyme and the NIH (Grant #GM43783-05) for funding this work.

Micro-Concentration/Desalting/Matrix-Addition Procedure for High Sensitivity Analysis of Peptides by Matrix-assisted Laser Desorption Ionization Mass Spectrometry

Haiying Zhang, Per E. Andren, and Richard M. Caprioli

Department of Biochemistry and Molecular Biology and Analytical Chemistry Center, University of Texas Medical School, 6431 Fannin, Houston, TX 77225, USA

Matrix-assisted laser desorption / ionization mass spectrometry (MALDI MS) is rapidly becoming a standard analytical technique for measuring the molecular mass of polypeptides and proteins. Because of the trace concentration nature of some biological analytes, there has arisen a corresponding need for the development of concentration methodologies in conjuction with this ionization technique. Biological extracellular neurosubstances from microdialysates, for example, are usually present at amole per μL levels and in relatively large (μL) volumes containing high concentration of salts. Consideration of high detection sensitivity requires working with concentration techniques optimized for small sample spotting. In addition, salts which may interfere with MALDI analysis should be removed instead of being allowed to accumulate during the concentration procedure.

We have used a C-18 packed capillary as an integrated micro-concentration/desalting/ matrix-addition device for the analysis of trace level peptides in samples containing physiological salts. This methodology provides low fmole / high amole sensitivity for peptides in amole per μL concentrations. A fused silica capillary (50 μm i.d.) containing about 1 cm C-18 coated support was used. Samples were loaded onto the C-18 column via a 10 μL loop of an injector, and salts were washed off the C-18 column within five minutes using water containing 2% acetic acid at a flow rate of 0.3 μL/min. The purified samples were eluted by a solvent containing MALDI matrix in 75% acetonitrile (0.1 μL/min). Eluents were spotted onto the multi-well sample holder for MALDI MS analysis. Removal of salts and reduction of the sample volume from a few μL to about 5 nL led to a MALDI-sensitive spot area of less than 0.3 mm^2. A sensitivity of 200 amole was achieved for neurotensin (NT) from a 20 amol/μL solution containing 0.2 M phosphate buffer (Fig. 1). In contrast, samples in the same salt solution, without any purification, could not be detected using direct analysis. The quantitative reproducibility of this pretreatment procedure for MALDI MS determination of trace peptide levels in physiological salt solution is shown in Figure 2 for the analysis of substance P in a solution containing 0.2M NaCl and neurotensin as the internal standard. A linear intensity relationship was achieved down to 100 amol/μL level, which is two orders of magnitude lower than that from direct analysis of the sample. As an example to show the validity of the procedure developed here for real biological samples, the metabolic fragments of NT, including NT1-8, 1-10, 1-11, 1-12 and 9-13, were readily detected from an *in vivo* microdialysate after an infusion of 100 fmol/μL NT into rat brain (Fig. 3).

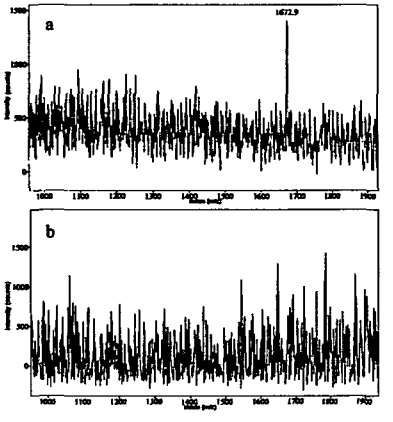

Figure 1. **(a)** MALDI mass spectrum obtained from C-18 packed capillary with 200 amole neurotensin loaded in 10 μL of 20 amol/μL solution containing 0.2 M phosphate (pH 7.0). **(b)** MALDI mass spectrum obtained from open capillary spotting with 100 fmole neurotensin from 1:1 mixture of 40 pmol/μL NT in 0.2M phosphate and MALDI matrix. In both cases, the volume spotted was 5nL.

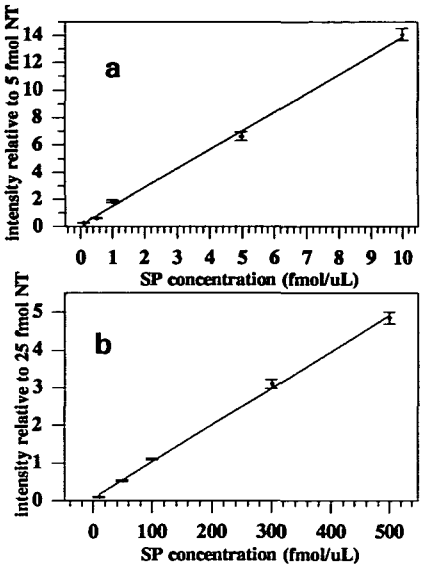

Figure 2. Peak height ratio *versus* substance P concentration: **(a)** obtained from C-18 packed capillary with 0.2M NaCl and with 5 fmol neurotensin as internal standard; n = 6 measurements. **(b)** obtained from direct MALDI analysis in pure water and with 25 fmol neurotensin as internal standard; n = 5.

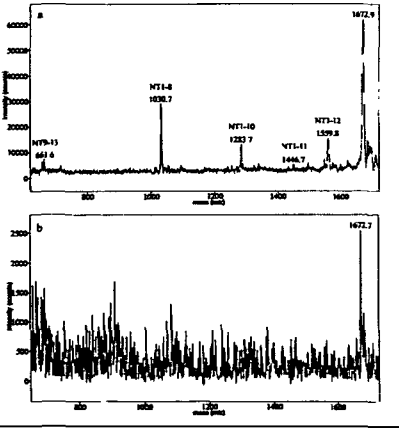

Figure 3. MALDI mass spectra of *in vivo* microdialysate obtained from the metabolism of exogenous neurotensin containing artifical cerebrospinal fluid: **(a)** from the C-18 packed capillary as 7 μL loading; **(b)** by direct MALDI analysis of 1 μL 1:1 mixture of sample and MALDI matrix without any concentration or purification treatment.

DIFFERENTIATION OF MULTIMERIC ANTIGENS BY MSIA AND ENZYMATIC MODIFICATION.

Jennifer R. Krone, Randall W. Nelson, David Dogruel, J. Kathleen Lewis and Peter Williams.
Department of Chemistry and Biochemistry
Arizona State University, Tempe, AZ 85287-1604.

INTRODUCTION

Mass spectrometric immunoassay (MSIA) provides a degree of specificity beyond that of conventional immunoassays through the direct detection of antigens at defined and characteristic mass-to-charge (m/z) values [Nelson, R.W. Krone, J.R.; Bieber, A.L.; Williams, P. *Anal. Chem.* **67**, 1153 (1995)]. While mass-specific detection in principle eliminates ambiguous identification of antigens, practical limits arise from an inability to determine the absolute molecular weight of the antigen to within a given accuracy and/or the inability to resolve antigen ion signals from those of interferences. These limitations are especially pronounced during the MSIA analysis of systems which contain alternate forms of the same antigen. If the isoforms are retained during the immunoaffinity capture step of MSIA, and the mass difference between the versions is small, antigen determination becomes ambiguous. One way to resolve this problem is to use monoclonal antibodies specific to only the relevant variant of the antigen (a reagent which is not always available).

An alternative is to devise methods which enable a more specific mass spectrometric identification of the antigen. We have found enzymatic treatment - capable of creating characteristic peptide maps of MSIA-isolated species prior to mass spectrometry - to be a practical means with which to differentiate between antigenic species. Further, we have developed a series of "enzymatically-active" mass spectrometer probe tips in order to perform the assays in the most efficient manner possible. The probe tips derive their activity through the (covalent) surface immobilization of select enzymes (see **Fig. 1**). Antigen is eluted directly (from MSIA reagent) onto the reactive surface of the probe tips and time given for proteolytic digestion. The reactions are then terminated with the addition of a MALDI matrix (allowed to dry), the probe tip inserted into the mass spectrometer and mass analysis performed.

The "enzymatically-active" probe tips have been found a rapid, sensitive and convenient means for the routine characterization of proteins and peptides. Further, when used in combination with MSIA, the probe tips have allowed low specificity immunoaffinity reagents, such as antisera, to be incorporated into the assay without a sacrifice in specificity.

RESULTS

The MSIA/peptide map method has been used to the characterize antigens retained from the venom of the *N.n. siamensis* (**Fig. 2, top**). The MSIA procedure was as in Fig. 1 using an affinity reagent of immobilized anti-α-cobratoxin antisera. The first step of the assay indicates the successful retrieval of α-cobratoxin from the whole venom (**Fig. 2, center**). Digestion on a trypsin-active probe tip yields a digestion pattern consistent (**Fig. 2, bottom**) with the native form of the toxin (**inset**).

CONCLUSION

We have developed a rapid, sensitive and convenient method of mass spectrometric immunoassay which combines micro-scale immunoaffinity capture of antigens with enzymatic mapping and MALDI mass analysis. To execute the assays in the fastest and most sensitive manner possible, "enzymatically-active" mass spectrometer probe tips were constructed *with which* to

perform the digestion, i.e., the probe tips were the enzymatic reagent. The approach contributed an additional degree of selectivity to the assay (mass spectral peptide mapping) which allowed the use of low-specificity immunoaffinity reagents (such as antisera) for antigen isolation.

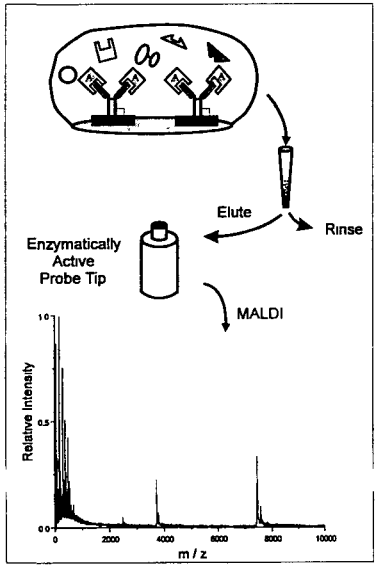

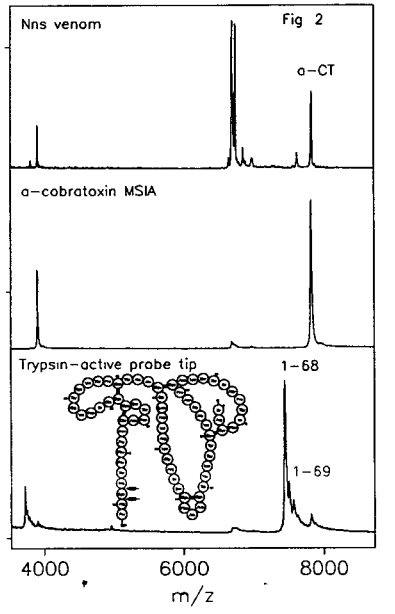

Fig. 1 General overview of the MSIA/peptide map process. Briefly, antigen retained during the MSIA process [1] is eluted onto an "enzymatically-active" probe tip where proteolytic digestion is allowed to occur. Digestion is terminated with the addition of a MALDI matrix

Fig. 2 Results of MSIA/peptide map process applied the whole venom of *N.s. siamensis*.**(top)** MALDI of whole venom. **(center)** MSIA using anti α-cobratoxin antisera as an affinity reagent. **(bottom)** Peptide map of MSIA isolated α-cobratoxin followed by proteolytic digest using a trypsin-active mass spectrometer probe tip. Peaks consistent with the native form of the toxin **(inset)** are observed.

Sequence Specific Fragmentation Generated by MALDI in Ion Trap/reTOF

Heewon Lee and David M. Lubman
Department of Chemistry, The University of Michigan, Ann Arbor, MI 48109

MALDI is generally a soft ionization method and has been thought to produce little fragmentation for structural analysis. Although prompt fragmentation is not observed in the MALDI process on the time-of-flight (TOF) MS time scale, it has been shown that extensive metastable decay does occur as a function of time. In this study, sequence-specific fragmentation for structural analysis has been generated by activation of ions via MALDI in an ion trap storage/reflectron time-of-flight device. The key to this work is that ion decay can be induced by MALDI activation but requires an extended period of time to occur in large peptides. This extended decay period, which may be in excess of 20 ms, is provided in these experiments using the long storage times of the ion trap device. The ions are stored until decay is complete and then rapidly pulsed into a reflectron TOF for analysis. Since the ions decay within the trap, they ultimately appear as stable ions in the reTOF rather than as metastable decay peaks.

The wavelength of 355 nm of the Nd:YAG laser was employed with 2,5-dihydroxybenzoic acid (DHB) as a matrix for MALDI. The desorbed ions were stored by the quadrupole ion trap for a determined time which varied from 1μs to 90 ms before being extracted into the time-of-flight drift tube. Peptides used in this study include Leu-enkephalin, angiotensin I, II and III, bradykinin and substance P.

The fragmentation typically provides a, b, y and internal fragment ions. However, no charge-remote fragmentation, which was reported for high energy CAD, was observed. The fragmentation pattern was compared with that of other desorption/ionization and fragmentation methods such as FAB, LSIMS, MPI and CAD.

MALDI fragmentation spectrum of Leu-enkephalin is shown in figure 1. The fragmentation obtained was most similar to that observed in FAB-low energy CAD. The ion fragmentation was found to depend strongly on laser power and the RF voltage placed on the ring electrode of the trap. Figure 2 shows the dependence of the peak intensity ratio of a_4/b_4 of Leu-enkephalin on the trapping time and the laser power density.

It was reported that a peptide with a terminal arginine, which is the most basic residue among common amino acids, prevents obtaining informative sequence-specific fragment ion spectra for FAB-MS. To investigate this arginine effect in MALDI experiments, bradykinin fragment 2-7 and substance P fragment 2-11 (figure 3) were studied. The peptide without a terminal arginine residue showed far more sequence-specific fragmentation peaks.

In this work it is demonstrated that rapid peptide sequence information can be obtained using an ion trap/reTOF mass spectrometer via its ability to store ions for an extended time period so that the unimolecular decay of ions can be observed.

43rd ASMS Conference on Mass Spectrometry and Allied Topics

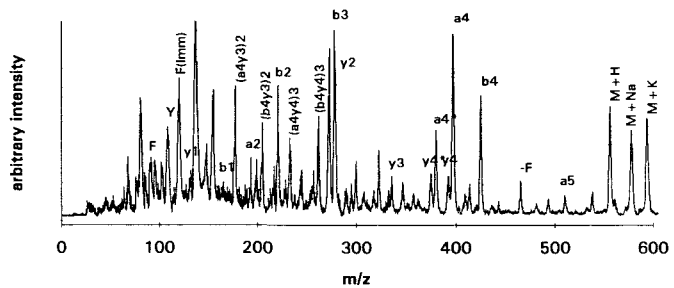

Figure 1. MALDI fragmentation spectrum of Leu-enkephalin

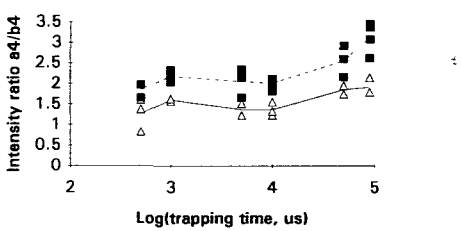

Figure 2. Dependence of the peak intensity ratio of a_4/b_4 of Leu-enkephalin on trapping time and laser power density. Δ points are obtained with laser power density of 2.6×10^6 W/cm^2 and ■ with 5.3×10^6 W/cm^2.

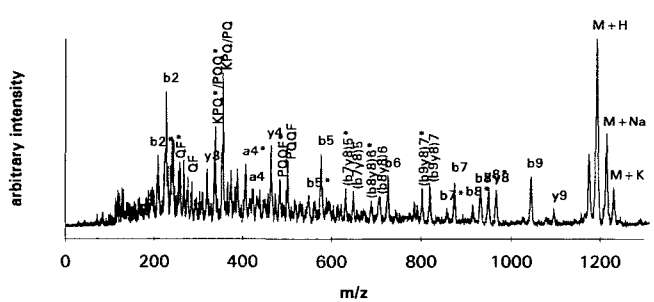

Figure 3. MALDI fragmentation spectrum of substance P fragment 2-11

A Strategy to Locate Cysteine Residues by Specific Chemical Cleavage Followed by MALDI-TOF MS

Jiang Wu*, Douglas A. Gage and J. Throck Watson
Department of Biochemistry and Chemistry*, Michigan State University
East Lansing, MI 48824

Characterization of a protein requires a determination of the number and location of cysteine sulfhydryls and cystine disulfide bonds, due to the diverse roles they play in both protein structure and function. Classical approaches usually involve alkylation of the free sulfhydryls before and after reduction of the protein, enzymatic digestion , HPLC separation and Edman degradation of resulting peptides.

We are developing a simple method to characterize the number and location of cysteine and cystine groups in peptides and proteins, using chemical modification and MALDI-MS peptide mass mapping. This approach employs a specific reaction between free sulfhydryls and 2-nitro-5-thiocyanobenzoic acid (NTCB) to selctively cyanylate free cysteine thiols. The peptide bond on the N-terminal side of the modified cysteinyl residues can then be cleaved under alkaline conditions to form an amino-terminal free peptide and a series of blocked 2-iminothiazolidine-4-carboxyl peptides which can then be mass-mapped [1,2].

To determine the free sulfhydryl groups, the protein is first allowed to react with NTCB to cleave at free cysteine sites. The resulting disulfide bond-linked protein is then reduced by tris(2-carboxyethyl)phosphine (TCEP) to obtain a series of peptides whose number and mass are dependent on the number and position of free cysteine residues present in the protein. To determine the total cysteines, the protein is first denatured and allowed to react with TCEP to reduce disulfide bonds. NTCB is then added to modify all cysteines. MALDI mass mapping of the cleavage products indicates total cysteine groups in the protein.

The figures show the MALDI-TOF mass spectra of ovalbumin after being processed under the above two procedures. The protonated molecular weights for the predicted products and experimental data found by the use of external calibration are listed below:

TCEP/NTCB treatment			NTCB/TCEP treatment		
fragment	predicted	found	fragment	predicted	found
1-10	1011.1		1-10	1011.1	
11-29	2378.7	2376.6	11-29	2378.7	2378.8
30-72	4762.5	4764.4	30-366	37684.7	
73-119	5427.1	5428.7	367-381	1715.1	1715.5
120-366	27581.1		382-385	429.5	429.4
367-381	1715.1	1714.8	1-29*	3371.8	3371.6
382-385	429.5	429.4		3312.8	3311.1
1-29*	3371.8	3371.0	367-385*	2126.6	2125 8
	3312.8	3311.6		2067.6	2068.0
367-385*	2067.6	2066.9			

* incomplete cleavage and/or β-elimination products

Most of the proteolytic peptides can be detected directly by MALDI without the need for previous separation. However, the high mass fragments are often suppressed and not seen in the spectrum. Incomplete cleavage and β-elimination products may occur but these are never the major products. Although the NTCB reaction is specific for free sulfhydryls, high molar excess of NTCB and longer reaction times should be avoided because this can result in a side reaction with disulfide bonds. The reaction can be performed on a Zetabind membrane allowing the removal of MALDI contaminants and reagents and thereby reducing the required sample size for proteins to the low picomole level[3].

This developing methodology shows great promise for recognizing the location of the free cysteines and characterizing the distribution of disulfide bonds in proteins.

We thank Dr. Eugene Zaluzec for his valuable contributions

1. Jacobson, G.R., Shaffer, M.H., and Stark, G.R. *J. Biol. Chem.*, 248,6583-6589(1973)
2. Papayannopoulos, I.A., and Biemann, K. *Protein Science.*, 1,278-288(1992)
3. Zaluzec, E.J., Gage, D.A., Allison, J., and Watson, J.T. *J. Am. Soc. Mass Spectrom.*, 5(4)230-237(1994)

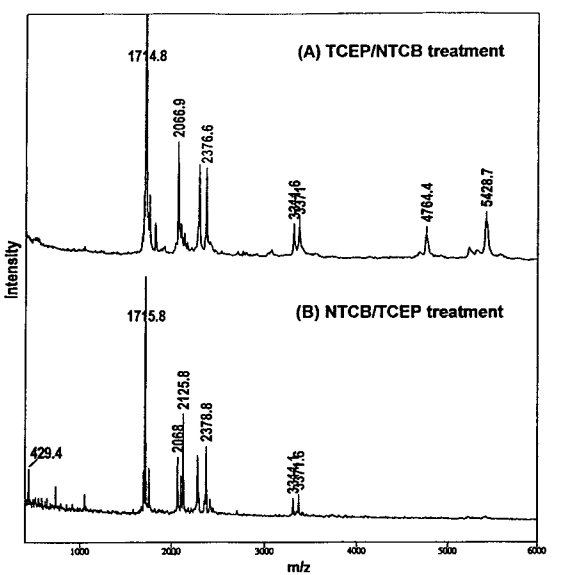

MALDI-MS of Proteins Electroblotted onto Membranes after 2D-PAGE-Separation

Kerstin Strupat, Christoph Eckerskorn*, Michael Karas, Friedrich Lottspeich*, Denis Hochstrasser§, Franz Hillenkamp,
Insitute for Medical Physics & Biophysics, University of Münster, 48149 Munster, FR Germany
* Max-Planck-Institute for Biochemistry, 82152 Martinsried, FR Germany
§ Medicine Department & Medical Computing Center, Geneva University Hospital, Geneva, Switzerland

It has been previously demonstrated that mass analysis of proteins immobilized onto polymer membranes is possible by MALDI-MS with IR-lasers (e.g Er-YAG-lasers) directly from the membrane.(1,2) It has been shown that proteins separated by SDS-PAGE with subsequent electroblotting of the separated proteins onto suitable blotting membranes and matrix incubation of the membrane in aqueous succinic acid solution for several minutes results in IR-MALDI-mass spectra of proteins taken directly from the immobilizing substrate

In continuation of this work, human plasma proteins were separated by (two-dimensional)-PAGE (2D-PAGE) according to Gorg *et al.* (3, 4) and Hughes *et al.*, respectively, and electrotransfered onto PVDF-membranes by a semi-dry procedure (Immobilon PSQ) The following matrix-incubation of the membrane was identical to the one found to be suitable for (one-dimensional) SDS-PAGE separated and electrotransfered proteins. One electroblot with 2D-separated plasma proteins was stained by Coomassie Blue and served as a reference blot, in order to locate the protein spots in the non-stained matrix-incubated blot. A home-built 1-stage reflectron time-of-flight mass spectrometer was used for this investigation An Er-YAG-laser at a wavelength of 2 94 µm and a pulse width of 100 ns was used to desorb the proteins.
Five protein spots were chosen in the mass range up to 20 kDa to demonstrate the feasibility of MALDI-MS to 2D-PAGE separated proteins Transthyretin (TTR, MW ca. 14 kDa) and the Haptoglobulins A, B, C (MW ca 16 kDa) of the α2-chain- differing in post-translational modifications - as well as an unknown spot D in close vicinity to the Haptoglobulin spot A were investigated by IR-MALDI-MS A MALDI-mass scan of the entire TTR-spot was performed in order to investigate the correspondence to the already known data of the laser densitometry of this spot

Figure 1 shows a MALDI-mass spectrum taken in the center of the TTR-spot. Its mass was determined to (13756±19) Da by external calibration using a 1D-separated Carbonic Anhydrase protein blotted onto PVDF-membrane as a reference protein on the same target. The standard deviation of this mass values results from 40 summed spectra of different locations, 10 single spectra were taken from each of the 40 different locations within the spot A comparison between the MALDI-mass data and the UV-laser densitometric data of the corresponding silver-stained TTR-spot in the gel shows excellent agreement with the local protein distribution. High MALDI-protein intensities are found in the center of the spot which decrease towards the edge.

Figure 2 shows MALDI-mass spectra of Haptoglobulin A-spot and its vicinity. Spot A has the lowest response in a silver-stained gel, among all investigated known proteins Its mass was determined to (16355±15) Da by external calibration The standard deviation of this mass values results from five summed spectra (10 single spectra) taken from five different positions in the spot. All spectra observed for the spots A, B and C of the Haptoglobins show a major component (slightly differing in their masses due to the post-translational modifications for the three Haptoglobulins) and a minor component

(shoulder) which is approximately 1240 Da lower in mass than the main component. The minor signal is found wherever the main component is found, its origin is not yet known. MALDI-mass analysis of areas in vicinity to spots A and C resulted in signals besides those from the Haptoglobin-modifications (see figure 2)

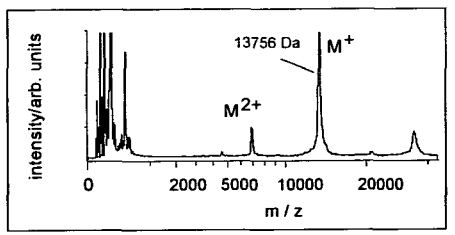

Fig. 1: MALDI-mass spectrum of the Transthyretin-spot taken in the center of the spot Membrane PVDF (Immobilon PSQ) Matrix succinic acid λ: 2 94 µm. Sum of 10 single spectra.
The mass of Transthyretin was determined to (13756±19) Da by external calibration using the protein carbon anhydrase (separated by SDS-PAGE) immobilized on PVDF-membrane From the literature the mass of the TTR-protein is 13762 Da.

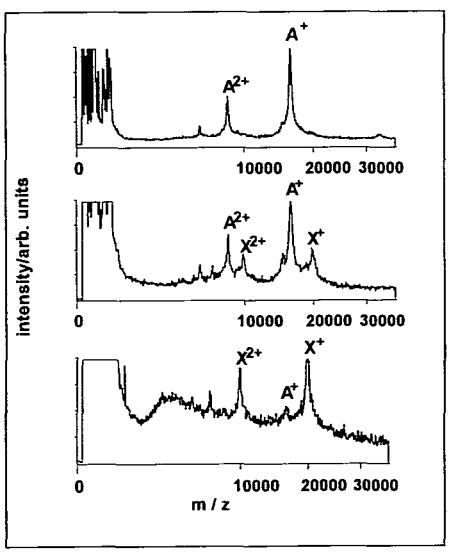

Fig. 2 MALDI-mass spectra of the of the Haptoglobulin spot A Membrane PVDF (Immobilon PSQ) Matrix: succinic acid.
λ 2 94 µm. Sum of 10 single spectra
top center of A
middle: between A and an adjacent, weak spot X
bottom. the adjacent, weak spot X
The mass of spot A (16355±15) Da, shoulder in spot A (15100±35) Da,
mass of spot X (19750±45) Da

References:

1 Kerstin Strupat, Michael Karas, Franz Hillenkamp, Christoph Eckerskorn, Friedrich Lottspeich, Anal Chem. 64 (1994) 464
2 Kerstin Strupat, Christoph Eckerskorn, Michael Karas, Franz Hillenkamp, Mass spectrometry in the Health and Life Sciences 1994, San Francisco
3 A Görg, W. Postel, S Günther; Electrophoresis 9 (1988) 531
4 G J Hughes, S. Frutiger, N. Paquet, F Ravier, C. Paquali, J.C Sanchez, R. James, J D Tissot, B Bellqvist, D Hochstrasser; Electrophoresis 13 (1992) 707

Acknowledgements: Financial support by Bundesministerium für Bildung und Forschung (BMBF, grant 325-4003-0310-720) is gratefully acknowledged

Analysis of Oligonucleotide And Protein Samples Using Membranes And Matrix-Assisted Laser Desorption/Ionization Mass Spectrometry

*Tracy I. Stevenson and Joseph A. Loo, Parke-Davis Pharmaceutical Research, Division of Warner-Lambert Company, 2800 Plymouth Road, Ann Arbor, MI 48105

INTRODUCTION One problem with matrix-assisted laser desorption/ionization (MALDI) mass spectrometry is that it is difficult to obtain accurate mass measurements for salt containing oligonucleotides and polypeptides due to adduct formation, causing broadening or skewing of the peaks, especially for samples over ~ 5 kDa. This problem can be minimized to some extent by sample cleanup and/or using an instrument with higher resolution capabilities to resolve the adducts, thereby allowing a more accurate mass determination. However, overall sensitivity is reduced because the ion signal is distributed over several ionic species.

Work has been performed in our laboratory to improve laser desorption and ionization of proteins and oligonucleotides while minimizing adduct formation and increasing resolution. Samples are applied to a specially prepared target plate membrane and allowed to dry. The samples are then washed to remove salts, which can form adducts, and then analyzed by MALDI time-of-flight (TOF) MS using an appropriate matrix for co-crystallization. The biological molecules bind to the membrane while the salts and buffers are washed away. Membranes tested to date include PVDF, Immobilon™-P, Immobilon™-CD, Nafion® 417, Nytran™, nitrocellulose, nylon 66, polyethylene, and Zitex®.

DISCUSSION Many biological samples are prepared or stored in buffer solutions which are very detrimental to obtaining high quality MALDI mass spectra. These buffer solutions can consist of mixtures of many species which mass spectrometrists have routinely avoided. An example of a typical mixture our laboratory receives is 50.0 mM HEPES + 10.0 mM CHAPS + 0.5 M NaCl + 10 % glycerol + 10.0 mM DTT. Some of the combinations are not a problem if sufficient protein is present in the solution enabling dilution, thereby lowering the concentration of the interfering species. However, others can cause problems even at extremely low levels such as sodium dodecylsulfate (SDS), which can completely suppress all ion signal at as low as 0.7 % (w/w) concentration.

To alleviate this problem, we investigated using membranes which have typically been used to bind proteins for sequencing, as well as some less traditional membranes. The sample containing membrane can be washed, removing the interfering species while retaining the analyte. To identify the best membrane for protein analysis, six different membranes were affixed to the sample plate and 10 pmol of bovine insulin applied to each membrane. The membranes were washed with copious amounts of deionized H_2O prior to the addition of matrix and MALDI analysis. PE (polyethylene) and Zitex® gave the strongest signals for the [M + H]+ ion of bovine insulin.

Figure 1 shows a very poor quality MALDI mass spectrum obtained for a HIV integrase sample in 20 mM HEPES + 10 mM CHAPS + 0.1 mM DPTA + 0.5 M NaCl and 20 % (w/w) glycerol (MW ~34,000 Da). The sample was cleaned-up by applying 2 µL of the protein solution to a PE membrane and washing away the buffer and salts with deionized H_2O. Once dry, 1.2 µL of sinapinic acid matrix was applied to the membrane and the sample was analyzed. The protein ion signal is now easily observed and its mass determined.

Oligonucleotides pose a similar problem for MALDI analysis. Salt adducts are very common and cause broadening of the ion peak which results in decreased mass accuracy and sensitivity. Figure 2 shows the negative ion mass spectra for oligothymidylic acid $d(pT)_8$ on Zitex® membrane. It can be seen in Figure 2b how Na+ adducts shift the mass of the oligonucleotide as well as cause a loss of resolution. However, after washing the membrane/sample with deionized H_2O, Na+ adduct formation has been greatly reduced and resolution restored, as shown in Figure 2c.

We have found in our laboratory that membranes can be used to quickly and efficiently clean-up peptide or protein samples which give no spectra or poor spectra due to contaminants present. This technique has proven to work well for samples ranging in molecular weights up to ~ 60,000 daltons. Polyethylene (PE) works best but is extremely fragile and difficult to work with in its presently available form (3M Disposable IR cards). Therefore, Zitex® is our membrane of choice due to its mechanical properties which make working with it very easy. Oligonucleotides have been much more difficult for our laboratory. We have not yet found a membrane for which we can obtain consistent results. DNA and RNA size appears to also play a crucial role in membrane selection and performance.

FIGURE 1: Spectra of HIV Integrase

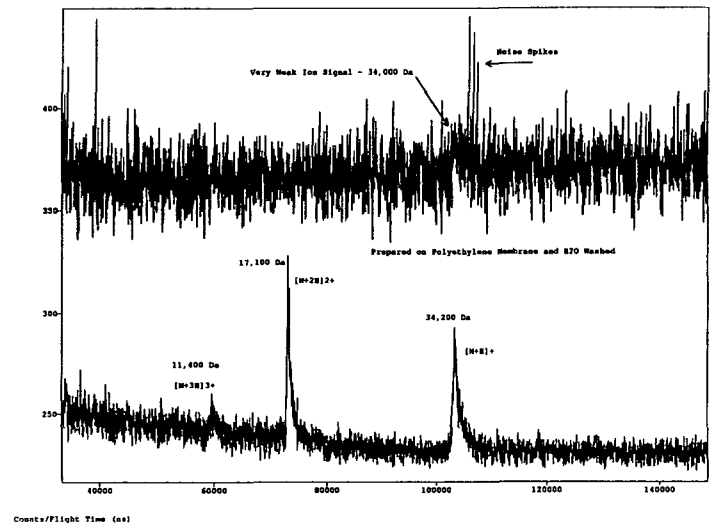

FIGURE 2: Oligonucleotide From Zitex Membrane

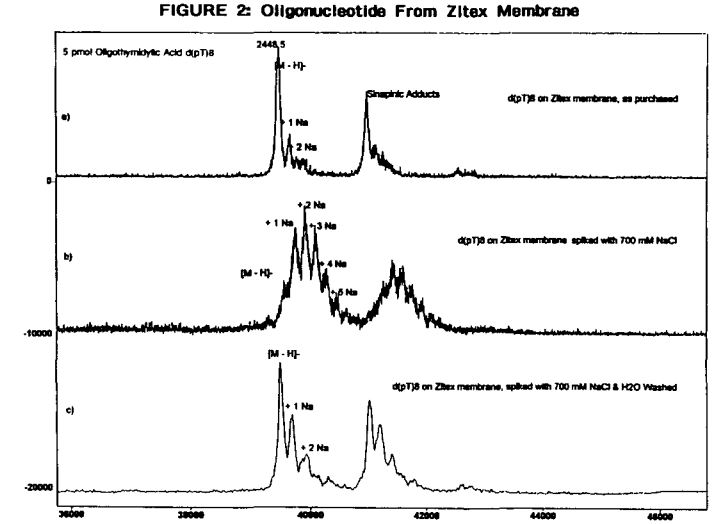

LDMS for Fast DNA Analysis and Disease Diagnosis*

C. H. Chen, N. I. Taranenko, S L. Allman, K. Tang,
K. J. Matteson, and L. Y. Ch'ang

Oak Ridge National Laboratory
P. O. Box 2008, Bldg 5500, Oak Ridge, Tennessee 37831-6378

Since the discovery of matrix-assisted laser desorption (MALD) for protein detection by Hillenkamp and his co-workers, matrix-assisted laser desorption mass spectrometry has been successfully used to detect various kinds of proteins. Proteins with molecular weights higher than 300,000 amu have been detected. However, when MALD was applied to DNA, the success was limited to small DNA segments Recently, by using a custom designed time-of-flight mass spectrometer with high ion energy combined with specific mixtures of organic compounds as matrices, we succeeded in detecting oligonucleotides up to 500 base pairs in size. Experimental results are shown in Fig. 1. In addition, double-stranded DNA using polymerase chain reaction (PCR) and DNA segments produced from enzyme digestions were also successfully detected DNA sequence is shown in Fig. 2. Experimental results are in Fig. 3. Since large DNA segments can be detected, with good sensitivity, the applications for disease diagnosis becomes feasible.

Cystic fibrosis is the most common autosomal recessive genetic disease of Caucasians. The gene responsible for cystic fibrosis is composed of 27 exons spanning 250,000 base pairs and encodes a protein by 1480 amino acids named the cystic fibrosis transmembrane conductance regulator (CFTR). In the North American population, about 70% of the cystic fibrosis carriers have a 3-base pair deletion in exon 10, resulting in the loss of a phenylalanine residue at codon 508 (ΔF508). We succeeded in using matrix-assisted laser desorption/ionization time-of-flight mass spectrometry to detect the codon 508 mutation in cystic fibrosis carriers and patients. Furthermore in a blind test, results from the normal and condon 508 mutation alleles in 30 clinical samples based on laser desorption mass spectrometry or the conventional gel electrophoresis of DNA were in total agreement.

In order to achieve MALDI for DNA sequencing, there are three critical requirements. They are (1) detection of large DNA segments, (2) detection sensitivity at a few femtomole region or better, and (3) resolution good enough to resolve DNA sizes of one nucleotide difference. Large DNA segments have been detected by MALDI with sensitivity at 100 femtomole. If the resolution can be improved, DNA sequencing by mass spectrometry should become feasible. Key factors to cause poor resolution of DNA segments by MALDI are (1) broad velocity spread, (2) chemical properties of matrices to cause fragmentation and adducts, (3) long ion production time and significant ionization volume, and (4) high laser fluence to cause ro-vibronic excited states that can lead to fragmentation. Major effort will be made to eliminate or reduce these factors.

*Research sponsored by the Office of Health and Environmental Research,
U. S Department of Energy under contract DE-AC05-84OR21400
with Martin Marietta Energy Systems, Inc.

43rd ASMS Conference on Mass Spectrometry and Allied Topics

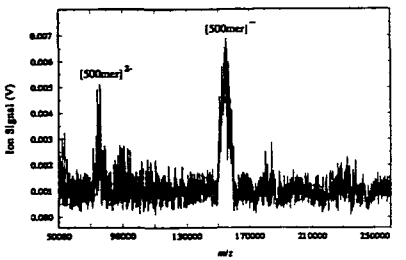

Figure 1. Negative ion spectrum of a 500-basepair DNA amplified from bacteriophage lambda genome. Total amount of DNA loaded was about 2.5 pmol. 2.4 μmol picolinic acid +0.3 μmol 3-HPA was used as a matrix. Laser wavelength was 266 nm and laser fluence was 200 mJ/cm². Both singly-charged and doubly-charged ions are observed.

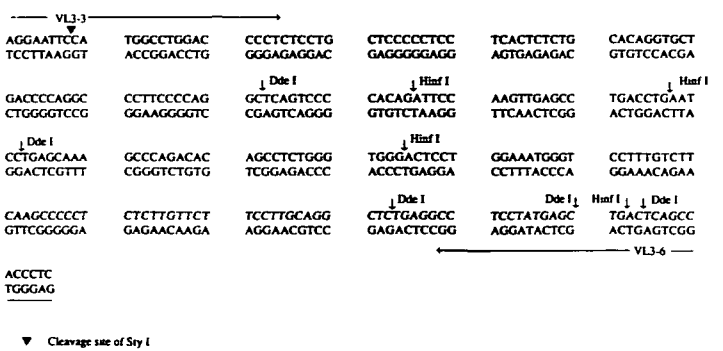

Figure 2. Sequence of DNA designated as pLB132. The sites for various enzymes to cut are also included.

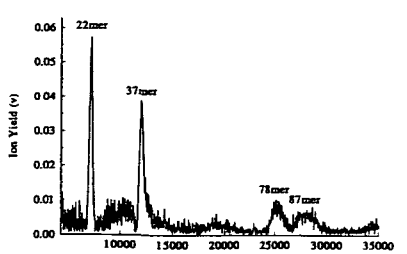

Figure 3. Negative-ion spectrum of DNA (LB132) cut with HinfI and StyI: 2 μL of DNA samples (~1-2 pmol of each fragment) were mixed with 2 μL of 3-hydroxypicolinic acid with a concentration of 0.3 M. The laser wavelength was 355 nm. The laser fluence was 70 mJ/cm². Data were obtained from the average of 20 laser shots.

MALDI MS for Rapid Screening of Genetic Polymorphisms Using Buccal Cell DNA

Yan-Hui Liu, Jian Bai, Xiaoli Liang, Mark G. Qian, and David M. Lubman, Department of Chemistry, The University of Michigan, Ann Arbor, MI 48109-1055

INTRODUCTION. Rapid and cost-effect methods for detection of DNA polymorphisms are the basis of genetic diagnosis and linkage study. The development of such methods will play an increasingly important role in the field of molecular pathology/genetics. MALDI MS employing nitrocellulose (NC) film substrate as an on-probe purification scheme is applied in this work for rapid and accurate detection of human genetic polymorphisms using DNA extracted from buccal cells.

EXPERIMENTAL. NC film substrate was produced by application of ~1 μL of NC solution (~16 mg/mL in acetone) onto a stainless steel probe tip and air-dried. DNA sample was then added onto the NC film and air-dried before the application of the matrix. MALDI MS was performed on a linear TOF with a 355 nm Nd:YAG laser for desorption/ionization. DNA extracted from buccal cells collected on a cytology brush has been employed as the primary source for PCR amplification. PCR, including multiplex PCR and PCR primer mutagenesis were used for amplification of genes of carbonic anhydrase (CA) II & III and of cystic fibrosis transmembrane conductance regulator(CFTR) on exons 6a and 12. For restriction-length polymorphism (RFLP) study, a restriction enzyme was added directly to the cycled PCR reaction to simplify the digestion process.

RESULTS AND DISCUSSION.

MALDI MS of PCR products based on DNA extracted from buccal cells. Although PCR products obtained from buccal cell DNA on cytology brushes are less than those from some other DNA sources (1), they are sufficient to support the MALDI MS analysis in this work. 1/4 to 1/3 of a PCR reaction product, which was around subpicomole level (~ 400 femtomole assuming 100% recovery after purification), was used for each MALDI MS analysis. Figure 1 shows the spectra of genes of CA II and CFTR on exon 6a and 12 under normal PCR conditions Products of multiplex PCR amplification and PCR primer mutagenesis were also detected by the MALDI MS method in this work

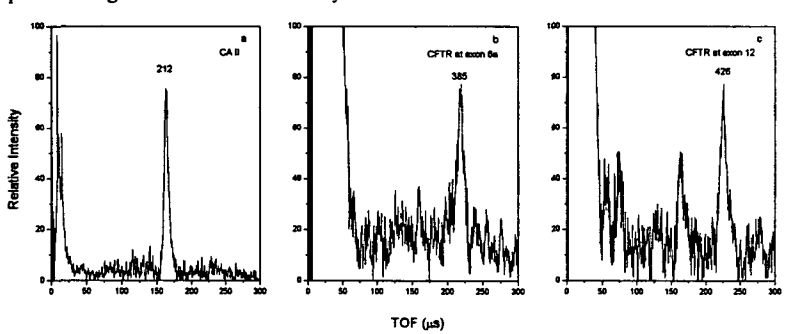

Figure 1. MALDI MS of PCR products of CA II (212 bp) and CFTR on exons 6a (385 bp) and 12 (426 bp)

Polymorphism study and disease diagnosis. RFLP of genes of CA II (Figure 2) and CFTR (Figure 3) on exon 6a and 12 was performed by direct digestion of PCR products with restriction enzymes followed by MALDI MS analysis.

MALDI MS of *BstN* I digest of CA II is shown in Figure 2. Individuals A and B are from homozygous population while individual C is form heterozygous population. Figure 3 shows an individual with both alleles normal for the CFTR genes on exon 6a and 12

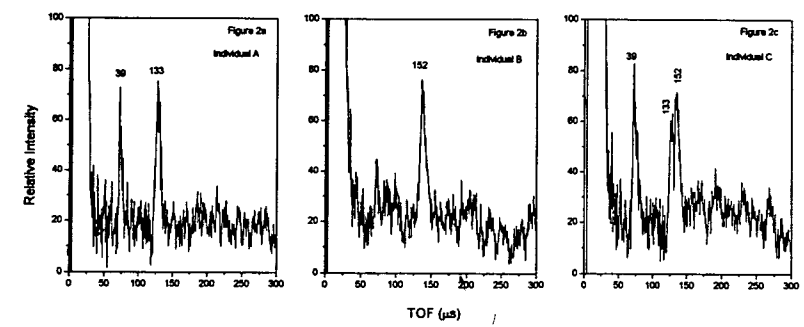

Figure 2 MALDI MS of *BstN* I digest of CA II gene

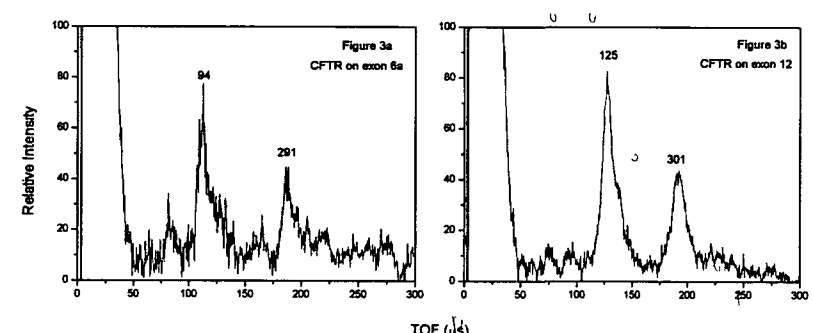

Figure 3 MALDI MS of (a) *Rsa* I digest of CFTR on exon 6a gene and (b) *Acc* I digest of CFTR on exon 12 gene.

CONCLUSION. MALDI MS with NC film substrate provides a fast, accurate and cost-effective method for detection of genetic polymorphisms following biological or clinical procedures. This method should also be readily extended to other areas which involve DNA mapping and screening

REFERENCE.

(1) Richards, B., Skoletsky, J., Shuber, A. P., Balfour, R., Stern, R. C , Dorkin, H., Parad, R. B., Witt, D., and Klinger, K. W. *Hum. Mol. Genet.* **1993**, *2*, 159-163.

Synthesis and MALDI Characterization of Electrophore-Labeled DNA

Gregory B. Hurst, Phillip F. Britt, and Michelle V. Buchanan, Chemical and Analytical Sciences Division, Oak Ridge National Laboratory, Oak Ridge, Tennessee 37831-6365

To speed up sequencing and other DNA analyses that yield information encoded as a "ladder" of DNA segments of different sizes, MALDI-MS detection methods are being developed [1-4] to replace currently-used gel electrophoresis methods. Enzymatic sequencing with MS detection offers the possibilities of increased speed [1] and improved accuracy [4] over gels.

One challenge in applying MALDI-MS to DNA detection is that the sensitivity falls off drastically with increasing molecular weight [1], although progress in detecting higher-molecular-weight DNA has been reported [2]. Our approach is to enhance ionization efficiency by derivatizing DNA sequencing primers with an ***electrophore*** to allow formation of negative ions by electron capture. An electrophore-labeled primer would be incorporated into each DNA segment produced in a sequencing reaction. Methods have been described for the preparation of DNA and RNA oligomers with covalently attached labels for fluorescent, chromophoric, or chemiluminescent detection [5,6]. The reaction is shown below for one of the electrophores evaluated in this study [7]. Isolated yields of electrophore-labeled M13(-40) primers (5'-GTTTTCCCAGTCACGAC-3') ranged from 11% to 74%.

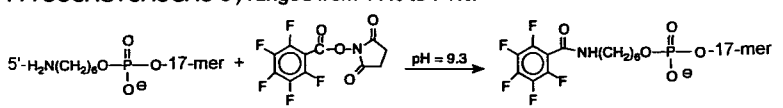

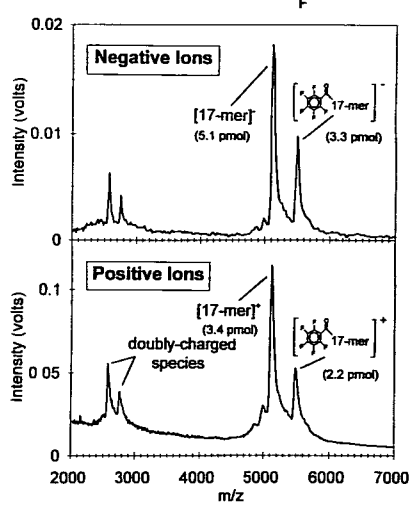

MALDI samples were prepared in the normal manner using a 3-hydroxypicolinic acid matrix, and analyzed using either a linear time-of-flight mass spectrometer [3] (Laser Photonics LN203C pulsed nitrogen laser) or an Extrel FTMS-2000 system [8] (3-Tesla magnet; Spectra Physics DCR-11 pulsed Nd:YAG laser, frequency-tripled line at 355 nm). The Figure shows positive- and negative-ion MALDI-TOF spectra of mixtures of the unlabeled and the pentafluorobenzoyl (PFB)-labeled M13(-40) primer. The measured m/z for the labeled primer is consistent with addition of one PFB group. Doubly-charged peaks appear in both positive and negative ion spectra for the labeled and unlabeled species. Similar results were obtained for the other electrophores studied (see Table 1.)

The electrophore-labeled primers retain the label during MALDI sample preparation and MALDI-TOF analysis, as demonstrated by spectra showing little or no fragmentation. As expected due to the longer time frame for the experiment [8], MALDI-FTMS of a PFB-labeled DNA tetramer (5'-ACTG-3') showed more extensive fragmentation to form sequence ions analogous to the unlabeled tetramer, although little loss of the label was observed. Because conditions for electron attachment by the labeled primer are not present in normal MALDI experiments, there is no enhancement in the signal due to the PFB-labeled primer in the Figure. We are modifying the MS measurement to improve conditions for electron capture by labeled DNA.

Compound	Calculated MW[a]	Observed m/z[b] (positve ions)	Observed m/z[b] (negative ions)
unlabeled 17-mer	5118.9	—	—
-17-mer	5476.9	5440±80	5464±35
-17-mer	5490.9	5493±18	5491±13
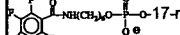 -17-mer	5503.0	5504	5497±30
-17-mer	5446.0	5441	5437±75

[a]Calculated monoisotopic mass for the neutral molecule, assuming that all phosphates are paired with protons.

[b]Uncertainties are 95% confidence interval based on the least squares fit to the mass calibration equation. For values with no uncertainty listed, only two calibration points (the singly- and doubly-charged 5'-OH primer) were used.

Table 1. Calculated molecular weights and observed m/z values for electrophore-derivatized M13(-40) primer.

1. Smith, L.M. *Science* **1993,** *262,* 530.
2. Tang, K.; Taranenko, N.I.; Allman, S.L.; Chang, L.Y ; Chen, C.H. *Rapid Commun. Mass Spectrom.* **1994,** *8,* 727.
3. Doktycz, M.J ; Hurst, G.B.; Habibi-Goudarzi, S.; McLuckey, S.A.; Tang, K.; Chen, C H.; Uziel, M.; Jacobson, K.B., Woychik, R.P.; Buchanan, M.V. *Anal. Biochem.*, submitted.
4. Schieltz, D.M.; Williams, P. 42nd ASMS Conference on Mass Spectrometry and Allied Topics, Chicago, Ill., May 29-June 3, 1994, p. 141.
5. Eckstein, F. (ed.) Oligonucleotides and Analogues, Oxford Univ. Press, New York, 1991
6. (a) Telser, J.; Cruickshank, K.A.; Morrison, L.E.; Netzel, R.L.; Chan, C.-K. *J. Am. Chem. Soc.* **1989,** *111,* 7226. (b) Smith, L.M.; Fung, S.; Hunkapiller, M.W., Hunkapiller, T.J.; Hood, L.E. *Nucleic Acids Res.* **1985**, *13*, 2399.
7 Britt, P.F ; Hurst, G.B.; Buchanan, M.V *Nucleic Acids Res.*, submitted.
8. Stemmler, E.A.; Hettich, R.L.; Hurst, G.B.; Buchanan, M.V. *Rapid Commun. Mass Spectrom.* **1993**, *7*, 828.

We thank Robert Foote (ORNL Biology Division) for primer synthesis, and Fred Sloop, Larry Waters, Robert Hettich (ORNL Chemical and Analytical Sciences Division) and Elizabeth Stemmler (Bowdoin College) for helpful discussions. Research sponsored by the National Institutes of Health, National Center for Human Genome Research, Grant No. 1 R55 HG/OD00819-01A1, under Interagency Agreement 1884-F026-A1 with the U.S. Department of Energy under Contract DE-AC05-84OR21400 with Martin Marietta Energy Systems, Inc.

Use of a Polymeric Substrate in MALDI MS for DNA Mapping and Screening

Yan-Hui Liu, Jian Bai, Xiaoli Liang, and David M. Lubman, Department of Chemistry, The University of Michigan, Ann Arbor, MI 48109-1055

INTRODUCTION. One major issue concerning MALDI MS analysis of DNA is the presence of impurities in biological sample and the inhomogeneous desorption of all fragments in a mixture. In this work we present the use of a nitrocellulose (NC) film as a substrate which allows for effective on-probe elimination of the interfering effects of salts, buffers and other contaminants. This method has been successfully applied in the detection of DNA mixtures for DNA mapping and screening.

EXPERIMENTAL. NC film was produced by application of ~1 μL of NC solution (10 ~ 32 mg/mL in acetone) onto a stainless steel probe tip and air-dried. A thin and homogeneous layer of NC film is essential for the successful detection of DNA mixtures in this work. 2 μL of DNA sample was added to the hydrophobic surface followed by air-drying. 4 μL of matrix was then applied to the sample spot and air-dried before MALDI MS analysis. The matrix used in this work is the saturated solution of the mixture of 3-HPA and PA with molar ratio of 4 to 1 in a 36% acetonitrile in water. A linear TOF with postacceleration and a 355 nm Nd.YAG laser were used for MALDI MS

RESULTS AND DISCUSSION. The use of the NC film substrate greatly enhances the ion yields of DNA fragments, the reproducibility of the signal and the signal persistence. This may be explained by the fact that NC binds alkali metal ions through electrostatic interactions (1) and some other buffer impurities by hydrophobic adsorption, so they are partially excluded from the matrix/analyte during crystallization. It is also possible that NC acts as a crystallization moderator. With the use of a NC substrate a much more homogeneous crystallization of the matrix/sample was obtained compared with the use of a stainless steel probe tip.

Analysis of enzyme digests of ds-DNA. *Msp* I digests of ds-DNA pBR322 with fragments ranging from 9 to 622 bp were detected with NC film substrate (Figure 1a), while only fragments < 100 bp can be detected by using stainless steel probe. A new mass calibration scheme was established that linear regression of the number of base pairs of the fragments and the corresponding TOF squared measured from mass spectrum was performed (Figure 1b).

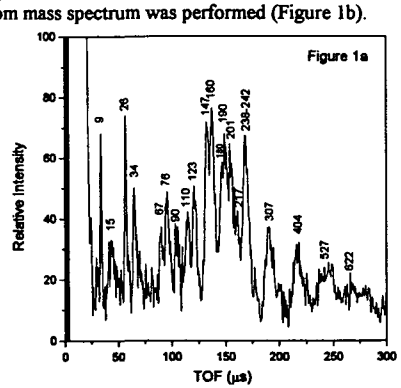

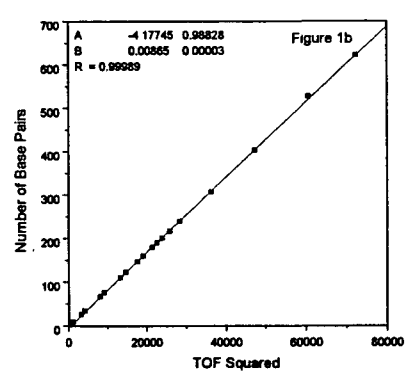

Polymorphism study. Variable number of tandem repeats (VNTR) polymorphism study of canine von Willeband's factor gene was performed by screening the PCR products directly by MALDI MS with NC film substrate. Figure 2a was from Siberian huskey which is homozygous with 9 repeats of AGGAAT on both alleles. Figure 2b was from a mixed breed dog which is heterozygous with 9 and 14 repeats of AGGAAT on each allele. Homogeneous and reproducible signal was obtained with the use of NC film substrate in MALDI MS analysis in this study.

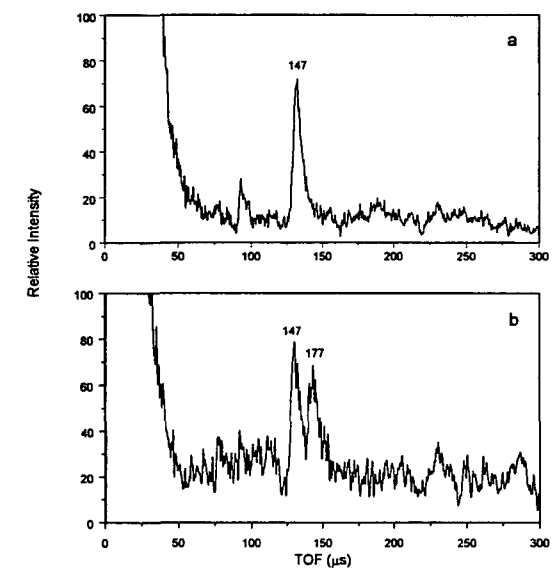

Figure 2. MALDI MS of PCR products of genes of (a) Siberian huskey and (b) mixed breed dog

CONCLUSION. The NC film substrate is demonstrated herein to enhance MALDI MS performance for DNA mixture analysis by effective elimination of impurities and by creation of a homogeneous crystallization of matrix/analytes. Desorption of all fragments in DNA mixtures were obtained by incorporating NC film substrate into MALDI process.

REFERENCE.

(1) Preston, L. M., Murray, K. K., Russell, D. H., *Biol. Mass Spectrom.* **1993**, 22, 544-550.

THE EFFECT OF IMPURITIES ON MALDI TOF MASS SPECTRA OF SINGLE-STRANDED OLIGODEOXYNUCLEOTIDES[1]

Thomas A. Shaler, Juanita N. Wickham, Kuang Jen Wu, Kristin A. Sannes, Joanna M. Hunter and Christopher H. Becker
Molecular Physics Laboratory, SRI International, Menlo Park, CA 94025

The effect of impurities on the matrix-assisted laser-desorption/ionization time-of-flight mass spectra of single-stranded DNA has been studied using the matrix 3-hydroxypicolinic acid and 355 nm pulsed light. The tolerance limits for impurities indicate that some preliminary purification of DNA is necessary to obtain good spectra. In addition, for some inpurities, the tolerance limits for DNA analysis differs significantly from the tolerance limits for protein analysis.[2]

By mixing the DNA oligomers with different concentrations of impurities and recording mass spectra, the tolerance limits are set for a given impurity in a sample. The tolerance limit for sodium chloride, sodium acetate, sodium fluoride, sodium dodecylsulfate (SDS), potassium chloride and manganese(II) chloride were found to be approximately 10 mM while the tolerance limit for magnesium (II) salts was found to be approximately 0.1mM (Table 1). In contrast, the tolerance limits of the organic compounds cyclohexane-N, N, N', N'-tetraacetic acid monohydrate (CDTA), ethylenediaminetetraacetic acid (EDTA) when present as its ammonium salt, dithiothreitol (DTT), glycerol, Tris(hydroxymethyl)aminomethane (Tris) and urea were 250-500 mM (Table 1). Given the significant degree of sample-to-sample variation, we estimate that these values are accurate to within about a factor of two.

Type I impurities (metal salts) degrade the signal by forming adducts with the DNA (Figure 1). Adduct formation causes a mass shift as well as a decrease in mass resolution. The simple *in situ* method of removing metal ions by adding chelating agents (i.e. EDTA and CDTA) did not improve the spectra significantly. Type II impurities (organic compounds) degrade the signal by disrupting the crystallization of the matrix and/or decreasing signal stability (Figure 2). For type I impurities, increasing the size of the DNA decreases the tolerance limit because the number of sites for adduct formation increases. For type II impurities, increasing the size of the DNA does not change the tolerance limit. For both type I and II impurities, changing the ion polarity does not change the tolerance limit.

1) submitted to Anal. Chem.

2) Mock, K. K.; Sutton, C. W.; Keane, A.; Cottrell, J. S.; Techniques in Protein Chemistry IV, Angeletti, R. H.; Academic Press, Inc., San Diego, CA:1993.

Table 1. Tolerance limits below which adequate mass spectra could be obtained for a DNA 21-mer in the positive ion mode by MALDI-TOF analysis.

Impurity	Type	Tolerance Limit
Na salts	I	20 mM
KCl	I	10 mM
Mg (II) salts	I	0.1 mM
$MnCl_2$	I	20 mM
NH_4OAc	II	100 mM
NH_4EDTA	II	250 mM
CDTA	II	500 mM
Dithiothreitol	II	500 mM
Glycerol	II	250 mM
Tris	II	500 mM
Urea	II	500 mM

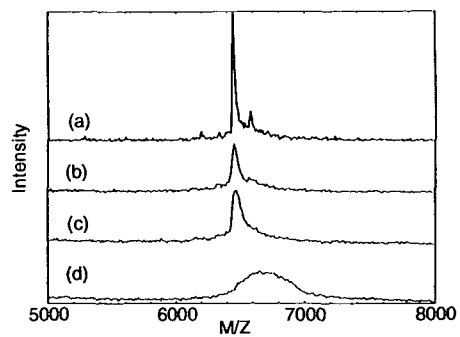

Figure 1. Positive-ion MALDI TOF mass spectrum of 21-mer ssDNA showing the effect of added NaCl: (a) control sample, (b) 5 mM, (c) 25 mM (tolerance limit), and (d) 250 mM.

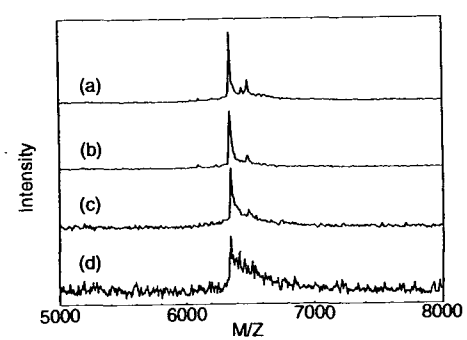

Figure 2. Positive-ion MALDI TOF mass spectrum of 21-mer ssDNA showing the effect of added DTT: (a) control sample, (b) 5 mM, (c) 250 mM (tolerance limit), and (d) 500 mM.

ANALYSIS OF ENZYMATIC DNA SEQUENCING REACTIONS BY MATRIX-ASSISTED LASER-DESORPTION TIME OF FLIGHT MASS SPECTROMETRY

Thomas A. Shaler, Juanita N. Wickham, Kuang Jen Wu, and Christopher H. Becker
Molecular Physics Laboratory, SRI International, Menlo Park, CA 94025

The products from base-specific, chain-termination DNA sequencing reactions, catalyzed by the modified T7 DNA polymerase Sequenase Version 2.0 (USB), have been analyzed by the technique of matrix-assisted laser-desorption/ionization (MALDI) time of flight mass spectrometry. Preliminary experiments were performed to determine detection limits for a synthetic mixture of mixed-base single-stranded DNA which contained a 14-mer, a 21-mer, and a 41-mer. Acceptable spectra, showing peaks for each component, were obtainable for samples that contained as little as 5 fmol per component. A spectrum obtained from such a mixture is shown in Figure 1.

In separate experiments, we had found that a synthetic 40-mer could easily be resolved from a 41-mer under conditions of continuous extraction. Initial sequencing reactions were therefore carried out on 2-pmol amounts of a short synthetic template that was 45 nucleotides in length, employing a 12-mer as the primer strand. Figure 2 shows spectra obtained from the four different dideoxynucleotide-terminated sequencing reactions. Nearly unambiguous sequence information can be read from the spectra out to 19 bases past the primer. A single false-stop in the ddT reaction at the position of the 14-mer provides the only source of ambiguity, which is possibly due to the relatively short length of the primer. Further improvements and optimization should make sequencing of templates in the 50- to 60-mer range possible.

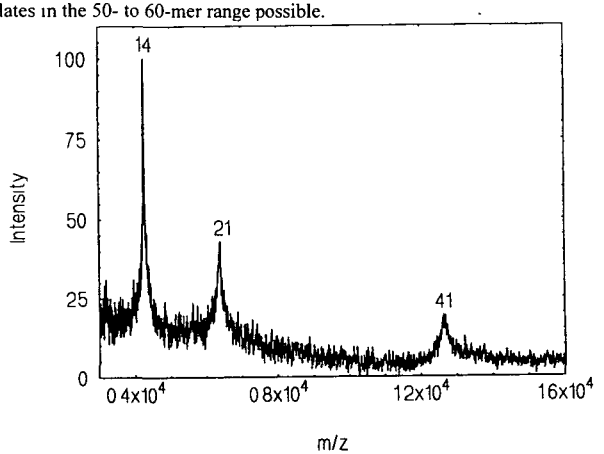

Figure 1. MALDI mass spectrum of a synthetic mixture of 14-, 21-, and 41-mer DNA containing 5 fmol each. The positive ion spectrum is the sum of 100 laser shots from 3-hydroxypicolinic acid matrix.

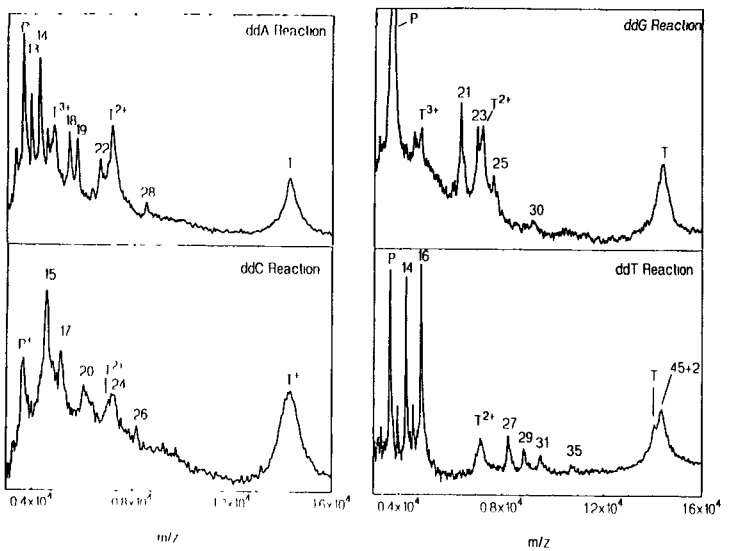

Figure 2. Mass spectrum of four dideoxy sequencing-reactions A,C,G, and T of a template (T) 45-mer with a 12-mer primer (P).

Acknowledgements. This work has been supported by the NIH National Center for Human Genome Research, and by NIST ATP program.

PROTOCOLS FOR IMPROVED LASER EJECTION/IONIZATION TOF-MS OF OLIGONUCLEOTIDES

Jannavi R. Srinivasan, Robert J. Levis
Department of Chemistry, Wayne State University
Detroit, MI-48202

Gas phase studies of biological molecules using laser mass spectrometry have provided new dimensions to the study of large molecules such as oligonucleotides. By replacing the gel electrophoresis step with mass spectrometry in the current sequencing methodology, enhanced sequencing rates may be obtained. For mass spectrometry to be a suitable substitute certain key factors such as the resolving power of the technique and the amount of material required for obtaining sequence information must be improved. This report deals with our efforts to improve laser ejection/ionization for oligonucleotide analysis.

The experiments are performed in a linear time of flight mass spectrometer as shown in Fig. 1 and a similar apparatus has been described in detail elsewhere(1). Oligonucleotide samples are prepared for laser analysis by premixing them with a UV absorbing matrix, 3-hydroxypicolinic acid(2). The substrates for laser ejection are 12mm quartz coverslips used in place of conventional metal substrates. The surface of the coverslips are chemically modified to provide a hydrophobic surface. The oligonucleotide/matrix sample is subject to a thermal processing step after being deposited on to the substrate. The resulting coverslip is mounted on one end of the sample rod that forms an integral part of the linear time of flight mass spectrometer. Laser ejection/ionization is performed by impinging a pulse of 355nm photons from a Spectra Physics GCR-11 Nd:YAG laser. The tripled output of the laser has a power density of 40mJ/cm^2 (unfocused, 2.7 ns) measured just before it enters the chamber. The ions formed during this event, both matrix and oligonucleotide, are extracted towards the detector by applying a potential of 5kV-8kV on the sample rod and maintaining a second grid (1.25 cm from sample) at ground. The positive ions are extracted into the field free time of flight region and detected by a hybrid detector placed 1.25m from the region of extraction. The current from the ions striking the detector is amplified and recorded by a LeCroy digital oscilloscope. The resulting data is then transferred to a 486 PC via GPIB.

The results reported here include investigations of the laser ejection process from glass substrates and improvements to the substrate surface to enhance key factors such as signal to noise ratios and detection limits. A unique detection system was tested for mixed base oligonucleotides of lengths greater than 50 bases. The sensitivity of the technique was determined for different oligonucleotide lengths. Fig. 2 is the laser ejection/ionization time of flight mass spectra recorded for a series of mixed base 32mer samples that were mounted on chemically modified glass and subjected

to thermal treatment prior to laser ejection. A detection level of 10 femtomol was achieved for this sample. This investigation was extended to the study of double stranded DNA that were obtained from a polymerase chain reaction. Fig. 3 is the laser ejection/ionization time of flight mass spectra of a 350mer (PCR product) comparing the effect of substrate treatment and detection system on the final data. The amount of DNA loaded on the substrate was 600 femtomol and 10 femtomol of the total sample was used to obtain the spectra shown here.

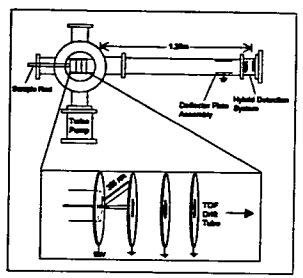

Fig. 1. Laser ejection/ionizaiton time of flight mass spectrometer.

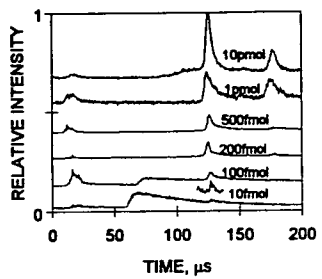

Fig. 2. Laser ejection/ionization TOFMS of mixed base 32mer.

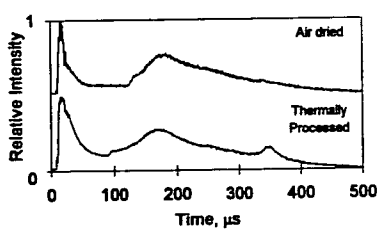

Fig. 3. Laser ejection/ionization TOFMS of ds 350mer (PCR).

References:

1. Schilke, D.and Levis, R. J., Rev. Sci. Inst., 65, 1903, (1994).
2. Wu, K. J., Steding, A., Becker, C. H., Rapid Comm. Mass Spectrom., 7, 142, (1993).

NON-COVALENT PROTEIN—OLIGONUCLEOTIDE INTERACTIONS MONITORED BY MATRIX-ASSISTED LASER DESORPTION IONIZATION MASS SPECTROMETRY

Xiaodong Tang[1], John H. Callahan[2], Ping Zhou[3], Joe Hayes[3], Akos Vertes[1]*
[1]Department of Chemistry, The George Washington University, Washington D.C. 20052
[2]Chemistry Division, Naval Research Laboratory, Washington D. C. 20375
[3]Cruachem, Inc., Dulles, VA 20166

The rapid development of new soft ionization techniques, such as matrix-assisted laser desorption ionization (MALDI), has made it possible to study the non-covalent protein oligonucleotide interactions by mass spectrometry. In this study our objective was to identify the amino acid and nucleotide residues involved in the interactions, and the matrix effects on the observation of protein-oligonucleotide complexes. The experiments were carried out on a linear time-of-flight mass spectrometer equipped with a nitrogen laser in positive ion mode.

Strong correlation was found between the presence of basic residues in proteins and the tendency to participate in complexation. Also, complex formation resulted in substantial improvement in mass resolution for DNA analysis. An example is shown in Figure 1, where MALDI-MS of $pd(T)_{10}$ and Arg-Lys—$pd(T)_{10}$ mixture are compared. When $pd(T)_{10}$ was measured alone, its molecular ion peak was broadened by the presence of sodium and potassium adducts (Fig. 1a). In the Arg-Lys—$pd(T)_{10}$ mixture, a large variety of complexes were produced containing up to six peptide units and four DNA units (Fig. 1b). The abundant $(1:1)^+$ complex was completely free from alkali adducts, leading to a trifold resolution improvement. In addition, $pd(T)_{10}$ formed complexes with other medium size proteins, including insulin, ubiquitin, lysozyme, ribonuclease A, and cytochrome C. It was demonstrated that Arg was distinguished from the other basic residues (Lys and His) by stronger interactions.

Further investigations proved the essential role of thymidylic acid in the DNA sequence for complex formation. We saw strong complex formation for the Arg-Lys—$pd(T)_{10}$ mixture (Figure 1b), whereas little or no interaction was observed between Arg-Lys and $pd(A)_9$, $pd(C)_{10}$, or $pd(G)_{10}$ homologues (Figure 2a, 2b, 2c). Under the same conditions, complexation occurred for Arg-Lys and a mixed DNA sequence, pd(AGCTCAGCTT) (Figure 2d). The interactions turned out to be specific to the properties of the base components and dependent on the pH value. In pH=1.7 DHB matrix solution, thymine stays in neutral form because an added positive charge can not be delocalized. The negative charge on phosphate group leads to strong ionic interactions with protonated sites on peptide molecules. Despite of the higher rigidity and spatial hinderance, extended chains of DNA can undergo similar ion pair formation with bulky proteins. On the other hand, positive charge attachment on adenine, guanine and cytosine is facilitated by delocalization. Therefore zwitterionic form is dominant in $pd(A)_n$, $pd(C)_n$, and $pd(G)_n$ systems, intermolecular ion pair formation is not feasible.

It was also found that the detection of complexes was strongly matrix dependent. The tested matrices included: 2,5-dihydroxybenzoic acid (DHB), sinapinic acid (SA), 3-hydroxypicolinic acid (3-HPA) and α-cyano-4-hydroxycinnamic acid (CHCA). The effects are shown in Figure 3 for lysozyme and $pd(T)_{10}$ mixture. In DHB matrix (Figure 3a), complex ions containing up to five $pd(T)_{10}$ and one lysozyme molecules were observed along with their doubly charged ions. In CHCA matrix, the mass spectrum was dominated by strong singly, doubly, and triply charged lysozyme ions, — no complex formation was found. Based on protein—oligonucleotide complex formation experiments the matrices can be divided into two groups: complex stabilizing (e.g., DHB and 3-HPA) and complex suppressing (e.g., CHCA and SA) matrices.

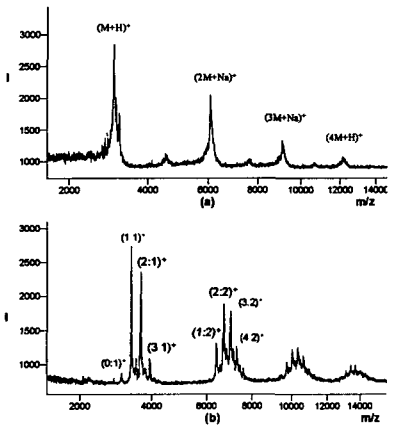

Figure 1.

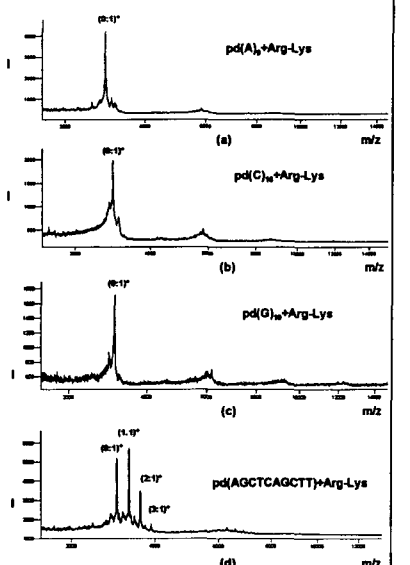

Figure 2.

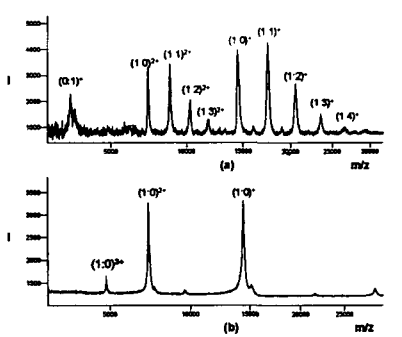

Figure 3.

Figure 1. MALDI mass spectra of (a) pure $pd(T)_{10}$, and (b) Arg-Lys/$pd(T)_{10}$ mixture in DHB matrix
Figure 2. Mass spectra of mixtures of Arg-Lys and (a) $pd(A)_9$, (b) $pd(C)_{10}$, (c) $pd(G)_{10}$ and (d) pd(AGCTCAGCTT) in DHB matrix
Figure 3. Mass spectra of lysozyme and $pd(T)_{10}$ mixture in (a) DHB and (b) CHCA matrix

MALDI POST SOURCE DECAY OF OLIGONUCLEOTIDES

L.J. Deterding and K.B. Tomer

Laboratory of Molecular Biophysics
National Institute of Environmental Health Sciences
Research Triangle Park, NC 27709

Matrix-assisted laser desorption ionization (MALDI) mass spectrometry is rapidly becoming an integral part of the characterization of biological compounds. This technique has several advantages, including, detection of molecular species in excess of 100,000 Da, sub-picomole detection limits, and the use of a reflectron for metastable ion analysis. It has been demonstrated that, in MALDI, a large fraction of the analyte ions undergo fragmentation after full acceleration. This process is called post source decay (PSD) (1,2). The activation energy for the PSD reactions arises from collisions of the analyte ion with matrix molecules during the ion acceleration process and collisions of the analyte ions with residual gas molecules in the drift path. In a single stage TOF instrument, these fragment ions have the same velocity as their parents. This yields increased sensitivity but the structural information contained in the PSD ions is lost. In a reflectron-based TOF instrument, the ions undergo deceleration in the mirror to the point of being repelled back into the flight tube. The deceleration/reacceleration is mass dependent. Thus, the PSD ions will reach the detector at a time different from the parent ion. In this manner, the structural information contained in the PSD ions can be obtained. The sequencing of peptides has been demonstrated with the use of MALDI-PSD (1,2). Application of this technique to nucleic acids could be useful in DNA sequencing analyses. Structural characterization of normal and modified oligonucleotides is important not only for DNA sequencing but also for the determination of DNA modifications induced by toxic compounds. The applicability of mass spectral analyses to the structural characterization of oligonucleotides has been previously been limited in many cases by poor sensitivities and lack of complete structural information (3,4). In this paper we report the PSD results of some synthetic oligonucleotides and of the enzymatic fragments of a digest of an oligonucleotide and a protein. For the enzymatic digestions, the timed ion selector device was used. This device allows only ions of a selected mass to pass to the detector. This is beneficial when matrix ions or additional sample component ions can cause interferences in the PSD/MS/MS acquisitions.

The PSD/MS/MS data from the oligonucleotides show that any of the cleavages along the phosphodiester chain are possible. Ions arising from cleavages at every nucleic acid residue were observed in all cases. Prominent ions due to loss of a base from the backbone cleavage ions, e.g a3-G in the PSD/MS/MS spectrum of the $(M-H)^-$ ion of pd(GTTAAC) (Figure 1.), are also observed. Similar data were acquired for the digest fragments from the 5' to 3' degradation of d(TCTAGA) using phosphodiesterase II from calf spleen.

The PSD/MS/MS data from glucagon tryptic fragments show that the most common cleavage ions observed are the *a* and *b* ions, which result from the retention of the charge by the N-terminus, and *y* ions, which result from retention of the charge by the C-terminus. In addition, abundant ions resulting from the loss of 17 from the *a*, *b*, and *y* fragments are observed. Figure 2 shows the PSD/MS/MS spectrum of the (M+H)+ ion of T3,4 of glucagon. These data show that the sequence of the digest fragment can be determined using this technique.

(1) Kaufmann, R., et al. *Rapid Commun. Mass Spectrom.* **1993**, 7, 902.
(2) Kaufmann, R., et al. *Int. J. Mass Spectrom. Ion Proc.* **1994**, 131, 355.
(3) Cerny, R.L., et al. *Anal. Biochem.* **1987**, 165, 175.
(4) McLuckey, S.A., et al. *J. Am. Soc. Mass Spectrom.* **1992**, 3, 60.

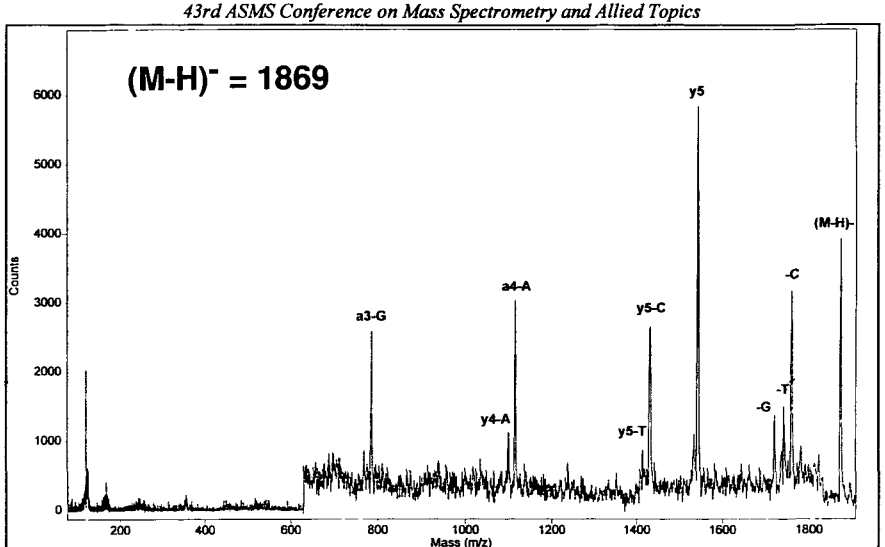

Figure 1. PSD/MS/MS spectrum of the $(M-H)^-$ ion of pd(GTTAAC).

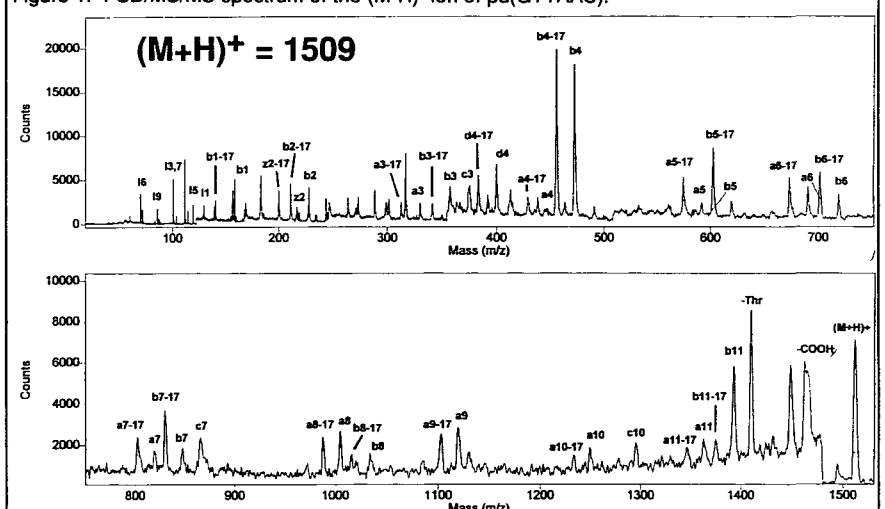

Figure 2. PSD/MS/MS spectrum of the (M+H)+ ion of tryptic fragment 3,4 of glucagon.

New Instrumental Approaches to TOF Mass Spectrometry of DNA

David Dogruel, Randall W. Nelson, Peter Williams
Department of Chemistry and Biochemistry
Arizona State University, Tempe, AZ 85287-1604

Introduction

The matrix-assisted laser desorption/ionization (MALDI) process has proven capable of producing intact vapor phase polypeptide molecules with molecular weights up to 1 MDa. Most proteins are routinely analyzed using MALDI/TOF mass spectrometry, however, nucleic acids (DNA and RNA), have presented more of a challenge; spectra obtained during MALDI/TOF analysis of DNA do not exhibit the quality, sensitivity, or reproducibility of spectra obtained from proteins. This suggests that the matrix behaves differently in the two cases, i.e. fails in either desorption or ionization, or both, during nucleic acid analysis.

Methods capable of separating the duality of the matrices (desorption and ionization) are needed to gain a better understanding of the poor performances observed during nucleic acid analysis. Analytes which ionize via alternate channels (other than proton exchange with the matrix) are desired. Synthetic polymers which preferentially ionize via fortuitous cationization are such a class of analyte, making it possible to qualify the desorption event independent of ionization. Further, it is possible to gain greater insight into the limitations of the matrices (with respect to ionization) by incorporating polypeptide analytes into the analysis.

We have chosen for study the polar polymer, poly (methyl methacrylate) (PMMA) on the basis of its ability to provide unique neat and matrix-assisted mass spectra. By altering the pH and ionic composition of the matrix, we have been able to determine the practical limits for both desorption and ionization

Experimental

Sample Preparation

Poly (methyl methacrylate) (PMMA4K), nominal MW= 4100, was obtained from American Polymer Standards Corporation and dissolved in methanol to 200 pmol/uL. The protein α-cobratoxin (MW 7822) was dissolved in 0.1% aqueous trifluoracetic acid to 200 pmol/uL.

Titration of Matrix

A sample of .4133 g of 2,5-dihydroxybenzoic acid (DHB) in 25 mL of deionized water was titrated with a 0.01 M solution of sodium hydroxide, the pH being monitored with a glass electrode/pH meter. For the MALDI experiments, DHB in methanol was titrated with KOH, and aliquots of 200 uL were removed at intervals of approximately every 1 pH unit

Mass Spectrometry

Mass spectrometry was performed on a linear time-of-flight mass spectrometer equipped with a Nd:YAG laser, using the third harmonic output (355 nm). Positive ions were accelerated to 30 kV using a two-stage source. An electrostatic ion guide was used over the nominal 1.5 m flight path. Detection was accomplished with a hybrid, microchannel-plate/discrete-dynode multiplier. Ion signal was monitored on a sampling oscilloscope and signal averaged with a 500 MS/s transient recorder. Data were transferred to an IBM compatible 486 computer and analyzed with PC compatible software utilizing external calibration.

Results

The generation of qualitatively different polymer distributions from neat and matrix-assisted analysis makes PMMA ideal for evaluating the ability of a matrix to desorb large molecules.

Use of the proteins in combination with PMMA allows the total functionality of the matrix to be investigated. A series of spectra are shown in **Fig. 1** of a sample containing PMMA and the protein α-cobratoxin. Several features are important to note:

1) The matrix functions as a desorption and ionization vehicle for the protein only in the low pH buffer region, with the best functionality occurring at the intrinsic pH of the matrix and a progressive loss in the ability to protonate as the pH increases.
2) In the region where the pH is changing most rapidly (no buffer capacity), the matrix suppresses all analyte signal for both the polymer and the protein.
3) At a basic pH the matrix loses the ability to desorb (indicated by the neat PMMA distribution).

The ionization of PMMA was also studied as a function of the available cation by addition of alkali metal salts. **Fig. 2** shows the distribution centroid of cesiated PMMA being ~ 750 Da higher (~20%) than that observed for the sodiated; beyond that expected from the difference in mass between the two cations. This indicates a need for further understanding of the cationization processes.

Conclusions

The most important aspects of MALDI matrices are the ability to desorb and ionize the analyte. It has been shown that the matrix functions best as a proton donor at its intrinsic pH and progressively loses the ability to desorb with increasing pH.

The use of polymers, like PMMA, which serve as qualifiers for matrix-assisted laser desorption and ionization can lead to a better understanding of the roles of the two processes involved in DNA and biopolymer analysis. Also, the dependence of the PMMA mass distribution on the available cation has implications in the choice of substrate and matrix composition for polymer analysis.

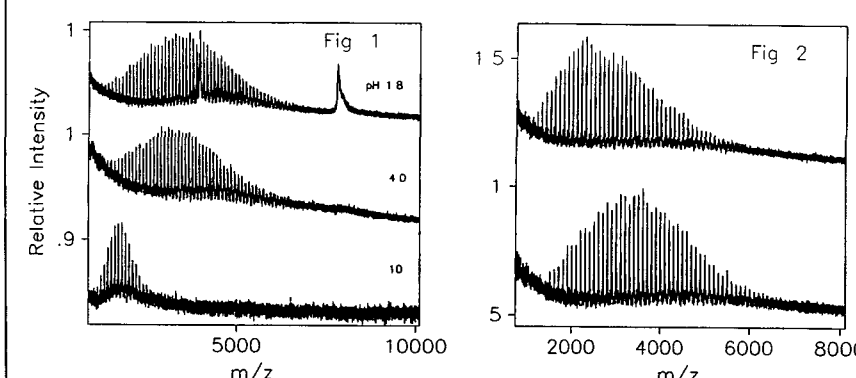

Figure 1: MALDI/TOF mass spectra of a mixture of PMMA and α-cobratoxin taken at different pH values
At the intrinsic matrix pH (1.8), strong protein signal is observed. As the pH increases, the ability of the matrix to ionize the protein via proton exchange is lost. At pH 10, the polymer distribution has reverted to neat desorption

Figure 2: PMMA molecular weight distributions obtained in the presence of different metal cations Top-Na^+ cationized PMMA, Bottom-Cs^+ cationized PMMA. The matrix DHB was used at its intrinsic pH (1.8) and the metal salts were doped into solution.

Progress in DNA Sequencing and Fundamental Studies Using MALDI-TOFMS

Chau-Wen Chou, Randall W. Nelson and Peter Williams
Department of Chemistry, Arizona State University, Tempe, AZ 85287-1604

A. The affinity cleaning-up of DNA sequencing fragments

MALDI has shown promise for a fast and accurate readout of DNA sequencing fragments. However, it seems probable that the final solution from the Sanger dideoxy method will be too much complex to be analyzed. Excess nucleotides, polymerase, buffers and other components may interfere with ablation or ionization. The impurities have to be removed rapidly and specifically.

The hybridization between two complementary strands is the most specific affinity force for DNA. Two experiments have been tried to select and separate the DNA fragments by using this feature:

(a). Agarose beads experiment. The complementary strand of primer is immobilized on the agarose beads. The fragments in the Sanger reaction solutions hybridize with the immobilized strand and can be separated by filtration.

(b). Biotin-streptavidin paramagnetic beads experiment. The complementary strand of the primer is labeled by biotin. It hybridizes with the fragments in the Sanger reaction solutions, and then is mixed with streptavidin paramagnetic beads. The strong affinity between biotin and streptavidin is used to select the biotinylated strand and then the fragments can be separated along with biotinylated strands.

The results showed that the hybridization yields between the DNA fragments and immobilized complementary strands on agarose beads were only about ~ 30%. It can be explained that the hybridization between solid and solution phase is not very efficient. On the other hand, the results from the biotin-streptavidin paramagnetic beads experiment were more encouraging. Fig.1 shows the spectra of DNA fragments (up to 52-mer) were captured from the solutions with possible impurities in the Sanger sequencing reaction. ~ 80% of DNA fragments can hybridize with biotinylated strands. After three washes and separations, only ~ 35% fragments were recovered. It indicates that the better protocols have to be developed to minimize the loss in the experiments.

B. The initial velocity measurements

The mechanism(s) of MALDI is (are) still not clear. Is it a thermal process or a photochemical process? The initial velocities of ablated matrix species and analytes may provide useful information on mechanisms. Here, the influence of laser wavelengths on the initial velocities of matrix have been studied carefully.

A modified Chait/Beavis [1] device was used to prevent field penetration derived the ground plate. Ions fly cross a 7.5 mm drift space mostly by their initial velocities. Small fields were applied to increase the signal intensity. We determined initial velocities and kinetic energies by comparing the flight time differences with flight time difference calculated for a range of initial energies of initial kinetic energies using the SIMION ion optics program.

Our results shows that the initial velocities of matrix ions are not affected by the small fields but vary due to the local conditions of sample spots. The results of anthranilic acid and co-matrix of nicotinic acid and anthranilic acid desorbed at 266 and 355 nm shows that initial velocities increase as the samples were desorbed by the photons with higher energy (Table 1). In addition, the laser desorption/ionization products of sinapinic acid are different at 266 and 355 nm. The wavelength discrimination is the characteristic of photochemical processes. It indicates that the photochemical processes play may more important roles than thermal processes in matrix-assisted laser desorption.

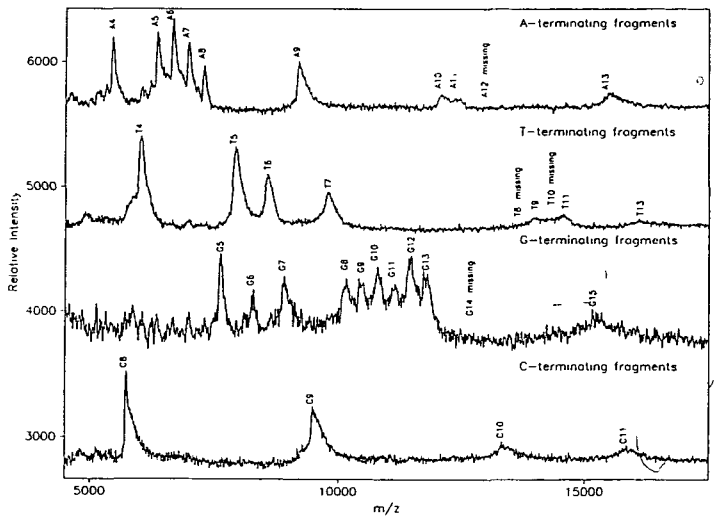

Table II Comparisons of initial energies of three different matrices at 266 and 355 nm

Anthranilic acid	
At 266 nm	At 355 nm
Average: ~1.9 eV ~ 1540 m/s	Average ~ 1.3 eV ~ 1370 m/s
Nicotinic acid and Anthranilic acid (1:1) mixture	
At 266 nm	At 355 nm
Average: ~ 1.3 eV ~ 1350 m/s	Average: ~ 0.7 eV ~ 970 m/s

1. Beavis, R. C.; Chait, B. T. *Chem. Phys. Lett.*, **1992**, *181*, 479.

MALDI of Drug Compounds from Intact Biological Tissue

*Christopher D. Reddick and Richard A. Yost
Department of Chemistry, University of Florida, Gainesville, FL 32611

Since its discovery in 1988 [1,2] matrix-assisted laser desorption ionization (MALDI) has played an increasingly important role in mass spectrometry. Most commonly, MALDI has been used to vaporize and ionize thermally labile and nonvolatile biomolecules, particularly peptides and proteins with masses between 1,000 and 50,000 Da. In our laboratory, we have investigated the potential of MALDI to detect smaller drug compounds (150 - 500 Da) from intact biological tissue. In this work, the MALDI process was optimized to enhance the production of analyte $(M+H)^+$ ions for the central nervous system (CNS) drug compounds, spiperone and ephedrine, in Matrigel model tissue. Experiments were also performed to evaluate the usefulness of MALDI for the detection of CNS drug compounds from actual biological tissue.

In all of the experiments performed, a Finnigan MAT™ Lasermat time-of-flight mass spectrometer was used. In the first optimization experiments, MALDI was performed on samples of spiperone and ephedrine in Matrigel using 2,5-dihydroxybenzoic acid (DHB) at analyte-to-DHB molar ratios of 1:100, 1:1,000, and 1:10,000 (*Figures 1 and 2*). For both compounds, increasing the concentration of the DHB matrix solution had the following effects: 1) ions from the Matrigel tissue were suppressed, 2) $(M+Na)^+$ and $(M+K)^+$ adduct ions were minimized, and 3) production of spiperone and ephedrine $(M+H)^+$ ions were improved. In the second set of optimization experiments, the effect of the MALDI matrix solvent polarity on the production of spiperone and ephedrine $(M+H)^+$ ions from Matrigel was investigated. The polarity of the matrix solvent was varied by using different mixtures of acetonitrile and water. Results of these experiments are shown in *Figures 3 and 4*. For both spiperone and ephedrine in Matrigel, production of the $(M+H)^+$ ion was improved by increasing the polarity of the MALDI matrix solvent. In the final optimization experiments with spiperone and ephedrine in Matrigel, the soak time of the MALDI matrix solution applied to the Matrigel samples was controlled by covering the Lasermat sample plate with a 2 mm thick Teflon disk. The disk was placed over the raised rim of the sample plate immediately after the MALDI matrix solution was applied, creating a miniature humidity chamber. Using this method, previously reported by Mock and co-workers (for MALDI of proteins adsorbed onto nitrocellulose membranes [3]), the matrix solution was prevented from crystallizing for intervals of 5-30 minutes From *Figure 5*, it can be seen that increasing the soak time from 1-10 minutes significantly increased the production of $(M+H)^+$ ions for both spiperone and ephedrine in Matrigel. At soak times beyond 15 minutes, no further increases were seen for either drug compound. These trends were attributed to the fact that at longer crystallization periods, the analyte was able to partition out of the Matrigel and into the MALDI matrix solution before it dried.

To evaluate the usefulness of MALDI for analytes in actual biological tissue, preliminary studies were performed with cerebral tissue from a male Spraige-Dawley rat. For analysis, thin slices of frozen cerebral tissue were incubated in a solution containing 100 ng of spiperone for 1 hr. MALDI was performed on the tissue samples by placing 1-2 µL of DHB matrix solution on top of the tissue *(Figure 6)*. These preliminary studies with rat cerebral tissue showed that MALDI was able to enhance the detection of spiperone from actual biological tissue.

The authors would like to thank Dr. Robert Perchalski for his helpful discussions pertaining to this work. Also, we would like to thank Dr. Robert Kennedy and the members of his research group for providing tissue samples for the final MALDI experiments. And finally, we would like to thank Bristol-Myers Squibb for their continued support and funding of this project.

[1] Karas, M. , Hillenkamp, F. *Anal. Chem* 1988, 60, 2299
[2] Tanaka, K , Waki, H. , Ido, Y. , Akita, S , Yoshida, Y. , Yoshida, T *Rapid Commun. Mass Spectrom.* 1988, 2, 151.
[3] Mock, K.K. , Sutton, C.W. , Cottrell, J.S. *Rapid Commun. Mass Spectrom.* 1992, 233-238.

Figure 1
Mass Spectrum of 100 ng Spiperone in 1 mg Matrigel

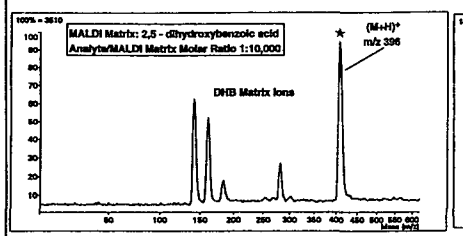

Figure 2
Mass Spectrum of 100 ng Ephedrine in 1 mg Matrigel

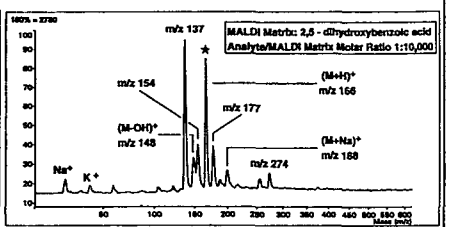

Figure 3
Effect of the MALDI Matrix Solvent Polarity on the $(M+H)^+$ Ion of Spiperone in Matrigel

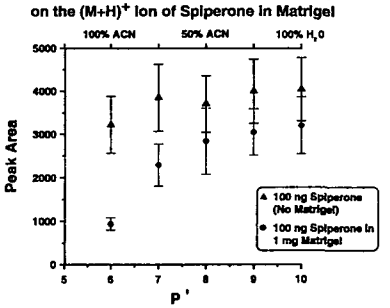

Figure 4
Effect of the MALDI Matrix Solvent Polarity on the $(M+H)^+$ Ion of Ephedrine in Matrigel

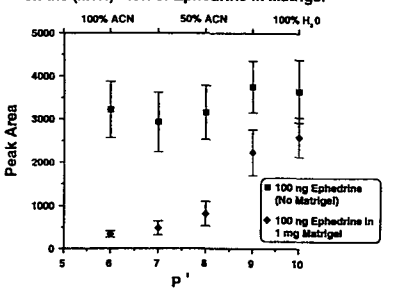

Figure 5
Effect of the MALDI Matrix Soak Time on the $(M+H)^+$ Ion of Spiperone and Ephedrine in Matrigel

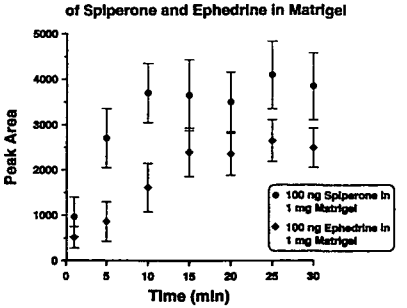

Figure 6
Mass Spectrum of Spiperone in Rat Cerebral Tissue

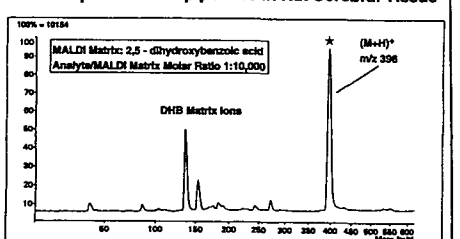

Application of MADLI TOFMS for Quantitation

R.R. Hensel[1], R. King[2], K. G. Owens, Department of Chemistry, Drexel University, Philadelphia, PA 19104

The successful MALDI TOFMS experiment may be broken down into five distinct processes: ***sample preparation, application, desorption, ionization, and detection.*** This presentation focuses on the importance of the first two processes in obtaining quantitative results. We have found that electrospray application may greatly improve the reproducibility of the recorded MALDI mass spectra.

In MALDI TOFMS, analyte is mixed with an excess concentration of matrix in a suitable solvent. In the solution phase the mixture is homogeneous. However, when this sample is applied to the MS probe and air dried, analyte is incorporated into the matrix crystals to varying degrees and the sample may no longer be homogeneous. This is not surprising since crystallization is a simple means of purification. When sample is electrosprayed onto the MS probe, analyte and matrix seem to be much more evenly distributed.

The two methods of sample application may be compared in a number of ways: by measuring the peak height ratios of analyte to internal standard (IS) of a sample applied to a single probe tip; by measuring signal intensity as the laser sweeps across the sample; and by fluorescent microscopy.

Desamino-[8-D-arginine] vasopressin (DDAVP) and the structural analog, arginine vasopressin (AVP), suitable for use as an internal standard (IS), were selected for these experiments. 2,5-dihydroxybenzoic acid (DHB) was used as the matrix in all experiments because DDAVP and AVP were ***soluble*** in the solvent/DHB system used. Samples (10^{-11} to 10^{-13} moles loaded onto the MS probe) and matrix were dissolved in the same solvent. The solvent consisted of nine parts methanol and one part acetonitrile/water/0.1% TFA (30/70 v/v).

Electrospray was accomplished by introducing approximately 25 µL of sample into a small bore stainless steel capillary. A potential of approximately +5 KV was applied to the capillary while the MS sample probe tip was held at ground. A flow rate of 2-5 µL/min was applied by an infusion pump. Between 1 and 2 µL of any given sample was electrosprayed on a single MS probe tip.

Experiments were conducted to compare the within-tip reproducibility and the tip-to-tip reproducibility of air dried versus electrosprayed sample. Between 25 and 50 laser shots were accumulated per sample site for air dried samples (once analyte signal was detected). Between 50 and 100 laser shots were collected as the laser swept the sample for electrosprayed samples.

Comparison of Within Probe Tip Reproducibility

Method	% CV (n) of Analyte to IS Ratios
Air Dried	6.27 (3) 49.6 (3) 39.2 (5)
Electrosprayed	3.70 (4) 9.31 (5) 4.56 (4) 9.66 (4) 15.1 (4)

Air dried and electrosprayed samples were next scanned in ***chromatogram*** mode on a Shimadzu, Inc., Kratos Kompact MALDI 3 mass spectrometer. The signal intensity collected over the mass range of the protein sample of each laser shot was recorded. This resulted in a chromatogram of intensity versus laser position. The results show that air dried samples exhibit considerable area with no signal. Presumably this is an area devoid of analyte. Electrosprayed samples showed more consistent signal intensity across the entire sample, with no areas of zero signal intensity.

A fluorescent molecular weight marker, fluorescein isothiocyanate labeled -lactalbumin from Bovine milk, (14,200 Daltons, Sigma Chemical Co.) was added to matrix. Samples were air dried or electrosprayed. The images obtained at a magnification of 200x indicate that air drying creates large crystals of matrix which seem to contain variable amounts of fluorescently labeled protein. Discernible microcrystals are observed from the electrosprayed sample which shows fluorescence to be detected across the sample area.

It has been our observation that matrix/analyte solution components tend to partition during the solvent evaporation process. This component segregation yields an inhomogeneous sample surface, resulting in highly variable analyte ion production. Methods that increase the rate of solvent evaporation, such as the selection of volatile solvents and/or rapid evaporation under vacuum, reduce component segregation. The electrospray process is one sample application method which reduces the segregation occurring during solvent evaporation. The small droplets that are formed by this process improve the homogeneity of the sample surface. The presence of cation adducts demonstrates that solution components are less segregated when electrosprayed. This increase in sample homogeniety decreases the within and between probe tip variability, resulting in a decrease in %CV for the analytical results.The electrospray sample application process has resulted in a more objective analysis which will be easily automated.

The within tip reproducibility was approximately 15% or better. However, tip-to-tip reproducibility is of much greater importance in the overall development of a quantitative analytical method. The coefficient of variation was less than 17% for standards between 32 and 400 ng/50 µL (6.0 x 10^{-13} to 7.5 x 10^{-12} moles loaded).

The presence of salt adducts creates cationized interference especially when analyte and internal standard are close in mass. Experiments are in progress to overcome these challenges:

- selection of an IS with a greater mass difference
- use of more than one IS in the quantitative method
- use of ion exchanged matrix
- selection of matrix materials other than DHB
- mathematical deconvolution of overlapping peaks in the raw data

MALDI TOFMS has been used for the quantitative analysis of DDAVP, using AVP as internal standard, from human plasma after solid phase extraction. The range of quantitation (2.0 to 10 µg/mL) is of limited value for bioanalytical application. However, lower limits of quantitation have been demonstrated by the analysis of neat standards. The limitation with respect to bioanalytical application seems to be with the solid phase plasma extraction methods we have used to date and not necessarily the MALDI TOFMS process. Experiments are in progress to lower the limits of quantitation for analytes in human plasma and to demonstrate the application of quantitative MALDI TOFMS for higher mass analytes.

1 Rhône-Poulenc Rorer, Department of Drug Metabolism and Pharmacokinetics, Collegeville, PA
2 Merck, Sharpe and Dohme, Inc., Department of Drug Metabolism, West Point, PA

Analysis of Synthetic Polymers and Copolymers by MALDI-MS

Martin Schaer
Ciba-Geigy Ltd., CH-4002 Basle, Switzerland

The analysis of synthetic polymers is of high importance in industrial laboratories. This creates a demand for a fast and accurate problem solving system.
Matrix-assisted laser desorption/ionisation mass spectrometry (MALDI-MS) has become a powerful tool for the analysis of synthetic polymers and copolymers and is used on a routinely basis in the industrial lab.

Most polymers investigated in our laboratory have weight distributions < 10,000 Da. MALDI-MS was successfully applied to study the following problems:
- End group determination
- Absolute M_n- and M_w-values
- Oligomeric additives: Detection of different oligomeric series and improvement of product purity
- Copolymer analysis: Determination of composition with the aid of numerical simulations (Figures 1 and 2)

In spite of this success a problem often occurs: For the characterisation of polymers the molecular weight distributions M_n and M_w have to be determined. They are defined by:

$$M_n = \frac{\sum N_i M_i}{\sum N_i} \qquad M_w = \frac{\sum N_i M_i^2}{\sum N_i M_i}$$

It is often observed that these values obtained by MALDI-MS are significantly *lower* than Size Exclusion Chromatography (GPC)- or other conventional technique-values.

- M_n and M_w are in agreement for:
  - PEG
  - PPG
  - PMMA
  - PS

  with narrow size distributions.
- M_n and M_w are lower than GPC-values for:
  - Oligomeric additives
  - Polysiloxanes
  - Oligomer mixtures which have not narrow Poisson-like size distributions.

Several problems can lead to the GPC/MALDI-discrepancy:

- MALDI-MS:
  - Ionisation/desorption efficiency
  - Limited dynamic range
  - Detection
  - Resolution
  - Fragmentation?
- GPC:
  - Relative measurement dependent on external standards
  - Solvent
  - Detection

Nevertheless the amount and quality of information that is obtained by a MALDI-MS analysis is very high as can be seen in Figures 1 and 2.
M_n- and M_w-values hide this information. They are "chromatographic" values and should not be used for the representation of the results of a mass spectrometric analysis.

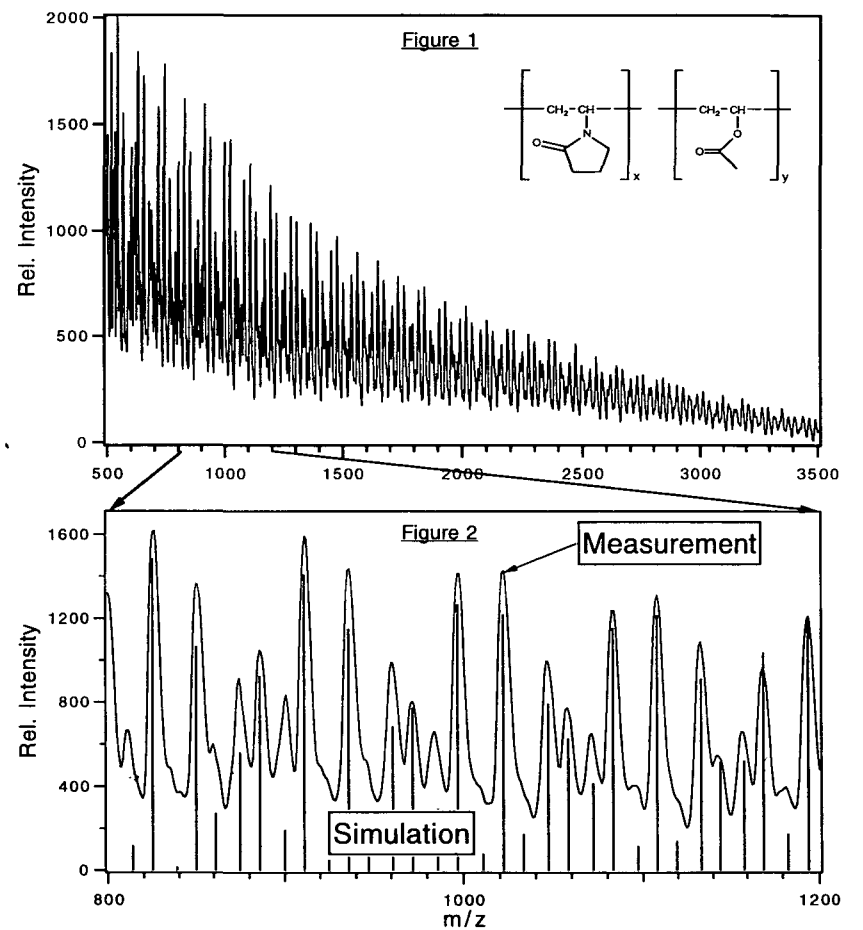

Figure 1: Positive ion mass spectrum of a copolymer consisting of N-vinylpyrrolidone and vinyl acetate.

Figure 2: The same mass spectrum in the range 800-1200 Da with a numerical simulation. A random sequence with x=0.2 and y=0.8 was assumed. Both, masses and ion signal intensities can be approximated with close agreement.

Characterization of Polyesters by Transesterification Using Matrix Assisted Laser Desorption Ionization Mass Spectrometry

John B. Williams, Arkady I. Gusev, and David M. Hercules
Department of Chemistry, University of Pittsburgh
Pittsburgh, Pennsylvania 15260

Introduction

Polyesters are a broad class of condensation polymers utilized in a variety of films, textiles, and, more recently, as thermoplastic molding material in the manufacture of blow molded containers. Knowledge of properties such as chemical structure, molecular weight distribution, and the presence of additives or impurities is crucial to the synthesis and performance of these materials. Matrix assisted laser desorption ionization time of flight mass spectrometry (MALDI-TOF-MS) has been applied to the analysis of many classes of synthetic and biological polymers. The method offers the advantages of generation of high mass ions (10^6 Da), high ion transmission through simultaneous monitoring of the entire mass range (multiplex advantage), ability to measure both mass and intensity, and production of spectra with limited fragmentation. These characteristics make MALDI-TOF-MS an ideal tool for analysis of synthetic polymers.

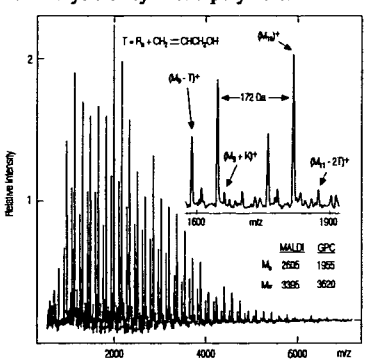

Figure 1. Oligomer distribution of poly(trimethylene glutarate) in IAA matrix.

The purpose of this research is to apply MALDI-TOF-MS to the characterization of polyesters. Molecular weight information can be obtained from the intensity and position of intact oligomers. Structural assessment is possible through evaluations of the position of oligomer and fragment peaks. Mechanisms of fragmentation may be investigated and compared to that seen in other mass spectrometric techniques. Tranesterification of these materials with trifluoroacetic acid (TFA) or chlorodifluoroacetic acid (CFA) will allow the acquisition of additional structural information from product oligomers and fragments as well as isotopic distribution. Transesterification also offers the potential for analysis of reaction products of intractable (insoluble, high molecular weight, or cross-linked) materials. Monitoring product formation with MALDI-TOF- MS should yield kinetic information on the transesterfication reaction.

Methods

The research was conducted on a LAMMA 1000 (Leybold-Heraeus Gmbh) modified with a Laser Science, Inc. nitrogen laser (VSL 337 ND). Matrices used are trans-3-indoleacrylic acid (IAA) and 2-cyano-5-phenyl-2,4-pentadienoic acid (CPPA). Mass calibration was achieved using poly(propylene glycol) (M_n = 440) as an internal standard.

Results

Figure 1 shows the oligomer distribution of poly(trimethylene glutarate) (PTG) in a crystalline IAA matrix. Intact sodium and potassium cationized oligomers, and corresponding sodium cationized fragments resulting from cleavage of the C-O bond are observed. Previous studies of fragmentation mechanisms using SIMS have suggested that C-O may be favored over C-C fracture.(1) This cleavage is accompanied by the transfer of hydrogen to form the acid terminated oligomers observed as fragments. Hydrogen migration has been shown by electron ionization mass spectrometric studies to occur by β-CH transfer (McLafferty rearrangement).(2) This mechanism may be responsible for the appearance of mono-, and sometimes di-, carboxylic acid fragments in the spectra of most compounds studied. Nuclear magnetic resonance (NMR) analysis of these materials indicated an absence of acid terminated impurities.

Transesterification results in formation diesters and diols of the reactant and TFA with a decrease in the molecular weight values of the material. Cleavage at the C-O bond also occurs in these products with fragments appearing at much higher intensity than corresponding product oligomers. Figure 2 allows observation of increase in intensity of a product fragment relative to the poly(butylene adipate) (PBA) oligomer in the 1400 to 2000 Da mass range from 15 minutes to 5 hours during transesterification with TFA. In addition to the possibility of obtaining kinetic data, the reaction also yields additional structural information for compounds, such as PBA, where fragmentation is not observed.

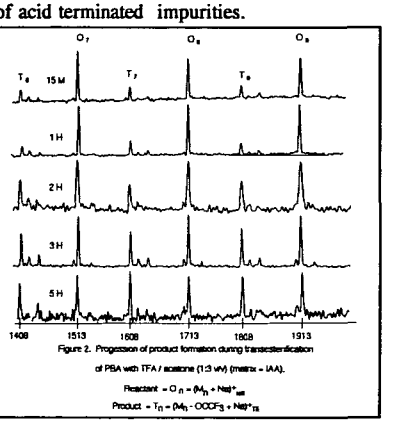

Figure 2. Progression of product formation during transesterification of PBA with TFA / acetone (1:3 v/v) (matrix = IAA).

Conclusions

MALDI spectra are useful for the determination of structure and molecular weight values for the seven experimental polyesters. Limited fragmentation, not observed in the MALDI analysis of many other polymer classes, occurs at the ester bond and is always accompanied by the transfer of a hydrogen to yield an acid terminated ion. Tranesterification of polyesters with TFA or CFA produces diesters that are readily identified as oligomers or fragments in MALDI spectra. These peaks, along with isotopic distribution pattern seen with CFA, yield additional structural information from the polyester. MALDI spectra can be used to monitor the growth of products in a reaction mixture. This ability encourages the implementation of more stringent controls to determine the feasibility of acquisition of quantitative kinetic information. The observed fragmentation of polyesters and derivatives arises from fracture of C-O bonds at unknown points in the polymer backbone. Experiments are being devised to determine if this cleavage is random or occurs at specific sites along the chain.

References

1. Hittle, L.R.; Altland, D.E.; Proctor, A.; Hercules, D.M. Anal. Chem. 1994, 66, 2302-2312.
6. McLafferty, F.W. Interpretation of Mass Spectra University Science Books: Mill Valley, CA, 1980;pp 201-205.

Accuracy of MALDI for Molecular Weight Characterisation of Synthetic Polymers

M. Koerner and R. Gerhards, Th. Goldschmidt AG, ZBF/Analytisches Labor, D-45127 Essen, Germany.
A. Keane, C. W. Sutton, and J. S. Cottrell, Finnigan MAT Ltd., Hemel Hempstead, Herts HP2 4TG, UK

Introduction: There is considerable interest in the use of mass spectrometry as an alternative to gel permeation chromatography (GPC) for the characterisation of synthetic polymers. The principal advantages of mass spectrometry for this application are speed of analysis, mass resolution, and the ability to measure accurate mass values. Using MALDI, the average molecular weight of a distribution can be measured without resolving individual oligomers. However, by resolving the distribution, not only is mass accuracy improved, but other characteristics such as the nature of the end group or groups can be determined. Using a reflectron instrument, such as the Vision 2000, mass measurement errors for individual, well resolved peaks of a few thousand daltons will generally be less than 200 ppm. However, the accuracy of the molecular weight of a distribution also depends on the accuracy with which the relative intensities of the peaks can be measured. This poster discusses the sources of error, both random and systematic, which affect such measurements.

Ionisation & Detection Efficiency: There are indications that systematic variations in ionisation efficiency across a distribution are relatively small, at least over a limited mass range. Good correlations have been obtained between GPC and MALDI data for samples with polydispersity values close to 1 by a number of groups [1; 2; 3]. However, there are also results which show discrepancies between GPC and MALDI data, particularly for polymers with large polydispersities [4; 5]. It is not clear to what extent this is attributable to variation in ionisation or detection efficiency with mass. Uniform detection efficiency across a wide mass range is largely a matter of having an adequate impact energy [6]. Since detector response should be largely independent of the chemical nature of the polymer, a detector response curve could be measured using standard mixtures and subsequently used to correct data from unknowns.

Peak Height or Peak Area?: Some investigators have taken mole fraction as corresponding to the intensity of a peak [4]. This may be a valid assumption if the time constant of the detector system is much longer than the true peak width. In general, the area under the peak would be expected to provide better precision. And, if individual oligomer peaks are not fully resolved, then molecular weights must be calculated by integrating across the entire distribution. To establish that mole fraction is indeed proportional to peak area, a series of mixtures of two polyethylene glycol standards were analysed. Aliquots of PEG1500 and PEG4600 solutions, which have negligible mass overlap, were mixed by volume in the ratios 3:1, 2:1, 1:1, 1:2, and 1:3. Graphs of peak area ratio versus composition yielded straight lines for both reflectron and linear mode, indicating that the proportionality between peak area and mole fraction holds, although the scatter on the measurements was quite large.

Sample Inhomogeneity: The variation in relative peak areas mentioned above can only be due to inhomogeneity in the deposit of matrix and sample. This is potentially a source of random errors, which will affect extended distributions most severely. If the sample is truly incorporated into the crystal lattice of the matrix , then it might be expected that some kind of sieving due to size exclusion processes would occur during crystallisation. The use of liquid matrices should avoid this problem [1] [7], but could

introduce artefacts due to variation in surface activity, (c.f. FAB). Clearly, more work is required to develop sample preparation methods which improve sample homogeneity. Possibly, the sample and matrix could be "frozen" into some kind of glassy solid solution, or electrosprayed onto the target so as to ensure rapid and uniform crystallisation.

Where's the Baseline?: One of the practical difficulties of integrating MALDI spectra of polymer distributions is knowing where to draw a representative baseline. Spectra of a series of polymethylmethacrylate (PMMA) standards illustrate this problem. A series of these standards was analysed using DHB matrix on a Vision 2000. The results are summarised below, together with data from GPC. Nevertheless, the agreement between the GPC and MALDI data is excellent, particularly above 10 kDa.

	GPC				MALDI			
Standard	M_n	M_w	M_p	D	M_n	M_w	M_p	D
pmma600 (PSS)	570	690	720	1.22	800	885	725*	1.10
mmg23040 (PSS)	890	1070	1210	1.20	1140	1290	1125*	1.12
20225-3 (MN)			1830	1.10	1570	1720	1525*	1.09
20225.4 (MN)			2010	1.10	1700	1880	1625*	1.11
mmg22107 (PSS)	1800	2000	2030	1.10	2240	2420	2225*	1 08
mmg27111 (PSS)	3250	3600	3500	1.10	3410	3560	3325*	1.04
mmg25111 (PSS)	6600	7000	7100	1.06	6680	6990	6600	1 05
mmg15107 (PSS)	7200	9500	11.3k	1.32	9840	11 1k	10.8k	1.13
mmg16127 (PSS)	12.3k	12.9k	13.1k	1.04	12.2k	12.4k	11.7k	1 02
20230-3 (MN)			15.1k	1.06	13.9k	14.9k	14.5k	1 07
20231-4 (MN)			22.2k	1.07	19 7k	20.5k	19.5k	1 04
6/2 (PSS)	26k	28k	28k	1.05	27.5k	28.2k	26.6k	1.02
mmg25040 (PSS)	27k	29k	30.5k	1.06	26.9k	27.9k	27.1k	1.04
mmbs12 (PSS)	35k	37k	37k	1.04	34.5k	35.1k	33.6k	1.02
mm11049 (PSS)	51.8k	52.2k	52.2k	1.08	50.2k	51.2k	49.0k	1.02

Note MALDI values for M_p are estimated from the point of maximum intensity, except for the values marked with an asterisk, which are the oligomer peaks of greatest area. Standards were purchased from Macherey-Nagel GmbH & Co , and Polymer Standard Service GmbH

1. Bahr, U., Deppe, A., Karas, M., Hillenkamp, F. and Giessmann, U. (1992) Anal. Chem., **64**, 2866-9.
2 Danis, P. O. and Karr, D. E. (1994) Proc of the 42nd ASMS, Chicago, Illinois, pp. 315.
3 Montaudo, G., Montaudo, M. S., Puglisi, C. and Samperi, F (1994) Rapid Commun. Mass Spectrom., **8**, 1011-5
4 Montaudo, G., Montaudo, M. S., Puglisi, C. and Samperi, F. (1995) Rapid Commun. Mass Spectrom., **9**, 453-60.
5. Lehrle, R. S. and Sarson, D. S. (1995) Rapid Commun. Mass Spectrom., **9**, 91-2.
6. Larsen, B. S., McEwen, C. N., Simonsick, W. and Peacock, P. M. (1994) Proc. of the 42nd ASMS, Chicago, Illinois, pp. 518.
7. Williams, J. B., Gusev, A. I. and Hercules, D. M. (1994) Proc. of the 42nd ASMS, Chicago, Illinois, pp. 981.

High Resolution MALDI Studies of Copolymers

David C. Schriemer, and Liang Li*
Department of Chemistry, University of Alberta
Edmonton, Alberta, Canada
T6G 2G2

Matrix assisted laser desorption ionization (MALDI) is finding increasing application in the area of polymer analysis. Success has been demonstrated in the determination of molecular weights and end-group analysis [1]. Polymers are arguably more difficult to analyze by MALDI than are biopolymers, due largely to their very diverse composition and chemistry.

Copolymer analysis by MALDI represents one of the more challenging applications. Proper matrix selection appears to be one of the most important parameters. In addition to commonly used matrices such as 2,5-dihydroxybenzoic acid and t-3-indoleacrylic acid, the following three matrices show promising general utility for a range of polymers:

1) 2-(4-hydroxyphenylazo)benzoic acid (HABA) [2]
   -for ether/hydroxyl containing polymers, allowing for alkali cationization

2) t,t-1,3-diphenylbutadiene (DPB) [3]
   -for unsaturated polymers, allowing for silver cationization

3) retinoic acid (all trans) [4]
   -useful for a wide range of polymer types, allowing for both alkali and silver cationization.

The MALDI experiments were carried out in a linear time-of-flight instrument, operated in time-lag focusing mode. This mode allows for routine achievement of an M/ΔM up to 3000, for lower molecular weight polymers. Two classes of copolymers were analyzed: alternating and block. Figure 1 displays the spectrum of the alternating copolymer poly[(o-cresyl glycidyl ether)-co-formaldehyde]. The spectrum was obtained from DPB in acetone with $AgNO_3$, and clearly demonstrates the mass of the repeat unit (176 amu). The secondary distribution arises from polymer with the loss of one epoxide. This is in keeping with the manufacturer's quote of 90% epoxide content.

Figure 2 contains an expansion of the spectrum of a block copolymer, poly(propylene glycol-b-ethylene glycol-b-propylene glycol)bis(2-aminopropyl ether). This spectrum was obtained from HABA in 1,4-dioxane doped with NaCl. This type of polymer places much greater demands on the resolution of the instrument, as any given number of the one monomer can have a distribution of the other, leading to overlap. In this mass range however, even isotope discrimination can be achieved, facilitating copolymer characterization.

43rd ASMS Conference on Mass Spectrometry and Allied Topics

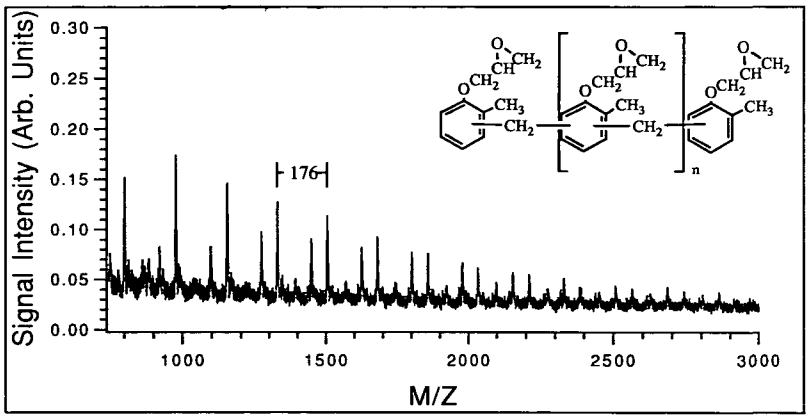

Figure 1

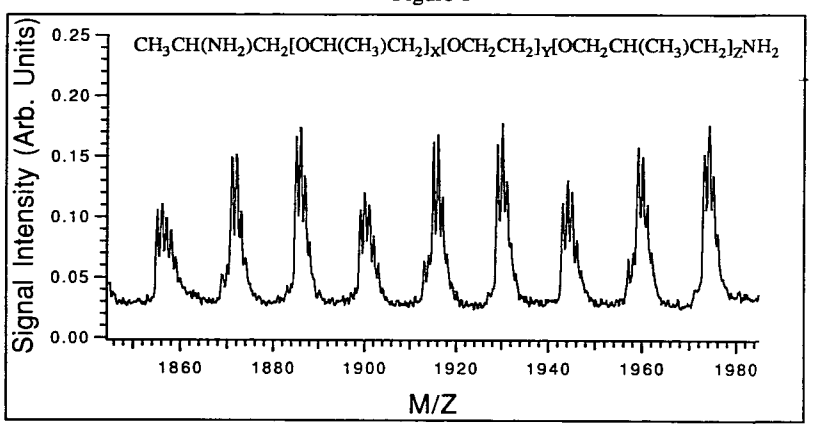

Figure 2

References:
[1] Strupert, K.; Karas, M.; Hillenkamp, F. *Int. J. Mass Spec. Ion Proc.*, **1991**, 111, 89-102.
[2] Juhasz, P.; Costello, C.E.; Biemann, K. *J. Am. Soc. Mass Spectrom.* **1993**, 4, 399-409.
[3] Cornett, D.S.; Duncan, M.A.; Amster, I.J. *Anal. Chem.* **1993**, 65, 2608-2613
[4] Walker, K.L.; Kahr, M.S.; Wilkins, C.L.; Xu, Z.; Moore, J.S. *J. Am. Soc. Mass Spectrom.* **1994**, 5, 731-739.

Analysis of GPC Standards by Matrix-Assisted Laser Desorption/Ionization

Scott D. Hanton, David M. Parees and Brian F. Hanley,
Air Products and Chemicals, Inc., Allentown, PA 18195
Richard C. King and Kevin G. Owens,
Department of Chemistry, Drexel University, Philadelphia, PA 19104

The application of matrix-assisted laser desorption/ionization (MALD/I) time-of-flight mass spectrometry (TOFMS) to analyze synthetic polymers can provide important chemical structure and molecular weight information, including the number average molecular weight (M_n), the weight average molecular weight (M_w), and the polydispersity (PD). Molecular weight directly influences many polymer physical properties: tensile strength, elongation, brittleness, abrasion resistance, chemical resistance, viscosity, adhesion, and solubility.[1] We investigated a range of polymers: polystyrene (PS), polyethylene glycol (PEG), polymethylmethacrylate (PMMA), and polydimethylsiloxane (PDMS). The goal of this work is to investigate the accuracy of molecular weight values obtained by MALD/I in comparison with classical methods (osmometry and light scattering) and gel permeation chromatography (GPC).

A significant advantage of MALD/I TOFMS is the direct measurement of the sample mass. TOFMS measures ion flight times, and these flight times can be calibrated to ion mass independent of analyte chemistry. To calibrate the TOFMS for these higher molecular weight polymer materials, we generated individual mass calibrations for each polymer from spectra with resolved oligomers. Each of these individual mass calibrations were very similar. We applied an average of the four individual results as our instrument mass calibration.

In three cases (PS, PMMA and PEG), the manufacturers' specified molecular weights agreed well with the MALD/I results. We plot the measured MALD/I molecular weight versus the manufacturer's specified molecular weight. Figure 1 shows the relationship for PS. Ideally, the line relating the MALD/I molecular weight to the manufacturer's specified molecular weight should have a slope of 1.00 and an intercept of 0.0. For PS we obtain a slope of 0.907 and a intercept of 763.

MALD/I MW vs Specified MW
Polystyrene

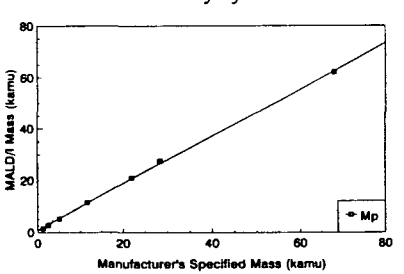

Figure 1

The PDMS MALD/I molecular weights appear to be approximately half of the manufacturer's specified molecular weights. In the plot of MALD/I molecular weight versus the manufacturer's specified molecular weight, we obtain a slope of 0.533 and an intercept of -286. Previous reports have indicated the ratio to be closer to one third.[2] In our MALD/I experiment, we employed a combination matrix consisting of 5-fluorosalicylic acid and an underlayer of trans-3-indoleacrylic acid. The use of the cooling underlayer is responsible for the larger (relative to the previous report) measured MALD/I molecular weights, which are in better agreement with NMR results.[2]

While most of the PMMA data show good agreement between the MALD/I, GPC and manufacturers' specified molecular weights, it appears that PMMA 9600 is considerably lower in mass than the specified value. Figure 2 shows a MALD/I mass spectrum of a mixture of PMMA 6300 and PMMA 9600. The two materials have very similar average molecular weights. We also observe longer GPC elution times than expected for PMMA 9600. While a lower MALD/I molecular weight has been previously reported for PMMA 9600,[3] it appears that the discrepancy may be due to a different end group, that may chemically affect the classical molecular weight measurements.

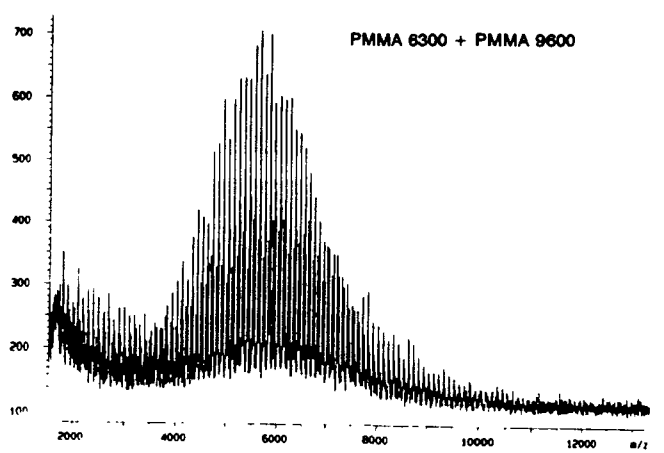

Figure 2

References
1 L. H. Sperling, Physical Polymer Science, New York: John Wiley & Sons, Inc., 1986.
2 M. P. Lacey and T. Keough, Proceedings of the 41st ASMS Conference on Mass Spectrometry, 1993.
3 P. O. Danis and D. E. Karr, Org. Mass Spectrom. 1993, 28, 923-925.

Structural Determination of Azo Dyes by Photoionisation Mass Spectrometry

Scott J. Wright, Michael J. Dale, Anita C. Jones and Patrick R. R. Langridge-Smith.
Department of Chemistry, The University of Edinburgh, King's Buildings, West Mains Road, Edinburgh, EH9 3JJ, UK.

Azo dyes are used extensively in industry as colourants for textiles, paper, leather and foodstuffs. The health hazards posed by their potential carcinogenicty mean that they are of significant environmental interest. Azo dyes have previously eluded routine mass spectrometric characterisation as a result of their thermal lability. Solid phase desorption/ionisation techniques, such as FAB and SIMS first enabled the analysis of such involatile species. However, fragmentation is difficult to control resulting in little or no molecular ion signal. Conversely, techniques such as thermospray ionisation generate essentially molecular weight information.

Laser desorption laser photoionisation time-of-flight mass spectrometry, L^2TOFMS, has been shown to be effective in the study of a wide range of thermally labile and involatile molecular species. This is due to separation of the desorption and ionisation events. An infra-red laser is used to desorb intact neutral species into the gas phase, which are then ionised by a UV laser and analysed in a reflectron time-of-flight mass spectrometer.

A series of azo dyes have been examined using two fixed ionisation wavelengths, 193 nm and 266 nm. A number of striking differences have been observed in the resulting mass spectra (see Figure 1).

Ionisation using 193 nm radiation generates predominantly molecular weight information via hydrogen and alkali metal adduct ions. The principal fragment ions observed correspond to cleavage of the C—N bonds adjacent to the azo functionality. Complementary structural information is obtained using 266 nm ionisation, where fragment ions corresponding to photolytic cleavage of the azo linkage dominate the mass spectra. This may be linked to trans-cis photoisomerism, in that both processes are thought to proceed via the same one photon excited intermediate state [1]. The results presented demonstrate that, using two ionisation wavelengths, it is possible to generate *both* molecular weight information *and* unambiguously determine the presence of an azo functionality.

It has also proved possible to differentiate between isomeric azo dyes. Two azo dyes, 4-[2-(amino) 4-(hydroxy) phenylazo] benzoic acid **(AHP)** and 3-[2-(hydroxy) 5-(amino)

phenylazo] benzoic acid **(HAP)**, have been investigated using 266 nm laser photoionisation. For **AHP**, the anticipated azo cleavage is observed. However, for **HAP** where the hydroxy group is ortho to the azo linkage, no azo cleavage products are detected. It is proposed that trans-cis isomerisation, and hence azo cleavage, is precluded by azo-hydrazone tautomerism. The resulting change in photochemistry allows for direct mass spectral differentiation between the two isomers using L^2TOFMS.

It has been further shown that the position of the carboxylic acid group, relative to the azo linkage, in isomers of methyl red can control the charge retaining fragment resulting from photolytic cleavage of the azo bond.

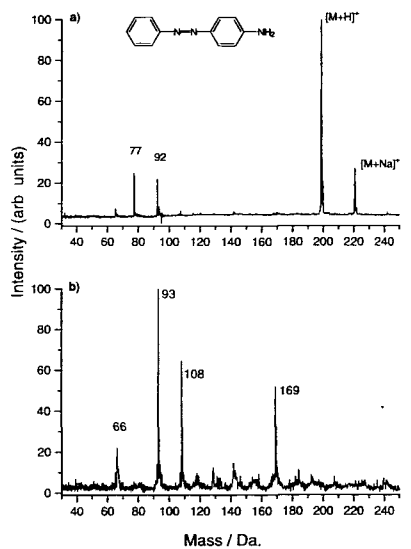

Figure 1: L^2TOF mass spectra of 4-phenylazoaniline using a) 193 nm and b) 266 nm ionising radiation.

[1] M. J. Dale, A. C. Jones, P. R. R. Langridge-Smith, P. G. Cummins, K. F. Costello, *Anal. Chem.*, **1993**, 65, 793.

TWO STEP LASER MASS SPECTROMETRY OF COPOLYMERISED INDOLE DERIVATIVES

J.Gordon Mackintosh, Scott J.Wright, Craig R.Redpath, Michael J.Dale, Andrew R.Mount and Patrick R.R.Langridge-Smith
Department of Chemistry, The University of Edinburgh, West Mains Road, Edinburgh, Scotland, United Kingdom. EH9 3JJ.

Over the last fifteen years there has been considerable interest in the electropolymerisation of heterocyclic molecules such as pyrroles and indoles to form electronically conducting polymers for a wealth of potential applications However the structural characterisation of these layers is made difficult by the fact they are generally insoluble and intractible The incorporation of solubilising functional groups into conducting polymers by the use of 5-substituted indole monomers, Figure 1, has been investigated.

Laser desorption laser photoionisation mass spectrometry (L2MS) has been used to investigate the products formed by the electropolymerisation of such substituted indoles[1,2] For each polymer studied to date, L2MS has revealed the presence of a trimeric species Further studies have shown that this trimeric species can be separated from other oligomers in the layer by differential solubility. The structure of species, Figure 2, has been elucidated using NMR spectroscopy[3] Electrochemical studies[4] have revealed that these trimer units, link together, to form polymer of linked trimer units.

Fig 1 where R=CN,COOH

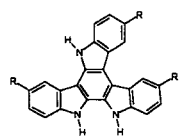

Fig 2 where R=CN or COOH

The copolymerisation of two different indole monomers would result in mixed functional trimers. If these trimers could be separated, polymers with mixed functional properties could be assembled from selected trimer units L2MS has been used to investigate the products of copolymerisation between an equimolar mixture of 5-cyanoindole (5CI) with indole-5-carboxylic acid (I5CA) It has also been used as a technique for monitoring the separation of these products

The polymer was grown on a platinum rotating disc electrode, and subsequently dissolved in dimethylformamide This solution was then cast onto a stainless steel rod and the solvent evaporated. An infrared laser was used to volatilise the neutral molecules, which were subsequently ionised using multiphoton ionisation and mass analysed using a reflectron time-of-flight mass spectrometer.

L2MS, Figure 3, reveals the presence of parent ions for 5CI and I5CA trimers, and also for two trimers of mixed functionality. This result confirms copolymerisation has taken place Extraction and separation of these four trimers was carried out by column chromatography This resulted in four fractions, the spectra of which are shown in Figures 4 to 7 Partial separation of the mixture is achieved. Fraction 1 shows mainly cyano trimer whilst fraction 4 shows mainly carboxy. Fractions 2 and 3 show a mixture although the relative proportion of each species does change These results were quantified by the spectrum shown in Figure 8, which results from an equimolar mixture of individually polymerised cyano trimer and carboxy trimer. Since, the trimers have similar ionisation efficiencies the relative abundance of each species can be estimated in the separated fractions It is clear from our work that L2MS is an invaluable tool for determining the structure of the products formed in this type of copolymerisation

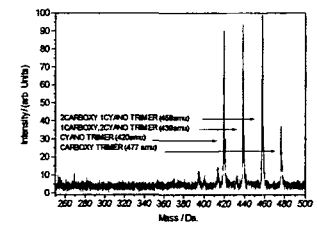

Figure 3

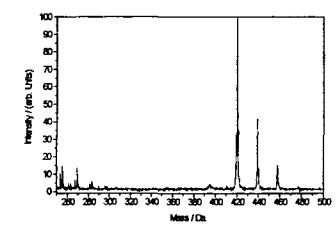

Figure 4

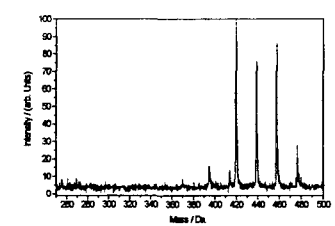

Figure 5

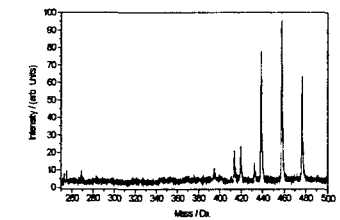

Figure 6

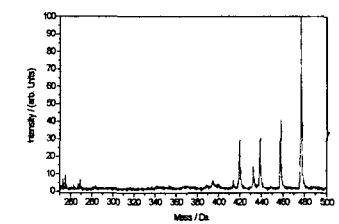

Figure 7

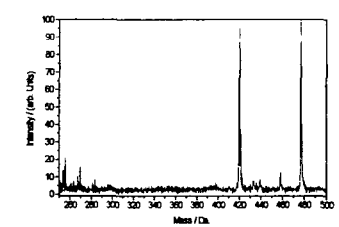

Figure 8

References

1. J G Mackintosh, C.R Redpath, A C Jones, P R R Langridge-Smith, D Reed and A.R Mount, J Electroanalytical Chem , 1994, 375, 163
2 J G Mackintosh, C R Redpath, A C Jones, P R.R Langridge-Smith and A.R Mount, J Electroanalytical Chem , 1995, in press
3 J G Mackintosh, A R Mount and D Reed, Magnetic Resonance in Chem , 1994, 32(9), 559
4 J G.Mackintosh and A.R Mount, J Chem.Soc.Faraday Trans , 1994, 90(8), 1121

Molecular Analysis From Organic Substrates Using Laser Desorption Mass Spectrometry

Michael J. Dale, Patrick R. R. Langridge-Smith, Qiao Zhan* and Renato Zenobi*
Department of Chemistry, The University of Edinburgh, King's Buildings, West Mains Road, Edinburgh, EH9 3JJ, UK
*Laboratorium für Analytische Chemie, Universitätstr. 16, ETH Zentrum, CHN C59, CH-8092 Zürich, Switzerland

The analysis of dyes and pigments on textiles is a major industrial imperative. Such materials are often resistant to removal from their organic substrates making conventional mass spectrometry difficult. The purpose of the present study was to determine the feasibility of using laser desorption laser photoionisation mass spectrometry (L2MS) for the direct analysis of molecular adsorbates on a variety of textiles.

Infrared laser desorption is used to volatilise neutral molecules. These are then postionised using multiphoton ionisation (MPI) and mass analysed using a reflectron time-of-flight mass spectrometer. The principal advantage of the technique lies in the spatial and temporal separation of the desorption and ionisation processes. This methodology has enabled us to generate readily interpretable mass spectra of a variety of model systems, such as porphyrin pigments, azo and phthalocyanine dyestuffs, directly from their host substrates [1]. However, the analysis of "real" systems using this approach, e.g. dyes or stains on fabrics, has been restricted by insufficient detection sensitivities.

The timescale and yield of the desorption process for complex samples such as fabrics may be different to those observed when desorbing from a dielectric or metal substrate. For example, desorption may take place over an extended timescale. The 10 ns ionisation laser pulse would then sample only a fraction of the desorbed material. For these systems we have employed a different approach involving laser desorption transfer. This is a rapid and effective method of depositing and accumulating intact dyestuffs from organic substrates onto a substrate suitable for L2MS, such as MACOR.

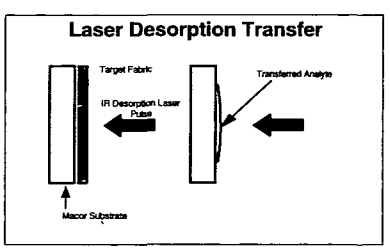

43rd ASMS Conference on Mass Spectrometry and Allied Topics

The spectra below show the L2MS mass spectra obtained on analysis of polyester dyed with Disperse Blue 1 using (a) direct L2MS and (b) laser desorption transfer followed by L2MS. It can readily be seen that the use of laser desorption transfer confers a substantial signal enhancement. The selectivity inherent in MPI also means that the spectra are relatively free from background signals from the ablated polyester. From this preliminary study it is apparent that laser desorption transfer coupled with L2MS is a rapid and effective method of determining analytes on organic substrates.

[1] M. J. Dale, *PhD Thesis*, The University of Edinburgh, 1994.

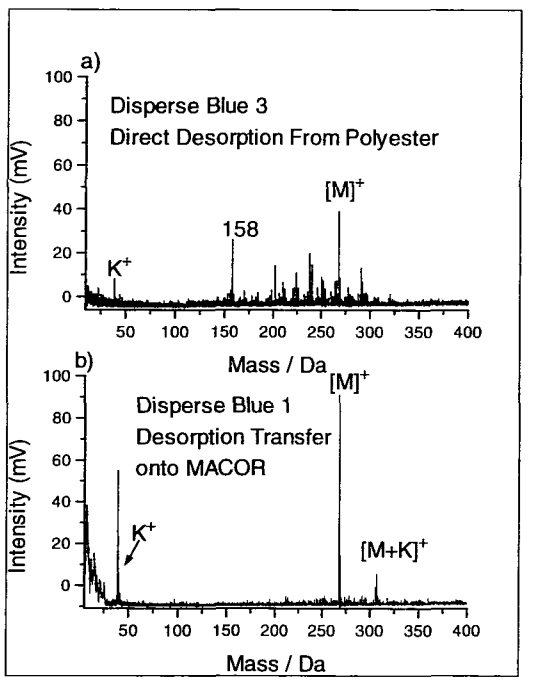

WAVELENGTH DEPENDENT PHOTOIONIZATION OF SOME AMINES AT METAL SURFACES

Robert Goldschmidt* and Kevin G. Owens, Department of Chemistry, Drexel University, Philadelphia, PA 19104

In the course of doing some laser desorption experiments, we observed ion signal for aniline at both 337 nm and 351 nm when the laser beam was directed onto a metal surface. This was unexpected since aniline's ionization potential is 7.7 eV while two photons of 337 nm light equals 7.36 eV and two photons of 351 nm light equals 7.06 eV. We observe signal only when the beam is incident on a metal surface; when the beam is allowed to pass through the instrument without hitting any metal surface we observe no signal. The signal has an easily observable laser repetition rate dependence which also indicates that this is a surface influenced ionization and not a gas phase multiphoton ionization.[1]

The photoionization behavior of molecules near or adsorbed to surfaces may differ from their behavior in gas or bulk phases.[2] For example, the surface interaction may lead to a perturbation of the allowed states of an adsorbate or of a molecule close to the surface and so to differences in the electronic absorption spectrum.[3] The substrate-adsorbate interaction may also lead to charge transfer between the substrate and adsorbate. Also, the interaction of the photon field with the substrate may influence ionization through processes such as photoemission and second harmonic generation, as well as through thermal effects.

We tested various compounds, introduced as vapors into the mass spectrometer, with the 337 nm beam incident on a stainless steel surface. Only amines are observed to give ion signal at 337 nm; aromatic amines give the molecular ion with little or no fragmentation, while aliphatic amines give the protonated molecular ion with fragmentation that increases with the laser intensity. Similar results were observed for compounds tested using 351 nm and a stainless steel surface. To better characterize the nature of this ionization, we are investigating the wavelength dependence of the ion signal in more detail.

Scanning experiments have been performed with aniline and toluene over the range 277.5 nm to 292.5 nm using a stainless steel surface. Spectra were acquired at laser energies between 3 and 40 μJ, or approximately 5×10^5 to 7×10^6 W/cm^2. Under these conditions both the aniline and toluene signal show a laser repetition rate dependence and no ions are observed if the metal surface is removed. There is no observable wavelength dependence of the aniline molecular ion signal in this range, though the fragment peaks do show a wavelength dependence. Toluene gives signal past where might be expected from its UV-visible absorbance spectrum, though it is likely close to its long wavelength threshold at 290 nm. The results are consistent with ionization by

absorption of two photons if one allows for electronic perturbation and thermal effects.[4]

Results at 337 nm and 351 nm show an influence of the metal substrate on the ion signal. The laser intensity threshold for aniline when using a stainless steel surface is about ten times higher than at the shorter wavelength experiments described above. With a copper surface, the signal level from aniline and other amines is noticeably reduced when 351 nm is used instead of 337 nm; no such reduction is observed with a stainless steel surface. With a silver surface, only small signal is observed even at 337 nm.

Laser energy dependence experiments were performed for aniline at 290 nm and at 337 nm, and for tripentylamine at 337 nm. The data was tested against three models: a linear, one photon ionization model (signal level vs. laser energy); a multiphoton ionization model (log signal vs. log laser intensity); and a thermally activated model (log signal vs inverse laser intensity). Statistical analysis does not lead to rejection of any of the models, though the linear model appears to be a poor fit in all cases except for the 290 nm aniline molecular ion. For aniline at 290 nm the multiphoton model gives a slope of 1.50 with a standard deviation of 0.19 for the molecular ion, a slope of 3.10 with a standard deviation of 0.22 for the mass 54 fragment, and a slope of 2.91 with a standard deviation of 0.29 for the mass 28 fragment. This suggests a two photon ionization of aniline and absorption of an additional photon to produce the fragments. For aniline at 337 nm the multiphoton model gives a slope of 6.39 with a standard deviation of 0.41 for the molecular ion, which is the only ion observed. A six photon absorption by aniline seems unlikely here, and the thermally activated model is more in agreement with the substrate effect described above. Thus aniline exhibits different ionization mechanisms at 290 nm and at 337 nm. For tripentylamine at 337 nm the multiphoton model gives a slope of 2.79 with a standard deviation of 0.16 for the protonated molecular ion. Absorption of 337 nm photons by tripentylamine would be surprising, and the substrate effect described above makes the thermally activated model more appealing.

References

1. J. R. Millard, M. Yang, J. P. Reilly, *J. Phys. Chem.* **95**, 4045 (1991).
2. T. J. Chuang, *Surf. Sci. Rep.* **3**, 1 (1983).
3. H. Gerischer In *Faraday Discussions of the Chemical Society No. 58, Photo-Effects in Adsorbed Species,* F. C. Tompkins, ed.;Chemical Society: London (1974).
4. J. R. Millard, M. Yang, J. P. Reilly, *J. Phys. Chem.* **91**, 4323 (1987).

Enhanced Detection Limits for High Molecular Weight PAHs Using Direct LD-TOF MS

B. Soloveytchik, J.H. Miller, A. Vertes
Department of Chemistry, George Washington University, Washington, D.C. 20052

Materials like shale oil, coal liquid, petroleum, asphalt, fly ash, soot, and engine-derived particulates contain high levels of carcinogenic PAHs. These products, formed during combustion are generally identified by one or more of the following techniques: GC, HPLC, supercritical fluid extraction [1], thermal desorption GC-MS [2], or laser mass spectrometry with postionization [3]. The method outlined here –direct laser desorption time-of-flight mass spectrometry (LD-TOF MS)– has several advantages: minimum sample preparation, low detection limits, and simple instrumentation.

GC-MS maintains good reproducibility and sensitivity for the lower molecular weight PAHs whereas its detection limit increases with decreasing volatility and increasing analyte molecular mass. Another problem related to the application of GC-MS and HPLC is the dependence of analyte response on the matrix. Traditional MS detection methods show better sensitivity than GC and a response free from matrix effects.

Here we describe the direct LD-TOF MS measurement of PAH standards and soot extracts. Our 2 m time-of-flight mass spectrometer (TOF-101, Comstock Inc.) was equipped with a laser desorption ion source and dual channel plate detector. An excimer laser (LEXTRA 50, Lambda Physik GmbH) operating at 308 nm was used to pump the dye laser (LPD 3000, Lambda Physik GmbH). The selected Coumarin 540A dye (Exciton Co.) emitted in the 513-588 nm range. Frequency doubling was used to generate the tunable UV radiation. Spectra were captured by a transient recorder (TR8828D, LeCroy) and down-loaded to a PC for processing. Toluene based standard solutions were prepared in the concentration range 100 ppm to 1 ppt. The following PAHs were investigated: 2,6-dimethyl phenol, naphthalene, biphenyl, fluorene, phenanthrene, dibenzothiophene, anthracene, fluorantene, pyrene, perylene, benz[a]anthracene, and dibenz[a,h]anthracene. Four soot samples were collected from automobile exhaust systems. 3-4 mg portions of the samples were extracted for 24 hours with 100 ml of n-pentane in a Soxhlet apparatus. 10 μl aliquots of the obtained extracts were analyzed without any additional processing.

The efficiency of the laser desorption and the sensitivity of the method depended on a number of parameters, such as molecular weight, volatility, and molar absorptivity of the analytes and irradiance and wavelength of the laser. The optimum ionization conditions were found to be at λ=280 nm excitation, thus all measurements were performed at that wavelength. Other critical parameters were explored by choosing PAHs with different molecular weights and melting points. The melting point correlated with the molecular mass and could be viewed as a quantitative measure of volatility (phenanthrene: 178.2 amu, Mp=100°C; pyrene: 202.3 amu, Mp=150°C; benz[a]anthracene: 228.3 amu, Mp=160°C; dibenz[a,h]anthracene: 278.4 amu, Mp=266°C). The dependence of the detection limit on the molecular mass of analytes for GC-MS and LD-TOF MS is compared in Figure 1. The increase of molecular weight resulted in a decrease of the detection limit for direct LD-TOF MS, whereas the trend was just the opposite for GC-MS. The lowest detected concentration for LD-TOF MS, 0.01 ppb, was observed for the higher molecular weight PAHs, i.e., perylene and dibenz[a,h]anthracene (see Figure 2).

Figure 3 shows the spectrum of a soot extract. The peaks in the 200-300 amu area belong to PAHs, namely m/z 228 to pyrene and/or crysene, m/z 252 to benzo[a]pyrene, m/z 276 to dibenzanthracene, and m/z 300 to coronene. For identification of structural and quantitative information —very important aspects for environmental analysis— additional techniques can be used. The lack of structural information is a major disadvantage of the direct LD-TOF MS. Fragmentation induced by even shorter wavelength may provide the solution to this problem.

A significant drawback of the commonly used GC-MS is that it gives poor response in the case of larger nonvolatile and more carcinogenic PAHs. In contrast, direct LD-TOF MS demonstrates increasing sensitivity and reproducibility for higher molecular weight condensed aromatic systems. Another important advantage of the used method is the fact that no preliminary sample processing is necessary unlike in the case of chromatographic analysis. The simplicity of sample preparation and the short time of analysis make direct LD-TOF attractive for further development for the analysis of PAH mixtures.

References:

[1] M. Burford, St. Hawthorne, D. Miller, *Anal. Chem.*, **65** (1993) 1497-1505.
[2] A. Robbat, T. Liu, B. Abraham, *Anal. Chem.*, **64** (1992) 1477-1483.
[3] M. Dale, A. Jones, S. Pollard, P. Langridge-Smith, *Environ. Sci. Technol.*, **27** (1993) 1693-1695.
[4] L. Vaek, W. Van Roy, R. Gijbels, F. Adams, In *Laser Ionization Mass Analysis*, A.Vertes, R. Gijbels, F. Adams, Eds.; Wiley: New York, 1993, pp.177-319.

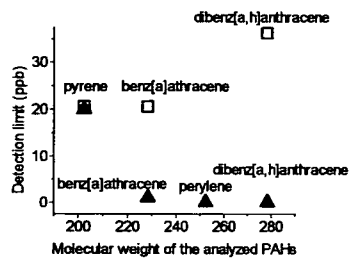

Figure 1. Detection limits as a function of molecular mass of PAHs for GC-MS (□) and direct LD-TOF MS (▲)

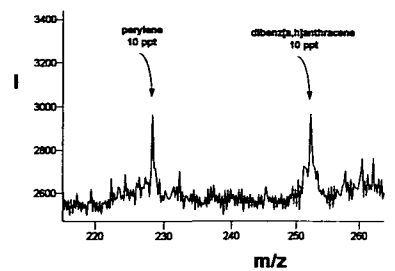

Figure 2. Direct LD-TOF MS spectrum of PAH standards (perylene and dibenz[a,h]anthracene) at 0.01 ppb

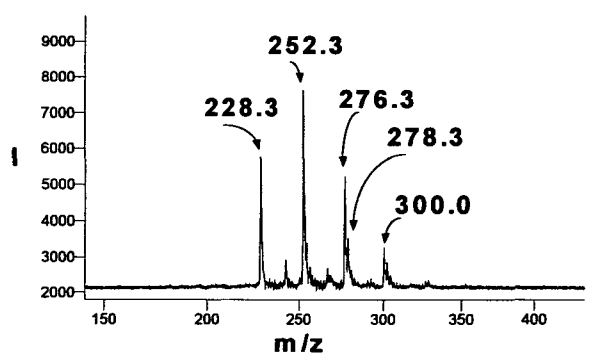

Figure 3. Direct LD-TOF MS spectrum of soot extract at 280nm.

REAL-TIME MONITORING OF AEROSOL REACTIONS

P.G. Carson, M.V. Johnston, Department of Chemistry and Biochemistry
A.S. Wexler, Department of Mechanical Engineering
University of Delaware Newark DE 19716

Rapid Single-Particle Mass Spectrometry has been used to monitor the reaction of ammonia and nitric acid vapor on sodium chloride aerosol particles. The reaction produces an ammonium nitrate surface layer. Sodium chloride particles (3.5μm dia.) were generated with a vibrating orifice aerosol generator and passed through a reaction chamber having constant partial pressure of nitric acid and ammonia. A portion of the particles leaving the reaction chamber were sampled directly into the mass spectrometer through a differentially pumped inlet. A particle beam was formed which then intercepted a continuous laser beam. The scattered radiation from each particle triggered an excimer laser which ablated the particle in flight. Ions produced by laser desorption/ionization were analyzed by time-of-flight mass spectrometry

In these experiments ammonia was the limiting reagent and its partial pressure determined the coating thickness. For a constant laser irradiance, increasing the partial pressure of ammonia caused a proportional increase in the ion signal intensities associated with the ammonium nitrate layer (O^-, OH^-, NO_2^- and NO_3^-). At the same time, the signal intensities of the ions associated with the sodium chloride core decreased (Cl^-, NaCl, $(NaCl)Cl^-$) Laser irradiance dependencies were used to probe the different layers of the coated particles A low laser irradiance preferentially formed ions from the ammonium nitrate surface layer while higher irradiances ablated a greater fraction of the particle and yielded a higher number of ions from the sodium chloride core.

To characterize the coating thickness, we plotted the signal intensity ratio of ions from the surface layer divided by the ions from the core as a function of the laser pulse energy (Figure 1). With a low laser pulse energy (0.2mJ), the spectra obtained from particles exposed to different partial pressures were indistinguishable within the experimental error. This result suggests that only the outer 50 nm of the particle is efficiently sampled by laser desorption/ionization. With pulse energies above 0.5mJ, a greater fraction of the particle is sampled and we can gain semi-quantitative information about the coating thickness from the NO_2^-/Cl^- signal intensity ratio. Figure 1 shows that this ratio increases with increasing coating thickness.

To accurately determine the average thickness of the ammonium nitrate coating, we collected the transformed particles on a teflon filter, removed them from the filter by dissolution in a phthalic acid solution and then determined the chloride to nitrate ratio by HPLC. Figure 2 results showed that the average coating thickness varied between 50 nm and 500 nm depending upon the ammonia partial pressure.

43rd ASMS Conference on Mass Spectrometry and Allied Topics

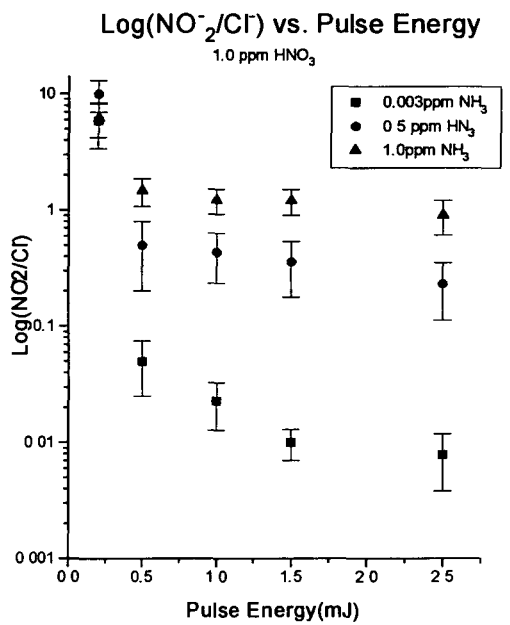

Figure 1

Average Coating Thickness of the Ammonium Nitrate Surface Layer on a 3.5 μm Diameter Sodium Chloride Particle

Ammonia Partial Pressure	Nitric Acid Partial Pressure	Coating thickness
0.003 ppm	1 ppm	50 nm
0.03 ppm	1 ppm	65 nm
0.3 ppm	1 ppm	75 nm
1.0 ppm	1 ppm	500 nm

Figure 2

LASER DESORPTION IONIZATION/FOURIER TRANSFORM MASS SPECTROMETRY FOR CHARACTERIZATION OF POLYMER STRUCTURES

[a]Kuangnan Qian*, [b]Tianlan Zhang, [b]Douglas P. Ridge,
[c]Longsheng Sheng and [a]Vladimir Jovanociceivic
[a]W.R. Grace & Co.-Conn., Washington Research Center, Columbia, MD 21044; [b]Department of Chemistry, University of Delaware, Newark, DE 19716; [c]Extrel FTMS, Madison, WI 53711

INTRODUCTION

The knowledge of polymer structure is important for understanding the chemical and physical properties of industrial polymers that are often manipulated via structural modifications. To analyze polymer structure by mass spectrometry, it is necessary to generate oligomer ions that are large enough to contain structural information by soft ionization techniques, such as laser desorption ionization (LDI). Using tandem mass spectrometry (MS/MS) and high resolution mass spectrometry (HRMS), one is able to obtain detailed chemical structures of homo- and co-polymers. For a copolymer, the relative abundance of oligomer ions provides useful information about its microstructure.

EXPERIMENTAL

Mass spectral data were collected by using an Extrel FTMS 2001 Fourier transform mass spectrometer equipped with a carbon dioxide laser (10.6 μm) probe. Two industrial polymers, poly(α-hydroxy acrylic acid sodium salt) (PHAS) and an ethylene oxide/propylene oxide (EO/PO) copolymer (Pluracol), were studied. PHAS was obtained from Nippon Peroxide Co. with an average molecular weight of 600 Daltons, as determined by gel permeation chromatography (GPC). Pluracol is a commercial product from BASF with an average molecular weight of 4000 Dalton (as determined by GPC). The EO/PO ratio of the polymer is 1.42 by NMR. PHAS was acidified by using HCl to pH≈3 prior to LDI/FTMS analysis. At the original pH, the sample showed no response to LDI. Pluracol was ionized directly by LDI without any matrix assistance.

RESULTS AND DISCUSSIONS

Structures of acidified PHAS by MS/MS and HRMS: Figure 1 shows the oligomer distribution of the acidified PHAS in negative ion mode. Direct examination of the spectrum reveals that there are at least three series of oligomers with a repeating mass of 70 amu, which appears to be consistent with CH_2=CH(COOH). The structure, however, was not confirmed by other analytical data. By using HRMS, we were able to determine that the elemental composition of one oligomer anion (m/z 261) to be $C_9H_9O_9$. Considering that no double bonds are present in the molecules (NMR), we can draw a lactone structure for the oligomer as shown in Figure 1. MS/MS further confirmed the lactone structure by examining a daughter ion spectrum of the oligomer. The combination of HRMS and MS/MS suggests that the acidified PHAS contains mostly polylactones. The repeating mass is 140 amu rather than 70 amu as suggested by the appearance of its mass distribution.

EO/PO copolymer microstructure by a Bernoullian model: The LDI mass spectrum of Pluracol shows oligomers with molecular weight much lower than that measured by GPC, suggesting that the observed species are either the low molecular weight oligomers or the thermal decomposition products of larger oligomers. A detailed examination of the mass spectral data using a multiple sorting procedure revealed the presence of two major oligomer series with molecular weight consistent with general formula (a) and (b).

CH_2=$CHCH_2$-(-OC_2H_4-)$_m$-(-OC_3H_6-)$_n$-OH (a) CH_2=$CHCH_2$-(-OC_2H_4-)$_m$-(-OC_3H_6-)$_n$-OCH_2COCH_3 (b)

The normalized oligomer intensities are compared with statistical calculation using a Bernoullian (random) model (Figure 2 (a)) under the assumptions that (a) the MS responses are uniform for all oligomer ions, (b) the distribution of EO and PO units are random and (c) the polymer dissociation is non-selective. The calculation matches with the experimental observation relatively well for the 11 and 12 mers but poorly for the 4 and 5 mers. To improve the fits for the small oligomers, a lower EO/PO ratio has to be assumed. Figure 2(b) shows that larger oligomers (N>9) have an EO/PO ratio close to the bulk ratio (1.42), implying that the copolymer indeed has a random distribution. The deviation increases as the oligomer size decreases suggesting that the EO/PO oligomer observed by LDI are from selective dissociation of larger oligomers.

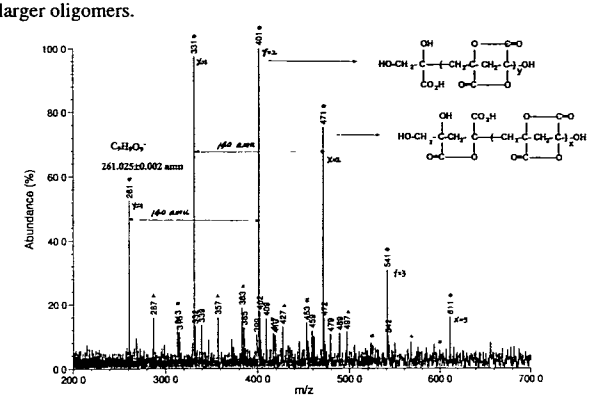

Figure 1. Negative ion mass spectrum of PHAS (acidified) by LDI/FTMS

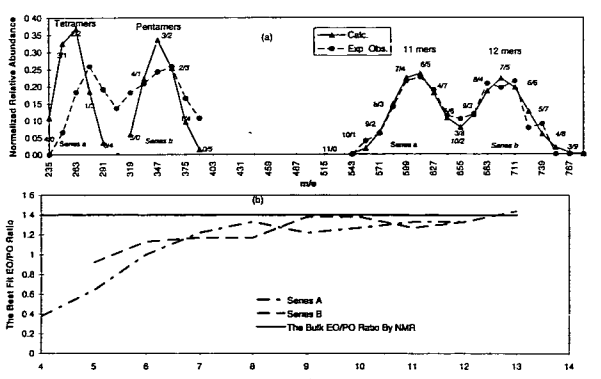

Figure 2. (a) Comparison of oligomer distribution measured by LDI/FTMS and calculated by a Bernoullian model (EO/PO=1 42), (b) The best fit EO/PO ratio as a function of oligomer size.

The electronic spectroscopy of some *p*-alkylphenols and catechols

Louis I. Grace*, Toni L.O. Barstis**, David M. Lubman and Thomas M. Dunn

The University of Michigan, Department of Chemistry, 930 North University Avenue, Ann Arbor, Michigan 48109

Dopamine is a very important neurotransmitter whose biological function has been studied rather extensively. Nevertheless, many questions still exist concerning the physical properties that cause dopamine to manifest its interesting biological behavior. Investigation of the electronic spectroscopy of a molecule often yields insight regarding such properties. In these studies, it is useful to examine the spectroscopy of a set of simpler compounds that are structurally related to the compound of interest, and then to draw analogies among them. To this end, we have studied a set of *p*-alkylphenols and catechols by means of supersonic jet resonant two-photon ionization (R2PI) with mass-selective detection. This technique permits one to obtain a spectrum of the sample in the vapor phase, in which the electronic states of the molecule are not perturbed as they would be in solution. It also yields spectra in which transitions to individual excited states may be resolved. In addition, the mass-selective detection, as compared to other detection schemes, affords one much greater confidence that the observed spectrum arises from the molecule of interest and not, for example, from a cluster species or a contaminant.

Although many studies have been made of the ultraviolet spectroscopy of dopamine in solution, so far, no one has obtained a vapor-phase spectrum for dopamine. We have obtained R2PI spectra for several compounds that are closely related to dopamine. Despite considerable effort, however, we have not been able to obtain a spectrum for dopamine itself. In the course of our studies, we have found that certain catechols exhibit unusual behavior regarding the conditions under which they yield R2PI spectra. This behavior may offer clues as to why the vapor-phase electronic spectrum of dopamine has not yet been observed.

The molecules we studied were *p*-ethylphenol, *p*-isopropylphenol, tyramine, tyrosine, cathechol, 4-methylcatechol, 4-ethylcatechol, dopamine and 3-methoxytyramine (3-O-methyldopamine). We made R2PI assignments for all of these except for dopamine. To aid us in the R2PI assignments, we used infrared and Raman data to make correlations among the ground states of these molecules, and between the ground-state data and the R2PI data. The ground state for *p*-cresol is well known,[1] and was useful as a guide for the *p*-alkylphenol assignments. The well-known

*Current address: University of California, Lawrence Livermore National Laboratory, P.O. Box 808, Livermore, California 94550.

**Current address: Saint Mary's College, Department of Chemistry and Physics, Notre Dame, Indiana 46556.

[1]R.J. Jakobsen, *Spectrochimica Acta*, **21**, 433-442 (1965).

catechol ground state[2] served as a guide for the catechol R2PI assignments. We assigned the 4-substituted catechols by analogy to existing assignments for other 1,2,4- trisubstituted benzenes.[3] 4-methyl- and 4-ethylcatechol yielded spectra only when the jet stagnation pressure was greatly reduced from the normal operating pressure (1atm absolute). An example of this behavior is shown in the accompanying panel.

R2PI spectra of 4-ethylcatechol with 90% neon/10% helium carrier gas at three different stagnation pressures

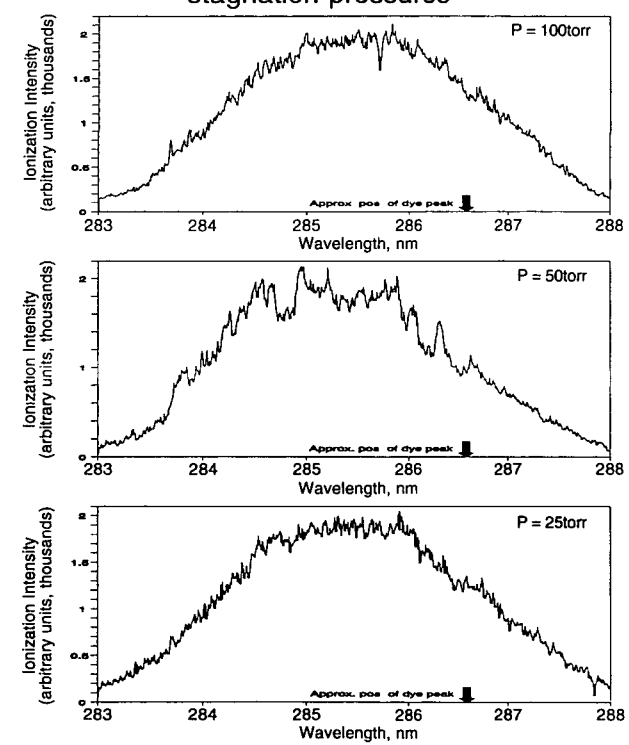

[2]Sarah J. Greaves and William P. Griffith, *Spectrochimica Acta*, **47A**(1), 133-140 (1991).
[3]G. Varsányi, *Assignments for Vibrational Spectra of Seven Hundred Benzene Derivatives* (New York: John Wiley and sons, 1974).

Laser Desorption/Ionization of Size Resolved Liquid Microdroplets

Bashir A. Mansoori* and Murray V Johnston, Department of Chemistry and Biochemistry
Anthony S. Wexler, Department of Mechanical Engineering
University of Delaware, Newark, DE 19716.

There is a continuing need for techniques that perform real time chemical characterization and quantitation of atmospheric aerosol particles Rapid single-particle mass spectrometry (RSMS) permits on-line analysis of aerosol particles by laser desorption/ionization. Particles are sampled directly into the source region of mass spectrometer where they are detected by light scattering from a continuous laser beam and then analyzed by laser desorption/ionization.

To understand the relationship between particle size and the resulting signal intensity, we have studied liquid microdroplets generated with a monodisperse aerosol generator. Liquid droplets have several advantages for quantitative work including well-defined morphology (spherical and homogenous), constant matrix composition surrounding the analyte, and straight forward preparation of calibration aerosol droplets having a known amount of analyte. The effects of droplet size, analyte concentration and laser irradiance on the signal intensity were systematically studied using two types of droplets glycerol droplets containing dissolved metal salts and 3-nitrobenzyl alcohol droplets containing the peptide leucine enkephalin.

For glycerol droplets containing inorganic cations and anions the threshold laser fluence for analyte ion detection is approximately 0.2 J/cm^2. With particles smaller than 5 µm diameter, the signal intensity is relatively invariant with increasing laser fluence Figure 1 shows plots of signal intensity vs. droplet diameter for glycerol droplets containing $FeCl_3$. This data was taken with a high laser fluence (3.4 J/cm)^2. As the droplet diameter increases, the signal intensity also increases but the relationship is nonlinear. However the signal intensity does increase linearly with volume. With low laser fluences and large (>5 µm) particles, the signal intensity correlates more closely with droplet surface area. Thus, high laser fluences appear to promote volume desorption, while low laser fluences appear to promote surface desorption. For a given particle size and laser fluence, the relationship between analyte peak area and analyte concentration is linear.

Matrix-assisted laser desorption/ionization (MALDI) can also be performed in liquid droplets For nitrobenzyl alcohol droplets containing leucine enkephalin the threshold for analyte signal detection is approximately 0.3 J/cm^2 Initially the peak area increases with laser fluence, but it reaches a plateau around 1 J/cm^2. Figure 2 shows the relationship between $(M+Na)^+$ peak area and concentration of leucine enkephalin in nitrobenzyl alcohol for 4.7 µm and 2.6 µm diameter droplets, respectively These plots indicate surface desorption and a surface preference for leucine enkephalin. The peak area increases with increasing concentration until a plateau is reached when monolayer coverage is achieved.

43rd ASMS Conference on Mass Spectrometry and Allied Topics

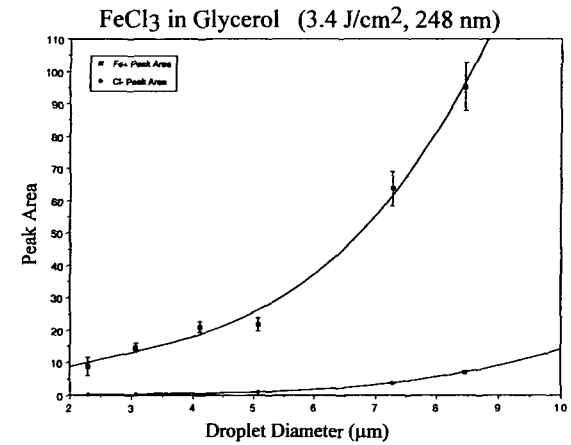

Figure 1

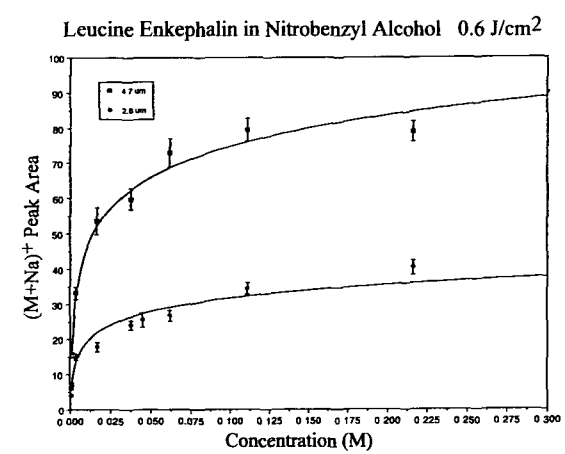

Figure 2

LASER DESORPTION IONIZATION T-O-F MASS SPECTROMETRY OF HYDROXY-NITROPAHs.

Dawit Bezabeh, and Peter B. Kelly, Department of Chemistry;
A. Daniel Jones, Facility for Advanced Instrumentation,
University of California, Davis CA 95616.

Introduction

Nitrated polycyclic aromatic hydrocarbons (NitroPAHs) are formed by reaction between PAHs and nitrogen oxides and/or nitric acids during incomplete combustion of organic matter. Analysis for nitroPAHs is complicated by the fact that their concentration are one to two orders of magnitude less than those of analogous unsubstituted PAHs. Our laboratory has been employing detection of negative ions for the purpose of selective detection of nitroPAHs over the large background of PAHs in environmental samples. In the environment, nitroPAHs are believe to further react with oxygen and/or hydroxyl radical to form hydroxy-nitroPAHs. Hydroxy-nitroPAHs, in general, are consider to be degradation products of nitroPAHs, hence we are investigating the negative ion laser desorption ionization of hydroxy-nitroPAHs.

Hydroxy-nitroPAHs are very difficult to analyze by other analytical methods, such as GC/MS, due to their acidity and polarity. Laser desorption ionization time-of-flight mass spectrometry has the potential to overcome the difficulty of analyzing polar hydroxy-nitroPAHs. The primary aim of the present study is to gain structural information about the photodegradation of hydroxy-nitroPAH and utilize these method to examine and investigate the chemistry of nitro-PAH photodegradation.

Experimental

Laser desorption ionization mass spectra were obtained using a custom-built time-of-flight mass spectrometry. A sample was prepared by depositing a small aliquot of the sample solution on a metal probe tip The sample was allowed to air-dry, forming a thin solid layer. Pulsed UV radiation at 266 nm was generated using the fourth harmonic of Quanta Ray DCR-3 ND:YAG laser with an 8 ns pulse width and focused in to the source region at a 45° angle of incidence on the surface of the sample. Spectra are obtained with a UV laser energy of 0.3 - 5 0 uJ/pulse

Results

Our initial work on the application of negative ion laser desorption ionization time-of-flight mass spectrometry of hydroxy-nitroPAHs yield structurally important peaks. The negative ion mass spectra of all hydroxy-nitroPAH standards gave $[M-H]^-$ as the most abundant peak. The hydroxyphenols show dimer and trimer anion formation with weak NO_2^- peak

As found in our earlier studies of nitroPAHs, characteristic CN^- and NO_2^- peaks were observed in the negative ion mass spectra of hydroxy-nitroPAHs with more than one benzene ring. The negative ion approach works well for analysis of mixtures of hydroxy-nitroPAHs. Good quantitative agreement between laser desorption ionization and electrospray ionization was found.

We gratefully acknowledge support from the National Institutes of Health "Superfund" program (Grant 2-P42-ES046699) and the California Air Resources Board (Grant No. A9-32-099).

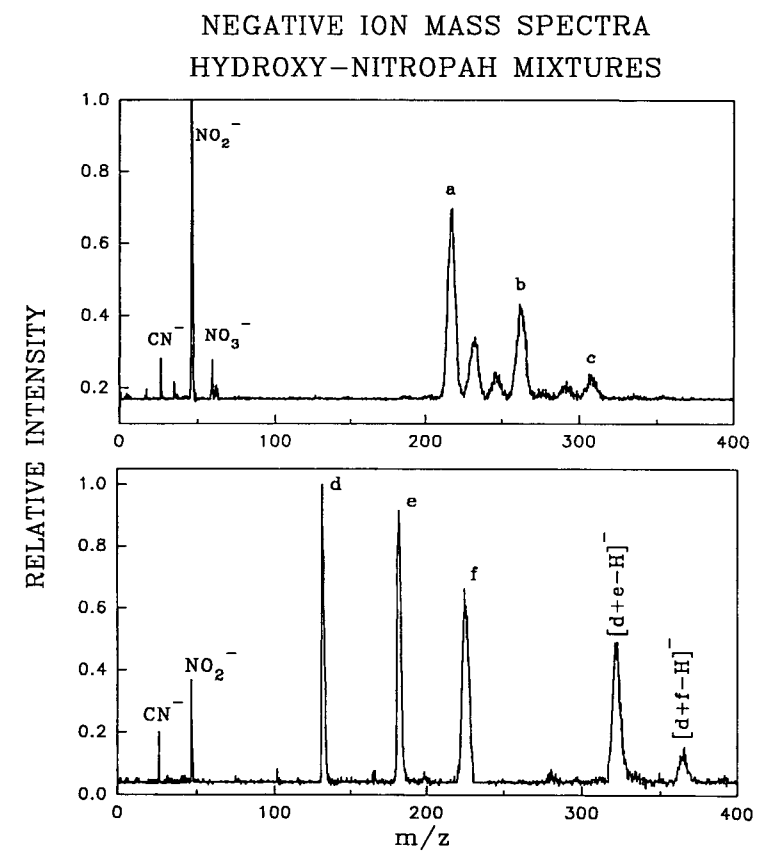

a = 1-HYDROXYPYRENE (217)
b = 1-HYDROXY-MONO-NITROPYRENE (262)
c = 1-HYDROXY-DI-NITROPYRENE (307)
d = 4-NITROPHENOL (138)
e = 2-NITRO-1-NAPHTHOL (188)
f = 9-HYDROXY-2-NITROFLUORENE (226)

Infrared Spectroscopy of Methanol attached to Gold Cluster Ions

G. Dietrich[1], H.-J Kluge[2], K. Lutzenkirchen[1], L Schweikhard[3], C. Walther[3], and J Ziegler[3]

[1]Johannes Gutenberg-Universität, Institut für Kernchemie, D-55099 Mainz, Germany
[2]Gesellschaft für Schwerionenforschung, D-64220 Darmstadt, Germany
[3]Johannes Gutenberg-Universität, Institut für Physik, D-55099 Mainz, Germany

Infrared spectroscopy is one of the standard applications for structural elucidation of molecules It delivers information about the bonds inside the examined molecule via excitation of the vibrational states. For molecules attached to cluster ions in the gas phase, the absorption of IR photons results in the dissociation of the complex Both the number and the energy of the absorbed photons yield information about the bond strength and the vibrational frequency of the excited bond, respectively [1].

We report first results on infrared multi-photon dissociation (IR MPD) of cluster ions consisting of Au_4^+ and up to three methanol molecules attached. The gold clusters are produced by laser vaporization and transferred into a Penning trap. Methanol gas is added into the trap ($p \approx 1\times10^{-5}$ mbar) and adsorbed on the clusters. The products with either one, two, or three alcohol molecules attached are selected by radial ejection of all unwanted species. The beam of a line-tunable pulsed CO_2-laser (930-982 cm^{-1} and 1035-1086 cm^{-1}) is focused axially into the trap. In resonance, the absorption of photons leads to an evaporation of one or several methanol molecules. For identification, the dissociation product ions are ejected out of the trap and detected by time-of-flight mass spectrometry. For a detailed description of the experimental setup see ref. [2].

Figure 1 shows the resulting TOF-spectra of the experimental sequence. The distribution of $Au_4^+\cdot(CH_3OH)_{0\text{-}3}$ (fig. 1a) is obtained by the reaction of Au_4^+ with methanol for the storage period of 700 ms. In figure 1b the complex $Au_4^+\cdot(CH_3OH)_3$ is selected by radial ejection of all unwanted ions. The resulting spectrum of the IR MPD is shown in figure 1c. the ion dissociates up to three alcohol molecules after the interaction with the CO_2-laser beam at a frequency of 957.9 cm^{-1} and a power of 300 mJ. The dissociation process can be interpreted as the result of the excitation of the CO stretching vibration of the methanol molecules This leads to the breaking of the weak bond between the cluster and the attached alcohol molecule. No fragmentation of the gold cluster has been observed.

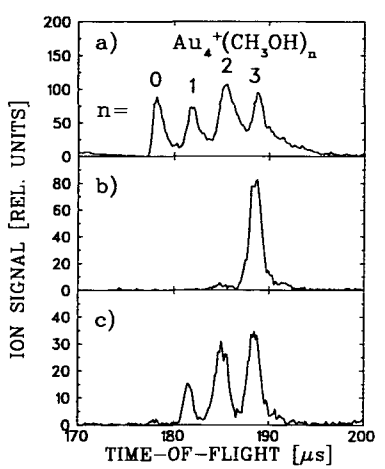

Fig. 1: Mass spectra showing the experimental sequence The reaction of the trapped Au_4^+ ions with methanol results in a distribution of attached alcohol molecules to the gold cluster ion (a) After selection of one of the ion-molecule complexes, e.g $Au_4^+\cdot(CH_4OH)_3$ (b), the dissociation of the complex is achieved by the exposure to the radiation of a CO_2 laser, e.g. 957.9 cm^{-1} (c).

In figure 2 the fragmentation yield of the IR MPD of $Au_4^+\cdot(CH_3OH)_{1\text{-}3}$ is plotted as a function of wavenumber. Compared to the frequency of the CO stretching vibration in the free methanol monomer at 1033.5 cm^{-1} [3] different red-shifts of the centers of the absorption bands for the three examined ions can be observed. The splitting of the bands for more than one methanol attached to the cluster can be explained by the formation of a hydrogen bonded methanol dimer on the surface of the cluster. The non-equivalent CO bonds absorb at different frequencies. A similar effect has been observed in a beam depletion spectroscopy experiment of size-selected methanol clusters [3]

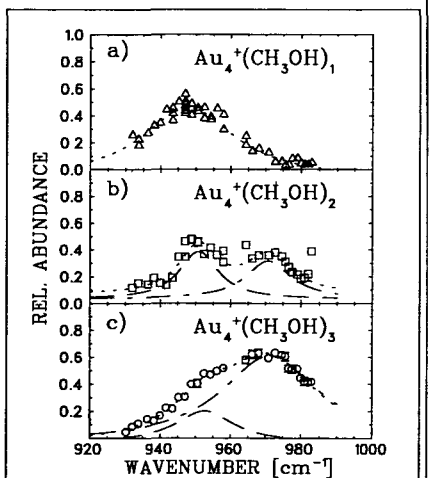

Fig. 2: Fragmentation yield as a function of the wavenumber of $Au_4^+\cdot(CH_4OH)_n$ (n = 1-3). The dashed lines are fitted Lorentzian curves, the dotted lines may guide the eye. The laser power was 472 mJ (n = 1) and 300 mJ (n=2,3)

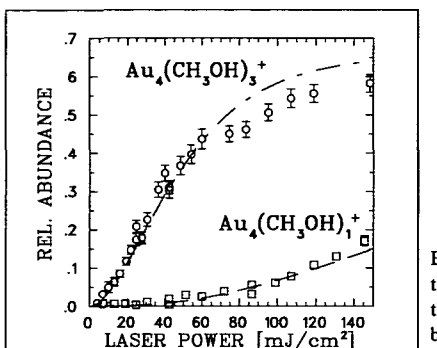

Fig. 3: Fragmentation yield as a function of the laser fluence of $Au_4^+\cdot(CH_4OH)_n$ (○ n = 3, ●: n = 1). The dashed lines represent processes due to 3 and 2 absorbed photons respectively.

By variing the laser power at a fixed wavenumber at the center of the depletion spectrum, the number of the absorbed photons required for fragmentation can be determined (fig 3). The data are fitted to multi-photon-fragmentation models [4] In the case of n = 2, 3 two photons were absorbed while for one adsorbed methanol molecules 3 photons were required. This indicates a larger bond strength for the $Au_4^+\cdot(CH_3OH)_1$ ion. Figure 3 shows the fragmentation yield depending on the laser power for n = 1, 3 In addition, the cross section of the photofragmentation could be determined to 2.3×10^{-19} cm^2 (n = 1, 947.0 cm^{-1}), 3.7×10^{-19} cm^2 (n = 2, 948.8 cm^{-1}) and 7.4×10^{-19} cm^2 (n = 3, 968 1 cm^{-1}).

This work was supported by the Deutsche Forschungsgemeinschaft and the Materialwissenschaftliches Forschungszentrum Mainz.

[1] M R. Zakin et al., J Chem. Phys **85** (1986) 1198
[2] St. Becker et al., submitted to Rev Sci Instrum.
[3] F. Huisken et al., Z. Phys. D - Atoms Molecules and Clusters **24** (1992) 277
[4] C Walther, Diploma Thesis, Universität Mainz (1994)

Laser Desorption / Resonant Laser Ablation - Trace Analysis of Solid Matrices

C. G. Gill*, A. W. Garrett, W. L. Earl, N. S. Nogar and P. H. Hemberger
CST-1, MS J565, Los Alamos National Laboratory, Los Alamos, NM, 87545

Laser desorption (LD) and ablation (LA) have been recognized for some time as potentially useful methods for chemical analysis, in particular as methods for sample introduction for both organic and inorganic mass spectrometry (MS). Quadrupole ion trap MS is well suited to pulsed ionization sources, such as LD and LA, making it a suitable mass analyzer for this type of experiment. LD-MS frequently involves sample desorption from a matrix material or a solid sampling support [1], with the intent of providing quantitative and qualitative information about the content and structure of a sample. LA-MS typically ablates material from a native solid sample [2] in order to provide elemental or isotopic information from the analysis. Although most LA has utilized fixed frequency lasers operating at relatively high irradiance (~10^9 W·cm^{-2}), there has been some recent interest in the use of resonant laser ablation (RLA) [3] which typically uses modest intensity laser pulses tuned to a one- or two-photon resonant transition in the analyte to enhance the ionization yield. To obtain useful mass spectrometric information about trace analytes in solid analytical samples, the chemical form of the analyte must be considered. Our approach to trace MS analysis of solid samples uses LD to generate intact molecular ions for analytes on a solid support matrix, and RLA to create atomic species from solid materials, either of which can then be analyzed by quadrupole ion trap mass spectrometry.

The analysis of organics by LD-MS is presented for several solid support matrices. This work presents quantification for LD of pyrene as a linear calibration curve over four decades of concentration from ppb-ppm, demonstrating the utility of LD-MS for quantitative work. In addition, a complex PAH Standard mixture was analyzed utilizing Ambersorb as a sampling support, illustrating the use of a sampling sorbent with LD-MS for characterizing complex mixtures. Current research includes the investigation of chemically modified silica support matrices, sol-gels, zeolites, and carbon based adsorbents as solid sampling supports for LD-MS.

Resonant Laser Ablation (RLA) provides significant advances, which are presented by this work. RLA increases the ionization yield for target analytes by tuning the ablation laser to a resonant one- or two-photon transition. This selectivity is demonstrated by Figure 1, which shows two mass spectra, one for the Cu(2+1) resonance, and one off resonance. The striking appearance of the copper ions in the RLA mass spectrum illustrates the utility of the method, in that analytes can be selectively ionized in the presence of a bulk sample matrix. By tuning the laser wavelength to desired resonant transitions, target analyte signals can be enhanced manifold (up to 22,000X) over non-resonant laser ablation. The "2+1" optical spectrum for several analytes was determined using the method, and it was observed (for copper) that the transitions were laser linewith limited at 1.11cm^{-1}. Figure 2 shows the RLA optical spectrum for the Cu(2+1) resonance. This was obtained by analyzing a SRM664 steel sample, using 463.507 nm laser light to excite neutral Cu from $[3d^{10}4s]^2S_{1/2}$ --> $[3d^{10}5s]^2S_{1/2}$ (two photons), using a third photon to ionize the atom from this resonant energy level. The effect of linewidth for the RLA process was investigated, the result of which was an inverse relationship between selectivity and linewidth. The etch rate for the RLA process was measured by using thin films of copper on silicon as being 3X10^{-13} g/shot, facilitating the determination of meaningful absolute detection limits in the attogram range.

References
1. Cisper, M.E., Earl, W.L., Nogar, N.S. & Hemberger, P.H. *Anal. Chem.* **66**, 1897-1901 (1994).
2. Gill, C.G. & Blades, M.W. *Journal of Analytical Atomic Spectrometry* **8**, 261-267 (1993).
3. Garrett, A.W., Hemberger, P.H. & Nogar, N.S. *Spectrochimica Acta*, **accepted** (1995).

Figure 1: RLA Selectivity for Cu in a NIST steel sample.

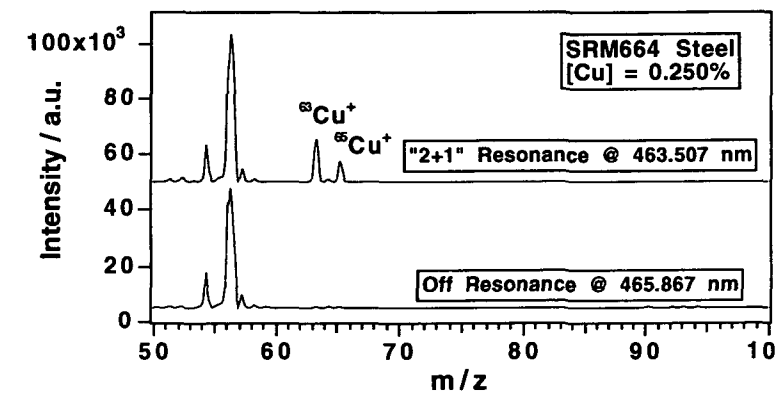

Figure 2: RLA optical spectrum for the Cu(2+1) resonance at 463.507 nm.

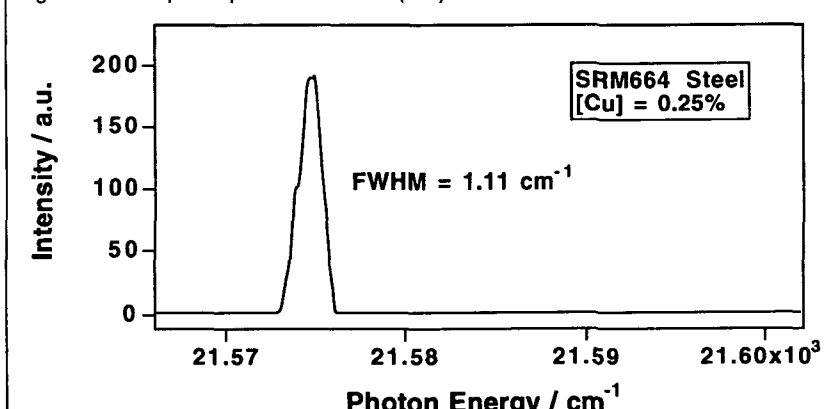

Lanthanide, Thorium, and Uranium Oxide Clusters Formed by DLV/FTICR

António Pires de Matos, Joaquim Marçalo, and João Paulo Leal
Departamento de Química, Instituto Tecnológico e Nuclear
P- 2686 Sacavém Codex, Portugal

In this work we report the formation of clusters of all the lanthanides (except promethium), thorium and uranium by direct laser vaporization (DLV) of surface oxidized metallic targets in a vacuum of about 2 x 10^{-8} Torr. The cluster ions were obtained using a Nd:YAG laser pulse (ca. 30 mJ at the fundamental 1064 nm wavelength) and the ions were stored in the trap of an Extrel (Waters) FTMS 2001-DT Fourier transform ion cyclotron resonance (FTICR) spectrometer.

We observed for all the lanthanides (Ln) that the clusters showed a sequential addition of Ln_2O_3 units in forming increasingly larger clusters, with two main series of the type $[Ln_mO_{(3m-1)/2}]^+$ (m odd) and $[Ln_mO_{(3m-2)/2}]^+$ (m even). Figure 1 shows the two series of oxide clusters for praseodymium. Work on lanthanide clusters has been reported by Gibson[1] using excimer laser abalation of lanthanide oxalates in a reflectron time of flight mass spectrometer, and by Kemp and Read [2], and Selbin et al [3,4] by fast atom bombardment (FAB) mass spectrometry of lanthanide salts. In some lanthanides, and due to the high resolution of the FTICR instrument, we could identify the two following clusters with hydrogen: $[Ln_2O_3H]^+$ and $[Ln_4O_6H]^+$ in which the fragment valence is 3 if H is present as OH. For Ce, with the 4 valence state accessible, we observed also clusters where the valence state is larger than 3, as for example in the series $[Ce_mO_{(3/2)m}]^+$.

For Eu, we observed clusters of the series of the type $[Eu_mO_{(3m-2)/2}]^+$ (m even), $[Eu_mO_{(3m-3)/2}]^+$ (m odd), $[Eu_mO_{(3m-4)1/2}]^+$ (m even), $[Eu_mO_{(3m-5)1/2}]^+$ (m odd), $[Eu_mO_{(3m-6)/2}]^+$ (m even) as previously reported by Gibson[1], but in addition we found clusters with hydrogen and in particular we mention here the clusters $[Eu_2O_2H]^+$, $[Eu_2O_3H_3]^+$ and $[Eu_3O_4H_3]^+$ in which all the Eu sites are in valence 2 if hydrogen is present as OH. Figure 2 shows the oxide clusters for europium.

For Th the clusters formed showed sequential addition of ThO_2, with the series $[Th_mO_{2m-1}]^+$ approaching a fragment valence 4 with increasing m. For U, five series of clusters were observed, $[U_mO_{2m}]^+$, $[U_mO_{2m-1}]^+$, $[U_mO_{3m-1}]^+$, $[U_mO_{3m-2}]^+$, and $[U_mO_{3m-3}]^+$, showing a sequential addition of UO_3 and UO_2, approaching fragment valences of 4 or 6, the most stable oxidation states in the case of uranium. While for U the largest cluster obtained was $[U_5O_{13}]^+$, for Th it was possible to obtain $[Th_{11}O_{21}]^+$. Figure 3 shows the oxide clusters obtained in this work for uranium. Thorium and uranium clusters have been previously obtained by Michiels and Gijbels (m = 1,2,3) using LAMMA [5] of oxides, and by Jennings et al [6], Tench et al [7], and Brown and Ismail [8] using FAB of thorium and uranium salts.

Summarizing, in all cases the cluster composition depends on the accessibility of the metal valence states, Ln(III) sites are dominant for the lanthanides, Ln(II) more easily accessible for Eu, M(IV) only for Ce, Th and U, and M(VI) for U.

Acknowledgment The authors thank JNICT (PBIC/C/CEN/1193) for financial support.

References [1] Gibson, J. K. *J. Phys. Chem.* **1994**, *98*, 11321. [2] Kemp, T. J. ; Read, P. A. *J. Chem. Soc. Dalton Trans.*, **1995**, 875. [3] Kahwa, I. A.; Selbin, J.; Hsieh, T. C.-Y.; Laine, R. *Inorg. Chim. Acta* **1988**, *141*, 131. [4] Kahwa, I.A.; Selbin, J.; Hsieh, T. C.-Y.; Evans D. W.; Pamidimukkala, K. M.; Laine, R. *Inorg. Chim. Acta* **1988**, *144*, 275. [5] Michiels, E.; Gijbels, R. *Anal. Chem.* **1984**, *56*, 1115. [6] Kemp, T. J. ; Jennings, K. R.; Read, P. A. *J. Chem. Soc. Dalton Trans.*, **1995**, 885. [7] Tench, R.J.; Balooch, M.; Bernardez, L.; Allen, M. J.; Siekhaus, W. J.; Olander, D. R.; Wang, W. *J. Vac. Sci. Technol.*, **1991**, *B9*, 820. [8] Brown, D. A.; Ismail, S. *Inorg. Chim. Acta* **1990**, *171*, 41.

43rd ASMS Conference on Mass Spectrometry and Allied Topics

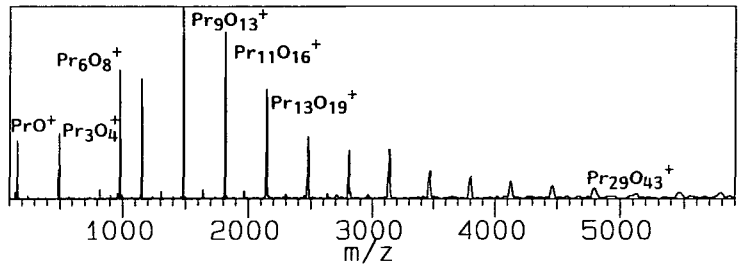

Fig. 1 DLV/FTICR spectrum of surface oxidized metallic praseodymium.

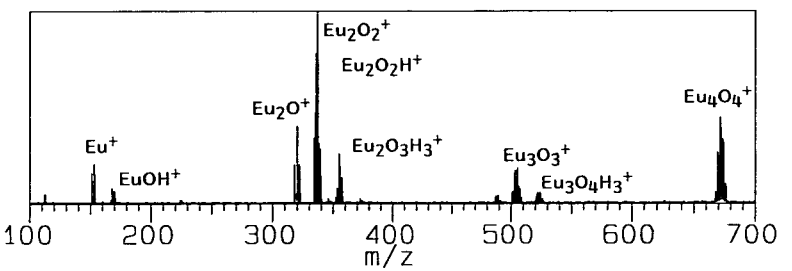

Fig. 2 DLV/FTICR spectrum of surface oxidized metallic europium.

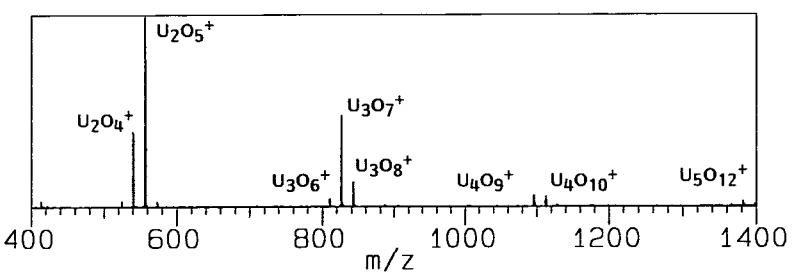

Fig. 3 DLV/FTICR spectrum of surface oxidized metallic uranium.

Photolabalisation of Fe Bound Phosphine Ligands: Laser Desorption FT ICR MS.

Robin Aplin, Stephen Davies, Tom McCarthy and W Carl Watkins, The Dyson Perrins Laboratory, Oxford University, South Parks Road, Oxford, OX1 3QY, UK, Dwight Evard and Garry Krupper, Bruker Inst., Inc. Billerica, MA 01821, USA.

Contrary to the accepted dogma that Fe complexes containing both phosphine and carbon monoxide ligands preferentially lose the latter on photolysis. Davies *et al*,[1,2,3,4] have shown by a series of elegant but complex experiments that the primary photoreaction in a number of cases is the loss of the phosphine ligand. Nitrogen laser desorption **without** a matrix on a Bruker 4.7 BioApex MALDI FT ICR MS instrument has been used to study the photolabalisation of two different classes of iron phosphine complexes (1-3 and 4-6). Photolysis followed by FT ICR MS analysis showed that the complexes (1-3) decompose by cleavage of the phosphine- Fe bond to form predominently non-Fe containing species

(1) ------- *hv* ---- m/z 277, Ph_3P^+Me and m/z 339, Ph_4P^+.
(2) ------- *hv* ---- m/z 339, Ph_4P^+.
(3) ------- *hv* ---- m/z 319, p-tolyl$_3P^+$Me and m/z 395, p-tolyl$_4P^+$.

A similar analysis of tri-phenylphosphine and tri-p-tolylphosphine produced similar quaternary species:

Ph_3P ---- *hv* ---- m/z 339, Ph_4P^+.
p-tolyl$_3$P ---- *hv* ---- m/z 395, p-tolyl$_4P^+$.

Photolysis followed by FT ICR MS analysis of the complexes (4-6) showed that they decomposed by loss of CO to form predominently two Fe containing species.

(4) ------- *hv* ---- m/z 383, $Ph_3PFe^+C_5H_5$ and m/z 399, $Ph_3FeO^+C_5H_5$.
(5) ------- *hv* ---- m/z 383, $Ph_3PFe^+C_5H_5$ and m/z 399, $Ph_3FeO^+C_5H_5$.
(6) ------- *hv* ---- m/z 425, p-tolyl$_3PFe^+C_5H_5$ and m/z 441, p-tolyl$_3PFeO^+C_5H_5$

The quaternary phosphines detected from the complexes (1-3) were also observed as was expected from the known phototransformation of these Fe-COR and Fe-COAr complexes into the corresponding Fe-R and Fe-Ar complexes[4]. These investigations show that the nitroger laser photolysis followed by desorption and FT ICR MS provides a facile and rapid approach to the study of the photochemical decomposition of organometallic complexes.

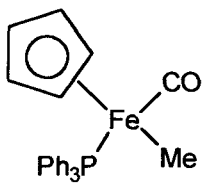

1

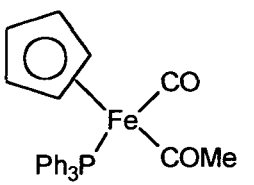

4

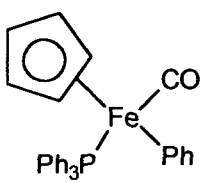

2

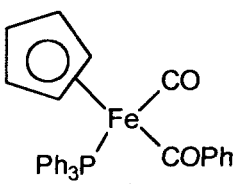

5

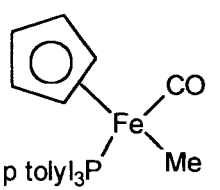

3

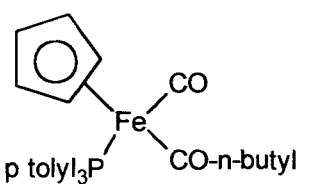

6

1. S.G.Davies, M.R Mitzer, K.Yanada and R Yanada, *J.Chem.Soc.,Chem.Commun.*, 1993, 658-659.
2. S G.Davies, M.R.Mitzer, W.Carl Watkins, R.G.Crompton, J.Boothand, J.C.Eklund, *J.Chem.Soc.,PerkinTrans*, 2, 1993, 1005-1007.
3 S.G.Davies, M.R.Mitzer, W.Carl Watkins, R.G.Crompton, J.Boothand, J C Eklund, *ibid.*, 1993, 1603-1609
4. S.G.Davies and W.Carl Watkins, *J.ChemSoc.,Chem.Commun.*, 1994, 491-492.

Laser Ablation Mass Spectrometry of Sodium Penetrated Petroleum Cokes

Gary D. Willett, F. G. Hopwood and K. J. Fisher, School of Chemistry, The University of New South Wales, Sydney, NSW 2052, Australia
Paul G. Greenhill, Comalco Research Centre, 15 Edgars Road, Thomastown, VIC 3074, Australia

Introduction: Potassium and sodium modification of metallurgical cokes and carbon anodes and cathodes is of considerable interest to the aluminium industry as it can ultimately lead to the destruction of these materials. We have undertaken a laser ablation Fourier transform mass spectrometry study of a variety of carbon based materials including graphite, thermal black, carbon fibre, pitch coke, petroleum coke and glassy carbons in an effort to obtain information concerning the mechanism of sodium modification of these materials. A systematic analysis of a series petroleum cokes and sodium penetrated petroleum cokes which have been graphitised to different extents over the temperature range 800-2100°C have revealed noticeable differences in their respective negative-ion laser ablation FT-mass spectra.

Results and Discussion: Fig. 1 shows the effect of sodium modification of the graphitised petroleum coke on the negative-ion laser ablation (1064 nm) FT- mass spectra.

The striking results from the negative ion experiment are that:

(i) The sodium modification of the petroleum coke alters the production of the negative ions. Fig. 2 shows that the mass average of the carbon anion clusters decreases as the laser power increases. The corresponding sodium penetrated coke sample shows the opposite effect with a slight increase in carbon cluster mass average.
The carbon cluster mass average was calculated as $\frac{\Sigma mI}{\Sigma I}$ *where m = mass of carbon cluster and I = mass spectral intensity of carbon cluster.*

(ii) For the coke graphitised at 800°C, the anion production ceased at a laser power of 1,000 MW/cm^2 whereas for the sodium penetrated coke it ceased at 5,100 MW/cm^2.

(iii) The sodium penetrated cokes produce a greater abundance of the larger (C_n^- n>16) carbon cluster anions.

(iv) At low laser powers (1,000 MW/cm^2) there is significantly more hydrogenation of the carbon clusters produced with the sodium penetrated coke than is observed for the unpenetrated coke. There are generally two peaks associated with the odd-numbered clusters; C_n^- and C_nH^- whereas the even-numbered clusters exhibit three peaks C_n^-, C_nH^- and $C_nH_2^-$.

(v) In a separate experiment, *for which the mass spectral results are not shown here*, less graphitised carbon has a larger uptake of sodium and consequently a greater disruption of the carbon lattice which results in a larger carbon cluster mass average.

The positive-ion laser ablation mass spectra of the sodium penetrated carbons did not reveal any unusual features besides the presence of Na^+ and a range of hydrogenated carbon clusters. However, as Fig. 3 reveals, at low laser powers (~50 MW/cm^2) the raw petroleum coke readily produces a distribution of fullerene cations. At higher laser powers (~300 MW/cm2) the fullerene ions give way to smaller carbon cluster ions.

The addition of KCl to the petroleum coke shows that KCl enhances the production higher mass carbon cluster anions (m/z 200-500 dalton). The electron affinity of Cl is -3.63 eV which is very similar to that of many carbon cluster ions. For example, the electron affinities C_{13} and C_{17} are -3.60 eV. Presumably then, this increase in the number of carbon cluster anions due to the addition of KCl to the petroleum coke arises because of charge transfer between chloride based anions and the neutral carbon clusters.

Metal containing carbon clusters: There is no evidence in the laser ablation FT-mass spectra of the sodium penetrated carbons for carbon clusters which contain sodium. However, some of the carbons when doped with metal oxides readily form both fullerenes and metallofullerenes. Fig. 4 shows the cation LA/FT-mass spectra of a La_2O_3 / thermal black mixture.

Anion carbon cluster reactions with sulfides: The anion carbon clusters produced from the laser ablation of the petroleum cokes have revealed some unexpected reactions with sulfur based compounds. For example, Fig. 5 shows that the reaction of the odd-numbered C_9^- anion cluster produces a range of reaction products including HS^-, C_8H^-, $C_5S_2^-$, $C_8H_3S^-$, C_9HS^-, $C_9H_3S_2^-$. The reaction of $C_8H_x^-$ anions with H_2S produces only a $C_8H_x^-$.....H_2S adduct. We are currently studying the kinetics of these reactions.

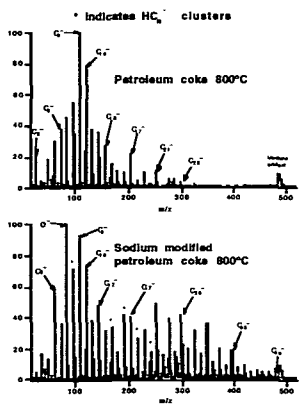

Fig. 1 Anion laser ablation mass spectra at a laser power of 600 MW/cm^2.

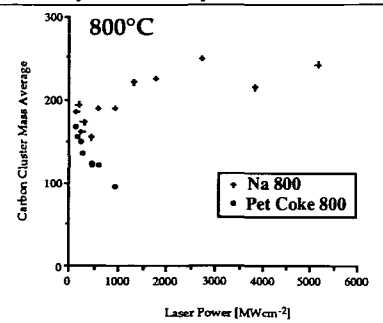

Fig. 2 Carbon cluster size versus laser power for pet-coke and sodium penetrated pet-coke.

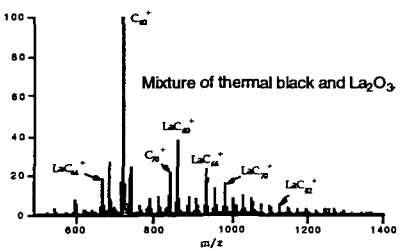

Fig. 4 Cation laser ablation mass spectrum of thermal black mixed with La_2O_3.

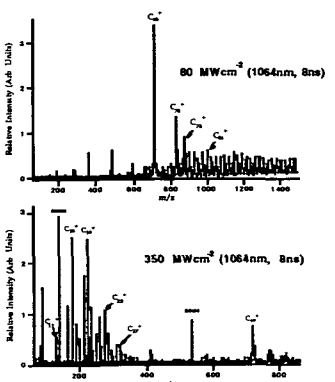

Fig. 3 Cation laser ablation mass spectra of petroleum coke at different laser powers.

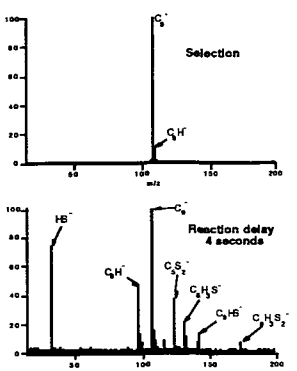

Fig. 5 Reaction of C_9^- and H_2S at 1x10^{-7} mbar.

LASER MASS SPECTROMETRY OF SYNTHETIC LINEAR AND DENDRITIC POLYMERS.

Ian A. Mowat, Robert J. Donovan, Morag Bruce and John J. Monaghan.
Department of Chemistry, University of Edinburgh, West Mains Road, Edinburgh, SCOTLAND, UK, EH9 3JJ.

(1) Introduction.

Laser mass spectrometry is an effective technique for the determination of the molecular weight distributions of a range of synthetic polymers (1-3). Previously this has been done using chromatographic methods such as Gel Permeation Chromatography or HPLC, or physical methods such as viscosity measurements. Unfortunately these methods require external calibration with a reference compound or significant information on the polymer's physical properties. Laser mass spectrometry enables large non-volatile molecules to be produced in the gas phase without significant decomposition or fragmentation. Time-of-flight analysis of the ions produced enables a complete mass spectrum to be obtained for all the ions produced in each laser pulse.

(2) Experimental.

A Nitrogen laser (337nm) was used to produce the ions, which were mass analyzed in a home built compact, linear, reflectron time-of-flight mass spectrometer (4). Spectra were acquired on a digital oscilloscope and transferred to a PC for storage and processing. Samples were prepared by a range of different methods, depending on the properties of the polymer being studied, e.g. either with or without a matrix, such as dithranol, or with or without added salts such as NaBr.

A wide range of polymers have been studied using this technique, including:- (i) Polar polymers and copolymers such as polyglycols, (ii) Non-polar polymers e.g. polystyrene, polyisoprene and polybutadiene; (iii) Polysiloxanes; (iv) Fluorinated polyethers e.g. Fomblin; (v) Mondisperse aryl ester dendrimers, and (vi) hyperbranched polyesters.

(3) Results.

Figure (1) illustrates the type of spectra obtained for an equimolar mixture of polyethylene glycol 1000 and 4600. Dithranol was used as the matrix and sodium bromide was used as the cationization agent. Spectra were acquired at a range of accelerating voltages from 400v to 20kV. This was to illustrate the vast change in sensitivity observed as the accelerating voltage (and hence the velocity) of the ions was increased. Information about the response factors of microchannel plates may also be obtained by this method.

The effect of increasing the accelerating voltage on the sensitivity of ion detection with respect to mass, can be illustrated such by taking the ratio of intensities of ions that were (a) far apart in terms of mass (i.e. the maximum peak of the PEG 1000 distribution, with several peaks in the PEG 4600 distribution; and (b) close together in terms of mass (i.e. several peaks in the PEG 4600 distribution).

It can be shown that for ions of similar masses, there is little change in relative sensitivity as the accelerating voltage is increased, i e. the ratio of peak intensities is fairly constant. However for ions that have different masses, there is a bias towards the detection of the faster, lighter ion at low accelerating voltages This bias decreases as the accelerating voltage is increased, and the difference in detection between low and high mass ions is reduced.

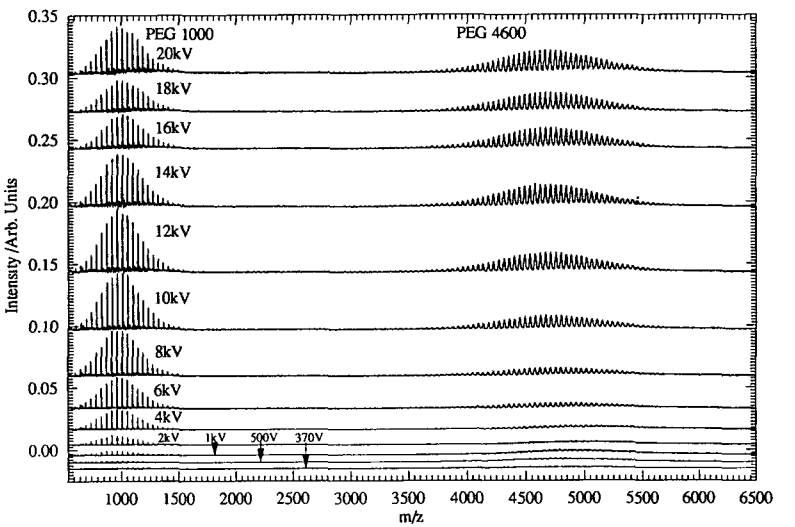

Figure (1) Equimolar mixture of PEG1000 and 4000, with a dithranol matrix and NaBr.

This work has been extended to a wide range of polymers, and experiments have been carried out to determine the important factors affecting the quality of MALDI spectra of synthetic polymers. Particularly useful compounds as an analytical probe of the MALDI process are dendritic polymers of a single molecular weight. These can then be used with a variety of different cationization agents to investigate the ionization process.

(4) Conclusions.

Laser desorption/ ionization mass spectrometry can quickly and successfully provide detailed information about synthetic polymers that is not otherwise available using other experimental techniques. However care must be taken in data interpretation as the behaviour of large molecules under laser desorption/ ionization conditions is not yet fully understood, and there are likely to be a range of properties which vary with molecular weight. This has important implications for the reliability of data obtained from the laser mass spectrometry of polymers.

References

(1) U Bahr, A Deppe, M Karas, F Hillenkamp, *Anal. Chem* **64**, 2866, (1992)
(2) PA Deans, RM O'Malley, *Rapid Commun. Mass Spectrom* , **7**, 53, (1992)
(3) MS Kahr, CL Wilkins, *J. Am. Soc. Mass Spectrom.*, **4**, 453, (1993)
(4) IA Mowat, RJ Donovan, *Rapid Commun. Mass Spectrom.*, **9**, 82, (1995)

Acknowledgements.
Thanks to Procter & Gamble (Newcastle) for financial support, to the EPSRC for the award of a grant to IAM, and to the British Mass Spectrometry Society for the award of a travel grant to IAM.

Effects of Protonation on the Structure and Entropy of Bifunctional Molecules.

J.E. Szulejko, T.B. McMahon, Dept. of Chemistry, U. of Waterloo, Waterloo, Ont. N2L 3G1, **CANADA**
H. Audier and A. Milliet, DCMR, Ecole Polytechnique, Palaiseau, **FRANCE**

Protonation of acyclic bifunctional molecules, $X\text{-}(CH_2)_n\text{-}Y$ in the gas phase gives rise to the interesting possibility of *intramolecular* hydrogen bonding. The formation of an intramolecular hydrogen bond may (i) increase the proton affinity (PA) over that of similarly sized monofunctional molecules and (ii) induce a considerable loss of entropy due to the loss of internal rotors. In this pulsed electron beam High Pressure Mass Spectrometric (HPMS) study, X and Y were different groups in most cases, unlike previously reported work in the literature[1]. The functional groups investigated, mainly by equilibrium proton transfer HPMS experiments, ranged from -OH, $-OCH_3$, Phenyl, $H_2C{=}CH$- to methyl ketones. The thermochemical data derived from proton transfer van't Hoff plots are presented in TABLE 1.

The proton affinities (PA) of the methoxy-1-alkanols can be reasonably approximated by the PA of methyl propyl ether which is estimated by an additivity scheme to be 195.5 kcal mol^{-1}. The difference between the HPMS determined PA and 195.5 kcal mol^{-1} can then be used as a measure of the *intramolcular hydrogen bond strength* (IHBS), see Table 2. The IHBS is observed to increase in the order of 2-methoxy-1-ethanol < 3-methoxy-1-propanol < 4-methoxy-1-butanol viz, 4, 18 and 24 kcal mol^{-1}. An *ab initio* study[2] on protonated bifunctional molecules has shown that a ring size of 6 is most favoured. Smaller or larger ring sizes lead to non optimal bond angles. The IHBS for 2-methoxy-1-ethanol is the least, due to non-optimal bond lengths and angles.

The non intramolecular hydrogen bonded PA's for acetic anhydride and acetophenone can be estimated from an O 1s binding energy (BE) versus PA correlation[3] for carbonyl type compounds to be 183.8 and 203.3 kcal mol^{-1} respectively. However, the O 1s BE's are not known for phenyl or benzyl acetone. Their PA's can be approximated by that of 3-Pentanone (199.5 kcal mol^{-1})[3]. The IHBS increases in the order; acetophenone (~ 0), phenyl acetone (~ 3) and benzyl acetone (~ 7). In the case of protonated benzyl acetone, there appears to be a significant interaction energy between the π cloud of the phenyl ring with the protonated carbonyl site ≈7 kcal mol^{-1}

The half reaction entropy change for a protonation reaction, $\Delta S_{1/2}$ is defined as the entropy difference between the protonated base (BH^+) and neutral base (B). $\Delta S_{1/2}$ (est) can be approximated by the difference in entropies of the protonated forms (comparable sized methyl cycloalkanes) and methoxy-1-alkanols (comparable sized n-alkanols). The agreement between experiment, $\Delta S_{1/2}$ (expt) and $\Delta S_{1/2}$ (est) is excellent for 3-methoxy-1-propanol, fair for 4-methoxy-1-butanol and very poor for 2-methoxy-1-ethanol, see Table 2. On an empirical basis, $\Delta S_{1/2}$ is observed to decrease with increasing IHBS[1], reflecting favourable geometric conditions for the formation of a strong IHBS and the efficient loss of internal rotors. A similar trend is also noted for acetophenone, phenyl acetone and benzyl acetone.

43rd ASMS Conference on Mass Spectrometry and Allied Topics

TABLE 1: SUMMARY OF EQUILIBRIUM PROTON TRANSFER THERMOCHEMICAL DATA

$$B_1H^+ + B_2 \rightleftharpoons B_2H^+ + B_1$$

B_1	B_2	ΔH^0	ΔS^0
3-Methoxy-1-Propanol	4-Methoxy-1-Butanol	-5.6	-1.8
Pyrrole	4-Methoxy-1-Butanol	-10.1	-17.0
Pyrrole	3-Methoxy-1-Propanol	-4.3	-14.5
Pyrrole	5-Hexen-2-one	-1.1	-1.9
Acetophenone	3-Methoxy-1-Propanol	-9.6	-13.0
Acetophenone	Pyrrole	-6.0	-0.5
3-Pentanone	Phenyl Acetone	-2.9	-1.6
Ethyl Acetate	Benzyl Acetone	-7.8	-18.5
Methyl Acetate	2-Methoxy-1-Ethanol	-4.8	-6.8
Acetone	Acetic Anhydride	-8.1	-16.5
i-Propyl Cyanide	Acetic Anhydride	-8.5	-12.3
i-Butene	Benzyl Acetone	-14.1	-19.5
i-Butene	2-Methoxy-1-Ethanol	-8.1	-8.0
i-Butene	Methyl Vinyl Ketone	-6.2	-3.7

TABLE 2. Summary of Protonation Thermochemical Data for the Molecules Studied

Base	PA_{ex}	$\Delta S^0_{1/2}$ expt.	$\Delta S^0_{1/2}$ est	IHBS
2-Methoxy-1-Ethanol	199.8	-2.5	-15.0	4
3-Methoxy-1-Propanol	213.5	-14.0	-15.0	18
4-Methoxy-1-Butanol	219.3	-16.0	-23.0	24
Acetophenone	203.7	1.5	.	v.small
Phenyl Acetone	202.3	-2.5	.	3
Benzyl Acetone	206.0	-14.5	.	7
Acetic Anhydride	202.0	-12.5	.	18
Methyl Vinyl Ketone	197.9	2.0	.	v.small
5-Hexen-2-one	210.4	-1.0	.	v.small

Note: The PA and entropy data were anchored to the PA and Entropy scales of ref.3
ΔH^0, PA_{ex}, IHBS in units of kcal mol^{-1} $\Delta S^0_{1/2}$ in units of cal mol^{-1} K^{-1}

1 G.R. Nicol and P. Kebarle, 40th. ASMS conference Proceedings, p160
2 S. Yamabe, K.Hirao and S. Wasada, J.Phys.Chem., 1992 *96* 10261
3 J.E. Szulejko and T.B. McMahon. J.Amer.Chem.Soc., 1993 *115* 7839

DETECTION AND CHARACTERIZATION OF GAS PHASE CYCLODEXTRIN COMPLEXES

C. Dejsupa and David V. Dearden
Dept. of Chemistry and Biochemistry, Brigham Young University, Provo, Utah 84602

Cyclodextrins, which are cyclic polysaccharides having a truncated cone shape with all the glucopyranose units in substantially undistorted conformation (Figure 1), have been widely studied as models of host molecules for targeted complexation and delivery of guest drug molecules, or as catalysts in various stereoselective reactions.[1] This is mainly due to their unique structural features: a nonpolar cavity and a series of hydroxyl groups, acting as polar counterparts, cyclically arranged around the exterior of both ends of the toroid. Extensive work has been performed to gain better understanding of cyclodextrin reactions, but little has been done utilizing a mass spectrometer, and virtually nothing is known of the gas phase chemistry of these ions.

All experiments employed an APEX 47e (Bruker Instruments) FTICR-MS instrument equipped with a 4.7 T superconducting solenoid magnet. Equimolar concentrations (typically 0.1 mg/ml) of mixtures of α- and β-cyclodextrins were prepared in water:methanol:acetic acid in a ratio of 48.5:48.5:3. Electrospray ions were generated using a newly-designed electrospray source (Analytica, modified by Bruker Instruments) and then guided into the "Infinity" trapping cell by a series of electrostatic lens voltages. Neutral amines (n-butylamine, cyclohexylamine, L-methylbenzylamine, 1-naphthylmethylamine, diethylamine, and triethylamine) were introduced into the cell through precision leak valves. The pressure of the amine was typically in the 10^{-8} mbar range, as determined with an ionization gauge (Balzers). Postacquisition data analysis was done on a SPARC computer station (Sun Microsystems) with XMASS processing software (Bruker Instruments). Experiments were designed so that both cyclodextrins experienced identical amine pressures. The relative reaction rates of the protonated α- and β-cyclodextrin ions are therefore highly accurate (± 15%). Absolute rates (and absolute efficiencies) have considerably higher uncertainties.

Figure 2 shows the relative reaction efficiencies of a number of amines with the two protonated cyclodextrins. Notably, β forms complexes more efficiently than α for all the amines investigated. The linear alkylamines complex most efficiently, while the cycloalkyl and cycloaromatic amines are more than an order of magnitude slower. Complexation with 1-(cyclohexyl)ethylamine with either cyclodextrin (not shown) was too slow to measure accurately. The series n-butylamine, diethylamine, triethylamine compares primary, secondary, and tertiary amines. Interestingly, efficiency decreases in the order primary > secondary > tertiary, perhaps reflecting the decreasing number of hydrogen bond donor sites through the series. Size effects are more clearly evident in Figure 3, which shows the α/β efficiency ratio. In the same series, the difference between α and β becomes more pronounced as the amine becomes bulkier around the nitrogen. The smaller cyclodextrin is only slightly less efficiently than β for relatively unhindered primary amines such as cyclohexyl- or n-butylamine, while amines with steric constraints around their hydrogen bonding sites, such as methylbenzyl- or triethylamine, show the largest differences between the two cyclodextrins.

On the basis of semiempirical electronic structure calculations, we believe the cyclodextrins are protonated on their lower rims, suggesting this is where the hydrogen bonding interactions occur. While these complexes are clearly hydrogen-bonded electrostatic adducts, an important question arises as to whether or not the amines are bound within the cyclodextrin cavities to form inclusion complexes.[2] At present this question cannot be answered conclusively, but the data suggest that at least some of the amines may be binding inside. For example, some of the least efficient complexation is for aromatic amines such as methylbenzyl- and naphthylmethylamine, which are known to form inclusion complexes in solution, and with amines with bulky *R* groups such as cyclohexylamine and 1-(cyclohexyl)ethylamine, which intuitively would have steric problems accessing the interior. Curiously, reaction with the very bulky triethylamine is fairly efficient, suggesting it may bind on the exterior, but β is much more efficient than α for this amine.

We are grateful for the support of NSF, PRF, and Bruker Instruments, and for the assistance of Dr. Gary Kruppa.

43rd ASMS Conference on Mass Spectrometry and Allied Topics

References

(1) Bender, M. L.; Komiyama, M. *Cyclodextrin Chemistry*; Springer-Verlag: Berlin, 1978.
(2) Cunniff, J. B.; Vouros, P. *J. Am. Soc. Mass Spectrom.*; **1995**, *6*, 437-447.

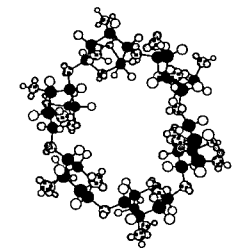

Figure 1. α-cyclodextrin

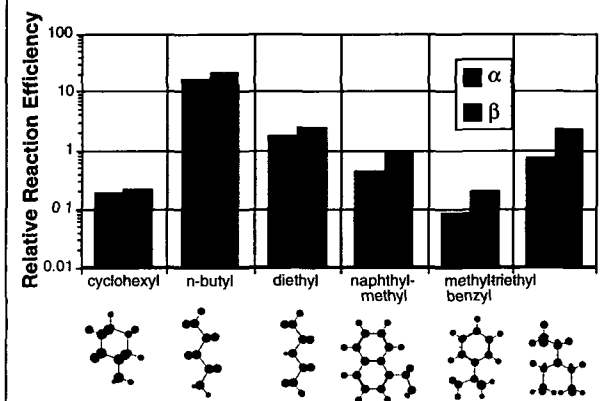

Figure 2 Reaction efficiencies of a series of amines with α- and β-cyclodextrins.

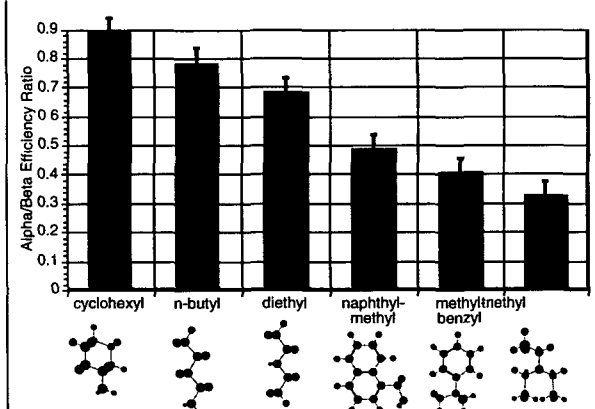

Figure 3. Ratio of reaction efficiencies, with α- and β-cyclodextrin, for a series of amines.

Probing Hydrogen-Bonding Interactions in an Ion Trap

Jennifer S. Brodbelt, Brad Hall, Jim Shen, and Armando Colorado, Department of Chemistry, University of Texas, Austin, TX 78712

Hydrogen-bonds are important stabilizing interactions in many types of protonated molecules and other types of gas-phase complexes. We have undertaken a systematic evaluation of the factors which mediate the strengths of hydrogen-bonds in many types of organic molecules. The methods used to study these interactions include energy-resolved collisional activation to measure critical energies of dissociation and the ligand exchange method to determine orders of relative cation affinities. The systems of greatest interest include a series of polyether/ammonium ion complexes, quinone/borinium ion complexes, and a variety of proton-bound heterodimers and homodimers.

Experimental: All experiments were performed in a Finnigan quadrupole ion trap mass spectrometer operated in the mass-selective instability mode. Complexes were formed by ion-molecule reactions between an appropriate cation and organic neutral. Energy-resolved collisional activation was performed by application of an appropriate ac voltage across the end-caps during a 10 ms interval. The amplitude of the voltage was varied from 0 - 500 mV, and the observation of fragment ions was monitored as a function of the amplitude. The ligand exchange method was performed by introducing two compounds into the trap and monitoring the transfer of a particular cation, such as the proton or borinium ion, in both forward and reverse directions.

Results and Discussion:

The ion trap was calibrated by evaluating the threshold activation voltage needed to dissociate a series of proton-bound dimers and correlating the known critical energies with the activation amplitude. After a suitable correlation was developed, the dissociation of a series of proton-bound dimers was examined. The critical energies determined for the dissociation of listed below, with the fragmentation schemes shown for the heterodimers. As predicted, the critical energies for the homodimers are higher than those for the heterodimers because the proton-bridges in the homodimers are equally strong, whereas the bridges in the heterodimers are non-equivalent. The molecule with the higher gas-phase basicity engages in a stronger bond to the proton, and thus the other proton-bridge is weakened.

Complex	Critical Energy (+0.1 eV)	
(urea + H+ + urea)	1.5 eV	37 kcal/mol
(urea + H+ + 2-aminoethanol)	1.3 eV	30 kcal/mol
(cyclohexanone + H+ + cyclohexanone)	1.3 eV	30 kcal/mol
(cyclohexanone + H+ + ethosuximide)	1.0 eV	23 kcal/mol

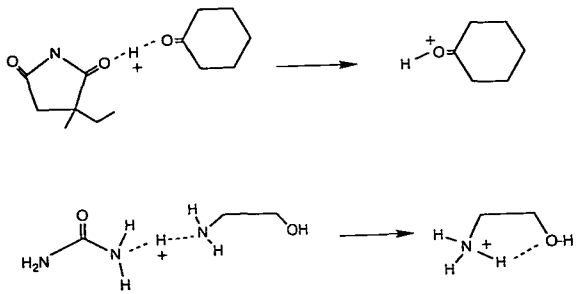

The critical energies for a series of polyether/ammonium ion complexes were also measured, and some of the results are summarized in the table below. The critical energy depends on two factors: the difference in basicities of the polyether and amine, and the number of potential hydrogen-bonds formed between the polyether and amine. For example, pyridine has a substantially lower gas-phase basicity than 18-crown-6, and it does not possess numerous hydrogen-bonding sites. On the other hand, ammonia has a relatively low gas-phase basicity, but it can participate in numerous interactions within the cavity of 18-crown-6. 1,3-Diaminopropane has a higher gas-phase basicity than 18-crown-6, and thus the interactions with 18-crown-6 become somewhat non-equivalent. Thus, the critical energy of the 1,3-diaminopropane/18-crown-6 complex is reduced relative to that of the 2-aminoethanol/18-crown-6 complex.

Complex	Critical Energy (+0.1 eV)	
(18-crown-6 + H+ + Pyridine)	1.4 eV	32 kcal/mol
(18-crown-6 + H+ + NH3)	2.1 eV	49 kcal/mol
(18-crown-6 + H+ + 1,3-diaminopropane)	2.1 eV	49 kcal/mol
(18-crown-6 + H+ + 2-aminoethanol)	2.8 eV	65 kcal/mol

Photoinduced Proton Transfer of H-Bonded Clusters

Yong Huang and David H. Russell
Department of Chemistry
LABORATORY FOR BIOLOGICAL MASS SPECTROMETRY
Texas A&M University
College Station, TX 77843

Gas phase proton transfer is one of the most fundamental reactions in chemistry, and proton transfer is of fundamental importance in matrix assisted laser desorption/ionization (MALDI). We have developed a cluster beam apparatus to study proton transfer reactions between substituted aromatic compounds and model bases. The objective of this study is to probe the mechanism and energetics of proton transfer reactions in clusters.

Experimental: A gas mixture of ammonia and nitrogen or argon at 3 or 4 atm. is admitted into the apparatus through an R. M. Jordan Pulsed Valve. Ferulic acid is desorbed by a 337 nm nitrogen laser and entrained into the gas mixture. The clusters formed in the supersonic jet are ionized by 355 nm radiation from a Nd:YAG laser between high voltage plates. Ions are accelerated perpendicular to the jet and separated in a 1.1 m TOF mass spectrometer and detected by a dual MCP detector.

Results and Discussion: A typical spectrum of ferulic acid and ammonia shows $H(NH_3)_n^+$ (n=1 to 4) and $M(NH_3)_n^{+\cdot}$ clusters (M is ferulic acid, n=0 to >20). NH_4^+ and $M^{+\cdot}$ are always the most abundant ions in their respective series in the mass spectrum. The gas phase reactions involved are as follows[1]

$$M(NH_3)_n^* \xrightarrow{h\nu} M^*(NH_3)_n \quad (1)$$
$$M(NH_3)_n^* \xrightarrow{h\nu} M(NH_3)_n^{+\cdot} \quad (2)$$
$$M(NH_3)_n^* \rightarrow (M\text{-}H)^{-*}(NH_3)_nH^+ \quad (3)$$
$$(M\text{-}H)^{-*}(NH_3)_nH^+ \xrightarrow{h\nu} (M\text{-}H)^- + (NH_3)_nH^+ \quad (4)$$
$$(M\text{-}H)^{-*}(NH_3)_nH^+ \xrightarrow{h\nu} (M\text{-}H)^{*\cdot}(NH_3)_n^+ \quad (5)$$
$$(M\text{-}H)^*(NH_3)_nH^+ \xrightarrow{h\nu} (M\text{-}H)^\cdot + H(NH_3)_n^+ \quad (6)$$

and simple evaporation

$$H(NH_3)_n^+ \rightarrow H(NH_3)_{n-y}^+ + (NH_3)_y \quad (7)$$
$$M(NH_3)_n^+ \rightarrow M(NH_3)_{n-y}^+ + (NH_3)_y \quad (8)$$

The branching ratio between reactions (2) and (3) depends on the kinetics and energetics of proton transfer. The energy of intracluster proton transfer is highly cluster size dependent. The energetically favored structures of the base-solvated acid clusters are all with the base molecules attached to the acidic functional group. Hydrogen bonding to the O or N atom is energetically favorable over hydrogen bonding to the π ring. H-bonding to the π ring stabilizes the system by 2 to 3 kcal/mol,[3] whereas OH...O and NH...N bonding is 3 to 6 and 2 to 5 kcal/mol, respectively. But the geometric probability to form the conventional H-bonding may be less than that to form a H-π hydrogen bonding considering the large area of the π ring. The π solvation lowers the energy requirement for out-of-plane $^1(\pi,\pi^*)$ transition. In addition, the H-π hydrogen bond energy may be increased by as much as twofold for S_1 than for S_0 state.[4] The first few base molecules will occupy the positions above and below the π ring so that proton transfer is essentially blocked while the excitation of ferulic acid through the out-of-plane transition is

enhanced. As the number of base molecules increases, the probability for binding to the OH increases energetically resulting in formation of the precursor of the ion pair leading to proton transfer.

The laser power dependence of proton transfer is determined by plotting ion intensity (I) vs. laser energy (E). When E < 4 mJ, $I = aE^m$ is fitted with data points with R^2 value = 0.94 to 0.97, where m is the number of photons for the reaction to occur and a is the reaction cross section. For the $H(NH_3)_n^+$ series, m = 3.6, 3.0, 3.7 and 3.4 for n = 1 to 4, respectively. For the $M(NH_3)_n^{+\cdot}$ series, m = 2.2, 2.0, 1.7, 1.7, 1.7, 1.8 and 1.7 for n = 0 to 6, respectively. For $H(NH_3)_n^+$, the reason m = 3 or 4 is that reactions (1), (3), (5) and (6) may be the major path. If (3) requires another photon, m = 4. For $M(NH_3)_n^{+\cdot}$, m is close to 2 (reactions (1) and (2)). We estimate the ionization potential of ferulic acid to be 8 eV or even lower since cinnamic acid is ca. 9 eV and usually a OCH_3 and a OH substituent reduce IP 0.5 eV each. When E is higher, the I vs. E curve reaches a plateau around n=8 for NH_4^+, n=6 for $H(NH_3)_2^+$. For the $M(NH_3)_n^{+\cdot}$ series, the curve slope decreases but doesn't reach a plateau in the current experiment.

Future Studies: The goal of all these studies is to explore the mechanism of MALDI. NH_3 will be replaced by a nonvolatile biological sample. Clusters will be generated by seeding the carrier gas with the peptide volatilized by laser ablation.

References

[1] J. A. Syage and J. Steadman, *J. Chem. Phys.*, **95**(4), 2497, 1991; J. Steadman and J. A. Syage, *J. Am. Chem. Soc.*, **113**(18), 6786, 1991; J. Steadman and J. A. Syage, *J. Phys. Chem.*, **95**(25), 10326, 1991
[2] O. Echt, P. D. Dao, S. Morgan and A. W. Castleman, Jr., *J. Chem. Phys.*, **82**(9), 4076, 1985
[3] D A. Rodham et al., *Nature*, **362**, 735, 1993; M. F. Perutz, *Phil. Trans. R. Soc. A*, **345**, 105, 1993; J. B. O. Mitchell et al., *J. Mol. Biol.*, **239**, 315, 1994
[4] H.-S. Im et al., *J. Am. Chem. Soc.*, **113**, 4422, 1991

Ferulic acid (M) entrained in 8 psi NH_3 + 38 psi Ar ionized at 355 nm.

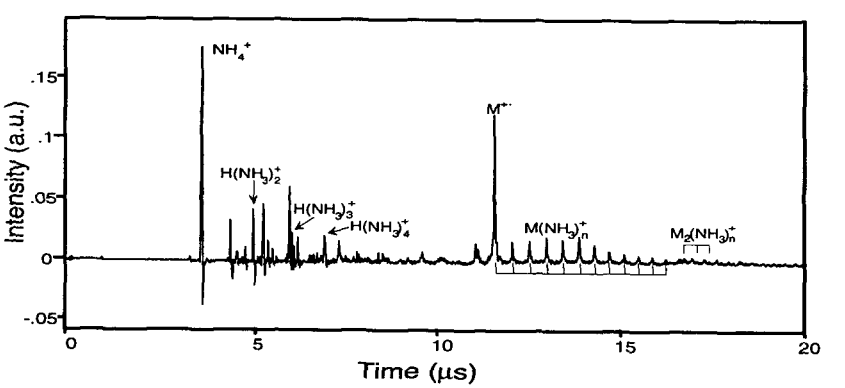

Investigation of a Chirality Effect in Proton Bound Dimers of Dimethyltartrate

E.N. Nikolaev* and T.B. McMahon†
* The Institute of Energy Problems of Chemical Physics; Russian Academy of Sciences; 117829 Leninski Prospect 38; Moscow; Russia
□ Department of Chemistry; University of Waterloo; Waterloo, Ontario; CANADA; N2L 3G1

In recent years, there has been a rapidly increasing interest in the influence of chirality on the biochemistry of chiral molecules. It has been found that the enantiomers of chiral bioactive molecules often differ in potency, toxicity, pharmacological actions, and metabolism[1]. It is also well known that important biopolymers are made up of monomer units having unique chiralities, with L-amino acid units in proteins and D-sugar units in DNA and RNA and chiral asymmetry is conserved in nature. The basis of this asymmetry conservation is chiral recognition. The molecular mechanism of recognition is not completely understood, however it is clear that it is based on enantioselective interactions of chiral molecules with monomers of a chiral matrix (stereoselective binding). A unique possibility now exists to investigate such chiral interactions in the gas phase.

Nikolaev and coworkers[2] have previously demonstrated a pronounced chirality effect in the unimolecular dissociation of proton bound dimers of dimethyl tartarate[2]. The present work extends the study of this chirality effect using high pressure mass spctrometry and using a high pressure ion source coupled to a FT ICR spectrometer. Additional chirality effects on unimolecular decomposition of the protonated dimethyltartrate (DMT) dimer as well as a hydrated proton bound dimethyltartarate dimer have been found.

Protonated monomers MH^+ and dimers M_2H^+ were produced by chemical ionization processes in methane. H_3O^+ adducts of tartarate monomers and dimers were produced from residual water and NH_4^+ adducts from ammonia which was added to the mixture in trace quantities. In order to distinguish L- and D- forms, the L- sample was deuterium labelled in each of the six hydrogen atoms of the ester methyl groups. To investigate the decomposition of dimers, they were isolated by ejection of all ions from the cell except the species of interest.

The protonated and hydrated dimer intensity distributions do not show a binomial distribution which would be expected for a statistical mixture of adducts. However the protonated ammonia adducts do exhibit such a statistical mixture. The pronounced deviation from a statistical intensity distribution is strong evidence of a substantial chirality effect. It can also be seen that nature of the chirality effect is strongly dependent on the adduct ion involved. In the case of the protonated dimers homochiral spicies dominate while in the case of the water adduct the heterochiral species is the most abundant.

This behaviour can be understood from the thermochemical data provided by high pressure mass spectrometric experiments. An analysis of the exchange of a ligand from the homochiral dimethyl tartarate dimer shows that the enthalpy change associated with replacement of a d,d ester by an l,l ester is +7.3 kcal/mole at temperatures below 60° C (Figure 1.). Thus the heterochiral species is of considerably lower stability and is disfavoured on thermodynamic grounds. A molecular modelling analysis shows that this lower stability likely arises from the opportunity to form a greater number of hydrogen bonds in the homochiral proton bound species (Figure 2.).

The thermochemical data then serve also to explain the kinetic data observed initially by Nikolaev et al. and in the current work using an external high pressure source to prepare the

various homo- and hetero- chiral dimers. By fitting the kinetic curves for the disappearance of the dimers to single exponential decay functions rate constants of k(DL)= 0.22 s^{-1} for heterochiral dimers and k(DD,LL)=0.027 s^{-1} for homochiral proton bound dimers are obtained. For water containing dimers the water loss rate constant and subsequent dimer decomposition into protonated monomers rate constant were found to be 2.0 s^{-1} and .05 s^{-1} for the homochiral dimers and 1.2 s^{-1} and .22 s^{-1} for the heterochiral species. These data then suggest that introduction of a water molecule into the proton bound dimers substantially alters the hydrogen bonding network.

1. Wainer,I.W.; Drayer, D.E. Drug Stereochemistry: Analytical Methods and Pharmacology; Marcel Dekker: NY, 1988.
2. Honovich, J.P.; Karachevtsev, G.V.; Nikolaev, E.N. Rapid Commun. Mass Spectrom. **6** *1992* 429.

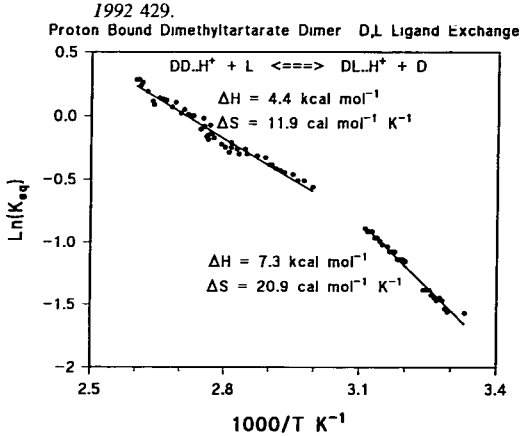

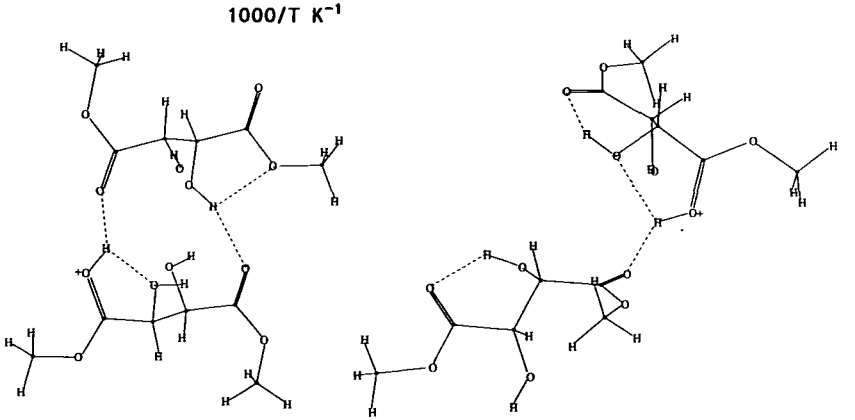

In Search of Non-Classical Ethyl Cation Stabilized by Organic Molecules.

Dmitri V. Zagorevski and John L. Holmes

Chemistry Department, University of Ottawa, Ottawa, Ontario K1N 6N5 Canada.

Onium ions play an important role in organic chemistry. Ethyl-containing onium ions, $R_nX^+C_2H_5$ (X - heteroatom), are of a special interest because in the gas phase they potentially may exist in several isomeric forms, such as the classical structure **I** and the symmetrical proton-bound dimer **II** (Scheme 1). The aim of this presentation is to summarize results on the structure and unimolecular reactivity of a variety of halonium and oxonium ions published in the literature and recently studied by the authors [1-7]. The following problems are discussed: how to generate ethyl-containing onium ions in the gas phase, how to identify isomeric species, and does interconversion of isomers take place?

Ions of interest can be generated by ion-molecule reactions (IMR) and unimolecular dissociations. The experiments were carried out on a tandem mass spectrometer operating with a chemical ionization ion source. Some IMR were identified by using ion cyclotron resonance spectrometry. Examples of reactions are shown below. Formation of stable adducts between cations and neutral molecules was observed in some cases (reaction 1) The most common IMR involved elimination of a molecule or radical (reactions 2 and 3). The use of the molecular ion of ethyl iodide as the reactant was very effective. Many of these reactions involved the formation of ionized dimers, which dissociated directly giving rise to onium ions (reaction 4). Unimolecular dissociation of molecular ions of various organic compounds can be used to generate onium ions having a formal carbon-heteroatom double bond (reaction 5).

$$BrCH_2CH_2^+ + O(C_2H_5)_2 \;\text{--->}\; BrCH_2H_2O^+(C_2H_5)_2 \qquad (1)$$

$$(C_2H_5)_2O^+H + IC_2H_5 \;\text{--->}\; (C_2H_5)_2O\cdots H^+\cdots C_2H_4 + HI \qquad (2)$$

$$C_2H_5I^+ + O(C_2H_5)_2 \;\text{--->}\; (C_2H_5)_3O^+ + I \qquad (3)$$

$$[C_2H_5I\ C_2H_5Br]^+ \;\text{--->}\; (C_2H_5)_2Br^+ + I^\cdot \qquad (4)$$

$$(CH_3)_3COC_2H_5^+ \;\text{--->}\; (CH_3)_2C{=}O^+C_2H_5 + CH_3^\cdot \qquad (5)$$

One of the most common arguments used in the identification of the non-classical structure **II** is the observation of hydrogen atom mixing prior to ethene loss. Isomer **II** is the key intermediate providing the exchange of hydrogen atoms between the carbon atoms of the ethyl

group. Non-symmetrical proton-bound isomers must also be introduced to complete the H-atom mixing (Scheme 1). The classical isomer may or may not be involved in this scheme.

Scheme 1.

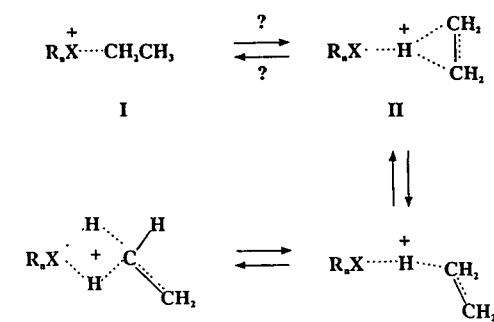

Structures **I** and **II** can be identified by other dissociations. For example, the formation of a (non-classical) ethyl cation is usually associated with isomer **II**, whereas C_2H_5 and RH (or C_2H_6) losses are consistent with isomer **I**. The latter two reactions do <u>not</u> involve hydrogen atom mixing.

In some cases (protonated ethanol and diethyl ether, diethylchloronium ion) classical and non-classical isomers can be co-generated and they easily intercovert. The triethyloxonium ion is an example of the separate existence of isomers. The classical structure was produced by reaction 2 and no H-atom mixing was observed in these species. Reaction 5 resulted in a proton bound dimer. This ion showed hydrogen atom mixing in the ethyl group originally attached to the iodine atom.

[1]. M. Sirois, M. George, J. L. Holmes, *Org. Mass Spectrom.*, **29**, 11 (1994)
[2]. C. Wesdemiotis, A. Fura, F. W. McLafferty, *J. Am. Soc. Mass Spectrom.*, **2**, 459 (1991).
[3]. A. G. Harrison, *Org. Mass Spectrom.*, **22**, 637 (1987).
[4]. R. D. Bowen, P. J. Derrick, *J. Chem. Soc. Perkin Trans. 2*, 1033 (1992).
[5]. D. V. Zagorevskii, S. P. Palii, J. L. Holmes, *J. Am. Soc. Mass Spectrom.*, **5**, 814 (1994).
[6]. D. V. Zagorevskii, J. L. Holmes, *Org. Mass Spectrom.*, **29**, 594 (1994).
[7]. D. V. Zagorevskii, M. Sirois, M. George, J. R. Cao, Ch. W. Ross III, J. L. Holmes, *European Mass Spectrom.*, in press.

Schistosome Surface Oligosaccharides Modulate Immune Response

Vernon N. Reinhold, Bruce B. Reinhold, Palanivel Velupillai, and Donald A. Harn
Boston University School of Medicine and Harvard School of Public Health

Successful parasites invade virtually every organ of their animal hosts, while evading nearly all of the host's immune defense responses. Why these parasites are successful is a question important not only to understanding and treating parasitic infections but also to other disease states in which the immune system is disabled or evaded. *Schistosoma mansoni,* appears to carry out this feat through carbohydrate signalling molecules on its egg's surface (1). Schistosomiasis is a chronic debilitating disease infecting 200-300 million people through out the world. In spite of the development of active and relatively safe drugs, prevention has remained a problem requiring repeat drug applications over a long period. Because of reinfection, there is a clear need for alternative control measures and in particular for an effective vaccine inducing significant levels of protection against the invasive stage of the parasite.

The most effective defense against schistosome parasites is considered to be the cell-mediated immune system, in which the macrophages are activated in response to the parasite and destroys the worms. But some worms survive which lay eggs that trigger an alteration of the lymphoid T-cell responses, shifting the immunity from cell-mediated to antibody-mediated (T-cell shifting), which is ineffective in combating the infection (2). In doing so they create their own environments in tissues and lay eggs where the worms hatch and thrive. In an effort to simulate this environment, Harn and colleagues (1) selected a battery of commercially available oligosaccharides, covalently bound them to human serum albumin and measured their lymphostimulatory effect. Lacto-N-fucopentaose III (LNFPIII), previously shown to be a stage specific antigen (3), stimulated splenic, non-T cells (B cells) to proliferate and produce IL-10 and prostaglandin E2 (PGE2), two mediators known to down-regulate CD4+ Th1 cells. This demonstrated a carbohydrate ligand dependent mechanism for cytokine production, and likely represents a novel mechanism for regulation of CD4+ T cell subsets. Other structurally related fucosylated, polylactosamine sugars appear to have similar lymphostimulatory properties as LNFPIII, and thus contribute to CD4+ T cell subset regulation.

To support this observation, we have isolated the egg surface enzyme (glutathione-S-transferase) from the *Schistosoma mansoni*. This glycoprotein gave rise to only O-linked glycans which were released by methylation and analyzed them by ES-MS (3). Within the distribution of glycoforms detected, fucosylation and Lewis X epitopes were detected by CID.

1. Velupillai, P. & Harn, D.A. (1994) *Proc. Natl. Acad. Sci.* USA **91**, 18-22.
2. Mosman, T.R. & Coffman, R.L. (1989) *Adv. Immunol.* **46**, 111-147.
3. Ko, A.I., Drager, U.C., & Harn, D.A. (1990) *Proc. Natl. Acad. Sci.* USA **87**, 4159-4163.
4. Reinhold, V.N, Reinhold, B.B, & Costello, C.E (1995) *Anal Chem* **67**, (June).

43rd ASMS Conference on Mass Spectrometry and Allied Topics

Identification of a Graft-vs-Host Disease associated Human Minor Antigen

Nicholas E. Sherman, Jeffrey Shabanowitz, and Donald F. Hunt
University of Virginia, Dept. of Chemistry, McCormick Road, Charlottesville, VA 22901

Joke M.M. den Haan, Els Blockland, Frits Koning, Jan Wouter Drijfhout, and Els Goulmy
Dept. of Immunohematology and Bloodbank, University Hospital, Bldg. 1 E3-Q, Rijnsburgerweg 10, 2333 AA, Leiden, The Netherlands

Eric Huczko, Jonathan Skipper, and Victor H. Engelhard
University of Virginia, Dept. of Microbiology, MR-4 Bldg. 4072C, Charlottesville, VA 22901

Human bone marrow transplants are performed as therapeutic treatment for severe aplastic anemia, leukemia, and immune deficiency disease. Even with the use of HLA matched siblings, aggressive pretransplant chemoradiotherapy, potent immunosuppressive drugs, and better antibiotics, bone marrow transplants can still result in 20-80% of cases of Graft-vs-Host Disease (1). It is believed that disparities for minor histocompatibility antigens between donor and recipient constitute a significant risk for graft failure, necessitating life long pharmacological immunosuppression of bone marrow transplant recipients. These minor antigens are peptides presented by the recipient on their HLA, and not the donor, due to slight differences in either protein sequence or antigen processing. Using electrospray tandem mass spectrometry, the first human minor antigen has been sequenced (2) This minor antigen was isolated from a patient suffering severe Graft-vs-Host Disease after a HLA identical bone marrow transplantation.

Peptides from B lymphocytes expressing this minor antigen were subjected to multi step fractionation beginning with immunoaffinity chromatography and then two dimensions of RP-HPLC. The single biologically active fraction obtained was then analyzed using a technique that allows for direct correlation of mass spectrometry and biological activity (3). The above approach reduced the number of peptide candidates from ~10,000 to only 5. Two peptides were then sequenced at the 25 fmol level using micro-capillary HPLC ESI tandem mass spectrometry on a Finnigan TSQ-7000. Only one of these peptides induced lysis by the minor antigen specific cytotoxic T-cell clone (see Fig. 1 CAD). The peptide sequenced was YXGEVXVSV. By co-elution, the Ile/Ile isoform was eliminated as the naturally processed peptide. The other three iosforms were tested for biological activity (see Fig. 2), and the Ile/Leu isoform was found to be more active by nearly two orders of magnitude (40 pM vs ~3 nM). This isoform was also the best binder to HLA-A2.1 with a 50% inhibition concentration of ~ 7 nM.

The naturally processed peptide was therefore determined to be YIGEVLVSV. This sequence was searched in protein and DNA databases. No 100% matches were found. However, thirteen proteins were similar with 6 matching 8 of 9 residues and 7 matching 7 of 9. The closest human sequence (YIGSVLISV), as well as the other twelve, are all from the same family of nonfilamentous class I myosins which are believed to be involved in cell and organelle locomotion. The strong homology between these sequences and the identified minor antigen provides strong evidence that the source protein is a member of this myosin family.

The minor antigen identified has potential as part of immunotherapy. This antigen is

restricted to the HLA-A2.1 population and has a frequency of 95%. Furthermore, It is tissue specific to hematopoietic, or white blood cell, including leukemic cells. In patients suffering from leukemia who express this antigen, cytotoxic T-cells raised against this minor antigen could be used to selectively rid the body of cancerous cells without damaging healthy tissue.

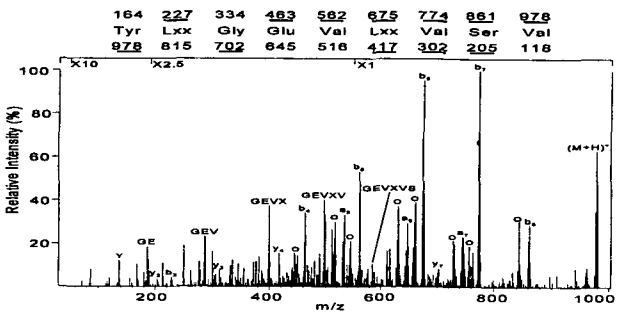

Figure 1 CAD of peptide (M=H)+ 978 using ~ 25 fmol material Predicted masses for fragments of b- and y-type are written above and below the sequence, respectively.

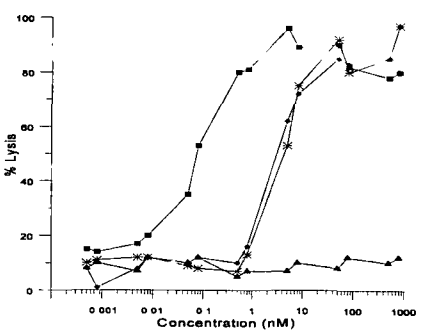

Figure 2 Dose response curves for peptides: YIGEVLVSV (squares), YLGEVLVSV (diamonds), YLGEVIVSV (stars), and SXDFGTXQV (triangles).

1. Beatty, P.G. et. al., 1991, *Transplantation* 51,443.
2. den Haan, J. et al., accepted to Science.
3. Cox, A.L. et al., 1994, Science 264, 716.

CE-MS AND MS-MS ANALYSES OF LIPOPOLYSACCHARIDES FROM *P.AERUGINOSA**

S. Auriola, P. Thibault, I. Sadovskaya[1], H. Masoud[1], E. Altman[1], J.C. Richards[1]
Institute for Marine Biosciences, National Research Council, 1411 Oxford St., Halifax, Nova Scotia, Canada, B3H 3Z1; [1]Institute for Biological Sciences, National Research Council, 100 Sussex Dr., Ottawa, Ontario, Canada, K1A 0R6.

Pseudomonas aeruginosa is a gram-negative bacterium recognised as an opportunistic pathogen among debilitated burn-wounded, and immunocompromised individuals. The major virulence factors of *P. aeruginosa* are associated with complex lipopolysaccharides (LPS) found on the outer surface of these bacteria. The LPS isolated from *P. aeruginosa* have been shown to contain a mixture of different polysaccharide lengths [1] and of different functionalities attached to the lipid A backbone [2]. At present, only partial or tentative structures of the core regions of these LPS are known, and detailed structural analysis including their heterogeneity is still fragmentary. Characterization of O-deacylated lipooligosaccharides (LOS) from core-deficient mutant strains of *P. aeruginosa* O6 was achieved using NMR spectroscopy [3], and provided for the first time a structural model for the complete core oligosaccharide of this serotype.

In order to investigate the sample heterogeneity often associated with substituents attached to the oligosaccharide backbone (i.e. fatty acids, phosphates, acetyl groups and substituted carbohydrate chains), the present investigation has focused on the development of on-line capillary zone electrophoresis coupled to electrospray mass spectrometry (CZE-ESMS). An example of a CZE-ESMS analysis is presented in Figure 1 for the injection of 20 ng of basic oligosaccharides arising from the complete deacylation and dephosphorylation of *P. aeruginosa* LPS. The total ion electropherogram is shown in Figure 1a, along with the two dimensional depiction of ion intensity as a function of both m/z and time (Figure 1b). The contour profile presented in Figure 1b clearly shows a series of at least five diagonal lines between 16 and 20 min, corresponding to doubly- and triply-protonated molecules. Members of series 4 consist of truncated core glycans, the highest member of which (oligosaccharide A) displays an $[M+2H]^{2+}$ ion at m/z 1017, and comprises a fully deacylated and dephosphorylated core having a glucosaminitol (GlcNol) at the reducing end. Diagonal lines of each series are formed of truncated glycans lacking alanine, rhamnose, and/or hexose residues. Series 1 differs from series 4 by the addition of a 3-hydroxy lauric acid on oligosaccharide A. Series 2 and 5 correspond to oligosaccharides of higher mobilities, lacking a side-chain KDO residue. The abstraction of an hexosamine residue from series 2 affords oligosaccharides of intermediate mobilities (series 3). Confirmation of individual oligosaccharide structures was facilitated using tandem mass spectrometry using either flow injection or on-line CZE-MS-MS analyses.

Combined CE-ESMS analyses also provided an efficient tool for monitoring the heterogeneity of substituents appended to either the O-chain (acetyl and formyl groups) or the core structure (phosphate and pyrophosphate groups) of LPS. Hydrophylic glycolipids arising from mild hydrazinolysis of *P. aeruginosa* LPS were successfully separated under anionic conditions using uncoated capillaries. The heterogeneity of the O-deacylated LPS arises mostly from substitution on the galactosamine residue of the O-chain, and from the number of phosphate groups appended to the core and lipid A structures. Based on electrophoretic measurements and MS-MS spectra, the incremental number of phosphate groups bonded to the core stucture was accounted for by the formation of pyrophosphate groups on the heptose residue. Further improvement in sample loadings was achieved using on-line capillary isotachophoresis (CITP) preconcentration prior to capillary zone electrophoresis, and enabled the on-column injection of up to 1 µL of O-deacylated LPS. An example of such application is shown in Figure 2 for the analysis of O-deacylated LOS from a core-deficient mutant of *P. aeruginosa*.

[1] M. Rivera, L.E. Bryan, R.E.W. Hancock, E.J. McGroarty, J. Bacteriol. 170, 512 (1988).
[2] D.N. Karunaratne, J.C. Richards, R.E.W. Hancock, Arch. Biochem. Biophys. 299, 368 (1992).
[3] H. Masoud, E. Altman, J.C. Richards, J.S. Lam, Biochemistry 33, 10568 (1994).

*NRCC#:38085

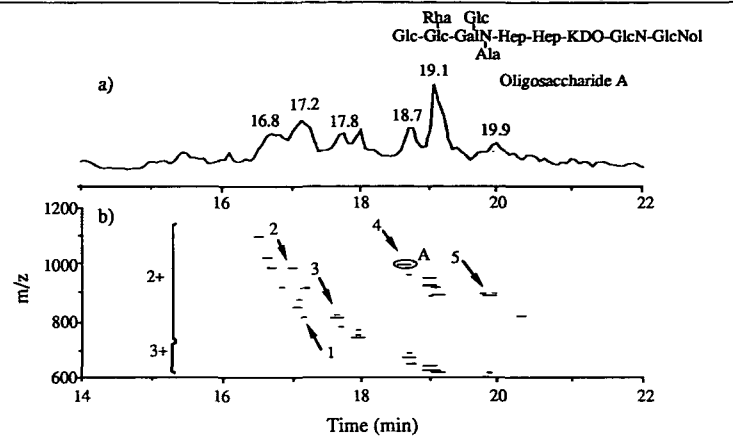

Figure 1: CZE-ESMS analysis (Pos. ion) of oligosaccharides arising from complete N,O deacylation, and dephosphorylation of LOS from *P. aeruginosa*. a) Total ion electropherogram for m/z 600-1300. b) contour profile of m/z vs. time showing characteristic heterogeneity patterns as indicated by arrows. Conditions: Polybrene coated capillary (100cm x 50µm I.D.), 1.0 M formic acid, -20 kV, 20 ng inj.

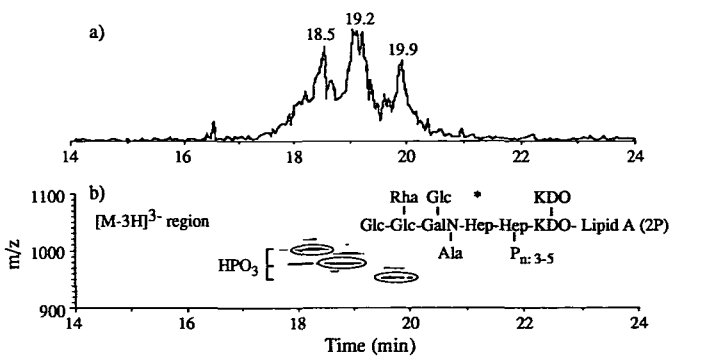

Figure 2: CITP-CZE-ESMS analysis (Neg. ion) of O-deacylated LOS from core-deficient mutant A28 from *P. aeruginosa*. a) Total ion electropherogram for m/z 600-1400. b) contour profile of m/z vs. time showing heterogeneity in the number of phosphate groups appended to the core structure. Conditions: Linear polyacryl. coated capillary (1.0m x 50µm I.D.), electrolyte: 50 mM NH_4 formate pH 4.5 terminator: MES pH 4.5, -25 kV, on-column inj. of 800 nL (16 ng total).

A Human Melanoma Antigen which Results from Post-Translational Modification

R. C. Hendrickson, J. A. Skipper, P. H. Gulden, J. Shabanowitz, Y. Chen, C. L. Slingluff, V. H. Engelhard, D. F. Hunt
Departments of Chemistry, Pathology, Surgery, Microbiology, and Berne Carter Center for Immunology, University of Virginia, Charlottesville, VA 22901

Killer T cells are part of the immune system that recognize peptide antigens derived from proteins expressed in tumor cells presented on the cell surface by major histocompatibility complex (MHC) class I molecules. The antigen processing mechanism involves protein synthesis and cytosolic proteolysis by the proteasome complex, followed by transport of peptides into the endoplasmic reticulum (ER) by the action of the transporter associated with antigen processing. In the ER, peptides are loaded into the MHC class I molecule and the resulting complex travels to the cell surface.

Most antigenic peptides have been predicted from a genetic sequence. Genomic libraries are generated from tumor cells and genetic fragments are transfected into cells that express the appropriate MHC molecule but not the tumor antigen. A combination of molecular subcloning and synthetic peptides based on the MHC binding motif and the proteins predicted sequence are used to identify the antigenic peptide.[1] Our approach is to isolate MHC class I associated peptides from the cell surface and then purify the mixture by multiple rounds of HPLC. A fraction containing peptide capable of reconstituting a T cell epitope is identified by ^{51}Cr release assays. Candidate peptides are identified and then sequenced by electrospray ionization tandem mass spectrometry (ESI-MS/MS).[2]

We identified a naturally occurring HLA-A2.1 associated peptide YMDGTMSQV in peptides extracted from melanoma cells. This peptide is identical to the antigenic peptide found using the genetic method except the amino acid residue at position three is an aspartic acid instead of an asparagine residue. Interestingly, the naturally occurring peptide YMDGTMSQV sensitized target cells for lysis at a 100 fold lower peptide concentration that the genetically encoded peptide YMNGTMSQV. The aspartic acid and the asparagine containing peptide bound to purified HLA-A2.1 molecules with similar affinity and therefore differences in binding affinity do not account for the differences in peptide recognition by the killer T cell clone.

We used mass spectrometry to determine whether the naturally occurring peptide epitope was a tyrosinase gene product that results from post-translational modification. HLA-A2.1 associated peptides extracted from the melanoma cell lines NA8mel, which does not express a tyrosinase gene, and NA8Mel+tyr, which has been transfected with a tyrosinase gene encoding the asparagine containing peptide were analyzed. Peptides were immunoaffinity isolated, concentrated, loaded onto a C18 micro capillary column (75 µm i.d. x 12 cm) and gradient eluted using acetonitrile and 0.1 M acetic acid with the concentration of acetonitrile increasing at 2%/minute into a Finnigan TSQ-7000 (San Jose, California) triple quadrupole mass spectrometer equipped with an electrospray ion source. Scans were acquired every 1.5 seconds over a mass range m/z 300-1400 and then plotted with intensities for m/z 1031 to 1032. Peptides YMNGTMSQV and YMDGTMSQV have molecular mass of 1031 and 1032 respectively. Analysis of the peptide mixture extracted from NA8mel failed to detect any species within the 1031 to 1032 mass window at greater than 0.2 fmol / 3 x 10^7 cells. The analysis of peptide extracts from NA8mel+tyr show one peptide within this mass window and was detected at a level of 200 fmol / 3 x 10^7. This peptide is therefore derived from the tyrosinase gene. When synthetic YMNGTMSQV was added to peptide extract from NA8mel+tyr two distinct peaks within this mass window were identified indicating that they do not have the same sequence. In contrast, when synthetic YMDGTMSQV was

[1] van der Bruggen, P., et al, Science, 254.1643-1647, 1991 December 13
[2] Cox, A. L.,et al., Science, 264·716-719, 1994 April 29.

added to the NA8mel+tyr extract the peptides co-elute suggesting that they are identical (Fig. 1). Proof for this conclusion was obtained by directly sequencing the naturally occurring tyrosinase peptide by mass spectrometry. To ensure that the conversion had not occurred during MHC purification and peptide extraction, HLA-A2.1+ T2 cells were pulsed with synthetic YMNGTMSQV prior to peptide extraction and purification and then analyzed (Fig. 3). These results establish that the peptide encoded by the tyrosinase gene has been post-translationally modified before presentation by HLA-A2.1 on the cell surface.

This is the first demonstration of a post-translational modification that results in the alteration of a peptides primary amino acid sequence. The alteration was directly identified by tandem quadrupole mass spectrometry and is relevant towards the identification and prediction of other peptide antigens. Further studies will investigate where the post-translational modification occurs within the cell and how this modification fits into the MHC class I antigen processing pathway.

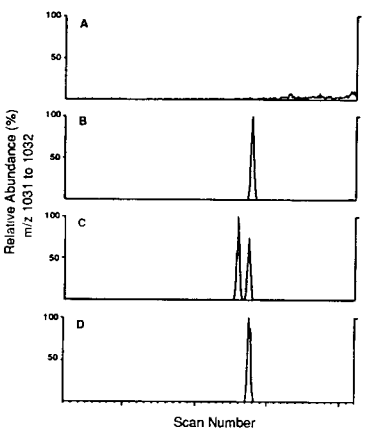

Fig. 1. Selected ion chromatograms for m/z 1031 to 1032 recorded on HLA-A2.1 associated peptides from NA8Mel and NA8Mel+tyr transfectant. (A) NA8Mel material equivalent to 1.3 x 10^8 cells. (B) NA8Mel+tyr material equivalent to 4 x 10^7 cells (C) NA8Mel+tyr material equivalent to 4 x 10^7 cells with synthetic YMNGTMSQV peptide added. (D) NA8Mel+tyr material equivalent to 4 x 10^7 cells with synthetic YMDGTMSQV peptide added.

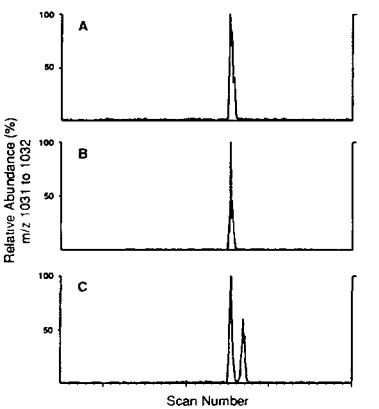

Fig. 2. Selected ion chromatograms for m/z 1031 to 1032 of peptides isolated from T2 cells pulsed with YMNGTMSQV prior to extraction and immunoaffinity purification of HLA-A2.1 molecules. (A) peptide extract material equivalent to 5 x 10^7 cells. (B) Synthetic YMNGTMSQV was added to an aliquot of peptide extract equivalent to that analyzed in panel A. (C) Synthetic YMDGTMSQV was added to an aliquot of peptide extract equivalent to that analyzed in panel A.

Tandem Mass Spectrometry and Data Analysis of Immunological Peptide Mixtures

John R. Yates, Ashley McCormack, Jimmy Eng, Paul DeRoos[1], and Alexander Rudensky[1]
Department of Molecular Biotechnology and [1]Department of Immunology, University of Washington, Seattle, WA 98195

Micro-column liquid chromatography electrospray ionization provides a rapid and sensitive method for the mass analysis of complex mixtures of peptides and proteins. Coupling the resolving power of reverse phase HPLC with direct sequence analysis by tandem mass spectrometry (µLC/ESI/MS/MS) is a useful strategy for the determination of amino acid sequences of peptides in mixtures, such as the antigens isolated from class I and class II major histocompatibility complexes (MHC) (Hunt et al *Science* **255** 1261-1263 (1992)). Class II antigens are derived from extracellular proteins or peptides. These molecules are bound to receptors on the surface of antigen presenting cells and then ingested into the cell. Ingested proteins are processed to a set of peptides of 11-25 amino acids in length prior to loading in the binding pocket of class II MHC antigens. This processing occurs in a series of fractions enriched in each type that can be distinguished by their densities. By structurally characterizing the antigens contained in each type of vesicle an understanding of the events involved in processing can be obtained. We have applied µLC/ESI/MS/MS and database *searching to the studies of antigen processing.*

A sucrose gradient is used to separate the vesicles by density. The vesicles are then assayed to determine the homogeneity of each fraction. The vesicles are lysed and contents of the vesicles are passed through Centricon filters with 3,000 and 10,000 molecular weight cutoffs. The fraction of peptides under 3 kDa are subjected to automated LC/MS/MS. The resulting tandem mass spectra are then used in the database searching algorithm described by Eng et al. (J. Am. Soc. Mass Spectrom. **5**, 976 (1994), Yates et al *Analytical Chemistry* **67**, 1426 (1995)). The peptide sequence represented in the tandem mass spectrum is identified by correlation to it's protein sequence in the database. From the sequence of the peptide, information relevant to the specificity of the protease involved in antigen processing can be inferred. Spectra are analyzed using the OWL database version 24.0 (88,823 entries). OWL is a non-redundant database comprising protein sequences from the GenBank (Release 84.0, National Center for Biotechnology Information, Washington, DC), SWISS-PROT (Release 29, Swiss Institute of Technology), Protein Information Resource (Release 41, National Biology Resource Foundation, Georgetown, Washington, DC), and National Research Laboratory (Release 14, Brookhaven National Laboratory, Brookhaven, NY) databases. All searches were performed on a DecStation 3000/900 (Maynard, MA) (Figure 3). A detailed description of the methods used for data reduction, preliminary scoring, and final scoring used in the computer algorithm have been presented elsewhere (Eng et. al. *J. Am. Soc. Mass Spectrom.* **5**, 976 (1994), Yates et al *Analytical Chemistry* **67**, 1426 (1995)).

Tandem mass spectrometry is performed on a Finnigan MAT TSQ700 equipped with electrospray ionization. Product ion tandem mass spectra were acquired during an LC/MS analysis by using a computer program written in the TSQ 700's Instrument Control Language (ICL). At the start of the program the instrument was configured to scan the second mass analyzer (Q_3) from an m/z of 400 to 1400 at 1.5 seconds/scan. When the ion current for a particular *m/z* value was above a preset threshold value of 250,000 counts, the program switched the instrument to scan in the product ion MS/MS configuration. The *m/z* value measured in the main beam mode was used to set the precursor ion *m/z* value in the first mass analyzer. The mass range was set at 50 u to 2 times the precursor ion *m/z* value with a scan time of 1.5 sec during acquisition of product ion tandem mass spectra. Five scans were

acquired and the instrument returned to the main beam mode of scanning. All analyses were performed with the collision cell filled with argon to a pressure of 3.5 mtorr. The collision energy for product ion scans was set by dividing the *m/z* value of the precursor ion by a constant (-35). This process was repeated throughout the LC analysis.

Shown in Figure 1 is the LC/MS/MS analysis of a low molecular weight fraction of high density fraction. All spectra were subjected to searches of the OWL database. Shown in Table 1 is a list of the peptide sequences identified in both the high density and medium density fractions. The cleavage patterns to produce these peptides is consistent with proteolysis by the enzyme cathepsin. In both analyses approximately 25-35 tandem mass spectra were acquired over the course of a 35 minute reversed-phase HPLC analysis. This permits the acquisition of spectra with a high probability of identifying peptides from known sequences, thus leading to rapid identification of the spectra.

This work was supported by the National Science Foundation, Science and Technology Center (DIR 8809710), NIH (GM52095), and Digital Equipment Corporation.

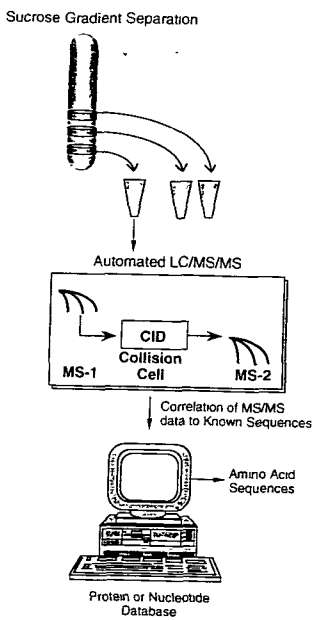

Figure 1

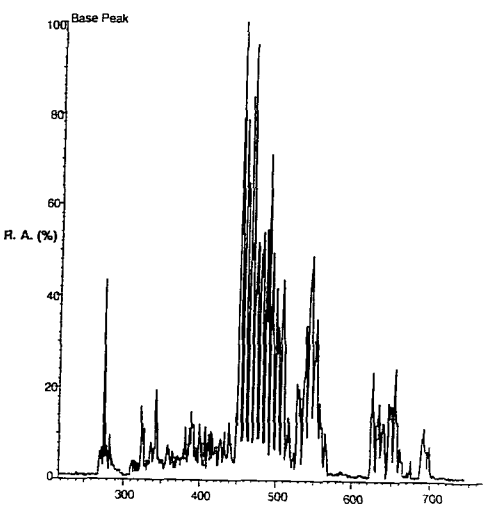

Figure 2

ES AND MALDI MS ANALYSIS OF GLYCOSYLATION-ENGINEERED α-1 ACID GLYCOPROTEIN

Mark F. Bean*, Michael J. Huddleston, Daniel J. O'Shannessy, and Steven A. Carr
SmithKline Beecham Pharmaceuticals, King of Prussia, PA 19460.

Genetic engineering control of protein expression can be carried beyond amino acid sequence to include posttranslational modifications of proteins such as glycosylation. This is achieved by expressing the recombinant protein in a cell-line tailored to produce the desired modification. Traditionally, verification of the success of such glycosylation engineering has depended on antibody recognition of the modifications. We have explored the use of mass spectrometry for the same purpose and found it to be a much superior means of analysis in terms of its ability to characterize microheterogeneity within the oligosaccharide structures and to associate protein modifications to specific amino acid sites.

In the present study, glycosylation engineering of alpha-1 acid glycoprotein expressed in the mutant Chinese hamster ovary Lec-11 cell line produced a variant that specifically antagonizes E-selectin mediated adhesive events *in vitro*. E-selectin is an adhesion lectin involved in the recruitment of leukocytes to sites of inflammation. LC-ESMS of the engineered and natural glycoproteins after removal of neuraminic acids, reduction, pyridylethylation, and tryptic digestion clearly revealed that the engineering was successful in coating the protein oligosaccharides with the blood group determinant sialyl-Lewis X (sLe^X) as well as VIM-2 type sugar structures (NeuAc2-3Gal1-4[Fuc1-3]GlcNAc, and NeuAc2-3Gal1-4GlcNAc1-3Gal1-4[Fuc1-3]GlcNAc respectively). Moreover, it was possible to describe the heterogeneity in the glycoforms at each of the five N-glycosylation sites (for example see Figure 1a) and to show that this was site-dependent.

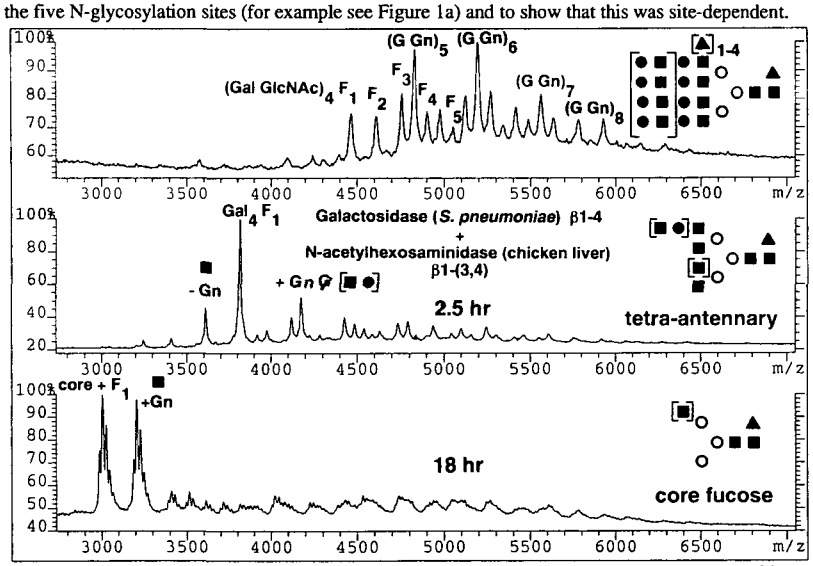

Figure 1. Time-course MALDI-MS of glycosidase treatment of a heterogeneous glycopeptide.

These particular oligosaccharide structures are of interest because they are the ones recognized by E-selectin in the inflammatory process. The natural human blood alpha-1 acid glycoprotein was shown by LC-ESMS to produce small amounts of multiply fucosylated and polylactosamine oligosaccharides, and thus probably has some sialyl-Lewis X constructs *in vivo*.

Through time-course MALDI MS analyses of glycosidase digests (galactosidase and N-acetyl glucosidaminidase) of one of the glycopeptides we were able to establish that the oligosaccharide was predominately tetra-antennary and that all of the other glycoforms possessed a core fucose unit (Figure 1, above). A further question was raised by the fact that two N-acetyl lactosamine units are isobaric with five fucoses (730 Da each). Certain peaks in the mass spectra thus had ambiguous structural assignments. One such spectral peak corresponded numerically either with a $(Gal\text{-}GlcNAc)_6\text{-}Man_3\text{-}GlcNAc_2\text{-}[Fuc]_1$-peptide or with a $(Gal\text{-}GlcNAc)_4\text{-}[Fuc]_5\text{-}Man_3\text{-}GlcNAc_2\text{-}[Fuc]_1$-peptide. This mass was selected for tandem ESMS fragmentation on a triple quadrupole using the new nanospray interface of M. Mann. The results are revealing (Figure 2); there can be no question that there are fucoses on some Gal-GlcNAc moieties (Lewis X constructs). Knowing also that all these oligosaccharides contained a core fucose, one is led to the unusual indication that some N-acetyl lactosamines are doubly fucosylated.

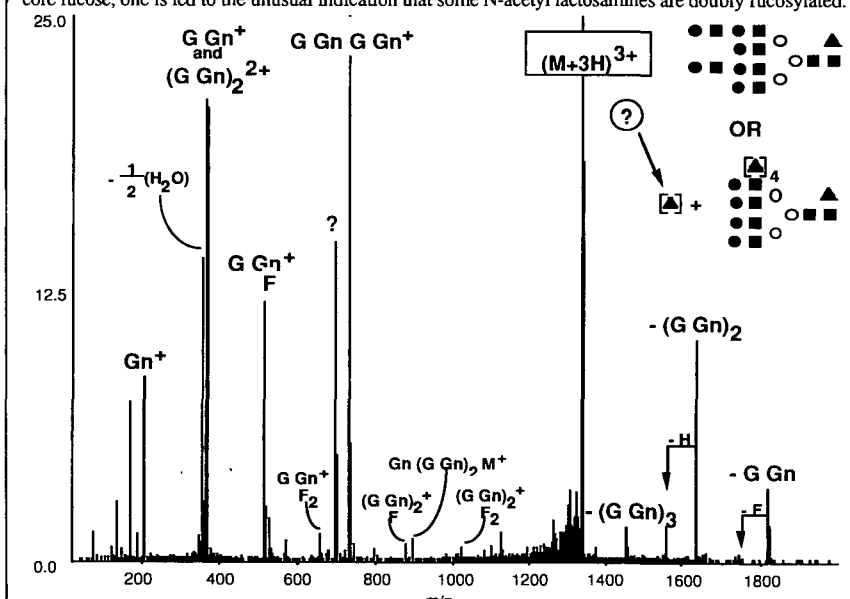

Figure 2. Nanospray tandem ESMS of one glycoform on one of the glycosylation sites isolated by LCMS of trypsinized sLe^X-α1-acid glycoprotein.

EPITOPE DETERMINATION BY MASS SPECTROMETRY: HIV p24

Kenneth B. Tomer, Damon I. Papac, Carol E. Parker

Laboratory of Molecular Biophysics
National Institute of Environmental Health Sciences
PO Box 12233
Research Triangle Park, NC 27709

Monoclonal antibodies are routinely used in vitro for diagnosis and in vivo for diagnosis and immunotherapy. The presence of specific monoclonal antibodies is also used to screen for the presence of the HIV virus in our nation's blood supply. Knowledge of the epitopes actually being screened for in these diagnostic kits is vital because sequence variations in the antigens being measured could lead to false negative results. This is particulary relevant with the HIV virus because the virus mutates constantly and, thus, avoids recognition by the host immune system.

One method for epitope determination is the proteolytic protection assay [Jemmerson et al , *Science* (**1986**) *232*:1001] in which the relative rates of enzymatic cleavage at specific residues are compared in the absence and presence of the antibody. Cleavages of the antigen occurring at residues involved in the binding with the antibody will occur at a slower rate in the bound state than in solution. Suckau et al. [*Proc. Natl. Acad. Sci. USA* (**1990**) *87*: 9848] incorporated the use of immobilized antibodies and PDMS product identification into this technique. We have recently developed a method to rapidly identify epitopes by using direct MALDI/MS analysis of the affinity bound proteolytic products [Papac et al., *Protein Sci.* (**1994**) *3*:1485]. A significant advantage the proteolytic protection assay has over other rapid approaches to epitope determination is that it is carried out under physiological conditions which permits the identification of conformationally and discontinuous epitopes.

The protein p24 is a core structural protein of the HIV virus It is a major target for antibody response, and antibodies to p24 are some of the first antibodies to appear during HIV infection. We have initiated a project to determine the epitope on recombinant p24 towards several monoclonal antibodies using the proteolytic protection assay combined with the direct analysis of products by MALDI/MS. The first step in this project involved the verification of the structure of several commercially available p24-based recombinant proteins. Several sources proved not to have molecular masses corresponding to the amino acid sequence provided for the sample. An authentic sample, however, was obtained from the NIH AIDS Research Resources Repository (donated by Dr. K. Steimer of Chiron Corp.) The binding of this material to three monoclonal antibodies under physiological conditions was then tested. One antibody did not bind the protein indicating that the antibody might be active towards denatured p24 (Fig. 1a). The other two antibodies did bind p24 (Fig. 1b). A LYS-C digest of the unbound p24 was analyzed by MALDI and all the expected fragments were found. This digest was then compared to a LYS-C digest of p24 affinity bound to a monoclonal antibody. The spectrum of the fragments from a LYS-C digest of p24 still affinity bound to one of the monoclonal antibodies is shown in Fig. 2. The presence of the ion at m/z3447 (L4 + 2H) suggests that the epitope may be discontinuous. These data show that mass spectrometry is useful for the determination of epitopes in their natural configuration.

43rd ASMS Conference on Mass Spectrometry and Allied Topics

FIGURE 1. Direct MALDI/TOF analysis of recombinant p24 affinity bound to monoclonal antibodies: A) no affinity binding was observed; B) affinity binding occurred.

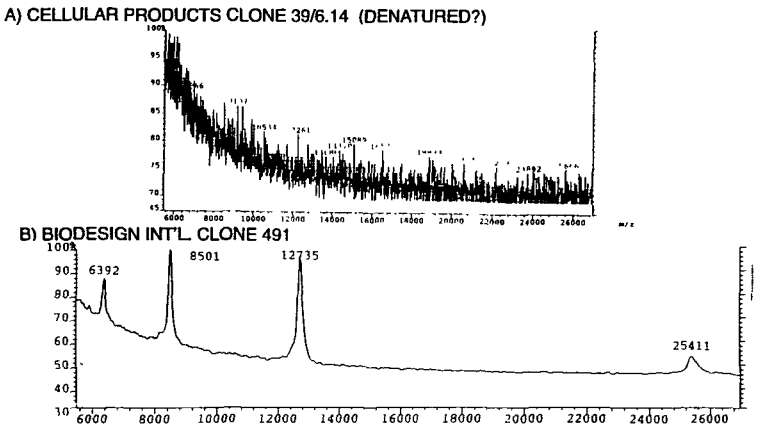

Figure 2. Direct MALDI/TOF analysis of peptide fragments remaining affinity bound to the monoclonal antibody after LYS-C digest.

...FYK I TLRAEQASQDVK I NWM..
171 182

M/Z 1346 (L8)

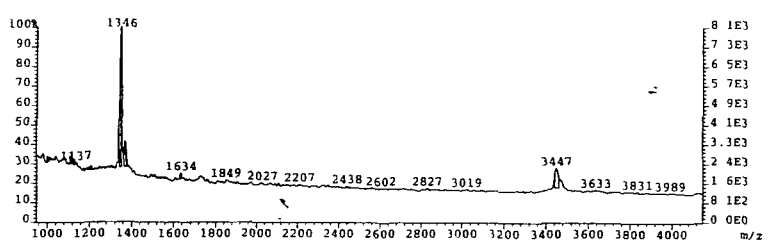

Probing the protein-ligand interactions by affinity-selected mass spectrometry

Yingming Zhao[1], Ruud Steenvoorden[1], Tom W. Muir[2], Stephen B.H.Kent[2] and Brian T. Chait[1]

[1]The Rockefeller University, 1230 York Avenue, New York, NY 10021, USA

[2]The Scripps Research Institute, La Jolla, CA 92037

Highly specific interactions between biological molecules, often within complex arrays, are critical to many cellular processes such as signal transduction and gene regulation. A comprehensive understanding of these processes requires detailed information about such interactions at the molecular level, in particular, precise identification of the sites of molecular recognition on the protein protagonists.

The interactions between antibodies and antigens can be investigated by affinity-selected mass spectrometry, a method that uses affinity purification in combination with mass spectrometry. The method is demonstrated to be very rapid for the localization of linear epitopes against the monoclonal antibodies[1,2]. The epitope can be quickly located to 10-15 amino acid residue region by proteolytic digestion of antigenic protein and affinity-selected mass spectrometric analysis of the digested products. If required, the antigenic site can be completely defined using the synthesis and mass spectrometric analysis of synthetic peptide ladders covering the region of interest.

We have applied the approach to identified antigenic epitopes of proteins and small peptides with binding affinity between 10^{-6} to 10^{-9}. Affinity-mass spectrometry proves to be an effective technique for assaying the interactions between antibodies and small peptides. The epitopes against anti-bFGF Mab#11.1 and anti-Ad-2 Mab-Dav-1 were accurately defined by the synthesis of ladder peptides and assaying the binding of the peptides to the antibodies by affinity-selected mass spectrometry. The method can also provide relative binding affinity when assaying the interaction between antibodies and peptide ladders. Therefore,affinity-selected mass spectrometry provide an alternative to ELISA (enzyme-linked immunosorbent assay) to detect antigens and assay the interactions between antibodies and antigens.

The method can also be applied to study other molecule-molecule interactions (such as protein-DNA, protein-RNA, receptor-ligand, and protein-protein interactions). For these studies, one of the interaction molecule (Such as DNA, RNA or ligand) is covalently or non-covalently immobilized to solid phase (such as agarose beads). The resulted complex is then used to affinity-purify its binding peptide fragments from proteolytic digestion of its interaction protein. The identities of the binding peptide fragments can be determined by mass spectrometry.

1: Zhao, Y; Chait, B.T., Protein Epitope Mapping by Mass Spectrometry, *Analytical Chemistry*, 1994, 66: 3723-3726

2: Zhao, Y; Muir, T; Kent, S.B.H.; Tischer, E.;Scardina, J.; Chait, B.T., Mapping of Protein-Protein Interaction by affinity-selected mass spectrometry, in preparation.

43rd ASMS Conference on Mass Spectrometry and Allied Topics

Strategy of Affinity-Selected MS for Linear Epitope Mapping

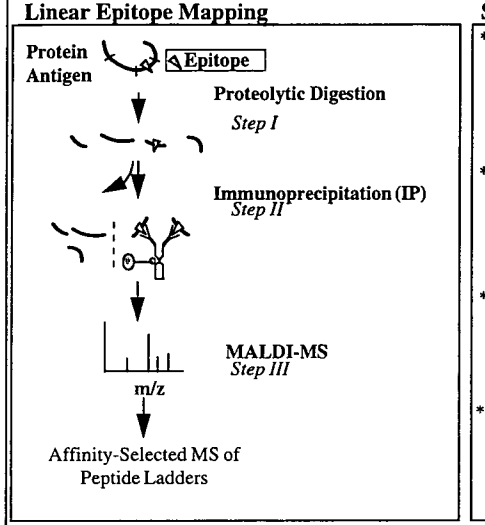

Strategy of Affinity-Selected MS for Studies of biomolecule Interactions

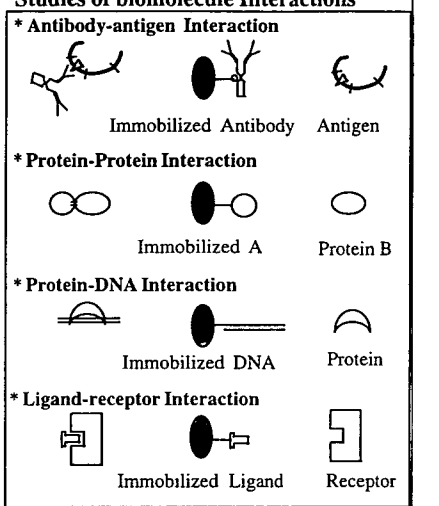

Affinity-Selected MS Also provide Relative binding Affinity When Assaying the Interactions between Antibodies and Peptide Ladders.

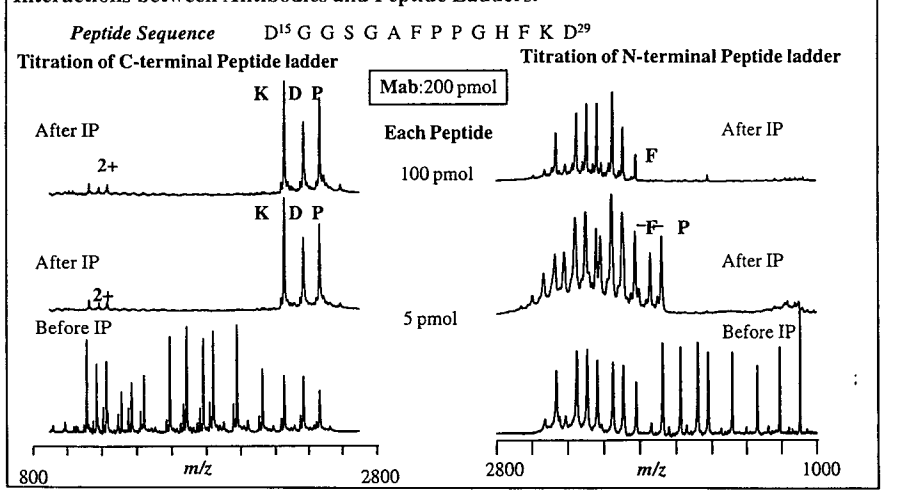

Resonant Excitation of Injected Atomic Ions in an Ion Trap Mass Spectrometer

G. C. Eiden, C. J. Barinaga, and D. W. Koppenaal, Materials and Chemical Sciences Center, Pacific Northwest Laboratory, Richland, WA 99352

Resonant excitation of ion motion in an ion trap mass spectrometer (ITMS) is not a new idea [1,2]. Most previous reports have characterized the resonant absorption profile (loss of observed ion signal versus excitation frequency) with respect to space charge, and the amplitude (V_{ac}) and duration (T) of the excitation pulse. These reports have often focused on (single frequency) resonant excitation to effect collisionally induced dissociation for MS/MS. We report studies of single frequency and broadband resonant excitation applied to selective ion accumulation or ejection in elemental mass spectrometry. We are using the ITMS to sample ions from an inductively coupled plasma (ICP) ion source [3]. ITMS performance degrades rapidly with increasing trapped charge. We have measured the selectivity with which a chosen ion can be ejected from the trap as a function of most of the relevant operating parameters: q_{eject}, total space charge, buffer gas pressure, the amplitude (V_{ac}), duration (T), and frequency of the resonant excitation pulse, and the spectral content (single frequency or broadband) of the excitation waveform. The instrument consists of a commercial ICP ion source coupled to an ITMS [3]. Ions are injected into the ITMS and collisionally trapped and cooled at buffer gas (He) pressures between 0.07 and 0.3 millitorr (measured outside the trap; pressure inside the trap is higher). Dipolar resonant excitation is effected either by the ITMS frequency synthesizer or by a broadband excitation source (HST-1000, Teledyne Hitachi, San Jose, CA). We report results for sample solutions of the systems: Ag, Cd (Cd at 1-10 ppb; the Ag:Cd ratio at 100-1000); Sr, Y, Zr (Sr and Zr at ~1 ppb each; Y at 100 ppb); and Cd neat at 0.1-0.5 ppm. We have focussed on systems in which we resonantly eject an abundant ion at m/z M and measure the loss of ions at M ± 1 amu. This represents a worst case scenario in that resonant excitation of a large ion cloud in the trap will necessarily perturb other trapped ions, especially those closest in m/z to the resonantly excited ions. Real samples will often have matrix ion m/z values much further removed from the m/z of the ions of interest, e.g. analysis of actinides from an argon plasma.

The resonant ejection process has been characterized by variations in the shape of the absorption profile with parameters such as buffer gas pressure, V_{ac}, T, and spectral content of the excitation waveform. We have found that the ejection efficiency increases as the excitation amplitude or duration is increased, as expected [1]. The data presented in this paper give a more detailed view of the dynamics of the ejection process. For example, on the low frequency side of the absorption profile, the increase in ejection efficiency is a bi-linear function of the duration of the excitation pulse (Figure). On the high frequency side of the profile, the signal shows a smoother variation with tickle time. These observations are consistent with the increase in resonant frequency with increasing displacement from the center of a trap with substantial non-linear field components [2], as in the Finnigan Corp. ITMS used here. We have also observed a stronger pressure dependence on the low frequency side of the profile. The profiles broaden dramatically on the low frequency side for changes in pressure of a factor of ~2 (broader at lower pressure). This is due to weaker dampening of the ion motion

by He collisions. Also, at low pressure (0.1 mTorr), the signal versus tickle time curves show the sharp break in slope (and a slope of ~zero at longer tickle times) regardless of excitation frequency. This is in contrast to the data shown in the Figure which was taken at 0.2 mTorr. These and other characteristics of the excitation process, and a more detailed comparison with theory [2], will be addressed in the near future [5].

1. a) J. V. Johnson *et al*, Anal. Chem. **62** (20), 2162 (1990); b) J. D. Williams *et al*, Anal. Chem. **66**, 725 (1994); c) M. J. Charles *et al*, J. Amer. Soc. Mass Spectrom. **5**, 1031 (1994); d) R. E. March et al, Org. Mass Spectrom. **28**, 499 (1993); e) J. M. Franklin *et al*, Proc. 41st ASMS Conf. on Mass Spectrom., 925a (1993).
2. J. Franzen, Intl. J. Mass Spectrom. Ion Proc. **125**, 165 (1993); ibid., **130** 15 (1994).
3. D. W. Koppenaal *et al*, Rapid Comm. Mass Spectrom. **8**, 71 (1994); D. W. Koppenaal, *et al*, J. Anal. At. Spectrom. **9**, 1953 (1994).
4. D. W. Koppenaal, *et al*, FACSS Conference, St. Louis, Oct. 1994.
5. G. C. Eiden *et al*, J. Amer. Soc. Mass Spectrom., to be submitted.

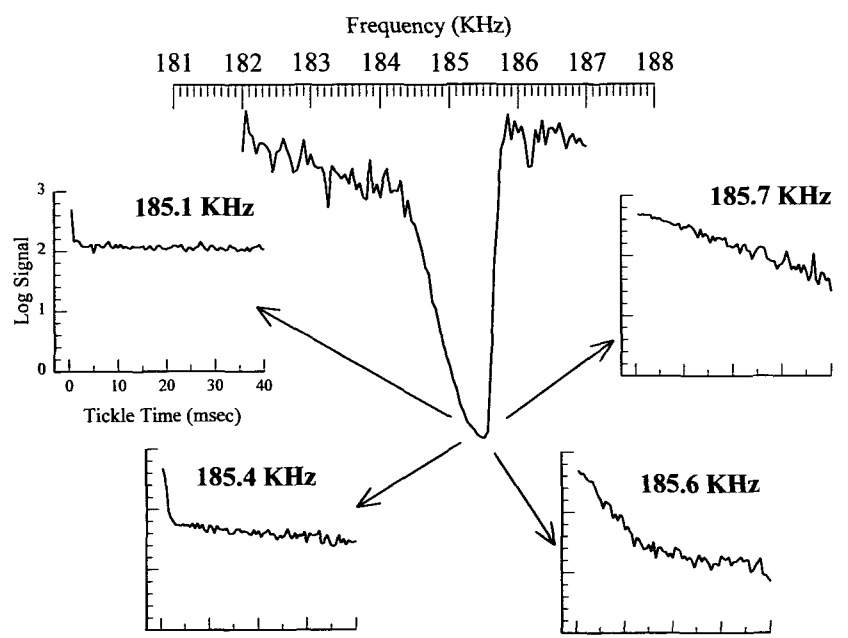

ION REMEASUREMENT IN THE RF QUADRUPOLE ION TRAP

Douglas E. Goeringer and Scott A. McLuckey
Chemical & Analytical Sciences Division, Oak Ridge National Laboratory

The development of the mass-selective instability mode of operation for the quadrupole ion trap has provided impetus for mass spectrometric applications of the device. In the technique, the amplitude of the confining rf voltage is increased linearly with time causing trajectories of stored ions to become unstable in the axial direction sequentially from low to high mass/charge. Ejected ions are subsequently detected by an external electron multiplier. Thus, the technique is straightforward but also destructive in nature; any further manipulations of the original ion packet are precluded by ion ejection and subsequent collision with the detector surface.

Trapped ions also can be detected by resonance absorption of energy from a supplementary excitation signal, and the varying, differential charge on the trap electrodes induced by resonantly excited, coherent ion motion produces fluctuating image currents detectable in an external circuit. Both of these *in situ* detection techniques have been used extensively in ion cyclotron resonance (ICR) mass spectrometry, although image current detection is now used almost exclusively due to its compatibility with Fourier transform signal processing. However, the first use of *in situ* ion detection in a mass spectrometry experiment was not made within the context of an ICR study but as part of the development of the rf quadrupole or Paul trap. Paul, Fischer, and Rettinghaus used such detection techniques in their early rf ion trap studies. In addition, image current detection and Fourier transform signal processing were later applied to ion trap mass spectrometry by Syka and Fies.

The nondestructive nature of image current detection was initially exploited for multiple remeasurement of ions[1] in FT-ICR mass spectrometry by Williams *et al.* Multiple excitation-detection-relaxation cycles were used to measure the **same** population of gramicidin D (*m/z* 1904) ions. With the remeasurement efficiency reaching up to 98%, signal averaging of spectra from 25 remeasurement cycles yielded a four-fold enhancement in signal-to-noise. The success with multiple remeasurement of ions in FT-ICR, along with the potential advantages of implementing the technique in the quadrupole ion trap, has led us to investigate adapting the method to the device.

We have modified a Teledyne 3DQ quadrupole ion trap mass spectrometer to allow for *in situ* detection and ion remeasurement via image current detection. Figure 1 is a block diagram of the signal processing configuration. A major obstacle to image current detection in the rf quadrupole ion trap, in contrast with the FT-ICR, is the trapping rf signal. This high voltage signal is coupled to the endcaps via the small ring-to-endcap capacitance producing a background signal level typically tens of volts in amplitude. Consequently, connecting the endcaps directly to the inputs of a differential amplifier, as is the normal practice in FT-ICR, is not practicable because the high background voltage overloads the inputs.

1. Williams, E.R.; Henry, K.D.; McLafferty, F.W. *J. Am. Chem. Soc.* **1990**, *112*, 6157-6162.

Thus, a center-tapped transformer was connected across the endcaps to circumvent the rf drive background. Coherent ion motion was induced by applying an excitation signal to the endcaps via the transformer; the excitation signal was tuned to the resonant frequency of the parallel LC circuit formed by the transformer and the endcaps. The signal voltage was generated by the resultant image current flow through the LC impedance. The signal LC circuit was connected to another reference LC circuit in a bridge configuration so that the excitation component of the overall signal could be nulled. Signals due to coherent ion motion were then low-pass filtered (cutoff frequency = 300 kHz) by an FET-preamplifier and processed by a lock-in amplifier which was phase-locked to the excitation signal generator. DC output signals from the lock-in were digitized and displayed by a digital sampling oscilloscope. Multiple image current measurements from a single population of trapped ions were performed by repeatedly ramping the trapping rf voltage. Figure 2 shows the signal corresponding to 24 remeasurement cycles for the m/z 131 ion of PFTBA. Analysis of the signal indicated the remeasurement efficiency was 99%.

Figure 1

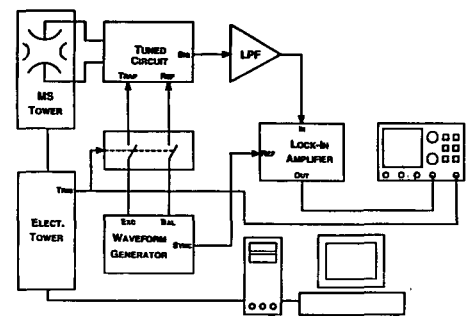

Figure 2

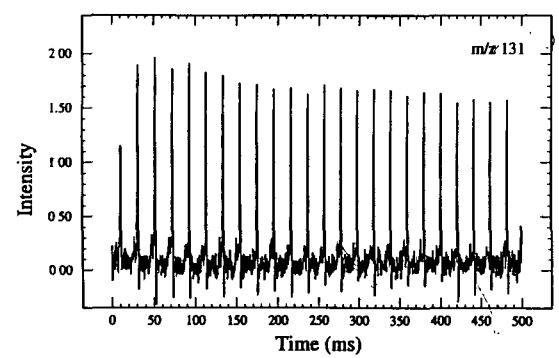

This work was supported by the United States Department of Energy, Office of Research and Development. Oak Ridge National Laboratory is managed for the United States Department of Energy by Martin Marietta Energy Systems, Inc. under Contract DE-AC05-84OR21400.

Buffer Gas and q_{eject} Effects on the Performance of an Ion Trap

Lammert, S.A., Wells, J.M.
Oak Ridge National Laboratory, P.O. Box 2008, Oak Ridge, TN 37831-6120

The transformation of the ion trap from ion storage device to mass spectrometer was assisted in no small part by the discovery that the addition of a helium buffer gas greatly improved the mass resolution and sensitivity.[1] Ions formed in the ion trap are kinetically cooled to the center of the ion trap by collisions with the helium buffer gas. In the earliest form of the experiment, these ions were then ejected from the trap via a mass instability scan. It was later discovered that the application of a resonant ac voltage could further improve the performance of the ion trap by resonantly ejecting ions as they approached the stability boundary in a process that was named "axial modulation". Until recently, it has been widely held that the ion trap must operate using a helium buffer gas. The development by Bruker-Franzen[2] of the Chemical and Biological Mass Spectrometer (CBMS) and later the Generic Detector (GD) for the US Army has demonstrated that ion traps can be operated without helium, using only air as the buffer gas. Attempts, however, to operate ion traps from Finnigan-MAT using an air buffer gas have not been successful. This research examines the role of the helium buffer gas in an ion trap mass spectrometer and explores the possibility of substituting ambient air as the buffer gas.

The study examines the dependence of resolution and sensitivity on the type (air or helium), pressure, and method of introduction of the buffer gas, as well as on the q_{eject}, the mass, and the sample pressure. It is shown that resolution and intensity depend not only on the pressure of the buffer gas, but also on the q-value used for resonant ejection. Figures 1 and 2 show the results obtained by varying the buffer gas pressure (helium and air, respectively) and the q_{eject}-value on the resolution of m/z 69 from perfluorotributylamine (PFTBA). There is clearly visible in Figure 1, the known resolution valley at a helium buffer gas pressures of ca. 1 millitorr. There is, however a second valley at a q_{eject}-value of ca. 0.85 which shows a significant decrease in peak widths over those obtained at a q_{eject}-value of 0.906 (near the stability boundary). Concurrent with the resolution improvement (but not shown in this abstract) is an increased signal intensity (although the total peak area remains relatively unchanged). Figure 2 demonstrates that by substituting air for helium, similar resolution performance can be obtained although the optimum region of the pressure and q_{eject}-value minimum is much narrower. Signal intensities using both buffer gases were determined using krypton as the sample in order to ensure that the measured mass ion intensities were the result only of ion storage and not skewed to low mass by collisions with the larger air buffer target mass. It was observed that a 50% reduction in signal intensity for m/z 84 from krypton was obtained when substituting air for helium. At higher sample pressures as well as for masses > 200 da., both the improvement in resolution using helium at a q_{eject}-value of 0.85, and the ability to substitute air for helium without performance degradation is diminished.

1. Stafford, G C , Jr., Kelley, P.E., Syka, J E.P , Reynolds, W.E , Todd, J F.J., *Int. J. Mass Spectrom. Ion Processes* **60** (1984) 85-98
2. Franzen, J., *Int. J. Mass Spectrom. Ion Processes* **130** (1994) 15-40

"The submitted manuscript has been authored by a contractor of the U.S. Government under contract No. DE-AC05-84OR21400. Accordingly the U.S. Government retains a nonexclusive, royalty-free license to publish or reproduce the published form of this contribution, or allow others to do so, for U.S. Government purposes."

43rd ASMS Conference on Mass Spectrometry and Allied Topics

FIGURE 1

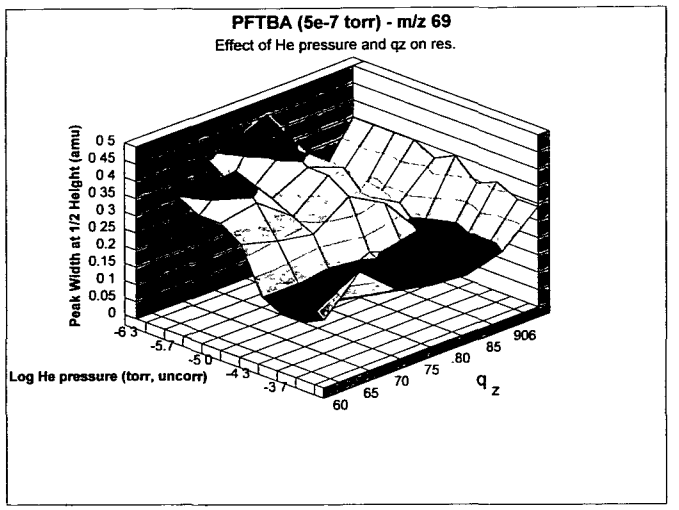

FIGURE 2

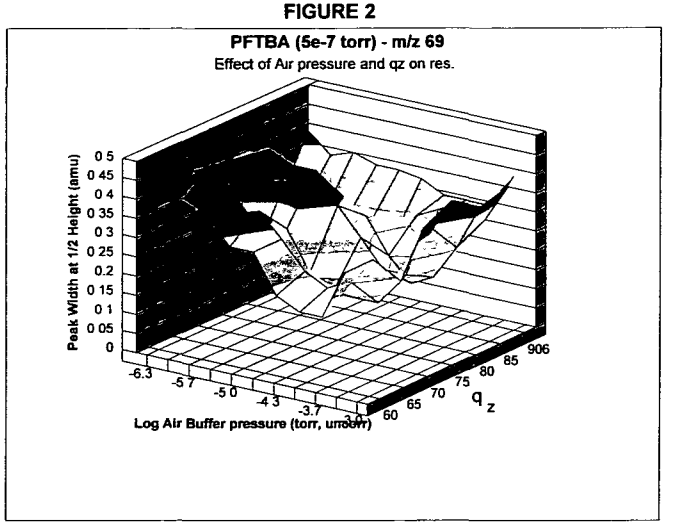

Effect of Ion Population Upon MS/MS Parameters in a Quadrupole Ion Trap Mass Spectrometer

Timothy P. Griffin, Richard A. Yost
University of Florida, Department of Chemistry
Gainesville, FL 32711

Ion frequencies have been observed to change with ion population [1] in the quadrupole ion trap mass spectrometer which has an effect upon single frequency collision-induced dissociation and isolation techniques that employ the use of frequencies. The shifting of the ion frequencies for varying ion populations have made it impossible to accurately predict the ion frequency for a specific set of a_z, q_z (DC, RF voltage) values, thus making it difficult to use an ion trap for routine GC/MS/MS. The interdependence of ion frequency and ion population makes it difficult to know the actual frequency of the ions without performing extensive, time-consuming experiments. Therefore, further studies examining the effect that the storage parameters have upon the ion frequency need to be performed.

These experiments focused on examining the ion frequency for different q_z values along the a_z=0.00 line. To perform these experiments a modified Finnigan MAT ITS-40 quadrupole ion trap mass spectrometer with both software to write custom scan functions (MS/MS) and an instrument-controlled frequency synthesizer have been developed in our laboratory and used for all experiments. In addition, the software enable the automatic acquisition of profile data. The $C_4H_8^+$ ion (m/z 56) from butanol was used as an ion probe and introduced into the manifold via a Graville-Phillips valve to give an uncorrected gauge reading of 4×10^{-7}torr. Helium was introduced through a modified transfer line to give an uncorrected gauge reading of 5×10^{-5} torr. The frequency of the ion motion was determined by use of the scan function depicted in Figure 1 As can be seen, the q_z value (RF voltage) is changed only during the time that the auxiliary frequency is to be applied. In addition, to minimize ionization and storage effects constant ion populations were used instead of constant ionization times.

The effect of q_z and ion population upon the ion frequency can is shown in Figure 2. The solid line in the figure denotes the theoretically predicted frequencies. Ion populations of 1, 5, and 30 thousand counts were examined. Notice that the frequencies deviate from the theoretically predicted values by a larger amount than the deviations due to differences in ion population. In addition, the frequencies deviate more at larger q_z values. The frequency shifts have been theorized to be due to an effective DC voltage being induced upon the ion cloud. This affectively causes the a_z value to move or shift away from the theoretical values. The shifting of the a_z for different ion populations and at different q_z values is shown in Figure 3. The experiment again used ion populations of 1, 5, and 30 thousand counts. It is interesting to note that as the q_z value increases the deviation of the a_z value away from zero increases. The deviations of the a_z value from zero is markedly larger than that observed for the varying ion populations.

1) Yates, N.A.; Yost, R.A.; Bradshaw, S.C.; Tucker, D.B. *Proceedings of the 39th ASMS Conference on Mass Spectrometry and Allied Topics*, Nashville, TN 1991, 132.

Figure 1
Ion Trap Scan Function

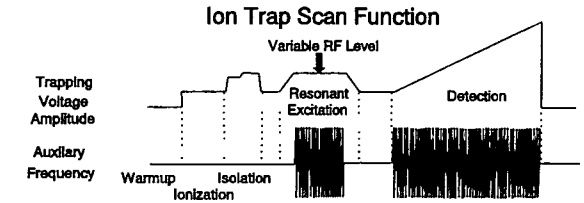

Figure 2
Freqency Dependence Upon Ion Population
q_z=0.00

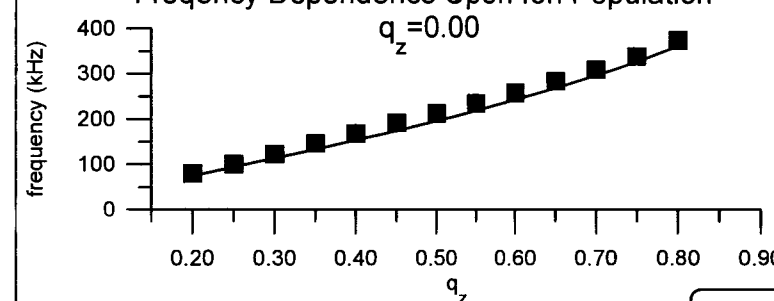

Figure 3
a_z Dependence on Ion Population and q_z values

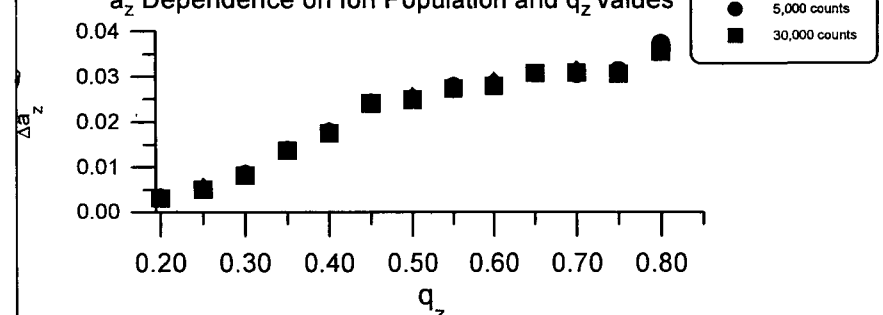

Fragmentation of Peptides by NanoES/Quadrupole Ion Storage (QUISTOR) MS

Roman Körner, Kenneth Morand, Matthias Wilm and Matthias Mann
Protein & Peptide Group – European Molecular Biology Laboratory
Meyerhofstr. 1, D-69012 Heidelberg, Germany

We have developed a nano electrospray (NanoES)/ion trap combination to allow long measurement times (>30minutes) on only 1µl of peptide solution. The long measurement time offers the possibility of time consuming experiments like MS/MS/MS and sequencing experiments on low amounts of digest mixtures .

The NanoES source features a finely drawn gold coated capillary, placed 1 to 2mm in front of the orifice (ref. 1,ref. 2). A differential pumped Analytica interface (Analytica of Branford, Inc.) transfers the ions to the ion trap (prototype of Esquire, Bruker-Franzen Analytic GmbH). Due to the short distance between the ion source and the orifice and the small size of the produced droplets it was possible to reduce the diameter of the orifice from 500µm (Analytica ES source) to 200µm resulting in an advantageous decrease of all pressures to about half the previous values.

On the ion trap it is difficult to obtain complete sequence information from a single collision induced MS/MS experiment.Firstly the internal energy of resonantly activated ions increases slowly via multiple collisions with He resulting in a cleavage of the weakest bonds of the ion before the internal energy for high energetic pathways is reached. MS/MS/MS can be helpful because less low energetic pathways are available for the second fragmentation .

The second reason is that to generate a sufficiently deep potential well for the fragmentation it is necessary to increase the RF amplitude resulting in the loss of fragment ions having masses below about one third of the parent ion mass. However,a subsequent fragmentation of a small fragment in a MS/MS/MS experiment often generates additional low mass fragments.

In the MS/MS/MS experiments the first fragmentation was performed in the interface region by increasing the potential difference between nozzle and skimmer. Stored Waveform Inverse Fourier Transformation (SWIFT, ref. 3) voltage pulses were applied during the injection time to accumulate a selected fragment in high intensity and good isolation in the trap for the resonance fragmentation.

As a model case the synthetic peptide HSIAGPPVPPR was fragmented. Due to the preferential cleavage on the N-terminal side of a proline the corresponding C-terminal peaks were not visible in the MS/MS spectrum, but the peptide could be sequenced completely by MS/MS/MS.

To examine the use of the ion trap for sequencing on peptide mixtures a tryptic digest of Cytochrome C was analyzed. A direct analysis of the digest yielded a sequence coverage of 64% (fig.1). This sequence coverage could be improved to 92% by selective storage of ions from approximately 150 Dalton broad mass windows using SWIFT pulses during the injection time. The ejection of ions outside this mass range permits increased accumulation of the required ions before space charge begins to negatively affect the spectrum. This leads to increased sensitivity. As an example fig. 2 shows that in the SWIFT selected mass range from 380 to 500 Dalton five additional tryptic peptides could be detected. The peptide (K73 K79)2+ was fragmented. A partial sequence of three amino acids could be determined from this MS/MS spectrum (fig. 3). Also in this case the peptide could be sequenced completely by MS/MS/MS (fig. 4) .

References

ref. 1: M.Wilm and M.Mann Int. J. Mass Spec. Ion Phys., (1994), 136 ,167-180
ref. 2: M.Wilm and M.Mann *Protein & Peptide Analysis by a Low-Flow High Sensitivity NanoES Source,* this Proceedings
ref. 3: L.Chen,T.-C.Wang,T.L.Ricca,A.G.Marshall Anal.Chem. 1987, 59 ,454-458

43rd ASMS Conference on Mass Spectrometry and Allied Topics

fig. 1
direct analysis of a tryptic Cyt. C digest

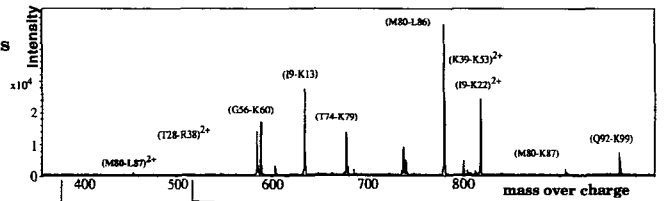

fig. 2
SWIFT isolation tryptic Cyt. C digest

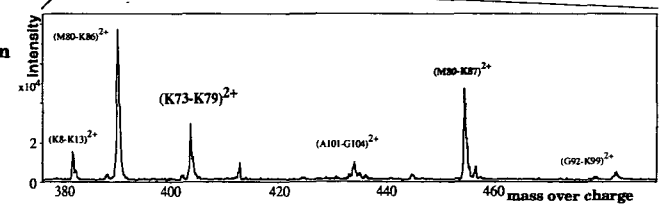

fig. 3
MS/MS of the peptide (K73-K79)2+ (KYIPGTK)

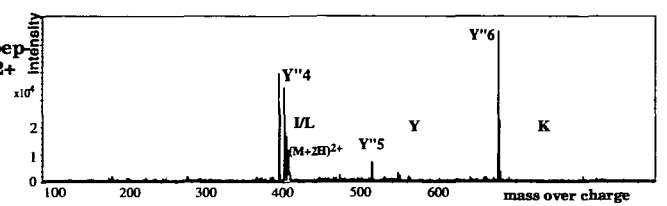

fig. 4
Orifice fragmentation of the Cyt. C digest & SWIFT isolation & Ion Trap fragmentation of the fragmentY"4

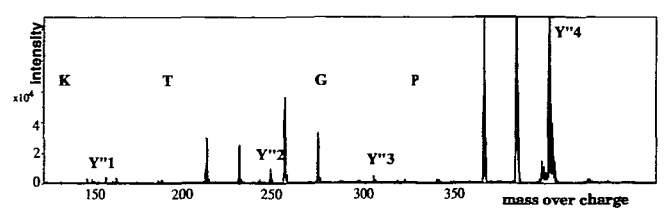

Peptide Sequencing Using Fast MS and MS/MS Scan Rates on a *uLC*/Quadrupole Ion Trap

Mark E. Bier*, Jae C. Schwartz, Joe Zhou, John E. P. Syka,
Dennis Taylor, Adrian P. Land, Mike James, and Bill Fies
Finnigan Corporation, 355 River Oaks Parkway, San Jose, CA 95134-1991

The quadrupole ion trap mass spectrometer may be operated at fast scan rates. The scan rate refers to the speed at which an amu is scanned out of the ion trap (amu/sec). Scan rates were first increased during the development of the prescan for variable ionization times. Years later at Purdue, the scan rate was increased by resonantly ejecting ions at a lower q_{ej}. (mass range extension) while maintaining the same Rf-amplitude scan rate . Fast scan rates can greatly improve detection limits because the ion current density over time is increased (i e. the signal height is increased), and the resulting shorter scan function allows for improved signal averaging.

Typically, the scan rate for ion trap mass spectrometers has been set at 5555-amu/sec (1X). In these experiments scan rates up to 177,778-amu/s, 32X the normal scan rate, have been tried, but we have primarily scanned at 16X the normal scan rate or less due to a data system limitation of the acquisition digital signal processor(DSP). In fact, to achieve these speeds the sampling rate was reduced from 10 at 1X to 4, 2, and 1 sample(s)/amu for the scan rate multipliers 4X, 8X, and 16X, respectively. The digital filter has been turned off at these higher scan rates to increase the bandpass. The q_{eject} was kept fixed at 0.83 for all scan speeds. A separate mass calibration file which included calibrated resonance ejection parameters was determined and loaded for each different scan rate. Initial investigations showed that a scan rate 16X the normal rate (i.e. 88880 Da/s) resulted in a resolution (m/Δm) reduction from 1100 to 250 at m/z=524.3 from MRFA and a signal height increase of *ca.* 6X. In one experiment it was possible to acquire 9 uscans at 16X the normal scan rate in the same time it would take to acquire 1 uscan at the normal scan rate from mass 80-1350 Da. In this case, the theoretical S/N ratio increases by 18 times over the normal scan rate data given there is no chemical noise. Chemical noise, however, will also increase in peak height with fast scan rates and will limit the S/N improvement to 3 times without background subtraction. Mass assignments at the faster rates, were found to be within an average of ca. ± 0.3 Da. Observations showed that there were reduced effects of space charge at higher scan rates. This suggests that a faster Rf scan rate allows for a larger number of ions to be ejected from the trap without causing a mass assignment increase.

Using capillary-LC(100um id x 15cm, POROS 10 R2 packing)(See Figure **1**), the low mass resolution MS/MS approach to peptide sequencing used by Hunt and coworkers at the University of Virginia, and fast Rf scan rates on a quadrupole ion trap we analyzed a mixture of five angiotensins: RVYVHPI, RVYVHPF, RVYIHPF, DRVYVHPFHL, and DRVYIHPFHL (Michrom Corp.). Both the MS (Figure **2**) and MS/MS scans were acquired to demonstrate the S/N enhancement. Background subtraction was also used to reduce the effects of chemical noise. Figure **3** shows the MS/MS spectrum of m/z 442.3^{+2} from RVYVHPI. We were able to acquire enhanced S/N spectra and make peptide fragment assignments at the 500 attomole level, however, unresolved adjacent mass peaks were given two fragment assignments. The (*) at m/z 385 in Figure **3** is believed to be a product ion from a coeluting parent.

Rapid scanning is limited by the acquisition rate of the processor, the degree of acceptable loss in mass resolution, the reduced S/N enhancement over slower rates as the duty cycle increases (i.e.

long ion times), and long scan functions such as MS^n that increases the time in which you are not looking at ions. The advantages of rapid scanning are: peaks have greater heights above non-chemical noise, signal averaging is improved, and space charge effects are reduced.

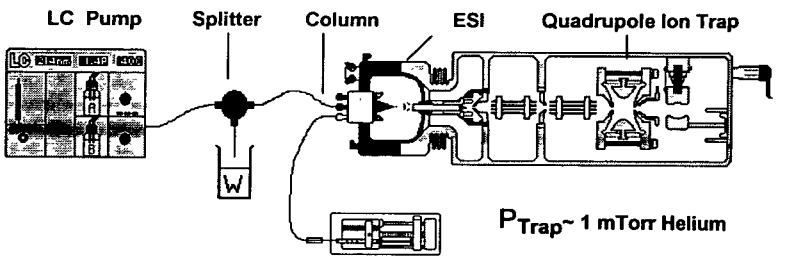

Figure 1

Signal-to-Noise Enhancement at Fast Scan Rates

µLC/MS of 10 fmoles RVYVHPI , 1X Normal Scan Rate= 5555 Da /sec

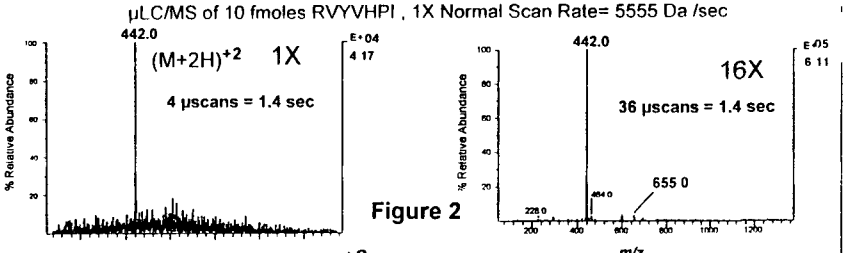

Figure 2

MS/MS of 442.3^{+2} from 550 attomoles of RVYVHPI

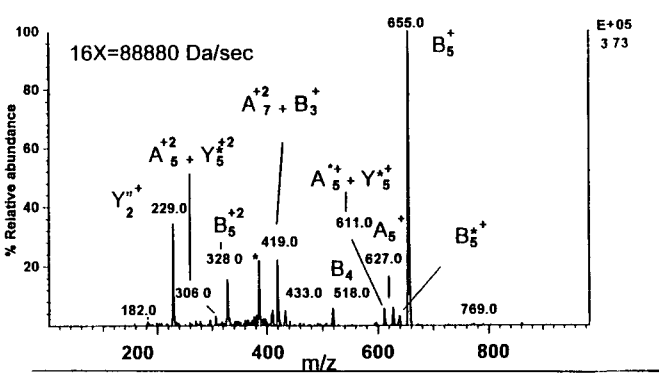

Figure 3

Practical Matrix-Assisted Laser Desorption/ Ionization Ion Trap Mass Spectrometry of Peptides

Jun Qin and Brian T. Chait
The Rockefeller University 1230 York Ave. New York NY 10021

Recent improvements in our understanding of the operation of the ion trap with an external matrix-assisted laser desorption/ ionization (MALDI) source have led to significant improvements in our ability to analyze peptides [J. Qin & B. T. Chait, paper in preparation]. A new excitation scheme [J. Qin & B. T. Chait, see companion paper at this conference.] allows for efficient collision-induced dissociation of peptide ions with m/z up to 3500. As a result of these improvements, MALDI/ITMS has become, in our laboratory, a routine and effective means for the sensitive characterization of proteins. We summarize here the performance of our MALDI/ITMS instrument and demonstrates its practicality through applications to a series of challenging biological problems.

The useful mass range (m/z) for peptides is up to 8 kDa. The resolution is both mass dependent and mass extension ratio dependent. For mass extension ratio of 10-15, the peak with (FWHM) is 2-5 Da for m/z < 3,500 and 5-7 Da for 3,500 < m/z < 8,000. Above m/z 8,000, the resolution deteriorates markedly. Single components as well as complex peptide mixtures (e.g. enzymatic digests; peptide ladders) can be mass analyzed with subpicomol sensitivity. Such mixtures can be readily analyzed without prior chromatographic separation. A mass accuracy of better than 200 ppm is routinely achieved with a simple three point external calibration over the whole mass range of interest.

MS/MS and sometimes MS/MS/MS can be performed with comparable sensitivity to single stage MS. Mass isolation is better than 3-5 Da for m/z < 3,000. MS/MS spectra (yielding useful sequence information) can be routinely obtained for all of the major proteolytic peptide fragments in a complex mixture without prior chromatographic separation using a loading of 0.5 pmol per component on the mass spectrometer probe. Such analysis was carried out for four different enzymatic digestions of E. Coli RecA protein (38 kDa).

In addition to its use as a sensitive tool for protein characterization, we have applied MALDI/ITMS to the identification of post-translational modifications, and have found the technique to be extremely useful for disulfide mapping and for the analysis of glycosylation and phosphorylation.

Inter-chain disulfide bonds dissociate spontaneously when disulfide-containing peptide ions are trapped. For a disulfide linked peptide composed of n (n >2) chains, a series of peptide ions containing n-i (i = 1, 2,..... n-1) disulfide bonds are observed in the positive ion spectra. In essence, this specific dissociation is equivalent to a controlled partial reduction of the disulfide bonds. This observation allows the disulfide connectivity to be defined. In disulfide mapping, intramolecular disulfide bonds are converted to interchain disulfide bonds by enzymatic or chemical cleavage of the peptide bonds between the cysteine residues. The unfractionated digestion is analyzed, and the disulfide linkages are determined. We have tested the strategy with synthetic C- terminal EGF-like domain in human blood coagulation factor XI, Iberiotoxin and αTGF. In addition, we have determined the disulfide linkages in earth worm hemoglobin linker chain L1(28 k Da), which contains a cystein-rich domain that has identical cysteine distribution pattern as that in the cystein-rich domain in the human LDL receptor.

In the ion trap, glycopeptides dissociate preferentially at the glycosidic bonds with charge retention on the peptide. These fragments allow a direct read-out of the composition (and sequence and branching in favorable cases) of the carbohydrate moiety. We have tested this strategy with synthetic glycopeptides and we have determined the sugar composition or sequence in some natural glycopeptides.

In the positive ion mode, we have observed that phosphopeptides lose ~ 98 Da upon trapping, providing an extremely convenient signature for phosphopeptides. Phosphoserine and phosphotyrosine are susceptible to this loss. Multiply phosphorylated peptides lose ~ 98 Da consecutively so that number of phosphate can be directly measured by the number of consecutive 98 Da losses. To determine the phosphorylation site within an enzymatic fragment(e.g., a tryptic fragment), the phosphoprotein is digested with the enzyme, then a peptide map is obtained by ITMS. The phosphopeptide is identified by the accurately measured mass, and further confirmed by the occurrence of ~ 98 Da loss. This method was tested with bovine β casein (23 k Da), a phosphoprotein containing 5 phosphates. We have determined the phosphorylation sites for bovine Synapsin I(74 k Da) as a substrate for the MAP kinase and CDC2 kinase (both are serine kinases). We have also determined the phosphorylation site for mouse lck (50 kDa) as a substrate for csk (a tyrosine kinase). In favorable cases, phosphorylation site can be determined to one amino acid by MS/MS if the phosphopeptide contains less than 15 amino acids. This capacity has been demonstrated with synthetic phosphopeptides.

In summary, we have developed a practical MALDI- ITMS instrument that can be used for the sensitive characterization of protein primary structures.

Analyzing Mixtures With a Hybrid Quadrupole/Ion Trap Mass Spectrometer

Karen R. Jonscher and John R. Yates, III
Dept. of Molecular Biotechnology, University of Washington, Seattle, WA 98195

Introduction: Tandem mass spectrometry has proven to be a versatile technique extending the mass spectrometry experiment to provide structural information for a number of different types of molecules. In this work we describe the construction of a hybrid quadrupole mass filter/quadrupole ion trap mass spectrometer interfaced to electron impact (EI), pulsed Cs^+ (LSIMS) and an electrospray ionization source (ESI) modified to incorporate a heated capillary. The goal of this work was to design a versatile instrument capable of analyzing complex mixtures of molecules.

Experimental: A quadrupole mass filter (mass range of 4,000 *m/z*), a focusing lens, a quadrupole ion trap mass spectrometer and a 20 kV collision dynode with an off-axis electron multiplier were aligned on a optical rail in the low pressure (~ 10^{-6}) region of a differentially pumped vacuum manifold. Operation of the ion trap was controlled by a PC interfaced to the ITMS™ (Finnigan MAT) electronics and operation of the quadrupole and vacuum system were controlled by a DECStation 2100 interfaced to a TSQ70 (Finnigan MAT). The mass analyzers were synchronized by triggering operation of the ion trap at the beginning of the quadrupole scan. The quadrupole was stepped through a given mass range in, typically, 10 u wide mass bins,and a scan window of 10 u was set in each mass bin. After triggering, the ITMS™ collected ions then a mass spectrum was acquired by resonant ejection at extended mass range. Data was displayed on a PC then ported to the DECStation 2100 for acquisition and data manipulation. Data porting time was on the order of 400 msec. The ITMS™ scan acquisition processor (SAP) board will not execute further instructions until the data porting is complete hence the duty cycle for the instrument is determined by the data porting time rather than by the ITMS™ scan time of ~ 120 - 220 msec. The minimum scan time for the quadrupole to scan in each mass bin was experimentally determined to be 0.57 sec, thus experiment scan times were typically on the order of 30 - 90 seconds to scan the quadrupole over a given mass range.

Results: Space-charge in the ion trap may limit the signal quality of ions present at low abundance in a mixture or in a matrix. Figure 1 provides an example of how the addition of the quadrupole mass filter, when scanned in small windows, significantly reduces space charge effects. Approximately 3 pmol of Glu-fibrinopeptide (MW 1571 u) were co-deposited onto a gold-plated probe tip with 1:1 glycerol:monothioglycerol and ionized by bombardment with 6 keV Cs^+ ions. Figure 1a shows suppression of the peptide in rf-only mode when all of the ions are being transmitted, while Figure 1b shows the reduction in space-charge effects obtained by scanning the quadrupole from 1450 *m/z* to 1650 *m/z*.

Electrospray ionization may be used to obtain LC-MS and LC-MS/MS information. Preliminary results are shown in Figures 2 and 3. Figure 2 illustrates the ion chromatograms resulting from electrospraying a mixture of angiotensin I (MW 1296 u) and ACTH 18-39 (MW 2466 u). Spectra obtained by summing scans under the peaks show excellent signal-to-noise obtained as well as some fragmentation upon injection into the ion trap. Figure 3 demonstrates the ability of this instrument to obtain fragmentation information "on-the-fly" for angiotensin I $(M+3H)^{+3}$. The capillary voltage is raised to promote source activation and the trap float voltage is decreased to increase the relative kinetic energy of the ions. Sufficient sequence information is obtained from the fragments to deduce the amino acid sequence for this peptide.

Conclusion: The hybrid instrument described in this work shows promise as a tool for the analysis of mixtures of molecules. The data porting time limiting the duty cycle may be eliminated by modification of the TSQ70 electronics to permit signal acquisition directly to the DECStation by way of the TSQ70 electrometer, bypassing the ITMS™ electronics. "On-the-fly" fragmentation may allow sequence information to be obtained for all ions in a mixture, reducing data loss due to co-elution during LC-MS.

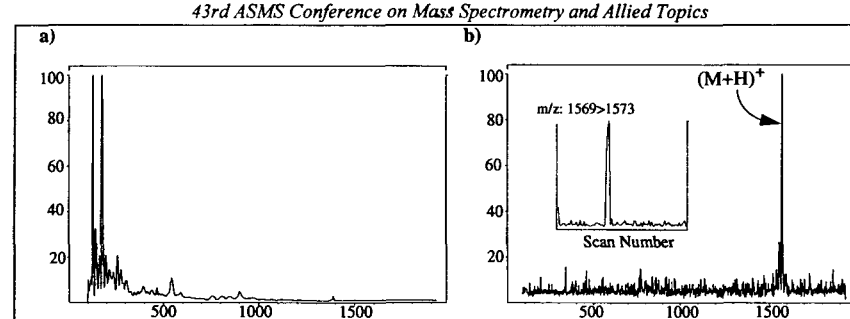

Figure 1: a) rf-only vs. b) scanning injection of Glu-fibrinopeptide ionized by LSIMS. Space-charge induced suppression was significantly reduced. Inset is the selected ion chromatogram.

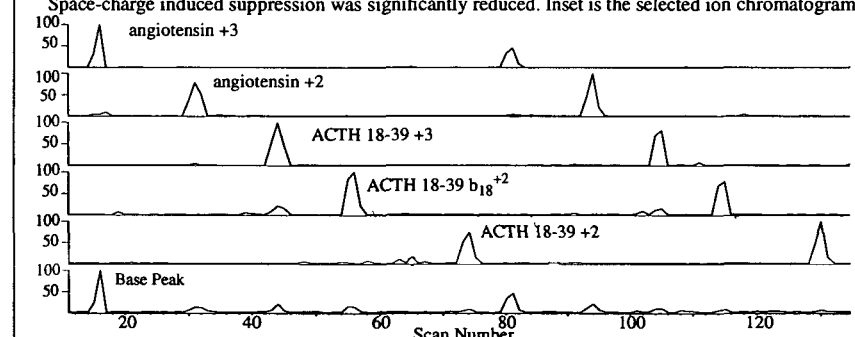

Figure 2: Selected ion chromatograms for a mixture of angiotensin I and ACTH 18-39 produced. by electrospray ionization and sequentially injected into the ion trap.

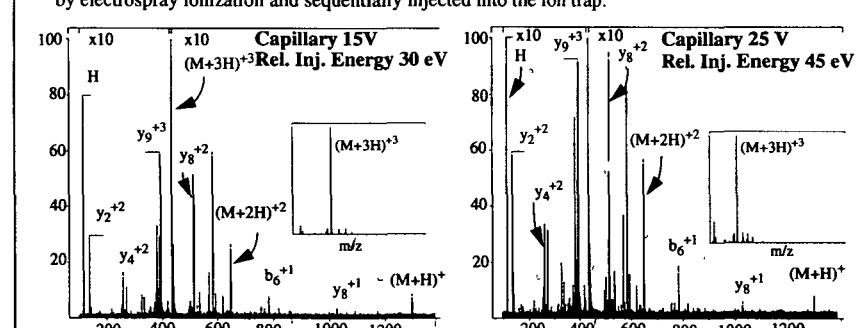

Figure 3: Mass spectra from angiotensin I +3 ion showing "on-the-fly" fragmentation achieved by decreasing the trap float voltage and increasing the capillary voltage. Insets show normalized mass spectra.

A Portable Atmospheric Sampling QUISTOR/reTOF- MS for Air Monitoring

Louis I. Grace, David M. Chambers, Stan W. Thomas and Brian D.Andresen

University of California Lawrence Livermore National Lab. P.O. Box 808, Livermore, California 94551

We are developing a portable mass spectrometer to detect volatile organic compounds in air. Given sufficiently low detection limits and high mass resolution, such an instrument will be useful in a wide array of air monitoring applications, for example, pollutant detection or plant maintenance and diagnostics. We chose a time-of-flight analyzer for its efficient ion transmission with virtually unlimited mass range. We use a quadrupole ion storage trap to create a pulsed source to provide a reference for ion flight times. Through its ion storage capability, the ion trap also lowers detection limits, enhances sensitivity and increases the duty cycle of the instrument. The flight tube houses a reflectron, which improves mass resolution by partially compensating for the kinetic energy spread of the ions. The ion trap is coupled to the flight tube via an einzel lens. An important feature of the new instrument is that the air sample is introduced directly. This eliminates the need for vacuum interlocks and various hardware associated with other types of sample inlet. Such a sampling system also reduces contact between the analyte and surfaces inside the instrument, thus greatly decreasing the loss of sample through adsorption onto the walls of the inlet, or through catalytic decomposition arising from such adsorption.

To aid the design of the portable instrument, we tested various features in a larger laboratory instrument. Based on these tests, we have chosen to use electron impact to ionize the sample. Also, we have designed an inlet which introduces the sample directly into the ion trap, so that the ions are formed within the trap instead of being injected externally. This may reduce the initial kinetic energy spread of the ions, and it offers lower detection limits. The various ion optics were modeled by means of the SIMION program and tested on the laboratory instrument. Then similar optics were designed for the portable instrument. To make the spectrometer portable, we have shortened the flight tube from 32in to 18in, and have made the ion trap envelope smaller.

For volatile organic compounds, the laboratory spectrometer has shown detection limits in the low to sub-ppb range (v/v) with mass resolution of 2000 or better (M/dM, FWHM). We are still making refinements to, and optimizing the tuning of, the portable instrument. At this point, the portable instrument shows detection limits of approximately 500ppb for a variety of volatile organic compounds. The mass resolution it achieves is routinely 1000 or better, and is often as high as 1250. The xenon spectrum in the accompanying figure is an example of the kind of data the new instrument yields. This spectrum shows a resolution of about 1000.

Xenon in Air

M/ΔM (FWHM) ≈ 1000, 100-ms ion accumulation time, average of 200 scans

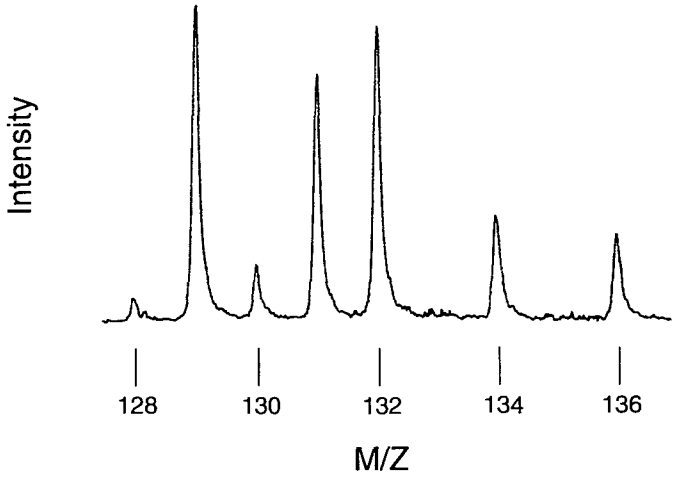

We find the performance of the portable instrument encouraging. Given the instrument's current capabilities, and based on our experience with the laboratory prototype, we expect to extend the detection limits of the new instrument into the part-per-trillion range and possibly also to improve the mass resolution.

This work was performed under the auspices of the U.S. Department of Energy by the Lawrence Livermore National Laboratory under contract W-7405-ENG-48.

IDENTIFICATION OF *IN VITRO* METABOLITES OF BUPROPION BY APCI LC-MS USING AN ION TRAP MASS SPECTROMETER.

Lester C.E. Taylor, Romi Singh, Sai Y. Chang, Robert L Johnson, Jae Schwartz‡.
Burroughs Wellcome Co , 3030 Cornwallis Road, R T P , NC 27709
‡Finnigan MAT, 355 River Oaks Parkway, San Jose, CA 95134

The drug bupropion (Wellbutrin®), Figure 1, *m*-chloro-a-*tert*-butyl-aminopropiophenone, shows activity as an anti-depressant (1) As part of continuing drug metabolism and structural characterization studies we have undertaken a series of mass experiments aimed at identifying the *in vitro* metabolites of bupropion

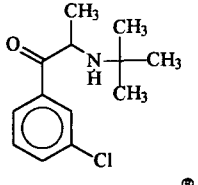

BUPROPION (WELLBUTRIN ®)

Mass spectrometry using atmospheric pressure ionization combined with triple quadrupole instruments has proven highly effective for identifying and quantitating drugs and drug metabolites in biological matrices such as plasma, urine and bile We report the use of APCI LC-MS for the identification of *in vitro* metabolites of bupropion using a quadrupole ion trap instrument fitted with an external atmospheric pressure ionization (API) source Preliminary experiments have shown that this instrument provides comparable sensitivity to conventional triple quadrupole instruments for metabolite identification while allowing further specificity for structural analysis by MS^n and is suitable for on-line coupling with HPLC

Ion Trap LC-MS

The quadrupole ion trap LC-MS system consisted of a Hewlett Packard HP1090 LC system using a Novapak C18 column. The column eluent was couple directly to a Finnigan APCI source operating at a nebulizer temperature of 500 °C, corona needle potential of approximately 4 kV A heated capillary interface to the mass spectrometer vacuum system was utilized operating at a capillary temperature of 150 oC and at a voltage of approximately 10 volts A linear gradient was run from 90% A to 60% A, where solvent A was a 50 mM ammonium acetate aqueous solution and solvent B was acetonitrile using a flow rate of 1 ml/min

The ion trap used for these studies was a prototype system configured especially for LC-MS applications. The ions exit the heated capillary and pass through a skimmer and are transferred by an RF only octopole which operates at a pressure of 1.3 x 10-3 torr through a 0.1 inch aperture lens into a second RF only octopole operating at a pressure of 2 x 10-5 torr This octopole transmits the ions into the ion trap through a 0 60 inch aperture in the entrance end cap of the ion trap The ion trap contains helium damping gas at a pressure of approximately 1 mtorr in order to trap injected ions and improve general performance of the trap The main components of the ion trap scan function consisted of ion injection times of between 5 to 1000 msec, single isolation using multifrequency waveforms applied for 15 msec per MS/MS stage, and spectrum generation using the mass selective instability mode with resonance ejection at a scan rate of 0 180 msec/amu. Total cycle times reached 1 5 sec/scan for MS^6 experiments The mass range of the ion trap is 2000 m/z and operates at a frequency of 760 kHz. A 15 kV conversion dynode along with a channeltron electron multiplier was utilized for optimum detection efficiency Being an early prototype, this system had several instrumental problems including a noisy dynode and some electronic instability which limited instrument performance for these studies

Results

We have followed the fragmentation pathways of several molecular ion species in a series of sequential $LC\text{-}MS^n$ experiments, extending as far as MS^6 with scan cycle times of less than 1 5 s Such experiments have provided insights into the structure of specific fragment ions. Bupropion was characterized in a series of MS^n experiments which established the fragmentation cascade of the parent compound This established the MS^6 pathway,(shown in Figure 1), MH^+ 240 to 184 to 166 to 131 to 130 to 103 The LC-MS analysis of human S9 incubation showed the presence of three isomeric monohydroxylated metabolites of bupropion These were further characterized in a series of MS/MS experiments which gave characteristic spectra for the three isomers. A minor dihydroxylated species (both hydroxyl groups located on the tertiary butyl group) was also identified in the human S9 sample and further characterized in a series of MS^n experiments Detailed structural information was generated by the use of on-line $LC\text{-}MS^n$ type experiments Additional metabolic products were identified in the rat liver microsome incubation sample

References

1. (a) N. B. Mehta, Fed Proc , 29, 650 **(1970)**, (b) S. Schroeder, J Clinical Psychia 44 (5, Sec 2), 60-62 **(1983)**

Figure 1

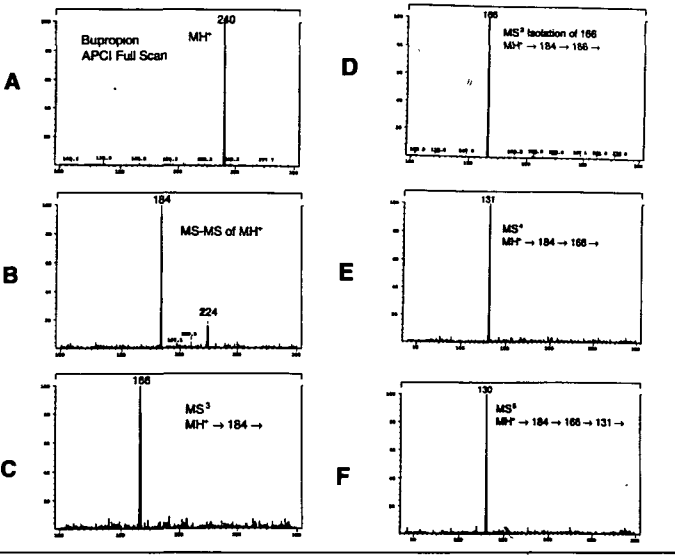

ANALYTICAL PROTOCOLS FOR ENVIRONMENTAL SUBSTANCES USING AN ION TRAP

J.B. Plomley, C.J. Koester, M. Lausevic, X. Jiang, F.A. Londry and R.E. March
Trent University, Department of chemistry, Peterborough, ON, Canada, K9J 7B8

The powerful capability of a capillary column for gas chromatographic separation of volatile organic compounds, complemented by the versatility of a mass-selective quadrupole ion trap detector operated in the tandem mass spectrometric mode, has been directed to the detection and identification of a variety of environmental pollutants. This GC/MS/MS combination with a choice of electron impact and chemical ionization offers both high sensitivity and high specificity. In order to establish an analytical protocol utilizing GC/MS/MS, it is necessary to ascertain ionization energies, proton affinities and the activation energy hierarchy of dissociation channels. With this information, one can then customize a scan function or functions wherein a molecular ion, protonated molecule or reagent ion is formed, stored preferentially, isolated, reacted, collisionally dissociated[1] and the fragment ions mass-analyzed.

Instrument

The instrument used in this study was a modified Varian Saturn III GC/QISMS (Quadrupole Ion Storage Mass Spectrometer) equipped with a Varian waveform generator and a Varian 8200 autosampler. Saturn Revision C software was used for data acquisition; Saturn version 5.0 software was used to define GC retention-time windows while "Toolkit" was used to define ion preparation methods (or customized scan functions) for individual retention-time windows. The waveform generator could be employed during and after ionization.

Within a single GC run, a series of customized scan functions can be synchronized with retention time so as to determine the concentrations of many compounds in rapid succession. A modified Saturn I instrument was used for high mass-resolution studies.[2,3]

ANALYTICAL PROTOCOLS

A major effort in this laboratory is being directed to the establishment of analytical protocols for the determination of PCBs, PCBEs, PCDFs and PCDDs, for a total of 628 isomers not counting ^{13}C- and D-labelled compounds used as standards.

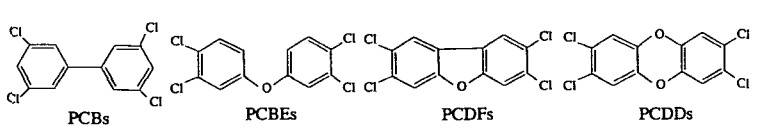

These compounds exhibit a range of toxicity from 1 - 10^{-13}. Toxicity correlates highly with both chlorine substitution and the absence of chlorine substitution in the *ortho* positions. The advent of the waveform generator, the development of software for multiple

43rd ASMS Conference on Mass Spectrometry and Allied Topics

scan functions, the loss of Cl and/or COCl upon dissociation and little variation of activation energies for dissociation among isomers combine to make us quite optimistic about the final outcome of this project.

Polychlorinated biphenyls (PCBs)

Two analytical protocols are being developed for PCB analysis; one is based on electron ionization (EI), the other on selected ion chemical ionization (SICI). The first protocol applies the EI method to congener-specific analysis using a customized scan function; the method is based on the difference between the fragmentation patterns of the highly toxic *(non* and *mono-ortho substituted)* congeners and those of the less toxic congeners.[4]

The second protocol applies the SICI method, using $C_2H_5^+$ reagent ions,[5] for the determination of total PCB content in a mixture and for differentiating between co-eluting congeners.

Polychlorinated biphenylethers (PCBEs)

The analytical protocol for PCBEs, which is under development, is based on the difference in fragmentation behaviour of *non* and *mono-ortho substituted* congeners and other congeners. All PCBEs exhibit loss of a chlorine atom from the molecular ion; *non* and *mono-ortho substituted* congeners exhibit also a characteristic loss of COCl.

Polychlorinated dibenzo-*p*-dioxins (PCDDs) and furans (PCDFs)

The analytical protocol for PCDDs[6] and PCDFs is now well developed. In this protocol, molecular ions formed by EI are isolated, dissociated resonantly, and daughter ions formed by the charateristic loss of COCl are mass analyzed. For a given degree of chlorine substitution, the apparent similarity of activation energy for loss of COCl among isomers is particularly fortunate given the complexity of rearrangement necessary. Switching of multiple scan functions permits determination of co-eluting dioxins, furans and their ^{13}C-isotopomers.

REFERENCES

1. P. Liere, T. Blasco, R.E. March and J.-C. Tabet, Rapid Commun. Mass Spectrometry, **8** (1994) 953.
2. F.A. Londry, G.J. Wells and R.E. March, Hyperfine Interactions, **81** (1993) 179.
3. R.E. March, F.A. Londry and G.J. Wells, 41st ASMS Conference on Mass Spectrometry and Allied Topics, 30 May - 4 June 1993, San Francisco, p 790.
4. M. Lausevic, X. Jiang, C.D. Metcalfe and R.E. March, Rapid Commun. Mass Spectrom. to be published.
5. M. Lausevic, J.B. Plomley, X. Jiang and R.E. March, Eur. Mass Spectrom. **1** (1995) in press.
6. J.B. Plomley, C.J. Koester and R.E. March, Anal. Chem. **66** (1994) 4437.

Time-of-Flight (TOF) Mass Spectrometry–Nearing the Half Century

K.G. Standing
Physics Dept., University of Manitoba,Winnipeg, MB Canada, R3T 2N2

It appears that the first published proposal for a TOF mass spectrometer was made by W.E. Stephens, a nuclear physicist at the University of Pennsylvania. The proposal was presented at a meeting of the American Physical Society in April 1946 [1], so it was probably submitted late in 1945; Fig. 1 shows the abstract. Thus we are about to celebrate the 50th anniversary of TOF mass spectrometry. In the present conference almost 10% of the presentations included TOF or TOF mass spectrometry in their keywords, so we may conclude that the field is flourishing. This is a pleasant contrast to the situation not too many years ago, when the TOF contingent at the ASMS meeting would have fit into a good-sized closet!

A few years passed before Stephens was able to report any measurements [2], and these showed "a peak width of two mass units at mass 40"-- not an impressive resolution compared to the values already obtained in sector instruments, but the spectrometer was expected to have other advantages, as pointed out in his abstract. Stephens' machine produced ions by a *pulsed* electron beam, then accelerated them across a *constant* potential difference, so it serves as the prototype for modern instruments using a simple DC accelerating voltage.

Soon afterwards Wiley and McLaren introduced a two-field source [3]. In their instrument, ions were produced in a field-free region, extracted by an accelerating *pulse*, then further accelerated across a constant potential difference. This was the basis of the Bendix TOF spectrometer, which dominated the field for many years. Wiley and McLaren gave a careful analysis of pulsed operation, including the effect of pulse delay, and their work still provides the foundation for instruments that employ pulsed extraction. They claimed a number of advantages for TOF spectrometers, including speed, ability to record the whole spectrum without scanning, and the absence of narrow slits. However, it is interesting to note that they did not mention the large m/z range of the instrument, a reflection of the inability of any existing technique to produce ions of high mass.

The first solution to the problem of producing large ions for TOF measurements was the dramatic discovery by Macfarlane and Torgerson that such ions could be desorbed from a solid surface by fission fragment bombardment [4]. In addition to a significant extension of mass range, their instrument introduced other important features; the ions were desorbed from a plane equipotential surface, thus providing small spatial dispersion, and modern (nsec) electronics were used, together with simple DC acceleration, which minimized stability problems. This was the basis for much of the TOF work in the next 10 or 15 years.

At the same time there were considerable improvements in TOF resolution as a result of the widespread adoption of various reflecting geometries, first proposed by Mamyrin [5]. A number of groups have reported values of $M/\Delta M_{FWHM}$>10,000 for simple inorganic compounds.

An even higher mass range became available with the discovery of matrix-assisted laser desorption/ionization (MALDI), the dominant TOF technique at present. Karas and Hillenkamp showed that the addition of a suitable organic matrix (initially nicotinic acid) to the sample made it possible to produce ions from a wide variety of biomolecules of masses up to 100,000 u and beyond with relative ease [6]. Since the lasers used are pulsed, the marriage with DC acceleration TOF is a natural one.

Electrospray ionization, the other new method for producing ions from high mass compounds, has only recently been coupled to TOF spectrometers, initially by Dodonov *et al* [7]. ESI/TOF instruments have a much larger m/z range than the quadrupole mass filters normally used with ESI, so they are particularly useful for examining interesting entities like non-covalent complexes [8]. They are also capable of giving spectra with considerably improved resolution, as illustrated by the spectrum of bovine insulin shown in Fig. 2.

Since ESI is a continuous method of ion production, it requires pulsed injection, so the ideas of Wiley and McLaren have acquired new relevance. If ES ions enter the spectrometer perpendicular to its axis ("orthogonal injection") [7], they can then be injected along a suitable flight path. It has recently been realized that pulsed methods can also give improved results for MALDI [8].

1 Proc. Am. Phys. Soc., Spring meeting at Cambridge, Mass., 25-27 April, 1946 {*Phys. Rev.* **69**, 691 (1946)}.
2 M.M. Wolff and W.E. Stephens, *Rev. Sci. Instrum.* **24**, 616 (1953).
3 W.C. Wiley and I.H. McLaren, *Rev. Sci. Instrum.* **26**, 1150 (1955).
4 R.D. Macfarlane and D.F. Torgerson, *Science* **191**, 920 (1976).
5 B.A. Mamyrin *et al*, *Soviet Physics JETP* **37**, 45 (1973).
6 M. Karas and F. Hillenkamp, *Anal. Chem.* **60**, 2299 (1988).
7 A.F. Dodonov *et al*, in *Time-of-Flight Mass Spectrometry*, Am. Chem. Soc. 1994.
8 See, for example, the contributions by Brown, by Ens, and by Reilly.

J1. A Pulsed Mass Spectrometer with Time Dispersion. W. E. STEPHENS, *University of Pennsylvania.*—Advances in electronics seem to make practical a type of mass spectrometer in which microsecond pulses of ions are selected every millisecond from an ordinary low voltage ion source. In travelling down the vacuum tube, ions of different M/e have different velocities and consequently separate into groups spread out in space. If the ions are collected in a fixed Faraday cage and the current amplified, then pulses of current corresponding to different ion M/e will be dispersed in time. If the amplified current pulses are put on the vertical plates of an oscillograph whose sweep is synchronized with the pulses, then an M/e spectrum of the ions will be exhibited. This type of mass spectrometer should offer many advantages over present types. The response time should be limited only by the repetition rate (milliseconds). The indication would be continuous and visual and easily photographed. Magnets and stabilization equipment would be eliminated. Resolution would not be limited by smallness of slits or alignment. Such a mass spectrometer should be well suited for gas composition control, rapid analysis, and portable use. A mass spectrometer of this type is being constructed

Fig 1 Stephens' abstract [1].

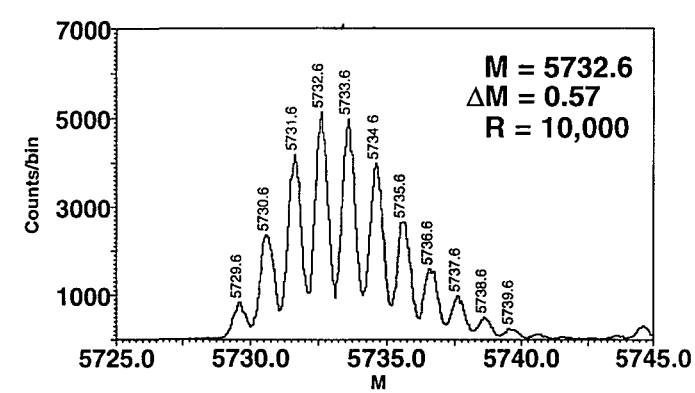

Fig. 2 Deconvoluted ESI/TOF mass spectrum of bovine insulin, from Krutchinsky *et al*, MPB 85

Organic Secondary Ion Imaging by Time-of-Flight Secondary Ion MS (TOF-SIMS)

Patricia M. Lindley[1] & Fraser Reich[2]

1. Charles Evans & Associates, 301 Chesapeake Dr., Redwood City, CA 94063
2. PHI Evans, 575 Chesapeake Dr. Redwood City, CA 94063

Time-of-Flight Secondary Ion Mass Spectrometry (TOF-SIMS) has now evolved to a state where commercial instrumentation is being used successfully in industries throughout the world for a variety of research and development projects, and also for powerful trouble-shooting of materials processing problems

In TOF-SIMS a pulsed, microfocused primary ion beam is scanned over a sample surface, generating secondary ions that are characteristic of that surface These secondary ions are created from the top few monolayers and are then extracted into a TOF spectrometer, where their masses are determined by precise measurment of their flight times to the detector. The resulting mass spectrum, however, is merely the starting point for the technique. The detector output is synchronized with the primary beam raster, so that secondary ion images may be obtained. Pulsed primary beams with probe sizes of 1000Å have recently been obtained using liquid metal ion guns (LMIG) While the experiment is running, the intensity of particular peaks in the mass spectrum may be monitored as a function of experiment time, and thus a 'time evolution of species' may also be obtained from the sample. Finally, secondary ion yields may be monitored as a function of depth for certain materials (inorganic), by sputter removal of material to reveal buried structures below the outer surface.

Although TOF-SIMS is capable of analyzing all vacuum-compatible solids, it is unique in its ability to characterize and image organic materials surfaces. This is due to the extremely high transmission and parallel detection capabilities of the TOF spectrometer Optimum use is made of the ionized material produced from the sample surface (>80% molecular ions created are transmitted to the detector), and a mass spectrum plus a full suite of secondary ion images may be acquired simultaneously before the top monolayer of material is consumed. This is extremely important for organic material analysis, since primary ion bombardment beyond this regime (known as the 'static SIMS' regime) results in the production of ever smaller fragment ions as the remaining surface becomes increasingly damaged by the incoming primary ions.

As the sample cannot be re-analyzed, it is important that maximum use be made of the information generated during the analysis, particularly if the analytical site is unique, as is often the case with defect analysis for instance. Accordingly, the TOF-SIMS technique has matured due to a combination of hardware and software interactions TOF-SIMS has seen the development of an interesting approach to data collection, in which the information concerning every secondary ion detected, its x, y position and time-of-flight (mass), can be saved to disk During the 'live' data acquisition, the analyst will examine the accumulating mass spectrum and initiate mapping of the species for which the lateral distributions need to be determined. Once the analysis is completed however, the 'raw' data set may be replayed any number of times off-line in order to finesse the data. This facility is surprisingly useful in a number of analytical situations Three examples serve to demonstrate this point:

(1) In the routine analysis of a homogeneous polymer film surface, a total positive ion image was acquired as a matter of course. At the end of the mass analysis and image acquisition, two small (1-2μm) particles were evident within the field of view. 'Regions of interest' mass spectra were acquired from the particles and a control area, by replay of the 'raw' data set Even after this stage however, the mass spectrum from the particles was not too dissimilar from the polymer sheet surface spectrum. Next, the two mass spectra were normalized, and the control spectrum was subtracted from the particles mass spectrum. Sole residuals after subtraction were identified as CF, CF_3, C_2F_4, C_3F_5 and so on, indicating that the particles were fluorocarbon-containing. A further replay, collecting an image from a combination of these species, then revealed locally intense signals of fluorocarbons from these small particles.

(2) A two layer paint on a wooden substrate was prepared in cross-section by microtoming, and analyzed in the TOF-SIMS instrument. The outer and inner layers were approximately 30μm and 60μm thick, respectively. Retrospective analysis permitted detailed investigation of the constituents and additives in the two layers of paint, that were not anticipated by the analyst from the outset. For instance, titanium (from a pigment) was found to be isolated within the top layer only, whereas sodium, although also present in this layer, had clearly diffused into the second layer When an image was acquired retrospectively from high mass fragments observed in the mass range 300-650 m/z, these species were all seen to be located in the lower paint layer, and are characteristic for a polymer paint additive. This mode of analysis is of great benefit to off-site clients, wishing to return with further questions concerning the original data so as to maximize the information from a single analysis.

(3) The mass resolution in the total mass spectrum acquired from a series of treated ceramic grains was severely degraded owing to the topography of the coarse crystals. Using the total ion image acquired during the analysis, individual grains approximately 10-75μm in diameter were easily identified. Mass spectra were then acquired retrospectively from individual grains whose surfaces were facing the analyzing beam at single, discrete heights in the secondary ion extraction region. The mass resolution following recalibration was seen to increase from approx 500 in the total surface spectrum to ~5000 (FWHM) in the spectra from individual grains For instance, a single peak at mass 43 was seen on individual grains to resolve into 3 peaks. This represents another example of how this type of off-line analysis permits the analyst to finesse the chemical information that is latent within these data sets

In conclusion, we have found that it is powerful to treat the TOF-SIMS data set as a very malleable entity which can be replayed and re-presented in a variety of ways to maximize the information available from the analysis. This is vital for samples which are unique and may be analyzed once only, and is very useful when it is not clear at the outset of analysis which species to map laterally on the sample.

Quantitative Analysis of Biomolecules by Time-of-Flight Secondary-Ion Mass Spectrometry: Fundamental Considerations

David C. Muddiman[1], Anthony J. Nicola, Andrew Proctor and David M. Hercules[2]

Department of Chemistry, University of Pittsburgh
Pittsburgh, Pennsylvania 15260

Present Addresses:

1. Pacific Northwest Laboratories
Chemical Sciences Department
Battelle Blvd. P.O. Box 999
Richland, WA 99352

2. Department of Chemistry
Vanderbilt University
Box 1822 Station B
Nashville, TN 37235

Static Time-of-Flight Secondary-Ion Mass Spectrometry (TOF-SIMS) has been applied to investigate an extensive assortment of analytical systems; from semiconductors to DNA sequencing. Recently, the TOF-SIMS method has been successfully applied to real biological systems [1,2]. This report focuses on some important aspects that must be taken into consideration when conducting measurements on biomaterials in order to observe the potential the TOF-SIMS method affords. The current data are presented using Cyclosporin A (CsA, 1202 Da) and cocaine (303 Da) as model compounds. CsA is observed in the TOF-SIMS mass spectrum predominately as a Ag-cationized species and cocaine as a protonated species; thus, they are complementary probe molecules.

Bioanalysis by TOF-SIMS is typically performed when the compound is supported on a chemically etched silver substrate resulting in a maximum secondary-ion (SI) yield. To obtain quantitative data for species requiring Ag-cationization, the Ag must be etched under identical conditions to avoid substrate variability introduced by the etching process (data not shown).

To define the dynamic range of the TOF-SIMS method, cocaine was used as a model compound due to its extraordinary SI yield. The TOF-SIMS detection system comprises a multi-stop TDC operating in the single-ion counting mode. The dynamic range of the TOF-SIMS method was limited using this detection configuration due to the probability of multiple ions arriving in a single primary ion pulse. Figure 1 shows the corrected standard curve for cocaine (using its deuterated analog as the internal standard) from 10 ng/mL - 100 μg/mL. Peak intensity corrections using a Poisson function (Eqn. 1)

$$I_{corr} = -n \times \ln\left(1 - \frac{I_{exp}}{n}\right) \quad (1)$$

where I_{corr} is the corrected intensity, n is the number of ion pulses and I_{exp} is the experimental peak area, extended the dynamic range of the TOF-SIMS method to over 4 orders of magnitude.

The therapeutic blood trough levels of CsA range from 25-2000 ng/mL; however, this is far from the maximum SI yield of CsA (*ca.* 500 μg/mL). Concentrating the sample has shown to decrease the SI yield which is attributed to an increase in the surface coverage (as a result of concentrating endogenous material present in the extract). Therefore, sample extracts must be of the highest purity prior to preconcentration and subsequent TOF-SIMS analysis to avoid an equal increase in coverage due to the presence of contaminants.

Enhancement of SI yield was observed utilizing a novel sample preparation technique. The initial observation was discovered when an allograft blood sample was analyzed on an etched Ag substrate that was soaking in a cocaine solution for *ca.* 2 months. The increase in SI yield was found to be over an order of magnitude (Figure 2). Attempts to reproduce the original experiment was done by applying 5 μL of a 20 μg/mL cocaine solution to an etched Ag substrate, allowing solvent evaporation, then applying either a CsA or polystyrene solution to the surface. These experiments resulted in about a 300% increase in SI yield. Taking into account the above mentioned results (except for the enhancement experiments), TOF-SIMS can provide quantitative information of drugs in real biological systems.

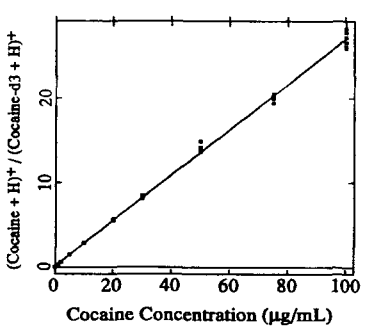

Figure 1: TOF-SIMS Corrected Standard Curve for Cocaine Hydrochloride

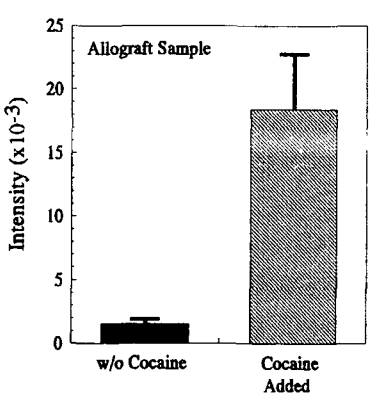

Figure 2: TOF-SIMS Data Obtained from a Normal and Modified Ag Substrate

References:

1. Muddiman, D.C., *et. al.*, These proceedings.
2. Muddiman, D.C.; Gusev, A.I.; Proctor, A.; Hercules, D.M.; Venkataramanan, R.; Diven, W. *Anal. Chem.*, **1994**, 66, 14, 2362-2368.

Peptide/Protein Sequencing by Exopeptidase Digestion Coupled with MALDI-TOF MS: Part of an Integrated Strategy

Dale H. Patterson, George E. Tarr, Fred E. Regnier and Stephen A. Martin
PerSeptive Biosystems, Framingham, MA 01701

Determination of the primary structure of peptides and proteins is critical as a support for molecular genetics, detection of secondary modifications, peptide/protein mapping, drug discovery and quality control Any single approach (instrumental or chemical) for deriving complete sequence information from all peptides and proteins is not viable as all methods possess inherent limitations. It is more advantageous to develop a number of integrated instrumental and chemical strategies that, when implemented as a whole, yield the desired structural information. MALDI-TOF is a tool around which these strategies can be built. Purely instrumental methods for deriving sequence information lie in MALDI-TOFs ability to deliver accurate molecular mass information over a wide mass range as well as MS/MS information in the form of post source decay (PSD). When coupled with enzymatically derived C- and N-terminal ladders, MALDI-TOF becomes a powerful tool to probe the primary structure of peptides as well as proteins.

Classical, solution-phase time-dependent carboxypeptidase Y (CPY) digestions have been performed on the ACTH 7-38 fragment and the resulting peptide ladders analyzed by MALDI-TOF. Optimization of this digestion has resulted in the sequencing of 19 amino acids from the C-terminus without gaps in 25 min. An improved strategy for performing the digestions was further developed wherein parallel CPY digestions of varying enzyme/substrate concentration ratios are carried out in the μL wells on the sample plate. This on-plate concentration-dependent strategy holds many advantages over the classical approach. Only sub-pmol amounts of total peptide are required; the manual labor of removing and quenching time aliquots is circumvented; and the total digestion time required is reduced to 10 min or less. Using the on-plate parallel digestion strategy has allowed the sequencing of numerous peptides of varying size, charge and polarity. Figure 1 shows the results for the ACTH 7-38 fragment.

To further the development of ladder sequencing, a strategy for applying statistical levels of confidence on residue assignments has been developed. The strategy involves the acquisition of multiple replicates, N, such that an experimental mean mass difference, x, with associated standard deviation, s, can be calculated. All possible assignments are used as the asserted mean mass, μ. Asserted means are deemed statistically improbable as calculated t-values for each μ are compared with a tabulated value for a desired confidence interval.

The integration of statistically accurate C- and N-terminal information via on-plate carboxypeptidase and aminopeptidase digestions offers a wealth of primary information from the termini of peptides. This approach often leaves the central portion of the peptide unexplored. Combining the terminal assignments with PSD data often proves sufficient for obtaining complete primary structural information. Figure 2 shows the results of on-plate carboxypeptidase Y and aminopeptidase 1 digestion coupled with PSD for the complete sequencing of renin substrate.

Delayed extraction (DE) MALDI-TOF has been shown to offer much improved resolution and mass accuracy due to its ability to significantly reduce the initial velocity distribution of extracted ions. DE MALDI-TOF holds advantages for the analyses of peptide ladders as its increased mass accuracy allows for a reduced number of replicates to be obtained in order to statistically deem improbable incorrect residue assignments. The much improved resolution of DE MALDI-TOF allows for the analysis of much larger ladders (*e.g* protein ladders) than does the continuous extraction technique. Figure 3 gives the DE MALDI-TOF analysis of an on-plate CPY digestion of pyridylethylated ribonuclease A, a 14,351 dalton protein.

43rd ASMS Conference on Mass Spectrometry and Allied Topics

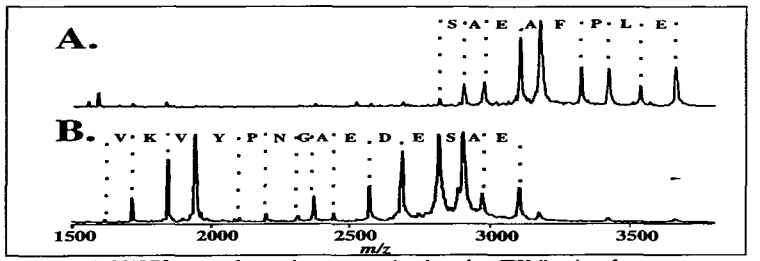

Figure 1. MALDI spectra of an on plate concentration-dependent CPY digestion of ACTH 7-38 yielding 19 amino acid residues from the C-terminus. Panels A and B represent the digestions from 6.10×10^{-4} and 1.53×10^{-3} units/uL CPY respectively.

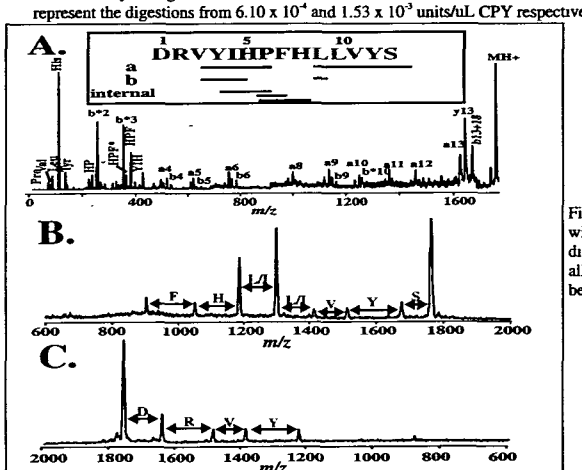

Figure 2. PSD data (A) combined with on-plate CPY (B) and AP1(C) digestions of renin substrate allow all primary sequence information to be obtained.

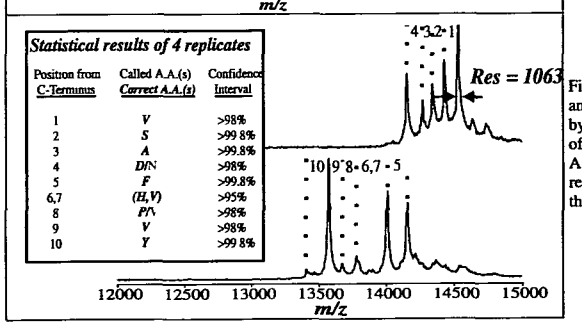

Figure 3. DE MALDI-TOF analysis of a ladded created by the on-plate CPY digestion of pyridylethylated RNAase A. The insert indicates the residue assignments based on the statistical analysis method.

MALDI Electrostatic Analyzer TOF Mass Spectrometry Studies of Biopolymers

K. J. Wu, E. P. Marsh and R. W. Odom

Charles Evans & Associates, 301 Chesapeake Drive, Redwood City, CA 94063

A new matrix-assisted laser desorption/ionization (MALDI) mass spectrometer has been constructed for biopolymer analysis. This new instrument is based on a mass spectrometer platform designed for time-of-flight secondary ion mass spectrometry (TOF-SIMS) applications. It features specialized stigmatic ion optics which extract and transport ions from the sample surface to the TOF mass analyzer. The time-of-flight mass analyzer consists of three 90° quasi-hemispherical electrostatic sector analyzers (ESA) in the ion flight path and a dual microchannel plate for ion detection. A schematic diagram of this apparatus is shown in Figure 1 These ESAs provide complete first order energy focusing of ion flight times. The design of the spectrometer corrects and compensates flight time variation due to kinetic energy aberration at the acceleration region as well as flight time differences arising from angular variances A fast sampling rate transient digitizer with speeds up to 500 psec/channel is used for ion signal acquisition.

A N_2 laser (λ=337 nm) with a pulse width of 600 psec is used for desorption/ionization. The laser beam is tightly focused onto the surface of the sample to ca 5 μm in diameter Such small desorption laser beam spots can in principle reduce the ionization volume which in turn would minimize the spatial distribution of MALDI ions and improve the mass resolution A micrometer controlled variable attenuator is employed for continuous adjustment of laser intensity.

The initial testing of the instrument included studies of known mass peptides, proteins, synthetic DNA oligomers and organic polymers. Detection sensitivity is comparable to the conventional MALDI-TOF apparatus, and typical amounts of analyte loaded for analysis are between 200 fmol to a few pmol The most improved feature of this instrument over conventional MALDI-TOFMS systems is its mass resolution and accuracy The routine mass resolution (M/ΔM, FWHM) has been demonstrated to be in the range of 5,000 - 7,000 for m/z up to ca 6,000. Resolution as high as 12,000 has been measured from bovine insulin on a single laser shot spectrum (Fig 2). Isotope distributions can not be definitively resolved for analyte compounds with mass over ~10,000 Da Instead, an envelop representing the isotopic distribution is measured and the mass resolution is determined by the width of the isotope profile The largest compound we tried and successfully measured was bovine trypsin (mw=23,311)

Mass accuracy measurements were carried out in two parts:
1) calibrate the mass constants of the instrument with four known mass standards 2,5-DHB (mw=154.1), leucine enkephalin (mw=555.6), substance P (mw=1347.7) and bovine insulin (mw=5733.5). The mass constants determined with these standards were kept unchanged throughout the following measurements
2) perform measurements on a mixture of three peptides: angiotensiongen (mw=1759 0), β-endorphin (mw=3465 4) and human growth hormone releasing factor (mw=5039 7) A total of 64 analyses over eight days were carried out in these measurements.

The mean of the measured molecular masses of these three analyte were compared with the calculated molecular masses The mass accuracy was determined to be ~ 40 ppm for analyzing compounds up to m/z = 6,000. Since this evaluation was performed with external calibration standards over extended period of time, it is expected that mass accuracy can be further improved with internal standards.

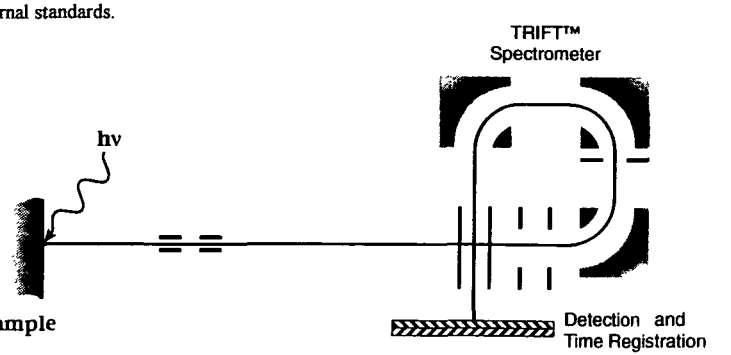

Fig. 1 - Schematic diagram of the MALDI triple ESA TOF mass spectrometer.

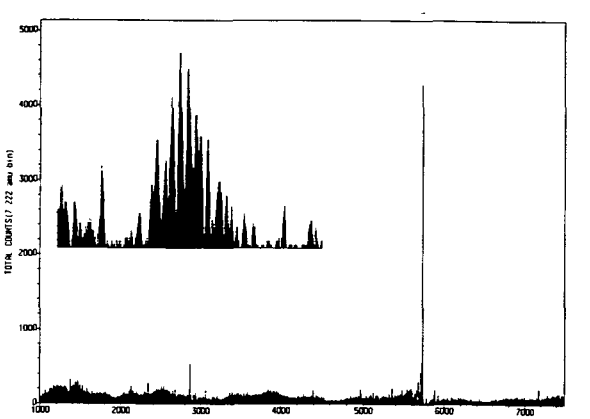

Fig. 2 - MALDI mass spectrum of bovine insulin with 2,5-DHB as matrix material. Spectrum was obtained with a single laser shot The insert shows isotopically resolved singly-charged mass peak distribution with a mass resolution of M/ΔM ~ 12,000 (FWHM).

* Financial support in part from National Science Foundation (NSF III-9310326) is gratefully acknowledged.

A Mass Analyzer for High Speed Liquid Chromatography

B. A. Andrien, J. F. Banks, J. G. Boyle, T. Dresch, P. J. Haren, and C. M. Whitehouse
Analytica of Branford, Inc., 29 Business Park Dr. , Branford, CT 06405

New fast liquid phase separation methods such as capillary electrophoresis allow complete separations to be performed in a few minutes with no loss in component resolution. Single constituent effluence peak widths of one second or even less have been demonstrated by optical detection methods. Conventional scanning mass spectrometers as detectors for chromatography are reaching their performance limits whenever a spectral mass range exceeding a few hundred amu has to be scanned at a rate exceeding one per second. On the contrary, time-of-flight mass spectrometry offers very high scan rates that can easily exceed 10^7 amu/s. It is therefore ideally suited as mass analyzer technology for the future high speed liquid phase chromatography.

The time-of-flight instrument developed in our laboratory is capable of recording more than 10 full mass range spectra per second with minimal dead time, each spectrum being the sum of multiple single scans. Orthogonal injection of the continuous ion beam from external atmospheric pressure ion sources and high repetition rates warrant high duty cycles and, hence, high sensitivity. Mass resolution of R(fwhm)=1000 has been achieved with a short linear configuration. When equipped with an ion mirror (reflectron) and an extended field free drift path of 130 cm total length, the instrument has a mass resolution of R(fwhm)=3000 .

The high speed capabilities of the instrument were demonstrated using an atmospheric pressure chemical ionization (APCI) source. 5 µl of a sample solution of Reserpine (in metha-

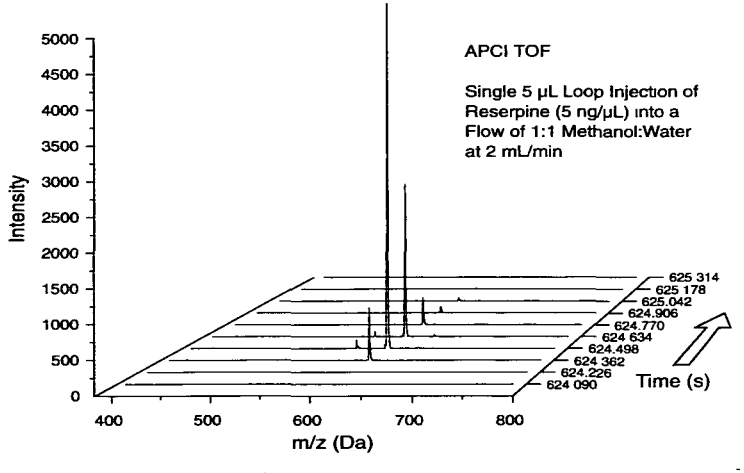

nol-water, total analyte amount 25 ng) were injected into the continuous flow of buffer liquid (methanol-water). At a flow rate of 2 ml/min the sample elution peak is only 0.2 seconds wide (fwhm). The linear time-of-flight spectrometer was operated at a repetition rate of 4096 Hz; summing 512 consecutive scans to form an averaged spectrum results in an acquisition rate of 8 spectra per second. Spectra were recorded for the mass range 250-1200 amu. Figure 1 displays the ten mass spectra around the sample elution peak, showing that the sub second peak is captured reliably.

The mass spectrometer was then coupled to a capillary electrophoresis (CE) separation system. The CE column was interfaced to the electrospray ion source by means of the sheath flow mechanism introduced by R. D. Smith et al.; in this setup a sheath liquid makes the electrical contact to the CE buffer solution and at the same time provides for a stable electrospray process. Figure 2 shows a results obtained with an amine coated column of 75 µm i.d. and 66 cm length, at electrophoresis field strengths of 300 and 450 V/cm. The buffer solution was 0.01 M acetic acid. The sheath liquid was methanol at a flow rate of 4 µl/min. A sample mixture of peptides in aqueous solution elutes from the column in about 100 seconds with well separated components. Time-of-flight mass spectra were acquired at a rate of 8 spectra per second, each spectrum being the sum of 1024 single scans. The recorded mass range extended from 100 to 1700 amu.

The displayed curves are the total ion currents calculated in real time from the acquired mass spectra. At 450 V/cm the single peak width is 2 seconds at the base and 1 second at half peak height. Within the scope of this experiment it was found that the peak widths scale with the elution time. Shorter columns and higher field strengths will allow even faster separations to be carried out, while the recording speed of the time-of-flight mass spectrometer guarantees adequate analyzer response.

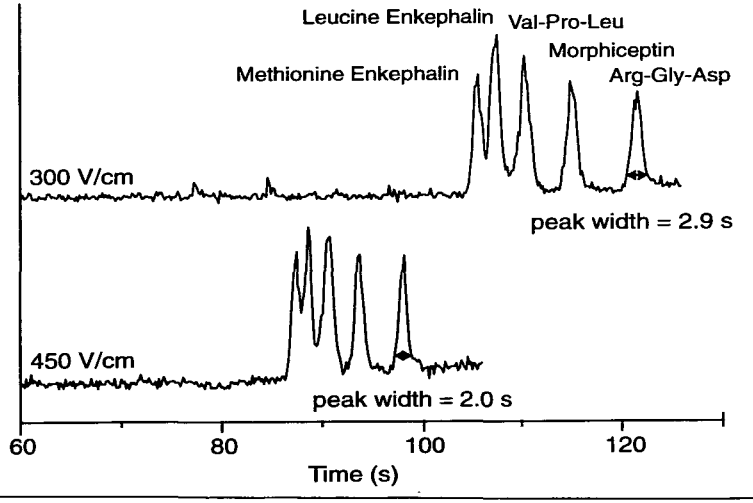

Achieving Linear Detector Response In TOF-MS

Dick Stresau and Kevin Hunter, ETP, Sydney, Australia
John Gray, ETP Scientific, Inc , Auburn, Ma., USA

Rapid development of Time-Of-Flight mass spectrometry is placing increased demands on detectors This challenge has been met using discrete-dynode electron multipliers designed specifically for TOF applications.

Our work has shown that three different issues are involved in achieving linear response in TOF detectors: linearity with large average output currents, linearity for large peaks, and gain recovery after a large peak. The flexibility of discrete-dynode technology allows us to achieve exceptional performance in each of these areas by adjusting and optimizing the ion and electron optics, individual dynode shapes, dynode voltage distribution, and inter-dynode capacitance. The result is a multiplier specifically tailored for TOF-MS applications

Linearity with large average output currents: Linear response for large output currents is similar to the considerations required in conventional mass spectrometry where one must be careful not to go beyond the linear limit for output current drawn from the multiplier

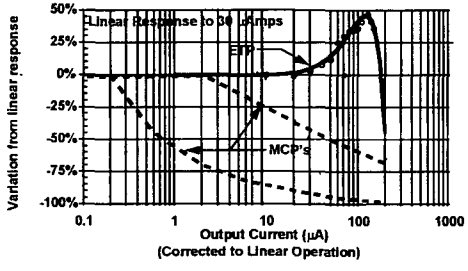

The above data is plotted as a percentage variation from linear response against the output current expected if things were perfectly linear. Notice that the **discrete-dynode multiplier is linear out to 30μA.** It is interesting to compare this to MCP performance. Even high current MCPs have only one tenth the current capacity of the new discrete-dynode TOF multipliers. Exceeding the linear limit will result in a loss of abundance calibration for the entire spectrum.

Linearity for large peaks: The linear limit for an individual peak in a TOF spectrum is several orders of magnitude greater than the average current limit. The new TOF multipliers exhibit linear operation with very large output pulses: 10^9 electrons or 500 mV (into 50 ohms, 10 nsec wide) Beyond this point space charge effects within the dynode structure begin to inhibit the flow of electrons between dynodes

Whereas excessive average-output-current affects the height of all peaks in a spectrum, an individual peak that exceeds the linear limit will be diminished without influencing the level of the smaller peaks This results in distorted abundance ratios

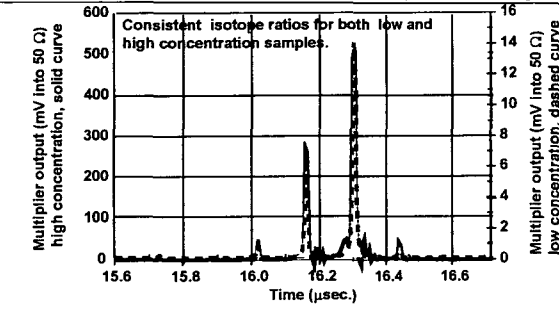

In the above figure two spectra are superimposed. The solid curve was taken with a very high concentration sample. The dashed curve is of the same compound but with 1/30th the concentration. The second spectrum is used as a "standard" to give an undistorted measure of abundance ratios. The two spectra are virtually identical. **The discrete-dynode multiplier shows no sign of non-linearity even with a 500 mV pulse!**

Gain recovery after a large peak: Achieving good linearity in a single pulse will have little advantage if the multiplier becomes saturated and effectively non-functional following the pulse Therefore it is important for a TOF detector to have very fast recovery after a large pulse.

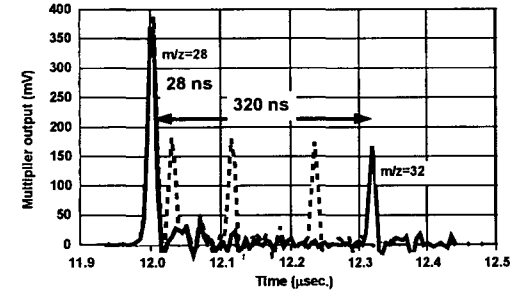

To demonstrate large pulse recovery speed, we used a double pulse on an orthogonal gate TOF system This produced two overlapping spectra in the same TOF scan The time between the two gate pulses was adjusted, allowing adjustment between the mass 28 peak from one pulse and the mass 32 peak of the other Four measurements have been superimposed so that the pulse height consistency is easily seen Note how the height of the mass 32 peak remains unchanged as the time between peaks is decreased. **The large pulse recovery time is less than 30 nanoseconds!**

The newly developed multipliers excel in all of the areas which are important for achieving large dynamic range in TOF systems: **linear output current up to 30μA, linear response for pulses up to 500 mV, recovery time after large pulse of less than 30 nsec.**

A Time Focusing Equation and a Classical Uncertainty Relation in TOFMS

Ronald Stein, Applied Physics Laboratory, University of Washington, Seattle, WA 98105

A time focusing equation is developed in which time (of flight) is the central variable rather than a parameter. The one-dimensional form of this equation is used to develop a classical uncertainty relation. This relation is used in conjunction with Liouville's theorem on the incompressibility of particles in phase space to better understand the function of time of flight mass spectrometers.

Perfect space focusing with respect to time is defined as $\partial t/\partial x_o = 0$, where t is the time of flight of an ion and x_o is it's starting position. Perfect velocity focusing with respect to time is defined as $\partial t/\partial v_o = 0$, where v_o is the ion's initial starting velocity.

Consider an ion in a one-dimensional system. It's time of flight t is a function of initial position x_o and initial velocity v_o only if the fields are constant in time, i.e., if $t = f(x_o, v_o, T)$. The total derative of the time of flight with respect to clock time T is

$$\frac{dt}{dT} = \frac{\partial t}{\partial x}\frac{dx}{dT} + \frac{\partial t}{\partial v}\frac{dv}{dT} + \frac{\partial t}{\partial T} \tag{1}$$

Note that $dx_o/dT = v_o$, $dv_o/dT = F_o/m$, and T increases as t decreases; i.e., $T + t =$ a constant that gives $dt/dT = -1$. Also, changes in time of flight with the changes in time are zero when x_o and v_o are held constant or $\partial t/\partial T = 0$. Therefore

$$v_o\frac{\partial t}{\partial x_o} + \frac{F_o}{m}\frac{\partial t}{\partial v_o} + 1 = 0 \quad \text{(Time Focusing Equation)} \tag{2}$$

(which is readily generalized to a three dimensional system [1]). This equation connects space and velocity focusing independently of the forces on the ions as the ions move toward the collector. The equation shows that space and velocity focusing cannot be perfect simultaneously ($\partial t/\partial x_o = 0$ and $\partial t/\partial v_o = 0$ together). If $\partial t/\partial x_o$ or $\partial t/\partial v_o$ is known, then the other quantity can be found if the initial conditions on the ions are known.

Consider an ion starting at x_0 and v_0 in a TOFMS using a time-independent conservative field. The change in time of flight with respect to initial position and velocity is given by

$$dt = \frac{\partial t}{\partial x_o}dx_o + \frac{\partial t}{\partial v_o}dv_o \tag{3}$$

For a collection of ions in a "small" region where $\partial t/\partial x_o$ and $\partial t/\partial v_o$ are approximately constant and the initial positions and velocities of the various ions are not correlated ($\sum_{i=1}^{n} dx_{o_i} dv_{o_i} = 0$), we can write

$$\Delta t = \left[\sum_{i=1}^{n} dt_i^2\right] = \left[\sum_{i=1}^{n}\left[\frac{\partial t}{\partial x_o}dx_{o_i}\right]^2 + \left[\frac{\partial t}{\partial v_o}dv_{o_i}\right]^2\right]^{1/2} \tag{4}$$

Using the time focusing equation (1), we can eliminate $\partial t/\partial v_o$ from equation (4) and minimize Δt as we vary $\partial t/\partial x_o$;we then find

$$\Delta t \Delta E_o \geq \Delta x_o \Delta p_o \tag{5}$$

where $\Delta p_o = m\Delta v_o$ and where Δx_o, Δy_o, Δt, and ΔE_o are the initial rms dispersions in the ion cloud's

43rd ASMS Conference on Mass Spectrometry and Allied Topics

position, velocity, time, and energy, respectively.

$$\Delta E_o = (F_o^2\Delta x_o^2 + m^2 v_o^2 \Delta v_o^2)^{1/2} = (\Delta PE_o^2 + \Delta KE_o^2)^{1/2} \tag{6}$$

where ΔPE_o and ΔKE_o are the cloud's initial rms potential and kinetic energy dispersions, respectively. The inequality sign in equation (5) becomes an equal sign when the ion cloud is time focused in space or the ions again become uncorrelated in position and velocity and have the following specific expression for space and velocity focusing:

$$\frac{\partial t}{\partial x_o} = -\frac{\Delta KE_o \Delta p_o}{\Delta E_o^2} \quad \text{and} \quad \frac{\partial t}{\partial v_o} = -\frac{\Delta PE_o \Delta x_o}{\Delta E_o^2} \tag{7}$$

Liouville's theorem states that if the forces on a particle are derived from any potential (time varying or not), the volume in phase space (position and velocity space) of an ion cloud is constant ($\Delta x \Delta p =$ constant is the one-dimensional form.).

As a consequence of Liouville's theorem, we can drop the requirement of equation (5) that the fields be independent of time. Also, since the initial location can be any location where the phase volume is uncorrleated, we can drop the initial location subscripts and write

$$\Delta t \Delta E \geq \Delta x \Delta p = K \quad \text{(Classical Uncertainty Relation)} \tag{8}$$

where $\Delta x \Delta p$ is the initial uncorrelated phase volume K of an ion cloud and $\Delta t \Delta E$ is the time of flight and energy of dispersion at some later time. The inequality in equation (8) becomes an equality at the initial instant in time and at any later time when the ions become time focused or $\Delta x \Delta p$ is again an uncorrelated ion cloud.

Let us investigate some of the consequences of the Classical Uncertainty Relation so as to better understand how a higher quality time focus (smaller Δt) can be obtained. We assume that a time focus where $\Delta x_o \Delta p_o = \Delta E_o \Delta t$ is achieved, which assumes that $\partial t/\partial x_o$ and $\partial t/\partial v_o$ have been optimized. If the initial conditions of the ions in time-independent fields are fixed, $\Delta x_o \Delta v_o$ is constant, and the average initial velocity is fixed, then we must increase ΔE_o to reduce Δt. This can be done by increasing ΔPE_o, by increasing the initial force F_o, which reduces the turn-around time. In time-varying fields, one could increase ΔE after the flight of the ions has started, but a good time focus independent of mass would now be very difficult to achieve. One could make the ions in a smaller phase volume $\Delta x_o \Delta v_o$ initially, or one could select ions from a larger phase volume but this would reduce the TOFMS sensitivity. Finally, one could operate under circumstances where Liouville's theorem is no longer true and hence circumstances where the Classical Uncertainty Relation no longer applies by putting in forces which are not completely derivable from potentials. Examples of such forces are dissipative forces of friction, collision forces to transfer momentum to other particles, and radiation reaction forces due to energy loss by radiation. Ions could collide with a neutral gas to reduce their momentum to the thermal values of the neutrals (by using a quadrapole trap ion source with a high neutral gas pressure in the trap). Ions could be entrained in a supersonic jet to take advantage of the expansion cooling of the gas jet stream. Ions could be passed close to conductive surfaces and be slowed down by the resistive heating of the image charges flowing in the conductive surface.

The Time Focusing Equation and the Classical Uncertainty Relation are very useful tools to help in the optimization of TOFMS time resolution.

1 R. Stein, Int. J. Mass Spectrom. Ion Processes, 132 (1994) 29

Analytical Form of Position Focusing in the Parabolic Electrostatic Field

Ronald Stein, Applied Physics Laboratory, University of Washington, Seattle, WA 98105

The parabolic electrostatic field can produce either perfect space or perfect velocity focusing in time (isochronous focusing). This well known result can be very desirable in a time of flight mass spectrometer to produce a quality time focus. The position (as opposed to the time) focusing properties of this field has been investigated by numerical methods for specific applications by others. Although some analytic results are in the literature [1, 2], the properties of this focusing are not generally well understood. Here, an analytical solution to the position focusing of charged particles in the parabolic electrostatic field is developed, with the solutions to the perfect space and perfect velocity focusing cases solved in some detail.

The only force field that will give perfect space and velocity focusing in one dimension over an extended region is one in which the force is attractive and directly proportional to the distance from the origin [3]. This force produces simple harmonic motion. For a charged particle q in an electric field E this force is given by $F_z=qE_z=-qAz$. The electrostatic potential V along the z axis is then given by $V=Az^2/2$ since $\vec{E}_z=-\partial V/\partial z$. If we have planar or cylindrical symmetry, and since $\nabla^2 V=0$, the potential in the neighborhood of the z axis is completely specified (see Fig. 1), or

$$V(z,x) = (V_o/L^2)(z^2-x^2/k) \tag{1}$$

where V_o is the potential on the hyperbolic surfaces shown and L is the distance form the origin to that surface along the z axis. In the planar case ($k=1$), the surfaces are hyperbolic rods perpendicular to the page. The same configuration is used in the quadrupole mass spectrometer. In the cylindrical case ($k=2$), the electrodes are hyperbolic surfaces of revolution which are used in the quadrupole trap. The parabolic potential can be generated by these electrode structures or with a wedge or cone along with one hyperbolic electrode to define a quarter space. The potential can be approximately produced along the z axis by a stack of coaxial parallel plates with the appropriate potentials on them and holes in their centers.

Since $\vec{E}=-\nabla V$, the electric fields are given by

$$E_z = -2(V_o/L^2)z \quad \text{and} \quad E_x = 2(1/k)(V_o/L^2)x \tag{2}$$

Since the force on the ions is given by $F=qE$ and F=ma, we have the equations of motion of $\ddot{z} = -\omega^2 z$, and $\ddot{x} = (1/k)\omega^2 x$, where $\omega=2qV_o/mL^2$. The forces in the z and x directions are independent. The ions are always forced away from the z axis (defocused) since E_x is always positive. The defocusing effect is twice as large in the planar case as in the cylindrical case.

Solving these equations of motion we find the position and velocity as

$$z = (z_o^2 + (\dot{z}/\omega)^2)^{1/2}\cos(\omega t-\phi) \quad \text{and} \quad \dot{z} = -\omega(z_o^2 + (\dot{z}/\omega)^2)^{1/2}\sin(\omega t-\phi) \tag{3}$$

$$x = x_o\cosh\omega' t + \dot{x}_o/\omega' \sinh\omega' t \quad \text{and} \quad \dot{x} = \omega' x_o \sinh\omega' t + \dot{x}_o \cosh\omega' t \tag{4}$$

where $\tan(\phi) = \dot{z}_o/\omega z$, $\omega'=\omega$ or $\omega/\sqrt{2}$ in the planar or cylindrical case, respectively, and at $t=0$ the initial distances and velocities are z_o, $\dot{z}_o$, x_o, and $\dot{x}_o$.

We now consider the two special cases where perfect space focusing ($\partial t/\partial z_o=0$) and perfect velocity focusing ($\partial t/\partial \dot{z}_o=0$) occur [4]. When ϕ is zero ($\dot{z}_o=0$) and the time t reaches $\omega t=\pi/2$, the z coordinate of the ion reaches zero independently of z_o (see Eq. (3)) and we have perfect space focusing for all z_o. Also, this time of flight is independent of x_o and $\dot{x}_o$. We analyze the special paraxial ray case where $\dot{x}_o=0$. The other initial conditions are $z_o=l$, $\dot{z}_o=0$, and $x_o=x_o$ (see Fig. 2). For the planar case at $\omega t=\pi/2$, we have $z=0$, $\dot{z}=-\omega l$, $x=x_o\cosh(\pi/2)=2.509x_o$, $\dot{x}=-\omega x_o\sinh(\pi/2)=-2.301\omega x_o$, and a focal length $F=l\coth(\pi/2)=1.090l$. In the cylindrical case we have $x=x_o\cosh(\pi/2\sqrt{2})=1.683x_o$, $\dot{x}=-(\omega/\sqrt{2})x_o\sinh(\pi/2\sqrt{2})=.975\omega x_o$, and a focal length of $\sqrt{2}\,l\coth(\pi/2\sqrt{2})=1.758l$. Referring to Fig. 2, the focal point is defined as the apparent point of origin of the ion if it's trajectory, on arriving at $z=0$, were extrapolated back in a straight line to the z axis. The focal length is independent of x_o.

To get perfect velocity focusing, we start an ion at $z_o=0$ and at some $\dot{z}_o=-\omega l$. Now $\phi=\pi/2$, and when the time t has gone from zero to $\omega t=\pi$, the ion has gone out to l and returned to $z=0$ with a velocity of $\dot{z}=-\omega l$. Since this time of flight is independent of $\dot{z}_o$, we have perfect velocity focusing. Also, t is independent of x_o and $\dot{x}_o$. We analyze the special paraxial ray case where $\dot{x}_o=0$. The other initial conditions are $z_o=0$, $\dot{z}_o=-\omega l$, and $x_o=x_o$ (see Fig. 3). For the planar case at $\omega t=\pi$, we have $z=0$, $\dot{z}=-\omega l$, $x=x_o\cosh(\pi)=11.592x_o$, $\dot{x}=-\omega x_o\sinh(\pi)=-11.549\omega x_o$, and a focal length $F=l\coth(\pi)=1.0037l$. In the cylindrical case, we have $x=x_o\cosh(\pi/\sqrt{2})=4.665x_o$, $\dot{x}=-(\omega/\sqrt{2})x_o\sinh(\pi/\sqrt{2})=3.222\omega x_o$, and a focal length of $F=\sqrt{2}\,l\coth(\pi/\sqrt{2})=1.448l$. Again, the focal length is independent of x_o.

A better understanding of the analytical form of the position focusing in the parabolic electric field should lead to improvements in time of flight mass spectrometer designs using this field.

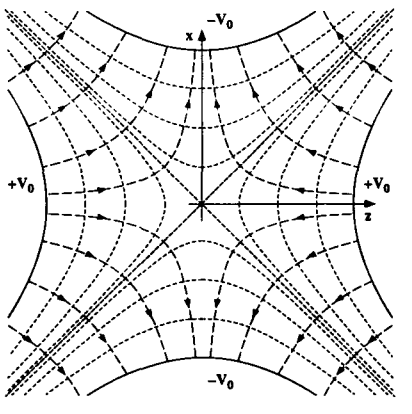

Fig 1. Perfect time focusing electric fields. The -Kz electric field is produced by using hyperbolic electrode surfaces.

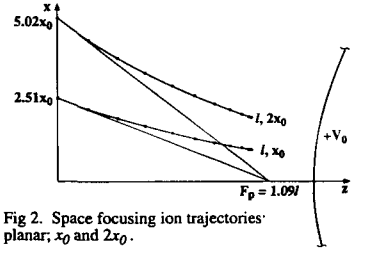

Fig 2. Space focusing ion trajectories: planar; x_0 and $2x_0$.

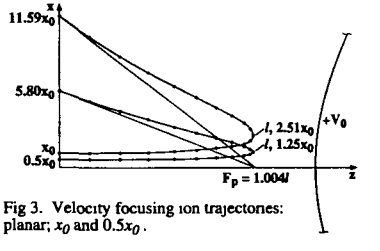

Fig 3. Velocity focusing ion trajectories: planar; x_0 and $0.5x_0$.

1 A. L. Rockwood, Proc. 34th Conf. Mass Spec. and Allied Topics, (1986) 173
2 L. D. Hulett Jr., D. L. Donohue, and T. A. Lewis, Rev. Sci. Instrum., 62 (1991) 2131.
3 W. D. MacMillan, Statics and Dynamics of a Particle, McGraw-Hill, New York, 1927, p. 225
4 R. Stein, Int. J. Mass Spectrum. Ion Processes, 132 (1994) 29

SPACE-VELOCITY CORRELATION FOCUSSING

Steven Colby and James P. Reilly
Department of Chemistry, Indiana University, Bloomington, IN 47405

Since their earliest development, time-of-flight mass spectrometers have suffered from limited mass resolution. The initial ion temporal, spatial and velocity distributions are the primary factors that must be understood, eliminated or compensated for in order to achieve enhanced mass resolution [1]. Perhaps the most significant improvements to linear time-of-flight mass spectrometers were introduced by Wiley and McLaren in 1955 [2]. To limit the deleterious effects that ion spatial and velocity distributions have on TOF mass spectral peakwidths, they introduced the concepts of space and energy focussing. Each of these was found to play a role in TOF mass spectrometer optimization. However, Wiley and McLaren found that the two could not be accomplished simultaneously. They noted that a compromise between space and energy contributions to resolution must be achieved.

We recently demonstrated that under certain conditions, the spatial and velocity distributions of ions in the source region of a time-of-flight mass spectrometer are not independent [3,4]. In these circumstances, an ion's position and velocity can be related mathematically and it is possible to accomplish simultaneous space and velocity (i.e. energy) focussing. An important example that illustrates this case is the MALDI ionization source. MALDI TOF mass spectra recorded with linear mass analyzers generally display very poor resolution that has often been attributed to the broad velocity distribution with which macromolecules are desorbed [5,6]. Assuming that MALDI ions are formed close to the surface from which desorption occurs, their positions and velocities at times following the desorption pulse are linearly related. If an ion drawout electric field is applied at an optimal time after the desorption light pulse, then the spatial and velocity distributions of the ions at the time of the drawout pulse can be simultaneously focussed. The optimal ion drawout time can be derived using a computer program that calculates ion flight time dispersion for a certain range of initial ion velocities and then optimizes instrument parameters so as to minimize this dispersion. Demonstrating the significance of these concepts, Figure 1A displays the range of flight times expected for lysozyme ions (m/z 14306) in our laboratory's short (21 cm drift length) MALDI instrument for initial ion velocities between 0 and 1200 m/sec if we apply DC drawout voltages of 25 kV and 0 V to the first two ion acceleration grids. In contrast, Figure 1B displays the range of lysozyme flight times when we set our first three grids at 25 kV, 25 kV, 21.3 kV and apply a pulsed voltage of 1.82 kV to the first grid at an optimal time. The predicted improvement in flight time dispersion is evidently dramatic. Figure 2A displays lysozyme experimental data recorded with a DC drawout voltage of 30 kV. Figure 2B presents a positive ion lysozyme spectrum recorded using pulsed ion drawout under conditions optimized for space-velocity correlation focussing, with post acceleration between the ion drift tube and the detector. A sharp parent ion peak is evident along with a background pedestal that derives from metastable fragmentation. The latter can be discriminated against using an electric field in the postacceleration region, as displayed in Figure 2C. Although not shown, data can also be recorded without postacceleration. In addition to the tall parent ion peak, small features associated with matrix adducts appear in this

spectrum. Mass spectral resolution, m/Δm, of about 1500 has been obtained for lysozyme using this method.

1. R.B. Opsal, K. Owens and J.P. Reilly, Anal. Chem. 57, 1884 (1985).
2. W.C. Wiley and I.H. McLaren, Rev. Sci. Instr. 26, 1150 (1955).
3. S. M. Colby, T. B. King and J. P. Reilly, Rapid Comm. Mass Spectrom. 8, 865 (1994).
4. T. B. King, S. M. Colby and J. P. Reilly, Int. J. Mass Spectrom. Ion Proc., accepted.
5. R.C. Beavis and B.T. Chait, Chem. Phys. Lett. 181, 479 (1991).
6. T.-W. Dominic Chan, et al., Chem. Phys. Lett. 222, 579 (1994).

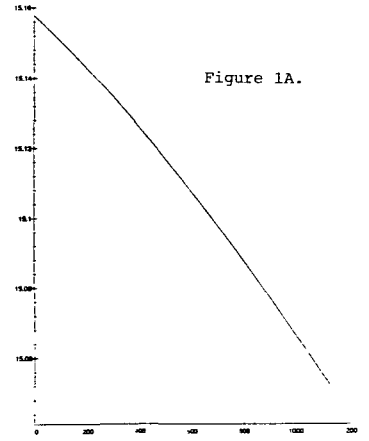

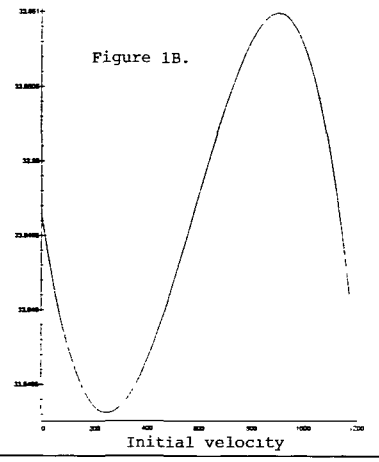

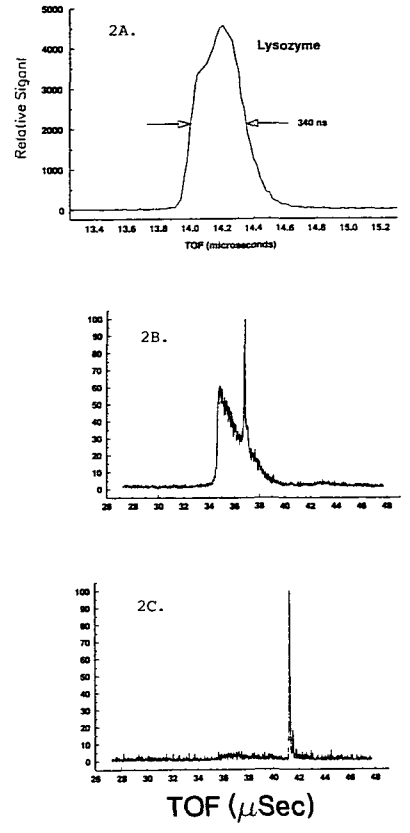

Tandem Mass Spectrometry on a Triple ESA Time-of-Flight SIMS Instrument

M. J Kristo, R. W. Odom, and K. J. Wu
Charles Evans and Associates, 301 Chesapeake Drive, Redwood City, CA 94063

Time-of-Flight SIMS is useful in the analysis of bio-organic compounds due to its high sensitivity, high mass resolution (up to 10,000), excellent mass accuracy (ppm range), and ability to form images of mass selected ions emitted from solid surfaces in the sputtering process Most TOF-SIMS instruments form ion images by rastering a finely focused ion beam across the sample surface and correlating the detected secondary ions with the position of the primary ion beam.

The TRIFT™ (TRIple focusing Time-of-flight) spectrometer[1-2] can generate ion images not only through rastering, but direct ion imaging as well. In direct ion imaging, the spatial relationship of ions leaving the sample surface is maintained and magnified by the spectrometer. Therefore, by measuring the time and position of each ion's arrival with a spatially sensitive detector, one can build up images of ion emission from the sample surface as well as mass spectra Even for non-imaging applications, the TRIFT™ instrument provides several advantages: 1) proper time-of-flight compensation for large energy and angular spreads, 2) excellent transmission, and 3) low non-mass specific background -- even low intensity peaks are significant

Nevertheless, normal TOF-SIMS has several disadvantages for bio-organic analysis First, static SIMS provides variable and sometimes poor ion yield for large bio-organic molecules. Second, static SIMS is a relatively soft ionization technique producing predominately ions characteristic of intact molecules. At m/z above ~1000 Da, the mass resolution and mass accuracy of high performance TOF-SIMS instruments often cannot unambiguously identify molecular ions By coupling tandem mass spectrometry to TOF-SIMS, we can provide structural information about these ions which is an invaluable aid for identification. Third, the SIMS spectra generated from real biological matrices can be extremely complex. With MS/MS and the proper choice of precursor/product ion pairs, interferences are minimized when imaging bio-organic molecules in complex matrices -- resulting in high contrast images

We have generated MS/MS data on metastable ions from met-enkephalin and substance P using the TRIFT™ instrument. To obtain this data, molecular ions were formed under energetic (11 keV) Cs^+ primary ion bombardment TRIKES (Time Resolved Ion Kinetic Energy Spectrometry)[3-4] was used to identify the precursor/product ion masses. By placing an energy slit after the first ESA and scanning the three ESA's in unison, we can select product ions of a certain energy which represent a specific product ion to precursor ion mass ratio. By measuring the flight time of the product ions, we determine the precursor ion mass since the precursor ion and product ion have essentially equal velocities The product ion mass was calculated from the precursor ion mass and the product ion to precursor ion mass ratio

We generate TRIKES data essentially as MS/MS maps by scanning the ESA's (the energy range being transmitted) and acquiring a time-of-flight spectra for each energy setting Surprisingly, we have found metastable decay to be a highly probable process and have measured metastable efficiencies (defined as the intensity of all metastable ions divided by the intensity of all normal SIMS ions) of roughly 12% for met-enkephalin and 40-50% for substance P. Therefore, useful TRIKES spectra can be acquired using reasonable integration times (typically 1 minute integration times for each energy setting) Of course, the metastable ion intensity encompasses many different precursor and product ion masses Peaks from low abundance precursor ions or improbable precursor to product ion transitions will require longer integration

times. With the large energy pass of the TRIFT™ spectrometer, we can use energy steps of 1% (no energy slit) to generate a map without losing peaks. Thus, depending on the region of interest, up to 100 spectra would be needed to build a complete map For acquiring detailed precursor ion spectra, we use smaller energy steps (0 1%), so more spectra are needed to define the same region

Typical product ion mass resolutions are approximately 1000. Figure 1 shows a TRIKES spectrum of the YGG (278) to YG (221) transition for met-enkephalin (mass resolution of 960). Despite the energy release of the metastable decay, the product ion resolution is impressive for two reasons First, the spectrometer provides excellent compensation for energy spread at any given ESA setting Second, as the ESA is scanned, the flight time of the peak (and the apparent mass) shift as one would expect, but this shift is canceled by the change in the energy fraction (product ion mass/precursor ion mass). Therefore, the product ion mass (the precursor ion mass times the product ion mass/precursor ion mass ratio) does not shift. On the other hand, the parent ion resolution is limited by the energy release in the metastable fragmentation. Figure 2 shows the precursor ion spectrum for mass 221 in met-enkephalin (mass resolution of 56). This spectrum is extracted from TRIKES spectra obtained at energies of 0.787 to 0 802 times the accelerating energy. The mass resolution corresponds to an energy release of approximately 0.9 eV.

1. Physical Electronics, Redwood City, CA 94063.
2. B W Schueler, Microsc Microanal Micostruct 3 (1992) 119
3. J D. Pinkston, M. Rabb, J. T. Watson, and J. Allison, Rev. Sci. Instrum 57 (1986) 583
4. J D Pinkston, Proc. of the 33rd ASMS Conference (1985), p. 721

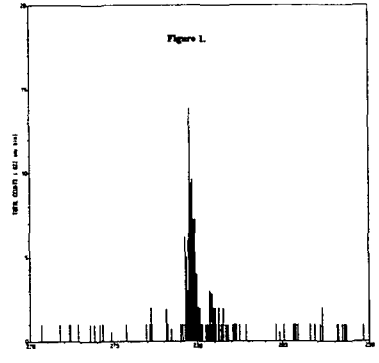

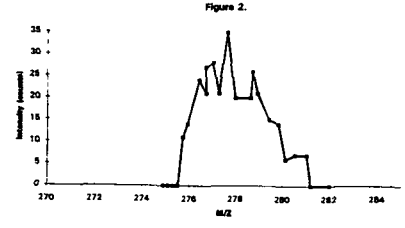

We gratefully acknowledge support of NIH under SBIR grant 1 R43 RR09217-01

Mass Spectrometric Studies on Porphyrins and Geoporphyrins

*Quirke, J. Martin. E.[1]; Yost, Richard A.[2]; and Van Berkel, Gary J.[3]

1) Department of Chemistry, Florida International University, Miami, FL 33199.
2) Department of Chemistry, University of Florida, Gainesville, FL 32611-7200
3) Chemical and Analytical Sciences Division, Oak Ridge National Laboratory, Oak Ridge, TN 37831

Porphyrins are among the more important compound classes, playing significant roles in such diverse areas as medicine, material sciences, catalysis and the petroleum industry. The most valuable property of the porphyrin macrocycle is its ability to chelate with any metallic element. In organic geochemistry, geologically-occurring porphyrins, geoporphyrins, are of both academic and commercial consequence.

Geoporphyrins occur as complicated mixtures of nickel(II) and vanadyl(II) [VO(II)] complexes in a wide range of sedimentary environments. They are believed to be formed by transformation of the functional groups of biologically-occurring cyclic tetrapyrroles, especially chlorophyll a into alkyl or hydrogen substituents coupled with the oxidation of the chlorin (dihydroporphyin) to the porphyrinic system. This proposal, the Treibs' hypothesis, is the cornerstone of molecular organic geochemistry.[1] The precise composition of geoporphyrin mixtures varies from crude oil to crude oil. For this reason, analysis of geoporphyrin mixtures is a valuable tool for the correlation of crude oils with other oils and/or source rocks.[2] Less happily, the geoporphyrins, especially the vanadyl complexes, poison catalysts in cracking of crude oil and other industrial processes.[3] Mass spectrometry is perhaps the most valuable tool for analysis of geoporphyrin mixtures. Such analyses present the mass spectrometrist with several challenging problems. Geoporphyrin mixtures are composed of overlapping pseudohomologous series of at least nine skeletal types. Carbon number ranges of C_{28}-C_{50} are not uncommon. The upper limit of the carbon number range is still unclear.

In this study, four facets of mass spectrometric analyses of porphyrins and geoporphyrins will be presented. First, the value of electron ionization tandem mass spectrometry (MS/MS) for identification of the various skeletal types of cycloalkanoporphyrins (CAP's)—porphyrins bearing an exocyclic ring—will be demonstrated[4]. Careful analysis of the $[M-40]^+$ to $[M-45]^+$ region of the daughter ion spectra of the molecular ions of CAP porphyrins may be used to identify the size of the exocyclic ring. For example, a CAP porphyrin bearing a 5-membered ring shows an intense diagnostic daughter ion, $[M-44]^+$. Second, electron ionization tandem mass spectrometry provides the best analytical method for the analysis of high carbon number ($>C_{33}$) porphyrins in crude oils.[5] The commercial and academic importance of these largely unexplored compounds will be discussed. Third, electrospray mass spectrometric analyses of geoporphyrins will be described.[6] This technique shows great promise for determining the carbon number range, and relative abundances of the geoporphyrins in intact mixtures. Electron ionization mass spectrometry is not well-suited to this task because fragment ions can coincide with lower molecular weight components of the mixture. Fourth, recent tandem mass spectrometric studies on nitrated porphyrins will be outlined[7]. These compounds, which are in many cases highly distorted, display novel fragmentation patterns in which the expected β-cleavage of alkyl substituents is often suppressed. The potential role of distortion on the fragmentation patterns of porphyrins will be commented on.

1. Treibs, A. *Angew. Chemie* **1936**, *49*, 682.
2. Filby, R.H.; Van Berkel, G.J. in *Metal Complexes in Fossil Fuels ACS Symposium Series*, 344, Filby, R.H. and Branthaver, J.F., Eds; American Chemical Society: Washington, D.C., 1987; pp. 2-39.
3. Branthaver, J.F. in *Metal Complexes in Fossil Fuels ACS Symposium Series*, 344, Filby, R.H. and Branthaver, J.F., Eds; American Chemical Society: Washington, D.C., 1987; pp. 188-204.
4. Laycock, J.D.; Yost, R.A.; Wang, L.; Quirke, J.M.E. submitted to *Energy & Fuels* (1995).
5. Johnson, J.V.; Britton, E.D.; Yost, R.A.; Quirke, J.M.E.; Cuesta, L.L. *Anal. Chem.* **1986**, *58*, 1325.
6. Van Berkel, G.J.; Quinones, M.A.; Quirke J.M.E. *Energy & Fuels* **1993**, *7*, 411.
7. Laycock, J.D. *Tandem Mass Spectrometric Studies of Porphyrins: Structural and Photochemical Studies*; Ph.D. dissertation, University of Florida, Gainesville, FL, 1994.

Mass Spectrometry of Porphyrins: Ionization and Appearance Energies

*James A. Ferguson[1], J. Martin E. Quirke[2], Jodie, V. Johnson[1], and Richard A. Yost[1]
[1]Department of Chemistry, University of Florida, Gainesville, FL 32611
[2]Department of Chemistry, Florida International University, Miami FL 33199

Porphyrins are of importance in petroleum as geomarkers, molecules which allow the origin of the compound to be traced, and, unfortunately, as potential poisons for cracking catalysts. In addition porphyrins are employed medically in photodynamic therapy, as catalysts for epoxidation reactions, as models for biological systems, and have potential applications in materials science as molecular wires and molecular machines. Approximately 5000 papers dealing with porphyrins are published each year. Despite this high level of scientific output, there is still much fundamental information on porphyrin chemistry to be learned.

The planar geometry of a porphyrin's tetrapyrrolic ring and inherent aromaticity give it great stability. This stability is seen in the high number and abundance of doubly charged (and even triply charged in some cases) ions observed in their mass spectra. The planarity of the ring can be distorted by metalating the porphyrin or by or adding substituents on the *meso*-bridges of the ring (Figure 1). Such distortions can alter the energies required to ionize the molecule and to break the bonds. Monitoring ion intensities while varying the electron energy used in electron ionization (EI) mass spectrometry provides a means of determining the ionization and appearance energies (IE and AE's). The mass spectrometric results may be compared with theoretical calculations predicting ionization energies and bond strengths.

Compared with other methods available for determining ionization energy, EI on the TSQ-70 provides the advantages of requiring only small amounts of sample, rapid determination (on the time scale of minutes as opposed to hours) and automated, real-time computer control of experimental parameters. One disadvantage is the electron beam is not monoenergetic and the energy spread of the electron beam makes absolute determination of the IE's and AE's difficult. While absolute values for IE and AE's are not simple to determine from the data, relative values are readily obtained.

In order to minimize electrical field gradients which would alter the electron energy, the instrument was tuned with the collector (COLL) and first extraction lens (L11) set to instrumental ground rather than the +15V and -5 to -15V respectively to which they are typically set. The electron energy (ELEN) was incremented in 0.1 V intervals under real-time computer control using instrument control language programs. To improve signal-to-noise, ten scans per ELEN value were collected using selected ion monitoring at a 0.5 second per amu scan rate and averaged. The ionization and appearance energies of a series of divalent-metal complexes (including vanadyl – VO) of octaethylporphyrin were determined by varying the voltage on the EI filament in the TSQ-70 under automated instrument control and monitoring the energies at which the molecular ions (M^+ and M^{2+} – first and second ionization energies), and fragment ions, (e.g., $[M-CH_3]^+$ and $[M-2CH_3]^+$ – appearance energies) first appear in the mass spectrum. The first ionization energies of metalated and non-metalated *meso*-substituted (mononitrooctaethyl-, tetranitrooctaethyl-, and tetraphenyl-) porphryins were also obtained. Changes in the EI filament over time affect the absolute values of the IE's and AE's however relative values remain fairly

constant. Results are shown in Table 1. The first section of the table shows the effect of metalating the porphyrin. Addition of the metals tabulated causes only a small distortion to the ring, explaining the small differences in the ionization and appearance energies shown. The effect of addition of a one nitro group a *meso*-bridge carbon is shown in the second section (OEMNP = octaethylmononitroporphyrin). The addition of one nitro group leads to only a small distortion of the ring and only small changes in the first ionization energy were observed. The effect of substitution on all four *meso*-bridge carbons is shown in the third section. Results for tetraphenyl porphyrin (TPP) and octaethyltetranitroporpyhrin (OETNP) show that the increased distortion from the steric effect of tetrasubstitution lead to a larger change in the ionization and appearance energies.

This technique provides a rapid, automated method for determining the relative ionization energies of porphyrins and appearance energies for their fragments which may be of use in predicting the catalytic activity of porphyrins.

Reference
1) Hobbs, J. D.; Majumder, S. A.; Luo, L; Sickelsmith, G. A.; Quirke, J. M. E.; Medforth, C. J.; Smith, K. M.; Shelnutt, J. A. *J. Am. Chem. Soc.* **1994**, *116*, 3261.

Table 1

Porphyrin	First IE	Second IE	AE for loss of CH_3	AE for loss of $2CH_3$
OEP	5.95	19.59	13.10	14.46
NiOEP	6.04	19.30	13.21	14.07
VOOEP	6.28	18.82	13.21	14.46
OEP	5.99	--	--	--
OEMNP	6.08	--	--	--
NiOEMNP	6.18	--	--	--
OEP	5.55	--	--	--
TPP	6.76	--	--	--
OETNP	8.45	--	--	--
NiOETNP	8.17	--	--	--

Figure 1

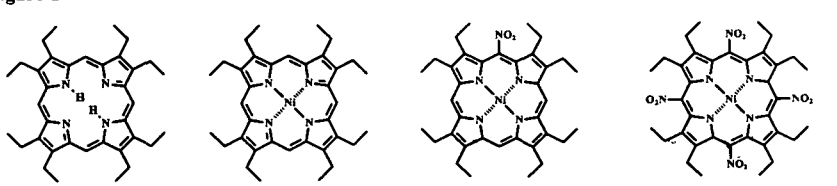

Octaethylporphyrin (OEP) | Nickel(II) octaethylporphyrin (NiOEP) | Ni(II) Mononitro-octaethylporphyrin (NiOEMNP) | Ni(II) Tetranitro octaethylporphyrin (NiOETNP)

Heavy Resid Asphaltene Characterization using High Resolution and Laser Desorption Mass Spectrometry*

Jerry E. Hunt[a], Yeonhee Kim[a], Randall E. Winans[a], Ken B. Anderson[a], Jeffrey T. Miller[b]

[a]Chemistry Division, Argonne National Laboratory, Argonne, IL 60439
[b]Amoco Corporation, Naperville, IL

Resid is the nondistillable portion of crude oil, generally thought to consist largely of unsaturated molecules of considerable size and ring number. Such molecules must be upgraded to more saturated compounds if they are to be used as fuel sources. Current processing of resid is performed though coking, thermal and catalytic cracking, deasphalting and hydroprocessing. Thermal treatments, however, produce large quantities of low-value coke and hydroprocessing is expensive.

Asphaltenes comprise the most process resistant portion of the resid. They contain high concentrations of heteroatoms and a high degree of unsaturation. Because these undesirable characteristics are concentrated in asphaltenes, finding an improved method of upgrading asphaltenes is a prerequisite to improving the upgrading of whole resid to viable fuel. Asphaltenes have, at present, only an operational definition. They are insoluble in straight chain saturated hydrocarbons. Very little is known about the structure of compounds in asphaltenes. They are a highly diverse group of compounds that are resistant to analysis by conventional methods. Conclusions about the structures of asphaltenes tends to be speculative.

In this study desorption electron impact (HREIMS), chemical ionization high resolution mass spectrometry (HRCIMS), and laser desorption mass spectrometry (LD) have been applied to deasphalted oils (DAO) and asphaltenes derived from heavy Maya resid. LD data should yield information on the high molecular weight aromatic compounds, while HRMS can provide molecular characterization.

Experimental

The resid was obtained by vacuum distillation of an asphaltene rich Maya crude oil. The HREIMS and HRCIMS data were acquired with a Kratos MS50TA at 12K dynamic resolution at a scan rate of 10s/decade. The ionization energy was 70eV for the EI spectra. Isobutane was the reagent gas for the CI experiments. A DCI probe was used to vaporize the samples into the gas phase with a maximum temperature of 700°C and a source temperature of 200°C. The laser desorption data were acquired on both a time-of-flight mass spectrometer constructed in-house and a Kratos MALDI III time-of-flight mass spectrometer fitted with a reflectron.

Results

A comparison HRCIMS data of the resid asphaltene and resid DAO are shown in figure 1. The average molecular weight distribution of the DAO is on average higher that of the asphaltene. Hydrocarbon and heteroatom-containing distributions as a function of hydrogen deficiency are obtained by DEIHRMS. The results show that the distributions of sulfur- and nitrogen-containing compounds in asphaltenes are different from those in DAO. As expected, the asphaltenes show an increase in heteroatom content, while the DAO show more abundant distribution of hydrocarbon series. Monosulfur containing compounds in the asphaltene and DAO are different. Interestingly, the DAO shows a series of peaks separated by methylenes up to a ring+double bond equivalent of 20, indicating aromatic species that are highly alkylated with long carbon chains. Monosulfur compounds in the asphaltenes range between 10 and 25. The distribution of nitrogen containing ions as a function of degree of unsaturation in the asphaltene and DAO fractions is shown in figure 2. A difference in abundance is apparent, with most of the nitrogen ending up in the asphaltene fraction with degrees of unsaturation chiefly in the range from 6 to 26.

Laser desorption is used to provide molecular weight distributions of heavy aromatic vacuum resid asphaltenes. High molecular weight aromatic model compounds show that laser desorption is a viable technique for obtaining molecular weight information from highly aromatic fused-ring compounds. The lack of any appreciable ion intensity in the high mass region (>800 u) is a good indication that most molecules in the asphaltene are lower molecular weight species. However, data from LD for use in molecular weight distributions needs to be interpreted with great care due to wide variations in ion sensitivities. For example, volatile compounds are not observed and aliphatic compounds are ionized only under conditions where cation attachment can occur.

Although the mass spectra indicate low molecular weight distributions (300-1000 u), other techniques, such as vapor phase osmometry and gel permeation chromatography, support higher molecular weights (>2500) for the resid asphaltenes. Recent data from small-angle neutron scattering of resid asphaltenes supports a temperature dependent aggregation process. Thus, the conventional view of asphaltenes as large polycyclic aromatic ring systems is not supported by our results. Future studies will focus on LD of further separated asphaltenes to search for high molecular weight species and more detailed HRCIMS of the nitrogen containing compounds as a function of process conditions.

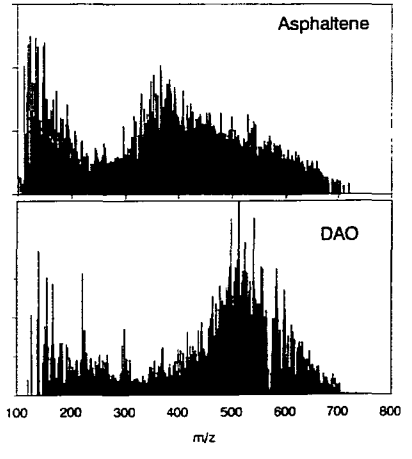

Figure 1. The desorption chemical ionization mass spectrum of the Maya resid asphaltene and deasphalted oil.

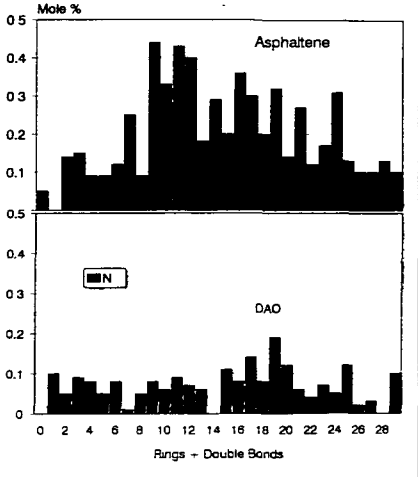

Figure 2. The distribution of nitrogen containing ions from HREIMS in Maya resid asphaltenes and deasphalted oil.

*This work was performed under the auspices of the Office of Basic Energy Sciences, Division of Chemical Sciences, U.S Department of Energy, under contract number W-31-109-ENG-38

Implementing the New EPA GC/MS Method for Total Aromatics in Reformulated Gasoline

D. Drinkwater and V. Nero
Texaco Research and Development
P. O. Box 509
Beacon, NY 12508

M. Cheng
Chevron Research and Technology Company
100 Chevron Way
Richmond, CA 94802-0627

The requirement that all reformulated gasoline (RFG) sold in the United States be analyzed by GC/MS for aromatic content presents a unique challenge and opportunity for petroleum mass spectrometry. A brief overview will be presented on the specifics of the method and the current regulatory requirements it entails. Details of the proposed ASTM implementation of this method will be examined from a mass spectrometry point of view, with emphasis on accuracy and precision considerations as well as the challenges presented by moving this technique into a refinery setting.

A number of extensions and improvements on the current method are proposed A fast chromatography version of the method is introduced, decreasing analysis time from the proposed 90 minute method to 10 minutes The special advantages of micro-bore and mini-bore capillary GC columns for GC/MS quantitation is discussed, including their use to extend the dynamic range and cleanliness of the mass spectrometer Extensions of the method for quantitating oxygenates and individual toxics is evaluated, as well as a proposal for the future use of this method as a complete method for aromatics, benzene (currently only D3606 GC/GC method is acceptable for RFG), and oxygenates (approved method is an OFID method). Data from these methods and the EPA GC/MS method, both measured at the refinery, are compared to show the excellent precision and lack of bias inherent in the GC/MS procedure

Figure I. shows the agreement between the mandated oxygenates method and the GC/MS method using fast chromatography (9 minute GC/MS method). Figure II. shows a sample calibration curve for benzene from 0 1 to 5 weight percent using the small bore capillary column to increase mass spectrometer linear dynamic range.

43rd ASMS Conference on Mass Spectrometry and Allied Topics

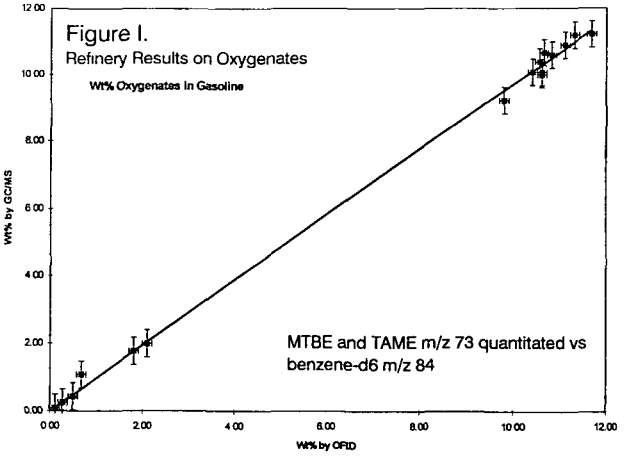

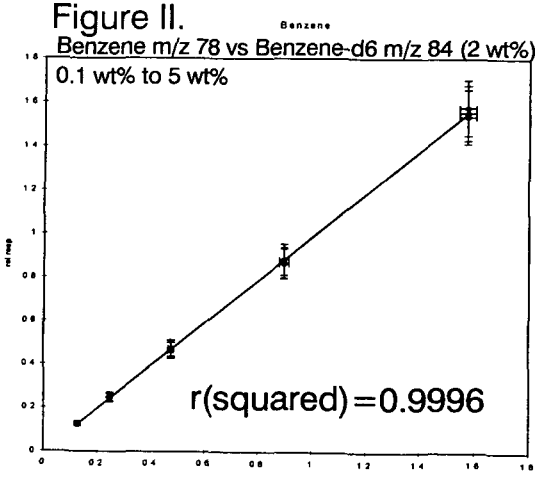

ANALYSIS OF GASOLINE FOR AROMATIC HYDROCARBONS BY GC/MS AND BY LOW EV-HR/MS

Ronald D. Grigsby and Ted B. McWilliams

BDM-Oklahoma, Inc.
National Institute for Petroleum and Energy Research
P.O. Box 2565, Bartlesville, OK 74005

The United States Clean Air Act requires that finished gasoline be formulated to reduce ozone-reactive emissions and to lower gasoline toxicity Mandated changes in gasoline composition include limiting the concentrations of benzene and total aromatics, as well as other restrictions on composition and volatility. A set of guidelines published by the U.S. Environmental Protection Agency has specified GC/MS for determining total aromatics content Based on the EPA guidelines, the American Society for Testing and Materials has proposed a standard method for determining aromatics in gasoline by GC/MS [1]

In our laboratory, the ASTM gasoline samples have been analyzed by GC/MS in a magnetic-sector instrument equipped with a capillary column In addition, they have been analyzed by low eV-high resolution mass spectrometry with sample introduction through an all-glass expansion-volume inlet. Nominal 10 eV electron ionization was used in the low eV analysis and 70 eV electron ionization in the GC/MS analysis The high-resolution data were obtained at a resolving power of 10,000 For both methods, internal standards were included with the samples and calibration curves were calculated using least squares with a spreadsheet program. As a further check, liquid chromatography was used to analyze the samples for benzene and toluene.

Figure 1 shows the low eV calibration curve for benzene in standard mixture No. 1 The ratio of molecular-ion intensities, Ai/As, for benzene and the internal standard, chlorobenzene is plotted vs. the ratio of weights for the two compounds, Wi/Ws. Theoretically, a straight line passing through zero should be obtained By least squares analysis, the intercept is -0.0095 and the slope is 1 4642.

The GC/MS calibration curve for benzene in standard mixture No. 1 is shown in Figure 2 For this curve, Ai/As is the ratio of the areas under the GC peaks for benzene and chlorobenzene The least-squares intercept is -0.0439 and the slope is 1 6641. Slopes for the two calibration curves are different because the response factors for benzene and chlorobenzene are not the same under low eV and 70 eV ionization conditions.

Table 1 shows a comparison of the analytical results obtained for benzene and toluene in QC sample C1 by the low eV, GC/MS, and HPLC methods.

A comparison of the analytical results obtained for sample RFA by the low eV and GC/MS methods is shown in Table 2. Weight percents of isomers, such as the xylenes and ethylbenzene, are reported together as C2-alkylbenzenes although most of the isomers are actually separated by the capillary-column GC used in the analysis.

In comparison with the low eV method, the GC/MS method provides more detail on the identification and quantification of specific compounds. However, it also requires more time to acquire the data followed by a more complex procedure for data analysis. The low eV method cannot distinguish between isomers. Thus, only compounds having a single isomeric form, e g., benzene and toluene, can be unambiguously identified and quantified. This is not necessarily a disadvantage, though, if only a total percentage of a compound type, such as the C4-alkylbenzenes, is desired.

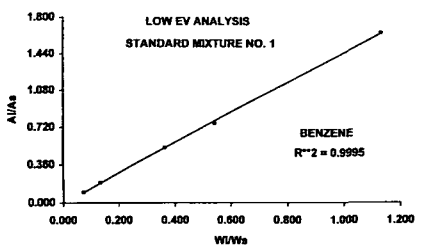

Figure 1. Calibration curve for benzene in standard mixture No. 1. Low eV analysis.

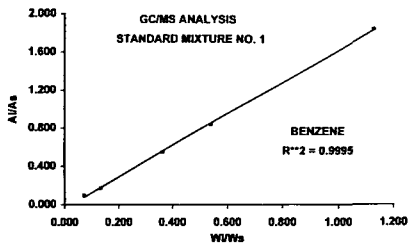

Figure 2. Calibration curve for benzene in standard mixture No. 1 GC/MS analysis

Table 1. Comparison of results from low eV, GC/MS, and HPLC methods. QC sample C1.

Compound	Low eV EV WT%	GC/MS WT%	HPLC WT%
Benzene	0.60	0.68	0 60
Toluene	10.74	11.73	11 92

Table 2. Comparison of results from low eV and GC/MS methods. Sample RFA.

Compound(s)	Low eV WT%	GC/MS WT%
Benzene	1.74	1.80
Toluene	5.86	5.11
C2-alkylbenzenes	13.07	13.12
C3-alkylbenzenes	8.41	9.63
Indan	0.26	0.48
C4-alkylbenzenes	3 21	3.29
C5- alkylbenzenes	0.48	1.14
Naphthalene	0 39	0.47
Methylnaphthalenes	0.64	0.67
Uncal alkyl-sub. indans	1.68	1.15
Uncal. C6-alkylbenzenes	0.15	0.21
Total aromatics	35 88	37.07

REFERENCE

1. "Proposed Standard Test Method for the Determination of Benzene, Toluene, and Total Aromatics in Finished Gasoline by Gas Chromatography/Mass spectrometry," Draft No. 5F, ASTM Subcommittee D02 04 Section M, American Society for Testing and Materials, Philadelphia, February, 1995.

Hydrocarbon Analysis Using An Ion Trap/MS With External Ionization

Siu T Teng, Finnigan MAT
355 River Oaks Pkwy, San Jose, CA 95134.

Introduction

Hydrocarbon analysis by mass spectrometry in the past few decades was performed on beam type instruments such as magnetic sector or quadrupole mass spectrometers Only recently have a few works of hydrocarbon analysis utilizing a quadrupole ion trap devices been reported. However, until recently, commercial ion trap mass spectrometers were operated conventionally, where the ion trap device was simultaneously used as ion source and mass analyzer The present work was conducted on the GCQ, which decoupling the ion source from the ion trap device as mass analyzer. This external ionization technique offers the leverage of temperature controlling of the ion source independently from the ion trap manifold The ions generated in the ion source are injected into the ion trap via a lens system and controlled by radio frequency (RF) using the waveforms technique The ion population is controlled by instrument software.

Experimental

The GC/MS analysis of normal alkanes was conducted by injecting 0.2 µL, 100·1 dilution of a standard mixture (Supelco) into a DB5MS (J&W) column. For the GC/MS analysis of the gasoline refinery standards (AccuStandard) a DB1 (J&W), 0 1 mm ID,0 40 µmm film thickness, 20 meters column was used For the analysis of the high boiler additives in diesel the DB5HT (J&W) column was used.

Results and Discussion

Typically, the analysis of aliphatic hydrocarbons may be hampered by the virtual absence of molecular ions and excessive fragmentation This is especially true for the most ion trap instrumentations with internal ionization Phinney [1] showed that varying the thermal energy imparted to the analyte molecules in the ion trap manifold could reduce fragmentation of C10 to C28 alkanes and enhance the abundance of molecular ions However, the most crucial condition is a temperature controlled ion source, which is achieved by the external ionization Figure 1 shows C30 (triacontane) as example of the results of saturated straight chain hydrocarbons analysis The molecular ion is well detected The result exhibits the primary characteristic of saturated hydrocarbon mass spectra with a smooth envelop of relative intensity distribution formed by the odd numbered series of m/z (14n+1), termed A^+ ions, where n is the number of carbon atoms in the fragment The exessive fragmentation due to the α-cleavage of the adjacent carbon-carbon single bond was not observed. The series of the $(A-1)^+$ and $(A-2)^+$ ions also appear to be matching the conventional quadrupole mass spectra in its intensity distribution. Figure 2 shows examples of the five point curve calibration of toluene and naphthalene of a refinery standards mixture required for the proposed ASTM method (draft #5) for quantitative gasoline analysis Figure 3 shows an MS/MS product ion spectra of hexadecyl diphenylamine at 1 ppm in diesel fuel. This demonstrates the sensitivity and specificity using MS/MS technique to identify and confirm low level concentration components in complex matrices.

Reference: [1] Phinney C S., Proceedings 41st ASMS Conf.,1993,632a/b.

43rd ASMS Conference on Mass Spectrometry and Allied Topics

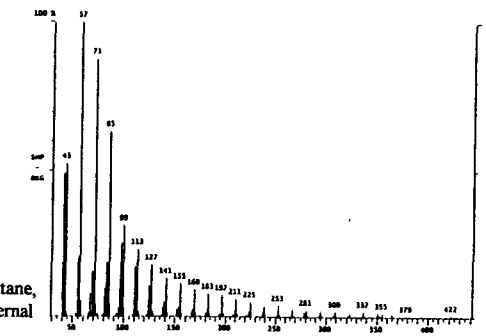

Figure 1
Mass spectrum of C30, triacontane, from an Ion Trap/MS with external ionization.

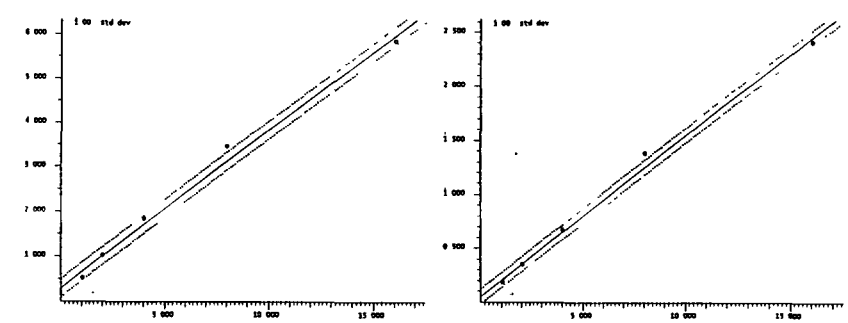

Figure 2
Five point curve calibration of toluene and naphthalene of a refinery standards

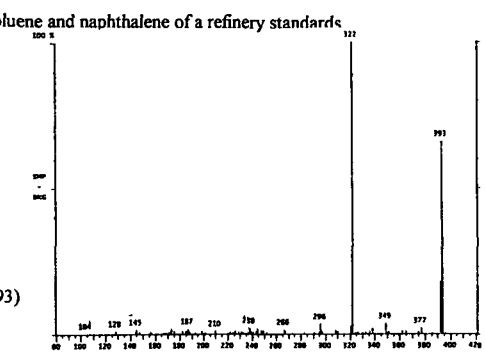

Figure 3
MS/MS product ion spectra of hexadecyl diphenylamine (MW393) at 1 ppm in diesel fuel

INDUSTRIAL APPLICATIONS OF FTMS: A PRESENT AND FUTURE PROSPECTUS

Joseph E. Campana, Extrel FTMS, Inc., 6416 Schroeder Road, Madison, WI 53711-2424

Petrochemicals include a wide variety of products from fuels, feedstocks derived from petroleum and natural gas, such as ethylene and butadiene; and large scale plastics and resins. We have reported how features of Fourier transform mass spectrometry (FT/MS), such as accurate mass determination (sub ppm) and ultra-high resolution can be applied to the analysis of hydrocarbons [1]. Figure 1 illustrates a relatively wide mass range (100 amu) ultra-high resolution (>200,000 resolving power) mass spectrum of a vacuum gas oil. The sub-ppm mass measurements were used to confirm the species identified in the inset. The mass errors for most peaks identified in Figure 1 are less than 1 mmu [1].

Other features of FT/MS include its compatibility with pulsed ionization techniques, such as laser desorption ionization (LDI) and matrix-assisted laser desorption; multistage mass spectrometry, high sensitivity, and compatibility with electrospray ionization, which will enable routine LC FT/MS. These features have application to the characterization of polymers and related materials, a necessity in today's petrochemicals industry.

LDI and MALDI FT/MS have been used to characterize many different classes of polymers ranging from polyols to glycol derivatives. Applications have been in structure determination, chemical composition, end-group identification, identifying variations in synthetic pathways, and average molecular weight determination. An example of MALDI FT/MS determination of average molecular weight with accurate mass measurement is illustrated in Figure 2 with polyoxyproplyenediamine, a product manufactured by a petrochemical company. There have been a wide variety of laser desorption FT/MS applications to polymer, plastics, and additives that have appeared in the chemical literature. Two recent review articles summarize such applications [2, 3].

These laser-based FT/MS techniques provide excellent molecular information and high sensitivity. High signal-to-noise ratio mass spectra can often be obtained in a single laser shot. This is very useful when a surface contaminant, a blemish, or impurity in a solid matrix has to be determined. The mass spectral results provide very high mass accuracy, and thus elemental compositions can be determined, unlike the results obtained on many time-of-flight mass spectrometers. Multistage mass spectrometry techniques can be applied if structural elucidation is necessary. Another important advantage of FT/MS is that high mass accuracy (less than 5 ppm error) can be routinely obtained without the use of an internal mass reference with laser desorption ionization. This is an advantage when probing solid and reactive materials where it is undesirable or at best, difficult to introduce an internal mass reference.

Advanced, state-of-the-art data acquisition hardware and software has improved the user friendliness of FT/MS for the non-specialist. It is also improving the performance and flexibility of the FT/MS technology as an analytical method. Expect to see further improvements in routine high mass measurement accuracy, higher resolution, the ability to perform ultra-high resolution accurate mass measurements over very wide mass ranges (1000 amu +) without internal mass references, and routine chomatography applications. These improvements will be a culmination of more powerful data stations and more people adopting FT/MS as the high-performance mass spectrometer of choice for analytical measurments.

References

1. Hsu, C.S.; Liang, Z.; Campana, J.E. *Anal. Chem.* **1994**, *66*, 859-855.
2. Sheng, L.-S.; Shew, S.L.; Winger, B.W.; Campana, J.E. in T. Provder, M. Urban and H.G. Barth (Eds.), Hyphenated Techniques in Polymer Characterization (ACS Symposium Series) American Chemical Society, DC, 1994.
3. Campana, J.E.; Sheng, L.-S.; Shew, S.L.; Winger, B.W. *Trends Anal. Chem.* **1994**, *13*, 239-247.

43rd ASMS Conference on Mass Spectrometry and Allied Topics

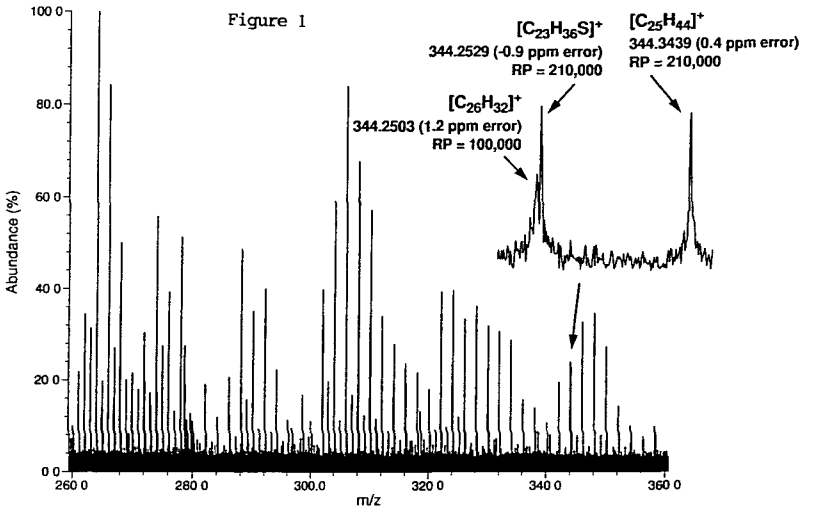

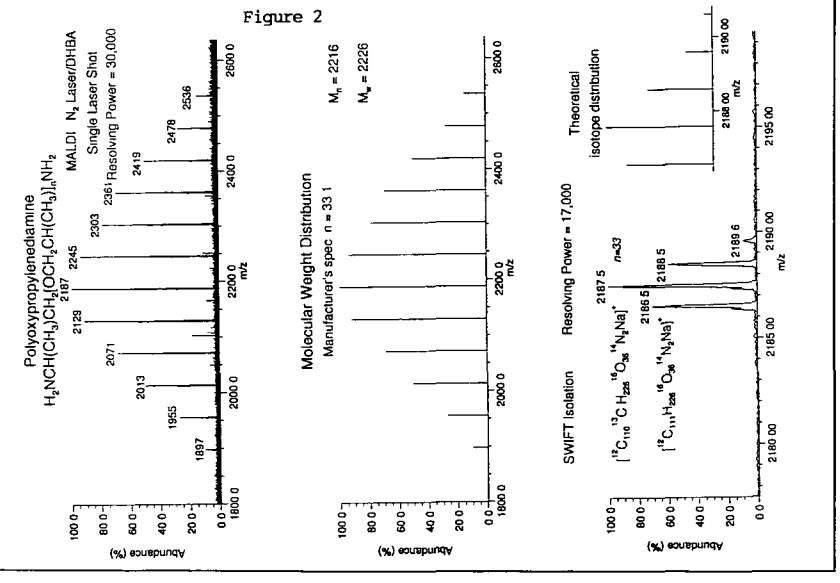

The Identification of Zinc Dialkyldithiophosphates in Lubricating Oils by Electrospray Ionization Mass Spectrometry

Vincent P. Nero and Donald D. Drinkwater
Texaco R&D, PO Box 509 Beacon, NY 12508

Electrospray Ionization Mass Spectrometry (ESI) was used to characterize the Zinc Dialkyldithiophosphates (ZDDPs), which are usually found in finished commercial motor oils. ZDDPs are detergent-like molecules consisting of the polar heteroatomic organometalic core surrounded with highly alkylated side-chains to increase their solubility in the base oil The core contains a central zinc atom coordinated to two dithiophosphate esters Generally two alkylated side chains, ranging from three to thirteen carbons, will be on each ester. ZDDPs are low cost additives which form protective films to reduce engine wear and prevent metal seizures. ZDDPs also serve as oxidation inhibitors. Their concentrations typically vary between 1% and 4%

ESI procedures have been developed, which can quickly characterize ZDDPs even in a fully formulated lubricant. The technique uses both positive and negative ion modes, and sometimes daughter ion analysis was also used to further elucidate composition The molecular ion distribution of the various types of alkyl groups and information concerning the nature of dimeric forms of the ZDDPs is obtained
In the positive ion mode, ESI sodium adducts form with the ZDDP molecular ions. This provides excellent information for identifying and quantitating their alkyl distributions. Figure I illustrates the alkyl distribution patterns of a zinc propyl hexyl dithiophosphate. This figure also clearly shows the characteristic zinc isotopic distribution of the individual alkyl clusters Under atmospheric pressure chemical ionization (APCI) conditions, ZDDPs form both protonated adducts to the molecular ions and fragment ions, but unfortunately, these fragment ions dominate the spectrum. The primarily fragmentation arises from the extensive loss of alkenes. Figure II illustrates a typical APCI spectrum. The major ion cluster around 322.6 amu represents complete loss of alkyl groups.
The negative ESI mode also provides excellent information. Under these conditions, the dialkyl dithiophosphate anion dominates the mass spectrum. Figure III shows the anions produced by zinc butyl pentyl dithiophosphate. Again, the alkyl groups can be easily identified and their distribution can be easily quantitated

Sample Preparation: All samples were either commercial additive packages consisting of ZDDPs in base oils or completely formulated commercial lubrication oils 100 ppm solutions of the additive package or 1000 ppm of the lubrication oil were prepared in various mixtures of MeCl2 / MeOH / hexane Solutions were infused directly into the MS interface at 30 ul/min.

Instrument Parameters: Both APCI and ESI experiments were performed on a Finnigan MAT TSQ 7000 MS. ESI parameters were: 80 psi nitrogen as a sheath gas pressure, 10 ml/min auxiliary nitrogen flow, 5 kV ionization spray voltage in both positive and negative ion modes, 250 °C capillary temperature, 20 V on the tube lens, 65 V on the skimmer region, and -3 V on the octapole lens, generally with no CID offset voltage. APCI parameters were 40 psi sheath gas, 150 °C capillary temperature, and 3-6 kV corona discharge voltage. Scan times were 4 sec. in the profile mode. MS/MS spectra were obtained using 60 V argon collisions.

Figure I

ESI (positive Ion) showing the Isotopic Distribution Patterns of the Sodium adduct to Zinc Propyl Hexyl Dithiophosphates

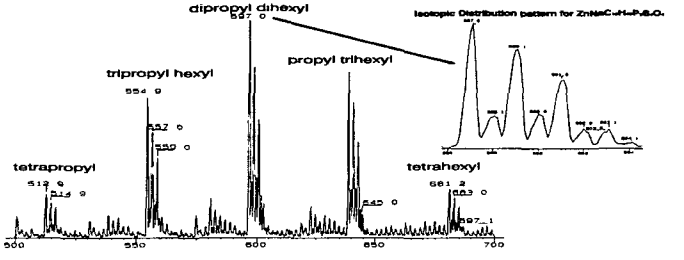

Figure II

Atmospheric Pressure Chemical Ionization (APCI) produces a Protonated Zinc Dithiodialkylphosphate and its fragment ions

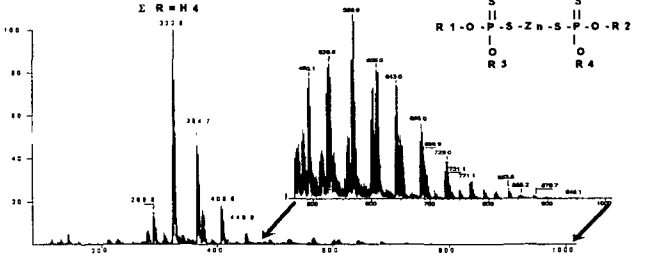

Figure III

Butyl Pentyl Dithiophosphate Anions (Negative Ion ESI/MS Spectrum of a C4C5ZDDP)

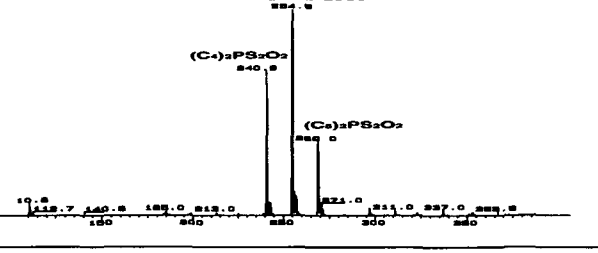

FLUID CATALYTIC CRACKING PRODUCTS CHARACTERIZED BY GCMS

Michael T. Cheng and James D. Hudson
Chevron Research and Technology Company
Richmond, California

Fluid catalytic cracking (FCC) products from the treatment of petroleum streams are important blending components for transportation fuels. There are many streams that can be the feedstocks to a FCC unit, therefore, FCC products are very complex and consist of many different types of compounds, such as alkanes, alkenes, cycloalkanes, and aromatic compounds. GCMS would be an ideal tool to characterize the FCC products, except that mass spectrometry is deficient as a tool to differentiate alkenes and cycloalkanes with same empirical formula, because they have very similar mass spectra. To fully characterize the FCC products, we describe in this report, a procedure in which the FCC products were analyzed before and after mild hydrogenation.

FCC products used in fuel blending are usually distilled, this sample was produced in the pilot plant and distilled at 343C. Initial GCMS run showed the presence of many peaks in the chromatogram. Most of the peaks can be identified unambiguously as alkanes (normal or branched C_5H_{10} to $C_{21}H_{44}$), or aromatic compounds, on the other hand, the alkenes and the cycloalkanes cannot be differentiated. Included in the aromatic compounds are alkylbenzenes, alkylindanes, alkylindenes, alkylnaphthalenes, alkylbiphenyls, and alkylphenanthrenes. The sample was then subjected to mild catalytic hydrogenation over 10% Pd on carbon at room temperature, and the hydrogen was supplied by a small party balloon. The hydrogenation was allowed to proceed until no hydrogen uptake was detected, however, the more definitive indication was by NMR. The proton NMR of the sample before hydrogenation showed olefinic protons and methyl groups attached to carbon-carbon double bonds, after hydrogenation the olefinic protons and the methyls attached to olefinic double bonds all disappeared, while the aromatic methyl groups are unchanged. This indicated that the olefinic double bonds were hydrogenated, while the aromatic double bonds were not changed.

This hydrogenated sample was then analyzed by GCMS. Many peaks present in the un-hydrogenated sample had disappeared upon hydrogenation, while no new peak was created upon hydrogenation. The disappearance of peaks was specially pronounce during the early part of the chromatogram, while the later part of the chromatogram was virtually unchanged. If a peak disappears upon hydrogenation, it then is an olefin; if it remains, a cycloalkane. Using this algorithm, all of the peaks in the un-hydrogenated sample can be identified. Using peak area from the total ion current trace, the following table summarizes the data.

	0-10 min	0-20 min	0-30 min	0-40 min	0-50 min	0-60 min
n-alkanes	8.8	5.3	3.9	3.6	4.0	4.5
branched alkanes	38.3	34.7	29.2	22.3	17.6	16.9
alkenes	49.2	32.5	19.9	13.7	10.8	10.4
cycloalkanes		17.7	19.0	13.0	10.3	9.9
cycloalkenes	3.7	2.8	1.9	1.2	1.0	1.0
dicycloalkanes			0.4	0.5	0.4	0.4
benzenes		6.9	24.4	28.1	23.0	22.1
indanes			1.0	12.8	11.6	11.2
indene			0.3	0.2	0.2	0.2
naphthalenes				4.4	17.1	16.8
biphenyls					4.0	5.6
anthracenes						0.9
total	100	99.9	100	99.8	100	99.9

Compounds with five or fewer carbons eluted in the 0-10 minute retention window, and in this window about 50% of the area was accounted for by the alkenes. In the 0-20 minute retention window, compounds with up to eight carbons elute; alkenes with five, six and seven carbon atoms account for about a third of the total area; cycloalkanes such as cyclopentanes and cyclohexanes, account for about 18% of the total; benzene and toluene are found in this window. In the 0-30 minute window, the benzenes account for about 25% of the total. Only small amount of alkenes with eight, nine, and ten carbons are found in the 20-30 retention window, the chromatograms for the sample before and after hydrogenation are very similar. From retention time of 30 minute until the end of the run, the TIC for before and after hydrogenation are essentially identical. In the 0-40 minute retention window, compounds with up to 13 carbon atoms are found. In the 0-50 minute window, compounds with up to 17 carbon atoms are found. And compounds with up to 21 carbon atoms are found in the last ten minute of the run.

From the table, one can then conclude that, the alkenes formed in a FCC unit are small alkenes, five, six, or seven carbon atoms species account for most of the alkenes, and they constitute about 10% of the total; benzenes are the most abundant species, they constitute about 22% of the total. This strategy can be applied to many refinery streams where it is necessary to distinguish alkenes from the cycloalkanes.

Coupling Field Ionization Mass Spectrometry with Liquid Chromatography for the Characterization of Heavy Saturated Hydrocarbons

Z. Liang, C. S. Hsu* and P. B. Grosshans
Exxon Research and engineering Company
Annandale, New Jersey 08801

We have successfully re-configured a commercial field ionization (FI) source to accommodate the moving belt interface for on-line LC operations. This novel combination allows us to characterize saturates with maximum chromatographic resolution and minimal sample preparation. Optimum FI operating conditions are obtained by comparing the carbon number distribution of a synthetic wax mixture by FI with that measured by gas chromatographic distillation (GCD). We found that it is important to apply a flash current onto the emitter between scans to avoid the condensation of high boiling components. Otherwise, the signals of high boiling components would be enhanced, resulting in a distorted quantitative measurement of the components in the mixture.

A SIMPLIFIED VIEW OF MOVING BELT LC/MS WITH FI SOURCE

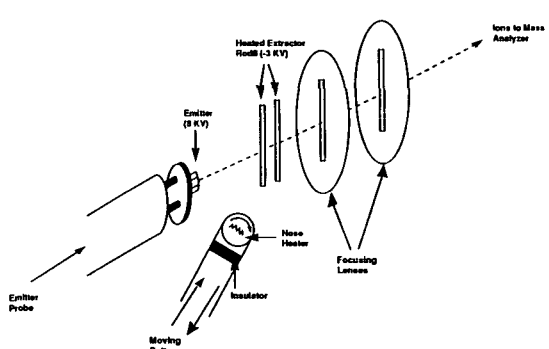

- EMITTER AND COUNTERELECTRODE - HIGH VOLTAGES
- MOVING BELT - POLYMERIC, INSULATED FROM GROUND
- LC NEBULIZER - GROUND POTENTIAL

ON-LINE LC/MS ALLOW MAXIMUM CHROMATOGRAPHIC RESOLUTION AND MINIMAL SAMPLE PREPARATION

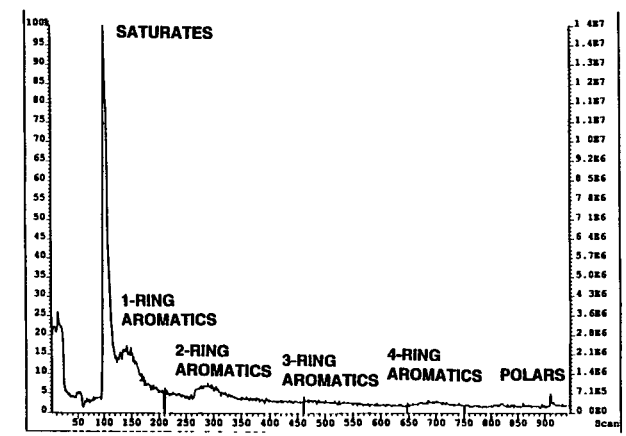

REMOVAL OF NORMAL PARAFFINS IS EVIDENT FROM THE FIMS MOLECULAR ION DISTRIBUTIONS

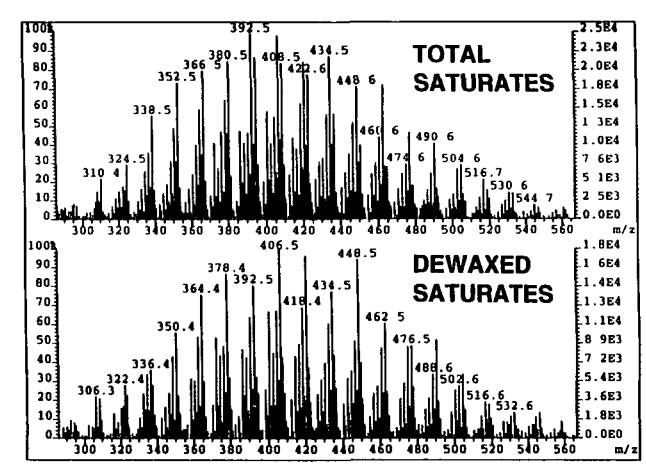

Why Do We Still Care about Dioxins?

Ronald A. Hites and Louis P. Brzuzy. School of Public and Environmental Affairs and Department of Chemistry, Indiana University, Bloomington, Indiana, USA, 47405.

Chlorinated dioxins and dibenzofurans (PCDD/F) are well-known environmental contaminants that have received prolonged attention by the scientific community and by environmental regulators. They enter the atmosphere primarily as byproducts from industrial combustion, waste incineration, metals production, and automobile emissions. PCDD/F are semivolatile, hydrophobic compounds; hence they accumulate in organic rich media such as soils, sediments, and biota .

In spite of our knowledge about the environmental behavior of PCDD/F, a significant problem remains: Deposition from the atmosphere is estimated to be roughly 10-25 times higher than estimated inputs from known sources.[1,2] There are three explanations for this mass balance discrepancy: **(a)** The depositional fluxes are overestimated because of sampling bias. **(b)** The input estimates are low because of unrecognized sources. **(c)** Both the sources are underestimated and the deposition is overestimated. We believe that depositional fluxes are overestimated because most PCDD/F measurements have been made in places of significant human industrial activity. Clearly, an expanded database of PCDD/F measurements from many geographical regions must be established before a realistic assessment of their mass balance can be made.

Measuring PCDD/F deposition directly is difficult, and there are few such measurements in the literature. Instead deposition is estimated from concentration measurements in other environmental matrices. For example, concentrations of PCDD/F in air and precipitation (usually rain) are used to estimate dry and wet deposition, respectively. Atmospheric deposition can also be estimated from PCDD/F concentrations in lake sediments. A sediment-derived estimate yields a sum of both wet and dry deposition.

Each of these techniques has practical limitations involving transporting and operating sampling equipment in rural and remote regions. To estimate fluxes on an expanded geographical scale, we have developed a technique using soils[3]. Soils are uniformly distributed, and they are relatively easy to collect and handle, providing a convenient matrix from which to estimate atmospheric deposition of PCDD/F.

Global Mass Balance for PCDD/F. We collected or had collected soil samples were collected from several areas of the world covering both the Northern and Southern Hemispheres. Over 300 samples were collected, and approximately 150 of these samples have been analyzed. From these data, fluxes have been estimated.

Atmospheric measurements of PCDD/F concentrations worldwide show that concentrations are within a fairly narrow range, between approximately 0.5 and 35 pg/m^3. This indicates that they are relatively mixed in the ambient atmosphere. Soil and sediment concentration values show greater variability. Sediment concentrations from the Great Lakes and Siskiwit Lake range

from 23 to 1500 pg/g. Literature values for background soil concentrations range from about 25 to 10000 pg/g.

Since PCDD/F are removed from the atmosphere by dry and wet deposition, then climatic factors that influence deposition might be controlling their concentrations in environmental sinks. We suggest that the deposition of PCDD/F from the atmosphere may exhibit some correlation to the various climatic zones of the world. If we consider these climatic zones as different depositional environments for atmospheric PCDD/F, we can estimate fluxes for each of these zones and revise the mass balance based on the flux and the geographical area of each zone.

Table 1. Area of the major climatic zones of the world, PCDD/F flux to, and estimated deposition to those areas.

Climate Zone	Area (10^{12} m^2)	Flux (ng/m^2 y)	Depostion (kg/yr)
Tropical Rainy	34.4	25	900
Dry	46.6	15	700
Humid Mesothermal NH	8.8	100	900
Humid Mesothermal SH	1.1	15	17
Humid Microthermal	16.4	70	1000
Polar	25.5	15	400
Undifferentialed Highlands	7.1	250	1800
Flux to Land			6000
Oceans	396 4	15	6000
Global Deposition			12000

Table 1 shows the major climatic zones of the world based on the designation of Trewartha[4], the areas of those zones, and the flux and the deposition of PCDD/F to those zones. Total deposition to these zones is about 6000 kg per year. However, this designation of climatic zones does not take into account the area of the global oceans. If we use a conservative depositional flux estimate of 15 ng/m^2 y, then the output rate to the global oceans is about another 6000 kg/yr. We estimate a total global deposition of PCDD/F at about 12,000 kg/yr, or about 12 kg/yr TEQ.

Based on current emission factor data from known combustion sources [5], we estimate global emissions of PCDD/F at about 5,000 kg/yr, which is about half of our estimate of deposition.

We conclude from this study that the global deposition of PCDD/F has been overestimated in the past. When deposition is estimated based on geographical regions, the mass balance between emissions and outputs improves. This indicates that most of the major sources of PCDD/F are known, and that PCDD/F contamination to the environment can be limited by controlling the emissions from these sources.

References

1) Rappe, C. In *Banbury Report 35: Biological Basis for Risk Assessment of Dioxins and Related Compounds.*, Cold Spring Harbor Press, 1990.
2) Harrad, S.J.; Jones, K.C. *Sci. Tot. Environ.*, **1992**, *126*, 89-107.
3) Brzuzy, L.P. and Hites, R.A., *Eniviron. Sci. Technol.*, submitted, February, 1995.
4) Trewartha, G.B, *Elements of Physical Geography*, McGraw-Hill Book Co., New York, 1957.
5) Thomas, V.M. and Spiro, T.G. *PU/CEES Report No. 285*, Princeton University, 1994.

Ultra sensitive and Very Fast Analysis of Halogenated Toxicants

Donald G Patterson, Jr , Zaiyou Liu, John R. Barr, Vaughn E. Green

Centers for Disease Control and Prevention
4770 Buford Highway, NE, Atlanta, GA 30341

Current sample cleanup and mass spectral methods for halogenated environmental toxicant analysis have recently generated a large amount of human and environmental data The impact of this new human data on analytical needs will be discussed However, the high cost ($1000 to $2000 per sample) and slow sample throughput of these methods (3 unknown samples per day) limits the size and statistical power of epidemiologic studies designed to assess any potential human health effects from exposure to these compounds In order to reduce the cost of these analyses and increase the sample throughput, we have developed a high speed, ultra sensitive, comprehensive two-dimensional separation system with high resolution mass spectrometric detection

Comprehensive two-dimensional separations differ from conventional heart-cutting multidimensional separations in that all substances are subjected to both dimensions of the separation process The theoretical peak capacity obtained from an orthogonal two-dimensional separation process is the product of the peak capacities obtained on each dimension. The same number of theoretical plates necessary to resolve the analytes of interest can be generated in a much shorter time with a comprehensive two-dimensional separation scheme than with a single dimensional approach. We have developed a prototype comprehensive two-dimensional gas chromatographic (C2D/GC) system utilizing a two-stage thermally modulated interface. This system has been interfaced to a Fisons/VG AutoSpec mass spectrometer and the combined C2D/GC/HRMS system used to determine polychlorinated dibenzo-p-dioxins (PCDDs), halogenated pesticides, and other environmental toxicants in human sample extracts The C2D/GC system utilizes two capillary columns (DB-5 and OV-1701) with a two-stage thermal modulation interface The Autospec mass spectrometer is operated in the SIR mode at 3000 resolving power while monitoring several ions for the native compounds and several ions for the carbon-13 labeled internal standard. Each of the second-dimension GC peak widths are about 60 msec at half-height giving about 5 data points over each second-dimension peak The thermal modulation system also generates an increase in sensitivity For example, summing four second-dimension peaks gave a signal/noise ratio of 12 for 500 attograms of 2,3,7,8-tetrachlorodibenzo-p-dioxin injected (See Figure) These data demonstrate the high sensitivity and specificity of the C2D/GC-HRMS system

Comprehensive 2D/GC-HRMS (3000RP) of 2,3,7,8-TCDD

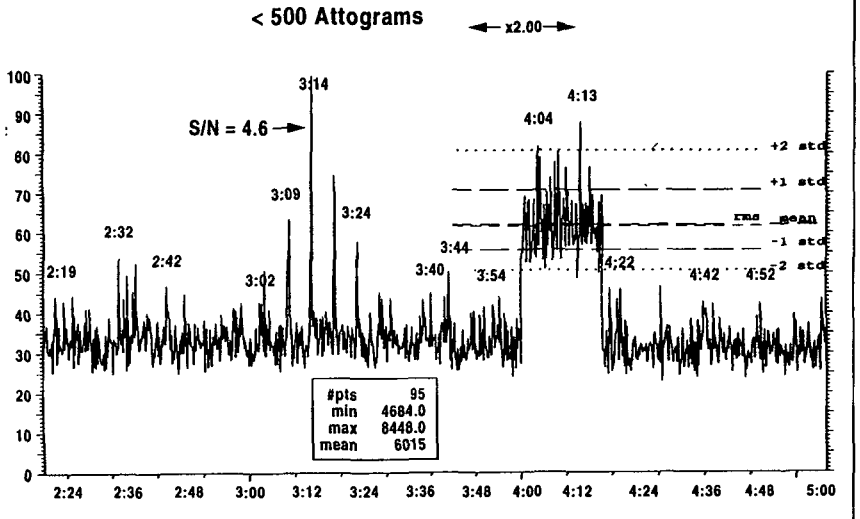

ACCUMULATIONS AND INVENTORIES OF ORGANOCHLORINES IN GREAT LAKES SEDIMENTS

D.L. Swackhamer, R.G. Pearson, University of Minnesota, Box 807 UMHC, Minneapolis, MN 55455; S.J. Eisenreich, Gray Freshwater Biological Institute, University of Minnesota, Navarre, MN 55392; D.T. Long, Geological Sciences, Michigan State University, E.Lansing, MI, 48108.

The Great Lakes are the largest reservoir of fresh water in the world They are home to more than 42 million people in the United States and Canada They also support an invaluable shipping industry, steel manufacturing, chemical industry, and commercial and sport fishery Unfortunately, they are also contaminated by more than 1000 chemicals The International Joint Commission has focused on 15 chemicals of concern, those that are persistent or have potential to bioaccumulate Included in this list of priorities are the pesticide toxaphene and the polychlorinated dibenzo-p-dioxins (PCDDs) and dibenzofurans (PCDFs) The state, provincial, and federal resource managers need to understand the history of these contaminants, and whether they are predominantly atmospheric or non-atmospheric, in order to best regulate the region

Toxaphene is a broad spectrum insecticide composed of hundreds of chlorinated bornanes and bornenes. Toxaphene was the replacement chemical for DDT, and was the most widely used organochlorine pesticide in North America It was mostly used in the southern U S., and was banned in the mid-1980's due to concerns of persistence and toxicity It is thought that toxaphene found in the Great Lakes is largely due to long range atmospheric transport from the south and atmospheric deposition into the lakes. The PCDDs and PCDFs are combustion products, and would be expected to have higher concentrations near urban and industrial regions.

Lake sediments accumulate over time, and particle-bound contaminants such as these will also accumulate over time in bottom sediments Thus sediments are useful to study in order to understand the history of inputs of contaminants to the Great Lakes We obtained several sediment cores from the Great Lakes, and used the data from them to determine current and past accumulations in the lakes, the time they first began to accumulate, the total integrated burden of contaminant in the lake, and evaluate the relative importance of atmospheric vs. non-atmospheric inputs. Cores were obtained from three sites in Lake Ontario in an east-west gradient, three sites in Lake Michigan in a north-south gradient; two sites in Lake Superior, one a depositional and one a non-depositional zone of the lake, and from two "control" lakes receiving only atmospheric deposition, one on Outer Island in the Apostle Islands, and Siskiwit Lake on the Bayfield penninsula Cores were sectioned in 1 cm or less intervals, and dated by ^{210}Pb. Sections were analyzed by Soxhlet extraction, silica gel and alumina cleanups, and gas chromatographic mass spectrometry in electron capture negative ion mode. Selected ions were monitored to quantitate homologs and total compound class

Accumulations of toxaphene in Lake Superior were two times greater than in the remote lakes (0.05 ng/cm2 yr), at all times. The homolog composition in the control lakes was constant throughout the cores and between cores, and showed a dominance of the heptachlorinated bornanes However, the composition in Lake Superior was significantly different, composed of mostly the octachlorinated bornanes. This composition more closely resembles the parent pesticide, while the control lakes are indicative of atmospherically weathered toxaphene. The inventories in Lake Superior are

approximately twice that of the control lakes. This evidence suggests that there has been and continues to be additional non-atmospheric inputs of toxaphene to Lake Superior.

Lake Michigan and Ontario accumulations are significantly greater than those in Lake Superior (5-10 times greater) The accumulations began in the 1940's, and maximized in Lake Michigan in 1980, except for the northern-most core In this core, the accumulations increased rapidly from the mid-1970's to the present Current accumulations here are higher than anywhere in the Great Lakes The homolog composition was similar for all three cores, however, and resembled the composition of parent toxaphene The inventories per unit area are 2-3 times greater than Lake Superior These data suggest that there has been a significant non-atmospheric source of toxaphene to Lake Michigan, and in particular there is a current source to the northern part of the lake

In contrast, accumulations in Lake Ontario increased to a maximum at about 1970 Accumulations increase from west to east in the lake The homolog compositions were similar in the western and central cores, having equal amounts of hexa-, hepta-, and octachlorinated bornanes, but the eastern-most core had a composition similar to parent toxaphene. Based on the hydraulics of Lake Ontario, this suggests an additional source of toxaphene from the New York side of the lake east of the Niagara River Inventories per unit area are slightly greater than those for Lake Michigan

PCDD and PCDF accumulations and inventories were similar in Lake Superior and the control lakes (1-3 pg/cm2yr), indicating that for these compounds, Lake Superior is an atmospherically-driven lake Accumulations were 5-10 times greater in Lake Michigan than in the control lakes, but they were not greater in the southern basin of the lake as was expected from the industrial and urbanized Milwaukee-Chicago-Gary corridor. Accumulations reached a maximum in the 1970's, except for the northern-most core which appears to have had constant accumulation since the 1970's The accumulations were another 3-5 times greater in Lake Ontario than in Lake Michigan, with a maximum in the 1970's.

The homolog composition of PCDDs was similar in all lakes and with depth The furan compositions were constant within a given lake and with depth, however, compositions differed among lakes In Lake Michigan and the control lakes, compositions were similar, and had a predominance of the less-chlorinated homologs (tetra- and penta-) In Lake Superior, the hepta-chloro homolog predominated The reason for the lack of agreement between Lake Superior and the control lakes is unclear In Lake Ontario, the furan composition was yet again different, having similar amounts of each of the homologs Furthermore, the relative proportion of furans to dioxins differed in Lake Ontario than in the other lakes, indicating a source of furans not linked to the source of dioxins

In summary, there are significant non-atmospheric sources of toxaphene to the Great Lakes, and current elevated accumulations in northern Lake Michigan. In general, accumulations maximized in the 1970's, but are still higher than in control lakes Lake Superior receives PCDDs and PCDFs almost entirely from the atmosphere, while much higher accumulations (order of magnitude) occur in Lake Michigan and Lake Ontario We do not see a sub-regional influence of PCDD and PCDFs on southern Lake Michigan as expected There appears to be an additional source of furans to Lake Ontario, decoupled from the sources of dioxins.

Characterization of Two Major Toxaphene Components in Lake Sediment.

G.A.Stern[1], M.D. Loewen[1], B.M. Miskimmin[2], D.C.G. Muir[1], D.W. Schindler[2] and J.B. Westmore[3]

[1] Freshwater Institute, Department of Fisheries and Oceans, Winnipeg MB R3T 2N6. [2]Department of Biological Sciences, University of Alberta, Edmonton AB T6G 2E9. [3]Department of Chemistry, University of Manitoba, Winnipeg MB R3T 2N2.

Toxaphene, a complex mixture consisting primarily of chlorinated bornanes (CHB's), was once widely used as a insecticide and briefly used as a fish toxin during the late 1950's and 1960's in many North American Lakes. The technical material is thought to consist of between two and three hundred penta- to undecachlorobornanes and camphene/diene isomers[1,2]. It is well known, however, that toxaphene residues extracted from biotic and abiotic samples do not resemble the technical material as analysed by HRGC, but instead consists of a more limited number of hexa-, hepta-, octa- and nonachlorobornanes[3]. In previous work[4,5], we structurally identified the two major CHB congeners, T2 (2-*exo*,3-*endo*,5-*exo*,6-*endo*,8,8,10,10-Octachlorobornane) and T12 its nonachloro- analog (2-*exo*,3-*endo*,5-*exo*,6-*endo*,8,8,9,10,10-Nonachlorobornane) found in beluga blubber. We report here the isolation of two more environmentally significant toxaphene congeners, a hexa- and heptachlorobornane (Hx-Sed and Hp-Sed, respectively), from the sediment of two lakes located in Alberta Canada[6] and their structures as determined by mass spectrometry (GC-ECNIMS, high and low resolution EIMS and linked field scanning) and ^{1}H-NMR. In the early 1960's both lakes were treated by addition of toxaphene to the water column at low ug/L concentrations. Sediments were collected from these lakes by freeze-coring, dated using ^{210}Pb and by counting varves and extracted with DCM. Highest toxaphene concentrations (~500-1600 ng/g dry wt.) were found in sediments of both lakes in slices dated to the early 1960's. In these slices the chromatographic pattern resembled that of the toxaphene standard while in more recent slices, the number of CHB peaks was greatly reduced with the two most prominant peaks corresponding to Hx-Sed and Hp-Sed.

The EI positive ion mass spectra of Hx-Sed and Hp-Sed are shown in Figure 1. In the mass spectra of both compounds, a 110 Da neutral species is eliminated from $[M\text{-}HCl\text{-}Cl]^+$ (m/z 271 for Hx-Sed, 305 for Hp-Sed) to yield the m/z 161 ion in the mass spectrum of Hx-Sed and the m/z 195 ion in that of Hp-Sed The observation of these decompositions, verified for both compounds by linked field scanning, provides us with important structural information because the neutral species lost are comprised of the bridging carbon (C7) and its two substituents *i e.* $CH_2ClC{:}CH_2Cl$ Observed decompositions involving the loss of CH_2Cl in the mass spectra of both compounds and the absence of corresponding decompositions involving the loss of $CHCl_2$ further support the positioning of two monochloromethyl moieties on C7. The group of peaks starting at m/z 306 and 307 in the mass spectrum of Hx-Sed and at m/z 340 and 341 in the mass spectrum of Hp-Sed correspond to the ions $[M\text{-}Cl]^+$ and $[M\text{-}HCl]^+$, respectively. Verified by linked-field scanning, the neutral fragment $C_2H_2Cl_2$ is eliminated from the latter ion giving rise to the even mass odd-electron ion $[M\text{-}HCl\text{-}C_2H_2Cl_2]^+$ (m/z 210 for Hx-Sed, 244 for Hp-Sed). In the mass spectrum of Hx-Sed loss of C_2H_3Cl is also observed and gives rise to the even mass odd-electron ion $[M\text{-}HCl\text{-}C_2HCl_3]^+$ (m/z 244). Losses of both C_2H_3Cl and $C_2H_2Cl_2$ in the mass spectrum of Hx-Sed suggest that there are three chlorines on the ring, two on one side and one on the other. In the mass spectrum of Hp-Sed, loss of only $C_2H_2Cl_2$ and not C_2H_3Cl, C_2HCl_3, C_2H_4 or C_2Cl_4 suggest a total of four ring chlorines, two on each side.

In the mass spectra of T2 and T12, competitive losses of Cl and HCl from the molecular ion were observed while those of toxicants A and B (2,2,5-*endo*,6-*exo*,8,8,9,10,10/8,9,9,10-Octachlorobornane and 2,2,5-*endo*,6-*exo*,8,9,10-Heptachlorobornane, respectively) showed an enhance elimination Cl

from the molecular ion[5]. It was suggested that the enhanced HCl elimination from the molecular ions in T2 and T12 with respect to that of toxicants A and B was to be expected from the greater acidity of the 5-*endo* and 6-*exo* hydrogen of T2 and T12 relative to the 5-*exo* and *endo* hydrogens of toxicant A and B, due to the electron-withdrawing properties of the 5-*exo* and 6-*endo* chlorines. This competitive loss of HCl and Cl from the molecular ion is also observed in the mass spectrum of Hp-Sed. This result along with conclusions drawn by Hainzl[2] with regard to relevant structures of CHB's suggest that Hp-Sed, like T2 and T12, has a 2-*exo*,3-*endo*,5-*exo*,6-*endo* ring conformation. The postulated structure for Hp-Sed is thus, 2-*exo*,3-*endo*,5-*exo*,6-*endo*,8,9,10-heptachlorobornane and was varified using ^{1}H-NMR. Positioning of the three ring chlorines on Hx-Sed required the use of ^{1}H-NMR. Based on these results and the mass spectral results discussed above, the structure of Hx-Sed was determined to be 2-*exo*,3-*endo*,6-*exo*,8,9,10-hexachlorobornane. The enhanced elimination of Cl from the molecular ion relative to that of HCl loss may result from the reduced acidity of the 5-*exo* proton in absence of the electron-withdrawing properties of a 5-*endo* chlorine.

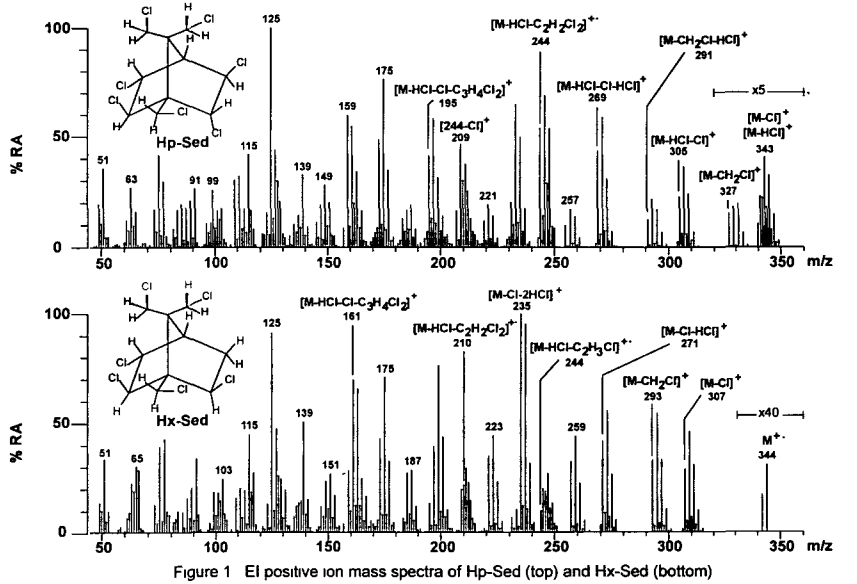

Figure 1 EI positive ion mass spectra of Hp-Sed (top) and Hx-Sed (bottom)

[1]J. Zhu, M.J. Mulvihill and R.J Norstrom, J.Chromatog. A, 669, 103 (1994).
[2]D Hainzl, J. Burhenne and H. Parlar, Chemosphere, 28, 245 (1994).
[3]D C.G. Muir and J. de Boer, Chemosphere 27(10), 1827, 1993.
[4]G.A. Stern, D C.G Muir, C. Ford, N.P Grift, E.Dewailly and T.F. Bidleman, Environ. Sci. Technol. 26, 1838 (1992).
[5]G.A. Stern, D.C.G. Muir, J.B. Westmore and W.D. Buchannon, Biological Mass Spec. 22, 19 (1993).
[6]B M Miskimmin, D.C.G Muir, D.W. Schindler and G A Stern, Environ. Sci. Technol. In press.

Dioxin and Furan Analysis by Ion Trap and Triple Quadrupole MS/MS and HRMS

Roger S. Mercer, Jennifer A. Townsend and Dave S. Waddell
Dioxin/Furan Unit, Laboratory Services Branch, Ontario Ministry of Environment and Energy
125 Resources Rd., Etobicoke, ON M9P 3V6

Jeffry B. Plomley and Raymond E. March
Department of Chemistry, Trent University
Peterborough, ON

Introduction: Polychlorinated dibenzo-*p*-dioxins and polychlorinated dibenzofurans are man-made compounds that have become widely distributed in the natural environment. These compounds are highly toxic to some species, exhibit a large inter-species variation in toxicity and have poorly characterized human toxicity. As a result, they are closely monitored in many jurisdictions.

Typical environmental levels for dioxins and furans range from parts-per-trillion and higher for soil and sediment samples to parts-per-quadrillion and lower for water samples. In many analytical methods ^{13}C-labelled surrogates are added to the samples for quantitation, necessitating the use of a detector more selective than low resolution mass spectrometry. In this laboratory we have employed both high resolution mass spectrometry (HRMS) using a sector mass spectrometer and tandem mass spectrometry (MS/MS) using a triple quadrupole mass spectrometer. These two types of instruments have comparable selectivity for dioxins and furans, but the HRMS instrument is approximately one order of magnitude more sensitive. HRMS and triple quadrupole MS/MS are also complementary with respect to interferences; an interfering compound observed by HRMS is rarely seen using MS/MS and vice versa.

We have recently begun analyzing dioxin and furan containing samples using an ion trap mass spectrometer equipped with a waveform generator to permit MS/MS operation. In MS/MS mode the parent ion is isolated in the trap, and collisionally activated dissociation (CAD) is performed by irradiating ions at their secular frequency. Ion trap MS/MS differs from triple quadrupole MS/MS in several respects that may influence the daughter ion spectra produced. For this reason we have conducted a comparison of the three instrumental techniques for dioxin/furan analysis.

Methods: All ion trap analyses were performed using: a Varian Saturn 4D system equipped with an rf waveform generator for MS/MS; Saturn version 5.0 and prototype "Toolkit" software. The ion trap was maintained at a temperature of 260°C. The GC flow rate was between 1.4 and 0.64 ml/min depending on GC column oven temperature. Only resonant irradiation techniques were examined in detail; non-resonant irradiation did not adequately fragment PCDD/Fs.

Three types of resonant excitation are possible using this instrument: single frequency irradiation (SFI), multi-frequency irradiation (MFI), and secular frequency modulation (SFM). Extensive optimization of all of these methods has been performed for PCDD/F; the details have been reported elsewhere.[1] Optimized irradiation conditions were used to produce all of the results discussed below.

43rd ASMS Conference on Mass Spectrometry and Allied Topics

Results and Discussion: We have compared the ion trap with HRMS and triple quadrupole MS/MS in three ways: CAD breakdown curves, isotope dilution quantitation and analysis of environmental field samples.

Breakdown Curves: Breakdown curves have been constructed for the three resonant irradiation modes of the ion trap and for the triple quadrupole using He collision gas. A comparison of the curves yields these observations: (1) the shape of the curves is similar for all irradiation modes of the trap. The irradiating voltage to produce a given product ion distribution varies with the mode. (2) The major product ions are the same for ion trap and triple quadrupole CAD, and are present in approximately the same proportions. (3) The onset of progeny ion production is much more rapid in ion trap CAD than in triple quadrupole CAD.

Isotope Dilution Quantitation: A set of calibration standards containing 17 native and 17 $^{13}C_{12}$-labelled PCDD/F at concentrations corresponding to USEPA Method 1613 were used to generate calibration curves using all three instruments. Typically, the HRMS and triple quadrupole instruments produce calibration curves with percent relative standard deviations (%RSD) of less than 20 percent for all 17 monitored congeners. On initial attempts, the ion trap produced %RSDs ranging from 16 to 80 percent. The worst results from the ion trap can be explained by poor chromatography caused by our use of a short GC column to decrease run times. Others, such as O_8CDD in the two most concentrated calibration solutions, produced poor results that appear to be concentration related. The ion trap produced a signal-to-noise ratio of 15:1 for 1 pg of 2,3,7,8-T_4CDD injected on the GC column.

Analysis of Environmental Field Samples: Several environmental samples of various matrices were examined. These samples were chosen because they contain multiple isomers in each congener group. The isomer pattern was similar for all congener groups in all of the samples examined. This indicates that the isomers have similar response relative to one another when examined using any of the three instruments. Some differences were observed in the ion trap chromatograms, but most of these are attributable to the lower resolution of the short GC column used on the ion trap. Quantitation of samples using the ion trap was not attempted, since not all of the required ions have been incorporated in the scan functions.

Conclusions and Future Work: In initial attempts, analysis of dioxins and furans by ion trap MS/MS produced results comparable to those obtained using HRMS and triple quadrupole MS/MS. The ion trap exhibits good sensitivity and selectivity. It appears that the CAD of dioxins and furans is similar in the ion trap and triple quadrupole. Calibration using isotope dilution quantitation standards was successful for several congeners, and poor calibration results for several others can be accounted for by chromatography. Future work will include: incorporation of additional ions in analytical scan functions; precise and accurate determination of isotope ratios; optimization of quantitation; and test stability of secular frequencies over time and with contaminated samples.

Reference

1. Plomley, J.B.; March, R.E.; Mercer, R.S. Proc. 43rd ASMS, Atlanta, GA (1995).

IONIZATION OF PCBs USING ION TRAP MASS SPECTROMETRY

M. Lausevic[1], X. Jiang[1], C.D. Metcalfe[2] and R.E. March[1]

[1]*Department of Chemistry, Trent University, Peterborough, ON, Canada K9J 7B8*
[2]*Environmental and Resource Studies Program, Trent University, Peterborough, ON, Canada K9J 7B8*

The toxicity of PCB mixtures is due principally to a small group of non-*ortho* and mono-*ortho* substituted congeners, usually present in environmental samples in lower concentrations than those of other congeners, thus the development of methods for toxic congener recognition is very important. The objectives of the present work were to compare quantitatively selected ion monitoring (SIM) of the electron impact (EI) mass spectra of PCBs with selected reagent ion chemical ionization (SRICI) mass spectra in terms of the detection limits achieved and to examine the possibility for distinguishing the more toxic congeners from those of lower toxicity. Since each ionization process determines the characteristics of the resulting mass spectrum, the task at hand was to identify from these mass spectra appropriate criteria for the determination of total PCB content and for differentiation of PCB congeners in order to determine the toxicity of PCB mixtures.

EXPERIMENTAL

The experiments were carried out with a modified Varian SATURN III Quadrupole Ion Storage Mass Spectrometer (QISMS™) coupled with a gas chromatograph and equipped with both a Varian waveform generator and a Varian 8200 autosampler SATURN revision C software was used for data acquisition in the EI and CI modes. The isolation of specific CI reagent ions, as well as isolation of molecular ions for resonant excitation experiments was achieved using a QISMS™ version 1.0 software package. A 30 m DB-5 chromatographic column was held at 38°C during the sample injection, than ramped to 260°C at 20°C/min and held at that temperature for 10 min.

RESULTS AND DISCUSSION

The relative responses of SIM of EI mass spectra and SRICI mass spectra of PCBs have been determined for some 60 PCBs contained in four standard mixtures.[1] The PCB congeners examined cover a wide range of toxicities. Average responses have been determined for PCBs as a function of the total number of chlorine substituents.

Relative responses and detection limits in CI and EI

In the CI mode, isolation of a specific CI reagent cation is carried out prior to protonation in order to ensure that a single reaction pathway predominates. In our previous study[2] it was shown that the reaction of PCBs with selected $C_2H_5^+$ ions isolated from methane yields CI mass spectra virtually free of contributions from charge exchange processes with the dominant product ion species being $[M+H]^+$. In addition, the enthalpy change for proton transfer is insufficient for fragmentation.

With selected $C_2H_5^+$ ions, the signal intensity per unit concentration decreases with increasing number of chlorine subsititutent atoms in the PCB molecule. The downward trend in average relative response in CI is due to the corresponding decrease in proton affinity (PA) with increased PCB electronegativity.

While the average relative response obtained in EI also shows a linear decrease with increasing number of chlorine atoms in the PCB molecule, the overall decrease observed with EI is much less pronounced than that observed with CI. The net decrease of the ionization efficiency is due to the corresponding increase in electronegativity of PCB isomers. Thus the increase in electronegativity with increasing degree of chlorination exerts a greater influence upon proton affinity than on ionization energy.

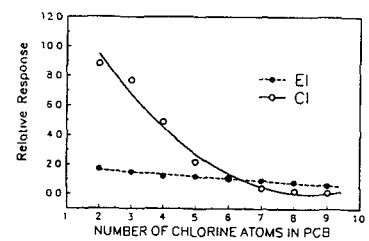

Fig. 1 The average responses of PCB isomers relative to hexa-chloro congener 153

The decreasing propensity for PCB ion formation (EI and CI) with molecular weight reflects the diminution of ionization efficiency for positive ion formation, and is opposite to that exhibited for electron affinity.

The detection limits for EI and CI were determined as the mass of congener 153 injected on column yielding a signal/noise ratio of 5:1. The detection limit with EI was found to be 0.8 pg; that with CI was found to be 30 pg. These detection limits reflect the efficiencies for positive ion (radical cation) formation and protonation, respectively.

An attempt to distinguish the more toxic congeners

An initial exploration has been carried out of the potential value of using a toxicity index.[3] Electron ionization, when combined with selected ion monitoring of both molecular and fragment ions, is the most sensitive mass-selective method for the determination of the most toxic PCB congeners. In our experiments, EI proved to be a reliable method for distinguishing between highly toxic non- and mono-*ortho* congeners and other PCBs. PCB ions with one or no chlorine atoms in the *ortho* position do not undergo one-chlorine atom loss from the molecular ion in EI. When there are two or more chlorine atoms in *ortho* positions, the loss of one chlorine atom is readily observed. Resonant excitation of isolated molecular ions suggests that losses of both one and two chlorine atoms can occur simultaneously and directly from the molecular ions. The typical fragmentation patterns can be recognised easily in selected ion chromatograms even when complex mixtures are analyzed.

REFERENCES

1. CLB-1(A,B,C and D) Released: January 1985, Documentation Revised: January 1991, *National Research Council of Canada, Institute of Marine Biosciences, Marine Analytical Chemistry Standards Program,* 1411 Oxford Street, Halifax, Nova Scotia, Canada B3H 3Z1
2. M. Lausevic, J.B. Plomley, X Jiang, R.E. March and C.D. Metcalfe, *Eur. Mass Spectrom.* **1** (1995) in press.
3. S. Safe, *Environ. Health Perspectives,* **100** (1992) 259.

Photoelectron Capture Negative Ion Mass Spectrometry of Organohalogens

Steven M. Colby, William A. Harris, Kent H. Hanser, and James P. Reilly
Dept. of Chemistry, Indiana University, Bloomington IN 47405

Photoelectrons, generated by directing a pulsed laser beam at a metal target, have recently been employed for electron impact ionization in time-of-flight mass spectrometry[1,2]. We have extended this concept to develop a new method in which laser induced photoemission is used as a source of electrons for electron capture negative ion mass spectrometry (ECNIMS)[3]. This technique has two principal advantages over conventional ECNIMS wherein electrons are generated from a heated filament. First, no mediating gas is required to thermalize the electrons. The electron energy is limited by the wavelength of the photons and the work function of the target material. It is therefore possible to select precisely the maximum electron energy. Some selectivity may even be achieved by tuning the electron energy to vibrational transitions of the analyte[4] This can dramatically increase the electron capture cross-section. The absence of a buffer gas eliminates several of the factors that can cause poor reproducibility and restrict the range of analytes. These include chemical reactions with the buffer gas and a strong temperature dependance on ion fragmentation patterns[5]. The absence of buffer gas also eliminates the pressure differential between the source region and the mass analyzer. This interface is responsible for a lack of reproducibility between instruments of differing design[5]. The second advantage to the generation of ions through photoemission is that electrons can be produced over a time period comparable to the laser pulse. This makes the method more easily adaptable to time-of-flight mass spectrometers. Because they are able to record an entire mass spectrum with each laser shot, these instruments are generally more sensitive than sector or quadrapole mass spectrometers.

The temporal duration of the emitted electron pulse depends on the mechanism of light interaction with the surface. Photoemitted electrons are produced only during the laser pulse while thermionic electrons, which require greater photon fluxes, may be observed for much longer periods. We have also found that it is possible for the laser light to be used for both electron generation and sample desorption. The technique can therefore be applied to samples whose vapor pressures are too low for conventional ECNIMS and Space-Velocity Correlation Focusing can be used to improve resolution[6,7].

It has previously been shown that a low energy electron beam may be used to generate negative ions from halogenated species[4]. However, this approach is limited by the low electron currents available. In contrast, laser induced photoemission may be quite efficient as has already been reported for Photoemission Electron Impact Ionization[1,2].

We have demonstrated Photoelectron Capture Negative Ion Mass Spectrometry with a number of halogenated organics. Figure 1 shows the mass spectrum of octafluoronaphthalene. The sample was introduced into the instrument through an effusive source and allowed to adsorb on a stainless steel surface within the source of the TOFMS. An ArF laser provided light to desorb the sample and generate electrons. By using the same surface for the trapping of analyte and as the laser target material we achieve good temporal and spacial overlaps between the molecules that are laser-desorbed and the generated photoelectrons. While parent ions are observed in Figure 1, extensive

fragmentation also occurs and the primary signal corresponds to halogen ions. This is in part due to the relatively high energy of the photoelectrons (up to 2.5 eV). When added to the electron affinity, this energy is sufficient to cause fragmentation. In future work we will attempt to reduce fragmentation by using longer wavelength lasers. We have also examined the sensitivity of this method by quantitatively introducing samples through a GC/MS interface. This interface, which is further described in another abstract at this conference[8], traps the GC effluent on a cryogenically cooled surface. Figure 2 shows a chromatogram of 10 ng of o-dichlorobenzene generated by monitoring the halogen atom signal. The width of the peak is due to a poorly heated valve between the chromatographic column and the GC-MS interface. This result is preliminary and further improvements in sensitivity are expected.

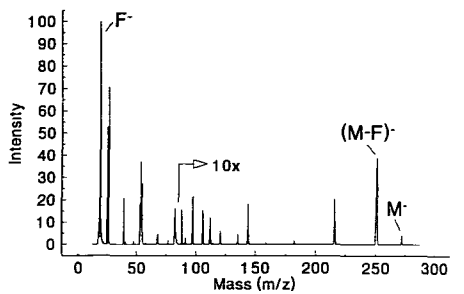

Fig. 1. The Photoelectron Capture Negative Ion Mass Spectrum of octafluoronaphthalene.

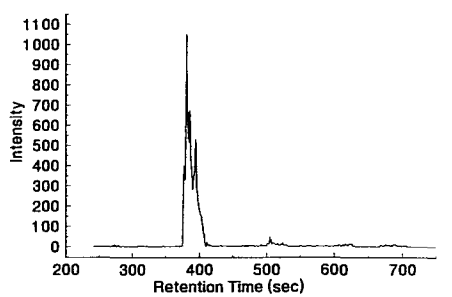

Fig. 2. A chromatogram of 10 ng of o-dichlorobanzene.

Refs:
1. S. M. Colby and J. P. Reilly; Int. J Mass Spectrom. Ion Process. 131 (1994) 125-138.
2. F. Moritz, M. Dey, K. Zipperer, S. Prinke, and J. Grotemeyer; Org. Mass Spectro. 28 (1993) 1467-1475.
3. S. M. Colby and J. P. Reilly; Pittsburg Conference, New Orleans, March, 1995, # 105.
4. J. M. Laramee, C. A. Kocher, and M. L. Deinzer; Anal. Chem. 64 (1992) 2316-2322.
5. V. S. Ong and R. A. Hites; J. Am Soc. Mass Spectrom. 4 (1993) 270-277.
6. S. M. Colby, T. B. King, and J. P. Reilly; Rapid Comm. Mass Spectrom. 8, (1994) 869-75.
7. T. B. King, S. M. Colby, and J. P Reilly; Int. J. Mass Spectr. Ion Process. In Press.
8. S. M. Colby, K. H. Hanser, W A. Harris, and J. P. Reilly; ASMS, Atlanta, May, 1995.

DETERMINATION OF PESTICIDES ON AGRICULTURAL SAMPLES BY STATIC SIMS ANALYSIS

J. C. Ingram, G S. Groenewold, A. D. Appelhans, D. L. Miller, J. E. Delmore
Idaho National Engineering Laboratory, P. O. Box 1625, Idaho Falls, ID 83415-2208

The development of methods to rapidly identify chemicals used in agriculture is important because detection is difficult using currently available technology Rapid screening of samples is needed in the areas of crop application, enforcement, food and environmental safety. SIMS instrumentation developed at the Idaho National Engineering Laboratory is demonstrating tremendous potential in this area through its ability to detect and identify chemicals of various types on environmental samples including vegetation, soil and rocks, stainless steel, glass, etc [i,ii,iii] SIMS is attractive as an analytical tool for application to agricultural and environmental problems due to the following· (a) no sample preparation is required, (b) no generation of waste, (c) rapid analysis (< 10 minutes), (d) amenable to almost any sample type, (e) ideal for involatile, ionic species (which can be difficult to detect by standard methods), (f) capable of "fingerprinting" (speciation), (g) non-destructive analysis allowing for additional analyses on the same sample Detection is achieved using a SIMS instrument equipped with a novel perrhenate primary ion gun, and pulsed extraction of secondary ions Together, these features allow analysis of insulating samples such as leaves and soils, which are not readily analyzed using conventional SIMS. Moreover, anion and cation spectra are acquired nearly simultaneously.

A scoping study was performed in order to evaluate the applicability of SIMS to detection of agrochemicals on various sample types. A matrix of 21 agrochemicals on four substrates were analyzed using a SIMS instrument utilizing a single quadrupole mass analyzer. These chemicals were applied to the samples at quantities approximating field usages (ca 5 $\mu g/cm^2$) Both the anion and cation SIMS spectra were collected for each sample. The results are summarized in the table. Strong detection indicates abundant quasi-molecular ions and/or abundant unique signature fragment ions. Medium detection indicates abundant signature fragment ions (no quasi-molecular ions). Weak detection indicates signature fragment ions observed in the SIMS spectrum at signal to noise values of 3 to 6. The results of this scoping study indicate that, in general, the more polar and less volatile agrochemicals are readily detected by SIMS. Additionally, in just over half the analyses, both the cation and anion SIMS spectra contained signature ions for the agrochemical analyzed.

Summary of Scoping Study Results				
	Dandelion	Grass	Soil	Stainless Steel
Alachlor	not detected	not detected	not detected	not detected
Atrazine	strong	strong	strong	strong
Captan	not detected	not detected	not detected	not detected
Carbofuran	strong	strong	medium	strong
Chlorpyrifos	medium	weak	weak	weak
Chlorsulfuron	strong	strong	medium	strong
DCMA	medium	medium	weak	medium
Cypermethrin	medium	medium	medium	strong
2,4 -D	strong	strong	weak	strong
Diuron	strong	strong	weak	strong
Glyphosate	strong	medium	not detected	strong
Malathion	strong	strong	strong	strong
Methomyl	strong	strong	medium	strong
M. Arsonic Acid	weak	weak	medium	weak
Mocap	not detected	not detected	weak	not detected
Norflurazon	medium	medium	medium	strong
Oxyfluorfen	strong	strong	strong	strong
Paraquat	strong	strong	strong	strong
Temek	weak	weak	medium	weak
Triallate	strong	strong	weak	strong

Further elucidation of the SIMS spectra for selected agrochemicals was provided through utilization of an ion trap SIMS instrument with MS/MS capabilities. One example is diuron, a herbicide used mainly for roadside applications. The SIMS cation and anion spectra of diuron on a dandelion leaf recorded using a single stage quadrupole SIMS instrument is shown in Figure 1. Both the cation $[M+H]^+$ and anion $[M-H]^-$ quasimolecular ions are observed. In order to identify the fragment ions observed in Figure 1, MS^n was performed using a ion trap SIMS instrument capable of investigating both the anions and cations In the case of the anion MS, the following sequence was performed (Figure 2): a) MS of the $[M-H]^-$ ion (*m/z* 233) resulting in an anion at *m/z* 186 which is interpreted as a loss of $NH(CH_3)_2$, b) MS of the *m/z* 186 anion resulting in an anion at *m/z* 150 which is interpreted as a loss of HCl, c) MS of the *m/z* 150 anion resulting in an anion at *m/z* 122 which is interpreted as a loss of CO. In the case of the cations, MS of the $[M+H]^+$ ion (*m/z* 233) results in a cation at *m/z* 72 which is interpreted as a loss of $C_6H_3Cl_2NH_2$ (Figure 2).

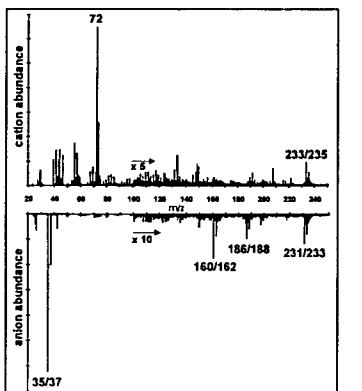

Figure 1

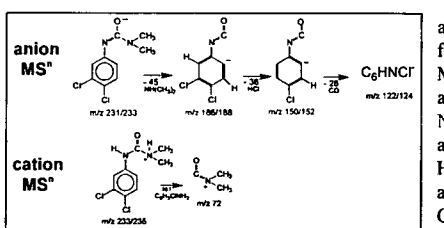

Figure 2

Comparing the ion trap results to the results recorded by the quadrupole SIMS instrument (Figure 1), it is clear that the anions at *m/z* 160/162 do not result from fragmentation of $[M-H]^-$ as this ion was not observed as a daughter ion during the ion trap (MS^n) experiments The *m/z* 160/162 ions are interpreted as originating from a cleavage of the N-C bond proximate to the aromatic ring of the neutral diuron molecule as illustrated in Figure 3 This interpretation together with the cation MS/MS results suggests that the cation at *m/z* 72 is a product of both fragmentation of the neutral diuron molecule and the $[M+H]^+$ quasimolecular ion The markedly abundant *m/z* 72 cation observed in Figure 1 is consistent with this explanation

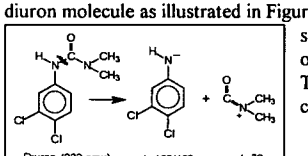

Figure 3

Funding of this work by LDRD Lockheed Martin is gratefully acknowledgment

[i] J. E. Delmore, A. D. Appelhans, *Bio Mass Spec.*, 1991, *20*, 237-246
[ii] J C. Ingram, G. S. Groenewold, A. D. Appelhans, J. E. Delmore, D A. Dahl, *Anal. Chem.*, 1995, *67*, 187-195.
[iii] G S. Groenewold, J. C. Ingram, J. E. Delmore, A. D. Appelhans, *Journal Am Soc Mass Spec.*, 1995, *6*, 165-174.

Real-time Analysis of Breath for Carbon Tetrachloride and its Metabolites

D. V. Kenny[1], K. D. Thrall[2], and P. J. Callahan[1]

[1]Battelle Memorial Institute
505 King Avenue
Columbus, Ohio 43201

[2]Pacific Northwest Laboratories
P.O. Box 999
Richland, Washington 99352

Real-time breath analysis offers a non-invasive method to detect exposure to toxic air pollutants. Breath measurements are useful in environmental exposure studies, and may provide evidence about previous long-term or repeated exposures in environments that are not easy to monitor. [1] If breath samples are collected during or immediately following a short term exposure, breath measurements can be used to predict the peak exposure. Previous breath sampling methodologies have been to collect repeated 1-minute breath samples at 5 minute intervals.[2] Although this method can aid in describing the rapid exponential emptying of the blood compartment that occurs following peak exposure, sampling 5 minute intervals still forces an approximation of the true shape of the clearance kinetics. We have developed a methodology to quantitively measure the concentration of exhaled volatile compounds in real-time using laboratory rats. Continously monitoring breath for a parent toxicant and its metaboloite(s) provides input into physiologically based pharmacokinetic (PBPK) models to describe the bio-kinetics of a chemical in the body. Real-time analyses are better than batch sampling methods because of the rapidly changing kinetics of elimination of some volatile chemicals from the body.

A Sciex TAGA 6000E MS/MS equipped with a low pressure chemical ionization source (LPCI), along with a Finnigan ITMS equipped with an atmospheric sampling glow discharge ionization source (ASGDI), and the Teledyne HST-1000 accessory kit (for filtered noise field (FNF) operation) were used for these experiments. The expired breath from 1 to 6 laboratory rats can be introduced separately into the two tandem mass spectrometers by way of a manifold. Figure 1 shows the schematic of the rat breath manifold. This device is a modification of a human breath interface patented by Battelle.[3] Carbon tetrachloride, its main metabolite, chloroform, and markers of lipid peroxidation; ethane and acetone, were simultaneously monitored in real-time, in the expired breath of the rats exposed to carbon tetrachloride. Figure 2 shows the results from the I.V. injection of a 0.6 mg/Kg dose of CCl_4. Figure 3 shows the results from a 25 mg/Kg dose of CCl_4 via oral gavage. The real-time concentration data was then input into a PBPK model to determine target tissue doses. The model accurately determined the dose of CCl_4 administered in each experiment. Since the methodology provides information on real-time metabolic processes and toxic responses, the implications for improving heath risk assessements are substantial.

---

[1] Bond, J.A., Wallace, L.A., Osterman-Golkar, S., Lucier, G.w., Buckpitt, A., Hendersen, R.F., *Fundam. Appl. Toxicol.*, (1992), 18 161-174.

[2] Raymer, J.H., Thomas, K.W., Cooper, S.D., Whitaker, D.A., Pellazzari, E.D., *J. Anal. Toxicol.* (1990) 14, 337-344.

[3] Kenny, D.V., Kelly, T.J., Apparatus and Method for Analysis of Expired Breath, U.S. Patent 5,042,501 (1991).

43rd ASMS Conference on Mass Spectrometry and Allied Topics

Schematic of Rat Breath Manifold Connected to Mass Spectrometer

Figure 1.

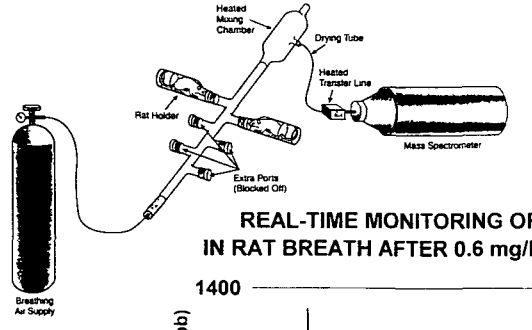

Figure 2.

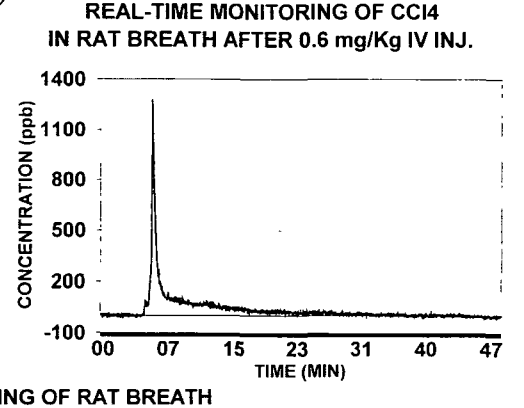

Figure 3.

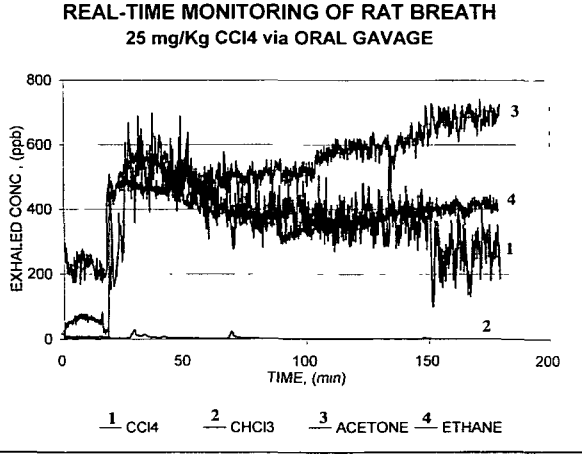

TUNABLE ENERGY (0.03-60 eV) ELECTRON CAPTURE NEGATIVE ION SPECTROMETRY

J.A. Laramee, P. Mazurkiewicz, P.C.H. Eichinger, and Max L. Deinzer
Department of Agricultural Chemistry
Oregon State University, Corvallis, OR 97331

The presence of environmentally persistent chlorinated-hydrocarbons, the use of organophosphate pesticides, and the production, storage and testing of explosives is extensive. Consequently there is considerable concern about residue levels in human, animal, and plant tissue, as well as ground water and air. Most recent efforts to improve both the detection sensitivity and quantification of these residues have been made using Electron Capture Negative Ion Mass Spectrometry (ECNIMS) since the method generally provides greater sensitivity for electron-loving compounds than is achieved by positive ionization methods (Knighton, *et al.*, 1994).

ECNIMS *without buffer gas* to moderate electron energies to thermal levels has been achieved by using an electron monochromator (Laramee *et al.*, 1992). This device has the advantage of being simple yet reliable and practical for the analysis of electron-loving compounds such as explosives and polychloro compounds from Arctic trout (Laramee and Deinzer, 1994). The electron energy is tunable to give just the right energy for ionizing specific compounds or isomers, and because no chemical ionization plasma is present the plethora of radicals, cations, anions and high-energy electrons is eliminated along with spurious adduct ions that are largely responsible for irreproducible spectra from ion/molecule reactions.

This methodology has now been refined into a prototype ion source for use on a JEOL DX-303 mass spectrometer. Construction of the electron monochromator was guided from particle trajectory calculations corrected for space-charge, electron-optical aberrations, and interlens field penetrations. A rectilinear beam is formed from a ribbon filament using a Pierce element. But magnetic field confinement does not completely overcome beam widening caused by the anode aperture lens action since the radial velocity vectors cause electron spiraling to occur. Hence the beam shape is maintained via a unique dual anode lens configuration with zero net lens action that produces a parallel beam with few radial velocity vectors. Electrons are dispersed in a crossed electric (E) and magnetic (B) field with drift velocity of $(E \times B)/B^2$. 0.03 eV electrons were produced with the ion source floated at -3000 eV (Figure 1). This performance compares well with that of the archetype instrument (Figure 2). The fractional electron energy distribution was measured to be $\pm$ 0.34 eV using the negative ion resonance at 0.03 eV from hexafluorobenzene (Fenzlaff and Illenberger, 1984).

Electron energy is another analytical dimension of information that can be used to distinguish among structurally similar compounds. Three-dimensional spectra readily show distinguishing spectral features of the sixteen organophosphates surveyed. These 3-D spectra are expected to provide a potentially useful means for identifying environmental unknowns, for example parathion and paraoxon are readily distinguished by this molecular fingerprinting system (Figure 3). Rapid detection is possible since the complete electron energy spectrum can be recorded in 3 milliseconds (Laramee and Deinzer, 1994).

ACKNOWLEDGEMENTS

This work was supported by NIEHS 00040, NIEHS 00210, and JEOL 6709.

REFERENCES

W.B. Knighton, R.S. Mock, D.S. McGrew, and E.P. Grimsrud (1994) *J. Phys. Chem.* **98**, 3770-3776.
J.A. Laramee, C.A. Kocher, and M.L. Deinzer (1992) *Anal. Chem.* **64**, 2316-2322.
J.A. Laramee and M.L. Deinzer (1994) *Anal. Chem.* **66**, 719-724.
H-P Fenzlaff and E. Illenberger (1984) *Int. J. Mass Spectrom. Ion. Proc.* **59** 185-202.

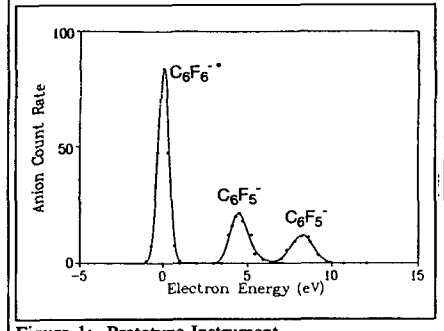

Figure 1: Prototype Instrument

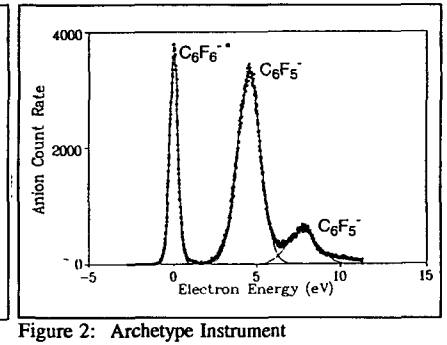

Figure 2: Archetype Instrument

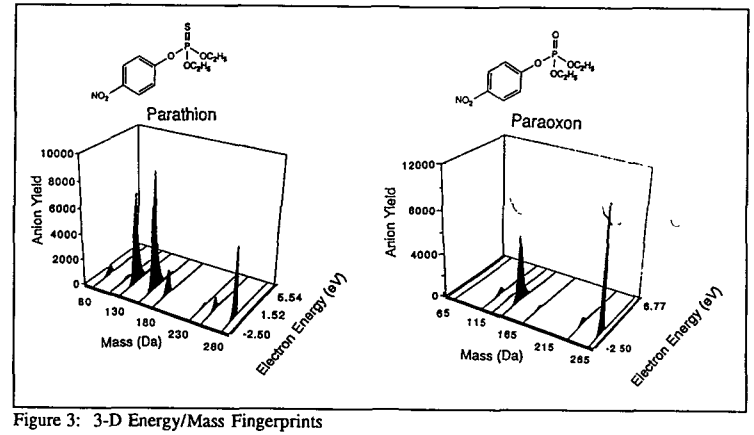

Figure 3: 3-D Energy/Mass Fingerprints

STRUCTURES AND ELECTRONIC PROPERTIES OF FULLERENE-RELATED COMPOUNDS*

Robert L. Hettich, Z. Charles Ying, and Robert N. Compton
Oak Ridge National Laboratory, Oak Ridge, TN 37831-6120

The synthesis and characterization of fullerene-related compounds has been the subject of active research both experimentally and theoretically since the discovery of C_{60} For example, endohedral fullerenes $M@C_n$ (carbon clusters containing a "trapped" atom M within their cage) can be generated for several different early transition metals and noble gases. The properties of these species have been modelled theoretically, and indicate that these species may have unusual applications. Likewise, the covalent attachment of hydrocarbon functional groups to a fullerene also alters its properties, opening up new applications as well The focus of this presentation is to describe how Fourier transform ion cyclotron resonance (FTICR) can be used not only for the detection and identification of fullerene-related compounds, but also the detailed structural interrogation of their properties. In particular, laser desorption FTICR was used to examine endohedral $La@C_n$ species and γ-radiolysis fullerene products Collisional dissociation and charge transfer processes were used to probe the structures and electronic properties of these nanoclusters in detail

Endohedral $La@C_n$ samples were generated by laser ablation of a lanthanum oxide-doped graphite rod in an argon atmosphere. The $La@C_n$ soot was deposited directly onto a stainless steel probe disk for subsequent examination by LD-FTICR LD-FTICR of the resulting samples revealed the presence of some C_{60} and C_{70}, although the most abundant species were $La@C_n^+$ for n = 60, 74, 82. Smaller peaks corresponding to $La@C_n^+$ for n = 70-100 were observed Three FTICR experiments were conducted to examine the $La@C_n^+$ species· 1) ion-molecule reactions with oxygen-containing species, 2) collision-induced dissociation reactions, and 3) charge exchange reactions to bracket the ionization potentials and electron affinities. The first two types of reactions were used to interrogate the structure of the $La@C_n^+$ species to verify that the metal atom was inside the cage (endohedral) and not attached to the outside of the cage (exohedral). No ion-molecule reactions were observed for $La@C_n^+$ and N_2O, and the collisional dissociation of $La@C_n^+$ for n = 60, 74, 82 revealed primarily sequential C_2 loss These results support the assumption that the La atoms are attached inside the fullerene cage. The third type of reaction (charge exchange) was used to bracket the ionization potentials of these endohedral species to ascertain the effect of the "trapped" heteroatom on the fullerene electronic structure $La@C_n^+$ was observed to charge exchange with decamethylferrocene (I P. = 5.8 ± 0.1 eV) and N,N,N,N-tetramethylphenylenediamine (I.P. =6 2 ± 0.05 eV), as shown in Figure 1 for $La@C_{60}^+$. Experimentally, this corresponded to a decrease in the $La@C_n^+$ signal and an increase in the ionized reagent with increasing reaction time $La@C_n^+$ is unreactive with ferrocene ((I.P. =6 75 ± 0 009 eV), implying that I.P. ($La@C_n$) < I.P. (ferrocene) Photoionization results of $La@C_n$ indicate that these species can be ionized with a ArF excimer laser, implying that I.P ($La@C_n$) < 6 4 eV. These experimental results imply that the I P. of $La@C_n$ is between 6.20 and 6.4 eV For comparison, the I.P (C_{60}) is 7 6 eV and the I P (La) is 5.577 eV Thus, the I P. of $La@C_n$ is between that of C_{60} and La. These measurements support the overall picture that the endohedral La atom transfers its three valence electrons to the lowest unoccupied molecular orbital (LUMO) of C_{60}. As a result, $La@C_n$ consists of a positively-charged La ion inside a negatively-charged C_{60} shell The molecular orbitals of C_{60} remain roughly the same, but are shifted downward in energy as a result of the Coulombic interactions between La^{3+} and C_{60}^{3-}.

Collaboration with Professor George Bakale (Case Western Reserve University) has been focused on identification of the γ-radiolysis product of C_{60} in cyclohexane Upon irradiation with γ-rays (1 42 krad/hr, total dose of 51 krad), the purple-colored C_{60} / cyclohexane solution turns muddy red. Positive ion LD-FTICR mass spectrometry (low laser power) of the resulting product reveals abundant ions in the m/z 1540-1560

region, shown in Figure 2a. Higher laser power densities reveal a series of fragment ions corresponding to loss of 82 Daltons from the ions stated above, shown in Figure 2b Accurate mass measurements and collisional dissociation experiments indicate that the radiolysis product consists of 10 cyclohexane groups attached to the C_{60}. This C_{60}(cyclohexane)$_{10}$ species fragments easily by sequential elimination of cyclohexene Apparently, the (C_6H_{11}) radicals formed by the gamma radiation of the cyclohexane solvent are efficiently captured by C_{60}, which is known to be a "radical sponge", until the terminal product of C_{60}(cyclohexane)$_{10}$ is generated Steric hindrance may prohibit attachment of more cyclohexyl groups to C_{60}.

* Research sponsored by an ORNL Director's R&D Program and the Office of Health and Environ. Research, U.S. Dept of Energy, under contract DE-AC05-84OR21400 with Martin Marietta Energy Systems, Inc

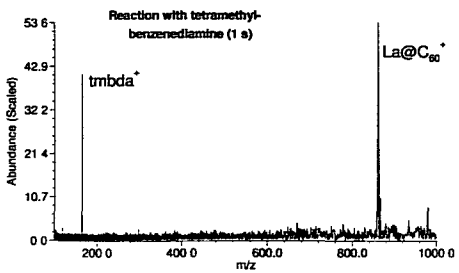

Figure 1

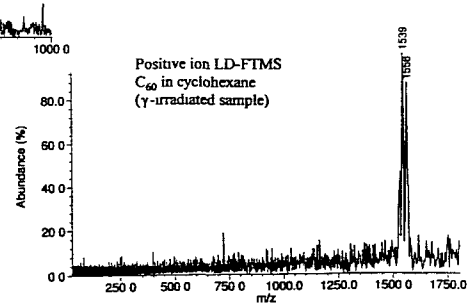

Figure 2a

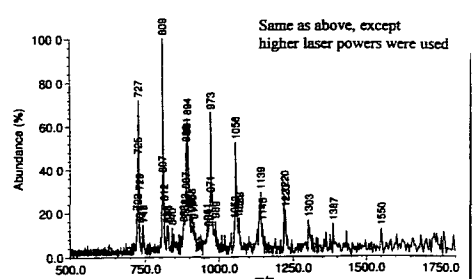

Figure 2b

"The submitted manuscript has been authored by a contractor of the U.S. Government under contract No. DE-AC05-84OR21400. Accordingly the U.S. Government retains a nonexclusive royalty-free license to publish or reproduce the published form of this contribution or allow others to do so for U.S. Government purposes."

Reactions of Fullerene Oxides in a Fourier-Transform Mass Spectrometer

Christopher Holliman and Stephen McElvany, Naval Research Laboratory, Code 6113, Washington, D.C. 20375-5342

High-intensity laser desorption of C_{60} fullerene results in the formation of larger fullerenes through coalescence. Fullerene coalescence appears to occur via the emission of small even-numbered carbon species. An understanding of the coalescence mechanism should provide insight into the fullerene growth process and may direct new synthetic routes to the macroscopic production of larger fullerenes.

The coalescence reactions of the fullerene oxides $C_{60}O_n$ (n = 1-3) proceed more efficiently and at a lower laser radiance than the coalescence of pure C_{60} [1]. The collisionally activated dissociation (CAD) spectra of CI-source produced $C_{60}O_n^-$ (n > 1) reveals that the loss of oxygen occurs exclusively with the disruption of the fullerene cage yielding odd- and even-numbered fullerene product ions [2]. The formation of similar product ions by laser irradiation or ozonolysis may be the first step in fullerene coalescence. The goal of this study is to produce possible fullerene coalescence precursors in the ion trap of a Fourier-Transform mass spectrometer. Once trapped, the structure and reactivity of the precursor can be probed via collisionally induced dissociation and ion-molecule reactions.

$C_{60}O_n$ neutrals are generated by bubbling ~6 % O_3 through a solution of C_{60} in toluene. The reaction mixture is separated by HPLC into five fractions (C_{60}, $C_{60}O$, $C_{60}O_2$, $C_{60}O_3$, $C_{60}O_{>3}$) using a Buckyclutcher column (Trident DNP).

The fullerene-oxide molecular anions are generated by MALDI from an acetylanthracene or dithranol matrix (~0.010 mg matrix / 1.0 mL THF) that is irradiated at the tripled-frequency (355nm) of a Nd-YAG laser. Ions are trapped in the source-side of a dual-cell FT-mass spectrometer and selectively focussed by quadrupolar axialization [3]. The ^{12}C isotopically pure ion is selected and submitted for CAD.

The MALDI-FTMS spectra of the $C_{60}O_2$ fraction that is obtained with the acetylanthracene matrix gives the expected isotopic abundances for $C_{60}O_2$. The CAD of $C_{60}O_2^-$ *m/z* 752 (Figure A) results in the loss of CO and the disruption of the fullerene cage. Further CAD of the product ion witf *m/z* 724 results in the loss of another CO unit and suggests that the C-O bonds of $C_{60}O_2$ are equivalent.

The CAD spectrum of the $C_{60}O_2^-$ ^{13}C isotopomer of *m/z* 753 (Figure B) reveals two new products corresponding to losses of 17 and 44u.

MALDI desorption of the $C_{60}O_2$ fraction from the dithranol matrix results in an increase in the abundance of *m/z* 753. Although the CAD spectrum of the dithranol-desorbed *m/z* of 752 is the same as that produced from the acetylanthracene matrix (Figure A), CAD of *m/z* 753 (Figure C) now produces abundant losses of 17u (OH) and 44u (CO_2). Figure C suggests the donation of a hydrogen atom from the dithranol matrix to produce $C_{60}O_2H^-$ *m/z* 753. Recall that the enol form of β-diketones are stabilized by intramolecular hydrogen bonding between the carbonyl oxygens. The product ion with *m/z* 736 loses oxygen upon further CAD indicating C-O bonding similar to that in $C_{60}O$ [2]. The product ion with *m/z* 753 loses a second CO unit upon further CAD indicating C-O bonding similar to that in $C_{60}O_2$.

The MALDI-FTMS spectra of the $C_{60}O_3$ fraction have been obtained. CAD of $C_{60}O_3^-$ *m/z* 768 results abundant losses of CO, CO_2 and C_2O_3 and the disruption of the fullerene cage.

$C_{60}O_n$ ions formed by CI and by MALDI of neutrals exhibit similiar CAD fragmentation. The addition of a second oxygen to the fullerene cage results in stronger C-O bonding than that observed in $C_{60}O$. The addition of hydrogen atom to $C_{60}O_2^-$ to form $C_{60}O_2H^-$ and the CAD spectra of both ions

support the proposed diketone structure of $C_{60}O_2$ MALD-FTMS followed by CAD is a viable route for the production and isolation of possible coalesenece precursors. Reactivity studies are now underway.

1.) Beck, R. D.; Stoermer, C.; Schultz, C.; Michel, R.; Weis, P.; Brauchle, G.; Kappes, M., *J Phys. Chem.*, **1994**, *101*, 3243-3249.

2.) Callahan, J. H.; McElvany, S. W.; Ross, M.M., *Int. J. Mass Spectrom. Ion Processes*, **1994**, *138*, 221-239.

3.) Schweikhard, L.; Guan, S.; Marshall, A. G., *Int. J. Mass Spectrom. Ion Processes*, **1992**, *120*, 71-84.

This research is supported by the Office of Naval Research.

Figure A

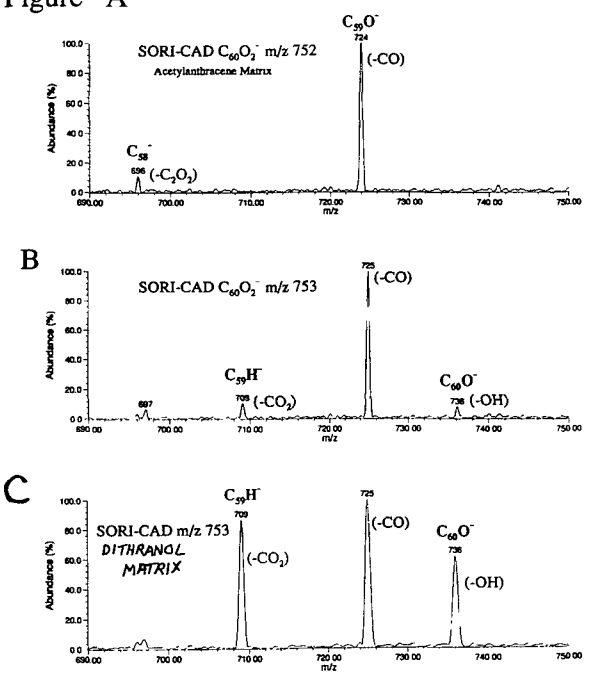

Collision experiments with fullerene ions and molecular target gases

Helen J. Cooper, Richard T. Gallagher and Peter J. Derrick

Warwick Institute of Mass Spectrometry and Department of Chemistry, University of Warwick, Coventry CV4 7AL, U.K.

Tore Vulpius

Department of General and Organic Chemistry, HC Orsted, University of Copenhagen, Copenhagen, Denmark.

Target capture is the process in tandem mass spectrometry in which the parent ion and the target gas do not separate following collision. It was predicted by Neumann *et al.* [1] and has been studied using Buckminster fullerene ions [2, 3, 4] and renin substrate ions [5].

The present study investigates the question of molecular target capture by $C_{60}^{+\cdot}$ ions. The gases employed were CH_4, CD_4, $^{13}CH_4$, N_2 and O_2. All of these gases form adducts with the $C_{60}^{+\cdot}$ ions and the mechanism of formation of these adducts has been studied by considering their translational energies.

Experiments were performed on a Kratos Analytical Concept IIHH four-sector mass spectrometer and a Jeol HX110A/HX110A four-sector mass spectrometer using EI ionisation and collision energies of 300-1000 eV. The gas pressure was sufficient to reduce the ion beam to 80% of its original intensity. Spectra were obtained by scanning the magnet of MS2.

At 1000 eV collision energy, the peak corresponding to $[M+13]^+$ is the most intense adduct for collisions of $C_{60}^{+\cdot}$ ions and methane. At 500 eV collision energy (figure 1), the $[M+14]^{+\cdot}$ peak is the most intense adduct. Also observed in this spectrum are peaks corresponding to $[M+1]^+$, $[M+12]^+$ and $[M+15]^+$. At 300 eV laboratory-frame collision energy the peaks $[M+14]^+$, $[M+15]^{+\cdot}$ and $[M+16]^+$ for $^{13}CH_4$ and $[M+14]^+$, $[M+16]^{+\cdot}$ and $[M+18]^+$ for CD_4 confirm that the adduct peaks with CH_4 are due to CHC_{60}^+, $CH_2C_{60}^{+\cdot}$ and $CH_3C_{60}^+$. At lower collision energies (ie less than 300 eV) no adduct peaks were observed.

Figure 2 shows the spectrum obtained with $C_{60}^{+\cdot}$ ions and nitrogen at a collision energy of 500 eV. A peak corresponding to $[M+28]^{+\cdot}$ is observed. This peak is also observed at 1000 eV collision energy. At 300 eV collision energy and below, no adduct peaks are observed. There is no evidence for the existence of an $[M+14]^+$ peak. Figure 3 shows the spectrum obtained with C_{60}^+ ions and oxygen at a collision energy of 500 eV. A peak corresponding to $[M+16]^+$ is observed. This peak is again observed at 300 eV although there is no evidence for its occurrence at higher collision energies (1000 eV). The full adduct $[M+32]^+$ is not observed.

The difference in translational energy between the parent ion and the adduct ion was measured and compared with predicted values. For the adducts $CH_2C_{60}^+$ and CHC_{60}^+, the measured and predicted values show good agreement. These adducts, therefore, may well be the result of fragmentation of a $CH_4C_{60}^+$ ion. A good correlation between predicted and measured values is also shown in the case of nitrogen. This is to be expected as the adduct ion observed was $[M+28]^+$ and could only be $N_2C_{60}^+$. The results obtained for oxygen are not consistent with the proposed mechanism i.e. $C_{60}O^+$ is not the result of fragmentation of $O_2C_{60}^{+\cdot}$.

43rd ASMS Conference on Mass Spectrometry and Allied Topics

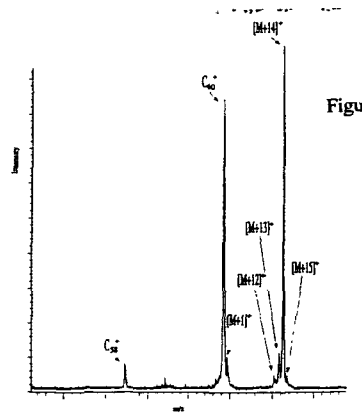

Figure 1

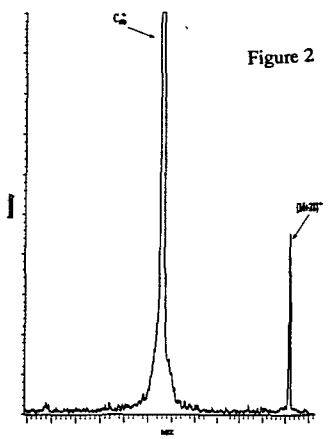

Figure 2

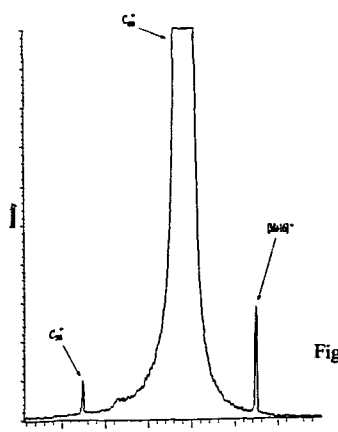

Figure 3

References

1. GM Neumann, MM Sheil, PJ Derrick; Z. Natursforsch., 39a, 584, (1984).
2. T Weiske, DK Böhme, J Hrusak, W Kratschmer, H Schwarz; Angew. Chem. Int. Ed. Engl., 30, 884, (1991).
3. MM Ross, JH Callahan; J. Phys. Chem., 95, 5720, (1991).
4. KA Caldwell, DE Giblin, ML Gross; J. Am. Chem. Soc., 114, 3743, (1992).
5. X Cheng, C Fenselau; J. Am. Chem. Soc., 115, 10327, (1993).

Intermolecular Nitrile Oxide Transfer in Fullerene Isoxazolines

R. T. Pogue, M. S. Meier, C. Thomas, V. Majidi
Department of Chemistry, University of Kentucky,
Lexington, Ky, USA 40506

INTRODUCTION

Mass spectrometric analysis of fullerene derivatives often requires very different conditions and produces very different results than are expected when examining underivatized fullerenes. Frequently, mass spectra of derivatives have relatively small molecular ion peaks and are dominated by fullerene ion peak at high masses. The need for reliable mass spectrometric methods is increasing as new classes of fullerene derivatives are introduced. One such class of derivatives, the fullerene isoxazolines, is examined in this presentation.

Fullerene isoxazolines are produced via a 1,3 dipolar addition of a substituted nitrile oxide to either C_{60} (1) or C_{70} (2), and examples of both aliphatic and aromatic substituents have been isolated. Mass spectrometry of these materials indicates that they are stable to different types of ionization. In addition, these new compounds have some unusual chemical properties which can be seen under laser desorption conditions.

Laser desorption mass spectrometry (LD-MS) is typically considered a soft ionization technique which provides molecular ions for unstable and thermally labile analytes. Recently, however, we have witnessed condensed phase reactions on the LD probe which are initiated by the rapid deposition of laser energy into the sample. Such reactions were observed upon LD-MS analysis of fullerene isoxazoline samples containing fullerene internal standards.

METHODS

Fast-atom-bombardment mass spectra were acquired with a Kratos Concept 1H double focusing mass spectrometer using a Saddlefield FAB gun. Laser desorption profiles were collected using a time-of-flight mass analyzer built at the University of Kentucky.

43rd ASMS Conference on Mass Spectrometry and Allied Topics

The third harmonic (355 nm) output of a Nd-YAG laser was used for desorption and ionization of the solid-phase samples.

RESULTS

Several of the isoxazolines studied were shown to undergo a fullerene-to-fullerene transfer of the entire derivative unit upon laser desorption of the isoxazoline with a fullerene internal standard. Subsequent fast-atom-bombardment (FAB) experiments, however, indicate that this reaction does not occur via a gas-phase recombination. Additional attempts at reproducing the reaction on the laboratory scale were unsuccessful. However by modifying the "trapping" material, it was possible to isolate nitrile oxide substituted materials not present in the original reaction mixture.

Thermogravimetric analysis (TGA) of several isoxazolines indicates that a mass loss occurs at 300-350°C which corresponds to the removal of the substituted nitrile oxide. This temperature may be similar to those temperatures which are present during the LD experiment (3). Additional heating to 900°C, in the TGA, causes loss of carbon from the fullerene cage.

Several authors have speculated that an "energy bottle neck" is responsible for the minimal fragmentation that is observed in laser desorption mass spectrometry. We believe that this bottle neck is useful in explaining the transfer of the in tact derivative moiety from one fullerene to another.

REFERENCES

1. Meier M. S.; Poplawska, M. *J. Org. Chem.*, **1993**, 58, 4524-4525

2. Meier, M. S.; Poplawska, M.; Compton, A. L.; Shaw, J. P.; Selegue, J. P.; Guarr, T. F. *J. Am. Chem. Soc.*, **1994**, 116, 7044-7048

3. Vertes, A.; Irinyi, G.; and Gijbels, R. *Anal. Chem.*, **1993**, 65, 2389-2393

Ion Mobilities from FT-ICR Mass Spectrometry

Ljiljana Paša-Tolić, Shenheng Guan,* and Alan G. Marshall*

Center for Interdisciplinary Magnetic Resonance, National High Magnetic Field Laboratory, Florida State University, 1800 E. Paul Dirac Dr., Tallahassee, FL 32310

* Department of Chemistry, Florida State University

In an experiment conceptually similar to condensed-phase gel electrophoresis, Bowers and coworkers have shown that ion size and shape may be inferred from ion mobility, based on the (constant) rate of forced drift of ions through a collision gas chamber.[1] By analogy to condensed-phase diffusion, similar ion mobility information is in principle available from FT-ICR measurements. For example, mass-spectral peak width for unapodized data acquired for several time-domain damping periods is simply the momentum transfer collision frequency. Specifically, if collisions are considered to produce a frictional damping force proportional to ion veleocity, then the detected time-domain ICR signal decreases exponentially with time, with a frictional damping time constant which is related to ion size and shape.

Here we report preliminary results obtained for ions generated by matrix-assisted laser desorption/ionization (MALDI), i.e., polyethyleneglycols and peptides, by two experimental methods. Immediately after generation, ions are cooled and axialized[2] by azimuthal quadrupolar irradiation in the presence of argon collision gas in the source compartment of a dual cubic trap. In the first experimental scheme, ^{12}C ions are isolated by stored-waveform (SWIFT) excitation and then transferred to the analyzer compartment where they are excited and detected at high pressure ($0.2 - 5 \times 10^{-6}$ Torr of Ar). Initial data show that reduced collisional frequency (ν_r), i.e., FT-ICR frequency-spectral peak width decreases with ion mass, $\nu_r \propto m^{-4/3}$, as expected from a hard-sphere model for ion/neutral collisions. However, inital experiments also show that the quantification of data in order to obtain ion size and shape from collisional cross-section, σ, is not easy, because spectral line widths are affected by a number of other factors, and signal-to-noise ratio is typically low in these experiments. Thus, we developed a second experimental scheme that allows ν_r determination without line width measurement (Fig. 1). After axialization, ions are excited to small ICR radius (~ 5 mm) and, after variable collisional relaxation period, t, (at $\sim 2 \times 10^{-7}$ Torr of Ar), transferred, excited and detected in the low-pressure ($\sim 2 \times 10^{-9}$ Torr) analyzer trap. Relative abundances of ions with (significantly) different m/z values are directly related to the contraction of the ICR radius during collisional relaxation prior to the ion transfer, and (relative) reduced collisional frequencies, i.e., the time-domain exponential damping constants, may be determined from a plot of relative ion abundances vs. relaxation period. The results from this experimental procedure agree with those obtained using the first method, i.e., a damping constant which increases with ion mass. Our preliminary results thus show that ion mobility data may be obtained by FT-ICR techniques. Work supported by NIH (GM-31683) and the National High Magnetic Field Laboratory at Florida State University.

1. G. van Helden, M.-T. Hsu, N. Gotts, and M. T. Bowers, *J. Phys. Chem.* **1993**, *97*, 8182-8192.
2. S. Guan, S. H. S. Kim, A. G. Marshall, M. C. Wahl, T. D. Wood, and X. Xiang, *Chem. Rev.* **1994**, *8*, 2161-2182.

43rd ASMS Conference on Mass Spectrometry and Allied Topics

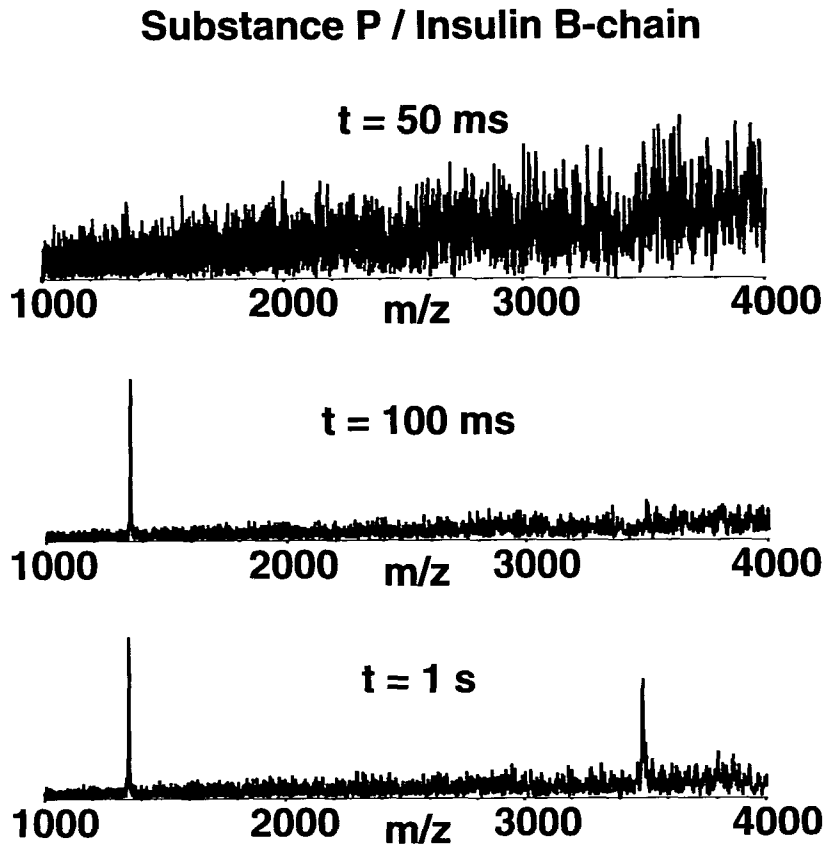

Figure 1. Magnitude mode MALDI FT-ICR mass spectra of a mixture of substance P and insulin B-chain. After axialization and isolation in the source trap, molecular ions are excited to small ICR radius (~ 5 mm) and, after 50 ms (top), 100 ms (middle), and 1 s (bottom) collisional relaxation periods at $\sim 2 \times 10^{-7}$ Torr, transferred, excited and detected in the low-pressure analyzer trap. Note that relaxation time increases as m/z increases!

Gas Phase Protonation of Aniline

* Michael J. Nold and Chrys Wesdemiotis
Department of Chemistry, The University of Akron, Akron, OH 44325-3601

Neutralization reionization (NR) mass spectrometry has been employed for the structural elucidation of protonated aniline in the gas phase. Via this method, the structure of an ion can be deduced by examination of the stability and reactivity of the corresponding neutral.

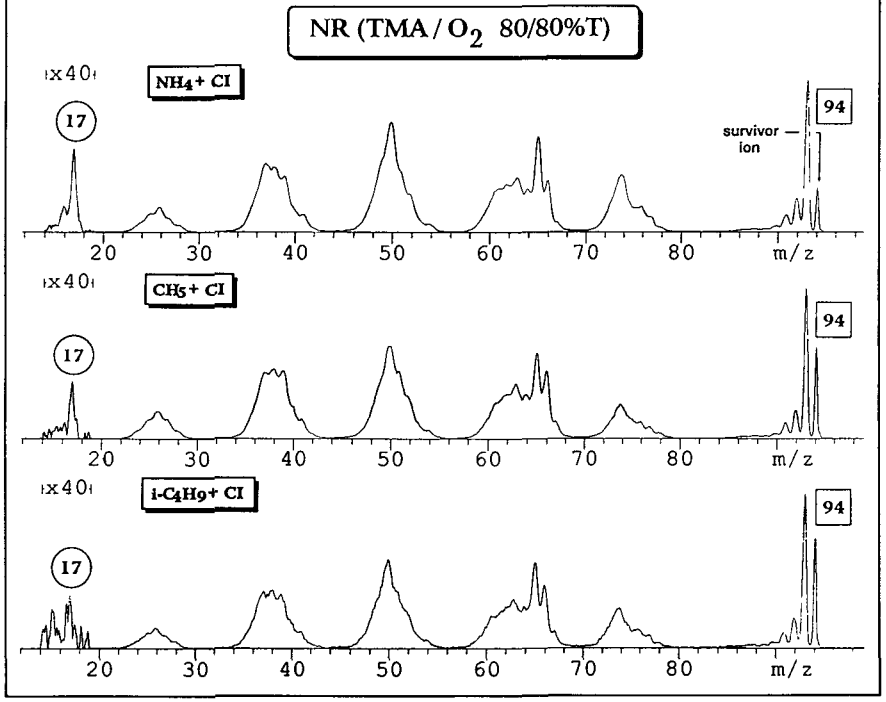

43rd ASMS Conference on Mass Spectrometry and Allied Topics

N-protonation and ring-protonation of aniline generate ions (m/z 94) that can interconvert before dissociation making it impossible to determine the actual protonation site. However, the stability of the corresponding neutrals is quite different.

Neutralization of N-protonated aniline produces a hypervalent nitrogen site which should dissociate immediately, either by loss of a hydrogen radical or by loss of ammonia to yield aniline or the phenyl radical respectively. The latter process is revealed by an m/z 17 peak in the NR spectrum which cannot arise from aniline. Neutralization of ring-protonated aniline, on the other hand, produces a stable, bound radical. Following reionization, an intact MH^+ ("survivor ion") should be observed only for the ring-protonated form. Thus, from the relative abundance of MH^+ in the NR spectra, the extent of ring-protonation can be determined.

Based on the [m/z 94] to [m/z 17] ratio in the respective NR spectra, N-protonation decreases as the protonating reagent is changed from NH_4^+ to CH_5^+ to $(CH_3)_3C^+$. This order suggests that both steric effects and the gas phase acidity of the protonating reagent influence the site of protonation. The increased yield of N-protonated isomer with the reagent of lowest acidity (i.e. NH_4^+) points out that this isomer (i.e. the anilinium ion) is the thermodynamically more stable. Nevertheless, with the reagents used, the less stable C-protonated species (an immonium cation) is always coproduced.

Synthesis and Characterization of 3,5-Dehydrophenyl Anion

Jun Hu and Robert R. Squires

Department of Chemistry, Purdue University, West Lafayette, IN47906

We have developed a general, regioselective method for producing biradical negative ions ("distonic" radical anions) in the gas phase, employing a flowing afterglow-triple quadrupole apparatus.[1] It involves reactions of trimethylsilyl substituted compounds with fluoride and molecular fluorine. During the reaction the trimethylsilyl groups are detached from the molecules and thus, radical anions are formed. Using this method we have synthesized the 3,5-dehydrophenyl anion as shown in Scheme 1.

Scheme 1

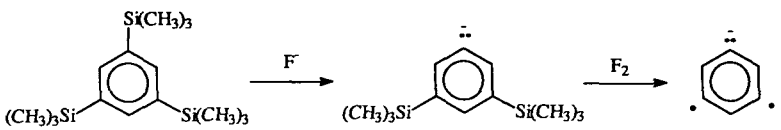

Simple molecular orbital theory predicts that this "triradical anion" will have an antiaromatic system for the three in-plane sigma orbitals, which are embedded in the 6π electron aromatic system of benzene. If the ion exists in a D_{3h} geometry, then it should be a ground-state triplet with a doubly degenerate HOMO(Scheme 2). While the synthesis of three-center 4π electron antiaromatic systems is a long-standing challenge in physical organic chemistry, there are no reports in the literature of previous attempts to synthesize sigma electron antiaromatic systems.

Scheme 2

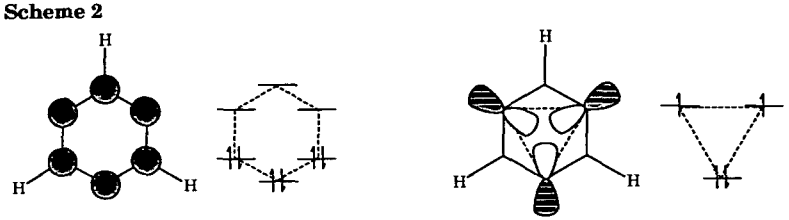

6 Huckel orbitals

3 Walsh orbitals

The reactivity of this ion has been probed with a variety of neutral reagents such as CO_2, CS_2, NO, NO_2, SO_2, O_2, *t*-butyl alcohol and cyclopentadiene. The observed behavior is compared to that of the 2,3-dehydrophenyl and 3,4-dehydrophenyl anions, which are synthesized in a similar manner from 3-trimethylsilyl- and 4-trimethylsilylphenyl anions, respectively.

The differing reactivity of the three ions is consistent with the assigned structures. Radical-type reactions of the $C_6H_3^-$ ions are not observed, suggesting singlet ground states. The electronic structures of these ions have also been investigated with *ab initio* molecular orbital theory.

References

1. Paul G. Wenthold, Jun Hu, and Robert R. Squires *J. Am. Chem. Soc.* **1994,** *116,* 6961.

Reactions of Radical Anions with Formally Distinct Radical and Anion Sites

Joseph J. Grabowski and Daniel Owusu
Department of Chemistry
University of Pittsburgh, Pittsburgh, PA 15260

Distonic radical cations are now well established; these are species in which the radical and charged sites are localized on distinct atoms, and which require structural reorganization to be isomerized to their conventional isomers. While radical anions are well known, radical anions with (at least) formal separation of charged and radical sites are relatively uncharacterized.

We have examined the thermally-equilibrated (298K) ion-molecule reactions of some distonic radical anions, {$(M\text{-}2H)^{\bullet -}$} with typical probe reagents in the gas phase using the flowing afterglow technique. The radical anions studied were generated from the reaction of their neutral precursors with the atomic oxygen radical anion which is available from the DET of nitrous oxide. The reactions of the radical anion were compared with that of the corresponding closed shell anion (M-H). The probe reagents used include carbon disulfide and ground state triplet molecular oxygen.

Carbanions react with CS_2 to give products of three pathways: a) addition, $(M\text{-}H+CS_2)^-$ b) sulfur transfer, $(M\text{-}H+S)^-$ and c) electron transfer to carbon disulfide, CS_2^-. Sufficiently exothermic addition reactions may lead to fragmentation giving $(M\text{-}H+CS_2\text{-}H_2S)^-$ and ions with fewer carbons than $(M\text{-}H)^-$. It is also known that the more basic an anion, the more it reacts by sulfur transfer. Results for the reaction of CS_2 with $(M\text{-}H)^-$ and with $(M\text{-}2H)^{\bullet -}$ are shown in Table 1.

Table of Nu^- + CS_2 Reaction Products

Nu-H	$PA(Nu)^-$	CS_2^-	NuS^-	$(Nu+CS_2\text{-}H_2S)^-$	$NuCS_2^-$
	400 7		Exclusive		
	390 8	Significant		Significant	Significant
	385 7	Trace			Major
	385		Trace	Trace	Major
	381 1				Exclusive
	378 0		Minor		Major
	354 1				Trace @ v long time

Qualitative Yield Descriptors: Major (>50%); Significant (20-50%); Minor (5-20%); Trace (<5%).

Table of $(M\text{-}2H)^{\bullet -}$ + CS_2 Reaction Products

Nu-H	$PA(Nu)^-$	CS_2^-	NuS^-	$(Nu+CS_2\text{-}H_2S)^-$	$NuCS_2^-$
	400 7	Exclusive			
	390 8	$(C_3H_4)^{\bullet -}$ only formed in 6% yield; has not been studied			
	385 7	Data not yet available			
	385	Major	Significant	Significant	
	381 1				Exclusive
	378 0	Major	Minor	Trace	
	353 9	Major	Significant	Trace	Trace

Qualitative Yield Descriptors: Major (>50%); Significant (20-50%); Minor (5-20%); Trace (<5%).

Table 1 . A Comparison of the reactions of $(M\text{-}H)^-$ and $(M\text{-}2H)^{\bullet -}$ with CS_2

We find that whereas electron transfer product is minor or absent in $(M\text{-}H)^-$ reactions, it tends to be the dominant one for the corresponding radical anion. The increased electron transfer to CS_2 shows that the radical anions have a lower electron binding energy than their anion counterparts. Also the sulfur transfer product can become more important in the radical anion than in the $(M\text{-}H)^-$ reaction. The observation in classical anions that the more basic the anion the more it abstracts sulfur is not always found between corresponding $(M\text{-}H)^-$ and $(M\text{-}2H)^{\bullet -}$. The $(M\text{-}2H)^{\bullet -}$ of 2,3-dimethyl-1,3-butadiene is less basic than the corresponding $(M\text{-}H)^-$ yet afforded more sulfur transfer.

It is known that carbanions react with ground-state molecular oxygen by electron transfer, hydride transfer or addition to oxygen . All the $(M\text{-}2H)^{\bullet -}$ examined lost signal intensity on reaction with triplet oxygen but none of the products corresponding to the above reactions were detected (Table 2). The signal loss may again reflec lower electron binding energy in the radical anion precursor compared to that of $(M\text{-}H)^-$.

Table of Nu^- + O_2 Reaction Products

Nu-H	$PA(Nu^-)$	Observations
	400.7	Slow reaction. Oxygen atom abstraction (m/z = 93).*
	390 8	90% O_2^-; 1% $C_2H_3O^-$, 8% HO^- k_{obs} = 2.8 x 10^{-10} cm^3 $molecule^{-1}$ s^{-1} [1]
	385.7	Fast reaction, major products $C_4H_5O^-$, $C_3H_3^-$
	385	Fast reaction, major product: $C_5H_7O^-$.
	381 1	99% HO^- (+ RCHO), Slow with $^3O_2$ [2]
	378 0	No reaction.
	354 1	No reaction observed to very long times.

* Another m/z = 108 is also observed.
1. Bohme *et al.*, *JACS*, 1976, *92*, 3301
2. Schmidt *et al.*, *JACS*, 1979, *101*, 6443

Table of $(M\text{-}2H)^{\bullet -}$ + O_2 Products

M	$PA(M\text{-}2H)^-$	Observations
	371	Signal loss (*o*-quinone?). k_{obs} = 2.78 x 10^{-10} cm^3 $molecule^{-1}$ s^{-1}
		$(C_3H_4)^{\bullet -}$ only formed in 6% yield, has not been studied.
		Signal loss.
	385	Signal loss; rapid reaction.
		Signal loss, k_{obs} = 1 05 x 10^{-10} cm^3 $molecule^{-1}$ s^{-1}
		Signal loss, slow, no O_2 detected
	353.9	Signal loss, rapid reaction

Table 2. A Comparison of the reaction of $(M\text{-}H)^-$ and $(M\text{-}2H)^{\bullet -}$ with ground state triplet oxygen

The formation of adduct with nitric oxide may reveal the radical character of the radical anions. Such adducts were observed for some (e.g m-xylene radical anion) but not for others (e.g isoprene or benzene radical anion)

It is apparent from the above that the distonic radical anions are unique and their reactivity cannot be predicted simply by analogy to conventional anions. Experiments are under way to better characterize their radical behavior.

Photodetachment of Solvated Ions

*Y.J. Yang[1], D.M. Peiris[1], J. M. Riveros[2] and J.R. Eyler[1]
[1]Department of Chemistry, University of Florida, Gainesville, FL 32611
[2]Instituto de Quimica, University of São Paulo, São Paulo, Brasil.

Several methods have been used to measure the binding energies of solvated ions, including equilibrium measurements in both high pressure[1,2] and ICR[3] mass spectrometers and photodissociation measurements in a TOF mass spectrometer[4]. An alternate way to study ion/neutral binding energies (BE's) is photodetachment measurement with ICR mass spectrometry. By measuring the depletion of the parent ion as a function of photon energy, the threshold of photodetachment, related directly to the binding strength of solvated ions, can be determined. We have studied UV-visible photodetachment of alcohol solvated halides using the output of a doubled dye laser pumped by a Nd:YAG laser. The photodetachment thresholds of methanol solvates were determined and the BE's measured using photodetachment and thermal-equilibrium methods were compared.

The experiment was performed in a FT-ICR mass spectrometer equipped with a 3T superconducting magnet, vacuum system and an Ionspec data system. Laser power output was *ca.* 8-15 mJ/pulse and was kept constant for each spectrum. The solvated halides were formed by the ion-molecule reactions[5]:

$NF_3 + e^- \rightarrow F^- + NF_2$ or $CF_4 + e^- \rightarrow F^- + CF_3$
$F^- + HCOOCH_3 \rightarrow \mathbf{CH_3OHF^-} + CO$

$COCl_2 + e^- \rightarrow COCl^- + Cl$ or $ClCOOC_2H_5 + e^- \rightarrow COCl^- + C_2H_5O$
$COCl^- + CH_3OH \rightarrow \mathbf{CH_3OHCl^-} + CO$

$CH_3ONO + e^- \rightarrow CH_3O^- + NO$
$CH_3O^- + C_6H_5X/CH_3OH \rightarrow \mathbf{CH_3OHX^-} + C_6H_4$ where **X = Br, I**

where the pressure of NF_3, CO_2Cl_2, and CH_3ONO, were about 4.0-5.0x10^{-7} torr and the total pressure was maintained at 0.8-1.0x10^{-6} torr. Ions were formed using an electron beam pulse, followed by a period for ion-molecule reaction to form solvated ions as well as relaxation of internal energy before firing of the laser. The intensity of ions was measured before and after laser firing.

Figure 1 shows photodetachment spectra of CH_3OHF^-, CH_3OHCl^-, CH_3OBr^- and CH_3OHI^-. Four photodetachment thresholds, which were determined using linear extrapolation, for CH_3OHF^-, CH_3OHCl^-, CH_3OHBr^- and CH_3OHI^- were 279.5, 280.6, 309.2 and 337.0 nm respectively. So the differences between thresholds and EA's were 1.04, 0.81, 0.65 and 0.62 eV respectively (Table 1).

No increase in the intensity of halide ions was seen upon laser irradiation for solvates, which means either only the photodetachment channel occurred or photodetachment involved with photodissociation channel occurred. Correct interpretation of the data depends on whether vertical photodetachment occurs to a bound or repulsive state (Fig. 2). Based on work of D. Neumark[6] and J. Brauman[7] et. al., the structures which correlate with the known relative acidities of alcohols and HF are alcohol-solvated halides (ROH...F^-) since the proton affinity of CH_3O^- is 381.2 kcal/mol higher than that of F^- (371.4 kcal/mol). Therefore $ROHX^-$ underwent an adiabatic transition to a near transition state of the neutral complex with a small barrier. An upper limit of 0.05-0.1 eV can be placed on the differences between thresholds and EA's (Table 1).

Table 1 Data Results

	F⁻	Cl	Br	I
EA (eV)	3 399	3 615	3 364	3 061
Exp. threshold[a] (nm)	279 5	280 6	309 2	337 0
(eV)	4.44	4 42	4 01	3 68
Thres.-EA (eV)	1 04	0.81	0 65	0 62
(Kcal/mol)	24 0	18 7	15.0	14 4
BE[b] (eV)	1 01	0 75	0 60	0 49
(Kcal/mol)	23 3	17.4	13.9	11 2
Estimated barrier (eV)	0 03	0.06	0 05	0 13
(Kcal/mol)	0 7	1.3	1 1	3.2

[a] the uncertainty for wavelength calibration is about ±0 5 nm (±0 005 eV) which is within the barrier

[b] experimental values of Hiraoka and Yamabe, using a thermal equilibrium method in HPMS (High pressure mass spectrometer)

Fig 1 Photodetachment of MeOHX⁻

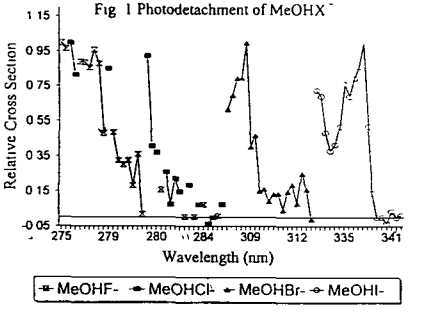

Fig. 2 Potential Curve of Photodetachment

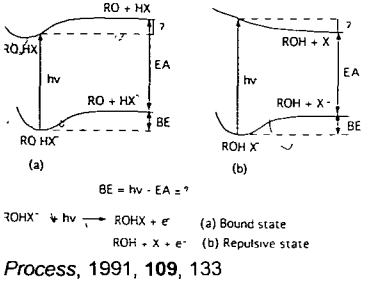

[1]K. Hiraoka and S Yamabe, *Int. J Mass Spec.; Ion Process*, 1991, **109**, 133
[2]R. Yamdagni, J D Payzant and P Kebarle, *Can. J. Chem*, 1973, **51**, 2507
[3]J.W. Larson and T B McMahon, *JACS*, 1988, **110**, 1087
[4]F. Misaizu, M.Sanekata, K Tsukamoto, K Fuke and S Iwata, *J.P.C*, 1992, **96**, 8259
[5]J M Riveros, *JACS*, 1973, **95**, 1057, *JACS*, 1991, **113**, 1053.
[6]S E Bradforth, D W. Arnold, R B Metz, A. Weaver and D.M. Neumark, *J P C*, 1991, **95**, 8066
[7]B.D Wladkowski, A.L East, J.E Mihalick, W.D. Allen and J. Brauman, *J.C P*, 1994, **100**, 2058

Advances in Applications of the Kinetic Method, G. Chen, C.D. Cleven, L. Horn, S. Ma, J.S. Patrick, S.S. Yang and R.G. Cooks, Department of Chemistry, Purude University, West Lafayette, IN USA 47907-1393

Since it's inception[1] the kinetic method has been used to obtain relative cation affinities for numerous compounds not easily studied by traditional methods.[2] These estimations are made based upon the relative extents of dissociation of an ion-bound dimer, such as a proton-bound dimer, of two compounds as is shown below.

$$B_1 + B_2H^+ \leftarrow [B_1\text{-}H^+\text{-}B_2] \rightarrow B_2 + B_1H^+$$

In the present work new applications and extensions of the kinetic method to unique classes of compounds are discussed. Studies using well-characterized dimer species such as the proton-bound dimer of n-propylamine and t-butylamine have provided insights into the mechanism of internal energy deposition during collision-induced dissociation (CID). Specifically, CID of this and other proton-bound dimer species with a variety of target gases has demonstrated a strong correlation between internal energy, measured as the effective temperature, and the center-of-mass collision energy. When the effective temperature is converted to a Boltzman energy, internal energy deposition is approximately 100% of center-of-mass, suggesting a collision complex or local collision effects in the CID mechanism.

Electron-bound dimer ions of polyaromatic hydrocarbons (PAHs) were formed under electron capture conditions using desorption chemical ioinization. The low energy collision-induced dissociation of these electron-bound dimer ions provides orderings and estimates of electron affinities for several PAHs ,including perylene (0.35 ± 0.1 eV), 1,2-benzanthracene (0.39 ± 0.1 eV), 1-methylanthracene (0.55 ± 0.1 eV), biphenylene (0.89 ± 0.1 eV) and benzo(ghi)perylene (0.42 ± 0.1 eV), whose values were previously unknown.[3] In addition, dissociations of electron bound dimer ions have been used to distinguish isomeric PAHs. For example, the isomeric PAHs 1,2-benzanthracene and triphenylene can be distinguished from the relative extents of dissociation of their respective electron-bound dimers with perylene.

The effects of steric hindrance have been investigated using the polyatomic $OCNCO^+$ cation as the binding ion in dimers of substituted and unsubstituted pyridines.[4] The relative extents of dissociation of proton- and $OCNCO^+$-bound dimer ions of substituted pyridines correlate well for meta- and para-substituted compounds. However, the relative dissociation of dimers containing ortho-substituted pyridines show substantial deviations from the behavior of the other pyridines. The plot of natural logarithm of the relative abundances from dissociation of $OCNCO^+$-bound dimer ions versus proton affinity shows this deviation.

43rd ASMS Conference on Mass Spectrometry and Allied Topics

The degree of deviation from the straight line is related to the steric hindrance displayed by the ortho-substituted pyridines.[4]

Dissociation of proton-bound heterodimers of amino acids showed small differences in the relative product ion abundance when stereoisomers of isoleucine (Ile) were paired with those of alanine (Ala). The natural logarithm of the ratio of $AlaH^+$ to $IleH^+$ observed was 5.185 and 5.345 for the l-/l- and d-/l- isomer pairs, respectively. The observed differences are attributed to entropic factors related to the chirality of the amino acid monomers.

The gas-phase basicity (GB) of the zwitterion betaine has been estimated as 232.9 ± 0.8 kcal/mol using the kinetic method. By comparison the gas-phase acidity of N,N-dimethylglycine was estimated as 337.1 kcal/mol. The difference of 104-116 kcal/mol between the values for betaine and those of acetic acid and the N,N-dimethylglycine anion is attributed to coulombic effects and represents the largest substituent effect yet observed for proton affinities. The plot of natural logarithm of the relative product ion abundances versus GB indicates two lines having similar slopes. The GB value for betaine is consistent with the proton affinity value recently obtained.[5] This result suggests that two species are present during ionization. Estimation of the lower GB provides a value of 220.4 ± 0.5 kcal/mol, which is indistingishable from the value of 219.8 kcal/mol obtained by the kinetic method for authentic N,N-dimethylglycine methyl ester, a known rearrangement product of betaine.[6]

In experiments performed using membrane introduction and a benchtop ion trap mass spectrometer the proton affinity of bicyclo-[3.3.0] oct-1(5)-ene was estimated as 200 ± 2 kcal/mol.

The studies discussed above further demonstrate the capabilities of the kinetic method in making thermochemical estimates of unusual species or species in reaction mixtures.

Acknowledgements NSF #CHE-92-23791, Purdue Univeristy/NIH Cancer Training Grant, Dr. W. Borden, Dr. S.H. Hoke II and Dr. M.N. Eberlin

1. Cooks, R.G. and Kruger, T.L., *J. Am. Chem. Soc.* **1977**, *99*, 1279.
2. Cooks, R.G.; Patrick, J.S.; McLuckey, S.A.; Kotiaho, T., *Mass Spectrom. Reviews* **1995**, in press.
3. Chen, G.; Cooks, R.G., *J. Mass Spectrom.*, submitted.
4. Yang, S.S.; Chen, G.; Ma, S.; Cooks, R.G.; Gozzo, F.C.; Eberlin, M.N., *J. Mass Spectrom.* **1995**, in press.
5. Beauchamp, J.L., presented at the 209th National Meeting of the American Chemical Society, Anaheim, CA, April 2-7, 1995.
6. Larsen, C.; Anthoni, U.; Nielsen, P.H.; Christophersen, C. *Org. Mass Spectrom.* **1987**, *22*, 117.

Gas Phase Ion Chemistry of Sulfonate Anions.

Jacob D. Smith* (a), Richard A. J. O'Hair (a), Joseph A. R. Schmidt (a), Todd D. Williams (b)

(a) Department of Chemistry, Kansas State University, Manhattan, Kansas 66506-3701.
(b) Mass Spectrometry Laboratory, University of Kansas, Lawrence, Kansas 66405.

Historically, a super acid has been defined as any acid which is stronger than sulfuric acid. The question: "what is the strongest neutral Bronsted super acid?" is difficult to answer in the condensed phase where solvation effects greatly affect the measured pK_as. This question can be answered by looking at intrinsic acidities in the gas phase.(1,2) We have used Cooks' kinetic method to study the relative acidities of sulfonic acids.(3) Dimer clusters with the general formula of $[RSO_3^- \cdots H^+ \cdots {}^-O_3SR']^-$ were formed via FAB (cesium ion gun operating at 25 kV, glycerol matrix) and then analyzed using unimolecular MIKES on a Fisons/VG (Manchester, UK) Autospec-Q instrument. The relative abundance of each sulfonate anion (RSO_3^- and $R'SO_3^-$) observed in the MIKE spectrum correlates with the relative acidities of RSO_3H and $R'SO_3H$.(3)

Based upon the experimental results, the following acidity scale is proposed (starting with the weakest acid): methane sulfonic acid, ethane sulfonic acid, methoxy sulfonic acid, sulfuric acid, m- and p-aminobenzene sulfonic acids, p-toluene sulfonic acid, benzene sulfonic acid, o-aminobenzene sulfonic acid, o-nitrobenzene sulfonic acid, cysteic acid, m- and p-nitrobenzene sulfonic acids, and triflic acid. This acidity ranking is similar to those of the analogous carboxylic acids except for the p-toluene and benzene sulfonic acids which show a reverse order.

In addition, *ab initio* studies on the acidities of the sulfonic acids RSO_3H (R = HO, CH_3, CF_3, F) have been performed up to the MP2(FC)/6-31+G*//HF/3-21+G* level of theory. The best correlation with the experimental literature values results from the HF6-31+G*//HF/3-21+G* level of theory, although the absolute ΔH°_{acid} *ab initio* values are poor. (1,2)

Using the same range of sulfonic acids, the fragmentation patterns of the monomer sulfonate anions (RSO_3^-) have been investigated via FAB/MS/MS techniques. CA/MIKES was performed using CAD (Ar gas) with attenuation of the parent ion beam by 70%. A general loss of R, resulting in the formation of radical anion of $SO_3^{\cdot -}$ is seen in all cases.(4) In agreement with Binkley et al, the loss of SO_2 is observed for those aromatic sulfonic acids bearing a H atom adjacent to the SO_3 group.(5) In those substituted aromatic sulfonate anions (when the substituent is either NH_2, CH_3, or NO_2) a general loss of the substituent at (NH_2, CH_3, or NO_2) to form the radical anion $C_6H_4SO_3^{\cdot -}$ was

observed. The ions $CH_3XSO_3^-$ (X = O and CH_2) also undergo loss of a $CH_3^\cdot$ radical. The fragmentation reactions of deprotonated cysteic acid and triflic acid are shown in equations 1 and 2.

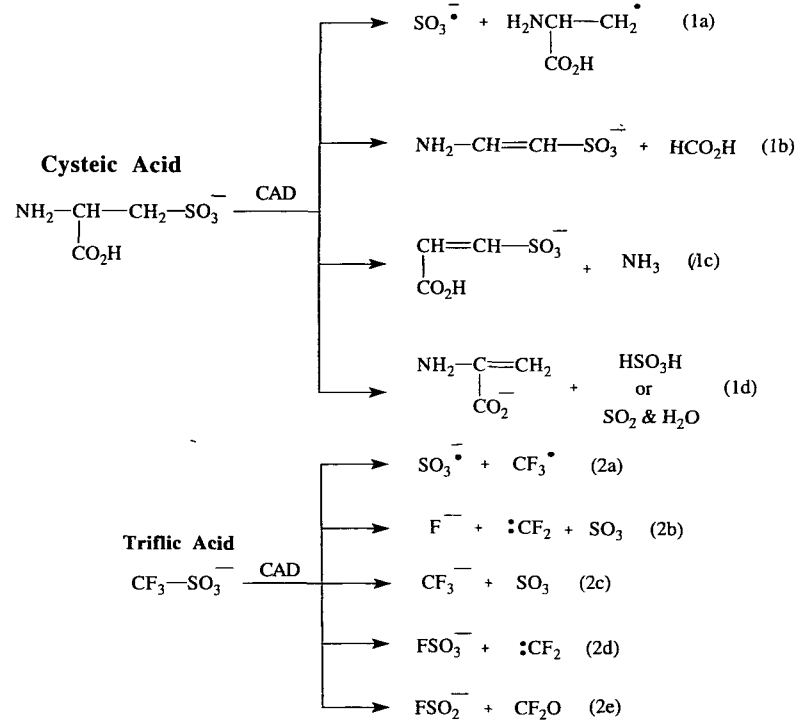

(1) A. A. Viggiano et. al., J. Am. Chem. Soc., **114**, 4299, (1992)
(2) I. A. Koppel et. al., J. Am. Chem. Soc., **116**, 3047, (1994)
(3) R. G. Cooks et. al., Mass Spectrom. Rev., in press.
(4) P. A. Lyon et. al., Anal. Chem., **57**, 2984 (1985)
(5) R. W. Binkley et. al., Org. Mass Spectrom., **28**, 769, (1993)

BOND-SELECTIVE PHOTODISSOCIATION: MECHANISMS AND APPLICATIONS

Craig W. Bookwalter, David L. Zoller, Philip L. Ross, Murray V. Johnston
Department of Chemistry and Biochemistry, University of Delaware, Newark, DE 19716

Many small molecules are known to photodissociate directly from an excited electronic state Depending upon the nature of the excited state, preferential cleavage at the chromophore may be observed. If similar processes occur in large molecules, then site-selective bond cleavage may be achieved. Nonselective dissociation may not be practical for the structural analysis of large (> 10 kDa) precursor ions. If the product ion current is spread over many m/z peaks, then the signal-to-noise ratio will be low and the mass resolution may not be sufficient to separate adjacent peaks. In contrast, bond selective photodissociation limits the precursor ion to a few, specific dissociation channels.

In our laboratory, photodissociation-photoionization mass spectrometry is used to study such process. Neutral molecules are photodissociated with an excimer laser and the products are softly photoionized with coherent vacuum ultraviolet radiation. Recently, we have performed a systematic study of the photochemistry of simple aliphatic disulfides to gain insight on the structural information that may be obtained by photodissociation of larger analogs such as peptides containing disulfide linkages

The primary photodissociation reactions are shown below.

		ΔH (rxn)	
RSSR $\xrightarrow{h\nu}$	2 RS·	280 kJ/mole	(1)
RSSR $\xrightarrow{h\nu}$	R· + RSS·	235 kJ/mole	(2)

(R = CH_3, C_2H_5, C_3H_7, C_4H_9)

Figure 1 shows the 9 68 eV photoionization mass spectra of di-n-dipropyl disulfide photodissociated with 248 nm and 193 nm radiation. At 248 nm, the spectra are dominated by photoionized RS• radicals that are produced by S-S bond cleavage (reaction 1). At 193 nm, the spectra are much more complex and show products of several processes Photoionized RS• radicals indicate cleavage of the S-S bond (reaction 1). Photoionized RS_2• and R• radicals indicate cleavage of the C-S bond (reaction 2). Photoionized S_2 (m/z 64) is a secondary decomposition product of the RS_2• radical. Molecular rearrangements are also observed.

Table 1 shows the change in relative yield of S-S versus C-S bond cleavage when going from 193 nm to 248 nm. For any given compound, the yield is directly calculated from the peak areas of the respective ions in the photoionization mass spectrum. The values show that the branching ratio for S-S bond cleavage relative to C-S bond cleavage is typically one to two orders of magnitude higher at 248 nm than 193 nm.

The observed wavelength dependence cannot be readily explained by photodissociation from the ground state. The ground state S-S bond energy (280 kJ/mole) is much larger than the C-S bond energy (235 kJ/mole). If dissociation occurred from the ground state, decreasing the photon energy (i.e. going from 193 nm to 248 nm) would be expected to favor the lower energy process. The opposite effect is observed. Also, dissociation from the ground state would mimic thermal decomposition

pathways. However, for disulfides, these thermal pathways are nonselective, showing both C-S and S-S bond cleavage Therefore, the selective cleavage of the S-S bond with 248 nm radiation is consistent with excited state photochemistry.

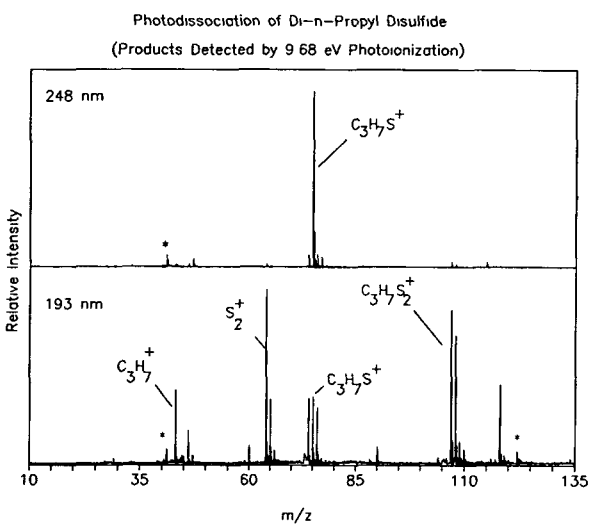

Figure 1

Compound	R_{248}/R_{193}
Dimethyl Disulfide	13
Diethyl Disulfide	240
Di-n-Propyl Disulfide	96
Di-n-Butyl Disulfide	13
Di-s-Butyl Disulfide	34
Di-t-Butyl Disulide	6

Table 1

COLLISION SPECTROSCOPY INVOLVING CHARGE PERMUTATION

Chrys Wesdemiotis, Sarka Beranova, Michael J. Polce, Yoojung Kim and Jody M. Talley

Chemistry Department, The University of Akron, Akron, OH 44325

A novel experimental approach for the study of gaseous ions and their decomposition mechanisms involves the use of neutralization-reionization mass spectrometry (NRMS).[1] With this method, which employs collisional charge permutation, it is possible to (i) identify the neutral fragments arising upon CAD of a mass-selected ion, (ii) determine ion structures and (iii) synthesize and characterize an ion's neutralized form, which can be an elusive neutral intermediate that is inaccessible by other means.

(i) Neutral losses are made detectable by collision-induced dissociative ionization (CIDI).[2] Their identification provides key insight on the dissociation mechanism of the precursor ion studied. This is demonstrated for $(CsI)_xCs^+$ and $(NaI)_xNa^+$ clusters (x = 2-4), whose CAD predominantly yields smaller cluster ions via evaporation of Cs_nI_n and Na_nI_n units ($n \leq x$), respectively, viz. eq 1 (illustrated with cesium). The identity of the evaporated neutrals has remained unknown.

$$(CsI)_xCs^+ \rightarrow (CsI)_{x-n}Cs^+ + Cs_nI_n \text{ [n times CsI, or } (CsI)_n \text{ multimer]} \quad (1)$$

Post-ionization of the neutral fragments from $(CsI)_3Cs^+$ to cations or anions gives rise to the neutral fragment-reionization ($^+N_fR^{+\cdot}$, $^-$) spectra of Figure 1. If the Cs_nI_n losses from this precursor ion (n = 1-3) exclusively consisted of CsI monomers, then the $^+N_fR^{+\cdot}$, $^-$ spectra should show no ions heavier than $CsI^{+\cdot}$ or $CsI^{-\cdot}$ (*m/z* 260). However, ions larger than $CsI^+/CsI^{-\cdot}$ do appear in both spectra. The product ions present in Figure 1 provide strong evidence that multimer moieties (i.e. smaller whole neutral clusters $(CsI)_n$) are evaporated in one step.[3] Note that, with the exception of $CsI^{+\cdot}/CsI^{-\cdot}$, radical ions are not observed in the $^+N_fR^{+\cdot}$, $^-$ spectra. Evidently, collisional ionization of $(CsI)_n$ preferentially yields closed-shell fragments $(CsI)_{n-y}Cs^+$ or $(CsI)_{n-y}I^-$ ($1 \leq y \leq n$). Analogous results are obtained for all other cesium and sodium iodide cluster ions investigated.

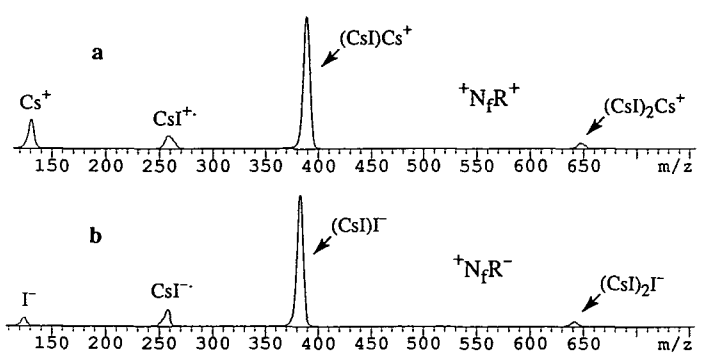

Figure 1. Neutral fragment-reionization ($^+N_fR^{+\cdot}$, $^-$) mass spectra of $(CsI)_3Cs^+$ precursor ions, acquired by subjecting $(CsI)_3Cs^+$ to CAD (with He) and later post-ionizing the so liberated neutral losses. (a) Post-ionization with O_2 to cations; (b) post-ionization with Xe to anions. The superscripts besides N and R denote the charges of precursor ion and ultimate product ions, respectively.

(ii) Neutralization-reionization (NR), a process entailing two successive charge changing collisions, offers an alternative means to study ion structures. This method is particularly useful whenever CAD induces rearrangement fragmentations, which may complicate structural assignments. For example, the CAD spectrum of $M^{+\cdot}$ from $CH_3OCH_2CH_2OH$ (2-methoxyethanol, ME) contains sizable fragments at *m/z* 47, $(CH_3)_2OH^+$,[4a] and 58, mainly $[CH_2OCH_2CH_2]^{+\cdot}$ [4b] (Figure 2a); such ions, which are also formed from metastable $ME^{+\cdot}$,[4] could imply that ionized 2-methoxyethanol has isomerized (at least partly) to the distonic isomers $CH_3(OH^+)CH_2CH_2O\cdot$ and $\cdot CH_2OCH_2CH_2OH_2^+$. The *m/z* 47 and 58 products are, however, suppressed in the corresponding $^+NR^+$ spectrum (Figure 2b). The dominant primary fragments in the latter are $CH_3OCH_2^+$ (*m/z* 45) and $^+CH_2OH$ (*m/z* 31), i.e. ions arising from structurally more diagnostic direct cleavages. The $^+NR^+$ spectrum of Figure 2b is consistent with retention of the original $ME^{+\cdot}$ structure and excludes any appreciable isomerization of (stable) $ME^{+\cdot}$ to distonic isomers.

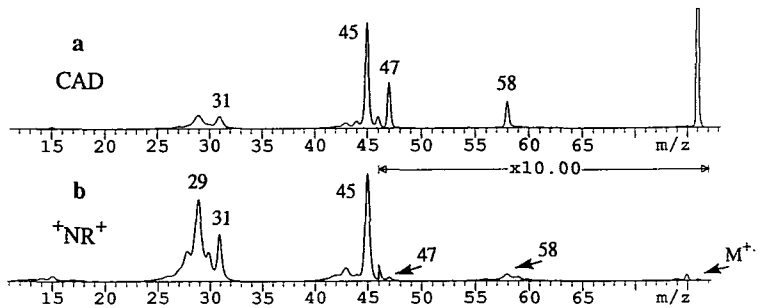

Figure 2. (a) CAD and (b) neutralization-reionization ($^+NR^+$) mass spectra of 2-methoxyethanol ion. Xe was used for neutralization and O_2 for CAD and reionization.

Rearrangements, which usually require lower critical energies than direct cleavages, are discriminated against upon neutralization-reionization because NR deposits higher average internal energies than CAD.[5] A large part of this energy originates in the reionization step, which involves collision-induced dissociative ionization (CIDI). This is shown to be true by comparison of the CAD and CIDI spectra of triethyl phosphate (TEP). The latter is measured by post-ionizing the TEP molecules eliminated from the proton-bound dimer TEP-H^+-TEP. The CIDI spectrum shows more direct fragmentations and more abundant lower mass fragments, pointing out that the nascent $\{TEP^+\}^*$ ions emerging from CIDI have gained higher average internal energies than the $\{TEP^{+\cdot}\}^*$ ions emerging from CAD.

(iii) The neutralization step also offers the potential to generate and study reactive neutral species from the corresponding cations or anions. Here, the carbene ion $HC-NH_2^{+\cdot}$ is used to prepare the elusive aminocarbene, $HC-NH_2$, a potential interstellar species. The $^+NR^+$ spectrum of $HC-NH_2^+$ includes an abundant molecular cation, indicating that the intermediate neutral, i.e. $HC-NH_2$, is stable towards dissociation. Moreover, the $^+NR^+$ spectrum is substantially different from that of the isomeric $H_2C{=}NH^+$ cation, indicating that the exothermic 1,2-H migration $HC-NH_2 \rightarrow H_2C{=}NH$ must surmount an appreciable barrier. Thus, aminocarbene must reside in an energy well and represents a bound molecule.

1. (a) C. Wesdemiotis and F. W. McLafferty, Chem. Rev. 87 (1987) 485. (b) J. L. Holmes, Mass Spectrom. Rev. 8 (1989) 513.
2. P. C. Burgers, J. L. Holmes, A. A. Mommers and J. K. Terlouw, Chem. Phys. Lett. 102 (1983) 1.
3. M. A. El-Sayed, J. Phys. Chem. 95 (1993) 1594.
4. (a) J. R. Cao, M. George, J. L. Holmes, M. Sirois, J. K. Terlouw and P. C. Burgers, J. Am. Chem. Soc. 114 (1992) 2017. (b) M. J. Polce and C. Wesdemiotis, J. Am. Soc. Mass Spectrom., submitted.
5. S. Beranova and C. Wesdemiotis, J. Am. Soc. Mass Spectrom. 5 (1994) 1093.

Collisionally Induced Emission Spectroscopy

Fred Wiedmann and Chrys Wesdemiotis
Department of Chemistry, University of Akron, Akron, OH 44325-3601

Collisionally Induced Emission (CIE) Spectra of small ions were first reported by Holmes et al. (J. L. Holmes, P. M. Mayer, and A. A. Mommers, JACS, 113, 9405 (1991)). Their results for $C_2H_4O^{+\cdot}$ and $C_2H_5^+$ isomers suggested that this method could become a viable alternative for structural analysis. Here we are continuing these studies.

The experiments are conducted with a VG Autospec EBE tandem mass spectrometer containing two collision cells between MS-1 (E1B) and MS-2 (E2). The tops of the cells and the cover of the instrument are equipped with quartz windows, permitting the detection of light emitted inside the cells. The light is measured by a photomultiplier tube that has been mounted onto the cover window. Cutoff filters can be placed between the PMT and the window to give a histogram. Early experiments used seven cutoff filters producing eight regions, while later experiments used ten cutoff filters producing eleven regions. The histograms have been corrected for the dark count, the ion abundance, and the filter transmittance, but not for the PMT response.

With this setup we have shown that the emission comes mainly from the projectile ion, its corresponding neutral, and any fragments. By looking at the emission spectra of a number of small ions, such as Cs^+, O_2^+, W^+, and Na^+, and comparing them to the published spectra of the ions and their neutralized forms, we know that the amount of emission from a projectile ion and its corresponding neutral change from one system to the next. For example, most of the emission from Na^+ appears in the region from 575-625 nm. This is the region that contains the Na lines at 589 and 590 nm, thus we see mainly emission from the sodium neutral. In contrast tungsten gives a dominant signal in the region from 200-300 nm. This corresponds well with the emission expected from W^+. The emission from Cs^+ also corresponds mostly to its ion, while the emission of O_2^+ is evenly distributed between the ion and its corresponding neutral.

As expected, the total emission is proportional to the total ion abundance. This is best seen with samples that decay relatively quickly. For example, the ion signal of $AlaH^+$(produced by FAB) decays over a period of about 20 minutes. The total emission spectrum is linearly related to the chromatogram. This relationship has been verified with several other ions.

While most of the emission comes from the projectile, both the choice of the target and its pressure effect the histogram. As expected, we have found that the total emission increases as the target pressure increases. The pressure of the target gas also has an effect on the relative intensity of the emission. For example, for Cs^+ projectiles and O_2 targets, the emission at 200 - 300 nm is very sensitive to pressure changes. This could be due to the fact that the O_2 target emits strongly in this region. Another explanation is that the more collisions the cesium ion has, the greater the probability that it is promoted to a highly excited state from which a higher energy UV photon is emitted upon the return to the ground state. Also, while different targets give the same peaks, each target gives a different relative intensity in a given band. These differences could be due to the emission of the target and/or the degree of projectile

excitation achievable with each target.

The total emission of several homologous ion series were measured under constant pressure. The results are summarized in the table below. The total ion counts have been normalized by the ion's abundance and are shown relative to the counts of the smallest ion in the homologous series. It was found that the total emission increases as the mass of projectile ion increases.

Ion	m/z	Total CIE	Ion	m/z	Total CIE
Na^+	23	1.0	Cs^+	133	1.0
Na_2I^+	173	1.2	Cs_2I^+	393	1.2
$Na_3I_2^+$	323	2.0	$Cs_3I_2^+$	653	2.7
$Na_4I_3^+$	473	2.9	$Cs_4I_3^+$	913	5.6
$Na_5I_4^+$	623	6.6			

Ion	m/z	Total CIE	Ion	m/z	Total CIE
$CuCl_2^-$	133	1.0	[Ala]H+	90	1.0
$Cu_2Cl_3^-$	231	0.9	$[Ala]_3H+$	232	4.3
$Cu_3Cl_4^-$	329	2.1	$[Ala]_5H^+$	374	8.7

A number of experiments have been run to determine the effect of different functional groups on the emission spectra. Below is a table listing the data for some of the molecules that were run. The total emission for each compound has been normalized to 100. At this time no definitive trends have been found. Several ions primarly (>65%) emit in the UV region, while others show significant near IR bands. There is very little or no emission found in the regions from 400-450 nm and from 575-625 nm.

Ion	200-400 nm	400-625 nm	625-900 nm
Acetone	73	19	8
Benzene	68	21	11
Toluene	78	15	8
Ethyl Benzene	26	28	46
Formic Acid	30	27	44
Acetic Acid	30	22	49
Benzaldehyde	39	25	36
Acetophenone	26	25	48
Aniline	30	31	39
Diethyl Ether	82	14	4
Ethanol	21	23	56

MATRIX ISOLATION OF MASS-SELECTED IONS FOR ANALYSIS BY FTIR SPECTROSCOPY

John Allison, Thomas M. Halasinski, Jerry T. Godbout and George E. Leroi
Department of Chemistry, Michigan State University, East Lansing, MI 48824

Using matrix isolation techniques, scientists have been able to generate trapped ionic species for spectroscopic analysis, usually by photoionizing molecules in the matrix. We have demonstrated that mass-selected cations can be directly deposited into growing inert gas matrices at low temperatures.[1] For some ions, several hours of ion deposition results in a total number of ions sufficient for detection using FTIR spectroscopy, allowing for structures of ions of interest in mass spectrometry to be determined. While the ability to use conventional structural tools for the analysis of ions generated in a mass spectrometer is exciting, the experiment clearly should not work. If cations alone are trapped in an inert gas matrix, within milliseconds the matrix should achieve a potential that will prohibit additional ion accumulation. Some mechanism must exist to maintain electrical neutrality. We will address this topic here. For example, when CF_3Cl is ionized be electron impact in the ion source of a quadrupole mass spectrometer, the vibrational spectrum of CF_3^+ can be obtained after several hours of accumulation of this ion. Small amounts of neutral CF_3Cl are also present in the matrix. If a mechanism exists for the generation of counterions in the matrix, then one may expect them to be Cl^-, which would be the probable product of electron attachment to CF_3Cl. However, atomic anions have no vibrational spectrum. When the cation-containing matrix is vaporized, cationic *and* anionic species are expelled into the gas phase and can be detected. How are the anionic components of the matrix formed?

We report here the first direct observations of counterions in matrices formed during the codeposition of mass-selected cations and neon. We have discovered that the addition of carbon dioxide to the neon matrix gas during deposition of a mass-selected ion beam results in two unique advantages. The first advantage is that it enhances positive ion accumulation - detectable signals can be achieved in noticeably shorter times. The second advantage is that detectable quantities of CO_2^- are observed. Figure 1 shows the spectrum obtained when CF_3^+ is mass-selected and deposited, using a matrix gas with a molar Ne:CO_2 ratio of 2300:1. Absorbances due to both CF_3^+ and CO_2^- are observed and their intensities correlate.

The spectroscopic detection of a counterion provides a means for investigating mechanisms of counterion generation. While we cannot yet eliminate or substantiate all possible mechanisms, we present here evidence towards a "surface bombardment" mechanism. In this mechanism, the collision of incoming ions with metallic surfaces surrounding the CsI sample window region appear to generate electrons and negative ions which are subsequently attracted to the matrix. When an isolated metallic grid is placed on the CsI matrix window and a +80 V potential is applied during ion deposition, an absorption due to CO_2^+ is observed. Figure 2 illustrates this result from an ion deposition involving

$C_7H_7^+$. We attribute the appearance of CO_2^+ to ionization of neutral CO_2 molecules in the matrix by electrons that have been formed by cation bombardment of surfaces, and accelerated towards the matrix by the potential applied to the grid. Improvements in the measurement of charged species of both sign from the matrix as it is vaporized by applying potentials on the collectors is also presented. This technique is useful for determining the presence of positively and negatively charged species in the matrix when spectroscopic signals are not observed.

1. Halasinski, T. M.; Godbout, J. T.; Allison, J.; Leroi, G. E. J. Phys. Chem. **1994**, *98*, 3930.

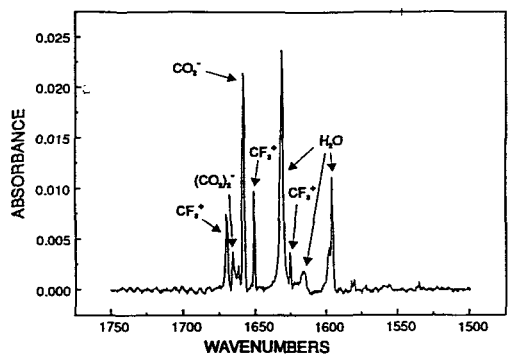

Figure 1. Infrared absorption spectrum of a 2300:1 Ne:CO_2 matrix in the 1750 - 1500 cm^{-1} region. 20 nA of CF_3^+ from EI of CF_3Cl was deposited for 13 hours.

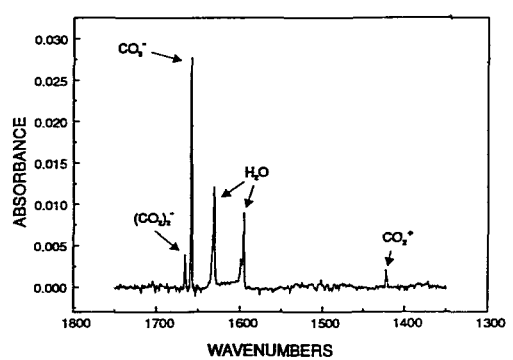

Figure 2. Infrared absorption spectrum of a 1500:1 NeCO_2 matrix in the 1750 - 1350 cm^{-1} region. 30 nA of $C_7H_7^+$ from EI of toluene was deposited for 18 hours. The copper grid on the CsI window was floated at a potential of +80 V during ion deposition.

SPECTROSCOPIC STUDIES OF THE ELECTRON RECOMBINATION OF SEVERAL SMALL IONS B. Lachele FOLEY, Nigel G. ADAMS, Lucia M. BABCOCK and Jeffery M. BUTLER, Chemistry Department, University of Georgia, Athens, GA 30602.

Dissociative electron-ion recombination is a critically important ionization loss process in many ionized gases including interstellar gas clouds and planetary ionospheres. Yet little data are available on this type of reaction and, in particular on the nature of the recombination products. To rectify this situation, we have used the chemical versatility of the flowing afterglow coupled with extensive spectroscopic facilities to identify recombination emissions from the recombination of H_3^+, HCO^+, N_2H^+, CO_2^+, CS_2^+, H_3O^+, NH_4^+ and CH_5^+. These emissions have been distinguished from those from other sources by adding a gas which rapidly attaches electrons (e.g., CCl_4, CH_3I or SF_6) upstream of the recombination region. Details of the technique have been discussed previously.[1]

For HCO^+ and N_2H^+, the electronic emissions CO(a→X) and N_2(B→A) have been observed and the individual vibrational bands have been separately identified. Using calculated Einstein A coefficients for the transitions, vibrational population distributions for the CO a and N_2 B states, resulting from recombination of HCO^+ and N_2H^+ respectively, have been determined. Comparison of these with the theoretical predictions of Bates,[2] for the *Impulse* and *Relic* mechanisms, has shown that the theory underestimates the degree of vibrational excitation. Further experimental studies with DCO^+ and N_2D^+ showed that there was little difference in the vibrational population distributions (≤10%) between the deuterated and undeuterated species whereas theory predicted a much greater effect.

For CO_2^+ and CS_2^+, CO (A→X), (a→X), (a'→a), (d→a) and CS (A→X) were observed. Note that the CO_2^+ recombination produces more emissions that CS_2^+ even though other states are energetically accessible in the latter case, presumably due to the availability of suitable curve crossings. The emission spectrum for the CO_2^+ recombination is remarkably similar to that observed from the Martian airglow[3], suggesting that this recombination should be considered as an emission source in addition to direct excitation by high energy electrons.

In the case of H_3^+ recombination, there has been controversy over the magnitude of the rate coefficient for the last ten years, the discrepancy being about an order of magnitude between the various workers. To try to determine the reason for this discrepancy, the emission spectrum of a recombining H_3^+/electron plasma was obtained over the available wavelength range (100 to 800 nm). The only significant emissions were in the range 110 to 170 nm with no emissions from H_3 Rydberg states[4] being observed. The observed emissions have been identified as H-atom Lyman α, H_2 (B→X) from v'=3 of the upper state to v"=9 to 11 of the lower state, and emissions from higher vibrational levels of the H_2 B state to the continuum of the X state.[5] None of there emissions are energetically possible with vibrationally relaxed H_3^+. Available potential curves for the H_3^+/H_3 system show that if the H_3^+ is excited to v~3 then curve crossings are available to produce H_2(X) + H(n=2) which emits L_α. Somewhat more excitation in the H_3^+ would be required to produce the H_2 B state emissions, however, potential curves for this are not presently available. A considerable effort was made to remove excitation in the H_3^+ by near resonant proton transfer with a large concentration of neutral H_2. Obviously, it is difficult to remove all of the excitation and this may be a contributor to the discrepancies

between the various measurements of the H_3^+ recombination coefficient. What is certain is that the recombination does not proceed via Rydberg states production followed by radiative decay, at least in the spectral range 100 to 800 nm.

Emissions have also been detected from recombining electron plasmas of H_3O^+, NH_4^+ and CH_5^+. For H_3O^+, no significant emissions were observed over the whole spectral range, even though several electronically excited states are energetically possible. Since the overall recombination coefficient is large (10^{-6} cm^3 s^{-1} [6]), and the OH X state is known to be a significant product (65% [7]), it appears that there are no suitable curve crossings to excited state products and that these crossings are inefficient compared with those to the ground state. For the other cases few emissions were observed, NH(A→X) for NH_4^+ and CH (A→X) and (B→X) for CH_5^+. A summary of the vibrational state distributions is given in the table below.

VIBRATIONAL STATE DISTRIBUTIONS OF DIATOMIC PRODUCTS OF ELECTRON-ION RECOMBINATION

Parent Ion	CO_2^+				HCO^+	CS_2^+	N_2H^+	N_2OH^+	O_2H^+
Product Neutral	CO				CO	CS	N_2	OH	OH
State v'	a(11)	a'(9)*	d(5)*	A(0)	a(7)	A(5)	B(5)	A(*)	A(*)
0	1.00	-	-	1.00	1.00	62	-	1.00	1.00
1	.56	-	~1	.88	.58	1.00	-	.47	.42
2	.26	-	~.94	.21	.83	.72	1.00	≤.22*	≤.19*
3	.22	-	~.88	.20	.46	.67	.28	-	-
4	.16	-	~.34	.15	.56	.34	.24	-	-
5	.16	1	≤.8	.12	.31	.17	.14	-	-
6	-	≤.2	≤.8	-	.26	-	.07	-	-
7	-	≤.2	≤.8	-	-	-	.013	-	-
8	-	≤.2	-	-	-	-	.007	-	-
9	-	-	-	-	-	-	.005	-	-

*Emission region is complex and values are only approximate.
* The OH A state predissociates at a high rotational level of v'=2

References:
1. Foley, B.L.; Adams, N.G.; Lee, H.S. (1993) J. Phys. Chem. 97, 5218.
2. Bates, D.R. (1993) Mon. Not. R. Astr. Soc. 263, 369.
3. Barth, C.A. et al. (1971) J. Geophys. Res. 78, 2213; Stewart et al. (1972) Icarus 17, 469.
4. Herzberg, G. (1987) Ann. Rev. Phys. Chem. 38, 27.
5. Dalgarno, A.; Herzberg, G.; Stephens, T.L. (1970) Ap. J. 162, L49.

Ab Initio Calculations of the $Ar{\bullet}CO_2^+$ Cluster Ion

Gregory I. Gellene
Department of Chemistry and Biochemistry
Texas Tech University, Lubbock, TX 79409-1061

Presently little detailed information is available on the structure of the $Ar{\bullet}CO_2^+$ cluster ion. In a photoionization study of $Ar{\bullet}CO_2$, Pratt and Dehmer[1] determined $D_0(Ar{\bullet}CO_2^+) = 0.26\pm0.03$ eV (2100 ± 320 cm^{-1}). They also concluded that the structure of $Ar{\bullet}CO_2^+$ involved major changes from the $Ar{\bullet}CO_2$ configuration which is known to be *T* shaped[2] with an Ar-C distance of 3.49Å.

Illies *et al.*[3] studied the photodissociation of $Ar{\bullet}CO_2^+$ and based on kinetic energy release measurements and the absence of rotational excitation in the CO_2^+ fragment concluded that the cluster ion was either linear or *T* shaped. Simple molecular orbital arguments were then presented in favor of a *T* shaped configuration.

Theoretically, the ion has been considered at the MP4(full)/G-31G*//MP2/6-31G* level of theory. Only linear and T shaped geometries were considered. It was found that the linear geometry was favored at the MP2 level while the T shaped geometry was favored at the MP4 level. However no frequencies were determined so the nature of the calculated stationary points is an open question.

Recent studies in this laboratory of Symmetry Induced Kinetic Isotope Effects in the formation of $Ar{\bullet}CO_2^+$ have made it essential that the ground state geometry of the ion be established. Thus we have undertaken the following high level *ab initio* calculations.

Method. Calculations were performed using the cc-pVDZ and cc-pVTZ basis sets without diffuse function augmentation for oxygen and carbon and with diffuse function augmentation for argon. The diffuse functions were included to provide an accurate description of the polarizability of Ar. This property is particularly important for the description of $Ar{\bullet}CO_2^+$ where the charge remains largely localized on CO_2^+.

Electron correlation was included using QCISD and QCISD(T) theory because the availability of QCISD analytical gradients allowed efficient geometry optimization. Harmonic force constants were determined with the double zeta basis sets by numerical differentiation of analytical QCISD first derivatives. To ensure accurate characterization of the stationary points in the presence of low frequency van der Waals modes, geometry optimizations were continued until all residual forces were less than 10^{-6} au. Calculations were performed using the GAUSSIAN 92 suite of programs.

Results. The major results ar summarized on the following figure. The relative energies were obtained from QCISD(T) calculations performed QCISD optimized optimized geometries using cc-pVTZ basis sets for carbon and oxygen and aug-cc-pVTZ basis set for argon. The vibrational frequencies were obtained at the QCISD level of theory using cc-pVDZ basis sets for carbon and oxygen and aug-cc-pVDZ basis set for argon.

Stationary Points on the CO_2^+/Ar Potential Energy Surface

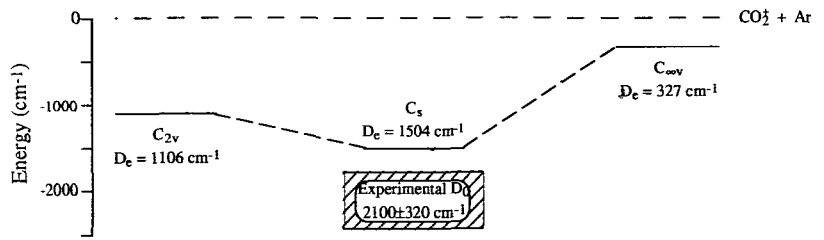

van der Waals Vibrational Modes

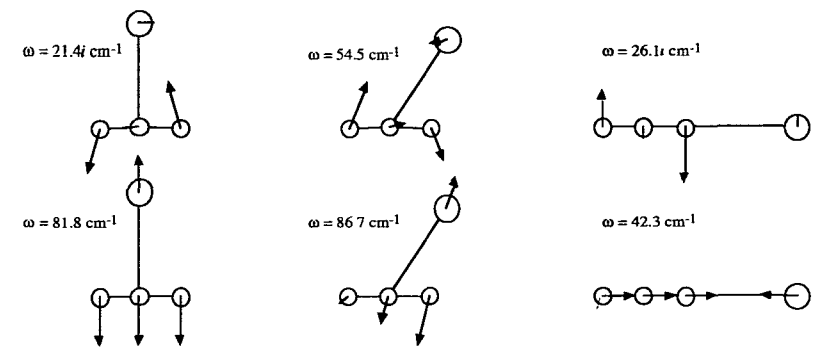

Conclusions

1. The $Ar{\bullet}CO_2^+$ cluster ion is neither *T* shaped nor linear but adopts an unsymmetrical C_s structure in its ground state.

2. It is interesting to consider whether thermal excitation and the double well nature of the potential energy well could give rise to the *T* shape-like photodissociation dynamics observed by Illies *et al.*

References

1. S. T. Pratt and P. M. Dehmer, *J. Chem. Phys.* **78**, 6336 (1983).
2. J. M. Steed, T. A. Dixon, and W. Klemperer, *J. Chem. Phys.* **70**, 4095 (1979).
3. A. J. Illies, M. F. Jarrold, W. Wagner-Redeker, M. T. Bowers, *J. Am. Chem. Soc.*, **107**, 2842 (1985).
4. W. L. Hwang, Y. S. Lee, and J. H. Kim, *Bull. Korean Chem. Soc.* **9**, 153 (1988).

The support of NSF (Grant no. CHE90-24091) is gratefully acknowledge.

SYMMETRY BREAKING AND ELECTRON CORRELATION IN O_2^+, O_2, AND O_2^-

Charu A. Chandrasekher, Gregory I. Gellene
Department of Chemistry and Biochemistry, Texas Tech University, Lubbock TX, 79409
K.S. Griffith, Department of Chemistry and Geology, Mankato State University, Mankato, MN 56002

Coupled-cluster (CC) theory provides one of the most powerful approaches available for building electron correlation onto a single determinant reference wave function. Two particularly attractive characteristics of the approach are that all CC methods are size-extensive and the hierarchical structure of the theory causes methods to become increasingly accurate as more excitations are considered. Most of the dynamical correlation of a system is accounted for by the CCD approach which considers only the double excitation cluster operator. The addition of the single excitation cluster operator to CCD defines CCSD which is exact for a two electron system. However, it is known that triple excitations are required for the correct description of many molecules, and a number of approximate treatments of the effects of triple excitation operator have been developed. An alternative size-extensive approach called quadratic configuration interaction (QCI) was developed which in the single-double space (QCISD) is exact for a two electron system. QCISD has been shown to be equivalent to CCSD with a Hartree-Fock reference wave function where specific operators are omitted from the doubles equation and from the singles and doubles equation. Considering that QCISD is an approximation to CCSD, it might be thought that QCISD would be less accurate than CCSD. However both CCSD and QCISD are inexact and that numerical comparisons are required to assess their relative merits. CCSD(T) and QCISD(T) (both of which treat the inclusion of triple excitations perturbatively) have been compared in terms of eighth order Møller-Plesset perturbation theory. Although this demonstrated that CCSD(T) contains more triple excitation terms than QCISD(T), a higher number of contributions does not guarantee the superior performance of a method because some terms may be more important than others. Numerical comparisons of QCISD(T) and CCSD(T) are required to assess their relative merits.

Calculations were performed using Dunning's aug-cc-pVDZ (double zeta quality) and aug-cc-pVTZ (triple zeta quality) basis sets for oxygen. The two basis sets were used in symmetry constrained and symmetry relaxed unrestricted Hartree-Fock (UHF) calculations for eight internuclear separations (r) for each species. Electron correlation was built onto each of these UHF wave functions using CCSD, CCSD(T), QCISD, and QCISD(T) producing various point-wise defined potential energy curves for each of the three species. Continuous curves were obtained by fitting the calculated energies to a polynomial in r from which the value for a variety of spectroscopic constants were extracted. This investigation compares the accuracy of CCSD to QCISD and CCSD(T) to QCISD(T) in determining potential energy curves for $O_2^+(X^2\Pi_g)$, $O_2(X^3\Sigma_g^-)$, and $O_2^-(X^2\Pi_g)$. This series of molecules was chosen for the following five reasons: (1) The open shell electronic structure of these molecules is not well described by a single configuration making electron correlation important and the relative importance of excited configurations varies with internuclear separation. (2) The calculation of accurate ionization potentials (IP) and electron affinities (EA) requires treating electron correlation in the neutral and the charged species in a balanced manner, particularly where the correlation energy is in fact larger than the EA. (3) Each of these species is subject to inversion symmetry breaking, and recovering from this artifactual symmetry breaking is a challenging test of approximate treatments of electron correlation. (4) The size of the molecules is compatible with the use of large basis sets. (5) Accurate experimental information is available for comparison with the calculations.

For O_2^+, symmetry breaking was favored for all r studied, but O_2^- and O_2 favored symmetry breaking only for r > 1.40 Å and r > 1.25 Å, respectively. When symmetry breaking is favored, a symmetry constrained ($D_{\infty h}$) and a symmetry relaxed ($C_{\infty v}$) UHF reference determinant are available for post-Hartree-Fock calculations. Values for adiabatic IP and EA of O_2 at the various levels of theory were determined by taking the appropriate difference in the respective minimum energy of O_2 and that of O_2^+ and O_2^-. The strategy was to compare symmetry constrained results to experimental values for various spectroscopic constants to evaluate accuracy and to compare symmetry relaxed results to the corresponding symmetry constrained results to evaluate recovery from symmetry breaking. ***r_e*** and ***ω_e*** The r_e values show two general trends which have been identified previously for other systems: extension of the basis set tends to decrease r_e, and inclusion of triples excitations tends to increase r_e, while the ω_e values show trends which are the reverse: basis set extension tends to increase ω_e and inclusion of triples excitations tends to decrease ω_e. Because the symmetry breaking does not occur for O_2^- and O_2 at bond lengths equal to their respective r_e, the ability of the different methodologies to overcome the use of a symmetry broken reference function with respect to r_e is best addressed by the O_2^+ results. For both r_e and ω_e the best recovery from symmetry breaking is provided by the CCSD method. ***D_J***: The D_J values can be assessed only for O_2 and O_2^+. For these two molecules, the value of D_J calculated by QCI methods with a symmetry constrained reference function is more accurate than the corresponding CC result. Comparison of corresponding D_J values calculated with symmetry constrained and symmetry relaxed reference functions further emphasizes the general superiority of CCSD in recovering from symmetry breaking. ***IP, EA, and D_e***: The accuracy of the IP of O_2 calculated at the UHF level of theory is quite high, so there is little opportunity for the various correlated methods to distinguish themselves in this regard. However, the situation is very different with respect to the accuracy of the calculated EA of O_2 where UHF calculations fail to predict a bound species. The EA calculated with QCI methods is consistently superior to the corresponding CC results for all basis sets and correlation levels considered. Finally, with respect to D_e values, the results indicate that with symmetry constrained reference functions, the QCI results are superior the the corresponding CC results for the range of basis sets and correlation levels investigated. ***$\omega_e x_e$*** and ***α_e***: The results show that when symmetry constrained wave functions are used, the calculated values of cubic and quartic force constants (upon which $\omega_e x_e$ and α_e depend) are remarkably insensitive to the basis set, level of correlation (including no correlation), and correlation method. When symmetry relaxed UHF wave functions are used the calculated values of k_3 and k_4 show a significant dependence on the level of correlation and the correlation method employed. With respect to calculating higher derivatives of the potential, CC methods appear to be superior to QCI methods in recovering from a symmetry relaxed UHF wave function.

Thus, In agreement with previous results obtained for closed-shell species, basis set extension tends to decrease r_e and increase ω_e while inclusion of triples excitations tends to increase r_e and decrease ω_e. Comparison of corresponding symmetry constrained and symmetry relaxed calculations indicates that the CCSD method is generally superior to CCSD(T), QCISD, and QCISD(T) in recovering from a symmetry broken reference function.

ACCURATE IONIZATION ENERGIES AND HEATS OF FORMATION OF SIMPLE ENOLS

František Tureček and Christopher J. Cramer
Department of Chemistry, Box 351700, University of Washington, Seattle, WA 98195-1700
Department of Chemistry and Supercomputer Institute, University of Minnesota, Minneapolis

Enols cation-radicals represent important intermediates in gas-phase ion chemistry *(1-3)*. Enol ions are typically more stable than their keto or aldehyde isomers, while an opposite order of stabilities is found for the neutral systems. The thermochemistry of enol ions relies on appearance energy measurements, which in combination with thermochemical cycles provide estimates of the ion enthalpies of formation *(4-6)*. The latter, when combined with threshold ionization energies, are further used to estimate the enthalpies of formation of neutral enols *(6-8)*. Ab initio calculations at intermediate levels of theory have also been used to estimate the relative stabilities of enols and ketones or aldehydes for both ion and neutral systems *(9-11)*.

We report on a systematic ab initio study of the thermodynamics of simple neutral enols, $CH_2{=}CHOH$ (**1**), $CH_2{=}C(OH)CH_3$ (**2**), *(E)*-$CH_3CH{=}CHOH$ (**3**), and *(Z)*-$CH_3CH{=}CHOH$ (**4**), and their cation-radicals. The stable geometrical forms of these species, i.e., the *syn* and *anti* rotamers for **1-4** and $\mathbf{1}^{+\bullet}$ - $\mathbf{4}^{+\bullet}$, have been obtained by MP2(FULL)/6-31+G(d,p) calculations. Single-point energies were calculated at the effective QCISD(T)/6-311+G(3df,2p) level based on single-point QCISD(T)/6-311G(d,p) and MP2/6-311+(3df,2p) calculations. Isogyric and zero-point corrections to the calculated total energies yielded the Gaussian-2(MP2) energies. Enthalpies and entropies were also calculated for the 250-600 K temperature interval to elucidate the equilibrium concentrations of the rotamers. Isodesmic reactions were used to relate the enol relative enthalpies to the corresponding standard heats of formation, which are summarized in Table 1 and compared with experimental data.

Table 1. Heats of formation of enols and enol cation-radicals in kJ mol^{-1}.

Enol	ΔH_f (exp)	$\Delta H_{f,298}$	*Ion*	ΔH_f (exp)	$\Delta H_{f,298}$
syn-$CH_2{=}CHOH$	-128	-122	*syn*-$CH_2{=}CHOH^{+\bullet}$		772
anti-$CH_2{=}CHOH$		-118	*anti*-$CH_2{=}CHOH^{+\bullet}$	757,768	764
syn-$CH_2{=}C(OH)CH_2$	-170	-167	*syn*-$CH_2{=}C(OH)CH_2^{+\bullet}$		680
anti-$CH_2{=}C(OH)CH_2$		-161	*anti*-$CH_2{=}C(OH)CH_2^{+\bullet}$	661	676
(E)-syn-$CH_3CH{=}CHOH$	-169	-149	*(E)-syn*-$CH_3CH{=}CHOH^{+\bullet}$		689
(E)-anti-$CH_3CH{=}CHOH$		-145	*(E)-anti*-$CH_3CH{=}CHOH^{+\bullet}$	(665)[a]	681
(Z)-syn-$CH_3CH{=}CHOH$	-174	-149	*(Z)-syn*-$CH_3CH{=}CHOH^{+\bullet}$		691
(Z)-anti-$CH_3CH{=}CHOH$		-148	*(Z)-anti*-$CH_3CH{=}CHOH^{+\bullet}$	(665)[a]	681

[a]Isomers unresolved.

Neutral enols **1-3** prefer *syn*-geometries, while *anti*-**4** is slightly more stable than *syn*-**4**. All enol ions prefer *anti*-geometries by 4-10 kJ mol^{-1}. The calculated standard enthalpies of formation are in reasonable agreement with the experimental values for **1**, **2**, and $\mathbf{1}^{+\bullet}$. The calculated enthalpies of formation for **3**, **4**, and $\mathbf{2}^{+\bullet}$-$\mathbf{4}^{+\bullet}$ are systematically higher than the experimental estimates. By comparison, the calculations gave accurate enthalpies for isodesmic reactions involving acetaldehyde ($\pm$0.5 kJ mol^{-1}), acetaldehyde cation-radical ($\pm$0.1 kJ mol^{-1}), ethylene ($\pm$0.0 kJ mol^{-1}), and ethylene cation-radical ($\pm$3.0 kJ mol^{-1}). The discrepancy between the experimental and ab initio data for $\mathbf{2}^{+\bullet}$-$\mathbf{4}^{+\bullet}$ may be due to the unknown temperature of the enol ions formed at the dissociation threshold.

Adiabatic and vertical ionization energies (IE) of **1-4** have been calculated and compared with experimental data from threshold electron impact measurements and photoelectron spectra. The *syn*-isomers show adiabatic ionization energies (IE_a) which are 0.09-0.11 eV higher than those for the *anti*-isomers. The latter IE show good agreement with the experimental threshold values, e.g. 9.14 versus 9.14-9.17 eV for **1**, 8.68 versus 8.61-8.67 eV for **2**, 8.60 versus 8.64 eV for **3**, and 8.62 versus 8.70 eV for **4**. The calculated IE_a of *syn*-**1** (9.51 eV) agrees with the value from the photoelectron spectrum.

Vibrational analysis of *syn*- and *anti*-$\mathbf{1}^{+\bullet}$ allowed us to identify the modes which are likely to be excited upon vertical ionization of neutral **1**. These correspond to the C=C stretch (a'_1) and in-plane bends involving the hydroxyl hydrogen atom (a'_3, a'_4, and a'_5). The calculated harmonic vibrational frequencies allow one to reinterpret the fine structure of the first band in the photoelectron spectrum of **1**.

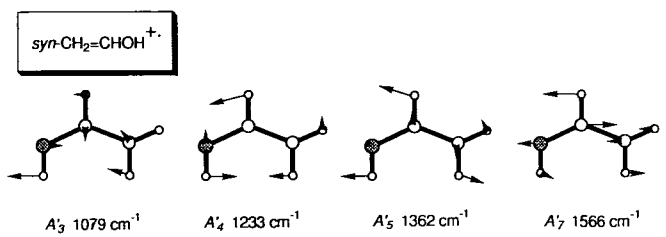

References

(1) H. Schwarz in *Adv. Mass Spectrom. 1985*, J. F. J. Todd, Ed.; Wiley: New York, 1986.
(2) G. Bouchoux, *Mass Spectrom. Rev.* **1988**, *7*, 1 and 203.
(3) F. Turecek in *The Chemistry of Enols*; Z. Rappoport, Ed.; Wiley: Chichester, 1990.
(4) J. L. Holmes and F. P. Lossing, *J. Am. Chem. Soc.* **1980**, *102*, 1591.
(5) G. Bouchoux, C. Alcaraz, O. Dutuit and M. T. Nguyen, *Int. J. Mass Spectrom. Ion Processes*, **1994**, *137*, 93.
(6) F. Turecek, L. Brabec and J. Korvola, *J. Am. Chem. Soc.* **1988**, *110*, 7984.
(7) F. Turecek, Z. Havlas, F. Maquin, N. Hill and T. Gaumann, *J. Org. Chem.* **1986**, *51*, 4061.
(8) F. Turecek and Z. Havlas, *J. Org. Chem.* **1986**, *51*, 4066.
(9) W. J. Bouma, J. K. MacLeod and L. Radom, *J. Am. Chem. Soc.* **1980**, *102*, 2246.
(10) N. Heinrich, W. Koch, G. Frenking and H. Schwarz, *J. Am. Chem. Soc.* **1986**, *108*, 593.
(11) Y. Apeloig in *The Chemistry of Enols*, Z. Rappoport, Ed.; Wiley: Chichester, 1990.

Theoretical Study of the Ring Closure of the 1,7-Octadiyne Cation.

* Ronny C. Robbins, James Jensen
U.S. Army
Aberdeen Proving Ground
Edgewood Area
APG, MD 21010-5423

The mass spectra of short chained alpha-omega diynes contain an intense ion at m/Z 91 and a minor peak at m/Z 45.5 indicating an aromatic type of structure for the m/Z 91 ion. Carbon-13 labeling experiments for 1,7-octadiyne, 1,8-nonadiyne and 1,9-decadiyne also indicate the formation of some type ring system before fragmentation. In table one, the mass spectrum of 1,7-octadiyne contains an intense peak at m/Z 91. This is a loss of a hydrogen followed by loss of a neutral CH_2. Also in table one, the mass spectrum of 1,2,7,8-^{13}C-1,7-octadiyne has a large m/Z 95 and a large m/Z 94 pointing to random carbon loss after ring formation.

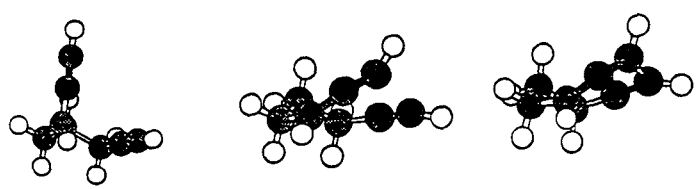

REACTANT SADDLE POINT PRODUCT

Figure One: 1,7 Octadiyne Cation After Cyclization and in Lowest Energy Congifuration.

The ring closure of the 1,7-octadiyne cation is studied using the GAUSSIAN92 program. The open structure rearranges to form an eight membered ring. The ring structure is more stable by approximately 4-5 kcal/mol. Geometries and Mullikan populations for both the open and ring structures are presented.

The transition state geometry is presented and the activation barrier calculated. The calculations were done at the SCF and CASSCF levels of theory using 6-31g*, 8 in 8 basis set, and a total of 1764 configurant ions. The "Thru-Space" interaction of the pi systems on two alkyne fragments is examined.

	REL.INT.			REL.INT.			REL.INT.	
M/Z	C-12	C-13	M/Z	C-12	C-13	M/Z	C-12	C-13
26	8	4	55	0	11	81	0	38
27	34	17	56	0	8	82	0	57
28	5	27	57	0	1	83	0	9
29	1	11	61	1	0	84	0	1
31	0	1	62	3	0	86	0	1
35	0	2	63	7	1	91	100	0
36	1	3	64	2	4	92	8	1
37	7	0	65	0	7	93	0	4
38	18	3	66	0	4	94	0	84
39	90	21	67	6	35	95	0	68
40	9	39	68	0	19	96	0	2
41	27	100	69	0	9	103	6	0
42	1	29	70	0	1	104	1	0
43	0	13	71	0	1	105	28	0
45	0	2	74	2	0	106	1	1
49	1	1	75	1	0	107	0	9
50	12	1	76	2	2	108	0	2
51	17	3	77	19	2	109	0	41
52	11	15	78	46	2	110	0	2
53	8	20	79	25	9			
54	7	13	80	3	23			

C-12 = Unlabelled 1,7-Octadiyne
C-13 = 1,2,7,8-^{13}C-1,7-Octadiyne

Table 1: Mass spectra for Unlabelled 1,7-Octadiyne, and 1,2,7,8-^{13}C-1,7-Octadiyne

References

1) Frisch, M.J., et. al., Gaussian 92, Revision B, Gaussian Inc, Pittsburgh, PA, 1992

2) Lifshitz, C., Gefen, S., "Time-Dependant Mass Spectra and Breakdown Graphs. I. 1,5-Hexadiyne", Int. J. Mass Specatrom. Ion Phys., 35, (1980), 31-37

3) Nagy-Felsobuki, E., Peel, J.B., Willett, G.D. Chem. "The Photoelectron Spectra of Some Non-Conjugated Acyclic Diynes", Phys. Lett. Vol. 68, No. 2,3, Pages 523-526, 1979

The Presence of Hydrogen Trioxide H_2O_3 in the Gas Phase

Toshihiro Fujii[1] and Hiroshi Kishi[2]

1) National Institute for Environmental Studies, 16-2 Onogawa,Tsukuba, Ibaraki 305, Japan, e-mail; t-fujii@nies.go.jp 2) Oyama National College of Technology. Oyama 323, Tochigi

This report is concerned with the presence of H_2O_3 in the gas phase. During the studies on the identification of the principal species produced by the CH_4/O_2 microwave (MW) discharge, I have succeeded in determining the presence of hydrogen trioxides H_2O_3 in the gas phase. The Li^+-adduct mass spectra of the discharge plasma, obtained by Li^+ ion attachment technique, clearly show the peak m/z 57 ($H_2O_3Li^+$), giving the direct evidence that H_2O_3 is formed in the plasma environment and detected mass spectrometrically.

A literature search made it possible to understand the controversial hypothesis on the possibility of the existence of hydrogen polyoxides H_2O_3 and H_2O_4. According to the literature, a pioneer in this field was the French chemist M. Berthelot, who suggested the formation of a trioxide during the decomposition of hydrogen peroxide in 1880. Fifteen years later D. Mendeleev suggested another intermediate, the tetraoxide, H_2O_4, in the same reaction. In the late 1920' s, the next development came experimentally from the use of electric discharge. G. I. Lavin and F. B. Stewart found that when the discharge H_2O vapor stream is chilled quickly on a cold trap (about -190°C), a glassy, active solid is obtained, yielding some hydrogen peroxides on warming. This finding gave rise to many hypotheses. Then, many scientists tested this glassy solid using many methods, including structure analysis , such as X-ray diffraction , ESR, electron diffraction and molecular spectroscopy.

It seems that the most significant results were obtained by Giguere and his co-workers. In 1970, they succeeded in confirming the existence of the two higher oxides of hydrogen, H_2O_3 and H_2O_4 by the isotope shift technique of the IR and Raman spectroscopy. It is concluded that the two polyoxides of hydrogen can be made only at very low temperature. On warming from liquid air temperature, H_2O_4 begins to decompose at -100°C and H_2O_3 at about -55°C. As expected, these compounds have not been detected in the gas phase to date.

EXPERIMENTAL The apparatus is shown in Fig. 1. The apparatus was basically the same as used before in detecting the hydrocarbon free radicals. Briefly a Shimadzu atmospheric pressure ionization quadrupole mass spectrometer with a Li^+ ion attachment reaction chamber (RC) was used. A stream of reaction products from a quartz discharge flow tube is directed into the alkali-metal ion attachment reaction chamber. The RC has a glass bead (Li^+ emitter). By heating this bead, lithium ions are produced. These parent ions, in turn, ionize the chemical products (M) by adduct formation ($M+Li^+$). ($M+Li^+$) complexes are formed by termolecular association reaction. Parent-daughter ion pairs [$Li^+/(M+Li^+)$] are measured to detect the intermediate species and to identify their possible sources.

The Results and Discussion A number of runs were made to broadly establish the operating characteristics of the apparatus designed and to increase the intensities of ions at m/z 57, issuing through the Li^+ ion attachment reactions. Fig. 2 shows the display trace of the mass spectra over regions m/z 5-9, 38-42 and 54-58. These Li^+-adduct data taken with the discharge on have additional peaks in the spectrum, compared with the data taken with the discharge off. Thus the additional peaks, for instance, the m/z 57 peak in the upper stage are attributed to ion attachment to chemical species effusing from the plasma.

The presence of the chemical species, whose molecular weight is 50 amu, is denoted by an increase in the current of the Li^+-adduct ions (m/z 57). According to the CAS-ONLINE search, there are, surprisingly, only 43 chemical species which have 50 amu as the molecular weight. Table I lists all these compounds. Under the present experimental conditions, the possible compounds are either H_2O_3 or C_2H_3LiO. It is concluded from two candidates that the peak m/z 57, due to the Li^+-adduct ions, is assigned to that of $H_2O_3Li^+$, since the isotopic abundance consideration of the m/z 56 peak relative to the m/z 57 peak indicates containing one Li atom and hence, rules out the possibility of $C_2H_3LiOLi^+$.

In conclusion, the direct proof of the presence of H_2O_3 in the gas phase was provided by the recently developed ion attachment technique incorporated with quadrupole mass spectrometry.

Table I. The retrieved compounds from the literature search, which have molecular weight of 50 amu.
HLi_3Si, H_2Mg_2, $\mathbf{H_2O_3}$, H_2OS, H_2Ti, H_3OP, H_4NS, H_5NP; $HeNO_2$, $He_{12}H_2$;Be_2O_2, Be_2H_8Mg; BF_2H, BFH_4O, $BLiO_2$, $BLiSi$, B_2N_2, B_4H_6; CAlB, CF_2, $CH_2B_2Li_2$, CH_3FO, CH_3LiN_2, CLiP, CH_6S, CH_7P, CMgN, C_2FLi, C_2H_2Mg, $\mathbf{C_2H_3LiO}$, C_2H_3Na, C_2H_8Be, $C_2H_4B_2$, C_3Li_2, C_3H_3B, C_3H_7Li, C_3N, C_4H_2; FHNO, FH_3N_2, FH_3Si, FP; AlLiO

Fig. 1

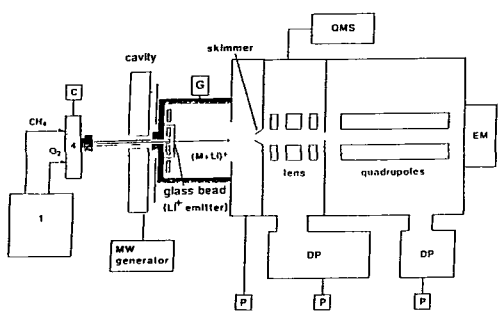

Fig.2

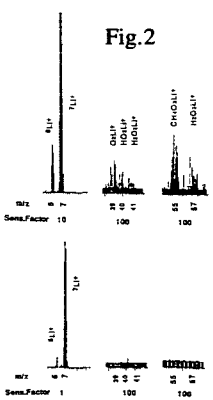

Ref; Fujii, T; Syouji, K. Phys. Rev. E, 1994, 49, 657-662.

Structure of Isomeric Gly-Pro b_2 Ions Calculated by Ab-initio Methods

Klaus Eckart, Max C. Holthausen§, Thomas Bräuninger§, Wolfram Koch§, and Joachim Spiess; Department of Molecular Neuroendocrinology, Max Planck Institute for Experimental Medicine, Hermann-Rein- Str. 3, D-37075 Goettingen; §Institute of Organic Chemistry, Technical University Berlin, Strasse des 17. Juni 135, D-10623 Berlin

INTRODUCTION

Acylium type dipeptide ions (b_2-ions) are expected to undergo cyclization to the corresponding protonated diketopiperazine. Recent investigations had shown that this expected process does not occur in the case of Gly-Gly (1) and Ala-Ala (2). More surprisingly, the cyclization could not be observed for the Gly-Pro b_2-ion, which should cyclize much easier due to the constraints introduced by the Pro pyrrolidine group (3). Furthermore, the amide bonds in the peptide backbone usually existing in the trans (Z) configuration do not possess a cis or trans preference for amide bonds involving the Pro pyrrolidine group as known from NMR data. Therefore, this sterical situation could not be responsible for the cyclization barrier.

It was speculated that this behavior depended on the structure of this particular dipeptide fragment ion, and some suggestions for the structures of the Gly-Pro dipeptide ion were made recently (3). These structures are based on the observed mass spectral fragmentation pattern, and it was therefore concluded, that the charged site must be localized on the pyrrolidine nitrogen. In the present work *ab-initio* molecular orbital calculations were performed in order to localize the most probable structure of this dipeptide fragment. The results will also be discussed with respect to production of b-ions in the course of peptide fragmentation. In addition different precursors to the Gly-Pro b_2 fragment ions are used to exclude a structural contribution from the neutral C-terminal leaving group.

METHODS

All mass spectral data were obtained on a VG Analytical AutoSpec-T tandem mass spectrometer equipped with a 3"-focal plane detector. Data were recorded and performed with the OPUS data system. Detailed experimental conditions were the same as reported earlier (3).

For the quantum chemical calculations the programs Spartan 3.0, Wavefunction, Inc. (semiempirical calculations) and DGauss 2.3, Cray Research, Inc. (DFT-calculations) were used. The global minimum in the conformational space of each respective isomer under investigation was located on the semiempirical (PM3) level. The geometry of each of the evolving structures has subsequently been optimized at the *ab initio* DFT level (BLYP, DZVP basis set employing a pseudopotential for the 1s electrons of C, O, N). The given relative energies refer to this correlated level of theory.

RESULTS AND DISCUSSION

The calculated relative energies of different isomeric Gly-Pro structures revealed a clear thermodynamic preference for the protonated diketopiperazine (Fig. 1). The small differences in the relative energies of **2**, **3**, and **4** suggested that these structures may contributed to the linear peptide fragment ion. Other alternative structures considered recently (3) exhibited relative energies above 100 kJ/mol. The Gly-Pro b_2-ions obtained through LSIMS induced fragmentation of Gly-Pro-β-naphthylamide and Gly-Pro-Gly were compared using high energy CAD. The resulting spectra demonstrated clearly that the C-terminal neutral leaving group does not significantly change the fragmentation pattern. Therefore, the structures of the investigated Gly-Pro b_2-ions may be almost identical.

The acylium ion type structure for the Gly-Pro b_2-ion could not be isolated as a global minimum. This localization ended up with the structure of **3**, which seemed to be the most likely

candidate. In this structure the positive charge is more effectively stabilized as in the acylium ion type structure. Furthermore, the constitution of **3** offers no structural possibility for forming the protonated diketopiperazine **1**. The same consideration appears for the alternative structure **2**.

Figure 1: Energies in kJ/mol from ab-initio MO calculations for the most stable Gly-Pro b_2 structures relative to protonated c[Gly-Pro].

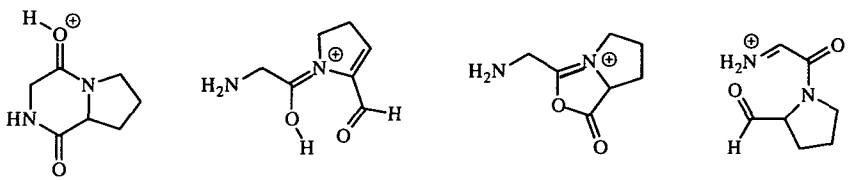

1 $E_{rel}=0$ **2** $E_{rel}=72$ **3** $E_{rel}=66$ **4** $E_{rel}=72$

Structure **4**, which is stabilizing the positive charge at the N-terminal Gly residue, was also considered as a potential structural candidate based on the thermodynamical results. **4** is supposed to be the most likely precursor for the Gly immonium ion (m/z 30) in the high energy CAD mass spectrum of the Gly-Pro b_2-ion. The formation of **1** from **4** is prevented by the absence of nucleophilicity on the N-terminal amino group of **4**. High energy CAD which favors direct bond cleavage is better suited than low energy CAD to correlate stable ionic structures with mass spectral fragmentation patterns. This makes it possible to correlate the mass spectral fragmentation patterns with the structures obtained from *ab-initio* MO calculations (Fig 1)

The similarity of the high energy CAD mass spectra of the Gly-Pro b_2-ions obtained from different precursors suggested, that the structure of this b_2-ions was not significantly influenced by the C-terminal neutral leaving group and was therefore reflecting the molecular properties of the charged fragment. From these considerations it is obvious that stabilization of the positive charge on the pyrrolidine nitrogen as shown in Fig. 1 is the driving force for the cleavage of the amide bond C-terminal to Pro.

These results may also belong to the formation of b-ions from larger peptides. This can be demonstrated by the effect of selective amide nitrogen methylation as reported for the peptide Pyr-Phe-Phe-Gly-Leu-Met(NH_2) (4). The positive ion FAB mass spectra of the peptide methylated selectively on each Phe nitrogen, the Gly nitrogen, or the Leu nitrogen showed a significant enhancement of the corresponding C-terminal b-ion over the remaining b-ions when compared with the pattern of the non-methylated peptide. It should be mentioned that the Pyr nitrogen does not exhibit a significant basicity as the N-terminal amino group of non-protected peptides. Nevertheless, in positive ion mass spectra the above described effect is commonly known for Pro residues in peptides, which contain no residues with basic side chains.

References:

1) Carroll, J. A.; Wu, J.; Do, T.; Lebrilla, *C. Proceedings of the 42nd ASMS Conference on Mass Spectrometry and Allied Topics* 475 (1994)
2) Cordero, M. M.; Houser, J. J.; Wesdemiotis, *C. Anal. Chem.* **65**, 1594 (1993)
3) Eckart, K.; Spiess, J., *Proceedings of the 42nd ASMS Conference on Mass Spectrometry and Allied Topics* 474 (1994)
4) Eckart, K.; Schwarz, H.; Chorev, M.; Gilon, C., *Eur. J. Biochem.* **157**, 209-216 (1986).

Fragmentation of Benzalacetones: Theory and Experiment

R. Heinicke, F. Moritz and J. Grotemeyer
Institut für Physikalische Chemie, Universität Würzburg
Marcusstr. 9-11, 97070 Würzburg, Germany

In order to understand the fragmentation reactions of cation radicals from certain organic compounds, cyclisation reactions via intramolecular substitution should be considered as a key step in the degradation of the molecular ions. This is important where the formation of an extended aromatic system is possible like in benzalacetones first observed by Williams et. al.[1]. In aromatic systems the facile loss of a hydrogen radical or another substituent from the aromatic ring of a molecular ion is unexpected in view of the strong bond of the sp^2 carbon atom to this atom/substituent. Thus it is reasonable to assume that there is at least a partial compensation of the energy needed for bond cleavage by bond formation via intramolecular aromatic substitution. Deuterium-labeling at the ortho position of the aromatic ring leads to a loss of hydrogen as well as deuterium. According to this results, there must be fast H-rearrangements prior to fragmentation in the aromatic ring. In further experiments Schaldach[2] und Grützmacher[3] investigated ortho-, meta- and para-substituted benzalacetones. In this paper we report some new results of the intramolecular aromatic substitution reaction of benzalacetones and substituted analogues. For investigation we used a Time-of-Flight-Mass-Spectrometer applying multi photon ionization (MUPI) with use of fs-laserpulses. Due to this ionization technique and the combination with supersonic beam the internal energies of the corresbonding molecular ions are comparatively well defined. Furthermore the fragmentation process yielding the loss of a hydrogen radical or in case of substituted benzalacetones the loss of the substituent leading to chromylium ions are studied.
Parallel to this experiments we performed semiempirical and ab initio calculations to determine the geometries and heat of formations of all structures and transition states taking part in the cyclyzation and fragmentation processes. The reaction dynamics are modelled with the help of RRKM-calculations.
The first efforts to ionize the molecule with ns-laserpulses failed. It was not possible to detect the molecular ion with reasonable intensities or to increase signal intensity by using different inlet systems. Using fs-laserpulses for ionization the signal intensity increased dramatically.

Figure 1 shows two spectra of unsubstituted benzalacetone obtained a) with ns-laserpulses (λ=255 nm, 20 μJ, pulse width 8 ns) and b) fs-ionization (λ~260 nm, 5.6 μJ, pulse width 500 fs).

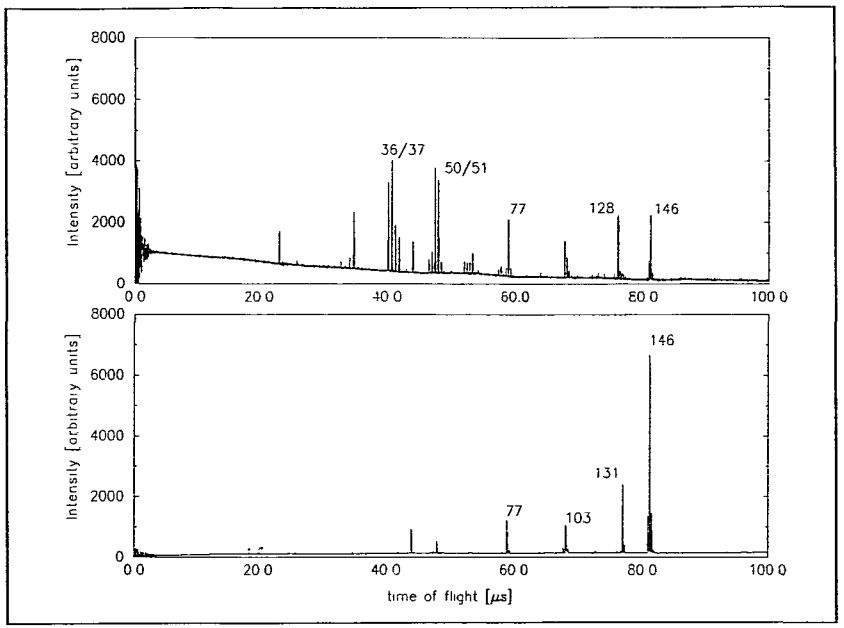

For all substituted benzalacetones the specific peak at m/z=145 was observed resulting from the loss of the substituent independant from the position of the substituent. The different possibilities of the excited molecule are described to explain the differences between ns- and fs-ionization. Only fs-ionization is fast enough to compete with depopulation of the excited state - propably via intersystem crossing.

[1] J. Royane, D.H. Williams, S. Lewis, A.L. Burlingame *Org. Mass Spectrom.* **1973**, *7*, 887.
[2] B. Schaldach, Dissertation, Fakultät der Universität Bielefeld, **1976**.
[3] H.-F. Grützmacher, *Org. Mass Spectrom.* **1993**, *28*, 1375.

Formation of $[M+H]^+$, $[M+Na]^+$, $[M-H]^+$, and $[M-H]^-$ Ions of Methyl Octadecanoate under Electron Impact Ionization Conditions: Does Surface Ionization Occur ?

Mitsuo Takayama[1], Kenzo Hiraoka[2], and Hisao Nakata[3]

1. Pharmaceutical Sciences, Toho University, 2-2-1 Miyama, Funabashi, Chiba 274, Japan.
2. Faculty of Engineering, Yamanashi University, 4 Takeda, Kofu-shi, Yamanashi 400, Japan.
3. Department of Chemistry, Aichi Kyoiku University, 1 Hirosawa, Igaya-cho, Kariya-shi, Aichi 448, Japan.

Introduction

Although the electron impact ionization (EI) behavior of methyl octadecanoate (**1**) has been extensively and intensively examined in connection with the McLafferty rearrangement (McR) reaction [1-3], here we report the formation of $[M+H]^+$, $[M+Na]^+$, $[M+K]^+$, $[M-H]^+$, and $[M-H]^-$ ions of **1** under low-impact energy EI (2~12 eV) conditions. Since the ionization energy (IE) of fatty acid esters lies in the range of 10~11 eV, this EI condition is unfavorable or critical for the formation of molecular ions M^+ and it could be expected that surface ionization (SI), thermal ionization (TI), and/or ion-pair formation from dimer M_2 under that EI conditions Our aims are to explain this strange ion formation and the following fragmentation behaviors

Experimental

Experiments were performed on a JEOL JMS-DX303 double focusing mass spectrometer equipped with a JMA DA5100 data system (JEOL, Tokyo, Japan). The sample was introduced into the ion source using a direct inlet probe with a glass sample tube of 16 mm x 2 mmø. The ionizing chamber temperature and ionizing current were 160 °C and 100 μA, respectively

Results and Discussion

The 2 eV/EI mass spectrum of **1** showed intense ion peaks of $[M+Na]^+$ at *m/z* 321, $[M+H]^+$ at *m/z* 299, $[M-H]^+$ at *m/z* 297, K^+ at *m/z* 39, and Na^+ at *m/z* 23, suggesting that the SI processes on the surface of a rhenium filament occur [4] (Fig.1). Generally speaking, the SI mass spectra of organic compounds show only few ion peaks together with intense $[M+H]^+$ and/or $[M-H]^+$ ions [5] On the other hand, the introduction of large amounts of the sample vapor into the ion source brought about the formation of preferential $[M+H]^+$ and abundant fragment ions in the vicinity of 8 to 15 eV impact energy though the spectral pattern fluctuated in intensity, while the M^+ ion disappeared at 10~11 eV when the small amounts of sample vapor. As shown in Fig.2a, positive-ion 12 eV/EI mass spectrum of **1** showed the McR ion at *m/z* 74 and related ions at *m/z* 75 and 87, but collision-induced dissociation (CID)

Fig.1 Positive-ion 2 eV/EI mass spectrum of 1.

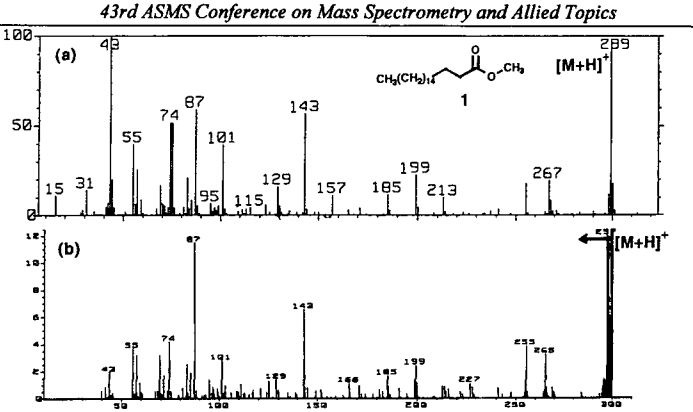

Fig.2 (a) Positive-ion 12 eV/EI mass spectrum of 1 and (b) collision-induced dissociation spectrum of the [M+H]+ ion produced under 12 eV/EI conditions.

spectrum (Fig 2b) of the $[M+H]^+$ ion did not show the peak of *m/z* 75 which may be originating from a hydrogen rearrangement like the McR reaction (Scheme 1)

It seems difficult to explain the formation of abundant fragment ions in the 12 eV/EI spectrum by the SI or a self-chemical ionization process. The resulted considerable fragmentation should be explained by the surface or thermal effect on the rhenium filament, or EI-induced fragmentation of the $[M+H]^+$ ions formed at 12 eV/EI conditions. Furthermore, negative-ion 8 eV/EI mass spectrum of **1** showed an intense peak of $[M-H]^-$ ion and it was almost independent of the impact energy (Fig.3).

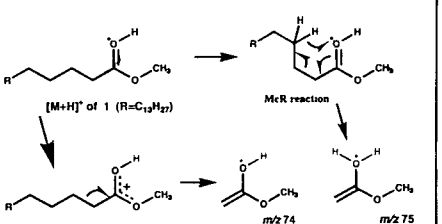

Scheme 1

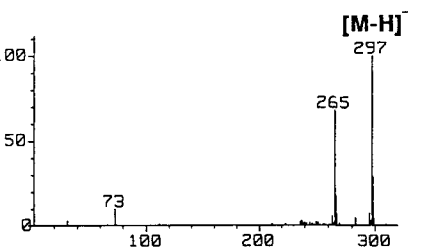

Fig.3 Negative-ion 8 eV/EI spectrum of 1.

References

1. Ryhage, R. and Stenhagen, E , *Mass Spectrometry of Organic Ions*, F.W. McLafferty (Ed.), Academic Press, New York, 1963, pp 399~452. 2. Zirroli, J A. and Murphy, R.C , *J. Am. Soc. Mass Spectrom*, **1992**, *4*, 223. 3 Vidavsky, I , Chorush, R.A., Longevialle, P and McLafferty, F.W., *J Am. Chem Soc.*, **1994**, *116*, 5865. 4. Fujii, T., *Int. J. Mass Spectrom. Ion Processes*, **1989**, *87*, 51. 5 Fujii, T., *Mass Spectrosc.* (Japan), **1989**, *37*, 259.

Gas-Phase Decomposition of Dimethyl(hydroxy)silyl Radical

Viet Q. Nguyen,[1] Scott A. Shaffer,[1] Frantisek Turecek,[1] and Cornelis E C A. Hop[2]
[1]Department of Chemistry, University of Washington, Seattle, WA 98195-1700
[2]Department of Chemistry, university of Wisconsin, Madison, WI 53706

Silicon radicals play an important role in chemical processes ranging from organic synthesis to microprocessor manufacturing.[1] Despite that extensive studies, both experimental and theoretical, have been conducted on radicals derived from silanes, alkyl silanes and halogenides,[2] much less is known about oxygenated silicon radicals

In this work, dimethyl(hydroxy)silyl radical $(CH_3)_2Si^{\cdot}OH$ (**1**) is generated and detected using neutralization-reionization mass spectrometry ($^{+}NR^{+}$) with dimethyldisulfide and oxygen as neutralization and reionization reagents, respectively. The tandem quadrupole mass spectrometer employed for our study was described in detail elsewhere [3] The cationic precursor for **1**, $(CH_3)_2SiOH^+$ ($\mathbf{1}^+$), is prepared as a stable fragment from either $(CH_3)_3SiOCH_2CH_3^{+\cdot}$ or $(CH_3)_3SiOH^{+\cdot}$. $(CD_3)_2SiOH^+$ ($\mathbf{2}^+$) and $(CH_3)_2SiOD^+$ ($\mathbf{3}^+$) are also generated from $(CD_3)_3SiOCH_2CH_3^{+\cdot}$ and $(CH_3)_3SiOCD_2CD_3^{+\cdot}$, to yield $(CD_3)_2Si^{\cdot}OH$ (**2**) and $(CH_3)_2Si^{\cdot}OD$ (**3**) upon neutralization, respectively

Upon $^{+}NR^{+}$, dimethyl(hydroxy)silyl radical **1** and/ or $\mathbf{1}^+$ from $(CH_3)_3SiOCH_2CH_3^{+\cdot}$ dissociates extensively on the μs timescale As a result, almost no survivor ion is detected. The $^{+}NR^{+}$ spectrum contains fragments of $CH_3SiOH^{+\cdot}$ (m/z 60), $SiOH^+$ (m/z 45), $SiO^{+\cdot}$ (m/z 44), $Si^{+\cdot}$, and CH_3^+ By contrast, $^{+}NR^{+}$ spectrum of $\mathbf{1}^+$ derived from $(CH_3)_3SiOH^{+\cdot}$ shows a portion of **1** that survives (1 2 % of ΣI_{NR}) Significant survivor ions of **2** and **3** are also detected in $^{+}NR^{+}$ spectra of both $\mathbf{2}^+$ and $\mathbf{3}^+$ at 1.3 and 2.4 % ΣI_{NR}, respectively. Ab initio calculations show substantial differences between the optimized geometries between **1** and $\mathbf{1}^+$ predicting large Franck-Condon effects that result from vertical neutralization of ground state $\mathbf{1}^+$ It is argued that increasing the fraction of higher energy $\mathbf{1}^+$ would result in a larger fraction of stable **1** upon neutralization, as in the case of $\mathbf{1}^+$ from trimethylsilanol Kinetic isotope effects and the increased fraction of vibrationally excited $\mathbf{2}^+$ and $\mathbf{3}^+$ due to the lower vibrational frequencies in the deuterated ions can account for the survivor ions of **2** and **3** observed in the $^{+}NR^{+}$ spectra The $^{+}NR^{+}$ spectrum of $\mathbf{1}^+$ shows conspicuous absence of m/z 47 (loss of C_2H_4) and m/z 74 (loss of $H^{\cdot}$), which both appear in the CAD spectrum of $\mathbf{1}^+$ This can be explained by the lack of the competitive pathway to lose C_2H_4 from reionized $\mathbf{1}^+$ Also, thermochemical arguments indicate that silanone$^{+\cdot}$ (m/z 74) is formed with high internal energy and dissociates readily.

References

(1) *Organosilicon Chemistry: From Molecules to Materials*, Auner, N; Weis, J Eds; VCH Publishers. Weiheim, 1994.
(2) Jasinski, J. M.; Gates, S. M *Acc. Chem. Res.* **1991**, *24*, 9
(3) Turecek, F *Org. Mass Spectrom.* **1992**, *27*,1087.

Neutral and Ion Optimized Geometries (HF/6-31+G*)

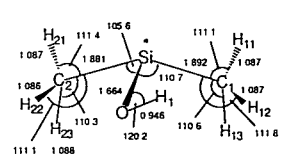

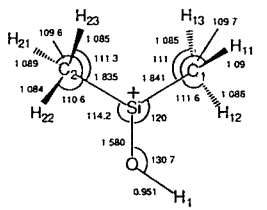

$^{+}NR^{+}$ (CH_3SSCH_3/O_2)

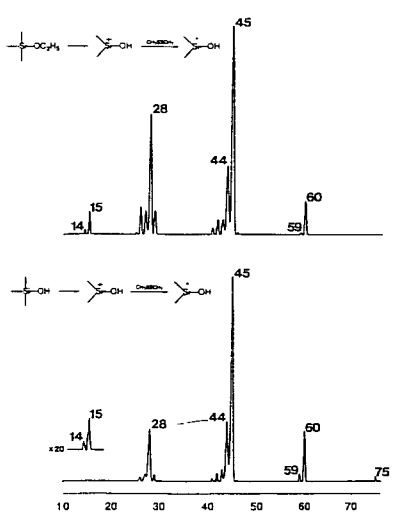

VERTICAL NEUTRALIZATION

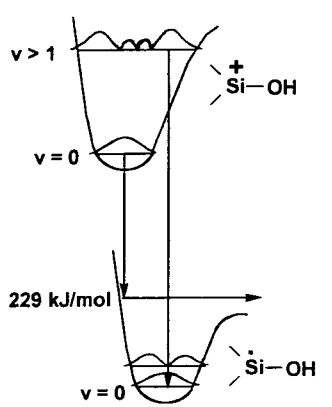

Study of the evolution of the m/z 91/92 ratio during CAD of butylbenzene molecular cations under multiple collision conditions

Beaugrand#, C.; Leymarie*, N.; Rolando*, C.; Sablier*, M.
(#) AIRND 35, rue Victor Hugo - 78230 Le Pecq (France)
(*) Ecole Normale Supérieure, Processus d'Activation Moléculaire U.R.A. 1679
24, rue Lhomond - 75231 Paris cédex 05 (France)

Fragmentation of the butylbenzene molecular cation is one of the most studied topics in mass spectrometry (1). The ratio of m/z 91 ion to m/z 92 ion has been used as a "thermometer" for studying the internal energy of precursor ions in many different processes: electron impact ionisation, photoionisation, CAD at low, intermediate and high energy. A set of thermochemical data has been established for this decomposition using PEPICO experiment and RRKM calculation (2). In all these processes, the decomposition of the excited molecular ion is unimolecular, and the fragments are not allowed to collide with a neutral gas. More recently the same concept has been applied to CAD under multiple collisions such as those occurring in an ion trap. However, ions of mass 91 and mass 92 exhibit very different behaviour.

Using our MS/MS/MS multiquadrupole, we have been able to perform CAD in the first collision cell on the butylbenzene molecular cation, then select the m/z 91 ion, m/z 92 ion or both for purpose of studying their CAD under multiple collision condition in the second cell. Results for the unselected m/z 91 and m/z 92 ions, and for selected m/z 92 ion are presented on the figures below.

Under multiple collision conditions the two fragment ions exhibit strongly different behaviour :

- the ion of mass 92 is more easily broken than that of mass 91 ion so the ratio m/z 91 to m/z 92 increases.
- One major breakdown pathway for the ion of mass 92 is the loss of hydrogen leading to m/z 91.

These two effects are cumulative, so the ratio of m/z 91 to m/z 92 ions is not constant and is very sensitive to additional collisions.

This ratio needs to be used carefully for estimating the transfer energy process to the precursor molecular ion under multiple collision conditions.

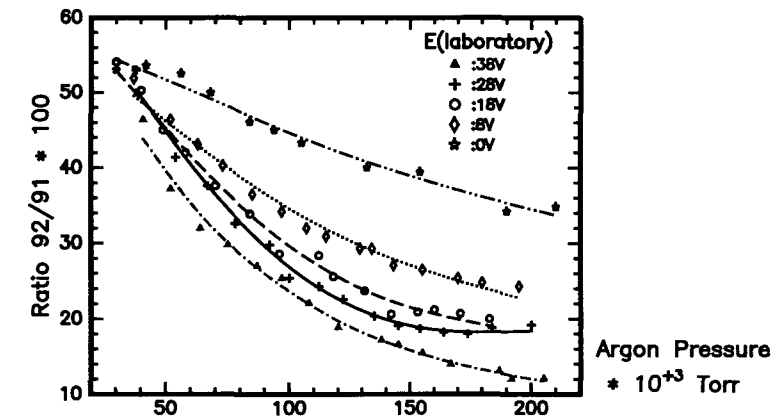

Variation of the m/z 92 to m/z 91 intensity ratio in function of the pressure of argon in the collision cell for various energy (laboratory frame) starting from a mixture of m/z 91 and m/z 92 ions :

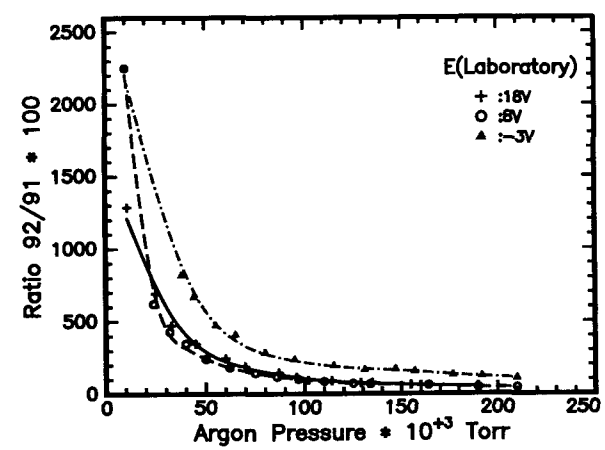

Variation of the m/z 92 to m/z 91 intensity ratio in function of the pressure of argon in the collision cell for various energy (laboratory frame) starting from m/z 92 ion :

(1) Kuck, D, Mass Spectrometry Review, 9, 187-234 (1990)
(2) Baer, T.; Dutuit, O.; Mestdagh, H. Rolando, C., J. Phys. Chem, 92, 5674-5679 (1988).

Can Protonated Peptides Fragment from Their Triplet States?

Árpád Somogyi, Vicki H. Wysocki
Department of Chemistry, Virginia Commonwealth University, Richmond VA 23284-2006, U.S.A.

István Mayer
Central Research Institute for Chemistry of the Hungarian Academy of Sciences, P. O. Box 17, H-1525 Budapest, Hungary.

Due to increasing numbers of experimental and theoretical studies, knowledge of peptide fragmentation is improving. Although there are some contradictory results and opinions, it is generally accepted that proton transfers within a protonated peptide can precede fragmentation. Our recent *ab intio* and MNDO bond order, as well as MNDO energy partitioning calculations[1,2] support this idea. Bond strength patterns (defined originally in Reference 2) show significant differences for different protonated forms of the same peptide. For example, in the energetically more stable amide oxygen protonated form, the strengthening of the amide bond indicates a non-fragmenting structure. In contrast, the energetically less favored amide nitrogen protonated form is a fragmenting structure, because the amide bond is significantly weakened. These results suggest that not all protonated forms undergo fragmentation and that thermodynamically less stable forms should also be considered in peptide fragmentation.

All the above conclusions were based on the assumption that protonated peptides fragment from their *ground (singlet) electronic* state. In the present study, *ab initio* (6-31G*) and MNDO bond orders and MNDO energy partitioning[3] values have been calculated and used to predict the bond strengths in protonated diglycines in their *triplet* states. For different protonated forms, several "triplet" UHF solutions were found that are close to each other in energy. This may indicate the existence of different close lying excited triplet states of these species. Comparisons with resent results for protonated peptides in *singlet* states show that the bond strength patterns are similar in singlet and triplet states in most cases. However, in one of the amide oxygen protonated triplets, the amide bond is predicted to be weakened; this could generate its easy cleavage (Figure 1). Nine different singlet → triplet excitations have been considered and characterized by using the MNDO energy partitioning method[3] for each of the protonated forms.

An energetic discussion based on MP2 6-31G*//6-31G* SCF total energies is also given for both singlet and triplet protonated diglycines. The formation of triplet protonated diglycines from the corresponding singlets requires an energy of 5.5-7.0 eV (Figure 2). The order of the relative stability of the singlet and triplet protonated forms is different; the most stable forms are the N-terminal protonated form for singlets, and the N-amide protonated form for the triplets (Figure 2). Although further experimental and theoretical evidence is necessary to prove (or exclude) the role of the triplet states in peptide fragmentation, the present results suggest that triplet states could be involved in the fragmentation of protonated peptides.

43rd ASMS Conference on Mass Spectrometry and Allied Topics

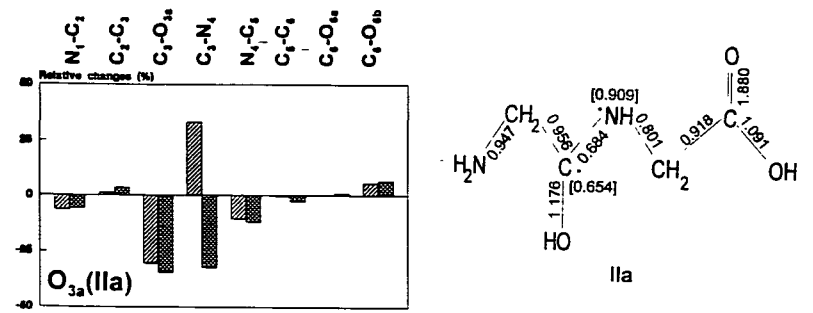

Figure 1 6-31G* bond strength pattern and bond orders and [free valences] for an amide-O protonated triplet.

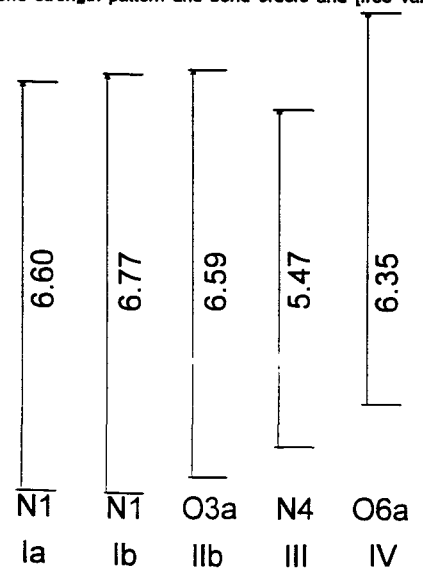

Figure 2 MP2 6-31G*//6-31G* SCF relative energies of singlet and triplet protonated diglycines (ev).

1 McCormack, A.L.; Somogyi, Á.; Dongré, A. R.; Wysocki, V. H. *Anal. Chem.* **1993**, *65*, 2859-2872.

2 Somogyi, Á.; Wysocki, V. H.; Mayer, I. *J. Am. Soc. Mass Spectrom.* **1994**, *5*, 704-717.

3 (a) Mayer, I.; Gömöry, Á. *Int. J. Quantum Chem., Symp.* **1993**, *27*, 599. (b) Mayer, I.; Gömöry, Á. *J. Mol. Struct. (Theochem)* **1994**, *311*, 331.

Elucidation of Mass Spectrometric Decomposition Mechanisms in the Compound 2,3-Difluoro-dimethyl-succinic Acid Diester

David M. Parees
Air Products and Chemicals, Inc., 7201 Hamilton Blvd., Allentown, PA 18195

The electron ionization spectrum of the title compound (Figure 1) contains a number of surprising ions and a significant number of the relatively intense ions obviously require rearrangements. This compound decomposes through interesting pathways, including losses of carbon dioxide, formaldehyde and methyl radicals. The molecular losses involve rearrangements of methyl (loss of carbon dioxide) and hydrogen (loss of formaldehyde) radicals. Succinic acid diesters have been studied before and a range of interesting losses and hydrogen and group migrations have been reported (1-4). In the present work, high resolution and exact mass analysis techniques defined the elemental composition of fragment ions. Low energy collision tandem mass spectrometry on a hybrid magnetic sector-quadrupole instrument provided data concerning the pathways of decomposition (see Figures 2, the precursors of m/z = 93, and 3, the progeny of m/z = 138).

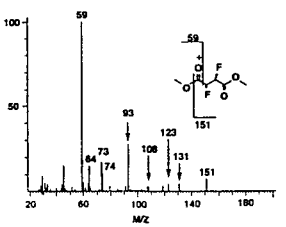

Figure 1

It appears that after initial loss of carbon dioxide, the ion at m/z = 138 (which is 0.15% relative to the base ion in the EI spectrum) can decompose with sequential losses of a methyl group (leading to the ion at m/z = 123) followed by loss of formaldehyde, to form the ion at m/z = 93. Similarly, these losses can occur in the reverse order, leading to the intermediate ion at m/z = 108. Analysis of a stable isotope labeled analog, in which all methyl hydrogens were replaced with deuterium, provided proof of radical movement from one part of the molecule to another. Shifts in the masses of some fragment ions, caused by the mass difference between hydrogen and deuterium, provided confirming evidence tracing migrations of hydrogen and methyl radicals. Exact mass analyses of some of these ions confirmed these rearrangements.

The ion at m/z = 74 was shown by exact mass measurement to not be a product of the decomposition of the ion at m/z = 93. The ion at m/z = 93 has two fluorine atoms and the ion at m/z = 74 has none. This decomposition pathway requires the shift of a methyl radical from one end of the molecule to the other, coupled with the loss of the middle portion of the molecule. The ion at m/z = 74 has the elemental composition $C_3H_6O_2$. This ion was examined by MS/MS and compared with the molecular ion of methyl acetate, which produced a significantly different spectrum.

Another fragment ion, containing only the fluorinated central portion of the molecule, was also surprising because of the required losses and its intensity in the spectrum.

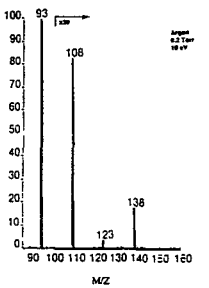

Figure 2

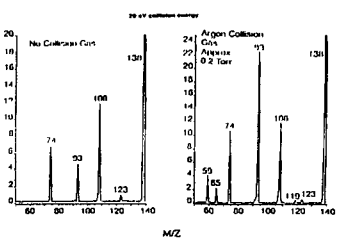

Figure 3

1. D. Bornstein, B. Domon, A. Mandelbaum, D. Mueller and W. J. Richter, Proceedings of the 34th Annual Conference on Mass Spectrometry and Allied Topics, June 8-13, 1986, Cincinnati, Ohio, pg. 95.

2. A. G. Harrison, R. K. M. R. Kallury, U. J. Krull and M. Thompson, Org. Mass Spectrom., **23**, 723 (1988).

3. I. Vidavsky, A. Mandelbaum, T. Tamiri and S. Zitrin, Org. Mass Spectrom., **26**, 287 (1991).

4. I. Vidavsky and A. Mandelbaum, Org. Mass Spectrom., **27**, 847 (1992).

Energy Resolved Mass Spectrometry of Organophosphonates

Michael W. Wensing, Brad E. Forch, Robert A. Fifer
U.S. Army Research Lab, Aberdeen Proving Ground, MD 21005
A. P. Snyder and C.S. Harden
U.S. Army, Edgewood Research Development and Engineering Center
Aberdeen Proving Ground, MD 21010

Organophosphonate compounds are a subgroup of the important organophosphorus compounds (OPCs). OPCs have been used in several applications including pesticides, plasticizers, pharmaceuticals, nerve gas agents, and lubricants. Their detection and differentiation is becoming a problem of increasing analytical importance. Detailed studies of the dissociation of OPCs can directly benefit the analyst who must detect and differentiate these compounds.

Energy resolved mass spectrometry (ERMS) is a very useful technique. Unlike MS/MS where collisions between a parent ion and an inert gas are usually carried out at a fixed parent ion energy, ERMS involved carrying out MS/MS at several parent ion energies. Parent ion energies are varied over a range which results in no dissociation of the parent ion to complete dissociation of the parent ion. The sequential nature of the dissociation of the parent ion is revealed directly in ERMS, but must be inferred in MS/MS. ERMS has been used to characterize the dissociation of odd electron molecular ions produced by electron ionization, however, ERMS has not been used extensively in characterizing the dissociation of even electron molecular ions produced by atmospheric pressure chemical ionization (APCI). Since very sensitive detection of OPCs is achieved by APCI due to the high proton affinity associated with these compounds, characterizing their dissociation pathways by APCI-ERMS has increased importance.

In this work, ERMS was used to characterize the dissociation pathways of two homologous series of phosphonate compounds. The first study involved the dissociation of diethyl alkyl phosphonates, specifically, diethyl methyl phosphonate (DEMP), diethyl ethyl phosphonate (DEEP), diethyl n-propyl phosphonate (DEPP), and diethyl n-butyl phosphonate (DEBP). All these compounds differ by the alkyl group which is directly attached to the phosphorus atom. The second study involve the dissociation of dialkyl methyl phosphonates, specifically, dimethyl methyl phosphonate (DMMP), diethyl methyl phosphonate (DEMP), diisopropyl methyl phosphonate (DIMP), and isopropyl methyl phosphonate (IMMP).

Neat samples of these compounds were analyzed via headspace analysis. Sample vapors were carried into the ion source aided by an exhaust motor and protonated via a corona discharge. The resultant parent ions traveled through a 2 mm orifice, a N_2 curtain gas region, a smaller orifice, and into the high vacuum region of a triple quadrupole mass spectrometer. The energy of the parent ions was increased by ramping the potential on the smaller orifice and keeping all the other lens elements at a fixed potential. Progeny ions were subsequently detected by scanning the first mass analyzer, Q1. The conventional collision cell, Q2, was not filled with Ar, and the third mass analyzer was operated in RF only mode.

The protonated parent ions of the diethyl alkyl phosphonates all undergo two sequential McLafferty rearrangements and produce two molecules of ethylene. The maximum intensity of the ion that is formed after the second McLafferty rearrangement is more intense than that of the ion that is formed after the first McLafferty rearrangement. This is consistent with what would be expected for two sequential and approximately equal, low energy pathways. The ion

resulting from the second McLafferty rearrangement further dissociates via either the loss of H_2O or the loss of R'OH where the R' group is the alkyl group that is directly attached to the phosphorus atom. The loss of H_2O is predominant at low parent ion energies for all compounds. This information is consistent with the more exothermic heat of formation of H_2O than the resulting alcohols. At higher parent ion energies the loss of R'OH becomes predominant for DEEP, DEPP, and DEBP.

The initial McLafferty rearrangement cannot be used to distinguish the dissociation of the parent ions of the diethyl alkyl phosphonates studied since all dissociate at similar energies. However, the ions that result from the second McLafferty rearrangement (protonated alkyl phosphonic acids) dissociate at resolvable energies. The protonated acid of DEBP is the most stable, dissociates least while the protonated acid of DEMP is the most stable and dissociates most. This leads to the conclusion that the R' group stabilizes the positive ion. The larger the R' group, the greater the electron-donating power and the more stable the ion.

Dialkyl methyl phosphonates where both alkyl groups are at least ethyl groups can be distinguished from their counterparts where the alkyl group attached to the phosphorus atom is larger than methyl. At high and low energies protonated methyl phosphonic acid which results from the CAD of DIMP and DEMP predominantly loses H_2O. At low energies, protonated alkyl phosphonic acids where the alkyl group is ethyl or larger predominantly lose water, while at high energies the these protonated acids predominantly lose R'OH.

DIMP and DEMP are distinguishable by ERMS. The McLafferty rearrangement that results in the loss of propylene occurs at a lower energy than the one the results in the loss of ethylene.

IMMP and DIMP are also distinguishable by ERMS. Both lose propylene via a McLafferty rearrangement, however, since IMMP cannot undergo another McLafferty rearrangement the intensity of its first generation product ion reaches a much larger maximum intensity than of the corresponding first generation product ion of DIMP.

DMMP is distinguishable from all the rest of the compounds studied in that it cannot undergo a McLafferty rearrangement. Therefore the protonated parent ion of DMMP is more stable than the protonated parent ion of any of the other compounds studied.

Energy Resolved Mass Spectrometry of Organophosphorus Esters

Michael W. Wensing, Brad E. Forch, Robert A. Fifer
U.S. Army Research Lab, Aberdeen Proving Ground, MD 21005
A. P. Snyder and C. S. Harden
U.S. Army, Edgewood Research, Development and Engineering Center
Aberdeen Proving Ground, MD 21010

Organophosphonate compounds are a subgroup of the important organophosphorus compounds (OPCs). OPCs have been used in several applications including pesticides, plasticizers, pharmaceuticals, nerve gas agents, and lubricants. Their detection and differentiation is becoming a problem of increasing analytical importance. Detailed studies of the dissociation of OPCs can directly benefit the analyst who must detect and differentiate these compounds.

Energy resolved mass spectrometry (ERMS) is a very useful technique. Unlike MS/MS where collisions between a parent ion and an inert gas are usually carried out at a fixed parent ion energy, ERMS involved carrying out MS/MS at several parent ion energies. Parent ion energies are varied over a range which results in no dissociation of the parent ion to complete dissociation of the parent ion. The sequential nature of the dissociation of the parent ion is revealed directly in ERMS, but must be inferred in MS/MS. ERMS has been used to characterize the dissociation of odd electron molecular ions produced by electron ionization, however, ERMS has not been used extensively in characterizing the dissociation of even electron molecular ions produced by atmospheric pressure chemical ionization (APCI). Since very sensitive detection of OPCs is achieved by APCI due to the high proton affinity associated with these compounds, characterizing their dissociation pathways by APCI-ERMS has increased importance.

In this work, ERMS was used to characterize the dissociation pathways of two series of organophosphorus compounds. The first series include dimethyl methyl phosphonate (DMMP), trimethyl phosphate (TMP), trimethyl phosphite (TMPI), and dimethyl phosphite (DMPI). All of these compounds have similar structures and lose similar neutrals. The second series of compounds included four trialkyl phosphates, specifically, trimethyl phosphate (TMP), triethyl phosphate (TEP), tripropyl phosphate (TPP), and tributyl phosphate (TBP).

Neat samples of these compounds were analyzed via headspace analysis. Sample vapors were carried into the ion source aided by an exhaust motor and protonated via a corona discharge. The resultant parent ions traveled through a 2 mm orifice, a N_2 curtain gas region, a smaller orifice, and into the high vacuum region of a triple quadrupole mass spectrometer. The energy of the parent ions was increased by ramping the potential on the smaller orifice and keeping all the other lens elements at a fixed potential. Progeny ions were subsequently detected by scanning the first mass analyzer, Q1. The conventional collision cell, Q2, was not filled with Ar, and the third mass analyzer was operated in RF only mode.

The first series of compounds have similar losses. DMMP and TMP which both have a phosphoryl moiety lose CH_3OH predominantly. TMPI loses CH_3OCH_3 predominantly, but also loses CH_3OH. DMMP and TMP both have stronger alkoxy P-O bonds than TMPI. These bond strengths have been measured by others. This presumably does not allow much interaction between the adjacent methoxy groups which should be necessary to lose CH_3OCH_3. Therefore, the loss of CH_3OH is the predominant loss observed. TMP is observed to lose more CH_3OCH_3 than DMMP, which would be expected since statistics favor the loss of CH_3OCH_3 by 3:1 for

TMP assuming the P-CH_3 moiety is not involved. When TMPI is protonated a dipole is set up which attracts the neighboring methoxy group. This assists in the loss of CH_3OCH_3. TMP and TMPI have statistically the same probability of losing CH_3OCH_3, however, the weaker alkoxy P-O alkoxy bond of TMPI favors the dimethyl ether loss with respect to TMP.

DMPI predominantly loses CH_3OH. This is a very suprising result since the loss of H_2O would normally be expected. However, DMPI when it undergoes multiple collisions may isomerize to dimethyl hydrogen phosphonate, and then would not be expected to lose H_2O. This would explain the observed predominant loss of CH_3OH. The main conclusion reached is that the loss of CH_3OCH_3 does not predominate when a phosphoryl moiety is present.

The second series of compounds undergo similar decomposition mechanisms. Trialkyl phosphates where both alkyl groups are larger than ethyl, undergo three sequential McLafferty rearrangements. The ion which results from the third McLafferty rearrangement reaches the largest maximum intensity which is consistent with this low energy mechanism. This ion appears to be very stable and dissociates only to a small extent losing H_2O.

Effect of Multiple and Single Collision Conditions on the Reproducibility of FAB-MS/MS Spectra Obtained using the Calibration Point Method

Sharon W. Lemire and Kenneth L. Busch, School of Chemistry and Biochemistry, Georgia Institute of Technology, Atlanta, GA 30332-0400

The reproducibility of product ion spectra in MS/MS is dependent on instrumental parameters such as type and pressure of collision gas, collision energy and rf tuning. These parameters are difficult to reproduce from instrument-to-instrument, or even from day-to-day on the same instrument. To compare MS/MS spectra from different instruments, or to develop a library-quality database, instrument-independent spectra must be reproducibly acquired. Generation of reproducible MS/MS spectra requires a calibration method that is simple, reliable, applicable to a wide range of compounds, and independent of type of collision gas. Several researchers have proposed calibration methods, but so far no one has developed a method that is easily applied to all types of instruments and to a wide range of compounds. The calibration method presented here uses an empirically determined calibration point based on a variable collision energy at a set target thickness to acquire product ion spectra from precursor ions ionized by LSIMS. A similar protocol for EI-MS/MS produced data with spectral similarities of 80-90% between a VG70-SEQ and Finnigan MAT TSQ-70. Spectral similarities of 85% were obtained under both single (SC) and multiple collision (MC) conditions.

The experimental setup has been previously described.[1] Product ions were produced by collision-induced dissociation in an rf-only quadrupole collision cell with argon as the collision gas. The precursor ion was attenuated by approximately 80% for MC conditions, giving a reading of 2.3 x 10^{-5} mbar on the ion gauge nearest the cell, and by approximately 25% for SC conditions, giving a reading of 5.4 x 10^{-7} mbar. These readings were corrected for argon response. The collision energy ranged from 25 to 43 eV for MC and from 162 to 185 eV for SC. The rf voltage was set at 75V.

The calibration point compound, 2-butyl-triphenyl-phosphonium bromide (2-BTPP), was used because it is easy to handle and produces a stable, long-lived signal. *Meta*-nitrobenzyl alcohol (*m*-NBA) was selected as the matrix because it readily solubilizes 2-BTPP and it provides long ion lifetimes in the ion source. Model compounds used previously[1] were of a mass equal to or less than the mass of the calibration compound (m/z 319). To determine the useful mass range of this technique, compounds with masses of up to m/z 726 were added to the trial set. The following additional compounds were chosen to represent classes of compounds commonly analyzed by FAB/LSIMS: thiamine hydrochloride (Vitamin B1), acridine orange-10 nonyl bromide (A-1372), diphenyl 4-dodecoxyfluorophenylsulfonium antimony hexafluoride (New Sulf), 1,1'-didodecyl-3,3,3',3'-tetramethylindocarbocyanine perchlorate (D-383), 3,3'-dihexadecyloxacarbocyanine perchlorate (D-1125).

The calibration point, which has also been previously defined[1], was determined prior to each run, and then the product ion spectrum for each compound was acquired. For each MS/MS spectrum, the seven most abundant ions in the spectrum were chosen for statistical evaluation. After the ion intensities were renormalized to the most abundant product ion, a comparison of the spectra obtained under MC and SC conditions for each model compound was made using the mean relative intensities (mean RI). The mean RI of the seven selected product ions for both conditions are shown in Table 1. Except for a few product ions, the mean intensities under the two conditions are similar. Even when the mean intensity of a product ion differs significantly between MC and SC conditions, the same general pattern relative to the other product ions is maintained. This pattern similarity was shown previously for spectra obtained from day-to-day under the same conditions. For compounds with masses from 269 to 726, approximately 60% of the product ions fell within 30% of the mean RI under MC conditions. Under SC conditions, approximately 80% of the product ions from compounds with masses from 153 to 465, fell within 30% of the mean RI.

The reproducibility of spectra obtained from day-to-day under both MC and SC conditions was also assessed based on the similarity index for the seven selected product ions. Two MC and two SC runs were randomly selected for this evaluation. A similarity index expresses the percent run-to-run difference for each ion:

$$(|I_a - I_b|)/[(I_a + I_b)/2] \times 100\% \qquad \text{(Eq 1)}$$

where I refers to the percent contribution of each ion to the total intensity and the subscripts refer to two separate runs. As shown in Table 1, most of the spectra is more reproducible under SC conditions, but the two compounds of highest mass are more reproducible under MC conditions. Compounds with masses similar to the calibration point compound (C^+ = 319) show similar reproducibilities under both conditions. As the masses of the model compounds deviate in either direction from that of the calibration compound, the reproducibility under SC conditions deteriorates. Under MC conditions, reproducibility worsens as the masses of the model compounds decrease but remains constant as the masses increase. Overall spectral reproducibility was assessed based on the percentage of ions that possessed a similarity index of less than 30%. SC conditions produced data with spectral similarities of 85% or better for model compounds with masses from 227 to 465 Da and MC conditions produced data with spectral similarities of 85% or better for model compounds with masses from 319 to 726 Da. Spectral reproducibility assessed by comparing percent deviation from the mean relative intensity and by comparing similarity indices for MC and SC conditions produced similar results. Both methods show that, in general, spectral reproducibility is better for SC conditions, but over a narrower mass range. Thus the primary limitation of this technique seems to be the deterioration of spectral reproducibility at masses significantly different from the calibration compound. This limitation may be overcome by using more than one calibration compound to cover the necessary mass range.

1. Lemire, S. W., Bartlett, M. G. and Busch, K. L., *Proceedings of the 42nd ASMS Conference on Mass Spectrometry and Allied Topics*, 508 (1994).

Table 1.
Comparison of Ion Intensities Under MC and SC Conditions

	m/z	Mean MC	Mean SC	Similarity Index MC	Similarity Index SC
m-NBA (MW = 153)	63	13	9	97	39
	77	33	55	36	38
	89	87	100	14	9
	95	7	7	44	24
	107	9	47	116	6
	124	7	50	140	80
	136	3	16	159	84
HMI (C+ = 227)	115	1	6	62	2
	143	1	3	33	2
	158	3	4	5	41
	169	9	37	33	4
	184	91	50	11	7
	197	2	10	5	26
	212	76	100	16	2
Vit B1 (C+ = 265)	81	16	17	44	29
	122	100	100	13	7
	144	37	20	34	7
	177	0.4	0.8	200	4
	182	0.8	0.8	69	22
	207	2.9	1.9	71	11
	224	0.7	1.5	111	7
Suf (C+ = 269)	77	3	28	68	46
	115	27	28	87	26
	128	29	13	94	7
	147	11	12	77	7
	154	7	4	19	10
	160	82	32	18	23
	192	89	100	38	19
n-BTPP (C+ = 319)	108	34	43	58	26
	152	6	6	17	10
	183	98	100	3	10
	185	40	45	3	4
	262	37	51	5	17
	263	57	22	17	1
	275	26	29	18	26
A-1372 (C+ = 392)	222	7	14	23	14
	223	15	17	6	11
	236	6	10	23	2
	250	36	70	30	4
	264	8	41	4	7
	265	47	91	9	11
	266	100	91	6	15
New Suf (C+ = 465)	77	0.8	6	20	20
	107	2	4	73	5
	141	0.5	1	73	30
	170	100	100	7	5
	220	16	27	22	34
	388	0.8	2	15	11
	465	8	66	60	1
D-383 (C+ = 666)	312	32	33	31	3
	336	66	55	20	70
	352	12	13	17	30
	481	12	17	14	131
	494	10	16	15	58
	636	93	59	21	91
	650	83	97	3	13
D-1125 (C+ = 726)	159	10	27	42	15
	196	12	14	18	52
	259	8	29	7	66
	277	66	80	5	75
	342	98	79	11	83
	368	49	47	23	6
	501	38	31	7	40

"SUPRESSION" OF α-AMINO ACIDS SIGNALS IN COAXIAL CF/FAB

Francisco M. L. Amado*, Pedro M. N. Domingues, Cristina M.F.Barros, M. Graça O. Santana Marques and A. J. Ferrer Correia

Department of Chemistry, Mass Spec. Lab., University of Aveiro, 3800-Aveiro, Portugal

The variation of the relative abundances of the protonated ions from several amino acids, isolated and in binary mixtures, using coaxial CF/FAB, is discussed and a general supression mechanism is suggested.

Data presents two well-defined series. In the first series (hydrophobic/high volatility amino acids), the RA decreases with the increase of the B.B. index (Figure 1). In the second series (hydrophilic/low volatility amino acids) the RA decrease with the proton affinities (Figure 2). In this serie correlation with BB values is not apparent. These data shows that the abundances of the protonated amino acids depend on the ability of neutral species for changing from the liquid-phase to a gas-phase like, i.e. of its concentration in that phase. Once there, the relative abundances of protonated ions are the result of a competition process determined by the proton affinities of the amino acids.

There is no significant variation of the total ion current whenever an amino acid sample is introduced using coaxial CF-FAB. The increase of the ion current of the protonated molecular amino acid isolated or within a mixture (Figure 3) is compensated by the decrease of the protonated glycerol (and cluster glycerol ions). Results of binary mixtures of amino acids, compared with the relative abundances of protonated ions when isolated, show not only a decrease in the glycerol ion signal but also a decay of the ion current of each amino acid within the mixture. In face of these results its possible to assume that there is a limit for the number of ions that can be formed at a given moment in FAB, under the same experimental conditions.

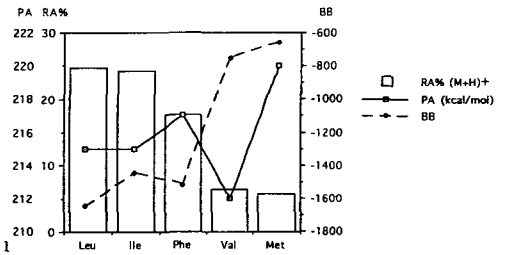

FIGURE 1

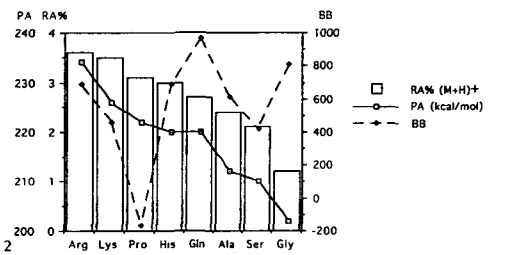

FIGURE 2

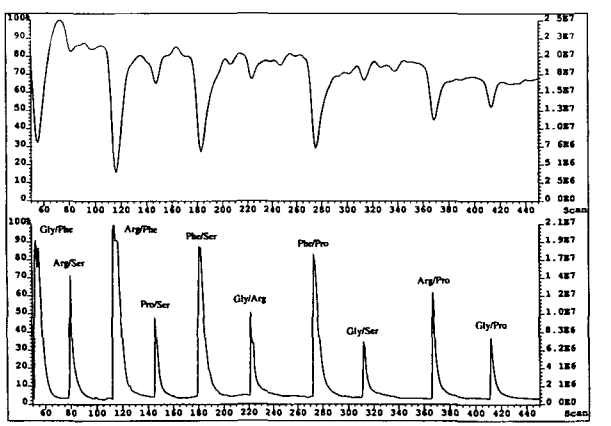

FIGURE 3- Ion current of the protonated molecular ions of glycerol and of binary mixtures of amino acids - a) non normalised ion current of psedomolecular ion of injected amino acids mixtures; b) ion current of psedomolecular ion of glycerol.

PDMS Analysis of Frozen Cycloalkenes

R. L. Betts, E. F. da Silveira† and E. A. Schweikert

Center for Chemical Characterization, Texas A&M University, College Station, TX 77843-3144, USA

† Departamento de Física, Pontifícia Universidade Católica, C P 38071 Rio de Janeiro 22452-970, Brazil

In order to determine the influence of stoichiometry on desorption mass spectra, frozen cyclohexane, cyclohexene, 1,3-cyclohexadiene and benzene surfaces have been bombarded with ^{252}Cf fission fragments Secondary ions were accelerated over 3 5 mm by a 2 8 kV potential difference and analyzed by a 62 cm long time-of-flight spectrometer Samples were leaked into the analyzing chamber and condensed on a plate cooled to liquid nitrogen temperatures. In spite of a base pressure of 8 x 10^{-8} mbarr, water peaks (e.g , m/z = 18, 10 and 37) are seen in the spectra

We have found that the desorption yields of the $C_nH_m^+$ secondary ions follow certain general trends a) even-electron species are generally more abundant than odd-electron species; b) more saturated ions are more abundant than less saturated ions if the sample is a more saturated compound, and vice-versa, c) these trends are observed for all $C_nH_m^+$ groups except for the molecular ion group Trends a and c are illustrated in Fig 1, where the PDMS positive ion mass spectra, corresponding to the most saturated sample (cyclohexane) and the least saturated sample (benzene), are presented Even-electron species are known to be generally more stable than odd-electron species and, for them, a relative high abundance is expected Molecular or quasi-molecular peaks are also expected to be abundant because they are formed relatively far from the impact site and may easily gain or lose a few hydrogen atoms Trend b is better observed by calculating the ratio of the two spectra, i.e , by dividing the desorption yield distribution corresponding to the benzene sample by that one obtained from cyclohexane This ratio is presented in Fig 2a for the $C_nH_m^+$ groups (C_1 to C_5) lighter than the molecular peak group (C_6) In Fig. 2b this ratio is shown for the desorbed hydrogen group (H^+, H_2^+ and H_3^+), for the molecular peak group and two heavier ones (C_6, C_7 and C_8) Data corresponding to water dusters are not represented. One sees clearly a general decreasing of the desorption yield rates when the hydrogenation increases The light $C_nH_m^+$ group yield ratio exhibits roughly an exponential decay with hydrogenation, while the heavier groups are more sensitive to the sample molecular structure

It is interesting to note that similar results are obtained when one compares PDMS desorption yields of hexane and benzene [1] These observations suggest that stoichiometry effects, for the light groups, are more dominant than effects due to the initial molecular structure Such results are compatible with a plasma model formation for the low mass $C_nH_m^+$ desorbed ions Stoichiometry alters not only the ratio between C and H

atoms in the gas phase but also density, melting point and stopping power for the ^{252}Cf fission fragments These factors modify the plasma temperature and, as a consequence, the relative abundance of the formed species before the beginning of the free-expansion process Calculations assuming a quasi-equilibrium plasma indicate that temperatures of 5000 - 7000K are necessary to reproduce qualitatively the observed relative desorption yields The ratio between charged and neutral species is predicted to be 3 x 10^{-4}

CONCLUSION

PDMS mass spectra of frozen C_6 cyclohydrocarbons were obtained and compared A gradual and systematic influence due to their stoichiometry is observed in the desorption yield of $C_nH_m^+$ ions Abundances of highly saturated emitted species increases with increasing saturation of the sample For emitted species lighter than the quasi-molecular ion peaks, the memory of the sample molecule structure appears to be lost, increasing evidences for intense chemical interaction after the projectile impact

Taking into account that different stoichiometry also corresponds to different density, melting point and stopping power for the ^{252}Cf fission fragments, the observed relative desorption yields are compatible with the production of low mass ions in a plasma.

Fig 1

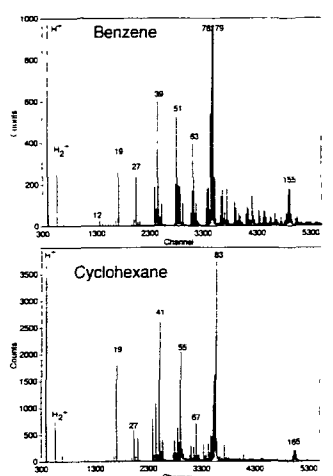

Fig 2a

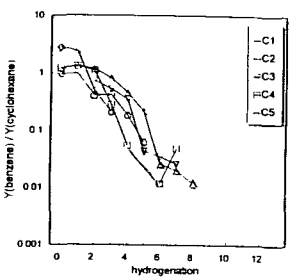

Fig 2b

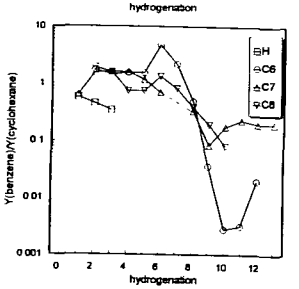

REFERENCES

1 M Wagner, K. Wien, B Curdes and E R. Hilf, *Nucl. Instrum and Meth.*, B 82 (1993) 362.

This work was supported by NSF Grant CHE-9208185 and by CNPq (Brazil)

Biomolecular Cluster Formation in PDMS

P. Demirev, J.Eriksson, P.Håkansson, R.Papaléo, B.Sundqvist, R.Zubarev,
Division of Ion Physics, Department of Radiation Sciences,
Uppsala University, box 535, Uppsala S-75121, SWEDEN

Non-covalent cluster ions of biomolecules are often observed with various ionization techniques. In desorption ionization, e.g. FAB, PDMS and MALDI, it is still an open issue whether clusters are ejected as intact species, pre-existing on the surface, or they are formed during the desorption process. This question is directly coupled to the successes of MS as an emerging method for probing non-covalent interactions between biomolecules, including immunological response monitoring.

We have studied the formation of heteroclusters - dimers and trimers - in PDMS from targets containing mixtures of biomolecules. The targets included aminoacids - Ile (MW 131), and Phe (MW 165), and nucleosides - cytosine (dC, MW 227), adenine (dA, MW 251), and guanine (dG, MW 267). The targets were prepared by depositing sample solutions on thick Si backing (frontside desorption), or 2 μm aluminized Mylar foils (backside desorption). Evaporation resulted in microcrystalline films with submicron thickness. The aminoacid and the nucleotide mixtures were dissolved in glacial acetic acid and water, respectively. This target preparation technique was chosen in order to alleviate the influence on cluster formation of other target preparation techniques, employed in PDMS, such as electrospraying or adsorption to a nitrocellulose membrane. The "Diploma" reflectron TOF spectrometer, coupled to one of the beam-lines of the Uppsala Tandem accelerator [1], or a commercial "Bioion" spectrometer, also fitted with a reflectron, were used for PDMS. Swift iodine ions (72.3 MeV) or ^{252}Cf fission fragments were used as primary ions, incident at 45° from the front, or normally from the back side, respectively. Initial radial velocity distributions of ejected molecular, homo- , and heterocluster ions were determined on the "Diploma" spectrometer by measuring the ion yield as a function of deflection in radial direction according to already described procedures [2]. Typically 2.10^6 start events provided satisfactory secondary ion statistics.

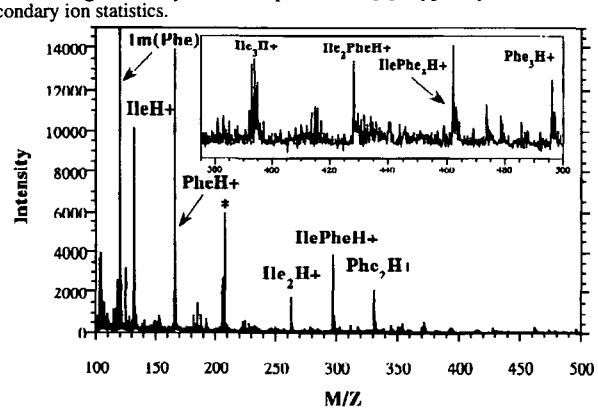

Fig. 1 PD mass spectrum from a Ile-Phe target;
inset : expanded view (m/z 370 to 500) of the trimer cluster region.

43rd ASMS Conference on Mass Spectrometry and Allied Topics

A characteristic mass spectrum of the Ile-Phe mixture is presented on fig. 1. Peaks, corresponding to the respective homo- and hetero- dimer and trimer ions are clearly discerned. Interstingly, an intense peak (denoted with * on Fig. 1) coinciding in mass to the complex of the two immonium ions is also observed. The heterodimer peak in this and in other cases examined (Val+Leu, Phe+Trp, Tyr+His, Val+Cys, Ser+Phe) had similar intensity as the homodimer peaks. The PD spectrum of the nucleoside mixture (dC, dA, and dG) contains peaks corresponding to the complementary pair (dCdG), as well as to the homodimers: (dC)2, and (dG)2. No dA-containing clusters, either the homo- or hetero- dimer, have been observed.

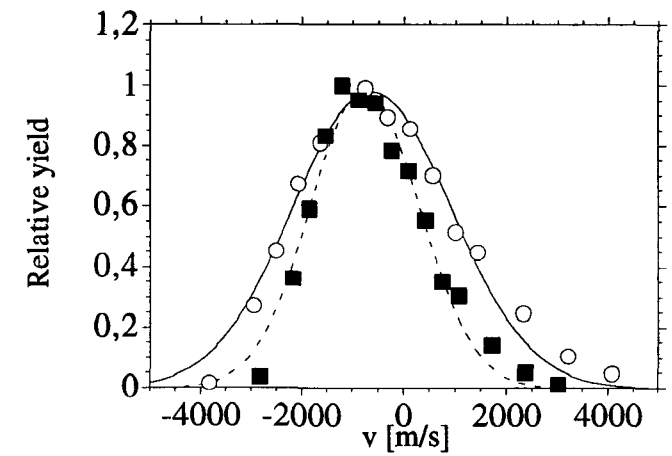

Fig. 2. Radial velocity distributions of dCH+ (o) and the mixed dCdGH+ cluster (■).

A comparison of the initial radial velocity distributions for the cluster and the monomer molecular ions reveals their remarkable similarity for both types of mixture samples studied - Fig 2. For instance, the respective values of $\langle v_x \rangle$ for IleH+, PheH+, Ile_2H+, IlePheH+, and Phe_2H+, are 578, 558, 559, 558, and 551 m/s. As typical for intact biomolecular ions both the homo- and the hetero-dimer clusters exhibit correlation with the direction of the incident MeV ion. The take-off angle of all these species is in a direction away from the trajectory of the impinging ion. In some favourable instances, e.g. for alkali cation attachment to peptides [3], initial radial velocity data can answer unequivocally the question whether cluster formation precedes or supersedes ion ejection. The data presented here, as well as data from coincidence experiments, cannot so far restore unambiguously the temporal (and spatial) sequence resulting in the observed cluster ions. Ejection of preexistent clusters as well as formation in the selvedge region are both plausible mechanisms, consistent with the current radial velocity data. Further experiments, including initial axial velocity determination and cluster formation specificity, may provide valuable additional clues.

References

[1] G.Brinkmalm et al., *Intern. J. Mass Spectrom. Ion Processes* **114** (1992) 183.
[2] G. Brinkmalm et al., *Phys. Rev.* **B47** (1993), 7560.
[3] P.Demirev et al., *Org. Mass Spectrom.* **26** (1991) 471.

^{252}Cf-PDMS of New Pyrazole Derivatives

C.R.Ponciano, W.O.Lin*, N.P. Pereira**, A.C.C. Freitas**, E.J.Barreiro**, E.F. da Silveira.
Physics Dept. Pontifícia Universidade Católica, PUC-Rio
Rua Marques de São Vicente, 225 C.P. 38071 - Brazil
*Chemistry Dept. PUC-Rio **Faculdade de Farmácia - UFRJ

The pyrazole derivatives are well-known for their analgesic and anti-inflammatory properties, specially the derivatives formed by replacing different functional groups in the C-5 position of pyrazole ring. A new series of eight 5-arylthio pirazole derivatives has been synthesized and analyzed through ^{252}Cf-PDMS and EI techniques. In this work the PDMS results are presented.

The PD mass spectra were obtained with a home-made time-of-flight spectrometer, having a 25 cm TOF tube and operated at 10 kV and - 7kV sample bias for positive and negative ions respectively. The spectrometer mass resolution is about 100. The samples were dissolved in acetone (around 7 μg/μl) and then electrosprayed on stainless steel electrodes. Data acquisition time was roughly 3 hours per sample.

The plane structure of the 5-arylthio derivatives is presented in figure 1. The positive and negative ion PD mass spectra for one of the compounds (R = H) are illustrated in figure 2.

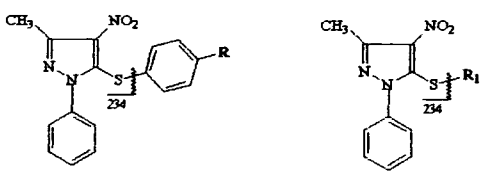

Fig. 1 - Plane structure of the compounds

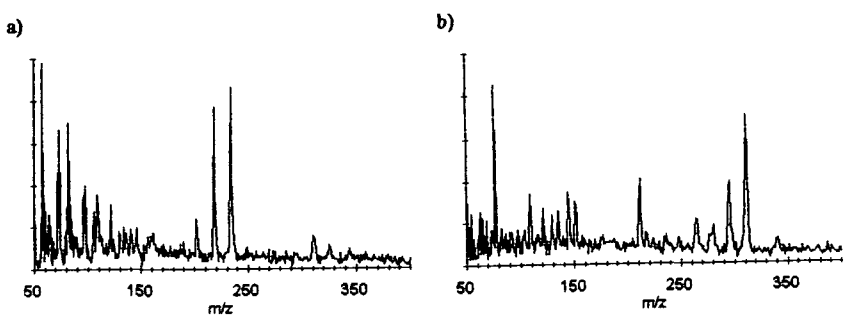

Fig 2 - a) negative and b) positive ion PDMS spectra of the compound (R = H)

In the **negative ion spectra** of the analyzed compounds, three peaks are always observed: m/z = 234, 218 and 202. The m/z = 234 peak may be attributed to the ion originated by the phenyl group loss bound to the sulfur atom, $[M - C_6H_5R]^-$ or $[M - R_1]^-$. Moreover, if this fragment loses either an oxygen atom or a sulfur atom, ions of m/z = 218 or 202 are formed.

The **positive ion spectra** show a pattern fragmentation characterized by the ions $[M - 17]^+$, $[M - 32]^+$, $[M - 46]^+$ and $[M - 100]^+$, attributed respectively to a loss of a hydroxyl group, a sulfur atom, a nitrogroup and a possible break across the pyrazole ring. Table I summarizes the percent desorption yield of those ions, normalized to the desorption yield of the molecular (or quasi molecular $[M + H]^+$) ion, corresponding to each R or R_1.

Table I - Desorption yield (%) normalized to the M^+ or $[M + H]^+$ peak

	R					R_1		
$[M - n]^+$ ions	H	OCH_3	Br	Cl	NO_2			
$[M - 17]^+$	53	53	67	77	42	33	48	19
$[M - 32]^+$	28	16	15	14	~ 0	~ 0	~ 0	8,6
$[M - 46]^+$	24	12	29	28	36	100	166	32
$[M - 100]^+$	27	2.5	43	62	25	26	37	4
MW =	311	341	389	345	356	312	313	352

Several observed trends can be noticed. The relative yield intensities for R = Br and R = Cl are very similar. Note that the yields of the $[M - 17]^+$ series are fairly constant and higher than those of the $[M - 32]^+$, probably because the loss of the sulfur atom requires the breaking of two bonds and a re-arrangement. In addition, the presence of nitrogen atom in R or R_1 substituent group stabilizes the bonding between carbon and sulfur resulting in the reduction of peak intensity of $[M - 32]^+$ and in the enhancement of the yield of $[M - 46]^+$ series. Thus, such observations give support to the proposed fragmentation pattern, i.e., the $[M - n]^-$ fragments are only differentiated by the substituent group (R or R_1).

A high mass resolution PDMS spectrum has been obtained only for the R = Br sample confirming the above results. It reveals a 3.6 ratio for the $[M(^{79}Br) + H]^+$ and $[M(^{79}Br)]^+$ peak yields.

Conclusion

The PDMS and EI measured mass spectra confirm the synthesis of the pyrazole derivatives. The molecular or quasi molecular peak of all the PDMS spectra are relatively more intense than the EI ones, showing that the latter process leads to a higher level of fragmentation. Positive and negative ion PDMS spectra of the different derivatives present a regular pattern corresponding the loss of the same fragments. This analysis illustrates PDMS as an useful method for structural determination of heterocyclic aromatic compounds.

Acknowledgment

The authors gratefully acknowledge Dr. S. Della-Negra and Dr. R.R. Pinho for running one of our samples with the IPN-Orsay PDMS reflectron. EFS acknowledges the Brazilian agency CNPq for financial support.

Matrix Effects on the Fragmentation of Vitamin B_{12} in PDMS

J. F. Blankenship, M.J. Van Stipdonk, and E.A. Schweikert
Center for Chemical Characterization, Texas A&M University
College Station, TX 77843

Recent MALDI studies by Castoro and Wilkins have shown that the addition of pyrolyzable sugars increase the yield of certain analyte ions by decreasing the desorbed ions' internal energy [1]. To examine the matrix-related internal energy decrease in MALDI, Kinsel et al. used the fragmentation pattern of vitamin B_{12} to qualitatively study various MALDI matrices [2]. By determining the yield of $[M+H]^+$ with prominent analyte fragment ion yields such as $[972]^+$ and $[M\text{-}CN]^+$, they were able to compare the ability of certain UV-absorbing matrices to produce low internal energy quasimolecular ions. In a similar manner, we use PDMS to probe matrix-related internal energy effects by small, aliphatic molecules on the fragmentation of B_{12}.

Samples consisting of B_{12} (analyte), methyl cellulose (binder), and various small (i.e. < 400 m/z) matrix compounds were co-deposited onto stainless steel plates and dried. Matrices included dextrose, maltose, cellobiose, fructose, and valine, each with matrix:analyte molar ratios ranging from 1:1 to 1000:1.

Figure 1 shows PDMS spectra from B_{12} samples with differing amounts of dextrose. High matrix/analyte conditions significantly affect the yield of $[M\text{-}CN+H]^+$ while only producing a small effect in $[M+H]^+$ yield. The other matrices examined gave similar results. Compared with the results from dextrose, there was no apparent steric effects from either the increase in dextrose units (mono vs. disaccharide) or the respective alpha and beta linkages of

43rd ASMS Conference on Mass Spectrometry and Allied Topics

maltose and cellobiose. Similarly, the inability of fructose to form a hemiacetal also did not affect the relative increase in yields. Also, changing the class of the matrix (saccharide vs. amino acid) by the addition of valine, resulted in analogous results. These suggest that the isolation of the analyte within the matrix is responsible for the yield improvements of $[M\text{-}CN+H]^+$.

References:

[1] J.A. Castoro and C.L. Wilkins, SPIE Lasers and Optics for Surface Analysis 1857, 51, (1993); J.A. Castoro and C.L. Wilkins, Anal. Chem. 65, 2621 (1993).
[2] G.R. Kinsel, L.M. Preston, and D.H. Russell, Biol. Mass Spectrom. 23, 205 (1994).

This work was supported by the National Science Foundation Grant No. CHE-9208185.

Figure 1

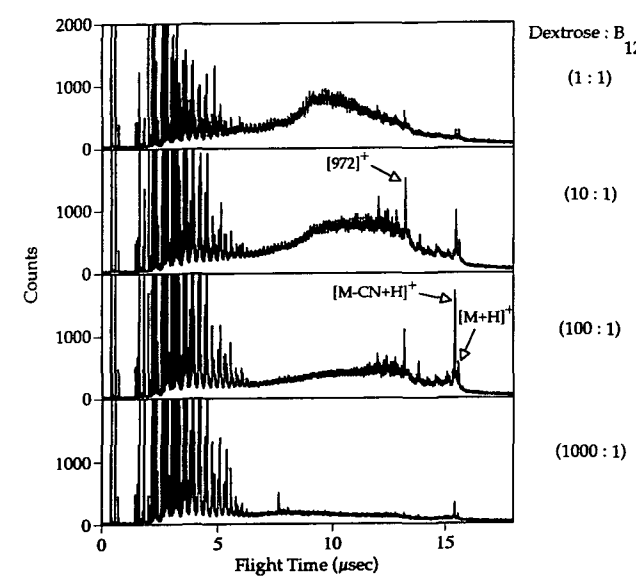

DESORPTION OF PEPTIDE IONS USING MALDI MATRICES IN CONJUNCTION WITH PDMS*

M J. Van Stipdonk, J. F Blankenship and E. A. Schweikert
Center for Chemical Characterization and Analysis, Department of Chemistry
Texas A&M University, College Station, TX 77843-3144

For several years, plasma desorption mass spectrometry (PDMS) has been an effective tool for the characterization of large biomolecules. The use of PDMS has declined with the advent of matrix assisted laser desorption/ionization mass spectrometry (MALDI), which offers higher sensitivity and higher accessible mass range than PDMS. Both MALDI and PDMS involve deposition of energy via electronic excitation of the sample matrix. The excitation is converted to translational motion and the desorption of molecules. Because of the similarity in excitation, a few groups are now investigating the use of UV and visible absorbing matrices similar to those used in MALDI to improve the performance of PDMS [1,2].

We have recently shown that the photons and ions from individual ion impacts (keV and MeV energy) can be collected simultaneously [3] This project was begun to determine whether MALDI matrices will improve the yield of intact peptide ions in PDMS, in order that we might later probe the fundamental processes that follow electronic excitation of MALDI samples by examining correlated photon and ion emission Because the emission of photons occurs on a time scale an order of magnitude faster than secondary ions, these studies may provide important information about the energetics of the desorption and ionization of molecules in both PDMS and MALDI

We present here the results of the desorption of two peptides, bradykinin and angiotensin II, using MALDI type matrices and PDMS. In these experiments, peptide and matrix were co-deposited along with a methylcellulose (MC) binder to produce thin homogeneous films. The matrices included 4-nitrophenol, 4-hydroxy-3-iodo-5-nitrobenzoic acid (HINB), Sinapic acid, α-cyano-4-hydroxycinnamic acid and others. In most cases, the matrices improved the yield of the $(M+H)^+$ ion from both peptides above a peptide/MC blank sample. HINB provided the largest improvement for bradykinin (**figure 1**), while α-cyano-4-hydroxycinnamic acid was the best matrix for angiotensin II.

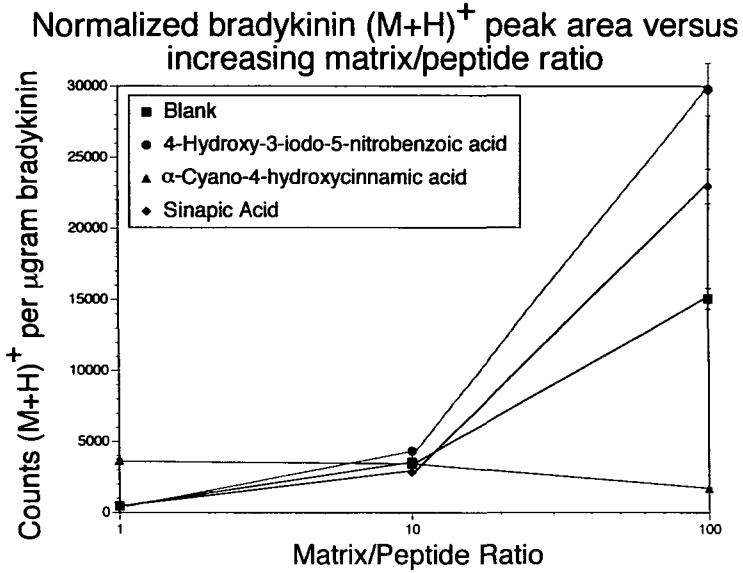

Figure 1

These results indicate that improved quasi-molecular ion yields in PDMS may be achieved by using acidic matrices. The positive influence of the MALDI matrices on ion yield in PDMS identifies a similarity in the ion formation process between the two techniques. Future experiments examining the ion and photon yields, and their relationship, should further the understanding of the chemistry and physics of ion formation for both methods of desorption.

*Work supported by NSF grant CHE-9208185

References

1) S. Bouchonnet, Y Hoppilliard, and C. Mauriac, Int. J. Mass Spectrom. Ion Process , 126 (1993) 163

2) W Tuszynski, R Angermann, J O Metzger, and R. Woisch, Nucl. Instrum Meth B 88 (1994) 184.

3) R. G. Kaercher, E. F. da Silveira, C. V Barros Leite, and E. A. Schweikert, Nucl Instrum Meth. B 94 (1994) 207.

Evaluation of Solvent Effects on MALDI Matrix Crystal Formation

Karen K. Campo, Ricky D. Edmondson, Lloyd W. Sumner, and David H. Russell
Laboratory for Biological Mass Spectrometry, Department of Chemistry, Texas A&M University, College Station, Texas 77843

The physical size and distribution of MALDI matrix crystals are dramatically effected by the solvent utilized in the preparation of matrix solutions. It is believed that smaller, more uniform crystals produce higher intensity MALDI ion signals and also improve mass resolution. Optimum reproducibility and surface homogeneity are directly linked to the solvent used in sample preparation.

In order to investigate these theories, the solvent, texture of the sample surface, and matrix were varied. The solvents used in this study were: acetone, 50/50 (v/v) acetonitrile and water, ethanol, methanol, and tetrahydrofuran. Alpha-cyano-4-hydroxycinnamic acid, 4-nitroaniline, and 3,5-dimethoxy-4-hydroxycinnamic acid (sinapic acid) were employed as matrices, with bovine insulin used as the analyte. The matrix/analyte samples were prepared on two stainless steel plates: one polished with 12000 grit sandpaper, the other polished with 1000 grit sandpaper. The dried droplet sample preparation method of a 50/50 (v/v) solution of both the analyte and matrix was used. The spectra were aquired at laser irradiances slightly above threshold, with the ion signal of each matrix/analyte/solvent being compared as to the solvent utilized. Each spectra were aquired at laser irradiances slightly above threshold. Three spectra were obtained from each sample spot. Three spots were obtained for each matrix/analyte/solvent. The crystal characteristics of each matrix/analyte/solvent sample were compared by using a Zeiss Auxiophot microscope.

From our results, ethanol used as the solvent in the matrix/analyte samples, gave the greatest ion signal in all three matrices, while methanol gave the lowest ion signal, as shown in Figure 1. Better sample-to-sample reproducibility was achieved on the more polished steel plate surface, as shown in Figure 2. Similar results have been obtained in aerosol MALDI experiments as well.[1]

Similar laser thresholds were seen for the three solvents, ethanol, methanol, and acetonitrile-water. Acetone had a lower threshold, while tetrahydrofuran had a higher laser threshold than the other solvents. Exact crystal size was undetermined due to the 800x magnification limit, yet, the crystal characterixtics could still be compared. In alpha-cyano-4-hydroxycinnamic acid, ethanol and methanol gave similar crystals, in 4-nitroaniline they did not. The same was true of acetone and tetrahydrofuran.

43rd ASMS Conference on Mass Spectrometry and Allied Topics

Figure 1: Ion Signal Intensities versus Solvent

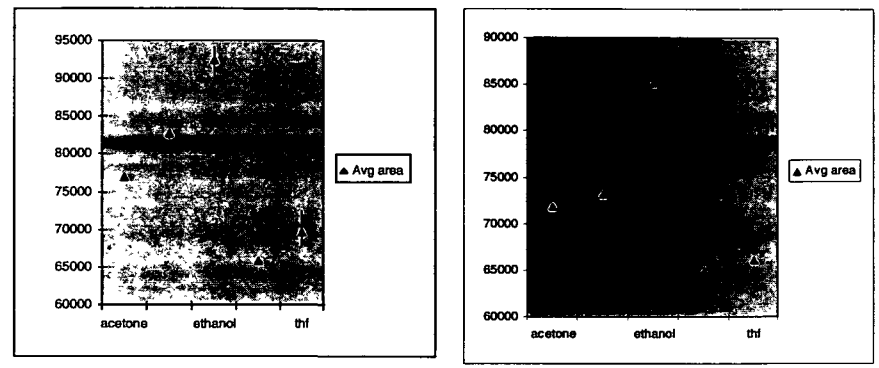

4-nitroaniline

Alpha-cyano-4-hydroxycinnamic acid

Figure 2: Comparison of Ion Signal Intensities and Reproducibility versus Solvent

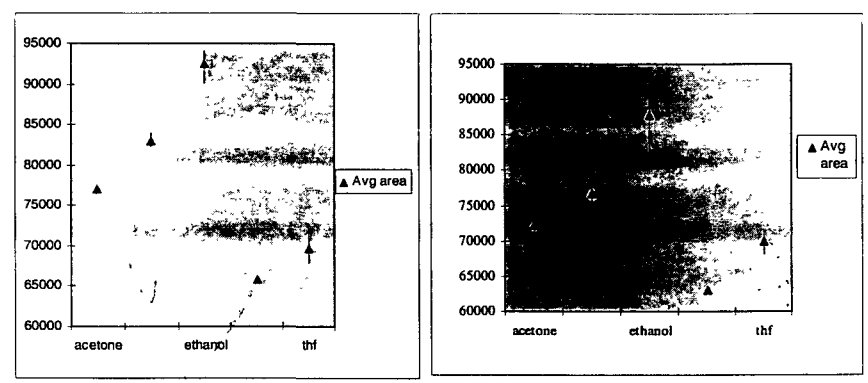

4-nitroaniline on a 12000 grit surface

4-nitroaniline on a 1000 grit surface

Infrared Matrix-Ass. Laser Des./Ion. (IR-MALDI) using a Free-Electron Laser

Cramer, Rainer, Haglund, Jr., Richard F., Hillenkamp, Franz
Department of Physics and Astronomy, Vanderbilt University, Nashville, TN 37235
Institute for Medical Physics and Biophysics, University of Muenster, Germany

At present a Free-Electron Laser (FEL) seems to be the most promising laser to help answer questions about the basic mechanisms of energy deposition, desorption or ionization in IR-MALDI. We use the Vanderbilt FEL for investigations in the 2-10 µm wavelength range and, along with an electro-optic switch, in the 100-5000 ns time regime of pulse duration.

Experimental: The mass spectrometer is a modified Comstock model TOF-101-MS with a microchannel plate detector. A high voltage (up to 30 kV extraction potential) ion source has been built allowing sample irradiation under 45 degree with both an UV-laser and the Vanderbilt FEL. By means of a dichroic mirror on the UV side, a video camera can be used for sample observation with a magnification of approximately 20. The IR side comprises a telescope optic to reduce the ~1 cm FEL beam diameter by a factor of 4 to an appropriate size for the aperture of the electro-optic switch, a broadband Pockels cell. The time structure of the FEL is shown in **Fig. 1**. Using the Pockels cell, the macropulse with a length of 2-5 µs can be continuously varied to achieve a pulse width between 100 and 5000 ns. In **Fig. 2** the wavelength range covered by the FEL is shown in comparison to other IR-lasers.

Measurements and Results: We were able to obtain spectra at wavelengths which were not used before in IR-MALDI (3.2 µm- 3.4 µm) and with different pulse lengths (100 ns - 2 µs). For the initial experiments shown here we only used succinic acid as matrix. **Fig. 3** shows the insulin peak of a single shot spectrum obtained by using a crystal as the sample. The wavelength is 3.25 µm, very close to the maximum absorption of the O-H stretch vibration of succinic acid. The insulin molecule ions could be detected for approximately the same period of time as the FEL macropulse, which was not shortened by the Pockels cell. **Fig. 4** shows a single shot spectrum of melittin. The laser parameters were the same as in **Fig. 3**. This time we used a standard MALDI sample preparation. The spectrum shows a melittin ion peak width slightly smaller than the FEL pulse width. It is noticeable that the maximum of the ion peak is reached earlier than in **Fig. 3**. **Fig. 5** shows a single shot spectrum of melittin obtained under basically the same conditions as in **Fig. 4** except the different FEL pulse length. In this case we used the Pockels cell to cut a 200 ns pulse out of the FEL macropulse. Compared to **Fig. 4** this spectrum has more background noise, less matrix ion signal intensity, the ion peak width is more than a factor of 3 smaller, and the mass resolution is increased by a factor of 3.

Discussion: Comparing **Fig. 3** and **Fig. 4** we note that the ion emission times are different. While in the first spectrum the insulin peak shape reflects the temporal FEL beam shape, in the latter the ion peak maximum is reached quite early and is followed by a decrease of the ion signal intensity. The most likely explanation for this disparity is based on the two different samples we used. When a crystal is used as in **Fig. 3**, within the laser spot the sample will not be totally desorbed by a 2 µs laser pulse whereas for the standard sample, which is at best 10-50 µm thick, almost all the sample will be gone. The pulse length we used in **Fig. 5** is close to pulse lengths of other IR-MALDI-lasers. Even if the quality of this spectrum is not state-of-the-art one can clearly see an improvement compared to the spectra with the longer pulse length.

Conclusions: Our first results with the Vanderbilt FEL support the assumption that the FEL is a promising laser to study IR-MALDI. Even with a macropulse of 2-5 µs we obtained IR-MALDI spectra. The substructure of the macropulse, the 1 ps micropulses, does not seem to be a problem. On the other hand it is quite rare to have all of the components (FEL, Pockels cell, TOF-MS) functioning at the same time. Therefore the FEL can be used as a research tool, but not as an IR-MALDI-laser for routine analysis. Once we know the parameters for best IR-MALDI performance one should rather develop an appropriate fixed-frequency laser or OPO.

43rd ASMS Conference on Mass Spectrometry and Allied Topics

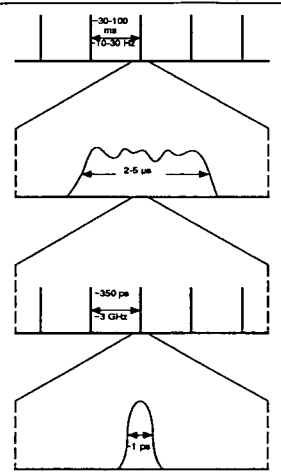

Fig. 1: Time structure of the Vanderbilt FEL

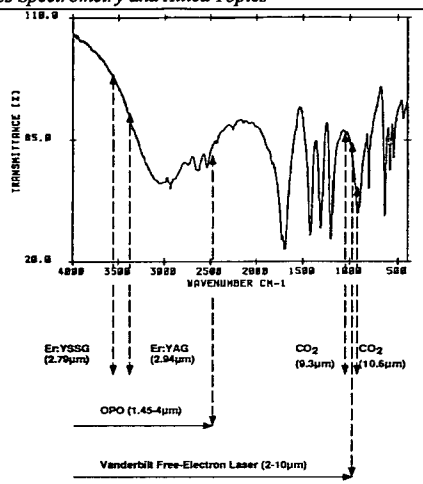

Fig. 2: FTIR-spectrum of succinic acid with IR-laser wavelengths marked

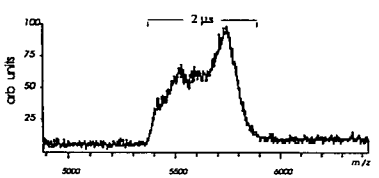

Fig. 3: Single shot spectrum of insulin from a crystal sample (wavelength: 3.25 µm, pulse length: ~ 2 µs)

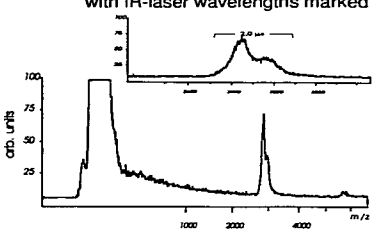

Fig. 4: Single shot spectrum of melittin from a standard sample with magnified analyte peak section indicating the peak width in time (wavelength: 3.25 µm, pulse length: ~ 2 µs)

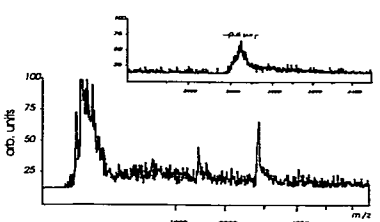

Fig. 5: Single shot spectrum of melittin from a standard sample with magnified analyte peak section indicating the peak width in time (wavelength: 3.25 µm, pulse length: ~ 200 ns)

Future Work: As the initial experiments indicate the FEL combined with our experimental set-up is suitable to carry out systematic investigations of fundamental aspects of the IR-MALDI.

We will study the correlation between sample absorption and desorption threshold as well as the effects of laser intensity and pulse duration on desorption and ionization.

Acknowledgement: Research is partially supported by the Medical FEL program administered by the ONR, contract N00014-91-0109. Rainer Cramer is supported by the DAAD through a doctoral stipend from funds of the Second University Special Program.

Effect of Analyte Hydrophobicity on Beam-induced Dehalogenation in LSIMS.

R. Théberge* and M.J. Bertrand, Regional Center for Mass Spectrometry, Department of Chemistry, University of Montreal, Montreal, Canada, H3C 3J7.

Dehalogenation reactions of organic compounds during their FAB/LSIMS analysis have been the object of several studies. The importance of these reactions lies in the fact that they can cause the presence of artefacts in the mass spectra. In a previous study[1] conducted in our laboratory, it was observed that the presence of an anionic surfactant additive can increase the extent of beam-induced dehalogenation of organic compounds. This observation was explained in terms of increased analyte surface concentration. In our continuing investigation of beam-induced dehalogenation, we have focused on how analyte surface activity (hydrophobicity) can affect the dehalogenation process through comparison of analogs of different surface activity. Mass spectral data were obtained using a VG Autospec-Q equipped with a caesium ion gun. The caesium ion beam energy and current were held constant at 22keV and 2μA, respectively. %Dehalogenation values were obtained from the first two minutes of analysis. Glycerol and 1,2,6-trihydroxyhexane were the matrices. The extent of dehalogenation was defined as

$$\%\text{Dehalogenation} = 100 \times [M_H H]^+ / [M_X H]^+ + [M_H H]^+ \qquad (1)$$

where $[M_X H]^+$ and $[M_H H]^+$ are the relative abundances of the protonated halogenated and dehalogenated species, respectively. In order to investigate the effect of analyte surface activity on dehalogenation, the analogous compound pairs 1-2 and 3-4 (**Fig. 1**) were used. The different surface activity of the analogs are based on the size of the alkyl side chain. For pre-formed ions, we can define analyte surface activity in terms of matrix surface coverage. As can be seen in **Fig. 2** and **3** from the intensity of the analyte ions with respect to the glycerol trimer $(gly)_3H^+$, the surface activity of compound 1 is much greater than 2. Compound 1 exhibits charge remote fragmentation which is characteristic of surfactants. The % dehalogenation for 1 is also greater than 2 (60 vs 44). A similar result was obtained for 3 and 4 (18 vs 24). These results *directly* support the contention that analyte surface activity can affect the observed extent of dehalogenation. This effect can be explained by the high concentration of beam-generated reductive species (thought to be electrons) near the surface. Hence, higher analyte surface concentration should result in an increased probability of reaction with beam-generated electrons and result in a greater % dehalogenation. The analyte surface concentration can also be affected by the surface tension of the matrix, particularly in the case of a surfactant such as 1. This hypothesis can be tested by using a matrix structurally analogous to glycerol with a lower surface tension such as trihydroxyhexane (THH). The relative abundance of analyte ions with respect to matrix ions as well as the extent of dehalogenation in THH (**Fig. 4**) is much smaller than in glycerol. The dependence of analyte signal strength on surface concentration is well known. Thus, analyte surface concentration is lower in THH and %dehalogenation is concomitantly lower (60 vs 45). It has recently been demonstrated that analyte signal increases with matrix surface tension[2]. It is understood that the LSIMS sensitivity (surface concentration) of a particular analyte is not governed solely by its surface activity and that other mechanisms, i.e. diffusion, may play an important role. It is also assumed that the beam-induced processes leading to dehalogenation occur to a comparable extent in glycerol and trihydroxyhexane.

An increase in analyte surface activity results in increased dehalogenation. The relationship between matrix surface tension and extent of dehalogenation was also established. These results support the hypothesis that analyte surface concentration can affect the extent of dehalogenation. It is proposed that this relationship might be applicable to other beam-induced reductions in FAB/LSIMS.

REFERENCES

(1) R. Théberge and M.J. Bertrand, *Proceedings of the 42nd ASMS Conference on Mass Spectrometry and Allied Topics*, **1994**, p.197.
(2) A. Santos, B. Saramago, F. Duarte and H.M. Florencio, *J. Chem. Soc. Faraday Trans.*, **1995**, 91, 1203.

Fig.1 Compounds used in this study

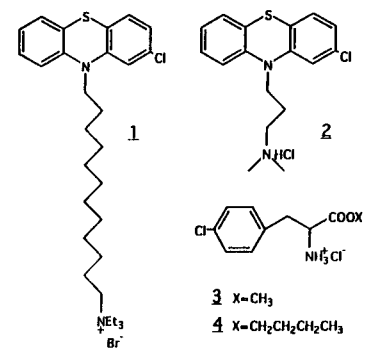

Fig 3. LSIMS mass spectrum of 2 in glycerol (0.0041M).

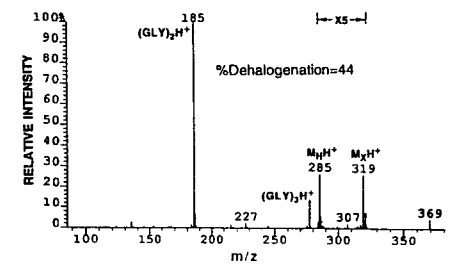

Fig 2. LSIMS mass spectrum of 1 in glycerol (0.0041M).

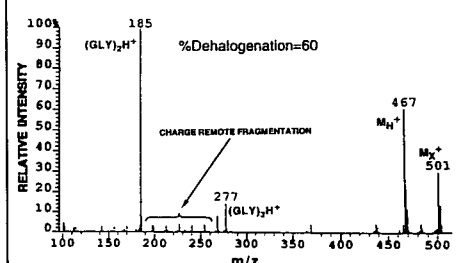

Fig.4 LSIMS spectrum of 1 in 1,2,6-trihydroxyhexane (0.0041M)

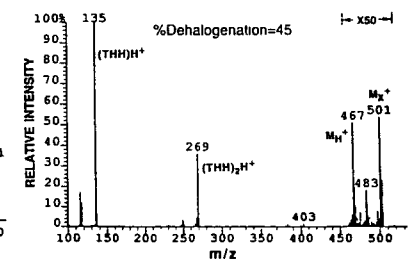

INVESTIGATION OF THE CLUSTERING PROCESSES OCCURRING IN LSIMS FOR A SERIES OF QUATERNARY ALKYL AMMONIUM SALTS

G. J. C. Paul[1], I. Marcotte[3], J. Anastassopoulou[1], T. Theophanides[1], M. Arkas[2], C. M. Paleos[2] and M. J. Bertrand[3],
[1]National Technical University of Athens, Chemical Engineering, Zografou 15780 and [2]NRC "Demokritos", 15310 Agia Paraskevi Attikis, Athens, Greece, [3]Regional Center for Mass Spectrometry, University of Montreal, Montreal, Canada, H3C 3J7.

The behaviour of quaternary alkyl ammonium salts in solution is of interest since they are amphiphilic molecules which are known to form micelles in solution. In this work, a series of quaternary alkyl dimethylammonium bromides, MBr, are studied by LSIMS. Pure glycerol was employed as the liquid matrix. The structures of these compounds are shown in Figure 1. Emphasis is placed on the clustering behaviour of these salts where the effect of structural changes is investigated.

A typical LSIMS mass spectrum for a quaternary alkyl dimethyl ammonium bromide is shown in Figure 2. The molecular ion, M^+, dominates the mass spectrum. The dimer, M_2Br^+, is the major cluster ion observed in LSIMS where X = H, CH_3 and CN. Negligible higher order clusters, $[M_xBr_{x-1}]^+$, where $x>2$, were detected in the analyte concentration range employed (0-0.35M). Different cluster ion formation of the general formula $[M_x-(x-1)H]^+$ where x = 1-4 is observed for X = COOH. Information on the clustering of these compounds in LSIMS was gained by investigating the relationship between the analyte concentration and the ion intensity ratio M_2Br^+/M^+ for X = H, CH_3 and CN. The plot for one of these ammonium salts is presented in Figure 3. At very low analyte concentrations, only M^+ is detected. Further addition of the analyte leads to dimerization where the M_2Br^+/M^+ ratio intensity increases until reaching a plateau where it remains constant. A similar trend was observed for X = COOH where the relation between $[M_2-H]^+$ and M^+ was investigated. The clustering behaviour of the quaternary alkyl dimethylammonium bromides in LSIMS with varying the analyte concentration can be explained in terms of equilibrium [1] for dimer formation and the corresponding equilibrium constant expression [1a]:

$$M^+ + MBr \rightarrow M_2Br^+ \qquad [1]$$
$$K = [M_2Br^+]/[M^+][MBr] \qquad [1a]$$

The plateau region of the plot where the M_2Br^+/M^+ ion intensity ratio remains constant is explained by the formation of an analyte monolayer at the liquid surface, where [MBr] remains constant and suggests a predominant sampling of ions originating from the surface in LSIMS. This explanation also holds for X = COOH compounds. The free energy of dimerization ($-\Delta G^\circ = RT\ln K$) can be related to the equilibrium constant expression by equation [2]:

$$-\Delta G^\circ = RT\ln [M_2Br^+]/[M^+][MBr] \qquad [2]$$

Consequently, values of M_2Br^+/M^+ for all the quaternary ammonium bromides provide relative dimer bond energies. Likewise, this can be performed for $[M_2-H]^+/M^+$ when X = COOH. These values are presented in Table 1. It can be seen from Table 1 that for m and X constant, increasing the alkyl chain length, n, decreases the M_2Br^+/M^+ (or $[M_2-H]^+/M^+$) intensity ratio. This

suggests that the hydrophobic interaction between alkyl chains in the dimer causes a destabilizing effect on the bond strength as n increases. It is also observed (Table 1) that for n and X constant, increasing the methylene spacer length, m, leads to a decrease in the dimer stability. This can be attributed to steric effects on the electrostatic interaction within M_2Br, as illustrated by the comparison of M_2Br^+/M^+ for X = CH_3 and X = H with n =12 and m = 0. Since H is a smaller substituent than CH_3, steric effects are lessened, permitting a stronger electrostatic interaction within the dimer. Comparing M_2Br^+/M^+ vs $[M_2-H]^+/M^+$ intensity ratios (Table 1) for X = COOH and X = CH_3, with n = 12 and m = 1, suggests stronger bonding energies for X = COOH Consistently, higher order clusters are observed for X = COOH. Formation of zwitterions for these ammonium salts is proposed through loss of proton from carboxylic acid, which forms stronger bonding than within M_2Br^+.

TABLE 1: EFFECT ON M_2Br^+/M^+ (OR $[M_2-H]^+/M^+$) UPON CHANGING THE ALKYL CHAIN (n) AND METHYLENE SPACER (m) LENGTHS

X	n	m	M_2Br^+/M^+ (x100)
H	12	0	47.39
H	14	0	44.40
H	16	0	31.38
CH_3	12	0	20.80
CH_3	12	1	17.96
CH_3	12	3	8.33
CH_3	14	0	13.13
CH_3	16	0	11.92
CH_3	16	1	9.62
CN	12	3	8.16
CN	14	3	5.69
CN	16	1	11.07
CN	16	3	3.85
CN	16	6	3.15
COOH	12	1	34.98
COOH	14	1	26.14
COOH	16	1	15.30
COOH	12	10	0.50

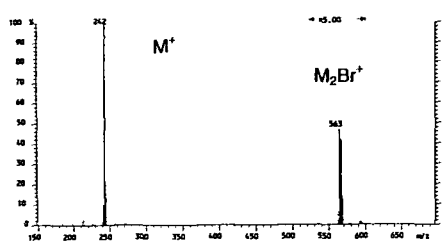

FIGURE 2: LSIMS MASS SPECTRUM OF n = 12, m = 1, X = CH_3

FIGURE 1: QUATERNARY AMMONIUM SALTS STUDIED BY LSIMS

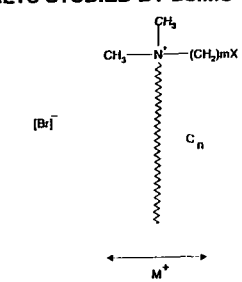

X = H, CH_3, CN, OH, COOH
m = 1-6
n = 12, 14, 16, 18

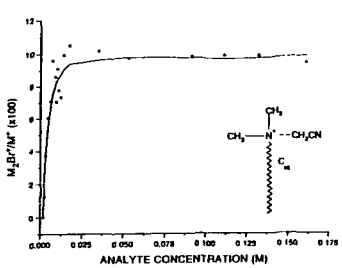

FIGURE 3: DEPENDENCE OF M_2Br^+/M^+ INTENSITY RATIO ON ANALYTE CONCENTRATION

ORGANIC SECONDARY ION EMISSION FROM SOLIDS AND LIQUIDS

John McMahon, Peter J. Todd, Richard J. Caimi[§], J. Thomas Brenna[§]
Oak Ridge National Laboratory, Oak Ridge, Tennessee, and
[§]Cornell University, Division of Nutritional Sciences, Ithaca, NY

Microprobe analysis targeted at spatial localization of organic compounds in complex, real samples, depends on efficient production of organic secondary ions. Glycerol is rare among organic compounds because its SIMS spectrum does not change with primary dose and the secondary ion yield from liquid glycerol is high. The bulk of published data on organic secondary ion emission from liquid glycerol bombarded by high intensity fast atom beams at ambient temperature. However, analysis of some classes of samples, particularly biologicals, may require analysis at cryogenic temperatures and with low primary beam doses to minimize damage of the molecular solid. We wanted to identify the reason that secondary ion emission from liquid glycerol is so intense and persistent. We therefore set out to characterize emission of secondary ions from glycerol and a non-freezing solid, high molecular weight polyethylene glycol (PEG), as temperature is adjusted between room temperature and near liquid N_2 (LN2) temperature.

This work was carried out using an imaging SIMS instrument that enables imaging of secondary ions along with simultaneous visual recording of the sample surface using a video cassette recorder (VCR). The latter capability facilitates unambiguous determination of phase changes in order to relate them to changes in secondary ion emission. Cs^+ (10 keV) were the primary ions. The charge compensation device in this instrument is a filament that floods the surface with low energy electrons during short periods when the extraction optics are turned off. Charge compensation permits us to distinguish changes in emissivity due to changes in bulk electrical conductivity.

Secondary ion emission from a glycerol droplet is nearly unchanged as temperature is lowered from ambient to its freezing point. As glycerol freezes, there is an abrupt and dramatic drop in secondary ions emission from the center of the droplet, while emission continues from the periphery. This effect is easily reproduced as the temperature is cycled multiple times.

Emission from the PEG droplet decreases with temperature with no charge compensation. However, signal is fully recovered with the charge compensation, indicating that lower molecular mobility in cold PEG results in higher electrical resistance and charge build-up at the surface during sputtering. The independence of secondary ion emission from the glassy PEG suggests that the crystalline character of solid bulk glycerol is the critical factor reducing ion emission.

Based on a consideration of the instrument geometry, the anomalous emission from the periphery of the glycerol droplet compared to emission from the droplet's center is unlikely to be a topographic effect. We hypothesized that emission was related to the

thickness of glycerol droplet. We tested this hypothesis by preparing a thin glycerol smear and characterizing its secondary ion emission as it freezes and thaws. Our data show that emission continues through the phase transition, consistent with that at the droplet periphery, and similar to the waxy PEG. We conclude that the effect is related to thickness. These results explain conflicting literature reports on the attenuation of emission from glycerol due to freezing.

An effect of crystallinity on ion emission referred to as "channeling" is well known in inorganic secondary ion emission studies and is used for determining crystalline features. Briefly, a decreased sputtering rate is observed when crystal planes line up with the incident primary ion beam, since the probability of impact in the first few atomic layers drops. This effect may be operative here, although simple channeling phenomenon is unlikely since a) emission from thick solid glycerol is always very low, even though the solid surface is clearly rough, and b) thin solid glycerol emits strongly. Further study will be required to explain this effect.

We summarize our results as follows: 1) Thick solid glycerol emits molecular secondary ions at a rate orders of magnitude lower than liquid glycerol. 2) Thin solid glycerol emits molecular secondary ions at rate similar to liquid glycerol. 3) Glassy PEG does not show an abrupt drop in ion emission as its temperature is lowered when charge compensation is provided. 4) Crystallinity affects molecular secondary ion emission in a complex way not fully reconciled with well known results in elemental crystals.

MECHANISTIC STUDIES OF HIGH VALENT IRON CATALYSTS

Susan T. Weintraub
The University of Texas Health Science Center at San Antonio
Michael J. Bartos, Scott Gordon-Wylie, James L. Wright and Terrence J. Collins
Carnegie Mellon University, Pittsburgh PA
Kathleen R. Noon
Michigan State University, East Lansing MI

Initial ESI/MS studies provided the key evidence for a novel chemical reaction that occurred when a model iron macrocyclic complex was exposed to an oxidant. Treatment of an iron(III) water complex with the oxidant *t*-butylhydroperoxide (TBHP) in acetonitrile yielded a product that could not be identified by traditional means. Through the use of ESI/MS it was ascertained that the nitrile solvent had been oxidized to release cyanide which was subsequently captured by the iron to give a deep blue iron(IV) cyanide complex. Although we were able to determine the structure of the product, two important questions remained. First, what was the origin of a significant infrared band at 1723 cm^{-1} that could not be attributed to any functionality in the iron(IV) cyanide complex? And second, what was the reaction mechanism for the C-H bond activation process?

After conducting extensive physicochemical analyses of the product exhibiting the 1723 cm^{-1} IR band, we concluded that a mixture must be present. But, we were unable to isolate a separate component responsible for the 1723 cm^{-1} IR band, using silica gel TLC with a variety of solvent systems. We found, however, that if the analogous tetraethyl-ammonium salt of the iron(III) water complex was employed in the reaction instead of the tetraphenylphosphonium salt, the product could be fractionated into two components: a blue compound that proved to be the purified iron(IV) cyanide complex (> 90% of the total mass) and a colorless compound that absorbed at 1723 cm^{-1} in the IR. We gave this compound the notation of **1723**.

^1H and ^{13}C NMR analysis of **1723** revealed that the compound was diamagnetic; while **1723** had clearly retained many of the structural features of the original macrocyclic tetraamide, a new alkene signal could be seen by NMR. This new metal-free species appeared to be produced by alteration of the diethyl-substituted region of the macrocyclic backbone. Initial characterization of **1723** by FAB/MS indicated that the monoisotopic molecular mass was 468 Da, as evidenced by the moderately intense ions at m/z 469, 471 and 472, with the appropriate relative intensities for 2 chlorine atoms. The EI mass spectrum of **1723** exhibited a relatively weak molecular ion cluster (less than 1% of the base peak) at m/z 468, 470 and 472 with the appropriate pattern for 2 chlorine atoms. The base peak in the EI mass spectrum was at m/z 97. Chlorine-containing fragments roughly equal in intensity to the molecular ion were seen at m/z 411/413/415 and m/z 399/401/403, representing loss of 57 and 69 mass units, respectively. Other significant fragments were observed at m/z 287/289/291 and m/z 154, with less intense signals found at m/z 182, m/z 140, m/z 84, m/z 69 and m/z 58. On the basis of the NMR and mass spectral data, we were able to postulate two different but related structures for **1723**: a dimethylhydantoin ring containing product and an eleven-membered ring species, as shown below.

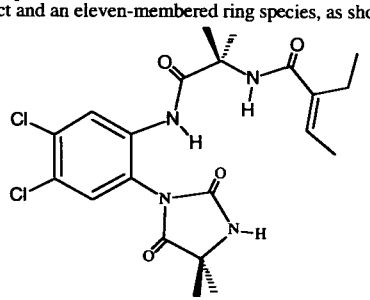

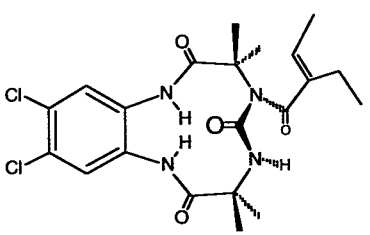

Examination of the hydantoin ring containing structure revealed that single bond cleavages along the enediamide chain could produce fragments with m/z values of 182, 154, 97 and 69. Formation of m/z 84, on the other hand, requires cleavage across the hydantoin ring in conjunction with hydrogen migration. The ion at m/z 140 is most likely produced by the loss of the elements of CH_2 from m/z 154. Inspection of the 11-membered ring containing product showed that it was also possible to generate the observed ions, although multiple bond cleavages, would be required. While these latter cleavages are decidedly less favorable than the ones associated with the hydantoin ring containing structure, the 11-membered ring product could not be ruled out on the basis of this evidence alone. Further evaluation by tandem MS and accurate mass analysis in addition to deuterium exchange studies were, therefore, conducted. In concert, the mass spectral analyses support the identity of **1723** as the product containing the hydantoin ring and rule out the 11-membered ring structure.

In an effort to determine the mechanism of formation of the cyanide ligand complex, mass balance analysis of the organic reaction products was undertaken. For these experiments, the oxidant was *t*-butyl-hydroperoxide and the solvent was isobutyronitrile. We suspected at the outset that free radical autoxidation might be involved in addition to metal-catalyzed processes and that these reactions might lead to thermally sensitive peroxide products. A technique was, therefore, devised to maintain component integrity in preparation for analysis. The TBHP-catalyzed reaction was allowed to proceed for 15 min and then the mixture was cooled to 0 °C. The organic products were vacuum-transferred to a liquid nitrogen cold trap, leaving behind the ligand-metal containing components as a solid residue in the reaction flask. The organic mixture was then analyzed by ^1H and ^{13}C NMR. After comparison with authentic standards, it was possible to unambiguously identify and quantify the following products: acetone, acetone cyanohydrin, *t*-butanol and di-*t*-butyl-peroxide. The identities of two additional products were also postulated: *t*-butylmethylperoxide and 2-*t*-butylperoxy-2-cyanopropane (termed the "mixed peroxide").

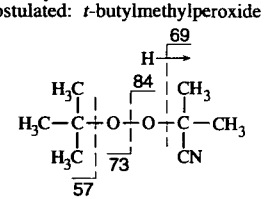

While assignment of the NMR signals for these latter products was straightforward, it was important to verify the structure of this unusual mixed peroxide. The structure of the mixed peroxide is shown to the left. From preliminary evaluation of standard di-*t*-butylperoxide and acetone cyanohydrin, appropriate conditions were found by which a 30 meter x 0.25 mm DB-1701 fused silica capillary column was able to resolve all of the components of interest. The mixed peroxide eluted from the GC in a sharp peak with a retention time of 6.9 min. Unlike di-*t*-butyl-peroxide which exhibits a molecular ion of modest intensity, no $[M]^+$ was detected for the mixed peroxide (M.W. 157 Da). The base peak in the EI mass spectrum of the mixed peroxide was m/z 57 ($[C_4H_9]^+$). Other structurally informative ions included m/z 73 (4% base peak) and m/z 84 (5%) representing the *t*-butanol and acetone cyanohydrin "halves" of the molecule; ions at m/z 69 (40%, $[(CH_3)_2CCN + H)]^+$), m/z 43 (42%) and m/z 125 (18%) were also observed. While the majority of the fragments could be readily interpreted on the basis of the proposed mixed peroxide structure, the peak at m/z 125 required further investigation. This ion represents the loss of 32 mass units from the molecular ion, and from inspection of the structure, this loss could only be a molecule of oxygen. Although there is precedent in the literature for loss of O_2 from organic peroxides, di-*t*-butylperoxide does not fragment in that way. Accurate mass analysis of the sample was, therefore, conducted. The high resolution mass of m/z 125 was found to be 125.1202, representing an elemental composition of $C_8H_{15}N$, with a difference of -0.3 mmu from the calculated value of 125.1205. The presence of oxygen in this ion was ruled out because the closest realistic oxygen-containing organic species ($C_7H_{11}NO$) has a mass of 125.0841, with a mass difference of 36 mmu that is greater than anticipated experimental error. The results also supported the assignment of m/z 73 as C_4H_9O (found, 73.0662; calculated, 73.0654; error, +0.8 mmu) and m/z 84 as C_4H_6NO (found, 84.0411; calculated, 84.0449; error, -3.8 mmu). In order to gain further insight into the mechanism by which these products were being formed, the reaction was then carried out in the presence of ^{18}O gas. It was quite surprising to find that while almost 50% of the acetone cyanohydrin molecules had become labelled, no more than 5% of the mixed peroxide was enriched in ^{18}O. Clearly, two different processes are involved in the formation of these products. Efforts are currently underway to elucidate these mechanisms.

Supported in part by NIH grant GM44867 and NSF grant CHE-9319505 to T. Collins and NIH grant RR00480 to the MSU Mass Spectrometry Facility.

New Axial Energy Analyzer for Secondary Ion Mass Spectrometry

Jian Wei and Richard A. Schaeffer
Extrel Corporation
575 Epsilon Drive, Pittsburgh, PA 15238

Introduction: Secondary Ion Mass Spectrometry (SIMS) has been widely used in depth profile analysis, surface contamination detection and the probing of the interactions between gas phase molecules and solid surfaces. Secondary ions are usually created by the bombardment of a substrate surface with a high energy primary ion beam and mass analysis of these ions will reveal some useful information about the chemical composition of the surface. However, the wide kinetic energy distribution in the secondary ions can severely degrade the resolution and abundance sensitivity of a quadrupole mass filter. In addition, both the high energy secondary ions and the neutral molecules generated by the ion bombardment on the surface will contribute significantly to the noises recorded by the spectrometer Thus, an energy analyzer with high transmission will be highly desirable in the SIMS applications.

Energy Analyzer Design and Working Principles: The energy analyzer reported here is coaxial with the quadrupole mass filter and can be used in tandem with a standard gas phase ionizer. There is a center stop in the analyzer to eliminate the high energy ions and the line-of-sight neutral molecules. Shown in Figure 1 is an example for the ion trajectories from SIMION simulations. The center stop inside the energy analyzer is omitted here for clarity. More detailed simulation results have demonstrated that the ions with energy outside a predetermined energy window will be rejected by the energy analyzer.

Experimental: The transmission of the tandem energy analyzer/ionizer was tested for both the RGA and SIMS applications using an Extrel 3/4" quadrupole mass at 2 1 MHz. The measurements were performed in a UHV chamber with the base pressure of 1.6×10^{-9} Torr. In the SIMS experiments, the energy of the primary Ar ions was 2 keV. The incident angle of on the samples is about 80° and the angle between the sample surface normal and the axis of the SIMS probe is about 10° Data acquisition was done through the INEL computer software.

Results and Conclusions: The RGA application to an Ar gas at $7\ 4\times10^{-7}$ Torr gave a sensitivity of 6 75 $\times10^{14}$ CPS/Torr (1.3×10^{-4} Amp/Torr) at the filament emission of 1.0 mA. This result from the new axial energy analyzer shows more than an order of magnitude improvement in transmission over the Bessel box energy analyzer. The detected background noise at this Ar pressure was 0.33 CPS, thus pushing the partial pressure detectability down to 1.0×10^{-15} Torr In the SIMS measurements, the new energy analyzer had also shown a 10X improvement in transmission. Figure 2 shows the spectrum from an unoxidized Al sample, where the Al^+ (27 amu) signal under the target current of 2 nA is 1.2 million counts per second. The band pass characteristics or the energy filtering effect of the energy analyzer can be seen through the low background noise and high abundance sensitivity in the SIMS spectrum. Figure 3 re-plots the data in Figure 2 to show this effect. The abundance sensitivity was measured to be better than 1×10^5 at 27 5 amu and the background noise was less than 1 CPS. Another application for the energy analyzer is to resolve the energy distribution of the ions being analyzed. The capability of the energy analyzer for fine energy scan is demonstrated in Figure 4

Simulated Secondary Ion Trajectories
Through The Energy Analyzer

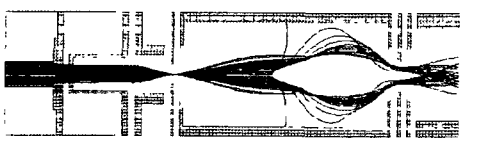

Figure 1

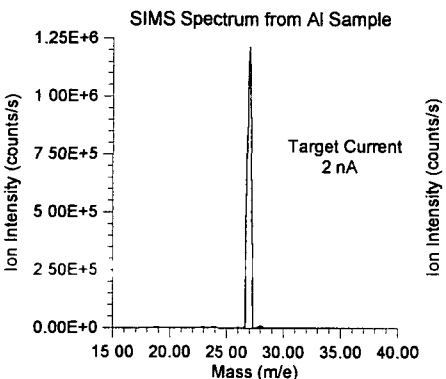

Figure 2

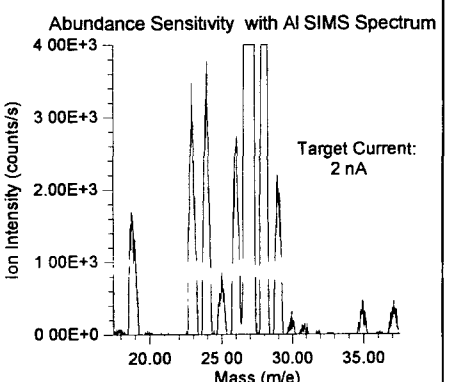

Figure 3

Fine Energy Scan for the Secondary Ions

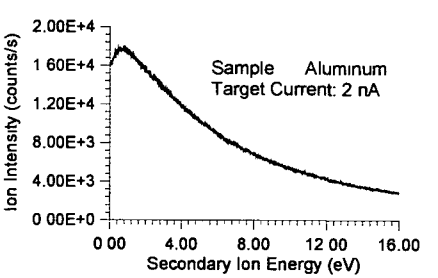

Figure 4

Quadrupole Mass Spectrometry Using the Second Mathieu Stability Region. Randall E. Pedder and Richard A. Schaeffer, Extrel Corporation, 575 Epsilon Drive, Pittsburgh, PA 15238

Introduction. The analysis of deuterium, tritium and helium for fusion applications requires extraordinary abundance sensitivity and mass resolution (900 FWHM for He^3 - HD, 3400 FWHM for HD-H_3) from a mass spectrometer, especially when the objective is to quantitate a very small relative concentration of one species in the presence of the others. Quadrupole mass spectrometers have been successfully applied to the analysis of hydrogen, helium and deuterium (1), with performance limited by the abundance sensitivity inherent in normal quadrupole operation (first stability region). More recently, the suitability of operation of a quadrupole in the second stability region for this application has been demonstrated.(2) In our laboratory, we have sought to characterize the operation of a quadrupole using the second stability region, specifically for high frequency operation with large diameter quadrupole rods (3/4", 19 mm) to yield extremely high resolution with excellent abundance sensitivity.

Experimental. Operation in the first stability region requires greater than 6:1 RF to DC voltage ratio (RF-only to unit-mass resolution). Operation in the second stability region requires an RF to DC voltage ratio slightly more than 2.1:1. This voltage ratio was effected through changing the gain resistor in the input buffer of the pole DC board by a factor of 2.9. The actual RF and DC voltages required to reach the high resolution tip of the second stability region are 4.6 and 13.4 times that required for the first stability region to reach the same mass. Experimental data was acquired using Extrel C-50 mass spectrometer electronics with an Extrel 150-QC quadrupole control electronics (300 Watt, 2.9 MHz), and a standard 3/4" quadrupole probe assembly with axial ionizer (Extrel 041-11) and analog electron multiplier.

Results and Discussion. Analysis of simulated ion trajectories reveals that the amplitudes of the higher harmonic frequencies in both the X and Y directions are much greater for the second stability region than the first, with a corresponding increase in ion velocity. This should translate into improved abundance sensitivity and resolution. Abundance sensitivity is a figure of merit of a mass spectrometer system which demonstrates the ability of a mass spectrometer to completely resolve adjacent peaks of widely varying intensities. For quadrupoles operated in the first stability region, it can be quite challenging to quantitate a low intensity peak which is adjacent to and at a lower mass than a very high intensity mass peak. This weakness is attributed to the weaker focusing of a quadrupole in the Y direction; the higher mass ions are not rejected effectively at the low frequency of ion motion boundary. Abundance sensitivity is demonstrated for the first and second stability regions in the figures to the right. Note that it is abundance sensitivity that limits quantitation in the first stability region. While high resolution (full width, half height FWHH) is demonstrated for the first stability region, the deuterium peak can be seen to leak over into the domain of the helium peak, making quantitation of low levels of helium in the presence of high concentrations of deuterium difficult. In contrast, the abundance sensitivity seen in the second stability region is limited only by system noise.

Ultra high resolution can be demonstrated using the second stability region, but as always, high resolution correlates with reduced transmission. The figure below represents typical resolution-transmission curves for deuterium for a quadrupole operated in the first and second stability regions. All resolutions are full width at half height. At the lowest resolution available for the second stability region the transmission is about forty percent that for equivalent resolution in the first region. At the lowest resolution available for the first stability region, the transmission is about eight times that of the highest transmission in the second region. At high resolution, the performance in the second stability region dominates, offering twice the ultimate resolving ability, with higher transmission than the first region at higher resolutions.

Conclusions. For applications requiring ultra-high resolution at very low mass with excellent abundance sensitivity, operation of a quadrupole in the second stability region offers clear advantages for maximum signal-to-noise. Operation in the second stability region allows for a factor of two or better usable resolution, higher transmission at extreme resolutions, and orders of magnitude better abundance sensitivity than operation in the first stability region. Indeed, abundance sensitivity measurements for the second stability region were immeasurable, effectively limited by system noise levels. One drawback of operation in the second stability region is the amount of DC voltage required (13.4 times as much as for the same mass in the first region). For the mass spectrometer configuration used, the mass range was limited from a standard sixty four amu to around eight amu.

(1) Ellefson, R.E.; Moddeman, W.E.; Dylla, H.F. *J. Vac. Sci. Technol.* **1981**, *18*, 1062-1067.
(2) Hiroki, S.; Abe, T.; Murakami, Y.; Yanagishita, K. and Nakamura, S. *J. Vac. Sci. Technol. A* **1994**, *12*, 2711-2715.

43rd ASMS Conference on Mass Spectrometry and Allied Topics

First Stability Region: Abundance Sensitivity

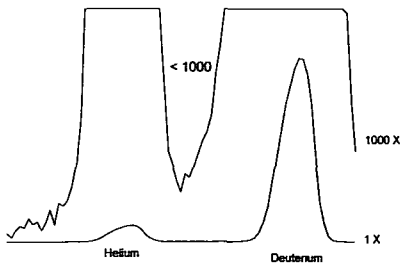

Second Stability Region: Abundance Sensitivity

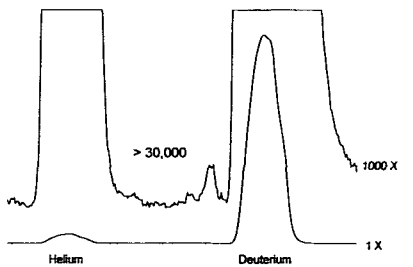

Second Stability Region: Separation of Helium and Deuterium

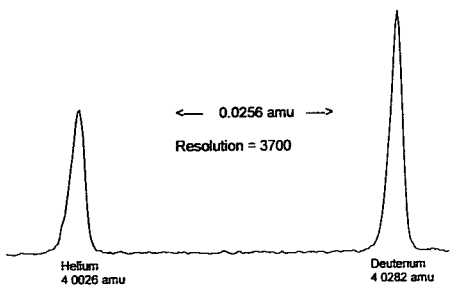

Deuterium Transmission as a Function of Resolution.
First and Second Stability Regions

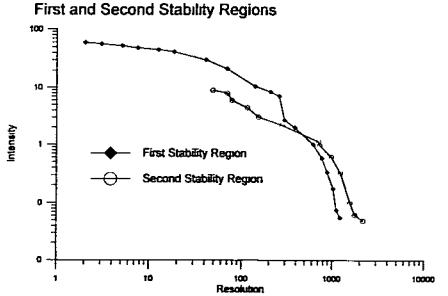

Resolution and Transmission of Quadrupoles: RF-DC and RF-Only Operation. Randall E. Pedder and Richard A Schaeffer, Extrel Corporation, 575 Epsilon Drive, Pittsburgh, PA 15238

Introduction. The mass range of a quadrupole mass spectrometer is dependent upon the RF frequency, the RF and DC voltages available, and the rod radius (for round rods), as well as the mode of operation (RF-only, first stability region, second stability region...). There is a variety of combinations of RF frequency, voltage and rod radii which yield equivalent mass ranges for a given input power. The resolving RF-only mode of quadrupole operation was identified and refined in the 1970's using retarding potentials and specialized ion detectors.(1,2,3) In contrast with normal RF-DC quadrupole operation, RF-only operation relies on the strong focusing fields at the a=0, q=0.906 edge of the first stability region, requiring 9/7 times as much RF voltage to get to a given mass. We have demonstrated high performance operation of a quadrupole using a retarding exit lens potential in our standard ion detector hardware.

Experimental. All experiments were performed in this study using standard Extrel EXM series probe assemblies consisting of a flange mounted analog electron multiplier, quadrupole in a grounded housing with entrance and exit lenses, and an Extrel 041-11 axial ionizer. All quantitative experiments utilized an emission current of 5.0 mA, and a partial pressure of perfluorotributylamine of 5 X 10^{-6} torr. The ion energy for experiments in each quadrupole size was kept constant, with the rest of the tune elements optimized for best sensitivity and peak shape at each frequency. The same 3/4" quadrupole probe assembly was used for both the RF-only and the RF-DC experiments, changing only the tuning of the ionizer and quadrupole entrance and exit lenses and the presence or absence of the resolving DC voltage.

Results and Discussion. From Mathieu Phase Space analysis, the transmission of a quadrupole is predicted to scale with the square of the rod radius, and increase marginally with increases in RF frequency. Indeed transmission does follow this trend experimentally, with small increases in absolute and relative transmission with increases in frequency, but four-fold increase in sensitivity with a two-fold increase in rod radius. Relative transmission for the 3/4" quadrupole is better at all frequencies than relative transmission for the 3/8" quadrupole. The following table contains the experimental results of the measurement of absolute transmission (measured on a Faraday collector) of various quadrupoles operated at various RF frequencies. All currents are in picoAmps.

m/z	3/8" 880 kHz	3/8" 1.2 MHz	3/8" 1.7 MHz	3/4" 880 kHz	3/4" 1.2 MHz	3/4" 1.7 MHz	3/4" 2.9 MHz
50	17	17	14.6	55	82	90	
69	840	860	800	3416	4670	5650	6140
131	154	160	208	881	1290	1148	
219	137	94	157	676	905		
414	4	3.87	9 4	40.7	31		
502	5	2.7	7	52.3	28.2		

In high resolution RF-only quadrupole operation, the transition from high pass mass filter to high resolution is controlled through changes in the exit lens 'retarding' potential, as can be seen in the separation of 664 and 665 from perfluorotributylamine. Note that the transmission as a function of resolution for high resolution RF-only mode is better than normal RF-DC operation, but that abundance sensitivity is better for RF-DC except for the highest RF-only resolutions.

Conclusions. Bigger is Better! Transmission scales roughly with the square of the rod radius. Larger diameter quadrupole rods require lower (more power efficient) frequencies to yield the same mass range. By increasing the rod radius instead of frequency, the same magnitude of applied voltage yields dramatically better transmission and resolution. For a well collimated ion source emittance, an increase in RF frequency yields increased resolution and relative transmission with marginal increase in sensitivity. For high mass ions, RF-only operation with a retarding potential offers twice the ultimate resolution and higher transmission at all resolutions albeit at sacrificed abundance sensitivity for the lower resolutions. Dramatic improvements in sensitivity are predicted for higher mass range systems (smaller diameter quadrupoles, lower RF frequencies). Predicted applications include cluster analysis and deposition and the analysis of large bio-molecules.

(1) Brinkmann, U. *Int. J. Mass Spectrom. Ion Phys.* **1972**, *9*, 161.
(2) Holme, A.E.; Sayyid, S.; Leck, J.H.; *Int. J. Mass Spectrom. Ion Phys.* **1978**, *26*, 191.
(3) Dawson, P.H.; Meunier, M.; Tam, W. *Adv. Mass Spectrom.* **1980**, *8B*, 1629.

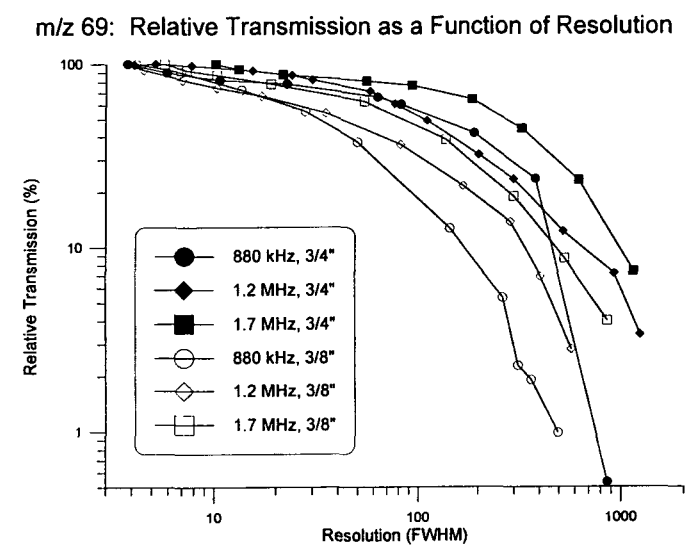

RF-Only Separation of m/z 664 and 665

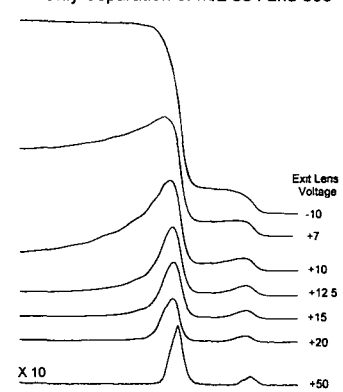

Exit Lens Retarding Potential Controls Resolution

RF-Only Versus RF-DC Operation: m/z 664

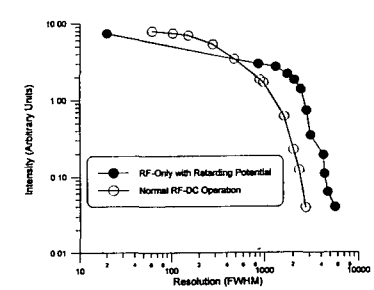

A.M. versus F.M. Quadrupole Mass Spectrometer

Beaugrand#, C.; Rolando*, C.; Sablier*, M., Simonneau*, G
(#) AIRND - 35, rue Victor Hugo - 78230 Le Pecq (France)
(*) Ecole Normale Supérieure, U R A. 1679 Processus d'Activation Moléculaire
24, rue Lhomond - 75231 Paris cédex 05 (France)

Quadrupoles are dynamic mass analyzers which currently use a constant DC voltage and a variable AC voltage at fixed frequency. Mass scanning is accomplished by varying the AC voltage, keeping the ratio AC / DC voltage constant (1). For a quadrupole mass filter, the standard scanning mode is obtained by amplitude modulation of the voltages U and V applied to the rods, but keeping their ratio constant in order to get a constant peak width ΔM (1,2). The reason for this unic way to scan is due to the available technology at the time of discovery. As a result, the resolution is variable with the mass, the frequency of the R.F. voltage is fixed and the mass span is linear.

However, the basic equation governing the motion of ions in a quadrupole field leaves the possibility of an other mode of scanning based on the use of a fixed DC and a fixed AC voltage, but with a variable frequency f (frequency modulation). Modern electronic components allow the construction of such power supply (3).

In this new scanning mode, U and V are kept constant but the frequency f is modified with time. As a consequence, the position of masses is not linear but the resolution is constant over the full mass range.

The new power supply provides a variable R.F. frequency at an adjustable constant amplitude. A tuned transformer cannot be used (in comparison with a standard scanning device) and the R.F. high voltage is only limited by the electronic component used. Our maximum value is 400V with a frequency scanning from 400 kHz to 1 MHz (400 kHz to 2 MHz for a 100V DC voltage). The DC voltage is kept constant and is adjustable in order to control the resolution. Off setting is also possible and permits to apply a polarisation along the quadrupole axis.

The new R.F. power supply has been installed on a quadrupole filter from a Finnigan Mat 3200 OWA (diameter : 6.35 mm, length : 140 mm). The R.F. amplitude and frequency control is done through a function generator (Philips PM 5132). 4-bromotoluene is used as reference compound and is directly injected into the open EI source of the mass spectrometer.

As a result, mass spectra at 150V (f=0.875MHz) and 200V (f=1.08MHz) for the mass 170-172 of 4-bromotoluene molecular ions are presented below (figures 1 and 2 respectively). These mass spectra are obtained using a frequency modulation scanning. The employed R.F. voltage can be sinusoïdal or not, the mass span is varying with f^2, the mass range depends on the dimensions of the filter and is only limited by the R.F. voltage applied to the rods. The positions of the peaks are in accordance with calculations.

At the present time, the available resolution is at least as good as that obtained in the standard scanning mode and lays around a value of $M/\Delta M \approx 1000$.

As predicted from theoretical calculations, the resolution is shown to increase with the applied AC voltage. To improve the resolution of our device further, we are now working on a new R.F. generator capable of delivering an AC voltage greater than 5 kV.

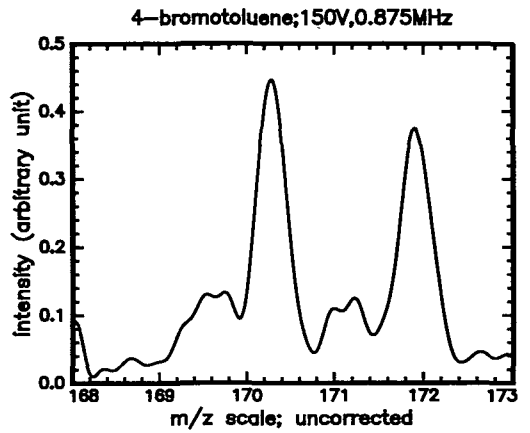

Figure 1

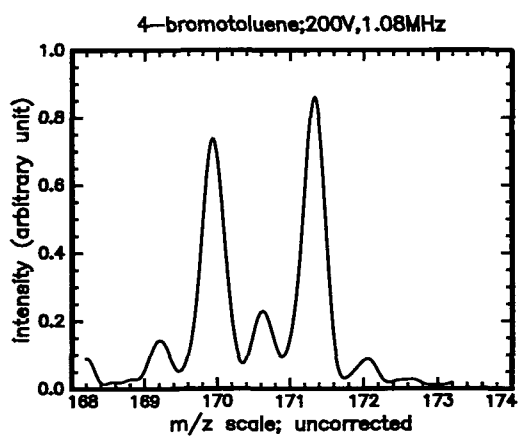

Figure 2

(1) Dawson, P.H. in *"Quadrupole mass spectrometry"*, Elsevier, **1976**.
(2) Miller, P.E.; Bonner Denton, M. *J. Chem. Educ.* **1986**, *63*, 617.
(3) Rolando, C. et al. *42nd ASMS Conference on Mass Spectrometry and Allied Topics*, Chicago, p 511.

Experimental Study and Modelisation of the Influence of a Low Frequency Component Added to the Standard RF Frequency of a Quadrupole Analyzer.

Claude Beaugrand[#], Lionel Poisson[*], Christian Rolando[*] and Michel Sablier[*],

(#) AIRND, 35 rue Victor Hugo, 78230 Le Pecq, France
(*) Ecole Normale Supérieure, Département de Chimie,
URA 1679, Procesus d'Activation Moléculaire
24 rue Lhomond, 75231 Paris Cedex 05, FRANCE

Addition of a low frequency component (ca 10 kHz to 100 kHz) of small amplitude (one hundredth to one thousandth of the main voltage) to the standard RF frequency (ca 1 MHz) of a quadrupole mass analyzer, has a strong influence on resolution, peak shape and transmission of ions.

Experimentally, by using a sinusoidal voltage we observed "weak" optimum conditions, which allow an increase of ion transmission, a better resolution at high mass and a wider tolerance on ion beam energy spread.

The most efficient frequency is inversely proportional to m/z (Figure 1) whereas the optimum voltage is nearly proportional to m/z. Those parameters are close to the solution used on the device called "Resolver" which is fitted on instrument from Nermag company.

In order to try to understand these complex experimental results, we have performed numerical simulations of ion trajectories using a classical Runge-Kutta numerical integration of the Mathieu equation. Calculations have been performed on an IBM Risc 6000 320 H computer, using 10^7 steps per trajectory.

Figure 1: Optimal frequency of the added voltage for increasing resolution in function of the inverse of the mass.

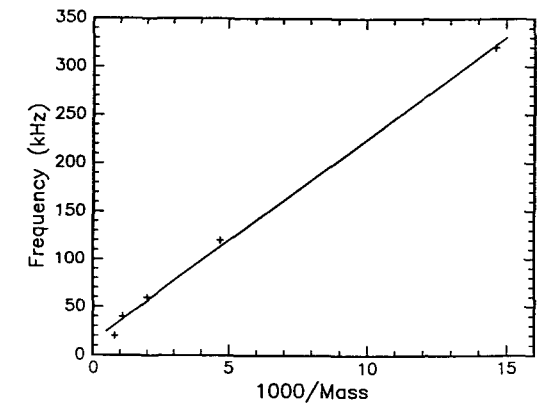

Figure 2: Numerical calculation of the stability diagram for a real quadrupole (r0=1", length 10", 1MHz), initial speed v=800 m.s^{-1}, perturbation q/1000, 10 kHz.

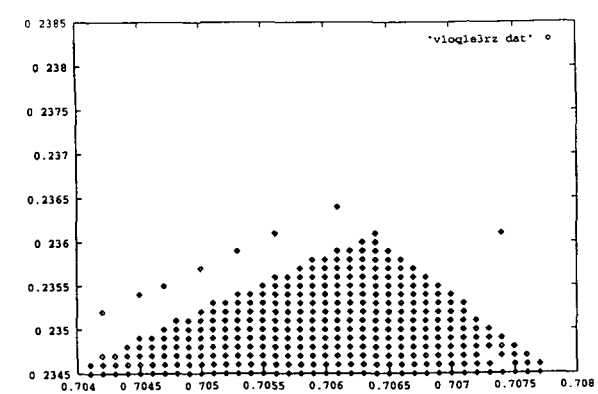

Numerical solutions are in good agreement with experimental results.

Preliminary analysis show that energy of ions (figure 2) and the finite dimensions of the quadrupole analyzer play a central role in the resolver effect.

CHARACTERISTICS OF A HIGH PRESSURE QUADRUPOLE COLLISION CELL#

P. Thibault[a], K. Whalen[b], R.K. Boyd[a], B. Shushan[c] and T. Sakuma[c]
a National Research Council, Halifax, Nova Scotia, Canada B3H 3Z1.
b Chemistry Dept., Dalhousie University, Halifax, Nova Scotia, Canada B3H 4J3.
c SCIEX, 71 Four Valley Drive, Concord, Ontario, Canada L4K 4V8.

Recently (1-3) an RF-only quadrupole collision cell $\mathbf{q_2}$, of a new design, was described for triple-quadrupoles $\mathbf{Q_1q_2Q_3}$. This new cell can operate at collision gas pressures up to 10 mTorr, about 10 times higher than most cells of this type. At these higher pressures an entirely new operating regime is accessed, *e.g.* the transmission efficiency for precursor ions is *increased* over that observed in the absence of collision gas. The useable resolving power of $\mathbf{Q_3}$ is also increased, with no requirement for linking the offset potential of $\mathbf{Q_3}$ to its mass filter function. The increased transmission and resolving power were ascribed (1-3) to a collisional focussing effect analogous to that exploited in quadrupole ion traps, consistent with trends observed (2) on varying the molecular mass of the target gas (larger effect when the target mass is a small fraction of that of the precursor ion). This focussing effect restricts all ions emerging from $\mathbf{q_2}$ to trajectories close to the central axis thus increasing the transmission efficiency (all ions now fall within the phase space acceptance of $\mathbf{Q_3}$). The low energies of the exiting ions (<< 1eV) implies that the problem of matching the offset potential to the ion energies, difficult for conventional $\mathbf{q_2}$ cells, has been circumvented and good resolution is now possible across the entire mass range. These advantages are offset to some extent by longer transit times (10-20 msec) through $\mathbf{q_2}$.

The present work extends the characterization of this new cell to a study of the chemical reactions which can be induced. Charge-site-remote (CSR) fragmentations (4) were chosen for study since it is known (5) that it is difficult to observe these using conventional $\mathbf{q_2}$ cells. The ion $C_{16}H_{33}N^+(CH_3)_3$ was chosen for initial study, in the hope that its simple chemistry would permit investigation of the desired effects with a minimum of complications. Argon was chosen as initial collision gas, since it was shown (2) that it provides the best compromise between collisional focussing (increased transmission and resolving power) and available (centre-of-mass) collision energy (CID efficiency). Figure 1 shows the effect of initial collision energy at the entrance to $\mathbf{q_2}$, at a fixed pressure of argon. The characteristic CSR fragments can be observed at energies below 20 eV, although they become clearly observable only at energies above this value. This contrasts with the observations on the same ion-target combination using a conventional low-pressure cell (5), where collision energies of 200 eV were required. It seems likely that this difference reflects the much longer residence times (2) in the new cell. It is known (4) that CSR fragmentations are observable at low collision energies provided that reaction times are correspondingly long. However, it is still necessary to show that the observed fragments (Figure 1) are truly CSR reaction products, rather than the mixed mechanism products described by Tuinman *et al.* (6). Use of xenon rather than argon led to much poorer transmission and resolving power (mass ratio of target:ion too large for effective collisional focussing). Surprisingly, at lower energies and higher pressures of xenon the CSR fragments were suppressed, and replaced by what appeared to be $Xe^{+\cdot}$ ions. At the highest pressures used there was even evidence for formation of $Xe_2^{+\cdot}$. Clearly the new cell needs further characterization.

(1) M. Morris, P. Thibault, R.K. Boyd, *Rapid Commun. Mass Spectrom.* **7**, 1136 (1993).
(2) M. Morris, P. Thibault, R.K. Boyd, *J. Am. Soc. Mass Spectrom.* **5**, 1042 (1994).
(3) B.A. Thompson, D.J. Douglas, J. Corr, J. Hager, C.L. Jolliffe, *Anal. Chem.* (in press).
(4) M.L. Gross, *Int. J. Mass Spectrom. Ion Proc.* **118/119**, 137 (1992).
(5) A.J. Alexander, P. Thibault, R.K. Boyd, *Rapid Commun. Mass Spectrom.* **3**, 30 (1989).
(6) A.A. Tuinman, K.D. Cook, L.J. Magid, *J. Am. Soc. Mass Spectrom.* **1**, 85 (1989).

NRCC No. 38086.

FIGURE 1. Hexadecyltrimethylammonium ion on argon; CGT 200

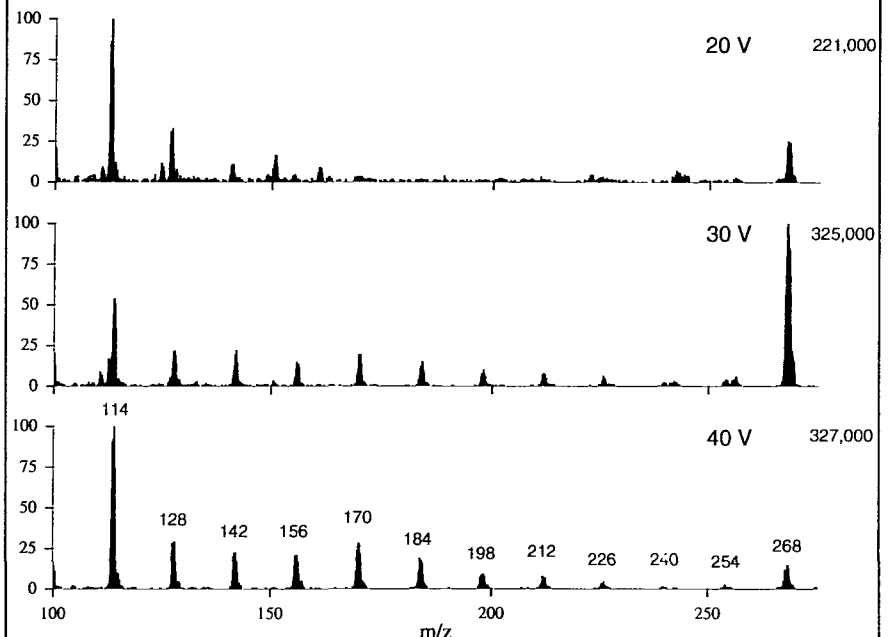

Fragment ion spectra of $C_{16}H_{33}N^+(CH_3)_3$ ions (m/z 284) in collision with argon in the high pressure regime of the new $\mathbf{q_2}$ cell. The collision energies noted are the initial values for ions just entering the cell (all ions exiting the cell have axial energies < 1 eV). The annotated fragment ions correspond to formal losses of (C_n,H_{2n+2}), and are products of CSR fragmentations (4) or of the charge-site induced reactions which lead to the same product ion masses (6). Deuterium labelling experiments will be conducted to distinguish between these possibilities.

A NEW DETECTOR FOR MAGNETIC SECTOR INSTRUMENTS BASED ON A SCANNING CCD

Jeffrey W. Finch[1], Brian D. Musselman[1], Gary R. Sims[2], and Fumio Kunihiro[3]

[1]JEOL USA Inc., 11 Dearborn Rd., Peabody, MA 01960, [2]Spectral Instruments, Suite 120 W. Grant Rd., Tucson, AZ 85745, [3]JEOL Ltd., Musashino 3-2-1, Akishima, Tokyo, Japan

Introduction: Static array detectors have been interfaced to magnetic sector instruments for the purpose of improving sensitivity over point detection [1,2,3]. These detectors have typically employed a Chevron MCP phosphor intensifier-photodiode array assembly placed at the focal plane of the mass spectrometer, which is integrated as the magnet is "jumped" in a stepwise fashion over the mass range of interest. While these detector systems have significantly higher sensitivty, there are many disadvantages including the complexity of the system, time required to acquire a single spectrum (due to settling times of the magnet), complex calibration routine, and limited dynamic range In order to overcome these disadvantages, a scanning array detector has been developed for magnetic sector instruments based on a charge-coupled device (CCD) with the goal of providing a simpler, more cost effective detector which can provide a significant improvement over point detection for ESI, LC/MS, and MS/MS 4-sector experiments

Methods: The point detector of an SX102A reverse-geometry (BE) instrument was removed and replaced with a custom CCD array detector [4] as shown in Figure 1. The detector consists of a Chevron intensifier coupled to a 1" CCD array, which is cooled to -40 °C. The detector has an effective center mass coverage of ~4%. As the magnet current is scanned exponentially from high mass to low mass, the ion images are "tracked" across the detector by operating the CCD in *time delayed integration* (TDI) mode In this mode, the speed at which charge is shifted across the CCD is synchronized with the speed of the ion image as it travels across the focal plane Therefore, the ion image is "integrated" as it passes over each detector element in the array, resulting in substantial improvement in signal-to-noise. Ion signals from the CCD detector are input into the APU and are processed in exactly the same fashion as data from the point detector External calibration of the SX102A with the CCD detector was accomplished by collecting a calibration spectrum of ultramark 1621 in FAB mode, and then processing the data using a JEOL Complement Data System running on a Hewlett Packard 32 bit workstation For electrospray measurements, samples were introduced via loop injection into a JEOL Generation 2 ESI source [5] with the ion source operating at 5 kV accelerating potential Gramicidin S and lysozyme (Sigma) were used directly without any further purification, and ESI solutions were made up by diluting stock solutions into a solvent of 1.1 water/methanol with 2% acetic acid

Results and Conclusions: Static images recorded for ultramark 1621 with the CCD array detector on the SX102A instrument indicate that resolution is as high as 6,500 (FWHM, m/z 1422) Scanning resolution of the device is as high as 3,500 at m/z 1422 (FWHM, ultramark 1621) at a scan speed of 60 sec/decade Figure 2 shows a single scan ultramark spectrum recorded at a scan speed of 5 sec/decade, indicating good mass resolution is achievable at scan speeds which are compatible with LC/MS applications, even at higher mass range Mass accuracy for ESI spectra recorded with the new detector at low resolution conditions (R~1,000) is within 0 02 to 0 2 amu. Calibration stability data of the mass spectrometer with the scanning CCD array is shown in Figure 3, where an ESI mass spectrum of gramicidin S was recorded each day over a four day period, using a single external calibration file acquired at the beginning of the first day Day to day calibration stability is excellent and is similar to that observable for point detection over periods of up to a week or longer. ESI spectra for loop injections of lysozyme recorded with the new CCD detector are

shown in Figure 4 Results indicate that sensitivity is a factor of 50 to 100 times greater than point detection, which is similar to ESI data recorded for lysozyme with a static photodiode array detector [2]

Diagram of the JEOL SX102A Double-focusing Mass Spectrometer with the Scanning CCD Array Detector

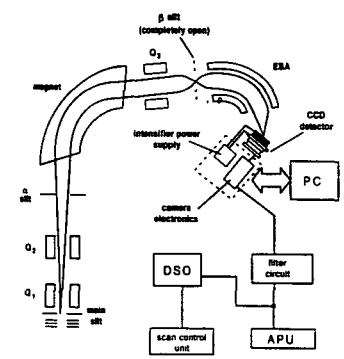

Figure 1

FAB Mass Spectrum with CCD Array Detector
Scan Speed = 5 seconds/decade
single scan of Ultramark 1621

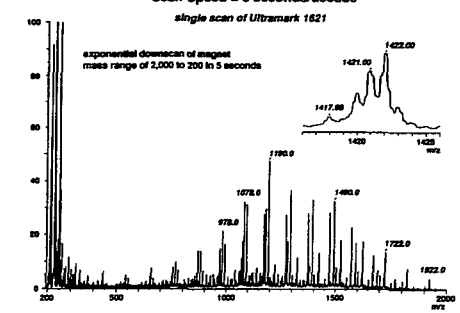

Figure 2

External Calibration Stability with CCD Array Detector
Electrospray spectra of Gramicidin S recorded over a four day period
standard deviation = ± 0 063 amu

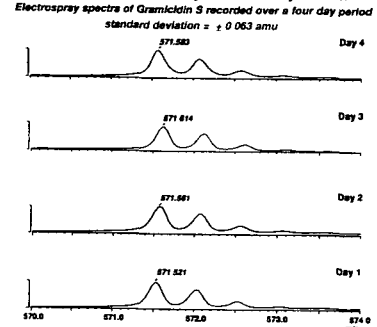

Figure 3

Electrospray with Scanning CCD Array Detector
loop injections of lysozyme
scan speed = 60 sec/decade, 20 sec/scan

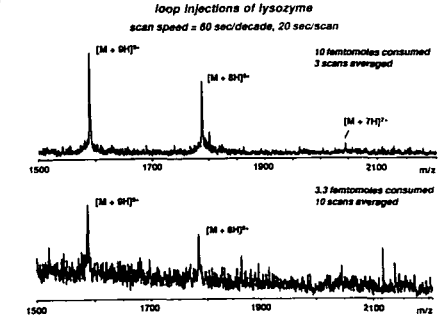

Figure 4

1 Hill, J A , Biller, J E , Biemann, K. *Int. J Mass Spectrom Ion Processes* **1991**, 111, 1-25
2 Cody, R B , Tamura, J , Finch, J W , Musselman, B D *J Am Soc Mass Spectrom* 1994, 5, 194-200
3 Kolli, V S.K , Orlando, R. *J Am Soc Mass Spectrom.* 1995, 6, 234-241
4. Finch, J W , Kunihiro, F., Sims, G R.; Musselman, B.D , Patent Pending
5 Finch, J W ; Cody, R B ; Tamura, J ; Musselman, B D , Proceedings of the 42nd ASMS Conference, 1994, Chicago, IL, p 753

SECONDARY ELECTRON MULTIPLIER OPERATING AT FORVACUUM PRESSURE

Alexander A. Makarov, Department of Chemistry and Institute of Mass Spectrometry, University of Warwick, Gibbet Hill Road, Coventry CV4 7AL, UK
Michael Y. Yablokov, Karpov's Institute of Physical Chemistry, Moscow, Russia

INTRODUCTION

Modern secondary electron multipliers (SEM) and microchannel plates (MCP) are acknowledged to operate reliably and effectively at residual gas pressures not exceeding 10^{-4}-10^{-5} torr However, as it is known from the practice of ion trap mass spectrometry, this limit is raised up to few millitorrs when vacuum chamber is filled with an inert gas such as helium. Unfortunately, the transition to similar pressures of air in conventional schemes of SEM or MCP unequivocally leads to breakdown and damage This obstacle results in the necessity of expensive high-vacuum system and seriously limits the perspectives of developing ultra-miniature mass-spectrometers for, e.g., field analysis

The objective of the present work has been the development of an ion-counting detector capable of working at forvacuum pressures of air (i e. up to several millitorrs).

The chosen concept envisaged the conversion of the incident ions into pulses of electrons by a single MCP operating at low gain, acceleration of the electrons to a phosphor and counting of light pulses by a photomultiplier

EXPERIMENTAL

To exclude the dependence of the detected current on residual pressure, the ion flux was simulated by ultraviolet radiation produced by hydrogen-filled UV lamp (Fig 1). Radiation intensity was attenuated by interchangeable diaphragms D of diameters d_1=0.3 mm, d_2=1 mm, d_3=1 5 mm located in atmosphere beyond UV window about 0 3 m away from the detector as well as by a hole of 8 mm diameter in the shielding electrode SE.

Electrons produced by photoelectron emission on MCP are multiplied inside MCP channels. The resulting flux of secondary electrons is accelerated in the gap between MCP and phosphor (both of the diameter 34 mm) and confined using electrode CE. Photon bursts produced on phosphor are detected by photomultiplier PMT (Hamamatsu R1635) and counted by ion counting electronics with adjustable discriminator level

UV lamp LGV-1, MCP 34-10 and phosphor KS-425 were produced by State Optical Institute, St.-Petersburg, Russia

During the optimisation of the detector, electrometer (V7-49, Minsk, Belarus) was also used.

Vacuum chamber is evacuated by turbomolecular pump TMP (TSH 180 H, Balzers) backed by a rotary pump RP. Pressure is measured by preliminary calibrated ionisation gauge IG (PMI-2) The increase of pressure is realised by opening leak connected directly to atmosphere

RESULTS

Firstly, multi-parametric optimisation of detector performance has been carried out at high vacuum (5 10^{-6} torr). The main criteria of optimisation has been minimum dark count rate and maximum counting effectiveness (close to 100%)

To obtain results independent of the nature of incident radiation (so that the results could be applicable not only to photon but to ion fluxes as well), secondary electron current was measured on electrode SE by applying small bias relatively to MCP and switching off bias on MCP. For the largest diaphragm d_3, it has appeared to be 5±1 fA.

The optimised voltages are represented in Fig. 1. Also, dependence of counting rate on MCP voltage is shown in Fig 2. It demonstrates that at MCP voltage of 600-650 V detection efficiency approaches 100% while at higher voltages false counts may occur (i e. signals from electron noise inside the channels may overcome the discriminator level). Analogous dependencies are observed for other voltages. Reproducibility of counting rate after opening to atmosphere and on day-to-day basis was about 10-15%

After optimal voltages has been established, pressure was gradually increased. It has been found that counting rate is independent of pressure within 10%, while dark count rate exhibit dependence shown in Fig. 3, i.e. it stays as low as 1-2 counts/second at air pressures as high as 3 millitorr!

CONCLUSION

On the basis of these experiments, it may be concluded that the main pre-requisites for successful ion counting at high air pressures (up to 1-3 millitorrs) are:

- low electric fields in front of MCP,
- the use of a single MCP in the low-gain regime so that electron currents are as low as possible, however sufficient for the reliable conversion into photons.

The developed multiplier may be used for reducing pumping requirements in miniature mass spectrometers with atmospheric-pressure ion sources as well as in portable mass spectrometers for field applications.

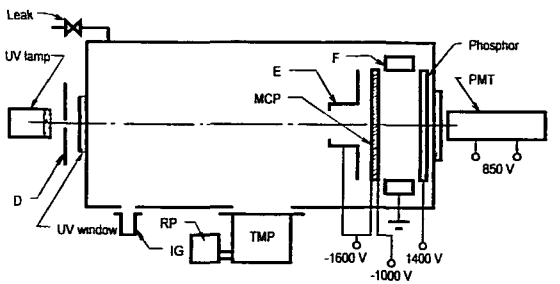

Fig.1 Scheme of the experimental setup.

D - diaphragm, IG - ionisation gauge, PMT - photomultiplier, RP - rotary pump, TMP- turbomolecular pump, SE- shielding electrode, CE- confining electrode,

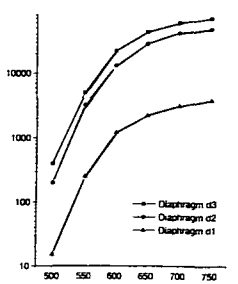

Fig 2. Dependence of counting rate S (cps) on MCP voltage V (in Volts)

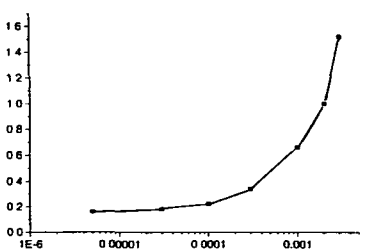

Fig. 3 Dependance of the dark count rate S (cps) on air pressure P (torr)

The Direct Imaging of Ions Using a Charge Injection Device (CID) Detector

Steven J. Christopher, Mark A. Parker, and R. Kenneth Marcus

Department of Chemistry
Howard L. Hunter Laboratory
Clemson University
Clemson, SC 29634-1905

Over the last two decades there have been rapid advances in mass spectrometry. In recent years, the majority of research has focused on ion source development, sample introduction schemes, and their coupling to many different mass spectrometer systems, depending on whether a solid, liquid, or gaseous sample is to be analyzed. One particular area of mass spectrometry which has not been emphasized is that of detector technology. Current research in this laboratory is focused on the direct detection and spatial imaging of ions emanating from a radio frequency glow discharge ion source using a charge injection device (CID) detector.

Charge injection devices are two dimensional X-Y addressable silicon detectors that have been successfully employed for the detection of photons and for the imaging of electron beams and soft X-rays.[1] CIDs as ion detectors for MS may offer a number of potentially advantageous characteristics over other detector systems, specifically MCPs coupled to CCDs. This is because direct ion detection eliminates the need for ion beam conversion/transduction into a photon image. Also, the inherent non-destructive readout, antiblooming, and random pixel integration properties of CIDs are well suited to the imaging of ions. Irrelevant data can be ignored or an area of weak ion signal intensity can be enhanced with extended pixel integration. Since the CID is functional to atmospheric pressure, it also holds an advantage over channeltrons and electron multipliers. The push towards portable MS systems may be inhibited by these detectors which have stringent vacuum and high voltage requirements.

A vacuum system devoted to ion imaging has been constructed in-house at Clemson University. This system employs two ion optic configurations and ion images were acquired in the presence and absence of plasma photons. Preliminary MacSIMION trajectory

calculations have shown that ions strike the CID surface with a kinetic energy of approximately 30 eV.

Figure 1 below is a background subtracted ion image acquired after correcting for plasma photon and dark current contributions. The upper line spectrum was acquired with -100 V placed on a wire screen approximately 3 mm from the CID surface. Plasma photons and ion intensity are present in the -100 V image. The background image (middle line spectrum in Figure 1) was obtained while the wire screen potential was held at 0 V. Photon contribution and dark current are present in the image. Subtracting the background image from the -100 V image corrects for photon and dark current contribution simultaneously, revealing the ion intensity component of the signal.

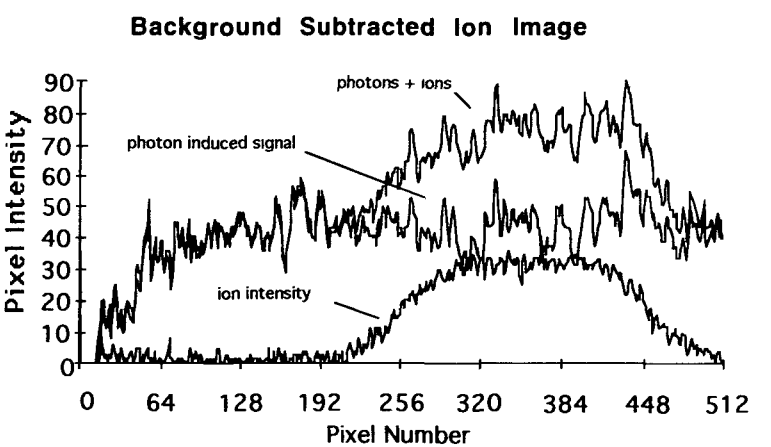

Figure 1. Background corrected ion image.

References:

1. R. Wentink, J. Carbone, Nuc. Inst. and Meth. in Physics Res., A 347 (1994) 522-528.

Development of a Hybrid Mass Spectrometer for Ion Investigations

U. Wilhelm, K. P. Aicher, M. Müller, J. Grotemeyer
Institut f. Phys. Chemie Marcusstr. 9-11, Universität Würzburg
97070 Würzburg, Germany

A hybrid mass spectrometer based on a quadrupole ion trap coupled with a reflectron time-of-flight mass spectrometer have been introduced recently. This hybrid instrument can be used widely for fundamental investigations of ions as well as for analytical purposes.

In this contrubution we demonstrate a new type of coupling of an ion trap with a reflectron- time-of-flight mass spectrometer. The system consists of three main stages: first a desorption chamber utilizing a supersonic jet together with gaseous or laser desorpted of neutrals, a hyperbolic ion trap and a reflectron-time-of-flight mass spectrometer with 1.2 m ion flight path. In our experiment the sample molecules are introduced as neutrals into the ion trap, where the ionization is done by a Nd:YAG pumped dye laser.

The main features of this instrument are long ion storage times, good ion optics in the coupling stage between both mass analysers and relatively high mass resolutions.

The mass resolving power of the hybrid instrument has been measured at Benzene to approximatly 1200. Details of the development and of the ion optics calculations will be shown. Experimental measurements demonstrate the ion storage time of small ions (i.e. Benzene). The storage time of ion masses in the trap can be extended up to 5 s and even longer.

The advantages of the electronic setup of the quadrupol ion trap (variable radio frequency, tunable endcap and ring electrode DC voltages) are presented and therefore the mass selectivity of the instrument is demonstrated (see figure 1). The mass limit of selecting only one ion mass for further storing in the ion trap goes up to about 80 Daltons. Hence the possibility of selecting and storing special ion mass ranges in the quadrupol ion trap will be possible up to a maximum mass of about 1600 Daltons.

Since we are interested in features like different ionization and fragmentation processes of neutrals and ions, a further feature of the instrument is the possibility of secondary activation of ions outside the ion trap. Here secondary activation of ions can easily be performed by induced photodissociation at the space focus of the drift region. The first results of photodissociation on Benzene are presented. The photodissociation was performed with an excimer laser running at 248 nm.

Using the reflectron-time-of-fligth mass spectrometer as an energy analysator there is the possibility to investigate the behaviour of metastable ions. First results on metastable ions are shown at Benzene. The mass resolution we reached in this experiment is about 100 Daltons.

For the desorption of neutral molecules an excimer laser running at 248 nm has been used.

Therefore first results on neutral desorped molecules are shown at Tryptophan.

Applying a jet system with subsequent ionization enables investigations about the trajectories of ions inside the trap (see figure 2). Therefore the reflectron-of-flight mass spectrometer is also handled as an energy analysator. Knowing the exact energy of the ions the starting position inside trap can be fixed.

Fig. 1: Fragment of Toluene (m/z = 39) selective storing

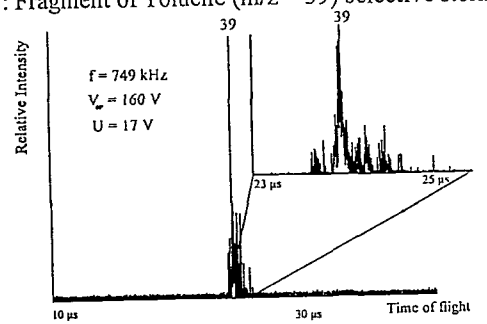

Fig. 2:

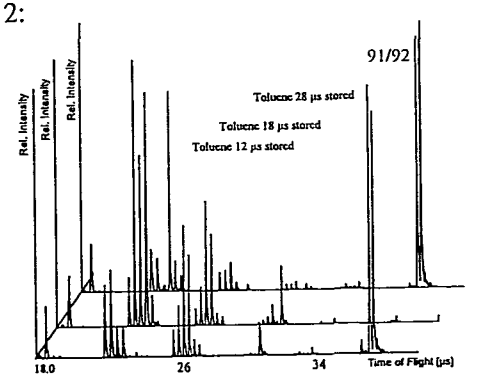

A Penning Ion Source-Quistor-Quadrupole Mass Spectrometer for Ambient Air Analysis

M. Gaelli and U.P. Schlunegger
University of Berne, Department of Organic Chemistry, Freiestrasse 3,
CH-3012 Berne, Switzerland

Introduction

In the 1980's an Environmental Protection Law was passed in Switzerland. Amongst other things, it set maximum limits for organic and inorganic substances in ambient air and emissions. To monitor the observance of these limits an intensive measurement campaign was started. It covered primarily inorganic substances, namely nitrous oxide NO_2, sulfur oxide SO_2 and Ozone O_3.
In the past few years, ozone, the so called summer smog, proved to be the most important problem. As organic substances play an important part in the formation of ozone, a fast and easy method is wanted to monitor these substances.

Commercially available methods usually show drawbacks as

- low time resolution
- low selectivity
- size of the instrument

With this in mind, a new instrument was planned to avoid the problems mentioned above. It is based on an penning ion source [1] and allows accumulation of ions in a quistor.

Instrumentation

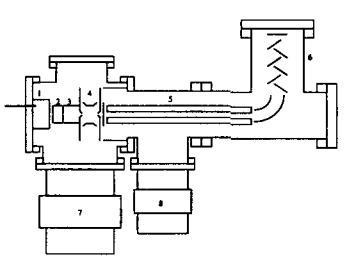

The instrument designed is shown in figure 1. The main parts are the inlet, the ion source, a transfer lens system, the quistor, the quadrupole mass filter and the detection system, a secondary electron multiplier (SEM). The system is differentially pumped at three stages.
Typical working pressures are about 5 mbar in the inlet, $4x10^{-4}$ mbar in the ion source /quistor compartment and 10^{-5} mbar in the analyzer compartment.

figure 1: the mass spectrometer. legend: 1 inlet, 2 ion source, 3 transfer lenses, 4 quistor, 5 quadrupole mass filter, 6 SEM, 7 turbo molecular pump, 8 molecular drag pump

The experiment

After ionization, the ions are stored for the desired time and then extracted towards the analyzer. After each extraction pulse, the mass value of the quadrupole mass filter is raised, normally by 0.2 Da. The acquisition is started at the extraction pulse and collecting data for 200 µs. Then a new sequence is started with another ionization pulse.
Pulse lengths are normally a 5 ms delay between extraction and ionization, 1 - 10 ms ionization, 100 - 500 ms storage and 100 µs extraction.

Discussion

Ionization time seems to have a very small influence on the signal intensity in the range investigated (1 - 1000 ms) whereas the signal varies rather strong with storage times. Substances show different "ideal" storage times. Acetone is most intensive after 50 ms, toluene after 500 ms storing.
The very small influence of ionization time displays the high ion yield of the penning ion source.

The spectrum of dichloromethane shows an interesting two-mass downwards shift of the molecular ion peak. As the dichloro-cluster still is visible, this must be due to loss of the two hydrogen atoms.

Literature

1 Kohler, M., Schlunegger, U.P.; Rapid Comm. Mass Spectrom.; 7; 1113-1117; 1993

Acknowledgment

This work was supported by the Swiss National Science Foundation.

Applications of Filtered Noise Fields in Ion Trap Mass Spectrometry

Dane Karr, Don Hoekman, and Alice Koski

Teledyne Electronic Technologies, Mt. View, CA

We have described a new method of operation for the Paul ion trap in which a Filtered Noise Field (FNF™) is used to perform Selective Ion Isolation[1]. The FNF is a waveform that is applied to the end electrodes of the trap during, and for a short time after, the creation of ions within the trap (or the introduction of ions into the trap). The waveform ejects undesired ions as they are created so that ions of interest may be accumulated without creating a space-charge condition. Since the trap is filled with only the ions of interest, the original sensitivity of the trap is maintained. The utility of FNF for the ejection of unwanted background ions during a full scan run and for Selected Ion Monitoring (SIM) analyses of low level components in a complex matrix is demonstrated.

We have removed phthalate peaks from the background in the system by employing FNF with "inverse-notches" and we show raw data to display this effect. We have also performed a GC/MS analysis of hexachlorobenzene (HCB) and used "inverse-notch" FNF to selectively remove background ions below 100 m/z, plus 207 m/z from column bleed, plus 281 m/z from column bleed, consecutively. The data show ability of FNF to markedly reduce the baseline in the total ion chromatogram and reduce the number of interfering ions in the mass spectrum.

For SIM analyses, we have isolated characteristic ions of caffeine using a three-notch FNF waveform. We have performed a direct probe analysis of coffee, with and without FNF isolation of caffeine ions. The full scan EI analysis of coffee results in significant space-charging by the end of the run whereas the FNF analysis is able to prevent space-charging throughout the run by retaining only the ions at 194, 109, and 82 m/z.

An additional SIM analysis was carried out isolating major ions from safrole. Safrole was spiked into a base/neutral and organochlorine pesticide mix at 1:10 and 1:100 dilution. The SIM analyses on these mixtures was performed using a four-notch FNF waveform and is compared to the full scan EI run. The figure below is the total ion chromatogram for safrole at a 1 100 dilution (30 pg safrole in 3 ng/component mixture) and detected via FNF by isolation of ions at 162, 131, 104, and 77 m/z. The figure below is the total ion chromatogram for the FNF analysis of safrole at a 1:100 dilution and the corresponding mass spectrum.

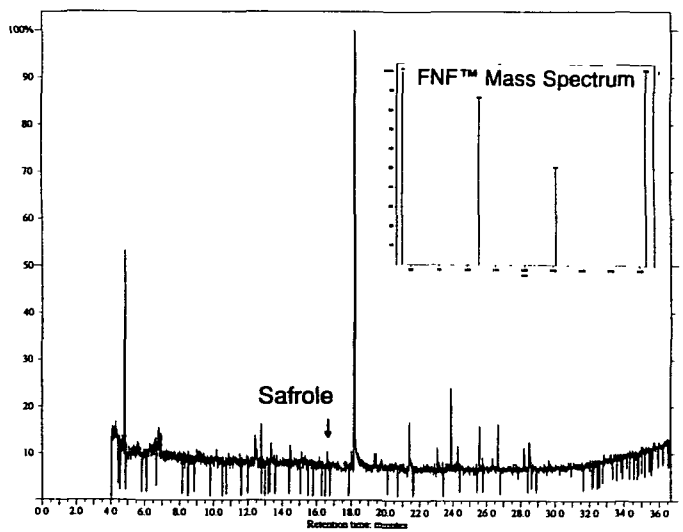

1) Tabone, V.; Yelton, R.O.; Kelley, P.E.; Stiller, S.W.; Proceedings of the 42nd ASMS Conference on Mass Spectrometry and Allied Topics; p 181.

DESIGN OF A HIGH FIELD FTICR FOR MALDI AND LD/CI STUDIES

Cynthia Pitsenberger, Paula Lei Qing, Michael Easterling, and I. Jonathan Amster
Department of Chemistry, University of Georgia, Athens, GA 30602

In 1989, an FT-ICR instrument was constructed in this laboratory for laser desorption studies. This instrument was designed primarily to examine the chemical ionization of laser-desorbed neutral peptide molecules, although it has subsequently been used for a number of other types of experiments. This instrument has a number of unique features which have proven useful for ion-molecule studies of laser-desorbed molecules. These features include (1) UHV vacuum with modest pumping. A 330 l/s turbomolecular pump provides a base pressure of 1×10^{-10} torr This low pressure permits reactive ions to be stored for several seconds, and allows ultrahigh resolution mass spectra to be recorded; (2) A two-stage solids sample introduction system to permit laser desorption studies of peptides under ultrahigh vacuum (10^{-10} - 10^{-9} torr); (3) Rapid response to the pulsed introduction of gases. Peak pressures of 10^{-4} torr can be achieved within 120 ms after the pulsed introduction of a gas, and the pressure is found to return to 10^{-9} torr or less within five seconds; (4) Dual laser ports for experiments that require two independent laser beams. This instrument has been used for a variety of experiments, such as chemical ionization of laser desorbed neutral molecules up to 1200 Daltons, MALDI of peptides up to 2000 Daltons, photodissociation and CAD studies of peptides, ion-molecule studies of peptides and amino acids, and measurements of their gas-phase basicities, and quadrupolar axialization and ion remeasurement studies of molecules up to 1200 Daltons. The principle drawback to this instrument has been its 1 tesla electromagnet. This low magnetic field strength leads to several limitations, such as a **low mass range** (the upper mass limit is 2000 Daltons); **rapid radial diffusion** of the ions from the cell at elevated pressures because of the low ratio of B/E (magnetic field to trapping voltage); **poor mass accuracy** at higher m/z values; coupling of the ion motion of closely spaced peaks, resulting in **poor isotope ratios**. Despite these limitations, this instrument has made a significant contribution in demonstrating several new techniques for peptide analysis, albeit with small, model peptides.

We have undertaken the redesign of this instrument to extend the mass range to 50 kDa or more, to apply the techniques that have been developed in this laboratory to biologically significant peptides and proteins. The new design seeks to incorporate many of the desirable features of the original instrument, while adding new high performance capabilities. Figure 1 shows an overhead view of the layout of the redesigned vacuum system. The new instrument has been designed to incorporate a shielded 4.7 tesla superconducting magnet with a 160 mm horizontal warm bore. The 4.7 tesla magnet will extend the mass range of this instrument by approximately a factor of 25, i.e. from m/z 2000 to m/z 50,000. This will permit techniques that we have demonstrated with small, model peptides to be applied to peptides and proteins of biological interest. The shielded magnet allows the turbomolecular pump, pulsed valves, ion gauge, and other integral parts of the vacuum system, to be operated within two feet of the open bore of the magnet. The new cell geometry is a open-ended cylindrical design, with capacitive coupling between the excitation plates and two quadrants of the trapping plates. This design, proposed and implemented by Laude and coworkers, has been shown to reduce the z-axis ejection of ions. The system for introducing solid samples for laser desorption and the design of the laser

optics has been improved. The new design maintains the capability to perform MALDI next to the analyzer cell while preserving ultrahigh vacuum conditions. A sample stub is transferred between the two linear motion sample manipulators outside of the magnetic field of the instrument. A linear motion feedthrough that is attached to the pump down chamber transfers the sample to a linear-rotary manipulator that is part of the ultrahigh vacuum main chamber. The linear-rotary manipulator is used to position the sample near the analyzer cell. Rotation of this manipulator allows different portions of the probe to be brought under the focus of the laser beam. A DC motor controls the rotary position of the manipulator, which can be placed under computer control. A video camera with telescopic optics can be mounted at the end of the main vacuum chamber, to allow the sample to be observed during laser desorption. An internal preamplifier that is mounted next to the analyzer cell, inside the vacuum system has been designed for this instrument by IonSpec. The internal preamplifier has been shown by McIver and Hunter to reduce the effects of distributed capacitance that decrease signal intensity and bandwidth. Quadrupolar excitation capabilities present with the original design have been retained in the new instrument. Two plate quadrupolar excitation, introduced by Laude and coworkers, is implemented in the new design. This allows the detector leads to remain static when switching between quadrupolar and dipolar excitation, and permits implementation of an internal preamplifier. Quadrupolar excitation capabilities present with the original design have been retained in the new instrument Data that illustrates the capabilities of the new instrument will be posted as it becomes available on the Amster home page of the World Wide Web. Come visit our laboratory at **http://amstersgi.chem.uga.edu/**.

We thank our FTICR colleagues for many of the ideas that have been implemented in this design. In particular, we acknowledge Alan Marshall, Robert McIver, David Laude, and Fred McLafferty. The generous support of the National Science Foundation (CHE-9412334) is gratefully acknowledged

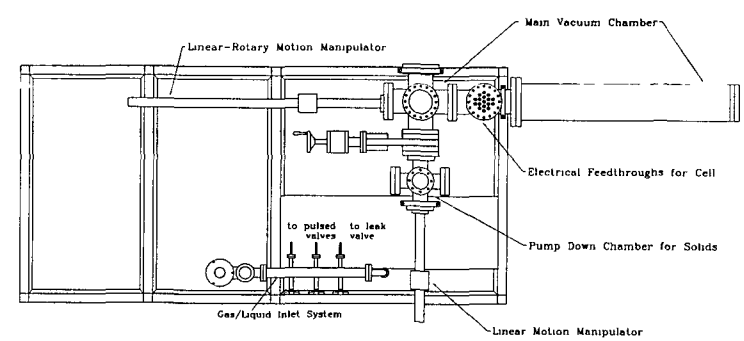

Figure 1. Overhead View of the Redesigned 4.7 Tesla FTICR

Design and Construction of an External Source Fourier Transform Mass Spectrometry Instrument

James A Carroll, Jiangyue Wu, Steven T. Fannin, Sharron Penn, and Carlito B. Lebrilla
University of California, Davis, Department of Chemistry, Davis, California 95616

The design and construction of an external source Fourier trasnform mass spectrometry (FTMS) instrument is described. The cost of the instrument was minimized by using only two stages of pumping and smaller vacuum components than previous designs Differential pumping is provided by a 190 L/s turbomolecular pump, which evacuates the source region, and a 2000 L/s cryogenic pump, which evacuates the analyzer region. Previous designs of FTMS instruments using external ionization sources typically used at least three stages of pumping.

The instrument is designed so that ionization sources can be exchanged quickly and easily. Electron impact (EI), secondary ion mass spectrometry (SIMS), matrix assisted laser desorption/ionization (MALDI), or electrospray ionization (ESI), sources can be coupled to the instrument simply by replacing the front flange of the source cube. The ions are transported from the source to the ion cyclotron resonance (ICR) cell by a single stage RF-only quadrupole ion guide, which focuses the ions through the fringing field of the magnet. The quadrupole rods are 0.78 m in length, which is shorter than previous instrument designs using a single stage quadrupole ion injection system. The ion tranmission efficiency through the rods was estimated to be about 50%, which compares well to the effieciency of similar instruments.

The ICR cell (2x2x4") is located in the homogeneous region of a 3 T superconducting magnet, which is shared with another instrument previously built in our laboratory. Sharing the magnet as well as the external circuitry and data system lead to a significant reduction is cost relative to construction of a separate instrument. Both instruments are secured on carts with wheels. When one instrument is not in use, the other can be rolled into place in the opposite bore of the magnet. This dual chamber design allows the original instrument in our laboratory, which has three stages of pumping, to be dedicated to electrospray ionization. ESI requires the higher pumping capacity of this instrument for adequate performance.

The new vacuum chamber is used mainly for MALDI, although LSIMS can be performed with the same source. Switching between the two ionization techniques requires no hardware modifications, so vacuum does not have to be broken. Simply using the appropriate sample preparation and rotating the sample probe 90° allows access for a laser beam to irradiate the sample for MALDI. The Omega data system (IonSpec. Corp., Irvine, CA) controls the experimental sequence and data processing. A schematic of the instrument is shown in Figure 1.

The performance of the instrument was evaluated using EI, SIMS, and MALDI ionization methods. The mass range is typical of a 3 T instrument. Cluster ions with mass-to-charge ratios up to about 9000 have been detected using SIMS ionization of CsI. Liquid SIMS of orgainc molecules such as oligopeptides and oligosaccharides showed results comparable to those from the original instrument in our laboratory Neither the reduced pumping capacity nor the shorter quadrupole rods have significantly decreased the performance of the instrument for LSIMS ionization.

MALDI performed in the external source provided excellent sensitivity for organic molecules. Figure 2 shows the MALDI Fourier transform mass spectrum of per-O-methyl β-cyclodextrin, which shows a strong signal corresponding to the sodium adduct at m/z 1451 and a signal corresponding to the potassium adduct at m/z 1467. The performance and versatility of the instrument make it a useful tool for the analysis of biological molecules.

43rd ASMS Conference on Mass Spectrometry and Allied Topics

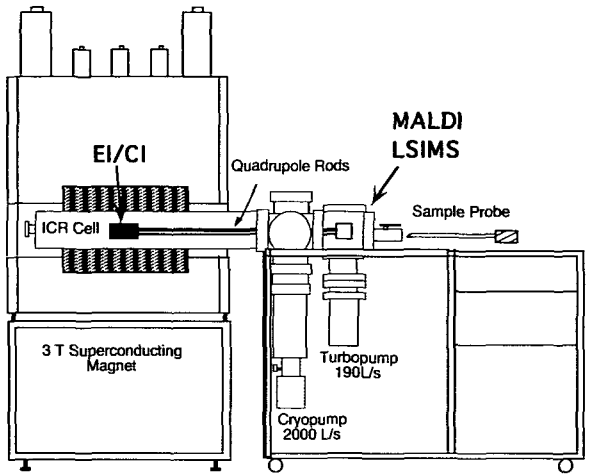

Figure 1. Schematic of the external source FTMS instrument for the analysis of biological molecules.

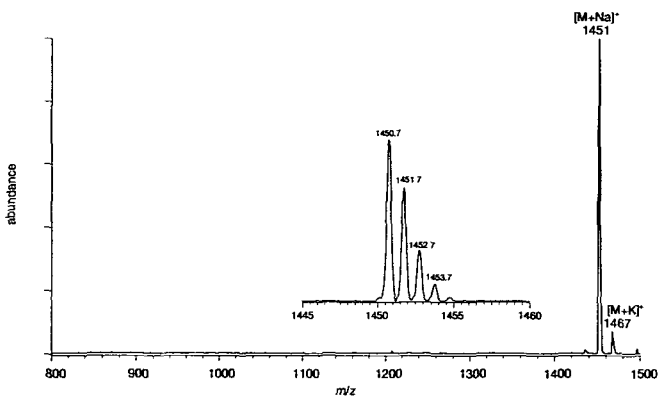

Figure 2. MALDI/FT mass spectrum of per-O-methyl β-cyclodextrin, a cyclic oligosaccharide.

In-Cylindrical-Cell MALDI with FT ICR Spectrometer

M.Knobeler, K P.Wanczek, F H Laukien*
Institute of Inorganic and Physical Chemistry, University, D-28334 Bremen, Germany
*Bruker Analytical Systems Inc., Billerica, MA 01821

The interest in the coupling of matrix assisted laser desorption/ionization (MALDI) and a Fourier transform ion cyclotron resonance (FT ICR) mass spectrometer increased in recent years. Several groups introduced different dual cell or near analyzer cell [1,2,3,4] and external [5,6] ionization techniques to take advantage of the features of MALDI and FT ICR. New methods as a gated deceleration potential at the rear trapping plate [1], ion cooling by pulsed gas inlet and axialization by quadrupolar excitation (QE) [2] and remeasurements of the ions [7] were introduced. Our new internal MALDI FT ICR instrument is a very direct method to produce the ions inside the cylindrical analyzer ICR cell.

The experiments were carried out with a modified Bruker CMS-47 spectrometer provided with a 7 T magnet, a pulsed nitrogen laser (337 1nm, 200µJ/pulse) and with one of our six homebuilt moveable vacuum systems This system is equipped with a special push rod system that allows to pump down to a pressure of 1 10^-8mbar in less than 3 min after introducing the sample into the vacuum system.

The target at the probe tip can directly be adjusted to the front trapping grid of the ICR cell. The target is electrically connected to the front grid and becomes a part of it. The center of the target is slight disaligned against the center of the front grid. During experiments the push rod has only to be rotated to hit with the laser different spots at the target.

Different matrices were used The best results were achieved with DHB in isopropanol/water with or without coadded fructose Concentrations of samples were 10^-4M to 10^-7M. 0.1µl to 10µl of the solutions was applied onto the target.

Ions with masses up to 2000 amu could be trapped without gated deceleration potential by asymmetrical trapping potential Spectra with resolved isotopes were achieved. This easier of use technique fulfills most of the requirements to analyze masses up to 2000 amu.

Trapping times up to 30s are achieved for bovine insulin at a background pressure of 1 10^-8mbar without any ion cooling technique.

Bovine insulin was detected at a permanent background pressure of 1 10-^3mbar and 1 10^-5mbar with a resolution of 60 and 450, respectively Spectra of melittin with a resolution of 4,500 at 1 10^-6mbar were achieved

Resolutions better than 50,000 and sensitivities of less than 1fmol were obtained without pulsed inlet of collision gas or quadrupolar excitation. Sensitivities of 10-100fmol and resolutions better than 10,000 were routinely achieved with masses up to 3,000 amu.

The target as a part of the front trapping grid enables a very efficient trapping of the produced ions including long trapping time, high sensitivity and high resolution. Essential are very carefully balanced deceleration voltage and time and trapping voltages at the front and rear grid. Nevertheless, techniques as axialization including remeasurements of one time generated ions should increase the sensitivity and resolution at least by one or two orders of magnitude.

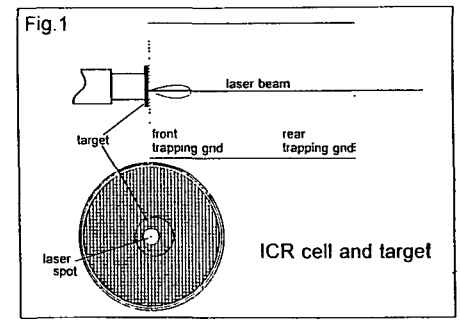

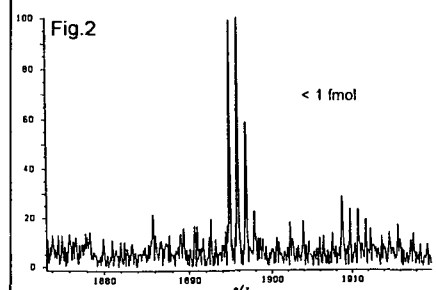

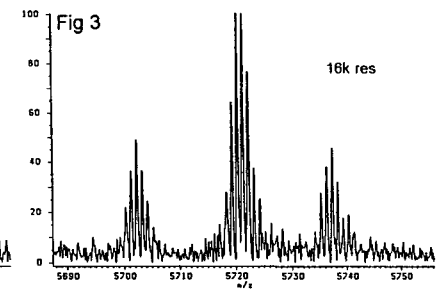

Figure 1: The cylindrical ICR cell. The target becomes a part of the front trapping grid.
Figure 2: Spectrum of gramicidin D after single scan. Less than 1 fmol was consumed. Over 100 comparable spectra were obtained with the 100fmol of sample applied onto the target.
Figure 3: Spectrum with 16,000 resolution of bovine insulin after single scan No ion cooling techniques as pulsed inlet of collision gas or quadrupolar excitation were used.

References:

[1] J A Castoro, C.Köster, C.L.Wilkins, Rapid Commun. Mass Spectrom. 1992, 6, 239
[2] S.Guan, H.S.Kim, AG Marshall, M.C Wahl, T.D.Wood, X.Xiang, Chem.Rev. 1994, 8, 2161
[3] T.Soloukı, D.H.Russel, Proc.Natl.Acad.Sci. USA 1992, 89, 5701
[4] J.S.Anderson, C.J.Harper, E.G.Schmidt, D.A.Laude, Proceed. 42nd ASMS Conf., Chicago 1994, 244
[5] M Mann, F H.Laukien, G.H.Kruppa, C.H.Watson, J Wronka, M.Knobeler, Proceed. 41nd ASMS Conf., San Francisco, 1993, 899
[6] R T.McIver,Jr , Y Li, R.L.Hunter, Int. J. Mass Spectrom. Ion Process 1994, 132, L1
[7] E.R.Williams, K.D Henry, F.W. McLafferty, J. Amer. Chem. Soc. 1990, 112, 6157

AN ELECTROSTATIC ION GUIDE INTERFACE FOR ELECTROSPRAY FTMS

Liang Tang, Michelle V. Buchanan, Robert L. Hettich and Gregory B. Hurst
Chemical and Analytical Sciences Division, Oak Ridge National Laboratory, Oak Ridge, TN 37831-6365

Introduction

The combination of electrospray (ES) technique with Fourier transform ion cyclotron resonance mass spectrometry (FTICR MS or simply FTMS) has distinct advantages for the analysis of biomolecules, including high analysis speed, high resolution and wide mass range. This report is the first demonstration of combining ES with FTMS using an electrostatic ion guide (EIG). Our approach to the combination of ES and FTMS is designing and constructing a perforated EIG, which is contained in a differentially pumped vacuum housing, to facilitate magnetic fringe field penetration, and establishing conditions for efficient trapping and detecting the ions in a cubic cell.

Experimental

A prototype instrument for coupling an electrospray ion source to FTMS is illustrated in Figure 1. The sample flow rate was typically 5 μL/min and the voltage on the ES tip (2) was 3 kV. A stainless steel capillary tubing (4) wrapped with a heating tape was used for the desolvation of the ES produced ion clusters. A skimmer (5) is opposite to the heated tubing to separate the first pumping stage from the higher vacuum region. The voltage on the skimmer may be varied from 0 to ±120 V, whereas the voltage on the heated tubing is held at ~100 V higher (i.e., more positive or more negative) than the skimmer. A specially designed ion guide was located 33 cm away from the skimmer. The ion guide consists of a stainless steel cylinder (6) and a central wire (7). The cylinder is 5-cm in ID and 75.9 cm in length. The first section of the cylinder (37.5-cm long) was perforated. The central wire (Nichrome) is 0.25 mm in diameter, and is attached to the cylinder. Two stainless steel electrodes were located at both ends of the ion guide. The typical voltages on the ion guide and two electrodes are 5V (cylinder), -15V (wire), 5V (front electrode) and 0V (rear electrode). The FTMS instrument is Nicolet 2000 (Extrel FTMS, Madison) with a 3T magnet. The pressures in the various regions are indicated in Figure 1.

Biochemicals were purchased from Sigma Chemical Co. (St. Louis, MO) and used as received. Protein and peptide solutions were made by dissolving the analyte in HPLC grade methanol. Acetic acid was added to the solutions, as noted in the figure captions. An aqueous solution of 2'-deoxycytidinyl-(3'-5')-2'-deoxyadenosine (dCA) was diluted in methanol [MeOH:H2O=99:1 (v/v)].

Results and Discussion

Marshall and his co-workers [1, 2] demonstrated that the transportation of externally produced ions from a rf glow discharge or thermionic source into an FTICR cell can be achieved by EIG, which can also be used in time-of-flight mass analyzer [3]. The characteristics of EIG include a wide acceptance angle for the externally produced ions, ion focus along the magnetic field lines, low cost in construction and high efficiency in operation. The features prompted us to investigate the use of an EIG for coupling ES with FTMS.

The novel ES-FTMS interface has shown efficacy in the analysis of biomolecules. Using static trapping plate accumulation, ions could be trapped with voltages as low as ±0.5 V (~0.2 seconds). It can be operated in both positive ion mode and negative ion mode, and has been evaluated with a number of peptides, proteins, and nucleic acid materials. The mass spectra of myoglobin and dCA are shown in Figure 2 and Figure 3.

43rd ASMS Conference on Mass Spectrometry and Allied Topics

Conclusions

We demonstrated the utility of using a single perforated EIG to introduce ions from an external ES source into FTMS. The interface requires only DC power supplies and can be installed on conventional FTMS instruments with relatively low cost. Ions could be detected without a pulse of buffer gas. The success with this EIG system has encouraged us to modify the interface to optimize ES-FTMS performance.

Acknowledgments

Research was sponsored by the Office of Health and Environmental Research, U.S. Department of Energy under contract DE-AC05-84OR21400 with Martin Marrieta Energy Systems, Inc. L. Tang acknowledges an appointment to the United States Department of Energy, Laboratory Cooperative Postgraduate Research Training Program, administrated jointly by the Oak Ridge Institute for Science and Education (ORISE) and ORNL.

References

1. P.A. Limbach, A.G. Marshall and M. Wang, *Int. J. Mass Spectrom. Ion Processes*, **125**, 135 (1993)
2. J.A. Marto, S. Guan and A.G. Marshall, *Rapid Commu. Mass Spectrom.*, **8**, 615 (1994)
3. P.W. Geno and R.D. McFarlane, *Int. J. Mass Spectrom. Ion Processes*, **74**, 43 (1986)

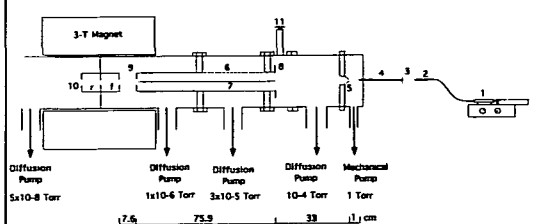

Figure 1. A schematic diagram of new ES-FTMS instrument. 1, syringe pump; 2, ES tip; 3, counter electrode; 4, heated capillary tubing; 5, skimmer; 6, ion guide cylinder; 7, ion guide central wire; 8, front electrode; 9, rear electrode; 10, dual cell, front (f) and rear (r); 11 gate valve.

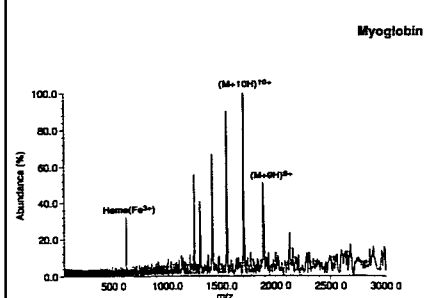

Figure 2. Positive ion ES-FT mass spectrum of myoglobin (10^{-5} M in 95% methanol:5% acetic acid). Spectrum was obtained with 0.5 V static trapping potential and 300 ms ion accumulation.

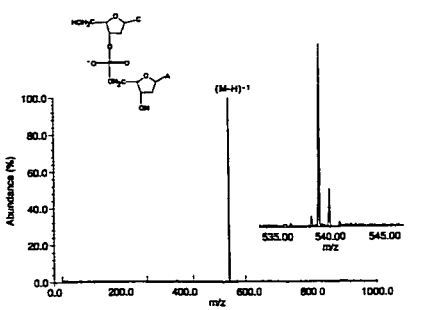

Figure 3. Negative ion ES-FT mass spectrum of dCA, (10^{-5} M in 99% MeOH:1% water). The insert is a mass range expansion showing the molecular ion and ^{13}C isotopes.

Interchangeable Electrospray Interface for the Study of Biomolecules using FTMS

M. Kirk Green, Eric Gard, Elvira Camara, Sharron G. Penn and Carlito B. Lebrilla
UC Davis, Davis CA 95616

A versatile, interchangeable electrospray interface has been constructed and installed on an external source quadrupole FTMS. This interface is readily interchangeable with FAB and MALDI sources, with the main requirement being the pump-down time. A heated capillary[1], two skimmers and a set of Einzel lenses are used to deliver ions to the RF-only quadrupole ion guide. Five stages of pumping are employed, using mechanical, turbo and cryopumps. A selenoid-driven shutter on the final lens blocks neutrals after injection of the ion packet.

Kinetic energy distributions of injected biomolecular ions were investigated. For large (10^4-10^5 Da), highly charged species, the kinetic energies were quite favourable to trapping, with sharp peaks at less than 10 eV. Thus lysozyme, for example, gives signals with high S/N using an ion injection tiime of 250 ms. The spectra obtained to date illustrate the ability of the instrument to handle biomolecules ranging from bradykinin (1060 Da) to bovine serum albumin (66,400 Da).

The ability of ESI to produce large gas-phase ions has allowed us to extend our studies of gas-phase H/D exchange of amino acids and peptides[2,3] to larger peptides and proteins, and to multiply-charged species. We have examined the kinetics of exchange for the different charge states of a series of bradykinin analogues and for the proteins lysozyme and cytochrome c reacting with CH_3OD. For the bradykinin analogues, apparent rate constants have been determined. Rates for singly charged species varied from $<10^{-14}$ to 2×10^{-12} cm^3 $molecule^{-1}$ sec^{-1} The rates for the doubly charged ions were always faster than for the corresponding singly-charged species, and fell in the range 6×10^{-14} to 1×10^{-11} cm^3 $molecule^{-1}$ sec^{-1}. The trends in rate constants can be explained in terms of the nature of the specific protonation sites in these peptides. For example, both charge states of bradykinin exchange slowly because the protonation sites are arginines, whose proton affinity is so high that exchange with CH_3OD is unfavourable. In Lys-1-bradykinin, the second protonation site is lysine, which exchanges rapidly[2,3], rendering the doubly-charged species relatively reactive.

Lysozyme undergoes H/D exchange at a much slower rate than cytochrome c. This is probably due to the large number (11) of highly basic arginine residues in lysozyme, which bind the protons so tightly that exchange with the deuterating reagent is strongly inhibited

1. Chowdhury, S. K., Katta, V. and Chait, B. T., *Rapid Commun. Mass Spectrom.* **4** (1990).

2. Gard, E.; Green, M. K.; Bregar, J.; Lebrilla, C. B., *Organic Mass Spectrometry*, **28**, 1632 (1993).

3. Gard, E.; Green, M. K.; Bregar, J.; Lebrilla, C. B., *J. Am. Soc Mass Spectrom.*, **5**, 623 (1994).

43rd ASMS Conference on Mass Spectrometry and Allied Topics

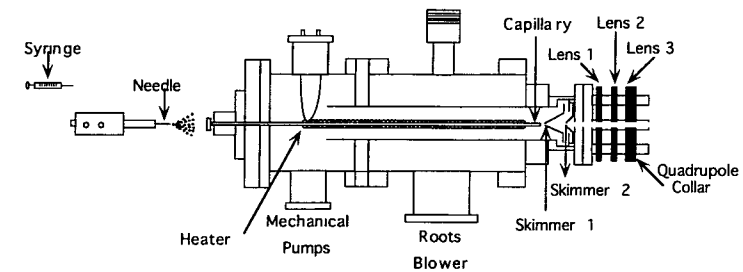

Figure 1· Schematic of the electrospray interface

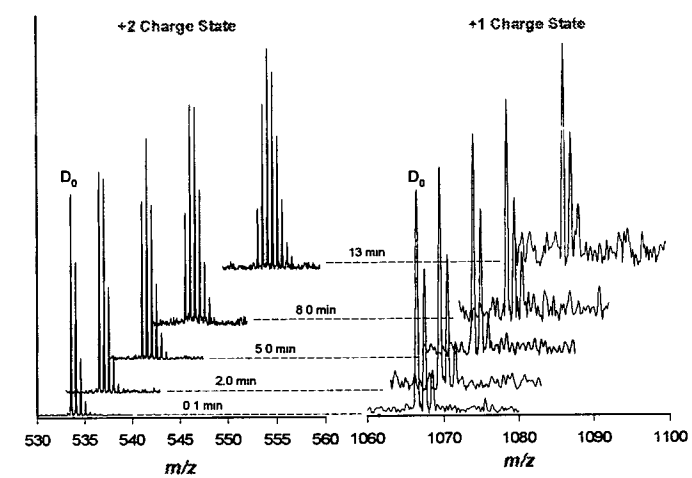

Figure 2: Changes in mass spectral peak intensity as a function of time for bradykinin ions undergoing H/D exchange with CH_3OD.

High-Field Electrospray FT-ICR Mass Spectrometer for Biopolymer Analysis

Ljiljana Paša-Tolić, Jarrod A. Marto, Michael W. Senko, Christopher L. Hendrickson, Forest M. White, Shenheng Guan,* and Alan G. Marshall*

Center for Interdisciplinary Magnetic Resonance, National High Magnetic Field Laboratory, Florida State University, 1800 E. Paul Dirac Dr., Tallahassee, FL 32310

* Department of Chemistry, Florida State University

Here we describe the design, construction, and characterization of a new high-field electrospray-ionization FT-ICR mass spectrometer. This instrument, shown schematically in Fig. 1, consists of a modified Vestec ESI source, a homebuilt two-section octupole ion guide, and a high-performance FT-ICR mass analyzer. The dual ion trap is housed within a 6"-diameter horizontal-bore, 6 T magnet (Oxford Instruments, Ltd.). An Odyssey data station Extrel Waters FTMS) is used for collection and analysis of the data. A completely modular differentially pumped vacuum system accomodates the high gas load of the ESI source (1 atm) and ultra-low pressure required for high performance ICR detection ($\leq 1 \times 10^{-9}$ torr).

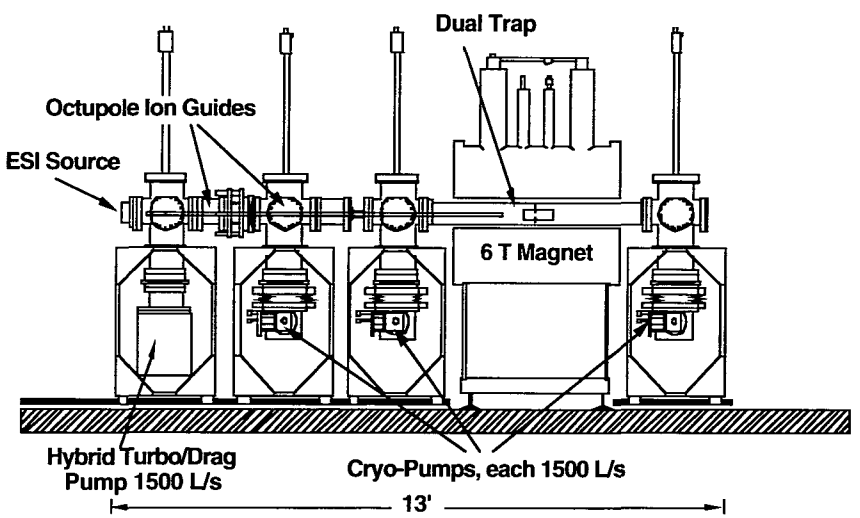

Figure 1. Schematic diagram of NHMFL external source ESI FT-ICR mass spectrometer.

43rd ASMS Conference on Mass Spectrometry and Allied Topics

The system described here is a prototype for a higher performance instrument built around an 8"-diameter horizontal-bore 9.4 T shielded magnet, which will be the highest field FT-ICR magnet in the world, and should demonstarte improved mass resolving power and mass accuracy (which scale as B), upper mass limit (which scales as B^2), maximum ion storage period (which scales as B^2), and other operating advantages. Our design offers two qualitative improvements relative to the currently available instruments: i) novel off-axis ion injection that provides for efficient trapping of a continuously-injected beam of ions having a large m/z and wide distribution in kinetic energy, and ii) simultaneous ion trapping and analysis, exploiting the dual trap for improved duty cycle.

We have characterized the ESI source ion kinetic energy distribution and transmission through the octupole guides. Figure 2 , left, is a mass spectrum collected in the source-side ion trap. After quadrupolar excitation to squeeze the ions to the central axis of the solenoidal magnet, the potential on the conductance limit trap plate was lowered to 0 V, and the ions were transferred to the low-pressure, high-resolution analyzer side of the dual ion trap. Broadband dipolar excitation and detection gave a time domain transient, which, when Fourier transformed and displayed in magnitude mode, demonstrates isotopic resolution of the +4 charge state of the insulin molecular ion (Fig. 2, right). This work was supported by NSF CHE-94-13008, NIH (GM-31683) and the National High Magnetic Field Lab at Florida State U.

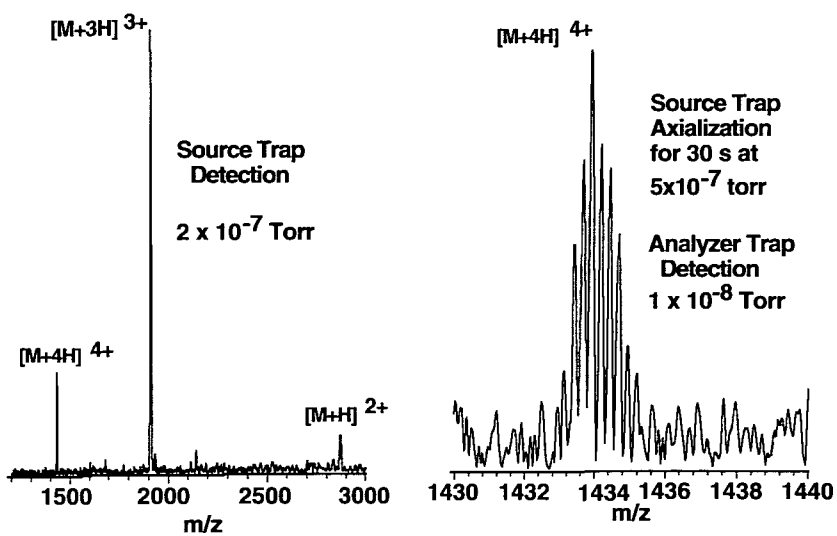

Figure 2. ESI FT-ICR magnitude-mode mass spectra of bovine insulin.

The Design and Performance of an In-Field ESI-FTICR Instrument

Qinyuan Wu, Harold R. Udseth, Gordon A. Anderson,, Michael G. Sherman, Steven Van Orden, Ruidan Chen, Steven A. Hofstadler, Dale W. Michell, Alan L. Rockwood and Richard D. Smith*
Pacific Northwest Laboratory, Richland, WA 99352

The coupling of electrospray ionization (ESI) with Fourier Transform Ion Cyclotron Resonance mass spectrometry (FTICR-MS) has been shown to be a promising tool for biological research. Most of the current schemes of combining ESI with FTICR involve forming ions outside the magnet and injecting into the magnetic field through either radio frequency ion guides or electrostatic lenses. Substantial ion losses occur during ion transportation for such external source ESI-FTICR, offsetting the high sensitivity in detection. Alternatively, ESI can be performed inside the magnet bore to significantly increase ion current in the cell [1]. However, such an in-field ESI scheme requires critical differential pumping and ion optics design to maintain ultra-high vacuum in the cell region in order to achieve resolution similar to that obtained from external source scheme.

In our in-field ESI-FTICR instrument (Fig. 1), a home-made ESI probe is inserted into a superconductor magnet (max. 4.7 T, but presently at 1 T) so that electrospray generated ions are confined by the magnetic field and are injected into the ICR cell located 20 cm from the ESI source. The system is equipped with five stages of differential pumping and the base pressure in the ICR cell region is 8×10^{-10} Torr. Injection of ions into the cell is controlled by an in-field shutter which also serves to maintain the ICR cell in ultrahigh vacuum when ESI probe is inserted. The ESI probe can be moved in x-y-z directions, allowing the relative positions of the spray needle to the heated capillary and the capillary to the first skimmer to be independently adjusted. Another feature of this system is that the magnet bore is 11" in diameter (with room-temperature shim) which allows cryo-panels to be inserted and a large 4" cubic ICR cell to be used. This design will also allow us to explore the use of other large and more complex cells to increase the size of the trapped ion population and the dynamic range, particularly in conjunction with the in-field ESI source.

In initial studies, we have obtained 2×10^6 resolving power (>12.5 sec transient) for N_2^+ ions generated by an electron impact source near the cell. Preliminary results show that the measured ESI ion current in the ICR cell increases by at least a factor of 10 when electrosprayed in the 1 T magnetic field. Fig. 2 shows spectra obtained for bovine ubiquitin (M.W.= 8565 Da) under a pressure of about 10^{-7} Torr. As the temperature on the inlet capillary increased (Fig. 2B), higher charge state ions were preferentially dissociated--a process referred to as thermally induced dissociation, or TID. More experiments are underway to optimize the performance of the system.

[1] S. A. Hofstadler and D. A. Laude, Jr. Anal. Chem. **1992**, 64, 569-572

This work was the U.S. Department of Energy. Pacific Northwest Laboratory is operated by Battelle Memorial Institute for the U.S. Department of Energy under Contract DE-AC06-76RLO 1830.

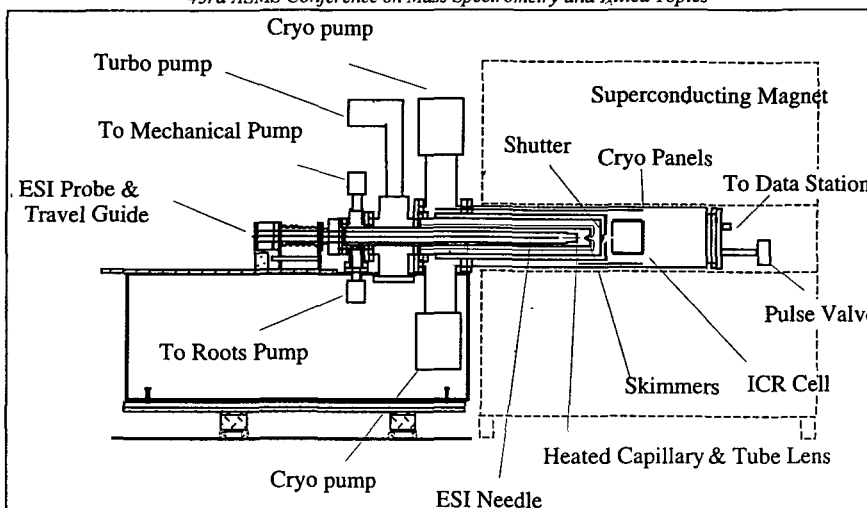

Fig. 1. An in-field electrospray ionization Fourier transform ion cyclotron resonance mass spectrometer.

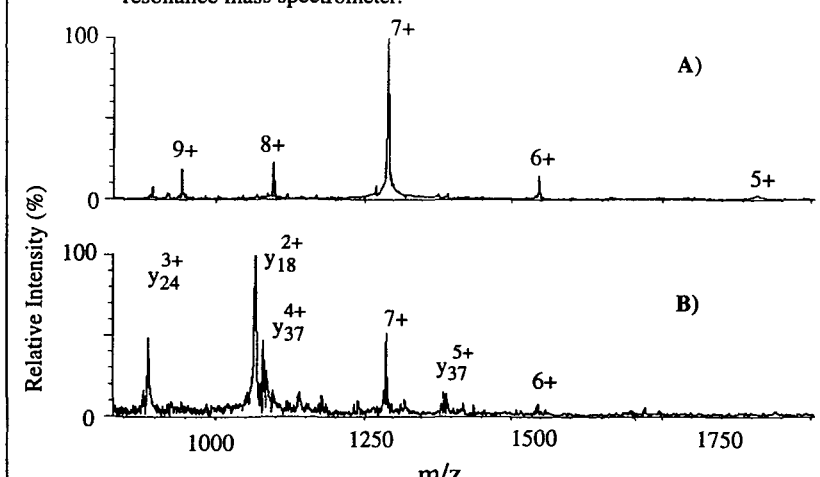

Fig. 2. ESI spectra of bovine ubiquitin (8565 Da, 1mg/ml in 5% HOAc). Capillary temperature at A) 140°C , and B) 170°C.

Performance of an External Cluster Ion Source and Electrostatic Ion Guide

Anthony M. DeSantolo, Mary L. Mandich, and William D. Reents Jr.
AT&T Bell Laboratories, 600 Mountain Ave., Murray Hill, NJ 07974

We have designed and constructed an instrument that produces cluster ions in an external source and transports them via an electrostatic ion guide to the FTICR cell of a 5 3T split-pair magnet A schematic of the cluster source and ion guide is shown in figure 1 Clusters are formed in the source by condensation of the elemental material of interest in a cooling gas The cluster source is a stainless steel block in which a 1/4" diameter target rod is positioned at the side of a channel through which flows 5-25 Torr of helium carrier gas at a rate of 100-500 sccm As the rod rotates and translates in the source, material is ablated off the rod and into the helium flow using the focused output of a XeCl excimer laser (308 nm, 12 nsec pulse width, 160mJ) A 500 mm focal length lens focuses the laser to a ~ 1 x 3 mm oval spot at the elemental target rod At these power densities, the laser creates a plasma above the surface of the rod that contains ionic and neutral species from the target plus electrons and ionized carrier gas species Clusters are formed by bimolecular association of neutral atoms and molecules with both charged and neutral atoms and molecules in the region of the source between the target rod and nozzle exit In the present source configuration, the growing clusters spend ~700μs in the source which allows for tens of thousands of cooling collisions with the helium carrier gas. In addition, the helium gas can be doped with various molecular reagents leading to the formation of multi-component clusters Although the initial plasma created by the laser creates a sufficient number of ionized clusters for detection, further ionization can be accomplished using the output of an electron gun positioned behind the source The clusters and carrier gas exit the source via a conical nozzle (1 mm diameter) into a vacuum of ~10^{-4} Torr Here, the clusters and carrier gas undergo a supersonic expansion and are translationally cooled to ~30K At this point, cluster growth stops and the particle size distribution becomes "frozen"

The high pressure operation of the source requires multiple stages of differential pumping to achieve the high vacuum required for FTMS, while at the same time high cluster ion densities are desired

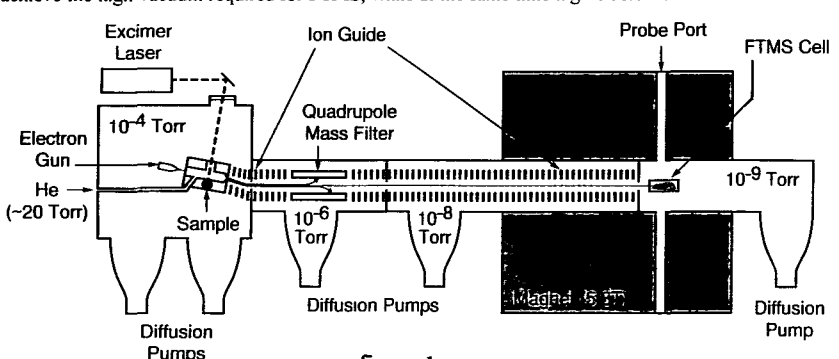

figure 1.

in the trapped ion cell We designed and built our own ion guide based on optimized ion trajectories. The design incorporates ion extraction, focusing, X/Y steering, and an exponential deceleration field to maximize ion throughput from the source, through the three variable(4-8mm) conductance limits separating four stages of differential pumping, to the trapped ion cell After exiting the source, the cluster ions drift for ~1cm at the source potential(+5V to +20V) after which they are accelerated(-100V to -1000V), focused, and steered through the first differential pumping aperture The cluster ions are refocused and steered (if necessary) through each conductance limit. After traversing the length of the ion guide(~2meters), the ions are retarded by an exponential deceleration lens to near thermal velocities and finally focused into the trapped ion cell The ion guide can incorporate a quadrupole mass filter for selecting out a portion of the mass distribution but it has not been used for the results described here Under typical operating conditions, the positive ion current from the source is ~500pA/laser pulse, about 15pA makes it to the trapping cell giving a transmission of ~3% for the entire system Further enhancement of the ion throughput, particularly for the higher mass ions, can be realized by increasing the ion guide voltage. Doubling the field from -500V to -1000V increases the number of C_{200}^+ ions reaching the cell a factor of 2 and the number of C_{288}^+ ions a factor of 4 However, no enhancement is observed for the lower mass clusters

Cluster ions arrive in a 300 - 5000μs wide pulse and are selectively loaded into cell by lowering the potential of the trapping plate nearest the ion guide for ~300μs. This gating sequence is synchronized to the output of the ablation laser Figures 2a and 2b show the positive ion mass spectra obtained from a carbon target rod, with 9 Torr helium in the source, +15V source bias, and a -950V field free voltage In figure 2a the delay between the laser pulse and the gating sequence is 150μs whereas in figure 2b the delay is 650μs clearly showing the higher mass carbon clusters arriving at the cell after the smaller ones

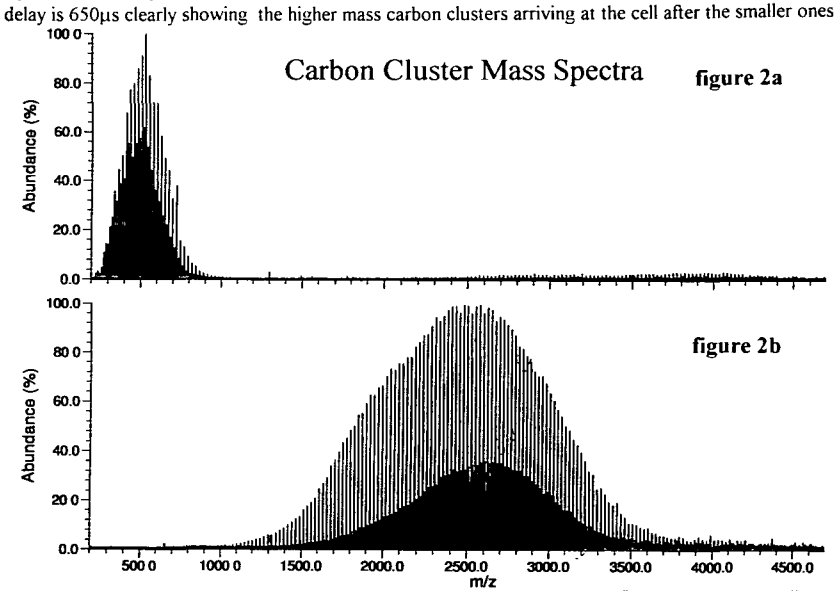

Construction of an ICP/FT-ICR Mass Spectrometer

Eric Milgram,* Cliff Watson, John Eyler
Department of Chemistry, University of Florida, Gainesville, FL 32611-7200

Introduction

Inductively coupled plasma mass spectrometry (ICP/MS) is a powerful technique for elemental analysis. The benefits of this technique include high sensitivity, wide linear dynamic range, relatively simple spectra, and isotopic information The vast majority of ICP/MS instruments are equipped with a quadrupole mass filter which offers a mass resolution no better than about 2,000 This severely limits most analyses due to the isotope of interest having the same nominal mass as a neighboring isotope, or some plasma by product Methods of dealing with this limitation have included chemical separation,[1] principle components analysis,[2] or more commonly, monitoring another isotope, often of much lower abundance. We are proposing construction of an ICP source for use with our Bruker BioApex 70e Fourier transform mass spectrometer If successful, it would be possible to routinely perform analyses that are inconceivable with existing instruments

Source Design

We opted to modify an existing commercial electrospray ionization (ESI) source design instead of designing an entirely new source This was done for several reasons·

1) existing design incorporates differential pumping
2) design and machining time greatly reduced
3) design will be easily adapted by other users with similar ESI sources

A torch support consisting of Delrin and Teflon was constructed to hold and translate the torch in three dimensions A water cooled heat shield/skimmer was designed to cover and protect the atmospheric pressure side of the ESI capillary Figure 1 illustrates a cut away view of the ESI source housing, capillary, and heat shield/skimmer showing insertion of torch support Upon successful completion of our initial studies, we plan to incorporate a quadrupole mass filter into our source to increase sensitivity and improve linear dynamic range if needed

Works Cited

1) Plantz, M R , Fritz J S , Smith, F G ; Houk, R S *Anal. Chem.* **1989**, 61, 149-153

2) Vaughn, M A., Templeton, D M. *Appl. Spectrosc.* **1990**, 44, 1685-1689

43rd ASMS Conference on Mass Spectrometry and Allied Topics

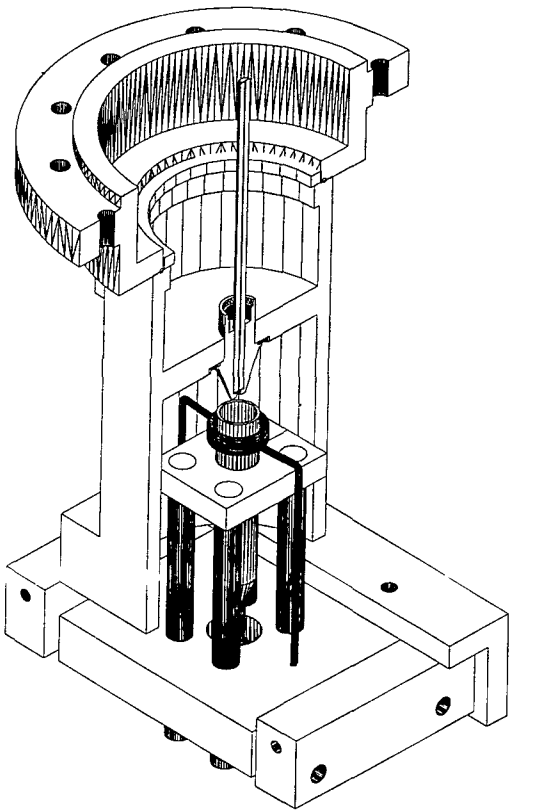

Figure 1: Cut-away view of ESI source housing, capillary, and skimmer/heat shield showing insertion of torch support

Characterisation of a Novel Ion-Emitter for FT-ICR

Iris Spiess[1], Imke Mass[1], Bernd Görtler[1], Albrecht Glasmachers[2] and Karl Peter Wanczek[1]
1 University of Bremen, Institut of Inorganic and Physical Chemistry, D-28334 Bremen, Germany
2 Ruhr University, D-44780 Bochum, Germany

Introduction :
For generation of ions from samples of low volatility and stability a variety of soft ionization methods are employd. The great advantage of these ionization methods is that samples of low stability like biological molecules and involatile organic and inorganic molecules can be ionized without destruction. A new improved electric pulse induced desorption EPID ionization method is presented. The multi-layer ion emitter of a high net heat capacity of EPID type is characterized by studying fragmentation of anthracene, 18-crown-6, 15-crown-5 with alkali metal and boron nitride.

Experimental:
A push rod of 900 mm length and 22.5 mm diameter is used to place the sample in front of the center of a ***screened ICR cell.*** Alternatively an ICR cell with ***open geomety*** is employed to inject the ions more directly in the center. The emitter is a thin aluminium filament deposited on a plate which also contains the two electrical connections. A short current pulse of 2 ns duration is produced by the discharge of a capacitor. Because of the high heat capacity of the emitter we exclude the possibility of a thermal ionization. In the present study boron nitride, anthracene and crown ethers were used to characterize the fragmentation behavior of the emitter. Anthracene is ionized by EPID and by simultaneous electron impact ionization with an electron energy of 50 eV. The spectra of 15-crown-5 and 18-crown-6 are recorded by emitter ionization and at 70 eV electron energy. The chemistry of the pure crown ethers and the reaction of 15-crown-5 with potassium and cesium ions is studied. Boron nitride is ionized with the new ion emitter. For the study solutions of $1x10^{-4}$ mol/l of anthracene in benzene and of 15-crown-5 and 18-crown-6 in water are prepared and a micro drop is fixed with a microsyringe on the aluminium filament. A dispersion of boron nitride in water is prepared in a ultrasonic bath and also fixed on the aluminium filament. The solvent is vaporized before introduction of the probe in the UHV system.

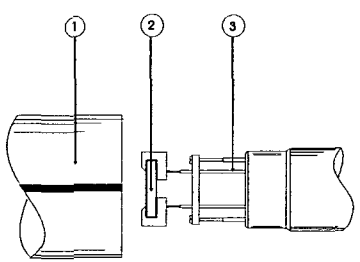

1 ICR cell

2 emitter

3 electrical feedthrough

Fig.1: *Arrangement of the ICR cell and the probe rod*

The investigation is performed with a Bruker Spectrospin FT-ICR spectrometer equipped with a superconducting magnet of 7.02 T. The control of the experiment and excitation/detection is performed by the Aspect 3000.

Results and discussion:
Anthracene
Figure 2 shows an ICR spectrum of anthracene ionized with the emitter. The only fragmentation that occurs is m/e=152,$C_{12}H_8^+$. The ion m/e=178, the molecular ion, is the most abundant ion. The peaks are compared with an ICR spectrum of anthracene ionized with the emitter and an electron energy of 50 eV. There are more fragment ions because of the high energy of the electrons. By electron impact, additional ions are formed from the neutral molecules also generated from the Epid emitter. Additional electron impact ionization increases the intensity of the molecular ion, m/e=178, by a factor of approximately two.
We used an ICR cell with open geometry to demonstrate the simultaneous trapping of positive and negative ions in combination with the EPID ionization technique. We acquired a spectrum of anthracene introduced by the emitter and methyl iodide.

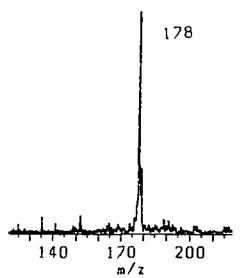

Fig.2: *ICR spectrum ionized with the emitter*

18crown-6 and 15-crown-5
Under our experimental conditions the protonated crown ether is a high abundant ion, due to proton transfer reactions, and not the molecular ion. Further on the experimental conditions do not allow to observe a signal with electron impact ionization only.
We also investigated the ion chemistry of 15-crown-5 with potassium and cesium ions.

Boron nitride
Boron nitride has a melting point of 3270 ^{o} C. With the new ionization method we obtained ICR spectra. The following cluster are detected: $B_{29}N_{29}$, $B_{33}N_{33}$. R.D. Barde et al predicted the bonnynall $B_{24}N_{36}$. We observe $B_{25}N_{37}$ and $B_{24}N_{38}$. In references there exist several theoretical concepts.

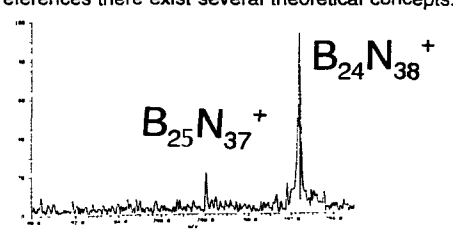

Fig.3: ICR spectrum of boron nitride

Fluorescence and Absorption Spectra of Mass-Selected Trapped Ions

George Jackson,* Yulin Huang, Shenheng Guan,*
Hyun Sik Kim, and Alan G. Marshall*

Center for Interdisciplinary Magnetic Resonance, National High Magnetic Field Laboratory, Florida State University, 1800 E. Paul Dirac Dr., Tallahassee, FL 32310

* Department of Chemistry, Florida State University

Ion structure and bonding has conventionally been inferred indirectly from measurements of ion mass and abundance following ion activation by photons or by ion-neutral collisions. Here we present the design and preliminary performance of an instrument designed for direct detection of uv/vis fluorescence and absorption spectra of mass-selected trapped ions. Figure 1 is a schematic representation of the experimental setup. Ions are generated by an off-axis electron beam, followed by azimuthal quadrupolar excitation and collisions with neutral gas to cool the ions and squeeze them toward the central axis of a 7 tesla magnet. Ions of interest are mass-selected and confined in a series of two coaxial open-ended cylindrical ICR ion traps. An excitation laser beam is introduced along the axis of the magnet through Brewster-angle windows located at each end of the vacuum chamber. The arm which contains the Brewster-angle window consists of a Woods horn to deflect scattered excitation laser light from the window and a series of baffles. Laser-induced fluorescence is conducted in a cylindrical mesh-walled trap. A pair of concave mirrors (one spherical and the other ellipsoidal) is mounted outside the mesh to focus fluorescence to the small opening located in the center of one of the mirrors (Figure 2). The fluorescence is then collected perpendicular to the Nd:YAG-pumped dye laser excitation beam by a mirror and prism assembly, and routed through a fiber-optic waveguide feedthrough to a photomultiplier detector located outside the vacuum chamber. The wavelength-dependent signal may be stored in a personal computer for later analysis.

Optical absorption will be detected by a recently developed highly sensitive cavity ringdown method. Highly reflective (99.999%) concave mirrors mounted on each end of the vacuum chamber serve as an optical cavity to trap photons. The ratio of the time constants for exponential decay of the photon leakage from the other end following an initial laser pulse in the absence and presence of absorber is a direct measure of I/I_0 in a Beer-Lambert law. An absorption spectrum is obtained by computer-controlled stepwise scanning of the incident photon wavelength. We shall attempt to measure the direct optical absorption spectrum of ~10^9 mass-selected ions. To date, we have verified experimentally the detection of more than 15 million ions confined in an open-ended cylindrical trap.

Work supported by the National Science Foundation (CHE-93-22824) and the National High Magnetic Field Laboratory at Florida State University.

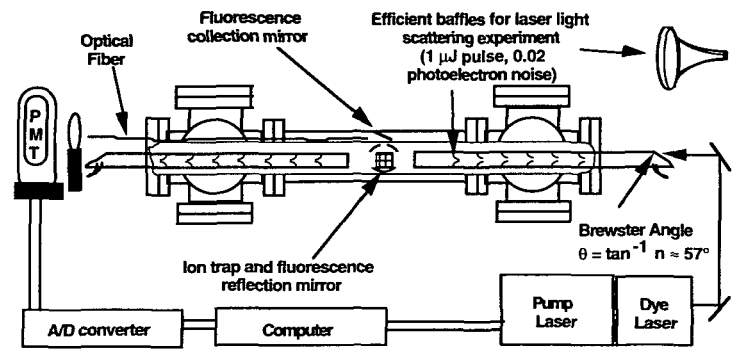

Figure 1. Laser-induced fluorescence in an ICR ion trap.

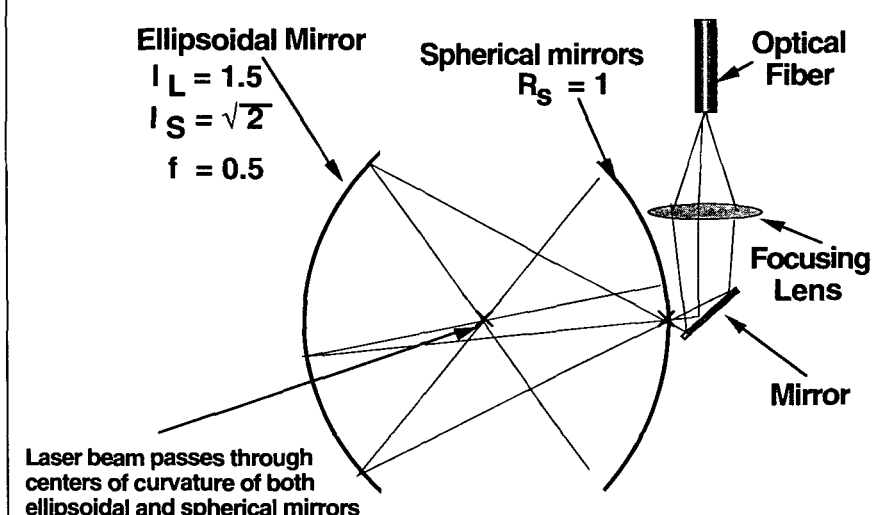

Figure 2. Elliptical and spherical mirror assembly for collection of laser-induced fluorescence signal.

FTICR Performance of a 5.3 Tesla Split-Pair Magnet

W. D. Reents, Jr., M. L. Mandich, and A. M. DeSantolo
AT&T Bell Laboratories, Murray Hill, NJ 07974 USA

A unique magnet is used for FTICR detection of particles formed in a pulsed laser vaporization source. This magnet was designed to achieve excellent FTICR performance with large ion populations containing broad ion distributions.

The magnet, built by Oxford Instruments, is a 5.3 Tesla split-pair design. The 2" split allows access to the homogeneous region of the magnet's bore via four perpendicular ports. This access can be used to probe the ion population in the cell, e.g. with photons or chemical reagents. Currently, a pulsed gas valve is attached to one of these ports.

The magnet has an 8" bore tube made of 316SS with metal-sealed flanges on each end. This tube comprises our vacuum chamber, with the homogeneous region located 15" from one end. This large, short bore coupled to our vacuum pumping station (4,000 l/s cryopump and 2,500 l/s LN_2-trapped diffusion pump) results in high conductance (3,000 l/s at cell). A gas pulsed in via the perpendicular access port momentarily raises the pressure in the cell to 0.01 - 1 torr, collisionally stopping all cluster ions injected from the attached laser vaporization source. The pressure returns to the background level (10^{-9} torr) within 3 sec.

The large homogeneous region and wide bore permit use of large cells for trapping large ion populations. This is necessary because of the "bright" pulsed laser vaporization source being used; ion currents of 200 - 600 pA/pulse are generated at the laser source output with 3-5 pA/pulse currently reaching the cell. The high pulsed gas pressure used (0.01- 1 torr) efficiently stops and traps these ions in the cell. A variety of trapped ion cell sizes and geometries have been examined, but the results from only one (4.5" ID x 3.5" long cylindrical cell) is discussed.

The split-pair magnet design conflicts with the high homogeneity magnetic field required for high performance FTICR. The specified homogeneity of 1 in 10^4 over a volume of 1" diameter by 5" in length is exceeded when shimmed (achieved a measured homogeneity of 8 in 10^5). This low homogeneity (actually lower over the full trapped ion cell volume) did not inhibit achieving 640,000 mass resolution at m/z 2786^+ ($^{12}C_{230}{}^{13}C_2{}^+$).

The instrument performs well in terms of detecting broad ion distributions. The performance, however, depends significantly upon rf excitation conditions. Although standard rf chirp produces reasonable mass spectral signals in our instrument with cubic and elongated cells, the short aspect ratio of the cell discussed here results in very irreproducable spectra which represent only a portion of the ion population present (see Figure 1; 331 summed scans). However, when SWIFT® excitation is used, a mass spectrum is attained that represents the broad carbon cluster ion distribution present in the cell (see Figure 2; 260 summed scans). This large ion population is shown in more detail in Figure 3 with additional mass scale expansions. In spite of the large ion population in the trapped ion cell, a mass resolution of 11,000 is easily attained at m/z 4,000.

Figure 1

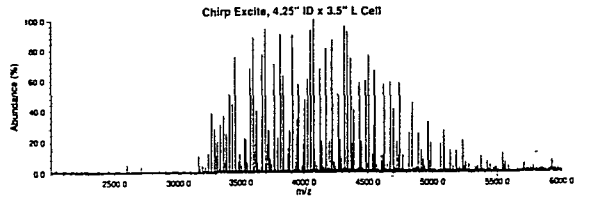

Figure 2

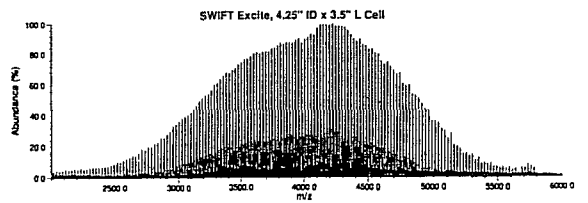

Figure 3

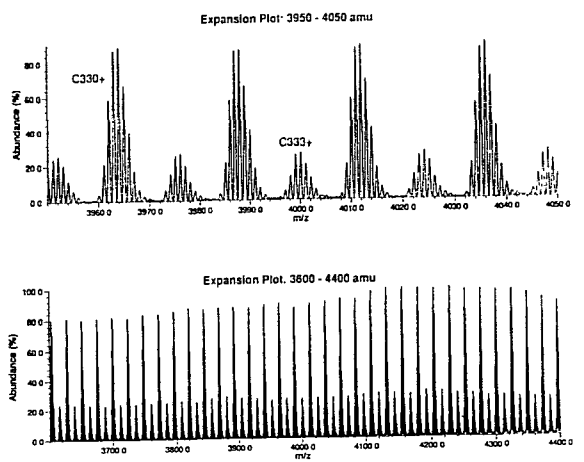

Performance of a Small Low-field FT/ICR Mass Spectrometer

James Pérez*, Diane T. Leeck, Brandon Beasley and Hilkka Kenttämaa
Department of Chemistry, Purdue University, West Lafayette, Indiana 47906-1393

The development of small Fourier transform mass spectrometers is driven by the potential for their implementation in routine analytical applications. We recently reported on the development of a small Fourier transform mass spectrometer, based on a low field (0.4 T) permanent magnet and an orthorhombic cell (~16 cm^3)[1]. The work presented here provides a systematic study of the base performance of this instrument, equipped with an unscreened cell and a screened cell. The screens used in this work consisted of 0.001 gauge tungsten wire arranged in a crosshatched configuration and with a wire density of 4 wires/cm (11-wire screens). The use of screens has the effect of reducing static electric fields in the cell[2] and this effect was studied by comparing the instrument performance factors with both cell configurations.

A notable difference in the performance between the screened and unscreened cell is the loss in sensitivity associated with the former. This was evident from the results of the ion trapping efficiency and the lower limit of detection experiments. Initial ion intensities originating from the electron ionization (EI) of benzene and carbon tetrabromide were reduced by ≥ 50% in the 11-wire screened cell. Ion trapping efficiency experiments based on the EI of these species suggest that the unscreened cell traps ions more efficiently.

The lower limit of detection was measured by electron ionization and chemical ionization of methyl stearate/methanol solutions of different concentrations. Results from both approaches suggest a sensitivity approximately in the picogram range for the unscreened cell. The sensitivity of the 11-wire screened cell was approximately in the nanogram range by EI of methyl stearate. Sensitivity measurements using the chemical ionization method did not enhance this measurement with the 11-wire screens.

The resolution was evaluated by measuring the heterodyne mode electron ionization mass spectra of the perfluorotributylamine fragment ion with m/z 131. At 16 k datapoints and a heterodyne frequency of about 47 kHz, the resolution was comparable with both cell configurations at about 55 k.

Performance factors which improve with the 11-wire screened cell include the mass range, mass accuracy and the dynamic range. The mass range was based on the EI mass spectra of tri(perfluoroheptyl)-1,3,5-triazine (MW = 1185 Da) and was extended from about m/z 866 to 1185 m/z in the screened cell. The mass accuracy was determined by repeated collection of the EI mass spectra of perfluorotributylamine (PFTBA) over time. The 11-wire screened cell achieves a nearly 50% improvement in the mass accuracy over the unscreened cell. The EI mass spectra of air samples were used to evaluate the dynamic range of the instrument, and was based on the component of air with the lowest detectable abundance. The dynamic range was greater by an order of magnitude in the 11-wire screened cell than in the unscreened cell. Table 1 summarizes the performance factors of this prototype instrument equipped with the screened and the unscreened cell.

Preliminary experiments were also performed using screens with a wire density of 8 wires/cm (20-wire screens). The results obtained to date support earlier SIMION data,

[3] which predicted that the 20-wire screens effect weak trapping potentials in the cell. The instrument performance with the 20-wire screened cell was poor.

Table 1. Comparison of the performance factors of the low-field instrument equipped with the unscreened cell and the 11-wire screened cell.

Performance Factor	Unscreened Cell	11-wire screened cell
Mass Range	4 to < 866 Da	4 to < 1186 Da
Resolution	54 k @ m/z 131 (NDP = 16 k)	58 k @ m/z 131 (NDP = 16 k)
Mass Accuracy	25 - 314 ppm (m/z 69 - 502)	13 - 277 ppm (m/z 69 - 502)
Ion Trapping Efficiency (50% of the initial total ion current)	≥ 1.0 seconds	≥ 0.5 seconds
Dynamic Range	10^2	10^3
Sensitivity (Methyl Stearate)	picogram range	nanogram range

References

1. L.C. Zeller, J.M. Kennady, J.E. Campana and H.I. Kenttämaa, *Anal. Chem.*, **65**, (1993) 2216.
2. M. Wang and A.G. Marshall, *Anal. Chem.*, **61**, (1989) 1288.
3. D.D Dahl and J.E. Delamore, SIMION PC/PS2 Version 4.0, EGG-CS- Rev. 2, April 1988; Idaho National Engineering Laboratory, EG&G, Inc.: Idaho Falls, Idaho.

Low Noise ICR Detection Electronics.

G.A. Anderson, J.E. Bruce, S.A Hofstadler, A.L. Rockwood, R.D. Smith Chemical Sciences Department
Pacific Northwest Laboratory Richland, WA 99352

FTICR signal detection offers many challenges; both wide bandwidth and low noise performance are required. Since, the input impedance of the amplifier is a very critical parameter, optimal performance of the preamplifier involves a careful balance of input impedance and noise performance through circuit design and component selection. The FTICR cell and its connections to the preamplifier are another critical parameter in FTICR detection sensitivity.

This work has investigated signal detection electronics for improved FTICR detection sensitivity. Amplifier noise sources are identified and their effect on detection sensitivity are evaluated. A high sensitivity, low noise preamplifier, developed in our laboratory, is presented and its performance is evaluated and contrasted with different preamplifier configurations. The detection circuit is analyzed and the effect of cell and wiring capacitance is discussed. The circuit sensitivity is calculated and compared with measured results. Component selection criteria are discussed and the present state-of-the-art components are evaluated. The effect of pre amplifier cooling is also investigated and the results are presented. Different detection frequency ranges result in different circuit optimization; these effects are analyzed and optimal component values and circuit configurations are shown for different frequency ranges.

Figure 1 shows the equivalent circuit for a FTICR detection circuit. This circuit illustrates the main noise components; amplifier voltage and current noise, and noise current due to input bias resistance Ri. The signal image current has been shown as[1]:

$$Is_{rms} = \frac{Nq^2 rB}{\sqrt{2}md} \qquad \omega = \frac{qB}{m} \qquad Is_{rms} = \frac{Nqr}{\sqrt{2}d}\omega$$

Given the image current and detection circuit capacitance and resistance, the detection system signal components are calculated, as shown in figure 2. This figure illustrates several interesting points; image current increases with frequency, signal voltage is constant with frequency and is inversely proportional to circuit capacitance. For low frequencies current noise dominates, for high frequencies voltage noise dominates. The equivalent input voltage noise is:

$$Vnt = \sqrt{en^2 + \frac{In^2}{\omega^2 Ct^2} + \frac{4kT}{Ri\omega^2 Ct^2}}$$

FETs offer low current noise due to their low input gate leakage currents and are well suited for low frequency operation. At higher frequencies bipolar transistors offer low voltage noise, their voltage noise is due primarily to Johnson noise in the base spreading resistance, which is low. Our work with large biomolecules results in frequencies of 50KHz for m/z 2000 and B equal 7 Tesla. FETs are the best choice for this region.

To support the large biomolecule studies at our laboratory, a FET input amplifier was design and built. The design is based on a cascode configuration proposed by Jefferts[2]. The differential casode amplifier has the following specifications:

Voltage noise	en = 1nv/Hz$^{1/2}$
Current noise	In = 4fA/Hz$^{1/2}$
Input resistance	Ri = 1G
Input capacitance	Cs = 34pF

Cooling the FETs improves the current noise by a factor of 10 and reduces bias current allowing the input resistor value to increase. Increasing Ri reduces the resistor noise current, due to Johnson noise in the resistor. Preamplifier performance shows good agreement with calculated system sensitivity. In conclusion, we have shown the basis for improved studies of large biomolecules through the use of optimal preamp electronics.

We thank the U.S. Department of Energy for support of this research through internal PNL Exploratory Research under contract DE-AC06-76RLO 1830.

Detection equivalent circuit

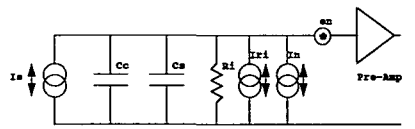

Cc = Cell capacitance + stray wiring capacitance
Cs = Pre-amp input capacitance
Ri = Pre-amp input resistance
Iri= Ri noise current
In = Pre-amp input current noise
en = Pre-amp input voltage noise

Figure 1

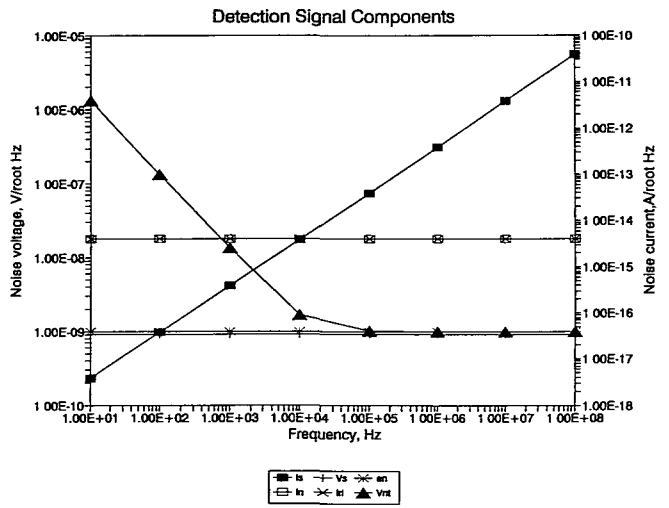

Figure 2

References:

(1) Commisarow,M.B. *J. Chem. Phys.* 1978,69(9),4097-4104.
(2) Jefferts,S.R.;Walls,F.L. Rev. Sci. Instrum. 1989, 60(6), 1194-1196.
(3) Winger,B.E.;Hofsadler,S.A.;Bruce,J.E.;Udseth,H.R.; Smith,R.D. J.Am.Soc.Mass Spectrom. 1993,4,566-577.
(4) Bruce,J.E.,Cheng,X.,Bakhtiar,R.;Wu,Q.;Hofstadler,S. A.;Anderson,G.A.;Smith,R.D. J. Am. Chem. Soc. 1994,116(17),7839-7847.
(5) Horowitz,P.;Hill,W. The Art of Electronics, 2nd ed.;Cambridge University Press: N.Y.,1989.
(6) Ott,H.W Noise Reduction Techniques in Electronic Systems, 2nd ed.; John Wiley & Sons: N.Y., 1988

Improved Performance of a LabVIEW-Based FTICR Data Station

J.J. Drader, C.L. Hendrickson, J.M. Robinson and D.A. Laude, Jr.; Department of Chemistry and Biochemistry, University of Texas at Austin, Austin, TX 78712

The increasing popularity of FTICR has been paralleled by a demand for a flexible data station which allows users to take advantage of new technological developments and to perform more intricate experiments. The natural approach to the problem is to build a data station which is tailored to the experimental requirements, and can also be easily modified to facilitate new experiments. In this work, we present a PC-based data station that uses LabVIEW software (National Instruments Corp., Austin TX). LabVIEW offers a high level graphical interface which allows operators with minimal programming experience to develop complex programs. Major improvements over previous data stations [1] include increased flexibility in waveform syntheses, sequence editing, and data processing.

The data station was set up as follows: the 486/DX66 PC contains both a National Instruments AT-AO-6 DAC card and a National Instruments GPIB interface card. The LeCroy 9100 arbitrary function generator (AFG) and the LeCroy 9410 digital storage oscilloscope (DSO) communicate with the PC through the GPIB interface. The system control, user interface, and data processing are implemented through virtual instruments (VI's) created LabVIEW 3.1 (graphical programming for instrumentation). VI's are used to create programs that resemble and perform like real instruments even though they are actually software based. The AFG provides two independent channels of arbitrary waveform output. One channel is connected to an amplifier and outputs the dipolar excitation, while the other is available for quadrupolar excitation (QE) or other waveforms. Four of the six DAC channels provide buffered output to control critically timed events. The remaining two DAC's provide the trap voltages. The board also has 8 digital I/O channels, four of which are used for TTL triggers. The signal from the differential amplifier is fed directly in the DSO for digitization before it is transferred over the GPIB interface to the PC where the transient data is processed.

The PC based data station was connected to a 3 Tesla ICR equipped with a concentric tube electrospray ionization source. The basic experimental sequence for ESI/FTICR under LabVIEW control was as follows:

Quench--->Open Shutter--->Pulsed Valve--->Accumulate Ions--->Close Shutter
--->Pump Down-->Excite-->Detect

Examples of the data system operation made use of electrosprayed horse heart myoglobin (MW = 16,951). The Spectrum Viewer was used to determine the frequencies of two charge states (m/z = 864 and m/z = 1234) found in the initial scan (Figure 1). These two frequencies were entered into the Waveform Generator where they were added together to form a double frequency excitation. Applying this excitation produced the spectrum in Figure 2.

SWIFT excitation was used to perform various manipulations of the charge state envelope. The SWIFT waveform is synthesized from a user defined notch spectrum and then stored to the AFG. Figure 3 illustrates the spectrum obtained after applying a notched excitation.

Selective broadband quadrupolar excitation (QE) was employed to cool desired charge states back to the center of the cell. In order to execute this QE remeasurement experiment, the following events were added to the above sequence:

(...Excite--->Detect)--->Pulsed Valve, Trigger QE Box--->QE cooling--->Pump Down
--->Excite---> Detect

As shown in Figure 4, this pulse sequence is an effective method for simultaneously isolating and selectively conditioning multiple ion packets in the ICR cell.

In conclusion, the PC-based data station has proven to be a viable approach for performing FTICR experiments. The LabVIEW software provides a secure foundation for future advances in data station technology. The high level graphical interface makes it simple to modify existing software while retaining the flexibility required to perform difficult programming tasks. National Instruments' continued development of new hardware drivers allows the user to easily upgrade computer peripherals and FTICR hardware.

The data station provides the potential for performing experiments which have not been possible on the commercial systems. For example, performing such experiments as simultaneous QE/SORI-CAD becomes a possibility by taking advantage of LabVIEW's flexible manipulation of FTICR hardware.

*Instrument drivers and software available upon request

References

1. C. L. Hendrickson, B. J. Bolanos, J. J. Drader and D. A. Laude, Jr.; Proceedings of the 42nd ASMS Conference on Mass Spectrometry and Allied Topics, Chicago, IL, 1994, p. 722a.

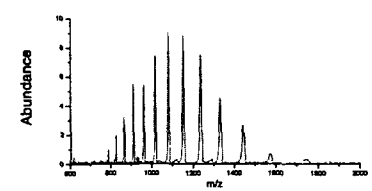

Figure 1

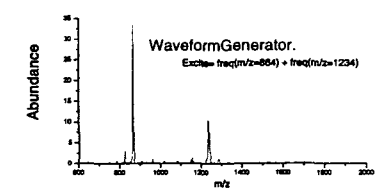

Figure 2

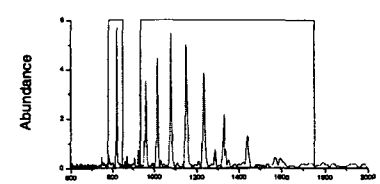

Figure 3

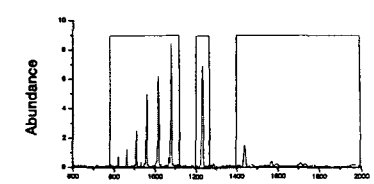

Figure 4

A New ICR-Cell for Simultaneous Trapping of positive and negativ Ions

R. Malek, K. P. Wanczek
University of Bremen, Inorganic Chemistry, PO Box 330440, D-28334 Bremen

The conventional setup [1] for **simultaneous trapping of positive and negative Ions** uses two pairs of trapping electrodes, which are at opposite potentials The outer trapping electrodes are solid plates, the inner are grids
A Fourier-Bessel series expansion is used for an **analytical model** of the trapping field. Possible **orbits** for positive and negative ions are identified.
The field is described by the equations:

$$\varphi = \sum_{n=1}^{\infty} B_{0n} \cosh(k_{0n} z)\, J_0(k_{0n}\rho) \qquad (1)$$

$$B_{0n} = \frac{2}{x_{0n}\cosh\left(x_{0n}\frac{L}{a}\right) J_1^2(x_{0n})} \left\{ (V_- - V_+)\frac{d}{a} J_1\left(x_{0n}\frac{d}{a}\right) + V_+ J_1(x_{0n}) \right\} \qquad (2)$$

(J_0: Bessel function; V_-, V_+: Trapping voltages; d: centre hole of the grid; L/a aspect ratio of the ICR cell)
After local linearizations of the electric field, the effective cyclotron frequencies are calculated for SF_5^+ and SF_5^- and compared with high resolution experiments.

Based on the theoretical model a **new ICR cell** is designed that can be described by the **same equations**. The astonishingly **simple** new trapping electrode structure is optimized for **better trapping efficiency and improved signal to noise ratio**. The **new ICR cell** needs a total of four trapping electrodes as well, but has two concentric electrodes in a plane at each side of the trapping cell (see **fig. 1**)
Experiments with a prototype Spectrospin CMS 47, and an additional DOS PC for control of the trapping voltages show the benefits of the new concept.
Broad band spectra show significant improvements in signal to noise ratio with the new cell. In **figure 2** spectra observed with the **old** (2a) and the **new** cell (2b) are **compared**.
Trapping-times, signal intensities and signal to noise ratio for simultaneously trapped positive and negative ions in the new ICR-cell are comparable to the circumstances in a conventional ICR-cell. The improved behavior for simultaneous trapping is mainly due to better charge separation and an advantageous potential distribution.
The mechanisms for simultaneous trapping of positive and negative ions in a cylindrical ICR cell are now completely understood. An analytical model allows predictions on stable ion movements and the detected frequencies. Improved trapping electrodes provide an electric field inside the ICR cell that is ideal for simultaneous trapping of positive and negative ions. Signal to noise ratio

and resolution are significantly improved and in the same range as for conventional ICR spectroscopy with positive **or** negative ions. The improved field and the detailed theory will allow new experiments· Separation of opposite charges can be controlled by changes of the trapping voltages and accelerations of axial movements. Thus total separation and total mixture of particles with opposite charges will be possible This allows ion/ion or electron/ion reactions with defined reaction times and Inverse Charge Collisional Dissociation experiments.

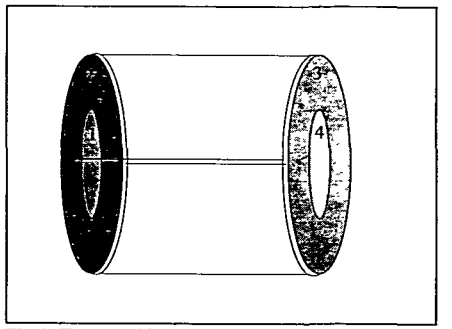

Fig.1: The new ICR cell with two pairs of concentric trapping electrodes.

Literature:

[1] M. Paul, R. Malek, Y. Wang, K. P. Wanczek; Proc 41st Conf. Mass Spectrom. AlliedTopics, East Lansing (1993)

Fig. 2· a) Spectrum of Air/SF_6 with the grid cell;
b) Spectrum of Air/Ar/SF_6 with the new ICR Cell

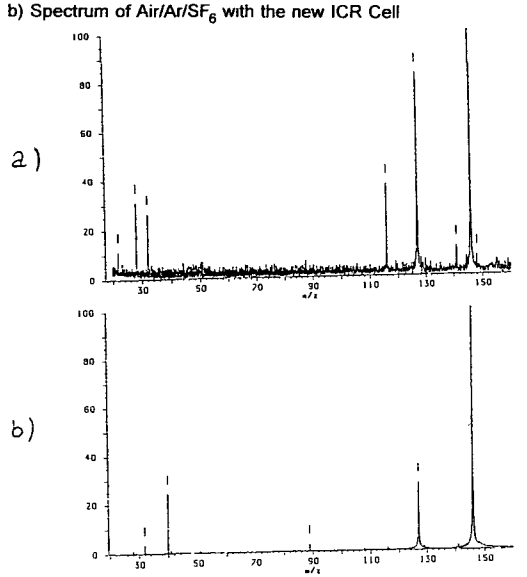

A Scheme for Feedback Excitation in FTICR-MS Based on Multielectrode Trap

Michael V. Gorshkov* **and Richard T. Kouzes**

Environmental Molecular Sciences Laboratory
Pacific Northwest Laboratory, Richland, WA 99352

*Member of the Institute of Energy Problems of Chemical Physics, Russian Academy of Sciences, Moscow, Russia 117829

One of the problems for FT-ICR is the change of the ion cyclotron frequency during the excitation process. There are several reasons for this frequency change: (i) relativistic mass increase, (ii) magnetic field inhomogeneity, (iii) space charge effects, and (iv) trapping electric field inhomogeneity. For example, in a magnetic field B (in Tesla), the cyclotron frequency of an ion of mass μ (in atomic units) will be shifted due to the relativistic effect by 90 $B^3 r_{cm}^2 \mu^{-3}$ Hz, where r_{cm} is the ion cyclotron radius (in cm). It is necessary to make the ion cyclotron radius large enough to generate a spatially coherent ion packet that passes sufficiently close to the detector electrodes to produce a measurable image current. On the other hand, the frequency shift effects increase with radius and present a problem for ion excitation. Excitation of ions of a given m/z by the use of fixed frequency excitation becomes difficult because the ions move out of the resonant condition as soon as their frequency shift becomes larger than the excitation bandwidth [1]. The measurement of the masses of light ions, light ion radial ejection, and the study of ion-molecule processes in the high energy region become difficult as well.

The method for ion cyclotron excitation via frequency capture is based on the use of a feedback loop [2] with a resonant LRC circuit to capture the instantaneous ion cyclotron frequency, plus a multi-electrode ICR trap [3,4]. In order to separate the frequency ranges in which (i) the ions are detected, (ii) cyclotron frequencies are captured, and (iii) the ion cyclotron motions are excited (Fig.1). Frequency multiples are used to avoid undesired feedback loop overload.

We find the following advantages of the proposed method for ion excitation in FT-ICR:(i) excitation of light ions up to extremely high kinetic energy (MeV and higher); (ii) "automatic" phase synchronization of the ions during detection which increases the resolving power; (iii) higher resolving power of the instrument because of the detection of the ion cyclotron signal in the high frequency domain; (iv) higher sensitivity in the case of detection of the ion cyclotron signal from heavy ions because of detection in the high frequency domain.

This work was supported by Associated Western Universities under the Grant DE-FG06-89ER-75522 with the Department of Energy and by The Laboratory Directed Research and Development program at Pacific Norhwest Laboratory.

1.S.Guan, M.V.Gorshkov, G.M.Alber, and A.G.Marshall, Phys. Rev. A47(1993), 2730.
2.L.Schweikhard and A.G.Marshall, J.Am.Soc.Mass Spectrom., 4(1993),433.
3.E.N.Nikolaev, M.V.Gorshkov, A.V.Mordehai, and V.L.Tal'rose, USSR Patent No.1307492, 1987.
4.A.L.Rockwood, Y.Pan, D.P.Ridge, and J.Wronka, USA Patent No.4,990,775, 1991.

43rd ASMS Conference on Mass Spectrometry and Allied Topics

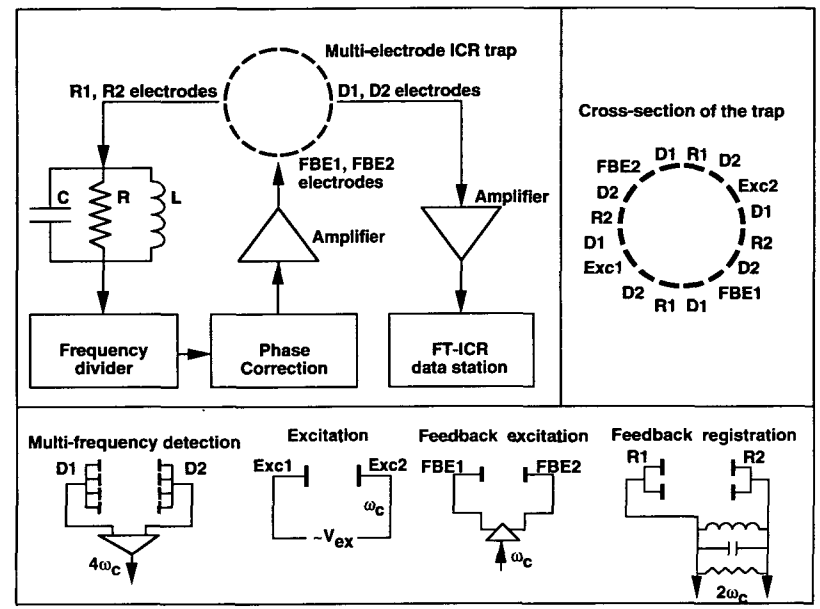

Figure 1. The scheme of the frequency capture excitation method. D1,D2 are the sets of electrodes which are used for ion detection at multiple frequency; Exc1,Exc2 are the electrodes which are used for regular cyclotron excitation; FBE1,FBE2 are the electrodes for feedback excitation signal; and R1,R2 are the sets of electrodes which are used to capture the frequency of ion cyclotron motion by feedback loop.

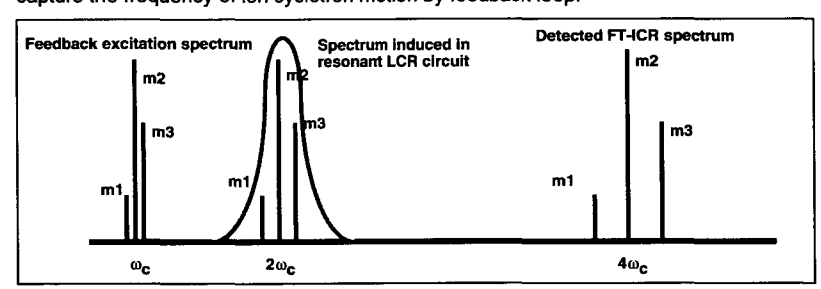

Figure 2. Frequency spectrum of the signal induced in the feedback loop, in the detection circuit of the FT-ICR spectrometer, and on the excitation electrodes of the ICR trap.

Universal ICR Ion Trap: Segmented and Optimized for Excitation, Detection and Trapping

George S. Jackson,* Shenheng Guan, and Alan G. Marshall*

Center for Interdisciplinary Magnetic Resonance, National High Magnetic Field Laboratory, Florida State University, 1800 E. Paul Dirac Dr., Tallahassee, FL 32310

* Department of Chemistry, Florida State University

Traditionally, ICR ion traps have been constructed from conductive electrodes, each of whose surfaces has the shape of a particular desired isopotential surface: e.g., 3-D axial quadrupolar "Penning" d.c. potential for ion trapping, 1-D linear a.c. potential for dipolar excitation, and 2-D azimuthal a.c. quadrupolar potential for ion axialization. Because no single trap geometry simultaneously optimizes all three such potentials, dozens of different compromised trap shapes are in use. A more general approach is to divide each each electrode into smaller segments and then apply appropriate potentials to each section, as for a recently reported ICR ion trap "linearized" for dipolar excitation and dipolar detection.[1]

Here we extend that idea to its logical extreme: a "universal" trap, consisting of a cubic trap, each of whose sides is divided into a 5 x 5 grid of square electrodes, each with independently controllable a.c. and d.c. voltages. Although there are 5 x 5 x 6 = 150 electrode segments, the high symmetry of the cubic geometry results in relatively few independent voltages: e.g., 7 for dipolar a.c. excitation or detection, 15 for azimuthal quadrupolar a.c. excitation, and 13 for three-dimensional axial quadrupolar d.c. trapping. In fact, only 48 independent voltages are needed to specify all three desired potentials. Thus, many of the electrodes may be wired together, with appropriate switching to change from one experimental event to another. Because the electrostatic trapping field usually remains in place throughout most experimental events, a simple resistive network may be used to switch between dipolar excitation/detection and azimuthal quadrupolar ion axialization.

Numerical simulations (Simion 6.0) confirm significant improvement in each of the three desired potential contour shapes, compared to an unsegmented cubic trap. For example, Fig. 1 demonstrates the much more accurate three-dimensional quadrupolar trapping potential of a segmented cubic trap (left) compared to an unsegmented cubic trap (right). Computer simulations also demonstrate a significant reduction in signal components at harmonic multiples of the fundamental ICR frequency, for a point charge excited to the same radius in cubic (Fig. 2) and "universal" (Fig. 3) traps. The "universal" trap allows for nearly distortion-free excitation and detection at a cyclotron radius extending almost to the radius of the trap itself. We therefore anticipate marked reduction in other non-linear effects (e.g., sidebands and mass-dependent axial ejection) as well as improved efficiency in ion trapping and dipolar or quadrupolar excitation, with corresponding improvement in mass resolving power, mass accuracy, and reproducibility. Work supported by NSF (CHE-93-22824), NIH (GM-31683), and the National High Magnetic Field Laboratory at Florida State University.

1. P. B. Grosshans, R. Chen, P. A. Limbach, and A. G. Marshall, *Int. J. Mass Spectrom. Ion Proc.* **1994**, *139*, 169-189.

43rd ASMS Conference on Mass Spectrometry and Allied Topics

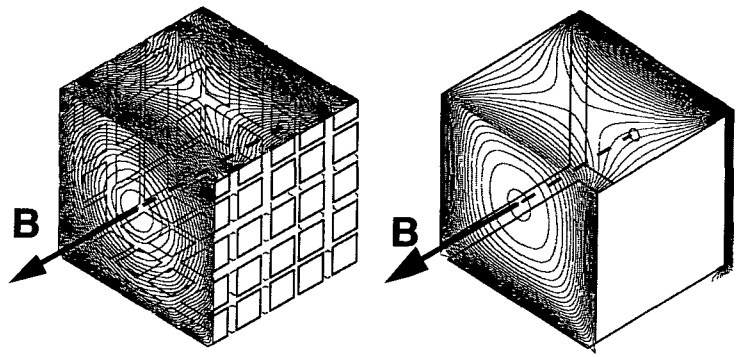

Figure 1. Isopotential contours on planes sliced just inside the endcap (left on both traps) and side (top) for the near-perfect 3-D quadrupolar trapping potential on left with the "universal" trap. Note the significant distortion with the regular cubic trap. B is the applied magnetic field.

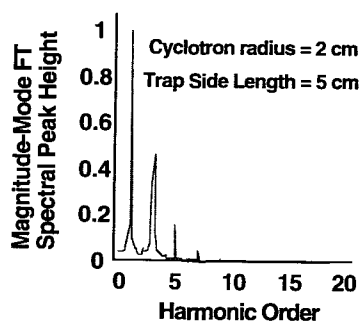

Figure 2. Harmonic signal magnitudes for a point charge in an unsegmented cubic trap.

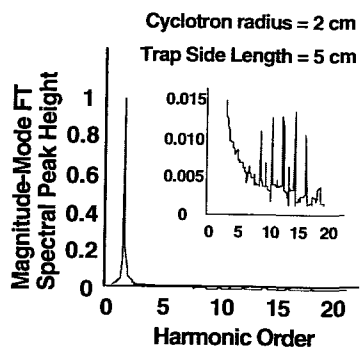

Figure 3. Harmonic signal magnitudes for a point charge in a segmented cubic trap.

Extending the Functionality and Performance of Commercial Ion Traps

McHugh, Sean; Hoekman, Don; Bradshaw, Stephen; Wilson, Ray; Li, Rebecca
Teledyne Electronic Technologies, Scientific Instruments, Mt. View, CA 94043

Due to its software intensive nature, the typical ion trap mass spectrometer may be functionally extended by connecting a smart instrument controller, and a relatively modest amount of additional electronics hardware, to the original instrument configuration.

By adding faster and higher resolution drive circuitry to the RF generator, a Filtered Noise Field (FNF) waveform generator to the end caps, a more sensitive A/D converter to the detector output, and parametric resonance scanning with direct frequency control to the RF drive circuitry, the standard ion trap will operate over a wider mass range, scan much faster, perform true Selective Ion Monitoring (SIM) and tandem mass spectrometry (MS/MS and MS^n), as well as execute multiple scanning modes of acquisition, such as: EI/CI, EI/SIM, EI/MS^n, etc.

The upgrade of the standard ion trap mass spectrometer (*Apogee*) involves the following:

1 - Replacement of the Scan and Acquisition Processor (SAP) with a new interface card, containing instrument control circuitry and programmable endcap drivers.

2 - Replacement of the existing DOS data system with a Windows data system to acquire, process, and display the data.

3 - Adding a smart instrument controller (the electronics tower), containing RF, instrument parameter, FNF waveform, parametric resonance scanning, and acquisition control of the ion trap.

Upgrading a commercial ion trap mass spectrometer has proven to add a tremendous amount of functionality to the basic instrument. In general, this has been achieved by the following:

1 - Direct analog control of the RF drive circuitry.

2 - Direct analog sampling of the multiplier output.

3 - Direct digital control of the instrument's non-scanning functions, such as: heaters, filament, emission current, multiplier, etc.

4 - Adding a smart instrument controller to handle scanning and acquisition.

Scan Report **Scan Function:** Full-Scan EI May-18-1995 3 46 pm
Conditions: FC43 Spectrum - Highlight on m/z 414 Peak
Instrument: Apogee on Saturn **Inlet:** Cal Gas **Scan Number:** 1328

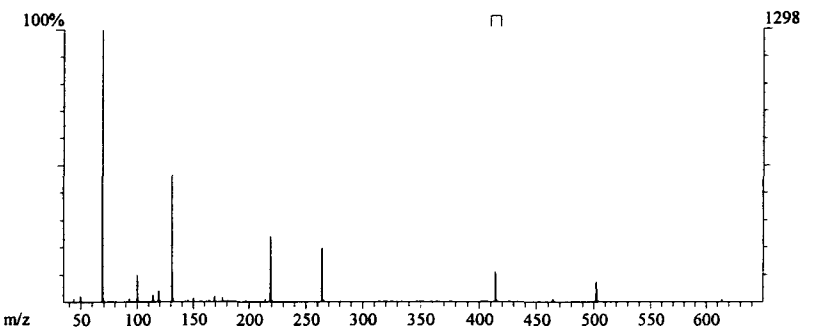

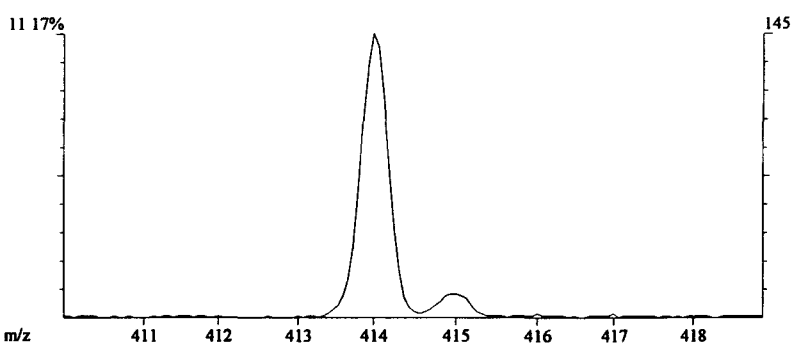

Scan Parameters

Low Scan Mass: 35.0 m/z
High Scan Mass: 650.0 m/z
Micro Scans: 20
Scan Rate: 8000 amu/sec
Ion Time: 600 µsec
Ion Level: 35.000 m/z

Instrument Parameters

Emission Current: 75 uamps
Multiplier: 1500 volts
Heater Temperature: 100 C
Electrometer Threshold: 82
Filament: 1
Cal Gas Inlet: On

Performance Enhancement for the HP 5971/5972

*Roy, Laura; Jehnsen, Chris; Hamerly, Thomas; Graves, Peter; Roy, Raymond
Detector Technology, Inc. Sturbridge, MA
Los Gatos Circuits, San Jose, CA

INTRODUCTION

As analytical chemistry advances, mass spectrometers are pushed to their limits in sensitivity and high mass detection. One approach to improving the performance in these areas is to improve the configuration of the continuous dynode electron multiplier(CDEM). Studies have been performed on the Hewlett Packard(HP) 5971/5972 utilizing a high energy dynode(HED) and a newly developed internal power pack. In house and field operations demonstrate the performance enhancement seen when using the HED Power 2000.

METHOD

The current HP configuration does not allow for an easy dynode upgrade. The HED Power 2000 utilizes an internal DC/DC converter which is packaged with the detector. The input to the converter comes from the high voltage applied to the CDEM. The converter output is -4.5KV, and is the voltage applied to the dynode. Because the converter and CDEM share the existing power supply, no additional modifications to the mass spectrometer are required. Upgrading the instrument is as easy as changing the detector.

RESULTS

Tests were performed on the original equipment multiplier and the HED Power 2000. Tests were done by Chris Jehnsen of LGC, San Jose, CA using an HP 5972 instrument. Standard Spectra Autotunes were run on both multiplier, see fig. 1 and fig. 2. After the autotunes were run a 1 microliter injection of .01 ppm Hexachlorobenzene was injected. The signal to noise when using the original equipment multiplier was 22.7:1, see fig. 3. The HED Power 2000 achieved a signal to noise of 62.3, see fig. 4.

APPLICATIONS

When testing at LGC was completed, the HED Power 2000 was ready for field operations. Steve Connor of the New York State Department of Health, Albany, NY used the upgrade to run dioxin tests. Before injecting any samples the HED Power 2000 was tuned using QuickTune. Figures 5 and 6 show the results. Injections of 2 ul were then run. The sample contained 6.92 pg/ul of 2378-TCDF, 7.86 pg/ul of 123478-HxCDF, 8.58 pg/ul of 123678-HxCDF, 8.38 pg/ul of 1234678-HxCDF, 7.36 pg/ul of 123789-HxCDF, and 9.92 pg/ul of 12346789-OCDF. The multiplier was run as 2300 V. Figure 7 shows the before and after results.

CONCLUSIONS

The data collected by Chris Jehnsen and Steve Connor indicated that there was significant improvement in signal to noise and high mass detection when using the HED Power 2000. This CDEM configuration not only enhanced the performance of the instrument but also provided for a quick and easy instrument upgrade. One issue was encountered during this investigation. When using the HP software a parameter must be adjusted. This is the target relative abundance of mass 502. This amount is configured to 3 - 8% and must be changed to 15 - 25% to maximize the performance of the HED Power 2000.

The results shown were selected from a variety of data. This data shows the average improvements seen when using the HED Power 2000 on a clean and uncontaminated instrument. Results may vary depending upon instrumentation and application.

43rd ASMS Conference on Mass Spectrometry and Allied Topics

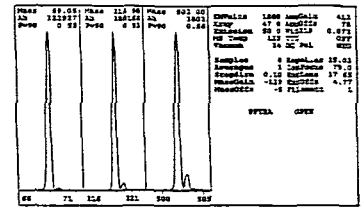

FIGURE 1 - BEFORE

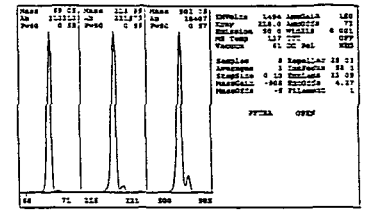

FIGURE 2 - AFTER

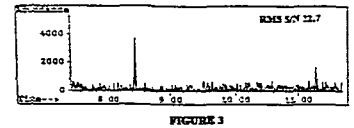

FIGURE 3
.01 ppm HCB (mass 284)
BEFORE

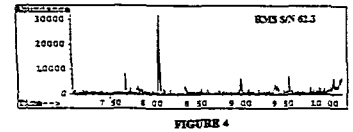

FIGURE 4
.01 ppm HCB (mass 284)
AFTER

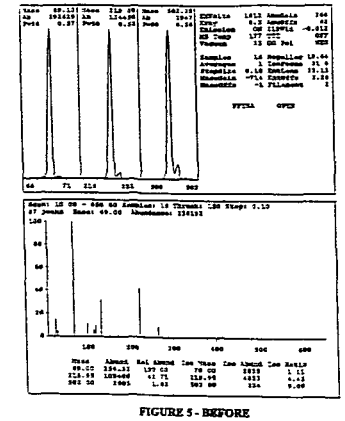

FIGURE 5 - BEFORE

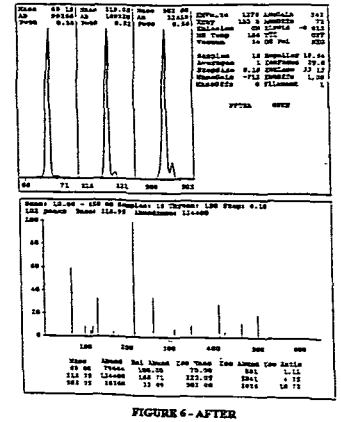

FIGURE 6 - AFTER

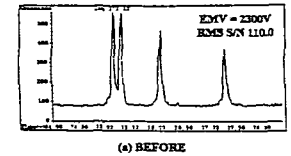

(a) BEFORE

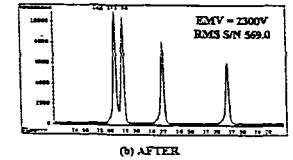

(b) AFTER

FIGURE 7
1234678-HxCDF, 123678-HxCDF
23478-HxCDF, 123789-HxCDF

Matrix-Assisted Laser Desorption/ Ionization Ion Trap Tandem Mass Spectrometry of Peptides: A New Excitation Scheme for CID

Jun Qin and Brian T. Chait
The Rockefeller University 1230 York Ave. New York NY 10021

One of the current limitations of MS/MS in the ion trap mass spectrometer is the limited internal energy that can be deposited by conventional resonance excitation. Extensive sequence specific fragmentation of peptide ions in the range of m/z 1000 to 3500 usually requires the deposition of large amounts of internal energy. To make the ion trap a useful analytical tool for protein characterization and identification of post-translational modifications, we need to devise means for inserting sufficient amounts of internal energy in peptide ions to achieve a high degree of fragmentation.

We report a new excitation scheme for collision-induced dissociation (CID) of peptide ions in an ion trap mass spectrometer. This new excitation scheme is capable of supplying large amounts of internal energy as compared with conventional resonance excitation so that peptide ions up to m/z 3,500 can be fragmented to generate extensive sequence specific ions. Fig. 1 shows the RF scan function that we devised to carry out the new excitation procedure. After ions are isolated by reverse- then- forward scan (only forward scan is shown here), the RF amplitude is raised to a higher level in 10 ms ("the slam scan segment") then abruptly dropped to a lower level where ions are excited for a period of between 30ms and 1s. The excitation frequency is ~ 5% red shifted from the resonance frequency and the excitation amplitude (the AC amplitude) is set at the maximum available value (21 V_{p-p}). The resulting product ions are cooled at the same RF level as that used during the excitation segment, and detected by resonance ejection. We term this new excitation scheme as red shifted off resonance large amplitude excitation (RSORLAE). Fig. 2 compares CID spectra of substance P taken with the conventional resonance excitation and the new excitation scheme (RSOLAE). The difference is dramatic. For conventional resonance excitation, only y_n type ions are observed. By contrast, for RSORLAE, both b_n and y_n type ions are observed. since dissociation channels that lead to y_n type ions are lower in energy compared with channels that lead to b_n type ions, the new excitation scheme (RSOLAE) inserts larger amounts of internal energy into peptide ions than the conventional resonance excitation.

Although we do not have a complete understanding of the new excitation scheme, the experiments illustrated in Fig. 3 give insights into the possible underlying principles. Fig. 3 compares the fate of bombesin ions as registered by the detector in the process of ion isolation, excitation and detection when the conventional resonance excitation and RSOLAE were carried out. Most of the isolated bombesin ions are ejected during the excitation process for the conventional resonance excitation at a frequency of 59124 Hz with an AC amplitude of 1.2 V_{p-p}; in contrast, none of the ions are ejected during the excitation process for RSOLAE at 59124 Hz and an AC amplitude of 21 V_{p-p}. The ability of the ions to be retained inside the trap over extended periods of time during the red shifted off resonance excitation process allows the build up of sufficient internal energy so that higher energy dissociation channels can be accessed.

Red Shifted Off Resonance Large Amplitude Excitation (RSORLAE)

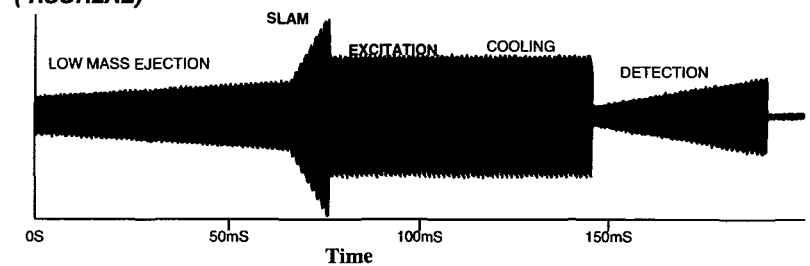

Fig. 1 The scan function of the new excitation scheme.

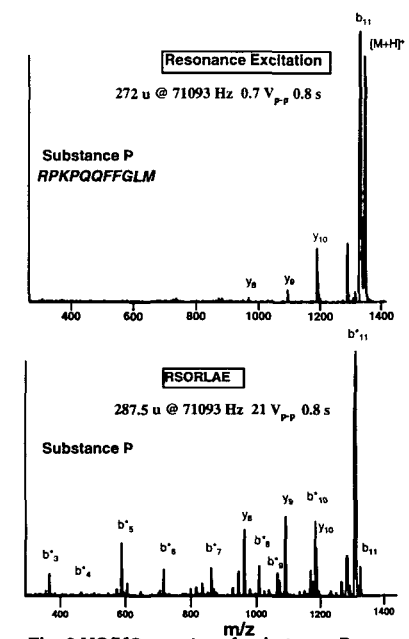

Fig. 2 MS/MS spectra of substance P taken with resonance excitation and RSORLAE.

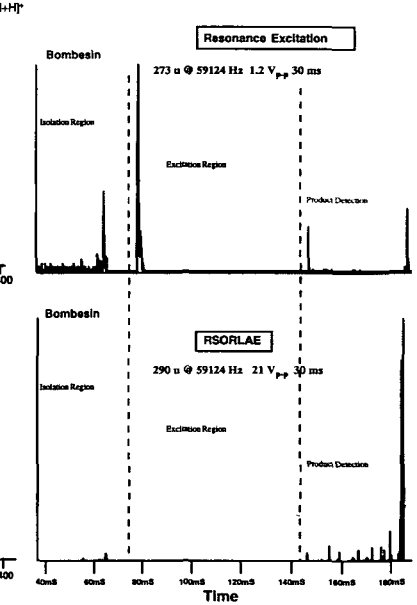

Fig. 3 The fate of the ions in isolation, excitation and detection for resonance excitation and RSORLAE.

Filtered Noise Fields in a Paul Ion Trap for Multiple MS Analyses

Dane Karr[1] and Clifford C. Walters[2]

[1]Teledyne Electronic Technologies, Mt. View, CA
[2]Mobil Research and Development Corp., Dallas TX

We have described a new method of operation for the Paul ion trap in which a Filtered Noise Field (FNF™) is used to perform Selective Ion Isolation[1]. The FNF is a waveform that is applied to the end electrodes of the trap during, and for a short time after, the creation of ions within the trap (or the introduction of ions into the trap). The waveform ejects undesired ions as they are created so that ions of interest may be accumulated without creating a space-charge condition.

Thus, low levels of components in a complex matrix may be identified by accumulating diagnostic ions for SIM or MS/MS analyses. In addition, since the trap is filled with only the ions of interest, the original sensitivity of the trap is maintained. The combination of high sensitivity (from the ion trap) with high selectivity due to SIM or MS/MS analyses makes it possible to detect minute quantities of material in very complex matrix. The utility of FNF for SIM and GC/MS/MS analyses are demonstrated here.

A GC/MS/MS analysis of sterane biomarkers[2] in the saturate fraction of crude North Sea oil was carried out. We performed Selected Reaction Monitoring (SRM) measurements for the 400 m/z and 414 m/z transition to the 217 m/z product ion. We have used alternating scans so these analyses may be completed in a single GC run. The 217 m/z mass chromatogram for the 400 → 217 m/z transition is shown below. An expansion which includes peak identification is also shown.

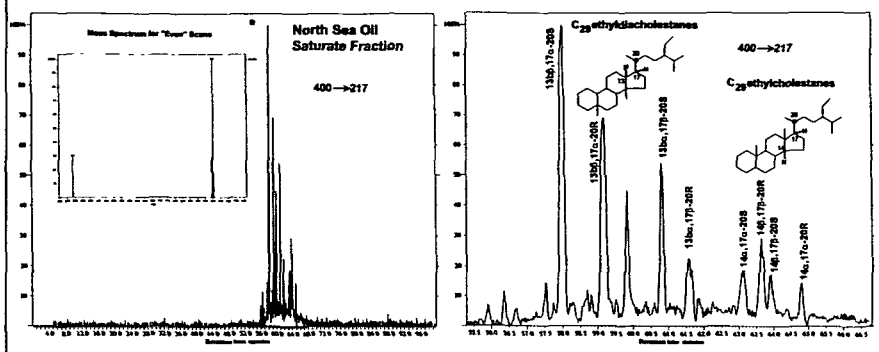

In addition, a GC analysis of atrazine spiked into orange juice at a concentration of 20 ppb was performed. We have collected data in full scan EI, an SIM EI analysis, and an SRM EI analysis. The SRM MS/MS analysis is very specific for atrazine in this matrix; the total ion chromatogram is displayed below (the corresponding mass spectrum is inserted).

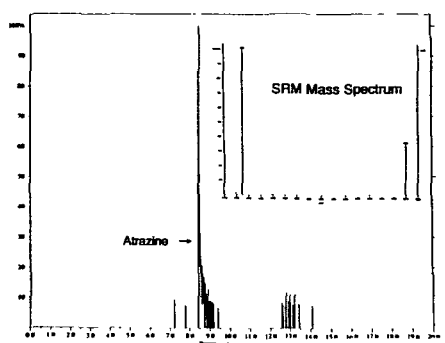

1) Tabone, V.; Yelton, R.O.; Kelley, P.E.; Stiller, S.W.; Proceedings of the 42nd ASMS Conference on Mass Spectrometry and Allied Topics; p 181.

2) Tissot, B.P.; Wells, D.H.; Petroleum Formation and Occurrence; Springer-Verlag: New York, 1978, Chapter 3.

ADVANCED SWIFT TECHNIQUE FOR MALDI / QUADRUPOLE ION TRAP MASS SPECTROMETER

Vladimir M. Doroshenko and Robert J. Cotter
The Johns Hopkins University School of Medicine, Baltimore, MD 21205

SWIFT (stored waveform inverse Fourier transform) and other related techniques are widely used for broadband excitation of ions in a quadrupole ion trap (QIT) mass spectrometer to perform mass selective accumulation of ions into the trap, ion isolation and fragmentation. With the introduction of nonlinear phase modulation to SWIFT technique, the ejection of ions from the trapping cell compared to that for unmodulated phase case is not *simultaneous* anymore. This fact has not been widely discussed. In this work we have used it to design function for phase modulation which allowed us to achieve unit mass resolution for ion isolation in the range m/z up to 1300. A high performance monoisotopic CID experiments have been demonstrated with the use of these techniques.

Some properties of SWIFT waveforms used can be observed from the data in Figure 1. Small number of points N=2048 was used to design waveformes in Fig. 1 to show the real structure of the SWIFT pulse (the sample interval is equal to 0.8 µs). The frequency band of pulses covers the range from 10 to 560 kHz with the notch of the width of 40 kHz in the waveform in Figure 1a. In many aspects the SWIFT pulse looks like frequency sweep chirp used in FTMS for ion excitation. One can expect from the "sweep" nature of the SWIFT signal that ejection of ions from the trap cell is not simultaneous. The same structure is observed for longer waveforms although it is observable at higher resolution only. Another type of SWIFT pulse used in this work is shown in Fig. 2. This pulse was designed for N=16000 and a 14 kHz frequency interval which is "stretched" in time-domain onto a ~6 ms time interval. On this background a 1 kHz narrow width notch in Figure 2b seems to be very broad. We use such "stretched" SWIFT pulses for increasing the mass resolution during ion isolation.

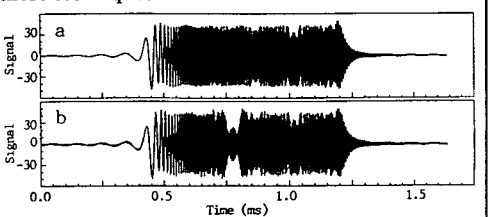

Fig. 1. Broadband SWIFT waveforms (f=10-560 kHz): a- without notches; b- notch at f=250±20 kHz.

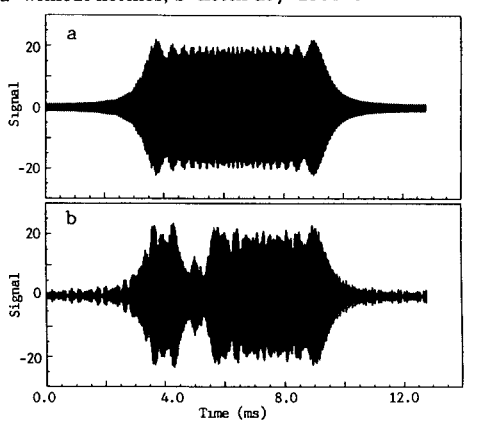

Fig. 2. Narrower band SWIFT pulses (f=208.6-222.3): a- without notches; b- notch at f=212.5±0.5 kHz.

Experiments were carried out on a modified Finnigan MAT ion trap detector. These modifications include additional hardware for interfacing of ITD with laser and external control of the instrument, and developed in-house *TrapWare* software (see *Rapid Commun. Mass Spectrom.* **1994**, *8*, 766). TrapWare designed and loaded waveformes to the memory of a Quatech (Akron, OH) WSB-100/WSB-A12M waveform synthesizer plug-in board connected to an IBM computer, and triggered them when it was necessary during experiment. The instrument scan functions and SWIFT pulses were designed simultaneously using the tables on the computer screen. Thus, the real mass values were used instead of frequencies for SWIFT pulse designing.

A significant increase of resolution for the ion isolation has been observed when after the first coarse isolation step using broadband SWIFT pulses shown in Fig. 1 a narrower band "stretched" pulses shown in Fig. 2 were applied. The example of isolation of monoisotopic species of the protonated ions of Angiotensin I (m/z=1296.7) is presented in Fig.3. A mass selective ion accumulation technique with the use of the SWIFT pulses and multiple laser shots was applied using the *ramped trapping voltage* method for trapping ions which involves ramping of the RF field from small to high trapping values during the ion flight into the center of the ion trap. The increase of resolution for ion isolation obtained for narrower frequency range SWIFT pulses is very similar to the phenomenon observed during the slowered mass scans. The asymmetry phenomenon has been also observed during application of normal and time-reversed SWIFT waveformes which is similar to asymmetry observed for forward and reverse mass scans in the resonance ejection technique. The unit mass resolution isolation technique has been successfully applied for SWIFT-activated CID mass spectrometry of peptides (Fig. 4).

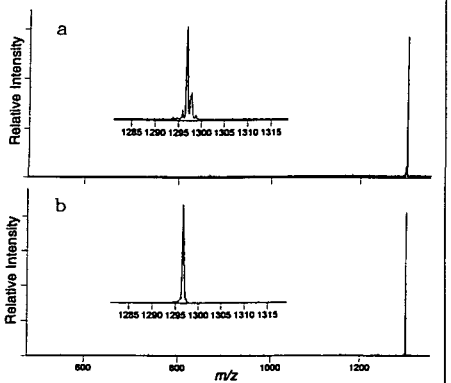

Fig. 3. MALDI mass spectra of isolated ions of Angiotensin I after the coarse (a) and fine (b) isolation steps.

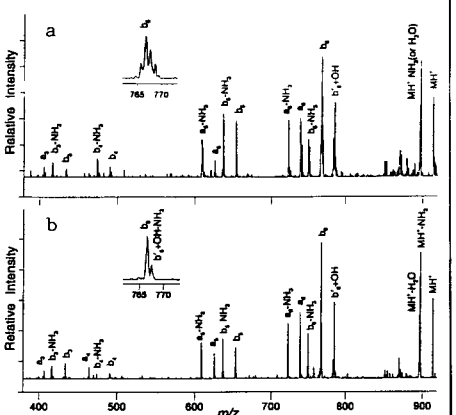

Fig. 4. CID spectra of α-Casein Fragment 90-96: a- after parent ion cluster isolation; b- after major isotopic form isolation at m/z=913.5.

APPLICATION OF TAILORED WAVEFORM GENERATION TO THE QUADRUPOLE ION TRAP

Dennis Taylor, Jae Schwartz, Joe Zhou, Mike James,
Mark Bier, Andy Korsak, George Stafford
Finnigan Corporation, San Jose, CA 95134

INTRODUCTION

A limitation of the ion trap mass spectrometer is the number of ions that can be stored in the quadrupole field at one time and maintain mass resolution Only storing selected ions of interest, or mass ranges of interest, allows the operator to eliminate unwanted background ions while concentrating the analytically useful ions The application of a supplementary AC field, at a predetermined frequency and amplitude, will resonantly excite ions in the axial direction and cause them to be ejected. If a supplementary signal is applied that contains a combination of frequencies (waveform), then mass ranges of ions can be excited and ejected at one time

RESULTS

The SWIFT method was used to produce the waveforms in the Fourier Transform Technique Notice the first half of the waveform contains mostly high frequency components, and the second half of the waveform contains mostly low frequency components Therefore, ion storage using this waveform technique depends on the time the ion is formed or injected in to the trap

Spectral coverage is the relative abundance of the frequency components making up the waveform. The Fourier technique yields a smooth measured abundance across the frequency range of the waveform

The Tailored waveform technique is achieved by summing together a plurality of spaced discrete frequencies covering the range of characteristic motion of the ions of interest This technique yields a much improved time coverage as compared to the Fourier technique This improvement will mean that all ions of interest will be excited and ejected continuously during the waveform application Tailored waveform spectral coverage results are similar to the results obtained using the Fourier technique

CONCLUSIONS

- Tailored waveforms give uniform frequency abundance over the entire time of waveform application
- Both Fourier and Tailored waveform techniques show good spectral coverage characteristics
- Waveforms generated by a Random Noise technique yield poor spectral coverage
- Tailored waveforms, using 500 Hz discrete frequency spacing, provide single mass ion isolation above 1000 m/z

REFERENCE

USP 5,324,939, 1994, John Louris and Dennis Taylor, Method and Apparatus for Ejecting Unwanted Ions in an Ion Trap Mass Spectrometer.

43rd ASMS Conference on Mass Spectrometry and Allied Topics

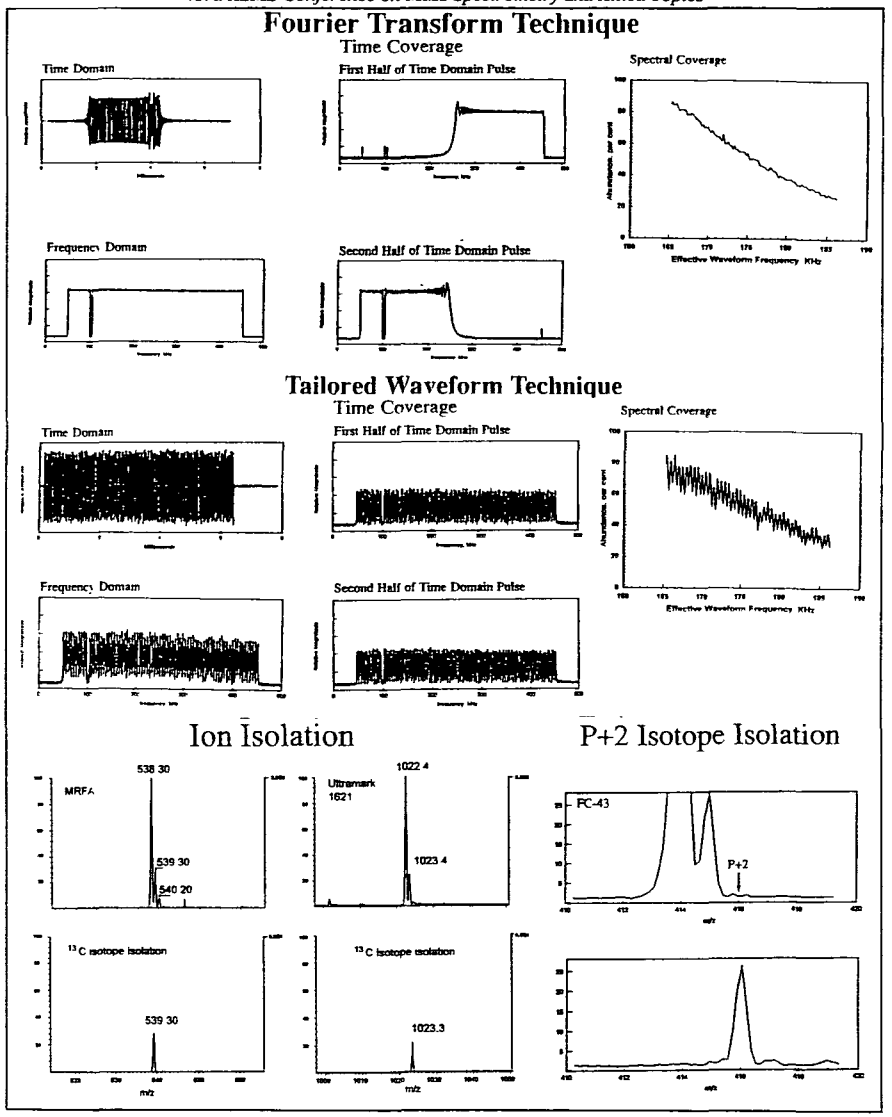

Selective Ion Accumulation in an ICP/ITMS using a Filtered Noise Field

G. C. Eiden, C. J. Barinaga, and D. W. Koppenaal, Materials and Chemical Sciences Center, Pacific Northwest Laboratory, Richland, WA 99352

Selective accumulation of ions in an ion trap mass spectrometer (ITMS) has been characterized using both single frequency and broadband resonant excitation. The goal of this work is to enhance selective accumulation of ions from plasmas and other external ion sources. The charge capacity of the ITMS is 10^6 to 10^7 ions, although the mass spectrum is distorted at much lower space charge. Detection of trace ions necessitates selective detection schemes such as selective trapping or optical detection. We report results of selective trapping studies for Sr, Y, and Zr solutions (100 ppb Y and 1 ppb each Sr, Zr). "Background" ions in mass channels adjacent to the channel of interest is a worst case situation with respect to selective ejection and abundance sensitivity. Real samples will often have matrix ion m/z values much further removed from the m/z of the ions of interest. Thus, we also give results for a multielement solution. Ions from an inductively coupled plasma ion source are endcap injected into the ITMS [1]. Broadband waveforms were generated by an HST-1000 (Teledyne MEC) instrument, using the filtered noise field (FNF) method [2]. The experiment is controlled by the ITMS electronics and ICMS software [3]. The sequence of experimental events is: ion injection at $q_z = 0.4$ (typical), collisionally cool ions, set trapping potential for resonant excitation ($q_z = 0.2$ to 0.6), analysis rf ramp.

The selectivity of the ejection process is determined by the ratio of the ejection efficiency of resonantly excited (target) ions to the ejection efficiency of ions in adjacent mass channels. Using single frequency or broadband excitation of cooled ions, we observe little or no decrease in the number of ions detected in mass channels adjacent to the target ion. A more precise estimate of the decrease is obtained from the slope of the signal versus the duration of the excitation pulse. The selectivity that we report is based on the error in these slopes from a linear regression fit, and thus provides a lower limit for the selectivity. Selectivity relative to ions further removed in m/z is even larger. In Fig. 1, the log of the ion signal is plotted for ^{88}Sr, ^{89}Y, and ^{90}Zr ions for the solution described above. We observe a ~2000-fold reduction in the intensity of the Y intensity and no observable reduction in the ^{88}Sr and ^{90}Zr peaks. Using the slope of the Sr signal versus time, we estimate a single frequency resonant excitation selectivity of ~10^5. Selectivities are much lower for "hot" ions, i.e., those that have not been collisionally cooled.

Figure 2 illustrates the efficacy of broadband excitation in reducing high space charge conditions in the trap. The top trace shows the mass spectrum of a multielement solution under high space charge conditions (~10^4 ions detected). The peaks are severely distorted and the signal at m/z 106 is completely obscured. The bottom trace demonstrates the recovery of mass resolution and sensitivity by selective ion ejection using broadband excitation. The FNF was targeted to remove all ions except for those in a window between 100 and 107 amu. The FNF waveform contained frequency components every 1000 Hz between 10 KHz and 500 KHz, except for a window at 270-295 KHz for which the amplitude of the waveform was zero. Comparison of the bottom

trace with the spectrum at low space charge conditions and no FNF applied (not shown) shows that nearly full sensitivity is retained for peaks between 100 and 106 amu.

We have also characterized single versus multiple frequency excitation with respect to buffer gas pressure and the frequency, amplitude, and duration of the resonant excitation pulse. We have found that the conditions for high selectivity include He buffer gas pressure ~0.2 mTorr (at, or slightly below, where the trapping efficiency versus pressure curve saturates); an excitation amplitude and duration of at least 450 mV (strongly pressure dependent) and 2 msec. Further design criteria for selective ejection and accumulation methods will be developed from these studies and reported in the near future [4].

1. C. J. Barinaga et al, Rapid Comm. Mass Spectrom. **8**, 71 (1994).
2. a) P. E. Kelley, US Patent Nos. 5,134,286 (1992) and 5,206,507 (1993); b) S. W. Stiller, *et al*, Pittsburgh Conference, Atlanta, GA, 1993, No. 267 and 1081; c) D. E. Goeringer *et al*, Anal. Chem. **66**(3), 313 (1994).
3. R. A. Yost and N. A. Yates, ICMS Ion Trap Software, Vers. 2.20, Gainesville, FL, 1992.
4 G. C. Eiden, C. J. Barinaga, and D. W. Koppenaal, J. Amer. Soc. Mass Spectrom., to be submitted.

Figure 1. Selectivity of single frequency resonant ejection

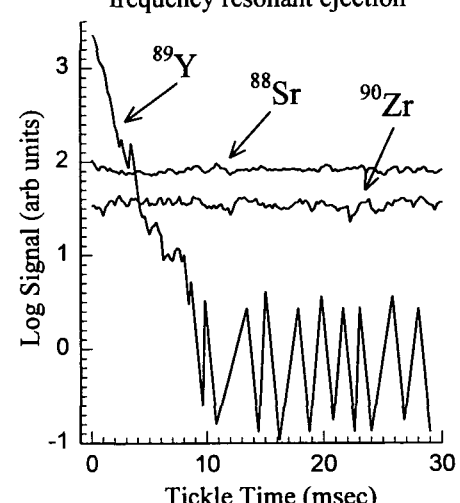

Figure 2. Space charge effects in a multielement mass spectrum

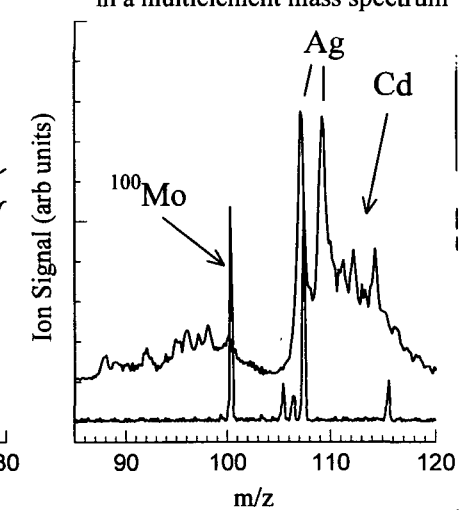

Automated Resonance Ejection in a Quadrupole Ion Trap Mass Spectrometer

J.Murrell*,P.Watts#, J.F.J.Todd *
*** The Chemical Laboratory, The University, Canterbury, Kent, CT2 7NH, UK**
 # CBDE, Porton Down, Salisbury, Wiltshire, SP4 0JQ, UK

The use of resonance ejection experiments within ion trapping instruments to aid in the deconvolution of complex ion/molecule reaction pathways was first demonstrated by Beauchamp *et al*[1]. They performed double resonance experiments upon an ICR mass spectrometer. A similar approach is taken within this poster whereby a radiofrequency excitation pulse is applied at the same frequency as the secular frequency of a particular *m/z* ratio during the reaction time; hence the ions at that value are ejected and thus prevented from undergoing further reaction. To remove the problem of tuning in the resonance frequency for each individual *m/z* value the performance of a set of resonance ejection experiments has been automated. This is accomplished using *dynamically programmed scans*[2]. The results not only aid in the understanding of the pathways of ion/molecule reactions, they also reveal some information about the physical characteristics of the ion trap. The reaction of the methanol dimer with cyclohexanol will be used to illustrate this technique and show some of the side reactions which may occur. All experiments were performed upon a Finnigan MAT Ion Trap Mass Spectrometer (ITMS) located at the University of Kent. The scan function utilised for each experiment is shown in Figure 1. The vapours of the methanol and the cyclohexanol were introduced into the manifold via leak valves to unadjusted gauge pressures of 2×10^{-6} and 1×10^{-6} Torr respectively. All the experiments were performed by using the same key sequence programme which was input and edited using a FORTH editor available within the ITMS software.

From this a technique a chromatogram-type plot is produced, as shown in Figure 2. Considering the profiles corresponding to the 65^+, 131^+, 133^+, 199^+, and 201^+, it can be seen that the decrease in intensities of the ions relate to the ejection of that particular ion or a precursor of it. When an ejection pulse is applied close to the secular frequency of the ion, normally termed off-resonance excitation, the ion being expelled may fragment which leads to its dissociation products being observed. These dissociation products are formed with a large amount of internal energy and may immediately react with the other neutrals present.

As can be seen in Figure 2, the ions are not ejected at their resonance frequencies but at lower values than expected, i.e. a higher *m/z* ratio or lower q_z value. This probably occurs because commercial ion traps do not possess a pure quadrupole geometry but are of a stretched type.[3] As can also been seen in Figure 2 the width of the resonances increases with the increasing m/z ratio, i.e. lower q_z values. This can be explained by considering both the depth of the potential well and the motion of the ions. At lower q_z values the well depths are shallower than those of higher q_z values and thus less energy is required to eject the ions. In respect to the motion of the ions, by considering the motion of the ion in the terms of a sine wave, for the low frequency, i.e. low q_z situation, the off-resonance excitation is in phase with the motion of the ion for a longer period of time than the higher q_z value case. Therefore at the lower q_z values the ions are excited for a longer periods of time. The combination of these two effects causes ions to be lost from the ion trap over a greater range at the lower q_z values than compared to the higher ones.

The program described within this poster provides another means by which the quadrupole ion trap may be used to understand ion/molecule reactions. There are some interference reactions, e.g. off resonance dissociation, which may occur and have been highlighted. The results also reveal some physical characteristics of the quadrupole ion trap: the ions not appearing at the q_z value at which they would be expected and the greater width of the resonances at lower q_z values as compared to higher ones. Future work will involve the use of this technique to better understand other complex ion/molecule reactions and the nature of ion motion within the ion trap.

1) L.R.Anders, J.L.Beauchamp, R.C.Dunbar and J.D.Baldeschwieler J.Chem.Phys. 45 (1966) 1062-1063
2) N.J.Clarke, A.M.Franklin, M.L.Langford, A.D.Penman, D.A.Thorner and J.F.J.Todd Rapid Commun. Mass Spectrom. Submitted
3) J.Louris, J.Schwartz, G.C.Stafford, J.E.P.Syka, D.Taylor, Proc. 40th ASMS Conf. Mass Spectrom. Allied Topics. Washington, DC, 1992, P.1003

Figure 1: Scan Function

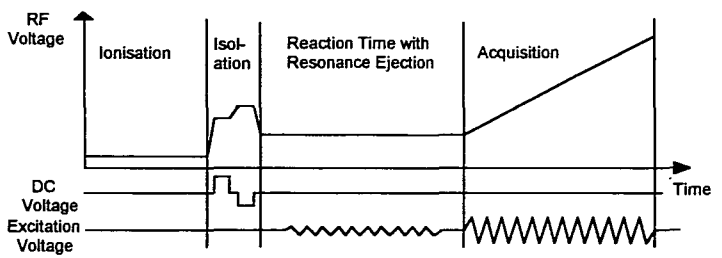

Figure 2: Reaction between Protonated Methanol Dimer and Cyclohexanol.

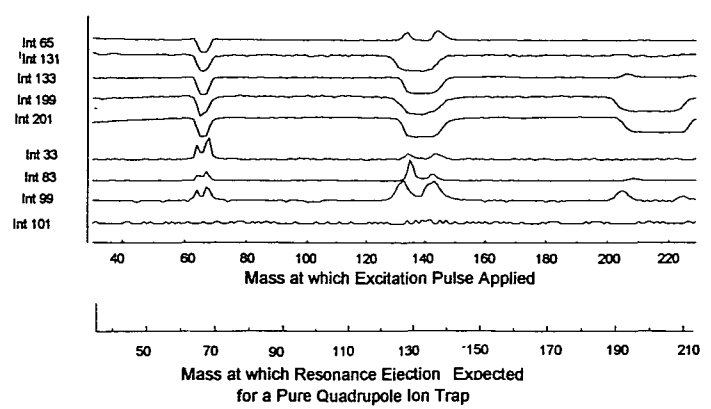

Enhancement of Ion Trapping Efficiency in an Ion Trap with a Pulsed Valve

Yang Wang, Michael Schubert and Jochen Franzen
Bruker-Franzen Analytik GmbH, 28359 Bremen, Germany

There is a high probability for ions, which are ionized within a three-dimensional quadrupole field, to be trapped. These ions are damped into the center of the ion trap by collisions with a buffer gas, for example He. The damping results in improvement of trapping efficiency and mass resolution. In practice the buffer gas is introduced into the ion trap with constant pressure. It is much more difficult, however, to trap ions which are produced externally and transferred into an ion trap with some excess energy. A method of enhancing the trapping efficiency for injected ions is the dissipation of the ions kinetic energy by collisional cooling with the buffer gas of increased pressure. However, the application of an increased buffer gas pressure constantly in time results in decreasing mass resolution. A good way to solve the problem is to use a pulsed valve. In addition, an appropriate buffer gas pressure, which may be different from that during the trapping and detecting periods, can improve the fragmentation and trapping efficiency of fragment ions in MS/MS experiments.

As a result of computer simulations, Fig. 1 shows the dependence of ion retention time on the initial phase ωt_0 of the rf voltage, for ions with mass $m = 1060$Dalton and two different He pressures 6.4×10^{-3}mbar (——) and 1.4×10^{-4}mbar (- - -). Although the curves are periodic with phase angle, only one period is shown. The calculation conditions are: trap geometry: $r_0 = 10$ mm, $z_0 = 0.707$ mm; rf frequency: $f = 0.781$ MHz; ion mass: $m = 1060$ Dalton; trapping parameter: $q_z = 0.103$; initial energy: $E_0 = 18$ eV; injection angle: $\theta = 11°$; initial phase of rf voltage: $\omega t_0 = 0.928 \times 2\pi$; initial position: $x_0 = 0$ mm, $z_0 = -0.707$ mm; He pressure: $P = 6.4 \times 10^{-3}$ mbar; time limit of calculation: $0 - 350\,\mu$s. It is clearly visible that ions can be trapped only in a very short time interval during a rf period. A higher pressure increases the ion trapping efficiency.

Experiments are performed in Bruker's ESQUIRE instrument with an electrospray ion source and a pulsed gas inlet system. A few peptide samples are measured, for example, Bradykinin, Cytochrome C and Leucine Enkephalin. The results demonstrate that the trapping efficiency can be enhanced without loss of the mass resolution by using a pulsed valve. Fig. 2 presents the doubly charged MH^{++} ion mass spectrum of Bradykinin ($m = 1060.2$ Dalton) and Fig. 3 the singly charged ion mass spectrum of Leucine Enkephalin (m= 555.6 Dalton). The He pressure is 1.4×10^{-4}mbar (lower peak) and the pulsed He gas pressure is 6.4×10^{-3}mbar (higher peak). With constant He pressure of 6.4×10^{-3}mbar, however, the mass resolution decreases (not shown in

Fig. 2 and Fig. 3).

With a higher He gas pressure in a pulsed mode, MS/MS spectrum of Bradykinin shows increased abundances of fragment ions.

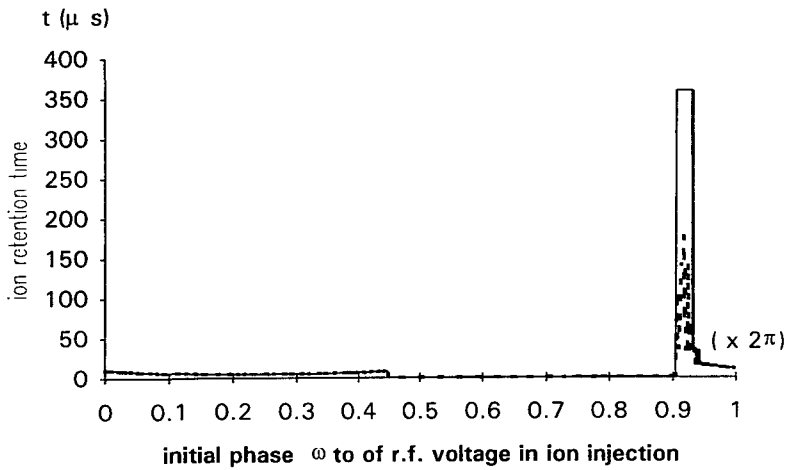

Fig. 1

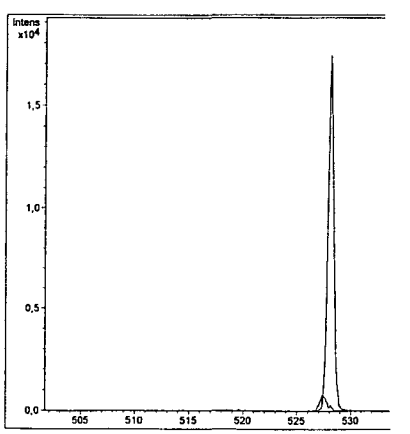

Fig. 2

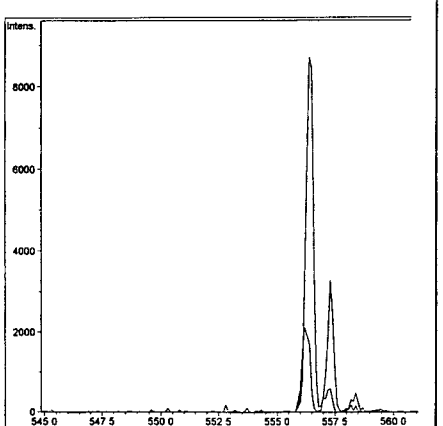

Fig. 3

Exciting Waveform Generation for Ion Traps

MICHAEL SCHUBERT · MARCUS NAGEL · YANG WANG · JOCHEN FRANZEN
Bruker-Franzen Analytik GmbH · Fahrenheitstraße 4 D – 28359 Bremen · Germany

For the mass selective collection and storage of ions in rf ion traps during ionization, dipolar excitation with special waveforms can be applied. The accumulation of ions with a selected *m/z*-value requires a narrow notch in the frequency distribution, otherwise ions of more than one *m/z*-value are stored.

It is the objective of this paper to compare the effects of two waveforms calculated by two different phase functions: The quadratic phase function used and preferred by MARSHALL et al., and a random phase function.

CHEN, WANG, RICCA, and MARSHALL proposed a phase-modulated Stored Waveform calculated by Inverse discrete FOURIER Transform (SWIFT) to generate a time-domain pulse for frequencies of preselected magnitude in the frequency-domain.

It is well-known by the work of these authors that the quadratic phase function solves best the problem of the dynamic range of the corresponding time-domain waveform. But this fact should not be overemphasized. Selecting a favorable random phase function and applying this favorable function repeatedly, the dynamic range problem can be solved sufficiently well.

The desired phase-modulated waveform pulse is calculated, by discrete inverse FOURIER transform, on a dedicated transputer board located inside the mass spectrometer. The waveform is stored in a separate memory and clocked out via a digitial-to-analog converter. The transmitted time-domain pulse is applied to the endcap electrode of the quistor.

The ions are generated by an external ion source and accumulated in the trap. Inside the trap, ions can be manipulated, isolated or fragmented and then mass selectively ejected towards an electron multiplier

When the gate is open for ion accumulation and ions enter the ion trap, the stored waveform pulse is clocked out to the endcap electrode. All ions except those of one *m/z*-value are ejected out of the trap by resonant excitation. In this way only desired ions are trapped and damped to the trap's center by the internal damping gas.

If the same favorable waveform pulse is used in subsequent experiments to eject ions of different *m/z* ratios, the RF amplitude of the ion trap has to be adjusted correspondingly. In each experiment the secular frequency of the desired ions must match the notch frequency of the waveform. — A calibration takes care of this adjustment.

A forable frequency spectrum for the stored waveform pulse could be easily imagined: The frequencies have constant amplitudes from 20 kHz to 500 kHz, the narrow notch starts at 151.4 kHz and ends at 154 3 kHz.

Fast FOURIER transform methods operate with discrete frequencies only. The length of the waveform pulse and the frequency differences are interconnected. In the experiences the frequency differences amount to $\Delta\nu$ = 976.6 Hz. The resulting time periode of the time-domain pulse is 1.024 ms. Four neighboring frequencies in the waveform spectrum are set to zero and form the notch.

The time-domain waveform pulses are calculated by discrete inverse Fast FOURIER Transform (FFT) by using the declared favorable frequency spectrum. Both phase functions, quadratic and random, are used. The resulting stored waveform pulse is reflected

43rd ASMS Conference on Mass Spectrometry and Allied Topics

about its time midpoint, equivalent to a time shift. The final time-domain waveform is normalized to the range of the digital-to-analog converter. For use during ionization, the individual waveform pulses are repeated as often as necessary. Apodization is not applied to single pulses, only the whole train of pulses is apodized.

The discrete Fast FOURIER Transform requires endless periodical repetition of the time-domain pulse to exactly reproduce the favorable frequency spectrum. In reality, this cannot be verified. The resulting frequency spectrum of a restricted train of pulses will differ from the original frequency spectrum.

The measured spectra with spectrum analyzer of the phase-modulated stored waveform with quadratic and random phase function differ in their spectral amplitudes by 6 dB. The somewhat lesser spectral amplitude of the random waveform pulse can be easily compensated for by higher amplification

In order to compare the results of quadratic and random phase modulation, a calibration gas is used. All mass-to-charge ratios from 50 u to 400 u are present. In the experiences, for example, the stored waveform pulses are used to isolate the ion with mass-to-charge ratio *m/z*=93 u.

First, the mass spectrum is acquired with a quadratic phased-modulated waveform pulse during the ionization time by exactly the same parameters. The RF-amplitude is set for isolation of ions with mass 93 u. It is interesting to note the raising intensity: The ratio of intensities of the original spectrum to the evaluated spectrum at mass 93 u is 1.8. This effect indicates that the space charge of all the ions in the full mass spectrum hinders the storage of further ions.

Application of the randomly modulated stored waveform, increased in amplitude to compensate for the lower spectral intensity, raises the abundance of the isolated ions of mass 93 u still more, by about 14% whereas all other ions are staying absent. The increase of roughly 14% from quadratic to random phase modulation is reproducible. This raise in intensity between quadratic and random phase modulation can only be explained by the incidental changes of frequencies with time.

In a following experiment, the ionization time is four times longer as usual. The intensity of the isolated ion is raising again with nearly the same factor. This factor is not just four times the intensity, indicating that space charge comes into effect. (If many ions are stored in the trap, the common electrical field cannot be ignored and the quistor is overloaded.) For much shorter ionization times, the proportionality of the ion intensity with ionization time has been verified.

For the selective storage of ions in quistor mass spectrometry with single mass resolution, a random phase-modulated stored waveform can be used with some advantage. The dynamic range and the spectral intensity of the waveform pulses are slightly lower as with quadratic phase modulation, but the storage efficiency is improved. The decrease in spectral intensity has to be compensated for by a slightly higher amplification. With otherwise exactly the same experimental conditions, about 14% more ions can be collected.

With random phase modulation, a single frequency is not just present during a short time period within the frequency sweep, as in the case of quadratic phase modulation. Unwanted ions are excited over longer periods of time, and are excited and ejected more selectively.

Ion Cloud Structure in a Quadrupole Ion Trap

*Gloria A. Bach, Efim A. Dynin, Nicholas J. Kirchner
Massively Parallel Instruments, Inc.

Introduction: We have simulated 1000 ions of three masses confined in a quadrupole ion trap. This work adds the explicit ion-ion repulsion force between each ion to the force on each ion from the Rf field for the three masses. We have quantified the existence of a shell structure consisting of mass separated layers. The spatial density of each layer is dependent upon q_z, damping gas pressure and the trap dimensions. The shell structure appears distinct when both effects of damping and explicit ion-ion repulsion are included in the calculation.

Theory: Calculations were performed on a desktop personal computer with an Intel 486 66 Mhz C.P.U. The analytical potential for the quadrupole ion trap was used, where the end cap electrodes are grounded and ϕ_O is the radio frequency voltage applied to the ring electrode. The potential field inside the trap, $\phi(r,z)$, is

$$\phi(r,z) = \frac{\phi_O}{2r_O^2}(r^2 - 2z^2) + \frac{\phi_O}{2} \qquad (1)$$

r and z in equation (1) are the distances of the ion from the center of the trap in cylindrical coordinate space. The ion / ion interaction force is calculated explicitly for each ion from the sum of all other ions in a given spatial range. The force is calculated from the equation $F = \frac{q_1 q_2}{4\pi\varepsilon_0 r^2}$. q_1 and q_2 are the coulomb charges on the two ions, r is the distance between the two ions, and ε_0 is the permittivity of free space. To speed up the calculation, a sorting algorithm was used to determine the relative closeness of all other ions to the ion of interest. All ions within a distance of 0.5 mm to the ion of interest were included in the ion / ion interaction force sum calculation.

Initial Conditions: 999 total ions were used in each calculation, 333 of mass 200, 300, and 400. Initial kinetic temperature of ions was 298 K, where individual ion temperatures were randomly chosen about a Boltzman distribution. Integration time step = 1×10^{-8} seconds. Collision gas was Helium, at a kinetic temperature of 298 K, with individual values randomly chosen about a Boltzman distribution. Collision probability was calculated using the Lengevin approximation, and collision time was assumed to be instantaneous relative to the integration time step. Starting radius for the ion cloud was 1 mm, where each ion was given a set of random starting coordinates such that the values of r and z for each ion fell between 0 and 1 mm. Initial entry of ions into the Rf field was randomized over the first Rf cycle by starting an equal number of ions into the trajectory loop during each time step of the first Rf cycle. The above initial conditions were stored to a file and re-used in each set of calculations.

Data Collection: Ion trajectories based on initial conditions were run for 1 millisecond before recording final positions. Data collection of final positions consisted of averaging the radial and axial position of each ion over a time period which included at least one cycle of secular motion for all masses. The chosen averaging time was 16 microseconds for the calculations done at 338 Volts, and 4 microseconds for those done at 1692 volts.

43rd ASMS Conference on Mass Spectrometry and Allied Topics

Conclusions: **Damping bath gas** causes the formation of a shell structure separated into mass layers in the quadrupole ion trap. **Ion / Ion interaction**, when combined with bath gas, causes the entire ion cloud to be shifted away from the center of the trap. More specifically, the ion cloud of lowest M/Z retains its shape and is shifted away from the center. The ion cloud of middle M/Z becomes compressed in shape, and its region of maximum density is shifted away from the center. The ion cloud of highest M/Z retains its shape and is shifted away from the center. **Higher effective potentials** cause a decrease in the effects of ion / ion interaction, because the force from the Rf field affects ion motion much more strongly than inter-ion coulomb forces. **In the limit of zero pressure** the shell structure disappears, and the effects of ion / ion interaction are minimized.

Histogram Plot; 338 Volts; Pressure = 1.5×10^{-2} Torr
(Number of ions within 0.01 mm increments at increasing distances from trap center)

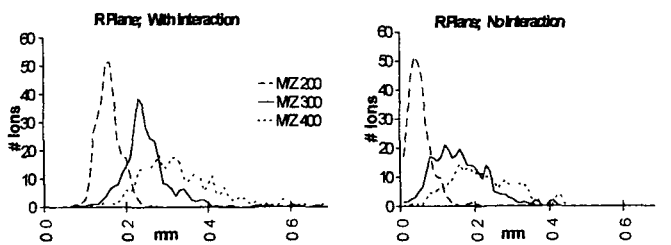

Position Scatter Plot; 338 Volts; Pressure = 1.5×10^{-2} Torr
(Z position vs R position for each ion)

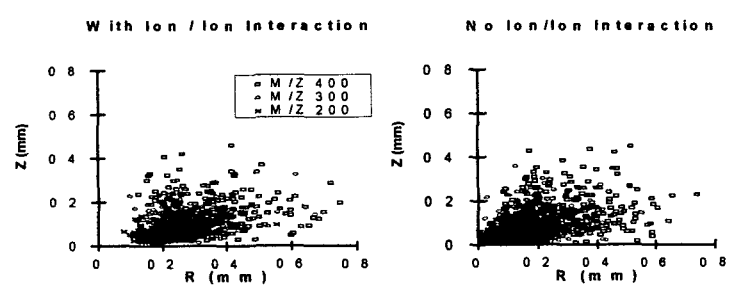

A Field-Portable Ion Trap for the Detection of Chemical Weapons Compounds

Palausky, M.A. , Lammert, S.A., Merriweather, R.
Oak Ridge National Laboratory, P.O. Box 2008, Oak Ridge, TN 37831-6120
Sarver, E.W. , Wasserman, M.B.
US Army ERDEC, AGP, MD 21010-5423

The pending ratification of the Chemical Weapons Convention Treaty imposes the almost immediate requirement of on-site inspections of chemical facilities worldwide. In support of this activity, the Defense Nuclear Agency has tasked Edgewood Research Development and Engineering Center (ERDEC) to develop a small, field portable mass spectrometer (the "Generic Detector") which is capable of unambiguous detection of chemical warfare agents and their associated precursors and by-products. Concerns by the chemical industry as to the disclosure of proprietary information necessitates the development of instruments which are specific only to the targeted compounds while remaining blind to proprietary compounds not covered by the treaty. Ion trap MS/MS, with its combination of high sensitivity and selectivity is uniquely suited for this role.

The Generic Detector is based on the Chemical and Biological Mass Spectrometer (CBMS) developed by Bruker-Franzen for the US Army to detect biological and chemical weapons in the battlefield. Analytical sampling inlets for heated direct injection, direct air sampling, thermal desorption and gas chromatography were added in order to accommodate a wider range of sample types. The Generic Detector ion trap mass spectrometer has been specifically designed to be a field portable mass spectrometer. It is small (75 x 43 x 35 cm), light (less than 45 kg) and operates on less than 500 watts of power at 24 V_{DC}. No gas cylinders are needed to operate the instrument because the Generic Detector has a unique electrode geometry and mass analysis scan that allows the instrument to be operated with air and not helium as the buffer gas as well as the gas chromatographic carrier gas. A summary schematic of these features is shown.

Chemical weapons precursors and by-products are typically more polar than the actual agent compounds and therefore analytically more challenging. In general, most of the compounds tested gave detectable responses for injected amounts in the low nanogram range. In addition, the response of the Generic Detector was linear over a range of injected amounts. These results are demonstrated in the calibration curves for 1,4-dithiane.

The GDMS gave a linear response for the compounds tested over ranges from (at the lower end) 0.025-25 ng up to 200 ng. Linearity was good (R > 0.97) for naphthalene, 1,4-dithiane, 2-diethylaminoethanethiol, and two of the phosphonates, DEMP and DEEP. Linearity of DMMP, trichloronitromethane and DIMP was lower, with R values of 0.96, 0.96 and 0.93, respectively. Detection limits for these compounds varied widely, from 0 1 to 35 ng; those for polar compounds were generally at least a factor of 10-100 greater than those for non-polar compounds. Although size considerations for a portable instrument have imposed limitations on the GDMS, in general, good analytical performance is obtained.

"The submitted manuscript has been authored by a contractor of the U.S. Government under contract No. DE-AC05-84OR21400. Accordingly, the U.S. Government retains a nonexclusive royalty-free license to publish or reproduce the published form of this contribution, or allow others to do so for U.S. Government purposes."

43rd ASMS Conference on Mass Spectrometry and Allied Topics

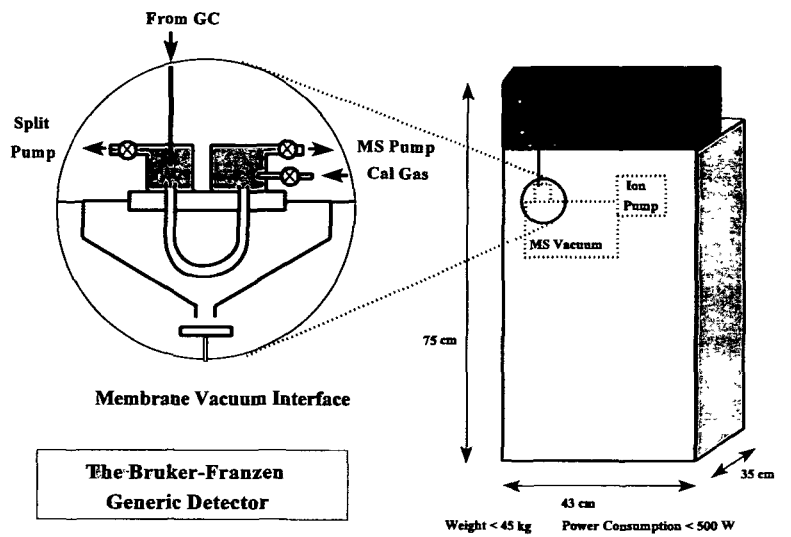

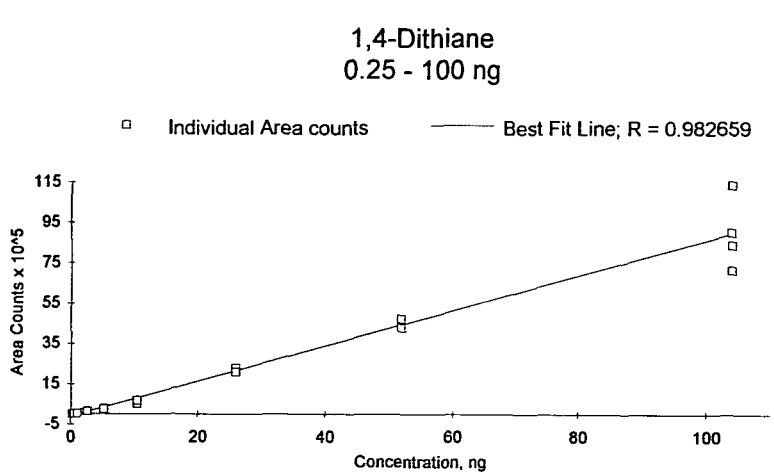

Ion Traps as Chemical Sensors

Kevin J. Hart
Chemical & Analytical Sciences Division
Oak Ridge National Laboratory
Oak Ridge, TN 37831-6120

Direct sampling ion trap mass spectrometers (DSITMS) have been developed or are in the process of being developed for monitoring of chemical components from a large number of sources including ground water wells, incinerator stacks, fugitive process emissions, automobile exhaust, explosives, chemical agents and illicit drugs [1]. With sufficient hardware and software support, automation of all aspects of sampling and ion trap operation is feasible. Thus, there is considerable potential for delivering a ***chemical sensor*** for a large range of organic compounds using ion trap mass spectrometers. Sensors are defined as a transducer with appropriate signal conditioning, computation and data transmission services [2]. Chemical sensors, of course, utilize transducers capable of measuring concentrations of chemical compounds.

The rationale behind using ion traps as the transducer in this scenario is based on the tremendous selectivity obtainable using selected reagent ion chemistry, mass spectrometry / mass spectrometry and/or MS^n and the very low detection limits (eg. sub-part-per billion) obtainable using these instruments. Significantly, many applications require the high selectivity and low detection limits the ion trap affords but can not support the personnel and financial requirements of an analytical laboratory equipped with a conventional mass spectrometer. In some cases, the limiting factor is the time scale in which final results must be logged and acted upon. One of the remaining hurdles for use of ion traps as chemical sensors is the development of a completely automated sampling, ionization, ion manipulation and data interpretation system. Another challenge in making ion traps a more effective detector for sensor applications is to reduce the overall size of the instrumentation which includes the vacuum chamber and all pumps, power supplies, electronics and computers.

The direct sampling interfaces developed at ORNL are an important step in achieving an automated ion trap system. These interfaces have been tested in a number of applications including, for example, incinerator stack monitoring. In one test, a volatile organic sampling train (VOST) was installed on a toxic waste incinerator. A sample stream, consisting of stack gas saturated with water, was pulled through a 100' heated transfer line to one of the field portable ion trap systems designed at ORNL. A heated, continuous air monitor constructed of stainless steel components served as the sampling interface. A T-connector was installed at the VOST / transfer line interface so a Tedlar bag containing VOC gas standards could be connected. The instrument response for 1000, 200 and 50 ppbv chloroform is shown in Figure 1. The exact split ratio between stack gas and standard is unknown. Consequently, the concentrations shown represent upper limits. The data shown do demonstrate the ability of the direct sampling ion traps to monitor VOC's in a real world process stream. Further testing of the ion trap as a VOC continuous emissions monitor is anticipated.

Other advances that will contribute to making an ion trap based chemical sensor a reality include automated gain control [3] and the ability to perform selective ion accumulation and broadband excitation using techniques such as filtered noise field [4]. These techniques will be used to address problems such as space charge and frequency shifts that can reduce the performance of the ion trap. One of the areas of ion trap based

sensor development that is lagging is the development of automated, customizable instrument control and data interpretation software. To alleviate this problem, an instrument control and data analysis system is being developed in LabVIEW, a popular, icon-based data acquisition and data analysis environment [5]. Thus, the ion trap, given a number of sampling, ionization, ion manipulation and interpretation parameters, will be able to output a series of voltages or numbers corresponding to the concentrations of a suite of analytes in a continuous monitoring application. These voltages or numbers can, of course, be used to trip alarms or displayed to the operator. The addition of advanced diagnostics with a number of performance standards to ensure that the ion trap is operating properly will provide a robust chemical sensor.

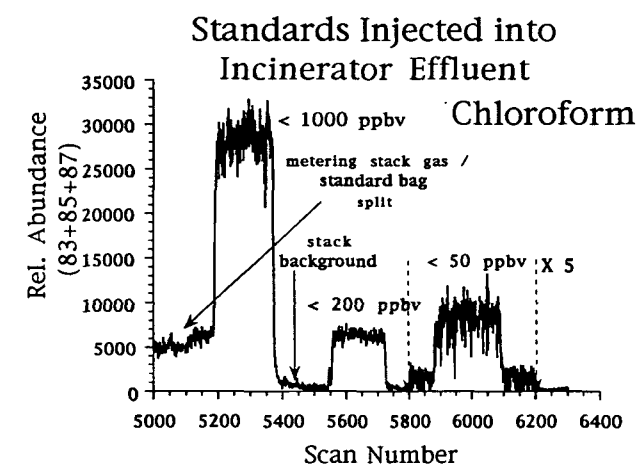

Figure 1: Summed RIC for m/z 83, 85 and 87 obtained for 3 concentrations of VOC standard metered into incinerator stack effluent.

References:
1. Wise, M.B., et. al., Spectroscopy, 1993, 8(5), p. 14.
2. Johnson, G.W., "LabVIEW Graphical Programming, Practical Applications in Instrumentation and Control", McGraw Hill, New York, 1994, p. 44.
3. Stafford, G.C., et. al., Proc. 35th ASMS Conference, Denver, CO, 1987, p. 775.
4. Kelley, P., Proc. 41st ASMS Conference,Chicago, IL, 1993, p. 453a.
5. National Instruments, Austin, TX.

The incinerator stack work was supported by the TSCA Incinerator Division, K-25 Site, Oak Ridge. This work was also supported by the U.S. Department of Energy, under contract DE-AC05-85OR21400 with Martin Marietta Energy Systems. Special thanks to Jim Dunn, TSCA Incinerator Division and Marc Wise, Mike Guerin, Rob Smith and Cyril Thompson, C&ASD, for their contributions to DSITMS and the incinerator work.

Electron Capture by Ions in a Quadrupole Ion Trap

Richard W. Vachet, Steven D. Clark, and Gary L. Glish
Department of Chemistry, University of North Carolina, Chapel Hill 27599-3290

Introduction: Electron capture has been implemented effectively as a selective ionization technique for various compounds. It has also been used to study physical apsects of ions. However, since electrons are not trapped under normal conditions in the quadrupole ion trap, reactions involving electron capture have not been investigated thoroughly using this instrument.

Electron capture by ions has been investigated as a function of several operating parameters. These parameters include bath gas pressure, time, type of ion, and number of ions. Electron capture will have implications on various experiments performed in the quadrupole ion trap. In fact the capture of electrons by ions may have analytical applications.

Experimental: Experiments were performed using a modified Finnigan MAT ITMS. Ions were generated by EI. The beam of electrons that served as the neutralization pulse was produced from the same filament used to generate ions. Samples were introduced via a pulsed valve. Since neutrals cannot be directly measured, three experiments were used to determine the extent of neutralization. One experiment served as the main experiment where the ions were generated and then neutralized with a second electron pulse after the unionized sample was pumped away. The second experiment provided the amount of ions generated during the first electron pulse and did not have a neutralization pulse. A third experiment had only the neutralization pulse. The third experiment provided the number of ions generated during the neutralization pulse. The extent of neutralization was determined by adding the intensities of ions from the second and third experiments and subtracting from this the intensity from the first experiment. The percent neutralized could then be calculated by taking this value and comparing it to the intensity from the second experiment.

Results and Discussion: Since electrons cannot be trapped under standard conditions in a quadrupole ion trap, the electrons that are captured are likely secondary electrons produced during the electron beam's interaction with background gases. Low energy primary electrons could also be produced by collisions with background gases or interactions with the RF field upon entering the trap. Figure 1 shows the percent neutralization of the radical molecular cation of dioxane with respect to neutralization pulse length at different pressures of Helium. This graph shows that the pressure of the background has plays a key role in the amount of neutralization. The trend on this graph seems to follow the equation: $I_n = I_o (1-e^{-\sigma N l})$ where I_n is the number of ions neutralized, I_o is the initial number of ions, σ is an electron capture cross section, N is the number of electrons, and l is the path length. If N and l are held constant then ions with different cross sections should be neutralized to different extents. Protonated dioxane which is an even electron species is neutralized to a smaller extent than the odd electron molecular ion of dioxane for a given neutralization period. It should be less likely for an even electron species to capture an electron and become a neutral radical than for a radical cation to capture an electron and become an even electron neutral. To see if smaller differences in electron capture cross sections could be noticed, N- butylbenzene was used. It has a lower neutralization percentage for a given neutralization period. This is attributed to the higher energy of N- butylbenzene's LUMO. Figure 2 shows the comparison of dioxane, protonated dioxane, and N-butylbenzene at a pressure of 1×10^{-3} Torr. It was also seen that varying the number of ions initially present did not change the neutralization percentage. This is expected from the equation above , where changes in I_o should not change the ratio of I_n / I_o.

Conclusions: Positive ions in a quadrupole ion trap capture electrons upon bombardment with an electron beam. The increases in neutralization follow increases in background gas pressure. This suggests that the low energy electrons needed are likely produced during interactions of the primary beam of electrons with background gases. The neutralization follows a typical Beer- Lambert type trend. These results indicate that increases in ionization times should not result in linear increases in ion intensity since some ions formed early in the ionization pulse will subsequently be neutralized. Also different ions show varying extents of neutralization, presumably due to differences in electron capture cross sections. Radical cations are neutralized to a greater extent than are their even electron counterparts. If this technique is sensitive enough to minor changes in electron capture cross sections, it may be useful as a means to differentiate ions, perhaps even isomers.

Figure 1

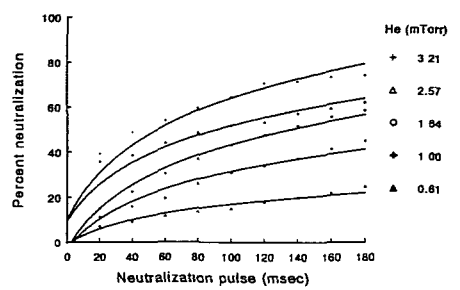

Figure 2

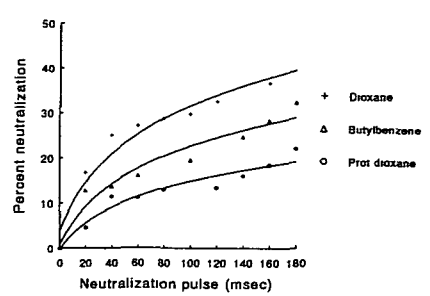

EXPERIMENTAL STUDIES OF SPACE CHARGE EFFECTS IN A QUADRUPOLE ION TRAP MASS SPECTROMETER

Barrie Ann Shaffer, Joe Karnicky, and S. E. Buttrill, Jr.
Varian Associates - Ginzton Research Center
3075 Hansen Way, Palo Alto, CA 94304-1025

In an rf quadrupole ion trap, ions experience an effective potential which is the sum of their coulombic interaction with other trapped ions and the trapping pseudopotential. We have experimentally probed the potential experienced by trapped ions by precisely measuring their secular frequencies as a function of the trapped ion population.

Isolated ion ejection spectra were observed by using an ion selection waveform to store a single ion mass before a resonant ion ejection process. For examining the effects of clouds of ions of various masses on one another we used ion selection waveforms to store multiple ion masses and observed the ion ejection profiles for each. These experiments were carried out using customized software and a standard Varian Saturn 3 GC/MS equipped with a Wave~Board. All experiments used FC-43 as the sample under conditions where there was no detectable broadening of the peaks in the mass spectrum.

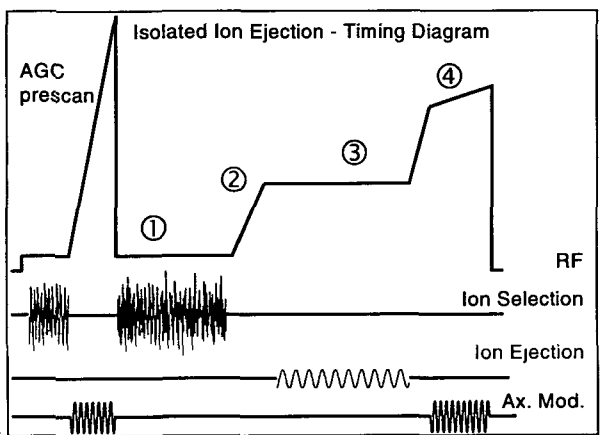

Figure 1.

The scan function for isolated ion ejection spectra is shown in Figure 1. Although an AGC prescan is provided by the software, in all of the experiments described here, the maximum ionization time and sample pressure were adjusted to ensure a constant ionization time. During ionization and for a short time thereafter (1) a tailored waveform is applied to the ion trap endcaps to accomplish selective ion accumulation [1]. The storage level is then raised (2) to establish the desired q_z value for the ejection spectrum. A single frequency waveform is used (3) for the ion ejection, then a narrow mass range scan (4) measures the number of ions remaining. The ejection profile is defined as the percent ion ejection as a function of applied frequency. The amplitude of the single frequency ejection waveform is adjusted to produce 70-90% ejection of the ion mass of interest. Data points are recorded across the ejection profile at 100 Hz intervals. The centroid of the profile is taken as the ejection frequency.

Different behavior is observed for a single mass isolated in the trap compared to a mass stored in the presence of ions of different mass. For a single isolated mass there is little shift in the ejection frequency as the number of stored ions is increased, and the amplitude necessary for ejection changes only slightly. When two different masses are stored, the ejection profile

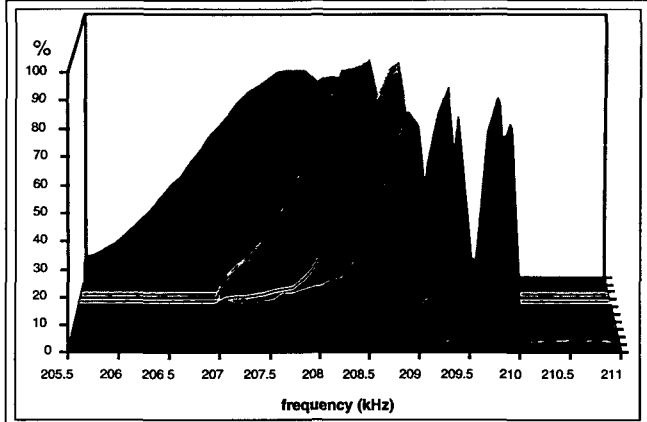

Figure 2. Ejection profile of m/z 364 in the presence of increasing amounts of m/z 264.

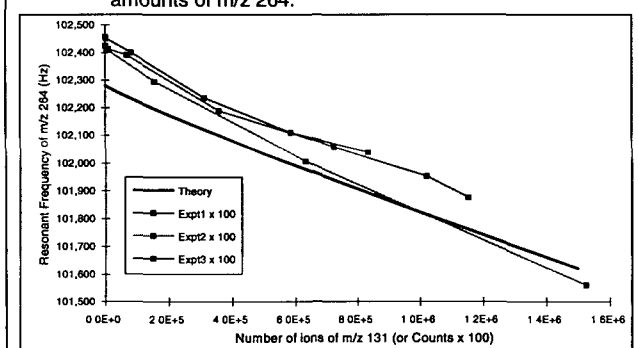

Figure 3. Comparison of predicted and experimental frequencies for m/z 264 in the presence of m/z 131

broadens and shifts to lower frequencies, as illustrated in Figure 2. The amplitude required to produce the ejection profiles of m/z 364 in Figure 2 increased from 0.25 Vpp to 2.40 Vpp as the amount of m/z 264 increased from 7 to 14,000 counts. The amount of m/z 364 was held constant at about 10,000 counts.

The potential due to an ion cloud of a single mass at equilibrium can be calculated using the approach of Guan and Marshall [2]. The potential seen by a high mass ion in the presence of a cloud of low mass ions is the sum of the psuedopotential for the heavy ion and the space charge potential of the light ions. The motion of the heavy ion in this potential may be integrated numerically to obtain the period of its secular motion. The calculated secular frequency for m/z 264 in the presence of increasing numbers of m/z 131 ions is shown as the heavy smooth line in Figure 3. Three sets of experimental data are plotted for comparison. The decrease in ejection frequency for m/z 264 with increasing numbers of m/z 131 and the slight upward curvature of the data are both reproduced by the model.

[1]. S. E. Buttrill, Jr. , B. A. Shaffer, J. Karnicky and J. T. Arnold, Proc. 40th ASMS Conf. on Mass Spectrometry and Allied Topics, May 31-June 5, 1992 pp. 1015-1016.
B. A. Shaffer, J. Karnicky, and S. E. Buttrill, Jr., Proc. 41st ASMS Conf. on Mass Spectrometry and Allied Topics, May 31-June 4, 1993 pp.802a-b.
[2]. S. H. Guan and A. G. Marshall, J. Am. Soc. Mass Spectrom., **5** (1994) 64-71.

ELECTROSPRAY / ION TRAP MS^n FOR STRUCTURE ELUCIDATION OF ANIONICS

Robert J. Strife, The Procter & Gamble Co, Miami Valley Laboratories,
P.O. Box 538707, Cincinnati, OH 45253-8707
&
Jae Schwartz, Mark Bier and Joe Zhou, Finnigan-MAT, 355 River Oaks Pkwy.
San Jose CA 95134

Electrospray ionization (ESI) is particularly useful in the analysis of aqueous or mixed organic / aqueous samples. Consumer products (CP's) are often formulated or used in the aqueous phase, and many of their components are amenable to electrospray analysis. Transformation of key components in CP's to other organic structures is a concern in many types of studies like environmental fate, shelf stability and metabolism / toxicology.

The combination of the ion trap with ESI provides several distinct advantages over linear arrays of quadrupoles for structure elucidation of these transformed products including: 1) ion integration capabilities, ideal for a "dim" ion source like ESI; 2) sequential product ion experiments in the time domain (MS^n) so that ions may be refragmented and probed for their organic structure; 3) efficient mass selective storage, via "notched" wave forms, for isolating a component from a mixture and 4) very efficient observed CID efficiencies.

EXPERIMENTAL -- Pure standards were diluted to 1-2 ng/µL for analysis using a prototype of the Finnigan-MAT LCQ. Samples were infused through the electrospray device at 220°C at a flow of 5 µL/min. Ion injection periods from 1 ms to 500 ms were used, with longer times being applied at higher stages of MS^n. Mass selective storage was accomplished by adjusting the q_z value of ions of the desired m/z value to 0.83. A notched wave form of variable amplitude was applied to eject ions of unwanted m/z values. CID was carried out at q_z of the parent ion of 0.2 - 0.3.

RESULTS & DISCUSSION -- C_{10}-linear alkyl sulfonate (C_{10}LAS) is a common component of detergent products eventually discharged into the environment. It is readily obtained as a pure compound, and possesses a "permanently" charged center in view of its high pk_a. We use it routinely to benchmark ESI performance. MS/MS (parent ion 297^-) using an ESI / triple quadrupole instrument (center-of-mass collision energy ~ 5 V), yielded predominantly m/z 183 (charge-remote elimination of octane) and 184 (loss of octyl radical, a "rule violation"). Less intense ions are observed at m/z 80 (sulfite radical anion) and 119.

MS^n analysis (Fig. 1) using the prototype LCQ instrument not only revealed the relationship between these ions but also generated other useful fingerprints for the fragmentation of this compound. Ions of m/z 184 were found to fragment only by loss of H radical to m/z 183. The ion of m/z 119 came from loss of 64 u (SO_2) from m/z 183 (**MS^3**), presumably by rearrangement to the 3-ethenyl phenoxide anion. This anion fragmented by two pathways (**MS^4**): 1) loss of CO with ring contraction to the aromatic ethenyl cylcopentadienyl anion (m/z 91) and 2) loss of acetylene to the phenoxide anion, m/z 93. When isolated and refragmented (**MS^5**), these anions collapsed by loss of acetylene or CO respectively to the aromatic cyclopentadienyl anion (m/z 65). Thus, a characteristic pattern is established for C_{10}LAS, useful for

investigating products of biodegradation (e.g., beta-oxidation of the alkyl chain). We then reapplied this approach to an aromatic polyphenol and generated an **MS^5** fragmentation map. The structure of an isolated impurity was investigated (**MS^6**) and a specific modification of an A-ring hydroxyl to an O-hydroxyethyl moiety was deduced. Furthermore, a second impurity of relatively high molecular weight was isolated ($[M-H]^-$ anion at m/z 579). MS/MS yielded mainly m/z 329 and 273. The ESI / Ion Trap combination allowed refragmentation of these ions (**MS^5**) and a partial structure of the impurity was deduced.

Finally, the LC/MS and LC/MS/MS sensitivity was benchmarked with C_{10}LAS and the prototype LCQ was found to be at least a factor of 20 (conservative estimate) more sensitive in the full-scan MS/MS mode than the ESI / triple quadrupole system (Fig 2). The product ion spectrum showed the principal fragments at m/z 183 and 184 at this low level (20 pg) of C_{10}LAS injected.

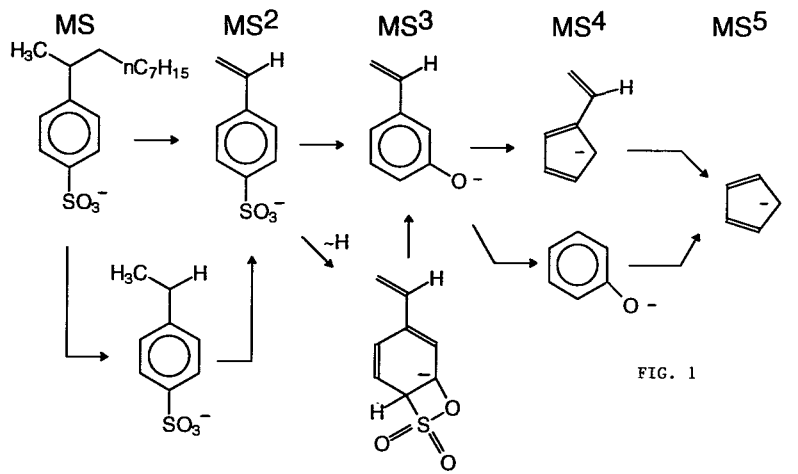

FIG. 1

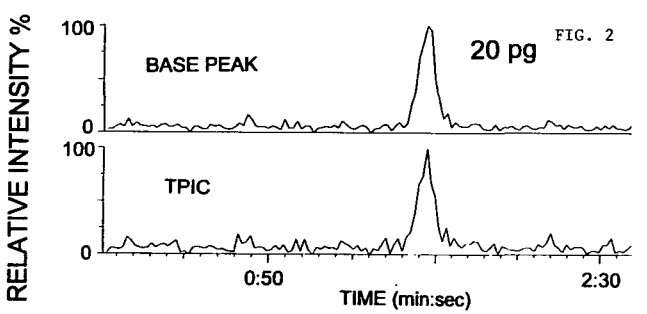

FIG. 2

Technological Aspects of a New LC/MS^n Quadrupole Ion Trap

Jae C. Schwartz, Mark E. Bier, Dennis M. Taylor, Joe Zhou,
John E.P. Syka, Mike S. James and George C. Stafford
Finnigan MAT, 355 River Oaks Pkwy, San Jose, CA 95134-1991

Inroduction: Most of the developments involving the quadrupole ion trap including ion injection, mass range extension, high resolution, and MS^n capabilities, have been performed on commercially available systems which were designed in 1982 and have pushed the existing hardware and software to their limits. A new ion trap system architecture has been developed which provides the utmost in versatility, programmability, and expandability. This architecture, incorporating a unique electronic and firmware design, has proven to be an ideal system for quadrupole ion trap instrument development. This system architecture provides the foundation for a new generation of commercial quadrupole ion trap products including a new LC/MS^n instrument shown in Figure 1 as well as a GC instrument. Innovations for implementing and putting into practice most of the latest developments into these commercial products were made using this novel system architecture .

Electronics: The digital electronics consists of an embedded 486 (or higher) microprocessor, acquisition and control digital signal processor (DSP) boards, two dual channel digital synthesizers (DDS), an arbitrary waveform generator, serial, IEEE, and ethernet communication boards. The analog circuitry includes a high stability RF amplifier, octopole RF amplifier, DC lens supplies, auxiliary and waveform amplifiers, electrometer, and main power supplies.

Firmware: An embedded Ion Trap instrument Control Language (ITCL) allows real time adjustment of instrument and scan function parameters and allows programming of experiments.

Operating Parameters: In developing the commercial quadrupole ion trap instruments, this powerful combination of hardware and firmware allowed in depth studies and therefore optimization of many fundamental ion trap parameters. In particular, the choice of operating parameters such as RF frequency, scan rate, resonance ejection **q** and amplitude, He pressure, and ring electrode r_0 have been studied both empirically and theoretically, in order to achieve the desired mass range of 2000 amu, maintain unit resolution throughout the mass range, and scan at 5555 amu/sec or faster. The information gained in these studies has also provided insight into how to best implement higher resolution scans. Automated experiments were performed and multidimensional data were acquired covering the data space of resonance ejection amplitude vs. resonance ejection **q** vs. peak width at a variety of fixed combinations of pressure, scan rate, r_0, and RF frequency. By choosing the optimum resonance ejection amplitude for each resonance ejection **q** the data can be simplified to a more informative format as in the example shown in Figures 2. This data shows the effects of scan rate on peak width vs. resonance ejection **q** at the specified values of the other parameters. Theoretical considerations in conjunction with these data suggest that the optimum **q** value for resonance ejection is at a point which maximizes frequency dispersion while keeping scattering effects minimized. The frequency dispersion is given in Equation 1. The theoretical resonance ejection voltage required to eject ions at a constant rate, k, at a constant **q**, neglecting He effects, is given by Equation 2 which indicates a linear relationship with mass and is experimentally demonstrated in Figure 3. A lower RF frequency of 760 Khz and a reduced r_0 of .707 cm can be used with minimum reduction of resolution and space charge limit, but yields a higher mass range.

Scan Functions: The control architecture allows for automated adjustment of the ion trap scan function for performing fully automated Full Scan MS, SIM, SRM, MS^n and higher resolution scans.

Results and Conclusions: A new quadrupole ion trap system architecture has been developed which is ideal for ion trap research and development. This architecture serves as the foundation for new commercial LC and GC MS^n quadrupole ion trap products. The combination of the electronics, firmware (ITCL), choice of operating parameters and scan function design result in many instrument capabilities

including, unit mass resolution throughout the 2000 m/z mass range (Figure 4), higher resolution scans (Figure 5), fully automatic MS^n, SIM, SRM, Zoom Scans, unit resolution isolation up to m/z 1200, single m/z or broad band activation, charge state identification, data dependent scanning and more!

$$\left.\frac{\partial f}{\partial m}\right|_{q_{eject}} = \frac{\omega}{4\pi}\left(\frac{d\beta}{dq}\right)_{q_{eject}} \frac{q_{eject}}{m}$$

Equation 1

$$V_{res} = \frac{k m \omega_0 z_0^2 W_{q_{res}}}{(sum\ C)_{q_{res}}}$$

Equation 2

LC-MS^n Quadrupole Ion Trap

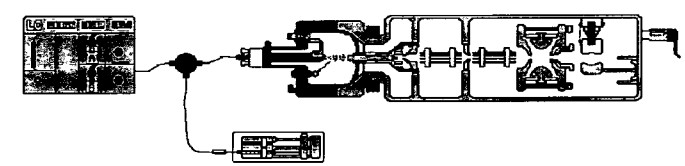

Figure 1

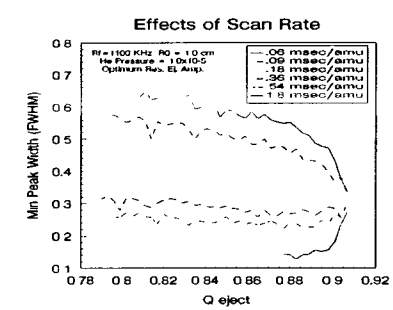

Figure 2

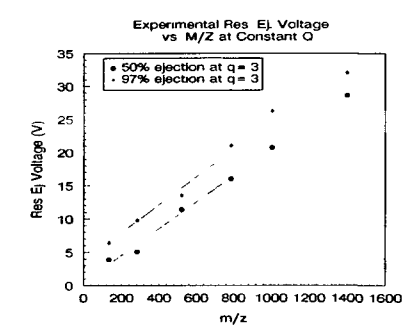

Figure 3

Full Scan Resolution

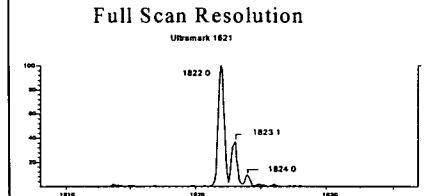

Figure 4

Zoom Scan Resolution

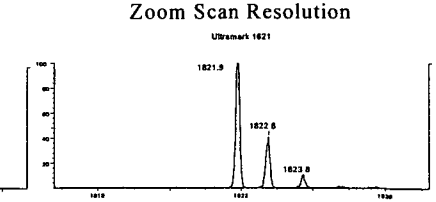

Figure 5

Novel Technologies and Enhanced Features for GC/MS/MS

Eric K. Johnson, Jae C. Schwartz, Dennis M. Taylor,
Mark E. Bier, John D. Ragsdale
Finnigan Corporation, 355 River Oaks Parkway, San Jose, CA 95134

Over the past ten years, much research and development has been devoted to the use of the quadrupole ion trap as a mass analyzer for analytical GC/MS and GC/MS/MS. These devices have principally used internal ionization with a pulsed electron ionization event, followed by ion ejection and detection with a continuous dynode electron multiplier. Although well developed for quantitative target compound analyses where the lowest limit of detection is required, these systems have yet to be fully utilized in some general applications where quadrupole mass filter technology remains dominant.

A novel device has been designed and constructed to test the practical performance of a combination of these two mass spectrometer systems, specific for gas chromatography detection. A conventional high energy electron ion source, a quadrupole ion trap mass analyzer operated in the mass selective instability with resonance ejection mode, and an off-axis post-acceleration dynode detector have been purposefully integrated with a modern instrument control architecture. A schematic of this architecture is represented in Figure 1.

With external ionization, ions are created outside the ion trap and then injected into the mass analyzer, where the analyte neutral population is dramatically reduced With a much lower probability of ion-molecule reactions, the resultant mass spectrum is virtually unaffected by increasing analyte concentration, producing the "classical" spectrum seen on conventional quadrupole filter mass spectrometers. An example of this effect is shown on Figures 2-4 The removal of this "self-protonation" process has been demonstrated for many other susceptible compound classes such as alcohols and esters.

Using this hybrid system, we have determined the operating conditions for the use of external ionization with a quadrupole ion trap that enables high efficiency ion storage and mass analysis over a 10-1000 dalton mass range in both MS and MS/MS modes. A novel technique to optimize the pseudopotential energy well of the quadrupole ion trap during ion injection, has resulted in the ability to quantitatively adjust the ion storage efficiency with increasing mass. The resultant ion ratios have proven to meet, and in many cases exceed the analytical quality of mass spectra derived using a quadrupole mass filter.

An example of this performance is demonstrated by the comparison of the EI spectra of straight chain hydrocarbons (Figure 5) with traditional quadrupole filter spectra (Figure 6). Standard hydrocarbon spectra with molecular ions present cannot be obtained with internal ionization traps It is this type of phenomena, combined with unwanted ion-molecule reactions that have prevented the older technology from routine qualitative unknown analyses. These problems are significantly addressed by the use of ion injection.

The use of resonance isolation and excitation to perform MS/MS and SRM experiments have been successfully demonstrated with this system. All modes, including full-scan and SIM exhibit a surprising increase in dynamic range and ion signal strengths explained in part, by the post-acceleration dynode detector. A further improvement to the limit of detection has been demonstrated by the sequential gating of the electron beam, post-injection, to reduce neutral noise. Combined with high pressure chemical ionization, the electron capture negative ion mode can surpass electron ionization results.

In summary, the data presented here demonstrate how external ionization and post-acceleration dynode detection, used in series with the quadrupole ion trap, have significantly improved the mass spectral performance compared with older methods of ion trap operation.

Figure 1 Externally Ionized Ion Trap

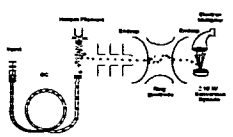

Figure 2 Triazines
Internal Ionization Trap

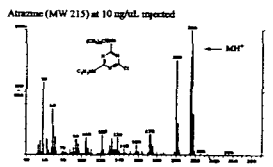

Figure 3 Triazines
External IonizationTrap

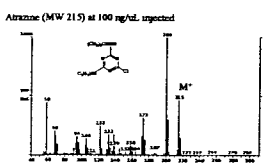

Figure 4 Triazines
Triple Stage Quadrupole

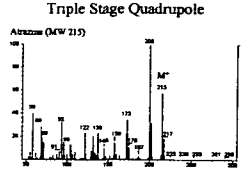

Figure 5 Normal Alkane
External Ionization Trap

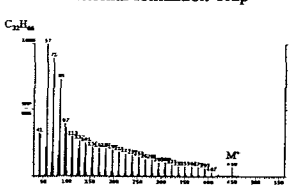

Figure 6 Normal Alkane
Triple Stage Quadrupole

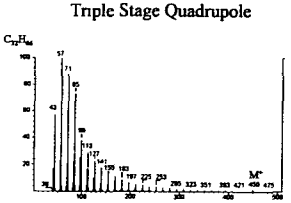

Quadrupole Ion Trap Control Language - Power in the Hands of Researchers

Joe Zhou and Jae Schwartz
Finnigan MAT, San Jose, CA 95134

Technical advances of the quadrupole ion trap during the last few years have made it a potentially powerful analytical instrument. Until now, however, software control of the device is still largely based on the old method developed over ten years ago. That is, by constructing scan functions through a series of scan descriptor tables. This method lacks the ability of building scan functions parametrically, *i.e.*, as a function of other parameters and also lacks infrastructures for general programmability, such as real-time decision making and execution flow control. Therefore, newer and more flexible concepts of ion trap control are needed. We developed an innovative technique, called the Ion Trap Control Language (ITCL), to overcome those deficiencies. This language was not only developed for ion trap research but also used as the basis for controlling Finnigan's new commercial ion trap products, *i.e.*, LCQ™ and GCQ™.

At the core of the digital control system are an embedded Intel 486 processor (running the pSOS real-time operating system), two digital signal processors (one dedicated for device control and scanning; the other for data acquisition and processing), and an arbitrary waveform signal generation board. The embedded real-time system communicates with the host computer (a Pentium-based PC with Windows NT operating system) through the Ethernet connection. Several real-time tasks, running on top of the pSOS operating system, are responsible for instrument operations. At the center of the control is the ITCL This language is the window (or interface) through which all ion trap mass spectrometer activities are controlled. It consists of two major tasks: an ITCL compiler task and an ITCL executor task. The compiler takes ITCL programs in ASCII text form as input and compiles them into an executable form. The compiled code is then passed to the executor for instrument control.

The Ion Trap Control Language is a procedural language that is syntactically similar to the popular computer programming language C It has some of the basic programming constructs as any computer language does; it also has system built-in variables and functions that can be used to control ion trap activities. Some of the key features are:

Flow Control Structures. ITCL provides basic constructs for modification of execution flow, such as 'if-else' statement for branching, 'while' loop for repetition, and 'break' statement for jump.

Variable and Function: All ion trap controls are performed through variable access and/or function calls. ITCL provides system built-in variables and functions for basic ion trap operations, such as for scan function creation, for scan execution, for data acquisition, and for data feedback. Users can define and access their own variables and functions as well.

Operators: The language has built-in operators for assignment (*e.g.*, =, +=, -=, *=, /=), arithmetic (*e.g.*, +, -, *, /), relational comparison (*e.g.*, <, >, <=, >=, ==, !=), logical relation (*e.g.*, ||, &&), and logical computation (*e.g.*, |, &).

Virtual Devices: All hardware components (*e.g.*, RF amplitude, DC voltage, *etc.*) that need to be controlled during a scan are treated the same and programmed in a similar fashion. Each device is assigned a unique numeric ID (fully configurable); no knowledge or distinction is made in order to create (through the scan matrix as will be described below) scan functions for a particular device.

Scan Matrix: This is an ITCL construct that is used as the building block to create scan functions for each virtual device. Description of the scan function of each device can be either independent of each other or linked by time events. All ion trap control activities are programmed through this mechanism. One powerful feature of defining scanning functions in this manner is that the scan description created is totally parametric, *i.e.*, can be a function of any ITCL variable

Real-time Data Feedback: Spectral feedbacks, such as the width, mass, or the height of a peak, calculated by the acquisition DSP are readily accessible through system variables or functions. This, in combination with the scan matrix, allows rapid data-dependent modifications of ion trap scan parameters.

Tailored Waveform Calculation: ITCL has the system built-in functions that are used to setup and to calculate arbitrary waveforms with any given number of frequency notches.

Math Calculation: System functions are provided by the language for frequently used math operations (*e.g.*, log, exp, sin, sqrt, *etc.*), and ion trap related calculations (*e.g.*, frequency to q conversion, q to beta conversion, Wronskian *etc.*).

Experiment Data Export: ITCL provides elements to export any experimental data of interest to the host computer numerically or graphically. Any experimental data of interest can be programmed to be plotted, in real-time, through a graph program provided on the host computer.

During the development of Finnigan's latest ion trap systems, the LCQ™ and GCQ™, many of the instrument parameters have been studied for optimum instrument operating conditions ITCL has proven to be a very powerful tool to accomplish this task. Experiments that normally require weeks or months were reduced to hours or days. Advanced scan capabilities of the system, such as data-dependent scans, are also programmed and controlled through ITCL procedures. The concept of achieving ion trap control through a procedural language, such as the Ion Trap Control Language, proves to be very powerful and provides a solid foundation upon which further ion trap research and development can be carried out.

Ion Optics and Design Considerations for a New LC/Quadrupole Ion Trap

Mark E. Bier*, Jae C. Schwartz, Joe Zhou, Dennis Taylor,
John Syka, Mike James, Bill Fies, and George Stafford
Finnigan Corporation, 335 River Oaks Parkway, San Jose, CA 95134-1991

We have coupled an atmospheric pressure ionization source (ESI/APCI) to a high performance quadrupole ion trap mass spectrometer (Figure **1**). The design is compact with the ion beam traveling less than 20 cm from the end of the heated capillary to the detector. The transfer optics, analyzer and electron multiplier are easily accessible by a removable top cover which includes a unique baffle for differential pumping. The rear chamber of the three chamber manifold is maintained at 1.5 X10e-5 Torr(uncorrected) by a unique dual stage turbo molecular pump. The mass range of the instrument was extended to M_{max}=2000Da. by reducing r_o to 7 mm, decreasing the main Rf frequency to 760 kHz, and by resonantly ejecting ions at a q_{eject}=0.83.

Several possibilities exist for gating ions into the ion trap. We have selected to gate ions using the tube lens. Positive ions are stopped by applying ca -140V to the tube lens. Tube lens/CAD is possible in this region. The skimmer lens is also a possible gating element but requires isolation from ground and an additional power supply. Gating with the interoctopole lens causes octopole 1 to trap ions. We transfer ions to the ion trap by using two short octopoles. We use octopoles because they are ion bunchers, especially at high pressures. We use two octopoles because of the need to differentially pump the system. The interoctopole lens serves three functions. One, to transfer ions into octopole 2 from octopole 1; two, to act as a differential pumping barrier; and three, to act as a potential barrier to charged particles that are produced in API sources even with an off-axis heated capillary. These charged particles cause noise spikes at the detector. We discovered that by placing +300 volts on the exit lens of the trap that this noise can be essentially eliminated (Figure **2**). For example, the ESI signal from cocaine $(M+H)^+$ was buried in noise **2a** with the exit lens=0V while **2b** shows a noise free spectrum. Placing several hundred volts on the interoctopole lens sufficiently reduces this noise during the mass analysis portion of the scan function. Once octopole 2 transfers ions directly into the trap, the Rf amplitude of both octopoles is switched off to avoid inducing Rf voltages onto the entrance end cap. Injected ions require helium pressures of ca. 1 mTorr for efficient ion trapping as well as an ion Rf level that is optimum. (Figure **3**). We calculate the optimum injection Rf level for trapping. We have found that if the exit optics are not designed properly the mass spectra may show mass discrimination. We have designed the exit optics with an off axis detector to respond equally to both low and 2000Da ions of high kinetic energy (e.g. 2000Da, 4keV)

Multiple reaction monitoring (MRM) of 10 pg reserpine shows that more than one reaction can be monitored with little loss in the ion trap duty cycle (scan out time is ca. 10 ms). Summing more than one ion current gives improved signal response and thus lowers detection limits. The capillary LC data shows MS/MS of 442.3^{+2} from 7.8 femtomoles of RVYVHPI (Figure **4**) (standard mix provided by Michrom Corp). The 10 fmole level at which this work was conducted is supported by the apparent loss of the two larger peptides of lessor abundance. At this low level, a large portion of these peptides may have adsorbed to a surface.

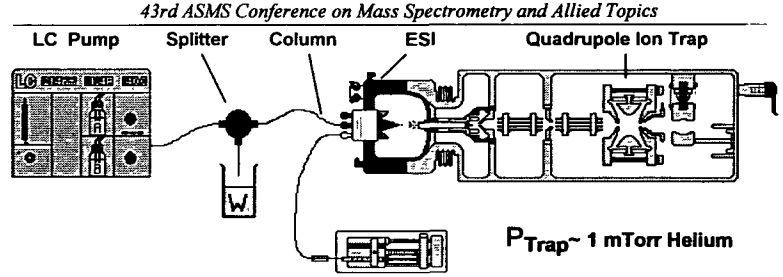

Figure 1

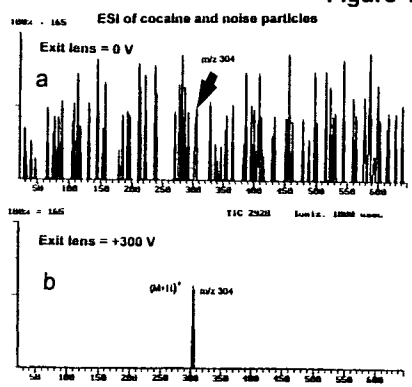

Figure 2

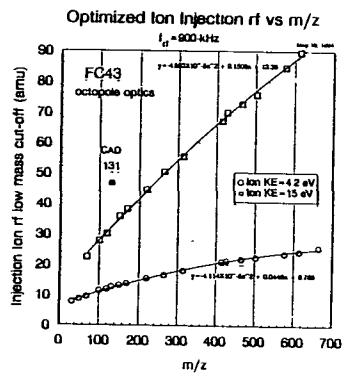

Figure 3

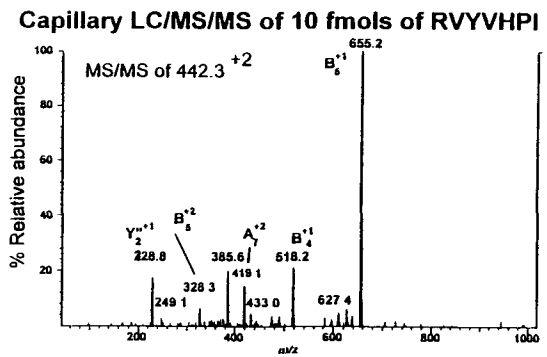

Figure 4

Particle Resonance's in "Monopole" and Quadrupole Electric Ion Traps

Ralph F. Wuerker
UCLA Plasma Physics Laboratory
Los Angles, CA 90024-1547
and
Paul Kelly
Teledyne Electronic Technologies
Mountain View, CA 94039-7127

A charged particle in a quadrupole electric trap ("Paul" or ion trap) can be resonated or selectively excited in two completely different ways. The most common method is via an AC signal across the end caps. Resonance occurs when the frequency of the applied signal is equal (tuned to) the natural frequency of the particle in the z direction. For this case, the particle amplitude (in absence of damping) grows linearly in time, until the end caps are reached. Off resonance, the two frequencies (particle and resonating) interact to produce a beat phenomena at one half the difference between the two frequencies, with the maximum excursion being proportional to the resonating voltage.

The second method of resonance has the resonating signal in series with the trapping source of frequency Ω. This is a true parametric resonance which occurs when the resonating frequency is equal to twice the natural frequencies of the particle in either the **z** or **r** directions. At resonance the particle orbit grows exponentially with time, and the particle can experience more oscillations before striking the electrodes. As a result, resolution should be higher. The scheme has the disadvantage that it must started, either by displacing the particle off origin by either end cap resonance or by pulsed excitation.

These resonance techniques are complicated by the mathematics of the ion trap which are Mathieu differential equations, with their own complexities. The resonating sources add additional terms to the equations of motion which further complicate the analysis. The first (end cap) resonating scheme results in a driven Mathieu equation. The second series or parametric resonating scheme results in a Mathieu equation with two different AC drives. Damping, due to background gas, adds further complexity.

The analysis of an ion trap can be greatly simplified by studying the behavior of a charged particle in the stable direction of a DC quadrupole or its equivalent a DC monopole. Such a system is not practical, but is important for the insight that it affords, since, a charged particle in a DC quadrupole obeys the differential equation of harmonic motion. For this case, the particle oscillates harmonically about the origin of the electrode structure at a characteristic frequency of;

$$\omega_{\beta_z} = \sqrt{\frac{2eV_{DC}}{m(Z_o)^2}}$$

where **e/m** is the charge to mass ratio of the particle, and V_{DC} is the trapping voltage between the origin and the end caps, a distance of Z_o away. Application of a resonating voltage across the end caps, results in the well known differential equation of driven harmonic motion, which at resonance ($\omega_d=\omega_{\beta z}$) has the following solution,

$$z = -\left[\frac{eV_d}{2m\omega_{\beta_z} Z_o}\right] t Cos\omega_{\beta_z} t = -\left[\frac{\omega_{\beta_z}}{4}\right]\left[\frac{V_d}{V_{DC}}\right] Z_o t Cos\omega_{\beta_z} t$$

showing that the amplitude grows linearly with time, at a rate proportional to the ratio of the resonating voltage to the trapping voltage. An expression for the resolution **R** of the resonance can be derived. Standard driven harmonic motion theory can be used to derive an expression for the off resonance amplitude. With damping, the amplitude of oscillation grows to a finite value while the frequency for maximum excursion is slightly above and below the $\omega_{\beta z}$ value.

When the resonating voltage is in series with the trapping voltage, one again realizes another Mathieu equation; namely, one which uses the first (**a**=1) unstable solution, the equation of parametric instability, with resonance occurring when the resonating frequency is $2\omega_{\beta z}$. The solution is of the form,

$$z \cong A_o\left[Sin\left(\frac{\omega_p t}{2} + \frac{\pi}{4}\right)\right]\exp\left(\frac{V_p}{4V_{DC}}\right)\left(\frac{\omega_p}{2}\right)t$$

showing that the amplitude in this case grows exponentially with time. If the particle is initially at the origin (A_o=0), the solution is zero for all time and the resonance never occurs, it must be started. Excessive damping will negate the parametric resonance, however the amplitude grows exponentially even in the presence of damping.

A particle in a real AC ion trap oscillates at a subharmonic of the drive frequency ;

$$\left(\omega_{\beta_z}\right)_{AC} = \sqrt{2}\left(\frac{e}{m}\right)\left(\frac{V_{AC}}{Z_o^2}\right)\frac{1}{\Omega}$$

This "resultant frequency" can be substituted into the resonance equations for the DC quadrupole and monopole deriving expressions for the growths of the particle orbit as a function of time for the two resonant situations in an AC ion trap. The effects of damping can be similarly included.

Implications of Ion Population for GC/MS/MS on a Quadrupole Ion Trap

*Scott T. Quarmby and Richard A. Yost
Department of Chemistry, University of Florida, Gainesville, FL 32611

The use of resonant excitation for collision-induced dissociation (CID) on the quadrupole ion trap relies upon accurate knowledge of the parent ion secular frequency. This frequency has been shown to shift as the number of ions stored in the ion trap changes, which causes the CID efficiency to vary significantly [1] GC/MS/MS presents an especially challenging problem because of the wide variation in sample concentration eluting from the GC As an alternative to broadband excitation [1], this work demonstrates the use of mass-selective automatic gain control (MSAGC) [2,3] to regulate the parent ion population for GC/MS/MS. MSAGC, derived from standard AGC [4], calculates an ionization time which will produce the desired parent ion population based upon the parent ion intensity detected during a prescan. By controlling the ion population, only a single resonant excitation frequency and voltage are needed over a wide analyte concentration range.

A Finnigan MAT ITS-40™ with Gatorware software, developed in our laboratory, was used which allowed custom scan functions. A computer controlled frequency synthesizer was coupled to the endcaps through an external balun circuit. Using a constant source of sample, the variations in the optimum resonant excitation frequency and voltage for CID were determined for ion populations from just above the noise to beyond the onset of space charge (loss of unit resolution). For a given ionization time and resonant excitation voltage, data were acquired for different frequencies to determine the most efficient frequency for CID. Plots of the optimum resonant excitation frequency versus the detected ion intensity can be seen in *Figure 1*. The optimum frequency decreased as the ion population increased. In *Figure 2* a plot of the CID efficiency at the optimum frequency versus the detected ion intensity shows that for larger ion populations, higher resonant excitation voltages produced more efficient CID.

The scan function utilized for GC/MS/MS using MSAGC is shown in *Figure 3*. Triplicate injections of the standard solutions were run; the calibration curves obtained are shown in *Figure 4*. For dimethyl disulfide and thiophene, linear dynamic ranges of 5 and 4 orders of magnitude were obtained, respectively. The linear dynamic range for thiophene was smaller because MSAGC was unable to control the ion population for the largest (100 ng) injection. To determine possible matrix effects on this technique, jet fuel spiked with dimethyl disulfide and thiophene was analyzed. The calibration curves obtained are shown in *Figure 5*. The analysis of dimethyl disulfide in jet fuel also had a linear dynamic range of 5 orders of magnitude. For thiophene, however, another compound that produced m/z 84 ions at the same retention time as thiophene was identified. Since the MSAGC prescan only monitored the total number of m/z 84 ions, MSAGC could not distinguish between m/z 84 parent ions from thiophene and from other jet fuel components. For low concentrations of thiophene, most of the fragment ions produced were from other jet fuel components, limiting the sensitivity of the analysis.

The optimum resonant excitation voltage increases as the number of ions stored in the ion trap increases whereas the optimum resonant excitation frequency decreases as the number of ions stored in the ion trap increases. Mass-selective automatic gain control keeps the ion population relatively constant for GC/MS/MS so that a single-frequency and voltage can be used over a wide sample concentration range. GC/MS/MS analysis with high sensitivity and a linear dynamic range of 4-5 orders of magnitude is possible with MSAGC.

The authors would like to thank Timothy Griffin for his work on the Gatorware software and James Stephenson for all of his ideas and helpful discussions. Partial funding for this project was provided by Finnigan MAT and the NASA Space Grant Fellowship supported through the Florida Space Grant Consortium.

(1) Yates, N.A.; Yost, R.A , Bradshaw, S.C ; Tucker, D.B. *Proceedings of the 39th ASMS Conference on Mass Spectrometry and Allied Topics*, 1991, Nashville, TN, pp. 132-133.
(2) Griffin, T.P., Yates, N.A.; Yost, R.A. *Proceedings of the 41st ASMS Conference on Mass Spectrometry and Allied Topics*, 1993, San Francisco, CA, p. 715.
(3) Quarmby, S T.; Griffin, T P.; Yost, R.A *Proceedings of the 42nd ASMS Conference on Mass Spectrometry and Allied Topics*, 1994, Chicago, IL, p. 706.
(4) Stafford, G.C.; Taylor, D.M ; Bradshaw, S C., Syka, J.E.P., Uhrich, M. *Proceedings of the 35th ASMS Conference on Mass Spectrometry and Allied Topics*, 1987, Denver, CO, p. 775-776.

43rd ASMS Conference on Mass Spectrometry and Allied Topics

Figure 1
Effect of Ion Population on Optimum CID Frequency
Effect of Resonant Excitation Voltage
Thiophene -- m/z 84

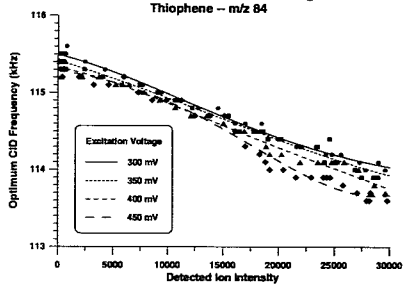

Figure 2
Effect of Resonant Excitation Voltage on CID Efficiency
CID Efficiency at Optimum Frequency
Thiophene -- m/z 84

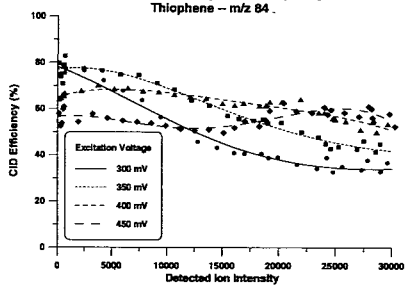

Figure 3
GC/MS/MS Scan Function with MSAGC Prescan

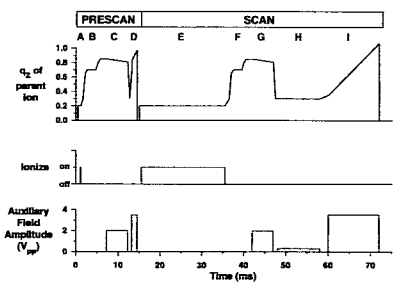

Prescan:
A=Fixed ionization time
B=Coarse two-step isolation [5]
C=Fine reverse-scan isolation [6]
D=Acquisition of 8 amu range centered at parent ion

Scan:
E=Variable ionization time
F=Coarse two-step isolation
G=Fine reverse-scan isolation
H=Single-frequency CID (10 ms)
I=Acquisition of m/z 35-100

[5] Yates, N.A., Yost, R.A.; Bradshaw, S.C.; Tucker, D.B. *Proceedings of the 39th ASMS Conference on Mass Spectrometry and Allied Topics*, 1991, Nashville, TN, pp. 1489-1490.
[6] Kaiser, R.E.; Cooks, R.G.; Syka, J.E.P.; Stafford, G.C. *Rapid Commun. Mass Spectrom.*, 4, 30 (1990).

Figure 4
Dimethyl Disulfide and Thiophene Standards
GC/MS/MS Calibration Curves
MSAGC -- Constant CID Frequency and Voltage

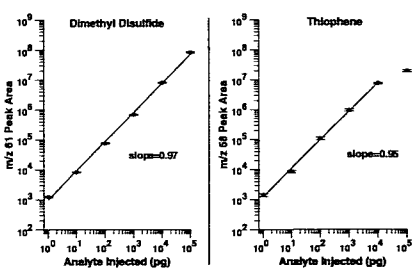

Figure 5
Dimethyl Disulfide and Thiophene in Jet Fuel
GC/MS/MS Calibration Curves
MSAGC -- Constant CID Frequency and Voltage

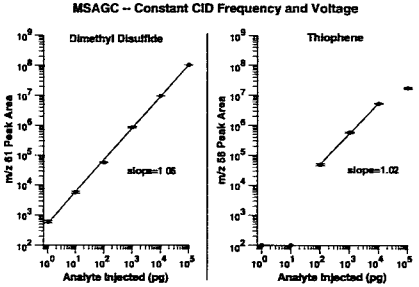

INVESTIGATIONS OF MASS SHIFTS IN THE ION TRAP MASS SPECTROMETER

J P DeGnore and R. A. Yost
Department of Chemistry, University of Florida, Gainesville FL 32611

It has been reported that under identical conditions, ions of exactly the same m/z, including positional isomers, will be detected at different m/z values [1] This phenomenon was called a mass shift because the mass, as assigned by the mass spectrometer, is shifted to a value either higher or lower than its nominal mass. Mass shifts would have serious implications for the practical use of ion trap mass spectrometers, particularly for high resolution and accurate mass assignment applications. Previous investigations have shown an apparent mass shift for the positional isomers of trifluoromethyl benzonitrile (TFBN) [1]. These mass shifts have been rationalized as originating from an interaction between the radio frequency (RF) fields of the ion trap and the polarizability of the analyte ion under investigation. Investigations by others have also reported this correlation between mass shift and polarizability of the analyte ion [3]. It has been suggested that ions of different polarizability would have different radial distributions in the ion trap and therefore would be ejected at different apparent masses [4].

Experiments were performed on a Finnigan MAT Ion Trap Mass Spectrometer (ITMS) to examine mass shifts of the M^+ ions of TFBN isomers All experiments used a standard stretched ion trap geometry (z_0 = 0 78311 cm) except for the experiments using the theoretical geometry. The experiments utilizing theoretical trap geometry had a reduced endcap to ring spacing (z_0 = 0.7071 cm) compared to the stretched geometry of a commercially available ion trap such as the ITMS. The results of these experiments are presented in the table below The apparent mass shift between the ortho and para isomers at normal scan rate is +0 8 DAC steps or approximately +0 14 u This mass shift was similar to that previously reported [1] At this scan rate isomeric peaks of m/z 171 are only characterized by only five data points Therefore, the centroid of this profile data may result in errors that would lead to anomalous mass shifts. Shifts of several DAC steps would be more convincing, to better characterize these mass peaks, and to produce shifts of greater than 1 DAC, experiments were performed using a reduced scan rate At a reduced scan rate, more data points can be acquired for improved peak characterization The method of employing an offset DAC summed to an attenuated RF DAC output was implemented for controlling the scan rate [6].

This theoretical trap geometry is expected to produce an increase in the mass shifts[5] The para isomers was shifted to slightly higher mass compared to the ortho isomer. This is in contrast to the results seen for the stretched trap geometry The magnitude of this mass shift at normal scan speed is similar to that in the normal scan rate experiments with a stretched trap geometry However, the reduced scan rate did not correlate well with our normal scan rate results nor with previous results [1]

To further examine if isomeric mass shifts are caused by the interaction of the isomeric polarizability and the RF field, the frequency of the ions were investigated The secular frequency of the ions was determined by varying the axial excitation frequency. This was repeated with various ionization times. The largest frequency difference between ortho and para at the same ion population was less than expected from previous investigations [1]. Also, in contrast to previous investigations, the para isomer is shifted to higher mass than the ortho isomer [1]. To exaggerate mass shifts, the theoretical trap geometry was also used in these experiments In agreement with previous reported results the ortho curve is lower in frequency than the para [1]. However, the largest frequency difference between ortho and para was less then expected from previous investigations [1]

Although the results of the normal scan rate experiment are similar in value to mass shifts previously reported, the results of the reduced scan rate experiments did not produce the same mass shift [1]. The degree of mass shift (in u) seen in previous investigations is much higher than the modest mass shifts seen in reduced scan rate experiments [1] The mass shifts seen in these investigations are small enough that they could be attributed to factors such as quantization noise in the DAC or instrumental calibration drift The axial resonant excitation experiments did not find the expected mass shifts for the same ion population. It is proposed that erroneous mass shifts could be caused by poor peak characterization, inconsistent ion population between isomers, and the error associated with determining a mass shift *based upon only one DAC step*

SOURCE	SCAN RATE	MASS SHIFT BETWEEN ORTHO AND PARA ISOMERS	
Traldi [1]	1	+0.7 DAC step	+0.12 u
Stretched	1	+0.8 DAC step	+0.14 u
Stretched	1/4	0.0 DAC step	0.00 u
Stretched	1/10	+1.9 DAC step	+0 32 u
Stretched	1/15	-1.0 DAC step	-0.17 u
Theoretical	1	-1 0 DAC step	-0.17 u
Theoretical	1/2	-0 1 DAC step	-0 02 u
Theoretical	1/4	-0 4 DAC step	-0.07 u
Theoretical	1/10	-1 0 DAC step	-0.17 u

[1] Traldi, P., Catinella, S., Bortolini, O , "Mass Displacements in Ion Trap Mass Spectrometer: Can They be Related to electronic Properties of Substituent Groups of the Ions Under Investigation?", *Organic Mass Spectrometry*, **27**, 927-8 1992).
[2] Mestdagh, H., Rolando, C., Sablier, M., Capron, L., Proceedings of the 42nd ASMS Conference, 1047, (1994)
[3] Cox, K. A , Cleven, C D , Cooks, R. G , Proceedings of the 42nd ASMS Conference, 224, (1994)
[4] Garrett, A. W , Hemberger, P. H., Cleven, C. D., Cooks R. G., Syka, J. E. P., Proceedings of the 42nd ASMS Conference, 89, (1994)
[5] Syka, J E P , "The Geometry of the Finnigan Ion Trap· History and Theory", Asilomar Conference on Mass Spectrometry, Pacific Grove, CA. Sept 27-Oct 1, 1992.
[6] Kaiser, R. E , Cooks, R G , Stafford, G. C., Syka, J E. P., Hemberger, P. H , *International Journal of Mass Spectrometry and Ion Processes*, **106**, 79 (1991)

The Effect of Scan Direction on Mass Resolution in Stretched and Compressed Traps

Mingda Wang

Varian Chromatography System, 2700 Mitchell Dr., Walnut Creek, CA 94598

It is well known that the mass resolution of resonance ejection in a stretched trap depends on rf scan direction [1] because of the introduction of octopole and the higher order electric fields. Frenzen has pointed out that ion secular frequency depends on its oscillation amplitude under such rf electric fields [2]. Bolton has reported that mass resolution gradually improves and reaches a limit when the two end caps are symmetrically stretching out [3].

In a stretched trap, mass resolution in a forward scan is much better than that in a reversed scan. In the presentation, a compressed trap with a positive octopole term, instead of with a negative octopole term in a stretched trap, is introduced. The relationship between the mass resolution and the scan direction is reversed when the sign of the octopole field is changed by replacing the stretched trap with the compressed trap. The reversed scan is created by adding a negative saw function to the sum point of the rf control amplifier during the analytical scan period. This modification enables Saturn data system to record the reverse scanned signal.

Figures 1-2 are the forward and reverse scans in the stretched and compressed traps. The mass unit widths in all scans should be the same though the mass peaks in the scans appear at different positions of mass axis. Comparing Figures 1 and 2, it is apparent that mass resolution depends not only on scan direction but also on the direction of octopole electric field. Figures 3-4 are the SIMION simulation of ion 69 trajectory in the stretched and compressed traps. The maximum step of the SIMION program is extended to 10 million. The trajectory is recorded more than 14 ms at the 0.84 μs/datum sampling rate while the trapping rf level is fixed. Then the time domain signal is subjected to the Fourier transform to obtain the ion secular frequency. The digital resolution of the frequency spectrum is better than 100Hz. Figures 3-4 clearly show **the shift of secular frequency with the amplitude in the stretched and compressed trap are in the opposite direction**. Figures 1-4 reveal that **the unit mass resolution can be easily achieved with normal scan speed (185 μs/amu) when the direction of ion frequency shift is in the same direction of the rf scan**.

It is observed that when the amplitude of the dipole excitation field increases, the absorption peaks become wider and their maxima are shifted. As expected, **the maximum in a stretched trap (top) shifts in the opposite directions to that in a compressed trap (bottom), which agrees with the shift directions of ion secular frequency.**

Reference:

1. J. D. Williams, K. A. Cox and R. G. Cooks, Anal Chem. 66, *725*, **1994**.
2. J. Freenzen, Int. J. Mass Spectrom. Ion Proc. 106, *63*, **1991**.
3. B. Bolton, Varian Chromatography System, Private Communication, **1992**.

43rd ASMS Conference on Mass Spectrometry and Allied Topics

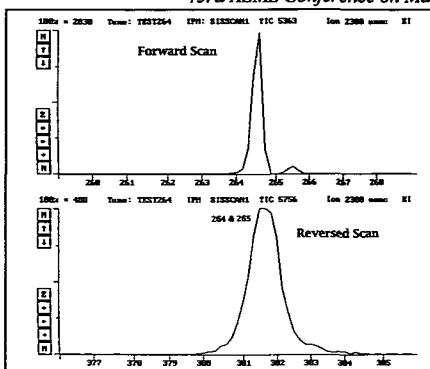

Figure 1: Forward and Reverse Scans in a Stretched Trap. The top and bottom figures are the forward scan and reversed mass spectra of ion 264 & 265 respectively. It is clear that **isotopic peaks of ion 264 and 265 are well resolved by the forward scan and can not be resolved by the reversed scan in the stretched trap.**

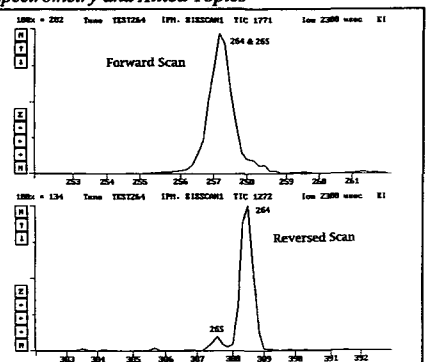

Figure 2: Forward and Reverse Scans in a Compressed Trap. In contrast to the stretched trap, the isotopic peaks of ion 264 & 265 can not be separated by the forward scan (top). But they are well separated by the reversed scan (bottom). It indicates that **mass resolution depends not only on scan direction but also on the direction of octopole electric field.**

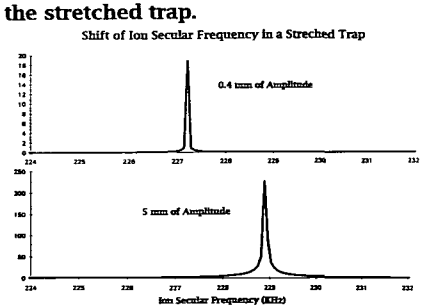

Figure 3: Ion Secular Frequency Shift in a Stretched Trap. Comparing the top and bottom figure, it is clear that in the stretched trap, the secular frequency **gains about 2 KHz** while ion oscillation amplitude increases from 0.4 mm to 5 mm. The secular frequencies are obtained from the Fourier transform spectrum of simulated ion z motion.

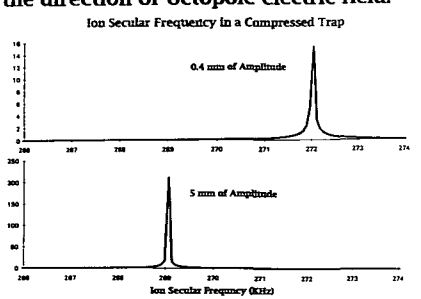

Figure 4: Ion Secular Frequency Shift in a Compressed Trap. The up and bottom figures show the secular frequency in the compressed trap lowers more than 2 KHz when ion oscillation amplitude increases from 0.4 mm to 5 mm. Figures 1-4 reveal that **the mass resolution depends on the direction of ion frequency shift.**

High Resolution Selected Ion Monitoring In An Ion Trap

Greg Wells and Chuck Huston

Varian Chromatography Systems
2700 Mitchell Drive
Walnut Creek, CA 94598

Selective ion monitoring in an ion trap was accomplished by isolating and detecting each target ion successively. The chromatogram could be divided into 200 time segments. In each time segment up to 10 different scan groups could be sequentially acquired. Each scan group could isolate and detect a different ion. In the example (Figure 1) two scan groups were used to alternately isolate selected ions from phencyclidine (PCP) and deuterated phencyclidine (D-5 PCP). The isolation of each mass occured at the same optimum operating point to ensure constant mass dispersion and resolution. The ionization time for each ion could be independently optimized to ensure the maximum sensitivity and dynamic range for each mass.

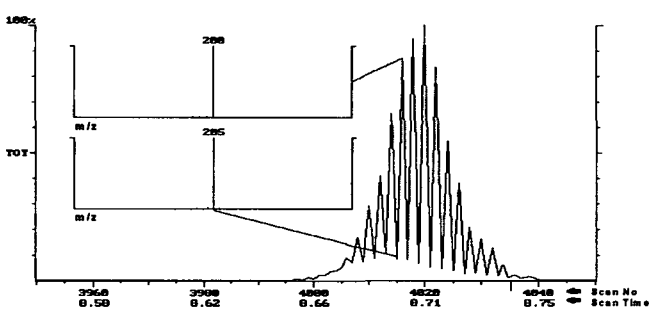

Figure 1

Each set of the 10 successive group spectra could then be merged into a single spectrum for data analysis (Figures 2 and 3).

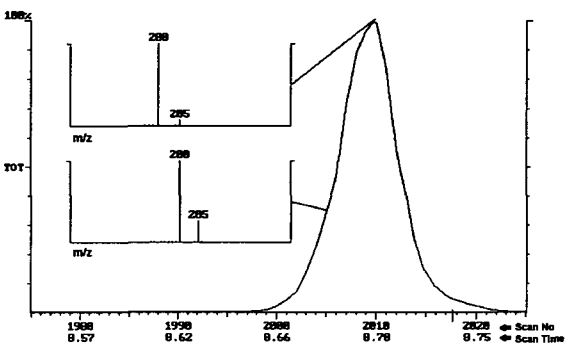

Figure 2

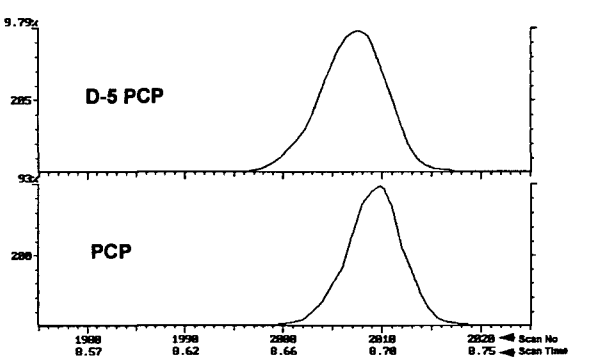

Figure 3

Field Modulated Selective Ion Storage In An Ion Trap

Greg Wells and Chuck Huston

Varian Chromatography Systems
2700 Mitchell Drive
Walnut Creek, CA 94598

Selective ion accumulation in an ion trap during the ionization period was accomplished by the combined application of a multi-frequency waveform to the end caps while the rf trapping field amplitude was modulated (Figure 1). The waveform was constructed from a minimal number of frequency components (<120 frequencies) that spanned the entire mass range and were spaced so that unwanted ions were resonantly ejected while target ions were accumulated during ionization. Modulation of the rf trapping field amplitude causes a frequency modulation of the secular motions of the ions in the trap; this periodically brings the ions into resonance with the frequencies of the supplemental waveform, causing the unwanted ions to be ejected.

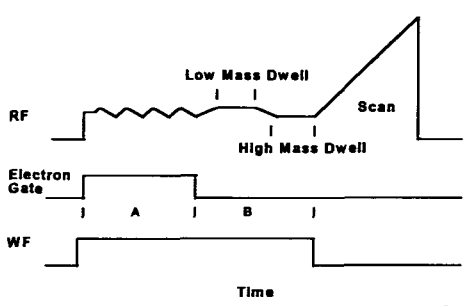

Figure 1

The technique can be extended to the selective accumulation of multiple ions. Figure 2 shows the isolation of m/z=100,131,264 and 414 from FC-43. The technique was used to analyze for Aldrin and Heptachlor Epoxide in an of bell pepper extract (Figure 3). These compounds were undetectable in the normal full scan EI mode.

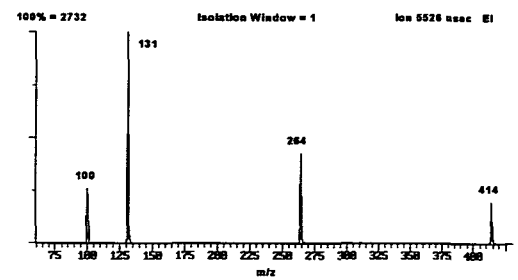

Figure 2

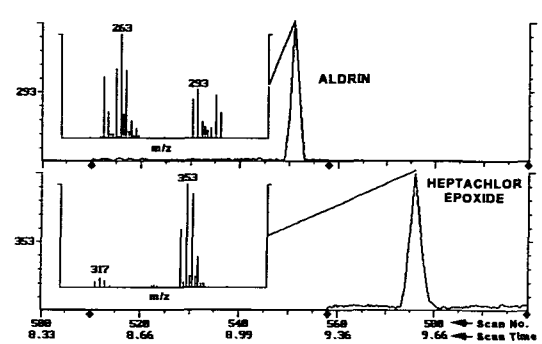

Figure 3

Mass Displacements Measured in a Quadrupole Ion Trap

F.A. Londry[1], R.J S Morrison[2] and R.E. March[1]

[1] Trent University, Peterborough, Ontario, Canada K9J 7B8 [2] Monash University, Melbourne, Australia 3168

Introduction

The mass intensity signals which are obtained when ions are ejected from an ion trap during a mass-selective instability scan can appear on the mass axis at positions which differ significantly from expected values. Several origins of this *mass displacement* have been proposed. Some, such as space-charge [1], affect all ions to approximately the same degree. Others, such as radial distribution [2], ion-ion interactions [3] and dipole moment [4], appear to be ion-specific and, consequently, are less amenable to correction. It is well known that ion-specific mass displacements observed with *stretched* ion traps are reduced substantially from those observed in traps of pure quadrupole geometry [5]. In both pure quadrupole and stretched traps three potential origins of mass displacement were evaluated: dipole moment, radial amplitude and ion fragmentation.

1) Dipole Moment

- Only the first term in the multipole expansion of a potential is independent of the choice of origin The dipole moment of an ion can vary from zero to infinity as the origin is moved away from the centre of charge.
- Rotational energy levels are populated at room temperature! Consequently, ions are rotating at a frequency greater than that of the RF drive by a factor of at least 10^5.
- *If* an ion had a *permanent* dipole moment comparable to that of the neutral species and *if* the dipole was aligned with the RF field, then the force experienced by an ion located at (0, 0, $0.1z_0$) would be increased by a factor of only 4×10^{-8}.
- Under maximizing conditions, the dipole moment *induced* in DCB by the trapping field would be smaller than the permanent dipole moment of the neutral by a factor of at least 10^4
- Neutral molecules of ortho- and para-dichlorobenzene (DCB) have permanent dipole moments of 2 5 and 0.0 debyes, respectively. To look for correlation between the permanent dipole moment of neutral molecules and mass displacement, the apparent mass difference between ortho- and para-DCB was measured a large number of times, under a broad range of experimental conditions, at intervals which spanned a one-month period Although the uncertainty in individual measurements was large, statistically significant results, were obtained by averaging all the data obtained for each electrode configuration. The mass difference (ortho - para) obtained by averaging the results of ~500 experiments for each trap geometry were 0.003±0.146 u and 0.000±0.066 u for quadrupole and stretched traps, respectively

Fig. 1. Axial Secular Frequency in a Stretched Trap

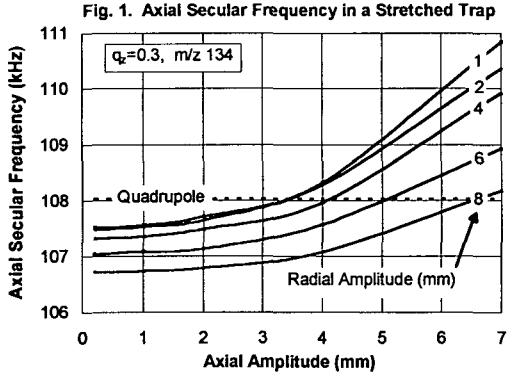

2) Computer Simulations

Frequency analysis of ion trajectory simulations in a stretched trap at q_z=0 3 demonstrated that an ion's secular frequency is a strong function of its amplitude in both the axial and radial directions Analysis of trajectories in a pure quadrupole trap yielded the theoretically predicted result indicated by the dotted line in Fig 1.

To establish the influence of radial amplitude on apparent mass, simulations were performed on ensembles of ten ions using both pure quadrupole and stretched geometries *M/z* 131 ions were cooled at q_z=0.2, radially excited to specific amplitudes and finally ejected during a mass-selective instability scan by two different methods: resonant excitation at β_z=0 5 and by crossing the stability boundary at β_z=1.0.

The major findings of these simulation studies were: i) Apparent mass at ejection is unaffected by initial radial position in both trap geometries ii) Ions in a stretched trap are held in a potential well which is significantly deeper than in a pure quadrupole trap. iii) Examination of radial position at ejection shows no significant difference in detection efficiency for either trap type, or ejection method, for initial radial amplitudes less than 3 mm.

3) Ion Fragmentation

The molecular ion of *n*-butylbenzene (NBB) exhibits a significant mass displacement [3,4]. Furthermore, this molecular ion undergoes fragmentation readily when subjected to resonance excitation in the presence of buffer gas. A shift to lower mass of the *m/z* 134 peak occurs when lower-mass fragments fall outside of the region of stability during resonance ejection of the molecular ion

The position of the *m/z* 134 peak of NBB was measured relative to the $C_3F_5^+$ (*m/z* 131) fragment of PFTBA in both quadrupole and stretched traps over a broad range of ionization times, ejection points, and helium pressures. These results have been summarized in Fig. 2 where the 134-131 (NBB - $C_3F_5^+$) mass difference, extrapolated to zero ion intensity, has been plotted as a function of helium pressure

Fig. 2. Mass Difference at Zero Ion Intensity

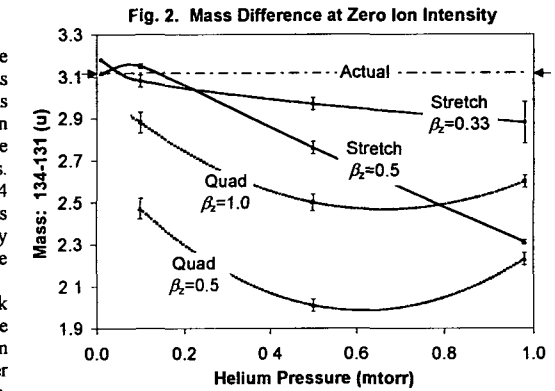

Conclusions

- The dipolar properties of ions provide an unlikely explanation for the mass displacements demonstrated by some compounds.
- Ion ejection from a stretched trap is delayed with respect to that from a quadrupole trap due to the greater trapping well-depth associated with the former. This ejection delay in the stretched trap is compensated by the tendency to premature ejection brought about by the shift in secular frequency associated with the amplitude of axial motion.
- Fragmentation of ions during resonance-excitation ejection can cause a significant shift to lower apparent mass. This shift can be reduced to zero in a trap of stretched geometry by a combination of one or more of the following conditions: i) reduce the pressure of the buffer gas; ii) eject at the βz=1 stability boundary and/or iii) eject resonantly at a sufficiently low value of qz that lower-mass fragments are trapped

Acknowledgements: The authors gratefully acknowledge the excellent technical support of A Kift and J.K. Fowler as well as the financial support of Varian Associates and NSERC

References

1. R.E. March and R.J. Hughes, *Quadrupole Storage Mass Spectrometry*, Chemical Analysis Series, Vol. 102, Wiley Interscience, New York, 1989.
2. A.W. Garrerr, P.H. Hemberger, C.D. Cleven, R.G. Cooks and J.E.P.Syka, *42nd ASMS Conference on Mass Spectrometry and Allied Topics*, Chicago, IL (1994) p 189.
3. K.A. Cox, C D Cleven and R.G. Cooks, *42nd ASMS Conference on Mass Spectrometry and Allied Topics*, Chicago, IL (1994) p. 224.
4. P. Traldi, D. Favretto, S. Catinella and O. Bortolini, Org. Mass Spectrom , 28 (1993) 745
5. J.E P. Syka, "The Geometry of the Finnigan Ion Trap History and Theory", 9th Asilomar Conference on Mass Spectrometry, Pacific Grove, CA, Sept. 27 to Oct. 1, 1992.

COOLING TIME AND PRESSURE EFFECTS ON COMPETITIVE THERMALIZATION/ACTIVATION PROCESSES BY RESONANCE EXCITATION ON ITMS.

P.Liere[1], T.Blasco[1], R.E. March[2], J.C. Tabet[1]
[1]Laboratoire de chimie organique structurale, Université Pierre et Marie Curie, Paris, FRANCE.
2Department of Chemistry, Trent University, Peterborough, ON, CANADA.

Mass spectrometers which permit MS/MS experiments involving collision-induced dissociation have been very useful for qualitative analysis as well as for the study of low-energy collision processes and ion/molecule reactions. The ion trap capabilities for MS/MS experiments have been described previously and have demonstrated a high sensitivity and CID efficiency; furthermore, several sequential stages of reaction, mass-selective isolation and excitation, $(MS)^n$, can occur in these instruments Moreover, the time parameter access in the ITMS presents an easy means to study the kinetic and thermodynamic properties of gas-phase ion/molecule reactions.

CID experiments were performed on an ITMS by using the resonance excitation process (or tickle process) whereby an auxiliary voltage was applied on the end-cap electrodes at the fundamental axial secular frequency of the previously isolated precursor ions. Some earlier studies have shown that the internal energy imparted into the parent ions can be changed by introducing a delay between the isolation period and the tickle period.[1] For this purpose, the classical model of n-butylbenzene was used as an "energy thermometer"[2] to estimate the average internal energy deposited into the molecular ion (m/z 134) according to the two product ions' relative abundances, m/z 91 ($C_7H_7^+$) and m/z 92 ($C_7H_8^{+\circ}$), produced from the direct cleavage and rearrangement pathways, respectively. Variation of helium and analyte pressures and of the cooling time before excitation (called t_{cb}) was investigated to have a better understanding of the energetic thermalization and activation processes by resonance excitation.

A Finnigan Ion Trap Mass Spectrometer (ITMS) was used. Helium buffer gas was introduced via a gas chromatograph and transfer line to the ion trap. n-Butylbenzene was introduced via a leak valve into the ion trap. All pressures were measured by a Penning gauge mounted to the vacuum chamber, as described recently [1] In Fig. 1 is shown the scan function used for the MS/MS experiments. The cooling time following isolation and prior to precursor ion (m/z 134) excitation was varied over a time scale 0-100 ms The tickle parameters were q_z (m/z 134) = 0.4, V_{tic} = 0.6 V and t_{ex} = 10 ms (V_{tic} and t_{ex} are defined as the peak-to-peak amplitude and duration of the tickle voltage, respectively).

Some recent studies[3] have shown that insertion of a cooling time in MS/MS experiments can play a great role in the degree of activation of the excited molecular ion. The cooling time causes an ion internal energy decrease in the time scale 0 to 20 ms, as is shown in Fig 2 This effect is due mainly to the thermalization of ion kinetic energy defined as a reduction of both molecular ion kinetic energy and spatial distribution as a result of momentum-exchange collisions with helium buffer gas. The initial internal energy, coming from the electron impact process, is likely thermalized in collisions between the molecular ion and neutral n-butylbenzene. The t_{cb} influence on molecular ion activation, when t_{cb} is prolonged to 100 ms has been discussed already and explained in terms of an accumulation of internal energy during both the cooling time before excitation and the tickle period as a result of collisions of increasing number between the molecular ion and buffer gas atoms.

Buffer gas pressure variation has a more marked effect on the average ion internal energy uptake by the resonance excitation process than does the cooling time variation. The resonance excitation activation process is more and more dominant as the helium pressure is increased. The I_{91}/I_{92} ratio increases from 1.6 to 4 and from 1 to 6 between $1.6.10^{-4}$ torr and $5.2.10^{-4}$ torr at t_{cb} = 0 ms and t_{cb} = 100 ms, respectively. Moreover, only the activation process is observed as P(He) = $5.2.10^{-4}$ torr and only the thermalization process is observed as the helium pressure is low (P(He) = $1.6.10^{-4}$ torr)

There are a number of points which can explain these results: (i) the number of collisions, either between low-kinetic energy molecular ion and helium, or between the excited molecular ions and

helium, is increased during the cooling and tickle periods, respectively, by increasing the helium pressure for a given t_{cb} value, (ii) the dual role of helium, as a target/buffer gas, favors ion dissociation over ion ejection; thus the irradiated ions, having the higher excursion amplitudes from the centre of the ion trap and the higher kinetic energy can be stored and decomposed rather that ejected as the helium pressure is increased (iii) The precursor ion excitation frequency bandwidth (generally measured when 10-20 % of the parent ions are fragmented or ejected) is decreased when the cooling time or helium pressure is increased in our experiments. This "frequency focusing" can play a major role in the tickle process efficiency. Indeed, if the applied tickle frequency and the precursor ion frequency are closer with a larger t_{cb} value or with a higher helium pressure, the average ion excursion amplitudes and ion kinetic energy will be higher for a constant excitation fluence. Thus, the CID process by resonance excitation will be more efficacious for internal energy deposition when the frequency distribution is narrow and overlaps the secular frequency for a given fluence.

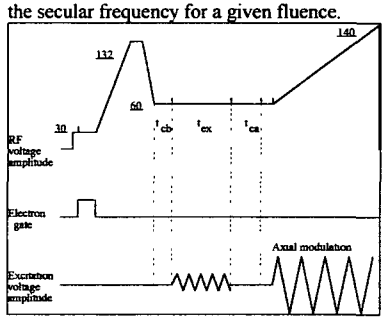

Fig 1- Scan function employed in the tandem mass spectrometry experiments showing cooling times before and after excitation period.

The influence of the analyte pressure and t_{cb} variations on the I_{91}/I_{92} ratio has been investigated, as is shown in Fig. 3. No helium was admitted into the ion trap The I_{91}/I_{92} ratio decreases as t_{cb} is increased to 20 ms and remains constant if tcb > 20 ms The initial internal energy thermalization does not seem to contribute significantly in these experiments despite the neutral pressure increase. This phenomenon is likely due to the space charge effects due to the ion/ion interactions of the molecular ion Thus, these repulsive forces cause ion excursion amplitudes to increase and, therefore, the ion kinetic energy increases thus preventing the thermalization process. On the basis of these experiments, this latter process seems to be optimum for a minimal analyte pressure in the ion trap

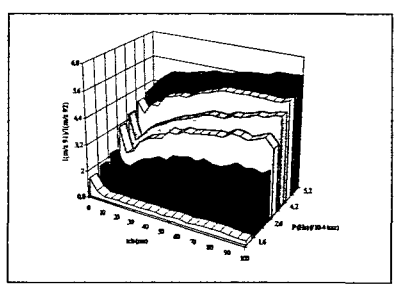

Fig. 2- Variation of I_{91}/I_{92} as a function of t_{cb} and helium pressure

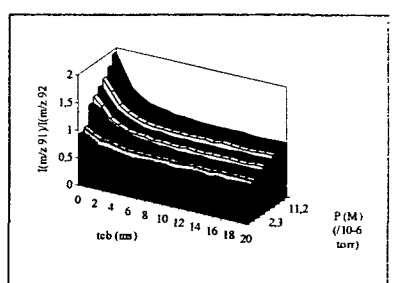

Fig 3- Variation of I_{91}/I_{92} as a function of t_{cb} and analyte pressure

1- P. Liere, T. Blasco, R.E. March and J.C. Tabet, *Rapid Commun. Mass Spectrom.* **8**, 953,(1994).
2- R.E March, M.R. Weir, F.A. Londry, S. Catinella, P. Traldi, J.A. Stone and W B. Jacobs, *Can. J. Chem.* **72**, 966, (1994).
3- A.G. Harrison and M.S. Lin, *Int. J. Mass Spectrom. Ion Phys.* **51**, 353, (1983)

QIT/TOF Analysis of Space Charge in a Quadrupole Ion Trap

Ventura,M.C.*, Aldalur,I., Laude,D.A., Department of Chemistry and Biochemistry,
The University of Texas at Austin, Austin,TX 78712-1167

Substantial efforts are made in the interest of avoiding high space charge conditions in performing quadrupole ion trap mass spectrometry. A potential due to space charge perturbs the electric field in the trap and thus the detected ion signal at a certain ion density level in the trap. The effects of peak distortion and mass shifting have been documented[1,2] In order to better characterize ion cloud behavior, a series of experiments was performed with a highly modified Finnigan ITD. A modified endcap electrode and masks are exploited to display information on the effects of space charge in the radial direction under high vacuum and collisional cooling conditions. Finally, the effects of collisional cooling on kinetic energy distributions within the trap may be calculated by employing TOF data from signals collected at various ion flight distances.

The system configuration is presented in Fig.1. The ITD has been oriented to permit horizontal TOF of ejected ions. The ion trap region and TOF region are connected but differentially pumped to maintain high vacuum conditions in the TOF region even during experiments using He buffer gas for collisional cooling. The illustration displays also the variable flight distance detection system. The channeltron detector has been removed from its mount on the ITD manifold wall and installed on the end of a probe translatable through the TOF region.

Fig.2 shows the altered endcap electrode and masks used to analyze ion signals from various radii within the trap. The outer two series of holes drilled into the endcap permit evaluation of the ion cloud at radial extents not available in commercial ion trap spectrometers. A LeCroy 9310 digital oscilloscope was used for high-precision peak shape analysis.

In all experiments, an essentially isolated naphthalene parent ion population (m/z=128) was examined. A q value of 0.23 was used in most experiments whereby background air and water ion trajectories are destabilized during storage, leaving only m/z=128 in the trap before mass-selective instability scanning. Peak shape data obtained from the use of four different masks are analyzed together to examine ion distributions and space charge phenomena in different areas of the trap. Experiments were run under low and high space charge conditions controlled by varying the sample pressure through a variable leak valve.

Kinetic energy distributions are calculated by measuring deviations in the peak width caused by varying ion flight distances necessary for an ejected ion bundle to reach the detector. Using a Gaussian model for the detected signal, a FWHM is measured on a peak, converted to σ, and the time deviation of σ from one flight distance to another yields a velocity relative to the peak centroid. This represents a velocity difference from the mean (a standard deviation) of the ion cloud velocity distribution. The value readily converts into a kinetic energy distribution.

The electrode/mask configurations were used to sample ion populations at various radii within the trap. Peak profiles were obtained for each electrode/mask configuration under low and high space charge conditions. Normal collisional cooling behavior was observed for low space charge conditions in all experiments where ions could be ejected from the center of the trap.

The ion storage time was varied in one experiment under high space charge conditions while monitoring the signal peak height. When no buffer gas was introduced, signal increased to equilibrium in ~10ms for the 7-hole and unmasked electrodes. Collisional cooling with sample neutrals apparently increases signal within these radii until it is counterbalanced by Coulombic effects. For the case where only the center hole radius was sampled, the signal continued to decrease with time. The Coulomb

1 March,R.E.,Hughes,R.J.,*Quadrupole Storage Mass Spectrometry*; Wiley; New York, 1989.

2 Cleven,C.D.,Cox,K.A. and Cooks,R.G., *Rapid Communications in Mass Spectrometry* vol.8: p.451-454, 1994.

concentration. When He buffer gas was added, however, the cooling effect was observed at this radius as well as the larger radii. The equilibrium signal level was reached at ~8ms in each case.

Resolutions were measured for both high and low space charge conditions for ions sampled from the various radii. Under high space charge, the 12 hole radial section had the best resolution though the signal level was poorer than for center trap samplings. Evidently space charge effects distort the signal in the 7-hole radius at some level, whereas this region exhibits the best resolution under low space charge.

In another experiment the relative mass shift was observed for the 1-, 7- and unmasked electrode configurations, with and without buffer gas. As the number of ions trapped increased from low to high space charge level, the shift of the peak centroid was measured, and relative values were plotted.The largest shift occurred for the center hole electrode where theoretically, the largest space charge exists. Also of note, no mass shift was observable using the unmasked electrode.

Finally, the evolution of the kinetic energy distribution of ions trapped for increasing delay times was determined using variable TOF. The data indicates an exponential focusing of the kinetic energy distributions as a function of the average number of collisions.

ION TRAP/TIME OF FLIGHT APPARATUS

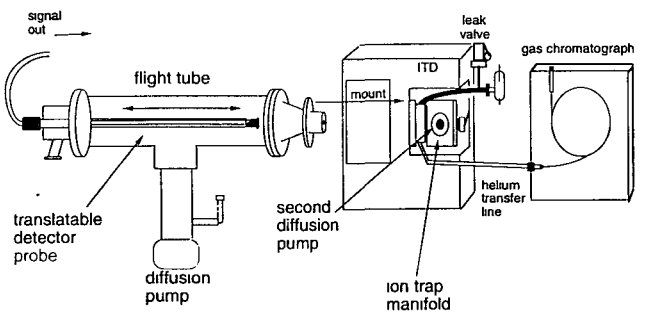

Figure 1

Endcap Electrode Masks

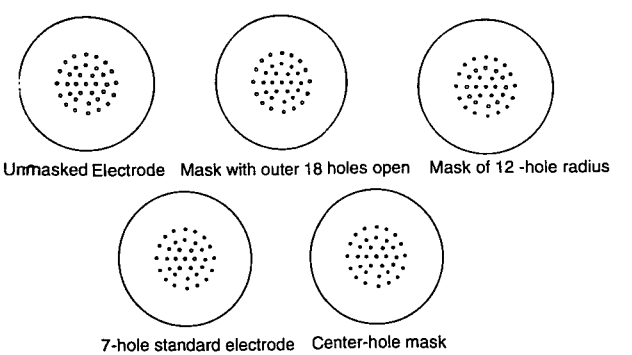

Figure 2

OPTICAL TOMOGRAPHY INSIDE QUADRUPOLE ION TRAPS

A.W. Garrett, N.S. Nogar, P.H. Hemberger. Chemical Science and Technology Division, Los Alamos National Laboratory, Los Alamos, NM 87545

C.D. Cleven and R.G. Cooks. Department of Chemistry, Purdue University, West Lafayette, IN 47907.

Operation of a quadrupole ion-trap mass spectrometer (ITMS) depends on details of ion motion in the trap such as spatial and velocity distributions, effects of gas pressure and ion density, the RF drive frequency, phase and amplitude, and additional (perturbing) fields. In spite of this, relatively few studies have experimentally addressed the motion of ions in ion traps. Trajectories can be calculated and plotted through computer simulations for idealized traps, but the accuracy of modeling real traps has yet to be established. [1,2] We have developed a methodology, based on spatially-resolved photodissociation, for the direct measurement of ion densities in the ITMS. [3-5] Both the ring electrode and/or the end caps can be slotted (>1 mm width) to allow optical access along the trap's axial or radial axes. Measurement of photodissociation products as a function of position and trap operational parameters then allows spatially resolved determination of the number densities of the parent ions.

Recently it has been shown that the mass resolution and mass measurement accuracy of the ITMS depend on both ion density and compound type. [6] Building on these experiments, we have used tomography to determine that ion radial distributions mirror these observations. Briefly, as the ion density increases, the mass peak increases in width, shifts to higher mass, and the radial distribution of the ion cloud increases (Figure 1). We have also found the magnitude of these effects to be dependent not only on ion density and compound but also on ion trap geometry (Figure 2). This data suggests that mass shifts are related to the expansion of the ion cloud in the radial direction. In addition, we have determined that field faults induced by slotting the electrodes for optical access can apparently be compensated for by "super-stretching" (z_0=0.870 cm, r_0=1.0 cm) the trap.

References
1. C. S. O, H. A. Schuessler, J. Phys. D, 14, 953 (1981).
2. R. K. Julian, Jr., H. P. Reiser, R. G. Cooks, Int. J. Mass Spectrom. Ion Processes, 123, 85 (1993).
3. P. H. Hemberger, N. S. Nogar, J. D. Williams, R. G. Cooks, J. E. P. Syka, Chem. Phys. Lett., 191,405 (1992).
4. J. D. Willlares, R. G. Cooks, J. E. P. Syka, P. H. Hemberger, N. S. Nogar, J. Am. Soc. Mass Spectrom, 4, 792 (1993).
5. A.W. Garrett, P.H. Hemberger, Proceedings of The 42nd ASMS Conference on Mass Spectrometry, 189, (1994).
6. C.D. Cleven, K.A. Cox, R.G. Cooks, RCMS, 8, 451, (1994).

43rd ASMS Conference on Mass Spectrometry and Allied Topics

Figure 1:
Radial Distribution (triangles) and Mass Shift (circles) of n-Butylbenzene

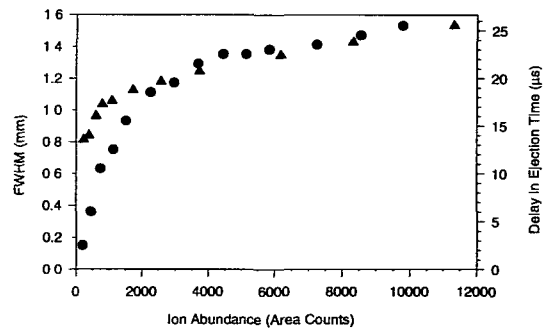

Figure 2:
Geometry Dependence of Radial Distributions
(triangles - ideal geometry, cicles - stretched, squares - super-stretched)

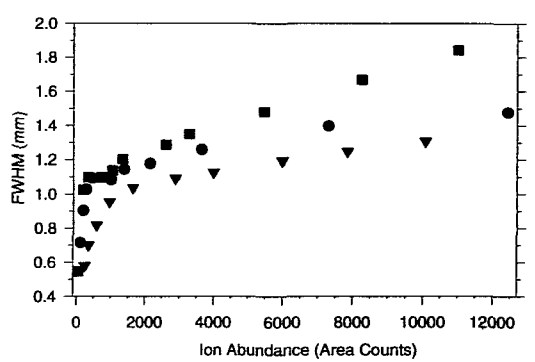

Ion Trap Mass Spectrometry: Variations in Electrode Size and RF Drive Frequency

A.W. Garrett, C.G. Gill, and P.H. Hemberger. Chemical Science and Technology Division, Los Alamos National Laboratory, Los Alamos, NM 87545

The use of smaller electrodes, reduced RF drive frequencies, resonance ion ejection, [1] and nonlinear resonance ion ejection [2] have all been used to increase the 650 amu mass/charge range of the standard Finnigan ion trap mass spectrometer. However, some of these techniques may have detrimental effects on other operational characteristics of the ITMS. Previous work has shown that mass resolution is dependent on ion density and electrode geometry [3]. Two sets of electrodes that are 0.8 (r_0 = 0.8 cm , z_0 = 0.566 cm) and 1.4 (r_0=1.40 cm, z_0=0.990 cm) scale versions of the Finnigan electrodes (r_0=1.0 cm, z_0=0.707 cm) have been machined at LANL in order to investigate the effect of size and RF drive frequency (900kHz-1.25MHz) on mass resolution and relative sensitivity. Comparisons of electrode geometries with endcap spacing for the specific cases of $r_0^2=2z_0^2$ and for a geometry stretched 10.7% in z have also been completed.

A direct drive digital synthesizer, used in place of the standard Finnigan oscillator, provided a means to control the frequency of the RF waveform applied to the ring electrode of each ion trap assembly. The RF circuitry was tuned at each drive frequency for minimum reflected power. The endcap electrodes were maintained at ground and a mass spectrum was generated via mass selective instability; axial modulation was not used. Signal from the preamplifier output (pin JA1) of the Finnigan analog board was directed to a digital oscilloscope where mass peak area and width were measured directly. RF scan rates were determined by the time difference between ejection of the m/z 69 and 131 peaks of FC-43. The RF level was adjusted at each RF drive frequency and electrode geometry to maintain a q_z value of 0.3 at m/z=131.

For each size trap, the width of a mass peak (Δm) increases as the ion abundance increases and as the RF drive frequency decreases (q_z remains constant). In addition, the slope of a Δm vs. ion abundance curve increases as the drive frequency increases (Figure 1). These results are consistent with ion tomography experiments which demonstrate that as ions are confined in a deeper potential well, the ion cloud is reduced in size and ion/ion interactions become more prominent.

As expected, normal sized (r_0=1.0 cm) electrodes stretched along the z axis by 10.7% provide better mass resolution than for the ideal ($r_0^2=2z_0^2$) spacing, but this trend was reversed for the smaller (r_0=0.8cm) electrodes. In addition, the normal sized-stretched electrode assembly provided better mass resolution than either the small-stretched or large-stretched assembly These observations indicate that the optimal separation of the endcap electrodes is electrode size dependent.

It is currently difficult to directly compare results between traps of different size because Δm depends on ion abundance and the correlation between mass peak area and ion abundance is uncertain for a given geometry. However, estimates indicate that the small ion trap is approximately two times less sensitive and the large trap is on the order of 5-10 times less sensitive than the normal sized trap. The sensitivity differences are

likely related to non-optimized spacing of the endcap electrodes for the small and large sized electrode assemblies. Perhaps there is some frequency optimization required also.

References

1. R.E. Kaiser, Jr., R.G. Cooks, G.C. Stafford, Jr., J.E.P. Syka, P.H. Hemberger, IJMSIP, 106, 79, (1991).
2. J.Frazen, R-H. Gabling, G. Henin, G. Weib, Proceeding of the 38th ASMS Conference on Mass Spectrometry, 417, 1990.
3. A.W. Garrett, P.H. Hemberger, C.Cleven, R.G. Cooks, Proceeding of the 43rd ASMS Conference on Mass Spectrometry, 1995.

Figure 1: Small Electrodes - Stretched Geometry

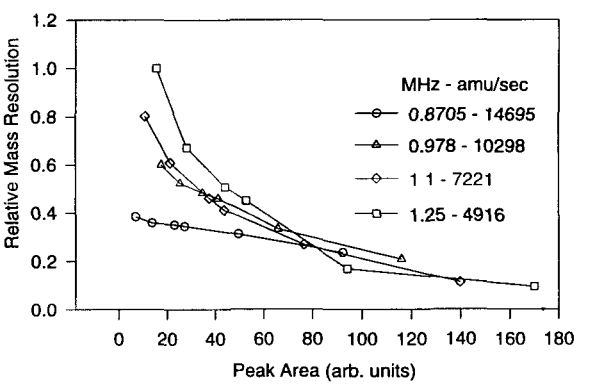

New Modes of Operation of an Ion Trap Mass Spectrometer

C.D. Cleven, C. Weil, M. Nappi, L.A. Horn and R.G. Cooks
Department of Chemistry, Purdue University, W. Lafayette, IN 47907
A.W. Garrett and P.H. Hemberger
Los Alamos National Laboratory, Los Alamos, NM 87545

The ion trajectory simulation program, ITSIM, has been used to investigate the use of quadrupolar dc pulses to manipulate the ion cloud in an ion trap mass spectrometer. Properly timed dc pulses can be used to optimize the shape and position of the cloud for different experiments. Manipulation of the ion cloud is important in photodissociation and in high-resolution experiments because the performance is dependent on the exact location of the ion cloud. Simulated data for both of these experiments are presented, as are experimental data for the photodissociation experiment.

Photodissociation Experiment

When utilizing photodissociation or other laser-based experiments, it is desirable to achieve the highest efficiency possible. In a trapped ion experiment, the photodissociation efficiency may be improved by repeating the irradiation step multiple times as long as the photofragment is not dissociated further. Alternatively, the shape of the target ion distribution can be manipulated so as to irradiate as many of the trapped ions as possible. This is achieved by shaping the ion cloud and in doing this, all ions of the same mass/charge ratio are forced to simultaneously intersect the laser beam. This feature of the quadrupolar pulse means that a mass-selective photodissociation is achieved without prior mass analysis.

Simulations indicate that a quadrupolar dc pulse can be used to force all ions of the same mass-to-charge ratio to be in phase with each other or phase-shifted by exactly 180 degrees. Hence, all the ions cross the z-axis simultaneously every 180 degrees of the radial secular cycle. If a laser beam is focussed collinearly with the z-axis and pulsed at an appropriate time following excitation, it will simultaneously irradiate all ions of a given mass. Besides improving the photodissociation efficiency, the experiment also provides the possibility to photodissociate ions of a particular mass present in a mixture of other ions. Figure 1 shows the spatial positions of ions of two different masses at a specific time following the quadrupolar dc pulse. When ions of a particular m/z ratio are focussed to the center of the trap, ions of different m/z ratios (and different secular frequencies) will still be dispersed in the axial and radial dimension. These experiments were performed using H_5- and D_5 -benzoyl cation at many different delay times (Figure 2), and the expected improvement in performance is achieved.

A New High-Resolution Experiment

Application of quadrupolar dc pulses during dipolar ac activation provides a new method of mass analysis as suggested by simulations of ion motion using ITSIM. The rf/ac signals are phase-locked and a dc pulse is applied at a specific time in the secular motion of a trapped ion population. Application of the pulse at the appropriate time results in increased separation from other ions of different mass-to-charge ratios (Figure 3). After the ions become spatially separated, another dc pulse is applied, again at an appropriate time in the secular period so that only ions of the mass of interest are axially ejected. The simulations show that isobaric ions are completely ejected in one rf cycle, and that complete separation of ions of m/z 344 80 and 344.83 is possible. Alternative experiments in which a series of dipolar dc pulses are used give comparable results, although with somewhat lower mass resolution.

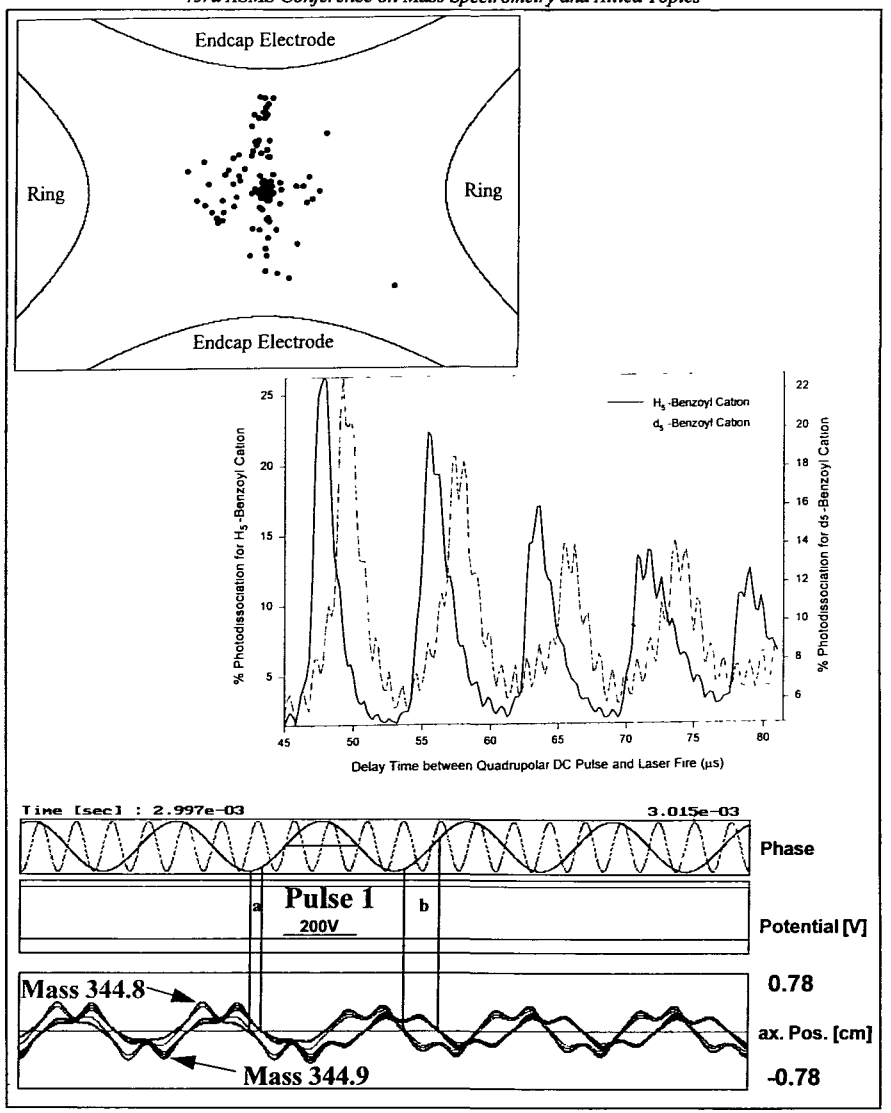

CALCULATION OF PARAMETRIC RESONANCE FOR NONLINEAR ION TRAP

Efim A. Dynin* and Nicholas J. Kirchner
Massively Parallel Instruments, Inc., 2030 Fortune Dr., Suite A, San Jose, CA 95131

The new method of parametric excitation enhances the performance of RF traps by applying pump voltage in series with drive source (1, 2) For linear trapping field the maximum efficiency is obtained when pumping frequency is equal to doubled frequency of secular motion and amplitude of ion oscillations increases without bound. However, nonlinear effects produce a detuning during excitation and modify an ion response. The purpose of present research is to investigate the influence of octupole anharmonicity on the parametrical resonance in the axial direction.

We report results of calculations for a time-dependent spatially inhomogeneous potential

$$\Phi(r,z,t)=\frac{c}{2z_0^2}\left(V_0\cos(\Omega t)-u\cos(\omega t)\right)\left[z^2-\frac{r^2}{2}+\frac{g}{z_o^2}\left(\frac{z^4}{3}-z^2r^2+\frac{r^4}{8}\right)\right].$$

Here r, z - cylindrical coordinates of ion, t - time, $2z_0$ - endcap separation, V_0 and u - trapping and pump voltages, Ω - trapping frequency, ω - pumping frequency Dimensionless parameters c and g depend on trap design

For pure quadrupolar field without pumping ($g = 0$, $u = 0$) the parameter $q = 2ecV_0/(mz_0^2\Omega^2)$ defines the behavior of ion with mass m and charge e. In particular, if $q << 1$ the trajectory is dominated by secular motion with frequency $\omega_0 = \Omega q/(2\sqrt{2})$ and constant amplitude The three additional small field parameters $\alpha = u/V_0$, $\varepsilon = (\omega - 2\omega_0)/\omega_0$, and g are included in numerical integration of the equations of motion for given potential Examples of simulations are presented in figures for the Finnigan MAT ion trap where, according to (3), $z_0 = 7\ 83$mm, $c = 2\ 17$, $g = 0\ 037$ Other parameters used in calculations are $V_0 = 50$ V, $u = 1$ V, $(\Omega/(2\pi)) = 1$ MHz, $(m/e) = 61$, $q = 0.142$ Initially ion has zero velocity and is located at r = 0 with axial coordinate z(t=0) which is shown at the figures.

The general conclusions from calculations are the following.

1- Besides micromotion and secular motion the ion is involved in oscillations with a frequency which may be significantly lower than the secular one (Fig a).

2- The period of these oscillations increases with decrease of $|\alpha|$, $|z(t=0)|$, and $|g|$.

3- The amplitude in resonance has a region of sharp dependence on the pump frequency (Fig b)

4- The maximum of amplitude has weak dependence on initial conditions and is close to $z_0\sqrt{|2\alpha/(gq)|}$

The last estimate was also derived by the analytical approach based on effective potential

$$U_{eff}=\frac{m\omega_0^2z^2}{2}\left(1-\frac{4\alpha}{q}\cos(\omega t)+\frac{8gz^2}{3z_0^2}\right).$$

The ability of such simple model to reproduce the qualitative characteristics may have important applications in the development of new schemes for nonlinear ion trap operation

References

(1) R.E. March, A W McMachon, E T Allinson, F A Londry, R L. Alfred, J. F J Todd, F Vedel, *Int. J. Mass Spectrom. and Ion Processes*, **99** 109 (1990)
(2) P Kelley, D Hoekman, S Bradshaw, L. Jones, J Louris, R Wilson, R Wuerker; Proceedings for the 42nd ASMS Conference on Mass Spectrometry and Allied Topics, p. 709, (1994).
(3) Y. Wang and J. Franzen; *Int. J. Mass Spectrom. and Ion Processes*; **132** 155 (1994).

43rd ASMS Conference on Mass Spectrometry and Allied Topics

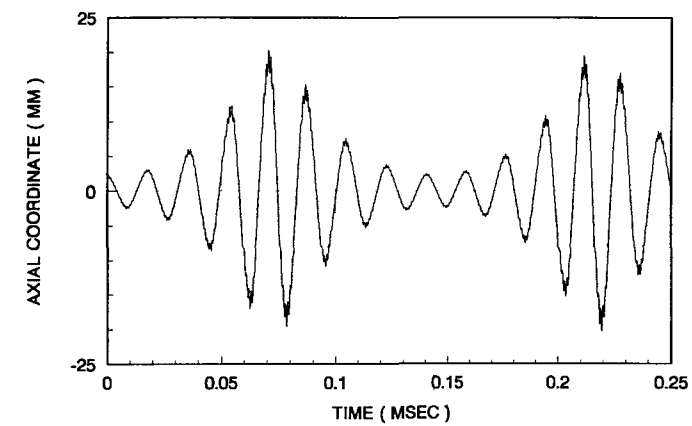

Figure A. Ion evolution for z(t=0) = 2 mm.

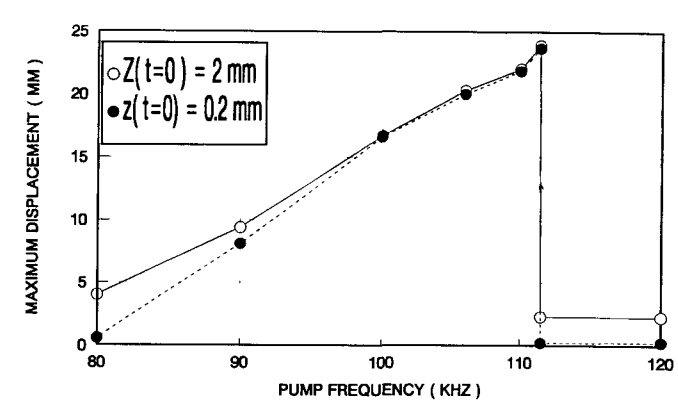

Figure B. Resonance curve.

The Use of Ion Trap Mass Spectrometry with FNF Waveforms for the MS/MS of Cocaine

Mark L. Miller
FBI, FSRTC, FBI Academy, Quantico, VA 22135

Quadrupole ion trap (IT) mass spectrometry with filtered noise field waveforms (FNF) should permit the trace detection of drugs of abuse in complex samples with high sensitivity and selectivity. The Teledyne 3DQ Discovery is equipped with FNF waveforms and this type of IT has numerous operational parameters. Because of this, extensive optimization is needed to develop mass spectrometry methods on it. An additional set of parameters which has a complex interplay with the performance of the IT is the connection of the gas chromatograph. Electronic pressure control on the GC allows for flexible control of the helium pressure for the carrier gas velocity and the buffer gas pressure in the IT. This was conducted to find the best conditions for the detection of cocaine to enable the trace analysis of drugs in difficult samples.

The difficulty of finding the right IT parameters was initially found when the switch was made from solution standards of cocaine to actual samples of hair extracts containing the drug. EI GC/MS spectra down to 100 pg were obtained on standards using FNF notch filters to block out unwanted ions but the spectrum was still hard to find in the extract analysis data. Similar problems were encountered in the GC/MS/MS mode with CAD FNF waveforms. It was also observed the CAD spectra changed with GC injector head pressure at the time of peak elution.

The FNF software is very flexible but the operational parameters are critical to the success of the experiment. FNF isolation of the cocaine ions after ionization resulted in $(M+H)^+$ at 304 which was much larger (4X to 5X) than the M^+ at 303 that could be isolated during ionization. The $(M+H)^+$ comes from self chemical ionization that occurs at the long ionization times used (50-800 ms). The CAD spectra of cocaine were very sensitive to the tickle voltage over a narrow range of 100-200 millivolts. Below this range few daughters are produced and above it all ions start to disappear. A tickle of 10 milliseconds worked best in that it gave 182 daughter intensities comparable to longer times but still left some 304 intensity. The RF mass for the tickle was less critical than other parameters but at low RF mass levels such as 40, no daughters were generated for cocaine. The FNF notch width was important to both the CAD spectrum and the blocking out of interfering ions. Narrow FNF notches gave the best

balance between parent/daughter intensities and minimum interference. Using the solid probe to optimize the scan function for CAD was helpful but was not sufficient for setting up high sensitivity GC/MS/MS scan functions on its own. Additionally, the scan functions required reoptimization any time the instrument was recalibrated. Attempts were made to overcome this problem by using a CAD "wiggle" where the RF mass is scanned over a narrow range (1-2 amu) during the tickle to compensate for slight changes in the tuning/calibration. However, the wiggle gave lower spectral intensities. Pre- and post-ionization times, and collisional cooling had little effect on the CAD spectral intensity of cocaine under the experimental conditions.

The optimum scan function found thus far is a two step tickle with FNF post-ionization isolation of 304. In the two step process the first CAD tickle uses an RF mass of 60 at 0.2v and the second tickle uses an RF mass of 75 at 2.15v. Another benefit of the two step tickle observed was the reduction in the amount of interfering ions that were not from the CAD process. The cocaine EI base peak of 82 (and other nonrelevant ions) appeared in spectra at much larger intensities than the parents or daughters if proper parameters were not used. With the best scan function found so far, 100 pg (on-column) of cocaine could be detected by MS/MS using a 800 ms ionization time and a split GC injection at 10 psi (0.25mm X 15m column). See figure below. This function was optimized using rapid/high temperature (240°C) split injections. However, the scan function was found to be sensitive to the chromatography because cocaine CAD spectra could not be detected in the splitless mode below 100 ng.

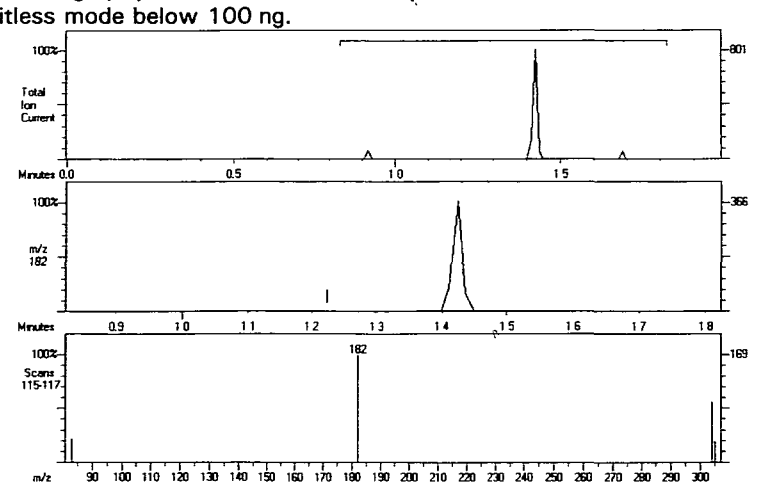

BIOMARKER DETECTION LIMITS UTILIZING A Py-QUADRUPOLE ION TRAP SYSTEM

Franco Basile, Curtis Mowry and Kent Voorhees*
Dept. of Chemistry, Colorado School of Mines, Golden, CO 80401

The Chemical/Biological Mass Spectrometer (CBMS) battlefield detector is composed of an impactor/pyrolyzer, transfer line, membrane interface, and a quadrupole ion trap mass spectrometer (QITMS). The CBMS is designed for real-time, field operation and uses an ion-getter pump and a non-linear quadrupole ion trap which allows operation with air as the buffer gas. Among the biomarker compounds used in the detection and identification of biological threats are isoprenoid quinones and fatty acids. The objective of this work is to characterize detection of these biomarkers with the CBMS system.

FATTY ACID METHYL ESTERS (FAMEs)

Detection Limits: The detection limit of a taxonomically significant methylated fatty acid, palmityl-methyl ester (C16:0 ME, FW: 270) was determined in the CBMS system. The detection limit for C16:0 ME is approximately 50 ng (19 nmol; MS Charge Control; m/z's used= 227, 199, 185, 171, 143; S/N= 10), with the sample injected through the IR pyrolyzer. The amount of "airborne" bacteria that can be detected with the CBMS system based solely on the detection of fatty acid biomarkers can be calculated. The CBMS system is designed to detect 60 CFU/L-air in 2 minutes of sampling (CFU = Colony Forming Units. 1 CFU ≥ 1 bacteria). The impactor has an air intake of 1000 L/s and collects bacteria with an overall efficiency of 50 %. At the 60 CFU/L-air limit, 5×10^6 CFU are collected in 2 min. If one assumes a single-cell mass of about 10^{-12} g, a 90 % water composition, and an average of 4 bacteria/CFU, the CBMS collects about 2 μg of dry cells in 2 min. For a Gram-negative bacteria like *Brucella*, 21% of its dry weight is cell wall, or 0.42 μg. The cell wall contains approx. 18 % lipid by weight or 76 ng of bound and free lipids. With an efficient *in situ* methylation of all bound and free lipids, the detection target of 60 CFU/L-air in 2 min can be accomplished solely based on lipid biomarkers like saturated fatty acids. This result was achieved without an optimization of the membrane interface in the CBMS system.

ISOPRENOID QUINONES

Two general types of isoprenoid quinones are found within eubacteria, benzoquinone-based Ubiquinones (Q-N) and napthoquinone-based Menaquinones (MK-N). Upon electron ionization, each type of quinone produces characteristic fragment ions. These fragments can be used as biomarkers (within the mass range of the CBMS) to aid in the identification of airborne bacteria. For example, Gram-positive bacteria contain only menaquinones, while Gram-negative may contain either type. Detecting the molecular ions of quinones will increase the probability of identification, as the distribution of quinones (with varying length of side chain and saturation) varies among bacteria. The top spectrum contains a full scan of an injection of Vitamin K2 (MK-4). The lower spectra demonstrate the utility of MS/MS in the ion-trap for biomarker detection. By isolating and then fragmenting m/z 225, the structure and therefore identity of this typical Menaquinone fragment can be confirmed.

Both types of biomarkers are sufficiently non-polar to be transmitted through the CBMS transfer line and membrane, and standard electron ionization/CID fragments were observed. Pyrolysis, transfer line, and membrane conditions still need to be optimized to improve detection limits for these important bacterial biomarkers.

ACKNOWLEDGEMENT

The authors are grateful for the generous support from the U.S. Army ERDEC (Grant: DAAL 03-92-G-003).

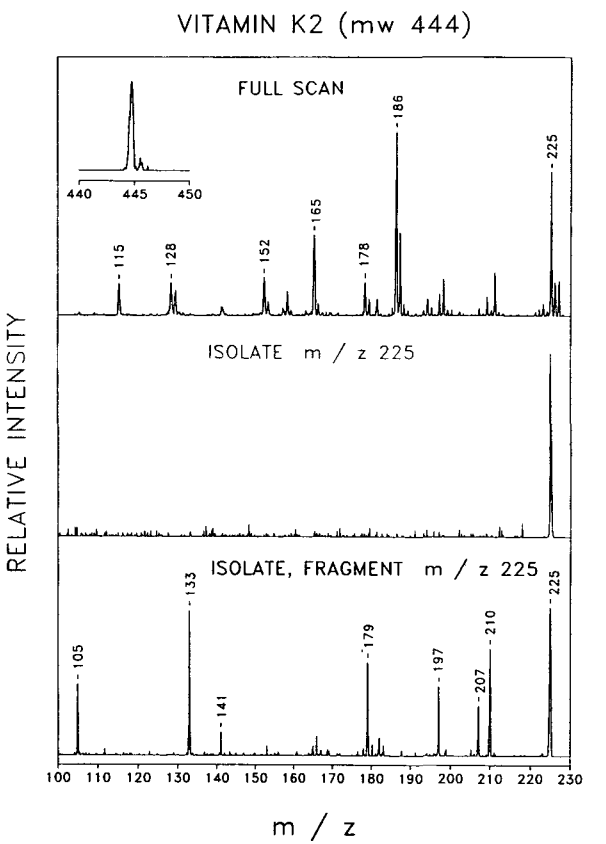

ION-MOLECULE REACTIONS OF NO IN THE QUADRUPOLE ION TRAP: IMPLICATIONS FOR BIOLOGICAL METABOLIC STUDIES

Susan F. Silverton, Jodie V. Johnson, Cecilia Basic and Richard A. Yost
University of Pennsylvania, Philadelphia, PA, Villanova University, Villanova, PA and University of Florida, Gainesville, FL

Quadrupole ion trap mass spectrometry (QITMS), with its excellent sensitivity, would seem to be an ideal instrument for real time monitoring of biological reactions in solution. In particular, the ability to monitor volatile products produced by cell populations could provide significant details of cellular metabolism during dynamic changes in cell function.

We have initiated a series of feasibility studies using a membrane interface to deliver gases dissolved in cell culture media to a QITMS. In addition to the compounds of interest, CO_2 and NO, significant amounts of H_2O, N_2, and O_2 are also introduced into the ion trap. Initial experiments showed that the presence of these other components lead to space-charging and ion-molecule reactions which affect the determination of CO_2^+ (m/z 44). However, the differences in ionization potential and proton affinities between CO_2 and NO led us to suspect that ion-molecule reactions of NO in the ion trap might interfere less with the determination of this volatile metabolic product. In these experiments, we have also attempted to reduce space-charging by controlling the ionization time and RF levels, and have investigated ion-molecule reactions of NO^+ (m/z 30) occurring during the chemical ionization of a mixture of water, nitric oxide, nitrogen, oxygen and carbon dioxide.

Methods

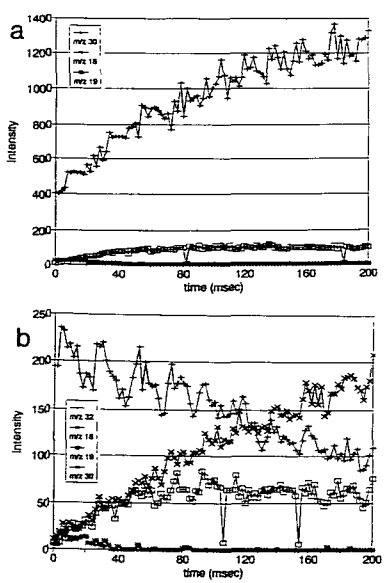

Figure 1 Mass selective CI and ion-molecule reactions of (a) NO (m/z 30) and (b) O_2 (m/z 32)

Ion-molecule reaction studies were performed on a Finnigan ITMS and gases were introduced via metering valves. Upon chemical ionization, N^+, H_2O^+, N_2^+ (or CO^+), NO^+, O_2^+, and CO_2^+ were the major ions produced. In separate experiments, each of these ions was mass-isolated and allowed to react with the gases present for periods up to 200 ms. Several sets of these experiments were performed with different amounts of NO and H_2O present. Note that helium was not present during these experiments.

Results

With only residual water and air present, the pressure in the quadrupole ion trap vacuum chamber was 5.3 $\times 10^{-7}$ torr, indicated. Nitric oxide was added to the vacuum chamber to yield an indicated pressure of 8.3 $\times 10^{-7}$ torr. Then water was added to the vacuum chamber to yield a total indicated pressure of 1.5 $\times 10^{-6}$ torr. Under these conditions, the mass selective reaction of H_3O^+ became the dominate ion following the mass selected CI reactions of H_2O^+, H_3O^+, N_2^+, and CO_2^+ . Based upon their higher ionization potentials, (Figure 2), N_2^+ and CO_2^+ underwent charge exchange with H_2O to form H_2O^+ which subsequently underwent self-CI, i.e. $H_2O^+ + H_2O \rightarrow H_3O^+$. As the proton affinity of NO (113 kcal/mole) is lower than that of water (166 kcal/mole), H_3O^+ did not protonate NO (Figure 1a). Also, as the ionization potential of O_2 is below those of H_2O, CO_2 and N_2, but above that of NO (Figure 2), the reaction of mass selected O_2^+ ions under these conditions yielded predominately NO^+ ions (Figure 1b).

IONIZATION POTENTIAL CHART

ION	M/Z	IE (eV)
N^+ (from N_2)	14	24.3
CO^+ (from CO)	28	19.5
Ar^+	40	15.8
N_2^+	28	15.6
CO^+ (from CO)	28	14.0
CO_2^+	44	13.8
H_2O^+	18	12.6
O_2^+	32	12.1
NO^+(from NO)	30	9.3

Figure 2 Ionization Potential Chart

Discussion

The ability to form and detect NO^+ successfully in the quadrupole ion trap in the presence of significant amounts of H_2O is in direct contrast to our previous attempts to form and detect CO_2^+ under similar conditions. This is due strictly to the relative ionization potentials of the neutral species determining what ion chemistry will occur and thus which ion will predominate in the quadrupole ion trap.

In these metabolism studies, the nitric oxide (NO) produced from the cell cultures will be significantly less abundant than H_2O, O_2, CO_2 and N_2. However, based upon the results above, NO would undergo charge exchange with all of these ionized species to form NO^+ and permit successful detection. Of more concern is the high concentration of water which is present. Although water does not undergo any significant ion-molecule chemistry with NO^+, the formation of abundant H_2O^+ and H_3O^+ ions during ionization leads to severe space charging, while the abundance of neutral water appears to lead to poor overall ion trap performance.

As far as future directions are concerned, the design and construction of a membrane introduction mass spectrometry (MIMS) interface for the on-line measurement of NO levels produced by functional cell cultures using an ITD ion trap mass spectrometer is currently underway. The MIMS is designed to accommodate a 1 ml stirred cell culture beaker and includes an injection port to allow the introduction of reagents to initiate cell events. The design will make use of a jet separator assembly with a coaxial flow of He similar to that reported by Dejarme, et al . [2]. However, in this design, the membrane will be placed directly within the cell culture fluid.

In order to reduce space-charge effects and increase the sensitivity of future NO analyses, stored wave form inverse Fourier Transform SWIFT wave form methods [3, 4] will be implemented to selectively eject all ions except those of the analyte during the ionization period.

1. Johnson, J.V., Silverton, S.F. Yost, R.A. Ion-Molecule Reactions of CO_2 in the Quadrupole Ion Trap: Implications for Biological Metabolic Studies. ASMS, 1994.
2. Dejarme, L.E., Bauer, S.J., Cooks, R.G., Lauritsen, F.R., Kotiaho, T. Graf, T. Rap Comm. Mass Sepctrom. 7 (1993) 935-942.
3. Julian, R.K., Cooks, R.G., Anal. Chem. 65 (1993) 1827
4. Soni, M.H., Cooks, R.G.Anal Chem. 66 (1994) 2488.

Barbiturate Analysis In A Quadrupole Ion Trap: Borinium Adduct Ion Formation

Armando Colorado and Jennifer Brodbelt, Department of Chemistry, University of Texas at Austin, Austin, Texas, 78712.

Introduction. Barbiturates are a powerful class of sedative/hypnotic pharmaceuticals with a diversity of uses, ranging from their utility as anesthetics, to treatment of anxiety, insomnia, and epilepsy. Barbiturate derivatives have a great degree of hydrogen-bonding activity, due to the fortuitous arrangement of hydrogen-bond donor and acceptor groups around the pyrimidine ring. Thus, there has been much use of barbiturates in the modelling and construction of supramolecular assemblies designed with an array of hydrogen bonding interactions. An understanding of the structural features which mediate hydrogen bonding participation in these types of compounds is essential. In the present study, both of these reasons are exploited in order to evaluate a new method for characterizing barbiturate derivatives based on selectivity of hydrogen-bonding interactions. In this report, we exploit the special reactivity of borinium ions to form strong hydrogen bonded adducts with barbiturate derivatives and then undergo characteristic dissociation reactions.

Experimental. Experiments were performed using a Finnigan ITMS operated in the mass selective instability mode. Barbiturates were introduced into the vacuum chamber via a heated solids probe at pressures ranging between 0.9-2.0 X 10^{-6} torr. TMB was introduced through a leak valve at a pressure corresponding to 6 X 10^{-6} torr. One mtorr of helium was added after the CI pressure had stabilized. Ion-molecule reaction periods ranged between 50 and 150 ms. The ion trap temperature was held at 120°C. For mass-selective isolation, a DC voltage was applied with an appropriate rf voltage to the ring electrode. Typical tickle voltages used were between 200 and 400 mV at a q value of 0.4. An activation time of 10 ms was utilized in all experiments.

CAD of the Borinium Adducts.. CAD of the borinium ion adduct $[M + 73]^+$ yields an array of fragment ions not observed in the dissociation of the protonated species. As in conventional EI and CI, the borinium adduct ion loses a side chain functional group, however, other numerous dissociation channels are followed and other products resulting from secondary ion-molecule reactions are generated For example, the borinium adduct of amobarbital dissociates by 14 pathways, whereas protonated amobarbital only produced three types of fragments. Likewise, the borinium adduct of hexobarbital dissociates by many more pathways than protonated hexobarbital. There are several possible explanations for the increased variety of fragmentation of the borinium adducts relative to the protonated structures. First, the borinium cation may tend to attack at several competing positions of the barbiturates, whereas protonation may occur only at one site. Second, the borinium adducts likely incorporate multiple hydrogen bonds that enhance specific types of rearrangements and secondary reactions.

One common neutral loss for each of the borinium adducts is the elimination of methanol. As shown later by the use of model compound studies, this pathway is an intramolecular rearrangement involving the elimination of a methoxy group from the borinium portion and an acidic proton from the barbiturate. The difference reflects whether the borinium cation is attached to an oxygen or nitrogen atom. In some cases, the elimination of methanol occurs in conjunction with the loss of the substituent found at the C5 position of the barbiturate.

The most interesting new product observed upon activation of the borinium/barbiturate adduct is the formation of a secondary ion-molecule reaction product, assigned as $[M + 73 - CH_3OH + TMB]^+$. Thus, the $[M + 73]^+$ adduct first undergoes the intramolecular elimination of methanol, then rapidly and spontaneously adds a molecule of trimethylborate. The unusual addition of TMB only occurs in conjunction with the loss of methanol, and attachment of TMB is not observed for the other fragments. This product is seen for barbital and thiamylal directly, and is observed for amobarbital and pentobarbital at long reaction times or higher reagent pressures. With the exception of thiamylal, the attachment of TMB to the $[M + 73 - CH_3OH]^+$ fragment also occurs along with the loss of the side chain functional group at the C5 position for all compounds. In general, the formation and stability of the $[M + 73 - CH_3OH + TMB]^+$ product appears to correlate with the availability of hydrogen bonding sites on the barbiturate ring.

CAD of Borinium Ion Adducts for Model Compounds. The reactions of strategically chosen, simple model compounds give new insight by restricting the number of functional groups in question, and selectively eliminating the interference of other reactive functionalities. Ten model compounds were chosen for this study: urea, uracil, glutaramide, piperidine, pyrimidone, cyclohexanone, barbituric acid, 1-methyluracil, 1,3 dimethylbarbituric acid, and 1,3 cyclohexadione. Upon reaction with the borinium ion, each forms the $[M + 73]^+$ adduct. Results show that six out of ten compounds form the $[M + 73 - 32 + TMB]$ adduct. Thus, the four compounds which fail to form the $[M + 73 - 32 + TMB]^+$ adduct include cyclohexanone, 1,3-cyclohexadione, urea, and 1,3 dimethylbarbituric acid. The functional group responsible for the formation of this interesting adduct apparently is the amine. If the amine is blocked by a methyl group as in the case of 1,3 dimethylbarbituric acid, then no TMB adduct is generated at $[M + 73 - 32 + TMB]^+$. Cyclohexanone is a compound in which methanol loss is not observed for the $[M + 73]^+$ adduct, and thus the secondary ion-molecule reaction product is prohibited. The 1,3 cyclohexadione-borinium ion adduct undergoes the loss of methanol but no TMB adduct is observed, probably due to weak hydrogen-bonding strength of the diketone. As proposed in Scheme 2, certain hydrogen-bonding interactions are critical for promoting the multi-step reaction. The four models that failed lacked one or more features deemed necessary for the reaction.

To characterize the nature of the $[M + 73 - 32 + TMB]^+$ adduct, this adduct was isolated and subjected to CAD. For 1-methyluracil, pyrimidone, and piperidine, the adduct eliminates TMB. This dissociation behavior is characteristic of a weakly bound adduct that simply disassembles when energized. In contrast, the adducts for glutarimide, uracil, and barbituric acid undergo numerous dissociation pathways, including elimination of methanol. This behavior typifies that found for strongly bound species. Therefore, the structures of the $[M + 73 - 32 + TMB]^+$ also seem to differ depending on the nature of the model compound, presumably because of its intrinsic basicity and positions of hydrogen-bonding sites. For example, uracil has two amine sites capable of participating in hydrogen-bonding, whereas in 1-methyluracil, one of the nitrogens is blocked by a methyl group so the acidic hydrogen is gone. This subtle difference may impact the stability of the resulting adducts, as shown in Scheme 1.

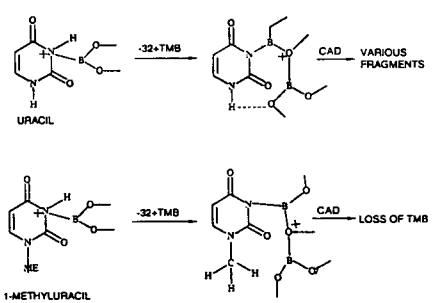

Scheme 1

Measurement Of Crtical Energies In A Quadrupole Ion Trap

Armando Colorado and Jennifer Brodbelt, Department of Chemistry, University of Texas at Austin, Austin, Texas, 78712.

Introduction Energy resolved mass spectrometry (ERMS) techniques have been in existence for over a decade. Applications include isomer distinction, evaluation of gas phase acidities , as well as the determination of critical energies (CE) for dissociation (1-4). Collisional activation dissociation (CAD) and photodissociation (PD) are two methods currently employed in obtaining CE's of gas phase ions. Quadrupole ion traps, in general, have never been viewed as optimal instruments for the measurement of critical energies due to the "non-zero" translational energy distributions of trapped ions, the potentially large spread in kinetic energies as ions are accelerated, and the multiple collision conditions in the case of quadrupole ion traps. Hart and McLuckey, however, from the Oak Ridge National Laboratory showed a logrithmic correlation between the threshold resonant excitation amplitudes (TREA) and literature critical energy values in a quadrupole ion trap by studying the kinetics of ion decomposition (5).

This paper introduces a facile and fast technique which allows CE's to be directly evaluated via threshold activation voltage (mV) measurements in a quadrupole ion trap utilizing calibration compounds with well defined dissociation energies. Also, the feasability of utilizing infrared multiphoton photodissciation in the measurement of CE's in a quadrupole ion trap will also be discussed.

Collisional Activation Experiment. All experiments were perfomed in a Finnigan Ion Trap Mass Spectrometer operated in the mass selective instability mode. Samples were introduced into the chamber via a leak valve or solids probe inlet at pressures between 6.0-8.0 X 10^{-6} torr (uncorrected), raised to 1.2 X 10^{-4} torr He (uncorrected) after sample pressures had stabilized. A q-value of 0.4 and an activation time of 10 ms were used for all experiments unless otherwise noted. Ion-molecule reaction times were in the range of 10-150 ms while a cooling time prior to activation was held at 10 ms. The trap temperature was kept at 120 °C. The range of tickle voltages applied across the endcaps were between 10-300 mV. For these sets of experiments, the threshold activation voltage was defined as that voltage where the daughter ion intensity is 10% of the total ion intensity. All samples were purchased from Aldrich Chemical Co. with the exception of anhydrous ammonia (MG Industries).

Collisional Activation of Calibration Compounds. The calibration compounds chosen for this study are tetraethylsilane (0.5 eV), nitromethane (0.7 eV), butylbenzene (1.1 eV), ethylbenzene (1.3 eV), toluene (1.7 eV), and styrene (2.4 eV). A plot of threshold activation voltage vs. literature CE's shows a linear function (Figure 1). A special case is the tetraethylsilane ion which spontaneously dissociates under the current operating conditions and is therefore considered the lower limit for which a threshold voltage can be measured. It is assigned a value of zero.

Effect of Instrument Parameters on Threshold Activation Voltage. The q-value appears to have little effect on the measured threshold voltages, but the activation time has a noticeable effect. Three activation times were utilized to examine the effect on the threshold voltage at three different q-values (0.3, 0.35, and 0.4). At an activation time of 10 ms, a linear relationship is exhibited between threshold activation voltage and critical energies. At 50 ms and 100 ms, however, a non-linear relationship is observed. At these long activation

times, other processes compete effectively with ion dissociation. Most importantly, ion-molecule charge-transfer reactions occur that deplete the fragment ion population.

Correlation of Threshold Activation Voltage and Degrees of Freedom. The energy required to excite a gas-phase ion into the quasi-continuum is highly dependent on the number of vibrational degrees of freedom, because of the ergodic energy distribution. This dependence was studied by measuring the threshold activation voltages of simple protonated aminoalcohols and dehydrated quinolone/aminoalcohol complexes. Results show dehydrated quinolone/aminoalcohol complexes do indeed have higher dehydration thresholds over simple protonated aminoalcohols. For example, protonated aminoethanol had a measured CE value of 1.1 eV versus 1.7 eV for the aminoethanol/nalidixic acid complex. Again, the increased number of degrees of freedom allows energy to be distributed over a larger number of bonds, thus increasing the dissociation threshold.

Collisional Activation of Hydrogen-Bonded Complexes. The determination of hydrogen-bonding interactions is particularly important in molecular recognition, where complexes may be assembled entirely by hydrogen-bonds. Thus, we wished to develop a quantitative analysis of model host-guest complexes. A series of crown ether/ammonium ion complexes were evaluated to correlate the stength of the hydrogen-bonding interactions with structural features. 12-crown-4, 15-crown-5, and 18-crown-6 were allowed to react with the ammonium ion to form the [L + NH_4^+] complexes. Activation experiments showed that the number of available binding sites and the geometry of the interactions affected threshold values. For example, the 12-crown-4/NH_4^+ complex dissociated at a critical energy value of 1.3 eV while the 18-crown-6/NH_4^+ complex dissociated at 2.2 eV. Increasing the basicity and the number of hydrogen-bonding sites of the guest also had an affect on the CE for dissociation. Activation of the 15-crown-5/aminoethanol dimer had a critical energy approximately 0.7 eV higher than the 15-crown-5/NH_4^+ dimer.

References:

1. Fetterloff, D. D.; Yost, R. A. *International Journal of Mass Spectrometry and Ion Physics.* **1982**, 44, 37.
2. Graul, S. T.; Squires, R. R. *J. Am. Chem. Soc.* **1990**, 112, 2517.
3. Dang, T. T.; Motell, E. L.; Travers, M. J.; Clifford, E. P.; Ellison, G. B.; Depuy, C. H.; Beirbaum, V. M. *International Journal of Mass Spectrometry and Ion Processes,* **1993**, 123, 171.
4. Hop, C. E. C. A.; McMahon, T. B.; Willet, G. D. *International Journal of Mass Spectrometry and Ion Processes.* **1990**, 101, 191.
5. Hart, K; McCluckey, S. A. *J. Am. Soc. Mass Spectrom.* **1994**, 5, 250.

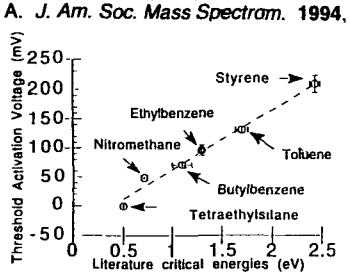

Evaluation of Cooperative Interactions of Quinones in an Ion Trap Mass Spectrometer

Brad J. Hall and Jennifer S. Brodbelt
University of Texas at Austin, Department of Chemistry and Biochemistry
Austin, TX 78712

This undertaking examines several aspects of the gas-phase reactivity of a selected group of primarily naphthoquinone and hydroxynaphthoquinones, a series possessing a variable degree of chelation ability. Gas-phase basicities and borinium cation affinities were determined to allow a correlation of the structural factors which mediate the strength of cooperative binding interactions. Selective ion-molecule reactions with dimethyl ether ions were used to evaluate structural aspects of reactivity. Finally, collisionally activated dissociation was used to characterize product structures and probe intramolecular rearrangements.

Selective Reactions of Dimethyl Ether Ions

Upon ionization, dimethyl ether forms a highly selective reactant, $CH_3OCH_2^+$, which promotes methylation or methylene substitution reactions of organic substrates, depending on the occurrence or absence of cooperative interactions. Illustrated in the table, there are clear preferences for formation of $(M + 15)^+$ vs. $(M + 13)^+$, depending on the presence of a hydroxyl group on the adjacent ring (a plus indicates formation). Methylation is a relatively general occurrence, requiring only the presence of a carbonyl oxygen. In contrast, compounds with a hydroxyl group on the ring adjacent to the quinone ring preferentially form $(M + 13)^+$ products. An intramolecular proton transfer is required for the formation of the $(M + 13)^+$ product, thus illustrating the cooperation involved in the process. A couple of interesting exceptions involve lapachol and 1,4 naphthoquinone. Lapachol may exclusively form $(M + 13)^+$ due to the formation of a stable cyclic structure with the reactivity centered around the unsaturated substituent and the hydroxyl group. 1,4 Naphthoquinone shows no reactivity with CH_3OCH_2; however, the molecular ion of this quinone forms an unusual $(M + 16)^+$ adduct upon reaction with neutral dimethyl ether.

Compound	$(M + 13)^+$	$(M + 15)^+$
Lawsone	o	+
Juglone	+	+
Plumbagin	+	+
Menadione	o	+
5,8 DHNQ	+	+
Lapachol	+	o
1,2 NQ	o	+
1,4 NQ	o	o
Chrysazine	+	+
α-tetralone	o	+

Collisionally Activated Dissociation of Protonated Quinones

Loss of one or two CO units is a common feature to many of the quinones, such as 1,2 naphthoquinone, 1,4 naphthoquinone, plumbagin, menadione, and lapachol. However when a hydroxyl substituent is placed on the ring adjacent to the carbonyl groups, loss of water is seen in addition to carbon monoxide loss. Fragmentation of the ring containing the carbonyl groups is activated when substituents are placed ortho to one of the carbonyl groups.

Relative Gas-Phase Basicities and Borinium Ion Affinities

The relative gas-phase basicity spans a wide range of basicities as evident from the anchor positions of some compounds of known basicity. Several definite distinctions can be seen for the two sets of isomers studied. 1,4 NQ is a weaker base than 1,2 NQ which may be due to charge stabilization over the two adjacent carbonyl groups in 1,2 NQ. Lawsone is much stronger in basicity than juglone, chrysazine, and plumbagin, indicating that the hydroxyl group ortho to the carbonyl stabilizes protonation. It is possible that intramolecular hydrogen-bonding occurring in the latter compounds between one carbonyl oxygen and the hydroxyl hydrogen on the adjacent ring is affecting their basicity. α-Tetralone, which has one of the highest basicities, clearly allows substantial delocalization of the positive charge throughout the phenyl ring. By contrast, in lawsone the proton may be stabilized by the interactive hydroxyl and carbonyl group, but the second carbonyl group withdraws electron density through the ring and effectively destabilizes the proton attachment.

1,4Dioxane(186.0kcal/mol)<1,4NQ<Juglone<5,8DHNQ<Menadione<Chrysazine<Plumbagin<Lawsone<1,2NQ<α-tetralone<pyrrole(200.3kcal/mol)<lapachol<2,5Dimethylpyrrole(210.6kcal/mol)

Borinium ion affinities of the quinones were measured because the borinium ion $(CH_3O)_2B^+$, represents a model of a bulky cation with special hydrogen-bonding capabilities. The borinium cations were generated from ionization of trimethylborate, and then ligand exchange experiments were performed in the usual way. The borinium cation affinity parallels the gas-phase basicity scale with two exceptions, lawsone and 1,2NQ For only those two ligands, the order of affinities is reversed This difference is attributed to the ability of the hydroxyl group of lawsone to undergo special secondary hydrogen-bonding with $(CH_3O)_2B^+$.

1,4NQ~Juglone<Menadione<1,2NQ<Lawsone<α-tetralone~Lapachol

Collisionally Activated Dissociation of $(M + 73)^+$ Adducts

In order to better evaluate the nature of the borinium ion adducts, CAD was used to characterize each $(M + 73)^+$ adduct. Loss of methanol is seen for those compounds that possess hydroxyl groups. Clearly the dissociation depends on intramolecular proton transfer, and is indicative of a complex with cooperative functional groups that can facilitate the rearrangement. In contrast the $(M + 73)^+$ adducts for 1,4 naphthoquinone and menadione break apart and regenerate $B(OCH_3)_2^+$. This behavior is indicative of those ligands which have no possibility of competitive intramolecular hydrogen-bonding interactions between one carbonyl oxygen and an adjacent hydroxyl hydrogen. Finally, the $(M + 73)^+$ adduct of 1,2 naphthoquinone shows the interesting elimination of 30 u, assigned as CH_2O. This adduct may be strongly bound due to the cooperative interactions of the adjacent carbonyl groups, yet it does not permit the simple elimination of CH_3OH due to the absence of an acidic hydrogen. Thus, an alternative hydrogen migration occurs with the subsequent loss of CH_2O.

METAL COMPLEXATION REACTIONS OF QUINOLONE ANTIBIOTICS IN A QUADRUPOLE ION TRAP

*Erwin J. Alvarez, Ming Tang, and Jennifer S. Brodbelt; Department of Chemistry and Biochemistry; The University of Texas at Austin; Austin, Texas 78712-1167.

INTRODUCTION

The field of gas-phase organometallic chemistry has generated increased interest and experienced extraordinary development in the last ten to fifteen years [1,2]. Metal complexation can be used as an analytical tool in several ways to enhance the characterization of complex organic molecules, such as drugs or proteins. First, metal ion attachment as an ionization method provides different ways to activate molecules, depending on the identity of the metal ion. Second, metal ionization alters the stabilities of the resulting products, therefore changing the dissociation pathways. In this study, a quadrupole ion trap mass spectrometer has been used to study the reactions between gas-phase monopositive cobalt, copper and nickel metal ions with a group of quinolone antibiotics, synthetic antibiotics that disrupt bacterial-gene replication [3], in order to compare the differences in product formation and trends in dissociation patterns.

EXPERIMENTAL

All experiments were performed in a Finnigan MAT Quadrupole Ion Trap Mass Spectrometer (ITMS). Ion-molecule reaction times ranged between 50 and 100 ms. Collisional activation was performed by the application of an ac voltage of 0.3-0.4 V_{p-p} at the axial frequency of motion of the ion of interest. Typical tickle voltages used were between 900 and 1000 mV. A q value of 0.3 was used; activation times were typically 10 ms. A Quanta Ray GCR-11 Nd:YAG laser (532 nm, 6-7 ns pulse width, 135-155 mJ/pulse) was used for desorbing a pure metal foil.

RESULTS AND DISCUSSION

Ion-molecule Reactions between Quinolone Antibiotics and Monopositive Metal Ions

Quinolone neutrals were allowed to react with Co, Ni and Cu ions formed by means of laser desorption. Metal ionization with copper and nickel ions resulted in adduct ions of the form $(M + Cu)^+$ and $(M + Ni)^+$ respectively while addition-elimination products of the form $(M + Co - 28)^+$ were typically observed when cobalt was employed. The elimination of the CO unit seems to be favored by the formation of a cyclized product which is stabilized by an intramolecular hydrogen bond (Scheme 1). The complexation of the metal ion by the quinolone allows the activation of certain regions of the charged molecule via insertion of the metal ion into particular bonds. This results in access to alternative dissociation channels.

Collision Activated Dissociation of $(M + Co - 28)^+$ Products

Collisional activation of the $(M + Co - 28)^+$ product revealed that dehydrogenation is the predominant fragmentation pathway for all the quinolones except flumequine; for enoxacin and piromidic acid it is the exclusive dissociation channel. The absence of an ethyl group seems to explain why flumequine does not exhibit this loss. Other fragmentation pathways can be rationalized as losses of organic units such as C_2H_2 or CH_4 in which the aromaticity and conjugation factors that provide such great stabilization to the quinolones are not compromised. Alternative fragmentations are viable depending upon the initial insertion point of the metal ion. For example, it is well-known that Co^+ may insert into C-O, C-C, and C-N bonds. For flumequine and oxolinic acid, the CAD patterns of the $(M + Co - 28)^+$ complexes are much more diagnostic than was noted for the CAD patterns of the protonated species. For oxolinic acid, the fragment ions can be used to identify the dioxolane ring, in addition to the ethyl and carboxylic acid substituents.

Collision Activated Dissociation of $(M + Ni)^+$ Products

The predominant fragmentation pathway for the $(M + Ni)^+$ product is the loss of 44 u, which can be rationalized as loss of CO_2 from the metallated quinolone. This process would occur by insertion of the metal ion into the carbon-carbon bond adjacent to the carboxylic acid moiety. In general, the CAD patterns for the $(M + Ni)^+$ ions are most informative (Table 1). For example, the loss of 101 u in the enoxacin spectrum can be assigned as the elimination of CO_2 and part of the piperazine ring. For oxolinic acid, the loss of 104 u represents the elimination of CO_2 and part of the dioxolane ring. For piromidic acid, the loss of 85 u may be assigned as the elimination of CO_2 and part of the pyrrolidine ring. Flumequine shows the loss of 64 u, which likely represents the loss of CO_2 and HF. These CAD patterns offer a highly diagnostic way to identify each quinolone.

Collision Activated Dissociation of $(M + Cu)^+$ Products

Again, loss of CO_2 is common, but there are generally fewer informative fragment ions in these spectra. The copper complexes of enoxacin, oxolinic acid, and piromidic acid all show the significant elimination of 110 u, which must represent the loss of half of the N-ethyl-pyrrolidinone containing the carboxylic acid substituent.

CONCLUSIONS

Metal ionization of quinolone antibiotics with copper and nickel ions resulted in addition products of the form $(M + Cu)^+$ and $(M + Ni)^+$ respectively while addition-elimination products of the form $(M + Co - 28)^+$ were observed when cobalt was used. In most cases, there may be several sites of metal ion insertion, and thus several different structures of cationized quinolones that may undergo diverse fragmentation processes. The CAD patterns of the nickel complexes proved to be the most structurally informative, more so than the fragmentation patterns of the protonated quinolones.

REFERENCES

1. Eller, K.; Schwarz, H. *Chem. Rev.* **1991**, 91, 1121-1177.
2. *Gas Phase Inorganic Chemistry*; Russell, D. H., Ed.; Plenum Press: New York, 1989.
3. Chu, D. T. W.; Fernandes, P. B. *Antimicrobial Agents and Chemotherapy*. **1989**, 33, 131-135.

Scheme 1: Formation of $(M + Co - 28)^+$ for Nalidixic acid

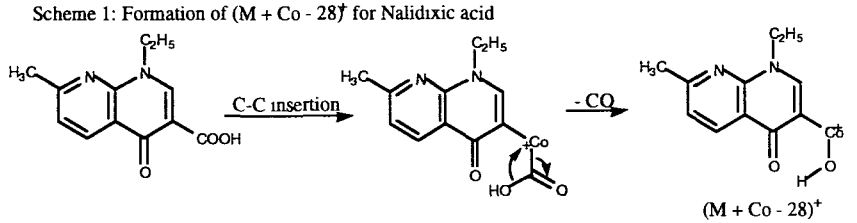

Table 1: CAD of $(M + Ni)^+$ Products

Quinolone (MW)	Product (m/z)	Fragments (m/z)	Neutral Losses (amu)
Enoxacin (320)	$(M + Ni)^+$ (380)	352, 336, 279	-28, -44, -101
Flumequine (261)	$(M + Ni)^+$ (319)	293, 291, 275, 255	-26, -28, -44, -64
Nalidixic acid (232)	$(M + Ni)^+$ (290)	264, 262, 246, 244, 236, 218, 190	-26, -28, -44, -46, -54, -72, -100
Oxolinic acid (261)	$(M + Ni)^+$ (321)	295, 277, 263, 217	-26, -44, -58, -104
Piromidic acid (288)	$(M + Ni)^+$ (346)	316, 302, 261	-30, -44, -85

ACKNOWLEDGMENTS

Financial support from the Welch Foundation, the National Institutes of Health, the National Science Foundation, the Dreyfus Foundation, and the Sloan Foundation are gratefully acknowledged. E. J. A. acknowledges a Fellowship from the National Institutes of Health.

The QUISTOR as a Pulsed-Extraction Source for Time-of-Flight Mass Spectrometry of VOCs in Air

David M. Chambers, Stan W. Thomas, Louis I. Grace and Brian D. Andresen
Lawrence Livermore National Laboratory, Livermore, California 94551

Introduction: Recently, we have been developing the ion trap/time-of-flight mass spectrometer (IT/TOF-MS) as a new instrument for real-time air analysis. The ion trap is an attractive pulsed-extraction source for TOF-MS because of its ion storage capability and its potential for high extraction efficiencies. In the IT/TOF-MS ion trap the entire ion cloud is extracted toward the exit endcap, as compared to 50% in an ion trap mass spectrometer. Moreover, the ion trap pulsed-extraction source can tolerate high background pressures and excessive space charge.

The work presented here focuses on the development of the ion trap to improve the overall performance of the IT/TOF-MS used for air monitoring. A number studies have been performed to determine the best conditions for extraction of the ion cloud with the proper spatial and velocity distributions for focusing in the TOF-MS. Results from these investigations have led to improvements in ion trap operation. Detection limits are generally in the low to sub-ppb (*v/v*) range for analysis between times 10 and 100 ms. Resolution exceeds 2000 m/Δm at FWHM. Mass accuracy is routinely 0.05% and scan-to-scan variations are less than 5%.

Experimental: The IT/TOF-MS instrument hardware was adapted from that available through R.M. Jordan Company (Grass Valley, CA), [1] except that it uses Finnigan-MAT trap electrodes. The ionization source used was an atmospheric sampling glow discharge ionization (ASGDI) source similar to that in reference [2]. Instrument electronics were constructed in house.

Results: The extraction process is the most critical function in the IT/TOF-MS operation because it defines transmission efficiency and resolution for the TOF-MS. Consequently, most of our work has been focused on optimizing ion trap conditions and the extraction procedure. Those changes that have produced the greatest improvement in signal and resolution include *bipolar extraction, rf phase synchronization* and *rf clamping.*

Bipolar Extraction - Ions can be extracted out of the ion trap by applying a positive pulse on the entrance endcap or a negative pulse on the exit endcap [1,3]. The extraction approach that we found to yield the best sensitivity and resolution involves applying an equal, but opposite pulse to both the entrance and exit endcaps. When an extraction voltage is applied to just one electrode, a parabolic field gradient is formed that focuses ions to a point outside the exit endcap. A bipolar field produces a linear accelerating field with little focusing as shown Fig. 1. The use of bipolar instead of unipolar extraction increased resolution from 750 to 2000 m/Δm at FWHM.

Phase Synchronization - Phase synchronization of the extraction pulse with the rf drive potential is performed by triggering the extraction pulse from the same clock used in the rf generator. The effect of rf phase on ion signal is shown in Fig. 2. The most favorable rf phase for ejection occurs between 0 and 90°, when ions are moving toward the center of the trap and are compressed axially. As the phase reaches 180° the ion peak shifts to longer flight times and forms a high-time tail. Longer flight times occur when the ring electrode potential swings low, which decelerates the ion packet. The high-time tail is greatest at 180° because the ion cloud is expanding from the center of the trap along the z-axis.

rf Clamping - Shown in Fig. 3 are spectra for the *m/z* 69 fragment from PFTBA **(a) with and (b) without** clamping of the rf potential on the ring electrode. Extraction was performed at an rf phase of 45°. Clamping the rf lengthens the flight time by 25 µs and narrows the peak width (FWHM) by 4 ns. With no clamping the rf drives to a greater positive potential while the ions are exiting the trap. This broadens the velocity distribution and accelerates ions during the extraction step.

[1] Michael, SM; Chien, M; Lubman, D *Rev. Sci. Instrum.* **63** (1992) 4277. [2] Chambers, DM; Glish, GL; McLuckey, SA, *Anal. Chem.* **65** (1993) 778. [3] Waldron, RM; Todd JFJ *Int. J.M.S.I.P.* **29** (1979) 315. [4] Todd, JFJ; Waldren, RM; Freer, DA; Turner, RB *Int. J. M. S. I. P.* **35** (1980) 107.

Figure 1
Ion Trajectory Model for Bipolar Extraction

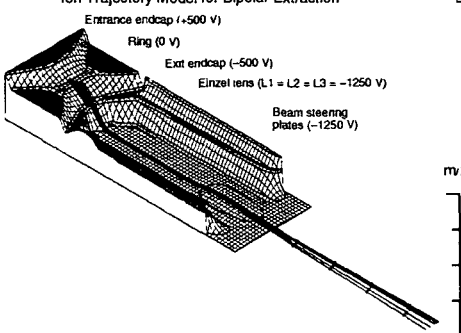

Figure 2
Effect of ring electrode rf phase on ion signal during pulsed extraction

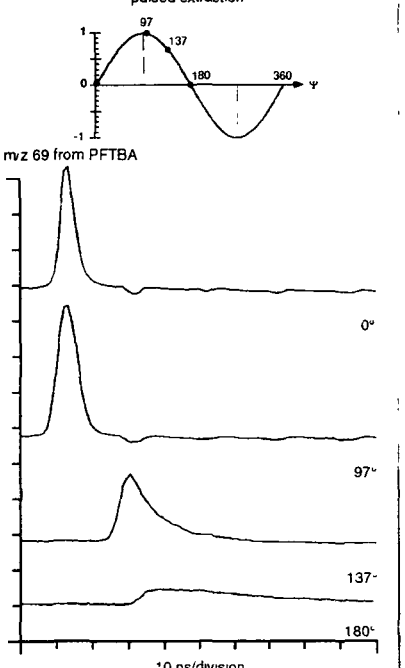

Figure 3
Effect of rf Clamping on Peak Shape for PFTBA at *m/z* 69

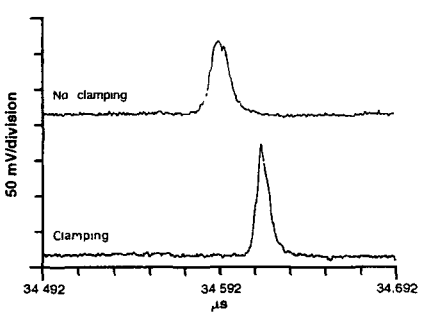

Work Performed under the auspices of the U.S. Department of Energy by the Lawrence Livermore National Laboratory Contract W-7405-Eng-48.

Oxidation of Dye Precursors: Gas Phase Reactions in an Ion Trap MS

Heewon Lee[a], Robert Voyksner[a], and L. Don Betowski[b]
[a] Research Triangle Institute, Research Triangle Park, NC 27709
[b] US EPA, Las Vegas, NV 89193

In the treatment of dye waste, often the most important parameter is the removal of color from the waste stream. Both reduction and oxidation can be performed which eliminate conjugated multiple bonds, removing the majority of the color. Since these approaches could generate a waste stream with higher toxicity than the initial dye waste in some cases, it is an important part of exposure assessment to characterize the reaction products. Previous work in our laboratory explored chemical reduction in solution followed by LC/MS and GC/MS characterization of the reduction products [1, 2]. However, the determination of oxidation pathway of dyes have been limited due to difficulties involved such as side reactions in solvent, sample adsorption, sample complexity, and lack of analytical methods to specifically detect the reaction products To overcome these difficulties the study of oxidation chemistry of dyes within the ion trap mass spectrometer (ITMS) is proposed.

Oxidation studies of nonvolatile compounds such as dyes are possible for ions formed by electrospray that are trapped in the ITMS. Most dyes do not have a significant vapor pressure to permit the study of neutral dye reactions with an oxidant by EI. In this study, the oxidation of dye precursors is performed as the initial stages of oxidation of dyes in the ITMS.

Ozone in oxygen stream is used as a major oxidant in this oxidation study. The compounds investigated include o-toluidine, cis- and trans-stilbene, and isoprene. The experimental parameters evaluated includes the pressure within the trap, reaction time, temperature, and oxidants. Oxidation reaction of o-toluidine, as shown in figure 1 and 2, produces extensive ring opening fragments (e.g. m/z 50 and 65), phenyl (m/z 77), benzyl (m/z 91), and high mass (e.g. m/z 120, 149) ions. The major product of cis- and trans-stilbene oxidation is almost exclusively benzaldehyde and isoprene seems to undergo polymerization followed by successive alkyl loss upon oxidation. It is demonstrated in this study that the MS/MS capability of the ITMS aids in the structure elucidation, and that the storage capability of the ITMS allows for monitoring of oxidation intermediates and products over a wide range of reaction rates. Further study on the oxidation of nonvolatile dyes will be performed using an electrospray ionization method in the ITMS.

[1] R. F. Straub, R. D. Voyksner, J. T. Keever, Anal. Chem. 65, 2131 (1993)
[2] R. D. Voyksner, R. F. Straub, J. T. Keever, H. S. Freeman, W N. Hsu, Environ. Sci. Tech., 27, 1665 (1993)

Acknowledgments
This work was supported by the Environmental Protection Agency, Cooperative Agreement Number CR-819555.

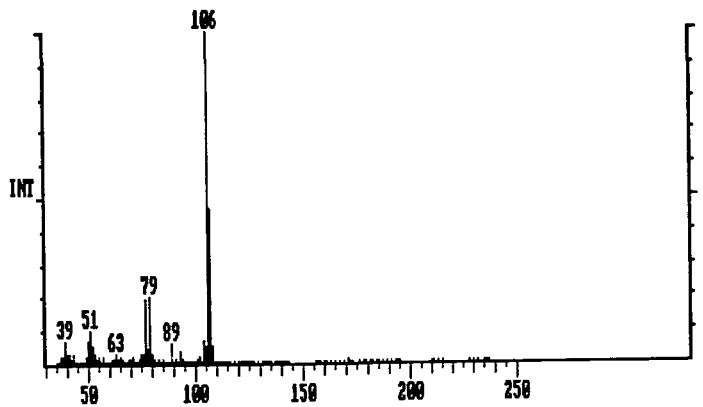

Figure 1. o-Toluidine: EI spectrum

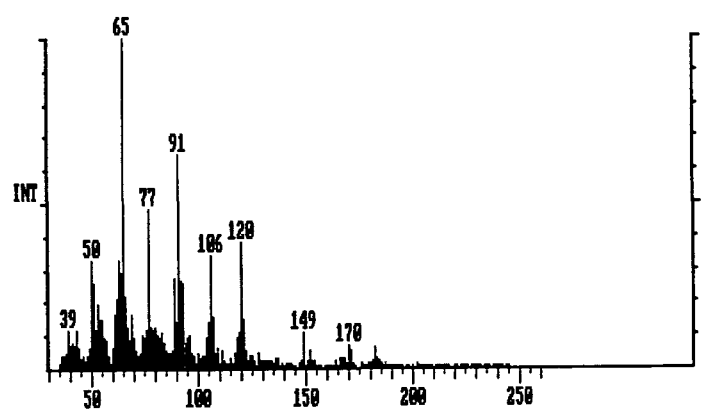

Figure 2. o-Toluidine: reaction with O_2/O_3

Developments in Explosives Vapor Detection by Glow Discharge/Ion Trap MS

Keiji Asano, Gopalakrishnan Vaidyanathan, Douglas Goeringer, and Scott McLuckey
Chemical and Analytical Sciences Division
Oak Ridge National Laboratory, Oak Ridge, TN 37831-6365

The quadrupole ion trap has found great utility in the analytical community due to its high sensitivity and MS^n capabilities. Problems associated with matrix ions filling ion traps have been addressed by mass-selective ion accumulation methods (1-3). The atmospheric sampling glow discharge ionization (ASGDI) source coupled to a quadrupole ion trap used for explosives detection is prone to matrix ion effects because of its large abundance of background ions at low mass. By using a mass selective ion accumulation method such as a filtered-noise field (FNF) (3), matrix ions are ejected allowing for the analyte ions to be concentrated in the trap. This paper will report on the detection limits found for explosives on the ASGDI/Finnigan ITMS using the FNF technology and on initial studies on the performance of the ASGDI/Teledyne 3DQ.

We have previously reported detection limits in terms of concentrations with respect to vapor detection with an estimated "mass" detection limit (4). In this paper, we have determined mass limits by depositing a known amount of explosives onto a capillary tube and placing the tube into a heated inlet leading directly into the ASGDI source. We have determined MS/MS detection limits in the low to sub-picogram range for three explosives, 2,4,6-trinitrotoluene (TNT), cyclo-1,3,5-trimethylene-2,4,6-trinitramine (RDX), and pentaerythritol nitrate (PETN). In all three cases, a FNF waveform (generated by the Teledyne-Hitachi HST-1000 module) was used to selectively accumulate the parent ion of interest which was then subjected to collisional activation. Figure 1 shows the MS/MS spectrum of 0.5 pg of RDX. Most of the parent ion, $(M-NO_2)^{-\cdot}$ has fragmented to the $(CH_2NCH_2NNO_2)^-$ anion. The background peak around m/z 170 could not be ejected without losing analyte ion intensity.

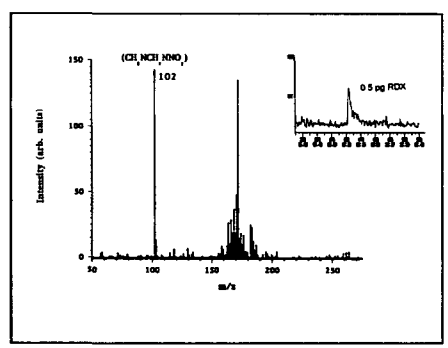

Figure 1

We have coupled an ASGDI source, designed in our laboratories, to the Teledyne 3DQ for continued work in explosives vapor detection. The combination of ion trap technology and FNF in the Teledyne 3DQ provides the capability to perform mass selective accumulation of multiple parent ions and simultaneous collisional activation. With additional FNF waveforms, MS^n experiments (n>2) are also possible. This parallel monitoring has the advantage of speed and improved duty cycle over instruments which perform multiple targeted compound analysis in series. The mass spectra in Figure 2 shows an example of parallel monitoring with three nitroaromatic compounds, DNT, TNT, and tetryl as the targeted compounds in air. Figure 2a shows the mass

spectrum acquired with the FNF set to accumulate the molecular anion of DNT (m/z 182) and TNT (m/z 227) and the $(M-NO_2)^-$ anion from tetryl (m/z 241). Figure 2b is the resulting MS/MS spectrum when a second FNF waveform with three frequencies corresponding to the secular frequencies of m/z 182, 227, and 241 is applied to the end-cap electrodes. Figure 2c shows the mass spectrum obtained when an FNF waveform is applied to isolate ions at m/z 165, 210, and 213 and Figure 2d is the resulting spectrum when an FNF for collisional activation (of m/z 165, 210 , and 213) is applied. The fragments are identified according to their genealogy which was determined by separate MS/MS and MS^3 experiments. The advantage of speed and duty cycle in parallel monitoring comes at the expense of specificity relative to MS^n experiments performed in series.

Figure 2

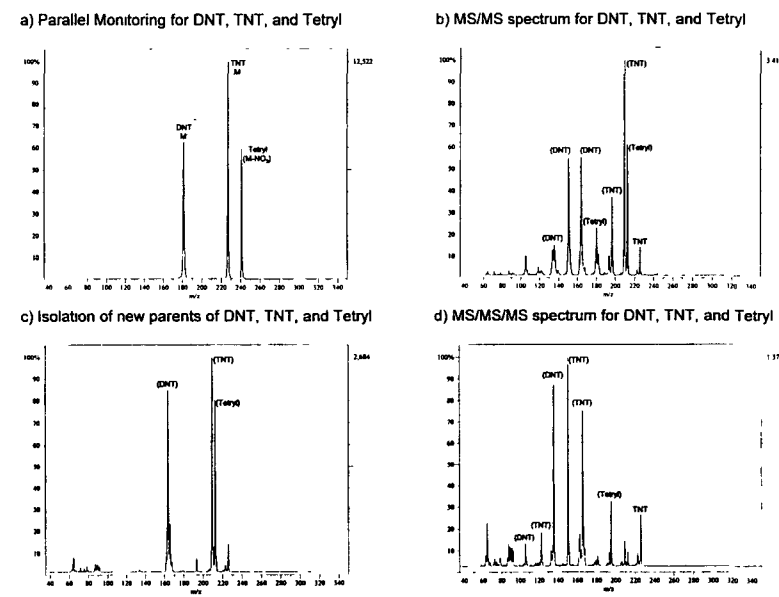

References:
1. Guan, S; Marshall, A.G. *Anal. Chem.* **1993**, *65*, 1288-1294.
2. Julian, R.K., Jr.; Cox, K; Cooks, R.G. *Anal. Chem.* **1993**, *65*, 1827-1833.
3. Kelley, P.E. U.S. Patent 5,134,286, 1992.
4. McLuckey,S.A.; Glish,G.L.; Asano,K.G. *Anal. Chim. Acta* **1989**, *225*, 25-35

Research sponsored by the U.S. Department of Energy, Office of Safeguards and Security, under contract DE-AC05-84OR21400 with Martin Marietta Energy Systems, Inc.

CAD Spectra of PAHs by Ion Trap and Triple Quadrupole Mass Spectrometry

Witold Winnik,*[φ] Leon Betowski, Robert D. Brittain,[ψ] Alvin Marcus[τ] and Steven Pyle.
United States Environmental Protection Agency, National Exposure Research Laboratory, Characterization Research Division, Las Vegas, Nevada 89193
[φ] National Research Council Associate at the U.S. EPA, Las Vegas, Nevada.
[ψ] Varian Co., Environmental Applications, 2700 Mitchell Drive, Walnut Creek, CA 94598.
[τ] Senior Environmental Employee at the U.S. EPA, Las Vegas, Nevada.

Polycyclic aromatic hydrocarbons (PAHs) are common products of many industrial and natural combustion processes. PAHs are found in grilled meat, tobacco smoke, air-borne particulates, used motor oil and soil. They are produced by practically any process involving combustion of fossil fuels. Because many PAHs are carcinogens, the U. S. Environmental Protection Agency (EPA), through its National Exposure Research Laboratory in Las Vegas, NV must develop analytical methods for determining these ubiquitous pollutants..

The Saturn 3 ion trap mass spectrometer, a recent commercial innovation, can detect analytes at the picogram level in the full-scan mode. This detector has the potential to eliminate or reduce sample preparation steps that would ordinarily be required to concentrate the analytes to levels suitable for detection by less sensitive means. For clean, simple matrices, direct injection of environmental samples would be sensitive, avoid pre-concentration steps or sample clean-up, and generate no waste solvent that would require disposal as hazardous waste.

In addition, ion trap detectors have been configured to perform tandem mass spectrometry (MS/MS). The MS/MS capability enables the ion trap to first isolate or "trap" an ion of interest and subsequently produce characteristic progeny ions. This allows the analyst to unambiguously distinguish the compound of interest from other compounds that yield ions of the same mass-to-charge ratio (m/z). The selective ionization mode of operation allows for the selective trapping of the analyte ions, thus eliminating a great portion of chemical noise. This feature combined with a GC/MS/MS capability of the Saturn 3 ion trap makes it an attractive detector for analysis of compounds in complex matrices.

The nonresonant ion-trap collisionally activated dissociation (CAD) spectra of 16 PAHs are characterized by a high abundance of lower m/z product ions (Fig. 1). Low picogram (or ppb) detection limits were achieved in the full-scan mode. Nonresonant CAD experiments are relatively easy to set up and typically exhibit excellent short-term and good long-term reproducibility. The nonresonant spectrum of pyrene was compared with the sequential, resonant $(MS)^n$ [where n=1-5] experiments performed on the prototype Finnigan ion-trap instrument.[1] The nonresonant pyrene CAD spectrum comprised simultaneously ***all*** the peaks observed in the $(MS)^n$ experiments {(n=2) **202**: 201, 200; (n=3) **200**: 199, 198, 174, 150; (n=4) **174**: 173, 148, 124; (n=5) **148**: 122, 98 m/z [1]}. This high-energy deposition attainable in the nonresonant technique is especially desirable in analyses of very stable molecules.

The nonresonant CAD breakdown curves obtained for the isomeric PAHs indicated a possibility of differentiation of some isomeric PAHs; (this capability was not possible in the experiments performed using the TSQ 700 mass spectrometer). The resonant ion trap CAD spectra of PAHs exhibited a relatively low degree of fragmentation and thus resembled those obtained using the triple quadrupole mass spectrometer (Fig. 1).

43rd ASMS Conference on Mass Spectrometry and Allied Topics

Figure 1

GC/Positive Ion CID Spectra of Pyrene (m/z 202). Comparison of Resonant, Nonresonant (Ion Trap), and Triple Quadrupole MS/MS Spectra.

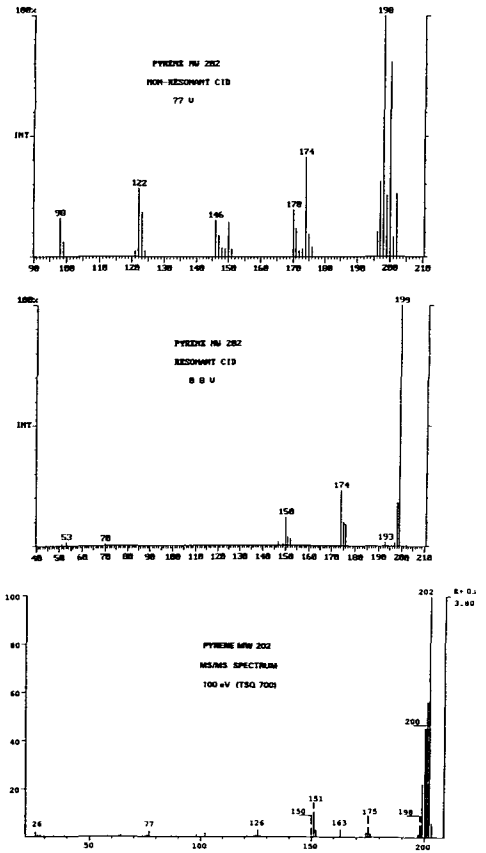

[1] B. D. Nourse, K. A. Cox, K. L. Morand, and R. G. Cooks, *J. Am. Chem. Soc.*, **1992** (114), 2010.

Notice: The U.S. Environmental Protection Agency (EPA), through its Office of Research and Development (ORD), prepared this abstract for a poster presentation. It does not necessarily reflect the views of the EPA or ORD.

Fragmentation Pathways of Triacylglycerols Deduced from Model Compounds

Stroobant V. and de Hoffmann E.

* Mass Spec. Lab., Univ. de Louvain, Pl. Pasteur 1, B-1348 Louvain-la-Neuve, Belgium.

We report a study on the fragmentation under low energy of esters anions from multifunctional alcohols, 1,2 ethanediol (ethyleneglycol), 1,3 propanediol and 1,2,3 propanetriol (glycerol) under DCI ionisation. A Finnigan MAT TSQ 70 was used. The ionisation gas was a mixture of CH4/N2O (75/25) while Xe was used as collision gas.

Fragmentation spectra of the studied multifunctional alcohols.

	Ethanediol diacetate	Ethanediol dipropionate	Propanediol diacetate	Propanediol dipropionate	Name of the fragments
$[M-H]^-$	145	173	159	187	$[M-H]^-$
A	103	117	117	131	$[M-H\text{-ketene}]^-$
B	101	129	101	129	β-ketoacid carboxylate
C	83	111	83	111	acylketene anion
D	61	61	75	75	$[M-H\text{-acylketene}]^-$
E	59	73	59	73	carboxylate
F	57	85	57	85	ketone enolate
G	41	55	41	55	ketene ynolate

The fragmentation spectra are listed in the Table. The main observed fragments can be explained as resulting from the formation in the first step of an internal β-ketoester by a new gas-phase rearrangement of these enolate anions. This rearrangement logically results from an intramolecular nucleophilic substitution reaction, where the enolic carbanion is the nucleophile (**Scheme, pathway a**). The fate of this rearranged anion depends on the two competitive fragmentation pathways leading to the ketone enolate or the acylketene anion, and is different for these diols esters.

The first pathway corresponds to a second nucleophilic substitution of the ketoester by the alkoxide that yields a neutral cyclic ether and the β-ketoacid carboxylate, an ion often observed in the spectra but at low intensities. The β-ketoacid carboxylate anion

then loses carbon dioxide and produces the enolate anion of the corresponding ketone (**Scheme, patway b**). The fragmentation pathway leading to the ketone enolate is sensitive to the relative positions (1,2 or 1,3) of the esters on the molecular backbone.

The second proposed pathway is stepwise (**Scheme, pathway c**). It starts with a proton transfer from the methylene group between the two carbonyls to the alkoxide anion, followed by the cleavage of the ester bond induced by the negative charge to yield an ion-dipole complex composed of a neutral acylketene and an alkoxide ion. The direct dissociation of this ion-dipole complex competes with a proton exchange inside the complex yielding a new complex constituted by an alcohol molecule and the anion of the acylketene.The fragmentation pathway leading to the acylketene anion is influenced by the presence of an alkyl group on the methylene group between the two carbonyls of the intermediate.

The same rearrangement also occurs in triglycerides. These fragmentations mechanisms allow to explain the structure of fragments observed from triglycerides and known to be useful in position elucidation.

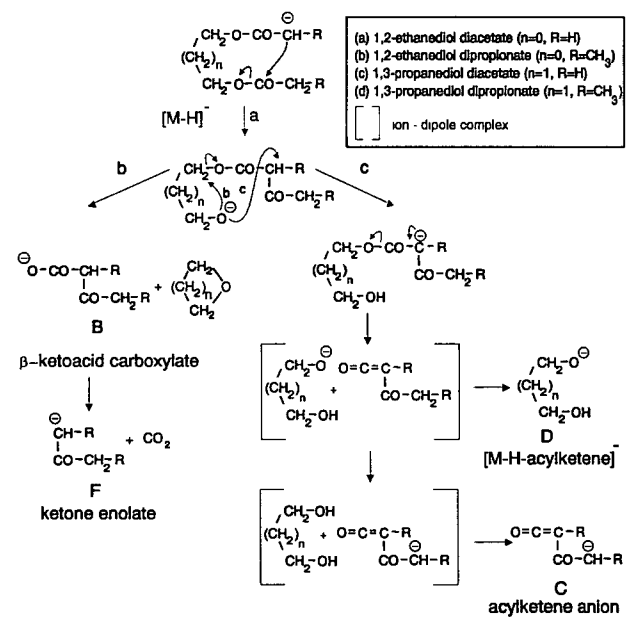

HPLC-MS ANALYSIS OF TRIACYLGLYCERIDES

P.J.W.Schuyl, T. de Joode, G.S.M.J.E. Duchateau and M.A. Vasconcellos
Physical and Analytical Sciences, Unilever Research Laboratory,
PO box 114, 3130 AC Vlaardingen, The Netherlands

Introduction

The Triacylglycerol (TAG) composition is very important for the physical characteristics of edible oils and fats.The degree of unsaturation and the structural configuration of the TAGs are important nutritional aspects.

A method is needed to get both qualitatively and quantitatively of the TAGs in a mixture, if possible in one single analysis:

- the degree and position of unsaturation
- geometry of the unsaturation (cis/trans)
- the Carbon Number (CN)
- length of each fatty acid chain
- sn position of each fatty acid chain

Experimental

HPLC

Separation of TAGs on a Ag silica HPLC-column depends on:

- the total number of double bonds
- the position of the most unsaturated fatty acid chain(s).
- the configuration of the double bonds (cis/trans).

MS

Electrospray is a suitable ionization method to determine the molecular masses of the TAGs.
Due to the apolar HPLC solvents used, methanol and sodium acetate have to be added to the column effluent to create $[M+Na]^+$ ions.

Apparatus

HPLC: Gilson 305/306/306/811B/805S.
column: home made Ag-phase,100x4.6 mm
particle size 3 µm, pore size 100Å.
gradient: ternary gradient of toluene/hexane/ethylacetate in 13 min.
flow: 1.5 mL/min.
post column split: 75:1 to 20 µL/min.
addition: 10 µL/min MeOH/0.1 mM NaOAc

MS: Fisons Trio-2000
ionization mode: positive electrospray
scan range: 500-1000 m/z
scan rate: 2 s/scan
total flow to source: 30 µL/min
source temperature: 100°C
pseudo molecular ions: $[M+Na]^+$

Parameters

Influence of the cone voltage on the response.
The cone voltage (CV) has a major influence on the response of the TAGs. The longer the fatty acid chains, the higher the cone voltage should be to give the highest signal.
At a cone voltage of 95 V the responses of saturated tri-C12 to tri-C18 were about the same, and therefore this value was selected in the further analyses.

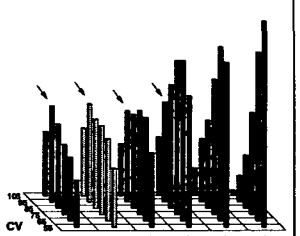

Dynamic range and linearity.
The dynamic range was tested with saturated tri-C8, tri-C12 and tri-C18 TAG at a cone voltage of 95 V. The dynamic range is limited by several factors: The higher the flow to the ESP source, the lower the dynamic range. The longer the fatty acid chain length, the lower the dynamic range. The dynamic range of co-eluting peaks is less than that of a single peak. When the source gets contaminated, the dynamic range and sensitivity will decrease.
By these combined factors the dynamic range is limited to about 10^2.

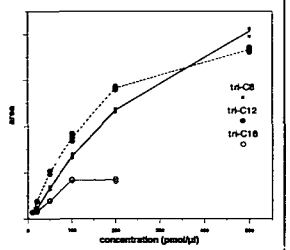

Results

Chromatogram

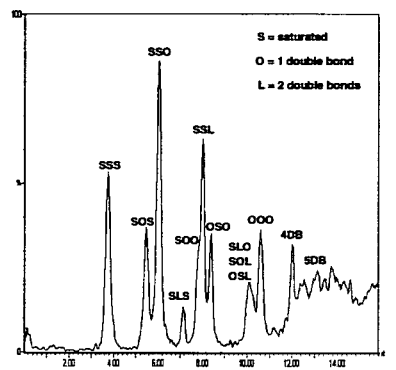

3D overview

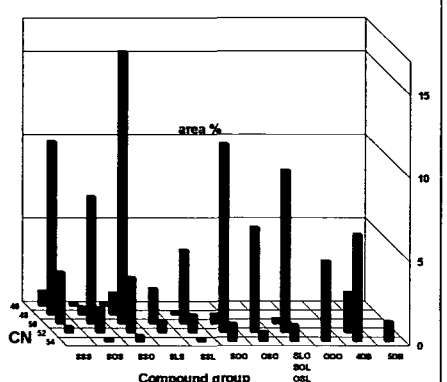

Quantitative results
The results by MS are quite comparable with the results from the by fatty acid methyl ester analysis calculated results and with the results obtained from HPLC-FID analysis, even without using response factors.

Conclusions

Ag-phase HPLC-MS is a suitable method for the analysis of TAGs in complex samples.
Information is obtained on CN and the sn-position of the unsaturated fatty acid
The quantitative results are comparable to the results obtained with the HPLC-FID method.
The detection limit is about 0.2 % for each individual TAG. The cone voltage has to be optimised to get equal responses of the TAGs present in the sample.
MS-MS will give information on the chain length of each individuel fatty acid in the TAG, but on line Ag-phase HPLC-MS-MS is not (yet) possible, because the $[M+Na]^+$ ions do not fragment.

Characterization of a Family of Brain Lipids with Sleep-Inducing Properties

G. Siuzdak, B. Cravatt, O. Prospero-Garica, S. Henrikson, N.B. Gilula, D. Boger, & R.A. Lerner

Departments of Chemistry, Neuropharmacology, and Cell Biology
The Scripps Research Institute
La Jolla, CA 92037

The bioanalytical techniques now available offer increased sensitivity in molecular characterizaton, allowing scientists to study biological fluids and the changes correlated with physical stimuli. Utilizing such techniques, researchers from five different laboratories at The Scripps Research Institute have taken a purely chemical approach to study sleep.

In this study, a compound associated with the sleep-wake cycle was isolated from the cerebral spinal fluid of sleep-deprived cats. In the initial stages of the isolation and characterization of this compound, liquid chromatography and mass spectrometry played an important role. Electrospray ionization, electron ionization, and fast atom bombardment allowed us to discern some of its functional characteristics, including: molecular formula, degrees of unsaturation, a long alkyl chain, and a nitrogen substituent capable of primary fragmentation as ammonia.

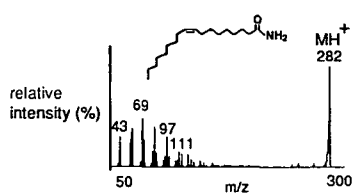

Figure 1. The CSF isolated product, *cis*-9,10-octadecenoamide, shown with ESI MS/MS data.

Initial electrospray mass analysis (PE SCIEX) of the natural compound revealed mass peaks of *m/z* 282 $[M + H]^+$, 304 $[M + Na]^+$, 320 $[M + K]^+$, and 564 $[2M + H]^+$, indicating that the molecular mass of the compound was 281 Da. High-resolution FAB-MS analysis allowed the exact mass measurement of the $[M + Na]^+$ ion, and the observed mass was *m/z* 304.2614 ± 0.0006 Da. This measurement allowed for determination of elemental composition and a best fit for the molecular formula $C_{18}H_{35}NO$, which has a calculated $[M + Na]^+$ *m/z* of 304.2616 Da. Furthermore, tandem mass analysis revealed a distinctive fragmentation pattern in the low molecular mass range consistent with other long chain alkanes, while sequential neutral loss of 17 and 35 from the parent ion indicated loss of ammonia followed by loss of water. Additional MS^3 experiments were performed on the daughter ions of *m/z* 265 and 247. Such MS^2 and MS^3 mass analyses were also performed on various synthetic candidate structures,

and while several products gave spectra quite similar to the spectra of the natural material, only the fragmentation patterns generated from monounsaturated fatty acid amide, *cis*-9,10-octadecenoamide, matched exactly those of the endogenous lipid. Especially useful was the loss of 17 mass units from the parent ion of *cis*-9,10-octadecenoamide, indicating the molecule first fragments at the carbon-nitrogen bond of its terminal amide group to release ammonia.

Table 1. Some evidence that led to the unknown's identity. Ultimately the identity was confirmed by independent synthesis and comparison of the spectral data.

DATA TYPE	SUMMARY OF DATA		
exact mass	$[C_{18}H_{35}NO + Na]^+$	observed actual	304.2614 304.2616
deuterium exchange	*m/z* = 285 $[M\text{-}2H^+\text{+}3D^+]^+$, 2 exchangeable protons		
isotope	Isotope pattern at *m/z* = 282 indicates that *m/z* 282 is not a multiply charged, nor does it have any elements with an unusual isotope pattern (e.g. Cl).		
cationization	Electrospray MS observation of *m/z* 304 $[M + Na]^+$ and *m/z* 320 $[M + K]^+$ confirms that M = 281.		
association	*m/z* 563.6 association product $[2M + H]^+$		
MS^2 data	Fragment ion *m/z* 265 corresponding to $[MH - NH_3]^+$. Fragment ion *m/z* 247 corresponding to $[MH - NH_3 - H_2O]^+$. Lipid fragments		
MS^3 data	Fragmentation of *m/z* 265 » *m/z* 247 (sequential loss) suggests *m/z* 247 fragment is related to *m/z* 265 fragment ion. Lipid fragments		
NMR data	Confirms lipid portion of molecule and configuration of double bond.		
ozonolysis with GC/MS	Identified the location of the double bond.		
IR data	Confirms identity of unknown as *cis* isomer		

We have also detected related compounds in the cerebrospinal fluid of rat and man indicating that *cis*-9,10-octadecenoamide is but one member of a family of fatty acid primary amides differing in the length of the alkyl chain and the position or configuration of the olefin. Mass analysis also identified a compound from the spinal fluid of man and rat with the molecular formula $C_{22}H_{43}NO$ whose MS^2 and MS^3 fragmentation patterns were found to be indistinguishable from those of synthetic *cis*-13,14-docosenoamide. Importantly, we now also show that synthetic *cis*-9,10-octadecenoamide demonstrates sleep-inducing properties in rats.

References: 1) Lerner, Siuzdak, Prospero-Garcia, Henriksen, Boger, and Cravatt, *PNAS*, 1994, 9505-9508.
2) Cravatt, Prospero-Garcia, Siuzdak, Gitula, Henriksen, Boger, and Lerner, *Science*, in press.
Acknowledge: This work was supported by The Lucille P. Markey Charitable Trust and NIH #1 S10 RR07273-01.

The Use of Nicotinates and Sulfoquinovosyl Monoacylglycerols in the Analysis of Monounsaturated ω3 Fatty Acids by Mass Spectrometry

Michael Keusgen, Jonathan M. Curtis*, and Stephen W. Ayer
Institute for Marine Biosciences, National Research Council of Canada, 1411 Oxford Street, Halifax, Nova Scotia B3H 3Z1, Canada.

EI mass spectra of picolinyl derivatives of fatty acids and nicotinate esters of long-chain alcohols have been used to locate carbon-carbon double bonds [1-3]. Induced by a hydrogen transfer to the aromatic nitrogen, a regular fragmentation series results due to radical cleavage along the alkyl chain. These derivatives have been tested for a number of standards but have not been fully evaluated for monounsaturated ω3 fatty acids (or the analogous alcohols) since they are not commercially available. We have studied a complex mixture of sulfoquinovosyl diacylglycerols (SQDGs) produced by the microalga *Heterosigma carterae*. One of the fatty acids liberated from these SQDGs was identified as cis 13-hexadecenoic acid (ie 16:1ω3), confirmed by ^{1}H and ^{13}C NMR. The EI mass spectrum of the nicotinate ester derivative suggested an ω4 unsaturation rather than ω3 as deduced from the NMR data. Here we explore this problem further in order to be able to correctly identify C=C double bonds at the ω3 position.

For the nicotinate ester of a saturated fatty alcohol (hexadecanol, figure (a)) a distinct series of charge remote radical cleavages along the alkyl chain is seen, giving ions from *m/z* 318 to *m/z* 178. The ion at *m/z* 332 due to loss of the terminal methyl group ($[M-CH_3]^+$) has a significantly lower intensity than the series from *m/z* 318 to *m/z* 178. Below *m/z* 178, rearrangement processes involving hydrogen transfer onto the ring dominate resulting in ions at *m/z* 137, 151, and 165. The base peak ion at *m/z* 124 is characteristic for nicotinate derivatives[2].

For the nicotinate ester of a fatty alcohol having an isolated double-bond near the centre of the chain (not shown), the mass spectrum shows minimum intensity at the point corresponding to formal cleavage at the double bond plus a mass differece of 26 between adjacent fragment ions. Vinylic cleavage gives low intensity fragment ions whilst allylic cleavage results in enhanced fragment ion intensity. Fragmentation resulting in loss of the alkyl chain terminus results in significant enhancement in intensity.

For the nicotinate ester of an ω3 monounsaturated fatty alcohol (cis 13-hexadecenol 16:1ω3, figure (b)) the minimum ion intensity at *m/z* 288-290 and mass difference of 26 between m/z 276 and 302 wrongly suggest unsaturation at the ω4 position. The fragment ion pattern is a result of two effects:

(i) for saturated alkyl chains $[M-CH_3]^+$ is a relatively weak fragment ion whereas $[M-C_2H_5]^+$ is much stronger. Thus *m/z* 316 has anomalously high intensity for a vinylic cleavage which normally produces low intensity fragments.

(ii) the fragment intensities resulting from cleavages at the isolated double bond as described above. In this case *m/z* 330 ($[M-CH_3]^+$, cleavage at the allylic position) is higher than $[M-CH_3]^+$ for hexadecanol.

The correct assignment is made by considering the regular fragment ion series from *m/z* 276 to *m/z* 178. This suggests that the ambiguous ions at *m/z* 288-290 are vinylic cleavage (expected

to be weak). Thus, the double bond is located in the ω3 position. For an ω4 unsaturation, the peak at *m/z* 276 would have a weaker intensity than the series *m/z* 262 to *m/z* 178 since it would represent cleavage at a vinylic position.

We have also used the sulfoquinovosyl moiety as a "natural derivative" for locating C=C double bonds in fatty acids *via* negative ion LSIMS MS/MS. Sulfoquinovosyl monoacylglycerols (SQMGs) were derived from the SQDG by an enzymatic reaction. Due to the negative charge localized on the sulfonate group, charge-remote fragmentation occurs along the alkyl chain in an analogous way to the charge-remote radical cleavage observed in the positive ion EI mass spectra of the nicotinates. For SQDGs, this type of fragmentation produces very complex MS/MS spectra [4]. For the SQMG which contains hexadecanoic acid, starting from *m/z* 555 (the deprotonated molecular ion) a series of fragment ions is clearly visible. For a saturated fatty acyl chain this series can be explained by the loss of C_nH_{2n+2}. A similar anomaly in the fragment ion intensities for ω3 unsaturation is seen for SQMGs as described above for the EI spectra. As with the latter case, this can be resolved by careful consideration of relative peak intensities [5].

[1] Harvey D.J. (1990) Spectros. Int. J. 8, 211-244.
[2] Vetter, W., Meister, W. (1981) Org. Mass Spectrom. 16, 118-122.
[3] Christie, W.W., Brechany, E.Y., and Holman, R.T. (1987) Lipids 22, 224-228.
[4] Gage, D.A., Huang Z.-H., Benning C. (1992) Lipids 27, 632-636.
[5] Keusgen, M., Curtis, J.M, Ayer, S.A. (submitted 1995) Lipids

The GC/EI mass spectra of the nicotinate derivatives obtained from (a) hexadecanol, and (b) *cis* 13-hexadecanol, by reductive cleavage of a SQDG followed by esterification.

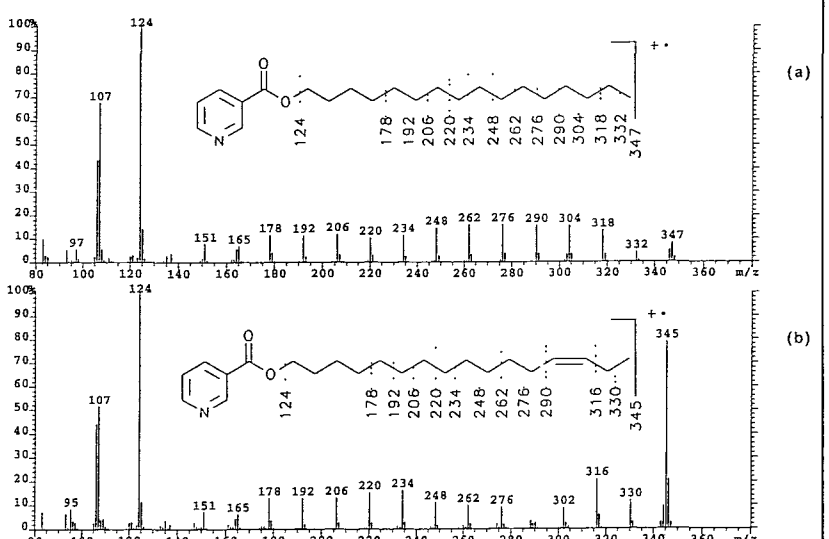

IDENTIFICATION OF FATTY ACIDS AND EICOSANOIDS USING ELECTROSPRAY MASS SPECTROMETRY

James L Kerwin[1] and Lowell H. Ericsson[2], Departments of Botany[1] and Biochemistry[2], University of Washington, Seattle, WA 98195-1330 USA

Introduction Hydroxy fatty acids and other oxygenated fatty acids are found in most major groups of organisms, including prokaryotic bacteria, fungi, molluscs, fish, green plants and mammals. Many of these compounds, especially derivatives of arachidonic acid (20:4ω6), collectively known as eicosanoids, are potent mediators of inflammatory and developmental processes. Since these fatty acid derivatives can be biologically active at nanomolar concentrations or less, there has been much interest in developing specific, sensitive spectrometric and other techniques for their structural identification and quantitation. Electrospray ionization MS and MS/MS is a relatively new technique extensively used in peptide and protein chemistry. Recently we and others have shown that a combination of positive and negative ion electrospray MS and MS/MS can be used with minimal sample preparation to identify intact glycerophospholipid molecular species and relative composition using subnanogram quantities of lipid. This report extends the utility of this mass spectrometric technique by describing spectra of fatty acids, eicosanoids and related oxygenated fatty acids using negative ion electrospray MS and tandem (collisional-induced dissociation) mass spectrometry (MS/MS), emphasizing its utility for rapid and sensitive analyses of biological samples

Results *Fatty acids.* The chain length and degree of unsaturation of fatty acids of complex mixtures of fatty acids can be determined using negative ion ESI MS. Analysis of base-hydrolyzed cod liver oil produced a fatty acid profile and relative composition similar to that found using GC-MS Minimal fragmentation of saturated and monounsaturated fatty acids was found, with progressively greater fragmentation occurring as the degree of unsaturation increased (spectra not shown).

Saturated monohydroxy fatty acids. The MS/MS spectrum of 2-OH stearic acid unexpectedly revealed a prominent peak 46 mass units less than the parent ion (*Figure 1*). This is in contrast to the loss of 44 from the parent ion most fatty acids, presumably from loss of CO_2 from the carboxyl moiety. The most likely explanation of the loss of 46 frrom the parent ion is from loss of CH_2O_2 from the carboxyl end of the compound, perhaps stabilized by resonance as outlined in *Figure 1*.

Unsaturated mono- and di-hydroxy fatty acids. Fragmentation of monohydroxyeicosatetraenoic fatty acids (HETE's) was comparable to that documented by other laboratories using fast atom bombardment MS/MS. Prominent ions found for 6 different HETE's were due to α-hydroxy fragmentation (*Figure 2* and unpublished observations). Fragmentation was confirmed using a d-8 analog of 5-HETE (*Figure 2*). Dihydroxy compounds showed similar fragmentation (*Figure 3*). By increasing the collision gas thickness (cgt) from 160 to 325 (one unit is equivalent to 10^{13} molecules argon/cm^2), additional structural information could be obtained.

Thromboxanes and prostaglandins. Cyclooxygenase products are also amenable to analysis by ESI. Thromboxane B_2 produced two ions using a low CID gas density that were possibly due to partial loss of the oxane ring (*Figure 4*). Six prostaglandins that have been examined produced spectra (not shown) dominated by loss of one or more H_2O molecules and CO_2 using low CID gas density, and fragmentation at carbons adjacent to hydroxyl groups and sites of unsaturation as the cgt was increased. Detection limits for prostaglandins were below 1 picogram.

Leukotrienes. Peptide-containing eicosanoids can be detected at levels near 20 picograms using negative ion ESI MS and less than 1 picogram can yield structurally useful spectra for

MS/MS analysis. Fragmentation of six leukotrienes were similar to those previously documented using FAB MS/MS (spectra not shown).

Soybean lipoxygenase. The well-characterized soybean lipoxygenase (LOX) enzyme was used to show the utility of ESI MS and MS/MS to screen for the presence of oxygenated fatty acids. Products formed by incubating linoleic and arachidonic acids were first identified using negative ion MS. Ions found in this spectrum were subsequently examined using MS/MS. Some peaks in the MS spectrum were shown to be due to decomposition of hydroperoxides formed by LOX metabolism of fatty acids. CID spectra consistent with the presence of both 9- and 13-OH and -OOH 18:2 and at least 3 different 20:4 metabolites were obtained (spectra not shown).

Conclusions Negative ion ESI MS and MS/MS were used to characterize fatty acids, hydro(per)oxy fatty acids, prostaglandins and leukotrienes. The versatility of this technique in examining biological samples using small amounts of material with minimal preliminary chromatographic separation provides an alternative approach to examining these lipid classes.

Acknowledgment. This research was supported in part by a grant from the National Institutes of Health (AI 22993).

Figure 1. 2-OH Stearic acid

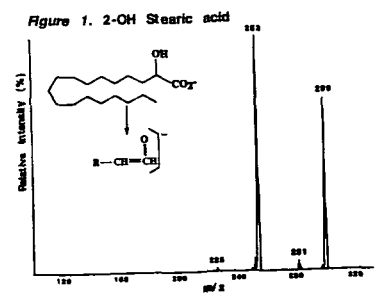

Figure 2. 5-HETE-d8

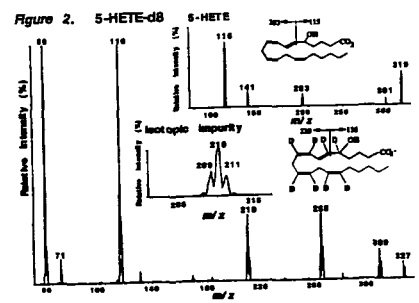

Figure 3. 14,15-diHETrE : cgt 160

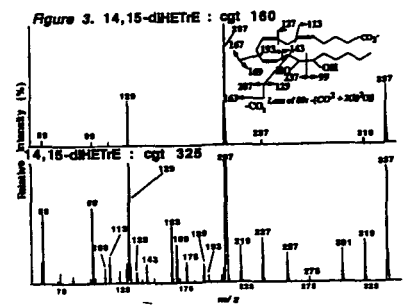

Figure 4. Thromboxane B_2 - cgt 300

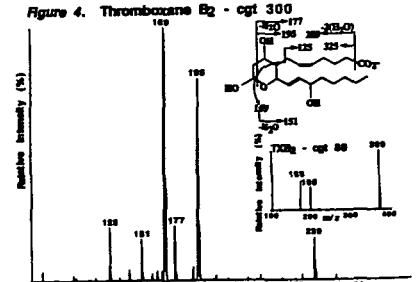

ESI-MS ANALYSIS OF PAF PRECURSORS IN HUMAN KERATINOCYTES AND CELL LINE

Kathleen A. Harrison, Jeffrey B. Travers, and Robert C. Murphy
National Jewish Center for Immunology and Respiratory Medicine
1400 Jackson Street
Denver, CO 80206

INTRODUCTION

Recent evidence has indicated that platelet activating factor (PAF), a phospholipid lipid mediator of inflammation, is produced by epidermal cells. Gas chromatography/mass spectrometry has been used to detect the stimulated production of PAF from the human keratinocyte-derived cell line called HaCaT cells (1). We have investigated the glycerophosphocholine (GPC) molecular species present in the membranes of HaCaT cells to determine the presence of the biochemical precursors of PAF and to determine their relative abundance in these cells.

RESULTS

Normal phase separation of phospholipid classes was monitored using online electrospray ionization mass spectrometry. The positive ions formed by ESI ionization of a typical glycerophosphocholine molecular species is shown in Figure 1 with the formation of an abundant ion at m/z 782 corresponding to MH^+. The abundance of this ion was found to be related to orifice potential as shown in Figure 2 where the orifice potential was varied between 55 and 150 volts. The MH^+ of this GPC, introduced at 5 μL/min at a concentration of 2 ng/μL, decreased in absolute abundance while GPC, the fragment ion corresponding to the phosphocholine moiety at m/z 184 increased correspondingly (Figure 2).

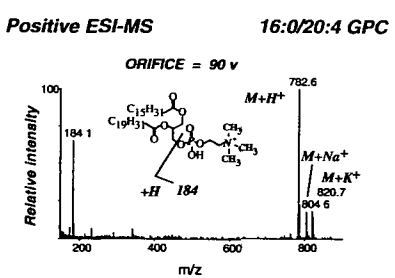

Figure 1 *Positive ions obtained by electrospray ionization mass spectrometry of 1-hexadecanoyl-2-arachidonoyl-GPC.*

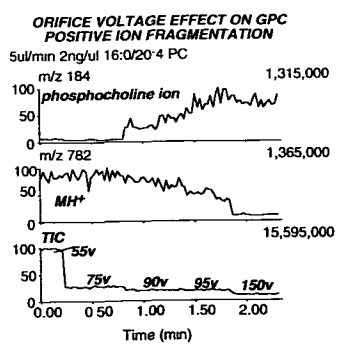

Figure 2 *The effect of orifice voltage potential on the positive ions obtained by electrospray ionization of 1-hexadecanoyl-2-arachidonoyl-GPC. The orifice potential was changed sequentially from 55-150 volts at the times indicated.*

Negative ions formed by electrospray ionization of GPC were also found to be dependent upon orifice potential (Figure 3). An abundant ion corresponding to $[M+acetate]^-$ was observed with the orifice at -55 volts. This ion was converted into the ion corresponding to $[M-CH_3]^-$ at -120 volts (Figure 3). Collision induced decomposition of $[M-CH_3]^-$ was found to be identical to that previously identified for this ion species obtained by fast atom bombardment ionization and tandem mass spectrometry.

The glycerophosphocholines from HaCaT cells were isolated by HPLC and analyzed by electrospray ionization mass spectrometry. From the relative intensities of the $[M+H]^+$, the overall profile of molecular species was determined (Table 1). The fatty acyl substituents were determined from the corresponding collision-induced decomposition of the $[M-CH_3]^-$ ions (data not shown). Based upon the relative abundances of the positive ions, the potential precursors of PAF (alkylacyl-GPC) were found to represent 28.5% of total GPC molecular species.

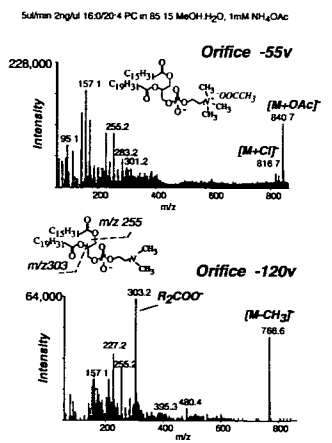

Figure 3 *(A) Negative ions obtained upon ESI/MS of 1-hexadecanoyl-2-arachidonoyl-GPC at an orifice potential of -55 V. (B) Negative ions obtained upon ESI/MS of 1-hexadecanoyl-2-arachidonoyl-GPC at an orifice potential of -120 V.*

Table 1 $[M+H]^+$ ions m/z values and relative intensities from ESI-MS analysis of HaCaT cell glycerophosphocholine

M/z	%relative abundance	molecular species
690 48	3.0	30 1 alkyl acyl
692.48	2.6	30 0 alkyl acyl
716.50	4 4	32:2 alkyl acyl
718 50	14 3	32 1 alkyl acyl
720 50	15 8	32 0 alkyl acyl
740 52	1.4	34 4 alkyl acyl
742.52	3.9	34 3 alkyl acyl
744 52	18.8	34 2 alkyl acyl
746 52	31.5	34:1 alkyl acyl
766 54	9 8	36:4 alkyl acyl
768 54	16 0	36 1 alkyl acyl
780 55	11 5	36 0 alkyl acyl
792.55	11.1	38 6 alkyl acyl
794.56	16 9	38 5 alkyl acyl
800 56	5 5	38:2 alkyl acyl
706.49	9.4	30 0 diacyl
730.51	9 5	32:2 diacyl
732.51	33 0	32:1 diacyl
734 51	28 8	32:0 diacyl
754 53	8.0	34 4 diacyl
756.53	16.5	34 3 diacyl
758.53	69 0	34:2 diacyl
760 53	100	34 1 diacyl
782.55	25.8	36 4 diacyl
784 55	47.8	36 3 diacyl
786.55	81.7	36 2 diacyl
806 56	6 6	38:6 diacyl
808 57	23 1	38:5 diacyl
814 57	10.7	38:2 diacyl
818.57	4 4	38.0 diacyl

ACKNOWLEDGEMENT - This work was supported by a grant from the National Institutes of Health (HL34303).

REFERENCE

1. Morelli, J.G., Travers, J.B., Harrison, K., Johnson, C., Clay, K.L., and Murphy, R.C.: Molecular species of platelet-activating factor biosynthesis induced by various stimuli in HaCaT keratinocytes. J. Invest. Dermatol. 104:562, 1995.

Identification of 20-Hydroxyeicosatetraenoic Acid in Rat Kidney Phospholipids

Ying Zhu, John C. McGiff and Michael Balazy
New York Medical College, Department of Pharmacology, Valhalla, NY 10595

Introduction 20-Hydroxyeicosatetraenoic acid (20-HETE) is a product of arachidonic acid and cytochrome P450 ω-hydroxylase and is an abundant microsomal eicosanoid in the rat kidney It is a potent constrictor of the renal vasculature and an inhibitor of renal potassium channels. The vasoactivity of 20-HETE is inhibited with indomethacin indicating that cyclooxygenase is required for its bioactivation. The isolated perfused kidney challenged with angiotensin II released 20-HETE into the perfusion fluid This hormone-mediated release of 20-HETE cannot be inhibited with cytochrome P450 inhibitors Incubations of rat renal slices with calcium ionophore also resulted in formation of 20-HETE, suggesting involvement of phospholipase A_2 in the release of this eicosanoid. We investigated the possibility that 20-HETE may be esterified within kidney phospholipid stores and released following an appropriate stimulus.

Methods Total lipids were extracted by the method of Bligh and Dyer from rat kidneys homogenized in methanol/water (2·3) and were hydrolyzed with and without potassium hydroxide (0 1N)/ethanol solution for 1 hr at 37 °C 20-HETE was quantitated by isotopic dilution electron capture GC/MS Kidney lipids were analyzed on normal-phase (NP) HPLC column (Spherisorb, 150x4 6 mm, 3 μm) eluted with hexane/2-propanol/ethanol/sodium acetate (50 mM)/acetic acid (400 260 100.30 1, pH 6.7). 20-HETE-containing phospholipids were prepared by incubating 20-HETE and *lyso*-phosphatidylethanolamine (*lyso*-PE) or *lyso*-phosphatidylinositol (*lyso*-PI) in the suspension of kidney microsomes for 1 - 4 hr at 37 °C Diacylglycerols (DAGs) were obtained by incubating phospholipids with 10 units of phospholipase C (B. cereus, type XI, Sigma) for 30 min at 37 °C DAGs were extracted with 10% ethyl acetate in hexane and derivatized with pentafluorobenzoyl (PFB) chloride and diisopropylethylamine in benzene The derivative was extracted with hexane and injected into a Hypersil column (20x2 1 mm) and eluted with 0.3% 2-propanol/hexane at 0.5 ml/min. The effluent from the column was mixed with helium (at 50 psi) in the nebulizer of the particle-beam LC/MS interface at the desolvation chamber temperature of 55 °C The interface was connected to the mass spectrometer (Hewlett-Packard 5989A) operating in the electron capture mode with methane flow into the ion source yielding a pressure of 1 3 torr

Results and Discussion Rat kidney total lipids contained endogenous 20-HETE of which 85-90% was in the esterified form The amount of free 20-HETE in the normal rat kidney was 0.26±0.08 ng/μmol phosphorus (P) and increased to 2 42±0 4 ng/μmol P upon alkaline hydrolysis of renal lipids (n=4) Analysis of these lipids by NP-HPLC followed by saponification and GC/MS analyses, revealed that 20-HETE occurred in two fractions· one coeluting with neutral lipids and the other, with fraction containing standard PI However, comparison of chromatographic mobility in NP-HPLC suggested that the endogenous phospholipid containing 20-HETE coeluted with biosynthetically prepared 20-HETE-PE Treatment of 20-HETE-PE with phospholipase C followed by PFB derivatization and analysis by electron capture LC/MS generated the mass spectrum (Fig 2) containing molecular anion at *m/z* 854 (M) and fragment ions at *m/z* 834 (M-HF), 816 (M-HF-H_2O), 814 (M-2HF) The cleavage of the ester bond at C-2 of the glycerol moiety produced anion at *m/z* 513 This spectrum was consistent with the structure of PFB derivative of 1-stearoyl-2-(ω-hydroxyarachidonoyl)-glycerol having the PFB group bound to the ω-hydroxyl of the arachidonate function. The results indicated that the negative ion particle beam LC/MS was a useful technique for characterizing the diglycerol derivative of 20-HETE.

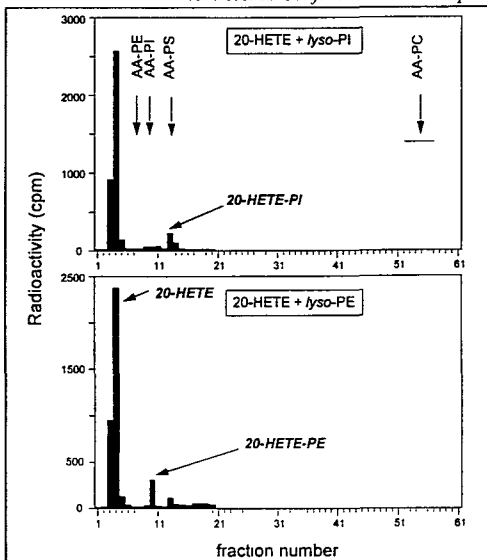

Figure 1. Effect of 1 hr (37 °C) incubations of radiolabeled 20-HETE (25 μM) with *lyso*-PI (top) and *lyso*-PE (bottom) in suspension of kidney microsomes containing CoASH (1 mM), ATP (1 mM) and ATP regenerating system (phosphocreatinine /phosphocreatinine kinase). Microsomes were preincubated with indomethacin (10 μM), baicalein (25 μM) and stilbene oxide (25 μM) for 15 min. After incubation, phospholipids were extracted with chloroform/methanol and analyzed by NP-HPLC. The amount of radioactivity in fractions was determined by scintillation counting In parallel experiments, radiolabeled arachidonic acid (AA) was incubated with microsomes and various *lyso*-phospholipids and analyzed by NP-HPLC Arrows indicate fractions which contained arachidonate-labeled phospholipids

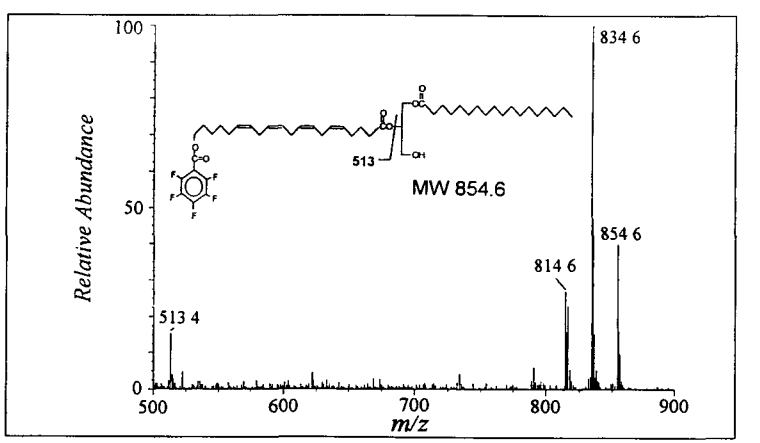

Figure 2 Electron capture spectrum of 1-stearoyl-2-(ω-hydroxyarachidonoyl)-3-pentafluorobenzoyl glycerol obtained by phospholipase C hydrolysis of a product in fraction 10 (Fig 1, bottom) followed by esterification with pentafluorobenzoyl chloride and analysis by particle beam LC/MS

Structural Characterization of Phospholipids by Matrix-assisted Laser Desorption Ionization FT-ICR Mass Spectrometry

Jarrod A. Marto†, Forest M. White, Staci Seldomridge, and Alan G. Marshall*

Center for Interdisciplinary Magnetic Resonance, National High Magnetic Field Laboratory, Florida State University, 1800 E. Paul Dirac Dr., Tallahassee, FL 32310

†Department of Chemistry, The Ohio State University
* Department of Chemistry, Florida State University

Here we report successful analysis of each of the four major classes of phospholipids (glycerophosphatidyl-choline, -ethanolamine, -serine, and -inositol) by use of matrix-assisted laser desorption Fourier transform ion cyclotron resonance mass spectrometry. Based on the relative size of the sample probe and laser spot, and assuming even sample distribution on the probe surface, we estimate that ~1.5 picomoles of lipid are desorbed per laser shot (total phospholipid on probe tip ≈ 3.5 nanomoles).

Both positive and negative molecular or quasi-molecular ions may be generated in high abundance. Isolated molecular ions are collisionally activated in the source half of a dual ion trap (~1.0 x 10^{-7} torr argon neutral collision gas), yielding fragments corresponding to polar-head group (positive-ions) or fatty acid side chains (negative-ions). Application of azimuthal quadrupolar excitation following collisionally activated dissociation (CAD) refocuses product ions close to the central z-axis; subsequent transfer of ions to the analyzer ion trap allows for high-resolution mass analysis.

Figure 1 shows representative negative-ion FT-ICR mass spectra for a 1,2-diacyl-glycerophosphoethanolamine (GPE), containing palmitic and oleic acids at the sn-1 and sn-2 positions respectively, generated from TCA matrix at a 5000:1 mole ratio with respect to the analyte. The top spectrum shows GPE molecular anion (m/z = 716) after isolation in the source ion trap, broadband axialization, and transfer to the analyzer trap. The middle and bottom spectra compare collisional activation of the molecular ion in the source side trap followed by either source side dipolar excitation and detection (middle), or broadband quadrupolar axialization and transfer to the analyzer trap (bottom). In each case, collisional activation was performed by sustained off-resonance dipolar irradiation at ~ 1 kHz below the reduced ion cyclotron frequency, ω_+, after optimizing the excitation amplitude and duration to maximize product ion signal magnitude. Collisional activation results in formation of abundant palmitic (m/z = 255) and oleic (m/z = 281) carboxylate anions. Product ion axialization and ion transfer to the low-pressure analyzer trap following CAD clearly results in much greater observed ion abundance and higher mass resolving power compared to CAD and detection in the source trap. For example, signal-to-noise ratio for the oleic carboxylate anion (m/z = 281) is at least 5 times higher and mass resolving power is ~15 times higher ($m/\Delta m_{50\%}$ ≈ 155,095 *vs.* $m/\Delta m_{50\%}$ ≈ 10,236) for analyzer trap detection than for source trap detection). Work supported by NSF (CHE 93-22824), NIH (GM-31683), The Ohio State University, and the National High Magnetic Field Laboratory at Florida State University.

43rd ASMS Conference on Mass Spectrometry and Allied Topics

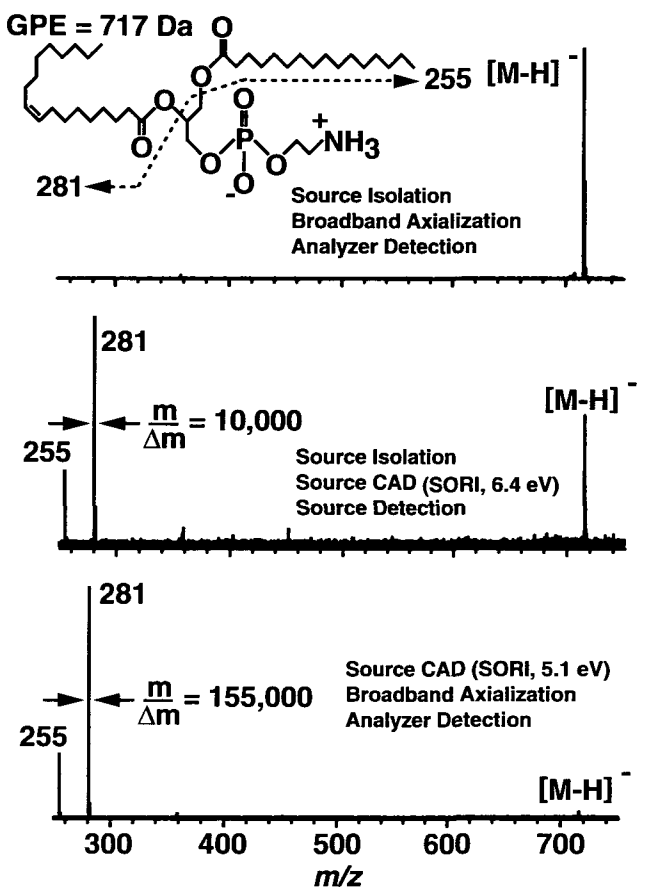

Figure 1. FT-ICR negative-ion mass spectrum (top) and MS/MS spectra (middle and bottom) of 1,2-diacylglycero-phosphoethanolamine (GPE), from which the palmitic and oleic acid side chains are readily identified (see text).

Detection of Phospholipid Molecular Species in U937 Cells using CF-LSIMS

Chun Li* and James A. Yergey
Merck Frosst Center for Therapeutic Research, P.O. Box 1005
Pointe Claire-Dorval, Quebec, H9R 4P8, CANADA

Phospholipids are important constituents of the lipid bilayer of all cell membranes, and are important sources of arachidonic acid for eicosanoid biosynthesis. The analysis of molecular species within a phospholipid class, however, has been a challenging and time consuming task.[1-3] Previously, we developed an LC/MS method using capillary HPLC / continuous-flow liquid secondary ion mass spectrometry (CF-LSIMS).[4] Phospholipid molecular species analysis by CF-LSIMS showed much better sensitivity compared with existing techniques such as static FAB and thermospray LC/MS. A full scan mass spectrum of <1 ng phospholipid injected on column can be easily obtained, in both positive and negative ion modes. Molecular weight, head group and fatty acid chain information can be readily obtained from the primary CF-LSIMS spectra.

Coupling capillary HPLC with CF-LSIMS is particularly useful for the identification of minor species within a complex mixture. Using this technique, molecular species within each phospholipid class isolated from both non-differentiated and DMSO-differentiated U937 cells were readily identified in a realtively short time, and MS/MS analysis was not always necessary. U937 cells and DMSO-differentiated U937 cells are important cell lines which have been used as our primary screening assays for PLA_2 inhibitors. DMSO-differentiated U937 cells released much more arachidonic acid upon Ca^+ ionophore challenge than non-differentiated U937 cells.[5] This dramatic difference in arachdonic acid release may due to the difference in phospholipid composition of the cell membranes or the PLA_2 enzyme activity. The analysis of phospholipid molecular species in the two cell lines using capillary HPLC / CF-LSIMS indicated that no significant difference in phospholipid composition was found between non-differentiated and DMSO-differentiated U937 cell membranes. Each phospholipid class PE, PI, PS and PC isolated from the two cell lines showed identical molecular species profiles. The difference in arachidonic acid release upon Ca^+ ionophore challenge, therefore, must due to the enzyme activity difference between the two cell lines, or the factors affecting the utilization of free fatty acid.

References:
1. K. Kayganich and R. C. Murphy **J. Am. Soc. Mass Spectrom** 2, 45,(1991)
2. K. Kayganich and R. C. Murphy **Anal. Chem.** 64, 2965, (1992)
3. H.Y.Kim, T. L. Wang and Y. C. Ma **Anal. Chem.** 66, 3977, (1994)
4. C. Li and J. Yergey **The 42nd ASMS Conference on Mass Spectrometry and Allied Topics**, Chicago, IL, (1994) p100.
5. C. Li, P. Weech and J. Yergey **The 39th ASMS Conference on Mass Spectrometry and Allied Topics**, Nashville, TN, (1991) p649.

43rd ASMS Conference on Mass Spectrometry and Allied Topics

Phosphatidylethanolamine (PE) Molecular Species

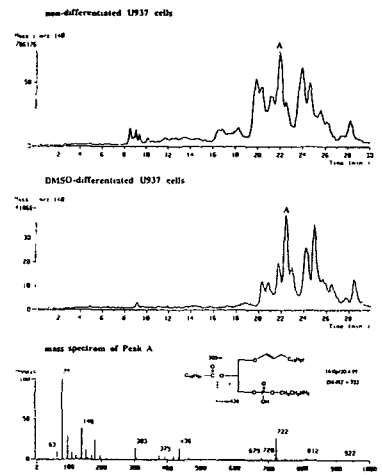

Phosphatidylinositol (PI) Molecular Species

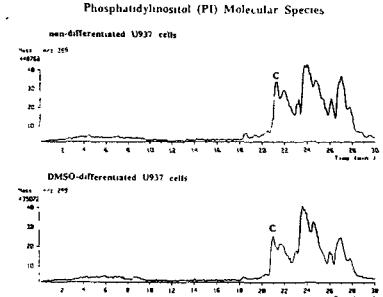

Identification of Molecular Species of Phosphatidylethanolamine (PE) Isolated from Human U937 Cells by CF-LSIMS

FAB [M-H]-	FAB+ [M+H]+	diacyl	alkylacyl	plasmalogen
660	662	14:0/16:1		
686	688	16:1/16:1		
760	762	16:1/22:6		
736	738	16:1/20:4		
712	714	16:1/18:2		
762	764	18:1/20:5		
694	696			14:0/20:4
720	722			36:5
736	738	16:0/20:5 *		
714	716	16:1/18:1		
720	722			16:0/20:5
688	690	14:0/18:1		
762	764	16:0/22:6		
788	790	18:1/22:6		
738	740	16:0/20:4		
764	766	18:1/20:4		
740	742	18:1/18:2		
790	792	18:1/22:5		
746	748			16:0/22:6
722	724			16:0/20:4
748	750			16:0/22:5
742	744	18:1/18:1		
716	718	16:0/18:1		
790	792	18:0/22:6		
766	768	18:0/20:4		
700	702			16:0/18:1
750	752			18:0/20:4
792	794	18:0/22:5		
768	770	18:0/20:3		
726	728		36:3	36:2
752	754		38:4	38:3
770	772	38:2		
744	746	18:0/18:1		

Phosphatidylinositol (PI) Molecular Species in Human U937 Cells

FAB [M-H]-	diacyl	alkylacyl	plasmalogen
805	14:1/18:1		
831	16:1/18:2		
833	16:1/20:5		
837	18:1/16:1		
853	32:1		
859	18:1/20:4		
861	18:1/18:2		
863	18:0/20:4		
865	18:0/18:1		
867	18:1/18:1		
863	18:1/20:3		
867	18:0/20:3		
863	18:0/18:1		
889	18:0/20:2		
891	18:0/20:1		

Phosphatidylserine (PS) Molecular Species in Human U937 Cells

FAB [M-H]-	diacyl	alkylacyl	plasmalogen
758	16:1/16:1		
732	32:1		
760	18:0/16:1		
786	18:1/18:1		
834	18:0/22:6		
836	18:0/22:5		
812	18:0/20:4		
788	18:0/18:1		

Phosphatidylcholine (PC) Molecular Species in Human U937 Cells

FAB [M-15]+ [M-60]+ [M-86]+	FAB+ [M+H]+	diacyl	alkylacyl	plasmalogen
714 669 643	730	16:1/16:1		
740, 695 668	756	16:1/18:2		
716, 671 645	732	16:0/16:1		
742 697 671	758	16:1/18:1		
766 721 695	782	16:0/20:4		
676, 631 605	692		30:0	
702, 657 631	718		32:1	32:0
732, 707 681	764		16:0/20:4	
744, 699 673	760	16:0/18:1		
770, 725 699	786	18:1/18:1		
718 673, 647	734	16:0/16:0		
730 685, 659	746		34:1	34:0
704 659 633	720		32:0	
798 753 727	814	18:1/20:1		
772, 727 701	788	18:0/18:1		

Analysis for Analogs of Phospholipids by FAB Mass Spectrometry

Chungping Yu, Jianxing Huang, and Theodore S. Widlanski
Indiana University, Chemistry Department
Bloomington, IN 47405

INTRODUCTION

Due to the inherent low volatility and thermal lability of naturally occurring diacylglycerylphospholipids, the conventional method for structural analysis of these lipids is to chemically derivatize these analytes to increase volatility, followed by electron impact or chemical ionization mass spectrometric analysis. However this procedure to obtain information of molecular weight, fatty acyl groups, and polar head groups of various lipid classes is sometimes impractical because a complicated chromatographic separation may be required after derivatization. Fortunately, a combination of positive ion and negative ion FAB has been used successfully for structural analysis of underivatized lipids.[1,2] In this paper we report the evaluation under both positive and negative ion FAB conditions of various analogs of phospholipids containing sulfur in the head group. To simplify the structural characterization of these molecules, each lipid is designed to include two identical esterified acyl groups.

EXPERIMENTAL

A Kratos MS80RFAQ was operated at an accelerating potential of 4 KV to collect all the FAB mass spectra. A primary atom beam of Xe was produced using a saddle field ion source operating with an emission current of 2 mA at voltage of 8-9 KV. All the samples were prepared by the following procedure with NBA as matrix. Samples (10-50 mg) were dissolved in either 50 mL of a mixture solvent of methylene and methanol (5:1) or 30 mL of methylene chloride. 2-3 mL of this solution was then mixed with 5 mL of NBA on the copper tip. For lipids **1-9**, an additional 1 mL of 2% sodium acetate solution in methanol was applied to the tip to yield significant sodium adduct ions.

DISCUSSION

Molecular weight information on lipids (**1-6**) can be derived from the abundant $[M+Na]^+$ ions in FABMS spectra. Spectra also show the presence of $[RCO]^+$ ions at m/z 155, 183, 211, and 265, corresponding to $[C_9H_{19}CO]^+$, $[C_{11}H_{23}CO]^+$, $[C_{13}H_{27}CO]^+$, and $[C_{17}H_{33}CO]^+$ ions, respectively. In addition, a few fragments produced either by the loss of one acyl group or by the partial elimination of the head group are observed in the middle mass range of the spectra. Because of the low abundance of these fragments, These ions were not used for the elucidation of any structural information. Under negative ion FABMS condition, these lipids lose the head group moiety, **X** group, to produce abundant sulfonate anions. Other anions recognized in these spectra correspond to the carboxylate anions of the acyl group providing further confirmatory analysis of the acyl group. As expected, the positive ion FAB spectra of **7-9** show the presence of abundant $[M+Na]^+$ ions and $[RCO]^+$ ions. In contrast to the absence or very

1. Matsubara, Toshiko and Hayashi, Akira *Prog. Lipids Res.* **30**, 301-322 (1991).
2. Murphy, Robert C. and Harrison Kathleen A. *Mass Spectrometry Reviews* **13**, 57-75 (1994).

low abundance of ions resulting from the cleavage of the carboxylate of the acyl group as seen in the spectra of other lipids, spectra of **7-9** show significant $[M-RCOO]^+$ ions at m/z 281, 365, and 297, respectively. These characteristic fragments can be used to distinguish lipids with sulfonyl head groups from lipids with other type of head groups. In negative ion FAB analysis, the only observed anion corresponds to the carboxylate anion of the acyl group. For lipids (**10-12**) containing serine in the head group, a rather intense $[M+H]^+$ ion is observed in the FABMS spectra without addition of sodium salt in the sample matrix. The basic nature of this zwitterion is probably responsible for the existence of significant $[M+H]^+$ ions. Additional ions are detected at m/z 439, 467, and 521 in the spectra of **10-12,** corresponding to the loss of the RCO fragment from the molecular species. In the negative ion mode, we observed cleavage of the oxygen-carbon bond between the sulfonate and serine to produce abundant sulfonate anions at m/z 533, 589, and 697 for lipids **10-12**, respectively. Once again, these spectra also show the characteristic carboxylate anion of acyl group.

CONCLUSION

In this work, we demonstrate that both positive and negative ion FABMS can be used together to identify the structure of sulfonyl-containing lipids and differentiate the lipids with different head groups. Solubility and concentration of analyte in the matrix and intrinsic properties of head group play an important role in affecting the mass spectrum quality and reproducibility. It is also noteworthy that different acyl groups do not have significant effect on the fragmentation pattern in both positive and negative ion modes. In future work by measuring the relative abundance ratio of the corresponding carboxylate anions, we may extend our study to a determination of the exact position of acyl group at the glycerol backbone of sulfur-containing lipids with two different acyl groups.

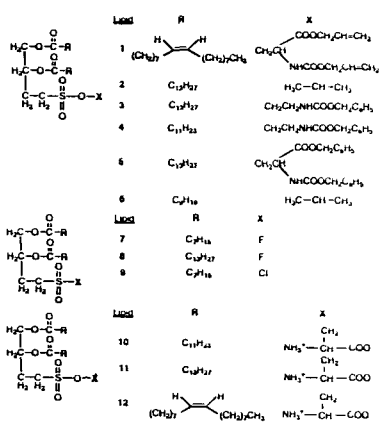

Analysis of Polyunsaturated Phospholipid Turnover by Electrospray LC/MS

*Ma, Yee-Chung; Ward Glen; Wang, Tao-Chin; Salem, Jr, Norman; Kim, Hee-Yong; Section of Mass Spectrometry, LMBB, NIAAA, NIH; NIMH, NIH, Bethesda, MD 20892

Phospholipids are not only the major constituents of biological membranes, but also play a role in many important biological functions. The distribution of individual phospholipid molecular species varies in different tissues, suggesting that their synthesis and turnover is differently regulated in various biomembranes. In the central nervous system, a very high abundance of polyunsaturated phospholipids was found. Since maintaining the balance of these polyunsaturated phospholipids is critical in normal brain development, understanding their dynamic changes in early postnatal life is important. In this study, polyunsaturates in the brain of mouse pups were labeled by feeding pregnant mice with deuterium labeled (d_5) linoleic (18:2n6) and linolenic (18:3n3) acid, the precursors of arachidonic (20:4n6) and docosahexaenoic (22:6n3) acid. The turnover of the 20:4n6 and 22:6n3 containing phospholipids in the brain of mouse pups can be assessed by monitoring the d_0/d_5 ratio using the electrospray LC/MS method we developed (1).

The mass spectrometers used in the study include an HP 5989 MS engine and a Finnigan TSQ70 triple quadrupole system, equipped with electrospray interface. The electrospray spectra of phospholipids produced simple MH^+ and $(M+Na)^+$. The response obtained for these phospholipids was similar within the same class but differed between classes. For phospholipids with a given fatty acyl composition, the electrospray technique was most sensitive for PC, followed by PE, PI and PS in descending order. By increasing capillary exit potential, characteristic diacylglyceride fragment ions (DG^+) were induced for all species except PC. Linear response curves were obtained for both MH^+ and DG^+ in the range of 10 pg to 10 ng when deuterium labeled compounds were used as internal standards (Figure 1).

In the animal study, pregnant mice were fed a diet containing deuterium (d_5) labeled 18:2n6 and 18:3n3 starting from 7 days of gestation and continuing throughout the pregnancy and lactation period. After weaning, pups were fed a diet in which most 18:2n6 and 18:3n3 were replaced by non-labeled 20:4n6 and 22:6n3. Ethanol (20 % cal) was introduced in the diet 10 weeks after birth for a duration of 2 weeks. At various time points, animals were sacrificed, the brain lipids were extracted, and both d_0 and d_5 20:4n6 and 22:6n3 containing phospholipids were analyzed by the reversed phase HPLC/electrospray MS method. The d_0/d_5 ratio of individual phospholipids obtained indicated that the turnover rate varied for different molecular species. In general, turnover of 20:4n6 containing phospholipids was faster than 22:6n3 containing phospholipids. Chronic ethanol consumption reduced the turnover of most 20:4n6 containing phospholipids while 22:6n3 containing phospholipids were not affected significantly. An exception was observed for 18:0/22:6-PC in which the turnover rate increased by about 25% (Figure 2).

REFERENCES:

(1) H.Y. Kim, T.C. Wang, and Y.C. Ma (1994) Anal. Chem. **66**, 3977-3982.

43rd ASMS Conference on Mass Spectrometry and Allied Topics

Figure 1 Calibration of PE using DG Ions

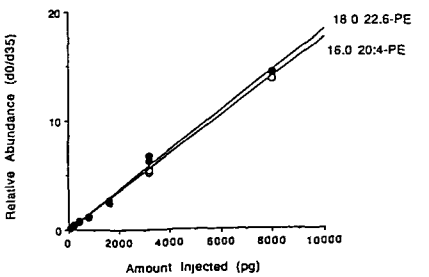

Calibration of PC using MH+

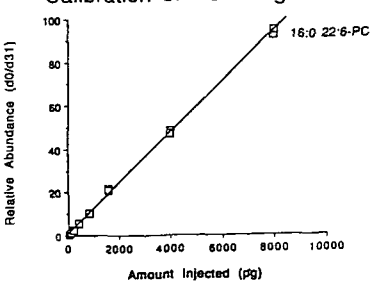

Figure 2 Effect of Ethanol on Turnover of Polyunsaturates

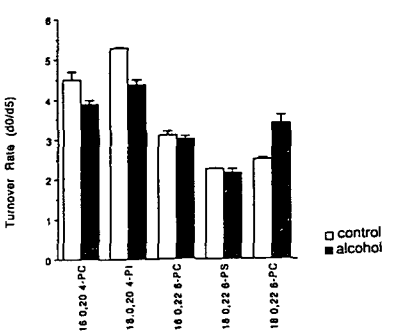

ISOLATION AND IDENTIFICATION OF PHOSPHOLIPIDS IN LIPID EXTRACTS BY ES/MS/MS

Kevin L. Duffin, Mark Obukowicz, and J.J. Shieh, Monsanto Corporate Research, Monsanto Company, St. Louis, MO 63198

Electrospray and tandem mass spectrometry were used to distinguish lipid compound classes and to identify the fatty acids that comprise the particular classes of lipid that were found in various tissue and cell extracts. Tissues and purified cell populations were extracted with chloroform:methanol solvent and the extract was analyzed directly after a simple centrifugation. Ammonium acetate was added to the extract solvent to assist in ionization of the nonpolar lipids that did not already possess a charge. Tandem mass spectrometry was used to fragment intact lipid ions to determine their class and to determine their fatty acid composition. Lipid standards were analyzed initially by these techniques to learn the expected fragmentation patterns of each class of lipid. Many of these results have already been published [1]. Results of these fragmentation studies then were used to identify the lipids found in mouse liver and footpad tissues, and in rat neutrophils. Common fragmentation patterns were observed in each of the different phospholipid classes, which aided in class identification and provided a means to separate phospholipid classes by classical parent ion or neutral loss MS/MS experiments without prior chromatographic separation. Product ion and neutral loss MS/MS experiments were then applied to the characterization of liver tissue, peritoneal leukocytes, and plasma of mice that were fed diets rich in linoleic acid (corn oil diet) or that were essential-fatty-acid-deficient. Lipids were separated and detected by MS/MS using the following fragmentation routes, which were generally applicable to those lipids that are listed:

Lipid	ES-MS/MS Characteristics
Cholesterol Ester	$(M+NH_4)^+$/ m/z 369 fragment ion
Sphingomyelin	M^+/ m/z 184 fragment ion
Phosphatidylcholine	M^+/ m/z 184 fragment ion
Phosphatidylethanolamine	$(M+H)^+$/ loss of 141
Phosphatidylglycerol	$(M+NH_4)^+$/ loss of 172 and 189
Phosphatidylserine	$(M+H)^+$/ loss of 185
Phosphatidylinositol	$(M+NH_4)^+$/ loss of 260 and 277
Phosphatidic Acid	$(M+NH_4)^+$/ loss of 98 and 115
Cardiolipin	$(M+NH_4)^+$/ fragments to form diacylglycerol

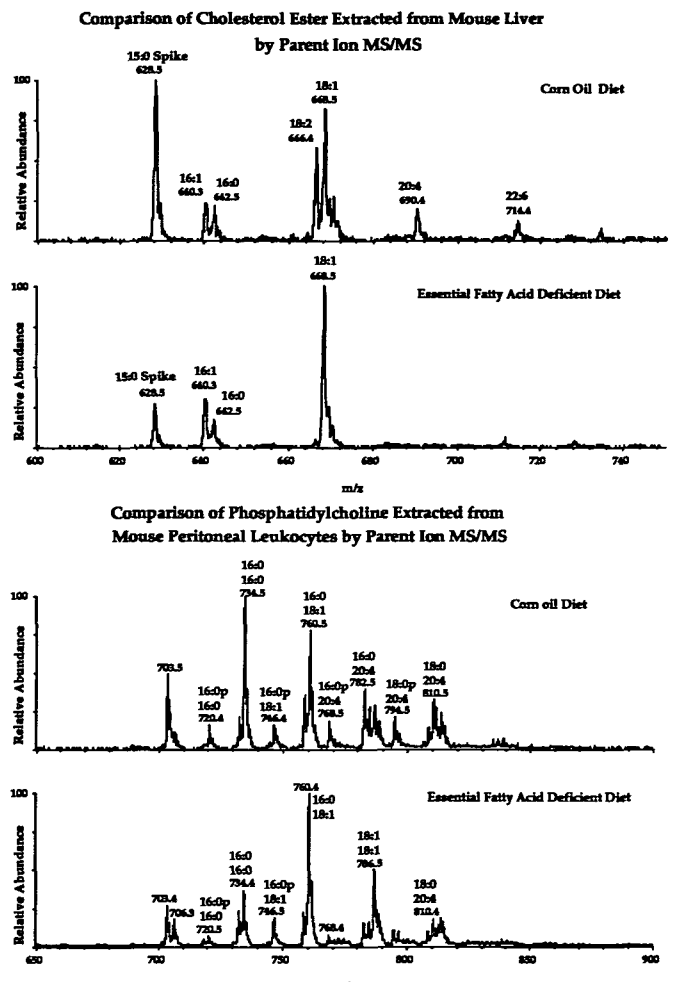

MASSIVE CLUSTER IMPACT IONIZATION OF PHOSPHOLIPIDS

Nyla N. Dookeran and Peter J. Todd
Chemical & Analytical Sciences Division
Oak Ridge National Laboratory
PO Box 2008, Bldg. 5510A
Oak Ridge, Tennessee 37831-6365

We used a massive cluster impact (MCI) gun as a source of primary ions to generate positive and negative secondary ions characteristic of phospholipids from three types of samples. These included reference phospholipids dissolved in glycerol and deposited neat on the FAB target of a JEOL SX102A mass spectrometer. We also obtained spectra from animal tissue deposited directly on the probe tip. Except for variations in total secondary ion yield, the mass spectral characteristics of lipids obtained from the three different types of samples are virtually identical. Furthermore, the fragmentation behavior of the ions formed is similar to that reported by others who have used FAB**[1]** and a liquid glycerol matrix. The obvious advantages of the MCI source include minimal sample preparation and secondary ion emission that persists for hours.

The MCI gun is a direct replacement for the JEOL Xe FAB gun. Its operation is based on electrohydrodynamic (EHD) ionization of glycerol, which is supplied from an integral reservoir via a stainless steel capillary. Glycerol cluster ions with a mass distribution extending to 10^7 u, charge distribution in the range of 10^2 and current of about 10-30 μA, are emitted from the gun when a potential of 15-20 keV are applied to the EHD emitter.**[2]** The beam of clusters is focussed and deflected onto the target by a series of lens elements/deflectors. Recent modifications to the original gun design have greatly improved the stability of the emitted beam, and the corresponding secondary ion current.

In the positive secondary ion mode, the presence of phosphatidylcholine is evident by an abundant m/z 184 ion. As with conventional FAB, virtually all the information about the lipids in a sample can be determined in the negative mode,. For example, abundant $[M-15]^-$, $[M-60]^-$ and $[M-86]^-$ are observed from phosphatidylcholine. Abundant $[M-H]^-$ from phosphatidylethanolamines are typically 40% of the base peak intensity, with peaks corresponding to either of the acyl groups as the base peak.

Most importantly, among the most abundant negative secondary ions detected are the acyl groups. Figure 1, for example, shows a region of the negative ion MCI spectrum obtained from a sample of 18:0/18:1 phosphatidylcholine. The two important features of the m/z 281 and the m/z 283 are their intensity in the spectrum and their intensity relative to each other. The former feature permits use of tandem mass spectrometry (MS/MS) to determine their structure, including position of double bonds and the latter permits assignment of the m/z 283 to the sn-1 and m/z 281 to the sn-2 positions of the glycerol backbone of the phospholipid.

Figure 2 shows the partial negative MCI mass spectrum obtained from a sample of 18:1/18:0 phosphatidylcholine deposited directly on the sample probe tip, without any other sample preparation. The abundant m/z 283 and 281 mark the sample as containing 18:0 and 18:1 lipids. Their abundance relative to each other indicate the 18:1 fatty acid is in the sn-1 position and the 18:0 fatty acid is in the sn-2 position. Importantly, the same spectrum was observed after continuous bombardment for more than one hour.

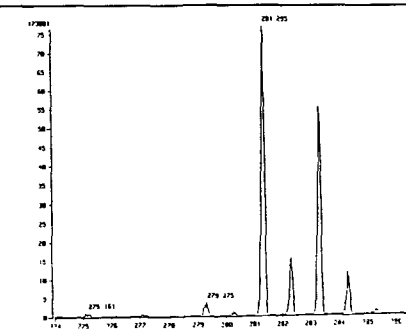

Figure 1. MCI Negative ion spectrum of 18:0/18:1 Phosphatidylcholine

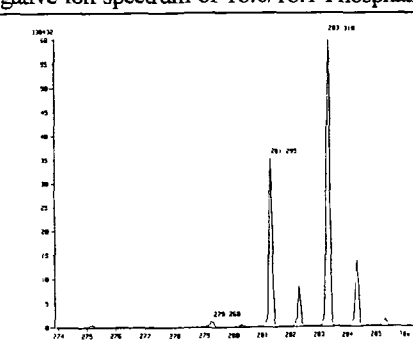

Figure 2 MCI Negative ion spectrum of 18:1/18:0 Phosphatidylcholine

1. Jensen, N. J.; Tomer, K. B.; Gross, M.L. *Lipids* **1986**, *21*, 580.

2. Mahoney, J. F.; Perel, J.; Ruatta, S. A.; Martino, P. A.; Husain, S.; Lee, T. D.; *Rapid Commun. Mass Spectrom.* **1991**, *5*, 441.

FORMATION OF THE $[M-H]^+$ ION IN THE LSIMS MASS SPECTRUM OF SPHINGOSINE

Eddie A. Chevis & Kenneth L. Busch
Department of Chemistry and Biochemistry, Georgia Institute of Technology, Atlanta, GA 30332

Abstract

The mass spectra of sphingosine and its saturated analogs were measured by electron ionization (EI), chemical ionization (CI), and liquid secondary ion mass spectrometry (LSIMS). In EI, the molecular ion can be observed intermittently. Self-chemical ionization predominates at all sample loadings and the protonated molecule $[M+H]^+$ is observed to the exclusion of the molecular ion M^+. The $[M+H]^+$ ion in EI is sometimes accompanied by an ion 2 Daltons lower in mass, $[M-H]^+$. Deuterium exchange experiments suggest that two hydrogens are lost from the hydrocarbon chain to form $[M-H]^+$. In chemical ionization, the choice of the reagent gas strongly influences the extent of fragmentation of $[M+H]^+$. The fragmentation processes observed are similar to those seen in EI, and the $[M-H]^+$ ion is now a constant 10-20% intensity relative to the protonated molecule. The relative intensity of the $[M-H]^+$ ion changes with the proton affinity of the reagent gas chosen for chemical ionization. Finally, in LSIMS, the intensity of the $[M-H]^+$ ion reaches its maximum relative intensity. The similarity of fragment ions in the LSIMS mass spectrum suggests that gas-phase dissociations are predominant.

Introduction

The long chain base sphingosine accounts for about 70% of all sphingolipid molecules isolated from cellular membranes [1]. Initially, the analysis of sphingosine and related compounds by mass spectrometry focussed on the completion of extensive work in the structural elucidation of gangliosides, glycosphingolipids, sphingomyelins, and sulfatides [2]. The development of new ionization methods has greatly aided this task. For example, Rubino *et al.* [2] demonstrated that FAB/MS and high-energy collision-induced dissociation allowed characterization of sphingosine without prior derivatization of the sample molecules. In their work, charge-remote fragmentation of the protonated molecule of sphingosine and its saturated analogs was used to confirm structure and elucidate fragmentation pathways. Sphingosine analysis by thermospray mass spectrometry has been discussed by Thakur and Smith as a potential method of early detection for Fumonisin toxicity. Thakur and Smith [3] demonstrated that native sphingosine and its saturated analogs in serum samples could be detected by thermospray mass spectrometry, with the mass spectra providing both qualitative and quantitative information.

Both FAB and the thermospray studies highlight fragmentation reactions useful for structural characterization of these compounds. The assumption has been that a desorption ionization method is required to produce a molecular ion from these compounds. There are several early reports of the electron ionization (EI) mass spectra of derivatized forms of sphingosine and its analogs [4-7]. However, we found that EI could occasionally be used to generate mass spectra from underivatized sphingosine. Initial results that showed the occurrence of a self-chemical ionization process to form $[M+H]^+$ suggested also that analogies to the mass spectra produced by chemical ionization and LSIMS/FAB could be explored. Such a comparison is one focus of this paper, and we measured chemical ionization (CI) mass spectra, also apparently without precedent in the literature. We completed this study with LSIMS mass spectra recorded in several different solvent matrices to complement and extend the work of Rubino *et al.*

One common feature of positive ion LSIMS/FAB mass spectra is the presence of an ion with mass two Daltons lower than the protonated molecule, viz $[M-H]^+$. A similar ion also often appears in the positive ion LSIMS mass spectra of precharged organic compounds, appearing there as $(C-2)^+$ where C is the mass of the cation. This ion formally corresponds to the product of a dehydrogenation reaction, and usually

appears with 10-20% intensity relative to the intensity of the cation or the protonated molecule. The mass spectra recorded by Rubino et al. contain this ion. The $[M-H]^+$ ion for the saturated compound corresponds in mass to the protonated molecule for unsaturated sphingosine. Another focus of this work is to confirm the origin of this fragment ion as a dehydrogenation reaction, and for the case of sphingosine and its saturated analogs, to explore the mechanism for its formation.

Conclusions

The ability of electron ionization to produce mass spectra for sphingosine was shown in this study. The fact that chemical ionization produces high quality mass spectra supports the assertion that the samples can be evaporated into the source without decomposition from a direct insertion probe. The strong basic nature of the sphingosine was apparent in the self-chemical ionization process observed in EI, and in the relative lack of fragmentation in CI and LSIMS. This study was also focussed on the production of the $[M-H]^+$ ion in each of the ionization methods, and deuterium exchange experiments suggest that the hydrogen that is lost in the dehydrogenation is derived from the alkyl chain of the molecule. There is no evidence for a beam-induced dehydrogenation reaction, and the appearance of the $[M-H]^+$ ion in all ionization methods confirms the origin of this peak in a gas-phase dissociation. Charge-remote fragmentation occurs not only in LSIMS but also in chemical ionization mass spectra.

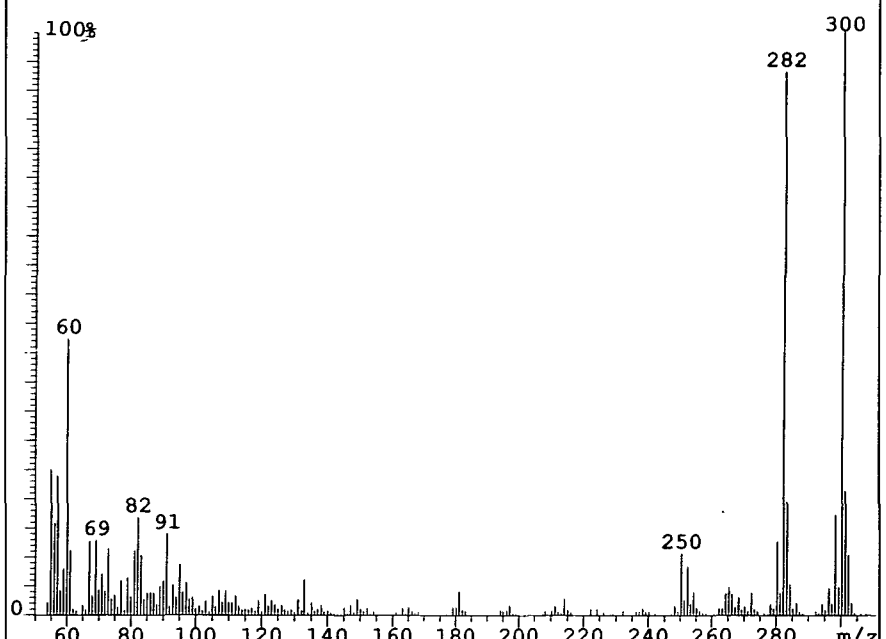

LSIMS Mass spectrum of Sphingosine in thioglycerol matrix.

Characterization of GS-15 and Biomarkers of the Helderberg Formation

Maria P.Ospina*, David H. Powell*, James E. Channel**, Richard A. Yost*
*Department of Chemistry, University of Florida
**Department of Geology, University of Florida

About 280 million years ago the magnetic properties of the sedimentary rocks in about one-half of the North American continent were changed. They were remagnetized over a very large area, and the process that caused this change is poorly understood[1].

In the case of the Helderberg Limestones in New York State, the remagnetization occurred 100 million years after the deposition of the sediment. The direction of the remanant magnetization indicates that the remagnetization occurred 280 million years ago, whereas the limestones were deposited 380 million years ago. The magnetic characteristics of these rocks, indicate that magnetite is the carrier of the magnetization. Estimates of the thermal conditions during burial eliminate the possibility of remagnetization by thermal processes and imply chemical growth of new magnetite. **QUESTION:** Where did the new magnetite come from and how did it get into the rock?

Geochemical models for post-depositional magnetite formation are controversial. It has been suggested that magnetite occurs the limestones as a result of hydrocarbon or associated brine migration[2,3] coeval with the Hercynian deformation of the Appalachian mountains. The grain size of the magnetite particles is in the range of several tens of nanometers with a quite narrow distribution. It is unlikely that the magnetite was formed from an inorganic source. A biological source is more likely.
Three possible biologically based mechanisms have been suggested:

1. Microbial attack of hydrocarbons leading to precipitation of magnetite from bitumen[4];
2. Microbial synthesis of magnetite with subsequent deposition after death as in bacteria that use magnetite particles for orientation
3. Production of magnetite as an end product of microbial metabolism by Fe(III) reducing bacteria.

An anaerobic, rod-shaped bacterium (GS-15) was isolated several years ago from the Potomac river and found to produce ultrafine-grained magnetite with a similar narrow distribution and size to those found in the Helderberg limestones. These magnetite grains are products of GS-15 metabolism. GS-15 can oxidize several aromatic compounds to CO_2 with Fe(III) as the sole electron acceptor[5]. These studies suggest that Fe(III) reducing organisms like GS-15 could be responsible for Fe(III) reduction and formation of post-depositional magnetite.

We have completed a preliminary GC/MS examination of the organic extractables from Helderberg limestone and the magnetite producing bacterium GS-15 in order to test whether a chemical fingerprint is present which may associate the new magnetite in the limestones with a bacterial source.

The dominant organic extractables in the Helderberg limestone are straight-chain aliphatic hydrocarbons ranging from C-15 through C-23 with both even- and odd-carbon numbers exhibited. We have detected the biomarker compounds pristane and phytane in the limestones and also ions that are markers for hopanes and steranes. The pristane:phytane ratio is about 0.5 which can indicate anaerobic environmental conditions. Since the Helderberg limestones have not experienced significant heating after deposition, the organic phase is considered geochemically immature and the pristane:phytane ratio is not conclusive with respect to the oxygenation conditions during deposition. The presence of pristane and phytane can indicate either a

chlorophyll based source or a bacterial origin. The lipids found in the outer membrane of certain bacteria that live only in strong salt solutions has been proposed as an indirect source for the isoprenoid alkanes .[9-13] This biological source is consistent with brine intrusions which have been associated with post-depositional magnetization.[2,3]

The GS-15 bacteria show only C-14 through C-16 fatty acids. The quantity of bacteria available for the extraction was less than half a gram due to the stringent conditions necessary to culture this organism. The analytes detected were therby restricted to the major components.

Future studies will employ larger quantities of GS-15 bacteria to examine the lower concentration fatty acids, terpenes, and precursors of hopanes and steranes. We will also use selected ion monitoring and tandem mass spectrometry to identify further marker compounds in GS-15 and the Helderberg limestone.

GC/EI Trace of an Extract of Helderberg Limestone

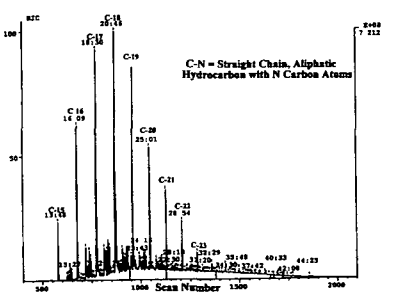

GC/EI Trace of an Extract of GS-15 Bacteria

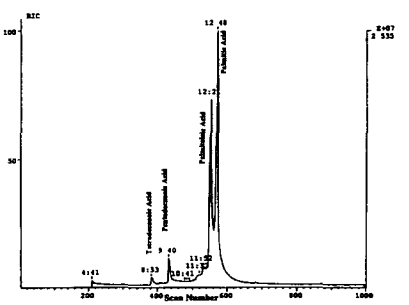

References

1. McCabe, C.; Van der Voo, R.; Peacor, D.R.; Scotese, C.R.; Freeman, R. **1983** *Geology,* 11, 221-223.
2. Donovan, T.J.; Forgey, R.L.; Roberts, A.A. **1979**, *Am Assoc Petroleum Geologists Bull* 63, 245-248.
3. Elmore, R.D.; Crawford, L. **1990**, *J. Geophys. Res.* 95, 4539-4549.
4. Elmore, R.D.; Engel, M.; Crawford, L.; Nick, K.; Imbus, S.; Sofer, Z. **1987** *Nature*, 325, 428-430.
5. Lovley, D.R.; Stolz, J.F.; Nord, G.L.; Phillips, E.J.P. **1987**, *Nature*, 330, 252-254.
6. Kates, M. *Techniques of Lipidology* **1986**, Elsevier, New York, pg. 106-107.
7. Zeng, X; Liu, S.; Ma, S. **1988** in *Geochemical Biomarkers*, Yen, T.F. and Moldowan, J.M. eds. Harwood Academic Publishers, New York, . pg. 25-49.
8. Henderson, W.; Wolrab, V.; Eglinton, G. **1968**, *Adv. Org Geochem.* 181 - 207.
9. Eglington, G.; Calvin, M. **1967**, *Scientific American*, 216, 32-43.
10. Sohn, M.L. **1986** in *Organic Marine Geochemistry*, American Chemical Society, Washington, DC, pg 10-30, 33-60.
11. Risati, J.B. *et al.* **1984** *Org. Geochem.* 6, 93-103.
12. Holzer, G. *et al.* **1979** *J. Chromatog.* 186, 795-809.
13. Volkman, J.K. *et al.* **1986** *Org. Geochem.* 10, 1-6: 371-681.

Py-MS FAME EXTRACT PROFILING OF PATHOGENIC MICROORGANISMS

Franco Basile, Ted L. Hadfield[1], Dave W. Sickenberger[2], and Kent J. Voorhees
Department of Chemistry, Colorado School of Mines, Golden, CO 80401; [1]Armed Forces Institute of Pathology, Washington, DC; [2]CBDCOM, ERDEC, Aberdeen Proving Ground, MD.

Pyrolysis-mass spectrometry (Py-MS) has been chosen for a new automated, field instrument for the detection of chemical and biological warfare agents (BWAs). Before this technology is implemented in field situations, its ability to identify and detect BWAs must be compared to established bacterial identification system. In this study, Py-MS of fatty acid methyl ester (FAME) extracts is compared to gas chromatography-FAME analysis [1]. The advantage of mass spectrometry over the chromatographic assay is speed of analysis without loss of taxonomic information. Py-MS offers the ability to perform bacterial-FAME analysis under 10 minutes, an order of magnitude decrease in total analysis time over the GC-FAME approach.

Py-MS Analysis of FAMEs from Pathogenic Bacteria

Representative FAME Py-mass spectra from the pathogenic microorganisms studied are shown **Figure 1**. PCA analysis of Py-mass spectra of FAMEs from these microorganisms is shown in **Figure 2**. Four clusters are obtained in this data set, and the large spread of these clusters is a direct result of the wide range of growth conditions used. *Bacillus anthracis* (Gram-positive) was characterized by branched, odd-carbon number fatty acids (br-C15:0 and br-C17:0). On the other hand, *Brucella, Francisella,* and *Yersinia* are all characterized by palmitic acid (C16:0) and mono-unsaturated fatty acids (C18:1 and C16:1). The monounsaturated fatty acid C24:1w15c is a characteristic biomarker present in *F. tularensis*[2]. Samples were analyzed with a mass range of 180-360 amu to include the M-32 fragment ion (m/z 348, loss of MeOH) of the methyl ester of this fatty acid. This important fatty acid is not identified in the MIDI system, which is unable to differentiate *Brucella* from *Francisella* (Only three clusters are obtained in the PCA plot of FAME-chromatograms). No taxonomic information is lost in the Py-MS analysis even though the GC-FAME analysis uses a total of 60 different FAMEs (retention times or ECLs) when compared to only 14 FAMEs (and their fragment ions) used in the Py-MS assay.

ACKNOWLEDGEMENT

The authors (FB, KJV, TLH) are grateful for the generous support from the U.S. Army Research Office/ERDEC (Grant#: DAAL03-92-G-003).

REFERENCES

1. Microbial ID, Inc. Microbial Identification System Operating Manual. Microbial ID, Inc., Newark, DE.

2. David C. White, et al., *J. Clin. Microbiol.* 5, 738-740 (1985).

43rd ASMS Conference on Mass Spectrometry and Allied Topics

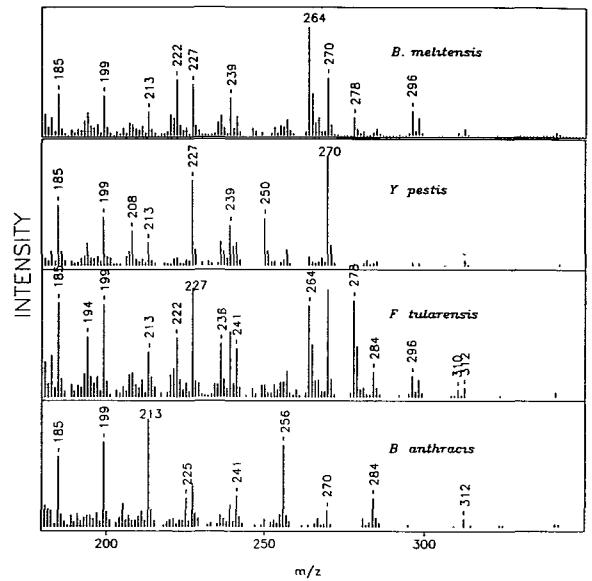

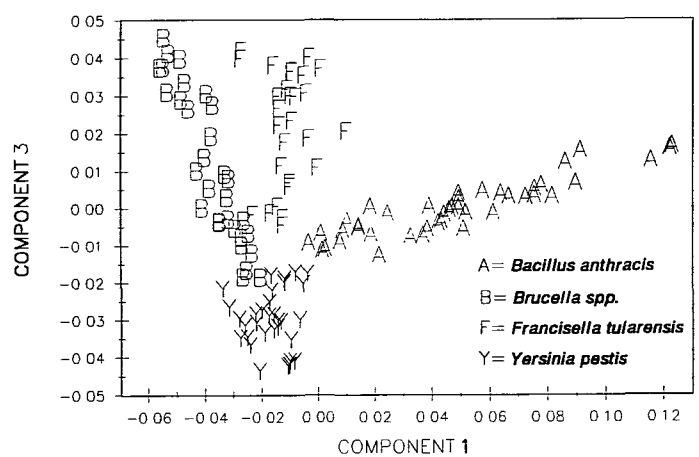

SPECIES DIFFERENTIATION OF BEESWAXES USING PYROLYSIS MASS SPECTROMETRY

Kent J. Voorhees, Paul T. Kay, and Michael B. Beverly, Dept. of Chemistry, Colorado School of Mines, Golden, CO 80401

The influx of Africanized honey bees, so called "killer bees", from South America has generated an interest and need for a technique to rapidly identify bee species Previous work using gas chromatographic (GC) methods [1,2] have shown chemical differences in beeswax that can be used for taxonomic identification. Curie-Point pyrolysis mass spectrometry (Py-MS) has been conducted on the waxes from several species of bees to determine the feasibility of using this technique as a method for bee identification. Pattern recognition analysis of the wax Py-MS spectra produced clusters that correlated to the bee species

EXPERIMENTAL

An Extrel ELQ-400 triple quadrupole mass spectrometer was used for all analyses All spectra were collected at 70ev ionization energy and over a scan range of 300-700 Da which matched the range of species specific compounds seen in GC analysis. Curie-point pyrolysis was performed at 510° C Wax samples were taken from honeycombs dissolved in chloroform (10 mg/ml) and sonicated for 5 min. An aliquot (3µL) of this suspension was applied to the pyrolysis wires and the solvent evaporated. Pattern recognition of the Py-MS spectra was done with the RESOLVE program developed at the Colorado School of Mines [3]

RESULTS

Principal component analysis of the Py-MS spectra from the waxes of seven species of bees resulted in the clustering of the spectra by their respective species (Figure 1) All of the spectra are clustered by their species except the spectra from the African, *Apis mellifera scutellata* (a), European, *Apis mellifera* (b), and hybrids of the two bees (m), which are enclosed by the inset box The overlapped grouping is expected as the waxes from African and European honey bees is very similar in composition (Figure 2).

A more detailed analysis was conducted on waxes from pure African bees (a), pure European bees (b), African/European hybrids from Texas (t), and African/European hybrids from Mexico (m). Using a pattern recognition technique called supervised rotations, separation of the European spectra from the African and hybrid spectra was achieved (Figure 3). Separation of African and European spectra was brought about by differences in the amounts of similar chemical compounds, an observation reported by other researchers using different analytical techniques[1,2]. That the African (a) wax could not be separated from the hybrid wax from Mexico (m) indicates that the latter wax more closely resembles the African wax (a) than does the hybrid wax from Texas (t). This result supports some theories that bees closer to their tropical origins demonstrate more African than European traits[1]

ACKNOWLEDGEMENTS

We wish to thank Raul Rivera at the USDA Bee laboratory in Weslaco, Texas, for providing African and Africanized wax, and Jerry Webb of Littleton, Colorado for wax samples from the European honey bee

REFERENCES

1 Daly, H.V. in *The "African" Honey Bee*; Spivak, M , Fletcher, D J C., Breed, M D , Eds.; Westview, Boulder, CO, 1991, pp13-45.

2. Carlson, D A., Roan, C., Yost, R.A , Hector, J , *Anal. Chem.*, **61** (1989) 1564-1571.

3. Harrington, P., Street, T E , Voorhees, K.J., Radicati di Brozolo, F., Odom, R.W., *Anal Chem* , **61** (1989) 715-719.

Figure 1

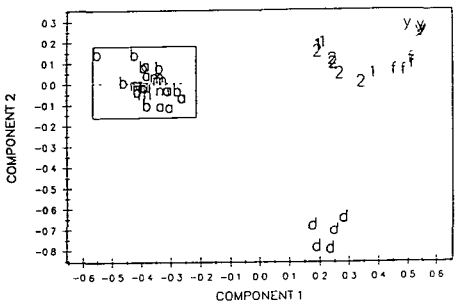

Figure 2

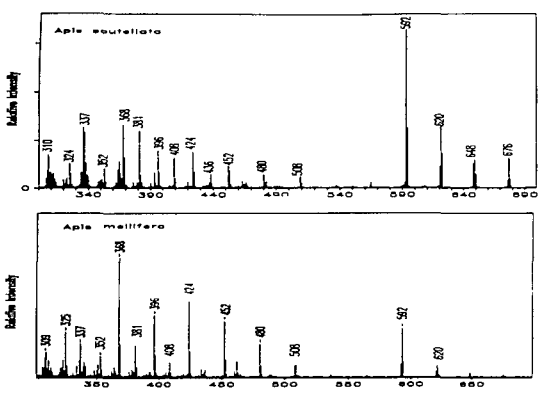

Figure 3

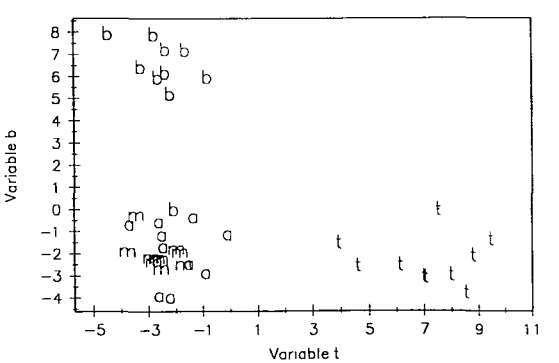

GC-MS TECHNIQUES USED IN EVALUATING ALCOHOL EFFECTS ON LIPID METABOLISM

Robert J. Pawlosky and Norman Salem Jr.
National Institute on Alcohol Abuse and Alcoholism, NIH, Rockville MD.

In the liver, alcohol consumption generally increases lipid peroxidation by generating hydroxyl radicals through the ethanol-induced monooxygenase, P450IIE1. The activation of this enzyme initiates events resulting in the production of aldehydes and F_2-isoprostanes. Both aldehydes and isoprostanes have biological activity which may be associated with some of the known effects of chronic alcoholism. High levels of lipid peroxidation may also lead to losses of polyunsaturated fatty acids, 20:4n-6 (arachidonic acid) or 22:6n-3 (docosahexaenoic acid). These losses may in turn reduce the function of certain cells (e.g. neural cells, platelets, erythrocytes).

Alcohol consumption may also reduce the uptake of essential fatty acids from the diet into the plasma and lower the production of polyunsaturated fatty acids by inhibiting enzymatic activity.

Gas chromatography-mass spectrometric techniques were used to evaluate lipid peroxidation by measuring 4-hydroxy-hexenal, 4-hydroxy-nonenal, and 8-isoprostane-PGF_2-alpha in the plasma of rhesus monkeys. The effects of alcohol on the uptake of deuterium-labeled 18:2n-6 (linoleic acid) and 18:3n-3 (linolenic acid) into the plasma was also evaluated using a stable isotope GC-MS method. The description of these methods is the subject of this presentation.

METHODS

Five rhesus monkeys were maintained on a low essential fat diet. Animals were given free access to a 7% artificially sweetened alcohol solution for 15 months. Four controls were maintained on the same diet and not given alcohol. The effects of alcohol consumption on plasma levels of lipid peroxidation products, 4-hydroxy-nonenal, 4-hydroxy-hexenal, and 8-isoprostane-PGF2-alpha were determined using negative ion GC-MS analysis. To determine whether alcohol had an effect on the uptake of the deuterium-labeled 18-carbon essential fatty acids, d_5-18:2n6 and d_5-18:3n3, into the plasma or the accumulation of deuterium-labeled long chain polyunsaturated fatty acids in the plasma, animals were given a single dose of 100 mg of the deuterium-labeled fatty acids and the blood was analyzed for the labeled fatty acids throughout a two week period.

Extraction-Derivative Formation

I. **Aldehydes.** Tissue samples (3-50 mg) were homogenized in a mixture of 400 ul methanol containing 50 ug/ml BHT, 200 ul of a 2 mM EDTA buffer, pH 7.0, and 200 ul of 0.1M PIPES containing 50 mM PFBHA.HCL, pH 6.5.

Samples were incubated at room temperature for 5 min. to form the O-PFB oxime derivatives. After incubation, 1 ml hexane was added, the mixture was vortexed for 1 min and centrifuged at 1000 g for 1 min. The hexane layer was collected and repeated twice. Hexane was evaporated under nitrogen and samples were dissolved in 50 ul pyridine and 50 ul BSTFA and incubated for 5 min at 80°.

II. **Isoprostanes.** *Solid phase extraction was used to extract the isoprostanes.* 1 ml Bond-Elute C-18 cartridges were conditioned with 2 ml methanol followed by 2 ml distilled water. Aqueous samples were applied and rinsed with 2 ml 80:20 water:methanol. Cartridges were dried under vacuum and rinsed with 2 ml dichloromethane. Isoprostanes were eluted with 1 ml methanol and solvent was evaporated under nitrogen. Samples were converted to PFB esters using 100 ul of PFB-bromide:diisopropylethlamine:acetonitrile 1:100:1000 @ 60°. The reagent was evaporated under nitrogen and 50 ul BSTFA and 50 ul CH_3CN were added to from TMS ether.

III. **Deuterated Fatty Acids:** The deuterated fatty acids were labeled at the ethyl terminal positions. The fatty acids were extracted using the Bligh and Dyer lipid extraction procedure, saponified in a 10% KOH methanolic solution, acidified with HCl, re-extracted into hexane and derivatized to the PFB esters using pentafluorobenzyl bromide.

GC-MS Conditions

I. **Aldehydes & Prostanes:** GC separations were performed on a 30 m X 0.25 mm DB-5 column (J&W) using helium. Samples were injected into a Hewlett-Packard 5989 GC using an on-column injection technique. The oven was at 110° and heated at 20°/min to 315°. Quantification was based on peak area ratios with d_4-PGF_2-alpha, d_3-4-hydroxynonenal, and d_3-4-hydroxyhexenal. Methane was used as the reagent gas (pressure was 4×10^{-4} torr). The source temperature was 200°.

II. **Deuterated Fatty Acids:** Deuterium-labeled fatty acids resolved from the non-labeled materials using a 25 meter polar FFAP capillary column using splitless injection with an oven temperature program of 80°-185°@20°/min, 185°-240°@10°/min and held for 30 min. The fatty acids were quantified using 23:0 as an internal standard.

RESULTS & DISCUSSION

1. The levels of both the 4-hydroxy-hexenal and nonenal were quantified in the plasma using the deuterium-labeled internal standards. The level of 4-hydroxy-nonenal was several orders of magnitude greater in the alcohol consuming animals compared to controls (alcohol mean 2800 pg/ml vs controls mean 150 pg/ml). The level of 4-hydroxy-hexenal was similar in both groups and this may be the result of several factors such as the high reactivity of this compound.

2. The level of 8-isoprostane-PGF_2-alpha was two fold higher in the plasma of monkeys consuming alcohol compared to controls (alcohol mean 170 pg/ml vs controls mean 90 pg/ml).

3. Alcohol did not appear to affect the uptake of either deuterium-labeled 18:2n6 or 18:3n3 into the plasma. This indicates that the loss of polyunsaturated fatty acids from tissues of alcohol exposed animals may not be due to the failure of animals to obtain essential fatty acids from the diet, however, production of long chain polyunsaturated fatty acids from these fatty acids may be affected by alcohol and must be determined.

The authors wish to thank Profs. Eric Van Kuijk for supplying the deuterium-labeled aldehydes and Hermann Esterbaurer for supplying the primary aldehyde standards.

A COMPARISON OF HIGH- AND LOW- ENERGY CID OF DERIVATIZED LIPIDS

W. J. Griffiths, Y. Yang, J. Zhang, J. Å. Lindgren and J. Sjövall
Department of Medical Biochemistry and Biophysics, Karolinska Institute, S-17177 Stockholm, Sweden.

Mass spectrometry has been extensively used in the past in the structure elucidation of lipids. Early work was done by Ryhage and Stenhagen at Karolinska Institutet on the electron impact ionization of fatty acid esters (*Ark. Kemi,* **13,** 523 (1959)), and subsequently GCMS has been extensively used in lipid analysis Since the discovery of FAB in the early 1980:s, this has become the ionization method of choice for the analysis of polar and sensitive lipids, although electrospray ionization is now gaining popularity. Both FAB and ES mass spectra are dominated by strong pseudomolecular ions, and little fragmentation occurs. To increase the amount of structural information, CID spectra are recorded. Gross and co-workers have carried out extensive studies on the CID of lipids (*Int. J. Mass Spectrom. Ion Processes,* **118/119,** 137 (1992)). They found that in keV CID reactions of fatty acids, charge-remote fragmentations (CRF) occur. CRFs also occur in the keV CID of bile acids. In this laboratory we have extensively used FAB and ES with keV CID, in the structural investigation of bile acids and other lipids. Bile acids derivatized with aminosulphonic acids give strong $[M-H]^-$ pseudomolecular anions upon FAB and ES ionization, and CRFs in keV CID reactions (*Rapid Commun. Mass Spectrom.*, **7,** 235 (1993)) Shown in Figs. 1a and 2a are the keV CID spectra of the $[M-H]^-$ pseudomolecular anions of (1a) taurocholic acid and (2a) prostaglandin $PGF_{2\alpha}$ derivatized with aminobenzenesulphonic acid, obtained when using He as the collision gas Charge-remote fragmentations are observed and described in the inset. Very recently we have purchased an OATOF sector, which has been added on to our VG AutoSpec FPD mass spectrometer. This hybrid instruments is described elsewhere at this conference. The collision energy for OATOF operation must be less than 12.5% of the accelerating potential energy When the accelerating potential energy is at 4 keV, as for electrospray operation, the collision energy must be below 500 eV. A point of immediate concern to us was, could CRF spectra be obtained on the OATOF at this collision energy? Shown in Figs 1b and 2b are 400 eV CID spectra of taurocholic acid and derivatized $PGF_{2\alpha}$ obtained using Xe collision gas. Clearly CRF occurs at this collision energy

Fig.1. CID spectra of taurocholic acid $[M-H]^-$ ions (m/z 514). Parent ions generated by electrospray. (1a) Collision energy 4 keV, He collision gas, constant B/E linked scans, ions detected on the focal plane detector. (1b) collision energy 400 eV, Xe collision gas, daughter ions analysed by the OATOF

Fig 2. CID spectra of $PGF_{2\alpha}$ derivatized with aminobenzenesulphonic $[M-H]^-$ (m/z 508). Parent ions generated by (2a) CF-FAB, Collision energy 8 keV, He collision gas, constant B/E linked scans, ions detected on the point detector

(2b) electrospray, collision energy 400 eV, Xe collision gas, daughter ions analysed by the OATOF.

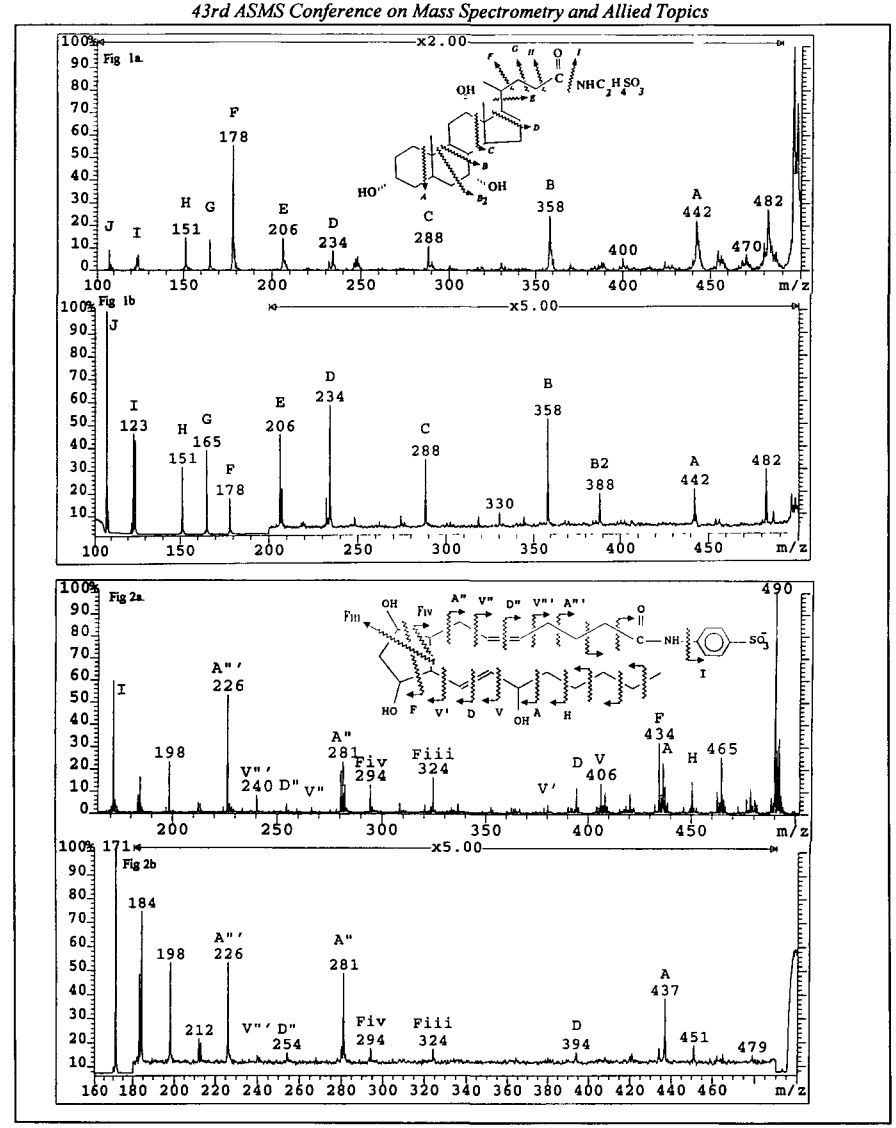

Electron Capture Mass Spectrometric Analysis of Lipid Peroxidation Products

Amy J. Grimsrud*, F. J. G. M. van Kuijk#, David W Thomas$, L. Joseph Sears*
Dept. of Chemistry, Montana State Univ , Bozeman, MT
Life Sciences Div., SRI International, Menlo Park, CA
#Dept of Ophthalmology, Univ. of Texas Medical Branch, Galveston, TX

INTRODUCTION. 4-hydroxyalkenals are the major aldehydic products of lipid peroxidation. These alkenals are responsible for many undesirable biological effects, such as inhibition of enzyme activity and inhibition of DNA synthesis. 4-hydroxynonenal can be used as a specific chemical indicator for lipid peroxidation (1). GC/MS electron capture ionization methods can be used for the determination of these compounds, if they are first modified to form PFB-oxime-TMS ether derivatives (1). The purpose of this study was to evaluate conditions that reduce fragmentation of the derivatives in HPEC/MS; and, where fragmentation does occur, to determine the origin of the observed ions

Increased fragmentation is often accompanied by the formation of noninformative ions, such as the O-PFB group at m/z = 196. In the course of the analysis of 4-hydroxynonenal derivatives, significant chromatographic peak tailing in the reconstructed ion chromatogram of m/z = 196 was observed (Fig. 1). EI experiments have shown that this tailing is not due to chromatographic effects The phenomenon of wall related processes has been previously documented by Sears, et.al. (2). Differences in temporal profiles of reconstructed ion chromatograms can be used to elucidate processes which lead to the generation of unexpected ions. Experimental parameters were varied to alter the observed EC spectra. These parameters were buffer gas (N_2, CO_2, CH_4, Ar, and NH_3), source temperature, source pressure, and ion exit slit width. Isotopically enriched $C^{18}O_2$ and $^{15}N_2$ were also used to elucidate the ion source wall related reactions.

DISCUSSION. It is expected that all ions generated from gas phase processes will have the same temporal profile. However, Figure 1 illustrates that the temporal profile of m/z = 196 does not coincide with that of other ions, such as m/z = 283 The extreme tailing chromatographic profile of m/z = 196 is indicative of a wall related process. We have used alternative buffer gases to elucidate the wall related reactions (3). Using NH_3 as a buffer gas gave comparable results to using CH_4 (i.e. tailing temporal profile and a prominent ion at m/z = 196)(Fig. 1).

Figure 2 shows the results from a series of experiments in which N_2 and isotopically enriched gases were used as buffer gases. A prominent ion appears at m/z = 198 when $^{12}C^{18}O_2$ is used in place of $^{12}C^{16}O_2$. Normal N_2 results in the formation of m/z=193, whereas isotopically labeled $^{15}N_2$ results in the emergence of an ion at m/z = 194. .The ^{18}O, ^{14}N, and ^{15}N in the respective spectra must come from the reaction of the analyte at the source wall with products generated from the irradiation of the labeled buffer gas. This provides clear evidence that the temporal distortion of the chromatographic profile of the O-PFB ion is not the result of a simple fragmentation.

Figures 3a and 3b show a comparison of chromatographic profiles and spectra obtained by varying the residence time of the analyte in the source by changing the ion exit slit dimensions. Condition **a** (small slit), results in a spectrum with an intense m/z = 196 peak and a tailing temporal profile. Condition **b** (large slit) yielded little m/z = 196 ion. Its chromatogram shows little tailing. We believe that the small amount of m/z = 196 ion present may be due to the expected gas phase fragment ion formation of O-PFB.

1. van Kuijk, F. J. G. M., Thomas, D. W., Stephens, R. J., and Dratz, E. A. (1986) Biochemical and Biophysical Research Communications. 139, 144-149
2. Sears, L. J., Campbell, J. A., and Grimsrud, E. P. (1987) Biomedical and Environmental Mass Spectrometry. 14, 401-415.
3. Sears, L. J , and Grimsrud, E. P. (1989) Analytical Chemistry. 61, 2523.

43rd ASMS Conference on Mass Spectrometry and Allied Topics

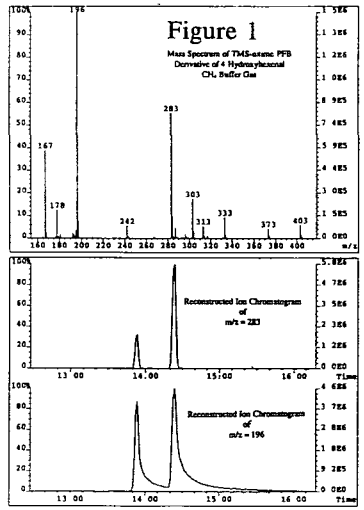

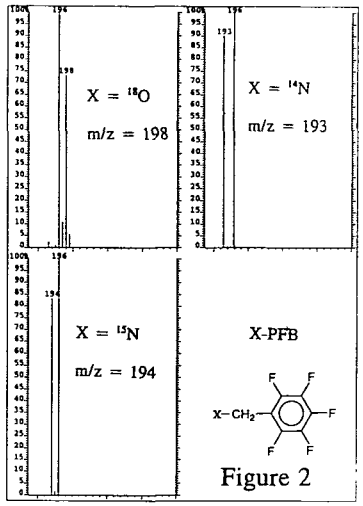

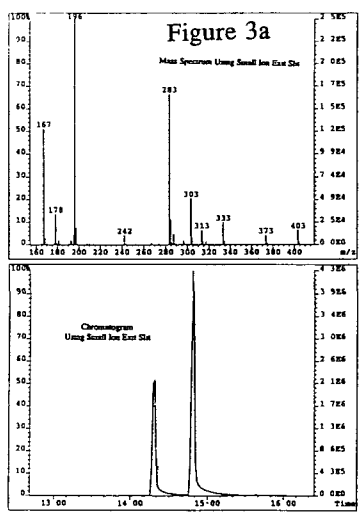

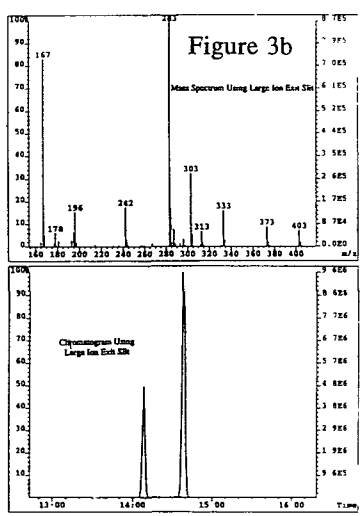

Analysis of Neurosteroids by Liquid Chromatography/Mass Spectrometry

Hee-Yong Kim*, Elena Romeo and Yee-Chung Ma
Section of Mass Spectrometry, LMBB, NIAAA, NIH
10 Center Dr. MSC 1256, Bethesda, MD 20892-1256

Progesterone and deoxycorticosterone have been shown to be metabolized in brain to 5a-pregnane-3a-ol-20-one (THP or Allopregnanolone) and 5a-pregnane-3a,21-diol-20-one (THDOC), respectively. Electrophysiological studies have indicated that these neurosteroids modulate the GABA/benzodiazepine binding sites. Anxiolytic and hypnotic effects have also been reported for these compounds when they were administered to laboratory animals. Therefore, analysis of these neurosteroids in the central nervous system may provide a biochemical understanding of stress-related situations in humans such as those observed in alcoholics during withdrawal. The best approximation of the brain concentration of these neurosteroids may be made by measuring their level in the cerebrospinal fluid (CSF). In order to develop a sensitive quantitative technique to analyze THP and THDOC along with several other neurosteroids which are normally present at trace levels in CSF, LC/MS techniques using thermospray (TSP), electrospray (ESI) and atmospheric pressure chemical ionization (APCI) were evaluated.

Finnigan TSQ-700 with TSP or ESI/APCI interface was used with following conditions.

TSP	Vaporizer temperature	70°C
	Source aerosol temperature	250°C
	Flow rate	0.5 mL/min
	Mobile phase	0.1M CH_3COONH_4 : methanol gradient
	Column	Waters Novapack-ODS column (2mm x 15cm)
ESI	Capillary temperature	280°C
	Flow rate	0.15 mL/min with approx. 4:1 split
	Mobile phase	H_2O : methanol gradient
	Sheath gas pressure	70 psi
	Auxiliary gas flow	15 flow unit
	Column	Prodigy-ODS column (1mm x 15cm)
APCI	Vaporizer temperature	500°C
	Capillary temperature	150°C
	Mobile phase	1% CH_3COOH : methanol gradient
	Sheath gas pressure	18 psi
	Auxiliary gas flow	5 flow unit
	Column	Waters Novapack-ODS column (2mm x 15cm)

CSF samples were extracted with ethyl acetate and were directly introduced to an LC/MS system.

Various neurosteroids including progesterone, dehydroepiandrosterone (DHEA), dihydroprogesterone (DHP), THDOC, THP, pregnenolone and pregnanolone were detected as $(M+H)^+$ or $(M+H-H_2O)^+$ (Figure 1). Among the three techniques examined, thermospray LC/MS appeared to be most sensitive, yielding a detection limit of 20-50 pg with column separation. Separation and detection of a steroid mixture by TSP at the 250 pg level are shown in Figure 2 as an example. The sensitivity of ESI and APCI was comparable with the detection limit in the range of 50-250 pg. The response curves, generated by selectively monitoring these ions in the presence of deuterated internal standards or 16-dehydropregnanolone (16-DP), were linear over two orders of magnitude with all three techniques. Using TSP LC/MS, pregnanolone, pregnenolone, DHP, THDOC and DHT were identified in human CSF. Their level ranged from 100 to 500 pM in normal CSF.

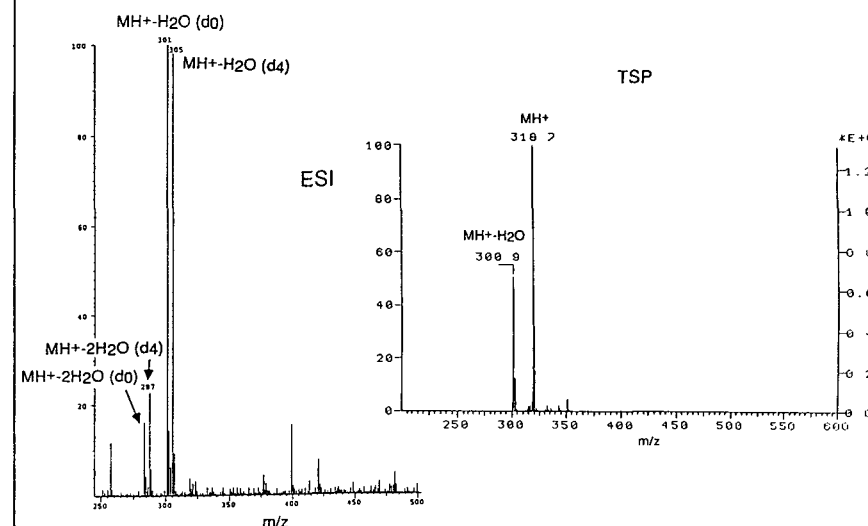

Figure 1. TSP and ESI mass spectra of allopregnanolone (mw=318).

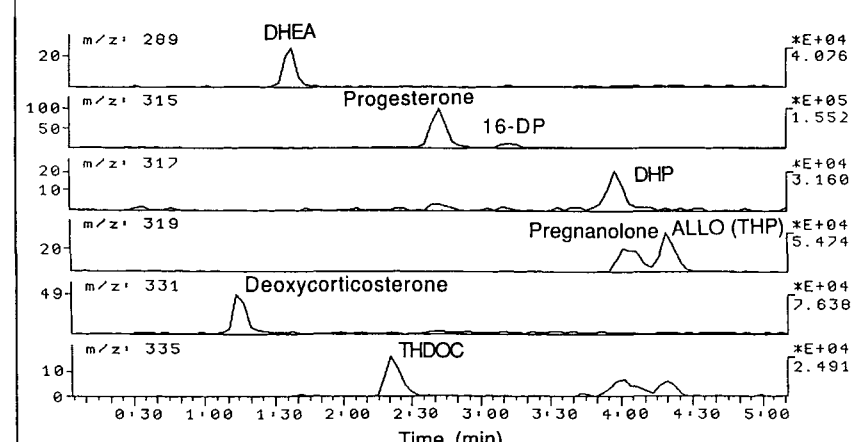

Figure 2. Separation and detection of a neurosteroid mixture by thermospray LC/MS.

MS/MS Study of PBN Spin Adducts from Rat Liver Microsomal Dispersions

Sang, Hong; Janzen, Edward G.; Arimura, Masana;
Kotake, Yashige; DuBose, Coit M.; Poyer, J. Lee
National Biomedical Center for Spin Trapping and Free Radicals,
Free Radical Biology and Aging Research Program,
Oklahoma Medical Research Foundation, 825 N.E. 13th Street, Oklahoma City, OK 73104, USA.

Spin-trapping has proved to be very useful for detecting short-lived radicals in chemical and biological systems. With the spin-trapping electron paramagnetic resonance technique (ST-EPR), determination of the spin adduct structures has been based mainly on the hyperfine splitting (hfs) pattern of the EPR spectra. In many cases, however, the structures of these spin adducts are difficult to determine based on their EPR spectra alone, because the hfs is often insensitive to the molecular structure of the spin-trapped radicals; for example C-phenyl- *N-tert*-butyl nitrone (PBN)-trapped carbon centered radicals all show six-line patterns with only small differences in hfs. Therefore EPR spectroscopy is often not sufficiently definitive to identify the structure of some free radicals, especially when unknown spin adducts are produced.

A combination of the mass spectrometric (MS) technique with ST-EPR is being developed to characterize the structures of free radicals involved in a variety of chemical and biochemical reactions. Analysis by gas chromatography mass spectrometry (GC-MS) of derivatized spin adducts was reported by Abe and coworkers [1]. They demonstrated that unstable spin adducts of PBN and 4-POBN may be derivatized by silylation to produce more thermally stable and volatile compounds for GC-MS. Some radical adducts, however, are stable only in solution. High performance liquid chromatography mass spectrometry (HPLC-MS) offers the advantage of keeping the radicals in solution at least until they enter the ion source. Tomer et al. have developed a technique for the identification of radical adducts in which HPLC/EPR and liquid chromatography thermospray mass spectrometry (LC/TSP-MS) or liquid chromatography electrospray ionization mass spectrometry (LC/ESI-MS) were performed under identical HPLC conditions [2]. In their HPLC/EPR system, in addition to using a UV detector, the EPR spectrometer was used to determine which peaks in the HPLC elution profile were EPR active.

Trichloromethyl free radicals ($\cdot CCl_3$) have been detected by the spin trapping method in rat liver when the animal is subjected to CCl_4 or when rat liver microsomes are treated with NADPH and CCl_4. With the use of HPLC and/or GC-MS, Janzen and coworkers studied the PBN-trichloromethyl adducts from rat liver extracts treated with CCl_4 *in vivo* and *in vitro* [3, 4].

This work has been extended using an MS/MS method to improve the detection of the trichloromethyl-PBN spin adduct from a hexane extract of rat liver microsomal dispersions. Compared to the earlier methods reported, the MS/MS method offers some distinct advantages. MS/MS reduces the need to carry out chromatographic separation. It also is simple, fast and especially useful for the

analysis of radical spin adducts which usually are present at low concentration and not very stable for chromatography.

Since PBN spin adducts usually produce an abundant fragment by EI, namely *m/z* 57 ($C_4H_9^+$), a scan of precursors of *m/z* 57 was recorded during MS/MS analysis to find ions potentially due to PBN spin adducts. Compared to the conventional mass spectra, precursor ion scan spectra can exclude most of the interfering ions derived from the mixture. This approach greatly reduces the number of peaks observed in the spectrum, because only ions which produce *m/z* 57 are detected. However, there are still many other peaks observed in the spectrum because *m/z* 57 is a very common fragment for many organic compounds. For the PBN-CCl_3 spin adduct, the relevant precursor ions are readily recognized because of the chlorine isotope pattern. But for other compounds with no abundant isotope pattern peaks or unknown spin adducts, a scan of precursors of *m/z* 57 may not distinguish which peaks in the spectrum are from PBN spin adducts.

To aid in the MS analysis of spin adducts, deuterated PBN (PBN-d_9) was used. The advantage of using PBN-d_9 is that a major fragment ion present in the mass spectra of any PBN spin adduct is $C_4D_9^+$. The fragment ion of *m/z* 66 (the deuterated *tert*-butyl group) is characteristic and, unlike *m/z* 57, it is not a common fragment for other compounds. The peaks at *m/z* 303, 305 and 307 are assigned to PBN-CCl_3, with a shift of 9 daltons compared to the non-deuterated PBN-CCl_3 (*m/z* 294, 296 and 298). The ions of *m/z* 249 and 251 are also from a PBN-d_9-spin adduct, since these two peaks shift 5 daltons when PBN-d_9 was replaced by PBN-d_{14}. When non-deuterated PBN was used, the peaks corresponding to the same spin adducts were also observed at *m/z* 240 and 242, with a relative intensity about 3: 1. These masses correspond to the PBN-COCl spin adduct, a molecule which was previously postulated as being formed in this incubation system.

The peak at *m/z* 202 corresponds to spin adducts if PBN-d_9 traps a free radical with 16 daltons. A peak at *m/z* 193 was observed in the same experiment when non-deuterated PBN was used. When PBN-d_{14} was used instead of PBN-d_9, this peak shifted only 4 daltons to *m/z* 206. Based on these mass spectra data, the only possible structure which fits these molecular ions (*m/z* 193, *m/z* 202 and *m/z* 206) is hydroxy-PBN, where the hydroxyl group is on the phenyl ring (ortho, meta or para) because the mass spectrum shows that this peak is shifted by 4 not 5 daltons to *m/z* 206 when PBN-d_{14} is used instead of PBN-d_9.

In this study EI with tandem MS, combined with the use of deuterated PBN, has been shown to be a useful technique for the identification of PBN-CCl_3 spin adducts and other PBN spin adducts. In the identification of PBN spin adducts, the scan of precursors of *m/z* 57 was useful as a screening step. The use of deuterated PBN with scanning of precursors of *m/z* 66 can provide more definitive information concerning PBN spin adducts including both known and unknown spin adducts.

[1] Abe, K.; Suezawa, H.; Hirota, M. *J. Chem. Soc., Perkin Trans. II* **1984**, 29-34.
[2] Iwahashi, H.; Parker, C. E.; Mason, R. P.; Tomer, K. B.; *Anal. Chem.* **1992**, 64, 2244-2252.
[3] Janzen, E. G.; Towner, R. A.; Krygsman, P. H. *Free Rad. Res. Comms.* **1990**, 9, 353-360.
[4] Krygsman, P. H.; Janzen, E. G.; Towner, R. A.; Haire, D. L. *Anal. Lett.* **1989**, 22, 1009-1020

Characterization of Glycosylation Sites in Recombinant Proteins by ES-MS/MS

An increasingly large number of recombinantly produced proteins of pharmaceutical interest are found to be glycoproteins. The biological activities of these glycoproteins are often significantly related to the carbohydrate structures on their surfaces. It is therefore important to develop facile and rapid procedures that will provide, beyond the site and type of linkage, sufficient structural information so that these glycans may be initially characterized and subsequently monitored for stability.

We have utilized a combination of procedures performed on a triple quadrupole electrospray instrument towards the detailed characterization of glycosylation sites. Low sample consumption is achieved by using capillary columns for LC / MS. Glycosylated peptides often do not elute as sharp or distinguishable peaks due to heterogeneity. These are readily located by application of stepped orifice and parent ion scan techniques which generate carbohydrate specific fragment ions. O-linked sites are recognized by comparison with a PNGase F deglycosylated sample (1).

We show that both the structure of an O-linked glycan and the peptide it is linked to can be identified from high orifice voltage LC / MS spectra. Several O-linked glycans were shown to be GNac-Hex-NANA and -(NANA)$_2$ (Fig.1). The identification of a peptide with N-linked carbohydrates of the complex type was achieved by matching the spectra of its glycoforms with a table of possible structures and the resulting masses. High mannose N-linked peptides are recognizable by the sequential loss of only hexoses. We show that with N-linked glycopeptides, a single stage fragmentation by CAD in MS2 typically results in a resistant fragment that is the peptide itself plus the GNac attached to an Asn. The sequence of the peptide and the Asn to which the GNac is attached can be obtained by first dissociating the carbohydrate moiety at the source with high orifice voltage. The remnant peptide plus GNac is than sequenced by fragmentation in MS2 (Fig.2).

(1) Huddleston,M.J., Bean,M.F. and Carr,S.A., Anal. Chem. 65, 877-884 (1993)

43rd ASMS Conference on Mass Spectrometry and Allied Topics

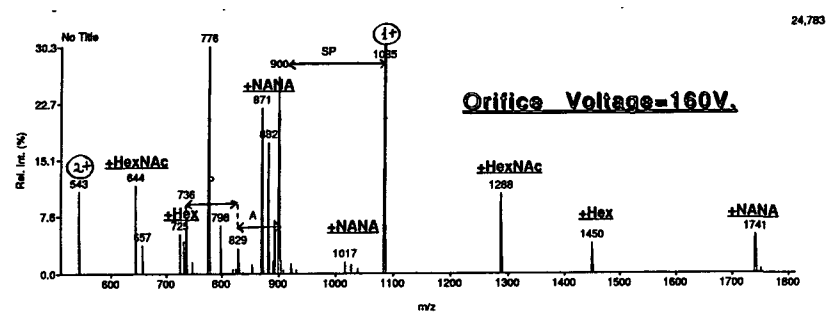

FIG. 1 High orifice voltage LC / MS. Fragmentation spectra of peptide A shows glcosyl moiety to consist of NANA-Hex-GNac. A second structure with an additional NANA was also identified. A partial amino acid sequence was observed.

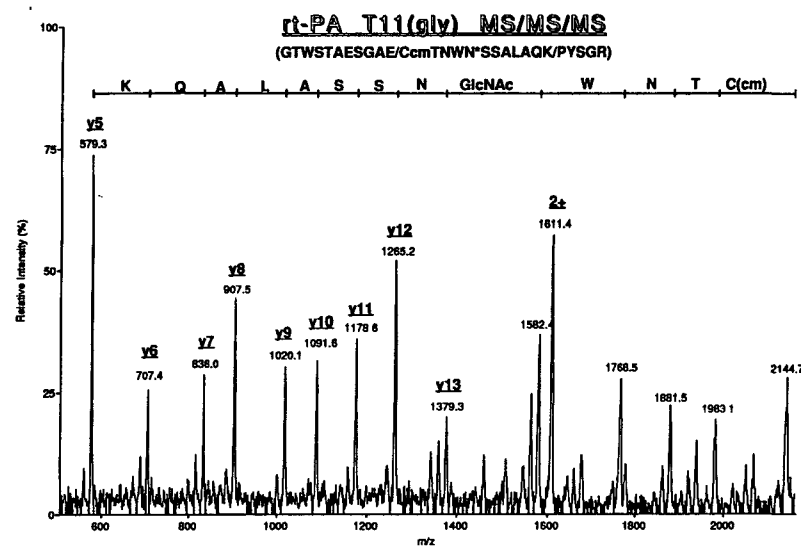

FIG. 2 Peptide sequence of N-glycosylated tPA T11 obtained by 2-step fragmentation process. Carbohydrate moiety was first removed by fragmentation at source using high orifice voltage. The resistant peptide plus GNac at 1612 Da wasthen fragmented by CAD in MS2. The GNac was shown to be attached to the Asn proximal to the C-terminus.

DETERMINATION OF *N*-LINKED GLYCOSYLATION IN EXTERNAL INVERTASE BY MALDI-TOF MS

Chenhui Zeng and Klaus Biemann
Dept. of Chemistry, Mass. Institute of Technology, Cambridge, MA 02139

Invertase (E.C.3 2.1.26, β-D-fructofuranoside fructohydrolase) from *Saccharomyces cerevisiae* is an enzyme that catalyzes the hydrolysis of sucrose into fructose and glucose The glycosylated form of invertase (external invertase) contains as much as 50% of its mass as polymannan (1) in 14 potential *N*-linked glycosylation sites (sequons) (2) Therefore, it has long been used as an ideal model for the study of the function of oligosaccharides in glycoproteins. The external invertase that we studied was purified from a commercial product presumably derived from the SUC2 gene (1) The amino acid sequence of invertase had been derived from the corresponding DNA sequence (1). It has also been reported that 13 of 14 potential sequons are either fully or partially glycosylated (3), and the glycosylation at four sequons had been found to contain long oligosaccharide chains ($GlcNAc_2Man_{>50}$), while other sequons contain short glycan chains ($GlcNAc_2Man_{8-14}$) except sequon 5 which is not glycosylated (4) The conformational structure of the short chain oligosaccharides (Man_{8-14}) isolated from invertase has been assigned by high-field one-dimensional ^1H NMR spectroscopy combined with α-1,2-linkage-specific mannosidase digestion (5).

In this report, we determined the degree of glycosylation by MALDI-TOF MS and, for the first time, present MALDI-TOF mass spectra to show the whole glyco-profile of the intact external invertase As shown in Figure 1, the signal of this glycoprotein covers mass range from 78 kDa to 115 kDa, and its average molecular weight was then determined to be 96 kDa. By combining enzymatic digestion and MALDI-TOF MS, we determined the distribution of glycosylation at each sequon. Our results generally agree with the published data (4), but some differences were noted and more detailed information has been obtained. For instance, sequons 1, 7, 9, and 11 were reported to be glycosylated with more than 50 mannoses (4). However, in this study, sequons 1, 7, and 11 were in fact determined to contain Man_{4-43}, Man_{8-80}, and Man_{6-64}, respectively, while sequon 9 was observed to contain only Man_{9-11}. Figure 2 shows an example of how MALDI-TOF MS reveals the distribution of high mannose oligosaccharides (Man_{8-80}) attached to a single glycosylation site.

During this study, Post-Source Decay (PSD) using a MALDI-TOF MS in the reflectron mode was also applied to sequence some enzymatic peptides to confirm and correct the amino acid sequence originally derived from the DNA sequence (1). To date, three amino acids have been found to be fully or partially modified; asparagine in position 65 is completely replaced by histidine, while the alanine and valine in positions 58 and 412 were observed to be partially replaced by threonine (~50%) and alanine (~40%), respectively The PSD spectra of the peptide (G^{56}-W^{66}) that contains two of the three modified amino acids are shown in Figure 3 Thus there must be two amino acid sequences In one, only one amino acid is modified (N^{65}-H^{65}) while the other one has threonine and alanine at 58 and 412, respectively. The amino acid sequence isotherwise almost identical with the one deduced from the SUC2 gene and that DNA sequence hasrecently been verified by Dr. F Maley. Therefore, these two invertase sequences must be derived from two modified DNA strains which may be called genes SUC2a and SUC2b

References

1. Gascon, S. and Lampen, J. D , *J. Biol. Chem.*, **1968**, 243, 1567
2. Taussig, R. and Carlson, M., *Nucleic Acid Res.*, **1983**, 11, 1943
3. Reddy, V A., Johnson, R. S., Biemann, K., William, R. S , Ziegler, F. D , Trimble, R. B and Maley F., *J. Biol. Chem.*, **1988**, 263, 6978
4. Ziegler, F. D., Maley, F. and Trimble, R. B., *J. Biol. Chem.*, **1988**, 263, 6986
5. Trimble, R. B and Atkinson, P. H , *J. Biol. Chem.*, **1986**, 9815

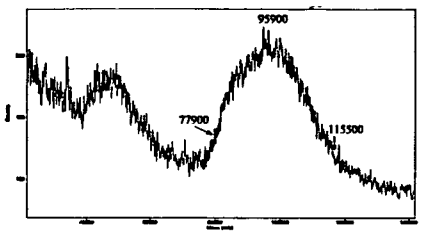

Figure 1. MALDI-TOF mass spectrum of intact external invertase

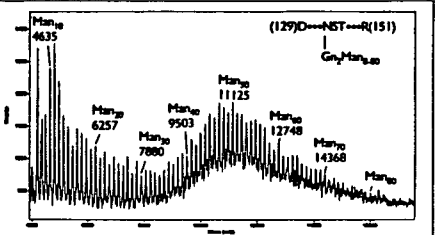

Figure 2. MALDI-TOF mass spectrum of glycopeptide Asp^{129}-Arg^{151} which contains sequon 7 at Asn^{146}

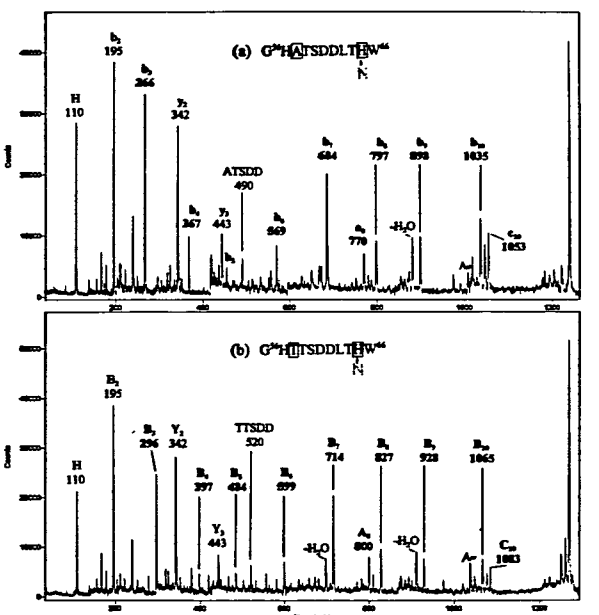

Figure 3. PSD spectra of precursor ions (a) at m/z 1240 and (b) at m/z 1270

Acknowledgements

This work was supported by NIH grant RR00317. Yeast external invertase was supplied by Dr. F Maley, NYS Dept. of Health, Albany, NY. C. Zeng especially acknowledges the support and always helpful discussionswith Dr. Catherine E. Costello.

Characterizing the N-Glycosylation of Corticotropin Releasing Factor-Binding Protein *A. G. Craig, S. W. Sutton, J. Vaughan, S. C. Koerber and W. H. Fischer. The Clayton Foundation Laboratories for Peptide Biology, The Salk Institute, P.O. Box 85800, San Diego, CA 92186-5800.

Corticotropin Releasing Factor-Binding Protein (CRF-BP) is a 35 kDa protein originally purified from human plasma which has been proposed to protect the maternal endocrine system from high levels of CRF produced by the placenta during pregnancy. CRF-BP inhibits CRF-induced ACTH release from pituitary cells in vitro (1). Based on the protein sequence, Asn180 was proposed as a site of N-linked glycosylation.

We have investigated the use of anti CRF-BP serum and matrix assisted laser desorption (MALD) to measure CRF-BP recombinantly expressed in Chinese Hamster Ovary Cells. We observed inhibition of ion formation in MALD spectra measured from rCRF-BP in a variety of forms (affinity and reverse phase purified) In contrast, immunoprecipitation of rCRF-BP (incubation overnight at 4°C in a 50 mM Hepes buffer with antisera raised against either an N-terminal CRF-BP peptide or the intact rCRF-BP) and rinsing of the pellet formed (20 min. centrifuge @ 15000 rpm) with 50 mM Hepes buffer (x2) and subsequent addition of 5 µl of 0.1 % aqTFA and application of an aliquot (0.5 µl) of this solution to a thin film of α-cyano-4-hydroxy cinnamic acid resulted in intact CRF-BP ion formation as shown in Figure 1(a), measured with a Bruker Reflex operated in the linear mode. It is possible that the elimination of MALD inhibition is due to the specificity of the immunoprecipitation resulting in a rinsing from the sample of contaminants or salts which are not removed by other purification procedures. Alternatively, the antibody precipitation may be altering a more intrinsic property of the protein relating to its amenability for ionization. Clearly, the presence of the antibody does not inhibit ion formation. Using this sample preparation technique we have measured the intact mass of recombinant CRF-BP after enzymatic treatment with peptide N-glycosidase-F (PNGase-F) as shown in Figure 1(b), indicating that the glycan molecule mass is approximately 1.5-2 kDa.

Figure 1(a) **N-Glycosidase-F treatment of CRF-BP**

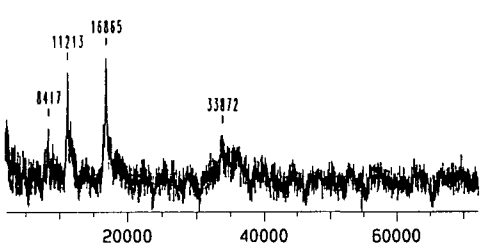

Figure 1(b) **CRF-BP (Untreated)**

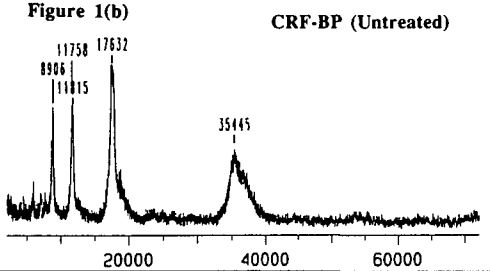

In addition, the CRF-BP glycopeptide has been identified from a tryptic map of CRF-BP in order to obtain more detailed information on the nature of the glycan structure and to verify that Asn180 is the only site of glycosylation. Figure 2(a) shows the MALD mass spectrum of the 180-192 fragment which was obtained after tryptic digestion followed by TCEP reduction (2), while Figure 2(b) shows the spectrum of the same fraction isolated after PNGase-F treatment. The mass shift observed indicates a more accurate mass of 2207 Da for the major glycan species, while the intense fragment ion is characteristic for the presence of sialic acid (3),. Using the previously proposed strategy of Huberty et al. (3), we searched for N-linked glycan structures containing sialic acid in The Complex Carbohydrate Structure Database (4, 5) and found that only two previously reported structures are consistent with the observed glycan mass. These two structures, $(Gal)_2(Man)_3(GlcNAc)_4(Neu)_2$ (2206 Da) and $(Fuc)_2(Gal)_2(Man)_3(GlcNAc)_4(Neu)$ (2207 Da), differ in the degree of sialic acid present (one or two sialic acid molecules). After treatment of the 180-192 glycopeptide with neuraminidase the MALD mass spectrum contained a species consistent with loss of two sialic molecules from the glycan (data not shown). On the basis of these measurements we propose that the glycosylation present on CRF-BP is consistent with the previously reported glycan structure $(Gal)_2(Man)_3(GlcNAc)_4(Neu)_2$.

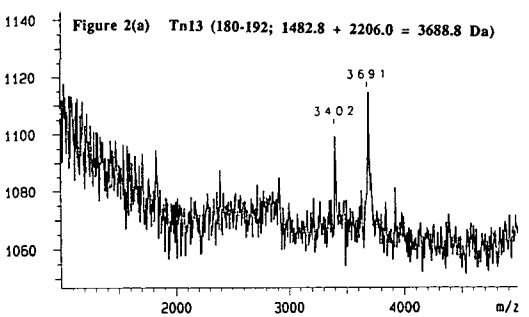

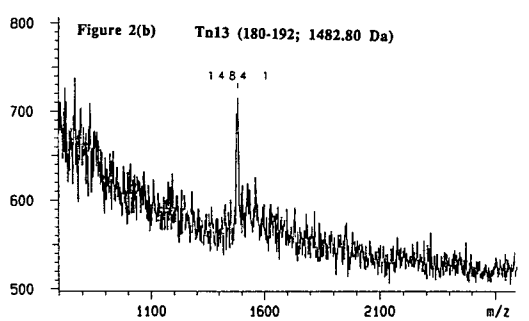

References
1. Potter, E.; Behan, D. P.; Fischer, W. H.; Linton, E. A.; Lowry, P. J. and Vale, W. W. (1991) *Nature* **349**, 423-426.
2. Fischer, W. H.; Rivier, J. E. and Craig, A. G. (1993) *Rapid Commun Mass Spectrom* **7**, 225-228.
3. Huberty, M. C.; Vath, J. E.; Yu, W. and Martin, S. A. (1993) *Anal Chem* **65**, 2791-2800.
4. Doubet, S. and Albersheim, P. (1992) *Glycobiology* **2**, 505-507.
5. Van Kuik, J. A. and Vliegenthart, J. F. G. (1992) *Trends Biotechnol* **10**, 182-185.

CHARACTERIZATION OF A PLASMINOGEN ACTIVATOR WITH LC, CE, ESI-MS AND MALDI-TOF MS

J. A. Chakel*, J. A. Apffel, R. R. Holloway, S. A. Swedberg, S. R. Udiavar and W. S. Hancock
Hewlett-Packard Laboratories, 3500 Deer Creek Road, Palo Alto, CA 94304
C. Souders, J. Johnson, T. M'Timkulu, and E. Pungor Jr.
Berlex Biosciences, Brisbane, CA 94005

The development of a glycoprotein as a new pharmaceutical is a challenging exercise as the heterogeneity of the carbohydrate can hinder analytical methods targeted at monitoring product consistency for regulatory agencies, such as the FDA. Desmodus Salivary Plasminogen Activator (DSPAα1) is a single chain plasminogen activator derived from Desmodus rotundus (vampire bat) salivary glands. DSPAα1 is a serine protease that plays a role in clot lysis. DSPA is known to be heterogeneous when expressed in CHO cells. It is a large (441 amino acids) complex molecule of calculated (non-glycosylated) average molecular weight 49,508 Da with six sites for potential glycosylation, four O-linked and two N-linked. It has been proposed, based on homology with other serine proteases that there are 28 cysteines forming 14 disulfide bridges.

In order to effectively characterize such a complex molecule, a variety of analytical techniques must be employed. The analytical approach used was to start at the gross level of intact protein and use analytical techniques applicable to such a complex, high MW sample. Following this characterization, the greater detail of the peptide map from an endoprotease Arg C digest was examined, followed by individual fractions from the digest. Thus the focus moved from more global properties of the sample to increasing degrees of detail. At each level, HPLC, LC/MS, HPCE and MALDI-TOF were applied. At the more global level, it is not possible to discern the detailed information of the specialized techniques. On the other hand, it is difficult to synthesize data from the more specific into a more global picture. This problem of context of scale of macromolecular analysis is at the heart of the need for multidimensional analysis. With samples of this complexity, no one technique yields the required depth of structure information combined with ready linkage to the overall structure of the macromolecule.

Initial examination of the intact glycoprotein (Figure 1) by HPLC shows that the sample is quite pure, and at least in terms of hydrophobicity, relatively homogeneous, although product variants may not be separated under the applied conditions. The HPCE separation (based on charge rather than hydrophobicity) is useful to further characterize the purity and homogeneity. The MALDI spectrum reveals that the protein has ~4600 Da due to glycosylation. The peak width of ~5 kDa relates to the degree of microheterogeneity of glycosylation. At higher levels of detail, LC/MS plays a crucial role in characterizing the peptide map generated by proteolytic digestion (Figure 2). Fractionation of the complex regions (areas containing glycosylated peptides) of the peptide map followed by HPCE and MALDI-TOF provide additional degrees of information. All of the techniques used have proven to be highly complimentary in the analysis of DSPAα1. More effective techniques are required for the integration of information from higher dimensional data generated by the combination of these techniques.

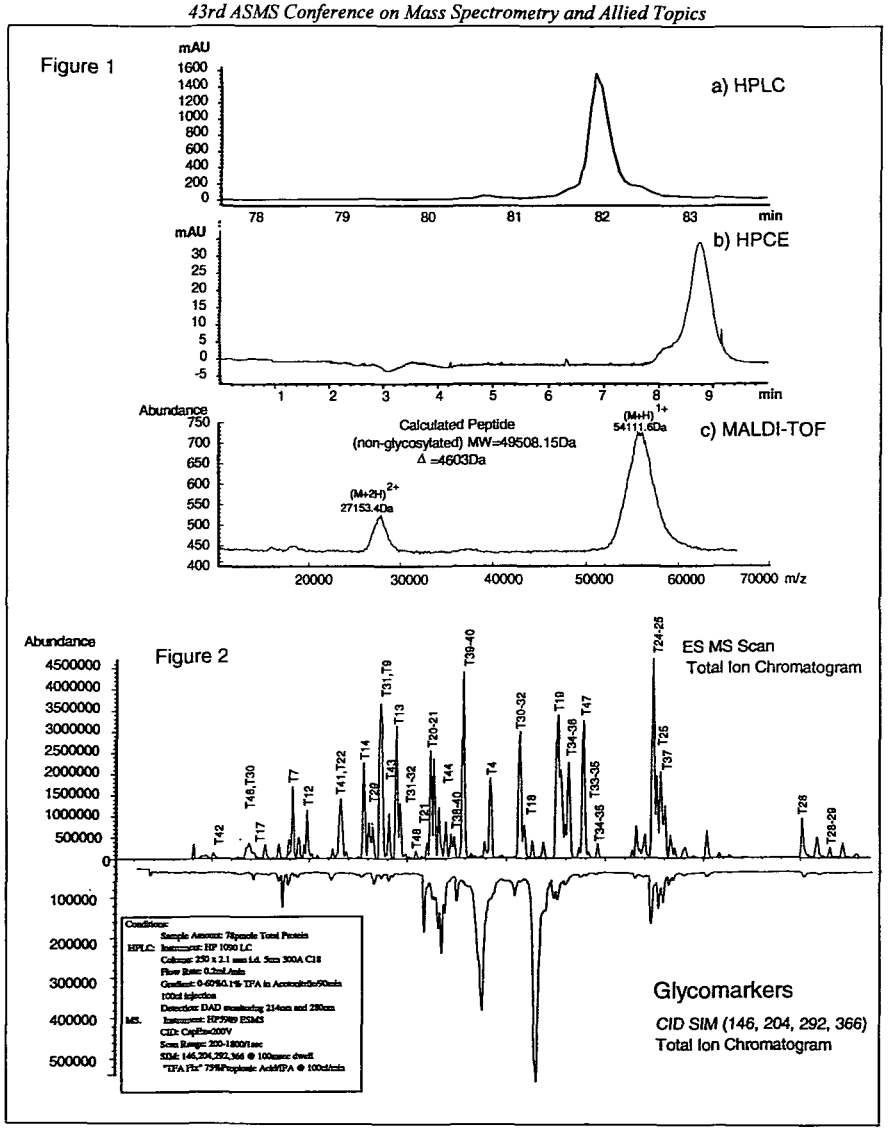

Analysis of parotid gland oligosaccharides by MALDI mass spectrometry

David R. Wing, Niall O'Donnell, Thomas J. P. Naven, David J. Harvey,

Oxford Glycobiology Institute, Department of Biochemistry, University of Oxford, South Parks Road, Oxford, OX1 3QU, UK.

Introduction

MALDI Mass spectra of complex oligosaccharides give abundant $[M + Na]^+$ ions which provide compositional information on the constituent monosaccharides, but no information on the sequence, branching or linkage patterns of these residues. Such information has previously been obtained by exoglycosidase digestion with the products being monitored by radioactivity following gel filtration chromatography. MALDI provides a more satisfactory solution to oligosaccharide detection by giving much higher resolution and by not requiring radioactive detection. In this report, MALDI and exoglycosidase digestion are used to examine the detailed structures of neutral *N*-linked oligosaccharides from human parotid gland glycoproteins.

Experimental

Oligosaccharides were released from the glycoproteins by hydrazinolysis and the neutral sugars were obtained by enzymatic removal of the sialic acids. These oligosaccharides were separated into 3 fractions by Bio-Gel P4 gel filtration chromatography and examined by MALDI (2,5-DHB matrix) using a Fisons VG AutoSpec-QFPD magnetic sector mass spectrometer fitted with an array detector. Fractions were then incubated successively with exoglycosidases (see Figure legend) with each product being examined by MALDI. Oligosaccharides were also converted into their 2-aminobenzamide derivatives and separated by normal-phase HPLC using a polyhydroxyethyl aspartamide column (200 x 4.6 mm). Fractions were examined by MALDI and FAB (as methylated derivatives) mass spectrometry and by MS/MS (linked scan).

Results and Discussion

Three crude fractions were obtained by Bio-Gel P4 chromatography, the fraction centred around 16 glucose units (GU) contained mainly biantennary oligosaccharides with from 1 to 5 fucose residues. Successive exoglycosidase digestion (Figure), FAB and MALDI mass spectra were consistent with these compounds having fucose substitution at position 6 of the reducing terminal GlcNAc residue and at positions α1-2 and α1-3 to the outer arm galactose and GlcNAc residues respectively. The 20 GU P4 fraction contained corresponding triantennary oligosaccharides with up to 7 fucose residues, and traces of the corresponding tetraantennary compounds. Fragment ions in the MALDI and FAB spectra of individual compounds separated by HPLC showed a preference for an asymmetrical distribution of fucose residues between the antenna in oligosaccharides where not all possible substitution positions were filled.

Figure legend. (a) MALDI mass spectrum of the parotid oligosaccharides in the 16 GU fraction from the BioGel-P4 column. (b-g) MALDI spectra of the products of successive incubation with (b) almond meal α-fucosidase, (c) *Charonia. lampas* α-fucosidase, (d) concentrated *C. lampas* fucosidase, (e) *Diplococcus pneumoniae* β-galactosidase, (f) *D. pneumoniae* β-*N*-acetylhexosaminidase, (g) Jack bean α-mannosidase.

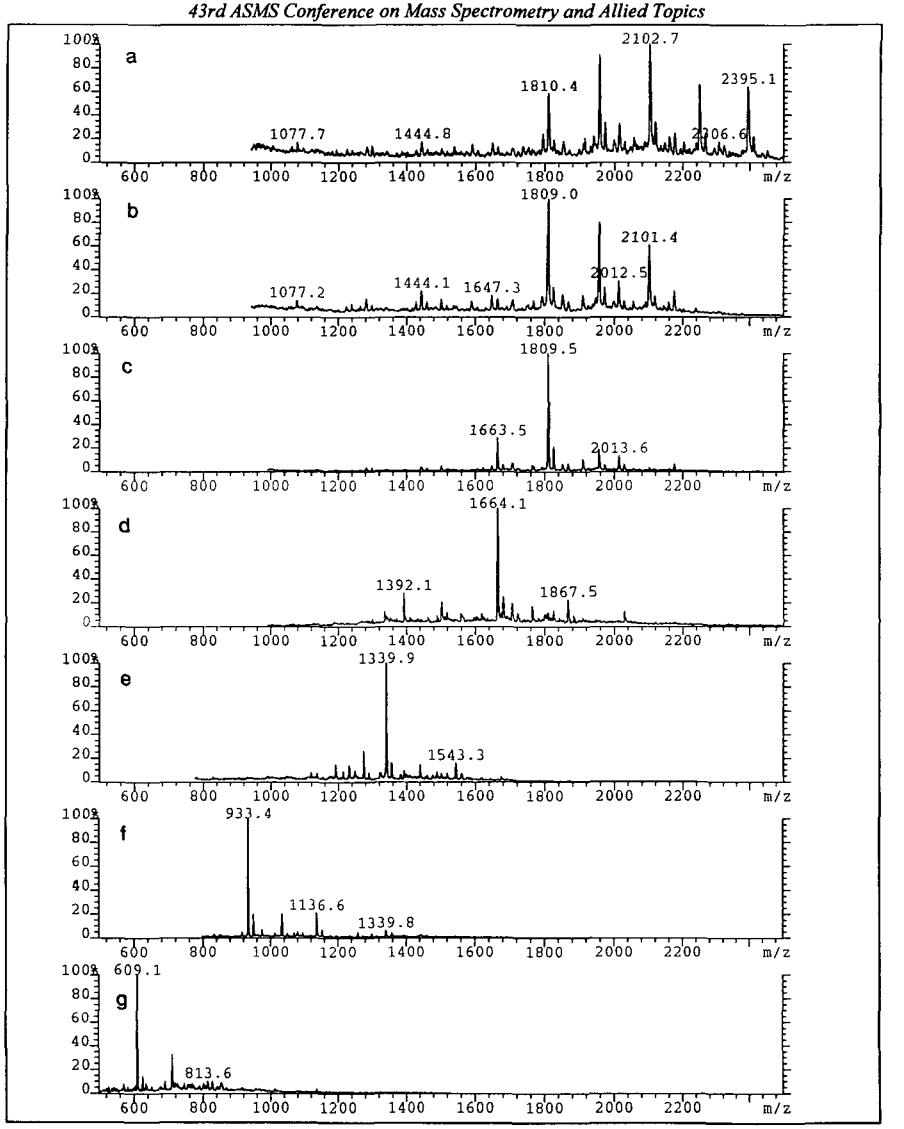

Analysis of the N-linked oligosaccharides of human C1s using electrospray ionisation mass-spectrometry

Y. Petillot[1], P. Thibault[2], N. Thielens[1], V. Rossi[1], M. Lacroix[1], B. Coddeville[3], G. Spik[3], V. Schumaker[4], J. Gagnon[1] and G. Arlaud[1].
[1]Institut de Biologie Structurale (CEA/CNRS), Grenoble, France. [2]Institute for Marine Biosciences, Halifax, Canada. [3]Université des Sciences et Technologies, Lille, France. [4]University of California, Los Angeles, U.S.A.

C1s, the serine proteinase responsible for the enzymic activity of human C1, the first component of the classical pathway of complement, bears two oligosaccharide chains linked to asparagine residues 159 and 391. With a view to gain information on the structures of these oligosaccharides, human C1s (**Fig.1**) and various of its fragments and peptides were subjected to electrospray ionisation mass spectrometry and monosaccharide analyses [1].

These analyses indicate that three major C1s species are observed (**Fig.2**), varying according to their oligosaccharides structure :

(i) species **A** (M=79,318 ± 8Da) contains a biantennary, bisialylated oligosaccharide at both positions 159 and 391 (calculated M=79,300);

(ii) species **B** (M=79,971 ± 8Da) contains a biantennary oligosaccharide at position 159, and a non-fucosylated triantennary oligosaccharide at position 391 (calculated M=79,957);

(iii) species **C** (M=80,131 ± 8Da) contains a biantennary oligosaccharide at position 159, and a fucosylated triantennary species at position 391 (calculated M= 80,103).

If one only takes into account these three major species **A**, **B**, and **C**, which are present in equimolar amounts and, altogether, represent approximately 75-80% of the C1s population, the average mass of C1s, determined experimentally, is 79,807 ± 8Da (calculated value=79,787).

The MS analyses performed on fragment C1sα (**Fig.3**) corroborate our previous data indicating that C1s undergoes only partial (about 50%) hydroxylation of Asn134. Together with the analysis performed on peptide C1sA 154-195 (**Fig.1**), they also provide indirect evidence for the occurrence of a third, minor post-translational modification (M=132± 2Da) taking place within the N-terminal region of C1s (positions 1-153), and which is therefore independent of the oligosaccharide linked to Asn 159.

[1] Y.,Pétillot, P. Thibault, N. Thielens, V. Rossi, M. Lacroix, B. Coddeville, G. Spik, V. Schumaker, J. Gagnon & G. Arlaud (1995) FEBS Letters 358, 323-328.

43rd ASMS Conference on Mass Spectrometry and Allied Topics

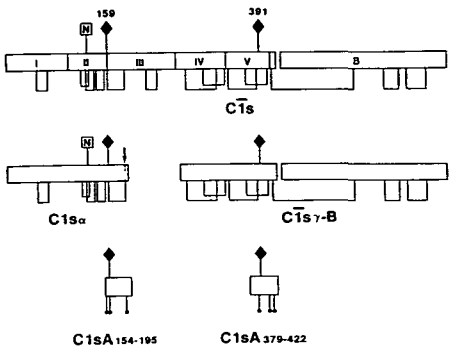

Fig.1. Schematic representation of the structure of C1s and of the various oligosaccharide-containing fragments and peptides used in this study.**I-V** indicate the modules of the N-terminal A chain and **N**, Asn134 that undergoes partial hydroxylation.The disulfide bridges present in C1s and its α and γ-B fragments are represented.The arrow shows the Arg-Cys bond that is partially cleaved in C1s α; (◆), Asn-linked oligosaccharides; (⊥), reduced and alkylated cysteine residues.

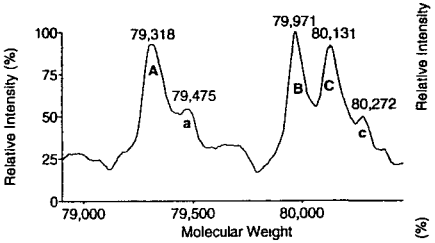

Fig.2. ESI-MS reconstructed molecular mass profile of intact C1s..

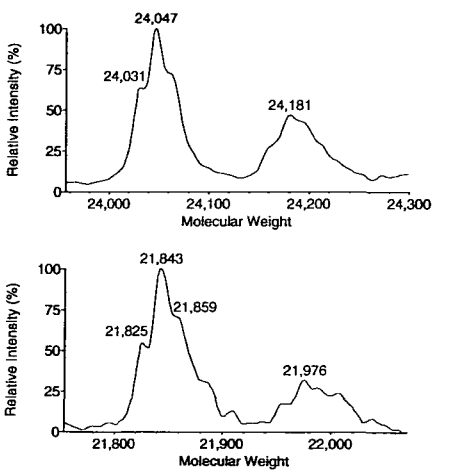

Fig.3. ESI-MS reconstructed molecular mass profile of fragment C1sα; (A) native fragment C1sα.; (B) fragment C1sα treated with PNGase F.

GLYCOSYLATED END-PRODUCTS OF BETA 2-MICROGLOBULIN IN SERUM BY MATRIX-ASSISTED LASER DESORPTION/ IONIZATION MASS SPECTROMETRY

P. A. DREIFUSS*, A. VERTES[1], X. TANG[1*], J. BRAATZ & D. PERU

W. R. Grace & Co.-Conn
7379 Route 32
Columbia, MD

[1]Department of Chemistry
George Washington University
Washington, DC 20052

Beta 2-Microglobulin (β_2M) is the protein precursor of amyloid deposits associated with dialysis-related amyloidosis (DRA), a major complication of chronic hemodialysis.[1] DRA patients suffer from degenerative bone and joint disease, including carpal tunnel syndrome. Recently, advanced glycosylated end-products (AGE) of β_2M have been potentially linked to DRA.[2]

Although there is a clear association between chronic hemodialysis and the development of amyloidosis, there is no clear correlation between β_2M serum levels and the occurrence of DRA. It is important then to address how β_2M may be present in the sera of DRA patients. Clinical measurements of β_2M species in serum, including AGEs, might identify patients at risk for developing DRA.

In this work, we demonstrate that matrix-assisted laser desorption/ ionization (MALDI)[3,4] mass spectrometry is an extremely useful and rapid means to investigate the nature of glycosylation of β_2M and can detect β_2M and β_2M-AGE in sera at low picomole levels. Previously, MALDI was used to determine the number of glucose molecules which can react with bovine serum albumin *in-vitro*.[5]

MALDI data were obtained on a linear time-of-flight mass spectrometer equipped with a 337 nm nitrogen laser. Serum samples were filtered through 30,000 MW cutoff microfilters. 1 µl samples were mixed with 10 µl of saturated matrix in 7:3 acetonitrile:water. Matrices included α-cyano-4-hydroxycinnamic acid and sinapinic acid. To prepare the β_2M-AGE, 2 mg/mL of β_2M was incubated at 37 °C for 1 month with 0.1M glucose in 100 mM phosphate buffer (pH 7.4) containing 200 units/mL penicillin.

The MALDI mass spectrum of the distribution of β_2M-AGE products from incubation of β_2M with glucose is shown in figure 1. The inset shows an expansion of the molecule ion region. The high mass end of the distribution can be seen to extend to the neighborhood of 12,868 D, expected for the condensation with 7 glucose molecules, consistent with the results of a detailed study by Miyata.[6] The MALDI mass spectra of an equimolar sample of β_2M and β_2M-AGE added to bovine serum and of an unspiked serum sample from a dialysis patient are shown in figures 2 and 3, respectively.

43rd ASMS Conference on Mass Spectrometry and Allied Topics

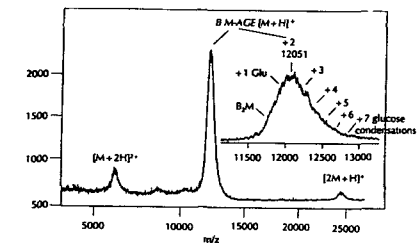

Figure 1:

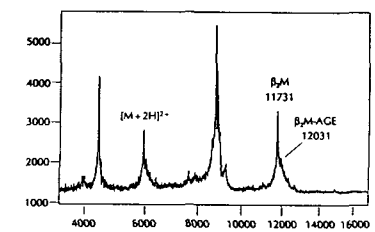

Figure 2:

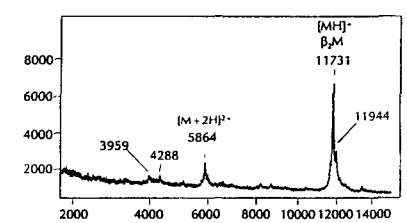

Figure 3:

[1] F. Gejyo, T Yamada, S Odani, et al. Biochem Biophys. Res Commun. 129, 701-706 (1985)
[2] T Miyata, et al., J. Clin. Invest, 93, 521-528 (1994)
[3] M. Karas & F Hillenkamp, Anal Chem., 60, 2299 (1988)
[4] K. Tanaka, H. Waki, Y. Ido, S Akita, Y. Yoshida and T Yoshida, Rapid Commun. Mass Spectrom. 2, 151 (1988)
[5] A Lapolla, C. Gerhardinger, L Baldo, D Fedele, A. Keane, R. Seraglia, S Catinella and P Traldi, Biochim et Biophys. Acta, 1225, 33-38 (1993)
[6] T. Miyata, R. Inagi, Y. Wada, Y. Ueda, Y. Iida, M. Takahashi, N. Taniguchi and K Maeda, Biochem, 33, 12215-12221 (1994)

Characterization of Human Chorionic Gonadotropin by HPLC/MS

Chaunliang Liu and Larry D. Bowers
Department of Patholoigy and Laboratory Medicine
Indiana University
Indianapolis, IN 46202-5120

Human Chorionic Gonadotropin (hCG) is a two subunit glycoprotein hormone of importance in some carcinomas and in athletic drug doping. The β-subunit (145 amino acids) is unique to hCG whereas there is identity of the alpha subunit with leutinizing hormone, thyroid stimulating hormone, and follicle stimulating hormone. Recent evidence suggests that the "nicking" of the β-subunit and the carbohydrate composition of the chain may help to identify the source of hCG. We are interested in the potential of HPLC/MS analysis of the β-subunit as a legally defensible identification of hCG in cases of athletic doping.

We have studied hCG using microbore HPLC/MS (Sciex, API III tandem mass spectrometer). The detection of the N-terminal portion of the β-chain was easily accomplished, and microheterogeneity of the carbohydrate could be localized more to the ^{13}Asn site. Observation of the C-terminal end of the molecule proved difficult, due to the presence of four closely associated O-linked carbohydrates. Using neuraminindase and O-glyconase, we were able to observe partially digested peptides from the C-terminal end.

We have characterized a number of different "nicked" and proteolytic species arising from β-hCG using HPLC/MS. The β-hCG was isolated using SPE, reductively alkylated with vinyl pyridine, digested with either trypsin or glu-C protease. Using the Glu-C protease, we studied the action of elastase on the β-hCG, which should "nick" the protein chain. HPLC/MS results suggest that elastase "nicks" hCG at 44,45 and 42,43; this does not agree with earlier work published on this hydrolysis using classical methodology.

43rd ASMS Conference on Mass Spectrometry and Allied Topics

Glycosylation Site Mapping of glycoproteins by MALDI-TOF MS

Yi Yang, Ron Orlando
Complex Carbohydrate Research Center, University of Georgia, Athens, GA 30602

A strategy based on MALDI-TOF MS was developed here as a sensitive, direct and fast way for the glycosylation site mapping of glycoproteins. Initially, the glycoprotein backbone was cleaved enzymatically, and a portion of the resulting peptide/glycopeptide mixture was analyzed directly by MALDI-TOF MS. A second aliquot of the trypsin-digested glycoprotein was further treated with N-glycanase to selectively release the N-linked carbohydrate chain, followed by MALDI-TOF analysis. The N-linked glycopeptides in this mixture can be easily identified by comparing these two MALDI-TOF spectra, since the molecular weights (MWs) of these glycopeptides decreased by the mass of their carbohydrate chains, while the MWs of both peptides and O-linked glycoepeptides were unaffected by this enzymatic digestion procedure. A third aliquot of the trypsin-digested glycoprotein was further treated by a combination of N-glycanase and O-glycanase, as well as neuraminidase if sialic acid was present, to remove both the N- and O-linked carbohydrate. The O-linked glycopeptides can then be identified by the comparison of the MALDI-TOF spectrum from this step to that from the N-glycanase treatment. These comparisons provided the mass of each carbohydrate chain and the peptide to which it was attached. Combined with standing Carbohydrate Structure Database (CarbBank), these comparisons can also be used to determine the possible structures and the heterogeneity of carbohydrate side chain. For example, Fig. 1 shown that peptides T7 (Asn-81), T11 (Asn-138) and T12 (Asn-158) in asialofetuin were identified as N-glycosylation sites and T19 as the O-glycosylation sites.

On the other hand, the total molecular weight of carbohydrate was approximated by anhydrous HF treatment of the intact glycoprotein, which cleaved both the N- and the O-linked oligosaccharides. This was shown by the shift in the molecular weight of avidin, which clearly demonstrated that avidin has only one N-glycosylation site (Fig. 2). This can be used to confirm that all of the oligosacchaide chains were found in the glycosylation site mapping procedure described in the preceding process.

The primary advantages of our MALDI-TOF approach towards glycosylation site mapping were its simplicity (no separation required) and sensitivity (1-10 picomoles).

ACKNOWLEDGMENT:

This research was supported by NIH Grant #2-P41-RR05351-06.

Figure 1: MALDI Analysis of Asialofetuin Digested with Trypsin

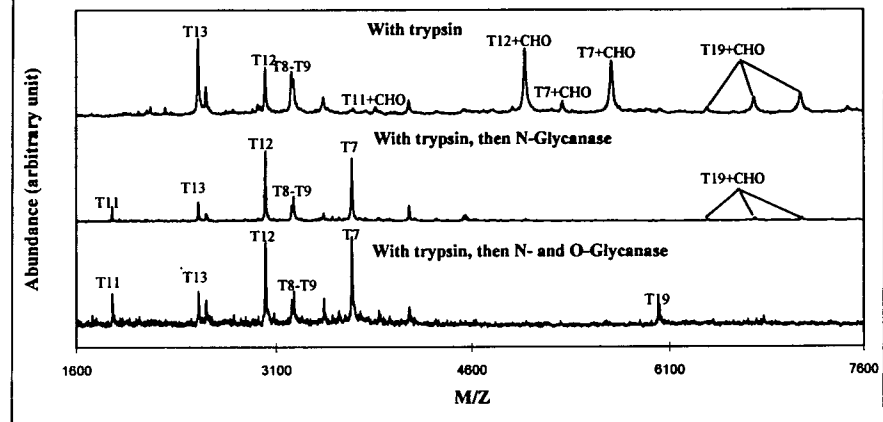

Figure 2: MALDI Analysis of Avidin Before and After HF Treatment

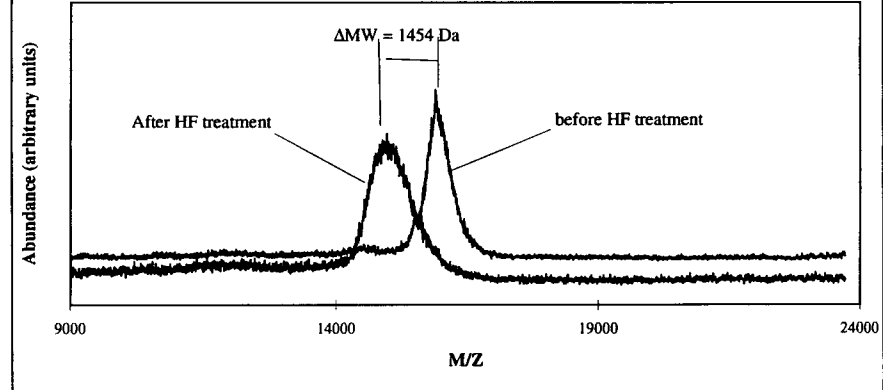

Characterizing the Carbohydrate Moieties of EPGs and PGIPs by MALDI-TOF

V.S.K. Kolli, C. Bergmann, C. Mohn, F. Thibaud, P. Albersheim, A. Darvill and R. Orlando
Complex carbohydrate Research Center and Department of Biochemistry and Molecular Biology, The University of Georgia, 220 Riverbend, Athens, GA 30602-4712.

Phytopathogenic fungi produce cell wall degrading enzymes (CWDEs) which they utilize during their colonization of host plants. Endopolygalacturonases (EPGs), considered to be among the first CWDEs released by an attacking fungus, hydrolyze homogalacturonan of the plant cell wall in to oligogalacturonide fragments. Polygalacturonase inhibiting protein (PGIP) is a plant cell wall associated protein that inhibits the activity of fungal EPGs and facilitates the formation of mid-sized oligomers of homogalacturonan that have been shown to elicit plant defense responses. Thus, the interactions of fungal EPGs and plant PGIPs are prime candidates for involvement in resistance to fungal attack. It is known that both EPGs and PGIPs exist in a variety of non-glycosylated and/or glycosylated states, depending upon the origin of these glycoproteins. It has been of interest to determine the possible role of the glycosylation in EPG -PGIP interactions. It is generally believed that knowledge of the carbohydrate structure(s) and their site-specificity from both EPGs and PGIPs will lead to a better understanding of the role of these glycoproteins in the resistance of plants to fungal attack. In this study, we used matrix assisted laser desorption/ionization time of flight (MALDI-TOF) mass spectrometry to characterize the glycoproteins and site specific glycoforms present in both EPGs and PGIPs which are isolated from *Fusarium moniliforme* and *Phaseolus vulgaris* respectively.

Mass spectra were run on Hewlett Packard LDI 1700XP time-of-flight mass spectrometer operated at an accelerating voltage of 30 kV, an extractor voltage of 9 kV, and a pressure of approximately 3.1 x 10^{-6} torr. A 1:1:1 mixture of equine heart cytochrome C (MW=12,360), equine heart myoglobin (MW=16,950), and bovine serum albumin (MW=66,465) was used to calibrate the MS to give a mass accuracy of approximately $\pm$ 0.1%. Samples were desorbed/ionized from the probe tip with a nitrogen laser (l=337nm) having a pulse width of 3 ns and delivering approximately 5.6 mj energy/laser pulse. The mass spectra of proteins were recorded over a mass to charge (m/z) range of 1-150,000, using a deflector to attenuate the detected abundance of ions below 2,000 m/z and α-cyano-4-hydroxycinnamic acid was used as a matrix.

The molecular weights obtained for HPLC (Fig.1) purified EPGs from SDS-PAGE were 48.5, 45, 41.5, 38 kDa respectively for four different glycoforms. Treatment of the intact glycoproteins with enzymatic and chemical deglycosylation methods followed by SDS-PAGE revealed that the EPGs are N-glycosylated, but provided no information about the size and number of glycosylation sites. In order to characterize and locate the carbohydrate moieties, different glycoforms of EPG separated by HPLC were analysed by MALDI-TOF. It is apparent from the spectra (Fig. 2) and the molecular weight (36,197Da) calculated from the nucleotide sequence that the mass differences between these different forms may each be accounted for by one N-glycosylated carbohydrate moiety. The mapping of the tryptic peptides (derived from trypsin digestion of EPGs) before and after N-glycanase treatment by MALDI-TOF is being used to locate the N-glycosylation sites in these EPGS.

Acknowledgment
This research work is supported by DOE grants, DE-F605-93ER20097 and DE-F605-93ER20114.

43rd ASMS Conference on Mass Spectrometry and Allied Topics

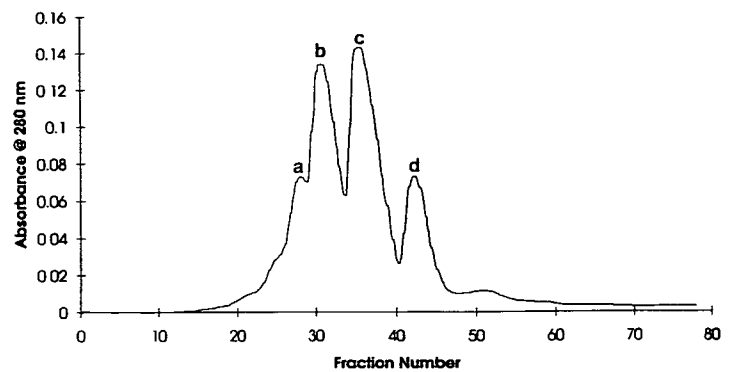

Fig.1. *F. moniliforme* EPG glycoforms separated by mono-S HPLC

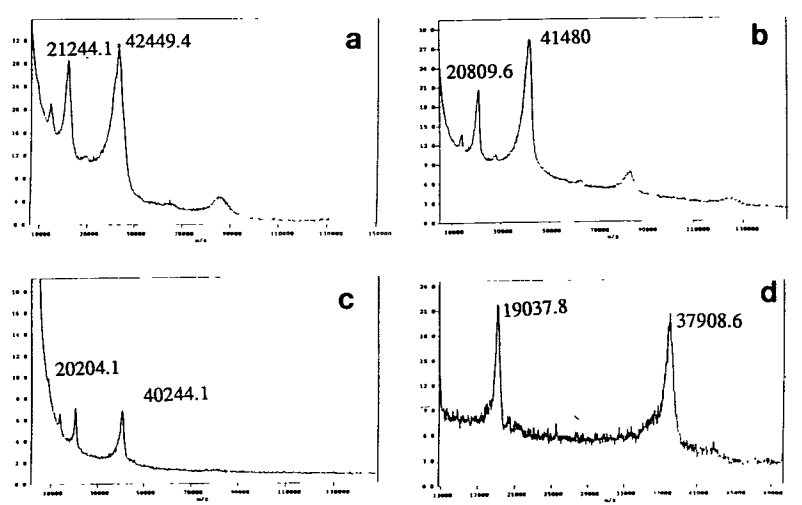

Fig. 2. MALDI spectra of different glycoforms of EPG

Characterization of the Nodulation Factors Produced by *Bradyrhizobium elkani*

V.S.K. Kolli[!], R.W. Carlson[!], N.K. Peters[+] and R. Orlando[!].
[!]Complex carbohydrate Research Center and Department of Biochemistry and Molecular Biology, The University of Georgia, 220 Riverbend, Athens, GA 30602-4712.
[+]Institute of Biology and geology, University of Tromsø, N-9037 Tromsø, Norway.

Gram-negative soil bacteria of the genera *Azorhizobium*, *Bradyrhizobium* and *Rhizobium* establish symbiotic relationships with leguminous plants through the formation of root nodules[1]. The nodulation process is controlled by both bacterial and plant genes. The expression of the bacterial nodulation genes is activated by flavanoids secreted by the plant roots. This activation leads to the synthesis of extracellular signals called the nod factors. The nod factors are chito-oligosaccharides of three to five 1,4-β-linked N-acetyl glucosaminosyl residues, which are N-acylated on the terminal non-reducing glucosaminosyl residue and may be further modified by the addition of another glycosyl residue or other modigying group such as sulfate, carbamyl, acetyl, and /or glycerol substituents (fig1). In the present study, we used FAB mass spectrometry and tandem mass spectrometry to characterize the low abundance lipo-oligosaccharides fractionated from the cell cultures of *Bradyrhizobium elkani.*

Mass spectra were run on a JEOL (Tokyo, Japan) SX/SX 102A tandem mass spectrometer operated at 10 kV accelerating potential. Ions were produced by JEOL FAB gun operated at 6 kV in a conventional FAB ion source. The samples were dissoved in dimethyl sulfoxide and 1μL aliquots were mixed with an equal volume of the FAB matrix, thioglycerol on the probe tip. Collisional activation was performed in the third field free region using helium as the collision gas. The helium pressure was sufficient to attenuate the primary ion by beam by 75%. The collision cell was floated at 3 kV providing a collision energy of 7 kV. All the mass spectra are averaged profiles of 3 scans as recorded by the JEOL complemnt data system.

The HPLC eluted various fractions of *Bradyrhizobium elkani* are subjected to FAB mass spectrometry for characterization of lipo-oligosaccharides. The MS results showed that some of the compouds have similar structrures previously reported for *Bradyrhizobium japonicum* and *Bradyrhizobium elkani*[2]. Four new lipo-oligosaccharides were identified from the FAB MS and MS/MS data (one of them is shown in fig2); they have the structures, NodBe-V(Cb,C16:0,MeFuc), NodBe-V(Cb,C16:0,Nme,MeFuc), NodBe-V(2Cb,C16:0,MeFuc) and NodBe-V(C18:1,Fuc,Gro).

References:

1. Nitrogen fixation, Vol. 2. *Rhizobium.* W.J. Broughton, ed. Clarendon Press, Oxford.
2. R. W. Carlson, J.Sanjuan, U.R. Bhat, J.Glushka, H.P. Spaink, H.W. Wijfjes, A.N. Van Brussel, T.J.W. stokkermans, N.K. Peters and G. Stacey, J. Biol. Chem. **268**, 1993, 18372.

Acknowledgments

This work was supported by NSF grant IBN 9291878 awarded to N.K.P., by USDA grant 9303956 awarded to R.W.C., and by the DOE grant DE-FG09-93ER20097 to the CCRC.

43rd ASMS Conference on Mass Spectrometry and Allied Topics

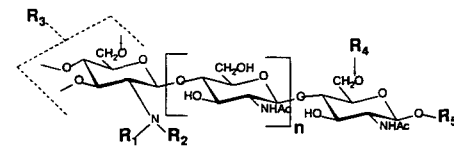

Fig. 1 Shows the lipo-oligosaccharides back bone and substituents.
R_1 = H, Me; R_2 = C16:0, C16:1, C16:2, C16:3, C16:4, C18:0, C18:1, C18:4; R_3 = H, Ac(O-6), Cb; R_4 = SO_3H, MeFuc, Fuc, AcMeFuc, MeFucS, D-Ara, H; R_5 = H, Gro.

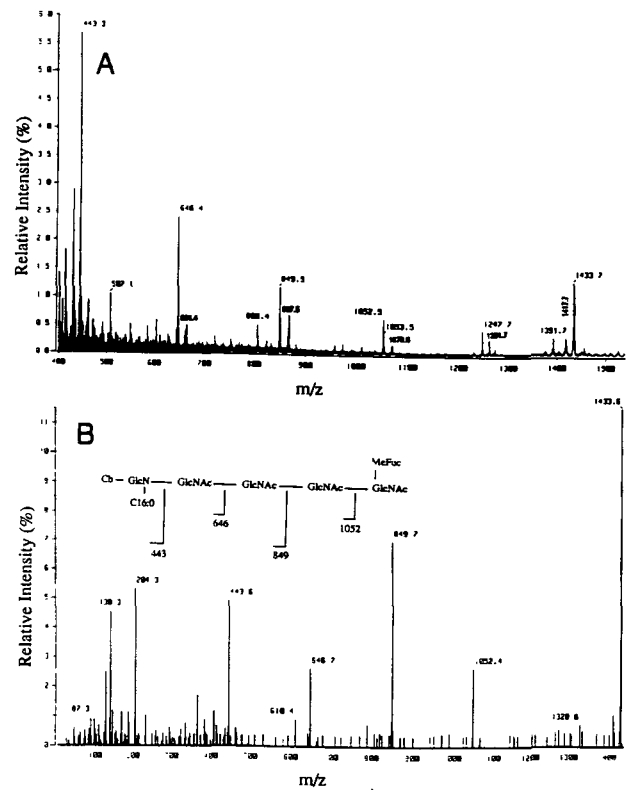

Fig. 2. FAB mass spectrum (A) of one of the HPLC fractions of low abundance lipo-oligosaccharides and MS/MS spectrum (B) of m/z 1442 ion.

FAB and ESIMS of Acidic Glycosphingolipids
---Le^x- and Le^a-derivatives

Y.Ohashi, T.Ii, S.Kurono, T.Ogawa and Y.Nagai
The Institute of Physical and Chemical Research (RIKEN)

Objective and Methods

Fucose-containing branched trisaccharide units, called Lewis-type sugar chains, are possible ligands to selectins if the position 3 of the non-reducing end galactose is substituted with an acidic group such as a sulfate or sialic acid. Fast atom bombardment (FAB) and electrospray ionization (ESI) were applied to synthetic glycosphingolipids to obtain basic fragmentation patterns. Once the methodology has been established, it will be applicable to determine the structure of trace amounts of biologically important real samples. ESI analyses were performed on the samples shown in scheme 1 using a Finnigan TSQ 700 mass spectrometer. These samples had typical concentrations of 100 pmol/μL in a 1:1 solution of CH_3OH and $CHCl_3$. FAB measurements were also carried out and in this case thioglycerol, for (+) FAB, and triethanolamine, for (-) ion modes, were used as the matrix. Argon gas of 40eV at 0.2 Pa was introduced as the collision gas for CID-MS/MS studies.

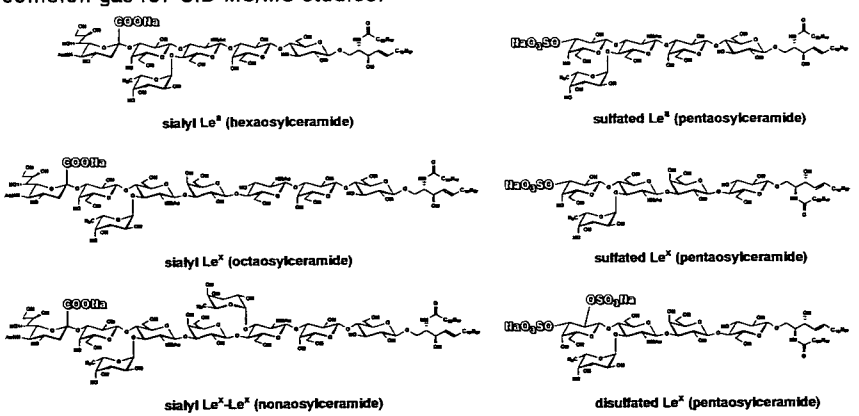

scheme 1
Le-type acidic glycosphingolipids

Results

a): Sulfated Le^x- and Le^a- glycosphingolipids; Positions of sulfate groups can be determined in the (+) as well as in the (-) mode according to the fragmentation patterns of Le-type oligosaccharides (to be published). Distinction of Le^x- from Le^a - type glycosphingolipids was successfully implemented by (-)FAB CID-MS/MS only by having the $[C_2\text{-Na+H}]^-$ ion, not by having the $[M\text{-Na}]^-$, as the precursor; the C3-linked fucose of Le^x is more readily eliminated as a neutral molecule in the negative ion mode generating the(Z1β-H-Na)$^-$ fragment ion in addition to the (Y1β +H-Na)$^-$. On the other hand, Le^a, which has a fucose group linked to C4 of GlcNAc, eliminates the fucose giving rise to the (Y1β +H-Na)$^-$ only (Fig. 1).

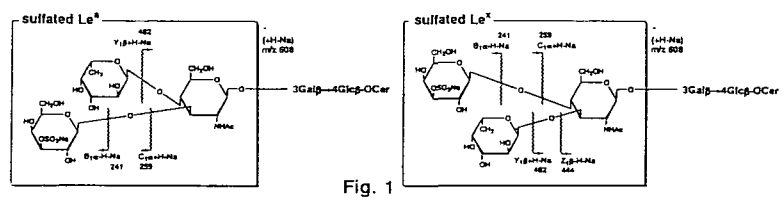

Fig. 1

b): Sialyl Le^x-glycosphingolipids; The above-stated fragmentation rule does not apply, however, to sialylated Le- sugar chains, because the less acidic carboxylate group fails to retain the negative charge at the reducing end, giving abundant ceramide-side ions (Y-ions) even in the negative ion mode. Thus the key ion corresponding to $(C_2\text{-Na+H})^-$ does not appear in the normal spectrum.

c): Positive Ion mode; Contrary to the general belief that acidic glycoconjugates give higher ion intensities in the negative ion mode, positive ion mode is also as informative and sensitive method as the negative ion mode.

d): Conclusions: Acidic glycoconjugates of high molecular weight can be analyzed by ESI and/or FAB mass spectrometry yielding information which sometimes exceeds NMR spectrometry. An interesting phenomenon in the (-)ESI spectra of these acidic glycolipids is that the second (-) charge to produce a double-charged ion is gained by an extra deprotonation or an attachment of an abnormal negative ion such as Cl^- or $(C_4H_9O_2)^-$, as reported previously for neutral glycolipids(1).

(1) T. Ii, Y. Ohashi and Y. Nagai, *Org. Mass Spectrom.*, **28**, 927 (1993).

MALDI-MS ANALYSIS OF GANGLIOSIDES FROM HUMAN GRANULOCYTES

Jasna Peter-Katalinic[1], Bernd Stahl[2], Michael Karas[2], Franz Hillenkamp[2], Franz-Georg Hanisch[3], Heinz Egge[1], Johannes Müthing[4]

[1] Institute for Physiological Chemistry, University of Bonn, Germany

[2] Institute for Medical Physics, University of Münster, Germany

[3] Institute for Immunobiology, University of Cologne, Germany

[4] Institute for Cell Culture, University of Bielefeld, Germany

INTRODUCTION:

Granulocytes are the second most abundant cells in peripheral blood. Their primary function is phagocytosis and the engulfing of pathogenic microorganisms. Peripheral blood lymphocytes, momocytes and granulocytes have distinct glycosphingolipid fingerprints [1]. The predominant ganglioside species of granulocytes belong to the neo-lactoseries (Galß1-4GlcNAcß1-3)nGalß1-4Glcß1-1Cer (where n=0-2) [2]. Terminally sialylated gangliosides were shown to be able to serve as receptors for influenza viruses A and Sendai virus via carbohydrate chains on their cell surfaces [3]. The carbohydrate structures of lower homologues were identified to belong to the unbranched neolacto-series by sequencing using (-)FAB-MS of the native gangliosides and the methylation analysis [4].

RESULTS:

In this contribution a structural study of ganglioside homologues of higher molecular weight by MALDI-MS after permethylation is presented. This approach was shown to be of excellent applicability for neutral glycosphingolipids [5] and for gangliosides [6] in subpicomole quantities of biological material.

2,5-Dihydroxybenzoic acid (DHB) was used as a solid matrix for analysis of up to tetradecasaccharide ceramide molecular ions in the mass region of 2000-4000 Da by (+)MALDI-MS. From the m/z values of molecular [M+Na]+ ions in pure fractions and in mixtures, the composition of the carbohydrate and ceramide portions were deduced and compared to the diagnostically significant fragment ion data, obtained by FAB-MS [7]. Due to the high sensitivity of MALDI-MS even minor components of ganglioside polar fractions - representing complex mixtures - were detected. The fucosylation and sialylation status was analysed.

Epitope analysis was performed using monoclonal antibodies CSLEX1 and CDw65 (VIM2), which allow the distinction of isomeric hexasaccharide structures sLe^x and VIM2:

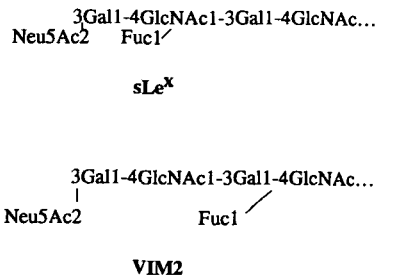

STRUCTURES:

NeuAcFuc(GalGlcNAc)$_3$GalGlc-O-Cer (16/18)

NeuAcFuc$_2$(GalGlcNAc)$_3$GalGlc-O-Cer (16/18)

NeuAcFuc$_3$(GalGlcNAc)$_3$GalGlc-O-Cer (16/18)

NeuAcFuc(GalGlcNAc)$_4$GalGlc-O-Cer (16/18)

NeuAcFuc$_2$(GalGlcNAc)$_4$GalGlc-O-Cer (16/18)

NeuAcFuc$_3$(GalGlcNAc)$_4$GalGlc-O-Cer (24/18)

REFERENCES:

[1] Kiguchi, K.; Henning-Chubb, C. B.; Hubermann, E., J. Biochem. 107, 8-14 (1990).

[2] Fukuda, M. N.; Dell, A.; Oates, J. E.; Wu, P.; Klock, J. C.; Fukuda, M., J. Biol. Chem. 260, 1067-1082 (1985).

[3] Müthing, J.; Unland, F.; Heitmann, D.; Orlich, M.; Hanisch, F.-G.; Peter-Katalinic, J.; Knäuper, V.; Tschesche, H.; Kelm, S.; Schauer, R.; Lehmann, J., Glycoconjugate J. 10, 120-126 (1993).

[4] Peter-Katalinic, J.; Unland, F.; Hanisch, F.-G.; Heitmann, D.; Müthing, J.; J. Cell Biochem. Suppl. 17A, 377 (1993).

[5] Egge, H.; Peter-Katalinic, J.; Stahl, B.; Karas, M., Pure Appl. Chem. 63, 491-498 (1991).

[6] Juhacz, P.; Costello, C., J. Am. Soc. Mass Spectrom. 3, 785-796 (1992).

[7] Peter-Katalinic, J.; Egge, H., Meth. Enzymol. 193, 713-733 (1990).

STRUCTURAL STUDIES ON SIALYLATION OF GANGLIOSIDES FROM DEVELOPING CHICKEN BRAIN BY ELECTROSPRAY MASS SPECTROMETRY

Jasna Peter-Katalinic[1], Alison E. Ashcroft [2], Brian N. Green [2], Franz-Georg Hanisch [3], Johannes Müthing [4]

[1] Institute for Physiological Chemistry, University of Bonn, Germany
[2] FISONS Instruments, VG BIOTECH, Altrincham, UK
[3] Institute for Immunobiology, University of Cologne, Germany
[4] Institute for Cell Culture, University of Bielefeld, Germany

INTRODUCTION:

Gangliosides constitute a heterogeneous group of sialylated glycosphingolipids differing in both the oligosaccharide and ceramide composition. The majority of brain ganliosides belong to the ganglioseries of glycolipids and contain invariable tetrasaccharide backbones with variable numbers of sialic acid residues [1]. The diversity of sialic acids has been well established. Despite the clear developmental changes noted in various organs, their biological role remains unclear [2]. The studies regarding the developmental regulation of Neu5Gc in isolated organs of various animals showed changes in the glycoconjugates, located mainly in the ganglioside fraction [3]. Gangliosides of embryonic chicken brain have been found to be expressed transiently during prehatching brain development [4]. The predominant "c"-type substitution pattern of sialic acids was revealed by sequencing using (-) FAB mass spectrometry of native [5] and (+)FAB-MS of permethylated [6] samples. The FAB-MS analysis of the permethylated G_{T1b}, G_{Q1b}, G_{Q1c}, G_{P1c} and G_{H1c} gave clear-cut fragmentation patterns concerning the carbohydrate sequence and the ceramide composition (C18:0 fatty acid and 4-sphingenine), but molecular ions were only of low abundance [6]. A carefull analysis of the sialic acids derived fragments at m/z=376 ($NeuAc^+$), 737 ($NeuAc_2^+$) and 1098 ($NeuAc_3^+$) gave rise to the assumption, that in 0-30% of the terminal sialic acid moieties NeuGc instead of NeuAc were present, as documented by specific shifts of 30 Da each [7]. In order to prove this very unusual assumption two control analyses of total sialic acids after release from parent gangliosides by hydrolysis using GC/MS and HPLC were performed [8,9] and the NeuGc level found to be lower than 1%. Direct sialylation analysis of the molecular ions in native material was necessary to clear this point and to explain the previously not reported expression of NeuGc sialic acid in perinatal chicken brain.

43rd ASMS Conference on Mass Spectrometry and Allied Topics

RESULTS:

In this contribution a sialylation analysis of native tri- to hexasialogangliosides using negative ionization electrospray mass spectrometry using picomol quantities of biological material will be presented. (-)ES-MS in MS1 of G_{T1b}, G_{Q1b}, G_{Q1c}, G_{P1c} and G_{H1c} were dominated by molecular ions of gangliosides or their sodium salts, singly charged at higher skimmer voltage and doubly and triply charged at decreased voltage. The lipid portion derived fragment ions were represented mainly by anions arising after loss of one-to-three sialic [Neu5Ac] acid moieties from the molecular ion(s), whereas the carbohydrate derived fragment ions were the monocharged mono-to-three sialic [Neu5Ac] acid residues after loss of one water molecule. The presence of functional modifications in sialic acid moieties like lactones, O-acetylation, O-methylation, N-glycolylation and others [2] would result in relative shifts of m/z values by -18, +42, +14, and +16 a.m.u. respectively. None of such shifts were observed in respective molecular and/or fragment ions in (-)ES-MS. The fragmentation tendancy as observed in MS1 was followed after low energy CID in MS2. Sugar ring cleavages were not observed. Quantitative differences in the daughter ion abundances were diagnostically used for assignment of positional isomers G_{Q1b} and G_{Q1c}.

REFERENCES:

[1] Stults, C. L. M.; Sweeley, C. C.; Macher, B. A., Meth. Enzymol. *179*, 167-214 (1989).

[2] Varki, A., Glycobiology *2*, 25-40 (1992).

[3] Gustafsson, B. E.; Karlsson, K.-A.; Larson, G.; Midtvedt, T.; Stromberg, N.; Teneberg, S.; Thurin, J., J. Biol. Chem. 261, 15294-15300 (1986).

[4] Rösner, H., Brain Res. *236*, 49-61 (1982).

[5] Rösner, H.; Rahmann, H.; Reuter, G.; Schauer, R.; Peter-Katalinic, J.; Egge, H., Biol. Chem. Hoppe Seyler *336*, 1177-1181 (1985).

[6] Peter-Katalinic, J., Sanibel Conference on Mass Spectrometry of Carbohydrates, Sanibel Island, Fla., USA, January 23-25, 1993.

[7] Peter-Katalinic, J.; Egge, H., Meth. Enzymol. *193*, 713-733 (1990).

[8] Hanisch, F.-G., Biol. Mass Spectrom. *23*, 309-312 (1994).

[9] Unland, F.; Müthing, J., Biomed. Chromatogr. 6, 155-159 (1992).

ESI-MS AND ESI-CID-MS/MS OF COMPLEX NEOLACTO-SERIES GLYCOSPHINGOLIPIDS

Steven B. Levery, PE-Applied Biosystems Division, 850 Lincoln Centre Drive, Foster City, CA 94404; **Mary Ellen K. Salyan, Mark R. Stroud**, The Biomembrane Institute, 201 Elliott Avenue West, Seattle, WA 98119

Studies on the structures of glycosphingolipids (GSLs) from both normal and pathological tissues have produced important findings on various aspects of cell surface biochemistry, including previously unsuspected details of ABO blood group immunochemistry and the aberrant glycosylation of tumor cells. The increasing complexity of compounds of interest has fostered a continuing need to examine the potential of state-of-the-art instrumentation for their analysis. Based on the promising results of other groups showing the efficacy of ESI-MS for solving glycan structural problems, we have explored its use for the analysis of more complex GSLs of interest.

Permethylated GSLs were analyzed on a PE-SCIEX API-III triple quadrupole mass spectrometer with an IonSpray source, operating in the positive ion mode. Samples dissolved in MeOH containing 1 mM of either ammonium acetate or formic acid were introduced by direct infusion. Single quadrupole MS produced abundant sodiated molecular ions as well as fragments originating from the non-reducing end of the glycan, similar to those observed previously in EI- and FAB-MS. In some cases, accompanying fragments also retained a sodium atom. Observed in CID tandem mass spectrometry of mono- and disodiated molecular species were numerous glycan sequence-related ions originating from both the reducing and non-reducing ends, as well as ions from internal sequences. These data were sufficient to deduce the complete "skeletal" sequence of complex GSLs, including a branched undecaglycosylceramide having an A blood group hapten on one arm and sialic acid on the other:

```
GalNAcα1→3
          Galβ1→4GlcNAcβ1→6
  Fucα1→2                    Galβ1→4GlcNAcβ1→3Galβ1→4Glcβ1→1Cer
NeuAcα2→3Galβ1→4GlcNAcβ1→3
```

In ESI-MS of the permethylated compound, a set of abundant disodiated, doubly charged pseudomolecular ions, at nominal monoisotopic m/z 1608, 1622, and 1636, represented deoxyHex•NeuAc•Hex_5•$HexNAc_4$ attached to ceramides predominantly consisting of d18:1 sphingenine combined with 20:0, 22:0, and 24:0 fatty acids, respectively. Also observed were less abundant trisodiated, triply charged pseudomolecular ions at nominal monoisotopic m/z 1079.67, 1089.00, and 1098.33, respectively. Non-reducing end sequence-related fragments were observed for the sialylated arm at nominal m/z 376, 344, and 312 (NeuAc, successive losses of MeOH); 580 (NeuAc•Hex); 825 and 793 (NeuAc•Hex•HexNAc); and for the A blood group hapten arm at nominal m/z 260 and 228 (HexNAc); 883 (deoxyHex•Hex•$HexNAc_2$). Fragments containing both arms and the branching Hex were observed weakly at m/z 1897 (deoxyHex•NeuAc•Hex_3•$HexNAc_3$) and abundantly at m/z 2142 (deoxyHex•NeuAc•Hex_3•$HexNAc_4$).

A typical MS-CID-MS pattern, in this case selecting via Q_1 for the disodiated pseudomolecular ion at nominal m/z 1622 (1624 measured), is reproduced below. Under these conditions, sodiated ions were predominant, with some persistence of disodiation in the

larger fragments. Unsodiated ions appeared only at measured m/z 376.5 (NeuAc); and 449.2 and 417.0 (internal -O-Hex-O-HexNAc-). Disodiated fragments include those at m/z 1436.5 (loss of NeuAc from the pseudomolecular ion); 1308.5 (loss of Cer); 1212.4 (loss of NeuAc•Hex•HexNAc); 1120.4 (loss of both NeuAc and Cer); 1095.4 (loss of -O-Hex-O-Hex-O-Cer). Monosodiated "A-type" fragments yielding the glycan sequence of two types of non-reducing terminals included those at m/z 660.9 (deoxyHex•Hex•HexNAc); 906.5 (deoxyHex•Hex•$HexNAc_2$); 398.5 and 366.5 (NeuAc); and 847.7 (NeuAc•Hex•HexNAc). Monosodiated internal fragments included those at m/z 472.5 (-O-Hex-O-HexNAc-); 1790.8 (loss of NeuAc and -O-Hex-O-Hex-O-Cer). Of particular interest is the fragment at m/z 458.3, which was observed abundantly in all spectra of branched neolacto-series gangliosides (three analogs, including the non-blood group core structure VI^3NeuAc-iso-nLc_8Cer), but not in any unbranched analogs (VI^3NeuAc-nLc_6Cer and IV^3NeuAc-nLc_4Cer). This ion is believed to arise from the sodiated fragment (m/z 1341.0) representing the blood group terminal tetrasaccharide attached (by its β1→6 linkage) to the internal -O-Hex-O-HexNAc-. Neutral loss of the tetrasaccharide branch, leaving the N-acetyllactosamine unit as -O-(HO-)Hex-O-HexNAc-, would yield a sodiated ion having the proper mass value.

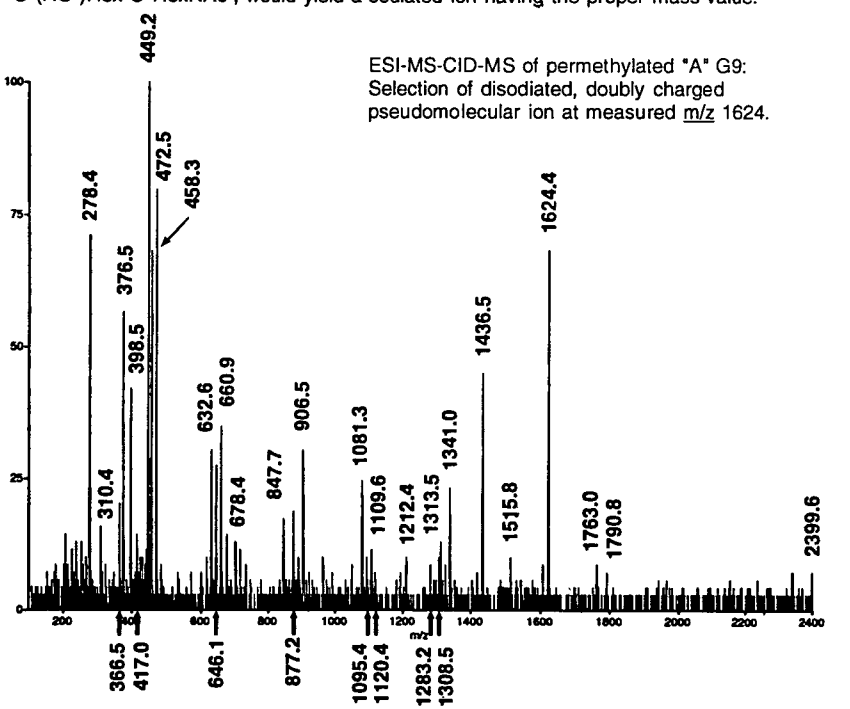

GLYCOSPHINGOLIPIDS FROM BOVINE RED BLOOD CELLS AND FOETAL CALF BRAIN

Hélène Perreault[1,3], Omanand Koul[2], Jacqueline Street[2], Robert H. McCluer[2] and Catherine E. Costello[1,4]

[1]Dept. of Chemistry, Massachusetts Institute of Technology, Cambridge, MA 02139; [2]Eunice Kennedy-Shriver Center for Mental Retardation, Waltham, MA 02154; Present addresses [3]Dept. of Chemistry, University of Manitoba Winnipeg, Manitoba, Canada R3T 2N2; [4]Dept. of Biophysics, Boston Univ. School of Medicine, Boston, MA 02118.

Introduction. Stage-specific embryonic antigen (SSEA) glycosphingolipids (GSLs) found in the central nervous system are involved in regulating cell-cell recognition, targeting and migration of cells during development. SSEA-1 (Lewis x) GSLs are biosynthesized in the brain by fucosylation of lipid substrates with the core structure [Gal-GlcNAc-Gal-Glc-Cer] and higher analogs through the action of fucosyltransferase enzymes. In order to optimize methodology to allow for the structural determinations of SSEA-type GSLs from foetal calf brain, potential substrates for the fucosyltransferases of this class were first isolated from bovine red blood cells and mouse kidney cells, purified using chromatographic techniques, derivatized and characterized by LSIMS, MS/MS and linear and PSD MALDI-TOFMS. The methods were then applied to fractions from foetal calf brain.

Experimental. Neutral glycolipid fractions were isolated from beef red blood cells[1] and mouse kidney cells[2] according to Li *et al*[1] and McCluer *et al*[2]. Complex neutral GSLs were isolated from foetal (1st trimester) calf brain according to Hakomori *et al*[3]. LSIMS and MS/MS experiments were performed with a JEOL HX110/HX110 (E1B1-E2B2) instrument, at +10kV accelerating voltage. High energy collisions with helium were induced at 7keV in a cell (helium) located between MS-1 and MS-2. For linear MALDI-TOFMS, modified VT2000 (Perseptive Biosystems Inc.) instrument was used. PSD MALDI-TOFMS experiments were conducted at Merck Co. (Rahway, NJ) by Dr. P. Griffin on a Vision-2000 instrument (Finnigan Corp.) For both types of MALDI-TOF experiments, a nitrogen laser source (337 nm) generated the radiation and the matrix was 2,5-DHB. Permethylation of the GSLs was effected as described by Ciucanu and Kerek[4]. The gas-to-solid method[5] was used for peracetylation.

Results. GSLs from bovine red blood cells (Fractions **7** and **PG**, ca. 10 nmol available) and mouse kidney cells (Fraction **6**, ca. 15 nmol) were examined prior to the feotal calf brain fractions. Microscale analysis was conducted to allow for determination of sugar content. Gas phase peracetylation of the fractions allowed for acquisition of structurally significant LSIMS and MS/MS spectra, and permethylated derivatives produced abundant Z_0-type ceramide ions which could be analyzed by MS/MS. Linear mode MALDI-TOFMS experiments on the native and derivatized compounds also played a major role in structure elucidation. The number of methyl and acetyl substitutions were helpful in distinguishing Hex, Fuc and HexNAc residues. Structures containing up to eight sugar residues were identified, and heterogenous ceramides were encountered, with modifications that include hydroxylation, additional sites of unsaturation and variation in alkyl chain lengths. The fractions from foetal calf brain (**r6, r8 and r10**) were available in much smaller quantities (ca. 1 nmol); MALDI-PSD (<1 pmol) experiments instead of MS/MS were acquired for fragmentation data. Gas phase peracetylation performed on 500 pmol of **r10** allowed for acquisition of structurally significant LSIMS data (250 pmol). LSIMS and MALDI-PSD data were complementary in some aspects. The fractions were found to be GSL mixtures with heterogeneity in the ceramide chains. Table 2 summarizes the results obtained from all mass spectrometric investigations. Details of structures of **r6** and **r8** are still uncertain; MALDI-PSD-TOFMS experiments are underway to clarify remaining features.

Carbohydrate structure, determined by mass spectrometry	**Ceramide structures based on MS (*proposed from total ceramide length) (Fraction N°-Component N°)**
Gal-GlcNAc-Hex-Hex-Cer	18:0-d18:1(**6-1**),18:0-d20:1(**6-2**),*16:0-d18:1(**PG-1**),*22:0-d18:1(**PG-2**),*24.0-d18:2(**PG-3**)
$(Hex)_4(HexNAc)_2Cer$	*24:0-d18:1(**6-3**)
Gal-HexNAc(Fuc)-HexNAc(Hex)-Hex-Hex-Hex-Cer	16:0-d18:1(**7-1**),22:0-d18:1(**7-2**), 22:0-d20:1(**7-3**),22:o-d20:1(OH)(**7-4**), 22:0-d20:1$(OH)_2$(**7-5**)
$(Hex)_3(HexNAc)_1Cer$	*18:0-d18:1(**r6-1**),*18:0-d18:1(OH)(**r6-2**)
$(Hex)_3(HexNAc)_1(Fuc)_1Cer$	*16:0-d18:1(**r6-3**),*18:0-d18:1(**r6-4**), *18:0-d18:1(OH)(**r6-5**)
$(Hex)_3(HexNAc)_2(Fuc)_2Cer$	*18:0-d18:1(**r6-6**),*18:0-d18:1(OH) (**r6-7**)
$(Hex)_4(HexNAc)_2(Fuc)_1Cer$	*18:0-d18:1(**r8**)
Hex-HexNAc(Fuc)-Hex-HexNAc(Fuc)-Hex-Hex-Cer	*16:0-d18-1(**r10-1**),*18:0-d18:1(**r10-2**), *18:0-d18:1(OH)(**r10-3**)

Table 1: Components identified in the GSL fractions investigated by mass spectrometry

Work accomplished at MIT was supported by NIH Grant no. RR00317 to K. Biemann, and work at EKS Center by NIH Grant no. HD005515 to R.H. McCluer

1. J. Chien, S. Li and Y Li, J. Biol. Chem. 253 (1978) 4031-4035.
2. M A. Williams, S.K. Gross, J.E. Evans and R.H. McCluer, J. Lipid Res , 29 (1988) 1613-1619
3. E. Nudelman, S. B. Levery and S. Hakomori, J. Biol. Chem., 261 (1986) 11247.
4 I. Ciucanu and F. Kerek, Carbohydr. Res., 131 (1984) 209-217
5 H. Perreault and C. E. Costello, Organic Mass Spectrom., 29 (1994) 720-735.

Detailed Characterization of Glycosphingolipids by ES-MS-CID-MS

Bruce B. Reinhold, Song Ye, Vernon N. Reinhold, John V. Brigande, and Thomas Seyfreid, Boston University School of Medicine and Boston College

Gangliosides are a family of sialic acid-containing glycosphingolipids which are amphiphillic compounds of the outer leaflet of plasma membranes. Although they are found in nearly all vertebrate tissues, gangliosides are most heavily concentrated in neurons of the central nervous system. They are thought to function in a variety of membrane mediated phenomena including cell-cell and cell-matrix interactions (Ledeen, 1989; Varki, 1993). Additionally, many studies indicate that ganglioside biosynthesis and expression are developmentally regulated, suggesting an important role in neuronal proliferation, migration, and differentiation.

Comparative studies on the occurrence and distribution of vertebrate brain gangliosides have revealed considerable variability in composition and concentration across phylogeny (Avrova, 1971; Rahmann and Hilbig, 1983). However, studies on vertebrate embryos have suggested similarities in ganglioside composition. Gangliosides GD3 and GM3, for example, dominate the early embryonic patterns of some vertebrates (Bouvier and Seyfried, 1989). Von Baer recognized in the early 19th century that highly diverse vertebrate morphologies develop from common vertebrate forms and Darwin proposed that the similarity in embryonic structure across different species is a reflection of a common descent. In this century, these observations are being translated into molecular terms. Due to their widespread distribution and complex molecular architecture, comparative studies of ganglioside structures should provide insights into fundamental biochemical homologies that exist in evolutionary and fetal development.

The gangliosides extracted from adult skate (*Raja erinacea*) brains provide a good example of the analytical challenge such studies represent. HPTLC analysis of these gangliosides (resorcinol staining) revealed many multiply-sialyted bands that did not migrate with known standards. Methylation and ES-MS of the total acidic glycolipid extract provided a complicated picture of ceramide and carbohydrate heterogeneity including structures containing up to seven sialic acid residues. ES-MS-CID-MS of doubly and triply charged ions using a TSQ 700 triple quadrupole provided extensive characterization of branching isomerism in the carbohydrate and allowed mass assignments for both the sphingosine and amide linked alkane chain (Reinhold, 1994). Collision spectra of skate brain gangliosides containing one, four and five sialic acid residues are illustrated.

43rd ASMS Conference on Mass Spectrometry and Allied Topics

Avrova, N.F. (1971) Brain Ganglioside Patterns of Vertebrates. ***J. Neurochem.*** **18**, 667-674

Bouvier, J.D. and Seyfried, T.N. (1989) Ganglioside Composition of Normal and Mutant Mouse Embryos. ***J. Neurochem.*** **52**, 460-466

Ledeen, R.W. (1989) Biosynthesis, Metabolism and Biological Effects of Gangliosides. In: ***Neurobiology of Glycoconjugates*** (Margolis, R.U. and Margolis, R.K., eds.) Plenum Press, New York, pp. 43-69

Reinhold, BB, Chan, S.-Y., Chan, S, and Reinhold, VN (1994) Profiling Glycosphingolipid Structural Detail: Periodate Oxidation, Electrospray, Collision-induced Dissociation and Tandem Mass Spectrometry. ***Organic Mass Spectrometry*****, 29,** 736-746.

Rahmann, H. and Hilbig, R. (1983) Phylogenetical Aspects of Brain Gangliosides in Vertebrates. ***J. Comp. Physiol.*** **151**, 215-224

Varki, A. (1993) Biological Roles of Oligosaccharides: All of the Theories are Correct. ***Glycobiology.*** **3**, 97-130

DETERMINATION OF THE GLYCOSYLATION POSITION IN MONO-*O*-GLYCOSYL FLAVONOIDS

Q. M. Li, H. Van den Heuvel and M. Claeys
University of Antwerp (UIA), Department of Pharmaceutical Sciences, Antwerp, Belgium

In a previous study we have shown how flavonoid O-diglycosides can be differentiated from flavonoid *O,C*- and *C*-diglycosides and how unambiguous information on the carbohydrate sequence can be obtained for *O*-diglycosides by performing low-energy CID on $(M + H)^+$ ions and tandem mass spectrometry [1]. In a continuation of this study we now demonstrate how these methods can be applied to characterize the aglycone part and obtain information on the glycosylation position in flavonoid *O*-glycosides.

The glycosylation site in *O*-glycosyl flavonoids is generally established rather indirectly by applying UV-spectroscopy and resorting to various specific shift reagents. A suitable analytical method has been reported previously by Sakushima and Nishibe [2], which involves methylation, chemical hydrolysis, isolation of the methylated aglycone, preparation of the trimethylsilyl derivative in order to derivatize the free hydroxyl group, and, finally, EI/MS analysis. Our more direct mass spectral approach is partly inspired by this method and also involves derivatization to the methyl phenolether derivative. Following methylation with diazomethane, the methylated mono-*O*-glycosyl flavonoid is ionized by fast atom bombardment, which results in the formation of protonated molecules, as well as protonated aglycone ions. In a subsequent step, a product ion spectrum of the protonated aglycone ions is obtained using low-energy collisional activation. The detailed analysis of the product ion spectrum allows to infer the position of the free hydroxyl group, which corresponds to the glycosylation position in the intact mono-*O*-glycosyl flavonoid.

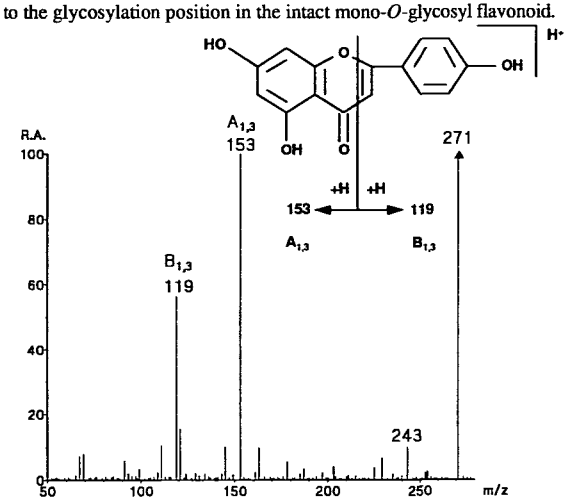

Fig.1. Low energy CID spectrum obtained for the protonated aglycone ions (Y_0^+) of apigenin 7-*O*-neohesperidoside.

Figure 1 illustrates the low-energy CID spectrum obtained on the FAB-generated Y_0^+ ions (*m/z* 271) of apigenin 7-*O*-neohesperidoside. The abundant product ions at *m/z* 119 ($B_{1,3}$) and *m/z* 153 ($A_{1,3}$) are rationalised by Retro Diels-Alder fragmentations in the C ring and are typical of the apigenin aglycone part (Scheme 1). With respect to the ion nomenclature used to denote fragment ions typical of the aglycone part, a systematic ion nomenclature is proposed in which the bonds broken in the C ring are indicated with subscripts.

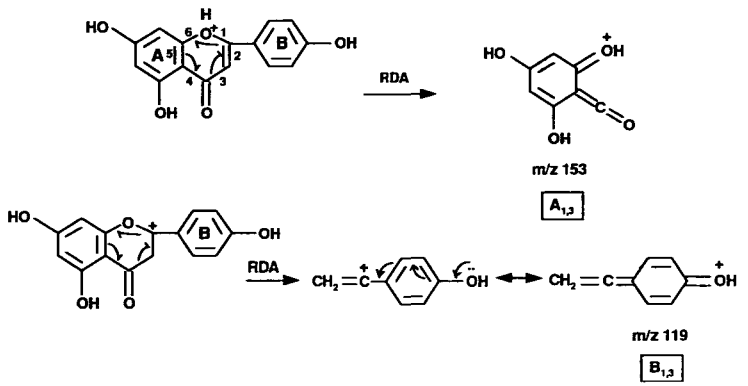

Scheme 1

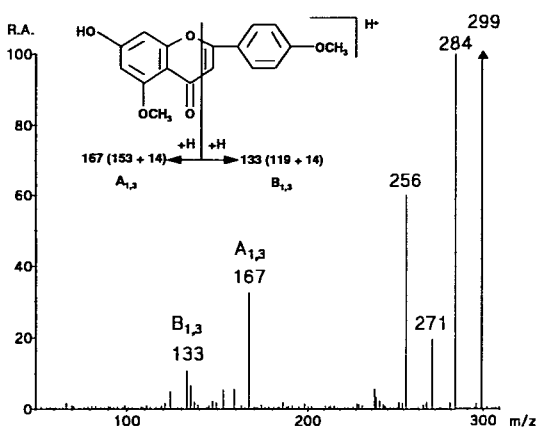

Fig.2. Low-energy CID spectrum obtained for the protonated aglycone ions (Y_0^+) of methylated apigenin 7-*O*-neohesperidoside.

Figure 2 shows the low-energy CID spectrum obtained on the Y_0^+ ions (*m/z* 299) of the sample of apigenin 7-*O*-neohesperidoside following methylation with diazomethane. The $B_{1,3}$ ions (*m/z* 133) have shifted by 14 u, indicating that the 4'-hydroxyl group of the B ring was free. The $A_{1,3}$ ions (*m/z* 167) also show a mass increase of 14 u which is consistent with glycosylation in the A ring. Taking into account the lower reactivity of the 5-hydroxyl group towards glycosylation, it is logical to propose glycosylation at the 7-*O* position. It is also pointed out that the Y_0^+ ions fragment by loss of a methyl radical; this rather uncommon transition from even-electron to odd-electron ions was found to be characteristic of phenolic methyl ether groups.

[1] Q. M. Li and M. Claeys, *Biol. Mass Spectrom.* 23, 406 (1994).
[2] A. Sakushima and S. Nishibe, *Phytochemistry* 27, 915 (1988).

MS AND LC/MS OF POLYPHENOLS

Jon D. Williams[1], Ronald L Belinger[2], Gerald B. Cohen[2]
Kraft Foods, Inc. - Analytical Chemistry
[1]801 Waukegan Rd., Glenview, Il 60030
[2]250 North Street, White Plains, NY 10625

Plant polypehnols, syn vegetable tannis, constitute one of the most distinctive groups of higher plant secondary metabolites.[1] Hydrolyzable tannins consist of polyesters based on gallic acid and/or hexahydrocyddiphenic acid and their derivatives (Figure 1). The propensity of polyphenols to bind with protein, nucleic acids, and carbohydrates protects the plant from both microbial and animal predators[2] Protein binding is thought to contribute to the astringent flavor notes found in beverages such as teas, cocoa, wines and beer[1] The extent of this interaction is governed by the number of phenolic moieties and how they are linked together Techniques to characterize both types of structural differences are necessary to elucidate these interactions This study reports the first application of direct introduction electrospray mass spectrometry, and reverse phase LC/MS to study the constituents of hydrolyzable tannins

Two Finnigan (San Jose, CA) TSQ-700s were used in this study The first was fitted with Finnigan electrospray ionization source which was held at 4 5 kV above ground potential to produce positively charged ions A sheath liquid of 2-methoxyethanol was flowed at 5 µL/ min Nitrogen sheath and auxiliary gas also were present. The temperature of the heated capillary was set at 190°C The resolution of the mass analyzers were opened to 2 Da wide to improve delectability The other TSQ was equipped with an EI/CI source Sample was introduced using a direct insertion probe or particle beam Negative chemical ionization with ammonia (1 3 Torr) generated sample ions The mobile phase for LC/MS experiments consisted of A (100% water + 0.1% NH_4OAc + 0.1% HOAc) and B (100% acetonitrile) and was delivered as a gradient The mobile phase was delivered to a 1 mm Hypersil C8 (Keystone, Bellefonte, Pa) at a rate of 50 µL/min Hydrolyzable tannins samples, derived from Aleppo (*Quercus infectoria*) and Chinese (*Rhus semialata*) galls and Tara (*Caesalpinia spinosa*) fruit, were obtained from Omichem (Belgium). Approximately 0 8 mg of sample were added to 1 mL of a solution containing 94% A 6%B

The number of gallic acid residues attached to each molecule was determined by 1) normal phase chromatography, 2) direct loop introduction of sample into mobile phase flowed into the electrospray ion source, and 3) negative chemical ionization with sample introduced on the DIP probe or by particle beam Similar results were obtained for electrospray and normal phase experiments while only fragment ions were seen in the chemical ionization experiments. Figures 2, 3 and 4 show the electrospray mass spectra obtained on each of the samples However, information on structural isomers were not obtained in these experiments. Some separation of isomers was observed when reverse phase HPLC and LC/MS was performed (Figure 5) Mass spectrometry made it easy to deduce the extent to which peaks with differing numbers of gallic acid residues overlap

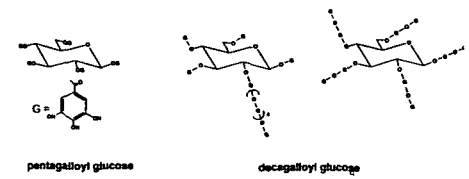

Fig 1 Structures of glucose galloyl tannins

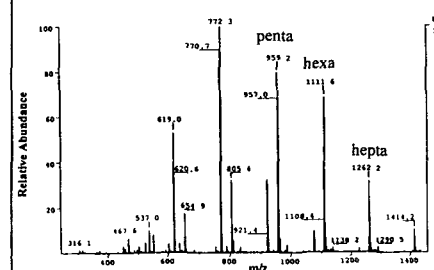

Fig 2 ESI-MS of Aleppo Gall

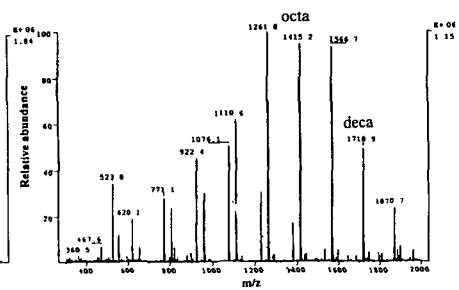

Fig 3 ESI-MS of Chinese Nut Gall

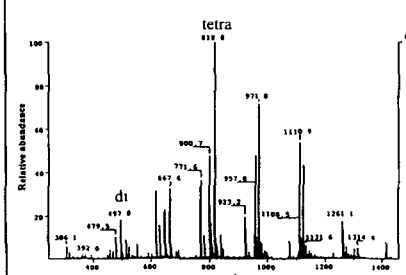

Fig 4 ESI-MS of Tara. note the presence of quinic acid as the central moiety

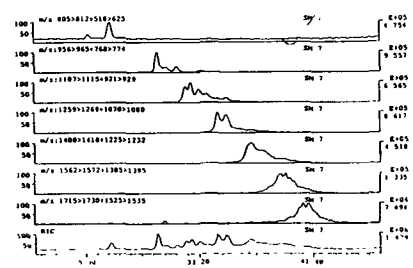

Fig 5 HPLC/MS of Chinese Nut Gall

References

1 E Haslam, Plant Polyphenols - Vegetable Tannins Revisted, Cambridge University Press (1989).
2 E C Bate-Smith, *Phytochemistry*, **25 (1973)** 903.

LOW-ENERGY COLLISION INDUCED DISSOCIATION OF PROTONATED GLYCOALKALOIDS AND RELATED AGLYCONES

M. Claeys[1*], H. Van den Heuvel[1], S. Chen[2], P. J. Derrick[2], F. A. Mellon[3] and K. R. Price[3]

[1]Department of Pharmaceutical Sciences, University of Antwerp (UIA), B-2610 Wilrijk, Belgium
[2]Warwick Institute of Mass Spectrometry, University of Warwick, Coventry, CV4 7AL, U.K.
[3]Institute of Food Research, Norwich Laboratory, Colney, Norwich NR4 7UA, U.K.

The glycoalkaloids are a group of nitrogenous, steroidal glycosides found in common food plants of the solanum species, including potatoes, tomatoes and aubergines, which are of biological interest and concern because of their toxicity. The high-energy collision-induced dissociation (CID) behaviour of protonated glycoalkaloids has recently been examined and has been shown to yield information on the linkages and the positions of the sugars in the carbohydrate part[1]. In a continuation of this study we have compared low- and high-energy CID of the $[M + H]^+$ ions of the nitrogenous steroids, tomatidine, solasidine, demissidine and solanidine, and of the glycoalkaloids, α-tomatine, α-chaconine and α-solanine, in order to determine to what extent these collisional activation methods can provide structural information on the aglycone and carbohydrate parts. The low-energy CID spectra were examined in an effort to define which particular fragmentations, among the many typically observed during high-energy CID, can also be induced by low-energy collisions. The low-energy CID spectra were recorded on a Fisons VG70SEQ mass spectrometer, equipped with a caesium ion source.

The mass spectral data obtained on the protonated aglycones show that low-energy CID gives rise to the formation of diagnostic product ions, which can be interpreted as the products of charge-driven reactions. In the case of demissidine and solanidine, abundant ions are present at m/z 150/151 and 204/205, which can be rationalised by rearrangement reactions and are most pronounced at very low collisional activation energies. Scheme 1 and Figure 1 give low-energy CID data obtained for the $(M + H)^+$ ions of α-tomatine and tomatidine respectively. A rationalisation for the formation of the ions at *m/z* 273 and 161 is given in Scheme 2. Low-energy CID of the protonated glycoalkaloids yields product ions which are characteristic both of the aglycone part and of the carbohydrate sequence. With respect to the carbohydrate sequence, Y_n^+ ions and low intensity Z_n^+ ions (ion nomenclature according to Domon and Costello[2]) are formed.

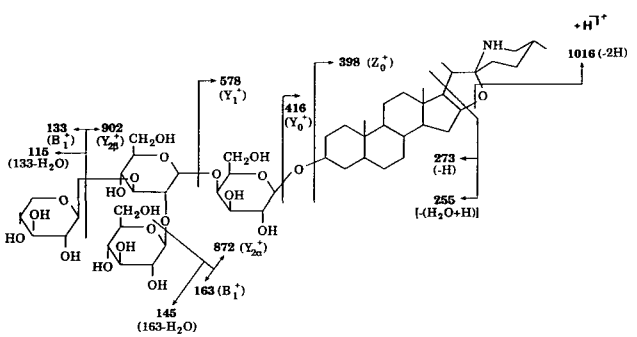

Scheme 1

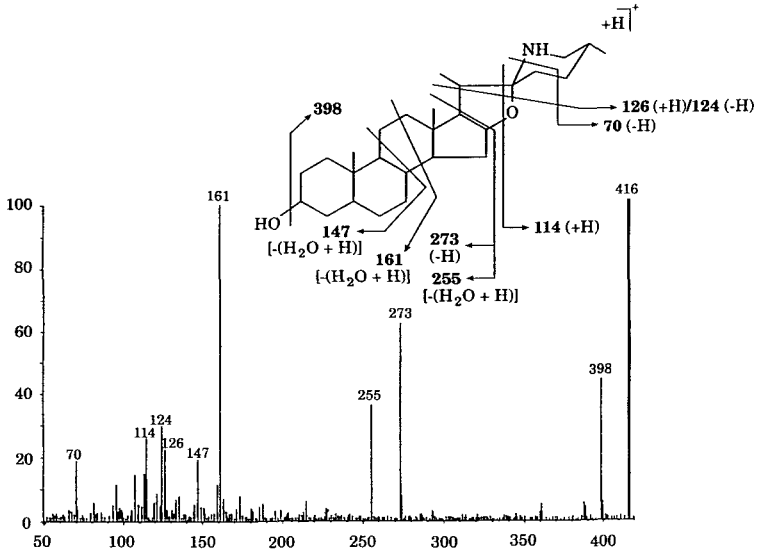

Fig. 1. Low-energy CID spectrum obtained for the $(M + H)^+$ ions of tomatidine.

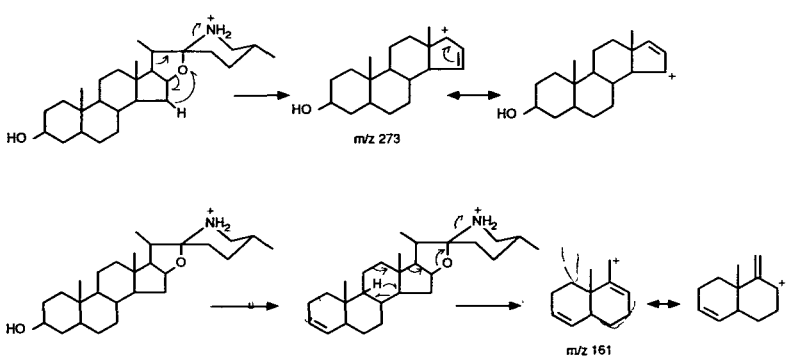

Scheme 2

[1]S. Chen, P. J. Derrick, F. A. Mellon and K. R. Price, *Anal. Biochem.* 218, 157-169 (1994).
[2]B. Domon and C. E. Costello, *Glycoconjugate J.* 5, 397-409 (1988).

MALDI-MS of Periplasmic Bacterial Glucans

Bernd Stahl[1]*, Philippe Talaga[2], Jianru Zeng[1], Michael Karas[1], Martin Steup[3], Franz Hillenkamp[1], and Jean-Pierre Bohin[2]

1 Inst. f. Med. Physics and Biophysics, Robert-Koch Str. 31, D-48149 Muenster, Germany
2 Lab. de Chimie Biol., Universite d. Sciences et Technol. de Lille, France
3 Inst. f. Biochem. and Molec. Physiol., University of Potsdam, Germany
* present address: MILUPA AG, Research Department, D-61381 Friedrichsdorf, Germany

Matrix-Assisted Laser Desorption/Ionization Mass Spectrometry (MALDI-MS) has been been established as a valuable tool in the analysis of glycans and glycoconjugates (1-3). Recently quantitative analysis of cyclic bacterial β1-2 glucans has been performed by MALDI-MS and HPLC (4). In this contribution a systematic analysis of periplasmic glucans is reported, including reference analysis using High Performance Anion Exchange Chromatography (HPAEC-PAD) and Fast atom Bombardement (FAB-MS). In *Escherichia coli* the synthesis of periplasmic glucans known as Membrane Derived Oligosaccharides (MDO) appears to be controlled by various enviromental factors (5). New analytical methods are needed for investigation of the products of this highly regulated process. UV-MALDI-MS was performed using 3-aminoquinoline and 2,5-dihydroxybenzoic acid as matrices MDO derivatives with acidic side groups were analyzed in both, positive and negative ion mode. The number and type of substituents of the oligosaccharides was determined by comparing the mass spectra before and after hydrogen fluoride / alkaline treatment. The pattern of neutral glucans of *Erwinia chrysanthemi* obtained by HPAE-chromatography was analyzed by MALDI-MS after fractionation of distinct peaks (Fig. 1). Each fraction was further analyzed by methylation analysis showing that differences in retention times are resulting from different numbers of β1-6 branches of the isomeric molecules (Tab. 1).

References:

1. Stahl, B., Steup, M., Karas, M., and Hillenkamp, F. (1991) *Anal Chem.* 63, 1463-1466.
2. Mock, K. K., Davey, M., and Cottrell, J.S. (1991) *Biochem. Biophys. Res. Commun.* 177,644-651.
3. Egge, E., Peter-Katalinic, J., Karas, M., and Stahl, B. (1991) *Pure Appl. Chem.* 63, 491-498.
4. Garozzo, D., Spina, E., Sturiale, L., Montaudo, G. and Rizzo, R (1994) *Rapid Commun. Mass Spectrom.* 8,358-360
5. Lacroix, J.M., Loubens, I., Tempête, M., Menichi, B., and Bohin, J.P. (1991) *Mol. Microbiol.* 5, 1745-1753

Figure 1: HPAEC-fractionation and subsequent analysis by MALDI-MS

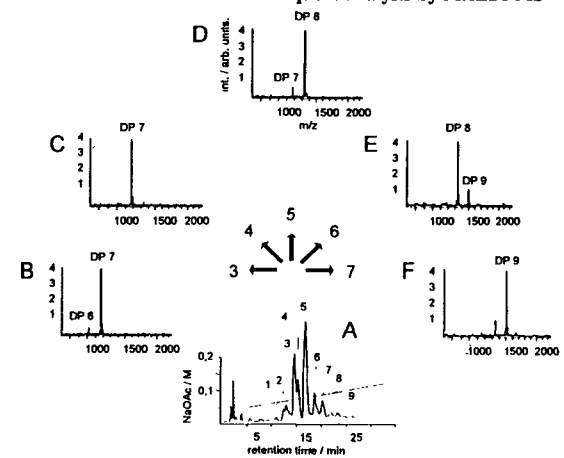

Fig. 1 HPAEC-Fractionation and MALDI-MS of neutral periplasmic glucans of *Erwinia chrysanthemi*.

A: HPAE chromatogram; Elution: 50 mM NaOAc in 150 mM NaOH for 5 min and a linear gradient of 50 mM to 200 mM NaOAc in 150 mM NaOH in 35 min

B-F: MALDI spectra of fractions 3 to 7, positive ion mode, VISION 2000, matrix: 2,5 dihydroxybenzoic acid. **B** and **C:** DP 7 (i.e. 7 glucose units). **D** and **E:** DP 8, **F:** DP 9, lower intensity oligomers with both lower and higher DP were observed

Table 1: Composition of several glucans of *E. chrysanthemi* as determined by HPAEC-, MALDI- and GC-MS analyses

Fraction no. (HPAEC).	DP (MALDI-MS)	No of β(1-6)-linkages (GC-MS)
1	5	nd
2	6	nd
3	7	2
4	7	1
5	8	3
6	8	2
7	9	2
8	nd	nd
9	10	nd

nd = not determined

EXAMINATION OF CHITIN-METAL INTERACTIONS BY ES AND MALD IONIZATION MASS SPECTROMETRY

Mona Shahgholi, Mark M. Ross and John H. Callahan, Code 6113, Chemistry Division
Naval Research Laboratory, Washington, DC 20375.

Marine algal exudates are rich in exopolysaccharides that can bind a variety of trace metal ions in their environment. The metal scavenging properties of these polysaccharides are important to study because they affect the bioavailability, toxicity, and biogeochemical fate of trace metal ions in the ecosystem (1). In this study, chitin is used as a model for the study of metal-organic interactions using electrospray (ES) and matrix-assisted laser desorption (MALD) ionization techniques. The objectives of this study were twofold. One is to develop proper sample preparation protocols for the analysis of this large heterogeneous biopolymer by ES and MALD. The second is to assess the utility of ES and MALD in addressing the metal binding processes.

Chitin is a (1-4)-2-acetamido-2-deoxy-beta-D-glucan commonly found in the exoskeletons and cuticles of many invertebrates and in the cell walls of most fungi and algae (2). Purified chitin must be first hydrolyzed into segments of reasonable mass range. Chitin oligosaccharides were prepared from chitin (Sigma) by hydrolysis in 11M HCl at 10 C for eight hours, conditions under which the chitin oligosaccharides remain N-acetylated (3). After the acid was neutralized by NaOH, the oligomers were purified on Bio-Gel P-2 (Bio-Rad). Under these conditions oligomers containing up to 8 N-acetyl glucosamine residues could be isolated. These hydrolysate mixtures were characterized directly by both MALDI and ESI. The hydrolysate thus prepared was mixed with dihydroxybenzoic acid (10 mg/mL in 90:10 v/v ethanol:water) for the MALDI experiments. For the ES experiments, the hydrolysate was diluted with methanol. After confirmation of the presence of chitin oligomers, the hydrolysate was subjected to on-line, microbore LC/ESIMS (4) using a capillary packed with 7 micron porous graphitic carbon. A variation of the on-line technique was used in off-line LC (with a graphitic carbon column from Shandon Scientific) to generate fractions containing each oligomer, which were then used for further study. These studies also focussed on the behavior of chitosan, which is the deacetylated form of chitin. Chitosan should bind metals with greater affinity than chitin.

Both oligosaccharides were evaluated by ES and MALD before and after addition of metal ions. Several metals from the transition group, alkali, and alkali earths were selected for these studies. Both doubly-charged and singly charged metal bound oligosaccharides are apparent in the ES spectra; however, the MALD spectra only show singly charged adducts. For example, ESI spectra showed the presence of both $[M+Cu]^{2+}$ and $[M-H+Cu]^{+}$ ions, but MALDI spectra only gave $[M+Cu]^{+}$ species (although it was not clear from the low resolution spectra obtained that proton loss had not occurred). CAD experiments were performed on various chitin adducts (H^+, Na^+, Mg^{2+}, Cu^{2+}, and Ni^{2+} were studied) using a triple quadrupole instrument, and the fragments generated were compared for the various metals. In general, collisional activation of the singly-charged species resulted in glycosidic bond cleavages. Fragments from protonated ions suggested that protonation occurred on the glycosidic oxygen. Sodium and magnesium adducts also gave primarily glycosidic bond cleavages, although the role of the ion is unclear. However, with the addition of Cu and Ni (to form $[M-H+Me]^{+}$ ions), the most abundant fragment ions observed involved cross ring cleavages. Moreover, a different cross ring cleavage was observed with each ion. The results suggest that specific chelation of each ion by the chitin may induce the cross ring cleavage. Fragmentation of doubly charged ions was also studied. Many of the same pathways were observed in the fragmentation of doubly charged ions as with singly charged species. However, doubly charged species also underwent charge separation upon activation. Future studies will focus on determining

whether specific chitin-metal interactions induce the observed cross ring cleavages and whether multiple metal addition can be observed by ESIMS. CAD studies of chitosan may help elucidate the role of metal interactions in fragmentation, as chitosan binds metals much more strongly than chitin.

1. Midorikawa, T.; Tanoue, E.; Sugimura, Y. (1990) *Anal. Chem.*, **62**, 1737.
2. Kafetzopoulos, D.; Martinou, A.; Bouriotis, V. (1993) *Proc. Natl. Acad. Sci. USA*, **90**, 2564.
3. Rupley, J.A. (1964) *Biochem. Biophys. Acta*, **83**, 245.
4 Hunt, D.F., et al. *Techniques in Protein Chemistry II*, Villafranc, J.J., ed. Academic Press: N.Y., 1991, pp 441-454.

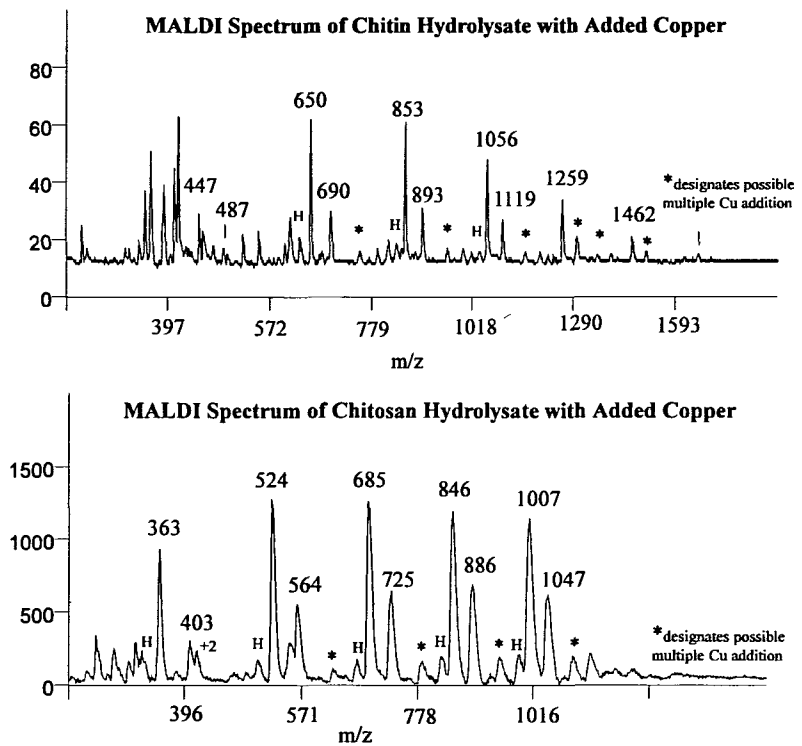

Figure 1. MALDI spectra of chitin and chitosan hydrolysates with added Cu. Major series in each spectrum is $[M+Na]^{+}$ and the next most abundant series is $[M+Cu]^{+}$. Asterisk denotes possible multiple Cu attachment.

FAB-MS/MS of Immunoreactive Tetrasaccharides from Chondroitin Sulfate

Mamoru Ohashi[a], Tadashi Ii[a], Masayuki Kubota[a], Takashi Hirano[a], Keiichi Yoshida[b] and Sakaru Suzuki[c]
[a] Department of Applied Physics and Chemistry, The University of Electro-Communications, Chofu, Tokyo 182, Japan
[b] Tokyo Research Institute, Seikagaku Corporation, Higashiyamato-shi, Tokyo 189, Japan
[c] Institute for Molecular Science of Medicine, Aichi Medical University, Nagakute, Aichi 480-11, Japan

In 1987 Yamagata et al. demonstrated that tetrasaccharide trisulfate and tetrasaccharide tetrasulfate fragments isolated from shark fin by chondroitinase AC digestion are the smallest chondroitin sulfate fragments that can inhibit the binding of the anti-chondroitin sulfate monochronal antibody MO-225 to various types of chondroitin sulfate proteoglycan derived from avian and mammalian tissues[1]. The structures of these compounds were deduced on the basis of the unsaturated disaccharide structures obtained by condroitinase ABC digestion. However, direct evidence to support the tetrasaccharide structures is still required Herein, we report that FAB CID-MS/MS of the molecule related ions and fragment ions has been successful in the confirmation of the proposed structures.

Materials and methods: Tetrasaccharide trisulfate(**1**) and tetrasulfate(**2**) were prepared according to the literature[1]. The mass spectra were measured with a Finnigan MAT TSQ 700 triple stage quadrupole mass spectrometer equipped with an Ion Tech FAB gun. A Xe beam with an energy of 8 keV was used. Thioglycerol and triethanolamine were used as the matrices in the positive- and negative-ion modes, respectively. The CID-MS/MS were recorded using argon as the collision gas typically at 1.0 mTorr to reduce the parent ion beam by approximately 30%. The collision energy was 5 eV or 30 eV.

Results and discussion:
Tetrasaccharide trisulfate(**1**): The structure of (**1**) and the fragmentation of the negative ion CID-MS/MS of (**1**) are shown in Scheme 1; (a) the $[M + 4K - 5H]^-$ ion (m/z 1149) as the parent ion; (b) the fragment ion that corresponds to $[Y_3 + 3K - 3H]^-$ (m/z 953) as the parent ion, (c) the fragment ion that corresponds to $[C_3 + 3K - 3H]^-$ (m/z 828) as the parent ion. These CID-MS/MS clearly indicate that a sulfate group is present at the C-2 position of the glucuronic acid moiety on the reducing end site of (**1**). The CID-MS/MS of the disaccharide ion at m/z 496 which corresponds to $[C_2 + K - H]^-$ is almost superimposable on the FAB CID-MS/MS of the molecular related ion $[M + K - 2H]^-$ of the potassium salt of 2-acetamido-2-deoxy-3-0-(β-D-gluco-4-enepyranosyluronic acid)-4-O-sulfo-D-galactose(ΔUA-GalNAc4S)[2]. This confirms the location of the sulfate group at C-4 in the galactosamine moiety on the non-reducing end site of (**1**). On the basis of these results the complete structure of the tetrasaccharide trisulfate(**1**) is now confirmed.

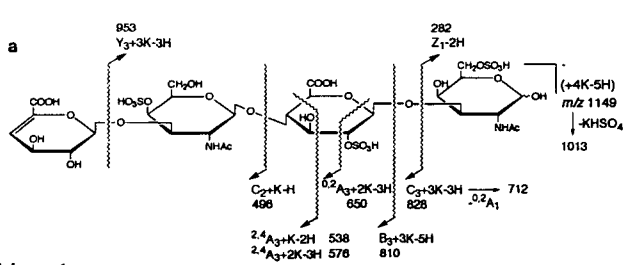

Scheme 1

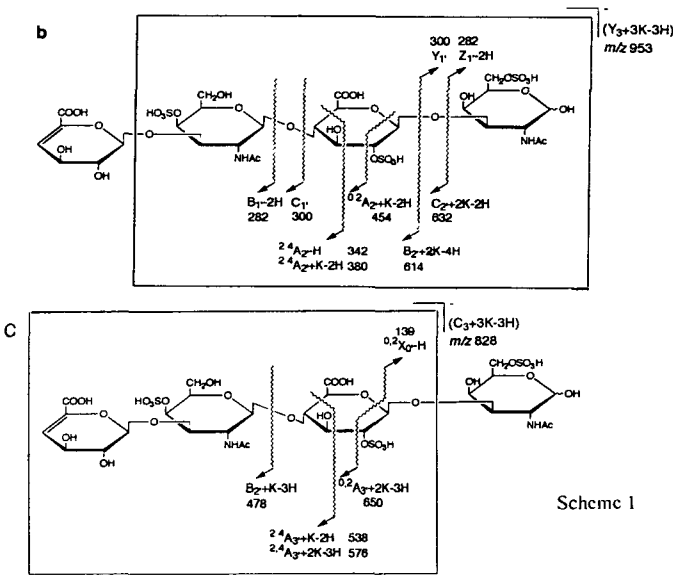

Scheme 1

Tetrasaccharide tetrasulfate(**2**), the fragmentation of the negative ion CID-MS/MS of the molecule related ion$[M + 5K - 6H]^-$ (m/z 1187) as the parent ion clearly confirms the structure of (**2**) as shown in Scheme 2. The CID-MS/MS investigation of the FAB fragment ions of (**2**) in a way similar to that of (**1**) also confirmed the location of the sulfate groups. These results confirm the structures of tetrasaccharide trisulfate and tetrasulfate as previously reported by Yamagata et al.

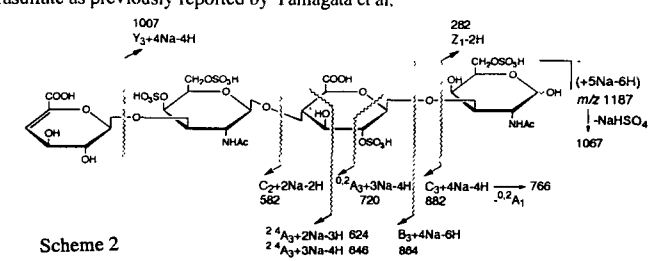

Scheme 2

This work was partially supported by a Grant-in-Aid for Scientific Research on Priority Area No. 04250106 from the Ministry of Education, Science and Culture of Japan.

References

1. Yamagata M, Kimata K, Oike Y, Tani K, Yoshida K, Shimomura Y, Yoneda M, Suzuki S (1987) *J. Biol. Chem.*, **262**; 4146-52.
2. Ii T, Okuda S, Hirano T, Ohashi M (1994) *Glycoconjugate J*, **11**; 123-32.

Mass Spectrometric Determination of an Octasulfated Disaccharide.

E. Watson, A. Termin, B. Shah., A. Bhide, T. Zamborelli and A.Venot.

Amgen Inc., Amgen Center, Thousand Oaks, CA 91320

Highly acidic compounds are difficult to analyse by matrix-assisted laser desorption ionization mass spectrometry. Very recently Juhasz and Biemann reported the use of arginine containing peptides to produce non-covalent complexes that survived as intact species when subjected to MALDI-MS (1). In this report we have used fully sulfated trehalose, (8 sulfate residues), as a model compound to evaluate the use of these arginine/lysine containing peptides as a means of forming stable noncovalent complexes for the characterization of these highly charged species by MALDI-MS. The extent and stability of complex formation is shown to correlate with the number of arginine groups present. No stable complexes were detected when lysine was substituted for arginine.
ESI mass spectrum of trehalose sulfate in 1% formic acid is shown in Figure 1. The mass spectrum was dominated by multiple sodium adduct containing species. The molecular weights of these various species were determined and are listed in Table 1. The relative intensity of these ions suggested that 3 species, containing 6, 7 and 8 sulfates were present in essentially equal amounts. From these results it was not possible to determine whether this represented the species distribution in solution or whether sulfite was being eliminated during ESI mass spectrometry.
The structures of the synthesized peptides used in this study are:

IRRERNKMAAAKSANAAAELTDTL	3 Arg
IRRERNKMAAAKSANARRELTDTL	5 Arg
IRRERNKMAAAKSRNRRRELTDTL	7 Arg
IRRERNKRRARKSRNRRRELTDTL	10 Arg
IRRERNRRRARRSRNRRRELTDTL	12 Arg
RIRRERNRRRARRSRNRRRELTRTLR	15 Arg

The mass spectra were all obtained using 2,5-DHB as the matrix. When the number of arginines was 10-15, the most abundant complex ion arose from a 1:1 complex with little or no elimination of sulfite, Figure 2.
There were no additional peaks due to sodium cationization. Ionic complexes were apparent using all of the peptides, with the exception of those containing only lysine, indicating the importance of arginines in forming these noncovalent complexes. These results demonstrate that the fragmentation decreases with increase in the number of arginines present.

References
(1) P. Juhasz and K. Biemann. Proc Natl Acad Sci, USA 1994, 91, 4333-4337.

43rd ASMS Conference on Mass Spectrometry and Allied Topics

Figure 1
Negative-ion Electrospray Mass Spectrum of Trehalose Octasulphate

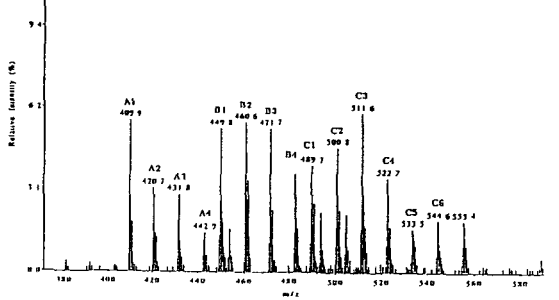

Table 1 Molecular Weights of Trehalose Sulphate Species

	Trehalose 8SO4	Trehalose 7SO4	Trehalose .6SO4
(M-H)	n d	901.6(B1)	821.8(A1)
(M-2H+Na)⁻	1003 1(C1)	923 2(B2)	843 4(A2)
(M-3H+2Na)⁻	1025 2(C2)	945 4(B3)	865 6(A3)
(M-4H+3Na)⁻	1047 2(C3)	967 4(B4)	887 8(A4)
(M 5H+4Na)⁻	1069 2(C4)	989 2(B5)	909 8(A5)
(M-6H+5Na)⁻	1091.2(C5)		
(M-7H+6Na)⁻	1112 8(C6)		

Figure 2
MALDI-MS

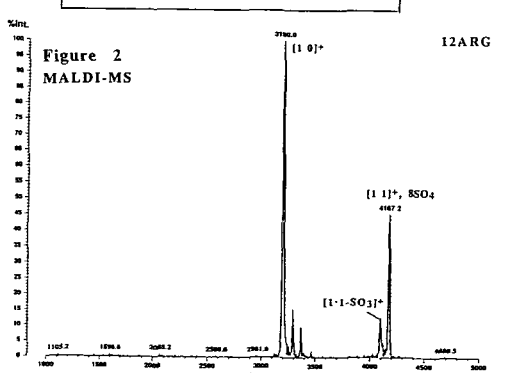

Electrospray Mass Spectrometry of Heparin-Derived Glycosaminoglycan Disaccharides

Eric Watson and Flora Yao

Amgen Inc., Amgen Center, Thousand Oaks, CA 91320

Heparin is a glycosaminoglycan that inhibits blood coagulation through the activation of antithrombin III (ATIII). It consists of sequences of uronic acid and glucosamine disaccharides in which the uronic acids could be O-sulfated at C2 and the glucosamines O-sulfated at C6 and/or C3. In addition glucosamine residues could also be N-acetylated or N-sulfated. As a result there are at least eight different dissacharide units, each characterized by a unique uronic acid and glucosamine residues.
We have evaluated the use of negative ion ESI mass spectrometry with CID in the free-jet-expansion region of the API interface as an alternate fragmentation technique to collision- induced ESI-MS/MS for obtaining structural information on heparin-derived GAGS.
The effect of orifice potential on the mass spectra was evaluated by increasing orifice potentials in steps of 20V from -50V to -220V. From -50V to -120V, a significant increase in the extent of fragmentation was observed. At orifice potentials from -120V to -250V, there was no further changes in the fragmentation pattern but there was a gradual decrease in sensitivity at the higher orifice potentials. Common fragmentations are seen to arise by simple cleavage on either side of the glycosidic oxygen accompanied by hydrogen attachment to the fragment bearing the charge. Other structurally significant ions arise from cross ring cleavages. The mass spectra of all of these species are sufficiently different such that they can be readily distinguished from one another. Figure 1 shows the negative-ion ESI spectrum of the disaccharide 11A at (A) -50V, (B) -120V and (C) CID-MS/MS.

The utility of the method has been evaluated using a series of authentic GAGS derived from heparin that differ solely in their degree of sulfation. All of the fragmentation patterns were sufficiently different such that they could be used for the identification of these disaccharides. These results show that positional isomers for the series 1A-1VA and 1S-1VS can be readily distinguished using the technique described here. The advantage of the described method is that a single set of instrumental conditions are used to fragment all of these species. Furthermore, the simplicity of this approach has the potential in characterizing GAGS introduced from an on-line separation technique such as capillary electrophoresis.

43rd ASMS Conference on Mass Spectrometry and Allied Topics

Figure 1 Negative-ion mass ESI spectra of 11A at (A) -50V, (B) -120V and (C) CID-MS/MS.

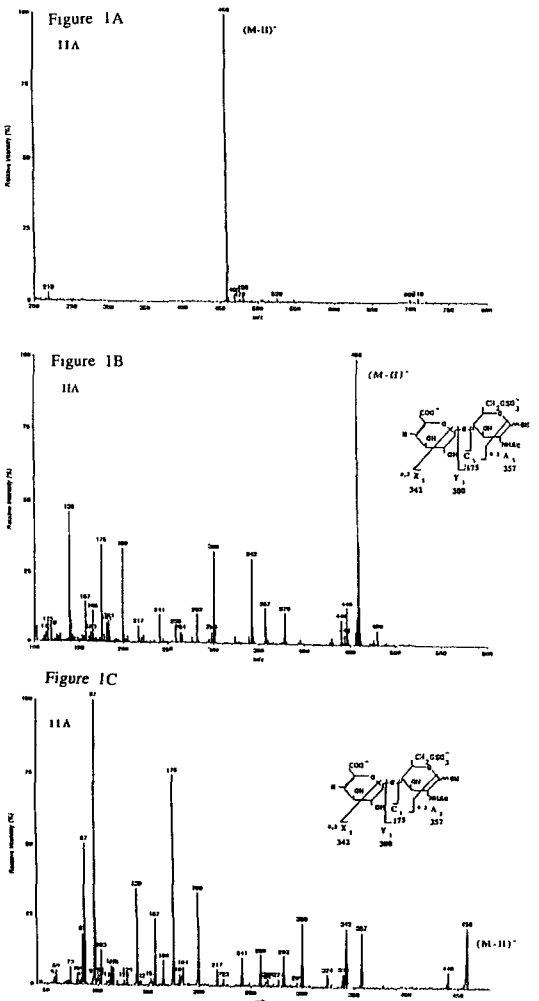

CE/MALDI - MS of Mixtures of Heparin Derived Oligosaccharides

A.Rhomberg, P.Juhasz[1)] and K.Biemann
Department of Chemistry, MIT, Cambridge 02139

Heparin and the closely related heparan sulfate are linear and highly acidic polysaccharides that are involved in a wide variety of biological phenomena. They interact with the components of the blood coagulation cascade, induce the formation of new blood vessels in wound healing and tumor metastasis, control the bioavailibility of many proteins and, as membrane bound coreceptors, control the specificity and binding of growth factors and other molecules involved in cell signalling [1]. Our interest focuses on biologically active oligosaccharides, 5-20 saccharide units in length. Heparin/heparan sulfate has a characteristic disaccharide repeat unit consisting of an uronic acid (iduronic or glucuronic acid) and glucosamine. Both can have different degrees of sulfation/acetylation. Sulfation and acetylation are carried out by a number of different enzymes This process leads to a high variability in sequence and complex mixtures of oligomers if the chain is degraded. We therefore employ capillary electrophoresis as a final purification step before performing enzymatic digestion and mass spectrometry. Capillary electrophoresis was carried out using a Beckman PAC/E 2050 and a Hewlett Packard ^{3D}CE. Fused silica (Polymicro) and LPA capillaries (Bio-Rad) of I.D /O.D.: 75/363 µm were used. The lengths were l/L 50.3/57.0 and 70/78.5 respectevly. Analytes were detected @200 nm (indirect detection), or @ 230/214 nm (direct detection). A voltage of 30 kV (reversed polarity) was employed. For fraction collection migration times (t_{det})were predetermined and elution times (t_{el})calculated based on the relationship $t_{el}=t_{det}*L/l$ Prior to the elution of an analyte the voltage was interrupted and each compound eluted at 30 kV into a modified microcentrifuge vial containing 5 µL of phosphate buffer (5 mM, pH=7,0). All steps were carried out fully automatic using the autosampler features of the CE instrumentation. For enzymatic digestions 1 µL of native heparinase I (Sigma) containing 1 unit activity was added to 3-5 µL CE-fraction and digested @30°C for 10 min-24 h. Mass spectrometry was performed on a Vestec VT2000, linear Time-of-Flight instrument. Samples were prepared by mixing 9 µL matrix solution (15 mg/mL caffeic acid or 25 mg/ml 3-hydroxypicolinic acid/D-fucose 90:10) with 1 µL of 0,1 mg/ml $(RG)_{15}$ solution (RG = arginylglycyl). 1 µL of CE-fraction or enzyme digest were added. 1 µL of the resulting mixture was deposited on the target.

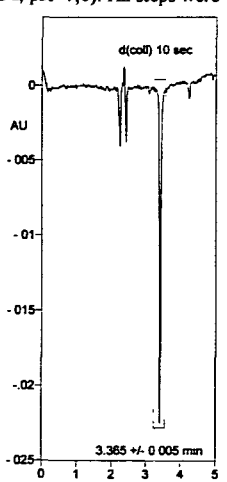

Figure 1

Results: Heparin/heparan sulfate oligosaccharides obtained by different procedures were purified by CE and collected fractions analyzed by MS. Oligosaccharides generated by enzymatic digestion contain α,β unsaturated acids (UV maximum: 232 nm). For a mixture of unsaturated hexasaccharides up to 20 components were resolved. Heparin oligosaccharides, prepared by nitrous acid degradation followed by borohydride reduction, have an anhydromannitol at the reducing end and do not adsorb in the UV. It is nevertheless possible to analyze such compounds by CE trough the use of indirect detection, for example with 1,5 naphtalenedisulfonic acid as background adsorber. A negative peak, generated by ionic displacement, results from the analyte ion. Figure 1 shows this for oligosaccharides prepared by nitrous acid treatment, and prepurified by ion exchange chromatography. The compound migrating at 3.37 min was isolated by pooling fractions from 10 runs into 5 µL of buffer. A 1 µL aliquot complexed with the sythetic peptide $(RG)_{15}$ was used to obtain the spectrum shown in Figure 2. From the molecular weight we calculated the molecule to contain 8 sulfate and no acetyl groups. Information on the stereochemistry of the uronic acids was obtained by digesting the remaining 3 µL of the CE-fraction with heparinase I After 10 min the hexasaccharide had been completely converted to a tetra- and a disaccharide [Figure 3] After prolonged digestion the tetrasaccharide was further cleaved into two disaccharides. Due to the specificity of the enzyme for iduronic acid, it can be deduced that no glucuronic acids were present in the molecule, because the hexasaccharide had been completely digested. Furthermore it was possible to assign the location of most sulfate groups.

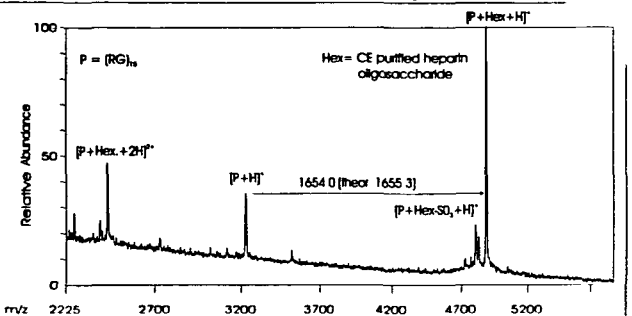

▲ Figure 2

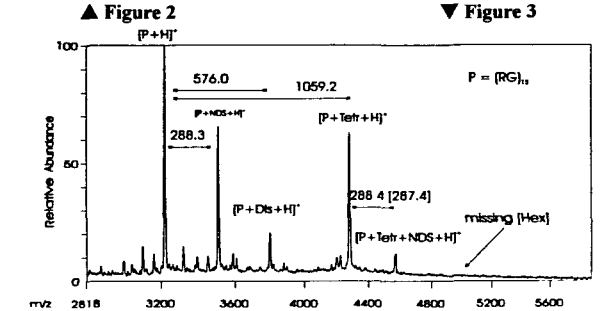

▼ Figure 3

Conclusions: The examples demonstrate that though CE is a microanalytical technique, it is possible to purify heparin oligosaccharides in quantities of 100 fmol -10 pmol and obtain mass spectra on the purified compounds and their enzymatic digestion products. Off-line coupling of CE and MS in this case is essential for obtaining both molecular weights for intact oligosaccharide and its enzymatic fragments Independent optimization of CE and MS conditions allows simultaneous achievement of optimum separational and spectral quality. The methodology should ultimately lead to the sequencing of defined heparin molecules to aid understanding of the biological action of this molecule.

References: [1]*Heparin.* Lane,D.A.; Lindahl,U.; Eds.; CRC Press, Boca Raton, Fl.; 1989
[2] Juhasz, P.; Biemann,K.; *Proc. Natl. Acad. Sci. U.S.A.* 1994, 91, 4333-37

Acknowledgments: This work has been supported by NIH grants RR00317 and GM05472. A. R. acknowledges financial support of Austrian government institutions and the Austrian-American Fulbright Commission. The gifts of ISMS-3 from D.J Tyrell (Glycomed), a mixture of unsaturated hexasaccharides from W.Herlihy (Glycan Pharm.) and LPA capillaries from Bio-Rad Laboratories are greatly appreciated.

[1)] present address: PerSeptive Biosystems, 500 Old Connecticut Path, Framingham, MA 01701

Ionspray (lc-)ms of synthetic sulphated oligosaccharides

* Peter L. Jacobs[1], Pieter Westerduin[1], Simona Marilena Rizea Savu[2] and Luigi Silvestro[2]

1. AKZO NOBEL, N.V. Organon, P.O. Box 20, 5340 BH Oss, The Netherlands,
2. IBMP - Inst. f. Biomed. and Pharmaceut. Res., Nürnberg-Heroldsberg, Germany.

INTRODUCTION

In a previous comparison of FAB, ^{252}Cf-PDMS and Ionspray ms for the direct analyses of synthetic sulphated pentasaccharides, FAB was favoured for the unambiguous assignment of molecular masses of unknowns although FAB was also the least sensitive of these techniques [1]. At that time the direct analyses of these pentasaccharides, all variants of the minimal pentasaccharide sequence exerting AT-III mediated anti-Xa activity, with Ionspray ms was complicated both by strong cationisation caused by the presence of up to 11 sodium counter-ions and the large influence on these spectra caused by small changes in instrumental parameters. In a novel Ionspray approach, a variety of oligosaccharides from an enzymatic digestion of glycosaminoglycans was analysed as ion-pairs with both TetraPropyAmmonium (TPA) and d_{28}-labelled TPA [2]. We now report an extension of the latter method applied for Ionspray ms analyses of various sulphated oligosaccharides obtained from a research program for the preparation of synthetic antithrombotics [3].

RESULTS AND DISCUSSIONS

The octa-sulphated pentasaccharide Org 31540 was desalted with Dowex.H$^+$ and flow injection Ionspray spectra were obtained both with d_{28}-labelled TPA and non-labelled TPA (Fig. 1). The ions shown are doubly charged (ΔM=93; TPA=186) and e.g. m/z 1031 contains 3 TPA groups as it shifts towards m/z 1073 with d_{28}TPA (((1073-1031)*2)/28). From these ions the molecular mass can be calculated and averaged (1507 Da). Similar Ionspray spectra were obtained by desalting during on-line reversed phase lc-ms using both TPA and d_{28}TPA as ion-pairs and an acetonitrile gradient on a 300Å C_4-column (not shown). On-line lc-ms desalting was not always effective for higher sulphated oligosaccharides with e.g. molecular masses > 2500 Da; the resulting Ionspray spectra could therefore not be used anymore to assign molecular masses unambiguously.

This problem was solved by post-column membrane ion suppression. With this method cations present (TPA$^+$ and Na$^+$) are replaced for H$^+$ from the regenerant and subsequently the (TPA) pairing reagent is added again. As an example of this technique the lc-ms spectra of an octadeca-sulphated decasaccharide are shown (fig. 2). With this approach TBA could be used instead of d_{28}-labelled TPA (fig. 2 top) as post-suppressor addition of TBA does not affect chromatography. With the combined spectra both the charge-state of the ions (-6), the number of counterions and, as a result, the molecular mass (4143 Da) could be calculated unambiguously. This example illustrates the successful application of this extended Ionspray approach for synthetic oligosaccharides with a larger molecular mass and sulphated at a higher degree than compounds obtained from digests of glycosaminoglycans before [2].

STRUCTURE OF ORG 31540

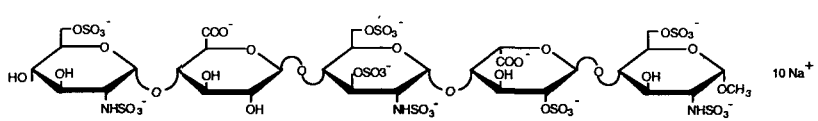

FIGURES

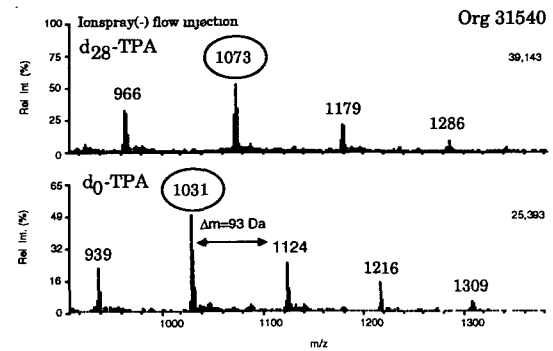

Fig. 1: Flow injection Ionspray(-) mass spectra of the pentasaccharide Org 31540 after Dowex desalting using both d_{28}-TPA (upper) and non-labelled TPA as ion-pairs.

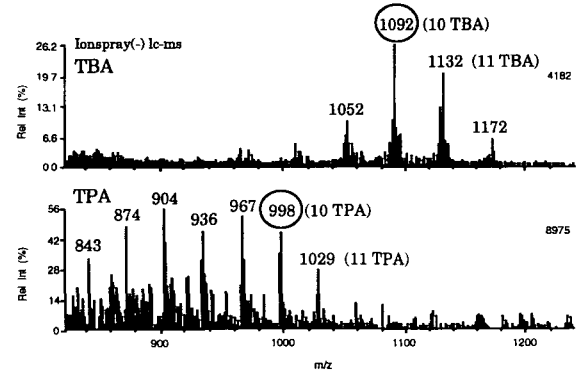

Fig. 2: Lc-ms Ionspray(-) spectra of an octadeca-sulphated decasaccharide using TPA (pH=4 formic acid) and an acetonitrile gradient with post-column membrane ion suppression and subsequent addition of TBA (upper) or TPA (lower).

REFERENCES

1. Jacobs P.L. et al., Ext. Abstr. of 12th Int. Mass Spectrom. Conf., Amsterdam (1991) 246.
2. Silvestro L. et al., J. of Chromatogr. 647 (1993) 289.
3. C.A.A. van Boeckel and M. Petitou, Angew. Chem. Int. Ed. Engl. 32 (1993) 1671.

MASSIVE CLUSTER IMPACT IONIZATION OF SACCHARIDES

Nyla N. Dookeran and Peter J. Todd
Chemical & Analytical Sciences Division
Oak Ridge National Laboratory
PO Box 2008, Bldg. 5510A
Oak Ridge, Tennessee 37831-6365

We studied the utility of ionizing saccharides by massive cluster impact (MCI), a form of secondary ionization wherein the primary ions are high molecular weight clusters. For a number of compounds and classes, MCI yields copious secondary ions without prior derivitization or the need to find a suitable matrix. In fact, MCI can be used for *in situ* ionization of some analytes directly from biologic tissue. For the simple sugars and disaccharides we studied, we found that *persistent* (e.g. > 2 h) positive and negative secondary ion emission could almost always be detected from pure samples. We characterized the secondary anions from a variety of saccharides by tandem mass spectrometry (MS/MS), and found the behavior of the MS/MS spectra to be consistent, sensible, diagnostic and invariant with the dose suffered by the sample.

The MCI gun is a direct replacement for the JEOL Xe FAB gun. Its operation is based on electrohydrodynamic ionization of glycerol, which is supplied from an integral reservoir via a stainless steel capillary. Glycerol cluster ions with a mass distribution extending to 10^7 u, charge distribution in the range of 10^2 and current of about 10-30 μA, are emitted from the gun when a potential of 15-20 keV are applied to the EHD emitter.[1] The beam of clusters is focussed and deflected onto the target by a series of lens elements/deflectors. The negative mass spectra produced by using the MCI gun show the anion series 151, 243, 335, ... etc, characteristic of glycerol clusters plus acetate.

Sample preparation for ionization of saccharides was minimal. Samples were mixed with conc. NH_4OH, and allowed to rest for about 0.5h. Generally secondary emission of anions characteristic of various saccharides was less intense than those of the cluster series. However, such emission typically persists for hours after continuous impact by massive clusters. The advantage of this persistence is that it permits MS/MS spectra to be obtained continuously and summed. For example, Figure 1 shows the MS/MS spectrum of sucrose m/z 341, $[M-H]^-$. Cleavage of glucose from fructose is clearly evident by the predominant peak at m/z 179. The MS/MS capability is essential for analysis of saccharides directly from plant tissue. Figure 2 shows the MS/MS spectrum of the m/z 341 obtained directly from a piece of banana placed on the probe tip and subjected to MCI.

1. Mahoney, J. F.; Perel, J.; Ruatta, S. A.; Martino, P. A.; Husain, S.; Lee, T. D.; *Rapid Commun. Mass Spectrom.* **1991**, *5*, 441.

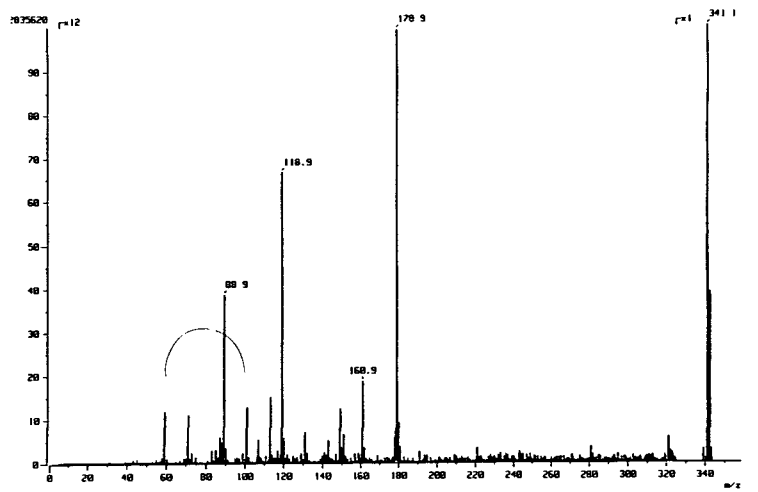

Figure 1. MS/MS spectrum of m/z 341 from sucrose mixed with NH_4OH.

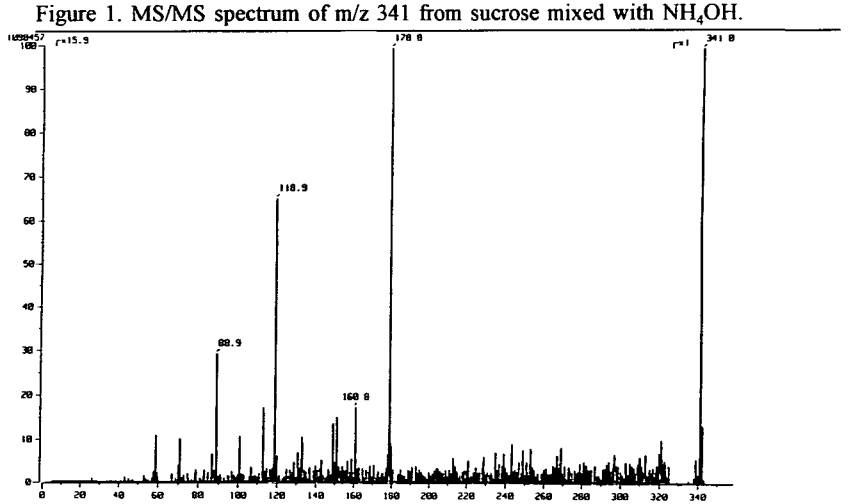

Figure 2. MS/MS spectrum of m/z 341 emitted from banana when subjected to MCI.

LC-ESIMS and In-source CID of Derivatized Oligosaccharides

Subhodaya Aduru and Kym F. Faull
Dept of Chemistry & Biochemistry and Psychiatry & Behavioral Sciences.
University of California Los Angeles, Los Angeles, CA 90024

Separation of oligosaccharides by conventional HPLC methods is complicated because of their high polarities and their detection is difficult because of the lack of UV absorbing groups To provide an easy and simple way to perform on-line LC-ESIMS of oligosaccharides trimethylaminophenyl ammonium (TMAPA) labeling (1) is used to enable the separation on a polyhydroxyethyl aspartamide column under hydrophilic interaction (HILIC) conditions and their detection by electrospray ionization mass spectrometry (ESIMS). TMAPA treatment provides a stable cation in ESI-MS even at high orifice potentials because of the permanent positive charge on them This in turn leads to good sensitivities during on-line LC-ESIMS.

Trimethylaminophenylammonium chloride (0.5 mg) and sodium cyanoborohydride (1.25 mg) were dissolved in 354 ul of water containing 41 ul of glacial acetic acid. 40 ul of this reductive aminating solution was added to the dry oligosaccharide (0.1-10 ug) and heated at 363 K for one hour and then dried in vacuum centrifuge. The dried residue was redissolved in 0.1% TFA /90% Acetonitrile, pH adjusted to 3 0 by ammonia (solvent A) and analyzed by mass spectrometry or injected onto polyhydroxyethyl aspartamide column (2.00 mm i.d , 25 cm length) equilibrated in solvent A The column was eluted with an increasing gradient of water (1%/min). The effluent from the column was connected directly to the electrospray ionization source of a Sciex API III mass spectrometer.

Figure 1 shows the total ion chromatogram for the resulting separation of a mixture of TMAPA tagged malto-oligosaccharides. The peaks A, B, C and D correspond to glucose, maltotriose, maltopentaose and maltoheptaose, respectively The corresponding ESI mass spectra for maltopentaose and heptaose show the singly charged TMAPA cations at m/z 963 and 1288 respectively. The intensity of the signals for the oligosaccharide TMAPA cations was found to be uninfluenced by orifice voltage above 35V indicating their high stabilities.

The TMAPA tagged oligosaccharides did not fragment under in-source CID conditions to give any structurally significant fragment ions. Therefore, peracetylation of the malto oligosaccharide TMAPA was carried out in an attempt to produce a derivative which might yield structurally significant fragment ions. Peracetylation of TMAPA labeled oligosaccharides was carried out by adding 50 ul of a 2:1 mixture of trifluoroacetic anhydride and glacial acetic acid. After sonicating for 10-15 minutes the reaction mixture was dried in a vacuum centrifuge, redissolved in 0.1% TFA/ 90% acetonitrile and analyzed on the Sciex instrument. ESI mass spectra of peracetylated oligosaccharide TMAPA at low orifice potentials show doubly charged, protonated molecular cations and no significant fragment ions. At high orifice potentials only doubly charged, sodiated molecular cations and sequence specific fragment ions are observed. Figure 2 shows the fragmentation of peracetylated maltoheptaose TMAPA at the glycosidic linkages at an orifice potential of 120V. The fragment ions observed are from the reducing end containing the glycosidic oxygen and one positive charge. Hence a mixture of oligosaccharides is tagged with TMAPA which facilitates their separation and detection and subsequently peracetylated to obtain structurally meaningful fragment ions.

References

1) A. Dell, N H.Carman, P.R.Tiller and J.E. Thomas-Oates; J. Biomed. Environ. Mass Spectrom, 16,19-24,1988

43rd ASMS Conference on Mass Spectrometry and Allied Topics

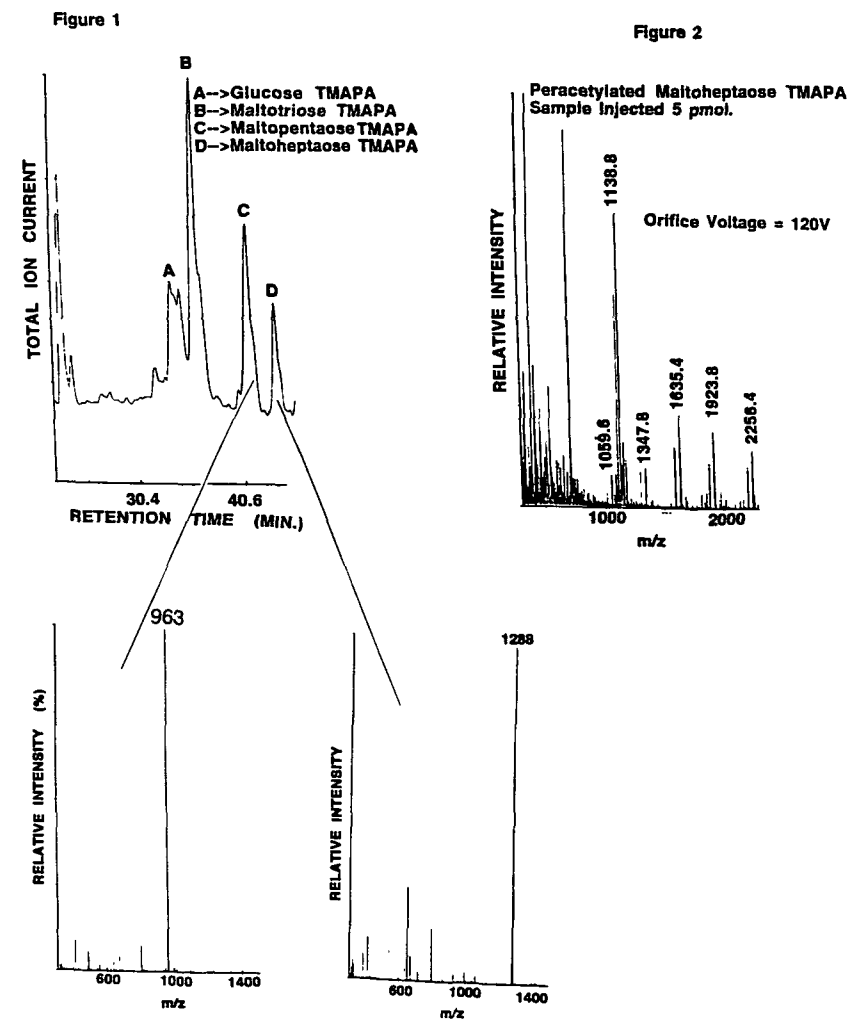

Improved MS Analysis of Oligosaccharides Derivatized as Fluorinated Glycosylamines

Huang, Z.H., Xu, Naxing, and Gage, D.A.

MSU-NIH Mass Spectrometry Facility, Department of Biochemistry, Michigan State University, East Lansing, MI 48824

Major methods currently used for the direct sequence determination of oligosaccharides involves the introduction of a chromophoric, lipophilic, or charged tag to the molecule prior to analysis by mass spectrometry. The derivatizing function is chemically bonded to the analyte at the reducing end either by direct condensation with an amine, e.g., 2-aminopyridine (glycosylamine-type) or by reductive amination using an amine, e.g., p-aminobenzoic ester and borohydride (amino-deoxyalditol)

Though successful in analytical practice, these methods are tedious and time-consuming, requiring subsequent purification and desalting by HPLC or other means. Sequence data can usually be provided by using PI-(glycosylamine) or NI-mode (amino-deoxyalditol) of ionization, however, only limited information was available regarding the connection pattern of parent sugars.

To overcome these difficulties, we describe here a simple protocol for oligosaccharide analysis based on the used of glycosylamines containing a fluorinated aniline residue.

Methods

Derivatization: The oligosaccharide, 10 µg was allowed to heat with an excess of m-tetrafluoroethoxyaniline (TFEA) in a mixture of HOAc in 8:2 MeOH-water at 80°C for 1-2 h. The resulting mixture was evaporated under reduced pressure at < 50°C to provide product for direct MS analysis.

Mass Spectrometry:

FAB-MS - JEOL JMS-HX110 double focusing mass spectrometer for FAB-MS. Matrix: glycerol-thioglycerol-dimercaptosuccinic acid (G+TG+DMSA) for PI-, thioglycerol-hydroxyethyl disulfide (TG+HEDS) for NI-FAB.

MALDI-MS - PerSeptive Biosystems Voyager Elite mass spectrometer equipped with a nitrogen laser (337 nm, 3 ns pulse). Matrix: alpha-cyano-4-hydroxycinnamic acid

Results

* The "one-vial derivatization" shows complete conversion, requiring no transfer and additional purification, and possible for handling low µg of analytes
* Strong and sustained ion signals (30-50 x increase in intensity) can be obtained, greatly facilitating MS/MS measurements.

* Unambiguous information regarding the sugar sequence (Y-ions) can be obtained under PI-FAB CID conditions. Using this method the sequence of xyloglucans obtained from cyclamen seed was determined and the results were in full agreement with that by NMR.
* Characteristic fragmentation patterns were obtained for disaccharides with different linkage position under NI-FAB CAD-MS, suggesting potential use for isomer discrimination purpose.
* Low picomole detection can easily be achieved under PI-MALDI, further studv on post-source degradation is in progress.

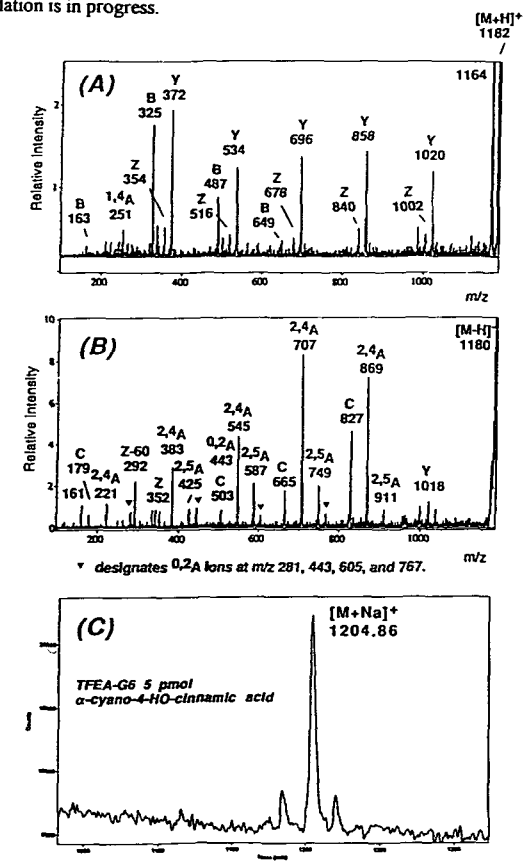

Fig. TFEA-G6-Glycosylamine (Mr 1181)
(A) PI-FAB-CAD-MS/MS,
(B) NI-FAB-CAD-MS/MS,
(C) MALDI-MS

MALD/I and electrospray mass spectrometery of cationic oligosaccharide derivatives.

T. J. P. Naven and David J. Harvey
Dept. Biochemistry, University of Oxford, Oxford, OX1 3QU, UK.

Oligosaccharides exhibit poor ionisation efficiencies in both MALD/I and electrospray (ESI) compared with peptides. We have investigated this poor ionisation efficiency by derivatising oligosaccharides with cationic compounds: Girard's T reagent and *p*-aminophenethyltrimethylammonium acetate (APTMA). The former proceeded by way of hydrazone formation whilst the latter via reductive amination (scheme 1a, b).

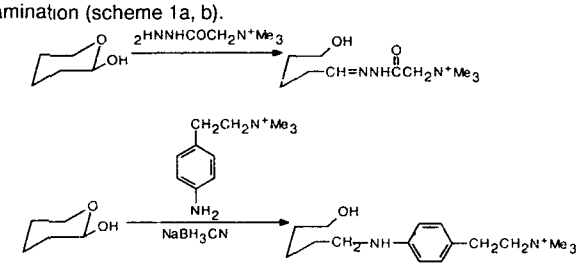

Scheme 1a, b (remaining hydrogens, hydroxyl groups and monosaccharides have been omitted for clarity)

The Girard's T derivatisation required no clean-up step prior to MALD/I and ESI, whereas the APTMA derivatisation employed separation on a normal phase amide column. Both compounds possessed a constitutive cationic site and this component enhanced the ionisation efficiency of the oligosaccharide derivative in both MALD/I and ESI. In MALD/I both derivatives formed the M^+ ion (as opposed to the sodium and potassium adduction observed for underivatised oligosaccharides), in ESI the Girard's T derivative formed only the singly charged ion M^+, whereas the APTMA derivative multiply charged, with the $[M^++H]^{2+}$ the most intense ion. The detection limits determined are shown in table 1.

Table 1 Comparison of detection limits obtained by MALD/I and ESI for derivatised and underivatised maltoheptaose. (- detection limit not determined any further because of the presence of the unreduced species).**

Derivative	MALD/I		ESI	
	Ion formed	(fmol)	Ion formed	(fmol)
Underivatised maltoheptaose	$[M+Na]^+$	400	no signal	
Girard's T	M^+	50	M^+	12
APTMA	M^+	800 **	$[M^++H]^{2+}$	3

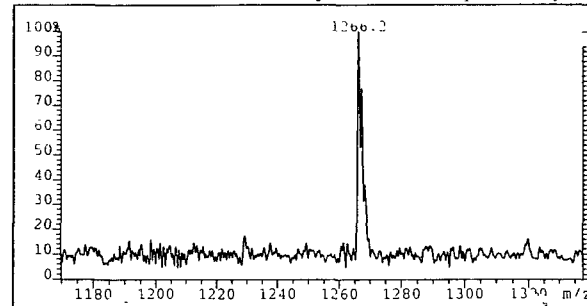

Fig. 1
MALD/I spectrum, acquired on a Fisons VG AutoSpec-FPD (E_1BE_2 geometry) fitted with a pulsed nitrogen laser (337 nm), of a Girard's T-maltoheptaose derivative (400fmol) using 2,5-DHB as the matrix with recrystallisation from ethanol

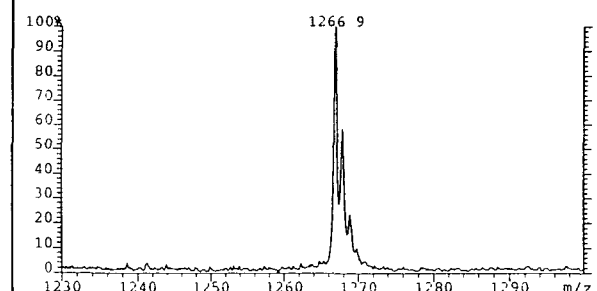

Fig. 2
MALD/I spectrum, acquired on the AutoSpec, of a Girard's T-maltoheptaose derivative [460 fmol consumed from 7 exposures, 1exposure/sec with a 0 01s delay between each each exposure ESI solvent water methanol (1 1,v v)

Mixtures of oligosaccharides released from glycopeptides by hydrazinolysis were derivatised with Girard's T and APTMA and analysed by MALD/I. Unique, quantitative fingerprint profiles of the derivatised mixtures were obtained.

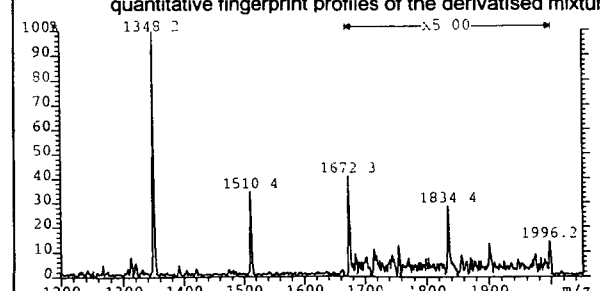

Fig. 3
MALD/I spectrum, acquired on a AutoSpec, of Girard's T derivatised bovine ribonuclease B-released sugars (45 pmol), using 2,5-DHB as the matrix with recrystallisation from ethanol.

Matrix Assisted Laser Desorption Ionization with an External Source Quadrupole FTMS for the Analysis of Oligosaccharides

Carlito B. Lebrilla, Steven T, Fannin, James A. Carroll, Jiangyue Wu
Department of Chemistry, University of California, Davis, CA 95616

Oligosaccharides have many diverse and important roles in biological systems It has been determined, for example, that saccharides (in the form of glycoconjugates) play important roles on the surfaces of cells such as recognition processes and binding of cells to antigens, hormones, enzymes, proteins and to other cells.[1] As a result, the interest for the development of analytical methods for their characterization has increased.

With the advent of new soft ionization techniques, e.g , Matrix Assisted Laser Desorption Ionization (MALDI), mass spectrometry has become an attractive method for the structural analysis of compounds with biological origin. The MALDI technique favors the production of pseudomolecular ions for large thermally labile compounds and therefore MALDI has proven to be particularly useful for biological applications

It has been shown that MALDI can be successfully coupled to an external source Quadrupole Fourier Transform Mass Spectrometer (FTMS) for the analysis of peptides and proteins.[2] Experiments in our laboratory have been performed to determine the utility of MALDI coupled with an external source Quadrupole Fourier Transform Mass Spectrometer (FTMS) for the analysis of various oligosaccharides

Figures 1 -4 show examples of MALDI/FTMS spectra of various oligosaccharides analyzed. The MALDI source was produced by simply removing a stainless steel mesh which functioned as part of a side electrode of a LSIMS source With this modification, either ionization method (LSIMS or MALDI) could be used without any other modifications to the hardware A nitrogen laser (337 nm) was mounted on the FTMS system frame, aimed and focused directly at the sample 2,4-Dihydroxybenzoic acid was used in ethanol. Oligosaccharide concentrations ranged from 0.5 to 2.5 mg/ml in methanol. Typical matrix/analyte molar ratios ranged from 300 1 To 1000:1. The analyte and matrix were applied (1μlit each) to a stainless steel probe tip and dried with a stream of air. The probe tip was inspected for proper crystal formation before each experiment

The spectra demonstrate that the combination of MALDI and external source FTMS is a promising technique for the analysis of oligosaccharides. Little fragmentation is observed, providing intense pseudomolecular ion signals. Most recently, we have begun an investigation for the analysis of branched oligosaccharides. Figure 5 shows a MALDI/FTMS spectrum for Trifucosyllacto-N-Hexaose extracted from human milk The spectrum indicates strong pseudomolecular ion signal, loss of fucose monomers and the presence of the characteristic $^{0,2}A$ fragments due to a reducing sugar

[1] Montreuil, J *Adv Carbohydr. Chem. Biochem.* **1980**, 37, 157 -223
[2] Mcrver, R.T.,Jr , Li, Y.; Hunter, R.L. *Int. J. Mass Spectrom. Ion Processes* **1994**, 132, L1 - L7

43rd ASMS Conference on Mass Spectrometry and Allied Topics

A linear Oligosaccharide
Maltohexaose (A Reducing Sugar)

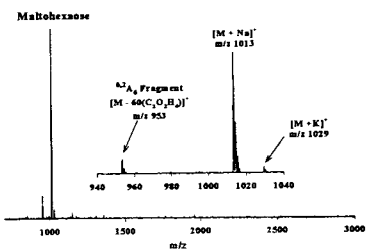

figure 1

A cyclic oligosaccharide
γ - Cyclodextrin (Cyclooctaamylose)

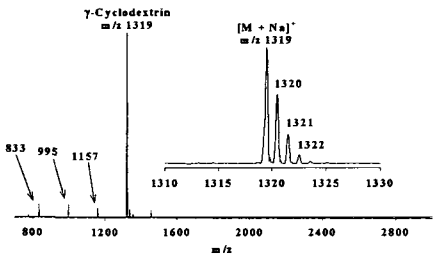

figure 2

A derivatized Cyclic Oligosaccharide
[Heptakis (2,3,6-tri-O-methyl)- β-cyclodextrin]

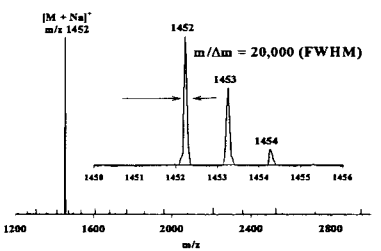

figure 3

Homologous Mixture
Asialo -G_{m1}-Ganglioside

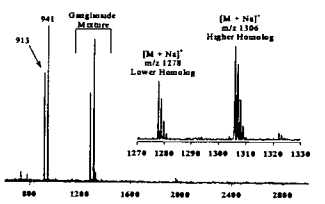

figure 4

Trifucosyllacto-N-Hexaose

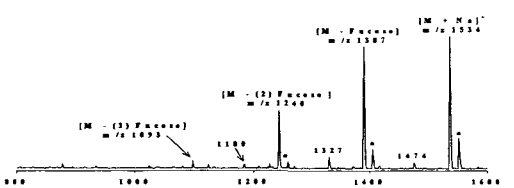

figure 5

MALDI-MS Applications: Carbohydrates

K. O. Börnsen, M.D. Mohr, H. M. Widmer; Ciba-Geigy Ltd., Basle, Switzerland

During the last years matrix assisted laser desorption and ionization mass spectrometry (MALDI-MS) has become a well established analytical method in biochemistry, especially in the field of peptides. High sensitivity, broad mass range, absence of any fragmentation (in linear time of flights instruments) and fast sample preparation are the main reasons for this success. However MALDI measurements of carbohydrates reached not the quality of peptides measurements. Therefore new methods and strategies have been developed in our laboratory to produce better spectra with a high reproducibility. Improvements, limitations and the behavior of carbohydrates with MALDI will be presented.

After a matrix evaluation it was found that a 3:1 mixture of dihydroxy benzoic acid (DHB) and hydroxy isoquinoline (HIC) /1/ as matrix yielded in best results for carbohydrates. This additive to the classic DHB matrix effects a much better crystallization behavior, but the original matrix properties of the DHB, however, are conserved. With this new matrix mixture it was possible to reach sample detection limits of 5 fmol/µl (equivalent to an amount of 0.5 fmol on the probe tip). By doing fast vacuum drying /2/ of the matrix/sample solution, a high reproducibility and quantitative data could be reached as well.

For further improvements, a desalting method of a few microliter on membrane, was applied to carbohydrate samples /3/. A membrane (Millipore, MF, pore size 0.0025 µm, diameter 25 mm) has been allowed to swim freely on a pure water surface. Five microliter were applicated by a micro pipette onto the membrane. After 30 to 120 minutes of dialysis the sample was sucked off again by the pipette. Especially dextran sulfates samples as examples for sulfated carbohydrates could been measured after desalting on a membrane swimming on water with 0.5% TFA easily. Figure 1 shows the spectra before and after a dialysis of this sample. The new matrix mixture together with this sample pretreatment was applied to dextran oligomers which could be determined up to n=90.

Nafion membranes demonstrate very interesting properties when used for ion exchange and purification of oligosaccharides from peptides. As an application for this, oligosaccharide libraries are measured. These samples derived from glycoproteins are often contaminated by huge levels of proteins as it is shown in Figure 2a. After a five minutes purification of 10 µl sample solution on a Nafion membrane all peptides are adsorbed onto the membrane surface. The resulting oligosaccharide solution is shown in Figure 2b.

These examples show how an optimal sample pretreatment and a good matrix can lead to strong improvements in MALDI experiments.

References:

1. U. Pieles, private communications
2. H. Görsch, Analytical Biochemistry 173, 393 (1993)
3. S. Weinberger, K.O.Börnsen, J.W. Finch, V.Robertson, B.D.Musselman, 41st ASMS Conference 1993

43rd ASMS Conference on Mass Spectrometry and Allied Topics

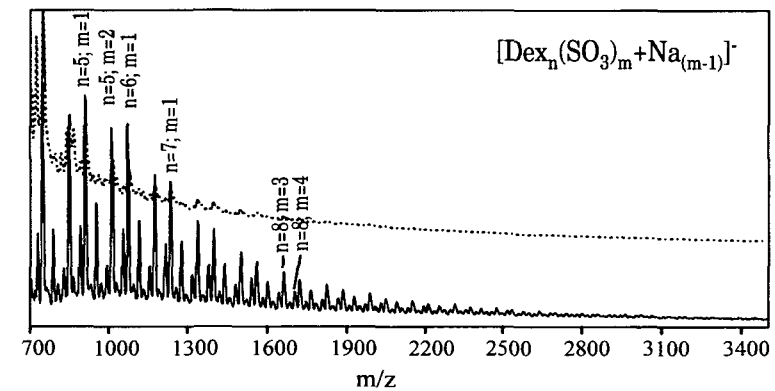

Fig. 1: Negative ion mass spectra of dextran sulfate. DHB/HIC mixture was used as matrix. In the upper spectrum the sample was measured directly. The bottom spectrum shows the result after a sample pretreatment of membrane dialyse of two hours.

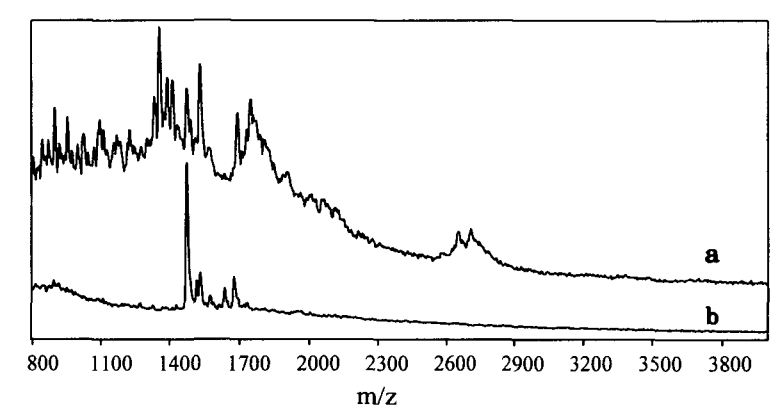

Fig. 2: Positive ion spectra of oligosaccharide library from rat IgG with DHB/HIC as matrix. Spectrum **a** was measured directly without any sample pretreatment. Spectrum **b** was measured after purification on a Nafion membrane.

ANOMERIC CONFIGURATION OF SUGAR NUCLEOTIDES BY FAB MS/MS

WOLUCKA, B. A., de HOFFMANN, E.

MASS SPECTROMETRY LABORATORY, UNIVERSITY OF LOUVAIN,
DEPARTMENT OF CHEMISTRY, PL. PASTEUR 1,
1348 LOUVAIN-LA-NEUVE, BELGIUM

Until now, the anomeric configuration of sugar nucleotides was usually determined either by non-destructive physicochemical methods, such as NMR and optical rotation measurements, or by different hydrolytic treatments, including alkaline hydrolysis or enzymatic cleavage with specific exoglycosidases and pyrophosphatases, followed by a comparison of the obtained degradation products with authentic sugar and glycosyl phosphates standards. We report here a method using FAB/MS/MS with a Finnigan TSQ70 mass spectrometer.

Very low energy collision induced dissociation, at 0.5 collision offset voltage, of the deprotonated molecules of glycosyl esters of nucleoside pyrophosphates results in distinct fragmentation patterns depending on cis/trans configuration of the phosphodiester and 2"-hydroxyl groups of the glycosyl residue. Sugar nucleotides with cis confguration produce, in MS/MS, only one, very intense fragment corresponding to nucleoside monophosphate, whereas those with trans configuration give weak signals of nucleoside di- and mono- phosphates and their dehydration products.

As shown by a study of twelve different sugar nucleotides, this empirical rule holds for sugar nucleotides having a free 2"-hydroxyl group and no alternative charge location. Owing to its simplicity, sensitivity and tolerance of impurities, the fast atom bombardment tandem mass spectrometry represents a suitable method for determining the anomeric linkage of glycosyl esters of nucleoside pyrophosphates if the absolute configuration of glycosyl residue is known and the compound fulfills the above mentioned requirements.

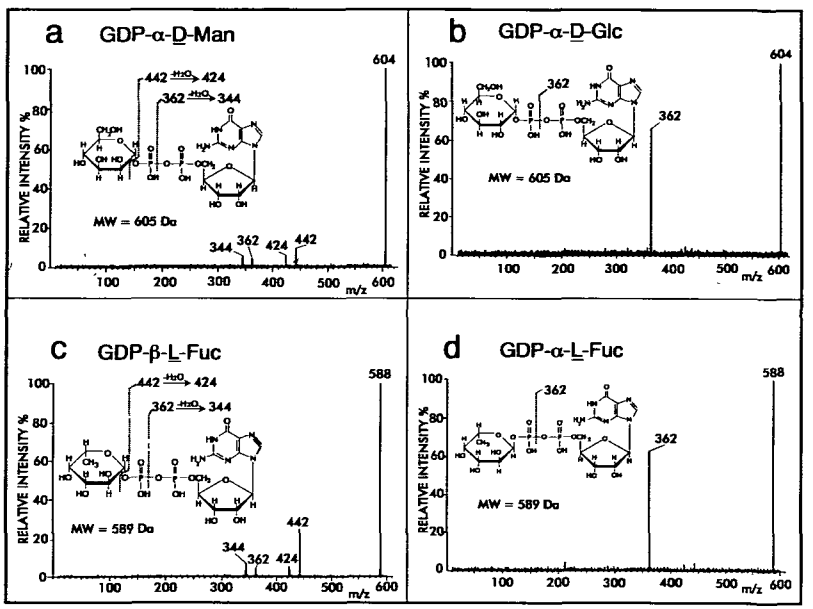

The figure displays negative ion FAB MS/MS product ion spectra from the $[M-H]^-$ deprotonated molecule of:
(a) guanosine 5'(α-D-mannopyranosyl pyro-phosphate) (GDP-α-D-Man);
(b) guanosine 5'(α-D-glucopyranosyl pyro-phosphate) (GDP-α-D-Glc);
(c) guanosine 5'(-L-fucopyranosyl pyro-phosphate) (GDP-β-L-Fuc);
(d) guanosine 5'(α-L-fucopyranosyl pyro-phosphate) (GDP-α-L-Fuc).
The collision-offset voltage in MS/MS experiments was 0.5 V.
In a and c, the 2" OH and phosphoester of the sugar moiety are in trans, while they are cis in c and d.

LC-MS/MS of Carbohydrates with Post Column Addition of Metal Chlorides using a Triaxial Electrospray Probe

Martin Kohler and Julie A. Leary, College of Chemistry*
University of California, Berkeley, CA 94720-1460

Introduction

The growing interest in the biological role and pharmaceutical application of carbohydrates has led to an increasing demand for faster and better analytical methodology [1]. Based on recent work in our laboratory on differentiating calcium and magnesium coordinated trisaccharides using ESI-MS/MS [2], a method for on-line formation of carbohydrate-metal complexes was developed. After purification by liquid chromatography, the sample is mixed with a metal chloride solution directly within the electrospray ion source, where a carbohydrate-metal complex is immediately formed. Depending on the metal chosen one observes either increased sensitivity in detecting the carbohydrate or informative MS/MS data for structural analysis. The work presented herein focusses on three issues using electrospray ionization: 1) sensitivity enhancement of the oligosaccharide-alkali metal complexes versus the protonated species, 2) the application of post column addition (PCA) of LiCl to enhance the detection limits in LC-MS, and 3) the use of post column addition of $CoCl_2$ and on-line LC-MS/MS in obtaining specific structural information.

Experimental

A commercially available triaxial electrospray probe (Fisons Instruments) was used for the experiments described. This probe consists of three coaxial stainless steel tubes. The sample is delivered to the innermost tube, the metal chloride solution flows through the tube in the middle and the nebulizer gas is delivered by the outermost tube. Conventional (MS) and tandem electrospray mass spectra (MS/MS) were collected on a VG-BioQ (Fisons Instruments) triple quadrupole electrospray mass spectrometer, equipped with an octapole collision cell. Argon was used as a collision gas at a pressure of 1.0–1.2 x 10^{-3} mbar. The collision energy (E_{lab}) was set between 20 and 80 eV.

Results and Discussion

Using a mixture of cellobiose, di-N-acetylchitobiose, Lewis X, and LNFP-V, the formation of oligosaccharide-alkali metal complexes by PCA of metal chlorides of lithium, sodium, potassium, rubidium, and cesium was investigated and their abundances were compared to the protonated species. As expected, a very high coordination affinity of these four oligosaccharides was found for lithium and sodium. For cellobiose, the signal of the $[M+Li]^+$ ion was found to be approximately 70 times more abundant than the corresponding $[M+H]^+$ signal. In an LC-MS experiment with 10 pmol of the carbohydrate mixture, the $[M+Li]^+$ ion was detected at a total sample consumption of 1.7 pmol. However, a sharp drop in affinity is found when alkali metals of larger ionic radii, such as potassium, rubidium, and cesium are used as the PCA reagent. All four oligosaccharides investigated show a gradual decline in affinity in going down the group I metals. The thresholds for the concentration of the PCA reagent and detection sensitivities of the oligosaccharide are in the same range, and in some cases better, than that obtained when an individual carbohydrate is premixed with LiCl without use of the triaxial probe.

In order to obtain linkage specific fragmentation for branched oligosaccharides and structures containing N-acetyl functionalities, experiments with post column addition of $CoCl_2$ were carried out. Since the affinity of cobalt to carbohydrates is considerably lower than that observed with alkali metals, the experimental conditions to form carbohydrate-cobalt complexes like $[M+Co-H]^+$ and $[M+CoCl]^+$ were investigated carefully. LC-MS/MS data were obtained for sample amounts ranging from 1 nmol (Lewis X, LNFP-V) down to 200 pmol (cellobiose and di-N-acetylchitobiose), corresponding to sample consumptions of 83 pmol and 17–33 pmol, respectively (see Figure). Post column addition of metal salts using a triaxial electrospray probe is a versatile technique to form metal complexes of carbohydrates for subsequent on-line MS and MS/MS analysis. The application of this technique for analysis of other compounds like peptides is considered to be straightforward.

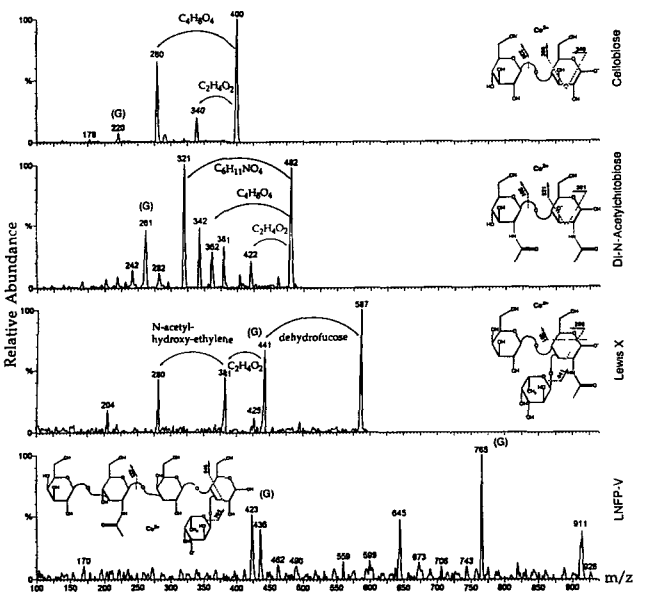

References: [1] Borman, S. C&EN **1993**, June 28, 27–34
[2] Fura, A.; Leary, J. A. *Anal. Chem.* **1993**, *65*, 2805–2811

M. Kohler thanks the Swiss National Science Foundation for fellowship support during 1994. J. Leary acknowledges NIH (GM 47356) for their support. This work has been submitted for publication to *Analytical Chemistry*.

Kinetic Energy Release Measurements of Oligosaccharide-Metal-Ligand Isomers Using FAB and ES Ionization

Glenn Smith, Geoffrey Bott†, and Julie A. Leary
Chemistry Dept., University of California, Berkeley, CA 94720
†G.B. Scientific, 701 DeLong Ave. Navato, CA 94945

Previous research in our laboratory has involved complexing $Co(acac)_3$ with various dialkyl tartrates and measuring the KER of ions generated from the unimolecular dissociation of the precursor complex (1) In so doing, we have shown that MIKES can be used to differentiate D- and L- enantiomers of these tartrates. By extending this methodology to mono- and di-saccharides we are capable of distinguishing α and β glycosidic linkages. Additionally, by measuring the KER following the unimolecular dissociation of various nickel complexes possessing monosaccharide-aminal ligands, differentiation of the stereochemistry of hydroxyl groups in isomeric hexose units is possible. The effects of different ionization methods (FAB and ESI) on the unimolecular KER values was also determined.

Two isomeric disaccharides, laminaribiose (β 1,3 glc-glc), and nigerose (α 1,3 glc-glc) were complexed with either racemic $Co(acac)_3$ in the presence of R,R or S,S threohydrobenzoin (THB), or with resolved Δ $Co(acac)_3$. In both cases the disaccharide displaces one of the acetylacetonate ligands to generate a positively charged complex consisting of Co^{3+}, two acetylacetonate ligands, (-1 charge each) and one neutral disaccharide. This precursor ion at m/z 599 is transmitted into the MIKES cell and allowed to undergo unimolecular dissociation. The KER of one of the product ions, m/z 500, is subsequently measured.

In the presence of the chiral resolving agent, R,R- or S,S-THB, a difference in KER accompanying the dissociation is observed for the two isomeric $Co(acac)_2$/disaccharide complexes. Table 1 lists all the KER values obtained for the $Co(acac)_2$/disaccharide complexes both with and without THB as well as for the complexes made with the resolved Δ $Co(acac)_3$. The difference in the KER values indicates a variance in the structure of the two disaccharides. Specifically the differentiation results from the presence of an α or β glycosidic bond between the otherwise identical monomers.

The THB appears to selectively complex one enantiomer of the $Co(acac)_3$, leaving the other free to complex with the disaccharide. The values obtained using the resolved Δ $Co(acac)_3$ suggest that the R,R-THB selectively complexes with the Λ form of $Co(acac)_3$ in the racemic mixture, thus leaving the delta form available for complexation to nigerose of laminaribiose. The use of optically resolved Δ $Co(acac)_3$ supports this hypothesis as observed in Table 1. This is evidenced by the fact that the KER for nigerose/Co(acac) in the presence of R,R-THB is the same as that of the nigerose/Δ Co(acac) complex. The same holds true for the value obtained for the laminaribiose complex in the presence of R,R-THB.

The identification of the stereochemistry of the C-2 hydroxyl group on a monosaccharide, and therefore the distinction between mannose and glucose, was also achieved by observing the unimolceular dissociation of an octahedral complex in which the monosaccharide was complexed to a transition metal ion. In this case, either mannose or glucose was reacted with the octahedral nickel tris-diamino propane complex, yielding the octahedral bis-monosaccharide aminal nickel complex (2). The precursor for this complex, m/z 529, and m/z 293 representing a $Ni(NH_2(CH_2)_3NH_2)$•monosaccharide complex were each analyzed by MIKES, and KER measurements determined for various product ions as shown in Table 2.

Both ESI and FAB ionization produce these precursors, which upon unimolecular dissociation give rise to two, three and four carbon neutral losses, some of which demonstrate different KER values when compared to its isomer. Since the stereochemical difference between mannose and glucose is in the axial vs equatorial positioning of the hydroxyl group at C-2, it seems likely that the monosaccharide coordinates differently to the nickel and this difference in structure is reflected in the different KER values obtained.

TABLE 1: FAB-MIKES Study of the Kinetic Energy Release of Various [Co(AcAc)2·disaccharide]+ Complexes (m/z = 599) Following Unimolecular Dissociation

	Racemic (Δ and Λ) $Co(AcAc)_3$		Resolved Δ-(+)-$Co(AcAc)_3$	
DISACCHARIDE	CHIRAL RESOLVING AGENT	KER (meV)	CHIRAL RESOLVING AGENT	KER (meV)
laminaribiose	R,R-THB	30 ± 1	none	33
	S,S-THB	40		
	none	32		
nigerose	R,R-THB	43 ± 1	none	43
	S,S-THB	29		
	none	32		

1 Standard deviations represent values calculated from the average of five separate experiments.

TABLE 2 FAB- and ES Ionization-MIKES Study of the Kinetic Energy Release of [Ni(DAP•monosaccharide)2-H]+ Complexes (m/z = 529) Following Unimolecular Decomposition

			FAB	ESI
monosaccharide	m/z of product ion	neutral fragment loss from m/z=529	KER (meV)	KER (meV)
mannose	469	$C_2H_4O_2$		
	439	$C_3H_6O_3$	43	
	409	$C_4H_8O_4$	51	
	293	DAP•man	65	67
glucose	469	$C_2H_4O_2$		
	439	$C_3H_6O_3$	32	
	409	$C_4H_8O_4$	34	
	293	DAP•glc	60	100

1 The product ion at m/z = 293 results from the loss of an entire neutral (DAP)-monosaccharide ligand.
2. The KER of the product ion at m/z=469 was not measured because it was obscured by another peak at m/z = 470.

1. Dang, T. T.; Pederson, S F.; Leary, J. A. *J. Am. Soc. Mass Spectrom.* 1994, *5*, 452.
2. Yano, S. *Coord. Chem. Rev* 1988, *92*, 133.

ESI-MS/MS Study of Co, Zn, Mn, Cu, and Ca Complexes of Oligosaccharides

Emily M. Sible, Steven P. Brimmer, and Julie A. Leary*
University of California, Department of Chemistry
Berkeley, CA 94720

Previous research in our laboratory has focused on the determination of linkage positions from the MS/MS spectra of linear and branched Ca^{2+} and Mg^{2+}-coordinated oligosaccharides(1). Our current study seeks to extend this methodology by investigating the difference in structural information obtained when various metals are coordinated to two structurally-related carbohydrates, a hexose trimer and a di-N-acetyl pentamer.

Complexes of the trimer, α1,3-α1,6 Mannotriose and the pentamer, Conserved Trimannosyl Core, with the chloride salts of Ca, Mn, Co, Cu, and Zn were made using electrospray ionization in a VG Bio-Q triple quadrupole mass spectrometer. The most abundant precursor ions and the most informative MS/MS spectra were obtained by optimizing variables such as the skimmer voltage, the metal to carbohydrate concentration ratios, the collision energy and the collision gas pressure.

The use of different metals had a significant effect on the optimum carbohydrate to metal ratio, the detection limit of the carbohydrate and the relative abundances of the [M + Metal Chloride]$^+$, [M + Metal - H]$^+$, and the [M + Metal]$^{2+}$, as can be seen in Table 1. For example, changing the concentration of mannotriose from 100 pmol/μl to 10 pmol/μl for either Co or Zn coordination causes the optimum ratio of metal to carbohydrate to change from 1:5 to 1:10 for Co and from 1:10 to 1:100 for Zn. The ionic radii of the metals appear to play an important role in the efficiency of coordination to the oligosaccharides. Ionic radii of 100-110 ppm form the best complexes to carbohydrates(2). The weakness of the Zn^{2+} and the Cu^{2+} complexes may be explained by the fact that their ionic radii are significantly smaller than these values. Table 2 demonstrates the amount of metal needed to produce the most abundant precursor ions and the effect the ionic radii of the metal may play on this ratio.

Examination of the data indicates that the metal used significantly changes the amount of structural and linkage information available from the MS/MS spectra. The Ca^{2+}-coordinated trimer at a concentration of 50 pmol/μl gave the most definitive linkage information for the mannotriose, thus supporting our previous work(1). This was in contrast to the pentamer which gave the most structural and cross-linkage information when coordinated to Mn^{2+}. However, this MS/MS of the pentamer did not permit the unambiguous assignment of the specific linkages in the carbohydrate. Because the dissociation pathways of these complexes were sufficiently different, further investigations of various pentamers, both with and without N-acetyl functionalities, are

currently underway to ascertain specific linkages as well as information regarding the effect the N-acetyl functionality has on metal coordination.

MS/MS of both the pentamer and the trimer when coordinated to Cu and Zn provided no significant structural or linkage information regardless of the collision energy, carbohydrate concentration, or gas pressure used. However, in all cases (even those with Cu or Zn coordination), the first loss observed is that of the hexose ring substituted at the C-3 position, as previously indicated in our studies(1).

References

(1) Fura, A., Leary, J.A., Anal. Chem., 65, 1993, 2805.
(2) Angyal, S.J., Adv. Carbohydr. Chem. Biochem., 47, 1989, 1.

Table 1

	Trimer			Pentamer		
Metal	Conc.	rel. abund. $-H^+/+Cl^-$	rel abund. $^{2+}/+Cl^-$	Conc.	rel abund. $-H^+/+Cl^-$	rel. abund. $^{2+}/+Cl^-$
Co^{2+}	100	4.5/1 0	8.4/1.0			
	50	3.3/1 0	0.8/1.0	50	0.3/1 0	1.2/1 0
	10	2.9/1 0	0.4/1.0			
Zn^{2+}	100	0 1/1 0	1.0/1.0			
	50	0.5/1 0	0.3/1.0	50	0.3/1 0	0.7/1 0
	10	0.3/1 0	$^{2+}$ NS			
Mn^{2+}	100	0.8/1.0	0.3/1.0			
	50	0.8/1 0	0.9/1.0	50	0.5/1 0	4.3/1 0
Cu^{2+}	100	3.5/1 0	1.5/1.0			
	50	2.5/1 0	1.6/1.0	50	1.5/1 0	1 0/1 0
Ca^{2+}	100	0 4/1 0	3.7/1.0			
	50	1.0/1 0	4.5/1.0	50	0 4/1 0	13 2/1 0

Table 2

		Trimer		Pentamer	
Metal	ionic radius (ppm)	concentration (carbo:metal) (in pmol/ul)	ratio	concentration (carbo:metal) (in pmol/ul)	ratio
Co^{2+}	92 (tet)	100:500	1.5		
	83 (oct)	50:250	1:5	50:250	1.5
		10:100	1 10		
Zn^{2+}	74 (tet)	100:1000	1.10		
		50:500	1:10	50:500	1 10
		10:1000	1 100		
Mn^{2+}	75 (oct)	100:500	1.5		
	106 (8-coord)	50:250	1.5	50:500	1:10
Cu^{2+}	74 (sq pl.)	100:1000	1.10		
	88 (oct)	50:500	1 10	50:500	1.10
Ca^{2+}	71 (tet)	100:500	1.5		
	114 (oct)	50:250	1.5	50:250	1.5

In-source and post-source decay fragmentation of oligosaccharides ionized by MALDI

David J. Harvey[1], Glen Critchley[2] and E. Anne Maisey[2]

(1) Oxford Glycobiology Institute, Department of Biochemistry, University of Oxford, South Parks Road, Oxford, OX1 3QU
(2) Fisons Instruments, VG Analytical, Floats Road, Wythenshawe, Manchester, M23 9LE, UK

Introduction

Ionization of complex oligosaccharides by MALDI on linear time-of-flight (TOF) instruments produces strong $[M + Na]^+$ ions with little or no apparent fragmentation. Although mass measurement of these ions can lead directly to a composition in terms of the isobaric monosaccharide content, there is no information relating to sequence, branching or linkage of the constituent sugar residues. When recorded on a magnetic sector instrument, on the other hand, weak fragments are observed which reveal much of this structural information. We have now examined these fragment ions and compared them with fragments observed by post-source decay (PSD) on a TOF instrument fitted with a reflectron.

Experimental

Oligosaccharides were of the type found in glycoproteins (*N*- and *O*-linked) and containing from 3 to 13 monosaccharide residues. In-source decay (ISD) was examined with a Fisons VG AutoSpec QFPD mass spectrometer fitted with an LSI nitrogen laser (20 Hz) and an array detector. TOF PSD spectra were examined with Fisons VG TofSpec E and SE instruments by stepping the ratio of acceleration voltage and reflectron voltage over the required mass range (7 segments were used) with the nitrogen laser (337 nM) firing at 50 shots/segment. 2,5-DHB was used as the MALDI matrix in both cases.

Results and Discussion

In-source fragmentation consisted mainly of glycosidic cleavages of the type common to FAB spectra, together with the production of a few ions that were formed by cleavages of the C_1-C_0 and C_2-C_3 bonds (loss of 101 Da) and cleavage of the C_2-C_3 and C_4-C_5 bonds (loss of 161 Da) of the reducing-terminal GlcNAc residue (Fig. 1). Glycosidic cleavage from the reducing terminus resulted in loss of intact monosaccharides [B-type cleavage, Domon and Costello nomenclature (1)], whereas loss from the non-reducing termini involved elimination of sugar moieties lacking one oxygen atom (Y-type cleavage). There was some evidence to suggest that loss of the sugar residues attached to the 3-position of the branching mannose occurred in preference to loss from the 6-position (Fig. 2) although the number of samples was limited.

The PSD spectra (Fig. 3) were similar in that glycosidic cleavages predominated but the ions produced by ring-cleavage of the reducing-terminal sugar residue were weaker than by ISD. Matrix ions were absent, thus allowing more low-mass fragments to be seen than with ISD.

Reference

1. B. Domon and C. E. Costello, *Glycoconjugate J.*, 1988, **5**, 397.

43rd ASMS Conference on Mass Spectrometry and Allied Topics

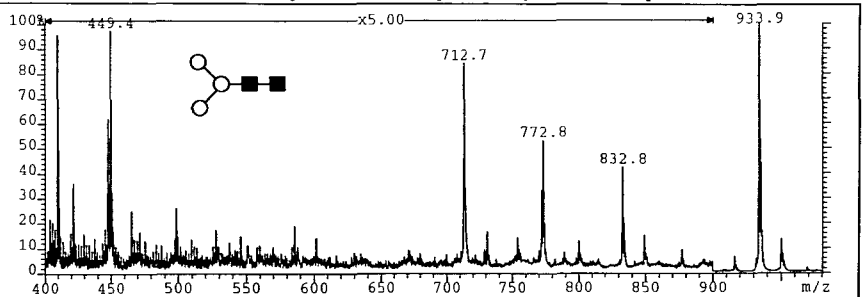

Fig. 1. MALDI ISD spectrum of $(Man)_3(GlcNAc)_2$. Through-ring cleavages are seen at *m/z* 832.8 (loss of 101 Da) and 772.8 (loss of 161 Da). Major glycosidic cleavages give *m/z* 771.8 (loss of Man) and 712.7 (loss of GlcNAc). Structural symbols: ○ = Man, ■ = GlcNAc.

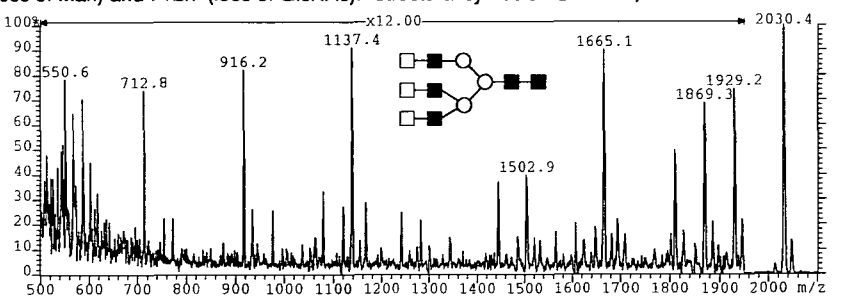

Fig. 2. MALDI ISD Spectrum of $(Gal)_3(GlcNAc)_5(Man)_3$. The ion at *m/z* 1136.4 is produced by loss of the $(Gal)_2(GlcNAc)_2Man$ fragment from the 3-position of the branching mannose. Structural symbols as Fig. 1 plus □ = Galactose

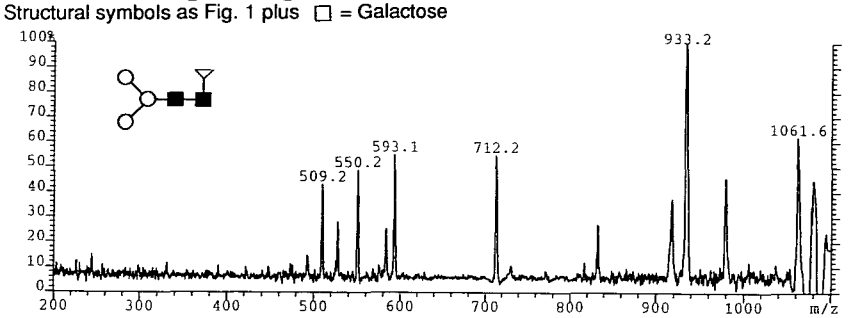

Fig. 3. MALDI PSD spectrum of $(Man)_3(GlcNAc)_2Fuc$. The ion at *m/z* 933 = $[M - Fuc]^+$,

Oligossacharide Structure Determination on an Ion Trap

Michael R. Asam & Gary L. Glish
Department of Chemistry
University of North Carolina
Chapel Hill, NC 27599

Introduction: Oligosaccharides are important elements in intra- and inter-cellular/molecular recognition mechanisms. Linkage types are part of the information that determine the tertiary structure of oligosaccharides and the tertiary structure is what determines specific recognition, so easily obtained linkage sequences will provide valuable information for computer and other modeling of cellular signalling interactions. Hofmeister et. al.[1] have shown that lithium cationized oligosaccharides have specific MS/MS dissociation patterns indicative of the carbohydrate linkage under low energy CID conditions in a hybrid mass spectrometer. We have used electrospray ionization on a quadrupole ion trap mass spectrometer to examine MS/MS disaccharide dissociation patterns under ion trap conditions. Our studies have concentrated on disaccharides complexed with lithium and sodium.

Experimental: The two sugars gentiobiose and sophorose were provided by Julie Leary of the University of California at Berkeley. The other disaccharides, trehalose, nigerose, lactose, and sucrose were obtained from the Sigma Chemical Company. All electrospray sample solutions were made by dissolving 0.85 mg of a disaccharide into 5 mL of a 75% methanol, 20% water, 5% acetic acid solution to make the concentration 500 μM. Lithium chloride and sodium chloride were dissolved in the 75% methanol, 20% water, 5% acetic acid solution to obtain 500 μM solutions as well. Prior to electrospraying, equal volume amounts of a disaccharide solution and an alkali cationic solution would be mixed on a vortex mixer and then taken into the electrospray syringe. A Harvard Apparatus syringe pump was used at a flow rate of 1μL per minute The electrospray source system is described elsewhere[2] with A1at 60 0 V, AL1 at 28 0 V, AL2 at 27.5 V, and A2 at ground. The instrument used was a Finnigan ITMS and the data collection software was from Finnigan (Revision B).

Results: The same dissociation patterns as those found by Hofmeister et. al. were observed for MS/MS experiments of the lithium cationized disaccharides (see Table 1) The same dissociations for MS/MS experiments of the sodium cationized disaccharides were observed with the exception that collision-induced dissociation (CID) was more difficult to effect, i.e., dissociation of the parent peak required more energy than in the lithium cationized case for all the disaccharides except gentiobiose and sucrose (see Table 2). MS^3 experiments on the $-C_2H_4O_2$ ion show dissociation to the $-C_4H_{10}O_5$ and $-C_6H_{12}O_6$ ions. MS^3 experiments on the $-C_3H_6O_4$ and $-C_4H_6O_4$ ions show dissociation to the $-C_6H_{12}O_6$ ion exclusively. MS^3 experiments on sodium cationized ions were far more sensitive than MS^3 on lithium cationized ions.

Discussion: It is interesting that the lithium cationized species behave differently than the sodium cationized species. If one imagines that the coordinating forces the alkali metals experience are similar it seems logical that the sodium cationized species should behave the same as the lithium cationized species and even loose their cations more readily, thus making CID fragmentation less efficient (due to sodium loss). The experimental data demonstrating that sodium cationized species are harder to dissociate suggests

[1]Hofmeister, G.E., Zhou, Z. & Leary, J.A. (1991) *J Am. Chem Soc. 113*, 5964-5970.
[2]Van Berkel,G.J , Glish, G.L., McLuckey, S.A (1990) *Anal. Chem. 62*, 1284-1294

that the coordinating forces experienced are different. The source of this difference has not been determined, but one possible suggestion is that the second ring of the disaccharide is coordinating to the sodium due to its larger size relative to lithium contributing additional stabilizing energy. Computer modeling experiments are underway to help determine if this suggestion is plausible. The mechanisms postulated by Hofmeister et. al. appear to be valid since MS^3 analyses show that $-C_2H_4O_2$ ions can dissociate to $-C_4H_{10}O_5$ ions.

Table 1: Lithium Cationized MS/MS Product Ions (*m/z*)

Compound	Linkage	289, $-C_2H_4O_2$	259, $-C_3H_6O_4$	229, $-C_4H_6O_4$	187, $-C_6H_{10}O_5$	169, $-C_6H_{12}O_6$
gentiobiose	β-1,6	X*	X	X	X	X
lactose	β-1,4	X		X	X	X
nigerose	α-1,3		X		X	X
sophorose	α-1,2			X	X	X
trehalose	α-1,1				X	X
sucrose**	α-1,2				X	X

*An X indicates the presence of an ion at that m/z resulting from the indicated neutral loss
**Sucrose is glucose-α(1,2)-fructose and the other sugars are glucose-x(x,x)-glucose (or galactose).

Table 2: Sodium Cationized MS/MS Product Ions (*m/z*).

Compound	Linkage	305, $-C_2H_4O_2$	275, $-C_3H_6O_4$	245, $-C_4H_6O_4$	203, $-C_6H_{10}O_5$	185, $-C_6H_{12}O_6$
gentiobiose	β-1,6	X*	X	X	x	x
lactose	β-1,4	x		x	x	x
nigerose	α-1,3		x		x	x
sophorose	α-1,2			x	x	x
trehalose	α-1,1				x	x
sucrose	α-1,2				X	x

*An X indicates the presence of an ion in comparable abundance to the lithium cationized product ion resulting from the indicated neutral loss. Smaller x's indicate the presence of the product ion, but at an abundance much lower than that for the lithium cationized product ion for that neutral loss.

Conclusions: Our results for lithium cationization corroborate Hofmeister et. al.'s findings and our results for sodium cationization show the same fragmentation patterns, but the conditions needed to obtain fragmentation of the sodium cationized disaccharides are somewhat different. In addition, we have been able to show through MS^3 experiments that the dissociation mechanisms postulated by Hofmeister et. al. are correct. The ion trap seems well suited for these types of analyses since MS^n is routine, i.e., as would be needed for tri-, tetra-, etc. saccharides. Such experiments will be undertaken in the near future.

High energy CID spectra of complex oligosaccharides ionized by MALDI.

Robert H. Bateman[1], Martin R. Green[1] and David J. Harvey[2]

(1) Fisons Instruments, VG Analytical, Floats Road, Wythenshawe, Manchester, M23 9LE.
(2) Oxford Glycobiology Institute, Department of Biochemistry, University of Oxford, South Parks Road, Oxford, OX1 3QU, UK.

Introduction

Complex oligosaccharides ionized by MALDI give spectra containing dominant $[M + Na]^+$ ions which are excellent for profiling oligosaccharide mixtures obtained from biological sources. Although such ions give some compositional information on the oligosaccharides, no information is present relating to the sequence, branching or linkage of the constituent monosaccharides. Fragments produced by post-source decay, examined on a time-of-flight instrument, provide only partial information. More information should be present in high energy collision spectra but such spectra are not obtainable on a scanned magnetic sector instrument because of the pulsed nature of the ion source. We have, thus, examined the high-energy collision spectra of $[M + Na]^+$ ions produced by MALDI (2,5-DHB matrix) from complex oligosaccharides using a magnetic sector instrument fitted with an orthogonal TOF analyser.

Experimental

Spectra of typical *N*-linked oligosaccharides (high mannose and complex) were examined with a VG AutoSpec-TOF mass spectrometer. This instrument has a double focusing magnetic sector and an orthogonal acceleration time-of-flight mass analyser in a tandem configuration. The MALDI source uses a pulsed 337 nm nitrogen laser and is held at 8 kV. The magnetic sector was used to select the precursor ion at a resolution of approximately 1500 (10% valley) and these ions were collisionally activated at 800 eV energy using xenon. The complete packet of precursor and product ions resulting from each laser pulse was orthogonally accelerated into the time-of-flight mass analyser and the product ion spectrum was recorded using a 1 GHz time-to digital converter. This process was repeated for each laser pulse at a repetition rate of 10 Hz until most of the sample loaded onto the target had been consumed.

Results and Discussion

The fragment ions in the high energy collision spectra were considerably different from those produced by either post-source decay (PSD) on a time-of-flight instrument or by in-source decay on a magnetic sector mass spectrometer. Ions in the high energy spectra were produced both by glycosidic cleavage and, more significantly, by ring cleavage. Major differences between the PSD and high energy spectra included a series of ions produced by cleavage of the C_1-C_2 and C_0-C_1 bonds of most constituent monosaccharides and which provided considerable structural information. These ions enabled branching patterns to be obtained from most oligosaccharides examined, particularly the high-mannose compounds (Fig. 2). Many more fragment ions, containing mainly the non-reducing terminal residues, appeared at low mass (Figs. 1-3) than in the PSD spectra. Ring cleavage also resulted in loss of carbon atoms 1 and 2 from the reducing-terminal GlcNAc. Complex oligosaccharides (see Fig. 3) produced major ions by cleavage adjacent to the GlcNAc residues of the antennae.

43rd ASMS Conference on Mass Spectrometry and Allied Topics

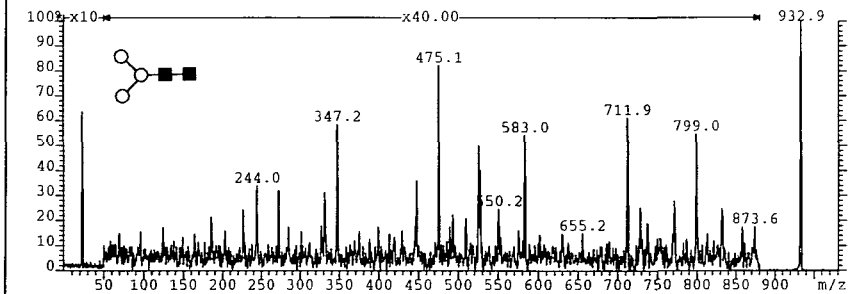

Fig. 1. MALDI OA-TOF spectrum of $(Man)_3(GlcNAc)_2$. ○= Mannose, ■= GlcNAc. Ions at *m/z* 799 and 475 are produced by cleavage of the C_1-C_2 and C_0-C_5 bonds of each mannose ring.

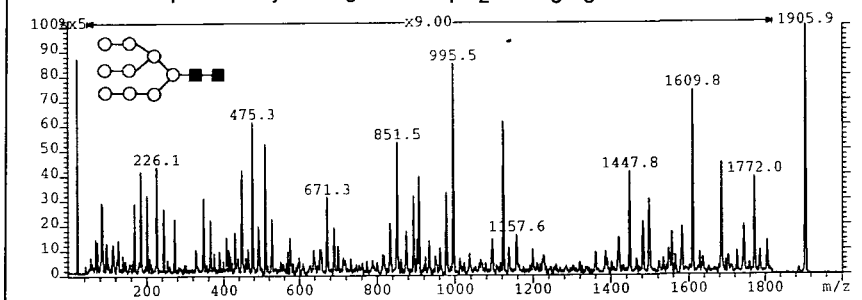

Fig. 2. MALDI OA-TOF spectrum of $(Man)_9(GlcNAc)_2$. Ions marked with an asterisk are formed by cleavage of the C_1-C_2 and C_0-C_5 bonds of each mannose ring,

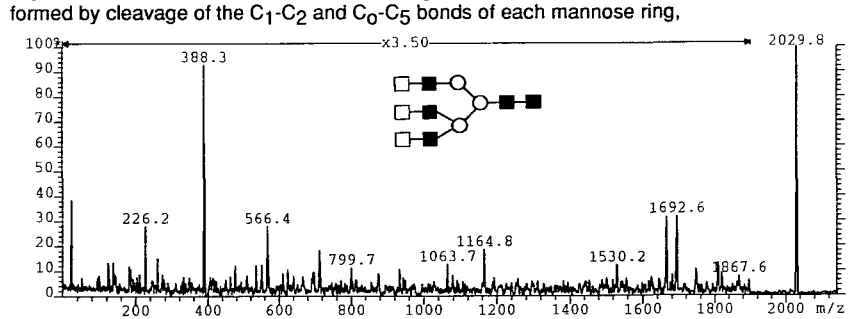

Fig. 3. MALDI OA-TOF spectrum of $(Gal)_3(GlcNAc)_5(Man)_3$ (symbols as Fig. 1 plus □= Gal). Ions at *m/z* 1664 and 1692 are formed by loss of Gal-GlcNAc by glycosidic and ring-cleavage (C_1-C_2 and C_0-C_5 bonds of GlcNAc) respectively. *m/z* 1164 is loss of $(Gal)_2(GlcNAc)_2Man$.

USING AEROSOLS FOR MALDI LIQUID INTRODUCTION

Gang Wei, Xun Fei, Lin He, and Kermit K. Murray
Department of Chemistry, Emory University, Atlanta, GA 30032

Aerosol matrix-assisted laser desorption/ionization was developed two years ago as a method for coupling direct liquid introduction with MALDI mass analysis.[1] The approach is simple: rather than depositing the solution of matrix and analyte on a solids probe, the matrix and analyte solution is sprayed directly into the mass spectrometer. A high speed pumping system and a heated drying tube are used to remove solvent and carrier gas, producing dried aerosol particles containing matrix and analyte. The collimated aerosol beam is irradiated with a 355 nm frequency tripled Nd:YAG laser and the resulting ions are mass analyzed in a linear time-of-flight mass spectrometer. The aerosol MALDI apparatus has been successfully coupled with liquid chromatography for on-line LC/MALDI-MS.[2]

A second aerosol MALDI apparatus, based on the original apparatus design,[3] has been constructed at Emory University. Two initial modifications have been made: one is the replacement of the metal nebulizer with a glass concentric nebulizer, and the second is delayed ion extraction. The glass nebulizer provides a reproducible spray as well as improved nebulization efficiency. A plot of pressure in the ionization chamber and the flight tube as a function of liquid flow rate is shown in Figure 1. The carrier gas flow rate was 0.25 L/min. Chamber pressures are acceptable up to a liquid flow rate of at least 1.5 mL/min. At a typical liquid flow rate of 0.5 mL/min., the chamber pressures are three to ten times lower with the glass concentric nebulizer than with the metal nebulizer.[3] Further improvements are currently being sought that will allow aerosol MALDI operation with a smaller and less expensive pumping system.

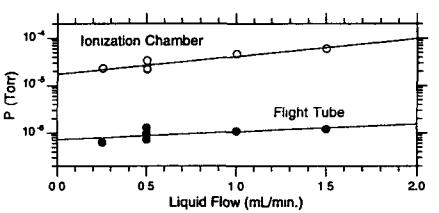

Figure 1. Operating pressures in the aerosol MALDI apparatus using a glass concentric nebulizer.

Aerosol MALDI delayed ion extraction provides information that is of fundamental interest as well as useful in designing instrument improvements. Figure 2 shows aerosol MALDI mass spectra of vitamin B-12 at successively larger delay times between the laser pulse and the 3 kV, 40 ns rise time pulsed extraction. The vitamin B-12 $[M\text{-}CN+H]^+$ and $[M\text{-}CN+Na]^+$ peaks occur at 70 µs flight time. Peak broadening results from ion velocities toward and away from the detector. A longer delay or a larger ion velocity will result in a greater ion spatial spread when the acceleration field is activated. The rate of peak broadening thus gives an indication of the velocities of the photoejected species.[4]

Peak widths for 21 vitamin B-12 data files (five of which are shown in Figure 2) are shown in Figure 3. The peak width was obtained from a fit to a gaussian functional form. Calculations show that the peak width at zero delay time is due almost entirely to the approximately 0.2 mm width of the ionizing laser beam. Additional broadening is due to the component of the ion velocity along the flight tube axis. A fit to these data was performed using an average ion velocity component to generate a gaussian peak width and convoluting this peak with the zero delay time peak. The average ion velocity was optimized in a least squares fit to the data and this fit is shown as a line in Figure 3. The resulting velocity for vitamin B-12 is 740 ± 100 m/s and is consistent with other determinations of the velocity of

MALDI formed ions.[5] Experiments are currently underway to limit the detector solid angle in order to resolve peaks corresponding to the forward and backward ejection velocity components.

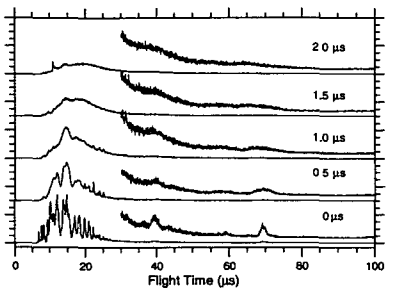

Figure 2. Aerosol MALDI mass spectra of vitamin B-12 at different delayed extraction times.

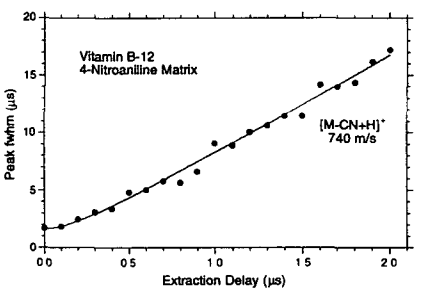

Figure 3. Vitamin B-12 $[M\text{-}CN+H]^+$ peak width as a function of extraction delay.

This work was supported by a grants from Emory University and the Emory University Research Committee. A Finnigan ASMS Research Award and SACP Starter Grant Award are gratefully acknowledged.

1. K. K. Murray and D. H. Russell, *Anal. Chem.* **65**, 2534, (1993).
2. K. K. Murray, T. M. Lewis, M. D. Beeson, and D. H. Russell, *Anal. Chem.* **66**, 1601, (1994).
3. K. K. Murray and D. H. Russell, *J. Am. Soc. Mass Spectrom.* **5**, 1, (1994).
4. H. J. Hwang and M. A. El-Sayed, *J. Chem. Phys.* **94**, 4877, (1991).
5. R. J. Levis, *Annu. Rev. Phys. Chem.* **45**, 483, (1994).

Design parameters of a gridless ion mirror for post source decay analysis

Jianru Zeng, Michael Karas, Franz Hillenkamp

Institute for Medical Physics and Biophysics
Robert-Koch-Straße 31, 48149 Münster, Germany

Although either linear or reflectron time-of flight instruments can be used with their respective advantages and disadvantages for the measurement of intact MALDI-ions, structure elucidation of analyte ions based on metastable-ion analysis (PSD-analysis) requires a reflectron instrument. All reflectron configurations, single-, double-stage and gridless ones, can be used, in principle, but, with differences in their practical performance, e.g. in the range of the usable "mass window" and thus, the number of steps required to register a complete PSD mass spectrum.
In this poster, the performance of a gridless ion mirror for PSD analysis is reported. For the configuration used (VISION 2000, Finnigan MAT) a potential distribution within the ion mirror can be chosen , which optimizes time- and space focusing relatively independently of each other. The ion optical calculations (SIMION) were verified experimenally, followed by an empirical optimization of the potential settings Under optimized conditions, a large usable mass window and good mass resolution can be achieved even with a standard small detector (20 mm diameter) (Fig. 1).

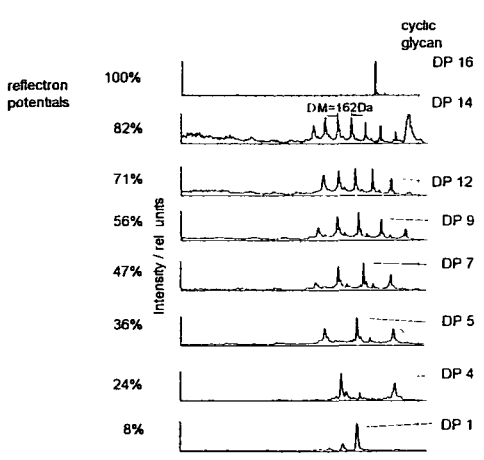

Figure 1: Post source decay spectra with different reflectron potentials for Vision 2000. "Mass window" is more than 40%. Analyte: cyclic glucan DP 16; Matrix: 2,5-DHB; Laser: 337 nm

In a single-stage RE-TOF-MS, a linear relationship exists between the flight time and metastable-fragment ion mass. In a two-stage reflectron TOF-MS, theoretical calibration based on instrument geometry and measurement of ion source and reflectron potentials is possible. In a gridless reflectron analyzer, however, this method of calibration is no longer applicable because of the penetration of the reflectron electric field into the "field-free" drift region. It appears straightforward to test an empirical calibration procedure. One concern is whether a calibration function indepent of the individual mass windows can be obtained. Figure 2 shows a window-independant calibration function: (M-Mc)/M= f[(t-to)/t]. In this figure, relative flight time differences are plotted vs. the relative mass difference. Using this calibration function combined with a correction factor for the postacceleration SEM detector, all fragment masses have been determined to better than 0.5 Da, resulting in average accuracy of better than 0.1%.

Precursor ion selection is also very important for post source decay analysis. The resolution of precursor ion selection is influenced not only by the geometry of blanker but also the TOF resolution at the location of beam blanker (which represented by linear TOF spectra). Delayed ion extraction can improve the resolution of linear TOF and thus the resolution of precursor ion selection, as shown in Figure 3. In this case the resolution is about 90 (Figure 3).

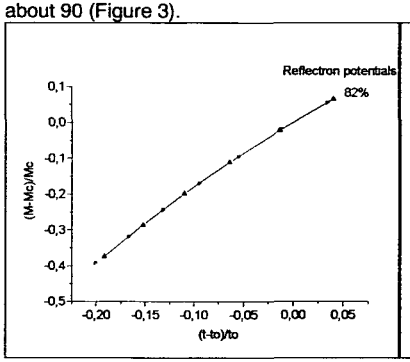

Fig. 2: A window-independent calibration function

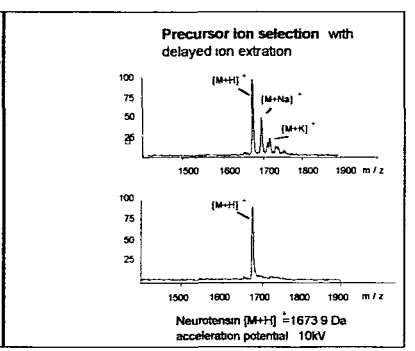

Fig. 3: Precursor ion selection

References:
1. B. Spengler, D. Kirsch, R. Kaufmann, Rapid Communication Mass Spectrom., 5, 198-202 (1991)
2. U. Bosel, H.J. Neusser, R. Weinkauf, J. Phys. Chem., 86, 4857 (1992)

A Method for Acquiring Daughter-Ion Spectra in a Reflecting TOF Instrument

G. Westmacott, W. Ens and K.G. Standing
Dept. of Physics, University of Manitoba, Winnipeg, Canada, R3T 2N2

Reflecting time-of-flight mass spectrometers provide an elegant method of obtaining daughter-ion spectra from metastable decay of selected parents [1]; the method is widely used in matrix assisted laser desorption/ionization (MALDI). For one- or two-stage mirrors, daughter ion peaks with molecular mass (m_d) near the parent mass (m_p) have comparable resolution to the parent and appear in the spectrum close to their correct mass according to the usual calibration preformed with known parent ion species. This is because the daughter ion energy is close to optimum for the mirror so it provides a compensation for the fraction of energy lost $(m_p-m_d)/m_p$ in the decay, as well as focusing for the energy spread. However, the energy of smaller daughters is further from the optimum, resulting in broader peaks and greater displacement from the usual mass position. For this reason, daughter ion spectra are normally acquired in segments with different mirror voltages. As the mirror voltage is reduced to optimize for a given daughter ion, the daughter ion flight time increases to that of the parent ion. This procedure requires a different calibration for each voltage which must be measured accurately, and a rather complicated algorithm to reassemble a single mass spectrum

We have developed an alternative method which is the same in principle but has practical advantages. Instead of leaving the target voltage constant and reducing the mirror voltage, the mirror voltage is left constant and the target voltage is increased. This has advantages because the flight time and the calibration depend strongly on the mirror voltage but only weakly on the target voltage; accurate measurement of the voltages is not necessary. As the target voltage is increased from the optimum for the parent ions, V_o, to V_a, to bring the average energy of a selected daughter ion mass to the optimum, its flight time is decreased to its correct m/z value predicted by the original parent ion calibration. That is, when V_a/V_o is close to m_p/m_d, the daughter ion energy is close to the optimum energy for the original mirror setting and so its mass can simply be determined from the original calibration. Of course, for ions within a segment that deviate from the optimum ratio, a small correction is still necessary, which for a single-stage mirror has a simple linear dependence on the flight time. Finally, since a single calibration applies at least approximately to all the segments, they may be simply joined together end-to-end to reassemble a single mass spectrum. Fig. 1 illustrates this for substance P.

For a single stage mirror the difference between the fragment ion apparent mass (the mass of the fragment as determined from the parent calibration) and the calculated fragment ion mass m_d is given by

$$\Delta m_d = (V_a/V_o)\, m_d{}^2/(4m_p) - m_d/2 + (V_o/V_a)(1/4)$$

where V_o is the acceleration voltage that optimizes the mirror for the parent ions Fig. 2 shows the results for substance P showing Δm_d versus m_d for four different V_a/V_o ratios. Fitting the above equation to the data gives effective ratios of the accelerating voltages. Applying the same correction Δm_d to the fragment ions of bradykinin, using the effective accelerating voltages as determined from the substance P data, gives corrected masses usually within ± 0 5 u of the calculated masses for similar steps in V_a as shown in Fig. 1.

[1] X. Tang et al, Rapid Comun Mass Spectrom. 3 (1989) 443.

43rd ASMS Conference on Mass Spectrometry and Allied Topics

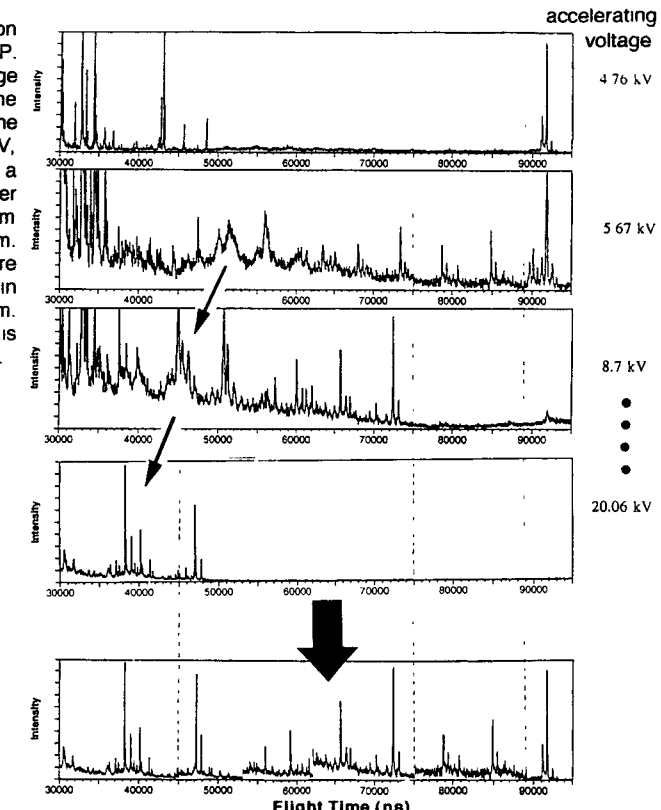

Fig 1. Fragment ion spectra for substance P. The accelerating voltage is increased from the optimum value for the parent ion V_o = 4 76 kV, bringing the energy for a segment of daughter ions in each spectrum close to the optimum. These segments are simply joined together in the bottom spectrum. The mirror voltage is constant at V_m = 5.6 kV.

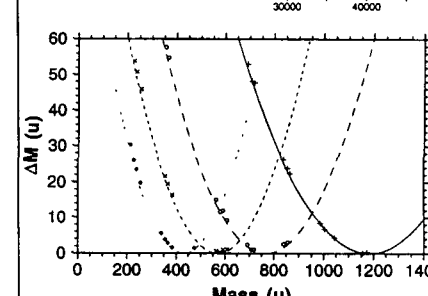

Fig 2. The difference between apparent and calculated fragment ion masses for substance P is plotted for four different accelerating voltages, V_a, correspond to ratios V_a/V_o = 1.19 (+), 1.83 (o), 2.46 (x) and 3.23 (♦), where V_o = 4.76 kV. Fitting the theoretical function for Δm_d gives effective ratios of the accelerating voltages V_a/V_o = 1 14, 1.76, 2.36 and 3 13 respectively. The mirror voltage is constant at V_m = 5.6 kV.

Time of Flight PSD Measurements with Precursor Ion Selection

Charles Hauer, Karen Roth, Robert Stack
New York Department of Public Health
Empire State Plaza
Albany, New York 12201

Paul Kowalski, D S. Cornett, Melvin Park
Bruker Analytical Systems, Inc.
Manning Park
Billerica, MA 01821

Introduction

MALDI TOF MS has been used successfully to obtain structural information from a variety of biological molecules, including peptides (1). To obtain useful post source decay information from a multi-component sample, such as an enzymatic digest of a protein, it is essential to devise a method that detects fragment ions which result from only a single parent ion in the mixture. To this end, an ion preselection devise has been designed with a transmission window resolution of at least 150 m/Δm. Presented here is an example of ion preselection, and peptide sequencing directly from a tryptic digest of myoglobin at the 100-500 fmol level with average mass errors of better than 0.05% for FAST™ PSD fragment ions.

Methods

All measurements were performed on a Bruker REFLEX TOF MS (Bruker Analytical Systems, Inc., Billerica, MA) configured with a Nitrogen 337nm laser. Reflectron mode spectra were acquired using a V-trajectory two stage gridless reflector

Horse heart myoglobin (Sigma) was denatured in a 30% methanol solution adjusted to pH approx 7.5 with ammonium bicarbonate. This solution was diluted with distilled water to 5% methanol, and the myoglobin was digested with sequencing grade modified trypsin (Boehringer Mannheim) overnight at room temperature. Aliquots of this digest were acetylated with acetic anhydride / methanol. Acetylation was performed on the sample stage. Aliquots of 100 and 500 femtomole were spotted on the sample stage with alpha-cyano-4-hydroxycinnamic acid (Sigma) matrix by the conventional dried drop method.

FAST spectra were acquired after the ion preselector was set to permit transmission of the parent ion of interest only. Preselection in the first field region is done with a pulsed deflection unit (FastFilter™) which has a set of deflection plates connected to a +/- 1 kV power supply and controlled with a fast pulse generator (Model DG 535, Stanford Research Sys., Stanford, CA)

Results

PreSelection of Ions using FastFilter A useful ion preselector provides a narrow transmission window to isolate a unique peptide ion, and its associated metastable species, only. It is also important to ensure that mass assignments are not altered by the preselection process. (Figure 1) shows a molecular weight spectrum of three synthetic peptides with nominal masses of 1425, 1434 and 1443 Da measured with and without the preselector. Note the baseline resolution of 160, without a mass shift, for preselection of the 1434 Da species.

FAST Analysis of Myoglobin Tryptic Peptides Despite the significant difference in precursor ion intensity resulting from a tryptic digest, FAST spectra obtained still contain many well resolved fragment ions even for low intensity tryptic peptides. Since only a very small portion of the

sample spot is consumed per FAST measurement, many tryptic peptides can be measured from the same 1 ul sample deposition to produce a quality FAST spectrum.

Assignment of post source decay ions is greatly facilitated through comparison with FAST spectra of the corresponding acetylated peptides. For example, comparison of the FAST spectra of the native 1854.8 Da peptide (Figure 2) and its acetylated version (Figure 3) unambiguously identifies the b3 to b8 ions. Clear assignment of b type ions also helps to identify the y type ions, such as y9 to y15 here, as well as "internal" fragment products.

Conclusions

The utility of FAST analysis for peptide sequencing from a unfractionated protein digest at the low femtomole has been shown. A precursor ion selector (FastFilter) capable of a transmission window resolution of at least 160 is now available for the Bruker REFLEX TOF MS. The FastFilter, combined with the low sample consumption of MALDI, permits the acquisition of multiple high quality peptide post source decay spectra from a single protein digest spot. Comparison of FAST spectra of native peptides with those of a simple derivative, such as amine terminal acetylation, affords true peptide sequencing from digests.

Figure 1

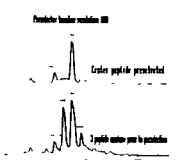

Figure 2

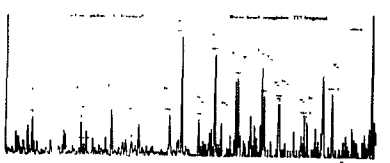

Figure 3

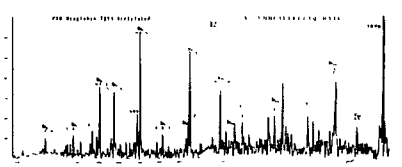

References: 1.Kowalski, P.; Kruppa, G.; Wronka, J.; Laukien, F.; 42nd ASMS Conference on Mass Spectromerty and Allied Topics, 679, 1994.

High Resolution Precursor Ion Selection for Post Source Decay Experiments

Armin Holle, Melvin A. Park, Detlev Suckau; Bruker-Franzen Analytik GMBH, Fahrenheitstr. 4, 28359 Bremen, Germany

In the past few years, matrix assisted laser desorption/ionization - time-of-flight mass spectrometry (MALDI-TOF) has grown rapidly in its importance in the analysis of biological molecules. As an extension of MALDI-TOF, post source decay (PSD) has become an accepted and frequently used method for obtaining sequence information for picomole amounts of low molecular weight (< ~2000 amu) peptides [1]. We have developed a precursor ion selector (preselector) which allows one to select ions on the basis of their time-of-flight (TOF), that is their mass. PSD analysis can then be performed on these ions free from the interference of other mixture components [2]. Such an experiment is in fact a tandem MS analysis.

Samples of 10000 Da MW poly(ethylene glycol)(PEG) were dissolved in sinapinic acid in a ratio of about 1:1000. Angiotensin II samples were prepared by dissolving the peptide in sinapinic acid in a ratio of 1:5000. Mass spectrometric analyses were performed in a Bruker Reflex™ TOFMS. The preselector we have developed is of the Bradbury-Nielson type. It consists of a set of electrodes which lay across the ion beam. Ions are gated by applying equal potentials of opposite polarities to adjacent electrodes.

As in any tandem mass spectrometer one of the key specifications is the mass resolution with which precursor ions can be selected. We measured the mass resolution of our preselector using samples of 10 kDa MW PEG. The PEG was measured in linear mode and produced ions at every flight time in the range of interest. As seen in the figure, the ion intensity can be used as a measure of transmission efficiency under various preselector conditions. Measured in this way, the resolution of our preselector was found to be about 120.

However, unlike other spectrometers, the useful mass resolution of the first stage of a tandem TOF mass spectrometer cannot be based simply on the parent ion signal. Although in general the useful resolution of the preselector decreases with decreasing daughter ion mass, we found that our preselector provides high resolution preselection (~100) over a wide mass range.

In practical terms, if one has a peptide mixture with, for example, peptides of mass 990 amu, 1000 amu, and 1010 amu, one can obtain a daughter ion spectrum of each peptide with nearly no interference from the other peptides in the mixture.

1. R. Kaufmann, D. Kirsch, B. Spengler, *Int. J. Mass Spectrom. Ion Process.* **131**, 355(1994).
2. M. Mann, P. Hojrup, and P. Reopstorff, Biol. Mass Spectrom. 22, 338-345(1993).

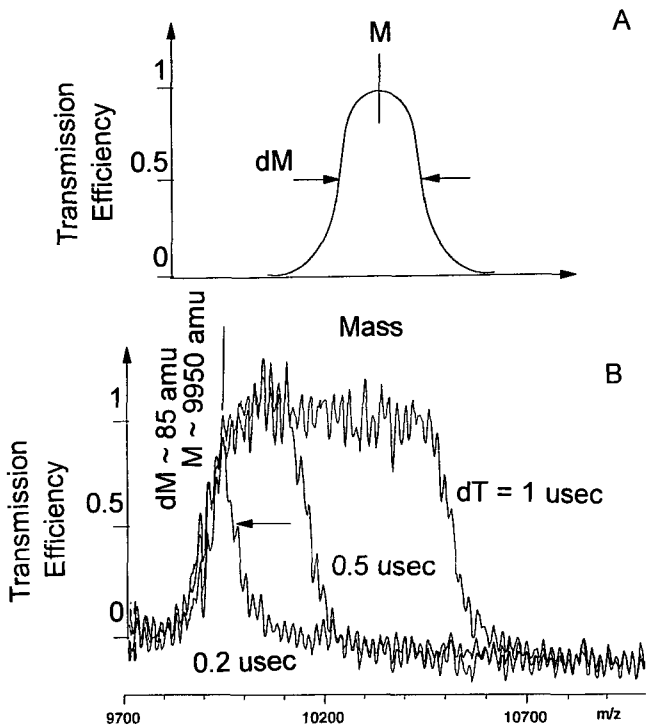

(A) Resolution defined as M/dM where dM is the full width at half transmission efficiency. (B) Measurement of the transmission efficiency of the FAST Filter™ using PEG 10000 and varying width preselection windows.

Probing the Outer Limits of Performance for MALDI-TOF MS and MS-MS

Marvin Vestal, Peter Juhasz, Calvin Blakely, and Stephen Martin
PerSeptive Biosystems, Inc., 500 Old Connecticut Path, Framingham, MA 01701

I. Background. In a very early work Wiley and McLaren [1] described a "time-lag energy focusing" technique for correcting initial velocity distributions in a two-field, pulsed ion source. In this instrument the ions are produced in a field free region, and the accelerating field is turned on by application of a fast pulse at a predetermined delay time after initial ion formation. More recently, Brown *et al.* [2] and Reilly *et al.* [3] have applied similar mass analyzers to MALDI, and have shown significantly improved resolution for selected masses as a function of the delay time and the pulsed field in the ion source. Following the approach of Wiley and McLaren theoretical expressions for the optimum time delay and maximum mass resolution have been derived. Most important prediction of the theory is that the maximum mass resolution scales linearly with the effective length of the TOF analyzer.

II. Experimental. Three geometries were compared in the present study: TOF analyzers of 1.3m (*RP*), 2.1m (*EL*), and 4.2m (*XL*) drift lengths. All of these analyzers were equipped with a single-stage coaxial ion mirror. The delayed extraction ion source had two-stage acceleration. Three high voltage power supplies, a delay generator, and a fast high voltage switch used for delayed ion extraction. This arrangement provided three independently variable parameters: the extraction delay, the field prior to ion extraction, and the extraction field. The high voltage supplies were independently variable up to 30kV *via* 16-bit DACs. The time delay is set by a computer controlled delay generator. The high voltage switch had a transition time of 20 nsec.

III Results. Significantly improved mass resolution was found in delayed extraction MALDI over static MALDI amounting to a factor of four in the linear mode and a factor of two in the reflector mode. Figure 1 compares mass resolution obtained on the 1.3m and the 4.2m analyzers in the linear mode. Although the resolution is clearly proportional with the drift length the proportionality is weaker than linear. In the reflector mode a closely linear relationship was observed as demonstrated in Figure 2. The maximum resolution observed on bovine insulin was in excess of 12000.

Mass accuracy also increased in proportion with the mass resolution. The increase over static MALDI is around 5-10fold.

Chemical noise due to ion fragmentation in the accelerating field is reduced in the delayed extraction experiments. An overall increase in ion stability was verified by the decreased level of metastable ions in the PSD spectra in delayed extraction mode. Signal-to-noise, however, remained the same as in static MALDI due to a less noisy background.

High resolution mass spectra can be obtained for peptide mixtures with delayed extraction in both linear an reflecting analyzers without the severe discrimination often encountered in static MALDI.

Applying a slightly retarding field in the ion source prior to ion extraction has the beneficial effect of substantially reducing the matrix background without compromising the resolution or sensitivity.

References:

1. Wiley and McLaren, *Rev. Sci. Instr.*, *26* (1953) 1150-1157.
2. R. S. Brown, J. J. Lennon, and D. Christie, *Desorption '94*, March 27-31, 1994, Sunriver Lodge, OR, p. 63
3. S. M. Colby, T. B. King, and J. P. Reilly, *Rapid Commun. Mass Spectrom* , *8* (1994) 865-868.

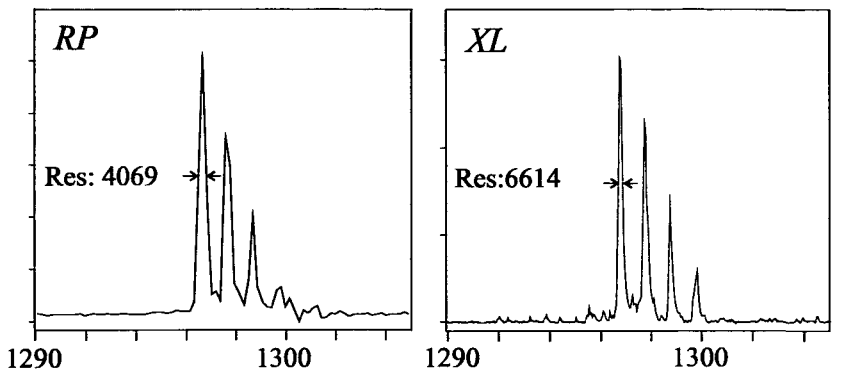

Figure 1 Improved mass resolution in linear MALDI TOF. Comparison of 1.3m (*RP*) and 4.2m (*XL*) analyzers. Sample: angiotensin I, matrix: α-cyano-4-hydroxycinnamic acid.

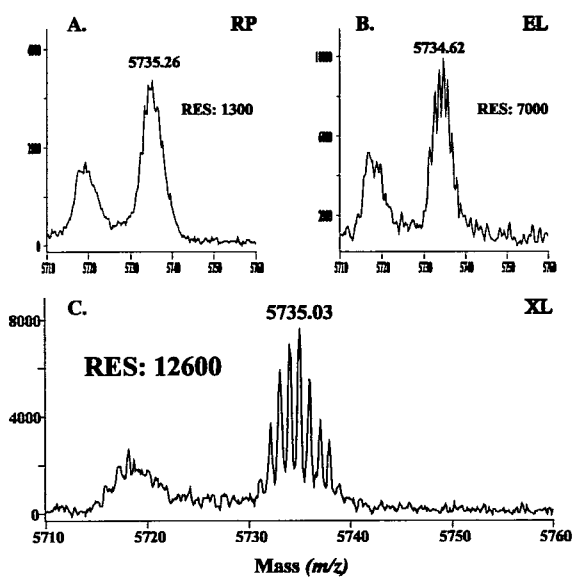

Figure 2 Improved mass resolution in the reflector mode. Comparison of 1.3m (*RP*), 2.1m (*EL*), and 4.2m (*XL*) analyzers. Sample bovine insulin, matrix: sinapinic acid.

ENHANCING RESOLUTION IN LINEAR MALDI-TOF MS

Scot Weinberger, James Kenny and Rich Kornfeld
Hewlett-Packard Company, Bay Analytical Operation, Palo Alto, CA. 94304

Introduction

Much of the popularity of matrix-assisted laser desorption/ionization time-of-flight mass spectrometry (MALDI-TOF MS) is due to its ability to determine molecular weights of polymers, especially biopolymers, present at femtomole levels in complex samples rapidly without significant operator expertise. In most cases linear MALDI-TOF MS produces spectra with resolution that may compromise the ability to assign molecular weight accurately or to differentiate between species of similar mass present in a mixture. One alternative is to use non-linear (reflectron) time-of-flight instruments to correct for peak broadening due to initial kinetic energy distributions. However, such approaches suffer from decreased sensitivity, increased system complexity and cost, and limited resolution improvements above 5 KDa.

This presentation discusses how optimizing sample preparation, laser spot profile , imparted kinetic energy, flight tube pressure, signal processing and data selection improves resolution in linear MALDI-TOF MS. The importance of these factors is tested across a broad molecular weight range(572-66430 Dalton) using the HP G2030A MALDI-TOF MS system and LeCroy 1 GHz oscilloscope

Results Summary

The Table below summarizes the importance of factors affecting resolution at low and high mass and provides a very brief description of the reason for the factor's importance.

Factor	Importance at Low MW (< 2000 Da.)	Importance at High MW (> 10000 Da.)
Sample Preparation	Prepare uniform, flat co-crystals	Minimize unresolvable adducts
Laser Spot Profile	Minimize multi-path trajectories, initial kinetic energy distribution	#
Kinetic Energy (see Fig 1 and 2)	Adjust for best peak profile definition	Maximize kinetic energy for improved sensitivity
Pressure(<10-6 torr)	#	Minimize free flight collisions
Signal Processing (see Fig 3 and 4)	Choose high bandwidth and high data acquisition rate	#
Data selection	Reject poor single shot data	#

- This factor is not of major significance in this mass range.

Resolution improvements range from a factor of five for VPDPR to virtually none for BSA.

Figure 1. Effect of imparted kinetic energy on resolution (100 megasamples/second)

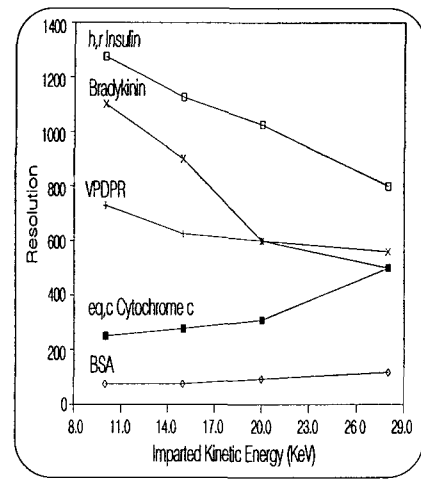

Figure 2. Effect of imparted kinetic energy on resolution (1 gigasamples/second)

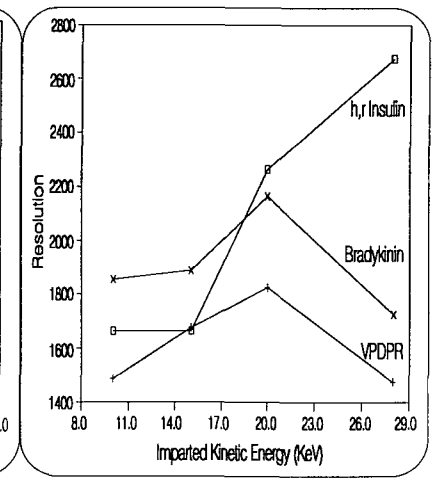

Figure 3. Spectra of VPDPR acquired at 1 gigasamples/sec DAR and 100 MHz(A) or 500 MHz(B) bandwidths

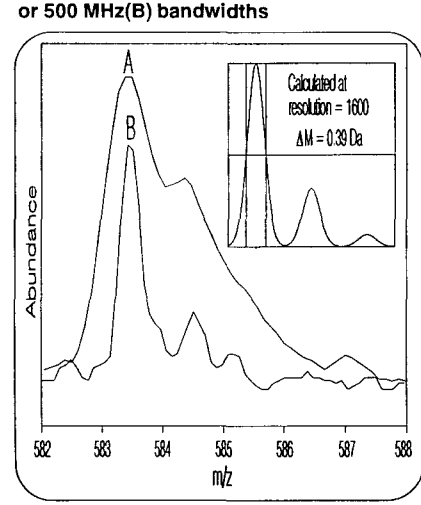

Figure 4. Spectra of bradykinin acquired at 1 gigasamples/sec DAR and 100 MHz(A) or 500 MHz(B) bandwidths

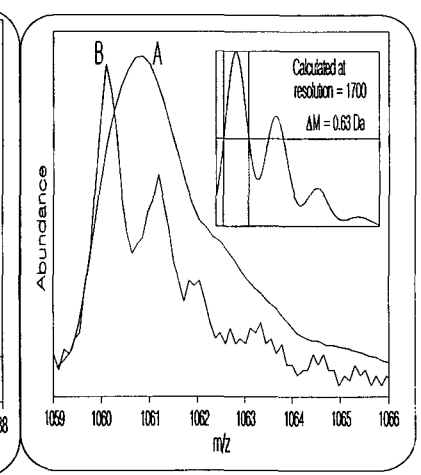

Strategies for LDI/MALDI on a Sector Instrument

John D. Lennon, III, David Shinn†, Richard W. Vachet, Gary L. Glish

Chemistry Department, University of North Carolina, Chapel Hill, NC 27599

†Chemistry Department, North Georgia College, Dahlonega, GA 30597

Introduction:

Laser Desorption Ionization (LDI) and Matrix Assisted Laser Desorption Ionization (MALDI) have both been demonstrated as very useful and sometimes essential ionization methods for studying cluster ions as well as in biological research. To combine the attributes of these ionization methods with those of a sector instrument would lead to several advantages, but is not a trivial matter. It has, however, been realized previously[1,2] through an iterative process by operating the magnet (B) in static mode with an array detector compiling small mass ranges until the complete spectrum is achieved. The work presented here demonstrates another strategy, which will allow for shorter analysis times and less sample consumption. It involves the incorporation of an inductive detector[3] between the electric (E) and magnetic sectors of an EB double focusing sector instrument. In this manner the electric sector can function as a crude time-of-flight (TOF). With the inductive detector triggered by the laser pulse, a complete TOF mass spectrum of the major components of the sample can be obtained with as little as one laser pulse. This quick assessment allows higher resolution spectra to be obtained by either of two methods. One is by operating the magnet in static mode with the Position and Time Resolved Ion Counter (PATRIC) collecting ions within the +/- 4% mass window passed by the magnet. This window is centered around the ion of interest determined from the inductive detector. The other method is by scanning the magnet over a small mass range around the ion of interest using the secondary electron multiplier (SEM).

Experimental:

A Finnigan MAT 900 double-focusing EB sector instrument was modified to include the inductive detector. A 3M fiber optic with a 600μm core diameter is introduced through the GC inlet of the ion volume. The FAB probe was used with a 30° stainless steel tip. A Tektronix TDS 420 oscilloscope was used to collect and display the signal from the inductive detector. A Continuum Surelite II Nd:YAG laser using the third harmonic (355nm) was used for all experiments. The power density was measured to be ~10^7W/cm^2. For the LDI studies, CsI and RbBr were analyzed (data not shown). For the MALDI studies, several small peptides were analyzed. The matrices used include saturated sinapinic acid (SA), 2.5M 2,5-dihydroxybenzoic acid (DHB) and 0.1M α–cyano-4-hydroxy(trans)cinnamic acid (4-HCCA). Trifluoroacetic acid was added to all matrices (0.1%).

Results:

Several known samples were run to obtain a calibration curve, shown in Figure 1, and also to demonstrate the use of the inductive detector to obtain LDI/MALDI spectra. Examples of an inductive detector trace and the corresponding higher resolution spectra (from the PATRIC) are shown in Figures 2a-2c for Substance P. Figure 2c shows the PATRIC spectra of an unknown which was observed in the inductive detector trace. This demonstrates the effectiveness of the strategy.

43rd ASMS Conference on Mass Spectrometry and Allied Topics

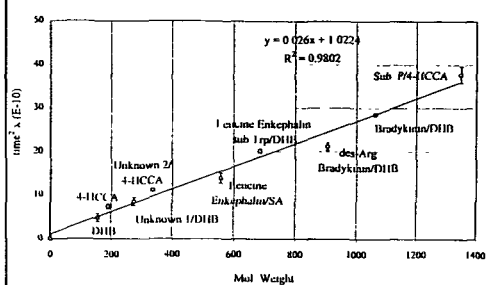

Figure 1. MALDI calibration plot

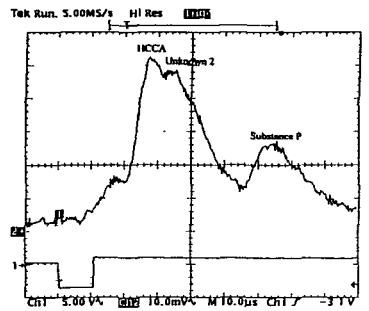

Figure 2a. Inductive detector trace of MALDI of Sub. P/4-HCCA (one laser pulse)

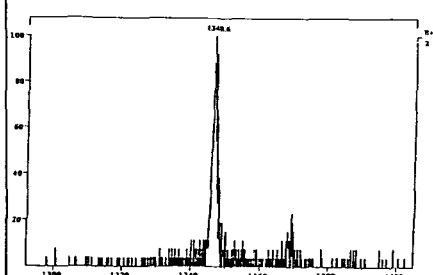

Figure 2b. PATRIC spectrum of Sub. P

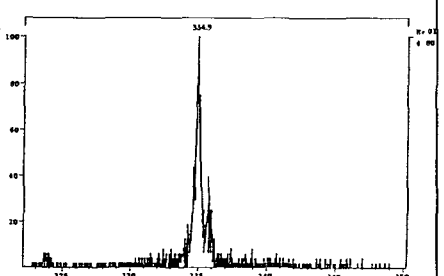

Figure 2c. PATRIC spectrum of an unknown seen in Figure 2a

Conclusion:

A new strategy for obtaining LDI/MALDI spectra on a sector instrument has been demonstrated. With the incorporation of an inductive detector, a quick assessment of the ions present in the sample can be obtained. This knowledge then allows high resolution spectra to be obtained with less analysis time and sample consumption. Although currently the time-of-flight resolution is notably poor, it is sufficient to elucidate the correct mass of the ions of interest with little or no need for adjusting the suspected mass range.

1. R.S. Anan, H.J. Kochling, J.A. Hill, K. Biemann, *Rapid Comm in Mass Spect*, **6**, 298, 1992.
2. R.S. Bordoli, K. Howes, R.G. Vickes, R.H. Bateman and D.J. Harvey, *Rapid Comm. in Mass Spect.*, **8**, 585, 1994.
3. M.A. Park and J.H. Callahan, *Rapid Comm. in Mass Spect.*, **8**, 317, 1994.

High Resolution Array Detection of the Ions Formed by MALDI

Y.Itagaki, T.Fujita, H,Naoki and T.Nakajima
Suntory Institute for Bioorganic Research
Mishima-gun Osaka, Japan 618

Introduction

Recently, Matrix Assisted Laser Desorption Ionization Time-of-Flight mass spectrometry (MALDI) has become important method for desorbing intact molecular ions of large molecules with high sensitivity and much less competition between hydrophilic and hydrophobic compounds in mixture However, the resolution obtained by TOF is low and can cause problem to differentiate mixtures which have small mass difference even at low mass range It has been discussed that the feasibility, the advantages and the disadvantages of the MALDI-array detector equipped double focusing mass spectrometer capability (1,2) to overcome the resolution problem of TOF. They have confirmed the usefulness of MALDI-sector MS observing the high resolution (R=4500 FWHM with substance P) and wide mass range (to 25,000) capabilities. We have also placed MALDI system at the position of ion source of the MS-2 of 4-sector tandem mass spectrometer combined with a focal plane array detector. This system was applied for the analysis of crude natural products such as neurotoxins extracted from spider venom which have mass range 500 to 3000 where monoisotopic separation are required Those data were evaluated together with FAB-sector MS and MALDI-TOF spectra.

Experimental

MALDI-sector MS experiments were performed on the MS-2 of JEOL HX110A/110A tandem mass spectrometer equipped with a focal plane array detector. Nitrogen laser 337nm with 3nsec pulse duration was used for the ionization One spider venom gland was homogenized in 2ml of 0.1% TFA/60% CH_3CN /H_2O solution. After the elimination of M.W. over 3000 using a microcon 3 (Amicon,Inc. Beverly,MA), Samples (1μl or 1/10th conc.1μl solution) were dissolved in a 5μl of saturated DHB in 50/50 (vol.%) EtOH/H_2O solution and potassium(K), oxalic acid or sucrose co-matrix DHB solutions. μ-Column HPLC/Continuous flow FAB/MS experiments were also performed on the same mass spectrometer with the 5μl/min. flow rate. MALDI-TOF spectra were measured on a PerSeptive Biosystems Voyager RP with linear and reflector mode

Results

A resolution of 6300(FWHM) has been achieved for acylpolyamine, $(M+H)^+$= m/z658 and the number of pixels between m/z 658 and 659 was 165 which allows to perform high resolution measurements As a screening method of acylpolyamines from single spider venom, we have established the μ-column HPLC-continuous flow (FRIT)-FAB/MS method (3) and confirmed 39 acylpolyamines were stored in the spider *Nehila clavata* venom gland (Fig.-1) MALDI spectra of the same crude extracts were obtained with the use of K containing DHB and sucrose co-matrix DHB. Both potassium(K) adduct and protonated acylpolyamines peaks were observed but minor substances and the compounds next to major acylpolysmine peaks were not easily identified from a K containing DHB matrix used MALDI spectrum Sucrose-comatrix used MALDI spectrum, on the other hand, the intensities of K attached molecular ions were reduced significantly and increased the intensities of protonated molecular ions. These signal intensity change allows to confirm the existence of minor acylpolyamines (Fig.-2).

Conclusions

MALDI-double focusing mass spectrometer equipped with an array detector was successfully used for the identifications of glutaminergic blocker neurotoxins (acylpolyamines) from crude extracts of a spider venom gland. The addition of K and (K+ sucrose or oxalic acid) to the matrix were effective to confirm the existence of minor toxic compounds because of the competitive formations of cluster ions between samples and sucrose or acid. In this case, clear monoisotopic resolution was necessary to differentiate minor toxic compounds from 1 to 2 Da different major toxins. MALDI-sector MS spectra were compared with the μ-column LC-FAB/MS, Static FAB/MS and MALDI-TOF spectra and showed its advantages and capabilities of a mixture analysis.

1) R.A.Annan, H.J.Kochling, J.A.Hill and K.Biemann, Rapid Commun. Mass Spectrom. **6**,298(1992)
2) R.S.Bordoli, K.Howes, R.G.Vickers, R.H.Bateman and D.J.Harvey, Rapid Commun. Mass Spectrom. **8**,585 (1994)
3) Y.Itagaki, T.Fujita, H.Naoki, Y.Naya and T.Nakajima, Proceedings of the 42nd ASMS Conference on Mass Spectrometry and Allied Topics, p162 (1994) Chicago Il

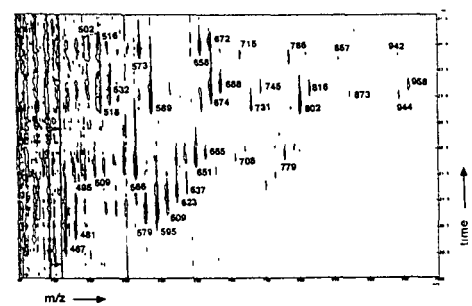

Fig.-1 2D Mass chromatogram of $(M+H)^+$ ions of *Nephila clavata* venom extracts

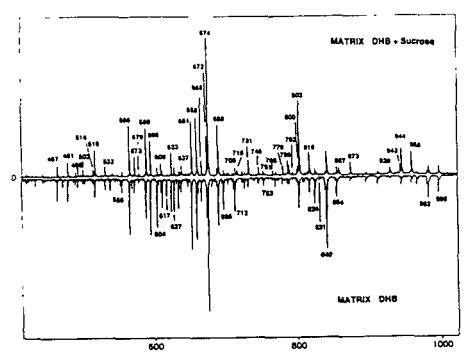

Fig.-2 Comparison of DHB and sucrose added matrices MALDI spectra of crude venom extracts

Accurate Mass Determination with MALDI/FTMS using Internal Standards

Carlito B Lebrilla, Steven T, Fannin, Jiangyue Wu, Melanie A. Franklin, Tadeusz F. Molinski
Department of Chemistry, University of California, Davis, CA 95616

An important feature of mass spectrometry is the capability for providing the exact mass of an ion and therefore allowing absolute identification of its elemental composition High resolution mass spectrometry is necessary for this type of analysis. Accurate mass determination is typically performed with multiple focusing instruments or Fourier Transform Mass Spectrometry (FTMS).

Experiments have been performed for the accurate mass determination on a group of biologically active cyclic bromotyrosine derivatives known as Bastadins. These compounds were extracted from *Ianthella Basta*, a marine sponge collected on the Great Barrier Reef.[1] Accurate mass measurements were performed on known and two unknown Bastadins using an internal standard, two calibrant technique with an external source Quadrupole FTMS system.[2,3] Matrix Assisted Laser Desorption Ionization (MALDI) was chosen as the ionization technique due to its inherent ability for producing very little fragmentation and instead favoring pseudomolecular ion formation of thermally labile compounds. In this regard MALDI has proven to be particularly useful for biological applications.

Accurate mass determinations in FTMS require that the frequencies of the ions be stable. If external calibrants are to be used, then the frequencies must remain constant for a long period of time. With internal calibrants, the frequencies must be stable only during the detection period (typically less than a few seconds). Such factors as the homogeneity of the magnetic field and the static electric field used for the trapping potential, can affect the stability of the ion's cyclotron frequency Although the 3 Tesla superconducting magnet used in our laboratory provides less than 20 ppm mass accuracy using external calibrants, it does not fulfill the rigorous requirement for publications of new compounds (5 ppm or less). In these cases, an internal calibration technique is necessary to obtain accurate masses

Figures 1 and 2 show examples of spectra using an internal standard, two calibrant technique for two unknowns, a newly isolated Bastadin (unknown # 1) and its permethylated derivative (unknown # 2), respectively. The internal standards used for these experiments were α-Cyclodextrin (maltopentaose for unknown # 1) and Gramicidin S These calibrants were chosen primarily for the mass range of interest and to bracket the mass of the sample as closely as possible. Rigorous experiments have not yet been performed to determine the largest possible mass range between the two calibrants that would still provide acceptable results.

Multiple mass measurements of the unknown permethylated Bastadin were performed (Table1) and an average value of the exact mass was obtained corresponding to 1014 9143. The closest molecular formula for the unknown is $C_{38}H_{36}Br_4N_4O_8Na$, which has a theoretical mass of 1014.9164 producing a deviation of only 2 1 +/- 1.5 ppm. Based on these results and NMR data this compound was determined to be the tetramethyl derivative of a new Bastadin, referred to as Bastadin 20.

[1] Mack, M.; Molinski, T F , Buck, E.D., Pessah, I N. *J Biol Chem.* **1994**, 269, 23236 - 248
[2] McCullough,S.M., Gard, E , Lebrilla, C.B *Int. J Mass Spectrom Ion Processes* **1991**, 107, 91 -102
[3] Wu, J.; Fannin, S.T.; Franklin, M.A., Molinski, T.F.; Lebrilla, C.B *Anal Chem.* **1995**, In Press

Figure 1 **Figure 2**

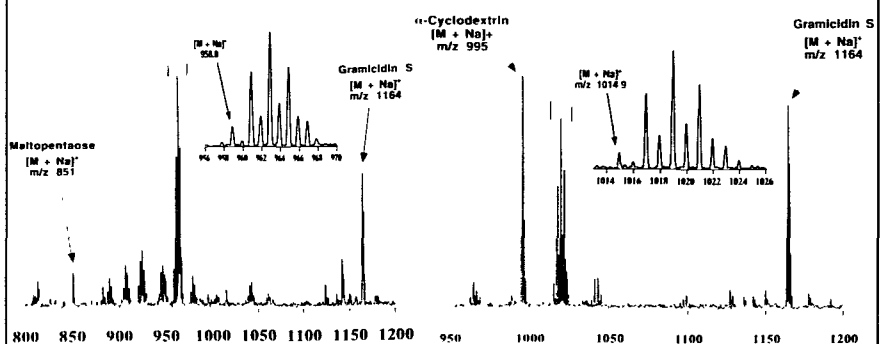

Unknown # 2 Results

For Unknown # 2 multiple determinations were used and a different internal calibrant (α-Cyclodextrin). The table below shows the results of three determinations for the $[M + Na]^+$ ion and four sodiated [A + 2] ions. This cluster represents a compound containing four Bromine atoms. The exact mass values in the table are for a compound with a molecular formula of $C_{38}H_{36}Br_4N_4O_8Na$.

Expected mass	Absolute Deviation(ppm) in each Determination #1	#2	#3	Average
1014.9164	-3.4	-0.4	-2.4	1014.9143
1016.9144	2.6	3.5	9.4	1016.9197
1018.9124	2.6	2.6	5.5	1018.9160
1020.9103	2.6	5.6	7.5	1020.9157
1022.9083	1.7	-3.2	-1.3	1022.9073

Table 1

Ion Coupling in High Resolution MALDI FT/ICR Mass Spectra of Biopolymers

Ljiljana Paša-Tolić, Shenheng Guan, George Jackson, Hyun Sik Kim,#
Yulin Huang and Alan G. Marshall*

Center for Interdisciplinary Magnetic Resonance, National High Magnetic Field Laboratory, Florida State University, 1800 E. Paul Dirac Dr., Tallahassee, FL 32310

* Department of Chemistry, Florida State University
#Department of Chemistry, The Ohio State University

Quasimolecular peptide $(M+H)^+$ and oligonucleotide $(M-H)^-$ ions, generated by matrix-assisted (DBA/fructose and HPA) laser desorption/ionization (frequency-tripled Nd:YAG or pulsed N_2 laser), are cooled and axialized[1] by azimuthal quadrupolar irradiation in the presence of argon collision gas in the source compartment of a dual cubic Penning trap. Following ion transfer to the low-pressure "analyzer" trap, and optimization of various experimental parameters (source trap gating; source trap pressure; source trap azimuthal quadrupolar excitation duration and amplitude; trapping potential) high FT-ICR mass resolving power and mass accuracy in the low ppm range are obtained for ions generated *inside* a 3.0 tesla selenoidal magnet (Fig. 1).

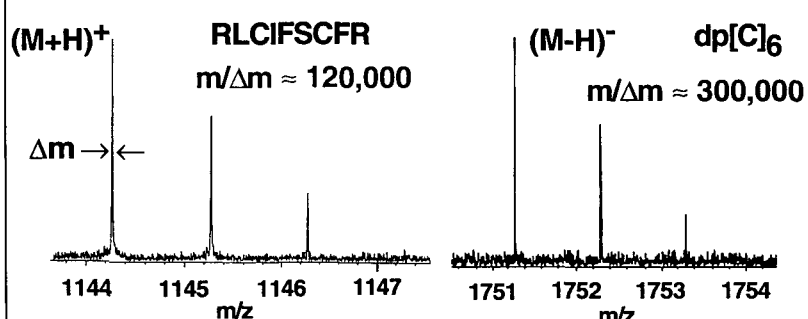

Figure 1. Representative high resolution MALDI FT-ICR magnitude-mode mass spectra of a nonapeptide, Arg-Leu-Cys-Ile-Phe-Ser-Cys-Phe-Arg (left), provided by S. Gaskel, and an oligonucleotide, pd[C_6], (right). The experimental event sequence and parameters work equally well for other samples in the same m/z range.

High mass resolution is important for resolving adducts and chemical modifications of a peptide/protein or oligonucleotide/DNA, and for facile determination of the degree of deuteration from an H/D-exchange experiment. Time-domain signal damping may arise from unimolecular decomposition, collisions of ions with background neutrals, and spatial inhomogeneity of the electric and magnetic fields inside the ICR trap. Here, ions are generated with laser power just above the threshold for ion formation; ions are then decelerated by gated trapping, and further cooled and axialized. After ion transfer to the analyzer half of the dual trap, collisional relaxation at ~1-2 x 10^{-9} torr is slow, and the time-domain ICR signal persists for approximately one minute. However, distortion of the overall electric potential in the trap from a three-dimensional axial quadrupolar potential, generated by the presence of many ions in a Penning trap, produces two undesirable effects. First, the FT-ICR mass spectral peaks are inhomogeneously broadened; for heavy ions, the instantaneous ICR frequency drifts during detection because the electric potential shape changes with ion radius. Frequency drift may be compensated and virtually eliminated[2] to yield ultrahigh mass resolving power. Second, ions of nearly equal cyclotron frequency couple by their Coulomb interaction to become synchronized to a single ICR frequency. Coalescence of closely-spaced resonances to form a single FT-ICR mass spectral peak whose width is less than the separation between its constituent ion resonances is illustrated (Fig. 2) by the high resolution spectrum of deuterated leucine enkephalin and a simulated spectrum for a Lorentzian peak with the same line width and degree of deuteration (deconvoluted from experimental data). Preliminary ion trajectory calculations (Simion 6.0) confirm that Coulomb-mediated interactions result in coupling of closely spaced resonances for high-mass ions under typical FT/ICR MS operating conditions. Coalescence may be counteracted by reducing the number of ions, and by increasing the magnetic field strength and/or ICR orbital radius.[3] Work supported by NSF (CHE-93-22824), NIH (GM-31683), and the National High Magnetic Field Laboratory at Florida State University.

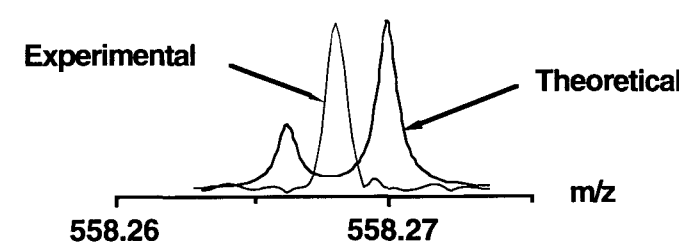

Figure 2. Coulomb-mediated coalescence in a MALDI FT-ICR high-resolution magnitude-mode mass spectrum of partially deuterated leucine enkephalin. Although experimental mass resolving power is high (m/Δm ~ 500,000), the $^{12}C^2H/^{13}C^1H$ doublet is not resolved (compare to the theoretical doublet computed from two magnitude-mode Lorentzians whose widths are the same as the experimental peak width), due to Coulomb interactions between ions of nearly identical mass-to-charge ratio.

1. S. Guan, H. S. Kim, A. G. Marshall, M. C. Wahl, T. D. Wood, and X. Xiang, *Chem. Rev.* **1994**, *8*, 2161-2182.
2. S. Guan, M. C. Wahl, and A. G. Marshall, *Anal. Chem.* **1993**, *65*, 3647-3653.
3. Y. Naito and M. Inoue, *J. Mass Spectrom. Soc. Jpn.*, **42**, 1 (1994).

Peptide Mapping and Sequence Analysis by MALDI FT-ICR Mass Spectrometry

Touradj Solouki, Ljiljana Paša-Tolić, George S. Jackson,* Shenheng Guan* and Alan G. Marshall*

Center for Interdisciplinary Magnetic Resonance, National High Magnetic Field Laboratory, Florida State University, 1800 E. Paul Dirac Dr., Tallahassee, FL 32310

* Department of Chemistry, Florida State University

One of the advantages of matrix-assisted laser desorption ionization (MALDI) is the ability to generate peptide and protein ions for the direct analysis of relatively impure samples such as enzymatic digest solutions. To date, most MALDI-based peptide mapping and sequence analyses of proteins have employed time-of-flight instruments. However, the low mass resolution of the TOF technique severely limits mass measurement accuracy. Here, we present MALDI FT-ICR mass analysis of enzymatic digest mixtures. In a simple extraction scheme, the tryptic digest solutions are crudely purified by using sep-pack C18 mini-extraction columns. The resulting mixtures are mass-analyzed with a 3 tesla Waters Extrel FTMS-2000 dual-trap FT-ICR mass spectrometer.

Apart from the direct information obtained from the high-resolution mass spectrum, the collision-induced dissociation (CID) and MS^n capabilities of FT-ICR help to determine the amino acid sequence of the fragment ions beyond what is obtained from enzymatic digestion. Moreover, by combined use of ion axialization excitation and remeasurement techniques,[1,2] mass spectra may be obtained from sub-femtomole quantities of peptide samples. Figure 1 shows MALDI FT-ICR mass spectra obtained from femtomole amounts of cytochrome c (horse) tryptic digest solution ionized by a single N_2 laser shot (Model VSL-33ND, Laser Science, Inc., Newton, MA) in the source-side trap (~2 x 10^{-7} torr argon collision gas). The top spectrum shows a representative positive-ion mass spectrum of tryptic digest products. The second spectrum from top shows a selected ion (at m/z 1616) after isolation by SWIFT excitation, axialization, and detection. The third remeasured mass spectrum contains a CID product (MS/MS) after SWIFT isolation (at m/z 1487, loss of lysine excluding NH_3) followed by axialization. Ion dissociation was induced by sustained off-resonance irradiation (SORI) at ~800 Hz below the reduced ion cyclotron frequency of the parent ion; excitation duration and amplitude were optimized for each experiment to maximize the product ion signal magnitude. Finally, a second SORI yielded CID products of the same batch of ions (at m/z 1487); after a series of axialization/remeasurement cycles the MS/MS/MS from the same initial batch of ions was obtained. *These are the first MS^n results that show real-time display of gas-phase fragmentation of the biomolecular ions for several stages of CID from a single batch of ions by use of repeated remeasurements.* Work supported by NSF (CHE-93-22824), NIH (GM-31683), and the National High Magnetic Field Laboratory at Florida State University.

1. R. R. Williams, K. D. Henry, F. W. McLafferty, *J. Amer. Chem. Soc.* **1990**, *112*, 6157-6162.
2. T. Solouki, S. Guan, J. A. Marto, F. M. White, and A. G. Marshall, this volume, ThPF 202.

All 4 Mass Spectra Obtained from a Single Laser Shot!

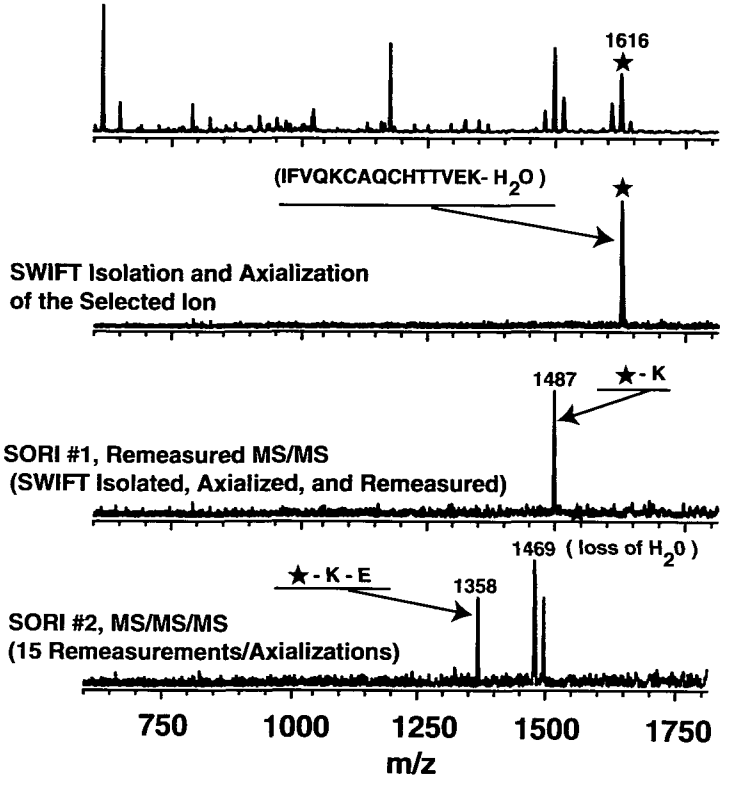

Figure 1. MALDI FT-ICR mass spectra of cytochrome c horse tryptic digest, with dihydroxybenzoic acid matrix (1000:1 molar ratio). Selected ions at m/z 1616 were isolated by SWIFT (second from top) radial ejection. MS/MS (third from top), and MS/MS/MS (bottom spectrum) were obtained from the same batch of ions as in the top mass spectrum; the product fragment ions (*viz.*,★ - K) of the selected parent ion (★) were axialized and remeasured. Finally, MS/MS/MS was performed and the product ions, were axialized, and remeasured. Note that for MS/MS/MS analysis, ions were remeasured 15 times and axialized between each remeasurement.

Attomole Biomolecule Detection by Remeasured MALDI FT-ICR Mass Spectrometry

Touradj Solouki, Shenheng Guan, Jarrod A. Marto#, Forest M. White*, and Alan G. Marshall*

Center for Interdisciplinary Magnetic Resonance, National High Magnetic Field Laboratory, Florida State University, 1800 E. Paul Dirac Dr., Tallahassee, FL 32310

* Department of Chemistry, Florida State University
#Department of Chemistry, The Ohio State University

We present a combination of two methods that significantly improve sensitivity for analysis of biomolecules by MALDI FT-ICR mass spectrometry: (a) sample deposition onto small indentation on the probe tip, and (b) multiple remeasurement of axialized ions. Laser desorption/ionization was performed with a Laser Science, Inc. cartridge-type pulsed N_2 laser (Model VSL-33ND, Newton, MA) operating at a wavelength of 337.1 nm with a pulse width of 3 ns. FT-ICR mass spectra were acquired at 3.0 tesla with a dual-trap Waters Extrel FTMS-2000 (Extrel-Waters, Madison, WI) instrument.

To reduce the amount of sample deposited on the probe tip, we constructed a probe tip with series of small indentations, such that attomoles of sample could be placed on these small spots. A Vickers microhardness tester (series 200 Wilson-Tukon) was used to confirm that the indentations were aligned with the laser beam. To mark the sample probe tip at the laser focal point, we applied a thin film of 4-nitroaniline on the probe tip and several laser shots were fired to remove the organic layer at different probe rotational positions; these laser spots were identified and marked under the diamond-tipped microhardness tester with 1000 kg load. The probe tip and indentation marks (~100 micron deep and ~5 x 10^{-4} mm^2 area) are shown schematically in Fig. 1. Two pins were used to lock the position of the probe tip onto Extrel's standard autoprobe. Results were highly reproducible from one marked spot to another, confirming the laser alignment accuracy and spot placement.

The FT-ICR detection limit was further reduced by combining azimuthal quadrupolar excitation in the presence of collisional cooling to axialize the ions,[1] with repeated ion remeasurement.[2,3] Ion multiple remeasurement enhances the signal-to-noise ratio and thus lowers the detection limit achievable with FT-ICR. Representative mass spectra for ~8 attomoles of substance P, applied to the sample probe, from a single data acquisition (top) and accumulation of time-domain signals from 40 repeated measurements (bottom) are shown in Figure 2. To date, eight attomoles is the lowest reported detection limit for MALDI FT-ICR/MS. Work supported by NIH (GM-31683) and the National High Magnetic Field Lab at Florida State University.

1. S. Guan, H. S. Kim, A. G. Marshall, M. Wahl, T. D. Wood, and X. Xiang, *Chem. Rev.* **1994**, *8*, 2161-2182.
2. E. R. Williams, K. D. Henry, and F. W. McLafferty, *J. Amer. Chem. Soc.* **1990**, *112*, 6157-6162.
3. J. P. Speir, G. S. Gorman, C. C. Pitsenberger, C. A. Turner, P. P. Wang, and I. J. Amster, *Anal. Chem.* **1993**, *65*, 1746-1752.

43rd ASMS Conference on Mass Spectrometry and Allied Topics

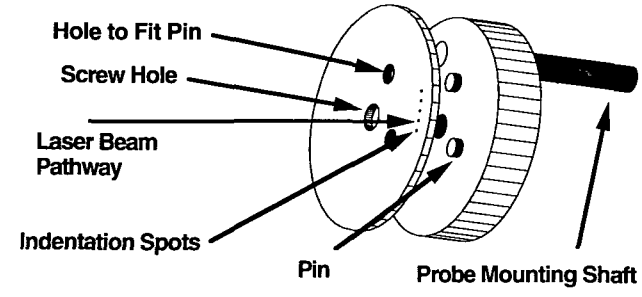

Figure 1. Modifications to a standard Extrel autoprobe. The indentation spots are located at positions 1-5 and are five degrees apart.

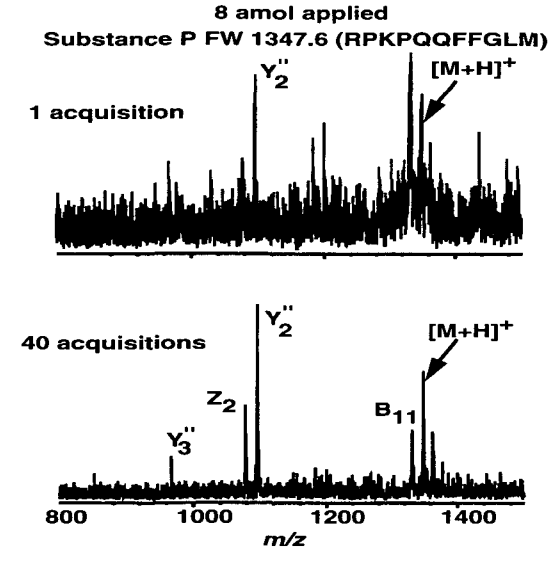

Figure 2. MALDI FT-ICR/MS for 8 attomoles of substance P applied to the sample probe. The sample solution contained 2,5-dihydroxybenzoic acid, fructose, and substance P with a relative molar ratio of ~10^9:10^8:1.

High Mass Analysis in Fourier Transform Mass Spectrometry

Jie Yao, Salvador J. Pastor, Charles L. Wilkins,
Department of Chemistry, University of California-Riverside, Riverside, CA 92521, USA

Matrix assisted laser desorption/ionization (MALDI) is a widely utilized technique allowing the detection of ions with masses as large as several hundred thousand daltons. In the past, time of flight mass spectrometers have been the instruments of choice for such applications. Recently, MALDI has been combined with Fourier transform mass spectrometry (FTMS), which is capable of high resolving power, precise mass measurement, ion remeasurement, and simultaneous detection of all ions. However, a current limitation of MALDI-FTMS mass spectral measurements is the inherent difficulty in trapping high mass species. Due to the MALDI desorption process, molecules and ions are ejected from the matrix surface with kinetic energies that scale directly with their mass.[1] As a consequence, ions of higher m/z and thus higher kinetic energies are inefficiently trapped by the low voltage trapping potentials that are standard to the FTMS experiment. The trapping problem was partially solved by introduction of a gated trapping protocol in which a 9-volt deceleration potential was applied to the rear trap plate of a cubic cell to slow ions that were entering the cell. Using this method, Castoro and co-workers[2,3] were able to show the successful analysis of singly charged biomolecules with molecular masses as great as that of carbonic anhydrase (MW = 29,000). For higher mass ions it was necessary to increase the trapping voltage and to average multiple spectra in order to improve the signal-to-noise ratio since very few ions were being trapped.

In an attempt to further extend the detectable mass range of singly charged ions using MALDI-FTMS, we have designed an electrostatic field deceleration method where decelerating voltages up to 75 volts are applied not only to the rear trap plate of the source side of a dual cubic cell, but also to the excitation and receiver plates of the cubic cell. This "five-plate" trapping method shows improved trapping efficiency during the ionization event. Simulations (MacSimion, Version 2.03, Montech Pty Ltd., Monash University, Victoria, Australia) show that application of voltages to five plates of the FTMS cell forms a "cuplike" electrostatic field in which ions can be more efficiently trapped. Simulated ion calculations show a much improved potential surface that is conducive to better trapping because off-axis ions are less likely to be ejected (neutralized on cell plates). Figure 1 is a simulation of the field map which results if 50 volts are applied to the rear trap plate and 20 volts to both the excitation and receive plates. The 5-plate trapping approach does not require cell modification. Instead, DC pulses and excitation pulses are separated in time and controlled by existing FTMS software. This setup allows maximum flexibility and control for an FTMS experiment without impairing the ability to do lower mass high resolution work.

When this 5-plate trapping method is applied, high mass ions with large translational kinetic energies can be trapped efficiently and detected. Using this approach, low resolution spectra of carbonic anhydrase (MW=29,000), egg albumin (MW=45,000), and bovine albumin (MW=66,000) have been obtained. Because the new decelerating method requires no modification to the existing cell, it is also possible to obtain high resolution spectra for compounds with masses of ca. 14,000 daltons and lower. Utilizing the 5-plate trapping method, a bovine insulin spectrum with a resolving power of 20,000 was obtained. It is not yet possible to obtain higher resolution for the higher mass proteins. Some of the probable causes of the poor mass resolution include the large collisions with neutrals, possible enhancement of metastable decay of the molecular ions as a consequence of internal excitation during the MALDI process, and difficulties in exciting high mass ions into coherence.

The axialization technique has provided particularly useful for enhancement in mass resolving power.[4,5] In a typical axialization experiment, a quadrupolar r. f. field at the unperturbed cyclotron frequency of ions is applied to the excitation and receive plates, thereby converting ion magnetron motion into

cyclotron motion. The present buffer gas cools the ions through ion-neutral collisions, thus driving ions to the center of the cell. In this paper, we combine the axialization technique and 5-plate trapping method to improve mass resolving power. High mass ions are formed by laser desorption/ionization and trapped by 5-plate trapping field. Then ions are axialized in the source cell in the presence of buffer gas and transfered to the analyzer cell for high resolution detection.

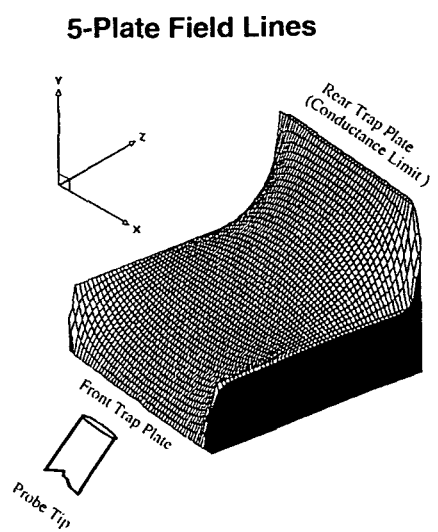

Figure 1: Five-plate trapping field lines calculated by MacSimion (Version 2.03, Montech Pty Ltd., Monash University, Victoria, Australia) for 50 V on the rear trap plate and 20 V on both the excitation (yz-plane) and receive (xz-plane) plates. The magnetic field lies along the z-axis.

1. Beavis, R.C.; Chait, B.T. *Chem. Phys. Lett.* **1991**, *181*, 479-484.

2. Castoro, J.A.; Koster, C.; Wilkins, C. L.*Rapid Commun. Mass Spectrom.* **1992**, *6*, 239-241.

3. Castoro, J.A.; Wilkins, C.L.; *Anal. Chem.* **1993**, *65*, 2621-2627.

4. Guan, S.; Wahl, M.C.; Marshall, A.G. *Anal. Chem.* **1993**, *65*, 3647-3653.

5. Pastor, S.J.; Castoro, J.A.; Wilkind, C.L. *Anal. Chem.* **1995**, *67*, 379-384.

Further improvement of Mass Accuracy in MALDI reTOF MS of Peptides

O. Vorm, P. Mortensen, and M. Mann
European Molecular Biology Laboratory (EMBL)

Introduction

We show how spectrum calibration can be carried out routinely and computer automated using only matrix peaks and giving no apparent error. Thus odd peak shapes becomes the main source of error. However, when "fast evaporation" sample preparation is used along with a reflecting TOF instrument, peptides in the mass range up to 2500 Da are usually analyzed with isotope resolution and well defined peak shapes.
In combination, a mass accuracy around 50 ppm is routinely obtained without the use of internal standards, even for demanding samples such as peptide maps obtained from subpicomole amounts of proteins isolated by SDS-PAGE.

Methods

Sample Preparation: Micro-crystalline matrix surfaces were prepared by the fast evaporation procedure (1, 2) we presented at ASMS '94.
Mass Spectrometry: All mass spectra were obtained on a modified Bruker REFLEX TOF Mass Spectrometer (Bruker-Franzen Analytik, Bremen, Germany). The original data acquisition system was replaced by a LeCroy 9350AM 1 gigasamples/sec digital storage oscilloscope (LeCroy Corporation, Chestnut Ridge, NY, USA) from where single shot spectra were transferred to a Macintosh PowerMac 7100/80 computer (Apple Computer Inc., Cupertino, CA, USA) via a National Instruments NI DAQ GPIB controller board (National Instruments, Austin, TX, USA). Control of all data acquisition parameters, the transfer and subsequent averaging of spectra as well as all further data processing was carried out using the computer program "LaserOne" developed in-house. LaserOne takes advantage of the features in AppleScript™ All automation of data recording, calibration and exchange of data with other computer applications was accomplished via scripts.
Detector Gating and Spectrum Calibration: Detector bias gating (3) has been developed in-house to avoid charge depletion in the detector. A further advantage is, that the lower value of the gated bias potential can be set to enable the clear and noise-free detection of the most prominent matrix ion signals while keeping these signals within the dynamic range of the device used for recording the TOF trace. This feature, when combined with the surface sample preparation procedure, yields well defined matrix ion signals with high resolution and symmetrical peaks. Consequently, a multi-point least-mean-squares fit to the measured flight times and calculated masses of several matrix peaks can be used for an accurate time to mass calibration of the spectrum. Since the low mass signals also appear highly reproducibly from sample to sample the fitting parameters were easily and reliably obtained by a computer algorithm without human control.

Conclusions

- The time to mass conversion of MALDI TOF spectra can be based on multiple matrix peaks. The procedure is easily automated and virtually always yields reliable calibration.
- The calibration contributes very little to the experimental error, and the remaining cause of error is poorly defined peak shape of the measured signal.
- Easy MALDI samples are usually measured with an accuracy better than 0.05 Da.
- Even for rather challenging samples, an accuracy better than 0.1 Da is typically achieved for the full range of isotope resolved peaks in MALDI reflector TOF spectra.

43rd ASMS Conference on Mass Spectrometry and Allied Topics

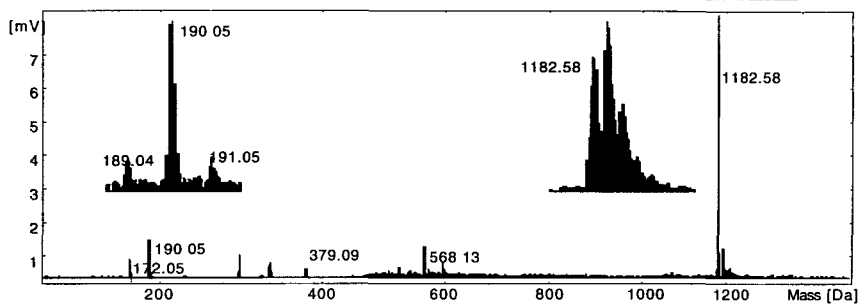

Fig. 1 MALDI reflector TOF spectrum of the peptide LHRH (calc. monoisotopic MH^+ 1182.581) recorded with detector gating, where the detector turned fully active after m/z 450. The left insert in the spectrum is a zoom of the matrix monomer peaks and the right insert is the isotope cluster of LHRH.

Fig. 2 Mass error (in Da) in peptide maps of proteins isolated by SDS-PAGE.

As a statistical example for calculating our mass accuracy for "real-life" samples, we examined all the peptide maps obtained from digests of proteins that were isolated by SDS-PAGE and subsequently identified by MALDI-MS and database search at EMBL from January to May of '95. This corresponds to roughly 500 identified peptides from around 50 identified proteins. In most cases subpicomole amounts of protein were present in the gel (as judged by the stain) and low femtomole amounts were applied to MALDI-MS. Several of the used peptide maps were recorded, calibrated and stored automatically as batch runs without operator interaction.

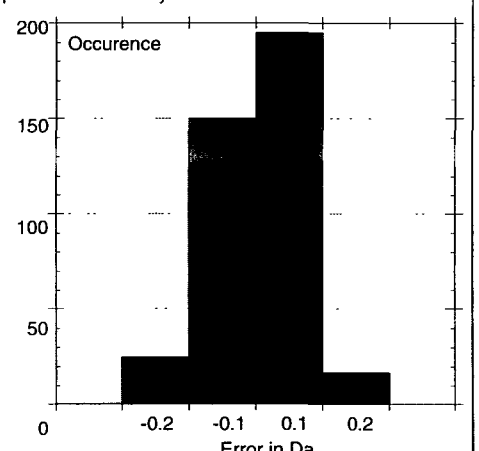

1) Vorm, O., Roepstorff, P., and Mann, M. "Improved resolution and very high sensitivity in MALDI TOF of matrix surfaces made by fast evaporation." Anal. Chem. (1994) 66, 3281-3287.
2) Vorm, O. and Mann, M. "Improved Mass Accuracy in Matrix Assisted Laser Desorption/Ionization Time-of-Flight Mass Spectrometry of Peptides" J. Am. Soc. Mass Spectrom. (1994) 5, 955-958.
3) Introduced for MALDI by B. T. Chait: "Matrix assisted laser desorption of proteins", at the 4th. Sanibel Conference on Mass Spectrometry, Jan. 25.-28 1992, Sanibel Island, Florida.

Orthogonal Injection MALDI

R. G. Dworschak, W. Ens, V. Spicer, K. G. Standing, A. V. Verentchikov
Dept. of Physics, University of Manitoba, Winnipeg, Manitoba, Canada, R3T 2N2

As described in an accompanying abstract [1] there is considerable advantage to decoupling the desorption process from the extraction process in matrix-assisted laser desorption/ionization by time-of-flight. This reduces the metastable decay caused by collisions in the plume, and allows time-lag focusing as described by Wiley and McLaren [2]. Improved resolution in the linear mode has already been demonstrated using delayed extraction in the axial geometry [1]. However, based on the success of orthogonal injection in our electrospray-TOF instrument [3], we believe even greater improvement is possible using orthogonal-injection in combination with an ion mirror. Since the plume in MALDI is forward-directed, the velocity and spatial spreads orthogonal to the plume should be considerably smaller than in the parallel direction. We have exploited the fact that a time-of-flight instrument is relatively insensitive to spreads orthogonal to its axis.

We have constructed a source geometry almost identical to the one used in our ES/TOF instrument [3], but with the final aperture of the ES apparatus replaced by a target probe integrated with the acceleration rings so as not to perturb the field. Ions are desorbed from the probe in zero field by a laser pulse and are allowed to drift to the axis of the spectrometer where they are injected into the DC extraction region by a pulse applied to the back electrode. The back electrode and the pulsing electronics may be floated up to 30 kV, and the final grid is grounded. Figure 1 shows a schematic of the source, acceleration and drift region of our instrument. The computer triggers the digital delay generator which simultaneously starts the transient recorder, fires the laser and triggers the extraction pulse. Note that the drift region is only 37 cm in this prototype instrument.

The source has recently been completed and spectra of molecular ions of matrix, benzoperylene, melittin, insulin and myoglobin have been extracted in a short linear TOF spectrometer. Figure 2 shows the minimum peak widths of 10, 20, 40 nS for the molecular ion peaks of matrix, insulin, and myoglobin respectively. These spectra were obtained by optimizing the extraction pulse voltage with a fixed acceleration voltage of 15 kV and a laser spot size of approximately 1 mm. In addition to the improved resolution, prompt fragmentation is observed with melittin.

1. W. Ens et al, these proceedings and references therein.
2. W C. Wiley and I. H. McLaren, Rev. Sci. Instrum. 26 (1955) 1150
3. A. N. Verentchikov et al, Anal. Chem. 66 (1994) 126

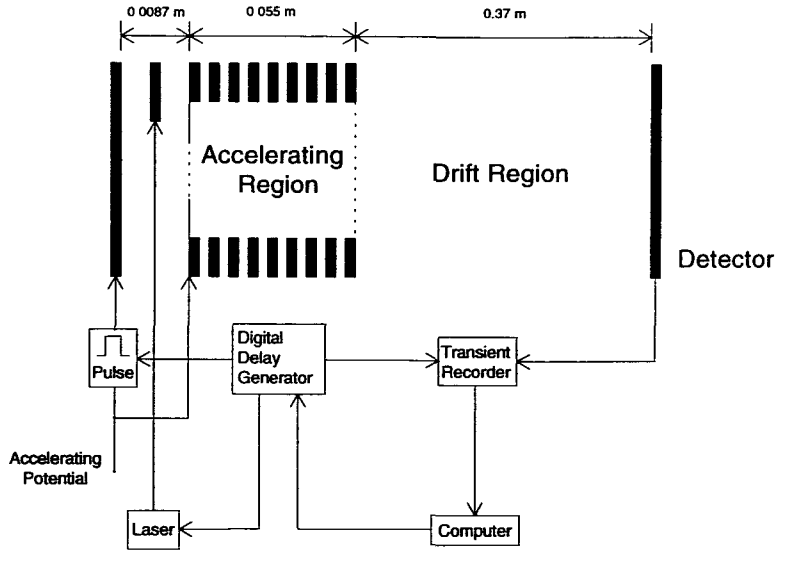

Figure 1 : Schematic diagram of the orthogonal injection MALDI spectrometer

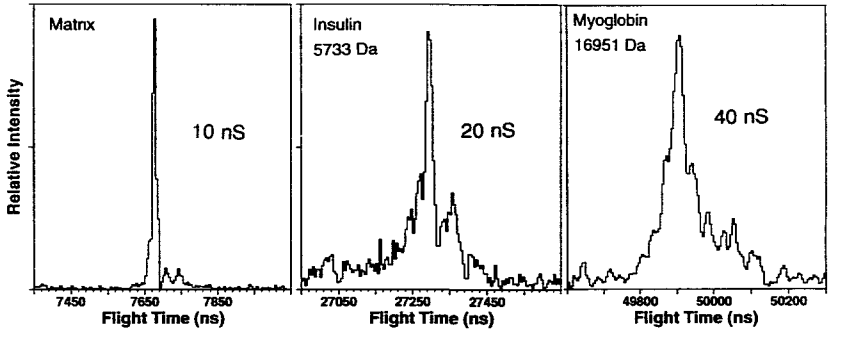

Figure 2: Molecular ion peaks of matrix, insulin, and myoglobin obtained with orthogonal injection MALDI shown with respective peak widths.

A Charge Detector for High Mass MALDI Ions

Carsten Lautz, Ute Bahr, Ulrich Röhling and Franz Hillenkamp

Institute for Medical Physics and Biophysics
University of Münster
48149 Münster, FR Germany

For several years the new ionisation method MALDI has been used for the analysis of large bioorganic molecules. In the case of MALDI the molecular ions - up to 300,000 Da - are for the most part singly charged and analyzed by time-of-flight (TOF) mass spectrometers. For detection of the ions, discontinuous secondary electron multipliers (SEM), microchannelplates (MCP) or combinations of both are used.

The major problem in the detection of high mass ions is the low efficiency of ion/electron conversion due to the low impact momentum of the ions on the detector surface. P W Geno et al [1] measured a "threshold" velocity of 10^4 m/s for an efficient ion/electron conversion for smaller ions, to achieve this velocity molecules of 10 kDa mass require an acceleration potential of 5 kV, molecules of 55 kDa mass (Albumin) already one of 30 kV. Using high acceleration voltages causes insulation problems and short flight times of the ions requiring fast and expensive A/D-converters. Postacceleration by conversion dynodes in front of the detector often decreases the mass resolution, because signals from ion/ion-conversion often overlap ion/electron-conversion and broaden the ion peaks

A detector is described here which, similar to a Faraday cup, measures all incoming charge and is fast enough for the analysis in a TOF mass spectrometer.

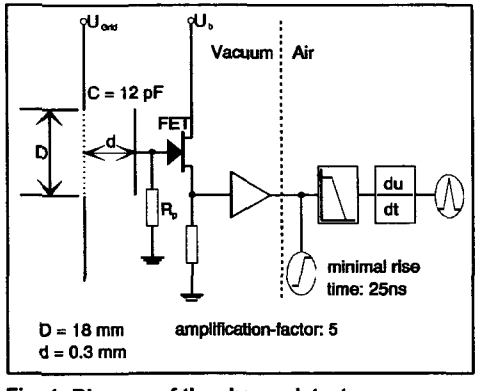

Fig. 1: Diagram of the charge detector

The 12 pF combined capacitance of the charge collector electrode and the FET imput paralleled by the FET imput resistance of 1 GΩ form the charge integrator. The FET functions as an impedance converter to the 1 KΩ imput of the amplifier The overall upper cutoff frequency of 6 MHz of the system, corresponding to a minimum risetime of 25 ns, is determined essentially by the amplifier. 18,000 ions are needed to obtain a step with signal-to-noise-ratio of 2.

The resulting staircase function must be differentiated electronically to obtain a normal mass spectrum (see fig. 2).

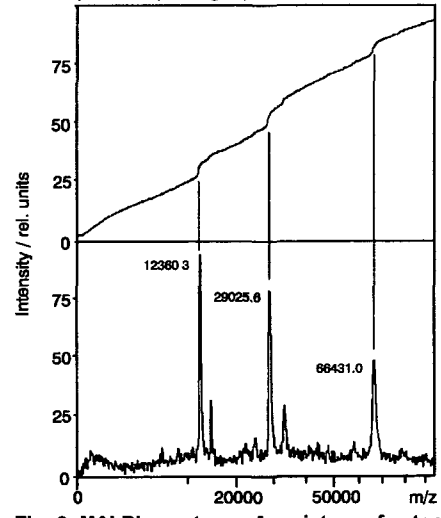

Built into the differentiator is another low-pass frequency filter to limit the high-frequency noise. For optimal performance this frequency should be variable: With increasing mass, the intrinsic mass resolution and thereby the intrinsic signal risetime decreases as does the signal intensity. For optimal performance (S/N and m/Δm) different differentiators were therefore used to receive spectra with signals in the range of 137 - 150,000 Da. A Finnigan MAT VISION 2000 intrument in the reflector configuration with a 5 kV acceleration energy was used.

For small ions (up to 2,000 Da) the mass resolution is limited by the rise time of the charge detector, up to 10,000 Da the mass resolution in the differentiated spectrum is limited by the

Fig. 2: MALDI-spectrum of a mixture of cytochrome C, carbonic anhydrase and bovine serum albumin with DHBs as matrix obtained with the charge detector
top: step function
bottom: electronically differentiated spectrum

cutoff frequency of the differentiator In the mass range between 10,000 Da and 30,000 Da the mass resolution obtained from the step function as well as the differentiated signal of the charge detector is superior to a SEM, for which the secondary ion signal of the post-acceleration SEM broadens the peaks. For higher mass ions the mass resolution is only negligibly affected by the secondary ion signal and mass resolutions are equal for both detectors.

At a mass of 1,000 Da the sensitivity of the SEM exceeds that of the charge detector by a factor of 1.6. At a mass of 70,000 Da this difference has shrunk to a factor of 1.1. These observation makes the charge detector particulary suited for the detection of high mass ions.

The absolute measurement of the ion charge by the detector allows the investigation of secondary surface effects in dependence on impact energy and ion mass by variation of the grid voltage

[1] P. W. Geno, R. D. Mcfarlane, Int. J. Mass Spectrom. Ion. Processes 92 (1989) 195

Application of MaxEnt to MALDI Mass Spectrometry

Xiaokui K. Zhang*, Anthony G. Ferrige** & Henry M. Fales*

*Laboratory of Biophysical Chemistry, NIH, Bethesda, MD 20892-1676

**MaxEnt Solutions Ltd, Isleham, Cambs. CB7 5QS, UK

MALDI coupled to time of flight mass spectrometry is recognised as one of the most powerful techniques for the study of large biologically important molecules. In comparison with other commonly used techniques, it is generally highly sensitive, is tolerant to solvents and buffers and is relatively easy to use. However, it does suffer the serious disadvantage that it is a low resolution technique, particularly for masses above 12000 Da where reflectron refocussing is not useful. This poor resolution performance arises from many factors including the initial energy of the ions, the location of ion formation and the strength and stability of the laser power. As a consequence, peaks may be very broad and, typically, in the range 20000-100000 Da peaks may have a full width at half-height of anything between 100 & 1000 Da, depending on their mass and the instrument operating parameters. Therefore, the spectra of mixtures of similar compounds may easily overlap to produce a poorly resolved peak envelope. Since peak maxima are dependent on the extent of peak overlap, it follows that some means of revealing the underlying structure is required. When internal standards are used as a means of improving the calibration accuracy, it is considered that calibration peaks must be cleanly separated from the peaks of interest for reliable mass measurement of either. This is unfortunate because it is obvious that the calibration peak should be as close as possible to the analyte peak for calibration extrapolation to be reliable.

Quantified MaxEnt is a well-known probabilistic method which is used to reconstruct the underlying sharp information contained in many types of spectra data and images. More recently, the mathematics have been developed further and the technique has been successfully applied to electrospray data for generating highly resolved zero-charge spectra and to ICP-MS data for automatically providing fully quantitative elemental analyses. Whatever the application, it is important to realise that the data are not processed in any way. They are only used for comparison with reconstructions of the data so that result quality may be assessed. Therefore, in the case of electrospray data, the reconstruction of the data is generated from trials which guide the computation to the best reconstruction of the zero-charge spectrum which, when convolved with the optimised peak profile model and an integer charge distribution, gives the best fit with the data. We present below a further practical development in applying the MaxEnt technique to MALDI-TOF data.

In this application, the sample is a mixture of four oligonucleotides. Peak overlap is severe and accurate mass assignment is impossible. Two experiments were performed - one using an external standard which was then combined with the sample acquisition and another which included an internal standard which overlapped with the analyte peaks. The data, reconstructed data and MaxEnt results for the two experiments are shown in Figures 1 & 2 respectively, along with the fully quantified masses.

In conclusion, it is clear that MaxEnt is capable of revealing the underlying sharp information contained in data and providing quantified results of high accuracy, even when (and preferably!) calibration peaks overlap the analyte. Of course, the information must be in the data to begin with and a potential future development could be a "quality meter" output from MaxEnt to guide the spectrometrist among compromises in spectral conditions to optimise the information from a given sample.

43rd ASMS Conference on Mass Spectrometry and Allied Topics

Figure 1: External Standard

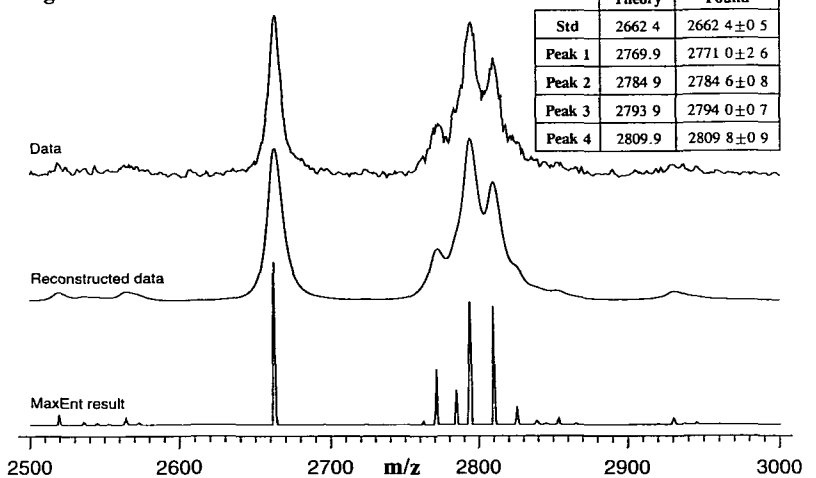

	Theory	Found
Std	2662 4	2662 4±0 5
Peak 1	2769.9	2771 0±2 6
Peak 2	2784 9	2784 6±0 8
Peak 3	2793 9	2794 0±0 7
Peak 4	2809.9	2809 8±0 9

Figure 2: Internal Standard

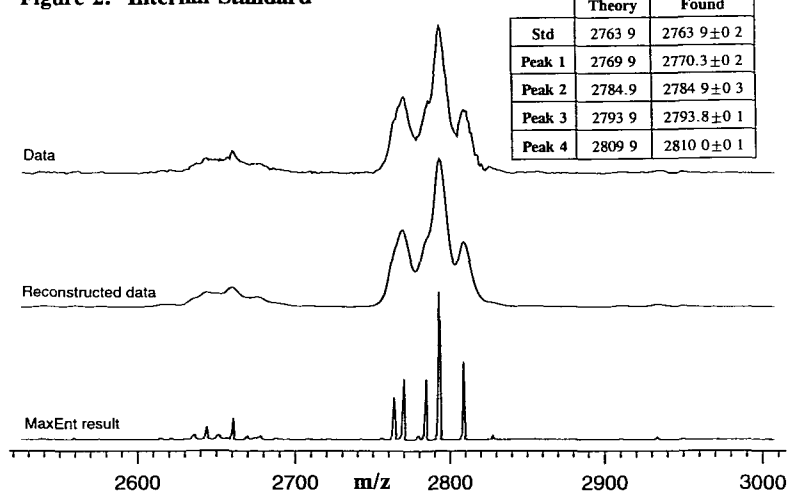

	Theory	Found
Std	2763 9	2763 9±0 2
Peak 1	2769 9	2770.3±0 2
Peak 2	2784.9	2784 9±0 3
Peak 3	2793 9	2793.8±0 1
Peak 4	2809 9	2810 0±0 1

Scanning Electron Microscopy as a Tool to Investigate Sample Morphology Effects in Matrix-Assisted Laser Desorption/Ionization Mass Spectrometry

A. Westman and E. Barofsky
Department of Agricultural Chemistry, Oregon State University, ALS 1007, OR 97331-7301, USA

One of the most important factors effecting matrix-assisted laser desorption/ionization (MALDI) is the method of sample preparation. Sample preparation involves co-crystallization of the analyte molecule with an excess of low mass, photoabsorbing, organic molecules – the matrix. Although it has been demonstrated that a number of compounds from different chemical classes are suitable as matrices in MALDI, there is still considerable uncertainty about the possible roles of the matrix. Factors such as morphology of the matrix-analyte film and molecular co-crystallization have been stressed as important for obtaining useful MALDI spectra [1, 2].

In this study samples for matrix-assisted laser desorption/ionization (MALDI) mass spectrometry have been prepared with several different techniques. The samples have been studied in a scanning electron microscope (SEM). The size, shape and surface density of the micro crystals formed was found to depend strongly both on the matrix material and on how the matrix/protein solution was applied to and dried on the metal backing. When a droplet of the matrix/protein solution is deposited on the metal backing and left to dry completely in ambient air, the result is a carpet of micro crystals of different size and orientation. Local crystal morphology varies considerably across the sample (fig. 1). When fast crystallization is induced immediately after the matrix/protein solution have been deposited on the metal backing a more homogeneous layer of smaller micro crystals is formed (fig. 2). All the samples investigated in this work (except the fast evaporation [3] samples) look the same in a light microscope However, the SEM micrographs reveal strikingly different sample morphologies. We suggest therefore that SEM micrographs of samples should more often be published together with the mass spectra This would make it easier to separate the effects of sample morphology from those of instrumentation and thereby make comparisons of performance between different experimental set-ups possible. Attempts are under way in our laboratory to further investigate the role of sample morphology in MALDI by directly comparing spectra from samples with different morphologies.

References

1. R.C. Beavis and J.N. Bridson, *J. Phys. D - Appl. Phys.*, **26** (1993) 442
2. K. Strupat, M. Karas and F. Hillenkamp, *Int. J. Mass Spectrom. Ion Proc.*, **111** (1991) 89
3. O. Vorm, P. Roepstorff and M. Mann, *Anal. Chem.*, **66** (1994) 3281

Acknowledgment

This study was supported in part by Grant 2P01 ES0040 from the National Institute of Environmental Health Sciences.
A. Westman was supported by fellowships from the Wenner-Gren Center Foundation and the Swedish-American Foundation

Fig. 1 SEM micrograph of a THAP sample. The sample is prepared by applying 1 µl matrix solution onto an aluminum probe.

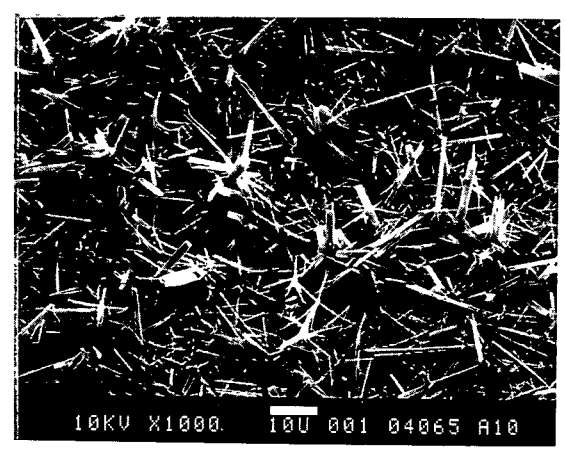

Fig. 2 SEM micrograph of a THAP sample. The sample is prepared by applying 1 µl matrix solution on an aluminum probe, gently wiping the sample with a kimwipe and applying 1 µl more of the matrix solution.

Nanoscale Sample Manipulation and Preparation Method for MALDI MS

Rafael E. Golding, Randy M. Whittal and Liang Li*
Department of Chemistry, University of Alberta, Edmonton, Alberta, Canada T6G 2G2

In a typical matrix-assisted laser desorption ionization (MALDI) experiment, 0.5 to 1.0 μL of a 1 μM solution is loaded to a sample probe for mass analysis. Sample is usually distributed over a 3 to 10 mm^2 area. However, only a small amount of sample is consumed. In order to preserve valuable samples available only in very small quantities (e.g. intracellular fluid), a reliable, reproducible and accurate sample delivery system is necessary to place the sample solution on the tip of the mass probe.

The system developed in this work is able to deliver volumes from 0.02 nL to 130 nL accurately depending on the length of the liquid column inside a capillary tube, and the I.D. of the tube. The delivery system is composed of a screw capped 2 mL glass vial connected to two fused silica capillary tubes and one PTFE tube (Figure 1). The connections are sealed using a silicone chromatographic septum. One of the capillaries has a tapered end and it is calibrated for the desired volume. The second capillary tube (50 μm I.D.) acts as a pressure attenuator. With the use of 10 μm to 200 μm I.D. capillaries, delivery of accurate volumes can be made over a large range. A disposable syringe is connected to the PTFE tube (300 μm I.D.) and provides the vacuum/pressure driving force necessary to move the sample inside the tube.

The matrix preparation technique of Vorm *et al.* [1] was used to prepare the matrix layer. α-cyano-4-hydroxycinnamic acid was dissolved in 99% acetone / 1% water at a concentration of 24 mg mL^{-1}. 0.7 μL of matrix solution was delivered to the stainless steel probe tip. An even solid matrix layer of very small crystals (0.5 - 2 μm in diameter) is formed.

All the operations of filling the capillary with the sample solution, and delivering the selected volume on the mass probe were performed under a microscope. A standard microscope slide holder was used for aligning the capillary tube and locating the sample on the center of the 4 mm diameter probe tip. The analyte solution spreads on the matrix layer instantly and dries in 1-5 seconds depending on the volume delivered. The evaporation of the liquid solution inside the capillary tube is very low. It ranges from 0.0017 nL/min for a 10 μm I.D. capillary to 0.60 nL/min for a 200 μm tube.

Figure 2 shows that a rapid decrease in the analyte spot area can be seen when the sample volume is reduced, especially under 0.4 nL. This behavior means that the sample will be confined in a smaller area producing higher analyte concentration per area unit.

The MALDI spectra were collected on a linear time-lag focusing time-of-flight mass spectrometer [2]. Two different samples were analyzed. A rhodamine labeled trisaccharide (B-MCO-TRSE) and the peptide bradykinin. A MALDI spectrum of B-MCO-TRSE is shown in Figure 3. The average spectrum was obtained from 0.1 nL of a 1 μM solution of the analyte delivered on the probe. This corresponds to 100 amol of the trisaccharide. In Figure 4, the average spectrum for 0.15 nL of a 1 μM solution of bradykinin is presented. The total amount in this case is 150 amol.

In conclusion, we have developed a method where exact and very small sample volumes can be accurately located on the mass probe tip. A smaller sample spot area produces higher analyte concentration per area unit on the solid matrix layer. Mass spectra for a total loading of 100 to 150 amol of material give spectra with signal to background ratios well above the detection limit. We plan to extend the use of this system to the analysis of single cell intracellular fluid.

References

[1] Vorm, O.; Roepstorff, P.; Mann, M. *Anal. Chem.* **1994**, *66*, 3281-3287.
[2] Whittal, R. M.; Li, L. *Anal. Chem.* in press.

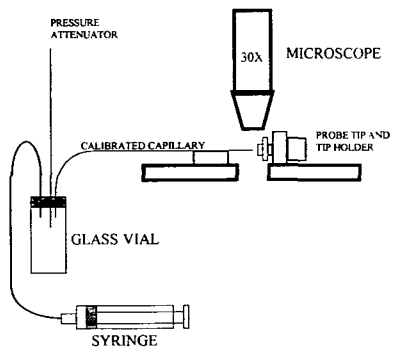

Figure 1

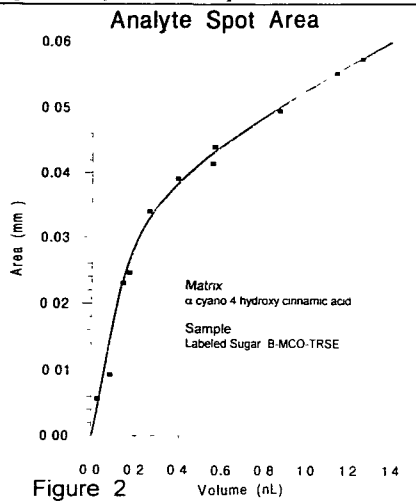

Figure 2

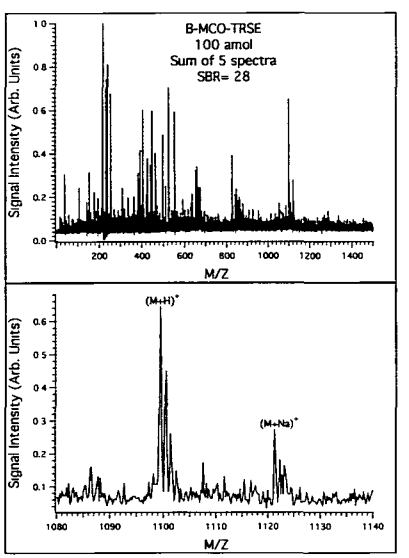

Figure 3

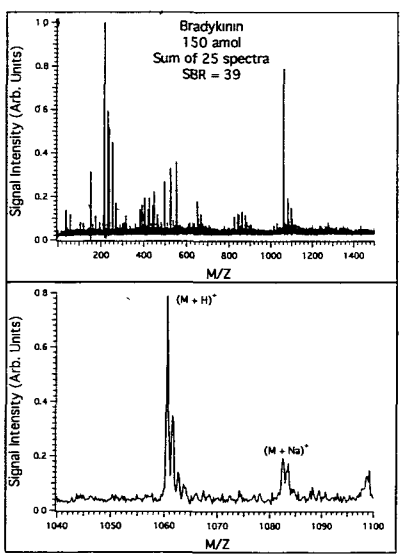

Figure 4

Methods for Modifying the MALDI Process by Jian Bai, Xiaoli Liang, Yan-Hui Liu, and David M. Lubman, Department of Chemistry, The University of Michigan, Ann Arbor, MI 48109

Introduction MALDI is characterized by a sharp threshold behavior, which implies that minimum laser energy needs to be absorbed by the microvolume of the matrix/analyte to result in the desorption/ionization process, and this is directly related to the density of matrix molecules probed by the laser beam. The MALDI sample preparation requires the mixing of analyte molecules with an excessive amount of matrix so that the density of the matrix molecules of a typical sample preparation is almost saturated. Additives to matrices/co-matrices have been used for improving the MALDI MS performance (1-3). This work reports the preliminary results of using additives to the commonly used matrices for the mediation of the MALDI process. The effect of additives of different physical and chemical properties and photoactivities on MALDI MS sample preparation and performance is evaluated, such as resolution, sensitivity. Initial results indicate that additives of various properties can serve as a general means of improving the MALDI MS performance for certain matrices

Experimental A linear TOF mass spectrometer with a microsphere plate detector was used for detection, and 355 nm laser radiation for LD/I. All the materials were used as purchased, and were dissolved in acetonitrile/water (1:1) at appropriate concentrations DHB and α-CHCA were used as two model matrices, and additives of different photoactivity, acidity, and volatility, including glutathione (GTTh), 4-nitroaniline (4-NA), and vanillin (VN), among others, were tested as additives. The analytes used were a peptide mixture and lysozyme.

Results and Discussions Obvious improvements were generally observed for additives to DHB, but not for α-CHCA. These results are dependent on the additives and the type of analyte. GTTh as an additive to DHB with a molar ratio of 1/4 provided the best results for all of the analytes, where enhanced resolution and reproducibility were achieved. 4-NA as an additive to DHB also improved the reproducibility of the MALDI MS signal, and tended to generate more multiply charged species for lysozyme. VN as the additive to DHB showed improvement in the analysis of lysozyme, but showed suppression effect on the larger peptides in the CNBr digest. The Figure shows the MALDI MS spectra obtained with GTTh and 4-NA as additives to DHB for the analysis of lysozyme (left) and the peptide mixture (right).

The improvements can be atributed to the homogeneous nature of the sample/matrix deposit from visual inspection when additives were used, where addition of the correct amount of GTTh or VN to DHB can result in very thin and homogenous film like sample/matrix deposit. Addition of 4-NA to DHB showed moderate improvement in the sample/matrix deposit homogeneity. Optimization of the molar ratio of additives to DHB was required in the case of GTTh or VN; an excessive amount of GTTh can result in total loss of the effectiveness of the DHB matrix. 4-NA, on the other hand, allows a much wider range of variation.

The MALDI MS spectra with DHB alone as the matrix showed dramatic variations in terms of resolution, intensity, and signal profiles as the laser spot was scanned over the probe tip by moving the focus lens laterally. This may be associated with the inhomogeneity of the sample deposit, but most importantly, may reflect the sensitive response of such a sample deposit to the laser intensity variations brought about by moving the focus lens. In fact, slight adjustment of the laser intensity can result in very different mass spectra when using DHB as the matrix (results not shown). These variations were almost totally eliminated when GTTh was added to DHB with a molar ratio of 1/4. We atribute this partly to the

dilution effect of GTTh on DHB, which makes the sample deposit less responsive to slight laser intensity variations.

Conclusion The initial results indicate that the use of additives to matrices may provide a general and simpler means of improving the current matrix systems Continuing efforts are needed to evaluate the effects of additives on the MALDI process, and to further characterize additives for such purposes.

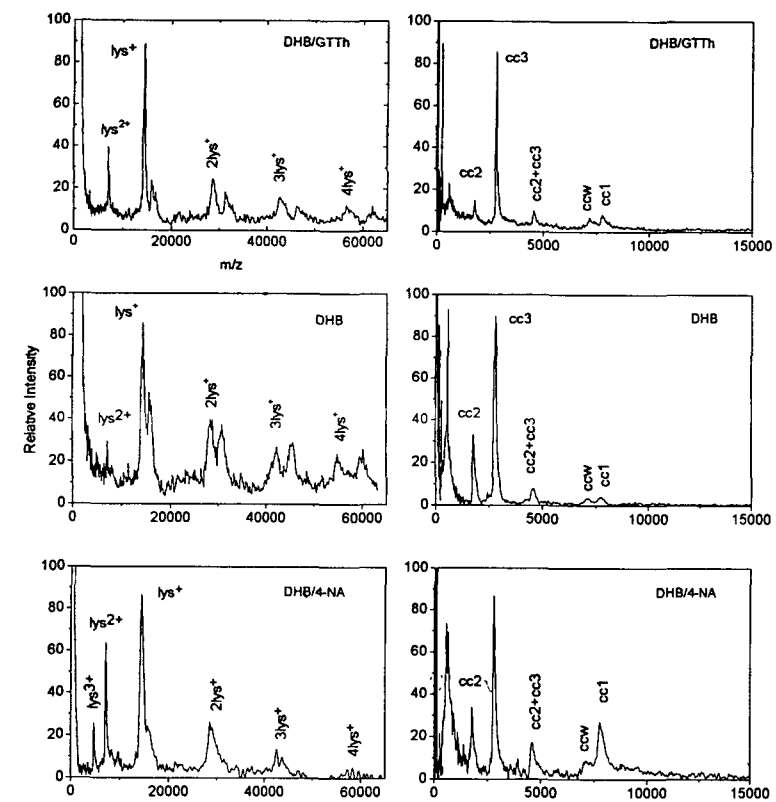

Ref: (1) Karas, M., Ehring, H , Nordhoff, E , Stahl, B , Strupat, K., Hillenkamp, F., Grehl, M., and Krebs, B. *OMS.* **1993**, *28*, 1476 (2) Koster, C., Castoro, J. A., and Wilkins, C L. *JACS.* **1992**, *114*, 7572. (3). Billeci, T. M. and Stult, J. T. *Anal. Chem.* **1993**, *65*, 1709.

Novel Sample Preparation for MALDI

H. J. Köchling and K. Biemann
Department of Chemistry, MIT, Cambridge, MA, 02139 USA

The widespread use of Matrix-Assisted Laser Desorption/Ionization (MALDI) within the mass spectrometry community has identified sample preparation as being critical for attaining optimal results. With the goal of achieving better control of sample preparation in MALDI, we have conducted experiments where the deposition of matrix has been separated from that of the analyte. Extremely homogeneous thin films were formed on Time-Of-Flight (TOF) mass spectrometer targets by pneumatic spraying of solutions containing only matrix. Both alpha cyano-4-hydroxycinnamic acid (αCCA) and 2,5-dihydroxybenzoic acid (DHB) were used to produce matrix films by this method. Aqueous solutions of analyte alone (without matrix) were then applied in the conventional manner onto the dry matrix films. As a demonstration of the versatility of the matrix films, a pre-prepared film of αCCA was sprayed with High Pressure Liquid Chromatography (HPLC) eluent and the resulting deposits were analysed by MALDI.

EXPERIMENTAL

Matrix films were produced by using a LC-TRANSFORM model 101 (Laboratory Connections, Marlborough, MA), introducing matrix solution with a syringe pump. Matrix solution was propelled by a nebulizing gas stream and the resulting spray dryed and focused by a heated sheath gas onto a rotating TOF target. Matrix films of αCCA were produced from a 5g/L solution in 1:1 (v/v) acetonitrile/water. For DHB films, a solution at one-half saturation (~10g/L) in water was used. HPLC experiments were performed by using the LC-TRANSFORM to spray the HPLC eluent onto a rotating TOF target previously coated with a matrix film of αCCA. All mass spectrometry experiments were conducted on a modified VT2000 linear TOF mass spectrometer (Vestec Corp., Houston, TX).

RESULTS AND DISCUSSION

The matrix films were deposited in the shape of an annulus. Both films had a center radius of 11 mm but were of different widths. The αCCA matrix film was 6 mm wide and was composed of two distinct layers, a light green bottom layer, which was very well adhered to the surface of the target, and a loose, powdery top layer, darker green in appearance although equally homogeneous. This top layer was removed by gentle wiping with a cotton swab to expose the lower layer, onto which samples were spotted for MALDI analysis. The DHB matrix film was composed of a single homogeneous layer, 4 mm in width and matte grey in color. It was also extremely well bonded to the target surface.

The principle benefits that the matrix films provided over the standard MALDI sample preparations derived from their much greater homogeneity. This resulted in superior MALDI spectra, as shown in Figures 1A and 1B for DHB by using bovine ubiquitin and in Figures 2A and 2B for αCCA by using ribonuclease A. Figure 3 shows the MALDI analysis of an αCCA matrix film sprayed with HPLC eluent from the separation of a three-component mixture. Mass spectra were acquired from regions of the matrix film corresponding to the HPLC peaks containing Substance P (Fig.3A), insulin (Fig.3B) and ubiquitin (Fig.3C).

CONCLUSIONS

Separating the deposition of matrix from that of analyte has been shown to allow better control of the sample preparation step in MALDI. A process based on pneumatic spraying was developed to produce stable, long-lived matrix films of αCCA and DHB. This process was shown to be capable of producing homogeneous matrix films regardless of the solubility characteristics of the matrix materials tested. The excellent homogeneity of the resulting matrix films facilitated the acquisition of MALDI spectra that exhibited increased sensitivity, larger signal/noise ratio and greater resolution than spectra acquired from corresponding conventionally prepared samples. The remarkable adhesion of the matrix films to the surface of the TOF targets and their ability to be pre-prepared allowed their use in an off-line HPLC detection experiment using MALDI. These same qualities permit their use in time studies and where extensive washing of MALDI samples is desired.

43rd ASMS Conference on Mass Spectrometry and Allied Topics

Fig. 1 Ubiquitin - 1pmol

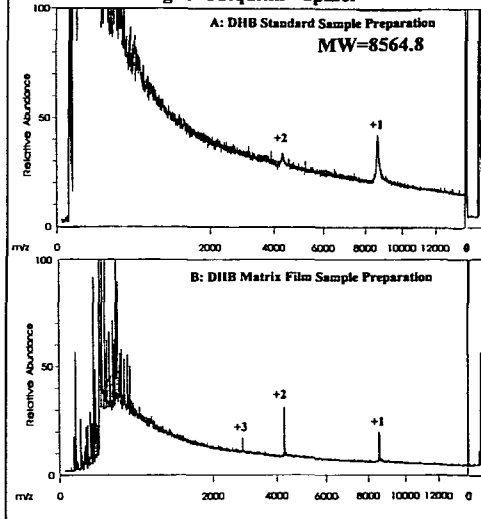

Fig. 2 Ribonuclease A - 1pmol

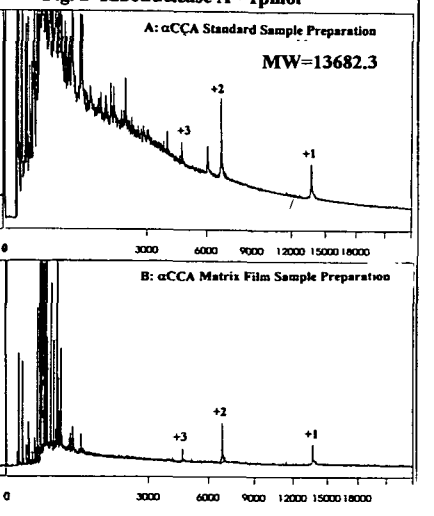

Fig. 3 MADLI Mass Analysis of HPLC EluentUsing αCCA Matrix Film

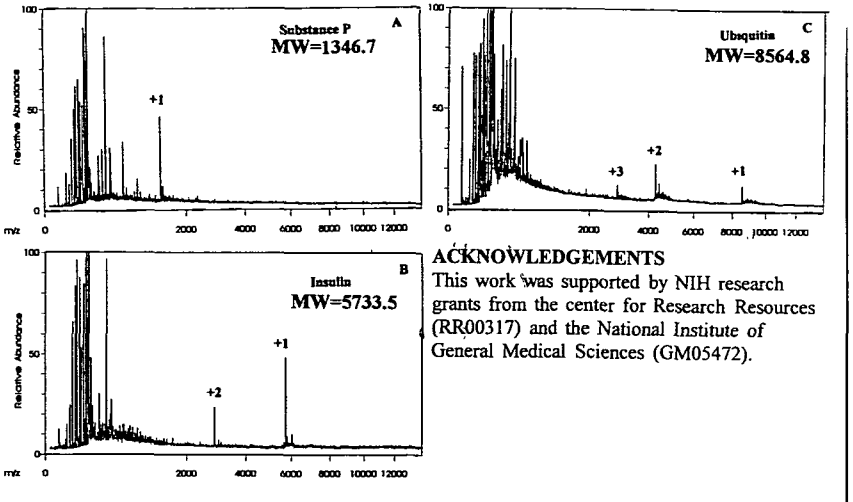

ACKNOWLEDGEMENTS

This work was supported by NIH research grants from the center for Research Resources (RR00317) and the National Institute of General Medical Sciences (GM05472).

Investigation of Sample/Matrix Preparation in MALDI by Confocal Microscopy

Yuqin Dai, Randy M. Whittal, and Liang Li*
Department of Chemistry, University of Alberta, Edmonton, Alberta, Canada T6G 2G2

Matrix-assisted laser desorption ionization (MALDI) mass spectrometry has become widely used for biomolecule analysis. In MALDI, the method of sample/matrix preparation plays a central role for achieving optimal performance. Detection sensitivity, selectivity, mass resolution, and other performance indicators are strongly dependent on the sample/matrix preparation. Thus, the understanding of chemical and physical phenomenon underlying the sample preparation process is very important. It is hoped that these studies would ultimately lead to rational design of improved methods for sample preparation in a wide range of applications.

We report herein a non-intrusive method to examine the sample/matrix preparation process. In this method, the analyte is tagged with a fluorescent group. The matrix and analyte samples are prepared under the same conditions as those used in conventional MALDI experiments. Laser confocal microscopy is then used to examine the matrix/analyte crystals The fluorescence and reflectance (or transmittance) images generated from the confocal microscope can provide information on the analyte and matrix crystal distribution, respectively.

In confocal microscopy, a laser beam is focused onto a small spot in an object. The illuminated spot is viewed with a specially designed optical system consisting of several lenses and apertures so that only signals emanating from this spot are detected By rastering the light beam, an image of the complete specimen can be obtained. Unlike conventional light microscopy, the confocal microscopy technique provides high contrast with the elimination of out-of-focus light interference. One can also slice very thin optical sections out of a thick sample specimen to obtain a 3-dimensional view at extremely high resolution (e.g , 200 nm lateral resolution and 400 nm axial resolution). The Molecular Dynamics Multiprobe 2001 confocal laser scanning microscope is used for the generation of all images reported herein.

In this presentation, we show that this method can be used to map the analyte distributions within the solid matrix crystals. For the samples prepared by using the dried-droplet method, we observe the analyte incorporation into small matrix crystals. More significantly, we find that the analyte is not uniformly distributed among many crystals formed on the sample surface This is shown in Figure 1 where the fluorescence image (analyte) and transmittance image (matrix) are reconstructed from multilayer scans and superimposed, representing a 3-dimensional image. In this case, the analyte is fluorescein isothiocyanate (FITC) labeled bovine insulin and the matrix is 2,5-dihydroxybenzoic acid (DHB). The MALDI spectrum of this chemical reveals that it is a mixture of insulin with one and two labeling groups attached. The bright area in the crystals shown in Figure 1 represents the fluorescence image of the analyte. As Figure 1 shows, several analyte domains are observed. By examining the entire sample/matrix regions on the substrate, it is also found that there is no direct correlation between the

43rd ASMS Conference on Mass Spectrometry and Allied Topics

location of the analyte domains and the physical appearance of the crystals. In contrast, large crystals grown by a slow process display much more uniform analyte distribution (figures not shown). This indicates that the speed of crystal formation plays an important role in entraining analyte. The same observations are found for other commonly used matrices such as sinapinic acid (SA) and several other fluorescent labeled oligosaccharides, peptides, and proteins. In addition, we have used the confocal microscopic method to examine sample/matrix containing two analytes with different labeling groups. By exciting and detecting fluorescence signals at different wavelengths, we can map the individual analyte distribution in the matrix crystals. We find that the analytes are not coherently distributed in the matrix. One type of analyte may reside in one region of a crystal and another region of the crystal may contain the other analyte only. There are regions where both analytes are present. This double-labeling imaging work is very useful for designing better internal standards for quantitative analysis by MALDI.

There is a report [1] indicating the possible correlation between the analyte distribution in the matrix crystals and MALDI analyte signals. Our confocal imaging results provide further evidence of this observation. Strong and much more reproducible analyte signals can be obtained from the crystals containing the analyte whereas the regions containing little or no analyte give only matrix peaks Thus, sample/matrix preparation methods that provide uniform analyte distribution would improve the signal reproducibility in MALDI. The sample preparation method reported by Vorm et al [2] is very effective in obtaining more reproducible signals. In this method, sinapinic acid matrix solutions are prepared in acetone. A drop of matrix solution is applied to the MALDI sample probe. The droplet spreads and dries very quickly, leaving a thin layer of matrix crystals. Analyte samples are then placed on top of the matrix layer and allowed to dry The color coded fluorescence and reflectance images (not shown) obtained by using confocal microscopy clearly show that the analyte is much more uniformly distributed on the sample surface. The use of confocal microscopy for developing more effective means of sample preparation for highly sensitive MALDI quantitation is currently underway.

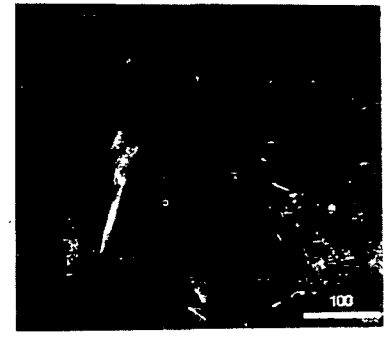

Figure 1. Confocal image of the analyte and matrix.

References

1. Gusev, A.I.; Wilkinson, W.R.; Proctor, A.; Hercules, D.M. Anal. Chem. 1995, 67, 1034.
2. Vorm, O.; Roepstorff, P.; Mann, M. Anal. Chem. 1994, 66, 3281.

Influence of Sample Preparation on Time-Dependent MALDI MS of Proteins

Gary Lavine and John Allison
MSU/NIH Mass Spectrometry Facility
Michigan State University
East Lansing, MICHIGAN

We have been developing a number of approaches for acquiring MALDI spectra, that may be more representative of the experiment than a single transient (from a single laser shot) or the sum/average of 20-200 transients. Using a larger laser spot size, "Big Spot MALDI", we have found that the experimental results are more reproducible. Also, many useful spectra can be obtained without having to move the laser. In addition, we realized that each MALDI mass spectrum, from each transient, is unique. With subsequent laser shots, resolution and composition of the spectra can vary. Thus, we generate and collect a number of "component spectra" from a MALDI experiment, where each is the sum of 10 successive transients. With this set of spectra, time-dependent variations can be more clearly realized. We use these tools here to investigate some approaches to MALDI target preparation.

In the past few years, a number of techniques have been described to yield improved MALDI performance, by changing the approach to sample and matrix deposition on a target. We compare three methods in this study. The first approach was our standard approach of codepositing a solution of α-cyano-4-hydroxycinnamic acid and 2 pmol each of bradykinin and insulin, and allowing the solvent to evaporate. The second was an approach to yield a layered target. The matrix is applied first in this technique, and a solvent system such as acetone selected to allow for very rapid evaporation, yielding smaller crystals. The analyte solution is then applied *on top* of these matrix crystals, and the solvent allowed to evaporate. It has been suggested that this leads to improved performance. A third approach we refer to as the crushed crystal method. Here, solid matrix is crushed into the target surface before solutions are applied. It is believed that this will place on the surface microcrystalline deposits which result in a more uniform surface, by seeding crystal growth evenly across the target.

We have analyzed the targets made in these ways at a number of laser power settings, collecting component spectra over a period of time. A more sensitive characterization method to allow for differences to be realized is what we call "power titrations". In this experiment, a series of component spectra are again collected from a single location on the target, although each component spectrum

is taken at a different laser power. Thus, a range of powers are sampled (constantly increasing, beginning at the power threshold for desorption/ionization of the matrix). The spectra are generated by beginning well-below the MALDI laser power threshold, and incrementing power after each set of 10 transients. The first spectrum shown was obtained with that power setting where matrix ions were first observed.

When these sets of spectra are compared, using targets prepared by the three methods selected for this study, it is clear that each yields different results. The mass spectra can be segmented into three regions. In the low mass region, there are peaks representing alkali ions and low mass ions derived from the matrix. All of these are clearly most intense when the standard method is used. In the "middle mass region", the three again yield different results. The standard method is best here, generating the smallest number of (and least intense) matrix-related peaks that lie above the peak representing the protonated matrix molecule. (This is particularly important when relatively low MW analytes are being analyzed.) At the high mass end of the spectra, where the two analyte peaks appear, the most surprising result is from the layered target. This case yields the largest difference in relative responses for bradykinin and insulin, with the signal representing protonated insulin being very weak, even at high powers.

Finally, we evaluated matrix additives and their influence on response. We were particularly interested in fucose as a nonabsorbing matrix additive. It had previously been reported that sugars can extend the signal duration for peptides. Our time-dependent data clearly support and show this observation.

While each approach yields unique spectra, and there are clear *differences* between them, we were unable to document major improvements over the results obtained for our standard preparation procedures. Surely, this is at least in part laboratory and instrument-dependent. When this comparison is reproduced on a reflectron-TOF instrument, more differences may be realized.

Dependence of Resolution on Laser Power in MALDI-TOF MS

Pao-Chi Liao and John Allison
Department of Chemistry, Michigan State University, East Lansing, MI 48824

Time-of-flight (TOF) mass spectrometry is most commonly used with matrix-assisted laser desorption ionization (MALDI). A dominant factor that influences the mass spectral resolution in a MALDI-TOF experiment is the laser irradiance [1]. It has been reported that the mass resolution dramatically decreases when laser powers much higher than threshold are used. For simplicity, we will discuss "power" instead of "irradiance" in this report. Most MALDI spectra reported in the literature represent the summation or average of 20-200 mass spectral transients, which may be obtained from multiple locations on the MALDI target or obtained using a variety of power settings (or, single shot spectrum may be presented). Conclusions such as the high power-low resolution relationship seem to evolve from the analysis of such summed spectra, or from the spectrum resulting from a single laser shot. We recently showed that the mass spectral transients of MALDI-TOF MS rapidly change with time, and an evaluation of the component spectra may yield different conclusions than evaluation of a single summed spectrum [2]. We use this tool of time-dependent MALDI data analysis to investigate details of the power-resolution relationship here.

All MALDI results were obtained on a ResearchTec TOF mass spectrometer (Vestec Corp., Houston, TX), used in linear mode, equipped with a nitrogen laser (model VSL-337ND, Laser Science, Newton, MA, 337 nm, 3-ns pulse, 250 μJ/pulse). Laser power is attenuated using a variable attenuator (model 935-5-OPT, Newport, Fountain Valley, CA) with a computer-controlled stepper motor, corresponding to an on-screen number ranging from 0 to 2,400. A larger number results in a higher laser power. Laser powers in this report are not expressed on an absolute scale, but relative to the value at the D/I threshold. The threshold laser power will be designated here as P_t (m, A), where P_t is the threshold power at which the analyte, A, generates observable signals (S/N > 5), using the matrix, m. The threshold laser power P_t (αCN, I), where αCN represents α-cyano-4-hydroxycinnamic acid and I represents insulin, corresponds in our instrument to a counter reading of 1200. When the stepper motor position was set at a point corresponding to a counter reading of 1800, the corresponding laser power is expressed in the text as 1.50 P_t.

If the typical approach of evaluating summed data is used, the resolution decreases considerably with increasing laser power. However, we have found that the resolution of all of the mass spectral transients accumulated, when a typical summed MALDI spectrum is obtained, is not constant. By collecting successive MALDI mass spectra, it is seen that the laser power/resolution relationship is more complex than is realized from a single spectrum representing many laser shots. When a sample is irradiated by a fixed laser power at the same spot, signal intensities decrease, and resolution increase with successive laser shots. As shown in Figure 1, the intensity of the insulin

signal decreases with component spectrum number (increasing number of laser shots), regardless of which laser power is used. The signal lasts longer when higher laser powers are used. The data in Figure 1a correlate with experience - signals "last longer" and are more intense at higher powers. The resolution in all of the component spectra is not constant. The data show that the resolution increases with component spectrum number. When the laser power is 1.80 P_t (αCN, I), the measured resolution starts at ~ 100 and increases to ~ 300, while the intensity falls, with increasing component spectrum number. That is, the "low power resolution" (300 ~ 400) can be realized when "high power" is used. The data also suggest that there may be a correlation between resolution and peak intensity.

[1]. R. C. Beavis and B. T. Chait, *Rapid Commun. Mass Spectrom.* **3**, 233 (1989).
[2]. P.-C. Liao and J. Allison, *J. Mass Spectrom.* (in press).

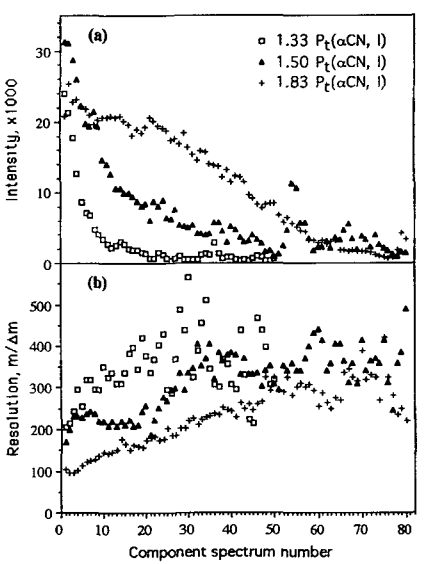

Figure 1 The (a) peak height and (b) resolution of the insulin signal obtained at different laser powers are plotted against component spectrum number. The experiment was configured so the laser fires 10 times in 2.5 seconds. Every 10 mass spectral trasients are summed as a component spectrum.

Big Spot MALDI- Advantages of Irradiating Large Portions of the Target

Joseph Hiller, Gabriella Szekely and John Allison
MSU/NIH Mass Spectrometry Facility
Michigan State University
East Lansing, Michigan 48824

MALDI evolved through a history of Laser Desorption and ablation techniques. It has continued to re-define itself into a separate, physically different method of encouraging molecules to acquire a charge and leave the solid state. Its present utility lies primarily in the ability to produce simple spectra which can be easily interpreted. In general, as the laser process becomes ablative with increasing pulse power, the complications of interpreting the spectra with increasing laser power grow rapidly.

To study a physical process, the physical situation should be such that the region studied ought to be as large and uniform as possible in order to exclude edge and other non-uniformity effects. Ignoring the issue of variable sample preparation, there are two classical options to accomplish this in MALDI: Locate the individual features that formed at the same time (approximately similar size and appearance crystals) and study many of those sites; or, Expand the spot size to cover a significant portion of the inhomogeneous surface. The observation that "sweet spots" exist that allow desorption at lower thresholds than others, suggests that better signal-to-noise may be obtainable with increased spot size to sample more "sweet spots" simultaneously. Increasing the spot size also helps ensure that if new features are encountered in samples, they will also be sampled.

The instrument is a VESTEC 2000 MALDI/TOF. The lens which is used to focus the light from a nitrogen laser, has been removed and placed on an XYZ translational stage. The translational stage is positioned such that the plane of the lens is perpendicular to the direction of the laser beam. In practice, this amounts to assuring that the laser continues to illuminate the same location of the sample as the lens is moved to new positions. Bradykinin has been purchased from Sigma. A concentration of 1,000 picomole/µl is prepared and 5,000 pM is deposited in a series of microcentrifuge vials. The vials are dried in a vacuum centrifuge and stored a -60°C until needed. MALDI surfaces are prepared from solutions of 10pM/µl of bradykinin in 0.1% trifluoroacetic acid. A solution of 1:1 0.1% trifluoroacetic acid to acetonitrile is saturated in the matrix, alpha-cyano-4-hydroxycinnamic acid is prepared and allowed to warm to room temperature. Each sample pin is prepared by placing 1µl of bradykinin on the probe tip, quickly followed by 1µl of matrix solution. Pins are then air dried and examined under a microscope. Those pins which have irregular coatings due to loss of solution over the edge, or other reasons, are discarded.

All spectra are taken from a fresh location so as to minimize damage to the sample surface. Spectra are the result of 10 individual TOF spectra which have been averaged on a Tektronix 520 digital oscilloscope prior to downloading to a computer. Each spectrum is saved and the next one taken as rapidly as possible using a digital device constructed to close the circuit for the joystick control provided with the VESTEC 2000. While the laser is pulsed at 4 Hz, the downloading of the spectra to the computer causes the time between spectrum acquisitions to be approximately 20 seconds. During this period, the laser beam is not moved from the initial spot. This produces a series of Time Dependent spectra which can be viewed in two or three dimensions using the GRAMS 386 software provided with the instrument.

Examining the spot area as a function of the lens position, the relationship of spot size to a fixed power/unit area required to produce ions (threshold power), can be deduced to be of the form:

$$P_{(thrsh)}^{1/2} = C_1 + C_2 * L$$

where L is the distance the lens is moved from the focal point, and C_1 and C_2 are constants for a particular lens' focal point (15 cm. for this instrument) and wavelength of light (337 nm). Determining the relationship between the lens position and the threshold power for a particular sample will determine the behavior of the instrument. For this system, the relationship between the lens position agrees with the above form.

Several spot sizes were examined for their Time Dependent MALDI spectra with intensity of the $(M+H)^+$ generated from the sample at the beginning of the analysis between 40 and 80% of the saturation level. All spot sizes examined produced acceptable MALDI spectra. As the spot size was increased, it became easier to predict the laser power at which the $(M+H)^+$ would be at near 75% of saturation for a new spot. This method of choosing the laser power for comparison was chosen to ensure the signal remained on scale during the measurement.

Increasing the spot size generally increases the length for which the Time Dependent experiment continues. Signal from the $(M+H)^+$ ion continues for a longer period, and appears more reproducible for the larger spot sizes. At very large spot sizes, however, where more than approximately 50% of the tip is illuminated, the signal again lasts less time. This observation may be due to heating of the pin surface by the laser.

At these larger spot sizes, the laser power used to illuminate the target is as much as ten times higher than that used for the focused spot. Upon removal of the sample holder from the vacuum, the temperature can be as much as 10°C higher. The longest lasting spot size corresponded to approximately 17 mm. along the translational stage, which places the sample at a position of 1.7 mm. from the focal point.

Using the Big Spot (L=1.7 cm) we have been able to acquire approximately 6-8 times as many spectra from the same point as can be acquired for the focused point. The Time Dependent spectra are also more uniform in profile along the time axis. For the first time we have found that we can readily reproduce the results of signal intensity, etc. for identically prepared sample. Threshold measurements have also become more reliable. The use of the Big Spot has provided the pathway for the development of other methods of sample diagnosis, such as Time Dependent MALDI and Power Titration MALDI, in which the laser power is increased linearly as spectra are acquired.

The Behavior of Peptide Mixtures in MALDI-MS

Joseph Hiller, Gary Lavine, Gabriella Szekely and John Allison
MSU/NIH Mass Spectrometry Facility
Michigan State University
East Lansing, Michigan 48824

We have been developing some new tools to characterize in greater detail the MALDI-TOF experiment. One goal is to understand in more detail the use of MALDI for mixture analysis, and to develop approaches that yield improved results. First, we increase the size of the laser spot used. This results in the irradiation of a more representative subset of the crystals on the surface, improving reproducibility, and allowing many spectra to be obtained without moving the laser during acquisition. This is important in experiments where multiple transients are accumulated. The second difference in our work, is that we can generate and collect a number of component spectra, for a given laser power. In our work, each successive set of 10 transients is summed into a single component spectrum. In subsequent component spectra, there are changes in resolution and relative intensities of the various peaks, clearly showing that all MALDI spectra are not the same - they change with time. A third approach that we use is called a power titration. In this technique, component spectra (again sums of 10 transients) are acquired at a number of increasingly higher laser powers. Thus, once one realizes that MALDI spectra are not all the same, and change in time (subsequent laser shots), we can work on a complex power/time/spectra surface. One can obtain time-dependent spectra at a fixed power, or change power and time simultaneously while acquiring spectra.
We have performed power titrations, acquiring a series of spectra with increasing power from a single large irradiated spot, for a synthetic mixture of peptides which include bradykinin (M_r = 1060), angiotensin (1297), melittin (2847), insulin b chain (3498), insulin (5734), cytochrome C (12446) and myoglobin (16891) - using alpha-cyano-4-hydroxycinnamic acid as the matrix, and a linear TOF instrument. The results are typical of MALDI analyses of mixtures of peptides. When equimolar amounts of each mixture component are used, signals representing bradykinin and insulin dominate. As power is increased, matrix peaks appear first. At higher powers there is a fairly regular trend indicating that desorption/ionization thresholds for each component vary with peptide molecular weight.

We have found several instances of suppression effects, where one component seems to suppress the signal of another, and frequently find melittin to be involved in such observations. In simple binary mixtures of melittin and bradykinin, clear

43rd ASMS Conference on Mass Spectrometry and Allied Topics

changes in relative response and desorption/ionization power thresholds are apparent as the amount of mellitin present is varied. When melittin is not present in the larger synthetic mixture, it is easier to detect the higher MW components of the mixture. In particular, melittin appears to dramatically suppress the signal for insulin in the synthetic mixture. We note that melittin is considered as a strongly basic polypeptide.

Using time-dependent spectral acquisition, and power titrations, we also note substantial differences in the responses of components of our synthetic mixture as a function of target preparation technique. In these experiments, we frequently start with separate solutions of matrix and analyte. Both use volatile solvent systems that can quickly be removed. Rather than mix them both prior to deposition on the probe, we can deposit some amount of each solution. If order is important, there are two possibilities. If one microliter of the peptide mixture is applied to the solid support first, followed by one microliter of the saturated matrix solution, this yields relatively poor performance. Application of the matrix solution first gives higher sensitivity for detecting the components of the synthetic mixture used here. In comparing these two approaches to solution deposition, we do note that, although application of the sample solution *first* resulted in a poorer representation of the mixture, it yielded the strongest signal for one particular component, angeotensin.

The power titration method for MALDI TOF MS is a very sensitive probe of the influence of various mixture components as well as the methods of preparation. It appears that, if the relative responses of components of a peptide mixture are to be used to determine relative amounts in the sample, spectra obtained at high power are preferable to use in such analyses. High powers increase the likelihood that minor components and larger analytes will yield signals, and represents conditions under which relative response factors are relatively constant.

MALDI Calibration and the Effect of Separate Layers of Sample and Standard

J. Zhou and T. D. Lee
Beckman Research Institute of the City of Hope
Duarte, CA 91010

The method most commonly used in MALDI to prepare samples is to evaporate a solution containing matrix and sample. When using this "dried droplet" method of preparing the sample, suppression of one protein signal often occurs in the presence of another. The degree of suppression depends on the molar ratio of proteins and matrices, the nature of the proteins, and the method of handling the sample. This suppression problem complicates the use of a internal protein standard to calibrate the mass scale. Often, samples must be prepared with different sample, standard ratios in order to obtain good ion intensities for each protein. When sample amounts are severely limited, it is not possible to prepare a number of samples with different concentrations of internal standard.

Recently, Xiang and Beavis developed a new sample preparation method to quickly grow a protein-doped polycrystalline matrix film [1]. Using our own variation of this technique, it is possible to deposit sample and standard in separate CHCA matrix layers. Samples were prepared by first depositing 0.5μl of a saturated solution of a-cyano-4-hydroxy-cinnamic acid (CHCA) in 1:1 water: acetonitrile onto the stainless steel sample stage of a Shimadzu Compact MALDI III TOF-MS. After 15s, the stage is washed leaving only a thin layer of matrix on the surface of the sample well. Additional matrix (~3 μl) is added to form a thick matrix pad. The first protein solution (0.5-5 pmole/μl in 1:1 0.1% aqu. TFA: acetonitrile) is added to the matrix pad and evaporated to dryness. The second protein is added in the same solution only containing 20% glycerol. After 3 min, the remaining solvent is removed from the sample pad by dipping the slide in water then air dried. Collected spectra are the average of a 100 laser shot scan across the sample.

Samples prepared using the layered method avoid the suppresion effects associated with the dried droplet method (Figure 1). With each successive scan, the signal of the protein in the top layer decreases. Thus, it is always possible to obtain a spectrum with good intensities for sample and internal standard ions. Thicknesses of the top protein layer were found to be inversely proportional to the molecular weight of the protein sample (~3μm for trypsin inhibitor, 20 kDa and ~0.4μm for BSA, 67 kDa). The observed mass value of the sample protein does not vary systematically with increasing scans over the sample. The mass measurement error for large proteins (> 15 kDa) was found to depend strongly on which order the proteins were layered in the sample (Figure 2). Proteins deposited in the bottom layer had a larger energy deficit as the result of increased numbers of collisions with neutral matrix ions during the MALDI process [2]. This complicates the use of the layered sample preparation method for internal calibrations, but does not entirely preclude its use. If the standard protein is always deposited in the top layer, using exactly the same proceedure, the calibration error increases with increasing molecular weight. A correction factor empirically determined for each standard protein can be used to adjust the value of the observed mass.

1. Xiang, F. and Beavis, R. C., *Rap. Commun. Mass Spectrom.* **1994**, 8, 199.
2. J. Zhou, W. Ens, K. G. Standing and A. Verentchikov, *Rap. Commun. Mass Spectrom.* **1992**, 6, 671.

43rd ASMS Conference on Mass Spectrometry and Allied Topics

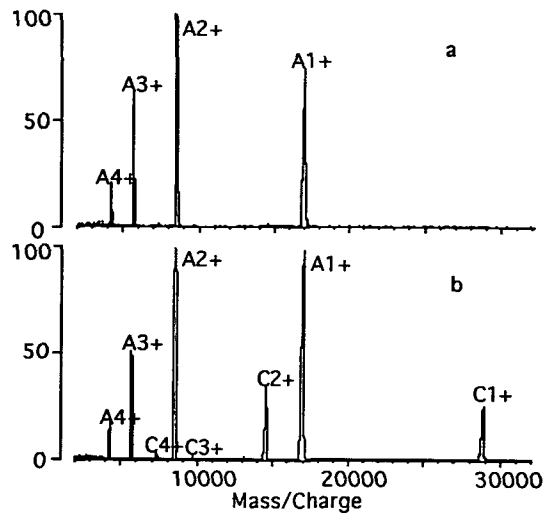

Figure 1. MALDI spectrum of apomyoglobin (4 pmol) and carbonic anhydrase (0.85 pmol) using the a) dried droplet and b) layered sample preparation

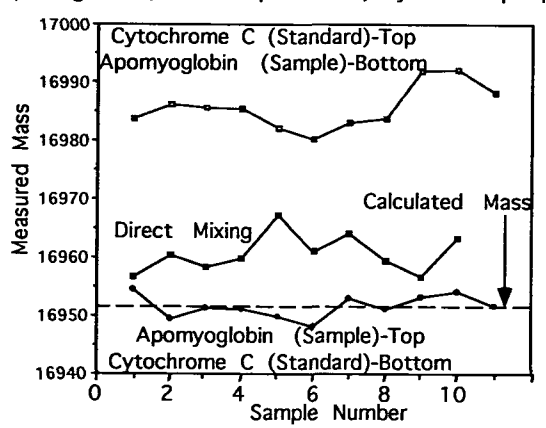

Figure 2. Comparison of Internal Calibration Using Direct Mixing vs. Layered Sample and Standard

Charge State Distribution Shifting of Protein Ions Observed in Matrix-Assisted Laser Desorption Ionization Mass Spectrometry

J. Zhou and T. D. Lee
Beckman Research Institute of the City of Hope
Duarte, CA 91010

Recently, Xiang and Beavis reported that a thin polycrystalline film, consisting of microcrystals of protein-doped matrix, could quickly form on a previously deposited layer of the same matrix (1). The film strongly adheres to the substrate so that it can be more easily washed and samples can be prepared in the presence of high concentrations of glycerol and even 6 M urea. While experimenting with our own version of Beavis method using the CHCA matrix, we observe significant increases in the intensities of higher charge state species for large proteins when the polycrystalline film was formed in the presence of glycerol or urea.

Experiments were conducted in a Kratos Compact MALDI III time-of -flight mass spectrometer (Shimadzu, Columbia, MD). All spectra were collected in the linear mode without using the reflectron. Spectra are an average of 100 laser shots over 2 mm long sample well. The CHCA matrix was prepared as a saturated solution in 0.1% TFA and acetonitrile (1:1 v/v). Proteins were dissolved in 0.1% TFA. Like the Beavis method, the initial layer of matrix was formed by drying about 4 ml of matrix solution on the sample well (2 mm x 1 mm). The matrix pad is then smeared with a microscope slide. Loose matrix powders were removed by tapping the sample slide. Protein solutions (a few pmole total amount) were mixed with matrix solution and applied to the matrix pad and allowed to dry completely. When glycerol was added to the sample-matrix solution (20% by volume), there was no obvious change in drop volume after a few minutes and the remaining liquid was removed from the pad by dipping the slide in room temperature water for two minutes.

The effect of effect of depositing the sample in the presence of glycerol is illustrated with the analysis of phosphorylase a (Fig. 1). When the sample is deposited on a preformed matrix pad (Fig. 1b), there is a noticable shift to higher charge states compared to the spectrum obtained by drying the sample, matrix solution directly on the bare stainless steel stage (Fig. 1a). In the presence of glycerol (Fig. 1c), a bimodal distribution is observed. With an increase in laser power, the higher charge state distribution decreases (Fig. 1d.). The bimodal distribution is generally not observed for most proteins, but the shift to higher charge states is a general phenomenon for many proteins larger than 30,000 Da. Other matrixes were studied (sinipinic acid, HABA) but no difference was observed when samples were prepared with glycerol. Depositing a thin layer of glycerol on samples already on the sample stage had no significant effect. These results indicate that glycerol is incorporated into the crystal structure along with the protein and either alters the structure of the protein or changes the chemistry responsible for charging the protein ions during the desorption process.

We were unable to obtain any evidence that differences in the spectrum reflected differences in the conformation of the protein in solution. Indeed, the fact that both glycerol and urea show the same effect would argue against that conclusion. As evidenced from CD data obtained on BSA, glycerol stabilizes the alpha helical structure while urea denatures the protein into a random coil. Using this sample preparation method, it may be possible to obtain MALDI spectra on magnetic sector or FTMS instruments that have limited mass ranges compared to time-of-flight analyzers.

1. Xiang, F. and Beavis, R. C., *Rap. Commun. Mass Spectrom.* **1994**, 8, 199.

43rd ASMS Conference on Mass Spectrometry and Allied Topics

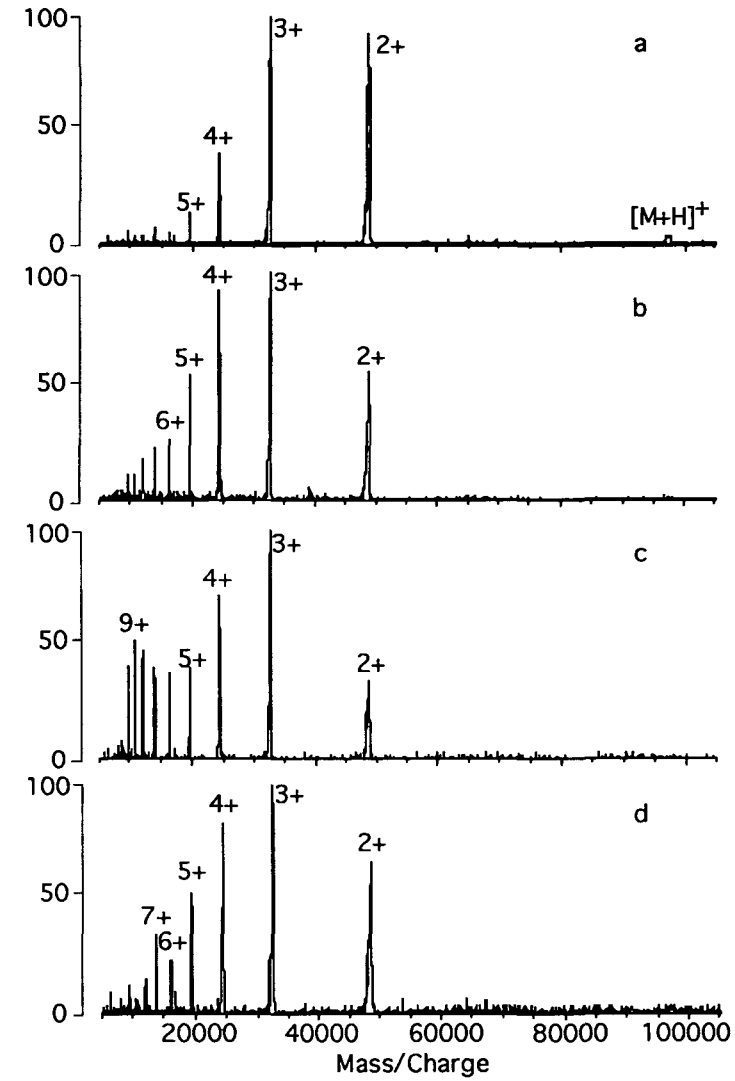

OPTICAL CHARACTERIZATION OF THE MALDI PLUME*

Gregory B. Hurst, Oak Ridge National Laboratory, Oak Ridge, Tennessee 37831-6365

The development of matrix-assisted laser desorption/ionization (MALDI) by Karas, Hillenkamp *et al.* has brought an entire new class of large-molecule applications within the reach of mass spectrometry [1]. However, the ionization efficiency and therefore the sensitivity of the technique could be improved if details of the ionization mechanism were understood more thoroughly. The environment in the MALDI plume may influence the ionization of the analyte, in analogy to the effect of pH on biomolecules in solution. Optical probing techniques, such as laser-induced fluorescence, allow some characteristics of the plume environment to be studied directly [2]. This paper describes measurement of wavelength-dispersed fluorescence produced in MALDI experiments in a time of flight mass spectrometer (TOF-MS).

An in-house-constructed linear TOF-MS for MALDI using a Laser Photonics LN203C pulsed nitrogen laser (337 nm) was modified to allow collection of the fluorescence related to the laser desorption event. A 5 cm quartz lens inside the vacuum chamber collimates the light emitted from the sample, and directs it through a quartz viewport. A second lens outside the chamber focuses the light into a UV-transmitting fiber optic (3M, FT-1.0-UMT) leading to a 0.5 meter focal length monochromator. Fluorescence spectra were obtained by scanning the monochromator while recording the output of an attached photomultiplier tube.

Samples investigated included 2,5-dihydroxybenzoic acid (DHB) and chrysene added to the probe tip as a solution or as a methanol slurry. Typical operating pressure in the mass spectrometer was in the 10^{-7} torr range. For obtaining desorption-laser-induced fluorescence spectra, the laser power density was approximately 10^{6} to 10^{8} W cm^{-2}. Solution-phase excitation and emission spectra of DHB in 1:1 (v:v) acetonitrile/water were obtained using a scanning fluorescence spectrophotometer (Perkin-Elmer model LS-5B) with slits set for 3 nm.

Figure 1 compares fluorescence spectra of DHB obtained by monitoring the emission resulting from laser desorption in the TOF-MS (Figure 1, A-C) and in acidic solution (Figure 1D) Spectra A-C were obtained consecutively by repeating a monochromator scan while illuminating the same sample spot with the desorption laser. Relatively narrow features are observed at 423 nm and 533 nm in A, which are less intense in B and nearly absent in C. This could be due to a laser-induced change in the sample, such as photochemical decomposition of the solid material on the probe, gradual removal of material from the sample by ablation, or changes in the crystal structure. The overall broad envelope of the emission observed in Figure 1 A-C matches the broad conventional fluorescence emission spectrum shown in Figure 1D for DHB in acidic solution. Because of potential complications due to the acid-base chemistry of DHB, desorption-laser-induced emission from chrysene, a polycyclic aromatic hydrocarbon with well known spectroscopic properties was examined (Figure 2.) Compared to the literature solution-phase fluorescence spectrum [3], the overall maximum is somewhat red-shifted, and the vibronic structure is obscured. In contrast to the DHB spectra, no narrow features are seen.

One possible explanation for narrow features in the DHB spectra in Figure 1 A-C is fragmentation of the organic molecule into smaller, highly-fluorescent species such as H, C_2, OH, etc. which have relatively narrow emission spectra. However, literature spectra of several such small molecules [4] do not match the observed narrow features in Figure 1 Another possibility is gas-phase fluorescence from DHB molecules or ions that have been cooled by expansion of the laser-produced plume into the vacuum subsequent to the desorption event. While the data presented here are preliminary, the presence of narrow features in the DHB spectra and their

43rd ASMS Conference on Mass Spectrometry and Allied Topics

absence in the chrysene spectrum suggests that the chemistry of the desorbed compound may determine whether such features are observed. An obvious difference between DHB and chrysene is the presence and absence, respectively, of -OH and -COOH functional groups. Further experiments to determine whether there is a correlation between presence of narrow emission features and the ability of a compound to perform as a MALDI matrix are planned.

*Research sponsored jointly by the U.S. Department of Energy, Office of Health and Environmental Research, and the Strategic Environmental Research and Development Program under contract DE-AC05-84OR21400 with Martin Marietta Energy Systems, Inc

1. (a) Karas, M ; Bachman, D , Bahr, U.; Hillenkamp, F. *Int. J. Mass Spectrom Ion Processes* **1987**, *78*, 53-68. (b) Hillenkamp, F.; Karas, M., Beavis, R.C.; Chait, B.T. Anal. Chem. 1991, 63, 1193A.
2. (a) Kimbrell, S.; Yeung, E. Applied Spectroscopy 1991, 45, 442. (b) Heise, T.W.; Yeung, E.S. Anal. Chem. 1992, 64, 2175. (c) Heise, T.W.; Yeung, E.S. Anal. Chem. 1994, 66, 355.
3. Berlman, I.B *Handbook of fluorescence spectra of aromatic molecules.* Academic Press, New York, 1965 p. 134.
4. (a) Lee, S.C ; Stanton, B J.; Eldridge, B.A.; Wehry, E.L. Anal. Chem 1982, 64, 268. (b) Pearse, R.W B, Gaydon, A.G. *The identification of molecular spectra.* Third ed., John Wiley, New York, 1963.

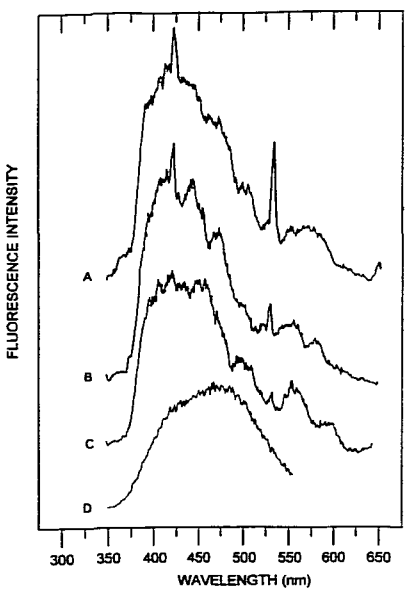

Figure 1

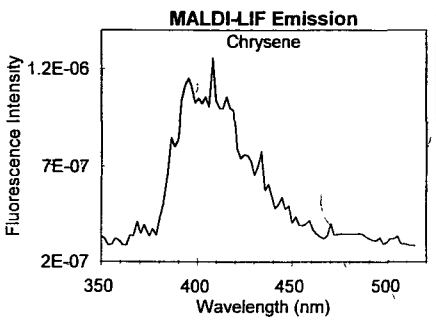

Figure 2

Optoacoustical Monitoring of Laser Absorption of MALDI Matrices in Solid State and in Aqueous Solution*

N. I. Taranenko, V. V. Golovlev, A. A. Puretzky, S. L. Allman, and C. H. Chen

Oak Ridge National Laboratory
P. O. Box 2008, Oak Ridge, Tennessee 37831-6378 USA

Recently matrix assisted laser desorption ionization (MALDI) mass spectrometry has been successfully applied for detection of DNA fragments with mass up to 500 mer[1,2]. This success was possible after finding a few matrices that play a key role in transporting analyte molecules and molecular ions into gas phase. Unfortunately, the search for new matrices is still an empirical procedure in view of the lack of detailed understanding of the complicated MALDI process However, it is generally accepted that the laser evaporation of the matrix with dissolved guest molecules is the starting point of MALDI The absorption of laser energy should be quickly and efficiently converted to heat to produce evaporation of the matrix substance Here we present a new technique involving broad band acoustical monitoring of solid state matrix samples as a method of investigation of the light-heat conversion process[3]. Generally, laser acoustic pulse generation can be treated as a result of thermal expansion of a thin layer of a substance heated by laser radiation. Therefore an acoustic signal can be used for calorimetric characterization of the thin layer of irradiated substance

In our experiments we investigated the amplitudes of an acoustic signals generated in 3-hydroxypicolinic acid (3-HPA), picolinic acid (PA), composite matrix (PA+3-HPA), and 3-aminopicolinic acid (3-APA) versus the laser pulse energy. A nonlinear dependence of the acoustical signal on laser fluence was found for PA, PA+3-HPA, and 3-APA matrices under irradiation by 7 nsec laser pulses at 266 nm Near linear dependence was found for 3-HPA at 266 nm There was no strong deviation from linear power dependence for any of these matrices at 355 nm. We found some correlation of the nonlinear acoustic pulse generation and the capability of the given compound to produce DNA ions in the MALDI experiment.

A comparative study of laser acoustic generation of solid matrices and their aqueous solutions showed that the observed acoustical nonlinearity is related to multiphoton (multistep) absorption rather than an ablation (desorption) process. We believe a multiphoton absorption involves high excited energy levels of matrix molecules leading to the process of light-heat conversion. Energy relaxation from high excited electronic states can occur through fast nonradiative transitions This can provide, probably, more efficient channels of laser heating of the matrix substance than one photon excitation through relatively long lived first singlet (or triplet) energy states.

Finally, one can expect the compounds that exhibit the characteristic of multiphoton absorption should be more promising for use as matrices in MALDI.

References

1. K. Tang, S. L. Allman, R. B. Jones, and C. H. Chen, *Rapid Comm. Mass Spectrom.* **7**, 142 (1993).
2. N. I. Taranenko, K. Tang, S. L. Allman, L. Y. Ch'ang, and C. H. Chen, *Rapid Comm. Mass Spectrom.* **8**, 1001 (1994).
3. N. I. Taranenko, V. V. Golovlev, A. A. Puretzky, S. L. Allman, and C. H. Chen, *Chem. Phys. Lett.* **234**, 165 (1995)

*Research sponsored by the Office of Health and Environmental Research, U S Department of Energy under contract DE-AC05-84OR21400 with Martin Marietta Energy Sytems, Inc.

Matrix-Assisted Laser Desorption/Ionization of Cytochrome c
λ = 337 - 450 nm

Xiangjun Chen and Ronald C. Beavis
Department of Chemistry
New York University Medical Center
550 1st Avenue
New York, NY 10016

The protein ion emission properties of MALDI matrices have been investigated quite carefully in the wavelength range of 250-350 nm, by a number of groups using a wide variety of lasers. These experiments have been unable to determine whether single or two photon absorption is responsible for protein ion emission. They have also shown that protein ion emission is not very sensitive to wavelength in this range.

This study presents the protein ion emission properties of MALDI matrices in the near ultraviolet, in the wavelength range of 337-450 nm. At these wavelengths, almost all biologically derived polymers are transparent, so all laser energy will be transferred to the matrix, without the possibility of simple resonance transfer of energy to the biopolymer. Most of the common matrices also become transparent in this wavelength range The behavior of protein ion threshold fluence has been studied as a function of wavelength and matrix.

The matrix-assisted laser desorption time-of-flight mass spectrometers commonly used in analytical laboratories currently use low power nitrogen lasers. The experimental setup allowed the easy comparison of longer wavelengths with a standard nitrogen laser. A linear time-of-flight mass spectrometer (custom built at New York University Medical Center) was used to detect protein ions. The laser illumination system was configured in two parts: a transmitter, which focused the light from the laser into a fiber optic; and a receiver, which focused the light emerging from the fiber optic into the ion source. Two transmitter assemblies were constructed and mounted at the output of the two lasers used in this study: a nitrogen laser (λ = 377 nm) and a tunable titanium:saphire laser with second harmonic generation (λ = 350 -450 nm). The receiver was mounted on the time-of-flight mass spectrometer, with the fiber optic mounted in chuck so that it could be easily removed. To change between the nitrogen and titanium:saphire laser, the only alteration was removing one fiber optic from the receiver chuck and replacing it with the fiber optic from the other laser.

Part of the results are shown below Three matrices were used in the study: α-cyano-4-hydroxycinnamic acid, indole acrylic acid, and 3,5-dimethoxy-4-hydroxycinnamic acid (sinapic acid). The wavelength maxima (λ_{max}) for protein ion production are shown in Table 1.

matrix	λ_{max} (nm)
α-cyano-4-hydroxycinnamic acid	434
indole acrylic acid	428
sinapic acid	398

Table 1. The maximum wavelength for producing cytochrome c ions in three common MALDI matrices.

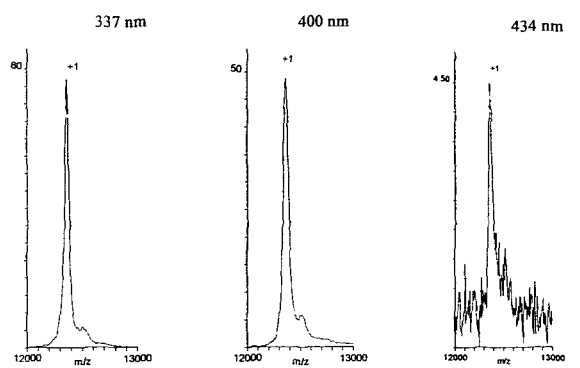

Figure 1 The molecular ion region of MALDI at three different wavelengths, using α-cyano-4-hydroxycinnamic acid as the matrix. Protein-doped matrix crystals were prepared using the dried droplet method, with using 0.5 µl droplets of 1 µM horse muscle cytochrome c in matrix-saturated 2.1 water:acetonitrile. Spectra were obtained near the ion production threshold laser fluence.

Influence of both esterification and target preparation on matrix-assisted laser desorption ionization time of flight mass spectrometry of an aromatic polyester.

J. Guittard[1], M. Tessier[2], J.C. Blais[1], G. Bolbach[1], L. Rozes[2], A. Brunot[1], E. Maréchal[2], J.C. Tabet[1].
1-Université Pierre et Marie Curie, Laboratoire de Chimie Structurale Organique et Biologique, CNRS EP 103, 4 place Jussieu, F-75252 Paris Cedex 05.
2-Université Pierre et Marie Curie, Laboratoire de Synthèse Macromoléculaire, CNRS URA 24, 4 place Jussieu, F-75252 Paris Cedex 05.

MALDI-TOF has been recognized as a powerful technique for the mass determination of large molecules [1] and for direct mixture analysis [2]. Polyesters are a challenge to the mass spectroscopist since they exhibit very broad asymmetrical molecular weight distributions and often a low solubility. We present results concerning the influence of both esterification with TFA and target preparation on the MALDI mass spectrum characteristics and on the molecular weight distributions of an aromatic polyester. MALDI mass spectra were performed on a home-built linear TOF (1,35m flight path -20KeV ion energy) using a pulsed N_2 laser.

Firstly, a « conventional » sample preparation method was used: matrix and analyte solutions were mixed and 1 µl was deposited onto the metal tip (« 1 step » method). Solubilization of the aromatic polyester requires the presence of TFA. The mass spectrum of compound 1 using 2,5-dihydroxybenzoic acid (2,5-DHB) as matrix and THF:TFA (0,1%) as solvent, exhibited the Na^+ and K^+ cationized oligomer peaks (fig.1).

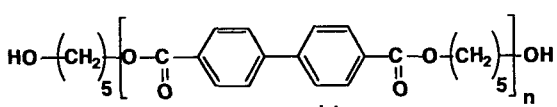

compound 1

The $\overline{M}_n$, $\overline{M}_w$ and I_p values determined from this spectrum, were respectively 2164, 2582 and 1,19. SEC values have not been obtained for this compound, due to its insolubility in THF, and NMR measurements gave $\overline{M}_n$=3200. A discrimination against the higher mass oligomers could originate from a poor incorporation of the polymer in matrix crystals. The mass spectrum of compound 1, using pure TFA as polymer solvent and 2,5-DHB in THF as matrix, shows peaks corresponding only to the Na^+ and K^+ cationized diesterified oligomers. The $\overline{M}_n$ and $\overline{M}_w$ values were lower than those obtained with THF:TFA (0,1%) despite the better solubility of the polyester in pure TFA.

So, we tried a « 2 steps » method [3] in which matrix and analyte handling are completely decoupled: 1µl of the matrix solution (0,1 M 2,5-DHB in THF or 0,1 M α-cyano-4-hydroxy-cinnamic acid (HCCA) in acetone) was deposited onto the probe tip ; then 1µl of compound 1 solution (10^{-4} M in TFA) was applied. For both matrices, the « 2 steps » method induced an increasing of the $\overline{M}_n$ and $\overline{M}_w$ values. Typically with HCCA (fig. 2), $\overline{M}_n$, $\overline{M}_w$ and I_p were respectively 4002, 5122 and 1,28.

In conclusion, the « 2 steps » method offers several advantages:
(i) sample surface becomes more homogeneous, leading to easier and faster data acquisition.
(ii) less discrimination against the higher mass oligomers.
(iii) the diesterification induces a shift toward higher masses (+192 uma), so matrix cluster peaks do not interfere with the lower mass oligomers peaks.

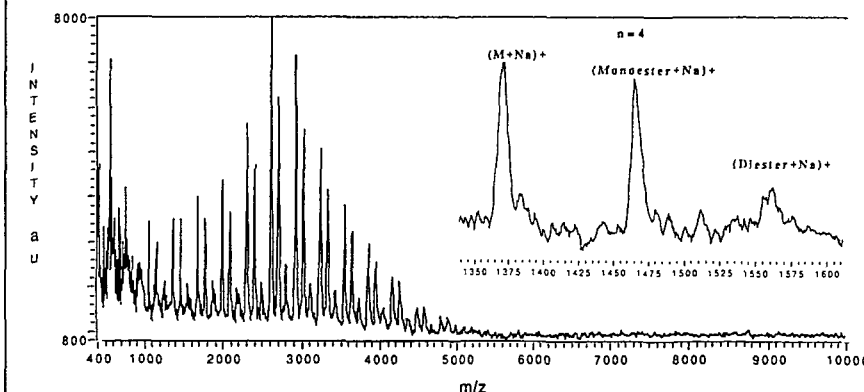

Fig. 1: MALDI mass spectrum of compound 1 obtained with the « 1 step » method

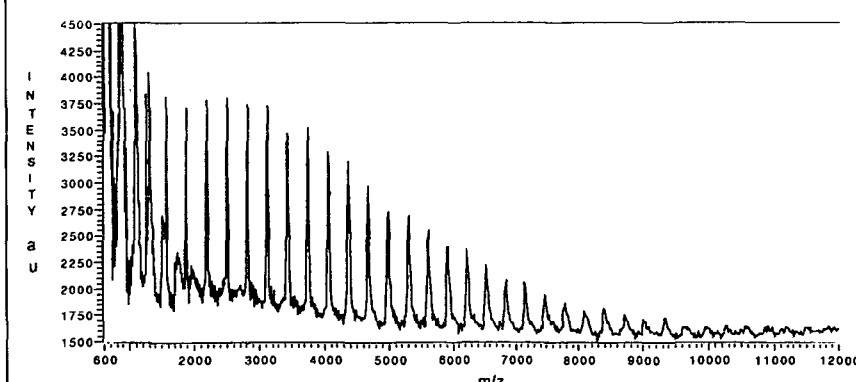

Fig. 2: MALDI mass spectrum of compound 1 obtained with the « 2 steps » method

1-M. Karas, F. Hillenkamp and U. Giessmann, Mass Spectrom. Reviews, 1991, *10*, 335
2-B.T. Chait, R. Wang, R.C. Beavis and S.B.H. Kent, Science, 1993, *262*, 89
3-O. Vorm, P. Roepstorff and M. Mann, Anal. Chem., 1994, *66*, 3281

Mechanistic Studies of the Cationization of Synthetic Polymers by Alkali Metals in the Matrix-Assisted Laser Desorption/Ionization Experiment

Richard C. King, Robert Goldschmidt, Yansan Xiong, and Kevin G. Owens*, Department of Chemistry, Drexel University, Philadelphia, PA 19104

Alkali metal cationization of several classes of synthetic polymers (notably the polyglycols and polymethacrylates) occurs via a gas-phase ion-molecule or excited state molecule-molecule reaction[1]. Laser post-ionization (and laser photodissociation) experiments of the neutrals desorbed during the MALDI process suggest that the alkali metal salt of the matrix (in this case 2,5-dihydroxybenzoic acid, DHB) is the preferred form of the ionizing reagent. Furthermore, the supersonic expansion conditions that occur as a result of disintegration of the matrix crystal provides the necessary collision frequency and relative energy distributions to virtually ensure the reaction of the neutral species in the plume and the cationization reagent.

Addition of the alkali metal salt of the matrix at the level of 10% was shown to effectively ionize materials without significantly affecting the desorption behavior of the protonated DHB material[2]. The matrix salt is not incorporated into the crystals with the analyte; proximity of the ionization reagent to the matrix dispersed analyte is sufficient for efficient ionization. When attempting to analyze a polymer sample by MALD/I, it would be advantageous to know whether matrix salt addition would be beneficial and if so, which salt would be best to use. In this work we examine the effect of added matrix salt for selected polymer samples to determine whether trends may be seen in the effectiveness of matrix salt addition and cation preference.

Results and Discussion

Cation Affinities: When a PEG 1000 sample is mixed with a single DHB salt (in all cases mixed at the level of 10% with the protonated form of the matrix), all of the observed PEG oligomer peaks are cationized by the expected alkali metal ions. In comparing the different alkali DHB ionization reagents, it appears that the largest peak intensity is found with potassium salt addition and the lowest from the lithium salt addition. Similarly, when a polytermethylene glycol (PTMEG) 1000 sample is mixed with a single DHB salt, all of the observed PTMEG oligomer peaks are cationized by the expected alkali metal ions. However, the largest peak intensity is observed with lithium salt addition and the lowest from potassium salt addition.

When an equimolar mixture of PEG 1000 and PTMEG 1000 is added to the potassium salt of the matrix, only PEG oligomers are observed. When this same equimolar mixture of PEG and PTMEG is added to the lithium salt of the matrix, however, strong lithium cationized PTMEG oligomers are observed while only weak lithium cationized PEG oligomers are apparent. From these data it appears that PEG has a higher affinity for or forms a more stable cationized species with potassium, whereas PTMEG has a higher affinity for lithium.

When the PTMEG sample is added to an equimolar mixture of the three alkali metal salts of DHB together, it is found that with increasing of laser intensity, the relative ratio of the various cationized species change. It appears that the potassium cationized oligomer peaks decrease in intensity, while the lithium cationized peaks remain constant or slightly increase. This change may be due to the laser intensity directly (changing the numbers of ions formed or destroyed during the laser pulse), or could a function of the spatial distribution of the salts in the solid crystal (as higher laser power may create ions from a larger or deeper sample spot). When the PEG 1000 sample is similarly added to an equimolar mixture of the three alkali metal salts of

DHB, the sodium and potassium cationized oligomers are easily observed, while the lithium cationized peaks are very weak.

Mechanism of ionization: There are at least two explanations for the results obtained when studying the method of cationization by the alkali metal salt of the matrix[1]:

- The bare cation is released from the gas phase matrix salt by a photodissociation reaction. In the expanding plume above the surface, there is a large amount of matrix neutral, matrix salt neutral and some polymer neutral which can collide with the reactive bare cation to produce the characteristic ion signals. The energetics provided by the high pressure gas expansion into the surrounding vacuum and kinetics of the two processes provide the necessary collision frequency and relative energy distributions to virtually ensure the reaction of the neutral species in the plume and the bare cation.

- Collisions between the excited state matrix salt and the neutrals in the expanding matrix plume may result in the formation of the cationized species seen in the spectra. Such collisions may also provide the energy needed to fragment the excited state matrix salt into the bare cation and the remaining $(M-H)^-$ ion observed in the negative ion spectra.

Conclusions

The addition of a small quantity of the alkali metal salt of the matrix (~10% of the level of the chosen matrix) is effective for producing abundant cationized samples of most oxygen containing polymers. The results shown here provide information concerning the mechanism of ionization and the relative affinity of different polymers for different cation species.

Cation Affinities: Experiments with mixed samples or mixed ionization reagents indicates that the two polymers studied show different affinity towards the different cations. PEG is preferentially cationized with potassium ions, while PTMEG is preferentially cationized with lithium. The affinity of the various polymers for different size cations is likely due to their differing chemical and gas-phase structures. These cation affinities will have a significant impact on the analysis of polymer blends if a limited number of sample preparation conditions are employed. Work is continuing to understand these affinity differences, and to uncover whether different sample preparation strategies may decrease this sampling discrimination.

Mechanism of ionization: Results obtained when studying the method of cationization by the alkali metal salt of the matrix[1] suggest that the bare cation may be released from the gas phase matrix salt through a photodissociation reaction. The expansion conditions then provide the necessary collision frequency and relative energy distributions of the analyte and cation to virtually ensure the reaction of the neutral species within the expanding plume. A second possibility is that the cation is transferred between the excited state matrix salt and the neutrals through collisions in the expanding matrix plume. Such collisions may also provide the energy needed to fragment the excited state matrix salt into the bare cation and the remaining $(M-H)^-$ ion observed in the negative ion spectra.

References

1 King, R.C., Owens, K.G., "Investigation of the Polymer Cationization Mechanism Occurring during the UV Matrix-Assisted Laser Desorption Experiment", Proceedings of the 42nd Annual Meeting of the American Society of Mass Spectrometry, p. 955, 1994.

2 Richard C. King, Kevin G. Owens, "Investigations of the UV Matrix-Assisted Laser Desorption Process", Proceedings of the 42nd Annual Meeting of the American Society of Mass Spectrometry, p. 977, 1994.

Separation of the Desorption and Ionization Events in the Matrix-Assisted Laser Desorption/Ionization Experiment

Richard C. King and Kevin G. Owens*, Department of Chemistry, Drexel University, Philadelphia, PA 19104
Scott D. Hanton, Air Products & Chemicals, Inc., Allentown, PA 18195

An understanding of the cationization mechanism operating in the matrix-assisted laser desorption/ionization (MALD/I) technique has allowed us to experimentally separate the desorption and ionization events. Several new matrix materials are demonstrated that effectively isolate and desorb several types of synthetic polymers, but do not ionize these materials. Separation of the desorption and ionization events allows the experimenter greater latitude to optimize each event independently and to either simplify or improve the information of the final MALD/I spectrum.

The likely functions that a successful MALD/I matrix must possess has been discussed by a number of authors[1-3]. Generally, a MALD/I matrix is something that disperses and isolates the analyte, absorbs the energy from the laser field, vaporizes to form gas phase materials, and provides an ionization route suitable to the chemistry of the polymer sample. Clearly the matrix needs to fulfill a number of different functions. We can demonstrate that the desorption and ionization functions can be separated, and that these functions can be accomplished by different chemical species in the functional matrix. Desorption reagents tend to absorb the laser energy efficiently and fragment producing a supersonic expansion of gas phase species from the sample surface. Good desorption reagents include: sinapinic acid, 2,5-dihydroxybenzoic acid, and thiourea. The ionization process is believed to be a gas-phase chemical ionization reaction that occurs just above the surface of the sample after the desorbing laser pulse. Different chemical functionalities are optimized with different ionization reactions. Unsaturated hydrocarbon polymers will readily silver cationize, oxygen-containing polymers (e.g., polyglycols, polyesters and polyacrylates) will cationize with the alkali metals, and amine functional polymers tend to protonate. For unsaturated hydrocarbon polymers silver acetylacetonate (AgAcAc) is used, while the alkali metal salts of 2,5-dihydroxybenzoic acid are utilized for oxygen-containing polymers. We have found that the ionization reagent needs only to be in close proximity to, not incorporated into the matrix crystals.

We can demonstrate that the desorption and ionization functions of the MALD/I matrix can be separated, and that these functions can be accomplished by different chemical species in a combination matrix. The combination matrix must contain functionality to perform all of its different roles. If any of the roles are not fulfilled, the MALD/I experiment will yield incomplete or no ion signal. We will show examples of the consequences of not fulfilling either the desorption or ionization role, and then show how to design single, double and triple reagent matrices to ensure desorption and ionization for these polymers.

The data on this poster demonstrate that desorption and ionization are separate events in the MALD/I experiment. Most importantly, it is not necessary for a single molecule to carry out all the functions of a MALD/I matrix. These functions can be carried out by separate components of a mixture of molecules, with each optimized for best MALD/I results.

References

1 F. Hillenkamp, M. Karas, R.C. Beavis, B.T. Chait, Anal. Chem., 63, 1193-1203, (1991).
2 P. Juhasz, C.E. Costello, K. Biemann, Am. Soc. Mass Spectrom., 4, 399-409, (1993).
3 A. Vertes, R. Gijbels, F. Adams, eds., Laser Ionization Mass Analysis, Chemical Analysis Series vol 124, New York: John Wiley & Sons, 1993.

43rd ASMS Conference on Mass Spectrometry and Allied Topics

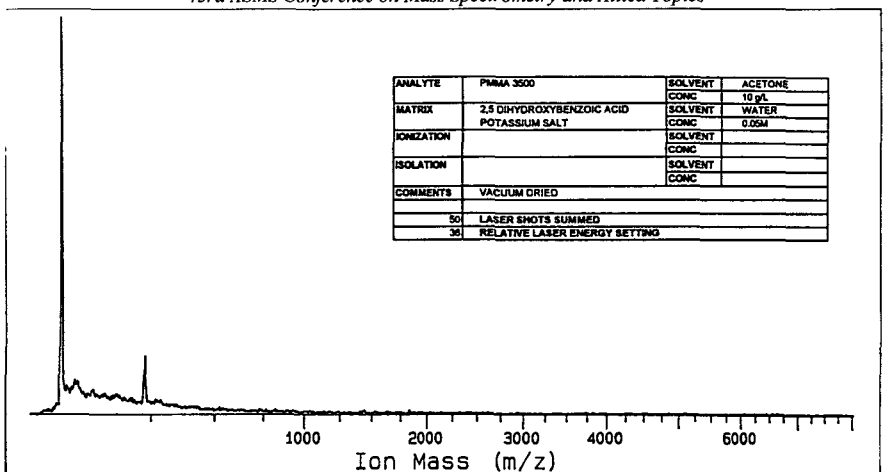

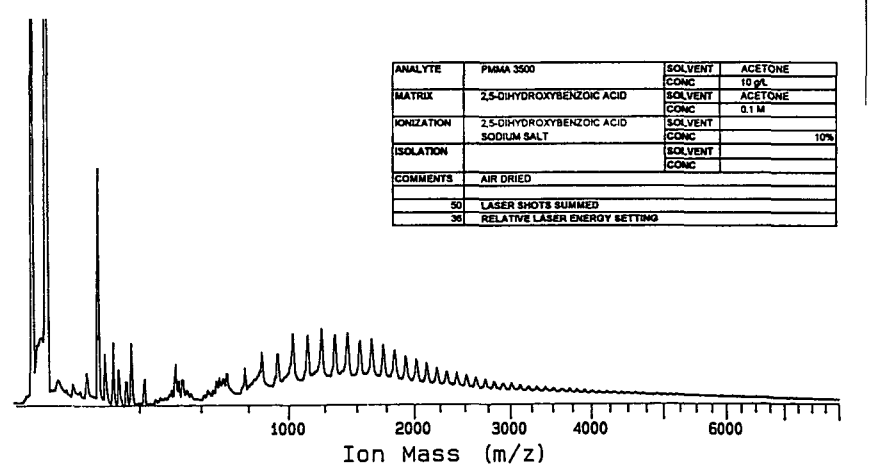

The alkali metal salts of the carboxylic acid matrix compounds acts as an efficient source for alkali metal reagent ions in the MALD/I experiment. The spectrum on top was obtained using the potassium salt of 2,5-dihydroxybenzoic acid (KDHB) as the matrix for a polymethylmethacrylate 3500 polymer sample. Although this absorbs 337nm light quite effectively, no oligomer ions are observed. When the system is modified by reducing the matrix salt concentration to 10% with the balance being the hydrogen form of the matrix, polymer ions are readily observed. In the former case the pure KDHB was unalbe to effectively desorb the analyte from the surface.

Evalution the Matrices used in MALDI by Their FAB Mass Spectra

Hsing-Long Chei and Jentaie Shiea*
Dept. of Chemistry, Natl Sun Yat-sen Univ.,Kaohsiung, Taiwan 804

The organic matrix used in matrix assisted laser desorption ionization (MALDI) play essential role both in ionization and desorption However, the choice of and search for the suitable matrix for protein analysis by MALDI is still a trial-and-error procedure. Since both FAB and MALDI are type of desorption ionization, the processes of phase transition and ion formation occurred in MALDI may be similar to those in FAB Therefore, the role of the matrix used in MALDI may be better understood by interpreting their FAB mass spectra. In this study, 25 organic compounds which are recognized as potential MALDI matrix were chosen as the analyte The FAB mass spectra of each analyte dissolved in glycerol was obtained. Since the laser desorption ionization (LDI) mass spectra of these compounds have been reported previously by Hillenkamp et al.[1], we then compared the mass spectra of the compounds obtained by FAB and LDI. It was found that except for four compounds, the major analyte ions found in FAB and LDI spectra are nearly identical. According to the type of the ions in FAB mass spectra, the investigated compounds can be divided into four classes. The classification of the first three classes is based on the value of $M^{\ddagger}/MH^{+}$ and the compounds in the last class produced both MH^{+} and MH_2^{+} ions

		As good MALDI matrix
Class 1	$M^{\ddagger}/MH^{+} > 1$	No
Class 2	$M^{\ddagger}/MH^{+} = 0$	No/Yes
Class 3	$M^{\ddagger}/MH^{+} < 1$	Yes
Class 4	$MH^{+}/MH_2^{+} > 1$	Yes

Except for few compounds, very similar classification of the organic matrixes has been suggested by Hillenkamp et al [1] by their LDI mass spectra. Table 1 indicates the usability of each compound as the matrix in MALDI for protein analysis. The data was quoted from the paper published by Hillenkamp et al. in 1992[1]. It can be seen that the compounds in class 3 and 4 are all good MALDI matrixes but all the compounds in class 1 and partial compounds in class 2 are not good MALDI matrixes. Since its very hard for the radical ion (class #1) and the ion with high gas phase basicity (some in class#2) to donate protone to the analyte, good MALDI spectra are imposible to obtain. It was also reported by Hillenkamp et al.[1] that for the compound such as indole-2-carboxylic acid the ratio of $M^{\ddagger}/MH^{+}$ on LDI mass spectra varied with the energy of the laser beam. Figure 1 show LDI mass spectra of indole-2-carboxylic acid at (a) 266 nm and (b) 337 nm. It can be seem that $M^{\ddagger}$ instead of MH^{+} was generated in the condition of higher energy deposition (i e. 266 nm, Figure 1a) To simulate the variation of energy deposition in FAB, the viscosity of the matrix was changed by 1) using more viscous FAB matrix such as diglycerol instead of glycerol (Figure 2) or by 2) lowering the glycerol matrix temperature by immersing the FAB probe into liquid nitrogen after sample application (Figure 3).

It can be seen when the viscosity of the matrix was increased the type of the indol-2-carboxylic acid ions on mass spectra was also changed from $M^{\ddagger}$ to $M^{\ddagger}/MH^{+}$ We have previously reported that as the viscosity of the FAB matrix increasing, the energy deposited on the molecule also increasing[2]. This will shorten the time of ion-molecule reaction which is responsible for the formation of MH^{+} ions. This is the reason why higher MH+ signal for the sample with lower viscosity is observed for there is enough time for ion-molecule reaction to be occurred. Owing to less ion-molecule reaction time is available for the sample with higher viscosity, more of the radical ions ($M^{\ddagger}$) shall be generated.

1. H. Ehring, M. Karas and F. Hillenkamp (1992) Org. Mass Spectrom., 27, 472.
2. J Shiea and J. Sunner (1990) Int. J. Mass Spectrom. Ion Processes, 96, 243.

43rd ASMS Conference on Mass Spectrometry and Allied Topics

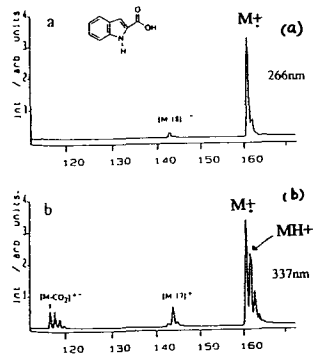

Figure 1. LDI mass spectra of indole-2-carboxylic acid previously reported by Hillenkamp et al. in 1992. Wavelength, (a) 266 nm and (b) 337 nm

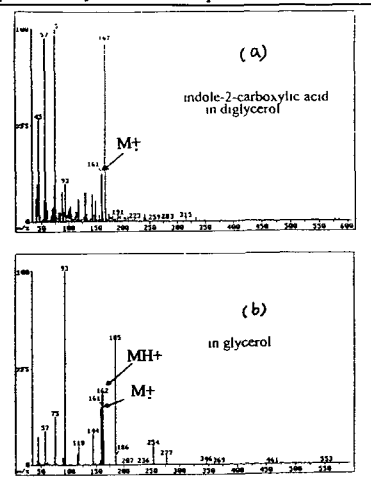

Figure 2 FAB mass spectra of indole-2-carboxylic acid dissolved in (a) diglycerol and (b) glycerol

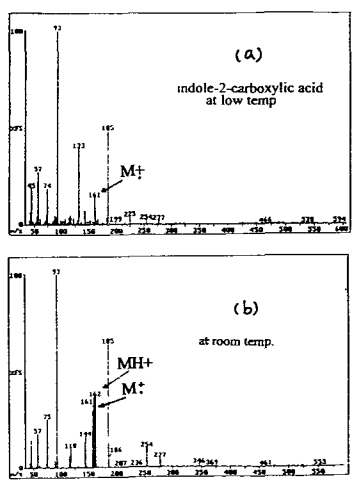

Figure 3. FAB mass spectra of indole-2-carboxylic acid dissolved in glycerol at (a) low temperature and (b) room temperature

Table 1. Classification of 26 organic compounds by their FAB mass spectra

			Major
class 1 $M^{\ddagger} \gg MH^{+}$		$(M^{\ddagger})/(MH^{+})$	Fragments
indole	-	2 88	(0)
1-naphthol	-	3 25	(F^{+})
indole-3-acetic acid	-	1 11	(F^{+})
4-aminobenzene sulphonic acid	-	X (radiational product)	
1,4-dihydroxybenzene	-	7 85	(0)
class 2 $[M+H]^{+} \gg M^{\ddagger}$			
adenine	-	-0	(0)
phenylalanine	-	0 16(radiational product)	
tryptophan	-	-0	(F^{+})
tyrosine	-	-0	(F^{+})
2-aminobenzimidazole	-	-0	(0)
aminonicotinic acid	0	-0	(F^{+})
nicotinic acid	++	-0	(C^{+})
uracil	0	-0	(0)
3-nitrobenzyl alcohol(1)	+	-0	$(F^{+}+F^{+}\cdot)$
indole-3-aldehyde(1)	0	-0	(F^{+})
class 3 $[M+H]^{+}/M^{\ddagger} < 1$			
2 5-dihydroxybenzoic acid	++	0 90	$(F^{+}+F^{+}\cdot)$
3,4 5-trihydroxybenzoic acid	0	0 66	$(F^{+}+F^{+})$
3,4-dihydroxycinnamic acid	+	0 52	$(F^{+}+F^{+})$
3 5-dimethoxy-4-hydroxycinnamic acid	+	0 71	(F^{+})
2-hydroxy-3-naphthoic acid	+	0 51	$(F^{+}+F^{+})$
1,3 5-trihydroxybenzene	0	0 86	(0)
2,3-dihydroxybenzoic acid(2)	+	0 45	$(F^{+}+F^{+})$
2 4-dihydroxybenzoic acid(2)	+	0 65	$(F^{+}+F^{+})$
class 4 $[M+H]^{+}/(M+2H)^{+} > 1$			
pyrazine-2 carboxylic acid	+	(3 42)	(F^{+})
tetrahydroxy-p-benzoquinone	+	(0 64)	(F^{+})

(F+) even electron fragment; (F+) : odd electron fragment
(0) : no fragment, (C+) even electron cluster
Key · ++, very strong protein signal, +, strong protein signal,
0, weak protein signal, -, no protein signal observed.

COMPARISONS OF PROTON TRANSFER REACTIONS OF MALDI MATRICES

Gary R. Kinsel, C. Mark Land, Angela Walker and Nan Li
The University of Texas at Arlington, Department of Chemistry, Arlington, TX 76019

The mechanism of matrix to analyte proton transfer during matrix assisted laser desorption ionization (MALDI) remains poorly understood. A variety of mechanisms have been suggested including excited state proton transfer, matrix ionization followed by proton transfer from the radical cation and matrix self-protonation followed by proton transfer to the analyte molecule. We have begun an investigation of the proton transfer reactions of a series of para substituted aniline molecules which serve as model MALDI matrices in a 3 T FT-ICR MS. This series of model matrices was chosen because the variations in the electron withdrawing and releasing ability of the para substituent should induce systematic and predictable changes in the proton affinities of the neutral and/or ionized matrices. Previously performed semiempirical calculations (PM3 type) of the heats of formation of the matrix neutrals and ions and proton affinities of the radical cations support the qualitative predictions.[1] Furthermore, the efficiencies of this same series of para substituted anilines as MALDI matrices has already been investigated experimentally.

Para substituent	Calculated M Proton Affinity (kcal/mol)
$-NO_2$	197.3
-CN	204.2
-COOH	205.7
-COOEt	207.4
-Cl	210.3
$-CH_3$	213.6
-OH	214.5

Initial studies focused on the self-protonation reactions of the substituted aniline compounds. These studies were performed by ionizing the matrix by electron impact in the ICR and then varying the delay between the end of the ionizing event and the excite and detect event During this time the radical

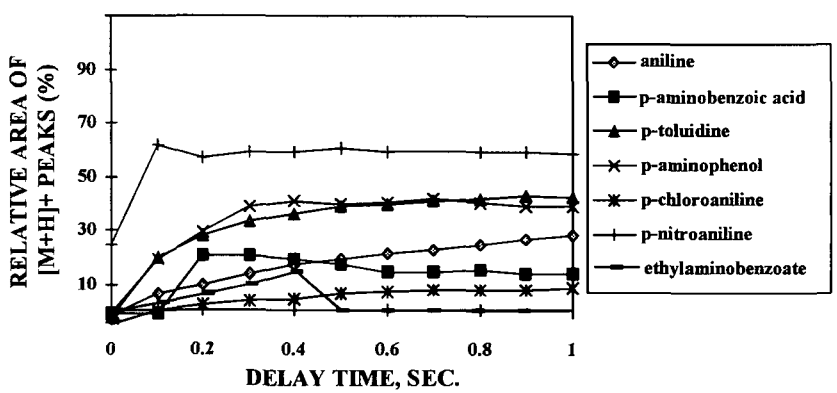

cations of the matrix could interact with residual neutral matrix molecules in the ICR and undergo proton

[1] Gimon-Kinsel, M., Preston-Schaffter, L.M , Kinsel, G.R., Russell, D.H. *J Am. Chem Soc* (manuscript in preparation)

43rd ASMS Conference on Mass Spectrometry and Allied Topics

transfer from the radical cation to the neutral molecule. For all matrices listed self-protonation is observed suggesting that in all cases the proton affinities of the neutral molecules are higher than the proton affinities of the radical cations. The highest degree of self-protonation is observed for 4-nitroaniline with the self protonation reaction occurring at the fastest rate. 4-nitroaniline also yields a very stable protonated molecule while the protonated 4-aminobenzoic acid, 4-aminophenol, 4-methylaniline and 4-chloroaniline undergo fragmentation following the self-protonation reaction. The trend in degree of self-protonation does not reflect the trend in calculated neutral molecule proton affinities. This result indicates that the trend in the differences in the proton affinities of the radical cation and neutral molecules do not reflect simply the proton affinities of the neutral molecules.

In order to assess the absolute proton affinities of the model substituted aniline matrices, mixed matrix studies were performed in order to determine the ability of the radical cation of one matrix to protonate the neutral molecule of another matrix. Thus far, it has been found that the proton donating abilities of the radical cations reflect the expected trend based on the relative electron withdrawing ability of the substituent in the para position *i.e* lowest proton affinity to highest: $-NO_2$, -CN, COOH, -COOEt, -Cl, CH_3, -OH. An example of this type of mixed matrix study is shown for a mixture of 4-nitroaniline and 4-aminoethylbenzoate. Note that the rate of protonation of the 4-aminoethylbenzoate increases to the rate of self-protonation of 4-nitroaniline when the two matrices are mixed.

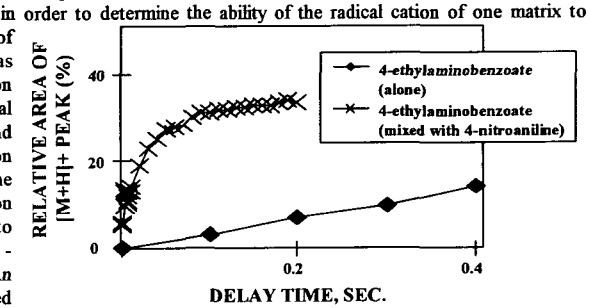

A significant question which has arisen in the course of this investigation relates to the ability of the 4-nitroaniline radical cation to protonate a peptide or protein. Our studies indicate that the 4-nitroaniline M^+ is a stable species with a proton affinity that must be less the neutral molecule value of 197 3 kcal/mol. If this numerical assignment is correct, the 4-nitroaniline $^{M+}$ should be readily able to protonate a peptide with an approximate average amino acid proton affinity of 212 kcal/mol.[2] However, studies of the wavelength dependence of MALDI suggest that at wavelengths where abundant radical cations are formed, less efficient proton transfer to the analyte occurs. Future studies of reactions of electron impact ionized matrices with laser desorbed neutral peptides will attempt to determine whether the M^+ of MALDI matrices do or do not have the ability to transfer a proton to an analyte protein in order to assess the involvement of this ion formation mechanism in the MALDI.

[2] Speir, J.P , Gorman, G S , Cornett, D S , Amster, I.J *Anal. Chem.* **1991**, *63*, 65-69.

Semi-Empirical Study of Proton Transfer in MALDI-MS of Small Peptides

Mehrnoosh Sadeghi and Akos Vertes
Department of Chemistry, The George Washington University, Washington D.C. 20052

The mechanism of ionization in matrix-assisted laser desorption/ionization (MALDI) is still not clearly understood. A theoretical study of hydrogen bond formation and proton transfer between the matrix and selected analytes in MALDI is presented. Different types of hydrogen bonds: a) bifurcated, b) intra, and c) intermolecular were investigated within the structure of the analytes alone and in complexes with the matrix. Proton affinities of the amino end group, the peptide bond, and the side chain of the peptides were investigated and compared.

In the large systems of our interest, ab initio calculations were not feasible. Among semi-empirical methods, AM1 developed by Dewar and coworkers, was chosen as an appropriate method for the study of hydrogen bonds in analyte-matrix systems [1]. Since hydrogen bonded structures and energies have been included in the parameterization of AM1, this method is successfully applied for the study of chemical reactions and mechanisms including hydrogen bonded systems. Geometry optimizations were carried out using the AM1 method as implemented in the MOPAC 6.0 package. The code was running on a 100 MHZ, R4000 workstation (IRIS Indigo XZ4000, Silicon Graphics, Mountain View, CA) Equilibrium geometries and dynamic reaction paths were visualized by the XMOL package (Version 1.3.1, Research Equipment Inc.).

The initial geometries of selected analytes (Gly-Gly, Gly-Ser, Gly-Gly-Gly, and His-His) and the matrix (3,5-dimethoxy-4-hydroxycinnamic acid or sinapinic acid, SA) were optimized separately. Geometries were defined in terms of internal coordinates and optimized for every relative configuration. For the optimization of the matrix-analyte complexes, the hydroxyl of the carboxylic group on the matrix was directed toward the site of interest on the analyte.

Investigation of the optimized geometries allowed us to locate intramolecular hydrogen bonds in the analytes. Bifurcated and intermolecular hydrogen bonds were observed between the analyte and matrix molecules. The intermolecular and bifurcated hydrogen bonds between Gly-Gly and SA are shown in Figure 1. In the case of His-His, in addition to these hydrogen bonds between matrix and analyte, an intramolecular hydrogen bond is also formed within the His-His molecule.

In order to study the energetics of hydrogen bond formation in the complexes, the sum of the heat of formations obtained separately for the analyte and matrix molecules was compared to the value obtained for the complex (Table 1) The difference is due to the intermolecular hydrogen bond formation in the complex. In every configuration the entire analyte was moved toward the matrix to obtain heat of formation diagrams. The presence and position of a minimum in the diagram revealed the formation of hydrogen bond between the two species (Figure 2). The calculated length and heat of formation of the hydrogen bonds are within the known range of 272 to 307 pm and -6 86 to -31.4 kJ/mol, respectively [2]

Proton affinity values were calculated for every dipeptide while the site of protonation was varied. These values were different depending on the site of protonation (see Table 2) The results seem to indicate that for every dipeptide the amino terminus is more susceptible to protonation than the peptide bond. As it has been shown, increasing the number of glycine residues leads to an increase in proton affinity [3]. For a basic dipeptide like His-His, the side chain has the highest proton affinity. The increased proton affinity of basic side chains points to their role in MALDI of proteins.

43rd ASMS Conference on Mass Spectrometry and Allied Topics

Compound	Investigated site	ΔH_f*
Gly-Gly+SA	peptide bond	-22.6
	amino group	-6.06
	peptide bond	-25.1
Gly-Ser+SA	side chain	-30.5
	amino group	-17.3
His-His+SA	side chain	-22.6

Table 1. Heat of formation of the hydrogen bonds formed between the analytes and matrix, SA.
*Values are in kJ/mol.

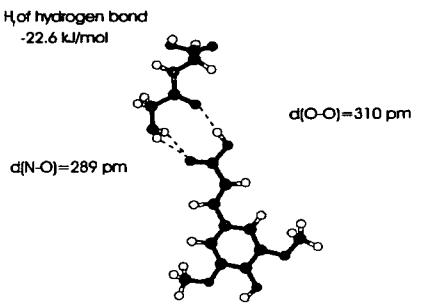

Figure 1. Intermolecular and bifurcated hydrogen bonds formed between Gly-Gly and SA.

Compound	Site of protonation	PA*
Gly-Gly	amino end group	860.65
	peptide bond	839.69
Gly-Gly-Gly	amino end group	870.15
	peptide bond	866.26
	peptide bond	878.56
His-His	amino end group	963.70
	peptide bond	948.39
	side chain	1001.0
Gly-Ser	amino end group	874.16
	peptide bond	851.99

Table 2. Comparison of proton affinity values for selected dipeptides protonated at different sites.
*Proton affinity: $PA(A) = \Delta H_f(A) + \Delta H_f(H^+) - \Delta H_f(AH^+)$ (values are in kJ/mol)

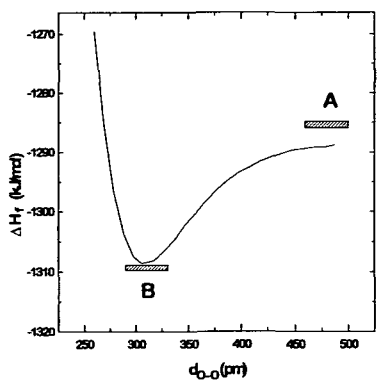

Figure 2. Hydrogen bond formation between Gly-Gly and SA. A compounded heat of formation B complex heat of formation.

References:
[1] Dewar, M. J. S.; Zoebisch, E. F.; Stewart, J. J. *J. Am. Chem. Soc.* **1985**, 107, 3902
[2] Vinogradov, S.; Linnell, *R. Hydrogen bonding*, Van Nostrand, New York, **1971**, 177-181
[3] Wu. Z.; Fenselau, K. *J. Am. Soc. Mass Spectrom.* **1992**, 3, 863

INTERNAL ENERGIES OF IONS FORMED BY MATRIX-ASSISTED LASER DESORPTION IONIZATION

Mary Gimon Kinsel, Kent J. Gillig, Lloyd W. Sumner, Ricky D. Edmondson, and David H Russell, Laboratory for Biological Mass Spectrometry, Department of Chemistry, Texas A&M University, College Station, Texas 77843

It is becoming increasingly clear that the internal energies of the analyte ions generated in MALDI vary significantly depending on the experimental parameters such as (1) matrix compound, (2) matrix additive (co-matrix), (3) laser irradiance and (4) sample preparation. The effect of these parameters is particularly evident in the amount of dissociation undergone by the analyte ions. Analyte metastable decay leads to poor resolution in linear TOF studies and analyte sequence information if the metastable decay product ions are separated and mass analyzed using an ion mirror. In an FT-ICR analyte dissociation limits the time that the analyte ion signal may be detected. We have used both TOF and FT-ICR experimental methods to characterize the internal energies of the analyte ions formed using several MALDI matrices.

TOF Experiment and Results

Retarding field experiments using a modified TOF mass spectrometer were performed to measure the contribution of metastable decay neutral products to the observed analyte signal. The corresponding metastable decay product ions were then separated and mass analyzed by scanning the voltage applied to the two-stage reflectron ion mirror. Figure 1 compares the metastable decay of the peptide RPPGFS (M_r = 659.3 Da) as a function of MALDI matrix. The common MALDI matrix α-cyano-4-hydroxycinnamic acid yields the mass spectrum shown in Figure 1a The product ions are referred to using the nomenclature suggested by Roepstorff and Fohlman.[1] The dominant ions correspond to sequence ions containing the C-terminus, y_4 and y_5. An almost complete series of b_n-ions is observed (b_1, b_2, b_3, b_5, and b_6) as well as a_n-17 ions. Several product ions containing neither the N- nor the C-terminus are observed in low abundance. Overall, 92% of the analyte $[M+H]^+$ ions decayed. In contrast, the metastable decay of RPPGFS is much reduced when 4-hydroxy-3-iodo-5-nitrobenzoic acid is used as matrix (Figure 1b). The dominant ion is the intact $[M+H]^+$ ion. The y_4 and y_5 remain the preferentially formed product ions. However, only 75% of the analyte $[M+H]^+$ ions have undergone metastable decay.

FT-ICR Experiment and Results

To further probe the internal energies of MALDI formed ions we implemented a series of FTICR experiments to obtain information regarding the chemical reactivities of laser desorbed species ($[M + H]^+$, M^+, or fragment ions). Ions fragment considerably on the millisecond time scale but the mechanism of positive analyte fragment formation is suppressed by specific collisional gases. The collisional gases most efficient at reducing fragmentation are Nitric Oxide and Oxygen.

---

[1] P. Roepstorff and J. Fohlman, *Biomed. Mass Spectrom.* **11**, 601 (1984).

43rd ASMS Conference on Mass Spectrometry and Allied Topics

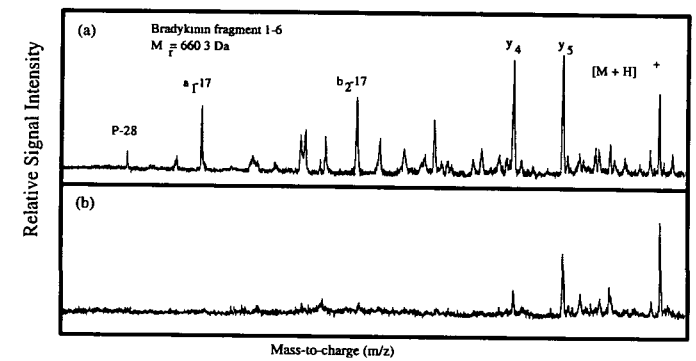

Figure 1: Metastable decay TOF mass spectra obtained from RPPRFS generated using the MALDI matrices (a) α-cyano-4-OH-cinnamic acid and (b) 4-OH-3-Iodo-5-nitrobenzoic acid.

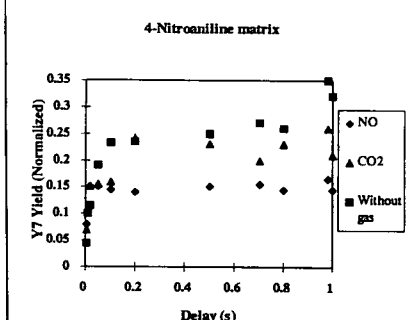

Figure 2: Collisional quenching of angiotensin II generated using 4-nitroaniline.

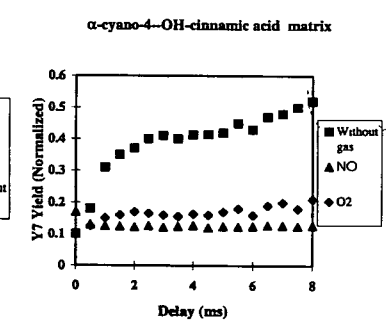

Figure 3 : Collisional quenching of angiotensin II generated using α-cyano-4-OH-cinnamic acid.

FACTORS INFLUENCING METASTABLE FRAGMENTATION IN MALDI TOF/MS

Steven Colby, Chris Houston, Noah Christian, Randy Arnold and James P. Reilly
Department of Chemistry, Indiana University, Bloomington, IN 47405

Time-of-flight mass spectra of proteins recorded using matrix-assisted laser desorption/ionization (MALDI) often appear remarkably simple. Parent ion peaks are dominant features, while signals corresponding to multiply charged or cluster ions are normally quite small. In early MALDI studies, it was believed that ion fragmentation is virtually non-existent. However, primarily through the work of Spengler and his collaborators, it has become evident that metastable fragmentation is a rather ubiquitous phenomenon [1,2]. The impact that metastable fragments have on TOF mass spectra obviously depends on whether or not they are separated from parent ions by electric fields outside of the source region of the instrument. Ion reflectrons are often employed to accomplish this separation. However, a simple postacceleration field at the end of the drift region of a linear TOF instrument can be similarly effective.

Figure 1 displays a diagram of our TOF mass spectrometer. Grid spacings are on the order of 1 cm and the drift tube is about 21 cm in length. MALDI generated ions are extracted from the source region of the instrument using a pulsed drawout field that is applied at an optimal time delay. Space-velocity correlation focussing [3,4] is used to establish the characteristics of this pulsed drawout field.

Figure 2 displays a positive ion MALDI TOF spectrum of lysozyme (m/z 14306). DC voltages applied to grids G0, G1, G2 and G4 were 15.0, 15.0, 12.06 and 0 kV, respectively. A 2 kV drawout pulse was applied to grid G0 3.6 microseconds after the desorption light pulse. The very sharp peak at 37.3 microseconds TOF corresponds to parent ions while the hump in front of this results from small fragment ions that move ahead of the parent ions in the postacceleration region of the instrument. In contrast, Figure 3 displays a negative ion MALDI TOF spectrum of lysozyme. A number of different voltage conditions were investigated, but in no case were we able to produce a spectrum quite like the positive ion version of Figure 2. Negative MALDI ions do not appear to break down into fragments that are as small as their positive ion counterparts. In addition, the parent to fragment abundance ratio is smaller in the negative ion case.

To demonstrate how much simpler the mass spectrum can appear when ions are not accelerated at the end of the drift region, we recorded data with a very different set of grid voltages. With G0, G1, G2 and G4 at -20 kV, -20 kV, -1.9 kV and -1.9 kV, respectively, and an optimized ion drawout pulse, we

observed the negative ion lysozyme spectrum of Figure 4. In this case, fragments formed in the drift tube are not sufficiently energetic to be detectable by our microchannel plates, so the broad underlying fragment ion pedestal that dominates the spectra in Figures 2 and 3 is not present.

References

1. B. Spengler, D. Kirsch and R. Kaufmann, Rapid Comm. Mass Spectrom. 5, 198-202 (1991).
2. B. Spengler et al., J. Phys. Chem. 96, 9684-9691 (1992).
3. S. M. Colby, T. B. King and J. P. Reilly, Rapid Comm. Mass Spectrom. 8, 865-868 (1994).
4. T. B. King, S. M. Colby and J. P. Reilly, Int. J. Mass Spectrom. Ion Proc., accepted.

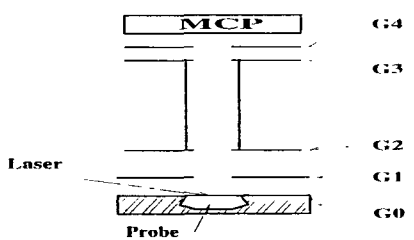

Figure 1.

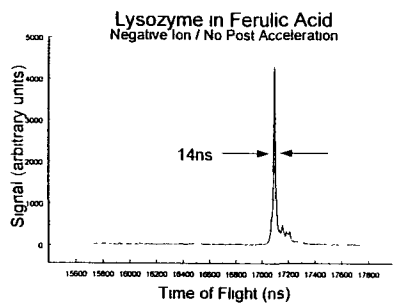

Figure 4.

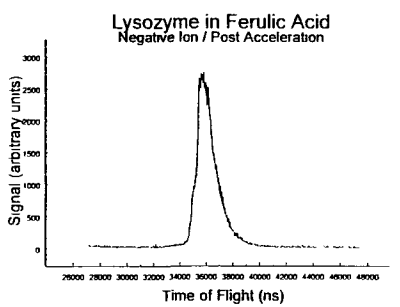

Figure 3.

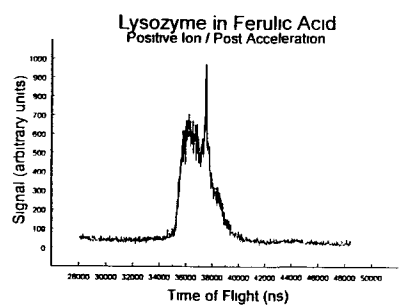

Figure 2.

Photodissociationexperiments and Investigations on the MALDI Process

Matthias Amft, Johann M. Grundwürmer, Roland Finsterer, Hou-Jun Yang and Jürgen Grotemeyer

Institut für Physikalische Chemie Universität Würzburg, Marcusstr. 9/11
D-97070 Würzburg, Germany

Subsequent fragmentation of molecular ions formed in the matrix assisted laser desorption and ionisation (MALDI) process can be induced by the absorption of photons. The experiments were performed in a home made linear-time-of flight-mass spectrometer that has been equipped with a postsource pulse focusing (PSPF) device[1]. Ion desorption was achieved by a frequency tripled (λ=355 nm) Quanta-Ray DCR11 Nd:YAG-laser. For fragmentation a "Laser Mark 960" CO_2-laser from Lumonics was used, that emitted light at 10.6 µm.

The molecular ions were fragmented in an additional field free drift region, which was placed in between the acceleration fields. This is advantageous, as an undefined fragmentation place, caused by a large laser focus, does not lead to different energies of the fragment ions.

Peptides like mellitine, gramicidine and insuline could be fragmented by CO_2-laser irradiation. Peaks can be made visible in the high mass region of mellitin spectra when PSPF is applied, however it is not clear at the moment, if these peaks are caused by CO_2-laser irradiation. Sometimes fragment ions are detected even when the fragmentation laser is switched off. Both, metastable decay in the field free region or ion formation at the desorption place could account for this observation. Calculations of the expected mass resolution for both processes seem to exclude metastable decay.

Additionally, the PSPF device opens up the possibility to split up the ion cloud in two parts at a given point of time. This is illustrated in figure 1. By varying the delay of the PSPF pulse, information about the ion distribution can be gained. Different matrix substances lead to different flighttimes and ion distributions.

Fig.1) Ion cloud separation using the PSPF-method

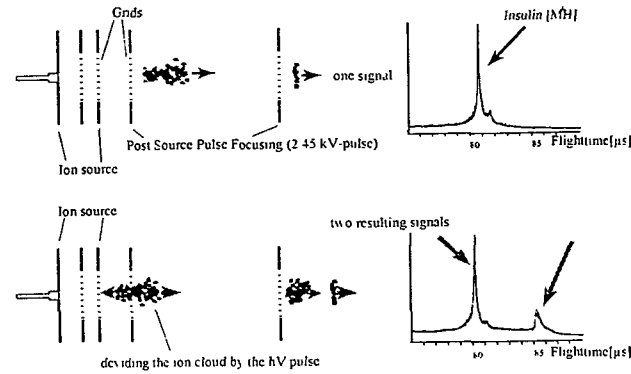

Furthermore effects on the focusing behaviour of ions caused by changing the ion source geometry and voltages were investigated by SIMION calculations[2]. The quality of the spectra could be improved either by increasing the field strength or by changing the desorption place. The experimental results can be explained by ion optic effects.

ACKNOWLEDGEMENT

This work is supported by the Deutsche Forschungsgemeinschaft (Grant Gr 917/6-2). The authors thank the Fonds der Chemischen Industrie for support.

REFERENCES

1) J. M. Grundwürmer, M. Bönisch, G. R. Kinsel, J. Grotemeyer, E. W. Schlag, *Int. J. Mass Spectrom. Ion Processes* **1994**, *131*, 139-148.

2) D. A. Dahl, J. E. Delmore, SIMION Version 4.0, Idaho National Engeneering Laboratory EG&G Idaho

Photochemical versus Thermal Mechanism for MALDI Probed by Backside Desorption

Hanno Ehring, Cesar Costa , Plamen A. Demirev, Bo U.R. Sundqvist
Division of Ion Physics, Department of Radiation Sciences, box 535,
Uppsala University, Uppsala, S-75121, SWEDEN

The exact nature of the MALDI of large biomolecules still remains under discussion. One of the important issues to resolve is the contribution of photochemical and photothermal effects in the formation and ejection of large biomolecular ions in the gas-phase as a result of UV or IR laser pulse irradiation. We have performed laser desorption in two laser beam incident geometries with respect to the sample surface - frontside and backside. To that end we use specially fabricated holders, onto which the samples are deposited. The sample holders consist of quartz glass onto which an Au layer with a thickness of 2000Å was evaporated. Different samples - small peptides (gramicidin S, and valinomycin) with and without a matrix (DHB), C_{60} fullerenes, or alkali halides - have been deposited on the Au layer. The home-built MALDI-TOF system with optical ports that allow irradiation of one-and-the-same sample both from the front and the backside, has been already described in detail [1]. A Nd - YAG laser (355 nm, 6 ns pulse width, 300 μm spot size), or a N_2 laser (337 nm, 4 ns, 200 μm) are used to irradiate the samples from the front or the back, respectively. The typical fluences are between 20 to 50 mJ/cm^2 for frontside, and 20 to 100 mJ/cm^2 for backside desorption. Since the absorption of the UV light at that fluence by 2000Å Au layer is complete, only thermal effects can contribute to the backside desorption.

Mass spectra of CsI obtained from the front and backsides are essentially indistinguishable, with a minor difference in the applied laser fluence (15 and 21 mJ/cm^2, respectively). Typical mass spectra for gramicidin S are shown on Fig. 1. While with a matrix the protonated molecular ion peak **[M+H]$^+$** is observed, without a matrix only the corresponding alkali cation adducts with the neutral molecule, **[M+Na]$^+$** and **[M+K]$^+$**, are detected in frontside desorption. Backside desorption of gramicidin S + DHB gives only the cationized species, which is indicative of a thermal desorprion process. Thermal effect is also observed in the backside spectrum of C_{60}, in which a broad shoulder, extending several μs after the main peak, is observed, due to the well-known phenomenon of delayed ionization of thermally-excited fullerenes. In contrast, the C_{60} molecular ion peak in frontside desorption is much sharper, indicative of prompt (multiphoton) ionization process.

While good quality spectra of peptides, like insulin and cytochrome C, with intense molecular ion peaks have been obtained in MALDI from the frontside, no such peaks corresponding to the molecular ions have been observed upon backside desorption of the same samples. All discussed results point to the conclusion that laser-induced photochemistry, e.g. protonation-deprotonation reactions between excited matrix molecules and the analyte [2], plays a major role in MALDI of peptides.

References

[1] A.Westman et al., *Rap. Commun. Mass Spectrom.* **8** (1994) 388.
[2] H.Ehring et al., *Org. Mass Spectrom.* **27** (1992) 472.

43rd ASMS Conference on Mass Spectrometry and Allied Topics

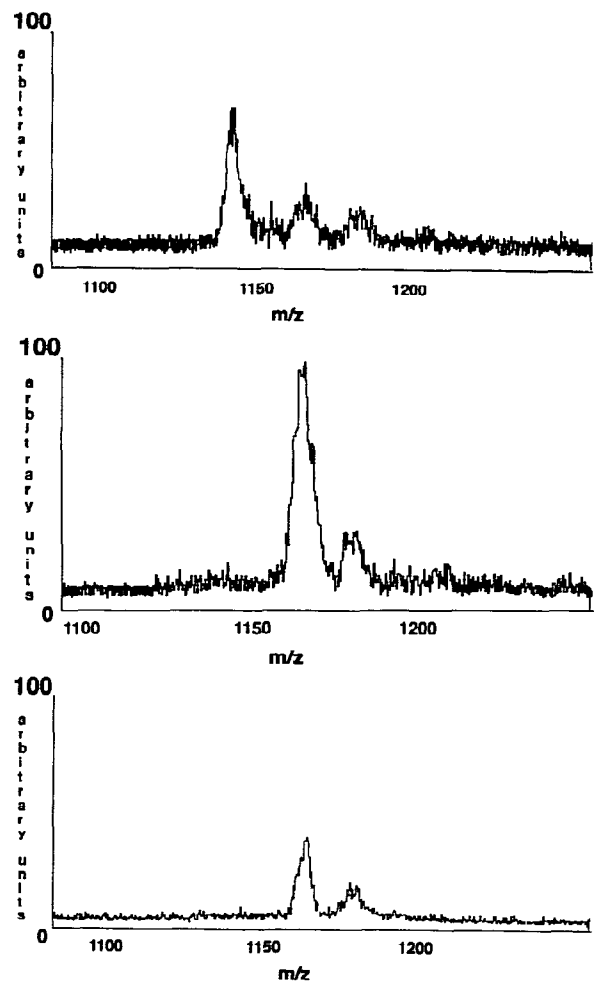

Fig. 1 Gramicidin mass spectra: upper trace - in DHB, frontside; middle - in DHB, backside; lower trace - no matrix, frontside. The three peaks are the **[M+H]$^+$**, **[M+Na]$^+$**, and **[M+K]$^+$**ions respectively.

Probing the Dynamics of MALDI Ion Formation

Ricky D. Edmondson, Karen K. Campo, and David H. Russell
Laboratory for Biological Mass Spectrometry
Department of Chemistry, Texas A&M University
College Station, TX 77843

We have observed that when thin films of matrix/analyte are prepared two thresholds exist for ion formation in MALDI. At low laser fluences(2mJ/cm^2) ions are produced from the first laser shot on each spot, but are then quickly depleted. In order to generate more ions from the same spot, fluences must be increased three to four times. Ions are then produced for many consecutive shots from that sample spot. This paper will discuss sample preparation techniques, along with the results of studies that compare the ions formed at the two thresholds.

The samples are prepared by depositing 1 µl of the matrix solution on a highly polished stainless steel surface and allowing it to dry. Twenty to 100 nl of analyte are then applied to the dried matrix. The analyte solution partially redissolves the matrix, but the undissolved matrix serves as nucleation sites for the matrix/analyte to crystallize. The outer circle seen in figure 1 shows where this recrystallization occurs. This sample preparation enhances the ion production at low laser fluences. Linear TOF spectra were taken of Vitamin B_{12} and mellitin with alpha-cyano-4-hydroxycinnamic acid at both ionization thresholds. When compared to the high fluence spectra , the low fluence spectrum of mellitin showed an abundance of analyte ions over matrix ions, in addition to higher resolution of the molecular ion region (5500 m/Δm).

The high fluence spectra of Vitamin B12 is consistent with previous studies as the most abundant ion is the loss of the cyano ligand, and no intact molecular ion is observed. However, in the low fluence spectrum

the intact molecular ion is a prominent peak. The results from these studies suggest that the ions formed at low laser fluences have more narrow energy distributions than ions formed at the higher fluences as well as lower internal energies. We have developed a model to explain the differences between the high and low threshold spectra. We would argue that the ions formed at the low laser fluence are related to a surface component. Whereas the high fluence threshold ion production is more related to the bulk sample. After the loosely held material from the surface is desorbed more energy is required to desorb material that is tightly bound to the bulk sample.

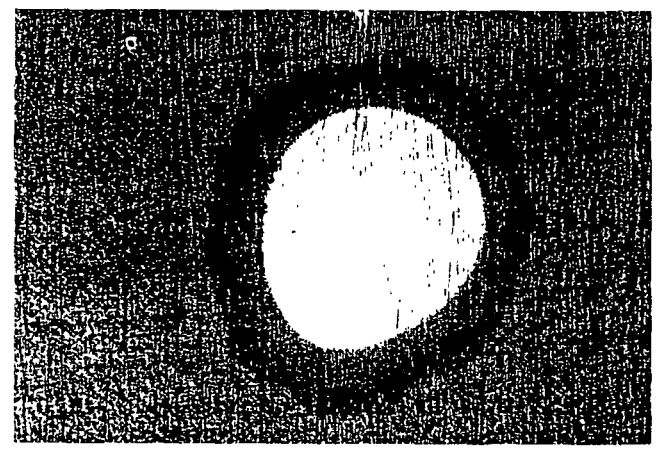

Figure 1

Sample plate with mellitin and alpha-cyano-4-hydroxycinnamic acid 50x magnification

Water as a Matrix in Infrared MALDI-MS

Stefan Berkenkamp, Michael Karas, Franz Hillenkamp
Institut für Medizinische Physik und Biophysik der
Westfälischen Willhelm Universitat Munster, FRG

Matrix-assisted Laser Desorption/Ionization mass spectrometry (MALDI-MS) has become a widely used technique for the analysis of large biological molecules Whereas UV-MALDI is now widely applied, Infrared MALDI-MS is still in a rather experimental stage with only a few laboratories working on its development Some advantages, such as better preformance in the mass range above 100kDa, have been reported Using Er-YAG-Lasers emitting at a wavelength of 2 94 µm a host of potential matrices are available with a strong absorption at this wavelength, primarily resulting from O-H and N-H stretching modes at ca. 3µm Among the potential advantages of IR-MALDI are the availibility of more or less physiological, non denaturating matrices with approximately neutral pH such as glycerol and Tris

Water, in the frozen state to provide compatibility with the vacuum requirements of the spectrometer, appears particulary attractive in this respect and was recognized early as a potential matrix because of its strong O-H stretching mode near 3 µm Interest in water as matrix derives primarely from the fact that it is the major constituent of most biological samples

A reflectron TOF instrument of 3 5 m equivalent flight length and a 12 kV acceleration potential was used for all experiments Working pressure in the sample chamber is 3×10^{-4} Pa Ions are detected by a conversion dynode (ion impact energy 20 - 27 kV, depending on ion mass) mounted 1 cm in front of a venetian blind secondary electron multiplier (EMI R2362) Single pulses of an ER-YAG laser (SEO 1-2-3, Schwartz Electro Optics, USA) of ca 150 ns duration at a wavelength of 2 94 µm are focused to a spot diameter of ca 180 µm with a 45° angle The instrument is equipped with a liquid nitrogen (LN) cooling stage. The temperature of the stainless steel substrate is monitored with a thermocouple with an absolute accuracy of ± 5 K

All attempts to obtain protein spectra from samples of bulk, frozen aqueous solutions by variation of all accessible parameters gave very poor results under almost all conditions predominantly water cluster signals up to a mass of ca 5000 Da were obtained Protein signals with poor signal-to-noise-ratios could only be obtained from the outermost rim of the sample and only in ca 5 - 20% of the exposures The situation changes dramatically if the samples (typically 3 µl of a 10^{-3} M solution) are first „dried" under ambient conditions (remaining the water of hydration at the protein) before being frozen to LN-temperature. Similarly, a few flakes of lyophilized protein can be frozen directly. The frozen samples are then introduced into the instrument and kept at low temperature The dried frozen samples form a thin, optically homogeneous and transparent layer, the rim of which is barely visible under microscopic observation. Spectra of superior quality and very good reproducibility can be obtained from all locations within the 3 mm diameter sample area Some temperature dependence is observed. Best results are obtained in the range of 170 - 200 K, but spectra can be obtained up to temperatures of 240 - 270 K, depending somewhat on the specific analyte under investigation Mass resolution (FWHM) of 300 - 350 is routinely obtained for proteins up to a mass of 20 kDa, selected spectra exhibit a mass resolution of up to 700 (Figure 1). This contrasts to a resolution of 150 - 200, obtainable with this instrument for standard preparations of the same proteins under optimal conditions in UV- and IR-MALDI Salt additions lead to a degradation of signal quality, as is also known for standard preparations, but even a physiological NaCl-concentration does not totally suppress the protein signals The threshold irradiance for protein detection is ca. 3×10^{6} W/cm^2, quite comparable to values needed for standard preparations in the UV as well as IR. Near threshold irradiance very little to sometimes no matrix signals are recorded in the low mass range These signals increase appreciably with increasing irradiance, as is commonly observed in MALDI-MS

The mass resolution of the protein signal, however, remains essentially unaffected with an up to eightfold increase in irradiance.

The practical application of MALDI with an ice matrix currently is still somewhat limited by accessable mass range (for pure air dried aqueous solutions, the upper mass limit so far is ca 30 kDa) and by sensitivity. Spectra have been obtained from air dried 10^{-5} M solutions, but with a substantially decreased signal-to-noise ratio and a strong low mass signal background compared with 10^{-3} M solutions. At the present state a minimum amount of ca. 1 pmol is needed for a successful protein analysis.

Since the exact amount of protein-hydration can not be predicted under experimental conditions, protein single crystals of Lysozyme were grown, frozen, and analysed by IR-MALDI-MS without matrix addition (Fig 2; since crystals are grown with $NaNO_3$ as precipitant, mass spectra obtained are of somewhat inferior quality due to salt content) The water content of protein crystals of Lysozyme is reported to be about 30% in vol The molar matrix/analyte-ratio therefore can be estimated to be ca 250, about three orders of magnitude lower than in a common MALDI preparation (10^5). Futhermore the „Matrix" is contributed by the analyte itself which again distinguishes the sample preperation with water as matrix from common matrix preparations

Very important information on the desorption/ionisation process can be gained from these experiments Theories and experimenatal evidences concerning mechanisms for desorption/ionisation and the concept of matrix-assistance in UV-MALDI can certainly not be adapted for IR-MALDI without reconsideration

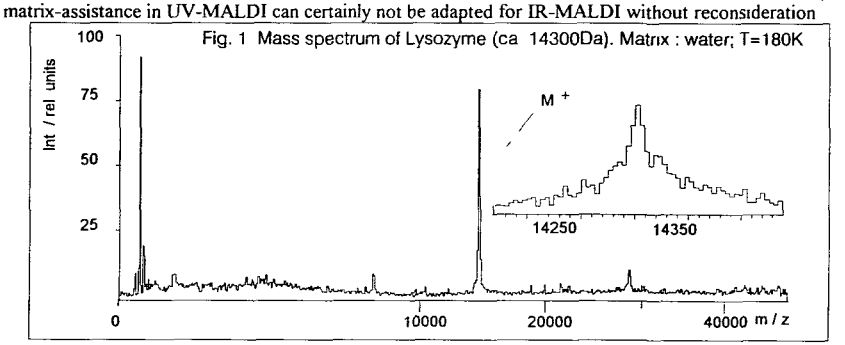

Fig. 1 Mass spectrum of Lysozyme (ca 14300Da). Matrix : water; T=180K

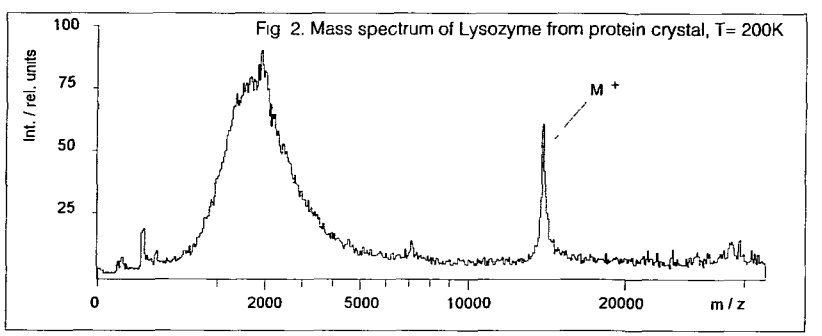

Fig 2. Mass spectrum of Lysozyme from protein crystal, T= 200K

AN INORGANIC MATRIX FOR USE IN MALDI-TOFMS

Koichi Tanaka[1], Shin-ichiro Kawabata[1], Martin Resch[2], Gerd Paulus[2],
Paul Humphrey[3] & David Dingley[3]
1 - Shimadzu Corporation, Kyoto, Japan, 2 - Shimadzu Europa GmbH, Duisberg, Germany,
3 - Kratos Analytical, Manchester, UK.

Initial experiments in the development of Matrix Assisted Laser Desorption/Ionisation[1,2] involved the use of an ultra fine metal powder (UFMP) to promote energy transfer. This was later largely superseded by the use of aromatic acids such as(sinapinic acid, 2,5-dihydroxybenzoic acid and a-cyano-4-hydroxycinnamic acid. These matrices all result in the generation of large numbers of ions particularly in the mass range 100-500 Da. For the analysis of small samples (m/z <500 Da) there can be considerable confusion and overlap of peaks making interpretation difficult.

As the laser is fired at an involatile, thermally labile sample competing reactions of vaporisation as opposed to decomposition occur. As is shown in figure 1, at low temperature decomposition will dominate whereas at higher temperatures vaporisation will be favoured.

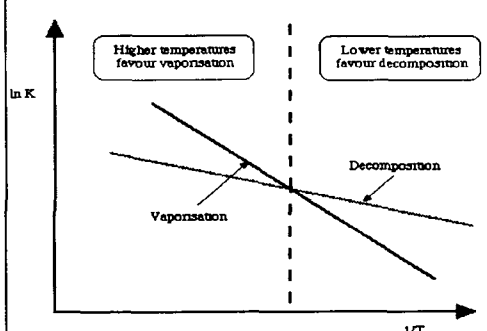

Figure 1 - Temperature dependance of rate constant

It therefore follows that raising the temperature as rapidly as possible to as high a value as possible will generate more and more gas-phase molecules and minimise decomposition. This is the first requirement for MALDI of thermally labile materials, to generate intact molecular ions.

The diameters of the UFMP particles are very small (100-1000 Å) which result in the absorbance being very efficient across a wide wavelength range. The material has a low heat capacity which combines with the absorbance to promote rapid heating. If the powder is mixed uniformly with a sample this will result in easy and immediate transfer of the laser energy.

The experiments were carried out on a KOMPACT MALDI III produced by Kratos Analytical. This is a

combined linear & reflectron bench-top system featuring a sealed unit nitrogen laser (λ = 337 nm) and optional extraction voltages of 6 or 20 kV Sample solutions were prepared having concentrations in the range 1 mg/ml to 1 µg/ml in a suitable solvent system (distilled water and/or methanol). A 1 µl droplet of this solution was placed on the multi-sample slide together with 1 µl of a matrix suspension. This latter was produced from a suspension of 10 mg/ml of 200 Å cobalt powder in ethanol or acetone. The mixture was allowed to dry for a few minutes in air to remove volatile solvents before the slide was introduced into the instrument.

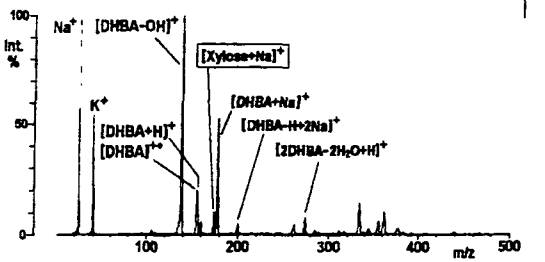

Figure 2 - MALDI spectrum of xylose using DHB as a matrix

The spectra in figure 2 show a comparison of spectra from xylose ($CHO(CHOH)_3CH_2OH$ - MW = 150.13 Da) acquired a) conventionally using a matrix of 10 mg/ml of 2,5-dihydroxybenzoic acid (DHBA) and b) using UFMP as a matrix. In each case the $[M+Na]^+$ ion dominates the xylose spectrum but in the spectrum with DHBA it is very difficult to identify this in the plethora of peaks due to matrix ions and attendant fragments, adducts and multimers. In the spectrum with UFMP greatly simplified and subsequently much easier to interpret.

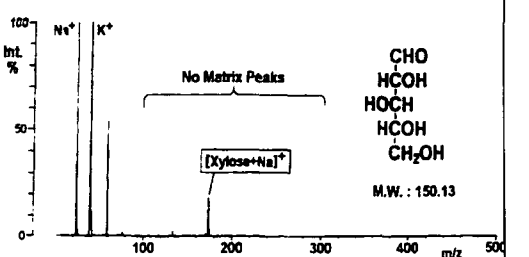

Figure 3 - MALDI spectrum of xylose using UFP as a matrix

Ultra-fine metal powder has the following advantages over conventional organic matrices -

(i) No background ions in the mass range 100 - 500 Da
(ii) Efficient energy absorption across a wide range of wavelengths (UV, Vis, IR)
(iii) Low chemical activity
(iv) Stable at room temperature and in ambient light

These factors make it an attractive alternative to more common matrices in the analysis of low mass (< 500 Da) materials.

Hydroxy Benzophenones: A New Class Of MALDI Matrices For Proteins/Peptides

*Duane Reiber and Robert S. Brown, Department of Chemistry and Biochemistry, Utah State University, Logan, UT 84322-0300

Matrix-assisted laser desorption/ionization (MALDI) has become a widely accepted technique for the mass spectrometric analysis of many classes of biomolecules. The identification of new matrices for MALDI is important both from a practical and mechanistic standpoint. While many of the most successful UV-MALDI matrices are aromatic carboxylic acids, a smaller number of matrices (such as 7-hydroxy coumarin) have been reported that may involve excited state enhanced proton transfer reactions. Benzophenones are known in the literature to exhibit long lived triplet states when excited in the UV. A series of multiply hydroxy substituted benzophenones (no carboxylic acid groups) have been utilized for UV-MALDI (337 nm) with various peptides and small proteins in a linear time-of-flight mass spectrometer (TOF-MS) equipped with delayed pulsed ion extraction. The more useful compounds as MALDI matrices included the following: 2,4-dihydroxy benzophenone; 4,4'-dihydroxy benzophenone; 2,4,4'-trihydroxy benzophenone; 4-hydroxy benzophenone and 2,2',4,4'-tetrahydroxy benzophenone.

Many of these compounds are equally as effective at protonating larger proteins such as cytochrome C as the more conventional aromatic carboxylic acid MALDI matrices (such as ferulic acid). The successful protonation by these hydroxy substituted benzophenones, given their lack of any acidic group to serve as a proton donator, suggest that for at least for this class of MALDI matrices, excited state processes must play an important role. In the excited state, the hydroxy substituents would be expected to become acidic enough to account for the proton transfer processes that are observed. Mass resolution obtainable with these hydroxy substituted benzophenones is also comparable to conventional MALDI matrices. This would suggest that the ionization time frame is not affected by any long lived triplet state. Given the collision rates expected from the dense plume model for MALDI, it is probably not surprising that excited state species would rapidly return to their ground state, thus rapidly quenching the ionization process. These hydroxy substituted benzophenones are also different from conventional MALDI matrices in that essentially no radical cations of the matrix are observed in the low mass region of the MALDI spectra. This region is dominated almost exclusively by protonated ions of the matrix. Almost no matrix degradation ions due to loss of water are observed for these hydroxy substituted benzophenones. This is in sharp contrast to what is observed for MALDI matrices such as sinapinic and ferulic acid. Dehydration is only significant in the 2,2' substituted benzophenones which can undergo intramolecular loss of water which is stabilized by formation of a six member ring. Significantly less (organic) matrix adducting to analytes is observed with the hydroxy substituted benzophenones when compared to may common MALDI matrices (i.e., ferulic acid or 2,5 dihydroxy benzoic acid). Cationization is, however, much more prevalent with the hydroxy substituted benzophenone matrices. Particularly troublesome have been iron (II) cation attachment species (i.e., $[M-H+Fe]^+$). These adduct ion species can be suppressed by the addition of a weak acid salt such as ammonium oxalate. These species are probably normally suppressed in acid MALDI matrices due to the large H^+ concentration favorably shifting the solution equilibrium.

The extent of rapid metastable ion decay is also significantly reduced with the hydroxy substituted benzophenones that have been studied. While the type of fast metastable ion decay is similar to conventional MALDI matrices (Table I), the extent and intensity is reduced. This trend is reversed in the negative metastable ion decay spectra obtained for the hydroxy substituted benzophenones (see figure 1). In addition, a series fragment ions are observed which are not typically produced in positive ion spectra.

Table 1 MALDI rapid metastable decay ions for the oxidized B chain of bovine insulin in various matrices

Residue	4-HBP[a]		2,4-DHBP[b]		4,4'-DHBP[c]		2,4,4'-THBP[d]		2,2',4,4'-THBP[e]		4-HCHAL[f]	
Phe			Y_{29}		Y_{29}		Y_{29}		Y_{29}		Y_{29}	
Val			Y_{28}		Y_{28}							
Asn			Y_{27}								Y_{27}	
Gln			Y_{26}						Y_{26}		Y_{26}	
His			Y_{25}		Y_{25}		Y_{25}		Y_{25}		Y_{25}	
Leu	Y_{24}		Y_{24}				Y_{24}		Y_{24}		Y_{24}	
Cys	Y_{23}		$\mathbf{Y_{23}}$		Y_{23}		Y_{23}		$\mathbf{Y_{23}}$		Y_{23}	
Gly			Y_{22}						Y_{22}			
Ser			Y_{21}	C_8	Y_{21}				Y_{21}	C_8	Y_{21}	
His			Y_{20}			C_9			Y_{20}		Y_{20}	C_9
Leu			Y_{19}		Y_{19}	C_{10}	Y_{19}		Y_{19}			
Val			Y_{18}	C_{11}	Y_{18}	C_{11}	Y_{18}	C_{11}	Y_{18}	C_{11}	$\mathbf{Y_{18}}$	
Glu	Y_{17}		Y_{17}		Y_{17}	C_{12}			Y_{17}		Y_{17}	C_{12}
Ala	Y_{16}		Y_{16}	C_{13}	Y_{16}	C_{13}			Y_{16}		Y_{16}	
Leu	Y_{15}		Y_{15}			C_{14}			$\mathbf{Y_{15}}$		Y_{15}	
Tyr	Y_{14}	C_{15}	Y_{14}	C_{15}	Y_{14}	C_{15}			Y_{14}		Y_{14}	C_{15}
Leu		C_{16}		C_{16}		C_{16}			Y_{13}			C_{16}
Val			Y_{12}	C_{17}	Y_{12}		Y_{12}		$\mathbf{Y_{12}}$		Y_{12}	C_{17}
Cys		C_{18}	Y_{11}	$\mathbf{C_{18}}$	$\mathbf{Y_{11}}$	$\mathbf{C_{18}}$	Y_{11}	C_{18}	$\mathbf{Y_{11}}$	C_{18}	Y_{11}	$\mathbf{C_{18}}$
Gly			Y_{10}		Y_{10}	C_{19}			Y_{10}			C_{19}
Glu			Y_9	C_{20}	Y_9		Y_9		Y_9		Y_9	
Arg				C_{21}								
Gly						C_{22}						
Phe		C_{23}		C_{23}		C_{23}						
Phe		C_{24}		C_{24}		C_{24}						
Tyr						C_{25}						
Thr		C_{26}				C_{26}						
Pro												
Lys						C_{28}						C_{28}
Ala		C_{29}		$\mathbf{C_{29}}$		$\mathbf{C_{29}}$		$\mathbf{C_{29}}$		$\mathbf{C_{29}}$		$\mathbf{C_{29}}$

a) 4-hydroxy benzophenone
b) 2,4-dihydroxy benzophenone
c) 4,4'-dihydroxy benzophenone
d) 2,4,4'-trihydroxy benzophenone
e) 2,2',4,4'-tetrahydroxy benzophenone
f) 4-hydroxy chalcone
g) most intense in bold

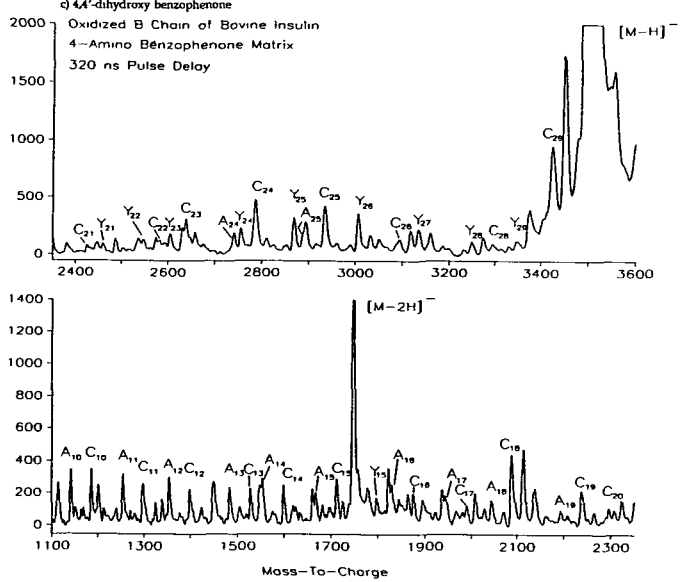

Synthesis of MALDI Matrices and Correlation with Ion/Neutral Populations

*Lloyd W. Sumner, Ricky D. Edmondson, Mary Gimon Kinsel, Rick Hammon, Gary Sulikowski, and David H. Russell
Laboratory for Biological Mass Spectrometry, Department of Chemistry, Texas A&M University, College Station, TX 77843

The ability to selectively utilize MALDI matrices to control the extent of internal energy transferred to the analyte during the ionization process would be highly useful. Ideally this parameter would be based on matrix structure and could enable the mass spectrometrist to select a matrix to meet his specific application Low energy transfer matrices could be used to obtain maximized quasi-molecular ion intensities while high energy transfer matrices could be used to promote prompt fragmentation or metastable decay in MS/MS experiments for structural elucidation. At present, our ability to predict energy transfer between the matrix and analyte is very limited. To probe this phenomenon in a systematic fashion we have attempted to synthesize a series of substituted cinnamic acid analogs to correlate matrix structure with the internal energy exchange occurring during the protonation reaction. The synthetic compounds compliment the limited quantity of compounds commercially available and both are listed in TABLE 1. Simultaneous positive-ion and neutral MALDI-TOF mass spectra of substance P and renin substrate were obtained on a Vestec Voyager Elite MALDI-TOF mass spectrometer operating at an acceleration voltage of 25kV. The instrument was equipped with an electrostatic particle guide and an ion mirror. Averaged MALDI mass spectra of 50 laser shots, obtained with a LSI nitrogen laser, were recorded on two separate oscilloscopes.

TABLE 1. MALDI Matrices

1.) 4-hydroxy cinnamic acid
2.) 4-hydroxy-methyl cinnamate
3.) alpha-aceto-4-hydroxy-ethyl cinnamate
4.) alpha-carboxy-4-hydroxy cinnamic acid
5.) 4-hydroxy-3,5-dimethoxy cinnamic acid
6.) alpha-cyano-4-hydroxy cinnamic acid
7.) alpha-cyano-3-hydroxy cinnamic acid
6.) alpha-cyano-4-hydroxy-3-methoxy cinnamic acid
9.) alpha-thio-4-hydroxy-3-methoxy cinnamic acid
10) alpha-phenyl-4-hydroxy cinnamic acid

The spectra were correlated to the internal energy transfer (i.e. fragmentation) to the analyte by measuring the ratio of the absolute intensities of the protonated to the neutral molecular species. A plot of these ratios is presented in Figure 1. Post source decay mass spectra were also obtained. Illustrative mass spectra of a low and high energy transfer matrix are presented in Figure 2a & 2b The lowest energy matrix observed was 4-hydroxy cinnamic acid. This compound had an ion/neutral ratio of about 32 which is three times higher than the commonly accepted low energy transfer matrix, 4-nitro aniline (ion/neutral ratio = 10) Several high energy transfer matrices were observed. These included the established hydroxy-alpha-cyano cinnamic acids, 4-hydroxy-3,5-dimethoxy cinnamic acid, and more interesting, the methyl synthetic esters Simple esterification of 4-hydroxy cinnamic acid to 4-hydroxy methyl cinnamate dropped it's ion/neutral ratio from 32 to 1.5. A similar observance was made for alpha-aceto-4-hydroxy ethyl cinnamate which also had a low ion/neutral ratio of about 0.5 Finally, the alpha-phenyl cinnamic acid also performed well as a high energy transfer matrix as suggested by Brown (Proceedings 42nd Annual ASMS conference).

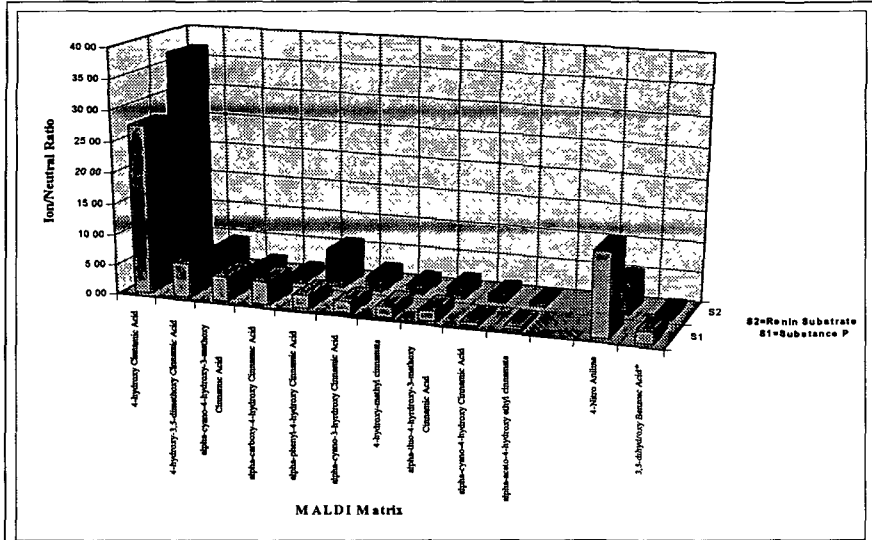

FIGURE 1

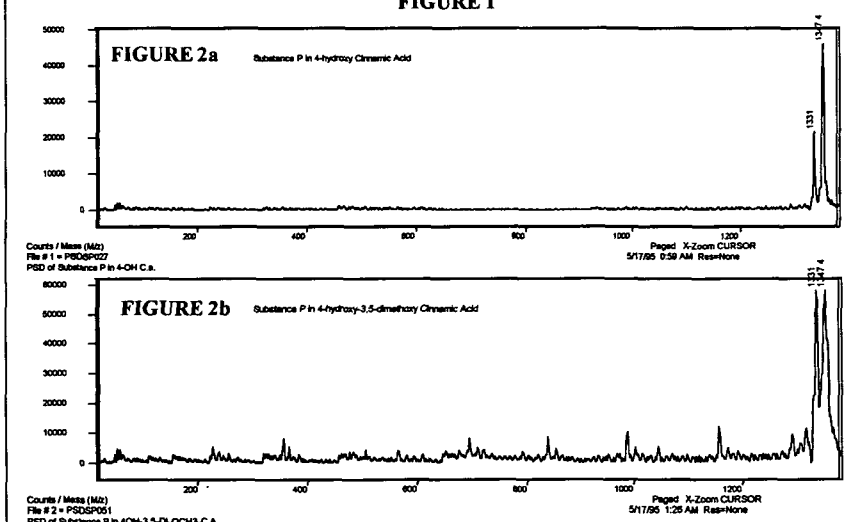

New Matrices for Matrix Assisted Laser Desorption/Ionization (MALDI) MS

Joern L. Krause and Urs P. Schlunegger

Institute of Organic Chemistry, University of Berne, Freiestr. 3, CH-3012 Berne / Switzerland

Introduction:

A large number of very different compounds have been tested with success as matrices for Matrix-Assisted Laser Desorption/Ionization (MALDI) MS since the introduction of this new technique into the MS field in 1988.

The UV-absorption is of special importance for the selection of new potential matrices. Compounds like salicylic acid, which contain a phenolic hydroxy group in ortho position to a carbonyl function often show a special behaviour under UV-irradiation [1,2]. UV-irradiation induces an intramolecular proton shift along the H-bond in these molecules, yielding a metastable excited state [3]. The excitation wavelength of those transitions is in general located in the ultraviolet region. With respect to this it is sensible to test compounds showing the described transition as new potential matrices.

Methods:

All presented MALDI-MS measurements have been carried out on a home built linear Time-of-Flight instrument. A pulsed nitrogen laser was used for desorption/ionization of the samples.

For the determination of the UV-absorption, UV-Vis spectra of all tested compounds have been measured in ethanolic solution (1 E-4 mole/l) on a Perkin-Elmer UV-Vis spectrophotometer).

Conclusions:

The results show that compounds which perform a proton transfer under UV-irradiation are actually usable as matrices for UV-MALDI MS. The resolution that can be achieved differs significantly from compound to compound. For substances like 5-methoxy-salicylic acid, salicylic amide, 5-chloro-salicylic amide or 5-chloro salicylic acid we obtained resolutions in the spectra of bovine insulin which are comparable to the resolution which can be achieved using sinapic acid as a matrix. In single shot spectra, salicylic amide allows a resolution of up to 1100 (m/Δm) for bovine insulin. We did not succeed to collect a spectrum with a similar or even better resolution with any other matrix. Regarding the measured absorption coefficients of matrices, showing the described transition under UV irradiation, it becomes obvious that the absorption of those compounds is significantly weaker as it is for compounds like sinapic acid or α-cyano-4-hydroxy-cinnamic acid. This could be the reason for the high ion intensity which may be achieved using a-cyano-4-hydroxy-cinnamic acid as a matrix. Such a high UV-absorption (200 times better as salicylic amide) leads to the high sensitivity of this matrix. The sensitivity of salicylic amide should be much better using radiation of about 300 nm wavelength. This was checked by using chlorinated salicylic amide (5-chloro-salicylic amide) as a matrix. 5-chloro-salicylic amide is absorbing the laser radiation about 8 times better as salicylic amide. This leads to a 3 times better sensitivity.

Whether the described proton transfer and the resulting metastable excited state is involved in the ionization process or if it just offers an absorption band in the used wavelength area is so far not clear. Further work is going on.

Acknowledgement:

This work was supported by the Swiss National Science Foundation. Grant No. 237'622.93/I.

Results:

The following table presents the results of our measurements with bovine insulin as an analyte, using different potential matrices. The structure of each matrix is given and the resulting ion intensities, resolutions and UV-absorption coefficients are listed.

Nr.	structure	chemical name	solvent	ε_{337}	intens.[1] $[M+H]^+$	resol.[2] [m/Δm]
1		sinapic acid	$EtOH/H_2O$ 1:1	14600	+ +	409
2		α-cyano-4-hydroxy-cinnamic acid	CH_3CN	21875	+ + +	418
3		2,5-dihydroxy-benzoic acid	H_2O	4250	+ +	240
4		trihydroxy-acetophenone	EtOH	2500	+	341
5		salicylic acid	$EtOH/H_2O$ 1:1	100	+	285
6		m-hydroxy-benzoic acid	$EtOH/H_2O$ 1:1	< 50	-	-
7		p-hydroxy benzoic acid	$EtOH/H_2O$ 1:1	50	-	-
8		5-chlor-salicylic acid	$EtOH/H_2O$ 1:1	750	+ +	260
9		5-chlor-salicylic acid methyl ester	$EtOH/H_2O$ 1:1	1150	+ -	< 200
10		5-methoxy-salicylic acid	$EtOH/H_2O$ 1:1	4000	+ +	290
11		salicylic amide	EtOH	100	+ +	360
12		5-chlor-salicylic amide	CH_3CN	900	+ +	382
13		p-hydroxy-acetophenon	$EtOH/H_2O$ 1:1	200	+ -	< 20
14		2,5-dihydroxy-diacetylbenzene	EtOH	1650	+ +	324
15		2,5-dihydroxy-terephthalic acid	$EtOH/H_2O$ 1:1	1250	+	91
16		p-hydroxy-benzoquinone	$EtOH/H_2O$ 1:1	900	+	55
17		7-hydroxy-1-indanone	$EtOH/H_2O$ 1:1	400	+ -	160

[1] Key for the measured ion intensities of $[M+H]^+$-signals:

+++	very intense signals
++	intense signals
+	good signals
+-	weak signals
-	very weak or no signals

[2] Resolution averaged over 10 single lasershots

References:

[1]

P.J. Thistlethwaite, G.J Woolfe, Chem. Phys. Lett. 63, 401(1979).

[2]

J. Catalan, F. Toribio, A.U. Acuna, J. Phys. Chem. 86, 303(1982)

F. Toribio, J. Catalan, F. Amat, A.U Acuna, J. Phys. Chem 87, 817(1983)

A.U. Acuna, F. Toribio, J Photochem. 30, 339 (1985).

A.U. Acuna, A. Costela, J.M. Munoz, J. Phys. Chem. 90, 2807 (1986).

[3]

M.E. Gimon, L.M. Preston, T. Solouki, M.A. White, D.H. Russell, Organic Mass Spectrom. 27, 827 (1992).

M.P. Chiarelli, A.G. Sharkey Jr., D.M. Hercules, Anal. Chem. 65, 307(1993).

P.C. Liao, J. Allison, J. Mass Spectrom. 30, 408(1995).

Amino Acid Composition and Wavelength Effects in Matrix-Assisted Laser Desorption Ionization

Zohra Olumee and Akos Vertes
Department of Chemistry, The George Washington University, Washington D.C. 20052

Despite the success of MALDI for molecular mass determination of large synthetic and bio-polymers, the mechanism of ion formation in the laser desorption process is not well understood. In extending the applications of MALDI-MS, low ion yield and variable ionization efficiency are two important limiting factors [1]. In order to examine the origin of these differences, we eliminated some of the complexities involved in the desorption of proteins. Short peptides of varied composition were used to explore the role of individual amino acid residues in the MALDI process. Our objective was to explore the efficiency of proton transfer, shot-to-shot variations of signal intensity, and the effect of excitation wavelength in ion formation. A linear time-of-flight mass spectrometer was used with two laser sources. Shot-to-shot variations of the laser pulse energy were measured by a pyroelectric joule meter. Fluctuations in the laser intensity were <5%. The ten different di- and tripeptides (listed in Table 1) and four peptides containing aromatic residues (Trp-Gly, Gly-Phe, Ala-Phe, and Tyr-Gly-Gly) were dissolved in 0.1% trifluoroacetic acid (TFAA). About 2μL aliquot of the analyte was mixed with 10 μL of saturated solution of the matrix (sinapinic acid, SA). To eliminate the effects of inhomogeneities, spectra were collected from randomly selected spots on the probetip.

Although several matrices and a large variety of irradiation conditions were used, attempts to obtain MALDI spectrum for N-methylacetamide (N-MAA) was unsuccessful. These negative results indicated that in short peptides the C=O of an isolated peptide bond was not the likely site of protonation. In the presence of end groups and in the case of longer peptides, however, one can not exclude the participation of the peptide bond in accommodating the proton. Table 1 summarizes the relative and absolute intensities and their standard deviations for the $[M+H]^+$ ions. Peptides containing non-polar amino acid residues (Gly-Gly and Ala-Ala) produced weak signal both in absolute and in relative intensities. As a general trend an enhancement of ion yields with increasing chain length was noticeable even for peptides with non-polar side chains. These observations were consistent with earlier FAB studies on gas phase proton affinities of short peptides [2]. Protonated molecular ions were abundant for short peptides containing basic and/or polar residues. The effect of basic residues (Arg and His) was very pronounced in absolute as well as in relative ion intensities. Lys-Lys however, showed very similar behavior to Gly-Gly indicating a profound departure from being the second most basic residue in liquid phase (pK=10.0).

Multiple shot MALDI flight time spectra of dipeptides Gly-Gly and His-His are presented in Fig. 1. Despite the large fluctuations in signal intensity, the response from His-His was consistently stronger and showed smaller relative error (see Table 1). In order to probe shot-to-shot variations in the signal, 50 consecutive spectra were analyzed in terms of analyte to matrix intensity ratios. The histogram of peak intensity ratios is shown in Fig. 2. The relative standard deviation of the ratios shows a dramatic drop from 50% for Gly-Gly to 18% in the case of His-His. This improvement in signal quality correlates with differences in proton affinity between the two dipeptides.

Shorter wavelength dye laser excitation (280 nm) resulted in substantial enhancement of ion formation from peptides containing aromatic side chains. Furthermore, stronger signal was observed for peptides containing non-polar amino acid residues. The sharp increase in the ion yield for peptides with aromatic residues points to the possible role of analyte excited states in ion formation. These observations are of importance in exploring the rules of selective ionization for different components in a protein mixture. The findings are especially relevant in sequencing studies, where digestion of proteins leads to relatively short peptide chains with an increased chance of lacking the residues promoting ionization.

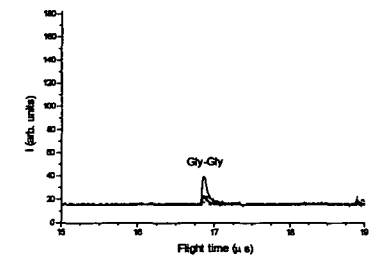

Figure 1a. Multiple shot positive-ion MALDI flight time spectra of Gly-Gly in SA matrix.

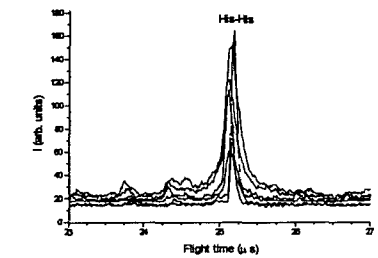

Figure 1b. Shot-to-shot variations in flight time spectra of His-His in SA matrix.

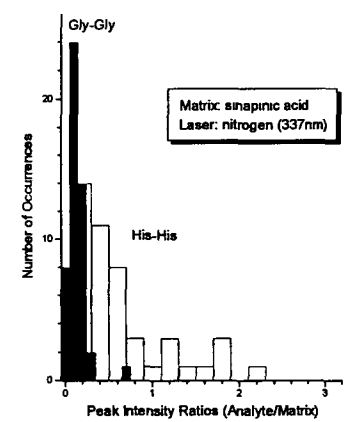

Figure 2. Shot-to-shot variations of peak intensity ratios for dipeptides of different character (Gly-Gly and His-His).

Table 1. Molecular ion intensities obtained using nitrogen laser excitation (337 nm) for different di- and tripeptides.

Compound	Char.of Side Chain	Relative* Intensity	Absolute Intensity
N-MAA**	N/A	0.00±0.00	0.00±0.00
Gly-Gly	np-np	0.08±0.04	3.60±2.09
Ala-Ala	np-np	0.17±0.06	4.60±2.69
Gly-Ser	np-p	0.17±0.03	5.69±0.77
Lys-Lys	b-b	0.06±0.02	3.61±0.92
His-Lys	b-b	0.19±0.05	7.34±3.05
His-His	b-b	0.44±0.08	21.1±1.9
Arg-Lys	b-b	0.47±0.07	26.0±4.5
Gly-Gly-Gly	np-np-np	0.23±0.05	10.9±2.6
Gly-His-Gly	np-b-np	0.30±0.09	11.5±5.2

* Relative intensity refers to the ratio of analyte and protonated matrix ion intensities.

** The abbreviations used in the table are: N-MAA= N-methylacetamide; b=basic; p=polar; and np=non-polar.

References

[1] Vertes, A; Gijbels, R. In: Laser Ionization Mass Analysis, Vertes, A; Gijbels, R.; Adams, F. (eds), Wiley, New York, **1993**, pp. 127-175.

[2] Wu. Z.; Fenselau, C. *J. Am. Soc. Mass Spectrom.* **1992**, *3*, 863-866.

Investigation of Selective Peptide Ionization with Various MALDI Matrices.

James A.Blackledge*, Anthony J. Alexander, and David W. Dodsworth
Bristol-Myers Squibb, PRI
P.O. Box 4755
Syracuse, NY 13221-4755

The excellent sensitivity, high sample throughput, and capacity for mixture analysis that is inherent in the technique of matrix-assisted laser desorption/ionization time-of-flight mass spectrometry (MALDI-TOF MS) has made it a popular method for the mapping of protein digests. In the course of such work, we have recently observed that certain MALDI matrices display a high degree of selectivity for individual peptides in a peptide mixture, which could potentially lead to erroneous conclusions about sample purity or result in certain mixture components being unobserved altogether. Previous reports have demonstrated that different matrices have varying degrees of sensitivity over different mass ranges (1), and that comatrix mixtures containing carbohydrate are effective in promoting simultaneous desorption and ionization of all components in a multicomponent mixture (2). Surprizingly, we observed that sinapinic acid (3,5-dimethoxy-4-hdroxy-cinnamic acid), which is not commonly used for peptide mapping, displayed the least amount of selective ionization in our peptide map, and therefore provided the best representation of the true sample mixture. In order to further investigate this phenomenon across different MALDI matrices, a series of three synthetic peptides were analyzed by MALDI-MS, both individually and as a mixture, using sinapinic acid (SA), α-CN sinapinic acid (α-CN SA), and a dihydroxybenzoic acid/fucose comatrix (DHB/Fuc).

Figure 1 displays the spectra of a representative RP-HPLC fraction from the protein digest, acquired in the three different MALDI matrices. Note that all of the ions above m/z ~ 3,000 Da., which are present at good intensity in SA, are severly reduced in both the DHB/Fuc. and α-CN SA matrices. The cluster of ions between m/z 2,000-3,000 in this fraction gives good signal intensity across all three matrices. However, comparison of the baseline noise reveals that the absolute signal for this cluster of ions, most especially the ion at m/z 2,380, is greatly enhanced in the DHB/Fuc. and α-CN SA matrices.

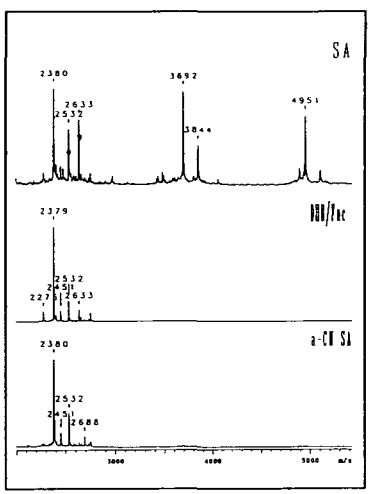

Figure 1. Representative digest fraction, analyzed in three different MALDI matrices.

Figure 2 contains the spectra acquired from a mixture of three synthetic peptides (see table), in the three different MALDI matrices. The same amount of material was loaded onto the sample stage for all three spectra. When analyzed individually, all three peptides gave good signals in all three matrices. However, when analyzed as a mixture, peptides B and C had reduced ion intensity. Peptide A also had a reduction in ion intensity as part of a mixture in α-CN SA, but was actually increased in SA and DHB/Fuc. All three components yielded discernable signals as part of a mixture, in all three matrices. Note the contaminant at m/z 1,819 Da., which is seen only in SA.

Out of some 50 different ions detected in the peptide map, only one species was not readily detected in SA. This fact, coupled with the observation that the relative intensity of the ions in the SA spectra correlated well with the relative concentrations of the peptides in the mixture, led us to conclude that SA was the matrix of choice for peptide mapping. However, the situation is somewhat different with the test peptide mixture. All of the test peptides gave good signals in all three matrices, when prepared as individual components. Unlike the trend seen in the digest fractions, where the enhancement/suppression of mixture components was consistent across both DHB/Fuc. and α-CN SA, with the test peptide mixture all three matrices gave different results. Our results show that, on the basis of "recovery" of signal intensity for the individual components in a mixture, SA is more effective than either DHB/Fuc. or α-CN SA as a matrix. Although none of the three peptides were completely suppressed in the test mixture, in any of the three matrices investigated, peptide C gave a very weak signal in both SA and DHB/Fuc., which is surprising considering that its composition is 50% arginine, the most basic amino acid residue. However, both SA and DHB/Fuc. resulted in strong suppression of at least one mixture component, clearly an undesirable situation. On this basis, the moderate suppression of all mixture components seen in α-CN SA may not be a severe limitation, as it reduces the possibility of a component being suppressed altogether.
Clearly, the choice of best matrix for the analysis of a peptide mixture must be determined experimentally.

Conclusions

- More than one matrix is often necessary to fully characterize a peptide digest fraction.
- Different matrices enhance/suppress different mixture components. This effect cannot be easily correlated with simple changes in basicity or hydrophobicity of individual peptides.
- For a given matrix the spectrum of a simple peptide mixture is not the sum of the spectra of the individual components. The underlying reasons for this are unclear.

Peptide	Sequence*	Molec. Wt.
A	LEMDVDRRGSAKEC	1,608 Da.
B	SRGNHVSPTHYVPQSDAAAR	2,151 Da.
C	TRQARRNRRRRWRERQR	2,439 Da.

* Bold-Face denotes a basic residue.

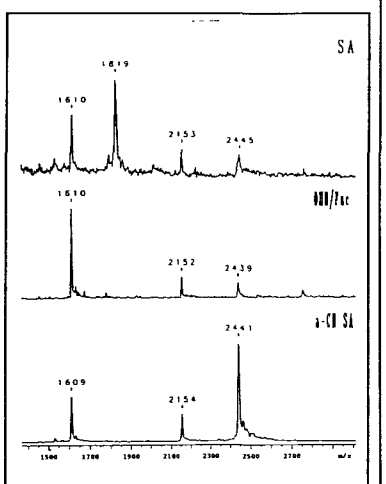

Figure 2. Synthetic peptide mixture analyzed in three different MALDI matrices.

1. Juhasz, P., Papayannopoulos, I A , Zeng, Ch.; Papov, V.; and Biemann, K.; Proceedings of the 40th ASMS Conference on Mass Spectrometry and Allied Topics, 1992, 1913-1914

2. Billeci, T.M., and Stults, J T., Anal. Chem 1993, 65, 1709-1716.

Effects of Substrates on the Ion Yields for Mixture Analysis by MALDI MS

Xiaoli Liang, Jian Bai, Yan-Hui Liu and David M. Lubman
Department of Chemistry, The University of Michigan, Ann Arbor, MI 48109-1055

Introduction

The suppression effect in which signals of certain components in a mixture are absent or indiscernible tends to be ubiquitous among desorption ionization techniques, such as FAB MS and PD MS. In MALDI MS, despite its tolerance to contaminants, the suppression effect caused by buffer or surfactants has been observed and the sample preparation has been addressed to increase the tolerance of MALDI toward contaminants through the use of a variety of schemes, such as simple washing, fabrication of matrix crystals and films, and the use of active substrates.

Several classes of compounds, such as gramicidin S and insulin, have also been found to suppress the ion signals of other components in a mixture. In this work, different substrates prepared from nitrocellulose (NC), Nafion, polystyrene (PS), polymethylmethacrylate (PMMA), and poly(styrene-co-2-acrylamide)sulfonic acid, have been used to alter the interactions among analytes, matrix and substrates, as well as the crystallization, thus to alleviate the suppression effect among analytes of interest in mixture analysis.

Method

Mixture of gramicidin S (gs), cytochrome *c* (cc), and lysozyme (ly) was used as a model system in this work. Polymer substrates were prepared by dissolving polymers in THF (NC in acetone). Both heating treated and untreated polymer substrates were tested and compared with the stainless steel probe. In the case of heating treatment, the polymer film was melted on a hot plate, and then cooled down to room temperature. The analyte mixture was added onto the stainless steel probe or the film, and allowed to incipient dryness before the application of matrix.

Results and Discussion

Signal of cytochrome *c* was indiscernible using CHCA as the matrix on a stainless steel probe tip with the traditional premixing method. When a thin NC film was used, the suppressed signal can be clearly observed. (Figure 1). The other substrates mentioned above generated similar results with CHCA as the matrix. Other matrix materials, were also tested on the polymer substrates. However, multiply charged ions were observed with caffeic acid matrix on these substrates; relatively poor

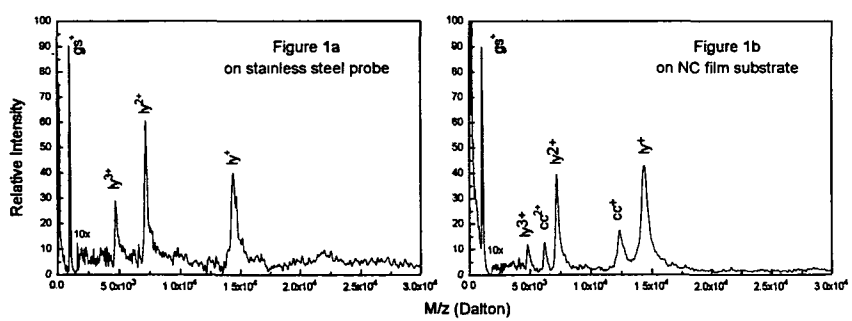

resolution was obtained with DHB matrix, while SPA provided different signal profile on different sample spots.

In the case of polymer substrates, heating of the films before application of the sample was found to improve the ion yields considerably (Figure 2), where the intensities of both singly- and doubly-charged ions of cytochrome *c* increased dramatically. It was found that without heating, PS can not form a homogeneous film , and the analyte mixture tended to scatter over the substrate upon application. After heating, a more uniform hydrophobic film was formed. Similar improvements were also experienced for the other two polymeric films. This phenomena may be due to the fact that more homogeneous hydrophobic film was formed during the heating treatment.

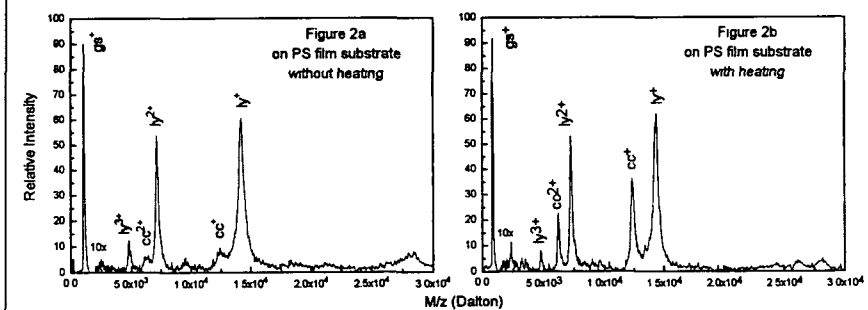

The mechanism of the suppression effect is not well understood yet. The fact that this effect can be alleviated by the use of hydrophobic film, indicates that the suppression effect may be related to the hydrophobicity properties of the analytes and the sample surface. It has been proposed that hydrophilic peptides were suppressed in the presence of hydrophobic peptides in FAB MS (1,2) and PD MS(3). If this is true in MALDI MS, it is easily understood that hydrophobic film can reduce the suppression effect, since the hydrophobic film will repulse the hydrophilic analyte to the sample surface and make it accessible for the MALDI MS analysis. Another possible explanation is that the films provide uniform sites for nucleation compared with the stainless steel probe (4). Therefore, the proteins with different properties can be incorporated into the matrix equally. However, more experimental evidence is needed to confirm this hypothesis.

Conclusion

The use of polymeric film as substrates improved the ion yields dramatically despite that the mechanism is not clear yet. Future work will focus on the mechanism studies and the application of polymeric substrates for the MALDI MS analysis of complex mixtures.

References

1. Naylor, S.; Findeis, A. F.; Gibson, B. W.; Williams, D. H. *J. Am. Chem. Soc.* **1986**, *108*, 6359-6363.
2. Caprioli, R. M.; Moore, W. T.; Fan, T. *Rapid Commun. Mass Spectrom.* **1987**, *1*, 15-18.
3. Wang, R.; Chen, L.; Cotter, R. J. *Anal. Chem.* **1990**, *62*, 1700-1705.
4. Preston, L. M.; Murray, K. K.; Russell, D. H. *Biol. Mass Spectrom.* **1993**, *22*, 544-550.

Surface Modification of Active Substrate Applied in MALDI MS

Yan-Hui Liu, Jian Bai, Xiaoli Liang, and David M. Lubman, Department of Chemistry, The University of Michigan, Ann Arbor, MI 48109-1055

Introduction. On-probe purification scheme of using active substrate such as Nafion has been employed in MALDI MS process to eliminate the deleterious effect of impurities and produce homogeneous desorption of all components in protein/peptide mixtures One particular concern is the possible adsorption of analytes of interest by the active substrate, which may lead to unrecoverable loss through various interactions, such as hydrophobic and ionic interactions associated with most polymeric surfaces. This is particularly true when analyzing relatively pure samples, where less impurities are competing for the possible adsorption sites. This work shows the effect of modification of the Nafion substrate on detection of protein/peptide mixtures.

Experimental. Nafion or modified Nafion substrate was obtained by applying 2 µl of the solution onto a stainless steel probe tip and air-dried. Modification of the Nafion substrate involved mixing of the Nafion solution with cetylpyridinium chloride (CPC), fucose, or tributyl phosphate (TBP). CNBr digest of cytochrome C (CC) was used as a model system in this work. Caffeic acid (CA) in 50% acetonitrile acquous solution was used as matrix. MALDI MS was performed on a linear TOF with postacceleration and a 355 nm laser was used for desorption/ionization.

Results and Discussion. Desorption of all fragments in a protein mixture from a Nafion substrate is more uniform than that from a stainless steel surface (1). However hydrophobic/ionic interactions between proteins and Nafion can prevent the sensitive detection of all fragments in a protein mixture. Figure 1 shows MALDI MS spectrum of ~ 1 pmol of cytochrome C digest on the Nafion substrate. No digest signal was obtained. By adding certain kinds of modification substances the adsorption effect can be alleviated.

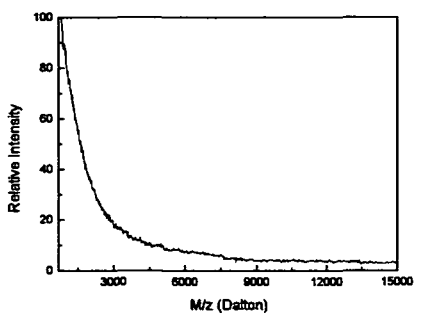

Figure 1. MALDI MS of CC digest on Nafion.

Figure 2 shows the effect of modification of Nafion with TBP by adding 1 µL of TBP to 10 µl of Nafion. Figure 2a is the spectrum obtained by adding CA before the sample was dried while 2b is by adding CA after sample was dried on the substrate. Similar results were obtained by modification of Nafion with fucose.

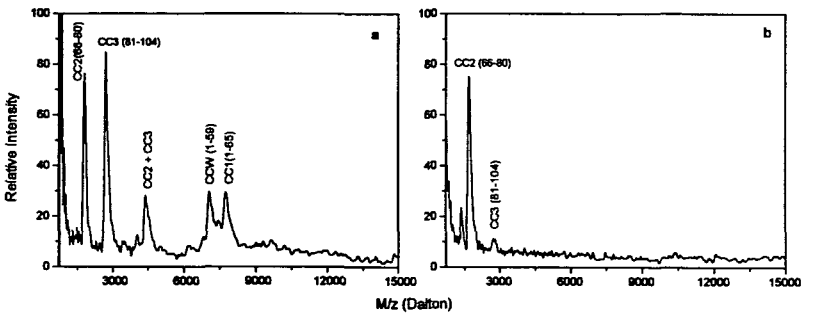

Figure 2. MALDI MS of CC digest on TBP modified Nafion.

Figure 3 is MALDI MS spectrum by modification of Nafion with CPC (20 mg/mL). No difference was observed by adding CA before or after the sample was dried These results show that CPC modified Nafion substrate can effectively eliminate the adsorption of proteins by Nafion

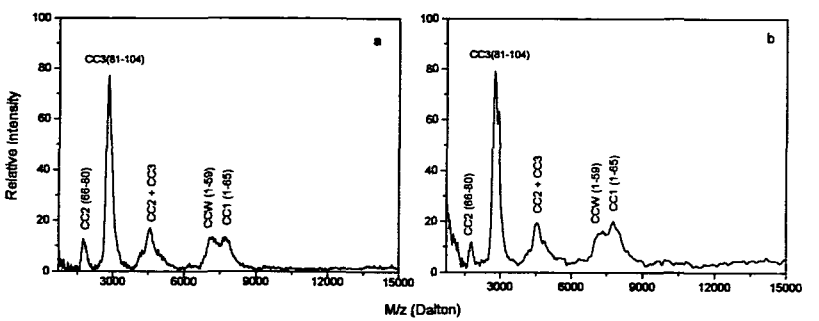

Figure 3. MALDI MS of CC digest on CPC modified Nafion.

Conclusion. This study shows that adsorption of proteins/peptides by active substrate can limit the sensitivity of MALDI MS detection. Modification of the sample loading surface in MALDI MS has the potential to alleviate the adsorption of proteins by the polymeric surfaces and hence enhance the sensitive and uniform desorption of all components in protein/peptide mixtures. Future work will focus on fabricating of composite substrates that retain the purification capability, but do not have adverse effect on MALDI MS detection.

Reference.

(1) Bai, J.; Liu, Y. H.; Cain, T. C.; Lubman, D. M. *Anal. Chem.* 1994, 66, 3423-3430.

Polymers as a Probe Element for Surface Enhanced Neat Desorption (SEND);

*Patrick Bardel and T. William Hutchens, Food Science and Technology Department, University of California at Davis, Davis, CA 95616.

BACKGROUND AND SIGNIFICANCE

Matrix-Assisted Laser Desorption/Ionization (MALDI) mass spectrometry has become a powerful tool for characterization of biological samples [1] In 1993, our laboratory has introduced new methods for the desorption of biopolymers into the gas phase using probe ***surfaces chemically defined***. This new strategy, involving probe elements with **Surfaces Enhanced for Neat Desorption (SEND)**, makes use of several different modes of EAM immobilization.[2] We have now investigated the relative importance of the phenolic ***OH*** and carboxylic ***COOH*** groups present in the 3 most used matrices (i.e., α-cyano-4-hydroxycinnamic acid (CHCA), sinapinic acid (SA) and 2,5-dihydroxybenzoic acid (DHBA)). Chemical information gathered in these experiments were subsequently used in the design and construction of laser desorption probe elements (i.e., polymers or solid phase) to be used in the SEND mode. Preliminary results based upon the ***covalent*** attachment of EAM to polymeric supports are presented here.

METHODS

α-cyano-4-acetylcinnamic acid, 3,5dimethoxy-4-acetylcinnamic acid, 2-acetyl-4-hydroxybenzoic acid, and α-cyano-4-methoxycinnamic acid and derivatized polymers were synthesized according to reported procedures.[3] Chemical composition of these products was verified by ^{1}H and ^{13}C Nuclear Magnetic Resonance Chemical modification of the solid phase compounds was ascertained by ^{13}C Cross Polarization Magic Angle Spinning (CPMAS) NMR analysis

The samples were analyzed with modified Hewlett Packard LDI 1700XP laser desorption/ionization time-of-flight mass spectrometers. Spectra shown have been accumulated from typically 50 laser shots.

RESULTS AND DISCUSSION

The OH and COOH groups present in most MALDI matrices were chemically altered and tested as potential MALDI matrices. Ether, oxirane, amide and ester bonds were formed. Of these four groups only the acetate derivatives of α-CHCA, SA and DHBA could be used as matrices. In particular, the acetylated α-CHCA (Figure1, 2) proved to be an efficient matrix due to the photochemical lability of this linkage Subsequent chemistry was attempted with solid phase compounds (Figure3, 4) and polymeric materials. Preliminary results confirmed previous trends and indicated that covalent attachment of α-CHCA to polymeric surface through its phenolic group can be exploited to design efficient SEND probe elements.

CONCLUSIONS

Chemical evaluations of the importance of OH and COOH groups present in most MALDI matrices led to several observations:

- the photochemical lability of some chemical bonds can be exploited to attach matrices to surfaces.
- appropriate design and construction of defined probe surface to enable desorption of intact macromolecules can be achieved through covalent linkage of usual MALDI matrices to a large variety of material (solid phase compounds, synthetic polymers).
- the use of different synthetic polymers should enable the development of a new variety of specifically designed probe elements containing the required number of EAM for desorption of large proteins.

REFERENCES

1. F. Hillenkamp, M. Karas, R. C. Beavis and B Chait, "Matrix-Assited Laser Desorption/Ionization Mass Spectrometry of Biopolymers" *Anal. Chem*, **1991**, *63*, 1193A.
2. T. W. Hutchens and T. T. Yip, "New Desorption Methods for the Mass Spectrometry Analysis of Macromolecules" *Rapid Commun. Mass Spectrom*, **1993**, *7*, 576.
3 A. I Vogel. "A Textbook of Practical Organic Chemistry", 4th Eds; Longman: London, 1993

43rd ASMS Conference on Mass Spectrometry and Allied Topics

FIGURE 4

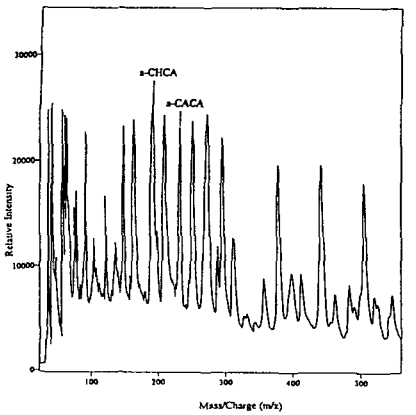

Low molecular weight region of bovine serum albumin from α-cyano-4-acetylcinnamic acid.

FIGURE 2

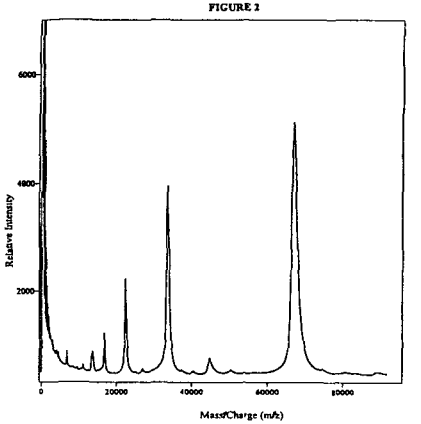

Bovine serum albumin mass spectra from α-cyano-4-acetylcinnamic acid

FIGURE 3

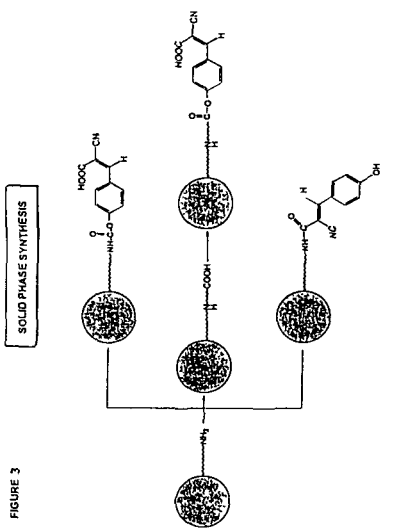

FIGURE 4a

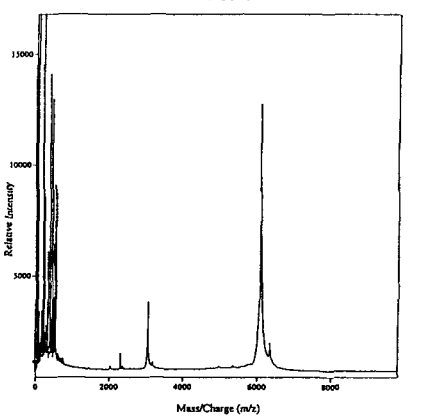

Oestrogen Receptor Dimerization domain (DD2) mass spectra from derivatized silica gel (Amino Propyl Silica gel derivative + α-CHCA)

Conformation of cytochrome c_2 mutants studied by H/D exchange using ESI-MS

F. Halgand[1], M. Jaquinod[1], M. Caffrey[1], J. Fitch[2], M.Cusanovich[2] and E. Forest[1].

[1] : Institut de Biologie Structurale, CEA/CNRS, 41 av.des Martyrs 38027 Grenoble, France.

[2] : Department of Biochemistry, University of Arizona, Tucson, USA.

Intoduction

In order to understand the functioning mechanisms of proteins, it is necessary to precisely characterize their structure. Nuclear magnetic resonance, circular dichroism as well as X-ray crystallography have been the most common techniques used to probe the three-dimensional conformation of these macromolecules. Mass spectrometry (MS), which has proved to be a powerful technique to study the primary structure of proteins, has been used only recently to probe conformational properties. Studying the charge state distributions by electrospray ionization (ESI) MS, several authors monitored conformational changes induced by organic solvents, pH, temperature or site-directed mutagenesis. Furthermore, the rate of hydrogen/deuterium (H/D) exchange, which depends on the solvent accessibility was recently probed by MS to get information on protein conformation or protein-ligand interaction.

To further investigate conformational changes induced by site-directed mutagenesis, we have adapted the H/D exchange procedure proposed by Zhang & Smith (1), using on-line HPLC/ESI-MS to carry out our experiments.

We compared *Rhodobacter capsulatus* cytochrome c_2 wild type with the P35A and G34S mutants, proteins expressed in a *Rb. capsulatus* strain that lacks a chromosomal copy of the cytochrome c_2 gene. The conformational properties of *Rb. capsulatus* cytochrome c_2 were characterized by the combined data obtained from hydrogen / deuterium exchange, protein chemistry and electrospray ionisation mass spectrometry.

1- Zhang Z. and Smith D.L. (1993), Protein Science, 2, 522-531.

Methods

After incubation in a deuterated solvant, proteins were digested with immobilized pepsin iunder conditions of low back-exchange and the resulting peptides where analysed using LC/ESI-MS.

Results and discussion

In an initial step we probed mutant stability by studying the charge state distribution in H_2O. We obtained approximately the same results for the WT and the mutants P35A and G34S with a maximum at +8.

To further investigate the influence of mutations we used H/D exchange. After one hour of incubation in D_2O, the H/D exchange equilibrium was reached. Mass increases showed that the conformational stability is influenced by the mutations, the G34S mutation having a stronger effect than the P35A one.

In order to characterize segments of the cytochrome c_2 influenced by the mutations, we have undertaken the H/D exchange studies of proteolytic peptides

using the previously described procedure. This procedure was developed and optimized on *Rb. capsulatus* cytochrome c_2 WT. The reproducibility of peptic cleavage and chromatographic profiles was useful to identify the peptides. Molecular mass analyses of deuterated peptides allowed the calculation of a mass increase, directly linked to the number of incorporated deuterium. Assignements of the sequences were realised using the MacBiospec software and Edman degradation. Three peptides were found with slow H/D exchange rates, five with medium H/D exchange rates and three with high H/D exchange rates. Our results were in good agreement with previous H/D exchange studies in NMR except for the N-terminal region. The N-terminal helix located within peptide [1-26] was found to be stable in the NMR studies. The medium exchange rate observed for this fragment could be explained by the length of the peptide which corresponds to the N-terminal helix ([3-13]) and the heme binding region ([14-26]).To better study the peptide [1-26] we performed a chymotryptic digestion and measured the H/D exchange rate after deuteration by LC/ESI-MS. Peptides [1-10] and [11-26] had slow and medium exchange rates, respectively, which is in good agreement with previous H/D NMR studies. Furthermore, overlapping peptides with different exchange rates provided detailed information about local H/D exchange rates. An example is presented by fragments [66-71] and [66-74]. Comparison of those two fragments allowed us to localize the additional deuterium on the three C-terminal residues. Therefore peptide [66-71] exhibits a slow H/D exchange rate whereas peptide [72-74] exhibits a high H/D exchange rate, results confirmed by H/D NMR studies.

Mutated amino-acids in cytochrome c_2 were chosen because they were highly conserved among the class-I cytochromes c and for their roles in the stability of the three-dimensional structure.

First, no significant modification of exchange rate was found for peptide [27-37] where the mutations are localized. The mass increase of 1 Da for P35A mutant is only due to one additional exchangable amide hydrogen, resulting from the mutation.

For both mutants, 3 peptides had an increase in their H/D exchange rate: [1-26], [38-51] and [52-59]. Both mutants seemed to induce the same conformational changes on these last two peptides, but in different ways. The decrease of stability in P35A mutant could be explained by the loss of the ß-turn which would probably induce a local modification of the backbone stability. G34S mutation induced the same modifications but it would be linked to the breaking of hydrogen bonds. Furthermore, both mutants showed an increase in H/D exchange rate of the peptide [1-26] indicating an influence on the N-terminal helix stability. This result is explained by the putative role of the N-terminal helix in the heme binding and in the conformational stability.

The methodology we developped on *Rhodobacter capsulatus* cytochrome c_2 is highly reproducible and sensitive. The use of this procedure has allowed the characterization of cytochrome c_2 regions influenced by mutations, in good agreement with previous NMR studies.

Association of H/D exchange and ESI-MS appears to be a very powerful way for screening the conformational changes induced in proteins by site-directed mutagenesis. It could also be applied to the characterization of regions implicated in protein-protein or protein-DNA interactions.

Probing Conformation and Dimerization in Yeast Hexokinase with ESIMS

Klaus Eckart and Joachim Spiess; Department of Molecular Neuroendocrinology, Max Planck Institute for Experimental Medicine, Hermann-Rein- Str. 3, D-37075 Goettingen

INTRODUCTION

Hexokinase is an important glycolytic enzyme catalyzing the ATP-dependent phosphorylation of glucose to glucose-6-phosphate. The enzyme has a molecular mass of 54,000 and may be present under non-denaturing conditions as monomer or dimer depending on the pH (1). Analysis of the hexokinase conformation with X-ray diffraction in solution revealed a reduction of the radius of gyration from 24.73 Å to 23.78 Å. This reduction was induced by glucose binding (2). Since it was demonstrated that the conformational streptavidin change induced by biotin binding could be analyzed with electrospray ionization mass spectrometry (ESIMS) (3), it was anticipated to establish such analysis for protein ligand systems exhibiting relatively low affinity. This would render this method applicable to many biologically interesting ligand protein systems such as neurotransmitter and neuropeptide receptors.

The possibilities and pitfalls for the detection of specific noncovalent complexes with ESIMS were reviewed recently (4). It was stated that the specificity has to be demonstrated by i. e. the formation of complexes with a certain stoichiometry, independence of the complex formation of concentration changes, and control experiments with altered complex components.

Detection of the hexokinase glucose noncovalent complex ($k_D=10^{-4}$ M) appeared to be difficult, because even the extremely stable biotin streptavidin noncovalent complex ($k_D=10^{-15}$ M) could be dissociated easily by skimmer CAD in the electrospray interface. The pH dependent dimer dissociation was therefore used to establish almost suitable conditions for the analysis of native hexokinase. With in those conditions the effect of specific ligand binding was than investigated.

METHODS

Mass spectral investigations were carried out on a VG Analytical AutoSpec-T tandem mass spectrometer. The instrument was fitted with the Fisons electrospray interface incorporating a hexapole lens for higher ion transmission and the stainless steel spray needle in combination with the pepperpot counter electrode for better stability when spraying buffered water solutions. The liquid was delivered with an infusion syringe pump. The hexokinase concentration was 10 µM. Samples were injected into a 20 µl loop of a Rheodyne 8125 injector. The spray chamber was not heated. The spray was stabilized with a 14 l/h oxygen stream and desolvated with a 300 l/h nitrogen stream. The sampling cone voltage offset was set to 300 V. The instrument was operated with a fully opened collector slit. The magnet was scanned over an appropriate mass range with a scan rate of 5 seconds/decade. Calibrations were performed with CsI. More conditions are given in the figure.

RESULTS AND DISCUSSION

The known pH dependent dissociation of the hexokinase dimer in solution (1) could also be detected with ESIMS. At pH 5 no significant dimer dissociation was observed, whereas at pH 10 the majority of the enzyme was dissociated into the monomer. It should be mentioned that the dimer is partially dissociated when the spray chamber was heated to 80°C. The lower sampling cone voltage offset needed in the case of a heated spray chamber did not compensate for the heat-induced dissociation.

These results provided strong evidence for the native conformation of the hexokinase investigated. In addition, the activity of the enzyme was assessed by glucose phosphorylation.

This test became important, because the commercially available hexokinase preparations had to be desalted with microcon 30 ultrafiltration devices for use in ESIMS. The activity assay revealed conservation of the enzymatic activity after desalting.

Addition of 2mM glucose to hexokinase in ammonium carbonate buffer, pH 9, enhanced M14 compared to M16 (Fig. 1). This effect was not detected with the same amount of lyxose, which is known not to be phosphorylated by hexokinase. The effect is more pronounced when mannose is added in comparison with glucose in the ammonium acetate buffering system. These differences may reflect the two times greater affinity of mannose to hexokinase compared with glucose.

Figure 1: The effect of 2mM glucose and 2mM lyxose to yeast hexokinase.
Conditions: flow rate: 5 ml/min; solvent: 10mM ammonium carbonate pH 9.

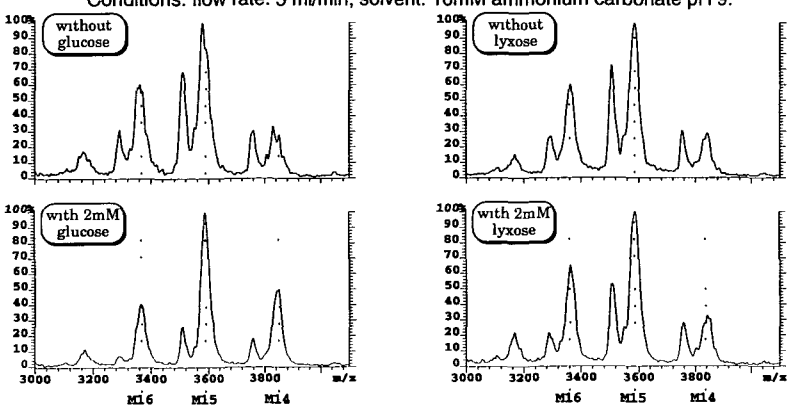

Beside the observed change in the charged state pattern of hexokinase, a small mass shift of the hexokinase signals to higher m/z values was observed (Fig. 1). Different k_D values for the dimer dissociation of the different isoenzymes may also serve as an explanation. It should be mentioned that four isoenzymes could be detected by comparison of different hexokinase preparations with ESIMS.

With the observation of the specific glucose effect on yeast hexokinase we demonstrated for the first time the use of ESIMS for the detection of a specific low affinity noncovalent interaction. The exclusive detection of the dimer at low pH in addition suggested that yeast hexokinase was not significantly denatured during the electrospray spray process.

The shift of the hexokinase multiply charge state pattern induced by glucose and mannose binding is compatible with the known decrease of the protein radius. Calculation of the differences in the molecular surface on the basis of the estimation of a ball type shape resulted in a reduction of 7% equivalent to reduction of the average charge from +15 to +14. The observed shift is much less, but it has to be considered that the model used for this estimation represents only an approximation to the real situation.

References:

1) Derechin, M.; Rustum, Y. M.; Barnard, E. A., *Biochemistry* **11**, 1793-1797 (1972).
2) McDonald, R.; Steitz, T. A.; Engelman, D., *Biochemistry* **18**, 338-342 (1979).
3) Eckart, K.; Spiess, J., *J. Am. Soc. Mass Spectrom.* **6**, in press (1995).
4) Smith, R. D.; Light-Wahl, K. J., *Biol. Mass Spectrom.* **22**, 493-501 (1993).

ESI-TOF-MS Studies of the Refolding and Assembly of Soybean Agglutinin

Xue-jun Tang*[1], Igor Chernushevich[2], Sanat Saha[1], C. Fred Brewer[1] and Kenneth G. Standing[2]
[1]Department of Biochemistry, Albert Einstein College of Medicine, Bronx, New York 10461, USA
[2]Department of Physics, University of Manitoba, Winnipeg, manitoba, Canada R3T 2N2

Soybean agglutinin (SBA) is a noncovalently bound tetrameric glycoprotein. Recent studies of SBA using ESI-MS [1]have revealed that native SBA consists of five major different subunits with four of them truncated at the C-terminus. The subunit composition of six isolectins, designated as SBA-I to VI, has been determined by ESI-MS and found to consist of two intact and two C-terminal truncated subunits composing the tetramers. More recently, we have demonstrated that the noncovalently bound SBA tetramers (~116,000 Da) can be detected using an ESI-TOF mass spectrometer [2]. Moreover, the ESI-TOF-MS technique allowed us to obtain information on the quaternary structure. In our present investigations, the refolding of a pure isolectin, SBA-I, which consists of two intact (α, MW 29438 Da) and two identical C-terminal truncated (β, MW 28001 Da) subunits in equal abundance, has been performed, and the refolding products were subject to analysis using ESI-TOF-MS.

On chromatofocusing using a PBE column at pH range of 7.4-6.5, native SBA-I gave a single peak at pH 6.95 (figure 1a). When the refolded SBA-I was subjected to chromatofocusing, at least four distinct peaks were eluted at pH values of 7.0, 6.4, 5.9 and 5.5 (figure 1b), indicating probable formation of new species. The first peak in the chromatofocusing profile of the refolded SBA-I, eluted at the pH value corresponding to native SBA-I, contains only about 25% of the total proteins eluted. The materials in the rest of three major peaks were pooled together and were designated as combined peak.

Figure 2 shows the ESI-TOF mass spectra of the native and the refolded SBA-I tetramers. The native SBA-I sample (figure 2a) gave only one series of multiply charged ions corresponding to the intact SBA-I tetramer. However, the 1st peak (figure 2b) yielded two sets of multiply charged ions, with one set corresponding to the native SBA-I and the other set representing a new tetramer. The new tetramer, is found mainly in the 1st peak and makes up about 25% of the tetramers eluted in the 1st peak. The measured mass of the new tetramer (113,812 Da) is about 1349 Da lower than that measured from the Native SBA-I (115,161 Da), a value close to the mass difference between the α and β subunit, suggesting the subunit composition of the new tetramer is $\alpha\beta_3$ The spectrum of the combined peak gave only one relatively broad peak with a mass (115,314 Da) corresponding to $\alpha_2\beta_2$ tetramer.

The pH shifts for the tetramers in the combined peak may, perhaps, be due to the tetramers in the combined peak incorporating extra amounts of buffers and salts during the refolding process, since the mass peak of the tetramers (figure 2c) is broad and shifted to higher mass compared with that of the native tetramer (figure 2a). The pH shifts may also be due to the different quaternary structures of the tetramers acquired in the refolding process. In order to address this question, we performed fragment ion analysis of these multiply charged tetramers. Figure 3 shows a segment (m/z 3600-4900) of each fragment ion spectrum obtained from the native SBA-I, the 1st peak and the combined peak. As can be seen, the $\alpha\beta$ heterodimers are dominant species in all the fragment ion spectra, suggesting that the α-β interactions are much stronger than α-α or β-β interactions, and that the spatial arrangement of the subunits α and β are similar in all the tetramers consisting of $\alpha_2\beta_2$. The $\alpha\alpha$ and $\beta\beta$ homodimers are present in low relative abundance except for the 1st peak. For native SBA-I (figure 3a), $\alpha\alpha$ and $\beta\beta$ homodimers are ~8-10% of the $\alpha\beta$ heterodimer, respectively, calculated using +13 and +15 charge states. $\alpha\alpha$ increases to 25% and $\beta\beta$ to 35% of the $\alpha\beta$ heterodimer for the 1st peak, consistent with the spectrum of the 1st peak (figure 2b), which suggests that the 1st peak contains ~25% of the $\alpha\beta\beta\beta$ tetramers.

The results obtained from ESI-TOF-MS analysis of the SBA-I refolding products shows that during refolding small amount of new isolectings were produced, most of which consists of three c-terminal truncated and one intact subunits, and they are also less stable than the native isolectins. However, the majority of the refolded isolectins have a quaternary structure similar to the native isolectins. The new peaks observed in chromatofocusing are probably due to isolectins with a different extent of incorporation of buffer and/or salt molecules during the refolding process.

[1] D. K. Mandal, E. Nieves, L. Bhattacharyya, G.A. Orr, J. Roboz, Q-T. Yu and C.F. Brewer *Eur. J. Biochem.* **221**, 547-553 (1994).
[2] X.-J. Tang, C.F. Brewer, S. Saha, I. Chernushevich, W. Ens, K.G. Standing, *Rapid Commun. Mass Spectrom.* **8**, 750 (1994).

43rd ASMS Conference on Mass Spectrometry and Allied Topics

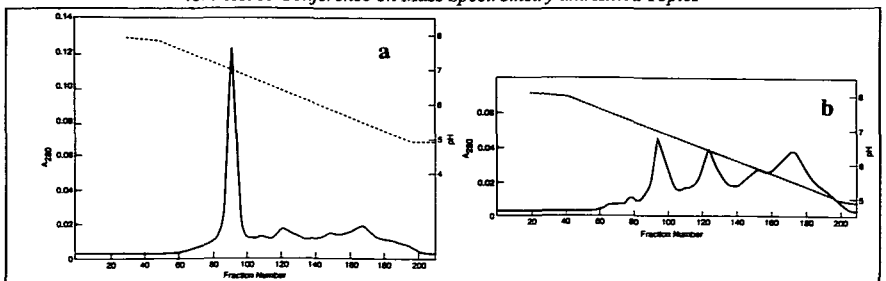

Figure 1. Chromatofocusing of native SBA-I (a) and refolded SBA-I(b) on a PBE column at a pH range of 5-8.

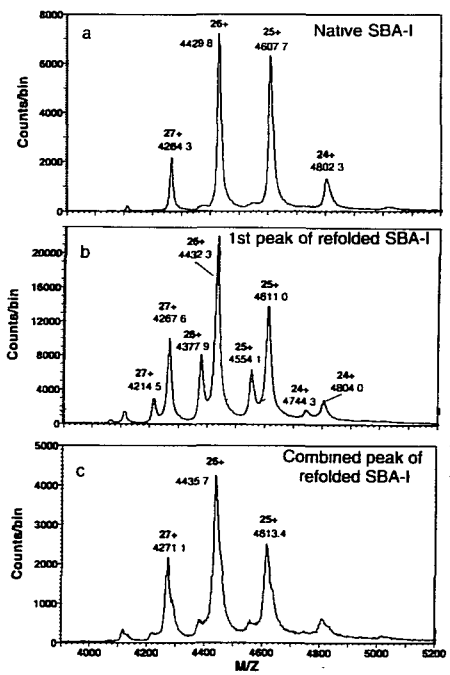

Figure 2. ESI-TOF m/z spectra of SBA-I tetramers in water.

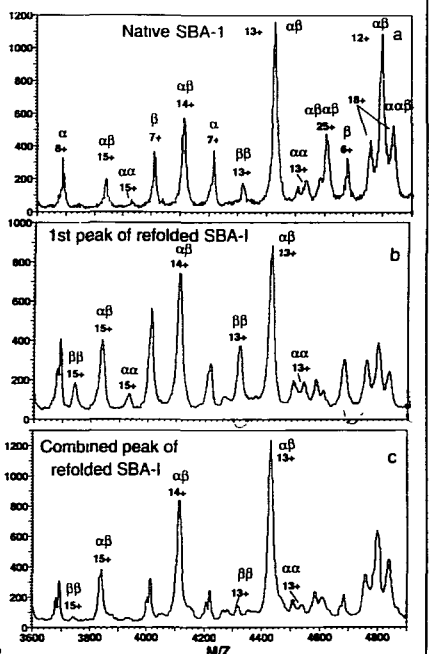

Figure 3. Segments of fragment ion spectra of SBA-I obtained with high capillary-skimmer potential.

Rapid Deuterium Exchange-in Time for Probing Conformational Change

Kuruppu Dharmasiri and David L. Smith, Department of Chemistry, University of Nebraska-Lincoln, Lincoln, NE 68588

Isotopic exchange of protein backbone amide hydrogens has been used extensively as a sensitive probe of protein structure. One of the salient features of hydrogen exchange is the vast range of exchange rates in one protein. Isotopic exchange methods have been used to study the structural features including protein folding and unfolding (1), functionally different forms of proteins (2), protein-protein complexation (3), and protein stability parameters (4). Many backbone amide protons that are surface accessible and are not involved in hydrogen bonding undergo rapid deuterium exchange. In order to study, fast exchanging amide protons, fast exchange-in times are necessary.

A rapid mixing apparatus has been developed which facilitates deuterium exchange experiment as rapid as 200 msec. The apparatus consists of an exchange chamber and digest region on-line. A flow of D_2O buffer solution (pD = 7.2) and protein enters the first mixing chamber in order to start the exchange reaction. Sample flow from the first mixing chamber flows through the length of tubing (length and diameter as well as flow rate determine the incubation time) At the end of the incubation time, the deutarated sample flows into a second mixing tee, where deutarated protein is mixed with a buffer solution (pH=2.2) to quench the exchange reaction and pepsin to digest the deuterated protein. The combined solution flows through another tubing section for 5 minutes while being digested. The resulting peptic digest is then separated by HPLC and analyzed by mass spectrometry for the deuterium content. The digest region and the HPLC column were cooled to 0°C to minimize the back-exchange. The total flow (50μL/min) from the microbore HPLC was introduced into the ESI source. The mass spectrometric analysis was accomplished with a VG Autospec high resolution mass spectrometer equipped with a focal plane array detector. The peptide fragments were identified by tandem mass spectrometry.

The cytochromes C are small globular proteins that involved in electron transfer reaction of the eukaryotic respiratory chain. Electrons in the heme group of the cytochromes C shuttled between the reduced (Fe (II)) and the oxidized (Fe (III)) states. It is believed that the reduced and oxidized cytochromes C have similar protein structures but different heme oxidation states. Another cytochrome C of interest is the apocytochrome C which is lacking heme group and tertiary structure In this study, reduced, oxidized, and apo cytochromes C have been studied by the rapid deuterium exchange methodology combined with mass spectrometry.

Various segments of the protein can be analyzed for deuterium incorporation with time. The exchange data provide the information about solvent accessibility of localized segments along the backbone of the protein. Figures 1a and b show the change in deuterium incorporation for two segments of the protein 95-104 and 83-94 respectively. Apocytochrome C shows the largest deuterium incorporation and reduced form shows the least for these two segments. Some segments show very little change in deuterium incorporation between reduced and oxidized forms (e.g.. segment 1-10).

In addition to the peptide fragments, undigested cytochrome C was observed during mass spectral analysis. As shown in Figure 2, the deuterium exchange curves for reduced and oxidized cytochromes C show that deuterium uptake is less in the reduced form. Difference in deuterium uptake shows the stability of reduced form over the oxidized form at pD = 7.2. Our results show that the on-line hydrogen exchange mass spectrometry coupled with proteolytic fragmentation can be used to rapidly (< 30 min.) identify localized conformational changes in proteins.

1. Roder, H ; Elove, G. A., Englander, S. W. *Nature* **1988**, *335*, 700
2. Englander, S. W. , Englander, J. J.; McKinnie, R E.; Jumer, G. J., Westrick, J. A., Gill, S. J *Science*, **1992**, *256*, 1684
3. Paterson, Y , Englander, S W.; Roder, R *Science*, **1990**, *249*, 755.
4. Yawen, B.; Milne, J S ; Mayne, L., Englander, S. W. *Proteins: Structure, Function, and Genetics* **1994**, *20* 4.

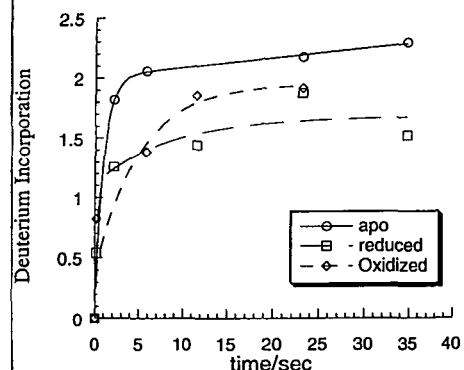

Fig. 1a. Deuterium exchange curve for segment 95-104 of apo, reduced (Fe^{+2}), and oxidized (Fe^{+3}) cytochrome C

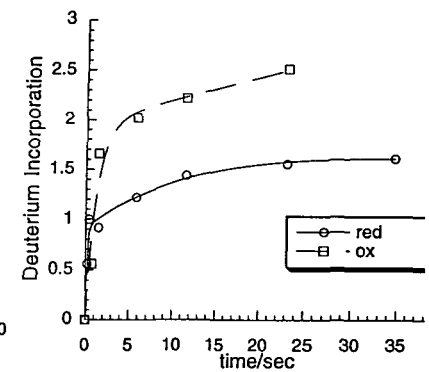

Fig 1b. Deuterium exchange curve for segment 83-94 of reduced (Fe^{+2}), and oxidized (Fe^{+3}) cytochrome C

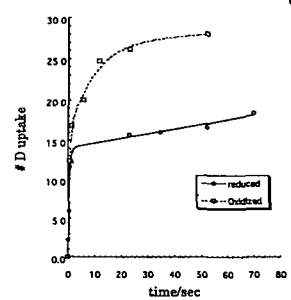

Fig. 2. Deuterium exchange curve for reduced (Fe^{+2}) and oxidized (Fe^{+3}) cytochrome C

ESI-MS OF PROTEIN NONCOVALENT TETRAMERIC ASSOCIATIONS AT HIGH *m/z*

Brenda L. Schwartz, David C. Gale, Ashutosh Chilkoti[1], Virginia F. Smith[2], Linda L. Randall[2], Patrick S. Stayton[1], and Richard D. Smith, Chemical Sciences Department, Pacific Northwest Laboratory, Richland, WA 99352
[1]Center for Bioengineering, University of Washington, Seattle, WA 98195
[2]Department of Biochemistry and Biophysics, Washington State University, Pullman, WA 99164

Electrospray ionization mass spectrometry (ESI-MS) has demonstrated broad applicability in the analysis of liquid-phase noncovalent complexes. Successful detection of these complexes by ESI-MS relies on the use of proper solution conditions and careful control of instrumental variables in the atmosphere-vacuum interface region. For large multisubunit proteins, electrospraying from near-neutral pH aqueous solutions, rather than from conventional acidic solutions, is often essential *in detecting the biologically active form of the protein. However, the limited gas-phase charging* typically observed for these proteins, presumably due to their compact quaternary structures, necessitates the use of mass spectrometers capable of extended *m/z* range detection (>3,000).[1]

The protein streptavidin (M_r ~ 53.1 kDa) exists in its active form as a noncovalent tetramer, which is comprised of four identical polypeptide-chain subunits, each containing a ligand binding site. Streptavidin, similar to avidin, exhibits an extremely specific and strong affinity ($K_D \sim 10^{-15}$M) for biotin (M_r = 244 Da). The intact tetrameric form of the avidin-biotin noncovalent complex has previously been observed utilizing a low rf frequency extended *m/z* range (~45,000) quadrupole mass spectrometer.[2] The ability to probe by ESI-MS relative noncovalent binding of two structurally similar ligands, biotin and 2'-iminobiotin (M_r = 243 Da, $K_D \sim 10^{-7}$M), to streptavidin was investigated.[3] The inherent variations in structural properties between these ligands give rise to their vast differences in binding affinities. Several protein:ligand molar ratios and incubation times were selected, in addition to altering conditions in the interface region (i.e., capillary temperature) to monitor the appearance of the specific complexes, and to subsequently induce their dissociation.

Solutions containing 1:10 streptavidin:ligand molar ratios in 10 mM NH_4OAc (pH 8.6) were analyzed by positive-ion ESI-MS following an incubation period of several minutes. The spectrum of the 1:10 streptavidin-iminobiotin sample (Fig. 1a) indicates that the intact noncovalent complex is not observed even under gentle ESI interface conditions. The experimental M_r of 53,128 ± 55 Da calculated from the tetramer charge states (Q^{16+} to Q^{13+}) corresponds in mass to the unbound streptavidin tetramer. Under identical conditions, a short incubation time for the 1:10 streptavidin-biotin sample (Fig. 1b) was sufficient to produce ions corresponding to the stoichiometrically specific association of four biotins binding to the protein, as indicated by the M_r of 54,081 ± 55 Da. Only under extremely mild interface conditions, combined with a larger iminobiotin concentration and longer incubation period, was significant binding for this complex detected. In addition, an intact noncovalent complex formed between streptavidin and a synthetic 5'-biotinylated 12-base pair oligonucleotide (5'-Biotin-dACTTATCTTTCT-3', M_r = 3956 Da) was observed. Negative-ion ESI-MS of a 1:5 protein:ligand solution in 20 mM NH_4OAc (pH 8.6) produces intense ions (Q^{17-} to Q^{14-}) for the complex (Fig. 2). The experimental M_r of 68,873 ± 70 Da is consistent with the predicted solution behavior for the binding of four biotin-oligonucleotides to the streptavidin *tetramer. These results demonstrate the ability of ESI-MS for probing relative stabilities of* noncovalent complexes, and prove that these complexes detected are structurally specific, and are not due to nonspecific interactions.

References:
1. K. J Light-Wahl, B. L. Schwartz, and R. D. Smith, *J. Am. Chem. Soc.* **116**, 5271 (1994).
2. B. L. Schwartz, K. J. Light-Wahl, and R. D Smith, *J. Am Soc. Mass Spectrom.* **5**, 201 (1994)
3. B. L. Schwartz, D. C. Gale, R. D. Smith, A. Chilkoti, and P. S Stayton, *J. Mass Spectrom.*, in press.

Pacific Northwest Laboratory is operated for the U. S. Department of Energy by Battelle Memorial Institute under contract DE-AC06-76RLO 1830.

43rd ASMS Conference on Mass Spectrometry and Allied Topics

Figure 1. Positive-ion ESI-MS of 1:10 Streptavidin-Ligand Solutions

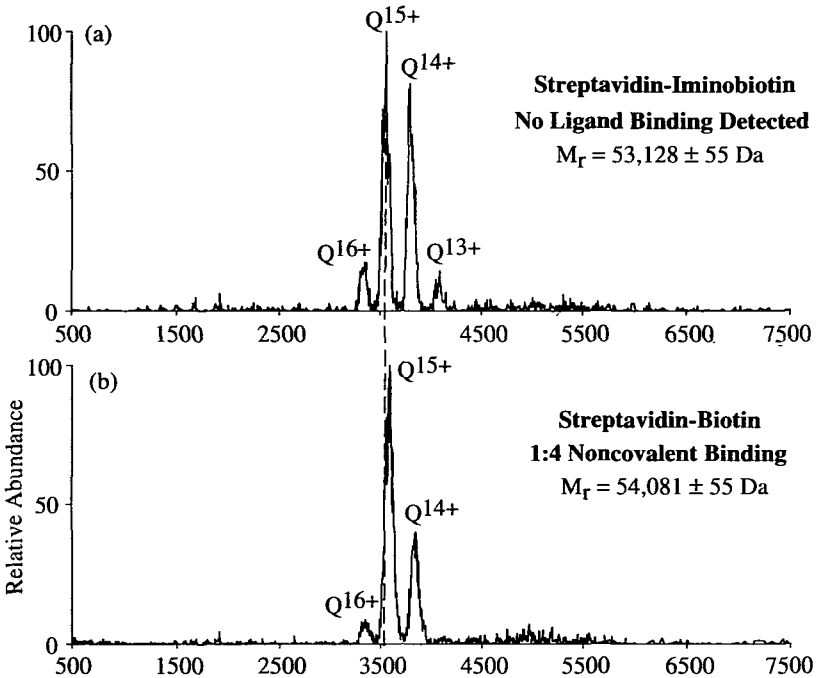

Figure 2. Negative-ion ESI-MS of Streptavidin-Biotinylated 12-bp Oligonucleotide

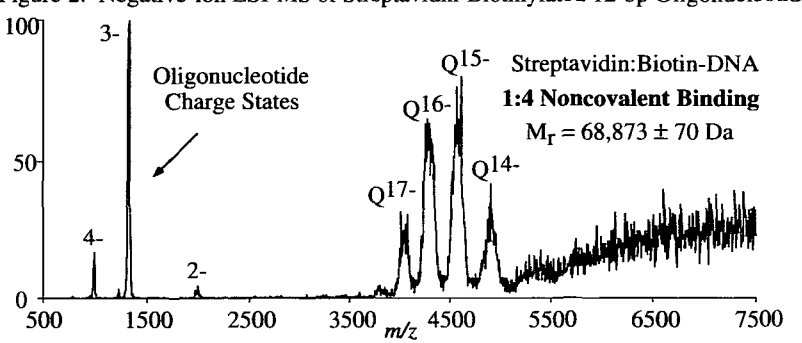

ESI-MS Analysis of the Transthyretin Tetramer and Some Non-Covalent Adducts.

B. N. Green, VG Organic, Tudor Road, Altrincham, Cheshire WA14 5RZ, UK.
R. W. A. Oliver, BMA Research Unit, University of Salford, Salford M5 4WT, UK

Introduction.

Alzheimers disease is a major social and health problem facing the developed countries because of the increasing longevity of their populations and hence is the subject of much current research. Amyloid β peptide (1-40) together with some smaller related peptides, are normal proteolytic products of a large transmembrane glycoprotein and are major components of the characteristic, practically insoluble, amyloid depositions found in the brains of Alzheimers patients *In vitro*, these peptides have been shown to readily aggregate and form insoluble amyloid fibrils similar to the brain depositions, but are also found in a soluble form in the cerebrospinal fluid and serum of subjects both with and without the disease

Recently, it was shown[1] that amyloid β peptides in these extracellular fluids do not normally aggregate because they are sequestered by one or more of the proteins, particularly transthyretin (TTR), present in these fluids Here, we summarise unsuccessful attempts to show similar sequestering of amyloid β peptides by TTR using electrospray mass spectrometry (ESI-MS)

Results and Discussion.

TTR samples from three sources were analysed by ESI-MS in the denatured state, i e. as the monomer, to check their authenticity and purity These analyses were carried out in 50% aqueous acetonitrile containing 0.2% formic acid All 3 samples showed substantial and different heterogeneity Furthermore, the peaks corresponding to the sequence mass of TTR (13761 4) indicated the unmodified TTR to be present only as a minor component in all 3 cases (Figure 1). Nevertheless, when the TTRs were analysed in water containing 5-10mM ammonium acetate at physiological pH, they produced 3 peaks corresponding approximately in mass-to-charge ratio to the expected non-covalent tetramer complex (55046) with 15-17 charges. It was only possible to approximately determine the mass-to-charge ratios of the tetramer due to the broad nature of the peaks. This latter was attributable, at least in part, to the heterogeneity of the monomer.

Amyloid β peptides (1-40), (1-28) and (12-28) were analysed by ESI-MS and found to be pure and to have molecular weights which agreed with those calculated from their sequences. However, when the amyloid peptides were incubated with TTR at 37°C and physiological pH, there was no evidence that the TTR sequestered the peptides (Figure 2), even though the peptides were added at levels up to 10 times molar excess over the TTR. The occurrence of complexes between the TTR and the amyloid peptides would have resulted in a substantial increase in mass-to-charge ratio However, in some cases, because of the broad nature of the tetramer peaks and the occurrence of 3 peaks with 15-17 charges, overlap of the complex ion, for example with 17 charges, could be expected to occur to some extent with the un-complexed TTR ion with 16 charges The use of more homogeneous TTR would be beneficial in obviating this difficulty

Ref. 1. Schwarzman et al, Proc Natl. Acad Sci. USA, 91, 8368-8372, 1994.

43rd ASMS Conference on Mass Spectrometry and Allied Topics

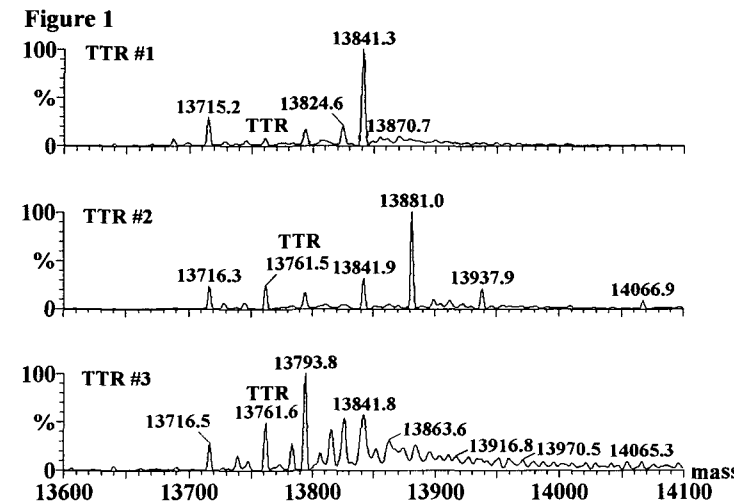

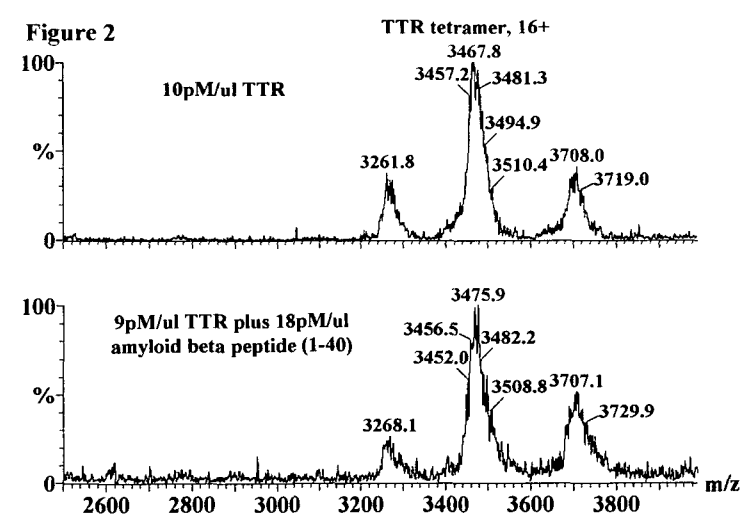

Conformational Changes and Molten Globule States of Proteins Detected by Matrix-Assisted Laser Desorption Mass Spectrometry

Houjun Yang, Xiaoling Li and Jürgen Grotemeyer*
Institut für Physikalische Chemie, Universität Würzburg, Marcusstr. 9/11, D-97070 Würzburg, Germany.

It is shown that simultaneous to the unfolding of hen-egg white lysozyme and horse heart cytochrome C the sequential conformational changes and molten globule states can be detected by the combination of proteolysis and matrix-assisted laser desorption/ionization mass spectrometry (MALDI-MS). This is demonstrated by the differences among the products and the time courses of native lysozyme as well as those unfolded in 1M and 3M guanidine hydrochloride (GuHCl) when they were proteolyzed by proteinase K and followed by MALDI-MS. Due to the absence of disulfide bonds in the cytochrome C molecule, it is more sensitive to the disturbance of the denaturant. The partially unfolded state as detected at low concentrations of guanidine hydrochloride in our experiment resembles in a way a molten globule state. One of the unique properties of the method described herein is to measure directly the peptide fragment liberated from proteolysis of the protein. It allows the identification of the sensitive sites susceptible to denaturation, which are subsequently cleaved by proteinase K proteolysis.

1. Conformation changes during unfolding.

Our results suggest strongly that the conformational changes happen in the lysozyme molecule while it is incubated with GuHCl at a concentration lower than 3 M. This is demonstrated by the differences among the time courses of native lysozyme, which unfolded in 1 M GuHCl and which in 3 M GuHCl while they were proteolyzed by proteinase K. Due to the abscence of disulfide bonds in cytochrome C molecule, it is more sensitive to the disturbance of the denaturant than lysozyme, the method can even to be employed to tell the differences between those unfolded in 0.5 M and 1 M GuHCl. The increase in rates and products of proteinase K digestion with the increase of GuHCl concentration suggests the gradual opening up of the molecule.

2. Relation of the partially unfolded to the molten globule state.

The partially unfolded state as detected in our experiment at low concentration of GuHCl before gross conformational changes occure resembles in a way the molten globule state[1,2,3]. If the unfolding of lysozyme in GuHCl occures by a simple two-state mechanism, all the time courses of proteinase K digestion of lysozyme in 0M, 1M, and 3M GuHCl would be coincident. The fact that this is not the case demonstrates unequivocally that partially structured intermediates are populated during unfolding at low concentrations of GuHCl. The molecule of lysozyme unfolded in dilute GuHCl is partially loosened up especially in the active site as indicated by the peptide fragments, Thr_{89}-Gly_{102} and/or Ser_{91}-Gly_{104} (in 1M GuHCl) as well as Ala_9-Phe_{34}, and thus open to attack by proteolytic hydrolysis without noticeable changes in its secondary structure. All the above is consistent with the concept of the molten globule state.
Cytochrome C takes stable conformation in the buffer without GuHCl, and denatured conformation at high concentrations of GuHCl (1 M and 3 M). The stable conformation induced by 0.5 M GuHCl represents such one as to have secondary structure and compactness similar to native protein but lack tertiary structure indicated by the more exposured conformation to be hydrolyzed, the concept of molten globule state holds also for cytochrome C.

3. Location of the area sensitive to denaturation

One of the unique properties of the method described herein is to measure directly the peptide fragment resulted from proteolysis of the protein. It allows to identify the sensitive sites susceptible to denaturant and subsequently to cleavage by proteinase K proteolysis. The results from proteinase K digestions of lysozyme at different concentrations of GuHCl indicate the active site to be easily disturbed by the denaturant at low concentrations of GuHCl. Both the fragments, Thr_{89}-Gly_{102} and/or Ser_{91}-Gly_{104} are related much to the binding sites of Asp_{101} and Asp_{103} in the active site, and the fragment Ala_9-Phe_{34} is released exactly by cleavage of the peptide bond of Phe_{34}-Glu_{35}, where the Glu_{35} is a residue in the active site. The results could be explained reasonably by conformational changes happening at the active site, and provide support to the suggestion that enzyme active sites are situated in a limited and flexible regions and are therefore more easily perturbed than the rest of the molecule [4]. The inhibition of lysozyme activity by GuHCl seems unreasonable because this would prevent the active site cleft to proteolysis.
A close examination of the peptide fragments generated from cytochrome C at various concentrations of GuHCl shows the β-turns and coiled area are susceptible to proteolysis. The peptide fragments produced from the unfolded states involve the heme group and the heme ligand His_{18} as indicated by Val_{11}-Val_{20}, $AcetylGly_1$-Gly_{34} and Phe_{10}-Gly_{41} in the case of proteinase K digestion of cytochrome C in 0.5 M GuHCl. This site-directed determination of the unfolding of the molecule induced by denaturant provides a sensitive way for detections of conformational changes.

Acknoledgement

This work was supported by grant from Deutsche Forschungsgemeinschaft (GR917/6-2). HJY gratefully acknoledges the fellowship support of the Alexander von Humboldt-Stiftung.

References

1. K. Kuwajima, Proteins: Struct. Funct. Genet. 6, 87-103 (1989).
2. V. N. Uversky, G. V. Semisotnov, H. R. Pain and O. B. Ptitsyn, FEBS Lett. 314, 89-92 (1992).
3. D. T. Haynie and E. Freire, Proteins: Struct. Funct. Genet. 16, 115-140 (1993).
4. H. J. Yang and C. L. Tsou, Biochem. J. 305, 379-384 (1995).

Unusually Strong Binding of A Noncovalent Gas-Phase Spermine-Peptide Complex and Its Dramatic Temperature Dependence

Rong Feng, American Cyanamid Co., P.O. Box 400, Princeton, NJ 08543

Naturally present polyamines, which play essential roles in various cell events, are known to cause conformational changes in nucleic acids. Spermine, in particular, has also been found to induce α-helix formation in an acidic peptide by forming a specific noncovalent complex with the peptide. In this study, electrospray ionization mass spectrometry (ESI-MS) and MS/MS techniques were utilized to characterize the complex formation between spermine and a spermine-binding peptide (SBP) having an amino acid sequence of AcYEQAAEQQEAAQEACONH$_2$ (MW$_{av}$ 1606.6 Da). The experimental data revealed an unusually strong binding complex between spermine and the peptide, and showed that the gas-phase stability of the complex was heavily influenced by the ESI interface temperature.

A Finnigan TSQ 700 triple quadrupole mass spectrometer was used for the ESI-MS and MS/MS studies. The peptide and spermine were dissolved in pure H_2O to form the complex and the samples were sprayed at a flow rate of 1 - 2 μl/min without organic modifier, unless otherwise noted. The ESI needle was held at ±4.0 kV and ambient temperature for positive and negative ion production. The electrosprayer was assisted by a coaxial pneumatic nebulizer to pulverize the aqueous sample solution; the coaxial liquid sheath makeup flow was not used. The temperature on the ion inlet capillary at the atmosphere/vacuum interface region was varied from 100 to 300 °C to probe the effects of thermal heating on the complex stability. The gas-phase dissociation patterns of the low- and high-temperature complexes were studied using MS/MS technique with the argon collision gas at 1.5 mTorr; the collision energy was varied from 10 to 60 eV.

SBP, an acidic peptide containing 4 glutamic acids, could be detected as either deprotonated negative ions or various cation adducts. Despite the weak binding constant (~10^4 M^{-1}) of the spermine-peptide complex in solution, its noncovalent gas-phase complex was readily detected using ESI-MS. The complex could be observed as positive ions but not as negative ions, indicating that the acidic residues in the peptide could no longer present themselves as free anions due to their active participation in complexing spermine.

In contrast to the weak binding in solution, the complex exhibited an unusually strong binding in the gas phase, as shown by collisionally-activated dissociation (CAD) studies of the complex ions in the Q2 collision chamber. In fact, the noncovalent complex would not dissociate until the cleavage of a covalent bond had occurred at high collision energy (Fig. 1). The gas-phase dissociation of the singly charged complex ion (*m/z* 1810) yielded a major product ion at *m/z* 1709, whose mass was 101 Da higher than the free peptide ion (*m/z* 1608). This indicated that the total binding energy of the complex in the gas phase exceeded that of a covalent bond (50 - 120 kcal/mol). This dramatically enhanced complex stability in the gas phase may be due to increased Coulombic stabilization energy of the opposite charges in the solvent-free environment. Although the effect of the dielectric constant of water (κ = 80) on the Coulombic interactions of closely placed charges (several Å in distance) is still not fully understood, it is expected that ion solvation stabilizes charges and reduces the attraction (or repulsion) between them. Therefore, the stability of a charge-coupled complex should increase upon transition from solution to the gas phase.

Interestingly, the gas-phase binding strength of the spermine-peptide complex could be greatly weakened by heating the ion flux in the capillary interface. At high interface temperature (>200 °C), the

43rd ASMS Conference on Mass Spectrometry and Allied Topics

collisional dissociation of the complex in the Q2 collision chamber occurred predominantly via breaking the noncovalent interactions, *i.e.*, shedding an intact spermine ion. The large difference in binding energies at different temperatures could be due to drastically different gas-phase conformations of the spermine-peptide complexes. The weak complex produced at high temperature might have significantly less α-helical structure than the strong complex produced at low temperature. Since the peptide α-helical structure plays the critical role in spacing the negatively charged acidic residues at appropriate intervals for coupling with the positive charges on spermine, heat-induced structural distortion in the peptide could cause significant charge decoupling in the complex, thus losing much of the strong binding interactions that hold the complex tightly together.

When the spermine-peptide complex was prepared in 1:1 CH_3OH/H_2O solution, the interface temperature required to weaken the complex to yield *noncovalent* collisional dissociation increased to 250 °C (*vs.* 200 °C in H_2O), reflecting a substantially enhanced complex stability in the presence of CH_3OH (Fig. 2). This is consistent with the known fact that organic modifiers such as CF_3CH_2OH or CH_3OH typically increase peptide α-helicity in solution. Circular dichroism and hydrogen/deuterium exchange experiments should shed more light on the complex conformations at low and high temperatures.

These ESI-MS data show that at least two conformations of the SBP-spermine complex exist in the gas phase, despite the absence of the stabilizing solvent molecules. The drastically different collisional dissociation patterns indicate that the low- and high-temperature complexes have very different gas-phase structures. The extremely strong binding of the low-temperature complex also demonstrates the greatly increased significance of the electrostatic stabilization in the gas phase *vs.* in solution.

Acknowledgment: The author thanks Jean Lefebvre for kindly providing the spermine-binding peptide for the ESI-MS studies and Pat Mowery for helpful discussions.

Figure 1

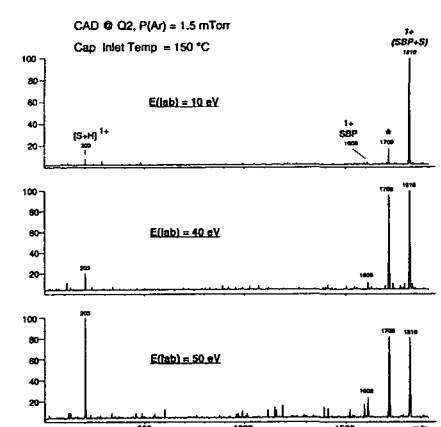

Figure 2

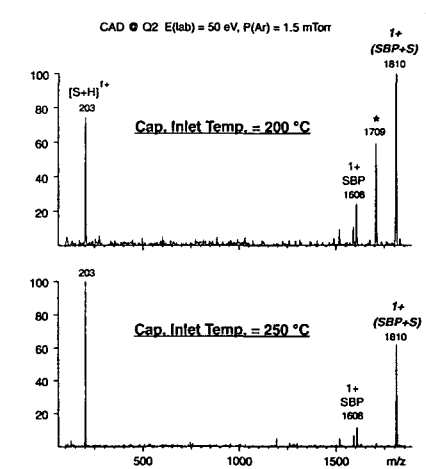

Conformation of Chaperone Bound Ligands Probed by ESI MS

Carol V. Robinson, Michael Groβ,
Christopher M. Dobson and Sheena E. Radford
Oxford Centre for Molecular Sciences,
South Parks Road, Oxford, OX1 3QT, UK.

Introduction

Protein folding in the cell is assisted by a host of helper proteins including the molecular chaperones which are thought to safeguard newly synthesised proteins from aggregation and other misfolding events. To unravel the molecular details defining the mechanism of action requires a novel approach to the problem of how to determine the conformational properties of a relatively small protein in the presence of the large 800KDa chaperone oligomer. Here we describe the development of one such approach, shown schematically in figure 1, and its extension to include other protein ligands and cofactors

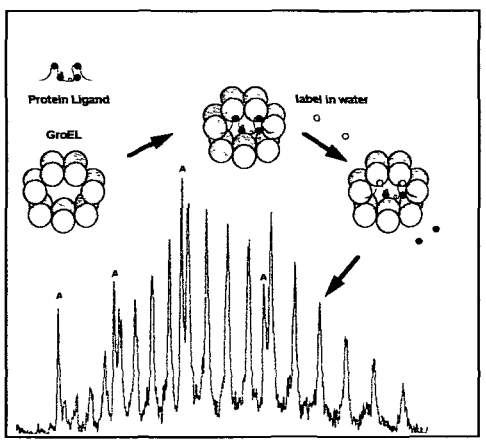

Figure 1:Schematic representation of the experiment designed to monitor hydrogen exchange in a chaperone-protein substrate complex. The black and open circles represent D and H respectively. The charge states labelled A represent the series of multiply charged ions arising from the substrate; the remaining peaks are from the GroEL monomer.

Results and Discussion

A number of control experiments were carried out to assess the feasibility of monitoring different conformational states by ESI MS. Measurement of hydrogen exchange from random coils, partially structured molten globules and native states were found to be in complete agreement with similar measurements by NMR. Such measurements are possible since conditions have been developed in order to preserve deuterium labelling even in extremely labile states such as molten globules (1).

Analysis of the hydrogen exchange kinetics and peak width data for an α-lactalbumin-GroEL complex have shown that the chaperone bound protein ligand is intermediate between the native and random coil states and most closely resembles the molten globule state.

More recently other chaperone - protein complexes have been examined. The stable complexes of dihydrofolate reductase (DHFR) and human α-lactalbumin with GroEL have been analysed using this technique. Furthermore, the non-covalent complex formed between GroEL with the co-factors GroES and ATP/ADP, has been examined and demonstrates that ATP/ADP is associated with the GroEL oligomer since the increase in mass associated with the attachment of ADP (+424) is seen only on the GroEL ion series.

Conclusion

Our recent results have demonstrate the feasabilty of detecting hydrogen exchange protection by ESI MS in the central cavity of GroEL. Further work will assess the hydrogen exchange protection of other ligands and the chaperone GroEL and examine conformational changes upon ligand and cofactor binding.

Reference

1. Robinson, C.V.; Groβ, M.; Eyles, S.J.; Ewbank, J.J.; Mayhew, M.; Hartl, F.U.; Dobson, C.M. & Radford, S.E. *Nature* **1994,** *372*, 645.

Studies of H/D exchange of Peptides by using aerosol MALDI

Xiaona Wei, Michelle D. Beeson, David H. Russell
Texas A & M University
Laboratory for Biological Mass Spectrometry
Department of Chemistry
College Station, Texas 77843

Hydrogen-deuterium (H/D) exchange measurements are becoming increasingly important in studies of the conformation and folding dynamics of proteins. The amide hydrogens of a peptide are labile to exchange with deuterium in solution but the exchange rates are related to the stability of secondary and tertiary structures. Mass spectrometry can be used to probe the conformation of the peptides/proteins by detecting the extent and/or rate of hydrogen-deuterium exchange[1].

One of the collaborative research project of the Laboratory for Biological Mass Spectrometry is to develop methods of investigation H/D exchange of model peptide (mw 1000-3000daltons)[2,3]. One of the methods we are evaluating for this project is aerosol-MALDI-TOF. The potential advantage of the method is the ability to sample directly the solution phase system, the aerosol MALDI mass spectra are less complex than the ESI spectra, typically only containing the $[M+H]^+$ ion, ion yield are insensitive to the presence of salts and buffers[4], and the experiment can be performed using a range of solution and solvent conditions[5].

Figure 1 are the spectra of Bradykinin H/D exchange. Bradykinin (mw=1060.2) contains a total of 17 labile hydrogens accessible. Three of the hydrogen atoms are involved in hydrogen-bonding that induce a β–turn and a partial helix. Fourteen hydrogen exchange was observed. Bradykinin spectra obtained in CH_3OH and CH_3OD indicate that the H/D exchange measurements are reproducible. Figure 2 are the H/D exchange spectra of Angiotensin II. An m/z shift of 22 was observed from 20 exchangeable protons. The H/D exchange efficiency was 110%. Spectra showed reproducibility in exchanges.

One major limitation of the current aerosol MALDI apparatus is the mass resolution. The mass resolution currently attainable on the aerosol MALD apparatus is not sufficient to distinguish between the exchange of ±1 hydrogen atom above m/z 1000. The $[M+H]^+$ ion signal corresponds to a distribution of deuterated species and the ^{13}C isotopic pattern. The incompletely resolved $[M+H]^+$ ion and the adduct ion signals may also contribute to the broadening. The number of exchanged hydrogens is determined by the mass increase of the peak centroid between the spectra before and after deuteration. The m/z resolution limit impedes accurate m/z assignment.

We are presently at the design stage of a second generation apparatus. The second generation instrument will consist of a microspray nebulizer, a wire ion guide system and a reflectron. Proof of concept experiments have been performed on our new PerSeptive Biosystems, Inc. Voyager Elite, and the Voyager Elite extended geometry instruments. Figure 3 and Figure 4 are MALDI-TOF mass spectra of Bradykinin and Melittin obtained using the Voyager Elite and the Voyager Elite Extended Geometry Instrument. The results for the experiment suggest that we can obtain unit mass resolution for peptides up to mass 5,000.

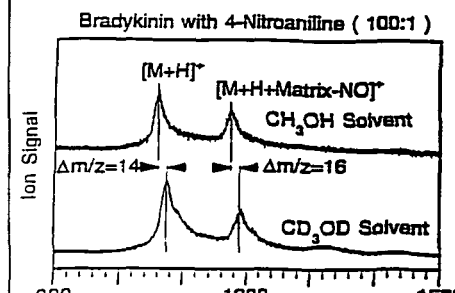

Figure 1

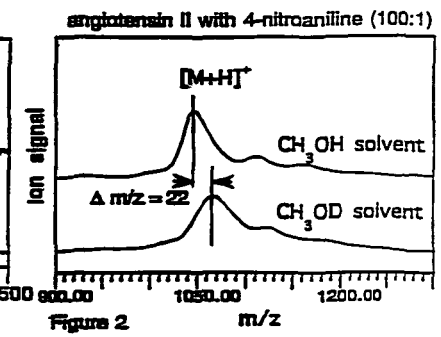

Figure 2

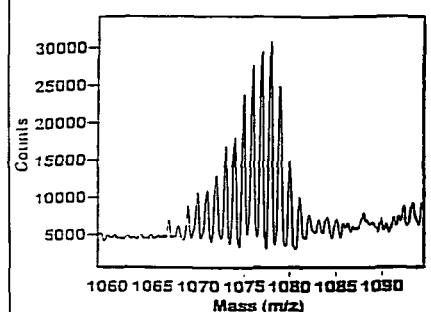

Figure 3

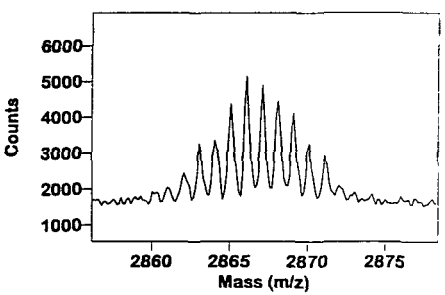

Figure 4

1. Miranker, A.; Robinson, C. V.; Radford, S. E.; Aplin, R. T.; Dobson, C. M. *Science* 1993, *262*, 896-900. 2. Rohl, C. A.; Scholtz, J. M.; York, E. J.; Stewart, J. M.; Baldwin, R. L. *Biochemistry* 1992, *31*, 1263-1269. 3. Englander, W. W. *Science* 1993, *262*, 848-849.. 4. Beeson, M. D., Wei, X.; Russell, D. H. ASMS TPB073, 1995. 5. Beeson, M. D.; Wei, X.; Russell, D. H. ASMS WPH226, 1995.

PROBING HIGH ORDER STRUCTURE OF PROTEINS BY H/D EXCHANGE/ESI-MS

Claudia S. Maier, Ok-Hee Kim and Max L. Deinzer
Department of Agricultural Chemistry, Oregon State University, Corvallis, OR 97331-7301

Very promising H/D exchange protocols in combination with mass spectrometric methods (especially ESI-MS) have been reported for probing global protein solution-conformations [1, 2], gas-phase conformations [3] and transient folding intermediates [4]. In these experiments all H/D exchange events were monitored by measuring the resulting mass increases during exchange-in reactions and the mass decreases during exchange-out experiments with deuterium labeled proteins. The resulting global structural information allowed distinguishing different conformations, but the methods possess limited ability to assign exchange rates to specific regions of the polypeptide chain. The mapping of exchange rates to specific regions of the polypeptide chain is a major assumption in correlating information obtained from H/D exchange experiments to structural features.

We evaluated two appoaches to increase the structural resolution of H/D using directly coupled microbore LC-ESI-MS and MSMS. The combination of chromatography and mass spectrometry provides flexibility in the choice of solvent systems during the labeling procedure. In the first approach, melittin was used as a model peptide because of its modest size and exclusive α-helical secondary structural elements (under conditions used). Fully deuterated melittin was injected onto a C8-column after prescribed incubation periods in methanol/water/acetic acid (pH 3 2) and the exchange-out events were directly monitored by on-line coupled ESI-MS. As evident from the obtained kinetic profile (figure 1), the exchange-out behavior is slowed down and this is the expected behavior of amide deuterons involved in hydrogen bonds [5]. The method presented here demonstates only the exchange-out behavior of the backbone amide deuterons. Microbore LC-ESI-MSMS experiments on fully-deuterated melittin enabled the direct localization of the two α-helical domains because the exchange-out of deuterons takes place relatively slowly during the chromatographic passage. Therefore, the observed fragment ions allowed the computation of the amide deuterons remaining at each residue By using the present method the number of deuterons remaining correlated directly with the degree of secondary structural stabilization at each backbone amide (figure 2). In previous work the number of exchangeable hydrogens are not specifically related to the amide hydrogens but includes the side chain hydrogens as well [6].

Secondly, the compatibility of the protein fragmentation method with directly coupled microbore LC-ESI-MS and MSMS was demonstrated using cytochrome c as a model system. This technique was first established by Rosa and Richards [7] and extended by Zhang and Smith by using FAB-MS for determination of deuterium content of the resulting peptides [8]. In the present procedure native cytochrome c was incubated in D_2O (pH 6) over different periods and immediately digested with pepsin at pH 2.5 at 0°C for 10 min. The digestion was terminated by freezing in liquid nitrogen, left frozen until it was injected onto the microbore C18-colum and eluted with aqueous acetonitrile/0.1 % trifluoroacetic acid gradient at 0°C over a period of 30 min. Because the incubation periods were varied, the complete analysis time (30 to 45 minutes depending on the retention time of the peptide) was fixed and the analysis condition were optimized to minimize back-exchange The molecular weight increase of the peptic peptides was determined after different incubation periods and the number of NH remaining was computed (figure 3). However, kinetic profiles [8] provide no information about regions in which amide hydrogen exchange takes place. Therefore, online microbore LC-ESI-MSMS was performed. This enabled us to locate domains with the highest content of amide hydrogens remaining within the polypeptide chain, e.g. in peptide 83 to 96 the region of residue 90 to 96 which represents the N-terminal part of the C-helix of cytochrome c (figure 4). A comparable labeling procedure was used to obtain compatible H/D exchange

maps for fully deuterated cytochrome c. The present H/D labeling experiments in combination with fragmentation method supplemented by MSMS provides detailed H/D exchange maps for the peptides which reflect the secondary structural construction of the protein.

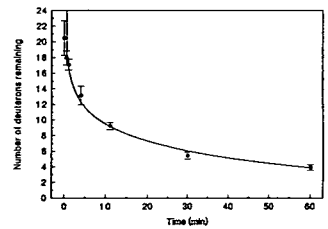

Figure 1

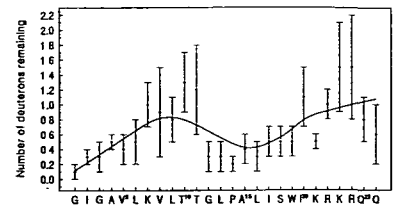

Figure 2

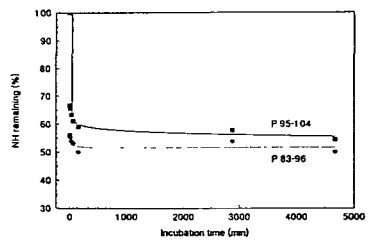

Figure 3

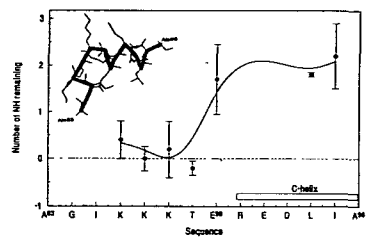

Figure 4

Acknowledgments

The Sciex API-III Electrospray Mass Spectrometer was purchased in part through grants from National Science Foundation (BIR-921 4371) and Anheuser-Busch Foundation. This study was funded in part by Grant No. 2P01 ES00040 from the National Institute of Environmental Health Sciences

References

[1] Katta, V., Chait, B.T. **Rapid Commun. Mass Spectrom.** 1991, 5, 214-217
[2] Wagner, D.S., Anderegg, R.J. **Anal. Chem.** 1994, 66, 706-711
[3] Suckau, D., Shi, Y., Beu, S C., Senko, M W., Quinn, J.P., Wampler, F.M. III, McLafferty, F W. **Proc. Natl. Acad. Sci. USA** 1993, 90, 790-793
[4] Miranker, A., Robinson, C.V., Radford, S.E., Aplin, R.T., Dobson, C.M. **Science** 1993, 262, 896-899
[5] Wagner, D.S., Melton, L.G, Yan, Y., Erickson, B.W., Anderegg, R.J. **Protein Science** 1994, 3, 1305-1314
[6] Anderegg, R.J., Wagner, D.S., Stevenson, C.L , Borchardt, R.T. **J. Am. Soc. Mass Spectrom.** 1994, 5, 425-433
[7] Rosa, J.J., Richards, F.M **J. Mol. Biol.** 1979, 133, 399-416
[8] Zhang, Z., Smith, D.L. **Protein Science** 1993, 2, 522-531

Studies of Partially Folded Proteins at Acidic pHs by H/D Exchange and ESI-MS

Xue-jun Tang* and Fang Wang
Department of Biochemistry, Albert Einstein College of Medicine, Bronx, New York 10461

A major experimental approach to understanding the protein folding process has been the structural characterization of partially folded equilibrium states using various experimental techniques including circular dichroism (CD) and NMR [1-3]. ESI-MS permits the accurate measurement of protein molecular mass (≤0.01%) at picomolar quantities, making H/D exchange in combination with ESI-MS an attractive choice for protein conformational studies [4,5]. In the present investigation, partially folded apomyoglobin (apo-Mb) and cytochrome c, induced by salts [3], detergents or hydrophobic solvent 2-propanol at pH 2, were characterized using CD and H/D exchange monitored by ESI-MS.

CD and H/D Exchange Rate Measurements of Acidic Compact States. Figure 1 shows the CD spectra of myglobin in H_2O at pH 6, in 10 mM HCl at pH 2 and in 10 mM HCl with the addition of CCl_3COONH_4 salt, and the H/D exchange rates of myoglobin in the corresponding deuterated solvents. The CD spectrum of myoglobin (holo-Mb) in 10 mM HCl at pH 2 (figure 1a), indicates a complete loss of α-helicity, suggesting that the protein was in a maximally unfolded state [3]. The addition of CCl_3COONH_4 salt to the acid unfolded protein solution induced a refolding transition with an increasing in the α-helical content as the concentration of the CCl_3COONH_4 increases. This transition reached a plateau at about 15.3 mM CCl_3COONH_4, having an ellipticity at 222 nm of -13,553 indicating a helical content of ~61% of Mb in H_2O, which is consistent with the findings of Goto et al [3]. Apo-Mb contains 153 amino acid residues with 121 residues in α helical conformation according to the X-ray crystallographic data, and a total of 262 exchangeable hydrogens. H/D exchange rates obtained for apo-Mb and holo-Mb are consistent with the CD measurements. Holo-Mb underwent the least exchange, and even after 30 min, 80 labile hydrogens remained unexchanged. Since the exchange of the labile hydrogens exposed to solvents are fast, the remaining hydrogens are expected to be those involved in hydrogen binding in α-helices or those located on side chains buried inside the hydrophobic core of the protein [2]. As the protein was denatured in 10 mM DCl (holo-Mb became apo-Mb), the number of hydrogens being exchanged increased considerably and only 13 backbone hydrogens remained after 35 min. The solutions containing CCl_3COOND_4 have exchange rates that decreases with an increase of CCl_3COOND_4 concentrations. For the solution containing 12.2 mM CCl_3COOND_4, the 61 unexchanged hydrogens at 34 minutes are ~50% of backbone hydrogens that are in the helical conformations of native myoglobin, which is in agreement with the CD data.

Effects of Different Salts and Detergents on Acid-Unfolded Proteins. Figure 2 shows the refolding transitions of apo-Mb and cytochrome c at pH 2 induced by salts or detergents. For the three salts selected, our CD results are consistent with those of Goto et al. who reported that the order of effectiveness for inducing the refolding transition was: ferricyanide > sulfate > trichloroacetate > thiocyanate > perchlorate > iodide > nitrate > trifluoroacetate > bromide > chloride. Our H/D exchange data, however, indicate that trichloroacetate (TCA) is more effective than sulfate in inducing folding. The discrepancy between the relative amount of the secondary structures derived from CD data and from H/D exchange data, is due to different principles of the two techniques. CD measures average amount of secondary structures at a given time. By contrast, H/D exchange monitored by ESI-MS reflects the amount of stable folded structure lasted through the time of exchange. Thus, the conformational information obtained from the H/D exchange is complementary to that from CD. For the three chosen detergents, the H/D exchange data agree with the CD data for both proteins and the order of effectiveness for induce folding is SDS > CTAB > CHAPS. It is noteworthy that the three detergents are of different classes, SDS being anionic, CTAB being cationic and CHAPS being zwitterionic, along with the hydrophobic solvent 2-propanol, are all effective in inducing the refolding transitions. Although both SDS and TCA are monovalent anions, the fact that SDS is about 100 times more effective than TCA, and that the monovalent cation CTAB is as effective as TCA or the divalent anion sulfate, in inducing protein refolding, suggests strongly that hydrophobic interactions may play an important role for bringing about the conformational transitions.

43rd ASMS Conference on Mass Spectrometry and Allied Topics

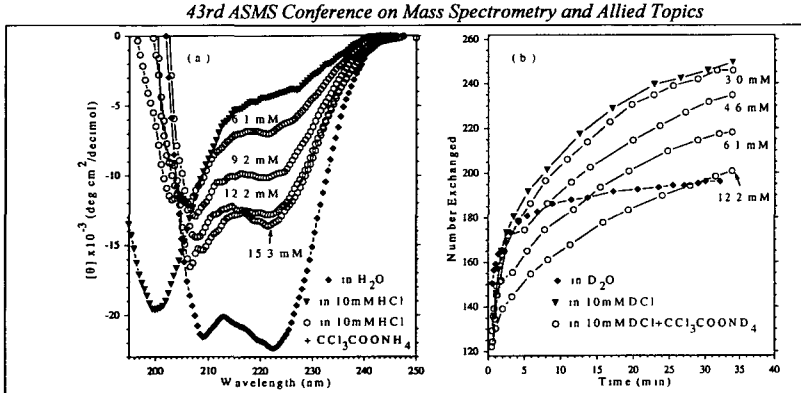

Figure 1. **(a)** CD spectra and **(b)** the hydrogen exchange rates of holo- and apo-myoglobin

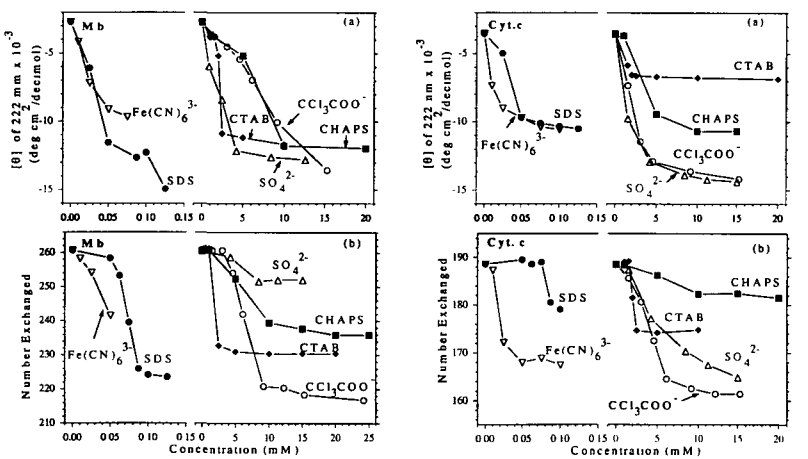

Figure 2. Salt and detergent induced refolding transitions of myoglobin (left) in the presence of 10 mM HCl and of cytochrome c (right) in the presence of 18 mM HCl measured by (a) the mean residue ellipticity at 222 nm and (b) the number of hydrogen exchanged after 2 hours at 20 °C.

[1] Kuwajima, K. (1989) *Proteins* **6**, 87-103.
[2] Englander, S.W. & Mayne, L., (1992) *Annu. Rev. Biophys biomol. Struct.* 21, 243-265
[3] (a) Goto, Y., Calciano, L.J. & Fink, A.L., (1990) *Proc Natl. Acda. Sci USA*, **87**, 573-577.
(b) Goto, Y., Takahashi, N. & Fink, A.L., (1990) *Biochemistry*, **29**, 3480-3488.
[4] Katta, V. & Chait, B.T., (1993) *J Am. Chem. Soc.*, *115*, 6317-6321.
[5] Wagner, D.S. & Anderegg, R.J. (1994) *Anal Chem.* **66**, 706-711.

—

Disulfide bridges assignments of homologous vegetable proteins

Guy P.[1], Saint-Pierre C.[1], Gagnon J.[1], Marion D.[2] and Forest E.[1]

1 Institut de Biologie Structurale, 38027 Grenoble, France.
2 INRA, 44072 Nantes, France.

We have studied a new family of cysteine-rich proteins of vegetable origin. These are single chain polypeptides of about a hundred amino-acid containing eight or ten cysteine residues involved in four or five disulfide bridges. The assignment of these disulfide bridges required the use of a rather complex strategy, in order to study cysteine residues in close proximity.

Puroindoline, the first protein studied, was extracted from wheat endosperm. The puroindoline sequence has been previously described as a 115 polypeptide chain containing ten cysteines all involved in disulfide bridges. Using electrospray ionization mass spectrometry (ESI-MS) we have shown that the protein is heterogeneous, composed of several forms with N- and C-terminal extensions and / or deletions [1]. To better characterize the structure of this protein, the topology of disulfide bridges has been assigned.

Puroindoline was digested with thermolysin and trypsin, then analyzed by µHPLC / ESI-MS. The resulting digest fragments were purified by reverse-phase high performance liquid chromatography (rp-HPLC).

The 2543 Da tryptic and 3854 Da thermolytic fragments were reduced with tris-(2-carboxyethyl)-phosphine (TCEP). Two disulfide bridges were assigned after ESI-MS-MS and Edman degradation analysis.

The 5830 Da and 6000 Da tryptic fragments were sequenced by Edman degradation. These fragments were composed of 5 peptides linked by 4 disulfide bridges. We submitted the 5830 Da tryptic fragment to endoprotease Glu-C sub-digestion. After rp-HPLC purification and ESI-MS analysis of the resulting sub-digested fragments before and after reduction, we have assigned a third disulfide bridge. The 6000 Da tryptic fragment was partially reduced with TCEP for 8 min at pH = 3.0. The 1944 Da partially reduced compound was purified by rp-HPLC and analyzed by both ESI-MS and MALDI-MS. Alkylation by iodoacetamide of free thiols, followed by Edman degradation analysis, provided explicit assignment of a fourth disulfide bond. Based on these results we have deduced the last disulfide bridge **(Fig. 1)**. We have observed that fragmentation of disulfide linked peptides occur under the MALDI process **(Fig. 2)** [2].

We are currently applying this strategy to a lipid transfer protein (LTP), another basic and cystine-rich protein of wheat endosperm, of known three-dimensional structure. A comparison of the disulfide bridge patterns between both proteins will give some elements of the three-dimensional structure of puroindoline.

[1] Blochet J-E, Chevalier C., Forest E., Pebay-Peroula E., Gautier M-F., Joudrier P., Pezolet M., Marion D., Complete amino acid sequence of puroindoline, a new basic and cystine-rich protein with a unique tryptophan-rich domain, isolated from wheat endosperm by Triton X-114 phase partitioning, *FEBS Lett.*, 1993, **3**, 336-340.

[2] Guy P., Jaquinod M. and Forest E., Fragmentation of disulfide linked peptides following MALDI-MS, submitted.

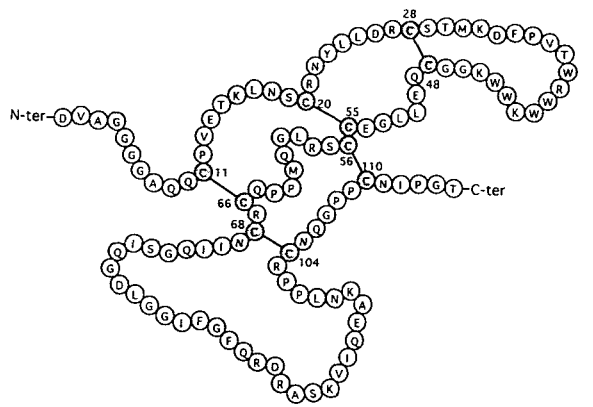

Fig. 1 Disulfide bridge assignment of puroindoline, a protein extracted from wheat endosperm.

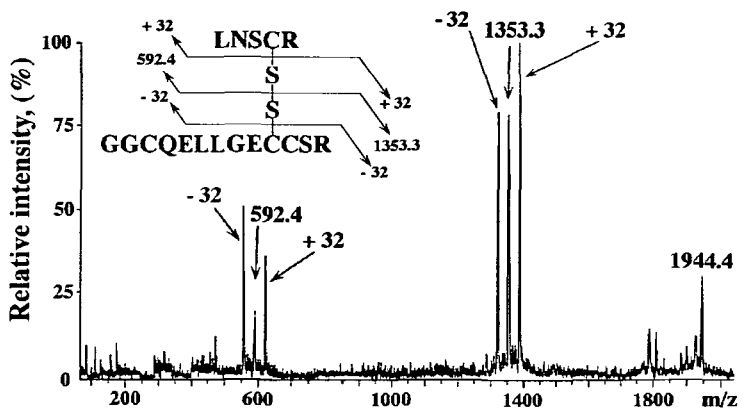

Fig. 2 PSD-MALDI mass spectrum of the 1944 tryptic parent ion.

DETERMINATION OF DISULFIDE BONDS IN PROTEINS WITH ABD-F

Umamaheswari Rajamani, Lewis Pannell, Danny Sackett, Han Le and Paolo Lecchi
Laboratories of Analytical Chemistry and Biochemical Pharmacology
NIDDK, NIH, Bethesda, MD 20892-0805

Objective

To develop a simple colorimetric method for the assay of free cysteines versus those involved in disulfide bonds The method should involve minimum manipulation of the protein, with all reactions ideally performed in the UV cell.

Method

4-(Aminosulfonyl)-7-fluoro-2,1,3-benzoxadiazole (ABD-F) reacts very readily with thiols It gives a colorimetric species, ABD-SR, which has a maximum absorbance at 385nm and fluoresces at 514nm. The reagent reacts with the free S-H and forms a new covalent bond with the elimination of H-F at slightly basic pH Traditional reducing agents are thiols themselves (dithiothreitol or mercaptoethanol) and will also react with ABD-F in the same way free cysteines do Therefore these must be removed after the reduction and before reaction with the ABD-F Tributylphosphine (TBP), while a little more difficult to work with, will readily reduce proteins and not react with ABD-F Therefore it is an ideal reagent for this work TBP may be added even after the ABD-F without problems

Reagents and Equipment

Denaturing buffer: Na_2HPO_4 (0 08M), EDTA (1 7mM), guanidine HCl (4M)

Proteins used Ribonuclease A, Superoxide dismutase, β-Lactoglobulin, Tubulin, Enolase

ABD-F 40mM in DMSO

TBP 12μl of TBP dissolved in 1ml methanol and stored under nitrogen

UV Cells Both 1ml and 50μl cells used were purchased from Hellma (Forest Hill, NY)

UV Measurements Beckman DV-65 UV/VIS at 385nm

Fluorescence Meas Perkin-Elmer MPF-66, excite 385nm; meas emission 514nm

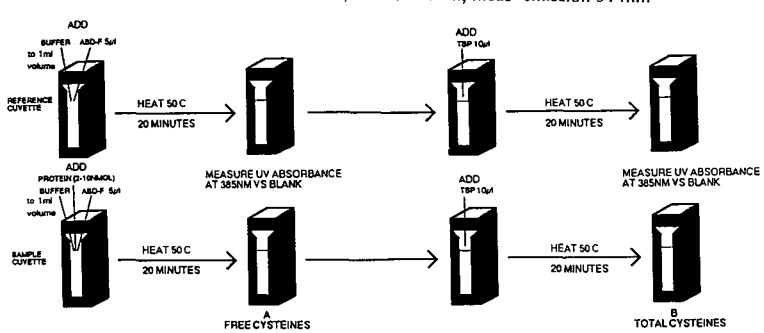

The ratio of the free cysteines is calculated from the ratio of absorbance A / absorbance B Increased sensitivity is possible with the use of smaller UV cells (50μl) with only 0 2-1 nmol of protein required Better still, using the fluorescence of the ABD-Cysteine adduct, only 100pmol of protein gives very consistent results When the sample is reduced to 10pmol, more variability occurred However the answer is still unambiguous at these low levels

Table I · Measurement of Protein Disulfide Bonds in 1ml UV Cells using ABD-F and TBP

Protein	Ribonuclease A	Superoxide-dismutase	β-Lactoglobulin	Tubulin	Enolase
Free / total Cysteines	0/8[1]	1/3[1]	1/5[1]	8/10[2]	1/1[3]
Free cysteine absorbance	-0 007	0 043	0 073	0 523	0 032
Total cysteine absorbance	0 337	0 148	0 395	0 649	0 032
Free / total measured	-0 02	0 29	0 18	0 81	1 0
Free cysteines calculated	-0 08[4]	0 87	0 92	8 1	1 0

[1]Reported in the Swiss Protein database
[2]Tubulin was reported to contain one disulfide and 8 free cysteines per monomer unit of 50kD Others have reported fewer disulfides
[3]Only single cysteine is present (Swiss protein database)
[4]The measured negative value is within experimental error of the correct value of "0"

Although this method determines the ratio of free cysteines to those in disulfide bonds, the free measurement along with a precise knowledge of the protein concentration will surfice as the ABD-cysteine absorbance at 385nm is ϵ_{385}7800 However, as the second step consumes no more protein, this is not a worthwhile savings Conversely, the concentration of the protein can be easily calculated from the absorbance of the reduced protein and a knowledge of the number of cysteines present

Conclusion

A method has been developed for the simple and rapid determination of the number of free versus disulfide bonded cysteines in a protein All reactions may be carried out in the UV cells and the same solution of protein is used for obtaining the number of free and total cysteines Using 1ml UV cells, the measurement is possible on 2-10nmol of protein By adapting the method to fluorescence assays, the amount of protein was reduced to 10-100pmol.

LOCATING DISULFIDE BONDS IN PROTEINS FROM AIDS RELATED RESEARCH

Lewis Pannell, Umamaheswari Rajamani, Han Le and Paolo Lecchi
Laboratory of Analytical Chemistry, NIDDK, NIH, Bethesda MD 20892-0805

Introduction Much of work has gone into the three dimensional structure of compounds targeted for their anti-HIV properties. This has been mainly performed by NMR and X-ray crystallography A good understanding of the "shapes" of compounds that are effective against AIDS allows for the development of designer drugs As a result, a number of requests have been made for identifying the disulfide bonds in proteins to help clarify the ambiguities that have been observed by other structural techniques

Method The method discussed in poster ThPG261, ABD-F/TBP is used to identify the number of cysteines involved in disulfide bonds If free cysteines are present, then the protein is capped with iodoacetic acid. Digestion of the protein (3-6nmol) with TPCK treated trypsin in ammonium bicarbonate or ammonium acetate buffer was performed overnight at 37°C The digest could be followed directly with CZE and was separated into 20+ fractions by HPLC MALDI (Kratos MALDI III) spectra were obtained on each fraction using 4-hydroxy-α-cyanocinnamic acid as matrix and the mass assignments were confirmed by FAB (JEOL SX102)

Human IL10 Mutant. A mutant 160 amino acid IL10 protein was studied as its mass was approximately 300 amu too high when examined by electrospray It was only modified from IL10 by the replacement of Tyr-153 by a cysteine An examination was made of the Wild-type protein first and all the non-cysteine containing pieces were identified From this fraction 11 was found to contain a peak at 2984.3 (MALDI and FAB) corresponding to a disulfide bond between Cys-12 and Cys-108, and the second disulfide peptide was located in fraction 20, corresponding to Cys-62 linked to Cys-114 This matched the previously reported disulfide bond locations The mutant protein was then examined Cysteine containing pieces are marked in bold

Ser Pro Gly Gln Gly Thr Gln Ser Glu Asn Ser Cys Thr His Phe Pro Gly
Asn Leu Pro Asn Met Leu Arg|Asp Leu Arg|Asp Ala Phe Ser Arg|Val Lys|
Thr Phe Phe Gln Met Lys|Asp Gln Leu Asp Asn Leu Leu Leu Lys|Glu Ser
Leu Leu Glu Asp Phe Lys|**Gly Tyr Leu Gly Cys Gln Ala Leu Ser Glu Met**
Ile Gln Phe Tyr Leu Glu Glu Val Met Pro Gln Ala Glu Asn Gln Asp Pro
Asp Ile Lys|Ala His Val Asn Ser Leu Gly Glu Asn Leu Lys|Thr Leu Arg|
Leu Arg|Leu Arg|Arg|**Cys His Arg**|**Phe Leu Pro Cys Glu Asn Lys**|Ser Lys|
Ala Val Glu Gln Val Lys|Asn Ala Phe Asn Lys|Leu Gln Glu Lys|Gly Ile
Tyr Lys|**Ala Met Ser Glu Phe Asp Ile Phe Ile Asn Cys Ile Glu Ala Tyr**
Met Thr Met Lys|Ile Arg|Asn

An examination of the wild-type IL10 by electrospray gave the correct mass of 18646 8 Da (theoretical 18647 6 Da) However the mutant gave 18894 4 Da (theoretical 18587 5) and from previous experience the extra mass (approx 305 amu) was predicted to come from a glutathione adduction The theoretical mass for the glutathione-mutant adduct is 18892.5 Da which agrees well with the measurement After digestion with trypsin, the fractions were analyzed as before and all the non-cysteine containing pieces appeared in the same

fractions No equivalent disulfide peptide was found in fraction 11 as with the wild-type protein suggesting that this connection did not exist Two disulfide pairings were identified in fraction 20, one matching the wild-type for Cys-62 to Cys-114 and the other corresponding to a disulfide bond between Cys-12 and Cys-153 (meas 4829.3, calc 4828.5) The remaining tryptic peptide, 108-110, was found in another fraction with glutathione attached The NMR determined structure had to be modified to accommodate the disulfide connections.

MALDI SPECTRUM OF FRACTION 20 FROM TRYPTIC DIGEST OF MUTANT

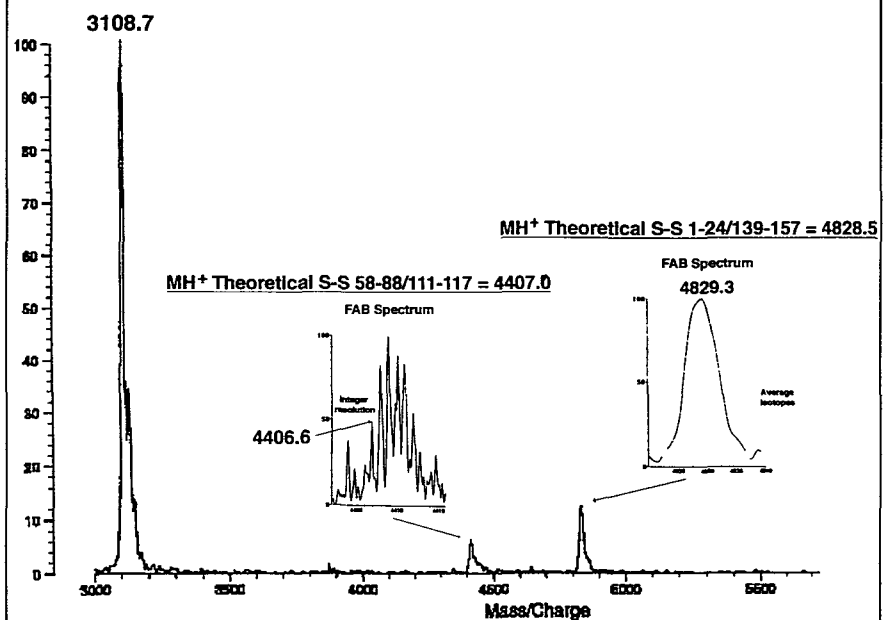

HGF N-Domain

As part of an examination of some mutant hepatocyte growth factor proteins, an initial examination of the disulfides in the N-domain of the protein was undertaken The spectra of the digest fractions revealed an ion at m/z1141 5 which could be assigned to the disulfide between Cys-44 and Cys-54 (calc MH⁺1141 6) and another fraction contained the other disulfide piece between Cys-40 and Cys-66 (meas 2820.6, calc MH⁺2820 8) A number of other intense peaks in the MALDI and FAB spectra could not be assigned and are still a mystery

A number of other proteins related to the AIDS research at NIH have been successfully studied

Identification of Cross-Linking Peptides Using ESI and MALDI-TOF MS

John C. Le [1], Mitsuru Haniu [1], Thomas Horan [2], Viswanatham Katta [1], Tsutomu Arakawa [2] and Michael F. Rohde [1]

[1] Protein Structure and [2] Protein Chemistry, Amgen, Inc., Thousand Oaks, California 91320

Information regarding the conformation of many recombinant proteins is important for understanding their structure-function relationships. This information often extends beyond the primary structure and thus relies on crystallization or NMR data. However, it is difficult to obtain conformational differences due to tertiary structure and carbohydrate complexities. Therefore, other analytical schemes to elucidate this essential information are of great interest.

In conjunction with peptide mapping and N-terminal sequence analysis to monitor possible conformation of proteins, the focus of this presentation was to implement both linear and reflectron modes of MALDI-TOF and ESI mass spectrometry for the identification of inter- or intramolecular cross-linking peptides by cross linkers such as disuccinimidyl suberate (DSS) and disuccinimidyl tartarate (DST) of recombinant human proteins.

To prepare and identify cross-linked peptides, several cross-linkers including DST were reacted with E.coli expressed protein. The cross linked proteins were subsequently digested by trypsin and fractionated by RP-HPLC according to the literature (1). Figure 1 shows the peptide map of the cross-linked protein. The peak at 29.6 min. was identified as DST- linked peptide (Mr= 1564) by electrospray ionization (ESI) mass spectrometry as shown in Figure 2a. We suspect that the DST-linker peptide has undergone nucleophilic attack by water, re-arrangement and dehydration. The fragmentation pattern of this cross-linked peptide obtained by collision induced dissociation (CID) of m/z 782.7, a doubly charged ion, verified that the DST linker was attached to the N-terminus (Figure 2b).

Recently a novel approach was developed to use cross-linkers to probe possible conformation and surface interaction of recombinant human proteins. This strategy was verified by the involvement of disuccinimidyl suberate (DSS), a 12 angstrom cross-linker, that reacts primarily with the ε-amine of lysine (K) side chains and links to the primary amine of methionine (M) **of synthetic peptides** (2). Figure 3 shows an ESI mass spectrum of a RP/HPLC fraction of this cross-linked peptide at Mr= 1245.38 and its proposed covalent structure (insertion).

Approximately 5 pmols of the above synthetic cross-linked peptide was subjected to mass and sequence determinations by MALDI-TOF-MS analysis. It is noteworthy that in sinapinic acid (SA) matrix only the molecular ion (m/z 1246.5) was observed (Figure 4a). Under similar instrument conditions and with significantly less laser power, alfa cyano-4-hydroxy cinnaminic (4HCCA) matrix generated both the molecular ion and apparent prompt fragmentation of the N-terminal amino acid residues [M+H] -X ions; The observed m/z 900.10 corresponds to the loss of tripeptide M-T-P (Figure 4b). This phenomenon is currently under investigation. Table 1 summarizes the calculated and the observed fragment ions. The MSMS spectrum of m/z 1246.5 by MALDI post- source decay (PSD) (Figures 5) showed a similar fragmentation pattern that supports the assignment sequence of this peptide.

The electrospray ionization spectra were obtained on a API Sciex III. The MALDI spectra were obtained on a PerSeptive Biosystems Voyager RP mass spectrometer.

43rd ASMS Conference on Mass Spectrometry and Allied Topics

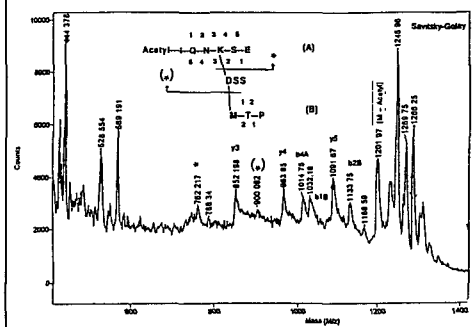

Figure 4b: MALDI-TOF linear mass spectrum of cross-linked peptide A-DSS-B, in alfa cyano-4-hydroxy cinnaminic acid (4HCCA) with LP=730 and its corresponding fragment ions

Table 1

Ions of X (underline A or B pep.)	m/z calc.	m/z obs.	Freq. Type
B pep. + linker	760.82	762.22	A pep. only
MTP (B pep.)	900.46	900.09	A pep +Linker
Acetyl	1203.57	1201.97	[M+H]-Acetyl
N-acetyl/Isoleucine (I)	1092.45	1091.67	Y5
N-acetyl/Glutamine (Q)	963.63	963.96	Y4
N-acetyl/Q/Asparagine(N)	851.59	852.19	Y3
Serine (S)/E	1013.76	1014.75	b4A (-)
	1028.41	1032.18	7c4A (-)
Threonine(T)/S-OH	1032.87	1032.18	b1B (-)
C-ter Proline (P)	1133.62	1133.76	b2B (-)
B pep./DSS and S/E	828.72	828.55	Non-specific

Acetyl-HN-IQNKSE (A) peptide chain MW= 759.82. Average mass is used for all calculation. Molecular ion of (Acetyl-A-DSS-B), [M+H] = 1246.82.
(-) Cleavage at peptide (A) or (B)

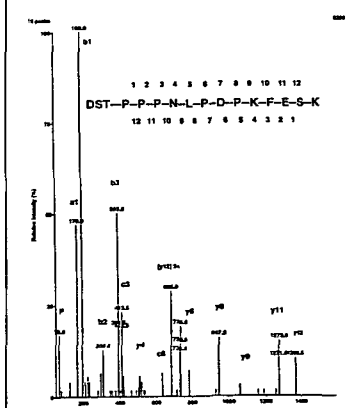

Figure 2b Collision induced dissociation (CID) of m/z 783.7, a [M+2H] ion of DST-peptide

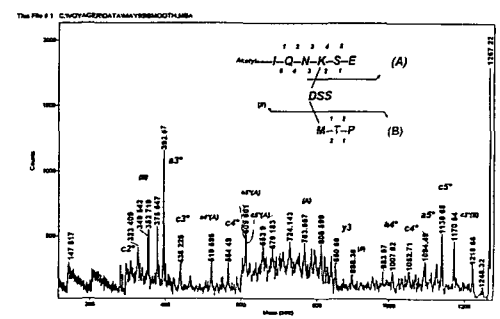

Figure 5: MALDI post-source decay (PSD) of cross-linked peptide A-DSS-B in 4-HCCA. [M+Na] =1267.22 is precursor ion. Cleavage at A or B peptide only is noted by ( ). Sodium adduct ions are noted by *

Reference:

1) M. Haniu, L.O. Narhi, T. Arakawa, S. Elliott, and M.F. Rohde, Protein Science (1993), 2, 1441-1451.
2) M. Haniu, John C. Le et al. submitted for publication.

Synthesis of Disulfide Linked ß-Actin Peptides.

F. Aladar Bencsath[1,4], Archil Shartava[2], Carlos A. Monteiro[2], and Steven R. Goodman[2,3]

[1]Department of Biochemistry and Molecular Biology, [2]Department of Structural and Cellular Biology, [3]USA Comprehensive Sickle Cell Center, University of South Alabama, Mobile, AL 36688; [4]Gulf Coast Seafood Laboratory, FDA, Dauphin Island, AL 36528

Identification of a specific disulfide linked peptide in the tryptic digest of irreversibly sickled cell (ISC) ß-actin has been facilitated by the availability of a reference peptide, which was characterized by liquid chromatography (LC) and mass spectrometry (MS). LC provided the peptide's retention time. MS (with fast atom bombardment ionization; FAB MS) provided the peptide's molecular ion mass and the masses of other diagnostic ions in the mass spectrum, and tandem MS provided a product ion pattern in the MSMS spectrum. The retention time and the masses of the diagnostic ions helped to locate the peptide among the LC fractions, and the product ion spectrum of the molecular ion proved identity.

While it is relatively easy to obtain linear peptides from advanced commercial biotechnology laboratories, modified (e.g., acetylated, glycosylated, phosphorylated, disulfide linked) peptides are harder to acquire. Such peptides may have to be specially prepared by the investigators themselves.

In earlier labeling and HPLC & MS studies, we found evidences (Shartava et al, J. Cell Biology, 1955; ASMS 1994, Proceedings p.1161) that the ^{284}Cys and the ^{373}Cys (and with them the tryptic peptides CDVDIR and KCF) are linked by a S-S bridge in the membrane protein ISC ß-actin, while they exhibit free sulfhydryl groups in the ß-actin from the normal red blood cell.

To isolate and identify this important disulfide linked peptide, we synthesized the corresponding model compound using, with some modification, a sulfhydryl labeling process for proteins which was introduced by Drewes and Faulstich (Anal. Biochem. 188:109, 1990). The first step of the synthesis was the activation: the thiol group in one of the two peptides (KCF) was transformed into the S-dinitrophenylthio derivative (S-DNPT-KCF) using the 2,4-dinitrophenyl sulfenylchloride reagent. The activated peptide was isolated from the excess reagent and the formic acid solvent by the help of the solvent mixture tetrahydrofuran/toluene, and centrifugation. The second step was the coupling: the dried activated peptide was dissolved in aqueous methanol and was allowed to react with the second cysteine-containing peptide (CDVDIR) in an aqueous ammonium hydrocarbonate buffer, to form the desired disulfide linked peptide KCF-CDVDIR. The bright yellow color of the liberated 2,4-dinitrothiophenol signaled the successful coupling, which was complete in minutes.

The first step of the synthesis was carried out in a conical centrifuge tube, the second step in an injection vial, and also on the MS/FAB probe tip. We optimized the

synthesis in preliminary experiments while preparing the cysteine-glutathione disulfide linked peptide. It seems that the method is generally applicable for the generation of asymmetric cystine peptides containing only one single S-S bridge.

The FAB mass spectrum of the disulfide linked peptide KCF-CDVDIR exhibits, beside an intense molecular ion m/z 1114, the molecular ions of the component peptides (m/z 397 and 720). Their presence in the spectrum must be the result of the often observed reductive process in the FAB-matrix glycerol.

HPLC separation of the raw product presented three components: the major product KCF-CDVDIR (fraction #29), the minor side-product S-DNPT-CDVDIR (fr#37), and the excess reactive intermediate S-DNPT-KCF (fr#38). We found in fr#29 of the tryptic hydrolyzate obtained from ISC-actin all three diagnostic ions. The MSMS product ion spectrum furnished from the molecular ion m/z 1114 contained identical fragment ion masses as the corresponding spectrum from the synthetic model compound, which proved identity. This is the first direct proof of the presence and location of an S-S bond in the ISC ß-actin, which seems to be the dominant factor causing the irreversible locking of the membrane skeleton into the sickled shape.

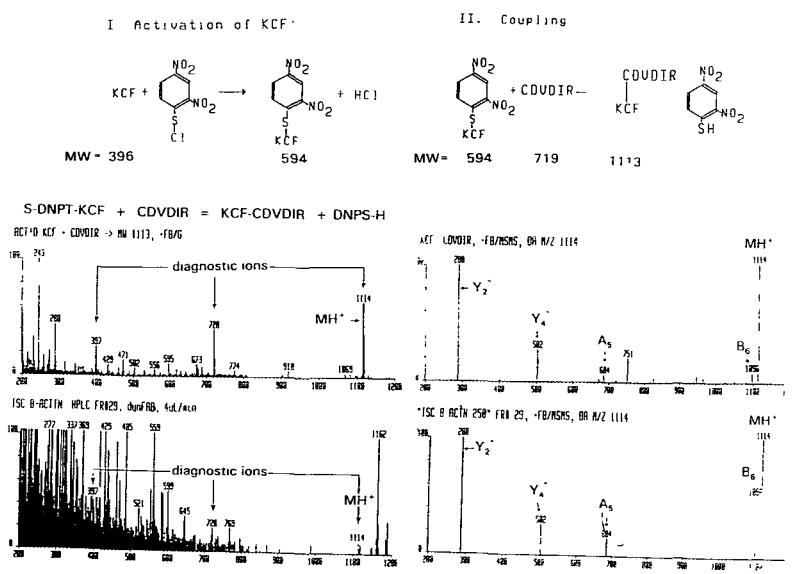

DETERMINATION OF THE LOCATION OF THE CYS IN PEPTIDES BY TANDEM MS/MS STUDIES.

* O. V. Nemirovskiy; M. L. Gross
Department of Chemistry, Washington University, One Brookings Dr., St. Louis, MO 63130

The interaction of transition-metal ions (especially Fe) and sulfides are common in all forms of life and are found at the active centers of a wide variety of redox and catalytic proteins, such as ferrodoxins, rubredoxins, and metalloenzymes. In most ferrodoxins, and in all rubredoxins, the protein ligands are cysteins, which provide thiolate donors to the Fe center.

On the basis of evidence that iron atoms are held in proteins by cystein ligands, we are using iron as an "indicator" of the location of Cys residues in peptides. This strategy was applied to series of cystein-containing pentapeptides with different position of the Cys residue along the peptide backbone. Upon FAB ionization metal-ion/peptides were readily desorbed into gas phase as (peptide - H + Fe)$^+$ complexes. Formation of iron-bis(pentapeptide) complexes was also observed under the same conditions.

Mass spectrometric experiments were performed with a VG ZAB-T, four-sector instrument of BEBE (reverse Mattauch-Herzog) design equipped with a Cs$^+$ gun operated at 30 kV. Data acquisition was carried out with OPUS V 3.1X data system and interfaced to mass spectrometer by a VG SIOS I unit. CAD spectra were collected with MS2 at 50% main beam suppression with helium as the collision gas and array detection. The collision cell was floated at 4kV. The matrix used for desorption of metal-peptide complexes was a 1·1 mixture of glycerol and thioglycerol containing 0.5 F solution of metal nitrate.

The position of the Cys residue in analyzed pentapeptides is a major influence on the fragmentations of the iron-bound peptide complexes [(M - H + Fe)$^+$]. Specific interaction of the iron atoms with the thiol group of the Cys side chain leads to the formation of the unique fragmentation patterns with abundant **(a_n - H + Fe)$^+$** ions, where *n* is the position of the Cys residue with respect to the N-terminus of the peptide backbone (Fig. 1). The formation of these ions may proceed by two different mechanisms which involve hydrogen transfer either from an amide group or from the side chain. Isotope labeling experiments show that only an amide hydrogen is involved in the formation of (a_n - H + Fe)$^+$ ions (Scheme I) When peptide contained two Cys residues an interesting internal ion was observed in CAD spectrum, and the expected, however less abundant, (a_n -H + Fe)$^+$ ions. The mechanism for the formation of an internal ion (*m/z* = 305) is suggested to require the interactions of the iron atom with both thiol groups of the Cys side chains. This strong interaction principally directs the fragmentation upon CA at the periphery of both cysteins.

Iron-bis(pentapeptide) complexes decompose upon CA overwhelmingly by losing a pentapeptide to form an iron-bound pentapeptide (*m/z* = 516). In addition, an abundant ion at *m/z* = 548 is observed, and corresponds to the formation of (peptide - H + Fe + S)$^+$ ions. The mechanism for the formation of these ions requires oxidation of the thiol groups to -S -$^{\cdot}$S- bond.

These preliminary results provide encouragement for the development of a method for the determination of the location of the disulfide bonds and total content of cystein residues in small proteins and peptide fragments in digests.

Acknowledgment.
This work was supported by the National Institutes of Health (Resource Grant. No. 2P41RR00954).

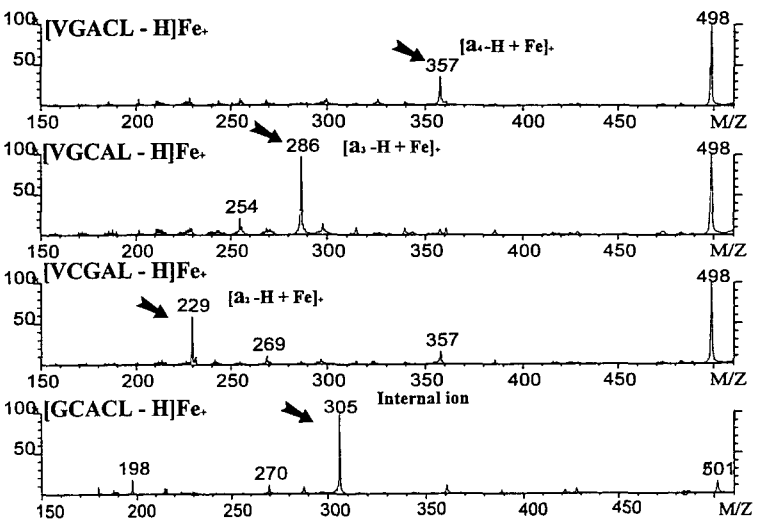

Fig. 1. The CAD spectra of iron-peptide complexes, m/z = 516.

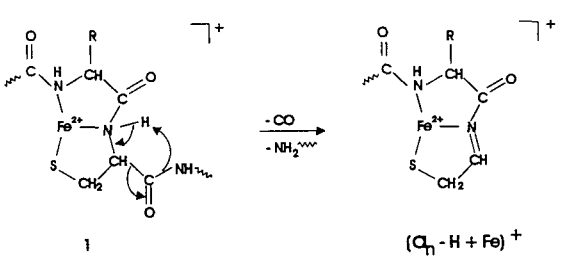

Scheme I. The mechanism for the formation of (a_n - H + Fe)$^+$ ions involves an amide hydrogen transfer.

Identification of a Cysteine Substitution in Recombinant Human Granulocyte Colony Stimulating Factor by Peptide Mapping-Electrospray Mass Spectrometry

Che-Hung Yeh, Nicole Tedeschi, and Alan C Herman
Amgen, Inc., Amgen Center, Thousand Oaks, CA 91320

Introduction

Several amino acid misincorporations have previously been identified in recombinant human proteins produced in *Escherichia coli* These have included norleucine substituted for methionine (Lu, *et. al*, 1988, Tsai, *et. al*, 1988) and glutamine substituted for histidine (Lu, *et.al*, 1993). In order to characterize trace amounts of heterogeneous forms of granulocyte colony stimulating factor (G-CSF) the unwanted chromatographic fractions from a routine purification were examined by reverse phase high pressure liquid chromatography (RPC). One of these column fractions contained a previously unobserved G-CSF form (Form X). RPC of this material followed by post-column derivitization with Ellman's reagent suggested that this form had only one disulfide bond instead of the two normally found in G-CSF This new G-CSF form was purified and further analyzed by a combination of LC-MS, peptide mapping, amino acid analysis and amino terminal sequencing. These analyses suggested that $cysteine_{64}$ had been replaced with an as yet unidentified amino acid.

Results and Conclusions

The data presented here suggest that in a small amount of G-CSF the $cysteine_{64}$ residue is substituted with another amino acid. This substituted form is subsequently removed from the product during the routine purification procedure. By collecting chromatographic fractions normally discarded, this form was obtained in suitable amounts for characterization. Although the data presented here clearly show a substitution of this cysteine, the nature of that substitution has not yet been confirmed. The amino acid composition data suggest no obvious amino acid substitution. The SV8 peptide is sufficiently large that it is difficult to achieve further analysis. Additionally, the sequence of the peptide is such that it does not lend itself to further digestion. One possible substitution is aminobutyric acid (Abu). It is feasible that the cysteinyl transfer RNA could charge with Abu in place of Cys. This would not, however, explain why the substitution only appears at the Cys_{64} position and not the other Cys positions. The replacement of a single cysteine would result in two free sufhydryl groups on the molecule. The elution of Peak X on RPC coincides with the elution of misfolded G-CSF containing only one disulfide (partially reduced). If the peak detected with Ellman's reagent were a mixture of Peak X and partially reduced G-CSF a free sufhydryl value of 2.5 would be obtained.

In data not presented, a secondary form of Peak X was identified in which the substitution of Cys_{64} was a glycine. This was determined by Edman sequencing

43rd ASMS Conference on Mass Spectrometry and Allied Topics

of the peptide and confirmed by mass spectrometry. Glycine represents a single base pair change from cysteine and is a wobble base.

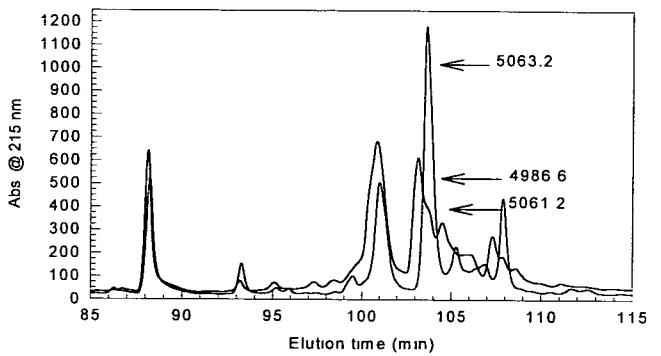

Figure LC-MS of carboxymethylated SV8 peptides. The region of the peptide map from 85 to 115 minutes is presented here in greater detail. The red trace is G-CSF standard protein, the blue trace is Form X. This area of the map was further analyzed by LC-MS to determine the mass of the individual peptides. Peptide A from the G-CSF standard has a mass of 5063.2 which is consistent with that predicted from its sequence. A corresponding peptide is present in Form X which is probably due to contamination with normal G-CSF A second peptide (Peptide B) elutes slightly earlier with a mass of 4986.6. Since this mass difference is greater than that found for the intact protein by 60 mass units, it suggests that the modification has occurred on one of the cysteine residues, preventing carboxymethylation

References

Lu,H. S., Tsai,L. B., Kenney, W.C. and Lai-P-H. Identification of unusual replacement of methionine by norleucine in recombinant interleukin-2 produced by *E. coli*. Biochem. Biophys. Res Commun. 1988 Oct 31 156(2). P 807-13

Lu, H S , Fausset, P. R., Sotos, L. S., Clogston, C. L., Rohde, M. F., Stoney, K. S. and Herman, A.C. Isolation and characterization of three recombinant human granulocyte colony stimulating factor His-->Gln isoforms produced in *Escherichia coli*. Protein. Expr. Purif. 1993 Oct. 4(5). P 465-72.

Tsai, L. B , Lu, H. S., Kenney, W. C , Curless, C. C., Klein, M L., Lai, P. H., Fenton, D.M., Altrock, B. W. and Mann, M B. Control of misincorporation of de novo synthesized norleucine into recombinant interleukin-2 in *E. coli*. Biochem Biophys. Res. Commun. 1988 Oct 31. 156(2). P 733-9.

The Location of S-S Bonds in Peptides by Partial Acid Hydrolysis and ESI-MS.

Robin Aplin and Kerry Anderson, The Oxford Centre for Molecular Sciences, The Dyson Perrins Laboratory, Oxford University, South Parks Road, Oxford, OX1 3QY, UK.

On line microbore HPLC-ES-MS (VG Biotech Platform) was used to follow the time course of the hydrolysis of the disulphide containing peptides (1 -4).

1 Oxytocin H-Cys-Tyr-Ile-Gln-Asn-Cys-Pro-Leu-Gly-NH_2

2 Tocinoic acid H-Cys-Tyr-Ile-Gln-Asn-Cys-OH

3 [Lys^8]-vasopressin H-Cys-Tyr-Phe-Gln-Asn-Cys-Prp-Lys-Gly-NH_2

4 Somatostatin H-Ala-Gly-Cys-Lys-Asn-Phe-Phe-Trp-Lys-Thr-Phe-Thr-Ser-Cys-OH

Hydrolysis proceeds very slowly (*eg.* Figure 1) with the initial deamidation being

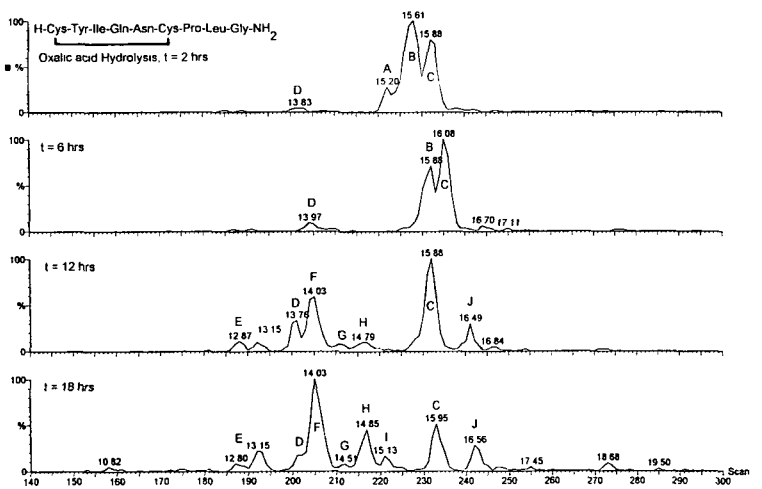

Figure 1: Microbore HPLC-ESI-MS Analysis of the products from the hydrolysis of Oxytocin in 250mM Oxalic acid. Base peak intensities (BPI).

followed by loss of residues from outside the S-S link and finally cleavage within the S-S link at the Asp- residue formed on deamidation Table 1. The structures of the peptides produced by cleavage within the S-S link were determined by MS-MS analysis (VG Biotech Quattro II). The peptides formed from tocinoic acid (2) and [lys8]-vasopressin (3) were analogeous to those obtained fron oxytocin (1, Table1) Somatostatin (3) gave a much more complex series of peptides due to both cleavage and varying degress of dehydration of its Ser- and Thr- residues. Cleavage within the S-S link again occuring at the Asp- residue formed on deamidation. In marked contrast to the results reported by Bauer *et al.*,(*J.Protein Chem.*1993,*12*,759-764.) where the majority of the small S-S linked peptides obtained from the oxalic acid hydrolysis of echistatin lacked the N-H and C-OH terminii from one chain, only one peptide of this type (MH^+, m/z 725) was observed in this study from both oxytocin (1) and tocinoic acid (2).

Peak	Exp. Mass / Da	Proposed Structure	Calc. Mass / Da
A	1006 9	Cys*-Tyr-Ile-Gln-Asn-Cys*-Pro-Leu-Gly-NH_2	1006 4
B	1008 9	Cys*-Tyr-Ile-Gln-Asp-Cys*-Pro-Leu-Gly-NH_2 and / or Cys*-Tyr-Ile-Glu-Asn-Cys*-Pro-Leu-Gly-NH_2 and / or Cys*-Tyr-Ile-Gln-Asn-Cys*-Pro-Leu-Gly-OH	1008 4
C	1009 8	Cys*-Tyr-Ile-Glu-Asp-Cys*-Pro-Leu-Gly-OH	1009.4
D	1027 4	Cys*-Tyr-Ile-Glu-Asp-Cys*-Pro-Leu-Gly-OH + H_2O	1027 4
E	742 9	Cys*-Tyr-Ile-Glu-Asp-Cys*-OH	742 2
F	912 3	Cys*-Tyr-Ile-Glu-OH Cys*-Pro-Leu-Gly-OH	912 4
G	970 7 1028 2	Cys*-Tyr-Ile-Glu-Asp-Cys*-Pro-Leu-OH + H_2O Cys*-Tyr-Ile-Glu-Asp-Cys*-Pro-Leu-Gly-OH + H_2O	970 4 1027 4
H	855 4	Cys*-Tyr-Ile-Glu-OH Cys*-Pro-Leu-OH	855 4
I	783 9	Cys*-Tyr-Ile-OH Cys*-Pro-Leu-Gly-OH	783 3
J	952 6 724 8	Cys*-Tyr-Ile-Glu-Asp-Cys*-Pro-Leu-OH Cys*-Tyr-Ile-Glu-Asp-Cys*-OH – H_2O	952 4 724 2

Cys* denotes participation in a disulphide bridge

Table 1 Products from the hydrolysis of Oxytocin (1) in 250mM oxalic acid

Disulfide Structure Study of EGF domain of Neu Differentiation Factor (NDF)

Viswanatham Katta, Naili Liu, Shi-Yuan Meng, Tom Zamborelli, John Mayer, Hsieng Lu and Shinichi Hara
Amgen Inc., Thousand Oaks, California 91320-1789.

Neu Differentiation Factor (NDF) was discovered as a ligand to stimulate autophosphorylation of Her-2 receptor expressed in mammary tumor cells. Form the cDNA sequence, precursor form of NDF (pro-NDF) was predicted to contain an immunoglobulin-like domain, epidermal growth factor (EGF) like domain, a single transmembrane domain, and a variable length cytoplasmic domain. It has been shown that NDF isoforms are generated by alternative splicing of the gene. α and β isoforms of EGF-domain peptides were expressed in E.coli and their structure studied. We discuss here the results for α-2 isoform.

The α-2 isoform is a 65-residue peptide with a calculated average mass of 7369.5 Da. It has six cystines forming three disulfide bonds. Both electorspray (Finnigan TSQ 7000) and MALDI (Perseptive Biosystems, Voyager RP) spectra exhibited the expected major species at 7369 Da and in addition a minor form at 16 Da higher (methionine oxidation), and two minor forms at -28 Da and -255 Da (C-terminal processing).

In order to study the disulfides, the protein was digested with endoproteinase Lys-C. The analysis of the digest mixture by linear MALDI-TOF showed the major disulfide containing peptides, but the map was not complete. The individual peptides were HPLC fractionated, Edman sequenced as well as analyzed by mass spectrometry.

The Post Source Decay (PSD) spectrum of a peptide at m/z 1838 (a predicted Lys-C peptide CQPGFTGARCTENVPMK with an internal disulfide bond) is shown in Figure 1. The fragmentation observed is typical to that observed in low energy CAD, i.e. sequential fragment ions were observed only upto the core disulfide, and no fragments of the peptide portion inside the loop are observed. This is in contrast to the prompt fragmentation at the S-S bond observed for intermolecularly disulfide bonded peptides (1). When the disulfide is internal, even at very high laser fluences, such fragmentation is not observed.

Figure 2a shows the linear MALDI spectrum of a peptide with two disulfide bonds obtained from 4HCCA matrix. Facile prompt fragmentation clearly identify that Lys-C peptides K2, K4, and K5 are disulfide bonded, but doesn't give a clue about the correct linkage. The PSD spectrum of the molecular ion (Fig 2b) showed, two groups of intense peaks with 32 Da spacing, similar to earlier observations (2). However, the center peak is weaker. Few fragment ions were observed, but assignments could not be made. To identify the actual linkages, on probe digestion of the peptide with endoproteinase Glu-C was carried out. The MALDI spectrum showed a new peak at m/z 2121, that indicated cys-14 is linked to cys-34 (Figure 2c). The PSD spectrum of m/z 2121 (not shown) verified that indeed these cystines are linked.

A minor form containing a mispaired disulfide also was identified and verified by PSD analysis.

1. Patterson S. D. and Katta V., *Anal. Chem.* 1994, 66, 3727-32.

2. Zhou J., Ens, W., Poppe-Schriemer N., Standing K. G., Westmore, J. B., *Int. J. Mass Spectrom. Ion Processes*, 1993, 126, 115-22.

43rd ASMS Conference on Mass Spectrometry and Allied Topics

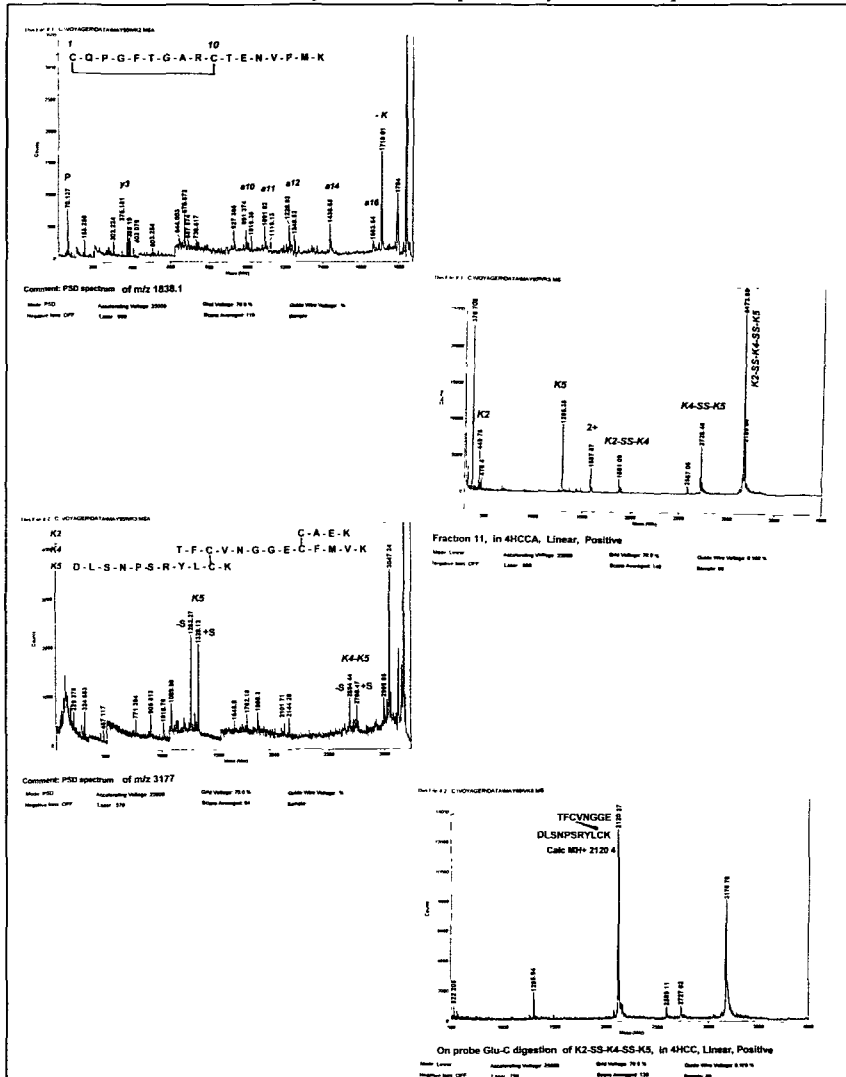

The Identification of Venomous Snakes using Electrospray Mass Spectrometry.

John R. Perkins[1], Dominique Despeyroux[1], Richard T. Gallagher[1], Peter J. Derrick[1], Keith R. Jennings[1] and Russell P. Newton[2]
1. Mass Spectrometry Research Unit, Department of Chemistry, University of Warwick, Coventry, CV4 7AL
2. Biochemistry Group, School of Biological Sciences, University of Swansea, Swansea, SA2 8PP

Introduction

All snake venoms contain multiple toxic principles which act in combination to produce the lethal action. The proportion and distribution of the active components varies from species to species and together with anatomical and morphological criteria, the activity profile of the venom can provide a means of species identification. As a generalization, the venoms from members of the *Elapidae* family of snakes (cobras and mambas) contain mainly neurotoxin activity while the venoms of rattlesnakes and vipers (*Crotalidae*) primarily affect cardiovascular and hemostatic mechanisms. Exceptions exist such as *Crotalus durissus terrificus* (tropical rattlesnake) which is a true rattlesnake applying biological criteria, but shows a similar venom activity profile to that of the cobras and mambas.

Molecular weight profiles of snake venoms can be of value to the biochemist to indicate the binding of enzymes in assays or to provide a confirmation for sequences of extracted peptides. Additionally, we were interested to see whether it was possible to provide a means of species identification for venomous snakes, based on the electrospray spectrum and resultant mass profile obtained for each venom.

MALDI-TOF-MS and electrospray-MS can provide complementary data for the determination of snake venoms MALDI-TOF-MS reveals inherent differences in the compositions of venoms from unrelated snakes but clusters of proteins with molecular masses greater than 10000 daltons could not be resolved. Flow injection electrospray-MS cannot provide a complete picture of the venom composition. However, electropsray profiles are markedly different between species so that the detail of this incomplete picture is sufficient to discriminate between species.

Results and Discussion

Flow injection (10 µL/min) spectra of 32 snake venom solutions (1mg/mL) were acquired using a VG Quattro II triple quadrupole mass spectrometer. MS analyses were performed over a mass range of 500 to 3500 at 10 sec/scan for 10 scans and MS/MS analyses were performed over a mass range of 50 to 2500 at 10 sec/scan.

Spectra from the venoms of the elapids were simple and typically dominated by peptides of molecular masses ca. 6000-9000 daltons (cobras and mambas) or ca. 13000 daltons (kraits, coral snakes, tiger snakes and brown snakes). A typical spectrum from the venom of *Bungarus fasciatus* (banded krait) is shown in Figure 1.

Spectra from the venoms of the crotalids were complex and were typically dominated by proteins of molecular masses ca. 14000 or 23000 daltons. Altering the cone voltage had a significant effect on the spectra obtained where low cone voltages (ca. 30 V) improved the response of proteins of molecular masses ca. 23000 daltons. For some venoms, high cone voltages (ca. 90 V) could improve the relative response for proteins of molecular masses ca. 14000 and 29000 daltons. A typical spectrum from the venom of *Bitis arietans* (puff adder) is shown in Figure 2.

Several venoms were chosen from closely related snakes. The spectra of three spitting cobras seemed to be virtually identical. Closer study revealed minor differences resulting from the presence of a few unique peptides or major differences in the relative ion abundances of toxins which were common to all three venoms.

A further tool for the investigation of common toxins is tandem mass spectrometry of the multiply charged ions within the flow injection electrospray spectrum. The identical product ion MS/MS spectra from the $(M+6H)^{6+}$ ions of higher abundance peptides in the venoms of *Naja naja* and *Naja naja atra* suggest the presence of common toxins and therefore some evolutionary relationship.

From these experiments we conclude that the electrospray spectra and resultant molecular mass profiles obtained for each venom can provide a basis for species identification of venomous snakes.

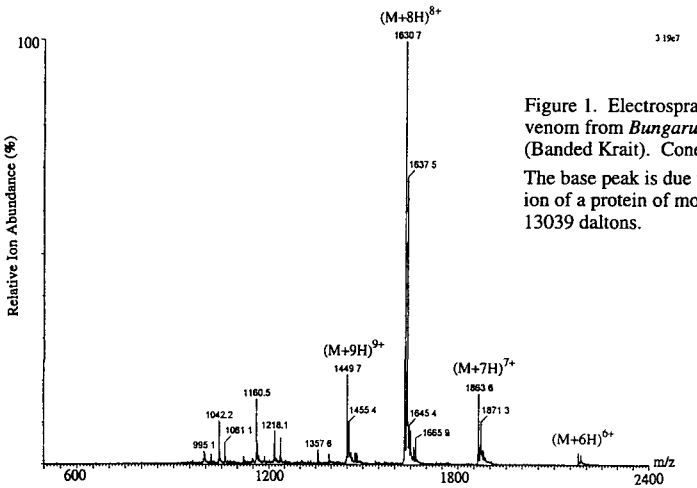

Figure 1. Electrospray Spectrum of the venom from *Bungarus fasciatus* (Banded Krait). Cone Voltage = 65 V. The base peak is due to the $(M+8H)^{8+}$ ion of a protein of molecular weight 13039 daltons.

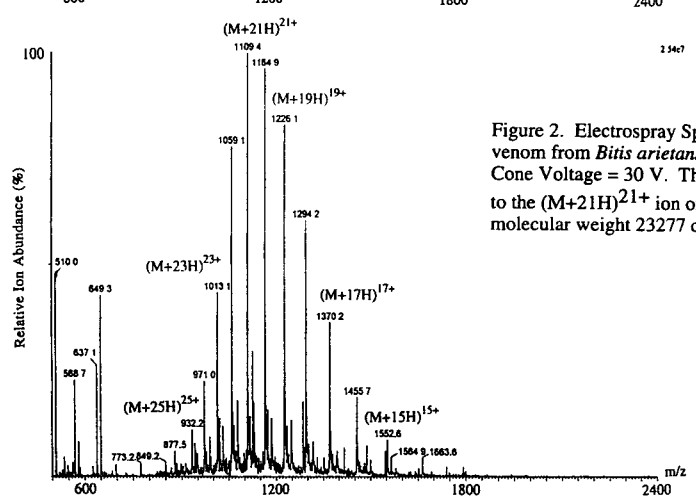

Figure 2. Electrospray Spectrum of the venom from *Bitis arietans* (Puff Adder). Cone Voltage = 30 V. The base peak is due to the $(M+21H)^{21+}$ ion of a protein of molecular weight 23277 daltons.

Current addresses:-
1. John R. Perkins, Advanced Bioanalytical Services, 15 Catherwood Services, Ithaca, NY 14850.
2. Dominique Despeyroux, Chemical & Biological Defence Establishment, DAD, Porton Down, Salisbury, SP4 0JQ

MS Investigation of the Molecular Mechanism of Action of Cytotoxin B

Matthias Wilm, Ingo Just*, Jörg Selzer*, Klaus Aktories* and Matthias Mann
European Molecular Biology Laboratory, Meyerhofstr. 1, 69 012 Heidelberg, Germany
**Institute for Pharmacology and Toxicology of the University of Saarland, 66 421 Homburg, Germany*

The toxins A and B from clostridium difficile cause antibiotic - associated pseudo membranous colitis. They act in cultured cell lines by inducing the disaggregation of the microfilament cytoskeleton. The GTPase RhoA plays an important role in the formation and regulation of the cytoskeleton. Toxin B treated RhoA loses its property to be a substrate for the ADP-ribosyltransferase C3 from Clostridium botulinum suggesting the possibility that RhoA is modified by toxin B. Recombinantly expressed RhoA was treated with toxin B and investigated mass spectrometrically[1].

The HPLC purified protein was measured on a tandem mass spectrometer (API III, Sciex, Ontario, Canada) equipped with a very stable, low flow NanoElectrospray source[2]. The protein was detected in its native and in a modified form. The mass difference of 162 Da suggested that a hexose was covalently bound to the protein. To localize the modification in the protein RhoA and ToxB treated RhoA were digested by Lys-C. The peptides were separated on a Sephasil RP-C18 column. The peptide (Asp28 - Lys51) had an altered retention time in the modified RhoA digest by the hexose modification as shown by electrospray mass spectrometry (fig.1). Tandem mass spectrometric sequencing localized the hexose to its N-terminal 16 amino acid (fig. 2). For a final localization the modified peptide was subdigested with pepsin. The unseparated peptide mixture was analyzed by NanoES and the modified peptide [(Asp28 - Glu40) + 162 Da] was found. MS/MS sequencing of this smaller peptide allowed the determination of threonine 37 as the modified amino acid (fig.3). Using radioactively labeled UDP-hexoses it could be shown that only UDP-glucose serves as co-factor for ToxB. Site directed mutagenesis confirmed the localization of the modification. A parallel investigation on toxin A exposed RhoA showed that the molecular mechanism of toxin A and toxin B from Clostridium difficile is the same[3].

(1) Just, I., J. Selzer, M. Wilm, C von Eichel-Streiber, M. Mann, K. Aktories (1995). "The cytotoxin from Clostridium difficile (toxin B) acts by glycosylation of the Rho proteins.", Nature, **in press**
(2) Wilm, M. S. and M. Mann (1994), Int J Mass Spectrometry Ion Processes **136**: 167 - 180
(3)Just, I., M. Wilm, et al. (1995). "The enterotoxin from Clostridium difficile (toxin A) mono glucosylates the Rho protein", JBC **in press**

43rd ASMS Conference on Mass Spectrometry and Allied Topics

Peptide Sequence: DQFPEVYVPTVFENYVADIEVDGK

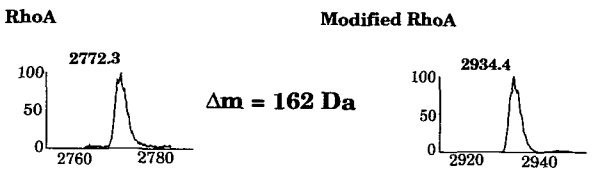

Figure 1 In the HPLC separation of a Lys-C digest of modified and unmodified RhoA the peptide (Asp28 - Lys51) was identified as containing the hexose modification.

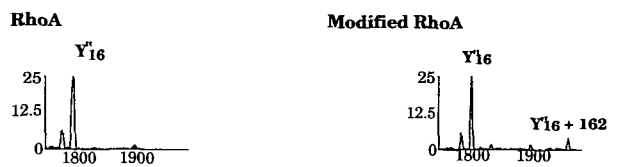

Figure 2 A MS/MS investigation of the modified Lys-C peptide localizes the hexose to the C-terminal amino acids (Pro 36 - Lys51).

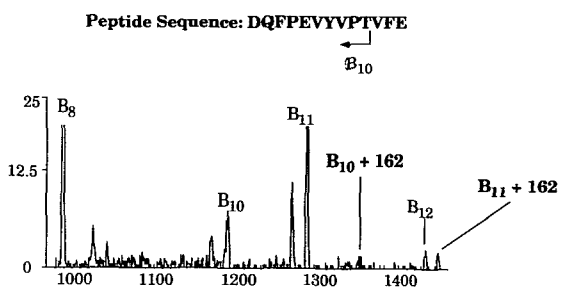

Figure 3 The MS/MS investigation of a peptide from a sub-digest of the Lys-C peptide localizes the hexose to the amino acids (Asp28 - Thr37). Thr37 is the only amino acid with a functional group which can be glycosylated.

THE ANALYSIS OF CYANOBACTERIAL TOXINS BY TANDEM MASS SPECTROMETRY

Vanessa C.M. Dale and Keith R. Jennings,
Institute of Mass Spectrometry and Department of Chemistry,
University of Warwick, Coventry, CV4 7AL, U.K.

Several cyanobacteria genera, including *Microcystis, Anabaena* and *Nodularia*, produce cyclic hepatotoxins. *Microcystis Aeruginosa* is known to be responsible for livestock death and human illness. The general structure of microcystins is cyclo (-D-Ala-L-X-erythro-D-methyl-aspartate-L-Z-Adda-D-isoglutamic acid-N-methyl-dehydro alanine). Five amino acids, including Adda, are invariable microcystin constituents, while the others, X and Z, are variable. X may be leucine (L), arginine (R) or tyrosine (Y); Z may be arginine (R), alanine (A) or methionine (M). The three microcystins -LR, -RR and -YR and Nodularin were studied of which only the microcystins are discussed here.

The CID spectra of the protonated precursors of the toxins yield only limited structural information because the proton binds at several sites on the peptide. Since a metal cation is larger than a proton, it normally co-ordinates with the heteroatoms of the amino acids, requiring the peptide to adopt a particular configuration thereby promoting more specific types of fragmentation that result in a CID spectrum that is both structurally more informative and is simpler than that given by the protonated molecule. A detailed study has been carried out of the CID spectra of ions produced by both the protonation and the cationisation of the cyanobacterial toxins some of which are presented and discussed.

High energy collision induced dissociation (CID) spectra were obtained using a Kratos 'Concept' II HH four sector instrument with an LSIMS source and floated collision cell Low energy CID spectra were obtained using a Fisons 'Quattro' II triple quadrupole mass spectrometer fitted with an ESI source. The high energy CID spectrum of the $[M+H]^+$ ion of mcyst-LR gives low mass ions at m/z 59, 70, 87, 100 and 112 that all arise from the Arg residue. The abundant ion at m/z 135 arising from cleavage of the Adda side-chain, has been assigned as $[PhCH_2CH(OCH_3)]^+$, indicating that the toxin contains this unusual amino acid residue A radical species of the same mass, 135 Da, can be lost to yield an ion of m/z 860 of lower abundance, resulting from homolytic cleavage of a C-C bond of the Adda side-chain. Cleavages through the peptide ring produce ions of m/z 155, 213 and 239. Mechanisms have been proposed which support the assignments Mdha+Ala+H^+, Glu+Mdha+H^+ and CO+Glu+Mdha+H^+ for these ions respectively. These amino acids, Glu, Mdha and Ala are all invariable in the microcystins. Although Mdha+Ala+H^+ has been postulated as the elemental composition of the m/z 155 ion, based on accurate mass measurement, we suggest $CH_3CH_2CH_2CO$+Mdha+H^+ as an alternative plausible assignment since a resolution in excess of 12,000 is required to distinguish between these possibilities.

For mcyst-RR and mcyst-LR, the most abundant adduct ions formed were $[M+Li]^+$ and $[M+2Li-H]^+$ respectively. The high energy CID spectra contain peaks due to ions formed by the loss of neutral species from the Adda and Arg side-chains. Losses from the latter give ions of m/z 985, 971 and 957 for mcyst-RR which result from heterolytic cleavages involving a 1,4-H-rearrangement, suggesting that Li^+ attachment occurs at a site removed from the Arg side-chain. Losses from the Adda side-chain produce ions of m/z 938, 922 and 909. Loss of 135 Da, described above, occurs by homolytic cleavage whereas losses of 106 and 122 Da are the result of rearrangements. The loss of 106 Da is thought to occur by a 1,2-elimination involving the movement of a methyl group to give $PhCH_2CH_3$; the loss of 122 Da occurs

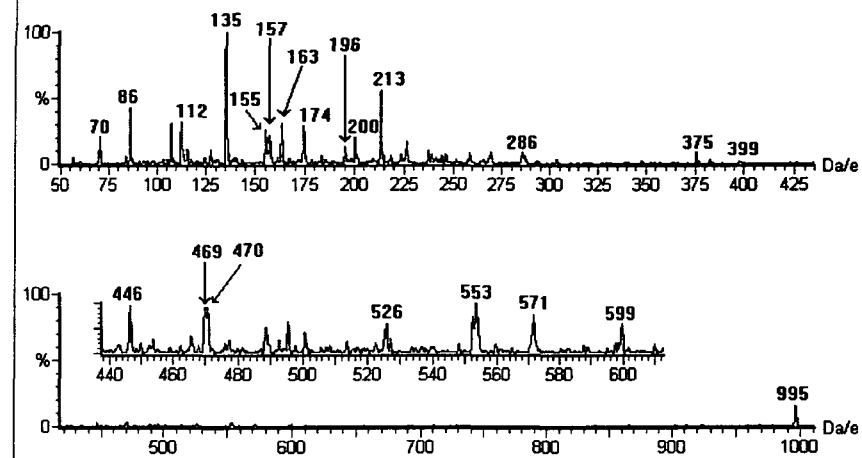

Fig. 1. Low energy CID spectrum of the $[M+H]^+$ ion of mcyst-LR obtained using ESI.

as a result of a further loss of CH_4 These losses are observed for all four toxins, indicating the presence of the Adda side-chain. Other high mass ions, resulting from partial losses of both the Adda and Arg side-chains result from homolytic cleavages that involve electron migration to form a closed-shell ionic species. All $[M+Li]^+$ ions, unlike $[M+H]^+$ ions, yield ions of m/z 189, and the $[M+2Li-H]^+$ species of mcyst-LR gives this ion and one of m/z 196, supporting the view that they contain the metal cation. Many other low mass ions originate from the ring of the cyclic peptide and contain the metal cation associated with the amino acid residues Glu, Mdha and Ala for which mechanisms have been proposed. In the CID spectrum of the $[M+2Li-H]^+$ ion of mcyst-LR, several low mass ions appear in which co-ordination of two lithium ions is postulated and the ions at m/z 31 and 56 correspond to $[LiOH]^+$ and $[LiCNO]^+$ respectively. These ions indicate that the basic side-chain of the Arg residue is a favourable site for Li^+ ion association.

The ESI-MS of cyanobacterial toxins has been reported previously. The low energy CID spectra given by the toxins contain peaks due to many fragment ions for which assignment is often difficult. Many ions formed under high energy CID conditions are not observed but fragmentations that arise from cleavages that occur around the Arg residue are very common. The ion of m/z 157 comprises the entire Arg side-chain together with the bound proton Other fragmentations in this region lead to the formation of the ions H_2N+Arg+H+H^+ and H_2N+Arg+CO-H+H^+, m/z 174 and 200 respectively, the mechanisms involving two sequential hydrogen transfers Those ions labelled in the above spectrum have been assigned structures and, in many cases, mechanisms to explain their formation have been proposed.

We thank the University of Warwick for financial support during this work.

STRUCTURAL ANALYSIS OF CONOTOXINS BY MASS SPECTROMETRY

Takemichi Nakamura[1], Michael Fainzilber[2], Eliahu Zlotkin[3], and A. L. Burlingame[1], 1. Dept. Pharmaceutical Chem., Univ. California, San Francisco, CA94143-0446; 2. Molecular Neurobiology, Free University of Amsterdam, The Netherlands; 3. Dept. Cell Animal Biology, Hebrew Univ. Jerusalem, 91904 Jerusalem, Israel

Conotoxins, a variety of peptide neurotoxins found in venom of *Conus* sea snails, are indispensable tools for neurophysiology and potential leads for structure based drug design [1]. Precise structural analysis of diverse conotoxins is an important task since the unique and specific biological activity of each toxin is directly related to unique structure of each molecule. Mass spectrometry is becoming an essential tool for structural study of these relatively small cysteine-rich peptides [2,3], typically consisting of 10 to 30 amino acid residues, partly because there are a number of possibilities for posttranslational modifications.

Many conotoxins have amidated C-termini as many other classes of bioactive peptides do. Finding and/or establishing the structures of those amidated peptides is usually a task for mass spectrometry. One practical way to do the job is to measure the molecular weight of the peptide of interest with an accuracy of better than a half unit mass and then compare the value with the calculated mass based on the peptide sequence. Although it is very simple, the requirement of knowing complete sequence is an obvious drawback of this method. Recently, we found that a combination of the CPase-Y ladder sequencing method and MALDI reflectron TOF mass spectrometry is another practical approach for establishing C-terminal amidation. Figure 1 shows a MALDI reflectron TOF spectrum of a CPase-Y treated Asp-N fragment from a conotoxin, TxVIIA. Thanks to the resolution and mass accuracy provided by an reflectron analyzer, one can confidently establish the C-terminal sequence of ---L(or I)F-NH_2 but not ---L(or I)F-OH by observing the mass differences of 146 and 113 from the "undigested peptide" at *m/z* 1529.9. Furthermore, a partial one unit mass upward-shift in the isotopic ion distribution of "undigested peptide" was observed (Fig. 1, inset), i.e., the relative intensity of "^{13}C-isotope peak" was visibly higher than that observed in the sample before CPase-Y treatment or in a theoretical pattern (data not shown). The partial one unit shift is attributable to a partial deamidation from the C-terminal residue by CPase-Y, which has amidase activity as well. This provided further support for the C-terminal amidated structure. It should be noted that this partial unit mass shift may be used to establish C-terminal amidated structures like -Glu-NH_2, -Asp-NH_2, or -Asn-NH_2, for which the mass of the amidated residue fits the mass of other residue.

γ-Carboxylation of Glu residue is another posttranslational modification frequently found in *Conus* peptides. Several strategies based on mass spectrometry have been used for identification and sequencing of γ-carboxyglutamic acid (Gla) residue in peptides and proteins [4,5]. However, those methods involve rather complex chemistries and are relatively time consuming. Recently, we found that it is possible to obtain structural information of a Gla containing peptide more directly by using a simple methylation procedure and high-energy CID tandem mass spectrometry. This allowed us to identify and sequence Gla residues rather easily with confidence. Figure 2 shows an example of the high-energy CID mass spectrum of a Gla containing conotoxin fragment after methylation. The intense immonium ion at *m/z* 174 (marked as γ) and the b-series ions clearly show presence and position of the Gla residue.

This work was supported by grants from NIH (RR01614) and NSF (DIR8700766).

43rd ASMS Conference on Mass Spectrometry and Allied Topics

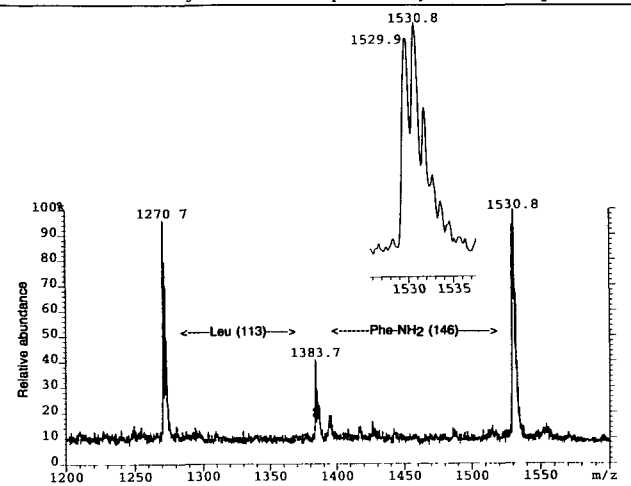

Fig. 1 CPase-Y/MALDI reflectron MS ladder sequencing of a C-terminal peptide from conotoxin TxVIIA.

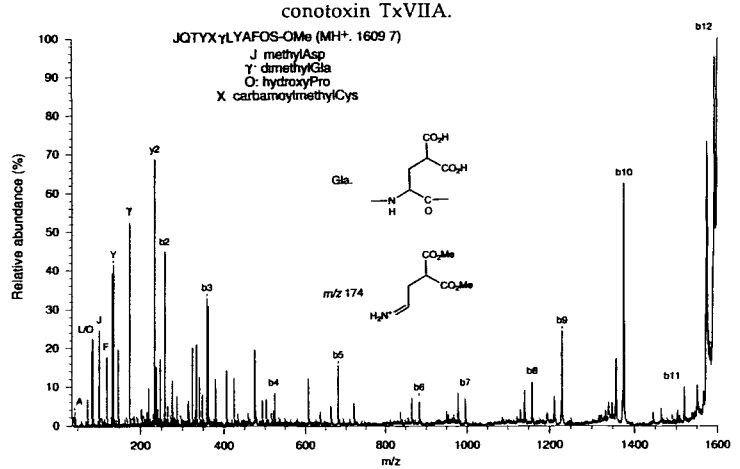

Fig. 2 High-energy CID spectrum of methyl tetra-ester of a Gla containing conotoxin digest.

1. Myers, Cruz, Rivier, Olivera *Chem Rev.* **1993**, 93, 1923; 2. Fainzilber, Hasson, Oren, Burlingame, Gordon, Spira, Zlotkin *Biochemistry* **1994**, 33, 9523; 3. Fainzilber, Nakamura, Gaathon, Lodder, Kits, Burlingame, Zlotkin *Biochemistry* **1995**, in press; 4. Morris, Dell *Biochem. J.* **1976**, 153, 663; 5. Carr, Hauschka, Biemann *J. Biol. Chem* **1981**, 256, 9944.

STRUCTURE-FRAGMENTATION CORRELATIONS OF PROTONATED ACTINOMYCINS#

D. Thomas, M. Morris, J.M. Curtis and R.K. Boyd, Institute for Marine Biosciences,
National Research Council, 1411 Oxford Street, Halifax, Nova Scotia B3H 3Z1, Canada.

The actinomycins are amongst the most effective anti-tumour agents known, but are highly toxic. Synthetic variants, which combine the therapeutic activity with lower toxicity, are highly desirable. The present work is devoted to understanding the MS/MS fragment spectra of actinomycins, to assist with structure determinations of new variants. Structurally, the actinomycins comprise two cyclodepsipeptide rings (5 residues per ring), each of which is attached to an aromatic chromophore by amide linkages. The chromophore structure appears to be invariant in nature, but synthetic variants with aromatic substitutions are known. Natural variants correspond to amino acid substitutions in the depsipeptide rings. Actinomycin D is shown as its protonated form (presumed ground state) in **I**.

Cyclic peptides present a challenge for MS/MS analysis due to difficulties in distinguishing a sequence from its *retro*-sequence (1). The present work adopted the strategy of Barber *et al.* (2), which assumes that the unknown structure is related to a known structure (*e.g.* actinomycin D) *via* one or more amino acid substitutions. In order to use this strategy effectively it is necessary to understand the fragmentation mechanisms, and to this end six actinomycin standards of established structures were studied by low-energy CID using a triple-quadrupole instrument (PE/SCIEX API III+). Some of these standards involved substitutions on the aromatic ring of the chromophore, while the others involved amino acid substitutions. From the resulting mass shifts, it was possible to propose chemically reasonable fragmentation mechanisms for protonated actinomycins, as extensions of previous work (2,3). Fragmentation of a cyclic peptide requires that at least two bonds be broken, and in the case of the depsipeptide rings in actinomycins we agree with earlier workers (2,3) that the lactone linkage appears to be the first cleaved. It is supposed that collisional activation mobilizes the ionizing proton from the most basic site (see **I**) to the one of the lactone linkages as in **II**, and that the primary product of ring opening is **III** where dhThr is the dehydro-threonine residue. In **III** the ionizing proton can readily move to more basic amide sites in the ring-opened peptide, and can thus initiate formation of the familiar **b** and **y** fragment ions. Some fragment ions were also observed which correspond to losses from both of the peptide moieties, and structures **IV** and **V** are postulated structures which rationalize the observed behaviour.

In addition to the mass shift information, the proposed mechanisms were supported by accurate mass measurements of fragment ions formed in the skimmer region of an electrospray source using a Fisons Instruments ZAB-EQ double focussing instrument operated at a resolving power (10% valley definition) of 7000. Sodiated polyethylene glycol ions were more suitable reference ions than their protonated counterparts, since they better survived the CID conditions in the skimmer region of the API source.

Fragment ion spectra of MH^+ ions of impurities in the standard actinomycin samples were then interpreted in terms of structure using the strategy of Barber *et al.* (2) and the present proposed mechanism. Some degree of success was achieved (4), but it seems appropriate to mention here the major limitations. The low-energy MS/MS approach can not distinguish between structural isomers (and gives no information on optical isomers). Since the chromophore ring is much more stable than the peptide moieties it is not possible to observe fragments in which the chromophore rings are separated and the peptides essentially intact. Therefore it is not possible to distinguish between the α and β rings (see **I**).

(1) K.B. Tomer *et al.*, *Anal. Chem.* 56 (1984), 880.
(2) M. Barber et al., *Talanta* 35 (1988), 605.
(3) J. Roboz et al., *Biomed. Env. Mass Spectrom.* 16 (1988), 67.
(4) D. Thomas *et al.*, *J. Mass Spectrom.* (in press).

NRCC No. 38084.

43rd ASMS Conference on Mass Spectrometry and Allied Topics

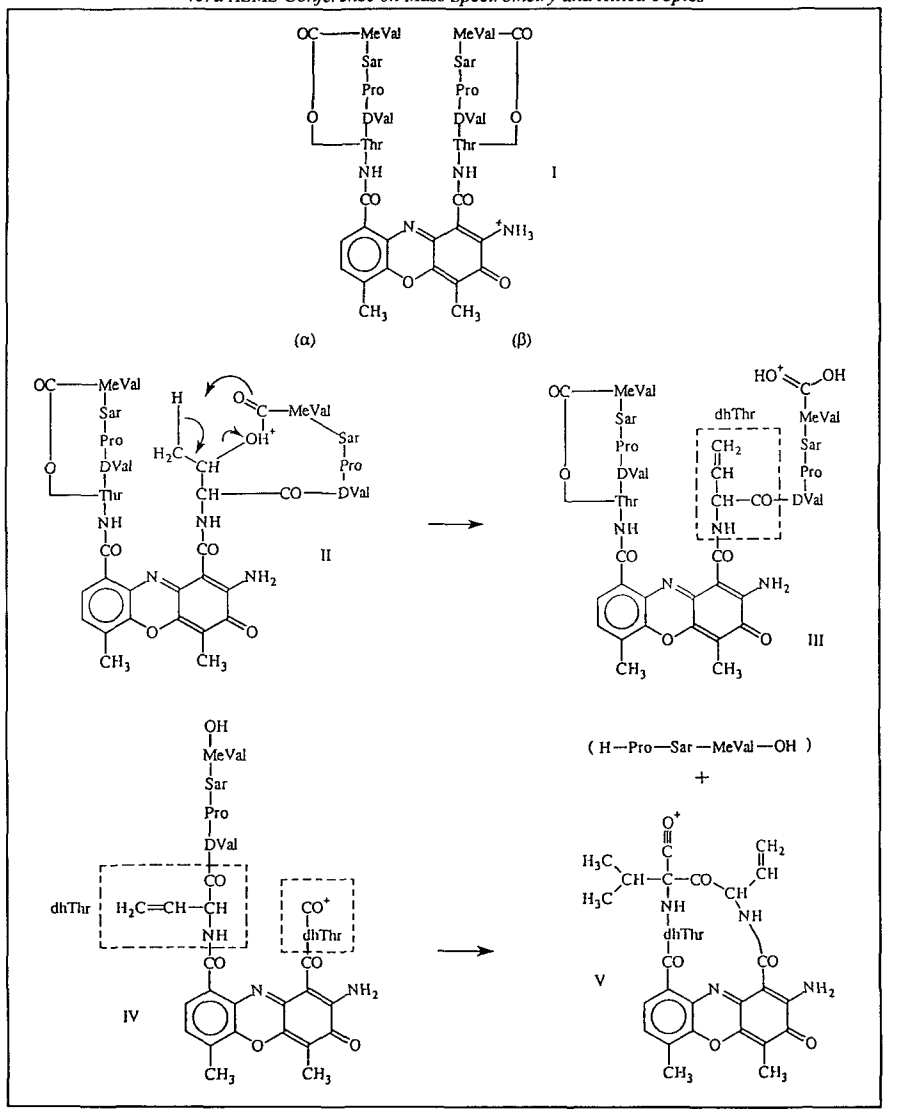

Characterization of Recombinant Forms of Adenylate Cyclase Toxin, CyaA

*Murray Hackett[1,2], Carthene B. Walker[1], Jeffrey Shabanowitz[1], Peter Sebo[5], Lin Guo[3], Erik L. Hewlett[3,4] Donald F. Hunt[1,2]

Departments of Chemistry[1], Pathology[2], Medicine[3] and Pharmacology[4], University of Virginia, Charlottesville, VA 22901; Institut Pasteur, Paris, France[5]

AC toxin (CyaA), a virulence factor from *Bordetella pertussis*, the bacteria which causes "whooping cough", is now known to be palmitoylated at residue Lys 983 (Hackett et al.,1994,*Science* 266, 433-435). This posttranslational modification is necessary for the biological activity of the177.5 kD protein, in order for it to catalyze the conversion of ATP to cAMP in eukaryotic target cells. AC toxin is also known to be hemolytic for sheep red blood cells. This activity is also dependent on the presence of the palmitoyl group. The acylation is believed to be catalyzed by an accessory protein, CyaC. To facilitate the production of large quantities of AC toxin for various structural and functional studies, the genes for CyaA and CyaC were expressed in a recombinant *E. coli* system. The recombinant AC toxin, in both its CyaC activated and its CyaC deficient form, was characterized by MALDI-TOF and triple quadrupole ESI mass spectrometry. The recombinant protein was found to differ slightly from the protein expressed naturally in *B. pertussis*. The CyaC active form was acylated at Lys 984 with myristate as well as palmitate, with about 13% of the active form myristoylated. About one third of K861 was palmitoylated, unlike the native toxin. The recombinant toxins possesed an extra Thr residue at the N-terminus, thus the slight difference in residue numbering between native and recombinant forms. *E. coli* expressed CyaC activated AC toxin has similar toxin activity, but reduced hemolytic activity, in comparison with AC toxin from *B. pertussis*.

At right, free acid CAD mass spectra from the tryptic digest of recombinant AC toxin. Figure A, myristoylated K984 tryptic peptide, EGVAT QTTAYGK$_{(MYR)}$R. Figure B, the tryptic peptide indicating the presence of unmodified K861, SEFTTFVEIVGK. Figure C, the palmitoylated K860 tryptic peptide, TGK$_{(palm)}$S-EFTTFVEIVGK. Abundant palmitoyated K984 was also isolated (data not shown).

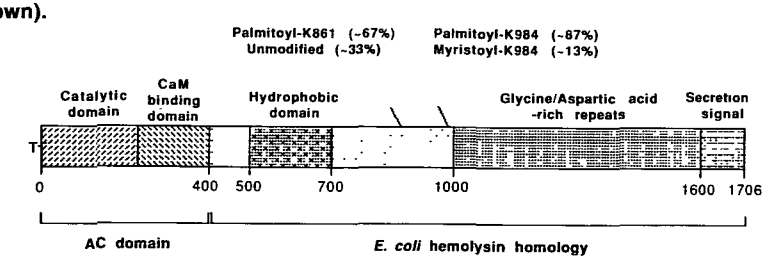

Structural representation of AC toxin expressed in *E. coli*

43rd ASMS Conference on Mass Spectrometry and Allied Topics

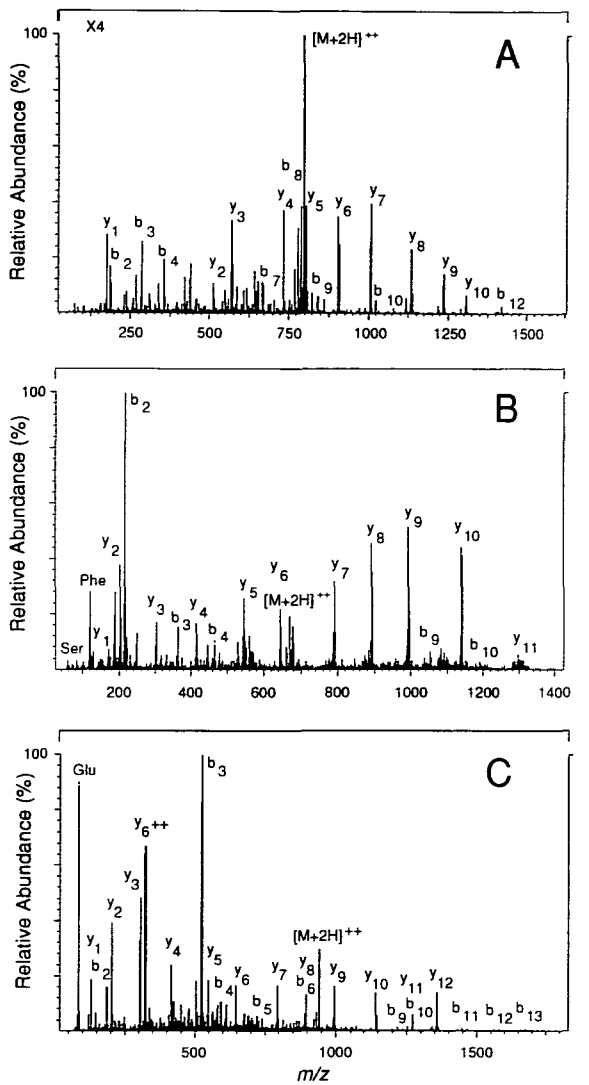

Identification of Post-translational Modifications for Cytochrome $P450_{lin}$

Rong Huang, Dipak Ghosh, Irwin C. Gunsalus, and Kenneth L. Rinehart
School of Chemical Sciences, University of Illinois at Urbana-Champaign, Urbana, IL 61801

Cytochrome P450 enzymes are a class of proteins involved in the oxidative synthesis and degradation of a variety of compounds. It has been reported that a number of hepatic P450s can be phosphorylated by purified protein kinases. Phosphorylation can also be stimulated *in vivo*. This modification may have potential importance for the control of enzyme activity, and perhaps also the regulation of P450 degradation. We first reported evidence of possible sulfation or phosphorylation for bacterial P450 enzymes, i.e., $P450_{lin}$ and $P450_{cam}$, at the 1993 ASMS conference [1]. For $P450_{lin}$, the ESIMS spectrum showed two components at 82 Da and 157 Da higher masses than the calculated molecular weight based on the amino acid sequence (i.e., 45,638 Da). Thus the number of phosphate or sulfate groups on the protein was initially suggested as two. In our continuing effort to characterize $P450_{lin}$, we have determined one modification site using mass spectrometric methods.

When native $P450_{lin}$ was digested with trypsin and separated by HPLC, two fractions both showed peaks at *m/z* 2338 in FABMS spectra (Fig. 1). The fraction eluting 2 min earlier also showed a peak at *m/z* 2418. It is well documented that phosphorylated or sulfated peptides tend to lose a phosphate or sulfate during the FAB ionization process. The typical pattern in Figure 1 indicates that the *m/z* 2418 peak corresponds to the phosphorylated or sulfated *m/z* 2338 peptide, which is at amino acid positions 27-46. It is supported by the fact that the modified peptide is eluted earlier than the normal peptide in reversed phase HPLC. Also, when both fractions are subjected to a secondary protease V8 digest, a common peptide at *m/z* 1194 (positions 35-46) is found in both fractions. This further supports the conclusion. Three residues Tyr^{31}, Ser^{36}, and Ser^{39} are therefore potential modification sites. The exact identity of the modification, i.e., phosphate or sulfate, has not been determined due to limited mass resolution.

The second assumed phosphate or sulfate, however, has never been found. The evidence obtained so far argues in favor of other explanations for the additional 157 Da in the ESIMS spectrum. It was noticed that the protein tends to lose ca. 160 Da from the molecular weight in urea solution. No intermediate mass loss (i.e., 80 Da) is observed. Phosphates and sulfates in general are stable under similar conditions. Also judged by their UV absorption, the modified peptide (*m/z* 2418) discussed above was in much smaller amount than the normal peptide. This indicated the majority of the protein components were not phosphorylated or sulfated. It was in line with the ESIMS spectrum of the intact protein, which indicated the minor component at 82 Da higher mass. One of the possibilities for the additional 157 Da was substrate binding. The substrate, linalool, has a molecular weight of 154 Da. It was ruled out based on spectral properties of P450 proteins. Substrate-bound P450 proteins have UV absorption at 390 nm compared to 419 nm for substrate-free proteins. The protein sample used to obtain the ESIMS spectrum was found to be substrate free. So far the instability of this modification (ca. 157 Da) has hindered its identification.

When native $P450_{lin}$ protein was digested with trypsin without denaturation, a peptide with molecular weight of 3801 Da was observed (Fig. 2). It did not correspond to any expected tryptic peptide based on the protein sequence. After the digest mixture was treated with dithiothreitol (DTT), this peptide disappeared while two new peptides with molecular weights of 1891 Da and 1912 Da were observed. They corresponded to amino acid positions 193-208 and 341-359, respectively, with Cys^{201} and Cys^{355} in the respective peptide. Apparently the two cysteines were linked by a disulfide bond (3801 + 2H = 1891 + 1912). However, an amino acid sequence homology analysis indicated that Cys^{355} was conserved in all P450 enzymes with known sequences and should be the heme binding residue [2]. The observed disulfide bond was likely due to partial denaturation.

In conclusion, one modification site for $P450_{lin}$ has been located within three possible residues. The other modification group is suggested as different from phosphate and sulfate. One disulfide bond is also observed.

1. Huang, R., Ghosh, D., Sun, F., Thompson, A.G., Gunsalus, I.C., and Rinehart, K.L. in *Proc. 41st ASMS Conf. Mass Spectrom. and Allied Topics*, San Francisco, CA, May 30-June 4, 1993.
2. Ropp, J. D., Gunsalus, I.C., and Sligar, S.G. *J. Bacteriol.* 1993, *175*, 6028.

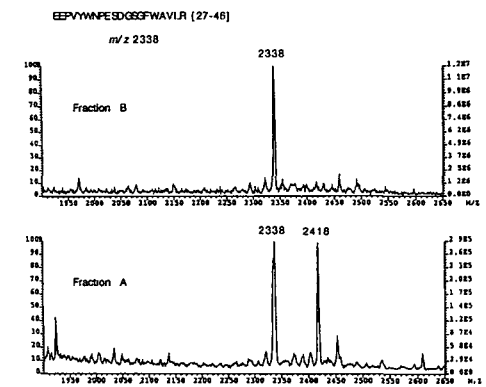

Figure 1. FABMS spectra for HPLC fractions A and B. Fraction A eluted 2 min earlier than Fraction B.

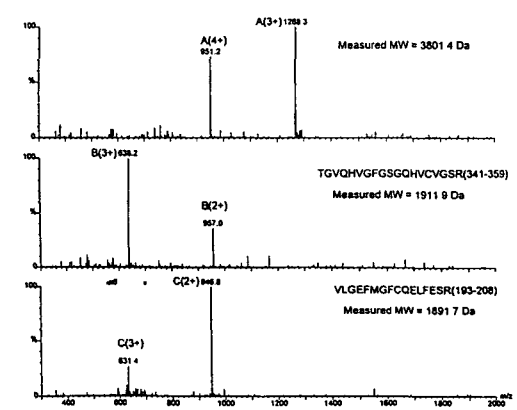

Figure2. Peptides observed before (A) and after (B & C) DTT reduction. Mass spectra were obtained by LC/ESIMS.

An ESI MS Study of the Soluble Methane Monooxygenase Enzyme System

Armelle Buzy, Amarbalita Bhambra, Patricia C. Wilkins, Howard Dalton and Keith R. Jennings
Departments of Chemistry and Biological Sciences, University of Warwick, Coventry CV4 7AL, UK.

Soluble methane monooxygenase (**sMMO**) is a multicomponent non heme iron-containing enzyme system present in methanotrophic bacteria. It catalyses the NAD(P)H- and O_2-dependent oxidation of methane to methanol [1]. Current interest in the enzyme resides in its broad substrate specificity such that it may be used *inter alia* for the biotreatment of halogenated hydrocarbon pollutants [2]. Detailed structural investigations of sMMO have therefore been undertaken in order to understand its enzymatic mechanism. In this work we report the application of electrospray ionization mass spectrometry (ESI MS) used in combination with data obtained from Edman degradation and molecular biology for the characterisation of soluble MMO from the methanotrophic bacterium, *Methylococcus capsulatus* (Bath), the first system to be purified [3].

The enzyme system consists of three proteins, **A**: the hydroxylase, (RMM 251 kDa), **B**: the regulatory protein (RMM 15.5 kDa), **C**: the reductase (RMM 38.6 kDa). All three proteins are necessary for enzyme activity. The hydroxylase is a non-heme diiron protein consisting of 3 non-covalently bound protein chains (α, 60 kDa; ß, 45 kDa and γ, 20 kDa) of $\alpha_2\beta_2\gamma_2$ stoichiometry. LC/MS analysis of **protein A** gave the profile shown in Fig. 1. The 3 subunits were identified in the 3 main peaks observed (Fig. 2). However, the spectrum extracted from the peak eluted at 37.5 min was shown to correspond to at least 3 proteins of measured RMM 60520 3, 59774.9 and 59972.9 Da. The first one was attributed to the α-subunit, as its RMM calculated from the DNA sequence is 60501.3 Da. The 2 other proteins were found to correspond in mass with proteins truncated after the 8th and the 6th residue (expected RMM 59757.5 and 59956.7 Da), respectively. The difference of about 18 Da observed for the 3 species remains to be explained (post-traductional modification, amino acid substitution, chemical modification, etc...). The ß- and γ-subunits give also RMM that disagree with the gene sequence data (measured RMM of 45000.2 and 19716.0 Da for expected RMM of 44875.6 and 19710.5 Da). The sequence deduced from molecular biology experiments suggested a RMM of 15886.8 Da for **protein B**, but SDS analysis of the purified protein showed the presence of two proteins of RMM ca. 16000, one being the expected protein and the other that obtained by truncating this protein after the 12th amino acid residue, inactive in native MMO assays. The ESI spectrum confirmed the presence of the truncated form but revealed an error in the expected protein sequence and demonstrated the presence of several minor species resulting from the loss of N- and C-terminal amino acid residues. Studies are currently being undertaken to investigate the role of the truncated form and to determine whether or not it exists in other methanotrophic bacteria. The measured RMM obtained for **protein C** was in good agreement with the mass of the protein containing 2 iron atoms linked to 4 cysteine residues and with at least 4 other cysteine residues linked by disulfide bridges. The fact that the metal centre is not removed during the mass analysis suggests that the iron atoms are very tightly bound in the native protein. This tight binding may account for the lack of inhibition of sMMO activity observed with most chelating agents.

[1] Colby, J.; Strirling, D I.; Dalton, H. 1977, *Biochem. J.*, 165, 395-402
[2] Pritchard, P. H.; Costa C. F. 1991, *Environ. Sci. Technol.*, 25, 372-379.
[3] Colby, J.; Dalton, H. 1978, *Biochem. J.*, 171, 461-468.

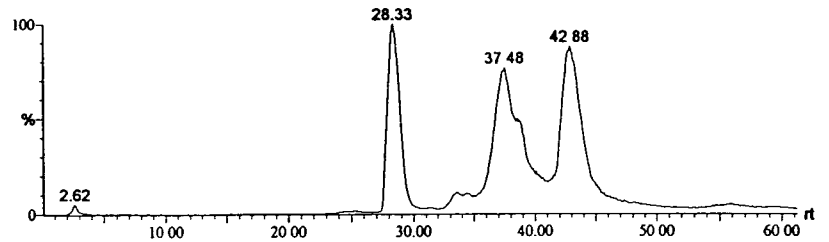

Figure 1· TIC (m/z 600-1900) of the LC/ESIMS analysis of the hydroxylase (protein A) of the Methane Monooxygenase from *Methylococcus capsulatus* (Bath). Brownlee Aquapore RP-300 HPLC column, linear gradient from 20-100% acetonitrile (0.1%TFA) in 50 min, split of 1:20 to MS.

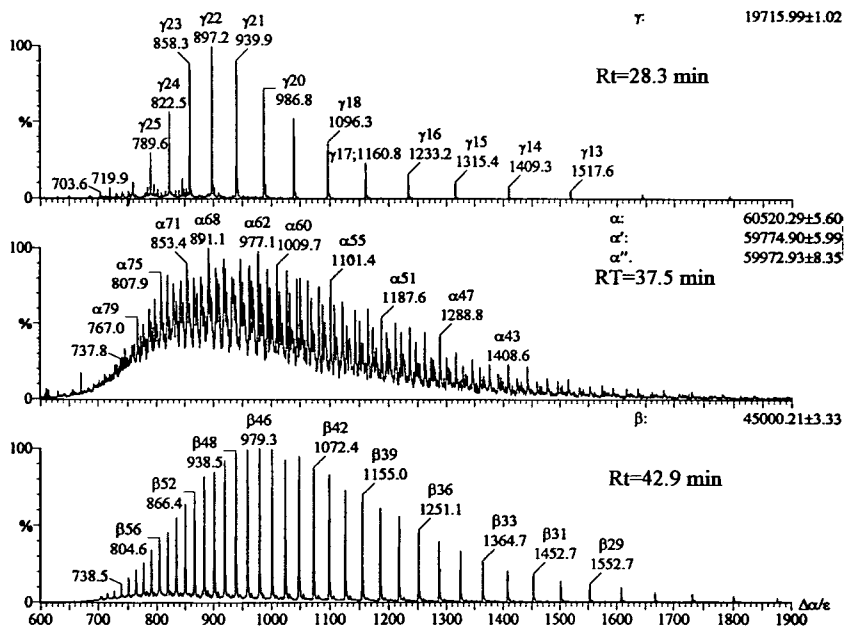

Figure 2: Extracted mass spectra from analysis shown in Figure 1.

ES-MS ANALYSIS OF RESORCINOL SUICIDE SUBSTRATE BINDING TO CYTOCHROME C PEROXIDASE

Daniel R. Doerge[1], Rao L. Divi[1] and Therese Hutton[2]
[1]National Center for Toxicological Research, Jefferson, AR 72079, U.S.A.
[2]VG Organic, Altrincham, Cheshire WA14 5RZ, U.K.

INTRODUCTION

Resorcinol and derivatives, consumed by humans through foodstuffs, food preservatives, drugs, hair dyes and groundwater, are toxic to the thyroid in humans and experimental animals causing goiter (enlargement of the thyroid) and, possibly, thyroid cancer. Yeast cytochrome c peroxidase (CcP) is a well studied enzyme (mw 34 kDa) known to differ from the classical peroxidase, horseradish peroxidase, by virtue of the formation of a catalytic amino acid radical upon reaction with H_2O_2. The present studies were undertaken to determine if the presence of a protein radical site(s) in oxidized CcP would confer susceptibility to inactivation by resorcinol, as observed previously for thyroid peroxidase, and provide support for the proposed mechanism of amino acid modification. In addition, we sought to use electrospray MS to provide evidence for the site and stoichiometry of covalent binding.

EXPERIMENTAL

Homogeneous yeast CcP was generously provided by Dr. James Erman (Northern Illinois University). MS measurements were performed using a VG Platform single quadrupole mass spectrometer (VG Organic, Altrincham, U.K.) or a Quattro II triple quadrupole mass spectrometer (VG Organic, Altrincham, U.K.). Protein samples (ca. 1 mg/ml in 10 mM ammonium acetate, pH 7.0) were diluted 2-fold into 50% aqueous acetonitrile containing 0.05% formic acid immediately before ES/MS analysis. Positive ion data were acquired over the range of *m/z* 500-2000 in MCA mode. The instrument was calibrated using the multiply charged ion peaks from a separate introduction of horse heart myoglobin (Sigma M-1882, M_r = 16,951.5 Da) at a concentration of 10 pmol/μl in 50% aqueous acetonitrile containing 0.2% formic acid and data were acquired under the same conditions as the CcP samples. Subtracted data were processed by MaxEnt to convergence using 1 Da/channel resolution.

RESULTS AND DISCUSSION

Incubation of CcP with resorcinol in the presence of H_2O_2 produced time-dependent loss of enzymatic activity (ca. 70%) that was not restored by dialysis or chromato-centrifugation as a treatment to remove all small molecules. Changes in the visible spectrum of the enzyme were also observed concomitant with resorcinol-mediated CcP inactivation. When CcP was similarly inactivated in the presence of ^{14}C-resorcinol, radiolabel became incorporated into the protein (7 mol/mol CcP). This suggested that amino acid residues of the apoprotein were modified concomitant to enzyme inactivation. This hypothesis was investigated using ES/MS analysis of native and inactivated CcP. Figure 1 (bottom panel) shows the results from MaxEnt processing of the ES mass spectrum for native CcP in acidic aqueous acetonitrile. The presence of two overlapping series with molecular weights of 33,432 Da and 34,048 Da was observed. These components were assigned to the apoprotein and the native heme-containing protein, respectively, corresponding to Δm = 616 Da for ferric protoporphyrin IX (mw = 615 Da). ES/MS analysis of resorcinol-inactivated CcP gave rise to a complex mixture of overlapping

components (see Figure 1) that upon MaxEnt processing gave a major component with molecular weight of 33,569 Da (Δm = 137, see Figure 1 top panel). This corresponds within experimental error to addition of one resorcinol unit ($\Delta m \approx 108$) and addition of two oxygens (Δm = 32). Smaller peaks that could correspond to native CcP (33,435 Da), oxidized CcP (33,451 Da, Δm = 16), addition of a second resorcinol unit to the major component (33,676 Da, Δm = 107) and addition of a third resorcinol unit to the major component (33,785 Da, Δm = 109) were also observed. The putative oxidations observed could be due to oxidation of methionine or tyrosine residues as previously observed following treatment of CcP with high concentrations of H_2O_2. However, no change in ES mass spectrum was observed upon addition of H_2O_2 at the levels used in this study (data not shown).

The visible spectral changes observed could be the result of perturbations in the protein ligands to the heme iron or direct binding to the porphyrin ring. The ES mass spectra of native CcP contains a peak consistent with ferric protoporphyrin IX ($M + H^+$ = 616 Da); however, the ES mass spectrum of resorcinol-inactivated CcP contains a small peak with a mass corresponding to addition of one resorcinol moiety (Δm = 108) in addition to a larger peak corresponding to the unmodified heme. These results suggest that binding to the apoprotein is primarily associated with CcP inactivation and that heme modification may be a secondary event.

In the proposed mechanism for suicide inactivation, the reaction of CcP compound ES with resorcinol would generate CcP compound II (1-electron oxidized above the native state) and a reactive resorcinol radical at the active site. Radical coupling would lead to a protein adduct. The observation of a major component in the ES mass spectrum of resorcinol-inactivated CcP corresponding to addition of one resorcinol moiety provides further support for the proposed mechanism. The present data do not permit identification of the residue(s) modified in the presence of resorcinol but future studies of peptides derived from modified CcP should be valuable in identifying amino acid radical intermediates.

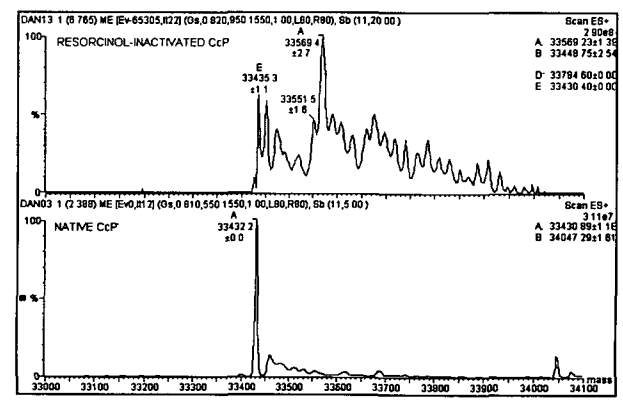

INTRODUCTION

Conidae are a group of venomous marine gastropods (~500 species) that are common in tropical and sub-tropical waters. Venom contained in the venom ducts of *Conus* species are used in conjunction with harpoon-like radular teeth to rapidly immobilize prey. These venoms have yielded a wide variety of *novel* bioactive peptides that act selectively on mammalian targets, including the sodium and calcium channels and nicotinic acetylcholine receptors [1-2]. For our studies venom is taken from individually dissected venom ducts and from the milking of certain species(Fig.1). The venom is typically subjected to reverse phase HPLC and the eluting conopeptides simultaneously monitored by UV and MS as depicted in Fig.2

EXPERIMENTAL

Mass spectra were acquired on a PE SCIEX API111 triple quadrupole mass spectrometer, equipped with an atmospheric pressure ionization source. When fractionation was not required TurboIonspray was used to allow the introduction of the complete eluant from the HPLC.

Reverse phase HPLC of the crude venom extracts and UV monitoring were affected on a Perkin Elmer Series 200 HPLC pump and a 785 UV detector respectively. Crude venom (1-2mg) was fractionated on a 250x4.6mm Vydac C_{18}, 300Å, 5µm column at 1mL/min using a gradient of 0-20%B over 5 min, 20-40%B over 45 min, 40-80%B over 5 min and finally 80%B for 10min, where A is 0.1%TFA and B is 90% acetonitrile/10% 0.09%TFA (aq).

Isolated conopeptides were characterized by a combination of Edman chemistry, MS, MS, MS/MS, chemical and enzymatic modification.

CONCLUSIONS

- LC/MS utilizing the Ionspray interface has proved a powerful tool to unravel the complexity of cone shell venoms.
- The sensitivity of the method allows for the first time the detailed analysis of crude venom from individual cone shells.
- Extensive venom composition variability observed within several species. This variability is seen between individuals on (i) the same reef (ii) distant reefs within the GBR complex and (iii) reefs from different hemispheres.
- Milked venom and duct venom exhibit great differences in complexity and composition.
- Milked venom composition changes with time in captivity.

1 Olivera, B.M.; et al., Science, **249**, (1990), 257-263.

2 Myers, R.A.; et al. Chem Rev., **93**, (1993), 1923-1936.

CHARACTERIZING PEPTIDES ISOLATED FROM *CONUS* VENOMS USING IONSPRAY HPLC/MS AND MS/MS

Alun Jones# Jon-Paul Bingham#, Richard J Lewis and Paul F Alewood#

#Centre for Drug Design and Development The University of Queensland Brisbane Queensland 4072, Australia.

*Southern Fisheries Centre, QDPI Deception Bay, Queensland, 4508, Australia.

43rd ASMS Conference on Mass Spectrometry and Allied Topics

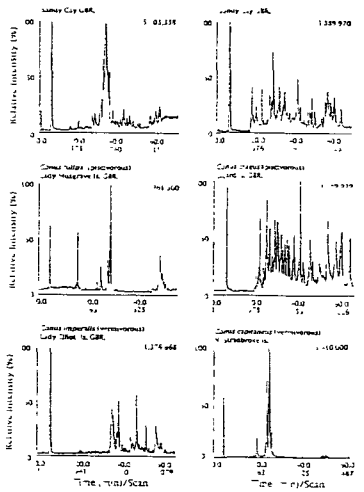

Example of mass profiling of the crude venom from the ducts of molluscivorous, piscivorous and vermivorous Conidae None of these species were found to contain the same peptides

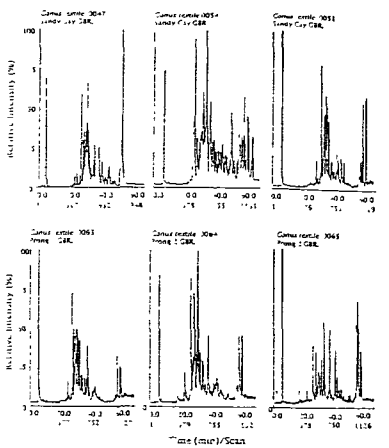

Variation of the peptides from the duct venom of six individual *Conus textile* Specimens were collected from two reefs on the Great Barrier Reef (GBR).

Comparison of Milked venom from *Conus striatus* over a period of one year

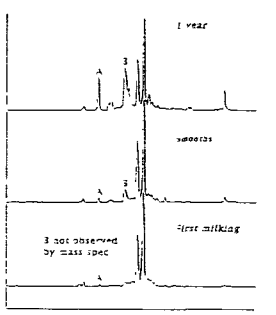

Variation in the composition of the milked venom from *Conus striatus* produced over a period of 12 months in an aquarium

MS/MS PnIB 2MaI,2PheMaI

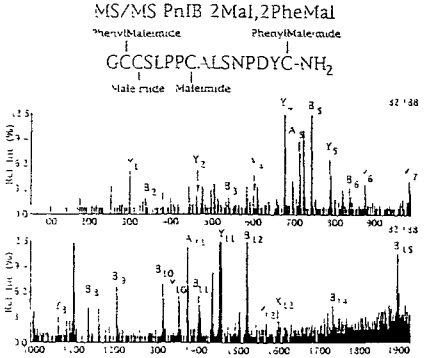

LC/MS/UV determination and fractionation of the different alkylated PnIB extracted from *Conus pennaceous* The disulfide bon were sequencially reduced (TCEP) and alkylated respectively with N phenyl Maleimide the Maleimide

ANALYSIS of HUMAN CYTOMEGALOVIRUS (HCMV) PROTEASE INHIBITION REACTIONS by ELECTROSPRAY IONIZATION MASS SPECTROMETRY (ESI/MS)

Marshall M. Siegel, Keiko Tabei, Geraldine A. Bebernitz, Jeffrey D. Hulmes, Ellen Z. Baum
American Cyanamid Company, Medical Research Division, Lederle Laboratories, Pearl River, NY 10965

INTRODUCTION HCMV is an opportunistic pathogen which can cause disease or death in immunocompromised patients. The 28 kDa protease encoded by the HCMV UL80 gene is essential for viral replication and is an appropriate target for an antiviral drug. Using random screening methods, compound CL13933 (a symmetrically-substituted disulfide with MW 568), was found to inhibit recombinant HCMV protease. To better understand the nature of the chemical reaction between the protease and inhibitor, ESI/MS was used as the detector for the reactions.

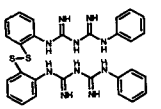

RESULTS & DISCUSSION The inhibition of HCMV protease A144L (MW 28,083) by CL13933 was found to be irreversible, as defined by the failure to recover enzymatic activity upon removal of the free compound either by gel filtration or by dialysis. Since CL13933 contains a disulfide bond, the mechanism of action for the compound suggested reaction(s) with the cysteine residue(s) of HCMV protease. Figs. 1A, B and C illustrate the transformed ESI mass spectra of A144L HCMV protease incubated with 0, 9, and 20-fold molar excess, respectively, of CL13933 (2h, 25°C). The masses of zero, one half, and three halves CL13933 adducts are indicated by 0D, 1/2D, and 3/2D, respectively. Peaks labeled ' are lacking the amino terminal methionine residue and behave exactly as their counterparts containing methionine. (The weak shoulders ~41 Da higher than the main peaks correspond to carbamylation of protease during purification from urea). At a molar ratio 9:1 of CL13933:protease, no changes in the spectra are observed (cf. Fig. 1A with B). At 20:1 of CL13933:protease, covalent adducts between CL13933 are observed (Fig. 1C). The protease contains 5 cysteine residues. To determine whether (and how many) cysteines reacted with CL13933, the free cysteines in these samples were quantitated by alkylation with iodoacetamide (IAM, Δ = 57). The resulting transformed ESI mass spectra are shown in Figs. 1D, E and F. The masses of one, three, and five alkyl groups are indicated by 1I, 3I, and 5I, respectively. Alkylation experiments demonstrate that less IAM-protease adducts are generated with increasing the molar ratio of CL13933 to protease (cf. Fig 1D with E) until only minor changes are observed (Fig 1F) relative to the unalkylated reaction (Fig. 1C). These results, and reduction experiments with β-mercaptoethanol, demonstrated that at 9:1 CL13933:protease, two intramolecular disulfide bonds were formed within the protease, and that at 20:1 CL13933:protease, a disulfide bond was formed between the protease and half a molecule of CL13933.

To identify the disulfide pairs which form in HCMV protease, tryptic digests of CL13933-treated A144L protease were prepared. The isolated fragments were analyzed by Edman sequencing and ESI/MS. The identified disulfide pairs were Cys138-Cys161 and Cys84-Cys87. These data suggest that specific pairing of cysteines occurred, as opposed to scrambling of the inter-

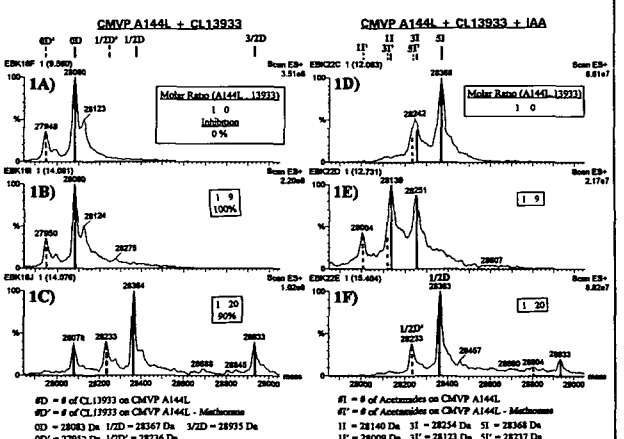

molecular disulfides. An adduct between Cys202 and a half molecule of CL13933 was also detected.

To elucidate the role played by each of the cysteines in HCMV protease in the inhibition of protease activity, each of the five individual cysteine residues was mutated to alanine (C84A, C87A, C138A, C161A, C202A). Each of the mutant proteases were found to be enzymatically active, but only mutants C138A and C161A were not inhibited by CL13933, suggesting that the disulfide between Cys138-Cys161 is responsible for the inhibition of the protease. The reactivity of the five different cysteine residues of HCMV protease was determined by incubating the mutant proteases with excess CL13933 (CL13933:protease, 6:1, 4h) and examining the products by ESI/MS (Fig. 2A). The proposed identity of the major (M) and minor (m) mass spectral peaks are illustrated in Fig. 2B. The HCMV protease is depicted as a line. Filled circles represent cysteines present in each protease; open circles are alanines substituted for cysteines. Filled rectangles are half molecules of CL13933. Disulfide bonds are indicated by bars (⌐¬) connecting two cysteines.

The proposed mechanism for the inhibition of HCMV protease by CL13933 uncovered a previously unreported feature of the enzyme: the presence of multiple reactive cysteines which are capable of thiol-disulfide exchange. The disulfide pairs are Cys84-Cys87 and Cys138-Cys161; Cys202 is unpaired. At low concentrations of CL13933, the thiols of Cys87, Cys138, and Cys161 react with CL13933, forming a transient covalent adduct. The other member of the pair (Cys84, Cys161, and Cys138, respectively) then displaces CL13933 by thiol-disulfide exchange, forming intramolecular disulfide(s). Cys84 is presumed to be non-reactive; it may be protonated or inaccessible to the compound in the native protease. At high concentrations of CL13933, covalent adducts between CL13933 and HCMV protease are observed, resulting from simultaneous reaction of Cys138 and Cys161 with CL13933, preventing thiol-disulfide exchange; also, Cys202 forms an adduct with CL13933 and does not participate in intramolecular disulfide bonding. Since Cys84 cannot react with CL13933 directly, but only acts to exchange adduct from Cys87, an adduct of five halves CL13933 is not observed.

Kinetics studies of A144L protease with CL13933 (1:20) by ESI/MS (Fig. 3) can be explained in terms of this model. At 10 minutes, the addition of 2/2 CL13933 adducts is observed but at later times it disappears, and 1/2 and 3/2 CL13933 adduct appear. This can be explained by the rapid simultaneous addition of 1/2 CL13933 at both Cys138 and Cys202 (2/2) and later addition of 1/2 CL13933 at Cys161 to the adducted protease (3/2) or the release of 1/2 CL13933 from Cys138 by producing a disulfide bond with Cys161 (1/2). This kinetics model is consistent with similar kinetics studies of C202A with CL13933.

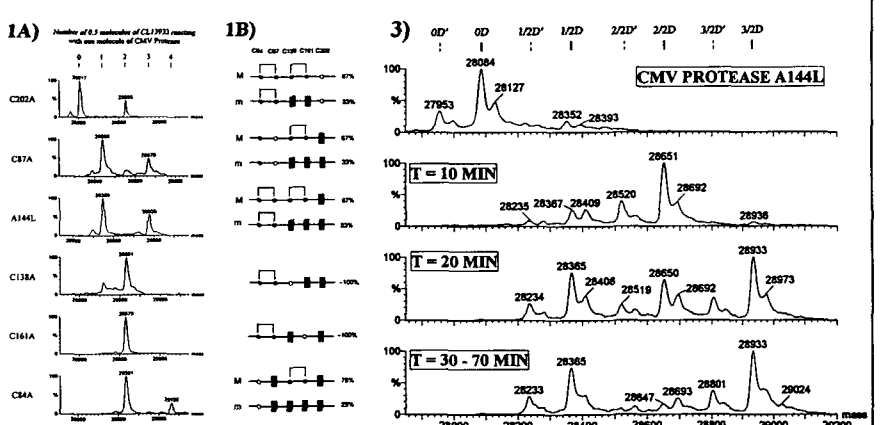

Evaluation of the Role of Hydrophobicity and the Role of Suppression in the Mass Spectrometry of MHC Peptides.

Amina S. Woods, Alex Huang, Robert Cotter, Drew Pardoll and Elizabeth M. Jaffee, Departments of Oncology and Pharmacology, Johns Hopkins School of Medicine, Baltimore, MD 21205

Recent advances have been made in the identification of specific gene products that represent tumor antigens. These antigens are peptide fragments of cytoplasmic proteins that are expressed bound to Class I MHC. In the case of human melanoma, the peptides were identified and sequenced by mass spectrometry. Our group has been utilizing MALDI in combination with exopeptidase digests as a method for sequencing MHC Class I antigens. Some modification of this approach have resulted in important visualization thereby allowing sequencing of the isolated peptides. In particular, we took advantage of the hydrophobicity of peptides to improve their detection.

To assess the role of hydrophobicity, equimolar solutions of synthetic MHC peptides of various hydrophobicity (as calculated by the Bull and Breese index [BBI]) were used.

peptide #1 FERFEIFPKE BBI= -3500, MW = 1341.7 Da
peptide #2 TYQTRALV BBI= -290, MW = 1107.3 Da
peptide #3 SIINFEKL BBI= -3790, MW = 963.3 Da
peptide #4 IYSTVASSL BBI= -3120, MW = 939.5 Da

Peptide Solutions: Peptides were diluted in 20% acetonitrile: 80% water: 0.1% TFA pH = 2.0. All solutions contained an equimolar amount of each of the 4 peptides. The following concentrations were prepared 10 pmoles/ul, 1 pmole/ul, 100 fmole/ul and 10 fmole/ul. Saturated solutions of Ammonium citrate dibasic (AC) and ammonium bicarbonate (AB), pH = 5.0 and 8.5 respectively, were used. Matrix: Saturated solution of α-cyano-4-hydroxy-cinnamic acid in 50% ethanol-water pH = 1.25. Each peptides solution was spotted 3 times on a sample slide, followed by the addition of matrix, or buffer and matrix, and left to dry at room temperature.

1: 0.3 ul peptides + 0.3 ul/matrix pH = 1.5
2: 0.3 ul peptides + 0.3 ul AC + 0.3 ul/matrix pH = 4.0
3: 0.3 ul peptides + 0.3 ul AB+ 0.3 ul/matrix pH = 7.2

Washes were done with 1ul of cold deionized water. The spectra were acquired before and after washing with water on a Kratos Kompact MALDI III (Manchester, England).

The analysis of the peptide mixture shows that hydrophobicity is not the only factor that plays a role in the desorption of the various peptides present in our mixture. The salt content, the pH of the solution as well as the concentration of the solutions played a role. The data from the 0.01 pmole/ul

solution was reported but should be considered unreliable because the spectra have an uneven base lines, and some molecular ions (MH^+) are barely above the noise level.

Salt contents: The washed samples showed an improvement in sensitivity and resolution and less suppression for the 10, 1 and 0.1 pmole/ul solutions.

Solution pH: The samples to which ammonium citrate was added (pH = 4.0), showed the most improvement in sensitivity, resolution and the least suppression. The samples to which ammonium bicarbonate was added showed some improvement in sensitivity and resolution and almost as much suppression as the non buffered samples, except for the washed samples, which showed less suppression than the ones that were only buffered.

Solution Concentration: The suppression increased as the sample concentration decreased. As a whole suppression was less marked in washed samples, regardless of their concentration.

The above results suggest that peptide suppression is not related to hydrophobicity.

- Salt content seems to aggravate suppression, and the washing of the sample matrix mixture after it is dried improves sensitivity and resolution as well as decrease suppression in spite of the possibility of sample loss.
- Solution pH seems to be the parameter that has the most significant effect on improving sensitivity and resolution as well as decreasing suppression. The most favorable results were obtained at pH 4.0 by addition of ammonium citrate buffer (pH = 5.0). The results generated at pH 7.2 by addition of ammonium bicarbonate showed some improvement. The non-buffered samples (pH 1.5), showed the most suppression. All samples regardless of pH were improved by salt removal.

In conclusion our data shows that pH and possibly the number of basic residues (arg, lys), do play a role in the desorption of peptides by MALDI. Peptide #2 contains 2 arg, peptide #1 contains an arg and a lys, peptide #3 contains one lys and peptide #4 contains none. We used both dibasic (pH 5.0) and tribasic (pH 7.5) ammonium citrate buffers. The effect of the tribasic buffer were similar to those obtained with ammonium bicarbonate, thus pointing that the improvements are probably due to the pH of the solution rather than the ammonium citrate *per se*.

1. C.J. Aldrich, A. DeCloux, A.S. Woods, R.J. Cotter, M.J. Soloski and J. Forman, **Cell 79** (1994) 649-658.

2. A.S. Woods, A.Y.C. Huang, R.J. Cotter, G.R. Pasternack, D.M. Pardoll and E.M. Jaffee, **Anal. Biochem. 226** (1995) 15-25.

Identification of Peptides Associated with Class II MHC Molecules

Theresa A Addona[1], Jeffrey Shabanowitz[1], and Donald F Hunt[2]
[1]Department of Chemistry, University of Virginia, Charlottesville, VA 22901
[2]Departments of Chemistry and Pathology, University of Virginia, Charlottesville, VA 22901

In the last few years, a number of different techniques have been applied to the sequencing of processed peptides in association with both class I and class II MHC molecules(1-5) These results include allele-specific motifs for various class I MHC molecules, and the general features of peptides bound to class II MHC molecules. Identifying these characteristics has led to considerable progress in understanding the pathways through which the peptides are produced and presented Given a known protein, sequence motifs for class I associated peptides have been used to predict optimal peptides for binding From these predictions, peptides responsible for eliciting an immune response have been identified (6).

The determination of sequence motifs for class II peptides is not as definitive Most of the class II associated peptides sequenced to date are nested sets derived from the same source protein, and share a common core sequence, but differ at both the amino and carboxyl terminal ends. Despite the lack of a length restriction, predictions for optimal peptide binding to class II molecules can be made, but presentation of these peptides on the cell surface is not known

The application of precursor ion scans on internal fragments in the core sequence of class II associated peptides was investigated as a general method for the identification of related, processed peptides in a complex mixture The complete sequences of twenty peptides extracted from class II molecules DR(w4,w14) were determined by microcapillary HPLC/electrospray ionization/tandem mass spectrometry The principal ion series in the product ion spectra recorded on triply and quadruply charged ions, consisted of multiply charged, high mass y ions and their internal cleavage fragments Precursor ion scans recorded on the internal cleavage fragment at *m/z* 1327 (DDTQFVRFDSD) of the synthetic peptide VDDTQFVRFDSDAASPRTEPR, showed that this fragment is derived predominately from the intact peptide and y_{20}^{+3}, and to a lesser extent, from the doubly charged internal fragment at *m/z* 1021. To test the application of this approach, precursor ion scans were recorded on a complex mixture from which DR(w4,w14) associated peptides had been sequenced. Figure 1 shows the ESI mass spectrum with the characterized peptides indicated by *. The complete sequences of these peptides are shown in Table 1. Those peptides that have already been identified to yield *m/z* 1327 by product ion scan are observed in the precursor ion scan and are also indicated by * (Figure 2) Most notably, peptide number 10 is not observed since this peptide cannot fragment to the selected product Other precursors that have not been identified, but contain a *m/z* 1327 in their product ion spectrum include *m/z* 733, 914, and 930

References

1 Hunt, D.F. et al 1992 *Science* 255:1261.
2 Falk, K. et al 1991 *Nature* 351:290.
3. Hunt, D.F. et al. 1992 *Science*. 256.1817.
4. Rudensky, A.Y. et al 1991. *Nature*. 353.622
5. Chicz, R.M et al. 1992. *Nature*. 358:764.
6. Pamer, E.G et al. 1992. *Nature*. 353:852.

Peptide Number	$(M+H)^+$	Observed *m/z*	Sequence
1	1925	642^{+3}	VDDTQFVRFDSDAASPR
2	1956	652^{+3}	VDDTQFVRFDSDAASQR
3	2155	718^{+3}	VDDTQFVRFDSDAASPRT
4	2255	752^{+3}	DTQFVRFDSDAASQRMEPR
5	2313	771^{+3}	VDDTQFVRFDSDAASQRMEP
6	2364	591^{+3}	VDDTQFVRFDSDAASPRGEPR
7	2408	602^{+4}	VDDTQFVRFDSDAASPRTEPR
8	2436	609^{+4}	VDDTQFVRFDSDAASPREEPR
9	2469	617^{+4}	VDDTQFVRFDSDAASQRMEPR

Table 1 List of peptides sequenced from the ESI spectrum shown in Figure 1

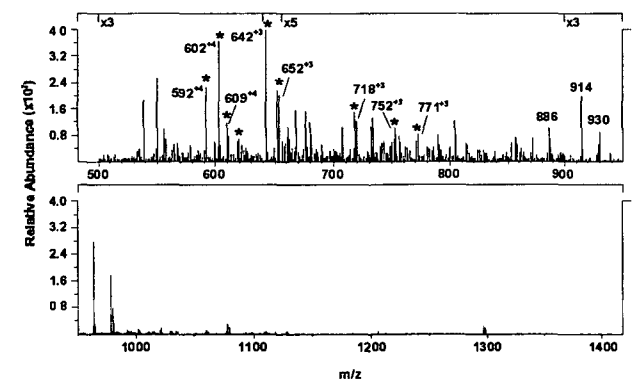

Figure 2. ESI spectrum of a complex mixture of DR(w4,w14) peptides. Peptides for which sequences are known are indicated by *.

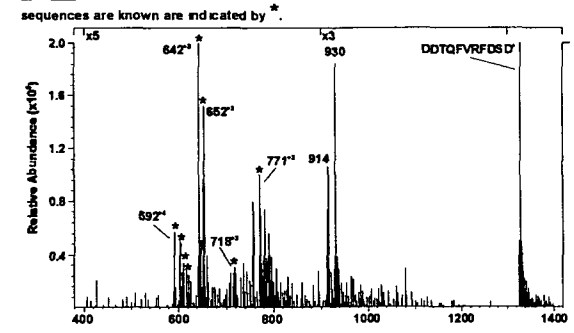

Figure 2. Precursor ion spectrum of a complex mixture recorded on the internal cleavage fragment at m/z 1327. Those peptides that have already been identified to yield m/z 1327 by product ion scan are indicated by *.

MHC CLASS II-ANTIGEN PROCESSING: CHARACTERIZATION OF THE MAJOR COMPONENTS IN SUBCELLULAR FRACTIONS

Ashley L. McCormack, Jimmy K. Eng, Paul DeRoos [1], Alexander Y. Rudensky [1], and John R. Yates, III
Department of Molecular Biotechnology and
[1]Department of Immunology, University of Washington, Seattle, WA 98195

In the past several years electrospray ionization tandem quadrupole mass spectrometry has made an impact in many areas of biology, especially immunology and the study of antigen presentation by major histocompatibility complex (MHC) class I and class II molecules (1). We are developing methodology to study the generation of MHC class II-peptide complexes. The cellular processing of MHC-peptide complexes has been studied extensively; however the exact mechanisms are unknown Previous research has suggested that MHC class II molecules move from the golgi complex to late endosomes (2) Then class II molecules accumulate in dense MIIC compartments where endogenous peptides bind to class II molecules. Finally the complex moves through the endosomal pathway to the cell surface. Exogenous peptides have also been found to accumulate in MIIC vesicles, where binding to class II molecules may occur. Here we present data from the analysis of peptide mixtures derived from subcellular fractions enriched with components of the endocytic pathway.

Our preliminary study focuses on utilizing µ-LC-MS/MS and database searching methodology to characterize the peptide components in subcellular fractions, including identifying protein origins and identifying the cleavage sites in the protein Lysed cellular material, including intact vesicles, was fractionated by density using a sucrose gradient (2). Fractions were assayed using known marker proteins and pooled accordingly Vesicles were lysed using acid conditions and components were fractionated using a 3,000 Da and/or 10,000 Da cut-off membrane filter. Peptide mixtures were analyzed directly with µLC-MS, automated µLC-MS/MS, and database searching.

Complex mixtures of peptides were found in all fractions, except those enriched in plasma membrane In the other fractions, large peptides, with molecular weight distributions of approximately 3.5 to 11.7 kDa were observed, as well as a complicated mixture of many smaller peptides. To facilitate sequencing, large molecular weight peptides were separated from smaller peptides using a 3000 Da cut-off membrane filter. The low molecular weight mixtures were analyzed using automated µLC-MS/MS, Figure 1. Uninterpreted spectra were used to search the *Mus musculus* subset of the OWL database, using the program SEQUEST as described by Eng and coworkers (3). Sequence data was obtained on peptides in fractions containing late endosomes and ER, Table1a, and in fractions containing MIIC, late endosomes and ER, Table 1b.

Each of these fractions contained over one hundred peptides. An average of 35 peptides per pooled fraction were analyzed by a single MS/MS experiment Currently we are adapting the automated MS/MS program, as well as the chromatography conditions to maximize the number of peptides analyzed. However, many of the peptides in these two fractions are present in higher charge states (greater than +3) and were not sequenced.

In most of the peptide sequences, the cleavage sites are consistent with an acid protease, such as cathepsin D or E. It has been suggested that acid proteases, such as cathepsin D and E, are important in the processing of MHC class II-peptide complexes (4). Peptides from human keratin and calreticulin were also identified; these proteins are common contaminants in protein samples handled by humans. It is interesting to note that these peptides also contain the correct cleavage sites, suggesting that these peptides were processed in the cells

µLC-ESI/MS/MS has proven to be a powerful technique for study of antigens presented by MHC molecules. Extending this approach to study antigen processing pathways provides insight into the mechanisms of antigen processing, selection, and presentation. Future studies will include pulsing the cells with hen egg lysozyme, followed by subcellular fractionation, and identification of lysozyme peptides in each pooled fraction by µLC-MS/MS.

References

1 Hunt,D F.,Henderson, R.A.; Shabanowitz, J , Sakaguchi, K , Michel, H , Sevilir, N , Cox, A L., Appella, E ; Engelhard, V H *Science* **1992**, 255, 1261.
2 Rudensky, A Y ; Maric, M.; Eastman, S ; Shoemaker, L., DeRoos, P C , Blum, J S *Immunity* **1994**, 1, 585
3. Eng, J., McCormack, A L , Yates, J R. III *J Am Soc Mass Spectrom* **1994**, 5, 976.
4 Maric, M A., Taylor, M D , Blum, J.S *Proc Natl. Acad Sci., USA* **1994**, 91, 2171

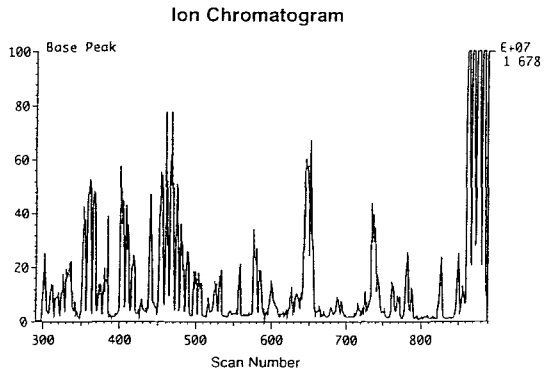

Figure 1 Reconstructed ion chromatogram obtained from automated µLC-MS/MS of an aliquot from a murine subcellular fraction conatining MIIC vesicles, late endosomes, and endoplasmic reticulum

Table 1a. Peptides Identified by µLC-MS/MS of Murine Subcellular Fractions Containing Late Endosomes and ER.

Sequence[a,b]	Protein
L - WQVKSGTIFDNF	Calreticulin precursor
L - LGLLPHTFTPTTQL	ATP synthase a chain
F - FDITADDEPLGRVSFEL	Peptidyl-prolyl cis-trans isomerase
G - AGFGGGFAGGDGLL	Human keratin

[a] The hyphen denotes the cleavage sight
[b] Amino acid sequences are shown using the single letter codes for the amino acids The isomers L and I and the isobaric amino acids Q and K cannot be differentiated using low-energy collision-induced dissociation and were assigned using the sequences retrieved from the database

Table 1b Peptides Identified by µLC-MS/MS of the Murine Subcellular Fractions Containing MIIC Vesicles, Late Endosomes, and ER

Sequence[a,b]	Protein
F - TLDDTWAKAHFAIMF	Cytochrome C oxidase polypeptide I
N - MTFFPQHFLGL	Cytochrome C oxidase polypeptide I
L - WQVKSGTIFDNF	Calreticulin precursor
F - AVLGLDL	Calreticulin precursor
L - LGLLPHTFTPTTQL	ATP synthase A chain
F - FDITADDEPLGRVSFEL	Peptidyl-prolyl cis-trans isomerase

[a] The hyphen denotes the cleavage sight
[b] Amino acid sequences are shown using the single letter codes for the amino acids The isomers L and I and the isobaric amino acids Q and K cannot be differentiated using low-energy collision-induced dissociation and were assigned using the sequences retrieved from the database

A Study of Analyzing Femtomole Amounts of Peptides with Continuous-Flow FAB

A. B. Whitehill,* I. Vidavsky, and M. L. Gross
Department of Chemistry, Washington University, One Brookings Drive, St. Louis, MO 63130

We have undertaken a study to investigate peptides isolated from major histocompatibility complex (MHC) molecules of the class II type, resulting in the need to be able to determine low picomole to femtomole amounts of peptides with 10 to 20 residues and corresponding molecular masses of approximately 1000 to 2000. To complement the biological experiments, mass spectrometric analysis needs to yield accurate molecular weight and structural information. Although the biological factors warranting such an endeavor are significant in their own right, this study will concentrate on our efforts to develop a mass spectrometric method for these peptides.

When dealing with small amounts of material, sample handling and detection must be scrutinized. In this study, samples were introduced with continuous flow-FAB via a commercially available VG probe. To optimize detection limits, a series of synthetic peptides were used to evaluate the following:

Sample analysis was performed with a VG ZAB-T four-sector mass spectrometer of BEBE design. Ions were created with a cesium ion gun and accelerated by an 8 kV potential. Molecular weight determination was accomplished by scanning MS1 (E_1B_1) with a mass resolving power of 2000 and at a rate of 15 seconds per decade over the appropriate mass range resulting in a scan time of approximately 11 seconds (two second delay between scans). Selected ion monitoring experiments were done by calibrating with a pair of known masses and stepping the voltage for the desired mass.

Samples were introduced with a continuous flow-FAB probe of screen and wick design. Peptides were dissolved in a 68% water/27% acetonitrile/3% glycerol/2% TFA matrix and introduced through a 350 μm O.D. x 50 μm I.D. fused-silica column. Solution flow was accomplished by inserting the capillary in a sample holder (bomb) pressurized to 23 p.s.i. with helium gas. Ionization and desorption occurred as the capillary delivered the solution to the screen where FAB occurred.

The first step in our analysis was to assure steady sample delivery at a flow rate of approximately 1.7 μL/min. This rate was chosen because the minimum sample volume that can be reproducibly handled with this technique is approximately 10 μL, resulting in a sample analysis time of six minutes. The water/glycerol/acetonitrile mixture is sufficient for steady matrix flow, but a protonating agent such as trifluoroacetic acid (TFA) must be added at an optimum level. This was evaluated by monitoring the molecular ion abundance for desorption from a series of 70% water/27% acetonitrile/3% glycerol matrices varying in TFA content from 0 to 3%. Two commercially available peptides (substance P and bradykinin) were monitored and both showed maximum signal to noise for matrices containing 2% TFA. For further experiments, a matrix of 67% water/27% acetonitrile/3% glycerol/2% TFA was used because the resulting ion current was steady and the extent of protonation was maximum.

After establishing the most effective matrix, selected ion monitoring (SIM) experiments were carried out to determine if samples were being spread while in the silica column, resulting in dilution and a higher limit of detection. A series of 20-s injections of hen egg white lysozyme peptide (HEL 52-61) at concentrations of 550 and 110 fmol/μL were analyzed and showed small amounts of peak tailing and spreading occur. In the 110 fmol/μl injections the sample consumption is 55 fmol, shorter injections and lower concentrations should yield detection limits of <10 fmol.

The detection limits for scanning experiments need to be evaluated for the analysis of fractions of unknown peptides. Different concentrations of various peptides were flowed for a fixed amount of time (approximately 1.8 minutes) and volume (3 μL) and spectra recorded. Table 1 is a summary of scanning

data for a series of peptides, and shows that a fairly wide range of detection limits (S/N = 3) are observed. One explanation for the range of detection limits is that hydrophobic peptides assemble on the surface of the matrix and are desorbed more effectively whereas hydrophilic peptides remain in the water-based matrix. Peptide hydrophobicity has been measured by a variety of experimental methods. Bull and Breese[1] measured surface tension of single amino acids whereas Hearns[2] et al. measured RP-HPLC retentions of peptides with a series of stationary and mobile phases. In both cases, a hydrophobicity index is established for single amino acids, and the peptide values are the sum for the sequence. Table 1 shows that detection limit decreases with increasing hydrophobicity, inferring that hydrophilic discrimination is occurring.

After determining that hydrophobicity affects detection limits of solutions containing single peptides, the effect of peptide mixtures on LOD was investigated. Full scan spectra were recorded for a series of peptide mixtures at known concentrations and summarized in Table 2.

Every peptide shows an increase in detection limit. This is probably due to a decrease in surface concentration of the peptide at the FAB probe tip, particularly for peptides of similar hydrophobicity. If true, the detection limit for a hydrophobic peptide in mixture with a hydrophobic peptide will not be affected. Table 2 shows that this is not the case as the detection limits of hydrophobic peptides, substance P and HEL 52-61, are made worse when the peptide is mixed with a more hydrophilic peptide. Although we have only limited sets of data, this suggests that hydrophobic/philic properties do not account for the behavior of mixtures of peptides in flow FAB.

Table 1. Scanning detection limits of various peptides.

Peptide	*m/z* $[M + H]^+$	Det. Limit (fmol/μL)	Amount (fmol)	B&B value[1]	Hearn value[2]
Bradykinin	1060.6	320	945	-940	5.3
HEL 52-61	1178.6	80	240	-1590	11.5
Lys-Bradykinin	1188.6	580	1740	-480	3.7
Substance P	1347.7	45	135	-1790	13.1
HEL 46-61	1753.8	750*		1720	12
Renin Sub. T.	1758.9	40	120	-7700	16.8

1. H. B. Bull; K. Breese *Arch Biochem Biophys*, **161**, *1974*, 665.
2. M. C. J. Wilce; M. I. Aguilar; M. T. W. Hearn *Anal. Chem.*, **67**, *1995*, 1210.

Table 2. Detection limits (for full scans) of peptides in mixtures.

Peptides		Concentrations (fmol/μL)		Est. LOD (3:1 S/N)	
Peptide 1	Peptide 2	Peptide 1	Peptide 2	Peptide 1	Peptide 2
RST	HEL 46-61	196	750*	90	>750
Substance P	HEL 52-61	125	183	125	140
Substance P	Lys-BKinin	187	560	190	1200
HEL 52-61	Bradykinin	550	945	330	945

*Impure sample

Identification of Influenza Epitopes Presented by Hemagglutinin Transfected Cells

Pamela H. Gulden*, Scott Tykodi#, Jeffrey Shabanowitz*, Thomas Braciale# & Donald F. Hunt*

*Department of Chemistry,and #Beirne Carter Center for Immunology Research and Department of Microbiology, University of Virginia, Charlottesville, VA 22901.

Major Histocompatibility Complex (MHC) membrane proteins present peptides to T cells of the immune system. Endogenously derived proteins, i.e., those produced inside the cell, are presented to $CD8^+$ T cells by Class I MHC. When an endogenously derived protein is either mutated by cancer or the result of a virus, peptides are produced that are foreign to the immune system. The recognition of a foreign peptide associated with Class I MHC by $CD8^+$ T cells initiates a Cytotoxic T Lymphocyte (CTL) response, resulting in death of the diseased cell.

The peptide sequence that elicits a CTL response when in complex with MHC is referred to as an epitope. Peptide epitopes are of use in the development of vaccines and therapies for viruses and cancer. Hemagglutinin, the major membrane-associated glycoprotein produced in cells as a result of influenza infection is known to contain epitopes recognized by CTL of individuals infected with the influenza virus.[1] Using cells transfected with hemagglutinin DNA, the goals of these studies were to 1) sequence influenza peptide epitopes derived from hemagglutinin, and 2) determine whether peptide affinity for MHC determines which foreign peptides are displayed on the cell surface.

Since Class I MHC proteins preferentially bind peptides with particular amino acids at certain positions (motifs)[2], it should be possible to predict which peptides of a foreign protein would bind to a particular Class I MHC allele. Peptides presented by Class I MHC molecules on the surfaces of hemagglutinin transfected cells were extracted and subsequently sequenced using a Finnigan-Mat TSQ 7000 instrument, following reverse-phase HPLC fractionation.

Of the eighteen synthetic K^d motif containing hemagglutinin peptides tested for K^d binding capacity, only the two that exhibited the greatest affinity, TYVSVGTSTL and LYQNVGTYV, were both present on the cell surface and able to stimulate a CTL response *in vitro*. These results indicate that peptide affinity for Class I MHC plays a crucial role in determining which peptides of a foreign protein will be presented to the immune system. Importantly, these data also show that the predicted influenza CTL epitopes are generated *in vivo*, lending support to the rational design of vaccines and therapies for intracellular pathogens employing synthetic peptides.

References:

1. Hahn, Y. S., et al. (1992) *J. Exp. Med.* **176,** 1335-1341.
2. Engelhard, V. H. (1994) *Annu. Rev. Immunol.* **12,** 181-207.

43rd ASMS Conference on Mass Spectrometry and Allied Topics

Table 1: Binding Capacity of Predicted Hemagglutinin K^d Epitopes

1st AA	1	2	3	4	5	6	7	8	9	10	IC50 (nM)
112	D	Y	E	E	L	K	H	L	L		200
204	L	Y	Q	N	V	G	T	Y	V		20
318	K	Y	V	K	S	E	K	L	V		400
433	T	Y	N	A	E	L	L	V	L		100
458	L	Y	D	K	V	R	M	Q	L		100
529	I	Y	A	T	V	A	G	S	L		40
156	S	F	F	R	N	M	V	W	L		40000
254	N	F	E	S	T	G	N	L	I		300
342	L	F	G	A	I	A	G	F	I		100
384	A	F	D	G	I	T	N	K	V		>100000
409	E	F	G	N	L	E	R	R	L		>100000
4	I	Y	L	I	L	L	F	T	A	V	60000
210	T	Y	V	S	V	G	T	S	T	L	20
318	K	Y	V	K	S	E	K	L	V	L	2000
9	L	F	T	A	V	R	G	D	Q	I	90
304	P	F	H	N	V	H	P	L	T	I	300
449	D	F	H	D	S	N	V	K	N	L	>100000
547	S	F	W	M	C	S	N	G	S	L	200

Table 1: Peptide sequences were chosen that fit the K^d binding motif Predominantly Y and sometimes F at position 2, L, I, or V at C-terminus. In the sequences listed, K^d anchor positions are underlined. Peptides were synthesized using standard FMOC chemistry with a Gilson AMS 422 peptide synthesizer Binding capacity was determined by binding inhibition of a known K^d influenza peptide epitope from nucleoprotein. The assay readout was Cr[51] release from lysed target cells

Table 2: Summary of HPLC, Mass Spectra, and CTL Assay Data

	Synthetic Peptide Data		HA Transfected Cell Extract Data	
	Elutes in HPLC Fr	CTL Activity?	In Corresponding HPLC Fr?	CTL Activity?
LYQNVGTYV:	20	Yes	Yes	Yes
TYVSVGTSTL:	20	Yes	Yes	Yes
IYATVAGSL:	21	Yes	No	Yes

Proteolytic Processing of Ovalbumin by the Murine Proteasome

Gina M. King, Jeffrey Shabanowitz, and Donald F. Hunt
University of Virginia, Charlottesville, VA 22901

Gabi Niedermann and Klaus Eichmann
Max-Planck-Institute for Immunology, Freiburg, Germany

A complex mixture of more than 10,000 peptide fragments derived from cellular proteins is displayed on the surface of nucleated mammalian cells by class I molecules of the major histocompatibility complex (MHC). Cytotoxic T lymphocytes (CTL), killer cells, bind to class I molecules, sample the peptides presented, and lyse those cells that display peptides derived from viral infection or other disease states. One mechanism for peptide presentation involves proteolysis of cellular proteins in the cytoplasm, followed by transport of peptides into the endoplasmic reticulum, a compartment where peptide-MHC I complexes are assembled. Once peptides become associated with class I molecules, the resulting complex moves to the cell surface. The initial degradation of proteins to peptides in the cytoplasm is thought to occur by a 700 kDa multi-component enzyme complex called a proteasome. The specificity of the enzymes in this complex determine, in part, which peptide fragments are generated from a particular protein and presented to the immune system. Cytokines such as interferon gamma and other cellular factors have been found to affect the cleavage specificity of the proteasome (1). Here we describe the use of mass spectrometry to follow the production of peptides from a portion of a 44 kDa glycoprotein, ovalbumin, by a murine proteasome.

Two different synthetic 22-mers, found in the ovalbumin amino acid sequence, were subjected to proteolytic degradation by the proteasome and sampled at various time points (only 36 hr. data shown). Digests were carried out in vitro with 20mM HEPES buffer, 5mM magnesium chloride, 1mM EGTA, 300 fmol of purified murine proteasome, and 5 nmol of peptide at pH=7 8 All degradation products were analyzed directly with a Finnigan TSQ700 mass spectrometer equipped with on-line microcapillary HPLC and electrospray ionization source. Peptide products were collisionally dissociated and sequenced. Relative abundances of peptides produced by the proteasome were determined by spiking known amounts of several peptide standards into the product mixture and performing co-elution experiments. The immunodominant peptide, SIINFEKL, generated from YVSGLEQLESIINFEKLTEWTS, was identified as the most abundant digestion product at all time points. This finding is consistent with other studies performed with ovalbumin derived peptides and proteasomes (2)(3). The SIINFEKL peptide binds with high affinity to the class I molecule and elicits a strong CTL response in vivo(2). The sub-immunodominant peptide, KVVRFDKL, generated from YTQINKVVRFDKLPGFGDSIEA, was identified as one of the least abundant digestion products at all time points. The KVVRFDKL peptide similarly binds with high affinity to the class I molecule but had not been detected on the cell surface as a processed antigen by CTL assays. Analysis of the products generated from the second 22-mer showed that the expected epitope was mostly cleaved in half by the proteasome, and only a very small amount of the KVVRFDKL peptide remained after the 36 hour digestion. KVVRFDKL was not present at detectable levels in the 72 hour digest (data not shown).

Since both peptides discussed bind with similar affinities to MHC-I molecules but only the SIINFEKL peptide is produced in large quantities after digestion with the proteasome, we conclude that peptides must be generated in sufficient quantities by the proteasome to be detected by the immune system. Our study demonstrates that the enzyme specificity of the proteasome complex contributes to the selection of protein fragments presented to the immune system. Studies on processing two synthetic 44-mers and the native protein are in progress.

43rd ASMS Conference on Mass Spectrometry and Allied Topics

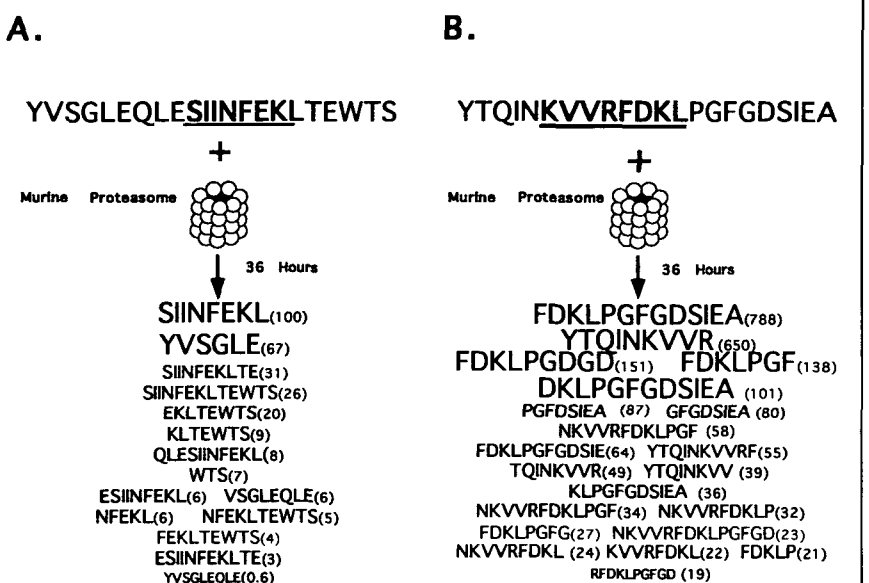

Fig. 1 **Murine Proteasome Digestion of Two Ovalbumin Derived Peptides**
A. An ovalbumin derived peptide containing SIINFEKL, the immunodominant epitope, digested with a murine proteasome for 36 hours. SIINFEKL is the most abundant peptide produced
B. A second ovalbumin derived peptide containing KVVRFDKL, the sub-immunodominant epitope, digested with a murine proteasome for 36 hours. KVVRFDKL is found only at a very low concentration relative to other peptide products. All digestion products are shown with relative total picomole concentrations in parentheses.

1. Akiyama, K. et al. (1994) Science, 265:1231-1234.
2. Niedermann, G. et al. (1995) Immunity, 2:289-299.
3. Dick, L. R. et al (1994) J. Immunol., 152:3884-3894.

Identification of endo-HEL Peptide Fragments Presented by MHC Molecules.

* I. Vidavsky†, A. B. Whitehill†, M. L. Gross†, C. A. Nelson‡, N. J. Viner‡, E. R. Unanue‡.

† Department of Chemistry, Washington University, St. Louis, MO 63130.
‡Department of Pathology, School of Medicine, Washington University, St. Louis, MO 63110.

The immuno response of T cells requires an antigen to be recognized. We have demonstrated before[1] with the model protein antigen Hen Egg Lysozyme (HEL), that this response to proteins involves unfolding and degradation to peptides that are recognized on the surface of antigen-presenting cells (APC) in association with the major histocompatibility complex (MHC) molecules. Previous results[2,3] showed that T-cells, after activation by I-A^k type APC, respond to a synthetic 10-mer residue, HEL 51-62. Similarly, T cells after activation by I-E^k type APC, respond to a 13-mer, HEL 84-96. HPLC chromatography of the mixture extracted from MHC class II complexes of APC after treatment with HEL gave the immuno active fractions that were analyzed by MALDI-TOF and cf-FAB MS. The major components were HEL 48-63, 48-62, 48-61 for I-A^k type APC and HEL 84-97, 84-98, 84-102 for I-E^k type APC.

To extend the understanding of the protein antigen processing mechanism producing the peptides that are presented to the T cells, we started working on characterizing peptides produced from a series of mutated HEL proteins. These m-HELs are engineered by oligonucleotide-directed mutagenesis of the cDNA that encodes the HEL, and produced by expression of HEL (or mutated HEL) genes in the APC. The mutation of HEL molecules was directed at altering the presentation of the 48-62 region, but preserving the structure and folding of wild HEL. The mutated HELs are modified also by adding a linker and a transmembrane segment. This strategy utilizes much lower amounts of protein(by several orders of magnitude) than used in external infusion, to allow study of mutated HELs.

To test the feasibility of this strategy, initial studies were done on peptides extracted from the MHC of I-A^k type APC expressing a gene encoded for wild type HEL, a 14 amino-acid linker and a 30 amino acid transmembrane segment. Two main peptide fractions were found to be immuno active. These fractions were studied by MALDI-TOF. Initial study by linear MALDI-TOF found the immuno active fractions to be cleaner than those from the experiment where HEL was infused externally, and the fractions contain one main peptide. The higher amount of immuno active peptide allowed reflectron-TOF measurements at unit resolution to confirm the molecular weight to within 100 ppm or better accuracy (when external calibration was used). Comparison of the measured M.W. to those of all the possible peptides containing the critical epitop gave us two candidates peptides, HEL 48-62 and HEL 48-63. PSD spectra of the two peptides and comparison to a synthetic analog allowed complete sequencing. The structure of these peptides was determined to be DGSTDYGILQINSRW and DGSTDYGILQINSRWW, which is HEL 48-62 and 48-63 (see figure 1). This result is nearly the same as that obtained previously[1].

Thus, sufficient amounts of HEL are generated and processed within the cell to allow characterization of the recovered fragments by this stategy. APC cells expressing mutated HELs proteins are currently being grown, and characterization of the peptides presented would allow detailed investigation of antigen processing and fragment binding to class II MHC molecules.

References
1. Vidavsky, I.; Whitehill, A.B.; Gross, M.L.; Nelson, C.A.; Viner, N.J.; Unanue, Emil R. Proc. 42nd Amer. Soc. Mass Spectrom. Conf., Chicago, 1994, p. 434.
2. Nelson, C.A.; Roof, R.W.; McCourt, D.W.; Unanue, E.R. Proc. Natl. Acad. Sci. USA 1992, 89, 7380.
3. Nelson, C.A.; Petzold, S.J.; Unanue, E.R. Proc. Natl. Acad. Sci. USA 1993, 90, 1227.

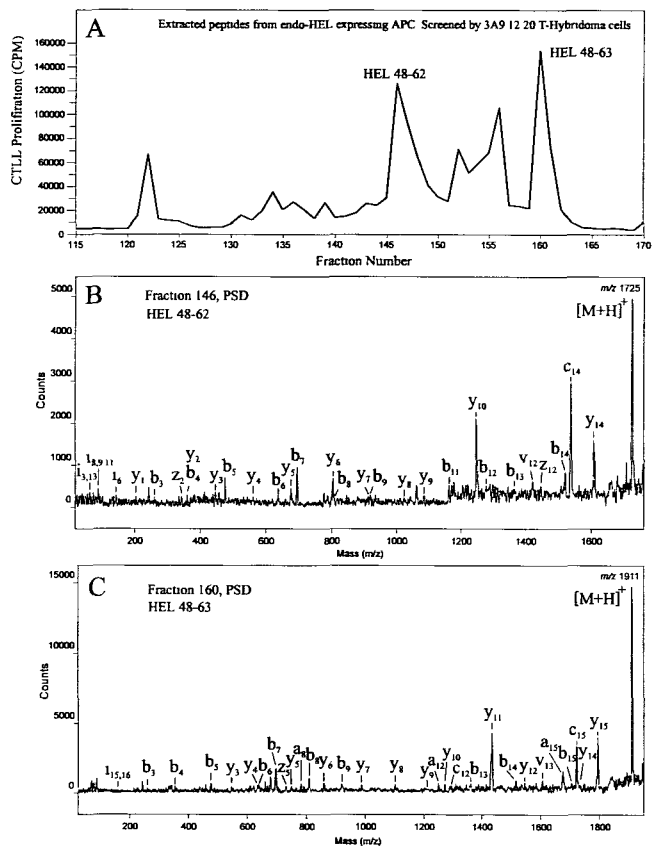

Fig. 1 A.HPLC of peptides from MHC. The PSD spectra are shown as B. and C.

Analysis of Invertebrate Hemoglobin Chains by ESI-MS and ESI-MS-MS.

B N Green, VG Organic, Tudor Road, Altrincham, Cheshire WA14 5RZ, UK.
S N Vinogradov, A. R Kuchumov, Biochemistry Dept, Wayne State University, Detroit, MI 48201, USA
R W. A. Oliver, BMA Research Unit, University of Salford, Salford, M6 4WT, UK

Annelid hemoglobins (Hbs) have a high mass (~3 5MDa) and consist of ~144 functional globin chains (16-18kDa) and ~36-40 linker chains (24-32kDa) necessary for the formation of the native structure Some of the different chains are monomeric but others form disulphide-bonded multimers e.g dimers (leech), trimers (earthworm) or tetramers Also, depending on the species, some chains are glycosylated. Thus the mixture of proteins produced from denatured annelid Hbs is generally complex e g denatured earthworm Hb contains ~15 major proteins and glycoproteins with molecular weights between 16 and 53kDa

A basic step in investigating the tertiary structure of these Hbs is to determine the precise masses of the non-covalently bound proteins present in the native molecule and also, by reducing and reducing/derivatising the native Hb, determine the masses of the chains which make up the multimers From such data, particular chains can be unambiguously associated with particular multimers and chain sequences (if known) validated. We have used electrospray ionisation mass spectrometry (ESI-MS) with maximum entropy (MaxEnt) processing of the m/z data to analyse several native annelid Hbs and their reduced/derivatised/ deglycosylated products without prior chromatographic separation MaxEnt automatically disentangles the complex multiply-charged data as it is originally produced by the mass spectrometer and presents each protein as a single peak on a true molecular weight scale The precision of mass measurement from ESI-MS-MaxEnt data is generally better than 0 01% MaxEnt also enhances the resolution

Samples (0 2-0 5μg/μl of 50% aqueous CH_3CN plus 0.2% HCOOH) were analysed on a VG Quattro II Scanning was from m/z 550-2500 (10sec/scan) and data collected over 5-10min Data were processed using the MaxEnt software supplied with the instrument.

Spectra from a marine worm (*Tylorrhynchus*) Hb are shown as typical examples in the Figure Panel (A) shows the m/z data from the native Hb and (B) after processing by MaxEnt Present are a monomer (M), linker degradation products (L3-L5), a trimer (T) and a dimer (D). Panel (C) is the result from mildly reduced Hb showing the appearance of 3 trimer chains (IIA, IIB & IIC) and 2 linkers (L1 & L2) which are dimeric in the native Hb. The reduced Hb (5μg/μl Hb in H_2O +2mM DTT) was analysed after simple dilution (x1/10) i.e without purification Panel (D) is the result from fully reduced/carbamidomethylated (Cam) Hb, showing all the chains, except the monomer, plus an appropriate number of Cam groups

Below are summarised the masses for *Tylorrhynchus* (3 determinations) derived from the reduced/Cam data (Reduced Mass) and are within 0.01% of the masses calculated from the sequences with Cys reduced (Sequence Mass) Measurements from the native Hb (Native Mass) agree well with the masses Calculated from Reduced Masses when allowance is made for the number of disulphide bonds present The measured mass of the monomer is outside experimental error of the sequence mass, inferring the sequence is incorrect

Chain	Reduced Mass	Sequence Mass	Subunit	Native Mass	Calc. from Reduced Masses
M	Not detected	15704 9	(M)	15575 4	
IIA	16601 9	16602 0			
IIB	16680 4	16680 0			
IIC	16794 0	16794.9	T	50068 4	T=IIA+IIB+IIC-10H=50066 2
L5	23243.8	23242 8	(L5)	23233 8	L5-10H=23233 7
L4	Not detected	24843 8	(L4)	24835.4	
L3	25336 0	25335 4	(L3)	25326.9	L3-10H=25325 9
L2	26317 2	26316.2	D2	52609.4	2L2-24H=52610 2
L1	28202 2	28200 5	D1	Not detected	

43rd ASMS Conference on Mass Spectrometry and Allied Topics

Results: *Tylorrhynchus heterochaetus* (marine worm)

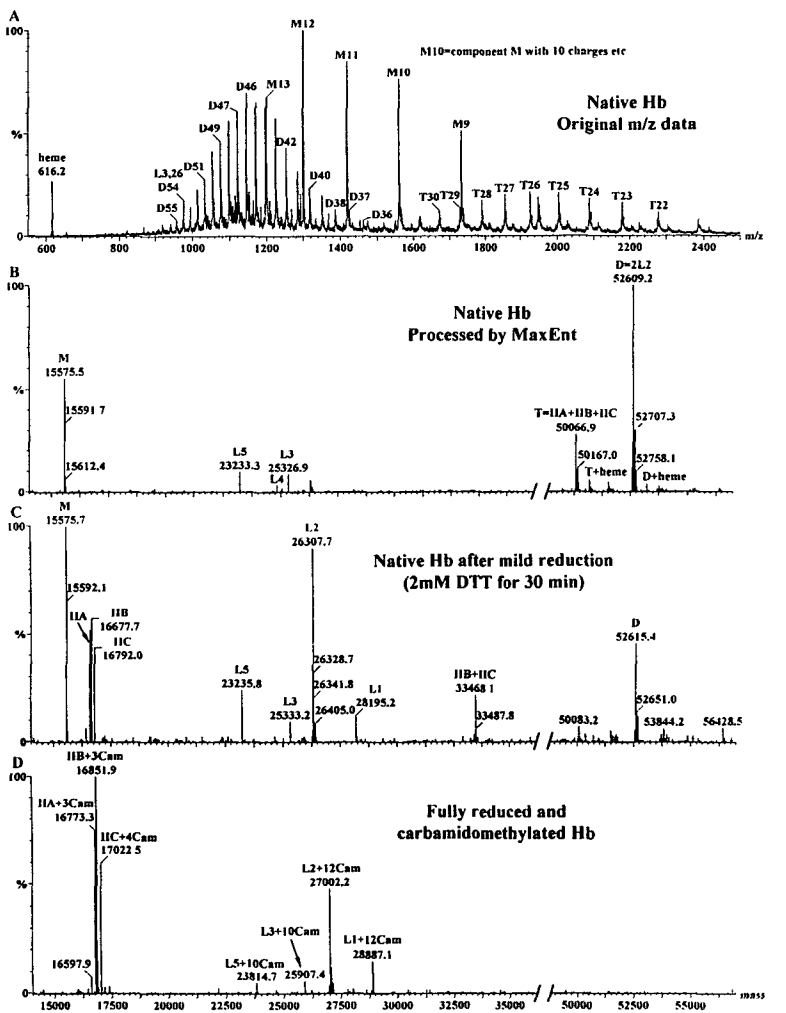

CHARACTERIZATION OF THE HEMOGLOBIN OF *CEBUS APELLA* BY MALDI-MS

Tun-Li Shen[1], Robert B. Johnson[2], Steven Buck[2], Morris Goodman[2], and Douglas A. Gage[1]
[1]Department of Biochemistry, Michigan State University, East Lansing, MI 48824
[2]School of Medicine, Wayne State University, Detroit, MI 48202

The primary function of hemoglobin, a tetrameric molecule that consists of four globin chains, is to transport oxygen in vertebrates. Hemoglobin in adult vertebrates has the structure $\alpha_2\beta_2$, and fetal hemoglobin has the structure $\alpha_2\gamma_2$. The timing and control of the expression of globin genes during development varies among different species[1]. Like humans, the primate *Cebus apella* has two γ-globin genes. Genetic analysis indicates both genes have potential to encode a complete γ-globin chain. The main objective of this work is to establish the identity of the γ-globin chain(s) expressed in the fetus of *C. apella*.

The primary structure of the *C. apella* γ-globin chains deduced from the cDNA sequence are shown below. The two γ-globin chains have the same structure except the amino acid residue 117 of the Cebus apella γ1-globin chains is Val rather than Ile; γ1: MW 15923, γ2: MW 15937.

1 MSNFTAEDKAAITSLWAKVNVEDAGGETLGRLLVVYPWTQRFFDSFGSLS
51 SPSAIMGNPKVKAHGAKVLTSLGEAIKNLDDLKGTFGQLSELHCDKLHVD
101 PENFRLLGNVLVTVLA*I*HHGKEFTPEVQASWQKMVAGVASALGSRYH

The γ-globin chains of *C. apella* were characterized by the following MALDI-MS experiments: molecular weight measurements, tryptic digestion and peptide mass mapping, and TCEP reduction of intact globins and tryptic peptides. All the MALDI spectra were obtained on PerSeptive Biosystems Voyager Elite mass spectrometer. Experiments were performed using α-cyano-4-hydroxycinnamic acid as the matrix. Tryptic digestion were carried out in 400 mM TrisHCl (PH 8.0), 6 M guanidine, 40 mM $CaCl_2$, sequencing grade modified trypsin was then added with a protein/enzyme ratio ~ 20 (W/W). Digestion mixtures were analyzed by MALDI-MS without further fractionation or purification. Tris(2-carboxyethyl)phosphine hydrochloride (TCEP) is an effective reagent for complete reduction of disulfide bonds[2]. Reduction of the globin chains were carried out with a fifty-fold molar excess of TCEP solution in a water bath at 37° C for half an hour.

The molecular weight of three rpHPLC-purified globin chains suggested that γ2-globin chains are the predominant polypeptide chain expressed in fetal *C. apella*. One peak CaE displayed MH^+ ion at 15137 close to the predicted mass of γ2 containing the initiator methionine. The MALDI spectrum of a second globin peak contained a MH^+ ion at m/z 15852, which is consistant with γ2 globin that is N-acetylated at ser-2 after loss of the initiator methionine. The MH^+ ion of a minor HPLC peak, CaD, did not correspond to the predicted mass of any globin chain. The observed MH^+ ion at m/z 16162 (see Figure 1) was approximately 300 Da higher than that expected for the γ2 chain (with ser-2 N-acetylated). Since this mass increment is close to that produced by a glutathione adduct (+305Da, γ-glu-cys-gly), we speculated that this modification could have produced the mass discrepancy. Therefore, a reduction experiment to remove the putative glutathione adduct which supported this hypothesis was carried out (see Figure 1 inset).

The key tryptic peptide that distinguishes the globin γ1- from γ2- globin is the fragment that encompasses the amino acid residue 117 (Val vs. Ile, Δ 14 Da). The sequences for the key peptide fragments of γ1-, and γ2- globin chain are: [106-121]

43rd ASMS Conference on Mass Spectrometry and Allied Topics

γ2: LLGNVLVTVLA*I*HHGK (MH^+ at m/z = 1684); γ1: LLGNVLVTVLA*V*HHGK(MH^+ at m/z = 1670)

The results from the tryptic digests show that all globins contain the MH^+ ion at ~ m/z 1684 and are thus γ2. Treatment of HPLC fraction CaD with TCEP, followed by MALDI-MS analysis supported. The TCEP reduction of the CaD tryptic digest produced a mass shift of ~ 300 Da for the m/z 2850.6 peak to m/z 2540.6 which corresponds to peptide [84-105] (calculated m/z 2542), which containing cysteine-94.

REFERENCES

1. K. Hayasaka, C G. Skinner, M. Goodman, and J. L. Slightom, *Genomic*, 18, 20 (1993).
2. E. J . Zaluzec, D. A. Gage, and J. T. Watson, *J Am. Soc. Mass Spectrom.* 5, 359(1994).

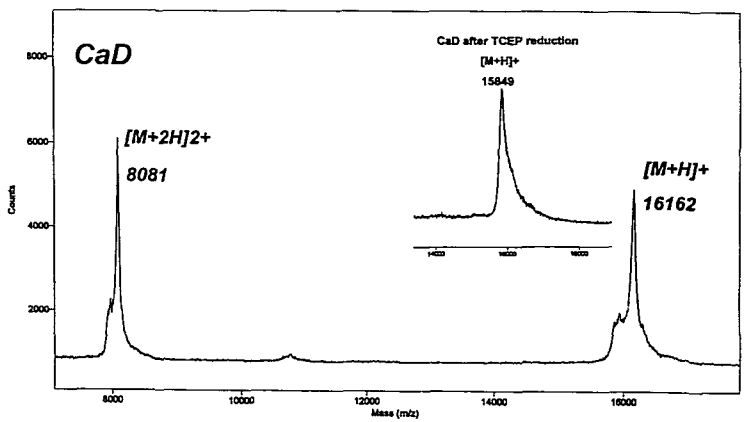

Figure 1. MALDI spectrum of CaD showing a prominent peak at m/z 16,162 for the protonated molecule, with a corresponding doubly-charged peak at m/z 8081. A shoulder is present on the low mass side of the $[M+H]^+$ peak which is close to m/z 15842. Reduction of the sample with TCEP produced a shift in the mass of the product from m/z 16,162 to 15189 (see inset). This shift in mass is close to that expected for the reductive cleavage of a glutathione adduct. Thus the peak at m/z 16,162 is interpreted to represent γ2 modified by glutathione addition.

CHARACTERIZATION OF THE HEMOGLOBIN FROM *BUENOA SCIMITRA*

Z. R. Kong,[§] K. L. Rinehart,[§] C. R. Vossbrinck,[†] R. Huang,[§] R. M. Milberg,[§] F. R. Sun [§]

[§] School of Chemical Sciences, University of Illinois, Urbana, IL 61801
[†] Office of Agricultural Entomology, University of Illinois, Urbana, IL 61801

Introduction

Hemoglobins have been found in the tissues of only four groups of insects: chironomids, gasterophilids, notonectids, and corixids. Because of their unusual functions, the hemoglobins from the Notonectidae, including *Buenoa* and *Anisops*, are particularly interesting,[1,2] but the structures, properties and functions of the hemoglobins in *Buenoa* remain unexplored. In order to understand the structure and function relationship of *Buenoa* hemoglobin, it is essential to know the protein sequence. The amino acid sequence of the hemoglobin's major component (Hb) from *B. margaritacea* was assigned previously.[3] Due to their similar functions in the insects' lives, it was assumed that the sequence of *Buenoa scimitra* Hb was similar to that of *B. margaritacea* Hb. In this work, we present mass spectrometric strategies and results in the characterization of the primary structure of *B. scimitra* Hb.

Experimental

Hemoglobin was collected from the insects' abdomens as described previously.[4] Purification of Hb was performed using reversed phase HPLC with CH_3CN (0.045% TFA and 10% H_2O) and H_2O (0.05% TFA) being used as delivery solvents.

Tryptic digestion of Hb was accomplished using trypsin in NH_4HCO_3 and urea solution (pH 8.4). *S. aureus* V8 digestion of Hb was accomplished using endoproteinase Glu-C in Na_2HPO_4 buffer (pH 7.7). The enzyme to substrate ratio was 1:50 (wt/wt).

ESIMS spectra were acquired on a VG Quattro mass spectrometer. LR/FAB spectra were obtained on a VG ZAB-SE mass spectrometer. MALDI spectra were acquired on a VG Tof-Spec time-of-flight mass spectrometer with a UV (337 nm) nitrogen laser. HR/FABMS data and FABMS/MS spectra were obtained on a VG 70-SE 4F mass spectrometer.

Results and discussion

Tryptic digestion of purified Hb yielded more than 20 peptides. Comparison of these results with those of *B margaritacea* revealed that most of peptides were expected, but some were unexpected $(M+H)^+$ ions. It was assumed that the expected peptides had the same amino acid sequences as those of *B. margaritacea*. These expected peptides were further characterized by MS/CID/MS and HR/FABMS.

For the unexpected $(M+H)^+$ ions, including *m/z* 2310, 1368, 933, 904, amino acid sequencing was only achieved on an ion at *m/z* 467.4, which was a doubly charged ion corresponding to the peptide at *m/z* 933. The amino acid sequence, H-TLQEMGVR-OH, was deduced from the CID spectrum (Figure 1). This sequence corresponded to amino acid positions 91-98, with Lys replaced by Arg at position 98 in the primary structure of *B. margaritacea* Hb.

S. aureus V-8 digestion was performed on Hb under specific conditions so that the protein was specifically cleaved at C-terminal aspartic acid and glutamic acid residues. The digest was analyzed by LC/ESIMS, ESIMS and MALDIMS. Comparison of these results with those from computer-assisted *S. aureus* V-8 digestion of *B margaritacea* Hb revealed that a peptide containing the amino acid homolog, Arg-98, showed up in the digest.

The enzymatic digestions provided two sets of Hb peptides. Proper alignment of these peptides was accomplished, which led to the Hb sequence. When Lys-98 in *B. margaritacea* Hb is replaced by Arg-98 in *B. scimitra* Hb , the molecular weight shifts to 17,707 Da by an increase of 28 mass unit. This molecular weight matches the experimental molecular weight determined by ESIMS, suggesting that there was only one amino acid difference between the two hemoglobin's major components.

Because the specificity of enzymes cannot be relied upon all the time, unexpected cleavages are frequently encountered. A computer-assisted search for the possible amino acid sequences of unexpected peptides was performed.

Conclusion.

The primary structure of *B. scimitra* Hb has been assigned by mass spectrometric methods. Comparison of this sequence with that of *B. margaritacea* Hb leads to the conclusion that there is only one amino acid difference. Their sequential similarity suggests that the Hb tertiary structures in the *Buenoa* genus are similar, which lead to similar functions and properties of the hemoglobins in the insects' lives. It has been reported that the functions of the hemoglobins are cooperative, that is, the binding of oxygen at one heme facilitates the binding of oxygen to the other hemes. Therefore, it is necessary to explore the hemoglobin's minor components. Protein sequencing of the hemoglobin's minor components is in progress.

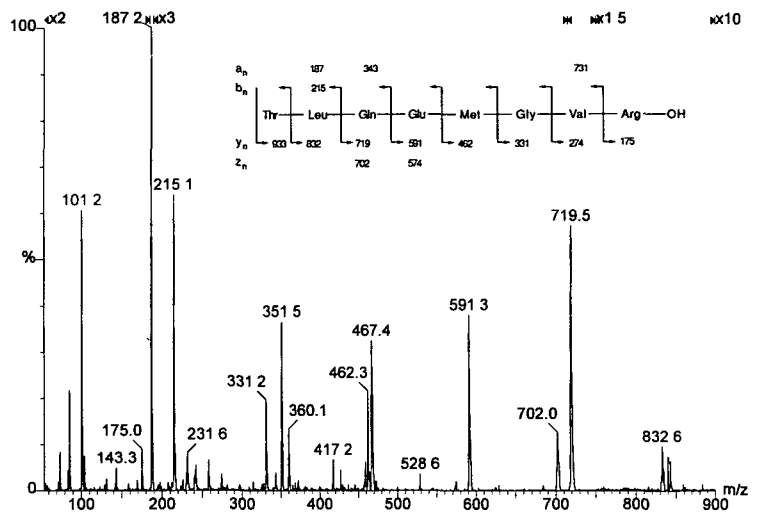

Figure 1. ESIMS/CID/MS spectrum of $(M+2H)^{2+}$ ion *m/z* 467.4

1. Hungerford, H.B. *Can. Entomol.* **1922**, *54*, 262.
2. Wells, R.M.G.; Hudson, M.J.; Brittain, T. *J. Comp. Physiol.* **1981**, *142*, 515.
3. Li, H. M.S. Thesis University of Illinois, **1994**.
4. Vossbrinck, C.R.; Odsmulski, P.A.; Debrunner, P.G. *Insect Biochem. Molec. Biol.* **1993**, *23*, 421.

HEMOGLOBIN ANALYSIS BY ELECTROSPRAY IONIZATION MASS SPECTROMETRY: QUADRUPOLE vs. MAGNETIC SECTOR.

Earl L. White, Mary S. Uhrig, Betsy A. Reed-Bombick and Inhou Chu, Product Evaluation Group, Research and Development Department, R.J. Reynolds Tobacco Co., Winston-Salem, NC 27102

INTRODUCTION

A method to detect relatively small changes in molecular weight of macromolecules was necessary to investigate intact hemoglobin molecules for possible adduct formation. Electrospray ionization mass spectrometry (ESI-MS) is a soft ionization technique whose utility is best suited for molecular weight determination of large molecules. Hemoglobin is a large tetrapeptide containing a pair of α- and non-α chains with 141 and 146 amino acid residues each, respectively. Hemoglobin is believed to form covalent adducts with several compounds commonly found in the environment. ESI mass spectrometry utilizing both quadrupole and electric/magnetic sectors for analysis can be used for studying macromolecules. Human hemoglobin samples were analyzed with both of these techniques and compared. The objective of this study was twofold. 1). To compare ESI-MS hemoglobin data from quadrupole and magnetic sector mass spectrometers. 2). To determine if relatively small molecular weight differences (~100 daltons) could be detected in intact hemoglobin from human lysate samples.

EXPERIMENTAL

Sample Collection and Preparation. Ten mL of blood sample were centrifuged to generate packed red blood cells, wash three times with 0.9% saline and lyse w/deionized water. The lysate was then washed with toluene to remove small organic compounds, centrifuged and dialyzed at 4 °C for 2 days. The hemoglobin lysate samples were diluted 1000 fold with a 0.1% formic acid-MeOH or $CH_3CN:H_2O$ (50:50) solution, filtered with a Amicon 10kDa cut-off filter and desalted with 200 μL of 0.1% formic acid.

Electrospray Ionization Mass Spectrometry. A Fisons Quattro II and AutoSpec EQFPD mass spectrometers were used for analyses. Ionization mode was positive ion electrospray. The scan range was 980-1300 amu and a scan time of 5 seconds/decade for the sector instrument. The sample was introduced by loop injection and the mobile phase was 50:50 $MeOH:H_2O$ + 1% acetic acid. The flow rate was 10 μL/min.

DISCUSSION

Quadrupole Data:

AFS Control (adult, fetal and sickle cell) was used for calibration of the instrument. Maximum entropy calculations (MaxEnt®) were performed to further enhance the resolution. The results of desalting was clearly demonstrated.

Magnetic Sector:

The expanded region of an ESI spectrum acquired at a resolving power of 15,000 (m/z = 1007-1012 amu, z≈15 for α-chain) depicted well resolved ^{13}C contributions. However, spectra acquired at nominal mass resolution closely resembled that of the quadrupole.

43rd ASMS Conference on Mass Spectrometry and Allied Topics

RESULTS

Molecular weights for adult human α- and β-hemoglobin chains were found to be 15,126.36±0.02 and 15,867.49±0.51 Da (quadrupole) and 15,126.01±0.48 and 15,867.48±0.92 Da (magnetic sector), respectively. Molecular weights for the heme plus α-chain (15,741 Da) and heme plus β-chain molecular weight (16,482 Da) were easily determined by both techniques. Glycated α- and β-chains (m/z = 15,288 and 16,029 Da, respectively) were detected with both systems, but with more interference in the quadrupole analysis. These results show that relatively small differences in the molecular weight of hemoglobin can be detected with this technique allowing exploration of adduct formation. Data from the magnetic sector instrument were superior, even at nominal-mass resolution. Maximum entropy calculations appeared to enhance resolution such that quadrupole analyses might be sufficient for exploring adduct formation.

SUMMARY

Electrospray ionization mass spectrometry was used to show that relatively small differences could be easily detected with this technique. The accuracy of the technique was found to be 0.003% (daltons), on the average. Molecular weight increments/decrements greater than 14 daltons could be easily detected. Deconvoluted/transformed spectrum for AFS sample indicates that a higher resolving power would significantly enhance the capabilities for detecting small molecular weight differences and would be required for detecting molecular weight changes less than ± 14 daltons. Desalting samples reduced Na^+ and K^+ adduct formation, therefore enhanced resolution for minor component detection.

Table 1. Expected vs. Observed Molecular Weights for Various Globulin Chains of Hemoglobin.

	Molecular Weight (Da)		
Hemoglobin Chain	Expected	Observed*	%RSD
α-Chain	15,126.4	15,126.9	0.003
β-Chain	15,867.2	15,868.1	0.006
A_γ-Chain (fetal)	15,995.3	15,995.4	0.001
G_γ-Chain (fetal)	16,009.3	16,009.2	-0.001
Mutation			
HbS - β-Chain [A_2 (β-6-Glu→Val)]	15,835.2	15,839.7	0.028
Glycated			
α-Chain	15,288.5	15,289.2	0.005
β-Chain	16,029.4	16,029.0	-0.003
+ Heme			
α-Chain	15,741.4	15,740.7	-0.004
β-Chain	16,482.2	16,481.4	-0.005

* - Observed include both quadrupole and magnetic sector analyses.

Electrospray Tandem Mass Spectrometry of Normal and Aberrant Haemoglobins.

Scott. G. Summerfield, Andrew Johnson* and Keith R. Jennings.
Department of Chemistry, University of Warwick, Coventry, CV4 7AL, U.K.
*Institute of Child Health, Guild St., London, WC1N 1EH, U.K.

Aberrant haemoglobins in the blood of humans may have a range of effects on the carrier from no abnormal activity to severe conditions such as sickle cell anaemia. Most clinical conditions are due to the variation of one or two amino acids along the alpha chain (141 residues, 15126.4 Da), the beta chain (146 residues, 15867.2 Da) or the delta chain (146 residues, 15924.3 Da) of the haemoglobin unit, altering both the primary structure of the protein, and in many cases, its mass. Multiply-charged ions of the intact chains may be observed by means of electrospray ionisation (ESI) and a quadrupole mass analyser

The masses of the alpha and beta chains can be measured to within 0.01% so that a shift in mass as low as 1 Da can be detected. Where variant and normal chains coexist, a difference of 6 Da can be detected. This study has led to the development of optimised conditions for the electrospray ionisation of a range of haemoglobins for both ESI/MS and ESI/MS/MS. Results are illustrated by CID of the human δ chain.

Low energy CID of the δ chain (15924.3 Da) of Hb A_2 is shown in Figures 1 and 2 for the $[M+17H]^{17+}$ ion where approximately 40% of the amino acid sequence may be identified from the C- and N-terminal ions. The sequence ion series b_2 to b_{47} and y_1 to y_{111} cover the entire δ chain so that the position of an amino acid substitution may be located along the molecule.

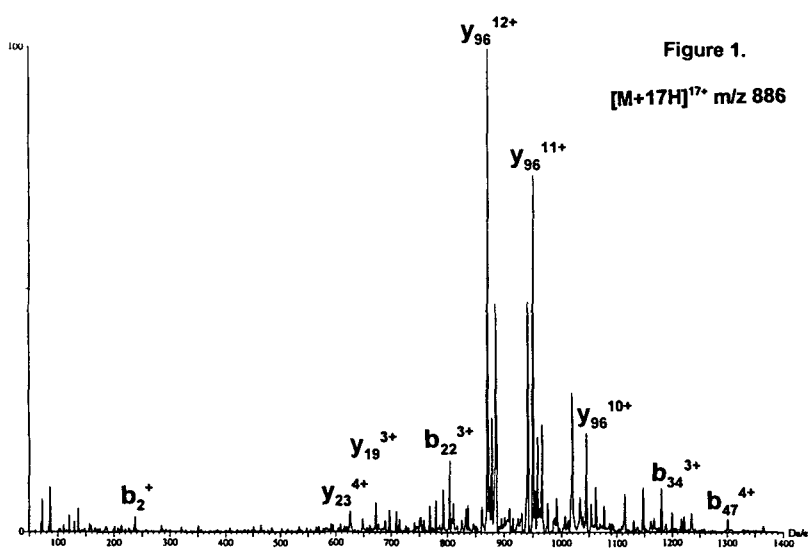

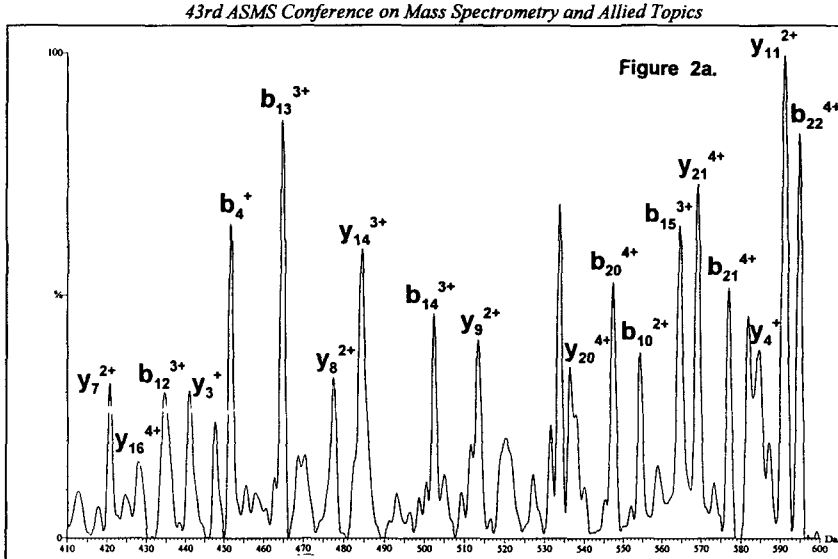

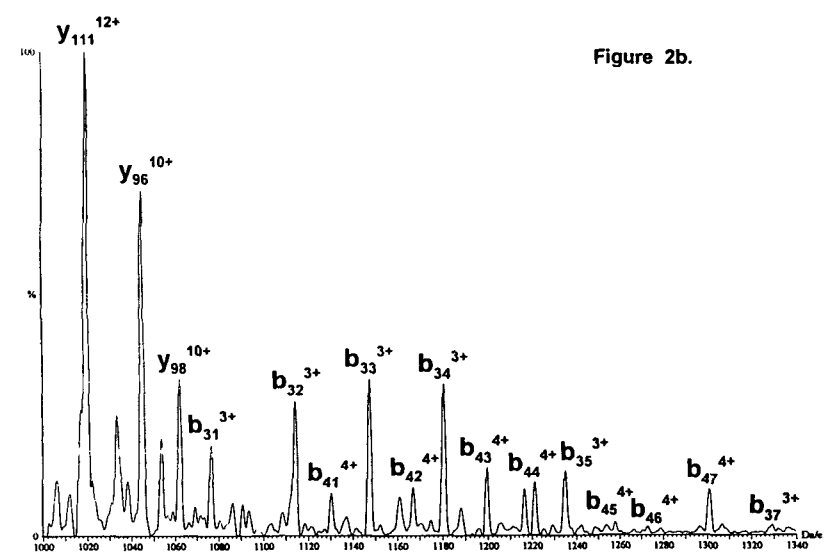

ISOLATION AND IDENTIFICATION OF GLOBULIN CHAINS OF HUMAN HEMOGLOBIN BY ELECTROSPRAY IONIZATION MASS SPECTROMETRY.

Inhou Chu* and Earl L. White, Product Evaluation Group, R.J. Reynolds Tobacco Company, Bowman Gray Technical Center, Winston-Salem, NC 27102

Introduction

Separation and quantification of hemoglobin adducts present a great challenge to many scientists [1]. GC/MS continues to be the method of choice for the analysis of hemoglobin adducts, even though laser-induced fluorescence spectrometry has shown some promising results [1]. In order to determine hemoglobin adducts by GC/MS, the adduct molecule has to be released from the hemoglobin and converted to a volatile form amenable to gas chromatography. This requires hydrolysis and derivatization of the samples which might be very destructive and sometimes, produces artificial results [1]. Aromatic amine adducts, for example, might generate free aromatic amines after the conversion which are indistinguishable from free amines that might arise from other sources.

We have initiated a systematic research program to study the interactions between hemoglobins and aromatic amines directly. Here, we present some of our initial results which include both isolation and identification of the globulin chains by HPLC/MS. Other approaches include enzymatic digestion of adduct molecules and synthesis of samples with higher hemoglobin/adduct ratios which are still under investigation.

Experimental

Sample Preparation Blood samples in this study were collected from both smoker and non-smoker volunteers. The samples were centrifuged to give packed red blood cells. The red blood cells were washed three times with 0.9% saline, lysed by the addition of deionized water and extracted with toluene to remove small organic molecules. The globulin chains were prepared by adding hemoglobin lysate samples to cold acidified acetone solution. The resulting white precipitates (globulin chains) were separated with a type-40 filter paper and washed several times with HPLC grade acetone.

Instrumentation The instrument used in this work is a high flow rate (up to 1 ml/min.) HPLC-electrospray mass spectrometry system. The column effluent was split approx. 1:1 to both a UV detector and the mass spectrometer for simultaneous detection. The multiply charged electrospray ionization/mass spectrometry (ESI/MS) spectra of separated hemoglobin or globulin chains were deconvoluted to molecular ions and the masses between smoker and non-smokers globulin chains were compared.

The LC/MS interface was a dual stage electrospray ion source purchased from Analytica of Branford, Inc., (Branford, CT) and recently upgraded to accommodate high flow rates. A HP5988A quadruple mass spectrometer (Palo Alto, CA) operating in the full scan mode with a scan range of 600-1500 amu at 0.1 s/scan was used in all experiments. Applied voltages for the electrical elements were optimized while constantly infusing sample solution into the electrospray source. The most sensitive capillary exit potential (EL) was determined by monitoring the ion signal of loop injections of human hemoglobin sample (1/100 dilution). The observed peak area was plotted against EL to determine the optimum capillary exit potential for this investigation.

Result and Discussion

The two major peaks observed in the LC/MS chromatograms of human hemoglobin samples (Figure 1) were identified by ESI-MS as the β- and α-chains, (molecular ions of 15,865

Da and 15,126 Da, Figure 2), respectively. Total ion chromatograms from lysate samples and those precipitated with the cold acidified acetone solution were essentially identical, which suggests that hemoglobins were denatured prior to detection, possibly in the HPLC column. The next step of our researches will be focused on the analyses of synthetic hemoglobin-aromatic amine adduct molecules. The positive identification of the active binding site(s) of the human globulin chains can be accomplished by analyzing the enzymatic digested hemoglobin adduct molecules utilizing the same techniques employed here.

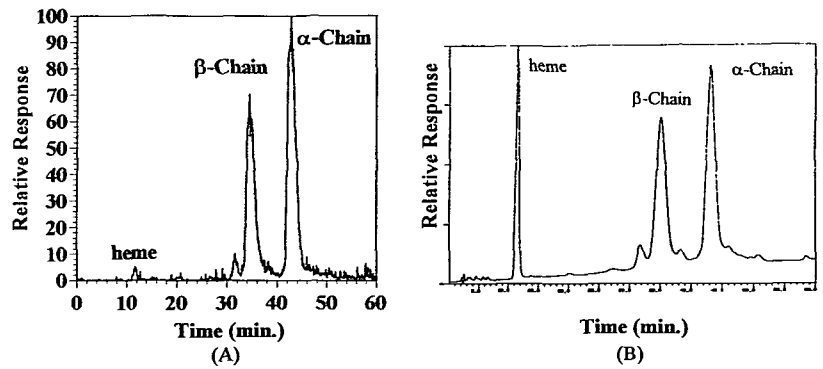

Figure 1. Chromatograms of (A) HPLC/MS and (B) HPLC/UV. Mobile phases: A: 60% CH3CN (0.1% TFAA) and B: 20% CH3CN (0.1% TFAA). Gradient: 50% A to 70% A in 15 min., followed by 70% A to 80% A in 30 min. HPLC column: Vydac C4 column.

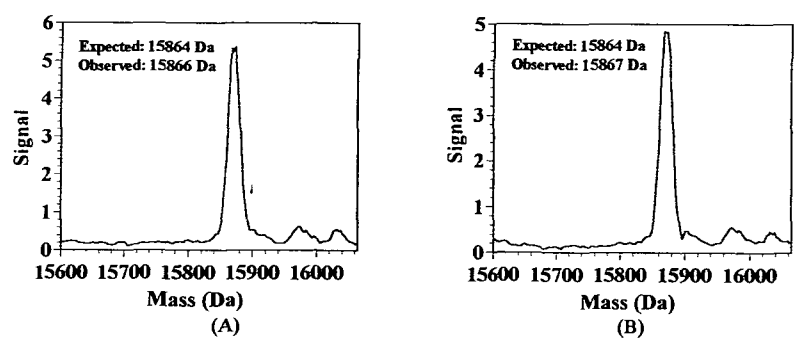

Figure 2. Deconvoluted spectra of (A) human α-chains (expected 15126 Da, observed 15126 Da) and (B) human β-chain (expected 15864 Da, observed 15867 Da).

1.Tannenbaum, S. R. and Skipper, P. L. Methods in Enzymology, 231, 625.

A Structural Assignment for a Stable Acetaldehyde-Lysine Adduct

[1]Karen P. Braun, [2]Robert B. Cody, [3]Dane R. Jones, and [1]Charles M. Peterson
[1]Sansum Medical Research Foundation, Santa Barbara, CA 93105
[2]JEOL USA, Inc., 11 Dearborn Rd., Peabody, MA 01960
[3]California Polytechnic State University, San Luis Obispo, CA

Introduction. Acetaldehyde is the first oxidation product of ethanol *in vivo*. Lysine residues in proteins such as hemoglobin have bee implicated as target structures for acetaldehyde adducts resulting from ethanol consumption. Although the presence of both stable and unstable acetaldehyde-hemoglobin adducts has been established, the structural characterization of the adducts has received relatively little attention. As a model for such adduct formation, we studied the peptide pentalysine *in vitro*. Pentalysine has several sites for adduct formation. The amino terminal amine group as well as the epsilon-amine groups of each lysine sidechain can serve as potential sites for modification by acetaldehyde. Mass spectrometry, nuclear magnetic resonance, and Raman spectroscopy were employed to demonstrate that acetaldehyde forms a stable linkage to lysine amine groups via a Schiff base.

Methods. *Sample preparation.* Pentalysine (1mM) was purified by reversed-phase HPLC prior to reaction with 1.5, 5, or 8 mM acetaldehyde and incubation at 37°C for 1 hour. Excess unreacted acetaldehyde was removed by ultrafiltration.

Mass spectrometry. Electrospray ionization (ESI) spectra were obtained by using a reverse-geometry double-focusing magnetic sector mass spectrometer (SX102, JEOL, Peabody, MA), equipped with an electrospray ionization source (Analytica, Branford, CT). Samples were diluted 1/10 with a 1:1 mixture of methanol/water containing 0.5% acetic acid and introduced into the ESI source by flow injection at 2µl/min. An unreacted sample of pentalysine was also analyzed as a blank. The ESI mass spectra were dominated by doubly charged species and a trace of singly charged species. Linked scan MS/MS spectra (He collision gas) were also obtained for the doubly charged species from the adduct ions by decreasing the accelerating voltage by 0.5.

Fast atom bombardment (6 keV Xe fast atom beam) mass spectra were also obtained for the samples by using another magnetic sector mass spectrometer (HX110, JEOL, Peabody, MA) and a glycerol matrix.

Results: When a 1.5:1 mole ratio of acetaldehyde to peptide was used, a monadduct was observed (data not shown). Likewise the deconvolved ESI mass spectrum of the model peptide (lys)5-OH following incubation with 20 µM acetaldehyde showed a single acetaldehyde adduct at mass 684 Da. However, when an excess of acetaldehyde was used, the number of

adducts observed increased. For the 8:1 mole ratio acetaldehyde:peptide mixture, five different adducts are observed with masses 684, 710, 736, 762, and 788 Da, respectively. The difference in mass in each case indicates a structure consistent with a Schiff base (a difference of 26 Da as shown in Figure 1, peaks labeled A,B,C,D, and E). Of particular interest is the decreasing relative abundance of adduct with increasing number of Schiff base adducts per molecule. In the sample shown, 40% of the peptide sample had at least 2 adducts, 20% of the molecules have at least 3 adducts, and less than 10% of the sample molecules have 4 or 5 adducts.

Linked scan MS/MS spectra were obtained to ascertain the points of acetaldehyde adduct formation (Table I). For these experiments, pentalysine-acetaldehyde adducts were generated by the addition of acetaldehyde in an 8:1 mole ratio (acetaldehyde to peptide). The pattern of y- and b-type fragment ions (y4+26 and b1+26 Da) is strongly suggestive of modification at the first and second positions of the N-terminus of the peptide. Weak b and y fragments for residues 3,4, and 5 suggest but do not confirm the presence of modifications on those sidechains.

Table 1. Observed product ions from linked scan for precursor m/z 684

N-terminal fragments	Observed b-ion mass	Observed b+adduct mass	C-terminal fragments	Observed y-ion mass	Observed y+adduct mass
b1	129.10	155.08	y1	147.11	-
b2	257.20	282.97	y2	275.21	-
b3	385.29	-	y3	403.30	429.41
b4	513.39	-	y4	531.40	557.37
b5	641 48	-	y5	659.49	-

Figure 1. Deconvoluted ESI mass spectrum of pentalysine reacted with acetaldehyde.

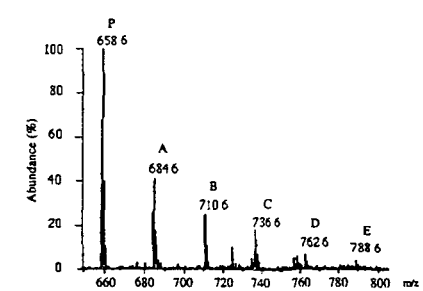

Variant Hemoglobin Characterisation by ES-MS/MS of Intact Globin Chains

Michael Morris, Brian N Green, H Ewa Witkowska[5] and Cedric H L Shackleton[5].
VG Organic, Tudor Road, Altrincham WA14 5RZ, UK
[5]Children's Hospital Oakland Research Institute, Oakland, CA 94609

Introduction

Mutations in the alpha and beta chains of human hemoglobins ('variant hemoglobins') may lead to serious physiological disorders in the host Mass spectrometry, in conjunction with separation techniques and/or enzyme digestion, has been in use for a number of years in the identification of hemoglobin variants [1,2] In using such methodologies, the structures of many known variants have been confirmed, and new variants have been characterised The advent of electrospray ionization, and its use in quadrupole-based instruments, now allows for the analysis of intact hemoglobin chains by analysing whole blood that has been diluted by a factor of 500 without other preparation

Methodology

Whole blood was diluted 500-fold in 1 1 acetonitrile water, containing 0 2% formic acid 10uL injections of the resultant solution were made into a solvent stream flowing at 5uL/min and passed to the ionization source of a VG Quattro II instrument Normal mass spectra were acquired by scanning from m/z980-m/z1400 in 8 seconds Product ion spectra were acquired after passing the mass-selected precursor ions of interest at appropriate resolution into a hexapole collision cell containing $2x10^{-2}$mbar of methane, and scanning the final quadrupole The collision voltage was typically ramped from 70V @ m/z50 to 45V @ m/z1500 during each 10 second scan in order to generate as much structurally-significant information as possible. Data were acquired for periods of up to 10 minutes

Results and Discussion

A sample was received from a patient believed to be the carrier of a variant hemoglobin beta chain Isoelectric focusing suggested that the variant was either Hb-Camden(Δm=+1) or Hb-Hope (Δm=+58), both of which were shown to be incorrect by mass spectrometry, which demonstrated a mass difference of +14Da, leading to 49 possible sites for single amino acid substitution Product ion spectra from the 16-protonated species from both the normal and the variants globins were compared and the mutation was determined to be in the first or second residue from the N-terminus from the comparison of the $\mathbf{b_2}$ ions in the partial spectrum shown in Figure 1 As the β_2 residue (His) cannot be replaced by single amino acid to give the necessary change in mass, the site of substitution was determined to the β_1 (Val→Leu/Ile) This is a previously unreported mutation, but is isobaric with Hb-Raleigh which shows a substitution at β_1 (Val→acAla). Further chemical analysis would be necessary to unequivocally determine the variant, although the number of possibilities is significantly reduced

An unknown hemoglobin variant was shown to contain a heterozygous alpha chain with a mass difference of 18Da, giving rise to 18 possible sites for single amino acid substitution of Met for Leu (human alpha globin contains no Ile) Product ion spectra from the 18-protonated normal and variant α-globins were compared and a difference was noted in the m/z values for the ion ascribed as $\mathbf{y_{12}}^{2+}$ (8 9Th) (Figure 2), locating the mutation in the final 11 residues of the molecule, at α_{136} Further evidence for the α_{136} mutation is derived from the presence of ions ascribed as $\mathbf{y_4}^+$ and $\mathbf{y_5}^+$ which are not shifted in the product ion mass spectrum of the variant Hemoglobin exhibiting the mutation α_{136} (Leu→Met) has previously been reported as Hb-Chicago

References

1 Y Wada *et al.*, Int. J Mass Spectrom Ion Processes, 122 (1992) 219-22
2 C H L Shackleton and H E Witkowska in D M Desiderio, Ed , 'Mass Spectrometry Clinical and Biomedical Applications', Plenum (1994) 135.

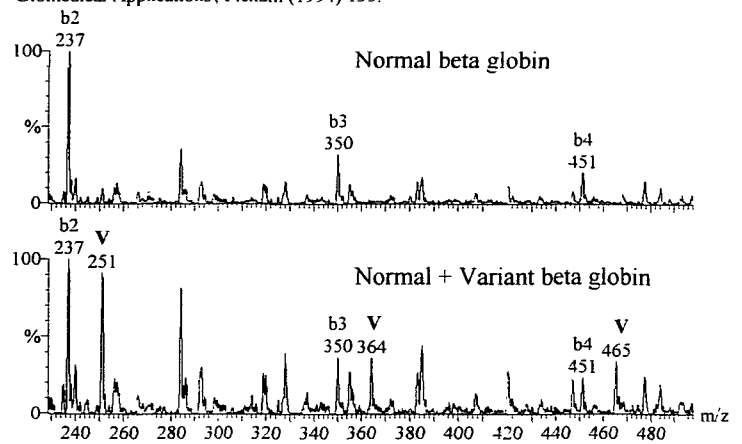

Figure 1 Comparison of the product ion spectra for Hb-Raleigh **V** = peak arising from variant

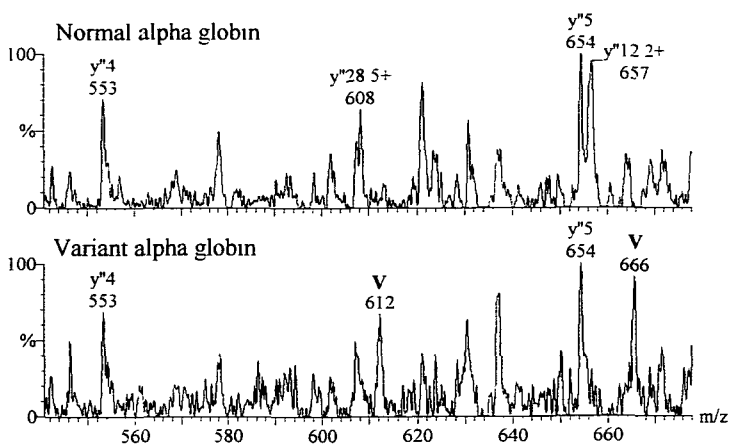

Figure 2 Comparison of product ion spectra for Hb-Chicago. **V** = peak arising from variant

Protein Mapping of Human Plasma Using Off-line HPLC-MALDI/TOF-MS

A. Ingendoh, H. Ikezawa, K. Seta, M Kanai, H Nakayama*, K. Uchida*, T Isobe and T. Okuyama*
Finnigan MAT Instruments Inc., 2-5-8 Hatsudai, Shibuya-ku, Tokyo 151, Japan
*Tokyo Metrop. University, Department of Biochemistry, Hachioji-shi, Tokyo 192-03, Japan

Introduction

For the analysis of complex physiological and biological samples that contain a large variety of different components, a highly resolved separation of the mixture is essential for the subsequent characterization of every single component. Common separation techniques for this purpose are SDS-PAGE, HPLC and CE Recently, Matrix-assisted Laser Desorption/ Ionization Time-of-Flight Mass Spectrometry (MALDI/TOF-MS) has been applied for mass determination of mixture components previously separated by the above methods Here, MALDI was used as a detector for the HPLC fractionation of human blood plasma The different fractions have been collected and mixed with matrix in the usual preparation, i.e. HPLC was coupled off-line to MALDI

Objective Human blood plasma contains a large variety of peptides and proteins in very different concentrations Is the combination of HPLC and MALDI capable to establish a protein map of such a complex mixture? Besides the number of detected proteins also the accuracy of their mass determination is a main criterion

Methods

Sample Preparation Human Blood Plasma was fractionated by two different modes

1. Reversed-Phase HPLC was used only, 29 fractions were collected.
2. The combination of Anion Exchange HPLC and Reversed-Phase HPLC was used, resulting in a more detailed separation into about 120 fractions

In both cases, 1µl of each fraction was mixed with 1µl matrix solution on the MALDI target Matrix was a 9:1 mixture of salicylic acid and 5-methoxysalicylic acid, dissolved at 10 g/l in 9 1 0 1% aeqeous TFA / acetonitrile The MALDI mass spectra were calibrated using Bovine Insulin, Cytochrome C or BSA regarding to the measured MW of the samples.

Exp Setup MALDI instrument was a VISION 2000 reflector-type TOFMS (Finnigan MAT)

Results

When human blood plasma is analyzed by MALDI directly, only a few proteins can be detected with a low signal intensity besides the main component, HSA (fig.1) This demonstrates that for a more detailed investigation a previous separation is essential. After reversed-phase HPLC (fig.3) each fraction still contained up to 10 different components (fig 2) to accelerate the MS analysis of the complete plasma and to avoid a too excessive dilution, that might lead to the loss of components with low concentrations Summarizing all fractions, about 80 diffferent peptides/proteins have been detected, among which ca 50 could be identified by comparison with databases (fig.4) The results of the more detailed fractionation by subsequent anion exchange and reversed-phase HPLC resembled those obtained by reversed-phase HPLC only. However, the latter, easier separation may even be more suited for off-line HPLC/MALDI, as more proteins could be detected MALDI provides for a high sensitivity for the detection of each species, as can be seen in the spectra of fractions that contain several proteins with quite different concentrations The biomolecules have been detected with an overall mass accuracy in the range of 0 033%

43rd ASMS Conference on Mass Spectrometry and Allied Topics

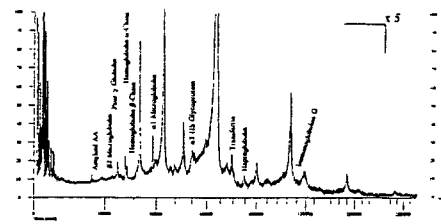

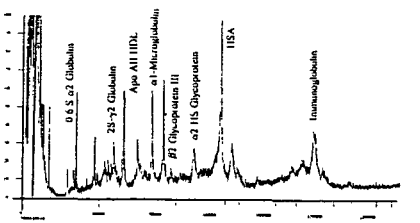

Fig. 1: MALDI analysis of the entire Human Blood Plasma (1.100 diluted in 1 3 MeCN/0.1% TFA) before separation by HPLC.

Fig. 2: MALDI spectra of the HPLC fraction #25 as example Each fraction still contained up to 10 different proteins

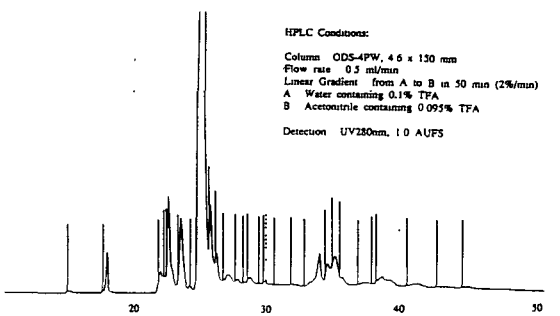

Fig. 3: Fractionation of Plasma proteins using a Reversed-Phase HPLC (preparation #1) Injection of 20 µl of Human Plasma into the column. 29 fractions have been collected

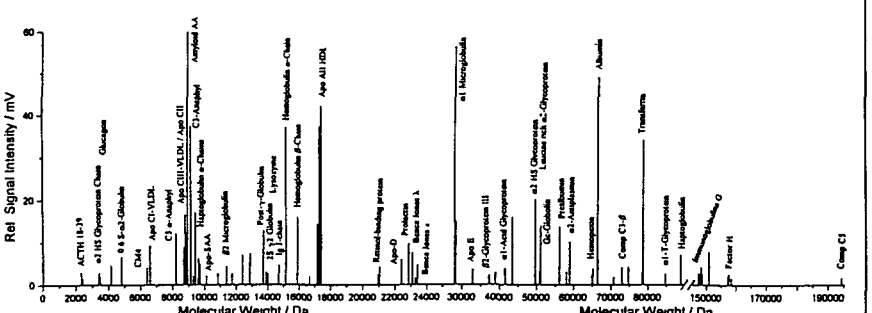

Fig. 4: Summary of the MALDI spectra of all 29 fractions. Ion signals are represented by columns. Among 80 detected components, about 50 could be identified by comparison with databases.

The Metal Ion Affinities of Biomolecules Determined by the Kinetic Method

Blas A. Cerda and Chrys Wesdemiotis
Department of Chemistry, The University of Akron,
Akron, Ohio, 44325-3601, U.S.A.

Since a great number of biomolecules require the presence of metal ions for their activity and/or their structural integrity, the role of metal ions in biological processes is varied and essential. One important factor that influences metal ion-biomolecule interactions is the relative intrinsic bond strength between the ionized metal and the various possible binding sites within the hydrophobic interior of the biomolecule. This important thermochemical property can be obtained based on the gas phase unimolecular dissociation of metal ion-bound heterodimers containing the biomolecules of interest (kinetic method).[1] Here we used this method to determine the relative copper (I) affinities (Cu^+A) of amino acids (a.a.) and the alkali metal ion affinities (M^+A) of DNA nucleobases.

Copper(I) affinities of amino acids. For the 20 common alpha-amino acids, we find the Cu^+ affinities to increase in the order Gly < Ala < Ser < Val < Leu < Ile < Thr < Pro < Asp < Asn < Glu < Phe < Tyr < Cys < Gln < Met < Trp < His < Lys < Arg and their values fall within <20 kcal/mol. For comparison, the proton affinities of amino acids cover a range of >33 kcal/mol. Correlation of the experimentally derived Cu^+A order to the reported proton[2] and sodium ion[3] affinity orders of amino acids points out that the Cu^+-A.A. bond is longer and less covalent in nature than the H^+-A.A. bond. Increasing the alkyl side chain of the amino acid, and hence inductive effects, augments the proton affinity substantially more than the Cu^+A. Further, soft donor groups, such as SH of cysteine, SCH_3 of methionine or the aromatic π-electrons of phenylalanine, stabilize Cu^+-A.A. bonds more than H^+-A.A. or Na^+-A.A. bonds

Alkali metal ion affinities of nucleobases. The kinetic method can provide absolute metal ion affinities, if reference bases of known M^+A are available. In such a case, heterodimers of the biomolecule of unkown M^+A (B) and the reference bases (B_i) are investigated (eqs 1 and 2):

$$B\text{-}M^+\text{-}B_i \xrightarrow{k} B\text{-}M^+ + B_i \quad (1a)$$

$$B\text{-}M^+\text{-}B_i \xrightarrow{k_i} B + M^+\text{-}B_i \quad (1b)$$

$$\ln (k_i/k) = [M^+A(B_i) - M^+A(B)] / RT \quad (2)$$

We used this relationship to appraise the Li^+ and K^+ affinities of the nucleobases, thymine, adenine, cytosine, and guanine, using aniline, pyridine, and n-propylamine as reference bases for the K^+A,[4] and pyridazine,[5] pyridine, dimethylformamide,[6] glycine, alanine, and valine,[3] for the Li^+A of the nucleobases.

Based on eq 2, plotting ln (k_i/k) vs. $M^+A(B_i)$ gives both RT and $M^+A(B)$. Such a plot for which B = cytosine is shown in Figure 1. From the slope and intercept of this graph, the effective temperature (T) and the K^+A of cytosine are found to be 442 K and 24.4 ± 0.3 kcal/mol, respectively. Similar plots for the other nucleobases and for heterodimers of Li^+

lead to the affinities summarized in Table 1. The proton affinities of these nucleobases[7] are also included for comparison. From the data in this table it can be seen that the proton and alkali metal ion affinities decrease in the order Gua > Cyt > Ade > Thy. This common behaviour is consistent with all three cations being hard Lewis acids. Finally, for a given nucleobase the affinities decrease in the order: PA > Li^+ > K^+A. Evidently, the bond strength decreases as the ionic radius of the Lewis acid increases, presumably because of lowered covalent bond character.

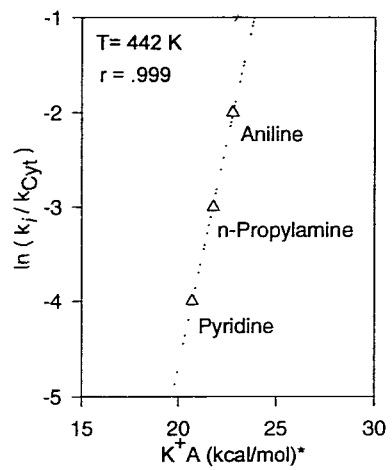

Figure 1. Effective temperature for cytosine.
* Reference 4

Table 1. Alkali Metal Ion vs. Proton Affinities of Nucleobases

Nucleobase	*PA**	*Li^+A*	*K^+A*
Thymine	209.9	54.8	22.7
Adenine	224.2	55.1	23.8
Cytosine	225.9	55.3	24.4
Guanine	227.4	57.3	25.7

All values in kcal/mol
*Reference7.

REFERENCES: 1. McLuckey, S. A.; Cameron, D.; Cooks, R. G. *J. Am. Chem. Soc.* 1981, 103, 1313. **2.** (a) Lias, S. G.; Bartmess, J. E.; liebman, J. F.; Holmes, J. L.; Levin, R. D.; Mallard, W. G. *J. Phys. Chem. Ref. Data* 1988, 17, Suppl. 1. (b) Isa, K; Omote, T.; Amaya, M. *Org. Mass Spectrom.* 1990, 25, 620. (c) Wu, Z.; Fenselau, C. *Rapid Commun. Mass Spectrom.* 1992, 6, 403. (d) Wu, Z.; Fenselau, C. *Rapid Commun. Mass Spectrom.* 1994, 8 777. (e) Bojesen, G.; Breindahl, T. *J. Chem. Soc. Perkin Trans. 2* 1994, 1029. **3.** Bojesen, G.; Breidahl, T.; Andersen, U. N. *Org. Mass Spectrom.* 1993, 28, 1448.**4.** Davidson, W. R.; Kebarle, P. *J. Am. Chem. Soc.* 1976, 98, 6133. **5.** Taft, R. W.; Anvia, F.; Gal, J. -F.; Capon, M.; Holmes, K.; Hosn, K.; Oloumi, R.; Vasanwala, R.; Yazdani, S. *Pure & Appl. Chem.* 1990, 62, 17. **6.** Staley, R. H.; Beauchamp, J. L. *J. Am. Chem. Soc.* 1975, 97, 5920. **7.**Greco, F.; Liguori, A.; Sindona, G.; Uccella, N. *J. Am. Chem.Soc.* 1990, 112, 9092.

METAL ION ASSISTED DERIVATIZATION OF BUCKMINSTERFULLERENE

Steven Z. Kan, Yong G. Byun, Samuel A. Lee, Young C. Xu and Ben S. Freiser
Department of Chemistry, Purdue University, West Lafayette, IN 47907 USA

The development of new materials and new chemicals based on C_{60} and other fullerenes is currently an area of intense study. In particular, a large effort has been focused on the production of fullerene derivatives through C-C bond formation.[1-3] Here we demonstrate that the derivatization of C_{60} can be catalyzed by a metal center through two potential routes - reactions of metallated C_{60} ions with neutral molecules and reactions of metal-ligated ions with C_{60}.

The study is carried out on an Extrel FTMS-2000 Fourier transform mass spectrometer. C_{60} is introduced by using a solids probe at 350 °C and the source temperature is kept at around 220 °C to maintain a static background pressure of C_{60}. Neutral reactants are introduced via either a leak valve or a pulsed valve. Argon at ~10^{-6} Torr is used as the collision gas for collisional activation experiments. FT-ICR ion ejection techniques are used to isolate ions and to determine ion/molecule reaction pathways.

Co^+ generated by laser desorption undergoes both charge transfer and attachment with C_{60}. **Figure 1** shows the reactions of CoC_{60}^+ with cyclopropane (c-C_3H_6) in which both metallated and unmetallated C_{60} derivatives are formed via reactions 1 and 2. Collision-induced dissociation (CID) experiments and ion/molecule reaction results indicate that C-C bonds are formed in these product ions.

$$CoC_{60}(CH_2)_n^+ + c\text{-}C_3H_6 \xrightarrow{n = 0-2} CoC_{60}(CH_2)_{n+1}^+ + C_2H_4 \quad (1)$$

$$\xrightarrow{n = 0-3} C_{60}(CH_2)_n^+ + CoC_3H_6 \quad (2)$$

$$Fe(C_6H_4)_n^+ + C_{60} \xrightarrow{n = 1-4} FeC_{60}(C_6H_4)_n^+ \quad (3)$$

$$FeC_{60}(C_6H_4)_n^+ + C_6C_5Cl \xrightarrow{n = 1,2} C_{60}(C_6H_4)_n^+ + [C_6C_5FeCl] \quad (4)$$

Figure 2 shows that the ligated ions $Fe(C_6H_4)_x^+$ (x=1-4), formed by reacting Fe^+ with chlorobenzene,[4,5] react with background C_{60} to form metallated and unmetallated C_{60} phenylene derivatives, reactions 3 and 4. A coupling mechanism that accounts for the formation of $FeC_{60}C_6H_4^+$ and $C_{60}C_6H_4^+$ is shown below. **1** also represents a new class of C_{60} derivatives with C_{60} being an η^1 ligand and suggests that it will be possible to prepare similar metallacyclic C_{60} derivatives in the condensed phase.

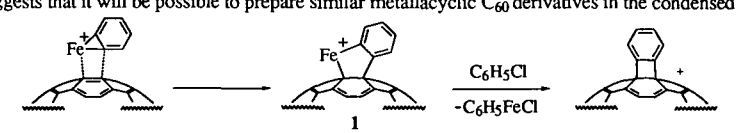

Figure 3 illustrates the reactions of RhC_{60}^+ with both iodomethane and diiodomethane, reactions 5 and 6. Upon CID, $C_{60}CH_3^+$ fragments at a center-of-mass energy of ~ 6 eV, while $C_{60}CH_2^+$ fragments at ~ 16 eV, suggesting that the former contains one C-C bond and the latter contains two C-C bonds.

$$RhC_{60}^+ + CH_3I \longrightarrow C_{60}CH_3^+ + RhI \quad (5)$$

$$RhC_{60}^+ + CH_2I_2 \longrightarrow C_{60}CH_2^+ + RhI_2 \quad (6)$$

1. Kan, S. Z.; Byun, Y. G ; Freiser, B. S. *J. Am. Chem. Soc.* **1994**, *116*, 8815.
2. Kan, S. Z.; Byun, Y. G.; Freiser, B. S. *J. Am. Chem. Soc.* **1995**, *117*, 1177.
3. Kan, S. Z.; Byun, Y. G.; Lee, S. A.; Freiser, B. S. *J. Mass Spectrom.* **1995**, *30*, 194.
4. Dietz, T. G.; Chatellier, D. S.; Ridge, D. P. *J. Am. Chem. Soc.* **1978**, *100*, 4905.
5. Huang, Y.; Freiser, B. S. *J. Am. Chem. Soc.* **1989**, *111*, 2387.

43rd ASMS Conference on Mass Spectrometry and Allied Topics

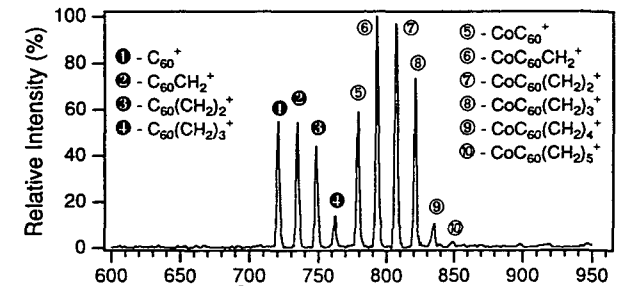

Figure 1. Pulsing in c-C_3H_6 (~ 10^{-5} Torr) to isolated CoC_{60}^+ and allowing 800 ms time delay.

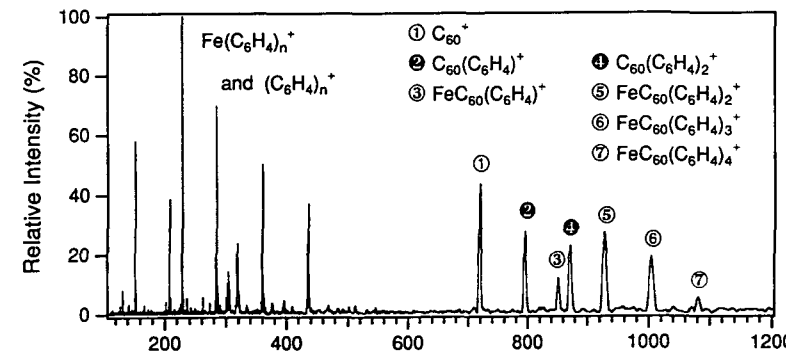

Figure 2. Mass spectrum illustrating the formation of $Fe(C_6H_4)_n^+$, $(C_6H_4)_n^+$, $FeC_{60}(C_6H_4)_n^+$, and $C_{60}(C_6H_4)_{1,2}^+$ in the $Fe^+/C_6H_5Cl/C_{60}$ system. C_6H_5Cl is leaked into the cell at a static background pressure of 7.9 x 10^{-7} Torr and 5.5 s time delay is allowed for the formation of the product ions.

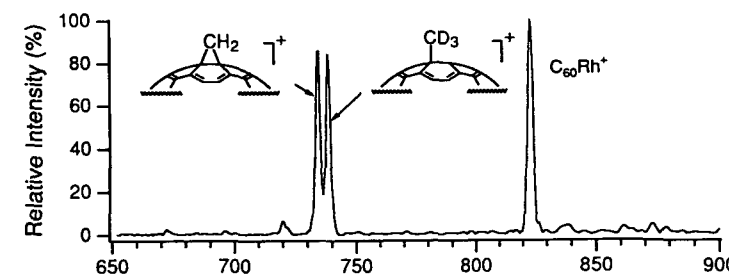

Figure 3. Sequentially pulsing CD_3I and CH_2I_2 to $C_{60}Rh^+$ - formation of $C_{60}CH_2^+$ and $C_{60}CD_3^+$.

Amino Acid and Peptide Reactions with Ground State Metal Ions Studied by FT-ICR

Q. Paula Lei and Jonathan Amster*

Department of Chemistry, University of Georgia

Athens, GA 30602

I. INTRODUCTION

Electrospray ionization and laser desorption are reliable methods for ionizing biomolecules to measure molecular weights, to obtain structural information for sequencing a protein or DNA, controlled fragmentation of the molecular ion would be useful. Collisional dissociation method such as SORI, VLE CAD, MECA and multiphoton dissociation of large molecules etc have been used in several groups. A great deal of work in gas phase chemistry has shown that transition metals exhibit high reactivity toward hydrocarbons, carbonyl compounds and amines. Based on the idea of using metal ions to fragment peptides and studying the chemistry of metal ion reactions, we have implemented a systematic study on the metal ions Cu^+ and Fe^+ reactions with 20 common amino acids, the building blocks of proteins, and two dipeptides, by laser desorption /chemical ionization - combined with FT-ICR.

II. EXPERIMENTAL

A Fourier transform mass spectrometer has been specifically designed and constructed for LD/CI experiments. The magnetic field used in the experiments was 1 tesla The analyzer cell of the mass spectrometer (4 4cm cube) was housed in a UHV chamber evacuated to a base pressure of $2x10^{-10}$ torr by a turbo molecular pump The solid samples, which are prepared by electrospray deposition, are first introduced into the antechamber and later to the main chamber by a magnetically coupled manipulator Metal ions formed by laser ablation were axialized by tens of thousands of thermalizing collisions with N_2 gas by using quadrupole excitation The neutral molecules are produced by the substrate assisted laser desorption method. Metal ions are then allowed to react with the neutral amino acid molecules in the ICR cell

III. RESULTS AND DISCUSSION

Figure 1 shows some representative spectra of amino acids reaction with Cu+ and Fe ions, and **Figure 2** summarizes the reaction pattern of amino acids and dipeptides A similar pattern of the amino acids reaction with the metal ions and dipeptide reaction with metal ions has been observed Metal attachment appears to be directed around the carbonyl function, with loss of CO, CO_2 or CO_2+H_2 For the dipeptides, fragmentation around the peptide bond with metal adduction such as (b1+metal)+ and (x1+metal)+ has have also been seen

References 1. Eller,K ,Schwarz,H *Chem. Rev.*, **1991**, 91, 1121-1177

2. Speir,J P , Gorman,G S , Cornett,D S , Amster,I.J. *Anal.Chem* **1991**, 63, 64-69

3 Speir,J P ; Gorman,G S , Amster,I J *J.Am.Soc.Mass Spectrom.* **1993**, 4, 106-110

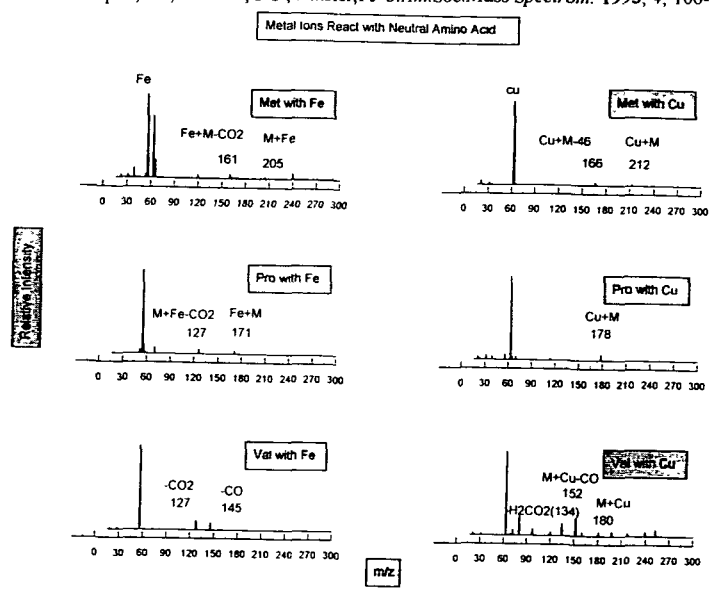

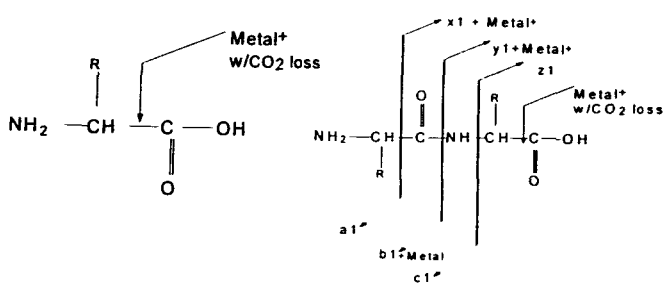

MS AND MS/MS OF COORDINATION BETWEEN NATIVE GANGLIOSIDES AND ALKALI METAL IONS

Lambert C. M. Ngoka and Catherine E. Costello, Department of Chemistry, Massachusetts Institute of Technology, Cambridge, MA 02139*

Complexation of gangliosides with alkali metal ions is involved in fundamental biological processes, control of ionic equilibria, neuronal signal transmission, regulation of transport enzymes, stabilization of secondary and tertiary structures of macromolecules, and long term adaptive processes such as learning, memory and ecophysiological adaptation[1,2]. Examination of ganglioside-metal complexes by mass spectrometry may provide some insight on the factors that govern selectivity in these interactions. Liquid SIMS and tandem mass spectrometry in conjunction with collisional activation on a four sector JEOL HX110/HX110 instrument have furnished novel structural and physicochemical data on gas phase complexes between gangliosides and alkali metal ions. The complexes were formed in the ion source by bombarding the appropriate ganglioside sample on the probe tip with a 25 keV Cs^+ beam from a cesium ion gun. The ganglioside sample was dissolved in a 1:1 glycerol/*m*-nitrobenzyl alcohol matrix which had been saturated with the appropriate alkali metal iodide(s). Gas phase complexes were accelerated to 10 keV and collided with helium gas in a collision cell (floated at 3 kV) located between MSI and MSII. Product ions were recorded on MSII during linked scans at constant B/E.

Both Liquid SIMS and MS/MS studies show that monosialogangliosides bind to two alkali metal ions with elimination of a proton to form $[M - H + 2m]^+$, where M is ganglioside and m is an alkali metal ion. Disialogangliosides form $[M - 2H + 3m]^+$ and trisialogangliosides form $[M - 3H + 4m]^+$. Free carboxyl groups of the sialic acids are required for the formation of these complexes.

Figures (a) and (b) show MS/MS spectra of $[M - H + 2Li]^+$ and $[M - H + 2Cs]^+$ of monosialoganglioside G_{M1}. Fragment ions arise from both carbohydrate and ceramide portions of the molecule, and represent glycosidic and ring cleavages. Ability to form complexes depends on the formation of metal dimers. In passing from Li to Cs, the ability to form dimers increases, the absolute abundances of all precursor and fragment ions increase, the degree of ring fragmentation decreases and the relative abundances of free metal cations increase. These studies have lent insights into (a) the coordination chemistry of the alkali metals with native gangliosides, (b) new aspects of the chemistry of the alkali metals, for example, trends in the formation of dimers. (c) information on possible origins of selectivity and mechanisms by which gangliosides regulate sodium and potassium ion fluxes across plasma membranes. Fundamental physicochemical data (affinities, for example) and improved structural determination of gangliosides are some of the new perspectives from these studies.

The MIT Mass Spectrometry Resource is supported by National Institutes of Health NCRR Grant RR00317 (to K. Biemann).

References

(1) Augustine, G. J.; Charlton, M. P.; Smith, S. J. *Annual Review of the Neurosciences* **1987**, *10*, 633.
(2) Smith, S. J.; Augustine, G. J. *Trends in the Neurosciences* **1988**, *11*, 458.

* Present Address: Boston University School of Medicine, Boston, MA 02118.

43rd ASMS Conference on Mass Spectrometry and Allied Topics

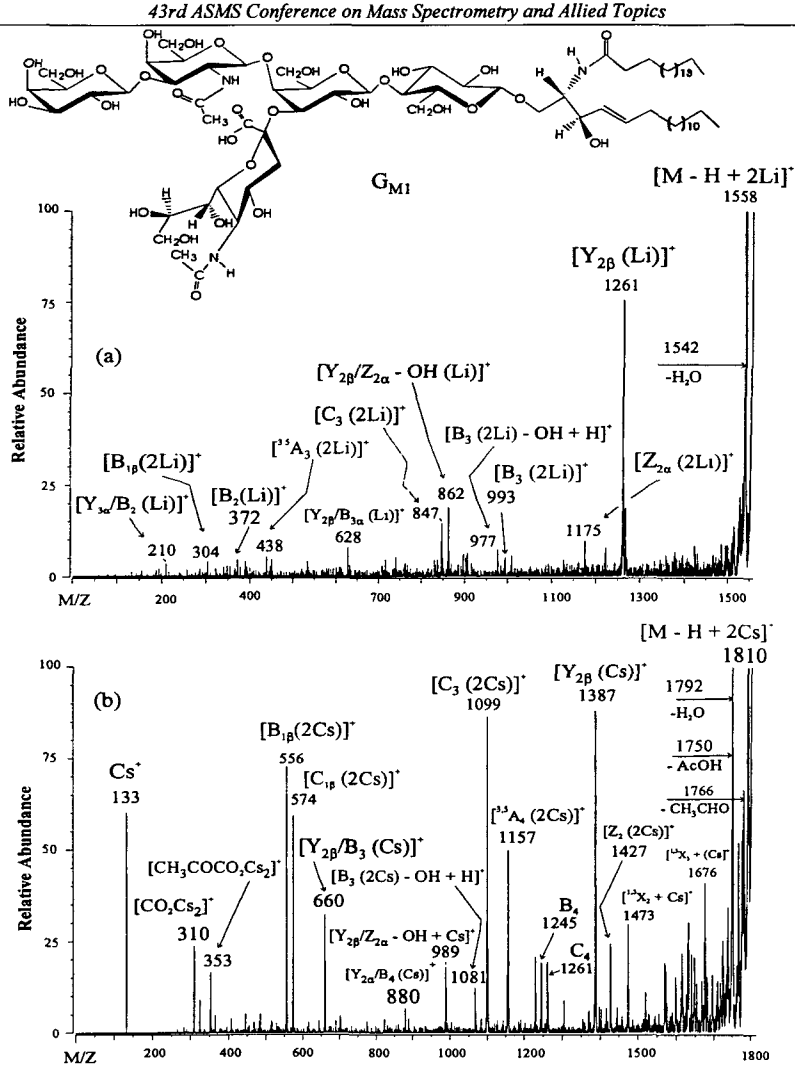

High Energy Collision Induced Dissociation Spectra of Monosialoganglioside (G_{M1}) Complexes with Lithium Ions (a), and Cesium Ions (b)

Electron Affinity and Catalytic Activity of Fe(octaethylporphyrin(NO_2)$_n$)

Lei Jin†, T. Wijesekera‡, P. E. Ellis, Jr‡., J. E. Lyons†,‡ and D. P. Ridge†

Department of Chemistry and Biochemistry and
Center for Catalytic Science and Technology
†University of Delaware, Newark, DE 19716, and
‡Sun Company, P. O. Box 1135, Marcus Hook, Pennsylvania 19061

Previous work in our laboratories has shown that the electron affinities of halogenated metal tetraphenyl porphyrins (TPP) are correlated with catalytic activities of those metalloporphyrins.[1] We also found that comparison of the electron affinities with the condensed phase reduction potential of the met TPPs revealed the nature of the LUMO of the neutral metal TPP. We report here the extensiion of our previous study to a different class of metalloporphyrins. Instead of tetraphenyl porphyrins with phenyl substituents in the meso positions, we examined octaethyl porphyrins (OEP) with ethyl substitutents in the β-pyrrole positions. The species examined are indicated below.

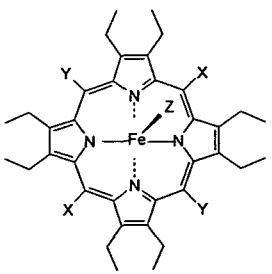

Fe(OEP)	X=Y=H, no Z
Fe(OEP)Cl	X=Y=H, Z=Cl
Fe(OEP(NO_2)$_2$)	X=H, Y=NO_2, no Z
Fe(OEP(NO_2)$_2$)Cl	X=H, Y=NO_2, Z=Cl
Fe(OEP(NO_2)$_4$)	X=Y=NO_2, no Z
Fe(OEP(NO_2)$_4$)Cl	X=Y=NO_2, Z=Cl

Electron Affinities were measured by examining charge reactions between the metalloporphyrins and species of known electron affinity. Using FTMS methods (FTMS 2000, Extrell FTMS, Madison Wisconsin) equilibrium constants and ΔG for the charge transfer processes could be determined. From ΔG, ΔH could be estimated giving an electron affinity difference. The resulting electron affinity ladder is shown in Fig. 1. Double headed arrows indicate equilibrium constant measurements and single arrows represent cases where all that could be determined was the sign of ΔG.
Fig. 2 shows the relationship between the catalytic activity and the electron affinity. The turn-over number (TON) is a measure of the rate constant for the catalytic oxidation of cyclohexane to cyclohexanol by O_2. The squares represent Fe(OEP(NO_2)$_2$)Cl, Fe(OEP(NO_2)$_4$)Cl and two halogenated

Fe(TPP)Cl species. These two families of catalysts follow the same correlation suggesting that electron affinity measures the electronic properties critical for catalytic efficiency. The crosses indicate unsubstituted Fe(OEP)Cl and Fe(TPP)Cl. In these cases the LUMO is thought to be a d orbital on the metal rather than a π orbital on the ligand. That these data point are not on the line suggests that the electronegativity of the ligand is the important factor in determining catalytic activity. This can be rationalized in terms of the stability of metal oxo species thought to be important in the catalytic mechanism.

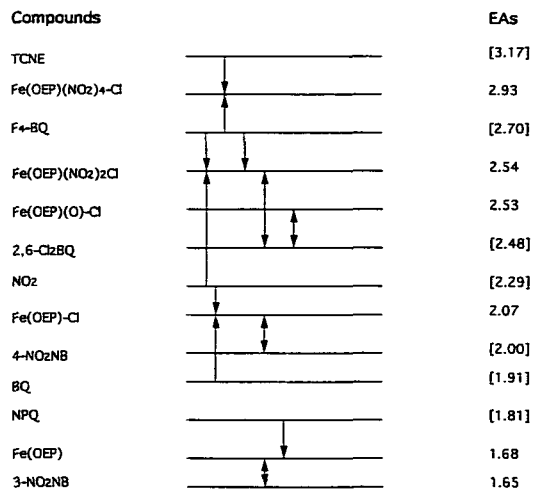

Figure 1

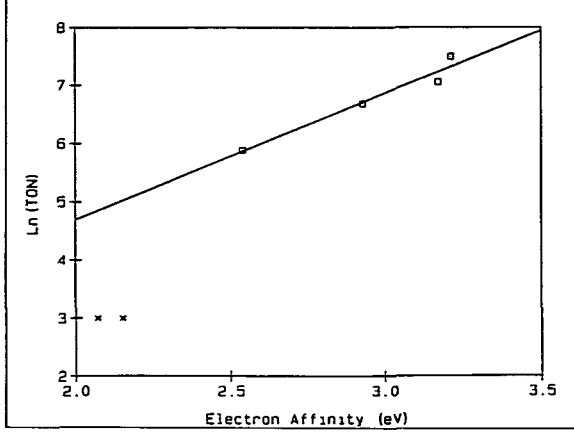

Figure 2

1. Chen, H. L.; Ellis, P. E., Jr.; Wijesekera, T.; Hagan, T. E.; Groh, S. E.; Lyons, J. E.; Ridge, D. P. *J. Am. Chem.*

Tandem Mass Spectrometric Study of $C_5H_5FeR^{+\cdot}$ Ions.

Dmitri V. Zagorevski and John L. Holmes

Chemistry Department, University of Ottawa, Ottawa, Ontario K1N 6N5, Canada.

Structure and unimolecular reactivity of $C_5H_5Fe^{+\cdot}R$ ions were studied by tandem mass spectrometry methods. All ions were generated in the ion source or from metastable precursors by reactions shown in Scheme 1. These reactions resulted in ions having cyclopentadienyl and R groups separately attached to the metal atom (structure **A**). Structure **A** may rearrange by the migration of group R to the hydrocarbon ligand producing structure **B** (Scheme 1), which may also undergo further isomerization.

Structures **A** and **B** exhibited different unimolecular reactivities (Scheme 1). Ion **A** dissociated by C_5H_5-Fe and Fe-R bond cleavages giving rise to $C_5H_5Fe^+$, RFe^+ and $C_5H_5^+$ ions The loss of HR (R=F, Cl, OH) also originated from isomer **A**. The major characteristic of ion **B** and related isomers was the formation of positively charged or neutral C_5H_5R and Fe. In addition, only isomer **A**, possessing the π-cyclopentadienyl and σ-R ligands strongly bound to the metal atom, had a realistic chance to survive neutralization-reionization (NR) conditions and to exhibit a recovery signal.

Scheme 1.

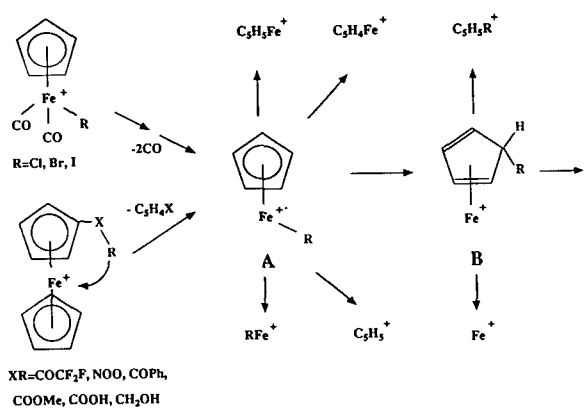

The behaviour of all halogen-containing derivatives was consistent with their existence as structure **A**. NR mass spectra of these ions showed intense recovery signals, demonstrating that stable neutral counterparts were generated in the gas phase. Collision induced dissociation (CID) mass spectra of ions generated in NR mass spectra were closely similar to that of ions before neutralization, indicating no isomerization in the course of NR.

Metastable ion (MI), CID and NR mass spectra of $C_5H_5FePh^+$ ions were dominated by ions corresponding to structure **B**. The dissociation of this isomer produced neutral or positively charged C_5H_5Ph and Fe. Fragmentation corresponding to isomer **A** was not found in the MI and CID mass spectra of ion source generated ions and a recovery signal was not observed in the NR mass spectrum. To identify isomer **A**, $C_5H_5FePh^+$ ions having low internal energies were generated by the decomposition of the metastable precursor. The CID mass spectrum of these species showed intense signals corresponding to $C_5H_5Fe^+$ and $PhFe^+$ ions.

All oxygen-containing $C_5H_5FeR^+$ ions (R=O, OH, OMe) underwent rearrangement of structure **A**. For the methoxy-derivative the initial reaction was a hydrogen atom shift from the methoxy group to the metal atom, followed by the migration of the H-atom to the cyclopentadienyl ring:

$$C_5H_5FeOCH_3^{+\cdot} \Rightarrow C_5H_5Fe(H)(OCH_2)^{+\cdot} \Rightarrow C_5H_6Fe(OCH_2)^{+\cdot}$$

The CID mass spectrum of $C_5H_5FeOH^+$ exhibited peaks due to $C_5H_5Fe^+$ and $HOFe^+$ ions, and the NR mass spectrum showed a recovery signal. All these data were consistent with structure **A**. The observation of intense signals corresponding to CO and Fe losses indicated a significant isomerization of these ions to structure **C**.

The loss of CO was the major dissociation of $C_5H_5FeO^+$ ions, which existed mostly as isomer **D**. No $C_5H_5Fe^+$ and OFe^+ ions, corresponding to structure **A**, were found in the CID mass spectrum, but they were present in the NR mass spectrum. The latter also exhibited a recovery signal demonstrating the formation of neutral counterparts of ion **A**.

C **D**

In conclusion, the behaviour of $C_5H_5FeR^+$ ions, originally formed as isomer **A**, was studied by tandem mass spectrometry and some other isomers were identified. Stable neutral counterparts of ion **A**, having no other ligands or solvent molecules in the coordination sphere of the metal atom, were generated by neutralization-reionization mass spectrometry It was the first observation of these extremely labile molecules. NR mass spectrometry was also successfully employed to characterize organometallic ion structures.

RAPID AND SENSITIVE SEQUENCING OF PROTEINS ISOLATED BY GEL ELECTROPHORESIS

M. Mann, M. Wilm, A. Shevchenko and T. Houthaeve
European Molecular Biology Laboratory (EMBL)
Postfach 10.2209, D-69012 Heidelberg, Germany

In recent years increasingly more sensitive mass spectrometric methods have been developed.for obtaining sequence information of peptides. Biological research demands such amino acid sequencing of extremely small amounts of proteins for their identification using sequence databases or for the cloning of the corresponding genes. However, the "raw material" is almost always proteins on polyacrylamide gels - a notoriously difficult medium to work off for mass spectrometrists. Here we describe sequencing of peptides from proteins isolated by one - dimensional or two - dimensional polyacrylamide gel electrophoresis at levels well below the micro gram level of protein starting material.

An *in gel* digestion procedure was developed which is optimized for the subsequent use of electrospray mass spectrometry and which can handle popular staining methods such as coomassie, reverse and silver staining:

- Excision of the protein band and a blank
- Washing of the gel plugs with water / acetonitrile and amm. bicarbonate / acetonitrile
- *In spot* reduction and alkylation with iodo-acetamide
- Washing with ammonium bicarbonate / acetonitrile
- Drying down in speed vac. Swelling of gel pieces in tryptic digest buffer at 4 oC
- Removing of excessive trypsin and overnight incubation at 37 °C
- Extraction of tryptic peptides with 5% formic acid /acetonitrile
- Drying down of pooled extracts

This procedure is followed by a transfer of the redisolved digest mixture into a specially prepared capillary which has been loaded with 100 nL of POROUS material (fig.1). Peptides are adsorbed onto this support and are then step eluted in one micro liter solution into a "NanoES" spraying needle[1]. The unseparated peptide mixture is then sprayed without pumping for 30 to 90 minutes and as many peptides as possible are sequenced. No electroblotting or high performance liquid chromatography is necessary in the sample preparation, reducing the risk of sample loss by transfer steps or non - specific adsorption to sample containers. Thus, the procedure is vastly simplified and, in our hands, more robust than current Edman or MS sample preparation protocols.

The procedure has been tested on Bovine serum albumine (fig 2) and has been applied to a wide variety protein micro characterization problems at EMBL. These examples showed that amino acid sequence data can now be obtained with extremely small quantities of sample by NanoES tandem mass spectrometry. Not only is the sensitivity up to hundred fold higher than what is practically obtainable by current techniques using Edman degradation, but the procedure is also much faster and involves fewer purification and manipulation steps. We anticipate that sequencing by NanoES tandem mass spectrometry will become a method of choice for many future protein sequencing projects.

1. Wilm, M.S. & Mann, M. *Int. J. Mass Spec. Ion Processes* **136**, 167 - 180 (1994).
2. Mann, M. & Wilm, M.S. *Anal. Chem.* **66**, 4390-4399 (1994).

43rd ASMS Conference on Mass Spectrometry and Allied Topics

Elution

Unseparated peptide mixture is step eluted (60% MeOH, 5% formic acid)

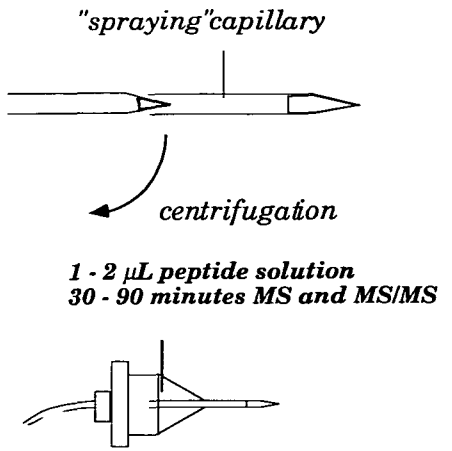

Operation

1 - 2 µL peptide solution
30 - 90 minutes MS and MS/MS

Figure 1. Elution and spraying of the unseparated peptide mixture.

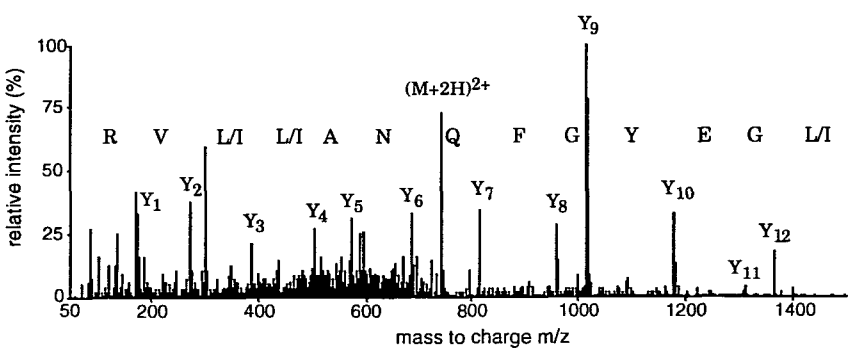

Figure 2. Model study on bovine serum albumine. 800 fmoles of BSA were applied to a 1D gel, excised, prepared as described above and the peptide mixture sequenced by NanoES. The figure demonstrates good sequence readability even at these low amounts.

In Situ Chemical Modification, Digestion, and Characterization of Proteins Utilizing a 2-D HPLC/MS Approach

R. K. Blackburn[1], J. Mark[2], and D. B. Kassel[1]

[1]Glaxo Wellcome, Inc., 5 Moore Drive, RTP, NC 27709
[2]PerSeptive Biosystems, Inc., Framingham, MA 01701

Introduction

Recent advances in MS instrumentation, particularly in the areas of matrix-assisted laser desorption and electrospray ionization, have lowered routine peptide/protein detection limits to the low picomole/femtomole levels. In order to take full advantage of these lowered detection limits, a 2-D HPLC system was investigated as a way to chemically and enzymatically manipulate proteins on-line in order to eliminate sample handling steps prior to MS analysis, thereby reducing sample losses from sample handling steps. Specifically, a technique has been developed in which a protein sample can be preconcentrated, reduced and alkylated, and tryptic digested on-line with no extraneous sample prep steps. Using the Poroszyme™ immobilized enzyme technology, these manipulations can be accomplished in minutes as opposed to hours or days. This approach can be applied to proteins in solution or proteins purified on SDS-PAGE gels. This approach was applied to the the Src Homology 2 Domain protein SH2.

Experimental

For all experiments, the 2-D Integral™ Microanalytical workstation was configured as shown in Figure 1. A solution containing SH2 was de-salted and preconcentrated onto a Poros R1 column in the first dimension. Alternatively, a gel purified sample of SH2 was electroeluted onto a Poros R1 cartridge using the method of Moyer and coworkers (1), and the Poros R1 column placed in the first dimension on the Integral. Next, a 40 µL plug of 4-vinylpyridine and DTT in a Tris/Guanidine Buffer, pH 8.6, was injected onto the immobilized protein and allowed to incubate at 37 °C for 15 min Following extensive washing, the protein was eluted from the Poros R1 column, thru a mixing tee for pH adjusting to 8.5, onto a Poroszyme™ trypsin column. After passing through the trypsin column, a third LC pump delivered a 0.5% TFA pH adjusting solution, and the digest was subsequently trapped on a Poros R2 or ODS trapping cartridge. After trapping, the trapping cartridge was connected to a longer Poros R2 analytical column, and the contents analyzed by LC/MS using a Sciex API-III mass spectrometer.

Results and Discussion

Initial experiments involved evaluating recovery of SH2 tryptic peptides when collected into an eppendorf or trapped on a reversed-phase cartridge after elution from the Poroszyme™ trypsin column. As shown in Table 1, recoveries of SH2 tryptic peptides collected into an eppendorf from a 20 pmol digest are < 50% compared with a 20 pmol trapped digest. These data demonstrate the importance of trapping rather than eppendorf collection to maximize recoveries of tryptic peptides in the 2-D approach.

Figure 2 shows a mass chromatogram comparison of tryptic maps of SH2 for a preconcentration/digestion/trapping experiment using 2-D system with and without an alkylation step. Note in Figure 2A and 2B that tryptic maps obtained with and without an alkylation step are comparable, with Cys-containing peptides shifting in retention time as well as molecular weight (data not shown) upon pyridylethylation. Other data (not shown) obtained after alkylating SH2 for 15 min without a tryptic digestion step showed full alkylation of the protein with no evidence of partial alkylation products.

Experiments with SH2 purified from an SDS-PAGE gel and electroeluted onto a Poros R1 cartridge and subjected to the alkylation/digestion/trapping procedure showed a 50% recovery of tryptic peptides relative to a standard SH2 sample without electroelution (data not shown). The 50% loss is consistent with losses reported for electroelution alone (1), showing that no significant sample losses occurred as a result of the alkylation/digestion procedure.

Summary

A rapid, 2-D HPLC approach has been developed which enables the pre-concentration/cleanup of protein samples, followed by on-line reduction/alkylation and tryptic digestion which eliminates sample handling steps prior to MS analysis. This elimination of sample handling steps greatly improves recoveries of tryptic peptides following digestion, allowing for smaller amounts of proteins to be analyzed. This approach should be particularly useful for generating high sensitivity MW maps of proteins to be used for database searching. Future plans include improving the robustness of the approach for applicability to proteins in general.

References

(1) Moyer et al., Techniques in Protein Chemistry V, (1994), pp. 195-204.

Table 1: Recovery of SH2 Tryptic Peptides after Poroszyme Digestion by Collection into an Eppendorff versus Trapping onto a Poros Reversed-Phase Cartridge

Tryptic Peptide	UV Peak Height After Collection (cm)	UV Peak Height After Trapping (cm)	Percent Recovery (Collected vs Trapped)
T9	0.3	0.3	100
T15	0.2	1.5	13
T5,T6	0.5	2.2	23
T12-T13	0.7	1.8	39
T8	0.1	1.8	6
T1	1.2	3.0	40
T14	0.4	1.9	21

Figure 1: Schematic of Integral Workstation for Alkylation/Digestion/Trapping Expts

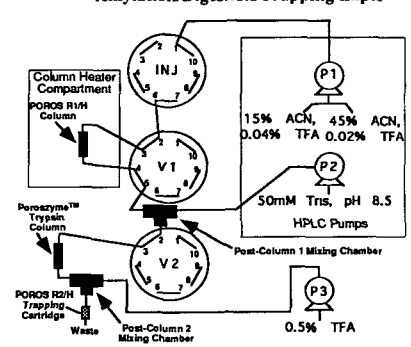

Figure 2: Comparison of SH2 Tryptic Maps Before and After Alkylation

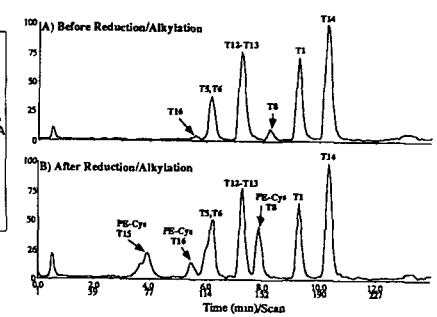

Identification of Peptides from Combinatorial Libraries with ACE-ESI-MS

Daniel P. Kirby*, Yen-Ho Chu, Yuriy Dunayevskiy, Barry L. Karger and Paul Vouros, The Barnett Institute and Department of Chemistry, Northeastern University, Boston, MA 02115

The use of on-line CE-ESI-MS has continued to expand since its introduction in 1987, and this growth has been stimulated by the incorporation of additional CE operational modes, such as CITP, into the combination. In this work, we report on the use of another CE mode, affinity capillary electrophoresis (ACE-MS), with the on-line system: ACE-ESI-MS.

ACE in its own right is a powerful technique and has been shown to be useful for the measurement of binding constants, estimation of kinetic rate constants, and determination of binding stoichiometries of receptor-ligand interactions. The technique has also been shown to be useful for selecting from a mixture a compound that binds most tightly to its receptor. By itself, however, ACE is limited in that no structural information is provided for the selected ligands. In this work we show that, upon coupling with MS, ACE is capable of not only selecting but also identifying peptidyl ligands from a combinatorial library of peptides.

We have developed a simple procedure using ACE-ESI-MS for the on-line separation and sequence determination of ligands from combinatorial libraries that bind most tightly to a receptor. In this procedure, the receptor is present in the CE buffer and the library is introduced as the sample. Ligands that bind tightly to the receptor are retained and, thus, separated from non-interacting species in the library. Then, ligands are detected and structurally identified by on-line MS-MS. Vancomycin-peptide binding with a library of 100 all-D, Fmoc-DDX(1)X(2) tetrapeptides was used as a model system. The technique is economical, rapid, experimentally straightforward and versatile, and, most significantly, is performed in homogeneous aqueous solution so that nonspecific interactions are minimized.

Figure 1 shows the reconstructed ion electropherograms (RIE) and selected ion electropherograms for ligands that were found in the retained peaks. The left side of the figure was for a buffer containing no receptor and the right side for buffer containing 70μM vancomycin. CID of each retained peak was performed to determine the sequence of the ligand An example is shown in Figure 2.

Under these experimental conditions, Fmoc-DDAA, the known ligand, was only slightly retained, whereas peptides with aromatic amino acids in the X_2 and alanine in the X_1 position bound more tightly--a previously unknown motif. Binding constants were verified separately for the discovered ligands. Note that the isobaric peptides Fmoc-DDAY, Fmoc-DDAF and Fmoc-DDAH (Figure 1A, B and D) did not bind to vancomycin under these conditions, showing clearly that binding is sequence specific.

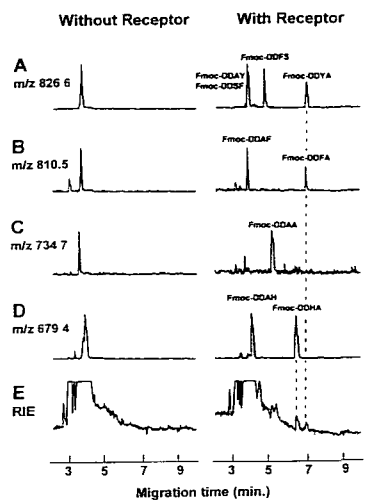

Figure 1. Affinity capillary electrophoresis-mass spectrometry (ACE-MS) of a synthetic all-D, Fmoc-DDXX library of 100 tetrapeptides using vancomycin as the receptor. A-D selected ion electropherograms of the masses indicated; E reconstructed ion electropherogram (RIE) for runs without (left) and with (right) vancomycin in the electrophoresis buffer. **ACE conditions: capillary:** 360μM O.D. x 50μM I.D. x 38cm long, coated with neutral hydrophilic polymer, **buffer:** 20mM Tris acetate (pH 8.1) containing no receptor (left) or 70μM vancomycin (right); **electric field:** -19.2kV (500V/cm), 5μamp; **sample:** hydrodynamically loaded, 10cm/8sec, ~10nL. **MS conditions: instrument:** Finnigan TSQ-700 with Finnigan API interface operated in +ESI mode, ESI: +4 2kV; gas sheath: 40cc/min N_2; liquid sheath 2μL/min 10mM tris acetate (pH 8.1) in H_2O-MeOH (25-75, v/v); **MS: scan range:** 525-925 amu in 2sec.

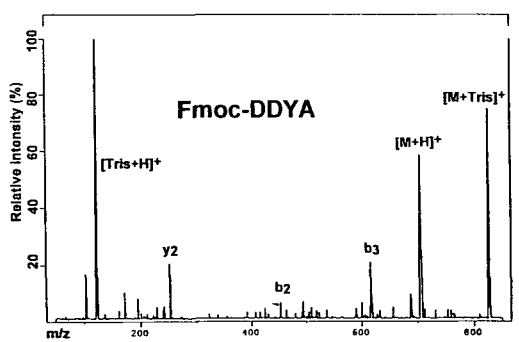

Figure 2. CID spectrum of a retained ligand.

CZE-ESMS of Peptides and Proteins using a Sheathless Interface*

J.F. Kelly[1,2], P.Thibault[1], L.R. Ramaley[2]

[1]Institute for Marine Biosciences, NRC, 1411 Oxford St., Halifax, Nova Scotia, B3H 3Z1; [2]Dept. of Chemistry, Dalhousie University, Halifax, Nova Scotia, Canada B3H 4J3.

Over the past six years, considerable advances have been made in the coupling of capillary zone electrophoresis (CZE) with electrospray mass spectrometry (ESMS). The most widely used interface utilizes a concentric flow of sheath liquid [1] in order to maintain electrical continuity at the interface and to ensure stable electrospray conditions. Low femtomole detection limits are typically obtained for the analysis of peptides and proteins using this interface. Significant improvements in sensitivity have been reported with sheathless interfaces using metallized capillary tips [2,3]. Original designs, however, suffered from a rapid erosion of the metal from the tip leading to the destabilization and eventual loss of electrospray. Recently, Kriger et al. [4] described a method for making a durable, gold-coated capillary tip and demonstrated its use as a sheathless interface.

This presentation describes the procedure we have developed for producing a durable gold-coating. The capillary tip was initially sputter-coated with gold. This coating was then augmented with gold by electrodeposition. Columns coated in this manner were used for 3-4 days without significant loss in performance. In addition, it was found that heat-tapering the capillary tip prior to coating provided the most sensitive and stable electrospray, though very small i.d. tips (i.e., < 10 μm) were prone to blockage. In practice, a tip i.d. of ≈20 μm provided the best compromise between sensitivity and prevention of blockage during production and use. Furthermore, by permanently derivatizing the inner capillary with a cationic polymer (MAPTAC) and using volatile acid electrolytes, efficient CZE separations can be realized without reconditioning the capillary surface which often leads to blockage of the capillary tip.

A comparison of the sheathless and co-axial CZE-ESMS interfaces revealed that the former was 10-50 times more sensitive for peptides smaller than 3500 Da (Figure 1). This improvement resulted from both an increase in analyte signal intensity and a reduction in background noise (usually by a factor of two or more). For a mixture of peptide standards ranging from 555 to 3495 Da the limit of detection was typically in the mid to low attomole range for SIR acquisition, and low femtomole range for full mass scan. Furthermore, the relatively strong acid electrolytes used for this work (up to 0.1M HCOOH) provided good peak resolution and separation efficiencies (150,000-200,000 plates). The present procedure was also applied to the analysis of complex digests of proteins such as α-casein and ovalbumin. Meaningful full scan mass spectra and electropherograms were obtained for 23 fmoles of CNBr digest of ovalbumin (a glycoprotein) using a strong acid electrolyte (0.5M HCOOH). Similar enhancements in sensitivity were observed for intact proteins.

An obvious benefit to the sheathless interface is the ability to obtain CZE-MS/MS data on significantly lower quantities of material. As an example, CZE separation followed by low energy CAD MS/MS was carried out on a mixture of peptides. On-column amounts ranged from 130 to 360 fmoles. The electric field strength across the capillary was reduced by a factor of about 3 just prior to the detection of the first peptide (Figure 2A). This reduced the rate at which the peptides eluted thus ensuring sufficient time to obtain full range mass scans for each peptide and at an acceptable resolution. Meaningful daughter ion spectra, displaying relevant sequence ions, were obtained for most of the peptides examined (Figure 2B).

[1] R.D. Smith, C.J. Barinaga, H.R. Udseth, Anal. Chem., 60, 1948 (1988).
[2] J.H. Wahl, D.R. Goodlett, H.R. Udseth, R.D. Smith, Anal. Chem., 64, 3194 (1992).
[3] J.H. Wahl, D.C. Cole, R.D. Smith, J. Chrom., 659, 217 (1994).
[4] S. Kriger, K.D. Cook, R.S. Ramsey, Anal. Chem., 60, 1948 (1995).

* NRCC No. 38083

43rd ASMS Conference on Mass Spectrometry and Allied Topics

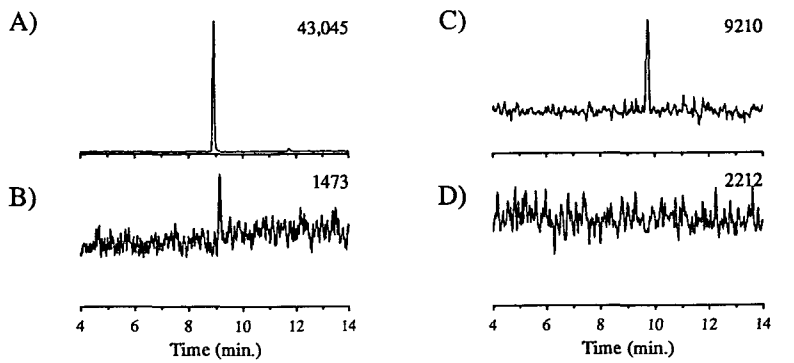

Figure 1: Sensitivity comparison of CZE-ESMS (SIR) for the peptide Leu-enkephalin (m/z 556.2) using a sheathless (A and B) and co-axial (C and D) interface. Conditions: 2pg for (A) and C), and 50 fg for (B) and (D), 1m x 50 µm i.d. capillary derivatized with MAPTAC, 50 mM HCOOH, -28.5 kV. Co-axial sheath liquid: 0.2% HCOOH in 25% MeOH at 2 µL/min. Numbers at top right are signal intensities.

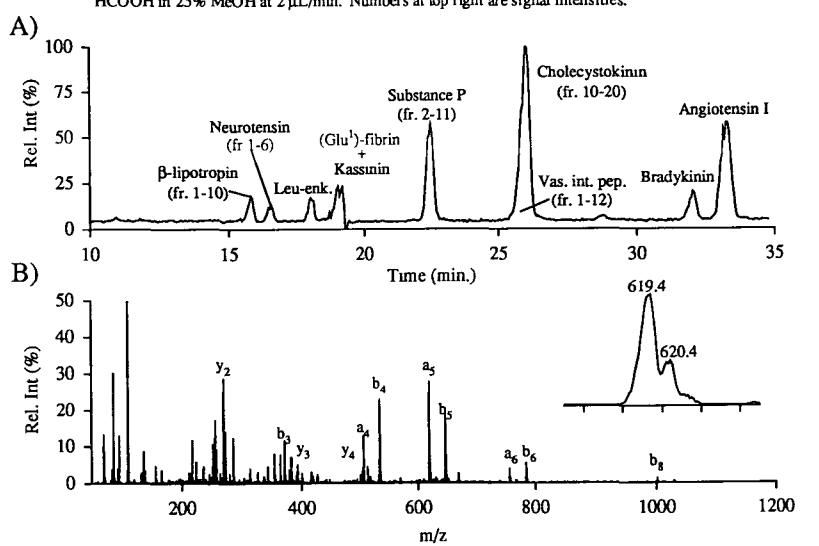

Figure 2: CZE-MS/MS of peptides using a sheathless interface. (A) Full scan TIE (m/z 300-1200). Conditions: 230pg each on column, 1m x 50 µm i.d., 0.1M HCOOH, -28.5 kV for 7 min., -8.5 kV thereafter. (B) CZE-MS/MS spectrum for Angiotensin I (m/z 433). Conditions: 154 fmoles on-column, 75 V (lab. frame), CGT = 4 x 10^{15} atoms.cm^{-2}, 0.1 Da step size, 3 msec dwell. Inset exhibits the m/z 615 to 625 range of this spectrum.

Novel Modifications and Clinical Applications of Membrane Preconcentration CE-MS

Andy J. Tomlinson, Linda M. Benson and Stephen Naylor
Biomedical Mass Spectrometry Facility, Mayo Clinic, Rochester, MN 55905, USA

On-line CE-MS is an emerging technique for the structural characterization of a wide variety of components in complex mixtures. However, the relatively poor concentration limits of detection (CLOD) of CE-MS reduces applicability for analysis of dilute analyte solutions. This is due primarily to the finite volume of the CE capillary (typically 1-2 µL) causing poor analyte focusing upon injection of large sample volumes. Electrophoretic focusing techniques such as analyte stacking, field amplification and transient isotachophoresis have been developed and clearly improve the CLOD of CE-MS. However, the analysis of several microliters of a sample by CE-MS is not possible even when such focusing techniques are used. Therefore, we have been developing preconcentration-CE-MS (PC-CE-MS). This technique uses a bed of adsorptive material at the inlet of the CE capillary. For convenience, we have developed a PC-cartridge (Figure 1) that contains the adsorptive membrane. This arrangement permits easy conditioning of the CE capillary and off-line activation of the adsorptive phase. We have found PC-CE-MS to be an effective means of analyte preconcentration and sample cleanup permitting the removal of salts, buffers, etc. from biologically derived matrices on-line with CE-MS and we term this mPC-CE.

Initially, we used a solid phase HPLC packing material at the CE capillary inlet. However, we have found that component elution from the solid phase PC-CE cartridge was a critical step. Large volumes of organic phase within the CE capillary results in anomalous behavior of EOF, leading to broad analyte zones and compromised component separations (Figure 2a). Reducing the volume of the organic elution buffer results in only a slight improvement in PC-CE-MS performance (Figure 2b). This obvious limitation of solid phase PC-CE-MS, can be only slightly improved using tITP after analyte elution from the solid phase (Figure 2c). Clearly, the bed volume of the solid phase had to be minimized. This was achieved by substituted the solid phase by a suitably impregnated membrane (mPC-CE-MS). This development improved the efficiency of analyte elution from the membrane PC-cartridge in a smaller volume of organic phase. However, while this leads to an enhanced performance, CE-MS was still superior. Therefore, we developed tITP conditions that are implemented after analytes removal from membrane. This enhanced the performance afforded by mPC-CE-MS such that component resolution and separation efficiency was comparable to that of CE-MS even for a sample loading of tens of microliters (Figure 3).

In addition to peptide analysis, mPC-CE-MS methods are applicable for investigation of small molecules (e.g., drug metabolites), polypeptides, and proteins. Figure 4 shows the detection of metabolites of the neuroleptic agent haloperidol by analysis of 10 µL of patient urine using mPC-CE-MS. We have also used mPC-CE-MS for clinical research by analysis of a patient urine for confirmation of the presence of Bence Jones protein (a 25 kDa protein that is indicative of multiple myeloma). Figure 5 shows the mPC-CE-MS analysis of a 24 hour urine collection from a patient diagnosed with multiple myeloma. The family of proteins observed in this sample confirmed that this patient was close to renal failure.

We thank Mayo Foundation for funding these studies. We also acknowledge the support of Finnigan MAT.

43rd ASMS Conference on Mass Spectrometry and Allied Topics

Figure 1 A Schematic of a membrane PC-CE Cartridge

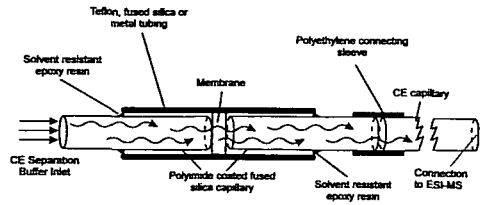

Figure 2 Analysis of Three Structurally Similar Peptides by Solid Phase PC-CE-MS

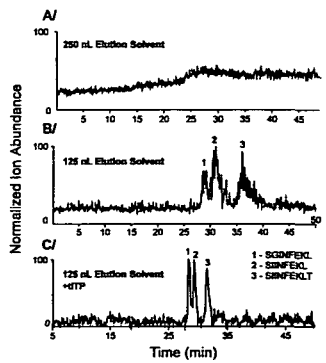

Figure 3 Analysis of a nine component synthetic peptide mixture by mPC-CE-MS with tITP

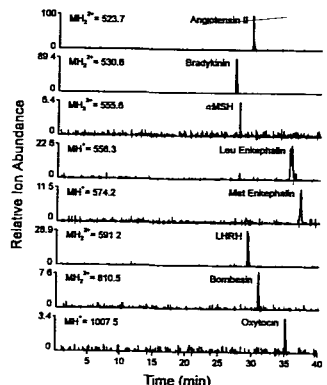

Figure 4 mPC-CE-MS Analysis of Urine From a Patient Taking 0.5 mg/day Haloperidol Using Full Scan Mass Spectrometry

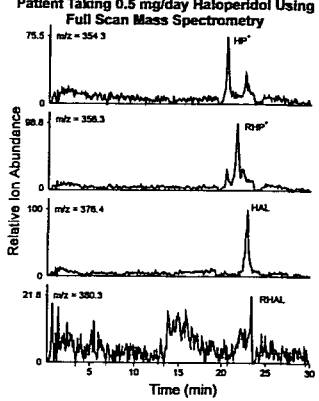

Figure 5 mPC-CE-MS analysis of urine from a patient diagnosed with multiple myeloma

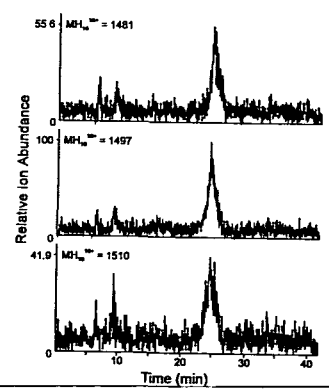

LC/MS Using an Ion Trap/reflectron Time-of-flight Mass Spectrometer

Mark G Qian, Jian Bai, Yan-Hui Liu, Kefei Zheng, and David M. Lubman

Department of Chemistry, The University of Michigan
Ann Arbor, MI 48109-1055

Introduction. The use of mass spectrometry as a detector for on-line separations of mixtures in solution has recently become an important method for characterization of proteins and peptides. Its use as a detector for on-line separations has become especially significant with the development of electrospray ionization (ESI) as a means of producing molecular ions of large proteins and peptides from solution The result is that large ions can be detected at a relatively modest mass/charge so that inexpensive quadrupole mass spectrometers have become widely-used detectors for chromatographic separations An inherent problem in interfacing on-line separations with scanning mass spectrometers such as quadrupole and sector devices is the duty cycle of the experiment Most of the ion signal is lost due to the poor duty cycle of these scanning instruments. Moreover, in the case of very narrow chromatographic peaks, a scanning mass spectrometer may provide a skewed response since the concentration changes during the scan time

In the work presented herein, we demonstrate the capabilities of the ion trap/reflectron time-of-flight mass spectrometer (IT/reTOFMS) as a fast and sensitive detector for microbore chromatography Microbore HPLC separations of tryptic digests of various proteins are separated and interfaced to an ion-spray version of the ESI source, operating at between 40-50 μL/min. Ion storage times of 500 ms are used to achieve long term ion integration for enhanced sensitivity of low concentration samples, with a resulting high duty cycle in detection Using the total ion storage capabilities of the trap, total ion chromatograms of tryptic digests of cytochrome C and bovine ß-casein are obtained with detection limits in the low picomole range In addition, using software developed in our laboratory the selected ion chromatogram can be displayed for enhancement of the S/N and for identification of a chromatographic peak with a particular mass Also the mass spectrum of each chromatographic peak can be displayed in order to search for unresolved chromatographic peaks. The entire data file can ultimately be displayed as a 3-D spectrum in analogy to a 2-D gel used for separations in the biological sciences

Methods. The experimental set-up consists of an HPLC separation system interfaced to an electrospray ionization source with detection using the IT/reTOF system. A gradient elution liquid chromatography system using reversed phase columns was initially used to optimize separation of mixtures of peptides and protein digests The liquid eluent of the separation is delivered through a fused silica capillary tube into an electrospray assembly where the sample is ionized The electrospray source utilizes gas on-axis nebulization methods or ionspray to accommodate higher flow rates The droplets produced are then sampled through a heated stainless steel (s.s.) capillary to desolvate the droplets leaving highly charged peptide ions The ions are then injected into a differentially pumped interface, where the on-axis component of the ion beam passes through a skimmer into the mass spectrometer region The ions are transported via a set of Einzel lens into the quadrupole ion trap storage device The ions are stored and accumulated to an optimal sensitivity for detection of electrospray-produced ions Ultimately, an extraction pulse is applied to the exit endcap and the ions are ejected into the reTOFMS for detection and mass analysis. The use of the reflectron device provides the enhanced resolution observed in these experiments. The ions are detected by a triple 40-mm microchannel plate assembly A data system based

on a high speed transient recorder is used to digitize and process the resulting mass-detected chromatogram that results.

Results. One example of the capabilities of the IT/reTOFMS for on-line analysis of a tryptic digest is demonstrated in Figure 1 and 2. In Figure 1a is shown a microbore HPLC separation of 100 pmol tryptic digest of bovine cytochrome C detected via a UV absorption detector. Figures 1b were obtained by monitoring the total ion current over a broad mass range (60-1500 u) as a function of time There are some differences in the relative peak heights of the corresponding peaks in Figures 1a and 1b, which is due mainly to the relative differences in UV absorption efficiency versus the detection of ion peaks by mass analysis. The data can be reprocessed by our computer software to provide the ion chromatogram for selected massed only. This procedure provides a selected ion chromatogram (SIC) for each mass in the spectrum detected. Figure 2a shows an SIC at *m/z* 634, which corresponds to the chromatographic peak at ~25 min. The relevant mass spectrum is shown in Figure 2b

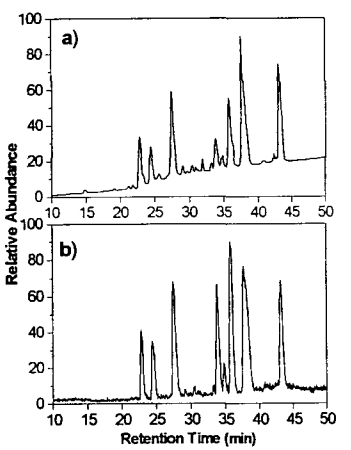

Figure 1

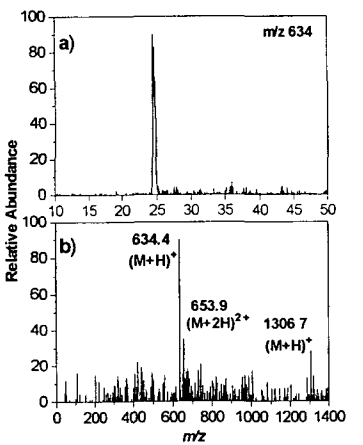

Figure 2

Acknowledgment: The work described herein received support under several sources which we wish to gratefully acknowledge including the National Science Foundation, Biological Instrumentation and Instrumental Develop program under grant #BIR-9223677, and Varian Associates, Inc , Ginzton Research Center

Direct Coupling of Thin Layer Chromatography with Matrix Assisted Laser Desorption Ionization

Arkady I. Gusev[a], Andrew Proctor[a], Yakov I. Rabinovich[b] and David M. Hercules[a,c]
[a] Department of Chemistry, University of Pittsburgh, Pittsburgh PA 15260.
[b] Center for Coal and Mineral Processing, Virginia Polytechnic Institute and State University, Blacksburg VA 24061.
[c] Present address: Department of Chemistry, Vanderbilt University, Nashville, TN 37235.

The use of thin layer chromatography (TLC) with mass-spectrometry (MS) combines the simple separation method of TLC with the specific detection capabilities of MS. Several MS methods have already been used for direct TLC/MS coupling, including secondary ion mass spectrometry, fast atom bombardment and laser desorption [1]. Although various applications, including several examples of two dimensional imaging have been reported, there are still several problems associated with such TLC/MS combinations i.e. fragmentation, poor detection limits and analyte spreading which degrade the image.

To compensate for these problems we employed the relatively new MS method of Matrix Assisted Laser Desorption Ionization (MALDI) [2]. The direct coupling protocol involves analyte extraction from inside the TLC plate and its transport to the surface followed by matrix deposition and crystallization. The extraction procedure was optimized to minimize analyte planar diffusion and to achieve high sensitivity.

Various MALDI matrices were evaluated for use with silica gel and cellulose TLC plates [3]. No signal was obtained from plate points without visible matrix crystals. The best detection limit was obtained with ferulic acid (FA), sinapinic acid (SA) and α-Cyano-4-Hydroxycinnamic acid (α-CHCA) matrices. These matrices also showed high sodium and potassium salt tolerance.

Figure 1 shows mass spectra of angiotensin II and III separated on a silica gel TLC plate. An absolute detection limit of 2-4 ng was demonstrated for angiotensin, bradykinin and enkephalin derivatives [3]. It should be noted that use of a wet TLC plate improved detection limits by a factor of 1.5-2. The method also worked for larger peptides and small proteins like bovine insulin chain B, insulin, horse heart cytochrome c and myoglobin, but TLC separation was poor. Only minor fragmentation was found for all analytes. The influence of ninhydrin on spectral quality was also investigated. Although the spectra were very complex, an increased signal was observed for several analytes when ninhydrin was applied to the TLC plate [3].

The TLC/MALDI method was found to be suitable for direct TLC imaging. However direct matrix deposition and matrix crystallization processes induced additional analyte planar diffusion of 0.5 -3 mm. Analyte spreading can be minimized by suitable matrix selection and controlling the matrix crystallization. Figures 2 A and B show the two dimensional image and contour plot of Rhodamine B obtained on a silica gel plate. Direct TLC imaging was carried out using the α-CHCA matrix with a spatial resolution of 250 μm. The Rhodamine B cation absolute intensities were used to plot the image.

Thus direct coupling of TLC separation and MALDI detection has been demonstrated. The major advantages of TLC/MALDI are low detection limits, minor fragmentation, high contamination tolerance and its suitability for imaging.

43rd ASMS Conference on Mass Spectrometry and Allied Topics

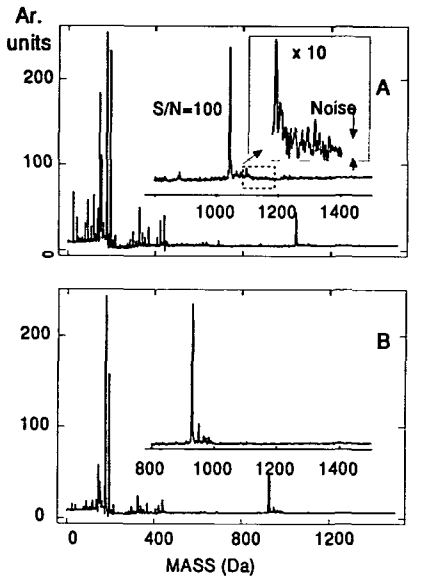

Figure 1

Mass spectra of (A) angiotensin II (150ng) and (B) Angiotensin III (250 ng) separated on a silica gel TLC plates

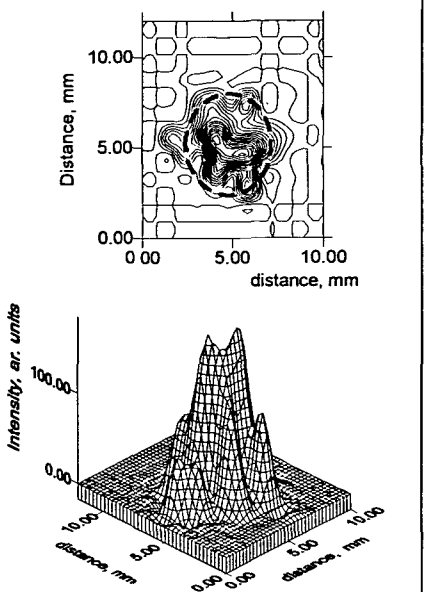

Figure 2
Contour plot and three dimensional image of Rhodamine B (5ng), separated on silica gel TLC plate.
- - - outline of the initial spot.

1. Busch, K.L., Thin layer chromatography coupled with mass spectrometry, in *Handbook of thin layer chromatography*, ed. by Sherma, J., Fried, B., Marcel Deker, New York, 1991, 183.
2. Hillenkamp, F.,; Karas, M.; Beavis, R.C.; Chait, B.T., *Anal.Chem.*, **1991**, 63, 1193A.
3. Gusev, A.I.; Wilkinson, W.R.; Proctor, A.; Rabinovich, Y.I, Hercules, D.M. *Anal.Chem.*,**1995**, (in press)

Flow Injection Analysis - Mass Spectrometry for In-Process Control of Drug Synthesis

Stephen T. Colgan, Thomas R. Sharp, Phillip D. Hammen,
Robert H. Reed, George J. Horan, Paul W. Gwiazda
Central Research Division, Pfizer Inc., Groton, CT 06340 U.S.A.

We describe the application of flow injection analysis coupled with an atmospheric pressure chemical ionization LC-MS interface (FIA-MS) to in-process control (IPC) procedures to support commercial synthesis of a drug substance -- CP-93,393. Its commercial synthesis entails nine steps. IPC procedures are needed to monitor completeness of reactions. Such procedures need to provide for rapid analysis, to be simple procedures, and to be usable for more than one synthetic step.

The production synthesis for this compound is shown in the accompanying reactions, and illustrates the variety of compound structures which must be accomodated by our procedure. Steps 7 and 8 of the process are not shown, as they are optical resolution and salt conversion steps rather than synthetic steps.

CP-93,393 itself (Figure 1) is an ideal molecule for APCI mass spectrometry. It produces an abundant $[M+H]^+$ and little fragmentation. Examination of the seven other molecules in the synthetic sequence shows that all respond nearly as well. A flow solvent of 50% H_2O and 50% methanol was used initially to test mass spectral performance of the compounds. Only one compound -- compound 1 -- requires the addition of a buffer salt to the flowing solvent to promote ionization. The flow solvent now in use contains 50% of a 0.05M aqueous solution of ammonium acetate. The rest of the compounds work equally well with and without the added buffer salt.

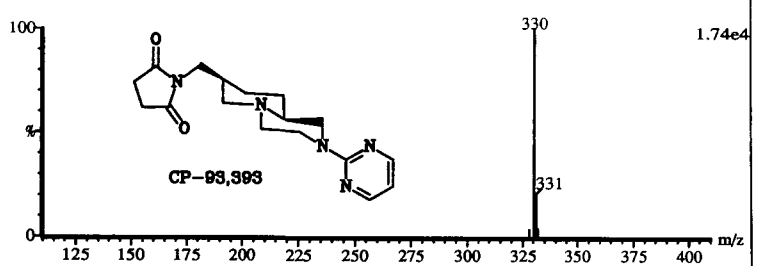

Figure 1: APCI mass spectrum of CP-93,393, $C_{17}H_{23}N_5O_2$, 329 daltons.

Compound 4 (Figure 2) exhibits the most extensive spontaneous fragmentation. A number of instrument operation parameters, solvent flow conditions and injection sizes were investigated in order to minimize this fragmentation. One instance (step 1), where one compound could generate a fragment which would be indistinguishable from the $[M+H]^+$ of the other compound, were found to present minimal interference and could be controllable by judicious choice of instrument operating parameters.

Step 6 in the synthesis presents the most difficulty regarding the development of an IPC method. Compound 6 is difficult to do by gas chromatographic assay. Compound 7 is not compatible with GC. The reaction introduces the pyrimidine chromophore into the product molecule, which allows its detection by UV-Vis in an HPLC assay. However, compound 6 does not have a chromophore. Both

compounds respond in APCI by producing exclusively $[M+H]^+$. They can now both be observed in a single assay, and by the same method as all of the other compounds.

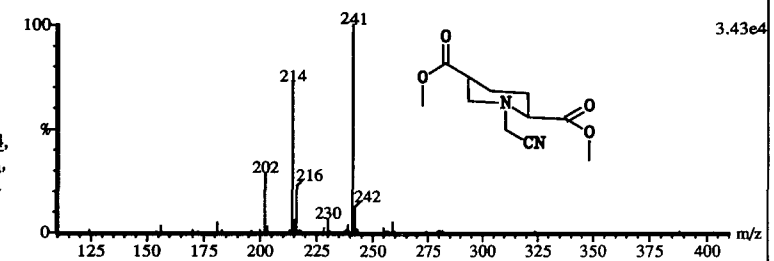

Figure 2: APCI mass spectrum of compound 4, $C_{11}H_{16}N_2O_4$, 240 daltons.

For this process synthesis, FIA-MS allows the use of a single analytical technique and a single instrument for IPC of the entire synthesis. The method replaces a gas chromatographic assay for the first five steps of the synthesis, HPLC assays for the latter steps, and provides an IPC procedure for step 6, in the middle of the reaction sequence, for which no other good IPC method exists. The only feature which our FIA-MS approach does not address is evaluation of the chirality of products of the optical resolution steps of the synthesis. Enantiomeric purity must still be evaluated by a conventional chiral procedure.

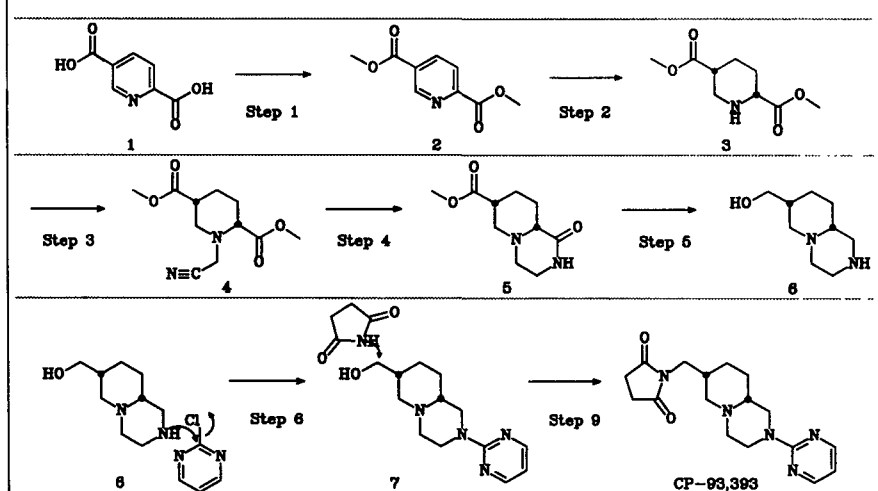

GLP FOR QUALITATIVE MASS SPECTROMETRY FROM AN ACADEMIC PERSPECTIVE,
Jack Henion, Analytical Toxicology, Cornell University, 927 Warren Dr., Ithaca, NY 14850.

INTRODUCTION

Mass spectrometers are now used in a wide variety of routine as well as research application areas As sophisticated measurement devices these systems provide information that may be important or even critical for analytical problem solving. Since any precise measurement device must be carefully maintained and monitored to assure reliable performance, we must all be reminded of the relevant factors that influence the performance of our mass spectrometer systems. We must then implement procedures in the routine use and operation of mass spectrometer systems that document and ensure the generation of reliable data.

In addition to the many aspects of good analytical chemistry including record keeping, equipment maintenance, and regular checks of accuracy and precision, we should all remember some of the fundamental factors that influence the data obtained from mass spectrometers. These include mass-axis accuracy and mass resolution as well as effects of matrix components on the ionization efficiency, etc. Since an error of just one dalton can negatively influence an unknown structural elucidation, it is imperative that the mass assignment of a mass spectrometer be accurate to within specified limits. For quadrupole mass spectrometers this is usually within ±0.1 Da. For a high resolution mass analyzer this could very well require mass accuracy measurements within just a few ppm. Routine performance verification and the determination of system suitability of the mass-axis accuracy is essential to ensure dependable measurements. The factors that affect mass accuracy include the electronic stability of the instrument, the mass resolution, and the peak mass assignment algorithm of the data system. Since mass accuracy also affects sensitivity for selected ion monitoring (SIM) and selected reaction monitoring (SRM) experiments, careful attention to these factors should be taken to ensure the required performance criteria.

Other factors that are important to control for reliable measurements include mass discrimination, relative abundances, space-charge effects upon ion peak shape, matrix suppression of ionization, artifacts of the ionization process such as in FAB, electrospray, and MALDI, factors associated with multiply charged ions from electrospray and MALDI, ion source and collision cell experimental conditions for MS/MS, and ancillary factors associated with coupled chromatography systems for GC/MS and LC/MS, etc. It is important to be aware of these issues which may influence the performance of mass spectrometric measurements.

DISCUSSION

An essential aspect of GLP procedures is record keeping regarding the "health" and performance of the mass spectrometer. Records should be maintained regarding regularly scheduled maintenance such as ion source cleaning, pump oil changes, detector replacement, etc. Non-scheduled maintenance should also be documented and explained in the normal course of record keeping. If performance problems begin to appear the operator should record observations to provide a history that can facilitate diagnosing a problem by service personnel. Records of data obtained under "normal" operation for the instrument should also be recorded on a regular basis and archived as a record of

performance characteristics for the instrument These data should include normal tuning results plus actual on-line GC/MS, LC/MS, LC/MS/MS, etc. results from reference compounds common to the laboratory's work. In the case of LC/MS the recorded experiments should not be obtained by simple "infusion" or flow injection. The latter do not adequately represent actual LC/MS conditions.

There is a developing tendency to "under-resolve" masses on mass analyzers of quadrupole mass spectrometers for certain analyses under SRM acquisition conditions. This is often done to achieve greater sensitivity or more stable ion current measurements. In some cases this may be appropriate provided control experiments indicate that there is no interference and that all requirements for an analysis are met. However, when one uses a mass resolution where the ion peak width at half-height is greater than one dalton, ion current differing by one dalton will also be measured resulting in reduced specificity This can occur in LC/MS/MS analyses when a co-eluting component differing by one dalton from the other component occurs. A specific example is when a mixture contains a sulfonic acid and its corresponding sulfonamide. If the two components coelute these two functionalities of the same parent compound cannot be distinguished by SRM using less than unit mass resolution conditions in the first mass analyzer. If they are chromatographically separated as shown in Figure 1 the CID ion current of one (RSO_3NH_2) can contribute ion current to the other (RSO_3H) under low mass resolution conditions (both Q1 and Q3 operated under low mass resolution conditions). In a full-scan mass spectrum obtained under less than unit mass resolution conditions the isotope ratios would also be inaccurate due to the lack of adequate mass resolution. To ensure that accurate and reducible data are routinely obtained mass spectrometry laboratories should address and monitor those factors which can affect the results desired from their equipment.

Figure 1

SRM LC/MS/MS Determination of RSO_3H and RSO_2NH_2

Effect of Mass Resolution Upon Selectivity*

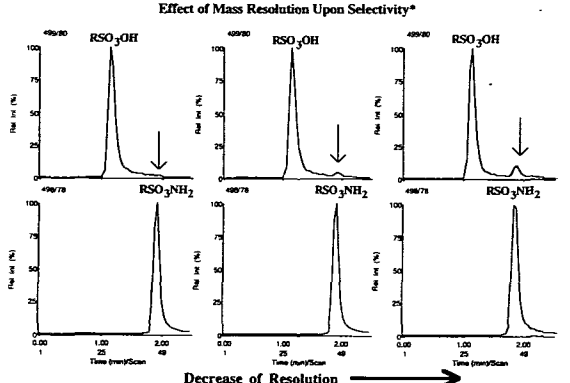

* Injections of a 1 2 mixture of RSO_3H and RSO_2NH_2 were made

ACKNOWLEDGMENT· The author thanks Dr. Y. Wu of Advanced BioAnalytical Services, Inc for providing Figure 1.

Providing Evidence Of Structural Validity As Part Of GALP Compliance

M Canales, Ph.D
R Coyle
T Hall
J Shofstahl, Ph D.

Summary

As pointed out in a recent ASMS workshop, validation of a mass spectrometer and the data system for the intended use is the end user's responsibility. Nonetheless, the vendor can be an important partner in assuring the success of that validation.

This talk discusses a software development process that is focused on providing evidence that quality was built-in and not just tested in. The focus is on structural validity, which is difficult for the end user to judge, rather than functional validity, which only the end user can determine.

As part of the ISO 9000-3 guidelines for software development, the vendor must show evidence of the following:

- Documented Product Development
- Management Oversight
- Peer Review
- Testing
- Product Documentation
- Change Control After Initial Release

The same information can provide evidence of the structural validity of the product in the Good Laboratory Practices or Good Automated Laboratory Practices environment.

The talk will suggest a Software Development Life Cycle that meets the user's need for quality while recognizing advances in software development since the invention of the "waterfall" model. It will describe a process for change control as well as a mechanism to revise existing applications to meet emerging quality standards.

The key phases of the life cycle are:

- Feasibility
- Software Requirements
- Rapid Prototypes → Visual Freeze
- Implementation
- Test Phases
  - Alpha
    Verifying the Functional Specification
  - Beta
    Validating the System for its intended use

Next the talk will make suggestions about what can be done with "mature" products. It will cover the issues of "Fix versus Enhance", change control, and "Use Validation"

Finally the talk will discuss the kinds of tools a vendor might provide to help the end user functionally validate the basic features of the system. Validation for the intended use can proceed from there with the assurance that the quality of underlying system is not a concern

Validation Aids A Vendor Might Provide At Factory

- Review of SOPs, Tool Descriptions, Coding Style Guides, System Life Cycle
- Review of Project Documentation
- Examples of Code Walk-throughs, Internal Documentation
- Review of Test Plans
- Examples of Test Reports
- Examples of Source Code (if you must)

Validation Aids A Vendor Might Provide At User Site

- Certificate of Compliance with internal factory procedures
- Release Notes
- List of Known Problems
- Manuals (on-line?)
- Test Suites (Procedures and files)

GOOD LABORATORY PRACTICE AND DATA MANAGEMENT

Steven M. Musser[1], James A. Sphon[1], Martin Browning Jr[2]. and Stan W. Woollen[2]

[1]Office of Scientific Analysis and Support, Division of General Scientific Support, U.S. Food and Drug Administration, Washington, DC 20204 and [2]Office of Regulatory Affairs, Division of Compliance Policy, U.S. Food and Drug Administration, Rockville, MD 20857

Compliance with good laboratory practice (GLP) regulations is required by the Food and Drug Administration (FDA) for conducting nonclinical laboratory studies as part of the safety evaluation submitted to FDA for a products' approval. The GLP regulations, 21 Code of Federal Regulations (CFR) Part 58, cover a wide variety of laboratory practices and are general in nature. Unfortunately, this generates considerable confusion when specifics are needed for technical operations such as mass spectrometry. This problem was clearly evident at the ASMS sponsored "Fall Workshop on mass spectrometry and GLP" where there were a number of questions regarding FDA's interpretation of GLP regulations as applied to mass spectrometry laboratories. Since many of the questions pertained to acquisition and storage of "raw data", some clarifications may be helpful.

What is raw data in the context of mass spectrometry applications? To better understand the interpretation of raw MS data and GLP regulations it is important to distinguish between detector output signal and recordable data (raw data). This is a rather fine point and some elaboration is necessary. Since the analog signal would be essentially meaningless in the modern MS laboratory, without first being digitized and in many cases averaged or smoothed before being written to magnetic disk (storage device) it is not considered to be raw data in the context of GLP. In order for the data to be considered raw data it must be in a recorded form. By this definition the information which is passed from the A/D converter and signal filters/averagers and recorded on disk (storage device) is the raw data. Raw data in this form is sometimes referred to as primary data. Transformations done to the data at this point are considered secondary data and would include: mass assignment based on a calibration file, background subtraction, integration results, or any other transformation done to the primary data.

The GLP requirements for storage of data are fairly straightforward, however there are several details which pertain to MS data that need to be addressed. First, data from a GLP study must be retained for 5 years after being submitted to the FDA. What this means for example is, if the data is not submitted to the FDA until 8 years after being originally reported, it must be retained for a total of 13 years. Second, it is not sufficient to simply file the data away, it must be in a readily accessible, readable format. Finally, all pertinent information needed to reconstruct the study results submitted with the final report, including calibration files, spectra used for background subtraction, the smoothing algorithm, integration results and the original chromatographic data must be saved. Because storage and retrieval of data in an electronic format over an extended period of time may be a problem, due to obsolescence of hardware and physical deterioration of the storage media, the data may be saved as a paper hard copy. Data may be stored electronically or in hard copy format, there is no preference as long as the data can be retrieved quickly and it is possible to generate the same findings as recorded in the final report. Regardless of how the data is stored, the following information must also be stored with the data; (a) general information including operator, date, time and calibration file used, (b) a calibration spectrum, (c) a mass spectrum of the test

43rd ASMS Conference on Mass Spectrometry and Allied Topics

article using the ionization method of the analysis, (d) if background subtraction is performed, then a copy of the background spectrum used for subtraction must be provided, (e) if the data is smoothed, then the amount of smoothing must be indicated, and (f) if the data is integrated, then the area to be integrated should be clearly marked and the integration results indicated. If the data is stored as a paper copy of the electronic data it must also include an authorized signature verifying that it is an exact representation of the raw data.

There are several other considerations which fall into the category of data management and they have to do with software control. While GLP regulations do not require the instruments' software programming code to be kept on site, the code must be accessible if needed. Additionally, a description (not the code) of transformations done to the primary data must be retained with the study results. For example, if the chromatographic data is smoothed, an explanation describing the algorithm used and how it was applied, along with the version of software used, would be required. This statement may be as simple as the following; using version 2.3.7 of brand X software (release date) a standard 3 point smooth was performed on the chromatographic data using the Einstein smoothing algorithm. This information would most likely be contained in the protocol describing post-acquisition processing of the data. Another important software control that needs to be addressed pertains to the integrity of data files. It is very important to be certain that the software cannot simply overwrite a previous data file of the same name without some record of the deletion being made. Ideally, it would not be possible to overwrite or delete any data file obtained in a GLP study, however in reality it is very difficult to provide this type of data security. There are two practical alternatives to assure this type of safety. First, the software developer designs the system such that files cannot be easily overwritten. Failing this, the facility must provide procedures to prevent files from being overwritten, ie. through the use of a standard operating procedure (SOP).

Validation of an On-Line Archiving System for Quantitative Mass Spec Data

Patricia M. Coleman, Thomas D. Oglesby, Robert J. White, Lisa P. Werdal
Taylor Technology, Inc., 107 College Road East, Princeton, NJ 08540

A typical problem encountered in any high volume Mass Spectrometry facility is the necessity of archiving large quantities of electronic data. Archiving procedures must be established to assure that all data is securely stored, and easy to identify, locate, and retrieve for an extensive period of time. Automating the archiving system is desirable from the standpoint of reducing personnel time requirements and, perhaps more importantly, eliminating some of the errors which occur in manual systems.

Installing an automated archiving system in a GLP facility requires compliance with FDA/EPA guidelines for the validation of computer systems. Validation is defined as "establishing documented evidence which provides a high degree of assurance that a computer system will consistently produce a product meeting its predetermined specifications and quality attributes"[1]. Two critical phrases of this definition are *documented evidence* and *meeting predetermined specifications*. It is clear from the definition that simply "testing" a computer system is not sufficient to meet regulatory requirements.

Proper validation of a computerized system requires the use of a System Development Life Cycle (SDLC) approach. A written Validation Protocol should be developed which describes all phases of this life cycle. Although ISO 9000, IEEE, and others have specified somewhat different terminologies in the SDLC, the basic framework remains the same. Each company should define the framework and terminologies which work best for them, making sure not to leave out any critical parts of the validation process.

Taylor Technology's framework for the SDLC is outlined as follows:

Phase I - Initiation
- A. System Overview
  - Describe System and its Context
  - Identify Responsibility for the System
- B. User Specifications
  - WHAT the system needs to do
  - User defined requirements

Phase II - Design
- A. Vendor Requirements
  - Adequate Market Experience
  - Quality Software Development Standards
- B. Design Specifications
  - HOW the System will do what is needed
  - Detailed system design by programmer/developer

Phase III - Testing
- A. Structural Testing (White Box Testing)
  - Verifies structural integrity of system
  - Performed by developer/programmer
- B. Functional Testing (Black Box Testing)
  - Verifies system's ability to meet User Specifications
  - Focus on outputs generated by selected inputs
  - Must follow written Test Plan and document results
    - Test Condition/Expected Result/Actual Result

Phase IV - Implementation
- A. Installation in Working Environment
  - Additional Functional Testing
  - User Approval
- B. On-going System Maintenance
  - Change Management / Periodic Review
  - System Documentation / Training Requirements
  - System Security / Backup Procedures

After the basic need for a new archiving system was agreed upon at Taylor Technology, a committee was formed to manage the project which included representation of Mass Spec Users, Information Systems, Quality Assurance and Management. General Requirements for the System were identified including the following:

Current Network Compatibility
Large Storage Capacity and WORM Media Compatibility
Minimal Hands-On Operation Requirements
Easy Retreival of Project/Client Specific Data

After several months of product research, a system was identified which had the potential of meeting the defined requirements. A period of Vendor qualification began which included a review of vendor's programming procedures and quality assurance program, two days of training for all members of the archiving committee and a test installation of a system prototype in our facility.

Because of the complexity of the project and the critical nature of the data involved, a decision was made to implement the system in two phases. In Phase 1, Data is manually identified for archive and then automatically collected by the system and stored to WORM media. An automatic byte by byte comparison of archived files is then performed and results reported. A Validation Protocol was started which described the Initiation of the project and the User and Design Specifications. A Test Plan for Phase 1 was written which identified the tests to be performed and the expected results. After testing was complete, the preliminary system was installed. The completed Validation Protocol included on-going maintenance information such as training, security and backup requirements, and references to internal SOP's and User's Documentation.

The Validation Protocol contains only a brief summary of Phase 2, in which Quantitative Mass Spec Data will be sent to the Archive System immediately after it is acquired. Specifications for Phase 2 are currently in development. When they are complete, the Protocol will be updated to include the second phase of the project.

Each Validation Project is unique. Meeting Regulatory Requirements mandates starting with a Systems Development Life Cycle approach and documenting the process using a Validation Protocol. Beyond that, common sense and logical decision making should guide the process.

[1] PhRMA's Computer System Validation Committee (CSVC) "Validation of Computer Systems", three day course, Baltimore, MD, April 24-26, 1995.

An Electronic Sample Logbook for the VG 11/250J Data System

Kenneth J. Rosnack and Thomas R. Sharp
Analytical R&D, Central Research, Pfizer Inc., Groton, CT 06340 U.S.A.

A significant part of conducting any chemical analysis is documenting the identity and source of the sample being analyzed. If such documentation is not done, the analysis may as well not have been conducted. This activity is even more important in situations where the results may be subject to regulatory and/or legal scrutiny. Quality assurance concerns also dictate that the information about the sample be accurately propagated from initial recording through to a final report. The multiple times such information is copied from analysis of sample to final report afford many opportunities to introduce simple transcription errors, which create complex information tracking problems. If such sample identity information could be recorded once, stored intimately with the analytical data, and propagated through the use of reliable computer systems, many of these quality assurance concerns can be addressed.

Toward this end, we have developed an electronic sample logbook system for our VG Analytical 11/250J mass spectrometer data system which provides for one-time entry of sample identification information, intimate association of this information with the analytical results, and at least sets the stage for further use of this information in archiving/retrieval and indexing of analytical results.

The system consists of several "macro programs" which make use of the RPG, MACRO, RUN and DBE features of the 11/250J data system software. Sample information is entered once into a spreadsheet format. A portion of a logbook page, showing the format we use, is reproduced below. The name to be used for the data file, identification of the sample submittor and of the sample itself, notes on operation and experimental conditions, and necessary accounting information are entered. The time and date are left blank. The contents of these fields are generated from the computer system time and date and recorded in the spreadsheet when data acquisition is initiated. While the time does not reflect the exact time that the data acquisition was started, it is reasonably close.

	0	1	2	3	4
	SAMPLE I.D.	RUN FOR ANALYST	CP-NUMBER	NOTEBOOK REFERENCE	RUN NUMBER
36	4211J3656	LOWE/QIAN		30933-174-01	0017244
37	4211J3657	LOWE		31061-77-16	0017245
38	4214W2315	CALIBRATION	FB+	H2SO4	0017246
39	4214J3658	MAGIC BULLET	TEST		0017247
40	4214J3659	B.L. BACON	CP-143,867	23568-71-1J	0017248
41	4214J3660	A.W. GROBIN	CP-88,059	24578-273-1H	0017249
42	4214J3661	A.W. GROBIN	CP-88,059-89	24578-287-1H	0017250
43	4214J3662	S.A. DIROMA	CP-122,721-1	24895-99-1F	0017251
44	4214J3663	S.A. DIROMA	CP-122,721-1	24895-109-1H	0017252
45					
46					
47					
48					
49					
50					

The identification fields in the data acquisition program are then filled in électronically from this spreadsheet by running a RUN program, thus eliminating a source of transcription errors. The data file name is filled in. An account number is generated. The program assembles a TXT field from the name of the sample submittor and the sample identification, the intials of the operator, and the instrument identification, and inserts it into the TXT field. The RUN program then terminates, leaving the system poised, ready to start the data acquisition run. After completing acquisition of data for a given sample, the process is repeated, filling in information for the next sample on the next available line of the logbook page. After the page is filled, a new page is crated, and the process repeated.

Hardcopy of the logbook pages can be generated. The computer files of logbook pages can be archived. With the appropriate additional software, these logbook page files could be used as the data source for indexing of analyses, generation of sample throughput statistics, and accounting purposes.

The updating of parameters can be extended for more involved experiments, such as GC-MS runs, by adding additional commands to the RUN program to modify parameters in the GCC parameter page.

This system has evolved and has been in use on our mass spectrometer data system for several years. It is reasonably robust, and has provided the means to decrease the amount of effort and improve the accuracy of our sample record keeping tasks.

5	6	7	8	9	10	11
COMMENTS	OPR	CHARGE NUMBER	TEST NUMBER	UNITS CHARGED	DATE CREATED	TIME CREATED
"/"/"/"/"/"	SVD	55260	80	1	11-FEB-94	10:39:47
"/"/"/"/"/"	SVD	55260	80	1	11-FEB-94	10:51:51
FB+/RP2K/1600-90/5SDEC/.5SINT	TRS	56330	80	1	14-FEB-94	13:39:54
"/"/"/"/"/MAGIC BULLET	TRS	56330	80	1	14-FEB-94	13:52:21
"/"/"/"/"/"	TRS	56330	80	1	14-FEB-94	14:01:12
"/"/"/"/"/"	TRS	56330	80	1	14-FEB-94	14:13:32
"/"/"/"/"/"	TRS	56330	80	1	14-FEB-94	14:26:48
"/"/"/"/"/"	TRS	56330	80	1	14-FEB-94	15:45:57
"/"/"/"/"/"	TRS	56330	80	1		

VALIDATION OF MASS SPECTROMETRY DATA SYSTEMS IN A REGULATORY ENVIRONMENT

Cynthia A. Palmer, Michael S. Alexander and Craig R. Abolin
Drug Metabolism and Pharmacokinetics, Sandoz Research Institute
59 Route 10, East Hanover, NJ 07936-1080
email: abolin.craig@ehccgate.sandoz.com

Regulatory pressures have been dramatically changing the extent, means of documentation, data archiving and report generation in quantitative mass spectrometry (MS) laboratories. An entirely new set of requirements beyond the presently accepted scope of Good Laboratory Practices is being placed on the MS laboratory, which must still attempt to meet ongoing analytical demands. In response to this need, we have initiated the development of a robust validation procedure for our specialized data acquisition and reporting system.

Our approach to validation is outlined as a flow diagram in Figure 1. There are two convergent pathways in the validation process: the creation of the overall validation framework with its supporting documentation, and the actual testing of the system with appropriate sets of data. The framework includes, but is not necessarily limited to, a comprehensive review of the current system, an outline of the rationale for the new system, predefined performance acceptance criteria, and provisions for security (physical and electronic), maintenance, data handling, system changes and upgrades, disaster recovery and training. The testing must demonstrate that the expected results with allowable tolerances (if any) are obtained. The actual data sets used must be able to test the system thoroughly.

The system must also be tested to determine its operating boundaries. If possible, the results should be compared to an acceptable standard method. Finally, the entire validation package must be audited and properly archived and a final validation document written.

The guiding principles of the MS data system validation are that: (1) all components of a data system must be thoroughly tested, both individually and in concert; (2) all steps in the generation and processing of analytical results must be unambiguously traceable to the raw data; (3) all steps in the process must be thoroughly documented. A validation plan example is presented for weighted nonlinear regression for LC/MS calibration curves, illustrating the development life cycle and system testing.

Validation can be achieved within reasonable cost and time constraints by breaking the overall validation process into a series of small steps. These goals are achievable without compromising laboratory productivity or quality by careful advance planning. We have found that validation can be performed in an incremental manner, with some portions in parallel (illustrated in Figure 2), and that basic questions about the actual mechanism of the data system validation process are not yet clearly defined in the MS user or regulatory community.

REFERENCES

"Red Apple Conference Center Book", September 1988. *Computerized Data Systems for Nonclinical Safety Assessment.* Drug Information Association, P.O. Box 3190, Maple Glen, PA 19002. 1988.

Computer Systems Validation for the Pharmaceutical and Medical Device Industries, Richard Chamberlain, Interpharm Press, Buffalo Grove, IL. (708) 459.8480. Second Edition, 349 pages. 1994.

Figure 1

Validation Flow Diagram

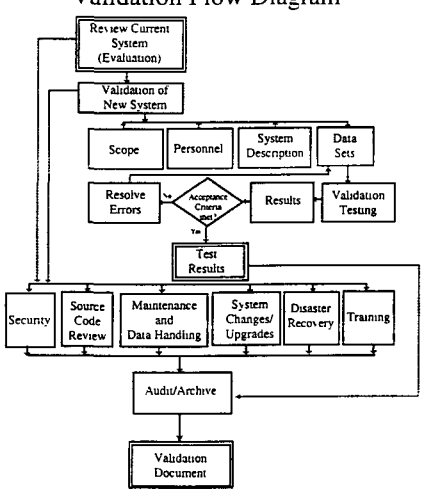

Figure 2

Sample Timeline for VALIDATION

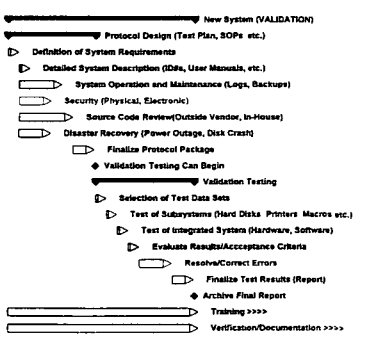

PROBING NONCOVALENT INTERACTIONS BY ION SPRAY MASS SPECTROMETRY

Bruce Ganem*

Department of Chemistry, Baker Laboratory
Cornell University, Ithaca, NY 14853-1301

Jack D. Henion

Analytical Toxicology, Diagnostic Laboratory
Cornell University
927 Warren Drive, Ithaca, NY 14850

With the advent of electrospray and ion spray interfaces, the analysis of macromolecules by mass spectrometry has emerged as an important tool in modern biological research. Four years ago, we reported the first studies in which noncovalent receptor-ligand and enzyme-substrate complexes were detected in the gas phase directly out of aqueous solution. That work established for the first time that the cumulative effect of weak intermolecular forces -- e.g. hydrogen bonding, charge transfer complexation, π-stacking, hydrophobic effects, charge-charge, charge-dipole, and dipole-dipole interactions -- could provide enough stabilization for such host-guest complexes to survive the gentle ion evaporation process.

Even though such intermolecular interactions are influenced differently by solvation, and display qualitatively different structural and distance constraints, it is now apparent from the efforts of numerous groups that electrospray and ion spray mass spectrometry can be used to detect molecular recognition phenomena in a wide variety of biologically important association complexes. Examples to date have included several active site directed enzymatic complexes (e.g. with substrates, products, and inhibitors), oligonucleotide duplexes, drug-nucleic acid complexes, heme-globin complexes, antibody-hapten complexes, hydrophobic leucine zipper peptide dimers, and carbohydrate association complexes on cell-surfaces.

These studies have paved the way for more ambitious applications of mass spectrometry designed to probe the higher order structure of macromolecular and supramolecular assemblies within biological systems. For example, the role of the modern mass spectrometer in unravelling the stoichiometry of multimeric chemical and biochemical architectures, in ascertaining the functional role of subunits in complex catalytic processes, and in studying the structures of membrane-bound proteins will be discussed.

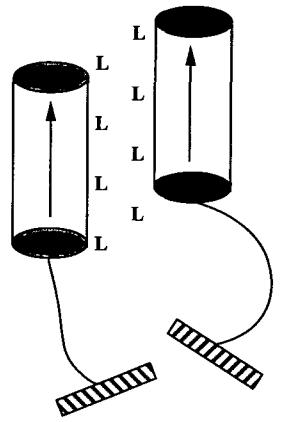

noncovalent leucine zipper interactions in transcriptional activator proteins

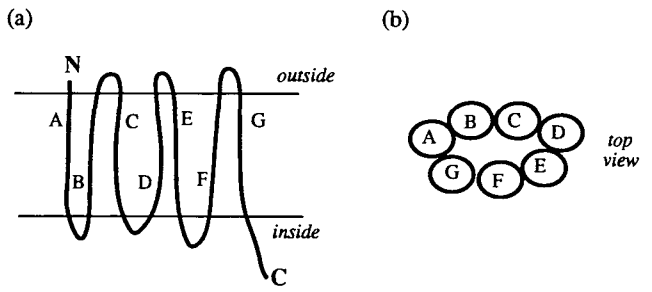

a transmembrane-spanning protein: (a) side and (b) top view

CHARACTERIZATION OF PROTEIN-DNA COMPLEXES USING ESI-MS

Xueheng Cheng, Amy C. Harms, Richard D. Smith, Paul E. Morin,* Paul N. Goudreau,** Thomas C. Terwilliger**

Chemical Sciences Department and Environmental Molecular Sciences Laboratory, Pacific Northwest Laboratory, Richland, WA 99352, USA
* Department of Medical Biophysics, University of Toronto, Toronto, Canada, M4X 1K9
** Genomics and Structural Biology Group, MS M880, Los Alamos National Laboratory, Los Alamos, NM 87545, USA

Protein-DNA interactions are crucial to the regulation and control of a host of functions within living organisms. Among the techniques for the study of protein-DNA interactions are x-ray diffraction, NMR, and electrophoresis (e.g., mobility shift assays). Electrospray ionization (ESI) has recently been shown to result in ionization of large biomolecules while preserving noncovalent biomolecular associations. The preservation of these associations is significant because mass spectrometry (MS) is a highly sensitive and structurally informative technique that is directly applicable to the analysis of mixture components.

We have made the first ESI-MS characterization of protein-DNA complexes. Gene V protein from bacteriophage f1 is known to bind strongly to single stranded DNA. Under mild interface conditions from solutions in 10 mM NH4OAc, gene V protein was observed as dimer ions from ESI. The binding stoichiometry was investigated using different lengths of ssDNA. Figure 1 shows a 4:1 protein:DNA complex was observed with a 16-mer ssDNA. A 12-mer ssDNA formed primarily a 2:1 protein:DNA complex. This indicates the protein binds as a dimer and with a stoichiometry of one dimer for eight nucleotides. The complex with 16-mer ssDNA was examined independently by gel filtration and a 4:1 complex was also found by this method.

PU.1, a member of the Ets family of transcription factors, is a sequence specific DNA binding protein that has a recognition sequence GGAA/T in double stranded DNA. Figure 2 shows a 1:1 complex is formed with a 17-bp dsDNA containing the recognition sequence. A competition experiment with a 19-bp dsDNA not containing the recognition sequence showed that only the 17-bp dsDNA formed complex with the protein, even when the 19-bp was present in 20 fold excess. A band shift assay confirmed the selectivity of the protein.

The results of these studies demonstrated the potential utility of ESI-MS in the characterization of stoichiometries and relative binding energies of protein-DNA complexes.

The research at PNL was supported through the U.S. Department of Energy. PNL is operated by Battelle Memorial Institute through Contract No. DE-AC06-76RLO 1830.

43rd ASMS Conference on Mass Spectrometry and Allied Topics

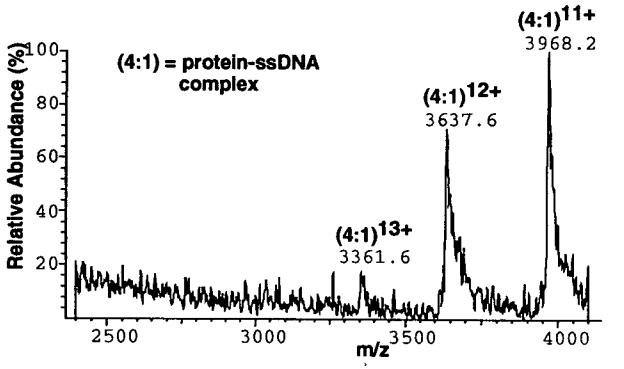

Figure 1. Gene V protein and 16-mer ssDNA

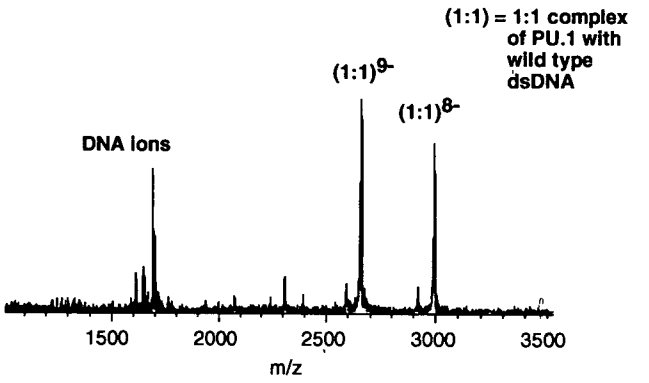

Figure 2. PU.1 Protein and 17-bp dsDNA with GGAA recognition sequence

Studies of Non-Covalent Interactions by Time-of-Flight Mass Spectrometry

I.V. Chernushevich[1*], W. Ens[1], K.G. Standing[1], P.C. Loewen[1], M.C. Fitzgerald[2], S.B.H. Kent[2], R.C. Werlen[3], M. Lankinen[3], X.-J. Tang[4], C.F. Brewer[4], S. Saha[4]
[1] University of Manitoba, Winnipeg, Manitoba R3T 2N2, Canada
[2] Scripps Research Institute, 10666 N.Torrey Pines Road, La Jolla, CA 92037
[3] Centre Medical Universitaire, 1 rue Michel Servet, CH 1211 Geneva 4, Switzerland
[4] Albert Einstein College of Medicine, 1300 Morris Park Ave., Bronx, New York 10461

The electrospray (ES) technique provides a suitably gentle ionization method for obtaining information on the higher-order structure of proteins and their interaction with other biomolecules [1,2], but the limited *m/z* range of most quadrupole mass spectrometers has been a major obstacle. This limitation is particularly significant when proteins and/or complexes of biomolecules are studied in their native conformations from solutions at near physiological conditions. We have interfaced an ES source to a time-of-flight mass spectrometer [3], which has in principle an infinite *m/z* range. Recent incorporation of nano-spray [4] and an RF-quadrupole ion guide [5] into the instrument has led to further improvements both in sensitivity and resolution and minimized mass and *m/z* discrimination. These features make the ES-TOF instrument suitable for studies of non-covalent complexes, as demonstrated by several examples below.

Studies have been carried out on the enzyme 4-oxalocrotonate tautomerase (~6810u), prepared by total chemical synthesis [6]; they showed that the enzyme forms a hexamer in solution at pH 7.5, which falls apart at pH<5. Ions of a site-specific immunoconjugate $F(ab')_2$-CPG2, prepared from an $F(ab')_2$-like fragment of the monoclonal anti-CEA murine IgG1 A5B7 and a mutant of the dimeric enzyme carboxypeptidase G2 [7], were recorded with m/z>6000 and were the dominant ions in these spectra, as shown in Fig.1. The complex was observed at pH ~6, and it fell apart at pH<4.5. Protein-protein non-covalent interactions in soybean agglutinin (SBA), a glycoprotein with monomer mass ~30,000 u, have been examined in this instrument [8]. Only monomer ions were observed in 30% acetonitrile, only tetramer ions (and tetramer clusters up to the 20-mer, M.W.~578,000 u) in pure water. Further information on the quaternary structure of SBA was obtained by collision-induced dissociation (CID) of the tetramer within the ion source. Although most of the experiments were carried out with a conventional ES source, nano-spray turned out to be very efficient in studies of non-covalent complexes. It produces a stable spray from almost any solution and allows use of as little as ~1 microL of solution. An example of a nano-spray spectrum of SBA is shown in Fig.2.

Catalase HP II from E.coli [9], a tetrameric protein with M.W.=339,100 u, was also studied with nano-spray. Earlier it was demonstrated that the performance of ES-TOF MS for heavy ions (>50,000 u) is deteriorated significantly by collision-induced dissociation inside the vacuum chamber at pressures ~10^{-6} Torr [10]. However, mass spectrum of HP II did *not* change when the pressure in the vacuum chamber was increased from $2*10^{-7}$ to $1.3*10^{-6}$Torr (Fig.3). The narrow peaks in this spectrum recorded at high declustering voltage (ΔU=200 V) allowed determination of the mass with an accuracy of 0.03%. At lower ΔU (Fig.4), the peaks became wider and clusters up to the 16-mer (M.W.>10^6 u) were clearly observed.

All the complexes mentioned above required observation of high *m/z* ratio (3,000 to 16,000), as provided by ES-TOF instrument.

1. R.D. Smith, K.J. Light-Wahl, *Biol. Mass Spectrom.* **22**, 493 (1993)
2. M. Przybylski, M.O. Glocker, *Angew. Chem. Int. Ed. Engl.*, in press.
3. A.N. Verentchikov *et al*, *Anal. Chem.* **66**, 126 (1994)
4. M.S. Wilm, M. Mann, *Int. J. Mass Spectrom. Ion Processes* **136**, 167 (1994).
5. A.N. Krutchinsky *et al*, 43rd ASMS Conference, MPB 085.
6. M.C. Fitzgerald *et al*, 43rd ASMS Conference, MPE 225; to be submitted to *JACS*.
7. R.C. Werlen *et al*, *Bioconjugate Chem.* **5**, 411 (1994)
8. X.-J. Tang *et al*, *Rapid Commun. Mass Spectrom.* **8**, 750 (1994); 43rd ASMS Conference, ThPG 249
9. I. Ossowski *et al*, *J. Bacteriology* **173**, 514 (1991).
10. I.V. Chernushevich *et al*, Proceedings of the 42nd ASMS Conference, p.989 (1994)

* on leave from the Institute of Energy Problems of Chemical Physics, Chernogolovka, Russia

43rd ASMS Conference on Mass Spectrometry and Allied Topics

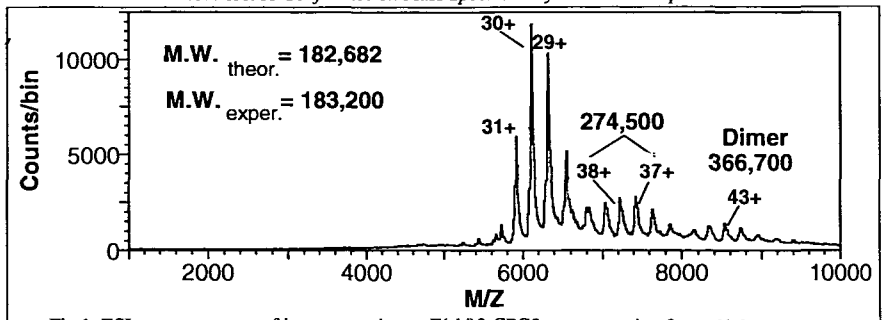

Fig.1. ESI mass spectrum of immunoconjugate F(ab')2-CPG2; concentration 2 pmol/µl.

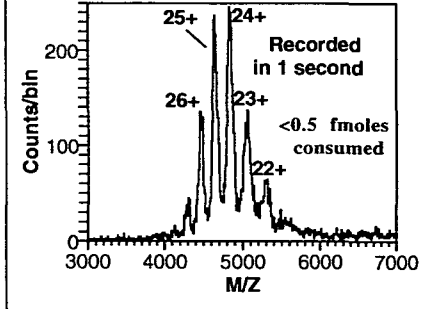

Fig.2. Nano-spray mass spectrum of native SBA; 10^{-6}M in water; 3µL (3pmoles) injected.

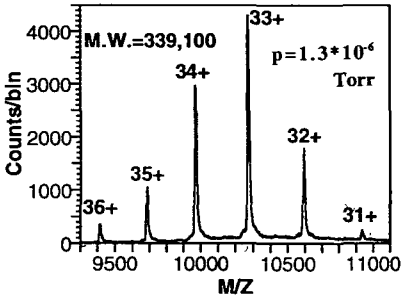

Fig.3. ESI mass spectrum of catalase HP II recorded at high pressure in the main chamber of the instrument.

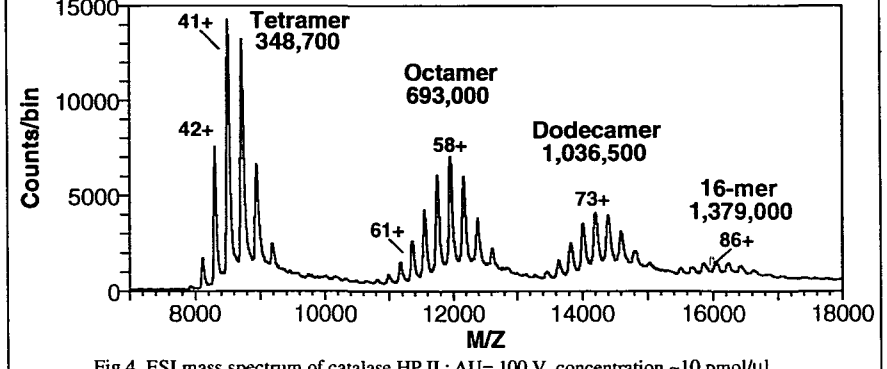

Fig.4. ESI mass spectrum of catalase HP II ; ΔU= 100 V, concentration ~10 pmol/µl

Detecting Conformational Changes in Cytochrome C upon Binding of Membranes

Paul W. Stoker, Jocelyn H. Ng-Ilag, and David L. Smith
Department of Chemistry, University of Nebraska, Lincoln, NE 68588-0304

Understanding the interaction of proteins with phospholipid membranes and the conformational changes caused by this membrane contact is necessary to ascertain the proteins' function. The binding of cytochrome C, an extrinsic mitochondrial membrane protein, to synthetic lipid membranes has been studied. One valuable technique employed is monitoring of the exchange of hydrogen for deuterium at the amide nitrogens all along the protein backbone. The incorporation of the deuterium for small proteins can be detected by NMR[1] and FTIR[2], but are not as useful for larger proteins and membrane bound proteins. In these more difficult cases, more useful information may be acquired by digestion of the deuterated protein followed by the analysis of the resultant peptide fragments by HPLC FABMS[3]. We have used the hydrogen exchange method HPLC ESIMS to examine the interaction of cytochrome C with a synthetic phospholipid membrane.

The synthetic phospholipid membrane was made to resemble the inner mitochondrial membrane upon which the cytochrome C is naturally bound. The composition of membrane consists of phosphotidylcholine, cardiolipin, phosphotidylethanolamine, and cholesterol. These lipids were purchased commercially and made into large unilamellar vesicles. Cytochrome C was added to the vesicles and allowed to complex for two hours. The cytochrome C-lipid complexes were washed with buffer to remove the unbound protein. Deuterated buffer at pD 6.0 was added to the complexes. To insure that little H_2O remained in the solution, the complexes were centrifuged and the buffer was removed, additional D_2O buffer at pD 6.0 was added, and then the tube was inverted several time to mix the sample. The complexes were incubated in the D_2O buffer for a prescribed time period (1-55 min). At the end of the time period the D_2O buffer at pD 6.0 was removed and the complexes were washed with cold D_2O buffer at pD 5.0 to remove any unbound cytochrome C and to slow the exchange reaction. After the removal of the cold D_2O buffer (pD 5.0), cold 200 mM $MgCl_2$ was added to the complexes, followed quickly by the addition of cold 1M D_2O buffer at pD 2.0. The resulting solution was filtered to remove the lipid membrane and the filtrate was frozen in liquid nitrogen and stored at -80° C until analysis. The samples were thawed quickly, digested by pepsin, and analyzed by HPLC ESIMS. In addition to the analysis of the membrane bound protein, control experiments were run with free cytochrome C for comparison.

Comparison of the results of the analysis of the peptide fragments for the free versus the bound cytochrome C indicate that there are two regions of the protein where a decrease in deuterium incorporation was observed. Figure 1 shows the peptide fragments that were analyzed and the regions of decreased incorporation. The largest region of decrease incorporation is in the 95-104 peptide fragment. The plot of the deuterium uptake versus time of the 95-104 fragment can be seen in Figure 2. In an earlier work this region of cytochrome C was postulate to be embedded in or on the surface of the lipid membrane[4]. The plot of the deuterium uptake versus time for a fragment in which very little difference is seen is also shown in Figure 3.

References:

1. Muga, Arturo; Mantsch, Henry H.: Surewicz, Witold K. *Biochemistry.* **1991**, *30*, 7219.
2. de Jongh, Harmen H.; Killian, J. Antoinette; and de Kruijff, Ben. *Biochemistry.* **1992**, *31*, 1636.
3. Zhang, Zhongqi and Smith, David L. *Protein Science.* **1993**, *2*, 522.

4. Lee, Seungcheol and Kim, Hyoungman. *Archives of Biochemistry and Biophysics.* **1989**, *271*, 188.

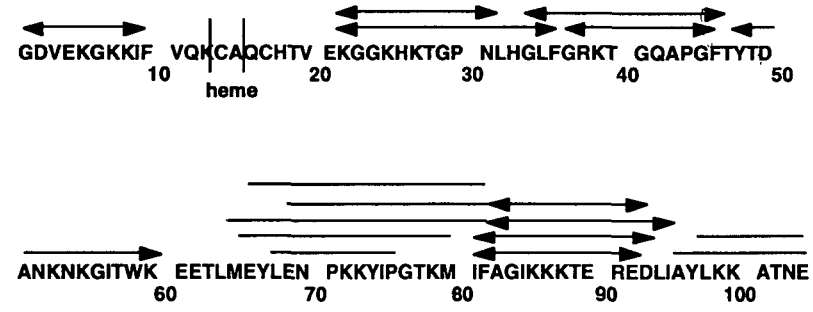

Figure 1. Peptide fragments formed by peptic digestion of cytochrome C. These peptide fragments were analyzed by HPLC ESIMS to determine the level of deuterium incorporation. The lines represent peptide fragments which showed a decreased incorporation of deuterium when bound to a phospholipid membrane as compared to free cytochrome C. The lines with arrowhead represent the peptide fragments which showed very little change in deuterium incorporation.

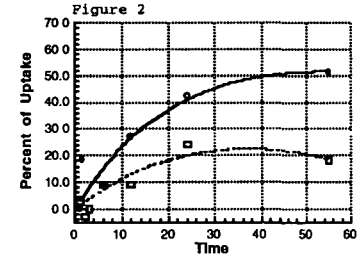

Figure 2: Plot of the deuterium uptake versus time for the peptide fragment 95-104 of the cytochrome C. The fragment is the result of pepsin digestion of the membrane-bound and free protein after the incubation period. The squares are the membrane-bound cytochrome C and the circles represent the free protein.

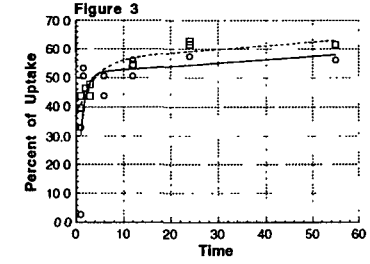

Figure 3: Plot of the deuterium uptake versus time for the peptide fragment 22-36 of the cytochrome C. Conditions and labeling of the data points are the same as described for Figure 2.

PROTEIN DENATURATION STUDIED BY HYDROGEN EXCHANGE AND MASS SPECTROMETRY

Zhongqi Zhang and David L. Smith
Department of Chemistry, University of Nebraska-Lincoln, Lincoln, NE 68588

The study of protein denaturation may provide important information for the mechanism of protein folding and unfolding, as well as the basis for the thermodynamic stability of proteins. Most of the studies of protein denaturation were done by differential scanning calorimetry, circular dichroism, fluorescence, infrared spectroscopy, etc., which give very limited space-resolved structural information. Some detailed information about protein denaturation has been obtained from NMR studies of several small proteins, but few studies have been done on structurally resolved denaturation of large proteins A new technique, based on protein fragmentation and mass spectrometry to determine hydrogen exchange behavior in a protein, provides a new tool for the studies of denaturation of large proteins (Zhang and Smith, *Protein Sci.* 2, 522, 1993). In this technique, deuterium labeled protein is digested by an acid protease, and the deuterium content on each peptide fragment is determined by directly coupled HPLC/mass spectrometry This presentation describes the results obtained when this technique was applied to the study of heat, acid and urea induced denaturation of rabbit muscle aldolase

In this study, a capillary perfusion column was connected directly to VG Autospec electrospray mass spectrometer equipped with an array detector. The perfusion column was used to reduce the time of analysis, and thus minimize the deuterium loss during analysis. The whole HPLC/ESIMS analysis can usually be finished within 5 minutes.

In the study of thermal denaturation of aldolase, aldolase was incubated in D_2O at different temperatures Because the amide hydrogens in a segment have much higher exchange rates when the segment is unfolded, the level of deuterium incorporation in each segment reflects the thermal stability of this segment The result shows that with the increase of temperature, loop areas loosen gradually, and α-helices and β-sheets unfold cooperatively at the denaturation temperature of 45-50 °C The last step of irreversible thermal denaturation of aldolase is the loss of its quaternary structure

In a mild denaturing condition, as shown in Fig 1, there is usually an equilibrium between the native state and a partially unfolded state. Hydrogen exchange occurs mostly in the unfolded state The distribution of deuterium labeling in an unfolded segment depends on the rates of the hydrogen exchange (k_2) and the refolding of the segment (k_{-1}). If $k_2 >> k_{-1}$, all amide hydrogens in the unfolded segment will be replaced with deuterium (EX1 mechanism) As a result, a bimodal isotopic pattern will be observed, and the unfolding rate constant of the segment k_1 equals the rate constant at which the envelope with high deuterium content increases with time

The study of acid induced denaturation of aldolase shows that at p^2H 4 0, aldolase is in an equilibrium between a folded state and an unfolded state, and the hydrogen exchange is through EX1 mechanism, as indicated by a bimodal isotopic pattern for most of the segments studied Further analysis of the patterns shows that most of the segments studied have unfolding rates of 0 2-0.4 hr^{-1}, suggesting that the unfolding of aldolase induced by acid is mostly cooperative When aldolase was incubated in D_2O with 4 M urea, it was found that the areas on the surface of the protein have an unfolding half-life of 1-2 minutes and the regions at the subunit interface have unfolding half-life of about 2 hours (see Fig 2 for examples) This tells us that urea induced denaturation of aldolase is a two-step process. The first step is the unfolding of the surface area and the second step is the unfolding of the subunit interface area

Mass spectrometry is very powerful in the study of protein folding and unfolding when combined

with the hydrogen exchange technique The technique described here can be used to study large proteins, and very importantly, to separate segments from different conformational states of the protein Since this technique has fewer restrictions than other methods and gives important information other methods fail to provide, it will become one of the most important methods for studies of protein folding and unfolding

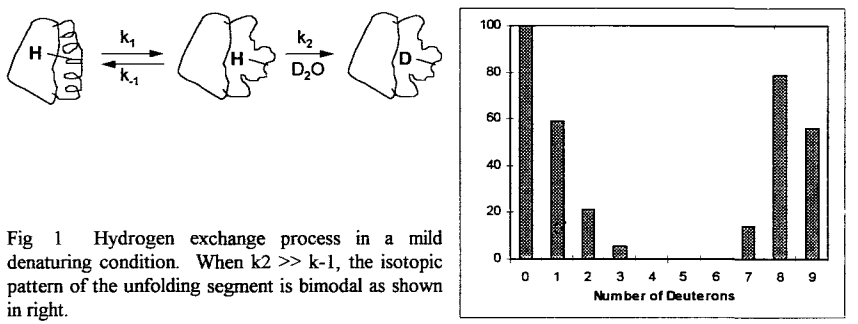

Fig 1 Hydrogen exchange process in a mild denaturing condition. When k2 >> k-1, the isotopic pattern of the unfolding segment is bimodal as shown in right.

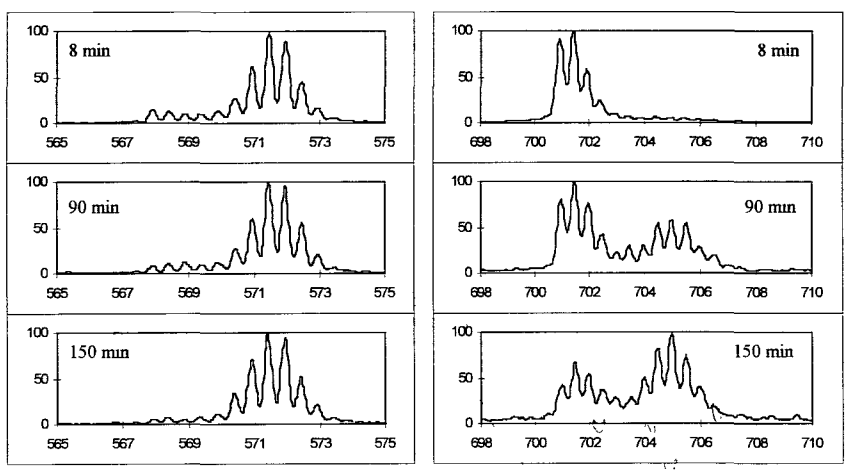

Fig. 2 Electrospray mass spectra of peptide 327-336 $(M+2H)^{2+}$ (left) and peptide 257-269 $(M+2H)^{2+}$ (right) when aldolase was incubated in D_2O with 4 M urea for different periods of time Peptide 327-336, with an unfolding half-life of 1-2 minutes, is from the surface of aldolase, and peptide 257-269, with an unfolding half-life of 2 hours, is from the subunit interface area

Mass Spectrometric Characterization of Non.covalent TT EF.Tu / Ts Complexes.

M.O. Glocker[1], S. Nock[2], M. Sprinzl[2] and M. Przybylski[1]

[1]University Konstanz, Faculty of Chemistry, P.O Box 5560 M732, 78434 Konstanz, Germany.
[2]University Bayreuth, Institute for Biochemistry, Universitätstr. 30, 95440 Bayreuth, Germany.

Bacterial elongation factor Tu (EF-Tu) is a GTPase which promotes the binding of aminoacyl-tRNA to the codon-programmed ribosomes EF-Tu from *Thermus thermophilus* consists of 405 amino acids and has a molecular weight of 44636 Da. The crystal structure of intact EF-Tu from *Thermus thermophilus* has been determined in the presence of a nucleotide GppNHp, a structural homolog of GTP [1]. It contains three domains, domain I (aa residues 1-211, GTP/GDP binding domain) carries the nucleotide binding region and consists of α-helical and β-sheet structure elements, while domain II (aa 212-311) and domain III (aa 312-405) show β-sheet secondary structural features. EF-Tu is an essential component of bacterial protein biosynthesis and forms a ternary complex with GTP and aminoacyl-tRNA. During its functional cycle it consecutively binds several ligands, GDP, elongation factor Ts, GTP, aminoacyl-tRNA and ribosomes [2] The common feature of ribosomal regulatory elongation cycles is the switch from an "inactive" GDP binding to an "active" GTP binding conformation of EF-Tu which is promoted by EF-Ts, a nucleotide exchange factor [3]. Elongation factor Ts (EF-Ts) is a homodimer and when isolated, forms an intermolecular disulfide bond. EF-Ts consists of 195 amino acids and has a molecular weight of 44618 Da for the homodimer. Not much is known about the regions through which both proteins are interacting and the tertiary structure of EF-Ts is unknown. Recently, mass spectometric methods were shown to be able to characterize protein tertiary structure features [4]. Also, mass spectrometric methods in combination with tertiary structure-selective chemical modification reactions were shown to present a useful tool for the characterization of protein surface topologies [5,6].

In this study we describe the use of protein tertiary structure-selective lysine acetylation combined with mass spectrometric analyses for the characterization of elongation factors EF-Tu and EF-Ts and their interacting regions. Acetylation reactions were carried out using EF-Ts, EF-Tu complexed with GDP (EF-Tu*GDP), and with non-covalent complexes formed between EF-Ts and EF-Tu*GDP The molecular weights of the proteins and partially acetylated derivatives were determined using electrospray mass spectrometry (ES-MS) and matrix assisted laser desorption / ionization mass spectrometry (MALDI-MS) and showed increasing molecular weights with increasing excesses of acetic anhydride. ES-MS, additionally, was used to study changes in

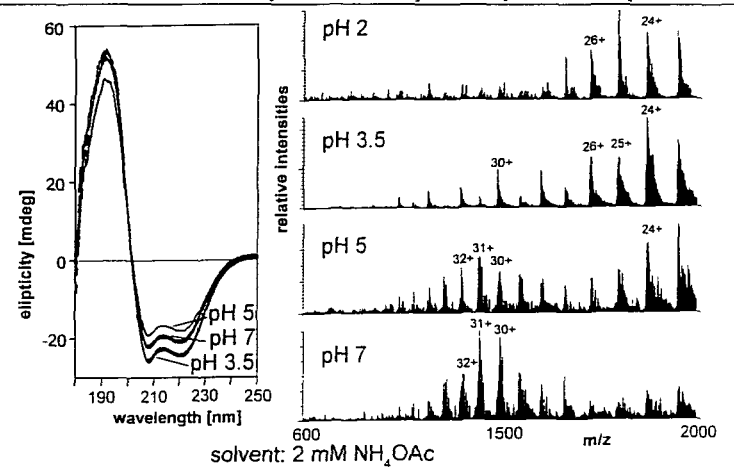

Figure 1. CD- and ES-MS spectra of EF-Ts at different pH.

protein conformations by comparison of charge structures of unmodified and acetylated EF-Tu and EF-Ts derivatives. Both, EF-Tu and EF-Ts derivatives with small degrees of acetylation showed similar charge structures than the unmodified proteins. In contrast, pH variation had extreme effects to the charge structure of EF-Ts (Fig. 1) At high pH EF-Ts showed a maximum around the 31+ molecular ion, while at low pH the maximum had shifted to the 25+ molecular ion. Mass spectrometric peptide mapping analyses of tryptic peptide mixtures of partially modified protein derivatives yielded the exact identification of acetylation sites Acetylation reactions with EF-Tu*GDP showed that lysine residues involved in nucleotide binding remained unacetylated. Differences in acetylation of EF-Tu*GDP alone in comparison to EF-Tu - EF-Ts complexes were observed for Lys45 and Lys52 in domain I, indicating that this region was shielded in the non-covalent complex. Also, acetylation reactions with EF-Ts alone enabled the differentiation between relative reactivities of all lysine residues Comparison of the acetylation pattern of the free EF-Ts with the acetylation pattern of the non-covalent complex of EF-Ts with Ef-Tu*GDP indicated that Lys119 of EF-Ts is shielded by the interaction with EF-Tu.

1) H Berchtold, L. Reshetnikova, C O A. Reiser, N K. Schirmer, M. Sprinzl and R. Hilgenfeld (1993) Nature 365, 126-132
2) D L Miller and H Weissbach (1977) in Molecular Mechanisms of Protein Biosynthesis (H Weissbach and S Petska eds) Academic press N Y , 323-373
3) M Sprinzl (1994) Trends in Biol Sci 19, 245-250
4) M Przybylski and M O Glocker (1995) Angew. Chem. Int. Ed., in press.
5) D Suckau, M. Mak, and M Przybylski (1992) Proc Natl Acad Sci USA 89, 5630-5634
6) M O Glocker, C. Borchers, W Fiedler, D Suckau and M Przybylski (1994) Bioconj. Chem 5, 583-590

Mass Spectrometry as a Tool for Protein X-ray Crystallographic Analysis

*S. L. Cohen, X. Xie, U. A. Mirza, S. K. Burley, and B. T. Chait
The Rockefeller University, 1230 York Avenue, NY, NY 10021

Mass spectrometry can complement as well as facilitate the structural characterization of proteins by X-ray crystallography and NMR spectroscopy. In this report we demonstrate the mass spectrometric contributions to a crystallographic structural study of a recently cloned pair of eukaryotic proteins, p42 and p62 [1]. The two proteins have been shown to associate with each other *in vitro* forming tight heterodimeric and weaker tetrameric complexes. The proteins may play an important role in activated transcription.

The proteins show sequence similarity to the oligomeric histone proteins. Initially, a sequence alignment with the histone proteins allowed for the design of truncated versions of p42 and p62 to facilitate the crystallization attempts (p42: 99 residues, 11.3 kDa; p62: 93 residues, 10.2 kDa). The truncated proteins were expressed and purified. ESI- as well as MALDI-MS verified the correct masses as well as the purity of the recombinant proteins.

Electrospray was also used to monitor the oligomerization of the proteins. Under moderately gentle electrospray conditions, a pure water solution of truncated p42/p62 exhibits strong multiple-charged peaks that correspond to the non-covalent p42/p62 complex (**Figure 1**). Monomer peaks are also observed in the spectrum but *no peaks corresponding to homodimers were measured.* Under even gentler conditions, there appear low intensity peaks that correspond to tetramers (i.e., a dimer of the heterodimers). Under harsh ESI conditions, the dimer peaks disappear leaving only the monomers. Taken together, these results suggest that the solution-phase non-covalent interactions between the truncated p42 and p62 can be maintained into the gas phase with high specificity.

Early attempts to crystallize the truncated p42/p62 yielded crystals that diffracted to low resolution. Coincidentally, MALDI-MS showed that the proteins slowly degraded from their N-and C-terminals in solution. This MALDI finding suggested that the terminals were "floppy" —a result which could account for the poor X-ray diffraction.

In an attempt to better define the minimal folding domains of the protein, the p42/p62 protein complex, formed from the truncated versions of the protein, was subjected to a limited proteolysis study. Three experiments were performed using trypsin, chymotrypsin and subtilisin proteases. MALDI-MS was used for rapid and accurate mapping of the proteolytic digestions. Results of the digestions are summarized in **Figures 2** and **3,** which show the observed sites of proteolytic cleavage superimposed on linear representations of the two proteins. The vertical arrows in both figures point to sites in the proteins which were proteolytically cleaved —the long arrows indicate rapid cleavage (minutes to hours), whereas the shorter arrows indicate sites of slower cleavage (hours to days). Based on the proteolysis results, we designed new constructs of the protein. For p42 this included two forms consisting of residues 1-94 and 10-94. For p62 one new construct consisting of residues 1-84 was planned. The new constructs were expressed and purified. ESI-MS verified that they retained a non-covalent heterodimeric association when sprayed from pure water. Using the the new constructs, we have succeded in growing stable crystals of the p42/p62 complex that diffract to high resolution.

[1] T. Kokubo *et al.* (1994) *Science* **367**, 484-487.

43rd ASMS Conference on Mass Spectrometry and Allied Topics

FIGURE 1

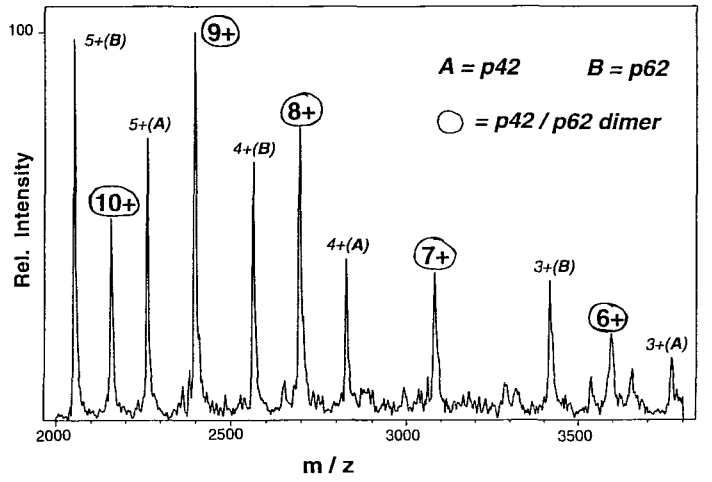

FIGURE 2: Proteolysis of p42 (1-99)

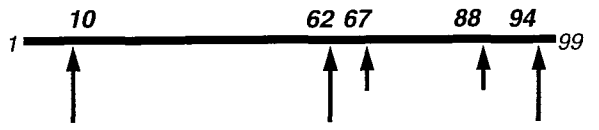

FIGURE 3: Proteolysis of p62 (1-93)

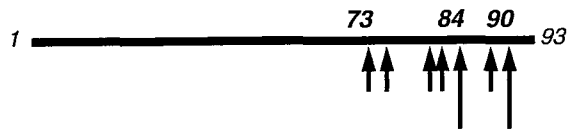

In-line SID Modes: Characterization and Comparison with High-Energy CAD

David A. Durkin and Kevin L.Schey, Dept. of Pharmacology, Medical University of South Carolina, 171 Ashley Ave, Charleston, SC 29425

A novel mode of operation for an in-line surface induced dissociation (SID) device has been evaluated with particular emphasis on comparison with high-energy collision activated dissociation (CAD). Ion optical considerations are discussed for several in-line SID modes using SIMION trajectory calculations. A series of ions ranging from small organic radical cations to cesium iodide clusters to peptides were used to evaluate both dissociation methods with respect to internal energy deposition and dissociation efficiency.

Ion/surface collisions were carried out in a JEOL HX110/HX110 tandem mass spectrometer equipped with an in-line SID device[1]. Precursor ions were generated by electron impact ionization, LSIMS ionization, and by electrospray ionization (ESI). Precursor ions selected by MS-1 were allowed to collide with a perfluoropolyether (Krytox) coated brass surface at collision energies ranging from 40-100 eV. Dissociation efficiencies were determined by dividing the sum of product ions signals (measured using detector three) by the precursor ion signal (measured with detector one). Differences in detector gains were taken into account in calculating dissociation efficiencies.

This new mode of operation causes ions to be deflected by two deflection electrodes which, according to SIMION trajectory calculations (Figure 1), delivers a focussed precursor ion beam to the target surface. SIMION calculations also predict that product ions are most efficiently extracted from the portion of the target closest to the extraction electrodes. Product ion signals are three to five times larger with the dual deflection mode compared to single deflection mode where ions collide with deflector 2 (as shown in Figure 1).

Typical ion/surface reaction products were observed with this device including extensive ion/surface reactions, chemical sputtering, and ion dissociation. Dissociation efficiencies measured using both SID and CAD are summarized in Figure 2. For radical cations, CAD efficiencies are slightly higher than SID efficiencies presumably due to the high probability of neutralization in SID. Efficiencies measured for CsI clusters are different for CAD and SID depending on the cluster examined. This result is likely due the high internal energy required to dissociate m/z 393 which is easily provided by SID. That is, internal energy deposition may play a role in observing efficient dissociation when high energy reactions are examined. Lastly, peptide ions are clearly dissociated more efficiently by SID.

SID spectra for leucine enkephalin produced by LSIMS and ESI are shown in Figure 3. Clearly, the SID process is efficient enough to produce abundant sequence information from lower ion currents provided by ESI.

In conclusion, SID compares favorably with high-energy CAD in terms of internal energy deposition and dissociation efficiency. Improvements in design and operation mode will continue to make SID a viable dissociation method in sector instruments.

References

1. Schey, K.L., Durkin, D.A., and Thornburg, K.R., J. Amer. Soc. Mass Spectrom. 6:257-263, 1995.

43rd ASMS Conference on Mass Spectrometry and Allied Topics

Figure 1.
SIMION trajectory calculations of double deflection mode of in-line SID.

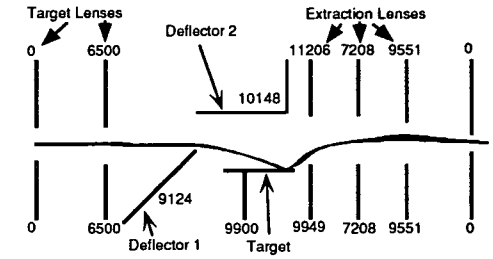

Figure 2.
CAD and SID dissociation efficiencies for EI, and LSIMS generated ions.

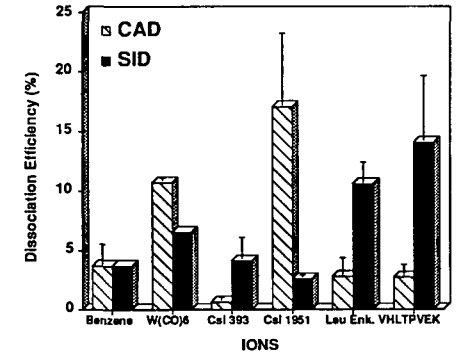

Figure 3.
SID spectra of leucine enkephalin generated by a) LSIMS (collision energy 60 eV) and by b) electrospray (collision energy 40 eV).

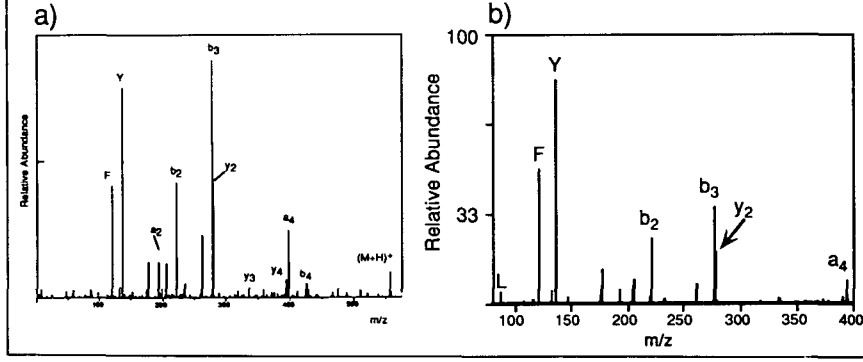

Influence of Peptide Sequence, Size and Basicity on ESI/SID Spectra

Jennifer L. Jones, Ashok Dongré, Hari Nair, Árpad Somogyi and Vicki H. Wysocki
Virginia Commonwealth University, Department of Chemistry, Richmond, VA 23284-2006

Electrospray ionization/surface-induced dissociation (ESI/SID) is used to investigate the effect of peptide sequence, size and gas-phase basicity on fragmentation efficiency. We recently reported results that show a sequence dependence of protonated peptides on fragmentation efficiency.[1] In summary, high energy onsets are detected when a protonated peptide is stabilized in any particular way (e.g., proton localization, intramolecular hydrogen bonding or structural rigidity) and shifts to lower energy are observed when the peptide is destabilized (e.g., proton randomization).

In the work presented here, synthetic peptides are used to systematically investigate the shift in fragmentation efficiency (e.g., AAAAA, PAAAA, KAAAA, and RAAAA) as a function of basicity. As the amino acid substituted at the first position is varied, differences in the onset energies for fragmentation are detected (see Figure 1). The shifts detected for each curve are in agreement with the order of increasing gas-phase basicity of the amino acid substituted as shown by the linear plot in Figure 2.[2,3] This figure is a plot of the internal energy at the inflection point for each peptide versus the reported gas-phase basicity[2] of the amino acid residue being substituted at the first position.

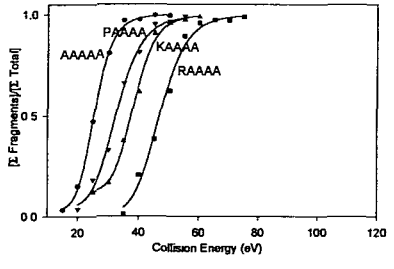

Figure 1.

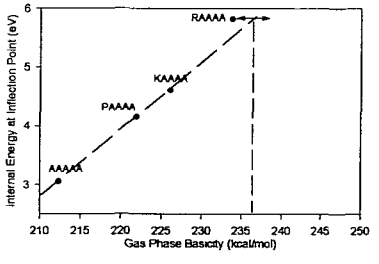

Figure 2

Other parameters that affect the overall position of the fragmentation efficiency curves are the size of the peptide and sequence effects (i.e., structural rigidity or intramolecular hydrogen bonding). Several oligomers of alanine plus other non-basic peptides are used to estimate the contribution of peptide size to the overall position of the fragmentation efficiency curves. As the size of the peptide increases, higher collision energies are needed to cause fragmentation. This effect is represented in Figure 3; the collision energy at the inflection point of the fragmentation

efficiency curves is plotted against the number of vibrational degrees of freedom for all non-basic residue-containing peptides investigated.

We can estimate the additional energy needed to fragment protonated peptides which contain a basic amino acid residue by using the shifts detected in Figure 1. We subtract out both the contribution of peptide size and gas-phase basicity on the overall position of the fragmentation efficiency curves; this allows an approximation of the influence of peptide sequence effects on the overall position of the fragmentation efficiency curves. The results are displayed in Figure 4; as the peptide sequence becomes more complex (i.e., various combinations of different amino acid residues), the more likely that secondary structure or intramolecular interactions within the peptide provide stabilization and require more energy to fragment

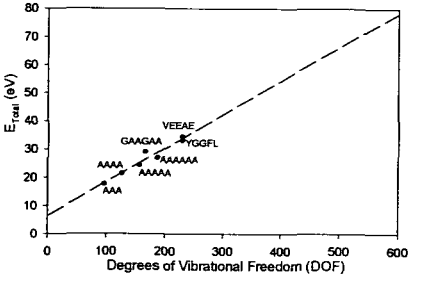

Figure 3.

For example, the bradykinin analogs (i.e., PPGFSP, PPGFSPFR and RPPGFSPF) have similar collision energies necessary to fragment the peptide as a result of structure. A logical explanation for this extra energy is that the prolines present in each bradykinin analog add structural rigidity to the peptide and also induce β-turns which allow the peptides to form more rigid structures than fully extended conformations. In agreement with a mobile proton model for fragmentation,[1] the extra rigidity hinders the proton transfers necessary to initiate charge-directed formation of typical sequence ions.

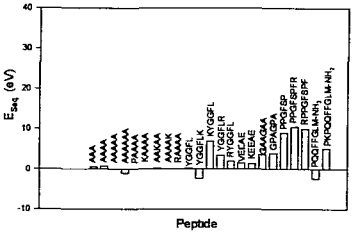

Figure 4

1. Jones, J.L.; Dongré, A.R ; Somogyi, Á.; Wysocki, V.H. *J Am. Chem. Soc.* **1994**, *116*, 8368-8369.
2. Gorman, G S.; Speir, J.P.; Turner, C.A ; Amster, I.J *J. Am. Chem. Soc.* **1992**, *114*, 3986-3988.
3. Wu, Z ; Fenselau, C. *Rapid Commun. Mass Spectrom.* **1994**, *8*, 777-780.

Ion/Surface Reactions: Towards a Better Understanding of Mechanisms, B. Feng, X. Jiang, S. Miller, J. Patrick, T. Pradeep, H. Rohrs, T. Ast and R.G. Cooks, Department of Chemistry, Purdue University, West Lafayette, IN 47907-1393

The goal of these studies is to provide insights into mechanisms involved in ion/surface reactions using ion/surface collisions by comparison with gas-phase ion/molecule reactive collisions. Reactions involving the collision of low energy beams of bare and ligated metal ions as well as small organic ions with a variety of surfaces have been investigated.[1,2] These studies have demonstrated the ability of various ions to abstract multiple ligands from surfaces which include liquid perfluorinated polymers, fluoroalkyl self-assembled monolayers (F-SAM), alkyl SAMs and others. Reactions include the abstraction of fluorine atoms by W^+, CH_nX^+ (X = Cl, Br or I) and other projectiles upon collision with an F-SAM.[3] Chemical sputtering is used after reactive collisions to explore the modified surface. For example, Xe^+ sputtering of an F-SAM after ion bombardment with CH_2Br^+ shows the presence of CF_2Br^+ (Figure 1), indicative of halogen exchange. Similar results have been obtained for SIMS-TOF analysis of an F-SAM surface after modification by $SiCl_4^+$.[4] Gas-phase studies have also been undertaken to evaluate the formation of WF_n^+ from complexes of $W(CO)_n^+$ with perfluorocarbons.[3,5] The above results lead to the proposal of a working mechanism for surface modification involving formation of a multi-center complex. For example, a four-centered complex is shown in Figure 2. Evidence supporting the proposed mechanism for ion/surface reaction is provided in the current work by experiments in which P, Si, W and I-containing ions, believed to cause surface modification, are collided at low energy with volatile neutrals in the second quadrupole of a triple quadrupole instrument. Experiments performed under single-collision conditions show product ions corresponding to abstraction of multiple fluorine atoms from fluorinated targets as well as complexes of the projectile with substituted alkyl groups. These findings parallel the observations from ion/surface collision experiments and suggest formation of a multi-center complex (analogous to an ion/molecule collision complex)of the projectile with the surface. The effects of chain length and the nature of the target were investigated using tetrafluoromethane, perfluoroethane, 1,1-difluoroethane, perfluorohexane, 1-fluorohexane, trichlorotrifluoroethane as targets. Competitive abstraction of species from gaseous targets show relative extents of adduct formation which correlate inversely with C-X bond strength (X=H,F,Cl,Br,I). The nature of the abstraction product observed is controlled by the number of fluorines the number of carbons (Figure 3; only 1 F abstracted from CF_4 (3A) while 2-3 F atoms are abstracted with perfluoroethane (3B)), and the nature of the substituents on the target. Specifically, multiple abstractions require longer carbon chains (n > 2) containing multiple fluorines. Furthermore, the observation of product ions corresponding to one-to-one complexes, and related fragments of the target molecules and projectiles under gas phase single collision conditions, supports the role of a long-lived collision-complex in the modification of surfaces through reactive ion/surface collisions.

The use of gas-phase collisions to explore the mechanisms for ion/surface reactions has been demonstrated and parallels between the two conditions have been found in the chemical systems examined here.

Acknowledgements NSF #CHE 92-233791; C.E.D. Chidsey and M.E. Linford; S.J. Pachuta

1. Cooks, R.G.; Ast. T.; Pradeep, T.; Wysocki, V.H. *Acc. Chem Res.* **1994**, *27*, 316.
2. Rabalais, J.W. (Ed.), *Low Energy Ion Surface Interactions*, Wiley, New York, 1994; Somogyi, A.; Kane, T.E., Ding, J-M.; Wysocki, V.H. *J. Am. Chem. Soc.* **1993**, *115*, 5275.
3. Riederer, D.E., Jr.; Miller, S.A.; Ast, T.; Cooks, R.G. *J. Am. Soc. Mass Spectrom.* **1993**,*4*,938.

4. Pradeep, T , Feng, B.; Ast, T.; Patrick, J.S ; Cooks, R.G ,Pachuta, S.J. *J. Am. Soc. Mass Spectrom.* **1995**, *6*, 187.
5. Chen, G , Hoke, S H II, Cooks, R.G. *Int. J. Mass Spectrom. Ion Proc.* **1994**, *139*, 87.

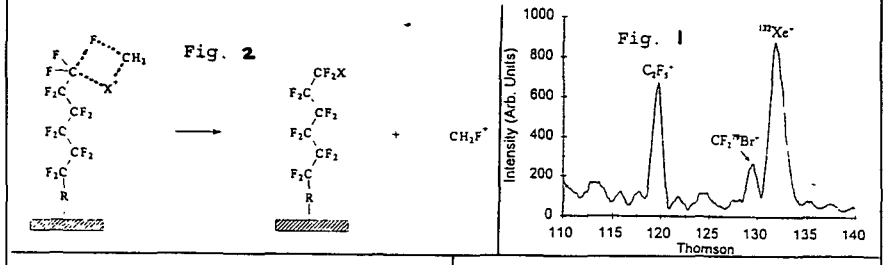

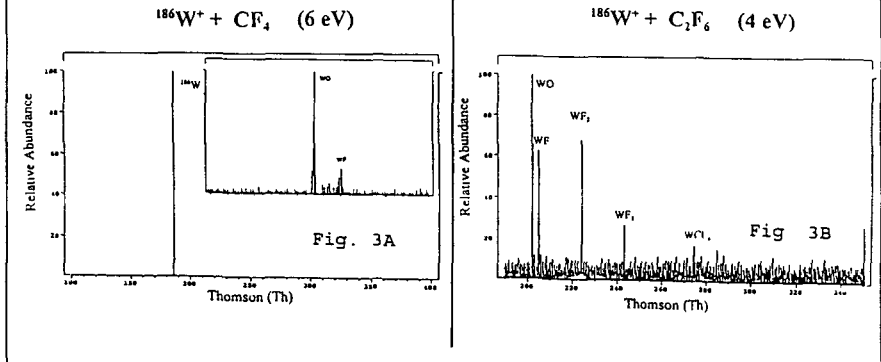

Construction of a Tandem Quadrupole Mass Spectrometer for the Study of Ion Surface Interactions Occurring Under Ultra High Vacuum (UHV) Conditions

Mark J. Hayward†‡, Frederick D.S. Park†, Lynn M. Manzella†, and Steven L. Bernasek†*
†Department of Chemistry - Princeton University - Princeton, NJ 08544 and
‡Agricultural Research Division - American Cyanamid Company - Princeton, NJ 08543

A new tandem quadrupole mass spectrometer has been constructed which allows the study of the interactions of mass selected ions with surfaces prepared and characterized at UHV. The entire surface induced dissociation (SID) tandem mass spectrometer is contained on a single 8" conflat flange (as shown in the accompanying figure) thereby permitting it to be combined with virtually any standard surface analysis system. The ion source and primary ion mass filter utilize two stages of differential pumping to allow mass selected ions produced by electron impact (EI) ionization to be delivered to the surface without affecting the pressure at the surface. This SID instrument has been combined with a surface analysis system which contains additional mass spectrometers (for desorption analysis of the surface and monitoring neutrals emerging from the surface during SID) and an Auger spectrometer. In the short time that the instrument has been operable, the following interesting results have been obtained:

1) Proton sputtering is a major process which results from the collision of ions with hydrocarbon surfaces.

2) Observation of proton sputtering is strong evidence of a charge exchange mechanism leading to hydrogen addition during SID.

3) There is little (if any) dependence on momentum transfer required for proton sputtering.

4) Protonation of neutralized molecular ions has a strong kinetic energy dependence which may be the result of a requirement for sufficient interaction time.

5) While there are many possible routes to the formation of $C_7H_7^+$ during SID of benzene molecular ions (see accompanying spectrum), the experimental evidence suggests that the primary mechanism involves the reaction of neutralized benzene with $C_3H_5^+$ sputtered from the hydrocarbon overlayer.

6) Ion surface reactions (at hydrocarbon covered surfaces) which lead to associative alkylation products take place in a manner that is like methane and/or isobutane CI. The use of CI as a model (where the CI reagent ions are considered equivalent to sputtered ions in SID) should facilitate greater understanding of alkylation reactions in future SID experiments.

43rd ASMS Conference on Mass Spectrometry and Allied Topics

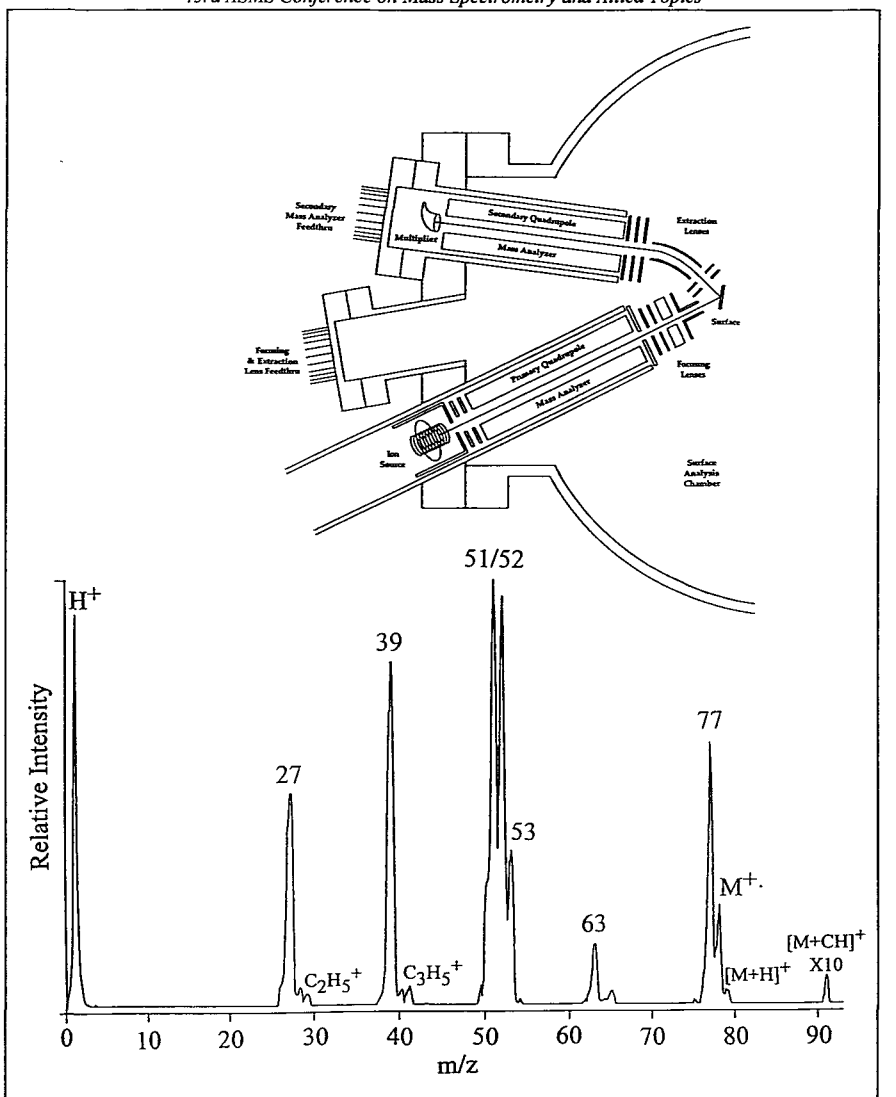

Strongly Enhanced Secondary Ion Yields in TOF-SIMS Studies with Very Highly Charged Primary Ions up to Th^{71+}

T. Schenkel, M. A. Briere, A. E. Schach von Wittenau and D. Schneider

Physics and Space Technology, Lawrence Livermore National Laboratory, Livermore, CA 94550 USA

The advent of new ion source technologies, such as the LLNL EBIT[1] (Electron Beam Ion Trap), has made low emittance (~0.2 π mm mrad) beams of slow (several keV/amu) very highly charged ions (up to U^{92+}) accessible for ion solid interaction studies. The prominent feature in the interaction of highly charged ions with surfaces, compared to conventional singly charged ions, is a dominance of electronic over collisional effects. Up to several hundreds of electrons (for Th^{70+} on Au[2]) are emitted from an area of a few square nanometers per incident ion. In insulators, this local disturbance of the charge equilibrium produces a "Coulomb explosion", resulting in the emission of large numbers of secondary particles, and the production of nanometer size defects[3]
Negative and positive secondary ion yields are determined using a single detector time of flight arrangement shown in Fig. 1. High pulses generated by the many secondary potential electrons and photons that are emitted at the impact of each highly charged ion provide the start signals; stop signals are given by the low pulses generated by single secondary ions Fig. 2 shows a typical pulse height distribution for this arrangement with the sample (SiO_2 on Si) biased at -2 kV and an incident Th^{65+} beam. The pulse height discrimination is accomplished via standard electronics, with a delay between the amplifier output and the start constant fraction discriminator allowing to determine the effect of the single hit TAC setup on the measurement of multiple ion production[4]
Fig. 3 shows a mass spectrum of negative secondary ions emitted from a SiO_2 film (100 nm on Si) for Th^{70+} impact. Clusters from two molecular series are present with masses up to 676 amu. The total positive and negative components of the secondary ion yield (detection efficiency and single hit[4] correction included), as a function of incident ion charge, are shown in Fig. 4. The yields increases linearly with incident ion charge above about 25+, with the total yield dominated in each case by the atomic species; O^+,Si^+,O^- Given a detection efficiency of ~5%, the total (i.e. sum of all positive and negative species) secondary ion production rate, for Th^{70+}, is in the order of 20-50, up from 10^{-4} to 10^{-2} for singly charged primary ions[5]. Theoretical estimates of the ionization probability for this process range from 5 to 20 % [6], suggesting that the total yield for highly charged ion induced sputtering can exceed 500 atoms/incident ion The enhanced ionization probability for both atomic and molecular species can be applied to improve the analysis of surfaces on micron and submicron scales

This work was performed under the Auspices of the US Dept. of Energy by Lawrence Livermore National Laboratory under contract No W-7405-ENG-48.

43rd ASMS Conference on Mass Spectrometry and Allied Topics

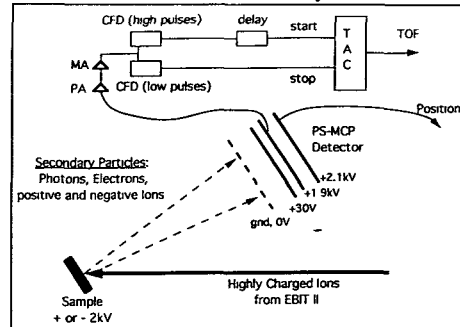

Fig. 1:
Scheme of the experimental setup for the single detector time-of-flight SIMS technique.
PA: preamplifier, MA: main amplifier,
CFD: constant fraction discriminator,
TAC: time-to-amplitude converte,
PS-MCD: position sensitive multi-channelplate detector

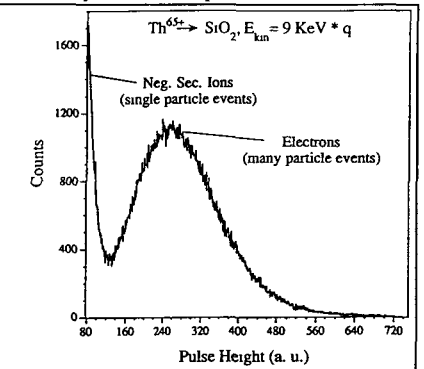

Fig. 2: Pulse height spectrum of the PS-MCD for 9 keV*q Th^{65+} on SiO_2 showing many electron events and events from single negative secondary ions.

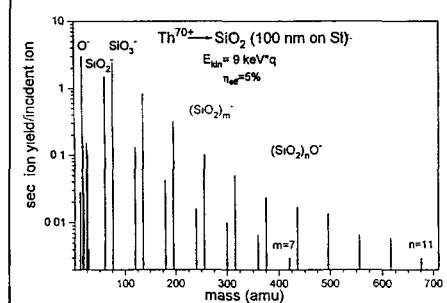

Fig 3: Mass spectrum of negative secondary ions emitted from a SiO_2 film (100 nm on Si) at Th^{70+} impact The total dose was $5*10^5$ ions The detection efficiency of η_{eff}=5% is included.

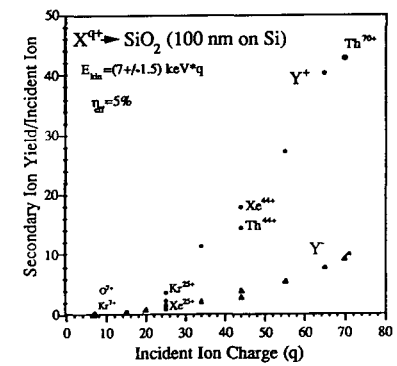

Fig.3: Positive and negative secondary ion yields from a SiO_2 film vs charge state of incident ions. The detection efficiency η_{eff} of 5% is included. The incident ions are: O:7+, Kr: 7+, 25+, 34+, Xe: 15+, 20+, 25+, 44+, Th: 44+, 55+, 65, 70+ ,and 71+.

References.
1. R. E. Marrs et al , Physics Today, Oct. 1994, 27
2 F. Aumayer et al , Phys Rev. Lett., 71(1993) 1943
3 D. Schneider et al., Surf. Sci , 294 (1993) 403
4 C. A Whitten Jr , Nucl. Instr. and Meth. A, 309, (1991), 264
5. A. Benninghoven, Surf. Sci., 53 (1975) 596
6. I. S. Bitensky et al., J de Physique, 50, (1989), C2-228

Ion Neutralization during Surface-Induced Dissociation at Ni(111) and NiO(111)

Samuel B. Wainhaus, John A. Burroughs, and Luke Hanley
University of Illinois at Chicago
Department of Chemistry, m/c 111
Chicago, IL 60607-7061

When a positive molecular ion is neutralized by the transfer of an electron from the surface, the scattered neutral can no longer be readily detected with a mass spectrometer. Such neutralization is a major problem in the surface-induced dissociation of molecular ions since it reduces the sensitivity of this method. Most polyatomic ions neutralize when scattered at low energies off clean metal surfaces. One approach to reducing charge transfer and increasing scattered ion yields is to form an oxide layer on the metal surface [1]. We examine here the neutralization of a typical organic ion, pyridine, when it was scattered at low energies off a clean metal surface, an oxygen adsorbed metal surface, and a well characterized oxide thin film. We also measured the relative neutralization efficiencies of $FeCp_2^+$ (Cp = cyclopentadiene) and $SiMe_3^+$ ions scattered off three different organic multilayers.

We measured the neutralization of a pyridine ion, $C_5H_5N^+$, when it was scattered at 20 and 40 eV off a clean metal surface, Ni(111); an oxygen adsorbed metal surface, p(2x2)O/Ni(111); and a well characterized oxide thin film, NiO(111)/Ni(111). These experiments used a tandem mass spectrometer coupled to an ultrahigh vacuum surface analysis chamber [2]. There was a large enhancement in the scattered ion signal upon going from the clean Ni(111) to the oxygen modified surfaces at both collision energies. At 20 eV, both modified surfaces showed a 30x enhancement of the scattered ion yields with respect to the clean surface. At 40 eV, the oxygen covered surface showed a 75x enhancement while the oxide showed a 150x enhancement (Figure 1).

These enhancements cannot be explained solely by changes in the surface work function or the surface dielectric layer thickness. These enhancements resulted from oxygen induced changes in the surface density of states which affected the resonant charge transfer of an electron from the surface to the scattered ion. Figure 2 is a schematic diagram of how the surface density of states changes with oxidation and how the ion state shifts when approaching the surface.

Other experiments support these arguments. The relative neutralization efficiencies of $FeCp_2^+$ and $SiMe_3^+$ ions scattered off organic multilayers do not follow the trend expected by consideration of the ionization potentials of the adsorbate molecules alone: the ionization potentials for C_3H_6, C_3F_6, and C_2Cl_4 are 9.73, 10.60, and 9.33 eV, respectively. One would expect from these values that the scattered ion yields in these experiments would have decreased as $C_3F_6 > C_3H_6 > C_2Cl_4$. However, we have observed the scattered ion yield trends to be $C_2Cl_4 \geq C_3F_6 > C_3H_6$.

Acknowledgment is made to the National Science Foundation (CHE-9220393) for support of this research. L.H. is supported by a National Science Foundation Young Investigator Award (1994-99).

43rd ASMS Conference on Mass Spectrometry and Allied Topics

1) S. Dagan and A. Amirav, J. Am. Soc. Mass Spectrom. 4 (1993) 869.
2) Q. Wu and L. Hanley, J. Phys. Chem. 97, 2677 (1993).

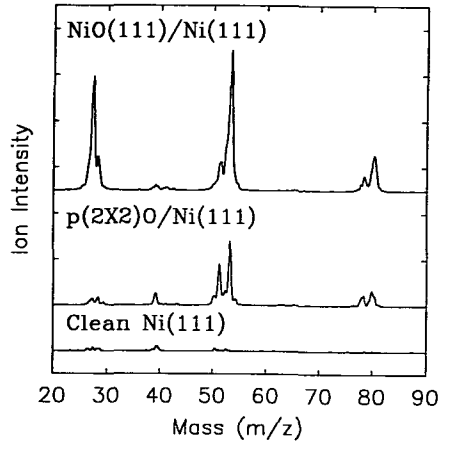

Figure 1: 40 eV mass spectra of $C_5H_5N^+$ scattered off NiO(111)/Ni(111), p(2x2)O/Ni(111), and clean Ni(111). The relative scattered ion signals off these three surfaces are 150, 75, and 1, respectively. The work functions are 4.3-4.6 eV, 5.8±.2 eV, and 5.1±.2 eV, respectively.

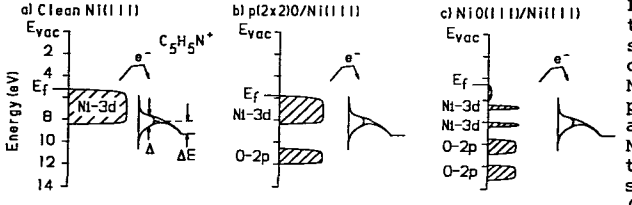

Figure 2: Charge transfer from the surface density of states of a) Ni(111), b) p(2x2)O/Ni(111), and c) NiO(111)/Ni(111) to the empty ion state of pyridine (see text).

Author	Page Number
Aaserud, David	650
Abashkin, V.M.	844
Abbott, Frank	524
Abian, Joaquin	463
Abney, Kent	47
Abolin, Craig	666, 671, 856 1324
Abrams, Garth	470
Abrams, Suzanne	470
Abramson, Fred P	875
Abushamaa, Amir	588
Acher, Mandelbaum	81
Ackermann, Bradley	443
Ackermans, P.	824
Ackley, Kathryn	764
Adams, Gregory W.	625
Adams, Jeanette	261, 280 281, 348, 378, 609
Adams, Nathan	135
Adams, Nigel G.	80, 693, 1040
Addona, Theresa A.	1290
Adrian P.	487
Aduru, Subhodaya	1192
Aebi, Beat	888
Afzaal, Sunia	710
Aggarwal, Suresht K.	169, 170
Agostara, Giuseppina	552
Ai, Jiu	167
Aicher, Klaus-Peter	1077
Akashi, Satoko	287, 288
Akbari, Nisar	547
Aktories, Klaus	1279
Al-Mahmoud, M. S.	514
Alain, Brunot	1236
Alameddin, N. G.	701
Albersheim, P	1173
Alcaraz, Armando	192
Aldrich, Jane V.	34
Aldridge, John	473
Alewood, Paul F.	1287
Alexander, Anthony J	438, 1253
Alexander, Michael	666, 1324
Aline, Leroy	406
Allanson, John	868
Allen, David	190
Allen, Mark	454, 646
Allen, T. A	772
Allison, John	356, 633, 642 691, 702, 1039, 1227, 1228
Allman, S L	268, 935, 1234
Altman, Elenora I-2	977
Alvarez, Erwin J.	1137
Amado, Francisco	90, 1056
Amarbalita, Marvy	1285
Ambrus, Gabor	303
Amft, Matthias	916, 1244
Amirav, Aviv	108, 482
Amster, I Jonathan	124, 798 797, 1080 1307
Amy, J., Stafford, G	1129
An, Yan	392
Anacleto, Joseph F.	454, 646
Anastasio, M B	319
Anastassopoulou, J.	608, 1065
Anders, M. W	93
Anderson, Gordon	682, 802 39, 355, 800, 801, 1086, 1093
Anderson, J. E.	772
Anderson, J S	791, 793
Anderson, Ken B.	1007
Anderson, Kerry	1276
Anderson, Mark	818
Anderson, Melissa	857
Anderson, Wayne	563
André, Tambuté	406
Andren, Per E.	274, 518
Andresen, Brian D.	192, 991 1138
Andrews, Glenn	312
Andrews, Kim	64
Andrews, Lori E.	617
Andrews, Philip	234, 924, 927
Andrews, Stuart R.	51
Andrien, Jr., Bruce	99, 999
Anex, Deon S.	24
Angeli, C.	705
Angelico, Vincent	417
Annan, Roland	620, 634
Anren, Hu	829
Anthony, Lowell	554, 555
Apffel, A.	1167
Aplin , Robin	237, 966, 1276
Appelhans, Anthony	843, 1022
Arakawa, Ryuichi	260, 601
Arakawa, Tsutomu	1272
Arata, Yoji	287, 288
Arimura, Masana	1163
Arisz, Peter W.	812
Arkas, M.	1065
Armentrout, P. B.	16, 696
Arnold, Elizabeth	835
Arnold, Randy	363, 1243
Baker, Chris	113
Bakhtiar, Ray	349
Balakin, A	107
Balazy, Michael	1148
Balcer, Jesse L	216, 217
Baldwin, Samuel W	487, 612 652
Ball, M.J.	271
Ballard, Kevin	382, 421
Ballinger, William	541
Bamberg, Michael	140
Banda, Phil	278
Banks, J Fred	455, 458, 999
Barbacci, Elsa	312
Barber, Michael	992
Barcel, Damia	463
Barcelo, D.	205
Barclay, Victoria	644
Bardel, Patrick	1256
Barinaga, Charles J	40 769 983, 1104
Barnidge, D. R.	310
Barofsky, Douglas F.	34, 495 413, 1222
Barofsky, Lilo	495
Barr, John R.	201, 344, 509 1016
Barrelro, Eliezer	1059
Barros, Cristina	1056
Barshick, C. M.	768, 775
Barshick, Stacy-Ann	816, 817
Barta, Istvan	303
Bartels, Micheal J	853
Bartlet-Jones, Mike	626

Author	Page Number
Bartlett, Michael	776, 777
Bartmess, John	57, 64, 799
Barton, Jacqueline K.	596
Bartos, Michael J.	1067
Baschky, Michael	12,. 368
Basic, Cecilia	1133
Basile, Franco	1132, 1157
Bateman, Robert	98, 117 137, 138, 625, 657, 1203
Bauer, Jan	153, 339, 823
Bauer, M D.	319, 386, 415, 615
Bauer, Scott	114, 153 339, 823
Bauerle, Gerald	223
Baum, Ellen	1288
Bauschlicher, Charles	706, 707
Bavda, Lalit	502
Bean, Karen	204
Bean, Mark	620, 980
Beasley, Brandon	1092
Beaugrand, C	668, 891, 1050 1071, 1072
Beavis, Ron C.	645, 623, 1235
Bebernitz, Geraldine	1288
Beck, Bret	679
Becker, Christopher	939, 940
Becker, St.	811
Becker, Stefan	679
Beckett, Malcolm	757
Beeson, Michelle D.	7, 445 904,.1266
Begley, Tadgh P	651
Behme, Robert	176
Behymer, Thomas D.	337, 822
Beiersdorfer, Peter	679
Belanger, Ronald	1182
Belas, Frank J.	536, 554, 555
Belenky, Alexi	582
Bell, David	317
Bencsath, F. Aladar	1273
Bencsura, Akos	922
Benkovic, Stephen J.	289
Bennett, C.B	615
Bennett, Samuel E.	34
Benoit, Frank M.	195, 227, 821
Benson, Linda M	510, 328
	1315
Bentzley, Catherine	580
Beranova, Sarka	377, 1037
Berg, Fred	156, 1044
Berg, J.M.	915
Bergman, Tomas	630
Bergmann, C.	1173
Bergmann, Frank	598
Berkenkamp, Stefan	179, 306 307, 308, 357, 1247, 1288
Bernasek, Steven L	1335
Bernier, Ulrich	537
Bertrand, J Aaron	777
Bertrand, M.	608, 1064, 1065 96, 154, 412, 585, 744
Bethem, Robert	222
Betowski, L Don	1139
Betowski, Leon	404, 1141
Betts, Robert	1057
Beussman, Douglas	134, 411
Beverly, Michael	1158
Beynon, Robert J	290
Bezabeh, Dawit	962
Bhavsar, J. H.	532
Bhide, Anjali	1187
Bi, Honggang	661
Biemann , Klaus	297, 627 896, 1165, 1189, 1225
Bier, M.E.	31, 160, 649, 653 302, 616, 652, 1103, 1113 1114, 1115, 861, 988, 1117
Bierbaum , Veronica	58, 374
Billedeau, Stanley M.	467
Binder, R.G.	340
Bingham, Jon-Paul	1287
Birken, Steven	270
Birkholz, Detlef	1020
Bischoff, Rainer	595
Blackburn , R.K.	1312
Blacken, Craig E.	46
Blackledge, James	438, 1253
Blackstock, Silas	369
Blair, I.A	536 554, 589, 593 555, 566, 607, 880
Blakley, Calvin	1209
Blanchard, David	264
Blankenship, James	1060 1061
Bluhm, Brian	805
Blum, Saul	1014
Bock, Cheryl	470
Bodor, Nicholas	272
Boger, Dale L.	1144
Bohin, Jean-Pierre	1184
Bohme, Diethard K.	79
Boismenu, Daniel	530
Bolanos, B. J.	131
Bolgar, Mark S	323, 546
Bolton, Barbara A	476, 477
Bombardt, Paul A.	869
Bond, L. A	48
Bondarenko, Pavel	892
Bonelli, Fabio	552
Bonner, Ron	644, 646, 739 740
Bookwalter, Craig	761, 1036
Boon, Jaap J	745, 746, 812 813
Bopp, H.	810
Borchers, Torsten	988, 1117
Borders, Montie	651
Bordoli, Robert	98
Borgerding, Anthony J.	183
Bori, Shushan	646
Börnsen, Klaus Olaf	1196
Borum, Peggy	537
Bothner, Brian	604
Bott, Geoffrey	1199
Boudjouk, Phil	699
Boue, Stephen M.	408
Bourque, Andre	582
Bowers, Larry	336, 576, 577 1171
Bowers, M.T.	448
Bowling, Donald J.	468
Box, Harold	449
Boyd, Robert	1073, 1282
Boyer, Scott	558
Boyle, James	999
Braatz, James	1170
Brach, Frank	505
Braddock, W. David	1315

Author	Page Number
Bradshaw, Stephen	1098, 1101
Brand, Willi A.	774, 828
Brauer, F P	48
Braun, Jennifer A.	62
Braun, Karen P.	1302
Breau, Alan	567, 850
Brenna, J. Thomas	46, 773, 1066
Brenneisen, Rudolf	574
Brewer, C. Fred	1259
Briere, Michael A.	1336
Brigande, John V.	1180
Brimmer, Steven, P.	1200
Brink, Christopher	44
Brinkmalm, Gunnar	413
Brinkman, U.A.Th.	205
Britt, Phillip F.	937
Brittain, Robert	1141
Brockmann, A.	292
Brodbelt, Jennifer	54, 223, 971, 1134, 1135, 1136, 1137
Brodsky, E.S.	825
Brooke, Dana	176
Brown, Bradley	488
Brown, Jeff	481
Brown, Paul W.	547
Brown, Richard	199
Brown, Robert	683, 1249
Brown, Stephen M	216, 217
Brown, Todd	852
Browner, Richard	425
Browning Jr., Martin	1321
Brozovich, Tara	847
Bruce, David	776, 777
Bruce, James	682, 802, 1093, 39, 355, 449, 459, 800, 801
Bruce, Morag	968
Brumley, William	231, 232, 346, 404
Brunet, Julie	836
Bryant, Duncan	435
Bryant, Matthew S.	334
Brzuzy, L	1015
Buchanan, Michelle	362, 816, 937, 1083
Buchbauer, Gerhard	142
Buchsbaum, J.C	915
Buck, Steven	1297
Buckel, Scott	322
Budde, William L.	337
Budzikiewicz, H	752
Budzinski, Ed	449
Bukowski, Nick	879
Bunk, David	660
Bunn, Alan	757
Burgoyne, Thomas	770
Burinsky, David	291
Burkhardt, Mark R.	342
Burlet-Schiltz, Odile	315
Burley, Stephen K	1331
Burlina, A.	882
Burlingame, Alma L	321, 617, 625, 1281
Burns, Scot	776
Burrell, Tim	188
Burroughs, John A.	389, 1337
Burton, Lyle	739, 740
Burton, Richard	82
Busch, Kenneth	419, 776, 777, 1055, 1155
Buseck, R. Peter	8
Busman, M.	318, 635
Butala, Pranay	559
Butelman, Eduardo	284
Butler, Jeffery M.	1040
Buttrill Jr., S. E.	122, 1112
Buzy, Armelle	749, 1285
Byrd, Michelle	70
Byun, Jaeman	587
Byun, Yong G.	710, 1306
Caffrey, Michael	1257
Cai, Jianyi	430, 573
Cai, Zongwei	208
Caimi, Richard	773, 1066
Cain, Teresa C.	919
Cairns, Stuart N.	168
Callahan, John	818, 942, 1185
Callahan, Patrick	1023
Camara, Elvira	678, 1084
Cameron, Andrew, S.	762
Cameron, Douglas	847
Camp II, David G.	244, 597
Campana, Joseph	414, 1011
Campbell, Clay	436
Campbell, Dale	212
Campbell, James A.	844, 846
Campbell, V. L	787, 792, 794
Campo, Karen K.	686, 1062, 1246
Campolmi, Laura	840
Canales, Ph.D., Mark	1320
Canova-Davis, Eleanor	1164
Cao, Jian-Ru	102
Cao, Ping	166, 456
Caprioli, Richard M	37, 274, 518, 928, 929
Capron, L.	700
Carazzato, Daniel	96
Carbonell, Ruben G.	282
Carell, Thomas	493
Carlsen, Steve	862
Carlson, Joel	193, 837
Carlson, R.W.	1174
Carlson, Rich	419
Carlson, Shannan	537
Carpenter, Stephen	505
Carr, Scott R.	354
Carr, Steven	492, 620, 634, 980
Carrier, Alain	96, 744
Carroll, James	678, 1081, 1195
Carson, Peter	2, 958
Cassady, Carolyn J.	351, 354
Cassidy, Ken C.	855
Castoro, John	414, 450
Castro, Lori	70
Catlow, John	525
Caudill, Doug	511
Cavalieri, Ercole	587
Cepa, Steven	502
Cerda, Blas	377, 1305
Cerniglia, C.E.	523
Cerny, Ronald	137, 208
Ch'ang, L Y.	935
Chace, Donald	240, 252
Chait, Brian T.	241, 269, 270, 284, 286, 286, 361, 643, 645

Author	Page Number
	921, 982, 982, 989, 1100, 1331
Chakel, J.	1167
Chamberlin, Edwin P	49
Chambers, David M.	991, 1138
Chan, Kelvin	532, 905
Chan, Stephen	291
Chandrasekher, Charu A.	1042
Chang, Sai	992
Channell, James	1156
Chao, Betty	277
Charbonnier, F	668, 891
Charles, M. Judith	189, 338, 247, 497
Chatman, Kelly	604
Chaudhary, A. K.	566, 593, 589, 607 880
Chauret, Nathalie	533
Chawla, Rahul	402
Check, Catherine E.	180
Chen, C. H.	268, 935, 1234
Chen, Guodong	1034
Chen, Hongwen	393
Chen, Jim	971
Chen, Ling	278, 605
Chen, Lorenzo H.	651
Chen, Ruidan	39, 355, 682, 800, 801, 802, 1086
Chen, Su	1183
Chen, Tom	36
Chen, Xiangjun	1235
Chen, Y.	978
Cheng, Michael	1013
Cheng, Xueheng	39, 349, 355, 376, 682, 800, 801, 802, 910, 1326
Chernushevich, I V.	126, 1327, 256, 1259
Chevis, Eddie A.	1155
Chiarelli, M. Paul	622
Chien, Benjamin	447
Chilkoti, Ashutosh	1261
Chin-Hsiung, Wang	912, 913
Chiu, Chung	197
Chiu, Rick W.	462
Chorush, Russell A.	87
Chott, Robert C	243, 914
Chou, Chau-Wen	945
Chou, Phillip	369
Chow, E Pingchang	301
Chow, Pauline	877
Chowdhury, Swapan	32
Christel , Bourhis	81
Christian, Noah	363, 1243
Christopher, Steven J.	1076, 698
Christova-Gueor, Nadia I.	497
Chu, Inhou	1299, 1301
Chu, Yen-Ho	1313
Chuang, C.H William	835
Chung, Henry	473
Churchwell, Mona I.	330, 572
Chyall, Leonard	52, 695
Cisper, M.E.	833
Claereboudt , Jan	824
Claeys, Magda	1181, 1183
Clark, C.R.	572
Clark, Steven D	1111
Clarke, Nigel J.	191, 735
Clauser, Karl R.	617
Clauss, Scott A.	6
Clauss, Therese W	845
Clench, Malcolm	190, 198, 199, 841
Cleven, C D.	1129
Cleven, Curtis	1127
Clifton, Carol	141
Cocknill, Steve	316
Coddeville, Bernadette	1169
Cody, R B	732, 1302
Cohen, Aharon	582
Cohen, Gerald	1182
Cohen, Steven L.	269, 1331
Colby, Steven	127, 363, 243, 1003, 1021
Cole, Mark	558, 559, 560, 562, 569
Cole, Richard B.	254, 453, 503, 516, 528, 672
Coleman, Patricia M.	1322
Colgan, S T.	1318
Collette, Timothy W.	826, 827
Collins, Terrence J	1067
Colorado, Armando	971, 1134, 1135
Compton, J L	593
Compton, Robert	1025
Consler, Thomas	29
Cook, Kelsey	144
Cooke, Gary	175
Cooke, Michael	198, 841
Cooks, R. Graham	56, 1127, 152, 1034, 1129, 1334
Coombes, R.C.	521
Cooper, Helen J	384, 1027
Coopersmith, Brad	671
Cordero, M.M.	619
Cordero, Marcela M	123, 358
Corley, Richard A.	853
Cornett, DS	1207
Cornio, L. J.	465
Cornish, Timothy J	123, 619, 133
Corr, Jay J.	848
Costa, Cesar	1245
Costello, Catherine	1179, 1308
Costello, Kevin	955
Cotter, Robert J	123, 133, 581, 271, 619, 358, 409, 915, 1102, 1289
Cottrell, J. S.	621, 950
Covey, Thomas	669
Cox, Kathleen A.	290, 381, 520
Coyle, Robert	1320
Craig, A. G.	384, 1166
Craik, Charles	321
Cramer, R.	584, 1063
Cravatt, Benjamin F	1144
Crea, Attilio	552
Creaser, Colin	73
Creasy, William R.	437
Critchley, Glen	18
Crowder, Cathy	64
Crutcher, Richard	984
Cui, Donghui	542
Cunniff, John	897
Curbishley, Steve	117
Cureton, G. H.	147

Author	Page Number
Curtis, Jonathan	1145, 1282
	781
Cusanovitch, Michael	1257
Cusworth, III, William	906
Cyr, Terry	529
D'Agostino, Paul A.	267
da Silveira, Enio	778, 1057
	1059
Dagan, Shai	108, 482
Dahl, David	717, 843
Dai, Yuqin	1226
Dalal, Nar S	807
Dale , Vanessa	1280
Dale, Michael	953, 954, 955
Dale, Mitchell W.	800
Dale, Vanessa	279
Dalene, Marianne	879
Dalton, A. Leigh	713
Dalton, Howard	1285
Dame, Amy D.	158
Damrauer, Robert	85
Danis, Paul O.	365
Darsey, Jerry	731
Darst, Seth	286
Darvill, A	1173
Dasgupta, K.	697
Dass, Chhabil	420
Davenport, Michael	118, 119
	134
Davico, Gustavo	85
Davidson, Susan	434
Davies, Stephen	966
Davis, Margaret R.	327
Davis, Michael T.	439, 719
Dawidski, Jean	449
Dawson, Brian	529
Dayton, David	407
de Gouw, Joost A	374
de Hoffmann, E.	1142, 1197
De Koster, Chris G.	746, 812
	813
de Vries, Mattanjah S.	24
Dear, Gordon	553
Dearden, David	53, 94, 347
	371, 970
Debbie, Armbrust	213
Dechert, Gary J	474
Deck, J.	523
Decker, Brian K.	693
DeCoster, Donna M.	27
DeGnore, Jon P.	1120
Deinzer, Max	206, 294, 1267
	258, 495, 1024
Dejsupa, Chadin	94, 347, 371
	970
Delacotte, J.-M.	747, 874
Delgado, Nelson	207
Dell, Anne	360
Delmore, James	843, 1022
DeMaio, William	549
Demirev, Plamen	1058, 1245
den Haan, Joke M.M	976
DeNoyer, Lyn	466
DePalma, Jr , Patrick	26
Depperman, Kevin L.	112
DePuy, Charles	85
DeRoos, Paul C	979, 1291
Derrick, Peter	130, 384, 1027
	726, 1183, 1278
DeRuiter, J	572
Des Rosiers, Christine	836
DeSantolo, Anthony	1091
	1087
Desiderio, Dominic	275
Despeyroux, Dominique	279
	1278
Destito, Rosalina	558, 560, 569
Deterding, Leesa	943
Detlev , Suckau	1208
Dharmasiri, Kuruppu	1260
Di Sacco, Sonia	165
Dickey, Robert	504
DiDonato, Gerald	432, 906
Dietrich, G	697, 809, 811, 963
Dindal, Amy B	834
Ding, Li N.	374
Ding, Wie-Dong	1288
Dingley, David	743, 1248
Diven, Warren	565
Divi, Rao L	1286
Dixon, Frank, Jr	423
Dobberstein, Peter	774
Dobbins, Richard	6
Dobson , Christopher	237, 681
	1265
Dodd, Jack	644
Dodonov, Alexander	107, 120
Dodsworth, David W	438
	1253
Doerge, Daniel R	1286
	330, 572
Dogruel, David	930, 944
Doktycz, Mitchell J.	362
Dollinger, Gavin	30
Dolnikowski, Gregory	721
Domingues, M. Rosario	469
Domingues, Pedro	90, 1056
Dong, Xia	748
Dongre, Ashok	353, 628, 1333
Donnelly, Brian	571
Donnelly, Joseph R	231, 232
	346
Donovan, Robert	968
Dookeran, Nyla	1154, 1191
Dormagen, Jonas	128
Doroshenko, Vladimir M	358
	409, 1102
Douce, David	198
Dougherty, Ralph C.	815
Douglas, Kenneth T	546
Dourdeville, Theodore	443
Downard, Kevin	896
Drabner, G	752
Drader, J. J.	787, 792, 1094
Draper, Sally	233
Dratz, E. A.	310
Dreifuss, Peter	21, 1170
Dresch, Tomas	99, 999
Drew, Barry	425
Driega, Alex	227
Drinkwater, Donald	759, 1006
	1012
Driskell, William J.	226
Drucker, Mark B.	1040
Duan, Yixiang	49
DuBose, Coit M.	1163
Duchateau, G.S.M.J.E.	1143
Duckworth, Douglas	41, 43

Author	Page Number
	767
Duebelbeis, Dennis	217
Duffin, Kevin	112, 659, 1153
	890
Duhr, Alexander	139
Dull, Gary	473
Dunayevskiy, Yuriy	493, 837
	1313
Dunbar, Robert C.	59, 370
	391, 716
Duncan, Mark W.	663
Dunn, Thomas M.	960
Dunphy, Jocelyn C.	345
Dunstan, David	470
Dupont , Annick	250
Durkin, David A.	1332
Dutky , Robert C.	238
Dutton, Walter	21
Duursma, Marc C	812, 813
Dworschak, R G	684, 1219
Dynin, Efim A	1108,1130
Dyson, H. Jane	289
Eades, Donald	500
Eanes, Ritchie C	698
Earl, W L	964
Easterling, Michael	797, 1080
Eckart, Klaus	320, 1046, 1258
Eckerskorn, Christoph	933
Edberg, Heather	111
Edini, C.	882
Edmondson, Ricky	690, 1242
	686, 1250, 1062, 1246
Egsgaard, Helge	78
Ehring, Hanno	1245
Eichinger, Dr. Peter	206
Eichmann, Klaus	1294
Eiden, Gregory C.	40, 769, 983
	1104
Eisenreich, Steven J.	1017
Eitzer, Brian	214
Elicone, Chris	442
Elliott, Steve	679
Ellis, Leroy	760
Ellis, P.E	1309
Emary, W. Bart	547
Emmett, Mark R.	37, 518
Eng, Jimmy	325, 641, 640
	979, 1291
Eng, Marian	1164
Engelhard, Victor H.	976, 1293
Engelmohr, Peter	783, 784
Engels, J. W.	594, 602
Englehard, V. H.	978
Enke, Christie G	118, 119, 129
	134, 411, 734, 780
Ens, W	126, 684, 1206, 1219
	1327
Epstein, Lois B.	617
Erickson, Tina A.	134, 411
Ericsson, Lowell	1146
Eriksson, Jan	1058
Ernest, Maréchal	1236
Ertes, Akos*1-1	942
Erve, John	495
Esaw, Barbara	551
Eshraghi, Jamshid	32
Ethier, Jean	529
Evans, Jason	76
Evans, Robert	109
Evans, William J	27
Evard, Dwight	966
Ewing, Andrew	459
Ewing, Nigel	351
Eyler, John	82, 257, 388, 637
	701, 768, 10331088
Fabio C. Gozzo,	56
Fabris, Dan	358
Facchetti, S.	602
Fagerquist, Clifton	352, 656
Fainzilber, Michael	1281
Falchetto , Rocco	441, 610
Fales, Henry M	238, 390, 1221
Falk, Nancy	159
Fannin, Steve	678, 1081, 1195
	1213
Farmer, Terry B	928
Farrell, Nicholas	403
Faubert, Denis	154
Faull, Kym F.	1192
Faye, T	874
Fearon, Karen	605
Federle, Thomas W	842
Fedora, Jim, W	763
Fei, Xun	1204
Feinberg, Thomas N	189, 338
Feistner, Gottfried J.	872
Felton, James	500
Fencl, Jennifer B	839
Feng, Bingbing	1334
Feng, Rong	1264
Fenn, John	102, 670
Fenselau, Catherine	55, 326
	358, 513
Fenyö, David	286, 645
Fergensen, David	1
Ferguson, James A	1006
Fernandez, Joseph	918
Ferrell, William	778
Ferrer Correia, A. J.	90, 469
	1056
Ferrige, Anthony G	1221
Fetterolf, Dean	571
Fields, Steven	443
Fies, Bill	988
Fifer , Robert A	1053, 1054
Figg, Deborah	44
Figliozzi, Gianine M	487
Filigenzi, Michael	194
Filosa, Angelo	178
Finch, Jeffrey W.	1074
Fink, Saul W.	143, 146
Fischer, Steven	424
Fischer, W.H.	1166
Fisher, Dixie	426
Fisher, Keith	967
Fitch, John	1257
Fitch, William	486, 909
Fitzgerald, Michael C	256
Fitzgerald, Robert	727
Fitzloff, John F.	428
Fletcher, Robert	6
Florance, James	276
Florio, Eugene	863
Flurer, Rick	332, 512
Foiles, Linda	224
Foley, B. Lachele	1040
Follansbee, J. C.	125
Foltz, Rodger L.	574

Author	Page Number
Forch, Brad E.	1053, 1054
Forde, Diane	32
Forest, Eric	309, 1257, 1269
Foret, Frantisek	105
Forssmann, Wolf-Georg	285
	611
Foster, Dale R.	220
Fouda, Hassan	541, 558, 559
	560, 561, 569
	578, 851
Fox, Alvin	830
Fox, Karen	830
Françoise , Fournier	81, 406
Frank, Samantha	72
Frankevich, V	1129
Franklin, Anthony, M	66, 84
Franklin, Melanie A.	1213
Franklin, Rebecca	418
Franzen, Jochen	1106, 1107
Fraser, Ian	868
Fregien, Kelly	576
Freiser, Ben	706, 707, 708
	709, 710, 1306
Freitas, Antonio	1059
Freitas, Michael A.	329
Freude, H.-Gerhard	552
Fruchter, John S	845
Frutos, Dinorah	780
Fuciarelli, Alfred F	592
Fuentes, Gary R.	484
Fujii, Toshihiro	398, 1045
Fujita, Tsuyoshi	1212
Fujiwara, Hideji	243, 914
Funenu, Daniel	250
Furlong, Edward T	196, 342
Fusciarelli, Al F.	597
Futrell, Jean H.	401, 402
G Neubauer	33
Gabeler, Stephen	613
Gaelli, Markus	1078
Gage, Douglas A.	633, 642
	932, 1193, 1297
Gagnon, Jean	1269
Gaines, Donald F	239
Galagan, Natalia	283
Gale, David	682, 802
	39, 244, 355, 459, 597, 1261
Gallagher, Richard	384, 1027
	726, 1278
Games, David E.	557
Ganem, Bruce	491, 1325
Gao, Q	125, 907
Gao, Quanyin	376, 910
Garbade, Klaus	67
Garcia, Edna	707
Gard, Eric	678, 1084
Gardner, Ben	132, 820
Garner, Carlos O.	536
Garrett, A. W.	964, 1127, 1129
Garrett, Aaron W	1128
Gaskell, Simon	290, 382, 421
	323, 381, 520, 546
Gates, Paul M.	196, 342
Gatlin, Christine L.	262, 263
Gauthier, Jeffrey	559, 560, 562
	569
Gedamke, Rich	908
Gellene, Gregory	375, 1041
	1042
Gelp, Emilio	463
Gérard, Bolbach	1236
Gerber, Nicholas	544
Geysen, H. Mario	488
Gharahdaghi, Farzin	918
Ghosh, Dipak	1284
Ghosh, Kris	36
Gibson, Bradford	273
Gibson, John K.	688
Gidden, Jennifer	83
Giese, Roger W	588
Gilbert, Anthony	736
Gill, C. G.	772, 833, 964
Gillece-Castro, Beth	302
Gillespie, Todd	525
Gillig, Kent	805, 920, 1242
Gimon-Kinsel, Mary	380, 723
	1242, 1250
Giordani, Anne B.	255, 898
Giordano, G.	882
Gisclon, Lee G	527
Glasmachers, Albrecht	1089
Glassmeyer, Susan	229
Gleich, Gerald J.	510
Glish, Gary L.	86, 385, 421
	655, 839, 1111, 1202, 1211
Glocker, Michael O.	294, 1330
Gobey, Jason	449
Gobin, Jovana	273
Gocs, Lisa *	781
Godbout, Jerry	1039
Goeringer, Doug	41, 91, 460
	410, 984, 350, 1140
Goetzinger, Wolfgang	105
Goheen, Steve C	845
Golding, Rafael E.	1223
Goldschmidt, Robert	19, 689
	956, 1237
Goldthwaite, Charles A.	554
	555, 566
Golovlev, V. V.	1234
Goodall, David M.	236
Gooden, Jonathon	586
Goodley, Paul C	424
Goodman, Keith J.	46
Goodman, Morris	1297
Goodman, Steven R	1273
Goodner, Kevin L	768
Goodwin, Mike	525
Gordon-Wylie, Scott	1067
Gorshkov, Michaël	720, 1096
Görtler, Bernd	1089
Gottschalk, Russell	1020
Goudreau, Paul N.	1326
Goulmy, Els	976
Grabowski, Joseph J.	62, 1032
Grace, Louis I.	960, 991, 1138
Graham, Elizabeth	856
Grande, H. Ray	504
Graner, Helena	588
Grange, Andrew H.	231, 232
	346
Grant, Karen E.	844
Grant, R.A.	615
Grant, Russell P	51, 557
Graves, Peter	1099
Gray, John	1000
Grayson, Michael	756
Greaves, John	27

Author	Page Number
Green, Brian	1177, 1262, 1303
	1296
Green, John Glass	145
Green, M. Kirk	678, 1084
Green, Martin	138, 625
Green, Vaughn E.	1016
Greenberg, Gerald E.	564
Greenhill, Paul	967
Gregg, Hugh	111
Greig, Michael J.	658
Griest, Wayne	817
Griffey, Richard H.	658
Griffin, J. B.	696
Griffin, Patrick	490
Griffin, Timothy	986
Griffith, Kelly S.	1042
Griffiths, William	60, 630, 1160
Grigorean, Gabriela	124
Grigsby, Ronald D.	1009
Grimm, Casey	480
Grimm, Deborah A.	451
Grimsrud, A.J.	1161
Grimsrud, E.P.	110
Groenewold, Gary	843, 1022
Gronert, Scott	153, 29
Gross, Deborah	89, 352, 656
Gross, M. L.	786
Gross, Michael	586, 587, 1265
	1274, 1292, 1295
Grosser, Robert	210
Grossert, S.	152
Grosshans, Peter	1014
Grote, William	766
Grotemeyer, Juergen	916
	1047, 1077, 1244, 1263
Grundwuermer, Johann	916
	1244
Gu, Ming	17
Guan, Shenheng	675, 733, 803
	806, 807, 808, 815, 1029
	1085, 1090, 1097, 1214, 1215
	1216
Guan, Ziqiang	87, 650, 680
Guarino, Bradley	312
GUENTHER, Clemens	881
Guentzel, M. Neal	506
Guerin, Michael	816, 819, 831
Guevremont, Roger	379, 674
	903
Guh, H. Y	177
Guido, David	331
Gulcicek, Erol E.	101
Gulden, Pamela H.	978, 1293
Gunsalus, Irwin	1284
Guo, Lin	1283
Guo, X. Q.	771
Guodong Chen,	56
Gusev, Arkady I	550, 565, 664
	665, 949, 1317
Guy, Philippe	1269
Gwiazda, P.W.	1318
Haapaniemi, Esa	157
Haas, George W.	760
Haas, Ruth	538
Habibi-Goudarzi, S.	362, 890
Hackett, Murray	441, 1283
Haddix, Martin	144
Haddon, William F.	340
Hadfield, Ted L.	1157
Haff, Lawrence	364
Haglund,Jr , R.F	584, 1063
Hahner, S.	584
Hahsmi, Mazzaz	93
Hail, Mark	148, 612, 908
Halasinski, Thomas	1039
Halgand, Frdric	1257
Hall , Brad	1136
Hall, Steven C.	617, 625
Hall, Trevor	1320
Halm, Kathy	867
Hamerly, Thomas	1099
Hamilton, Brenda	671, 856
Hamilton, Jill	609
Hamm, H. E.	318
Hammen, P.D.	1318
Hancock, James R	267
Hancock, W. S	1167
Hanisch, Franz-Georg	1176
	1177
Haniu, Mitsuru	1272
Hankin, Joseph	85
Hanley, Brian	952
Hanley, Luke	389, 1337
Hansen, Jr , E.B	523, 572
Hanser, Kent	127, 1021
Hanson, Curtiss	72, 74, 135
	188
Hanson, Stewart	736
Hanton, Scott	19, 136, 689
	952, 1238
Hara, Shinichi	1277
Harden, Charles S.	373, 1053
	1054
Harden, Leslie A.	340
Harder, Andreas	69
Harding, Robert H.	758
Haren, Patrick	99, 999
Hargiss, Leonard O	755
Harms, Amy C.	596, 597, 907
	1326
Harn, Donald A.	975
Harnick, Barry J.	220, 221
Harper, C. J.	787
Harris, Frank	51, 60
Harris, Wes	852
Harris, William	127, 1021
Harrison, Alex. G.	383, 714
	715
Harrison, Evan	843
Harrison, Kathleen	871, 1147
Harrison, M.	621
Hart, Kevin	734, 1110
Hart, Robert	849
Harvey, David J.	1168, 1194
	1201, 1203
Hass, J. Ronald	171
Hassila, Heikki	157
Hatcher, Joey	799
Hathout, Yetrib	326
Hauer, Charles	1207
Hauer, Michael J.	869
Havel, Jim	865
Hawley-Fedder, Ruth	224
Hayes, Joe	942
Hayes, Michael J	862
Hayes, T. W.	701
Hayes, Timothy	920
Hayward, Mark	116, 150, 628

Author	Page Number
	151, 1335
He, Lin	1204
He, Ling	446, 447. 687
He, S.	295
Headley, John V.	215
Hedley, Julie	753, 754
Heeler, Kevin **	487
Heeren, Ron M.A	812, 813
Heikes, David	209
Heimark, L.	293
Heine, Gaby	285
Heinicke, Ralf	1047
Heinze, T.M.	523
Hemberger, P.H.	769, 833, 964
	1127, 1128, 1129
Hemling, Mark	492, 620
Hendrickson, C. L.	792, 1094
Hendrickson, Ronald C.	441
	978
Henion, Jack	103, 150, 204
	212, 430, 573, 857, 859, 860
	873, 888, 890, 491, 1319,1325
Henrikson, Steven J	1144
Henry, Michael S.	503
Hensel, Russell	947
Hentschel, Rosemary T	468
Hercules, David	550, 565, 748
	664, 665, 949, 996, 1317
Herman, Alan	1275
Herold, Christopher	727
Herold, David	727
Herron, Nelson	232
Herron, William J	350, 410
Hertzberg, Robert	492
Hettich, Robert	677, 1025
	1083
Hewlett, Erik L.	1283
Hieftje, Gary	770
Hieshima, Glenn B	474
Higgins, Cecil E.	834
Higgins, Priscilla	57
Hildebrandt, J. D.	318
Hileman, Fred	162, 766, 852
	112, 890
Hill, Howard	233
Hill, Robert	226, 341
Hill, Susan E.	176
Hillenkamp, F	179, 307, 584
	306, 308, 357, 925, 933, 1063
	1176, 1184, 1205, 1220, 1247
	1288
Hiller, Joseph	691, 1229, 1230
Hilliard, George	620
Hillman, Steven	240, 252
Hilvert, Don	289
Hines, Wade	387
Hipp, Travis L.	1250
Hirabayashi, Atsumu	884
Hirano, Takashi	1186
Hiraoka, Kenzo	1048
Hirayama, Kazuo	287, 288
Hirayama, Shigeki	95
Hirose, Keiji	95
Hirsh, S.	292
Hites, R A.	1015
Hites, Ronald	229, 770
Hkansson, Per	1058
Hlavac, Allan	32
Ho, Yen-Peng	716
Ho, Z. Stacy	425
HŒkansson, Per	413
Hoekman, Don	737, 738, 1079
Hoekman, Don	735, 1098
Hofmann, Bernhard	100
Hofstadler , Steven	347, 682
	802, 1093, 355, 449, 39, 376
	459, 800, 801, 1086
Hogge, Lawrence	470
Holbert, Anthony	100, 456
Holland, John	119, 132, 820
Holland, Ricky	622
Holle, Armin	926, 1208
Holliman, Christopher	1026
Holloway, B.	1167
Holmes, Christopher	486
Holmes, John L.	13, 392, 393
	394, 974, 1310
Holthausen, Max C.	1046
Honing, M.	205
Honing, Maarten	463
Hop, Cornelis	17, 239
Hop, Marcel, C.E.C.A	1049
Hopfgartner, Gerard	335, 538
Hopkinson, Alan C.	79
Hopwood, Femia	967
Horan, G.J.	1318
Horan, Thomas	1272
Horn, L., Nappi, M	1129
Horn, Lynn	1034
Horvath, Thomas	128
Horwitz, Marcus	273
Hostettmann, Kurt	548
Houalla, Marwan	665
Houston, Chris	363, 1243
Houthaeve, Tony	314, 638
	987, 1311
Howald, Markus	181, 182
Howard, Jack	422
Howard-Lock, Helen E.	522
Howarth, Oliver	779
Howdeshell, Michael	229
Hoyes, John	117, 620
Hsieh, Feng-Yin	566
Hsieh, Frank	387, 442, 613
Hsing-Long, Chei	1239
Hsu, Chang Samuel	474, 1014
Hu, Jun	1031
Hu, Peifeng	35, 322
Hua, Yousheng	503
Huang, A.Y.	1289
Huang, Chao-Ran	428
Huang, E.	293
Huang, Jianxing	1151
Huang, Lee	245
Huang, Rong	1284, 1298
Huang, S-wan	911
Huang, Yong	723, 972
Huang, Yulin	806, 808, 1090
	1214
Huang, Zhi-Heng	1193
Hubbard, Natalie	925
Huby, Francois	365
Huddleston, Michael	980
Hudson, James	1013
Huebner, Vreni	30
Hull, Clifford	21, 1170
Hull, R. Delon	226
Hulse, James	865

Author	Page Number
Humphrey, Paul	743, 1248
Hunt, Donald F.	441, 610, 626
	976, 978, 1283, 1290, 1293
	1294
Hunt, Jerry E.	760, 1007
Hunter, Kevin	1000
Hunziker, Heinrich E.	24
Hurlbut, Jeff	870
Hurst, Gregory B.	362, 937
	1083, 1233
Husser, Christophe	335, 538
Huston, Chuck	478, 1122
	1123
Hutchens, T.William	1256
Hutton, Therese	1286
Hwang, Thomas	70
Iannucci, Robert	883
Iden, Charles R.	591, 606, 603
Ier, Mark E. **	487
Ii, Tadashi	1175, 1186
Ijames, C. F.	238, 796
Ikonomou, Michael, G.	703
Illies, Andreas	83, 372
Ingedoh, Arnd	179
Ingemann, Steen	400
Ingendoh, A.	621, 950
	304, 305, 624, 1304
Ingram, Jani	843, 1022
Inoue, Masayuki	106
Inskeep, Phil	541
Isabelle, Daoust-Maleval	406
Isakson, Peter	659
Isbell, John	54
Ishikawa, Keiichiro	601
Ismail, Yasser	588
Isobe, Toshiaki	304, 305, 316
	624, 1304
Isola, Mauro	165
Issakova, Olga	483
Itagaki, Yasuhiro	1212
Jackson , George S.	1097
Jackson, Alan K.	112
Jackson, Christian	23
Jackson, Edwin K.	664
Jackson, George	1090, 1214
	1215
Jackson, Kenneth	636
Jackson, Tony	18, 750, 751
Jacobs, Peter L.	1190
Jacobson, Denley	699
Jacobson, Myron K.	158
Jacoby, Cliffton B.	366
Jacquy, Dissard	406
Jaffee, E.M.	1289
Jalonen, Jorma	157
James, John	838
James, Mary A	83
James, Mike	988, 1103, 1114
	1117
Janning, P.	248
Janssen, Hans-Gerd	481
Janzen, Edward, G	1163
Jaquinod, Michel	1257
Jardine, I	649
Jarman, M	507, 521
Jayasimhulu, Koka	210
Jean-Claude , Blais	1236
Jean-Claude , Tabet	81, 1125
	406, 1236
Jedrzejewski, Paul	324, 632
Jeffrey, William	626
Jehnsen, Chris	1099
Jenkins, Roger A.	834
Jenkins, Yonchu	596
Jennings, Keith	279, 749, 750
	751, 779, 1280, 1285, 1300
	1278
Jennings, Richard	757
Jensen, James	1044
Jensen, Ole N	34, 638
Jentaie, Shiea	570, 829, 912
	913, 1239
Jerina, Donald	599
Jesaitis, A J.	310
Ji, Qinchung	119
Jiang, Kate	277
Jiang, Xudong	1334
Jin, Lei	1309
Jirovetz, Leopold	142
Joëlle, Guittard	1236
Joensuu, Päivi	157
Johnson , Eric	1115
Johnson, Andrew	1300
Johnson, Deborah	766
Johnson, Jennifer	820
Johnson, Jodie	405, 537, 1006
	1133
Johnson, Kenneth L	543, 629
	648
Johnson, Robert B	992, 1297
Johnson, Walter	492
Johnston, David	32
Johnston, Murray	2, 5, 580
	761, 958, 961, 1036
Johnston, Paul F	844
Jones, A.D.	498, 962
Jones, Alun	1287
Jones, Anita	953
Jones, Anne	553, 868
Jones, Dane R.	1302
Jones, David	692, 743
Jones, Jennifer	1333
Jones, Patrick	321
Jonscher, Karen R.	990
Joode, T. de	1143
Joshi, Jill C	862
Jourdan, Thomas	571
Juhasz, Peter	364, 1189, 1209
Juneau, Paul L	898
Jurima-Romet, Malle	529
Just, Craig	135
Just, Ingo	1279
Kaesermann , Donald	311
Kage , David	257
Kahr, Michael	44, 47
Kalinoski, Henry T.	159, 755
Kalkum, Markus	294
Kaltashov, Igor	55
Kamada, Kimiko	95
Kambouris, Sara J.	607, 880
Kamel, Amin	563, 578, 887
Kan, Steven	708, 709, 710
Kan, Steven Z	1306
Kanain, Michiko	304, 305, 616
	624, 1304
Kane, Thomas	417
Kaneko, Takeo	106
Kaplan, David L.	193, 300

Author	Page Number
Karas, Michael	357, 933, 1176, 1184, 1205, 1247
Kardash, Dawn	699
Karger, Barry L.	105, 1313
Karnicky, Joseph F.	122, 1112
Karr, Dane	737, 832, 1079, 1101
Kass, Steven	12, 368
Kassel, D.B.	29, 1312
Kasthurikrishna, N.	152
Kaswan, R.	292
Kato, Koichi	287, 288
Kato, Shuji	374
Katritzky, Alan	82
Katta, Viswanatham	1272, 1277
Katzmann, Jerry A.	1315
Kaur, Surinder	30
Kawabata, Shin-ichirou	1248
Kay, Paul	1158
Ke, Fu	379
Keane, A.	621, 950
Keevers, Jeff	427, 444
Keiko, T	307
Kelleher, Neil L	650, 651
Keller, Douglas	505
Kelley, J M.	48
Kelley, Paul	1101, 1118
Kelly, John	1314
Kelly, Michele A.	564
Kelly, Peter B	772, 962
Kemp, Craig	175
Kemp, Terry	749
Kenny, Donald	1023
Kenny, James	1210
Kent, Steven B.H.	256, 982
Kenttamaa, Hilkka	70, 71, 369, 52, 1092
Kenyon, George H	651
Keough, T.	386, 415, 615
Keough, Thomas	484
Kerns, Edward	148, 176, 433, 174, 489, 568
Kerr, Kelly E.	80
Kershner, Karen M.	345
Kerwin, James	1146
Keusgen, Michael	1145
Khandke, Kiran	306
Kidd, L. R.	499
Kiddy, R. A.	48
Kiesel, Jennifer R.	112
Killinger, William E.	25
Kilpatrick, Peter K.	282
Kim, Hee-Yong	1152, 1162
Kim, Ho-Seung	272
Kim, Hyun Sik	815, 1090, 1214
Kim, Jin Young	172
Kim, Ok-Hee	1267
Kim, Sung Ho	172
Kim, Tamen	889, 893
Kim, Yeonhee	1007
Kimura, Cliff	15
King, Fred	42
King, Gina M.	1294
King, Kathy	31
King, Richard	19, 136, 689, 947, 952, 1237, 1238
Kinkead, Scott	47
Kinsel, Gary	690, 1240
Kinumi, Tomoya	636
Kirby, Daniel P.	104, 105, 1313
Kirchner, Nicholas J.	1108, 1130
Kirpekar, F	584
Kishi, Hiroshi	398, 1045
Klatt, Tracey	490
Kleintop, Brent	905
Klinger, George S	845
Klohr, Steven E.	174, 433, 489
Kloos, Steve	699
Klopchin, Patrick G.	658
Kluge, H -J.	697, 809, 811, 963
Klujev, N.A.	825
Klunk , Lewis J.	566
Knapp, D R.	635, 647
Kneen, Kurt	702
Knighton, W.B.	110
Knobeler, Markus	1082
Knochenmuss, Richard	8
Knudsen, Jen	237
Ko, Chan Y	177
Koch, Wolfram	1046
Kochling, Heinrich	1225
Kocis, Petr	483
Koepke, Andreas K. E.	320
Koerber, S.C.	1166
Koester, Carolyn	224, 993
Kofel, Peter	121
Koga, Yoshinori	601
Kohler, Martin	1198
Kohn, Harold	520
Koizumi, Hideaki	452, 884
Kok, G.L.	833
Koleis, Janece C.	196
Kolli, V.S K.	1173, 1174
Kong, Zhengrong	1298
Konteatis, Zenon	490
Koppenaal, David W.	40, 769, 983, 1104
Korfmacher, Walter	334, 858, 859
Kornfeld, Rich	1210
Kornig , Stefan	142
Korsak, Andy	1103
Koski, Alice	1079
Köster, Claus	926
Koster, Hubert	581
Kotake, Yashige	1163
Koudrikova, Tatiana	544
Koul, Omanand	1179
Koupai-Abyazani, M.R.	551
Kouzes, Richard T.	720, 1096
Kowalski, E.M	589
Kowalski, Paul	1207
Kraft, Andreas	120
Kragelund, Birthe	237
Krahmer, Mark	830
Krause, Joern L.	121, 1251
Krebs, Joseph F	289
Kreek, Mary Jeanne	284
Krishnamurthy, M.	402
Kristo, Michael	1004
Krmer, Roland	250
Krol, George J.	860
Krone, Jennifer R.	876, 930
Kruppa, Gary	681, 886
Krutchinsky, A.N.	126

Author	Page Number
Kryak, David D.	337, 822
Kšrner, Roman	987
Kubis, Alan	36
Kubota, Masayuki	636, 1186
Kuchumov, Askar R.	1296
Kuehl, Douglas	200, 515
Kuell, Chris	266
Kuhnen, Florian	782, 785
Kulkarni, Sandhya	34
Kunihiro, Fumio	1074
Kunz, Arthur	307, 308
Kurono, Sadamu	1175
Kuzmich, Sandra	564
Kvalo, Loretta T	854
Kwok, David	877
Labdon, James	36
Lacey, M P.	386, 415, 615, 484
Lacroix, Monique	1169
Lafleur, Arthur	422
Lafont, R	557
Lafontaine, Felix	151
Laiko, Victor	120
Laine, Roger	242
Lam, Zamas	505
Lamaat, Shalaby	213
Lamb, Diane	514
Lammert, Stephen	985, 1109
Land, A P.	649, 653
Land, Adrian	31, 302, 616, 652, 861
Land, Mark	1240
Lander , Harry M.	241
Lane, W.S.	649
Langevin, Carolyn N.	334, 858
Langford, Marian	60, 97, 168, 66
Lango, Jozsef	303, 396
Langridge-Smith, Patrick	953, 954, 955
Lapiguera, Amelia P.	334, 858
Laramee, James	206, 1024
Larsen, Barbara	23, 485, 580
Larson, Michael	194
Lasater, M A.	88
Laskey, Rachel	331
Laude, D A.	88, 131, 787, 788, 789, 790, 791, 792, 793, 794, 795, 1094, 1126
Laukien, Frank	886, 1082
Laurence, Rozes	1236
Lausecker, Berthold	335, 538
Lausevic, Mila	993
Lautz, Carsten	1220
Lavine, Gary	691, 1227, 1230
Laviolette, Barbara	551
Lawrence, David L.	842
Lay, Jack	115, 501, 622, 731
Le Blanc, J.C. Yves	903
Le, Han	583, 599, 1270, 1271
Le, John C.	1272
Leal, João Paulo	704, 965
Leano, Hector	838
Leary, Julie, A.	1198, 1199, 1200
Leathard, David	199
Lebedev, Albert	171, 825
LeBel, Guy L.	821
LeBlanc, Daren J.	522
LeBlanc, Yves	252
Lebrilla, Carlito	678, 1081, 1084, 1195, 1213
Lecchi, Paolo	583, 599, 1270, 1271
Leclercq, Piet A.	481
Lee, Hack Sung	58
Lee, Heewon	931
Lee, K. L.	268
Lee, Michael	432
Lee, Mike	148, 612, 908
Lee, Mike S.	176, 433, 568, 174, 489
Lee, S	448
Lee, Sam	706, 708, 709, 710, 1306
Lee, Terry D.	439, 719, 1231, 1232
Lee, Yin-Yu	61
Leeck, Diane	52, 70, 1092
Lehman-McKeeman, L.D.	511
Lehmann, Wolf D.	324, 632
Lehn, Jean-Marie	250, 251
Lei, Qing Paula	1080, 1307
Leize, Emmanuelle	250, 251
Lemire, Sharon	1055
Lemoine, Jérôme	993
Lennon, III, John D	1211
Lennon, John	683
Leone , Stephen R.	61, 374
LePage, Guy	545
Lepine, Francois L.	63, 531
Lerner, Jeremy	727
Lerner, Richard A	1144
Leroi, George E.	702, 1039
Levendis, Yiannis	837
Levery, Steven B.	1178
Levis, Robert, J.	941
Levsen, Karsten	463
Lewer, Paul	216
Lewis, J. Kathleen	876, 930
Lewis, Richard J	1287
Leymarie, N.	705
Li, Chun	1150
Li, Guo-Zhong	807, 808, 889, 893
Li, Hongwei	461
Li, Kai-Ming	587
Li, Liang	22, 885, 923, 951, 1223, 1226
Li, Lily Y.-T.	212, 860, 873
Li, Nan	1240
Li, Qimin	1181
Li, Rebecca	737, 738, 1098
Li, Ruomei	52
Li, Xia-Ling	1263
Li, Xuhui	461, 687
Li, Yaming	106
Li, Yiao-Ling	916
Li, Yunzhi	676
Liang, Li	446, 447, 687
Liang, Xiaoli	579, 614, 919, 936, 938, 1224, 1254, 1255
Liang, Yongjiang	94
Liang, Zhenmin	1014
Liao, Pao-Chi	633, 642, 691, 1228
Lias, Sharon	141

Author	Page Number
Lidgard, Ray	663
Lim, H.K.	532, 905
Limbek, Belá	122
Limero, Thomas	838
Lin, C.C.	859
Lin, Chin-Chung	334, 858
Lin, Chuan-Yuan	391
Lin, Peiping	440
Lin, Tong	655
Lin, Whei	1059
Linberg, Leonid	883
Linden, H. Bernhard	140
Linder, Christopher	712, 713
Lindgren, Jan Åke	1160
Lindh, Ingemar	630
Lindinger, M.	697, 809, 811
Lindley, Chris E.	342
Lindley, Patricia M	995
Lindsey, Jean	111
Ling, Victor	1164
Link, Andrew	325
Linnert, Harrald V.	65
Linscheid, M.	248, 249
Lipsky, James J.	543
Liston, Theodore	558, 560
Liston, Theodore	562, 569
Little, Daniel P.	38, 651, 680
Little, James L.	730
Liu, Chuanliang	1171
Liu, Fei	118
Liu, Naili	1277
Liu, Yan-Hui	579, 614, 919
	936, 938, 1255, 1224, 1254
Liu, Yuanhui	1316
Liu, Zaiyou	1016
Lloyd, Patrick	184
Lloyd, Steven	480
Lloyd, Thomas	867
Lock, Colin J.L.	522
Loewen, Mark	228
Loftus, Neil	879
Lombardo, Christian	29
Londry, Frank A	993, 1124
Long, Austin	870
Long, David T.	1017
Lonning, P.E.	507
Loo, Joseph A.	35, 235, 322
	934
Look, Gary	486
Lopata, Ronald J.	151
Loran, John S.	236
Lorenz, Peter	632
Louris, John	1101, 1118
Lowen, M.	1018
Lowes, Steve	534, 824
Lu, Hsieng	1277
Lu, Lin	736
Lu, Taiwei	727
Lu, Weining	6
Lu, Wenzhe	254, 453, 503
	528
Lu, Zhi-Zhen	428
Lubman, David	447, 461, 687
	931, 938, 1224, 579, 614, 919
	1254, 1255, 446, 654, 936
	960, 1316
Lucke, Richard B	845, 846
Ludicky, Robert	814
Lund, Anders L	296
Lundberg, David	661
Luo, Wendy	567, 850
Luther, Elbridge	558, 578, 559
	560, 569
Luther, Michael	29
Lützenkirchen, K.	697, 809
	810, 811, 963
Lykins, Jr ,Benjamin W.	826
	827
Lyons, L.E.	1309
Ma, Cheng-Yu	834
Ma, Li	201, 509
Ma, Nina	483
Ma, Yee-Chung	1152, 1162
Maass, Imke	1089
MacDonald, Linda,M.	219
Macfarlane, Ronald	316, 892
Mackintosh, J. Gordon	954
MacLean, Matthew	
MacMillan, Denise	
Maden, Amy J.	116
Magarotto, M.	882
Maggio, Vincent L.	201, 344
Magiera, Daniel	588
Mahon, Andrea	749
Maier, Claudia S.	1267
Maisey, Anne	18, 625, 1201
Majidi, Vahid	764, 1028
Major, Hilary J	534
Makarov, Alexander	130, 1075
Mäkelä, Mauri	157
Makino, S	732
Malaiyandi, Murugan	227
Malek, Robert	1095
Malfatti, Michael	500
Malis, Greg M.	866
Mallis, Larry M	146, 431
Malspeis, Louis	163, 878
Mamer, Orval	63, 531, 836
Mammen, Mathai	910
Mandich, Mary	1087, 1091
Mann, Matthias	28, 33, 314
	594, 638, 639, 739, 886
	987, 1218, 1279, 1311
Mansoori, Bashir	2, 961
Manura, John	113, 149
Manzella, Lynn M.	1335
Marçalo, Joaquim	704, 965
March, Raymond E.	79, 230
	993, 1124, 1019
Marchese, Alfredo	661
Marcos Eberlin,	56
Marcotte, I.	608, 1065
Marcus, Alvin	1141
Marcus, R. Kenneth	26, 45
	466, 698, 1076
Margalit, Alon	659
Marie-Claude, Perlat	81
Marion, Didier	1269
Mark, J	1312
Markey, S.P.	238, 465, 472
Markham, Dan A.	853
Marnett, L. J.	593
Marques, M. Graa	90, 469
	1056
Marquez, Cristina D.	556
Marquis-Rigault, Annie	250
Marrero, Carlos	151
Marsh, Eugene	998

Author	Page Number
Marshall, Alan G.	92, 675, 711
	733, 803, 806, 807, 808, 815
	1029, 1085, 1090, 1097, 1149
	1214, 1215, 1216
Martin, Charles	124
Martin, Gilbert	299
Martin, Millie	838
Martin, Stephen	364, 442, 613
	997, 1209
Martin, Steve	387
Martine, Tessier	1236
Marto, Jarrod A.	1085, 1149
	1216
Masoud, Hussein I-2	977
Masson, Jean-Michel	315
Matassa, Luca C.	855
Mathews, Kimberly	100
Mathews, W. Rodney	331
Mathur, Chandra	854
Matimba, Henri E. K.	400
Matsui, Neil	617
Matsumoto, Hiroyuki	636
Matsumoto, Richard	850
Matsuo, Takekiyo	260
Matteson, K J	935
Mattina, Mary Jane	214
Maunit, B.	
Mayeno, Arthur N.	510
Mayer, Istvan	1051
Mayer, John	1277
Mayol, Robert F.	566
Mays, Dennis C.	543
Mazurkiewicz, Paul	206
McCandless, Jacqueline	278
McCarthy, Dennis J.	
McCloskey, James A	600
McCluer, Robert	1179
McClure, P Cheryl	201, 344
	509
McCormack, Ashley L.	979
	1291
McDowell, Roy A.	360
McElvany, Steve	818, 1026
McEwen, Charles	23, 485
McGiff, John C	1148
McGilvery, D. C.	718
McGown, Steven	207
McGuire, Lisa	30
McHugh, Charles	661
McHugh, Sean	737, 738, 1098
McIntire, W. E.	318
McIver, Jr., Robert	676
McKay, Richard	485
Mckee, Michael	372
McKenna, Rosemary	331
McKown, Linda A	527
McLafferty, Fred	38, 87, 650
	651, 680, 806
McLean, Matthew	278, 605
McLuckey, Scott	91, 984, 1140
	41, 362, 410, 350, 460
McMahon, John	1066
McMahon, Terry	11, 969, 973
McMarthy, Tom	966
McNett, Debra A.	220
McSpadden, William M.	730
McVeety, Bruce D	845
McWilliams, Ted B.	1009
Medzihradszky, Katalin F.	625
Meier, Mark	1028
Meisels, Gerry	399
Mello, Charlene M.	300
Mellon, Fred A.	1183
Meltzer, Michael	111
Menacherry, Stanley	502
Meng, Shi-Yuan	1277
Mentzer, Mary	492
Menzies, Allan	529
Mercer, Roger S.	230, 1019
Merriweather, Roosevelt	819
	1109
Mertens, Thomas R	345
Mesmer, Mantai	464
Mestdagh, H.	700, 705
Meyer, Jacques	309
Meyer, Timothy,R.	219
Michael, Wadsley	213
Michel, Hanspeter	598
Micke, Mel	1230
Migdalof, Bruce H	880
Mikaya, Anzor	141
Miles, Walter	197
Milgram, Eric	1088
Miller, Cathy M.	484
Miller, David	1022
Miller, Jeffery	1007
Miller, John	957
Miller, Mark L.	1131
Miller, Scott	1334
Milliet, Ariel	969
Millington, David	240
Milot, Sylvain	63
Miranker , Andrew	681
Mireault, Pascal	154
Mirza, Urooj A.	241, 270, 1331
Mische, Sheenah, M	918
Miskimmin, B.M.	1018
Mitchell, Charles	927
Mitchell, Dale W.	804
Mitrovich, Samuel	673
Miyares, Paul H	129
Mo, Wenjun	66, 84
Mohn, C	1173
Mohr, Martin	1196
Moini, Mehdi	100, 166, 456
Molinski, Tadeusz F	1213
Monaghan, John	968
Mong, Gary M.	846
Moniatte, Marc	299
Monnig, Curtis A.	236, 462
Montanarella, L.	602
Monteagudo, Edith	552
Monteiro, Candida	259
Monteiro, Carlos A	1273
Montgomery, Jane	530, 836
Moon, Hong-sik	520
Moore, Christopher	273
Moore, Colin	214
Moore, Robert B.	889, 893
Moore, Theresa A.	869
Mordehai, Alex	122
Morgan, E.D.	557
Morgon, Nelson H.	65
Mori, Brian	877
Morin, Paul E.	1326
Moritz, Fritz	1047
Morrall, Stephen W.	842
Morrical, Bradley	1, 187

Author	Page Number
Morris, A. Kirk	597
Morris, F X	147
Morris, Howard R.	360
Morris, III, Samuel J	345
Morris, Jackie	190
Morris, Michael	1282
Morris, Mike	1303
Morrison, R. J. S.	718
Mortensen, Peter	638, 1218
Morton, George	549
Morton, Shelby	43
Morton, Thomas Hellman	14
Mosbaugh, Dale W.	34
Moseley, Arthur	519, 849
Mosely, Jackie A	384
Moshkarina, N A.	825
Moss, M. Lee	867
Mouget, Yves	412
Moulis, Jean-Marc	309
Mount, Andrew	954
Mowat, Ian	968
Mowry, Curtis	1132
Moyer, James	312
Moyer, Michael D.	526
Muddiman, David C	550, 565
	996
Mueller, Matthias	1077
Muenster, H.	248, 249
Muething, Johannes	1176
	1177
Muir, D C.G.	1018
Muir, Derek	225, 228
Muir, Tom	982
Mulder, Patrick	587
Muller, Odilo	105
Mullis, James	426
Munch, Jean W	337
Munchausen, Linda	480
Munson, Burnaby	75, 76
Murphy, Robert C.	333, 871
	539, 1147
Murray, Kermit K.	1204
Murrell, Jason	1105
Murthy, Satya S	854
Murugaiah, Veeravagu	588
Musselman, Brian D	1074
Musser, Steven M	504, 1321
Myers, James D	725
Myers, Tanya	229
Mylari, Larry	541
Mylchreest, Iain	173, 436, 653
Nadeau, Ronn	243, 914
Naemura, Koichiro	95
Nagabhushan, T L	293
Nagai, Yoshitaka	1175
Nagel, Marcus	1107
Naim, Abdul	588
Nair, Hari	417, 1333
Naito, Yasuhiro	601
Nakajima, Terumi	1212
Nakamura, Takemichi	1281
Nakata, Hisao	1048
Nakayama, Hiroshi	304, 616
	1304
Naoki, Hideo	1212
Narayanaswami, Gowri	941
Nardo, Cymbelene L.	334
Natale, David	36
Nauman, David	422
Naven, Thomas J P.	1168
	1194
Navetta, Kim	578
Nawrocki, Joseph	388, 637
Naylor, Stephen	328, 510, 543
	629, 648, 1315
Nedved, Michael L.	491
Needham, Larry L.	344
Needham, Shane	561
Neidermann, Gabi	1294
Neitz, Susanne	285
Nelson, Chad C.	574
Nelson, Christopher A	1295
Nelson, Randall W.	876, 930
	944, 945
Nemirovskiy, Olga	1274
Nero, Vince	759, 1008, 1012
Neubauer, Kenneth	5
Newman, Carolyn M.	344
Newman, Michael	873
Newton, Russell P.	1278
Ng, Ken	266
Ng-Ilag, J	1328
Ngoka, Lambert	1308
Nguyen, Viet	1049
Ni, Jinsong	714, 715
Ni, Zhi-Jie	486
Nibbering, Nico M. M	400
Nichol, Greg	232
Nicol, Gordon	76
Nicola, Anthony J	664, 996
Nicoll-Griffith, Deborah	533
Nigam, Somesh	36
Nigel Adams	693
Nikiforov, Alex	142
Nikolaev, Eugene	973
Niwa, Yoshio	106
Nobes, Brian J.	566
Noble, Christopher	1, 186
Noble, Dick	278
Nock, Steffen	1330
Nogar, N. S.	772, 964, 1127
Noggle, F T.	572
Noguchi, Kazuyoshi	287, 288
Nold, Michael	1030
Noon, Kathleen R.	356, 1067
Norberg, Peter	766
Nordhoff, E.	584
Nordmeyer, Trent	1, 184
Norwood, Daniel	426
Novikova, L	107
Nugent, Kerry	487, 861
Nuwaysir, Lydia	278, 605, 646
Nyberg, Fred	274
O'Connor, Peter B.	680
O'Donnell, Niall	1168
O'Hair, Richard A.J.	329, 1035
O'Shannessy, Daniel	980
Oberth, C.H.	498
Obukowicz, Mark	1153
Oda, Robert P.	1315
Odom, Robert	998, 1004
Ogawa, Tomoya	1175
Oglesby, Thomas	856, 905
	276, 334
Oglesby, Thomas D.	858, 1322
Ogorzalek Loo, Rachel R	234
	235, 924
Oh, Chang-Hwan	591

Author	Page Number
Ohashi, Mamoru	636, 1186
Ohashi, Yoko	1175
Ohorodnik, Susan	818
Okuyama, Tsuneo	304, 304
	616, 624, 1304
Olberding, Edward L	220, 221
Olivares, Jose A	47, 49
Oliver, Ronald	1262, 1296
Olson, Douglas	470
Olumee, Zohra	1252
Omori-Satoh, Tamotsu	305
	624
Onigbinde, Adebayo	75
Orians, Kristin J.	703
Orkiszewski, Ralph	382, 421
Orlando, R.	292, 295
	1172, 1173, 1174
Osborn, Blaire L.	875
Ospina, Maria	1156
Ostrovskaya, Galina	283
Ott, Istvan	303
Ottinger, Sean E.	506
Overberg, A.	621, 950
Overney, Gregor	734
Overton, Santford	113, 149
Owens, Gary	610
Owens, Kevin	19, 136, 689
	947, 952, 956, 1237, 1238
Owusu, Daniel	1032
Painter, Sherry	369
Paiva, Tony	245
Paleos, C. M.	1065
Palmer, Cynthia A.	1324
Palmer, Peter T	832
Panagiotou, Thomai	837
Pan, S.	295
Panico, Maria	360
Pannell, Lewis	583, 599, 1270
Pannell, Lewis	1271
Papac, Damon	917, 981
Papaleo, Ricardo	1058
Papayannopoulos, I A	277
	301
Papov, Vladimir	297
Pappin, Darryl	626
Pardoll, D.	1289
Parees, David	19, 952, 1052
Park, Frederick D S.	1335
Park, Hyeung-geun	520
Park, Melvin	1207, 1208
Park, SungAe	291
Parker , Mark A.	1076
Parker, Carol	917, 981
Parlar, H.	228, 1018
Parry, David. E.	51
Pasa-Tolic, Ljiljana	92, 1029
	1085, 1214, 1215
Pastel, Michael	179
Pastor, Salvador J.	416, 1217
Pastor, Steve	266
Pastorova, Ivana	746
Patkin, Adam	742
Patrick, Jeffrey	1034, 1334
Patterson, Dale	997
Patterson, Donald Jr	201,1016
	344, 509
Patterson, Kathleen	826, 827
Paul, G. J. C.	608, 1065
Paulino, Jose	50
Paulus, Gert	1248
Pawlosky, Robert	1159
Pearson, Paul G.	508, 869
Pearson, Richard	832
Pearson, Roger	1017
Pedder, Randall E.	1069, 1070
Peiris, Dil	1033
Pellascio, Bernhard	311
Peltier, John	387
Penn, Sharon G.	236, 1084
Pepinsky, R. Blake	301
Pereira, Neila	1059
Perez, James	1092
Perkins, John R.	1278
Perreault, Helene	1179
Peru, Kerry M.	215
Pesch, R.	248, 249
Peschke, Michael	83, 372
Peter-Katalinic, Jasna	1176
	1177
Peterman, Scott	74
Peters, N.K.	1174
Petersen, Mary	865
Peterson, Charles M.	1302
Peterson, Kent	12
Petitou, Maurice	259
Petrosyan, V S	825
Philip Wong,	56
Philippe, Lière	1125
Phillips, Andy	481
Phillips, D.H	507
Phillips, Eugene	188
Phillips, Lawrence R	163, 878
Phillips, Mark A	554
Picard, Claudine	259
Picotte, Pierre	517
Pierce, Richard H.	503
Pincock, J A.	152
Pinkston, J. David	468
Pires de Matos, António	704
	965
Pirhalla, Jill	661
Pitsenberger, Cynthia	798
	1080
Plante, Sylvie	585
Pleasance, Stephen	553, 868
Plomley, Jeffry B	230, 993
	1019
Pogue, Robert	764, 1028
	169, 170
Poisson, L	1072
Pokrovskiy, Valeriy	283, 765
Polce, Michael J	395, 1037
Pomerantz, Steven C	600
Ponciano, Cassia	1059
Poon, G K.	507, 521, 528
Pope, Marshall	53, 347, 371
Potier, Noelle	595
Poulsen , Fleming	237
Poutsma, John	50
Povey, William T.	97
Powell, David	1156
Powell, Mark	862, 883
Powers, Daniel D	282
Poyer, J Lee	1163
Pozniak, Boguslav P	370
Pradeep, Thallapil	1334
Pragnell, Charlton	198
	542, 563, 887

Author	Page Number
Pramanik, B.	293
Prather, Kimberly	1, 184, 185, 186, 187
Preece, Steve	535
Prell , George D. (2)	606
Preston, Andrew	736
Price, John M.	725
Price, Keith R.	1183
Prockop, Darwin	601
Proctor, Andrew	550, 565, 664, 665, 748, 996, 1317
Prokai, Laszlo	253, 257, 272
Prokai-Tatrai, Katalin	272
Prom, Jean-Claude	259, 315
Prospero-Garcia, Oscar	1144
Provost, Lionel R.	267
Przybylski, Michael	618, 1330
Ptillot, Yves	309, 1169
Pucci, Sergio	165, 840
Pugh, Jonathon	657
Pullen, Frank	434
Pungor Jr., E.	1167
Purdon, Michael P.	511
Puretzky, A. A.	1234
Pureveen, Jos	745
Purves, Randy	885
Pykäläinen, Mika	77
Pyle, Steven	1141
Pylypiw Jr., Harry	214
Pyne, David A.	898
Pyrek, Jan St	158, 169, 170
Qian, Kuangnan	25, 758, 959
Qian, Mark G	446, 579, 614
Qian, Mark G	654, 936, 1316
Qin, Jun	989, 1100, 403
Quarmby, Scott T	1119
Quirke, J. Martin E.	1005, 1006
Rabinovich, Yakov I	1317
Radford, Sheena	1265
Radom, Leo	10
Raffaelli, Andrea	165, 840
Ragsdale, John	1115
Raida, Manfred	285, 611
Rainbird, B.J.	219
Rajamani, Umamaheswari	1270, 1271
Ralitsch, Milan	1020
Ramadas, Bhat	245
Ramaley, Louis I-2	1314
Ramanathan, Ragulan	253
Ramesh, Rao	211
Ramsey, J.M.	155, 775
Ramsey, Michael	3
Ramsey, Roswitha S.	460
Ranasinghe, Asoka	496
Ranasinghe, Yasmin A	86
Randall, Linda L.	1261
Rappmund, Andreas	68
Raptakis, Emmanuel	130
Ray , March	1125
Ray, Kenneth	223, 456
Rebek, Julius Jr.	493
Reddick, Christopher	946
Reddy, D. Meghanath(1)	606
Reddy, G R	593
Redpath, Craig	954
Reed, Don	495
Reed, R.H.	1318
Reed-Bombick, Betsy	1299
Reents, William	4, 1087, 1091
Reeve, Jr , Joseph	273
Regert, M.	747, 874
Regg, Brian	443
Regnier, Fred	442, 997
Reiber, Duane	683, 1249
Reich, Fraser	995
Reichlmaier, Stefan	20
Reilly, James	127, 363, 1003, 1021, 1243
Reinhold, Bruce B.	975, 1180
Reinhold, Vernon N.	975, 1180
Reiter, Alex	280, 281, 348
Remberg, Barbara	142
Rempel, D. L.	786
Resch, Martin	1248
Rettenmeier, Albert W.	853
Reuschel, Scott A.	574
Reynolds, David J.	726
Rhomberg, Andrew	1189
Rich, Jennifer	72
Rich, Michaela	74, 188
Richard, Martin	233
Richards, Don	434
Richards, James I-2	977
Richardson, D. E.	701
Richardson, Susan	338, 826, 827
Ridder , Gregg M.	484
Ridge, D. P.	75, 93, 959, 1309
Rieger, Robert A.	603, 606
Riggs, B. Lawrence	1315
Rimando, Agnes	428
Rindgen, Diane	590
Rinehart, Kenneth	1284, 1298
Rippy, Allyson	712
Riveros, José M.	65, 397, 1033
Robbins, Ronny	156, 1044
Robbins, Winston	1014
Robert, Croes	213
Roberts, Gerald	492, 620
Robertson, Duncan H L	290
Robertson, Philmore	564
Robinson, Carol	237, 681, 1265
Robinson, J. M.	131
Robinson, Kevin	692
Roboz, John	246, 303
Robson, John	233
Rockwood, A. L.	125, 907
Rockwood, Alan	801, 1093
Rockwood, Alan W.	725
Rodebaugh, Ron	266
Rodgers, M. T.	696
Rodriguez-Cruz, Sandra	352, 89, 656
Roehling, Ulrich	1220
Roepstorff, P	314, 584
Rohde, Michael	1272
Roher, Alex	271
Rohrbaugh, Dennis	218
Rohrs, Henry	1334
Rolando, C.	668, 700, 705, 747, 874, 891, 1050, 1071, 1072
Romeo, Elena	1162
Rontree, John	824
Rosazza, J. P N	514
Rosell, Joan	102, 670
Roskey, Mark	364
Rosnack, K.J.	312, 1323

43rd ASMS Conference on Mass Spectrometry and Allied Topics

Author	Page Number
Ross III, Charles	92
Ross, Andrew R.S.	703
Ross, Mark M.	298, 1185
Ross, Philip	1036
Rossi, Vronique	1169
Rourick, Robyn	148, 433, 568, 489
Rouse, Jason C.	359
Rousseau, Caroline	178
Roussis, Stilianos, G	762, 763
Roy, Laura	1099
Roy, Tim	835
Roybal, Jose	870
Rudensky, Alexander Y	979, 1291
Ruiz, Migdalia	151
Russell, David	380, 690, 723, 805, 920, 1242, 7, 445, 686, 146, 904, 972, 1062, 1246, 1250, 1266
Russell, John W.	864
Russell, K.C	251
Rybal'chenko, Vladimir	283
Ryzhov, Victor	59
Sablier, M	668, 700, 705, 747, 874, 891. 1050, 1071, 1072
Sackett, Danny	1270
Sadeghialavijeh, M.	1241
Sadilek, Martin	694
Sadoun, Aladin	15
Sadovskaya, Inna I-2	977
Saegesser, Martin	258
Saha, Sanat	623, 1259
Sakairi, Minoru	452, 884
Sakuma, Takeo	222, 252, 517, 545, 1073
Salat, Janos	303
Saleh, Samir A.	880
Salem, Norman	1152, 1159
Salt, Kimberly	185, 186
Salt, Salt	1
Salvadori, Piero	840
Salyan, Mary Ellen K	1178
Samama, Jean-Pierre	315
Samuel, Mitrovich	494
Sanaullah,	336
Sanchez, Gabriel	517, 545
Sanchez, Stephanie C.	880
Sander, Peter	724
Sanders, Mark	173
Sandersson, Katarina	274
Sang, Hong	1163
Sannes, Kristin	940
Sarkisian, Molly	604
Saru, F.	668, 891
Sarver, Emory W.	1109
Sasaki, Tania A	479
Satsangi, Neera	540
Satzger, Duane	332, 464, 512
Saulys, Dovas A.	239
Saves, Isabelle	315
Sawada, Masami	95
Sayer, Jane	599
Scarberry, R E	647
Schaaff, Thomas	403
Schachterle, Steve	475, 476, 477
Schaefer, William	423
Schaeffer, Richard	1068, 1069, 1070
Schaer, Martin	948
Schaffter, L M.	147
Schaller, Johann	311
Schaps, Marlene E.	474
Scheller, Nova	496, 497
Schenkel, Thomas	1336
Scherer, Stefan	128
Schey, K. L.	318, 635, 1332
Schieltz, David	325, 640, 641
Schindler, D.W.	1018
Schlunegger, Urs P.	121, 181, 182, 311, 1078, 1251
Schmehl, Russell H.	451
Schmidt, E. G	790
Schmidt, Joseph A R.	329, 1035
Schneider, Dieter H.	1336
Schneider, Joanne	210
Schneider, Klaus	361
Schneider, Rick	578, 851
Schnier, Paul D.	656, 902
Schnier, Paul S	352
Schnolzer, Martina	324, 632
Schorno, Karl S.	662
Schrader, W.	248, 249
Schreurs, Jolanda	294
Schriemer, Dave C	923, 951
Schubert, Michael	458, 1106, 1107
Schuerch, Stefan	181, 182
Schuhmacher, Martina	618
Schultz, Birgit	313
Schumaker, Verne	1169
Schurz, Helen	341
Schuyl, P J.W.	755, 1143
Schwartz, Brenda	39, 355, 682, 802, 1261
Schwartz, Jae	160, 861, 992, 1103, 1113, 1114, 1115, 1116, 276, 988, 1117
Schwartz, Jay	519, 849
Schweikert, Emile	778, 1057, 1060, 1061
Schweikhard, L.	697, 809, 810, 679, 811, 963
Schweingruber, Hans	242
Scoble, Hubert	359, 685
Scott, Gary	138
Scrivener , Elaine	726
Scrivens, Jim	18, 750, 751, 753, 754, 757
Scullion, Simon	841
Sears, L.J	1161
Sebo, Peter	1283
Seedorf, Ronald	828
Segal , John	18
Selzer, J	1279
Sena, Marcelo	397
Senko, Michael W	733, 806, 1085
Sepetov, Nikolai	483
Serrano, Jose	200, 515
Seta, Kazuo	304, 305, 616, 624, 1304
Severinov, Konstantin	286
Severinova, Elena	286
Seyfreid, Thomas, N.	1180
Shabanowitz, Jeffrey	441, 610

Author	Page Number
	626, 976, 978, 1283, 1290, 1293, 1294
Shackleton, Cedric H L	1303
Shaffer, Scott, A	1049
Shaffer, Barrie A.	1112
Shaffer, Scott	17
Shah, Bhavana	1187
Shah, Nikhil	486, 909
Shahgholi, Mona	1185
Shalaby, Lamaat	925
Shaler, Thomas	939, 940
Sharp, T.R.	164, 1318, 1323
Shartava, Archil	1273
Shaw, Angela	470
Shaw, R.W.	775
Shay, Brian J	159, 755
Shealy, Dana B.	226
Sheehan, Edward	673, 894, 895
Shen, Nanzhu	371
Shen, Shida	99
Shen, Tun-Li	1297
Sheng S. Yang,	56
Sheppard, Robin	103, 150
Sherman, Michael	907, 1086
Sherman, Nicholas E.	626, 976
Sherman, Paul	162
Shevchenko, A.	33, 638, 1311
Shew, Sandy	414
Shick, Jr., Charles	26, 45
Shiea, Jentaie	911
Shieh, J.J.	1153
Shimada, Ichio	287, 288
Shinn, David	1211
Shofstahl, James	1320
Short, R. T	771
Short, Robert	9
Shu, Chi-Kuen	473
Shuguang Ma,	56
Shukla, Anil K.	401, 402
Shum, Sai	266
Shushan, Bori	222, 252, 517, 545, 903, 1073
Shyong, Bao-Jen	927
Sible, Emily, M	1200
Sickenberger, Dave W	1157
Siegel, Marshall	179, 306, 307, 308, 1288
Siethoff, C.	249
Silverton, Susan F	1133
Silvestro, Luigi	1190
Sim, P. Greig	195
Simanek, Eric E.	910
Simay, Antal	303
Simon, Jerald	451
Simonneau, G.	1071
Simpson, J.T.	472
Sims, Gary R.	1074
Singh, Padma	242
Singh, Rajendra. K.	914
Singh, Romi	992
Singleton, David	312
Sinimanne, Sarath R.	201, 509
Sisenwine, Samuel	532, 905
Sisk, Ellen C.	597
Siu, K.W. Michael	848, 903, 379, 674
Siuzdak, Gary	289, 604, 1144
Sjövall, Jan	630, 1160
Skarping, Gunnar	879
Skeen, Todd T.	834
Skipper, Jonathon	978, 1293
Slawson, Matt H.	574
Slayback, John	143, 146, 431
Slingluff, C. L.	978
Smelyanskiy, Yanina	234
Smirnoff, Igor	364
Smith , David L.	296
Smith , Jean B.	296
Smith, Brian	721
Smith, Claudia A.	468
Smith, D	1328
Smith, D.H	775
Smith, David H.	41, 767, 768
Smith, David L.	137, 440, 1260, 1329
Smith, Diana M.	617
Smith, Glenn	1199
Smith, Jacob D.	1035
Smith, Jean B.	440
Smith, Philip C.	556
Smith, R. D.	125, 907
Smith, Rebecca	70, 71
Smith, Richard	682, 802, 1093
Smith, Richard D	39, 244, 349, 355, 376, 449, 457, 459, 592, 596, 597, 800, 801, 804, 910, 1086, 1261, 1326
Smith, Richard W.	522, 901
Smith, Steve	736
Smith, Virginia F.	1261
Snider, C.E.	319
Snider, Neil S.	866
Snyder, A. Peter	373, 1053, 1054
Sochacki, Marek	598
Solouki, Touradj	92, 711, 805, 1215, 1216
Soloveytchik, Boriana	957
Solsten, R. Thomas	243
Somani, H.	521
Somogyi, Arpad	353, 417, 418, 1051, 1333
Song, Siqing	316
Song, Ye	1180
Soni, M H , Weil, C.	1129
Sorensen, Daniel	64
Sorokine, Odile	299
Souders, C.	1167
Sovocool, G. Wayne	231, 346
Spalding, Roy	208
Spanbroek, Rainer	1176
Sparkman, O. David	728, 820
Speakman , Alison	879
Spear, Kerry L.	487
Sphon, James A.	1321
Spicer, V	126, 684, 1219
Spier, J. Paul	886
Spiess, Iris	69, 782, 785, 1089
Spiess, Joachim	320, 1046, 1258
Spik, Genevive	1169
Spreen, R C.	147
Sprinzl, Mathias	1330
Squires, Robert	50, 695, 1031
Srinivasan , Jannavi, R.	941
Srinivasan, N.	152
St-Germain, François	836

Author	Page Number
St Claire, Bob	849
Stacey, Catherine	458, 886
Stack, Robert	1207
Stadlmann, Jens	139
Stafford, George	1103, 1114, 1117
Stahl, Bernd	925, 1176, 1184
Stahl, Douglas C	719
Standing, K G	684, 1206, 1219, 126, 994, 1327, 1259
Starrett, Anne	148, 432
Stavinoha, William B.	540
Stayton, Patrick S	1261
Ste-Marie, Line	530
Steenwyk, Rick C.	869
Stein, Ronald	1001, 1002
Stein, Stephen E.	141, 729
Steiner, Robert	42
Stemmler, Elizabeth	677
Stephane, Bouchonnet	1125
Stephenson, James	367, 408
Stern, Gary	225, 228, 1018
Steup, Martin	1184
Stevens, K.L.	340
Stevens, Robert	240
Stevenson, Tracy I.	934
Stewart, Jon D.	289
Stillwell, W G.	499
Stockton, Brian	73
Stoeckli, Markus	121
Stoffel(s), J. J.	48
Stoker, Paul	1328
Stoney, Ken	612, 652, 861
Stout, Howard	414
Stracke, Patric	139
Streeper, Rob	508, 540, 556
Street, Jacqueline	1179
Stresau, Dick	1000
Strife, Robert	160, 1113
Strobel, Fred	348
Stroh, Justin	312
Stromatt, Robert	264
Stroobant, Vincent	1142
Stroud, Mark R.	1178
Strupat, Kerstin	933
Strupp, Christian	289
Stults, John	31, 302, 676
Subramanian, Periyasamy	471
Suleiman, Ahmad A.	254
Sullards, Cameron	261, 378
Summerfield, Scott	279, 779, 1300
Sumner, Lloyd	1062, 1242
Sumner, Lloyd W.	1250
Sun, Furong	1298
Sun, Y.	319, 386, 415, 615
Sundqvist, Bo	413, 1058, 1245
Sunner, J.	310
Supko, Jeffrey G.	163, 878
Sutton, C	621, 950
Sutton, S. W.	1166
Suzuki, Sakaru	1186
Swackhamer, Deborah L	1017
Swanek, Frank D.	459
Swanson, Steve	525
Swedberg, S.	1167
Swenberg, James A.	496, 497
Swenson, David	242
Swiderek , Kristine M	719
Syka, John	988, 1114, 1117
Szekely, Gabriella	1229, 1230
Szulejko, Jan	969
Tabei, Keiko	179, 306, 308, 1288
Tachiyashiki, Satoshi	260
Tagami, Uno	287, 288
Taghizadeh, Koli	422
Takach, Ed	364
Takada, Yasuaki	452, 884
Takai, Yoshio	95
Takayama, Mitsuo	1048
Talaga, Philippe	1184
Talrose, V	107
Tam, Steve	598
Tanaka, Koichi	1248
Tang, Dazhi	30
Tang, K.	268, 935
Tang, Kai	581
Tang, Liang	1083
Tang, Ming	1137
Tang, Wei	524
Tang, X	21, 1170
Tang, Xiaodong	942
Tang, Xue-jun	1259, 1268
Tang-Liu, Diane	567, 850
Tannenbaum, S R.	499
Taranenko, N. I.	268, 935, 1234
Tarr, George	442, 997
Tata, Prasad	550, 565
Tayler, Paul	757
Taylor, Dennis	988, 1103, 1114, 1115, 1117
Taylor, Lester	992
Taylor, Mike	18, 753, 757
Taylor, Paul	276, 492
Taylor, Steven	298
Taylor, Susan	148, 432, 612
Taylor, William	712, 713
Tchekhovskoi, Dmitrii V.	729
Tedeschi, Nicole	1275
Teesch, Lynn	471, 514
Teklehaimanot, Bibi	399
Teng, Siu	1010
Termin, Andreas	1187
Terunuma, Hideya	601
Terwilliger, Thomas C	1326
Thoberge, Roger	1064
Thanabal, Venkataraman	35
Theophanides, T.	1073
Thibault, Pierre	977, 1169, 1314
Thierry, Blasco	1125
Thilens, Nicole	1169
Thomas, Angela	217
Thomas, Boban	606
Thomas, Craig	1028
Thomas, D W.	1161
Thomas, Darren	195, 233, 1282
Thomas, Stan W.	991, 1138
Thomas, Susan	777
Thompson, Cyril	831
Thompson, Harold C	467
Thompson, Stephen	692
Thompson, Toni	544
Thompson, William	148
Thompson, William L.	174, 433, 143
Thomson, Michael L.	151

Author	Page Number
Thorne, Jacqueline	105
Thorne, Peter S.	471
Thorpe, Colin	93
Thrall, Karla	1023
Thruston, Jr., Alfred D.	826, 827
Tianlan, Zhang	959
Tippin, Tim	519, 849
Tobe, Yoshito	95
Tobias, Herbert J.	46
Todd, John F. J.	97, 168, 191, 66, 84, 735, 1105
Todd, Peter	9, 1066, 1154, 1191
Tomany, Michael	613
Tomer, Kenneth	917, 943, 981
Tomlinson, Andy J.	328, 629, 648, 1315
Tomlinson, John	332, 512
Tomy, Gregg	225
Tong, Huayi	266
Torok, D.S.	472
Torres, T. A	789, 791
Tosh, R.E.	401
Townsend, Jennifer A	1019
Tran, Huu M.	617
Travers, Jeffrey	1147
Tretyakova, Natalia	171
Tria, John	766
Trimble, Laird	533
Triolo, Antonio	552
Truong, Long	1164
Tsao, Rushung	179
Tseng, Jih-Lie	275
Tsuchiya, Masahiko	106
Tsuneyoshi, Toshihiro	601
Turecek, Frantisek	17, 262, 263, 694, 906, 1043, 1049
Turesky, Robert J	499, 590
Turner, Wayman E.	344
Turnipseed, Sherri	870
Tykodi, Scott	1293
Uchida, Kazuhisa	304, 1304
Udiavar, S.	1167
Udseth, H R.	125, 457, 907
Udseth, Harold R.	597, 801
	1086
Uhrich, Mark	276, 519, 849
Uhrig, Mary	1299
Unanue, Emil R.	1295
Urban, Jan	631
Urford, Neil	781
Uzabiaga, Françoise	259
Vachet, Richard	386, 421, 1111, 1211
Vachon, Benoit	836
Vachon, Luc	530
Vaidyanathan, G	1140
Vainiotalo, Pirjo	77
Vaisar, Tomas	262, 263, 631
Valaskovic, Gary A.	650, 680
Valero, Gustavo	832
Valiga, Robert E.	767
Van Baar, B. L. M.	205
Van Berkel, Gary	43, 667, 899, 460, 900, 1005
van Breemen, Richard B.	282, 428, 429
Van den Heuvel, Hilde	1181, 1183
van der Doelen, Gisela	745
Van Dorsselaer, Alain	250, 251, 299, 595
van Grevenstein, A.	745
Van Hoof, F.	824
van Kuijk, F J.G.M.	1161
van Ocht, J.	745
Van Orden, Steven	349, 725, 1086
van Rooij, Gerard J.	813
van Soest, Remco	573
Van Stipdonk, Michael	778, 1060, 1061
van Vyncht, Gery	535
Van Ysacker, Peter G.	481
Vartanian, V H.	788, 791, 795, 971, 1137
Vasconcellos, M.A.	1143
Vath, James	359, 685
Vatsadze, Sergey	171
Vaughan, J.	1166
Velupillai, Palanivel	975
Venesky, John S.	174
Venkataramanan, Raman	565, 550
Venot , Andre	1187
Ventura, M. C.	1126
Verentchikov, A V	613, 1219
Vertes, Akos	21, 922, 957
Vertes, Akos	1170, 1241, 1252
Vestal, Marvin	364, 613, 1209
Vestling, Martha M.	358
Veverka, Karen A.	543
Vidavsky, Ilan	587, 1292, 1295
Viger-Chougnet, Antoinette	538
Vigushin, D	521
Vincent , Gervat	81
Viner, Nicholas J.	1295
Vinogradov, Serge N.	1296
Visentini, Josie	178
Vlasak, Paul R.	134
Vogt, Volker M	301
Volk, Kevin J.	174, 176, 433, 489, 568
Vollmer, David	501, 622
Volmer, Dietrich	463, 115, 202, 203
von Helden, G	448
von Wittenau, A.S	1336
Voorhees, Kent	115, 1132, 1157, 1158
Vorm, Ole	314, 638, 1218
Vossbrinck, Charles	1298
Vouros, Paul	105, 193, 300, 493, 544, 590, 837, 897, 1313
Voyksner, Robert	427, 444, 1139, 247, 839
Vrbanac, James	421, 508
Vulpius, Tore	1027
Wachs, Timothy	103, 857
Waddell, Dave S.	1019
Wagner, David	488
Wagner-Redeker, Winfried	548
Wahl, Karen	264
Wainhaus, Samuel	389, 1337
Waite, Herb	298
Wakefield, Michael	173, 436, 741

Author	Page Number
Walker, Carthene	441, 1283
Walker, Kathleen L.	462
Walsh, John	519
Walther, C.	809, 811, 963
Wanczek, Karl Peter	67, 68, 69, 783, 784, 782, 1082, 785, 1089, 1095
Wang, Bing	582
Wang, Dingneng	109, 407
Wang, Fang	1268
Wang, Guangdi	672
Wang, HangQi	442
Wang, Jia-shen	161, 722
Wang, Jianyao	379, 674
Wang, Jin	847
Wang, Liping	93
Wang, Mingda	1121
Wang, Rong	270, 921
Wang, T -C. L.	465
Wang, Tao-Chin	1152
Wang, Wei	1293
Wang, Weimin	889, 893
Wang, Wen-shyang	911
Wang, Xiaomin	79
Wang, Yajun	920
Wang, Yan	516
Wang, Yang	1106, 1107
Wang-Iverson, David	864
Ward, Glen	1152
Warrack, Bethanne	612
Warshawsky, David	210
Wasserman, Michael B	1109
Watkins, Carl	966
Watkins, Layle	72
Watson, C. H.	701
Watson, Cliff	82, 257, 637, 388, 1088
Watson, Eric	1187, 1188
Watson, J. Throck	575, 932
Watts, Heath	847
Watts, Peter	1105
Waugh, Russell J	333
Wedge, P.	152
Wei, Gang	1204
Wei, Jian	1068
Wei, Xiaona	7, 445, 904, 1266
Weil, David A.	366
Weinberger, Scot	1210
Weinsotck, Joseph	492
Weintraub, Susan T.	540, 556, 1067
Weiss, Christian	881
Weissenberg, Klaus	741
Welch, Michael	660
Wells, Greg	478, 1122, 1123
Wells, J. Mitchell	985
Wen-Shyang, Wang	912
Wendling, Jay	162
Wensing, Michael W.	373, 1053, 1054
Werdel, Lisa P.	1322
Wesdemiotis, Chrys	377, 395, 1030, 1037, 1038, 1305
West, Andrew	317
Wester, Dennis W.	844
Westerduin, Pieter	1190
Westmacott, G R	1206
Westman, Ann	1222
Westmore, J.B.	1018
Westmore, John	225, 228
Wexler, Anthony	2, 5, 958, 961
Whalen, Kevin I-1	1073
Wheelan, Pat	539
Wheeler, K P.	653
Wheeler, Kevin	436, 652, 861
Wheeler, Patrick D	658
White, Dineen J	864
White, Earl	1299, 1301
White, Forest M	711, 1085, 1149, 1216
White, John	199
White, Mark	777
White, Robert	856, 276, 1322
Whitehill, Andy B.	1292, 1295
Whitehouse, Craig	99, 886, 101, 999, 455
Whitehouse, Larry	529
Whitesides, George M.	910
Whiting, Andrew	381
Whitman, Christian P	256
Whitney, Jeffrey	148, 433, 568, 489
Whittal, Randy M.	22, 923, 1223, 1226
Whitten, William	3
Whitton, Margie	322
Wiberg, Karin	158
Wickham, Juanita	939
Widger, William R.	520
Widlanski, Theodore S.	1151
Widmer, H. Michael	1196
Wiedmann, Fred	1037, 1038
Wilcox, M D	318
Wilhelm, Jeffrey A.	276, 854
Wilhelm, Ulf	1077
Wilkerson, Charles W.	183
Wilkes, Jon G.	115, 202, 203, 467
Wilkins, Charles L	416, 462, 479, 1217
Wilkins, Pat	1285
Wilkinson, William R.	665
Willett, Gary	967
Williams, David T.	821
Williams, Evan R.	89, 352, 656, 902
Williams, John B.	949
Williams, Jon	1182
Williams, Peter	876, 930, 944, 945
Williams, Ted L.	693
Williams, Todd D.	329, 1035
Williams, Tracie L	367
Williamson, Brian	73
Williamson, D H.	110
Willoughby, Ross	494, 673, 466, 894, 895
Wilm, M. S.	33, 594
Wilm, Matthias	28, 638, 739, 987, 1279, 1311
Wilner, Keith	563
Wilson, Ian.D.	534, 557
Wilson, Ray	737, 738, 1098
Wilson, Terry	176
Wilton, Amanda N.	546
Winans, Randall E.	760, 1007
Winders, Andrew	385
Wing, David R.	1168

Author	Page Number
Winger, Brian	414, 450
Winnik, Witold	404, 1141
Winslow, L. D.	662
Winters, Conrad	178
Wintner, Edward A.	493
Wise, Marc B.	734
Wise, Marcus	819, 831
Wishnok, J S.	499
Witkowska, H Eva	1303
Wolf, Susan	627
Wolfe, Henry	32
Wolfe, Tracy L.	163
Wolfender, Jean Luc	548
Wollnik, Hermann	120, 128,139
Wolter, M. A.	594, 602
Wolucka, B A.	1197
Wong, Carla	832
Wong, Diane	273
Wong, Mel	245
Wong, P.	152
Wong, R.Y.	340
Wood, Troy D	87, 651, 680
Woods, A.S.	915, 1289
Woods, Amina	271
Woods, James	284
Woolen, Stan W.	1321
Woolfitt, Adrian	98, 657
Worrall, Timothy	581
Worthy, Suzanne	817
Wright, Adrian	434
Wright, L. James	1067
Wright, Scott	953, 954
Wronka, John	124, 1207
Wu, Henry Y.	859, 860
Wu, Jiangyue	678, 932, 1081 1195, 1213
Wu, Jingtao	461
Wu, K.	295
Wu, Kuang Jen	939, 940, 998
Wu, Kuen Yuh	496
Wu, Qinyuan	349, 376, 1086
Wu, Wu-Nan	526, 527
Wuerker, Ralph	1118
Wulser, Kurt W.	137
Wunderlin, Markus	618
Wysocki, Vicki	353, 403, 417 418, 628, 1051, 1333
Wyttenbach, T	448
Xia, Ming	100
Xiang, Xinzhen Jane	177
Xiao, Guang	564
Xie, Xiaoling	1331
Xin, Tianpei	711
Xiong, Yansan	689, 1237
Xu, Allan	865
Xu, Linxiao	588
Xu, Ming	815
Xu, Naxing	575
Xu, Xiaoming	254
Xu, Yaodong	265
Xu, Young	706, 707, 710
Xue, Weiling	210
Xuewu, Jiang	993
Yablokov, Michail	1075
Yakovlev, B	107
Yalcin, Talat	383
Yamada, Hitoshi	95
Yamakawa, Yoshio	305, 624
Yamamoto, Ralph	294
Yan, Lin	275
Yang, George	453
Yang, Hou-Jun	916, 1244,1263
Yang, Lily	838
Yang, Mo	3, 155
Yang, Sheng	1034
Yang, Y	1172
Yang, Yang	1160
Yang, Yarjing	388, 1033
Yao, Flora	1188
Yao, Jie	416, 1217
Yates, Hilary	18, 753, 754, 757
Yates, John	325, 640, 641 990, 979, 1291
Yates, Nathan A.	626
Yeh, Che-Hung	1275
Yeh, Chen-Sheng	710
Yen, Ten-Yang	247, 497
Yeola, Suresh N.	880
Yergey, Alfred L.	265
Yergey, James	533, 1150
Yeung, Bernice	300
Yhard, G. Bradley	781
Ying, Z. Charles	1025
Yinon, Jehuda	343
Yongwu, Liang	451
Yoo, Jong Shin	172
Yoo, Ryong	375
Yoshida, Keiichi	1186
Yoshidome, K.	732
Yost, Richard	537, 946, 986 367, 405, 1156, 408, 1005 1006, 1119, 1120, 1133
You, Jianzhang	466
Young, J.P.	775
Young, Larry	877
Youngquist, R. Scott	484
Yousef, Ibrahim	545
Yu, Chungping	1151
Yu, Jim	284
Yu, Qitao	246, 303
Yu, Wen	685
Yu, Zhonghua	321
Yuan-Ping, Yang	570
Yuji, Reiko	287, 288
Zacchello, F	882
Zagorevski, Dmitri	974, 1310
Zaia, Joseph	513
Zaikin, Vladimir	141
Zamborelli, Tom	1187, 1277
Zamecnik, Jiri	863
Zefirov, Nikolay	171
Zell, Manfred	335, 538
Zembrowski, William	541
Zeng, Chenhui	1165
Zeng, Jianru	925, 1184, 1205
Zenobi, Renato	8, 955
Zhan, Qaio	8, 955
Zhang , Wenzhu	643
Zhang, Haiying	929
Zhang, J	907
Zhang, Jian	920
Zhang, Jie	1160
Zhang, Tian-lan	75, 93
Zhang, X. Kate	390, 1221
Zhang, Xin	265
Zhang, Yu	654
Zhang, Z.	647
Zhang, Zhongqi	1329

43rd ASMS Conference on Mass Spectrometry and Allied Topics

Author	Page Number
Zhao, Jamie	859, 873
Zhao, Sean	727
Zhao, Xinjin	758
Zhao, Yingming	982
Zhao, Zhiyang	508
Zhao, Zhongxi	449, 459, 457 592
Zheng, Kefei	1316
Zhong, Wenquing	418
Zhou, Feimeng	43, 667, 899 900
Zhou, Jie	1231, 1232
Zhou, Joe	160, 988, 1103, 1113, 1114, 1116, 1117
Zhou, Ping	942
Zhu, Y. F.	268
Zhu, Ying	1148
Zidarov, Dimo	744
Ziegler, J.	697, 809, 810, 811 963
Zilg, Harald A.	313
Zlotkin, Eliahu	1281
Znamirovschi, Calin G.	780
Zoller, David	761
Zubarev, Roman	1058
Zuckerman, Ronald N.	487
Zyk, Nikolay	171

Key Word	Page Number
2-D gel	636
Absorption Spectroscopy	1090
Abstraction	1334
Acetylation	636
Acid-base Equilibria	57, 64, 90, 672
Acids	10, 337, 473, 822, 909, 1035
Acids, Amino	32, 243, 252, 262, 297, 321, 377, 383, 388, 453, 472, 531, 1034, 1056, 1058, 1252, 1275, 1307,169
Acids, Bile	170, 545
Acids, Fatty	167, 524, 1145, 1146, 1149, 1152, 1153, 1157, 1159, 1160
Acids, Nucleic	588, 590, 595, 601, 939
Acids, Organic	218, 431, 723
Acylcarnitines	537
Adduct(s)	197, 200, 201, 373, 496, 507, 515, 585, 586, 588, 909, 1027, 1045, 1065, 1134, 1137, 1185, 1302
Adduct(s), Protein	36, 321, 326, 379, 384, 495, 520, 543, 648, 1268, 1299
Adduct(s), Radical	589, 1163
Aerosols	1, 2, 3, 4, 5, 7, 184, 185, 186, 187, 445, 668, 904, 958, 961, 1204, 1266
Affinity	982
Affinity, Binding	29, 30, 39, 244, 250, 322, 355, 596, 651, 682, 971, 1256, 1305, 1313
Affinity, Cation	11, 54, 56, 968, 1045, 1237, 1305, 1308
Affinity, Electron	65, 1034, 1042, 1309
Affinity, Metal	1136
Affinity, Proton	10, 13, 55, 65, 80, 90, 406, 695, 699, 969, 971, 1034, 1056, 1136, 1240
Aggregates	910
Alcohols	163, 472, 727, 911
Aldehydes	838, 1043, 1159, 1161
Alkaloids	526
Alkynes	156, 321, 1044
Amides	367, 77, 150, 243, 390, 467, 500, 872, 914, 956, 1030
Amino Acids	166, 420
Anabolic Steroids	511, 575, 577
Anion	159, 1147, 1151
Anion(s)	64, 65, 243, 316, 426, 604, 635, 779, 799, 814, 863, 867, 962, 1035, 1038, 1113, 1142, 1177
Antibiotics	172, 308, 315, 317, 332, 427, 502, 520, 544, 863, 866, 1137, 1282
Antibodies	289, 291, 292, 925, 981, 982
Aromatics	474, 530, 746, 759, 900, 960, 1008, 1059
Aromatics, Polycyclic	200, 201, 509, 515, 667, 815,. 957, 962
Artificial Intelligence	727, 731
Atm.Press Chem Ioniz'n (API)	99, 147, 195, 207, 222, 226, 233, 311, 330, 334, 335, 341, 373, 422, 423, 424, 426, 452, 485, 504, 510, 521, 535, 541, 551, 561, 570, 572, 578, 666, 669, 781, 841, 858, 867, 869, 890, 992, 999, 1053, 1054, 1078, 1318
Atmo Press. Ionization	100
Automation	112, 143, 147, 240, 335, 478, 569, 649, 719, 735, 739, 743, 856
Azo-dyes	161, 953, 1139
Benzynes	1031
Binding	637
Biodegradation	210, 506, 842
Biomarkers	200, 474, 495, 530, 747, 830, 919, 923, 1023, 1132, 1156, 1157, 1315
Biomolecules	7, 115, 137, 298, 329, 416, 445, 453, 484, 606, 637, 663, 678, 680, 684, 885, 925, 927, 930, 931, 937, 960, 990, 994, 996, 997, 1060, 1061, 1084, 1148, 1153, 1181, 11831, 202, 1223, 1261, 1266, 1278, 1285, 1303, 1305, 1315, 1326
Biopolymers	39, 125, 301, 448, 940, 998, 1085, 1176, 1210, 1235, 1247, 1255, 1256, 1275
Biotransformation	284
Biradicals	369, 1031
Blood	284
Bond Strengths	11, 16, 52, 53, 696, 1006, 1033, 1051, 1305
Bond, Peptide	1051
Breakdown Curves	388, 399, 766
Calculations	118, 722, 786, 1106, 1130
Calculations, Ab Initio	10, 12, 15, 17, 50, 56, 65, 71, 72, 74, 262, 329, 368, 372, 383, 695, 710, 1031, 1041, 1042, 1043, 1046, 1051
Calculations, Molecular Orbital	157, 723, 1047, 1241
Calculations, RRKM	1047
Calculations, Trajectory	717, 1070, 1095, 1108
Capillary Electrophoresis	103, 104, 105, 124, 236, 248, 249, 328, 449, 452, 453, 454, 455, 456, 457, 458, 459, 460, 461, 462, 493, 528, 590, 592, 629, 890, 977, 999, 1167, 1189, 1313, 1314, 1314
Carbamates	205, 211, 222, 327, 463, 879
Carbazoles	210
Carbohydrates	170, 245, 359, 360, 620, 812, 830, 925, 975, 1168, 1173, 1174, 1175, 1176, 1177, 1178, 1180, 1184, 1186, 1187, 1188, 1191, 1193, 1194, 1196, 1197, 1198, 1200, 1201

Key Word	Page Number
	1203, 1021, 1131
Carbonyls	189
Carboxylic Acids	486, 522, 606, 821, 901
Carboxypeptidases	297
Carcinogens	197, 329, 501, 586, 957
Carotenoids	429
Catalysis	701, 758
Cation(s)	82, 85, 160, 655, 696
Charge Exchange	417, 1025, 1037
Charge Remote	630, 1073
Charge Transfer	51, 60, 72, 76, 350, 374, 375, 899, 1309, 1337
Charge-State Distribution	234, 245, 255, 347, 672, 902, 1232, 1268, 1330
Chelates	264, 273, 609, 703
Chemical diversity	488
Chemical Ionization	166
Chemical Ionization (CI)	73, 75, 76, 77, 86, 108, 152, 153, 218, 329, 371, 474, 567, 575, 631, 776, 834, 879, 882, 883, 901, 1045
Chemical Ionization, Negative	215, 472, 556, 877, 880
Chemical library	488
Chemometrics	142, 144, 906
Chiral Recognition	94, 95, 434, 973, 1199
Chromatography	572, 611, 746, 952
Chromatography, Affinity	292, 430, 491, 573, 640, 917, 981
Chromatography, Anion Exchange	117, 1184
Chromatography, Capillary Liquid	300, 325, 890, 981, 929, 988
Chromatography, Gas (GC)	113, 127, 149, 167, 183, 220, 221, 232, 398, 479, 480, 481, 496, 721, 736, 820, 874, 1016
Chromatography, Liquid	275, 304, 435, 604, 610, 1304
Chromatography, Liquid (LC)	7, 122, 233, 238, 310, 435, 438, 444, 445, 497, 503, 509, 543, 554, 744, 773, 849, 904, 913, 927, 1147
Chromatography, Liquid -, Capillary	430, 439, 441, 443, 444, 533,. 573, 616, 1150
Chromatography, Liquid -, High Pressure (HPLC)	203, 295, 296, 311, 296, 337, 422, 423, 434, 441, 442, 443, 458, 491, 495, 519, 536, 547, 555, 566, 787, 822, 920, 976
Chromatography, Liquid -, Microcapillary	302, 440, 441, 470, 626, 660, 872, 979, 1290, 1291
Chromatography, Liquid -, Nanoscale Capillary	441
Chromatography, Supercritical Fluid	96, 468
Chromatography, Thin layer	1317
Chromophores	411, 1038, 1233
Circular Dichroism	1330
Cluster Formation	88, 109, 164, 375, 463, 688, 708, 709, 778, 1058, 1065, 1087
Cluster(s)	6, 67, 83, 164, 370, 811, 963, 972, 1029, 1048, 1069, 1091, 1336
Cluster(s), Ionic	11, 56, 107, 239, 696, 907, 965, 1087, 1154
Cluster(s), Proton Bound	11, 15, 55, 164, 406, 723, 969
Collision(s)	1106
Collision(s), High Energy	60, 130, 273, 750, 1027, 1037, 1280, 1308
Collision(s), Low Energy	61, 300, 402, 443, 498, 629, 631, 750, 975, 992, 1029, 1050, 1073, 1125, 1180, 1298
Collision(s), Reactive	78, 81
Collision(s), Surface	628, 1332
Collision-Induced Diss'n	57
Collision-Induced Diss'n. (CID)	14, 16, 41, 50, 61, 77, 79, 83, 92, 106, 117, 123, 137, 157, 225, 230, 246, 253, 262, 263, 266, 279, 327, 343, 349, 351, 367, 376, 377, 379, 381, 382, 383, 385, 386, 388, 392, 395, 396, 401, 402, 404, 405, 407, 409, 414, 415, 495, 513, 539, 548, 557, 574, 600, 620, 625, 630, 634, 646, 647, 654, 677, 695, 702, 711, 750, 753, 780, 839, 871, 906, 926, 986, 1019, 1034, 1049, 1050, 1073, 1100, 1101, 1119, 1131, 1141, 1160, 1175, 1183, 1197, 1215, 1216, 1259, 1264, 1280, 1300, 1303, 1327, 1332
Collision-Induced Diss'n. (CID) Collisional Stabilization	78, 80, 985, 1125
Collisions	788
Complex	165, 319, 403, 1135
Complex, Endohedral	1027
Complex, Ion/Neutral	15, 375, 392, 400, 698, 777, 907, 974, 1033, 1041, 1136, 1142
Complex, Non-Covalent	35, 39, 95, 178, 235, 236, 244, 250, 251, 253, 289, 294, 355, 595, 596, 597, 800, 910, 928, 942, 1259, 1261, 1262, 1264, 1325, 1326, 1327, 1330, 1331
Complex, Sandwich	699
Complexation	266, 780, 852
Computational Methods	10, 15, 51, 340, 720, 724, 726, 729, 731, 806, 979
Computer	638, 639, 719, 728, 730, 732, 734, 739, 741

Key Word	Page Number
	1116, 1218
Computer Modeling, Simulation	771, 1070, 1108, 1112, 1124, 1129, 1130, 1214
Computer Program	142, 641, 643, 644, 645, 647, 721, 725, 732, 733, 734, 735, 737, 738, 740, 741, 744, 1320
Computer Validation	1322
CONJUGATES	308
Conjugation	72, 524, 546
Corona Discharge	99, 102
Coulomb Effect	89, 348, 352, 378, 788, 1034, 1214, 1336
Cross Sections	60, 696, 1029
Cross-linking	326, 928, 1330
Cyclization	156, 969, 1044, 1046
Cyclodextrin	178, 236, 253, 257, 434, 970
Data	141, 736, 1321, 1324
Data Analysis	92, 142, 645, 665, 685, 691, 719, 720, 721, 724, 729, 730, 733, 736, 740, 742, 744, 757, 898, 959, 1110, 1221, 1320
Data Archive	1322
Data Systems	112, 141, 480, 724, 728, 730, 733, 734, 737, 738, 740, 1093, 1094, 1098, 1320, 1323, 1324
Database	25, 141, 617,638, 640, 641, 643, 645, 728, 729, 730, 918
Dechlorination	63, 1064
Decomposition	155, 188, 473, 765
Deconvolution	144, 690, 1301
Degradation	148, 172, 174, 175, 176, 218, 343, 433, 471, 473
Deoxynucleotides	449
Derivatization	157, 163, 166, 189, 353, 472, 513, 626, 630, 746, 847, 853, 881, 949, 1193, 1194, 1273, 1281
Desorption	765, 829, 835, 1235, 1238, 1244, 1245
Desorption Chemical Ionization (DCI)	404, 405, 523, 574
Desorption Ionization (DI)	282, 356, 419, 945, 964, 1057, 1060
Desorption, Thermal	111, 149, 761, 763, 834
Detector	136, 398, 1000, 1093
Detector, Array	1076, 1168, 1194, 1211
Detector, Focal-plane	1212
Detector, High Mass	135, 1099, 1220
Detector, Scanning Array	1074, 1292
Detergent	234, 918
Dication(s)	51, 60, 61
Dienes	68
Digests	643
Digests, Enzymatic	312, 610, 612, 629, 916, 917, 927,1165, 1168, 1172, 1215, 1270, 1277, 1284, 1312
Digests, Proteolytic	33, 36, 269, 290, 310, 313, 323, 657, 981, 1171, 1253, 1260, 1297, 1329
Digests, Tryptic	29, 495, 1271
Dimer	768
Dioxins	162, 230, 825, 993, 1016, 1019
Dipeptides	390, 1046
Direct Inlet Probe	25,114, 153, 1089
Dissociation	394, 716, 802, 902, 1332
Dissociation, Thermal	391, 397, 410, 463
Dissociation, Unimolecular	55, 74, 215, 393, 396, 397, 399, 400, 406, 407, 412, 414, 809, 811, 963, 973, 1035, 1049, 1310
Distonic Ions	353, 369, 392, 395, 1031, 1032
Disulfide	36, 312, 313, 1036, 1269, 1270, 1271, 1274, 1276, 1277, 1281, 1284
Disulfide Bonds	656
DNA	38, 361, 362, 363, 496, 579, 583, 584, 585, 589, 591, 592, 593, 601, 605, 607, 935, 937, 938, 945, 1234
Drift Tube	674, 712
Drinking Water	827
DRUG DISTRIBUTIONS	308
DRUG LOADING	308
Drug(s)	147, 171, 233, 246, 303, 326, 330, 332, 334, 424, 513, 517, 519, ,520, 522, 523, 528, 529, 534, 540, 541, 542, 543, 544, 547, 550, 553, 554, 555, 561, 563, 564, 565, 571, 572, 573, 576, 578, 661, 850, 851, 856, 857, 858, 865, 867, 868, 869, 873, 877, 878, 883, 887, 946, 996, 1059, 1131, 1134, 1190
Drugs	551
Dyes	839, 870, 955
Dynorphin	284
Eicosanoids	333, 536, 539, 659, 871, 1146, 1148, 1150, 1159
Electrochemistry	43, 254, 667, 899, 900, 954
Electron Beams	797, 1024
Electron Capture	63, 206, 215, 229, 472, 575, 588, 880, 937, 1021, 1111, 1161
Electron Energy	206, 1024
Electron Monochromator	206, 1024
Electron Multiplier	112, 136, 1075, 1099
Electron, Secondary	1111, 1243
Electron-Capture NCI	197, 225, 340, 727, 1017
Electrophoresis	31, 181, 534

Key Word	Page Number
	610, 617, 618, 933, 1311
Electrospray Ionization (ESI)	23, 28, 29, 32, 34, 35, 36, 37, 38, 39, 82, 88, 89, 98, 101, 102, 103, 104, 105, 112, 120, 122, 125, 126, 138, 148, 159, 160, 172, 177, 178, 189, 193, 202, 203, 205, 207, 208, 216, 217, 234, 235, 236, 238, 239, 240, 241, 243, 244, 245, 246, 247, 248, 249, 250, 251, 252, 253, 254, 255, 256, 257, 258, 260, 261, 262, 263, 264, 265, 266, 267, 270, 272, 273, 274, 275, 276, 277, 285, 290, 298, 300, 301, 303, 309, 311, 312, 313, 315, 317, 318, 320, 323, 324, 332, 335, 337, 345, 347, 348, 349, 350, 351, 352, 354, 355, 362 ,376, 378, 379, 381, 388, 390, 403, 408, 410, 425, 426, 427, 428, 429, 435, 436, 437, 439, 440, 443, 444, 446, 450, 451, 453, 454, 455, 456, 457, 460, 461, 483, 485, 488, 492, 493, 497, 498, 499, 500, 501, 502, 507, 512, 516, 518, 519, 520, 522, 524, 525, 528, 529, 534, 536, 538, 539, 544, 546, 547, 548, 554, 555, 557, 566, 592, 593, 594, 595, 596, 597, 598, 601, 602, 604, 605, 606, 607, 610, 612, 616, 618, 621, 623, 628, 630, 631, 632, 634, 635, 646, 648, 650, 651, 655, 657, 658, 659, 660, 661, 667, 668, 669, 671, 672, 673, 674, 678, 680, 703, 744, 749, 755, 779, 780, 787, 789, 794, 800, 801, 822, 824, 839, 849, 851, 853, 856, 857, 862, 863, 866, 871 ,872, 885, 886, 891, 892, 894, 895, 896, 898, 899, 900, 901, 902, 903, 905, 906, 907, 908, 909, 910 ,911, 912, 913, 975, 976, 977, 978, 980, 987, 988, 994, 999, 1005, 1012, 1074, 1083, 1084, 1085, 1086, 1113, 1117, 1143, 1144, 1146, 1147, 1152, 1153, 1160, 1164, 1167, 1169, 1175, 1177, 1178, 1180, 1185, 1188, 1192, 1193, 1194, 1198, 1199, 1200, 1202, 1257, 1258, 1259, 1261, 1262, 1264, 1267, 1268, 1269, 1271, 1272, 1275, 1278, 1279, 1282, 1283, 1285, 1286, 1290, 1293, 1294, 1296, 1297, 1299, 1300, 1301, 1302, 1303, 1304, 1311, 1312, 1313, 1314, 1316, 1325, 1326, 1327, 1328, 1329, 1331, 1333
Elemental Analysis	4, 40, 41, 42, 43, 45, 49, 127, 722, 767, 768, 769, 770, 772, 775, 848, 964, 1088, 1099
Energy	17, 673, 770, 1135
Energy Defect	895
Energy Transfer	922
Energy, Activation	72, 382, 397, 756, 894, 1073, 1125
Energy, Binding	16, 236, 257, 716, 1033, 1264
Energy, Dissociation	13, 677, 803, 1014
Energy, Internal	415, 1027, 1060, 1242, 1250
Energy, Kinetic	348, 398, 894, 895, 1084, 1231
Energy, Kinetic -, Distribution	126, 684, 686, 690, 998, 1125, 1246
Energy, Kinetic -, Release	55, 421, 1199
Enolates	93, 1043
Environmental	1, 4, 44, 48, 116, 151, 162, 180, 181, 182, 183, 185 ,186, 187, 188, 189, 190, 191, 193, 194, 195, 196, 198, 199, 200, 207, 208, 210, 212, 214, 215, 218, 219, 220, 221, 222, 227, 228, 229, 231, 264, 337, 338, 339, 340 ,342, 343, 344, 345, 346, 404, 437, 476, 479, 515, 724, 815, 816, 817, 818, 819, 821, 822, 823, 825, 826, 827, 828, 829, 830, 832, 836, 838, 840, 841, 842, 843, 844, 845, 847, 848, 957, 962, 964, 1009, 1017, 1019, 1020, 1021, 1022, 1078, 1109, 1110, 1141, 1299
Enzymes	182, 286, 301, 306, 315, 506, 531, 584, 611, 615, 925, 997, 1165, 1166, 1285
Epoxides	505
ESI LC/MS	532
ESI/MS	179, 306, 1288
Essential Oils	142
Ester(s)	93, 152, 746, 949, 1052
Ester(s), Fatty Acid	76, 157, 514, 516, 882, 1048, 1145
Ethers	74, 81, 400
Ethylchloroformate	166
Exact Mass Measurement	32, 175, 231, 346, 676, 1213
Excitation	803, 1102, 1103, 1130
Excited State(s)	1040, 1051
Exhaust Analysis	197
Experimental Design	784, 912, 990, 1081, 1093, 1095
Explosives	155, 193, 342, 1140
Extraction	107, 192, 196, 204, 837, 847, 857
FAB (Fast Atom Bombardment)	90, 95, 164, 165, 169, 170, 277, 282, 283, 356, 404, 419, 451, 471, 514, 549, 599, 603, 606, 609, 678, 714, 715, 746, 844, 1035, 1038, 1055, 1066, 1151, 1156, 1174, 1175, 1176, 1181, 1183, 1186, 1193, 1239, 1274
FAB, Continuous Flow	469, 533, 585, 1056, 1150, 1212, 1273, 1292, 1295

Key Word	Page Number
FAB, Dynamic	1154, 1191
FAB/MS	179
Faraday Cup	770, 1076
Filtered noise field	1104
Flames	6, 78
Flavanol Glycosides	258
Flow Injection	150, 194, 823, 1318
Flowing Afterglow	12, 50, 58, 62, 85, 368, 374, 693, 695, 713, 1031, 1032, 1040
Fluorescence Spectroscopy	1090
Forensic Chemistry	571
Fourier Transform IR (FTIR)	1039
Fourier Transform MS	656, 794, 795, 1094
Fourier Transform MS (FTMS)	38, 39, 52, 70, 71, 75, 87, 92, 93, 188, 347, 349, 351, 354, 355, 366, 376, 414, 416, 449, 450, 459, 637, 650, 651, 675, 676, 677, 678, 679, 680, 681, 682, 699, 701, 704 ,706, 707, 708, 709, 710, 711, 733, 783, 786, 787, 789, 790, 791, 792, 793, 796, 797, 798, 800, 801, 802, 803, 804, 805, 806, 807, 808, 812, 813, 814, 815, 886, 902, 959, 965, 966, 967, 973, 1011, 1025, 1026, 1080, 1081, 1083, 1084, 1086, 1088, 1090, 1091, 1092, 1093, 1097, 1215, 1216, 1217, 1240, 1306, 1307, 1309
Fragmentation	140, 156, 169, 170, 213, 225, 227, 246, 318, 359, 377, 405, 494, 694, 722, 748, 926, 1005, 1006, 1044, 1049, 1050, 1059, 1144, 1151, 1161, 1164, 1177, 1192, 1203, 1244
Fragmentation Mechanism/Pathways	63, 74, 92, 161, 171, 333, 382, 403, 483, 486, 498, 539, 627, 681, 683, 761, 872, 974, 1035, 1047, 1052, 1053, 1054, 1142
Fragmentation, Chg.-Remote	353, 415, 1145, 1160
Fragmentation, Peptide	316, 380, 381, 382, 383, 384, 385, 625, 627, 628, 631, 632, 635, 683, 886, 920, 931, 1249, 1263, 1274, 1333
FTMS	720, 1096, 1195
Fuel	758, 761, 1009, 1010, 1013
Fullerenes	422, 899, 967, 1025, 1026, 1027, 1028, 1306
Functional Groups	748
Fundamentals	136, 280, 281, 348, 375, 389, 494, 671, 672, 689, 785, 798, 896, 956, 986, 1030, 1063, 1119, 1120, 1128, 1226, 1237, 1238, 1319, 1337
Furans	230, 399, 993, 1016, 1019
GC/MS	166, 727
Geology	1156
Glow Discharge	41, 42, 45, 66, 96, 168, 466, 767, 768, 775, 1176, 1140
Glutathione conjugates	532
Glycerol	283, 1066
Glycines	265
Glycoconjugates	213, 336, 1178, 1184, 1186
Glycolipids	516, 1178, 1179, 1180, 1308
Glycoproteins	299, 359, 360, 646, 975, 980, 1164, 1165, 1166, 1167, 1169, 1171, 1172, 1173, 1221, 1296
Glycosides	754, 1181, 1183
Glycosylation	245, 299, 1166, 1172
Good Laboratory Practice (GLP)	1319, 1320, 1321, 1323, 1324
Halocarbons	50, 62, 84, 694, 1023, 1036
Hard and soft ionization	154
Herbicides	151, 204, 208, 209, 213, 215, 405, 914
Heterocyclic Compounds	190, 195, 486, 500, 540
High Mass Ions	786, 810, 1069, 1084, 1085, 1087, 1099 1217
High Resolution	720
Histones	33
HPLC/ESIMS	636
Hydrocarbons	58, 704, 714, 758, 760, 762, 1009, 1010, 1011, 1014, 1057
Hydrogen/Deuterium Exchange	58, 85, 86, 87, 175, 1257, 1260, 1266, 1267, 1268, 1328, 1329
Hydrogen/Deuterium Exchange, Labeling	46, 237, 523, 631, 1265
Hydrolysis	216, 582
ICP MS (Inductively Coupled Plasma MS)	40, 43, 44, 769, 770, 983, 1088, 1104
ICR	64, 67, 68, 69, 697, 782, 785, 788, 799, 809, 810, 811, 963, 1082, 1085, 1088, 1089, 1095
ICR MS (Ion Cyclotron Resonance MS)	52, 59, 257, 369, 370, 637, 675, 679, 680, 716, 733, 797, 804, 805, 806, 967, 1011, 1090, 1097, 1149, 1213, 1242
Imaging	9, 20, 1226, 1317
Imide	756
Immunoassay	204, 294, 876, 930, 976, 1295
Infrared Spectroscopy (IR)	357
Insecticide	219, 228
Instrumentation	4, 46, 97, 104, 105, 111, 114, 118, 120, 125, 129, 132, 134, 135, 140, 154, 357, 447, 467, 481, 675, 717, 732, 738, 771, 801, 802, 807, 808, 888, 891, 897, 984, 986, 991, 998, 1069, 1070, 1071, 1072, 1077, 1080, 1081, 1082, 1086, 1091, 1092, 1093, 1096, 1098, 1103, 1109, 1110, 1114, 1115, 1116, 1118, 1121, 1128, 1233
Internal Standard	162, 1231
Ion Acceleration	717, 1096, 1219, 1246
Ion Adduct	178, 776, 777
Ion Clouds	788, 1088, 1127
Ion Cooling	416, 796, 807, 1091, 1106, 1217
Ion Desorption	69, 106, 897, 1057, 1061
Ion Detection	125, 790, 984, 1000, 1075, 1076, 1096, 1097, 1121, 1211, 1220
Ion Ejection	107, 135, 790, 1105, 1112, 1118, 1129
Ion Energetics	385, 399, 690, 702, 1250
Ion Focusing	717, 1001, 1002
Ion Imaging	20, 717, 995, 1076
Ion Injection	102, 168, 892, 1117, 1140
Ion Isolation	134, 801, 802, 1102, 1107
Ion Isomeric	392, 393, 394
Ion Loss	417, 810
Ion Mirror	130, 133, 413, 771, 1205, 1209
Ion Mobility	571, 674, 889, 1029
Ion Optics	130, 786, 1001, 1002
Ion Pairing	242, 247, 431, 903, 1048, 1190
Ion Reactivity	62, 369, 370, 697, 702, 704, 712, 1025, 1026
Ion Solvation	250, 410, 674, 907
Ion Source	96, 97, 100, 102, 107, 109, 110, 119, 364, 463, 466, 567, 670, 891, 892, 1210
Ion Storage	119, 782, 785, 1077, 1092, 1108, 1112, 1118, 1123, 1128, 1138, 1316
Ion Structure	77, 171, 380, 393, 394, 407, 699, 700, 974, 1310
Ion Suppression	255
Ion Trajectories	140, 798, 808, 1118, 1127, 1130
Ion Transport	101, 102, 126, 132, 135, 892, 1083, 1087, 1138
Ion Trap	97, 118, 122, 168, 276, 325, 391, 408, 444, 446, 447, 458, 460, 487, 519, 530, 576, 577, 626, 652, 655, 675, 734, 737, 738, 784, 792, 795, 797, 819, 831, 833 ,836, 849, 861, 885, 992, 1019, 1077, 1078, 1079, 1094, 1098, 1101, 1103, 1107, 1114, 1120, 1121, 1126, 1130, 1134, 1135, 1140, 1141, 1202
Ion Trap -, Electrodynamic	119
Ion Trap -, ICR	675, 788, 791, 795, 804, 805, 807, 808, 1029, 1090, 1097
Ion Trap -, Quadrupole	3, 40, 41, 54, 73, 79, 84, 86, 91, 121, 153, 155, 160, 191, 223, 230, 302, 358, 367, 409, 410, 461, 475, 476, 477, 478, 548, 616, 641, 649, 653, 654, 687, 735, 769, 775, 783, 803, 808, 816, 817, 818, 832 ,839, 888, 890, 931, 936, 946, 964, 971, 983, 984, 985, 986, 987, 988, 989, 990, 991, 993, 1010, 1100, 1102, 1104, 1105, 1106, 1107, 1109, 1110, 1111, 1112, 1113, 1114, 1115, 1116, 1117, 1118, 1119, 1121, 1122, 1123, 1124, 1125, 1127, 1128, 1129, 1131, 1132, 1133, 1137, 1138, 1139
Ion(s)	348, 350, 390, 426, 619, 644, 658, 670, 679, 1151, 1242
Ion(s), Metastable	624, 1048
Ion(s), Product	133
Ion, Metastable	68, 83, 86, 383, 387, 392, 395, 400, 412, 413, 514, 581, 683, 1205
Ion, Molecular	10, 66, 70, 80, 82, 374, 693, 714, 715, 1040, 1176
Ion, Multiply Charged	55, 89, 91, 239, 245, 265, 267, 351, 352, 353, 354, 410, 600, 725, 768, 789, 892, 896, 903, 1200, 1232, 1336
Ion, Precursor	421, 1207
Ion, Product	502
Ionization	49, 64, 106, 141, 251, 400, 451, 494, 667, 679, 776, 881, 884, 895, 900, 1005, 1048, 1155, 1163, 1245
Ionization Efficiency	49, 108, 482, 772
Ionization Energy	13, 52, 60, 1006, 1043
Ionization Mechanism	97, 243, 247, 282, 668, 670, 683, 884, 896, 901, 914, 922, 1240, 1241, 1248, 1249, 1252
Ionization Process	90, 686, 690, 1056, 1246
Ionization, Field	107, 757, 1014, 1089
Ionization, Penning	42
Ionization, Pulsed	889
Ionization, Single Photon	761, 1036
Ionization, Surface	48, 108, 398, 417, 482, 692
Ionspray	143, 146, 150, 165, 174, 278, 431, 435, 517, 526, 527, 545, 563, 564, 594, 600, 604, 615, 662, 840, 848, 864, 888, 889, 893, 903, 1171, 1190, 1276

Key Word	Page Number
Isomerization	319
Isomers	66, 144, 145, 157, 715, 1037, 1145, 1175, 1177, 1197
Isotachophoresis	449, 459
Isotope	47, 242, 828
Isotope Dilution	208
Isotope Distributions	283,725
Isotope Effects	375, 508
Isotope Enrichments	47, 875
Isotope Exchange	852
Isotope Ratio MS	44, 46, 47, 48, 49, 773, 774, 775, 828
Isotope, Isotope	806
Isotope, Stable	156, 508, 566, 666, 722, 852, 875, 1044, 1152, 1159
Ketones	77, 1043
Kinetics	59, 391, 694, 701, 713, 765, 899, 973
Labeling	177, 251, 324, 531, 1052
Labeling, C-13	875
Labeling, Deuterium	27, 46, 95, 287, 336
Laser	21, 411, 809, 811, 963, 1021, 1229
Laser Ionization	6, 8, 127, 686, 956, 959, 965
Laser Spray	1204
Laser Vaporization	688, 941, 965
Laser, Ablation	3, 44, 688, 772, 944, 945, 967, 1087
Laser, Desorption	2, 5, 8, 24, 124, 155, 187, 360, 366, 692, 708, 709, 711, 760, 764, 789, 791, 814, 815, 918, 946, 947, 953, 954, 955, 956, 957, 958, 959, 960, 961, 962, 966, 968, 1007, 1028, 1063, 1080, 1136, 1168, 1170, 1176, 1194, 1201, 1211, 1221, 1231, 1232, 1239, 1248, 1256, 1271, 1307
Laser, Tunable	807, 1063, 1235
LC/MS	540
Levodopa	551
Library Searching	643, 728, 729, 730, 1055
Linked Scan	145, 169, 170, 225, 228, 258, 328, 412, 421
Lipid	331, 514, 721, 773, 1142, 1143, 1144, 1146, 1150, 1152, 1154, 1155, 1156, 1159, 1160, 1161
Lipopolysaccharides	516, 917, 1174
Local Area Network	742, 1324
Macrocycles	53, 94, 255, 347, 371, 780, 970
Magnetic Sector MS	35, 98, 138, 145, 248, 266, 267, 358, 372, 386, 648, 657, 732, 770, 846, 1074, 1211, 1292, 1299, 1302
MALDI	7, 445, 904, 1266
MALDI/MS	179, 306, 1288
Mass	1236
Mass Accuracy	305, 438, 492, 805, 950, 1092
Mass Calibration	579, 1127, 1205, 1206
Mass Discrimination	131, 134
Mass Displacement	1059, 1120, 1124
Mass Range	1071
Mass Resolution	364, 581, 985, 1003, 1069, 1070, 1071, 1092, 1097, 1121, 1128, 1205, 1209, 1228, 1243
Mass Spectrometer	99, 119, 447, 494, 853, 879, 1000, 1081, 1098, 1116, 1213, 1322
Mass Spectrometer -, Double Focussing	231, 346, 385, 412, 481, 763
Mass Spectrometer -, Gas Chromatograph (GC/MS)	113, 149, 158, 162, 181, 192, 196, 198, 209, 214, 218, 220, 221, 224, 225, 227, 474, 475, 476, 477, 481, 506, 529, 576, 577, 721, 742, 745, 747, 759, 820, 821, 830, 832, 834, 835, 837, 846, 870, 877, 882, 1010, 1017, 1109, 1119
Mass Spectrometer -, High Resolution	232, 602, 732, 1003, 1016, 1085
Mass Spectrometer -, Infrared (IR/MS)	479, 1063, 1247
Mass Spectrometer -, Liquid Chromatograph (LC/MS)	122, 173, 176, 195, 200, 202, 203, 212, 222, 238, 258, 274, 285, 293, 296, 313, 330, 334, 422, 425, 427, 428, 429, 432, 433, 434, 436, 437, 439, 444, 450, 465, 468, 469, 491, 494, 502, 503, 512, 515, 524, 525, 527, 541, 542, 547, 552, 554, 555, 561, 563, 564, 568, 589, 611, 612, 660, 662, 671, 673, 744, 781, 824, 840, 854, 855, 856, 857, 858, 860, 866, 867, 870, 873, 887, 894, 895, 905, 980, 1074, 1114, 1117, 1143, 1152, 1162, 1171, 1190, 1192, 1301
Mass Spectrometer -, Neut.-Reioniz'n	17, 377, 395, 694, 1030, 1037, 1049, 1310
Mass Spectrometer, Double Focussing	1212
Mass Spectrometer, Energy-Resolved	16, 1053, 1054
Mass Spectrometer/LC	29, 31, 33, 36, 37, 143, 172, 174, 177, 199, 204, 205, 208, 270, 293, 295, 336, 342, 430, 431, 432, 438, 446, 464, 466, 467, 487, 499, 503, 505, 508, 510, 517, 518, 538, 545, 548, 553, 557, 558, 559, 560, 562, 569, 570, 578, 632, 646, 652, 661, 739, 753, 754, 774, 841, 842, 846, 851, 859, 861, 862, 864, 868, 875, 992, 999, 1014

Key Word	Page Number
1148, 1267, 1282, 1298, 1316	
Mass Spectrometry, GC	76, 108, 128, 129, 145, 190, 219, 220, 221, 223, 228, 229, 333, 337, 340, 471, 473, 479, 480, 481, 482, 511, 531, 537, 571, 575, 724, 728, 737, 815, 816, 817, 819, 826, 827, 829, 838, 844, 845, 846, 847, 878, 880, 881, 883, 993, 1008, 1009, 1013, 1020, 1079, 1099, 1101, 1115, 1123, 1156, 1161
Mass Spectrometry, High Resolution	210, 214, 231, 267, 346, 396, 496, 725, 760, 786, 844, 951, 1007, 1009, 1011, 1020, 1074, 1120, 1124, 1129
Mass Spectrometry, LC	213, 216, 278, 288, 291, 440, 551, 556, 567, 573, 719, 848, 865, 885, 1260, 1277, 1329
Mass Spectrometry, LC Matrix	32, 148, 163, 332, 335, 424, 426, 442, 504, 572, 613, 687, 822, 850, 863, 884, 1012, 1163, 1182, 1301, 1312
Mass Spectrometry-CE	103
Massive Cluster Impact	465
Matrix Assisted Laser Desorption/Ionization	1195
Matrix Effects	269, 462, 685, 951, 1060, 1062, 1191, 1196, 1222, 1224, 1225, 1227, 1240, 1243, 1244, 1247, 1248, 1250, 1251, 1254
Matrix Isolation	43, 316, 1039, 1061
Matrix-Ass'd Laser Desorp. Ion. (MALDI)	18, 19, 21, 22, 23, 34, 117, 121, 123, 124, 131, 133, 138, 182, 268, 269, 270, 271, 284, 285, 286, 287, 288, 291, 292, 297, 298, 299, 304, 305, 310, 314, 323, 324, 326, 357, 358, 359, 361, 362, 363, 364, 365, 366, 414, 447, 448, 451, 462, 484, 490, 492, 520, 550, 565, 579, 580, 582, 583, 584, 586, 598, 614, 615, 617, 624, 625, 633, 642, 663, 664, 665, 676, 678, 683, 684, 685, 686, 687, 689, 690, 691, 692, 726, 743, 751, 755, 791, 793, 805, 812, 813, 876, 915, 916, 917, 919, 920, 921, 922, 923, 924, 925, 926, 927, 928, 929, 931, 932, 933, 934, 935, 936, 937, 938, 939, 940, 942, 943, 946, 947, 948, 949, 950, 951, 952, 961, 968, 980, 981, 982, 989, 990, 994, 997, 998, 1003, 1026, 1062, 1063, 1081, 1082, 1100, 1102, 1149, 1165, 1166, 1167, 1170, 1172, 1173, 1179, 1184, 1185, 1187, 1189, 1193, 1196, 1204, 1205, 1206, 1207, 1208, 1209, 1210, 1211, 1212, 1213, 1214, 1215, 1216 ,1217, 1218, 1219, 1220, 1222, 1223, 1224, 1225, 1226, 1227, 1228, 1229, 1230, 1233, 1234, 1235, 1236, 1237, 1238, 1239, 1240, 1241, 1242, 1243, 1244, 1245, 1246, 1247, 1248, 1249, 1250, 1251, 1252, 1253, 1254, 1255, 1263, 1272, 1277, 1283, 1289, 1295, 1297, 1304, 1317, 1331
Membrane Introduction	114, 116, 118, 151, 152, 153, 191, 339, 818, 823, 833, 836, 934, 1133
Metabolic Profiling	148, 240, 432, 433, 524, 541, 542, 545, 553, 558, 560, 562, 564, 568, 569, 872, 887
Metabolism, Metabolites	93, 226, 252, 272, 327, 328, 334, 432, 498, 499, 500, 505, 507, 508, 517, 519, 521, 523, 525, 527, 528, 529, 531, 533, 534, 535, 536, 538, 539, 541, 543, 544, 546, 549, 550, 551, 552, 553, 558, 560, 562, 563, 564, 565, 566, 567, 574, 582, 842, 849, 850, 854, 858, 859, 860, 874, 878, 882, 992, 1133, 1315
Metal Ion Chemistry	238, 260, 261, 262, 263, 280, 281, 378, 379, 403, 609, 698, 700, 702, 703, 704, 705, 708, 709, 710, 711, 714, 715, 779, 780, 1198, 1199, 1200, 1306, 1307, 1308, 1309
Metal Ions	608
Metalloprotein	309, 319, 322
Metals	42, 43, 47, 53, 279, 376, 377, 589, 596, 697, 712, 713, 777, 847, 900, 1137, 1305
Micelles	1065
Microanalysis	489, 1223
Microdialysis	37, 274, 518, 530, 568
Microparticle Analysis	1, 2, 5, 187, 765, 958, 961
Microprobe	9
Microsomes	511, 529, 542, 887
Microwave Plasma	100, 705, 1045
Mixture Analysis	106, 115, 118, 144, 192, 283, 285, 290, 433, 456, 462, 489, 682, 731, 757, 819, 906, 923, 990, 1143, 1158, 1162, 1189, 1207, 1296
Molecular Beams	24, 109, 407, 960
Molecular Dynamics	922
Molecular Recognition	53, 94, 250, 251, 253, 682, 970, 971
Molecular Weight Distribution	19, 22, 23, 366, 755, 806, 950, 952, 1007
Monitoring, Air	183, 766, 831, 835, 991, 1078, 1138
Monolayer	417, 418

Key Word	Page Number
MS/MS	3, 16, 30, 31, 32, 37, 56, 66, 79, 81, 84, 92, 109, 117, 123, 130, 134, 137, 138, 139, 146, 159, 160, 161, 165, 168, 171, 176, 177, 191, 194, 202, 203, 209, 212, 214, 217, 223, 226, 230, 233, 238, 240, 244, 249, 252, 274, 276, 277, 296, 302, 318, 321, 322, 326, 328, 329, 341, 342, 343, 345, 355, 358, 378, 380, 382, 384, 386, 387, 390, 394, 395, 396, 401, 402, 405, 406, 409, 411, 412, 415, 421, 425, 430, 433, 436, 442, 449, 457, 459, 470, 475, 476, 477, 478, 483, 486, 487, 489, 491, 492, 493, 502, 505, 510, 513, 514, 518, 525, 526, 527, 532, 535, 537, 538, 542, 544, 545, 549, 552, 553, 554, 555, 557, 558, 559, 560, 562, 563, 568, 569, 573, 574, 576, 577, 587, 592, 594, 597, 607, 617, 621, 624, 625,626, 627, 629, 635, 640, 647, 649, 650, 651, 652, 654, 659, 661, 662, 671, 714, 715, 722, 750, 751, 754, 757, 781, 824, 832, 839, 840, 850, 851, 856, 859, 860, 861, 862, 865, 866, 868, 869, 887, 943, 974, 975, 976, 977, 987, 1004, 1023, 1030, 1052, 1055, 1073, 1101, 1106, 1107, 1113, 1117, 1119, 1131, 1139, 1141, 1142, 1145, 1149, 1153, 1163, 1164, 1174, 1178, 1179, 1181, 1183, 1186, 1197, 1198, 1200, 1201, 1202, 1203, 1209, 1273, 1274, 1278, 1279, 1281, 1282, 1283, 1290, 1291, 1293, 1294, 1296, 1303, 1310, 1311, 1313, 1314, 1325, 1337
Multi-photon Ionization	24, 772, 953, 954, 955, 960, 964, 1047
Multipoles	101
Natural Products	148, 181, 182, 273, 428, 429, 526, 540, 548, 1144, 1148, 1158,1181, 1182
Nebulization, Nebulizer	425, 668, 1204
Network	1324
Neuropeptides	37, 272, 274, 275, 518, 556, 1262
Nitroaromatics	66, 197
NMR	146, 549, 720
Non-polar Solvents	910
Nonvolatiles	338, 817
Nucleobases	158, 247, 587, 591
Nucleosides	247, 552, 608
Nucleotides	28, 34, 38, 361, 420, 457, 590, 594, 602, 609, 935, 1197
Oligomers	22, 75, 776, 928
Oligonucleotides	244, 248, 249, 350, 361, 362, 364, 376, 580, 581, 582, 583, 593, 594, 595, 596, 597, 598, 599, 600, 601 602, 603, 604, 658, 677, 934, 935, 936, 939, 940, 941, 942, 943, 1214, 1261, 1326
Oligosaccharides	182, 359, 923, 1166, 1168, 1185, 1187, 1189, 1190, 1191, 1192, 1195, 1199, 1201, 1202, 1203
On-line Analysis	5, 116, 152, 153, 186, 260, 339, 446, 457, 461, 510, 543, 592, 773, 890, 958, 961, 1198
Organic analysis	154
Organometallics	106, 127, 165, 266, 451, 699, 701, 706, 707, 781, 848, 966, 1012, 1067, 1306, 1310
Organophosphorus Esters	206, 373, 406, 1053, 1054
Organosilanes	17, 391, 908
Oxidation	69, 189, 190, 254, 270, 331, 333, 338, 429, 567, 591, 871, 1139
Parmacokinetics	158, 852, 854, 855, 861, 1023
Particle Beam	199, 205, 211, 464, 465, 466, 467, 566, 841, 870
Particles	184
Penicillins	315, 909
Penning Ionization	154
PEPICO	399
Peptide hormone	924
Peptide Structure	256, 271, 277, 279, 300, 312, 313, 381, 387, 458, 490, 598, 620, 647, 743, 896, 916, 922, 979, 989, 1046, 1051, 1100, 1206, 1272, 1281, 1300, 1307
Peptide(s)	28, 123, 124, 241, 261, 263, 265, 267, 268, 269, 270, 276, 280, 281, 282, 283, 285, 302, 303, 310 ,311, 314, 325, 347, 354, 363, 379, 384, 386, 439, 443, 447, 454, 455, 456, 460, 513, 611, 612, 619, 621,623, 624, 626, 627, 630, 634,639, 640, 641, 654, 655, 664,665, 669, 726, 743, 906, 908,918, 921, 924, 926, 927, 929,942, 976, 978, 988, 989, 1038,1061, 1214, 1216, 1218, 1225, 1228, 1230, 1249, 1252, 1274,1276, 1289, 1290, 1291, 1292, 1293, 1294, 1295, 1298, 1302, 1314, 1316, 1332, 1333
Peptide(s), Cyclic	628, 1046, 1213, 1280, 1282
Peptide(s), MAP	287, 288, 291, 614, 652, 676, 685, 1208, 1253
Peptide(s), Modified	30, 34, 278, 323, 498, 629, 1272, 1281, 1283, 1284, 1302
Peptide(s), Support-bound	483, 484, 490
Peptide(s), Synthetic	30, 34, 277, 278, 312, 487, 490, 873, 1273

Key Word	Page Number
Peroxidase	532
Pesticides	202, 203, 206, 211, 214, 216, 217, 219, 220, 221, 222, 223, 226, 343, 344, 404, 471, 482, 824, 1016, 1022
Petroleum	474, 758, 760, 762, 967, 1005, 1007, 1008, 1010, 1012, 1013, 1014
PFB Derivatives	496
Pharmaceutical(s)	112, 143, 146, 147, 173, 174, 175, 178, 432, 434, 435, 475, 486, 508, 512, 527, 533, 549, 552, 662, 739, 855, 858, 862, 865, 878, 909, 1136, 1318
Phenols	1182
Phosphates	431, 1284
Phospholipids	331, 841, 1147, 1148, 1149, 1154, 1216
Phosphopeptides	420
Phosphorylation	29, 33, 302, 632, 633, 635, 636, 637, 646
Photochemistry	152, 202, 260, 338, 501, 966, 1036
Photocleavable	488
Photodissociation	61, 680, 388, 408, 411, 953, 1033, 1077, 1129, 1244
Photodynamic Theropy	179
Plasma	26, 857, 864, 1088
Plasma Desorption	316, 413, 618, 778, 994, 1057, 1058, 1059, 1060, 1061
Plasma Source	775, 983, 1104
Plasma, Human	158, 880, 881, 1170, 1304
Pollutant	196, 227, 838, 1017
Polyamines	595, 1212
Polyaromatic Hydrocarbons	6, 108, 195, 196, 198, 199, 254, 585, 587, 588, 837, 1141
Polychlorinated Biphenyls (PCBs)	63, 232, 993
Polyethers	53, 95, 371, 503, 711
Polyethylene glycols	75
Polymer Structure	19, 20, 365, 753, 756, 949
Polymer(s)	18, 19, 21, 22, 23, 24, 25, 26, 69, 156, 179, 365, 366, 468, 689, 747, 749, 751, 755, 756, 764, 813, 814, 912, 948, 949, 950, 951, 952, 954, 959, 968, 995, 1011, 1236, 1237, 1238
Polymer, Additives	18, 750, 813, 948
Polymer, Nonpolar	27, 948
Polyols	159
Polypeptides	645, 923
Polysiloxanes	468, 748
Polysulfides	749
Porphyrins	469, 667, 1005, 1006
Post Source Decay (PSD)	625, 943
Principal Component Anal	115
Probe	124, 1079
Probe, Continuous-Flow	687
Product Ion Scans	1206
Prostaglandins	331, 333, 1146
Protease	1288
Protein Analysis	28, 35, 235, 286, 292, 293, 295, 296, 301, 305, 314, 320, 323, 324, 357, 358, 440, 441, 442, 458, 459, 610, 611, 612, 613, 616, 618, 622, 623, 638, 639, 642, 643, 648, 649, 660, 676, 685, 719, 787, 794, 886, 916, 919, 933, 934, 947, 987, 989, 1100, 1170, 1208, 1218, 1253, 1258, 1263, 1273, 1275, 1278, 1279, 1283, 1285, 1295, 1296, 1297, 1303, 1311, 1312, 1314
Protein Conformation	87, 234, 237, 256, 286, 289, 294, 310, 320, 352, 656, 681, 794, 915, 981, 1257, 1258, 1260, 1262, 1263, 1264, 1265, 1267, 1268, 1326, 1327, 1328, 1329, 1330
Protein modification	636
Protein Reactions	1288
Protein Refolding	1259
Protein Semi-Quantitation	306
Protein(s)	31, 33, 241, 263, 268, 269, 289, 290, 291, 297, 304, 306, 309, 311, 317, 318, 319, 322, 349, 439, 454, 455, 460, 633, 644, 645, 650, 651, 653, 692, 739, 852, 875, 903, 917, 921, 928, 932, 942, 980, 1004, 1170, 1208, 1215, 1221, 1225, 1249, 1261, 1269, 1271, 1276, 1284, 1286, 1288, 1298, 1325, 1328, 1331
Proton Transfer	15, 89, 351, 354, 371, 374, 656, 723, 902, 972, 1241, 1246, 1252
Protonation	94, 901, 969, 970, 1030
Purification	318, 919
Pyridines	54, 158
Pyrolysis	25, 115, 181, 188, 473, 745, 761, 763, 764, 1157, 1158
Quadrupolar Axialization	416, 680, 682, 790, 793, 796, 798, 803, 1080
Quadrupolar Excitation	792, 793, 796, 798, 799, 802, 1080, 1217
Quadrupole MS	26, 45, 47, 49, 114, 144, 180, 438, 454, 466, 480, 522, 613, 767, 849, 908, 1053, 1069, 1070, 1071, 1072, 1078, 1262
Quadrupole MS)	272, 905, 1299
Quadrupole, Triple	30, 78, 109, 150, 167, 373, 407, 487, 578, 652, 653, 830, 861, 908, 978, 1006, 1054, 1180
Quantitative Analysis	2, 173, 194, 217, 223, 276, 335, 336, 427, 470, 497, 499, 556, 559

Key Word	Page Number
	561, 578, 580, 591, 658, 659, 660, 661, 663, 664, 665, 666, 671, 737, 741, 742, 759, 768, 821, 850, 851, 854, 855, 862, 863, 864, 865, 868, 869, 874, 880, 947, 950, 996, 1008, 1143, 1162
Quaternary Ammonium	1065
Radiation	391
Radicals	13, 17, 71, 190, 372, 530, 694, 1036
Rare Earths	27, 688, 965
Rate Constants	59, 110, 370, 716
Reaction	52, 65, 73, 79, 83, 713
Reaction Mechanisms	12, 62, 85, 368, 393, 401, 402, 713, 969, 1064, 1334
Reaction Monitoring	150, 241, 289, 332, 489, 561
Reaction Products	241, 294, 368, 547, 1045
Reaction, Association	14, 54, 370
Reaction, Bimolecular	712, 1032
Reaction, Electron/Ion	1040, 1095, 1111
Reaction, Gas Phase	70, 71, 80, 161, 188, 693, 700, 705, 1040, 1044, 1155
Reaction, Ion/Atom	705
Reaction, Ion/Ion	350, 1095
Reaction, Ion/Molecule	11, 12, 50, 51, 54, 56, 58, 59, 61, 62, 68, 69, 70, 71, 75, 76, 78, 80, 81, 83, 84, 85, 86, 89, 91, 93, 94, 110, 265, 352, 367, 368, 369, 371, 372, 373, 374, 402, 693, 695, 696, 698, 700, 701, 704, 706, 707, 708, 709, 710, 716, 800, 970, 1032, 1091, 1105, 1133, 1137, 1139, 1306
Reaction, Ion/Surface	418, 1334, 1336
Reaction, SN2	81, 110
Reaction, Solution Phase	239, 1064
Reaction, Surface	765
Reaction,Gas-Phase	656
Reactive drug intermediates	532
Real-Time Monitoring	1, 2, 5, 185, 766, 831 ,958, 991, 1023, 1110, 1133, 1318, 1325
Rearrangement	12, 14, 372, 396, 1052
Receptor	294, 1313
Reduction	161, 608, 1064, 1155
Reference Spectra	1055
Resolution	91, 113, 140, 357, 363, 421, 438, 613, 684, 1210, 1219, 1221, 1247, 1251
Resonant ejection	1104
Resonant Excitation	983
RF Glow Discharge	26, 45, 97, 698
RNA	584
RRKM	59
Sacchandes	754
Salts	185, 239, 255, 599, 1038, 1196
Sampling	689, 813, 816, 820, 833, 991, 1318
Saponins	428
Scattering	186, 401
Secondary Ion Emission	465, 778, 1336
Secondary Ion Imaging	20, 1004
Selected Ion Monitoring	128, 232, 497, 632, 800, 801, 818, 821, 866, 878, 1079, 1122, 1162
Selected Reaction Monitoring	167, 217, 536, 659, 868
Self-Assembled Monolayer	1334
Separations	129, 440, 462, 480, 491, 570, 787, 1301
Sequencing	28, 31, 38, 248, 278, 297, 299, 300, 322, 324, 361, 363, 364, 387, 442, 484, 580, 584, 588, 598, 600 ,601, 615, 617, 619, 620, 621, 622, 623, 624, 627, 647, 649, 650, 655, 725, 814, 921, 940, 987, 988, 997, 1207, 1208, 1253, 1275, 1279, 1285, 1290, 1294, 1311
Silanes	428
Siloxanes	1049
SIMS	20, 240, 252, 413, 748, 1004, 1022, 1068
SIMS, Liquid	273, 275, 419, 420, 470, 533, 608, 751, 776, 777, 1055, 1064, 1065, 1066, 1150, 1154, 1155, 1179, 1280, 1308
SIMS, Organic	9, 843, 1066
SIMS, Static	565, 771, 843, 996, 1022, 1066
Solvation	35, 235, 723, 1033
Solvents	836, 894, 911, 1062
Space Charge	674, 804, 893, 1108, 1112, 1127
Spray ionization	7, 445, 904, 1266
Sputtering	712
Stable Isotopes	853
Steroids	169, 334, 336, 464, 482, 557, 662, 1162
Structure Determination	70, 137, 146, 160, 175, 176, 228, 249, 299, 301, 349, 381, 448, 475, 483, 489, 492, 526, 587, 589, 603, 677, 729, 916, 953, 954, 973, 1025, 1032, 1037, 1067, 1113, 1144, 1164, 1186, 1263, 1277, 1328, 1331, 1333
Substitution	260, 608
Supercritical Fluid (SCF)	96
Supercritical Fluid Extraction	232
Supramolecules	910
Surface	1256

Key Word	Page Number
Surface Analysis	9, 44, 282, 692, 778, 843, 1022, 1068, 1334
Surface-Induced Dissociation (SID)	139, 353, 389, 403, 416, 417, 418, 628, 1332, 1333, 1337
Surfactants	159, 234, 345, 468, 755, 840, 841, 842
Terpines	227, 470, 745
Tertiary Structure	1267
Thermospray	163, 194, 205, 213, 342, 437, 463, 854,1163
Thioesters	471
Time-of-Flight	131, 748, 790
Time-of-Flight MS (TOF)	1, 4, 6, 18, 19, 21, 22, 24, 42, 88, 119, 120, 121, 122, 123, 125, 126, 127, 128, 129, 130, 131, 132, 133, 134, 135, 136, 137, 138, 139, 140, 183, 184, 185, 186, 187, 256, 268, 316, 362, 380, 386, 387, 411, 413, 415, 446, 461, 565, 579, 582, 586, 613, 614, 615, 619, 622, 654, 663, 664, 665, 684, 686, 687, 697, 743, 756, 771, 772, 778, 809, 810, 811, 820, 885, 918, 919, 931, 933, 935, 936, 937, 938, 941, 943, 944, 946, 951, 952, 955, 957, 962, 963, 968, 994, 995, 996, 997, 998, 999, 1000, 1001, 1002, 1003, 1004, 1021, 1077, 1126, 1138, 1179, 1201, 1203, 1204, 1206, 1207, 1209, 1210, 1219, 1222, 1223, 1224, 1225, 1233, 1234,1236, 1242, 1243, 1248, 1250,1251, 1254, 1255, 1259, 1292, 1316, 1327
Toxicology	327, 331, 340, 341, 467, 497, 504, 505, 510, 511, 512, 516, 517, 525, 572,574, 576, 577, 587, 590, 867, 1279
Toxins	503, 504, 1280
Trace Analysis	116, 151, 172, 176, 204, 219, 231, 338, 339, 346, 430 ,568, 573, 817, 823, 828, 829, 843, 870, 955
Transfer Line	113, 115, 831
Transition Metal Complex	1067
Treatment	284
Tunable energy	154
Velocity Distribution	1219
Volataile Organic Analysis	114, 142, 149, 183, 339, 766, 816, 818, 819, 820, 823, 829, 831, 832, 833, 834, 836, 838, 845
Work Function	398, 1337
Xenobiotics	63, 210, 327, 424, 499, 506, 511, 515, 523, 590, 877, 881
Zwitterion	48

LC/MS Workshop

Thomas Covey (PE/Sciex) and Mike Balogh (Waters)

The workshop had the following agenda designed to cover the broad interests of the LC/MS interest group.

A. Non-Scanning Mass Analyzers
  1. Ion Traps by Adrian Land, Finnigan
  2. Ion Traps vs Quads by Jack Henion, Cornell University
  3. Electrospray TOF by Fred Banks, Analytica
B. Vacuum System Maintenance by Kevin Bentley, Inland Vacuum Industries
C. Novel Mechanisms in APCI by Paul Goodley, Hewlett-Packard
C. Environmental LC/MS
  1. Bob Betham, Alta Analytical
  2. Paul Winkler, Quanterra Environmental Services
D. Pharmaceutical Open-Access MS by Lester Taylor, Burroughs-Wellcome
E. Micro-Chromatographic Techniques by Jean-Pierre Salzman, LC Packings

There were ≈ 450 attendees, as indicted from the return of questionnaires that were distributed. Adrian Land spoke about the new LCQ electrospray ion trap system emphasizing its ease of use, multiple experiment capability (triple play), and MS^n capability for structure elucidation. Some examples of quantitation of pharmaceuticals in plasma by MSMS were also highlighted.

Jack Henion showed a comparison between a modified Varian ion trap with electrospray and a benchtop triple quad, the LC 300 from PE/Sciex. Performance in the single MS mode appeared to be roughly similar based on the signal to noise in full scan total ion current traces of some small molecular weight drugs.

Fred Banks of Analytica gave a presentation of the orthogonal ESP TOF with particular reference to the fast scanning capabilities for high resolution chromatographic separations such as CZE. One hundred full scans/second could be achieved.

Kevin Bentley presented some very practical information regarding vacuum system maintenance, a topic not usually discussed but of daily interest to mass spec facilities. His emphasis was on pump oils and the extreme conditions LC/MS ion sources put on this weak link in the system. The relationship between the chemical properties of the oil and expected lifetime were detailed

Paul Goodley described some novel observations they had made regarding the introduction of liquids at high flow rates (>1mL/min). No discharge voltages to initiate chemical ionization or liquid charging voltages to assist the electrospray process were used. Impressive sensitivities were shown. It was explained that the liquid was charging as a result of the triboelectric effect (static charge accumulation) thus promoting the ion evaporation process. This effect can be demonstrated with glancing blows between two ice cubes which will generate sparks.

Bob Betham gave a crisp overview of the growth of LC/MS in the environmental field, with reference to regulatory implications and future application areas. It appears that there is a shift in the focus of environmental analyses in the future toward LC/MS techniques. Paul Winkler showed an excellent example from the pesticide field.

Lester Taylor gave a presentation of the open access mass spectrometer concept. Atmospheric pressure ionization instruments have been appropriately software configured so that synthetic and medicinal chemists can drop a sample in an autosampler, log in an appropriate identifier, and obtain a molecular weight within minutes. An average of 80-100 samples per day have been run over the past 9 months. A significant increase in the use of

mass spectrometry for structural elucidation has occurred with the introduction of this approach.

A questionnaire was distributed in order to gather information pertaining to the format, content and direction of this session next year. There were more than 100 respondents. Below is a summary of the results.

The first question, "If LC is common in your lab which of the following do you use?" was clearly carried by ESI/MS/MS by 3:1 over thermospray and particle beam. The interest areas for applications to be presented were strongly centered on drug discovery and natural products, as one selection, and toxicology, pharmacology and metabolism as the other (68% and 53% respectively). Environmental and industrial chemistry followed at 23% and 10%.

Future presentations were requested from LC generally in both practice (65%) and theory (42%) with the interest between microcapillary and techniques using flow rates above 50 ul/min evenly divided. CZE and quantitation were both highly requested (approximately 50% each). Other areas on the form received less interest. There was little interest in software and interpretation specifically.

The practical application of hardware was highly requested in both categories available on the form (Applications-hardware and Hardware-analyzers/interface design). In addition, we received comments indicating a better knowledge of hardware and design could be useful toward increasing performance.

Overall the comments we received on the format indicated a shorter session with a more limited focus was needed but was evenly divided as to whether it should be held at lunch or during the evening. A panel of experts focusing on audience questions was suggested although many were satisfied with the current format.

The group, like ASMS itself, reflects changes in its constituency and we are attempting to identify and respond to it. Numerous individuals took the time to express their thoughts in detail and the effort is greatly appreciated by the organizers. We hope you will see the benefits of your efforts in next year's program.

ION TRAP INTEREST GROUP WORKSHOP

The topic of the (Quadrupole) Ion Trap Interest Group Workshop was "Theory vs. Reality". This was an informal workshop based around informal contributions from the attendees. Doug Goeringer of Oak Ridge National Laboratory was drafted to start the discussions and presented some recent work concerning modeling of the ion temperatures in the ion trap. He noted that due to the relatively high helium pressure used for normal operation that a boltzman temperature distribution provided a good model for the ion temperature. The theory is based on the ion transport in gases and provides a useful model for the kinetics of CID in the ion trap. These results suggest that heating the ion trap will lower the resonant excitation energy required to effect dissociation in the ion trap. A bit more discussion ensued concerning the internal and kinetic temperatures of ions in the trap.

Richard Morrison, from Australia but currently working with Ray March at Trent University, initiated a discussion of the mass displacement in the ion trap. He showed theoretical results in which the secular frequency of an ion depends upon the radial and axial amplitudes of ion, which can lead to mass shifts in the detected mass spectrum. Work was done with both an ideal quadrupole trap and the stretched trap which is commonly used. The stretched trap introduces a component of higher order fields. Vladimir Doroshenko, Johns Hopkins University, then discussed their approach and basis for varying the amplitude of the resonant ejection voltage with mass to provide a better calibration for the ion trap. Curt Clevin, Purdue University, then discussed some of their pertinent experimental results which indicated that the stretched geometry reduced mass shifts in the ion trap. These results were obtained by performing photodissociation of ions as a function of their position in the ion trap.

Frank Londry of Trent University was the next discussion volunteer and he talked about work involving practical high resolution in the ion trap. The most significant problem for obtaining high resolution is unstable peak position. A significant improvement can be obtained by phase locking the various rf and ac voltages associated with the ion trap. When this is done, the practical limit of resolution seems to be peak widths of 30 millimass units, achieved at a scan rate of 100 u/s. The mass accuracy improves as the helium pressure is reduced but is variable over the mass range.

The next volunteer speaker was Sohrab Habibi from Jack Henion's lab at Cornell. He addressed the issue of comparing the ion trap with triple quadrupoles. He stressed the importance of making sure that comparable experimental conditions were used. Jenny Brodbelt then discussed work in her lab on determining critical energies of ion dissociation. This worked focussed on the study of H-bonding. The final speaker was Steven Boue from Rick Yost's group at the University of Florida. He presented some preliminary data on their electrospray system combined with photodissociation. The systems they are exploring include oligosacharrides and oligonucleotides.

After the technical session, a short business meeting was held. The major topic of discussion was defining the focus of the interest group, since this is a new interest group. This discussion centered on whether the focus should be narrowly described as pertaining only to quadrupole ion traps or should it be more inclusive, including other types of ion trapping techniques. A vote was taken and it was decided that all ion trapping techniques should be included but there was enough opposition so that it was agreed that this topic would be revisited next year.

43rd ASMS Conference on Mass Spectrometry and Allied Topics

FTMS INTEREST GROUP WORKSHOP

MOST RECENT RESULTS IN FTMS

The second annual workshop of the FTMS users group focused on recent results from FTMS research, preferably work performed after the submission of ASMS abstracts in January. A variety of chemists from both industry and academics gave short presentations. The lead-off speaker was Cliff Watson from the University of Florida, who discussed a method for apodizing the beat pattern in the free inductance decay (FID) that is associated with interfering frequencies from equally spaced ^{13}C isotope peaks in electrospray FTMS. This pattern results in dead areas of the FID that contain only noise; apodizing these areas to zero increases the signal-to-noise ratio of the spectrum. Jared Drader from David Laude's group at the University of Texas at Austin then spoke on the LabView data system that is being developed for interfacing with the group's FTMSs. This is a graphical software with an open architecture that facilitates addition of peripherals to the system. The third speaker of the evening, Pete O'Connor from Fred McLafferty's group at Cornell University, discussed dissociation studies on multiply charged ions produced by electrospray. Among the data presented were spectra for ion isolation of a single ^{13}C isotope for large proteins using the stored waveform inverse Fourier transform (SWIFT) technique. CID was then performed on this isolated isotope peak. Ron Heeren of the Institute for Atomic and Molecular Physics in Amsterdam then described his group's recently acquired Bruker FTMS. The group has modified the vacuum system using turbodrag pumps in order to obtain a very fast pump down time and an ultimate base pressure of 10^{-11} mb. Ron also discussed recent MALDI-FTMS results obtained for polymers and microprobe LD-FTMS for studying artworks.

The evening's fifth speaker, Chris Hendrickson from the High Field Magnet Laboratory at Florida State University, discussed the FTMS facilities at this laboratory. Chris invited audience members to be external users of the facility, indicating that in years 2-5 75% of the site's funding is earmarked for external users. He indicated that long term visitors, for example graduate students, may be eligible for airfare, tuition, or lodging funds. The following speaker, Bill Reents of Bell Laboratories, discussed a unique FTMS that utilizes a split-pair 5.3 T superconducting magnet. This design features ports on the side of the magnet to allow easy access to the cell for light sources. Bill's presentation centered on the best cell design to maintain decent performance and avoid space charge effects. Cell design was also the topic of the next talk, which was presented by Kent Gillig from David Russell's group at Texas A&M University. Kent discussed an ICR cell with a wire ion beam guide running through its center; this is a modified electrostatic Kingdon trap. Kent was followed by the first ion chemistry talk of the evening. Young Xu from Ben Freiser's group at Purdue University discussed the first known example of a metal-containing distonic ion, an iron pyrobenzene species.

Brian Winger spoke on Extrel FTMS's work in peptide analysis by electrospray. He presented examples of using SWIFT to eject ions from the cell in order to increase the resolving power and m/z accuracy. Brian's colleague at Extrel FTMS, Sanford Shew, then discussed FTMS on the Internet. There is a usernet MS group and Extrel FTMS has a world-

wide web (WWW) page and a bulletin board. The evening's eleventh speaker, Karl-Peter Wanchez from the University of Breman, spoke on his group's research in the area of in-cell MALDI. The sample target was positioned as a part of the grid on the trapping plate electrode and spectra exhibiting very nice resolution were obtained. This was followed by another instrument company representative, Steve van Orden, from Bruker. Steve discussed several recent Bruker instrumental developments including a pneumatic assist in electrospray and the coupling of a massive cluster ionization (MCI) source to FTMS. The MCI source bombards the sample with extremely large matrix clusters (e.g., glycerol clusters) and produces singly and mutliply charged ions from species as large as ubiquitin (MW 8565).

David Weil from 3M Corporation then lead a discussion of industrial problems related to FTMS. One question that he asked the audience dealt with m/z discrimination in laser desorption. In general, this had not been observed by many audience members which could mean that it is not a problem or that it has not been specifically looked for. Dave also asked for input on the need to standardize experimental FTMS parameters from lab to lab. The general audience view was that this was not feasible due to the many different configurations of FTMS instruments that exist. The final speaker of the evening was Ben Freiser of Purdue University. Ben first spoke on metallocarbohedrenes and their adduct formation, yielding, for example, $V_8C_{12}(CH_3CN)_4^+$. He concluded by describing a pulse-leak valve system developed in his laboratory in order to admit a constant pressure of a gas for a pulse of time into the FTMS vacuum chamber. In this system, the gas inlet was connected to a leak valve that was then connected to a tee. One part of the tee went to a pulsed valve that then went to the main MS vacuum chamber; this allowed a static pressure to be introduced when the pulse valve was open. The second part of the tee went to another pulse valve that was also connected to a pump; opening this valve allowed the reservoir between the leak and pulsed valves to be pumped out thus preventing pressure buildup.

Users group members are encouraged to provide feedback to Carolyn Cassady (CCASSADY@MIAMIU.ACS.MUOHIO.EDU or 513-529-2494) by late next fall concerning topics that they would like to see discussed at the 1996 workshop.

Carolyn J. Cassady

Submitted by Carolyn J. Cassady
Workshop Organizer

GOOD LABORATORY PRACTICES (GLP) WORKSHOP
Thursday, May 25, 1995

This is a follow-up to the extremely successful 1994 ASMS Fall Workshop on "Mass Spectrometry and Good Laboratory Practices" organized by Robert K. Boyd and Jack D. Henion. From the Fall workshop, it was clear that, unlike the rigid regulations put forth by the US EPA, GLP required by the US FDA is highly subjective to interpretation. In the 1994 Fall Workshop, we had heard "The viewpoint on GLP for Mass Spectrometry" from a FDA scientist, Dr. Steven M. Musser. Therefore, one objective of this workshop is to invite a representative from the FDA Compliance branch to present his view of GLP. The second objective is to facilitate an exchange of views on this evolving subject amongst mass spectrometry practitioners.

The workshop began with an announcement by Dr. Robert Boyd that a report on the Fall Workshop had been drafted and submitted to JASMS for publication. To obtain the draft version of the report, one simply needs to contact Dr. Robert K. Boyd at National Research Council, 1411 Oxford Street, Halifax, NS, B3H 3Z1, Canada. Dr. Boyd's e-mail address is BOYDRK@IMB.LAN.NRC.CA.

Five scientists from the academia, agricultural and pharmaceutical industries were invited to give a 5 to 10 minutes presentation on a specific GLP related topic to stimulate discussion. These topics have been chosen because they were raised or not addressed at the 1994 Fall Workshop.

Dr. Jane Gale of Bristol-Myers-Squibb (BMS) led the discussion on "Automation and GLP: RECORD, RECORD, RECORD!!". Dr. Gale described the automated sample login, storage, and retrieval system at BMS. The system included a LIMS, robotics apparatus, autosamplers for GCMS, LC/MS, or other analytical instruments, and electronic data transfer and archive. Dr. Gale stressed the importance of documentation of the sample's progress from generation to discard, which can easily be done by the computers in an automated system. The steps that are documented for GLP purposes include sample generation, unique identifier assigned via bar coded label, shipment from study site to BMS analysis site, receipt at BMS, log in, decontamination, storage, retrieval, analysis, return to storage, and discard.

Professor Jack Henion of Cornell University / Advance Bioanalytical Services (ABS) led the discussion on "Operator Training". Dr. Henion emphasized that it is essential to properly train personnel to understand the fundamental physico-chemical principles underlying the operation of the various instruments. He also advocated the importance of recurrency training (every six to twelve months) to refresh the understanding and to update with new developments. To train operators in his laboratory, Dr. Henion listed 19 items ranging from ions productions, ion optics and energetics, detections, calibrations, data acquisitions, and different type of mass spectrometric experiments. For GLP purposes, these training are documented by the signature of a well qualified senior personnel on the checklist of the 19 training items for the trainee.

Dr. Tom Oglesby of Taylor Technology led the discussion on "Instrument Validation for Quantitative Analysis". Dr. Oglesby employs, as suggested at the 1994 Fall Workshop, the performance base full system validation method. He validates the entire GC or LC/MS/MS/DS as one unit by meeting a specified set of performance criteria such as injecting a certain amount of a standard would result in a chromatographic peak with certain S/N ratio. Dr. Oglesby also indicated that instrument validation is an on-going process. In a bioanalytical assay, standards and quality control samples (QCs) are analyzed with unknowns in each set of samples. Criteria on the performance of the standards and QCs are established and documented in the analytical method or standard operating procedure for the laboratory. These criteria must be met in order to accept the data from the analysis of unknown samples. Therefore, one is essentially validating the instrument in each analytical run For GLP compliance, documentation of the instrument performance and in process validation is essential.

Dr. Steve Unger of Glaxo addressed the issues related to "GLP vs. Non-GLP Work in the Same Laboratory". Dr. Unger indicated that whenever possible, laboratory functions supporting GLP and non-GLP studies are separated. However, this separation may not be practical because the same resources often support both GLP and non-GLP studies. At Glaxo, all work are done in the "spirit-of-GLP". Developmental toxicological

studies are conducted with GLP compliance. Discovery support and metabolite identification are considered non-GLP work. Laboratory practices, whenever possible, adhere to the higher (GLP) standard. However, acceptance criteria are often relaxed in non-GLP studies since speed and volume is more important. This common sense approach represents the general view of the audience.

Dr. Joe Snodgrass of American Cyanamid described the approach to GLP in the agricultural industry, which is also regulated by the US FDA. In general, there is no different in how the agricultural and the pharmaceutical industries view GLP. "The Nine Pillars of the GLPs" described by Dr. Snodgrass are 1) Personnel, 2) Facilities & Equipment, 3) SOPs and Protocols, 4) Quality Control, 5) Documentation, 6) Management Oversight, 7) Quality Assurance Unit, 8) Test Substances & Reference Substances, and 9) Archives.

The highlight of the workshop was a keynote lecture on "GLP: The Viewpoint from FDA Compliance" by Dr. Charles A. Snipes, an inspector for US FDA. Dr. Snipes described the two types of inspection: routine and directed. Routine inspections may involve general surveillance or study specific audit. Directed inspections usually are study specific or for a specific purpose. The content of Dr. Snipes' presentation are similarly general as in the published Code of Federal Regulations, Title 21, Part 58 : "Good Laboratory Practice for Nonclinical Laboratory Studies." However, Dr. Snipes did stress the importance of the availability of organization chart, master study schedule, personnel training record, and audits by internal quality assurance unit.

In his lecture, Dr. Snipes indicated that computer software validation is necessary and invited further question. This was the major topic of discussion after the lecture. Upon questioning, Dr. Snipes did agree that validation of the performance of the complete system (the "black box" approach) as suggested by S. Musser in the 1994 Fall Workshop and described by T. Oglesby earlier in the session is acceptable. Dr. Snipes indicated that, although he is asking the user to have access to the source codes or to perform validation of computer software, he understands that it may not be possible, especially for older software. The consensus at the workshop among the users, FDA scientists, and mass spectrometer manufacturers in the audience is that mass spectrometer data system software should be validated by the manufacturers and that documentation of the validation should be available to the end users.

On issues related to data archive, Dr. Snipes indicated that it is imperative to be able to reproduce the raw data. For example, the area of a chromatographic peak must be exactly the same in archived data. This raised the concern that new hardware or software of mass spectrometer data system, or manual integration, may not be able to re-integrate electronic data to the exact same number. Thus, the consensus amongst workshop participants is to keep the paper copy of raw data for archive purpose.

Dr. Snipes ended his lecture with a description of the FDA Form 483. This is a written report of the inspection. The Form 483 is formally named "Inspectional Observations". Dr. Snipes indicated that this is purely documentation of the observations made by the inspector. The Form is not a citation nor would it necessary invalidate the study being audited. Furthermore, the recipient of Form 483 can contact the FDA office for clarification or correction of the observations.

The workshop was very well received as evidenced by the approximately 180 attendees and the lively and spirited discussion which lasted until about 11:00 pm. The workshop was very useful for the organizer because I got the opportunity to ask the question which a FDA inspector asked during a study specific audit. The question is whether any laboratory has a SOP for manual chromatographic peak area integration. Among the 180 attendees of the workshop, no one has such a SOP. This is probably due to the almost impossible task of describing all possible chromatographic interference or anomalous situation in the chromatographic/mass spectrometric analysis of biological samples. Finally, I would like to thank all the speakers for leading the discussion, the participants for their active interactions, and ASMS for sponsoring the travel of Dr. Snipes. I would also like to acknowledge Professor Jack Henion for his encouragement to organize this workshop.

Respectfully submitted,
Kelvin Chan, Workshop Organizer

ELEMENTAL INTEREST GROUP WORKSHOP

"Comparison of Mass Analyzers for ICP and GD Ion Sources"

The objective of the workshop was to compare the benefits and limitations of various plasma-analyzer combinations, primarily focusing on attributes of the combinations, rather than the well-known benefits of the analyzers itself. Efforts to address noted limitations were described, as well as future expectations for each. The presenters and plasma mass analyzer combinations addressed are shown below.

Panelist	Affiliation	Plasma/Analyzer Combination
Sam Houk	Iowa State University	ICP / Quadrupole
Ken Marcus	Clemson University	GD / Quadrupole
Fred King	West Virginia University	GD / Time-of-flight
Pat Mahoney	Indiana University	ICP / Time-of-flight
John Eyler	University of Florida	GD / FT-ICR
David Koppenaal	Pacific Northwest Laboratory	ICP / ITMS
Doug Duckworth	Oak Ridge National Laboratory	GD / ITMS

Presentations

ICP / Quadrupole
This combination is the tried and proven mainstay in ICP-MS and enjoys the benefits of quadrupole mass filters — robustness, simplicity, and reliability. Limitations include sequential data acquisition (a problem when using very limited sample sizes), unit mass resolution, and mass discrimination (bias). New means of improving transmission and reducing mass bias are under development. Improvements in transmission are observed with a variable potential lens system, which operates at the optimum voltage for the element of interest. Mass bias is being addressed through the extraction of ions from a shock wave set up by the collision of the ions with a barrier.

GD / Quadrupole
As in ICP-MS, GD applications enjoy the benefits inherent with quadrupole mass filters. This is particularly true for depth profiling applications, which exploit their rapid scanning capabilities. In quadrupole GDMS, isobaric interferences are often the limiting factor in terms of sensitivity and accuracy. Many efforts have been made to eliminate or reduce polyatomic species — heating/cooling the ion source, variation in discharge parameters, optimization of sampling position, and collisional dissociation. Recent efforts at ORNL have concentrated on improving the purity of the discharge gas through appropriate conditioning of the getter purification system. Sub-ppm detection limits for problematic elements (e.g., Si, Fe, Cr) are observed.

GD / Time-of-flight
TOF instruments perform nicely in terms of selectivity, sensitivity speed and simplicity. Inherently, they are the most simple mass analyzer, providing a large mass range and rapid spectral acquisition. Limitations observed in current GD / TOF instruments include limited

dynamic range (~10^4), abundance sensitivity, detection limits (low ppm), mass (temporal) resolution, and duty cycle. It was stressed that the limitations in these areas lie in the detection system and stressed the need for development, particularly for the low mass (fast event) range.

ICP / TOF
The multiplex advantage of ICP-TOF instruments was demonstrated in the isotopic analysis of laser ablated material. Precision better than 2% was observed. Using boxcar averaging, $^{206}Pb/^{208}Pb$ ratio precision reached the statistical limit (0.2%). The need for better data acquisition systems was reiterated. Detection limits could be improved by approximately 100x by limiting the divergence of the ion beam.

GD / FTICR
The primary advantage of this combination is the ability to mass resolve polyatomic and atomic isobaric interferences. Mass resolutions of 2 million ($m/\Delta m_{1/2}$) have been observed on instruments with very high magnetic fields (7 Tesla). Clearly such resolution is not needed for most applications; permanent magnet systems may provide mass resolving powers on the order of 50,000 in the low mass range. Other advantages are the possibility of using gas-phase ion chemistry and the multiplex advantage. Disadvantages are the limited dynamic range (~10^4-10^6), cost, complexity, and sensitivity. Dynamic range can be improved through the ejection of majors and axialization/remeasurement techniques. Resulting sensitivity has been demonstrated to be on the single to sub ppm level.

ICP / ITMS
The ion trap, new to atomic mass spectrometry, appears to have several real and potential advantages. It is potentially the most sensitive of all mass analyzers; detection limits are in the low part-per-trillion. Its ability to dissociate polyatomic species and neutralize highly electronegative species (Ar in particular) are notable benefits. The possibility for high mass resolution exists. It was stressed that the ITMS is not a panacea for ICP-MS, however. For example, oxide and hydroxide formation can be problematic (though reduced with a Zr getter pump in the analyzer). The ion trap is a reaction cell and the reactions occurring therein can be advantageous or disadvantageous.

GD / ITMS
The ion trap hold promise for the analysis of glow discharge generated ions. Fortuitous ion-molecule reactions, analogous to the ICP / ITMS observations, in which argon and argon-related species are removed through charge transfer reactions are observed in the GD / ITMS system. Loosely bound polyatomic species tend to dissociate upon collision with the He bath gas. Dissociation of strongly bound polyatomics (MS/MS) has been demonstrated with efficiencies of ~100%. As a new mass analyzer for atomic ions, the ion trap has many parameters remaining to be evaluated. Dynamic range, abundance sensitivity and abundance precision were identified as the most critical issues for highly sensitive multi-element analysis. To this end, the use of highly selective methods of ion accumulation become important. The use of filtered noise fields was presented as a highly selective means of accomplishing this.

Submitted by,
Douglas C. Duckworth

PROCESS MASS SPECTROMETRY WORKSHOP

"On-Line Mass Spectrometry for Process Control and Diagnostics"

Organized by Steven J. Doherty[1] and Mark A. LaPack[2]

[1] The Dow Chemical Company, Analytical Laboratories, Freeport, TX 77541
[2] The Dow Chemical Company, Analytical Sciences Laboratories, Midland, MI 48667

This was the second workshop on process mass spectrometry at ASMS. The goal of these workshops is to discuss the experiences and challenges encountered by those who develop, apply, and commercialize on-line mass spectrometric applications. Approximately fifty people were in attendance representing industry, academia, national laboratories, and instrument manufacturers. As with last year, the workshop was structured around three informal presentations, separated by periods of discussion. Following the final discussion period, several people remained for over thirty minutes to discuss specific topics of interest.

Most attendees of last year's workshop had suggested that future workshops address novel ways to deal with complex samples and future directions for process monitoring. The underlying message from this year's workshop supported the trends revealed in the literature. Smaller, less expensive, and more powerful mass spectrometers are making their way out of the laboratory and into the field and production areas. These non-traditional uses of mass spectrometry to solve non-traditional problems are driving the use of hyphenated techniques such as membrane introduction-mass spectrometry (MI-MS) and gas chromatography-mass spectrometry (GC-MS).

Anthony J. Borgerding (Los Alamos National Laboratory, Los Alamos, NM) began this workshop with a review of the current state of the art for fast gas chromatography and fast GC-MS as well as his own current work in the area. Tony described the problems and some solutions associated with the application of fast GC-MS for on-line applications. The goal was to produce GC-MS data at one-tenth the time of conventional chromatographic separations. By producing ten millisecond injections and using short, small diameter columns, five compounds could be reproducibly separated in five seconds. With peak widths of a few hundred milliseconds, scan rates of 100 scans per second are required. Quadrupole, ion trap, and time of flight (TOF) mass analyzers were discussed, with TOF described as the most promising for this application. Ideally, ions would be stored in the ion source prior to mass analysis to optimize the sensitivity of the technique. Parts per million detection limits were reported for halogenated solvents with parts per billion detection limits easily obtainable with improvements in the technology. This approach appears promising as it provides a very good compromise to the inevitable trade-off between speed and selectivity for on-line techniques.

Mary E. Cisper (Los Alamos National Laboratory, Los Alamos, NM) presented an overview of recent studies performed at Los Alamos for developing methods to monitor volatile organic compounds (VOC's). For monitoring VOC's in air using an ion trap, it was found that MI-MS provided at least

ten times better detection limits when compared with introducing the sample via a molecular leak valve. Both flat sheet and hollow fiber membrane separators were described. A configuration in which the membrane separator was interfaced to the mass spectrometer through a jet separator was shown to further enhance the introduction of VOC's relative to air in the analyzer. With this configuration, sub-parts per billion detection limits were reported. A variety of experimental parameters were varied to determine the optimum operating conditions of the analyzer. During these studies, it was found that higher air pressures in the ion trap resulted in a charge exchange process that enhanced the sensitivity of the VOC's by a factor of 150. Mary also provided a preliminary report on work being performed to compare results from a field analysis using a portable analyzer with conventional lab analyses of VOC's in soil and water samples. Although the results have not yet been finalized, one of the goals of this study is to demonstrate to the regulatory agencies that the two methods are at least equivalent so that the "near-real-time" technique may be accepted for reporting purposes.

Mark Dearth (The Ford Motor Company, Dearborn, MI) presented a description of Ford's interactions with government agencies, national laboratories, universities, and various business consortia to address environmental issues. The auto industry is using a great deal of resources to measure the components of auto emissions. Historically, techniques such as total organic carbon, optical spectroscopies, mass spectrometry, and chromatographic techniques have been used for on-line and off-line studies. A tremendous challenge has arisen from requirement to determine parts per billion levels of specific "reactive" (i.e., unsaturated and aromatic) hydrocarbons and oxygenated species in auto exhaust. On-line analysis is expected to provide the most reliable data and to reduce development and testing time. Mark stated that sampling is a key component to these studies. The analyzer for this application should possess the following characteristics: twenty parts per billion detection limits, one to ten samples per second acquisition rate, robust, small, and inexpensive. An analyzer is currently being developed in cooperation with Oak Ridge National Laboratory that is expected to meet many of these criteria. This analyzer is based on ion trap technology with glow discharge ionization, which will provide the combination of soft ionization, good analyzer signal to noise, and tandem mass spectrometry capabilities. We look forward to future updates from all three speakers.

Those who remained for continued discussion following the presentations agreed that the needs are diverse for on-line and environmental field monitoring. Instrument manufacturers do not currently meet these needs with standard, commercially-available instrumentation. The manufacturers in attendance concurred that there is a large market that is as yet untapped, but as for the technology that will satisfy that market, the picture remains cloudy.

Finally, the growing interest in the field of on-line mass spectrometry was demonstrated again when it was announced that one - and possibly two - up-coming volume of the *Journal of Process Control and Quality* will be devoted to applications and developments of on-line mass spectrometry. A call for papers was formally issued by the organizers of the workshop.

DESORPTION / IONIZATION INTEREST GROUP WORKSHOP

"MICRO-ELECTROSPRAY: CAN LESS GIVE MORE?"

The workshop was held on Tuesday evening, May 23, with about 300 attendees. Panel members were Richard M. Caprioli (University of Texas Medical Center), Kelsey D. Cook (University of Tennessee), Matthias Mann (EMBL, Heidelberg, Germany), Jean-Pierre Salzmann (LC Packings), and Richard D. Smith (Pacific Northwest Laboratories). In addition, presentations were made by Tom Covey (Perkin-Elmer Sciex) and Gary Valaskovic (Cornell University).

Workshop organizer Richard Cole (University of New Orleans) introduced the topic of 'micro-electrospray', which he referred to as the 'miniaturization' of the electrospray technique to accomodate submicroliter/min flow rates and accompanying small sample volumes. Electrospray ionization MS at higher flow rates is often termed a "concentration-sensitive" technique, i.e., for quantitative purposes, signal response is related to analyte concentration. Moreover, increasing the flow rate of solution (thereby increasing the absolute quantity of analyte entering the mass spectrometer per unit time) does not usually augment the signal. For ultra-trace analyses, increasing the analyte concentration via solvent evaporation can improve detection ability. However, the analyst may be left with a sample volume of only one microliter or less, thereby necessitating special handling to introduce it into the mass spectrometer. Equally challenging may be a low volume sample which contains a high level of competing analytes or impurities, thus necessitating a micro-scale separation or clean-up to avoid signal suppression by these competing species.

Interest in micro-electrospray has surged in the past year, spurred primarily by work presented at the 1994 ASMS meeting by Matthias Mann, Kelsey Cook, and Richard Caprioli who independently reported 10-100 fold gains in sample utilization efficiency. Dick Smith, whose work with low flow rate systems dates back even further, reminded the audience that low flow rate electrospray ionization mass spectrometry is a concept that has been with us for a while, attributing the statement that the optimum flow is "as low as possible" to John Fenn's early electrospray work of one decade ago.

Matthias Mann and colleague Matthias Wilm described different approaches to micro-flow systems. They presented their version of a micro-electrospray device which is readily distinguished from other approaches because the sample is introduced in a discrete portion at the beginning of the experiment, as opposed to continuous sample introduction via direct infusion, HPLC, or CE. In their method a small volume of sample (~ 1 µl) is deposited into a 1 mm i.d. borosilicate glass pipette which had been drawn out to a 1 micron i.d. tip, then gold plated by vapor deposition. The electrospray process itself sustains a flow of about 20 nL/min enabling measurements to be made for ~ 50 min. Attomole sensitivity for MS-MS experiments on peptides was achieved by employing signal averaging techniques. The issue of capillary blockage was raised, but it was noted that *in situ* protein digests taken off 2-D gels could be run with these sprayers without problems. A list of equipment and suppliers was distributed to those interested in using the method.

The remaining speakers described continuous introduction devices. Kelsey Cook described a procedure for preparing gold coated fused silica capillaries with the unique feature of being extremely durable. The tip of the capillary is first tapered to a fine point, then treated with (3-mercaptopropyl)trimethoxysilane, afterwhich a thin film of gold is vapor-deposited on the outer surface. These spray devices can be made from commercially available fused silica capillaries having inner diameters of 10 µm or greater. High voltage contact is made directly on the gold coating. Sample utilization efficiency was shown to improve by a factor of 30 with the 10 µm i.d. capillary, relative to a 32 gauge needle. The advantages of this system for on-line CE-MS were discussed. However, a 25 µm i.d. was suggested to be the best compromise between sensitivity improvements and blockage problems.

Dick Smith showed a low flow rate sprayer comprised of a small diameter fused silica capillary whose tip had been tapered via etching using 40% HF. Electrical contact was made at the capillary tip which had been coated with a conductive silver epoxy. The capillary inner diameter may be as small as 10 µm. The improved sensitivity of the reduced flow sprayer was discussed, with the ion sampling efficiency estimated to be > 10 %. Other data was presented showing improved sample utilization efficiency with decreasing capillary inner diameter. The use of microsprayers for sheathless CE-MS was predicted to allow the lowering of detection limits from the (current) attomole level into the zeptomole range.

Jean-Pierre Salzmann described practical aspects of interfacing micro-flow liquid chromatography (200-400 nL/min) to electrospray MS. He described the advantages and disadvantages of various injector, pumping and gradient configurations. He also discussed low volume sample handling, and stressed the importance of avoiding dead volumes to minimize band broadening outside of the column. It was evident that the low flow rates delivered to the 50-320 µm i.d. capillary LC columns were ideally suited to coupling to the micro-sprayers discussed in the workshop. It was pointed out that nanoliter/min flow rates are often achievable using hardware intended for higher flow delivery when flow splitting is employed.

Richard Caprioli's version of micro-electrospray utilizes fused silica of greater than 10 µm i.d. and 150 µm o.d.. The voltage is not applied directly to the sprayer tip, so no metal adhesion is required. Instead, voltage is applied to a metal junction made a few centimeters away from the spray tip. For capillary LC-MS, the stationary phase can be packed directly into the spray capillary itself. This minimizes dead volumes which have proven to be lethal at these low flow rates. The use of 10 µm C-18 particles as packing material created an integrated de-salting / preconcentration / fractionation set-up for use at 50-500 nL/min flow rates allowing attomole/µL detection levels for peptides.

Tom Covey presented work evaluating several of the above micro-sprayer systems employing inner diameters from 2 to 100 µm. The Mann/Wilm discrete sprayers were reported to give the highest sample utilization efficiency, providing flows in the 10-25 nL/min range. This flow hovers just above the lower limit to workable flow rates, while providing close to the upper limit of sample utilization efficiency when working at concentrations below 100 fm/µL (~ 1 in 10 analyte molecules present enter the mass spectrometer). The improvement in efficiency likely originates from increases in both ionization efficiency and transfer efficiency through the atmospheric pressure-to-vacuum orifice. With very small aperture sprayers, resistance to flow is minimized when the restriction length is kept as short as possible.

Lastly, Gary Valaskovic presented some micro-electrospray data obtained using higher analyte concentrations. Each presenter entertained questions and comments by workshop participants.

In summary, there was a general consensus among the panel members that micro-electrospray is only worth doing if the added sensitivity is truly needed. Additional problems (e.g., capillary plugging and high back pressure) complicate analyses, so if sensitivity is adequate at higher flow rates, micro-electrospray is probably unnecessary. A capillary inner diameter of about 20 µm seemed to represent the point where sensitivity improvements became overshadowed by added headaches originating from excessive back pressures and capillary blockage. Plugging often can be directly linked to poor solubility. It was noted that the 'Taylor cone' (from which charged droplet formation originates) is no longer stable at very low flow rates (e.g., < 20 nL/min). Below this level, the Taylor cone retracts into the electrospray capillary. For low flow LC and CE coupling, unions and other dead volumes must be avoided.

Submitted by Richard B. Cole
Workshop Organizer

Workshop Report
Computer Applications Interest Group

David D. Stranz, Coordinator

Tuesday, May 23, 1995
Atlanta, GA

Validation of Mass Spectrometry Data Systems

This workshop provided a follow-up to the successful ASMS 1994 Fall Workshop on *Mass Spectrometry and Good Laboratory Practices, but with a tighter focus, that of* validation of the data systems and software provided with modern mass spectrometers. Among the issues which surfaced at the Fall Workshop was, "To what degree are end users and data system vendors required to validate the computer hardware and software provided with their instruments?" Auditors from the US Food and Drug Administration have great flexibility when assessing GLP compliance, leading study directors to often prepare for the worst, possibly a line-by-line validation of the vendor's *data system source code.*

In the ensuing seven months, the FDA's Office of Regulatory Affairs has had time to consider some of these problems. The FDA spokesman at the Fall Workshop, Steve Musser, was invited back to speak at this evening workshop. Representatives from the software development groups at four instrument vendors were also invited to describe their software development efforts.

Steve Musser distributed copies of an FDA technical report furnished to auditors investigating software development activities, and summarized the report with seven key points. A software validation package must contain these critical elements:

- Design specifications, both high and low level
- A test plan, covering module, worst case, and typical use testing
- Test results evaluation, with emphasis on demonstration that the specifications have been met
- Procedures for controlling changes and revalidation
- Documentation of the individuals responsible for approving and executing the validation plan
- Risk analysis for critical software functions
- An archive of the whole of the above, including all versions of specifications and specific details of test results

If a vendor of a mass spectrometry data system can provide the end user a sufficiently detailed summary of this validation package, then this will generally satisfy an auditor's requirements. Steve stressed, however, that individual auditors were still free to require additional documentation.

Gerry Bentley (PE-Sciex), David Stranz (VG Organic), Mark Canales (Finnigan MAT), and Wayne Duncan (Hewlett-Packard) *each described the software development* process at their respective companies. All of these vendors are ISO-9000 and TickIT compliant, and all follow a similar procedure. Modern software development activities

focus on what is called the "software lifecycle", the flow of activities from a software product's inception through its commercial lifetime. The software lifecycle generally begins as a proposal for a new product or application. This proposal is formally investigated for feasibility, commercial potential, and resource requirements. If the investigation results in approval, a functional requirements document is produced, which describes all of the features the product must have. Next, one or more technical specification documents are written, detailing how the functional requirements must be implemented in software and providing procedures for testing that the resulting code meets both technical and functional specifications. Finally, the actual code is written, reviewed, debugged, and tested, first at the module level, then integrated at the system level, and finally as a finished product. Most vendors perform both in-house and external testing to uncover defects in the software and in the design and functional requirements. These testing programs evaluate software under worst-case as well as typical use conditions. All vendors have in place a defect and change request tracking process, with only certain individuals able to assign responsibility for and approve changes. Priorities are assigned to changes, and statistics are computed to help improve the process of finding and correcting defects, and avoiding new defects.

The software lifecycle is generally not a linear process; the various steps may run in parallel at times. There is generally iteration between design, implementation, and testing stages, as problems or alternatives are uncovered. It is nearly impossible to completely specify a complex software product from the outset of the project, because new requirements are constantly being introduced as the field or market changes. The lifecycle and its accompanying documentation must remain flexible enough to cope.

Following the presentations, the workshop opened to a lifely discussion among the thirty or so attendees. While most comments were favorable regarding the FDA's recommendations and the vendors' procedures, there was considerable concern about the FDA auditors' flexibility and whether the vendors could provide appropriate documentation, particularly for older systems.

While Steve acknowledged the open-endedness of an auditor's potential requirements, he stressed that the FDA is looking at the overall quality and documentation of a study, and that a sufficiently detailed vendor-supplied validation package would usually suffice.

The vendors present acknowledged that, while this modern software development lifecycle was being followed in the development of new software products, such *procedures were generally not in place five to ten years ago, when older data systems* were being developed. All agreed that they would work with the end user and the FDA to provide acceptable documentation in the event of an audit of an older system, and all stated that the seven points presented by Steve were being met in their current practices and could be documented in the summary validation package.

Progress and Prospects for TOF Mass Spectrometry

A Workshop Sponsored by the Time-of-Flight Interest Group
Monday, May 22, 1995; 8-10:20 PM

A brief business meeting introduced this new interest group. **Robert J. Cotter** (Johns Hopkins University) encouraged members to suggest topics for 1996 oral sessions, plenary lecturers and possible recipients of the Distinguished Contributions to Mass Spectrometry Award. Attendees were recorded on a mailing list that will enable the group to construct a TOF bulletin board and listserver on the Internet. Finally, Dr. Cotter noted that the ASMS will shortly have a homepage on the Web.

Marvin Vestal (PerSeptive Biosystems) then gave an informal presentation of a *delayed extraction MALDI* technique for improving mass resolution. Using an extended (15 meter) geometry his group has been able to achieve mass resolutions of 5000 for insulin and 1050 for a DNA 50mer. **Jack Holland** (Michigan State) and **Rebecca O'Malley** (University of South Florida) both reminded the attendees that delayed extraction techniques had first been developed by Wiley and McLaren in 1955. **Marshall Siegel** (American Cyanamid) asked whether there were any calibration problems associated with pulsed extraction. Vestal replied that timing is based upon the extraction pulse rather than the laser pulse.

Liang Li (University of Edmonton) described a *time-lag focusing* scheme using a 280ns delay that is not adjusted with mass. Using a 1 Gsample/second digitizer he achieved a mass resolution of 4072 for bradykinin.

Werner Ens (University of Manitoba) described an orthogonal injection electrospray TOF mass spectrometer that achieved 10,000 resolution for insulin using pulsed extraction. In response to a question by **Ron Stein** (Applied Physics Laboratory), Ens noted that timing in this instrument was also based upon the extraction pulse. **Marvin Vestal** (PerSeptive Biosystems) noted that resolution is in many cases limited by the bandwidth (generally 50 MHz) even on 1 Gsample/second digitizers.

Scott Weinberger (Hewlett-Packard) stressed the importance of developing small, simple-to-use instruments and keeping the background pressure low. He also described in detail the problems associated with the poor beam profile of nitrogen lasers. He noted that people tend to define the *desorption threshold* differently, and that combined bandwidth limits of 100 to 500MHz in detectors and digitizer preamplifiers are common.

Timothy Cornish (Johns Hopkins University) described improvements to a coaxial, dual-channelplate detector that enable one to record peak widths of as little as 1.5 ns without ringing. **Ron Stein** (Applied Physics Laboratory) asked about the coaxial cables used; and **Marvin Vestal** (PerSeptive Biosystems) asked whether the interleaving mode was used on the digitizer. Cornish replied that the peak was recorded as a single transient for a single ion.

Steve Thompson (Kratos Analytical) described a new detector manufactured by Ballatini, that consisted of small, fused glass spheres with the active surface on the outside of the spheres. These 1 mm thick detectors can be made in any size and in any shape. **Winston Chen** (Oak Ridge National

Laboratories) noted that these had been described in the most recent issue of *Vacuum Science*.

Robert J. Cotter (Johns Hopkins University) described *post-source decay* mass spectra using a *curved-field reflectron*. This reflectron eliminates the need for acquiring and stitching together spectra obtained at different reflectron voltages, and therefore provides *seamless* amino acid sequencing spectra.

Douglas Beussman (University of New Mexico) described *photon-induced dissociation* (PID) fragmentation of alkanes at 193 nm. **Marvin Vestal** (PerSeptive Biosystems) asked about the possibility for background CID resulting from laser vaporization of background material from surfaces. Contributions from CID were determined by firing the laser early and were minimal.

Jack Holland (Michigan State University) described the technique known as *time-compressed chromatography* using time array detection on an integrating transient recorder.

Kai Tang (Sequenom, Inc) described work with oligonucleotides, including high mass resolution (1000 for 20mers) and spectra of an exonuclease digestion mixture. **Chris Becker** (SRI International) described progress in the Sanger approach using 5 fmol of 14, 21 and 41mers on a 12mer primer scheme in which the 40 and 41mers can be resolved at a resolution of 200.

Mark T. Qian (University of Michigan) described results on the CID spectra of bradykinin and the M_2H^{+2} peak of angiotensin 1, using an electrospray, reflectron TOF mass spectrometer

James Reilley (Indiana University) returned the discussion to the subject of delayed extraction. He described the technique as different from that of Wiley and McLaren in that they were not attempting to simultaneously focus both kinetic energy (velocity) and spatial distributions. Rather, they converted the initial kinetic energy distributions common in MALDI to a spatial distribution Mass spectra were shown for lysozyme using a 4500V drawout pulse. He noted that at longer delay times there was considerable metastable decay in the source. **Rebecca O'Malley** (University of South Florida) commented that pulsed, delayed extraction had previously been used by Cotter for both IR laser desorption and MALDI of peptides, and by her group for the analysis of polymers.

The workshop then adjourned at 10:20 PM.

Respectfully submitted,

Robert J. Cotter

Robert J. Cotter
TOF Interest Group Coordinator
June 5, 1995

Historical Interest Group Report

The meeting was called to order on Wednesday, 24-MAY-95. A brief report was presented by Mike Grayson, Archivist for the Society, regarding an increase in financial support of the Chemical Heritage Foundation (CHF) in Philadelphia. Based on the fact that CHF has acquired a new facility for their offices, the Beckman Center for the History of Chemistry and the Othmer Library, space for a museum of chemical instrumentation will be made available. The increased level of support by ASMS provides one seat on the CHF Board and two seats on the Chemical Instrumentation Group Board.

The new home of CHF is in the heart of the historic district of Philadelphia. Sometime during 1996, 1400 square feet of space will be made available for a display of instrumentation. The long-range plan is to devote approximately 12,000 square feet to the instrumentation museum.

Plans for 1996 meeting were discussed. It was decided that the historical interest group would submit a request to the vice-president for programs for one oral session and one poster session at the Portland meeting. The theme would be history of various mass separation techniques:

Magnetic Sector
Time-of-Flight
Quadrupole Mass Filters
Preparative Scale Instruments (Calutrons)

An oral presentation would be planned for each of these topics with the presentor giving an overview of the history of the separation technique in general terms. Poster presentations would be solicited that focused on particular instruments or instrument manufacturers such as CEC 110, Bendix TOF, etc. Presentors will be encouraged to make use of all available resources including oral histories of significant individuals. History session authors will be provided four pages in the bound volume for their manuscript instead of the usual two pages and longer articles will be encouraged for submission to JASMS. Several individuals volunteered to make presentations.

Ken Busch made a timely suggestion that the Historical Interest Group begin to plan for the 50th anniversary of the Society which is now seven years away. This suggestion was met with enthusiasm and volunteers for a planning committee were solicited. The following individuals offered their services in planning for the 50th anniversary of the Society:

Ken Busch
Mike Grayson
Burnaby Munson
Larry Phillips
G. Siuzdak
Mike Story
Al Yergey

Mike Grayson will chair the 50th anniversary planning committee during the coming year.

Several suggestions were made for topics for future meetings between now and the 50th anniversary meeting:

- Timelines for instrument companies and/or instruments
- History of various techniques and applications
- History of mass spectrometry societies both in US and abroad
- Pre-history of mass spectrometry (Aston to Nier)
- History of important mass spectroscopists
- History of important developments in mass spectrometry

Besides topics for future meetings, a number of other suggestions were made to commemorate the 50th anniversary of the Society:

- Reissue J. J. Thomson's book
- Create a multi-media CD-ROM of historical highlights in mass spectrometry
- Gather Accounts and Perspectives from JASMS and publish as a book
- Publish a collection of important works in the field

These various ideas will be discussed among the planning committee in the coming year to form a plan for review by the Historical Interest Group, the ASMS Board and the Editor of JASMS.

Larry Phillips is completing his two year term as Chairman of the Historical Interest Group. Charles Judson and Burnaby Munson were nominated to chair the group in the coming two years. Their names were submitted to the President for appointment.

Any ASMS member interested in participating in the Portland Historical session is encouraged to contact any member of the planning committee. Contributions, ideas, and volunteer labor are needed and welcome.

Larry Phillips (301) 846-1234
Mike Grayson (314) 233-2541

BIOMEDICAL APPLICATIONS INTEREST GROUP WORKSHOP

"PROBING BIOMOLECULAR NON-COVALENT INTERACTIONS: TRICKS AND TRAPS"

The workshop was held on Thursday evening June 1, with about 120 attendees present. Prior to beginning the workshop, opening comments were offered by the current interest group chairperson, Pam Crain, who noted that about 1300 registrants at the previous ASMS meeting (Chicago) had declared the Biomedical Applications Interest Group to be their first or second interest group, thus making this the largest of ASMS's interest groups. She informed the attendees how interest groups are formed and how they are intended to function, and solicited volunteers for the position of chairperson, who will be appointed by the board summer 1995 to a two-year term. The chairperson solicited suggestions about what specifically the interest group could do to be of greater use to affiliates who may analyze biomolecules but who may not be experienced with the chemistry and properties of biomolecules. Such assistance could take the form of compilations, tutorials, or the like. There was some discussion of the utility of a tutorial or workshop on handling biomolecules (properties, preparation etc.) The chairperson noted that because of the size of the interest group and of the importance of biomedical applications as reflected in the large number of presentations in the biomedical area, the ASMS Board will listen, and she urged attendees to make their wishes and needs known to them and to the incoming chairperson, to be appointed.

Attendees were polled regarding the effectiveness of JASMS as a vehicle for scientific communication of results in our area of interest. As evidenced by a show of hands, more than half of the audience had published in the journal, and no dissatisfaction was expressed with any aspect of the journal. It was noted that our group generally tends to represent end users, not innovators, of mass spectrometric techniques, and generally publishes where our findings, themselves, are what is relevant. Suggestions for plenary lecturers and symposium topics for next year's meeting were solicited and all were given to Veronica Bierbaum (V-P, Programs).

The workshop was structured as an informal open discussion, with topics selected from written questions submitted from the attendees, and it was intended to emphasize practical aspects of using the mass spectrometer to determine the nature and extent of non-covalent ligand:biomolecule (or other bi-molecular) interactions. It soon became readily apparent that the audience was rather strongly divided into two opposing camps. One consisted of skeptics with generic concerns (or direct experience) that one could (or actually does) obtain different ligand:biomolecule ratios according to how the mass spectrometer is tuned. There was an equally fervent group of proponents testifying that if the samples and selected controls are prepared carefully, and appropriate tuning and solvent considerations are adopted, then valid measurements can be made mass spectrometrically. It was noted that an actual example of an interaction for which the stoichiometry was unknown was

correctly determined mass spectrometrically, and was subsequently confirmed by "classical" methods. Several in the audience suggested that perhaps too many papers reporting these kinds of measurements are being reviewed by mass spectrometrists and that we might decline to do so with the suggestion that these papers be reviewed by experts in binding measurements by more conventional methods. There was unanimous agreement that great care should be exercised before undertaking these kinds of analyses, with regards to tuning and using the proper controls, although in the latter matter, there was no agreement on any "universal" control sample. Audience participation was notable, and although the discussion was at times spirited, a uniformly high level of civility was maintained by all. The workshop adjourned at 10:00 p.m.

Respectfully submitted

Pam Crain

Pam Crain
(pamela.crain@rna.pharm utah.edu)

ASMS BUSINESS MEETING, ATLANTA, GA

May 24, 1995

The Business Meeting, which was held in conjunction with the ASMS Annual Conference, was chaired by President Christie G. Enke who opened proceedings at 8:15 a.m. by welcoming all present. A number of presentations by members of the ASMS Board of Directors were made, summaries of which are given below.

President's Report (Chris Enke)

The Society is continuing its healthy growth, both in size and in membership services offered. The 1995 Conference in Atlanta broke new records in attendance (about 2,500, up 304 from Chicago) and in number of presentations (1,461 vs. 1,266 in Chicago). The Board is actively working to find ways to accommodate this growth and to better serve the now over 3,000 members of ASMS. Board members' responsibilities are being redefined and extended and the role of the interest groups, in providing activities of value to their constituents, is being expanded.

In an effort to allow the non-member conference attendees an opportunity to enjoy full and continuous membership status, starting with the 1996 Conference, non-member registrants had the option of becoming full members for the period May 1, 1995 through March 30, 1996 by paying $20 dues (in addition to the non-member registration fee). A total of 70 non-member registrants took advantage of this opportunity. Conference registrants who joined ASMS at the time of the Annual Conference will receive all 12 issues of *JASMS*. Membership will expire March 1 of the following year. They will be able to renew their full membership by the same arrangement at the 1996 Annual Conference or by paying the regular annual membership dues before March 30, 1996

Treasurer's Report (Chris Enke for Charles Evans)

ASMS is perhaps one of the most literally non-profit organizations around. It has been our aim to have each activity self-sustaining. Roughly, the general income from dues and interest pay for the operating expenses (Society office and expenses) and journal costs (currently $27 per member.) The conference registrations and short course fees generally cover current conference costs and a small fraction of the operating expenses. The fall workshop and the Sanibel and Asilomar conferences are planned to have break-even budgets. However, the 1994 Conference in Chicago resulted in a lost of $4,174 which led to a net loss for the year of $12,029. This is a small amount compared to the total 1994 Society expenses of $777,977, but represented a continuing trend of increased operating and conference expenses. This observation led to the Board's action to adopt a modest raise in 1995 dues and conference registration fees.

Vice President for Programs' Report (Veronica Bierbaum)

The Vice President for Programs thanked all participants in the Conference, and the Program Review Committee in particular (who had reviewed some 1,500 abstracts), for making the Meeting such a success. She also acknowledged the efforts of the oral session chairs and co-

chairs, workshop organizers, mass spectrometry tutorial organizers and chair (Brian Musselman), poster session chair (Herman Bierbaum) and the ASMS office staff for all of their hard work

Vice President for Arrangements' Report (Brian Musselman)

The presentation from the Vice President for Arrangements confirmed that Portland, OR will be the site of our next meeting in 1996 (May 12-16, 1996). The Conference dates were presented, along with the identities of the cities for future meetings Those cities included: Palm Springs, CA which replaces Kansas City (June 1-6, 1997); Orlando, FL (May 31-June 5, 1998) and the newest site, Dallas, TX (June 13-18, 1999).

Ms. Carol Gibbs, a representative of the Portland Oregon Visitors Association, made a short presentation on the virtues of Portland at our meeting site. She encouraged the members to attend the 1996 Meeting and include time for a vacation in Oregon

Members-at-Large for Measurements and Standards' Report (Sharon Lias)
Meeting of the Measurements and Standards Committee

The Measurements and Standards Committee met at 12:30 p m. on Monday, May 22, in the Presidential Suite. Attending were Committee members: Sharon Lias (Chair), John Bartmess, Anne Giordani, James Little, Phil Price and guests Jane Gale (who will replace Anne Giordani in July) and Jack Henion (previous Chair).

Discussion included: (1) projected Committee work on again updating the list of keywords used in ASMS Conference abstracts (revisions to be submitted to Sharon Lias by August 1); (2) a discussion (led by Jack Henion) of an activity he initiated while on the Committee - the possible development of a generic "suggested" SOP for mass spectrometry; (3) the planned update of the 1991 ASMS article, "Standard Definitions of Terms Relating to Mass Spectrometry," and (4) a discussion (led by John Bartmess) about the problems brought about by the fact that thermodynamic conventions used by mass spectrometrists are non-standard. (Sharon Lias and John Bartmess will examine possible solution to the problem).

Meeting of the Sanibel Committee

The Sanibel Committee met at 12:30 p.m. on Tuesday, May 23, in the Vice Presidential Suite. Attending were Sanibel Committee members Rebecca O-Malley (Chair,), Lester Taylor (Budget Officer), Susan Graul, Thomas Covey, and Sharon Lias (representative to the ASMS Board and Secretary), as well as 1996 Meeting Organizers Jonathan Amster and Jennifer Brodbelt. Details of the 8th Sanibel Conference on "Metal Containing Ions and Their Applications in Mass Spectrometry" were discussed with the organizers All planning appears to be on schedule, with a complete list of speakers and topics already available, with a preliminary budget in preparation.

The Business Meeting of the Sanibel Conference Committee followed, with the Committee choosing Ion Traps as the subject to be proposed to the ASMS Board for the 1997 Sanibel Conference. A list of possible organizers was drawn up, and Lester Taylor, as the new Chair of

the Committee, will line up organizers for the conference once the topic has been approved by the Board.

At the end of the meeting, Rebecca O'Malley stepped down as Chair of the Committee. Lester Taylor is the new Chair and Susan Graul is the new Budget Officer.

Members-at-Large for Education Report (Robert Boyd)

The major undertakings of the Education Committee are the Fall Workshop and the Short Courses offered prior to the Annual Conference. In 1994, the subject of the Fall Workshop was "Good Laboratory Practices for Mass Spectrometry," organized by Jack Henion. This turned out to be a highly successful workshop, reflecting current concerns of the mass spectrometry community involved in activities regulated by the EPA and, in particular, by the FDA. A report of this Workshop has been submitted for publication in *JASMS*. Four Short Courses were offered prior to the 1995 conference in Atlanta, namely "GC/MS for Environmental Analysis," "Interpretation of Mass Spectra," "Practical MS/MS," and "Liquid Chromatography - Mass Spectrometry." The dates for the Fall Workshop are October 13 and 14, 1995 and will be held at the Ramada Hotel in Alexandria, VA. The Committee thanks all those colleagues who contributed to the success of the 1994 Workshop and of the 1995 Short Courses. The subject of the 1995 Fall Workshop will be "Capillary Electrophoresis- Mass Spectrometry," to be organized by Pierre Thibault. New Short Courses for 1996 will include one on biological applications of mass spectrometry and one on ion optics

Member-at-Large for Publications' Report (Mark Ross)

The Member-at-Large (MAL) position for the *Proceedings* on the ASMS Board of Directors has changed and will now be referred to as MAL for Publications. The responsibilities of this position have been expanded beyond that for the extended abstracts, which are published in the *Proceedings*. The new duties include assisting the Society Office with Society publications such as announcements, brochures and the *Spektaker*. Second, this MAL will be responsible for identifying, developing and disseminating pre- and post - conference publicity. Finally, the MAL will serve as the liaison between the ASMS Board and *JASMS* The liaison efforts will focus on working with ASMS Board and *JASMS* Editor, with Society Member suggestions, to make efficient use of *JASMS* for Society information, encourage contributions and in general enhance the connections between the Society and the *Journal*.

***JASMS* Editor-in-Chief's Report (Mike Gross)**

Mike Gross briefly reviewed the status of *JASMS* and pointed to a number of reasons why Members should publish their work in the Society's *Journal*. These included the widespread circulation (>4,000 copies) and modest institutional subscription rate ($326 for 1995). *JASMS* is a journal of wide scope which has grown from 6 issues per year to 12 at present. Gross noted that the number of submissions continues to increase steadily, and the ISI Impact Factor of *JASMS* in its field is second only to *Analytical Chemistry*.

Secretary's Report (Tom Baillie)

The Secretary announced the result of the elections for the three Board positions which will become vacant on July 1, 1995. The new board members are Hee-Yong Kim (Secretary), Charles McEwen (Vice President for Arrangements) and Anne Giordani (Member-at-Large for Publications). A motion was made by President Enke to accept these candidates for office, and was seconded by past President Fales. The vote was unanimous in favor of the motion The Secretary then thanked the unsuccessful candidates for their willingness to stand for election, and members of the Nominating Committee for their efforts in connection with the election.

Following the above reports, President Enke thanked and made a presentation to each of the outgoing Board Members, (Brian Musselman, VP for Arrangements; Tom Baillie, secretary; and Mark Ross, MAL for Publications), and also acknowledged the efforts of Judith Sjoberg and her staff at the ASMS office for their continued outstanding service to the Society President Enke then introduced the winner of the ASMS Research Award (Kermit Murray), made possible by a generous grant from Finnigan Corporation (award presented by Phil Warren), and the ASMS and Corporate Member Research Award (Lee Sunderlin), which was funded by contributions from a number of ASMS Corporate Members and the Society itself. These presentations were followed by the announcement of Student Travel Awards (of which there were 24 this year) and of the Best Student Paper Awards for articles published in the *International Journal of Mass Spectrometry and Ion Processes* The recipients of the latter awards (sponsored jointly by Elsevier and Finnigan) were Matthias Wilm and Massimiliano Aschi (award presented by Mike Bowers and Egbert van Wezenbeek).

Finally, President Enke called for any new business There being none, the Meeting was formally closed at 9:05 a.m.